DOC.20080312.0001

QA: QA

MDL-WIS-PA-000005 REV00

January 2008

Total System Performance Assessment Model/Analysis for the License Application

Volume I

THIS DOCUMENT CONTAINS THE FOLLOWING, LOCATED AT THE BACK OF THE DOCUMENT:
1) ADDENDUM 001, DATED 03/11/2008

Prepared for:
U.S. Department of Energy
Office of Civilian Radioactive Waste Management
Office of Repository Development
1551 Hillshire Drive
Las Vegas, Nevada 89134-6321

Prepared by:
Sandia National Laboratories
OCRWM Lead Laboratory for Repository Systems
1180 Town Center Drive
Las Vegas, Nevada 89144

Under Contract Number
DE-AC04-94AL85000

DISCLAIMER

This report was prepared as an account of work sponsored by an agency of the United States Government. Neither the United States Government nor any agency thereof, nor any of their employees, nor any of their contractors, subcontractors or their employees, makes any warranty, express or implied, or assumes any legal liability or responsibility for the accuracy, completeness, or any third party's use or the results of such use of any information, apparatus, product, or process disclosed, or represents that its use would not infringe privately owned rights. Reference herein to any specific commercial product, process, or service by trade name, trademark, manufacturer, or otherwise, does not necessarily constitute or imply its endorsement, recommendation, or favoring by the United States Government or any agency thereof or its contractors or subcontractors. The views and opinions of authors expressed herein do not necessarily state or reflect those of the United States Government or any agency thereof.

QA: QA

Total System Performance Assessment Model/Analysis for the License Application

Volume I

MDL-WIS-PA-000005 REV00

January 2008

Sandia National Laboratories

Model Signature Page/Change History

Complete only applicable items.

1. Total Pages: ~3,500

2. Type of Mathematical Model

☐ Process Model ☐ Abstraction Model ☒ System Model

Describe Intended Use of Model

The TSPA-LA Model is intended to be used for postclosure total system analyses for the License Application.

3. Title

Total System Performance Assessment Model/Analysis for the License Application

4. DI (including Rev. No.):

MDL-WIS-PA-000005 REV00

	Printed Name	Signature	Date
5. Originator	TSPA Department	Jerry A McNeish	1/31/08.
6. Independent Technical Reviewer	Mel Marietta	M. L. Marietta	1/31/08
7. Checker	Robert Zimmerman (Lead)	R. S. Zimmerman	1/31/08
8. QCS	John Devers (Lead)	John R Devers	02/01/08
9. Responsible Manager/Lead	Jerry McNeish	Jerry A McNeish	2/1/08.
10. Responsible Manager	Kathryn Knowles	K. Knowles	2/1/08

11. Remarks

This document is comprised of 3 Volumes.

Change History

12. Revision No.	13. Description of Change

INTENTIONALLY LEFT BLANK

ACKNOWLEDGEMENTS

This work was performed in an environment that required close coordination, cooperation, communication, and teamwork. The effort cuts across organizational boundaries, discipline boundaries, geographic boundaries, and cultural boundaries. The team that created and produced the TSPA-LA Model/Analysis for the License Application document consisted of analysts, authors, checkers, reviewers, graphic specialists, technical editors, word processing specialists, reference checkers, and other technical support staff.

The outcome is a direct result of the long and hard hours the team devoted to the development of this product. The dedication demonstrated by the team enabled the production of a high-quality product under very tight deadlines and, therefore, is acknowledged.

Sincere thanks go to the following contributors:

AUTHORS
R. Baca
A. Behie
K. Brooks
B. Bullard
Y. Chen
V. Chipman
T. Dale
N. Deeds
J. Groves
T. Hadgu
C. Hansen
J. Helton
W. Hintze
S. Hommel
K. P. Lee
B. Lester
M. Lord
R. MacKinnon
P. Mattie
J. McNeish
S. Mehta
D. Miller
S. Miller
J. Min
S. Mishra
B. Mukhopadhyay
M. Nutt
L. Pincock
C. Sallaberry
G. Saulnier
S. D. Sevougian
R. Senger
A. Smith
W. Statham
C. Stockman
C. Thom
K. Turnham
P. Vo.
Y. Wang
E. Zwahlen

CHECKERS
R. Zimmerman–Checker Lead
J. Devers–QCS Lead
B. Arnold
C. Beach
S. Darnell
J. Cunnane
R. Dockter
J. Duguid
M. Gross
C. Haukwa
K. Helean
J. Houseworth
G. Keating
J. Lee
J. Leem
P. Mariner
S. Mishra
B. Mitcheltree
W. Mitcheltree
D. Mohr
K. Mon
J. Pickens
B. RamaRao
B. Robinson
D. Sassani
J. Schreiber
A. Smith
R. Spencer
C. Stockman

REVIEWERS
P. Brady (EBS)
N. Brown (WP)
R. Finch (EBS)
S. Finsterle (NS)
D. Franklin (Navy)
E. Hardin (NFE)
C. Ho (NS)
C. Howard (ES)
J. Linhart (DOE-EM)
H. Loo (DOE-EM)
M. Marietta (ITR)
P. Nair (Licensing)
L. Price (FEPs)
R. Quittmeyer (Seismic)
G. Valentine (Igneous)
M. Zhu (PASIT)

TECHNICAL/MGMT REVIEWERS
K. Knowles
J. McNeish
S. D. Sevougian
P. Swift

SHAREPOINT/FILE MGMT
D. Miller–Document Coordinator
L. Winzer

GRAPHIC COORD/PRODUCTION
D. Miller - Lead
R. Danat
K. Loo
R. McKinley
J. Sandgren
R. Sandgren
J. Scott
D. Young

DOCUMENT PRODUCTION
D. Miller-TSPA Production Lead
C. Beglinger
P. Gibson
V. Kelly
D. Nurse
M. Shrivastava
L. Winzer

CONTENTS

Page

ACKNOWLEDGMENTS v

ES1. SCOPE ES-1
ES1.1 Introduction ES-1
ES1.2 Governing Regulations ES-2
ES2. TOTAL SYSTEM PERFORMANCE ASSESSMENT METHODOLOGY ES-3
ES3. TSPA-LA MODEL DEVELOPMENT PROCESS ES-5
ES3.1 Features, Events, and Processes Analysis ES-5
ES3.2 Development of the Scenario Classes ES-6
ES3.3 Incorporation of Uncertainty ES-7
ES3.4 Natural and Engineered Model Components ES-8
ES3.5 Alternative Conceptual Models ES-8
ES3.6 Configuration Management for the TSPA-LA Model ES-9
ES4. YUCCA MOUNTAIN SITE DESCRIPTION ES-10
ES4.1 Physiographic Setting and Topography ES-10
ES4.2 Climate ES-10
ES4.3 Geology ES-11
ES4.4 Regional Tectonic Setting ES-11
ES4.5 Local Volcanism ES-11
ES4.6 Hydrology ES-12
ES5. THE REPOSITORY SUBSURFACE FACILITY AND ENGINEERED BARRIER SYSTEM ES-12
ES5.1 Layout ES-12
ES5.2 Engineered Barrier System ES-13
ES6. NATURAL AND ENGINEERED BARRIERS ES-15
ES6.1 Upper Natural Barrier ES-16
ES6.2 Engineered Barrier System ES-17
ES6.3 Lower Natural Barrier ES-20
ES7. GENERAL DESCRIPTION OF THE TSPA-LA MODEL ES-22
ES7.1 Model Components for the Nominal Scenario Class Modeling Case ES-22
ES7.2 Model Components for the Early Failure Scenario Class ES-24
ES7.3 Model Components for the Disruptive Events Scenario Classes ES-26
ES7.4 TSPA Input Database ES-28
ES8. VERIFICATION/VALIDATION OF THE TOTAL SYSTEM PERFORMANCE ASSESSMENT MODEL ES-29
ES8.1 Verification and Validation Strategy ES-29
ES8.2 Computer Code and Input Verification ES-30
ES8.3 Stability Testing ES-31
ES8.4 Uncertainty Characterization Reviews ES-32
ES8.5 Surrogate Waste Form Validation ES-34
ES8.6 Corroboration of Abstraction Model Results with Validated Process Models ES-34
ES8.7 Auxiliary Analyses ES-35

CONTENTS (Continued)

Page

ES8.8 Confidence Building: Natural Analogues ES-37
ES8.9 Summary of Technical Reviews ES-38
ES9. SYSTEM PERFORMANCE ANALYSES ES-40
ES9.1. Total Mean Annual Dose to the Reasonably Maximally Exposed Individual for the Repository System ES-40
ES9.2. Results of the Scenario Class Modeling Case Simulations ES-40
ES9.3 Comparison of Annual Dose with Postclosure Individual and Groundwater Protection Standards ES-45
ES9.4. Human Intrusion ES-47
ES10. SUMMARY OF THE RESULTS OF THE TSPA-LA MODEL ES-47

1. PURPOSE 1-1
1.1 INTRODUCTION 1-1
1.1.1 Governing Regulations 1-1
1.1.2 Total System Performance Assessment Methodology 1-6
1.1.3 Treatment of Uncertainty 1-8
1.2 TSPA-LA MODEL DEVELOPMENT PROCESS 1-8
1.2.1 Features, Events, and Processes Analysis 1-9
1.2.2 Development of the Scenario Classes 1-9
1.2.3 Incorporation of Uncertainty 1-10
1.2.4 Alternative Conceptual Models 1-11
1.2.5 Configuration Management for the TSPA-LA Model 1-11
1.3 YUCCA MOUNTAIN SITE DESCRIPTION 1-13
1.3.1 Physiographic Setting and Topography 1-13
1.3.2 Climate and Precipitation 1-14
1.3.3 Geology 1-15
1.3.4 Hydrogeology 1-17
1.4 DESIGN OF YUCCA MOUNTAIN REPOSITORY SUBSURFACE FACILITIES 1-18
1.4.1 Repository Layout 1-19
1.4.2 Features of the Engineered Barrier System 1-19
1.4.3 Waste Emplacement Approach 1-21
1.5 GENERAL DESCRIPTION OF THE TSPA-LA MODEL 1-21
1.5.1 Model Components and Modeling Case for the Nominal Scenario Class 1-22
1.5.2 Model Components and Modeling Cases for the Early Failure Scenario Class 1-24
1.5.3 Model Components and Modeling Cases for the Igneous Scenario Class 1-25
1.5.4 Model Components and Modeling Cases for the Seismic Scenario Class 1-27
1.5.5 Model Components for the Human Intrusion Scenario 1-28

CONTENTS (Continued)

Page

1.6 CONCEPTUAL DESCRIPTION OF PROCESSES RELEVANT TO AN EVALUATION OF POSTCLOSURE PERFORMANCE IN THE ABSENCE OF DISRUPTIVE EVENTS 1-28
1.6.1 Water Movement in the Unsaturated Tuffs above the Repository 1-29
1.6.2 Water and Water Vapor Movement around the Repository Drifts 1-30
1.6.3 Water Movement and Radionuclide Transport within and through the Engineered Barrier System 1-32
1.6.4 Water Movement and Radionuclide Transport through the Unsaturated Tuffs below the Repository 1-34
1.6.5 Water Movement and Radionuclide Transport through the Saturated Zone Aquifers to the Biosphere 1-35
1.7 CONCEPTUAL DESCRIPTION OF PROCESSES RELEVANT TO AN EVALUATION OF POSTCLOSURE PERFORMANCE AFTER THE OCCURRENCE OF DISRUPTIVE EVENTS 1-36
1.7.1 Water Movement in the Unsaturated Tuffs above the Repository 1-36
1.7.2 Water Movement around the Repository Drifts 1-37
1.7.3 Water Movement and Radionuclide Transport within and through the Engineered Barrier System 1-37
1.7.4 Water Movement and Radionuclide Transport through the Unsaturated Tuffs below the Repository 1-39
1.7.5 Water Movement and Radionuclide Transport through the Saturated Zone Aquifers to the Biosphere 1-39
1.7.6 Atmospheric Transport and Redeposition of Radionuclides 1-39
1.8 CONSERVATISMS AND LIMITATIONS RELATED TO THE TSPA-LA MODEL 1-40
1.8.1 Conservatisms Incorporated in the TSPA-LA Model 1-40
1.8.2 Limitations of the TSPA-LA Model 1-42
1.9 DESCRIPTION OF THE TOTAL SYSTEM PERFORMANCE ASSESSMENT MODEL/ANALYSIS FOR THE LICENSE APPLICATION 1-48
1.10 DOCUMENT ORGANIZATION 1-50
1.10.1 Volume I 1-50
1.10.2 Volume II 1-51
1.10.3 Volume III 1-52

2. QUALITY ASSURANCE 2-1
2.1 CONFIGURATION MANAGEMENT 2-1
2.1.1 Configuration Management of Software 2-2
2.1.2 Configuration Management of the Development of the TSPA-LA Model 2-2
2.1.3 Configuration Management for the TSPA-LA Model Input 2-6
2.2 MODEL VALIDATION 2-7

3. USE OF SOFTWARE 3-1
3.1 INTRODUCTION 3-2

CONTENTS (Continued)

Page

3.2 ASHPLUME_DLL_LA 3-3
3.2.1 Description of Software 3-3
3.2.2 Relationship to the TSPA-LA Model 3-3
3.2.3 Software Documentation 3-3
3.2.4 Range of Validation 3-3
3.3 CWD 3-4
3.3.1 Description of Software 3-4
3.3.2 Relationship to the TSPA-LA Model 3-4
3.3.3 Software Documentation 3-4
3.3.4 Range of Validation 3-4
3.4 EXDOC_LA 3-4
3.4.1 Description of Software 3-4
3.4.2 Relationship to the TSPA-LA Model 3-5
3.4.3 Software Documentation 3-5
3.4.4 Range of Validation 3-5
3.5 FAR 3-5
3.5.1 Description of Software 3-5
3.5.2 Relationship to the TSPA-LA Model 3-5
3.5.3 Software Documentation 3-6
3.5.4 Range of Validation 3-6
3.6 FEHM 3-6
3.6.1 Description of Software 3-6
3.6.2 Relationship to the TSPA-LA Model 3-6
3.6.3 Software Documentation 3-6
3.6.4 Range of Validation 3-7
3.7 GETTHK_LA 3-7
3.7.1 Description of Software 3-7
3.7.2 Relationship to the TSPA-LA Model 3-7
3.7.3 Software Documentation 3-7
3.7.4 Range of Validation 3-7
3.8 GOLDSIM 3-8
3.8.1 Description of Software 3-8
3.8.2 Relationship to the TSPA-LA Model 3-8
3.8.3 Software Documentation 3-8
3.8.4 Range of Validation 3-8
3.9 INTERPZDLL_LA 3-9
3.9.1 Description of Software 3-9
3.9.2 Relationship to the TSPA-LA Model 3-9
3.9.3 Software Documentation 3-9
3.9.4 Range of Validation 3-9
3.10 MFCP_LA 3-10
3.10.1 Description of Software 3-10
3.10.2 Relationship to the TSPA-LA Model 3-10
3.10.3 Software Documentation 3-10

CONTENTS (Continued)

Page

3.10.4 Range of Validation 3-10
3.11 MKTABLE AND MKTABLE_LA 3-11
3.11.1 Description of Software 3-11
3.11.2 Relationship to the TSPA-LA Model 3-11
3.11.3 Software Documentation 3-11
3.11.4 Range of Validation 3-11
3.12 MVIEW 3-12
3.12.1 Description of Software 3-12
3.12.2 Relationship to the TSPA-LA Model 3-12
3.12.3 Software Documentation 3-12
3.12.4 Range of Validation 3-12
3.13 PASSTABLE1D_LA 3-12
3.13.1 Description of Software 3-12
3.13.2 Relationship to the TSPA-LA Model 3-13
3.13.3 Software Documentation 3-13
3.13.4 Range of Validation 3-13
3.14 PASSTABLE3D_LA 3-13
3.14.1 Description of Software 3-13
3.14.2 Relationship to the TSPA-LA Model 3-13
3.14.3 Software Documentation 3-14
3.14.4 Range of Validation 3-14
3.15 PREWAP_LA 3-14
3.15.1 Description of Software 3-14
3.15.2 Relationship to the TSPA-LA Model 3-14
3.15.3 Software Documentation 3-14
3.15.4 Range of Validation 3-14
3.16 SCCD 3-15
3.16.1 Description of Software 3-15
3.16.2 Relationship to the TSPA-LA Model 3-15
3.16.3 Software Documentation 3-15
3.16.4 Range of Validation 3-15
3.17 SEEPAGEDLL_LA 3-16
3.17.1 Description of Software 3-16
3.17.2 Relationship to the TSPA-LA Model 3-16
3.17.3 Software Documentation 3-16
3.17.4 Range of Validation 3-16
3.18 SOILEXP_LA 3-17
3.18.1 Description of Software 3-17
3.18.2 Relationship to the TSPA-LA Model 3-17
3.18.3 Software Documentation 3-17
3.18.4 Range of Validation 3-17
3.19 SZ_CONVOLUTE 3-17
3.19.1 Description of Software 3-17
3.19.2 Relationship to the TSPA-LA Model 3-18

CONTENTS (Continued)

Page

3.19.3 Software Documentation 3-18
3.19.4 Range of Validation 3-18
3.20 TSPA_INPUT_DB 3-18
3.20.1 Description of Software 3-18
3.20.2 Relationship to the TSPA-LA Model 3-18
3.20.3 Software Documentation 3-19
3.20.4 Range of Validation 3-19
3.21 WAPDEG 3-19
3.21.1 Description of Software 3-19
3.21.2 Relationship to the TSPA-LA Model 3-19
3.21.3 Software Documentation 3-19
3.21.4 Range of Validation 3-20
3.22 CORROBORATIVE SOFTWARE USED 3-20

4. INPUTS 4-1
4.1 DIRECT INPUTS 4-1
4.2 TSPA-LA MODEL GENERATED PARAMETERS 4-2
4.3 PARAMETER ENTRY FORMS 4-2
4.4 TRACEABILITY OF INPUTS 4-3
4.5 CRITERIA 4-4
4.6 CODES AND STANDARDS 4-4
4.7 TSPA INPUT DATABASE 4-4
4.7.1 Database Structure 4-5
4.7.2 Database Operation Login 4-5
4.7.3 Parameter Identification Form 4-5
4.7.4 Parameter Documentation Form 4-6
4.7.5 Parameter Value Entry Form 4-6
4.7.6 Parameter Entry Form Information Entry Form 4-6
4.7.7 Parameter Verification Form 4-6
4.7.8 Database Reports 4-7
4.7.9 Database Support of GoldSim 4-8

5. ASSUMPTIONS 5-1
5.1 NOMINAL SCENARIO CLASS 5-1
5.1.1 Unsaturated Zone Flow 5-1
5.1.2 Engineered Barrier System Environment 5-2
5.1.3 Waste Form Degradation and Mobilization 5-4
5.1.4 Engineered Barrier System Flow and Transport 5-4
5.1.5 Unsaturated Zone Transport 5-6
5.1.6 Saturated Zone Flow and Transport 5-6
5.1.7 Biosphere 5-7
5.2 EARLY FAILURE SCENARIO CLASS 5-7
5.2.1 Drip Shield Early Failure Modeling Case 5-7
5.2.2 Waste Package Early Failure Modeling Case 5-8
5.3 IGNEOUS SCENARIO CLASS 5-8

CONTENTS (Continued)

Page

5.3.1 Igneous Intrusion Modeling Case 5-8
5.3.2 Volcanic Eruption Modeling Case 5-9
5.4 SEISMIC SCENARIO CLASS 5-10
5.5 HUMAN INTRUSION SCENARIO 5-11

6. TSPA-LA MODEL DESCRIPTION 6-1
6.1 CONCEPTUAL DESIGN 6.1-1
6.1.1 Features, Events, and Processes Screening and Scenario Development 6.1.1-1
6.1.2 Calculation of Dose for the TSPA-LA Model 6.1.2-1
6.1.3 Treatment of Uncertainty in the TSPA-LA Model 6.1.3-1
6.1.4 TSPA-LA Model Structure and Design 6.1.4-1
6.1.5 TSPA-LA Model File Architecture 6.1.5-1
6.2 ALTERNATIVE CONCEPTUAL MODELS 6.2-1
6.3 TSPA-LA MODEL FOR THE NOMINAL SCENARIO CLASS 6.3-1
6.3.1 Mountain-Scale Unsaturated Zone Flow 6.3.1-1
6.3.2 Engineered Barrier System Thermal-Hydrologic Environment 6.3.2-1
6.3.3 Drift-Scale Unsaturated Zone Flow 6.3.3-1
6.3.4 Engineered Barrier System Chemical Environment 6.3.4-1
6.3.5 Waste Package and Drip Shield Degradation 6.3.5-1
6.3.6 Engineered Barrier System Flow 6.3.6-1
6.3.7 Waste Form Degradation and Mobilization 6.3.7-1
6.3.8 Engineered Barrier System Transport 6.3.8-1
6.3.9 Unsaturated Zone Transport 6.3.9-1
6.3.10 Saturated Zone Flow and Transport Model Component 6.3.10-1
6.3.11 Biosphere 6.3.11-1
6.4 TSPA-LA MODEL FOR THE EARLY FAILURE SCENARIO CLASS 6.4-1
6.4.1 Drip Shield Early Failure Modeling Case 6.4-2
6.4.2 Waste Package Early Failure Modeling Case 6.4-5
6.4.3 Treatment of Uncertainty 6.4-7
6.4.4 Model Component Consistency and Conservatisms in Assumptions and Parameters 6.4-7
6.5 TSPA-LA MODEL FOR THE IGNEOUS SCENARIO CLASS 6.5-1
6.5.1 Igneous Intrusion Modeling Case 6.5-2
6.5.2 Volcanic Eruption Modeling Case 6.5-10
6.6 TSPA-LA MODEL FOR THE SEISMIC SCENARIO CLASS 6.6-1
6.6.1 TSPA-LA Model Components and Submodels for the Seismic Scenario Class 6.6-2
6.6.2 Interaction of Seismic Scenario Class Submodels with other TSPA-LA Submodels 6.6-31
6.6.3 Model Component Consistency and Conservatisms in Assumptions and Parameters 6.6-35
6.6.4 Alternative Conceptual Model(s) for Seismic Scenario Modeling Cases 6.6-37

CONTENTS (Continued)

Page

6.7 TSPA-LA MODEL FOR THE HUMAN INTRUSION SCENARIO 6.7-1
6.7.1 TSPA-LA Model Components and Submodels for the Human Intrusion Scenario 6.7-2
6.7.2 Evaluation of the Earliest Time of Waste Package Penetration by Human Intrusion 6.7-3
6.7.3 TSPA-LA Model Implementation 6.7-17
6.7.4 Model Component Consistency and Conservatism in Assumptions and Parameters 6.7-22
6.7.5 Alternative Conceptual Model(s) for the Human Intrusion Scenario for TSPA-LA 6.7-23

FIGURES

Page

ES-1. Yucca Mountain Area FES-1
ES-2. Timeline of Legislative and Regulatory Events: 1980 to 2010 ..... FES-2
ES-3. Structure of the Process of the TSPA-LA FES-3
ES-4. Major Steps in a Generic Performance Assessment FES-4
ES-5. Iterative Application of the TSPA Process FES-5
ES-6. Performance Assessment Pyramid Showing the Steps Involved in Developing a Total System Model FES-6
ES-7. Schematic of Attributes of Repository Performance FES-7
ES-8. Schematic Representation of the Development of the TSPA-LA Model, Including the Nominal, Igneous, and Seismic Scenario Classes FES-8
ES-9. TSPA-LA Principal Model Components and Submodels FES-9
ES-10. Principal Components of the Yucca Mountain Repository System FES-10
ES-11. Geographic and Prominent Topographic Features of the Death Valley Region FES-11
ES-12. Topographic Map of the Yucca Mountain Site Showing in Slope Characteristics FES-12
ES-13. Overall Water Flow Behavior in the Unsaturated Zone, Including the Relative Flux Magnitudes of Fracture and Matrix Flow Components in the Different Hydrogeologic Units FES-13
ES-14. Distribution of Faults in the Yucca Mountain Site Area and Adjacent Areas to the South and West FES-14
ES-15. East-West Structure Section across Yucca Mountain Site Area FES-15
ES-16. Location and Age of Post-Miocene (less than 5.3 million years) Volcanoes (or clusters where multiple volcanoes have indistinguishable ages) in the Yucca Mountain Region FES-16
ES-17. Regional Map of the Saturated Zone Flow System Showing Direction of Flow and Outline of the 3-D Saturated Zone Site-Scale Flow Model Domain FES-17
ES-18. Subsurface Facility Layout FES-18
ES-19. Cross-Section Illustration of the EBS FES-19
ES-20. Conceptual Drawing of Mountain-Scale Flow Processes FES-20
ES-21. Illustration of the Four Climate Periods Used in the TSPA-LA Model and the Analogues for the Monsoon and Glacial-Transition Climates FES-21
ES-22. Schematic Illustration (not to scale) of Thermal-Hydrologic Processes in the Vicinity of the Emplacement Drifts Due to Repository Heating FES-22
ES-23. General EBS Design Features and Materials, Water Movement, and Drift Degradation FES-23
ES-24. Conceptual Drawing of Unsaturated Zone Transport Processes FES-24
ES-25. Conceptualization of Features and Processes Important to Saturated Zone Transport FES-25
ES-26. Schematic Design of the Drip Shield and Waste Package FES-26
ES-27. Three Waste Types Grouped into Two Representative Waste Packages: CSNF and CDSP WPs FES-27
ES-28. Schematic of CSNF Waste Form Degradation Mechanisms at Various Scales FES-28

FIGURES (Continued)

Page

ES-29. Overview of the Biosphere Groundwater Scenario Showing Groundwater Transport of Radionuclides and Uptake by the RMEI FES-29
ES-30. Schematic Diagram of the Intersection of an Igneous Dike with the Repository and Waste Packages FES-30
ES-31. Schematic Representation of a Volcanic Eruption at Yucca Mountain Showing Transport of Radioactive Waste in a Tephra Plume FES-31
ES-32. Model Validation Approach for the TSPA-LA Model FES-32
ES-33. Stability of Seismic Ground Motion Modeling Case for 20,000 Years: (a) Comparison of Expected Annual Dose for Three Replicates and (b) Confidence Interval Around Mean Annual Dose FES-33
ES-34. Expected Annual Dose Over 20,000 Years for Seismic Ground Motion Modeling Case Considering Additional Specified Event Times and Damage Fractions FES-34
ES-35. Annual Dose from a Seismic Ground Motion Event at 1,000 Years with Damage Fraction 10^{-6} for Three Timestep Schemes FES-35
ES-36. Comparison of Ash-Fall Thickness at Cerro Negro with ASHPLUME Simulated Results FES-36
ES-37. Location of Peña Blanca Nopal I Ore Deposit in the Sierra Peña Blanca FES-37
ES-38. Geologic Characterization of Nopal 1 Ore Body FES-38
ES-39. Uranium Concentration Determined in Groundwater Samples from Wells at and near the Nopal I Ore Deposit FES-39
ES-40. Total Expected Annual Dose for 10,000 Years after Closure FES-40
ES-41. Total Expected Annual Dose for 1,000,000 Years after Closure FES-41
ES-42. Contribution of Individual Radionuclides to Total Mean Annual Dose for 10,000 Years after Repository Closure FES-42
ES-43. Contribution of Individual Radionuclides to Total Mean Annual Dose for 1,000,000 Years after Repository Closure FES-43
ES-44. Annual Dose for the Nominal Scenario Class Modeling Case for the Post-10,000-Year Period FES-44
ES-45. Mean Annual Dose Contributions from Major Radionuclides for the Nominal Scenario Class Modeling Case for the Post-10,000-Year Period FES-45
ES-46. Expected Annual Dose for the Drip Shield Early Failure Modeling Case for (a) the First 10,000 Years after Repository Closure and (b) Post-10,000-Year Period FES-46
ES-47. Mean Annual Dose Contributions from Major Radionuclides for the Drip Shield Early Failure Modeling Case for (a) the First 10,000 Years after Repository Closure and (b) Post-10,000-Year Period FES-47
ES-48. Expected Annual Dose for the Waste Package Early Failure Modeling Case (a) the First 10,000 Years after Repository Closure and (b) Post-10,000-Year Period FES-48
ES-49. Mean Annual Dose Contributions from Major Radionuclides for the Waste Package Early Failure Modeling Case for (a) the First 10,000 Years after Repository Closure and (b) Post-10,000-Year Period FES-49

FIGURES (Continued)

Page

ES-50. Expected Annual Dose for the Igneous Intrusion Modeling Case for (a) 10,000 Years after Repository Closure and (b) Post-10,000-Year Period FES-50
ES-51. Mean Annual Dose Contributions from Major Radionuclides for the Igneous Intrusion Modeling Case for (a) the First 10,000 Years after Repository Closure and (b) Post-10,000-Year Period FES-51
ES-52. Expected Annual Dose for the Volcanic Eruption Modeling Case for (a) 10,000 Years after Repository Closure and (b) Post-10,000-Year Period FES-52
ES-53. Mean Annual Dose Contributions from Major Radionuclides for the Volcanic Eruption Modeling Case for (a) the First 10,000 Years after Repository Closure and (b) Post-10,000-Year Period FES-53
ES-54. Expected Annual Dose for the Seismic Ground Motion Modeling Case for (a) 10,000 Years after Repository Closure and (b) Post-10,000-Year Period FES-54
ES-55. Mean Annual Dose Contributions from Major Radionuclides for the Seismic Ground Motion Modeling Case for (a) the First 10,000 Years after Repository Closure and (b) Post-10,000-Year Period FES-55
ES-56. Expected Annual Dose for the Seismic Fault Displacement Modeling Case for (a) 10,000 Years after Repository Closure and (b) Post-10,000-Year Period FES-56
ES-57. Mean Annual Dose Contributions from Major Radionuclides for the Seismic Fault Displacement Modeling Case for (a) 10,000 Years after Repository Closure and (b) Post-10,000-Year Period FES-57
ES-58. Total Mean Annual Dose and Median Annual Doses for Each Modeling Case for (a) 10,000 Years after Repository Closure and (b) Post-10,000-Year Period.. FES-58
ES-59. Combined ^{226}Ra and ^{228}Ra Activity Concentrations, Excluding Natural Background, for Likely Features, Events, and Processes Using Nominal, Early Failure, and Seismic Ground Motion Damage Processes FES-59
ES-60. Combined Activity Concentrations of All Alpha Emitters (including ^{226}Ra but without radon and uranium isotopes), Excluding Natural Background, for Likely Features, Events, and Processes Using Nominal, Early Failure, and Seismic Ground Motion Damage Processes FES-60
ES-61. Mean Annual Drinking Water Dose from Combined Beta and Photon Emitters for Likely Features, Events, and Processes using the Nominal, Early Failure, and Seismic Ground Motion Damage Processes FES-61
ES-62. Expected Annual Individual Dose at the RMEI Location from Human Intrusion 200,000 Years after Repository Closure FES-62

1-1. Performance Assessment Pyramid Showing the Steps Involved in Developing a Total System Model F1-1
1-2. Performance Assessment Pyramid Showing How Detailed Underlying Information Builds the Technical Basis for the TSPA-LA Model F1-2
1-3. Schematic Representation of the Development of the TSPA-LA Model, Including the Nominal, Igneous, and Seismic Scenario Classes F1-3
1-4. Geographic and Prominent Topographic Features of the Death Valley Region F1-4

FIGURES (Continued)

Page

1-5. Topographic Map of the Yucca Mountain Site Showing Differences in Slope Characteristics North and South of Drill Hole Wash....F1-5
1-6. Overall Water Flow Behavior in the Unsaturated Zone, Including the Relative Flux Magnitudes of Fracture and Matrix Flow Components in the Different Hydrogeologic Units....F1-6
1-7. Distribution of Faults in the Yucca Mountain Site Area and Adjacent Areas to the South and West....F1-7
1-8. East-West Structure Section across Yucca Mountain Site Area....F1-8
1-9. Location and Age of Post-Miocene (less than 5.3 million years) Volcanoes (or clusters where multiple volcanoes have indistinguishable ages) in the Yucca Mountain Region....F1-9
1-10. Subsurface Facility Layout....F1-10
1-11. Cross Section Illustration of the Engineered Barrier System....F1-11
1-12. Conceptual Drawing of Mountain-Scale Flow Processes....F1-12
1-13. Illustration of the Four Climate Periods Used in the TSPA-LA Model and Analogues for the Monsoon and Glacial-Transition Climates....F1-13
1-14. Schematic Design of the Drip Shield and Waste Package....F1-14
1-15. Three Waste Types Grouped into Two Representative Waste Packages: CSNF and CDSP WPs....F1-15
1-16. Schematic of CSNF Waste Form Degradation Mechanisms at Various Scales....F1-16
1-17. General EBS Design Features and Materials, Water Movement, and Drift Degradation....F1-17
1-18. Conceptualization of Unsaturated Zone Transport Processes....F1-18
1-19. Overview of the Biosphere Groundwater Scenario Showing Groundwater Transport of Radionuclides and Uptake by the RMEI....F1-19
1-20. Schematic Illustration of the Processes Affecting Ambient Drift Seepage....F1-20
1-21. Schematic Illustration (not to scale) of Thermal-Hydrologic Processes in the Vicinity of the Emplacement Drifts Due to Repository Heating....F1-21
1-22. Conceptualization of Features and Processes Important to Saturated Zone Transport....F1-22
1-23. TSPA-LA Principal Model Components and Submodels....F1-23

2-1. Flowchart Illustrating the Management Control Process for the TSPA-LA Model....F2-1
2-2. Example of the TSPA-LA Model Change Approval Form....F2-2
2-3. Example of the TSPA-LA Model Change Checklist....F2-3
2-4. Example of the TSPA-LA Model Implementation Checklist....F2-4
2-5. Example of the TSPA-LA Model Concept Checklist....F2-7

3-1. Hardware Configuration for TSPA-LA Modeling....F3-1
3-2. TSPA-LA Software Architecture....F3-2

4-1. Control of Information for TSPA-LA Model Development and Analysis....F4-1
4-2. Development and Revision of Parameter Entry Forms....F4-2

FIGURES (Continued)

Page

4-3. Structural Framework (Schema) for the TSPA Input Database Showing Relationships between Tables F4-3
4-4. Example of a Parameter Identification Form for the TSPA Input Database F4-4
4-5. Example of a Parameter Documentation Form for the TSPA Input Database F4-5
4-6. Example of a Parameter Value Entry Form for a One-Dimensional Data Table in the TSPA Input Database F4-6
4-7. Example of a PEF Information Entry Form in the TSPA Input Database F4-7
4-8. Example of a Parameter Verification Form for the TSPA Input Database F4-8

6-1. TSPA-LA Principal Model Components and Submodels F6-1

6.1.1-1. Steps in the Features, Events, and Processes Analysis and Scenario Selection Process F6.1.1-1
6.1.1-2. Schematic Illustration of the Features, Events, and Processes Analysis Method F6.1.1-2
6.1.1-3. Schematic Representation of the TSPA-LA Model Components for the Nominal Scenario Class F6.1.1-3
6.1.1-4. Schematic Representation of the TSPA-LA Model Components for the Early Failure Scenario Class F6.1.1-4
6.1.1-5. Schematic Representation of the TSPA-LA Model Components for the Igneous Intrusion Modeling Case F6.1.1-5
6.1.1-6. Schematic Representation of the TSPA-LA Model Components for the Volcanic Eruption Modeling Case F6.1.1-6
6.1.1-7. Schematic Representation of the TSPA-LA Model Components for the Seismic Scenario Class F6.1.1-7
6.1.1-8. Schematic Representation of the TSPA-LA Model Components for the Human Intrusion Scenario F6.1.1-8

6.1.4-1. Information Transfer Between the Model Components and Submodels of the TSPA-LA Nominal Scenario Class F6.1.4-1
6.1.4-2. Repository Percolation Subregions Used in the TSPA-LA Model (based upon the 10th percentile percolation flux case, glacial-transition climate) F6.1.4-2
6.1.4-3. Information Transfer Between the Model Components and Submodels of the TSPA-LA Early Failure Scenario Class F6.1.4-3
6.1.4-4. Information Transfer Between the Model Components and Submodels of the TSPA-LA Igneous Intrusion Modeling Case F6.1.4-4
6.1.4-5. Information Transfer Between the Submodels of the TSPA-LA Volcanic Eruption Modeling Case F6.1.4-5
6.1.4-6. Information Transfer Between the Model Components and Submodels of the TSPA-LA Seismic Scenario Class F6.1.4-6
6.1.4-7. Information Transfer Between the Model Components and Submodels of the TSPA-LA Human Intrusion Scenario F6.1.4-7

FIGURES (Continued)

Page

6.1.5-1. Illustrated Overview of all the Various Elements that Make Up the Framework for Initializing and Running the TSPA-LA Model F6.1.5-1
6.1.5-2. Illustration Depicting Elements Required for Loading of Initial Parameter Values and Dynamically Linked Libraries for the TSPA-LA Model F6.1.5-2
6.1.5-3. Illustration Depicting Elements Active When Information from the Multiscale Thermohydrologic Model is Preprocessed by PREWAP_LA F6.1.5-3
6.1.5-4. Illustration Depicting Elements Active When Preprocessing for the Localized Corrosion Initiation Analysis F6.1.5-4
6.1.5-5. Illustration Depicting Elements Active when Sampling of Uncertain Unsaturated Zone Parameters and Generation of Input Files F6.1.5-5
6.1.5-6. Illustration Depicting Elements Active in the Execution of the TSPA-LA GoldSim Model File and the TSPA-LA Volcanic Eruption GoldSim Model File F6.1.5-6
6.1.5-7. TSPA-LA Software Configuration Illustrating Software Run with GoldSim ... F6.1.5-7
6.1.5-8. Details of the Software Configuration for the Localized Corrosion Initiation Analysis F6.1.5-8
6.1.5-9. Layout of Calculation Containers that Define the Highest Level of Organization of the TSPA-LA Model File F6.1.5-9
6.1.5-10. Levels of Discretization of Engineered System Representation in the TSPA-LA Model File F6.1.5-10
6.1.5-11. Schematic of the Five Repository Percolation Subregions Showing the Implementation of the Levels of Discretization Shown on Figure 6.1.5-10 .... F6.1.5-11

6.3.1-1. Information Flow Diagram for the Mountain-Scale Unsaturated Zone Flow ... F6.3.1-1
6.3.1-2. Inputs, Outputs, and Basis for Model Confidence for the Climate Analysis F6.3.1-2
6.3.1-3. Illustration of the First Three Climate States Used in the TSPA-LA Model and the Analogues for the Monsoon and Glacial-Transition Climates F6.3.1-3
6.3.1-4. Inputs, Outputs, and Basis for Model Confidence for the Infiltration Model F6.3.1-4
6.3.1-5. Schematic Illustration Showing the Variation of Precipitation and Consequent Infiltration with Respect to Elevation at Yucca Mountain F6.3.1-5
6.3.1-6. Inputs, Outputs, and Basis for Model Confidence for the Site-Scale Unsaturated Zone Flow Process Model F6.3.1-6
6.3.1-7. Comparison of Net Infiltration, Percolation Flux at the Repository Horizon, and Percolation Flux at the Water Table in the Tenth Percentile Infiltration Scenario During the Glacial-Transition Climate State F6.3.1-7
6.3.1-8. General Stratigraphy at the Yucca Mountain Site Observed at Borehole SD-6 ..... F6.3.1-8

6.3.2-1. Information Flow Diagram for the EBS Thermal-Hydrologic Environment Submodel F6.3.2-1
6.3.2-2. Inputs, Outputs, and Basis for Model Confidence for the Multiscale Thermohydrologic Process Model F6.3.2-2
6.3.2-3. Inputs, Outputs, and Basis for Model Confidence for the EBS Thermal-Hydrologic Environment Submodel F6.3.2-3

FIGURES (Continued)

Page

6.3.2-4. The Distribution of the Four Primary Host-Rock Units is Shown for the Repository Layout Considered in the Multiscale Thermohydrologic Model Calculations for the TSPA-LA Model F6.3.2-4
6.3.2-5. Thermal-Hydrologic Conditions for the PWR1-2 Waste Package Plotted for 10th, 30th, 50th and 90th Percentile Percolation-Flux Cases at a Location near the Center of the Repository F6.3.2-5
6.3.2-6. Thermal-Hydrologic Conditions for the PWR1-2 Waste Packages Plotted for 10th Percentile Percolation Flux Case at a Location Near the Center of the Repository F6.3.2-6
6.3.2-7. Repository Percolation Subregions Used in the TSPA-LA Model (based upon the 30th percentile infiltration case, glacial-transition period) F6.3.2-7
6.3.2-8. Thermal-Hydrologic Time History Parameter Inputs to the TSPA-LA Model F6.3.2-8

6.3.3-1. Information Flow Diagram for the Drift Seepage and Drift Wall Condensation Submodels F6.3.3-1
6.3.3-2. Inputs, Outputs, and Basis for Model Confidence for the Drift Seepage Submodel F6.3.3-2
6.3.3-3. Schematic Illustration (not to scale) of Thermal-Hydrologic Processes in the Vicinity of the Emplacement Drifts Due to Repository Heating F6.3.3-3
6.3.3-4. Schematic Illustration of the Processes Affecting Ambient Drift Seepage F6.3.3-4
6.3.3-5. Procedure for Probabilistic Calculation of Seepage at Selected Timesteps in the TSPA-LA Model F6.3.3-5
6.3.3-6. Inputs, Outputs, and Basis for Model Confidence for the Drift Wall Condensation Submodel F6.3.3-6
6.3.3-7. Schematic Illustration of the Processes Affecting Drift-Wall Condensation F6.3.3-7
6.3.3-8. Schematic Depicting Approximate Locations of Disposal Drifts Chosen for Condensation Analysis F6.3.3-8

6.3.4-1. Information Flow Diagram for the EBS Chemical Environment Submodel F6.3.4-1
6.3.4-2. Inputs, Outputs, and Basis for Model Confidence for the EBS Chemical Environment Submodel F6.3.4-2
6.3.4-3. General EBS Design Features and Materials, Water Movement, and Drift Degradation F6.3.4-3
6.3.4-4. Schematic Diagram of EBS Flow Pathways (arrows) and Critical Locations (labels) F6.3.4-4

6.3.5-1. Schematic Design of the Drip Shield and Waste Package F6.3.5-1
6.3.5-2. Information Flow Diagram for Waste Package and Drip Shield Degradation F6.3.5-2
6.3.5-3. Inputs, Outputs, and Basis for Model Confidence for the Waste Package and Drip Shield Degradation Submodel F6.3.5-3

6.3.5-4. Schematic of Waste Package Implementation in the Waste Package Degradation Model Showing a Waste Package in a Dripping Environment

FIGURES (Continued)

Page

After a Drip Shield Failure and Patches Degrading from General Corrosion on the Surface of the Waste Package F6.3.5-4
6.3.5-5. Exposure Conditions and Degradation Processes for the Drip Shield and Waste Package F6.3.5-5
6.3.5-6. Effect of Scaling the General Corrosion Distribution by a Size Factor of Four F6.3.5-6
6.3.5-7. Schematic of Waste Package Closure Lid Design F6.3.5-7
6.3.5-8. Process and Data Flow for the Waste Package and Drip Shield Degradation Model Component F6.3.5-8
6.3.5-9. Integration of Submodels for Localized Corrosion Initiation Analysis F6.3.5-9
6.3.5-10. Computational Organization of Localized Corrosion Initiation Analysis for Crown Seepage F6.3.5-10

6.3.6-1. Information Flow Diagram for the EBS Flow Submodel F6.3.6-1
6.3.6-2. Inputs, Outputs, and Basis for Model Confidence for the EBS Flow Submodel F6.3.6-2
6.3.6-3. Cross Section of Typical Emplacement Drift F6.3.6-3
6.3.6-4. Schematic Diagram of Water Flow Pathways in the EBS F6.3.6-4

6.3.7-1. Information Flow Diagram for Waste Form Degradation and Mobilization F6.3.7-1
6.3.7-2. Inputs, Outputs, and Basis for Model Confidence for Waste Form Degradation and Mobilization F6.3.7-2
6.3.7-3. Three Waste Types Grouped into Two Representative Waste Packages: CSNF and CDSP WPs F6.3.7-3
6.3.7-4. Decay Chains of the Actinide Elements F6.3.7-4
6.3.7-5. Implementation of the In-Package Chemistry Submodel F6.3.7-5
6.3.7-6. Schematic of CSNF Fuel Waste Form Degradation Mechanisms at Various Scales F6.3.7-6
6.3.7-7. Implementation of the DSNF Degradation Submodel F6.3.7-7
6.3.7-8. Connections between the Dissolved Concentrations Limits Submodel and Other TSPA-LA Submodels F6.3.7-8
6.3.7-9. Illustration of Type I and Type II Out-of-Bound Conditions Using the Plutonium Solubility Model as an Example F6.3.7-9
6.3.7-10. Comparison of the Solubility-Limited Dissolved Concentration Model for Plutonium F6.3.7-10
6.3.7-11. Schematic Representation of Colloid Suspension Stability as a Function of pH and Ionic Strength for (a) Groundwater and Glass Degradation Colloids (montmorillonite), (b) CSNF Residue Colloids (ZrO_2), (c) Uranium Mineral Colloids (meta-autunite), and (d) Steel Degradation Colloids (hematite) F6.3.7-11
6.3.7-12. Logic Diagram for Computing the Concentration and Stability of All Colloids in the Waste Package F6.3.7-12

6.3.8-1. Information Flow Diagram for the EBS Transport Submodel F6.3.8-1

FIGURES (Continued)

Page

6.3.8-2. Inputs, Outputs, and Basis for Model Confidence for the EBS Transport Submodel F6.3.8-2
6.3.8-3. Cross Section of Idealized Drift Showing EBS Transport Submodel Domains for a CSNF Waste Package F6.3.8-3
6.3.8-4. Schematic Representation of CSNF Waste Package Showing its Relationship to the Cell Pathway Network Used to Implement the EBS Transport Submodel F6.3.8-4
6.3.8-5. Setup of a Cell Pathways for a CSNF Waste Package Used in the EBS Transport Submodel F6.3.8-5
6.3.8-6. Setup of Cell Pathways for a CDSP Waste Package Used in the EBS Transport Submodel F6.3.8-6
6.3.8-7. Setup of Invert Cell Pathways Used in the EBS Transport Submodel and their Relationship to the Actual Invert Geometry F6.3.8-7
6.3.8-8. Setup of Dual-Continuum EBS-UZ Interface Cell Pathway Network and its Relationship to the Near-Field Unsaturated Zone F6.3.8-8
6.3.8-9. Schematic Representation of the Computational Grid for the EBS-UZ Interface Model F6.3.8-9
6.3.8-10. Simple Model Setup Using Cell Pathways with Different Diffusive Areas F6.3.8-10

6.3.9-1. Information Flow Diagram for Unsaturated Zone Transport F6.3.9-1
6.3.9-2. Inputs, Outputs, and Basis for Model Confidence for the Unsaturated Zone Transport Submodel F6.3.9-2
6.3.9-3. Conceptualization of Unsaturated Zone Transport Processes F6.3.9-3
6.3.9-4. Illustration of Radionuclide Diffusion Into and Out of Matrix Pores F6.3.9-4
6.3.9-5. Illustration of Colloid-Facilitated Transport Processes F6.3.9-5
6.3.9-6. Location of Repository Release Nodes for Five Percolation Subregions F6.3.9-6

6.3.10-1. Information Flow Diagram for Saturated Zone Flow and Transport F6.3.10-1
6.3.10-2. Inputs, Outputs, and Basis for Model Confidence for the Saturated Zone Flow and Transport Model Component F6.3.10-2
6.3.10-3. Conceptualization of Features and Processes Important to Saturated Zone Transport F6.3.10-3
6.3.10-4. Illustration of Colloid-Facilitated Transport Processes F6.3.10-4
6.3.10-5. Regional Map of the Saturated Zone Flow System Showing Direction of Flow and Outline of the 3-D Saturated Zone Site-Scale Flow Model Domain F6.3.10-5
6.3.10-6. Source Regions for Radionuclide Release in the Saturated Zone Flow and Transport Abstraction Model F6.3.10-6
6.3.10-7. Map of the 3-D Saturated Zone Model Domain Showing Simulated Particle Paths F6.3.10-7
6.3.10-8. Radionuclide Decay Chains Considered in Saturated Zone Transport Calculations F6.3.10-8
6.3.10-9. Conceptualization of the 1-D Saturated Zone Flow and Transport Abstraction F6.3.10-9

FIGURES (Continued)

Page

6.3.10-10. Simulated Particle Paths for Different Values of Horizontal Anisotropy in Permeability F6.3.10-10
6.3.10-11. Flowchart of the Implementation of the Saturated Zone Flow and Transport Submodel in the TSPA-LA Model F6.3.10-11

6.3.11-1. Information Flow Diagram for the Biosphere Model Component of the TSPA-LA Model F6.3.11-1
6.3.11-2. Inputs, Outputs, and Basis for Model Confidence for the Biosphere Model Component of the TSPA-LA Model F6.3.11-2
6.3.11-3. Overview of the Biosphere Groundwater Exposure Case Showing Groundwater Transport of Radionuclides and Exposure to the Reasonably Maximally Exposed Individual F6.3.11-3
6.3.11-4. Schematic Representation of the Transport of Radioactive Waste in the Volcanic Ash Exposure Case F6.3.11-4
6.3.11-5. Relationship among Biosphere Submodels for the Groundwater Exposure Case F6.3.11-5
6.3.11-6. Relationship among Biosphere Submodels for the Volcanic Ash Exposure Case F6.3.11-6

6.4-1. Schematic Representation of the TSPA-LA Model Components for the Early Failure Scenario Class F6.4-1
6.4-2. Information Flow Diagram for the Early Failure Scenario Class in the TSPA-LA Model F6.4-2
6.4-3. Inputs, Outputs, and Basis for Model Confidence for the Early Failure Scenario Class F6.4-3

6.5-1. Location and Age of Post-Miocene (less than 5.3 million years) Volcanoes (or clusters where multiple volcanoes have indistinguishable ages) in the Yucca Mountain Region F6.5-1
6.5-2. Schematic Drawing of the Processes Associated with a Dike Intrusion or Eruption through the Repository F6.5-2
6.5-3. TSPA-LA Model Components for the Igneous Intrusion Modeling Case F6.5-3
6.5-4. Information Flow Diagram for the TSPA-LA Igneous Intrusion Modeling Case F6.5-4
6.5-5. Inputs, Outputs, and Basis for Model Confidence for the TSPA-LA Igneous Intrusion Modeling Case F6.5-5
6.5-6. Schematic Diagram of the Intersection of an Igneous Dike with the Repository and Waste Packages F6.5-6
6.5-7. TSPA-LA Model Components for the Volcanic Eruption Modeling Case F6.5-7
6.5-8. Information Flow Diagram for the TSPA-LA Volcanic Eruption Modeling Case F6.5-8
6.5-9. Inputs, Outputs, and Basis for Model Confidence for the TSPA-LA Volcanic Eruption Modeling Case F6.5-9

FIGURES (Continued)

Page

6.5-10. Schematic Diagram of the Intersection of an Igneous Dike and Eruptive Conduit with the Repository F6.5-10
6.5-11. Number of Waste Packages Hit by Conduits from a Volcanic Eruption F6.5-11
6.5-12. Schematic Representation of a Volcanic Eruption at Yucca Mountain, Showing Transport of Radioactive Waste in a Tephra Plume F6.5-12
6.5-13. Schematic Diagram of Tephra Redistribution Model F6.5-13
6.5-14. Comparison of Dose to the RMEI for Post-Eruptive Processes and Dose to the RMEI During a Volcanic Eruption F6.5-14

6.6-1. Schematic Representation of the TSPA-LA Model Components for the Seismic Scenario Class F6.6-1
6.6-2. Information Flow Diagram for the Seismic Scenario Class in the TSPA-LA Model F6.6-2
6.6-3. Inputs, Outputs, and Basis for Model Confidence for the Seismic Scenario Class F6.6-3
6.6-4. Schematic Illustration of the Seismic Scenario Class, the Seismic Effects within a Drift, and Subsequent Radionuclide Releases to the Accessible Environment F6.6-4
6.6-5. Schematic Representation of Future Configurations of EBS Components for Seismic Damage Abstraction F6.6-5
6.6-6. Hazard Curve for Seismic Scenario Class F6.6-6
6.6-7. Comparison of Mean Rockfall Volumes for Lithophysal (a and b) and Nonlithophysal (c and d) Zones F6.6-7
6.6-8. Drip Shield Plate Fragility as a Function of Rockfall Load: (a) 10 Percent, (b) 50 Percent, and (c) 100 Percent F6.6-8
6.6-9. Drip Shield Framework Fragility as a Function of Rockfall Load: (a) 10 Percent, (b) 50 Percent, and (c) 100 Percent F6.6-9
6.6-10. Probability of Damage for a CSNF WP under and Intact Drip Shield: (a) 23 mm OCB with Intact Internals, (b) 23 mm OCB with Degraded Internals, and (c) 17 mm OCB with Degraded Internals F6.6-10
6.6-11. Probability of Damage for a CDSP WP under an Intact Drip Shield: (a) 23 mm OCB with Intact Internals, (b) 23-mm OCB with Degraded Internals, and (c) 17-mm OCB with Degraded Internals F6.6-11
6.6-12. Quadratic Fit for Mean Damaged Area on a CSNF WP with Degraded Internals under an Intact Drip Shield: (a) 23-mm OCB and (b) 17-mm OCB F6.6-12
6.6-13. Quadratic Fit for Mean Damaged Area on a CDSP WP under an Intact Drip Shield: (a) 17-mm OCB with Degraded Internals, (b) 23-mm OCB with Degraded Internals, and (c) 23-mm OCB with Intact Internals F6.6-13
6.6-14. Probability of Incipient and Immediate Rupture for (a) CSNF and (b) CDSP WPs under Intact Drip Shields F6.6-14
6.6-15. Probability of Damage for a CSNF WP Surrounded by Rubble: (a) 23-mm and (b) 17-mm F6.6-15

FIGURES (Continued)

Page

6.6-16. Quadratic Fit for Mean Damage Area on a CSNF WP with Degraded Internals Surrounded by Rubble: (a) 23-mm and (b) 17-mm F6.6-16
6.6-17. Probability of Puncture for a CSNF WP Surrounded by Rubble..... F6.6-17

6.7-1. Schematic Representation of the TSPA-LA Model Components for the Human Intrusion Scenario F6.7-1
6.7-2. Information Flow Diagram for the Human Intrusion Scenario in the TSPA-LA Model..... F6.7-2
6.7-3. Inputs, Outputs, and Basis for Model Confidence for the Human Intrusion Scenario..... F6.7-3
6.7-4. Unconfined Compressive Strength versus Young's Modulus in Tptpll Zone..... F6.7-4
6.7-5. Conceptualization of the Human Intrusion Scenario for the TSPA-LA and Subsequent Radionuclide Releases to the Accessible Environment..... F6.7-5
6.7-6. Schematic Depiction of Borehole (map view) with a Bisecting Fracture F6.7-6
6.7-7. Schematic Illustration of the Implementation of Human Intrusion in TSPA-LA F6.7-7

TABLES

		Page
1-1.	Principal Documents that Support the TSPA-LA Model	T1-1
2-1.	Configuration Control Documents for the TSPA-LA Model	T2-1
3-1.	TSPA-LA Model Software Codes	T3-1
3-2.	ASHPLUME_DLL_LA Software Documents	T3-3
3-3.	CWD Software Documents	T3-3
3-4.	EXDOC_LA Software Documents	T3-3
3-5.	FAR Software Documents	T3-4
3-6.	FEHM Software Documents	T3-4
3-7.	GetThk_LA Software Documents	T3-4
3-8.	GoldSim Software Documents	T3-5
3-9.	InterpZdll_LA Software Documents	T3-5
3-10.	MFCP_LA Software Documents	T3-6
3-11.	MKTABLE/MkTable_LA Software Documents	T3-6
3-12.	MVIEW Software Documents	T3-6
3-13.	PassTable1D_LA Software Documents	T3-7
3-14.	PassTable3D_LA Software Documents	T3-7
3-15.	PREWAP_LA Software Documents	T3-7
3-16.	SCCD Software Documents	T3-8
3-17.	SEEPAGEDLL_LA Software Documents	T3-8
3-18.	SoilExp_LA Software Document	T3-8
3-19.	SZ_Convolute Software Documents	T3-9
3-20.	TSPA_Input_DB Software Documents	T3-9
3-21.	WAPDEG Software Documents	T3-10
4-1.	Direct Inputs	T4-1
4-2.	TSPA Generated Data Tracking Numbers Referenced by Parameter Entry Forms	T4-10
4-3.	Requirements	T4-11
6-1.	TSPA-LA Model Discretization	T6-1
6.1.2-1.	Effect of Combinations of Scenario Classes on Total Mean Annual Dose	T6.1.2-1
6.1.3-1.	Aleatory Uncertainties in the TSPA-LA Model	T6.1.3-1
6.1.3-2.	Examples of Epistemic Uncertainties in the TSPA-LA Model	T6.1.3-2
6.1.4-1.	Percolation Subregion Information	T6.1.4-1
6.1.5-1.	Location of Implementation Description in the GoldSim TSPA Model File	T6.1.5-1

TABLES (Continued)

Page

6.2-1. Table of Alternative Conceptual Models T6.2-1

6.3.1-1. Durations of Climate States in First 10,000 Years T6.3.1-1
6.3.1-2. Net Infiltration Rates Averaged over the Unsaturated Zone Model Domain and Probability-Weighting Factors for the Infiltration Scenarios T6.3.1-1
6.3.1-3. Alternative Conceptual Models Considered for the Mountain-Scale Unsaturated Zone Flow T6.3.1-2

6.3.2-1. Parameter Distribution for Host-Rock Thermal-Conductivity Uncertainty T6.3.2-1
6.3.2-2. Percolation-Based Probability Subregion Quantile Ranges T6.3.2-1
6.3.2-3. Probability Weighting for the 12 Percolation Flux and Host-Rock Thermal-Conductivity Combinations T6.3.2-1
6.3.2-4. List of Thermal-Hydrologic Variables Predicted by the MSTHM Process Model and Used in the TSPA-LA Model T6.3.2-2
6.3.2-5. Alternative Conceptual Model Considered for the Engineered Barrier System Thermal-Hydrologic Environment T6.3.2-2

6.3.3-1. Spatial Variability and Uncertainty Distributions for $1/\alpha$ for Method A as Defined in the Abstraction of Drift Seepage T6.3.3-1
6.3.3-2. Spatial Variability and Uncertainty Distributions for Fracture Permeability (log (k [m^2])) T6.3.3-1
6.3.3-3. Inputs Passed by the TSPA-LA Model to the Seepage Dynamically Linked Library T6.3.3-2
6.3.3-4. Drift-Wall Condensation: 1,000 Years; High Dispersion Coefficient, Low Invert Transport Properties, Well-Ventilated Drip Shield T6.3.3-4
6.3.3-5. Parameter Distributions for Drift Wall Condensation Abstraction T6.3.3-5
6.3.3-6. Alternative Conceptual Models Considered for the Drift Seepage and Drift-Wall Condensation Submodels T6.3.3-6

6.3.4-1. Illustration of the Form of the Mean Water-Rock Interaction Parameter Table T6.3.4-1
6.3.4-2. Illustration of the Form of an In-Drift Precipitated Salts Look-up Table for Each Unique Set of Values of Carbon Dioxide Partial Pressure, Pco_2, and Temperature T6.3.4-2
6.3.4-3. Illustration of Estimated Model Uncertainty Ranges for In-Drift Precipitated Salts Submodel Outputs of pH and Ionic Strength T6.3.4-4
6.3.4-4. Summary of Chemistry for Seepage and Condensation in the TSPA-LA Model T6.3.4-5
6.3.4-5. Alternative Conceptual Models Considered for EBS Physical and Chemical Environment T6.3.4-6

6.3.5-1. Drip Shield and Waste Package Degradation Mechanisms and Their Disposition for Implementation in the TSPA-LA Model T6.3.5-1

TABLES (Continued)

Page

6.3.5-2. Alternative Conceptual Models Considered for Drip Shield and Waste Package Degradation T6.3.5-1
6.3.5-3. Uncertain Inputs to the TSPA-LA Model for Generalized Corrosion of the Drip Shield and Waste Package and Stress Corrosion Cracking of the Waste Package T6.3.5-3
6.3.5-4. Uncertain Inputs to Localized Corrosion Initiation Stand-Alone Model T6.3.5-6

6.3.6-1. The EBS Flow Abstraction within the TSPA-LA Model T6.3.6-1
6.3.6-2. Drip Shield and Waste Package Flow Splitting Parameters T6.3.6-2
6.3.6-3. Alternative Conceptual Models Considered for the EBS Flow T6.3.6-2

6.3.7-1. Waste Package Configurations T6.3.7-1
6.3.7-2. Radionuclides Included in TSPA-LA T6.3.7-2
6.3.7-3. Nominal Grams of Radionuclides per Waste Package for Each Type of Waste T6.3.7-3
6.3.7-4a. Radionuclide Inventory Per Waste Package Showing the Amount of Decay and Ingrowth Experienced During the Preclosure Period T6.3.7-4
6.3.7-4b. Supplemental Radionuclide Inventory Per Waste Package due to Mixed Oxide Fuel and Lanthanide Borosilicate Waste Showing the Amount of Decay and Ingrowth Experienced During the Preclosure Period T6.3.7-5
6.3.7-5. Initial Radionuclide Inventories and Initial Radionuclide Activities Per Waste Package Type in the TSPA-LA Model T6.3.7-6
6.3.7-6. Disposition of Radionuclides for Groundwater Release Modeling Cases: Nominal, Igneous Intrusion, and Seismic T6.3.7-7
6.3.7-7. Uncertainty Multipliers for Grams per Waste Package of Radionuclides for Each Waste Type T6.3.7-11
6.3.7-8. Summary of In-Package Chemistry Abstraction (Vapor or Liquid Influx) T6.3.7-11
6.3.7-9. In-Package Ionic Strength Abstraction for Vapor Influx Case T6.3.7-11
6.3.7-10. In-Package Ionic Strength Abstraction for CSNF Cell 1 of Liquid Influx Case (log I (molal)) T6.3.7-12
6.3.7-11. In-Package Ionic Strength Abstraction for CDSP Cell 1A of Liquid Influx Case (log I (molal)) T6.3.7-13
6.3.7-12. In-Package Ionic Strength Abstraction for CDSP Cell 1B of Liquid Influx Case (log I (molal)) T6.3.7-14
6.3.7-13. In-Package Ionic Strength Deviation for CSNF Cell 1 of Liquid Influx Case (log I (molal)) T6.3.7-15
6.3.7-14. In-Package Ionic Strength Deviation for CDSP Cell 1A of Liquid Influx Case (log I (molal)) T6.3.7-16
6.3.7-15. In-Package Ionic Strength Deviation for CDSP Cell 1B of Liquid Influx Case (log I (molal)) T6.3.7-17
6.3.7-16. Maximum pH for CSNF Cell 1 of Liquid Influx T6.3.7-17
6.3.7-17. Maximum pH for CDSP Cell 1A of Liquid Influx T6.3.7-18
6.3.7-18. Maximum pH for CDSP Cell 1B of Liquid Influx T6.3.7-18
6.3.7-19. Minimum pH for CSNF Cell 1 of Liquid Influx T6.3.7-18
6.3.7-20. Minimum pH for CDSP Cell 1A of Liquid Influx T6.3.7-18

TABLES (Continued)

Page

6.3.7-21. Minimum pH for CDSP Cell 1B of Liquid Influx T6.3.7-19
6.3.7-22. Maximum pH for CSNF Cell 1 of Vapor Influx T6.3.7-19
6.3.7-23. Maximum pH for CDSP Cell 1A of Vapor Influx T6.3.7-19
6.3.7-24. Maximum pH for CDSP Cell 1B of Vapor Influx T6.3.7-19
6.3.7-25. Minimum pH for CSNF Cell 1 of Vapor Influx T6.3.7-20
6.3.7-26. Minimum pH for CDSP Cell 1A of Vapor Influx T6.3.7-20
6.3.7-27. Minimum pH for CDSP Cell 1B of Vapor Influx T6.3.7-20
6.3.7-28. Log K Temperature Interpolation Functions for Use in the Total Carbonate Concentration Abstraction T6.3.7-20
6.3.7-29. Initial Release Fraction Percentage Distributions T6.3.7-21
6.3.7-30. Linear Regression Model Alkaline Case ($pH \geq 6.8$) T6.3.7-21
6.3.7-31. Linear Regression Model for Acid Case ($pH < 6.8$) T6.3.7-22
6.3.7-32. Dissolution Rate Parameters for High-Level Radioactive Waste Glass T6.3.7-23
6.3.7-33. Solubility-Controlling Solid Phases Used in the Dissolved Concentration Limits Model Abstraction T6.3.7-24
6.3.7-34. Base Americium Solubility Look-Up Table (log[Am], mg/L) T6.3.7-25
6.3.7-35. Base Neptunium (Np_2O_5) Solubility Look-Up Table (log[Np], mg/L) T6.3.7-26
6.3.7-36. Base Neptunium (NpO_2) Solubility Look-Up Table (log[Np], mg/L) T6.3.7-27
6.3.7-37. Base-Case Plutonium Solubility Look-Up Table (log[Pu], mg/L) T6.3.7-28
6.3.7-38. Base Protactinium Solubility Look-Up Table (log[Pa], mg/L) T6.3.7-30
6.3.7-39. Base Thorium Solubility Look-Up Table (log[Th], mg/L) T6.3.7-31
6.3.7-40. Base Tin Solubility Look-Up Table (log[Sn], mg/L) T6.3.7-32
6.3.7-41. Uncertainty in Americium Solubility Model T6.3.7-33
6.3.7-42. Uncertainty in Neptunium (Np_2O_5) Solubility Model T6.3.7-34
6.3.7-43. Uncertainty in Neptunium (NpO_2) Solubility Model T6.3.7-35
6.3.7-44. Uncertainty in Plutonium Solubility Model T6.3.7-36
6.3.7-45. Uncertainty in Protactinium Solubility Model T6.3.7-36
6.3.7-46. Uncertainty in Thorium Solubility Model T6.3.7-37
6.3.7-47. Uncertainty in Tin Solubility Model T6.3.7-37
6.3.7-48. Multiplication Factor, N(pH), Used to Modify Fluoride Concentration Uncertainty Terms (ε_2) for Americium T6.3.7-38
6.3.7-49. Multiplication Factor, N(pH), Used to Modify Fluoride Concentration Uncertainty Terms (ε_2) for Neptunium (Np_2O_5) T6.3.7-39
6.3.7-50. Multiplication Factor, N(pH), Used to Modify Fluoride Concentration Uncertainty Terms (ε_2) for Neptunium (NpO_2) T6.3.7-40
6.3.7-51. Multiplication Factor, N(pH), Used to Modify Fluoride Concentration Uncertainty Terms (ε_2) for Plutonium T6.3.7-41
6.3.7-52. Multiplication Factor, N(pH), Used to Modify Fluoride Concentration Uncertainty Terms (ε_2) for Thorium T6.3.7-42
6.3.7-53. Uranium Solubility Look-Up Table (log[U], mg/L) for CSNF WPs Breached under Nominal Conditions or by Seismic Activity T6.3.7-43
6.3.7-54. Uncertainty in Log K Values for Base-Case Uranium Solubility Model (CSNF WP Nominal and Seismic Scenario Classes) T6.3.7-44

TABLES (Continued)

Page

6.3.7-55. Multiplication Factor, N(pH), Used to Modify Fluoride Concentration Uncertainty Terms (ε_2) for Uranium (CSNF WP, Nominal and Seismic Scenario Classes) T6.3.7-45
6.3.7-56. Schoepite Controlled Uranium Solubility Look-Up Table (log[U], mg/L) for CDSP WPs Breached Under any Scenario, CSNF WPs Breached in by an Igneous Intrusion, and in the Invert (all locations and scenarios) T6.3.7-46
6.3.7-57. Na-Boltwoodite and $Na_4UO_2(CO_3)_3$ Controlled Uranium Solubility Look-Up Table (log[U], mg/L) for CDSP WPs Breached under Any Scenario, CSNF WPs Breached by an Igneous Intrusion, and in the Invert (all locations and scenarios) T6.3.7-47
6.3.7-58. Uncertainty in Uranium Solubility Model in CDSP WPs Breached Under Any Scenario, CSNF WPs Breached by an Igneous Intrusion, and in the Invert (all locations and scenarios) T6.3.7-48
6.3.7-59. Multiplication Factor, N(pH), Used to Modify Fluoride Concentration Uncertainty Terms (ε_2) for Uranium in CDSP WPs Breached under Any Scenario, CSNF Waste Packages Breached by an Igneous Intrusion and in the Invert (all locations and scenarios) T6.3.7-49
6.3.7-60. Actinide Caps (mg/L) Between an Ionic Strength of 3 and 10 Molal for CSNF Packages T6.3.7-50
6.3.7-61. Actinide Caps (mg/L) Between an Ionic Strength of 3 and 10 Molal for CDSP Packages, Cell 1b T6.3.7-50
6.3.7-62. Parameters for TSPA-LA Glass Waste Form Colloid Abstraction T6.3.7-51
6.3.7-63. Parameters for TSPA-LA CSNF Waste Form Irreversible Colloid Abstraction T6.3.7-54
6.3.7-64. Parameters for TSPA-LA SNF Waste Form Reversible Colloid Abstraction T6.3.7-56
6.3.7-65. Parameters for TSPA-LA Iron Oxyhydroxide Colloid Abstraction T6.3.7-58
6.3.7-66. Parameters for TSPA-LA Groundwater Colloid Abstraction T6.3.7-60
6.3.7-67. Alternative Conceptual Models Considered for In-Package Chemistry T6.3.7-61
6.3.7-68. Alternative Conceptual Models Considered for CSNF Waste Form Degradation T6.3.7-61
6.3.7-69. Alternative Conceptual Models Considered for High-Level Radioactive Waste Glass Degradation T6.3.7-62
6.3.7-70. Alternative Conceptual Models Considered for Dissolved Concentration Limits T6.3.7-63
6.3.7-71. Alternative Conceptual Models Considered for Colloids T6.3.7-64

6.3.8-1. Summary of EBS Transport Abstraction T6.3.8-1
6.3.8-2. Parameters for EBS Transport Abstraction T6.3.8-2
6.3.8-3. Sampled Parameter Ranges and Distributions Used for Kinetic Sorption on Stationary Corrosion Products T6.3.8-8
6.3.8-4. Sampled Model Inputs Used in the EBS Radionuclide Transport Abstraction T6.3.8-10

TABLES (Continued)

Page

6.3.8-5. Unsaturated Zone Saturation and Flux Inputs Used in the EBS Radionuclide Transport Abstraction T6.3.8-12
6.3.8-6. Summary of CSNF Rind Volume Calculation Parameters for TSPA-LA T6.3.8-13
6.3.8-7. Alternative Conceptual Models Considered for EBS Transport T6.3.8-14

6.3.9-1. Radionuclide Half-Life and Daughter Products Used in the TSPA-LA Model T6.3.9-1
6.3.9-2. Matrix Sorption Coefficient Distributions for Unsaturated Zone Units in the Unsaturated Zone Transport Submodel T6.3.9-3
6.3.9-3. Species Dependent Free Water Diffusivities Used to Calculate the Effective Matrix Diffusion Coefficients for Unsaturated Zone Transport T6.3.9-5
6.3.9-4. Parameter Distributions for Tortuosities Used to Calculate the Effective Matrix Diffusion Coefficients for Unsaturated Zone Transport T6.3.9-6
6.3.9-5. Fracture γ Parameter Distribution for all Rock in the Unsaturated Zone Transport T6.3.9-6
6.3.9-6. Parameter Distributions for Fracture Porosity for Unsaturated Zone Transport T6.3.9-7
6.3.9-7. Parameter Distributions for Fracture Frequency for Unsaturated Zone Transport T6.3.9-8
6.3.9-8. Colloid Size and Concentration Distributions for Unsaturated Zone Transport T6.3.9-8
6.3.9-9. Cumulative Probability Distributions for Colloid Transport at Matrix Interfaces for Unsaturated Zone Transport T6.3.9-9
6.3.9-10. Colloid Size Exclusion Factor Used in the Compliance Model T6.3.9-10
6.3.9-11. Radionuclide Sorption Coefficients onto Colloids for Unsaturated Zone Transport (revised groundwater colloid mass concentration parameters for TSPA-LA Model) T6.3.9-11
6.3.9-12. Colloid Retardation Factors (Colloidal_Retard_Factor_dist) for Unsaturated Zone Transport T6.3.9-12
6.3.9-13. Lower Triangular Matrix for all Species Except Uranium and Selenium as Generated from the Correlation (Covariance) Matrix by Cholesky Factorization Using MathCad T6.3.9-12
6.3.9-14. Lower Triangular Matrix for Uranium and Selenium as Generated from the Correlation (Covariance) Matrix by Cholesky Factorization Using MathCad T6.3.9-13
6.3.9-15. Alternative Conceptual Models Considered for the Unsaturated Zone Transport Model T6.3.9-13

6.3.10-1. Radionuclides Transported in the Saturated Zone Flow and Transport Submodel T6.3.10-1
6.3.10-2. Uncertain Model Inputs Used in the 3-D Saturated Zone Flow and Transport Process Model and 1-D Saturated Zone Flow and Transport Abstraction T6.3.10-2
6.3.10-3. Constant TSPA Parameters for Saturated Zone Flow One-Dimensional Transport Model T6.3.10-7

TABLES (Continued)

Page

6.3.10-4. Flow Path Lengths of Pipe Segments T6.3.10-7
6.3.10-5. Average Specific Discharge in Flow Path Segments T6.3.10-7
6.3.10-6. Summary of Alpha Concentration Results in Amargosa Valley Groundwater T6.3.10-8
6.3.10-7. Alternative Conceptual Models Considered for Saturated Zone Flow and Radionuclide Transport T6.3.10-8

6.3.11-1. Pathways for the Groundwater Exposure Case T6.3.11-1
6.3.11-2. Pathways for the Volcanic Ash Exposure Case T6.3.11-1
6.3.11-3. Groundwater BDCF Uncertainty Representation in the TSPA-LA Model, GoldSim Model File for the Present-Day Climate T6.3.11-2
6.3.11-4. Alternative Conceptual Models Considered for the Biosphere T6.3.11-4

6.4-1. Early Failure Unconditional Probability Values T6.4-1
6.4-2. Uncertain Inputs Used in the Early Failure Scenario Class T6.4-1

6.5-1. Waste Form Temperatures Inside Intrusive Body T6.5-1
6.5-2. Annual Frequencies of Intersection of Repository by a Dike for the License Application Footprint T6.5-2
6.5-3. Cumulative Distribution Function for the Number of Waste Packages Hit by Conduits T6.5-3
6.5-4. Key Parameters for the ASHPLUME Code T6.5-4
6.5-5. Key Input Parameters to the Tephra Redistribution Submodel T6.5-6

6.6-1. Expected Waste Package Failure Due to Fault Displacement T6.6-1
6.6-2. Uncertain Inputs Used in the Seismic Scenario Class T6.6-2
6.6-3. Seismic Ground Motion and Fault Displacement Modeling Cases Using Pre-Specified Parameters T6.6-5
6.6-4. Alternative Conceptual Models Considered for the Seismic Scenario Class T6.6-6

6.7-1. Waste Package Specification and Design Dimensions T6.7-1
6.7-2. Specifications of Drilling Components T6.7-1
6.7-3. Uniaxial Compressive Strength and Young's Moduli by Rock Unit T6.7-2
6.7-4. Material Properties for Drip Shield and Waste Package Fabrication T6.7-2
6.7-5. Borehole Properties used in UZ Flow and Transport Calculations T6.7-3
6.7-6. Borehole Fracture Properties used in UZ Flow and Transport Calculations T6.7-4
6.7-7. Fraction of SZ Source Region Nodes in each Percolation Subregion Bin T6.7-4

INTENTIONALLY LEFT BLANK

EXECUTIVE SUMMARY

ES1. SCOPE

ES1.1 Introduction

Total System Performance Assessment Model/Analysis for the License Application (TSPA-LA) describes the method, structure, validation or confidence building, and application of a computational model of the performance of the repository system. This model, the Total System Performance Assessment Model, was developed to evaluate the safety of the Yucca Mountain repository for the safe disposal of spent nuclear fuel (SNF) and high-level radioactive waste (HLW). The TSPA-LA is one of an iterative series of performance assessments conducted during the progress of the Yucca Mountain Project. The TSPA-LA Model evaluates the ability of the repository to adequately isolate nuclear waste meeting standards for exposure following repository closure, according to the U.S. Nuclear Regulatory Commission (NRC) Proposed Rule.

The NRC Proposed Rule 10 CFR 63, Parts E and L, consists of proposed changes to the existing rule, published as Implementation of a Dose Standard after 10,000 Years (70 FR 53313 [DIRS 178394], pp. 55313 to 55320), and the unrevised portions of the existing rule, published in the Federal Register as Energy: Disposal of High-Level Radioactive Wastes in a Geologic Repository at Yucca Mountain, Nevada (10 CFR Part 63 [DIRS 180319]). General references to the NRC Proposed Rule will cite both 70 FR 53313 [DIRS 178394] and 10 CFR Part 63 [DIRS 180319]. References to specific articles from either the proposed changes to the existing rule (e.g., 10 CFR 63.321 [DIRS 178394]) or to parts of the existing rule that have not changed (e.g., 10 CFR 63.322 [DIRS 180319]) will use, as shown here, only the DIRS reference number that applies. The same convention is followed when referring to the proposed and existing rules from the U.S. Environmental Protection Agency (EPA). The EPA Proposed Rule 40 CFR Part 197, Subpart B, was published as Public Health and Environmental Radiation Protection Standards for Yucca Mountain, NV (70 FR 49014 [DIRS 177357], pp. 49014 to 49065). The existing rule, as published in the Federal Register, is 40 CFR Part 197, Public Health and Environmental Radiation Protection Standards for Yucca Mountain, NV; Final Rule (66 FR 32074 [DIRS 155216], pp. 32074 to 32135).

The NRC Proposed Rule standards apply to the first 10,000 years following repository closure (10 CFR 63.311(a)(1) [DIRS 178394]), and include additional standards within the period of geologic stability (10 CFR 63.311(a)(2) [DIRS 178394]), defined as one million years after repository closure (10 CFR 63.302 [DIRS 178394]). Figure ES-1 shows the Yucca Mountain area and the entrance to the underground facilities, which will become part of the repository after a license to construct the repository is granted. Figure ES-2 shows a timeline of the major legislative and regulatory actions bearing on the Yucca Mountain Project from 1980 to the present. Among the regulatory mandates of NRC Proposed Rule 10 CFR Part 63 ([DIRS 178394] and [DIRS 180319]) is the requirement to demonstrate, by means of risk-informed assessment, the reasonable expectation of waste isolation after closure of the repository (NRC Proposed Rule 10 CFR 63.304 [DIRS 180319]).

The TSPA-LA Model evaluates the performance of engineered and natural components of the Yucca Mountain repository system for the expected natural conditions prevailing at the Yucca

Mountain site (referred to as the Nominal Scenario Class), considers the effect on repository performance of unexpected early failure of the engineered components of the repository system, and evaluates the impact on repository performance due to natural disruptive events, such as igneous activity and seismic events, and evaluates the impact of an inadvertent human intrusion from drilling into the repository. The technical basis for the TSPA-LA Model includes field, laboratory, and natural-analogue data obtained during site characterization investigations at Yucca Mountain and analogue sites. The development of the process models, submodels, and other components included in the TSPA-LA Model can be found in the supporting analysis model reports that are referenced in appropriate sections of this report.

ES1.2 Governing Regulations

The TSPA-LA Model supports evaluations of the performance of the Yucca Mountain repository system under the relevant postclosure regulatory requirements promulgated in NRC Proposed Rule 10 CFR 63, Subparts E and L ([DIRS 178394] and [DIRS 180319]). The TSPA-LA Model was also used to address the criteria related to postclosure performance described in *Yucca Mountain Review Plan, Final Report* (NRC 2003 [DIRS 163274], Section 2.2), and agreement items associated with the NRC's Key Technical Issues (Reamer 2001 [DIRS 158380], Attachment 1). The TSPA-LA Model serves as part of the overall U.S. Department of Energy (DOE) strategy to provide for the safe disposal of SNF and HLW, a process comprising the following five steps, as illustrated by Figure ES-3:

Step 1: Define the goals and boundary conditions of the TSPA-LA Model according to regulations promulgated by the U.S. government.

Step 2: Develop the design for the Yucca Mountain repository so that the repository will meet the regulatory standards, including the contributions to repository performance of both natural and engineered barriers to radionuclide migration from the repository.

Step 3: Identify and evaluate features, events, and processes (FEPs) potentially relevant to the long-term performance of a waste-disposal repository, screen the identified FEPs, and use relevant FEPs to establish scenario classes for use in assessing estimated repository performance.

Step 4: Develop and use the TSPA-LA Model to estimate repository performance.

Step 5: Analyze and interpret the results of the model simulations of repository performance with respect to the performance measures established by the regulations.

The TSPA-LA Model addresses Step 4 of that process, as informed by the preceding steps, to provide information for Step 5, which describes the results.

In particular, the TSPA-LA Model calculates estimates of the:

a. Annual doses to the reasonably maximally exposed individual (RMEI) from releases from the undisturbed Yucca Mountain disposal system (NRC Proposed Rule 10 CFR 63.311 [DIRS 178394])

b. Annual doses to the RMEI from releases from the Yucca Mountain disposal system resulting from human intrusion (NRC Proposed Rule 10 CFR 63.321 [DIRS 178394])

c. Annual levels of radioactivity in the representative volume of groundwater of 3,000 acre feet (NRC Proposed Rule 10 CFR 63.331 [DIRS 180319])

d. Annual doses to the RMEI for early drip-shield (DS) and waste-package (WP) failures

e. Annual doses to the RMEI for igneous and seismic scenarios (NRC Proposed Rule 10 CFR 63.342(c)(1) [DIRS 178394]).

ES2. TOTAL SYSTEM PERFORMANCE ASSESSMENT METHODOLOGY

The general performance assessment (PA) process adopted by the DOE follows the methodology developed by Cranwell et al. (1990 [DIRS 101234], Sections 2 and 3). Over time, the methodology has been enhanced, including input from the NRC, and applied to numerous projects by various international organizations involved in radioactive waste management. Figure ES-4 shows the major steps in the PA process. Previous PAs and related supplemental analyses of the performance of the Yucca Mountain repository were conducted to meet various regulatory milestones, following the publication of the Nuclear Waste Policy Amendments Act of 1987, Public Law No. 100-203 [DIRS 100016]. The Yucca Mountain PAs have been iterative, with each succeeding PA building on and extending the scope and results of the previous PAs by incorporating both an improved understanding of the processes affecting performance and, through additional field observations and laboratory analyses, better identification and quantification of the parameters used in the TSPAs. Figure ES-5 illustrates the evolution of the PA iterations for the Yucca Mountain Project and identifies the corresponding TSPAs. The most recent TSPA documents were *Total System Performance Assessment for the Site Recommendation* (TSPA-SR) (CRWMS M&O 2000 [DIRS 143665]) and the application of the TSPA-SR Model to *Total System Performance Assessment – Analyses for Disposal of Commercial and DOE Waste Inventories at Yucca Mountain – Input to Final Environmental Impact Statement and Site Suitability Evaluation* (Williams 2001 [DIRS 157307]). The TSPA-LA Model is built on the foundation of those earlier PAs and has been enhanced by updated analyses of the processes affecting Yucca Mountain and the design elements of the repository, including a comprehensive consideration of the FEPs that are relevant to repository system performance.

Figure ES-6 represents the PA process as a pyramid. The foundation of the pyramid consists of a system characterization involving assimilation of the information collected by scientists and engineers involved in site characterization and engineering design. The repository system and site characterization provides information regarding waste properties, facility design, regional geology, regional hydrology, and environmental characteristics of the Yucca Mountain site. The

broad foundation of the pyramid represents the more than 20-year body of knowledge, collected in the field and in the laboratory, regarding the Yucca Mountain repository system. These data were used to identify the set of possible FEPs that may be part of and affect the performance of the repository system. This body of knowledge also provides the basis for the second stage of the PA pyramid.

The second stage of the PA pyramid consists of the development and testing of process models that include the retained FEPs, and their outcomes regarding repository performance. The process models consist of sets of hypotheses, assumptions, simplifications, and idealizations that, together, describe the essential aspects of a system or subsystem of the repository relative to performance. An example of such a process model is one that describes the movement of water and dissolved radionuclides by diffusive flow in rock pores or by advective flow in fracture openings in the unsaturated bedrock surrounding the repository and through the saturated zone (SZ) below the repository. Because the PA methodology deals with future outcomes and includes uncertainty in both descriptions of processes and parameter values, an essential element of the PA methodology is to capture uncertainty in probabilistic analyses that represent likely outcomes, based on the best available values of process model parameters and the processes involved.

The third stage of the PA pyramid involves the development of abstracted models. These abstractions are progressive simplifications of the detailed models of physical and chemical processes to more compact, efficient numerical models. Abstractions consist of statistical or mathematical abstractions, including look-up tables, equations representing response surfaces, probability distributions, linear transfer functions, or reductions of model dimensionality. The abstractions used to analyze the projected evolution through time of the various components of the repository system are compact but still capture the salient features of the process models, along with their associated uncertainties.

The top level of the PA pyramid consists of the integrated total system models. The total system model is a numerical model that is used to simulate the integrated behavior of the entire Yucca Mountain repository system. The TSPA-LA Model incorporates the abstracted detailed models that describe the TSPA-LA Model components, and their submodels, from their development to their implementation, including information from the analysis model reports. The abstractions and associated process models and submodels describing various repository attributes in a series of analysis model reports form the technical basis for the TSPA-LA Model.

The attributes of both natural and engineered systems comprising the total repository system, as illustrated on Figure ES-7, include:

- Limited water entering emplacement drifts and coming into contact with the WPs and, subsequently, the waste forms
- Prolonged lifetimes of WPs and DSs
- Gradual and limited radionuclide mobilization and release from the repository's engineered barrier system (EBS)

- Retarded radionuclide transport by means of retardation and dilution in natural hydrogeologic systems after release from the EBS

- Low mean annual dose to receptors, even considering the potential occurrence of disruptive events.

Use of the TSPA-LA Model to simulate Yucca Mountain repository behavior and project future outcomes is aided by the development of scenario classes to assist in the analysis of repository performance and provide the framework for the TSPA-LA Model analyses. The TSPA-LA Model is structured to address a specific set of scenario classes that span the range of possible FEPs for both expected conditions and disruptive events. The TSPA-LA Model scenario classes include the Nominal Scenario Class, the Early Failure Scenario Class, two disruptive event scenario classes, the Igneous Scenario Class and the Seismic Scenario Class, and a human intrusion scenario.

This document contains references to the supporting analysis model reports for the model abstractions that are included in the TSPA-LA Model. Other information from the documents supporting the process models and their abstractions is included in the electronic GoldSim model file for the TSPA-LA Model, along with additional references to the parameter values and distributions of parameter values that are incorporated in the TSPA-LA Model.

ES3. TSPA-LA MODEL DEVELOPMENT PROCESS

The TSPA-LA Model was developed to support the evaluation of a geologic repository for the safe disposal of SNF and HLW at Yucca Mountain, Nevada, and evaluates the ability of the natural and engineered systems of the Yucca Mountain repository to isolate nuclear waste from the biosphere. The TSPA-LA Model evaluates repository performance for the first 10,000 years following repository closure and for the period of geologic stability, understood at NRC Proposed Rule 10 CFR 63.302 [DIRS 178394] to be one million years after repository closure.

ES3.1 Features, Events, and Processes Analysis

The development of the TSPA-LA Model for the Yucca Mountain repository system began, as is shown on Step 3 of Figure ES-3, with a thorough analysis and screening of the FEPs that could affect repository performance after closure. The results of the FEPs analyses led to the development of process models and abstractions that address the attributes necessary to allow the TSPA-LA Model to assess repository safety and determine whether or not the repository meets regulatory standards. These process models and their abstractions considered FEPs that could affect the Yucca Mountain repository system and, in turn, FEPs that could be affected by the presence of the repository.

Figure ES-8 is a schematic representation of the development of the TSPA-LA Model and describes, for analysis purposes, the repository system divided into individual model components. Each individual model component represents a major process or set of processes of the total repository system. Figure ES-9 shows the model component areas as well as the event scenario classes that are included in the analyses of repository performance. Figure ES-10 shows the principal components and supporting submodels of the Yucca Mountain repository system.

ES3.2 Development of the Scenario Classes

A scenario is a well-defined, connected sequence of FEPs that describes a possible future condition of the repository system. A scenario class is a set of related scenarios that share sufficient similarities that they can usefully be aggregated for the purposes of screening or analysis. The objective of scenario development for the TSPA-LA Model is to define a limited set of scenario classes that are representative of the range of future FEPs that are potentially relevant to the licensing of the facility.

The TSPA-LA approach focuses on a set of scenario classes that are distinguished by initiating events. The Nominal Scenario Class includes all possible future outcomes except those initiated by early failure of the DSs or WPs, igneous or seismic activity, and inadvertent human intrusion into the repository. The Igneous Scenario Class includes all possible future outcomes initiated by igneous activity. The Seismic Scenario Class includes all possible futures initiated by seismic activity. In addition to the analyses of the scenario classes, the TSPA-LA Model also simulates a Human Intrusion Scenario according to the scenario and criteria described in NRC Proposed Rule 10 CFR 63.322 [DIRS 180319].

Modeling cases are used in the TSPA-LA Model to represent scenario classes and to calculate estimates of performance measures for the repository system. The TSPA-LA Model starts with the Nominal Scenario Class, which incorporates all expected FEPs describing the fundamental processes at work under ambient conditions without disruptive events, early failures, or a human intrusion, as well as possible changes to those processes. The Nominal Scenario Class is analyzed with the Nominal Modeling Case.

The Early Failure Modeling Cases, the DS Early Failure Modeling Case and the WP Early Failure Modeling Case, address FEPs that describe early DS and WP failure due to manufacturing and material defects and pre-emplacement operations, including improper heat treatment of the WPs.

Igneous disruption of the repository is addressed by two modeling cases. The Igneous Intrusion Modeling Case addresses the FEPs for the possibility that magma, in the form of a dike, could intrude into repository drifts, potentially destroying DSs and WPs in those drifts intruded by the magma, exposing the waste forms to percolating water that could mobilize radionuclides from the waste forms and transport the radionuclides through the unsaturated zone (UZ) and SZ to the RMEI. The Volcanic Eruption Modeling Case addresses FEPs that describe a volcanic conduit (or conduits) that invades the repository, destroys WPs, and erupts at the land surface. The volcanic eruption disperses volcanic tephra and entrained waste under atmospheric conditions and deposits the contaminated tephra on land surfaces where the contaminated tephra becomes subject to redistribution by soil and near-surface hydrogeologic processes.

Seismic disruption of the repository is addressed by two modeling cases that analyze possible seismic disruption of the repository and its effect on repository performance. The Seismic Ground Motion (GM) Modeling Case addresses FEPs concerning damage to WPs and DSs due to vibratory ground motion. The Seismic Fault Displacement (FD) Modeling Case includes the effects of fault displacement on WPs and DSs. FEPs that describe localized corrosion of WPs and DSs are also considered in this modeling case because disruption of the DSs could possibly

result in crown seepage that, in turn, could induce localized corrosion. This modeling case includes advection and diffusion of mobilized radionuclides out of the WP breaches.

The TSPA-LA Model considers a Human Intrusion Scenario in a stylized calculation that simulates a future drilling operation in which an intruder drills a land-surface borehole using a drilling apparatus operating under the common techniques and practices currently employed in exploratory drilling for groundwater in the region around Yucca Mountain. During drilling, the drilling apparatus directly intersects a degraded DS and WP causing a release of waste and continues into the SZ underlying Yucca Mountain. The TSPA-LA Model simulated a Human Intrusion Scenario occurring approximately 200,000 years after repository closure.

ES3.3 Incorporation of Uncertainty

Uncertainty in the expected behavior of the Yucca Mountain repository system requires that the TSPA-LA Model analyses be probabilistic in order to capture the full range of potential outcomes.

Uncertainty in the TSPA-LA Model is characterized as either epistemic or aleatory uncertainty where:

- **Epistemic Uncertainty,** also referred to as "reducible" uncertainty, concerns the state of uncertainty in knowledge about a parameter value due to limited data or alternative interpretations of the available data. Epistemic uncertainty can be reduced, in principle, using the results of experimental testing and additional data collection.

- **Aleatory Uncertainty,** also referred to as "irreducible" uncertainty, concerns whether or not there is a chance occurrence of a FEP. No amount of exploratory work will allow determining whether or not a chance event will or will not occur at any given time, but determining a range of likelihoods-of-occurrence for a given timeframe is generally supportable through using various formalized means for combining scientific insights from experts in the field.

The TSPA-LA Model calculates future outcomes for multiple realizations using distributions of values for uncertain parameters that may be important to performance, rather than deterministic or single-value calculations for each parameter in the repository system. The model realizations are performed using various combinations of parameter values obtained from the parameter-value distributions in the TSPA Input Database, which contains parameter values obtained from field observations, laboratory data, data from established technical literature, and process-model analyses as described in Section 6.3. Each of the combinations of parameter values is representative of a subset of the full range of potential outcomes. These probabilistic analyses thus reflect an appropriate range of process behaviors or parameter values, or both, of the inherently variable Yucca Mountain repository system, given that complete knowledge of the system is not attainable.

ES3.4 Natural and Engineered Model Components

The TSPA-LA Model for the Yucca Mountain repository system is based on several natural and engineered model components. These principal model components of the TSPA-LA Model function as follows (Figure ES-9):

- UZ Flow describes fluid flow through the unsaturated welded and nonwelded tuffs above and below the repository.
- The EBS Environment describes the coupled processes in the environment surrounding and within the engineered elements of the repository.
- WP and DS Degradation describes the responses of these engineered systems to heat, humidity, seepage, and the geochemical environment of the EBS.
- Waste Form Degradation and Mobilization describes the degradation and dissolution of the waste forms and the release of radionuclides from the WPs.
- EBS Flow and Transport describes the flow of water and the transport of radionuclides from the repository to the UZ below the repository.
- UZ Transport describes the transport of radionuclides released from the repository through the UZ below the repository to the SZ.
- SZ Flow and Transport describes water flow and radionuclide transport from beneath the repository and downgradient through saturated rocks and alluvium, to the RMEI.
- Biosphere describes the biologic uptake of radionuclides, including inhalation, ingestion, and water consumption by humans at the site of the RMEI. The biosphere model component also includes consumption of bio-accumulated radionuclides in plants and animal food products.

In addition, the TSPA-LA Model considers early DS and WP failures, a human intrusion scenario, and describes the potential effects on the repository and the surrounding environment in response to igneous and seismic events.

ES3.5 Alternative Conceptual Models

A conceptual model is a set of working hypotheses and assumptions that provide an acceptable description of a system for its intended purpose. Because the TSPA process deals with future outcomes and includes uncertainty in both process descriptions and parameter values, there may be alternative conceptual models (ACMs) that provide reasonable descriptions of a particular system or subsystem. Considering ACMs helps build confidence that plausible changes in modeling assumptions or simplifications will not change conclusions regarding subsystem and total-system performance. Each model component and submodel discussion includes a summary evaluation of ACMs. For example, the development of the EBS Physical and Chemical Environment process model included consideration of an alternate initial water chemistry and the potential effect of feldspar equilibrium on seepage water composition, and the potential for

carbonate exchange to affect CO_2 composition in the UZ. All these ACMs were considered during development of the EBS Physical and Chemical Environment process model. Because ACMs must be compatible with all known data and established facts, their number is limited. Typically, when two or more models exist for the same phenomena and data, the more conservative one from a total-system perspective has been chosen for implementation.

ES3.6 Configuration Management for the TSPA-LA Model

The description of the TSPA-LA Model indicates how the supporting parameter values, along with the process-model abstractions representing many different aspects of the Yucca Mountain repository system, were integrated into one comprehensive PA model and used to estimate future repository performance. Appropriate restrictions were built into the TSPA-LA Model during its development to help ensure that the process-model abstractions were used only within their range of applicability.

The numerical abstractions of the process models were integrated in the TSPA-LA Model using software called GoldSim. The GoldSim software implements the TSPA-LA Model and simulates repository performance and calculates potential annual dose to the RMEI. The software used for the TSPA-LA Model is subject to the Yucca Mountain Project Quality Assurance program and controlled through the Software Configuration Management system to ensure that calculations are traceable to controlled software. The TSPA-LA Model simulations are conducted on computers and servers in a controlled environment. The TSPA-LA Model simulations are recorded, and the results are stored in the Yucca Mountain Technical Data Management System.

A number of software codes were implemented to support the development of the TSPA-LA Model. Some of these codes were used to provide supporting information, and some codes were directly implemented in the TSPA-LA Model using the GoldSim simulation software. Supporting software codes, including process models, were developed and operated externally before running the TSPA-LA Model. Software codes directly implemented as dynamically linked libraries (DLLs) in the TSPA-LA Model are generally referred to as abstractions and are run within the TSPA-LA Model. All software codes used to support the TSPA-LA Model are qualified and are under configuration control. Each qualified software code is uniquely identified with the software name, tracking number, version number, hardware platform, and operating system under which the code was qualified. All software documentation, including the software media, is linked to the unique tracking number.

Input parameter values are controlled through the TSPA Input Database. The database supports the TSPA-LA Model by providing the parameter values and distributions of these parameter values necessary for the TSPA analysis of the repository. The TSPA Input Database categorizes, stores, and retrieves fixed and distributed values of the TSPA-LA Model parameters and allows qualified, authorized analysts to review and update parameter values. The TSPA Input Database has strict user controls, featuring read and write access and audit trails that ensure the security, integrity, and traceability of the information used in the TSPA-LA Model analyses.

The TSPA-LA Model handles both the multiple-realization requirement and can accommodate the maximum size of coupled submodels. The GoldSim software fulfills these requirements

using an efficient solver that minimizes run time for each individual realization. The Monte Carlo sampling structure in GoldSim along with GoldSim's distributed processing capability allows the software to simultaneously run multiple realizations, then reassembles the results from these realizations into an ensemble result from the entire probabilistic run. Further, GoldSim acts as a driver, or integration software, that can couple other large pieces of software for those process models and submodels that were not converted to response surfaces, but are run concurrently in the TSPA-LA Model. A separate software code, EXDOC 2.0 (EXDOC_LA V. 2.0. 2007 [DIRS 182102]), uses the GoldSim results to compute mean and median dose histories.

ES4. YUCCA MOUNTAIN SITE DESCRIPTION

The Yucca Mountain repository system consists of natural and engineered systems that together will ensure the safe disposal of radioactive materials. The following provides a brief overview of the Yucca Mountain site and context for the development of the TSPA-LA Model.

The characteristics of the natural systems at Yucca Mountain that affect repository performance include climate, site geology, and site hydrogeology. The characteristics of the site geology and hydrogeology that affect repository performance include groundwater flow through the UZ and SZ, radionuclide transport, and disruptive events caused by igneous and seismic activity. The Yucca Mountain repository system lies in the Great Basin physiographic province. Characteristics of the natural system at Yucca Mountain that aid in repository performance include a semiarid climate, relatively stable site geology, a deep water table, and limited groundwater flow through the UZ and SZ. The Yucca Mountain area has a low incidence of large magnitude seismic activity. Volcanic activity in the Yucca Mountain region has declined through recent geologic time as described in *Igneous Activity at Yucca Mountain: Technical Basis for Decision Making* (NRC 2007 [DIRS 182132], Sections 2 and 3).

ES4.1 Physiographic Setting and Topography

Yucca Mountain is located within a transition zone between the northern boundary of the Mojave Desert and the southern boundary of the Great Basin Desert. The topography in this region is characterized by isolated, long and narrow, roughly north-south-trending mountain ranges and broad intervening valleys (Figure ES-11). The topography in the Yucca Mountain vicinity was shaped by erosional processes on the eastward-sloping ridge of the mountains and along faults and fault scarps that have created a series of washes downcut to varying degrees into different bedrock formations (Figure ES-12).

ES4.2 Climate

Current climatic conditions for the repository site and the Yucca Mountain region are discussed in *Yucca Mountain Site Description* (BSC 2004 [DIRS 169734], Section 6.3). The Yucca Mountain Project environmental program collected site climate and meteorological data using a network of nine automated weather stations (BSC 2004 [DIRS 169734], Section 7.1.3.2). The climate data show that the mountains west of Yucca Mountain cause a rain shadow effect, causing the present-day Nevada climate to be semiarid to arid, with dry winds and low precipitation. The climatic factors that most affect water-transport processes in the Yucca Mountain UZ are solar radiation-intensity flux; diurnal and seasonal temperature cycles; relative

humidity; and precipitation, in the form of either rain or snow as well as extended periods of drought.

ES4.3 Geology

Yucca Mountain is an uplifted, block-faulted ridge of alternating layers of Miocene age welded and nonwelded volcanic tuffs. The major Yucca Mountain geologic units are the volcanic tuff formations of the Paintbrush Group, the Calico Hills Formation, and the Crater Flat Group. For purposes of hydrogeologic studies, including infiltration, *Yucca Mountain Site Description* (BSC 2004 [DIRS 169734], Tables 3-1, 3-5, and 7-1) provides a separate stratigraphic nomenclature based on the degree of welding and hydrologic property distributions. The major hydrogeologic units are divided into the Tiva Canyon welded; the Paintbrush nonwelded, which consists primarily of the Yucca Mountain and Pah Canyon members and interbedded tuffs; the Topopah Spring welded; the Calico Hills nonwelded; and the Crater Flat undifferentiated units (Ortiz et al. 1985 [DIRS 101280], pp. 10 to 14, Table 1). Figure ES-13 shows the spatial relationship of the major hydrogeologic units of the UZ in both perspective and north-south and east-west cross-sectional views.

ES4.4 Regional Tectonic Setting

Igneous Activity at Yucca Mountain: Technical Basis for Decision Making (NRC 2007 [DIRS 182132], Section 2) describes the tectonic setting in terms of the geologic framework or structural geologic configuration (or both) of the different rock masses in the Yucca Mountain vicinity. The overall tectonic setting of the Great Basin physiographic province, including Yucca Mountain, is extensional, generally consisting of fault-bounded basins and mountain ranges that have been modified by volcanic activity during the past 15 million years. Typically, faults in the Great Basin include normal and strike-slip faults that reflect the extensional deformation caused by plate tectonic interactions at the western margin of the North American continent. The structural geology of Yucca Mountain and its vicinity is dominated by north-stretching normal faults with movement down to the west (Figures ES-14 and ES-15). Some of the faults on Figure ES-14 show evidence of quaternary activity (i.e., within the last 1.8 million years). Figure ES-15 shows that Yucca Mountain is a large eastward tilting block bounded by the Solitario Canyon fault to the west and the Bow Ridge fault to the east.

ES4.5 Local Volcanism

Two types of volcanism have occurred in the Yucca Mountain region. An early phase of Miocene silicic volcanism in the southwestern Nevada volcanic field culminated between 11.8 and 12.4 million years ago with the eruption of four voluminous ash-flow tuffs of about 1,000 km^3 each (Sawyer et al. 1994 [DIRS 100075], pp. 1311 and 1312). One of the silicic ash-flow tuffs that erupted from the Timber Mountain Caldera Complex (Figure ES-16) is the Topopah Spring Tuff, which forms the repository horizon planned for waste emplacement. Yucca Mountain is an uplifted, erosional remnant of these ash-flow tuff deposits.

Small-volume basaltic volcanism continued into the Quaternary Period. In terms of eruption volume, the 15-million-year history of volcanism in the region is viewed as a magmatic system that peaked between 11 and 13 million years ago, with the eruption of over 5,000 km^3 of

ash-flow tuffs. Following this peak of eruptive activity, relatively minor volumes of basalt have erupted in the last 11 million years (BSC 2004 [DIRS 169989], Section 6.1.1.1). Considered in terms of total eruption volume, frequency of eruptions, and duration of volcanism, basaltic volcanic activity in the region, including Yucca Mountain, defines one of the least active basaltic volcanic fields in the western United States (e.g., *Synthesis of Volcanism Studies for the Yucca Mountain Site Characterization Project* (CRWMS M&O 1998 [DIRS 105347], Chapter 2)).

ES4.6 Hydrology

ES4.6.1 Surface Hydrology

Yucca Mountain is located in the Amargosa River drainage basin, which is the major tributary drainage area to Death Valley (Figure ES-11). Stream flow from Yucca Mountain is captured by local drainages to the Amargosa River. The Amargosa River and its tributaries are ephemeral streams that are dry most of the time, with surface water-flow occurring rarely in direct response to precipitation. In some cases, groundwater discharges at springs in stream channels. During episodic flooding, flow occurs along the Amargosa River and flows to and fills much of the Death Valley playa to depths of 0.3 m (1 ft) or more (Miller 1977 [DIRS 105462], p. 18). During periods of cooler and wetter climate periods, such as 140,000 to 175,000 years ago, Death Valley was filled with water to depths of 175 m. Throughout the Yucca Mountain region and the Death Valley basin, perennial flow is only observed downgradient from spring discharges and around the margins of playas, where the groundwater discharges at land surface.

ES4.6.2 Groundwater Hydrology

Yucca Mountain is located in the Death Valley Regional Groundwater System (Figure ES-17). Groundwater below Yucca Mountain and in the surrounding region flows generally south toward discharge areas in the Amargosa Desert and Death Valley. The area around Yucca Mountain is in the central subregion of the Death Valley Regional Groundwater System, which has three groundwater basins: Pahute Mesa-Oasis Valley, Ash Meadows, and Alkali Flat-Furnace Creek. The primary sources of groundwater recharge are infiltration on Pahute Mesa, Rainier Mesa, Timber Mountain, and Shoshone Mountain to the north and the Grapevine and Funeral Mountains to the south (Figures ES-11 and ES-17). Recharge in the immediate Yucca Mountain vicinity is low, consisting of water reaching Fortymile Wash (Figure ES-17) as well as precipitation that infiltrates into the subsurface.

ES5. THE REPOSITORY SUBSURFACE FACILITY AND ENGINEERED BARRIER SYSTEM

ES5.1 Layout

Note: The following information regarding the repository subsurface facility and the EBS describes the design analyzed by the TSPA-LA Model and may be updated. The design layout of the Yucca Mountain repository subsurface facility is illustrated on Figure ES-18 and aspects of the design are described in *Total System Performance Assessment Data Input Package for Requirements Analysis for TAD Canister and Related Waste Package Overpack Physical Attributes Basis for Performance Assessment* (SNL 2007 [DIRS 179394]) and in *Total System Performance Assessment Data Input Package for Requirements Analysis for Subsurface*

Facilities (SNL 2007 [DIRS 179466], Table 4-1, Parameter Number 01-02). The waste emplacement drifts will be excavated to a diameter of 5.5 m and a nominal length of 600 m (actual lengths will range from 300 to 800 m) using a tunnel boring machine. Emplacement drifts will accommodate the 70,000 metric tons of heavy metal waste inventory scheduled for emplacement in the repository and are planned with a uniform spacing of 81 m between their centerlines. Each emplacement drift will have a capacity of approximately 100 WPs. An area in the southern section of the repository will be constructed to allow for contingencies during emplacement. The emplacement drift area will be excavated in the Topopah Spring Tuff upper lithophysal unit, Topopah Spring Tuff middle nonlithophysal unit, Topopah Spring Tuff lower lithophysal unit, and the Topopah Spring Tuff crystal-poor lower nonlithophysal unit of the repository host horizon. Eighty percent of the excavation will be in the lower lithophysal unit. The lithophysal rock units contain numerous cavities (lithophysal) of varying size and, consequently, high porosities. The nonlithophysal rock units are highly fractured and are characterized by fewer cavities, lower porosities, and have longer fractures than the lithophysal rock units.

ES5.2 Engineered Barrier System

The principal features of the EBS are a titanium-alloy DS and a two-layer WP to contain the waste. Figure ES-19 is a cross-section illustration of an emplacement drift and the major components of the EBS. The EBS includes ground support, a corrosion-resistant waste-emplacement supporting pallet, and an invert at the base of the drift filled with crushed welded tuff, which will have a steel infrastructure.

ES5.2.1 Ground Support

The repository subsurface ground-support system will be used to maintain drift stability in lithophysal and nonlithophysal rocks. Ground support will consist of friction-type, nongrouted rock bolts and a perforated steel sheet covering the upper 240 degrees of the drift-wall circumference above the invert. The perforations in the steel-sheet liner will provide flexural strength and allow air circulation for moisture removal behind the perforated sheet. Cementitious materials will not be used for the emplacement drifts ground support because of uncertainties related to potential chemical effects on the long-term performance of the repository. However, cement may be used in the turnouts from the access ways to the emplacement drifts. Analyses of the effects of the corrosion of ground support materials indicate only a negligible effect on the composition of seepage waters (SNL 2007 [DIRS 177412], Section 6.8).

ES5.2.2 Drip Shield

The emplacement drifts will be equipped with titanium interlocking DSs designed to reduce the effects of rockfall and seepage dripping on the WPs. The linked DSs will form a single continuous barrier for the entire length of each emplacement drift. The DSs will be fabricated from Titanium Grade 7 plates, with Titanium Grade 29 for structural support, and Alloy 22 for the base plates, which will prevent direct contact between titanium and the steel members of the invert.

ES5.2.3 Waste Package

The WPs will consist of an outer shell and an inner shell. The 25-mm-thick outer shell will be composed of corrosion-resistant Alloy 22. The 50-mm-thick stainless-steel inner shell will serve three functions: (1) the inner shell will provide structural strength to resist rockfall, support the internal waste form components, allow the WPs to be supported by the emplacement pallets, and facilitate handling; (2) the inner shell will provide radiation shielding to reduce the exterior surface contact dose rate; and (3) the inner shell will provide limited containment for the radioactive waste inside the WPs, although the TSPA-LA Model analyses do not consider this containment. The commercial spent nuclear fuel (CSNF) reference WPs also contain a stainless steel transport aging and disposal canister that is 25 mm thick and designed to hold a 21 pressurized water reactor or 44 boiling water reactor SNF assemblies. The co-disposal (CDSP) WP is designed to contain five defense HLW glass canisters surrounding a central canister of DOE-owned spent nuclear fuel (DSNF).

ES5.2.4 Emplacement Pallet

An emplacement pallet will support each WP placed in the repository. The emplacement pallets will prevent the WPs from coming in contact with the invert and any invert moisture. The emplacement pallet will be constructed of Alloy 22, a material that will provide long-term corrosion resistance and is the same material as the WP outer shell.

ES5.2.5 Invert

The invert will provide support for the WP emplacement pallets and the DSs. The invert will consist of a steel support structure and a crushed welded tuff ballast derived from the repository host rock. The ballast will be placed in and around the steel invert infrastructure to an elevation just below the top of the pallets' longitudinal and transverse support beams. The invert ballast will be compacted to prevent long-term settlement.

ES5.2.6 Waste Form

CSNF is composed of irradiated uranium oxide contaminated with fission and neutron induced activation products and their daughters. DSNF consists of a variety of uranium and plutonium compounds, including oxides, metals, and carbides packaged in seal-welded canisters. HLW will be mixed and solidified in a high-temperature, borosilicate glass for storage in stainless-steel canisters. Following breaching of the CSNF WPs and CDSP WPs and exposure of the waste to water infiltrating the WPs, the waste forms will be subject to aqueous dissolution and release of radionuclides. All waste forms will release radionuclides at different rates depending on their integrity and the solubility of the constituents of the waste.

ES5.2.7 Waste Form Cladding

SNF generally is encased in a metallic protective cladding. After the cladding is breached, the waste forms can degrade and release radionuclides to the EBS environment. The TSPA-LA Model takes no barrier credit for CSNF cladding. In addition, DSNF cladding is considered to be failed upon receipt. Therefore, the TSPA-LA Model does not take credit for waste-form cladding.

ES5.2.8 Emplacement Drift

The WPs will be placed in 5.5-m diameter, circular emplacement drifts that will serve to enhance the role of the natural barriers and the EBS. The presence of the circular underground drifts will result in the formation of a capillary barrier at the drifts' walls during the thermal and ambient postclosure periods. In addition, the decay heat from the waste in the WPs will lead to the development of a dry-out zone around the drifts that will help to prevent percolation from entering the repository and contacting the waste forms during the thermal period. The effectiveness of the drifts in providing a barrier will depend on the strength of the capillary pressure close to the drifts, host-rock permeability, the local percolation flux above the drifts, the temperature of the rock near the walls of the drifts, and the shape of the drift openings. An analysis of the presence of ground support and rock bolts indicated that these elements of the repository construction will not alter the role of the capillary barrier (SNL 2008 [DIRS 181244], Section 6.4.2.5).

ES5.2.9 Internal Waste Package Components

The WPs will have internal steel components and stainless-steel inner WP liners. These internal steel components are expected to degrade to iron oxyhydroxides following WP failure. These iron oxyhydroxides degradation products could potentially sorb radionuclides released from the degradation of the waste forms.

ES5.2.10 Thermal Loading and Waste Package Spacing

The WPs will be placed in the emplacement drifts in a line-load configuration with a WP-to-WP spacing of approximately 10 cm and a line-averaged heat load of 1.45 kW/m. Preclosure forced ventilation will be active from the start of emplacement, continuing until 50 years after the last WP is emplaced.

ES6. NATURAL AND ENGINEERED BARRIERS

The repository horizon is a minimum of 200 m beneath the land surface with a mean depth from the surface of approximately 300 m. The waste forms are solids (with minor gaseous constituents). Unless there is a volcanic eruption, the means for the radioactive constituents of the waste to reach the biosphere will be along groundwater pathways. The waste forms will pose risks to humans if, and only if, all of the following processes were to occur:

- Breaching of the DSs
- Breaching of the WPs
- Exposure of the waste forms to water
- Dissolution of the waste forms releasing radionuclides into the water
- Release of dissolved or colloid-associated radionuclides from the repository, through the UZ, and subsequent aqueous and colloidal transport of radionuclides through the SZ
- Natural or pumped discharge of radionuclide-containing water from the SZ

- Biosphere uptake of released radionuclides by humans or any part of the food chain.

Sections 7.1.8 and 7.3.1.2 describe other pathways to the biosphere as part of the volcanic eruption modeling case.

Three repository subsystems constitute barriers to radionuclide transport from the repository to the natural environment. The engineered components and natural processes of the Yucca Mountain repository system that are expected to combine to provide long-term waste isolation and act as barriers to radionuclide release, flow, and transport are:

- The Upper Natural Barrier—Limits water movement in the UZ above the repository
- The EBS—Limits water movement, radionuclide release, and radionuclide transport within and through the repository
- The Lower Natural Barrier—Reduces rate of water movement and delays radionuclide transport through the UZ below the repository and radionuclide transport through the SZ, and delays subsequent uptake by the biosphere.

ES6.1 Upper Natural Barrier

Figure ES-20 illustrates the key concepts associated with water movement in the UZ at Yucca Mountain. The source of water in the UZ at the repository horizon is precipitation at the land surface (SNL 2007 [DIRS 184614], Section 6.1.4). Climate controls the range of precipitation and land surface temperature conditions. Three potential climates, present-day, monsoon, and glacial-transition, are identified as likely during the first 10,000 years after repository closure, as illustrated on Figure ES-21. The durations of the 10,000 year climate periods used in the TSPA-LA Model were based on the most reasonable sedimentation rates at analogue climate sites as described in Section 6.3.1.2. The present-day climate is characterized by the relatively warm temperate conditions now observed at Yucca Mountain. The monsoon climate is characterized by hot summers with higher summer rainfall relative to the present-day climate. The glacial-transition climate has cooler and wetter summers and winters relative to the present-day climate. The climate durations used in the TSPA-LA Model for simulating the next 10,000 years at Yucca Mountain are the present-day climate for 600 years, followed by a warmer and wetter monsoon climate for 1,400 years, followed by a cooler and wetter glacial-transition climate for the remaining 8,000 years (Section 6.3.1.2). The climate from 10,000 years after repository closure to the period of geologic stability, defined as 1,000,000 years in NRC Proposed Rule 10 CFR 63.302 [DIRS 178394], is based on specifications regarding deep percolation rates provided in NRC Proposed Rule 10 CFR 63.342(c)(2) [DIRS 178394].

Precipitation on the surface of Yucca Mountain that does not run off, evaporate, or transpire infiltrates downward through the soil horizon and into the matrix and fractures in the bedrock as described in the site-scale UZ flow submodel. Net infiltration is spatially and temporally variable and higher on side slopes and ridge tops where bedrock is exposed. The net infiltration flowing downward to the UZ, the percolation flux, provides the water for groundwater flow and transport that could allow radionuclide transport from the repository to the water table. Flow at the repository horizon is included in the TSPA-LA Model using the drift seepage and drift-wall

condensation submodels. Flow into the repository is modeled with consideration of the capillary effect resulting from the presence of the repository underground opening.

ES6.2 Engineered Barrier System

The EBS includes the engineered components and the physical and chemical environment surrounding and within the engineered elements of the repository. Figure ES-19 illustrates the primary components of the EBS that are the WPs containing the waste, the DSs that protect the WPs from dripping water and falling rocks, and the crushed-tuff invert and support structures beneath the WPs and DSs. The barrier functions of the EBS are to isolate the waste forms from migrating water and chemical conditions leading to mobilization of the radionuclides in the waste forms. The EBS helps divert water from the UZ above the repository to the invert and to the UZ below the repository. The WP and DS Degradation Model Component simulates the response of these engineered systems to heat, humidity, seepage, geochemical environment, and moisture. The Waste Form Degradation and Mobilization Model Component simulates the dissolution of the waste forms and the amount of water released from breached WPs. The EBS Flow and Transport Model Component simulates the flux of fluid and radionuclides from the repository to the UZ below the repository.

ES6.2.1 Water Movement and Radionuclide Transport Within and Through the Engineered Barrier System

Figure ES-22 illustrates the key concepts associated with thermal-hydrologic (TH) processes affecting the EBS, including water vapor movement around the drifts, in the postclosure environment. WP and DS temperatures will be elevated, and some WPs and DSs may approach the boiling point of water immediately after emplacement. However, the heat output from the SNF and HLW will decline continuously because of radioactive decay. Heat output from the WPs will be at a maximum during the nominally 50-year preclosure period, but the emplacement drifts will be ventilated to remove most of the heat (SNL 2007 [DIRS 181383], Section 6.1.3). However, the warming of ventilation air will ensure that preclosure conditions will have relatively low humidity. At permanent closure of the repository, ventilation will cease, and a small zone of boiling to above boiling conditions is expected to form. At the same time, a condensation zone is expected to develop outside the boiling zone, resulting in continuous drainage of condensate and percolation in the near-drift region (SNL 2007 [DIRS 181383], Sections 6.1.3 and 6.1.4). However, the end-to-end WP spacing, coupled with the nonuniform heat output from the relatively hotter CSNF WPs and the relatively cooler CDSP WPs, which contain DSNF and HLW glass, makes it likely there will be direct heat flow toward cooler areas and around the drifts rather than through the drifts. In the drifts, vaporized water will tend to move away from hotter regions within the drifts and condense at cooler locations on the drift walls. The condensed water would then be available to drip directly onto an underlying DS (SNL 2007 [DIRS 181383], Section 6.3.11).

The titanium DSs will provide exceptional structural strength and corrosion resistance in saline environments that may evolve on the DS surfaces. The DSs will shield the WPs from damage due to rockfall as the emplacement drifts degrade over time. The titanium DSs are expected to degrade by general corrosion, which is a slow process. Except for a limited number of early

failures, the first DS failure is not projected to occur until between 200,000 and 310,000 years after repository closure.

The temperature of the WP surfaces, the chemistry of the water in contact with the WP surfaces, and the degradation characteristics of Alloy 22 will affect the degradation rates of the WPs. Degradation of the WPs because of general corrosion is not expected during the preclosure period. During the postclosure dry-out period, drift-wall temperatures are expected to be greater than the boiling point of seepage water. During this time, potential high-temperature modes of degradation include stress corrosion cracking (SCC), dry oxidation, and localized corrosion in response to deliquescence formed by hygroscopic minerals in dust deposited on the WPs and DSs as described in *Engineered Barrier System: Physical and Chemical Environment* (SNL 2007 [DIRS 177412], Section 6.10). Three main types of WP degradation were considered under nominal conditions-general corrosion, SCC, and seepage induced localized corrosion. An additional corrosion process, microbially induced corrosion, was considered to provide enhanced general corrosion on the WPs. The TSPA-LA Model also included mechanical failure of the DSs and WPs in the Seismic Scenario Class. Failure mechanisms that the analyses considered included collapse of DSs, SCC, and rupture of DSs and WPs. Under nominal conditions, the time of the first breach of a WP ranges from 100,000 years to one million years, with breaches caused by SCC in the weld of the outer closure lid. General corrosion failures would occur after 400,000 years.

Liquid water can enter WPs by advection when WP failure is by general corrosion or rupture. Water vapor is present at equilibrium with the relative humidity after all modes of WP failure. Degradation will begin after water contacts the waste forms. Following degradation and the start of dissolution of the waste forms, the concentrations of dissolved radionuclides in the water in the WPs will depend on their solubility limits. In case of high solubility limits, the concentration will depend on the waste form degradation rate. In addition, some radionuclides may attach to mobile colloids in the water. Radionuclides released from the solid waste forms into the solution will be available for transport. Figure ES-23 illustrates radionuclide transport through the EBS as either dissolved species or adsorbed onto colloidal particles. Radionuclide transport through the EBS will depend upon the distribution of water on the waste form surfaces and between the waste form surfaces and the outer edges of the degraded WPs. If water has dripped into the WPs through general corrosion breach, there could be advective transport of radionuclides to the edges of the WPs. If water has not dripped into the WPs then diffusive radionuclide transport could occur in an assumed continuous, interconnected water film.

Radionuclides may be transported through the invert by advection if there is mobile seepage water or by diffusion through the water into the pores of the invert materials. The radionuclides transported through the invert would ultimately be released to the fractures and matrix of the UZ below the repository, as shown on Figure ES-23. The dissolved and colloidally attached radionuclides will then be available for transport through the matrix and fractures in the UZ rock and ultimately released to the SZ.

The TSPA-LA Model simulates the release of radionuclides from the repository, depending on:

- The degradation rates of the components of the engineered barrier

- The dissolution rates of the waste forms
- The solubilities of the radionuclides
- Whether or not the released radionuclides are dissolved or attached to colloids
- Whether or not the radionuclides are sorbed onto corrosion products or invert material, or both
- The rate and volume of water flowing through the engineered barrier system
- The assumed existence of continuous water-film pathways allowing diffusion.

ES6.2.2 Water and Water-Vapor Movement around the Engineered Barrier System

The heat generated by the decay of waste (SNL 2007 [DIRS 181383], Section 6.1.2, Figure 6.1-1) will result in elevated rock temperatures for thousands of years after emplacement. For the TSPA-LA repository design concept, these temperatures will be high enough, in most locations, to cause boiling conditions in the vicinity of the drifts, thus giving rise to local water redistribution and altered groundwater flow paths in the UZ. As water approaches within a distance of one to several meters above the ceiling or crown of an emplacement drift, changing conditions may affect the amount of water that can drip into the drifts. In the early postclosure period, the water in the vicinity of the drifts will first encounter a dry-out zone. Under boiling conditions, water reaching the dry-out zone will vaporize, thus preventing liquid water from reaching the drifts. Vaporized water in the host rock will tend to move away from the drifts and through the permeable fracture network, driven primarily by the altered pore pressure conditions caused by boiling. In cooler regions away from the drifts, the water vapor will condense in the cooler fractures, where it will have the potential to drain either toward the heat source from above or migrate around the drifts to the UZ below the heated drifts. In addition, water percolating through the repository horizon will be partly diverted around the repository drifts, reducing the amount of liquid water available to enter the drifts and the development of a capillary barrier in the rocks around the drifts may prevent dripping into the drifts.

There may be considerable spatial and temporal variability of the TH conditions in and around the repository (SNL 2007 [DIRS 181383], Section 8.1). The spatial variability will be caused by heterogeneity in the rock properties and variations in the ambient percolation flux. In addition, differences in the thermal output of different WPs may cause a range of TH conditions in the repository. For example, cooler regions are expected along the edges of the repository and near low-thermal output WPs. The temporal variability in water movement around the drifts is caused, in the short-term, by the thermal output of the waste. Eventually, the waste heat output will decline, resulting in hundreds of years of drying and several thousand years of cooling and rewetting of the bedrock surrounding the drifts. Percolation encountering the dry-out zone could still be prevented from dripping into the drifts because of the capillary conditions in the bedrock matrix. The rate of water dripping into an emplacement drift is expected to be considerably less than the local percolation rate because the dry-out zone around the drift is expected to reduce liquid water flow, potentially preventing water from reaching the drift walls for a considerable period. The modeling approach to these phenomena in the long-term repository safety

calculations is conservative, however, and percolation is allowed to reach and even enter drifts soon after the boiling front is no longer in the rock. The uncertainty and variability in TH conditions is included in the parameter value distributions as part of the stochastic simulations conducted with the TSPA-LA Model.

ES6.3 Lower Natural Barrier

ES6.3.1 Flow and Transport in the Unsaturated Zone below the Repository

Figures ES-23 and ES-24 illustrate radionuclide transport of the dissolved or colloidally attached radionuclides released from the EBS to the UZ beneath the repository. Radionuclide transport within the UZ is expected to be principally by advection, but matrix diffusion and colloid-facilitated transport are considered as well. The effectiveness of these transport mechanisms will depend on sorption/desorption and radioactive decay that are included in the TSPA-LA Model. In the welded tuff units, advection of liquid water through fracture networks is expected to dominate radionuclide transport. Advection is also an important mechanism for transport between fractures and the rock matrix, especially at interfaces between nonwelded and welded tuff units, where there will likely be transitions between dominant advective fracture flow and dominant diffusive matrix flow. Dominant fault-and-fracture flow in welded tuffs will provide relatively short transport times through these units, whereas dominant matrix flow in the vitric nonwelded tuffs will result in much longer transport times. Mass transfer between fractures and the tuff matrix may play an important role in transport within Yucca Mountain and the transfer of radionuclides from fractures to the matrix may retard the overall transport of radionuclides to the water table. Also, the TSPA-LA Model includes variable flow paths, such as through perching horizons, which may affect the direction, distance, and time of radionuclide transport.

Sorption describes the combination of chemical interactions between dissolved solutes and solid phases such as immobile rock matrix or colloids, including adsorption, ion exchange, and surface complexation. Radionuclide transport in the UZ will also likely involve colloid-facilitated transport. Radioactive decay will lead to changes in radionuclide concentrations with time. In simple parent-progeny decay, the activity of the parent radionuclide will decrease with time. Chain decay will add additional complexity to the mix of transported material because of the ingrowth of radionuclide daughter products created from the decay of parent radionuclides. Further, some daughter products may have different sorption characteristics than their parent radionuclides and may have different transport characteristics.

Because the characteristics of the natural environment, along with the processes controlling transport, are variable in space and time, radionuclide transport will also be variable. Part of the temporal variability may involve long-term climatic changes that will not only change the percolation flux but could also cause the water table beneath Yucca Mountain to rise due to wetter climates or fall in response to drier climates.

ES6.3.2 Flow and Radionuclide Transport through the Saturated Zone to the Biosphere

Radionuclides transported through the UZ below the repository will be released to the SZ beneath the repository. Figure ES-25 illustrates the key concepts associated with flow and transport in the SZ beneath and downgradient from the Yucca Mountain site, as well as the pathways by which dissolved radionuclides may come into contact with the biosphere, including potential human uptake of and exposure to radionuclides.

Radionuclides reaching the SZ will be subject to flow and transport processes in the general direction of groundwater flow to the southeast, and then to the south and southwest. The groundwater flow processes determine the rate of water movement within the SZ and the flow paths through which groundwater is likely to travel. The groundwater flow paths extend from where the radionuclides may enter the SZ through volcanic tuff and alluvium to the boundary of the accessible environment and beyond.

Advective transport will be determined by the rate of groundwater flow and the effective porosity of the media through which the flow occurs and processes that relate to interactions between the dissolved or colloidal radionuclides and the aquifer materials. Dispersive processes will be affected by the effective porosity of the host rock and by small-scale velocity heterogeneities that allow some dissolved constituents to travel faster or slower than the average advective transport time.

Dissolved radionuclide transport may be retarded by diffusion from fractures into the rock matrix. The effectiveness of matrix diffusion in retarding radionuclide transport will depend on the diffusive properties of the matrix and the degree of spacing between the flowing fracture zones.

Some radionuclides that are potentially important to repository performance may be sorbed by the matrix of the SZ rocks. Carbon, technetium, and iodine do not sorb (SNL 2008 [DIRS 183750], Sections 6.5.3.1, 6.6.2, 6.6.2[a], 6.7.1, and 6.7.1[a]) and are modeled considering only advection, dispersion, and matrix diffusion processes. Other radionuclides, such as neptunium, uranium, and plutonium, will be sorbed to varying degrees onto colloids, which could subsequently diffuse into the matrix pores of fractured tuffs and alluvium (SNL 2008 [DIRS 183750], Sections 6.5.3.1, 6.7.1, 6.7.1[a], and 8.1). The stronger the sorption, the longer the radionuclide transport time when compared with advective-dispersive transport times.

The time for radionuclides to reach any specified point in the SZ downgradient from the repository, such as the boundary of the controlled area, described as 18 km in the primary direction of groundwater flow (10 CFR Part 63 (66 FR 55732 [DIRS 156671], III Public Comments and Responses, 3.5, p. 55750)), will depend primarily on the groundwater velocity and the potential retardation of radionuclides by sorption on the mineral surfaces within the bedrock or alluvial aquifers of the SZ.

Radionuclides in the SZ downgradient from the repository could enter biosphere pathways, including uptake by the local human population. The principal biosphere pathways to humans consist of the following:

- Direct consumption of water containing dissolved radionuclides
- Consumption of crops produced using water containing dissolved radionuclides
- Consumption of meat or dairy products from livestock watered with contaminated water or fed with contaminated crops, or both
- Direct exposure to contaminated soil
- Inhalation of dust that may contain attached radionuclides.

ES7. GENERAL DESCRIPTION OF THE TSPA-LA MODEL

The development of the TSPA-LA Model began with the identification and screening of the relevant FEPs that could affect the performance of the repository. The FEPs that were screened in were used to develop scenario classes for the TSPA-LA Model analyses. Figure ES-8 is a schematic representation of the development of the TSPA-LA Model showing the individual model components of the repository system. Figure ES-9 shows the hierarchy of the abstractions and submodels of the TSPA-LA Model. Each of the following individual model components represents a major aspect of the total repository system.

ES7.1 Model Components for the Nominal Scenario Class Modeling Case

The Nominal Scenario Class modeling case for the TSPA-LA Model encompasses all screened-in FEPs except those FEPs related to early failure, human intrusion, and igneous or seismic activity. The Nominal Scenario Class modeling case includes the potentially important effects and system perturbations caused by climate change and repository heating that are projected to occur after repository closure. In addition, the Nominal Scenario Class modeling case considers that the WPs and DSs will be subject to EBS environments and will degrade with time until they are breached and expose the waste forms to percolating groundwater. The degraded waste forms will release and mobilize radionuclides for transport out of the emplacement drifts. Radionuclides released from the emplacement drifts will be transported through the UZ below the repository by percolating groundwater and ultimately released to the SZ where they will be available for groundwater flow and transport to the accessible environment. The TSPA-LA Model's calculated annual dose to the RMEI also includes FEPs associated with the biosphere.

ES7.1.1 Unsaturated Zone Flow

The UZ Flow Model Component of the TSPA integrates five processes that contribute to flow in the UZ as shown on Figures ES-8 and ES-9: climate, infiltration, site-scale UZ flow, drift seepage, and drift-wall condensation. The UZ Flow Model Component defines the temporal and spatial distribution of water flow from the ground surface through the unsaturated tuffs above and below the repository horizon and the temporal and spatial distribution of seepage into the

waste emplacement drifts. Figure ES-20 provides a conceptual illustration of the mountain-scale flow processes at Yucca Mountain. Water at the repository horizon is derived from precipitation in the form of rainfall and snow at the land surface above the repository. Long-term temporal variability is included in the TSPA-LA Model by specifying four successive climate states: present-day, monsoon, glacial-transition, and a long-term climate based on specifications regarding deep percolation rates provided in NRC Proposed Rule 10 CFR 63.342(c)(2) [DIRS 178394] (Figure ES-21).

ES7.1.2 Engineered Barrier System Environment

The EBS Environment Model Component encompasses environments that may affect the performance of the EBS, including the mountain-scale TH environment and the chemical environment within the emplacement drifts as shown on Figures ES-8, ES-9, and ES-10. These environments are important to repository performance because they help determine the degradation rates of the EBS components, quantities, and species of mobilized radionuclides, as well as the transport of radionuclides and fluids through the emplacement drifts and into the UZ below the repository. Figure ES-20 shows the position of the repository drifts and WPs with respect to the Yucca Mountain flow system. Water percolating into the repository environment will be affected by heat from the emplaced waste and waste heat, and geochemical processes and conditions will determine the chemical environment of the EBS.

ES7.1.3 Waste Package and Drip Shield Degradation

The WPs and DSs will be the primary engineered components of the EBS (Figure ES-26). The WP and DS Degradation Model Component describes the degradation of the WPs and DSs as a function of time, presence of water, and repository location (Figures ES-8, ES-9, and ES-10). The WP and DS Degradation Model Component simulates general corrosion of the WPs and DSs, general corrosion and localized corrosion of the WP outer surface, SCC of the DSs and WPs, microbially influenced corrosion (MIC) on the WP outer surface, and early WP failure.

ES7.1.4 Waste Form Degradation and Mobilization

The Waste Form Degradation and Mobilization Model Component simulates waste-form degradation and the release of CSNF, DSNF, and HLW radionuclide inventories (Figure ES-27). Figure ES-28 illustrates the mechanisms related to the degradation of CSNF, as well as the release of dissolved and colloidal radionuclides from the waste forms to the EBS Transport Submodel. The Waste Form Degradation and Mobilization Model Component accounts for in-package water chemistry; matrix degradation rates for CSNF, DSNF, and HLW waste forms; radionuclide solubilities; and the types and concentrations of waste form and in-drift colloids.

ES7.1.5 Engineered Barrier System Flow and Transport

The EBS Flow and Transport Model Component calculates the rate of radionuclide release from the EBS to the UZ, which is determined by seepage into the emplacement drifts, condensation on the drift walls, WP and DS degradation, the presence of water films on in-package internals, waste-form degradation, and the TH environment of the EBS. The EBS Flow and Transport Model Component simulates the rate of water flow through the EBS, diffusive and advective transport, sorption, and colloid-facilitated transport.

ES7.1.6 Unsaturated Zone Transport

The UZ Transport Model Component describes the migration of radionuclides from the EBS and through the UZ to the water table. Consistent with the Mountain-Scale UZ Flow Submodel, the conceptual model for UZ transport (Figure ES-24) simulates coupled advective and diffusive transport through fracture and matrix continua using a dual-continuum approach. The UZ Transport Model Component simulates advective, dispersive and diffusive transport; sorption; colloid retardation, filtration, and exclusion; radioactive decay and ingrowth; and changes in water-level elevation.

ES7.1.7 Saturated Zone Flow and Transport

The SZ Flow and Transport Model Component simulates the transport of radionuclides from their introduction at the water table below the repository to the regulatory boundary 18 km downgradient from the Yucca Mountain repository (66 FR 55732 [DIRS 156671], III Public Comments and Responses, 3.5, p. 55750). Radionuclides are transported through the SZ either as solutes or sorbed to colloids. The SZ Flow and Transport Model Component simulates advection, dispersion, and diffusion in fractures; matrix diffusion; colloid retardation and exclusion; and sorption (Figure ES-25).

ES7.1.8 Biosphere

The Biosphere Model Component simulates radionuclide transport in the biosphere and the resulting exposure of the RMEI to radionuclides released from the repository after closure (Figure ES-29). The TSPA-LA Model includes the two dominant mechanisms of radionuclide release to the biosphere: (1) release through the SZ via groundwater, and (2) release through the air by ash dispersal from a volcanic eruption.

ES7.2 Model Components for the Early Failure Scenario Class

The Early Failure Scenario Class addresses FEPs that describe the potential for DS and WP early failure in the absence of disruptive events. The early-failure scenarios include DSs and WPs that fail prematurely due to material defects or improper manufacturing conditions or pre-emplacement operations and practices, such as improper heat treatment or welding flaws. Early DS and WP failures are analyzed using the Drip Shield Early Failure (EF) Modeling Case and the Waste Package EF Modeling Case. The DS and WP Early Failure Modeling Cases address FEPs that describe the potential for DS and WP early failure that could affect repository performance in the absence of disruptive events. The Drip Shield EF Modeling Case analyzes the possibility that DSs could fail prematurely, thus failing to protect the underlying WPs from seepage and possible localized corrosion. The Waste Package EF Modeling Case analyzes WPs that fail prematurely due to material defects, manufacturing errors, or pre-emplacement operations and practices, such as improper heat treatment or welding flaws that could affect WP performance and longevity.

ES7.2.1 Drip Shield Early Failure Modeling Case

Analysis of Mechanisms for Early Waste Package/Drip Shield Failure (SNL 2007 [DIRS 178765], Section 6.1.6) identified numerous potential mechanisms that could result in the

early failure of DSs. The following mechanisms were identified as potentially leading to early DS failure in TSPA-LA Model analyses:

- Improper heat treatment
- Base metal selection flaws
- Improper weld filler material
- Emplacement errors.

The probabilities of occurrence for the four DS early failure mechanisms were combined to develop a probability distribution for the rate of occurrence of undetected defects in DSs where an undetected defect was assumed to result in the early failure of a DS. The occurrence of undetected defects is assumed to be independent between DSs and, therefore, DS early failure is also independent between DSs. The Drip Shield EF Modeling Case considers DSs as associated with the waste forms in CSNF and CDSP WPs. Also, the TSPA-LA Model uses the simplifying assumption that each DS early failure affects a single WP and removes the overlying DS as a barrier to seepage at the time of repository closure, thus allowing the full volume of seepage to contact the affected WP. The TSPA-LA Model then assumes that a WP beneath an early failed DS experiences localized corrosion if it is contacted by seepage, completely compromising the WP outer barrier at the time of repository closure, thus allowing both advective and diffusive transport of radionuclides.

ES7.2.2 Waste Package Early Failure Modeling Case

Analysis of Mechanisms for Early Waste Package/Drip Shield Failure (SNL 2007 [DIRS 178765], Section 6.1.6) identified numerous potential mechanisms that could result in the early failure of WPs. The following mechanisms were identified as potentially leading to early WP failure in TSPA-LA Model analyses:

- Weld flaws
- Improper heat treatment of the outer corrosion barrier
- Improper heat treatment of outer corrosion barrier lid
- Improper stress relief of outer corrosion barrier lid (low plasticity burnishing)
- WP mishandling damage
- Improper base metal selection
- Improper weld filler material.

The TSPA-LA Model calculates the characteristics of weld flaws using distributions for the size and number of potentially undetected weld flaws based on industrial analogue studies, which are then used to form the per WP closure weld volume and weld thickness. The TSPA-LA Model simulates the critical flaw orientation probability and an applicable depth factor to model where undetected flaws might remain and might result in SCC that could penetrate the WP closure welds.

The analysis of the other early WP failure mechanisms determined that the occurrence of an undetected defect could result in early failure of a WP. The probability distribution for the rate of occurrence of undetected defects is equivalent to a probability distribution for the rate of WP

early failures. The occurrence of undetected defects is assumed to be independent between WPs; therefore, WP early failure is also independent between WPs regardless of the type of WP.

ES7.3 Model Components for the Disruptive Events Scenario Classes

Igneous events and seismic activity are possible sources of repository disruption. The TSPA-LA Model assumes that igneous activity will cause EBS damage from magma intersecting and intruding into the repository drifts and/or from an eruption from a volcanic vent passing through the repository. Seismic activity in the form of vibratory ground motion and/or fault displacement will disrupt DSs resulting and allow dripping water to contact WPs, and that could lead to localized corrosion of the WP outer barrier.

The modeling cases described below do not mention the likelihood of these events. Rather, these descriptions indicate how such an event is considered in the TSPA-LA Model if it were to occur.

ES7.3.1 Igneous Scenario Class Modeling Cases

ES7.3.1.1 Igneous Intrusion Modeling Case

The Igneous Intrusion Modeling Case describes the performance of the repository system if igneous activity disrupts the repository. The Igneous Intrusion Modeling Case assumes that a dike intersects the repository and destroys DSs and WPs in those drifts intruded by magma, exposing the waste forms to percolating water and mobilizing radionuclides for transport out of the repository, down through the UZ to the SZ, and then to the accessible environment as shown on Figure ES-30. The Igneous Intrusion Modeling Case uses the following model components to simulate repository performance following an igneous intrusion:

- UZ Flow
- EBS Environment
- WP and DS Degradation
- Waste Form Degradation and Mobilization
- EBS Flow and Transport
- UZ Transport
- SZ Flow and Transport
- Biosphere.

ES7.3.1.2 Volcanic Eruption Modeling Case

The Volcanic Eruption Modeling Case simulates the fraction of igneous events in which a volcanic eruption through the repository also occurs. In this case, waste from WPs intersected by flowing magma is transported to the land surface through one or more eruptive conduits, and tephra and entrained waste are discharged into the atmosphere, transported by wind currents, and deposited at the land surface as shown on Figure ES-31. The Volcanic Eruption Modeling Case also evaluates the hillslope and fluvial redistribution of the contaminated tephra deposited on the land surface using the code FAR (FAR V. 1.2. 2007 [DIRS 182225]).

The TSPA-LA Model uses the following processes and model components to calculate repository system performance for the Volcanic Eruption Modeling Case:

- Volcanic interaction with the repository
- Atmospheric transport
- Tephra redistribution
- Biosphere.

ES7.3.2 Seismic Scenario Class Modeling Cases

The Seismic Scenario Class evaluates repository performance for seismic activity that disrupts the repository drifts and the EBS and uses the same TSPA-LA Model components as the Nominal Scenario Class to evaluate the mobilization and transport of radionuclides exposed to seeping water, release from the EBS, transport in the UZ, and transport in the SZ to the location of the RMEI. The effects of seismic events are taken into account in the EBS but not in the natural system. The Seismic Scenario Class modeling cases simulate damage to DSs and WPs as a function of the magnitude of a seismic event, including Seismic GM and Seismic FD Modeling Cases using mean hazard curves for peak ground velocity (PGV) and fault displacement. Each mean hazard curve is defined as the mean estimate or average of a distribution of hazard curves and typically represents the 80th or greater percentile of the distribution because the average is dominated by the larger values of the distribution.

The Seismic Scenario Class modeling cases use the following model components to estimate total system performance:

- UZ Flow
- EBS Environment
- WP and DS Degradation
- Waste Form Degradation and Mobilization
- EBS Flow and Transport
- UZ Transport
- SZ Flow and Transport
- Biosphere.

ES7.3.2.1 Ground Motion Modeling Case

The Seismic GM Modeling Case includes WPs that fail solely due to ground motion damage from a seismic event. The Seismic GM Modeling Case uses nominal processes because nominal corrosion processes can affect the repository's susceptibility to damage during a seismic ground motion event.

The TSPA-LA Model simulates the effects of vibratory ground motion on both lithophysal and nonlithophysal rock using rockfall analyses. The large rock blocks that could be ejected from the nonlithophysal units of the repository horizon during vibratory ground motion, could fill emplacement drifts during the period of geologic stability. The drifts in the lithophysal zone are predicted to collapse into small fragments with particle sizes of centimeters to decimeters, whereas the large blocks in nonlithophysal zones may be shaken loose from the drift walls and

fall onto DSs. Drift collapse could lead to increased temperature and relative humidity of the outer surface of WPs in lithophysal regions, where rubble filling the collapsed drift could form a thermal blanket covering the WPs. Drift collapse could also affect seepage flux and drift-wall condensation in the emplacement drifts in the lithophysal zones.

ES7.3.2.2 Fault Displacement Modeling Case

The Seismic FD Modeling Case includes only those WPs that fail due to fault displacement damage from known and hypothetical faults in the repository. The projected number of WPs that could fail due to fault displacement is a small fraction of the total number of WPs in the repository. A fault displacement that occurs in an emplacement drift may cause one portion of a drift to be displaced vertically or horizontally relative to an adjacent section, possibly causing shearing of an overlying WP and DS if the fault displacement exceeds the available clearance in the EBS. The TSPA-LA Model simulates direct shear failure of a WP if fault displacement exceeds one-quarter of the outer diameter of the WP OCB (about 0.4 meters to 0.5 meters), allowing advective flow through the sheared WPs. If a WP is sheared, the TSPA-LA Model also assumes that the overlying DS is failed

ES7.3.2.3 Human Intrusion Scenario Modeling Case

The Human Intrusion Modeling Case simulates a single drilling intrusion at 200,000 years that intersects a single waste package, creating a pathway for water flow into the waste and for radionuclide movement out of the EBS. The Human Intrusion Modeling Case uses the following model components to estimate total system performance:

- UZ Flow
- EBS Environment
- WP and DS Degradation
- Waste Form Degradation and Mobilization
- EBS Flow and Transport
- UZ Transport (stylized to represent presence of a borehole)
- SZ Flow and Transport
- Biosphere.

ES7.4 TSPA Input Database

The TSPA Input Database provides the parameter values and distributions of parameter values necessary for the TSPA-LA Model. All input data, including the parameter values and their distributions, are stored and controlled. The TSPA-LA Model was developed concurrently with the supporting models and analyses and tracks and ensures traceability of data and data sources. The TSPA Input Database also categorizes and stores fixed and distributed values of the TSPA-LA Model parameters under strict user controls that ensure the security, integrity, and traceability of the information used in the TSPA-LA Model analyses using signed and catalogued Parameter Entry Forms.

ES8. VERIFICATION/VALIDATION OF THE TOTAL SYSTEM PERFORMANCE ASSESSMENT MODEL

Procedures IM-PRO-003, *Software Management,* Section 6.9.12, and SCI-PRO-006, *Models*, Section 6.3, respectively, were utilized to support verification and validation of the TSPA-LA Model, providing confidence that the TSPA-LA Model adequately represents the physical processes in the repository system and properly transfers outputs between the TSPA-LA Model modules and submodels. Figure ES-32 provides an illustration of the major activities conducted for TSPA-LA Model validation. The model validation activities provide confidence in the TSPA-LA Model and its results. Using these activities ensures that the TSPA-LA Model is valid for its intended use of calculating mean annual dose and other performance measures with respect to radionuclide releases from the repository and compliance with NRC Proposed Rule 10 CFR Part 63, Subparts E and L ([DIRS 178394] and [DIRS 180319]).

ES8.1 Verification and Validation Strategy

TSPA-LA Model verification activities were designed to establish confidence that the calculated results were achieved properly using the modeling tools, submodels, and a given set of controlled inputs. TSPA-LA Model verification included verification of the integrated TSPA-LA Model software (GoldSim), verification of DLL implementations within the TSPA-LA Model, verification of model inputs entered into the TSPA Input Database, and verification of the implementation of the submodel abstractions within the TSPA-LA Model. Coupling between submodels within the TSPA-LA Model was verified by ensuring that information generated by one submodel was fed correctly to successive submodels.

A typical model validation compares the model's results with experimental measurements and/or field observations. However, such measurements are impossible to obtain for the TSPA-LA Model at the temporal and spatial scales of interest for postclosure repository performance. Therefore, the TSPA-LA Model was validated using corroboration, technical review, and natural analogues.

The TSPA-LA Model inputs were checked, controlled, and documented to maintain traceability and transparency. Confidence in the methodology of and inputs to the TSPA-LA Model is provided through:

- Selection of input parameters and/or input data from validated supporting analysis model reports
- Model calibration activities and/or evaluation of the initial boundary conditions for the TSPA-LA Model, establishing model convergence
- Evaluation of the impacts of uncertainties on model results.

These three activities demonstrate that: (1) the TSPA-LA Model's input parameter values from source documents, as well as those parameter values that are calculated by the TSPA-LA Model, are correctly propagated throughout the model; (2) the TSPA-LA Model is stable in terms of the number of realizations, the length of model timesteps, and spatial discretization; and (3) that the

uncertainty in model inputs is propagated through and correctly accounted for in the TSPA-LA Model.

The following post-development methods were used to demonstrate TSPA-LA Model validation with respect to intended use and desired level of confidence:

- Corroboration of TSPA-LA Model results with analogue studies or other relevant observations not previously used to develop or calibrate the model
- Confidence building through incorporation of the recommendations and observations provided by technical reviews conducted by external experts regarding the TSPA-VA, the TSPA-SR, and a draft version of the TSPA-LA
- Corroboration of abstraction or submodel results to the results of the validated mathematical models from which the abstraction or submodel was derived
- Corroboration of TSPA-LA Model results with the results obtained from auxiliary analyses as a means of providing additional confidence.

ES8.2 Computer Code and Input Verification

The verification of computer codes from outside sources and model inputs used in the TSPA-LA Model included: (1) verification of the integrated system software, GoldSim, the software platform on which the TSPA-LA Model is based; (2) verification of DLLs from source documents and DLLs that are generated within the TSPA-LA Model; and (3) verification of model inputs from the TSPA Input Database. Submodels from source analysis and/or model reports were verified by comparing submodel results calculated by the TSPA-LA Model with the results in the analysis and/or model reports. Coupling between submodels was examined by verifying that the information generated by one submodel was input correctly to successive submodels and that the information never exceeded the applicable range of validity of the next successive submodel. The following model verification activities apply and demonstrate that incorporation of information and submodels from other sources into the TSPA-LA Model has not altered the validity of the information, the submodels, or both:

- The TSPA-LA Model software, GoldSim, was qualified per a well defined process following program procedure SCI-PRO-003.
- Outputs from DLLs from other sources, including analysis/model reports and data tracking numbers, were correctly replicated in the TSPA-LA Model.
- Outputs from DLLs calculated within the TSPA-LA Model were found to be within established acceptance criteria.
- Individual submodels were validated in their respective analysis/model reports.
- Results from submodels within the TSPA-LA Model were compared to results contained in analysis/model reports and were found to agree within selected acceptance criteria.

- Feeds from one submodel to another submodel were found to be correctly transferred, and these feeds either did not exceed the valid range of the successive submodel or the values used were fixed within the range or at the upper bound of the range of the successive submodel.

- Inputs from the TSPA Input Database were verified to correspond with source data.

ES8.3 Stability Testing

The stability of the model was evaluated in the following areas:

- Statistical stability of mean and median annual dose
- Numerical accuracy of expected dose calculations
- Adequacy of temporal discretization
- Adequacy of spatial discretization
- Stability of the FEHM UZ transport submodel

The uncertainties represented in the TSPA-LA Model are characterized as either epistemic or aleatory uncertainty, and the numerical evaluation of repository performance treats the two categories of uncertainty separately. This technical approach follows advice given by the NRC and the EPA in their publications, and reflects an internationally accepted way to conduct complex, long-term analyses of this type as indicated by the acceptance of the TSPA methodology by an International Peer Review (*An International Peer Review of the Yucca Mountain Project TSPA-SR* (OECD/IAEA 2002 [DIRS 158098]). Appendix E contains summary comments and recommendations provided by the International Peer Review.

For each modeling case, the TSPA-LA Model calculates a distribution of expected annual doses for each epistemic realization, where the expectation is over the aleatory uncertainty in the modeling case. For brevity these quantities are simply termed expected annual dose. The mean and median of the distribution of expected annual dose is termed the mean annual dose and median annual dose, respectively. Section 6.1.2 provides a formal definition of these quantities and describes the calculations for each modeling case.

The stability of the mean and median annual dose is demonstrated for each modeling case by means of replicated sampling. Three sets of calculations were performed for three independent samples of epistemic uncertainty, termed replicates. Each set of calculations results in estimates of the mean and median annual dose, along with the 95th and 5th percentiles of expected annual dose. Comparison of these statistics resulting from each replicate demonstrates that the sample size is sufficient to obtain statistically stable estimates of mean and median annual dose. Figure ES-33a shows the three estimates of mean annual dose, median annual dose, along with the 95th and 5th percentiles of expected annual dose, for the Seismic GM Modeling Case for 10,000 years postclosure. Figure ES-33a demonstrates that there is very little variation between the results for each replicate, therefore, the results are statistically stable. The three estimates for the mean annual dose for each replicate were then used to calculate a confidence interval (Figure ES-33b). Figure ES-33b shows that the true value of the mean annual dose is contained in the narrow confidence interval for the values of the calculated mean annual dose for each replicate.

In general, these calculations involve numerical evaluation of one or more integrals. Because each modeling case addresses different aleatory uncertainties, the methods of calculating expected annual dose differ for each modeling case. Figure ES-34 illustrates numerical accuracy of the calculated expected annual dose for the Seismic GM Modeling Case for 10,000 years postclosure. Figure ES-34 shows that the expected annual dose does not change when the numerical integration is refined by considering additional specified event times and damage fractions. Therefore, the TSPA-LA Model provides a sufficiently accurate value of expected annual dose. Section 7.3.2 demonstrates that the calculation of expected annual dose is sufficiently accurate for each modeling case.

The temporal discretization of the TSPA-LA Model affects its ability to estimate the future behavior of water and radionuclide movement. Timestep size was evaluated for the Waste Package EF, Igneous Intrusion, Seismic GM and Human Intrusion Modeling Cases, which collectively span the range of processes and events that influence repository performance. The analyses demonstrate that the TSPA-LA Model results are stable with respect to the temporal discretization employed. The degree of stability shown in the graphical comparisons of the results of the stability analysis, see Figure ES-35, indicated that a statistical comparison of timestep changes was not necessary.

The TSPA-LA Model deals with the variability associated with spatial discretization of the various model domains which operate at different scales with spatially dependent information. The TSPA-LA Model also represents variability in environmental conditions among WP by means of representative WPs. The spatial discretization utilized in the TSPA-LA Model accounts for the variable scales of the submodels while avoiding undue computational burdens. Analyses were conducted to examine the effect on TSPA-LA Model results of representing large populations of WPs by a few select WPs. The analyses demonstrate that the TSPA-LA Model results are not sensitive to the use of representative WPs. Therefore, the spatial variability in the environmental conditions among WPs is adequately represented.

Additional stability analyses were conducted for the FEHM UZ Transport Submodel. The FEHM UZ Transport Submodel employs a particle-tracking technique to determine transport of radionuclides through the UZ. Stability was examined by varying the number of particles used to simulate radionuclide transport. The analyses demonstrate that TSPA-LA Model results are not sensitive to the number of particles used. Therefore, the UZ Transport Submodel produces stable results.

ES8.4 Uncertainty Characterization Reviews

10 CFR 63.114 (a)(2) [DIRS 178394] requires that a repository PA include an appropriate treatment of the uncertainty and variability of the values of uncertain parameters. The Lead Laboratory conducted a risk-informed review of the parameters used in the TSPA-LA Model, including sensitivity analyses that focused on the effects of the uncertainty and variability in these parameters on the results provided by the TSPA-LA Model. Fifteen formal reviews were performed to scrutinize the uncertainty characterizations of the values of 40 TSPA-LA Model input parameters and their associated abstractions. The technical reviews focused on: (1) confirming that the values of TSPA-LA Model parameters appropriately reflect the major sources of uncertainty and/or variability in those values; (2) verifying that the probability

distributions were derived using sound statistical methods and interpretations; and (3) ensuring that model parameter probability distributions are reasonable and defensible and do not underestimate dose risk. One result of the reviews was that fifteen probability distributions were subsequently corrected, modified, or independently derived to improve their treatment of uncertainty and variability. The approach of the uncertainty characterization and propagation was generally based on *Guidelines for Developing and Documenting Alternative Conceptual Models, Model Abstractions, and Parameter Uncertainty in the Total System Performance Assessment for the License Application* (BSC 2002 [DIRS 158794]).

The reviews included a risk-based ranking of TSPA-LA Model scenario classes and modeling cases to focus the reviews on the most important component model abstractions for the Nominal Scenario Class, the Early Failure Scenario Class, the Igneous Scenario Class, and the Seismic Scenario Class. The Human Intrusion Scenario was excluded from the ranking because the relevant model parameters (for release, flow, and transport) are addressed in the Nominal Scenario Class.

Based on insights and results from previous TSPAs, the following ranking (from highest to lowest) of the scenario modeling cases was obtained:

1. Seismic Scenario Class, Seismic GM Modeling Case
2. Igneous Scenario Class, Igneous Intrusion Modeling Case
3. Igneous Scenario Class, Volcanic Eruption Modeling Case
4. Early Failure Scenario Class, Waste Package and Drip Shield EF Modeling Cases
5. Seismic Scenario Class, Seismic FD Modeling Case
6. Nominal Scenario Class, Nominal Modeling Case.

The magnitudes of the projected dose risk indicated that the first three modeling cases dominated the projected total dose. The analysis provided a list of key TSPA-LA Model parameters whose uncertainty or variability was anticipated to have the greatest influence on the mean and variance of the dose distribution.

Sensitivity analyses were performed during the development of the TSPA-LA Model to investigate the propagation of uncertainty throughout the TSPA-LA Model and to identify uncertain inputs that may be important to the uncertainty in the calculated results. The during-development sensitivity analyses generally confirmed that the uncertainty reviews of the TSPA-LA Model had identified the key uncertain inputs, confirmed that important uncertain inputs were propagated appropriately in the process models and submodels, demonstrated that the effects of these uncertainties were consistent with underlying physical principles, and identified implementation inaccuracies that were subsequently resolved.

Appendix K presents sensitivity analyses performed with the TSPA-LA Model that were used to identify the dominant sources of uncertainty in total expected dose to the RMEI, and in the contributions to the expected dose from key radionuclides such as ^{239}Pu, both dissolved and sorbed to colloids, ^{237}Np, and ^{99}Tc. The post-development TSPA-LA Model sensitivity analyses also investigated uncertainty in selected process model results such as the time of DS failure and the chemical environment in the repository drifts. These sensitivity analyses confirm that uncertain inputs have been appropriately propagated through the TSPA-LA Model consistent

with physical principles, and the analyses are illustrated using selected causal explanations of the relationships between the input and output variables.

ES8.5 Surrogate Waste Form Validation

The waste forms included in the TSPA-LA Model are CSNF (stainless steel and zirconium-based Zircaloy cladding), DSNF, and HLW. Because all waste forms have some amount of variability in form and radionuclide inventory, the CSNF,DSNF, and HLW waste forms are analyzed in the TSPA-LA Model using surrogates that are generally represented by mean characteristic values. For example, DSNF has 11 categories of DSNF and their individual representation in the TSPA-LA Model would dramatically increase simulation time. The naval spent fuel (Category 1) in the TSPA-LA Model is represented by Zircaloy-clad CSNF. The remaining DSNF (Categories 2 through 11) is represented by a single DOE surrogate spent fuel that has a radionuclide inventory that is the weighted average of the radionuclide inventories of Categories 2 through 11. The dissolution rate of the DOE surrogate spent fuel is instantaneous, based on the rapid dissolution of Category 7 DSNF (i.e., uranium metal) under in-package chemistry conditions. The results of all the analyses show that the use of surrogates to represent naval spent nuclear fuel, as well as CSNF, HLW, and the remaining DSNF is appropriate.

ES8.6 Corroboration of Abstraction Model Results with Validated Process Models

Development of the TSPA-LA Model required the abstraction of process models to provide submodels as well as parameter values for direct input to the TSPA-LA Model. Corroboration of the results provided by the abstractions used in the TSPA-LA Model with their respective process models provides confidence that the direct input parameters implemented in the TSPA-LA Model are technically sound for their intended purpose.

The consistency between the TSPA-LA Model and submodels and the source process models is achieved by ensuring that the individual abstractions are validated for their intended use in the TSPA-LA Model, performing input-verification activities during their implementation in the TSPA-LA Model and performing TSPA-LA Model stability-testing activities during development. Certain post-development validation and confidence building activities unrelated to the TSPA-LA Model development activities need to be performed in order to determine that the TSPA-LA Model is appropriate for its intended use. These confidence-building activities were performed after ensuring the integrity of the underlying process models through abstraction validation and TSPA-LA Model implementation processes, and after the abstractions were shown to be functioning correctly when applied together as TSPA-LA Model components. These activities ensure the stability of the TSPA-LA Model, and they constitute the first steps towards defining and executing follow-up post-development validation and confidence-building activities.

To corroborate the abstraction models with the validated process models, the abstraction results were qualitatively and quantitatively compared with the results obtained by the respective process models. The corroboration was performed for the process models and analyses that served as and provided direct inputs to the TSPA-LA Model. The results demonstrate that the process model abstractions are validated and corroborated with their underlying process models (Section 7.6). The results of the corroboration analysis confirm that the abstractions

implemented in the TSPA-LA Model corroborate qualitatively and quantitatively with their underlying validated process models and analyses.

ES8.7 Auxiliary Analyses

Auxiliary analyses were used to assist in validating the TSPA-LA Model. The auxiliary analyses helped to determine the reasonableness of and provide confidence in the results calculated by the TSPA-LA Model. Four different auxiliary analyses were performed: (1) single realization analysis; (2) comparison of the results of the TSPA-LA Model with a Simplified TSPA Analysis; (3) comparison of the results of the TSPA-LA Model with the TSPA independently developed by the Electric Power Research Institute (EPRI); and (4) a Performance Margin Analysis (PMA) of the TSPA-LA Model's modeling cases.

Single Realization Analysis

Single realization analyses (Section 7.7.1) demonstrate proper functioning of TSPA-LA Model and coupling of its submodels. Single realization analyses were performed on four modeling cases that cover the range of WP failure mechanisms considered in the TSPA-LA Model, and highlight the processes affecting and controlling radionuclide releases under varying thermal-physical-chemical conditions: (1) the Waste Package EF Modeling Case; (2) the Drip Shield EF Modeling Case; (3) the Igneous Intrusion Modeling Case; and (4) the Seismic GM Modeling Case. The Drip Shield and Waste Package EF Modeling Cases emphasize the transport at early times when the repository is at an elevated temperature, as well as the effects of climate change on the intact DSs. The Igneous Intrusion and Seismic GM Modeling Cases show the effects of late-time processes when the DSs have been breached and there is variable damage to the WPs.

The single realizations represent unique combinations of epistemic and aleatory uncertainty. The aleatory uncertainty for each modeling case represents (1) spatial location in the Waste Package and Drip Shield EF Modeling Cases, (2) timing of an event in the Igneous Intrusion Modeling Case, and (3) randomly generated seismic events of varying magnitudes in the Seismic GM Modeling Case. The single realization analyses qualitatively and quantitatively illustrate mass transport of various selected radionuclides with respect to the upper natural barrier, the EBS, and the lower natural barrier.

These analyses help explain the relationship between DS and WP failure mechanisms and failure openings, waste-form degradation under varying thermal-physical-chemical conditions, the partitioning of the released mass between the UZ fractures and UZ matrix at the EBS-UZ boundary, and the transport characteristics of the EBS, UZ, and SZ, including sorption, radioactive decay, decay-chain ingrowth, dispersion, and dilution. In all modeling cases analyzed, early-time release following the WP failure is dominated by non-sorbing and non-solubility limited radionuclides such as ^{99}Tc and ^{129}I, whereas late-time release is dominated by solubility-limited radionuclides that undergo sorption such as ^{242}Pu, ^{237}Np, and ^{239}Pu.

Comparison with Simplified TSPA Analysis

TSPA-LA Model results were compared to results calculated using a stand-alone Simplified TSPA Analysis of the Yucca Mountain repository (Section 7.7.2 and Appendix L) that was

developed to corroborate the TSPA-LA Model using a higher level abstraction than that used in the TSPA-LA Model. The simplification involved removing detail from the TSPA-LA Model to capture spatial and temporal variability, and treating the repository system using a more average representation of processes and parameter values. Although the Simplified TSPA Analysis is different than the TSPA-LA Model in both its structure and computational method, the simplified model has identical technical bases. The Simplified TSPA Analysis simulated: (1) the Nominal Modeling Case; (2) the Waste Package EF Modeling Case; (3) the Seismic GM Modeling Case; and (4) the Igneous Intrusion Modeling Case.

The results of the Simplified TSPA Analysis show that for the Seismic GM and Igneous Intrusion Modeling Cases, the total mean annual dose and the mean annual dose from individual radionuclides are similar in magnitude to those obtained for the corresponding modeling cases using the TSPA-LA Model. The Simplified TSPA Analysis of the Waste Package EF Modeling Case calculated a higher mean annual total and individual radionuclide doses than those calculated with the TSPA-LA Model. The Simplified TSPA Analysis for the Seismic GM Modeling Case indicated a similar trend in the mean annual dose for the key radionuclides, although the magnitude of their mean annual doses were slightly different. The Simplified TSPA Analysis for the Igneous Intrusion Modeling Case indicates that the total probability-weighted mean annual dose is similar in magnitude to that obtained for the nominal scenario simulated over a 1,000,000-year period with the TSPA-LA Model, with minor differences in radionuclide concentrations.

Comparison with EPRI TSPA Analysis

The TSPA-LA Model results were compared to results obtained with the EPRI TSPA analyses obtained using the EPRI Integrated Multiple Assumptions and Release Code (IMARC). Section 7.7.3 and Appendix M describe the similarities and differences between the EPRI TSPA Analysis and the TSPA-LA Model. The EPRI TSPA Analysis used data available in the analysis model reports that were primarily used for preparation of the TSPA for the Site Recommendation (TSPA-SR), and did not use the information used in the TSPA-LA Model. The EPRI Analysis does not explicitly consider aleatory uncertainty, whereas the TSPA-LA Model considers both epistemic and aleatory uncertainty. Compared to the TSPA-LA Model, the EPRI Analysis represents a more simplified implementation of the various process models and their associated uncertainties. To help understand the basis for the doses obtained with the EPRI TSPA Analysis and TSPA-LA Model, the EPRI TSPA nominal modeling case was compared to the corresponding TSPA-LA nominal modeling case. Also, the TSPA-LA Model mean annual doses for the Nominal Modeling Class and Waste Package EF Modeling Case were compared with the corresponding mean annual doses obtained with the EPRI model.

A comparison of the calculated results between those from the EPRI model and those from the TSPA-LA Model indicates similar values of dose and similar radionuclides that contribute most to dose. Although both models predict a similar increase in dose after 100,000 years, after about 1,000 years postclosure, the TSPA-LA Model calculates a greater increase in dose due to early-failure. The early-failure increase in dose occurs later in the EPRI TSPA Analysis. The maximum annual dose calculated by the EPRI TSPA Analysis at one-million years postclosure is about 0.02 mrem/yr as compared to the approximately 0.4 mrem/yr at one million years calculated by the TSPA-LA Model. The differences in the respective results can broadly be

accounted for by differences in: (1) seepage rates through the repository; (2) the representations of early-failure of EBS components; (3) waste form and radionuclide inventory; and (4) solubility limits and sorption characteristics in the UZ and SZ.

Performance Margin Analysis

The Performance Margin Analysis (PMA) (Section 7.7.4 and Appendix C) was used to quantitatively evaluate conservatisms in the TSPA-LA Model to (1) confirm that they are conservative with respect to the calculated mean annual dose; (2) quantify the extent to which the conservatisms, individually and collectively, overestimate the mean annual dose; and (3) assess whether or not the conservatisms introduce any inappropriate risk dilution. The PMA addressed a select set of TSPA-LA modeling cases for both 10,000-year and 1,000,000-year time periods, and utilized modified representations of selected TSPA-LA Model submodels and selected sets of conservative parameter values. The PMA results for peak mean annual dose for the 10,000 year and 1,000,000 year are lower than the doses calculated for the same modeling cases using the TSPA-LA Model. The largest mean annual doses calculated using the PMA are more than an order of magnitude lower for the 10,000 years postclosure period, and are lower by a factor of two for the 1,000,000 years postclosure period. Also, for the PMA results, different modeling cases contribute most to the total mean annual dose than indicated by TSPA-LA Model results. When compared to the total mean annual dose calculated with the TSPA-LA Model, the lower total mean annual dose calculated by the PMA demonstrates that the conservatisms incorporated in the TSPA-LA Model do not introduce risk dilution.

ES8.8 Confidence Building: Natural Analogues

Corroboration of the results of the TSPA-LA Model can be gained, in part, through comparison with natural analogues. Natural analogue results were used in the validation process for the model components and submodels for several of the analysis model reports supporting the TSPA-LA Model. The natural analogues relevant to the Yucca Mountain repository are discussed in *Natural Analogue Synthesis Report* (BSC 2004 [DIRS 169218]) and include natural analogues to materials intended for use in the Yucca Mountain repository as well as the results of some investigations of analogues to geologic processes. The information from natural analogues has contributed to the understanding of drift stability, degradation of the waste forms and elements of the EBS, seepage, UZ flow and transport, coupled processes, SZ transport, the biosphere, and disruptive events, such as volcanism and seismic events. Natural analogue information was used in the development of the supporting submodels of the TSPA-LA Model as provided by the analysis/model reports. The use of natural analogues helps ensure that these submodels are grounded in reality and provides confidence that the TSPA-LA Model provides reasonable results. In addition to the confidence provided in general by the examples of natural analogues on a qualitative basis, performance comparisons with two selected analogues, the Cerro Negro volcanic eruption and the Nopal I uranium mine at Peña Blanca, provide additional confidence in the TSPA-LA Model.

The ASHPLUME software was used to simulate ash-fall thickness from the 1995 eruption of the Cerro Negro volcano. The results show that ASHPLUME can reasonably predict the spatial distribution of ash-fall thickness from the eruption of a basaltic cinder cone volcano similar to Cerro Negro (Figure ES-36). The Cerro Negro ash-fall calculation method was used to simulate

eruptive releases of ash from volcanic vents in the vicinity of the Yucca Mountain repository or from a volcanic vent passing through the repository and resulting in WP destruction and aerial distribution of waste particles containing radionuclides.

Radionuclide transport by groundwater is the most likely off-site transport pathway for the Yucca Mountain repository. The Peña Blanca natural analogue site (Figure ES-37) offers a unique opportunity to examine the groundwater flow and transport of uranium and some of its daughter products in a climatic and geologic setting very similar to that of Yucca Mountain. Both the Peña Blanca and Yucca Mountain sites are set in volcanic tuff in an oxidizing UZ and are in similar desert environments. Figure ES-38 shows the geologic structure at the Nopal I mine, the position of the ore deposit above the water table, and the low westerly to easterly groundwater gradient. The Nopal I mine at Peña Blanca was originally comprised of uraninite, which is chemically similar to nuclear fuel. The Nopal I deposit was analyzed using a modified version of the metal-fuel dissolution submodel used in the TSPA-LA Model. The observed uranium concentrations at observation wells PB1, PB2, PB3, clustered within 50 m of the ore deposit, and PB4, approximately 0.75 km downgradient from the ore deposit shown on Figure ES-39. The concentration values of uranium in the groundwater downgradient from the Nopal I ore deposit indicate that radionuclides released from the deposit appear to have been retarded by the natural geologic system. The relatively high uranium concentrations shown on Figure ES-39 are due to the disturbance caused by drilling the observation wells PB1, PB2, and PB3 in 2002. Successive well cleaning and sampling removed the excess uranium from these wells and uranium concentrations returned to values similar to the concentrations observed in PB4. The results of field investigations at the Nopal I mine and analyses of rock and water samples demonstrate the ability of natural systems to provide a sink for radionuclides released from the deposit.

ES8.9 Summary of Technical Reviews

Technical reviews of PA models form an important part of model validation. During the past decade, the Yucca Mountain Project has developed successive TSPA models as well as accompanying input process models, all of which have been subject to technical reviews by external experts as part of their validation. Each milestone PA for the Yucca Mountain repository was subject to external reviews. The Total System Performance Assessment for the Viability Assessment (TSPA-VA) was the subject of a peer review as described in Section 7.9.1. An International Review Team (IRT) conducted an evaluation of the Total System Performance Assessment for the Site Recommendation (TSPA-SR), and the accompanying TSPA-SR performance-assessment model. Appendix E summarizes the comments provided by the IRT review of the TSPA-SR Model, and the responses to those comments. An Independent Validation Review Team (IVRT) reviewed a draft version of the TSPA-LA Model and the accompanying IVRT report provided comments as described in Section 7.9. The comments from the IVRT technical review of the draft TSPA-LA Model were addressed, and the TSPA-LA Model incorporates the material contained in the responses to those comments.

TSPA-VA Peer Review

The TSPA-VA peer provided a two-year, formal, independent evaluation and critique of the development and completion of the TSPA-VA. The TSPA-VA peer review panel's key

conclusions were as follows. (1) The peer review found that TSPA-VA utilized an overall sound approach for assessing the postclosure performance of the Yucca Mountain repository. (2) The peer review found that the TSPA-VA's descriptions of the long-term probable behavior of the Yucca Mountain repository was not supported by adequate evidence that the TSPA-VA Model represented the systems, components, and processes that they were designed to represent. The peer review found that because the TSPA-VA Model contained both conservative and non-conservative submodels, decisions based on the TSPA-VA Model results should be made cautiously. (3) The peer review concluded that the TSPA-VA was a necessary and useful step in the evolving understanding of the performance of the Yucca Mountain repository. The panel also felt that the TSPA-VA provided valuable insights into the performance of the various repository components and helped identify issues where additional data and analyses could improve the understanding of repository performance. (4) The peer review noted the inherent difficulty in the ability of the TSPA-VA Model to predict the repository behavior during the postclosure regulatory period mandated at that time. (5) The peer review noted that the planned future activities at Yucca Mountain would provide valuable information for confirming, calibrating, and/or validating the process models describing repository performance.

The Yucca Mountain Project fully implemented the recommendations provided by the peer review, resulting in major revisions to the components of the TSPA-VA Model. Using expanded site-scale test data, revisions to the TSPA-LA Model resulted in the TSPA-SR Model, and the associated analyses that supported the Final Environmental Impact Statement.

International Review Team Peer Review

The IRT review provided an independent assessment of the methodology used in the TSPA-SR. The IRT review was based on international standards and guidance. The IRT made several recommendations regarding the application of the TSPA-SR Model and its methodology to the development of the TSPA-LA. The IRT's key conclusions were as follows. (1) The TSPA-SR Model's methodology was sound and implemented in a competent manner. (2) The performance assessment approach provided an adequate basis for suggesting likely compliance with the 10,000 years regulatory standard, and, thereby, for the site recommendation decision. (3) The IRT stated that future TSPA iterations should emphasize that the understanding of the repository system and its performance and provides for safety both during and beyond the postclosure regulatory period. The IRT provided 27 specific recommendations for future improvements to be included in the preparation and submission of the LA (Appendix E).

IVRT Technical Review

The IVRT review scope was defined by the then available TSPA Technical Work Plan for the draft TSPA-LA Model according to two model validation goals: (1) describe the postclosure performance of the repository system for the Nominal, Igneous, and Seismic Scenario Classes; and, (2) produce an estimate of mean dose (and other performance measures, as appropriate) consistent with the degree of conservatism representative of the component abstraction models and parameters values and their uncertainty. The IVRT provided seven recommendations that were implemented in the current TSPA-LA Model (Sections 7.9.3.2 and 7.9.3.3).

ES9. SYSTEM PERFORMANCE ANALYSES

The TSPA-LA Model was used to conduct a PA of the Yucca Mountain repository system. The analyses provide mean and median annual dose to the RMEI for the first 10,000 years after repository closure and for the period of geologic stability (one million years) specified in NRC Proposed Rule 10 CFR 63.303 [DIRS 178394]. The TSPA-LA Model calculated evaluated modeling cases representing nominal conditions, early DS and WP failures, and disruptive events. The TSPA-LA Model analyses also address both the individual and groundwater protection requirements of NRC Proposed Rule 10 CFR 63.311 [DIRS 178394] and 10 CFR 63.331 [DIRS 180319], respectively.

The analyses account for uncertainties in the representations of FEPs that could affect the annual dose. The PA analyses address the effect of alternative parameters, submodels, and approaches to FEPs. The calculations are probabilistic in the sense that the results are for multiple realizations, carried out using sampled values from the probability distributions for the values of the uncertain model parameters.

ES9.1. Total Mean Annual Dose to the Reasonably Maximally Exposed Individual for the Repository System

Figure ES-40 displays the total expected annual dose for first 10,000 years after repository closure and shows that the greatest mean annual dose for this period is less than 0.23 millirem. Figure ES-41 displays the total expected annual dose for the postclosure period from 10,000 to one-million years after repository closure and shows that the greatest median annual dose for this period is less than 1 millirem. These total expected annual dose values represent the sum of the expected dose calculations for each of six scenario class modeling cases considered for the TSPA-LA Model. Figures ES-40 and ES-41 show the distribution of the doses calculated from multiple realizations of the TSPA-LA Model and thus display the uncertainty in the total expected dose resulting from epistemic uncertainty about the repository system.

Figure ES-42 shows the radionuclides that contribute most to the estimate of mean annual dose and indicates that ^{99}Tc, ^{14}C, ^{129}I, and ^{239}Pu dominate the estimated mean annual dose during the first 10,000 years after repository closure. In a similar manner, Figure ES-43 shows that ^{239}Pu, ^{129}I, and ^{226}Ra generally dominate the mean annual dose for the first 100,000 years of the postclosure period; and that ^{226}Ra, ^{242}Pu, and ^{237}Np generally dominate the mean annual dose for the postclosure period from 100,000 to one-million years.

ES9.2 Results of the Scenario Class Modeling Case Simulations

Following are descriptions of the results provided by the scenario class modeling cases used to simulate repository performance. Figures ES-44 through ES-57 present the expected annual dose calculated for the individual modeling cases. The following describes these results by modeling case.

ES9.2.1 Nominal Scenario Class Modeling Case

The results for this modeling case show zero mean annual dose for the first 10,000 years because no WPs are estimated to fail (by general corrosion, localized corrosion, or SCC) in this period.

The first WP failure (by nominal SCC) would occur at approximately 30,000 years, and the DSs would begin to fail by general corrosion at approximately 260,000 years. As shown on Figure ES-44, the estimated maximum mean and median annual doses for the postclosure period from 10,000 to one-million years would be 0.5 and 0.3 millirem, respectively. Figure ES-45 shows the radionuclides that dominate the estimate of mean annual dose for the Nominal Scenario Class Modeling Case. The main contributors to mean annual dose would be the highly soluble and mobile radionuclides ^{129}I and ^{99}Tc.

ES9.2.2 Early Failure Scenario Class Modeling Cases

The Early Failure Scenario Class Modeling Cases include FEPs that relate to early WP and DS failure due to manufacturing, material defects, or pre-emplacement operations that would include improper heat treatment. Radionuclide mobilization and transport for the Early Failure Scenario Class is similar to the Nominal Scenario Class, but differs from the Nominal Scenario Class in that the Early Failure Scenario Class considers only WPs affected by early DS and WP failures.

ES9.2.2.1 Drip Shield Early Failure Modeling Case

The defective DSs were modeled as being failed at the time of repository closure, and WPs underlying any failed DSs and exposed to seepage are conservatively considered as failed. Figure ES-46 shows the expected annual dose histories for the first 10,000 years after closure and the postclosure period from 10,000 to one-million years. The expected annual doses account for aleatory uncertainty about the number of early failed DSs, types of WPs under failed DSs, and their locations in the repository. The mean, median, and 5th and 95th percentile curves in this plot show the uncertainty in the expected annual dose due to epistemic uncertainty from incomplete knowledge of the behavior of the repository system. The calculations for the first 10,000 years show a projected mean annual dose of approximately 0.0003 millirem at 2,000 years after repository closure. The mean annual dose then decreases steadily and is less than 0.0002 millirem during the postclosure period from 10,000 to one-million years.

Figure ES-47a shows the radionuclides contributing most to the total mean annual dose during the first 2,000 years after repository closure are soluble and mobile radionuclides, in particular ^{99}Tc, ^{129}I, and ^{14}C. During the postclosure period from 10,000 to one-million years, Figure ES-47b shows that ^{239}Pu, ^{242}Pu, ^{226}Ra, and ^{237}Np dominate the mean annual dose.

ES9.2.2.2 Waste Package Early Failure Modeling Case

The WPs are assumed to be failed at the time of repository closure. However, intact DSs overlying early failed WPs will degrade by general corrosion after repository closure. Figure ES-48 shows the expected annual dose histories for the first 10,000 years after repository closure and for the postclosure period from 10,000 to one-million years. The expected annual dose accounts for aleatory uncertainty about the number of early failed WPs, types of early failed WPs, and their locations in the repository. The mean, median, and 5th and 95th percentile curves on Figures ES-48a and ES-48b reflect the epistemic uncertainty in the expected annual dose.

Figure ES-48a shows that the calculated mean annual dose is about 0.004 millirem at about 9,800 years. The mean annual dose during the first 10,000 years postclosure results from early failed CDSP WPs. The relative humidity in the CDSP WP emplacement locations tends to be

higher and forms an aqueous layer suitable for radionuclide diffusion earlier than in the CSNF WPs. Because the CDSP WPs contain DOE SNF and the TSPA-LA Model does not take credit for the canister, cladding, or fuel matrix, diffusive transport of radionuclides can start as soon as the humidity in the breached CDSP WPs is greater than 95 percent (Section 8.2.2.2). The increase in mean annual dose at about 9,800 years postclosure, as shown on Figure ES-48a, is due to the beginning of diffusive transport from early-failed CSNF WPs. Figure ES-48b shows that the estimated mean and median annual doses are about 0.02 and 0.006 millirem, respectively, before 15,000 years, and the doses gradually decrease thereafter until about 300,000 years postclosure. At about 300,000 years postclosure, the DSs begin to fail from general corrosion, and the expected annual dose increases during the period from 300,000 to 400,000 years postclosure because of advective transport of radionuclides through failed WPs.

Figure ES-49a shows that in the first 10,000 years after closure, the more soluble and mobile radionuclides, ^{99}Tc, ^{129}I, and ^{14}C, dominate the estimate of mean annual dose. Figure ES-49b shows that during the postclosure period from 10,000 to one-million years, ^{239}Pu, ^{242}Pu, ^{226}Ra, and ^{237}Np dominate the expected mean annual dose.

ES9.2.3 Igneous Scenario Class Modeling Cases

The Igneous Scenario Class addresses the set of FEPs that describe igneous events that could affect repository performance. The Igneous Scenario Class is represented by: (1) the Igneous Intrusion Modeling Case that represents a magma dike that intrudes into the repository causing subsequent release of radionuclides to the groundwater in the UZ, and (2) the Volcanic Eruption Modeling Case that represents a hypothetical volcanic eruption from a volcanic conduit that passes through the repository and emerges at the land surface with the release of radionuclides to the atmosphere.

ES9.2.3.1 Igneous Intrusion Modeling Case

After a magmatic dike intersects the repository, radionuclide release and transport away from the repository would be similar to the Nominal Modeling Case. All of the DSs and WPs would be damaged, exposing the waste forms to percolating groundwater with subsequent degradation, radionuclide mobilization, and transport through the UZ to the SZ. The Igneous Intrusion Modeling Case considers that the remnants of the DSs, WPs, or cladding do not divert any water from the waste.

Figure ES-49 shows calculated expected annual dose histories that account for aleatory uncertainty in igneous intrusions such as the number of future events and the time at which they may occur. The mean, median, and 5th and 95th percentile curves on Figure ES-50 indicate epistemic uncertainty in expected annual dose resulting from incomplete knowledge of the behavior of the physical system during and after the disruptive event. The calculated mean annual dose for the first 10,000 years postclosure is less than 0.06 millirem, and 1.3 millirem during the postclosure period from 10,000 to one-million years. The median projected annual dose for during the postclosure period from 10,000 to one-million years is less than 0.4 millirem.

Figure ES-51a shows that ^{99}Tc and ^{129}I dominate the estimate of the expected mean annual dose for the first 4,000 years, and ^{239}Pu, ^{99}Tc, and ^{240}Pu dominate the estimate of the mean annual

dose for the first 10,000 years postclosure. Figure ES-51b shows that ^{239}Pu dominates the estimate of the mean for the next 170,000 years, and ^{226}Ra, ^{242}Pu, and ^{237}Np dominates expected mean annual dose for the during the postclosure period from 10,000 to one-million years.

ES9.2.3.2 Volcanic Eruption Modeling Case

Volcanic eruptions may occur at Yucca Mountain if an igneous dike rises through the Earth's crust, intersects one or more repository drifts, and forms an eruptive conduit. WPs in the direct path of the conduit would be destroyed, and the waste in those packages would be entrained in the eruption. Contaminated volcanic ash would be erupted, transported in the atmosphere, deposited at land surface, and subject to potential redistribution by hillslope and fluvial processes. The RMEI could receive a radiation dose from exposure to the contaminated ash.

Figure ES-52 shows the expected annual dose for first 10,000 years after closure and the post-10,000-year period. The expected annual dose considers aleatory uncertainty in the numbers and times of eruptions, the number of WPs intersected by the eruption, the fraction of waste that is ejected, eruptive power, the duration of the eruption, wind direction, and wind speed. The distribution of the expected annual dose is due to epistemic uncertainty with respect to incomplete knowledge of the behavior of the repository system during and after an eruption. The mean annual dose for the first 10,000 years postclosure is less than 0.0002 millirem, and decreases to less than 0.0001 millirem for the postclosure period from 10,000 to one-million years.

Figure ES-53a shows that for the first 1,000 years postclosure, the d mean annual dose is dominated by ^{241}Am. Between 1,000 and 10,000 years postclosure, the radionuclides that dominate the mean annual dose are ^{239}Pu and ^{240}Pu. Figure ES-53b shows that^{239}Pu, ^{240}Pu, and ^{226}Ra are the dominant contributors until approximately 100,000 years after closure when ^{226}Ra and ^{229}Th, ^{126}Sn, and ^{237}Np are the primary dose contributors for the postclosure period from 100,000 to one-million years.

ES9.2.4 Seismic Scenario Class Modeling Cases

The Seismic Scenario Class represents the direct effects of vibratory ground motion and fault displacement associated with seismic activity affecting repository performance. The Seismic Scenario Class modeling cases include seismic-related changes in seepage, the performance of WPs and DSs, and flow in the EBS. The Seismic Scenario Class is represented by the Seismic GM Modeling Case and the Seismic FD Modeling Case.

ES9.2.4.1 Ground Motion Modeling Case

The Seismic GM Modeling Case considers the possible failures of DSs and WPs due to mechanical damage associated with seismic vibratory ground motion, including: accumulation of rockfall on DSs; collapse of the DS framework; SCC of WPs; and rupture or puncture of WPs. Figure ES-54 presents calculated expected annual dose histories for the Seismic GM Modeling Case for the first 10,000 years after closure and the postclosure period from 10,000 to one-million years. The distribution of the expected annual dose takes into account aleatory uncertainty associated with the number of seismic ground motion events, the time and magnitude of each event, and the effects of each event on WPs, DSs, and the emplacement drifts.

The mean, median, and 5th and 95th percentiles of the distribution of expected annual dose shown on Figure ES-54 reflect epistemic uncertainty due to incomplete knowledge of the behavior of the repository system during and after seismic events. Figure ES-54 shows that the largest mean annual dose for first 10,000 years after closure is approximately 0.2 millirem. The median annual dose for the postclosure period from 10,000 to one-million years is less than 0.5 millirem. The smoothness of the plot of the expected annual doses shown on Figure ES-54a is due to the use of a quadrature method to numerically integrate over the aleatory uncertainty for the first 10,000 years after repository closure. Alternatively, the uneven plot shown on Figure ES-54b is due to the use of a Monte Carlo method to numerically integrate over aleatory uncertainty for the postclosure period from 10,000 to one-million years, as well as the inclusion of general corrosion in the Seismic GM Modeling Case.

The results on Figure ES-55a show that ^{99}Tc, ^{14}C, ^{129}I, and ^{239}Pu dominate the estimate of the mean for the first 10,000 years after closure. Figure ES-55b shows that radionuclides ^{99}Tc and ^{129}I, with lesser contributions from ^{79}Se and ^{239}Pu and ^{226}Ra, and ^{135}Cs, dominate the calculated expected mean annual dose during most of the postclosure period from 100,000 to one-million years, with ^{242}Pu and ^{237}Np increasingly prominent after 800,000 years postclosure. The expected mean annual dose due to ^{14}C decreases completely within the first 100,000 years postclosure because of radioactive decay. The CDSP WPs would be the primary WPs damaged during the first 10,000 years after closure because the CSNF WPs are stronger and more failure-resistant. The CSNF WPs will be more robust than CDSP WPs because they include two inner stainless-steel vessels instead of one: the inner vessel and its lid similar to the CDSP WPs, and the CSNF WPs are placed in an outer, tightly fitting stainless-steel transportation, aging, and disposal (TAD) canister. The stainless steel, waste-containing canisters in the CDSP WPs do not fit as tightly and could move more freely under the influence of ground motion. The predominant mechanism that would cause damage to CDSP and CSNF WPs is SCC resulting in diffusive releases of radionuclides.

ES9.2.4.2 Fault Displacement Modeling Case

The Seismic FD Modeling Case includes disruption of WPs and DSs by the displacement of faults. Figure ES-56 shows the expected annual dose histories for the Seismic FD Modeling Case for the first 10,000 years after closure and for the postclosure period from 100,000 to one-million years. The expected annual dose accounts for aleatory uncertainty about the number, type, and locations of disrupted DSs and WPs. The mean, median, and 5th and 95th percentile curves on Figure ES-56 show uncertainty in the distribution of expected annual dose, due to epistemic uncertainty regarding the behavior of the repository system during and after fault displacement events. These figures show that the mean annual dose for the first 10,000 years after closure is less than 0.002 millirem, and less than 0.02 millirem for the postclosure period from 10,000 to one-million years. The median projected dose for the postclosure period from 10,000 to one-million years is approximately 0.01 millirem.

Figure ES-57a shows that ^{99}Tc, ^{239}Pu, and ^{129}I dominate the estimate of the mean annual dose for the first 10,000 years after closure. Figure ES-57b shows that ^{239}Pu, dominates the mean annual dose up to 100,000 years postclosure, and ^{242}Pu, ^{226}Ra, and ^{237}Np dominate the mean for the remainder of the postclosure period from 100,000 to one-million years.

ES9.2.5 Total Mean Annual Dose to the Reasonably Maximally Exposed Individual for the Repository System

Figure ES-58 shows the contribution to the total mean annual dose histories for the Drip Shield EF, Waste Package EF, Igneous Intrusion, Volcanic Eruption, Seismic GM, and Seismic FD Modeling Cases. Figure ES-58 shows that the Seismic GM and Igneous Intrusion Modeling Cases provide the largest contributions to the total mean annual dose for the postclosure period from 10,000 to one-million years. The Seismic GM Modeling Case includes general corrosion processes for the postclosure period from 10,000 to one-million years. Figure ES-58 shows that the events that most affect repository performance are seismic ground motion, igneous intrusions, and WP failure due to general corrosion.

ES9.3 Comparison of Annual Dose with Postclosure Individual and Groundwater Protection Standards

ES9.3.1 Individual Protection Standard

The results provided by the TSPA-LA Model include calculations of the total mean annual dose to the RMEI in any year during the next 10,000 years after repository closure (NRC Proposed Rule 10 CFR 63.303(a)) and the total median annual dose to the RMEI in any year from 10,000 years after repository closure through the period of geologic stability (NRC Proposed Rule 10 CFR 63.303(b)). Per NRC Proposed Rule 10 CFR 63.311 [DIRS 178394] the postclosure individual protection standard is 15 millirem up to 10,000 years postclosure and 350 millirem after 10,000 years, but within the period of geologic stability (one million years). The TSPA-LA Model results, shown on Figure ES-40 and ES-41, which refer to distribution of total expected annual dose, show that the highest projected total mean and total median annual doses to the RMEI are estimated to be about 0.23 millirem (Figure ES-40) and 0.99 millirem (Figure ES-41), respectively. These results demonstrate that the total mean annual dose to the RMEI in any year during the next 10,000 years after repository closure is less than the individual protection standard of 15 millirem per NRC Proposed Rule 10 CFR 63.311(a)(1) [DIRS 178394]. In addition, the highest projected dose values, mean or median, throughout the period of geologic stability are more than two orders of magnitude below the individual protection limit of 350 millirem per 10 CFR 63.311(a)(2) [DIRS 178394].

Uncertainty/Sensitivity Results

For different time frames in the analysis, different epistemic parameters emerge as important to the overall uncertainty in the results. Table ES-1 lists summary results of the sensitivity analysis. The important parameters listed on Table ES-1 are as follows:

- *IGRATE*. This parameter is the probability of an igneous event, expressed as the annual frequency of an intersection of the repository by a volcanic dike. Uncertainty in this parameter arises from epistemic uncertainty about igneous activity that may affect the repository.

- *SCCTHRP*. This parameter is the residual stress threshold for the Alloy-22 WP outer barrier, expressed as a percentage of the yield strength. If the residual stress in the WP

outer barrier exceeded this threshold value, stress corrosion cracks could form, which could allow radionuclides to migrate from the WP. The primary causes of residual stresses in the WP outer barrier would be high-peak ground velocity seismic ground motions, which may cause impacts from WP to WP, from WP to emplacement pallet, and from WP to DS. These impacts could cause dynamic loads that could dent the WP, resulting in structural deformation with residual stresses that could make the material susceptible to SCC.

- *WDGCA22*. This parameter relates to the temperature dependence of the Alloy 22 WP outer barrier general corrosion rate. This uncertainty parameter determines the magnitude of this temperature dependence and directly influences the short-term and long-term general corrosion rates of the Alloy 22. Larger values of *WDGCA22* result in earlier, higher general corrosion rates during the thermal period, and lower long-term corrosion rates when the repository temperatures are near the ambient in-situ temperature.

The parameters in Table ES-1 that most affect the total uncertainty in the TSPA-LA Model are factors that govern degradation of the WPs, the occurrence of damage from seismic events, and the frequency with which igneous intrusions occur.

Table ES-1. Top-Ranking Uncertainty Importance Parameters

Time After Closure (years)	Two Most Important Parameters	
3,000	SCCTHRP	IGRATE
5,000	SCCTHRP	IGRATE
10,000	SCCTHRP	IGRATE
125,000	IGRATE	SCCTHRP
250,000	WDGCA22	IGRATE
500,000	IGRATE	WDGCA22
1,000,000	IGRATE	WDGCA22

Source: Output DTN: MO0709TSPAPLOT.000_R0 [DIRS 183010].

ES9.3.2 Groundwater Protection Standard

The groundwater protection standard in NRC Proposed Rule 10 CFR 63.331 [DIRS 180319] stipulates that the releases of radionuclides in groundwater at the location of the RMEI should not cause the level of radioactivity in the representative water volume of 3,000 acre-feet of water (10 CFR 63.332(a)(3) [DIRS 180319]) to exceed the groundwater protection standard. The regulation does not require that evaluation of the groundwater protection standard include very unlikely events. Therefore, igneous and seismic events are not included in applying this standard.

Figure ES-59 shows the estimates of groundwater protection performance measures taken from the simulation for the Early Failure Modeling Cases and the Seismic GM Modeling Case. The first groundwater protection performance measure is the annual maximum concentration of ^{226}Ra and ^{228}Ra in the representative volume of 3,000 acre-ft of water. The second groundwater protection performance measure is gross alpha activity (excluding radon and uranium) in that volume (Figure ES-60). The third is the dose from beta- and photon-emitting radionuclides in

the groundwater, expressed in terms of annual dose to the whole body or any organ of a human receptor resulting from drinking two liters of this water per day (Figure ES-61). The TSPA-LA Model results show that releases from the repository will meet the groundwater protection standard.

ES9.4. Human Intrusion

The TSPA-LA Model was used to simulate a Human Intrusion Scenario in order to address the second requirement of the human intrusion standard (10 CFR 63.321(b) [DIRS 178394]). To calculate dose for all environmental pathways per 10 CFR 63.321(c) [DIRS 178394], the TSPA-LA Model used a probabilistic approach analogous to that used to evaluate conformance with the individual protection and groundwater protection standards.

The estimates of WP degradation suggest that, using current technology, a degraded WP could not be penetrated by drilling before about 200,000 years postclosure. Consequently, the analysis considered the effects of a drilling intrusion at 200,000 years. Figure ES-62 shows the expected annual dose that could result from a drilling intrusion 200,000 years after repository closure. The expected annual dose accounts for aleatory uncertainty about the type of WP intersected by the drill and location of the intersected WP. The mean, median, and 5th and 95th percentiles of the distribution of expected annual dose reflect epistemic uncertainty due to incomplete knowledge of the behavior of the physical system during and after the drilling intrusion.

The values on Figure ES-62 represent the dose from a single WP and are not combinations of releases from other WPs that may fail due to other processes. The mean and median annual doses from human intrusion are estimated to be less than 0.01 millirem. These results indicate that releases from a human intrusion would result in doses well below the human-intrusion individual protection standard of 350 millirem annual individual dose to the RMEI during the postclosure period from 10,000 to one million years.

ES10. SUMMARY OF THE RESULTS OF THE TSPA-LA MODEL

The TSPA-LA Model was applied to the assessment of total system performance of the Yucca Mountain repository based on FEPs that could affect total system performance. The TSPA-LA analyses incorporate uncertainty in input data and submodel performance and use the validated TSPA-LA Model.

The TSPA-LA Model simulation/analysis periods cover 10,000 years after repository closure and the 1,000,000-year period of geologic stability. The 10,000-year simulations were extended an additional 10,000 years to assess whether or not the trends present at the end of 10,000 years continue. The results of the analyses showed that the period between 10,000 years to 20,000 years after repository closure did not display any significant changes to the trends observed from 0 to 10,000 years, providing confidence in the conclusions reached regarding the 10,000-year period.

The TSPA-LA Model results demonstrate that the projected highest mean dose to the RMEI in any year during the next 10,000 years after repository closure is less than the individual protection standard in NRC Proposed Rule 10 CFR 63.311(a)(1) [DIRS 178394], which describes the limits on radionuclides in the representative volume. The TSPA-LA Model

analyses also indicate the performance of the repository system provides significant protection to groundwater. The results show concentrations in the groundwater are likely to be well below the groundwater protection standard in NRC Proposed Rule 10 CFR 63.331 [DIRS 180319] and its Table 1. Likewise, the results suggest the mean annual drinking water dose to any organ and to the whole body from beta- and photon-emitting radionuclides is likely to be well below the applicable standards in the proposed rule.

The physiographic setting, topography, climate, area geology, and soil characteristics at the site of the Yucca Mountain repository are favorable for restricting the amount of infiltration of precipitation into the subsurface. The reduced infiltration along with rock characteristics, ambient and perturbed subsurface environmental conditions, and the geometry of emplacement drifts will further limit the amount of liquid water available to enter the drifts. Features of the waste form and other components of the EBS, together with limitations due to the solubility of radionculides and the subsurface geology and hydrology, will limit the release, rate of release, and transport of radionuclides to the SZ beneath the repository. Only a small fraction of the radionuclide inventory is projected to be released from the EBS, move down through the UZ beneath the repository, and enter the SZ. Sorption and diffusion of radionuclides into the UZ will further reduce the concentrations of radionuclides entering the SZ. After the migrating radionuclides enter the SZ, the TSPA-LA Model results indicate that the characteristics of the rock, soil, and the hydrologic and geochemical environmental factors in the SZ will combine to retard radionuclide transport and reduce the rate of radionuclide transport to the accessible environment. Including the disruptive events such as igneous and seismic phenomena, the TSPA-LA Model analysis indicates that the repository will, with a high degree of confidence, perform in a manner that protects the natural environment and future human populations in the area.

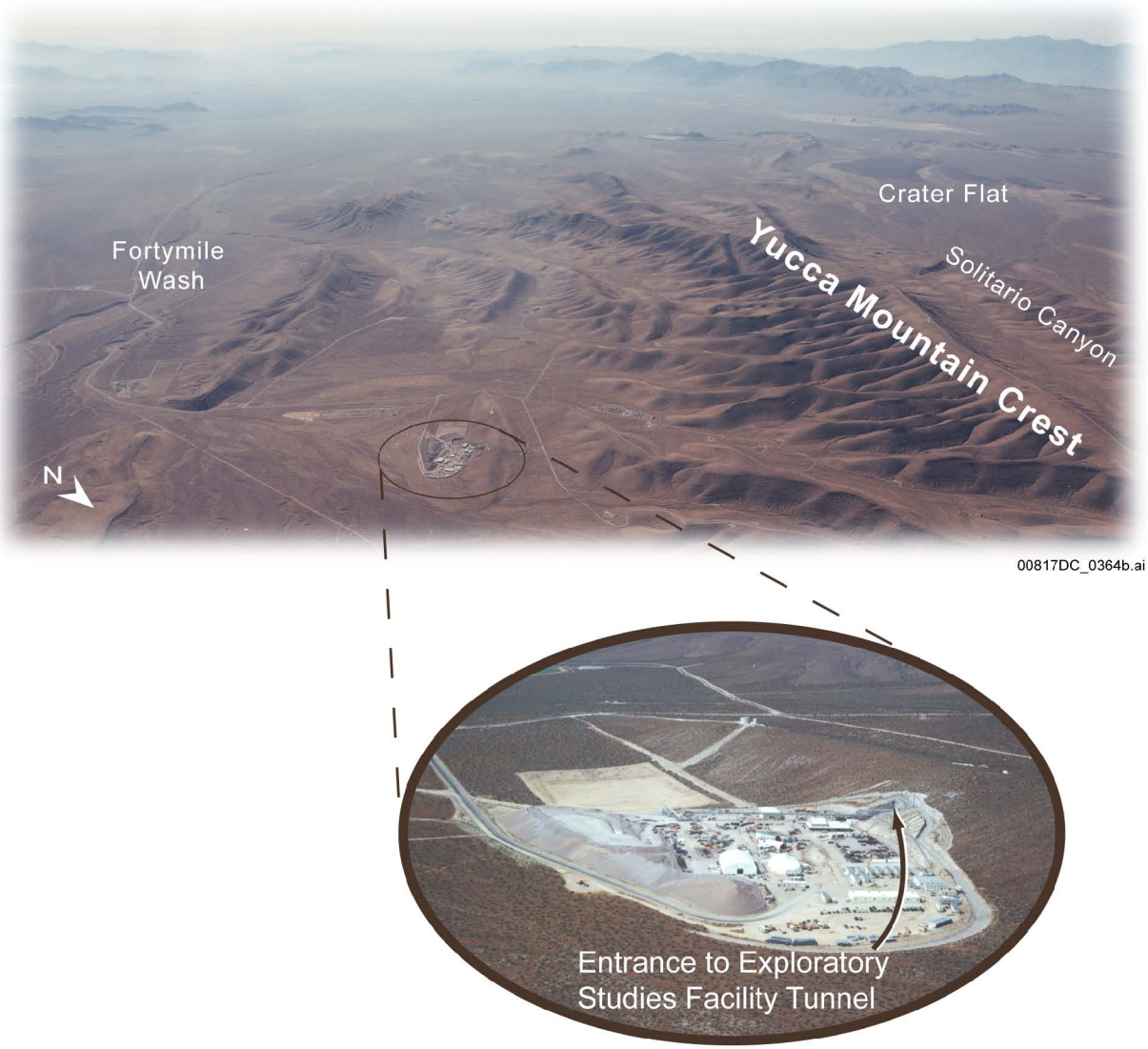

Figure ES-1. Yucca Mountain Area

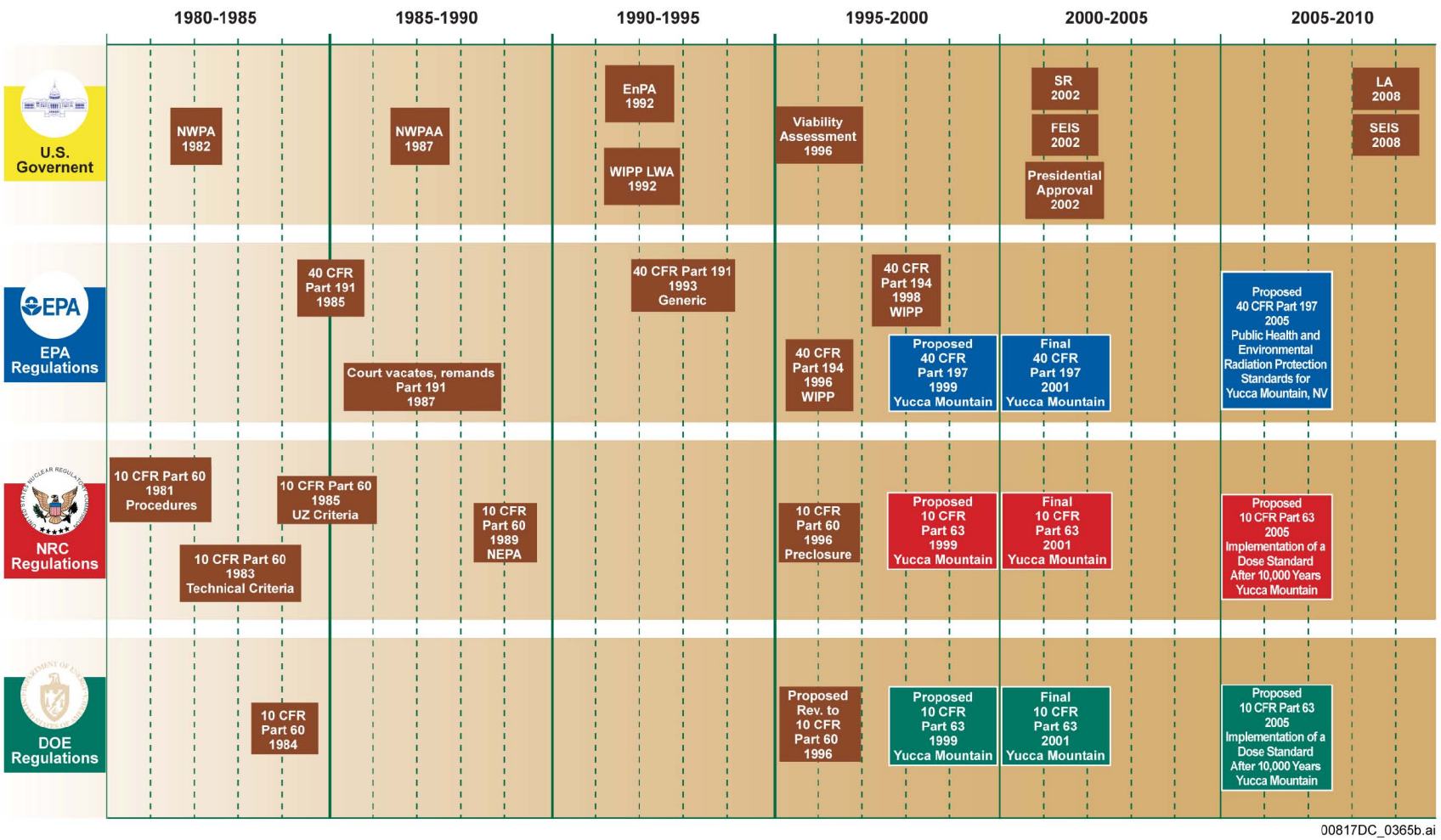

Figure ES-2. Timeline of Legislative and Regulatory Events: 1980 to 2010

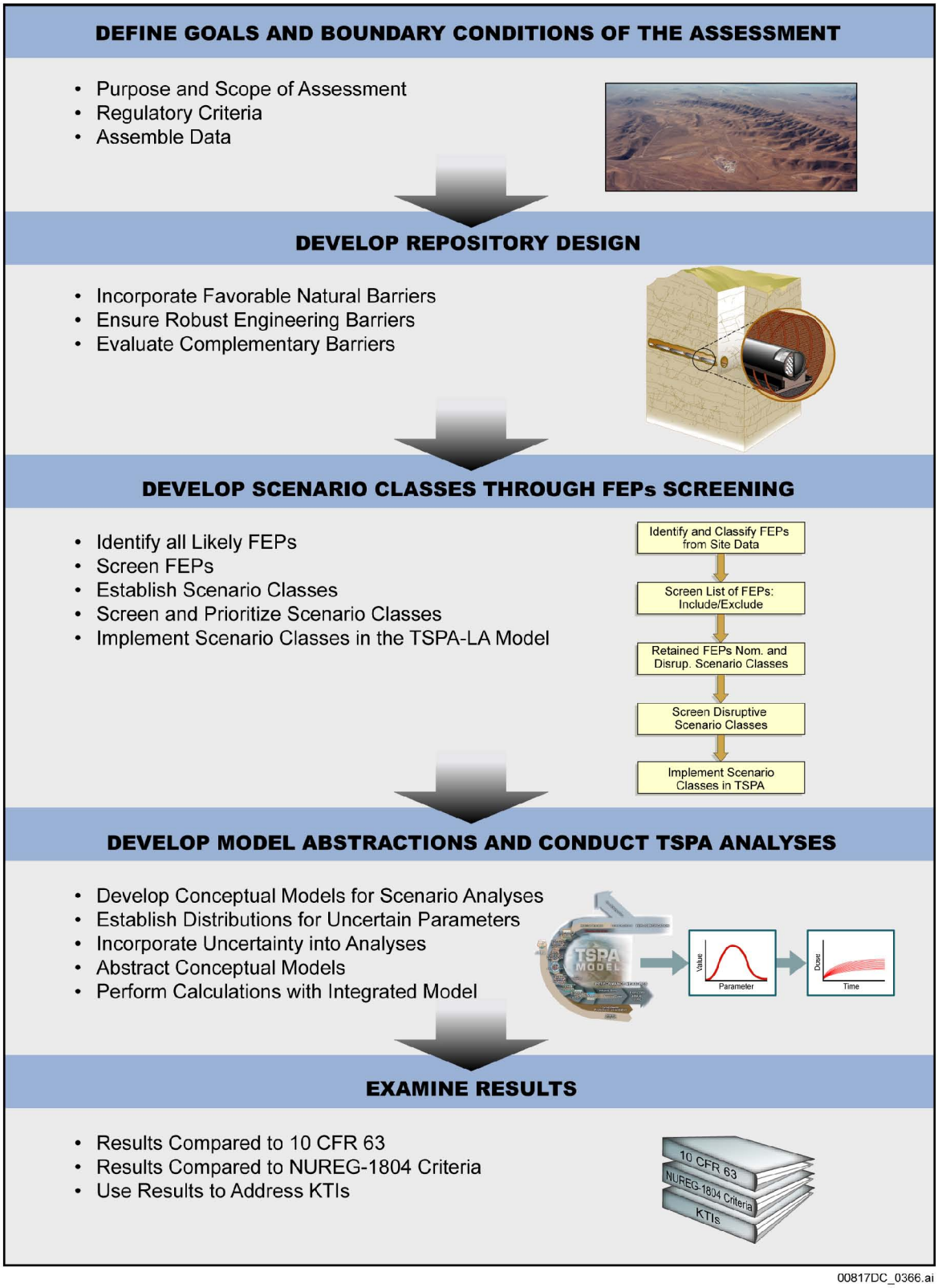

Figure ES-3. Structure of the Process of the TSPA-LA

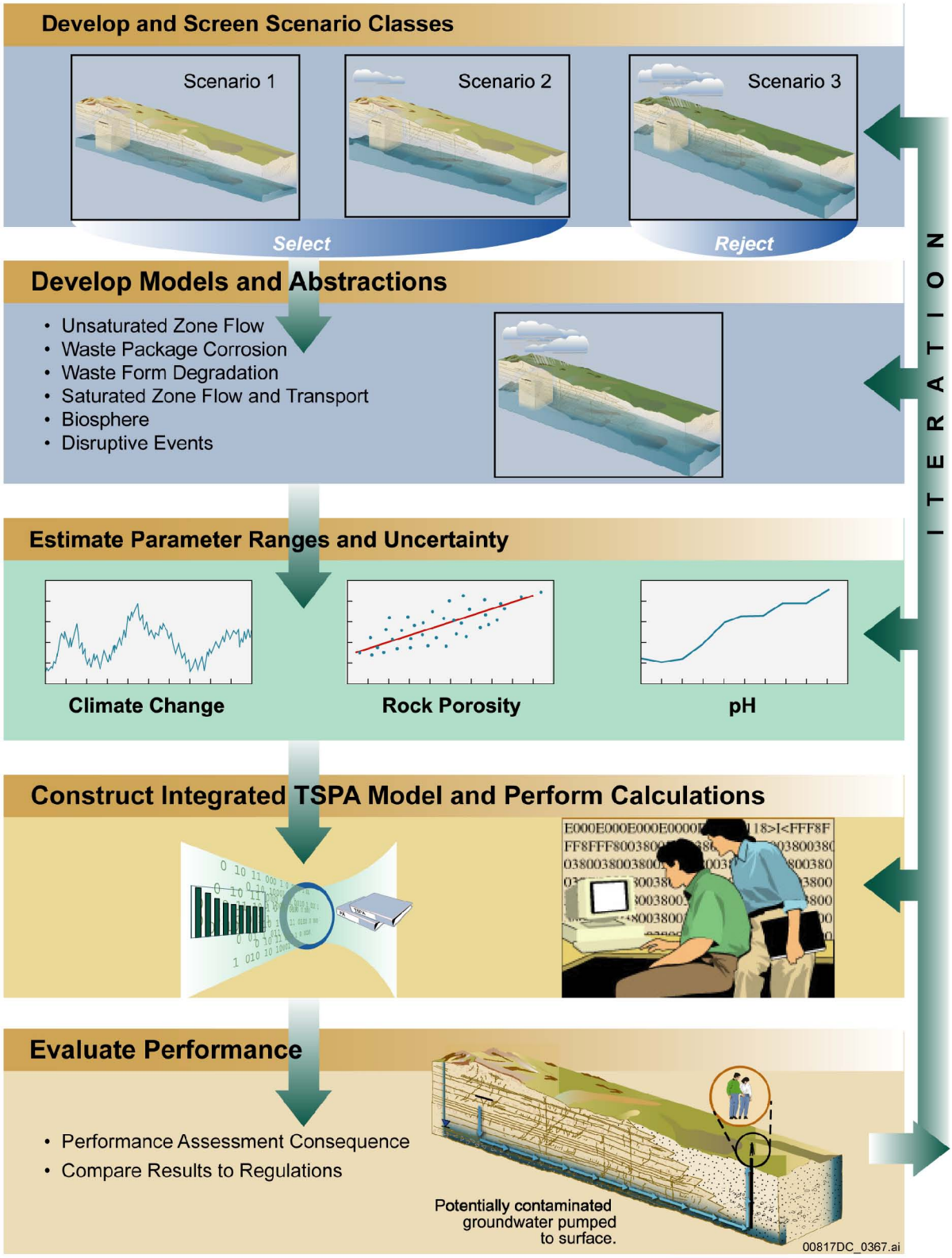

Figure ES-4. Major Steps in a Generic Performance Assessment

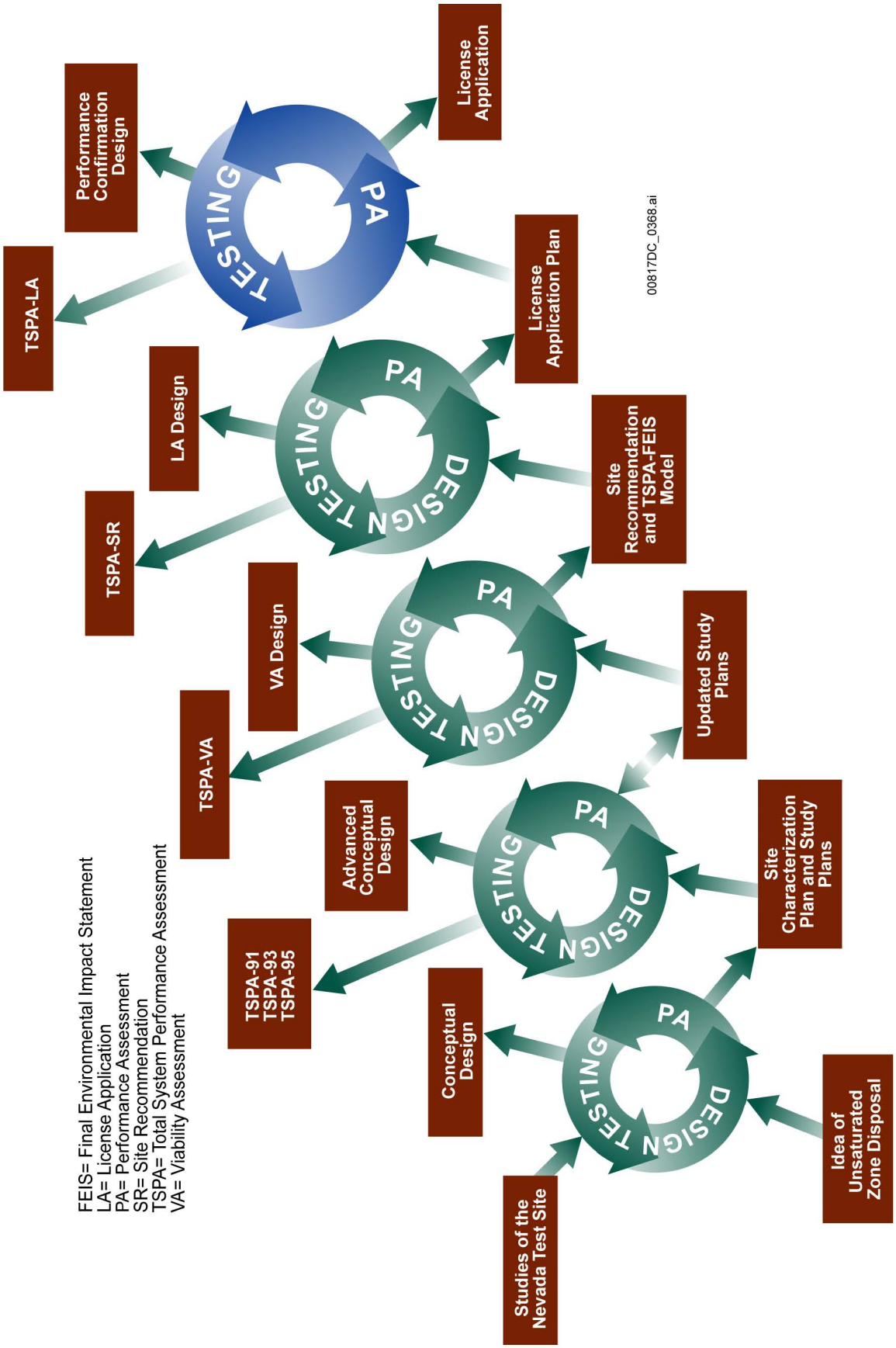

Figure ES-5. Iterative Application of the TSPA Process

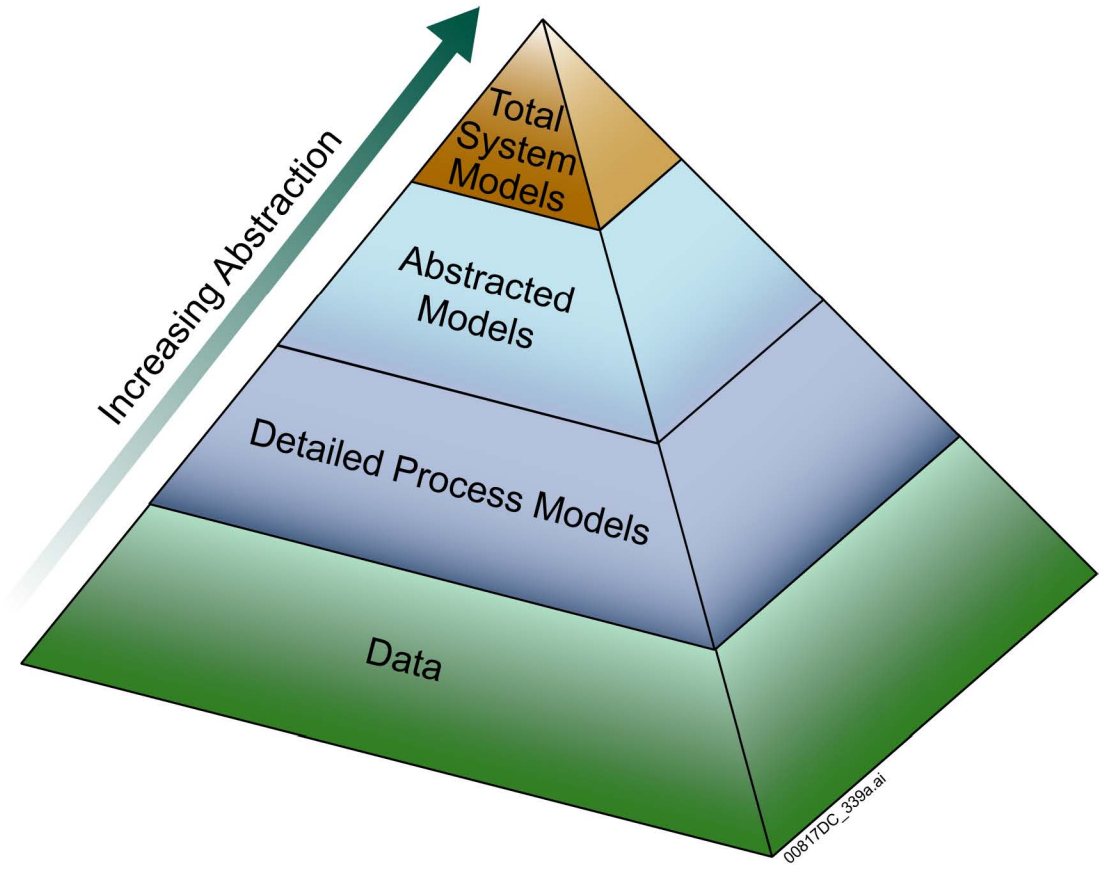

Figure ES-6. Performance Assessment Pyramid Showing the Steps Involved in Developing a Total System Model

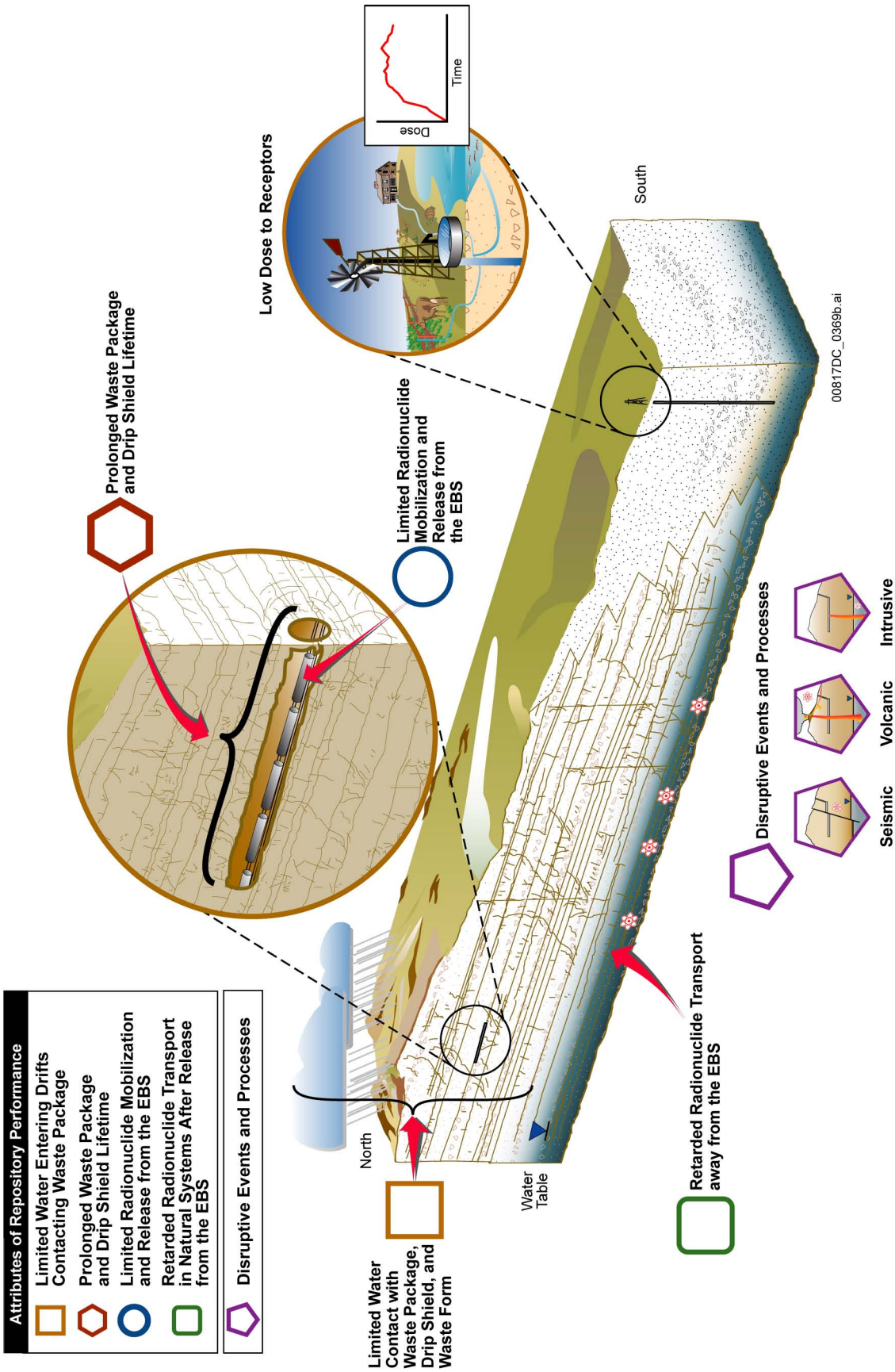

Figure ES-7. Schematic of Attributes of Repository Performance

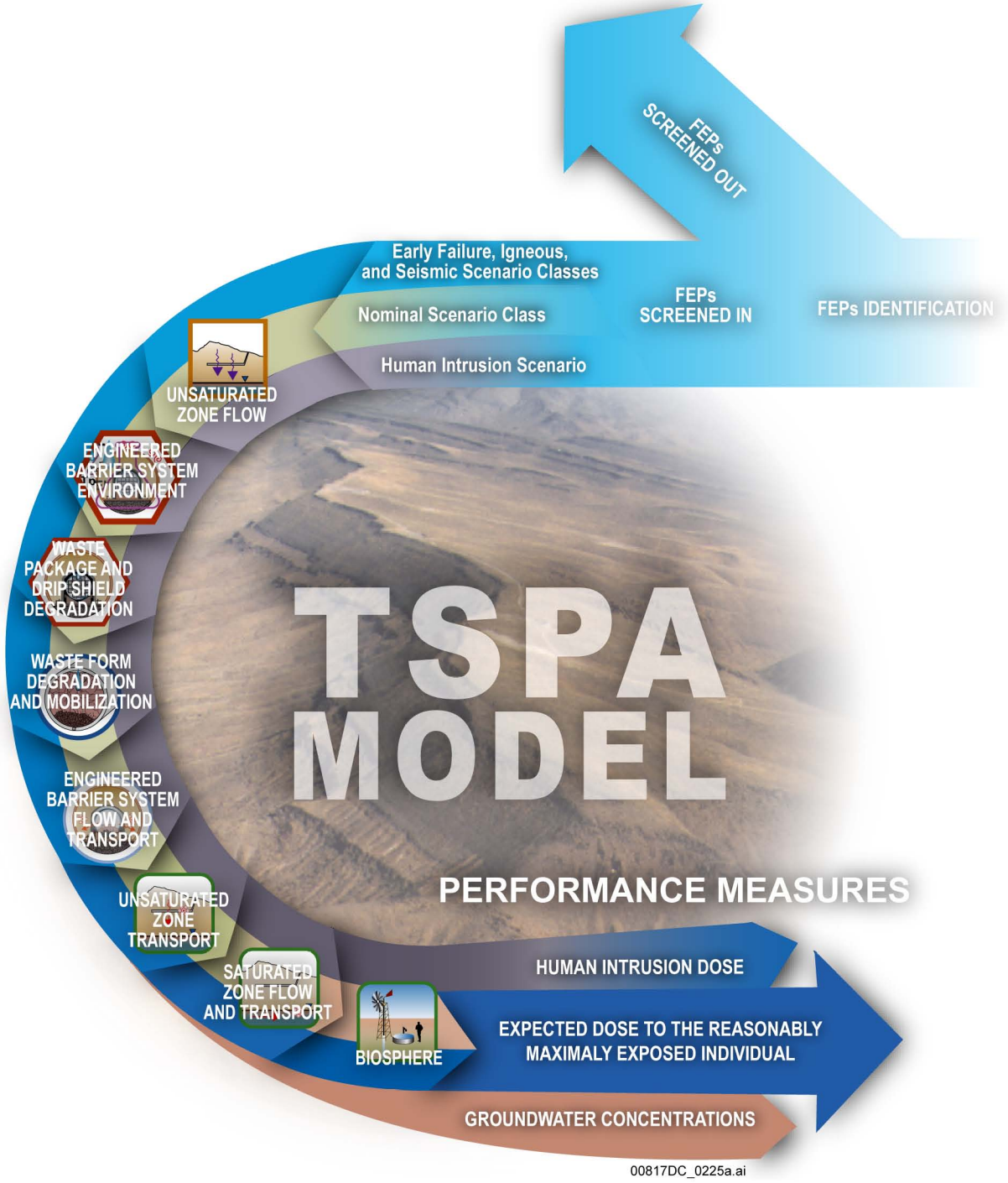

Figure ES-8. Schematic Representation of the Development of the TSPA-LA Model, Including the Nominal, Igneous, and Seismic Scenario Classes

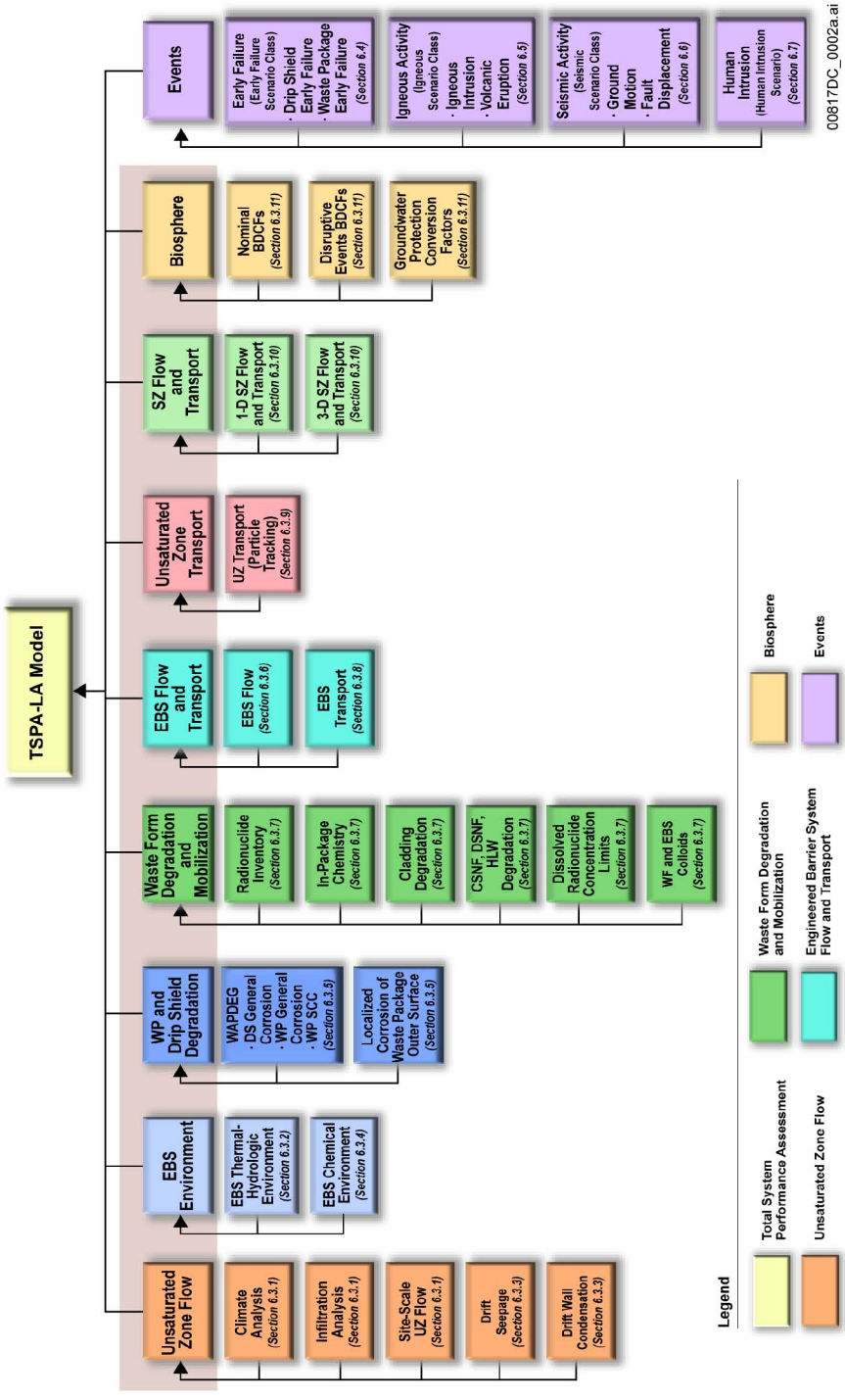

Figure ES-9. TSPA-LA Principal Model Components and Submodels

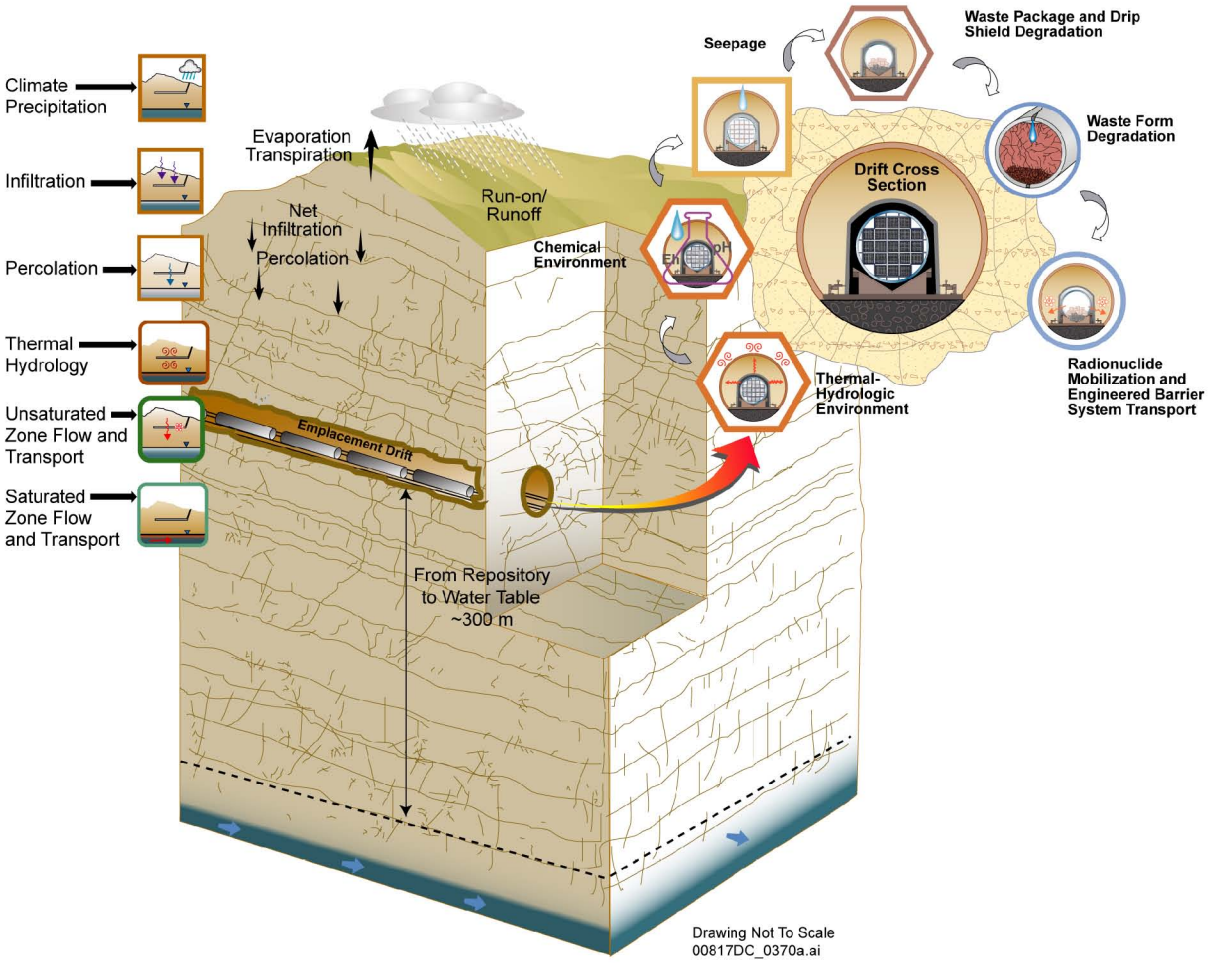

Figure ES-10. Principal Components of the Yucca Mountain Repository System

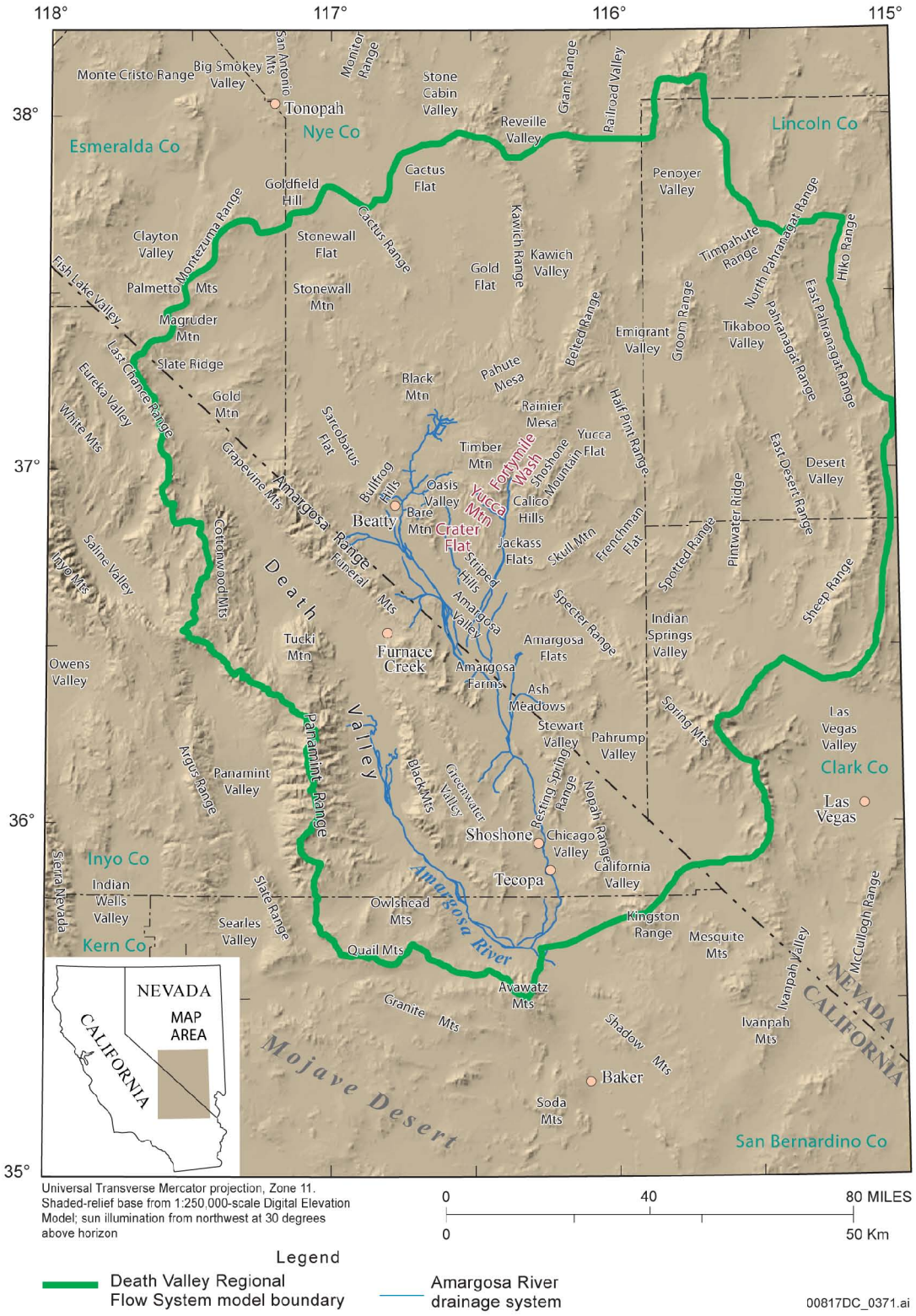

Source: Modified from BSC 2004 [DIRS 169734], Figure 8-2.

Figure ES-11. Geographic and Prominent Topographic Features of the Death Valley Region

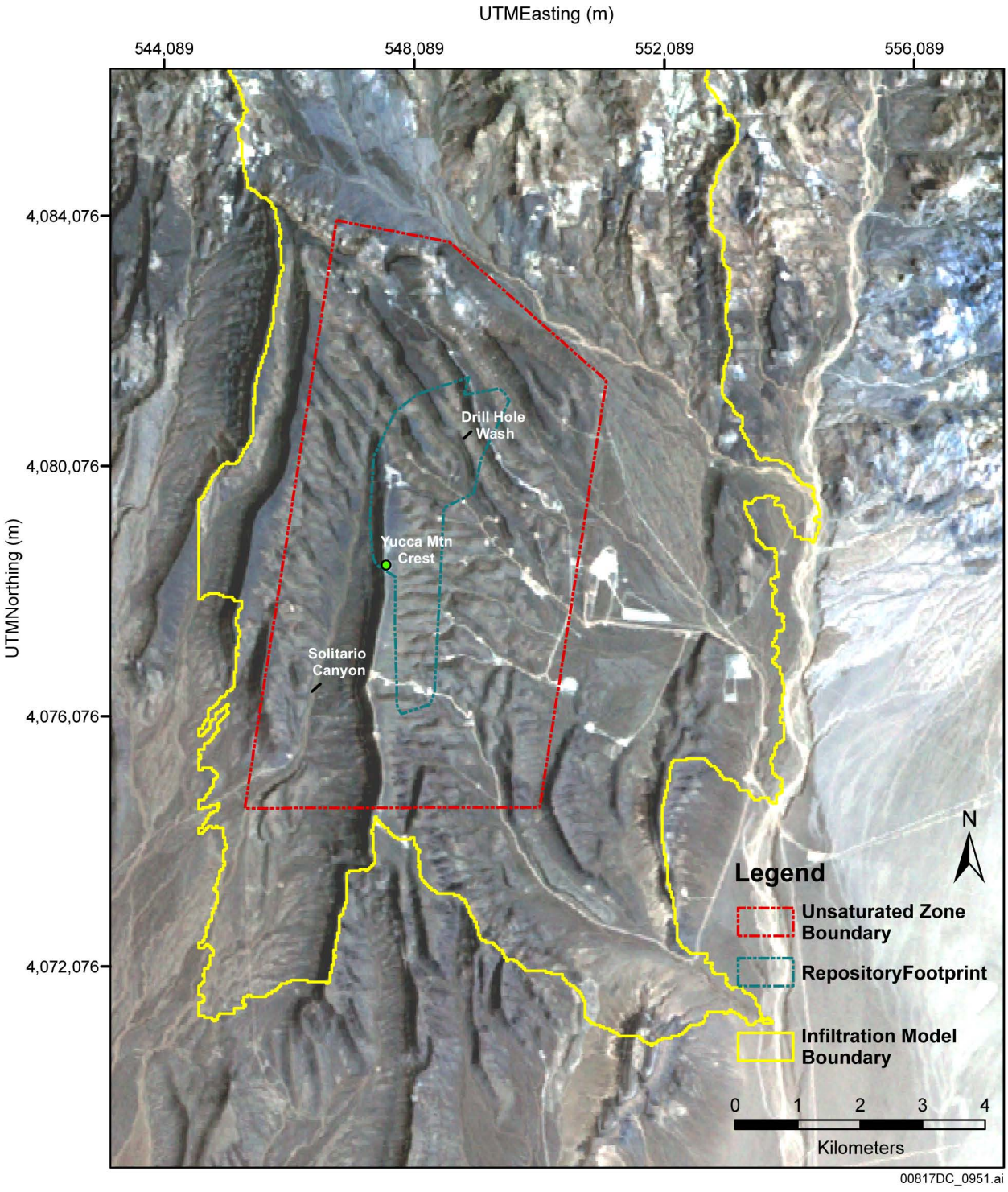

Source: Modified from SNL 2007 [DIRS 182145], Figure 6.5.2.1-1[a].

NOTE: The model boundary is the same as the 1999 unsaturated zone flow model domain of the TSPA-SR.

Figure ES-12. Topographic Map of the Yucca Mountain Site Showing in Slope Characteristics

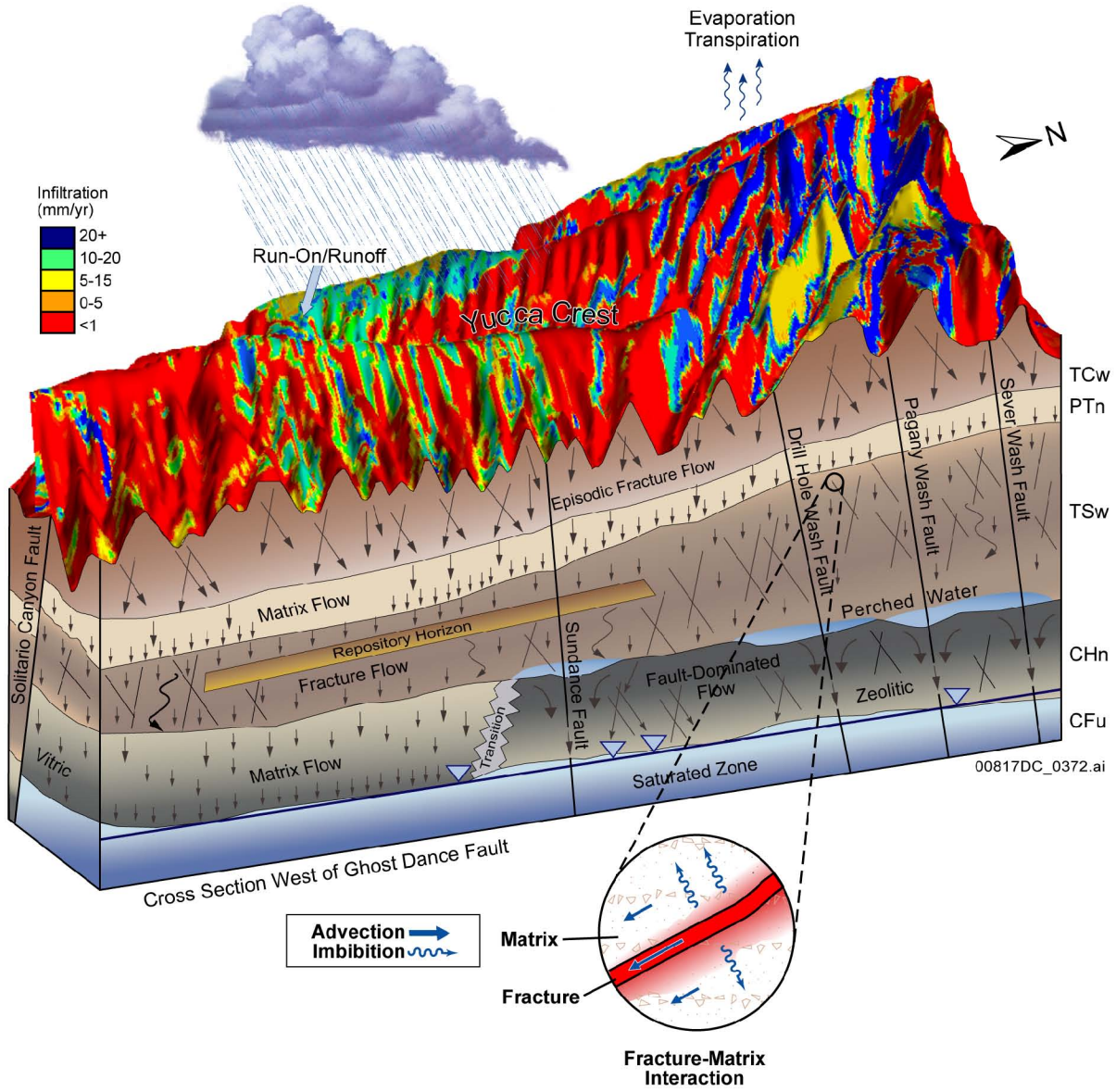

Source: Modified from BSC 2004 [DIRS 170035], Figure 6-1.

Figure ES-13. Overall Water Flow Behavior in the Unsaturated Zone, Including the Relative Flux Magnitudes of Fracture and Matrix Flow Components in the Different Hydrogeologic Units

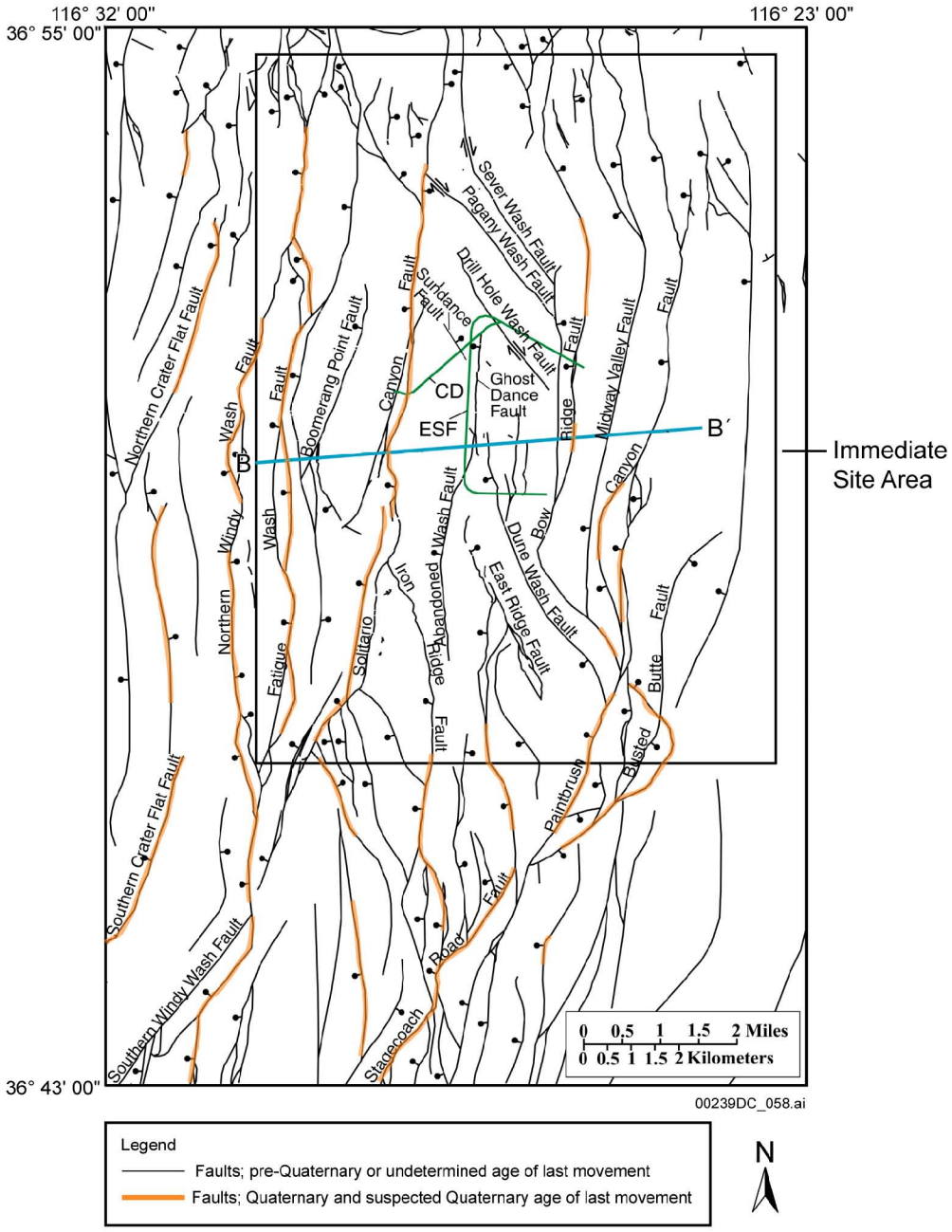

Source: Modified from BSC 2004 [DIRS 169734], Figure 3-20.

NOTES: The following faults have demonstrable Quaternary activity: Northern Crater Flat, Southern Crater Flat, Northern Windy Wash, Southern Windy Wash, Fatigue Wash, Solitario Canyon, Iron Ridge, Bow Ridge, Paintbrush Canyon, and Stagecoach Road. All faults are shown with solid lines, although many segments are concealed or inferred.

Symbols and acronyms: bar and bell: downthrown side of fault; arrows: relative direction of strike-slip movement; ESF = Exploratory Studies Facility (green line); CD = Cross-Drift; blue line: approximate location of section on Figure ES-15.

Figure ES-14. Distribution of Faults in the Yucca Mountain Site Area and Adjacent Areas to the South and West

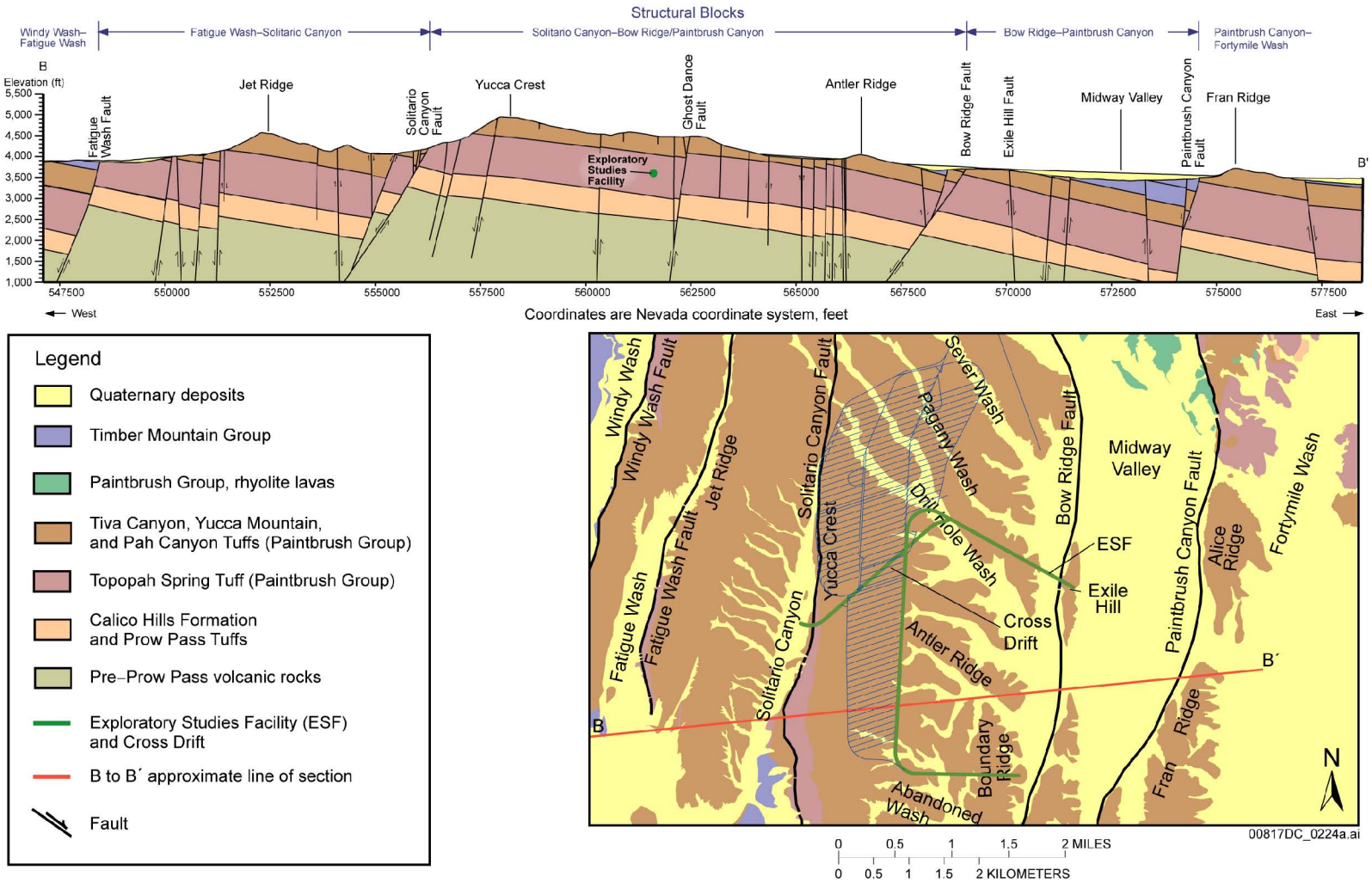

Source: Simplified from Day et al. 1998 [DIRS 100027], Cross Section B-B'.

NOTE: ESF = Exploratory Studies Facility, location of intersection along the approximate line of section, also shown on Figure ES-14.

Figure ES-15. East-West Structure Section across Yucca Mountain Site Area

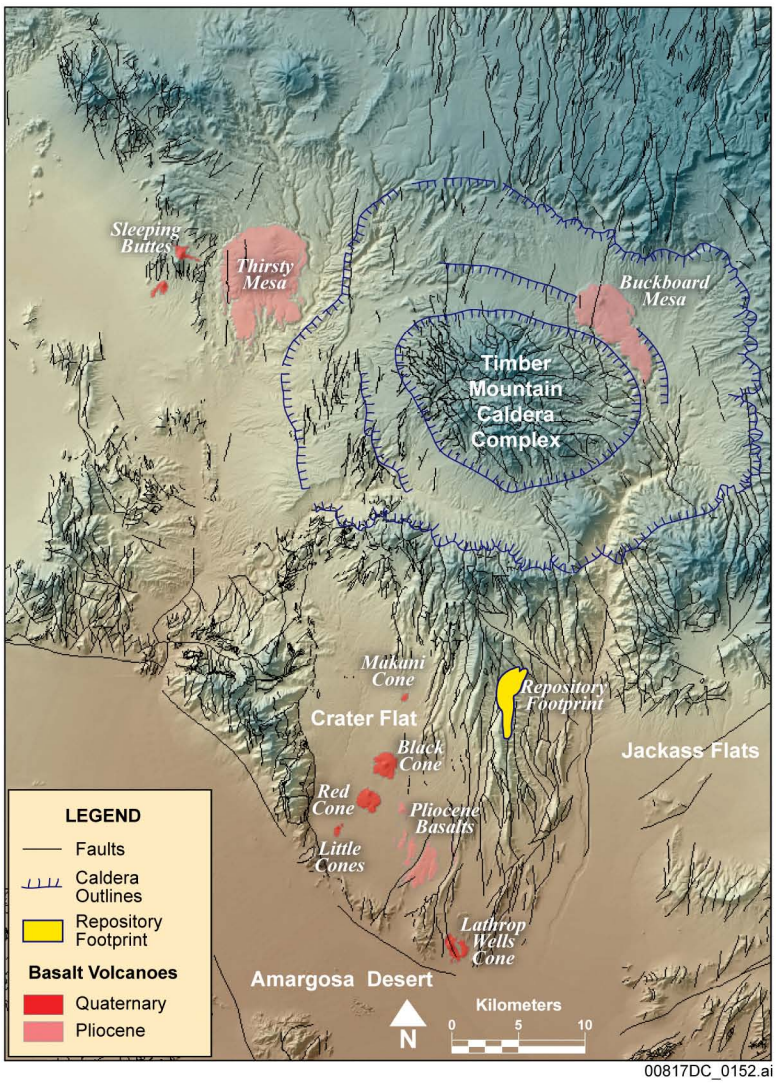

Source: Modified from CRWMS M&O 1998 [DIRS 123196], Figure 2.1.

Figure ES-16. Location and Age of Post-Miocene (less than 5.3 million years) Volcanoes (or clusters where multiple volcanoes have indistinguishable ages) in the Yucca Mountain Region

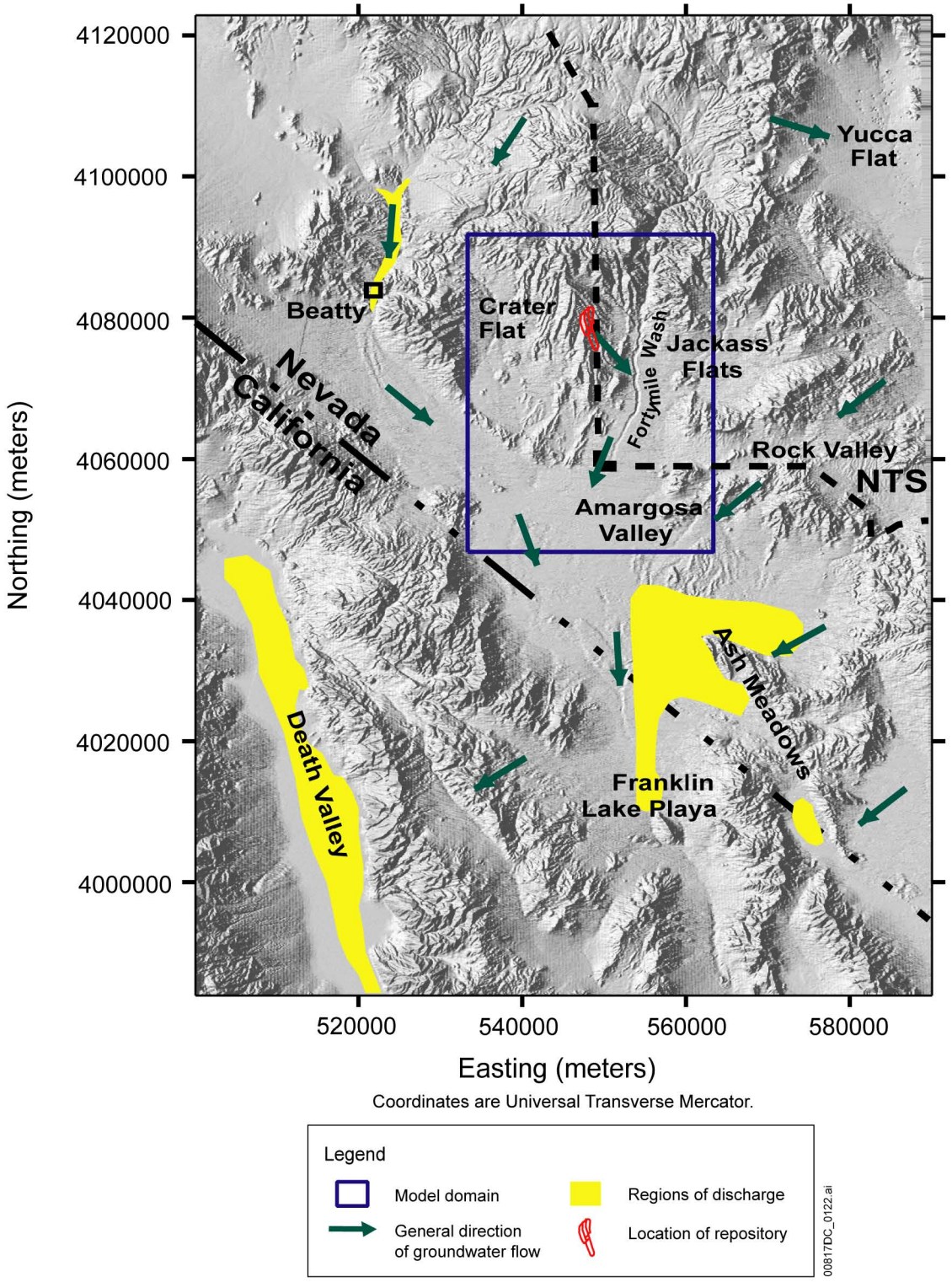

Source: Compiled from BSC 2004 [DIRS 169734], Figures 8-2, 8-5, and 8-6.

Figure ES-17. Regional Map of the Saturated Zone Flow System Showing Direction of Flow and Outline of the 3-D Saturated Zone Site-Scale Flow Model Domain

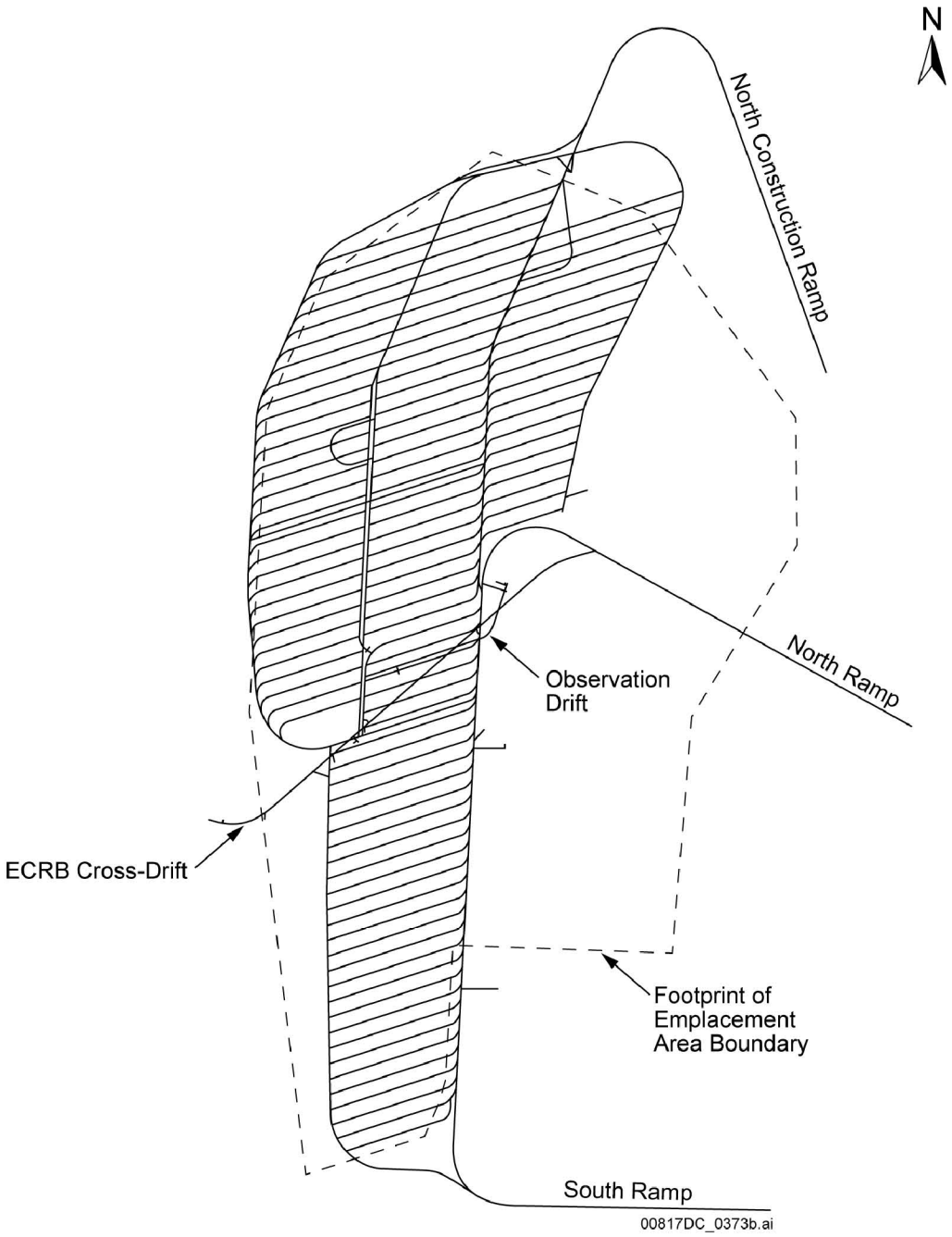

Source: Modified from SNL 2007 [DIRS 179466], Table 4-1, Parameter 01-02.

Figure ES-18. Subsurface Facility Layout

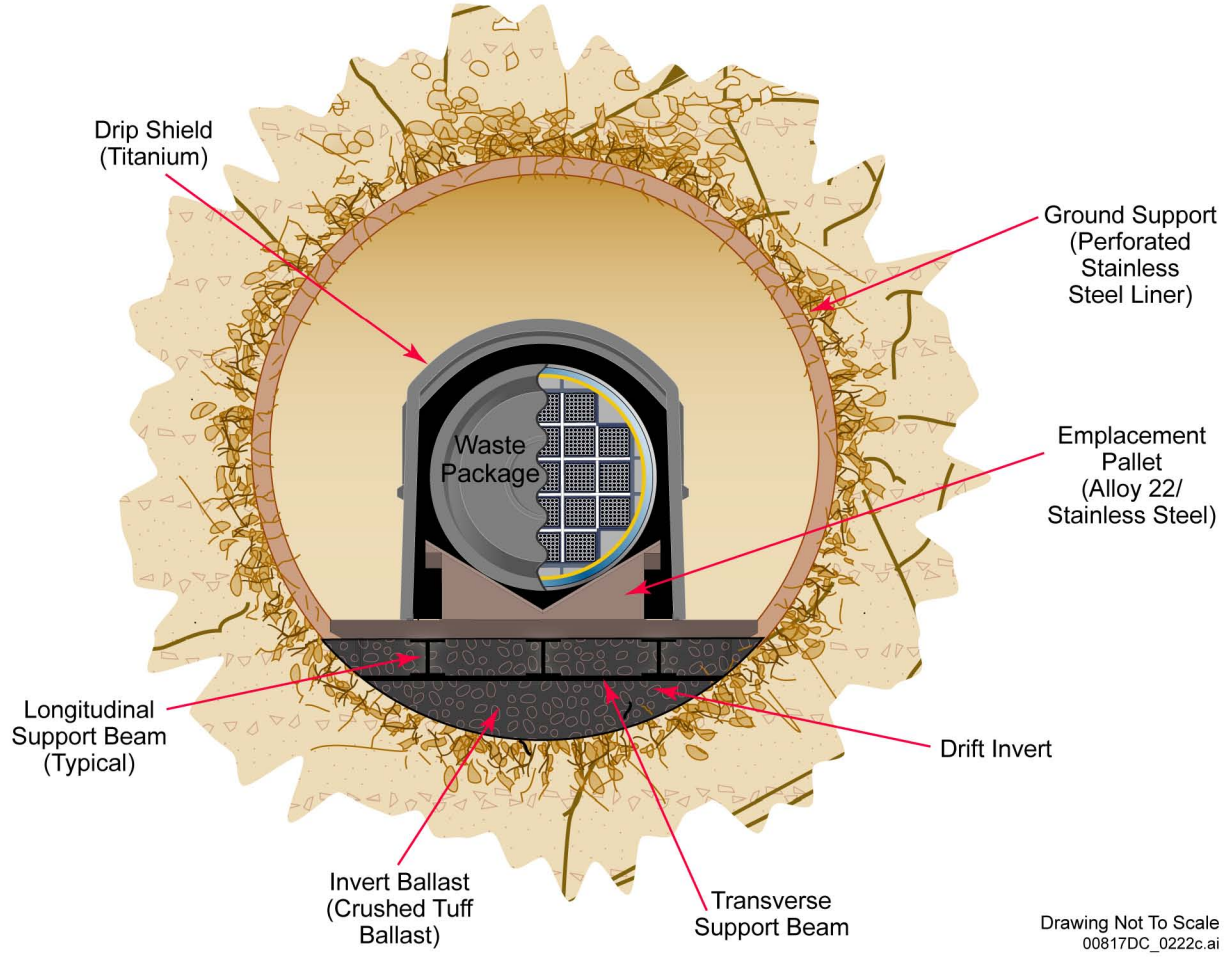

Source: Modified from SNL 2007 [DIRS 179354], Figure 4-1.

Figure ES-19. Cross-Section Illustration of the EBS

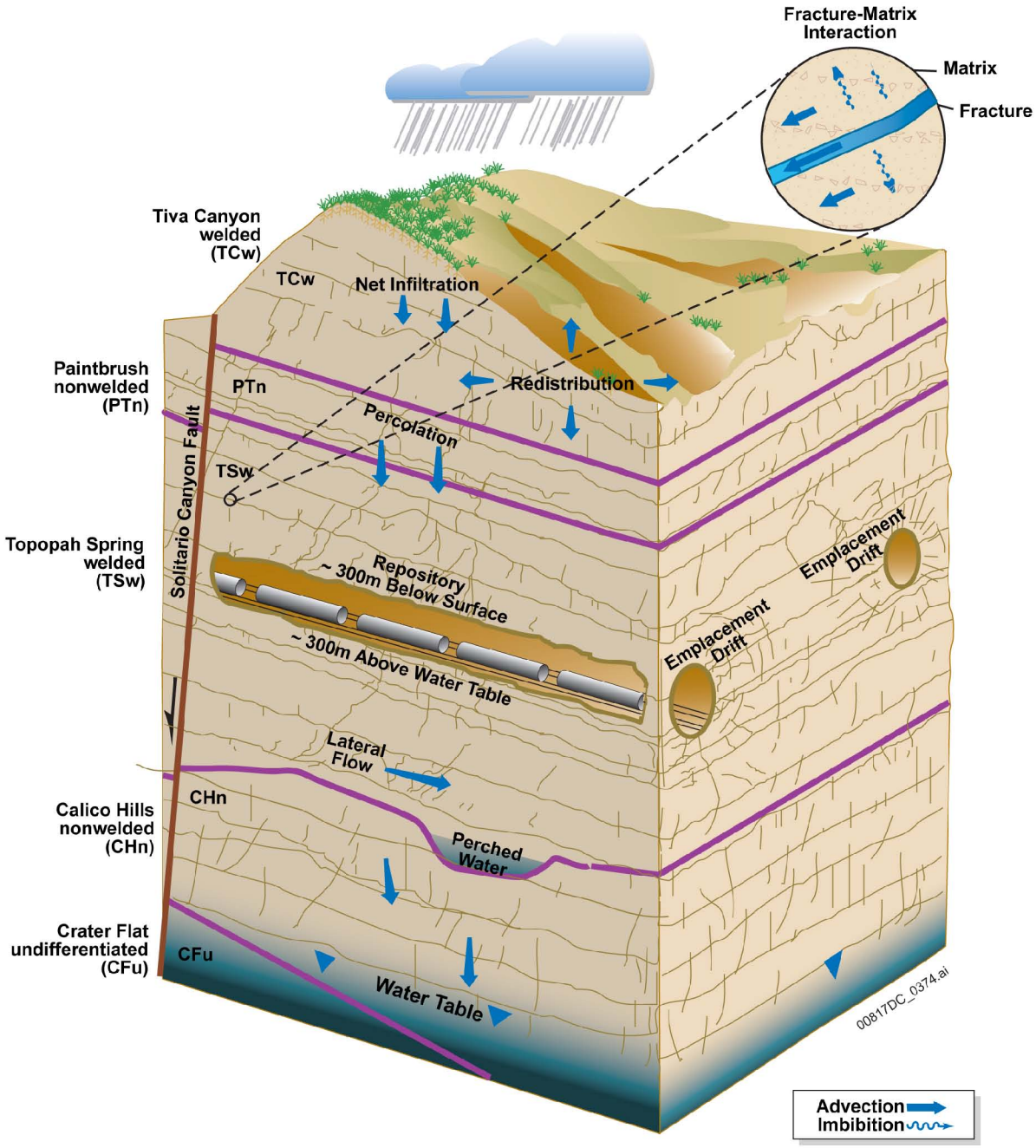

Figure ES-20. Conceptual Drawing of Mountain-Scale Flow Processes

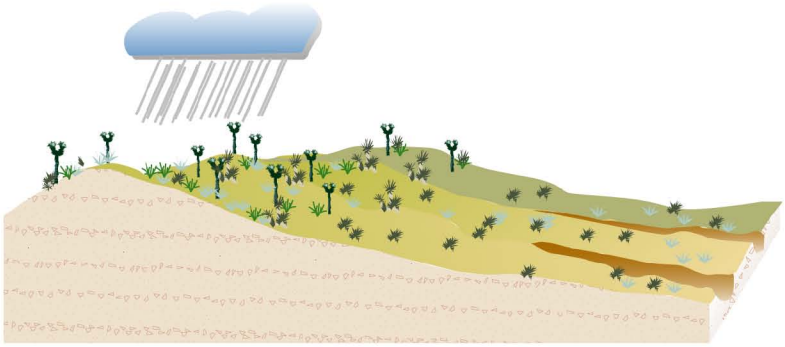

Present-Day Climate

Yucca Mountain:
Regional Meteorological Stations

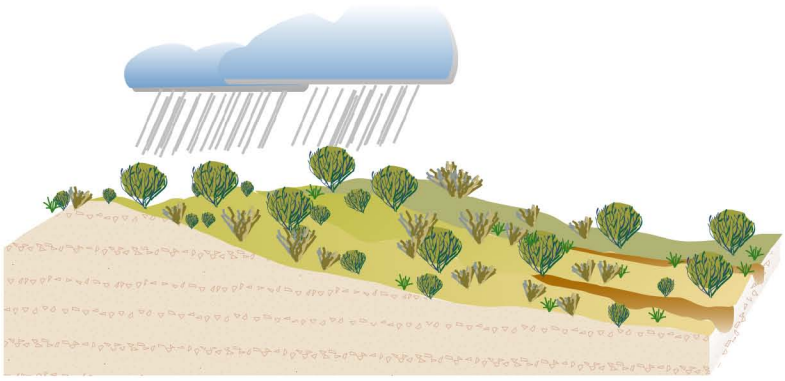

Monsoon Climate

Lower-bound analogue: Yucca Mountain
Upper-bound analogue: Nogales, AZ
Higher precipitation and temperature
than present-day climate

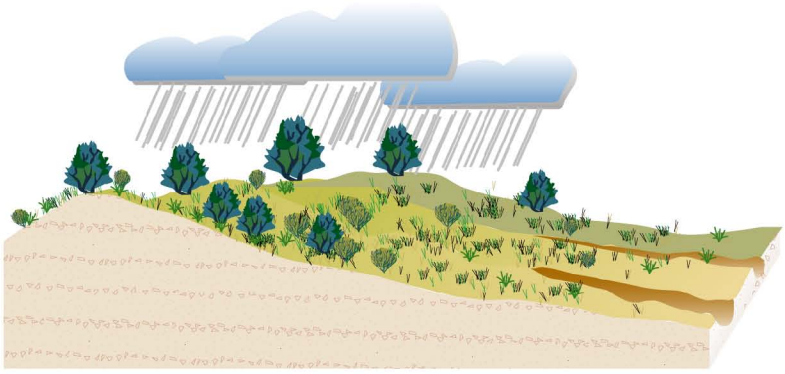

Glacial-Transition Climate

Lower-bound analogue: Delta, UT
Upper-bound analogue: Spokane, WA
Higher precipitation and lower
temperature than present-day climate

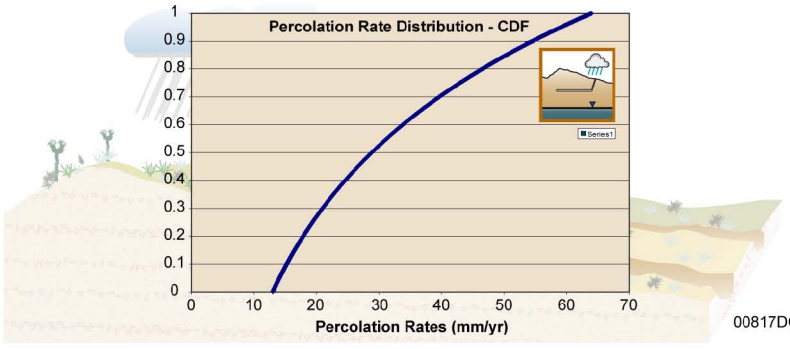

Post-10,000 Year Climate

Sampled value based on a log-uniform
probability distribution for deep percolation
rates from 13 to 64 mm/yr
(10 CFR 63.342(c)(2) [DIRS 178394])

Figure ES-21. Illustration of the Four Climate Periods Used in the TSPA-LA Model and the Analogues for the Monsoon and Glacial-Transition Climates

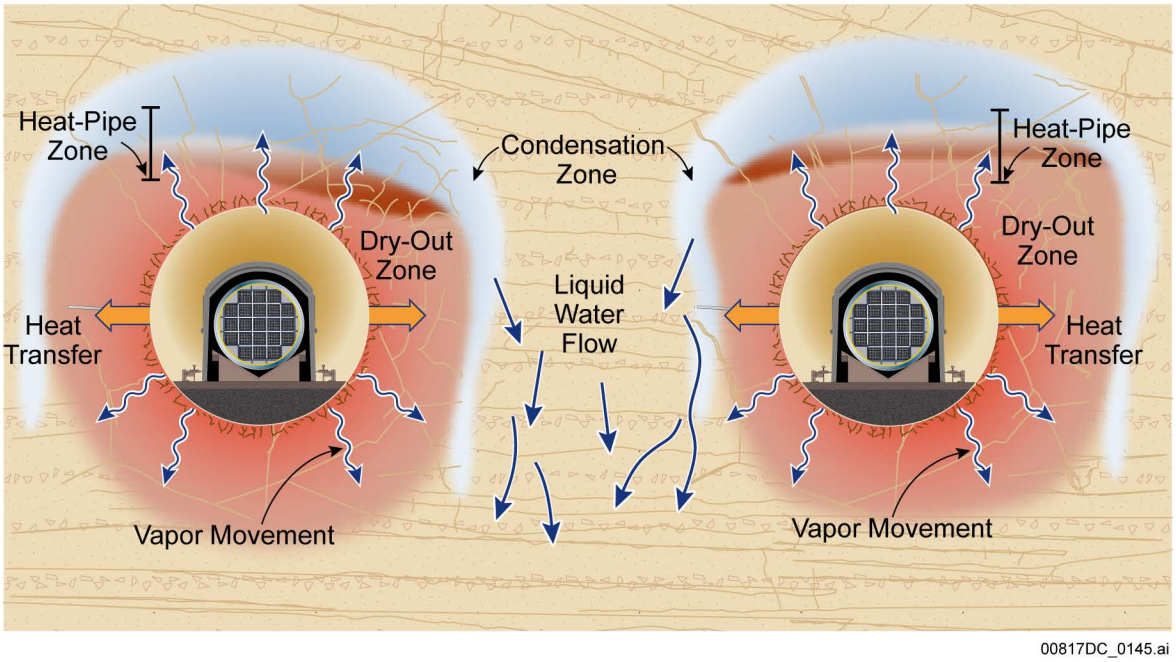

Source: Modified from BSC 2004 [DIRS 169734], Figure 5-81.

Figure ES-22. Schematic Illustration (not to scale) of Thermal-Hydrologic Processes in the Vicinity of the Emplacement Drifts Due to Repository Heating

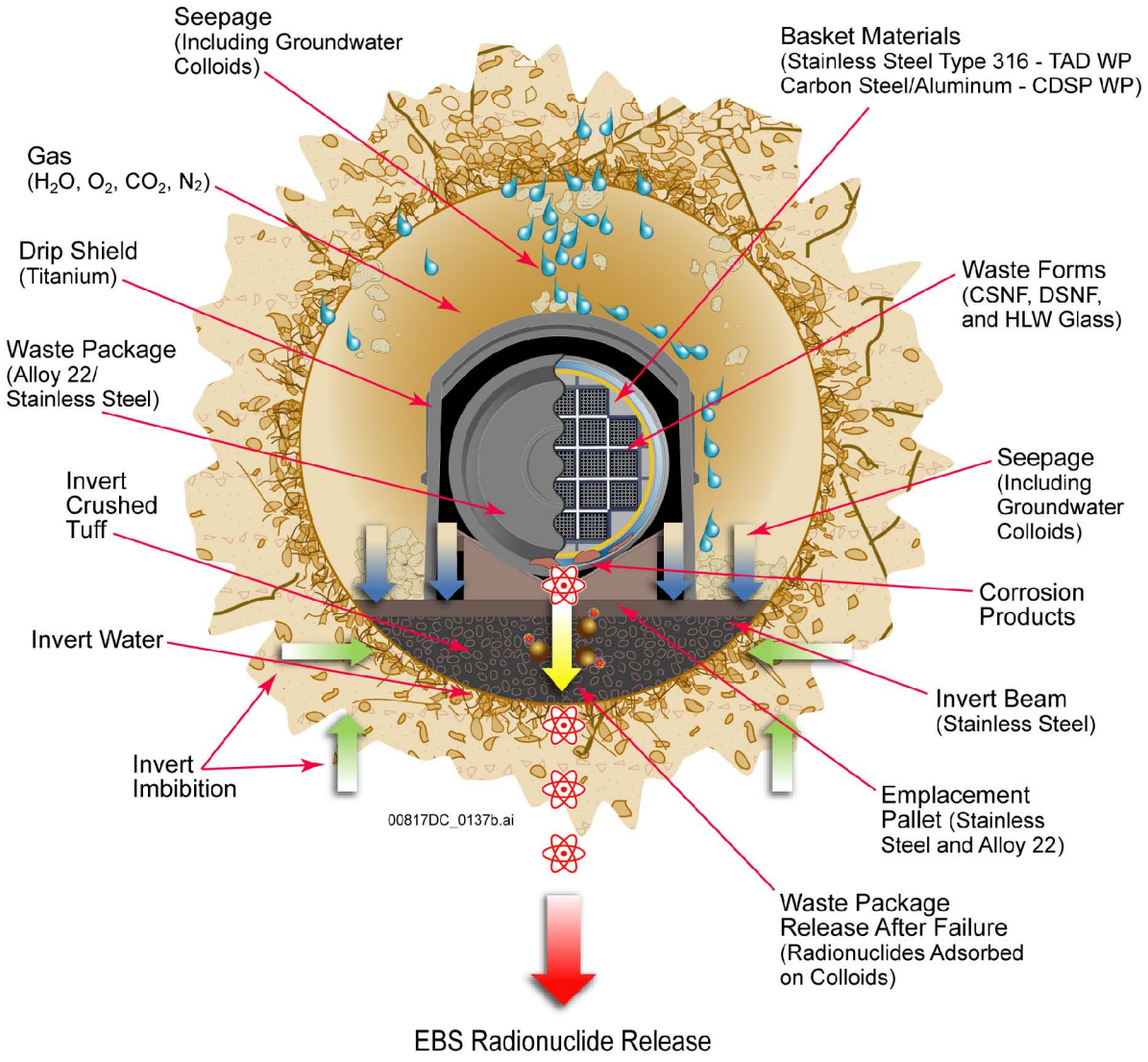

NOTE: Discussion and analysis of the features and processes illustrated on this figure can be found in *EBS Radionuclide Transport Abstraction* (SNL 2007 [DIRS 177407]), Section 6.1.1, Figure 6.1-1).

Figure ES-23. General EBS Design Features and Materials, Water Movement, and Drift Degradation

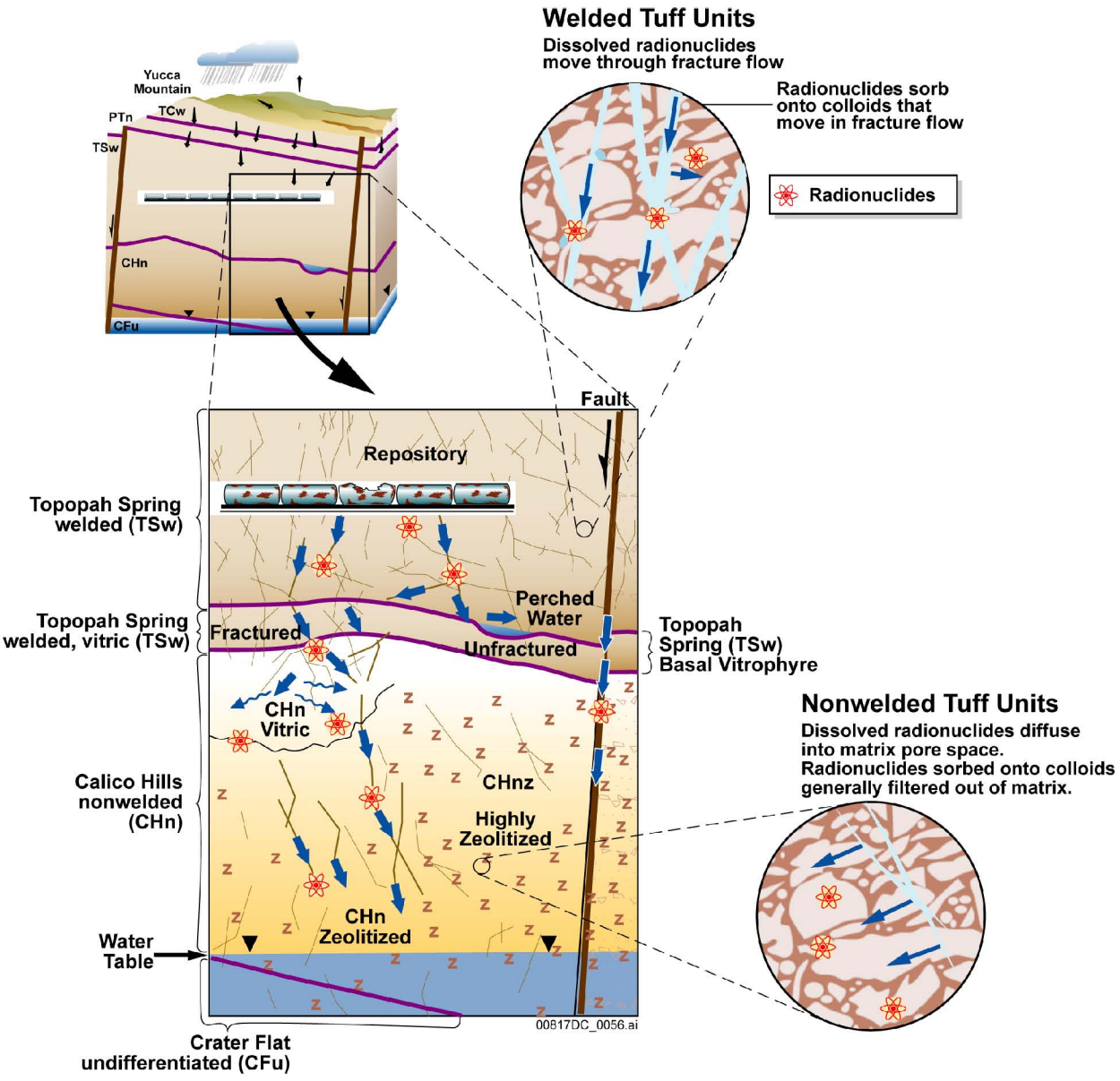

Figure ES-24. Conceptual Drawing of Unsaturated Zone Transport Processes

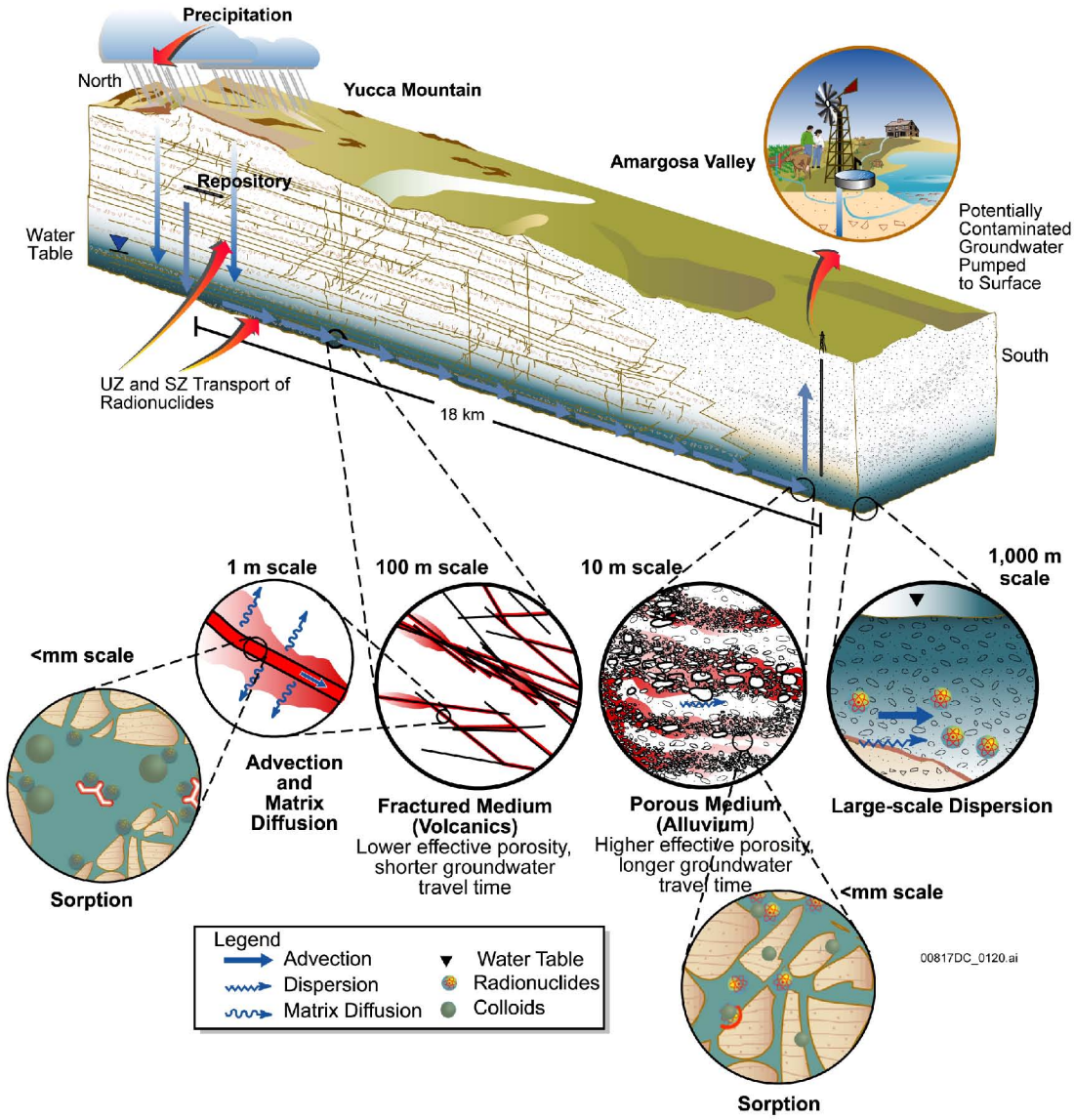

Figure ES-25. Conceptualization of Features and Processes Important to Saturated Zone Transport

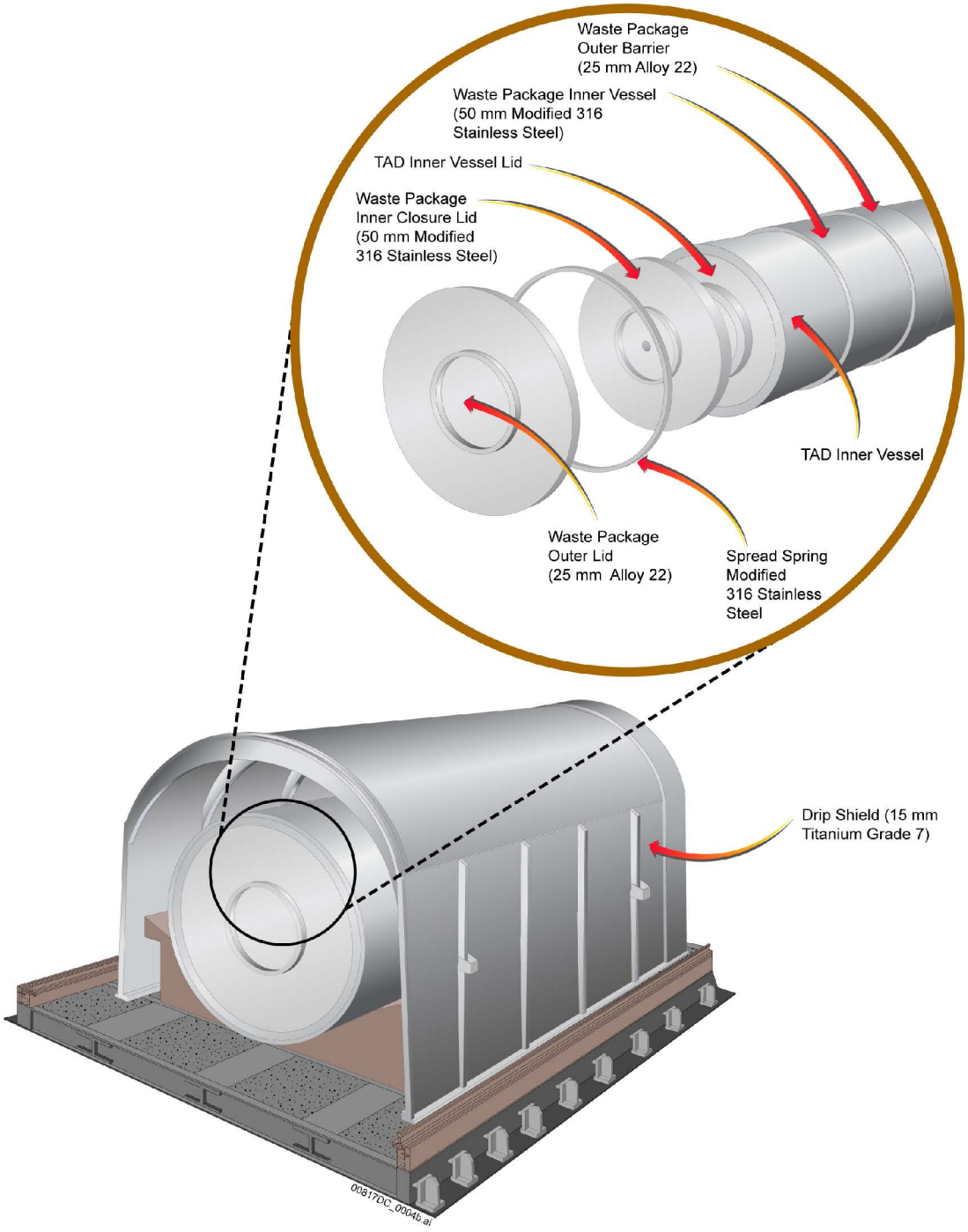

NOTE: SNL 2007 [DIRS 179394] and [DIRS 179354].

Figure ES-26. Schematic Design of the Drip Shield and Waste Package

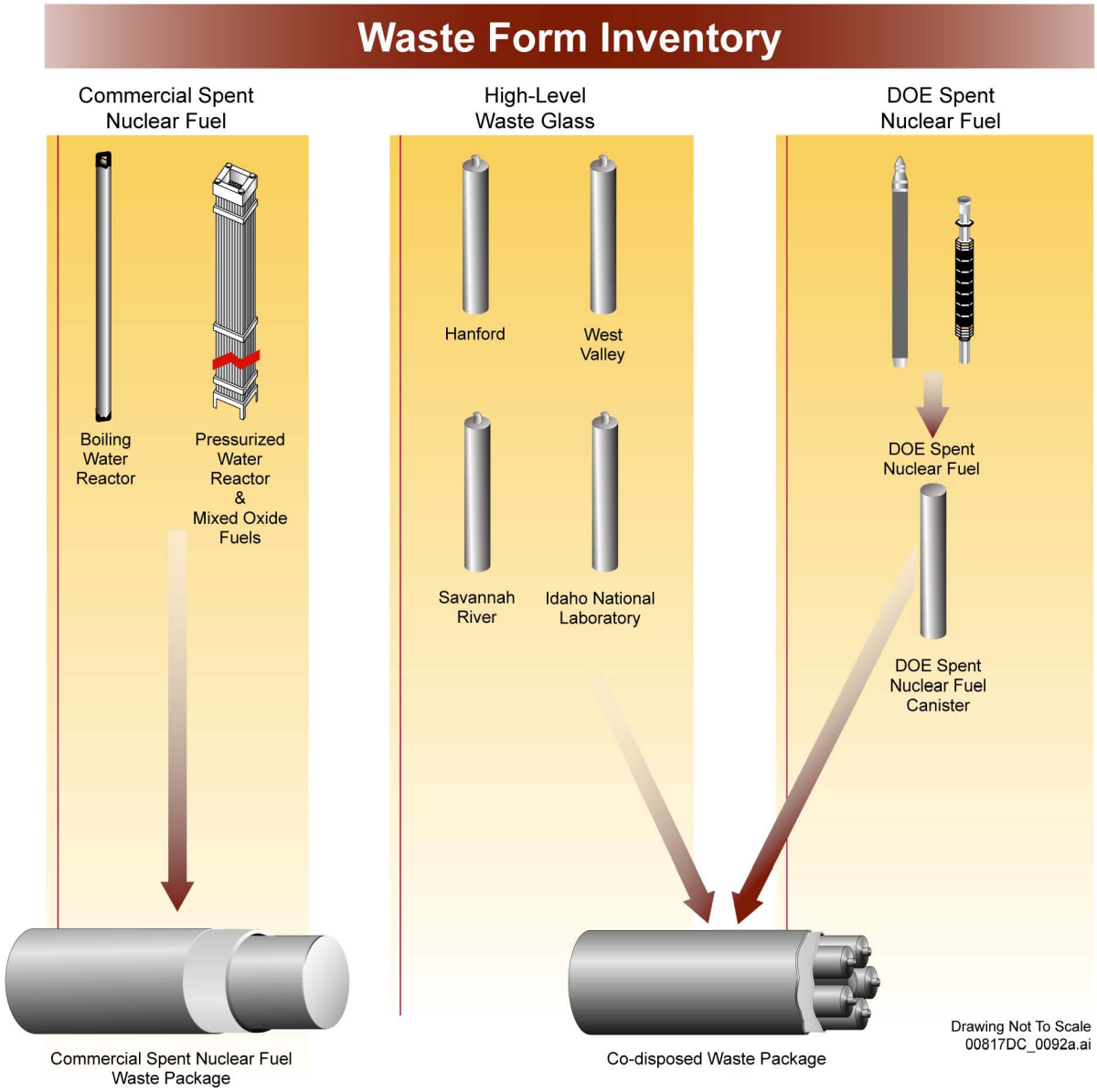

Source: Modified from SNL 2007 [DIRS 180472], Figure 6-1.

NOTE: For modeling purposes, the naval fuels are treated as commercial spent nuclear fuel.

Figure ES-27. Three Waste Types Grouped into Two Representative Waste Packages: CSNF and CDSP WPs

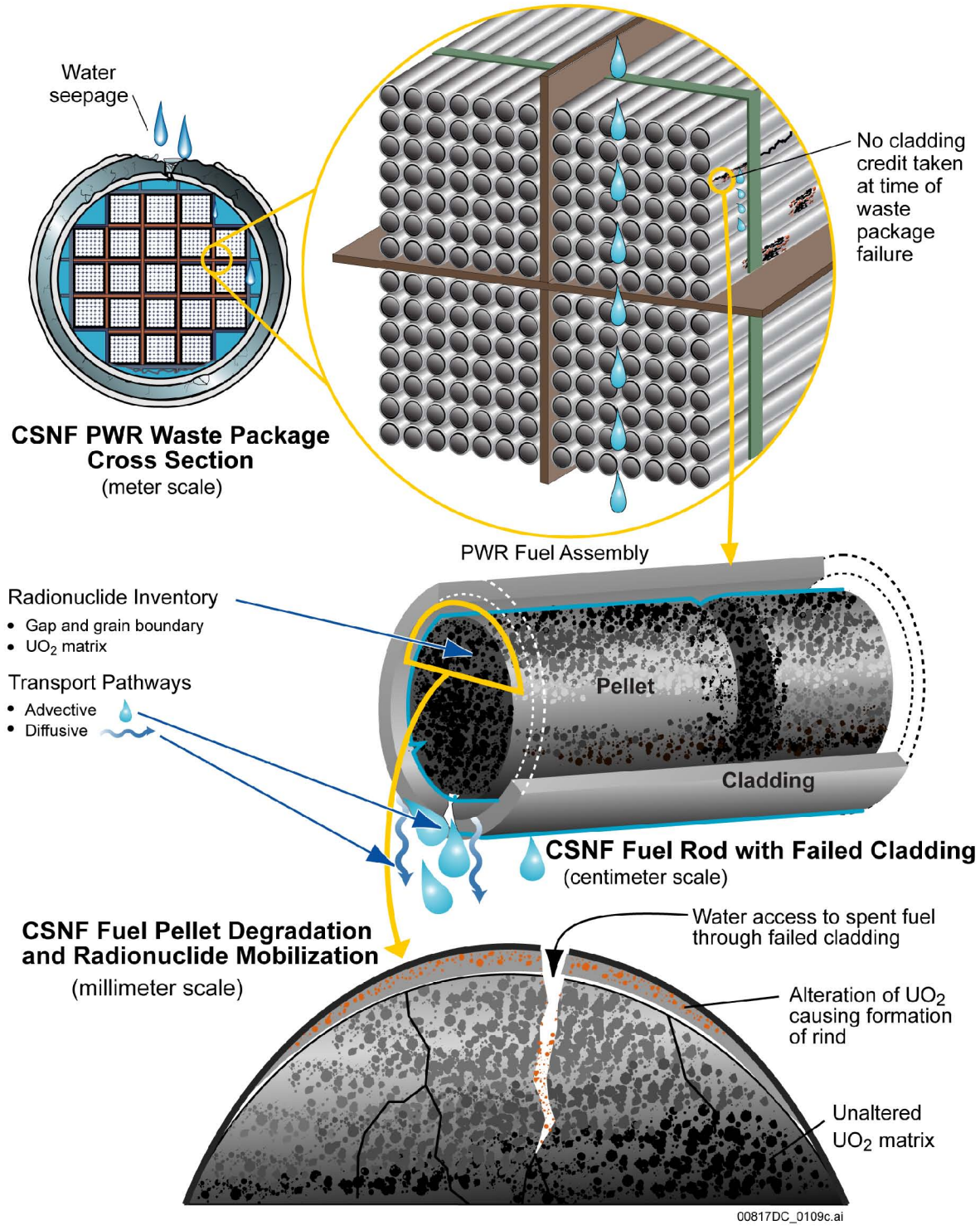

Figure ES-28. Schematic of CSNF Waste Form Degradation Mechanisms at Various Scales

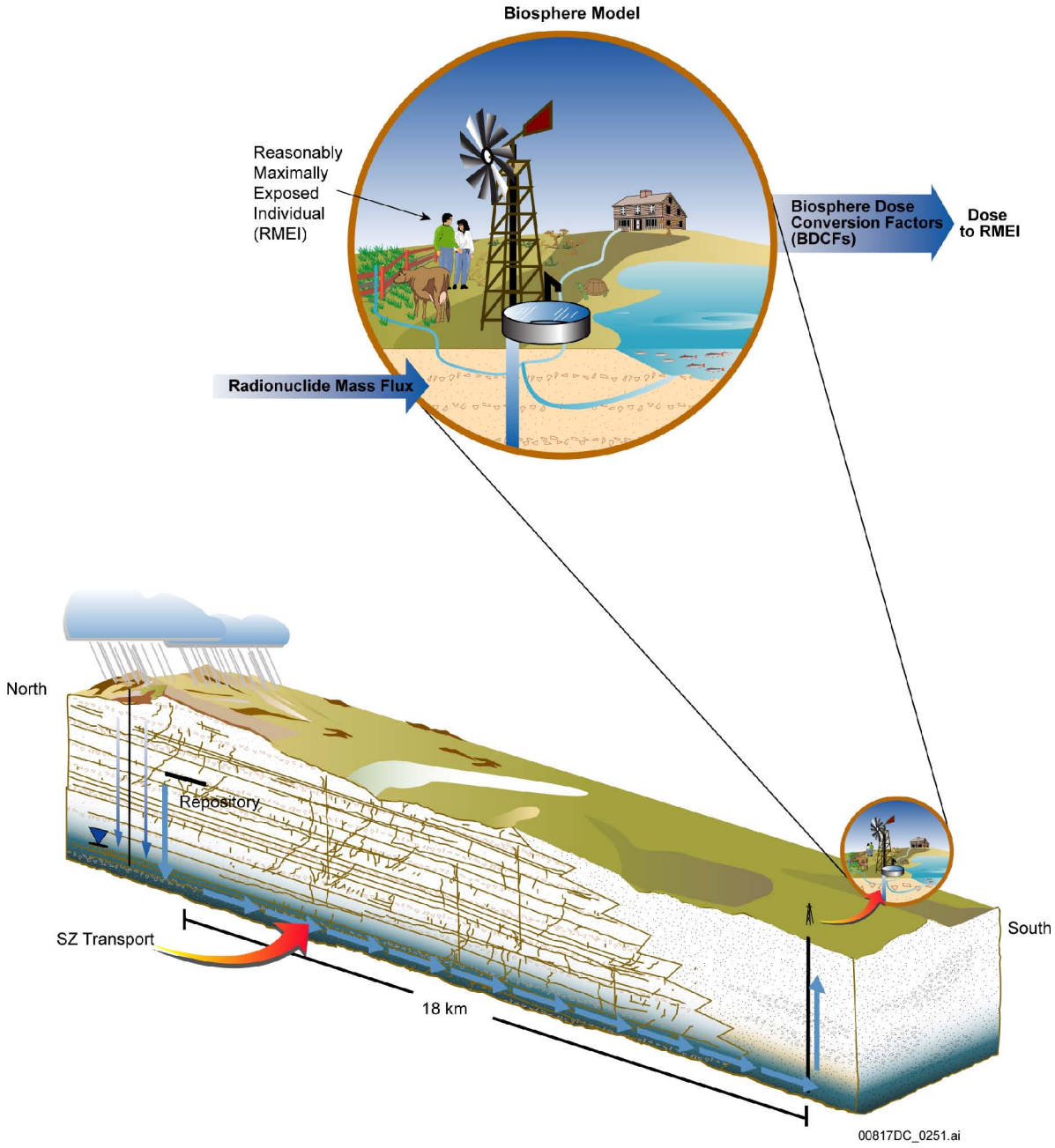

Figure ES-29. Overview of the Biosphere Groundwater Scenario Showing Groundwater Transport of Radionuclides and Uptake by the RMEI

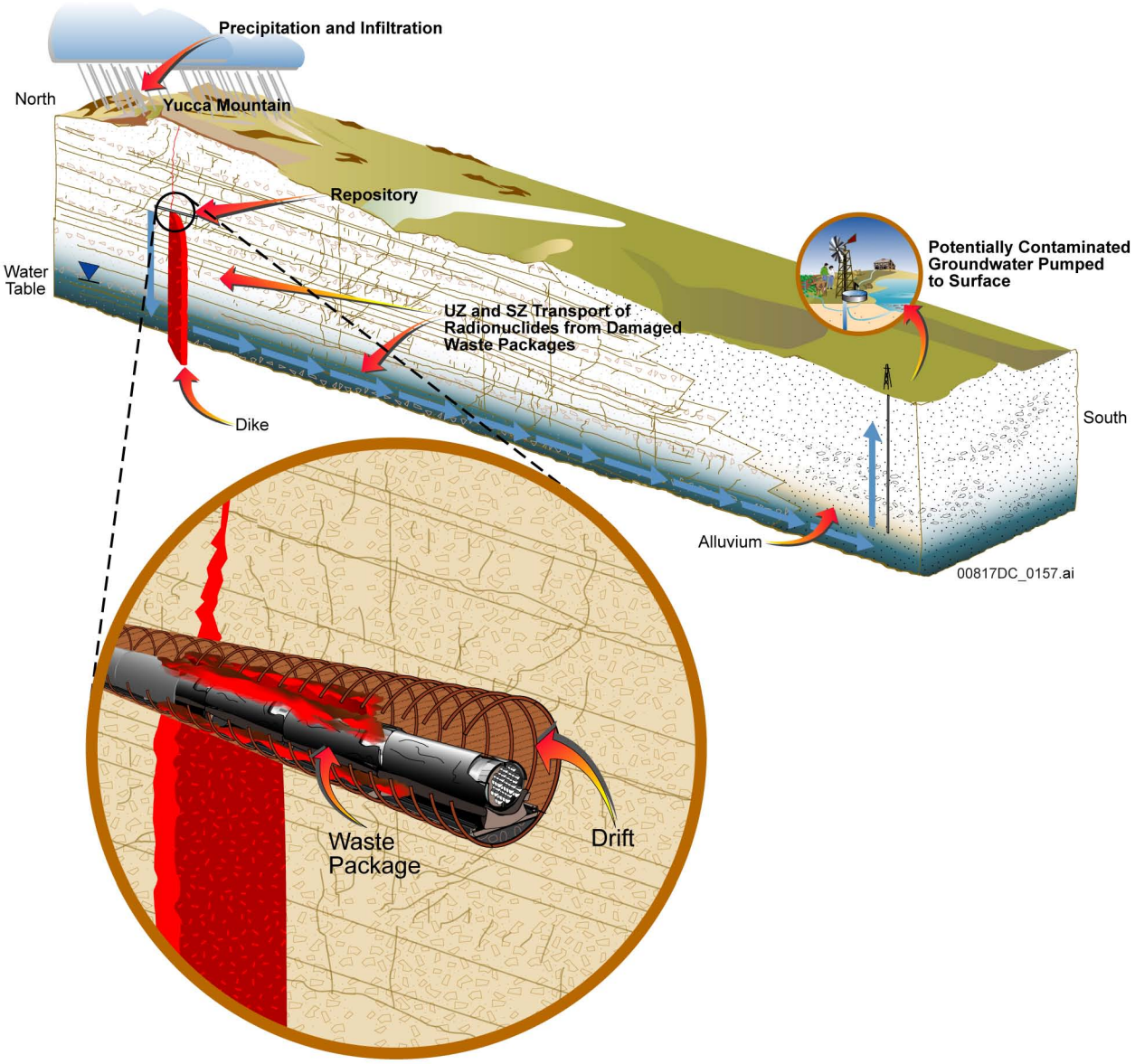

Figure ES-30. Schematic Diagram of the Intersection of an Igneous Dike with the Repository and Waste Packages

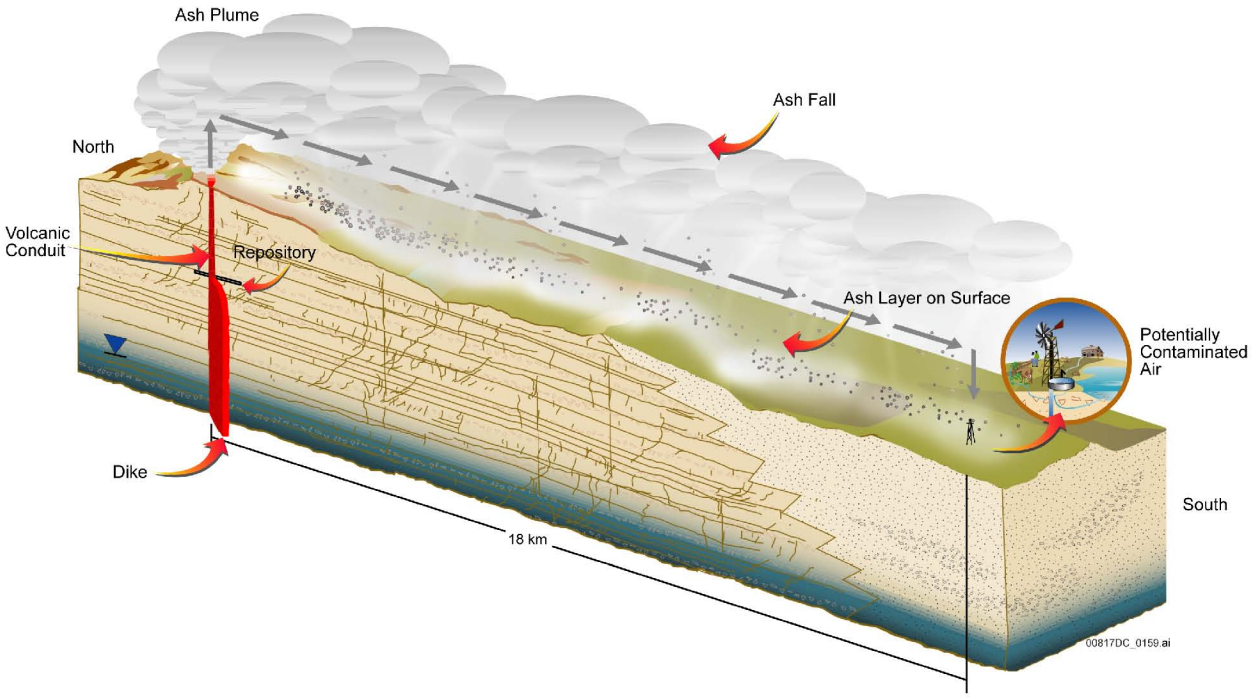

Figure ES-31. Schematic Representation of a Volcanic Eruption at Yucca Mountain Showing Transport of Radioactive Waste in a Tephra Plume

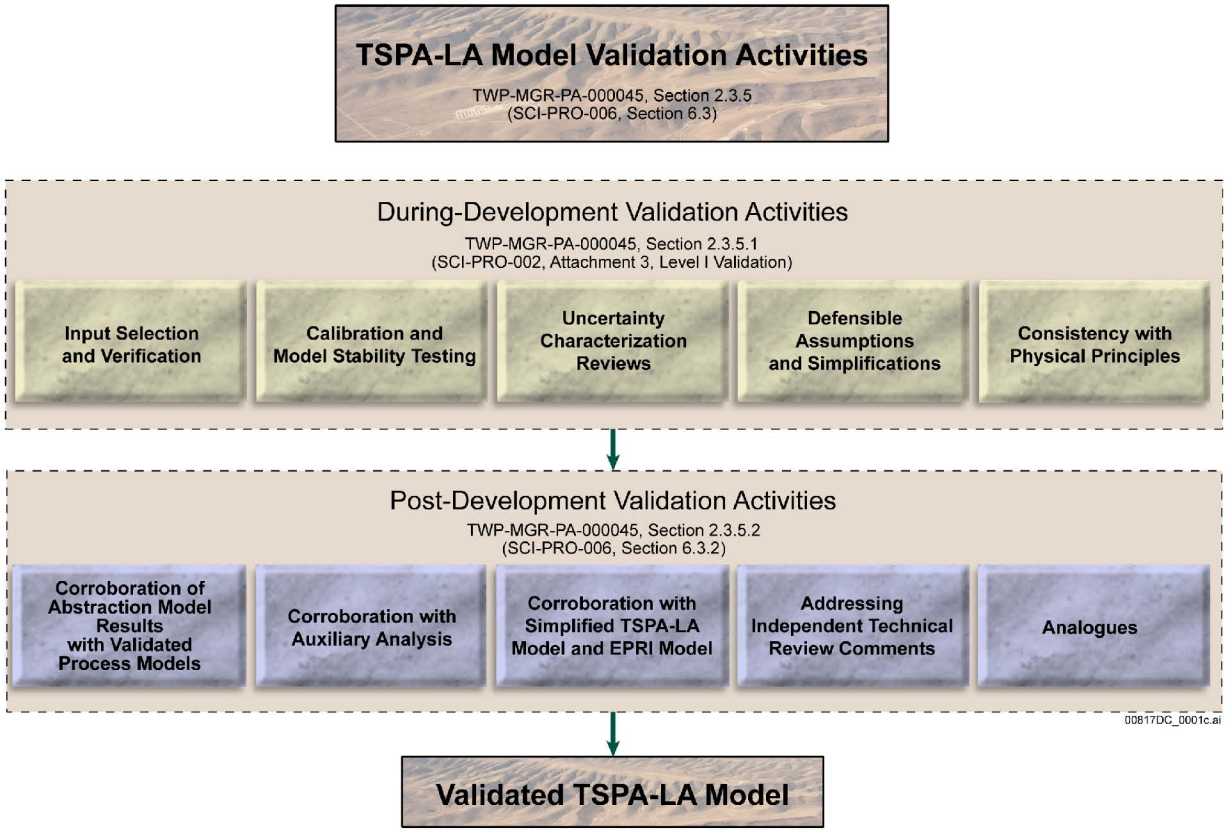

Figure ES-32. Model Validation Approach for the TSPA-LA Model

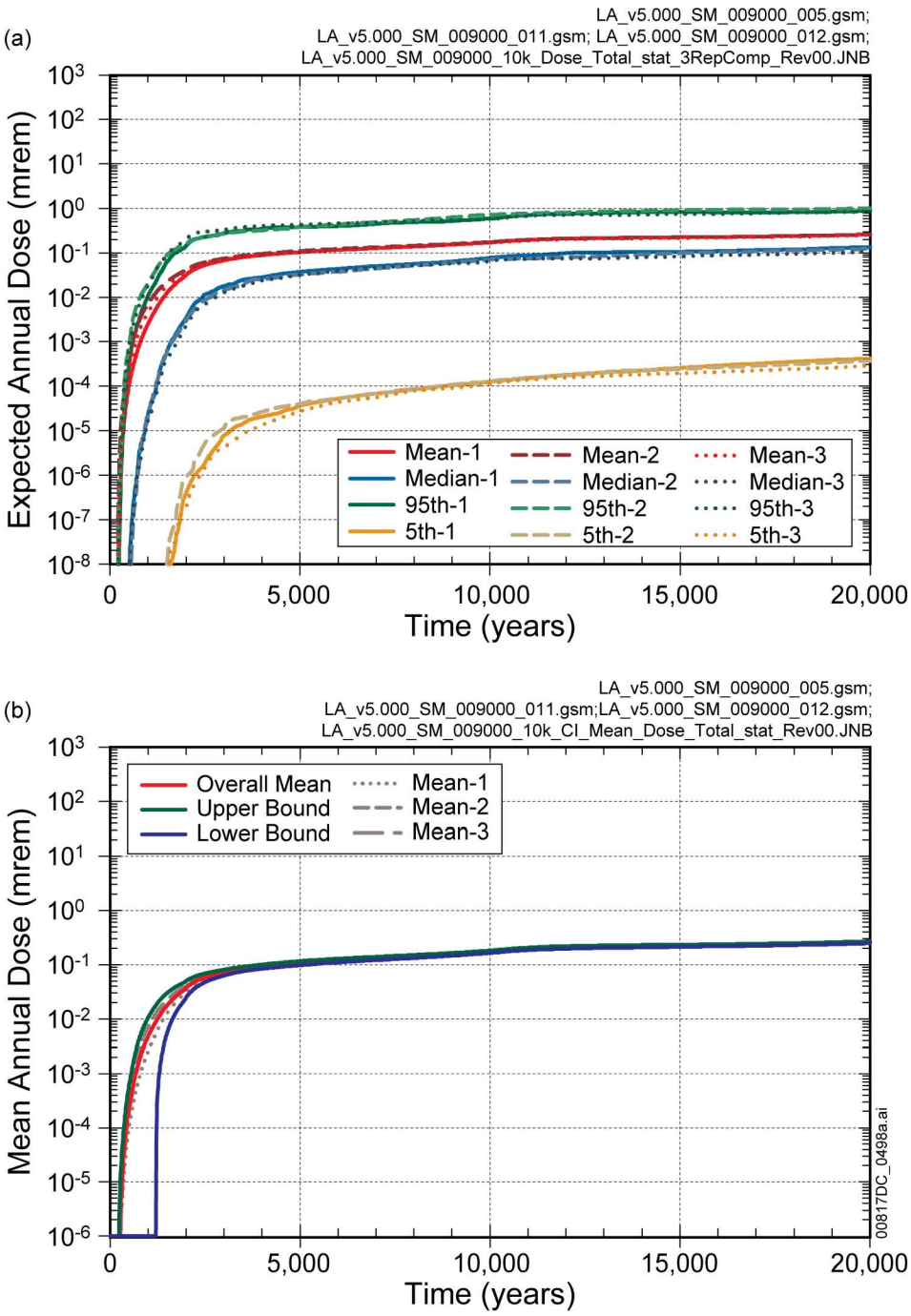

Source: Output DTN: MO0709TSPASTAB.000 [DIRS 182983].

Figure ES-33 Stability of Seismic Ground Motion Modeling Case for 20,000 Years: (a) Comparison of Expected Annual Dose for Three Replicates and (b) Confidence Interval Around Mean Annual Dose

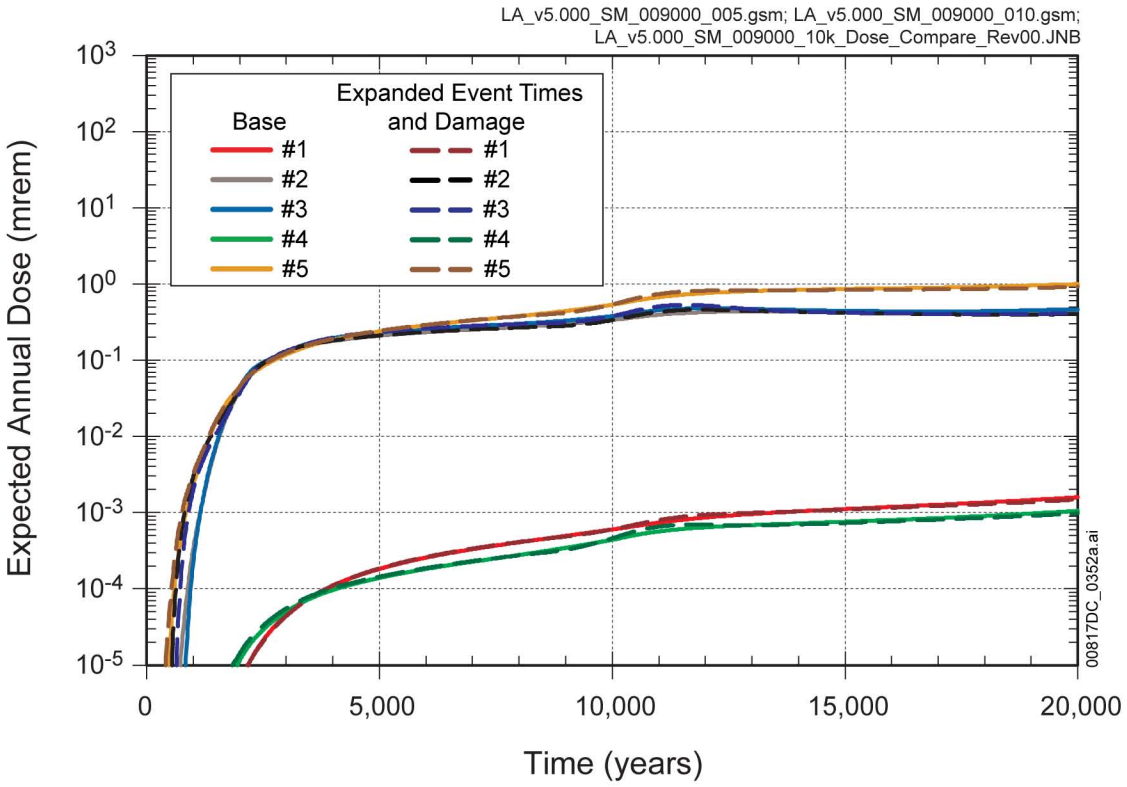

Source: Output DTNs: MO0708TSPAVALI.000 [DIRS 182985] and MO0709TSPAREGS.000 [DIRS 182976].

Figure ES-34. Expected Annual Dose Over 20,000 Years for Seismic Ground Motion Modeling Case Considering Additional Specified Event Times and Damage Fractions

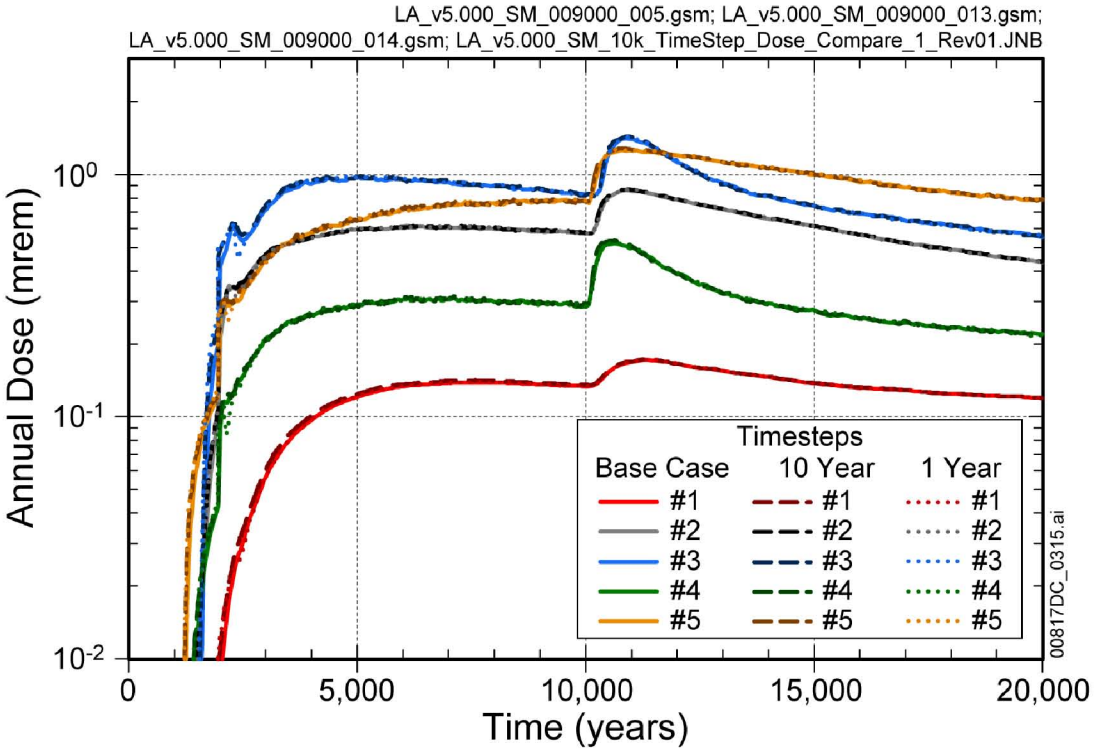

Source: Output DTN: MO0708TSPAVALI.000 [DIRS 182985]

Figure ES-35. Annual Dose from a Seismic Ground Motion Event at 1,000 Years with Damage Fraction 10^{-6} for Three Timestep Schemes

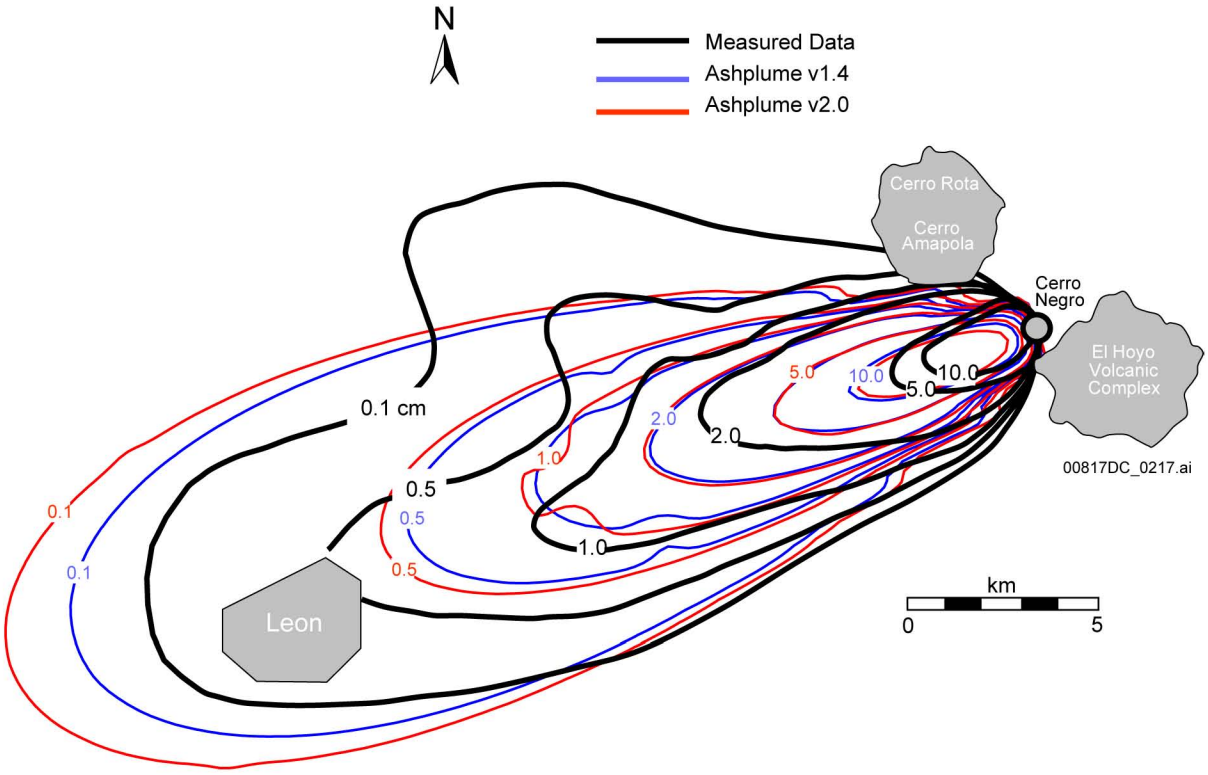

Source: SNL 2007 [DIRS 177431], Appendix L.

Figure ES-36. Comparison of Ash-Fall Thickness at Cerro Negro with ASHPLUME Simulated Results

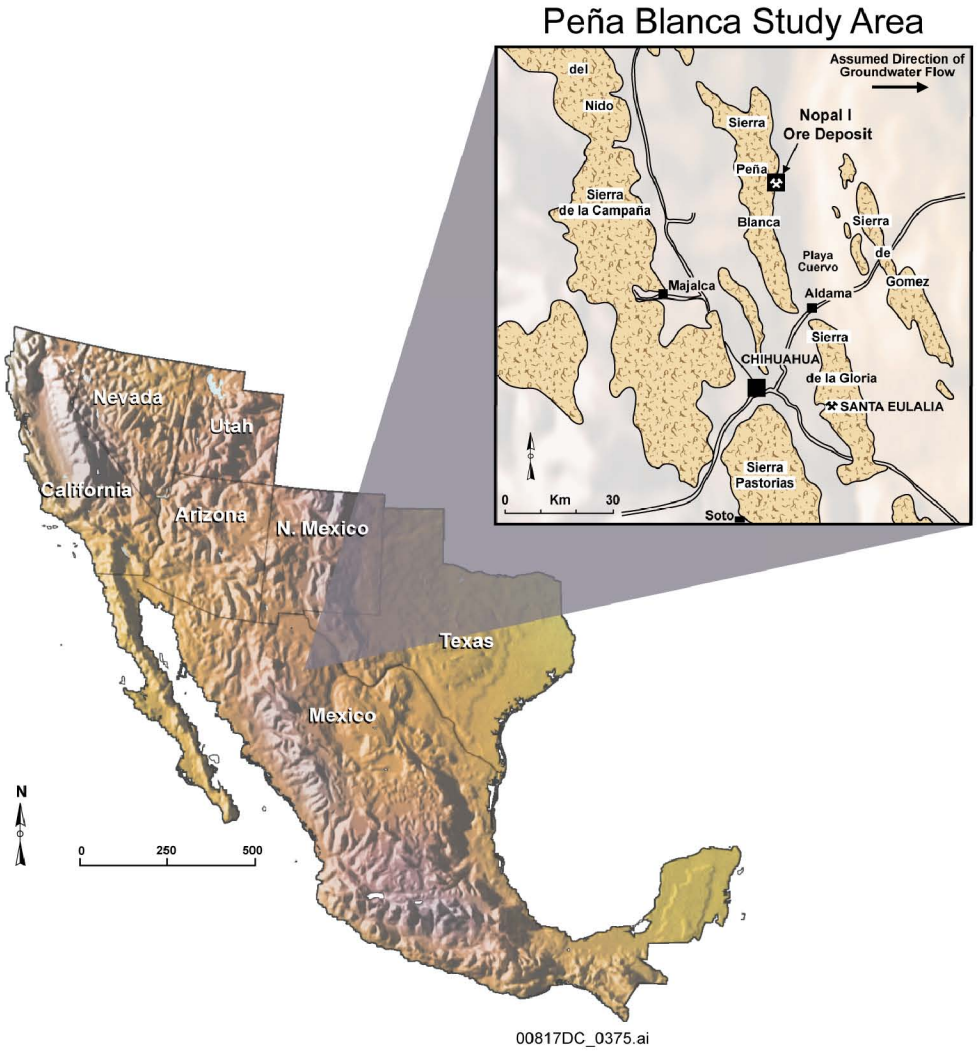

Source: Modified from George-Aniel et al. 1991 [DIRS 105636], Figure 1.

Figure ES-37. Location of Peña Blanca Nopal I Ore Deposit in the Sierra Peña Blanca

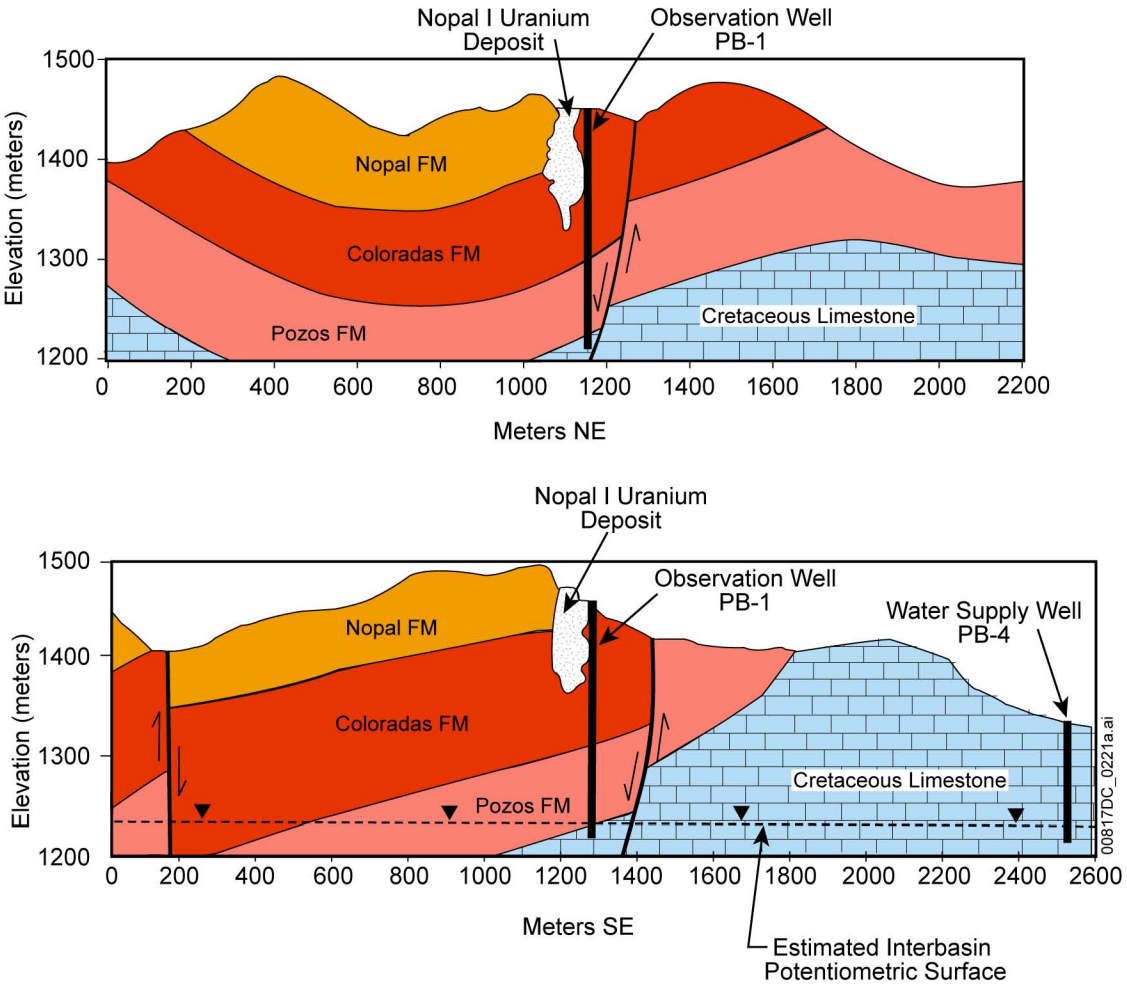

Source: Modified from Pearcy et al. 1993 [DIRS 151774], p. 1-4.

Figure ES-38. Geologic Characterization of Nopal 1 Ore Body

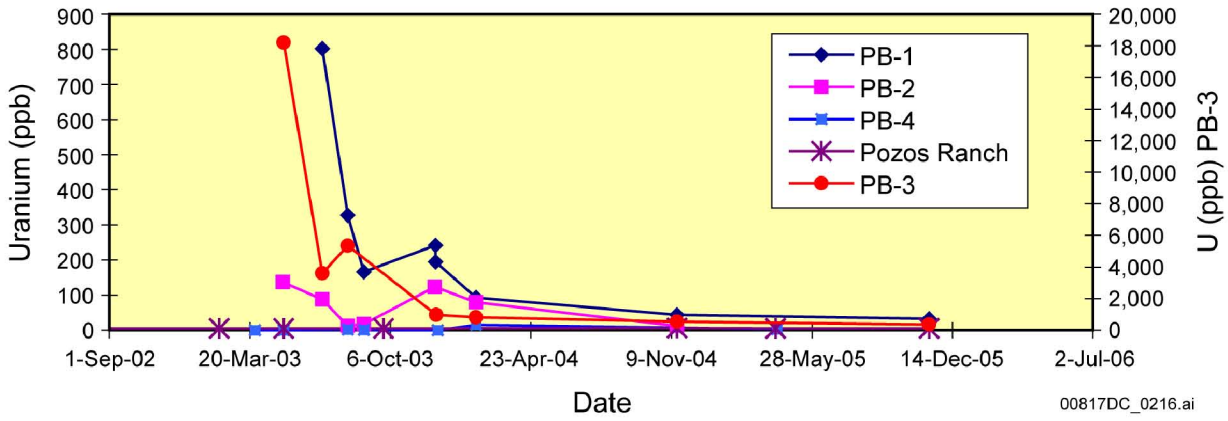

Source: Data from Goldstein et al., 2006 [DIRS 181364], p. 217.

Figure ES-39. Uranium Concentration Determined in Groundwater Samples from Wells at and near the Nopal I Ore Deposit

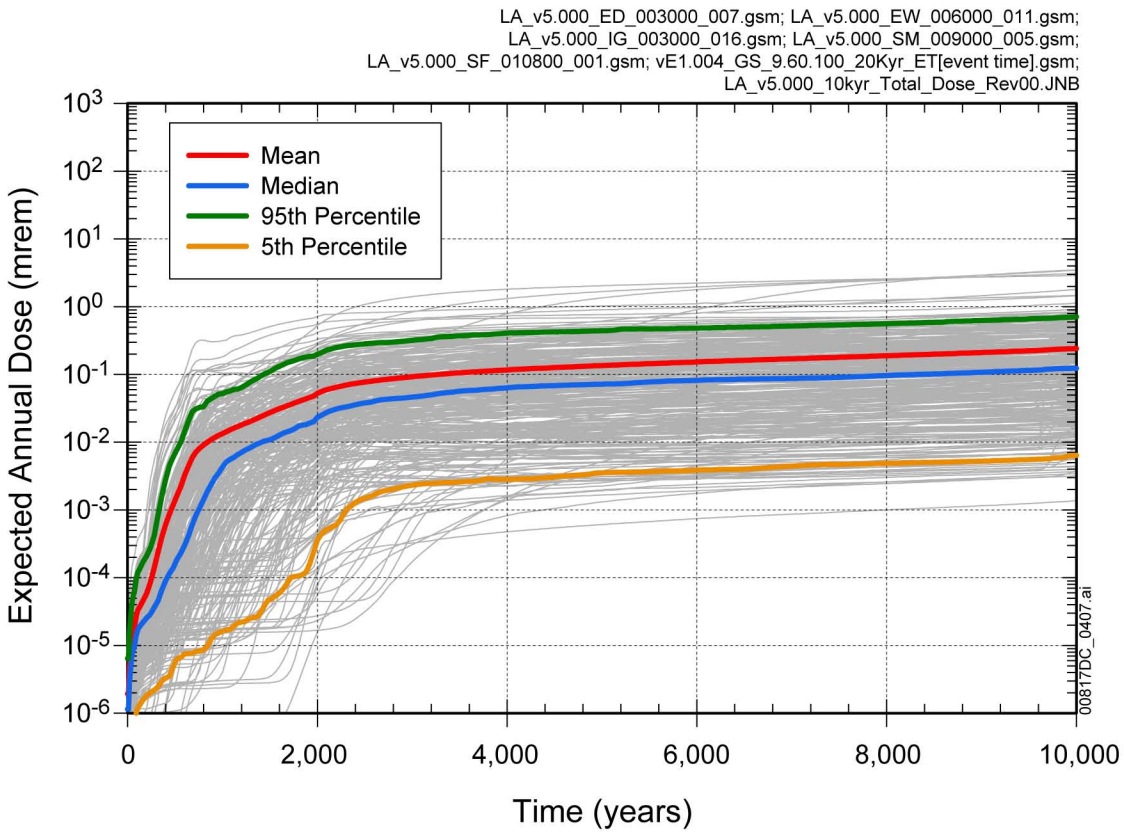

Source: Output DTN: MO0709TSPAREGS.000 [DIRS 182976].

Figure ES-40. Total Expected Annual Dose for 10,000 Years after Closure

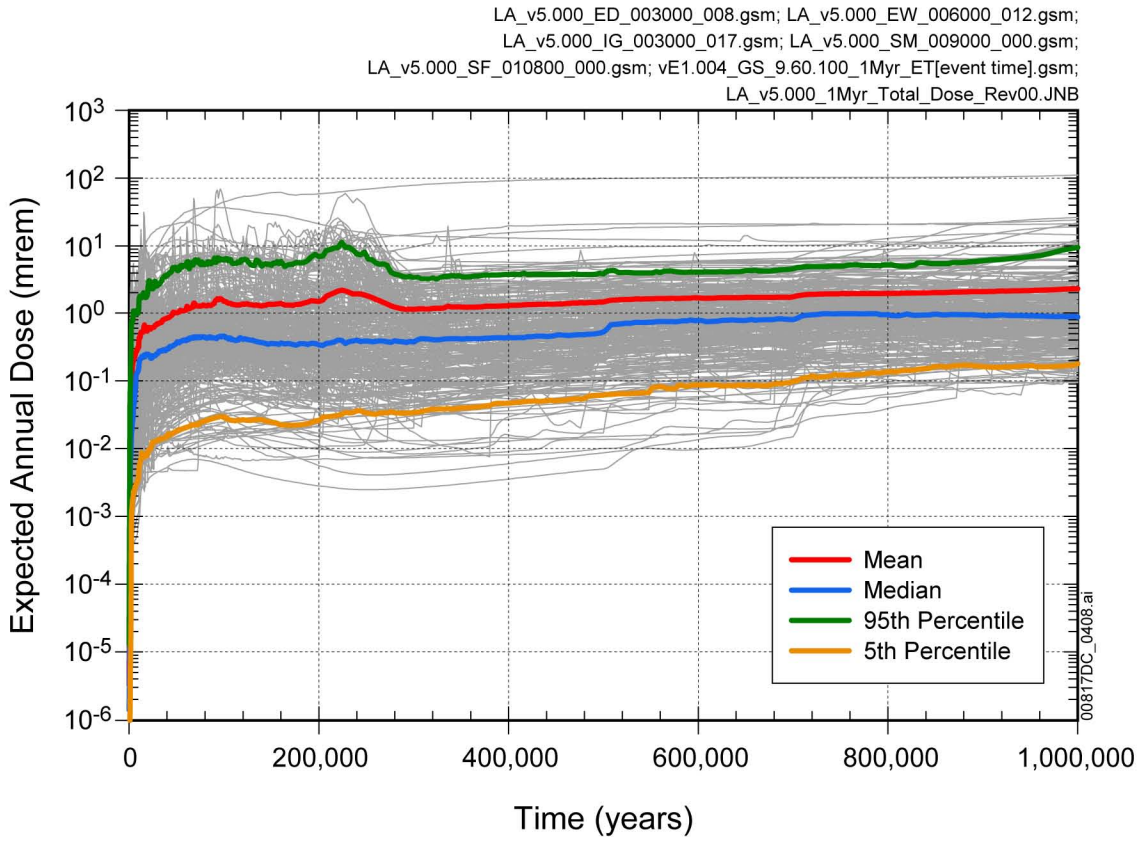

Source: Output DTN: MO0709TSPAREGS.000 [DIRS 182976].

Figure ES-41. Total Expected Annual Dose for 1,000,000 Years after Closure

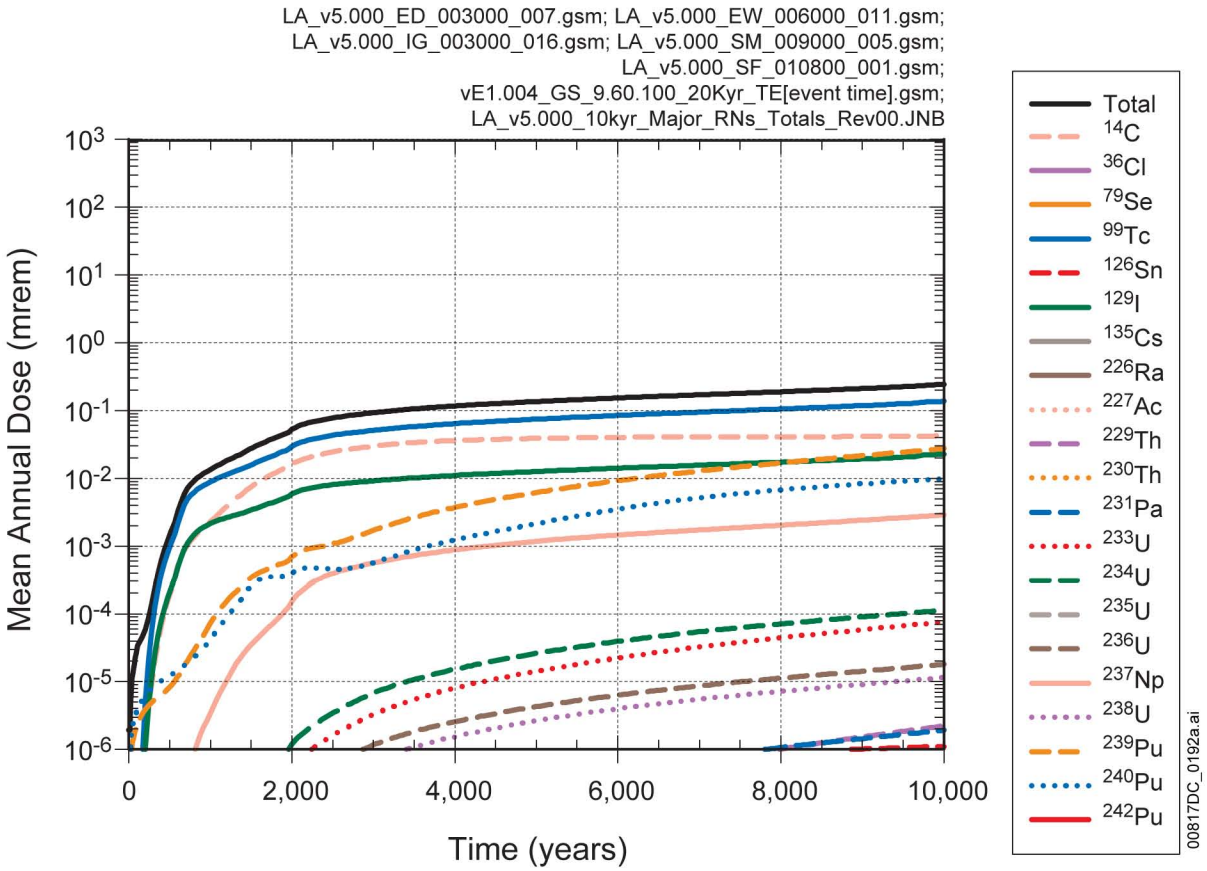

Source: Output DTN: MO0709TSPAREGS.000 [DIRS 182976].

Figure ES-42. Contribution of Individual Radionuclides to Total Mean Annual Dose for 10,000 Years after Repository Closure

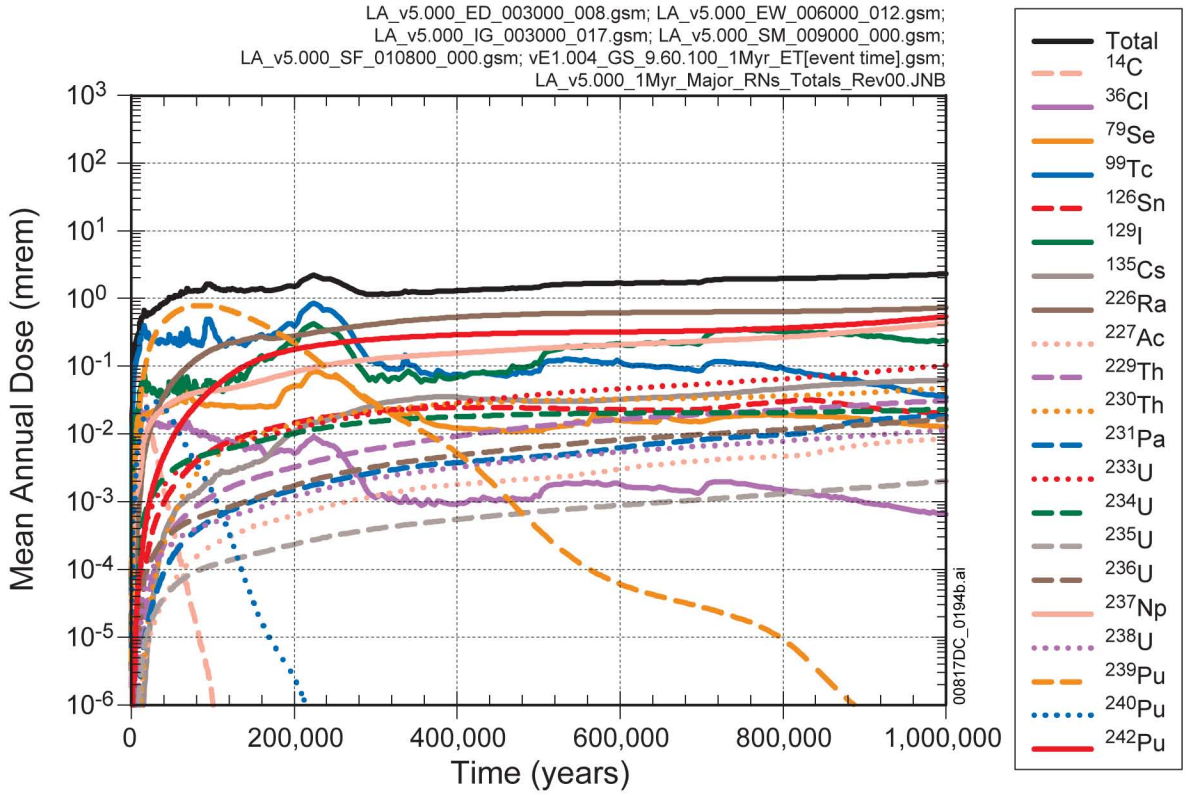

Source: Output DTN: MO0709TSPAREGS.000 [DIRS 182976].

Figure ES-43. Contribution of Individual Radionuclides to Total Mean Annual Dose for 1,000,000 Years after Repository Closure

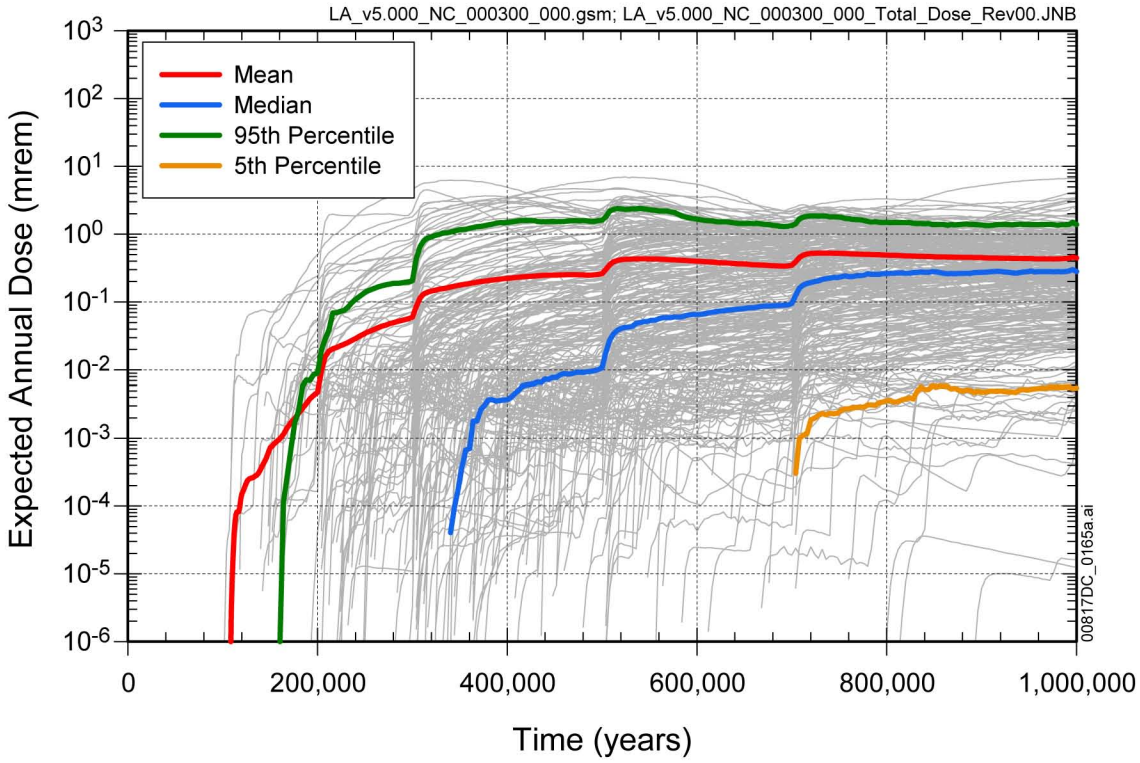

Source: Output DTN: MO0709TSPAREGS.000 [DIRS 182976].

Figure ES-44. Annual Dose for the Nominal Scenario Class Modeling Case for the Post-10,000-Year Period

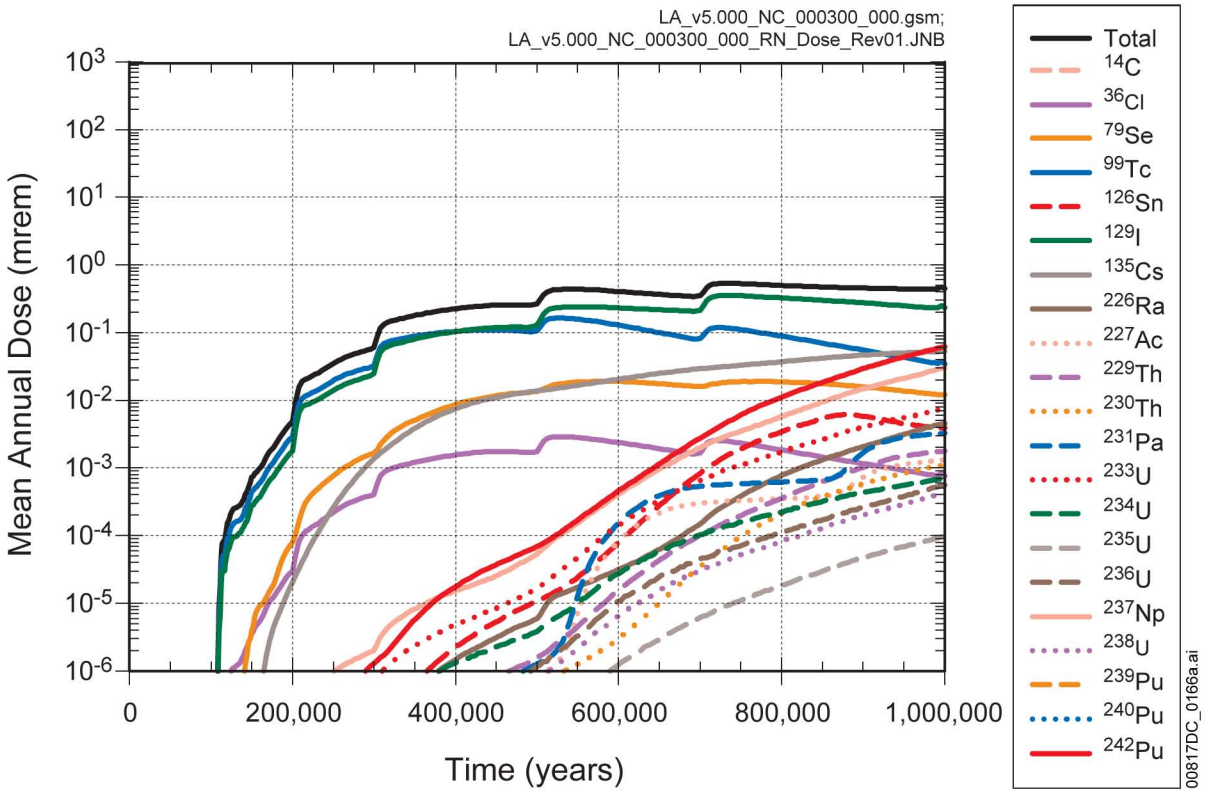

Source: Output DTN: MO0709TSPAREGS.000 [DIRS 182976].

Figure ES-45. Mean Annual Dose Contributions from Major Radionuclides for the Nominal Scenario Class Modeling Case for the Post-10,000-Year Period

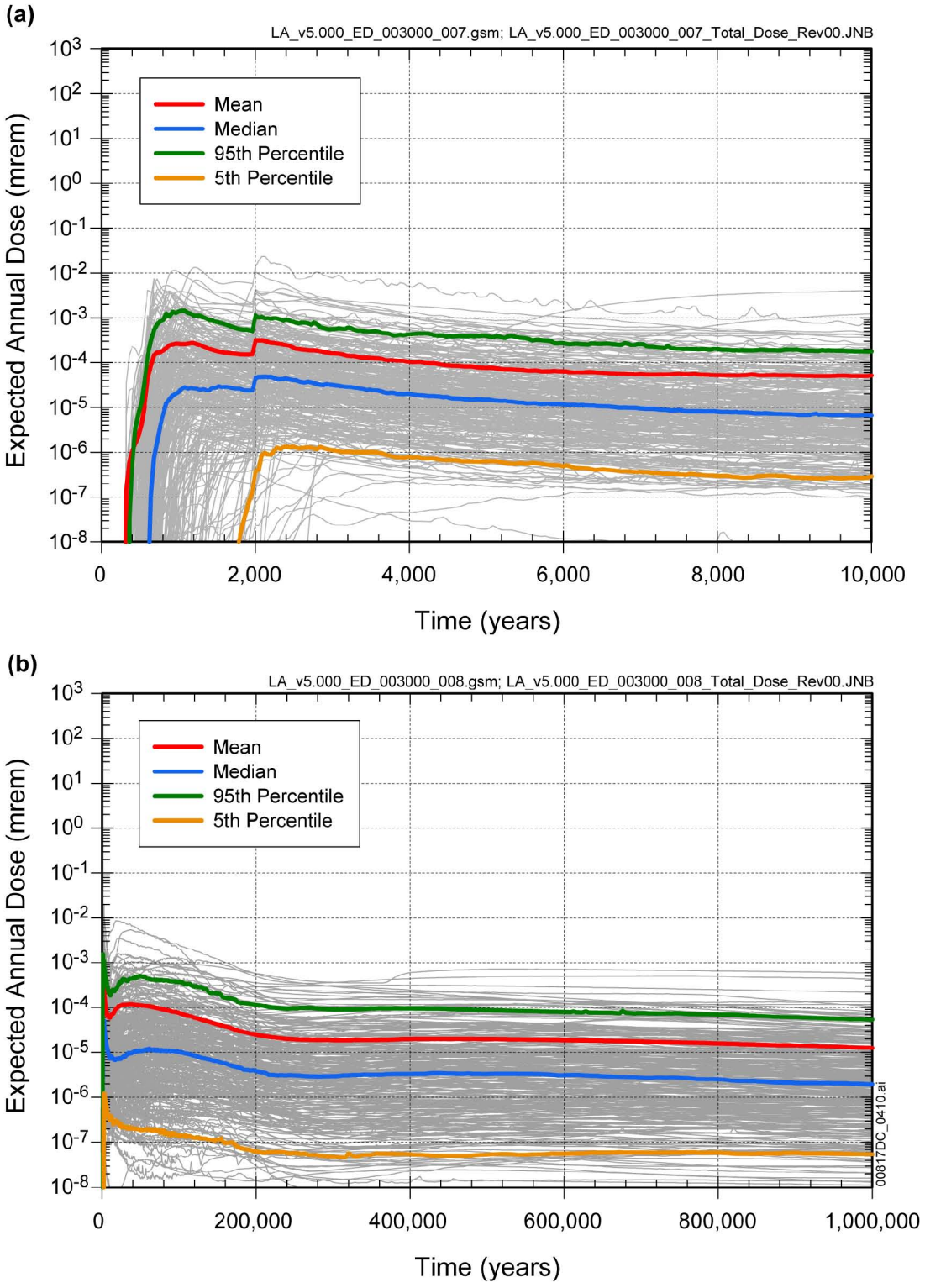

Source: Output DTN: MO0709TSPAREGS.000 [DIRS 182976].

Figure ES-46. Expected Annual Dose for the Drip Shield Early Failure Modeling Case for (a) the First 10,000 Years after Repository Closure and (b) Post-10,000-Year Period

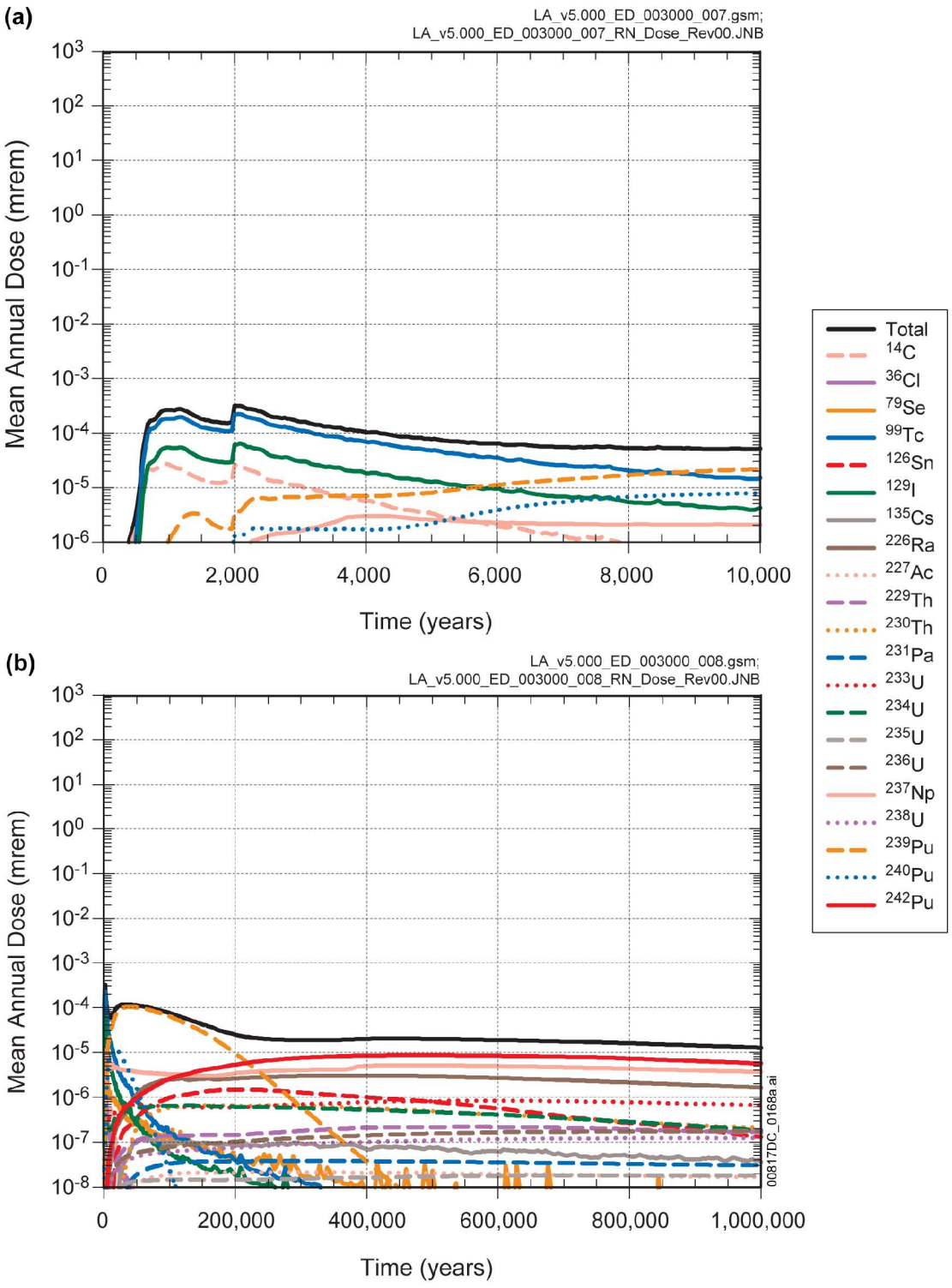

Source: Output DTN: MO0709TSPAREGS.000 [DIRS 182976].

Figure ES-47. Mean Annual Dose Contributions from Major Radionuclides for the Drip Shield Early Failure Modeling Case for (a) the First 10,000 Years after Repository Closure and (b) Post-10,000-Year Period

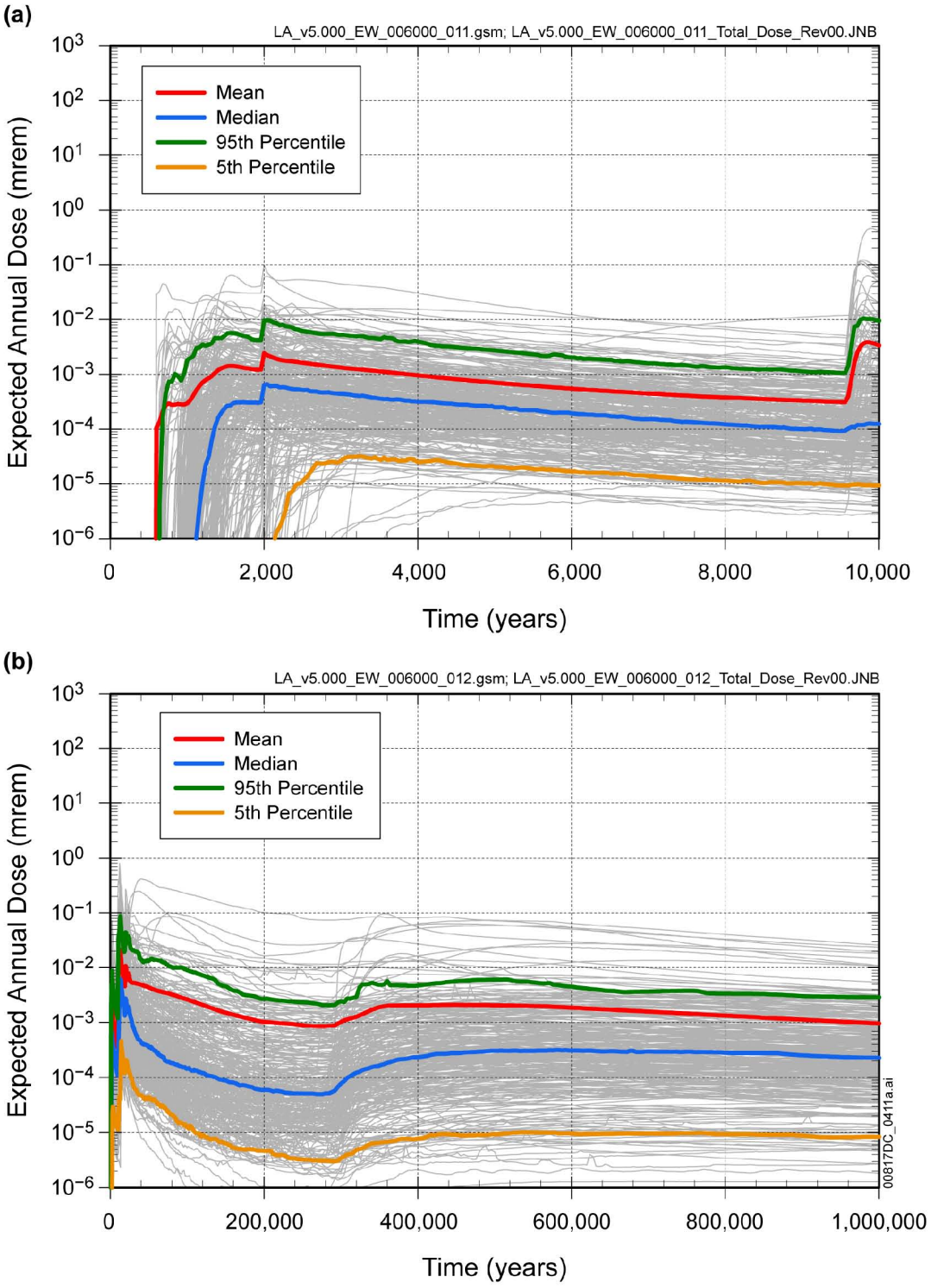

Source: Output DTN: MO0709TSPAREGS.000 [DIRS 182976].

Figure ES-48. Expected Annual Dose for the Waste Package Early Failure Modeling Case (a) the First 10,000 Years after Repository Closure and (b) Post-10,000-Year Period

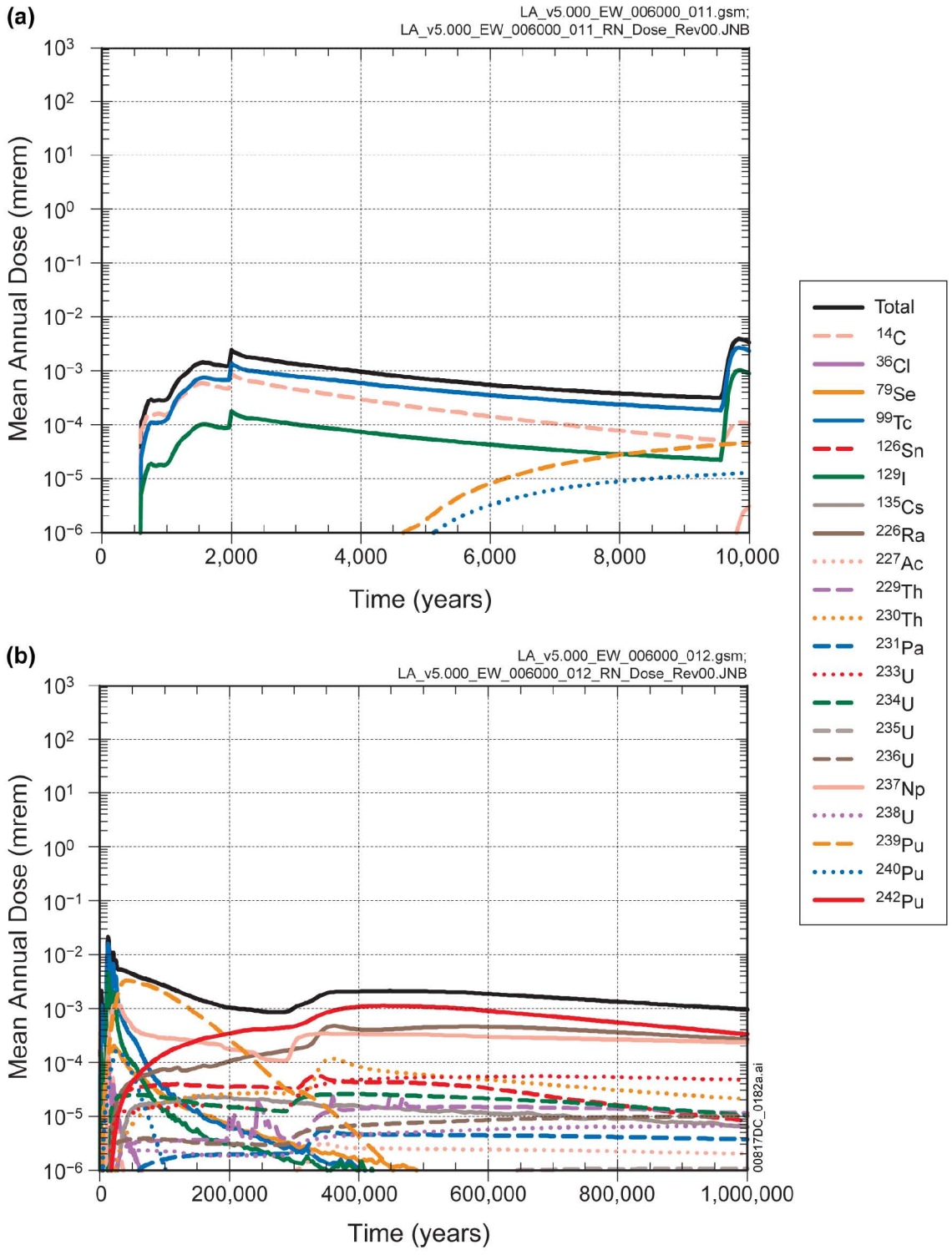

Source: Output DTN: MO0709TSPAREGS.000 [DIRS 182976].

Figure ES-49. Mean Annual Dose Contributions from Major Radionuclides for the Waste Package Early Failure Modeling Case for (a) the First 10,000 Years after Repository Closure and (b) Post-10,000-Year Period

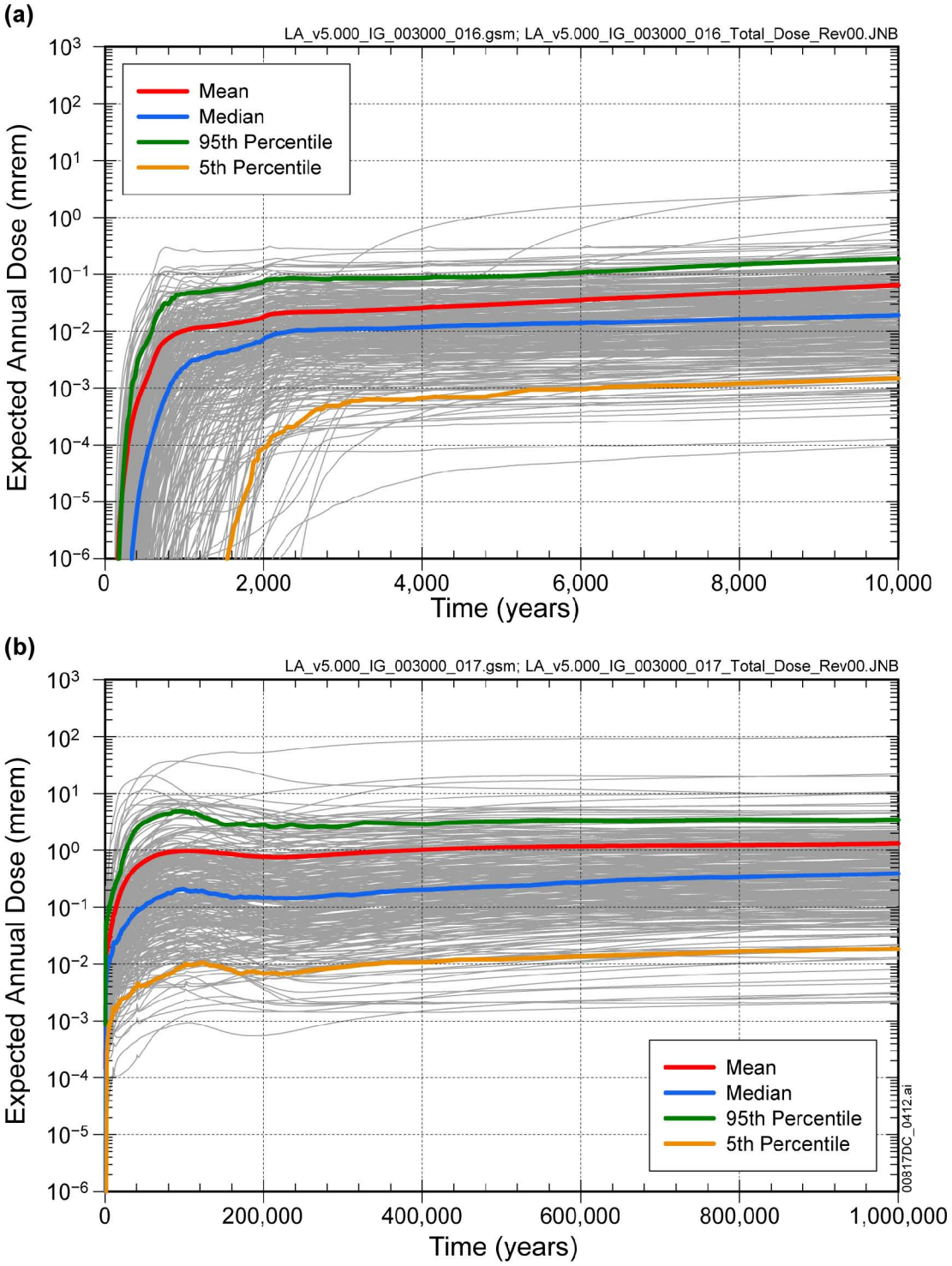

Source: Output DTN: MO0709TSPAREGS.000 [DIRS 182976].

Figure ES-50. Expected Annual Dose for the Igneous Intrusion Modeling Case for (a) 10,000 Years after Repository Closure and (b) Post-10,000-Year Period

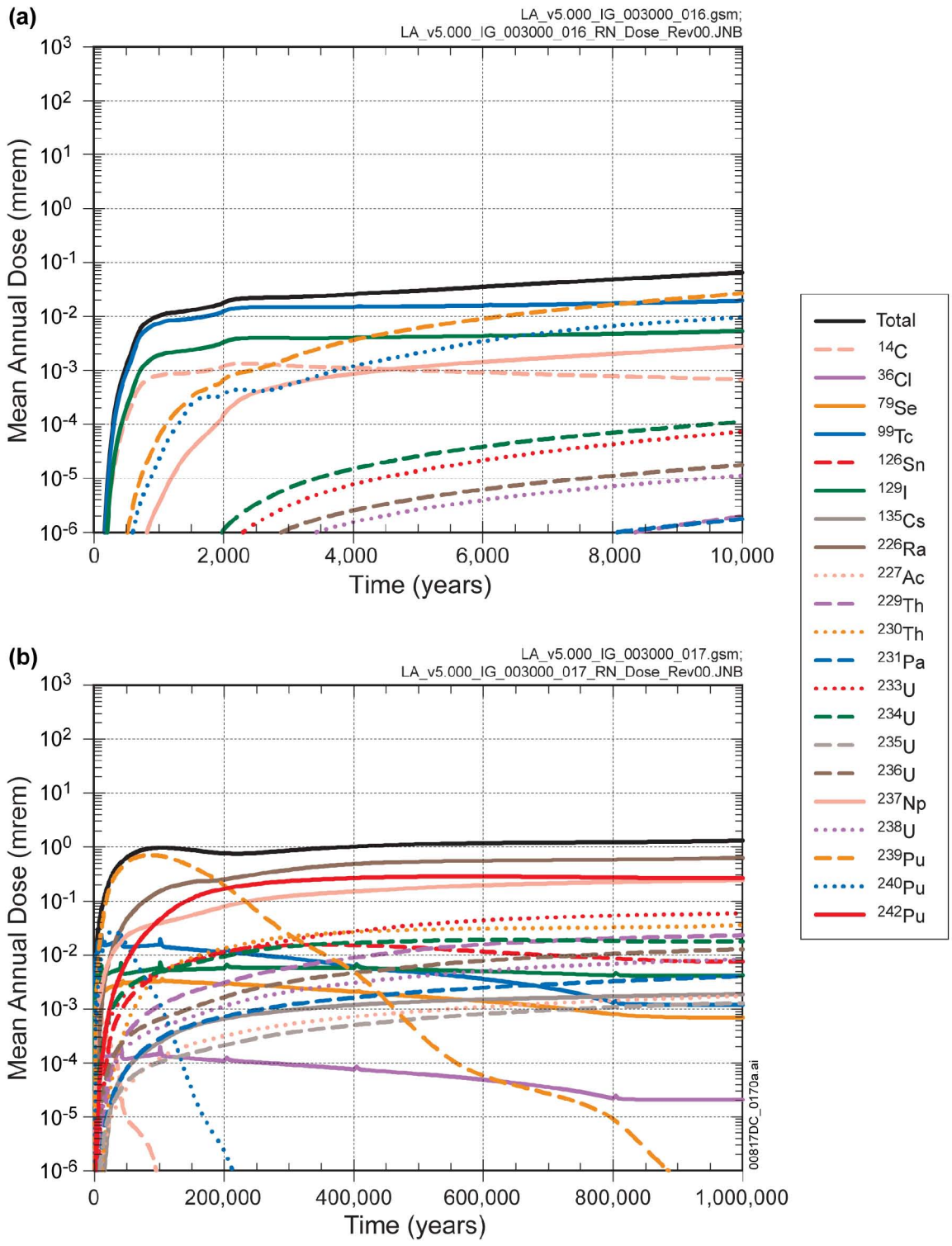

Source: Output DTN: MO0709TSPAREGS.000 [DIRS 182976].

Figure ES-51. Mean Annual Dose Contributions from Major Radionuclides for the Igneous Intrusion Modeling Case for (a) the First 10,000 Years after Repository Closure and (b) Post-10,000-Year Period

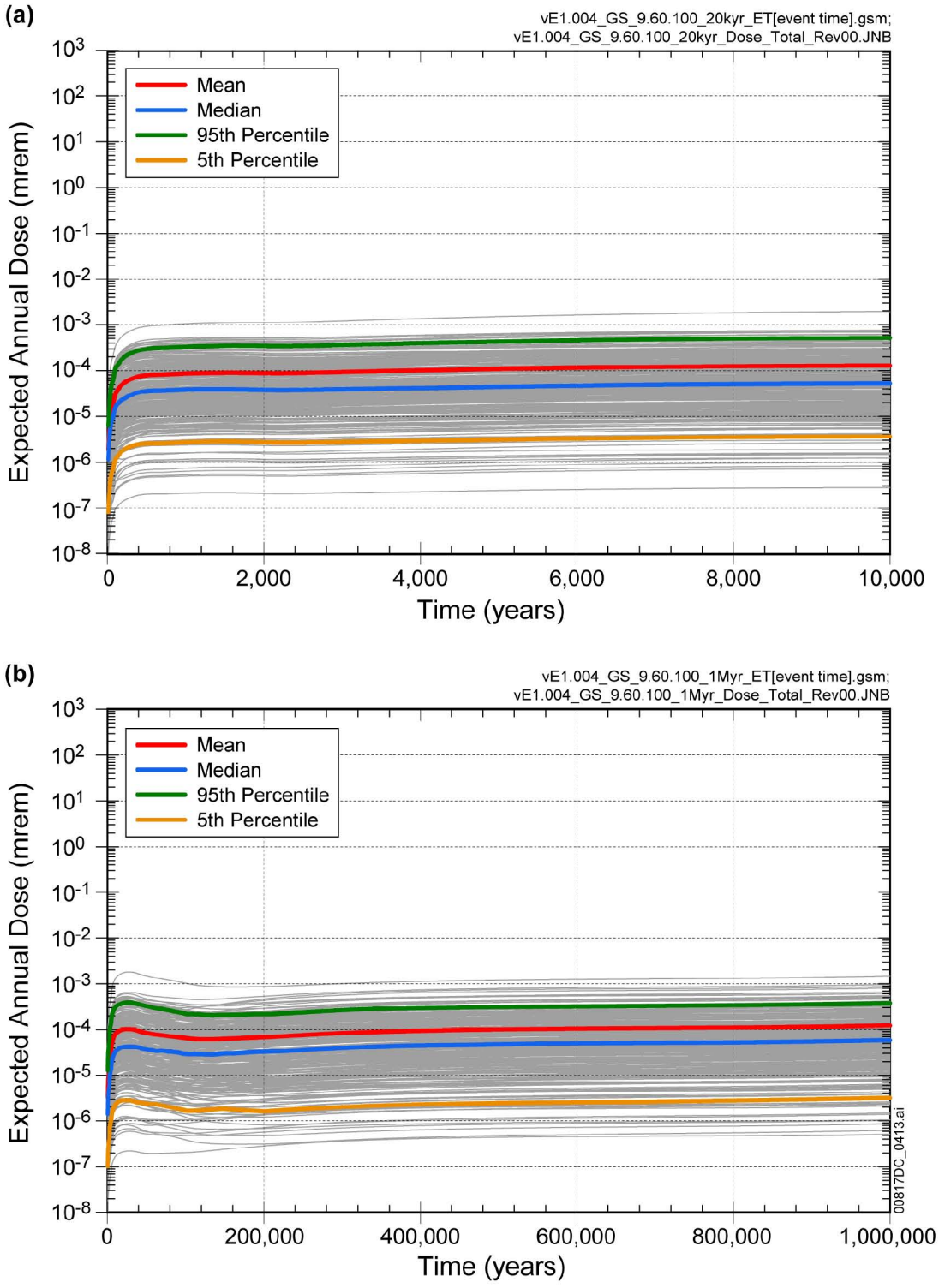

Source: Output DTN: MO0709TSPAREGS.000 [DIRS 182976].

Figure ES-52. Expected Annual Dose for the Volcanic Eruption Modeling Case for (a) 10,000 Years after Repository Closure and (b) Post-10,000-Year Period

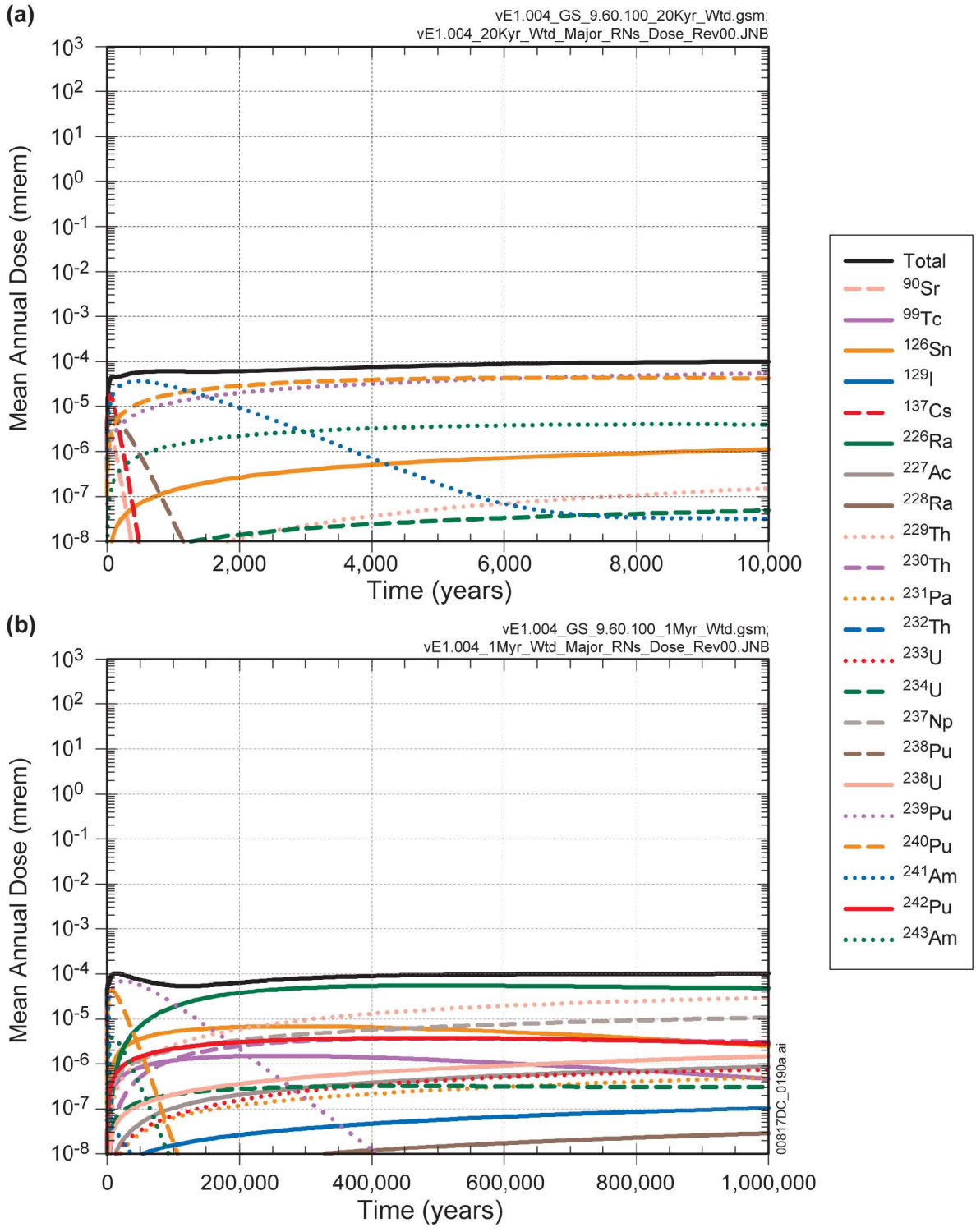

Source: Output DTN: MO0709TSPAREGS.000 [DIRS 182976].

Figure ES-53. Mean Annual Dose Contributions from Major Radionuclides for the Volcanic Eruption Modeling Case for (a) the First 10,000 Years after Repository Closure and (b) Post-10,000-Year Period

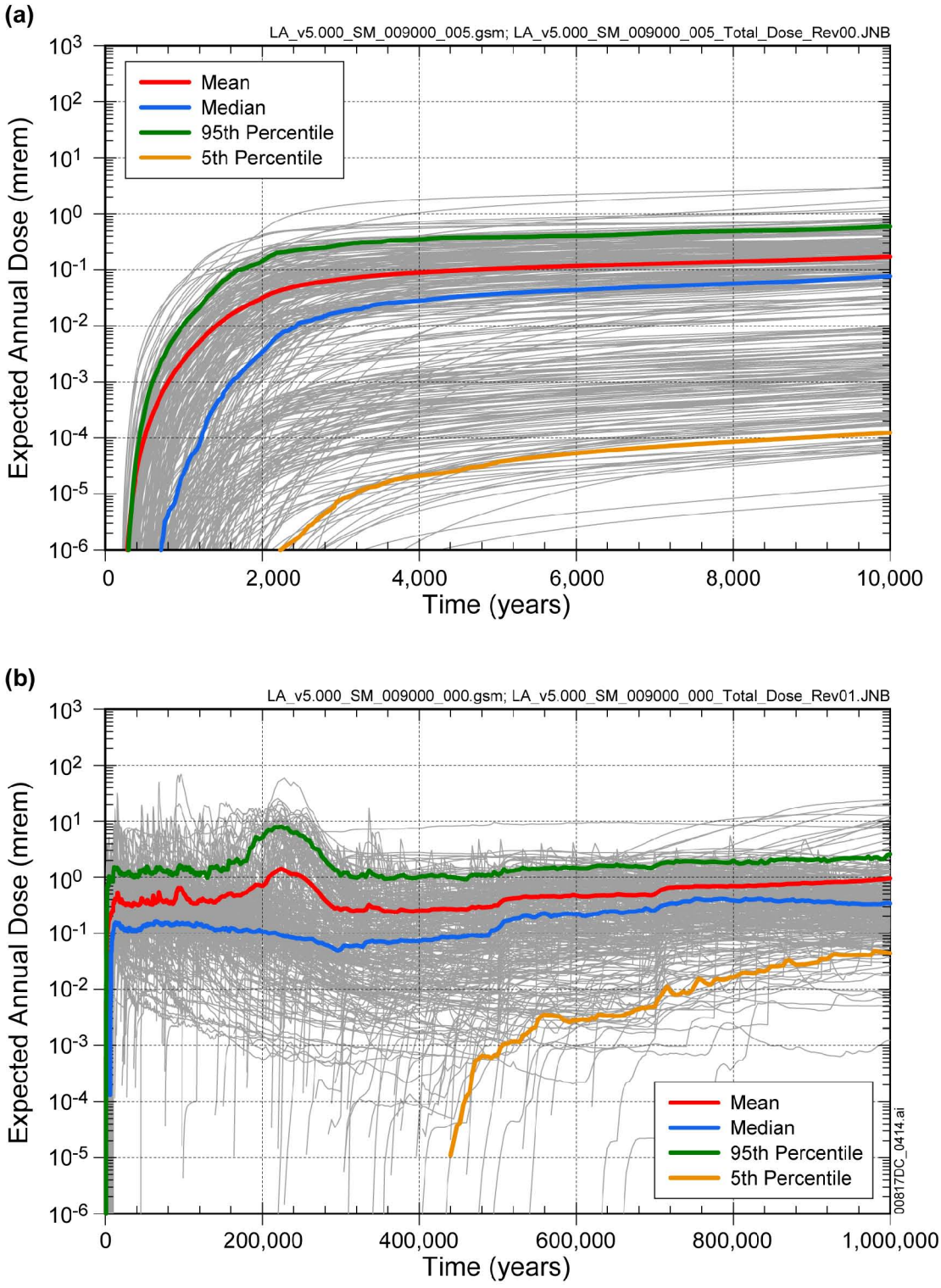

Source: Output DTN: MO0709TSPAREGS.000 [DIRS 182976].

Figure ES-54. Expected Annual Dose for the Seismic Ground Motion Modeling Case for (a) 10,000 Years after Repository Closure and (b) Post-10,000-Year Period

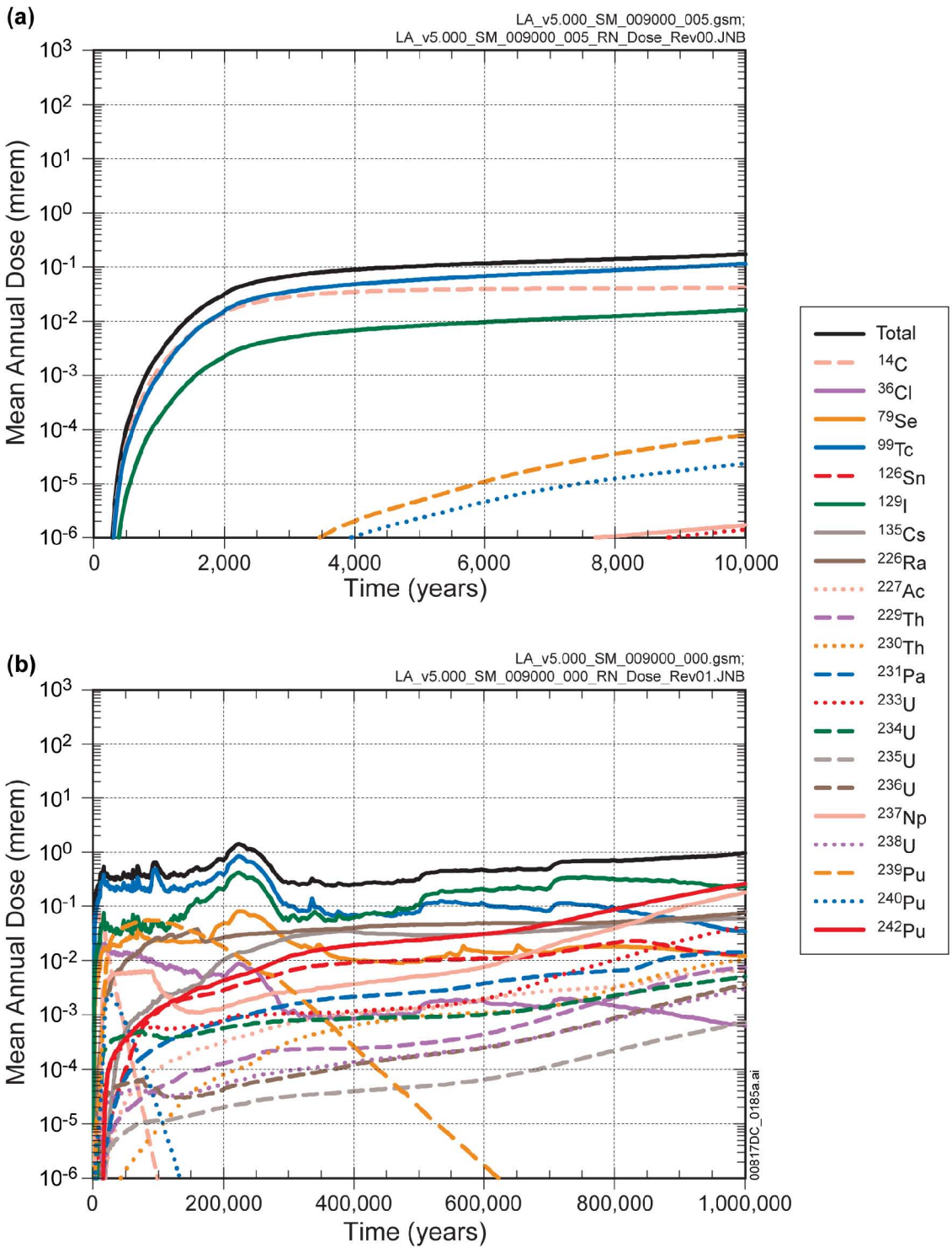

Source: Output DTN: MO0709TSPAREGS.000 [DIRS 182976].

Figure ES-55. Mean Annual Dose Contributions from Major Radionuclides for the Seismic Ground Motion Modeling Case for (a) the First 10,000 Years after Repository Closure and (b) Post-10,000-Year Period

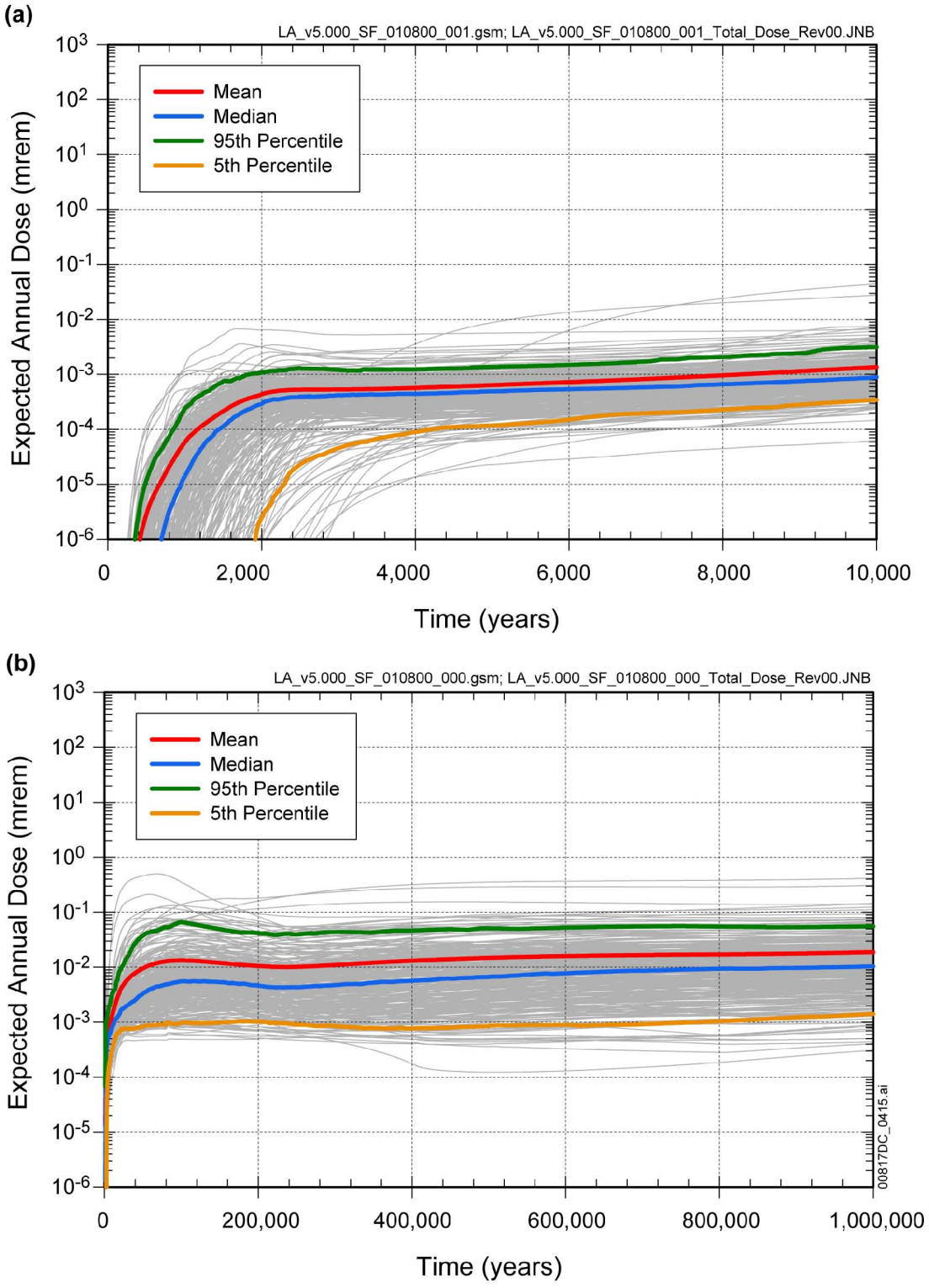

Source: Output DTN: MO0709TSPAREGS.000 [DIRS 182976].

Figure ES-56. Expected Annual Dose for the Seismic Fault Displacement Modeling Case for (a) 10,000 Years after Repository Closure and (b) Post-10,000-Year Period

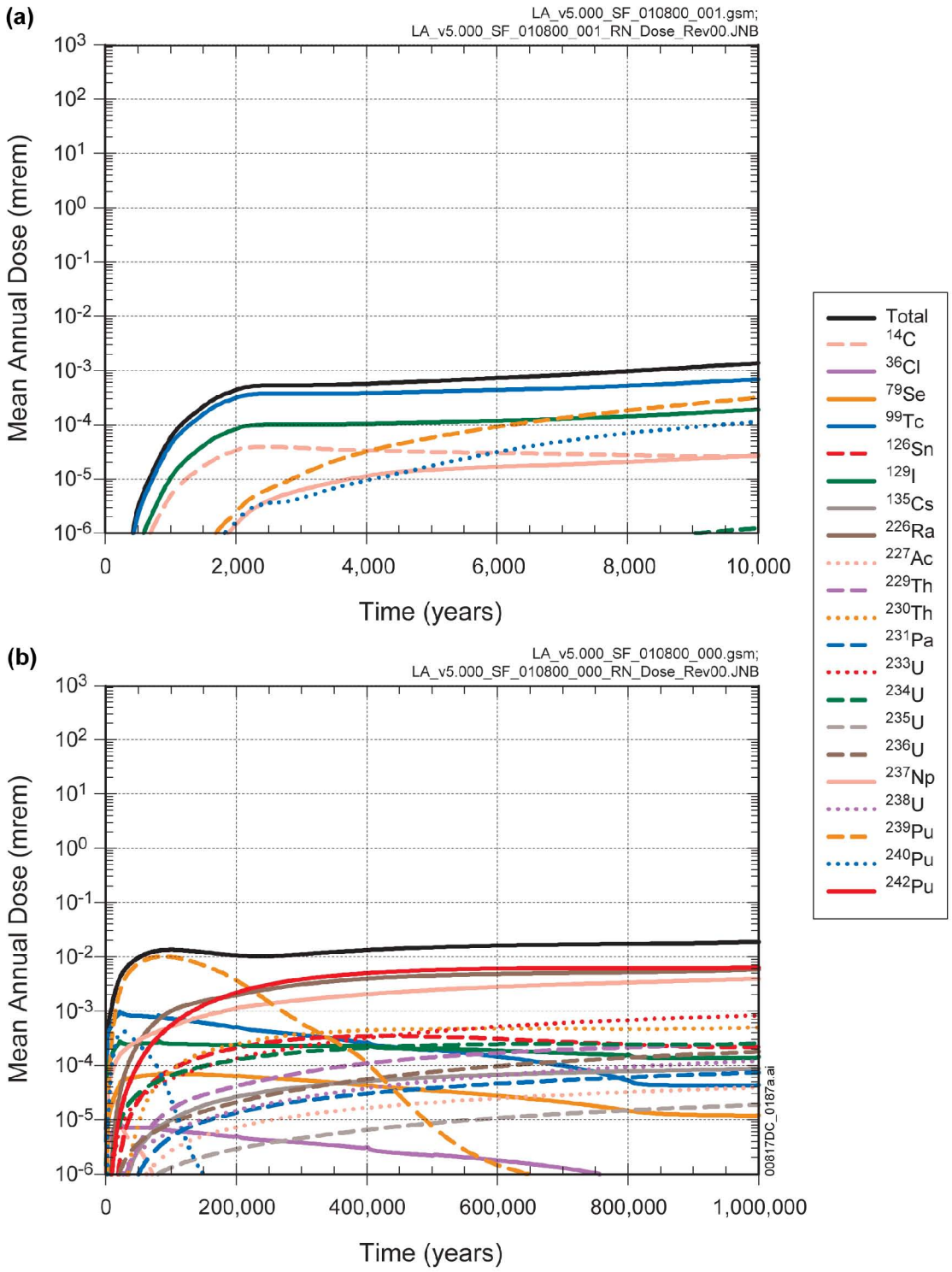

Source: Output DTN: MO0709TSPAREGS.000 [DIRS 182976].

Figure ES-57. Mean Annual Dose Contributions from Major Radionuclides for the Seismic Fault Displacement Modeling Case for (a) 10,000 Years after Repository Closure and (b) Post-10,000-Year Period

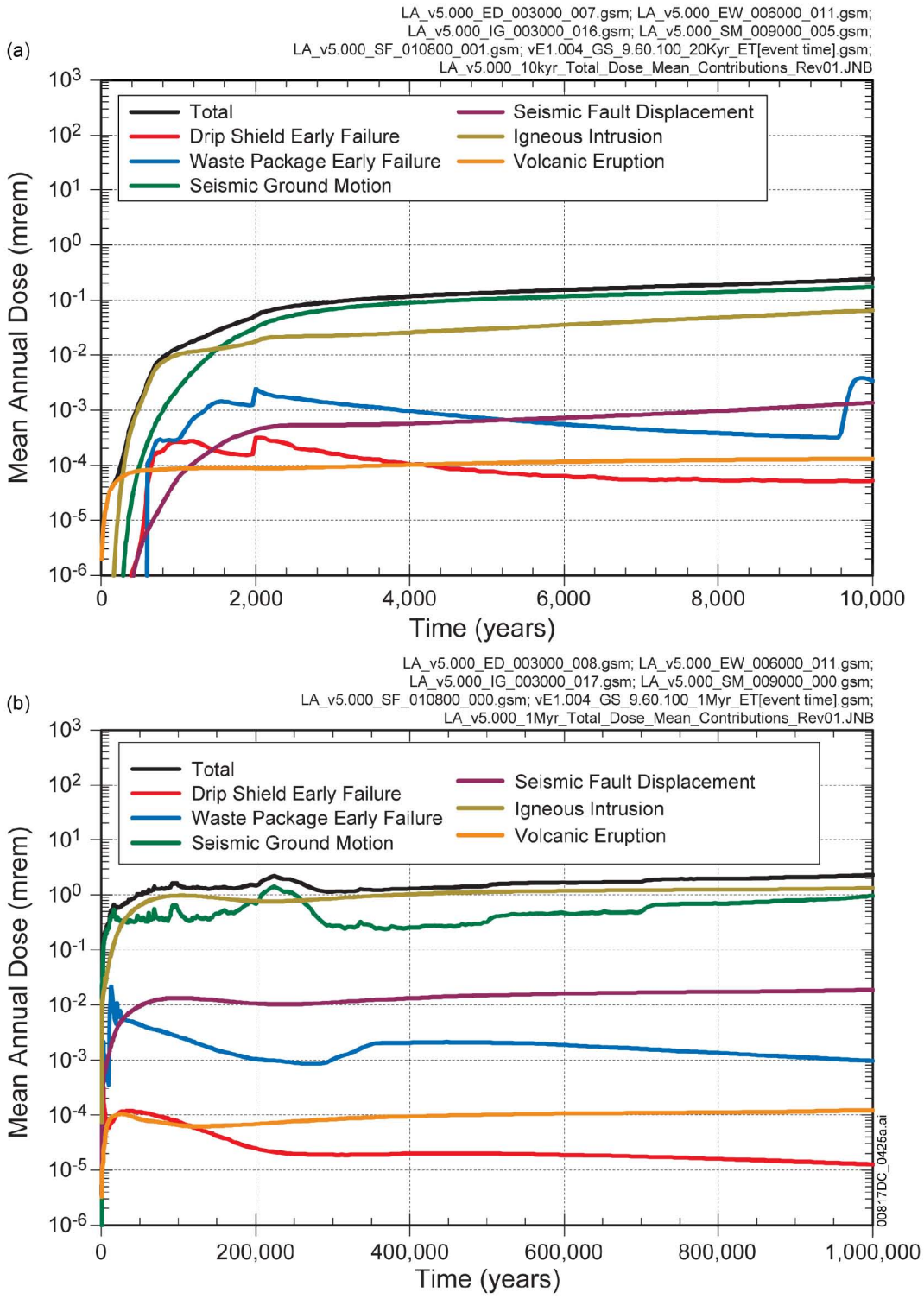

Source: Output DTN: MO0709TSPAREGS.000 [DIRS 182976].

Figure ES-58. Total Mean Annual Dose and Median Annual Doses for Each Modeling Case for (a) 10,000 Years after Repository Closure and (b) Post-10,000-Year Period

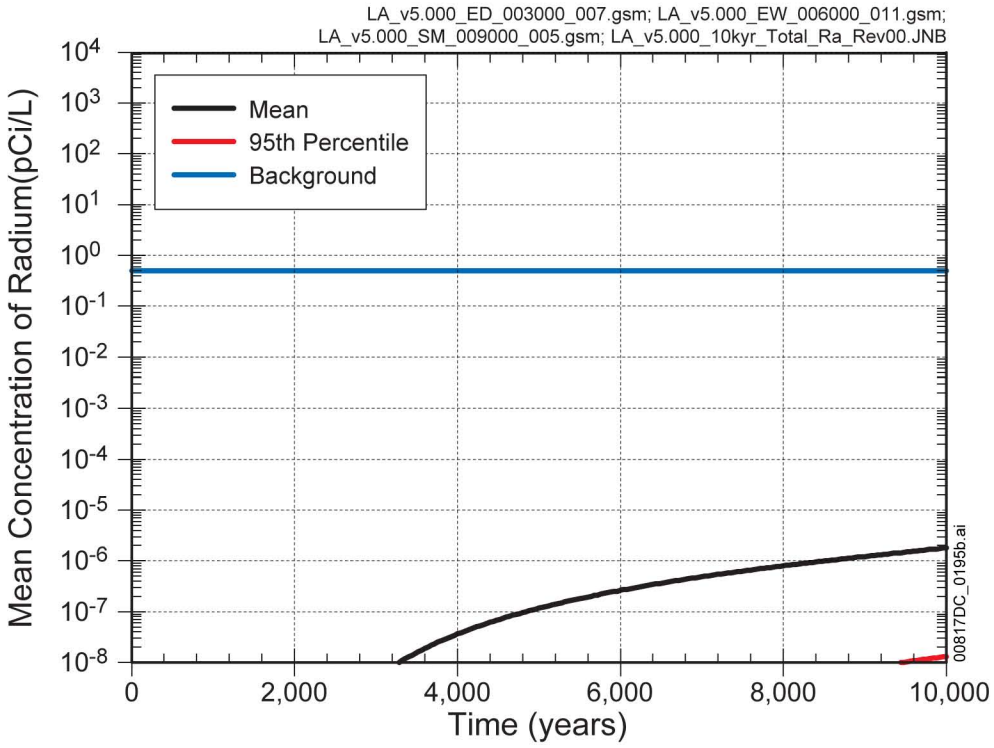

Source: Output DTN: MO0709TSPAREGS.000 [DIRS 182976].

Figure ES-59. Combined ^{226}Ra and ^{228}Ra Activity Concentrations, Excluding Natural Background, for Likely Features, Events, and Processes Using Nominal, Early Failure, and Seismic Ground Motion Damage Processes

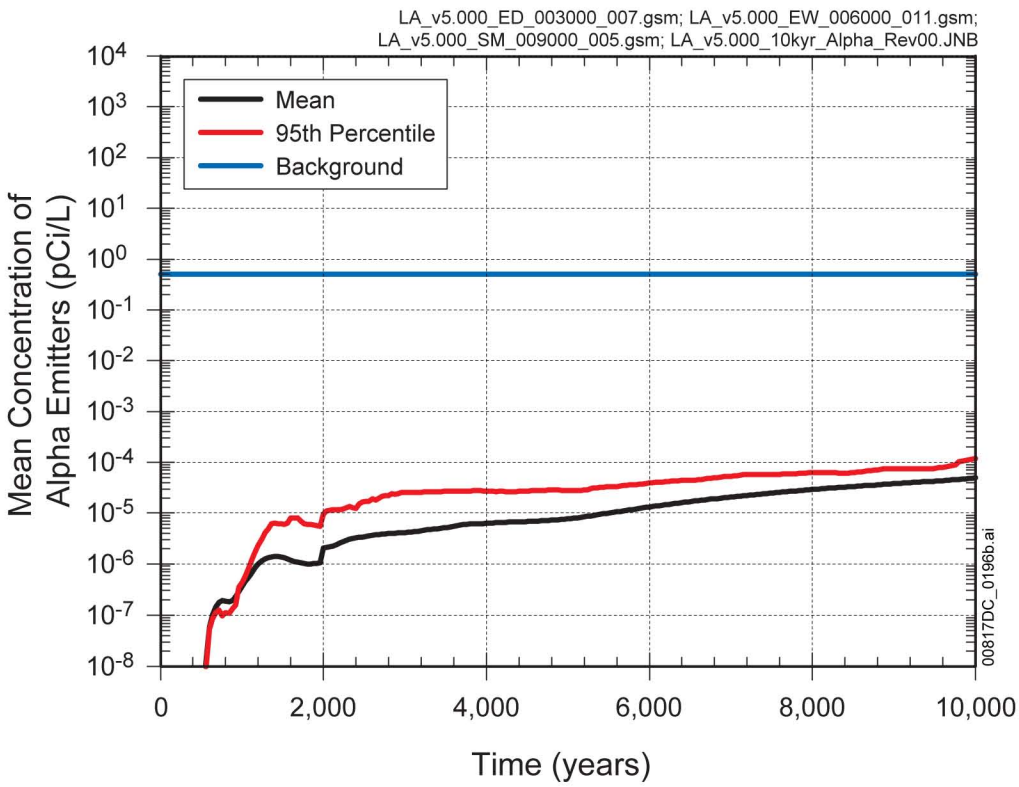

Source: Output DTN: MO0709TSPAREGS.000 [DIRS 182976].

Figure ES-60. Combined Activity Concentrations of All Alpha Emitters (including ^{226}Ra but without radon and uranium isotopes), Excluding Natural Background, for Likely Features, Events, and Processes Using Nominal, Early Failure, and Seismic Ground Motion Damage Processes

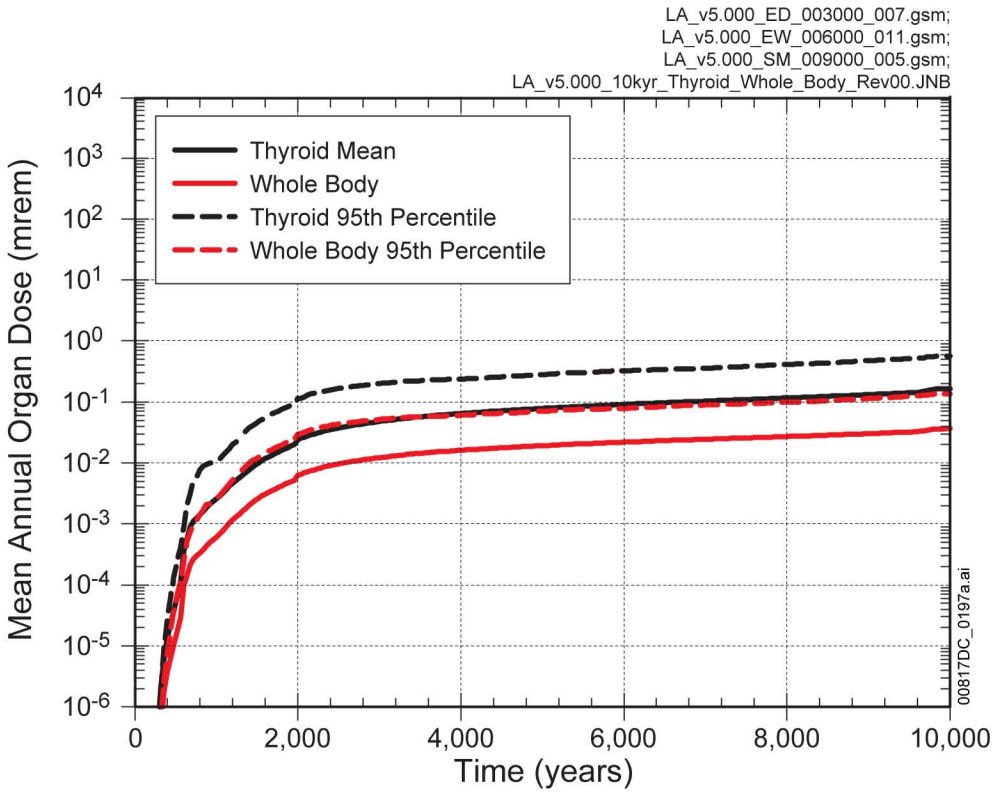

Source: Output DTN: MO0709TSPAREGS.000 [DIRS 182976].

Figure ES-61. Mean Annual Drinking Water Dose from Combined Beta and Photon Emitters for Likely Features, Events, and Processes using the Nominal, Early Failure, and Seismic Ground Motion Damage Processes

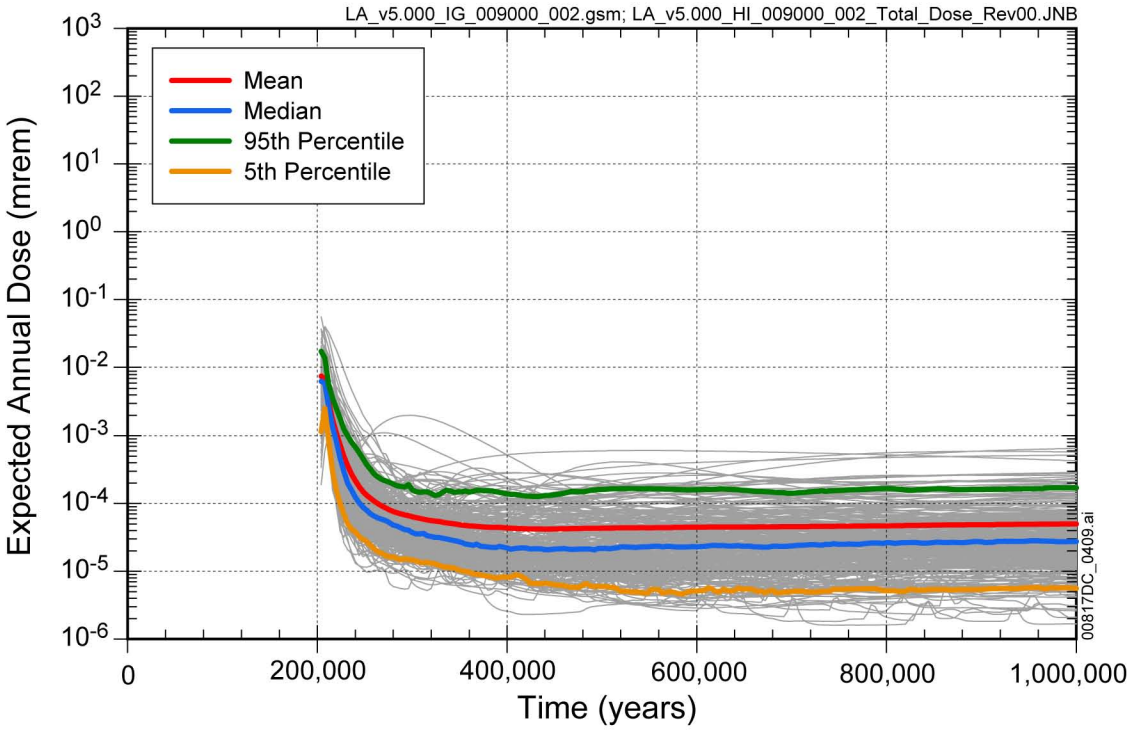

Source: Output DTN: MO0709TSPAREGS.000 [DIRS 182976].

Figure ES-62. Expected Annual Individual Dose at the RMEI Location from Human Intrusion 200,000 Years after Repository Closure

1. PURPOSE

Total System Performance Assessment Model/Analysis for the License Application describes the methodology, structure, validation, and application of the Total System Performance Assessment for the License Application (TSPA-LA) Model that has been developed to support the License Application (LA) to the U.S. Nuclear Regulatory Commission (NRC) for construction of a geologic repository for the safe disposal of spent nuclear fuel (SNF) and high-level radioactive waste (HLW) at Yucca Mountain, Nevada. The TSPA-LA is one of a series of iterative performance assessments (PAs) conducted over the life of the Yucca Mountain Project. The TSPA-LA Model evaluates the ability of the repository to adequately isolate nuclear waste following repository closure, as described in NRC Proposed Rule 10 CFR Part 63 ([DIRS 178394] and [DIRS 180319]).

1.1 INTRODUCTION

The TSPA-LA Model was developed to analyze the ability of the natural and engineered components of the Yucca Mountain Repository system to contain and isolate nuclear waste following repository closure. PAs and related supplemental analyses of the Yucca Mountain Repository have been conducted following the publication of the Nuclear Waste Policy Amendments Act of 1987, Public Law No. 100-203 [DIRS 100016]. Total System Performance Assessments (TSPAs) of the Yucca Mountain Repository have been iterative and periodically updated, each succeeding assessment building on and extending the scope and results of the previous TSPA. The iterative PAs incorporate both an improved understanding of the processes affecting repository performance and, through additional field observations and laboratory analyses, better identification and quantification of the values of the parameters used in the TSPAs. The most recent TSPA document applied the TSPA methodology to the Final Environmental Impact Statement for the Yucca Mountain Repository (Williams 2001 [DIRS 157307]).

The TSPA-LA Model was also used to perform analyses to address criteria contained in *Yucca Mountain Review Plan, Final Report* (NRC 2003 [DIRS 163274], Section 2.2) and in the Key Technical Issues related to a performance assessment (PA) identified in agreement with the NRC (Reamer 2001 [DIRS 158380], Attachment 1). The TSPA-LA Model evaluates the potential consequences of nuclear waste disposal at Yucca Mountain in terms of dose to potential receptors. The analyses presented in this document demonstrate the validity of the TSPA-LA Model in terms of its ability to represent the natural and engineered systems in and around the repository environment and the effects of possible disruptive events that could affect the performance of the Yucca Mountain Repository system.

1.1.1 Governing Regulations

Final rules from the U.S. Environmental Protection Agency (EPA) and NRC concerning the disposal of waste at Yucca Mountain have not yet been published. Until the final rules are published, the EPA and NRC rules are assumed, for the purposes of this document, to be unchanged from the proposed rules published in the Federal Register. Therefore, the analyses described in this report have been designed and executed consistent with the expectation that the final rules will be identical in all regards to the proposed rules. The discussion in this section is consistent with that expectation.

The NRC Proposed Rule 10 CFR 63, Parts E and L, consists of proposed changes to the existing rule, published as Implementation of a Dose Standard after 10,000 Years (70 FR 53313 [DIRS 178394], pp. 55313 to 55320), and the unrevised portions of the existing rule, published in the Federal Register as Energy: Disposal of High-Level Radioactive Wastes in a Geologic Repository at Yucca Mountain, Nevada (10 CFR Part 63 [DIRS 180319]). General references to the NRC Proposed Rule will cite both 70 FR 53313 [DIRS 178394] and 10 CFR Part 63 [DIRS 180319]. References to specific articles from either the proposed changes to the existing rule (e.g., 10 CFR 63.321 [DIRS 178394]) or to parts of the existing rule that have not changed (e.g., 10 CFR 63.322 [DIRS 180319]) will use, as shown here, only the DIRS reference number that applies. The same convention is followed when referring to the proposed and existing rules from the EPA. The EPA Proposed Rule 40 CFR Part 197, Subpart B, was published as Public Health and Environmental Radiation Protection Standards for Yucca Mountain, NV (70 FR 49014 [DIRS 177357], pp. 49014 to 49065). The existing rule, as published in the Federal Register, is 40 CFR Part 197, Public Health and Environmental Radiation Protection Standards for Yucca Mountain, NV; Final Rule (66 FR 32074 [DIRS 155216], pp. 32074 to 32135).

The conceptual structure of the TSPA-LA Model and analysis of the Yucca Mountain Repository, as presented in this document, is based on regulatory requirements in NRC Proposed Rule 10 CFR Part 63 ([DIRS 178394] and [DIRS 180319]). The NRC Proposed Rule adopts the EPA Proposed Rule 40 CFR Part 197, Subpart B ([DIRS 177357] and [DIRS 155216]) regarding public health and safety standards for radioactive material for the Yucca Mountain Repository. The core requirement in the NRC Proposed Rule that ultimately gives rise to the conceptual structure of the TSPA-LA is the individual protection standard in 10 CFR 63.311 [DIRS 178394], specifying the dose standard for the reasonably maximally exposed individual (RMEI):

> "(a) DOE must demonstrate, using performance assessment, that there is a reasonable expectation that the reasonably maximally exposed individual receives no more than the following annual dose from releases from the undisturbed Yucca Mountain disposal system:
>
> (1) 0.15 mSv (15 mrem) for 10,000 years following disposal; and
>
> (2) 3.5 mSv (350 mrem) after 10,000 years, but within the period of geologic stability.
>
> (b) DOE's performance assessment must include all potential environmental pathways of radionuclide transport and exposure."

The NRC proposed rule requires that an application for a license to operate an HLW disposal facility at Yucca Mountain include a PA analysis, including the PA objectives for the geologic repository after permanent closure. Accordingly, 10 CFR 63.114(a) [DIRS 178394] states that any PA prepared in compliance with 10 CFR 63.113 [DIRS 180319] must:

"(1) Include data related to the geology, hydrology, and geochemistry (including disruptive processes and events) of the Yucca Mountain site, and the surrounding region to the extent necessary, and information on the design of the engineered barrier system used to define, for 10,000 years after disposal, parameters and conceptual models used in the assessment.

(2) Account for uncertainties and variabilities in parameter values, for 10,000 years after disposal, and provide for the technical basis for parameter ranges, probability distributions, or bounding values used in the performance assessment.

(3) Consider alternative conceptual models of features and processes, for 10,000 years after disposal, that are consistent with available data and current scientific understanding and evaluate the effects that alternative conceptual models have on the performance of the geologic repository.

(4) Consider only features, events, and processes consistent with the limits on performance assessment specified at § 63.342.

(5) Provide the technical basis for either inclusion or exclusion of specific features, events, and processes in the performance assessment. Specific features, events, and processes must be evaluated in detail if the magnitude and time of the resulting radiological exposures to the reasonably maximally exposed individual, or radionuclide releases to the accessible environment, for 10,000 years after disposal, would be significantly changed by their omission.

(6) Provide the technical basis for either inclusion or exclusion of degradation, deterioration, or alteration processes of engineered barriers in the performance assessment, including those processes that would adversely affect the performance of natural barriers. Degradation, deterioration, or alteration processes of engineered barriers must be evaluated in detail if the magnitude and time of the resulting radiological exposures to the reasonably maximally exposed individual, or radionuclide releases to the accessible environment, for 10,000 years after disposal, would be significantly changed by their omission.

(7) Provide the technical basis for models used to represent the 10,000 years after disposal in the performance assessment, such as comparisons made with outputs of detailed process-level models and/or empirical observations (e.g., laboratory testing, field investigations, and natural analogs).

(b) Any performance assessment used to demonstrate compliance with § 63.113 for the period of time after 10,000 years through the period of geologic stability must be based on the performance assessment specified in paragraph (a) of this section."

Thus, the requirements state that any PA used to demonstrate compliance with the regulations should include a site description, considerations of uncertainty, alternative conceptual models (ACMs), and a features, events, and processes (FEPs) analysis as described in NRC Proposed Rule 10 CFR 63.114 [DIRS 178394]. Further, the FEPs identified as pertinent to the repository were screened for the postclosure 10,000-year compliance period as specified in NRC Proposed

Rule 10 CFR 63.342(a) [DIRS 178394], "DOE's performance assessments conducted to show compliance with §§ 63.111(a)(1), 63.321(b)(1), and 63.331 shall not include consideration of very unlikely features, events, or processes, *i.e.*, those that are estimated to have less than one chance in 10,000 of occurring within 10,000 years of disposal (less than one chance in 1,000,000 per year)." The NRC Proposed Rule 10 CFR 63.114(a)(2) [DIRS 178394] requires the PA to include concepts related to uncertainty in the estimates of the values of the parameters used in the TSPA-LA Model. The uncertainties used to provide the estimates of parameter values for the TSPA-LA Model address: (1) uncertainty in the epistemic or subjective sense related to knowledge about the appropriateness of assumptions used in an analysis, (2) spatial variability, and (3) uncertainty in the aleatory sense related to events that may or may not occur in the future. The regulation indicates that a PA analysis shall calculate outcome in terms of dose to the RMEI but include an uncertainty analysis that evaluates "how uncertainty in parameter values affects uncertainty in the estimate of dose" (66 FR 55732 [DIRS 156671], p. 55747, Supplementary Information III, Section 3.1).

The U.S. Department of Energy (DOE) must demonstrate, using a PA, that there is a reasonable expectation that, for 10,000 years following disposal, the RMEI receives no more than an annual dose of 15 mrem from releases from the undisturbed Yucca Mountain disposal system. DOE analysis must include all potential pathways of radionuclide transport and exposure. NRC Proposed Rule 10 CFR 63.303 [DIRS 178394] also adopts the EPA performance measures quoted from EPA Proposed Rule 40 CFR 197.13 [DIRS 177357] as follows:

> "(a) The NRC will determine compliance based upon the arithmetic mean of the projected doses from DOE's performance assessments for the period within 10,000 years after disposal."
>
> "(b) NRC will determine compliance based upon the median of the projected doses from DOE's performance assessments for the period after 10,000 years of disposal and through the period of geologic stability:"

The TSPA-LA Model calculates dose to the RMEI from the simulated release of radioactive materials from the Yucca Mountain Repository to the accessible environment, as specified in 40 CFR Part 197 ([DIRS 155216], p. 32133). The RMEI is located in the accessible environment where the groundwater path of the highest concentration of the contaminant plume would cross the southernmost boundary of the controlled area of the repository (at a latitude of 36° 40′ 13.6661″ North). This location is approximately 18 km from the repository footprint (66 FR 55732 [DIRS 156671], III Public Comments and Responses, 3.5, p. 55750).

The NRC Proposed Rule 10 CFR 63.305(b) [DIRS 180319] also describes specifications which indicate that: (1) the reference biosphere should incorporate FEPs consistent with present conditions in the Yucca Mountain region; (2) the PA should not project future demographic or biosphere conditions other than climate; (3) the PA should include reasonable assumptions about future geologic, hydrologic, and climatic conditions that could affect future conditions at the Yucca Mountain disposal site after repository closure; and (4) the PA should include biosphere pathways consistent with arid or semiarid conditions. Regarding climate, NRC Proposed Rule 10 CFR 63.342(c)(2) [DIRS 178394] states that,

> "DOE must assess the effects of climate change. The climate change analysis may be limited to the effects of increased water flow through the repository as a result of climate change, and the resulting transport and release of radionuclides to the accessible environment. The nature and degree of climate change may be represented by constant climate conditions. The analysis may commence at 10,000 years after disposal and shall extend to the period of geologic stability. The constant value to be used to represent climate change is to be based on a log-uniform probability distribution for deep percolation rates from 13 to 64 mm/year (0.5 to 2.5 inches/year)."

The NRC Proposed Rule 10 CFR 63.303(b) [DIRS 178394] states that, "Compliance is based upon the median of the projected doses from DOE's performance assessments for the period after 10,000 years of disposal and through the period of geologic stability for: . . ." The National Academy of Sciences considers the period of geologic stability at Yucca Mountain as approximately one million years (National Research Council 1995 [DIRS 100018], p. 72). To comply with this stipulation in the regulation, the TSPA-LA Model provides analyses that provide estimates of repository performance for one million years, where one million years is considered to be the period of geologic stability. According to NRC Proposed Rule 10 CFR 63.302 [DIRS 178394], "Period of geologic stability means the time during which the variability of geologic characteristics and their future behavior in and around the Yucca Mountain site can be bounded, that is, they can be projected within a reasonable range of possibilities. This period is defined to end at one million years after disposal." The one-million-year analyses are thus consistent with the NRC Proposed Rule 10 CFR 63.342 [DIRS 178394] and the EPA Proposed Rule at 40 CFR 197.25 [DIRS 177357]. The TSPA-LA Model developed for the FEPs screened for the 10,000 year time period was also applied to the one-million-year time period of geologic stability. The period of one million years after repository closure includes the peak dose from the Yucca Mountain Repository (Section 8).

The NRC proposed rule also requires DOE to assess a Human Intrusion Scenario and 10 CFR 63.321 [DIRS 178394] provides the individual protection standard for the Human Intrusion Scenario as follows:

> "(a) DOE must determine the earliest time after disposal that the waste package would degrade sufficiently that a human intrusion (see § 63.322 [DIRS 180319]) could occur without recognition by the drillers.
>
> (b) DOE must demonstrate that there is a reasonable expectation that the reasonably maximally exposed individual receives, as a result of human intrusion, no more than the following annual dose:
>
> (1) 0.15 mSv (15 mrem) for 10,000 years following disposal; and
>
> (2) 3.5 mSv (350 mrem) after 10,000 years, but within the period of geologic stability.

(c) DOE's analysis must include all potential environmental pathways of radionuclide transport and exposure, subject to the requirements at § 63.322 [DIRS 180319]."

1.1.2 Total System Performance Assessment Methodology

The TSPA process is represented on Figure 1-1 as a series of pyramid levels. Figure 1-2 separates the levels of the TSPA pyramid showing the information flow, the reports, and the feedback loops involved in the development of the TSPA-LA Model. The foundation of the TSPA pyramid consists of a repository-system characterization involving the assimilation of the information collected by scientists and engineers involved in site characterization and engineering design. The repository system and regional characterization entails data collection regarding waste properties and design of the repository facilities, as well as the regional geology, regional hydrology, and environmental characteristics of the Yucca Mountain site. The broad foundation of the pyramid represents the more than 20-year body of knowledge collected in the field and in the laboratory regarding the repository system. This accumulated body of knowledge was used to identify the set of possible FEPs that may affect the repository system after repository closure and also provide the basis for the second stage of the TSPA pyramid. The TSPA-LA Model is built on the family of analyses of the identified FEPs, including analyses related to the exclusion of FEPs that are either very unlikely, are not required for regulatory reasons, or that have a low impact on performance (Section 1.1.1).

The second stage of the TSPA pyramid consists of the development and testing of detailed models used to conceptually describe retained and probable FEPs and their outcomes regarding repository performance. The detailed conceptual models consist of sets of hypotheses, assumptions, simplifications, and idealizations that, together, describe the essential aspects of a system or subsystem of the repository relative to its performance. Model conceptualization identifies and selects FEPs that collectively comprise the scenarios considered in the conceptual models. An example of such a model or set of interconnected models is the description of the movement of water molecules and dissolved radionuclides by diffusive flow in rock pores or by advective flow in fracture openings in the unsaturated bedrock surrounding and below the repository and through the saturated zone (SZ) below the repository. Furthermore, because the TSPA process deals with future outcomes and includes uncertainty in both process descriptions and parameter values, there may be more than one ACM that provides a reasonable description of a particular system or subsystem. Therefore, the development and documentation of the supporting analyses are essential elements of the TSPA process. The supporting analyses capture uncertainty in probabilistic analyses that represent likely outcomes, based on the best available parameter values and the processes involved. This information serves as the foundation and source of input for the TSPA-LA Model. The documentation of the processes involved in the incorporation of uncertainty, the evaluation of ACMs, the treatment of conservatism, and the evaluation of FEPs in the supporting analyses provides input to the TSPA-LA Model.

The third stage of the TSPA pyramid involves the development of mathematical representations or abstractions of the conceptual models of the FEPs or scenarios, or both, that contribute to overall repository performance. The mathematical models consist of quantitative expressions of the process models developed in such a way that they can be used together to simulate repository performance. The mathematical models might include algebraic expressions, ordinary

differential, partial differential, or integral equations characterizing accepted conservation laws, such as the conservation of mass, energy, or momentum, as well as appropriate constitutive equations that describe material behavior in the domain of the conceptual model. An example of one of the process models abstracted in mathematical and numerical form is a model describing the flow of water infiltrating into the bedrock and then percolating through the unsaturated zone (UZ) above the water table. Such a model would incorporate equations describing fluid flow and probable fluid interactions between the rock matrix and fractures in the rock, as well as descriptions of any other hydrologic, physical, and chemical processes needed to describe how water flows throughout the rock mass of the UZ.

The TSPA-LA Model includes a numerical representation of water flow through Yucca Mountain as an abstraction consisting of a series of statistical or mathematical expressions, including look-up tables, equations representing response surfaces, probability distributions, linear transfer functions, or reductions of model dimensionality. These inputs developed by the abstraction process were either implemented directly into the TSPA-LA Model or through a series of simplifying steps, depending upon the relative complexity or importance, or both, of the FEPs being abstracted. This abstraction, or progressive simplification of the conceptual models to more compact and usable numerical models, is the essence of this level of the TSPA pyramid. The models eventually used to analyze the projected evolution through time of the various components of the repository system are abstracted models that capture the salient features of the process models, along with their associated uncertainties.

The top level of the TSPA pyramid consists of the integrated total system model. The total system model is a numerical model used to simulate the behavior of the Yucca Mountain Repository system. The TSPA-LA Model incorporates the abstracted process models and/or the analyses that describe the model components and their submodels from their development to their implementation. Together these form the basis for the TSPA-LA Model.

The TSPA-LA Model integrates conceptual, mathematical, and computational models of the relevant FEPs that may affect repository performance as informed by site-specific information, relevant laboratory data, and natural analogues that assist in building the confidence in the long-term processes evaluated in TSPA-LA Model analyses. The TSPA-LA approach to the analysis of the repository system appropriately incorporates parameter distributions used to quantify uncertainty. Incorporating this uncertainty in multiple stochastic realizations of the TSPA-LA Model produces a long-term projection of repository performance. The simulations of repository performance thus provide a means for the defensible analysis of system behavior, incorporating process models and parameters based on scientific observations. The TSPA-LA Model then uses the parameter values and process models to assess the capability of the Yucca Mountain Repository System to comply with applicable radiation-protection standards contained in the governing regulations.

The use of the TSPA-LA Model to simulate Yucca Mountain Repository behavior and project future outcomes is aided by the development of scenario classes to assist in repository performance analyses. A scenario class is a set of related scenarios, incorporating groups of possible FEPs, that describe possible future repository conditions and share sufficient similarities that can be aggregated for performance analysis. The TSPA-LA scenario classes represent a wide range of future outcomes, including the Nominal, Early Failure, Igneous, and Seismic Scenario Classes, as well as a Human Intrusion Scenario.

The TSPA-LA Model builds on the family of analyses related to FEPs. The resulting TSPA-LA Model includes the results of analyses of the FEPs that were screened and included in the TSPA-LA Model development process. In addition, the TSPA-LA Model development was affected by the exclusion of FEPs that are either very unlikely, are not required for regulatory reasons, or that have a low impact on performance.

Probabilistic simulations provide a useful tool for the LA process and address issues raised by previous TSPAs conducted for the Yucca Mountain Repository. The TSPA-LA Model also provides results useful in addressing questions raised by internal and external reviews, such as those conducted by the U.S. Nuclear Waste Technical Review Board and the Performance Assessment International Review Team (OECD and IAEA 2002 [DIRS 158098]).

1.1.3 Treatment of Uncertainty

The TSPA-LA Model incorporates uncertainty in parameter values and event occurrence. Uncertainty in the TSPA-LA Model is characterized as either epistemic or aleatory uncertainty according to the following definitions (Hoffman and Hammonds 1994 [DIRS 107502]):

- **Epistemic Uncertainty**—Epistemic uncertainty pertains to the state of uncertainty in the state of knowledge concerning parameter values because there are limited data or there are alternative interpretations of the available data. The state of knowledge about the exact value of the parameter can increase through testing and data collection. Therefore, epistemic uncertainty can also be referred to as 'reducible uncertainty.'

- **Aleatory Uncertainty**—Aleatory uncertainty concerns whether or not there is a chance of occurrence of a feature, event, or process. For example, there can be uncertainty about whether or not a volcanic disruption can occur or not occur. Aleatory uncertainty may also be referred to as 'irreducible uncertainty' because no amount of knowledge will determine whether or not a chance event will or will not occur.

Maintaining a separation between aleatory and epistemic uncertainty strongly affects the design of the PA analyses conducted with the TSPA-LA Model. It may also strongly affect the design of individual TSPA-LA submodels. However, some parameters may have elements of both types of uncertainty. For example, UZ flow is modeled as occurring as an epistemically uncertain constant rate during each climate period, although percolation is dependent on the aleatory uncertainty in rainfall. The aleatory uncertainty in rainfall is accounted for in the calculation of the distribution of UZ flow rates. The manner in which the two forms of parameter uncertainty are handled in the TSPA-LA Model will ensure that the distributions of parameter values accurately reflect their development in the supporting process models and submodels.

1.2 TSPA-LA MODEL DEVELOPMENT PROCESS

The TSPA-LA Model analyses were conducted in a probabilistic framework. The TSPA-LA Model was used to calculate estimates of repository performance, including expected annual dose to receptors, groundwater concentrations at selected distances from the repository, and effects of disruptive events. The calculated results are consistent with the abstraction model inputs provided by analyses of the processes governing flow and transport of radionuclides

expected to be released from the repository upon failure of the waste packages (WPs) containing SNF and HLW. The TSPA-LA Model uses Monte Carlo simulation techniques to address the uncertainty and/or variability in the values of the input parameters of the model. The TSPA-LA Model provides multiple realizations of the model's output by sampling input parameter values from assigned probability distributions spanning their defined ranges. To assist in TSPA-LA Model validation, several hundred to more than 1,000 realizations were simulated to ensure stochastic convergence and stability of the results. The simulations of each realization provided time histories of the annual dose or other performance measures. These results were analyzed for uncertainty and sensitivity with respect to the values of the input parameters at both total system and subsystem levels.

1.2.1 Features, Events, and Processes Analysis

The development of the TSPA-LA Model includes the identification and screening of FEPs that could affect the repository for up to one-million years after repository closure, although most FEPs are screened considering the first 10,000 years postclosure. Appendix I provides a mapping between the FEPs documentation and the TSPA-LA Model. The FEPs that were screened in were used to develop scenario classes for the TSPA-LA Model analyses. Figure 1-3 is a schematic representation of the development of the TSPA-LA Model and describes, for analysis purposes, the repository system divided into individual model components. Each individual model component represents a major process or set of processes of the total repository system. Figure 1-3 shows the model component areas as well as the scenario classes that were used to analyze repository performance under all expected conditions identified in the FEPs analysis, including a possible human intrusion into the repository.

1.2.2 Development of the Scenario Classes

The processes included in the principal model components in the TSPA-LA Model shown on Figure 1-3 were combined to evaluate the repository system performance for four scenario classes, seven modeling cases, and a stylized analysis of possible human intrusion into the repository. The underlying TSPA-LA Model incorporates all FEPs describing the fundamental processes governing repository performance and additional FEPs that describe disruptive events, as well as possible changes to those fundamental processes. The Nominal Scenario Class encompasses all processes affecting the integrity of the WPs containing SNF and HLW in the absence of disruptive events. These processes include WP degradation because of corrosion mechanisms, including general corrosion, stress corrosion cracking (SCC), localized corrosion, and microbially influenced corrosion (MIC). The Early Failure Scenario Class addresses FEPs that describe the potential for drip shield (DS) and WP early failure in the absence of disruptive events. The early failure scenarios include DSs and WPs that fail prematurely due to material defects or improper manufacturing conditions or pre-emplacement operations and practices, such as improper heat treatment or welding flaws. Early DS and WP failures are analyzed using the Drip Shield Early Failure (EF) Modeling Case and the Waste Package Early Failure (EF) Modeling Case.

The TSPA-LA Model includes two scenario classes that address the possibility that disruptive events may occur at or near the repository and that these events may affect repository performance. The Igneous Scenario Class comprises two modeling cases that address FEPs that

describe igneous activity that could affect the repository. The Igneous Intrusion Modeling Case includes FEPs that account for the possibility that a dike containing magma could intrude into the repository and disrupt repository performance. The Igneous Intrusion Modeling Case includes all nominal flow-and-transport processes involving radionuclides after their release from WPs affected by an igneous intrusion. The Igneous Scenario Class also includes the Volcanic Eruption Modeling Case that addresses FEPs that describe a volcanic conduit(s) that invades the repository, destroys WPs, and erupts at land surface. The volcanic eruption disperses volcanic tephra and entrained waste into the atmosphere and deposits the contaminated tephra on land surfaces where the contaminated tephra becomes subject to redistribution by near-surface hydrogeologic processes.

The TSPA-LA Model also includes a Seismic Scenario Class, which is used to analyze possible seismic disruption of the repository and the disruption's effect on repository performance. The Seismic Scenario Class considers two modeling cases: (1) the Seismic Ground Motion (GM) Modeling Case addresses FEPs concerning damage to WPs, DSs, and commercial spent nuclear fuel (CSNF) due to vibratory ground motion; and (2) the Seismic Fault Displacement (FD) Modeling Case addresses the effects of fault displacement on WPs and DSs. The modeling cases simulate the degraded performance of damaged DSs and the release of radionuclides from WPs that are damaged due to seismic events. The transport of released radionuclides will be simulated using all the nominal processes that apply.

The NRC Proposed Rule 10 CFR 63.322 [DIRS 180319] requires DOE to assess a Human Intrusion Scenario, and 10 CFR 63.321 [DIRS 178394] provides the performance standard for the Human Intrusion Scenario. The TSPA-LA Model considered the Human Intrusion Scenario in a calculation that simulates a future drilling operation. The Human Intrusion Scenario considers an intruder drilling a land-surface borehole using a drilling apparatus operating under the common techniques and practices currently employed in exploratory drilling for groundwater in the region around Yucca Mountain. While drilling a borehole, the drilling apparatus directly intersects a degraded WP and continues subsequently into the SZ underlying Yucca Mountain. The human intrusion causes the subsequent compromise and release of waste in the penetrated WP. The TSPA-LA Model simulated the Human Intrusion Scenario occurring approximately 200,000 years after repository closure.

1.2.3 Incorporation of Uncertainty

The TSPA-LA contains over 300 parameters with uncertain parameter values that are described by probability distributions. In some cases, if there is significant uncertainty in parameter values, the TSPA-LA Model uses conservative estimates of the parameter values so as not to bias the results toward potentially optimistic projections of total system performance. To the extent practical, the TSPA-LA Model uses probability distributions to quantify uncertainty in parameter values.

A multi-disciplinary team of scientists and engineers was formed to conduct parameter uncertainty/variability reviews. The team identified parameter-value distributions using the most recent and relevant data and information about the repository system that was available from all sources. The information was used to quantify uncertainties in parameter values; provide insights for updating conceptual and numerical models, submodels, and abstractions; and provide

additional lines of evidence about the possible future behavior of the repository. To the extent possible, the data and information regarding the parameter-value distributions have been incorporated into the TSPA-LA Model database.

The process used to evaluate unquantified uncertainties in parameter values contained in the parameter-valued distributions involved: (1) identifying the unquantified uncertainties to be evaluated; (2) developing more representative, quantified descriptions of those uncertainties; and (3) evaluating the implications of those newly quantified uncertainties with respect to repository performance. The impacts of these representations of parameter values to previously unquantified uncertainties were then evaluated using revised process models and supplemental TSPA-LA Model analyses using the revised uncertainty treatments. The results were documented accordingly in the TSPA-LA Model database. A Performance Assessment Systems Integration Team evaluated the review team's findings and recommended appropriate implementation using a risk-informed perspective.

The TSPA-LA Model analyses are probabilistic in order to capture the full range of possible future outcomes and the uncertainty and variability in the expected behavior of the repository system. The TSPA-LA Model calculates multiple realizations using distributions of values for uncertain parameters, and the model realizations are performed many times using many combinations of the distributed parameter values. Each combination of parameter values represents a subset of the full range of future outcomes.

1.2.4 Alternative Conceptual Models

ACMs are a means to specifically acknowledge model form uncertainty. An ACM is a set of working hypotheses and assumptions that provide an acceptable description of a system for the intended purpose. Because the TSPA process deals with future outcomes and includes uncertainty in both process descriptions and parameter values, there may be several ACMs that provide reasonable descriptions of a particular system or subsystem. Considering ACMs helps to build confidence that plausible changes in modeling assumptions or simplifications will not change conclusions regarding subsystem and total system performance. Also, ACMs are used to ensure that the nominal model adequately captures the range of plausible and reasonable uncertainty in the conceptual model of the repository system. Each model component and submodel discussion in Section 6.3 includes a summary evaluation of ACMs.

1.2.5 Configuration Management for the TSPA-LA Model

The development of the TSPA-LA Model required organization, control, and accountability. Configuration control was implemented for software, input parameter values, and model architecture. The result is enhanced transparency and traceability for the TSPA-LA Model.

A number of software codes were implemented to support the development of the TSPA-LA Model. Some of these codes were used to provide supporting information and some codes were directly implemented in the TSPA-LA Model using the GoldSim simulation software (GoldSim V. 9.60.100, software tracking number (STN): 10344-9.60-01 [DIRS 181903]). Supporting software codes, including process models, were developed and operated externally before running the TSPA-LA Model. Software codes directly implemented in the TSPA-LA

Model are generally referred to as abstractions and are run within the TSPA-LA Model. All software codes used to support the TSPA-LA Model are qualified and are under configuration control through Software Configuration Management (SCM) per IM-PRO-003, *Software Management*. Each qualified code is in SCM and is uniquely identified with a tracking number. The SCM database also includes information on the software name, version, hardware platform, and operating system under which the code was qualified. All software documentation, including the software media, is linked to this tracking number.

Input parameter values are controlled through the TSPA Input Database. The database supports the TSPA-LA Model by providing the parameter values and distributions necessary for the PA analysis of the repository. The TSPA Input Database categorizes, stores, and retrieves fixed and distributed values of the TSPA-LA Model parameters, and allows qualified, authorized analysts to review and update the values. The TSPA Input Database has strict user controls, featuring read and write access and audit trails that ensure the security, integrity, and traceability of the information used in the TSPA-LA Model analyses.

The TSPA-LA Model integrates several model components and submodels to simulate the performance of the repository. A numerical representation is used to implement the TSPA-LA Model with GoldSim software, which was developed by GoldSim Technology Group (GoldSim V.9.60.100, STN: 10344-9.60-01 [DIRS 181903]). The inputs used by this numerical representation of the TSPA-LA Model are obtained from controlled sources maintained by the Office of Civilian Radioactive Waste Management (OCRWM) data and information systems, such as OCRWM Program Documents, the Technical Data Management System (TDMS), the Technical Information Center, or other available sources such as NRC Proposed Rule 10 CFR Part 63 ([DIRS 178394] and [DIRS 180319]).

The TSPA-LA Model was designed and developed to run in a reasonable time on readily available computer hardware, using appropriate software. However, the size and complexity of the TSPA-LA Model makes it subject to some hardware limitations, including limiting the number of realizations that can be performed. The TSPA-LA Model was tested and provided stable results that met the validation criteria in the areas of statistical and temporal stability, spatial variability, and discretization.

The probabilistic, multiple-realization requirement necessitates that the hardware configuration has several hundred nodes. Each node is a separate processor capable of running one realization of the TSPA-LA Model. Each individual node, or central processing unit, was purchased with the largest hardware, with 3.2 gigahertz (GHz) processor speed, 3 or 4 gigabytes (GB) of random access memory (RAM) per processor, and high-speed hard drives to access virtual memory. The TSPA-LA Model uses individual central processing units with 32-bit Intel Xeon processors, which have a maximum allowable process size of 3 GB using the flexible 32-bit Windows 2003 operating system. The UZ Transport Submodel was designed to maximize the use of the 3 GB process size. More information on the hardware platform for the TSPA-LA Model is provided in Section 3.0.

The TSPA-LA Model handles both the multiple-realization requirement and the maximum size of individual coupled submodels. The GoldSim software (V. 9.60.100, STN: 10344-9.60-01 [DIRS 181903]) fulfilled all of these requirements, having an efficient solver that minimized its

run time for each individual realization. The Monte Carlo sampling structure in GoldSim allows the software to simultaneously run multiple realizations by distributing the realizations to individual nodes on the (approximately) 750-node TSPA-LA Model's Computational Cluster, then reassemble the results from these realizations into an ensemble result from the entire probabilistic run. Further, GoldSim acts as a driver, or integration software, that can couple other large pieces of software for those process models and submodels that were not converted to response surfaces, but are run concurrently in the TSPA-LA Model. Examples of such software include WP degradation software, UZ transport software, FEHM, seepage software (SEEPAGEDLL_LA V. 1.3, STN: 11076-1.3-00 [DIRS 180318]), and SZ transport software (SZ_CONVOLUTE V. 3.10.01, STN: 10207-3.10.01-00 [DIRS 181060]). Because of GoldSim's ability to run each submodel software in its own process space (particularly GoldSim itself and FEHM), it can maximize the use of the computer memory, subject to a soft limitation on the amount of virtual memory that should be used on any particular node (i.e., it is generally faster to run processes in 3 or 4 GB of RAM per processor than to run on the hard disk virtual memory).

1.3 YUCCA MOUNTAIN SITE DESCRIPTION

The Yucca Mountain Repository system consists of natural and engineered systems that together will ensure the safe disposal of radioactive materials. The following information is provided as a general overview of the Yucca Mountain site, giving a context for the development of the TSPA-LA Model that is discussed in detail in the remainder of this document. The understanding and analysis of FEPs relevant to postclosure performance is described in the supporting analyses that contain the abstractions used as input to the TSPA-LA Model. Detailed information on the direct inputs to the TSPA-LA Model is provided in Section 6 with full references and traceability.

The characteristics of the natural systems at Yucca Mountain that affect repository performance include climate, site geology, and site hydrogeology. The characteristics of the site geology and hydrogeology that affect repository performance include groundwater flow through the UZ and SZ, radionuclide transport, and disruptive events caused by igneous and seismic activity. This section provides a brief description of the current understanding of the Yucca Mountain natural system and the repository design. Information on Yucca Mountain site characteristics, along with descriptions of field and laboratory investigations conducted at Yucca Mountain, can be found in *Yucca Mountain Site Description* (BSC 2004 [DIRS 169734]), which contains comprehensive descriptions of the repository site and the surrounding region.

1.3.1 Physiographic Setting and Topography

Yucca Mountain is located within a transition zone between the northern boundary of the Mojave Desert and the southern boundary of the Great Basin Desert (BSC 2004 [DIRS 169734], Section 3.2.1, and BSC 2004 [DIRS 169734], Sections 6, 7, and 8). The topography is characterized by isolated, long and narrow, roughly north-south-trending mountain ranges and broad intervening valleys (Figure 1-4). The Yucca Mountain physiography consists of steep and narrow V-shaped highland valleys that grade into flat alluvial floors in their lower reaches (BSC 2004 [DIRS 169734], Section 1.3.1).

The local topography is described in *Yucca Mountain Site Description* (BSC 2004 [DIRS 169734], Section 7.1.3.3) and has the following characteristics. Landforms include about 5 to 10 percent ridgetops, 45 percent side slopes (including footslopes), about 45 percent terraces, and less than 5 percent active channels. The surface elevations above the repository site are approximately 1,400 m above mean sea level . Terraces and channels are located at lower elevations of the primary washes and have thinner soil cover in the upper washes and thicker soil cover further downgradient. Yucca Mountain is a generally north-to-south-trending ridge with a relatively gentle eastward slope and a steep, westward facing escarpment. The topography in the Yucca Mountain vicinity is shaped by erosional processes on the eastward-sloping ridge of the mountain and along faults and fault scarps that have created a series of washes downcut to varying degrees into different bedrock layers. Slopes are locally steep on the west-facing escarpments eroded along the faults and in some of the valleys that cut into the more gentler eastward-facing dip slopes. As described in the *Yucca Mountain Site Description* (BSC 2004 [DIRS 169734], Section 7.1.1.1), narrow valleys and ravines are cut in bedrock; wider valleys are covered by alluvial deposits, with terraces cut by intermittent streams. Locally, small sandy alluvial fans extend down the lower slopes and spread out on the valley floors. East of the Yucca Mountain crest, drainage is into Fortymile Wash. West of the crest, streams flow southwestward down fault-controlled canyons and discharge into Crater Flat (Figure 1-4). The topography is different to the south and north of Drill Hole Wash. The washes south of Drill Hole Wash trend eastward, are relatively short (less than 2 km), and have erosional channels with gently sloping sides (Figure 1-5). The washes north of Drill Hole Wash trend northwest and are relatively longer (3 to 4 km) because they are controlled by fault features and have steeper side slopes.

1.3.2 Climate and Precipitation

In general, the present-day Nevada climate is characterized as semiarid to arid, with dry winds and low precipitation. The Pacific side of the mountain system to the west of Nevada causes a rain shadow effect, which in turn, causes moisture-loaded winds traveling east from the Pacific Ocean to rise, cool, and drop precipitation on the Pacific mountain system. The climatic factors affecting water-transport processes in the UZ at Yucca Mountain are solar radiation flux, diurnal and seasonal temperature cycles, relative humidity, and precipitation, in the form of either rain or snow, as well as extended periods of drought. The Yucca Mountain Project environmental program collected site meteorological data using a network of nine automated weather stations (BSC 2004 [DIRS 169734], Section 7.1.3.2). Current climatic conditions for the site and the Yucca Mountain region are discussed in detail in *Yucca Mountain Site Description* (BSC 2004 [DIRS 169734], Section 6.3).

The analysis of data from 114 weather stations measuring precipitation in the Yucca Mountain region, providing at least eight years of complete records, indicates a strong positive correlation between average annual precipitation and station elevation (BSC 2004 [DIRS 169734], Figure 7-7). These results indicate that the zones of maximum precipitation are likely to correspond to the zones of higher elevations in the mountain ranges. Average annual precipitation over the area of the Nevada Test Site ranges from a maximum of 370 mm in the Belted Range to a minimum of 100 mm in the Amargosa Desert. Annual precipitation in the Yucca Mountain vicinity ranges from a minimum of about 100 mm at low elevations along the southern boundary of the repository area to a maximum in excess of 300 mm at high elevations in the north (BSC 2004 [DIRS 169734], Figure 7-6).

1.3.3 Geology

1.3.3.1 Surficial Deposits

The dominant surficial deposits in the general vicinity of Yucca Mountain are fluvial sediments and fluvial debris-flow deposits found in basins, washes, and alluvial fans. These deposits have varying degrees of soil development and thickness and have a gravelly texture, with rock fragments constituting between 20 and 80 percent of the total volume (BSC 2004 [DIRS 169734], Section 3.3.7.2). The deposits range from 100-m thick in the valleys to less than 30-m thick in the mouths of the washes. Halfway up the washes, alluvial fill generally is less than 15-m deep in the center of the channels and well-developed, cemented, calcium-carbonate soil horizons are common. On the more stable surfaces, generally on the ridgetops, soils are 0.5- to 2-m thick with a high clay content. Overall, the thickness of surficial deposits was classified into 4 categories: 0 to less than 0.5 m, 0.5 m to less than 3.0 m, 3.0 m to less than 6.0 m, and greater than or equal to 6.0 m, which encompass about 50 percent, 5 percent, 5 percent, and 40 percent of the site area, respectively (BSC 2004 [DIRS 169734], Section 3.3.7). Soil thickness tends to be well correlated to local topography, with the upland areas generally having thin soils and the lower washes and alluvial fans having thicker soils (surficial materials). The deeper deposits are present on the shallower slopes of the ridges, in washes, and underlying alluvial fans, whereas the deposits on the steeper side slopes, if present, consist of colluvium from rock slides. For the infiltration modeling, mapped surficial, unconsolidated deposits were reconfigured into five surficial soil classes based on differences in soil texture (SNL 2007 [DIRS 182145], Sec. 6.5.2.4). *Simulation of Net Infiltration for Present-Day and Potential Future Climates* (SNL 2007 [DIRS 182145], Tables 6.5.2.4-2 and 6.5.2.4-3) describe the five soil classes and their nominal soil depths as follows: Class 1, Very deep soils, 95 m; Class 2, Moderately deep soils, 16.47 m; Class 3, Intermediate depth soils, 3.26 m; Class 4, Shallow soils, 0.25 m; and Class 5, Exposed bedrock, 0 m. Soil types account for bare rock and disturbed ground, consistent with the geologic mapping. Soil storage capacity is determined mostly by soil thickness and porosity. Soil porosity and permeability, along with various other hydrologic properties, such as residual water content and field capacity, can be correlated to soil type (BSC 2004 [DIRS 169734], Section 7.1.3.4).

The maximum erosion during the first 10,000 years after repository closure is expected to be on the order of centimeters (BSC 2004 [DIRS 169734], Section 3.4.6), which is within the range of existing surface elevation irregularities, and would not affect the processes in the hundreds of meters of UZ at Yucca Mountain. Similar conditions can be expected to be in effect throughout the one-million-year period of geologic stability (NRC Proposed Rule 10 CFR 63.302 [DIRS 178394]). Therefore, the effects of soil erosion on infiltration are considered negligible and are reasonably excluded from the TSPA-LA Model calculations (Data Tracking Number (DTN): MO0508SEPFEPLA.002_R0 [DIRS 175064]).

1.3.3.2 Bedrock Geology

Yucca Mountain is an uplifted, block-faulted ridge of alternating layers of welded and nonwelded volcanic tuffs of Miocene age. The major Yucca Mountain geologic units are the volcanic tuff formations of the Paintbrush Group (Tp), the Calico Hills Formation (Tac), and the Crater Flat Group (Tc). The lithostratigraphic nomenclature divides the Paintbrush Group into

the Tiva Canyon (Tpc), Yucca Mountain (Tpy), Pah Canyon (Tpp), and Topopah Spring (Tpt) tuffs. The Crater Flat Group is divided into the Prow Pass (Tcp), Bullfrog (Tcb), and Tram (Tct) tuffs. For the purposes of hydrogeologic studies, including infiltration, a separate stratigraphic nomenclature was developed based on the degree of welding and the distribution of the hydrologic properties of the hydrogeologic units (BSC 2004 [DIRS 169734], Tables 3-1, 3-5, and 7-1). The main geologic units are divided into the Tiva Canyon welded (TCw), the Paintbrush nonwelded (PTn) (consisting primarily of the Yucca Mountain and Pah Canyon members and the interbedded tuffs), the Topopah Spring welded (TSw), the Calico Hills nonwelded (CHn), and the Crater Flat undifferentiated (CFu) units (Ortiz et al. 1985 [DIRS 101280]). Figure 1-6 shows the spatial relationship of the geologic units of the UZ in both perspective and east-west cross-sectional views.

1.3.3.3 Tectonics

1.3.3.3.1 Tectonic Setting

Tectonic setting refers to the geologic framework or structural configuration of the different rock masses in the Yucca Mountain vicinity. The overall tectonic setting of the Great Basin physiographic province generally consists of fault-bounded basins and mountain ranges (including Yucca Mountain) that have been modified by volcanic activity during the past 15 million years. Typically, faults in this setting include normal and strike-slip faults that reflect the extensional deformation caused by the tectonic interactions of crustal plates at the western margin of the North American continent. Studies of the extensional tectonics in the central Basin and Range tectonic province (Snow and Wernicke 2000 [DIRS 159400]) conclude that approximately 250 to 300 km of extension have occurred by a west-northwest motion of the Sierra Nevada block away from the Colorado Plateau, at rates initially as great as 2 cm/yr, and at 1.5 to 1 cm/yr during the last 5 million years. Research suggests that most of the current extension, as indicated by strain measurements and seismicity, is concentrated along the eastern and western margins of the Basin and Range tectonic province (Thatcher et al. 1999 [DIRS 119053]; Martinez et al. 1998 [DIRS 159031]).

1.3.3.3.2 Structural Geology

The structural geology of Yucca Mountain and its vicinity (BSC 2004 [DIRS 169734], Section 3.5) is dominated by a series of north-striking normal faults (Figure 1-7), along which Tertiary volcanic rocks were tilted and displaced hundreds of meters. Movement occurred during a period of extensional deformation in the middle-to-late Miocene time, but has continued at a low level into the Quaternary Period, which consists of the last 1.8 million years before the present. These faults extend through the Yucca Mountain vicinity and divide the site area into several blocks, each of which is further deformed by minor faults. Block-bounding faults within the Yucca Mountain site area are spaced from 1 to 6 km apart and include, from east to west, the Paintbrush Canyon, Bow Ridge, Solitario Canyon-Iron Ridge, Fatigue Wash, and Windy Wash faults (BSC 2004 [DIRS 169734], Section 3.5, Figures 1-7 and 1-8), which commonly dip from 50° to 80° to the west. Displacements along these block-bounding faults are mainly dip-slip, down-to-the-west, with subordinate strike-slip or oblique-slip components of movement exhibited along some faults. Numerous intrablock faults occur within the individual structural blocks, representing local adjustments in response to the stress created, for the most part, by the

large displacements that took place along the block boundaries (BSC 2004 [DIRS 169734], Section 3.5).

1.3.3.3.3 Volcanism

Two types of volcanism have occurred in the Yucca Mountain region. An early phase of Miocene silicic volcanism in the southwestern Nevada volcanic field culminated between 11.8 and 12.4 million years ago with the eruption of 4 voluminous ash-flow tuffs of about 1,000 km^3 each (Sawyer et al. 1994 [DIRS 100075], pp. 1311 and 1312). One of the silicic ash-flow tuffs that erupted from the Timber Mountain Caldera Complex (Figure 1-9) is the Topopah Spring Tuff, which forms the horizon that will be used for waste emplacement. Yucca Mountain is an uplifted, erosional remnant of these voluminous ash-flow tuff deposits.

The early caldera-forming, silicic volcanism was approximately coincident with the major period of crustal extension, which occurred primarily between 13 and 9 million years ago (Sawyer et al. 1994 [DIRS 100075], pp. 1314 and 1316). The onset of basaltic volcanism in the Yucca Mountain region occurred as extension rates waned during the latter part of the caldera-forming period of silicic volcanism. Small-volume basaltic volcanism continued into the Quaternary Period. In terms of eruption volume, the 15-million year history of volcanism in the Yucca Mountain region is viewed as a magmatic system that peaked between 13 and 11 million years ago, with the eruption of more than 5,000 km^3 of ash-flow tuffs. Following this peak of eruptive activity, volcanism has been in decline, characterized by eruptions of relatively minor volumes of basalt since 11 million years ago (BSC 2004 [DIRS 169989], Section 6.2). Approximately 99.9 percent of the volume of the southwestern Nevada volcanic field erupted before about 7.5 million years ago, culminating with the eruption of tuffs from the Stonewall Mountain volcanic center, which is the last active caldera system of the southwestern Nevada volcanic field. The last 0.1 percent of eruptive volume of the volcanic field consists of basalt that erupted since 7.5 million years ago (BSC 2004 [DIRS 169989], Section 6.2). Considered in terms of total eruption volume, frequency of eruptions, and duration of volcanism, basaltic volcanic activity in the Yucca Mountain region comprises one of the least active basaltic volcanic fields in the western United States (e.g., *Synthesis of Volcanism Studies for the Yucca Mountain Site Characterization Project* (CRWMS M&O 1998 [DIRS 105347], Chapter 2)).

Post-caldera basalts in the Yucca Mountain region can be divided into 2 episodes: Miocene eruptions, between approximately 9 and 7.3 million years before present, and post-Miocene eruptions, between approximately 4.8 and 0.08 million years ago. The time interval of about 2.5 million years between these episodes is the longest hiatus of basaltic eruptive activity in the Yucca Mountain region during the last 9 million years (CRWMS M&O 1998 [DIRS 105347], Chapter 2). This eruptive hiatus also marks a distinct shift in the locus of post-caldera basaltic volcanism to the southwest in the Yucca Mountain region (BSC 2004 [DIRS 169989], Section 6.2). Thus, the Miocene basalts and post-Miocene basalts are both temporally and spatially distinct.

1.3.4 Hydrogeology

1.3.4.1 Surface Hydrology

Yucca Mountain is located in the Amargosa River drainage basin, which is the major tributary drainage area to Death Valley (Figure 1-4). Streamflow from Yucca Mountain can extend from local drainages to the Amargosa River and then to Death Valley. The Amargosa River and its tributaries are ephemeral streams that are dry most of the time, with surface water flow rarely occurring in direct response to precipitation. In some cases, groundwater discharges at springs in stream channels. During episodic flooding, flow occurs along the Amargosa River, filling much of Death Valley to depths of 0.3 m or more (Miller 1977 [DIRS 105462], p. 18). During periods in which the climate has been cooler and wetter, such as 140,000 to 175,000 years ago, Death Valley was filled with water to depths of 175 m (BSC 2004 [DIRS 170002], Section 6.2, p. 6-6). The entire Death Valley drainage basin and several closed drainage basins are hydrologically interconnected through the groundwater system (D'Agnese et al. 1997 [DIRS 100131], Figure 9, pp. 20 and 22). About 10,000 km^2 of watershed area drain directly into Death Valley (Miller 1977 [DIRS 105462], p. 18). The Amargosa River drains almost 9,100 km^2 north and east of Death Valley. Like the streams, the playas are mainly ephemeral and contain water only after heavy runoff periods, and perennial flow is only observed downgradient from spring discharges and around the margins of playas and saltpans, where the groundwater discharges to the land surface.

1.3.4.2 Groundwater Hydrology

Yucca Mountain is located within the larger Death Valley Regional Groundwater System (Figure 1-4). The groundwater flow system of the Death Valley region is complex, involving many local groundwater systems. There is groundwater movement between aquifers in some areas. In other areas, low-permeability confining units support artesian conditions. The groundwater below Yucca Mountain and in the surrounding region flows generally south toward discharge areas in the Amargosa Desert and Death Valley. The area around Yucca Mountain is in the central subregion of the Death Valley Regional Groundwater System, which consists of the Pahute Mesa-Oasis Valley, Ash Meadows, and Alkali Flat-Furnace Creek groundwater basins. The primary sources of groundwater recharge to the regional system are infiltration on Pahute Mesa, Rainier Mesa, Timber Mountain, and Shoshone Mountain to the north, and the Grapevine and Funeral Mountains to the south (Figure 1-4). Recharge in the immediate Yucca Mountain vicinity is low, consisting of water reaching Fortymile Wash (Figure 1-4), as well as precipitation that infiltrates into the subsurface (BSC 2004 [DIRS 169734], Section 7.1.2).

1.4 DESIGN OF YUCCA MOUNTAIN REPOSITORY SUBSURFACE FACILITIES

Following is a description of the design and layout of the repository subsurface facility and engineered barrier system (EBS). Descriptions of the repository subsurface facility are found in *Total System Performance Assessment Data Input Package for Requirements Analysis for TAD Canister and Related Waste Package Overpack Physical Attributes Basis for Performance Assessment* (SNL 2007 [DIRS 179394]) and in *Total System Performance Assessment Data Input Package for Requirements Analysis for Subsurface Facilities* (SNL 2007 [DIRS 179466]).

1.4.1 Repository Layout

The layout of the subsurface facility is illustrated on Figure 1-10 (SNL 2007 [DIRS 179466], Table 4-1, Parameter Number 01-02). The emplacement drifts will be excavated using a tunnel boring machine to a diameter of 5.5 m; with a nominal length of 600 m (actual lengths will range from 355 to 808 m). Emplacement drifts will be excavated in a sequence of 4 panels, which will contain 70,000 metric tons of heavy metal waste. Emplacement drifts will be arranged with a uniform spacing of 81 m between their centerlines. The repository design used in the TSPA-LA Model calls for approximately 100 WPs to be placed in a single emplacement drift with a nominal length of 600 m. There is an area in the southern section of the repository that will be constructed to allow for contingencies during waste emplacement. The repository's host-rock units contain both lithophysal and nonlithophysal units. The lithophysal rock units are characterized by numerous cavities (lithophysae), which result in high porosities. The lithophysal rock units are highly fractured and the fractures have short trace lengths. In contrast, the nonlithophysal rock units are characterized by few cavities, lower porosities, and fractures with generally longer trace lengths. Approximately 80 to 85 percent of the emplacement drift area will be excavated in lithophysal units, and 15 to 20 percent will be excavated in nonlithophysal units of the repository host horizon (SNL 2007 [DIRS 179466], Table 4-1, Parameter Number 01-01).

1.4.2 Features of the Engineered Barrier System

The subsurface facility system includes ground support, such as rock bolts, steel liner, cement, and wire mesh. The EBS design (SNL 2007 [DIRS 179354], Figure 4-1) includes a DS, a two-layer WP, a corrosion-resistant emplacement pallet (made of Alloy 22 and stainless steel on which the WPs will be placed), and an invert, consisting of a steel support structure and crushed, welded tuff, at the base of the emplacement drifts. The TSPA-LA Model analysis of the EBS does not include the degradation of the subsurface facility system's ground-support material. Figure 1-11 presents a cross-section illustration of an emplacement drift and the major components of the EBS. The following provides a more detailed description of each of the EBS components and repository thermal loading.

1.4.2.1 Drip Shield

The DSs will be composed of a corrosion-resistant titanium alloy. The function of the DSs is to reduce the effect of rockfall and dripping on the WPs. The DSs are designed to link together, forming a single continuous barrier for the entire length of the emplacement drifts. The DSs will be fabricated from Titanium Grade 7 plates, with Titanium Grade 29 for structural support. The base plates will be composed of Alloy 22 to prevent direct contact between titanium and the steel members of the invert.

1.4.2.2 Waste Package

WPs will consist of an outer layer and an inner layer (Figure 1-11). The outer layer is 25-mm thick corrosion-resistant Alloy 22. The WPs will be treated to minimize the possibility of SCC, and the outer closure weld will be stress mitigated. The inner layer is 50-mm thick stainless steel and serves 3 functions. First, the inner layer provides structural strength to resist rockfall, to

support the internal waste form components, to allow the WPs to be supported by the emplacement pallets, and to facilitate handling. Second, the inner layer provides radiation shielding to reduce the exterior surface contact dose rate. Third, because of sorption of radionuclides on corrosion products from the degradation of the inner layer, it acts as a limited containment part of the EBS barrier for the radioactive waste inside the WPs. The inner layer is not considered to be a barrier to flow. In order to calculate radionuclide transport through the WPs, the TSPA-LA Model uses the transportation, aging, and disposal (TAD) canister with 21-PWR fuel assemblies as the representative CSNF WP, and the 5-DHLW/DOE Long WP as the representative configuration for the co-disposed (CDSP) WPs that contain both DOE spent nuclear fuel (DSNF) and HLW glass. These CSNF and CDSP WPs are planned to be the most common two types of WPs in the repository (SNL 2007 [DIRS 177407], Section 6.3.3.1).

1.4.2.3 Emplacement Pallet

An emplacement pallet will support each WP (Figure 1-11). The emplacement pallets are designed to prevent the WPs from coming in contact with the invert of the emplacement drifts and, therefore, prevent direct exposure to invert moisture or materials that may induce accelerated corrosion of the WPs. The material supporting the WPs will consist of Alloy 22, providing long-term corrosion resistance and an identical material in contact with the outer surfaces of the WPs. To reduce the possibility of SCC, the emplacement pallets will also be annealed to remove stresses from welding and fabrication.

1.4.2.4 Invert

The invert will provide support for the WP emplacement pallets and the DSs. The invert consists of two components: a steel invert structure and a crushed tuff fill. The granular crushed tuff will be composed of crushed welded tuff produced from the excavation of the repository's underground openings with the tunnel boring machines, and will be placed in and around the steel invert structure to an elevation just below the top of the longitudinal and transverse support beams. The crushed tuff will be compacted to prevent long-term settlement.

1.4.2.5 Waste Form

SNF consists of fuel removed from nuclear reactors after its useful heat-generating capacity has been spent. The TSPA-LA Model analyzes the disposal of WPs containing CSNF and CDSP WPs, containing both DSNF and HLW. CSNF consists primarily of uranium oxide, some of which has been enriched with surplus plutonium to create a mixed-oxide fuel (MOX). DSNF is fuel associated with DOE's defense programs and research and development programs. The majority of DSNF consists of a uranium-metal compound SNF with zirconium cladding, which accounts for approximately 86 percent of the mass of the DSNF inventory . However, there are 11 categories of DSNF representing a variety of uranium-based waste forms (Sections 7.5.2 to 7.5.4). Naval spent nuclear fuel, a category of DSNF, is classified material and, as such, cannot be included in the unclassified TSPA-LA Model. Naval fuel is represented as CSNF for modeling purposes (Section 7.5.2). HLW consists of by-products of nuclear reactions, material generated during fuel preparation and reprocessing, and sludges and residues recovered from nuclear-waste storage tanks. HLW will be mixed and solidified in a high-temperature, borosilicate glass for storage in stainless-steel canisters. CDSP WPs typically contain five HLW canisters surrounding one DSNF canister.

Following breaching of the CSNF WPs and CDSP WPs and exposure of the fuel, the waste forms will be subject to aqueous dissolution at various rates followed by release of radionuclides to the EBS.

1.4.2.6 Waste Form Cladding

Nuclear fuel generally consists of stacked pellets of uranium-based fuel encased in a metallic protective cladding. However, for the PA analyses, the TSPA-LA Model assumes that CSNF cladding is failed at the time the WPs are breached. In addition, DSNF cladding is in poor condition and is considered to be failed upon receipt. Therefore, the TSPA-LA Model does not take credit for spent-fuel cladding.

1.4.2.7 Emplacement Drift

The nuclear waste will be placed in 5.5-m diameter, circular emplacement drifts excavated with tunnel boring machines. The drifts will serve to enhance the role of the natural barriers and the EBS due to two processes: (1) the formation of a capillary barrier at the drifts' walls that will be active during the thermal and ambient postclosure periods, and (2) the formation of a dry-out zone helping to prevent percolation from reaching the repository during the thermal period. The effectiveness of these processes depends on the strength of the capillary pressure in the fractures close to the drift, the host rock's permeability close to the drifts, the local percolation flux above the drifts, the temperature of the rock near the drifts' walls, and the shape of the drift openings.

1.4.2.8 Internal Waste Package Components

The WPs will have internal steel components consisting primarily of carbon-steel basket guides and basket tubes, steel canisters for HLW and DSNF, and stainless-steel inner WP liner. All these internal steel components are expected to degrade to iron oxyhydroxides upon exposure to water and repository atmospheric conditions following WP failure. These degradation products could potentially sorb radionuclides released from the degradation of the waste forms.

1.4.3 Waste Emplacement Approach

WPs will be placed in the emplacement drifts in a line-load configuration with a WP-to-WP spacing of approximately 10 cm, and a line-averaged heat load of 1.45 kW/m per 12 WPs (SNL 2007 [DIRS 179354], Table 4-4, Parameter Numbers 05-02 and 05-03). Preclosure ventilation will be activated for at least 50 years from the start of waste emplacement.

1.5 GENERAL DESCRIPTION OF THE TSPA-LA MODEL

The development of the TSPA-LA Model began with the identification and screening of all FEPs that could affect the repository (Section 1.2.1). Appendix I contains additional information on all FEPs that have been included in the TSPA-LA Model. This information provides a mapping between the FEPs documentation, the TSPA-LA Model, and the associated GoldSim software (GoldSim V. 9.60.100, STN: 10344-9.60-01 [DIRS 181903]) model file. The FEPs that were screened in were used to develop the scenario classes for the TSPA-LA Model analyses (Section 1.2.2). Figure 1-3 is a schematic representation of the development of the TSPA-LA Model. The Figure illustrates how the TSPA-LA Model, for analysis purposes, divides the

repository system into individual model components. Each individual model component represents a major process or set of processes of the total repository system. Figure 1-3 indicates these model component areas as well as the scenario classes that are included in analyses of repository performance.

GoldSim software (GoldSim V. 9.60.100, STN: 10344-9.60-01 [DIRS 181903]) integrates the model components and submodels of the TSPA-LA Model allowing simulation of repository performance for each realization of uncertain parameters. GoldSim manages the flow of information between and among the external process models, the model components and submodels, and the abstractions provided to the TSPA-LA Model. A separate software code, EXDOC 2.0, uses GoldSim results to compute mean and median dose. The principal model components of the TSPA-LA Model are described in the following sections.

1.5.1 Model Components and Modeling Case for the Nominal Scenario Class

The TSPA-LA Model is based on the Nominal Scenario Class, which incorporates all expected FEPs to describe the most likely fundamental processes at work under ambient conditions, as well as possible changes to those processes after repository closure. The Nominal Scenario Class represents the most likely FEPs under the expected natural conditions prevailing at the repository. The Nominal Scenario Class describes WP failure during expected repository performance without the occurrence of early failure of EBS components or of disruptive events. The Nominal Scenario Class includes a single modeling case, the Nominal Modeling Case, that addresses FEPs that describe WP degradation due to corrosion mechanisms including general corrosion, SCC, localized corrosion, and MIC. The TSPA-LA Model components for the Nominal Modeling Case are the nominal modeling components, namely:

- UZ Flow
- EBS Environment
- WP and DS Degradation
- Waste Form Degradation and Mobilization
- EBS Flow and Transport
- UZ Transport
- SZ Flow and Transport
- Biosphere.

1.5.1.1 Unsaturated Zone Flow

The UZ Flow Model Component defines the temporal and spatial distribution of water flow from the ground surface through the unsaturated tuffs above and below the repository horizon and the temporal and spatial distribution of water dripping into the waste emplacement drifts. The UZ Flow Model Component of the TSPA-LA Model integrates five processes that contribute to flow

in the UZ. These processes include: climate-induced precipitation, infiltration, mountain-scale UZ flow, drift seepage, and drift-scale coupled processes. Figure 1-12 provides a conceptual illustration of the Yucca Mountain mountain-scale flow processes. The UZ Flow Model Component provides a representation of the hydrogeologic processes above and below the repository. Water that reaches the repository horizon has its source in precipitation at the land surface above the repository. This precipitation occurs in the form of rainfall and snow. The temporal variability in precipitation that occurs is included in the TSPA-LA Model by specifying four successive climate states: present-day climate and three future climate states (Figure 1-13). The climate from 10,000 years after repository closure to the period of geologic stability is based on specifications regarding deep percolation rates described in NRC Proposed Rule 10 CFR 63.342(c)(2) [DIRS 178394] (Sections 1.1.1 and 1.6.1).

1.5.1.2 Engineered Barrier System Environment

The EBS Environment Model Component includes the EBS mountain-scale thermal-hydrology and the EBS chemical environments within the emplacement drifts. These environments are important to repository performance because they help determine the degradation rates of EBS components, quantities and species of mobilized radionuclides, and transport of radionuclides and fluids through the repository and drifts, and their release into the UZ below the repository. Figure 1-12 shows the position of the repository drifts and WPs with respect to the flow system within Yucca Mountain. The percolation moving into the repository environment will be affected by heat from the emplaced waste. The waste heat and geochemical processes and conditions will determine the EBS chemical environment.

1.5.1.3 Waste Package and Drip Shield Degradation

Together, the WPs and DSs are the key engineered components of the EBS (Figure 1-14). The WP and DS Degradation Model Component describes the degradation of the WPs and DSs as a function of time, presence of water, and repository location. The WP and DS Degradation Model Component is described in Section 6.3.5. The WP and DS Degradation Model Component includes the implementation of WAPDEG.DLL (WAPDEG V. 4.07 [DIRS 181774]) within GoldSim and supporting submodel implementations. The WP and DS Degradation Model Component accounts for the following degradation processes: general corrosion of the DSs; general corrosion and localized corrosion of the outer surfaces of the WPs; SCC of the WPs; MIC on the outer surfaces of the WPs; and early DS and WP failure.

1.5.1.4 Waste Form Degradation and Mobilization

The Waste Form Degradation and Mobilization Model Component establishes the radionuclide inventories for representative CSNF and CDSP WPs (Figure 1-15) using the radionuclide inventories for the CSNF, DSNF, and HLW waste forms, and then calculates the rates of degradation of these waste forms. Figure 1-16 provides an overview of the mechanisms included in the Waste Form Degradation and Mobilization Model Component, as well as the concentrations of radionuclides released from the CSNF waste forms to the EBS Transport Submodel. The Waste Form Degradation and Mobilization Model Component accounts for the following processes and conditions: in-package water chemistry, matrix degradation rates for CSNF, DSNF, and HLW waste forms, radionuclide solubilities, and the types and concentrations

of waste form and in-drift colloids.

1.5.1.5 Engineered Barrier System Flow and Transport

The EBS Flow and Transport Model Component calculates the rate of radionuclide release from the EBS to the UZ. This quantity is determined by seepage into the emplacement drifts, condensation on the drift walls, WP and DS degradation, the presence of water films on in-package internals, and the EBS thermal-hydrologic (TH) environment (Figure 1-17). The EBS Flow and Transport Model Component accounts for the following processes: the rate of water flow through the EBS, diffusive and advective transport, sorption, and colloid-facilitated transport.

1.5.1.6 Unsaturated Zone Transport

The UZ Radionuclide Transport Model Component describes the migration of radionuclides from the EBS of the repository, through the UZ, to the water table. Consistent with the Mountain-Scale UZ Flow Submodel, the conceptual model for UZ transport (Figure 1-18) uses a dual-continuum representation to couple advective and diffusive transport through fracture and matrix continua. The UZ Transport Model Component accounts for the following processes: advection, dispersion, matrix diffusion, sorption, colloid facilitated transport (retardation, filtration, and size exclusion), radioactive decay and ingrowth, climate change, and water table rise.

1.5.1.7 Saturated Zone Flow and Transport

The SZ Flow and Transport Model Component evaluates the transport of radionuclides from their introduction at the water table below the repository to the regulatory boundary 18 km downgradient from the Yucca Mountain Repository (Figure 1-19). Radionuclides move through the SZ either as solutes or sorbed to colloids. The SZ Flow and Transport Model Component accounts for the following processes: advection and dispersion, matrix diffusion, colloid retardation and exclusion, radioactive decay and ingrowth, sorption, climate change, and water table rise.

1.5.1.8 Biosphere

The Biosphere Model Component evaluates radionuclide transport in the biosphere and the resulting exposure of the RMEI (NRC Proposed Rule 10 CFR 63.312 [DIRS 180319]) for releases of radioactive material after closure of the repository (Figure 1-19). The Biosphere Model Component analyzes two dominant mechanisms of radionuclide release to the biosphere: (1) release through the SZ via groundwater, and (2) release through the air by ash dispersal from a volcanic eruption. These two release mechanisms correspond to the two modes by which radionuclides may be introduced into the biosphere.

1.5.2 Model Components and Modeling Cases for the Early Failure Scenario Class

The Early Failure Scenario Class addresses FEPs that describe WP failures due to materials and/or manufacturing defects or pre-emplacement operations and practices that could affect the performance of the EBS. The Early Failure Modeling Cases address FEPs that describe the

potential for DS and WP early failure that could affect repository performance in the absence of disruptive events. The Drip Shield EF Modeling Case analyzes the possibility that DSs could fail prematurely, thus failing to protect the underlying WPs from seepage and possible localized corrosion. The Waste Package EF Modeling Case analyzes WPs that fail prematurely due to material defects, manufacturing errors, or pre-emplacement operations and practices, such as improper heat treatment or welding flaws that could affect WP performance and longevity. The TSPA-LA Model components for the Early Failure Scenario Class modeling cases are the nominal modeling components, namely:

- UZ Flow
- EBS Environment
- WP and DS Degradation
- Waste Form Degradation and Mobilization
- EBS Flow and Transport
- UZ Transport
- SZ Flow and Transport
- Biosphere.

The Early Failure FEPs are addressed by specifying initial conditions for the TSPA-LA Model, which represent WPs and/or DSs that experience early failure.

1.5.3 Model Components and Modeling Cases for the Igneous Scenario Class

The Igneous Scenario Class addresses FEPs that describe igneous activity that could affect repository performance. The Igneous Scenario Class includes the Igneous Intrusion Modeling Case that addresses the FEPs for the unlikely possibility that magma, in the form of a dike, could intrude into the repository and disrupt expected repository performance. The Igneous Scenario Class also includes a Volcanic Eruption Modeling Case that addresses FEPs that describe a volcanic conduit that invades the repository, destroys WPs, and erupts at the land surface. The volcanic eruption disperses volcanic tephra and entrained waste under atmospheric conditions and deposits the contaminated tephra on land surfaces where the contaminated tephra becomes subject to redistribution by soil and near-surface hydrogeologic processes.

1.5.3.1 Igneous Intrusion Modeling Case

The Igneous Intrusion Modeling Case assumes that a dike intersects the repository and destroys all DSs and WPs, exposing the waste forms to percolating water and mobilizing radionuclides that may then be transported out of the repository and down through the UZ to the SZ, and then transported to the accessible environment. The TSPA-LA Model uses the following model components to calculate total system performance for the Igneous Intrusion Modeling Case:

- UZ Flow
- EBS Environment
- WP and DS Degradation
- Waste Form Degradation and Mobilization
- EBS Flow and Transport
- UZ Transport
- SZ Flow and Transport
- Biosphere.

Prior to the time of the first intrusion, the TSPA-LA Model for the Igneous Intrusion Modeling Case is the same as the model for the Nominal Modeling Case. The TSPA-LA Model changes the representation of the EBS components (WPs and DSs) at the time of the first intrusion to represent damage to the EBS caused by the intrusion of magma. The TSPA-LA Model assumes that the entire repository is damaged at the time of the first intrusion and that subsequent intrusions cause no significant additional damage.

1.5.3.2 Volcanic Eruption Modeling Case

The Volcanic Eruption Modeling Case represents the fraction of igneous intrusions in which the conduit for a volcanic eruption also intersects a repository drift. In this case, waste from WPs is transported to the land surface through one or more eruptive conduits, and tephra and entrained waste are discharged into the atmosphere, transported by wind currents, and deposited at land surface. The Volcanic Eruption Modeling Case also evaluates the fluvial and eolian redistribution of contaminated tephra deposited on the land surface. The TSPA-LA Model uses the following processes and model components to calculate repository system performance for the Volcanic Eruption Modeling Case:

- Volcanic interaction with the repository
- Atmospheric transport
- Tephra redistribution
- Biosphere.

The TSPA-LA Model does not include any nominal processes other than radionuclide decay prior to the occurrence of an eruptive event.

1.5.4 Model Components and Modeling Cases for the Seismic Scenario Class

The Seismic Scenario Class evaluates repository performance in the event of seismic activity capable of disrupting repository emplacement drifts and the engineered components of the EBS through ground motion and fault displacement. The Seismic Scenario Class includes damage to DSs and WPs as a function of ground motion or fault displacement associated with a seismic event. Radionuclides in breached WPs may be mobilized and transported out of the repository, transported through the UZ to the SZ, and then to the accessible environment. The TSPA-LA Model uses the following model components to estimate total system performance for the Seismic Scenario Class:

- UZ Flow
- EBS Environment
- WP and DS Degradation
- Waste Form Degradation and Mobilization
- EBS Flow and Transport
- UZ Transport
- SZ Flow and Transport
- Biosphere.

The Seismic Scenario Class includes two modeling cases: (1) Seismic GM Modeling Case and (2) Seismic FD Modeling Case. The Seismic GM Modeling Case addresses FEPs concerning damage due to vibratory ground motion, which include:

- Potential buckling and/or rupture of the DS due to accumulated rockfall and dynamic loading during seismic events
- Potential SCC damage and/or rupture of WPs due to seismic events
- Diffusion and/or advection of mobilized radionuclides from failed or ruptured WPs.

The Seismic FD Modeling Case addresses FEPs that describe damage due to fault displacement, including rupture of WPs and the overlying DS components. FEPs that describe localized corrosion are also included in both Seismic Modeling Cases because rupture of the DS leads to the possibility of crown-seepage induced localized corrosion of WPs.

Prior to the first seismic event, the TSPA-LA Model for the Seismic GM Modeling Case is the same as the model for the Nominal Modeling Case. After the first seismic event, rockfall may affect seepage into a drift, damage to DS components may affect seepage contacting WPs, and damage to WPs may result in radionuclide release. Rockfall and damage may accumulate as additional seismic events occur, increasing the effects on flow and transport processes. Seismic

events that include fault displacement will affect an uncertain number of WPs. Subsequent fault displacement events will not increase damage to WPs already damaged by preceding fault displacement events, although additional WPs may be damaged. If a WP is damaged by a fault displacement event, the overlying DS is considered to be ruptured and is no longer a barrier to seepage.

1.5.5 Model Components for the Human Intrusion Scenario

The TSPA-LA Model considers a stylized Human Intrusion Scenario based on a simulated future exploratory drilling operation that penetrates the repository. The scenario considers a drilling operation that utilizes the most sophisticated drilling apparatus currently available. Using current technology, if the drilling apparatus encountered a WP, it would easily be detected by a driller because of the combination of the WP or DS resistance to penetration and the presence of metal in the drilling cuttings. Encountering DSs or WPs would not only alert the driller to the presence of non-natural materials, but the strength of the DSs and WPs would be enough to prevent the penetration of the WP by the drilling apparatus. However, if the drilling apparatus were to directly intersect a degraded WP, and the borehole were deepened to the SZ, then the borehole could become an avenue for aqueous waste transport. The stylized scenario in NRC Proposed Rule 10 CFR 63.322 [DIRS 180319] supposes that waste from the penetrated WP is transported to the SZ and available to the RMEI. Because only a degraded WP would be penetrated, the TSPA-LA Model for the Human Intrusion Scenario would include simulation of nominal processes until the time of the WP penetration. However, following the penetration, only the waste transported down the borehole would be evaluated for dose to the RMEI, and the waste transport would be simulated by only the SZ and biosphere model components. Therefore, the Human Intrusion Scenario Modeling Case would involve the following TSPA-LA Model components:

- UZ Flow
- EBS Environment
- WP and DS Degradation
- Waste Form Degradation and Mobilization
- SZ Flow and Transport
- Biosphere.

1.6 CONCEPTUAL DESCRIPTION OF PROCESSES RELEVANT TO AN EVALUATION OF POSTCLOSURE PERFORMANCE IN THE ABSENCE OF DISRUPTIVE EVENTS

The following sections describe processes relevant to the evaluation of repository system performance. Information relevant to the technical basis for this conceptual description can be found in *Yucca Mountain Site Description* (BSC 2004 [DIRS 169734], Sections 6, 7, and 8).

Because the repository horizon will be approximately greater than 200 m beneath the land

surface (SNL 2007 [DIRS 179466], Table 4-1, Parameter Number 01-06) and the waste forms are solids (with minor gaseous constituents), the primary means for the mobile radioactive constituents of the waste forms to reach the biosphere, in the absence of an unlikely volcanic eruption, will be along groundwater pathways. The waste forms will pose minimal risks to humans, unless all of the following processes were to occur:

- The WPs are breached.
- The waste forms are exposed to water.
- Radionuclides within the waste forms are dissolved in the water.
- Dissolved or colloid-associated radionuclides are released from the repository and transported with the water in the SZ.
- Radionuclide-containing water is discharged, either naturally or at a pumping well, from the SZ.
- Humans or any part of the food chain uses water containing the released radionuclides.

The following sections describe how these processes might occur and how the major components and processes of the Yucca Mountain Repository system could act to affect long-term waste isolation. The discussion is divided into five topics:

- Water movement in the unsaturated tuffs above the repository in the upper natural barrier
- Water and water vapor movement around the repository drifts
- Water movement and radionuclide transport within and through the EBS
- Water movement and radionuclide transport through the unsaturated tuffs, below the repository
- Water movement and radionuclide transport through the SZ aquifers and biosphere.

1.6.1 Water Movement in the Unsaturated Tuffs above the Repository

The following concepts are excerpted from *UZ Flow Models and Submodels* (SNL 2007 [DIRS 184614], Section 6.1.4). Figure 1-12 illustrates the key concepts associated with water movement in the UZ at Yucca Mountain. The source of water in the UZ at the repository horizon is precipitation at the land surface. Climate will control the range of precipitation and land surface temperature conditions. Four potential climate periods, present-day, monsoon, glacial-transition, and a post-10,000-year climate, were identified as being likely from repository closure to the period of geologic stability (Figure 1-13). The present-day climate state is equivalent to the current climate in the Yucca Mountain area as determined from regional meteorological stations. The monsoon climate state is characterized by hot summers, with increased summer rainfall relative to the present-day climate. The glacial-transition climate state

has cooler and wetter summers and winters, relative to the present-day climate state. Climate forecasting indicates that, during the next 10,000 years at Yucca Mountain following repository closure, the present-day interglacial climate may persist for 400 to 600 years, followed by a warmer and wetter monsoon climate for 900 to 1,400 years, followed by a cooler and wetter glacial-transition climate for the remaining 8,000 to 8,700 years (BSC 2004 [DIRS 170002], Section 6.6 and Table 6-1). Per the NRC Proposed Rule 10 CFR 63.342(c)(2) [DIRS 178394], the post-10,000-year climate after repository closure until the period of geologic stability will be modeled by sampling a log-uniform probability distribution for deep percolation rates from 13 to 64 mm/year.

A large portion of the precipitation on the Yucca Mountain land surface either runs off into the washes that are cut into the mountain, evaporates from the surface, or transpires from the native plants in the area. The remaining water infiltrates downward through the soil horizon and into the rock. The net amount of total precipitation that infiltrates is called net infiltration. Net infiltration is the source of percolation flux within the UZ, and it provides the water for flow and transport mechanisms that may move radionuclides from the repository to the water table and into the SZ. Net infiltration is spatially and temporally variable because of the nature of the storm events that supply precipitation, and because of the variation in soil cover and topography. Infiltration is believed to be high on side slopes and ridgetops, where bedrock crops out and fracture flow in the bedrock is able to move moisture away from zones of active evapotranspiration.

The net infiltration moves downward through the UZ, driven primarily by gravity. The downward movement of water in the UZ is called percolation. Percolation flux in the unsaturated fractured tuffs occurs in the rock matrix and in the fractures of the rock. Generally, the welded tuff layers have more of the total flux within the fractures because the permeability of the matrix is low, whereas the nonwelded lithologic layers have more of the total flux within the matrix. Water flows through the welded and densely fractured TCw unit mainly through fractures. Within the more porous PTn unit, most of the water flows through the matrix, where the high storage capacity causes a dampening of the infiltration pulses. Small amounts of flowing water preferentially flow along faults that cut through the PTn. Unsaturated flow in the TSw unit occurs primarily through fractures. In addition, some lateral diversion of water occurs as it moves downward from the soil horizon through the UZ. This lateral diversion is caused by the eastward dip of the geologic strata and heterogeneities in the rock because of the different permeabilities of the welded and nonwelded tuffs between land surface and the repository horizon.

1.6.2 Water and Water Vapor Movement around the Repository Drifts

Figure 1-20 illustrates the key concepts anticipated to be associated with water movement around the repository drifts after waste emplacement at Yucca Mountain. Water is one of the principal determining factors of: (1) corrosion of the EBS, (2) waste dissolution, and (3) radionuclide transport from the repository to the accessible environment. The amount and chemical composition of water seeping into waste-emplacement drifts will affect the long-term performance of the repository system.

In the UZ, percolating water encountering a large underground opening will be partly diverted

around the cavity. This effect would reduce the amount of liquid water that could enter a waste-emplacement drift or prevent dripping altogether and is due to the formation of a capillary barrier around the cavity. Moreover, during the early stages after closure, the heat from decaying radionuclides will likely vaporize water that approaches the waste-emplacement drifts. The presence of a capillary barrier and a zone of vaporization would limit the amount of water that could potentially contact the WPs.

The heat generated by the decay of radioactive wastes is anticipated to result in elevated rock temperatures in the repository environment for thousands of years after emplacement (SNL 2007 [DIRS 181383], Figure 6.1-1). For the TSPA-LA repository design concept, these temperatures will be high enough, in most locations, to cause boiling conditions in the vicinity of the drifts, thus giving rise to local water redistribution and altered flow paths. Conditions one to several meters above the ceilings of the emplacement drifts could change in several ways that could affect the amount of water seeping into the drifts. Within 50 years after repository closure, the water will first encounter a dry-out zone above the repository drifts. Under boiling conditions, water reaching the dry-out zone would vaporize, thus preventing liquid water from reaching the drifts. Water vapor would tend to move away from the drifts and through the permeable fracture network, driven primarily by a pressure increase caused by boiling. In cooler regions away from the drifts, the vapor would condense in the fractures, where it could drain either toward the heat source from above or shed around the drifts into the zone below the heat source. Condensed water could also imbibe from fractures into the matrix, leading to increased liquid saturation in the rock matrix.

For the TSPA-LA repository design concept, the dry-out zone around drifts may extend from a few to more than 25 m from the walls of the drifts. Boiling conditions in the rock are anticipated to range from no boiling to boiling for over 2,000 years after emplacement (SNL 2007 [DIRS 181383], Section 8.2[a] and Table 6.3-39), reflecting the spatial and temporal variability of possible TH conditions in the repository system. The spatial variability would be caused by heterogeneity in the rock properties and variations in the ambient percolation flux. In addition, differences in the thermal output of different WPs could cause a range of TH conditions in the repository environment. For example, cooler regions are expected along the edges of the repository and near low-thermal output WPs. The temporal variability in water movement around the drifts could be caused, in the short-term, by the thermal output of the wastes that will eventually decline to minimal values. Hundreds of years of drying and several thousand years of cooling and rewetting are anticipated. In the long-term, water movement will be controlled by the climatic variability (BSC 2004 [DIRS 170002], Sections 6.6) and percolation flux at the repository horizon. If water ultimately penetrates the dry-out zone as the repository cools and reaches the immediate vicinity of the walls of the drifts, most of it will still be prevented from seeping into the drift because of the capillary barrier effect.

The characteristics of the rock around the repository openings may change with time. The fracture permeability could increase because of mechanical stress relaxation following the construction of the repository drifts, and ultimately, the drifts could collapse. The fracture permeability may also change because of rock thermal expansion and mineral precipitation. The capillarity of the fractures could either increase or decrease because of these same processes. However, these changes are not expected to significantly affect seepage into emplacement drifts (DTN: MO0706SPAFEPLA.001_R0 [DIRS 181613], FEPs 2.1.08.01.0A, 2.1.08.02.0A,

2.2.01.01.0A, 2.2.01.01.0B, and 2.2.01.03.0A).

In summary, the rate of water dripping into an emplacement drift is expected to be significantly less than the local percolation rate because of the following:

- The dry-out zone around the drifts will reduce liquid water flow while the temperatures in the drifts are elevated, potentially preventing water from reaching the drift surfaces.
- The capillary barrier will divert water around the drifts.

1.6.3 Water Movement and Radionuclide Transport within and through the Engineered Barrier System

Figures 1-21 and 1-17 illustrate the key concepts associated with TH processes, including water movement within the drifts and water contacting the WPs that may experience water dripping from the walls of the emplacement drifts.

The heat output from the SNF and HLW will decline continuously because of radioactive decay. WP heat output will be highest during the nominal 50-year preclosure period, but the emplacement drifts will be ventilated to remove most of the heat (SNL 2007 [DIRS 179466], Table 4-2). Temperatures of the WPs and DSs will be elevated, and some WPs and DSs may approach the boiling point of water immediately after emplacement, depending on ventilation. However, the warming of ventilation air will ensure that preclosure conditions will be relatively dry with low humidity. At permanent closure, ventilation will cease. The temperature of the drift-wall rock will be below boiling initially, but will increase sharply within a few decades (SNL 2007 [DIRS 179466], Table 4-2). The maximum postclosure temperatures of a WP and DS at any location will be determined by the history of heat output from the waste, the resistance to dissipation of heat in the host rock, heat transfer from the WPs to the DSs and to the walls of the drifts, and the relationship to other nearby heat sources.

Vaporized water within the drifts will tend to move away from hotter regions within the drifts and will condense at cooler locations on the walls of the drifts or in the adjacent rock. Some of this condensed water could then drip directly onto an underlying DS or move along the walls of the drifts to the invert.

Evaporation of dripping water could result in the evolution of highly saline brines on the surfaces of the DSs. The dominant degradation mode of the titanium DSs may be by general corrosion. Because this process is anticipated to be very slow, DS failure is not expected to occur during the 10,000-year period after repository closure. Therefore, the integrity of the DSs could reduce any damage to WPs in the event of rockfall as the emplacement drifts degrade over time.

Significant degradation of the WPs is not expected during the preclosure period. In the postclosure dry-out regime, when drift-wall temperatures are greater than the boiling point of seepage water, potentially relevant high-temperature modes of degradation include SCC and localized corrosion, and dry oxidation is conservatively accounted for by applying aqueous general corrosion rates. In the transition regime, the temperatures of the walls of the drifts are estimated to be approximately equal to the boiling point of the seepage water, and evaporation could cause seepage waters to become concentrated on the surfaces of the WPs if the DSs were

to fail. These concentrated brines could result in localized corrosion of the WPs. In lower temperature regions, seepage waters could enter the drifts, but the thermal driving force for localized corrosion would be less and general corrosion, SCC, and MIC may lead to WP failure.

The temperatures of the surfaces of the WPs, the chemistry of the water in contact with the surfaces of the WPs, the mechanical stress, and the degradation characteristics of the metals themselves will affect the degradation rates of Alloy 22 and stainless steel (no credit is taken for the stainless-steel portions of the WPs relative to the corrosion failure of the WPs). Because these environmental parameters are spatially variable, and because the metal fabrication could be variable, WP degradation is also expected to be variable in space and time. Although degradation will occur, WPs are not anticipated to be breached during the first 10,000 years after repository closure. The only exceptions may be a small number of potential early WP failures because of manufacturing defects.

Until a WP has been sufficiently degraded to allow an opening to form through its two metallic liners, there is no potential for water to come into contact with the waste forms. During this period, the waste forms are completely contained within the WPs. If there is a breach of a WP, some of the water vapor or dripping water could enter a WP. When cracks develop in WPs, available water may enter WPs by diffusion through the cracks. However, if there are larger WP failures such as patches, and if there is DS failure that allows water to fall directly on the WPs and the patches, then water may enter the WPs by advection.

Figure 1-17 illustrates the key concepts associated with water moving into the WPs and contacting the waste forms. Figure 1-17 also illustrates the transport of radionuclides through the EBS. These radionuclides may be mobilized as either dissolved species or they may be adsorbed onto colloids.

Water may enter breached CSNF WPs and contact the waste forms, which are assumed to have failed cladding. CDSP WPs will contain HLW glass placed in stainless-steel pour canisters and DSNF fuel assemblies in stainless-steel canisters. Because DSNF cladding may or may not be fully intact, DSNF is modeled as not having any cladding.

The rate at which radionuclides may be released from the repository will depend on the following:

- Degradation rates of the components of the EBS
- Dissolution rate of the waste forms
- The form of the released radionuclides (colloidal versus dissolved)
- Sorption of radionuclides onto corrosion products and invert material
- The solubility of the radionuclides
- The rate of water movement and volume of water that flows or diffuses through the EBS.

1.6.4 Water Movement and Radionuclide Transport through the Unsaturated Tuffs below the Repository

Figure 1-18 illustrates the key concepts associated with water movement in the unsaturated rocks beneath the repository and the migration and transport of radionuclides in these rocks. After the dissolved or colloidally attached radionuclides are released into the UZ beneath the repository, they may be transported with the water to the SZ.

Radionuclide transport within the UZ is strongly related to UZ flow through advective transport. Advective transport (advection) refers to the movement of dissolved or colloidal materials because of the bulk flow of fluid. In the welded units, advection through fractures is expected to dominate transport, mainly because liquid water largely flows through fracture networks in these units. Advection is also an important mechanism for transport between fractures and matrix, especially at interfaces between nonwelded and welded units where there is a transition between dominant matrix flow and dominant fracture flow, respectively.

Liquid water flow paths below the repository horizon will affect advective transport of released radionuclides, particularly in perched water bodies, where lateral transport of radionuclides is likely to occur. Dominant fault-and-fracture flow provides relatively short transport times for transport to the water table, whereas dominant matrix flow leads to much longer transport times. In addition to advection, radionuclide transport within the UZ will be affected by several other mechanisms, such as matrix diffusion, sorption, colloid-facilitated transport, and radioactive decay. Matrix diffusion refers to solute transport from fracture networks to surrounding matrix blocks resulting from molecular diffusion. Mass transfer between fractures and matrix may play an important role in transport within Yucca Mountain. Because flow velocity in the matrix is much slower than in fractures, the transfer of radionuclides from fractures to the matrix by matrix diffusion could retard the overall transport of radionuclides to the water table.

The transport of radionuclides may also be affected by sorption and colloid attachment. Sorption describes a combination of chemical interactions between dissolved radionuclides and the solid phases (immobile rock matrix or colloids), including adsorption, ion exchange, surface complexation, and chemical precipitation. Radionuclide transport in the UZ also involves a colloid-facilitated transport mechanism. Colloids are particles small enough to become suspended (and thus transportable) in a liquid. Radionuclides can be sorbed onto colloids. Unlike the sorption of radionuclides to the rock matrix, however, the radionuclides sorbed on colloids are potentially mobile.

Radioactive decay can also affect the concentration of radionuclides during transport through the UZ. For simple decay, radionuclide concentration decreases exponentially with time, thereby creating stable decay products. Chain decay adds additional complexity because of the ingrowth of new radionuclides created from the decay of a parent radionuclide. Daughter products from chain decay may have different sorption characteristics than their parent radionuclides, therefore exhibiting different modes of transport.

Because each of the characteristics of the natural environment and the processes controlling transport are variable in space and time, radionuclide transport is also variable. Part of the temporal variability relates to long-term climatic changes that not only affect the percolation flux

through the repository system but could also cause the water table beneath Yucca Mountain to rise during wetter climates or fall during drier climates. A rise in water table elevation would be accompanied by a potentially increased flow through the repository in response to a wetter climate. Also, a higher water table could shorten transport times through the UZ below the repository, depending on the height of the water level rise.

1.6.5 Water Movement and Radionuclide Transport through the Saturated Zone Aquifers to the Biosphere

Radionuclides that are transported through the UZ below the emplacement drifts are released to the SZ beneath the repository. Figure 1-22 illustrates the key concepts associated with water movement and the transport of radionuclides in the SZ beneath and downgradient from the Yucca Mountain site. Figure 1-22 also illustrates the pathways by which dissolved radionuclides and colloids may come into contact with the biosphere.

When radionuclides released from the repository reach the SZ, they will be transported laterally within the SZ. The general direction of groundwater flow in the SZ is to the southeast, and then to the south and southwest. The processes that affect the performance of the SZ barrier include both groundwater flow and radionuclide transport processes. The groundwater flow processes determine the rate of water movement within the SZ and the flow paths. Dissolved radionuclides diffuse from fractures in which they are advectively transported into the matrix, which has little advective flux and tends to slow the transport time of these species. The effectiveness of this process depends on the diffusive properties of the matrix and the degree of spacing between the flowing fracture zones. Larger diffusion coefficients or smaller spacing between flowing fracture zones result in slower transport times within the fractured rock.

Many radionuclides that are potentially important to repository performance may be sorbed within the matrix of the rock mass. The degree of sorption depends on the individual radionuclide. Carbon, technetium, and iodine are not sorbed (SNL 2008 [DIRS 183750], Sections 6.5.3.1 and 6.7.1) and are transported considering only advection, dispersion, and matrix diffusion processes. Other radionuclides, such as neptunium, uranium, and plutonium, are sorbed in the matrix of the fractured tuffs and alluvium (SNL 2008 [DIRS 183750], Section 6.7.1). The stronger the sorption, the longer the radionuclide transport time compared with advective-dispersive transport times. However, radionuclide transport could be enhanced by colloid-facilitated transport when radionuclides are sorbed onto mobile colloids whose size allows transport along fractures.

The TSPA-LA Model calculates the time for radionuclides to reach the boundary of the controlled area (10 CFR 63.302 [DIRS 180319]) downgradient from the repository. The time required depends primarily on the groundwater velocity and the retardation of radionuclides that may sorb on the mineral surfaces within the volcanic or alluvial aquifers. A rise in the water table elevation could cause a change in the locations of downgradient discharge points and possibly alter transport times if formations of differing transmissivity are encountered by the higher water table.

If radionuclides were to reach a location downgradient from the repository where water is being pumped from the aquifer, the potential exists for radionuclides to come into contact with humans

through biosphere pathways. The TSPA-LA Model calculates dose to the RMEI based on an annual water demand of 3,000 acre-feet. In addition, the biosphere submodel includes the potential effect of a rise or fall in water table elevation because the TSPA-LA Model calculates biosphere dose conversion factors (BDCFs) based on a unit concentration in water, regardless of origin.

The principal biosphere pathways to humans consist of the following in approximate order of importance:

- Direct consumption of water containing dissolved radionuclides
- Inhalation of dust that may contain attached radionuclides
- Inhalation of aerosols from evaporative coolers
- Raising fish in contaminated water and subsequent consumption of the fish
- Watering of livestock with contaminated water or feeding of livestock with contaminated crops, or both, and the subsequent consumption of meat, milk, or eggs
- Consumption of crops produced using water containing dissolved radionuclides
- Direct exposure to contaminated soil.

1.7 CONCEPTUAL DESCRIPTION OF PROCESSES RELEVANT TO AN EVALUATION OF POSTCLOSURE PERFORMANCE AFTER THE OCCURRENCE OF DISRUPTIVE EVENTS

Section 1.6 describes processes relevant to repository performance in response to nominal conditions. The following sections describe processes relevant to the evaluation of repository system performance likely to occur in response to natural disruptive events that may affect the repository system. Natural disruptive events that may affect the repository include an igneous intrusion intersecting the repository, a volcanic eruption from a volcanic conduit that intersects repository drifts, and seismic activity that produces vibratory ground motion and/or fault displacement that affects the EBS.

As described in Section 1.6, the primary means for radionuclide transport to the biosphere, in the absence of an unlikely volcanic eruption, will be along groundwater pathways. If disruptive events occur and if these events affect the EBS, the disrupted parts of the EBS will transport radionuclides through the UZ using the nominal processes described in Section 6.3. The following sections describe how these processes might differ from those described in Section 1.6 because of disruptive events.

1.7.1 Water Movement in the Unsaturated Tuffs above the Repository

Figure 1-12 illustrates the key concepts associated with water movement in the UZ at Yucca Mountain. Disruptive events are not expected to affect precipitation at the land surface, which is the source of water in the UZ at the repository horizon (SNL 2007 [DIRS 184614],

Section 6.1.4). Likewise, flow fields in the UZ above the repository will not be affected by disruptive events. The climate states incorporated in the TSPA-LA Model are the same for all modeling cases and scenario classes (Section 1.6.1).

1.7.2 Water Movement around the Repository Drifts

As described in Section 1.6.2, in the absence of disruptive events, the rate and chemical composition of seepage into the repository's emplacement drifts is expected to be substantially less than the local percolation rate because of the early-time dry-out zone around the drifts that will reduce liquid water flow while the temperatures in the drifts are elevated, and the strength of the capillary barrier around the drifts. In addition, changes in mechanical stress coupled with the mechanical properties of the rock surrounding the repository will eventually cause drifts to collapse and alter the quantity and location of seepage.

The Igneous Intrusion Modeling Case considers the case where magma that intrudes every drift in the repository emplacement drifts damages all CSNF WPs and CDSP WPs in the intruded drifts, and solidifies. The waste forms are instantly degraded and radionuclides become available for transport through normal dissolution processes when seepage re-enters the drifts. The radionuclide transport to the UZ is controlled by the amount of seepage and radionuclide solubilities, and the solidified magma has hydrologic characteristics similar to the local bedrock.

The Seismic Scenario Class modeling cases include disruptive events in which there are expected changes in the UZ above the repository that will affect the factors controlling seepage into the drifts. The principal changes to these modeling cases are expected to be in the distribution and quantity of seepage as described in *Abstraction of Drift Seepage* (SNL 2007 [DIRS 181244], Section 6.7). Seepage into the repository depends on the integrity of the drifts, the surface area of the drifts, the value of capillary strength, and whether or not a drift lies in the lithophysal or non-lithophysal zone. The more degraded a drift becomes, the more seepage enters the repository. Seismic disruptive events will degrade the repository drifts by causing a loss of integrity of the walls and ceiling of the emplacement drifts. In general, the greater that loss of integrity, the greater the seepage. The most extreme variance in seepage into the repository drifts is expected to occur when a seismic event triggers complete collapse of the repository drifts in the lithophysal zone, increasing the seepage to the value of the percolation flux with no assumed physical retardation of seepage. Collapse of the non-lithophysal areas of the drifts will also increase seepage but not to the value expected for the lithophysal zones.

1.7.3 Water Movement and Radionuclide Transport within and through the Engineered Barrier System

Section 1.6.3 illustrates and describes the TH processes related to the movement of seepage water within the drifts and seepage contacting WPs under the influence of nominal processes. The disruptive events expected to have the most influence on aqueous geochemical processes in the repository environment are seismic events and a possible igneous intrusion that enters the repository drifts. There are two modeling cases that analyze responses to seismic events and one modeling case that is concerned with an igneous intrusion into the repository.

Section 1.7.2 briefly describes the disruption of the pattern of seepage into the repository that can

occur in response to seismic events. In addition, rock and seepage responses to seismic events can affect fluid flow within the EBS after seismic activity. Enhanced seepage into the repository, coupled with disruption of the EBS, WP and DS degradation, and waste-form degradation processes in the EBS as described in Section 1.6.3. Further, water flow in rubble in the repository in response to seismically influenced rockfall would encounter little resistance because of the relatively high porosity and permeability of the rubble. However, the repository invert is not expected to be as disrupted under the seismic modeling cases. Therefore, although there could be enhanced degradation and release of waste from the EBS following seismic ground motion or fault displacement, transport of waste following liberation from the WPs would follow nominal processes through the invert.

The rate at which radionuclides may be released from the repository due to seismic activity will depend on the following:

- The number and extent of WP damage
- Dissolution rate of the waste forms in the failed WPs
- Whether or not the released radionuclides are dissolved or colloidally attached
- Whether or not the released radionuclides are sorbed onto corrosion products and invert material
- The solubility of the released radionuclides.

The Igneous Intrusion Modeling Case simulates the number of WPs damaged and failed when portions of the repository are affected by magma that reaches the repository environment through a dike that breaches the repository as described in *Number of Waste Packages Hit by Igneous Events* (SNL 2007 [DIRS 177432], Section 7.1). This modeling case assumes that for any drift intersected by a dike, all WPs in the drift will be failed by contact with magma. All waste from the failed WPs will be incorporated in the cooled magma or otherwise available for transport out of the repository subject to nominal processes.

The rate at which radionuclides released from the failed WPs may be released from the repository will depend on the following:

- Whether or not and at what rate the radionuclides released from the failed WPs are available to be dissolved
- Whether or not the released radionuclides are dissolved or colloidally attached
- Whether or not and at what rate the radionuclides released from the failed WPs are available for sorption onto corrosion products and invert material
- The solubility of the released radionuclides
- The rate of water movement and volume of water that flows or diffuses through the cooled magma and/or the damaged EBS.

1.7.4 Water Movement and Radionuclide Transport through the Unsaturated Tuffs below the Repository

Section 1.6.3 illustrates and describes the processes related to the movement of water and transport of radionuclides released from the repository under the influence of nominal processes. The principal difference between the nominal scenarios and scenarios that include disruptive events is the impetus for the release of radionuclides from the WPs and waste forms. Section 1.7.3 describes the factors relevant to the mobilization of radionuclides as a result of disruptive events. After disruptive events have mobilized radionuclides as a result of igneous or seismic events, radionuclide transport of dissolved or colloidal materials within and through the UZ will be governed by the same nominal processes described in Section 1.6.4.

1.7.5 Water Movement and Radionuclide Transport through the Saturated Zone Aquifers to the Biosphere

Section 1.6.3 illustrates and describes the processes related to the movement of water and transport of radionuclides released from the repository under the influence of nominal processes. Section 1.7.3 describes the factors relevant to the mobilization of radionuclides after disruptive events. Section 1.7.4 describes radionuclide transport of dissolved or colloidal materials by nominal processes within and through the UZ after release from the EBS by disruptive events. In a similar way, radionuclide transport of dissolved and colloidal materials through the SZ to the biosphere will be governed by the same nominal processes described in Section 1.6.5. The TSPA-LA Model treats SZ flow and transport in the same way for both the Nominal Modeling Case and modeling cases that include disruptive events. In addition, the TSPA-LA Model uses the nominal BDCFs for the both the Igneous Intrusion Modeling Case and the Seismic Scenario Class modeling cases.

1.7.6 Atmospheric Transport and Redeposition of Radionuclides

The TSPA-LA Volcanic Eruption Modeling Case simulates the fate and transport of radionuclides deposited on the land surface and dispersed into the atmosphere as a result of a volcanic eruption that intersects the repository. The Volcanic Eruption Modeling Case is described in Section 6.5.2. This modeling case considers waste from WPs that fail when a volcanic conduit intersects the repository environment as described in *Number of Waste Packages Hit by Igneous Events* (SNL 2007 [DIRS 177432], Section 7.2). The Volcanic Eruption Modeling Case considers the WPs that are intersected by a volcanic conduit to be fragmented and directly released by a volcanic eruption at land surface and that a portion of that waste will be incorporated with tephra erupted into the atmosphere. The atmospheric transport and dispersal of tephra and waste particles in the eruptive cloud released during the volcanic eruption is described in *Atmospheric Dispersal and Deposition of Tephra from a Potential Volcanic Eruption at Yucca Mountain, Nevada* (SNL 2007 [DIRS 177431]). The dispersal and deposition is simulated using ASHPLUME (ASHPLUME_DLL_LA V. 2.1, STN: 11117-2.1-01 [DIRS 180147]). The ASHPLUME conceptual model accounts for incorporation and entrainment of waste fuel particles associated with a hypothetical volcanic eruption through the repository and downwind transport and deposition of contaminated tephra. ASHPLUME describes the conceptual model in mathematical terms to predict radioactive waste/ash deposition on land surface.

The contaminated tephra on the land surface is then subject to redistribution and dilution by hillslope and fluvial processes. The conceptual and mathematical model of redistribution processes implemented by the TSPA-LA Model is described in *Redistribution of Tephra and Waste by Geomorphic Processes Following a Potential Volcanic Eruption at Yucca Mountain, Nevada* (SNL 2007 [DIRS 179347]). The tephra redistribution conceptual model is implemented with FAR V. 1.2 (STN: 11190-1.2-00 [DIRS 182225]). Three major processes are considered by the tephra redistribution conceptual model to predict waste concentration at the RMEI location for the Volcanic Eruption Modeling Case: (1) mobilization from hillslopes, (2) mixing and dilution with uncontaminated sediments during channel transport, and (3) diffusion into the soil column at the RMEI location.

The waste inventory in the CSNF and CDSP WPs hit by the erupting magma provides the radionuclides in the waste-contaminated tephra. Radionuclide concentrations in the waste-contaminated tephra are proportional to those in the waste inventory, subject to radionuclide decay. The biosphere component of the Volcanic Eruption Modeling Case contains appropriate BDCFs to calculate the annual dose associated with predicted radionuclide concentrations at the RMEI location due to three exposure pathways: (1) short-term inhalation exposure, (2) long-term inhalation exposure, and (3) ingestion and radon exposure. The Biosphere Model Component of the Volcanic Eruption Modeling Case is described in Section 6.3.11.

The TSPA-LA Volcanic Eruption Modeling Case considers only the post-eruption situation where volcanic tephra has already been deposited on the ground surface. The Volcanic Eruption Modeling Case does not include evaluation of the annual dose received during the volcanic eruption phase when the ash is transported and dispersed in the atmosphere. Section 6.4.2.5 presents an analysis showing that the mean annual dose during the eruption phase is much lower than the mean annual dose after the eruption.

1.8 CONSERVATISMS AND LIMITATIONS RELATED TO THE TSPA-LA MODEL

1.8.1 Conservatisms Incorporated in the TSPA-LA Model

The submodels incorporated into the TSPA-LA Model are representations of the repository system. The guiding principles during the development of these submodels were to: (1) ensure that representations were not optimistic (i.e., leading to an underestimation of the dose results), and (2) incorporate all included FEPs. Although these representations were developed to be as realistic as possible, some conservative (reasonable and technically defensible based on supporting analyses) representations were required for complete development of the TSPA-LA Model. These conservatisms and models are appropriate and within the regulatory guidelines for the TSPA-LA effort, as found in NRC Proposed Rule 10 CFR Part 63 ([DIRS 178394] and [DIRS 180319]). Conservatisms incorporated in the TSPA-LA Model, if present, are not functions of the TSPA process, but are a result of the approach, methodology, and assumptions used in the abstractions found in the supporting analyses and process models described therein.

The NRC Proposed Rule 10 CFR 63.114(a)(2) [DIRS 178394] requires that a PA:

> "Account for uncertainties and variabilities in parameter values, for 10,000 years after disposal, and provide for the technical basis for parameter ranges, probability distributions, or bounding values used in the performance assessment."

Also, NRC Proposed Rule 10 CFR 63.304 [DIRS 180319] requires that the ranges of parameters and performance-assessment calculations provide a Reasonable Expectation of repository performance in the following way:

> *"Reasonable expectation* means that the Commission is satisfied that compliance will be achieved based upon the full record before it. Characteristics of reasonable expectation include that it:

1. Requires less than absolute proof because absolute proof is impossible to attain for disposal due to the uncertainty of projecting long-term performance;

2. Accounts for the inherently greater uncertainties in making long-term projections of the performance of the Yucca Mountain disposal system;

3. Does not exclude important parameters from assessments and analyses simply because they are difficult to precisely quantify to a high degree of confidence; and

4. Focuses performance assessments and analyses on the full range of defensible and reasonable parameter distributions rather than only upon extreme physical situations and parameter values."

Accordingly, because 10 CFR 63.304(4) [DIRS 180319] does not preclude the use of conservative parameter values, the approach used for the TSPA-LA Model was to use full ranges of 'reasonable and defensible' distributions of estimates of parameter values that also could include conservative estimates of their values as provided by the supporting analyses. The TSPA-LA Model approach integrates the abstraction models developed in the supporting analyses to describe the relevant FEPs and appropriately propagate uncertainty in these abstractions. The TSPA-LA Model embodies all the assumptions, limitations, differences, and conservatisms of the underlying abstractions, process models, and related analyses.

The intended purpose of the TSPA-LA Model (SNL 2008 [DIRS 184920], Section 1.1.1) is to provide a defensible basis for an evaluation for compliance with the adopted postclosure regulatory standards (e.g., NRC Proposed Rule 10 CFR Part 63 [DIRS 178394] and [DIRS 180319]). Defensibility includes, but is not limited to, reasonable and technically defensible conservative estimates of expected dose or other performance measures. The development of the TSPA-LA Model employed the following measures in providing defensible estimates of repository performance:

- Providing the best available estimates of parameter values while covering their ranges of uncertainty, including conservative estimates, where appropriate.

- Documenting the full range of uncertainty and sensitivity analyses and other supporting analyses conducted to evaluate the significance of alternative assumptions to provide confidence in the overall results.

- Providing probabilistic estimates of mean dose, including conservative approaches only where knowledge of a process is limited.

The TSPA-LA Model includes an assemblage of the best available estimates of the parameters and parameter values, including, only when necessary, conservative estimates of parameter values and conservative assumptions related to the underlying process models and submodels. The TSPA-LA Model then uses this information to calculate the best available estimate of repository performance. The descriptions of the TSPA-LA Model components in Section 6.3 include the conservatisms applicable to each of the model components and include, as applicable, conservative values in the ranges of estimates of parameters values.

The preparation for the TSPA-LA Model involved the development of parameter-value distributions to account for uncertainty in parameter values. The TSPA process includes a Parameter Review Team that is responsible for evaluating parameter uncertainty, including the use of conservative parameter values. The Parameter Review Team meets with the authors of each supporting analysis, process model, and submodel that served to develop inputs to the TSPA-LA Model. The Parameter Review Team's goal was to develop realistic parameter-value distributions that appropriately characterize uncertainty. However, in cases where there was insufficient information available to support realistic characterizations, subject matter experts (SMEs) and the Parameter Review Team jointly concurred on conservative treatments of uncertainty. The TSPA-LA Model's parameter distributions are described in Section 4.8 and Appendix M, and further documented in the TSPA Input Database (Section 4.8) and on Parameter Entry Forms (PEFs) (Section 4.4).

1.8.2 Limitations of the TSPA-LA Model

Constraints that influence the TSPA-LA Model relate to the physical system, computer software, computer hardware, input data and knowledge, and limitations of the process models. The physical system is constrained by the given initial conditions, which reflect the complexity of the systems and processes being analyzed. Assessing the performance of a nuclear waste repository, which is sited in the UZ geologic setting at Yucca Mountain, involves numerous coupled physical and chemical processes. The constraints evolve through time, for example, with the gathering of additional scientific data and with advances in computer hardware and software.

The primary limitations on the TSPA-LA Model are described in the following sections. These limitations do not affect the utility of the TSPA-LA Model for achieving its intended purpose of providing a defensible evaluation of repository performance in compliance with applicable regulatory standards.

1.8.2.1 Software Limitations

The TSPA-LA Model uses GoldSim software (GoldSim V. 9.60.100, STN: 10344-9.60-01 [DIRS 181903]). The GoldSim software has the following general capabilities:

- Addresses variability and uncertainty by using Monte Carlo simulation
- Superimposes the occurrence and consequences of discrete events onto continuously varying systems
- Uses model 'containers' that facilitate the simulation of large, complex systems
- Dynamically links external process models and/or abstractions directly to the GoldSim software
- Directly exchanges information between any Open Database Connectivity compliant database and the software.

The limitations of the GoldSim software do not affect its ability to achieve its intended purpose of providing a defensible evaluation of repository performance in compliance with applicable regulatory standards.

When developing and integrating the process models that comprise the model components of the TSPA-LA Model, hardware and software limitations were an important consideration in the model abstraction process. Hardware limitations include the speed and number of computer processors available, while software limitations include limits on the size of individual processes and threads in a 32-bit operating system. For Yucca Mountain, the judgment of scientists involved in developing the TSPA-LA Model is that the computational size and efficiency of the underlying process models do not allow direct coupling of most process models. Examples include the process-level TH, thermal-hydrologic-chemical (THC), UZ flow, and biosphere models. Some process models, such as EBS transport, have been built directly into the TSPA-LA Model but most have been abstracted in one form or another, as described in Section 6. The decoupled process models were run separately and converted to abstractions, such as response surfaces and look-up tables, which serve as direct input to the TSPA-LA Model.

1.8.2.2 Computational Limitations

The regulatory requirement to include the effects of model and data uncertainty in the PA of the repository means that the TSPA-LA Model must have the capability of modeling the repository system in a probabilistic fashion, which involves multiple realizations of the future system behavior. Furthermore, there must be a sufficient number of model realizations of the future behavior of the repository system to produce a stable estimate of the mean annual dose. This probabilistic requirement thus places a constraint on the size of the TSPA-LA Model and the run time for individual simulations of repository performance using the hardware configuration described in Section 1.2.5. These software and hardware constraints affected the size of the various pieces during the development of the TSPA-LA Model, including the number of nodes in the three-dimensional UZ flow fields, the number of particles per radionuclide used in the UZ

Transport Model Component, the number of unique radionuclides in all parts of the TSPA-LA Model and software, and also the spatial discretization of the EBS.

For example, the TSPA-LA Model simulates a few strategically defined groups of WPs that share common attributes rather than representing each WP individually. The chemical and thermal conditions for each WP in a group are generally defined by spatial averages or by a single member of the group. For example, the flow rate of seepage is a spatial average across the WPs in a group, and the temperature history is that of a WP selected as representative of the group. This technique reduces the computational requirements on the TSPA-LA Model and still allows simulation of repository performance. In contrast, modeling the full spatial variability in the repository by representing every WP individually in a probabilistic framework would require more computational time than practical with available technology and would provide only minor improvements to the estimates of repository performance.

1.8.2.3 Data Limitations

The TSPA-LA Model utilizes a large amount and variety of field and laboratory data. Source documents for these data, cited in Section 4 and elsewhere in this report, describe the limitations in these data, indicate where additional data could lead to further refinements of the process models and submodels, and provide the bases for the conclusion that the currently available data supporting the TSPA-LA Model are defensible and suitable for their intended use. The limitations on the field and laboratory data used in the TSPA-LA Model do not affect the utility of the model for achieving its intended purpose of providing a defensible evaluation of repository performance in compliance with applicable regulatory standards. In addition, the TSPA-LA Model uses the TSPA-LA Input Database that includes the results of the evaluation of uncertainties in parameter values, and the TSPA-LA Model propagates those uncertainties throughout the analyses.

1.8.2.4 Process Model Limitations

The TSPA-LA Model is a representation of the total repository system, including both natural and engineered components. The model components shown on Figure 1-3 are represented by separate process models, which were based on an analysis of FEPs affecting postclosure repository performance. In most cases, these process models are mathematical representations of physical and chemical processes that will occur in the natural and engineered systems over the life of the repository. The principal investigators who have developed these process models have also developed abstractions, or simplifications, of the process models to be used in the TSPA-LA Model. The abstraction models may be response surfaces, one-dimensional or two-dimensional look-up tables, or software linked to GoldSim as dynamically linked libraries (DLLs). The abstraction models capture the principal features of the process models. Therefore, the TSPA-LA Model is subject to the limitations of the supporting process models. However, although the TSPA-LA Model is subject to the limitations of the process models and submodels contained in supporting analyses, these limitations do not affect the ability of the TSPA-LA Model to achieve its intended purpose of providing a defensible evaluation of repository performance in compliance with applicable regulatory standards. Further, the uncertainty in the TSPA-LA Model is incorporated through the use of distributions of parameter values in Monte Carlo techniques for stochastic model realizations to simulate repository performance.

1.8.2.5 Condition Reports

The *Total System Performance Assessment Model/Analysis for the License Application* addresses the issues raised in the following condition reports (CR):

- *Condition Report-11049* (Use of Unqualified Software)—CR-11049 identifies the in-process TSPA-LA Model's GoldSim outputs, along with the analyses and graphical presentations of those outputs, in the draft TSPA-LA. These model outputs were produced with in-process software that was unqualified at the time and, thus, appear to be noncompliant with current quality assurance procedures. The in-process software has been qualified. During development use of GoldSim is discussed in Section 3.0. Impact analyses will compare the TSPA-LA Model results prepared with the qualified software to the preliminary results prepared using the in-process software. The condition report will evaluate and document whether or not the use of the preliminary in-process software was contrary to procedure and constitutes a condition adverse to quality. The qualified version of GoldSim and its software qualification documentation may be found in Section 3.8, and Table 3-8.

- *Condition Report-11152* (Updates for Draft SEIS-TSPA)—CR-11152 identifies several issues in the TSPA-LA Model relating to the Supplemental Environmental Impact Statement (SEIS). The evaluation and/or resolution of these issues is documented in Appendix P of this TSPA-LA Model/Analysis report.

- *Condition Report-11357* (Pallet Chemical Degradation FEP Status Change)—CR-11357 identifies that FEP 2.1.06.05.0C, 'Chemical Degradation of Emplacement Pallet' has been added to Appendix I of this TSPA-LA Model/Analysis report and the status is listed as included rather than excluded.

- *Condition Report-11382* (OCS Expectations for TSPA)—CR-11382 identifies the following expectations of the Office of Chief Scientist: (1) provide an addendum to the TSPA-LA to address issues identified in the development of the TSPA-LA Model, and (2) address the proposed changes to the regulations governing the preparation of the TSPA-LA Model in this TSPA-LA Model/Analysis report. The planned addendum to this report will document the first issue and will be completed upon approval of this TSPA-LA document. The second issue is documented in Section 1.1.1, Governing Regulations.

- *Condition Report-11424* (Waste Form and In-Drift Colloids-Associated Radionuclide Concentrations: Abstraction and Summary Rev03 Typographical Errors)—CR-11424 identifies and tracks the correction of minor typographical errors discovered during the Licensing/Data Qualification review of the TSPA Uncertainty and Sensitivity Analysis. The condition identified in CR-11424 only affects file names and not parameter values. Therefore, the condition has no material effect on TSPA-LA Model calculations.

- *Condition Report-11572* (Issue with Decay Chain Transport in UZ Transport Abstraction Model)—CR-11572 concerns the way in which decay species and decay chains are simulated in fault-zone nodes in the UZ Transport Abstraction. The issue

only affects the UZ transport model and a southern release location located on a fault zone. The transport model at these nodes does not include diffusion into the matrix resulting in excessively long transport times to the UZ for decay-chain daughters. The issue affects only 7 percent of the nodes in the model. The issue was resolved by specifying a different southern release location in *Total System Performance Assessment Model/Analysis for the License Application*, as described in Appendix P, Section P21.

- *Condition Report-11581* (Issues Associated with Characterize Eruptive Processes at Yucca Mountain, Nevada Rev03)—CR-11581 concerns a surveillance audit of primary sources for Characterize Eruptive Processes at Yucca Mountain, Nevada. The audit found discrepancies regarding the sources and traceability of primary input data as well as incorrect DIRS referencing. The issues raised in CR-11581 involve record keeping and the quality of the data is not in question. Therefore, CR-11581 is judged to have no material impact on TSPA-LA Model calculations.

- *Condition Report-11584* (Issues Associated with Number of Waste Packages Hit by Igneous Event Rev03)—CR-11584 concerns a surveillance audit of three primary sources for Number of Waste Packages Hit by Igneous Events. The audit found that not all values of the input data could be verified and that some data input values were either not traceable or incorrectly entered into the analysis in Number of Waste Packages Hit by Igneous Events. The documentation issues raised in CR-11584 do not involve the quality of data used in the TSPA-LA Model. Therefore, CR-11584 is judged to have no material impact on TSPA-LA Model calculations.

- *Condition Report-11589* (Issues Associated with Dike/Drift Interactions Rev02)—CR-11589 concerns a surveillance audit of primary sources for *Dike/Drift Interactions.* The audit identified issues associated with the traceability of some data input values, inaccuracies in some data input values, and the Q status of some software used in the analysis in *Dike/Drift Interactions*. Because CR-11589 indicates that the technical information in question is correct, CR-11589 is judged to have no material impact on TSPA-LA Model calculations.

- *Condition Report-11655* (Addenda Planning Documentation)—CR-11655 concerns the issue that the current Technical Work Plan does not address the need for the scope of the addendum that is planned for *Total System Performance Assessment Model/Analysis for the License Application.* In addition, there is no documentation in the records package for the analyses nor is there any documentation in the supplemental records package for the Technical Work Plan.

- *Condition Report-11657* (Addenda Input Inconsistencies)—CR-11657 concerns the issue that although all inputs were listed in the DIRS system report: (1) two references were listed in the DIRS report as direct input but were not included in Section 4 of the Addendum and (2) two references listed in the addendum were identified as established fact current but the DIRS report listed these references as data. The issues raised by CR-11657 involve record keeping only, and data quality is not in question. Therefore, CR-11657 is judged to have no material impact on TSPA-LA Model calculations.

- *Condition Report-11658* (Addenda Records Deficiencies)—CR-11658 concerns three issues: (1) there are two second backcheck copies but only one refers to the SCI-PRO-003 review, (2) there is no concurrence documentation from the Lead or Lead Checker in the records package, and (3) there is no documentation of any deviations to the Technical Work Plan. The issues raised by CR-11658 involve record keeping only, and data quality is not in question. Therefore, CR-11658 is judged to have no material impact on TSPA-LA Model calculations.

1.8.2.6 Other Limitations of the TSPA-LA Model

In addition to the limitations related to software, computational constraints, data, and process models that are discussed in the previous sections, there are the following additional limitations that derive from choices made in the design and implementation of the TSPA-LA Model.

Conservatism—The decision to implement reasonable and technically defensible conservative approaches may cause the TSPA-LA Model to tend to underestimate the overall performance of the repository system or its model components. This limitation does not affect the utility of the TSPA-LA Model for achieving its intended purpose of providing a defensible evaluation of compliance with applicable regulatory standards, because the TSPA-LA Model tends to overestimate, rather than underestimate, radionuclide releases from the repository system and subsequent doses to the RMEI. However, effects of conservative assumptions at the model component level should be considered in interpretations of the realistic behavior of the repository system and its components. Not all conservative assumptions made at the model component level necessarily result in conservative outcomes at the system level: conservatisms that have the potential to increase radionuclide release (or dose) may have little or no impact on overall performance if the model component or process model in which the conservatisms are applied result in only a minor contribution to performance. At any level within the repository system modeled with the TSPA-LA Model, conservative assumptions may tend to mask the relative importance of other processes or parameters, and conclusions regarding the importance, or lack thereof, of aspects of the TSPA-LA Model should be understood as having been made consistent with the conservatisms embedded in the model.

Some abstractions used in the TSPA-LA Model are based on process level models that are limited to conditions under which Darcy's law and its extensions and generalizations are applicable. These abstractions are limited in the TSPA-LA Model to situations in which the differential equations describing fluid flow can be uncoupled from those that describe the mass transport of colloids or dissolved species in the UZ, SZ, and through the EBS, including corrosion products and the invert. The uncoupling is appropriate as long as the density and viscosity of the fluids in the TSPA-LA Model do not change with concentration in such a manner as to significantly alter the flow fields. Density and viscosity values reported for solutions with comparably high concentrations of uranium indicate that the use of Darcy's law and the uncoupling of flow and transport equations under the condition commonly encountered in the TSPA-LA Model are reasonable and appropriate for the model's intended use.

The TSPA-LA Model utilizes some numerical model abstractions from process level models that are limited to conditions under which Fick's first law of diffusion is applicable. This is true for describing diffusive transport in the UZ, SZ, and through the EBS, including the WPs, corrosion products, and the invert. Fick's first law states that mass transport is proportional to the

concentration gradient and mass is transported from high to low concentration in such a way as to tend to minimize the gradient. The second and third order effects can contribute to additional diffusive mass transfer under unique situations such as thermal diffusion, pressure diffusion, and external forced diffusion (e.g., under an imposed electrical current). The models invoked in the TSPA-LA either directly or indirectly are limited to situations dominated by ordinary concentration diffusion. Fick's law for mass transport is as fundamental as Fourier's law of heat conduction, which states that the flow of heat by conduction is proportional to the temperature gradient.

Limitations inherent in mathematical modeling and uncertainty analysis—Because the TSPA-LA Model represents complex natural or engineered systems, insights that can be drawn from the model's calculations are limited to those based on processes that have been included in the model. Processes that have been omitted from the TSPA-LA Model, either through the FEP screening process (Section 6.1.3) or through simplifications made as part of the abstraction process (Section 6.3), are not evaluated in detail. This limitation is inherent in mathematical models that simplify complex systems to allow predictive analysis, and does not affect the utility of the model for achieving its intended purpose of providing a defensible evaluation of compliance with applicable regulatory standards. Insights into processes that have been omitted from the TSPA-LA Model or simplified through the abstraction process can be obtained by consulting underlying reports describing analyses that document the FEP screening process and the development of relevant process models, as cited in Section 6.

Similarly, conclusions drawn from sensitivity and uncertainty analyses (Section 9 and Appendix K) are dependent on the design of the TSPA-LA Model and the treatment of uncertainty in its inputs. Because the TSPA-LA Model is based on Monte Carlo uncertainty analysis, the results are sensitive only to those processes and parameters that are included in the model. Sensitivity to uncertainty in parameter values will be directly related to both the roles of the parameters in the mathematical models, and to the distribution of values assigned to the parameters to represent uncertainty. Parameters for which no uncertainty is assigned will not appear as important in the results of standard sensitivity analyses, regardless of their function in the TSPA-LA Model.

1.9 DESCRIPTION OF THE TOTAL SYSTEM PERFORMANCE ASSESSMENT MODEL/ANALYSIS FOR THE LICENSE APPLICATION

Total System Performance Assessment Model/Analysis for the License Application describes how the supporting parameters and parameter values, along with process-model abstractions representing many different aspects of the repository system, were integrated into one comprehensive model to describe the total repository system. Modeling activities were conducted and documented in accordance with SCI-PRO-006, *Models*.

Figure 1-23 shows the principal model components of the TSPA-LA Model and the hierarchy of the submodels that support and/or are contained within these model components. References to the documents that describe the development of model components and submodels used to analyze the repository system, and/or provide direct inputs to the TSPA-LA Model, can be found in Table 1-1 and in the list of references in Section 9 of this document. Section 6.1.4 describes the overall approach used to assemble the representations of the individual model components and their submodels into a description of the entire repository system. Descriptions of the model

components and submodels used in the TSPA-LA Model, and the scientific bases for these model components and submodels, are presented in Section 6.3.

The TSPA-LA Model documentation consists of four key information sources: (1) *Total System Performance Assessment Model/Analysis for the License Application* (i.e., this report), (2) the numerical model files within the GoldSim model file, (3) the TSPA-LA Input Database, and (4) DTNs submitted to document TSPA-LA Model calculations and analyses. GoldSim allows all linked operations of the abstracted process models and submodels to perform complex calculations, thereby incorporating the natural geochemical and hydrogeologic processes and engineered-design elements of the repository. There are several GoldSim model files developed and documented herein. Appendix B contains DTNs with the results calculated using these various model files. Nominally, the discussion in this document will refer to the GoldSim model file, meaning all related model files.

Total System Performance Assessment Model/Analysis for the License Application describes work performed according to *Technical Work Plan for: Total System Performance Assessment FY 07-08 Activities* (SNL 2008 [DIRS 184920]). Any deviations from the Technical Work Plan (TWP) during the documentation of the TSPA-LA Model, and the subsequent analyses conducted using the TSPA-LA Model, are identified and discussed at the appropriate location. The following exceptions to the TWP also apply:

- Section 7.3 will not contain the entropy analyses described in the TWP.
- Section 7.3 does not explore the sensitivity of parameters with constant values that are chosen from a range of values.
- There were minor immaterial deviations from some desktop protocols referenced in the TWP. These deviations consisted of some changes in naming conventions that did not materially affect the TSPA-LA Model calculations.
- The use of unqualified software for some of the model validation activities described in Section 7.7.2 is documented in corroborative DTNs: MO0708SIMPLIFI.000 [DIRS 182980] and SN0704PMASZFTA.001 [DIRS 182560].
- The Yucca Mountain Acceptance Criteria listed in Table 3.3-1 of the TWP are also discussed in Appendix H.

TSPA-LA Model Analysis Time Period—Two time periods were used for the analysis of repository performance. NRC Proposed Rule 10 CFR 63.311 [DIRS 178394] states the following:

> "(a) DOE must demonstrate, using performance assessment, that there is a reasonable expectation that the reasonably maximally exposed individual receives no more than the following annual dose from releases from the undisturbed Yucca Mountain disposal system:
>
> (1) 0.15 mSv (15 mrem) for 10,000 years following disposal; and

(2) 3.5 mSv (350 mrem) after 10,000 years, but within the period of geologic stability indicates that performance assessment cover a compliance period of 10,000 years after repository closure."

The TSPA-LA Model analyses presented in Volume III satisfy the 10,000-year requirement of the NRC proposed rule. Some validation analyses in Volume II extend the analysis period to 20,000 years postclosure to allow evaluation of whether or not the trends present at the end of 10,000 years continue, or if uncertainties in results affect the conclusions regarding the 10,000-year performance period and beyond. These extended results do not display any significant changes to the trends observed from 0 to 10,000 years, providing confidence in the conclusions reached regarding the 10,000-year performance period.

The time period for the TSPA-LA Model analyses presented in this document to satisfy the 'period of geologic stability' requirement in 10 CFR 63.311(a) (2) [DIRS 178394] is one million years after repository closure. The one-million-year analyses comply with NRC Proposed Rule 10 CFR 63.302 [DIRS 178394], which indicates that, "This period is defined to end at one million years after disposal." The one-million-year analyses are thus consistent with the proposed NRC Proposed Rule 10 CFR 63.342 [DIRS 178394] and the EPA Proposed Rule 40 CFR 197.25 [DIRS 177357]. The graphical representations of the TSPA-LA Model simulations show the mean annual dose to the REMI observed during the one-million-year postclosure time period.

1.10 DOCUMENT ORGANIZATION

Total System Performance Assessment Model/Analysis for the License Application is organized in three volumes so that the TSPA-LA Model's GoldSim model file and sources of supporting information are fully integrated. The GoldSim model file contains in-depth descriptions of the submodels and descriptions of their implementation. Direct inputs to the TSPA-LA Model are available in the TSPA-LA parameter database, which is the controlled source for the direct inputs to the GoldSim model file. The database allows the user to review most parameter values by accessing a single source location. The information found in Volumes I, II, and III provides cross-referencing that allows investigation of the structure and operation of the TSPA-LA Model's GoldSim files used to perform performance-assessment calculations.

1.10.1 Volume I

Volume I provides a road map to the information required to use the TSPA-LA Model, including detailed information regarding direct inputs, parameters, and submodel descriptions, as required to describe the TSPA-LA Model calculations, and to trace the sources of the TSPA-LA Model's direct inputs. Volume I also contains appropriate references to source information.

Section 1: **Purpose**—Section 1 describes the FEPs process that led to the development of the scenario classes used in analyzing the performance of the repository system. Section 1 also describes the regulatory framework for the TSPA-LA Model as well as an overview of the natural and engineered barriers in the repository system, including site-description information, descriptions of the elements of the EBS, processes affecting water movement through the UZ and SZ, descriptions of the model components, and a general description of the architecture of

the TSPA-LA Model.

Section 2: **Quality Assurance**—Section 2 describes the applicable quality assurance (QA) procedures of *Quality Assurance Requirements and Description* (QARD) (DOE 2007 [DIRS 182051]), along with descriptions and references to the methods used for the electronic management of information.

Section 3: **Use of Software**—Section 3 lists and briefly describes the software used in the development of the TSPA-LA Model. The primary software used to run the TSPA-LA Model is GoldSim (V. 9.60.100 [DIRS 181903]). Analysis of the results developed with the TSPA-LA Model is aided by the use of additional postprocessing software. Section 3 identifies and briefly describes all auxiliary software and software routines that were developed for the TSPA-LA Model, including those developed external to, and incorporated into, the TSPA-LA Model.

Section 4: **Inputs**—Section 4 identifies the direct inputs used in the TSPA-LA Model, either by direct tabulations included in this document or through linkage to the appropriate sections of the GoldSim model file or TSPA-LA Model database. Section 4 also identifies all applicable criteria, codes, and standards.

Section 5: **Assumptions**—Section 5 lists the assumptions directly used to perform the TSPA-LA Model analyses along with their bases. Section 5 also includes key assumptions from supporting documents that are used in the TSPA-LA Model.

Section 6: **Model Description**—Section 6 describes the TSPA-LA Model representation of the repository system, presents the scenario classes being analyzed, describes the modeling cases used to analyze the scenario classes, and provides references to the applicable sections of the TSPA-LA Model, the GoldSim model file, and supporting analyses. Section 6 includes detailed descriptions of the conceptual models, mathematical formulations, implementations of the submodels in the TSPA-LA Model, conservatisms, and ACMs.

1.10.2 Volume II

Volume II contains the information supporting the TSPA-LA Model validation.

Section 7: **Validation**—Section 7 describes the validation of the TSPA-LA Model as required by Section 6.3 of SCI-PRO-006, *Models*. Model validation provides confidence that the TSPA-LA Model correctly represents both the natural and engineered systems that constitute the repository. Validation of the TSPA-LA Model involves three stages:

- Validation of the TSPA-LA Model formulation
- Confirmation of the validity of the inputs to the TSPA-LA Model, including verification that the GoldSim software and supporting software codes are correctly implemented and that the inputs are free of errors
- Validation of the simulated repository performance for the postclosure time periods specified in NRC Proposed Rule 10 CFR 63.303 (b) [DIRS 178394].

The model validation of the TSPA-LA Model is consistent with the intended use of the TSPA-LA Model and the required level of confidence. The specific model validation activities documented in Volume II include the following:

- Validation of the interaction of the model components, abstractions, and submodels to ensure that they are working correctly and interfacing properly
- Validation testing the temporal discretization for the TSPA-LA Model scenario classes
- Validation of the statistical stability of the TSPA-LA Model by analyzing the results of a large number of model realizations
- Analysis of the spatial discretization of the TSPA-LA Model, using multiple model realizations to verify that the TSPA-LA Model uses an appropriate number of collection 'bins'
- Validation of the surrogate waste form used to represent DOE-owned spent fuel
- Corroboration of the results of the abstraction models with validated process models
- Corroboration of the TSPA-LA Model results with natural-analogue information
- A summary of previous technical reviews of the TSPA-LA Model.

1.10.3 Volume III

This volume contains the results of analyses performed with the TSPA-LA Model, inputs and references, and the appendices. These are detailed below.

Section 8: **Analyses**—Section 8 includes conclusions of the analyses as required by SCI-PRO-006. However, the order of presentation and scope of the material presented deviates from the suggestions provided in SCI-PRO-006, Attachment 2. Section 8 contains the results of TSPA-LA Model performance analyses evaluating the postclosure performance of the repository and its compliance with NRC Proposed Rule 10 CFR 63.113 [DIRS 180319] and the performance measures defined in 10 CFR 63.311 (a) (1) and (2) [DIRS 178394]. The probabilistic analyses account for uncertainty and address FEPs that could affect total system performance. Volume III presents the results of analyses and calculations in the following areas:

- System and subsystem performance analyses for the Nominal Scenario Class, including the Nominal Modeling Case; the Early Failure Scenario Class, including the Drip Shield EF and Waste Package EF Modeling Cases; the Igneous Scenario Class, including both Igneous Intrusion and Volcanic Eruption Modeling Cases; and the Seismic Scenario Class, including the GM and FD Modeling Cases
- Groundwater and individual protection analyses consistent with regulatory guidelines in NRC Proposed Rule 10 CFR 63.331 [DIRS 180319] and 10 CFR 63.311 (70 FR 53313 [DIRS 178394]), respectively

- Analysis of the Human Intrusion Scenario
- Analyses of the capabilities and importance of the upper and lower natural barriers and the EBS that have been identified as contributing to repository performance.

Section 9: **Inputs and References**—Section 9 provides the sources of inputs, software, data tracking numbers, and cited references.

Appendices

A. Acronyms and Abbreviations—Appendix A contains a list of acronyms and abbreviations used in this document.

B. Data Tracking Numbers for the TSPA-LA Model—Appendix B describes the contents of the output DTNs for the TSPA-LA Model and the interrelation among the DTNs in the TSPA-LA Model.

C. Performance Margin Analysis—Appendix C describes the PMA, a separate set of TSPA calculations conducted parallel to those of the TSPA-LA Model in order to quantitatively evaluate the model's explicit and implicit conservatisms (Section 6.3). The PMA provides insights into the appropriateness of the TSPA-LA Model's use in satisfying regulatory standards and supports validation of the TSPA-LA Model.

D. Parameter Listing—Appendix D refers to the TSPA Input Database which contains the list of parameters used in the TSPA-LA Model. The database provides a listing of all parameters and identifies the parameter entry form (PEF) that includes each parameter.

E. Response to Review Comments from the International Review Team—An International Review Team (IRT) evaluated the most recent performance assessment of the Yucca Mountain Repository, and provided recommendations for future investigations. Appendix E provides a summary of, and responses to the IRT's recommendations.

F. Dynamically Linked Libraries Description and Feeds—Appendix F provides a brief description of the DLLs used in the TSPA-LA Model, and includes a detailed description of the input files used by the model DLLs.

G. Wiring Diagrams for Model Information Feeds—Appendix G provides a set of color-coded flow charts that illustrate information flow between model components and submodels within the TSPA-LA Model.

H. Yucca Mountain Review Plan Acceptance Criteria—Appendix H evaluates *Total System Performance Assessment Model/Analysis for the License Application* with respect to 10 CFR Part 63, Subpart E (Technical Criteria) ([DIRS 178394 and [DIRS 180319]).

I. Features, Events, and Processes Mapped to TSPA-LA Model—Appendix I provides summary information describing how FEPs relevant to the Yucca Mountain Repository are included and implemented in the TSPA-LA Model. Appendix I also includes

descriptions of the screening criteria applied to the identified FEPs and summaries of the screening decisions.

J. Conceptual Structure of TSPA-LA—Appendix J presents a formal description of the conceptual structure of the TSPA-LA Model, including the mathematical description of uncertainty, and derives the equations used to calculate mean annual dose.

K. Uncertainty and Sensitivity Analysis Results—Appendix K presents the distributions of results for each modeling case (uncertainty analyses) and identifies the uncertain parameters that predominantly contribute to the uncertainty in each modeling cases' results (sensitivity analyses).

L. Simplified TSPA—Appendix L describes the 'Simplified TSPA Analysis', a simplified, stand-alone, numerical analysis that corroborates and provides confidence in the results of the TSPA-LA Model.

M. Comparison with Electric Power Research Institute Analysis—Appendix M presents a comparison of the TSPA-LA Model and the TSPA of the Yucca Mountain Repository conducted by the Electric Power Research Institute. The comparison provides an independent means of validation of the TSPA-LA Model.

N. Derivation of Implementing Equations for Waste Package Parsing and Average Damage Area—Appendix N describes the calculations implemented in the TSPA-LA Model that divide the entire set of WPs into smaller groups to mitigate unintended model responses introduced by assigning averaging WP failure properties to WPs with very different properties.

O. Localized Corrosion Initiation Uncertainty Analysis—Appendix O describes the implementation and results of the Localized Corrosion Initiation Uncertainty Analysis, which calculates the chemical conditions on the surfaces of WPs to determine whether or not there are sufficient conditions for the initiation of localized corrosion.

P. Impact Assessments—Appendix P describes post-TSPA-LA Model development activities related to correcting implementation decisions, identification of undocumented conservatisms, and revised parameter values. Appendix P also includes an evaluation of the sensitivity of expected mean annual dose with respect to igneous event frequency, which is not documented elsewhere.

Table 1-1. Principal Documents that Support the TSPA-LA Model

Topic	Title	Document Identifier
UZ Flow		
Climate	*Future Climate Analysis*	ANL-NBS-GS-000008 [DIRS 170002]
Infiltration	*Simulation of Net Infiltration for Present-Day and Potential Future Climates*	MDL-NBS-HS-000023 [DIRS 182145]
Mountain-Scale UZ Flow	*UZ Flow Models and Submodels*	MDL-NBS-HS-000006 [DIRS 184614]
Drift Seepage	*Abstraction of Drift Seepage*	MDL-NBS-HS-000019 [DIRS 181244]
	In-Drift Natural Convection and Condensation	MDL-EBS-MD-000001 [DIRS 181648]
	Seepage Model for PA Including Drift Collapse	MDL-NBS-HS-000002 [DIRS 167652]
EBS Environment		
EBS Thermal-Hydrologic	*Multiscale Thermohydrologic Model*	ANL-EBS-MD-000049 [DIRS 181383]
EBS Chemical Environment	*Engineered Barrier System: Physical and Chemical Environment*	ANL-EBS-MD-000033 [DIRS 177412]
WP and DS Degradation		
WP, General Corrosion, and Localized Corrosion	*General Corrosion and Localized Corrosion of the Drip Shield Barrier*	ANL-EBS-MD-000004 [DIRS 180778]
WP, General Corrosion, and Localized Corrosion	*General Corrosion and Localized Corrosion of Waste Package Outer Barrier*	ANL-EBS-MD-000003 [DIRS 178519]
	Stress Corrosion Cracking of Waste Package Outer Barrier and Drip Shield Material	ANL-EBS-MD-000005 [DIRS 181953]
	Analysis of Mechanisms for Early Waste Package/Drip Shield Failure	ANL-EBS-MD-000076 [DIRS 178765]
Waste Form Degradation and Mobilization		
Radionuclide Inventory	*Initial Radionuclide Inventories*	ANL-WIS-MD-000020 [DIRS 180472]
In-Package Chemistry	*In-Package Chemistry Abstraction*	ANL-EBS-MD-000037 [DIRS 180506]
Cladding Degradation	*Cladding Degradation Summary for LA*	ANL-WIS-MD-000021 [DIRS 180616]
Waste Form Degradation	*CSNF Waste Form Degradation: Summary Abstraction*	ANL-EBS-MD-000015 [DIRS 169987]
	Defense HLW Glass Degradation Model	ANL-EBS-MD-000016 [DIRS 169988]
	DSNF and Other Waste Form Degradation Abstraction	ANL-WIS-MD-000004 [DIRS 172453]
Dissolved Radionuclide Concentration Limits	*Dissolved Concentration Limits of Elements with Radioactive Isotopes*	ANL-WIS-MD-000010 [DIRS 177418]

Table 1-1. Principal Documents that Support the TSPA-LA Model (Continued)

Topic	Title	Document Identifier
Waste Form and EBS Colloids	*Waste Form and In-Drift Colloids-Associated Radionuclide Concentrations: Abstraction and Summary*	MDL-EBS-PA-000004 [DIRS 177423]
EBS Flow and Transport		
EBS Flow and Transport	*EBS Radionuclide Transport Abstraction*	ANL-WIS-PA-000001 [DIRS 177407]
UZ Transport		
UZ Particle Tracking	*Particle Tracking Model and Abstraction of Transport Processes*	MDL-NBS-HS-000020 [DIRS 184748]
	Calibrated UZ Properties	ANL-NBS-HS-000058 [DIRS 179545]
	Radionuclide Transport Models Under Ambient Conditions	MDL-NBS-HS-000008 [DIRS 177396]
Transport Interface	*Drift-Scale Radionuclide Transport*	MDL-NBS-HS-000016 [DIRS 170040]
SZ Flow and Transport		
SZ Convolute 1-D SZ Transport SZ Flow and Transport	*Saturated Zone Flow and Transport Model Abstraction*	MDL-NBS-HS-000021 [DIRS 183750]
Biosphere		
Biosphere	*Biosphere Model Report*	MDL-MGR-MD-000001 [DIRS 177399]
Disruptive Events		
Seismic Activity	*Seismic Consequence Abstraction*	MDL-WIS-PA-000003 [DIRS 176828]
Igneous Intrusion Modeling Case	*Number of Waste Packages Hit by Igneous Intrusion*	ANL-MGR-GS-000003 [DIRS 177432]
	Dike/Drift Interactions	MDL-MGR-GS-000005 [DIRS 177430]
	Characterize Framework for Igneous Activity at Yucca Mountain, Nevada	ANL-MGR-GS-000001 [DIRS 169989]
Volcanic Eruption Modeling Case	*Atmospheric Dispersal and Deposition of Tephra from a Potential Volcanic Eruption at Yucca Mountain, Nevada*	MDL-MGR-GS-000002 [DIRS 177431]
	Redistribution of Tephra and Waste by Geomorphic Processes Following a Potential Volcanic Eruption at Yucca Mountain, Nevada	MDL-MGR-GS-000006 [DIRS 179347]
	Characterize Framework for Igneous Activity at Yucca Mountain, Nevada	ANL-MGR-GS-000001 [DIRS 169989]

Source: *Technical Work Plan for: Total System Performance Assessment FY 07-08 Activities* (SNL 2008 [DIRS 184920], Table 1-1).

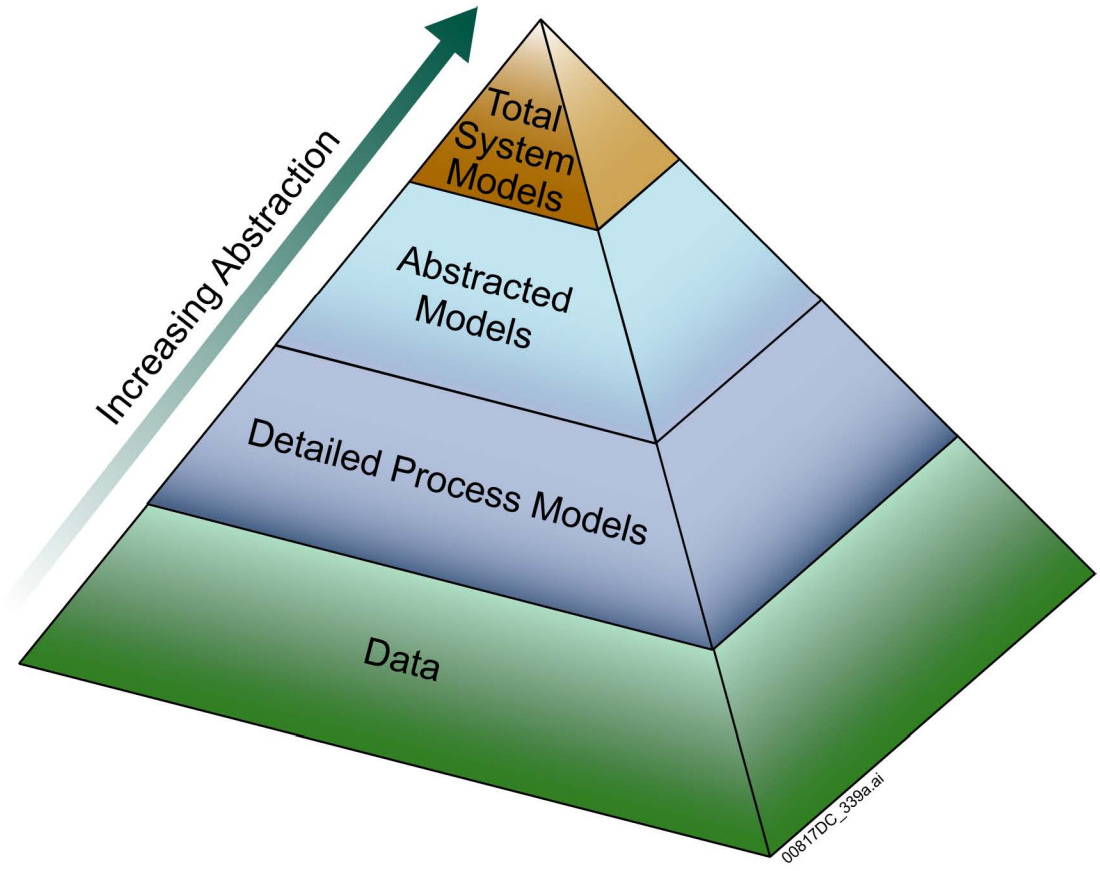

Figure 1-1. Performance Assessment Pyramid Showing the Steps Involved in Developing a Total System Model

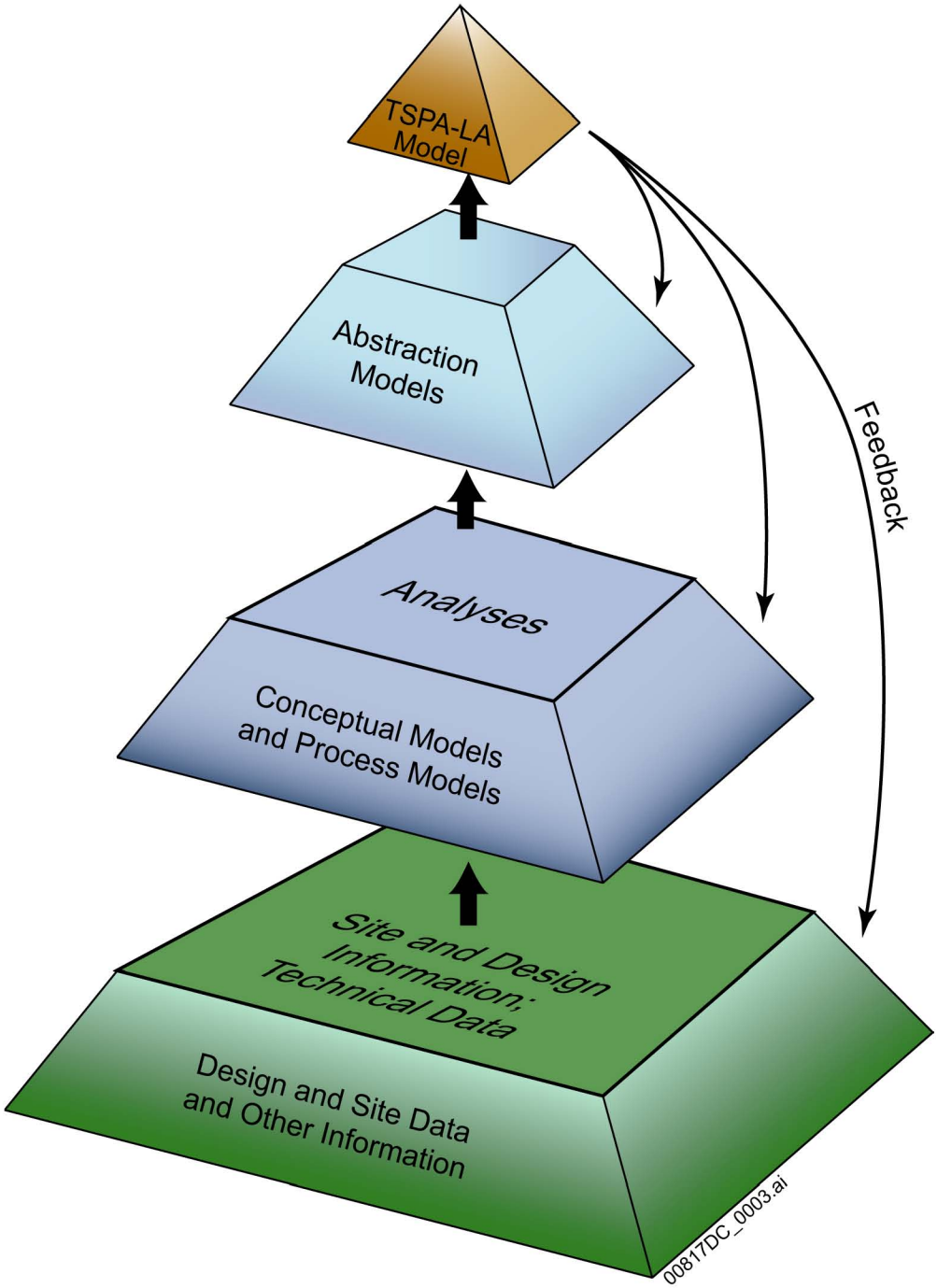

Figure 1-2. Performance Assessment Pyramid Showing How Detailed Underlying Information Builds the Technical Basis for the TSPA-LA Model

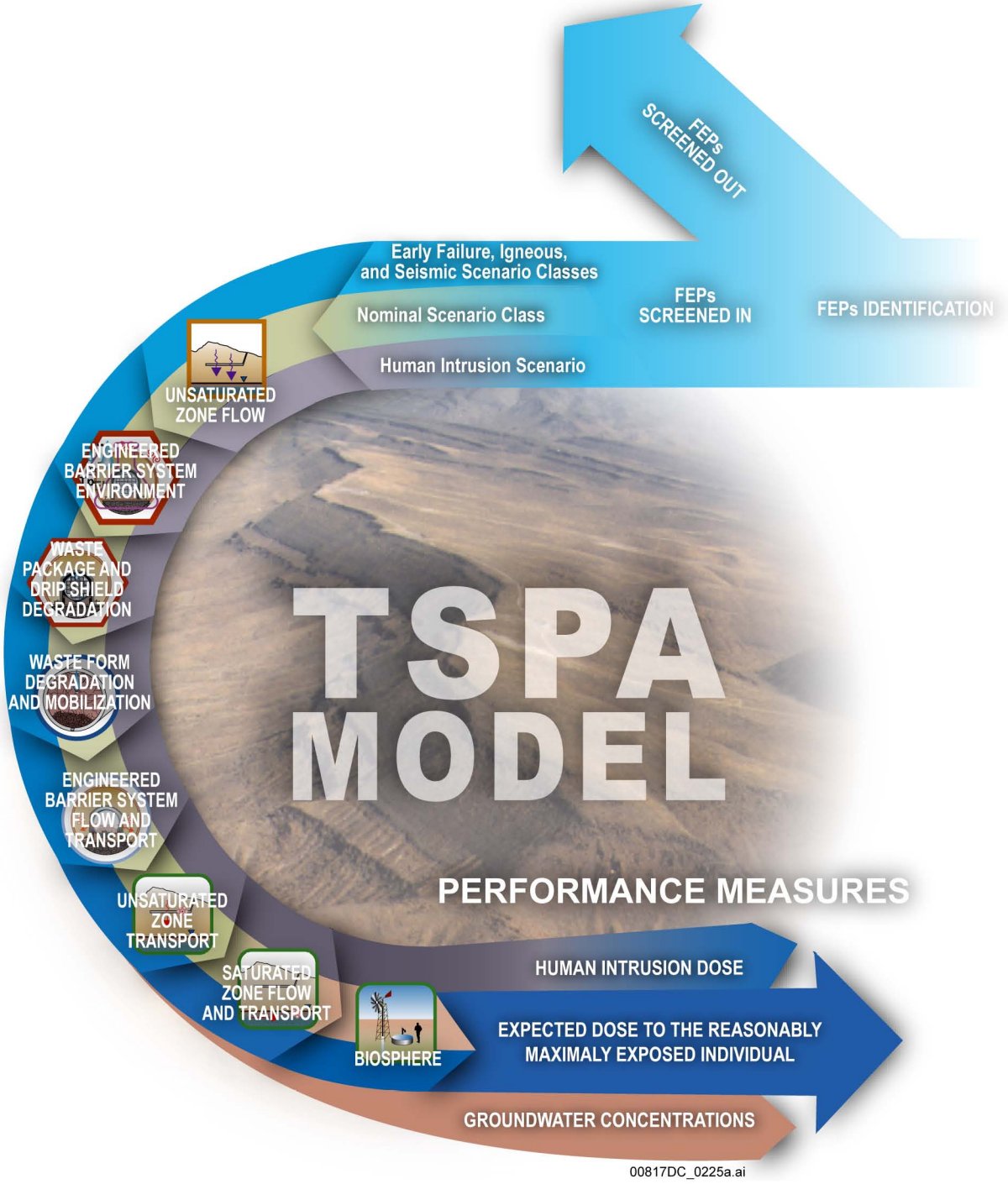

Figure 1-3. Schematic Representation of the Development of the TSPA-LA Model, Including the Nominal, Igneous, and Seismic Scenario Classes

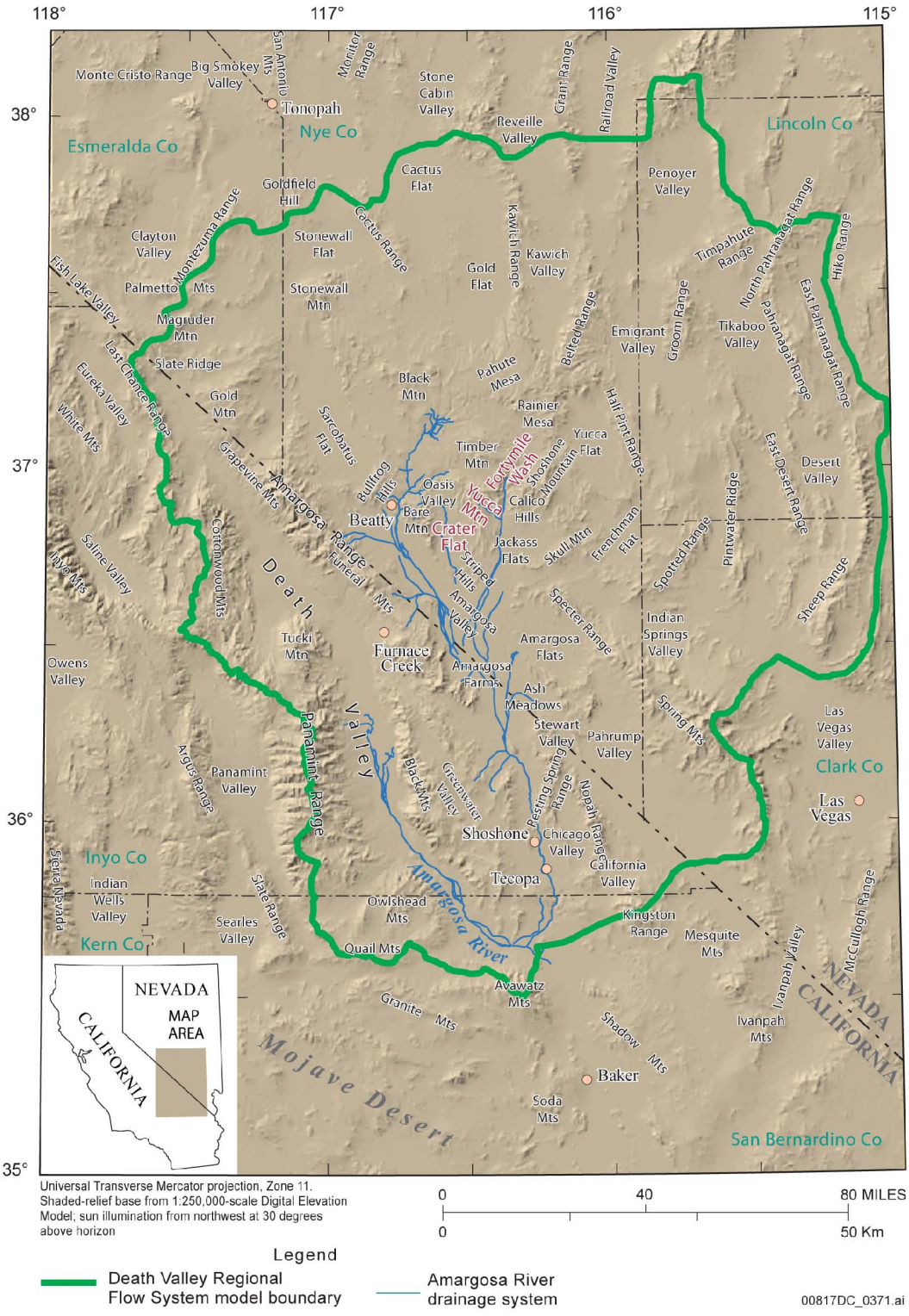

Source: Modified from BSC 2004 [DIRS 169734], Figure 8-2.

Figure 1-4. Geographic and Prominent Topographic Features of the Death Valley Region

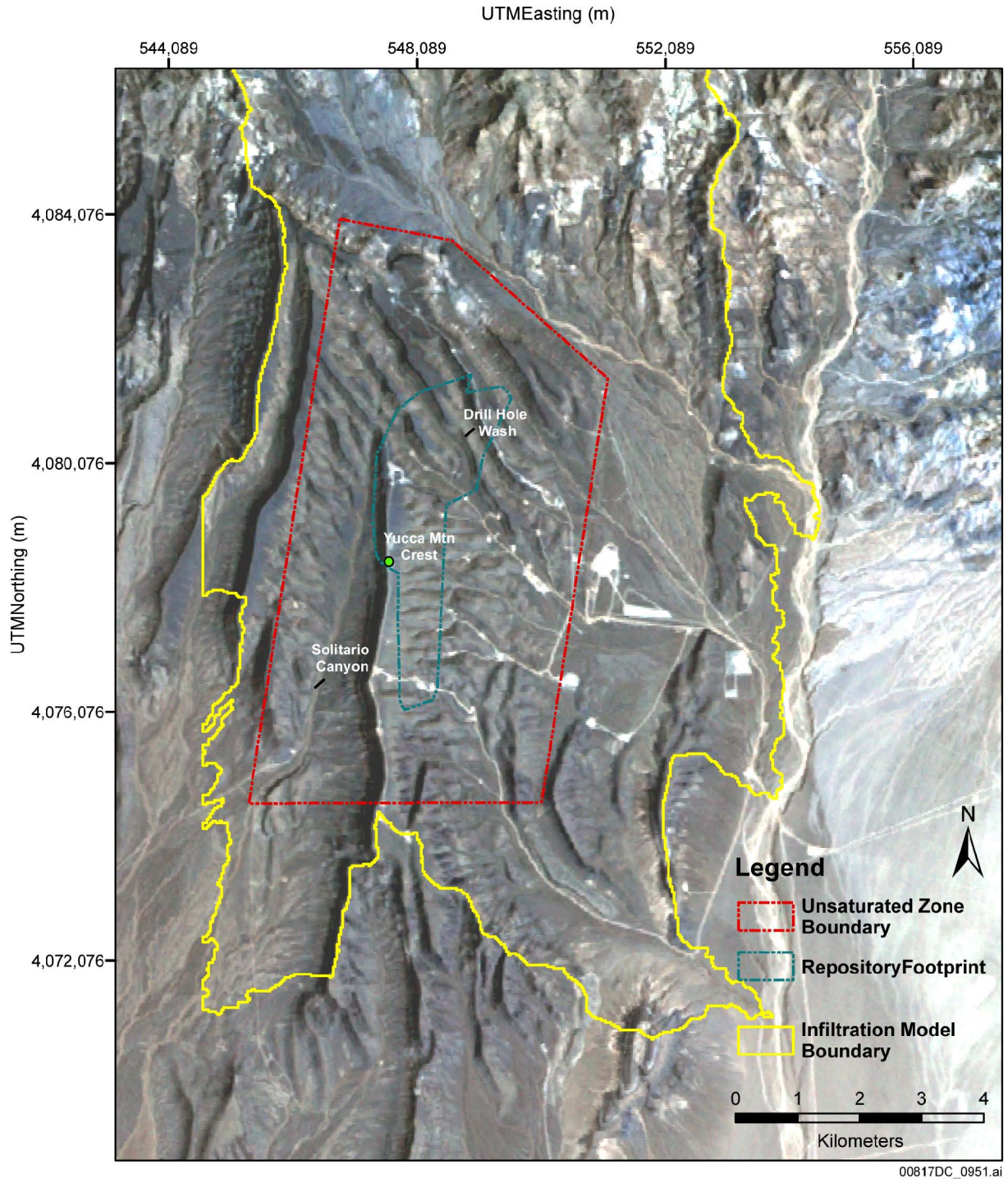

Source: Modified from SNL 2007 [DIRS 182145], Figure 6.5.2.1-1[a].

NOTE: The model boundary is the same as the 1999 unsaturated zone flow model domain of the TSPA-SR.

Figure 1-5. Topographic Map of the Yucca Mountain Site Showing Differences in Slope Characteristics North and South of Drill Hole Wash

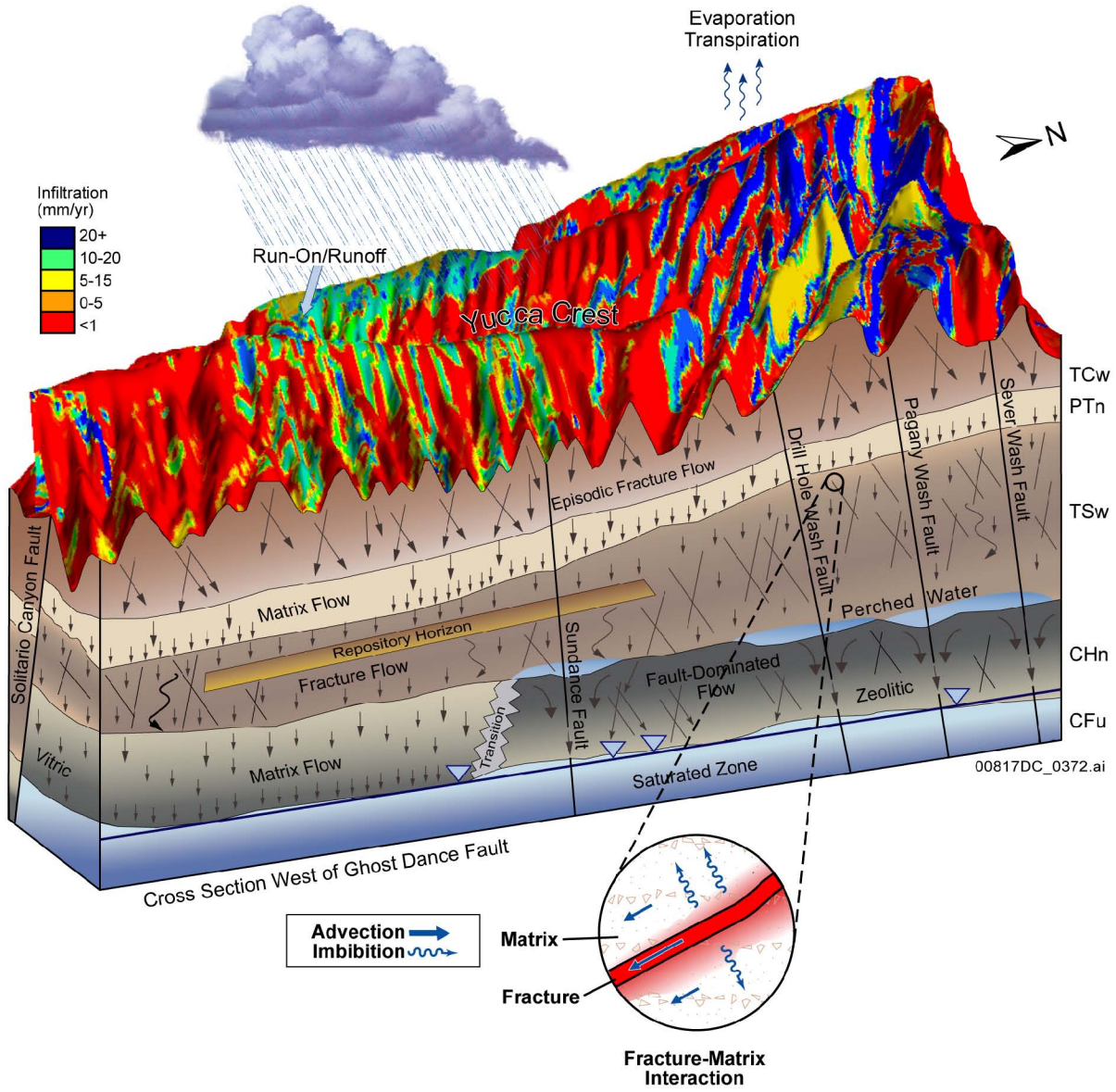

Source: Modified from BSC 2004 [DIRS 170035], Figure 6-1.

Figure 1-6. Overall Water Flow Behavior in the Unsaturated Zone, Including the Relative Flux Magnitudes of Fracture and Matrix Flow Components in the Different Hydrogeologic Units

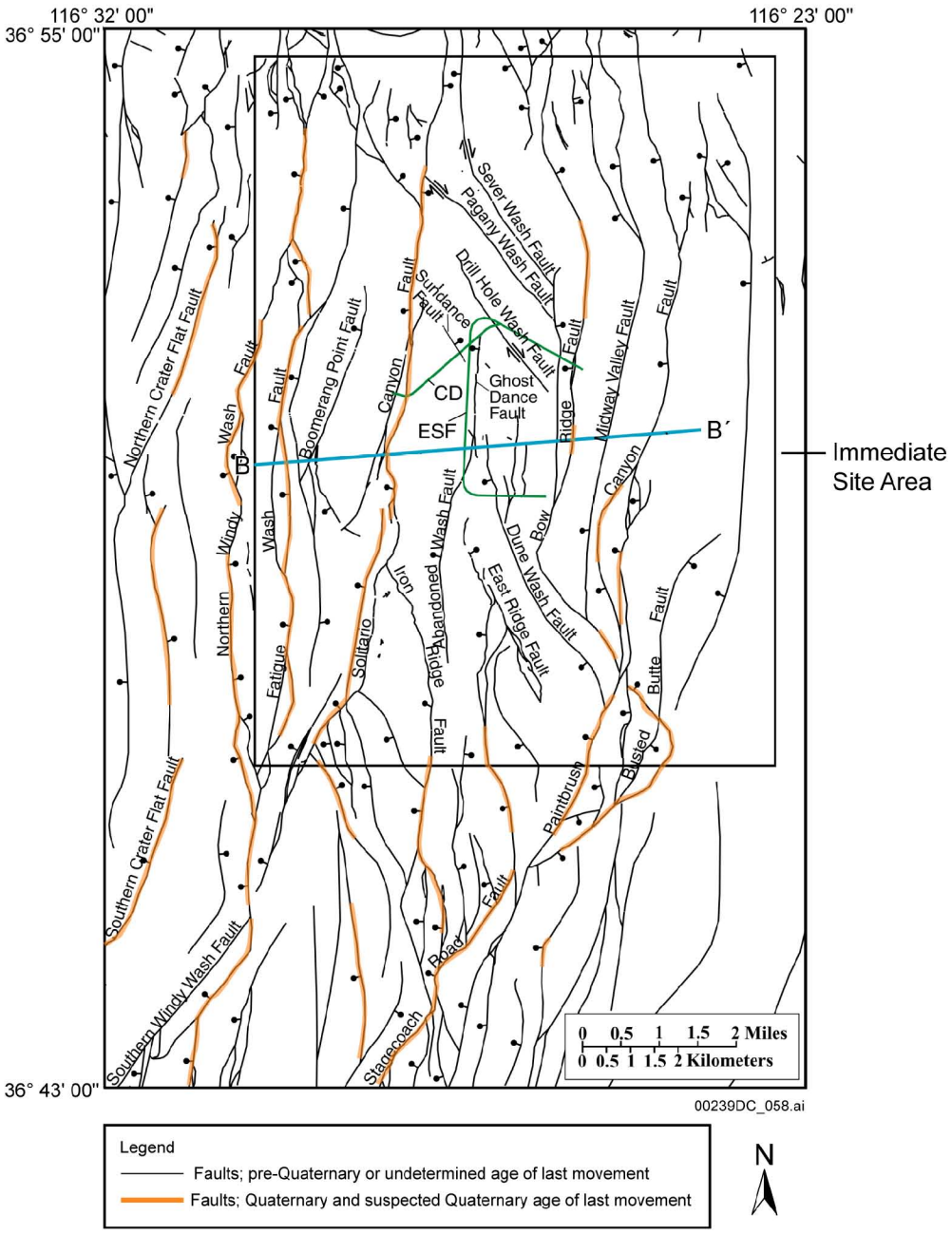

Source: Modified from BSC 2004 DIRS 169734], Figure 3-20.

NOTES: The following faults have demonstrable Quaternary activity: Northern Crater Flat Fault, Southern Crater Flat Fault, Northern Windy Wash Fault, Southern Windy Wash Fault, Fatigue Wash Fault, Solitario Canyon Fault, Iron Ridge Fault, Bow Ridge Fault, Paintbrush Canyon Fault, and Stagecoach Road Fault. All faults are shown with solid lines, although many segments are concealed or inferred.

Symbols and acronyms: bar and bell: downthrown side of fault; arrows: relative direction of strike-slip movement; ESF = Exploratory Studies Facility (green line); CD = Cross-Drift; blue line: approximate location of line of section shown on Figure 1-8.

Figure 1-7. Distribution of Faults in the Yucca Mountain Site Area and Adjacent Areas to the South and West

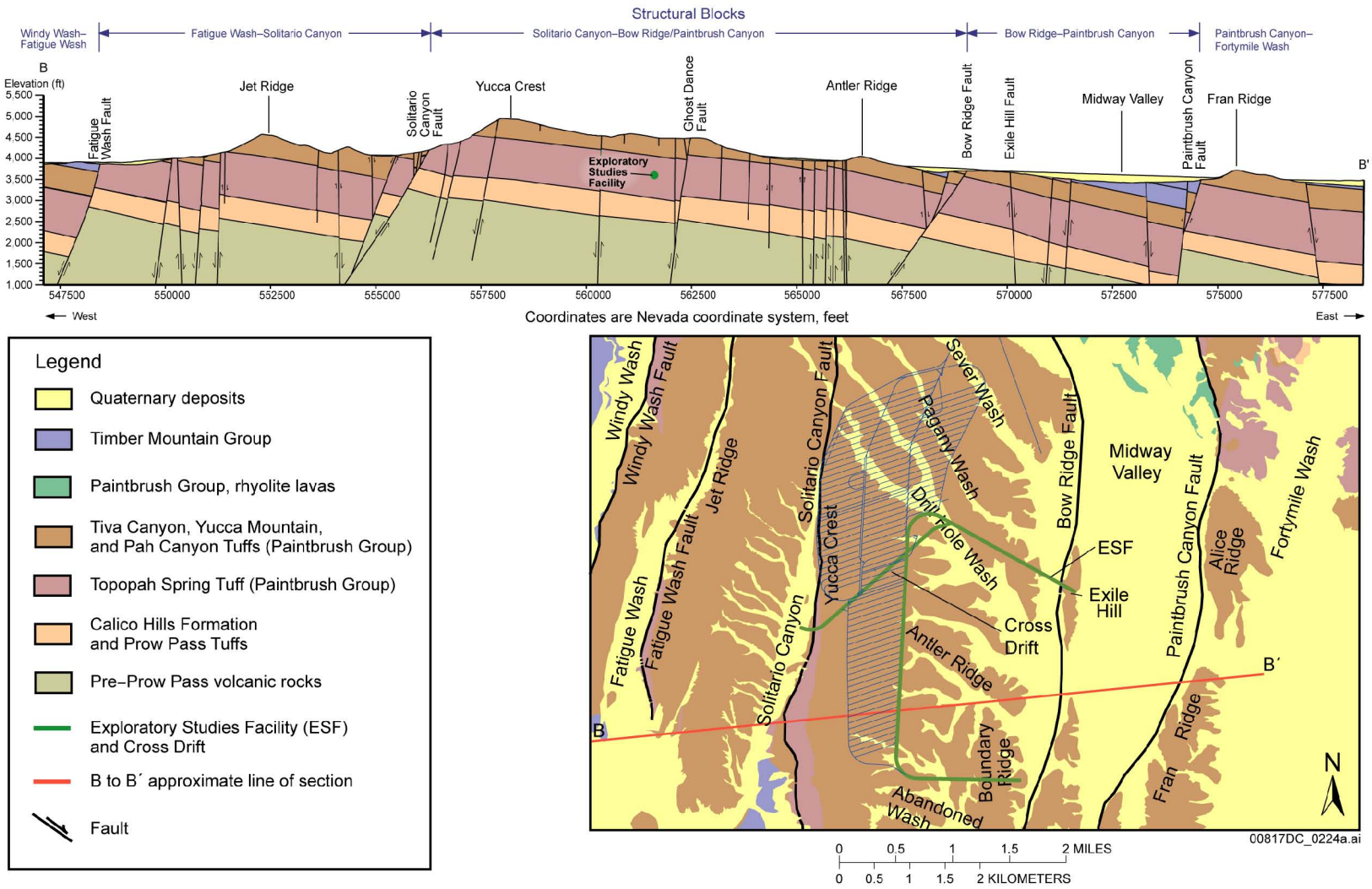

Source: Simplified from Day et al. 1998 [DIRS 100027], Cross Section B-B'.

NOTE: ESF = Exploratory Studies Facility, location of intersection along the approximate line of section, also shown on Figure 1-7.

Figure 1-8. East-West Structure Section across Yucca Mountain Site Area

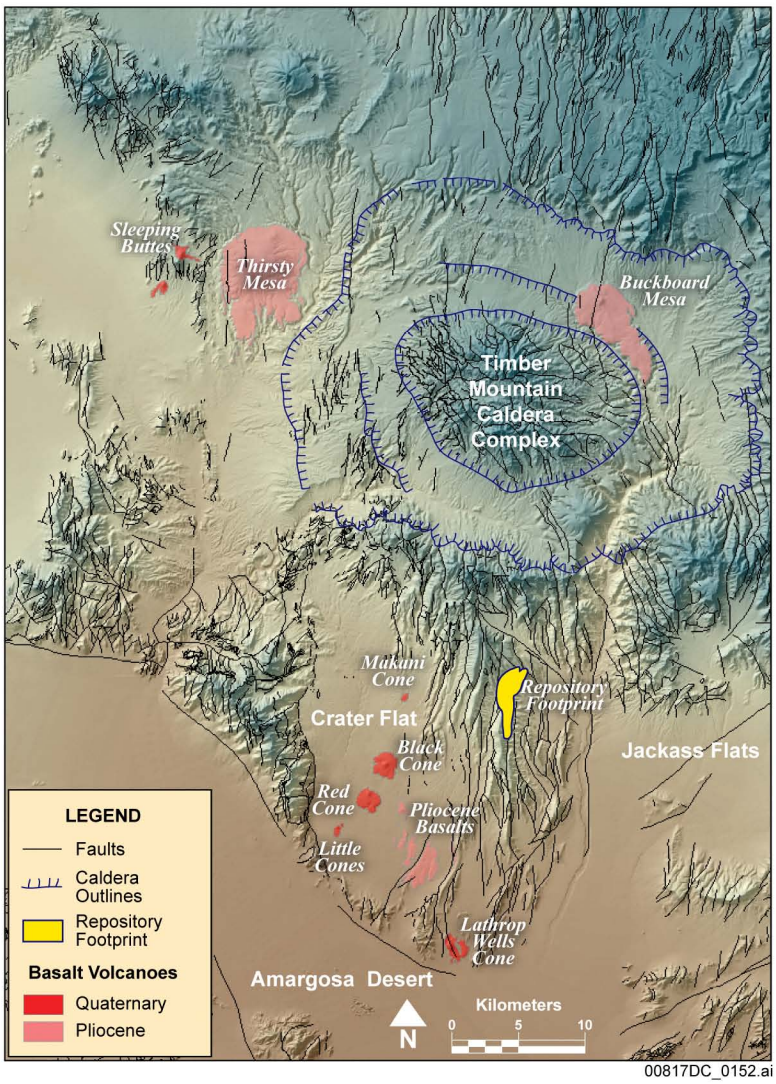

Source: Modified from CRWMS M&O 1998 [DIRS 123196], Figure 2.1.

Figure 1-9. Location and Age of Post-Miocene (less than 5.3 million years) Volcanoes (or clusters where multiple volcanoes have indistinguishable ages) in the Yucca Mountain Region

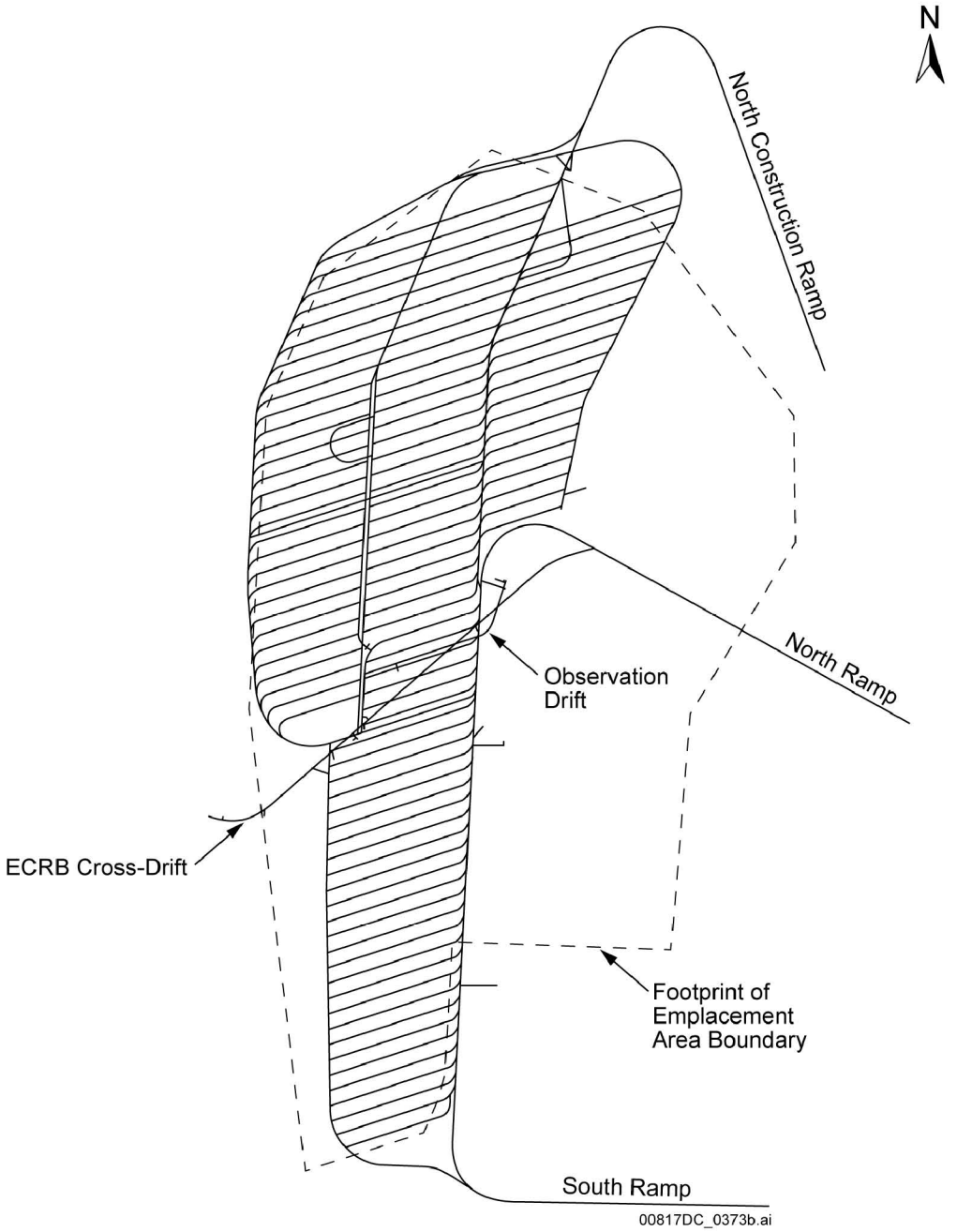

Source: Modified from SNL 2007 [DIRS 179466], Table 4-1, Parameter 01-02.

Figure 1-10. Subsurface Facility Layout

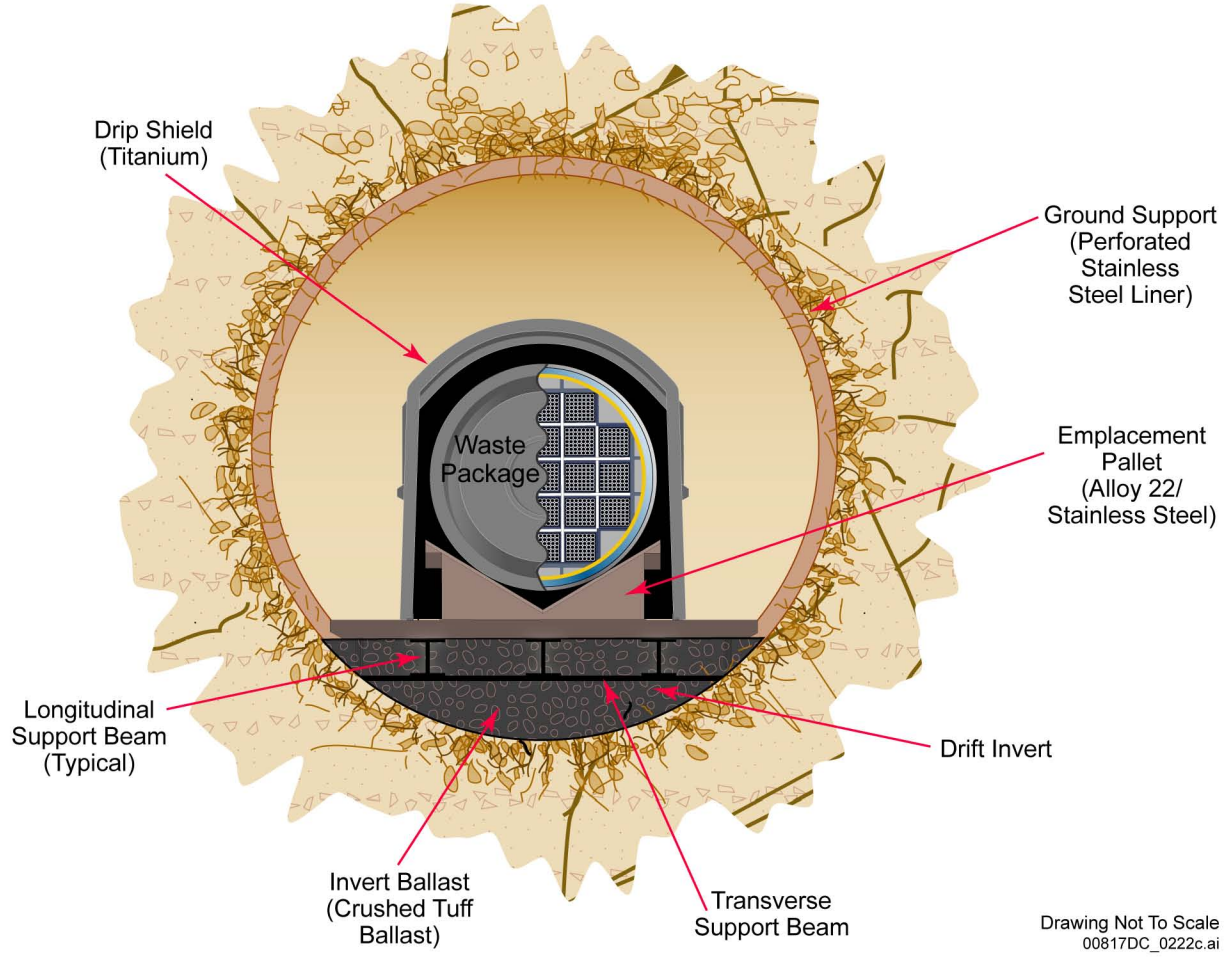

Source: Modified from SNL 2007 [DIRS 179354], Figure 4-1.

Figure 1-11. Cross Section Illustration of the Engineered Barrier System

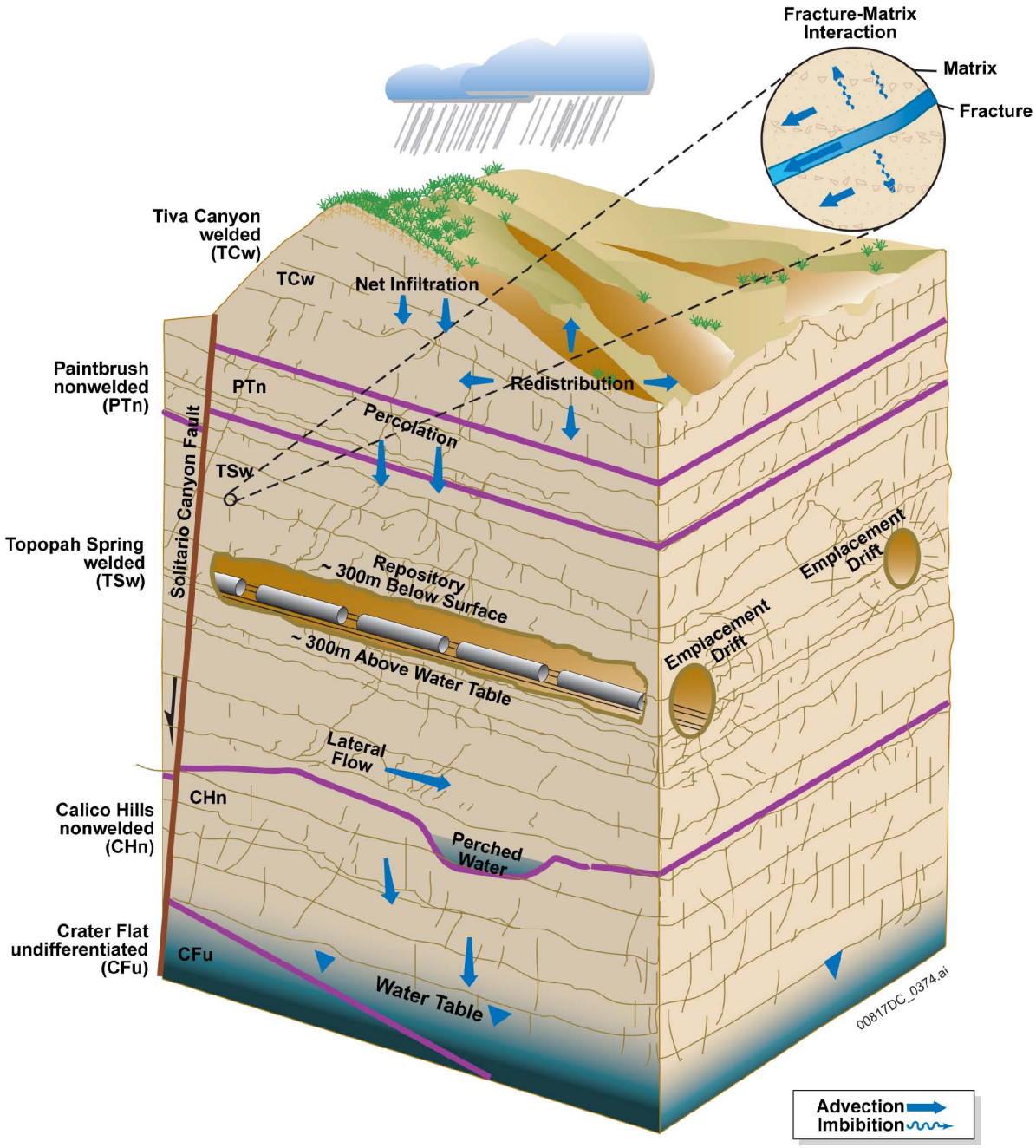

Figure 1-12. Conceptual Drawing of Mountain-Scale Flow Processes

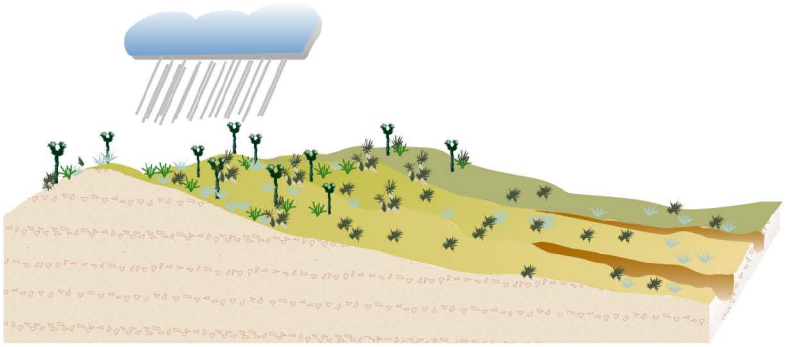

Present-Day Climate

Yucca Mountain:
Regional Meteorological Stations

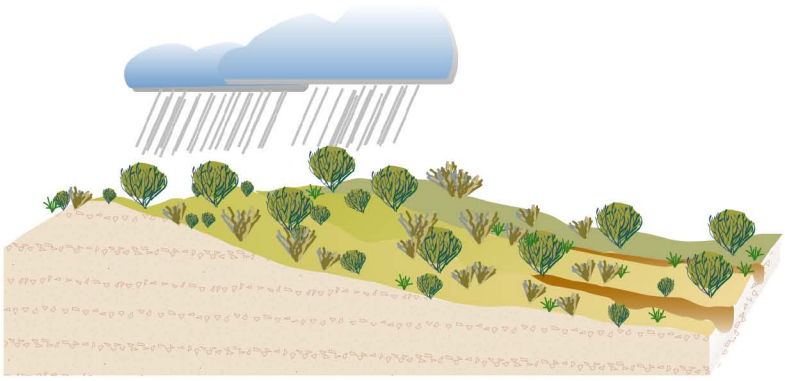

Monsoon Climate

Lower-bound analogue: Yucca Mountain
Upper-bound analogue: Nogales, AZ
Higher precipitation and temperature
than present-day climate

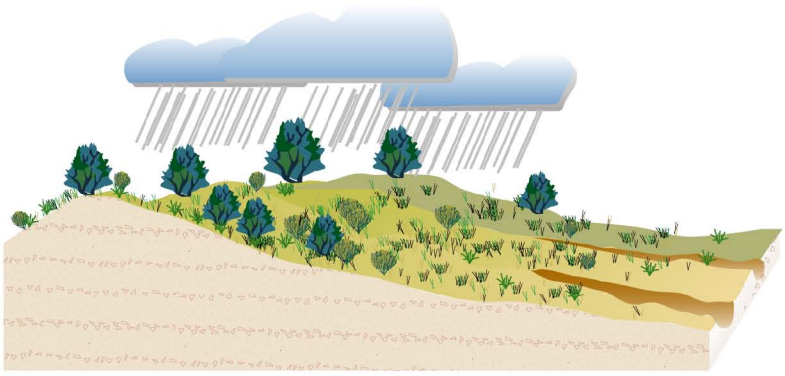

Glacial-Transition Climate

Lower-bound analogue: Delta, UT
Upper-bound analogue: Spokane, WA
Higher precipitation and lower
temperature than present-day climate

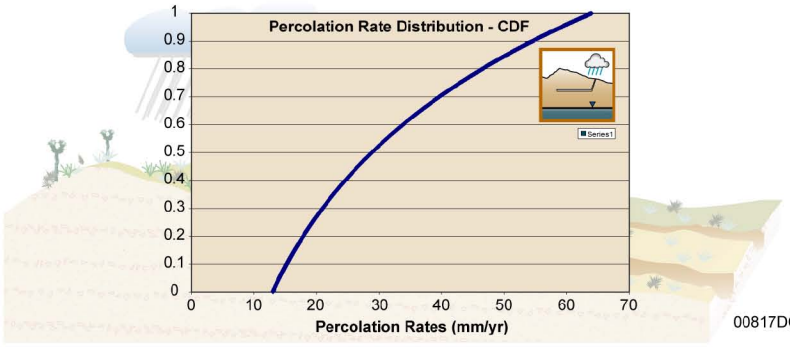

Post-10,000 Year Climate

Sampled value based on a log-uniform
probability distribution for deep percolation
rates from 13 to 64 mm/yr
(10 CFR 63.342(c)(2) [DIRS 178394])

Figure 1-13. Illustration of the Four Climate Periods Used in the TSPA-LA Model and Analogues for the Monsoon and Glacial-Transition Climates

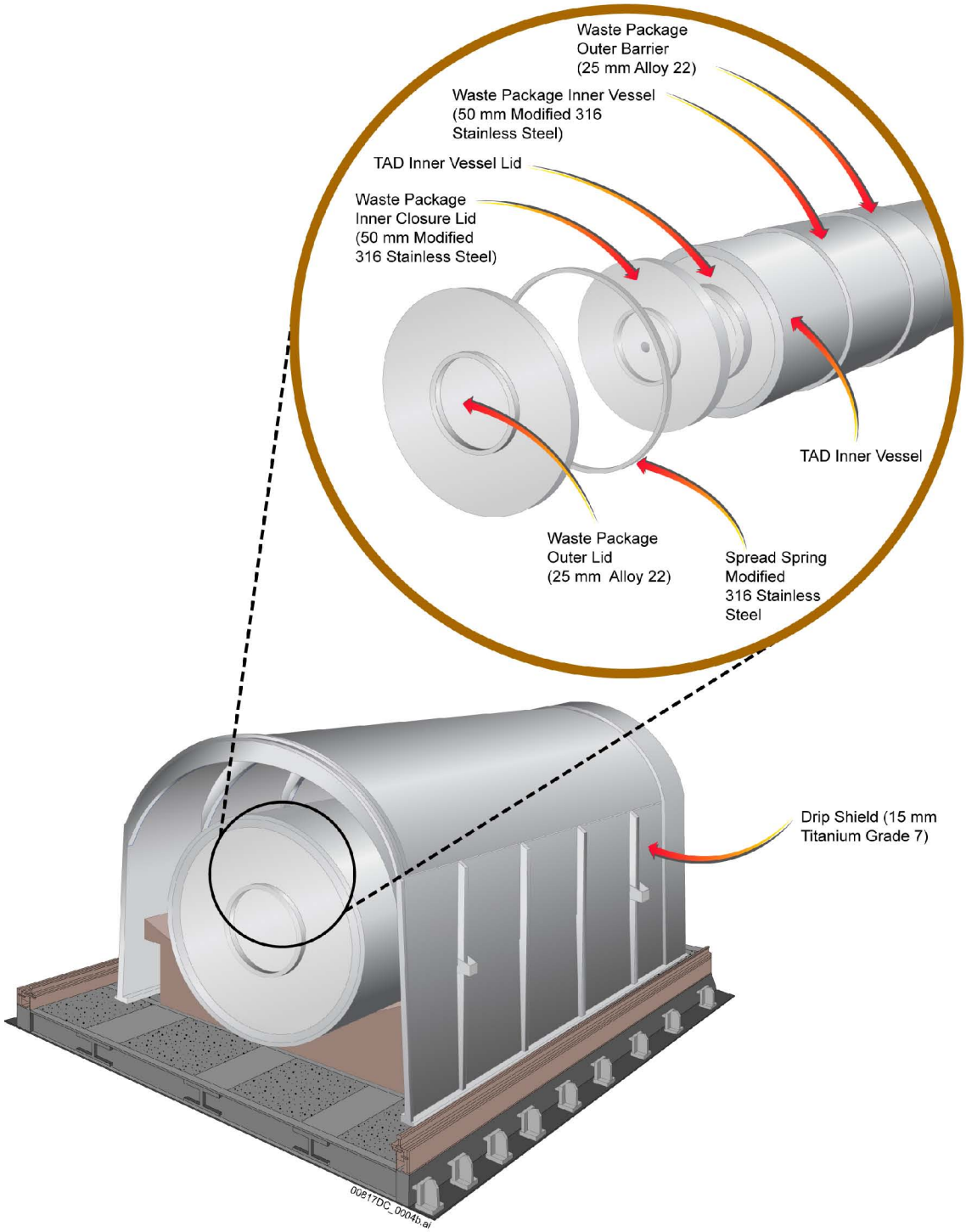

Source: SNL 2007 [DIRS 179394] and [DIRS 179354].

Figure 1-14. Schematic Design of the Drip Shield and Waste Package

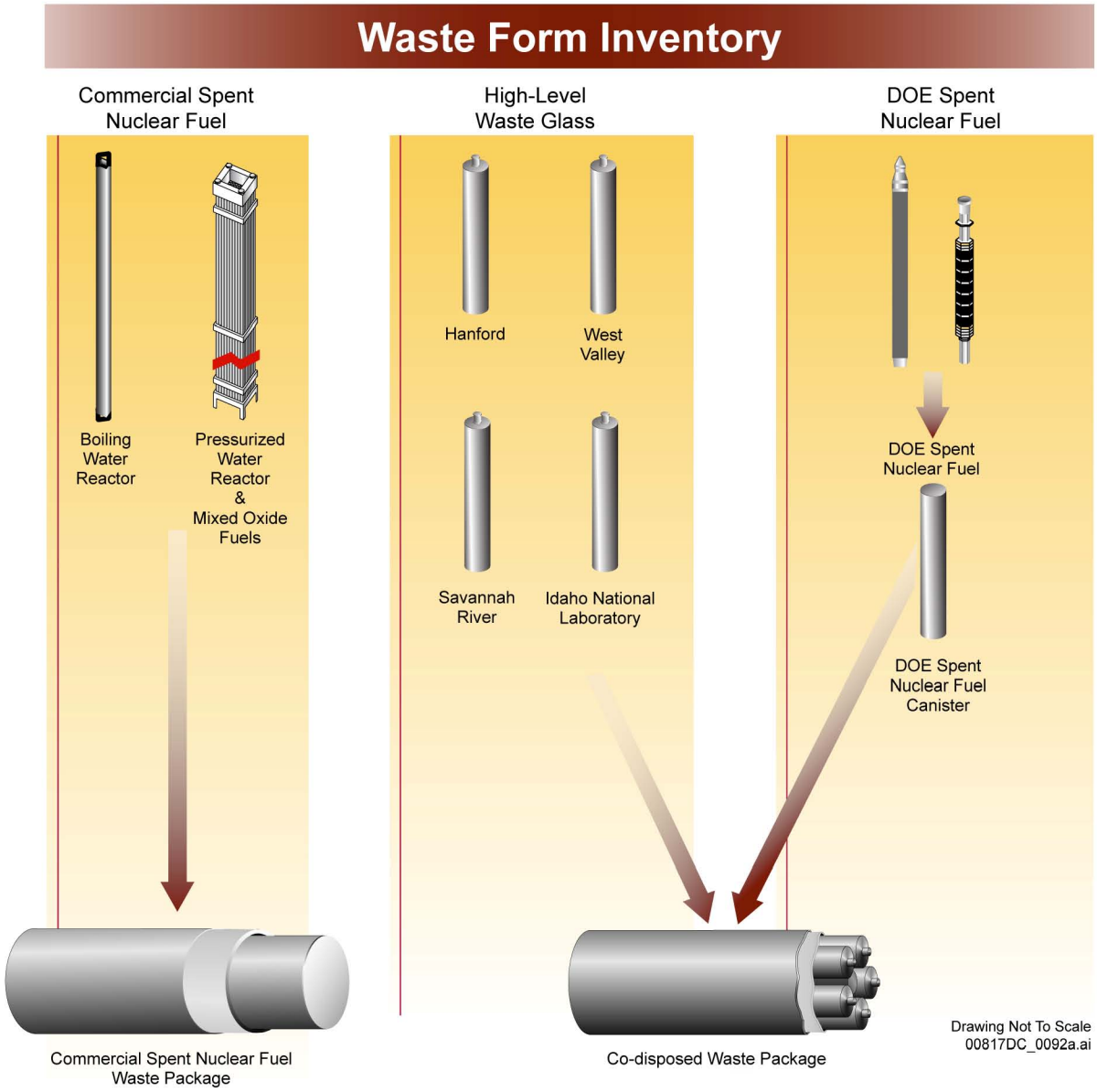

Source: Modified from SNL 2007 [DIRS 180472], Figure 6-1.

NOTE: For modeling purposes, the naval waste packages are modeled as commercial waste packages.

Figure 1-15. Three Waste Types Grouped into Two Representative Waste Packages: CSNF and CDSP WPs

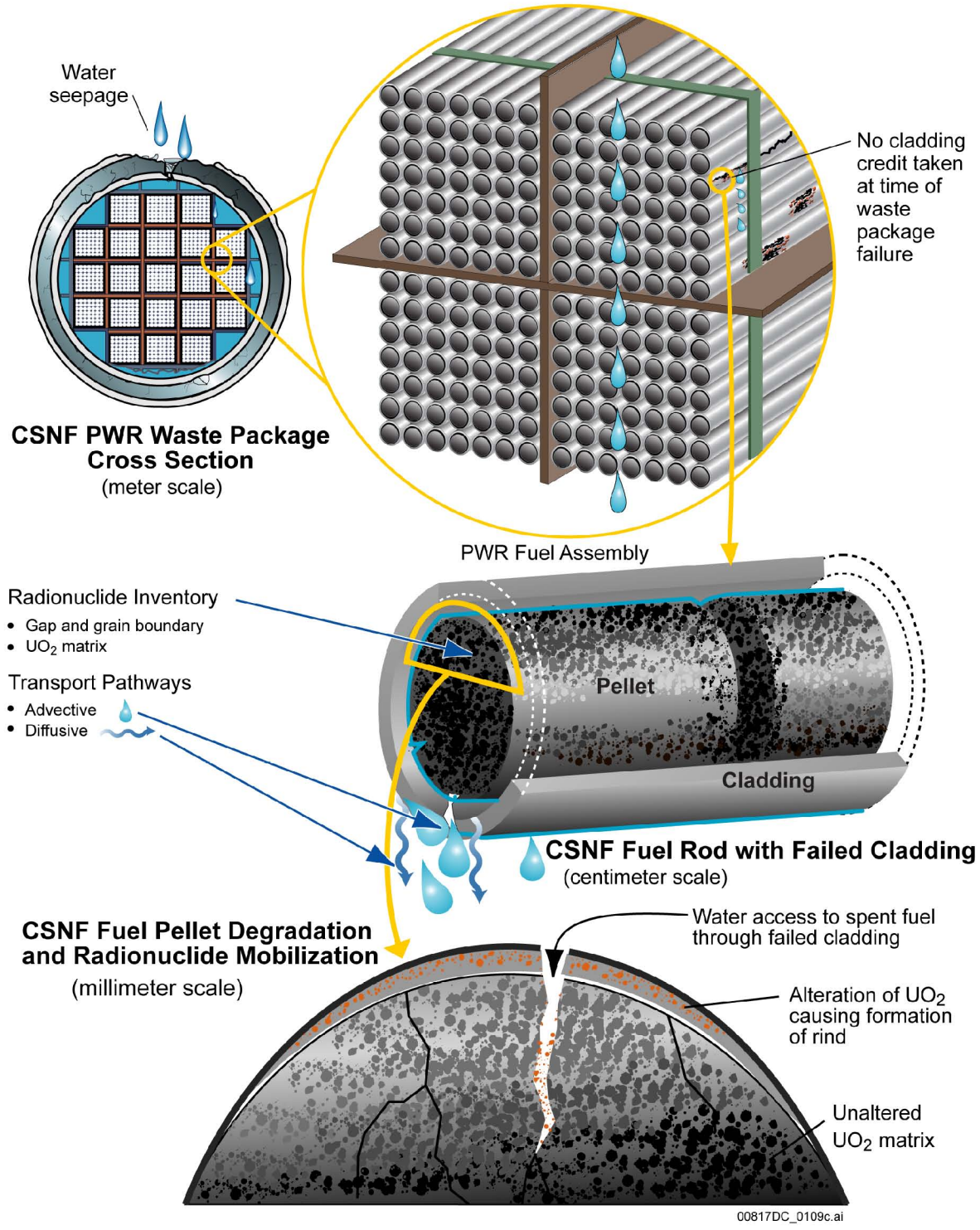

Figure 1-16. Schematic of CSNF Waste Form Degradation Mechanisms at Various Scales

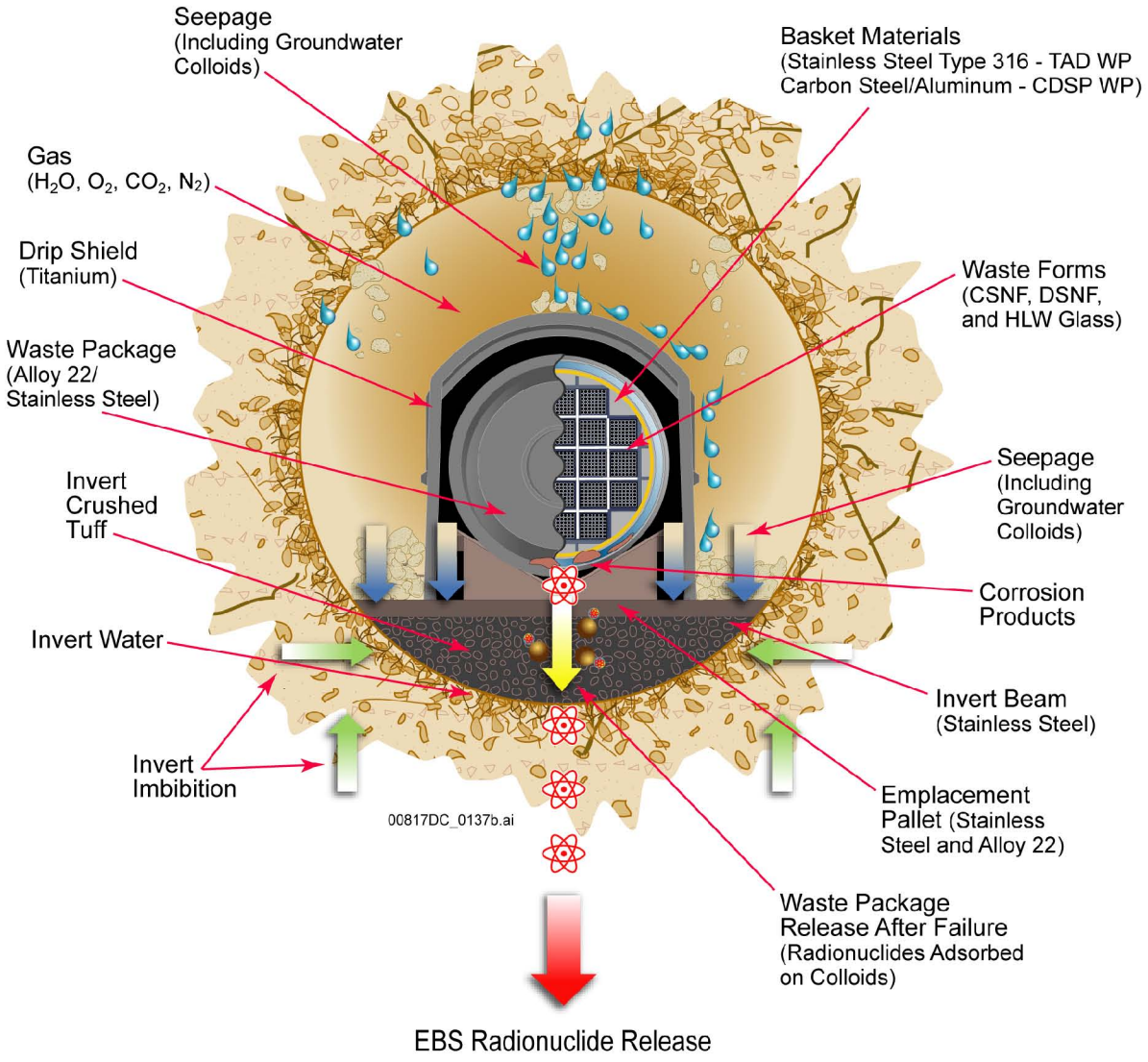

NOTE: Discussion and analysis of the features and processes illustrated on this figure can be found in *EBS Radionuclide Transport Abstraction* (SNL 2007 [DIRS 177407], Section 6.1.1, Figure 6.1-1).

Figure 1-17. General EBS Design Features and Materials, Water Movement, and Drift Degradation

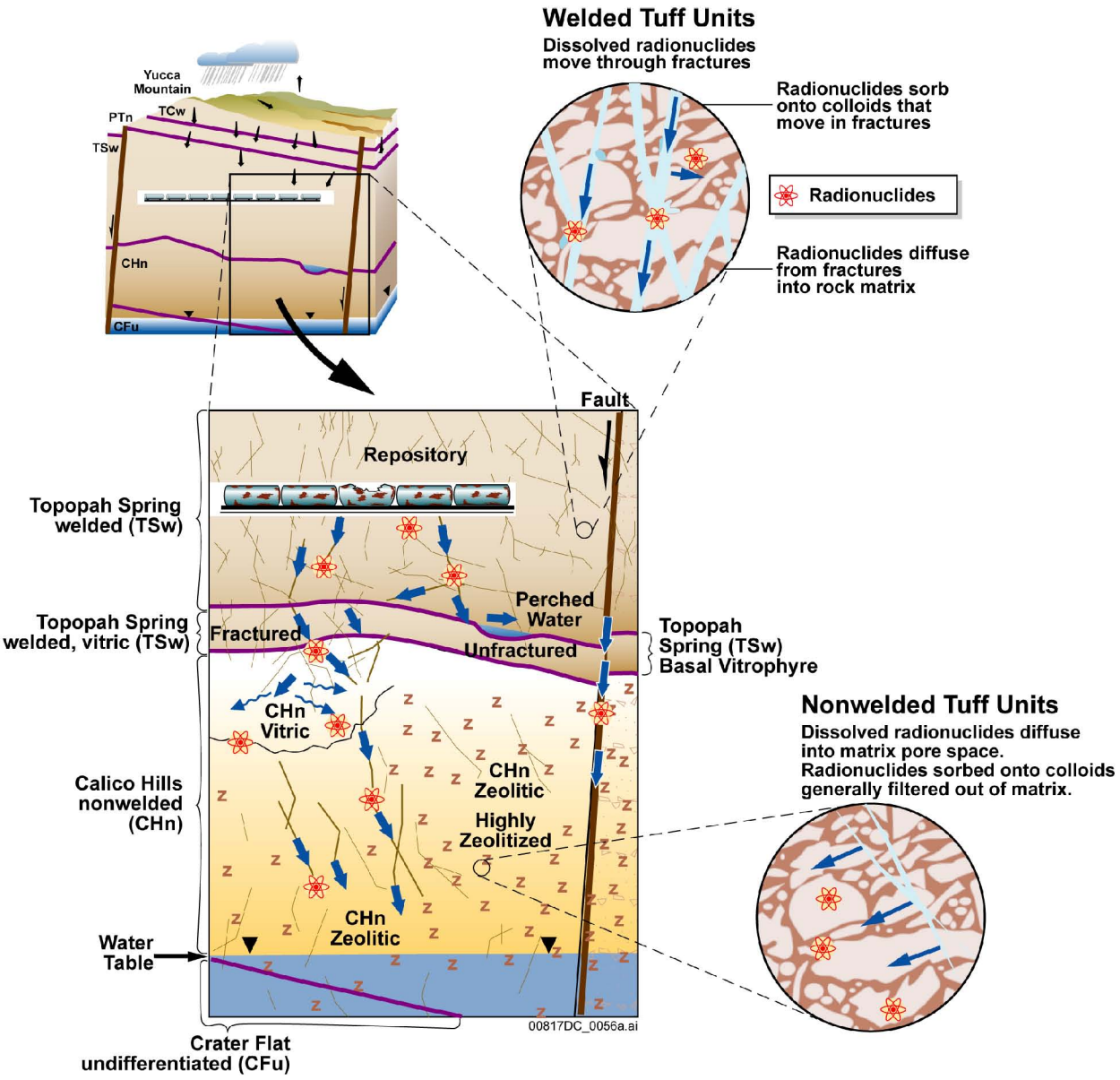

Figure 1-18. Conceptualization of Unsaturated Zone Transport Processes

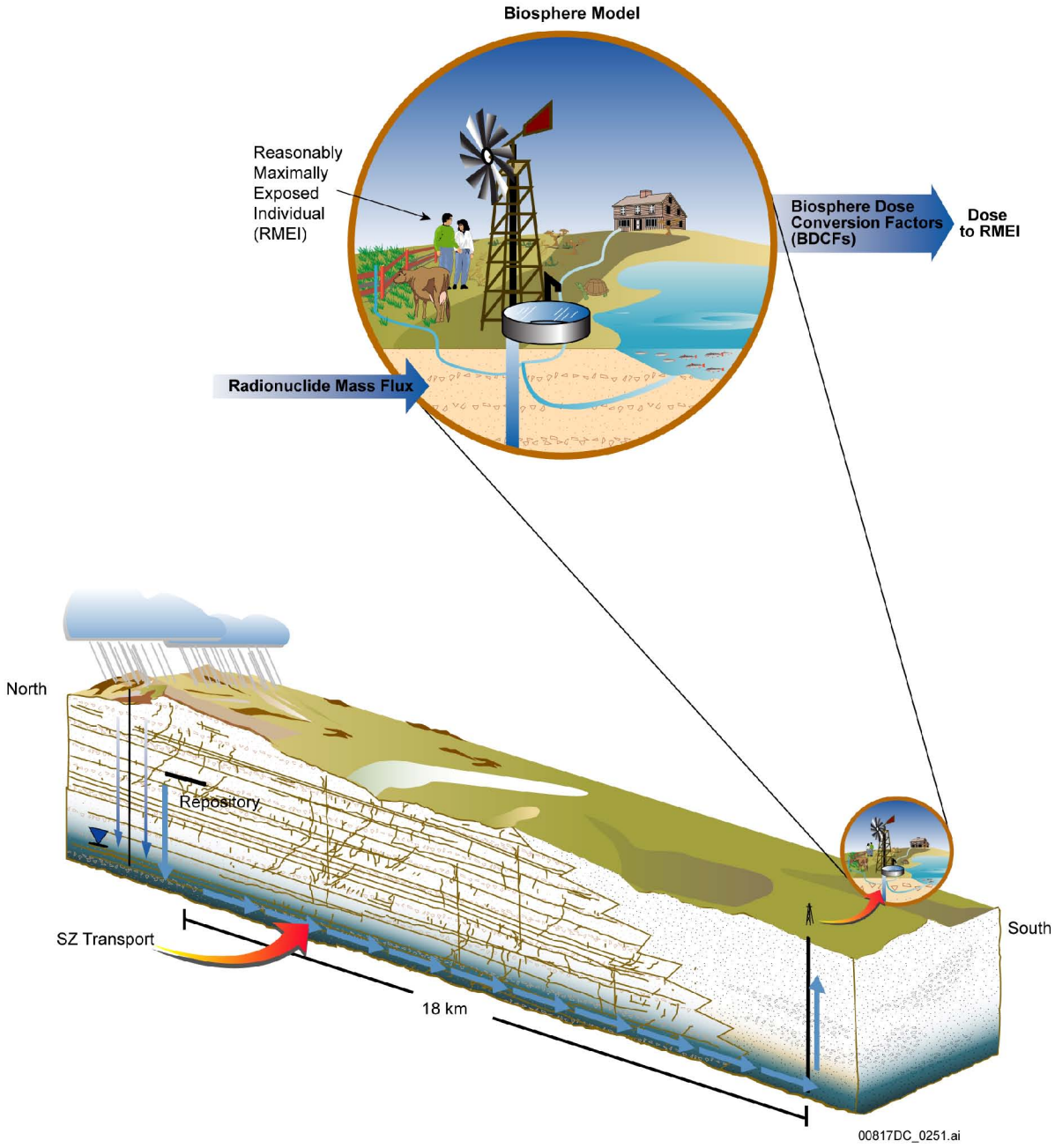

Figure 1-19. Overview of the Biosphere Groundwater Scenario Showing Groundwater Transport of Radionuclides and Uptake by the RMEI

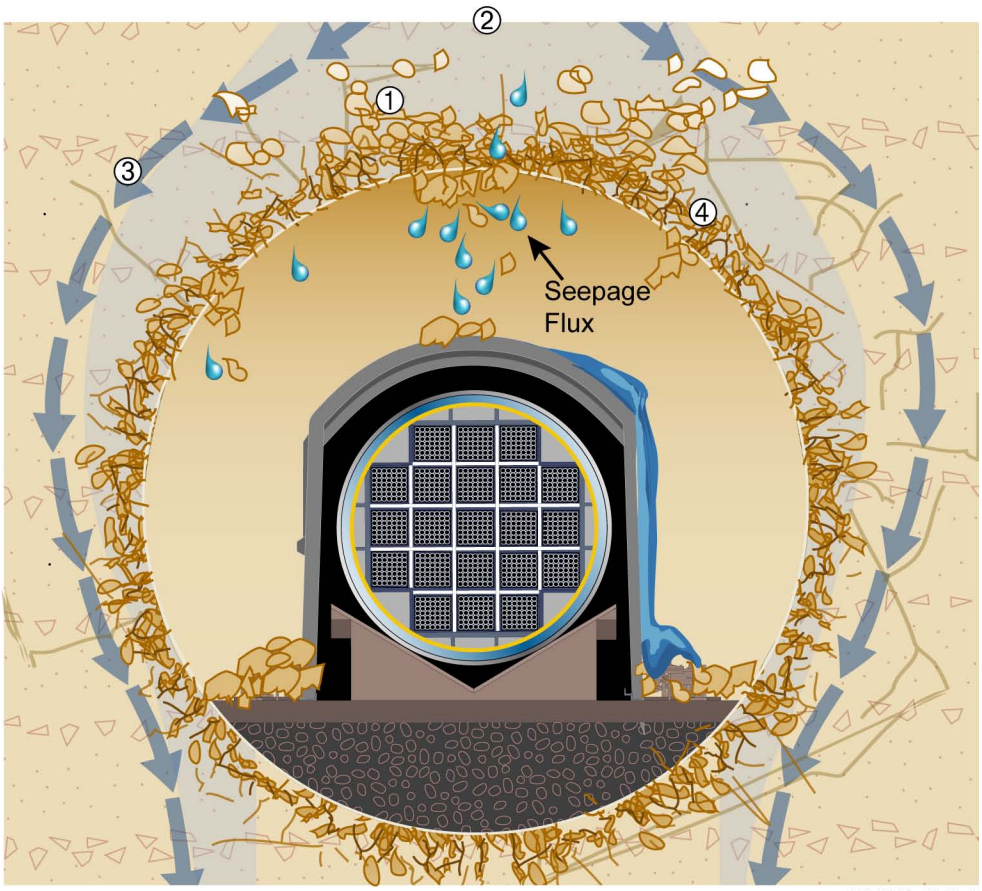

Source: Modified from SNL 2007 [DIRS 181244], Figure 6.3-1.

Figure 1-20. Schematic Illustration of the Processes Affecting Ambient Drift Seepage

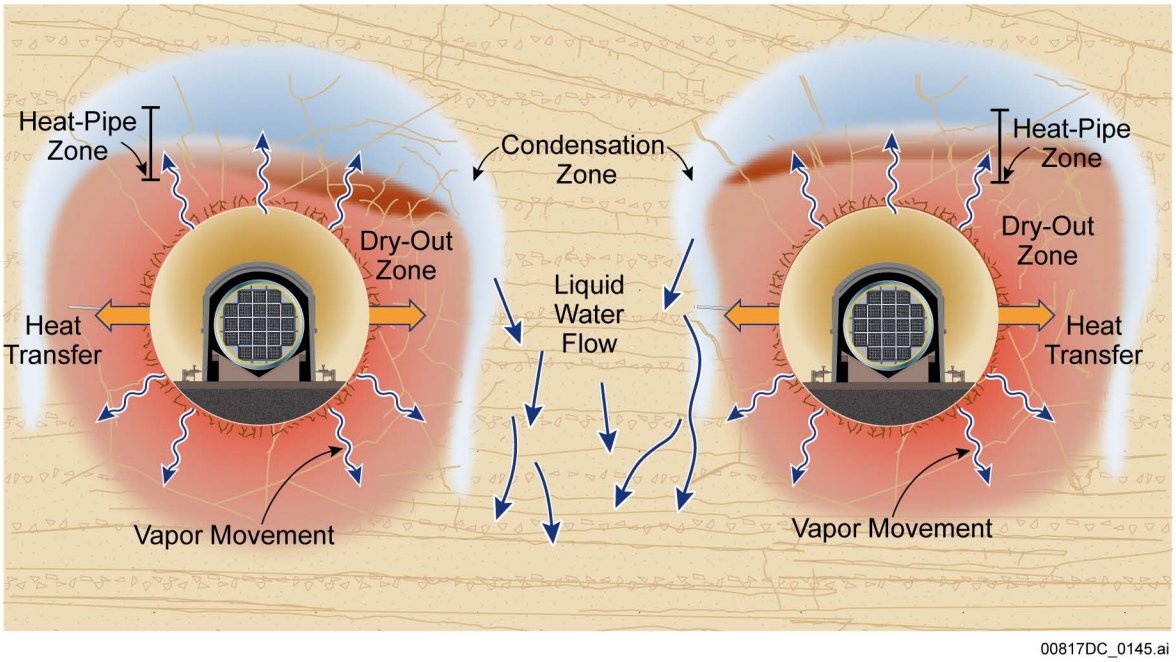

Source: Modified from BSC 2004 [DIRS 169734], Figure 5-81.

Figure 1-21. Schematic Illustration (not to scale) of Thermal-Hydrologic Processes in the Vicinity of the Emplacement Drifts Due to Repository Heating

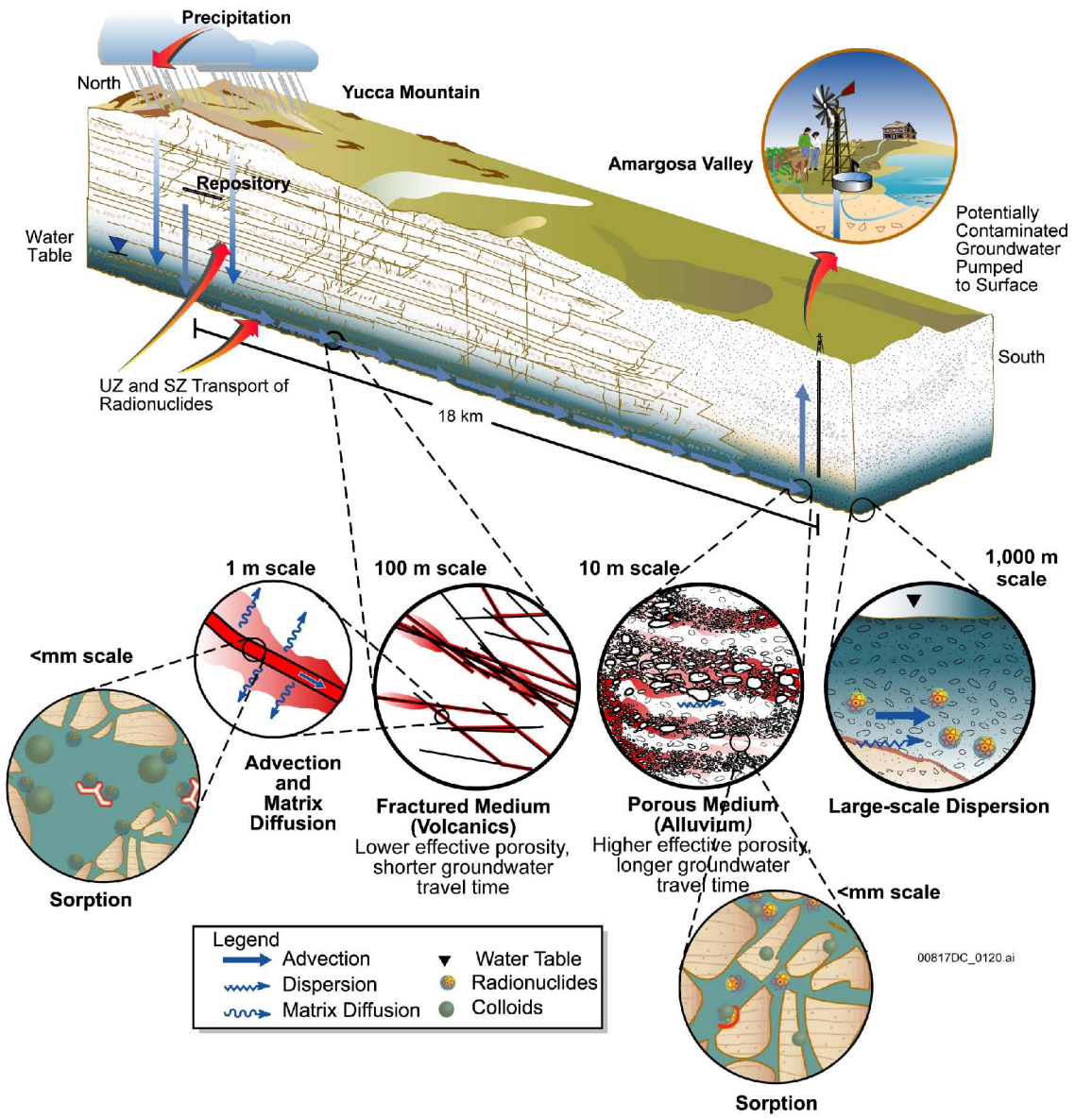

Figure 1-22. Conceptualization of Features and Processes Important to Saturated Zone Transport

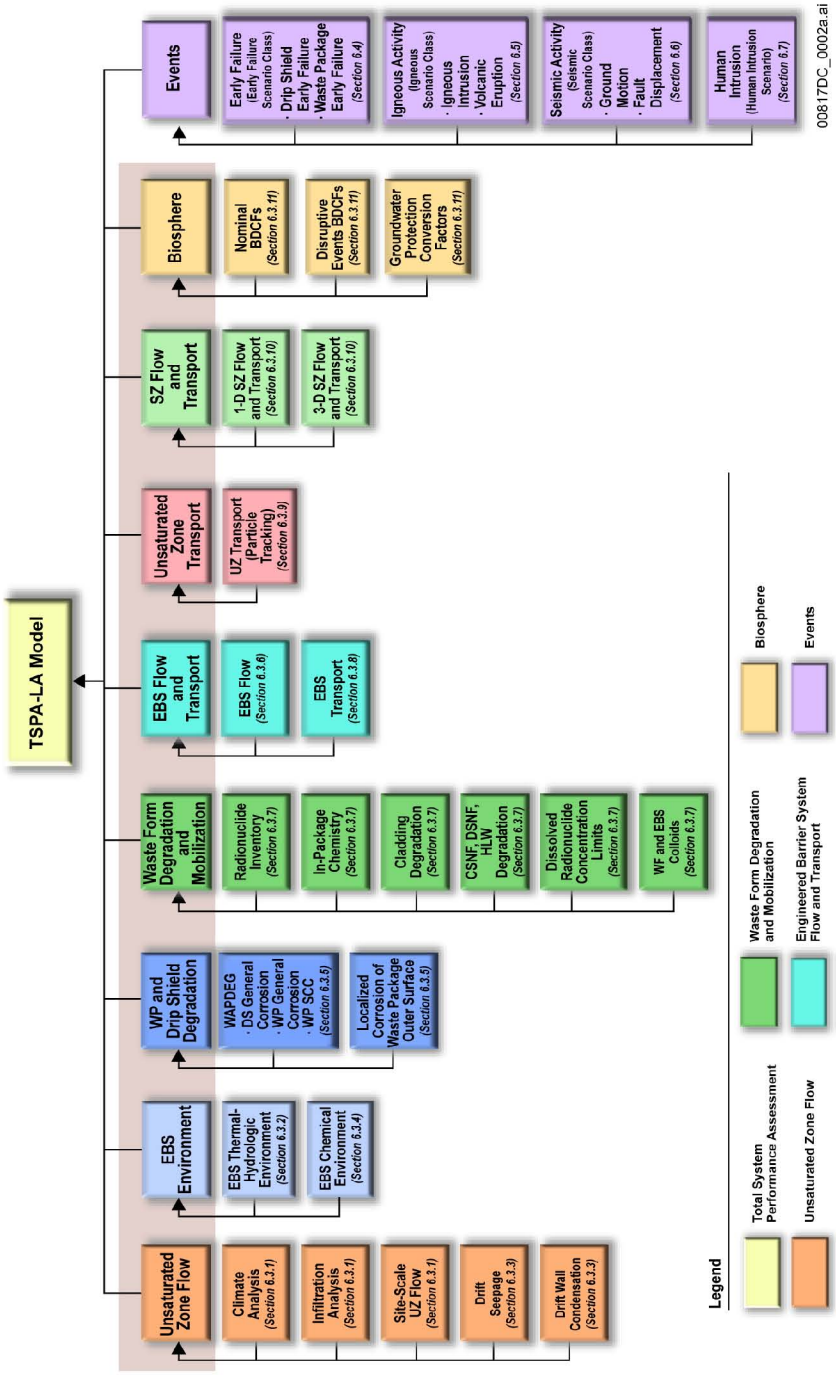

Figure 1-23. TSPA-LA Principal Model Components and Submodels

INTENTIONALLY LEFT BLANK

2. QUALITY ASSURANCE

The OCRWM QA program is first codified and implemented in the *Quality Assurance Requirements and Description* (QARD) (DOE 2007 [DIRS 182051]). The QARD applies to this technical product.

Technical Work Plan for: TSPA-LA FY 07-08 Activities (SNL 2008 [DIRS 184920]) describes in more detail the implementation of the QA program and contains the following:

- The conclusion that the work scope related to the completion of this technical product is subject to the requirements of the QARD (DOE 2007 [DIRS 182051])
- The list of QA procedures used to complete this technical product
- The processes used to control the electronic management of data used to complete this technical product.

2.1 CONFIGURATION MANAGEMENT

The development of the TSPA-LA Model required organization, control, and accountability. In the language of Configuration Management, this translated into implementing the following four processes:

1. **Configuration Identification**—This is the unique identification of all the items to be managed in the system. Configuration identification consists of selecting the items to be managed and recording their functional and physical characteristics.

2. **Configuration Change Control**—This is the mechanism used to approve or disapprove all proposed changes to the system that is being managed. Configuration change control ensures that changes to any configuration items are approved and controlled so that consistency among components is maintained.

3. **Configuration Status Accounting**—This is used to ensure that information contained in the status accounting system documents the evolution of the TSPA-LA Model in a transparent and traceable manner.

4. **Review**—The review process checks the configuration items to verify that they are uniquely identified, described, and managed in the system.

The software development procedures (i.e., IM-PRO-003, *Software Management*; IM-PRO-004, *Qualification of Software*; IM-PRO-005, *Software Independent Verification and Validation*; and IM-PRO-006, *Software Independent Verification and Validation of Legacy Code*) implement these Configuration Management processes for software development. However, to efficiently manage the development of the TSPA-LA Model, the same configuration management processes (e.g., Configuration Identification and Configuration Change Control) mentioned previously were used in the form of workplace controls. Summaries of the controls placed on software development, model development, and input development are provided in the sections that follow.

2.1.1 Configuration Management of Software

All software codes used to support the TSPA-LA Model were qualified in accordance with project software development procedures. These procedures establish the roles and responsibilities for the organizations responsible for implementing the four configuration management processes described previously. The first three processes below were administered by the SCM organization. The fourth process below was administered by the Software Independent Verification and Validation organization.

1. **Configuration Identification**—Each piece of software and its supporting documentation was uniquely identified with a software tracking number (STN) and document number, respectively.

2. **Configuration Change Control**—After software was qualified in accordance with the software development procedures and placed on the software baseline, only then approved changes were made.

3. **Configuration Status Accounting**—This process kept track of the status of software during software development and operations. The following are examples of the items tracked: (a) descriptions of the primary function of the software; (b) versions of documents and media; (c) software users; (d) software status, such as active, retired, or canceled; and (e) descriptions of operating platforms and systems.

4. **Review**—The details of the review process are established in IM-PRO-005, *Software Independent Verification and Validation* (for earlier code qualifications, LP-SI.13Q-BSC, *Software Independent Verification and Validation,* and AP-SI.3Q, *Software Independent Verification and Validation*). This review ensures that software requirements are adequately written and traced through the software documentation and that each requirement is verified by validation testing. Additionally, the review ensures that the documentation is reviewed by a qualified individual without recourse to the originator.

The specific codes used in the TSPA-LA Model are discussed in detail in Section 3. Section 3 also expands the discussion of the SCM functions mentioned in Items 1 through 3.

2.1.2 Configuration Management of the Development of the TSPA-LA Model

The development of the TSPA-LA Model required modifications from time to time for a number of reasons. This section presents the management control system that was implemented to track and maintain a record of these changes, as illustrated on Figure 2-1.

New or revised analysis and/or model reports were developed for the TSPA-LA. During the development of new or revised analysis and/or model reports, the TSPA Analysts consulted with the SMEs to define the technical output of their analysis and/or model reports for use in the TSPA-LA Model. Draft information, such as preliminary DTNs and preliminary TSPA Data Input Packages, was provided for initial implementation and inserted into the TSPA-LA Model. This information included relevant process models, model abstractions, and submodels that are contained in the analysis and/or model reports. The appropriate SMEs have reviewed the results

of the initial implementation to ensure that the implementation is consistent with each SME's intent. Discrepancies were addressed by changing the implementation of the submodels or model abstractions in the TSPA-LA Model and/or by changing the supporting analyses and/or model reports and/or DTNs prior to their approval.

In addition, new or revised analysis and/or model reports developed for the TSPA-LA Model were reviewed by the TSPA Department according to SCI-PRO-003, *Document Review*. Part of this review determined whether or not changes to the TSPA-LA Model were needed and if the changes were within the TSPA-LA Model development scope and schedule.

Internal TSPA-LA Model changes, such as a change in model logic to select specific parameters for individual modeling cases, were identified as part of TSPA-LA Model development. The TSPA Department Manager reviewed and approved changes to the TSPA-LA Model development scope and schedule to accomplish required revisions to the analyses and/or model reports and/or the TSPA-LA Model inputs developed by the analysis and/or model reports. Changes outside the TSPA-LA Model development scope and schedule elevated the issue(s) to the appropriate management level for resolution. Management approval of changes to the TSPA-LA Model were based in part on whether or not a change was necessary to comply with regulatory requirements, regardless of the final input feed date for the requested change, or whether the TSPA-LA Model was finalized or frozen for performing TSPA-LA analyses.

Changes to the TSPA-LA Model were tracked by the TSPA Department. Figure 2-2 shows the TSPA Model Change Approval Form used to track the changes to the TSPA-LA Model. During the development stage of the TSPA-LA Model, TSPA Analysts were required to obtain written approvals from the TSPA Department Manager, TSPA Model Calculations Lead, and TSPA Configuration Management Lead, to change and/or introduce new process models, model abstractions, or parameters into the TSPA-LA Model. The written authorization specified the source(s) (e.g., analysis and/or model reports, DTNs) of the process models, analyses models, model abstractions, or input parameters.

Another important aspect regarding the control of the TSPA-LA Model is ensuring consistent, well-documented inputs. The supporting organizations provide abstractions and technical product output to the TSPA-LA Model according to a scope and schedule review. The most recent scope and schedule reviews were led by the Performance Assessment System Integration Team. The reviews resulted in the addition of detailed requirements and specifications to the TWPs for each work package containing an analysis and/or model report. Additional requirements were incorporated into revisions to the TWPs that specified content for FEPs, ACMs, parameters, and characterization of uncertainty for the TSPA-LA Model.

Additional product management emphases and controls included:

- A consistent model hierarchy and structure supporting the TSPA-LA Model architecture
- A consistent treatment and documentation of model abstractions supporting the TSPA-LA Model
- A consistent treatment and documentation of ACMs

- A consistent treatment and documentation of FEPs included in the TSPA-LA Model, as well as how the FEPs were included and where their inclusion was documented
- A consistent evaluation of the definition and performance of the natural and engineered barriers of the repository system and the basis for the projection of barrier performance
- A consistent evaluation of parameter uncertainty and how that uncertainty is propagated through the model hierarchy to the TSPA-LA Model and how the significance of that uncertainty is evaluated
- A consistent documentation of how the TSPA-LA Model components and submodels are integrated and how the information flows between the submodels and the analyses, including roadmaps of information supporting the TSPA-LA Model
- A consistent basis for determining the appropriate amount of confidence required for model validation
- A consistent evaluation of the parameter values that were used to develop parameter distributions and why those parameter values are sufficient to capture the range of possible observations.

The above emphases determined much of the content of the analysis and/or model reports that support the TSPA-LA Model and postclosure safety case for presentation in the LA. These analysis and/or model reports remain the primary supporting documentation for the TSPA-LA Model. Updated TWPs for each of the supporting analysis and/or model reports ensured that the scope was assigned appropriately (i.e., FEP by FEP, model by model, and parameter by parameter).

The more detailed scope definitions that resulted from the above process yielded a much more consistent and comprehensive treatment of, not only parameter uncertainty, but also FEP uncertainty and ACM uncertainty. The process also allowed for early definition of the scope and content of the TSPA-LA Model within the context of the document, as agreed to in several Total System Performance Assessment Integration Key Technical Issue agreements. This more detailed scope definition has allowed the authors of analysis and/or model report authors to focus on the key performance-related aspects of their models and analyses in a more risk-informed way.

Physical Control of Files—The TSPA-LA Model input files, DLLs, and the database were controlled by their storage in a set of controlled subdirectories on the TSPA file server.

Input Files—Input files for the TSPA-LA Model were stored in a controlled subdirectory on the TSPA file server. Read access to this subdirectory was limited to the TSPA Department staff. Write access was limited to the TSPA-LA Configuration Management staff and the System Administrator. The TSPA-LA Configuration Management staff established a baseline list of files. Any subsequent changes to the input files were documented as changes to the baseline list.

DLLs—DLLs for the TSPA-LA Model were obtained from SCM and installed in a controlled subdirectory on the TSPA file server by the TSPA-LA Configuration Management staff. Read access to this subdirectory was limited to the TSPA Department staff. Write access was limited to the TSPA-LA Configuration Management staff and the System Administrator. The TSPA-LA Configuration Management staff established a baseline list of DLLs, and any subsequent changes to the DLLs were documented by the TSPA-LA Configuration Management staff as changes to the baseline list.

Input Parameters—Both fixed-value and uncertain input parameters for the TSPA-LA Model were controlled in the TSPA Input Database described in Section 4.4. The database was stored in a controlled subdirectory on the TSPA file server. Read access to this subdirectory was limited to the TSPA Department staff. Write access was limited to the TSPA-LA Configuration Management staff and System Administrator. Changes to the database were controlled via the change control and checking process used for the TSPA-LA Model.

Change Control and Checking—Table 2-1 summarizes the forms, checklists, descriptions, and logs used to manage the change control and checking of the TSPA-LA Model.

The TSPA-LA GoldSim model file was checked by qualified individuals assigned by the TSPA Model Calculations Lead. The checker for a model change and/or model run is another TSPA Analyst who was not involved in modifying the model file or input file(s).

Two types of checks were performed on updated versions of the TSPA-LA GoldSim model file: implementation checking and conceptual model checking. Implementation checking verifies that all of the changes to the TSPA-LA Model file and/or external files were performed correctly. Conceptual model checking considers whether the TSPA-LA Model implementation correctly reproduces the conceptual process model or model abstraction from the associated analysis and/or model report, submodel, or scientific analysis.

Implementation Checking—Implementation Checking was completed by reviewing the changes identified by the analyst in a checklist similar to Figure 2-3 and then documenting completion to the following steps in a second checklist similar to Figure 2-4. The primary steps involved in Implementation Level checking included:

- Checking modified GoldSim elements against their source information to verify that they were changed correctly
- Verification that the input links of added elements were correct
- Verification that the output links of added parameters were correct
- Checking that the links to and from any deleted elements were appropriately reconnected
- Verification (by inspecting source references for changes) that each change to an external file was correct.

Concept Level Checking—The Concept Level Checking process considers whether the changes to the TSPA-LA Model correctly reflect conceptual model changes using a checklist similar to Figure 2-5. The conceptual description includes a general description of changes made to the TSPA-LA Model. Any development and testing work to support changes to the TSPA-LA Model were documented in the conceptual description.

Any differences between the results of the initial and modified modeling case(s) were explained and properly documented by the checker and/or analysts in terms of the changes made to the TSPA-LA Model.

The details of the Implementation and Concept checks are described in a series of Desk Guides used by the TSPA Department. The completed Desk Instruction forms are contained in the output DTNs for the TSPA modeling runs listed in Section 8.

2.1.3 Configuration Management for the TSPA-LA Model Input

The TSPA-LA Model was developed by making incremental changes to the TSPA Final Environmental Impact Statement Model (Williams 2001 [DIRS 157307]). Each of these incremental changes had a set of input files and parameters that were saved and/or archived on the designated TSPA Department server. The DLLs and their associated input files were not embedded in the TSPA-LA Model file but were saved or archived separately as file sets, whereas the input parameters used for each TSPA-LA Model run were captured in each of the incremental TSPA-LA Model files and in the final TSPA-LA Model file, upon which this document is based. The TSPA-LA Model file and all associated inputs were submitted to the TDMS database in accordance with TST-PRO-001, *Submittal and Incorporation of Data/Technical Information to the Technical Data Management System*.

The input files are necessary to run each of the DLLs. The DLL input files used during the development of the TSPA-LA Model were numbered (e.g., Input File Set 1, Input File Set 2, and so on). The Input File Set used for each model change was documented on the TSPA-LA Model Change Approval Form (Figure 2-2). An electronic copy of each file set was saved on the designated TSPA Department file server (see Appendix F for detailed information on DLL input files).

The TSPA Input Database, which is described in Section 4.7, is electronically linked at run time to the TSPA-LA Model. The TSPA Input Database is a controlled warehouse of all of the input parameters used to run the TSPA-LA Model. An important configuration management feature of the TSPA Input Database is that the TSPA Input database supports the independent verification of every value used in the TSPA-LA Model. For example, a TSPA Analyst is assigned the task of verifying that for a given parameter value or set of values, the reference information used to find the value is within the reference. Once the TSPA Analyst has confirmed the value in the database is the same as the value in the reference, then the TSPA Analyst clicks a verification button in the TSPA Database for the given parameter, thereby indicating that the parameter is verified. If the parameter value or reference information is edited, then the TSPA Input Database indicates that the parameter is no longer verified. The TSPA Input Database verification feature ensures that any preliminary input parameters are confirmed to be consistent with the formal reference such as an analysis and/or model report or DTN.

The parameter values are obtained from controlled sources maintained by the project data and information systems, such as project documents, TDMS, and Technical Information Center. The TDMS database is a project-wide database, whereas the TSPA Input Database is used only for the TSPA-LA Model. Each of the parameter sets used in the TSPA Input Database has a DTN to provide the link to the TDMS database or a reference to the controlled source of the information, such as an analysis and/or model report. The TDMS maintains the qualification status of all of its contents. In closing, the TSPA Model inputs are controlled and well documented by using the TSPA Input Database. Additional details on the control and documentation of the sources of the data can be found in Section 4.

2.2 MODEL VALIDATION

The assessment of the validation status of the TSPA-LA Model for its intended use is based on: (1) the compilation of the information developed according to the activities documented in Section 7 following criteria in SCI-PRO-006, *Models*; (2) the summary of the validation work developed by the Independent Technical Reviewer (ITR); and (3) the determination of the Performance Assessment Systems Integration Manager.

The ITR is required per SCI-PRO-006 (Section 6.4.12) to provide a review of the model validation documentation (Volume 2, Section 7) and then document the review. The documentation must include the validation criteria and the information used in determining whether the criteria were met.

SNL (2008 [DIRS 184920], Section 2.3.5) indicates that the final determination regarding model validation is made by the Performance Assessment Systems Integration Manager:

> The complete body of information developed for validation of the TSPA-LA model, including the process model validation information for the supporting submodels, will be provided to the Performance Assessment Systems Integration Manager for determination of the model's validation status.

The signature of the Performance Assessment Systems Integration Manager on this document signifies that the TSPA-LA Model is found valid for its intended purpose.

INTENTIONALLY LEFT BLANK

Table 2-1. Configuration Control Documents for the TSPA-LA Model

Figure Number	Name	Purpose
2-2	TSPA-LA Model Change Approval Form	Provides management control of all changes to the TSPA-LA Model. Summarizes the extent of the change.
2-3	TSPA-LA Model Changes Checklist	Initiated by the TSPA analyst. Documents the specific changes made to the TSPA-LA Model (parameter checking). Checker uses this list of changes to check.
NA	Conceptual Description	Provides overview of the changes that were incorporated into the TSPA-LA Model. May also include development and checking work that was performed to support the change.
2-4	TSPA-LA Model Implementation Checklist	Documents the answers to parameter check questions. Conceptual checking and Configuration Management check.
NA	GoldSim Version Report (Run Log)	Provides record of specific changes made to the GoldSim model file (generated by GoldSim).
2-5	TSPA-LA Model Concept Checklist	Documents the answers to concept check questions.

INTENTIONALLY LEFT BLANK

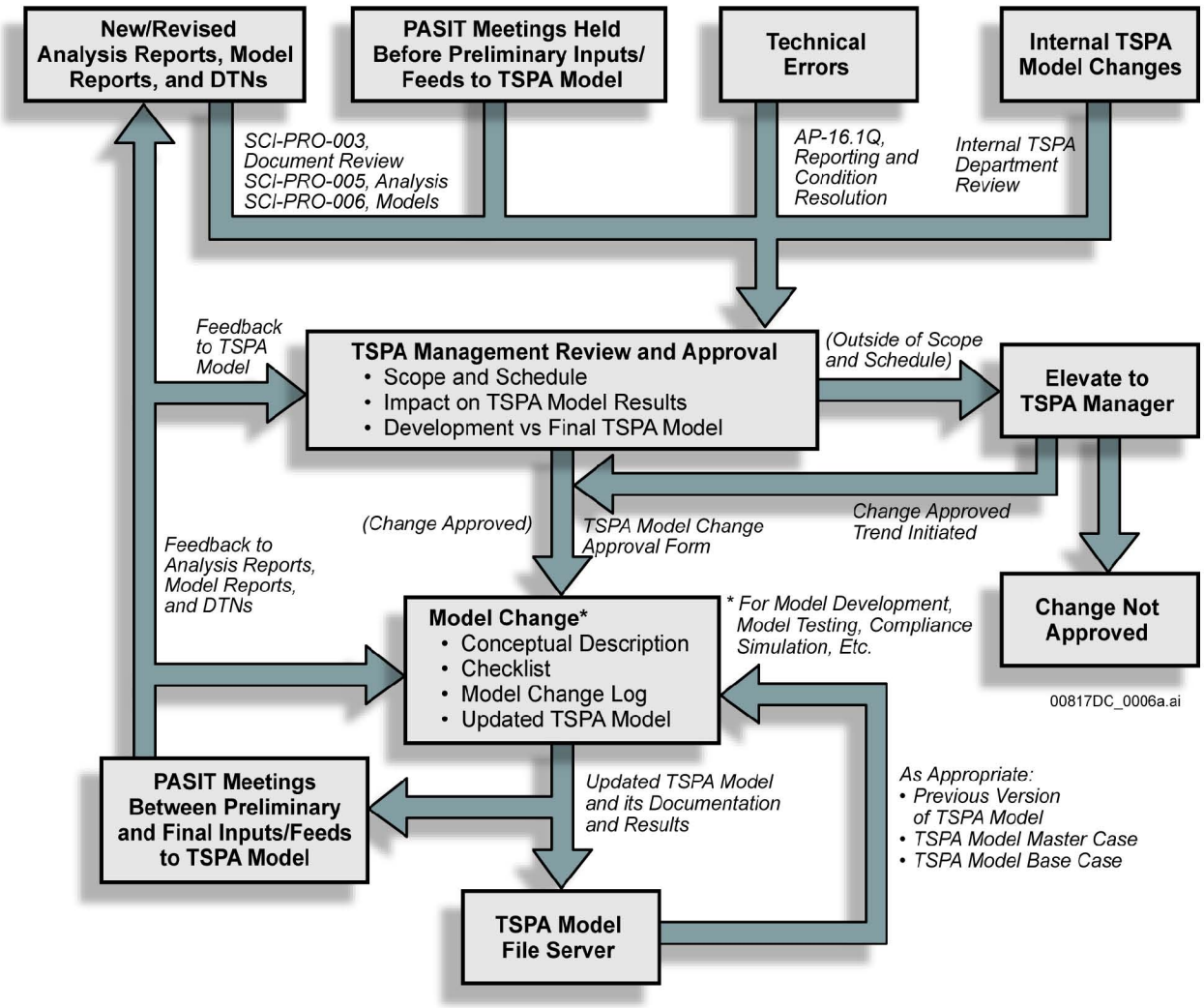

Figure 2-1. Flowchart Illustrating the Management Control Process for the TSPA-LA Model

TSPA Analyst:	Date:
Input File Set:	DLL Set:
Change to TSPA Database?	Change due to Parameter Source?
Change Number:	Model Version:
Basis for Proposed Change:	
Description of Proposed Change:	
Model Freeze Date:	Expected Change Date:
Modeling Stage: ___ Development ___ Production ___ Post-production	

Reviewer Signatures	Date	Approval (yes/no)
TSPA Model Calculations Lead		
TSPA Configuration Management Lead		
TSPA Department Manager		
Performance Assessment Manager		
Comments Attached?		

00817DC_0007.ai

Figure 2-2. Example of the TSPA-LA Model Change Approval Form

Model ID:				
TSPA Analyst:		Date:		
Checker:		Date:		
Parameter, Element, etc.	Location	Description of Change	Comment / Resolution	Correct? Y/N /Initials
Background color denotes changes are made within the **Epistemic_Params** submodel.				
Background color denotes changes are made within the **Aleatory_Params** submodel.				
Background color denotes changes are made within the **EBS_Submodel** submodel.				

00817DC_0008.ai

Figure 2-3. Example of the TSPA-LA Model Change Checklist

Model ID:			TSPA Analyst Name: Signature:
Checker Name: Signature:			Date:
No.	Check Questions	Y, N, or NA	Notes
1.00	**Master Case Folder**		
1.01	Are the change approval form(s) included? (Both the word file and the signed PDF file)		
1.02	Is the conceptual description file included? (Both the word file and the signed PDF.)		
1.03	Is the version report included?		
1.04	Is the Master Case Change Checklist file included? (Both the word file and the signed PDF)		
1.05	Is the Master Case GoldSim file included without results?		
1.06	Are all other files, if any, placed in the Additional_Information directory (including all external files modified for the Master Case and all Base Cases)?		
2.00	**Nominal Base Case Directory or Directories**		
2.01	Is/are the GoldSim file(s) included with results?		
2.02	Is/are the Change Checklist file(s) included? (Both the word file and the signed PDF file)		
2.03	Is/are the version report(s) included?		
2.04	Do all entries in the version report(s) match the checklist(s)?		
2.05	If there are any additional files associated with the Nominal Base Case(s), is/are they located in the Additional_Information directory?		
2.06	Compared to the Master Case, are there any additional scenario specific changes, other than simulation settings, required to run the Nominal Base Case(s) from the Master Case?		
3.00	**Human Intrusion Base Case Directory or Directories**		
3.01	Is/are the GoldSim file(s) included with results?		
3.02	Is/are the Change Checklist file(s) included? (Both the word file and the signed PDF file)		
3.03	Is/are the version report(s) included?		
3.04	Do all entries in the version report(s) match the checklist(s)?		
3.05	If there are any additional files associated with the Human Intrusion Case(s), is/are they located in the Additional_Information directory?		
3.06	Compared to the Master Case, are there any additional scenario specific changes, other than simulation settings, required to run the Nominal Base Case(s) from the Master Case?		
4.00	**Early Failure Base Case Directory or Directories**		
4.01	Is/are the GoldSim file(s) included with results?		
4.02	Is/are the Change Checklist file(s) included? (Both the word file and the signed PDF file)		
4.03	Is/are the version report(s) included?		
4.04	Do all entries in the version report(s) match the checklist(s)?		
4.05	If there are any additional files associated with the Early Failure Case(s), is/are they located in the Additional_Information directory?		
4.06	Compared to the Master Case, are there any additional scenario specific changes, other than simulation settings, required to run the Nominal Base Case(s) from the Master Case?		

00817DC_0009.ai

Figure 2-4. Example of the TSPA-LA Model Implementation Checklist

Model ID:			TSPA Analyst Name: Signature:
Checker Name: Signature:			Date:
No.	Check Questions	Y, N, or NA	Notes
5.00	**Igneous Base Case Directory or Directories**		
5.01	Is/are the GoldSim file(s) included with results?		
5.02	Is/are the Change Checklist file(s) included? (Both the word file and the signed PDF file)		
5.03	Is/are the version report(s) included?		
5.04	Do all entries in the version report(s) match the checklist(s)?		
5.05	If there are any additional files associated with the Igneous Base Case, are they located in the Additional_Information directory?		
5.06	Compared to the Master Case, are there any additional scenario specific changes, other than simulation settings, required to run the Igneous Base Case(s) from the Master Case?		
6.00	**Seismic Base Case Directories**		
6.01	Is/are the GoldSim file(s) included with results?		
6.02	Is/are the Change Checklist file(s) included? (Both the word file and the signed PDF file)		
6.03	Is/are the version report(s) included?		
6.04	Do all entries in the version report(s) match the checklist(s)?		
6.05	If there are any additional files associated with the Seismic Base Case(s), are they located in the Additional_Information directory?		
6.06	Compared to the Master Case, are there any additional scenario specific changes, other than simulation settings, required to run the Seismic Base Case(s) from the Master Case?		
7.00	**Change Control Check**		
7.01	Does/Do the Change Approval Form(s) need to be revised to address additional scope discovered during version change?		
7.02	Does the Master Case originate from the previous Master Case?		
7.03	Are all input file transfers controlled by the Input Database and associated file elements?		
7.04	Are all DLL file transfers controlled by the Input Database and associated file elements?		
7.05	Was the Master Case versioned before the Base Cases were run?		
7.06	Was a database download performed before running the Base Cases?		
7.07	If this Master Case requires changes to an external file, are copies of the modified files placed in the Additional_Information directory for the Master Case?		
7.08	Is the Master Case checklist consistent with the Master Case Goldsim version report?		
7.09	Are all changes associated with input changes and conceptual model changes documented with sufficient source information in the checklist? (i.e. TMRB proposal #, DTN change, error log entry, new AMR etc.)		
7.10	Are the Base Case checklists consistent with the Base Case Goldsim version reports?		

00817DC_0010.ai

Figure 2-4. Example of the TSPA-LA Model Implementation Checklist (Continued)

Model ID:			TSPA Analyst Name: Signature:
Checker Name: Signature:			Date:
No.	Check Questions	Y, N, or NA	Notes
8.00	**Element Level Check**		
8.01	Are all new inputs, if any, added to the Input Database? Are new input elements connected to the Input Database?		
8.02	Have all changed/added Goldsim elements been checked against their source information to verify that they were changed correctly?		
8.03	If a cloned element was changed, was the changed element and at least one of its clones checked to be identical?		
8.04	Are the input links of added elements correct?		
8.05	Are the output links of added parameters correct?		
8.06	Are the links to and from any deleted elements appropriately reconnected?		
8.07	Are all changes to external files correct?		
9.00	**Conceptual Level Check**		
9.01	Is the conceptual description consistent with the change approval form?		
9.02	Is the Master Case Change Checklist consistent with the conceptual description?		
9.03	Are all conceptual model changes made in the Master Case?		
9.04	Is mass conserved within each major subsystem?		
9.05	Can each entry in the GoldSim run log be shown to have no/negligible impact on the run?		
10.00	**Error Tracking**		
10.01	Are there any model errors in this case that will be addressed in a future version of the model?		
10.02	Are errors noted by 10.01 adequately described in the error log, including a proposed correction?		
10.03	Are there any previously logged model errors addressed in this case?		
10.04	If errors noted by 10.03 are addressed in this case, is their treatment adequately documented in this case's conceptual description and Master Case checklist.		
10.05	If errors noted by 10.03 are addressed in this case, has the error log entry been updated to reflect that the correction has been made?		

00817DC_0011.ai

Figure 2-4. Example of the TSPA-LA Model Checking Implementation Checklist (Continued)

Concept Analyst Checklist for TSPA Model Version:			
Analyst (name): Analyst (sig): Date:		Checker (name): Checker (sig): Date:	
1.00	**Conceptual Level Check**	**Y,N, or n/a**	**Notes**
1.01	Is the objective adequately and clearly stated?		
	Are the conceptual descriptions sufficiently detailed to:		
1.02	Understand it's purpose?		
1.03	Explain what is intended to be done?		
1.04	Explain how it is intended to be done?		
1.05	Explain why it is being done?		
1.06	Properly designed for each relevant scenario?		
1.07	Does the implementation address the conceptual design in detail and intent for each scenario?		
1.08	Does the conceptual design, it's implementation, and analysis of results accomplish the stated purpose?		
1.09	Does the modified portion of the model respond appropriately to its inputs?		
1.10	Do the model components downstream from the modifications respond appropriately?		
1.11	Are model inputs and outputs within their specified ranges?		
1.12	Can the final dose results be explained in terms of upstream parameters (e.g., waste package/drip shield failure curves, seepage flow, pH, solubilities, EBS release rates)?		
1.13	Did the modification(s) invalidate or bring into question assumptions of an upstream or downstream conceptual model?		
1.14	Is the model implemented correctly for all scenario classes?		
1.15	Are there any unintended behaviors that cannot be explained?		
1.16	Is there additional work needed or outstanding issues generated as a result of this work?		

00817DC_0033.ai

Figure 2-5. Example of the TSPA-LA Model Concept Checklist

INTENTIONALL LEFT BLANK

3. USE OF SOFTWARE

A number of software codes were implemented to support the development of the TSPA-LA Model. Some of the software codes were used to provide supporting information and some were directly implemented in the TSPA-LA Model using the GoldSim simulation software code. Supporting software codes, including process models, were developed and operated externally before running the TSPA-LA Model. Software codes directly implemented in the TSPA-LA Model are generally referred to as abstractions and are run within the TSPA-LA Model. All software codes used to support the TSPA-LA Model are qualified and have been placed under the control of SCM per IM-PRO-003, *Software Management*. Each qualified software code is in SCM and uniquely identified with a tracking number. The SCM database also includes information on the software name, version, hardware platform, and operating system under which the software code was qualified. All software documentation, including the software media, is linked to this tracking number.

The software codes used to support the TSPA-LA Model are listed in Table 3-1 along with their unique STNs. A few of the software codes (e.g., GoldSim, SEEPAGE, and FEHM) are identified here in Section 3 with several versions, because they were used for the development and prototyping of the TSPA-LA Model. The software codes used in the TSPA-LA Model that are validated in Section 7 and used to develop the results and conclusions presented in Section 8 are identified in Table 3-1 and individually discussed in Section 6. Brief descriptions of the primary function(s) of the software codes are also provided in Sections 3.1 through 3.22. The software codes used to support the TSPA-LA Model were selected because they were either developed specifically for use with the TSPA-LA Model or considered to be the most suitable software codes on the Yucca Mountain Project Software Baseline. As a result, there are no limitations on the outputs of any of the software codes used to support the TSPA-LA Model. All software codes used for the TSPA-LA were qualified in accordance with the procedures that were in place at the time of their qualification.

Qualification documentation for each software code is available in SCM as well as the Records Processing Center. All software codes were obtained from SCM, were appropriate for use in this analysis, and each was used within the software's range of validation. Unless noted otherwise, the software codes described below are directly linked to the GoldSim software code used during the TSPA-LA analyses.

Installation of Qualified TSPA-LA Software Codes on TSPA-LA Department Computers—The installation process for each software code listed in this section was followed to ensure that there was a proper, qualified (i.e., in accordance with governing project procedures and controlled by SCM) installation by personnel authorized by SCM. Because installation procedures have changed during the course of developing the TSPA-LA Model, the installation process is described in one of the following types of documents: Installation Test Process, Software Management Report, or User Information Document.

In order to run the TSPA-LA Model, two types of installations were performed: the GoldSim installation and supporting DLL installations. The installations for GoldSim and callable DLL software routines have the following similarities: (1) both types of installations are qualified, (2) both document the installations using a procedurally required form called a Software User

Request, and (3) both collect the objective evidence of the installation and forward it to SCM. SCM then submits the installation documentation to the Records Processing Center.

One key difference between GoldSim and the callable DLLs is that GoldSim is installed on all master computers, remote processors, and local (desktop) computers, whereas DLLs are only installed on a single computer identified as the PA_Cronus. The PA_Cronus is a TSPA-LA computer that serves as a file server to all the other computers in the TSPA-LA Department. The single installation of the DLLs on the PA_Cronus is possible because of the nature of the GoldSim qualification.

When GoldSim was qualified, the qualification process verified and tested that the DLLs, input files, and database parameters were obtained from the PA_Cronus file server and properly distributed to remote processors as part of the GoldSim distributed processing environment.

In summary, the TSPA-LA Model was run on TSPA-LA Department distributed processing network computers using qualified installations of GoldSim and the DLLs.

TSPA-LA Model Computing Environment—The computer system utilized for the TSPA-LA Model is based on a TSPA-wulf personal computer cluster consisting of more than 752 processors (Figure 3-1) with 6 to 16 GB of RAM available to each processor (note that TSPA-wulf is a TSPA-LA phrase that refers to building a supercomputer by interconnecting a cluster of off-the-shelf personal computers). Realizations are fed from a central server to the processors to accomplish the distributed processing. When this report was prepared, run time for the TSPA-LA Model was approximately two hours for each realization.

This system has evolved and become more powerful with each successive iteration of the TSPA-LA. The numbers of processors utilized, processor speed, and physical memory have increased by an order of magnitude. This allows the TSPA-LA Model to incorporate more detail and provide rapid turnaround as analyses are developed. The architecture of the computing environment is shown on Figure 3-2. The system has 30 master servers for distributing jobs or analyses. A large file server contains storage for input and output files and the TSPA-LA Input Database. The system has a backup power supply and is capable of remote access, if necessary.

3.1 INTRODUCTION

The sections that follow identify the following types of information: (1) name of software; (2) brief description of software; (3) relationship to the TSPA-LA Model (i.e., used for model development only, model development and final model, or final model only); (4) location of software documentation; and (5) statement regarding use of code within range of validation. The sections are listed in alphabetical order. The tables that contain the software documents are numbered to match the section number in which they are described.

3.2 ASHPLUME_DLL_LA

3.2.1 Description of Software

All versions of ASHPLUME_DLL_LA used in the TSPA-LA Model documented in this report have the following general capabilities:

- Are called from another program that conforms to the external interface method and function calls described in *User's Guide, GoldSim Probabilistic Simulation Environment* (GoldSim Technology Group 2007 [DIRS 181727]) listed in Table 3-8
- Provide GoldSim with the ability to perform calculations not included in the standard capabilities of GoldSim
- Calculate the waste and ash areal depositional densities on the ground surface from a hypothetical volcanic eruption through the repository (Section 6.5.2)
- Transfer information back and forth to the GoldSim software running the TSPA-LA Model.

3.2.2 Relationship to the TSPA-LA Model

ASHPLUME_DLL_LA V2.0 (STN: 11117-2.0-00 [DIRS 181034]) was used for the TSPA-LA Model development.

ASHPLUME_DLL_LA V2.1 (STN: 11117-2.1-00 [DIRS 181035]) was used for the TSPA-LA Model development and TSPA-LA Model validation and analysis cases.

ASHPLUME_DLL_LA V2.1 (STN: 11117-2.1-01 [DIRS 180147]) was used for the TSPA-LA Model development and TSPA-LA Model validation and analysis cases.

3.2.3 Software Documentation

The software documents for the versions of ASHPLUME_DLL_LA mentioned in Section 3.2.2 are listed in Table 3-2.

3.2.4 Range of Validation

The range of validation for the versions of ASHPLUME_DLL_LA listed in Section 3.2.2 is defined by the documented functionality (i.e., requirements) and range(s) of acceptable inputs. The requirements are located in the respective requirements documents listed in Table 3-2. The range(s) of acceptable inputs is discussed in the respective design and user documents listed in Table 3-2.

3.3 CWD

3.3.1 Description of Software

All versions of CWD used in the TSPA-LA Model documented in this report have the following general capabilities:

- Are called from another program that conforms to the external interface method and function calls described in *User's Guide, GoldSim Probabilistic Simulation Environment* (GoldSim Technology Group 2007 [DIRS 181727]) listed in Table 3-8
- Provide GoldSim with the ability to perform calculations not included in the standard capabilities of GoldSim
- Implement the abstraction results of the probability of occurrence and size of manufacturing defects in the closure lid welds of the Alloy 22 WP outer surface
- Transfer information back and forth to the GoldSim software running the TSPA-LA Model.

3.3.2 Relationship to the TSPA-LA Model

CWD V2.0 (STN: 10363-2.0-00 [DIRS 162809]) was used for the TSPA-LA Model development and TSPA-LA Model validation and analysis cases. CWD V2.0 (STN: 10363-2.0-01 [DIRS 181037]) was used for the TSPA-LA Model development and TSPA-LA Model validation and analysis cases.

3.3.3 Software Documentation

The software documents for the versions of CWD mentioned in Section 3.3.2 are listed in Table 3-3.

3.3.4 Range of Validation

The range of validation for the versions of CWD listed in Section 3.3.2 is defined by the documented functionality (i.e., requirements) and range(s) of acceptable inputs. The requirements are located in the Software Management Report listed in Table 3-3. The range(s) of acceptable inputs is discussed in the respective design and user documents listed in Table 3-3.

3.4 EXDOC_LA

3.4.1 Description of Software

EXDOC_LA V2.0 (STN: 11193-2.0-00 [DIRS 182102]) calculates the expected annual dose, as well as, statistics for expected annual dose (i.e., mean and quantiles) for each modeling case.

3.4.2 Relationship to the TSPA-LA Model

EXDOC_LA V2.0 was used for the TSPA-LA Model development and TSPA-LA Model validation and analysis cases. A controlled version of EXDOC_LA V2.0 was used prior to a qualified version.

3.4.3 Software Documentation

The software documents for the version of EXDOC_LA V2.0 mentioned in Section 3.4.2 are listed in Table 3-4.

3.4.4 Range of Validation

The range of validation for the version of EXDOC_LA listed in Section 3.4.2 is defined by the documented functionality (i.e., requirements) and range(s) of acceptable inputs. The requirements are located in the requirements document listed in Table 3-4. The range(s) of acceptable inputs is discussed in the design and user documents listed in Table 3-4.

3.5 FAR

3.5.1 Description of Software

All versions of FAR used in the TSPA-LA Model documented in this report have the following general capabilities:

- Are called from another program that conforms to the external interface method and function calls described in *User's Guide, GoldSim Probabilistic Simulation Environment* (GoldSim Technology Group 2007 [DIRS 181727]) listed in Table 3-8
- Provide GoldSim with the ability to perform calculations not included in the standard capabilities of GoldSim
- Implement the Fortymile Wash volcanic ash redistribution (Section 6.5.2) into the TSPA-LA Model
- Transfer information back and forth to the GoldSim software running the TSPA-LA Model.

3.5.2 Relationship to the TSPA-LA Model

FAR V1.1 (STN: 11190-1.1-00 [DIRS 180002]) was used for the TSPA-LA Model development. FAR V1.2 (STN: 11190-1.2-00 [DIRS 182225]) was used for the TSPA-LA Model validation and analysis cases.

A controlled version of FAR V1.2 was used prior to a qualified version. After qualification, FAR V1.2 was obtained from SCM in accordance with the governing procedure (IM-PRO-003) and installed. The FAR V1.2 installation package documents the confirmation that the

controlled version of FAR V1.2 is identical to the qualified version of FAR V1.2 obtained from SCM.

3.5.3 Software Documentation

The software documents for the versions of FAR mentioned in Section 3.5.2 are listed in Table 3-5.

3.5.4 Range of Validation

The range of validation for the versions of FAR listed in Section 3.5.2 is defined by the documented functionality (i.e., requirements) and range(s) of acceptable inputs. The requirements are located in the respective requirements documents listed in Table 3-5. The range(s) of acceptable inputs is discussed in the respective design and user documents listed in Table 3-5.

3.6 FEHM

3.6.1 Description of Software

All versions of FEHM used in the TSPA-LA Model documented in this report have the following general capabilities:

- Are called from another program that conforms to the external interface method and function calls described in the *User's Guide, GoldSim Probabilistic Simulation Environment* (GoldSim Technology Group 2007 [DIRS 181727]) listed in Table 3-8
- Provide GoldSim with the ability to perform calculations not included in the standard capabilities of GoldSim
- Calculate the transport of radionuclides through the UZ
- Transfer information back and forth to the GoldSim software running the TSPA-LA Model.

3.6.2 Relationship to the TSPA-LA Model

FEHM V2.23 (STN: 10086-2.23-00 [DIRS 173139]) was used for the TSPA-LA Model development.

FEHM V2.24-01 (STN: 10086-2.24-01-00 [DIRS 179419]) was used for the TSPA-LA Model validation and analysis cases.

3.6.3 Software Documentation

The software documents for the versions of FEHM mentioned in Section 3.6.2 are listed in Table 3-6.

3.6.4 Range of Validation

The range of validation for the versions of FEHM listed in Section 3.6.2 is defined by the documented functionality (i.e., requirements) and range(s) of acceptable inputs. The requirements are located in the respective requirements documents listed in Table 3-6. The range(s) of acceptable inputs is discussed in the respective design and user documents listed in Table 3-6.

3.7 GETTHK_LA

3.7.1 Description of Software

GetThk_LA V1.0 (STN: 11229-1.0-00 [DIRS 181040]) has the following general capabilities:

- Is called from another program that conforms to the external interface method and function calls described in the *User's Guide, GoldSim Probabilistic Simulation Environment* (GoldSim Technology Group 2007 [DIRS 181727]) listed in Table 3-8
- Provides GoldSim with the ability to perform calculations not included in the standard capabilities of GoldSim
- Reads WAPDEG output for the Seismic Scenario Class and calculates statistics (Section 6.6)
- Transfers information back and forth to the GoldSim software running the TSPA-LA Model.

3.7.2 Relationship to the TSPA-LA Model

GetThk_LA V1.0 was used for the TSPA-LA Model validation and analysis cases.

3.7.3 Software Documentation

The software documents for the version of GetThk_LA V1.0 mentioned in Section 3.7.2 are listed in Table 3-7.

3.7.4 Range of Validation

The range of validation for the version of GetThk_LA listed in Section 3.7.2 is defined by the documented functionality (i.e., requirements) and range(s) of acceptable inputs. The requirements are located in the respective requirements documents listed in Table 3-7. The range(s) of acceptable inputs is discussed in the respective design and user documents listed in Table 3-7.

3.8 GOLDSIM

3.8.1 Description of Software

All versions of GoldSim used in the TSPA-LA Model documented in this report have the following general capabilities:

- Address the inherent variability and uncertainty that is present in real-world systems by using Monte Carlo simulation
- Superimpose the occurrence and consequences of discrete events onto continuously varying systems
- Build top-down models using hierarchical containers that facilitate the simulation of large, complex systems that are easy to understand and navigate
- Dynamically link external programs or spreadsheets directly to the GoldSim software
- Directly exchange information between any Open Database Connectivity (ODBC)-compliant (Yucca Mountain Structured) database and GoldSim.

3.8.2 Relationship to the TSPA-LA Model

GoldSim V9.60. (STN: 10344-9.60-00 [DIRS 180224]) was used for the TSPA-LA Model development.

GoldSim V9.60.100 (STN: 10344-9.60-01 [DIRS 181903]) was used for the TSPA-LA Model development and TSPA-LA Model validation and analysis cases.

A controlled version of GoldSim V9.60.100 was used prior to a qualified version. After qualification, GoldSim V9.60.100 was obtained from SCM in accordance with the governing procedure (IM-PRO-003) and installed. The GoldSim V9.60.100 installation package documents the confirmation that the controlled version of GoldSim V9.60.100 is identical to the qualified version of GoldSim V9.60.100 obtained from SCM.

3.8.3 Software Documentation

The software documents for the versions of GoldSim mentioned in Section 3.8.2 are listed in Table 3-8.

3.8.4 Range of Validation

The range of validation for the versions of GoldSim listed in Section 3.8.2 is defined by the documented functionality (i.e., requirements) and range(s) of acceptable inputs. The requirements are located in the respective requirements documents listed in Table 3-8. The range(s) of acceptable inputs is discussed in the respective design and user documents listed in Table 3-8.

3.9 INTERPZDLL_LA

3.9.1 Description of Software

All versions of InterpZdll_LA used in the TSPA-LA Model documented in this report have the following general capabilities:

- Are called from another program that conforms to the external interface method and function calls described in *User's Guide, GoldSim Probabilistic Simulation Environment* (GoldSim Technology Group 2007 [DIRS 181727]) listed in Table 3-8
- Provide GoldSim the ability to perform calculations not included in the standard capabilities of GoldSim
- Provide interpolation capabilities for the EBS Chemical Environment Submodel of the TSPA-LA Model (Section 6.3.4)
- Transfer information back and forth to the GoldSim software running the TSPA-LA Model.

3.9.2 Relationship to the TSPA-LA Model

InterpZdll_LA V1.0 (STN: 11107-1.0-00 [DIRS 167885]) was used for the TSPA-LA Model development and TSPA-LA Model validation and analysis cases.

InterpZdll_LA V1.0 (STN: 11107-1.0-01 [DIRS 181043]) was used for the TSPA-LA Model development and TSPA-LA Model validation and analysis cases.

3.9.3 Software Documentation

The software documents for the versions of InterpZdll_LA mentioned in Section 3.9.2 are listed in Table 3-9.

3.9.4 Range of Validation

The range of validation for the versions of InterpZdll_LA listed in Section 3.9.2 is defined by the documented functionality (i.e., requirements) and range(s) of acceptable inputs. The requirements are located in the Software Management Report listed in Table 3-9. The range(s) of acceptable inputs is discussed in the respective design and user documents listed in Table 3-9.

3.10 MFCP_LA

3.10.1 Description of Software

All versions of MFCP_LA used in the TSPA-LA Model documented in this report have the following general capabilities:

- Are called from another program that conforms to the external interface method and function calls described in *User's Guide, GoldSim Probabilistic Simulation Environment* (GoldSim Technology Group 2007 [DIRS 181727]) listed in Table 3-8
- Provide GoldSim with the ability to perform calculations not included in the standard capabilities of GoldSim
- Control the selection of input files for various DLLs that are part of the TSPA-LA Model
- Transfer information back and forth to the GoldSim software running the TSPA-LA Model.

3.10.2 Relationship to the TSPA-LA Model

MFCP_LA V1.0 (STN: 11071-1.0-00 [DIRS 167884]) was used for the TSPA-LA Model development and TSPA-LA Model validation and analysis cases.

MFCP_LA V1.0 (STN: 11071-1.0-01 [DIRS 181045]) was used for the TSPA-LA Model development and TSPA-LA Model validation and analysis cases.

3.10.3 Software Documentation

The software documents for the versions of MFCP_LA mentioned in Section 3.10.2 are listed in Table 3-10.

3.10.4 Range of Validation

The range of validation for the versions of MFCP_LA listed in Section 3.10.2 is defined by the documented functionality (i.e., requirements) and range(s) of acceptable inputs. The requirements are located in the Software Management Report listed in Table 3-10. The range(s) of acceptable inputs is discussed in the respective design and user documents listed in Table 3-10.

3.11 MKTABLE AND MKTABLE_LA

3.11.1 Description of Software

All versions of MkTable and MkTable_LA used in the TSPA-LA Model documented in this report have the following general capabilities:

- Are called from another program that conforms to the external interface method and function calls described in *User's Guide, GoldSim Probabilistic Simulation Environment* (GoldSim Technology Group 2007 [DIRS 181727]) listed in Table 3-8
- Provide GoldSim with the ability to perform calculations not included in the standard capabilities of GoldSim
- Control the selection of input files for various DLLs that are part of the TSPA-LA Model
- Transfer information back and forth to the GoldSim software running the TSPA-LA Model.

3.11.2 Relationship to the TSPA-LA Model

MkTable V1.00 (STN: 10505-1.00-00 [DIRS 174528]) was used for the TSPA-LA Model development.

MkTable_LA V1.0 (STN: 11217-1.0-00 [DIRS 181047]) was used for the TSPA-LA Model development and TSPA-LA Model validation and analysis cases.

MkTable_LA V1.0 (STN: 11217-1.0-01 [DIRS 181048]) was used for the TSPA-LA Model development and TSPA-LA Model validation and analysis cases.

3.11.3 Software Documentation

The software documents for the versions of MkTable_LA mentioned in Section 3.11.2 are listed in Table 3-11.

3.11.4 Range of Validation

The range of validation for the versions of MkTable_LA listed in Section 3.11.2 is defined by the documented functionality (i.e., requirements) and range(s) of acceptable inputs. The requirements are located in the Software Management Report and the respective requirements documents listed in Table 3-11. The range(s) of acceptable inputs is discussed in the respective design and user documents listed in Table 3-11.

3.12 MVIEW

3.12.1 Description of Software

MVIEW V4.0 (STN: 10072-4.0-01 [DIRS 181049]) is a stand-alone executable program that transforms text output describing numeric model geometry and numeric model output into two-dimensional and three-dimensional visual representations.

3.12.2 Relationship to the TSPA-LA Model

MVIEW V4.0 is not part of the TSPA-LA Model. Rather, MVIEW is used to interpret the results of the TSPA-LA Model using two-dimensional and three-dimensional visual representations. MVIEW V4.0 is also used to statistically analyze the TSPA-LA Model output.

3.12.3 Software Documentation

The software documents for the version of MVIEW 4.0 mentioned in Section 3.12.2 are listed in Table 3-12.

3.12.4 Range of Validation

The range of validation for the version of MVIEW listed in Section 3.12.2 is defined by the documented functionality (i.e., requirements) and range(s) of acceptable inputs. The requirements are located in the requirements document listed in Table 3-12. The range(s) of acceptable inputs is discussed in the design and user documents listed in Table 3-12.

3.13 PASSTABLE1D_LA

3.13.1 Description of Software

All versions of PassTable1D_LA used in the TSPA-LA Model documented in this report have the following general capabilities:

- Are called from another program that conforms to the external interface method and function calls described in *User's Guide, GoldSim Probabilistic Simulation Environment* (GoldSim Technology Group 2007 [DIRS 181727]) listed in Table 3-8
- Provide GoldSim with the ability to perform calculations not included in the standard capabilities of GoldSim
- Read one-dimensional tabular information from an input file and pass that information into GoldSim in a format that is compatible with the external definition of a one-dimensional look-up table element
- Support the evaluation of localized corrosion on the WPs.

3.13.2 Relationship to the TSPA-LA Model

PassTable1D_LA V1.0 (STN: 11142-1.0-00 [DIRS 169130]) was used for the TSPA-LA Model development.

PassTable1D_LA V1.0 (STN: 11142-1.0-01 [DIRS 181050]) was used for the TSPA-LA Model development.

PassTable1D_LA V2.0 (STN: 11142-2.0-00 [DIRS 181051] was used for the TSPA-LA Model development and TSPA-LA Model validation and analysis cases.

3.13.3 Software Documentation

The software documents for the versions of PassTable1D_LA mentioned in Section 3.13.2 are listed in Table 3-13.

3.13.4 Range of Validation

The range of validation for the versions of PassTable1D_LA listed in Section 3.13.2 is defined by the documented functionality (i.e., requirements) and range(s) of acceptable inputs. The requirements are located in the Software Management Report and respective requirements documents listed in Table 3-13. The range(s) of acceptable inputs is discussed in the respective design and user documents listed in Table 3-13.

3.14 PASSTABLE3D_LA

3.14.1 Description of Software

All versions of PassTable3D_LA used in the TSPA-LA Model documented in this report have the following general capabilities:

- Are called from another program that conforms to the external interface method and function calls described in *User's Guide, GoldSim Probabilistic Simulation Environment* (GoldSim Technology Group 2007 [DIRS 181727]) listed in Table 3-8
- Provide GoldSim with the ability to perform calculations not included in the standard capabilities of GoldSim
- Read three-dimensional tabular information from an input file and pass that information into GoldSim in a format that is compatible with the external definition of a three-dimensional look-up table element
- Support the evaluation of localized corrosion on the WPs (Sections 6.3.5).

3.14.2 Relationship to the TSPA-LA Model

PassTable3D_LA V1.0 (STN: 11143-1.0-00 [DIRS 168980]) was used for the TSPA-LA Model development and TSPA-LA Model validation and analysis cases.

PassTable3D_LA V1.0 (STN: 11143-1.0-01 [DIRS 181052]) was used for the TSPA-LA Model development and TSPA-LA Model validation and analysis cases.

PassTable3D_LA V2.0 (STN: 11143-2.0-00 [DIRS 182556]) was used for the TSPA-LA Model development and TSPA-LA Model validation and analysis cases.

3.14.3 Software Documentation

The software documents for the versions of PassTable3D_LA mentioned in Section 3.14.2 are listed in Table 3-14.

3.14.4 Range of Validation

The range of validation for the versions of PassTable3D_LA listed in Section 3.14.2 is defined by the documented functionality (i.e., requirements) and range(s) of acceptable inputs. The requirements are located in the Software Management Report and the respective requirements documents listed in Table 3-14. The range(s) of acceptable inputs is discussed in the respective design and user documents listed in Table 3-14.

3.15 PREWAP_LA

3.15.1 Description of Software

PREWAP_LA V1.1 (STN: 10939-1.1-00 [DIRS 181053]) has the following general capabilities:

- Implements the processing of output files produced by the Multiscale Thermal-Hydrologic Abstraction software, MSTHAC V7.0 (STN: 10419-7.0-00 [DIRS 164274]).
- Processes files from MSTHAC V7.0 as input for DLLs (e.g., WAPDEG) (STN: 10000-4.07-00 [DIRS 181774]), which are components of the TSPA-LA Model.

3.15.2 Relationship to the TSPA-LA Model

PREWAP_LA V1.1 was used for the TSPA-LA Model development and TSPA-LA Model validation and analysis cases.

3.15.3 Software Documentation

The software documents for the version of PREWAP_LA V1.1 mentioned in Section 3.15.2 are listed in Table 3-15.

3.15.4 Range of Validation

The range of validation for the version of PREWAP_LA listed in Section 3.15.2 is defined by the documented functionality (i.e., requirements) and range(s) of acceptable inputs. The

requirements are located in the requirements document listed in Table 3-15. The range(s) of acceptable inputs is discussed in the design and user documents listed in Table 3-15.

3.16 SCCD

3.16.1 Description of Software

All versions of SCCD used in the TSPA-LA Model documented in this report have the following general capabilities:

- Are called from another program that conforms to the external interface method and function calls described in *User's Guide, GoldSim Probabilistic Simulation Environment* (GoldSim Technology Group 2007 [DIRS 181727]) listed in Table 3-8
- Provide GoldSim with the ability to perform calculations not included in the standard capabilities of GoldSim
- Implement the abstraction results of the stress and stress-intensity factor profiles in the closure-lid welds of the Alloy 22 WP outer surface
- Transfer information back and forth to the GoldSim software running the TSPA-LA Model.

3.16.2 Relationship to the TSPA-LA Model

SCCD V2.01 (STN: 10343-2.01-00 [DIRS 181157]) was used for the TSPA-LA Model development and TSPA-LA Model validation and analysis cases.

SCCD V2.01 (STN: 10343-2.01-01 [DIRS 181054]) was used for the TSPA-LA Model development and TSPA-LA Model validation and analysis cases.

3.16.3 Software Documentation

The software documents for the versions of SCCD mentioned in Section 3.16.2 are listed in Table 3-16.

3.16.4 Range of Validation

The range of validation for the versions of SCCD listed in Section 3.16.2 is defined by the documented functionality (i.e., requirements) and range(s) of acceptable inputs. The requirements are located in the Software Routine Report listed in Table 3-16. The range(s) of acceptable inputs is discussed in the respective design and user documents listed in Table 3-16.

3.17 SEEPAGEDLL_LA

3.17.1 Description of Software

All versions of SEEPAGEDLL_LA used in the TSPA-LA Model documented in this report have the following general capabilities:

- Are called from another program that conforms to the external interface method and function calls described in *User's Guide, GoldSim Probabilistic Simulation Environment* (GoldSim Technology Group 2007 [DIRS 181727]) listed in Table 3-8
- Provide GoldSim with the ability to perform calculations not included in the standard capabilities of GoldSim
- Implement the Drift Seepage Abstraction (Section 6.3.3.1.2) into the TSPA-LA Model
- Transfer information back and forth to the GoldSim software running the TSPA-LA Model.

3.17.2 Relationship to the TSPA-LA Model

SEEPAGEDLL_LA V1.2 (STN: 11076-1.2-00 [DIRS 173435]) was used for the TSPA-LA Model development.

SEEPAGEDLL_LA V1.3 (STN: 11076-1.3-00 [DIRS 180318]) was used for the TSPA-LA Model development and TSPA-LA Model validation and analysis cases.

SEEPAGEDLL_LA V1.3 (STN: 11076-1.3-01 [DIRS 181058]) was used for the TSPA-LA Model development and TSPA-LA Model validation and analysis cases.

3.17.3 Software Documentation

The software documents for the versions of SEEPAGEDLL_LA mentioned in Section 3.17.2 are listed in Table 3-17.

3.17.4 Range of Validation

The range of validation for the versions of SEEPAGEDLL_LA listed in Section 3.17.2 is defined by the documented functionality (i.e., requirements) and range(s) of acceptable inputs. The requirements are located in the respective requirements documents listed in Table 3-17. The range(s) of acceptable inputs is discussed in the respective design and user documents listed in Table 3-17.

3.18 SOILEXP_LA

3.18.1 Description of Software

SOILEXP_LA V1.0 (STN: 10933-1.0-00 [DIRS 167883]) has the following general capabilities:

- Is called from another program that conforms to the external interface method and function calls described in *User's Guide, GoldSim Probabilistic Simulation Environment* (GoldSim Technology Group 2007 [DIRS 181727]) listed in Table 3-8
- Provides GoldSim with the ability to perform calculations not included in the standard capabilities of GoldSim
- Calculates the cumulative redistribution factors used to calculate the radionuclide concentration in volcanic ash after it is deposited
- Transfers information back and forth to the GoldSim software running the TSPA-LA Model.

3.18.2 Relationship to the TSPA-LA Model

SOILEXP_LA V1.0 was used for the TSPA-LA Model development.

3.18.3 Software Documentation

The software document for the version of SoilExp_LA V1.0 mentioned in Section 3.18.2 is listed in Table 3-18.

3.18.4 Range of Validation

The range of validation for the version of SoilExp_LA listed in Section 3.18.2 is defined by the documented functionality (i.e., requirements) and range(s) of acceptable inputs. The requirements are located in the Software Management Report listed in Table 3-18. The range(s) of acceptable inputs is discussed in the design and user documents listed in Table 3-18.

3.19 SZ_CONVOLUTE

3.19.1 Description of Software

All versions of SZ_Convolute used in the TSPA-LA Model documented in this report have the following general capabilities:

- Are called from another program that conforms to the external interface method and function calls described in *User's Guide, GoldSim Probabilistic Simulation Environment* (GoldSim Technology Group 2007 [DIRS 181727]) listed in Table 3-8

- Provide GoldSim with the ability to perform calculations not included in the standard capabilities of GoldSim
- Calculate the radionuclide mass-flux rates in accordance with the three-dimensional SZ Flow and Transport Abstraction (Section 6.3.10)
- Transfer information back and forth to the GoldSim software running the TSPA-LA Model.

3.19.2 Relationship to the TSPA-LA Model

SZ_Convolute V3.0 (STN: 10207-3.0-00 [DIRS 164180]) was used for the TSPA-LA Model development.

SZ_Convolute V3.10.01 (STN: 10207-3.10.01-00 [DIRS 181060]) was used for the TSPA-LA Model development and TSPA-LA-LA Model validation and analysis cases.

3.19.3 Software Documentation

The software documents for the versions of SZ_Convolute mentioned in Section 3.19.2 are listed in Table 3-19.

3.19.4 Range of Validation

The range of validation for the versions of SZ_Convolute listed in Section 3.19.2 is defined by the documented functionality (i.e., requirements) and range(s) of acceptable inputs. The requirements are located in the respective requirements documents listed in Table 3-19. The range(s) of acceptable inputs is discussed in the respective design and user documents listed in Table 3-19.

3.20 TSPA_INPUT_DB

3.20.1 Description of Software

All versions of TSPA_Input_DB used in the TSPA-LA Model documented in this report are a Microsoft Access database that is used as a quality-controlled storage area for the TSPA-LA Model input parameters. The parameter values are maintained as originally entered (i.e., no manipulations or post-processing of the parameter values are performed). The database is capable of interfacing via ODBC for automated download to the TSPA-LA Model.

3.20.2 Relationship to the TSPA-LA Model

TSPA_Input_DB V2.2 (STN: 10931-2.2-00 [DIRS 181061]) was used for the TSPA-LA Model development and TSPA-LA Model validation and analysis cases.

TSPA_Input_DB V2.2 (STN: 10931-2.2-01 [DIRS 181062]) was used for the TSPA-LA Model validation and analysis cases.

3.20.3 Software Documentation

The software documents for the versions of the TSPA_Input_DB mentioned in Section 3.20.2 are listed in Table 3-20.

3.20.4 Range of Validation

The range of validation for the versions of TSPA_Input_DB listed in Section 3.20.2 is defined by the documented functionality (i.e., requirements) and range(s) of acceptable inputs. The requirements are located in the respective requirements documents listed in Table 3-20. The range(s) of acceptable inputs is discussed in the respective design and user documents listed in Table 3-20.

3.21 WAPDEG

3.21.1 Description of Software

All versions of WAPDEG used in the TSPA-LA Model documented in this report have the following general capabilities:

- Are called from another program that conforms to the external interface method and function calls described in *User's Guide, GoldSim Probabilistic Simulation Environment* (GoldSim Technology Group 2007 [DIRS 181727]) listed in Table 3-8
- Provide GoldSim with the ability to perform calculations not included in the standard capabilities of GoldSim
- Implement the general corrosion, SCC, and MIC abstractions used in the TSPA-LA Model
- Calculate DS and WP failure profiles
- Transfer information back and forth to the GoldSim software running the TSPA-LA Model.

3.21.2 Relationship to the TSPA-LA Model

WAPDEG V4.07 (STN: 10000-4.07-00 [DIRS 181774]) was used for the TSPA-LA Model development and TSPA-LA Model validation and analysis cases.

WAPDEG V4.07 (STN: 10000-4.07-01 [DIRS 181064]) was used for the TSPA-LA Model development and TSPA-LA Model validation and analysis cases.

3.21.3 Software Documentation

The software documents for the versions of WAPDEG mentioned in Section 3.21.2 are listed in Table 3-21.

3.21.4 Range of Validation

The range of validation for the versions of WAPDEG listed in Section 3.21.2 are defined by the documented functionality (i.e., requirements) and range(s) of acceptable inputs. The requirements are located in the respective requirements documents listed in Table 3-21. The range(s) of acceptable inputs are discussed in the respective design and user documents listed in Table 3-21.

3.22 CORROBORATIVE SOFTWARE USED

Volume III, Appendix L, describes how computer code written in FORTRAN 90 was used to develop a simplified model. The FORTRAN code used for this work scope will be controlled in corroborative DTN: MO0708SIMPLIFI.000 [DIRS 182980].

Table 3-1. TSPA-LA Model Software Codes

Code	Version	Software Tracking Number	Operating System	DIRS Number
ASHPLUME_DLL_LA[a1]	2.0	STN: 11117-2.0-00	Windows 2000	DIRS 181034
ASHPLUME_DLL_LA[a2]	2.1	STN: 11117-2.1-00	Windows 2000	DIRS 181035
ASHPLUME_DLL_LA[a2]	2.1	STN: 11117-2.1-01	Windows 2003	DIRS 180147
CWD[a2]	2.0	STN: 10363-2.0-00	Windows 2000	DIRS 162809
CWD[a2]	2.0	STN: 10363-2.0-01	Windows 2003	DIRS 181037
EXDOC_LA[b1]	2.0	STN: 11193-2.0-00	Windows 2000 Windows 2003 Windows XP	DIRS 182102
FAR [a1]	1.1	STN: 11190-1.1-00	Windows 2000 Windows 2003	DIRS 180002
FAR [a2]	1.2	STN: 11190-1.2-00	Windows 2000 Windows 2003	DIRS 182225
FEHM[a1]	2.23	STN: 10086-2.23-00	Windows 2000	DIRS 173139
FEHM[a2]	2.24-01	STN: 10086-2.24-01-00	Windows 2000 Windows 2003 Windows XP	DIRS 179419
GetThk_LA [a2]	1.0	STN: 11229-1.0-00	Windows 2000 Windows 2003	DIRS 181040
GoldSim[a1]	9.60	STN: 10344-9.60-00	Windows 2000 Windows 2003 Windows XP	DIRS 180224
GoldSim[a2]	9.60.100	STN: 10344-9.60-01	Windows 2000 Windows 2003 Windows XP	DIRS 181903
InterpZdll_LA [a2]	1.0	STN: 11107-1.0-00	Windows 2000	DIRS 167885
InterpZdll_LA [a2]	1.0	STN: 11107-1.0-01	Windows 2003	DIRS 181043
MFCP_LA[a2]	1.0	STN: 11071-1.0-00	Windows 2000	DIRS 167884
MFCP_LA[a2]	1.0	STN: 11071-1.0-01	Windows 2003	DIRS 181045
MkTable[a1]	1.00	STN: 10505-1.00-00	Windows 2000	DIRS 174528
MkTable_LA[a2]	1.0	STN: 11217-1.0-00	Windows 2000	DIRS 181047
MkTable_LA[a2]	1.0	STN: 11217-1.0-01	Windows 2003	DIRS 181048
MView[b1]	4.0	STN: 10072-4.0-01	Windows XP	DIRS 181049
PassTable1D_LA[a1]	1.0	STN: 11142-1.0-00	Windows 2000	DIRS 169130
PassTable1D_LA[a1]	1.0	STN: 11142-1.0-01	Windows 2003	DIRS 181050
PassTable1D_LA[a2]	2.0	STN: 11142-2.0-00	Windows 2000 Windows 2003	DIRS 181051
PassTable3D_LA[a1]	1.0	STN: 11143-1.0-00	Windows 2000	DIRS 168980
PassTable3D_LA[a1]	1.0	STN: 11143-1.0-01	Windows 2003	DIRS 181052

Table 3-1. TSPA-LA Model Software Codes (Continued)

Code	Version	Software Tracking Number	Operating System	DIRS Number
PassTable3D_LA [a2]	2.0	STN: 11143-2.0-00	Windows 2000 Windows 2003	DIRS 182556
PREWAP_LA[b1]	1.1	STN: 10939-1.1-00	Windows 2000	DIRS 181053
SCCD[a2]	2.01	STN: 10343-2.01-00	Windows 2000	DIRS 181157
SCCD[a2]	2.01	STN: 10343-2.01-01	Windows 2003	DIRS 181054
SEEPAGEDLL_LA[a1]	1.2	STN: 11076-1.2-00	Windows 2000	DIRS 173435
SEEPAGEDLL_LA[a2]	1.3	STN: 11076-1.3-00	Windows 2000	DIRS 180318
SEEPAGEDLL_LA[a2]	1.3	STN: 11076-1.3-01	Windows 2003	DIRS 181058
SoilExp_LA [a1]	1.0	STN: 10933-1.0-00	Windows 2000	DIRS 167883
SZ_Convolute[a1]	3.0	STN: 10207-3.0-00	Windows 2000	DIRS 164180
SZ_Convolute[a2]	3.10.01	STN: 10207-3.10.01-00	Windows 2000/ Windows 2003	DIRS 181060
TSPA_Input_DB[a2]	2.2	STN: 10931-2.2-00	Windows 2000	DIRS 181061
TSPA_Input_DB[a2]	2.2	STN: 10931-2.2-01	Windows 2003	DIRS 181062
WAPDEG[a2]	4.07	STN: 10000-4.07-00	Windows 2000	DIRS 181774
WAPDEG[a2]	4.07	STN: 10000-4.07-01	Windows 2003	DIRS 181064

[a1] Codes are used only for the TSPA-LA Model development (See Note Below).

[a2] Codes used in the TSPA-LA Model that are used for the TSPA-LA Model development (See Note Below) and to develop results and conclusions in Section 8.

[b1] Code is a pre- or post-processor that does not require GoldSim to run codes that are used for the TSPA-LA Model development (See Note Below) and to develop results and conclusions in Section 8.

Note: TSPA model development should not be confused with model development as described in SCI-PRO-006. TSPA model development is merely a phrase to represent the draft model versions (i.e., v4.001 to v4.047) that were created before finalizing the model (e.g., v5.000) presented in this document. These draft model versions will be submitted as part of the records package for this document. All software codes used for the results presented in this document are on the software baseline.

Table 3-2. ASHPLUME_DLL_LA Software Documents

Version 2.0 Windows 2000 (STN: 11117-2.0-00)			
Description	**Document ID**	**DIRS Number**	**Tracking Number**
Requirements Document (RD)	11117-RD-2.0-00	DIRS 167601	MOL.20031212.0438
Design Document (DD)	11117-DD-2.0-00	DIRS 167603	MOL.20031212.0439
User Manual (UM)	11117-UM-2.0-00	DIRS 167607	MOL.20031212.0444
Installation Test Process (ITP)	11117-ITP-2.0-00	DIRS 167606	MOL.20031212.0440
Validation Test Process (VTP)	11117-VTP-2.0-01	DIRS 167604	MOL.20031212.0441
Validation Test Report (VTR)	11117-VTR-2.0-00	DIRS 166506	MOL.20031212.0443
Version 2.1 Windows 2000 (STN: 11117-2.1-00)			
Description	**Document ID**	**DIRS Number**	**Tracking Number**
Requirements Document (RD)	11117-RD-2.1-00	DIRS 181073	MOL.20061106.0385
Design Document (DD)	11117-DD-2.1-00	DIRS 181075	MOL.20061106.0387
User Information Document (UID)	11117-UID-2.1-00	DIRS 181076	MOL.20070102.0242
Software Validation Report (SVR)	11117-SVR-2.1-00-WIN2000	DIRS 181077	MOL.20070102.0246
Version 2.1 Windows 2003 (STN: 11117-2.1-01)			
Description	**Document ID**	**DIRS Number**	**Tracking Number**
Requirements Document (RD)	Same as above	NA	NA
Design Document (DD)	Same as above	NA	NA
User Information Document (UID)	Same as above	NA	NA
Software Validation Report (SVR)	11117-SVR-2.1-01-WIN2003	DIRS 181275	MOL.20070223.0261

Table 3-3. CWD Software Documents

Version 2.0 Windows 2000 (STN: 10363-2.0-00)			
Description	**Document ID**	**DIRS Number**	**Tracking Number**
Software Management Report (SMR)	10363-SMR-2.0-00	DIRS 167564	MOL.20030501.0182
Version 2.0 Windows 2003 (STN: 10363-2.0-01)			
Description	**Document ID**	**DIRS Number**	**Tracking Number**
Software Management Report (SMR)	Same as above	NA	NA
Software Validation Report (SVR)	10363-SVR-2.0-01-WIN2003	DIRS 181079	MOL.20070209.0021

Table 3-4. EXDOC_LA Software Documents

Version 2.0 Windows 2000 (STN: 11193-2.0-00)			
Description	**Document ID**	**DIRS Number**	**Tracking Number**
Requirements Document (RD)	11193-RD-2.0-01	DIRS 182906	MOL.20070723.0260
Design Document (DD)	11193-DD-2.0-01	DIRS 182907	MOL.20070723.0262
User Information Document (UID)	11193-UID-2.0-00	DIRS 182908	MOL.20070723.0264
Software Validation Report (SVR)	11193-SVR-2.0-00-WIN2000	DIRS 182909	MOL.20070723.0266
Software Validation Report (SVR)	11193-SVR-2.0-00-WIN2003	DIRS 182910	MOL.20070723.0268
Software Validation Report (SVR)	11193-SVR-2.0-00-WINXP	DIRS 182911	MOL.20070723.0270

Table 3-5. FAR Software Documents

Version 1.1 Windows 2000 and Windows 2003 (STN:11190-1.1-00)			
Description	**Document ID**	**DIRS Number**	**Tracking Number**
Requirements Document (RD)	11190-RD-1.1-00	DIRS 181080	MOL.20070323.0326
Design Document (DD)	11190-DD-1.1-00	DIRS 181081	MOL.20070323.0328
User Information Document (UID)	11190-UID-1.1-00	DIRS 181084	MOL.20070417.0336
Software Validation Report (SVR)	11190-SVR-1.1-00-WIN2000	DIRS 181085	MOL.20070417.0338
Software Validation Report (SVR)	11190-SVR-1.1-00-WIN2003	DIRS 181087	MOL.20070417.0340
Version 1.2 Windows 2000 AND 2003 (STN: 11190-1.2-00)			
Description	**Document ID**	**DIRS Number**	**Tracking Number**
Requirements Document (RD)	11190-RD-1.2-00	DIRS 183117	MOL.20070919.0325.
Design Document (DD)	11190-DD-1.2-00	DIRS 183118	MOL.20070919.0327
User Information Document (UID)	11190-UID-1.2-00	DIRS 183116	MOL.20070919.0332
Software Validation Report (SVR)	11190-SVR-1.2-00-WIN2000	DIRS 183120	MOL.20070919.0334
Software Validation Report (SVR)	11190-SVR-1.2-00-WIN2003	DIRS 183121	MOL.20070919.0336

Table 3-6. FEHM Software Documents

Version 2.23 Windows 2000 (STN: 10086-2.23-00)			
Description	**Document ID**	**DIRS Number**	**Tracking Number**
Requirements Document (RD)	10086-RD-2.23-00	DIRS 174616	MOL.20050301.0040
Design Document (DD)	10086-DD-2.23-00	DIRS 173440	MOL.20050301.0043
User Information Document (UID)	10086-UID-2.23-00	DIRS 173441	MOL.20050301.0046
Software Validation Report (SVR)	10086-SVR-2.23-00-WIN2000	DIRS 173442	MOL.20050301.0049
Version 2.24-01 Windows 2000 and 2003 (STN: 10086-2.24-01-00)			
Description	**Document ID**	**DIRS Number**	**Tracking Number**
Requirements Document (RD)	10086-RD-2.24-00	DIRS 181094	MOL.20061127.0272
Design Document (DD)	10086-DD-2.24-01-00	DIRS 181095	MOL.20070309.0032
User Information Document (UID)	10086-UID-2.24-01-00	DIRS 181096	MOL.20070309.0037
Software Validation Report (SVR)	10086-SVR-2.24-01-00-WIN2000	DIRS 181097	MOL.20070309.0047
Software Validation Report (SVR)	10086-SVR-2.24-01-00-WIN2003	DIRS 181098	MOL.20070309.0045

Table 3-7. GetThk_LA Software Documents

Version 1.0 Windows 2000 and 2003 (STN: 11229-1.0-00)			
Description	**Document ID**	**DIRS Number**	**Tracking Number**
Requirements Document (RD)	11229-RD-1.0-00	DIRS 181100	MOL.20060915.0163
Design Document (DD)	11229-DD-1.0-00	DIRS 181101	MOL.20060915.0165
User Information Document (UID)	11229-UID-1.0-00	DIRS 181102	MOL.20060915.0169
Software Validation Report (SVR)	11229-SVR-1.0-00-WIN2000	DIRS 181104	MOL.20060915.0173
Software Validation Report (SVR)	11229-SVR-1.0-00-WIN2003	DIRS 181105	MOL.20060915.0171

Table 3-8. GoldSim Software Documents

Version 9.60 Windows 2000, Windows 2003, and Windows XP (STN: 10344-9.60-00)			
Description	**Document ID**	**DIRS Number**	**Tracking Number**
Requirements Document (RD)	10344-RD-9.60-00	DIRS 181106	MOL.20070416.0330
Design Document (DD)	10344-DD-9.60-01	DIRS 181107	MOL.20070416.0338
User Information Document (UID)	10344-UID-9.60-00	DIRS 181108	MOL.20070416.0339
User's Guide, GoldSim Probabilistic Simulation Environment, V. 9.60	NA	DIRS 181727	TIC: 259221
Software Validation Report (SVR)	10344-SVR-9.60-00-WIN2000	DIRS 181109	MOL.20070416.0341
Software Validation Report (SVR)	10344-SVR-9.60-00-WIN2003	DIRS 181110	MOL.20070416.0343
Software Validation Report (SVR)	10344-SVR-9.60-00-WINXP	DIRS 181111	MOL.20070416.0345
Version 9.60.100 Windows 2000, Windows 2003, and Windows XP (STN: 10344-9.60-01)			
Description	**Document ID**	**DIRS Number**	**Tracking Number**
Requirements Document (RD)	Same as above	NA	NA
Design Document (DD)	Same as above	NA	NA
User Information Document (UID)	Same as above	NA	NA
User's Guide, GoldSim Probabilistic Simulation Environment, V. 9.60	Same as above	NA	NA
Software Validation Report (SVR)	10344-SVR-9.60-01-WIN2000	DIRS 182913	MOL.20070711.0250
Software Validation Report (SVR)	10344-SVR-9.60-01-WIN2003	DIRS 182914	MOL. 20070711.0252
Software Validation Report (SVR)	10344-SVR-9.60-01-WINXP	DIRS 182915	MOL. 20070711.0254

Table 3-9. InterpZdll_LA Software Documents

Version 1.0 Windows 2000 (STN: 11107-1.0-00)			
Description	**Document ID**	**DIRS Number**	**Tracking Number**
Software Management Report (SMR)	11107-SMR-1.0-00	DIRS 168988	MOL.20040130.0403
Version 1.0 Windows 2003 (STN: 11107-1.0-01)			
Description	**Document ID**	**DIRS Number**	**Tracking Number**
Software Management Report (SMR)	Same as above	NA	NA
Software Validation Report (SVR)	11107-SVR-1.0-01-WIN2003	DIRS 181092	MOL.20070220.0471

Table 3-10. MFCP_LA Software Documents

Version 1.0 Windows 2000 (STN: 11071-1.0-00)			
Description	**Document ID**	**DIRS Number**	**Tracking Number**
Software Management Report (SMR)	11071-SMR-1.0-00	DIRS 167597	MOL.20030529.0258
Version 1.0 Windows 2003 (STN: 11071-1.0-01)			
Description	**Document ID**	**DIRS Number**	**Tracking Number**
Software Management Report (SMR)	Same as above	NA	NA
Software Validation Report (SVR)	11071-SVR-1.0-01-WIN2003	DIRS 181113	MOL.20061218.0126

Table 3-11. MKTABLE/MkTable_LA Software Documents

Version 1.00 Windows 2000 (STN:10505-1.00-00)			
Description	**Document ID**	**DIRS Number**	**Tracking Number**
Software Management Report (SMR)	10505-SMR-1.00-00	DIRS 167572	MOL.20010712.0055
Version 1.0 Windows 2000 (STN:11217-1.0-00)			
Description	**Document ID**	**DIRS Number**	**Tracking Number**
Requirements Document (RD)	11217-RD-1.0-00	DIRS 181114	MOL.20060413.0349
Design Document (DD)	11217-DD-1.0-00	DIRS 181115	MOL.20060413.0351
User Information Document (UID)	11217-UID-1.0-00	DIRS 181116	MOL.20060413.0354
Software Validation Report (SVR)	11217-SVR-1.0-00-WIN2000	DIRS 181117	MOL.20060413.0357
Version 1.0 Windows 2003 (STN: 11217-1.0-01)			
Description	**Document ID**	**DIRS Number**	**Tracking Number**
Requirements Document (RD)	Same as above	NA	NA
Design Document (DD)	Same as above	NA	NA
User Information Document (UID)	Same as above	NA	NA
Software Validation Report (SVR)	11217-SVR-1.0-01-WIN2003	DIRS 181118	MOL.20070208.0274

Table 3-12. MVIEW Software Documents

Version 1.0 XP (STN: 10072-4.0-01)			
Description	**Document ID**	**DIRS Number**	**Tracking Number**
Requirements Document (RD)	10072-RD-4.0-01	DIRS 174593	MOL.20050712.0023
Design Document (DD)	10072-DD-4.0-00	DIRS 174594	MOL.20050712.0025
User Information Document (UID)	10072-UID-4.0-00	DIRS 174595	MOL.20050712.0027
Software Validation Report (SVR)	10072-SVR-4.0-01-WINXP	DIRS 181119	MOL.20070417.0382

Table 3-13. PassTable1D_LA Software Documents

Version 1.0 Windows 2000 (STN: 11142-1.0-00)			
Description	**Document ID**	**DIRS Number**	**Tracking Number**
Software Management Report (SMR)	11142-SMR-1.0-00	DIRS 168978	MOL.20040310.0105
Version 1.0 Windows 2003 (STN: 11142-1.0-01)			
Description	**Document ID**	**DIRS Number**	**Tracking Number**
Software Management Report (SMR)	Same as above	NA	NA
Software Validation Report (SVR)	11142-SVR-1.0-01-WIN2003	DIRS 181120	MOL.20061218.0107
Version 2.0 Windows 2000 and 2003 (STN: 11142-2.0-00)			
Description	**Document ID**	**DIRS Number**	**Tracking Number**
Requirements Document (RD)	11142-RD-2.0-01	DIRS 181121	MOL.20070420.0357
Design Document (DD)	11142-DD-2.0-01	DIRS 181122	MOL.20070420.0359
User Information Document (UID)	11142-UID-2.0-00	DIRS 181123	MOL.20070420.0361
Software Validation Report (SVR)	11142-SVR-2.0-00-WIN2000	DIRS 181124	MOL.20070420.0363
Software Validation Report (SVR)	11142-SVR-2.0-00-WIN2003	DIRS 181125	MOL.20070420.0365

Table 3-14. PassTable3D_LA Software Documents

Version 1.0 Windows 2000 (STN: 11143-1.0-00)			
Description	**Document ID**	**DIRS Number**	**Tracking Number**
Software Management Report (SMR)	11143-SMR-1.0-00	DIRS 168981	MOL.20040317.0127
Version 1.0 Windows 2003 (STN: 11143-1.0-01)			
Description	**Document ID**	**DIRS Number**	**Tracking Number**
Software Management Report (SMR)	Same as above	NA	NA
Software Validation Report (SVR)	11143-SVR-1.0-01-WIN2003	DIRS 181126	MOL.20070208.0286
Version 2.0 Windows 2000 and 2003 (STN: 11143-2.0-00)			
Description	**Document ID**	**DIRS Number**	**Tracking Number**
Requirements Document (RD)	11143-RD-2.0-00	DIRS 182916	MOL.20070816.0245
Design Document (DD)	11143-DD-2.0-00	DIRS 182917	MOL. 20070816.0247
User Information Document (UID)	11143-UID-2.0-00	DIRS 182918	MOL. 20070816.0252
Software Validation Report (SVR)	11143-SVR-2.0-00-WIN2000	DIRS 182919	MOL. 20070816.0254
Software Validation Report (SVR)	11143-SVR-2.0-00-WIN2003	DIRS 182920	MOL. 20070816.0256

Table 3-15. PREWAP_LA Software Documents

Version 1.1 Windows 2000 (STN: 10939-1.1-00)			
Description	**Document ID**	**DIRS Number**	**Tracking Number**
Requirements Document (RD)	10939-RD-1.1-00	DIRS 181127	MOL.20060418.0163
Design Document (DD)	10939-DD-1.1-00	DIRS 181128	MOL.20060418.0165
User Information Document (UID)	10939-UID-1.1-00	DIRS 181129	MOL.20060418.0169
Software Validation Report (SVR)	10939-SVR-1.1-00-WIN2000	DIRS 181130	MOL.20060418.0171

Table 3-16. SCCD Software Documents

Version 2.01 Windows 2000 (STN: 10343-2.01-00)			
Description	**Document ID**	**DIRS Number**	**Tracking Number**
Software Routine Report (SRR)	10343-SRR-2.01-00	DIRS 152499	MOL.20010205.0113
Version 2.01 Windows 2003 (STN: 10343-2.01-01)			
Description	**Document ID**	**DIRS Number**	**Tracking Number**
Software Routine Report (SRR)	Same as above	NA	NA
Software Validation Report (SVR)	10343-SVR-2.01-01-WIN2003	DIRS 181277	MOL.20070209.0013

Table 3-17. SEEPAGEDLL_LA Software Documents

Version 1.2 Windows 2000 (STN:11076-1.2-00)			
Description	**Document ID**	**DIRS Number**	**Tracking Number**
Requirements Document (RD)	11076-RD-1.2-00	DIRS 173465	MOL.20050406.0437
Design Document (DD)	11076-DD-1.2-00	DIRS 173464	MOL.20050406.0440
User Information Document (UID)	11076-UID-1.2-00	DIRS 173463	MOL.20050406.0425
Software Validation Report (SVR)	11076-SVR-1.2-00	DIRS 173462	MOL.20050406.0429
Version 1.3 Windows 2000 (STN:11076-1.3-00)			
Description	**Document ID**	**DIRS Number**	**Tracking Number**
Requirements Document (RD)	11076-RD-1.3-00	DIRS 181131	MOL.20060525.0294
Design Document (DD)	11076-DD-1.3-00	DIRS 181132	MOL.20060525.0296
User Information Document (UID)	11076-UID-1.3-00	DIRS 181133	MOL.20060525.0300
Software Validation Report (SVR)	11076-SVR-1.3-00-WIN2000	DIRS 181134	MOL.20060525.0302
Version 1.3 Windows 2003 (STN: 11076-1.3-01)			
Description	**Document ID**	**DIRS Number**	**Tracking Number**
Requirements Document (RD)	Same as above	NA	NA
Design Document (DD)	Same as above	NA	NA
User Information Document (UID)	Same as above	NA	NA
Software Validation Report (SVR)	11076-SVR-1.3-01-WIN2003	DIRS 181135	MOL.20070223.0249

Table 3-18. SoilExp_LA Software Document

Version 1.0 Windows 2000 (STN: 10933-1.0-00)			
Description	**Document ID**	**DIRS Number**	**Tracking Number**
Software Management Report (SMR)	10933-SMR-1.0-00	DIRS 168977	MOL.20040227.0046

Table 3-19. SZ_Convolute Software Documents

Version 3.0 Windows 2000 (STN:10207-3.0-00)			
Description	**Document ID**	**DIRS Number**	**Tracking Number**
Requirements Document (RD)	10207-RD-3.0-00	DIRS 167587	MOL.20030717.0478
Design Document (DD)	10207-DD-3.0-00	DIRS 167588	MOL.20030717.0479
User Manual (UM)	10207-UM-3.0-00	DIRS 167591	MOL.20030717.0483
Installation Test Process (ITP)	10207-ITP-3.0-00	DIRS 167590	MOL.20030717.0480
Validation Test Process (VTP)	10207-VTP-3.0-00	DIRS 167589	MOL.20030717.0481
Validation Test Report (VTR)	10207-VTR-3.0-00	DIRS 167593	MOL.20030717.0484
Version 3.10.01 Windows 2000 and Windows 2003 (STN:10207-3.10.01-00)			
Description	**Document ID**	**DIRS Number**	**Tracking Number**
Requirements Document (RD)	10207-RD-3.10-00	DIRS 181284	MOL.20061106.0218
Design Document (DD)	10207-DD-3.10-00	DIRS 181286	MOL.20061106.0219
User Information Document (UID)	10207-UID-3.10-00	DIRS 181288	MOL.20070223.0313
Software Validation Report (SVR)	10207-SVR-3.10.01-00-WIN2000	DIRS 181289	MOL.20070501.0392
Software Validation Report (SVR)	10207-SVR-3.10.01-00-WIN2003	DIRS 181290	MOL.20070501.0394

Table 3-20. TSPA_Input_DB Software Documents

Version 2.2 Windows 2000 (STN:10931-2.2-00)			
Description	**Document ID**	**DIRS Number**	**Tracking Number**
Requirements Document (RD)	10931-RD-2.0-00	DIRS 173449	MOL.20050131.0427
Design Document (DD)	10931-DD-2.0-00	DIRS 173450	MOL.20050131.0430
User Information Document (UID)	10931-UID-2.2-00	DIRS 181137	MOL.20060222.0419
Software Validation Report (SVR)	10931-SVR-2.2-00-WIN2000	DIRS 181139	MOL.20060222.0422
Version 2.2 Windows 2003 (STN:10931-2.2-01)			
Description	**Document ID**	**DIRS Number**	**Tracking Number**
Requirements Document (RD)	Same as above	NA	NA
Design Document (DD)	Same as above	NA	NA
User Information Document (UID)	Same as above	NA	NA
Software Validation Report (SVR)	10931-SVR-2.2-01-WIN2003	DIRS 181140	MOL.20061011.0198

Table 3-21. WAPDEG Software Documents

Version 4.07 Windows 2000 (STN:10000-4.07-00)			
Description	**Document ID**	**DIRS Number**	**Tracking Number**
Requirements Document (RD)	10000-RD-4.07-00	DIRS 167545	MOL.20030409.0228
Design Document (DD)	10000-DD-4.07-00	DIRS 167547	MOL.20030409.0229
User Manual (UM)	10000-UM-4.07-00	DIRS 162606	MOL.20030409.0233
Installation Test Plan (ITP)	10000-ITP-4.07-01	DIRS 167548	MOL.20030409.0231
Validation Test Plan (VTP)	10000-VTP-4.07-00	DIRS 167542	MOL.20030409.0232
Validation Test Report (VTR)	10000-VTR-4.07-00	DIRS 167554	MOL.20030409.0234
Version 4.07 Windows 2003 (STN:10000-4.07-01)			
Description	**Document ID**	**DIRS Number**	**Tracking Number**
Requirements Document (RD)	Same as above	NA	NA
Design Document (DD)	Same as above	NA	NA
Validation Test Plan (VTP)	Same as above	NA	NA
Installation Test Plan (ITP)	Same as above	NA	NA
User Manual (UM)	Same as above	NA	NA
Software Validation Report (SVR)	10000-SVR-4.07-01-WIN2003	DIRS 181141	MOL.20070417.0371

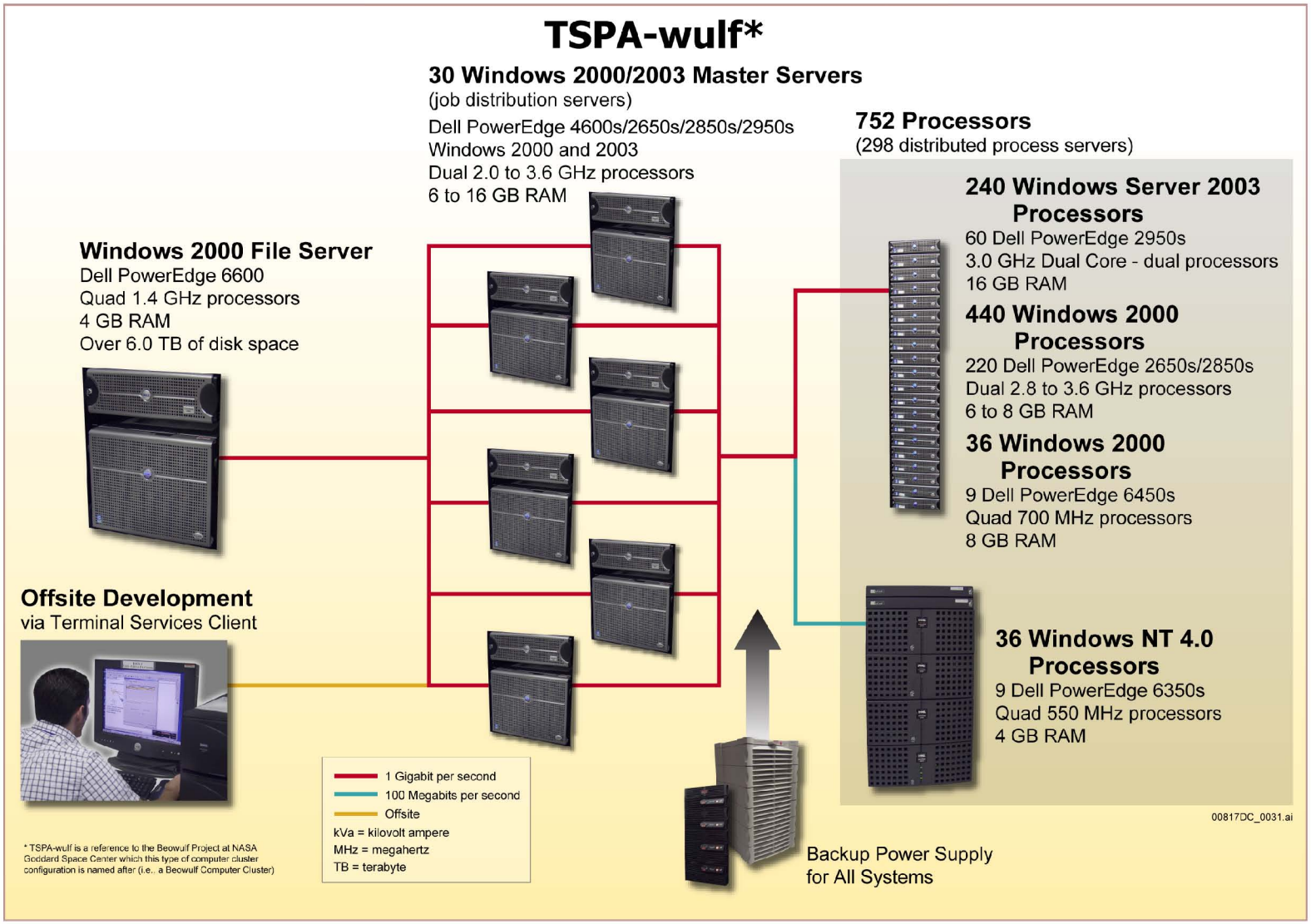

Figure 3-1. Hardware Configuration for TSPA-LA Modeling

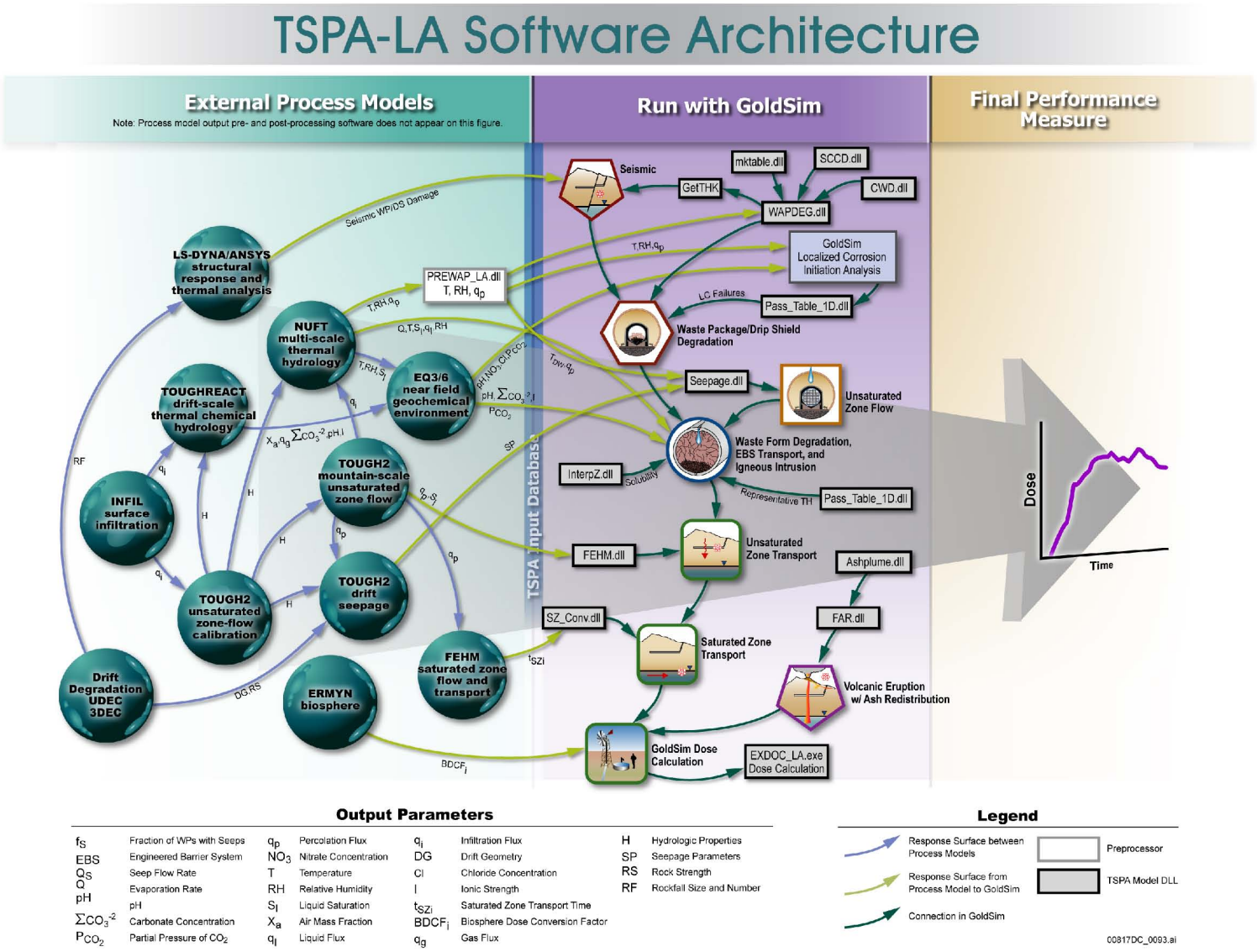

Figure 3-2. TSPA-LA Software Architecture

4. INPUTS

The TSPA-LA Model integrates several model components and submodels to simulate the performance of the repository. A numerical representation was used to implement the model with GoldSim software (see Table 3-1 for specific versions used). Inputs used by this numerical representation of the TSPA-LA Model were obtained from controlled sources maintained by the OCRWM data and information systems, such as the Controlled Documents Information System, TDMS, Technical Information Center, and other available sources such as NRC Proposed Rule 10 CFR Part 63 [DIRS 178394 and 180319]. Figure 4-1 provides an overview of the information flow for the TSPA-LA Model development and analysis. This figure illustrates the control of information as it flows from initial data collection and generation to external process models, to the GoldSim software, and finally to the TSPA-LA Model output that is submitted to the TDMS.

This section provides descriptions of the TSPA-LA Model inputs, criteria, codes and standards, and the TSPA Input Database. Model inputs consist of both direct and indirect inputs per SCI-PRO-004, *Managing Technical Product Inputs*.

4.1 DIRECT INPUTS

Direct inputs are only those parameters and their values that are used by the TSPA-LA Model to develop results and conclusions presented in this report. This information is stored in the TSPA Input Database described in Section 4.7. Table 4-1 lists the direct inputs and associates each with a reference (source) and a Parameter Entry Form (PEF) number. The respective PEF (see Section 4.3 for an overview of PEFs) contains a list and descriptions of the parameters used as input and their sources. The references shown in Table 4-1 are primarily analysis and/or model reports and DTNs associated with analysis and/or model reports. Since the direct inputs used by the TSPA-LA Model are considered technical product output and not experimental or raw field data, then in accordance with SCI-PRO-006, Attachment 2, Section 4.1, the statement in the next sentence can be accurately stated. The TSPA-LA Model does not use any data to develop the model.

When a direct input is referenced from an analysis and/or model report rather than a DTN, Table 4-1 lists the document title, document identifier (DI) number, revision number, and Document Input Reference System (DIRS) reference number for the analysis and/or model report. Similarly, when a direct input is referenced from an analysis and/or model report output DTN, Table 4-1 lists the DI, document title, DTN, and DIRS reference number for the DTN. In these cases, the DI and document title are listed to provide the connection to the analysis and/or model report that generated the DTN. The revision number for the analysis and/or model report is deliberately not shown because the Technical Database Information Form (TDIF) for the DTN will indicate the current analysis and/or model report revision number that is the source of the DTN.

In some instances, parameters are incorporated into input files or DLLs. The parameters that fall into these categories are specifically identified in the TSPA Input Database described in Section 4.7. Consequently, not all parameters in the TSPA Input Database are direct inputs, as defined by SCI-PRO-004. Thus, the PEFs containing these parameters are not presented in

Table 4-1 or Table 4-2. For example, PEF 80, shown in Table 4-2, contains parameters that are actually all of the DLLs identified in the TSPA Input Database and used in the TSPA-LA Model.

4.2 TSPA-LA MODEL GENERATED PARAMETERS

The TSPA-LA Model requires the generation of many parameters (often incorporated into large data files) that are created by preprocessing methods (i.e., created prior to running the TSPA-LA Model). These parameters are captured in output DTNs along with explanations for how they were generated. Use of these DTNs in the TSPA-LA Model is described at various locations in this document, such as Appendix F. The PEFs that reference the DTNs created by this document are listed in Table 4-2. In addition, Appendix B lists and describes all output DTNs generated by the TSPA-LA Model.

4.3 PARAMETER ENTRY FORMS

All parameter names, parameter values, and parameter references used in support of the TSPA-LA Model are documented in PEFs and contained in the TSPA Input Database. PEFs document both parameters that were downloaded from the TSPA Input Database and parameters that were entered directly into the TSPA-LA Model. Figure 4-2 provides an overview of the PEF development and update process.

Concurrent with the TSPA-LA Model development, inputs changed as analyses and/or model reports and DTNs were revised. These changes caused some PEFs to be added and others were retired from further use. As a result, some PEF numbers do not appear in Tables 4-1 and 4-2.

Generally, PEFs provide the following information:

1. List of parameters, parameter descriptions, parameter values, and references
2. Directions or roadmaps to the location(s) of the information in the references
3. Explanations of any transformations, files, or parameters created by a TSPA analyst
4. Signatures documenting that inputs were appropriately selected from analysis and/or model reports and used in the TSPA-LA Model.

The PEF contains signature lines for purposes of approval as represented on Figure 4-2. Approvals indicate the following:

- The Parameter Team Lead indicates that the PEF contains appropriate information, including the list of parameters, parameter descriptions, references where the parameters were obtained, and roadmaps describing the location of the parameters within the references.
- The TSPA analyst indicates that the PEF contains the parameters (and their associated parameter values) used as direct input to the TSPA-LA Model and any conversions made to the parameter values necessary for model input.

- The SME indicates that the PEF accurately represents the parameters (and their associated parameter values) and the references intended for TSPA-LA Model input. SMEs are generally the principal investigators that are most knowledgeable about the input parameters and their uncertainties for use in the TSPA-LA Model.

- The database administrator indicates that the parameters and parameter values are available in the TSPA Input Database in the appropriate formats defined by the software documents listed in Table 3-20.

4.4 TRACEABILITY OF INPUTS

Traceability of inputs is provided by using one or more of the following tools:

1. **DIRS Database**—DIRS is a database that contains the technical product input sources, such as direct and indirect inputs and their status.

2. **TSPA Input Database**—The TSPA Input Database (Section 4.7) provides detailed information for each parameter, such as parameter name, parameter description and type, source reference, parameter value, and verification status. When the database is downloaded into the TSPA-LA Model, this traceability information is embedded in the TSPA-LA Model as a model element.

3. **Table 4-1**—Table 4-1 lists all direct inputs used in the TSPA-LA Model and associates each direct input with a PEF.

4. **PEFs**—The PEFs collectively contain all parameters used as input to the TSPA-LA Model. Each PEF references the specific locations of the parameters within a reference document or DTN to aid in the traceability of the direct inputs. The original signed PEFs are in the records package for this document; however, the TSPA Input Database can be used to generate any PEF, as described in Section 4.7.

5. **TSPA-LA Model**—The TSPA Input Database information listed in Item 2 of Section 4.4 is embedded in the TSPA-LA Model file (e.g., parameter name, type of parameter, source reference, and parameter value).

The following examples show how the tools described above can be used to obtain documentation and demonstrate traceability:

1. **Source of any Parameter**—The source of a parameter may be obtained by accessing the reports in the TSPA Input Database.

2. **Listing of Direct Inputs**—The DIRS database can provide a list and associated status of all direct inputs. Table 4-1 also contains a list of all direct inputs and corresponding DIRS reference numbers.

3. **Location of a Parameter within the TSPA-LA Model**—A particular parameter within the TSPA-LA Model file can be located using the GoldSim search utility. Enter all or part of the parameter name in the *search* field adjacent to the binocular icon in the upper left hand corner of the TSPA-LA Model file. Pressing F3 or the Search button (i.e., the binoculars) finds the next item (element) in the browser that matches the search string.

4. **Parameters Associated with a PEF**—The list of parameters for any designated PEF can be obtained from the records package in the Records Information System (RIS) or by generating a report from the TSPA Input Database.

4.5 CRITERIA

In 10 CFR 63.102(j) [DIRS 180319], the NRC requires the DOE to complete "a performance assessment to quantitatively estimate radiological exposures to the reasonably maximally exposed individual at any time during the compliance period." The TSPA-LA Model was developed to meet this requirement.

The requirements to be addressed by this TSPA-LA are identified in the *Technical Work Plan for: Total System Performance Assessment FY 07-08 Activities* (SNL 2008 [DIRS 184920]). This subset of requirements shown in Table 4-3 was established based on the *Yucca Mountain Review Plan, Final Report* (NRC 2003 [DIRS 163274]) and is discussed in Appendix H.

4.6 CODES AND STANDARDS

No codes or standards are required for this document other than those identified in Section 4.5.

4.7 TSPA INPUT DATABASE

This section provides a summary of the TSPA Input Database. Additional detail on its design and operation can be found in the software documents listed in Section 3. The TSPA Input Database supports the TSPA-LA Model by providing the parameter values and distributions necessary for the PA analysis of the repository. The database is used to categorize, store, and retrieve fixed and distributed values of the TSPA-LA Model parameters. The database is programmed with user controls featuring read and write access and audit trails. These controls were designed to ensure the security, integrity, and traceability of the information used in the TSPA-LA Model analyses. The following sections provide a brief overview of:

- Database structure
- Database operation login
- Database forms
  - Parameter Identification Form (PIF)
  - Parameter Documentation Form (PDF)
  - Parameter Value Entry Form (PVEF)
  - PEF Information Entry Form
  - Parameter Verification Form (PVF)

- Database reports
- Database support of GoldSim.

4.7.1 Database Structure

The TSPA Input Database was developed using a commercially available desktop database manager, Microsoft Access 2000. It is a multi-user, Microsoft Windows based, relational database solution that allows data entry, viewing, and querying, as well as report preparation. The TSPA Input Database was designed and qualified in accordance with IM-PRO-004, *Qualification of Software*. The software documents listed in Table 3-20 provide details of the software design and implementation of the database. In a relational database, related information can be stored in separate tables, reducing the likelihood of redundant entries. Referential integrity relationships among tables in the TSPA Input Database are used where there is information in one table that must refer to information in another table.

Figure 4-3 illustrates the structured framework (schema) of the TSPA Input Database and the relationships among the three fundamental elements of data flow and data storage in the database. The three principal operational elements of the database are the PIF, parameter documentation form, and parameter value entry form. Each of these three database elements appears as a separate interactive screen image when the database is electronically accessed. The relationship line between these elements (Figure 4-3) automatically enforces database referential integrity by creating a foreign key constraint on the related tables. In this manner, parameter information is not duplicated across multiple tables.

4.7.2 Database Operation Login

The initial point of entry to the TSPA Input Database is the login screen, which contains a password entry feature to control access of authorized users. (Note: the database that is included with the electronic version of this document does not have password entry because it is read-only.) Each authorized user is assigned a user name, and each user name has an established password and user level. The user level (i.e., 1, 2, or 3) determines user privileges. A Level 1 user is allowed to perform data entry and updates but is not allowed to perform data verifications. A Level 2 user is allowed to view data and perform data verifications. A Level 3 user has read-only privileges.

4.7.3 Parameter Identification Form

Following login into the TSPA Input Database, the PIF (Figure 4-4) appears as the first interactive, menu-driven screen image. The PIF serves as the primary means to view existing parameters and to enter new parameters into the database. All parameters have an associated PIF accessible by selecting a parameter name from the list on the left side of the PIF. The database ensures that each parameter is assigned a unique parameter name and parameter identification. The PIF presents the PEF number that the parameter is assigned, a description of the parameter, and other attributes. The Primary Model Location field identifies the location in which the parameter is first introduced into the TSPA-LA Model as a data element. In contrast, the Other Locations field identifies the other locations in which the parameter is introduced into the

TSPA-LA Model. These locations are often difficult to ascertain due to the complexity of the model and should be viewed as general assignments.

4.7.4 Parameter Documentation Form

The parameter documentation form (Figure 4-5) is accessible from the PIF via the Documentation button. This form presents the reference information from which the parameter was obtained. The appearance of the parameter documentation form differs depending on the parameter type recorded on the PIF. For example, if the parameter type is file, two additional fields are displayed. The File Element Pathway field contains the external file pathway to the controlled data file, and the Document Signature field contains the associated audit-tracking signature number. This information is required by the GoldSim software in order to perform external file and DLL transfers. For details, see *User's Guide, GoldSim Probabilities Simulation Environment* (GoldSim Technology Group 2007 [DIRS 181727]). The effective date on the form indicates the date the parameter was entered into the TSPA Input Database. Finally, the parameter documentation form contains a hyperlink to the Automated Technical Data Tracking system to provide access directly to the DTN from which the parameters were obtained.

4.7.5 Parameter Value Entry Form

The parameter value entry from (Figure 4-6) is accessible from the parameter documentation form via the Value button. This form presents the parameter value(s). The appearance of the parameter value entry form differs depending on the parameter type recorded on the PIF. Each parameter type has a corresponding parameter value format. In addition, each parameter value has a unique component identification. For data tables, each row of data has its own component identification. For one-dimensional and two-dimensional data tables and multiple-row stochastic values, two separate forms are required. Figure 4-6 is an example of a parameter value entry form for the 1-D Table parameter type, with multiple-row stochastic values. A sequential code is assigned to each row of values in the input tables. This code is read by the GoldSim software to ensure that downloads from the TSPA Input Database are performed in the correct order.

4.7.6 Parameter Entry Form Information Entry Form

The PEF Information Entry Form (Figure 4-7) is accessible from the PIF via the Enter PEF Information button. For each PEF number, this form presents the name of the analyst(s), roadmap information, and PEF revision history. The contents and purpose of the PEF are described in more detail in Section 4.3.

4.7.7 Parameter Verification Form

The parameter verification form (Figure 4-8) is accessible from the PIF form, parameter documentation form, and parameter value entry form via the Verify button. This form presents the checker's name, date and time of verification, and any checker comments. The Editing History field shows all users and the dates and times for modifications made to the parameter information. The verification status is cleared when any parameter form is modified that affects a parameter. A cleared verification status indicates that the parameter needs to be reverified. Before downloading parameter values to the TSPA-LA Model for a PA analysis, each parameter undergoes verification to ensure that all information was correctly and completely entered. Only

users with the appropriate, controlled access to the TSPA Input Database can perform data verification (Section 4.7.2).

4.7.8 Database Reports

TSPA Input Database reports are accessible from the PIF via the Report button. The following reports can be produced:

- **Alphabetized Parameter Listing**—This report is an alphabetic list of all parameters and includes parameter description, primary model location, PEF number, and reference information.
- **Parameter Listing by Analyst(s)**—This report lists all parameters for a specified TSPA analyst. The report is grouped by PEF number and primary model location and includes parameter description, input type, other model locations, reference information, and verification status.
- **Complete Parameter Listing by PEF**—This report lists all parameters by PEF number and includes parameter description, units, type, distribution, primary model location, and reference information. A count of parameter entries is displayed for each PEF grouping and for the entire database.
- **Print a PEF**—This report displays the PEF information for a selected PEF number and includes TSPA analyst, roadmap, and revision history; all parameters associated with the PEF parameter description; reference information; and any associated to be verified (TBV) references. A count of the total number of parameter entries for the PEF is printed at the end of the parameter listing.
- **List by All Locations in TSPA-LA Model**—This report lists all parameters associated with the specified TSPA-LA Model location, which includes both primary and other locations. The list includes PEF number, parameter description, input type, reference information, and whether the model location is primary. The number of parameter entries for the TSPA-LA Model location requested is reported at the end of the list.
- **List by Primary Locations in TSPA-LA Model**—This report lists all parameters associated with the specified primary model location and is grouped by reference document. The report includes parameter description, PEF number, and any associated DTN(s).
- **Report and DTN Listings**—This report lists all references cited in the PEFs and includes analysis and/or model reports by DI and document title and all associated DTNs.
- **DI–PEF List**—This report lists all parameters grouped by PEF for the selected DI. The information presented includes parameter description, primary model location, and input type. The end of each DI list includes a count of the number of PEFs and parameter entries.

- **List All Data**—This report lists all information about the selected parameter, including the parameter values.
- **List by Input Type**—This report lists all parameters associated with the selected input type. The information presented includes PEF, parameter description, primary model location, and reference information. The number of parameter entries is reported at the end of the report.

4.7.9 Database Support of GoldSim

The TSPA Input Database serves as the quality-controlled repository for the input parameters before the parameter values are downloaded to the TSPA-LA Model. The database is designed to interface with GoldSim, via ODBC, for automated downloads to the TSPA-LA Model. Upon download of the database to the TSPA-LA Model, designated content from the database is embedded in a model element.

The TSPA Input Database download provides two primary functions: (1) ensures the most recent data are being used, and (2) ensures that the correct DLLs and input files are moved from a controlled directory to the directory for the current GoldSim run.

Table 4-1. Direct Inputs

Line #	Document_ID	Reference_Document	Document DIRS	DTN	DTN DIRS	PEF
1	10 CFR 63	10 CFR 63. Energy: Disposal of High-Level Radioactive Wastes in a Geologic Repository at Yucca Mountain, Nevada	180319	NA	NA	81
2	70 FR 53313	Implementation of a Dose Standard After 10,000 Years	178394	NA	NA	90
3	ANL-EBS-MD-000003	*General Corrosion and Localized Corrosion of Waste Package Outer Barrier*	NA	MO0703PAGENCOR.001_R4	182029	5
4	ANL-EBS-MD-000003	*General Corrosion and Localized Corrosion of Waste Package Outer Barrier*	NA	MO0703PAGENCOR.001_R4	182029	7
5	ANL-EBS-MD-000003	*General Corrosion and Localized Corrosion of Waste Package Outer Barrier*	NA	MO0703PAGENCOR.001_R4	182029	85
6	ANL-EBS-MD-000003	*General Corrosion and Localized Corrosion of Waste Package Outer Barrier*	NA	MO0703PAGENCOR.001_R4	182029	117
7	ANL-EBS-MD-000004	*General Corrosion and Localized Corrosion of the Drip Shield*	NA	SN0704PADSGCMT.001_R2	182122	3
8	ANL-EBS-MD-000004	*General Corrosion and Localized Corrosion of the Drip Shield*	NA	SN0704PADSGCMT.002_R1	182188	105
9	ANL-EBS-MD-000005	*Stress Corrosion Cracking of Waste Package Outer Barrier and Drip Shield Materials*	NA	MO0702PASTRESS.002_R2	180514	4
10	ANL-EBS-MD-000005 REV 04	*Stress Corrosion Cracking of Waste Package Outer Barrier and Drip Shield Materials*	181953	NA	NA	131
11	ANL-EBS-MD-000015	*CSNF Waste Form Degradation: Summary Abstraction*	NA	MO0404ANLSF001.001_R0	169007	31
12	ANL-EBS-MD-000015 REV 02	*CSNF Waste Form Degradation: Summary Abstraction*	169987	NA	NA	82
13	ANL-EBS-MD-000016	*Defense HLW Glass Degradation Model*	NA	MO0502ANLGAMR1.016_R0	172830	32

Table 4-1. Direct Inputs (Continued)

Line #	Document_ID	Reference_Document	Document DIRS	DTN	DTN DIRS	PEF
14	ANL-EBS-MD-000033	*Engineered Barrier System: Physical and Chemical Environment*	NA	SN0701PAEBSPCE.001_R1	180523	75
15	ANL-EBS-MD-000033	*Engineered Barrier System: Physical and Chemical Environment*	NA	SN0701PAEBSPCE.002_R0	179425	76
16	ANL-EBS-MD-000033	*Engineered Barrier System: Physical and Chemical Environment*	NA	SN0703PAEBSPCE.006_R2	181571	77
17	ANL-EBS-MD-000033	*Engineered Barrier System: Physical and Chemical Environment*	NA	SN0703PAEBSPCE.007_R2	184141	78
18	ANL-EBS-MD-000033	*Engineered Barrier System: Physical and Chemical Environment*	NA	SN0706PAEBSPCE.016_R0	181837	104
19	ANL-EBS-MD-000033 Rev 06	*Engineered Barrier System: Physical and Chemical Environment*	177412	NA	NA	119
20	ANL-EBS-MD-000037	*In-Package Chemistry Abstraction*	NA	MO0502SPAINPCA.000_R0	172893	79
21	ANL-EBS-MD-000037	*In-Package Chemistry Abstraction*	NA	SN0702PAIPC1CA.001_R2	180451	12
22	ANL-EBS-MD-000037	*In-Package Chemistry Abstraction*	NA	SN0702PAIPC1CA.001_R2	180451	102
23	ANL-EBS-MD-000037 Rev 04 AD 01	*In-Package Chemistry Abstraction*	180506	NA	NA	136
24	ANL-EBS-MD-000049	*Multiscale Thermohydrologic Model*	NA	LL0702PA027MST.082_R0	179590	15
25	ANL-EBS-MD-000049	*Multiscale Thermohydrologic Model*	NA	LL0702PA027MST.082_R0	179590	86
26	ANL-EBS-MD-000049	*Multiscale Thermohydrologic Model*	NA	LL0703PA011MST.006_R0	179853	16
27	ANL-EBS-MD-000049	*Multiscale Thermohydrologic Model*	NA	LL0703PA011MST.006_R0	179853	108
28	ANL-EBS-MD-000049	*Multiscale Thermohydrologic Model*	NA	LL0703PA012MST.007_R0	179854	17
29	ANL-EBS-MD-000049	*Multiscale Thermohydrologic Model*	NA	LL0703PA012MST.007_R0	179854	108
30	ANL-EBS-MD-000049	*Multiscale Thermohydrologic Model*	NA	LL0703PA013MST.008_R0	179855	18
31	ANL-EBS-MD-000049	*Multiscale Thermohydrologic Model*	NA	LL0703PA013MST.008_R0	179855	108
32	ANL-EBS-MD-000049	*Multiscale Thermohydrologic Model*	NA	LL0703PA014MST.009_R0	179856	19
33	ANL-EBS-MD-000049	*Multiscale Thermohydrologic Model*	NA	LL0703PA014MST.009_R0	179856	108

Table 4-1. Direct Inputs (Continued)

Line #	Document_ID	Reference_Document	Document DIRS	DTN	DTN DIRS	PEF
34	ANL-EBS-MD-000049	*Multiscale Thermohydrologic Model*	NA	LL0703PA015MST.010_R0	179857	20
35	ANL-EBS-MD-000049	*Multiscale Thermohydrologic Model*	NA	LL0703PA015MST.010_R0	179857	108
36	ANL-EBS-MD-000049	*Multiscale Thermohydrologic Model*	NA	LL0703PA016MST.011_R0	179858	21
37	ANL-EBS-MD-000049	*Multiscale Thermohydrologic Model*	NA	LL0703PA016MST.011_R0	179858	108
38	ANL-EBS-MD-000049	*Multiscale Thermohydrologic Model*	NA	LL0703PA017MST.012_R0	179859	22
39	ANL-EBS-MD-000049	*Multiscale Thermohydrologic Model*	NA	LL0703PA017MST.012_R0	179859	108
40	ANL-EBS-MD-000049	*Multiscale Thermohydrologic Model*	NA	LL0703PA026MST.013_R0	179981	50
41	ANL-EBS-MD-000049	*Multiscale Thermohydrologic Model*	NA	LL0703PA034MST.016_R0	179982	23
42	ANL-EBS-MD-000049	*Multiscale Thermohydrologic Model*	NA	LL0703PA034MST.016_R0	179982	108
43	ANL-EBS-MD-000049	*Multiscale Thermohydrologic Model*	NA	LL0703PA035MST.017_R0	179985	24
44	ANL-EBS-MD-000049	*Multiscale Thermohydrologic Model*	NA	LL0703PA035MST.017_R0	179985	108
45	ANL-EBS-MD-000049	*Multiscale Thermohydrologic Model*	NA	LL0703PA036MST.018_R0	179986	25
46	ANL-EBS-MD-000049	*Multiscale Thermohydrologic Model*	NA	LL0703PA036MST.018_R0	179986	108
47	ANL-EBS-MD-000049	*Multiscale Thermohydrologic Model*	NA	LL0703PA037MST.019_R0	179989	26
48	ANL-EBS-MD-000049	*Multiscale Thermohydrologic Model*	NA	LL0703PA037MST.019_R0	179989	108
49	ANL-EBS-MD-000049	*Multiscale Thermohydrologic Model*	NA	LL0703PA038MST.020_R0	179992	27
50	ANL-EBS-MD-000049	*Multiscale Thermohydrologic Model*	NA	LL0703PA038MST.020_R0	179992	108
51	ANL-EBS-MD-000049	*Multiscale Thermohydrologic Model*	NA	MO0505SPAROCKM.000_R0	173893	28
52	ANL-EBS-MD-000049	*Multiscale Thermohydrologic Model*	NA	MO0703PAHYTHRM.000_R1	182093	29
53	ANL-EBS-MD-000076	*Analysis of Mechanisms for Early Waste Package/Drip Shield Failure*	NA	MO0701PASHIELD.000_R2	180508	2
54	ANL-EBS-MD-000076	*Analysis of Mechanisms for Early Waste Package/Drip Shield Failure*	NA	MO0701PASHIELD.000_R2	180508	118
55	ANL-EBS-MD-000076 REV 00	*Analysis of Mechanisms for Early Waste Package/Drip Shield Failure*	178765	NA	NA	130

Table 4-1. Direct Inputs (Continued)

Line #	Document_ID	Reference_Document	Document DIRS	DTN	DTN DIRS	PEF
56	ANL-MGR-GS-000001	*Characterize Framework for Igneous Activity at Yucca Mountain, Nevada*	NA	LA0307BY831811.001_R0	164713	60
57	ANL-MGR-GS-000002	*Characterize Eruptive Processes at Yucca Mountain, Nevada*	NA	LA0612DK831811.001_R1	179987	62
58	ANL-MGR-GS-000003	*Number of Waste Packages Hit by Igneous Events*	NA	SN0701PAWPHIT.001_R2	182961	30
59	ANL-MGR-GS-000003	*Number of Waste Packages Hit by Igneous Events*	NA	SN0701PAWPHIT.001_R2	182961	61
60	ANL-NBS-GS-000008	*Future Climate Analysis*	NA	GS000308315121.003_R0	151139	33
61	ANL-NBS-HS-000031	*Saturated Zone Colloid Transport*	NA	LA0303HV831352.003_R0	165624	84
62	ANL-NBS-HS-000058	*Calibrated Unsaturated Zone Properties*	NA	LB0610UZDSCP30.001_R0	179180	116
63	ANL-WIS-MD-000004 REV 04	*DSNF and Other Waste Form Degradation Abstraction*	172453	NA	NA	83
64	ANL-WIS-MD-000010	*Dissolved Concentration Limits of Elements with Radioactive Isotopes*	NA	MO0702PADISCON.001_R0	179358	9
65	ANL-WIS-MD-000010	*Dissolved Concentration Limits of Elements with Radioactive Isotopes*	NA	MO0702PADISCON.001_R0	179358	107
66	ANL-WIS-MD-000010	*Dissolved Concentration Limits of Elements with Radioactive Isotopes*	NA	MO0702PAFLUORI.000_R1	181219	10
67	ANL-WIS-MD-000010	*Dissolved Concentration Limits of Elements with Radioactive Isotopes*	NA	MO0704PASOLCAP.000_R0	180389	11
68	ANL-WIS-MD-000020	*Initial Radionuclides Inventory*	NA	MO0702PASTREAM.001_R0	179925	72
69	ANL-WIS-MD-000020	*Initial Radionuclides Inventory*	NA	MO0702PASTREAM.001_R0	179925	113
70	ANL-WIS-MD-000020	*Initial Radionuclides Inventory*	NA	SN0310T0505503.004_R0	168761	74
71	ANL-WIS-MD-000021	*Cladding Degradation Summary for LA*	NA	MO0411SPACLDDG.003_R1	180755	1
72	ANL-WIS-MD-000021 REV 03 ADD 01	*Cladding Degradation Summary for LA*	180616	NA	NA	92
73	ANL-WIS-PA-000001	*EBS Radionuclide Transport Abstraction*	NA	SN0703PAEBSRTA.001_R3	183217	59

Table 4-1. Direct Inputs (Continued)

Line #	Document_ID	Reference_Document	Document DIRS	DTN	DTN DIRS	PEF
74	NA	*Fundamentals of Heat Transfer, 5th Edition*	163337	NA	NA	47
75	MDL-EBS-MD-000001	*In-Drift Natural Convection and Condensation*	NA	MO0703PAEVSIIC.000_R2	181990	73
76	MDL-EBS-MD-000001	*In-Drift Natural Convection and Condensation*	NA	MO0702PALOVERT.000_R2	180377	70
77	MDL-EBS-MD-000001	*In-Drift Natural Convection and Condensation*	NA	MO0702PALV010K.000_R2	180376	71
78	MDL-EBS-MD-000001 Rev 00 ADD 01	*In-Drift Natural Convection and Condensation*	181648	NA	NA	99
79	MDL-EBS-PA-000004	*Waste Form and In-Drift Colloids-Associated Radionuclide Concentrations: Abstraction and Summary*	NA	MO0701PACSNFCP.000_R1	180439	53
80	MDL-EBS-PA-000004	*Waste Form and In-Drift Colloids-Associated Radionuclide Concentrations: Abstraction and Summary*	NA	MO0701PAGLASWF.000_R1	180393	54
81	MDL-EBS-PA-000004	*Waste Form and In-Drift Colloids-Associated Radionuclide Concentrations: Abstraction and Summary*	NA	MO0701PAGROUND.000_R0	179310	55
82	MDL-EBS-PA-000004	*Waste Form and In-Drift Colloids-Associated Radionuclide Concentrations: Abstraction and Summary*	NA	MO0701PAIRONCO.000_R1	180440	56
83	MDL-EBS-PA-000004	*Waste Form and In-Drift Colloids-Associated Radionuclide Concentrations: Abstraction and Summary*	NA	MO0701PAKDSUNP.000_R1	180392	57

Table 4-1. Direct Inputs (Continued)

Line #	Document_ID	Reference_Document	Document DIRS	DTN	DTN DIRS	PEF
84	MDL-EBS-PA-000004	*Waste Form and In-Drift Colloids-Associated Radionuclide Concentrations: Abstraction and Summary*	NA	MO0701PASORPTN.000_R1	180391	58
85	MDL-MGR-GS-000002	*Atmospheric Dispersal and Deposition of Tephra from a Potential Volcanic Eruption at Yucca Mountain, Nevada*	NA	LA0702PADE03GK.002_R1	179980	63
86	MDL-MGR-GS-000002	*Atmospheric Dispersal and Deposition of Tephra from a Potential Volcanic Eruption at Yucca Mountain, Nevada*	NA	MO0408SPADRWSD.002_R0	171751	64
87	MDL-MGR-GS-000002 Rev 03	*Atmospheric Dispersal and Deposition of Tephra from a Potential Volcanic Eruption at Yucca Mountain, Nevada*	177431	NA	NA	62
88	MDL-MGR-GS-000005	*Dike/Drift Interactions*	NA	LA0702PADE01EG.001_R0	179495	13
89	MDL-MGR-GS-000005	*Dike/Drift Interactions*	NA	LA0702PADE01EG.002_R0	179496	14
90	MDL-MGR-GS-000006	*Redistribution of Tephra and Waste by Geomorphic Processes Following a Potential Volcanic Eruption at Yucca Mountain, Nevada*	NA	MO0605SPAFORTY.000_R1	182281	65
91	MDL-MGR-GS-000006	*Redistribution of Tephra and Waste by Geomorphic Processes Following a Potential Volcanic Eruption at Yucca Mountain, Nevada*	NA	MO0702PAFARDAT.001_R3	182578	66
92	MDL-MGR-GS-000006	*Redistribution of Tephra and Waste by Geomorphic Processes Following a Potential Volcanic Eruption at Yucca Mountain, Nevada*	NA	MO0704PASCOURD.000_R1	182149	87
93	MDL-MGR-MD-000001	*Biosphere Model Report*	NA	MO0702PAGBDCFS.001_R0	179327	67
94	MDL-MGR-MD-000001	*Biosphere Model Report*	NA	MO0702PAGWPROS.001_R0	179328	68

Table 4-1. Direct Inputs (Continued)

Line #	Document_ID	Reference_Document	Document DIRS	DTN	DTN DIRS	PEF
95	MDL-MGR-MD-000001	*Biosphere Model Report*	NA	MO0702PAVBPDCF.000_R0	179330	69
96	MDL-NBS-HS-000006	*UZ Flow Models and Submodels*	NA	LB0612PDFEHMFF.001_R0	179296	38
97	MDL-NBS-HS-000006	*UZ Flow Models and Submodels*	NA	LB0701GTFEHMFF.001_R0	179160	39
98	MDL-NBS-HS-000006	*UZ Flow Models and Submodels*	NA	LB0701MOFEHMFF.001_R0	179297	40
99	MDL-NBS-HS-000006	*UZ Flow Models and Submodels*	NA	LB0702PAFEM10K.002_R0	179507	43
100	MDL-NBS-HS-000006	*UZ Flow Models and Submodels*	NA	LB0701PAWFINFM.001_R0	179283	42
101	MDL-NBS-HS-000008	*Radionuclide Transport Models Under Ambient Conditions*	NA	LA0408AM831341.001_R0	171584	34
102	MDL-NBS-HS-000008	*Radionuclide Transport Models Under Ambient Conditions*	NA	LA0408AM831341.001_R0	171584	98
103	MDL-NBS-HS-000008	*Radionuclide Transport Models Under Ambient Conditions*	NA	LB0701PAKDSESN.001_R0	179299	41
104	MDL-NBS-HS-000019	*Abstraction of Drift Seepage*	NA	LB0702PASEEP01.001_R0	179511	44
105	MDL-NBS-HS-000019	*Abstraction of Drift Seepage*	NA	LB0702PASEEP02.001_R1	181635	45
106	MDL-NBS-HS-000019	*Abstraction of Drift Seepage*	NA	LB0407AMRU0120.001_R0	173280	37
107	MDL-NBS-HS-000019 REV 01 ADD 01	*Abstraction of Drift Seepage*	181244	NA	NA	135
108	MDL-NBS-HS-000020	*Particle Tracking Model and Abstraction of Transport Processes*	NA	LA0701PANS02BR.003_R2	180497	35
109	MDL-NBS-HS-000020	*Particle Tracking Model and Abstraction of Transport Processes*	NA	LA0701PANS02BR.003_R2	180497	98
110	MDL-NBS-HS-000020	*Particle Tracking Model and Abstraction of Transport Processes*	NA	LA0702PANS02BR.001_R1	180322	36
111	MDL-NBS-HS-000020	*Particle Tracking Model and Abstraction of Transport Processes*	NA	LA0702PANS02BR.001_R1	180322	114
112	MDL-NBS-HS-000020	*Particle Tracking Model and Abstraction of Transport Processes*	NA	LB0702PAUZMTDF.001_R1	180776	46
113	MDL-NBS-HS-000020	*Particle Tracking Model and Abstraction of Transport Processes*	NA	LB0702PAUZMTDF.001_R1	180776	98

Table 4-1. Direct Inputs (Continued)

Line #	Document_ID	Reference_Document	Document DIRS	DTN	DTN DIRS	PEF
114	MDL-NBS-HS-000020	*Particle Tracking Model and Abstraction of Transport Processes*	NA	MO0704PAFEHMBR.001_R3	184647	48
115	MDL-NBS-HS-000020	*Particle Tracking Model and Abstraction of Transport Processes*	NA	MO0704PAFEHMBR.001_R3	184647	101
116	MDL-NBS-HS-000020	*Particle Tracking Model and Abstraction of Transport Processes*	NA	MO0704PAPTTFBR.002_R0	180442	49
117	MDL-NBS-HS-000020 Rev 02 AD 01	*Particle Tracking Model and Abstraction of Transport Processes*	184748 181006*	NA	NA	100
118	MDL-NBS-HS-000021	*Saturated Zone Flow and Transport Model Abstraction*	NA	SN0702PASZFTMA.001_R0	179504	51
119	MDL-NBS-HS-000021	*Saturated Zone Flow and Transport Model Abstraction*	NA	SN0702PASZFTMA.002_R1	183471	52
120	MDL-NBS-HS-000021	*Saturated Zone Flow and Transport Model Abstraction*	NA	SN0702PASZFTMA.002_R1	183471	89
121	MDL-NBS-HS-000021 Rev 03 AD01	*Saturated Zone Flow and Transport Model Abstraction*	183750 181650*	NA	NA	128
122	MDL-WIS-PA-000003	*Seismic Consequence Abstraction*	NA	MO0703PASEISDA.002_R4	183156	6
123	MDL-WIS-PA-000003	*Seismic Consequence Abstraction*	NA	MO0703PASEISDA.002_R4	183156	132
124	MDL-WIS-PA-000003	*Seismic Consequence Abstraction*	NA	MO0703PASEISDA.002_R4	183156	133
125	MDL-WIS-PA-000003 Rev 03	*Seismic Consequence Abstraction*	176828	NA	NA	134
126	TDR-TDIP-ES-000006 Rev 00	*Total System Performance Assessment Data Input Package for Requirements Analysis for TAD Canister and Related Waste Package Overpack Physical Attributes Basis for Performance Assessment*	179394	NA	NA	109

Table 4-1. Direct Inputs (Continued)

Line #	Document_ID	Reference_Document	Document DIRS	DTN	DTN DIRS	PEF
127	TDR-TDIP-ES-000009 Rev 00	*Total System Performance Assessment Data Input Package for Requirements Analysis for DOE SNF/HLW and Navy SNF Waste Package Overpack Physical Attributes Basis for Performance Assessment*	179567	NA	NA	110
128	TDR-TDIP-ES-000010 REV 00	*Total System Performance Assessment Data Input Package for Requirements Analysis for Engineered Barrier System In-Drift Configuration*	179354	NA	NA	129

* DIRS not currently in the TSPA Input Database. The new reference is evaluated in Appendix P.

Table 4-2. TSPA Generated Data Tracking Numbers Referenced by Parameter Entry Forms

Line#	Document ID	Document Title	Document DIRS	DTN	DTN DIRS	PEF
1	MDL-WIS-PA-000005	*Total System Performance Assessment Model/Analysis for the License Application*	NA	MO0707EMPDECAY.000_R0	182995	113
2	MDL-WIS-PA-000005	*Total System Performance Assessment Model/Analysis for the License Application*	NA	MO0707PERCFLUX.000_R0	183001	108
3	MDL-WIS-PA-000005	*Total System Performance Assessment Model/Analysis for the License Application*	NA	MO0707PREWAPMS.000_R0	183002	16, 17, 18, 19, 20, 21, 22, 23, 24, 25, 26, 27, 108
4	MDL-WIS-PA-000005	*Total System Performance Assessment Model/Analysis for the License Application*	NA	MO0707UZKDCORR.000_R0	183003	41, 98
5	MDL-WIS-PA-000005	*Total System Performance Assessment Model/Analysis for the License Application*	NA	MO0707WPDRIPSD.000_R0	183005	88, 93, 96, 103, 117, 118
6	MDL-WIS-PA-000005	*Total System Performance Assessment Model/Analysis for the License Application*	NA	MO0708TSPAGENT.000_R0	183000	7, 8, 47, 61, 75, 86, 89, 91, 94, 95, 97, 98, 101, 102, 106, 107, 111, 112, 114, 115, 120, 121, 122, 123, 124, 125, 126, 127, 132, 133, 134

NOTE: See Appendix B for a complete listing of all DTNs that support the TSPA-LA Model.

Table 4-3. Requirements

Title	Requirement Source
Performance Objectives for the Geologic Repository after Permanent Closure	10 CFR 63.113
Requirements for Performance Assessment	10 CFR 63.114
Requirements for Multiple Barriers	10 CFR 63.115
Separate Standards for Protection of Groundwater	10 CFR 63.331
Representative Volume	10 CFR 63.332

NOTE: Requirement sources are found in 10 CFR Part 63 [DIRS 180319].

INTENTIONALLY LEFT BLANK

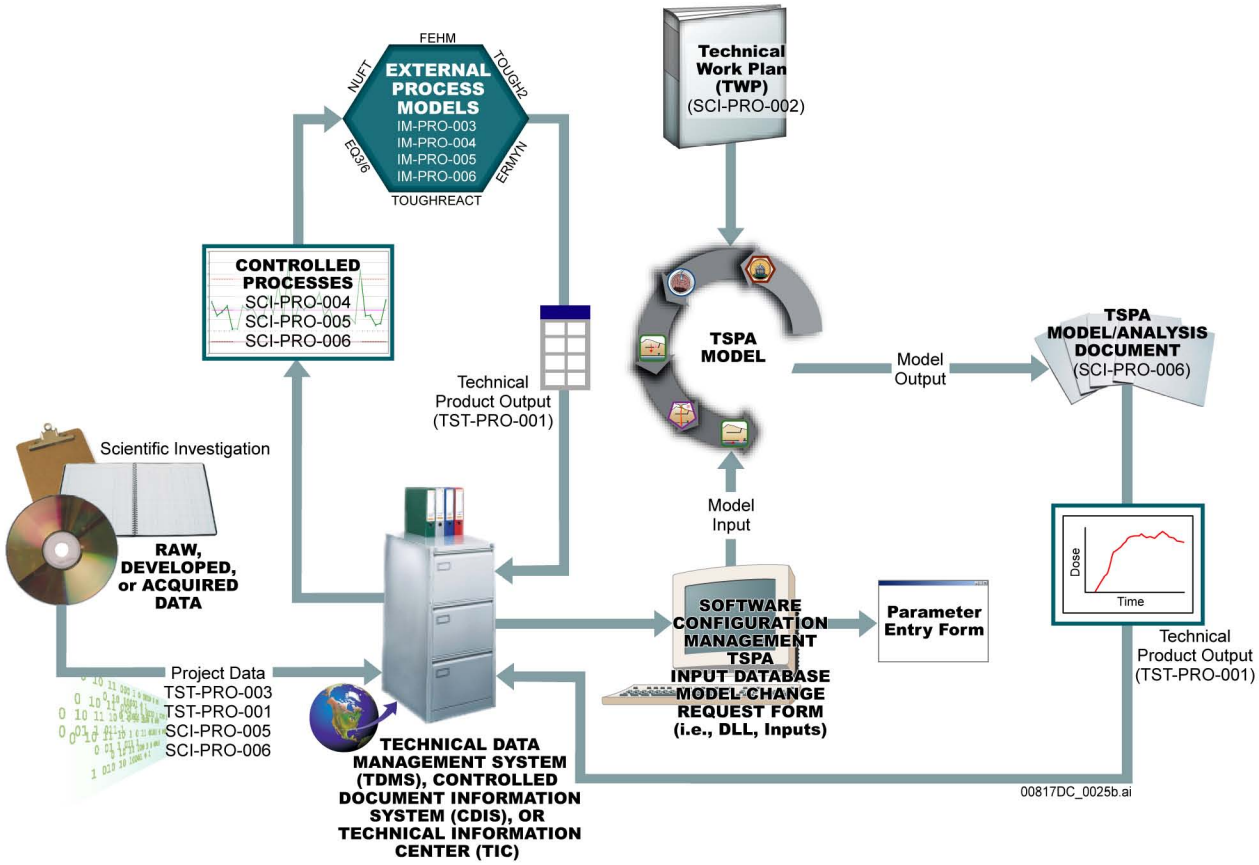

Figure 4-1. Control of Information for TSPA-LA Model Development and Analysis

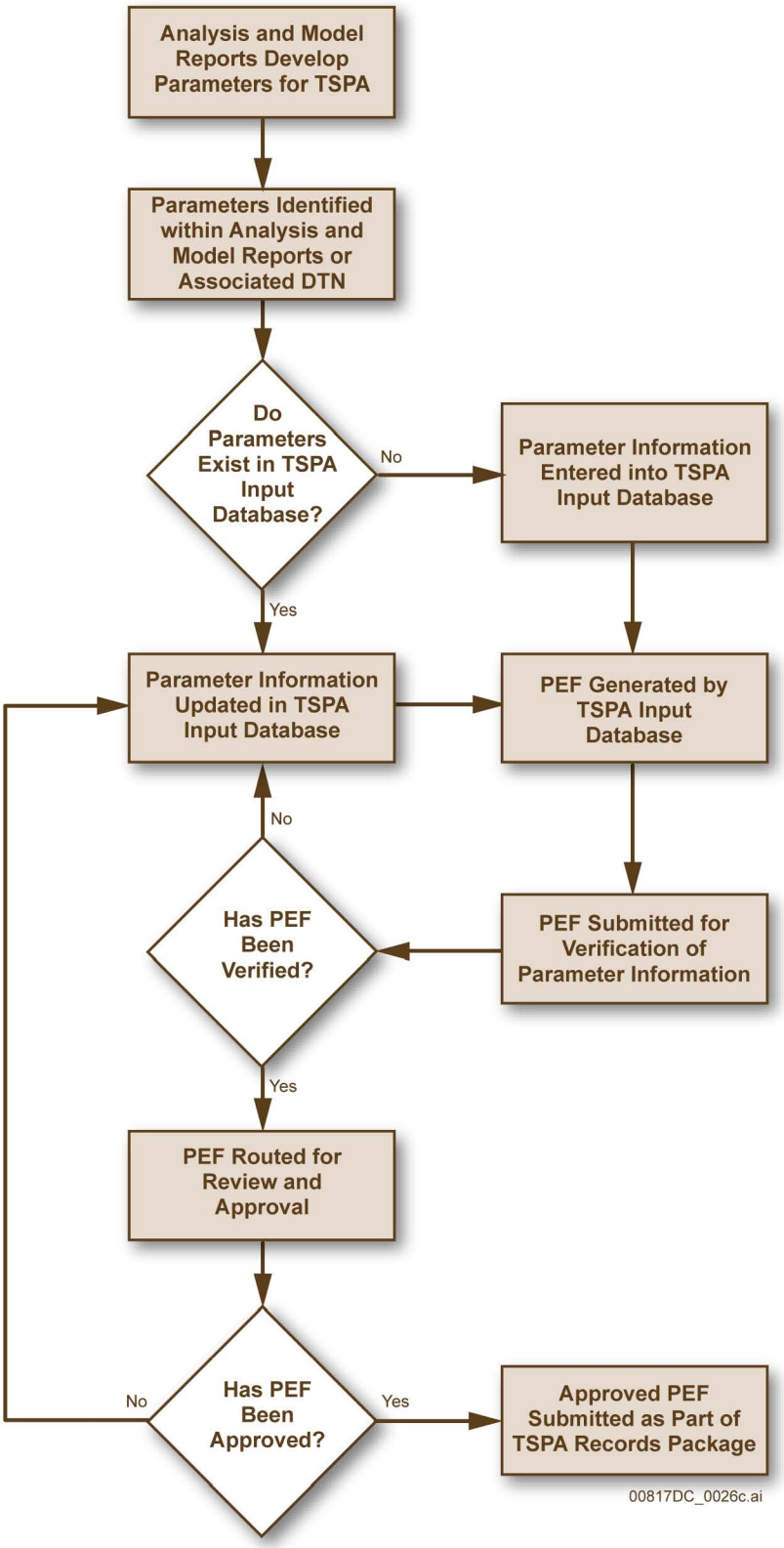

Figure 4-2. Development and Revision of Parameter Entry Forms

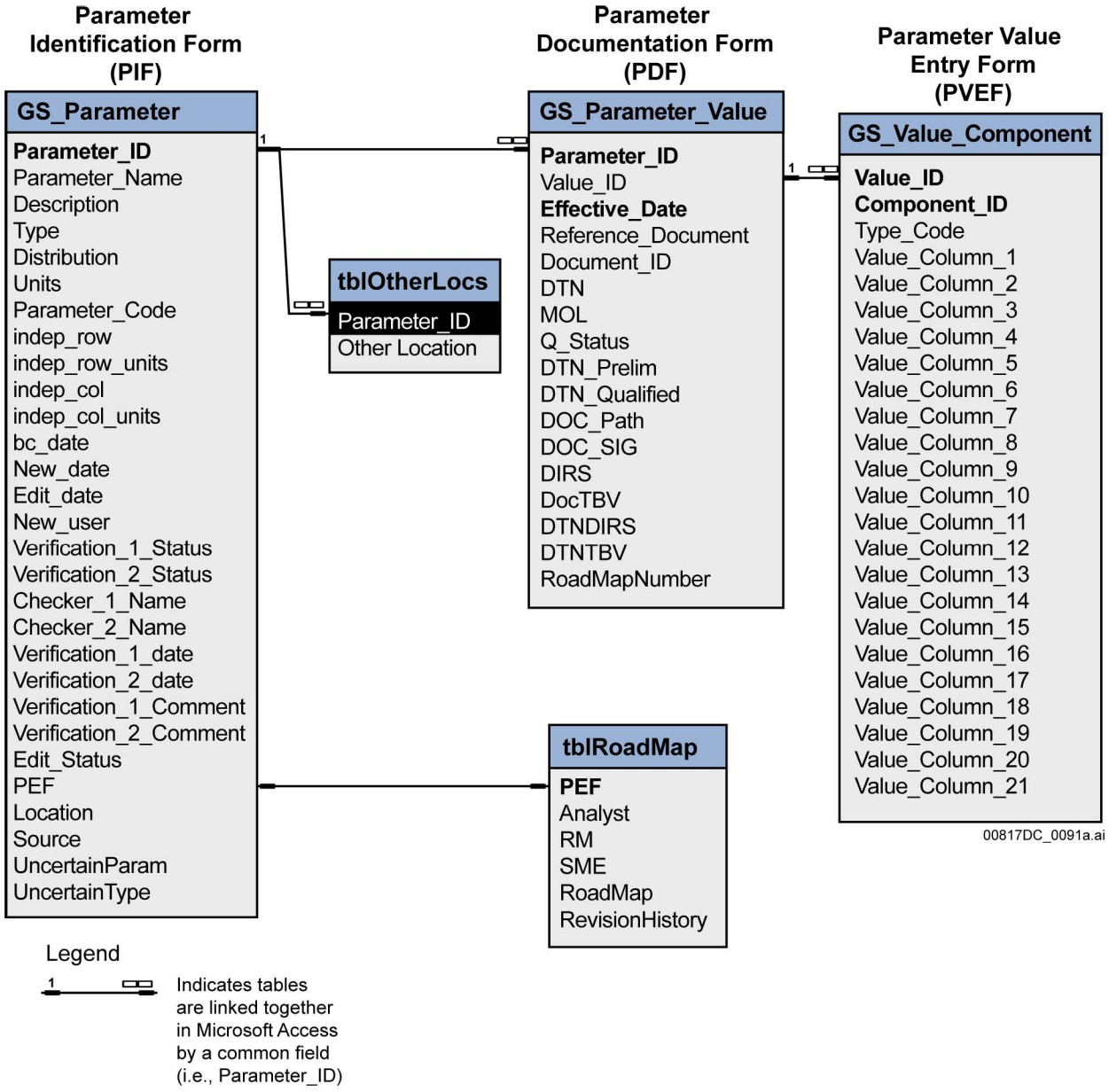

NOTE: These tables are described in detail in the TSPA Input Database documents listed in Section 3.

Figure 4-3. Structural Framework (Schema) for the TSPA Input Database Showing Relationships between Tables

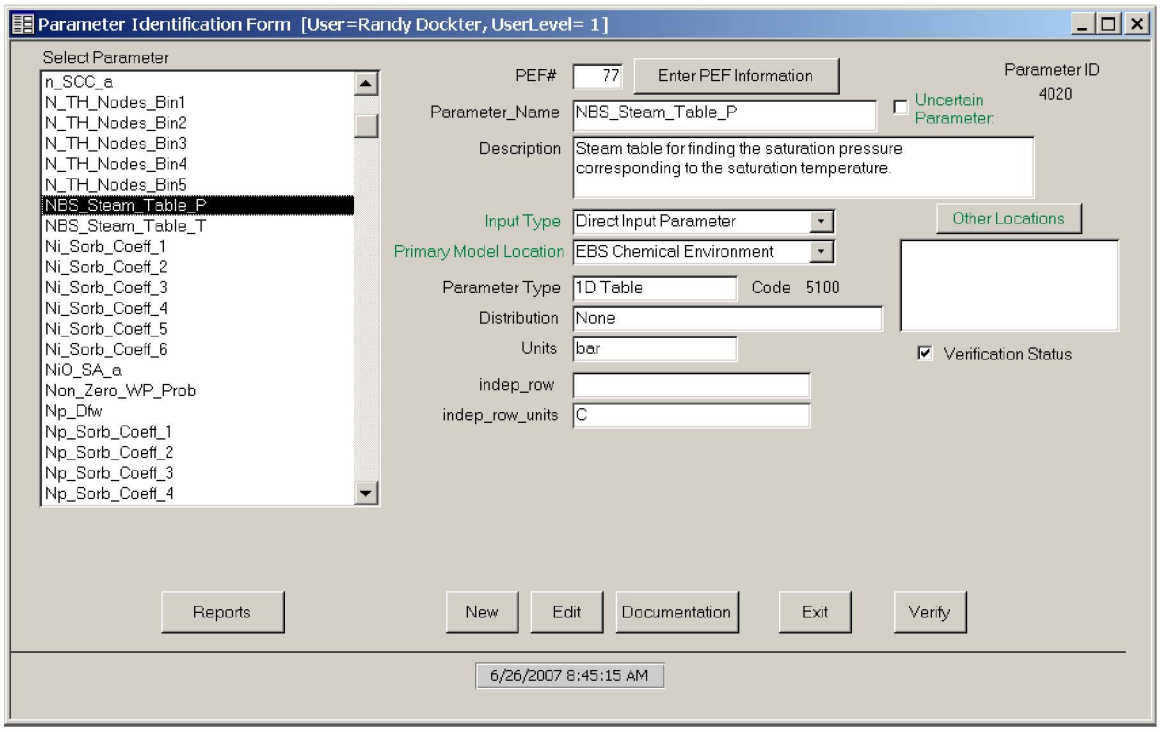

Figure 4-4. Example of a Parameter Identification Form for the TSPA Input Database

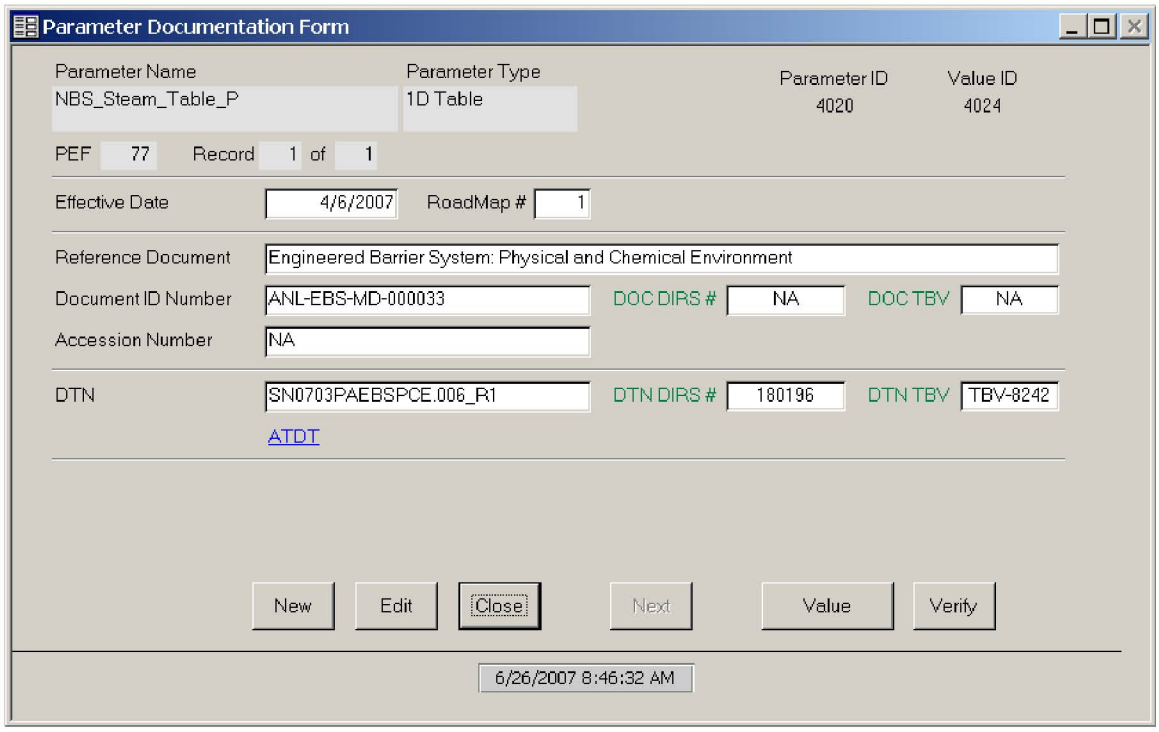

Figure 4-5. Example of a Parameter Documentation Form for the TSPA Input Database

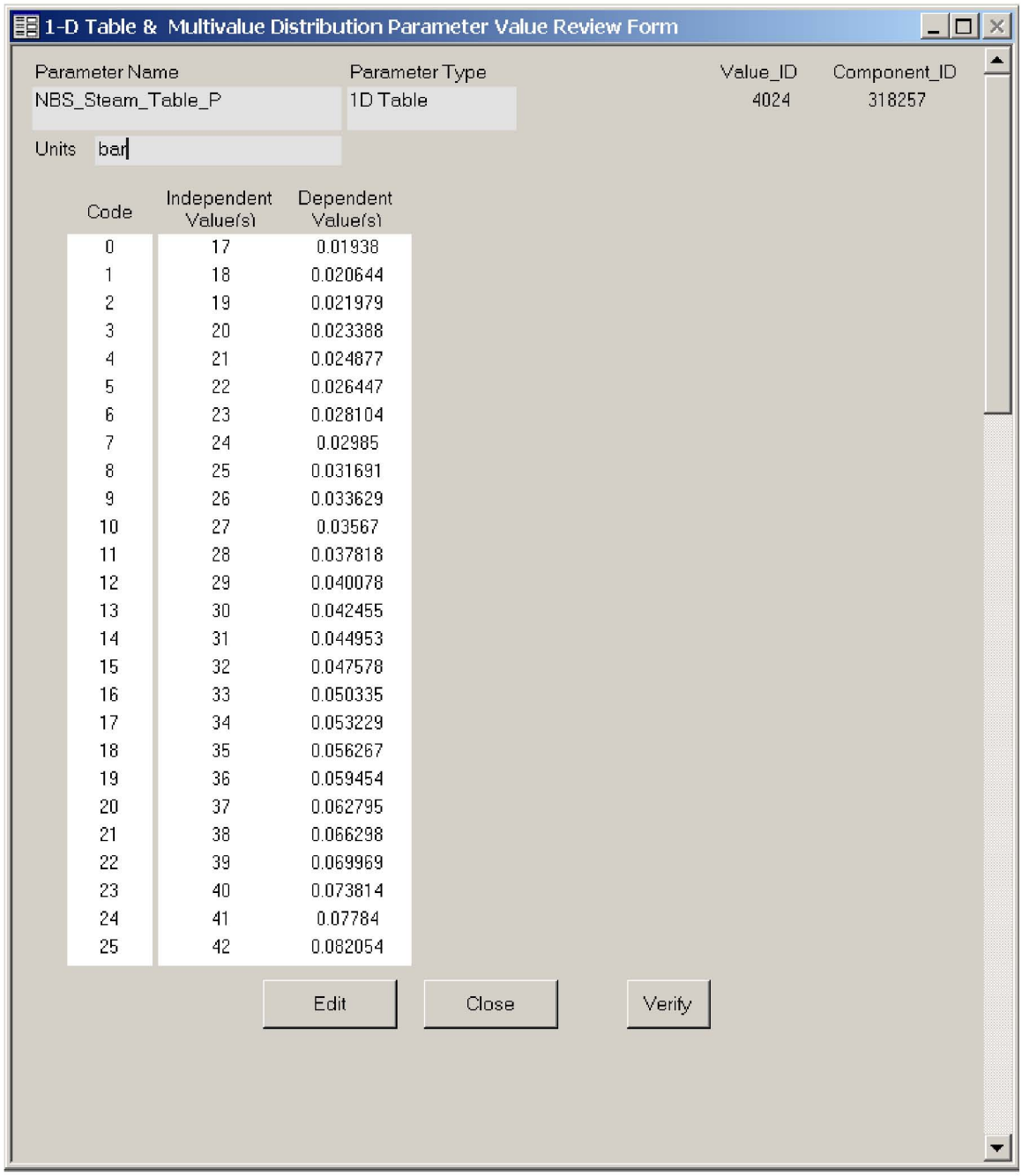

Figure 4-6. Example of a Parameter Value Entry Form for a One-Dimensional Data Table in the TSPA Input Database

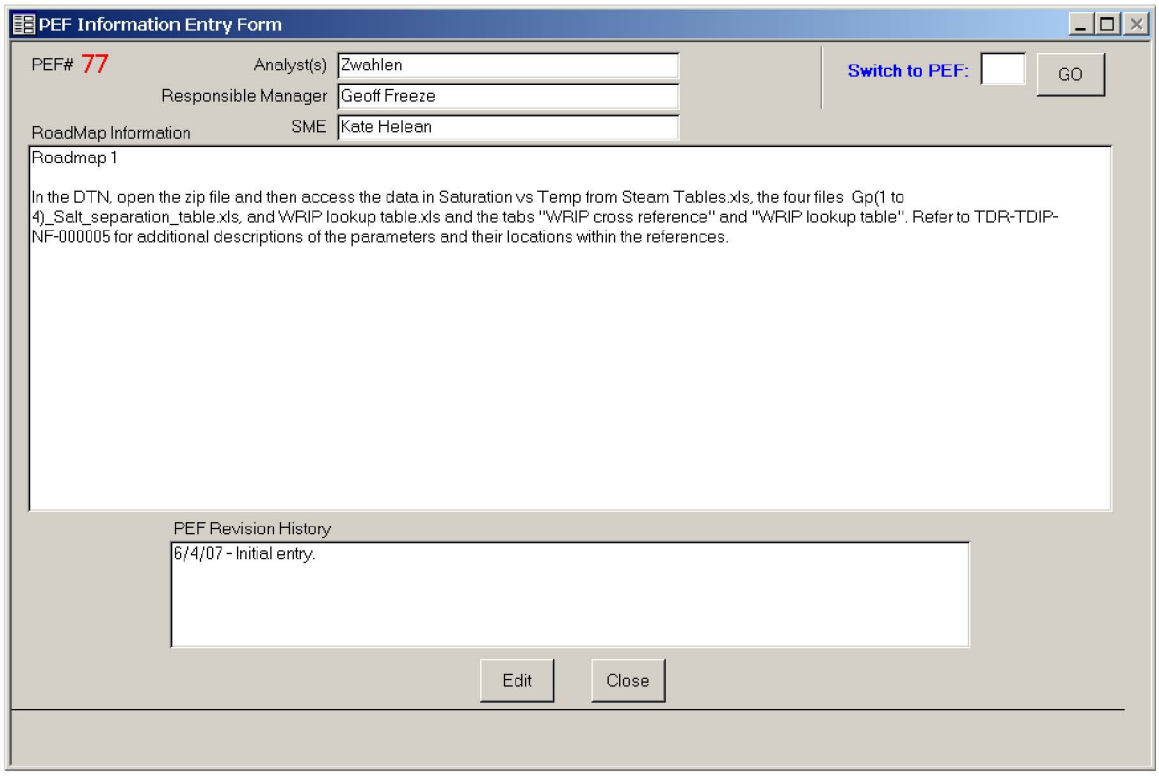

Figure 4-7. Example of a PEF Information Entry Form in the TSPA Input Database

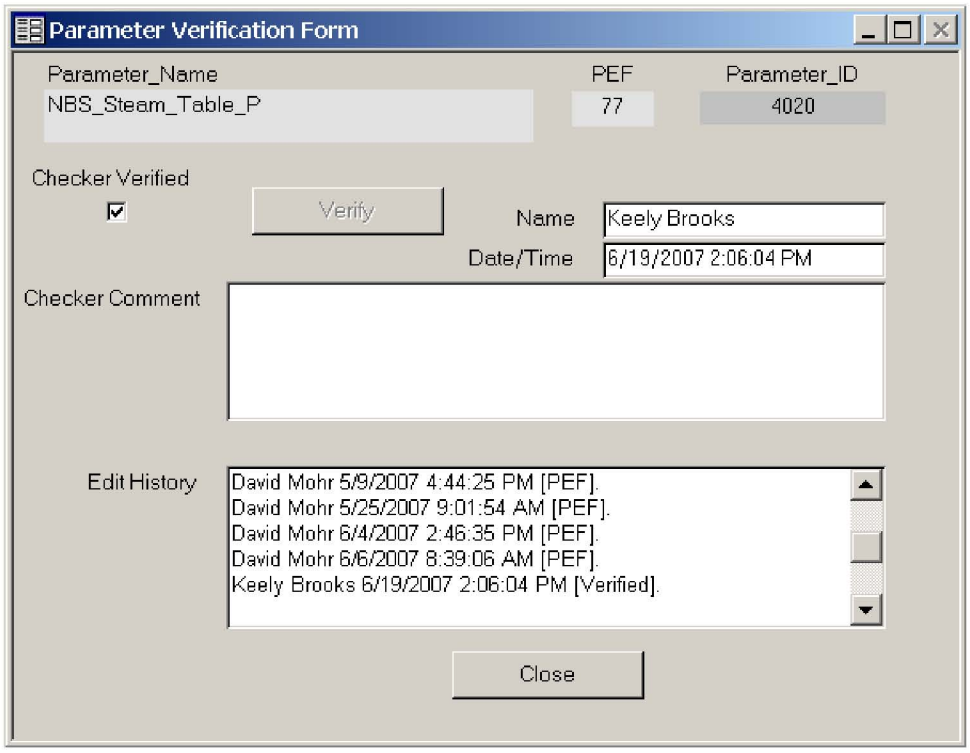

Figure 4-8. Example of a Parameter Verification Form for the TSPA Input Database

5. ASSUMPTIONS

Section 5 presents assumptions for the TSPA-LA Model. The assumptions are as defined and described in SCI-PRO-006, *Models,* Attachment I, Definitions: "***Assumption***–A statement or proposition that is taken to be true or representative in the absence of direct confirming data or evidence, or those estimations, approximations, and/or limitations made during model development (such as when expanding the range of variables to achieve conservatism)." The TSPA-LA Model was developed by integrating assumptions, process models, abstractions, and the results of analyses documented in other project documents.

The assumptions that support the TSPA-LA consist of a subset of the assumptions from supporting analyses that, in turn, support the TSPA-LA Model. The assumptions below were judged to be either required by SCI-PRO-006 or represent assumptions not covered in Section 6.3 that describe the technical bases for the TSPA-LA Model and its submodels. In addition, Section 6.1.4 describes how the process models and submodels from the supporting analyses were integrated into the TSPA-LA Model and the reasoning behind that integration. Modeling implementation decisions (i.e., assumptions) covered in Section 6.3 are not included here because they are not considered essential to the understanding of the results of the TSPA-LA Model.

The assumptions from supporting analyses provide the conceptual underpinning of the TSPA-LA Model and show the key supporting results of these analyses that were assimilated into the TSPA-LA Model.

These assumptions are organized by scenario class, beginning with the Nominal Scenario Class and followed by the Early Failure Scenario Class, the Igneous Scenario Class, and the Seismic Scenario Class. In addition, Section 5.5 includes the assumptions for the Human Intrusion Scenario. Because the assumptions from supporting analyses were not changed in applying them to the TSPA-LA Model, the bases for these assumptions are described in the supporting analyses or are included in the descriptions of the following assumptions. Sections 6.3.1 to 6.7 discuss the conservatisms assumed to apply to the TSPA-LA Model components and scenario classes.

5.1 NOMINAL SCENARIO CLASS

5.1.1 Unsaturated Zone Flow

Assumption—Climate changes can be considered in an approximate way by imparting an instantaneous jump from one steady-state flow field to another, with a corresponding rise or fall in the water table representing the base of the UZ Transport Model Component. Shorter-term transients, such as wet and dry years or individual storm events, are assumed to be adequately captured with a model that assumes such transients can be averaged to obtain a long-term, effective, steady-state climate.

Basis—This assumption and its rationale/basis are described in *Particle Tracking Model and Abstraction of Transport Processes* (SNL 2008 [DIRS 184748], Section 5, Assumption 6).

Supports Total System Performance Assessment Model/Analysis for the License Application in: Section 6.3.1.3

Assumption—The effect of uncertainty regarding the influence of the duration of climate periods on repository performance is negligible and, for simulation purposes, the range of durations estimated for the present-day climate state and the monsoon climate state can be simplified to the longest predicted duration of each climate state. For the present-day climate, a duration range of 400 to 600 years after emplacement and 550 years after closure is projected, and only the longest duration of 600 years after emplacement is simulated in the TSPA-LA Model. The monsoon climate period is predicted to have a duration of between 900 to 1,400 years. The TSPA-LA Model simulations use a duration of 1,400 years for the monsoon climate state.

Basis—The effect on performance is negligible based on the impact that the ranges of the durations of these climate periods have on total infiltration that is applied to the Site-Scale UZ Flow Process Model. The difference of estimated total infiltration when using the minimum climate durations as compared to the maximum projected durations of these climate periods is only about 3 percent during the 10,000-year simulation period (Section 6.3.1.2). When considering the minimum and maximum transition times, the small impact of these maximum climate-period durations on the amount of total infiltration is not likely to have a significant effect on radionuclide releases from the repository or the travel times of these radionuclides to the RMEI.

Supports Total System Performance Assessment Model/Analysis for the License Application in: Section 6.3.1.2

Assumption—Per regulatory guidance, with the exception of factors related to geology, hydrology, and climate, and for the purposes of performance assessment, future conditions at the Yucca Mountain site are assumed to be the same as current conditions.

Basis—This assumption is described in NRC Proposed Rule 10 CFR 63.305(c) [DIRS 178394].

Supports Total System Performance Assessment Model/Analysis for the License Application in: Section 6.3.1.2

5.1.2 Engineered Barrier System Environment

Assumption—It is assumed that the NFC (near field chemistry) model results, calculated using averaged rock properties (mineralogy, porosity, saturation, grain density) for the four repository host units to evaluate the degree of water-rock interaction and thermal properties for the Tptpll (Topopah Spring Tuff lower lithophysal unit) lithologic unit to model development and evolution of the thermal field, are applicable to all lithologies intersected by the repository drifts.

Basis—This assumption and its rationale/basis are described in *Engineered Barrier System: Physical and Chemical Environment* (SNL 2007 [DIRS 177412], Section 5.2.1).

Supports Total System Performance Assessment Model/Analysis for the License Application in: Section 6.3.2.2

Assumption—The NFC/physical and chemical environment (P&CE) model simulations using the four starting waters adequately represent all possible seepage waters.

Basis—This assumption and its rationale/basis are described in *Engineered Barrier System: Physical and Chemical Environment* (SNL 2007 [DIRS 177412], Section 5.2.2).

Supports Total System Performance Assessment Model/Analysis for the License Application in: Section 6.3.4.2

Assumption—The ambient percolation-flux distribution above the repository horizon is assumed to be unaffected by mountain-scale, repository heat-driven, TH effects. Therefore, the estimated repository-scale percolation-flux distribution is assumed to be the percolation-flux distribution from the PTn to the upper Topopah Spring welded tuff (TSw) UZ Flow Model Component layer.

Basis—This assumption and its rationale/basis are described in *Multiscale Thermohydrologic Model* (SNL 2007 [DIRS 181383], Section 5.1.2).

Supports Total System Performance Assessment Model/Analysis for the License Application in: Section 6.3.2.1

Assumption—The entire WP inventory of the repository is assumed to be emplaced at the same time.

Basis—This assumption and its rationale/basis are described in *Multiscale Thermohydrologic Model* (SNL 2007 [DIRS 181383], Section 5.2.3).

Supports Total System Performance Assessment Model/Analysis for the License Application in: Section 6.3.2.1

Assumption—The EBS is assumed to be in a state of local metastable equilibrium. All aqueous and gas constituents in the TSPA-LA Model achieve and maintain local equilibrium, and most mineral phases achieve and maintain local equilibrium upon saturation. Because the reaction rates of some minerals likely to form under the Yucca Mountain geochemical conditions are slower than the scale of the modeled processes in the TSPA-LA Model, these minerals would not precipitate despite local conditions of saturation or supersaturation. However, using the assumption of metastable equilibrium, the TSPA-LA Model can be used to make steady-state predictions for nonequilibrium conditions concerning mineral stability with respect to relative humidity, provided the appropriate inputs are used.

Basis—This assumption and its rationale/basis are described in *In-Drift Precipitates/Salts Model* (SNL 2007 [DIRS 177411], Section 5.2) and applied in Section 6.6.2.6 with respect to local equilibrium and in Section 6.6.3.3 with respect to relative humidity.

Supports Total System Performance Assessment Model/Analysis for the License Application in: Section 6.3.2.2

5.1.3 Waste Form Degradation and Mobilization

Assumption—Plutonium and americium sorption on HLW derived waste form colloids, steel corrosion derived iron oxyhydroxide colloids, and CSNF derived waste form colloids is modeled as irreversible.

Basis—This assumption and its rationale/basis are described in Waste Form and In-Drift Colloids-Associated Radionuclide Concentrations: Abstraction and Summary (SNL 2007 [DIRS 177423], Sections 5.4, 5.5, and 6.3.12.2).

Supports Total System Performance Assessment Model/Analysis for the License Application in: Section 6.3.7.6.2

Assumption—It is assumed that physical filtration and gravitational settling of colloids will not occur within the WPs and repository drifts.

Basis—This assumption and its rationale/basis are described in *EBS Radionuclide Transport Abstraction* (SNL 2007 [DIRS 177407], Section 5.7).

Supports Total System Performance Assessment Model/Analysis for the License Application in: Section 6.3.7.6

5.1.4 Engineered Barrier System Flow and Transport

Assumption—It is assumed that the seepage locations in the emplacement drifts are random with respect to the locations of the WPs, but after seepage occurs, its location does not change with time. It is also assumed that fragments of the DSs that may rest on WPs, or fallen rock that may rest on DSs or WPs, do not divert any seepage flux. In addition, it is assumed that all seepage into the emplacement drifts falls on the crowns of the DSs, and in the absence of a DS, all seepage falls on the crowns of the WPs.

Basis—This assumption and its rationale/basis are described in *EBS Radionuclide Transport Abstraction* (SNL 2007 [DIRS 177407], Section 5.1).

Supports Total System Performance Assessment Model/Analysis for the License Application in: Section 6.3.6.1

Assumption—It is assumed that there is no evaporation of the seepage water from the surfaces of the DSs.

Basis—This assumption and its rationale/basis are described in *EBS Radionuclide Transport Abstraction* (SNL 2007 [DIRS 177407], Section 5.2).

Supports Total System Performance Assessment Model/Analysis for the License Application in: Sections 6.3.6.1 and 6.3.6.4.1

Assumption—It is assumed that evaporation of water from the surface or interior of a WP does not occur.

Basis—This assumption and its rationale/basis are described in *EBS Radionuclide Transport Abstraction* (SNL 2007 [DIRS 177407], Section 5.3).

Supports Total System Performance Assessment Model/Analysis for the License Application in: Sections 6.3.6.1 and 6.3.6.4.1

Assumption—The TSPA-LA Model assumes that under low water conditions inside a WP, defined as having a relative humidity below 95 percent and a liquid influx of less than 0.1 L/year, bulk water in the WP is assumed to be unavailable for in-package chemistry calculations, and the water films are assumed to be discontinuous and not allow diffusive transport. Similarly, at and above the boiling point of water in the repository (100°C), no bulk water will be present and, thus, no transport of radionuclides could take place. For all other conditions in the repository, a thin film of adsorbed water is assumed to be present on the surfaces of internal WP components and corrosion products in a breached WP. This water film is assumed to be continuous and to behave as a bulk liquid, thus allowing radionuclides to dissolve in the water film and diffuse. Colloids are also assumed to diffuse in this water film.

Basis—This assumption and its rationale/basis are described in *In-Package Chemistry Abstraction* (SNL 2007 [DIRS 180506], Section 6.10.9.1[a]) and in *EBS Radionuclide Transport Abstraction* (SNL 2007 [DIRS 177407], Section 5.5).

Supports Total System Performance Assessment Model/Analysis for the License Application in: Section 6.3.7.2

Assumption—Under low-water conditions, defined as having a relative humidity below 95 percent and a liquid influx of less than 0.1 L/year, the HLW degradation rate is calculated from the aqueous degradation equations assuming a pH of 10, and the CSNF degradation rate is calculated from the aqueous degradation equations assuming a pH between 6 and 7. These pH ranges are based on limited solubility data under conditions where there is water vapor condensation on HLW and CSNF.

Basis—This assumption and its rationale/basis are described in *In-Package Chemistry Abstraction* (SNL 2007 [DIRS 180506], Sections 5.5[a] and 6.10.9.1[a]).

Supports Total System Performance Assessment Model/Analysis for the License Application in: Section 6.3.7.2

Assumption—The partial pressure of O_2 in the WPs is a constant value of 0.2 bar and is equated to the partial pressure of O_2 in the emplacement drift environment, which is equal to atmospheric O_2.

Basis—This assumption and its rationale/basis are described in *In-Package Chemistry Abstraction* (SNL 2007 [DIRS 180506], Section 6.3.1.1).

Supports Total System Performance Assessment Model/Analysis for the License Application in: Section 6.3.7.4.1.3

Assumption—It is assumed that no corrosion products exist in the invert.

Basis—This assumption and its rationale/basis are described in *EBS Radionuclide Transport Abstraction* (SNL 2007 [DIRS 177407], Section 5.6). Assuming that no corrosion products exist in the invert is a bounding assumption that reduces the potential effectiveness of the invert as a transport barrier by ignoring the potential for radionuclide sorption onto steel corrosion products.

Supports Total System Performance Assessment Model/Analysis for the License Application in: Section 6.3.8.2.4 and 6.3.8.4.2

5.1.5 Unsaturated Zone Transport

Assumption—Radionuclide releases at the location of the repository can be represented stochastically by identifying regions on the basis of the predicted water flux through the medium, and placing particles randomly within this region to represent the release.

Basis—This assumption and its rationale/basis are described in *Particle Tracking Model and Abstraction of Transport Processes* (SNL 2008 [DIRS 184748], Section 5, Assumption 4).

Supports Total System Performance Assessment Model/Analysis for the License Application in: Section 6.3.9.3

Assumption—For the purposes of computing radionuclide transport, flow through the UZ can be approximated assuming that the system (rock mass and flow conditions) has not been influenced by repository waste heat effects or drift shadow effects. Durable changes to the rock mass hydrologic properties are also assumed to be negligible.

Basis—This assumption and its rationale/basis are described in *Particle Tracking Model and Abstraction of Transport Processes* (SNL 2008 [DIRS 184748], Section 5, Assumption 5).

Supports Total System Performance Assessment Model/Analysis for the License Application in: Section 6.3.9.4

5.1.6 Saturated Zone Flow and Transport

Assumption—The change in groundwater flow in the SZ from one climatic state to another occurs rapidly and is approximated by a shift from one steady-state flow condition to another steady-state flow condition over one timestep.

Basis—This assumption and its rationale/basis are described in *Saturated Zone Flow and Transport Model Abstraction* (SNL 2008 [DIRS 183750], Section 5, Assumption 5).

Supports Total System Performance Assessment Model/Analysis for the License Application in: Section 6.3.10.1

5.1.7 Biosphere

Assumption—Per regulatory guidance, it is assumed that the RMEI has a diet and living style representative of the people who now reside in the town of Amargosa Valley, Nevada.

Basis—This assumption is described in NRC Proposed Rule 10 CFR 63.312(b) [DIRS 180319]. Information on the consumption of radionuclides for the RMEI is described and tabulated in *Characteristics of the Receptor for the Biosphere Model* (BSC 2005 [DIRS 172827], Sections 6.4 and 7.1.2.2).

Supports Total System Performance Assessment Model/Analysis for the License Application in: Section 6.3.11

Assumption—The average concentration of radionuclides in the groundwater supply of the hypothetical community of the RMEI is an appropriate estimate of radionuclide concentration for the calculation of radiological dose. To comply with 10 CFR Part 63, the average concentration of radionuclides in groundwater is calculated by considering all of the radionuclides exiting the controlled area (10 CFR 63.302 [DIRS 180319]) in a year and those contained (10 CFR 63.332(a) [DIRS 180319]) in an annual groundwater volume of 3,000 acre-feet (10 CFR 63.312(b) and 10 CFR 63.332 (a)(3) [DIRS 180319]).

Basis—This assumption and its rationale/basis are described in *Saturated Zone Flow and Transport Model Abstraction* (SNL 2008 [DIRS 183750], Section 5, Assumption 3).

Supports Total System Performance Assessment Model/Analysis for the License Application in: Section 6.3.11

5.2 EARLY FAILURE SCENARIO CLASS

Analysis of Mechanisms for Early Waste Package/Drip Shield Failure (SNL 2007 [DIRS 178765]) describes calculations related to the number of early DS and WP failures and summarizes all the assumptions related to those calculations. The assumptions for both DSs and WPs concern flaws related to Alloy 22 (UNS N06022) and titanium composition, welding, improper heat treatment, improper laser peening, improper handling, surface contamination, and incorrect DS emplacement/interlocking in the repository.

5.2.1 Drip Shield Early Failure Modeling Case

Assumption—The early-failed DSs are assumed to fail at time zero and are independently placed within the repository. In addition, it is assumed that the underlying WP fails at time zero due to localized corrosion.

Basis—The occurrence time for the early-failed DSs is a simplifying assumption used in the TSPA-LA Model in the absence of a model that explicitly accounts for the propagation of DS failures from the flaws, contamination, and improper treatment of the DSs. Furthermore, the

as-received and undetected flaws, contamination, and improper treatment of the DSs are due to manufacturing and handling, and precede placement in the repository. Therefore, these assumptions are part of the as-received condition or emplacement of the DSs and are imposed as initial postclosure conditions in the TSPA-LA Model. After DS failure, there is a finite probability that the underlying WP will fail due to the initiation of localized corrosion as described in Appendix O. Instead of explicitly modeling WP failure for the situation of an early-failed DS, the TSPA-LA Model considers the bounding condition that the underlying WP is failed due to localized corrosion at the same time as the DS.

Supports Total System Performance Assessment Model/Analysis for the License Application in: Section 6.4.1

5.2.2 Waste Package Early Failure Modeling Case

Assumption—The early-failed WPs are assumed to fail at time zero and are independently placed within the repository.

Basis—The occurrence time for the early failed WPs is a simplifying assumption used in the TSPA-LA Model that explicitly accounts for the propagation of WP failures from the as-received and undetected flaws, contamination, and improper treatment of the WPs. Furthermore, the flaws, contamination, and improper treatment of the WPs are due to manufacturing and handling, and precede placement in the repository. Therefore, these assumptions are part of the as-received condition of the WPs and are imposed as initial postclosure conditions in the TSPA-LA Model.

Supports Total System Performance Assessment Model/Analysis for the License Application in: Section 6.4.2

5.3 IGNEOUS SCENARIO CLASS

5.3.1 Igneous Intrusion Modeling Case

Assumption—The permeability of any cooled igneous rock that has invaded emplacement drifts is assumed to be the same as that of the bulk host rock, and does not impede flow.

Basis—Natural analogs indicate that a number of different processes could lower permeabilities in the intrusions immediately in contact with a host rock (Lichtner et al. 1999 [DIRS 121006], pp. 8 and 9; Frankel 1967 [DIRS 168717]). However, the extent or uniformity of any changes to the permeability of the intrusion is not known locally. Therefore, it is assumed that hydraulic properties of the cooled intrusion are the same as those of the host rock. This assumption is necessary for the EBS and UZ flow submodels. This assumption is reasonable, technically defensible, and conservative and does not need further justification.

Supports Total System Performance Assessment Model/Analysis for the License Application in: Section 6.5.1

Assumption—In the Igneous Intrusion Modeling Case, when any main, drift, turnout, or other extension in the repository is simulated to be hit by a dike, then all WPs in the entire repository are considered to fail.

Basis—This assumption is described in *Number of Waste Packages Hit by Igneous Events* (SNL 2007 [DIRS 177432], Section 5.1).

Supports Total System Performance Assessment Model/Analysis for the License Application in: Sections 6.5.1.1

Assumption—In the Igneous Intrusion Modeling Case, the DOE-owned high-level waste glass waste form is assumed to instantaneously degrade releasing radionuclides from the glass matrix.

Basis—During an igneous intrusion, glass is expected to melt and resolidify as the drift cools (SNL 2007 [DIRS 177430], Section 6.4.8.3.3). During the melting process, volatile radionuclides may be released. As the glass cools, new crystalline and glass phases may form that may degrade slower or faster than the original glass phase (BSC 2004 [DIRS 169988], Section 6.5.5). To bound the uncertainty in the release fraction of the volatile radionuclides and in the degradation rates of radionuclide-containing phases, it is assumed that the glass will degrade instantaneously during an igneous intrusion.

Supports Total System Performance Assessment Model/Analysis for the License Application in: Section 6.5

5.3.2 Volcanic Eruption Modeling Case

Assumption—In the Volcanic Eruption Modeling Case, when a waste emplacement drift is hit by a conduit, then only the number of waste packages that can fit within the profile (footprint) of the conduit are considered to fail.

Basis—This assumption is described in *Number of Waste Packages Hit by Igneous Events* (SNL 2007 [DIRS 177432], Section 5.2).

Supports Total System Performance Assessment Model/Analysis for the License Application in: Sections 6.5.2.1.1

Assumption—The ASHPLUME code (ASHPLUME_DLL_LA V.2.1, STN: 11117-2.1-01 [DIRS 180147]) assumes that volcanic eruptions in the Yucca Mountain repository are violent Strombolian eruptions for the entire duration of the explosive phase. Erupted magma is presumed to be fragmented and dispersed in the convective plume for the entire duration of the eruption. This assumption is conservative in that it maximizes the potential for ash and waste dispersal during Strombolian activity.

Basis—This assumption and its rationale/basis are described in *Atmospheric Dispersal and Deposition of Tephra from a Potential Volcanic Eruption at Yucca Mountain, Nevada* (SNL 2007 [DIRS 177431], Section 5.1.1).

Supports Total System Performance Assessment Model/Analysis for the License Application in: Section 6.5.2

Assumption—The waste entrained in a volcanic eruption is assumed to be instantaneously fragmented and dispersed in the same manner as the erupted magma.

Basis—For the purpose of estimating waste-particle diameters in the eruptive environment, all waste is assumed to be unaltered CSNF physically disaggregated to a size range that approximately relates to fuel form grain size. If partly or wholly assimilated into the magma melt, the unaltered glass waste forms are likely to have particle diameters comparable to those of the ash particles, which are larger than the values used for spent fuel. The waste particles are transported by combining with ash particles of equal size of larger, and the ash-dispersal model assumes that fuel in the affected WPs is available for entrainment in the ash plume as finely-divided particles with diameters in the range of 1 to 2,000 μm, with a mean of 30 μm. The waste mass is distributed among the ash mass based on relative particle sizes. These assumptions are described in *Atmospheric Dispersal and Deposition of Tephra from a Potential Volcanic Eruption at Yucca Mountain, Nevada* (SNL 2007 [DIRS 177431], Sections 1, 5.1.2, 5.2.4, 5.2.5, and 6.5.2.6).

Supports Total System Performance Assessment Model/Analysis for the License Application in: Section 6.5.2 and the GoldSim Model File

Assumption—Climatic change is assumed not to significantly affect wind speed and direction. The magnitude of short-term variability in wind speed and direction, which is included in the data that characterize present wind conditions, is assumed to be significantly greater than long-term variability introduced by potential future climatic changes.

Basis—This assumption and its rationale/basis are described in *Atmospheric Dispersal and Deposition of Tephra from a Potential Volcanic Eruption at Yucca Mountain, Nevada* (SNL 2007 [DIRS 177431], Section 5.2.1).

Supports Total System Performance Assessment Model/Analysis for the License Application in: Section 6.4.2

5.4 SEISMIC SCENARIO CLASS

Assumption—Seismic events occur in a random manner, following a Poisson process, over long periods of time.

Basis—This assumption and its rationale/basis are described in *Seismic Consequence Abstraction* (SNL 2007 [DIRS 176828], Section 5.2).

Supports Total System Performance Assessment Model/Analysis for the License Application in: Section 6.6.1.3

Assumption—Waste package internals are assumed to degrade as structural elements after the outer corrosion barrier (of a WP) is first damaged by a seismic event. More exactly, the internals degrade as a structural component for the TSPA-LA Model by the time of the next seismic event after the first seismic event that breaches a WP.

Basis—This assumption and its rationale/basis are described in *Seismic Consequence Abstraction* (SNL 2007 [DIRS 176828], Section 5.4).

Supports Total System Performance Assessment Model/Analysis for the License Application in: Sections 6.6.1.1 and 6.6.1.2

5.5 HUMAN INTRUSION SCENARIO

Assumption—The NRC adopts language from the EPA Proposed Rule 40 CFR 197.26 [DIRS 155216] that describes the assumptions related to a stylized human intrusion scenario. The DOE used the following assumptions leading to an estimate of the dose to any RMEI from a human intrusion (NRC Proposed Rule 10 CFR 63.322 [DIRS 180319]):

a. "There is a single human intrusion as a result of exploratory drilling for ground water;

b. The intruders drill a borehole directly through a degraded waste package into the uppermost aquifer underlying the Yucca Mountain repository;

c. The drillers use the common techniques and practices that are currently employed in exploratory drilling for ground water in the region surrounding Yucca Mountain;

d. Careful sealing of the borehole does not occur, instead natural degradation processes gradually modify the borehole;

e. No particulate waste material falls into the borehole;

f. The exposure scenario includes only those radionuclides transported to the saturated zone by water (e.g., water enters the waste package, releases radionuclides, and transports radionuclides by way of the borehole to the saturated zone); and

g. No releases are included which are caused by unlikely natural processes and events."

Basis—These assumptions are described in NRC Proposed Rule 10 CFR 63.322 [DIRS 180319]. Information on the consumption of radionuclides for the RMEI is described and tabulated in *Characteristics of the Receptor for the Biosphere Model* (BSC 2005 [DIRS 172827], Sections 6.4 and 7.1.2.2).

Supports Total System Performance Assessment Model/Analysis for the License Application in: Section 6.7

INTENTIONALLY LEFT BLANK

6. TSPA-LA MODEL DESCRIPTION

This *Total System Performance Assessment Model/Analysis for the License Application* (TSPA-LA) of the Yucca Mountain repository system is a systematic probabilistic analysis that synthesizes site characterization data, repository design information, process models, abstractions, and analyses. More specifically, U.S. Nuclear Regulatory Commission (NRC) Proposed Rules 10 CFR 63.2 (1) [DIRS 178394] and 10 CFR 63.2 (2) and (3) [DIRS 180319] define three activities as part of performance assessment (PA):

"*Performance assessment* means an analysis that:

1. Identifies the features, events, processes (FEPs) (except human intrusion), and sequences of events and processes (except human intrusion) that might affect the Yucca Mountain disposal system and their probabilities of occurring;

2. Examines the effects of those FEPs, and sequences of events and processes upon the performance of the Yucca Mountain disposal system; and

3. Estimates the dose incurred by the reasonably maximally exposed individual, including the associated uncertainties, as a result of releases caused by all significant FEPs, and sequences of events and processes, weighted by their probability of occurrence."

The first activity determines what representations of possible future states of the repository (i.e., scenario classes) are sufficiently important to warrant quantitative analysis. For the TSPA-LA, nominal and event scenario classes are analyzed. The Nominal Scenario Class incorporates all FEPs (Appendix I), except those FEPs associated with early failures of the waste packages (WPs) or drip shields (DSs) and disruptive events. The Early Failure Scenario Class addresses FEPs that describe the potential for DS and WP early failure in the absence of disruptive events. The TSPA-LA Model includes two scenario classes that address the possibility that disruptive events may occur at or near the repository and that these events may affect repository performance. In addition, the NRC Proposed Rule 10 CFR 63.322 [DIRS 180319] requires the U.S. Department of Energy (DOE) to assess a Human Intrusion Scenario and 10 CFR 63.321 [DIRS 178394] provides the performance standard for the Human Intrusion Scenario. Section 6.1.1 summarizes the scenario class development process adopted for the TSPA-LA, including the basis for identification and screening of potentially relevant FEPs. Section 6.1.2 summarizes the selection of the scenario classes. The following scenario classes are included in the TSPA-LA.

Nominal Scenario Class (Section 6.3)—The Nominal Scenario Class uses the TSPA-LA Model components to describe all included FEPs that are nominally expected to occur. The Nominal Scenario Class encompasses all processes affecting the integrity of the WPs containing spent nuclear fuel (SNF) and high-level (radioactive) nuclear waste (HLW) in the absence of disruptive events. These processes include WP degradation because of corrosion mechanisms including general corrosion, stress corrosion cracking (SCC), localized corrosion, and microbially influenced corrosion (MIC).

Early Failure Scenario Class (Section 6.4)—The Early Failure Scenario Class describes performance of the repository system in the event of early failures of the DSs or WPs due to

manufacturing or material defects or to pre-emplacement operations including improper heat treatment. Early failure events are addressed by two modeling cases: (1) the Drip Shield Early Failure (EF) Modeling Case that includes an early failure of one or more DSs that then assumes localized corrosion of the WP(s) beneath the failed DS(s) and the subsequent release of radionuclides to the groundwater, and (2) the Waste Package EF Modeling Case that includes an early failure of one or more WPs and the subsequent release of radionuclides to the groundwater.

Igneous Scenario Class (Section 6.5)—This class considers those FEPs associated with igneous activity. This scenario class includes two modeling cases: (1) the Igneous Intrusion Modeling Case with releases of radionuclides to groundwater, and (2) the Volcanic Eruption Modeling Case with releases of radionuclides to the atmosphere. The Igneous Intrusion Modeling Case assumes that a dike intersects the repository and destroys DSs and WPs in those drifts intruded by magma, exposing the waste forms to percolating water and mobilizing radionuclides. The Volcanic Eruption Modeling Case represents the fraction of igneous intrusions in which a volcanic eruption also occurs.

Seismic Scenario Class (Section 6.6)—The Seismic Scenario Class describes performance of the repository system in the event of seismic activity capable of disrupting repository emplacement drifts and the engineered barrier system (EBS). This scenario class includes processes captured in the Nominal Scenario Class, as well as damage to DSs and WPs as a function of the magnitude of the seismic event(s). Seismic disruption of the repository is addressed in two modeling cases. The first modeling case represents the DSs and WPs that fail from nominal processes, as well as mechanical damage associated with seismic vibratory ground motion. This modeling case is referred to as the Seismic Ground Motion (GM) Modeling Case. The Seismic GM Modeling Case includes drift degradation and subsequent effects of accumulating rubble. The Seismic GM Modeling Case also includes the effects of SCC of the WPs and diffusion of mobilized radionuclides through WP cracks and WP rupturing with the potential to have both advection and diffusion of mobilized radionuclides through the rupture opening. The second modeling case considers the WPs that are breached because of fault displacement. This modeling case is referred to as the Seismic Fault Displacement (FD) Modeling Case. The Seismic FD Modeling Case includes breaching of WPs and DSs by the displacement along faults, as well as nominal failures of the DSs and WPs. Seismic ground motion damage of the DSs and WPs is excluded from this modeling case. This modeling case includes advection and diffusion of mobilized radionuclides out of the breached WP.

Human Intrusion Scenario (Section 6.7)—The Human Intrusion Scenario describes performance of the repository system in the event that subsurface exploratory drilling disrupts the repository. Human intrusion disruption of the repository is addressed by a single modeling case.

The second and third PA activities defined by the NRC Proposed Rule 10 CFR 63.2 (2) and (3) [DIRS 180319] require the development of a TSPA Model that describes overall system behavior and clearly displays the extent to which uncertainty in the understanding of the repository system affects the description of system behavior. The Yucca Mountain repository system is a combination of integrated processes that are conceptualized and modeled as a collection of coupled model components. For the TSPA-LA Model, eight principal model

components are combined to evaluate repository system performance for Nominal, Early Failure, Igneous, and Seismic Classes and the Human Intrusion Scenario. The model components are:

- Unsaturated Zone (UZ) Flow
- EBS Environment
- WP and DS Degradation
- Waste Form Degradation and Mobilization
- EBS Flow and Transport
- UZ Transport
- Saturated Zone (SZ) Flow and Transport
- Biosphere.

The TSPA-LA Model components and their supporting abstraction models and analyses are illustrated on Figure 6-1. The model components are in the top row of the figure, with submodels and abstractions below the model component level. As shown, model components are composed of a collection of submodels (e.g., process models, analyses, or abstractions) that together represent a key component of the repository system. Submodels are implemented in the TSPA-LA Model to represent each abstraction, analysis, or process model included in the TSPA-LA Model. Note that submodels have arrows on the left side illustrating links to the parent model component. Figure 6-1 also illustrates specific information that is used to analyze the disruptive event scenario classes. Note that the Nominal, Early Failure, Igneous (except volcanic eruption), and Seismic Scenario Classes and the Human Intrusion Scenario use many of the same submodels and parameters. Each of the model components included in the TSPA-LA Model quantifies uncertainty in the underlying processes and input parameters, or bounds that uncertainty appropriately by selecting parameters and parameter values that bound potential consequences of the TSPA-LA Model from an overall performance perspective (i.e., that bound the expected dose to the receptor). Input uncertainty in the TSPA-LA Model is explicitly represented by assigning probability distributions to parameters representing epistemic and aleatory uncertainty. Because many of the TSPA-LA Model inputs are uncertain, the TSPA-LA Model uses a probabilistic framework to implement the model components and submodels. The treatment of uncertainty and the probabilistic framework used in implementing the TSPA-LA Model is discussed further in Section 6.1.3.

Section 6 Structure—The primary goals of Section 6 are to describe: (1) how the model components and their submodels, illustrated on Figure 6-1, are integrated in the TSPA-LA Model, and (2) how the TSPA-LA Model is implemented to estimate the dose incurred by the reasonably maximally exposed individual (RMEI) due to radionuclide releases in the Nominal, Early Failure, Igneous, and Seismic Scenario Classes and the Human Intrusion Scenario. The contents of Section 6 are summarized as follows.

Section 6.1 develops the basis for a detailed description of the TSPA-LA Model and its implementation for the Nominal, Early Failure, Igneous, and Seismic Scenario Classes and the Human Intrusion Scenario. The following topics are presented:

- FEP analysis for the TSPA-LA Model and the formation and screening of scenario classes (Section 6.1.1)

- Descriptions of scenario classes and their treatment in the TSPA-LA Model (Section 6.1.2)
- Treatment of uncertainty in the TSPA-LA Model analyses (Section 6.1.3)
- A description of the TSPA-LA Model structure and design (Section 6.1.4)
- TSPA-LA Model file architecture (Section 6.1.5).

Section 6.2 introduces alternative conceptual models (ACMs) for the TSPA-LA Model, including a general discussion of ACMs. Detailed evaluations of the ACMs are included in Sections 6.3, 6.4, 6.5, 6.6, and 6.7.

Section 6.3 provides detailed descriptions of the TSPA-LA Model components and submodels. The model component and submodel descriptions include:

- A discussion of how submodels are connected to other submodels and model components in the TSPA-LA Model.
- A description of the conceptual model on which the submodel is based.
- A description of the submodel abstractions.
- A description of how the abstractions are implemented in the TSPA-LA Model.
- An evaluation of the consistency and reasonable and technically defensible conservatism in assumptions and parameters used in the TSPA-LA Model. Assumptions and parameter values that are different among submodels in the TSPA-LA Model are documented.
- A summary of ACMs that were considered in the development of the conceptual model.

The focus of Section 6.3 is on the TSPA-LA Model components and submodels and their implementation in the Nominal Scenario Class. The majority of these submodels are applied in the same manner to evaluate the consequences of the Early Failure, Igneous, and Seismic Scenario Classes and the Human Intrusion Scenario.

Section 6.3 provides a discussion on the consistency of modeling assumptions for each model component. This section also includes explanations of the differences in model assumptions between different model abstractions, and it discusses their impact on the TSPA-LA Model.

Section 6.3 discusses reasonable and technically defensible conservatisms associated with the TSPA-LA Model for each model component. The list of reasonable and technically defensible conservatisms in each subsection focuses on those aspects of the TSPA-LA Model that result in estimates of performance that either:

- Overestimate the consequences of processes that have potential to degrade subsystem performance

- Underestimate the effects of processes that might result in improved subsystem performance.

The reasonable and technically defensible conservatisms presented in Sections 6.3, 6.4, 6.5, 6.6, and 6.7, in respect to how they impact the TSPA-LA Model at the submodel level, are primarily associated with assumptions from supporting analysis and model reports rather than on the overall TSPA-LA Model performance. These reasonable and technically defensible conservatisms may or may not have a direct impact on the performance of the TSPA-LA Model. Validation of the TSPA-LA Model consists of a sequence of activities that are designed to build confidence in the results of the model (Section 7, Volume II). An important function of the TSPA-LA Model is to assimilate the conservatisms identified in the supporting analysis and model reports to evaluate their significance (either quantitatively or qualitatively) to performance. The Performance Margin Analysis (PMA) presented in Section 7.7.4 quantifies the impact of submodel representations and assumed conservatisms with respect to the overall performance. Additionally, TSPA-LA Model uncertainties identified in Sections 6.3, 6.4, 6.5, 6.6, and 6.7 will affect the assessment of total system performance and must be taken into account. A discussion presented in Section 7.4 and Appendix K includes information regarding the impacts of these uncertainties on those estimates (e.g., uncertainty in the estimate of mean annual dose).

Sections 6.4, 6.5, 6.6, and 6.7 describe how the consequences of the Early Failure, Igneous, and Seismic Scenario Classes and the Human Intrusion Scenario, respectively, are evaluated, including modifications to the model components described in Section 6.3. Each scenario class section includes discussions that are specific to each case that outline the differences between the Nominal Scenario Class model components and submodels and those used to model the Early Failure, Igneous and Seismic Scenario Classes, and the Human Intrusion Scenario. Sections 6.4, 6.5, 6.6, and 6.7 also include a discussion of the consistency of model assumptions and conservatisms specific to each scenario class.

Model Terminology—A variety of model components and submodels are discussed in Section 6. Use of the word model, without any qualification, will be restricted to the TSPA-LA Model itself. A number of elements were identified within the TSPA-LA Model. The elements shown on Figure 1-3, commonly referred to as the TSPA wheel, have been identified by the TSPA-LA modeling team as particularly important. The items indicated by icons on Figure 1-3 will be referred to as model components. These model components were chosen because they provide a useful framework for discussing and reviewing the TSPA-LA Model and the process level models that support the TSPA-LA Model. All other parts of the TSPA-LA Model will be referred to as submodels. The distinction between the terms model components and submodels are, to a certain extent, arbitrary, but they have been introduced to try to improve the clarity of the discussion within Section 6. Submodels in the TSPA-LA Model are composed of one or more process models, analyses, or abstractions. Table 6-1 maps the principal model components of the TSPA-LA Model from Figure 6-1 to each submodel discussed in Sections 6.1.4, 6.3, 6.4, 6.5, 6.6, and 6.7. Additionally, the process model, analysis, or abstraction that feeds each submodel is listed in Table 6-1 and discussed in Sections 6.3, 6.4, 6.5, 6.6, and 6.7. The term process model is used throughout Section 6.0 as a generalized term for a mathematical model that represents an event, phenomenon, process, or component, evaluated within an analysis and model report. The process model moniker is used here to identify the detailed computational

models that form the basis of the data, analysis, and abstractions implemented with the TSPA-LA Model.

Table 6-1. TSPA-LA Model Discretization

Figure 6-1		Section 6				Referenced Analyses/Models	
TSPA-LA Principal Model Components		Subsection			Submodel for TSPA-LA	Abstraction/Process Model(s)/Analysis(es)	Reference
Unsaturated Zone Flow Model Component	Site-Scale UZ Flow	Mountain-Scale UZ Flow	6.3.1		UZ Flow Fields Abstraction	UZ Flow Fields Abstraction	1
						Site-Scale UZ Flow Process Model	
						Active Fracture Model	
						Dual-Permeability UZ Flow Model	
	Infiltration Analysis				Infiltration Submodel	Infiltration Model Abstraction	2
						Infiltration Process Model	2
	Climate Analysis				Climate Submodel	Future Climate Analysis	3
	Drift Seepage	Drift-Scale UZ Flow	6.3.3	6.3.3.1	Drift Seepage Submodel	Drift Seepage Abstraction	4,5
						Drift Seepage Abstraction including Drift Collapse	
						TH Seepage Process Model	
	Drift Wall Condensation			6.3.3.2	Drift Wall Condensation Submodel	In-Drift Natural Convection and Condensation Process Model	7
						Drift Wall Condensation Abstraction	
EBS Environment Model Component	EBS Thermal-Hydrologic Environment	EBS TH Environment	6.3.2		EBS TH Environment Submodel	MSTHM Process Model	6
						MSTHM Abstraction	
	EBS Chemical Environment	EBS Chemical Environment	6.3.4		EBS Chemical Environment Submodel	EBS P&CE Abstraction	8
						IDPS Process Model	15

Table 6-1. TSPA-LA Model Discretization (Continued)

Figure 6-1		Section 6				Referenced Analyses/Models	
TSPA-LA Principal Model Components		Subsection			Submodel for TSPA-LA	Abstraction/Process Model(s)/Analysis(es)	Reference
WP and DS Degradation Model Component	WAPDEG	WP and DS Degradation	6.3.5	6.3.5.1	WP and DS Degradation Submodel	WP General Corrosion Abstraction	10,11,12
						WP MIC Abstraction	
						WP SCC Abstraction	
						DS General Corrosion Abstraction	
	Localized Corrosion on WP Outer Surface			6.3.5.2	Localized Corrosion Initiation Submodel	Localized Corrosion Initiation Abstraction	
						Localized Corrosion Penetration Rate Abstraction	
Waste Form Degradation and Mobilization Model Component	Radionuclide Inventory	WF Degradation and Mobilization	6.3.7	6.3.7.1	Radionuclide Inventory Submodel	Initial Radionuclide Inventory Screening Analysis	20,35
						Initial Radionuclide Inventory Abstraction	20,35
	In-Package Chemistry			6.3.7.2	In-Package Chemistry Submodel	In-Package Chemistry Abstraction	21
	Cladding Degradation			6.3.7.3	Cladding Degradation	Cladding Degradation Abstraction	22
	CSNF, DSNF, HLW Degradation			6.3.7.4	Waste Form Degradation Submodel	CSNF WF Degradation Abstraction	23
						DSNF WF Degradation Abstraction	24
						HLW Glass Degradation Abstraction	25
	Dissolved Radionuclide Concentration Limits			6.3.7.5	Dissolved Concentration Limits Submodel	Dissolved Concentration Limits Abstraction	26
	WF & EBS Colloids			6.3.7.6	Engineered Barrier System Colloids Submodel	WF and In-Drift Colloid Concentration Abstraction	27

Table 6-1. TSPA-LA Model Discretization (Continued)

Figure 6-1		Section 6			Referenced Analyses/Models	
TSPA-LA Principal Model Components		Subsection		Submodel for TSPA-LA	Abstraction/Process Model(s)/Analysis(es)	Reference
EBS Flow and Transport Model Component	EBS Flow	EBS Flow	6.3.6	EBS Flow Submodel	EBS Flow Abstraction	13
	EBS Transport	EBS Transport	6.3.8	EBS Transport Submodel	EBS Transport Abstraction	13
					Single Continuum Invert Abstraction	
					Mass of Corrosion Products Abstraction	
					Waste Form Water Volume Abstraction	22,25
				EBS-UZ Interface Submodel	EBS-UZ Interface Abstraction	13
Unsaturated Zone Transport Model Component	UZ Transport (Particle Tracking)	UZ Transport	6.3.9	UZ Transport Submodel	Active Fracture Model Abstraction	14
					Particle Tracking Model Abstraction	
					Dual-Continuum Transport Model Abstraction	
					UZ Transport Abstraction	
SZ Flow and Transport Model Component	3-D SZ Flow and Transport	SZ Transport	6.3.10	SZ Flow and Transport Submodel	3-D SZ Flow and Transport Process Model	17,18
					3-D SZ Flow and Transport Abstraction	16
	1-D SZ Flow and Transport				SZ Convolute Abstraction	
					1-D SZ Flow and Transport Abstraction	
Biosphere Model Component	Nominal BDCFs	Biosphere	6.3.11	Biosphere Submodel	Biosphere Process Model	19
	Groundwater Protection Conversion Factors				Groundwater Exposure Case Abstraction	
	Disruptive Events BDCFs				Volcanic Ash Exposure Case Abstraction	

Table 6-1. TSPA-LA Model Discretization (Continued)

Figure 6-1		Section 6				Referenced Analyses/Models	
TSPA-LA Principal Model Components		Subsection			Submodel for TSPA-LA	Abstraction/Process Model(s)/Analysis(es)	Reference
Events	Early Failure	Early Failure Scenario Class	DS Early Failure	6.4.1	DS Early Failure Submodel	Abstraction of DS Failures from Undetected Defects	28
			WP Early Failure	6.4.2	WP Early Failure Submodel	Abstraction of WP Failures from Undetected Defects	28
	Igneous Activity	Igneous Scenario Class	Igneous Intrusion Modeling Case	6.5.1	Igneous Intrusion Submodel	Igneous Activity Analysis	29
					Igneous Event Time and Probability Submodel	Annual Frequency Abstraction	
					Igneous Intrusion EBS Damage Submodel	Number of WP Hit by Igneous Events Abstraction	30
					EBS TH Environment Submodel Modifications for Igneous Intrusion	Dike Drift Interactions Analysis	9
					EBS Chemical Environment Submodel Modifications for Igneous Intrusion	Unevaporated Seepage Chemistry Abstraction	
						Basalt Chemistry Abstraction	
					Mean Annual Dose for Igneous Intrusion	Calculation of Expected Dose	Section 6.1.2 Appendix J

Table 6-1. TSPA-LA Model Discretization (Continued)

Figure 6-1		Section 6				Referenced Analyses/Models	
TSPA-LA Principal Model Components		Subsection			Submodel for TSPA-LA	Abstraction/Process Model(s)/Analysis(es)	Reference
Events (continued)	Igneous Activity (continued)	Igneous Scenario Class	Volcanic Eruption	6.5.2	Volcanic Eruption Submodel	Eruptive Processes Analysis	31,32
					Volcanic Interaction with the Repository Submodel	Number of WP Hit by Eruptive Conduits Analysis	30
					Atmospheric Transport Submodel	Atmospheric Dispersal and Deposition of Tephra Analysis	32,33
						ASHPLUME Model Abstraction	
					Tephra Redistribution Submodel	Redistributed Tephra Abstraction	
					Volcanic Ash Exposure Submodel	Mean Annual Dose for Volcanic Eruption Abstraction	31
	Seismic Activity	Seismic Scenario Class		6.6.1	Ground Motion Damage	Seismic Damage Abstraction	34
					Fault Displacement Damage		
				6.6.2.1	Drift Seepage Submodel and Drift Wall Condensation Submodel Modifications for Seismic Disruption	Drift Seepage Abstraction including Drift Collapse	4,5

Table 6-1. TSPA-LA Model Discretization (Continued)

Figure 6-1		Section 6				Referenced Analyses/Models	
TSPA-LA Principal Model Components		Subsection			Submodel for TSPA-LA	Abstraction/Process Model(s)/Analysis(es)	Reference
Events (continued)	Seismic Activity (continued)	Seismic Scenario Class (continued)		6.6.2.2	EBS TH Environment Submodel Modifications for Seismic Disruption	Collapsed Drift TH Abstraction	6
				6.6.2.3	WP and DS Degradation Submodel Modifications for Seismic Disruption	WP and DS Degradation Submodel	10,11,12
				6.6.2.4	WP Localized Corrosion Initiation Submodel for Seismic Disruption	Localized Corrosion Initiation Analysis	10
	Human Intrusion	Human Intrusion Scenario		6.7	Human Intrusion Submodel	10CFR Part 63.322 & 63.321	36

Table 6-1. TSPA-LA Model Discretization (Continued)

Figure 6-1	Section 6		Referenced Analyses/Models	
TSPA-LA Principal Model Components	**Subsection**	**Submodel for TSPA-LA**	**Abstraction/Process Model(s)/Analysis(es)**	**Reference**

NOTES:

1 UZ *Flow Models and Submodels* (SNL 2007 [DIRS 184614]).
2 *Simulation of Net Infiltration for Present-Day and Potential Future Climates* (SNL 2007 [DIRS 182145]).
3 *Future Climate Analysis* (BSC 2004 [DIRS 170002]).
4 *Abstraction of Drift Seepage* (SNL 2007 [DIRS 181244]).
5 *Seepage Model for PA Including Drift Collapse* (BSC 2004 [DIRS 167652]).
6 *Multiscale Thermohydrologic Model* (SNL 2007 [DIRS 181383]).
7 *In-Drift Natural Convection and Condensation* (SNL 2007 [DIRS 181648]).
8 *Engineered Barrier System: Physical and Chemical Environment* (SNL 2007 [DIRS 177412]).
9 *Dike/Drift Interactions* (SNL 2007 [DIRS 177430]).
10 *General Corrosion and Localized Corrosion of Waste Package Outer Barrier* (SNL 2007 [DIRS 178519]).
11 *Stress Corrosion Cracking of Waste Package Outer Barrier and Drip Shield Materials* (SNL 2007 [DIRS 181953]).
12 *General Corrosion and Localized Corrosion of the Drip Shield* (SNL 2007 [DIRS 180778]).
13 *EBS Radionuclide Transport Abstraction* (SNL 2007 [DIRS 177407]).
14 *Particle Tracking Model and Abstraction of Transport Processes* (SNL 2008 [DIRS 184748]).
15 *In Drift Precipitates/Salts Model* (SNL 2007 [DIRS 177411]).
16 *Saturated Zone Flow and Transport Model Abstraction* (SNL 2008 [DIRS 183750]).
17 *Saturated Zone Site-Scale Flow Model* (SNL 2007 [DIRS 177391]).
18 *Site-Scale Saturated Zone Transport* (SNL 2007 [DIRS 177392]).
19 *Biosphere Model Report* (SNL 2007 [DIRS 177399]).
20 *Initial Radionuclides Inventory* (SNL 2007 [DIRS 180472]).
21 *In-Package Chemistry Abstraction* (SNL 2007 [DIRS 180506]).
22 *Cladding Degradation Summary for LA* (SNL 2007 [DIRS 180616]).
23 *CSNF Waste Form Degradation: Summary Abstraction* (BSC 2004 [DIRS 169987]).
24 *DSNF and Other Waste Form Degradation Abstraction* (BSC 2004 [DIRS 172453]).
25 *Defense HLW Glass Degradation Model* (BSC 2004 [DIRS 169988]).
26 *Dissolved Concentration Limits of Radioactive Elements* (SNL 2007 [DIRS 177418]).

Table 6-1. TSPA-LA Model Discretization (Continued)

Figure 6-1	Section 6		Referenced Analyses/Models	
TSPA-LA Principal Model Components	**Subsection**	**Submodel for TSPA-LA**	**Abstraction/Process Model(s)/Analysis(es)**	**Reference**

27 *Waste Form and In-Drift Colloids-Associated Radionuclide Concentrations: Abstraction and Summary* (SNL 2007 [DIRS 177423]).

28 *Analysis of Mechanisms for Early Waste Package/Drip Shield Failures* (SNL 2007 [DIRS 178765]).

29 *Characterize Framework for Igneous Activity at Yucca Mountain, Nevada* (BSC 2004 [DIRS 169989]).

30 *Number of Waste Packages Hit by Igneous Events* (SNL 2007 [DIRS 177432]).

31 *Characterize Eruptive Processes at Yucca Mountain, Nevada* (SNL 2007 [DIRS 174260]).

32 *Atmospheric Dispersal and Deposition of Tephra from a Potential Volcanic Eruption at Yucca Mountain, Nevada* (SNL 2007 [DIRS 177431]).

33 *Redistribution of Tephra and Waste by Geomorphic Processes Following a Potential Volcanic Eruption at Yucca Mountain, Nevada* (SNL 2007 [DIRS 179347]).

34 *Seismic Consequence Abstraction* (SNL 2007 [DIRS 176828]).

35 *MOX Spent Nuclear Fuel and LaBS Glass for TSPA-LA* (SNL 2007 [DIRS 177422]).

36 NRC Proposed Rule at 10 CFR 63.321 [DIRS 178394] and 63.322 [DIRS 180319].

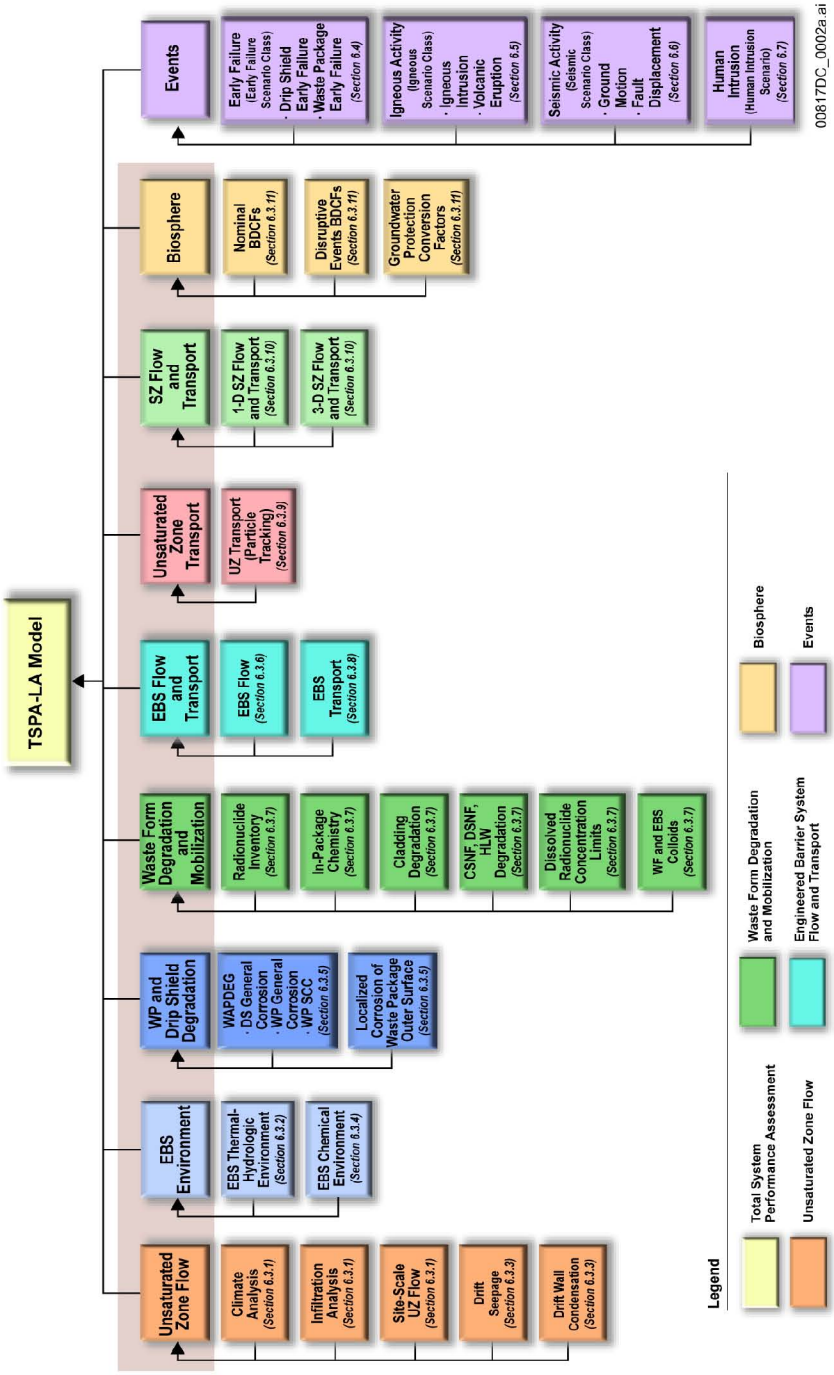

Figure 6-1. TSPA-LA Principal Model Components and Submodels

INTENTIONALLY LEFT BLANK

6.1 CONCEPTUAL DESIGN

The TSPA-LA Model evaluates the repository system performance for four scenario classes and for a human intrusion scenario. The TSPA-LA Model is exercised using modeling cases (discussed in detail in Section 6.1.2) that represent the scenario-specific conditions over which the repository performance can be assessed. The remainder of Section 6.1 provides a conceptual overview of the FEPs related to the TSPA-LA Model (Section 6.1.1), the scenario classes and modeling cases (Section 6.1.2), a discussion on the treatment of uncertainty in the TSPA-LA Model (Section 6.1.3), the individual model components and submodels that comprise the model scenario classes and modeling cases (Section 6.1.4), and the architecture of the TSPA-LA Model (Section 6.1.5). As noted in *Yucca Mountain Review Plan, Final Report* (NRC 2003 [DIRS 163274], Section 2.2), the model abstraction review process ends with a review of how the abstracted submodels are implemented in the TSPA-LA Model. This section provides overview information to facilitate this review and, in particular, an overview of the integration of model components and submodels that describe processes and conditions in different parts of the Yucca Mountain repository system.

Section 6 provides a text-based description of the TSPA-LA Model. For a complete representation of the conceptual basis and mathematical implementation of the TSPA-LA Model, and for full traceability to the source information used to develop the model, the reader should use the text of Section 6 in conjunction with complementary tools that are provided in this report and on the accompanying digital video disk (DVD). The following information tools should be used together while reading Section 6:

- Model Components and Submodels, listed in Table 6-1
- Model Implementation Descriptions, mapped in Table 6.1.5-1
- The GoldSim model file (available on DVD)
- The TSPA Input Database (available on DVD)
- Parameter Entry Forms (PEFs) (available within the TSPA Input Database on DVD)
- Appendix I—FEPs Mapped to TSPA-LA GoldSim model file.

Understanding the conceptual basis for the TSPA-LA Model begins with a review of the FEPs development and screening process, described in Section 6.1.1. Potentially relevant FEPs are identified and evaluated, consistent with available field and laboratory data for the Yucca Mountain site, for inclusion into process models documented in a suite of analysis and model reports. Appendix I provides a roadmap between the conceptualization represented by included FEPs and the mathematical implementation in the GoldSim model file. Appendix I identifies one or more locations where included FEPs are implemented within the GoldSim model file. The appendix also identifies documentation that provides additional information on the conceptualization and mathematical representation of each included FEP.

Table 6-1 provides the roadmap through the conceptual structure of the TSPA-LA Model. The table identifies the process models and associated analyses that support the TSPA-LA Model and gives the principal references. The table also identifies the abstractions that were developed for implementation into the TSPA-LA Model. These elements are mapped to the conceptual structure of the TSPA-LA Model, as defined in Section 6.3. All of this information is mapped to the conceptual structure provided by the TSPA wheel (Figure 1-3), illustrating how the details of

the TSPA-LA Model conceptualization relate to the high-level conceptual structure that has formed the basis for analysis and discussion of the Yucca Mountain repository system for many years.

The mathematical implementation of the conceptualization presented in Table 6-1 is discussed in Section 6.3 and documented in the GoldSim model file. Table 6.1.5-1 presents the suite of submodels that were developed to implement the abstractions identified in Table 6-1. Table 6.1.5-1 includes the locations within the GoldSim model file, to view the actual implementation of the submodels. The model file also includes documentation of the submodel implementation. Decisions made during the implementation of the submodels have resulted in slight differences between the model structure defined in Table 6.1.5-1 and the model structure defined in Section 6.3, and these differences are resolved in Table 6-1. Collectively, stepping from Figure 6-1 to Table 6-1 to Table 6.1.5-1 and Section 6.3 associates an increase in the detail provided by looking at smaller and smaller logical segments of the model. The basic idea is that the principal model components from Figure 6-1 may be comprised of one or more submodels (listed on Figure 6-1 and in Table 6-1), which may be comprised of one or more abstractions, analyses, or process models (listed in Tables 6-1 and 6.1.5-1). The reader can follow the roadmap, terminating in the model file, which provides the greatest detail of the implementation.

The annual dose results generated from the GoldSim model file undergo further processing to calculate the distribution of expected annual doses for each scenario class, where the term "expected annual dose" refers to the expectation of annual dose over aleatory uncertainty conditional on each epistemic realization. Section 6.1.2 outlines these calculations, which are implemented in the EXDOC_LA software [DIRS 182102]. The representation of the two types of uncertainty is discussed in Section 6.1.3. The distributions of expected annual dose from each scenario class are combined to form a distribution of total expected annual dose. The mean of this distribution of total expected annual dose is the quantity compared to the regulatory standard specified in 10 CFR 63.303(a) [DIRS 178394] for the period within 10,000 years after disposal, and the median of this distribution is the quantity compared to the regulatory standard specified in 10 CFR 63.303(b) [DIRS 178394] for the period after 10,000 years of disposal.

Parameters connect the model, as implemented in the GoldSim model file, to the field and laboratory measurements that provide the basic data for the TSPA-LA Model. All parameters included in the TSPA-LA Model are documented in the TSPA Input Database, which is a Microsoft Access Database included in the DVD. The parameter database provides the linkage between the description of the parameter, the parameter values used by the model, and the model structure defined in Table 6.1.5-1. Information provided for each parameter includes a brief description, the identification of parameter type (i.e., constant, table, or stochastic), and information on parameter source. The source information includes the source data tracking number (DTN) or the analysis and model report, as well as information on any modifications made to the source information. Traceability to the specific location of source values is provided by the PEFs that are included in the database. The PEFs provide a roadmap to a specific location within a DTN or the analysis and model report where a parameter value can be found.

The database also identifies the submodel where the parameter is implemented within the model file. Many parameters are included in calculations at multiple locations within the model file,

but the database identifies at least one location, which is the primary location where the parameter value is brought into the model.

Most of the information from the TSPA Input Database is also captured in the GoldSim model file. At the location where a parameter is implemented in the model file, the information from the database about DTNs or analysis and model report sources and parameter types can be obtained by moving the cursor over the parameter icon. Thus, information from the database and the PEFs is linked through the GoldSim model file. The database description on page 6.1-2 provides details.

There are differences in assumptions and parameter sets used in the TSPA-LA Model that have arisen in the development of the abstractions and process models. Most of these differences are due to the use of conservative assumptions in the process model or analysis when uncertainty is difficult to quantify. Assumptions made within the TSPA-LA Model are consistent between the various submodels, assumptions, and parameter values that differ between submodels and are documented as part of the discussion of each submodel implementation in Section 6.3. Evaluating potential impacts from these assumptions with respect to the mean annual dose is conducted through a series of processes described in Section 7.4 (Uncertainty Characterization), Section 7.7.1 (Analysis of Single Realizations), Section 7.7.4 (Performance Margin Analysis), and Section 8.3 (Results of Barrier Capability). To enhance understanding of the complex interactions within the TSPA-LA Model, a discussion of consistency among model components and submodels and identification of conservative assumptions in abstractions, process models, and parameter sets is presented, along with each submodel described in Section 6.3.

The tools discussed above, in conjunction with review of Section 6.0, all provide the reader with a complete representation of the conceptual basis and mathematical implementation of the TSPA-LA Model, and full traceability to the source information used to develop the model.

INTENTIONALLY LEFT BLANK

6.1.1 Features, Events, and Processes Screening and Scenario Development

This section describes the identification and screening of features, events, and processes (FEPs) for the TSPA-LA Model and the development of scenario classes used to estimate repository performance in the TSPA-LA.

For the TSPA-LA Model, FEP analysis and scenario development follows a five-step approach (Figure 6.1.1-1):

Step 1. Identify and classify the FEPs potentially relevant to the long-term performance of the disposal system.

Step 2. Evaluate the FEPs to identify those FEPs that should be included in the TSPA-LA and those that can be excluded from the TSPA.

Step 3. Form appropriate scenario classes from the FEPs that were included in the TSPA. Disruptive events are used to form scenario classes.

Step 4. Construct the calculation of total mean annual dose.

Step 5. Specify the implementation of the scenario classes in the computational modeling for the TSPA-LA and document the treatment of FEPs that were included.

FEP analysis, which includes Steps 1 and 2 above, addressed scenario analysis acceptance Criteria 1 and 2, respectively, as outlined in *Yucca Mountain Review Plan, Final Report* (NRC 2003 [DIRS 163274], Section 2.2.1.2.1.3). Scenario development, which includes Steps 3 and 4 above, addressed scenario analysis acceptance Criteria 3 and 4, respectively, as outlined in *Yucca Mountain Review Plan, Final Report* (NRC 2003 [DIRS 163274], Section 2.2.1.2.1.3). Section 6.1.2 outlines the calculation of total mean annual dose using the scenario classes, addressing Step 4 above. Sections 6.1.3 and 6.1.4 describe the implementation of each scenario class in the model components and submodels incorporated into the TSPA-LA Model (Step 5 above).

6.1.1.1 Features, Events, Processes, Scenarios, and Scenario Classes

Features are physical, chemical, thermal, or temporal characteristics of the site or repository system. For the purposes of screening FEPs for the TSPA-LA, a feature is defined as an object, structure, or condition that has the potential to affect disposal system performance (SNL 2008 [DIRS 179476], Appendix A). Examples of features are the WP and fracture systems or faults.

Processes are phenomena and activities that have gradual, continuous interactions with the system being modeled. For the purposes of screening FEPs for the TSPA-LA Model, a process is defined as a natural or human-caused phenomenon that has the potential to affect disposal system performance and that operates during all or a significant part of the period of performance (SNL 2008 [DIRS 179476], Appendix A). Percolation of water into the unsaturated rock layers above the repository is an example of a process.

Events are occurrences that have a specific starting time and, usually, a duration shorter than the time being simulated in a model. Events are also defined as uncertain occurrences that take place within a short time relative to the time frame of a model. For the purposes of screening FEPs for the TSPA-LA Model, an event is defined as a natural or human-caused phenomenon that has a potential to affect disposal system performance and that occurs during an interval that is short compared to the period of performance (SNL 2008 [DIRS 179476], Appendix A). An earthquake is an example of an event.

The identification, classification, and screening of a comprehensive list of FEPs potentially relevant to the postclosure performance of the Yucca Mountain Repository was an iterative process based on site-specific information, design, and regulations. The iterative FEP analysis process was initiated to support the TSPA for the Site Recommendation (TSPA-SR) and continued through the TSPA-LA FEP analysis, as described in *Features, Events, and Processes for the Total System Performance Assessment: Methods* (SNL 2008 [DIRS 179476], Section 6.1.4.1).

A scenario is a well-defined, connected sequence of FEPs that can be thought of as describing possible future conditions in the repository system. Scenarios can be undisturbed where the performance is the expected or nominal performance of the system, or disturbed if altered by events such as volcanism or seismicity (NRC 2003 [DIRS 163274], Section 3). There is an infinite number of possible future states, and for scenario development to be useful, the process must generate scenarios that can be aggregated into a manageable number of scenario classes representative of the range of futures potentially relevant to the PA of the repository (SNL 2008 [DIRS 179476], Section 6.3).

A scenario class is a set of related scenarios that share sufficient similarities to usefully aggregate them for the purposes of analysis. The number and breadth of scenario classes depend on the resolution at which scenarios were defined. Coarsely defined scenarios result in fewer broad scenario classes, whereas narrowly defined scenarios result in many scenario classes. The objective of scenario development is to define a limited set of scenario classes that can be quantitatively analyzed while maintaining comprehensive coverage of the range of possible future states of the repository system. The process of scenario development is described by Cranwell et al. (1990 [DIRS 101234], Section 2.4).

The following sections provide summaries of the TSPA-LA FEP analysis and scenario development steps.

6.1.1.2 Step 1: Identification and Classification of Features, Events and Processes

In Step 1 of the FEP analysis and scenario development process, FEPs potentially relevant to postclosure performance are identified and classified. The primary objectives of FEP identification and classification are to develop a comprehensive set of FEPs for subsequent screening, to uncover missing FEPs and interactions, and to provide a framework for developing and organizing scenario classes.

An initial list of FEPs relevant to Yucca Mountain was developed from a comprehensive list of FEPs from radioactive waste disposal programs in other countries (BSC 2005 [DIRS 173800],

Section 2.1.1). The list was supplemented with additional Yucca Mountain-specific FEPs from project literature, technical workshops, and reviews (BSC 2005 [DIRS 173800], Sections 2.1.1). This process is illustrated on Figure 6.1.1-2. This initial FEP list, developed to support TSPA-SR, contained 328 FEPs (BSC 2002 [DIRS 159684], Table FEPS). This list was revised for TSPA-LA in part with an application of a hybrid procedure that included reclassification, refinement, and audits against other recently published international lists. Additional analyses and refinements were conducted during the transition from the TSPA-SR FEP list to the TSPA-LA FEP list (DTN: MO0706SPAFEPLA.001_R0 [DIRS 181613]).

The TSPA-SR FEP classification was derived from a Nuclear Energy Agency classification scheme (NEA 1999 [DIRS 152309], pp. 28 to 34) that was based on a combination of the classification schemes listed in *Development of the Total System Performance Assessment-License Application Features, Events, and Processes* (BSC 2005 [DIRS 173800], Section 2.1.2). The TSPA-SR classification was a layered scheme, with different layers categorized by cause, field of effects, and causative factors, location, scientific discipline, radionuclide transfer agent, and/or radionuclide mobilization. As a check on comprehensiveness, TSPA-SR FEPs were also classified according to technical subject area (i.e., a combination of locations and physical field of effect). The alternate classification did not result in the identification of any additional FEPs. For TSPA-LA, yet another classification scheme was applied based on a mapping between Yucca Mountain Project (YMP) specific features (i.e., locations and fields of effect) and processes (i.e., radionuclide mobilization and causative factors). The revised approach improved traceability by relating FEPs directly to YMP specific technical subject areas rather than to generic international groupings.

These FEP identification actions resulted in a comprehensive TSPA-LA FEP list containing 374 FEPs (DTN: MO0706SPAFEPLA.001_R0 [DIRS 181613]).

6.1.1.3 Step 2: Screening of FEPs

In Step 2 of the FEP analysis and scenario development process, the list of FEPs identified and classified in Step 1 was screened to determine which FEPs should be included or excluded from the TSPA-LA analysis. A FEP can be excluded based on any one of the following three FEP screening criteria, which derive from NRC Proposed Rule 10 CFR Part 63 ([DIRS 178394] and [DIRS 180319]), as described below:

1. Low Probability (10 CFR 63.342(a) and (b) [DIRS 178394])—Performance assessments shall exclude events that have less than one chance in 10,000 of occurring over 10,000 years. FEPs meeting this criterion may be excluded (screened out) from the TSPA-LA on the basis of low probability. For example, the impact of large meteorites was excluded because of low probability.

2. Low Consequence (10 CFR 63.114(e) and (f) [DIRS 178394])—FEPs may be excluded (screened out) from the TSPA-LA on the basis of low consequence if the omission of a FEP would not significantly change the magnitude or time of radiological exposures or radionuclide releasesFor example, gas generation from waste form decay is excluded because of low consequence, even though the process is certain to occur.

3. By Regulation—FEPs may also be excluded if they are inconsistent with regulations that specify repository system characteristics, concepts, and definitions. The regulations most commonly used for screening TSPA-LA FEPs are those pertaining to the characteristics, concepts, and definitions of the reference biosphere, geologic setting, RMEI, and human intrusion ((NRC 2003 [DIRS 163274], Section 2.2.1.2.1.3, Acceptance Criterion 2) and (SNL 2008 [DIRS 179476], Section 6)).

In addition, according to 10 CFR 63.342(c) [DIRS 178394], PAs conducted to show compliance of FEPs with individual protection standards following permanent closure and affected by human intrusion shall project the continued effects of all included FEPs beyond 10,000 years after closure until the period of geologic stability, including seismic and igneous events covered under the probability limits of 10 CFR 63.342(a) [DIRS 178394].

The FEP screening process included input from subject matter experts, as documented in the *LA FEP List and Screening* (DTN: MO0706SPAFEPLA.001_R0 [DIRS 181613]). The FEP screening process is described in *Features, Events, and Processes for the Total System Performance Assessment: Methods* (SNL 2008 [DIRS 179476], Section 6). A second report, *Features, Events, and Processes for the Total System Performance Assessment: Analyses* (SNL 2008 [DIRS 183041]), contains tables that identify the relevant FEP analysis reports for each FEP and indicate whether or not each FEP is included in the TSPA-LA Model or was screened out.

Appendix I contains additional information on all FEPs that were included in the TSPA-LA Model. This appendix provides a mapping between the FEPs documentation and implementation of the FEP in the TSPA-LA Model. Table I-2 identifies each included FEP, by FEP number, and provides a brief explanation of how the FEP is included. The actual inclusion of the FEP may be by direct implementation in the TSPA-LA Model file, implementation within a dynamically linked library (DLL), or by inclusion in a process model abstraction. Table I-2 identifies a path to the location of each included FEP within the TSPA-LA Model file. Table I-2 includes information on how each FEP was implemented and identifies supporting documentation where additional information is available, explaining the implementation of the included FEP.

6.1.1.4 Step 3: Formation of Scenario Classes

All FEPs screened in during the formal identification and screening for Step 1 and Step 2 are used for TSPA-LA scenario development and are incorporated into scenario classes (Sections 6.3, 6.4, 6.5, 6.6, and 6.7). For the purpose of scenario class formation, features and processes generally are present in all possible repository futures. In contrast, events may or may not occur in every future of the repository system. For this reason, scenario classes are distinguished by events, while the features and processes are generally applicable across all scenario classes.

The three retained events that have been identified for inclusion in the TSPA-LA are:

- Early failure
- Igneous
- Seismic.

These three events lead to the definition of three corresponding scenario classes for the TSPA-LA, and one additional scenario class accounting for repository futures in which none of the three events occur:

- Early Failure Scenario Class, A_E: the set of futures each of which includes one or more early failure events (i.e., one or more early failed WPs and/or one or more early failed DSs).
- Igneous Scenario Class, A_I: the set of futures each of which includes one or more igneous events.
- Seismic Scenario Class, A_S: the set of futures each of which includes one or more seismic events.
- Nominal Scenario Class, A_N: the set of futures each of which includes nominal features and processes (e.g., corrosion processes, such as general corrosion, localized corrosion, and SCC) but *no* events (i.e., no igneous and no seismic events and no early WP or DS failures).

The first three scenario classes are not mutually exclusive. Because the three types of events occur independently, many potential futures of the repository include events of different types, and such futures are included in more than one of the sets listed above. Section 6.1.2 explains how the four scenario classes listed above are aggregated from a set of mutually exclusive scenario classes and how total dose to the RMEI is correctly calculated using these four scenario classes.

6.1.1.5 Description of Scenario Classes and Modeling Cases

The scenario classes addressed by the TSPA-LA Model are distinguished by the type of event included in each scenario class. For example, the Early Failure Scenario Class accounts for all possible futures in which one or more early failures of DSs or WPs occur, the Igneous Scenario Class accounts for all possible futures in which one or more igneous events occur, and the Seismic Scenario Class accounts for all possible futures in which seismic events occur. In contrast, the Nominal Scenario Class accounts for all possible futures in which no early failures, igneous, or seismic events occur.

Each scenario class is implemented in the TSPA-LA Model by one or more modeling cases. The modeling cases that implement a scenario class are distinguished by different modes and extent of damage to the repository that could result from the occurrence of the events represented by the scenario class. The Early Failure Scenario Class is implemented in two modeling cases, the

Waste Package EF Modeling Case and the Drip Shield EF Modeling Case, because early failure of a DS has a different effect on the repository performance than early failure of a WP. Similarly, the Seismic Scenario Class is implemented in two modeling cases, one accounting for damage due to ground motion, and a second accounting for damage due to fault displacement. The Igneous Scenario Class also comprises two modeling cases, one for igneous intrusion and one for volcanic eruption.

Each scenario class accounts for FEPs that remain screened in after Step 2. The FEPs addressed by each scenario class, and the modeling cases used for each scenario class, are described below. In general, FEPs that describe a feature, such as the WP, or a process, such as flow in the UZ, are relevant to, and included in, more than one scenario class. In contrast, FEPs that describe an event, such as the occurrence of an igneous intrusion, are only included in the scenario class and modeling case that accounts for the effects of the event on repository performance. Thus, there is not a one-to-one association between FEPs and modeling cases.

A single FEP or related FEPs may be implemented differently in different scenario classes, model components, or portions of a model domain. These differing implementations are not inconsistencies; rather, they are reasonable simplifications that focus the model on things that matter and allow reasonable and technically defensible conservatism where information is controversial or lacking. In cases where a FEP is treated differently in different parts of the model, it is important that the impacts on the overall performance of any simplifications can be shown to be neutral or conservative for the purposes of each model component. For example, flow in fractured basalt is represented realistically for the purposes of a FEP screening argument (screening out hydrologic effects of the vertical dike on the grounds that flow in the dike will be insignificant), whereas flow through magma-filled drifts is represented conservatively. In another example, a radionuclide solubility model is applied in the WP and invert but is conservatively neglected in the UZ and SZ.

Nominal Scenario Class—The Nominal Scenario Class for the TSPA-LA Model includes all of the FEPs that were screened in according to the FEP screening process described in Section 6.1.1, except for those FEPs that are related to early failures, igneous activity, seismic activity, or a human intrusion. This scenario class, therefore, incorporates the important effects and system perturbations caused by climate change and repository heating that are projected to occur after repository closure. In addition, the Nominal Scenario Class considers that the WPs and DSs are subject to the EBS environment and will degrade with time. If the WPs and DSs breach and the waste forms are subsequently exposed to water, radionuclides may be mobilized and eventually be released from the repository. These radionuclides can then be transported by groundwater percolating through the UZ to the SZ and then to the accessible environment by water flowing in the SZ. The TSPA-LA Model includes FEPs associated with the biosphere in order to calculate annual dose to the RMEI. Accordingly, the TSPA-LA Model explicitly includes the following model components (Figure 6.1.1-3):

- UZ Flow
- EBS Environment
- WP and DS Degradation
- Waste Form Degradation and Mobilization
- EBS Flow and Transport

- UZ Transport
- SZ Flow and Transport
- Biosphere.

The FEPs included in these model components are addressed in one modeling case. This modeling case represents those WPs that fail because of corrosion processes (e.g., general corrosion, SCC, or localized corrosion). This modeling case is referred to as the Nominal Modeling Case. The Nominal Modeling Case quantifies repository performance in the absence of early failures or disruptive events before 10,000 years. For repository performance 10,000 years after closure, nominal processes are included in the Seismic GM Modeling Case, described below.

Early Failure Scenario Class—The Early Failure Scenario Class describes performance of the repository system in the event of early failures of the DSs or WPs due to manufacturing or material defects or to pre-emplacement operations including improper heat treatment. Early failure events are addressed by two modeling cases: (1) the Waste Package EF Modeling Case that considers the early failure of one or more WPs and the subsequent release of radionuclides to the groundwater; and (2) the Drip Shield EF Modeling Case that considers the early failure of one or more DSs that results in localized corrosion of the WPs beneath the failed DSs and the subsequent release of radionuclides to the groundwater.

The Waste Package EF Modeling Case accounts for the consequences of one or more WP failures at the time of repository closure due to manufacturing defects or damage during emplacement. WP early failure compromises the WP, exposing the waste forms to percolating water and mobilizing radionuclides. The released radionuclides may then be transported out of the repository, moved down through the UZ to the SZ, and then transported through the SZ to the accessible environment. The TSPA-LA Model components needed to calculate total system performance for the Waste Package EF Modeling Case include the following (Figure 6.1.1-4):

- UZ Flow
- EBS Environment
- WP and DS Degradation
- Waste Form Degradation and Mobilization
- EBS Flow and Transport
- UZ Transport
- SZ Flow and Transport
- Biosphere.

The FEPs associated with DS early failure and corrosion failure of WPs are not addressed in the Waste Package EF Modeling Case. Instead, these FEPs are accounted for in the Drip Shield EF and Nominal Modeling Cases.

The Drip Shield EF Modeling Case accounts for the consequences of one or more DS failures at the time of repository closure due to manufacturing defects or damage during emplacement. The WPs beneath the early failed DSs are assumed to be susceptible to localized corrosion, which compromises the WPs, exposing the waste forms to percolating water, and mobilizing radionuclides. The released radionuclides may then be transported out of the repository, moved down through the UZ to the SZ, and then be transported through the SZ to the accessible environment. The TSPA-LA Model components needed to calculate total system performance for the Drip Shield EF Modeling Case include the following (Figure 6.1.1-4):

- UZ Flow
- EBS Environment
- WP and DS Degradation
- Waste Form Degradation and Mobilization
- EBS Flow and Transport
- UZ Transport
- SZ Flow and Transport
- Biosphere.

The Drip Shield EF Modeling Case assumes that a WP underneath a failed DS experiences localized corrosion.

Igneous Scenario Class—The Igneous Scenario Class describes performance of the repository system in the event of igneous activity that disrupts the repository. Igneous disruption of the repository is addressed by two modeling cases: (1) the Igneous Intrusion Modeling Case that represents the interaction of intrusive magma with the repository and the release of radionuclides to the groundwater, and (2) the Volcanic Eruption Modeling Case that represents an eruption at the land surface and the release of radionuclides to the atmosphere.

The Igneous Intrusion Modeling Case models a dike intersecting the repository and compromising DSs and WPs in those drifts intruded by magma, exposing the waste forms to percolating water and mobilizing radionuclides. The released radionuclides may then be transported out of the repository, moved down through the UZ to the SZ, and then be transported through the SZ to the accessible environment. The TSPA-LA Model components, needed to calculate total system performance for the Igneous Intrusion Modeling Case, include the following, given that a certain number of WPs are destroyed by the intrusion (Figure 6.1.1-5):

- UZ Flow
- EBS Environment
- WP and DS Degradation
- Waste Form Degradation and Mobilization
- EBS Flow and Transport
- UZ Transport
- SZ Flow and Transport
- Biosphere.

The FEPs associated with corrosion failure of WPs prior to the disruption are included in the Igneous Intrusion Modeling Case. The FEPs associated with corrosion failure of WPs of undisrupted WPs after the disruption occurs are not included in the Igneous Intrusion Modeling Case. Instead, these FEPs are accounted for in the Nominal Modeling Case.

The Volcanic Eruption Modeling Case represents the fraction of igneous intrusions in which a volcanic eruption also occurs. For this modeling case, waste from WPs intersected by eruptive conduits is transported to the land surface, and tephra and entrained waste are discharged into the atmosphere, transported by wind currents, and deposited on the surface. The Volcanic Eruption Modeling Case also evaluates the fluvial and eolian redistribution of contaminated tephra deposited on the land surface. The TSPA-LA Model uses the following processes and model components to calculate repository system performance for the Volcanic Eruption Modeling Case (Figure 6.1.1-6):

- Volcanic interaction with the repository
- Atmospheric transport
- Tephra redistribution
- Biosphere.

Seismic Scenario Class—The Seismic Scenario Class describes performance of the repository system in the event of seismic activity capable of disrupting repository emplacement drifts and damaging the EBS. Radionuclides in damaged WPs may be mobilized and transported out of the repository, transported to the water table by the groundwater percolating through the UZ, and then transported to the accessible environment by water flowing in the SZ. The TSPA-LA Model components needed to calculate total system performance for the Seismic Scenario Class include the following (Figure 6.1.1-7):

- UZ Flow
- EBS Environment
- WP and DS Degradation
- Waste Form Degradation and Mobilization
- EBS Flow and Transport
- UZ Transport
- SZ Flow and Transport
- Biosphere.

Seismic disruption of the repository is addressed in two modeling cases. The first modeling case is the Seismic GM Modeling Case, which represents the consequences of mechanical damage associated with seismic vibratory ground motion. The Seismic GM Modeling Case includes: drift degradation and the effects on the EBS of accumulated rubble, the effects of SCC of the WPs and diffusion of mobilized radionuclides through WP cracks, and the effects of WP rupture with the potential to have both advection and diffusion of mobilized radionuclides through the rupture opening. Because corrosion processes accounted for in the Nominal Scenario Class have the potential to alter the repository's susceptibility to damage during a seismic ground motion event, the Seismic GM Modeling Case includes these nominal processes when calculating consequences after 10,000 years.

The second modeling case is the Seismic FD Modeling Case, which represents advection and diffusion of mobilized radionuclides out of WP breaches caused by a fault displacement. Seismic ground motion damage of the DSs and WPs is excluded from this modeling case.

6.1.1.6 Human Intrusion Scenario

In addition to the four scenario classes described above, the TSPA-LA considers a Human Intrusion Scenario as defined in NRC Proposed Rule 10 CFR 63.322 [DIRS 180319]. The Human Intrusion Scenario considers the intrusion of a single water or exploratory well into the repository, through the DS and WP, and into the underlying SZ. Human intrusion is not expected to occur during the first 10,000 years after repository closure (Section 6.3.7). NRC Proposed Rule 10 CFR 63.321 [DIRS 178394] describes the Individual Protection Standard for a Human Intrusion.

The Human Intrusion Scenario in implemented in a single modeling case, the Human Intrusion Modeling Case. This modeling case describes performance of the repository system in the event that subsurface exploratory drilling disrupts the repository. The Human Intrusion Modeling Case assumes that subsurface exploratory drilling activities intersect the repository and destroy a single DS and WP without being recognized by the drillers. After penetrating a thinned DS and WP, the drillers continue to bore a conduit through to the SZ. The drillers penetrate a DS and WP with an opening the size of the drill bit, thereby exposing the waste forms to percolating water and mobilizing radionuclides. The released radionuclides may then be transported out of the repository, move down through the borehole to the SZ, and then be transported through the SZ to the accessible environment. The TSPA-LA Model components needed to calculate total system performance for the Human Intrusion Modeling Case include the following, given that a certain WP is destroyed by the intrusion (Figure 6.1.1-8):

- UZ Flow
- EBS Environment
- WP and DS Degradation
- Waste Form Degradation and Mobilization
- EBS Flow and Transport
- UZ Transport (stylized)
- SZ Flow and Transport
- Biosphere.

The FEPs associated with corrosion failure of WPs prior to the disruption are not included in the Human Intrusion Modeling Case. The FEPs associated with corrosion failure of WPs and of undisrupted WPs after the disruption occurs are also not included in the Human Intrusion Modeling Case.

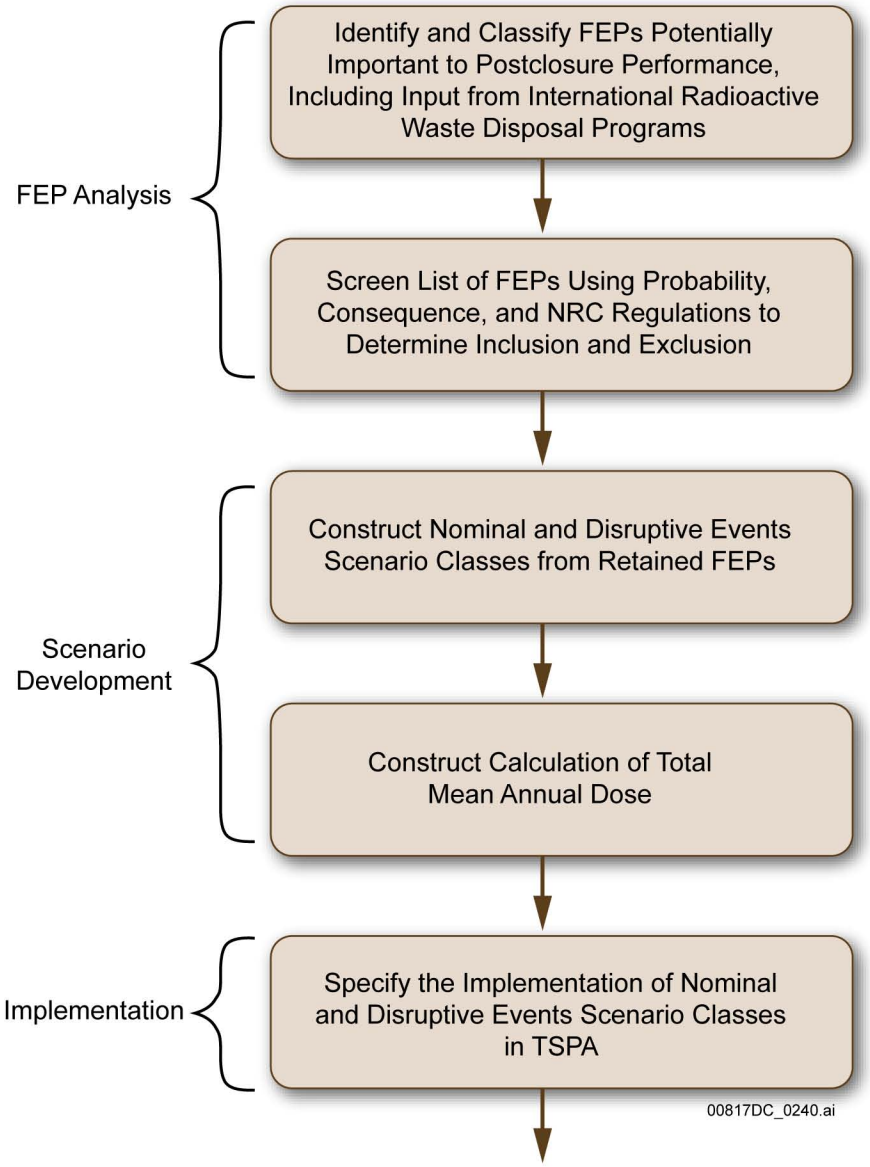

Figure 6.1.1-1. Steps in the Features, Events, and Processes Analysis and Scenario Selection Process

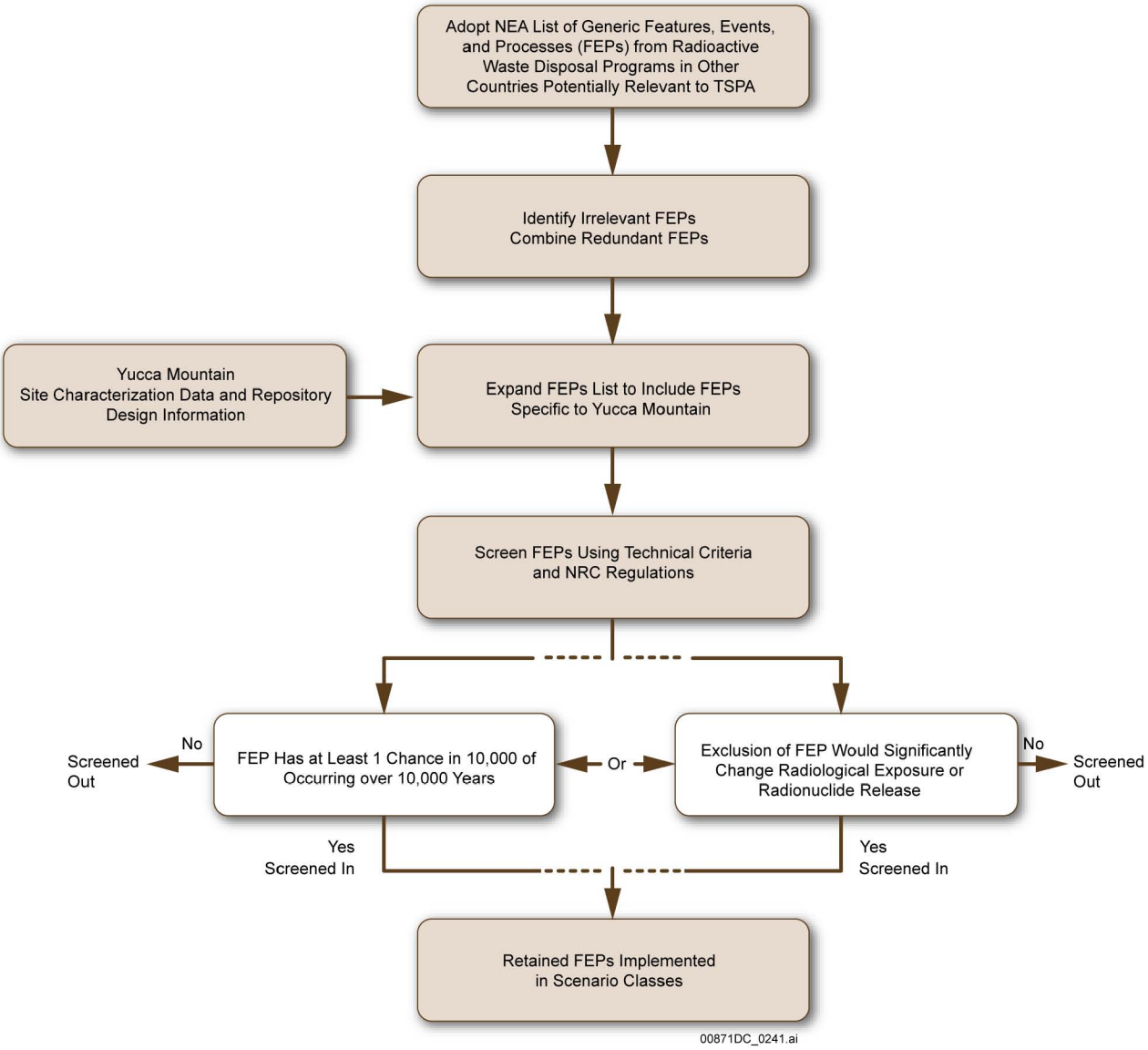

Figure 6.1.1-2. Schematic Illustration of the Features, Events, and Processes Analysis Method

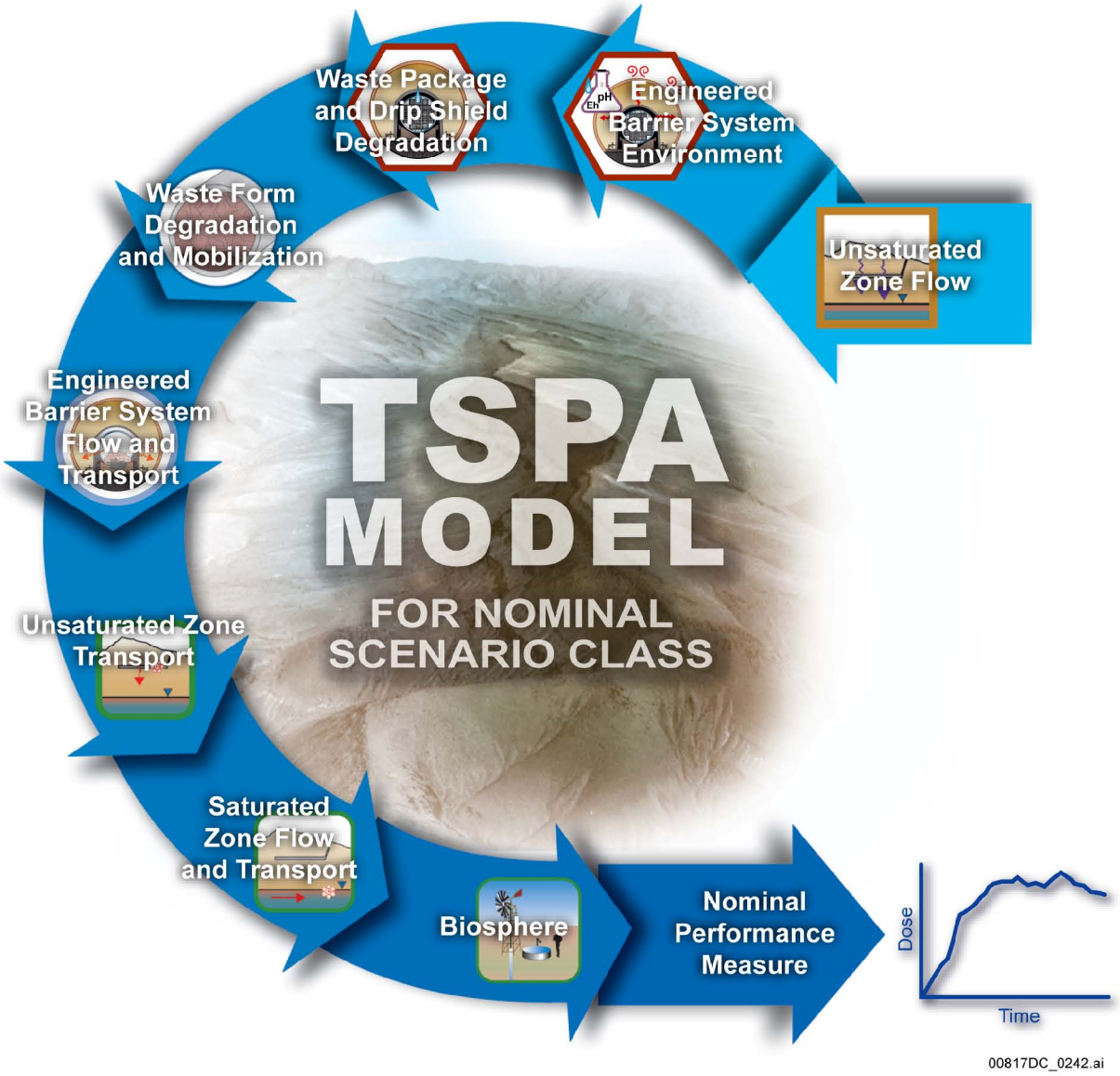

Figure 6.1.1-3. Schematic Representation of the TSPA-LA Model Components for the Nominal Scenario Class

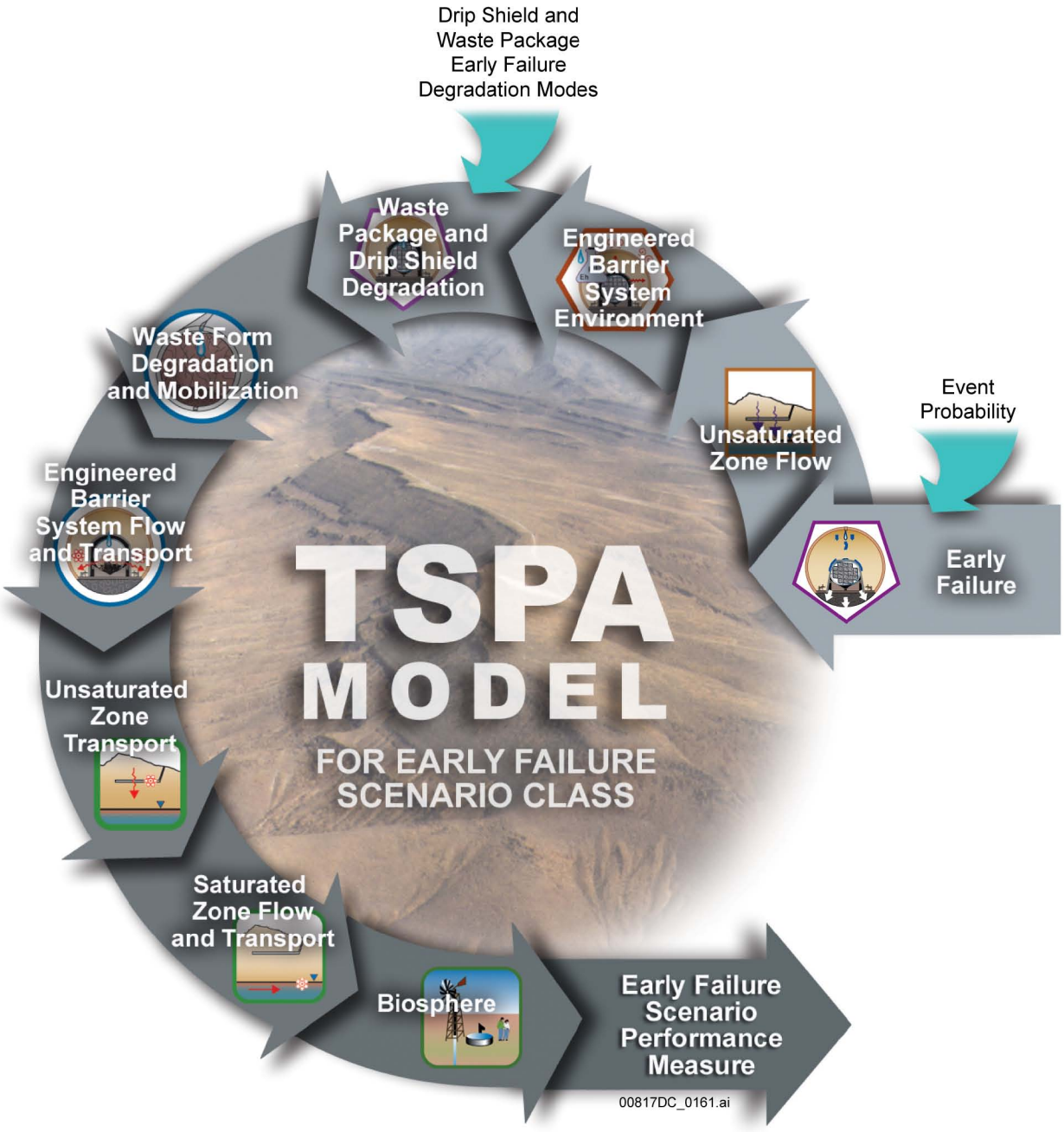

Figure 6.1.1-4. Schematic Representation of the TSPA-LA Model Components for the Early Failure Scenario Class

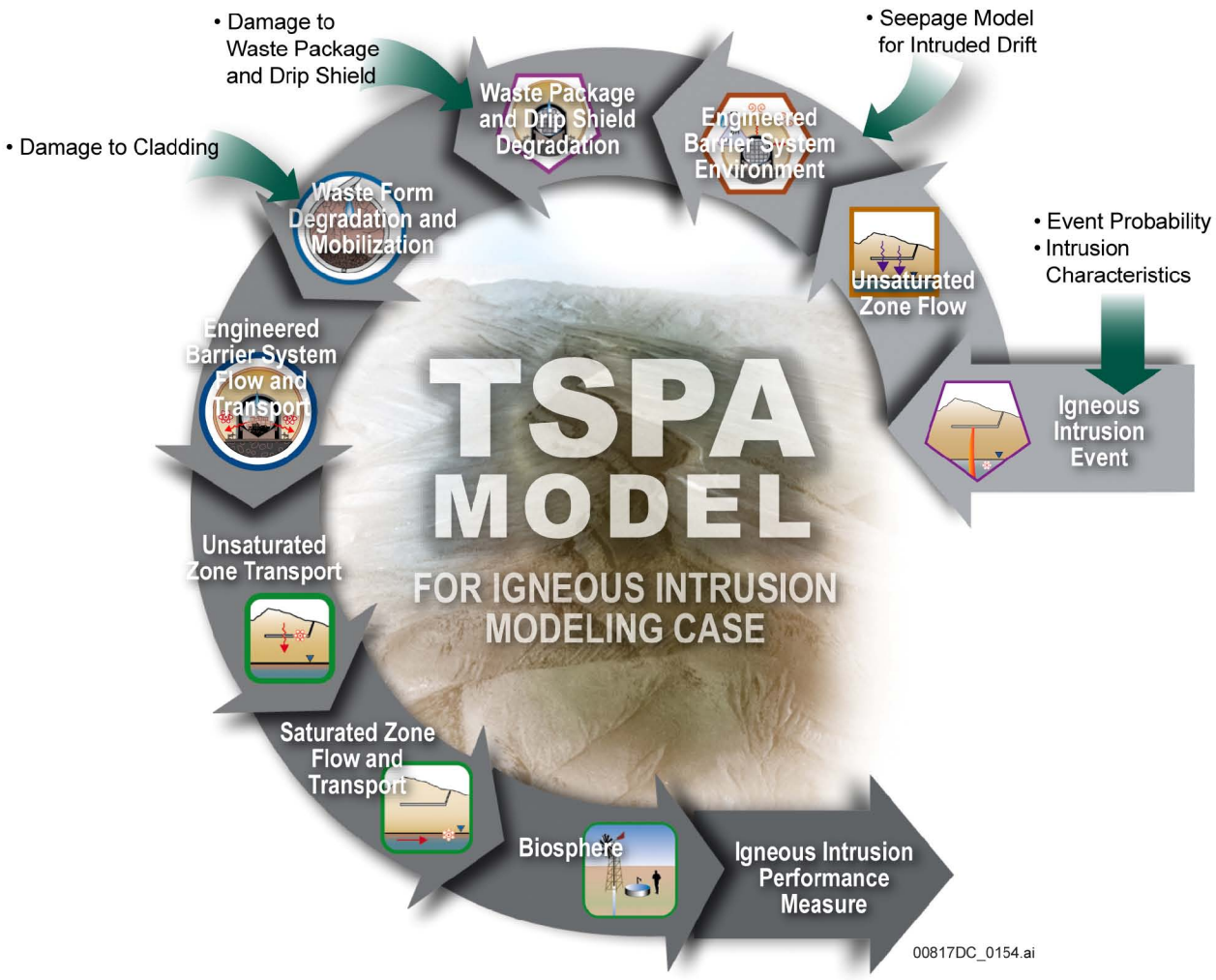

Figure 6.1.1-5. Schematic Representation of the TSPA-LA Model Components for the Igneous Intrusion Modeling Case

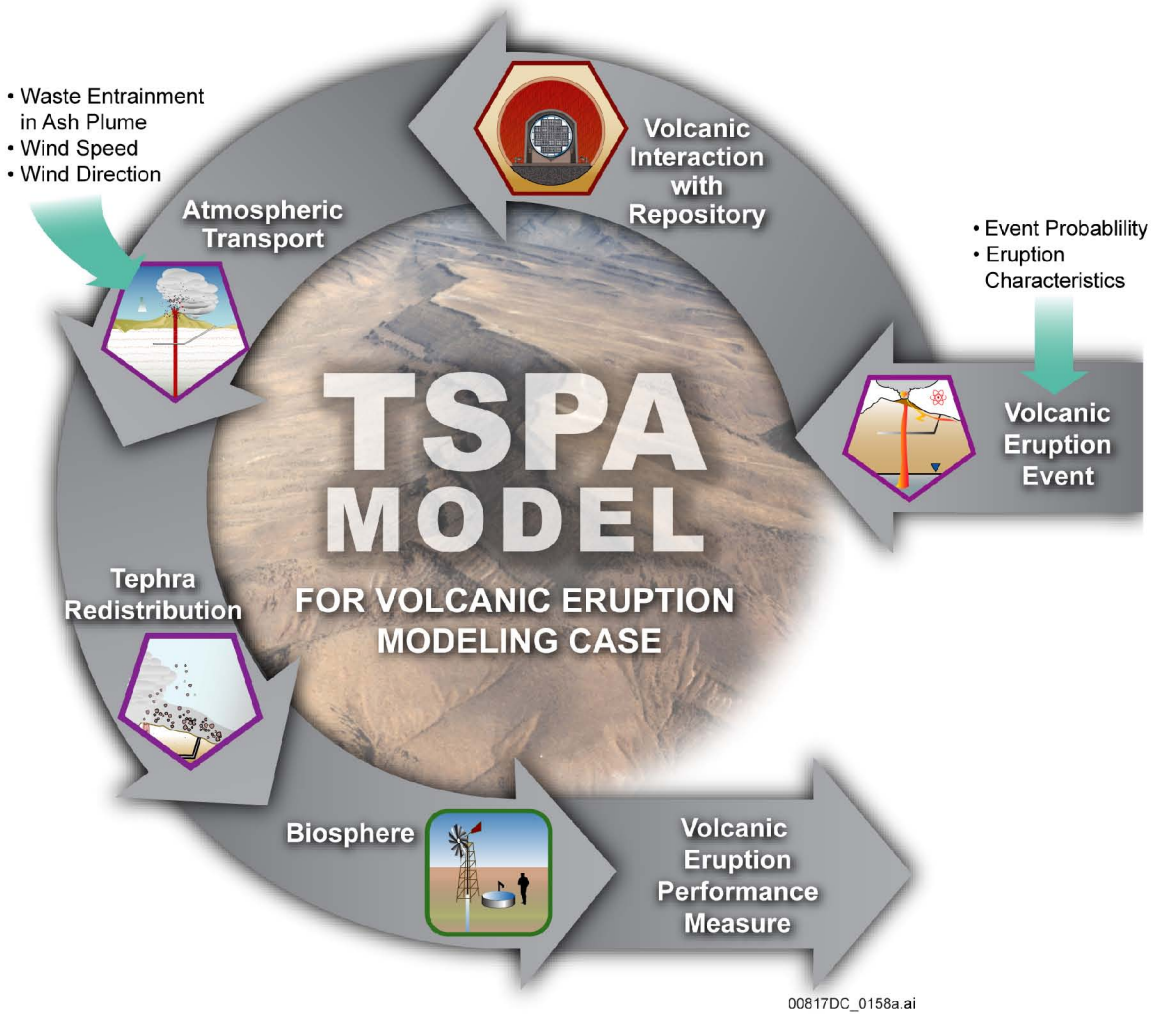

Figure 6.1.1-6. Schematic Representation of the TSPA-LA Model Components for the Volcanic Eruption Modeling Case

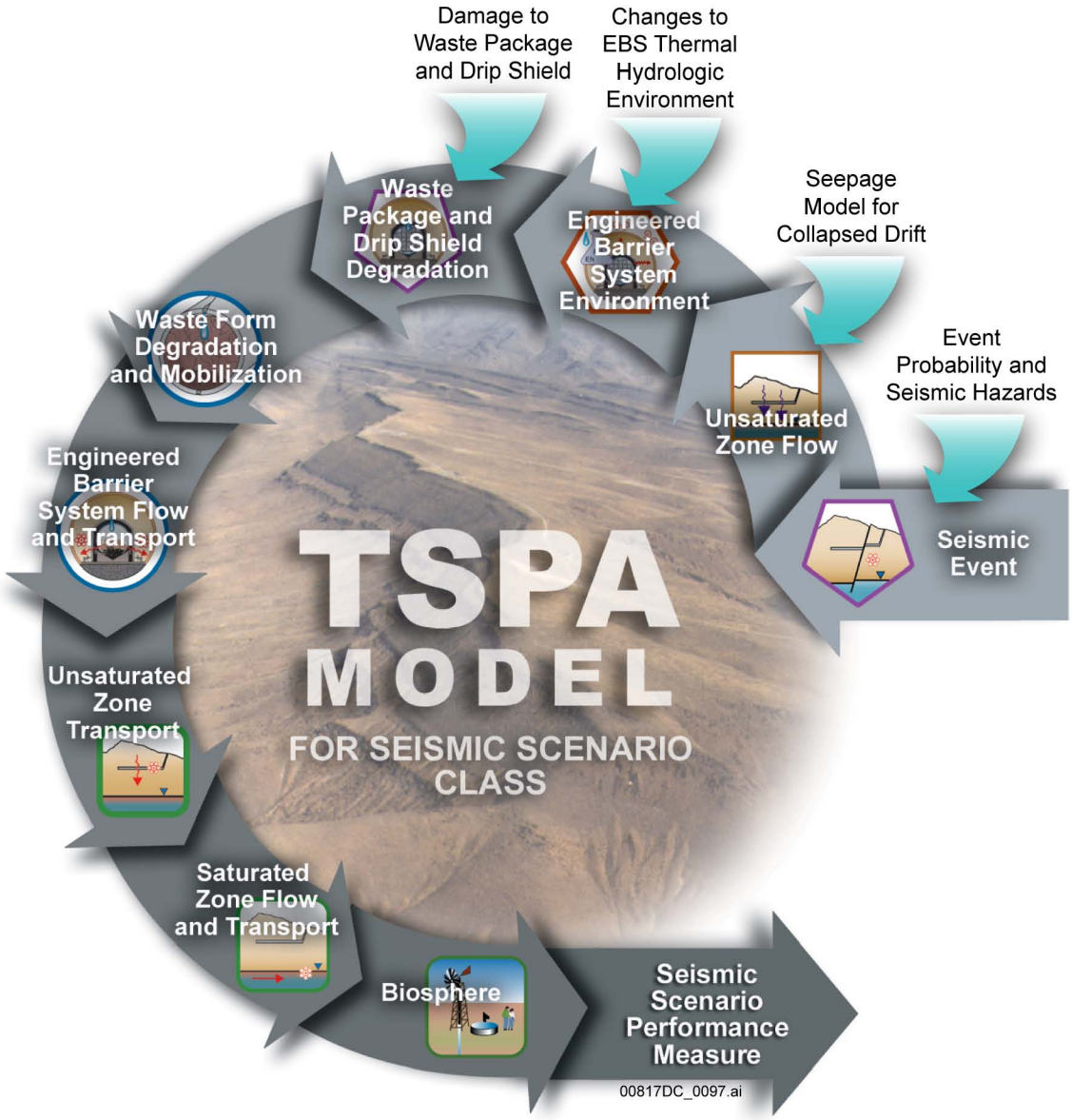

Figure 6.1.1-7. Schematic Representation of the TSPA-LA Model Components for the Seismic Scenario Class

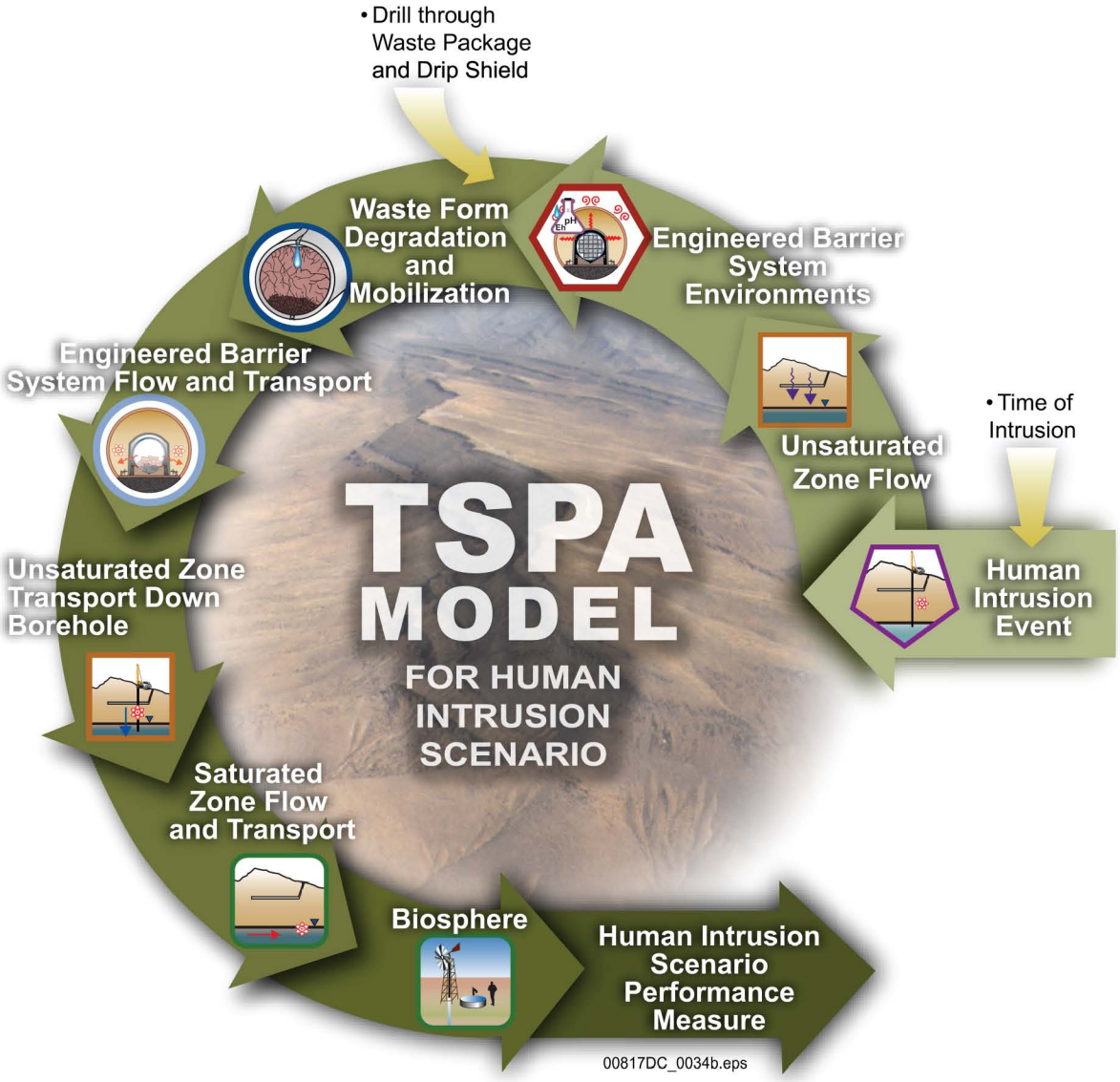

Figure 6.1.1-8. Schematic Representation of the TSPA-LA Model Components for the Human Intrusion Scenario

6.1.2 Calculation of Dose for the TSPA-LA Model

The identification and screening of FEPs is discussed in Section 6.1.1. The screening resulted in three retained events that are used to define scenario classes: early failure events, igneous events, and seismic events. Section 6.1.1 describes the scenario classes used to estimate repository performance in the TSPA-LA Model. The scenario classes are the Nominal Scenario Class, Early Failure Scenario Class, Igneous Scenario Class, and Seismic Scenario Class. A separate Human Intrusion Scenario is also described.

This section outlines the calculation of total mean annual dose and total median annual dose using the scenario classes defined in Section 6.1.1. Section 6.1.2.4 describes calculations for each of the individual modeling cases used in the TSPA-LA Model. Appendix J presents formal derivations for calculation of total mean annual dose and total median annual dose and the calculations performed for each modeling case.

6.1.2.1 Description of Uncertainty

The treatment of aleatory and epistemic uncertainty in the TSPA-LA Model is of particular importance to this discussion. In general, aleatory uncertainty derives from inherent uncertainty about future events, and epistemic uncertainty derives from lack of knowledge about quantities, models, or assumptions. Formally, aleatory uncertainty is characterized by a set $\mathcal{A} = \{\mathbf{a} : \mathbf{a} = [a_1, a_2, \ldots, a_{nA}]\}$ in which each vector $\mathbf{a} \in \mathcal{A}$ represents a possible future of the repository, and each a_j is a specific property of the future $\mathbf{a}$ (e.g., number of WP early failures, time of a seismic event). Each individual element a_i is described by a probability distribution, which conceptually leads to a density function $d_A(\mathbf{a})$ for the set $\mathcal{A}$. In this text it is useful to group the elements a_i of $\mathbf{a}$ into subsets corresponding to the modeling cases (e.g., denote by A_E the subset of elements that describe early failure events).

Similarly, epistemic uncertainty is characterized by a set $\mathcal{E} = \{\mathbf{e} : \mathbf{e} = [e_1, e_2, \ldots, e_{nE}]\}$ where each element e_i of $\mathbf{e}$ is an uncertain parameter (e.g., uncertainty in radionuclide solubility). Associated to each element e_i of $\mathbf{e}$ is a probability distribution, which taken together lead to a density function $d_E(\mathbf{e})$ for the set $\mathcal{E}$. Certain elements of $\mathbf{e}$ are used to characterize distributions for elements of $\mathbf{a}$ and thus are specific to certain modeling cases (e.g., the rate of occurrence for igneous events); other elements characterize uncertainty that applies to all modeling cases (e.g., uncertainty in radionuclide solubility). Where the distinction is important, it is useful to denote by $\mathbf{e}_A$ the subset of elements that influence aleatory uncertainty and to denote by $\mathbf{e}_M$ the elements e_i of $\mathbf{e}$ that are common to all modeling cases. The density function $d_A(\mathbf{a})$ is more correctly expressed as $d_A(\mathbf{a}|\mathbf{e}_A)$ to show the dependence of $\mathbf{a}$ on $\mathbf{e}_A$.

6.1.2.2 Calculation of Total Mean and Median Annual Dose

Total mean annual dose is defined as the expected value of dose to the RMEI, where the expectation is taken over both aleatory and epistemic uncertainty (Section 6.1.3). Total median

annual dose is estimated as the median of the distribution of expected dose to the RMEI, where the expectation is taken only over aleatory uncertainty. As specified in the proposed revision to 10 CFR 63.303 [DIRS 178394], total mean annual dose is the quantity compared to the regulatory standard for the period within 10,000 years after disposal, and total median annual dose is the quantity compared to the regulatory standard specified in 10 CFR 63.303(b) [DIRS 178394] for the period after 10,000 years of disposal. The calculations of total mean annual dose and total median annual dose are formally described in Appendix J Section J.4, which presents the mathematical definition of aleatory and epistemic uncertainty, the conceptual structure for the treatment of uncertainty, and the computational approach to the calculation of mean annual dose for each scenario class.

Calculation of total mean annual dose proceeds in a four-step process. First, a set of realizations of epistemic uncertainty are sampled from $\mathcal{E}$ consistent with the density function $d_E(\mathbf{e})$. Next, for each scenario class, a set of realizations of aleatory uncertainty, or futures, are selected from the set from $\mathcal{A}$ consistent with the density function $d_A(\mathbf{a})$. The contribution to total dose from each scenario class, $D_J(\tau|\mathbf{a},\mathbf{e})$, is computed as a function of time τ for each future $\mathbf{a}$ and each epistemic realization $\mathbf{e}$, where the subscript J in $D_J(\tau|\mathbf{a},\mathbf{e})$ indicates a particular scenario class. Third, for each scenario class and for each epistemic realization $\mathbf{e}$, the expected annual dose $\bar{D}_J(\tau|\mathbf{e})$ is computed where the expectation is taken over aleatory uncertainty. This expectation over aleatory uncertainty accounts for the probabilities that define each scenario class; thus, in the vernacular of previous TSPA analyses, $\bar{D}_J(\tau|\mathbf{e})$ is probability-weighted. Finally, total expected annual dose $\bar{D}(\tau|\mathbf{e})$ is computed for each epistemic realization $\mathbf{e}$ by summing expected annual doses over scenario classes, and total mean annual dose $\bar{\bar{D}}(\tau)$ is calculated as the expectation over epistemic uncertainty.

Total median annual dose $Q_{0.5}(\bar{D}(\tau|\mathbf{e}))$ is calculated as the median of the distribution of expected dose, where the expectation is taken only over aleatory uncertainty. Formally, at each time τ, the calculation of total expected annual dose produces a distribution $\{\bar{D}(\tau|\mathbf{e})\}$ of values of total expected annual dose, one value for each epistemic realization $\mathbf{e}$. The TSPA-LA Model estimates the total median annual dose to the RMEI by the median of the distribution $\{\bar{D}(\tau|\mathbf{e})\}$.

The quantity $\bar{D}(\tau|\mathbf{e})$ is formally described as the total expected annual dose conditional on epistemic uncertainty. For convenience, this text uses the less cumbersome term total expected annual dose to refer to $\bar{D}(\tau|\mathbf{e})$. The quantity $\bar{\bar{D}}(\tau)$ is technically also an expected value. Again, for convenience, and to distinguish this quantity in the text from the total expected annual dose $\bar{D}(\tau|\mathbf{e})$, this text uses the term total mean annual dose to refer to $\bar{\bar{D}}(\tau)$.

For an arbitrary future $\mathbf{a}$ and epistemic realization $\mathbf{e}$, total annual dose, $D(\tau|\mathbf{a},\mathbf{e})$, is approximated as:

$$D(\tau|\mathbf{a},\mathbf{e}) \cong D_N(\tau|\mathbf{a},\mathbf{e}) + D_E(\tau|\mathbf{a},\mathbf{e}) + D_I(\tau|\mathbf{a},\mathbf{e}) + D_S(\tau|\mathbf{a},\mathbf{e}) \quad \text{(Eq. 6.1.2-1)}$$

where

$D_N(\tau|\mathbf{a},\mathbf{e})$ = Dose at time τ resulting from nominal processes

$D_E(\tau|\mathbf{a},\mathbf{e})$ = Additional dose at time τ resulting from any early failures occurring in the future $\mathbf{a}$

$D_I(\tau|\mathbf{a},\mathbf{e})$ = Additional dose at time τ resulting from any igneous events occurring in the future $\mathbf{a}$

$D_S(\tau|\mathbf{a},\mathbf{e})$ = Additional dose at time τ resulting from any seismic events occurring in the future $\mathbf{a}$.

Equation 6.1.2-2 approximates total annual dose as the sum of dose resulting from nominal process and from events. The approximation relies on the simplifying assumption that the dose resulting from a combination of events is the sum of the doses resulting from each separate event; this approximation is justified in Section 6.1.2.3.

Total expected annual dose, $\bar{D}(\tau|\mathbf{e})$, is calculated as the expected value of $D(\tau|\mathbf{a},\mathbf{e})$ where the expectation is over the uncertainty in $\mathbf{a}$ (aleatory uncertainty). Written simply,

$$\begin{aligned}
\bar{D}(\tau|\mathbf{e}) &= \int_{\mathcal{A}} D(\tau|\mathbf{a},\mathbf{e}) d_A(\mathbf{a}) dA \\
&= \int_{\mathcal{A}} \left(D_N(\tau|\mathbf{a},\mathbf{e}) + D_E(\tau|\mathbf{a},\mathbf{e}) + D_I(\tau|\mathbf{a},\mathbf{e}) + D_S(\tau|\mathbf{a},\mathbf{e}) \right) d_A(\mathbf{a}) dA \\
&= \int_{\mathcal{A}} D_N(\tau|\mathbf{a},\mathbf{e}) d_A(\mathbf{a}) dA + \int_{\mathcal{A}} D_E(\tau|\mathbf{a},\mathbf{e}) d_A(\mathbf{a}) dA \\
&\quad + \int_{\mathcal{A}} D_I(\tau|\mathbf{a},\mathbf{e}) d_A(\mathbf{a}) dA + \int_{\mathcal{A}} D_S(\tau|\mathbf{a},\mathbf{e}) d_A(\mathbf{a}) dA \\
&= \bar{D}_N(\tau|\mathbf{e}) + \bar{D}_E(\tau|\mathbf{e}) + \bar{D}_I(\tau|\mathbf{e}) + \bar{D}_S(\tau|\mathbf{e})
\end{aligned} \quad \text{(Eq. 6.1.2-2)}$$

where the dependence of $d_A(\mathbf{a})$ on $\mathbf{e}$ is omitted for brevity of notation. The quantity $\bar{D}_N(\tau|\mathbf{e})$ is the expected annual dose resulting from nominal processes. The quantities $\bar{D}_E(\tau|\mathbf{e})$, $\bar{D}_I(\tau|\mathbf{e})$, and $\bar{D}_S(\tau|\mathbf{e})$ are the expected values of the additional annual dose resulting from the occurrence of early failure, igneous, and seismic events, respectively. For brevity these quantities are frequently referred to as the expected annual dose for each scenario class, and the term "additional" is omitted for convenience.

Total mean annual dose, $\overline{\overline{D}}(\tau)$, is calculated as the expected value of $\overline{D}(\tau|\mathbf{e})$ where the expectation is over the uncertainty in $\mathbf{e}$ (epistemic uncertainty). $\overline{\overline{D}}(\tau)$ is calculated by:

$$\begin{aligned}\overline{\overline{D}}(\tau) &= \int_{\mathcal{E}} \overline{D}(\tau|\mathbf{e}) d_E(\mathbf{e}) dE \\ &\cong \frac{1}{N}\sum_{k=1}^{N} \overline{D}(\tau|\mathbf{e}_k)\end{aligned} \qquad \text{(Eq. 6.1.2-3)}$$

where $\{\mathbf{e}_k\}$ is a Latin hypercube sample (LHS) of the epistemic variables of size N consistent with the distributions defining each of the elements e_i of $\mathbf{e}$.

Due to the complexity of $D(\tau|\mathbf{a},\mathbf{e})$, evaluation of the integral in Equation 6.1.2-2 requires that the set of all futures A be divided into subsets, for which the integral can be numerically evaluated. The set A is first divided into eight mutually exclusive, or disjoint, sets of repository futures, defined by the events retained in the TSPA-LA Model (early failure, igneous, and seismic). A sequence of re-arranging terms in the integral, presented below, leads to the calculation of total expected annual dose as the sum of the expected annual dose for each of the four scenario classes $\{A_N, A_{EF}, A_I, A_S\}$ identified in Section 6.1.1.

The three retained events lead directly to the first three disjoint sets of repository futures:

- Early failure scenario set, S_{EF}: the set of futures each of which includes one or more early failure events (i.e., one or more early failed WPs and/or one or more early failed DSs), but no seismic or igneous events, and also includes nominal features and processes.

- Igneous scenario set, S_I: the set of futures each of which includes one or more igneous events, but no seismic or early failure events, and also includes retained nominal features and processes.

- Seismic scenario set, S_S: the set of futures each of which includes one or more seismic events, but no igneous or early failure events, and also includes retained nominal features and processes.

The three sets listed above describe only those futures in which a single type of event occurs, thus they are subsets of the scenario classes defined in Section 6.1.1. Because the events occur independently, there are many future states of the repository in which more than one type of event may occur. Therefore, four additional sets are defined to account for futures that include combinations of the three types of events:

- Early failure/Igneous scenario set, S_{EF+I}: the set of futures each of which includes one or more early failure events and one or more igneous events, but no seismic events.

- Early failure/Seismic scenario set, S_{EF+S}: the set of futures each of which includes one or more early failure events and one or more seismic events, but no igneous events.

- Igneous/seismic scenario set, S_{I+S}: the set of futures each of which includes one or more igneous events and one or more seismic events, but no early failure events, and also includes nominal features and processes.

- Igneous/seismic/early failure scenario set, S_{EF+I+S}: the set of futures each of which includes one or more early failure events and one or more seismic events and one or more igneous events, and also includes nominal features and processes.

Each of the four scenario sets listed above can also be defined in terms of intersections of the scenario classes listed in Section 6.1.1. Finally, it is possible that no events occur in the future of the repository. One more set of repository futures, defined as the complement of the union of the sets above, accounts for the futures in which no event occurs:

- Nominal scenario set, S_N: the set of futures each of which includes nominal features and processes (e.g., corrosion processes, such as general corrosion, localized corrosion, and SCC) but *no* events (i.e., no igneous or seismic events and no early WP or DS failures).

The eight sets of futures defined above partition the set of all futures of the repository into a collection of disjoint sets. The set of all futures is formally a probability space with a probability measure p_A derived from the distributions of the individual elements a_i of $\mathbf{a}$. Hence, a probability can be calculated for each of the eight disjoint sets $\{S_{EF}, S_I, S_S, S_{EF+I}, S_{EF+S}, S_{I+S}, S_{EF+I+S}, S_N\}$. Because the union of the eight sets equals all of A, and the eight sets are disjoint, the probabilities associated with each of the eight sets sum to exactly one.

These eight sets $\{S_{EF}, S_I, S_S, S_{EF+I}, S_{EF+S}, S_{I+S}, S_{EF+I+S}, S_N\}$ form a collection of scenario classes in and of themselves. Since these sets are disjoint and their union covers all futures of the repository, these sets meet the acceptance criteria for scenario classes specified in the *Yucca Mountain Review Plan, Final Report* (NRC 2003 [DIRS 163274]). Total expected annual dose could be calculated separately for these eight scenario classes, and then combined appropriately to estimate repository performance. However, the TSPA-LA Model calculation of total expected annual dose is simplified by aggregating these eight disjoint sets into the scenario classes identified in Section 6.1.1.

Partition the set of futures A into $\{S_{EF}, S_I, S_S, S_{EF+I}, S_{EF+S}, S_{I+S}, S_{EF+I+S}, S_N\}$ as defined above. Next, separate the integral in Equation 6.1.2-2 into a sum of eight integrals over the separate disjoint sets:

$$\begin{aligned}\bar{D}(\tau|\mathbf{e}) &= \int_{\mathcal{A}} D(\tau|\mathbf{a},\mathbf{e}) d_A(\mathbf{a}) dA \\ &= \int_{S_N} D(\tau|\mathbf{a},\mathbf{e}) d_A(\mathbf{a}) dA + \int_{S_{EF}} D(\tau|\mathbf{a},\mathbf{e}) d_A(\mathbf{a}) dA \\ &\quad + \int_{S_I} D(\tau|\mathbf{a},\mathbf{e}) d_A(\mathbf{a}) dA + \int_{S_S} D(\tau|\mathbf{a},\mathbf{e}) d_A(\mathbf{a}) dA \\ &\quad + \int_{S_{EF+I}} D(\tau|\mathbf{a},\mathbf{e}) d_A(\mathbf{a}) dA + \int_{S_{EF+S}} D(\tau|\mathbf{a},\mathbf{e}) d_A(\mathbf{a}) dA \\ &\quad + \int_{S_{I+S}} D(\tau|\mathbf{a},\mathbf{e}) d_A(\mathbf{a}) dA + \int_{S_{EF+I+S}} D(\tau|\mathbf{a},\mathbf{e}) d_A(\mathbf{a}) dA \\ &= \int_{\bigcup_J S_J} D(\tau|\mathbf{a},\mathbf{e}) d_A(\mathbf{a}) dA\end{aligned} \quad \text{(Eq. 6.1.2-4)}$$

where, for convenience in the presentation, $J = 1, 2, \ldots, 8$ is an index and the collection $\{S_J\}$ are the eight disjoint sets $\{S_{EF}, S_I, S_S, S_{EF+I}, S_{EF+S}, S_{I+S}, S_{EF+I+S}, S_N\}$.

Next, use Equation 6.1.2-1 in Equation 6.1.2-4 to obtain

$$\begin{aligned}\bar{D}(\tau|\mathbf{e}) &= \int_{\bigcup_J S_J} D(\tau|\mathbf{a},\mathbf{e}) d_A(\mathbf{a}) dA \\ &= \int_{\bigcup_J S_J} \left(D_N(\tau|\mathbf{a},\mathbf{e}) + D_E(\tau|\mathbf{a},\mathbf{e}) + D_I(\tau|\mathbf{a},\mathbf{e}) + D_S(\tau|\mathbf{a},\mathbf{e}) \right) d_A(\mathbf{a}) dA \\ &= \int_{\bigcup_J S_J} D_N(\tau|\mathbf{a},\mathbf{e}) d_A(\mathbf{a}) dA + \int_{\bigcup_J S_J} D_E(\tau|\mathbf{a},\mathbf{e}) d_A(\mathbf{a}) dA \\ &\quad + \int_{\bigcup_J S_J} D_I(\tau|\mathbf{a},\mathbf{e}) d_A(\mathbf{a}) dA + \int_{\bigcup_J S_J} D_S(\tau|\mathbf{a},\mathbf{e}) d_A(\mathbf{a}) dA\end{aligned}$$

(Eq. 6.1.2-5)

Consider first the integral involving $D_E(\tau|\mathbf{a},\mathbf{e})$. If a future $\mathbf{a}$ does not include any early failure events, there is no additional dose that can result from early failure. Thus, the quantity $D_E(\tau|\mathbf{a},\mathbf{e})$ is zero for any future $\mathbf{a}$ that does not include any early failure events. Using this observation, the term in Equation 6.1.2-5 that involves $D_E(\tau|\mathbf{a},\mathbf{e})$ is expanded as

$$\begin{aligned}\int_{\bigcup_J S_J} D_E(\tau|\mathbf{a},\mathbf{e}) d_A(\mathbf{a}) dA &= \sum_J \int_{S_J} D_E(\tau|\mathbf{a},\mathbf{e}) d_A(\mathbf{a}) dA \\ &= \int_{S_{EF}} D_E(\tau|\mathbf{a},\mathbf{e}) d_A(\mathbf{a}) dA + \int_{S_{EF+I}} D_E(\tau|\mathbf{a},\mathbf{e}) d_A(\mathbf{a}) dA \\ &\quad + \int_{S_{EF+S}} D_E(\tau|\mathbf{a},\mathbf{e}) d_A(\mathbf{a}) dA + \int_{S_{EF+I+S}} D_E(\tau|\mathbf{a},\mathbf{e}) d_A(\mathbf{a}) dA\end{aligned}$$

(Eq. 6.1.2-6)

since the integral of $D_E(\tau|\mathbf{a},\mathbf{e})$ over any of the sets $\{S_I, S_S, S_{I+S}, S_N\}$ is zero. Finally, by using the definition of the Early Failure Scenario Class, A_E, and the eight disjoint scenario sets, $\{S_{EF}, S_I, S_S, S_{EF+I}, S_{EF+S}, S_{I+S}, S_{EF+I+S}, S_N\}$, write $A_E = S_{EF} \cup S_{EF+I} \cup S_{EF+S} \cup S_{EF+I+S}$. Equation 6.1.2-6 becomes

$$\begin{aligned}
&\int_{S_{EF}} D_E(\tau|\mathbf{a},\mathbf{e}) d_A(\mathbf{a}) dA + \int_{S_{EF+I}} D_E(\tau|\mathbf{a},\mathbf{e}) d_A(\mathbf{a}) dA \\
&\quad + \int_{S_{EF+S}} D_E(\tau|\mathbf{a},\mathbf{e}) d_A(\mathbf{a}) dA + \int_{S_{EF+I+S}} D_E(\tau|\mathbf{a},\mathbf{e}) d_A(\mathbf{a}) dA \\
&\qquad = \int_{S_{EF} \cup S_{EF+I} \cup S_{EF+S} \cup S_{EF+I+S}} D_E(\tau|\mathbf{a},\mathbf{e}) d_A(\mathbf{a}) dA \qquad \text{(Eq. 6.1.2-7)} \\
&\qquad = \int_{A_E} D_E(\tau|\mathbf{a},\mathbf{e}) d_A(\mathbf{a}) dA \\
&\qquad = \bar{D}_E(\tau|\mathbf{e})
\end{aligned}$$

where $\bar{D}_E(\tau|\mathbf{e})$ is the expected annual dose due to early failures. Similar sequences of operations lead to the following expressions for the expected annual dose due to igneous events, $\bar{D}_I(\tau|\mathbf{e})$, and the expected annual dose due to seismic events, $\bar{D}_S(\tau|\mathbf{e})$:

$$\bar{D}_I(\tau|\mathbf{e}) = \int_{A_I} D_I(\tau|\mathbf{a},\mathbf{e}) d_A(\mathbf{a}) dA \qquad \text{(Eq. 6.1.2-8)}$$

$$\bar{D}_S(\tau|\mathbf{e}) = \int_{A_S} D_S(\tau|\mathbf{a},\mathbf{e}) d_A(\mathbf{a}) dA \qquad \text{(Eq. 6.1.2-9)}$$

where

$A_I = S_I \cup S_{EF+I} \cup S_{I+S} \cup S_{EF+I+S}$	is the Igneous Scenario Class.
$\bar{D}_I(\tau|\mathbf{e})$	is the expected annual dose due to igneous events.
$A_S = S_S \cup S_{EF+S} \cup S_{I+S} \cup S_{EF+I+S}$	is the Seismic Scenario Class.
$\bar{D}_S(\tau|\mathbf{e})$	is the expected annual dose due to seismic events.

The final quantity required for calculation of total expected annual dose is $\bar{D}_N(\tau|\mathbf{e})$, the expected annual dose for the Nominal Scenario Class. The Nominal Scenario Class excludes the occurrence of any events, and thus does not depend on any of the aleatory uncertainties that describe future events. The Nominal Scenario Class addresses other types of aleatory uncertainty describing the time, location and extent of damage to WP caused by corrosion processes. Moreover, these corrosion processes occur in every future of the repository. Hence,

$$\bar{D}_N(\tau|\mathbf{e}) = \int_{A} D_N(\tau|\mathbf{a},\mathbf{e}) d_A(\mathbf{a}) dA \qquad \text{(Eq. 6.1.2-10)}$$

where the aleatory uncertainty in Equation 6.1.2-10 describes spatial and temporal variability in waste package failure by corrosion processes. Using Equation 6.1.2-7 through Equation 6.1.2-10, Equation 6.1.2-5 becomes

$$\begin{aligned}\bar{D}(\tau|\mathbf{e}) &= \int_{\bigcup_J S_J} D_N(\tau|\mathbf{a},\mathbf{e}) d_A(\mathbf{a}) + \int_{\bigcup_J S_J} D_{EF}(\tau|\mathbf{a},\mathbf{e}) d_A(\mathbf{a}) \\ &\quad + \int_{\bigcup_J S_J} D_I(\tau|\mathbf{a},\mathbf{e}) d_A(\mathbf{a}) + \int_{\bigcup_J S_J} D_S(\tau|\mathbf{a},\mathbf{e}) d_A(\mathbf{a}) \\ &= \int_A D_N(\tau|\mathbf{a},\mathbf{e}) d_A(\mathbf{a}) + \int_{A_{EF}} D_{EF}(\tau|\mathbf{a},\mathbf{e}) d_A(\mathbf{a}) \\ &\quad + \int_{A_I} D_I(\tau|\mathbf{a},\mathbf{e}) d_A(\mathbf{a}) + \int_{A_S} D_S(\tau|\mathbf{a},\mathbf{e}) d_A(\mathbf{a}) \\ &= \bar{D}_N(\tau|\mathbf{e}) + \bar{D}_{EF}(\tau|\mathbf{e}) + \bar{D}_I(\tau|\mathbf{e}) + \bar{D}_S(\tau|\mathbf{e})\end{aligned} \qquad \text{(Equation 6.1.2-11)}$$

Section 6.1.2.4 describes in further detail the calculation of each term in Equation 6.1.2-11. The results of these calculations are presented in Section 8.

6.1.2.3 Screening of Scenario Classes

As outlined in Section 6.1.2.2, the calculation of total annual dose as the sum of annual dose from each scenario class relies on the simplifying assumption that the occurrence of an early failure or other event has no effect on the consequences of a later event. This simplifying assumption allows the TSPA-LA Model to approximate the dose from a future involving a combination of events, such as a seismic event followed by an igneous intrusion, as the sum of the dose from the seismic event and the dose from the igneous event. In general, this method of approximation affects the TSPA-LA Model results in a conservative way, by overestimating the resulting dose. Table 6.1.2-1 summarizes the effect of each combination of events on the calculation of total mean annual dose; these effects are discussed below.

6.1.2.3.1 Nominal Scenario Class with Other Scenario Classes

During the period before 10,000 years, the corrosion processes included in the Nominal Scenario Class have no consequences that affect the consequences of any early failure or disruptive event. Thus, no combinations of the Nominal Scenario Class with other scenario classes are relevant before 10,000 years.

During the period after 10,000 years, the corrosion processes described by the Nominal Scenario Class affect the consequences of seismic ground motion events, so these processes are included in the Seismic GM Modeling Case. As explained in Section 6.1.2.4.1 and Section 6.1.2.4.3, the inclusion of these processes means that dose due to nominal processes is combined with the additional dose due to seismic ground motion events, and this combined quantity is calculated by the Seismic GM Modeling Case. The corrosion processes are included in the Igneous Intrusion Modeling Case so that the inventory remaining in the WPs at the time of the intrusion is reduced by the radionuclides released due to general corrosion processes prior to the intrusion. In order to avoid double-counting the dose from radionuclides released due to general corrosion processes prior to the intrusion, any observed dose prior to the time of the first intrusion is not included in

the results of the Igneous Intrusion Modeling Case. Nominal corrosion processes are not included in the Seismic FD, Igneous Eruption, or Early Failure Modeling Cases, which results in over counting of radionuclides released in these modeling cases. However, these modeling cases affect only a small fraction of the WPs (at most two percent in the Seismic FD Modeling Case), so the resulting effect on total mean annual dose is minor.

6.1.2.3.2 Early Failure Scenario Class with Other Scenario Classes

In the TSPA-LA Model, early failures are assumed to take place at the time of repository closure. Since an early failure cannot follow any disruptive event, these combinations are not relevant and are not listed in Table 6.1.2-1. In the TSPA-LA, if a disruptive event follows an early failure, the inventory released as a consequence of the disruptive event is estimated without subtracting the inventory that may have been released from the WPs affected by early failure. However, on average less than 2.46/11,629 = 0.02 percent of the WPs are affected by early failure (Output DTN: MO0707WPDRIPSD.000_R0 [DIRS 183005]), so not more than 0.02 percent (on average) of the inventory is counted twice, and the net effect on total mean annual dose of the combination of early failures and disruptive events is negligible.

6.1.2.3.3 Igneous Scenario Class with Other Scenario Classes

The combinations of an igneous intrusion and volcanic eruption with other scenario classes are considered separately.

Igneous Intrusion with Seismic Scenario Class—The TSPA-LA Model assumes that all components of the EBS suffer maximum damage from an igneous intrusion. After the intrusion, the EBS components (DSs and WPs) no longer function as a barrier to advective or diffusive transport of radionuclides. Since the effects of a seismic event (either vibratory ground motion or fault displacement) are damage to components of the EBS, a seismic event following an igneous intrusion should not have any effect on the repository performance.

The TSPA-LA Model overestimates total dose by not excluding the dose resulting from seismic events occurring after an igneous intrusion. However, during 1,000,000 years, the average probability of an igneous intrusion is roughly $\left(1.7\times10^{-8}\ \text{yr}^{-1}\right)\times\left(10^{6}\ \text{yr}\right)=1.7\times10^{-2}$ (Section 6.5.1.1), so the over-estimate of dose affects roughly 2 percent of the realizations of the Seismic GM Modeling Case, and the overall effect on total mean annual dose is minor.

Volcanic Eruption with Seismic Scenario Class—The TSPA-LA Model overestimates total dose by not reducing the inventory that could be released by seismic events, by the amount of inventory released by any volcanic eruptions. However, on average an eruptive event affects less that 0.03 percent of the WPs, so not more than 0.03 percent (on average) of the inventory could be counted twice, and the net effect on total mean annual dose of the combination of volcanic eruptions and seismic events is negligible.

Combinations of Igneous Intrusions with Volcanic Eruptions—The TSPA-LA Model overestimates total dose by not reducing the inventory that could be released by intrusions or eruptions by the amount of inventory released by any preceding igneous event. However, on average an eruptive event affects less that 0.03 percent of the WPs, so the effect on total mean

annual dose of an eruptive event preceding other igneous events is negligible. The TSPA-LA Model accounts for multiple igneous intrusion events and for multiple volcanic eruption events in the calculation of total mean annual dose.

6.1.2.3.4 Seismic Scenario Class with Other Scenario Classes

The TSPA-LA Model overestimates total dose by not subtracting the inventory released due to preceding seismic ground motion events from the inventory available at the time of an igneous event. During 1,000,000 years, essentially all future states of the repository include releases due to seismic ground motion damage; thus, essentially all realizations of the Igneous Modeling Cases overstate releases by the amount of inventory released by seismic ground motion events prior to an intrusion. This interaction is conservative in the sense that the consequences of the Igneous Modeling Cases are always overstated. Additional discussion of the magnitude by which these consequences are overstated is provided in Appendix J, Section J.10.

The inventory released from a fault displacement event is not subtracted from the inventory that could be released by a later disruptive event. In addition, the inventory that could be released from WPs affected by fault displacement is not reduced by releases from any preceding disruptive events. However, a fault displacement affects at most 212/11,629 = 1.8 percent of the WPs, so at most 1.8 percent of the inventory is counted twice, and the net effect on total mean annual dose of the combination of fault displacements, with other disruptive events, is negligible.

6.1.2.4 Calculation of Expected Annual Dose for the Modeling Cases

Equation 6.1.2-11 shows the calculation of total expected annual dose as the sum of expected annual dose for each scenario class. In turn, the expected annual dose for each scenario class is the sum of the expected annual dose for the modeling cases comprising the scenario class. Appendix J presents the formal derivation of expected annual dose for each modeling case. This section summarizes that discussion and gives the equations used to evaluate expected annual dose for each of the modeling cases.

6.1.2.4.1 Nominal Scenario Class

The Nominal Scenario Class includes one modeling case, the Nominal Modeling Case. By definition, the Nominal Scenario Class excludes the occurrence of any early failures or of any events. Thus, there is no aleatory uncertainty in the Nominal Modeling Case related to the occurrence of early failures, igneous or seismic events. Conceptually, the time, location and degree of damage to each WP that fails by nominal corrosion processes are aleatory uncertainties that could be described by appropriate elements of the vector for aleatory uncertainty, $\mathbf{a}$. However, these aleatory quantities are not explicitly represented in the TSPA-LA Model in the same manner as aleatory quantities related to early failures or events. Rather, these aleatory quantities are addressed through a number of averaging operations within submodels that determine time, location and degree of damage occurring by corrosion processes. Section 6.3.5 describes these submodels; Appendix N outlines the averaging operations that account for the aleatory uncertainty in these submodels. Thus, the Nominal Modeling Case computes the expected annual dose $\bar{D}_N(\tau \mid \mathbf{e})$ directly by the models described in Section 6.3.

The expected annual dose for the Nominal Modeling Case, $\overline{D}_N(\tau \mid \mathbf{e}_i)$, is calculated for both 10,000 years and for 1,000,000 years. However, for estimating total expected annual dose for 1,000,000 years, $\overline{D}_N(\tau \mid \mathbf{e}_i)$ is not used directly in Equation 6.1.2-11. Instead, as described in Section 6.1.2.4.4, the dose due to nominal processes is calculated as part of the Seismic GM Modeling Case, and addresses the aleatory uncertainty in corrosion processes using the techniques outlined in Appendix N.

6.1.2.4.2 Early Failure Scenario Class

The Early Failure Scenario Class includes two modeling cases: the Waste Package EF Modeling Case, and the Drip Shield EF Modeling Case. For the Early Failure Scenario Class, expected annual dose at time τ is computed as:

$$\overline{D}_E\left(\tau|\mathbf{e}_i\right) = \overline{D}_{EW}\left(\tau|\mathbf{e}_i\right) + \overline{D}_{ED}\left(\tau|\mathbf{e}_i\right) \qquad \text{(Eq. 6.1.2-12)}$$

where $\overline{D}_{EW}\left(\tau|\mathbf{e}_i\right)$ is the expected annual dose from early failed WPs, and $\overline{D}_{ED}\left(\tau|\mathbf{e}_i\right)$ is the expected annual dose from early failed DSs. Equation 6.1.2-12 is justified because early failure is modeled as occurring independently for each WP and DS.

Waste Package EF Modeling Case—The Waste Package EF Modeling Case estimates the dose resulting from the occurrence of early failure of WPs. The aleatory uncertainties in this modeling case include:

- The number of WP early failures
- The type of each WP having early failure
- The location of each WP having early failure, described in terms of the seepage conditions at each location.

For each realization $\mathbf{e}_i$ of epistemically uncertain parameters, the expected dose $\overline{D}_W\left(\tau|\mathbf{e}_i\right)$ is calculated by

$$\overline{D}_{EW}\left(\tau|\mathbf{e}_i\right) = \sum_{r=1}^{2}\sum_{s=1}^{5}\sum_{t=0}^{1} pW_i\, fWT_r\, fBN_s\, pDRP_{rsti}\, nWP\, D_{EW}\left(\tau|[1,r,s,t],\mathbf{e}_i\right) \qquad \text{(Eq. 6.1.2-13)}$$

where

pW_i is the probability of a randomly chosen WP having early failure (element of $\mathbf{e}_i$)

fWT_r is the fraction of WPs in the repository of type r (co-disposed [CDSP WP] or transportation, aging, and disposal [TAD] canister)

$fDRP_{rsi}$ is the fraction of WPs of type r in percolation bin s (Section 6.3.2) that experience dripping conditions (function of elements of $\mathbf{e}_i$)

$$pDRP_{rsti} = \begin{cases} 1 - fDRP_{rsi} & \text{if } t = 0 \\ fDRP_{rsi} & \text{if } t = 1 \end{cases}$$

fBN_s is the fraction of WPs in the repository that are in percolation bin s

nWP is the number of WPs in the repository

$D_{EW}\left(\tau \left| [1, r, s, t], \mathbf{e}_i \right.\right)$ is the dose at time τ that results from early failure of one WP of type r in percolation bin s with dripping ($t = 1$) or non-dripping conditions ($t = 2$), and is calculated using the GoldSim component of the TSPA-LA Model.

For derivation of Equation 6.1.2.13, see Appendix J Section J.6.2.

Drip Shield EF Modeling Case—The Drip Shield EF Modeling Case estimates the dose resulting from the occurrence of early failure of DSs. The aleatory uncertainties in this modeling case include:

- The number of DS early failures
- The location of each DS early failure, described in terms of the seepage and conditions at each location
- The type of WP located beneath each DS early failure.

The calculation of expected annual dose for the Drip Shield EF Modeling Case is very similar to Equation 6.1.2-13 for expected annual dose for the Waste Package EF Modeling Case. For each realization $\mathbf{e}_i$ of epistemically uncertain parameters, the expected dose $\bar{D}_D\left(\tau \left| \mathbf{e}_i \right.\right)$ is calculated by

$$\begin{aligned} \bar{D}_{ED}\left(\tau \left| \mathbf{e}_i \right.\right) &= \sum_{r=1}^{2} \sum_{s=1}^{5} \sum_{t=0}^{1} pD_i \, fWT_r \, fBN_{rs} \, pDRP_{rsti} \, nWP \, D_{ED}\left(\tau \left| [1, r, s, t], \mathbf{e}_i \right.\right) \\ &= \sum_{r=1}^{2} \sum_{s=1}^{5} pD_i \, fWT_r \, fBN_{rs} \, pDRP_{rs1i} \, nWP \, D_{ED}\left(\tau \left| [1, r, s, 1], \mathbf{e}_i \right.\right) \end{aligned} \qquad \text{(Eq. 6.1.2-14)}$$

where

pD_i is the probability of a randomly chosen DS having early failure (element of $\mathbf{e}_i$)

fWT_r is the fraction of WPs in the repository of type r (CDSP or TAD canister)

nWP is the number of WPs in the repository

$fDRP_{rsi}$ is the fraction of WPs of type r in percolation bin s (Section 6.3.2) that experience dripping conditions (function of elements of $\mathbf{e}_i$)

fBN_{rs} fraction of WPs of type r in percolation bin s

$$pDRP_{rsti} = \begin{cases} 1 - fDRP_{rsi} & \text{if } t = 0 \\ fDRP_{rsi} & \text{if } t = 1 \end{cases}$$

$D_{ED}\left(\tau \middle| [1, r, s, t], \mathbf{e}_i\right)$ is the dose at time τ that results from early failure of one DS over a WP of type r in percolation bin s with dripping ($t = 1$) or non-dripping conditions ($t = 0$), and is calculated using the GoldSim component of the TSPA-LA Model.

The second line in equation 6.1.2-14 results because no WP failure is assumed to occur under an early failed DS unless dripping conditions are present. For derivation of Equation 6.1.2.14, see Appendix J Section J.6.3.

6.1.2.4.3 Igneous Scenario Class

The Igneous Scenario Class includes two modeling cases: the Igneous Intrusion Modeling Case, and the Volcanic Eruption Modeling Case. For the Igneous Scenario Class, expected annual dose at time τ is computed as:

$$\bar{D}_I\left(\tau \middle| \mathbf{e}_i\right) = \bar{D}_{II}\left(\tau \middle| \mathbf{e}_i\right) + \bar{D}_{IE}\left(\tau \middle| \mathbf{e}_i\right) \qquad \text{(Eq. 6.1.2-15)}$$

where $\bar{D}_{II}\left(\tau \middle| \mathbf{e}_i\right)$ is the expected annual dose from igneous intrusions, and $\bar{D}_{IE}\left(\tau \middle| \mathbf{e}_i\right)$ is the expected annual dose from eruptions. Although the occurrence of intrusions and eruptions is not independent, Equation 6.1.2-15 is justified because effects of an intrusion and an eruption are independent.

Igneous Intrusion Modeling Case—The Igneous Intrusion Modeling Case estimates the dose resulting from groundwater transport of radionuclides as a consequence of an igneous intrusion into the repository. The Volcanic Eruption Modeling Case estimates the dose that results from an eruption that occurs during an igneous event. The time of the igneous event is the single aleatory uncertainty in this modeling case. The TSPA-LA conservatively assumes that an igneous intrusion affects all WPs, and that maximum damage occurs to each WP; thus, the extent of damage is not treated as an aleatory uncertainty.

For each realization $\mathbf{e}_i$ of epistemically uncertain parameters, the expected annual dose $\bar{D}_{II}\left(\tau \middle| \mathbf{e}_i\right)$ at time τ is formally calculated by

$$\bar{D}_{II}\left(\tau \middle| \mathbf{e}_i\right) = \int_0^{\tau} D_{II}\left(\tau \middle| [1, t], \mathbf{e}_i\right) \lambda_I\left(\mathbf{e}_i\right) dt \qquad \text{(Eq. 6.1.2-16)}$$

where, $D_{II}\left(\tau \middle| [1, t], \mathbf{e}_i\right)$ is the dose conditional on one intrusion occurring at time t, and $\lambda_I\left(\mathbf{e}_i\right)$ is the frequency of igneous events for realization $\mathbf{e}_i$. Equation 6.1.2-16 accounts for the possibility of more than one igneous intrusion occurring in the future of the repository. Because the first intrusion damages the repository to the maximum extent, subsequent intrusions should not

contribute additional radionuclides to the expected annual dose. However, on average, only 2 percent of realizations include more than one intrusion, so the over-counting of dose is minor.

Nominal corrosion processes are included in the Igneous Intrusion Modeling Case for calculation of dose to 1,000,000 years. However, the calculation of $D_{II}\left(\tau|[1,t],\mathbf{e}_i\right)$ does not accumulate the dose from radionuclides released by corrosion processes prior to the intrusion. The dose from the radionuclides released prior to the intrusion is not included in $D_{II}\left(\tau|[1,t],\mathbf{e}_i\right)$ to avoid counting these radionuclides twice in the calculation of total annual dose by Equation 6.1.2-1. The dose from radionuclides released prior to the intrusion by corrosion processes is accounted for as part of the Seismic GM Modeling Case, as described in Section 6.1.2.4.3.

The integral in Equation 6.1.2-16 is approximated by employing a quadrature technique to integrate over time t

$$\bar{D}_{II}\left(\tau|\mathbf{e}_i\right)=\sum_{k=0}^{N-1}D_{II}\left(\tau|[1,t_k],\mathbf{e}_i\right)\lambda_I\left(\mathbf{e}_i\right)\Delta t_k \qquad \text{(Eq. 6.1.2-17)}$$

where

T is the time period of interest (10,000 or 1,000,000 years)

$[t_0,t_1,\ldots,t_N]$ is a sequence of times of igneous intrusions occurring in $[0,T]$, for which $D_{II}\left(\tau|[1,t],\mathbf{e}_i\right)$ has been computed using GoldSim results

$\Delta t_k = t_{k+1}-t_k$

For derivation of Equation 6.1.2-16 and Equation 6.1.2-17, see Appendix J Section J.7.2.

Volcanic Eruption Modeling Case—The Volcanic Eruption Modeling Case estimates the annual dose resulting from eruptions. The aleatory uncertainties in this modeling case include:

- Number of igneous eruptive events
- Time of each eruptive event
- Eruptive power, eruptive velocity, duration, wind speed, and wind direction for each eruptive event
- Number of WPs affected and fraction of WP content that is ejected into the atmosphere.

For each realization $\mathbf{e}_i$ of epistemically uncertain parameters, the expected annual dose $\overline{D}_{IE}(\tau|\mathbf{e}_i)$ at time τ is formally calculated by

$$\overline{D}_{IE}(\tau|\mathbf{e}_i) = pE\,\lambda_I(\mathbf{e}_i)\,\overline{N}_{IE}\,\overline{F}\int_{U_{IE}}\left[\int_0^{\tau} D_{IE}(\tau|[1,t,1,\mathbf{u}],\mathbf{e}_i)\,dt\right] d_U(\mathbf{u})\,dU \qquad \text{(Eq. 6.1.2-18)}$$

where

pE	is the probability that an igneous event includes one or more eruptive conduits that intercept waste
$\lambda_I(\mathbf{e}_i)$	is the frequency of igneous events for realization $\mathbf{e}_i$
$\overline{N}_{IE}$	is the mean number of WPs affected by an eruptive conduit
$\overline{F}$	is the mean fraction of WP content ejected into the atmosphere
U_{IE}	is the vector space of all values of eruptive power, eruptive velocity, duration, wind speed, and wind direction
$\mathbf{u}$	is a vector of values sampled from the distributions for eruptive power, eruptive velocity, duration, wind speed, and wind direction
$d_U(\mathbf{u})$	is the probability density function (pdf) on U_{IE} formed from the individual probability distributions for eruptive power, eruptive velocity, duration, wind speed, and wind direction
$D_{IE}(\tau\|[1,t,1,\mathbf{u}],\mathbf{e}_i)$	is the dose calculated by GoldSim conditional on one eruption occurring at time t, which affects one WP, with eruptive power, eruptive velocity, duration, wind speed, and wind direction described by $\mathbf{u}$.

The calculation of expected dose in Equation 6.1.2-18 accounts for the possibility that more than one igneous eruption occurs in the future evolution of the repository. The calculation conservatively assumes that each eruption event affects a different set of WPs, thus the consequence of two or more eruption events is the sum of the consequences of each individual event.

Due to the relatively large number of aleatory uncertainties in Equation 6.1.2-18, calculation of expected annual dose employs a Monte Carlo technique. A LHS of size nU is generated from U_{IE}, and the quantities $D_{IE}(\tau|[1,t,1,\mathbf{u}_l],\mathbf{e}_i)$ are computed using GoldSim. The expected dose is calculated using a quadrature technique to integrate over time t

$$\overline{D}_{IE}(\tau|\mathbf{e}_i) = pE\,\lambda_I(\mathbf{e}_i)\,\overline{N}_{IE}\,\overline{F}\sum_{k=0}^{N-1}\left[\sum_{l=1}^{nU} D_{IE}(\tau|[1,t_k,1,\mathbf{u}_l],\mathbf{e}_i)/nU\right]\Delta t_k \qquad \text{(Eq. 6.1.2-19)}$$

where

$\mathbf{u}_l$ are the sampled vectors from U_{IE}

T is the time period of interest (10,000 or 1,000,000 years)

$[t_0, t_2, \ldots, t_N]$ is a sequence of times of igneous eruptions occurring in $[0, T]$, for which $D_{IE}\left(\tau \middle| [1, t, 1, \mathbf{u}_l], \mathbf{e}_i\right)$ has been computed using GoldSim results

$\Delta t_k = t_{k+1} - t_k$

For derivation of Equation 6.1.2-18 and Equation 6.1.2-19, see Appendix J Section 7.3.

6.1.2.4.4 Seismic Scenario Class

The Seismic Scenario Class includes two modeling cases: the Seismic GM Modeling Case, and the Seismic FD Modeling Case. For the Seismic Scenario Class, expected annual dose at time τ for 10,000 years is computed as:

$$\bar{D}_S\left(\tau \middle| \mathbf{e}_i\right) = \bar{D}_{SG}\left(\tau \middle| \mathbf{e}_i\right) + \bar{D}_{SF}\left(\tau \middle| \mathbf{e}_i\right) \qquad \text{(Eq. 6.1.2-20)}$$

where $\bar{D}_{SG}\left(\tau \middle| \mathbf{e}_i\right)$ is the expected annual dose from seismic ground motion events, and $\bar{D}_{SF}\left(\tau \middle| \mathbf{e}_i\right)$ is the expected annual dose from seismic fault displacement events. Equation 6.1.2-20 is justified because the occurrence of ground motion and fault displacement events is modeled as independent.

For 1,000,000 years, the expected annual dose for the Nominal and the Seismic Scenario Classes are combined, and are computed as:

$$\bar{D}_N\left(\tau \middle| \mathbf{e}_i\right) + \bar{D}_S\left(\tau \middle| \mathbf{e}_i\right) = \bar{D}_{N+G}\left(\tau \middle| \mathbf{e}_i\right) + \bar{D}_{SF}\left(\tau \middle| \mathbf{e}_i\right) \qquad \text{(Eq. 6.1.2-21)}$$

where $\bar{D}_{N+G}\left(\tau \middle| \mathbf{e}_i\right)$ is the expected annual dose resulting from the combination of nominal processes and seismic ground motion events.

Seismic GM Modeling Case—The Seismic GM Modeling Case calculates annual dose from radionuclides released from the EBS due to damage to WPs resulting from vibratory ground motion. In addition, this modeling case accounts for damage to the DS due to vibratory ground motion, and the effects of this damage on radionuclide releases from WPs. The occurrence of seismic events is modeled as a Poisson process with the smallest events of consequence having an annual frequency of 4.287×10^{-4} yr^{-1}. During the first 10,000 years after closure, only a few seismic ground motion events will occur; however, during the 1,000,000-year peak dose period, the TSPA-LA must account for the effects of a sequence of a few hundred seismic events. In addition, because corrosion processes alter the response of the engineered barrier components to seismic events, corrosion processes are included in the Seismic GM Modeling Case calculation for 1,000,000 years, and the dose from radionuclides release due to corrosion processes is

calculated as part of the Seismic GM Modeling Case for 1,000,000 years. Due to these differences, different numerical techniques are used to calculate expected annual dose for 10,000 years and for 1,000,000 years.

The *Seismic Consequence Abstraction* (SNL 2007 [DIRS 176828]) outlines a probabilistic model for effects on the EBS due to seismic ground motion events. The abstraction provides different probability models for:

- the occurrence and extent of SCC damage to CDSP WP and TAD canister WPs
- the occurrence and extent of rupture of CDSP WP and TAD canister WPs
- the occurrence and extent of rockfall in the lithophysal and non-lithophysal zones
- the state of the DS and its supporting framework as a function of time.

The abstraction also accounts for the change in susceptibility of each EBS component to damage, and, if damage occurs, the change in the extent of damage, due to general corrosion taking place.

For 10,000 years, the consequences of seismic ground motion events can be approximated by examining only the occurrence of SCC damage to CDSP WPs with the DS intact and without rockfall, and without considering the effects of corrosion processes. Section 7.3.2 provides justification for the simplifications to the seismic consequences abstraction that lead to this approximation.

The aleatory uncertainties in the Seismic GM Modeling Case for 10,000 years include:

- the number of seismic events that cause SCC damage to CDSP WPs
- the time of each damaging seismic event
- the amount of damage caused by each seismic event.

For each realization $\mathbf{e}_i$ of epistemically uncertain parameters, the expected annual dose $\bar{D}_{SG}\left(\tau|\mathbf{e}_i\right)$ at time τ for $\tau < 10{,}000\,\text{yr}$ is formally calculated by

$$\bar{D}_{SG}\left(\tau|\mathbf{e}_i\right) = \int_0^{\tau}\left(\lambda_1\left(\mathbf{e}_i\right)e^{-\lambda_1(\mathbf{e}_i)t}\left(\int_{A_{\min}}^{A_{\max}} D_{SG}\left(\tau\left|[1,t,A],\mathbf{e}_i\right.\right)d_{A1}\left(A|\mathbf{e}_i\right)dA\right)\right)dt + \int_0^{\tau}\left(\lambda_1\left(\mathbf{e}_i\right)e^{-\lambda_1(\mathbf{e}_i)t}\left(\int_t^{\tau}\int_{B_{\min}}^{B_{\max}} D_{SG}\left(\tau\left|[1,\tilde{t},B],\mathbf{e}_i\right.\right)d_{A2}\left(B|\mathbf{e}_i\right)\lambda_2\left(\mathbf{e}_i\right)d\tilde{t}\right)\right)dt \quad \text{(Eq. 6.1.2-22)}$$

where

$\lambda_1\left(\mathbf{e}_i\right)$ is the frequency of seismic ground motion events that cause SCC damage to CDSP WPs with intact internals

$\lambda_2\left(\mathbf{e}_i\right)$ is the frequency of seismic ground motion events that cause SCC damage to CDSP WPs with degraded internals

$d_{A1}(A|\mathbf{e}_i)$ is the density function that describes the probability of damage area equal to A occurring on CDSP WPs with intact internals, given that a seismic event that causes damage occurs

$d_{A2}(B|\mathbf{e}_i)$ is the density function that describes the probability of damage area equal to B occurring on CDSP WPs with degraded internals, given that a seismic event that causes damage occurs

$D_{SG}(\tau|[1,t,A],\mathbf{e}_i)$ is the annual dose at time τ resulting from a seismic ground motion event occurring at time t that causes damaged area equal to A.

Two frequencies ($\lambda_1(\mathbf{e}_i)$ and $\lambda_2(\mathbf{e}_i)$) and density functions ($d_{A1}(A|\mathbf{e}_i)$ and $d_{A2}(B|\mathbf{e}_i)$) for damaged area are used in Equation 6.1.2-22 because *Seismic Consequence Abstraction* (SNL 2007 [DIRS 176828]) specifies different probability models for the occurrence and the extent of damage depending on whether the internals of the WP are intact or degraded. The TSPA-LA Model assumes that WP internals degrade rapidly after the first seismic event that damages the WP outer barrier. The calculation of expected annual dose in Equation 6.1.2-22 accounts for the possibility that more than one damaging event occurs in the future of the repository, using the conservative assumption that the annual dose from a sequence of events causing cumulative damage to WPs is reasonably approximated by the sum of the annual dose resulting from the individual events. This assumption of linearity in seismic consequences is justified in Section 7.3.2.

The integral in Equation 6.1.2-22 is approximated by employing quadrature techniques to integrate over time t and damaged areas A and B.

For derivation of Equation 6.1.2-22 and description of its numerical solution, see Appendix J Section J.8.3.

For 1,000,000 years, the full *Seismic Consequences Abstraction* (SNL 2007 [DIRS 176828]) is considered, including both the effects of corrosion processes on EBS components, and the dose resulting from corrosion processes. Because the corrosion processes are included with the Seismic GM Modeling Case for 1,000,000 years, the annual dose calculated by this modeling case is expressed as

$$D_{N+G}(\tau|\mathbf{a},\mathbf{e}) = D_N(\tau|\mathbf{a},\mathbf{e}) + D_{SG}(\tau|\mathbf{a},\mathbf{e}) \quad \text{(Eq. 6.1.2-23)}$$

where $D_N(\tau|\mathbf{a},\mathbf{e})$ represents the dose at time τ resulting from radionuclides released due to corrosion processes, and $D_{SG}(\tau|\mathbf{a},\mathbf{e})$ represents the dose at time τ resulting from radionuclides released due to seismic events. The aleatory uncertainties in corrosion processes is the same as described in the discussion of the Nominal Modeling Case, and is treated by means of the averaging operations described in Appendix N. The aleatory uncertainties in seismic events include:

- The number of seismic events
- The time of each seismic event
- The amount of rockfall in the lithophysal zone caused by each seismic event
- The effect of rockfall on the structure and function of DSs at the time of each seismic event
- The occurrence and extent of damage to each type of WP (CDSP WP and TAD) for each seismic event
- The occurrence and extent of rupture of the outer barrier for each type of WP (CDSP WP and TAD canister) for each seismic event.

Owing to the complexity of the abstraction and numerous seismic events that could occur in the future of the repository, a Monte Carlo technique is used to calculate expected annual dose. Denote by A_G the set of all sequences of seismic events that could occur in the future of the repository. A member $\mathbf{a} \in A_G$ is a vector, the elements of which describe the aleatory quantities listed above that define each seismic event. For each realization $\mathbf{e}_i$ of epistemically uncertain parameters, the expected annual dose $\bar{D}_{SG}\left(\tau \middle| \mathbf{e}_i\right)$ at time τ for $\tau \leq 1{,}000{,}000\,\text{yr}$ is formally calculated by

$$\bar{D}_{N+G}\left(\tau \middle| \mathbf{e}_i\right) = \sum_{j=1}^{n} D_{N+G}\left(\tau \middle| \mathbf{a}_{ij}, \mathbf{e}_i\right) \Big/ n \qquad \text{(Eq. 6.1.2-24)}$$

where

$\mathbf{a}_{ij}, j = 1, \ldots, n$ is a random sample from A_G generated in consistency with the distributions that describe each of the elements of a member $\mathbf{a}$ of A_G,

$D_{N+G}\left(\tau \middle| \mathbf{a}_{ij}, \mathbf{e}_i\right)$ is the combined dose from seismic events and corrosion failures described by sample element $\mathbf{a}_{ij}$.

The quantity $\bar{D}_{N+G}\left(\tau \middle| \mathbf{e}_i\right)$ is calculated directly by the GoldSim component of the TSPA-LA Model; results of these calculations are used to compute total expected annual dose, as reported in Chapter 8. It is important to note that the quantities $D_N\left(\tau \middle| \mathbf{a}, \mathbf{e}\right)$ and $D_{SG}\left(\tau \middle| \mathbf{a}, \mathbf{e}\right)$ are not computed separately. The expected dose due to nominal corrosion processes, $\bar{D}_N\left(\tau \middle| \mathbf{e}_i\right)$, is computed separately for the purpose of model validation and analysis and is presented in Section 8.3. For 1,000,000 years, the expected dose due to seismic events only (excluding dose due to nominal corrosion processes) is not calculated separately.

The derivation of Equation 6.1.2-24 is discussed in Appendix J Section J.8.4. For a complete description of A_G and the distributions that describe the elements of a member $\mathbf{a}$, see Appendix J Section J.8.2.

Seismic FD Modeling Case—The Seismic FD Modeling Case calculates annual dose from radionuclides released from the EBS due to damage caused by fault displacements. The aleatory uncertainties in this modeling case include:

- Number of fault displacement events
- Time of each fault displacement event
- Number of WPs of each type (CDSP WP or TAD canister) damaged by each fault displacement event
- The location of each WP damaged by each fault displacement event, described in terms of the seepage conditions at each location
- Area opened in the outer barrier of each WP type by each fault displacement event.

The TSPA-LA Model conservatively assumes that each fault displacement event affects a different set of WPs that have not been damaged by prior fault displacement events. When a fault displacement event occurs, the DS above the affected WPs is assumed to be ruptured by the event.

The calculation of expected annual dose for fault displacements does not explicitly treat the aleatory uncertainty for the location of each affected WP. Instead, to save computational resources, expected annual dose is estimated by modeling 100 WPs of each type, placed proportionally into the percolation bins, and within each bin, into dripping or non-dripping locations. Results are calculated for the set of 100 WPs and then scaled to the expected number of packages affected by a fault displacement event.

For each realization $\mathbf{e}_i$ of epistemically uncertain parameters, the expected annual dose $\overline{D}_{FD}(\tau|\mathbf{e}_i)$ at time τ is calculated by

$$\overline{D}_{SF}(\tau|\mathbf{e}_i) = \sum_{r=1}^{2}\left[\overline{N}_r \lambda_{Fr}/100\right]\left[\int_0^{\tau}\left(\int_{A_{\min}}^{A_{\max}} D_{SFr}(\tau|[1,t,100,A_r],\mathbf{e}_i)\, d_{Ar}(A_r)\, dA_r\right) dt\right] \quad \text{(Eq. 6.1.2-25)}$$

where

r indicates each type of WP (CDSP WP or TAD canister)

$\overline{N}_r$ is the expected number of WPs of type r damaged by one fault displacement event

λ_{Fr} is the frequency of fault displacement events that cause damage to WPs of type r

$D_{SFr}\left(\tau\middle|[1,t,100,A_r],\mathbf{e}_i\right)$ is the annual dose resulting from a fault displacement occurring at time t which damages 100 WPs of type r, causing an opening with an area equal to A_r on each WP

$d_{Ar}(A_r)$ is the density function describing the probability of a fault displacement creating an opening of area A_r on WPs of type r.

The quantity $D_{SFr}\left(\tau\middle|[1,t,100,A_r,1],\mathbf{e}_i\right)$ is calculated directly by the GoldSim component of the TSPA-LA Model. The integrals in Equation 6.1.2-25 are approximated using quadrature techniques similar to those employed in Equation 6.1.2-23. For derivation of Equation 6.1.2-25 and the quadrature techniques used in its evaluation, see Appendix J Section J.8.6.

6.1.2.5 Calculation of Expected Annual Dose for the Human Intrusion Modeling Case

The Human Intrusion Modeling Case estimates repository performance in the event that a drilling intrusion intersects the repository. Unlike the other modeling cases, the Human Intrusion Modeling Case is not a component of the calculation of total mean annual dose (Section 6.1.2.2). Rather, the results of the Human Intrusion Modeling Case are compared against the regulations specified in 10 CFR 63.321[DIRS 178394].

Calculation of expected annual dose for the Human Intrusion Modeling Case resembles the calculation in the other modeling cases. The aleatory uncertainty in this modeling case is the type of WP intersected and the location of the drilling intrusion. The time of the intrusion is fixed at 200,000 years (Section 6.7.2), and the Human Intrusion Scenario specifies a single drilling intrusion.

The Human Intrusion Scenario uses a Monte Carlo technique to calculate expected dose. For each realization $\mathbf{e}_i$ of epistemically uncertain parameters, the expected annual dose $\bar{D}_{HI}\left(\tau\middle|\mathbf{e}_i\right)$ at time τ is calculated by

$$\bar{D}_{HI}\left(\tau\middle|\mathbf{e}_i\right)=\sum_{j=1}^{nA} D_{HI}\left(\tau\middle|\left[1,r_j,q_j,SR_j\right],\mathbf{e}_i\right)\Big/nA \qquad \text{(Eq. 6.1.2-26)}$$

where

nA is the number of aleatory realizations

r_j is the type of WP (CDSP WP or TAD canister) intersected in the jth aleatory realization

q_j is the percolation rate in the percolation bin selected in the jth aleatory realization (Section 6.3.2)

SR_j is the SZ source region selected in the jth aleatory realization (Section 6.3.9)

$D_{HI}\left(\tau\left|\left[1, r_j, q_j, SR_j\right], \mathbf{e}_i\right.\right)$ is the annual dose resulting at time τ from a human intrusion that intersects 1 WP of type r_j that experiences percolation rate q_j and intersects the SZ in source region SR_j.

The quantity $D_{HI}\left(\tau\left|\left[1, r_j, q_j, SR_j\right], \mathbf{e}_i\right.\right)$ is calculated directly by the GoldSim component of the TSPA-LA Model.

Table 6.1.2-1. Effect of Combinations of Scenario Classes on Total Mean Annual Dose

Preceding Event	Later Disruptive Event			
	Igneous Intrusion	**Volcanic Eruption**	**Seismic Ground Motion**	**Seismic Fault Displacement**
Early Failure Waste Package	Very minor (~0.02%) overcounting of inventory. Negligible effect on total mean annual dose.	Overcounting of inventory in WPs affected by the eruption event. Negligible effect on total mean annual dose.	Very minor (~0.02%) overcounting of inventory. Negligible effect on total mean annual dose.	Overcounting of inventory in WPs affected by the fault displacement event. Negligible effect on total mean annual dose.
Early Failure Drip Shield	Very minor (~0.01%) overcounting of inventory. Negligible effect on total mean annual dose.	Overcounting of inventory in WPs affected by the eruption event. Negligible effect on total mean annual dose.	Very minor (~0.01%) overcounting of inventory. Negligible effect on total mean annual dose.	Overcounting of inventory in WPs affected by the fault displacement event. Negligible effect on total mean annual dose.
Igneous Intrusion	Included in calculation of Mean Dose for the Igneous Scenario Class $\overline{\overline{D}}_I(\tau)$.	Conservative overstatement of the consequences of the igneous eruption event. Negligible effect on total mean annual dose.	Conservative overstatement of the consequences of the seismic ground motion event. Minor effect on total mean annual dose.	Conservative overstatement of the consequences of the seismic fault displacement event. Negligible effect on total mean annual dose.
Volcanic Eruption	Very minor (~0.03%) overcounting of inventory. Negligible effect on total mean annual dose.	Included in calculation of for the Igneous Scenario Class $\overline{\overline{D}}_I(\tau)$.	Very minor (~0.03%) overcounting of inventory. Negligible effect on total mean annual dose.	Very minor (~0.03%) overcounting of inventory in WPs affected by the fault displacement event. Negligible effect on total mean annual dose.
Seismic Ground Motion	Conservative overcounting of inventory and consequences of an intrusion. Minor effect on total mean annual dose.	Overcounting of inventory in WPs affected by the eruption event. Negligible effect on total mean annual dose.	Included in calculation of mean dose for the Seismic Scenario Class $\overline{\overline{D}}_S(\tau)$.	Overcounting of inventory in WPs affected by the fault displacement event. Negligible effect on total mean annual dose.
Seismic Fault Displacement	Very minor (~2 %) overcounting of inventory. Negligible effect on total mean annual dose.	Overcounting of inventory in WPs affected by the eruption event. Negligible effect on total mean annual dose.	Very minor (~2 %) overcounting of inventory. Negligible effect on total mean annual dose.	Included in calculation of mean dose for the Seismic Scenario Class $\overline{\overline{D}}_S(\tau)$.

INTENTIONALLY LEFT BLANK

6.1.3 Treatment of Uncertainty in the TSPA-LA Model

Sources of Uncertainty—Uncertainties are inherent in projections of the geologic and environmental conditions surrounding the Yucca Mountain repository into the future. Assessment of total system performance over this period must take these uncertainties into account. In addition, the discussion of the quantitative estimates of this performance (e.g., estimates of mean annual dose) will include information regarding the impacts of these uncertainties on those estimates (e.g., uncertainty in the estimate of mean annual dose).

The TSPA-LA Model accounts for uncertainty in two categories: aleatory uncertainty and epistemic uncertainty. Aleatory uncertainty arises from inherent uncertainty about the occurrence of future events that may affect the repository and the effect of these events on repository performance. Because aleatory uncertainty cannot be reduced by the acquisition of additional data or knowledge, this kind of uncertainty is also referred to as irreducible uncertainty. Examples of aleatory uncertainty considered in the TSPA-LA Model include the number and location of early failed WPs, time and amplitude of seismic ground motion events, and occurrence of igneous events. Aleatory uncertainties included in the TSPA-LA Model are listed in Table 6.1.3-1.

The second category is referred to here as epistemic uncertainty. Epistemic uncertainty stems from a lack of knowledge about a quantity that is believed to have a fixed (or deterministic) value. Sources of epistemic uncertainties include incomplete data, measurement errors, and estimates based upon expert judgment. Unlike aleatory uncertainty, epistemic uncertainty is potentially reducible with additional data and knowledge. In the TSPA-LA Model, epistemic quantities are generally inputs to specific submodels, with the submodels having been developed to use single values for these quantities. A particular epistemic quantity can be a parameter for a probability distribution or density function (e.g., adsorption coefficients for transport of radionuclides in the UZ), a field of values selected from alternative sets (e.g., the flow field in the UZ), or a factor added to a parameter to represent the uncertainty (e.g., the uncertainty term added to the model for actinide solubilities). Examples of epistemic uncertainties included in the TSPA-LA Model are indicated in Table 6.1.3-2.

During development of the TSPA-LA Model, a number of technical reviews were conducted to ensure consistent and appropriate treatment of uncertainty and variability for parameters identified as key uncertain inputs to the model (Section 7.5). These technical reviews focused on: (1) confirming that the major sources of uncertainty and/or variability were appropriately represented, (2) verifying that probability distributions were derived using sound statistical methods and interpretations, and (3) ensuring model parameter representations (i.e., probability distributions) are reasonable and defensible, as opposed to depicting extreme variations that could potentially introduce risk dilution (i.e., wider distribution and lower peak mean annual dose).

Probabilistic Framework for Implementing the TSPA-LA Model—Both aleatory and epistemic uncertainties are quantified using probability distributions. However, in the TSPA-LA Model, the numerical treatment of the two categories of uncertainty is different. Because the aleatory uncertainties vary between modeling cases, treatment of aleatory uncertainties also

varies among modeling cases. The subsections of Section 6.1.2 describe the treatment of aleatory uncertainty for each modeling case of the TSPA-LA Model.

In general, epistemic uncertainties are addressed by means of a Monte Carlo technique employing an LHS of the epistemically uncertain quantities. The same LHS is used in each of the modeling cases. This method allows a thorough mapping of the uncertainty in model inputs (parameters) to the corresponding uncertainty in model output (estimates of performance) and also allows results from each modeling case to be combined into an estimate of total mean annual dose. Uncertainty in the model outcome is quantified via multiple model realizations, using LHS to select values for uncertain parameters. The benefits of probabilistic modeling include: (1) obtaining a representative range of possible outcomes (and the likelihood of each outcome) to quantify predictive uncertainty, and (2) analyzing the relationship between the uncertain inputs and uncertain outputs to provide insight into the effect of the uncertainties.

Propagation of Uncertainty—The Monte Carlo analysis for the TSPA-LA Model involves the following four steps (see Appendix J for more detail of each step):

- **Select Imprecisely Known Input Parameters to be Sampled**—The TSPA-LA Model includes several thousand parameters, several hundred of which are treated as uncertain. The magnitude of uncertainty, type of probability distribution used to characterize the uncertainty, and guidance on sampling values for the parameters are developed in the individual process models or abstractions or both, as documented in their respective model reports.

- **Construct Probability Distribution Functions for Each Parameter**—The probabilistic framework employed in Monte Carlo simulations requires that the uncertainty in the TSPA-LA Model inputs be quantified using probability distributions. Examples of such representations can be found in the descriptions of various TSPA-LA submodels in Section 6.3. These distributions are specified in terms of either empirical distribution functions or coefficients of parametric distributions.

- **Generate a Sample Set by Selecting a Parameter Value from Each Distribution**—The next step in the Monte Carlo process requires the generation of a number of parameter distributions that are sampled in the course of an analysis. The TSPA-LA Model uses LHS, where the range of each parameter is divided into intervals of equal probability, and a value is selected at random within each interval. LHS helps achieve a more complete coverage of the range of values of an uncertain parameter than unstratified sampling.

- **Calculate Outcomes for the Sample Set and Aggregate Results for All Samples**—In this step of the Monte Carlo methodology, the modeling case for the scenario class of interest is evaluated for each of the randomly generated parameter sets. This is an operation consisting of multiple model realizations where the outcome (i.e., annual dose as a function of time) is computed for each sampled parameter set. The aggregation of all results produces distributions of system performance measures for the modeling case. After all of the required model realizations have been completed, the overall uncertainty

in the model outcome can be characterized by probability distributions of the system performance measures.

Correlation Methods—The TSPA-LA Model employs several techniques to account for correlations between uncertain input parameters. In some cases, correlations among variables are addressed in the development of the process models and implicitly accounted for in the TSPA-LA Model abstractions. In other cases, correlations among variables are explicitly addressed within the TSPA-LA Model. The GoldSim software provides functionality for correlating pairs of variables when the correlation between each pair is 100 percent. Because GoldSim's stochastic functions only allow correlation between a single pair, Cholesky factorization (Press et al. 1992 [DIRS 103316], Section 2.9) is used to induce the desired rank correlation in sets of three or more random variables while maintaining their marginal distributions. This method is applied to normally distributed variables by using a linear combination of independent normal variables to produce a multivariate normal vector with the correct correlation structure (Iman and Conover 1982 [DIRS 124158], pp. 313 to 320; Anderson 1984 [DIRS 169668], Section 2.4). The random vector is created using a linear combination of independent standard normal random variables. Multiplying this random vector by the lower triangular matrix resulting from the Cholesky factorization of the covariance matrix, results in a vector from a multivariate-normal distribution with mean vector zero and honors the covariance matrix. By extending this method to nonnormal distributions, the marginal distributions are used in a way such that the rank correlation structure is preserved in the transform.

INTENTIONALLY LEFT BLANK

Table 6.1.3-1. Aleatory Uncertainties in the TSPA-LA Model

Scenario Class	Aleatory Uncertainties
Nominal (Section 6.3)	Time and location of general corrosion failures for each type of waste package
Early Failure (Section 6.4)	Number of early failed waste packages
	Type and location of each early failed waste package
	Number of early failed drip shields
	Type of waste package under each early failed drip shield
	Location of each early failed drip shield
Igneous (Section 6.5)	Number of igneous events
	Time of each igneous event
	Number of waste packages affected by eruption
	Eruptive power, height, and duration of each eruption
	Wind speed and wind direction during eruption
Seismic (Section 6.6)	Number of seismic events
	Type of each seismic event: ground motion or fault displacement
	Time of each seismic event
	Peak ground velocity of each ground motion seismic event
	Occurrence and extent of damage to each type of waste package caused by ground motion
	Occurrence and extent of rupture or puncture of each type of waste package caused by ground motion
	Volume of rockfall caused by ground motion for lithophysal and non-lithophysal zones
	Occurrence of failure of drip shield framework caused by ground motion and accumulated rockfall
	Occurrence of failure of drip shield plates caused by ground motion and accumulated rockfall
	Number of waste packages of each type affected by fault displacement
	Failed area on each type of waste package caused by fault displacement

Table 6.1.3-2. Examples of Epistemic Uncertainties in the TSPA-LA Model

Model Component	Epistemic Uncertainties
Unsaturated Zone Flow	Infiltration Submodel (Section 6.3.1): • Infiltration scenario Unsaturated Zone Flow Fields Abstraction (Section 6.3.1): • Hydrologic properties • Ratio of porosity to fracture aperture Drift Seepage Submodel (Section 6.3.3.1): • Permeability and capillary strength parameters • Factor accounting for local heterogeneity in flow-focusing and permeability Drift Wall Condensation Submodel (Section 6.3.3.2): • Correlation parameters for abstraction for fraction of waste package locations with dripping condensation and condensation water flow rate
EBS Environment	EBS Thermal-Hydrologic Environment (Section 6.3.2): • Thermal conductivity of surrounding rock EBS Chemical Environment Submodel (Section 6.3.4): • Ambient waste composition • pCO_2, ionic strength, and pH of in-drift seepage water • Water-rock interaction for seepage water
Waste Package and Drip Shield Degradation	Waste Package and Drip Shield Degradation Submodel (Section 6.3.5.1): • Corrosion rates of Alloy 22 and drip shield components • Temperature and relative humidity at drip shield and waste package • pH, NO_3^-, and Cl^- of crown seepage
Waste Form Degradation and Mobilization	Waste Form Degradation and Mobilization (Section 6.3.7): • Radionuclide inventory for CSNF, DSNF, and HLW • Temperature and relative humidity at waste package • pCO_2, ionic strength, and pH in waste package • Waste form degradation rates • Radionuclide solubility • Colloid concentrations • Mass of Pu and Am embedded in waste form colloids from HLW glass • Forward rate constant for kinetic sorption of radionuclides onto iron oxyhydroxide surfaces • Coefficient for sorption onto colloids for each radionuclide

Table 6.1.3-2. Examples of Epistemic Uncertainties in the TSPA-LA Model (Continued)

Model Component	Epistemic Uncertainties
EBS Flow and Transport	EBS Flow Submodel (Section 6.3.6): • Drip shield and waste package flux splitting factors • Representative subregion typical liquid saturation in invert • Representative subregion typical imbibition flux in invert • Representative subregion typical liquid saturation and flux through the EBS-UZ interface EBS Transport Submodel (Section 6.3.8): • Steel corrosion rates • Specific surface area of steel corrosion products • Adsorption isotherm for water vapor sorption onto degraded waste form and onto steel corrosion products • Density of radionuclide sorption sites in steel corrosion products
Unsaturated Zone Transport	Unsaturated Zone Transport Submodel (Section 6.3.9): • • Fracture aperture • Active Fracture Model gamma parameter • Tortuosity • Rock Matrix K_ds for each radionuclide • Coefficient for sorption onto colloids for each radionuclide • Colloid retardation factors
Saturated Zone Flow and Transport	Saturated Zone Flow and Transport Submodel (Section 6.3.10): • Groundwater specific discharge multiplier • Flowing interval spacing in volcanic units • Colloid retardation in alluvium
Biosphere	Biosphere Submodel (Section 6.3.11): • Biosphere dose conversion factors for groundwater modeling cases • Inhalation biosphere dose conversion factors for Volcanic Eruption Modeling Case
Events	DS Early Failure Submodel (Section 6.4.1): • Probability of early failure for a single drip shield WP Early Failure Submodel (Section 6.4.2) • Probability of early failure for a single waste package Igneous Activity, Igneous Intrusion Submodel (Section 6.5.1): • Igneous event probability (event frequency) Igneous Activity, Volcanic Eruption Submodel (Section 6.5.2): • Igneous event probability (event frequency) • Ash and waste particle size • Radionuclide diffusivity in soils Seismic Activity, GM Damage Submodel (Section 6.6.1.1): • Residual stress threshold for Alloy 22

NOTE: Additional information concerning uncertainty and the distribution of TSPA-LA Model parameters and parameter values can be found in the GoldSim model file.

INTENTIONALLY LEFT BLANK

6.1.4 TSPA-LA Model Structure and Design

This section provides an overview of how model components and submodels are connected within the TSPA-LA Model and how information flows between them. The primary focus of this section is on the description of the TSPA-LA Model for the Nominal Scenario Class. The Nominal Scenario Class reflects the initial starting conditions expected for the proposed repository system and therefore is a natural starting point for presenting the model structure and design. A summary of the TSPA-LA Model structure and information flow for the Early Failure, Igneous, and Seismic Scenario Classes and the Human Intrusion Scenario is presented following the Nominal Scenario Class description.

For all scenario classes, the separation of aleatory and epistemic uncertainty with respect to parameter values was maintained as described in Section 6.1.3. The structure of the model components and submodel reflect this requirement. Connections between the model components and submodels are presented, as well as inputs differentiated between aleatory and epistemic when applicable.

The TSPA-LA Model components and submodels for the following process areas are briefly discussed here and in more detail in Section 6.3:

- Mountain-Scale UZ Flow
- EBS Thermal-Hydrologic (TH) Environment
- Drift-Scale UZ Flow
- EBS Chemical Environment
- WP and DS Degradation
- EBS Flow
- Waste Form Degradation and Mobilization
- EBS Transport
- UZ Transport
- SZ Flow and Transport
- Biosphere.

This list corresponds to model components and submodels previously presented on Figure 6-1 and in Table 6-1. This list is a combination of model components and submodels that represent the order in which these TSPA-LA Model components are discussed in Section 6.3. The intent here is to list the models in the order that information flows within the TSPA-LA Model. Therefore, it is necessary to list the submodels of the EBS Environment and EBS Flow and Transport Model Components separately. For example, as will be described in the next section, the EBS Flow Submodel provides the Waste Form Degradation and Mobilization Model Component with the flow rate of water through a failed WP as a function of time. This information is used by the Waste Form Degradation and Mobilization Model Component to calculate waste form degradation and radionuclide concentrations in WPs. This information in turn is used as input to the EBS Radionuclide Transport Submodel that calculates radionuclide transport through the WP and EBS. Thus, following the flow of information in Section 6.3 requires an expansion of the eight principal model components (and their respective submodels) compared to what is displayed on Figure 6-1. Table 6-1 maps the outline of Section 6.3 to the

eight principal model components depicted on Figure 6-1. The general philosophy used in this document is that the TSPA-LA Model is composed of eight principal model component areas (UZ, SZ, Biosphere, etc.) that represent a part of the natural system or EBS. Each model component area is composed of one or more submodels. A submodel can be either a detailed process model developed, tested, and validated in a supporting document, a simple or detailed abstraction of the process model, an abstraction of the process model results, or direct process model input (e.g., a look-up table or distribution of values). These process models and/or abstractions are defined within the supporting documents. They are developed for use within the TSPA-LA Model to represent the EBS or a natural system process.

Figure 6.1.4-1 schematically depicts the flow of information between the TSPA-LA Model components and submodels for the Nominal Scenario Class. A more detailed representation of information flow within the TSPA-LA Model can be found in Appendix G. TSPA-LA Model components implemented outside of the GoldSim model file are shown outside of the dashed border on Figure 6.1.4-1. The abstraction information provided by external models is input to the TSPA-LA Model GoldSim model file. Information transferred via internally generated outputs that are used as downstream inputs between model components and submodels within the TSPA-LA Model GoldSim model file are shown within the dashed border on Figure 6.1.4-1. The primary output from each submodel and abstraction is denoted by a numerical index and described in the following sections.

6.1.4.1 Mountain-Scale Unsaturated Zone Flow

Mountain-scale UZ flow in the TSPA-LA Model refers to the percolation of groundwater through the unsaturated rocks between the land surface and the water table and includes the future climates, infiltration changes, and site-scale UZ flow. The conceptual model and TSPA-LA Model implementation for these three processes are discussed in detail in Section 6.3.1 and are briefly described in this section. As given in *Future Climate Analysis* (BSC 2004 [DIRS 170002], Table 6-1) and appended by governing regulations, four climates are used in the TSPA-LA Model: (1) present-day climate for the first 550 years after repository closure; 600 years after emplacement, (2) monsoon climate for the period 550 to 1,950 years after repository closure, (3) glacial-transition climate for the period 1,950 to 10,000 years after repository closure, and (4) post-10,000-year climate for the period 10,000 to the modeling time frame of 1,000,000 years after repository closure (Section 1, Governing Regulations). For the present-day, monsoon, and glacial transition climates, a distribution of net infiltration is estimated by the Infiltration Model (SNL 2007 [DIRS 182145]). From this distribution, four infiltration scenarios are selected and provided to the Site-Scale UZ Flow Process Model as the upper boundary condition. These infiltration scenarios correspond to the 10th, 30th, 50th and 90th percentiles of the distribution of spatially-averaged infiltration. For the post-10,000-year period, proposed 10 CFR 63.342(c)(2) [DIRS 178394] specifies that the average percolation flux through the repository follows a log-uniform probability distribution from 13 to 64 mm/yr. Four infiltration rates representing the 31st percentile, 70th percentile, 86th percentile, and 97th percentile values of the distribution are used as target values for the four post-10,000-year period flow fields. The 12 infiltration maps generated for the present-day, monsoon, and glacial transition climates are used as a basis for the spatial variability for the post-10,000-year climate (SNL 2007 [DIRS 184614], Section 6.1.4). For the 12 infiltration maps, the average infiltration through the repository footprint was calculated. The four infiltration maps with average infiltration rates that most closely matched

the chosen average target infiltration rates were used as a basis for generating the flow-fields. The closest infiltration rate maps for the post-10,000-year climate determined by the analysis were the present-day 90th percentile, the 50th percentile glacial transition, the 90th percentile glacial transition, and the 90th percentile monsoon maps. The four infiltration maps were then scaled so that the average infiltration through the repository footprint would match the target values. The Site-Scale UZ Flow Process Model simulates three-dimensional, dual-permeability, steady-state flow conditions, and generates a total of 16 three-dimensional flow fields: 1) four flow fields for each of the 10th percentile, 30th percentile, 50th percentile, and 90th percentile infiltration boundary-condition scenarios, corresponding to the present-day, monsoon, and glacial transition climates within each infiltration scenario, and 2) four flow fields based on the scaled versions of the present-day 90th percentile, the 50th percentile glacial transition, the 90th percentile glacial transition, and the 90th percentile monsoon maps, corresponding to the post-10,000-year period.

Four UZ hydrologic property sets and 16 flow fields generated by the Site-Scale UZ Flow Process Model are used by the Multiscale Thermohydrologic Process Model (MSTHM) (SNL 2007 [DIRS 181383]) for the development of EBS environment TH conditions and are accessed directly by the UZ Transport Submodel (SNL 2008 [DIRS 184748], Sections 6 and 8). In both internal and external applications using the flow fields, the four different infiltration scenarios represent epistemic uncertainty in UZ flow conditions. These scenarios are sampled in the TSPA-LA Model once per realization based on the probability-weighting factors, excluding the contingency area, of 0.62, 0.16, 0.16, and 0.06 for the 10th percentile, 30th percentile, 50th percentile, and 90th percentile infiltration scenarios, respectively. An infiltration index corresponding to the sampled infiltration scenario is applied in the TSPA-LA Model to correlate the sampled infiltration scenario to downstream submodels that are infiltration dependent. The weighting factors are derived from *UZ Flow Models and Submodels* (SNL 2007 [DIRS 184614], Table 6.8-1). Climate change is implemented within the TSPA-LA Model UZ calculations by assuming a series of step changes in boundary conditions for UZ flow and utilizing the flow field corresponding to the selected infiltration scenario and climate. This implementation is based on the assumption that changes in flow fields due to climate apply instantaneously in the MSTHM Process Model and UZ Transport Model Component (see assumption in Section 5.1.1).

Figure 6.1.4-1 shows that 16 flow fields and UZ hydrologic properties generated by the Site-Scale UZ Flow Process Model are also used by the MSTHM Process Model. These flow fields are used to specify the percolation flux, consisting of liquid flux in fracture and matrix continua at the base of the PTn above the repository horizon, as a boundary condition. In addition, these data are used within the TSPA-LA Model for the simulation of the transport of radionuclides in the UZ Transport Submodel, as shown on Figure 6.1.4-1. The description for Output #1, discussed below, pertains to arrow #1 on Figure 6.1.4-1.

Output 1—For each infiltration scenario and climate (Section 6.3.1), the following are outputs from the Site-Scale UZ Flow Process Model (SNL 2007 [DIRS 184614], Section 6.6.3).

The following outputs are passed to the MSTHM Process Model (Section 6.3.2):

- The three-dimensional numerical grid
- The percolation flux at the base of PTn unit above each subdomain location for each infiltration condition and climate period
- UZ hydrologic properties including matrix and fracture properties, such as material type, permeability, porosity, and residual saturation, for the different infiltration property sets, and temperature and gas phase pressures at the lower and/or upper boundary.

The following outputs are passed to the UZ Transport Model Component (Section 6.3.9) of the TSPA-LA Model:

- The three-dimensional numerical grid representing the model domain
- UZ hydrologic properties for each of the four infiltration scenarios (Section 6.3.1) including:
  - The active fracture parameter for each computational cell in the numerical grid
  - Three three-dimensional steady-state flow fields including:
    - Fracture continuum liquid flux
    - Matrix continuum liquid flux
    - Water table levels
    - Fracture continuum liquid saturation
    - Matrix continuum liquid saturation
    - Liquid flux between matrix and fracture continua.

6.1.4.2 Engineered Barrier System Thermal-Hydrologic Environment

The EBS TH Environment Submodel implements the MSTHM Abstraction in the TSPA-LA Model. The MSTHM Abstraction is provided by the MSTHM Process Model, as shown on Figure 6.1.4-1. The MSTHM Abstraction is described in detail in *Multiscale Thermohydrologic Model* (SNL 2007 [DIRS 181383], Section 6.2[a] and Appendix III[a]). The conceptual model and TSPA-LA Model implementation for the EBS TH environment are discussed in detail in Section 6.3.2. The following paragraphs summarize its application for the development of the EBS TH Abstraction and how this abstraction is used in the TSPA-LA Model.

The MSTHM Process Model subdivides the repository footprint into 3,264 equal-area subdomains. Each of the 3,264 MSTHM Process Model subdomains is equally sized in area, 81 m in width by 20 m in length, where the length component is along the waste emplaced drift axis (SNL 2007 [DIRS 181383], Section 6.2.12.1[a]). The MSTHM Process Model performs simulations for the four percolation flux cases and three host-rock thermal conductivity cases (low, mean and high). The four percolation flux cases result from the application of four different infiltration scenarios, termed 10th-, 30th-, 50th-, and 90th-percentile

infiltration scenarios, in the TSPA-LA Model. For the possible combinations of percolation flux case and thermal conductivity case, the MSTHM Process Model calculates time-dependent TH variables, temperature, and relative humidity, for six representative commercial spent nuclear fuel (CSNF) WPs and two representative CDSP WPs, and DS pairs at each subdomain location. In addition, the MSTHM Process Model calculates time-dependent values for average drift-wall temperature, duration of boiling at the drift wall, invert temperature, invert saturation, and invert liquid flux at each of the 3,264 subdomain locations. Before any information is passed to downstream submodels, three sets of analyses are performed. First, the 10th percentile infiltration scenario, glacial-transition values of percolation flux at the base of the PTn at each of the 3,264 MSTHM Process Model subdomain locations are used to group each of the locations into one of five repository percolation subregion quantile ranges of 0.0 to 0.05, 0.05 to 0.3, 0.3 to 0.7, 0.7 to 0.95, and 0.95 to 1.0 (SNL 2007 [DIRS 181383], Section 6.2.12.1[a]). The five repository percolation subregions are shown on Figure 6.1.4-2. In the second analysis, the MSTHM Process Model subdomain locations and associated TH information are designated as belonging to repository percolation subregions one through five, respectively. The third analysis involves determining a single representative CSNF WP and a single representative CDSP WP for each percolation subregion. Representative WPs are selected for each percolation subregion for the purposes of reducing the computational burden of the TSPA-LA Model calculations and adequately representing the spatial variability in repository conditions that control radionuclide release from the repository (Section 7.3.3). The determination of the repository subregions and the selection of the representative WPs are described in Section 6.3.2. The grouping of the repository percolation subregions and the number of subdomain locations in each percolation subregion are summarized in Table 6.1.4-1.

The MSTHM Abstraction produces two sets of outputs that are indexed by fuel type and percolation subregion. Each set contains output for each combination of four infiltration scenarios and three host-rock thermal conductivity conditions. One set contains the comprehensive MSTHM Process Model output (e.g., DS and WP temperature and relative humidity, drift-wall temperature, percolation flux, and fraction of lithophysal unit) at each subdomain location in each percolation subregion for each fuel type. The WP and DS Degradation Model Component and the Drift Seepage Submodel use this information to account for spatial variability in the WP groups. The other set only contains the DS and WP temperature and relative humidity; the drift-wall temperature; and the invert temperature, relative humidity, liquid flux, and saturation for the representative CSNF WP and CDSP WP in each percolation subregion. The data in these two sets are compiled in text files that give parameter values at discrete timesteps. The representative WP data in the text files are read into look-up tables at run time to provide time-dependent parameter values to other submodels within the TSPA-LA Model. The data in representative WP file set are accessed by the EBS TH Environment Submodel to provide representative TH responses for each subregion. These TH responses serve as input to the Drift Wall Condensation Submodel, the EBS Chemical Environment Submodel, the EBS Flow Submodel, the Waste Form Degradation and Mobilization Model Component, and the EBS Transport Submodel. For ease of presentation, the WP and DS Degradation Model Component and the Waste Form Degradation and Mobilization Model Component are shown on Figure 6.1.4-1 rather than the individual submodels that comprise these model components (Sections 6.3.5 and 6.3.7, respectively).

The MSTHM Process Model accounts for the impact of percolation-flux and host-rock thermal conductivity uncertainty on the TH environment conditions, using simulations conducted for the 10th, 30th, 50th, and 90th percentiles of percolation flux with the mean host-rock thermal conductivity values for the host-rock units. Three additional cases are used in conjunction with the four mean host-rock thermal conductivity cases to capture the impact of host-rock thermal conductivity uncertainty: 10th percentile percolation flux with low- and high-thermal conductivity, and 90th percentile percolation flux with high-thermal conductivity. The TH data sets associated with the remaining five of the 12 possible combinations of percolation flux and host-rock thermal conductivity are provided to the TSPA-LA Model as surrogates from the previously identified seven cases. These five cases use their associated values of percolation flux, but refer to one of the other seven cases for the TH data (SNL 2007 [DIRS 181383], Section 6.3.15[a]). Within each realization of the TSPA-LA Model, the infiltration scenario and host-rock thermal conductivity condition are sampled. There are four choices for the infiltration scenario, resulting from the application of four infiltration fields. There are three host-rock thermal conductivity conditions, low, mean and high. These two distributions represent epistemic uncertainty and are sampled once per realization. The resulting values for these two parameters determine which of the 12 TH data sets are applied in downstream calculations of the TSPA-LA Model.

Output 2—The following outputs are passed from the MSTHM Process Model through the MSTHM Abstraction to the EBS TH Environment Submodel (Section 6.3.2):

- Definition of the five repository percolation subregions
- Percolation flux at the base of the PTn
- In-drift TH environment (e.g., DS and WP temperature and relative humidity, drift-wall temperature for each fuel type, CSNF, and CDSP WP).

Output 3—The following outputs are passed from the EBS TH Environment Submodel (Section 6.3.2) to the Drift Seepage and Drift Wall Condensation Submodel (Section 6.3.3):

- For each of the five percolation subregions (Section 6.3.2):
  - The percolation flux at the base of the PTn for each infiltration scenario and climate at each MSTHM subdomain location (Drift Seepage Submodel)
  - The average percolation flux at the base of the PTn for each infiltration scenario and climate (Drift Wall Condensation Submodel)
  - The drift-wall temperature surrounding each of the eight WPs (two CDSP WPs and six CSNF WPs) at each subdomain location (Drift Seepage Submodel)
  - Time-dependent temperature for the drift wall for the representative CDSP WP and the representative CSNF WP (Drift Wall Condensation Submodel)
  - The fraction of lithophysal unit at each location.

Output 4—The following outputs are passed from the EBS TH Environment Submodel (Section 6.3.2) to the WP and DS Degradation Model Components (Section 6.3.5), which then calculates WP and DS failures, including localized corrosion WP failures:

- For each of the five percolation subregions:
  - Time-dependent WP surface temperature on each of the eight WPs (two CDSP WPs and six CSNF WPs) at each subdomain location
  - Time-dependent WP surface relative humidity on each of the eight WPs (two CDSP WPs and six CSNF WPs) at each subdomain location.

Output 5—The following outputs are passed from the EBS TH Environment Submodel (Section 6.3.2) to the EBS Chemical Environment Submodel (Section 6.3.4):

- For each of the five percolation subregions (Section 6.3.2):
  - Time-dependent temperature for the invert for the representative CDSP WP and the representative CSNF WP
  - Time-dependent relative humidity for the invert for the representative CDSP WP and the representative CSNF WP
  - Time-dependent temperature for the drift wall for the representative CDSP WP and the representative CSNF WP
  - Averaged glacial-transition percolation rate for each infiltration scenario for each percolation subregion.
- For the Localized Corrosion Initiation Analysis (Section 6.3.4.3.2):
  - Time-dependent WP surface temperature on each of the eight WPs (two CDSP WPs and six CSNF WPs) at each subdomain location in each percolation subregion
  - Time-dependent WP surface relative humidity on each of the eight WPs (two CDSP WPs and six CSNF WPs) at each subdomain location in each percolation subregion.

Output 6—The following outputs are passed from the EBS TH Environment Submodel (Section 6.3.2) to the EBS Flow Submodel (Section 6.3.6):

- For each of the five percolation subregions (Section 6.3.2):
  - Time-dependent WP surface temperature for the representative CDSP WP and the representative CSNF WP
  - Time-dependent temperature in the invert for the representative CDSP WP and the representative CSNF WP

- Time-dependent liquid flux for the representative CDSP WP and the representative CSNF WP.

Output 7—The following outputs are passed from the EBS TH Environment Submodel (Section 6.3.2) to the Waste Form Degradation and Mobilization Model Component (Section 6.3.7):

- For each of the five percolation subregions (Section 6.3.2):
  - Time-dependent WP surface temperature for the representative CDSP WP and the representative CSNF WP
  - Time-dependent WP surface relative humidity for the representative CDSP WP and the representative CSNF WP.

Output 8—The following outputs are passed from the EBS TH Environment Submodel (Section 6.3.2) to the EBS Transport Submodel (Section 6.3.8):

- For each of the five percolation subregions (see Section 6.3.2):
  - Time-dependent WP surface temperature for the representative CDSP WP and the representative CSNF WP
  - Time-dependent WP surface relative humidity for the representative CDSP WP and the representative CSNF WP
  - Time-dependent temperature in the invert for the representative CDSP WP and the representative CSNF WP
  - Time-dependent saturation in the invert for the representative CDSP WP and the representative CSNF WP.

The TH conditions for each representative WP are identical for dripping and non-dripping environments.

6.1.4.3 Drift Seepage and Drift Wall Condensation

This section describes the implementation of the Drift Seepage and Drift Wall Condensation Submodels. The simulated drift-seepage flux is calculated within the TSPA-LA Model for both ambient and waste-heat-generated thermal periods using responses surfaces abstracted over a heterogeneous fracture-permeability field for a range of representative percolation flux rates, and for ranges of fracture permeability log(k) and fracture capillary-strength parameter ($1/\alpha$) values (SNL 2007 [DIRS 181244]). The conceptual model and TSPA-LA Model implementation for drift seepage are discussed in detail in Section 6.3.3.1. The drift-seepage analysis performed external to the TSPA-LA Model provides two response surfaces: (1) mean seepage flux into the drift as a function of long-term percolation flux, k, and $1/\alpha$, and (2) the standard deviation (SD) of seepage flux into the drift as a function of long-term percolation flux, log(k), and $1/\alpha$. Figure 6.1.4-1 shows that drift-scale seepage is modeled externally in the Seepage Process

Model (BSC 2004 [DIRS 167652]). For the TSPA-LA Model, the results are then abstracted as described in *Abstraction of Drift Seepage* (SNL 2007 [DIRS 181244]), and imported into the TSPA-LA Model before performing the PA simulations.

Abstraction of Drift Seepage (SNL 2007 [DIRS 181244], Section 6.7.1.1) also provides spatial variability distributions for both k and 1/α and the flow focusing factor (f_{ff}) for the percolation flux, as well as uncertainty (epistemic) distributions for Δlog(k) and Δ1/α. The TSPA-LA Model samples these uncertainty distributions once per realization to account for parameter uncertainty in both k and 1/α. Using values of percolation flux at the base of the PTn, provided by the MSTHM Abstraction, seepage rates are calculated for each of the 3,264 MSTHM Process Model's subdomain locations. The spatial variability distributions are evaluated for log(k), 1/α, and f_{ff} at each location. The log(k) and 1/α values are adjusted for uncertainty by adding the values of Δlog(k) and Δ1/α, sampled from the uncertainty distributions for each realization. The adjusted log(k) and 1/α values, along with the percolation flux that is adjusted for flow focusing, are used to evaluate the response functions for ambient mean seepage and the SD of ambient seepage. These two quantities are used to form a uniform distribution for ambient seepage that ranges between mean seepage -1.7321 SD and mean seepage + 1.7321 SD (SNL 2007 [DIRS 181244], Section 6.5.1.3). This distribution is sampled to yield the ambient seepage for each WP at each location.

The thermal seepage condition at each WP location (e.g., no seepage when the drift-wall temperature is greater than 100°C, otherwise ambient seepage) is then used to appropriately modify the calculated ambient seepage. This results in a calculated drift-seepage flux for every WP at every subdomain location for the given infiltration scenario and climate. An average seepage flow rate is calculated for the WPs that have seepage, along with the fraction of WPs that have seepage, for each percolation subregion. The details of the seepage submodel calculations for TSPA-LA are discussed in Section 6.3.3.1, and seepage impacts on EBS flow are discussed in Section 6.3.6.

Process modeling (SNL 2007 [DIRS 181648], Section 6.3.7.2.2) has shown that there is a potential for water vapor in the drift atmosphere to condense on cooler portions of the drift walls. Condensation on drift walls and its effects on EBS flow are modeled in the TSPA-LA. The conceptual model and TSPA-LA Model implementation for drift wall condensation are discussed in detail in Section 6.3.3.1. The rate of condensation at a location on the drift wall depends on the availability of water at that location. The rate at which water is available generally increases with an increase in percolation flux, increasing water transport through the invert, and decreasing axial dispersion within the drifts (SNL 2007 [DIRS 181648], Section 8.3.1.1). The TSPA-LA Model's Drift Wall Condensation Submodel calculates the fraction of DS/WP pairs dripped on by drift-wall condensate and the average rate of condensation in each percolation subregion for each WP type. These quantities are determined from two correlations: (1) a correlation for average condensation rate versus average percolation flux, and (2) a correlation for the fraction of DS and WP pairs dripped on by drift-wall condensate versus average percolation flux. The average percolation flux for each of the five repository percolation subregions modeled in the TSPA-LA Model is calculated by averaging the percolation fluxes at the base of the PTn at each MSTHM subdomain location in that percolation subregion using the comprehensive MSTHM Abstraction data (Section 6.3.2). The impact of DS ventilation and axial dispersion uncertainty on condensation are accounted for by selecting between four cases with an equal

probability: (1) ventilated DS-low axial dispersion, (2) ventilated DS-high axial dispersion, (3) unventilated DS-low axial dispersion, and (4) unventilated DS-high axial dispersion. For each TSPA-LA Model realization, the drift-wall condensation case is sampled as an epistemic uncertainty, and the average rate of condensation and fraction of DS/WP pairs dripped on by drift-wall condensate at simulation time t is calculated for each percolation subregion and WP type. The average rate of condensation dripping from drift walls is combined with drift seepage to increase the dripping flow rate through the EBS.

Output 9—The following outputs are passed from the Drift Seepage (Section 6.3.3.1) and the Drift Wall Condensation Submodels (Section 6.3.3.2) to the EBS Flow Submodel (Section 6.3.6):

- For each percolation subregion:
  - Time-dependent drift-seepage rate for the DS-representative CDSP WP pairs and DS-CSNF WP pairs
  - The fraction of DS-CDSP WP pairs and DS-CSNF WP pairs in dripping (seepage) environments
  - The average time-dependent condensation rate for the DS-representative CDSP WP pairs and DS-representative CSNF WP pairs
  - The fraction of DS-CDSP WP pairs and DS-CSNF WP pairs in dripping (condensate) environments.

6.1.4.4 Engineered Barrier System Chemical Environment

The time-dependent evolution of the chemical-environment variables, pH and ionic strength, in the invert is determined by the time-dependent composition of water and gas entering the emplacement drift and how these water and gas compositions evolve as the water evaporates under the prevailing TH conditions within the invert. Time histories of seepage water and gas compositions are computed in the TSPA Model in each percolation subregion, based on the EBS P&CE Abstraction response surfaces (SNL 2007 [DIRS 177412]), using temperature, relative humidity, and percolation flux inputs from the EBS TH Environmental model. The evolution of the chemistry of the incoming seepage in the invert in terms of pH and ionic strength is modeled within the TSPA-LA Model using response surfaces in the form of look-up tables for these two variables as a function of percolation rate, the amount of water-rock interaction, temperature, relative humidity, and Pco_2. These response surfaces are provided by the EBS P&CE Abstraction (SNL 2007 [DIRS 177412], Section 6.9.2) and are based on calculations that simulate the evaporation/condensation evolution of each of the four seepage water types and gas compositions for a range of representative EBS TH conditions. The conceptual model and TSPA-LA Model implementation for the chemical environment in the EBS are discussed in detail in Section 6.3.4.

The first step in determining values of pH, ionic strength, chloride concentration, and nitrate concentration is selecting a starting water. In each realization, one of four water types is randomly sampled, and this water type is implemented for each representative WP in each

repository percolation subregion. Once the starting water has been selected, the Pco_2 time history, as a function of the temperature, the water-rock interaction and the selected starting water, is determined. The water-rock interaction is a function of the average percolation rate in each percolation subregion. Once the Pco_2 is determined, the chemical compositions are found in the look-up tables as a function of water-rock interaction, Pco_2, temperature, and relative humidity. For each realization, the TSPA-LA Model determines the pH and ionic strength in the invert for each representative WP at any point in time during the postclosure period. The pH and ionic strength are adjusted for epistemic uncertainty and variability by sampling uncertainty distributions for each parameter once per realization.

The EBS Chemical Environment Submodel also provides look-up tables and implementation instructions to determine abstracted values of time-dependent parameters, chloride and nitrate concentrations, and chloride-to-nitrate ratios. These abstracted variables are used to assess the potential for localized corrosion on the WP outer surface. However, this application of the EBS Chemical Environment Submodel is implemented in the ancillary Localized Corrosion Initiation Analysis for the TSPA-LA Model, as summarized in the next section and described in detail in Section 6.3.5.2.3. This flow of information is shown on Figure 6.1.4-1, but is not captured by an output number in Figure 6.1.4-1.

Output 10—The following outputs are passed from the EBS Chemical Environment Submodel (Section 6.3.4) to the Waste Form Degradation and Mobilization Model Component (Section 6.3.7):

- Outputs from this model component are provided for each percolation subregion and each representative WP, in dripping and non-dripping environments:
  - The time-dependent pH in the invert
  - The time-dependent ionic strength in the invert
  - The time-dependent Pco_2 in the drift.

6.1.4.5 Waste Package and Drip Shield Degradation

Time-dependent WP and DS degradation are implemented within the TSPA-LA Model. For the Nominal Scenario Class, the conceptual model and TSPA-LA Model implementation for the WP and DS degradation in the EBS are discussed in detail in Section 6.3.5. The flow of information between the WP and DS Degradation Model Component and other model components of the TSPA-LA Model are summarized below.

For the Nominal Scenario Class, general corrosion is the only degradation mode modeled for DS degradation. General corrosion rates for the inner and outer surfaces of the DSs are represented by two independent CDFs of the general corrosion rate because the environments above and below the DSs are not expected to be similar (SNL 2007 [DIRS 180778], Section 6.5.2, and 8.1[a]). These distributions represent epistemic uncertainty in DS general corrosion rates. For each realization, a single general corrosion rate is sampled from each distribution of the general corrosion rate and applied to all DSs. In the Nominal Scenario Class, the DSs are failed as a barrier to flow when the corroded thickness equals or exceeds the initial thickness of the DS plates. The status of the DS, intact or damaged, is an input to the EBS Flow submodel that determines the flow rate of water through a damaged DS and then onto a WP.

The TSPA-LA Model for the Nominal Scenario Class includes four WP degradation modes: general corrosion, MIC, and SCC, which are modeled using the Waste Package Degradation Model, and localized corrosion (SNL 2007 [DIRS 178519], Section 6.4.4), which is modeled using the Localized Corrosion Initiation Submodel.

The Nominal Scenario Class is represented by a single modeling case. This modeling case considers those WPs that fail as a result of corrosion processes (e.g., general corrosion, SCC, and/or localized corrosion). The TSPA-LA Model implementation of the WP degradation modes for the Nominal Scenario Class Modeling Case is briefly described as follows.

Nominal Scenario Class Modeling Case: WPs that Degrade by Corrosion—general corrosion rates of the WP outer surface are temperature-dependent and include epistemic uncertainty and variability. The temperature dependence is treated as an epistemic uncertainty that is sampled once per realization. The general corrosion rate, for low, medium, and high uncertainty levels, is sampled for every patch on every WP simulated in a percolation subregion. The uncertain temperature dependence for the realization, and each general corrosion rate on a patch, are used to calculate the temperature-dependent general corrosion rate (as a function of time) for every patch on every selected WP in a percolation subregion.

MIC is represented by an enhancement factor applied to the general corrosion rate of the WP outer surface (i.e., general corrosion rate × enhancement factor). The MIC factor is applied to the general corrosion rate when the relative humidity at the WP outer surface is above a relative humidity threshold. The MIC threshold represents epistemic uncertainty and is sampled once per realization.

Another potential failure mode considered for WPs is SCC in the closure lid. SCC can be initiated on a smooth surface (incipient cracks) or at an existing weld flaw (due to manufacturing defects). Two characteristics of weld flaws are treated as epistemic uncertainties sampled once per realization: flaw-size distribution and flaw-count distribution. SCC is determined by stress and stress intensity factor profiles in the closure-lid weld regions, and subsequent crack growth from the flaw sites. The uncertainty in stress and stress intensity profiles is represented by a scaling factor that is sampled independently, once for each realization. The uncertainty in crack growth rate is a function of the repassivation slope, n, which is also sampled once per realization.

The results for general corrosion, MIC, and SCC are compiled by the WAPDEG DLL (WAPDEG V4.07, STN: 10000-4.07-00 and 10000-4.07-01 [DIRS 181774 and 181064]). In the TSPA-LA Model Nominal Modeling Case, 10 WAPDEG DLL simulations are run per realization, one for each representative WP type (CSNF and CDSP) in each of the five repository percolation subregions. The EBS TH Environment Submodel provides temperature and relative humidity histories for eight WP and DS pairs (six CSNF WPs and two CDSP WPs) at each of the 3,264 subdomain locations. The process begins by randomly sampling a maximum of 500 DS/WP pairs from all of the pairs for a given fuel type in a percolation subregion. If the percolation subregion contains fewer than 500 DS/WP pairs, then all pairs in the percolation subregion are used. At the start of each EBS calculation, the WAPDEG DLL reads in the temperature and relative humidity histories for each selected WP and calculates time-dependent degradation. This information is used by the WAPDEG DLL to calculate the following output: (1) the cumulative number of WP failures as a function of time, (2) the average number

of patches per failed WP as a function of time, and (3) the average number of cracks per failed WP as a function of time.

Localized corrosion on WPs may occur when a WP is contacted by deleterious brine (SNL 2007 [DIRS 178519], Section 8.1, Figure 8-1). Two mechanisms may cause deleterious brine formation on the WP: seepage from dripping at the emplacement drift crown and dust deliquescence. In the TSPA-LA Model, only crown seepage water chemistry has the potential to fail WPs due to localized corrosion (SNL 2007 [DIRS 181267], Section 7.1.5). Only WPs that have DS plate failures coincident with deleterious brine contacting the WP are susceptible to localized corrosion failures. Localized corrosion of the WP is a process that is included in the Nominal Scenario Class. Localized corrosion of the WPs is calculated in the ancillary Localized Corrosion Initiation Analysis for the TSPA-LA Model using a response surface for localized corrosion initiation. The response surface is a function of the pH, chloride concentration, nitrate concentration, and WP temperature. Additionally, the criteria that seepage water must contact the WP for localized corrosion initiation is imposed. Thus, this separate GoldSim model file includes the Drift Seepage submodel, the EBS TH Submodel and EBS Chemical Environment Submodel. In addition, the ancillary model file also includes the general corrosion of the DSs and considers the consequences of seismic activity on the DSs.

Output 11—The following outputs are passed from the WP and DS Degradation Model Component (Section 6.3.5) to the EBS Flow Submodel (Section 6.3.6) for the Nominal Modeling Case:

- For each percolation subregion and each WP type (CDSP WPs and CSNF WPs):
  - The time-dependent average number of patch penetrations per failed DS
  - The time-dependent average number of patch penetrations per failed WP.

Output 12—The following outputs are passed from the WP and DS Degradation Model Component (Section 6.3.5) to the Waste Form Degradation and Mobilization Model Component (Section 6.3.7):

Nominal Modeling Case:

- For each percolation subregion and each fuel type (CSNF WPs):
  - The time-dependent fraction of WPs failed.

Output 13—The following outputs are passed from the WP and DS Degradation Model Component (Sections 6.3.5) to the EBS Transport Submodel (Section 6.3.8) for the Nominal Modeling Case:

- For each percolation subregion and each fuel type (CDSP WPs and CSNF WPs):
  - The time-dependent fraction of WPs failed

– The time-dependent average number of crack penetrations per failed WP
– The time-dependent average number of patch penetrations per failed WP.

6.1.4.6 Engineered Barrier System Flow

The following discusses the implementation of the EBS Flow Submodel (SNL 2007 [DIRS 177407], Section 6). The EBS Flow Submodel is implemented within the TSPA-LA Model and determines the volumetric flow rate of seepage water (including seepage into the drifts and drift-wall condensation) at different locations as seepage water moves through breached DSs, breached WPs, and the invert. In addition, the EBS Flow Submodel determines the fraction of WPs that are dripped upon, either by drift seepage and/or drift-wall condensation. The conceptual model and TSPA-LA Model implementation for flow in the EBS are discussed in detail in Section 6.3.6.

The TSPA-LA Model includes two dripping environments for each percolation subregion: (1) the seeping environment, which includes dripping above the WP from drift seepage and may also include drift-wall condensation; and (2) the non-seeping environment, which includes the WPs that are not exposed to drift seepage, but may or may not be exposed to drift-wall condensation. Inputs to the EBS Flow Submodel include the drift-seepage rate and the drift-wall condensation rate and the fraction of WPs exposed to drift-seepage and the drift-wall condensation from the UZ Flow Model Component. Both rates are combined to yield a total dripping rate. The flow rate of water through each breached DS or WP is proportional to the total dripping rate and the average number of patch penetrations on each DS or WP from the WP and DS Degradation Model Component. EBS flow is calculated for WPs of each type located in seeping and non-seeping environments. Flow in the seeping environments combines drift seepage and drift-wall condensation above and below the WP and includes the imbibition flux in the invert. Flow in the non-seeping environments includes drift wall condensation above and below the WP and includes the imbibition flux in the invert. Inputs to the EBS Flow Submodel for each WP type and repository percolation subregion include:

- The average total dripping rates due to seepage and drift-wall condensation
- The fraction of WPs dripped upon due to seepage and drift-wall condensation drift-wall condensation
- The average number of patch penetrations per failed CSNF DS and CDSP DS
- The average number of patch penetrations per failed CSNF WP and CDSP WP.

The EBS Flow Submodel does not use the average number of crack penetrations per failed WP because stress corrosion cracks are too small to allow advective water flow through these cracks (DTN: MO0706SPAFEPLA.001_R0 [DIRS 181613], FEP Number 2.1.03.10.0A).

The EBS Flow Submodel introduces two uncertain (epistemic) flux-splitting parameters to characterize the fraction of flow that enters breaches on DSs and on the WPs. These two parameters are sampled once per realization and are applied to all representative DS and WP pairs located in the dripping environments. Outputs from the EBS Flow Submodel are used

by: (1) the Waste Form Degradation and Mobilization Model Component, which uses the flow rate through a failed WP to calculate pH and ionic strength in the WP; and (2) the EBS Transport Submodel, which uses the flow rate through a failed WP and volumetric flow rate through the invert to calculate advective transport of radionuclides through a failed WP and through the invert to the host rock.

Output 14—The following output is passed from the EBS Flow Submodel (Section 6.3.6) to the Waste Form Degradation and Mobilization Model Component (Section 6.3.7):

- For each representative WP group, as applicable, in a seeping and non-seeping environment, in each percolation subregion:
  - The volumetric flow rate of water through the WP as a function of time.

Output 15—The following outputs are passed from the EBS Flow Submodel (Section 6.3.6) to the EBS Transport Submodel (Section 6.3.8):

- These outputs are provided for each representative WP in a seeping and non-seeping environment, in each percolation subregion:
  - The flux through the invert pore space as a function of time
  - The flow rate of water through the WP as a function of time
  - The fraction of WPs in a seeping environment
  - The fraction of WPs in a non-seeping environment.

6.1.4.7 Waste Form Degradation and Mobilization

The Waste Form Degradation and Mobilization Model Component, shown on Figure 6.1.4-1, includes submodels for radionuclide inventory, in-package chemistry, cladding failure, waste form degradation, dissolved concentration limits of radioactive elements, and EBS colloids. The conceptual models and TSPA-LA Model implementations for the submodels of the Waste Form Degradation and Mobilization Model Component are discussed in detail in separate subsections of Section 6.3.7. The flow of information between submodels of the Waste Form Degradation and Mobilization Model Component and other submodels of the TSPA-LA model are described below.

In-package chemistry is modeled within the TSPA-LA Model using simplified expressions to define the bulk chemistry consisting of pH, ionic strength, and total carbonate concentration ($\sum CO_3$) as a function of time inside a WP. Chemistry outputs are used to set conditions for waste form degradation, colloid stability, and to determine dissolved concentration limits inside the WPs. Within the TSPA-LA Model, no performance credit is taken for zircaloy or stainless steel cladding as a mechanism to prevent radionuclide release or inhibit CSNF waste form degradation (SNL 2007 [DIRS 180616], Section 6.2[a]). Waste form degradation is modeled within the TSPA-LA Model using empirical degradation rate formulas developed for the three different waste form types: CSNF, DOE spent nuclear fuel (DSNF), and HLW. DSNF and HLW glass are combined and disposed in CDSP WPs. Dissolved concentration limits of radionuclides (i.e., solubility limits for radioactive elements in the TSPA-LA Model) are

modeled using look-up tables, distributions, or single values. The formation, stability, and concentration of radionuclide-bearing colloids in the WP and EBS, as well as reversible and irreversible sorption of dissolved radionuclides, are modeled using empirical relationships and uncertainty distributions for sorption coefficients.

The three waste form categories (CSNF, DSNF, and HLW glass) are contained and disposed in two types of WPs: CSNF WPs and CDSP WPs. The CDSP WPs will contain both DSNF and HLW glass. The inclusion of mixed oxide SNF and lanthanide borosilicate (LaBS) glass HLW in the TSPA-LA Model is accomplished by adding radionuclide-specific inventories to the GoldSim source term (SNL 2007 [DIRS 180472]). WPs containing naval SNF WPs are conservatively represented as CSNF WPs containing CSNF inventory (see discussion in Section 6.3.7.1). Each percolation subregion environment represents a group of WPs in that subregion of the same type and in the same environment. Assigning individual WPs into WPs groups is discussed in detail in Section 6.1.5. The total radionuclide inventory (Section 6.3.7.1) in each WP group available for degradation and transport is calculated for each percolation subregion by taking into account the number and type of failed WPs.

The In-Package Chemistry Submodel is implemented using response surfaces and parameter distributions for four different abstraction conditions: CSNF and CDSP WPs that are dripped on, and CSNF and CDSP WPs that are not dripped on. Due to the contribution of drift-wall condensation, a WP can be dripped on if it is in a seeping or non-seeping environment, but only if its DS has failed. The In-Package Chemistry Submodel is implemented by sampling seepage rate-dependent uncertainty distributions and Pco_2-dependent response surfaces for pH. Ionic strength is determined by sampling uncertainty distributions whose range is a function of the relative humidity within the breached WP for non-dripping conditions and by sampling uncertainty distributions whose range is a function of the seepage rate through a breached WP for dripping conditions. The sampled values of pH and ionic strength represent epistemic uncertainty and are sampled once per realization. The $\sum CO_3$ for each abstraction condition is calculated using a temperature, Pco_2, and pH-dependent equation. This calculated value includes no additional uncertainty. Inputs to the In-Package Chemistry Submodel include volumetric flow rates of seepage into a failed WP as provided by the EBS Flow Submodel, the Pco_2 provided by the EBS Chemical Environment Submodel, and the temperature and relative humidity provided by the EBS TH Environment Submodel.

Outputs from the In-Package Chemistry Submodel are provided for each representative WP and each representative early-failed WP, if available, in dripping and non-dripping environments in each percolation subregion and consist of:

- The pH as a function of time
- The ionic strength as a function of time
- The $\sum CO_3$ as a function of time.

These outputs are used internally in the TSPA-LA Model by the Waste Form Degradation and Mobilization Model Component as inputs to the rate equations for the Waste Form Degradation Submodels, the dissolved concentration limits look-up tables, and EBS colloids stability criteria.

Most of the CSNF is encased in zirconium-alloy cladding, with only 1 percent of CSNF encased in stainless-steel cladding (DTN: MO0411SPACLDDG.003_R1 [DIRS 180755]). No performance credit is taken for zirconium-alloy cladding or stainless-steel cladding in the CSNF WP. The cladding does not reduce the amount of water that can contact the spent fuel in the CSNF WP nor does it reduce the release rate of the inventory when the waste form degrades. Both zirconium-alloy cladding and stainless-steel cladding are modeled as being perforated upon emplacement of the WPs in the repository. Perforated rods are modeled as instantly split down the rod length after the WP has failed (SNL 2007 [DIRS 180616], Section 6.2.4[a]).

No performance credit is taken for CSNF cladding; therefore, all of the CSNF inside a failed CSNF WP is exposed and available for degradation. Waste form degradation is modeled within the TSPA-LA Model using empirical formulas for the degradation rate developed for the three different waste form types: CSNF, DSNF, and HLW.

CSNF is isolated from repository environmental conditions until the WP is breached. Since no performance credit is taken for CSNF cladding, after the WP is breached, the CSNF may be exposed to humid air or dripping water. Upon exposure to moisture, radionuclides can be released by two mechanisms: (1) instantaneous release of the gap fraction and grain boundary inventory, and (2) matrix dissolution under alkaline or acidic conditions (BSC 2004 [DIRS 169987], Section 6). The fraction of the inventory emplaced in the repository that makes up the initial release inventory is determined by sampling distributions representing epistemic uncertainty. These distributions are sampled once per realization. For the CSNF inventory that is not part of the initial release inventory, matrix dissolution is modeled using two rate formulas, one for $pH < 6.8$ and one for $pH \geq 6.8$ (BSC 2004 [DIRS 169987], Section 8.1). Both CSNF degradation rate formulas are a function of specific surface area of exposed fuel, temperature, $\sum CO_3$, P_{O_2}, and in-package pH. Epistemic uncertainty in a specific surface area of exposed fuel is sampled once per realization. The CSNF degradation rate is calculated using input provided by two submodels: the EBS TH Environment Submodel provides the time-dependent temperature of the CSNF, and the In-Package Chemistry Submodel provides time-dependent pH and total carbonate concentration inside the failed WP. As the CSNF waste form degrades, the EBS Transport Submodel calculates the mass and saturated volume for the degraded CSNF rind and a rind thickness. These parameters are used to determine radionuclide concentrations in the fuel rind and to model transport from the CSNF rind into the WP.

The DSNF is modeled as being immediately available for dissolution and mobilization after a WP containing DSNF is breached. Because of this simplification, no rate equation or rate parameters are necessary to implement the DSNF Waste Form Degradation Abstraction for DSNF in the TSPA-LA Model (BSC 2004 [DIRS 172453], Sections 6.2 and 8.1). Each time a CDSP WP fails, the DSNF inventory associated with the failed WP, after accounting for decay and ingrowth, is made immediately available for transport (subject to solubility constraints) in the volume of water associated with the degraded DSNF and WP corrosion products (see Section 6.3.8.2). Once released, radionuclides are available for transport through the WPs to the EBS.

Degradation of HLW glass inside a damaged CDSP WP is included in the TSPA-LA Model. The rate equation is a function of an effective rate constant, temperature, pH, and the exposed surface area of the HLW glass (BSC 2004 [DIRS 169988], Section 8.1). The effective rate

constant is treated as an epistemic uncertainty, and is represented by two distributions, one for acidic conditions and one for alkaline conditions. These distributions are sampled once per realization. The exposed surface area of the glass is calculated as the product of the specific surface area of the glass and the glass exposure factor. The exposure factor is treated as an epistemic uncertainty and is sampled once per realization. The HLW Glass degradation rate is calculated using input provided by two submodels: the EBS TH Environment Submodel provides the time-dependent temperature of the CDSP WP, and the In-Package Chemistry Submodel provides time-dependent pH inside the failed WP. As the HLW glass degrades, the EBS Transport Submodel calculates the mass and saturated volume for the degraded HLW rind and a rind thickness. These parameters are used to determine radionuclide concentrations in the HLW rind and to model transport from the rind into the WP.

Outputs from the Waste Form Degradation Submodel for HLW glass, CSNF, and DSNF degradation are provided for each representative WP and each representative early-failed WP, as applicable in seeping and non-seeping environments, and in each percolation subregion, as follows:

- The degradation rate of HLW glass
- The degradation rate of CSNF fuel
- The instantaneous degradation of DSNF fuel.

These outputs are used internally in the Waste Form Degradation and Mobilization Model Components to determine the concentration of radionuclides in water in the associated degraded fuel rind.

The Dissolved Concentration Limits Submodel determines radionuclide concentration limits. The Dissolved Concentration Limits Submodel is used to calculate the solubility of certain radionuclides in the WP and in the invert that are potentially important to dose. The Dissolved Concentration Limits Submodel is implemented in the TSPA-LA Model in the form of: (l) look-up tables for plutonium, neptunium, uranium, thorium, americium, and protactinium, plus one or more epistemic uncertainty terms; (2) constant values over two pH intervals for radium; or (3) undefined values for technetium, carbon, iodine, cesium, and strontium (SNL 2007 [DIRS 177418], Sections 6 and 8.1). The look-up tables provide radioelement solubility as a function of pH and CO_2 fugacity (fCO_2). Solubilities are evaluated as a function of time to account for the evolution of pH and fCO_2 during the postclosure period. One or more epistemic uncertainty terms are evaluated by sampling their respective distributions once per realization and are added to each tabulated solubility value. These uncertainty terms represent uncertainty in the solubility constants of phases that control the solubility of plutonium, neptunium, uranium, thorium, and americium; uncertainty of the fluoride concentration in water that controls the solubilities of neptunium, uranium, thorium, americium, and protactinium; and uncertainty in the chemical analogy in the case of protactinium. The In-Package Chemistry Submodel and the EBS Chemical Environment Submodel provide the pH, ionic strength, and fCO_2 inputs to the Dissolved Concentration Limits Submodel when the Dissolved Concentration Limits Submodel is implemented in the WPs and in the invert, respectively (SNL 2007 [DIRS 177418], Executive Summary, Sections 1 and 6.4).

Outputs from the Dissolved Concentration Limits Submodel are provided for each representative WP, as applicable in seeping and non-seeping environments, and for each percolation subregion, as follows:

- The time-dependent solubilities for plutonium, neptunium, uranium, thorium, americium, and protactinium
- The time-dependent value of radium solubility, which can be one of two values depending on pH.

These outputs are used by the EBS Transport Submodel to calculate radionuclide concentration limits that are in the volumes of water associated with the CSNF rind, in the DSNF rind, in the HLW glass rind, in the in-package corrosion products, and in the invert.

The TSPA-LA Model's EBS Colloids Submodel calculates the types and concentrations of colloids potentially generated after WP failure. Three types of colloids are considered: (1) waste form degradation colloids, which are generated from degradation of the glass waste form and SNF waste forms; (2) colloids produced from the steel components of the WPs and invert; and (3) colloids present in natural seepage water entering the EBS. Nine radionuclides can potentially sorb on the colloids: plutonium, americium, cesium, protactinium, thorium, tin, radium, uranium, and neptunium. Inputs to the colloid-associated EBS Colloids Submodel include pH and ionic strength in the WP provided by the In-Package Chemistry Submodel, dissolved radionuclide concentrations in the WP and invert from the EBS Transport Submodel, and pH and ionic strength in the invert provided by the EBS Chemical Environment Submodel.

At each timestep in the TSPA-LA Model calculations, the EBS Colloids Submodel uses in-package ionic strength, pH, and dissolved radionuclide concentrations to evaluate the formation and stability of colloids in the WP. Besides reversible sorption, irreversible (kinetic) sorption of plutonium and americium onto iron oxyhydroxide colloids and waste form colloids derived from HLW glass and CSNF is also considered. A competitive sorption model with a sorption capacity is implemented for the reversible sorption onto the three colloid types.

The EBS Chemical Environment Submodel (Section 6.3.4) calculates the ionic strength and pH of the invert water. Based on the values of ionic strength and pH in the invert, the EBS Colloids Submodel determines colloid stabilities and concentrations for the invert conditions and redistributes available radionuclide mass based on the distribution coefficients and the total mass of each type of colloid. These colloids and associated radionuclides are then subject to transport through the invert and into the UZ.

Several epistemic uncertainties, related to colloid stability and colloid-associated radionuclide concentrations, are represented by distributions that are sampled once per TSPA-LA Model realization. These uncertain parameters include the equilibrium sorption distribution coefficients, the specific surface area of corrosion-generated colloids, the groundwater colloid concentration, and the forward rate constant for irreversible (kinetic) sorption.

Output 16—The following outputs are passed from the Waste Form Degradation and Mobilization Model Components (Section 6.3.7) to the EBS Transport Submodel (Section 6.3.8):

- Outputs from the Waste Form Degradation and Mobilization Model Component are provided for each representative WP in seeping and non-seeping environments. For each percolation subregion, they provide:
  - The mass of radionuclides available for transport through the EBS
  - The concentrations limits of radionuclides inside a failed WP and in the invert
  - The concentrations of radionuclides, plutonium and americium, irreversibly attached (embedded in) waste form colloids
  - The concentrations of radionuclides, americium and plutonium, which are irreversibly attached to iron oxyhydroxide colloids
  - The concentrations of radionuclides: americium, plutonium, protactinium, cesium, thorium, tin, radium, uranium, and neptunium, which are reversibly attached to colloids.

6.1.4.8 Engineered Barrier System Transport

The EBS Transport Submodel is described in *EBS Radionuclide Transport Abstraction* (SNL 2007 [DIRS 177407], Section 6). The conceptual models and TSPA-LA Model implementations for the EBS Transport submodel are discussed in detail in Section 6.3.8 and are summarized below.

EBS transport is modeled directly within the TSPA-LA Model at run time, using a one-dimensional, finite-difference numerical solution algorithm that is embedded in the GoldSim operating software (GoldSim V9.60.100, STN: 10344-9.60-01 [DIRS 181903]) of the TSPA-LA Model. Each representative WP group in each repository percolation subregion is modeled. The modeled system uses a linked series of mixing cells that represent the waste form as the source of radionuclides and colloids, corrosion products as a source of iron oxyhydroxide colloids and stationary corrosion products in the WP that sorb radionuclides, and the invert crushed tuff as a sorbing medium. The EBS Transport Submodel describes the transport of both dissolved radionuclides and radionuclides sorbed onto colloids through the TSPA-LA Model's mixing cells via diffusion and advection. The outputs from the EBS Transport Submodel are mass flux of dissolved radionuclides and mass flux of colloid-associated radionuclides into the host-rock fractures and host-rock matrix below the repository. The total mass flux into the UZ host rock and the fraction going into the fractures and the matrix in the UZ is computed based on modeling approximately 18 m of dual continuum below the repository as part of the EBS Transport Submodel. The calculated radionuclide mass flux as a function of time at the EBS-UZ interface is passed to the UZ Transport Model Component of the TSPA-LA Model. The UZ Transport Model Component applies a three-dimensional, dual-permeability UZ Transport model that uses a finite element, heat and mass (FEHM) software code (FEHM V2.24, STN: 10086-2.24-01-00 [DIRS 179419]).

Several epistemic uncertainties related to transport in WPs and the invert are represented by distributions that are sampled once per realization. In the WPs these include: (1) the water adsorption isotherm parameters, (2) the surface properties such as specific surface area and sorption site density of the stationary corrosion products, (3) the corrosion rate of in-package stainless-steel and carbon-steel components, (4) diffusive path length from a WP to the invert, and (5) the uncertainty in pH from surface complexation calculations. In the invert, these include radionuclide reversible sorption coefficients and an invert diffusion coefficient for radionuclide diffusion.

Implementation of the EBS Radionuclide Transport Submodel requires transport connections between the single-continuum invert and the dual-continuum host rock. For each representative waste-emplacement drift, these connections determine the fraction of radionuclide mass flux transported into the host-rock matrix continuum, and the fraction transported into the host-rock fracture continuum after release from the EBS. The diffusive transport connections are derived by enforcing mass flux continuity between the invert and the host rock, which determines the split of invert diffusive releases between the UZ fracture and matrix continua. However, the split for advective mass flux is imposed. The total advective mass flux leaving the invert is based on the combined fluid flux in the invert (a combination of seepage, condensation, and imbibition flux), but when the advective mass flux is passed to the UZ, it is partitioned such that the advective fraction carried by the imbibition flux is sent to the UZ matrix, while the remainder is sent to the UZ fractures. Mass partitioning fractions are also passed from the EBS Transport submodel to the UZ Transport Model Component.

The following time-dependent outputs are calculated for each WP group in each percolation subregion.

Output 17—The following outputs are passed from the EBS Transport Submodel (Section 6.3.8) to the UZ Transport Submodel (Section 6.3.9):

- Outputs from the EBS Transport Submodel are provided for each representative WP and each representative early-failed WP, as applicable, in seeping and non-seeping environments, for each percolation subregion, as follows:
  - The radionuclide mass release rate to the UZ.
  - The diffusive and advective release fractions from the EBS into the UZ below the repository.

6.1.4.9 Unsaturated Zone Transport

UZ transport is modeled within the TSPA-LA Model by the UZ Transport Submodel. The conceptual models and TSPA-LA Model implementations for the UZ Transport Submodel are discussed in detail in Section 6.3.9 and are summarized below.

The UZ Transport Submodel implements the three-dimensional, dual-permeability, finite-element software code FEHM (FEHM V2.24, STN: 10086-2.24-01-00 [DIRS 179419]) particle tracker (SNL 2008 [DIRS 184748], Sections 6 and 8). The UZ flow fields for each combination of infiltration scenario and climate change are accessed directly by the UZ

Transport Submodel. The FEHM particle tracker transports particles with the same dual-permeability spatial grid as used in the Site-Scale UZ Flow Process Model (SNL 2007 [DIRS 184614]), including the same water flux and liquid saturation values. When climate changes, the TSPA-LA Model uses the UZ flow fields associated with the new climate for the given infiltration scenario.

As noted in Section 6.1.4.8, Output 17, the mass of dissolved radionuclides and reversibly sorbed radionuclide mass on colloids from the EBS are combined and released to the UZ as a total radionuclide mass. This mass is equilibrated within the UZ between the aqueous phase and the groundwater colloids present in the UZ. Americium and plutonium isotopes that are irreversibly sorbed onto colloids are transported separately as fast and slow fractions. The following UZ transport processes are simulated:

- Advective and diffusive transport of dissolved and colloid bound radionuclides in the fractures and rock matrix
- Fracture-matrix interaction and matrix diffusion
- Sorption of dissolved radionuclides in the matrix continuum
- Retardation of colloids, on which radionuclides are irreversibly sorbed, in the fracture continuum
- Colloid filtration at interfaces between matrix units
- Colloid size exclusion at fracture-matrix continua interfaces
- Radioactive decay and ingrowth.

The release of radionuclides from the EBS to the UZ is calculated as follows: The radionuclide mass flux, calculated by the EBS Transport Submodel and released from the five repository percolation subregions, enters the FEHM grid nodes that reside within the subregions. The number of FEHM grid nodes receiving released radionuclides depends on the number of WPs that have failed. At each timestep, there are a number of failed WPs from each representative group in each repository percolation subregion. The radionuclide mass flux released from each failed WP in a group is equal to the mass flux from the representative WP group divided by the number of failed WPs in that group. To simulate WPs failing at different locations, the FEHM release nodes in the UZ are randomly selected for each group, without replacement (to prevent a node from being selected more than once), from the available UZ FEHM grid nodes within each percolation subregion. If the number of failed WPs in a group exceeds the number of FEHM grid nodes in a percolation subregion, releases are allocated evenly to all FEHM grid nodes in the percolation subregion.

For each realization, a set of uncertain material properties for UZ transport is sampled and the values or parameters generated from the sampled values are used in the UZ transport particle tracking analysis. These epistemic uncertainties are represented by distributions and include matrix adsorption coefficients, matrix diffusion coefficients (as generated from sampled values

of tortuosities and species-dependent values of free-water diffusion coefficients), fracture apertures (as generated from sampled values of fracture porosity and fracture frequency), active fracture model gamma parameters, colloid equilibrium sorption parameters (as generated from sampled values of sorption coefficients onto colloids and colloid concentrations), and colloid retardation factors for UZ transport. In addition, colloid filtration sizes for rock units are sampled and compared to sampled values of colloid size for each particle during the particle tracking process. This information is accessed by the UZ Transport Submodel during TSPA-LA Model simulations. Note that because UZ transport processes tend to be more sensitive to rock property uncertainties, some UZ rock properties (e.g., the AFM gamma) are sampled for the UZ Transport Submodel, whereas they are not sampled for the Site-Scale UZ Flow Process Model. Outputs from the UZ Transport Submodel at each timestep are radionuclide mass release rates from the fractures and matrix to four UZ collector regions at the water table. When the climate changes, the elevation of the water table is instantaneously set to the elevation associated with the new flow field. Any radionuclides in the UZ below the new and higher water table elevation at the time the climate changes are immediately removed from the UZ and provided as inputs to the SZ Flow and Transport Submodel. The immediate change in the water table which decreases the transport length to the SZ and the immediate application of mass residing between the old and new water table to the SZ, represents a reasonable, technically defensible conservative implementation (SNL 2008 [DIRS 184748], Section 6.4.8).

Output 18—The following outputs are passed from the UZ Transport Model Component (Section 6.3.9) to the SZ Flow and Transport Submodel (Section 6.3.10):

- The mass release rate of dissolved radionuclides (or, where applicable, combined dissolved radionuclides and radionuclides reversibly sorbed onto colloids) from each collector region to the SZ
- The mass release rate of radionuclides irreversibly sorbed onto retarded (slow) and unretarded (fast) colloids from each collector region to the SZ
- The cumulative potential mass release of ingrowth products associated with inventory boosting (see Section 6.3.10.3).

6.1.4.10 Saturated Zone Flow and Transport

The SZ Flow and Transport Submodel is described in *Saturated Zone Flow and Transport Model Abstraction* (SNL 2008 [DIRS 183750]). The conceptual models and TSPA-LA Model implementations for the SZ Transport Submodel are discussed in detail in Section 6.3.10 and are summarized below.

The SZ Flow and Transport Submodel of the TSPA-LA Model evaluates the transport of radionuclides, from their introduction at the water table below the repository, to the accessible environment 18-km downstream from the repository (66 FR 55732 [DIRS 156671], p. 55753). The groundwater used by the hypothetical farming community is conservatively assumed to contain all radionuclide mass in the SZ that crosses the boundary of the accessible environment. The captured radionuclide mass is homogeneously distributed in 3,000 acre-ft/yr of groundwater (10 CFR 63.312(c) [DIRS 180319]). The TSPA-LA SZ Flow and Transport Submodel uses two

abstractions to describe SZ flow and transport: (1) a 3-D SZ Flow and Transport Abstraction of individual radionuclides that are important to dose and (2) a 1-D SZ Flow and Transport Abstraction that calculates the transport of second-generation daughter radionuclides (Figure 6.3.10-8).

The 3-D SZ Flow and Transport Abstraction and the 1-D SZ Flow and Transport Abstraction receive inputs from two other sources. The Climate Analysis (BSC 2004 [DIRS 170002]) provides the duration of climates. The Infiltration Model (SNL 2007 [DIRS 182145]) provides the net infiltration flux (Section 6.3.1) to scale groundwater flux for the future climates considered for the TSPA-LA Model. Changes in recharge and groundwater flux in the SZ, associated with climate variations, are approximated as step changes from one steady-state flow condition to the next. Note although the data from the new Infiltration Model described in SNL 2007 [DIRS 182145] is reflected in the groundwater flux scaling factors, the new infiltration rates were not used to update the recharge in the repository area. The use of the old recharge data is not expected to make a marked difference since even though the weighted flow through the UZ Flow Model footprint has increased 49 percent over the previous net infiltration, the recharge is a small portion (13 percent) of the infiltration budget and the flow budget (1 percent) (SNL 2007 [DIRS 177391], Section 6.4.3.9).

Using 12 representative radionuclide groups, the 3-D SZ Flow and Transport Process Model (SNL 2008 [DIRS 183750]) is run outside the TSPA-LA Model. It is used to perform a series of probabilistic transport simulations for a unit mass source rate to obtain unit mass breakthrough curves at the 18-km boundary of the accessible environment, for each of the 12 representative radionuclide groups. For each realization, parameters containing epistemic uncertainty are sampled and used in the three-dimensional and one-dimensional SZ Flow and Transport Models (SNL 2008 [DIRS 183750], Table A-1[a]). The uncertain parameters include: (1) effective porosity in the alluvium; (2) values of the distribution coefficient, K_d, in the tuff and alluvium; (3) parameters used for irreversible and reversible sorption onto colloids; (4) longitudinal dispersivity; (5) transverse dispersivity; (6) coordinate offsets for the point source locations within each of the four SZ capture regions; (7) horizontal permeability anisotropy; (8) fraction of the groundwater flow path within the alluvium; and (9) parameters related to matrix diffusion in the tuff (SNL 2008 [DIRS 183750], Table 7.1[a]).

The unit mass breakthrough curves generated by the 3-D SZ Flow and Transport Process Model, in combination with the convolution integral method, are used by the 3-D SZ Flow and Transport Abstraction in the TSPA-LA Model to calculate transport in the SZ to the accessible environment. For a given timestep, the convolution integral method takes a point-source radionuclide mass from the bottom of the UZ Transport Submodel from four capture regions (SNL 2008 [DIRS 183750], Section 6.5.2.13). The total radionuclide mass release rate, for both matrix and fracture continua in each of these four capture regions, is released to a single location that is randomly selected in each capture region. The location of the random release point in each SZ capture region was selected during the generation of the SZ Convolute Abstraction breakthrough curves for each realization. The location of the UZ release point (Figure 6.3.9-6) used in each realization is, therefore, implicit to the sampled breakthrough curve used in the SZ convolution integral approach. The randomly selected point source location is determined by applying sampled offset values to known coordinates within each of the four SZ capture region. The sum of the fracture and matrix radionuclide mass release rates is released to

four SZ capture regions (Figure 6.3.10-6) and then fed to the SZ convolution integral model, SZ_Convolute (SZ_Convolute V3.10.01, STN: 10207-3.10.01-00 [DIRS 181060]), and to the one-dimensional SZ pipe model (SNL 2008 [DIRS 183750], Section 6.3) at each TSPA-LA Model timestep. The 3-D SZ Flow and Transport Abstraction combines this source with the appropriate unit mass breakthrough curve for that radionuclide to determine the mass flux of radionuclides across the 18-km boundary. The breakthrough curves reside in files in the GoldSim software run-time directory and are accessed when needed by the SZ_Convolute DLL. The SZ_Convolute method convolves the source term with the SZ_Convolute library of unit breakthrough curves.

For some of the daughter radionuclides that are considered in the TSPA-LA Model, a 1-D SZ Flow and Transport Abstraction is used to account for decay and ingrowth during transport for four decay chains. The 1-D SZ Flow and Transport Abstraction is incorporated directly in the TSPA-LA Model as three one-dimensional pipe segments for each SZ source region using GoldSim pipe pathway elements. The simplified 1-D SZ Flow and Transport Abstraction is required because the radionuclide transport methodology used in the 3-D SZ Flow and Transport Abstraction does not calculate ingrowth by radioactive decay. The rates of groundwater flow within individual pipe segments are adjusted to match the flow rates in the 3-D SZ Flow and Transport Abstraction. The flow path length of the first segment is constant and represents a distance for which the properties of the volcanic medium and gradient are relatively uniform. The flow path lengths of the second and third segments are a function of two uncertain parameters: the first represents uncertainty in the horizontal permeability anisotropy, and the second represents uncertainty in the northwestern boundary of the alluvium. These two parameters are sampled once per SZ realization. Values of transport parameters in the one-dimensional SZ pipe segments correspond to the values used in the 3-D SZ Flow and Transport Abstraction on a realization-by-realization basis.

Results from the 3-D SZ Flow and Transport Abstraction are combined with the results of the 1-D SZ Flow and Transport Abstraction to produce a radionuclide mass release rate at the boundary of the accessible environment. The TSPA-LA Model coordinates the consistent, random selection of radionuclide breakthrough curves and properties for the one-dimensional transport calculation for each realization.

Output 19—The output passed from the SZ Flow and Transport Submodel (Section 6.3.10) to the Biosphere Submodel (Section 6.3.11) is the mass flux of radionuclides (in 3,000 acre-ft of water) at the 18 km boundary of the accessible environment (66 FR 55732 [DIRS 156671], p. 55753).

6.1.4.11 Biosphere

The annual dose to the RMEI is modeled using BDCFs that convert radionuclide concentrations in groundwater, or in volcanic ash to dose. The two exposure cases considered in the TSPA-LA Model are the groundwater exposure case and the volcanic ash exposure case. For the groundwater exposure case, radionuclides enter the accessible environment from wells that extract contaminated groundwater from the SZ aquifer. Human exposure arises from using the contaminated water for domestic and agricultural purposes. Groundwater BDCFs apply to the Nominal Scenario Class, the Early Failure Scenario Class, the Seismic Scenario Class, the

Igneous Intrusion Modeling Case of the Igneous Scenario Class, and the Human Intrusion Scenario. In the volcanic ash exposure case, radionuclides are released as contamination in volcanic ash that is dispersed into the atmosphere with possible redistribution by fluvial processes leaving a contaminated layer on surface soil. Human exposure occurs in the accessible environment with the transport of radionuclides from surface soil to other environmental media such as foodstuffs, inhalable contaminated atmospheric particulate matter, and groundshine. Volcanic Ash BDCFs apply to the Volcanic Eruption Modeling Case of the Igneous Scenario Class. The BDCFs are developed outside the TSPA-LA Model, using the Biosphere Process Model (SNL 2007 [DIRS 177399]).

Using the methods developed in *Biosphere Model Report* (SNL 2007 [DIRS 177399]), BDCFs for the groundwater exposure cases and the volcanic ash exposure cases were calculated, using probabilistic analysis, in a series of simulations for each of the primary radionuclides tracked in the TSPA-LA Model (DTN: MO0702PAGBDCFS.001_R0 [DIRS 179327], DTN: MO0702PAVBPDCF.000_R0 [DIRS 179330]). In the case of the Volcanic BDCFs, the results were insensitive to climate change and were provided for only the present-day climate. For the Groundwater BDCFs, climate has an influence on the BDCFs as a result of changes in agricultural practices and swamp cooler usage. For each primary radionuclide, one thousand stochastic BDCFs were developed for each of the three climates (present-day, monsoon, and glacial transition) anticipated to occur over the next 10,000 years (SNL 2007 [DIRS 177399]). The present-day accessible environment, being the warmest and driest, uses the largest volume of contaminated groundwater and generates higher BDCFs than the other climates. To prevent speculation about climate changes over the 1,000,000-year period, TSPA used these conservative, present-day BDCFs for all simulation time periods. In a similar vein, the BDCFs for the Volcanic Eruption Modeling Case were generated stochastically using 1,000 realizations. In the TSPA-LA Model, a discrete distribution whose output is an integer from 1 to 1,000, inclusive, is used to randomly select a particular set of values from these BDCF tables. The selected BDCFs for each radionuclide are then multiplied by the appropriate radionuclide concentrations and summed over all radionuclides to compute annual dose to the RMEI. In the SZ, radionuclide concentrations are calculated from the annual radionuclide mass flux provided by the SZ Flow and Transport Model Component uniformly dispersed in the 3,000 acre-feet of water. For the Volcanic Eruption Modeling Case, the BDCFs are multiplied by the appropriate concentrations, one concentration is that in the resuspendible soil layer, and the other is the concentration appropriate for crop uptake (i.e., averaged over the tillage depth).

In addition to the annual dose calculation, the Biosphere Model Component also includes the calculations of activity concentration in groundwater and beta-photon doses for evaluating compliance with the groundwater protection limits (SNL 2007 [DIRS 177399]; DTN: MO0702PAGWPROS.001_R0 [DIRS 179328]). Three items, including the gross alpha concentration in groundwater, the radium concentration in groundwater, and the annual dose from beta- and photon-emitting radionuclides ingested by daily consumption of two liters of groundwater are evaluated for compliance. These calculations are based on the activity concentration of each primary radionuclide in groundwater, as calculated from radionuclide concentrations that are provided by the SZ Flow and Transport Model Component. They use the conversion factors (DTN: MO0702PAGWPROS.001_R0 [DIRS 179328]) for calculating the annual beta and photon dose, and the number of alpha particles as per the requirement in

10 CFR 63.331 [DIRS 180319], emitted per decay of the primary radionuclides, as TSPA-LA Model inputs provided by the Biosphere Model Component.

The Biosphere is the last component in the chain of TSPA-LA Model components and, thus, has no output coupling; rather, the Biosphere component outputs are the time evolution of stochastic dose histories and other parameters (alpha activity and organ/whole body doses) required by 10 CFR 63.331 ([DIRS 180319], Table 1) to evaluate repository system performance.

Output 20—The following outputs are passed from the Biosphere Model Component at each timestep (Section 6.3.11):

- The annual dose incurred by the RMEI for every radionuclide under consideration for both groundwater exposure and volcanic ash exposure cases
- The gross alpha concentration in groundwater
- The radium concentration in groundwater
- The annual whole body and individual organ doses from beta- and photon-emitting radionuclides by daily consumption of two liters of groundwater.

6.1.4.12 Events

In addition to the analysis of the Nominal Scenario Class described in Sections 6.1.4.1 through 6.1.4.11, the TSPA-LA Model is used to analyze early failure events and other disruptive events. The early failure events analyses consider early failure of WPs and DSs. The early failure events are captured in two separate modeling cases: (1) Waste Package EF Modeling Case, and (2) Drip Shield EF Modeling Case. The disruptive events analyses consider igneous events, including an igneous intrusion into the repository and a volcanic eruption through the repository, seismic events, with either ground motion affecting the repository or fault ruptures intersecting the repository, and a human intrusion. The Igneous Scenario Class includes two modeling cases: (1) Igneous Intrusion Modeling Case, with groundwater transport; and (2) Volcanic Eruption Modeling Case, with atmospheric transport. The Seismic Scenario Class includes two modeling cases: (1) Seismic GM Modeling Case, and (2) Seismic FD Modeling Case. The Human Intrusion Scenario includes one stylized Human Intrusion Modeling Case.

6.1.4.12.1 Early Failure Scenario Class

The two early failure Scenario Class modeling cases, mentioned above and considered for the TSPA-LA Model, are discussed below.

The Waste Package EF Modeling Case considers all WPs that fail early due to manufacturing or material defects, including improper pre-emplacement operations. The implementation of early WP failures in the TSPA-LA Model consists of sampling or specifying aleatory quantities associated with the early failure events. These include: the number of WPs that fail early in a realization and how these WPs are distributed among the different WP types (Section 6.4), and the percolation subregion and dripping environment type containing the EF WPs. Like the Nominal Scenario Class, in the TSPA-LA Model's early failure WP analysis, two types of WPs

are considered: (1) CDSP WPs, and (2) CSNF WPs; five percolation subregions are considered; and two dripping environments, seeping and non-seeping are considered. Localized corrosion and general corrosion of the WPs are considered in the Waste Package EF Modeling Case; however, these two mechanisms would not introduce any additional damage to the early-failed WPs because the entire surface area of the early failure WP is damaged at the time of the early failure. General corrosion of the DS is included in the Waste Package EF Modeling Case. Other than the Waste Package Degradation Model Component, the Waste Package EF Modeling Case invokes the same modeling components and submodels used in the Nominal Scenario Class.

The Drip Shield EF Modeling Case considers all DSs that fail early due to manufacturing or material defects including improper pre-emplacement operations. The implementation of early DS failures in the TSPA-LA Model consists of sampling or specifying aleatory quantities associated with the early failure events. These include: the number of DSs that fail early in a realization and how these DSs are distributed among the different WP types (Section 6.4), and the percolation subregion and dripping environment type containing the EF DSs. Like the Nominal Scenario Class, in the TSPA-LA Model's early failure DS analysis, two types of WPs are considered: (1) CDSP WPs and (2) CSNF WPs; five percolation subregions are considered; and two dripping environments, seeping and non-seeping are considered. In order for WP releases to occur under an early-failed DS, a WP beneath the early-failed DS is modeled as a WP in a seeping environment that fails immediately by localized corrosion once seepage contacts the WP. In the absence of localized corrosion, the WP under an early-failed DS would not be subject to releases before nominal processes result in WP failures. The implementation of placing the early- failed DS in a seeping environment requires that the resulting dose be weighted by the probability of at least one early-failed DS occurring in a seeping environment. Localized corrosion of a WP under an early-failed DS is assumed to be instantaneous once seepage contacts the WP. As a result of localized corrosion, general corrosion of a WP is considered in the Drip Shield EF Modeling Case; however, this mechanism would not introduce any additional damage to a WP beneath an early-failed DS because localized corrosion damages the entire surface area of the WP. General corrosion of the DS is excluded in the Drip Shield EF Modeling Case. Other than the WP and DS Degradation Model Component, the Drip Shield EF Modeling Case invokes the same modeling components and submodels used in the Nominal Scenario Class.

Figure 6.1.4-3 schematically depicts the flow of information between the principal TSPA-LA Model components and submodels for the early failure modeling cases. The flow of information between submodels in these two modeling cases is similar to the Nominal Scenario Class Modeling Case depicted on Figure 6.1.4-1 with some exceptions that are described below and described in detail in Section 6.4.

The WP and DS Degradation Model Component, which combines the localized corrosion and general corrosion processes in the Nominal Scenario Class, is replaced with early failure degradation modes for the WPs and/or DSs. As discussed above, localized corrosion and general corrosion of WPs provide no additional damage to the early-failed WP, and therefore the WP damage and failure areas calculated by the WP and DS Degradation model component are not applicable in the Waste Package EF Modeling Case. DS degradation by general corrosion is still applicable in the Waste Package EF Modeling Case. As discussed above, general corrosion of DSs provides no additional damage to early-failed DSs, and therefore the DS damage and failure

areas calculated by the WP and DS Degradation model component are not applicable in the Drip Shield EF Modeling Case. WP degradation by localized corrosion is assumed to occur instantly once a WP beneath an early-failed DS is contacted by seepage water.

6.1.4.12.2 Igneous Scenario Class

The two Igneous Scenario Class modeling cases, mentioned above and considered for the TSPA-LA Model, are discussed below (Section 1.5.3).

The following events occur in the Igneous Intrusion Modeling Case, as described in *Dike/Drift Interactions* (SNL 2007 [DIRS 177430], Section 6). The Igneous Intrusion Modeling Case considers an igneous event in which a fracture with magma rising in it (dike) intersects the repository drifts. The magma flows into and fills the drifts, cooling in place with no eruption to the surface unless the magma is within an eruptive conduit. The intruding magma engulfs all WPs and DSs in those repository drifts that are intersected by the dike. In response to the heat and corrosive gases, the WPs and fuel cladding fail, exposing the radioactive waste to the magma. After the magma-filled drifts cool to ambient conditions (i.e., temperatures prior to magma emplacement), the water moving into the intruded drifts is altered by the chemistry of the basaltic rock. This affects the mobility (solubility) of the radionuclides in the exposed waste. Radionuclides exposed to water moving into the magma-intruded drifts are transported by the groundwater downward through the UZ to the water table and then out to the accessible environment by flow and transport processes in the SZ.

Figure 6.1.4-4 schematically depicts the flow of information between the principal TSPA-LA Model components and submodels for the Igneous Intrusion Modeling Case. The flow of information between submodels in this modeling case is similar to the Nominal Scenario Class Modeling Case depicted on Figure 6.1.4-1 with some exceptions that are applied after the igneous intrusion occurs. These exceptions are described below and described in detail in Section 6.5.

- The Igneous Intrusion Modeling Case allows for all nominal processes to occur before the igneous intrusion occurs.
- As a result of the igneous intrusion, the Igneous Intrusion Modeling Case fails all WPs and DSs in the repository.
- The Igneous Intrusion Modeling Case does not include drift-wall condensation after the igneous intrusion.
- The TSPA-LA Model uses a seepage flux equal to the local percolation flux and neglects capillary diversion at the drift wall after the igneous intrusion. Therefore, the Drift Seepage Submodel response surfaces for seepage are not implemented after the igneous intrusion. The seepage response surfaces provide the seepage flow rates and seepage fractions applicable for the nominal conditions, which prevail prior to the igneous intrusion.

- For approximately the first 100 years after intrusion, waste form temperatures are perturbed by the hot intruded magma. A temperature abstraction is applied, as described in *Dike/Drift Interactions* (SNL 2007 [DIRS 177430], Section 6.7). This abstraction is used to specify waste form and invert temperatures during this period.

In addition to the changes affecting the information flow noted above, the following submodel changes are also implemented:

- In the Igneous Intrusion Modeling Case, the DSs and WPs in intruded drifts provide no further protection; therefore, DS and WP degradation, as calculated by the WP and DS Degradation model component, are no longer applicable in the intruded drifts.

- The TSPA-LA Model exposes waste that is contained in the failed WPs directly to the intruding magma. Radionuclides are then transported through the failed WPs and released to the invert where they are transported to the EBS-UZ interface.

Additional information developed to support the TSPA-LA Model in igneous intrusion groundwater transport includes the following:

- Mean annual frequency of a dike intersecting the repository.

The Volcanic Eruption Modeling Case models: (1) damage to the EBS and the amount of waste erupted to the surface, (2) the atmospheric transport and eventual deposition of the waste-contaminated ash on the land surface, (3) redistribution of the contaminated tephra, and (4) the estimate of dose to the RMEI in the Biosphere Model Component. Figure 6.1.4-5 schematically depicts the flow of information for the Volcanic Eruption Modeling Case. The volcanic eruption is modeled using the numerical code ASHPLUME (SNL 2007 [DIRS 177431]), via the ASHPLUME DLL (ASHPLUME_DLL_LA V2.1, STN: 11117-2.1-01 [DIRS 181035]) that is dynamically linked to the TSPA-LA Volcanic Eruption Model at run time. The consequences of a volcanic eruption also include the change in dose at the location of the RMEI from the transport of radioactive waste-contaminated ash through sedimentary processes that include both eolian and fluvial transport mechanisms. The Redistributed Tephra Abstraction calculates source term multipliers that are used to account for this effect at the location of the RMEI, for both interstream divide areas and distributary channels. The tephra redistribution calculations for a probability-weighted volcanic event are performed using the FAR (FAR V1.2, STN: 11190-1.2-00 [DIRS 182225]).

6.1.4.12.3 Seismic Scenario Class

This Seismic Scenario Class considers seismic disruptions (i.e., fault displacement and ground motion) as additional events that occur during the time period of evaluation. This scenario class includes two modeling cases: (1) a ground motion case for the vibratory ground motion damage to the WPs, and (2) a fault displacement case for the fault displacement damage to the WPs and DSs.

The Seismic Scenario Class describes the performance of the repository system in response to seismic events with a mean annual exceedance frequency in the range of 4.287×10^{-4} to 1×10^{-8}

per year (SNL 2007 [DIRS 176828], Table 6-88). This modeling case includes the effects of ground motion and fault displacement on the host rock, DSs, and WPs. The Seismic Scenario Class takes into account changes in seepage flux and TH on the WP surface that might occur as a result of emplacement drift degradation in the lithophysal region due to seismic events. Figure 6.1.4-6 schematically depicts the flow of information between principal TSPA-LA submodels for the Seismic Scenario Class. The flow of information between submodels in the Seismic Scenario Class is very similar to the Nominal Scenario Class, as depicted on Figure 6.1.4-1.

The majority of the submodels for the Seismic Scenario Class are the same as those implemented for the Nominal Scenario Class, with two exceptions:

- Ground motion and fault displacement damage to DSs and WPs is calculated as a function of the seismic events, in addition to the damage determined by calculations with the WAPDEG DLL for expected degradation and corrosion processes. This information is provided by *Seismic Consequence Abstraction* (SNL 2007 [DIRS 176828]).

- Drift seepage in the lithophysal and non-lithophysal units is calculated for degraded drifts. Therefore, the Drift Seepage Abstraction, including drift collapse, is implemented. In addition, drift-wall condensation ceases once the drift is fully collapsed.

Additional information that is developed to support the TSPA-LA Model for seismic damage to the DSs and WPs includes an annual frequency of occurrence for seismic events, the hazard curve for mean ground motion at a depth of 300 m beneath the surface of Yucca Mountain, and the mean hazard curves for fault displacement. Multiple seismic events over the modeled duration are included, with the impacts of each event being additive to previous events.

6.1.4.12.4 Human Intrusion Scenario

The Human Intrusion Scenario includes one Human Intrusion Modeling Case. The Human Intrusion Scenario considers the intrusion of a single water or exploratory well into the repository, through a DS and WP, and into the underlying SZ as required by 10 CFR 63.322 (DIRS 180319).

Figure 6.1.4-7 schematically depicts the flow of information between principal TSPA-LA submodels needed to calculate total system performance for the Human Intrusion Modeling Case. The flow of information between submodels in the Seismic Scenario Class is very similar to the Nominal Scenario Class, as depicted on Figure 6.1.4-1.

The majority of the submodels for the Human Intrusion Scenario are the same as those implemented for the Nominal Scenario Class (described in Section 6.3), with four exceptions:

- Mechanical damage to WPs, DSs, and cladding
- Drift seepage for the Human Intrusion Scenario
- UZ Transport for the Human Intrusion Scenario

- EBS flow for the Human Intrusion Scenario.

At the time of the human intrusion, mechanical damage to the single WP and DS is conceptualized as a patch opening the size of the drill bit. DS and WP openings due to general corrosion, MIC, SCC, and localized corrosion are not included in the Human Intrusion Scenario, instead outputs calculated by the WP and DS Degradation Model Component are replaced with a patch opening the size of the drill bit once the human intrusion has occurred. Seepage and water flow through the borehole and into the WP occurs at the percolation rate at the base of the PTn, without consideration of flow focusing. The Drift Seepage Submodel is used to calculate the seepage flux down the borehole. The EBS Flow submodel calculations that determine how much seepage penetrates the DS and WP is replaced with the assumption that all the water that flows down the borehole also flows into the WP. UZ Transport through the borehole from the WP boundary down to the water table occurs using a GoldSim pipe pathway element. The water flux through the UZ is the same as that through the EBS. UZ releases are randomly assigned to one SZ capture region. Once assigned to a capture region, the SZ and Biosphere Model Components treat the UZ releases from the borehole like UZ releases from the UZ Transport Model Component of the Nominal Scenario Class.

Additional information that is developed to support the TSPA-LA Model for inadvertent Human Intrusion through a DS and a WP includes probability of occurrence for earliest time a WP could be penetrated by drilling.

Table 6.1.4-1. Percolation Subregion Information

Percolation Subregion Number	Percolation Subregion Quantile	Number of Locations in Percolation Subregion
1	0 – 0.05	163
2	0.05 – 0.3	816
3	0.3 – 0.7	1306
4	0.7 – 0.95	816
5	0.95 – 1.0	163

Source: SNL 2007 [DIRS 181383], Section 6.2.12.1[a]

NOTE: The number of locations in each percolation subregion is calculated by multiplying the total number of locations, 3,264 (SNL 2007 [DIRS 181383], Section 6.2.12[a]), by the quantile range. Percolation subregions 1 and 5 are rounded down, while percolation subregion 3 is rounded up.

INTENTIONALLY LEFT BLANK

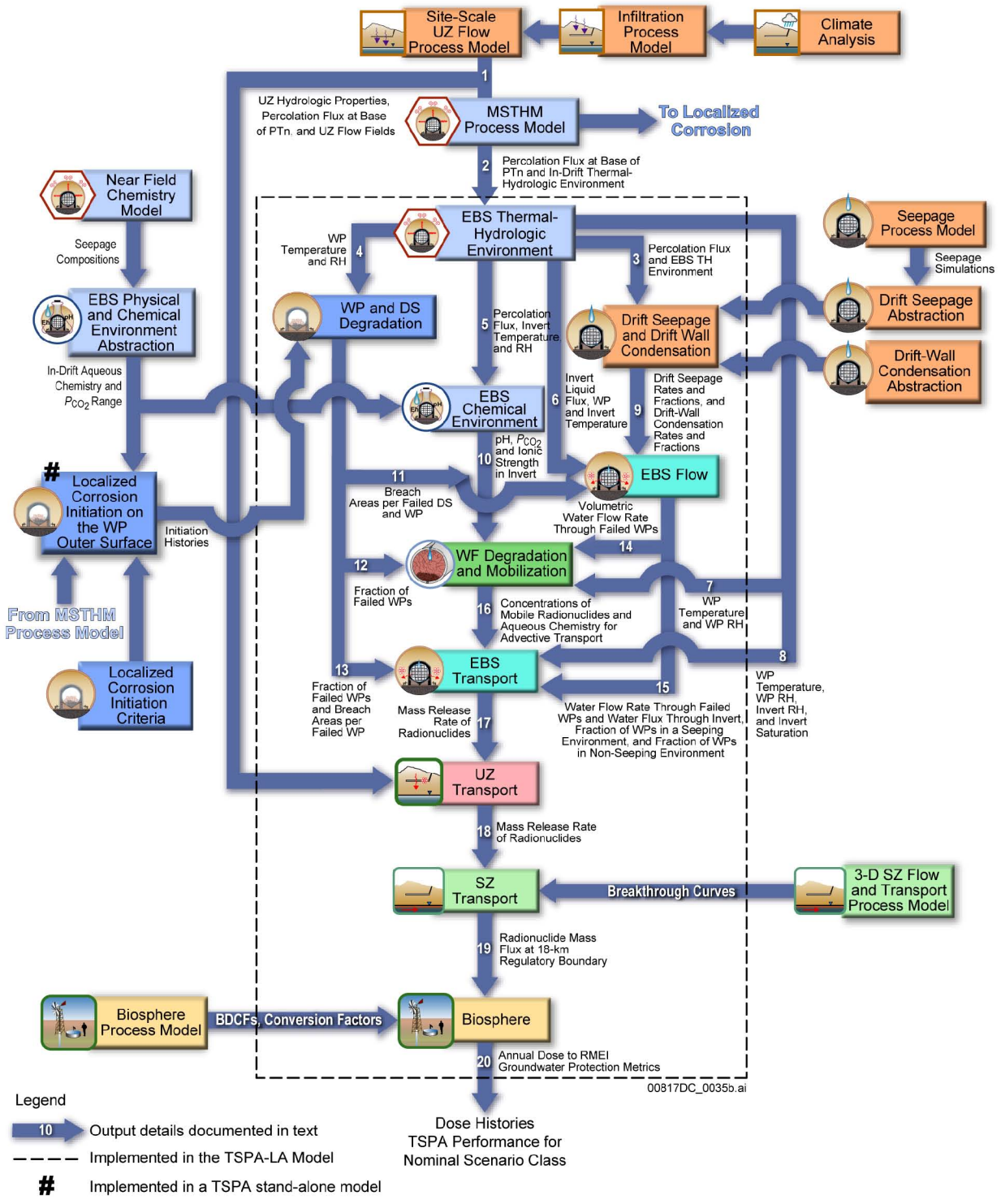

Figure 6.1.4-1. Information Transfer Between the Model Components and Submodels of the TSPA-LA Nominal Scenario Class

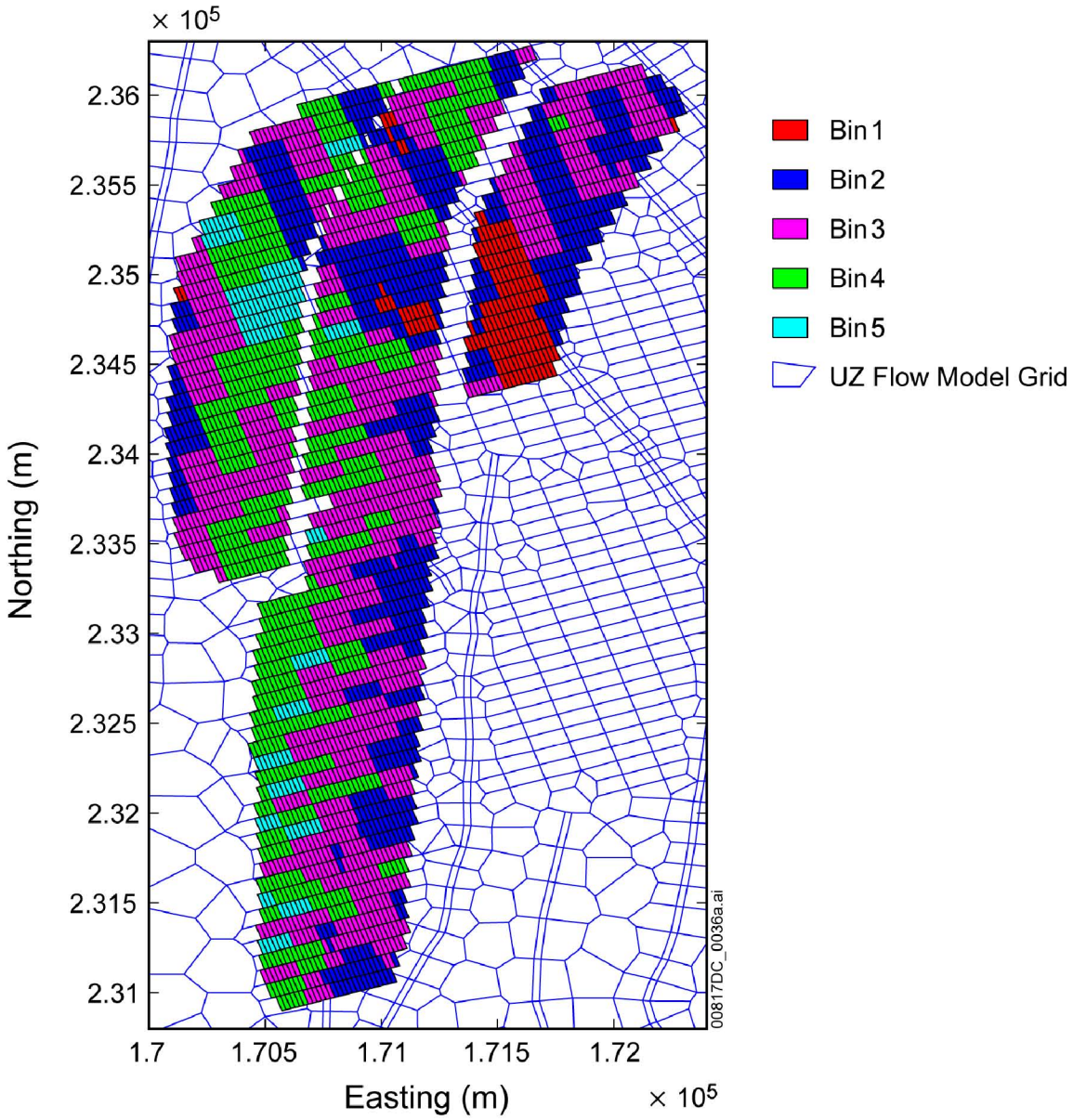

Sources: SNL 2007 [DIRS 181383], Figure VIII-1[a].

Figure 6.1.4-2. Repository Percolation Subregions Used in the TSPA-LA Model (based upon the 10th percentile percolation flux case, glacial-transition climate)

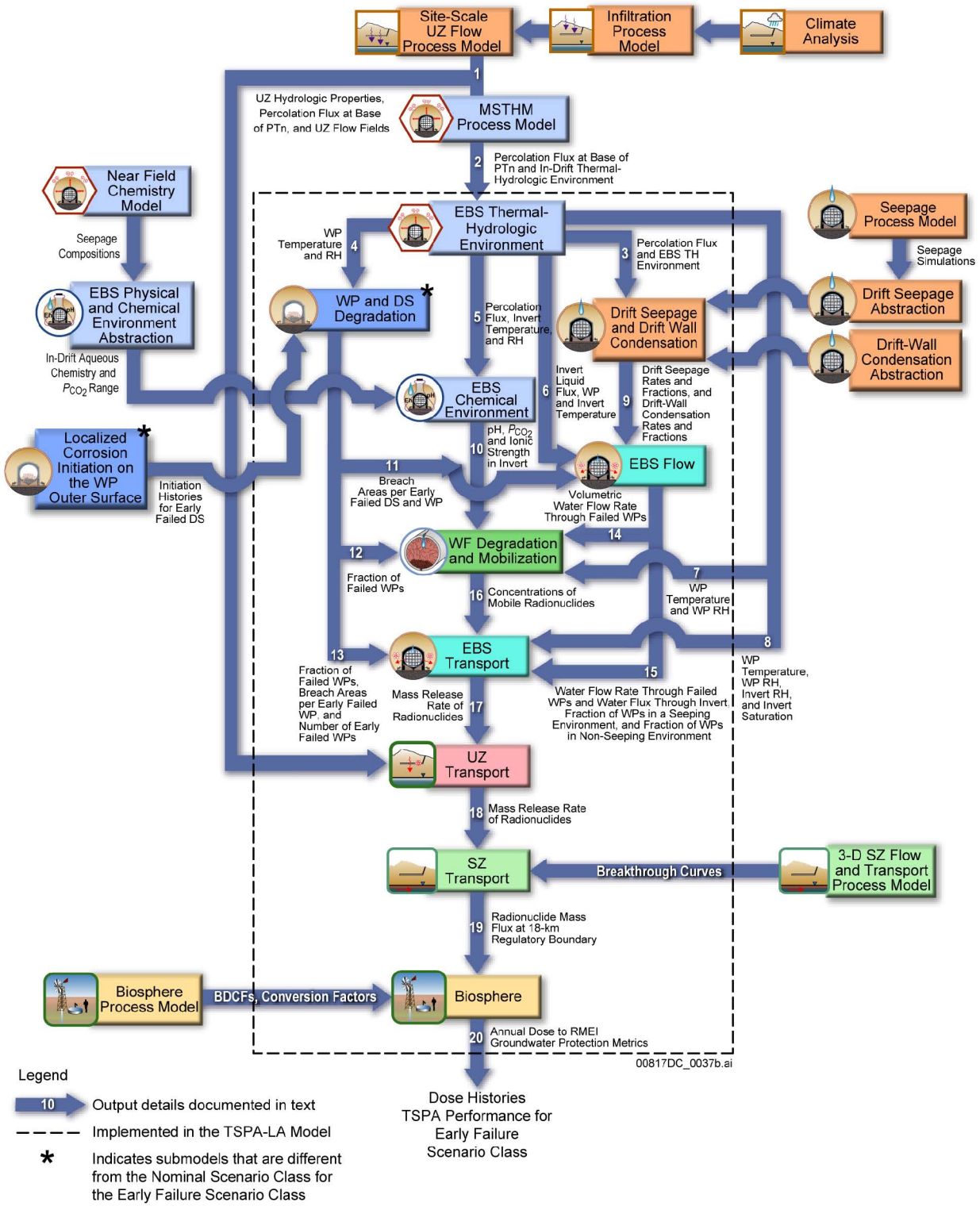

Figure 6.1.4-3. Information Transfer Between the Model Components and Submodels of the TSPA-LA Early Failure Scenario Class

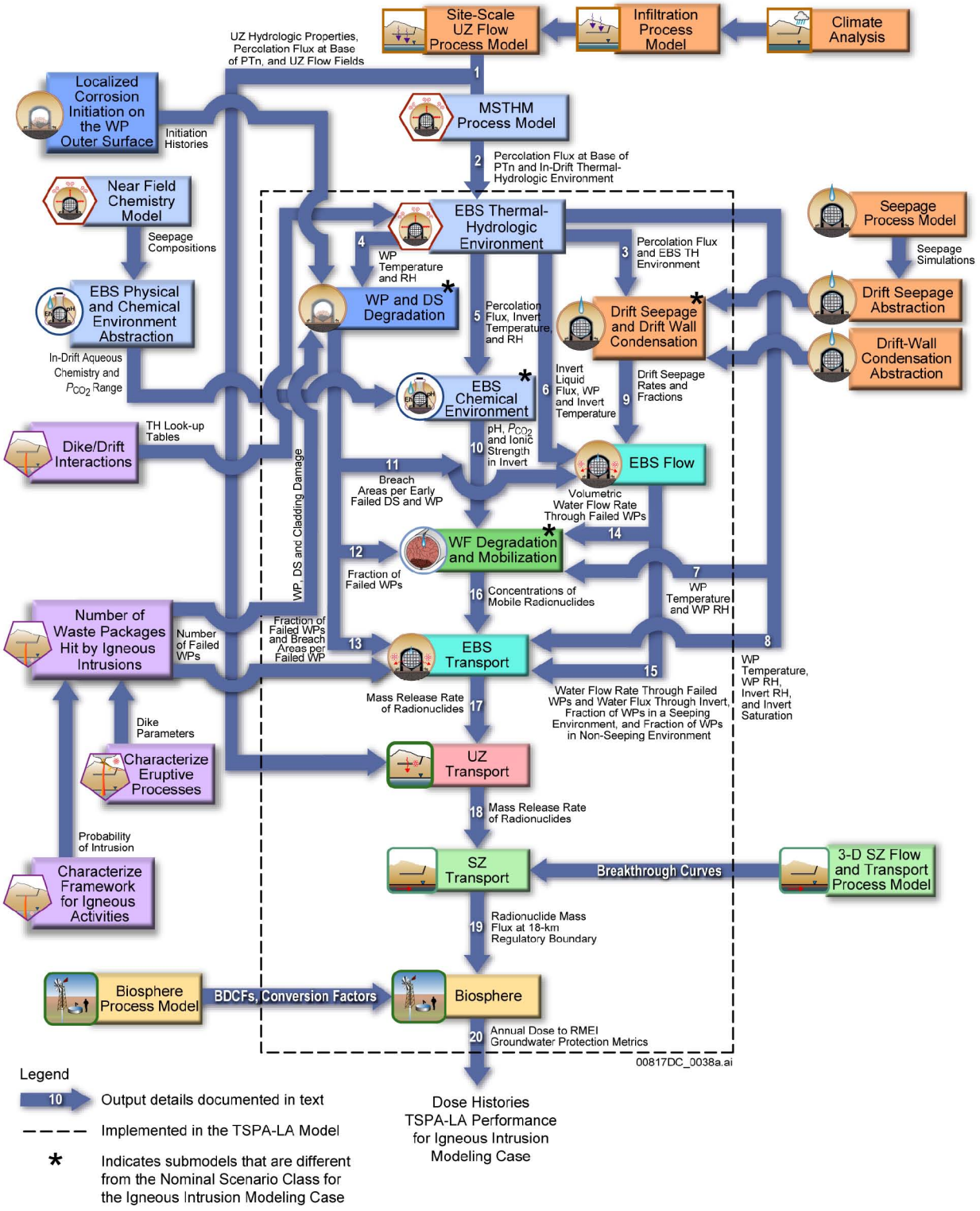

Figure 6.1.4-4. Information Transfer Between the Model Components and Submodels of the TSPA-LA Igneous Intrusion Modeling Case

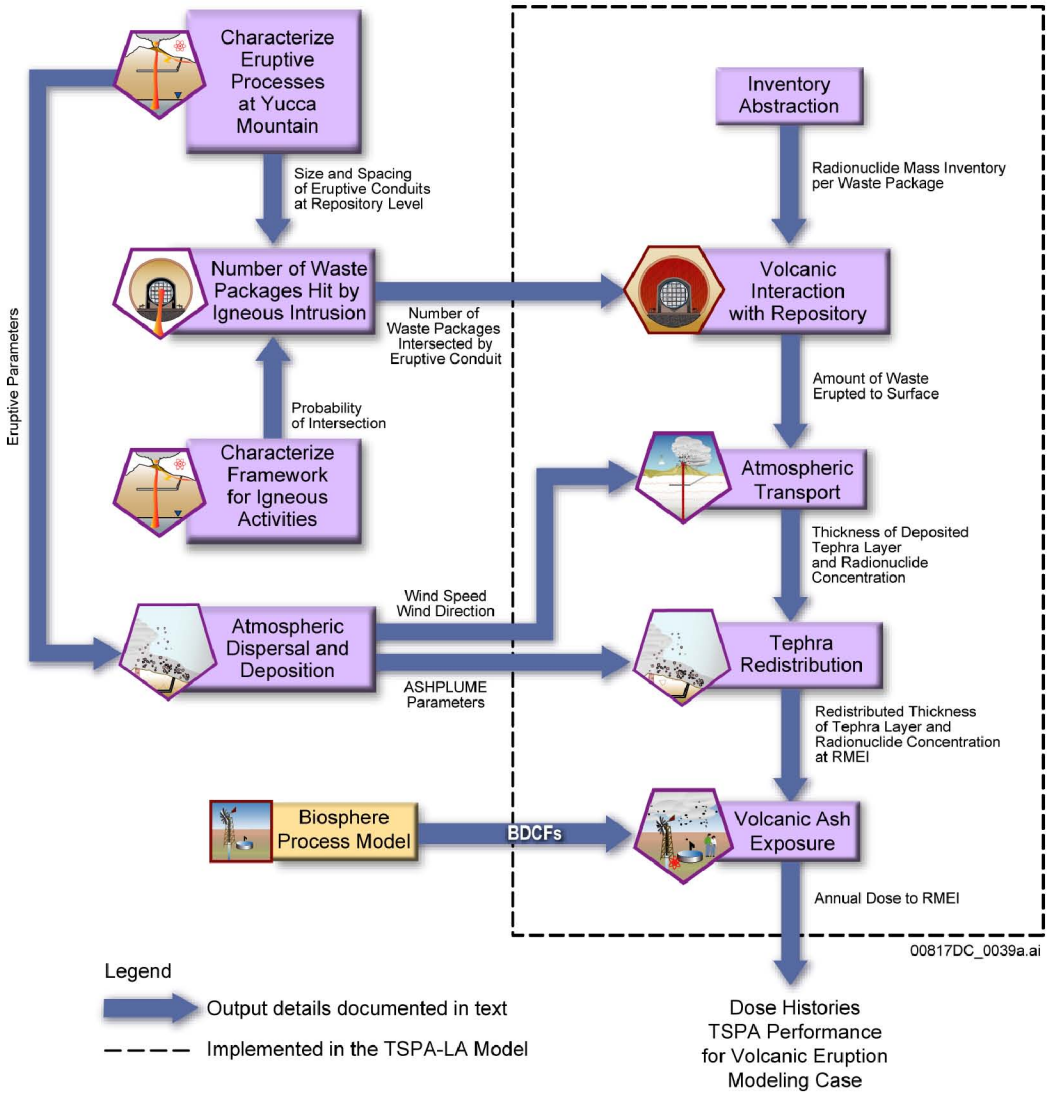

Figure 6.1.4-5. Information Transfer Between the Submodels of the TSPA-LA Volcanic Eruption Modeling Case

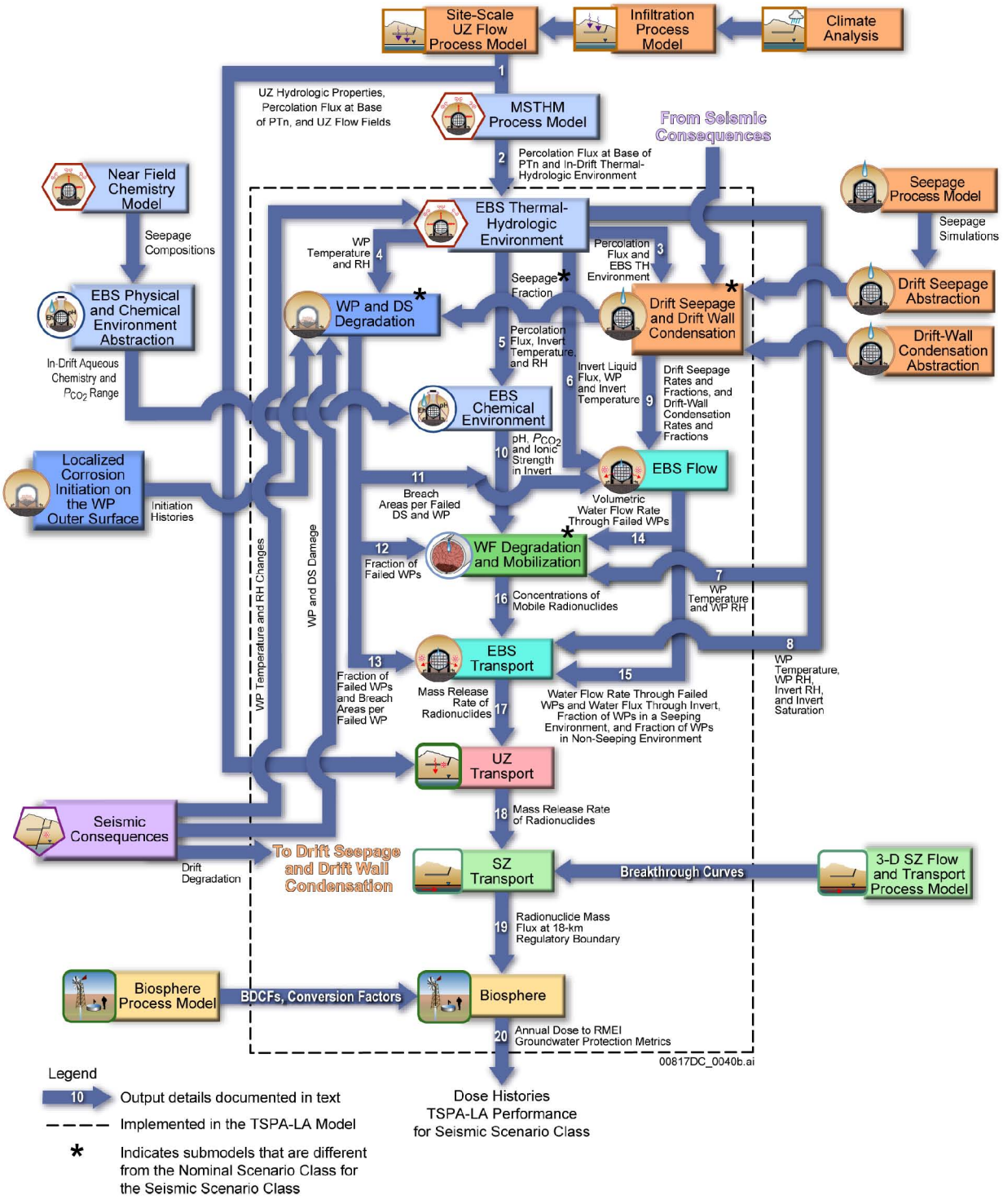

Figure 6.1.4-6. Information Transfer Between the Model Components and Submodels of the TSPA-LA Seismic Scenario Class

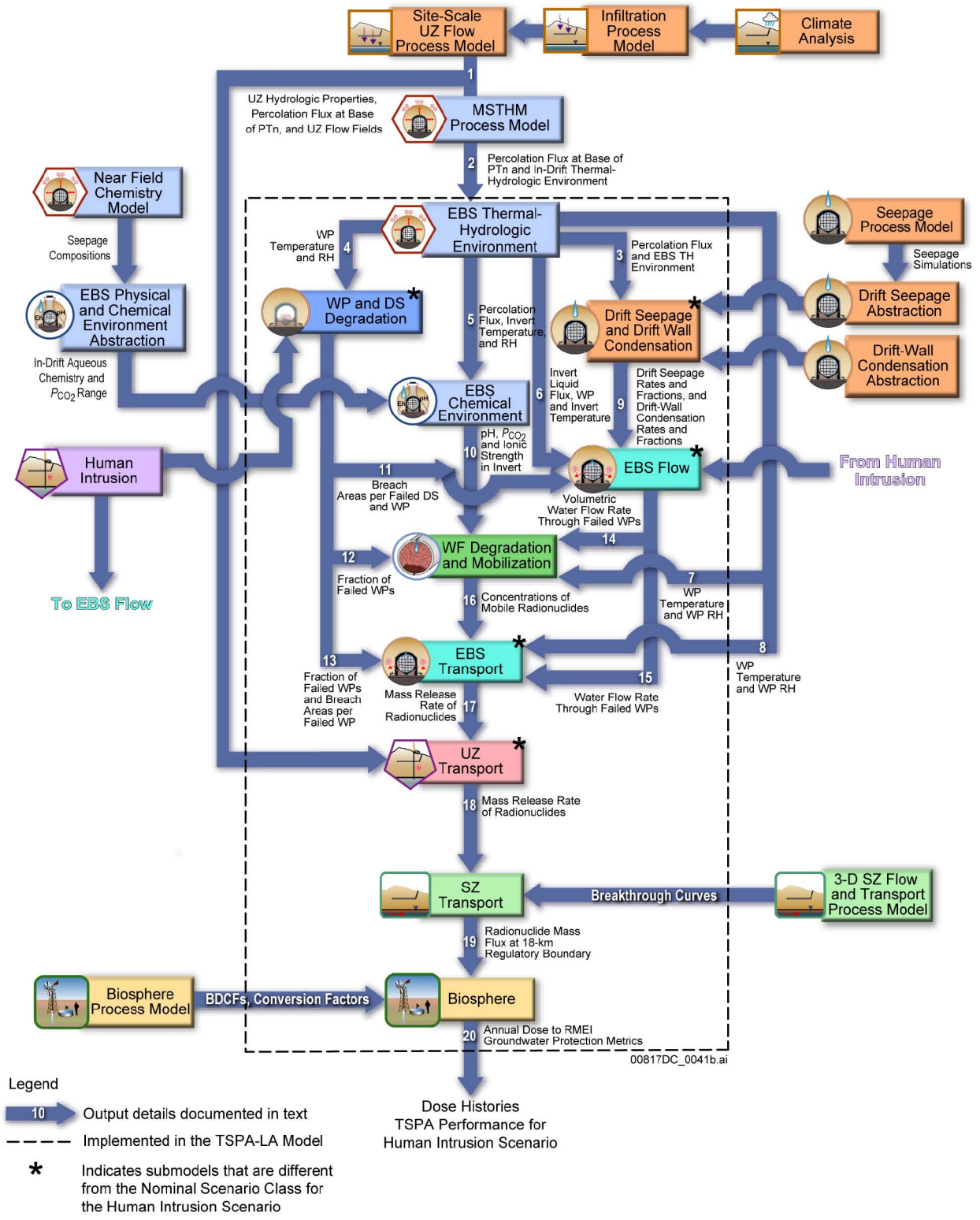

Figure 6.1.4-7. Information Transfer Between the Model Components and Submodels of the TSPA-LA Human Intrusion Scenario

INTENTIONALLY LEFT BLANK

6.1.5 TSPA-LA Model File Architecture

The overall information flow discussed above forms the basis for the TSPA-LA computational model architecture. GoldSim V9.60.100 (STN: 10344-9.60-01 [DIRS 181903]) simulation software serves as the integrating shell that links various submodels and codes that comprise the TSPA-LA Model. For many modeling cases, the TSPA-LA Model GoldSim output is further processed with EXDOC_LA V2.0 (STN: 11193-2.0-00 [DIRS 182102]) to determine the expected dose for each modeling case and a total expected dose combining all of the modeling cases.

GoldSim is a stochastic sampling program that integrates all the submodels, codes, and response surfaces together into a coherent structure that allows for consistent sampling of parameter values among the submodels. The GoldSim program is used to conduct multi-realization simulations of the entire repository system. Values of stochastic parameters for each realization are sampled from uncertainty distributions. Thus, each realization of the total system has a unique set of the values of the input parameters. In addition, each realization is considered to be equally likely, unless importance sampling is used to emphasize some realizations (usually to increase the likelihood of sampling an unlikely event or parameter value). Multiple realizations of the TSPA-LA Model yield a probability distribution of dose rate in the biosphere that shows uncertainty in dose rate based on uncertainty in all of the submodels. When an uncertain parameter appears in more than one GoldSim file (e.g., the sampled infiltration scenario is used in both the Localized Corrosion Initiation Analysis model file and the TSPA-LA Model file), replicate sampling in the two GoldSim files can be achieved by copying the distribution from one model file into the other. This feature allows for different model files to share the exact same sampling for common parameters.

GoldSim was used for five work products: (1) the TSPA-LA Model, (2) the Localized Corrosion Initiation Analysis, (3) waste form inventory decay calculation, (4) eruptive phase dose calculation, and (5) TSPA-LA Model post-implementation verification tests. Different qualified versions of GoldSim were used over the two-year period when these work products were under development.

Much of the computational work for the TSPA-LA Model is done a priori using separate software codes whose results are integrated within the GoldSim software as response surfaces, DLLs, look-up tables, and inputs. For example, the UZ flow fields are computed using the software code Transport of Unsaturated Groundwater and Heat V1.6 (TOUGH2 V1.6 (STN: 10007-1.6-01 [DIRS 161491])). This is a three-dimensional, finite-volume numerical simulator, representing the entire UZ model domain for the dual-permeability Site-Scale UZ Flow Process Model. Details of the calculation results using detailed process models are presented in analysis model reports that support the TSPA-LA Model and are described in Section 6.3. Many of the results of these detailed process-level calculations are provided to the TSPA-LA Model as multidimensional tables that are read into GoldSim at run time. Examples of these multidimensional tables include: (1) liquid flux and velocity fields for the UZ as a function of x, y, z, t, and infiltration flux, as well as other uncertain UZ rock property parameters; and (2) temperature and relative humidity as a function of time and location within the repository.

Once the GoldSim runs are completed and the modeling case dose results are exported to text files, additional software is required to calculate the expected dose for a subset of the modeling cases. The GoldSim runs provide the inputs into these additional dose calculations, which are performed by EXDOC_LA V2.0. The EXDOC_LA V2.0 code calculates the expected dose, conditional on an event occurring. The overall purpose is to separate aleatory and epistemic uncertainty. The solution is integrated over the aleatory uncertainty, for fixed values of the epistemic parameters, to calculate an expected value, conditional on one epistemic element. This operation is repeated for each sample element, to obtain a group of expected results. Statistics (i.e., mean and percentiles) are calculated for these results. The treatment of aleatory uncertainty can be thought of as an inner loop in the calculation and the treatment of epistemic uncertainty as an outer loop. Moreover, EXDOC_LA V2.0 calculates the related complementary cumulative density functions (CDFs) (and associated statistics) for a selected timestep, to allow presentation of both aleatory and epistemic uncertainty on the same graph. In order to produce representative output to be used as input to the EXDOC_LA V2.0 calculations, the TSPA-LA Model in GoldSim is configured with separate sampling of epistemic and aleatory quantities. For computing efficiency, the TSPA-LA GoldSim model is performed with specified aleatory quantities and EXDOC_LA V2.0 is used to calculate the expected dose from these GoldSim runs. As an example, the GoldSim calculations for the Igneous Intrusion Modeling Case are performed for 10 specified event times and EXDOC_LA V2.0 is used to determine the expected dose accounting for event times between these specified values. Thus, GoldSim and EXDOC_LA V2.0 are both required to generate the expected dose.

6.1.5.1 TSPA-LA Model Implementation in GoldSim

The GoldSim V9.60.100 software program is flexible in representing the various component processes in the TSPA-LA Model. The four ways that submodels may be coupled into GoldSim, from most complex to least complex, include the following:

- External function calls to detailed process software codes, such as the UZ transport software, FEHM V2.24 (STN: 10086-2.24-01-00 [DIRS 179419]), or the WP degradation software, WAPDEG V4.07 (STN: 10000-4.07-00 [DIRS 181774] and STN: 10000-4.07-01 [DIRS 181064])

- Cell or Pipe Pathway Elements in GoldSim, which are basically equilibrium batch reactors, which when linked in series, provide a description of transport through selected parts of the repository system, such as in EBS transport

- Response surfaces, which take the form of multidimensional tables, representing the results of modeling with detailed process models that are run before running the TSPA-LA Model (e.g., inputs to the EBS TH Environment, such as temperature and relative humidity in the invert)

- Functional or stochastic representations of a submodel directly built into the GoldSim code, such as seismic ground motion damage or BDCFs.

The details of implementation for specific submodels are best understood by direct review of the TSPA-LA Model implementation within GoldSim, also known as a GoldSim model file. The

text within the GoldSim model files described in this report was updated after the models were run. The updated GoldSim models with the descriptive text are part of output DTN: MO0708GWEFINAL.000_R0 [DIRS 182977].

While Sections 6.3.1 to 6.3.9 include a detailed conceptual description of the submodels included in the TSPA-LA Model, each subsection also includes a discussion of TSPA-LA Model implementation of the submodel discussed in that section with a model pathway to the appropriate location in the GoldSim model file, allowing a detailed review of the implementation. In addition, the GoldSim model file includes a description of the inputs and calculations being performed within each submodel. A summary of the locations of submodel documentation within the GoldSim model file is provided in Table 6.1.5-1.

6.1.5.2 Controlled Data: TSPA Input Database and Data Control Processes

The TSPA Input Database provides all inputs to the TSPA-LA Model. The input database captures values for fixed and uncertain parameters, coefficients in response surface equations, look-up tables, time series data, stochastic distributions, and external files used by TSPA-LA software. To ensure direct inputs to the TSPA-LA Model file are documented, they were also captured on PEFs. Inputs captured by the TSPA Input Database and PEFs consist of three general types and are documented in output DTNs (i.e., output DTN: MO0709TSPAREGS.000_R0 [DIRS 182976]). The three types of inputs are:

1. Direct inputs from controlled sources used directly in the TSPA-LA Model
2. Inputs from controlled sources, but adapted for use in the TSPA-LA Model
3. Inputs generated and used by TSPA in the TSPA-LA Model.

Inputs of the first type are acquired by TSPA analysts from the Yucca Mountain Project Technical Data Management System (TDMS) or from the analysis model reports that provide input to the TSPA-LA Model. These inputs are used directly in the TSPA-LA Model without modification. These parameter values are entered in the TSPA Input Database and captured on a PEF.

Inputs of the second type are also acquired by TSPA analysts from the Yucca Mountain Project TDMS or from the analysis model reports that provide input to the TSPA-LA Model. These inputs are used directly in the TSPA-LA Model with minor formatting. In some instances, prior to entering inputs into the TSPA Input Database, input values are modified by a TSPA analyst to be compatible with the form required by TSPA-LA software or applicable submodels. Such modifications are simple modifications and may include rounding to a specified number of significant digits, removing duplicate input values in defined look-up tables, sorting input values numerically, or converting inputs to units required by the appropriate TSPA-LA submodel or analysis. The changes made by the TSPA analyst are captured on PEFs.

Inputs of the third type are acquired by TSPA analysts from the Yucca Mountain Project TDMS or from the analysis model reports that provide input to the TSPA-LA Model and are processed by TSPA analysts before being captured in the TSPA Input Database and on a PEF. Inputs of the third type include formatting direct inputs through the use of TSPA Department-generated software, manipulating inputs from controlled sources to be consistent with TSPA-LA

conceptual models, and correlating and sampling of the values of the uncertain parameters used both internally by the TSPA-LA Model and TSPA-LA Localized Corrosion Initiation Analysis GoldSim files, and externally by TSPA-LA Model and TSPA-LA Localized Corrosion Initiation Analysis DLLs. In addition, TSPA analysts generate input files used external to the TSPA-LA Model and TSPA-LA Localized Corrosion Initiation Analysis GoldSim files by other qualified software. Like inputs of the first and second type, the changes made by TSPA are captured on PEFs. In the event that substantial preprocessing is required by the TSPA Department, a TSPA analyst performs the preprocessing calculations, submits the information to the Yucca Mountain Project TDMS, including all pertinent documentation, and retrieves the information from the TDMS or a controlled source for use in the TSPA-LA Model.

Figures 6.1.5-1 through 6.1.5-6 depict a sequence of process steps that take place in order to initialize and run the TSPA-LA Model. The initial figure (Figure 6.1.5-1) provides an illustrated overview of all the various elements that make up the framework required for initializing and running the TSPA-LA Model. The framework includes project documents and databases (i.e., analysis model reports and TDMS), as well as elements that are specific to the TSPA-LA Model (i.e., controlled files on the TSPA-LA Model file server and in the TSPA Input Database). PEFs are the most important documents for ensuring traceability of information for all inputs, whether from sources supporting TSPA or intermediate inputs produced during the execution of the TSPA-LA Model. A full discussion of PEFs can be found in Section 4.3. The arrows on the figure illustrate the transfer of information or software. Information transfers include input parameter values and files generated as part of a preprocessing step. Figures 6.1.5-2 through 6.1.5-6 describe the succeeding steps in the processing input data to the TSPA-LA Model. For each figure, the elements in use for the step being discussed will be shown in the lighter of the two colors. The dashed lines on the figure indicate cases where the location of files and software are stored in the TSPA Input Database, but the information or software are actually accessed from the TSPA-LA Model file server.

Input parameter values are loaded into the TSPA Input Database (Figure 6.1.5-2). Parameter values that are in files (e.g., UZ flow fields) are placed in a controlled directory on the TSPA-LA Model file server. The locations of those files are stored in the TSPA Input Database, along with the MD5 digital signature identifying the file. The majority of the input parameters are taken from analysis model reports and the TDMS. Inputs are also taken from other sources (e.g., NRC Proposed Rule 10 CFR Part 63 [DIRS 178394] and [DIRS 180319]) or are generated by the TSPA Department. DLLs are obtained from Software Configuration Management and are installed in a controlled directory on the TSPA-LA Model file server. The locations of those DLLs are stored in the TSPA Input Database, along with the MD5 digital signature identifying the DLL. The traceability of the values of the input parameters and DLLs is documented on PEFs. Any modifications to the original source input (e.g., a change in significant figures, unit conversion) are documented as part of the PEF.

The TH information provided by the MSTHM Abstraction is preprocessed by the PREWAP_LA V1.1 code (STN: 10939-1.1-00 [DIRS 181053]) and the resultant preprocessed PREWAP TH files are documented by a PEF (Figure 6.1.5-3). The set of PREWAP TH files are placed in the TDMS and also placed in a controlled directory on the TSPA-LA Model file server and the location of the files is stored in the TSPA Input Database.

Input parameters values are downloaded from the TSPA Input Database to the localized corrosion analysis in the GoldSim model file (Figure 6.1.5-4). The file is then run for the same number of realizations as the TSPA-LA Model to generate localized corrosion failure histories for each modeling case that includes localized corrosion. A database download is performed to transfer input files (e.g., PREWAP TH files) and the DLLs (i.e., PassTable3D_LA V2.0 (STN: 11143-2.0-00 [DIRS 182556])) associated with the files to the directory where the localized corrosion analysis file runs. The file is run three times, once for the Nominal Modeling Case, once for the Seismic GM Modeling Case, and once for the Seismic FD Modeling Case (Section 6.3.5.2.3). The values of uncertain parameters sampled in the Localized Corrosion Initiation Analysis model file are perfectly correlated to the same distributions sampled within the TSPA-LA Model file. Therefore, each realization of the Localized Corrosion Initiation analysis matches up to the same realization of the TSPA-LA Model GoldSim file. The information for the localized corrosion initiation files is extracted from the localized corrosion analysis file. A PEF is generated to document the production of the localized corrosion initiation files. Then, the localized corrosion analysis files are placed in the TDMS and also placed in a controlled directory on the TSPA-LA Model file server. The locations of the files are stored in the TSPA Input Database.

UZ_PARAMS_MULTI_LA_COMPLIANCE files contain samples of the values of uncertain parameters used in the UZ Transport Model Component (Section 6.3.9) and are generated by running the TSPA-LA Model GoldSim model file (Figure 6.1.5-5). Input parameters values are downloaded from the TSPA Input Database to the TSPA-LA Model GoldSim model file. The database download also transfers input files and the DLLs associated with the file to the directory from which the TSPA-LA Model GoldSim model file is run. Because the TSPA-LA Model is run only to sample the values of uncertain UZ parameters needed for the UZ_PARAMS_MULTI_LA_COMPLIANCE file, it can be configured to run for only the first two timesteps. TSPA-LA Model runs are made for the number of epistemic realizations that the TSPA-LA Model is configured to run (i.e., 300 and 1,000 realizations) (Section 6.3.9.3). The values of the UZ uncertain parameters required for a UZ_PARAMS_MULTI_LA_COMPLIANCE file are extracted and put into the UZ_PARAMS_MULTI_LA_COMPLIANCE files. A PEF is generated to document the production of the UZ_PARAMS_MULTI_LA_COMPLIANCE files. Those files are then placed in a controlled directory on the TSPA-LA Model file server. The locations of those files are stored in the TSPA Input Database. Once all the input parameters to the TSPA-LA Model are pre-processed for use by the TSPA-LA Model, the input parameter values are downloaded from the TSPA Input Database to the TSPA-LA Model (Figure 6.1.5-6). The database download also transfers input files, and the DLLs associated with the files, to the directory from which the TSPA-LA Model GoldSim model file is run.

Figure 6.1.5-7 illustrates the linkages between the software that supports the execution of the TSPA-LA GoldSim model file and the separate GoldSim model file for the Volcanic Eruption Modeling Case. Most of the software consists of DLLs that are called by GoldSim at run time. The software and their functions are described in Section 3. The Localized Corrosion Initiation Analysis is a separate GoldSim model file (Figure 6.1.5-8). This figure illustrates the linkages between the software and the relation of the software to the TSPA-LA Model components discussed in Section 6. The submodels for EBS thermal-hydrology, EBS chemistry, drift seepage, DS degradation, and seismic consequences for the Seismic GM and FD Modeling Cases

and the associated DLLs are implemented in both the GoldSim model file and in the GoldSim model file for the Localized Corrosion Initiation Analysis.

6.1.5.3 Implementation File Structure for the TSPA-LA Model

The layout of calculation containers in GoldSim provides a framework for discussing the implementation of the TSPA-LA Model in GoldSim. Understanding the roles of the containers and their contents is essential for navigating through the TSPA-LA Model files. The layout of containers in the GoldSim software generally follows the Section 6.3 discussion of the model components and submodels, but there are differences at the detail level.

The container structure represents the end result of the construction and evolution of the GoldSim model file developed by TSPA analysts. The end result is a complex file structure that meets the requirements of the TSPA-LA Model. This section is designed to provide information that will facilitate investigation of the TSPA-LA Model and the associated GoldSim model file.

GoldSim Submodels—The TSPA-LA Model implemented in GoldSim contains three GoldSim submodels embedded in one main GoldSim model. Each GoldSim submodel is a completely separate model within the main model and each has it own simulation settings. A GoldSim submodel is a special GoldSim element that performs a complete simulation and passes calculated results to the main model. The three GoldSim submodels in the TSPA-LA Model are: (1) the Epistemic Parameters GoldSim Submodel, (2) the Aleatory Parameters and Dynamic Calculations GoldSim Submodel, and (3) the EBS GoldSim Submodel. A description of each GoldSim Submodel is presented below. The main model sets the simulation settings for these three embedded models and then calls upon each model to perform its simulation. Once all three embedded models have performed their simulation, the main model receives the results and then performs the calculations for the UZ Transport, SZ Flow and Transport, and Biosphere Model Components using these results.

The Epistemic Parameters GoldSim Submodel is a static model that samples distributions of the values of parameters that characterize epistemic uncertainty. The Epistemic Parameters GoldSim Submodel (GoldSim element name: Epistemic_Params) is located in the Epistemic_Uncertainty container shown on Figure 6.1.5-9 and is one containment level below the Epistemic_Uncertainty container level inside the GoldSim model file. Table 6.1.5-1 provides the GoldSim model file pathway to the Epistemic Parameters GoldSim Submodel. The output of the Epistemic Parameters GoldSim Submodel is a suite of values for all parameters that are characterized by epistemic uncertainty. No additional distributions characterize epistemic uncertainty within the TSPA-LA Model or any of the other two GoldSim submodels. These values may be determined by sampling uncertain distributions or may be determined by the evaluation of time-independent calculations that include values sampled from uncertain distributions. The Epistemic Parameters GoldSim Submodel is a small GoldSim model embedded in a larger model and hence it has its own Monte Carlo simulation settings. Because it has its own Monte Carlo simulation settings, the Epistemic Parameters GoldSim Submodel can perform a unique Latin Hypercube Sampling for all realizations performed by the TSPA-LA Model, or it can repeat sequences of sampled values. Within the suite of modeling cases that are performed, the TSPA-LA Model invokes both sampling options within the Epistemic Parameters GoldSim Submodel. In order of calculation hierarchy, the Epistemic Parameters GoldSim

Submodel provides values to both the Aleatory Parameters and Dynamic Calculations GoldSim Submodel and the EBS GoldSim Submodel, as well as to the calculations for the UZ Transport, SZ Flow and Transport, and Biosphere Model Components performed in the main model.

The Aleatory Parameters and Dynamic Calculations GoldSim Submodel is a dynamic model that samples distributions of the values of parameters that characterize aleatory uncertainty and performs additional dynamic calculations utilizing these sampled values. The Aleatory Parameters and Dynamic Calculations GoldSim Submodel (GoldSim element name: Aleatory_Params) is located in the Time_Zero container shown on Figure 6.1.5-9 and is one containment level below the Time_Zero container level inside the GoldSim model file. Table 6.1.5-1 provides the GoldSim model file pathway to the Aleatory Parameters and Dynamic Calculations GoldSim Submodel. The output of the Aleatory Parameters and Dynamic Calculations GoldSim Submodel is a suite of calculated values and time histories for all of the parameters that are characterized by aleatory uncertainty. No additional distributions characterize aleatory uncertainty within the TSPA-LA Model or any of the other two GoldSim submodels. These values may be determined by sampling uncertain distributions or by calculations that include values sampled from uncertain distributions. Because the Aleatory Parameters and Dynamic Calculations GoldSim Submodel is a dynamic model, it has a simulation clock and can perform time-dependent calculations. If a calculation includes an epistemic quantity, the value of the epistemic quantity is first determined in the Epistemic Parameters GoldSim Submodel and then passed into the Aleatory Parameters and Dynamic Calculations GoldSim Submodel. The Aleatory Parameters and Dynamic Calculations GoldSim Submodel is a small GoldSim model embedded in a larger model and hence it has its own Monte Carlo simulation settings. Because it has its own Monte Carlo simulation settings, the Aleatory Parameters and Dynamic Calculations GoldSim Submodel can perform a unique Latin Hypercube Sampling for all realizations performed by the TSPA-LA Model, or it can repeat sequences of sampled values. Within the suite of modeling cases that are performed, the TSPA-LA Model invokes both sampling options within the Aleatory Parameters and Dynamic Calculations GoldSim Submodel. The Aleatory Parameters and Dynamic Calculations GoldSim Submodel provides calculated values to the EBS GoldSim Submodel, discussed next, but does not provide values to the Epistemic Parameters GoldSim Submodel and does not directly provide any transport-related values to the UZ Transport, the SZ Flow and Transport, or the Biosphere Model Components performed in the main model. In order of calculation hierarchy, the Aleatory Parameters and Dynamic Calculations GoldSim Submodel receive values from the Epistemic Parameters GoldSim Submodel and provide values to the EBS GoldSim Submodel.

The EBS GoldSim Submodel is also a dynamic model. With the exception of some static calculations that determine the size of the WP groups modeled by the GoldSim source term elements and the fractional failure history of each WP group, this embedded model performs all of the EBS-related calculations that support the UZ Flow, EBS Environment, WP and DS Degradation, Waste Form Degradation and Mobilization, and EBS Flow and Transport Model Components. The EBS GoldSim Submodel (GoldSim element name: EBS_Submodel) is located in the Time_Zero container shown on Figure 6.1.5-9 and is three containment levels below the Time_Zero container level inside the GoldSim model file. Table 6.1.5-1 provides the GoldSim model file pathway to the EBS GoldSim Submodel. The output of the EBS GoldSim Submodel provides the time histories of radionuclide flux from the bottom of the invert into the UZ beneath the repository, taking into account all repository-related processes. The EBS

GoldSim Submodel does not sample any uncertain distributions. Inputs to the EBS GoldSim Submodel include sampled values of epistemic parameters from the Epistemic GoldSim Submodel and all of the values of the aleatory parameters and associated time history results from the Aleatory Parameters and Dynamic Calculations GoldSim Submodel. In addition, the TSPA-LA Model performs additional calculations between performing the calculations of the Aleatory Parameters and Dynamic Calculations GoldSim Submodel and the EBS GoldSim Submodel. These calculations are static calculations that populate the number of WPs in each GoldSim source term within the EBS GoldSim Submodel and also determine the fraction of WPs that are exposed to drift seepage and the time history of WP failures from general and localized corrosion. These static calculations involve external DLLs that perform the related calculations necessary to model the EBS.

Looping Containers—Unlike the Epistemic GoldSim Submodel and the Aleatory Parameters and Dynamic Calculations GoldSim Submodel, the EBS GoldSim Submodel is placed within looping containers. A looping container is another special GoldSim element that allows the calculations within the container to be repeated in a DO-WHILE loop. The EBS GoldSim Submodel simulation is performed in 15 loops within one realization of the TSPA-LA Model, one loop for each of 15 WP groups. Each of the 15 WP groups is described by a set of average properties for the entire group. Combining groups of WPs that have similar properties results in average properties that are derived from a subset of WPs that have less variation. For the TSPA-LA Model, the WP properties that define the different WP groups are: (1) the percolation flux rate above the WP location, (2) the occurrence of drift seepage above the WP location, and (3) whether or not drift seepage-induced localized corrosion damages the WPs at a WP location. Choosing the number of WP groups to model balances computational efficiency against the most important processes that govern releases from the EBS. Using a looping container over each WP group ensures that the calculations that are performed for each WP group are consistent with the calculations performed for the other groups. Therefore, the TSPA-LA Model models the EBS GoldSim Submodel in 15 different loops, each loop models a different WP group. The 15 loops are actually performed in two loops, an outer loop (called EBS_PS_Loop in the GoldSim model file), referred to as the percolation subregion loop, and an inner loop (EBS_PSE_Loop in the GoldSim model file), referred to as the percolation subregion environment loop. The outer loop is performed five times, once for each percolation subregion. These five loops account for spatial variability in the percolation flux above the repository. This discretization is described in detail in Section 6.3.2 of this report. Within each of these five percolation subregion loops, the EBS GoldSim Submodel performs calculations for three additional loops, bringing the total number of loops to 15. These three loops consider two different drift seepage conditions above each WP location and two different damage mechanisms to the WP. The first loop considers all the WPs in a percolation subregion that are not exposed to drift seepage. The fraction of WPs that are exposed to drift seepage is determined by the Drift Seepage Submodel of the UZ Flow Model Component. The second loop models all WPs that are exposed to drift seepage and do not experience localized corrosion in the modeled duration. The third loop models all WPs that are exposed to drift seepage and experience localized corrosion in the modeled duration. The distinction between seepage locations and non-seepage locations is important because advection and diffusion from a failed WP can result in greater mass release than for diffusion release alone. Advection from the WP can only occur if there is a water source dripping onto a failed WP. The distinction between localized corrosion packages and non- localized corrosion packages is important when considering the opening area on the WP. The rate of advection and diffusion

from a failed WP is proportional to the opening area on the failed WP. In the absence of localized corrosion, crack damage from SCC (Section 6.3.5) and/or seismic ground motion (Section 6.6.1) has a different release rate than a WP with localized corrosion patch openings that completely penetrate the WP. Appendix N presents the derivation of the equations used to calculate the number of WPs (referred to as WP parsing) modeled by each WP group.

High Level Containers—The highest level of the GoldSim model file is a set of containers that define the overall organization of the GoldSim model file (Figure 6.1.5-9). These containers are not all of the same type or size. Global_Model_Input (Figure 6.1.5-9) stores the configuration properties for the TSPA-LA Model and other inputs referenced throughout the TSPA-LA Model. Epistemic_Uncertainty (Figure 6.1.5-9) contains the Epistemic Parameters GoldSim Submodel. Time_Zero (Figure 6.1.5-9) contains both the Aleatory Parameters and Dynamic Calculations GoldSim Submodel and the EBS GoldSim Submodel. This container is a conditional container that performs dynamic calculations prior to advancing the simulation clock controlling the calculations performed for the UZ Transport, SZ Flow and Transport, and Biosphere Model Components in the main model. The calculations for these model components are captured within the TSPA_Model (Figure 6.1.5-9) container. In general, within these high-level containers or the GoldSim Submodels embedded directly beneath them, the model elements that define the input parameters and perform calculations are grouped into nine containers, one for each of the eight principal model components, shown on Figure 6-1, and one for events. Understanding the containers and their organization is important for navigating through the GoldSim model file and finding information, but they do not always correspond to the conceptual organization of the TSPA-LA Model discussed elsewhere in this report. For instance, within the Aleatory Parameters and Dynamic Calculations GoldSim Submodel, the Aleatory_Calcs_Seismic container contains information related to the Seismic Scenario Class, discussed in Sections 6.1.4.12.2 and 6.5, but does not contain all of the submodels involved in representing the Seismic Scenario Class. Additional inputs and calculations are defined in the Epistemic Parameters GoldSim Submodel and within the EBS GoldSim Submodel where radionuclide releases from seismic-damaged WPs are modeled.

The conceptual TSPA-LA Model discussion focuses on model components and submodels that can be divided, at the highest level, between natural system models and engineered system models. The following discussion will define, at a high level, the implementation of these models in the GoldSim model file.

Submodel Organization—The TSPA-LA Model is a system of scientific models and abstractions sharing numeric information and linked together in the GoldSim software. In general, the TSPA-LA Model is composed of eight principal model components and an event scenarios component. Each model component is itself a system of dynamic calculations performed by one or more submodels. Within a model component container, the submodels that comprise the model component are organized into separate containers. Each submodel may be a function of the calculated values from other submodels within the same model component or another model component. To enhance transparency, each submodel is further organized into separate containers for inputs, calculations, and outputs. The inputs to a submodel may include parameter definitions and results from other submodels. These two types of inputs are segregated into Model_Input and Model_Feed containers, respectively. The calculations for each submodel are performed in a Model_Calcs container. The outputs of the submodel that are

passed to other submodels are captured in a Model_Output container. The elements within the Model_Feeds container of one submodel are linked to the elements within the Model_Output container of another.

Representation of the Natural System above the Repository—The natural system above the repository includes the land surface, the soil and rock near the land surface, and the UZ above the repository. The information pertaining to this part of the repository system is located in three locations in the TSPA-LA Model. Uncertain inputs are captured in the Epistemic_Params_UZ_Flow and Epistemic_Calcs_UZ_Flow containers within the Epistemic Parameters GoldSim Submodel. Additional input parameters and UZ flow calculations are located in the Time_Zero container. Static calculations to obtain the fraction of WPs that are exposed to drift seepage, which is used to determine the number of WPs to model in each WP group, are located in the Static_Calcs_UZ_Flow container. These static calculations are located in the percolation subregion (outer) loop of the EBS calculations. Therefore, the UZ Flow calculations in the Static_Clacs_UZ_Flow container are performed five times, once in each percolation subregion loop. Within each percolation subregion loop, the inputs to the UZ Flow calculations are appropriate for the active percolation subregion and thus the calculated values of the UZ Flow Model Component will vary in each percolation subregion loop. The rest of the calculations that are part of the UZ Flow Model Component are found within the Global_UZ_Flow, Seep_Params and Condensation_Model containers within the EBS GoldSim Submodel. The calculations inside these three containers are performed 15 times, once for each outer loop and inner loop pair of the EBS GoldSim Submodel. For each loop, implementation using IF…THEN…ELSE functions allows the inputs to the UZ Flow calculations to change to the appropriate values for the active percolation subregion and seeping environment type. However, because WP damage by localized corrosion does not affect UZ Flow properties, the calculated values of the UZ Flow Model Component within one percolation subregion loop will be the same in the second and third percolation subregion environment loops. Combining all of this information, the UZ Flow Model Component includes information on climate state, infiltration, seepage into drifts, and drift-wall condensation.

Representation of the Engineered System—The calculations that model the performance of the Engineered_System are located in four locations in the TSPA-LA Model. Uncertain inputs are captured in the Input_Params_Epistemic container within the Epistemic Parameters GoldSim Submodel. Within this container, the input parameters are further organized into containers defined for each EBS Model Component, EBS Environment, WP and DS Degradation, Waste Form Degradation and Mobilization, and EBS Flow and Transport. Within each of these model component containers, the uncertain inputs may be further organized into separate containers for each submodel of the model component. The level of discretization within the Epistemic Parameters GoldSim Submodel increases with increasing complexity of the model component. Additional input parameters and EBS calculations are located in the Time_Zero container. Dynamic calculations related to the chemical interaction between seepage water and the host rock and the integrity of the DS under nominal conditions are performed in the Aleatory Parameters and Dynamic Calculations GoldSim Submodel. The water-rock interaction calculation is discussed in detail in Section 6.3.4. The nominal corrosion of the DS is discussed in Section 6.3.5. Static calculations that are used to determine the number of WPs to model in each WP group, the WP Parsing Submodel, and localized corrosion and general corrosion failures of the WP are located in the Static_Calcs_PS_Loop container. Two of the four EBS-

related model components have calculations within this container, WP and DS Degradation and EBS Flow and Transport. These calculations are located in the percolation subregion (outer) loop of the EBS calculations. Therefore, the EBS calculations in the Static_Calcs_PS_Loop container are performed five times. Each time the inputs to the calculations are appropriate for the active percolation subregion and thus the calculated values will vary in each loop. The rest of the calculations that model the EBS are found within the EBS GoldSim Submodel. The EBS GoldSim Submodel container includes a greater variety of information than any of the other containers. The overall discretization of WP groups and the structure of the container are shown on Figure 6.1.5-10. Some aspects of the implementation of the EBS submodels can be characterized as global and are independent of details such as fuel type or location within the repository. Much of the implementation, however, is dependent on the discretization of the submodel by waste type, percolation flux subregion or bin, and seepage environment.

The first level of discretization is by waste type. The TSPA-LA Model considers two types of WPs: CSNF and CDSP WPs. These WPs represent all of the WP types considered in the TSPA-LA Model. Details of how this representation is developed are found in Section 6.3.2.2.2. Within the TSPA-LA Model, discretization by waste type is handled explicitly by implementing different GoldSim elements to perform the fuel type-specific calculations.

The second level of discretization is by percolation subregion. The magnitude of infiltration varies spatially across the land surface above the repository footprint and percolation flux varies spatially at the repository level. This spatial variability is captured in a CDF of percolation flux values that are calculated for 3,264 locations (SNL 2007 [DIRS 181383], Section 6.2.12.1[a]). This CDF provides the basis for the TSPA-LA Model representation by percolation subregions, as described in Section 6.3.2. Percolation subregion locations are shown on Figure 6.1.4-2.

The third level of discretization is by seeping environment (i.e., seepage with or without drift-wall condensate) and localized corrosion failure mode. The CSNF and CDSP WPs that are in each percolation subregion are identified as either having seepage above each WP location or not. Those that have seepage are further discretized into two groups, those that experience localized corrosion damage and those that do not experience localized corrosion damage.

The three levels of discretization result in the 30 environments in the TSPA-LA Model (two fuel types × five percolation flux subregions × three seepage/ localized corrosion states) that are used to represent all of the WPs in the repository.

Figure 6.1.5-11 illustrates how the repository is conceptualized with the three levels of discretization discussed above. The representation is purposely a schematic to emphasize the conceptually important aspects of the discretization. The left portion of the figure shows the percolation flux subregions, as defined in Section 6.1.4.2, superimposed on the repository footprint. The rest of the figure shows a schematic representation of these subregions (the boxes) and illustrates the discretization by waste type and seeping/localized corrosion conditions. The levels of discretization shown on Figure 6.1.5-10 together with the repository conceptualization shown on Figure 6.1.5-11 lead to the implementation found in the GoldSim model file.

The discretization structure determines the type of information that is included in the containers at each level. Containers at the highest level of Global_Inputs_and_Calcs in the EBS GoldSim

Submodel, the Global_WP_DS_Deg, Global_EBS_Environ, Global_WF_Deg_Mob, and Global_EBS_F_and_T containers, include global inputs, such as the corrosion rate for Alloy 22, the chemistry inside a failed WP under seeping or non-seeping conditions, and the regression coefficients in the waste form degradation rate equations. This is information used for all percolation flux subregion environments.

At the level of discretization by waste type, the CSNF_Packages and CDSP_Packages containers within the EBS GoldSim Submodel, GoldSim containers include information needed to evaluate processes that are specific for each fuel type.

The next level of discretization is by percolation subregion environment and refers to the 30 environments defined on Figure 6.1.5-10. As stated earlier, the TSPA-LA Model captures the required EBS calculations for all 15 CSNF environments in one container and for all 15 CDSP WP environments in another container. These two calculation containers accommodate the 30 environments by using IF…THEN…ELSE functions to vary the calculation inputs to those specific for each of the 30 environments. The detailed source term calculations are performed within each of these two percolation subregion environment containers. Parameter values identified here include the temperature and relative humidity of the invert and WP surface, reading WAPDEG V4.07 DLL output to determine crack and patch failures, and chemical parameters for the WP and invert for dripping and non-dripping conditions, solubilities of radionuclides in the invert and in the WPs, which are values that are determined from look-up tables that are defined elsewhere. At this level, the TSPA-LA Model also calculates the mass flux of radionuclides at the base of the invert.

Once calculated, results of EBS conditions and radionuclide mass flux rates are passed from each loop to TS_PROC.DLL. This is a specialized GoldSim DLL that stores and segregates results for each outer loop of a GoldSim submodel. For results that differ for each inner loop, the DLL can be configured to add or average the results of each inner loop. The model components that comprise the EBS are discussed in additional detail in Sections 6.3.2 through 6.3.8.

Representation of the Natural System Below the Repository—The natural system below the repository includes the UZ, the SZ, and the biosphere. Related model components are shown on Figure 6-1 and are present in the TSPA_Model container at the highest level of the GoldSim model file. Within the TSPA_Model container there are six high level containers. The UZ_Flow container is a repeat implementation of the Climate Submodel of the UZ Flow Model Component. This information is used by the UZ Transport and SZ Flow and Transport Model Components. The Engineered_System container captures the radionuclide mass flux from the bottom of the invert into the UZ beneath the repository and the number of failed WPs. This information is fed directly into the UZ Transport Model Component from within this container. In addition, this container also captures EBS-related results that are useful for model analysis. The calculations for the model components representing the natural system below the repository are captured in the UZ_Transport, SZ_Transport, and Biosphere containers. Each of these containers is briefly discussed below. Finally, all model results that are useful for model analysis are captured within the results container.

Similar to the organization discussed previously, the uncertain parameters that characterize epistemic uncertainty for the UZ Transport, SZ Flow and Transport, and Biosphere Model

Components are captured in separate containers within the Epistemic Parameters GoldSim Submodel. Many of the uncertain parameters used in the UZ Transport Model Component are shared by the EBS Flow and Transport Model Component. The uncertain parameters used by both models are sampled within the EBS Flow and Transport Model Component. Additionally, all uncertain parameters used in the UZ Transport Model Component are pre-sampled and written to an external file accessed by the FEHM V2.24 DLL during UZ transport calculations. Because a large number of uncertain parameters are shared between the EBS and UZ transport Submodels, all uncertain parameters used in UZ transport calculations have been co-located with parameters of the EBS Flow and Transport Model Component so that the elements that generate the UZ external file are co-located. Similarly, the epistemic uncertainties in the SZ Flow and Transport Model Component are correlated to input files accessed by the SZ_Convolute V3.10 DLL (STN: 10207-3.10.01-00 [DIRS 181060]). Thus, these parameter values are pre-sampled and stored in look-up tables. The pre-sampled values in the look-up tables share an index value with the external files. The index is randomly sampled in the Epistemic Parameters GoldSim Submodel, ensuring consistency between the calculations performed inside the GoldSim model and those performed by the SZ_Convolute V3.10 DLL. The epistemic uncertainties in the Biosphere Model Component are reflected in BDCFs. The BDCFs for different radionuclides may be highly correlated and are provided to TSPA as look-up tables of correlated values. Each look-up table shares a common index variable. The index is randomly sampled in the Epistemic Parameters GoldSim Submodel, ensuring that the desired correlation among BDCFs is applied.

The model calculations addressing the performance of the Natural System below the Repository are calculated in the TSPA_Model container of the TSPA-LA Model. Within this container, separate containers exist for the three model components comprising the natural system below the repository. The UZ Transport Model Component receives the radionuclide mass flux from the bottom of the invert. Time histories of releases from the bottom of the invert into the fractures and matrix beneath the repository are captured in the Engineered_System container. Additional EBS outputs are also captured within this container. These results are used by the TSPA analysts to analyze the performance of the EBS.

The UZ_Transport container includes a call to the FEHM V2.24 DLL, as well as input parameters needed by the FEHM V2.24 DLL and outputs from the calculations done by the FEHM V2.24 DLL. 16 flow fields are calculated using TOUGH2 V1.6. These flow fields represent four infiltration scenarios for each of four climate states. These 16 flow fields are used for calculations made in the UZ_Transport container. The UZ_Transport container contains input parameters such as fracture porosity and matrix diffusion coefficients. The FEHM V2.24 DLL calculates radionuclide release rates from the UZ fractures and matrix to the SZ. The UZ Transport Model Component is discussed in additional detail in Section 6.3.9.

The SZ_Transport container includes outputs from the 3-D SZ Flow and Transport Model Component, consisting of radionuclide breakthrough curves that provide the information needed to perform one-dimensional calculations that account for radionuclide decay and the growth of radionuclide daughter products during transport through the SZ. The SZ_Transport container includes parameter values needed for the three-dimensional and one-dimensional calculations, inputs of radionuclide mass from the UZ, the calculations of radionuclide transport through the SZ, and outputs of radionuclide mass to the biosphere. The 3-D SZ Flow and Transport Model

Component is performed using the SZ_Convolute V3.10 DLL. The SZ Flow and Transport Model Component is discussed in additional detail in Section 6.3.10.

The Biosphere container includes information needed to calculate dose to the RMEI, due to the radionuclides released from the repository and transported through the UZ and SZ. The Biosphere container includes BDCFs, groundwater protection conversion factors, and radionuclide mass flux inputs from the SZ. The Biosphere Model Component is discussed in additional detail in Section 6.3.11.

Events—Early failures of the WP and DS and other disruptive event scenarios are addressed in the TSPA-LA Model using distinct scenario classes. The implementation of these scenario classes is integrated into the TSPA-LA Model's GoldSim model file, along with the implementation of the Nominal Scenario Class. In general, parameters relating to the event scenarios use separate containers to segregate the Nominal Scenario Class calculations from the Early Failure Scenario Class, the Seismic Scenario Class, the Igneous Scenario Class, and the Human Intrusion Scenario. Similar to the calculations supporting the Nominal Scenario Class, much of the information used for the events scenario classes can be found throughout the TSPA-LA Model's GoldSim model file in containers used for calculations for the Nominal Scenario Class.

Within the Epistemic Parameters GoldSim Submodel, the Aleatory Parameters and Dynamic Calculations GoldSim Submodel, and the EBS GoldSim Submodel, separate containers hold the input parameter definitions and calculations that are applicable in the event scenarios. An events container is placed alongside the other model component containers in each of these locations. Within this container, inputs and calculations are further segregated into containers for each event type. Performing a GoldSim model run for an event scenario is similar to running the Nominal Scenario Class model file. The TSPA-LA Model has been built using GoldSim selector elements to pass submodel outputs from one submodel to another. The default result for these output elements is the sampled or calculated value for the Nominal Scenario Class. When configured to run an event scenario, these submodel output elements use IF…THEN…ELSE functions to replace or augment a Nominal Scenario Class result with the event-specific calculation result (if appropriate).

Modeling early failure event scenarios includes the conditions of early failures of the DSs or WPs. The Early Failure Scenario Class is discussed in detail in Section 6.4. The Drip Shield EF and Waste Package EF Modeling Cases model the performance of the repository following an early failure event. Submodels of the WP and DS Degradation Model Component from the Nominal Scenario Class are augmented with additional processes that are applicable for an early failure event. The Drip Shield EF Modeling Case is discussed in greater detail in Section 6.4.1. The Waste Package EF Modeling Case is discussed in greater detail in Section 6.4.2.

Modeling seismic events includes conditions resulting from seismic ground motion activity and fault displacement. The Seismic Scenario Class modeling cases model the performance of the repository following one or more seismic events. Consequences to the drift, DS, and WP from seismic activity are included. Submodels of the UZ Flow, EBS Environment, WP and DS Degradation Model Components from the Nominal Scenario Class are augmented with additional processes that are applicable for the repository following seismic activity. The

Seismic GM Modeling Case and the Seismic FD Modeling Case are discussed in detail in Section 6.6.1. The Seismic Scenario-related containers include the parameters needed to characterize a potential seismic event, and the potential consequences to the drift, WPs, and DSs, including levels of ground motion, rockfall potential, and the potential for fault displacement.

The Igneous Scenario-related containers include information for the Igneous Intrusion Modeling Case. The Igneous Intrusion Modeling Case models the performance of the repository following an igneous intrusion. Submodels of the UZ Flow, EBS Environment, WP and DS Degradation, and Waste Form Degradation and Mobilization Model Components from the Nominal Scenario Class are augmented with additional processes that are applicable after the igneous intrusion. The Igneous Intrusion Modeling Case is discussed in greater detail in Section 6.5.1. The Volcanic Eruption Modeling Case is performed in a separate GoldSim model file and is discussed in detail in Section 6.5.2. However, in general, this model file is organized similar to the TSPA-LA Model, but with less complexity because the modeling case excludes a number of the EBS and groundwater-related model components. The information in this model file includes parameter inputs for ASHPLUME, as well as the call to the ASHPLUME_DLL_LA V2.1 DLL (STN: 11117-2.1-00 [DIRS 181035] and STN: 11117-2.1-01 [DIRS 180147]), and the calculations for tephra redistribution and the probabilistic weighting of the source term used to determine dose.

Modeling a human intrusion event includes groundwater drilling operations that intersect the repository, resulting in a breach to a DS and a WP, followed by subsequent radionuclide transport down the borehole and into the SZ. Submodels of the UZ Flow, WP and DS Degradation, EBS Flow and Transport, and UZ Transport Model Components from the Nominal Scenario Class are augmented with additional processes that are applicable for a human intrusion event. The Human Intrusion Modeling Case is discussed in greater detail in Section 6.7.1.

INTENTIONALLY LEFT BLANK

Table 6.1.5-1. Location of Implementation Description in the GoldSim TSPA Model File

Submodel	Documentation Location(s)
Epistemic Parameters GoldSim Submodel	\Epistemic_Uncertainty\Epistemic_Params
Aleatory Parameters and Dynamic Calculations GoldSim Submodel	\Time_Zero\Aleatory_Params
EBS GoldSim Submodel	\Time_Zero\EBS_PS_Loop\EBS_PSE_Loop\EBS_Submodel
Natural System below the Repository	\TSPA_Model
Climate	Epistemic: NA Aleatory: NA EBS: \Global_Inputs_and_Calcs\Global_UZ_Flow\Climate Other: \TSPA_Model\UZ_Flow\Climate
Infiltration	Epistemic: \Input_Params_Epistemic\Epistemic_Params_UZ_Flow\Uncertain_Params_Infiltration Aleatory: NA EBS: \Time_Zero\EBS_PS_Loop\Static_Calcs_PS_Loop\Static_Calcs_UZ_Flow\Infiltration \Global_Inputs_and_Calcs\Global_UZ_Flow\Infiltration
Drift Seepage	Epistemic: \Input_Params_Epistemic\Epistemic_Params_UZ_Flow\Input_Params_Seepage_Uncert \Input_Params_Epistemic\Epistemic_Params_UZ_Flow\Uncertain_Params_Seepage Aleatory: NA EBS: \Time_Zero\EBS_PS_Loop\Static_Calcs_PS_Loop\Static_Calcs_UZ_Flow\Drift_Seepage \Global_Inputs_and_Calcs\Global_UZ_Flow\Drift_Seepage
Drift Wall Condensation	Epistemic: \Input_Params_Epistemic\Epistemic_Params_UZ_Flow\Uncertain_Params_DWC Aleatory: NA EBS: \Global_Inputs_and_Calcs\Global_UZ_Flow\Drift_Wall_Condensation
EBS TH Environment	Epistemic: \Input_Params_Epistemic\Epistemic_Params_EBS_Environ\Uncertain_Params_TH Aleatory: NA EBS: \Global_Inputs_and_Calcs\Global_EBS_Environ\EBS_Environment\ThermoHydrology

Table 6.1.5-1. Location of Implementation Description in the GoldSim TSPA Model File (Continued)

Submodel	Documentation Location(s)
WP and DS Degradation	Epistemic: \Input_Params_Epistemic\Epistemic_Params_WP_DS_Deg\ Aleatory: \Model_Calcs_Aleatory\Aleatory_Calcs_WP_DS_Deg EBS: \Time_Zero\EBS_PS_Loop\Static_Calcs_PS_Loop\Static_Calcs_WP_DS_Deg \Global_Inputs_and_Calcs\Global_WP_DS_Deg\Global_IWPD
Localized Corrosion	Epistemic: \Input_Params_Epistemic\Epistemic_Params_WP_DS_Deg\ Aleatory: NA EBS: \Time_Zero\EBS_PS_Loop\Static_Calcs_PS_Loop\Static_Calcs_WP_DS_Deg \Global_Inputs_and_Calcs\Global_WP_DS_Deg\Global_LC
Radionuclide Inventory	Epistemic: \Input_Params_Epistemic\Epistemic_Params_WF_Deg_Mob\Uncertain_Params_RN_Inventory Aleatory: NA EBS: \Global_Inputs_and_Calcs\Global_WF_Deg_Mob\RN_Inventory
In-Package Chemistry	Epistemic: \Input_Params_Epistemic\Epistemic_Params_WF_Deg_Mob\Uncertain_Params_InPkg_Chem Aleatory: NA EBS: \Global_Inputs_and_Calcs\Global_WF_Deg_Mob\In_Package_Chemistry
Waste Form Degradation	Epistemic: \Input_Params_Epistemic\Epistemic_Params_WF_Deg_Mob\Uncertain_Params_CSNF_WF Aleatory: NA EBS: \Global_Inputs_and_Calcs\Global_WF_Deg_Mob\WF_Degradation\CSNF_WF_Dissolution
	Epistemic: \Input_Params_Epistemic\Epistemic_Params_WF_Deg_Mob\Uncertain_Params_HLW_WF Aleatory: NA EBS: \Global_Inputs_and_Calcs\Global_WF_Deg_Mob\WF_Degradation\Input_Params_HLW_WF
	Epistemic: NA Aleatory: NA EBS: \Global_Inputs_and_Calcs\Global_WF_Deg_Mob\WF_Degradation\Input_Params_DSNF_WF

Table 6.1.5-1. Location of Implementation Description in the GoldSim TSPA Model File (Continued)

Submodel	Documentation Location(s)
Cladding Degradation	Epistemic: NA Aleatory: NA EBS: \Global_Inputs_and_Calcs\Global_WF_Deg_Mob\Clad_Degradation
EBS Chemical Environment	Epistemic: \Input_Params_Epistemic\Epistemic_Params_EBS_Environ\Uncertain_Params_EBS_CE Aleatory: \Input_Params_Aleatory\Input_Params_EBS_Environ\Input_Params_EBS_CE EBS: \Global_Inputs_and_Calcs\Global_EBS_Environ\EBS_Environment\EBS_Chemical_Environment
Dissolved Concentration Limits	Epistemic: \Input_Params_Epistemic\Epistemic_Params_WF_Deg_Mob\Uncertain_Params_Solubility Aleatory: NA EBS: \Global_Inputs_and_Calcs\Global_WF_Deg_Mob\Global_Solubility
EBS Colloids	Epistemic: \Input_Params_Epistemic\Epistemic_Params_EBS_F_and_T\Uncertain_Params_Colloids Aleatory: NA EBS: \Global_Inputs_and_Calcs\Global_EBS_F_and_T\Model_Input_EBS_Transport\Input_Params_Colloids
EBS Flow	Epistemic: \Input_Params_Epistemic\Epistemic_Params_EBS_F_and_T\Uncertain_Params_Flux_Split Aleatory: NA EBS: \Time_Zero\EBS_PS_Loop\Static_Calcs_PS_Loop\Static_Calcs_EBS_F_and_T\EBS_Flow \Global_Inputs_and_Calcs\Global_EBS_F_and_T\Model_Feeds_EBS_Flow
EBS Transport	Epistemic: \Input_Params_Epistemic\Epistemic_Params_EBS_F_and_T Aleatory: NA EBS: \Global_Inputs_and_Calcs\Global_EBS_F_and_T\Model_Input_EBS_Transport
EBS-UZ Interface	Epistemic: \Input_Params_Epistemic\Epistemic_Params_EBS_F_and_T\Uncertain_Params_EBS_UZ_Trans Aleatory: NA EBS: \Global_Inputs_and_Calcs\Global_EBS_F_and_T\EBS_UZ_Transport_Inputs
UZ Transport	Epistemic: \Input_Params_Epistemic\Epistemic_Params_UZ_Transport Aleatory: NA Other: \TSPA_Model\UZ_Transport
SZ Flow and Transport	Epistemic: \Input_Params_Epistemic\Epistemic_Params_SZ_Transport Aleatory: NA Other: \TSPA_Model\SZ_Transport

Table 6.1.5-1. Location of Implementation Description in the GoldSim TSPA Model File (Continued)

Submodel	Documentation Location(s)
Biosphere	Epistemic: \Input_Params_Epistemic\Epistemic_Params_Biosphere Aleatory: NA Other: \TSPA_Model\Biosphere
Early Failure Scenario Class	Epistemic: \Input_Params_Epistemic\Epistemic_Params_Events\Epistemic_Parameters_EF Aleatory: \Input_Params_Aleatory\Aleatory_Params_Events\Aleatory_Params_EF EBS: \Time_Zero\EBS_PS_Loop\Static_Calcs_PS_Loop\Static_Calcs_Events\Static_Calcs_EF \Global_Inputs_and_Calcs\Global_Events\Global_EF
Igneous Scenario Class	Epistemic: \Input_Params_Epistemic\Epistemic_Params_Events\Epistemic_Params_Igneous_Intr Aleatory: \Input_Params_Aleatory\Aleatory_Params_Events\Aleatory_Params_Igneous_Intr EBS: \Time_Zero\EBS_PS_Loop\Static_Calcs_PS_Loop\Static_Calcs_Events\Igneous_Intrusion \Global_Inputs_and_Calcs\Global_Events\Igneous_Scenario
	Epistemic: \Model_Uncertainties\EU Aleatory: \Model_Uncertainties\AU EBS: \Eruptive_Model
Seismic Scenario Class	Epistemic: \Input_Params_Epistemic\Epistemic_Params_Events\Epistemic_Params_Seismic Aleatory: \Input_Params_Aleatory\Aleatory_Params_Events\Input_Params_Seismic_Uncert \Input_Params_Aleatory\Aleatory_Params_Events\Input_Params_Seismic_FD_Uncert EBS: \Time_Zero\EBS_PS_Loop\Static_Calcs_PS_Loop\Static_Calcs_Events\Seismic_Fault_Displacement \Global_Inputs_and_Calcs\Global_Events\Seismic_Scenario
Human Intrusion Scenario	Epistemic: NA Aleatory: \Input_Params_Aleatory\Aleatory_Params_Events\Aleatory_Params_HI EBS: \Time_Zero\EBS_PS_Loop\Static_Calcs_PS_Loop\Static_Calcs_Events\Human_Intrusion_Events \Global_Inputs_and_Calcs\Global_Events\Human_Intrusion Other: \TSPA_Model\UZ_Transport\UZ_Transport_Calculations\HI_Borehole_Transport

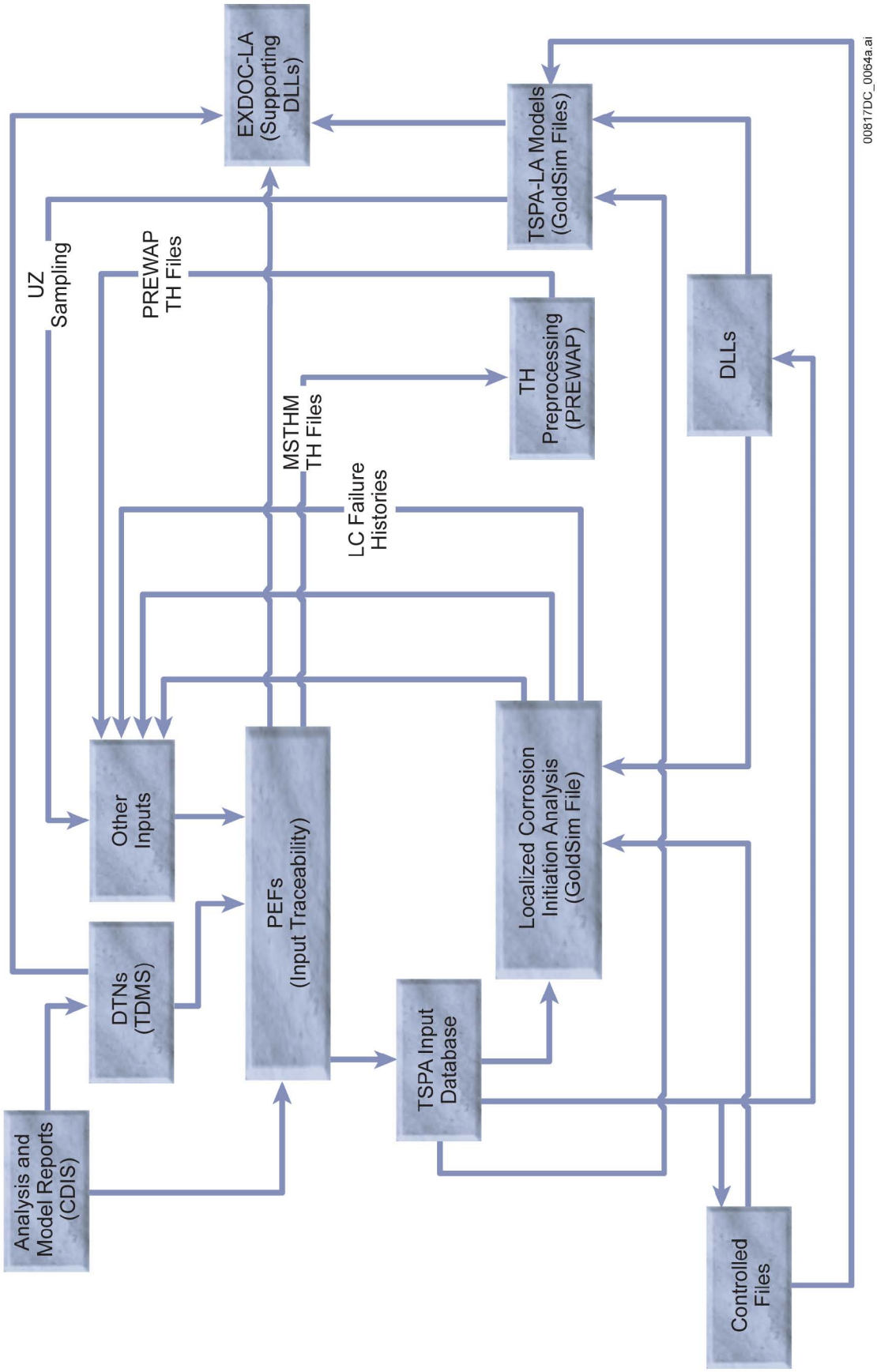

Figure 6.1.5-1. Illustrated Overview of all the Various Elements that Make Up the Framework for Initializing and Running the TSPA-LA Model

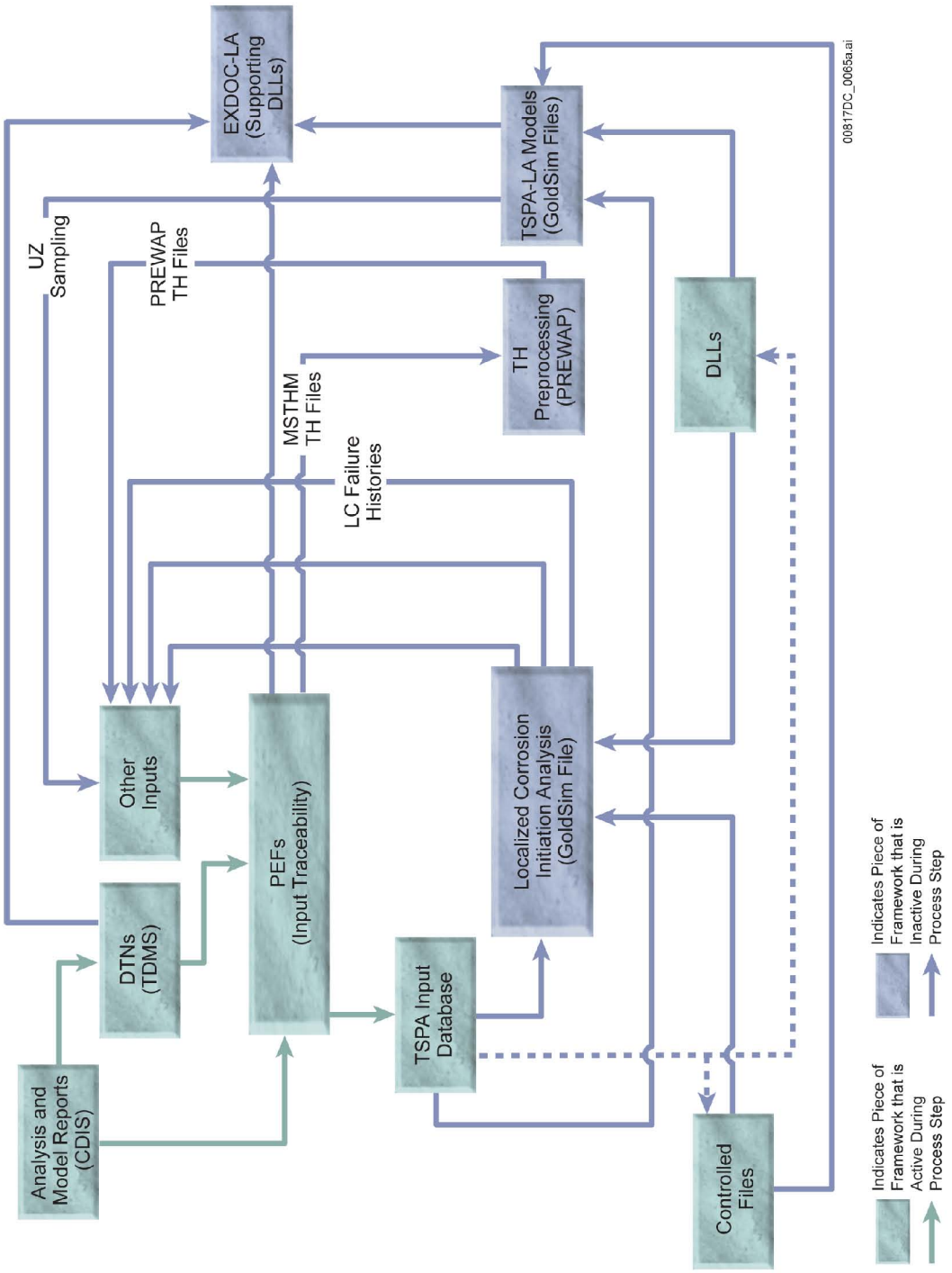

NOTE: Dashed lines indicate cases where location of files and software are stored in the TSPA Input Database, but the information is actually accessed from the TSPA-LA Model file server.

Figure 6.1.5-2. Illustration Depicting Elements Required for Loading of Initial Parameter Values and Dynamically Linked Libraries for the TSPA-LA Model

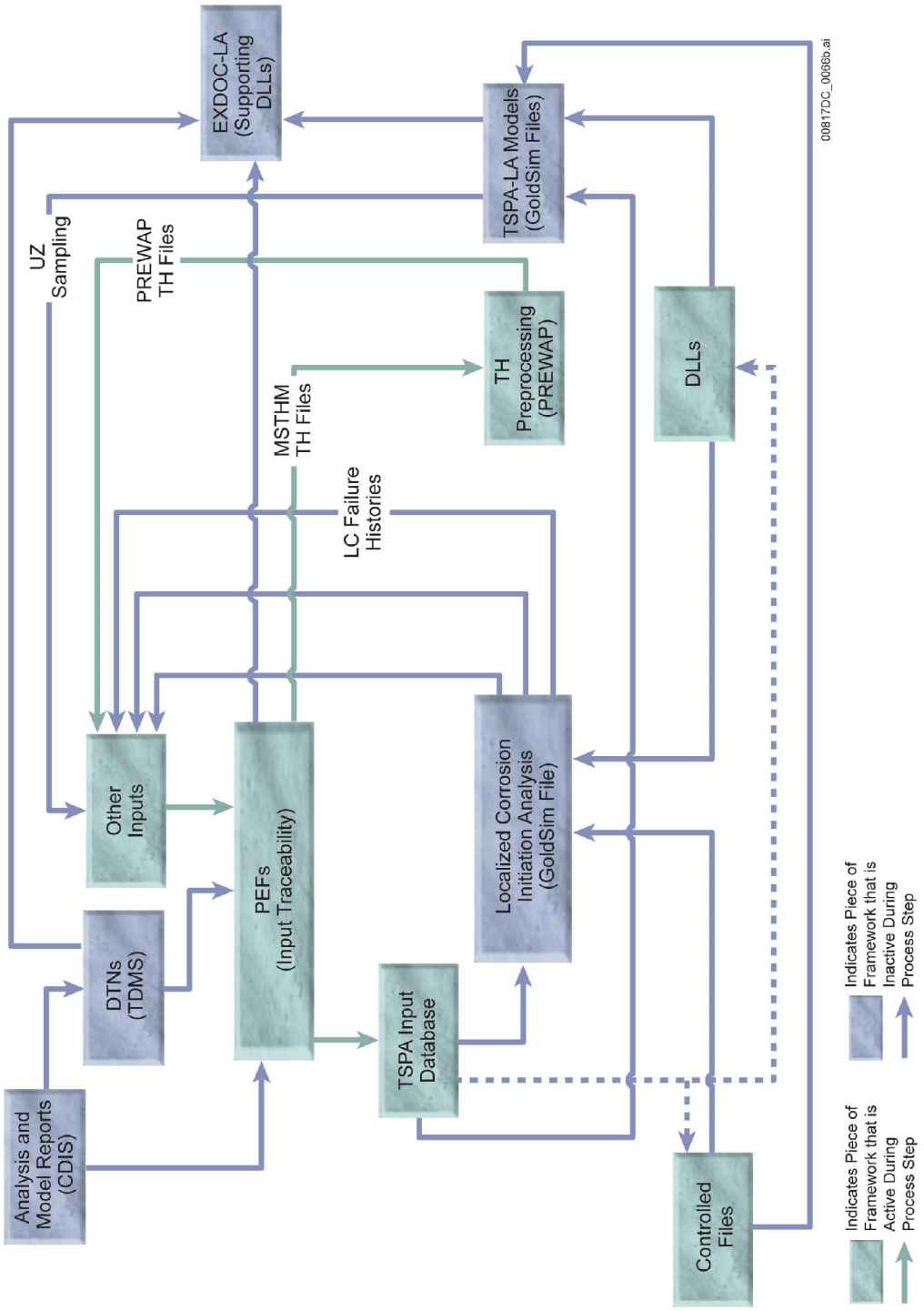

NOTE: Dashed lines indicate cases where location of files and software are stored in the TSPA Input Database, but the information is actually accessed from the TSPA-LA Model file server.

Figure 6.1.5-3. Illustration Depicting Elements Active When Information from the Multiscale Thermohydrologic Model is Preprocessed by PREWAP_LA

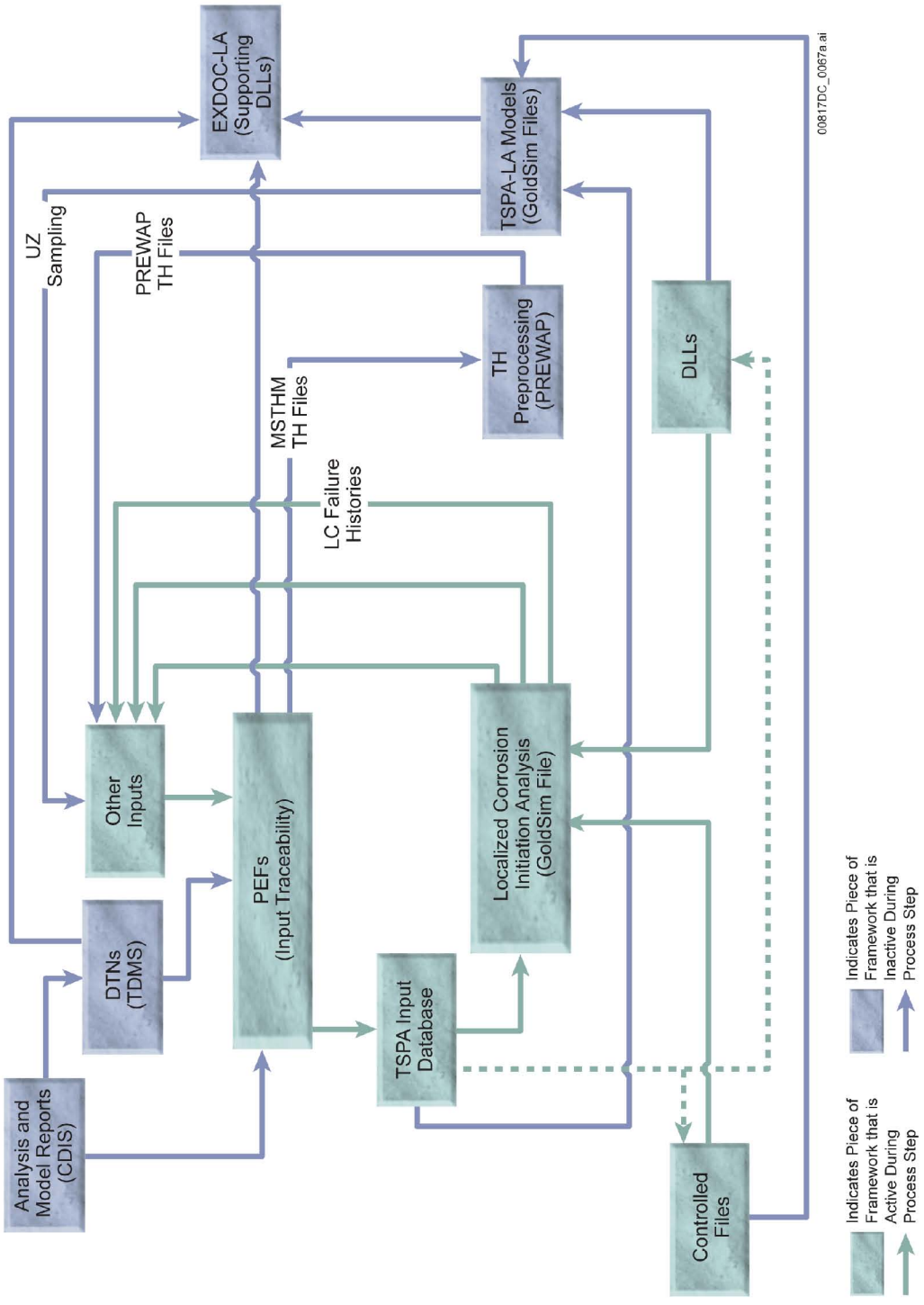

NOTE: Dashed lines indicate cases where location of files and software are stored in the TSPA Input Database, but the information is actually accessed from the TSPA-LA Model file server.

Figure 6.1.5-4. Illustration Depicting Elements Active When Preprocessing for the Localized Corrosion Initiation Analysis

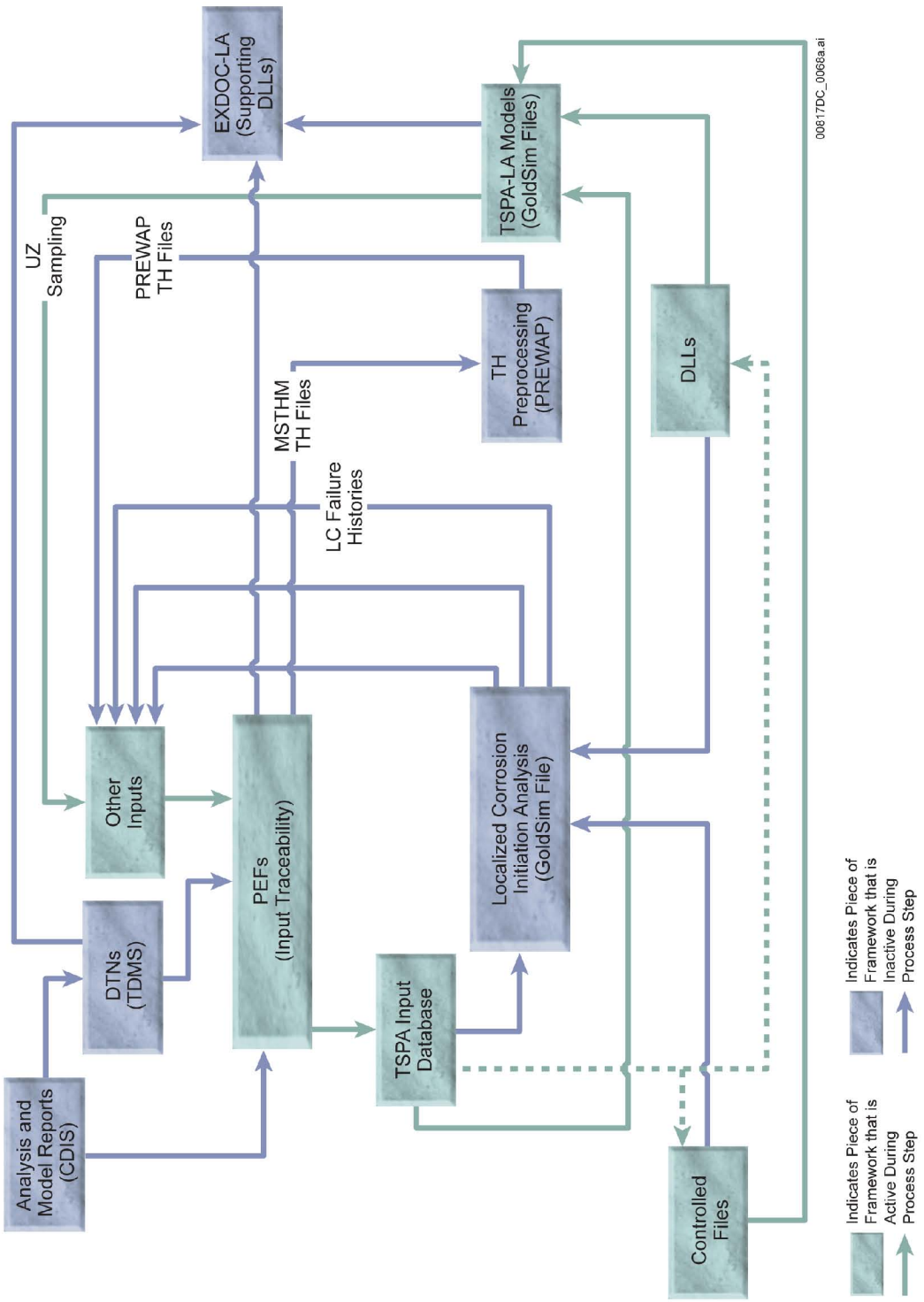

NOTE: Dashed lines indicate cases where location of files and software are stored in the TSPA Input Database, but the information is actually accessed from the TSPA-LA Model file server.

Figure 6.1.5-5. Illustration Depicting Elements Active when Sampling of Uncertain Unsaturated Zone Parameters and Generation of Input Files

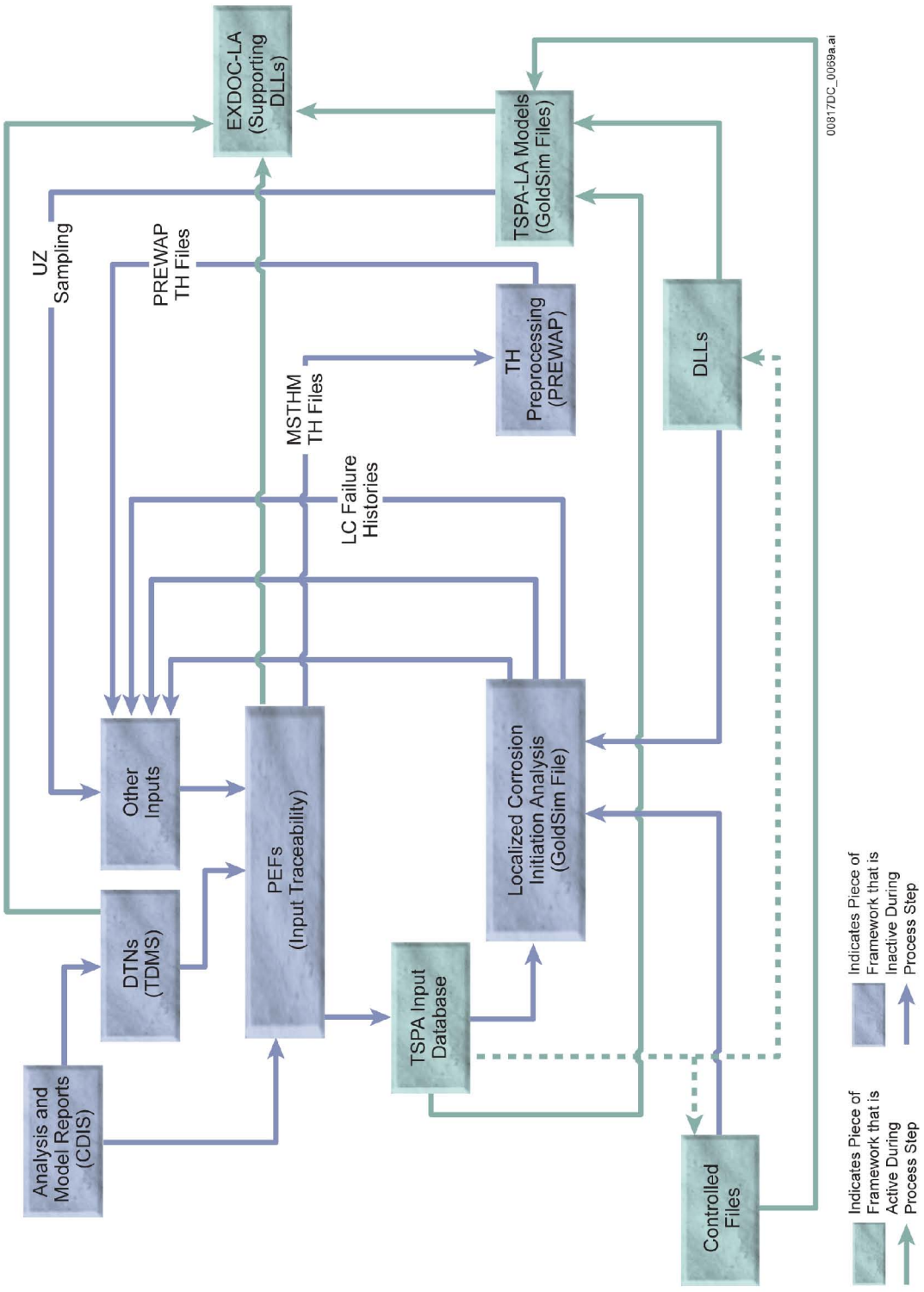

NOTE: Dashed lines indicate cases where location of files and software are stored in the TSPA Input Database, but the information is actually accessed from the TSPA-LA Model file server.

Figure 6.1.5-6. Illustration Depicting Elements Active in the Execution of the TSPA-LA GoldSim Model File and the TSPA-LA Volcanic Eruption GoldSim Model File

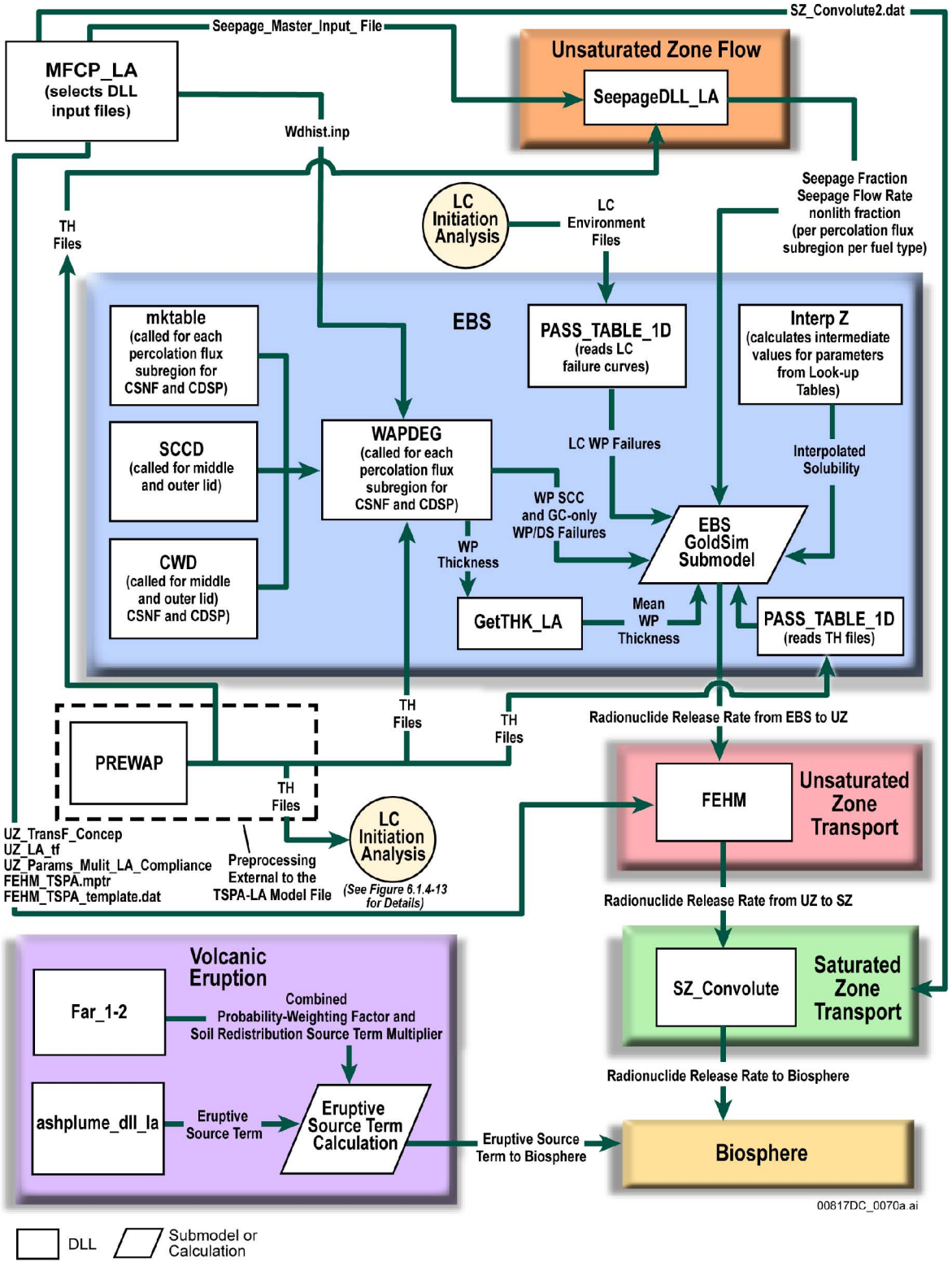

Figure 6.1.5-7. TSPA-LA Software Configuration Illustrating Software Run with GoldSim

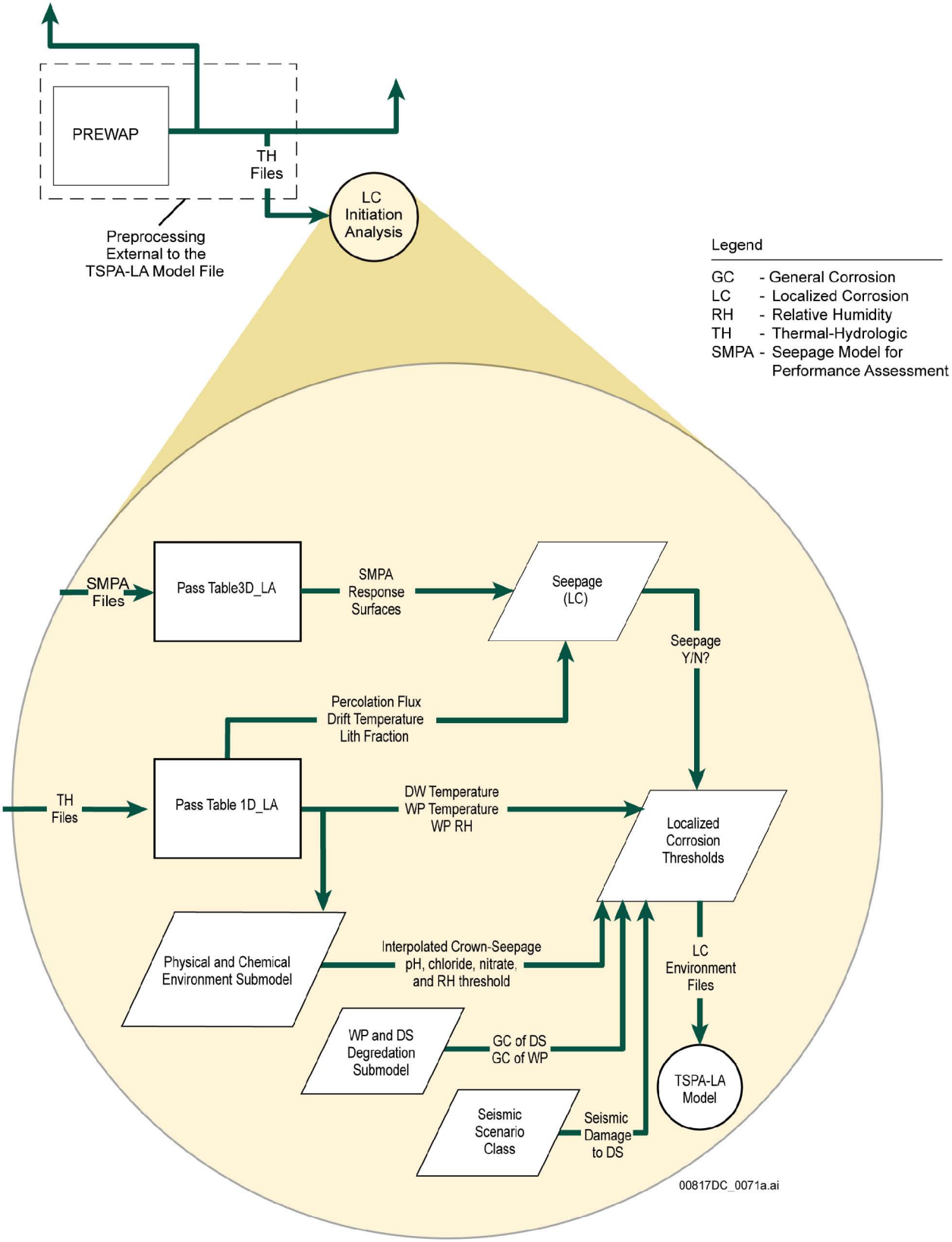

Figure 6.1.5-8. Details of the Software Configuration for the Localized Corrosion Initiation Analysis

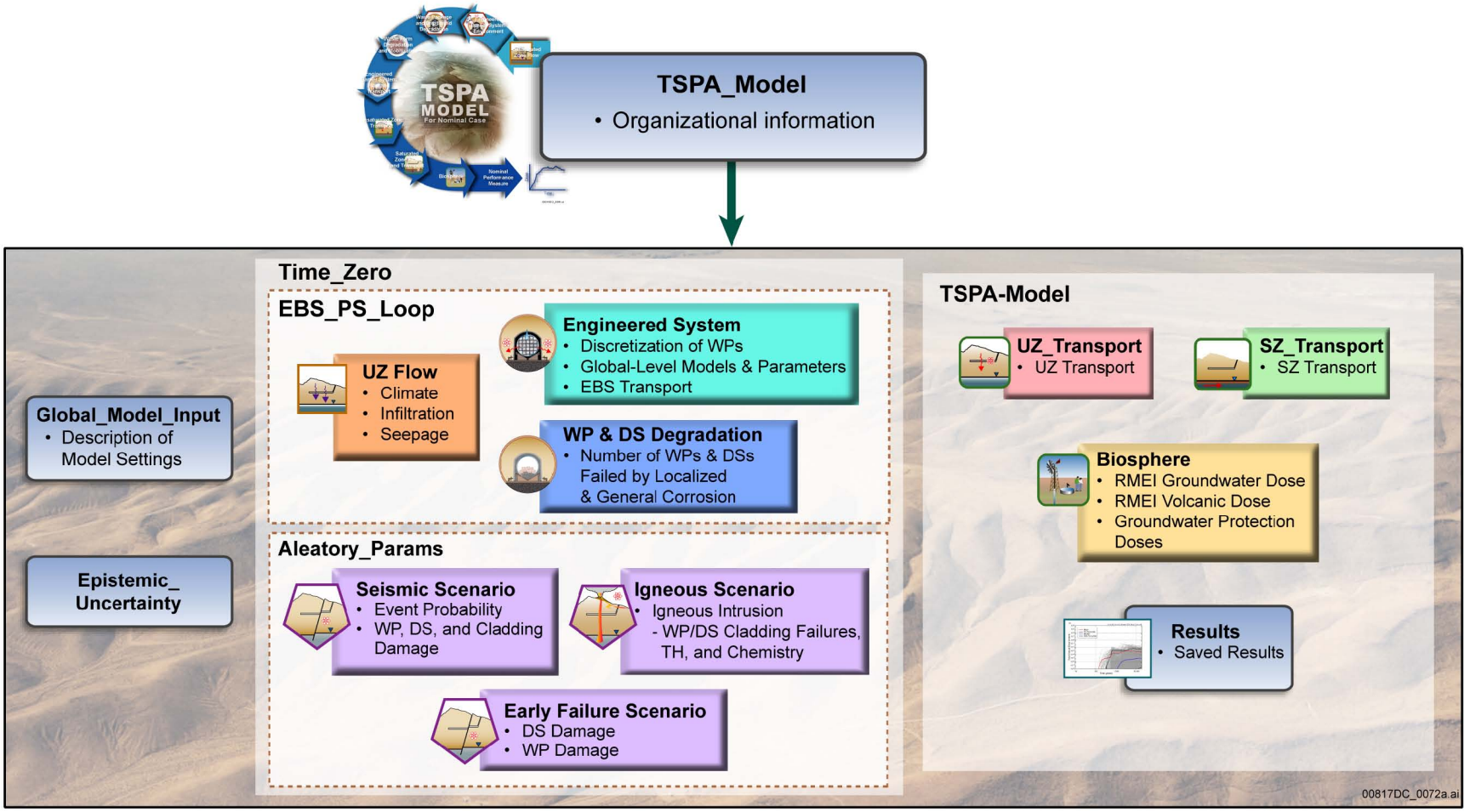

Figure 6.1.5-9. Layout of Calculation Containers that Define the Highest Level of Organization of the TSPA-LA Model File

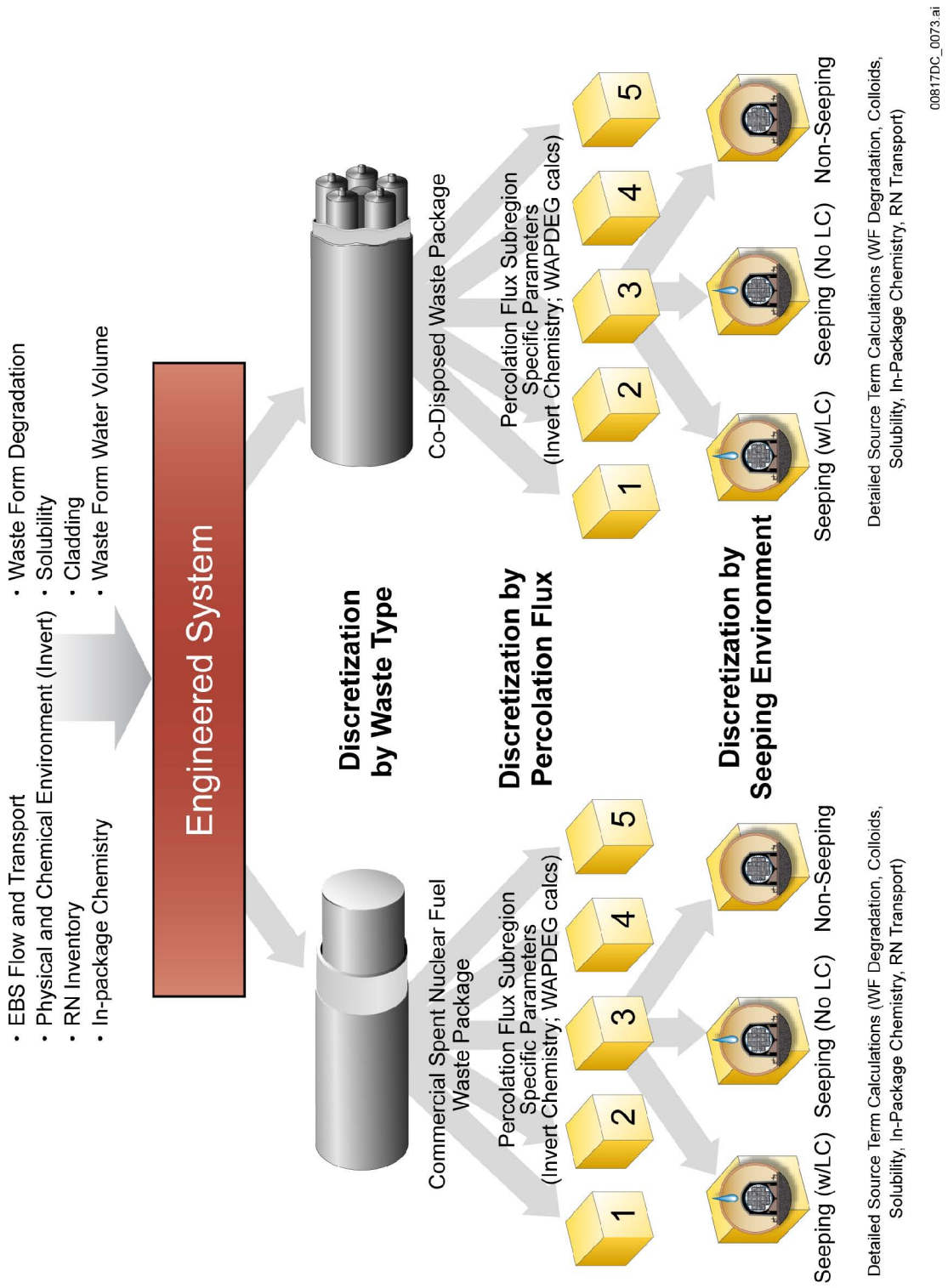

Figure 6.1.5-10. Levels of Discretization of Engineered System Representation in the TSPA-LA Model File

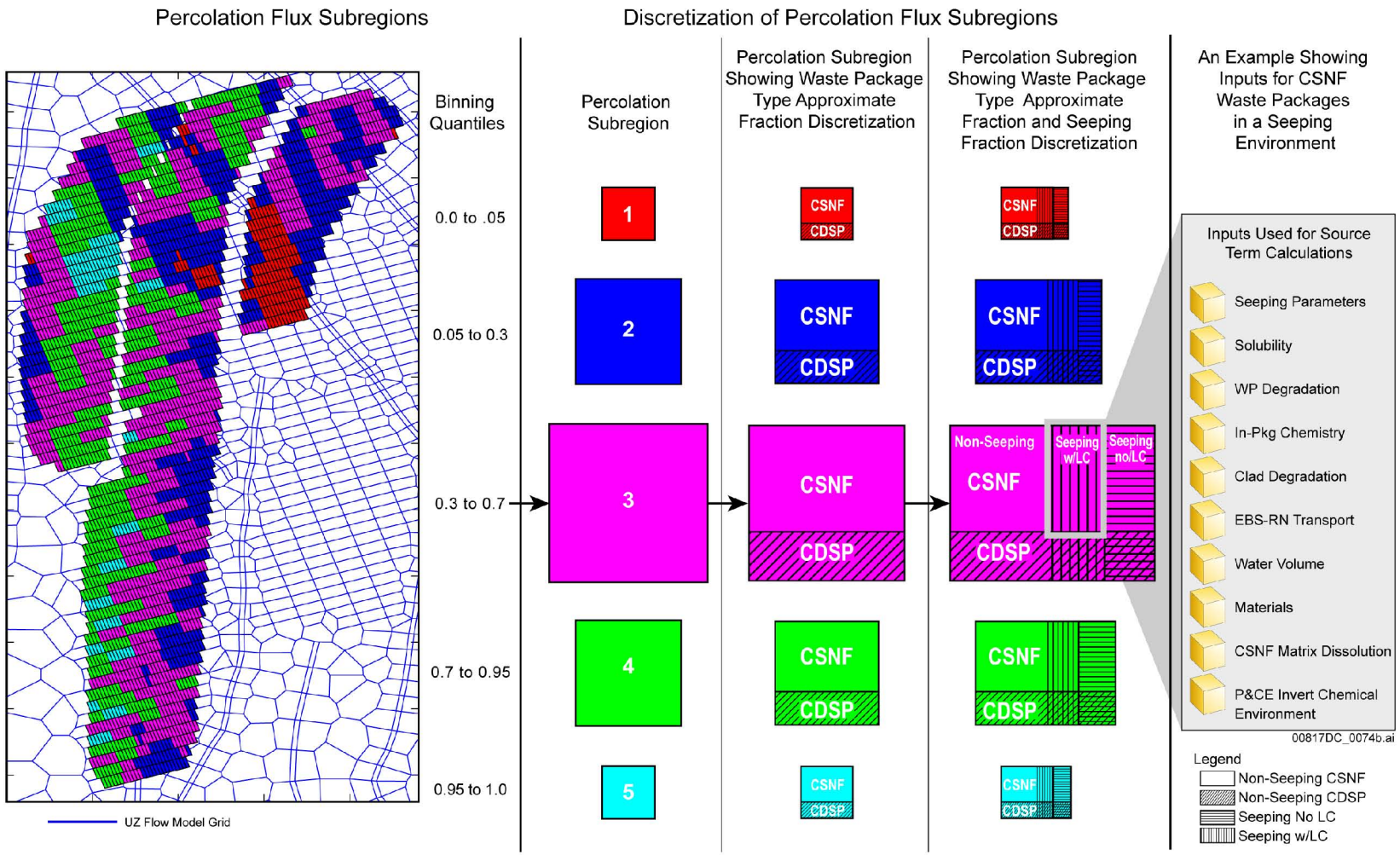

Source: Percolation Flux Map from SNL 2007 [DIRS 181383], Figure VIII-1[a].

NOTE: The early failure packages are randomly set in one of the five repository percolation subregions at the start of a realization.

Figure 6.1.5-11. Schematic of the Five Repository Percolation Subregions Showing the Implementation of the Levels of Discretization Shown on Figure 6.1.5-10

INTENTIONALLY LEFT BLANK

6.2 ALTERNATIVE CONCEPTUAL MODELS

Alternative conceptual models (ACMs) are a means to specifically acknowledge model form uncertainty. A model is a set of working hypotheses and assumptions that provide an acceptable description of a system for the intended purpose. The hypotheses and assumptions must be logically consistent with one another, in agreement with existing information, able to predict system behavior, and able to be tested. In 10 CFR 63.114(c) [DIRS 178394], the NRC specifically requires the DOE to, "Consider alternative conceptual models of features and processes that are consistent with available data and current scientific understanding and evaluate the effects that alternative conceptual models have on the performance of the geologic repository."

A model that is evaluated and chosen to represent a system is called the base-case model. Any remaining models that meet the above criteria are then designated ACMs for the system. In addition to ACMs, the TSPA-LA Model contains various conservative assumptions that played an important role in enhancing the confidence and defensibility of the model. These conservatisms and their impact on the TSPA-LA Model are documented in Appendix C.

General Consideration of Alternative Conceptual Models

As suggested by the statements in 10 CFR 63.114(c) [DIRS 178394], a conceptual model can be truly alternative only if it meets the following criteria:

- It must differ significantly from the initial (or base-case) conceptual model.
- It must be consistent with available data and current scientific understanding.
- It must be reasonable (i.e., there is a reasonable physical basis for the alternative).

The ACMs in all model components, submodels, and process models that provide inputs to the TSPA-LA Model were considered according to a process that included the identification, screening, and evaluation of potential ACMs as part of the analysis documented in the model reports that feed the TSPA-LA Model. Reasonable and technically defensible conservatism at the subsystem level has been used to select the best ACM to use rather than quantitatively propagate multiple ACMs to the TSPA-LA Model. Generally, additional uncertainty is incorporated into the selected conceptual model if more than one ACM is deemed appropriate for use rather than considering multiple ACMs in the TSPA-LA Model. If an ACM appears to be significant at the subsystem level, an appropriate abstraction is developed for that ACM for consideration within the TSPA-LA Model. The result of the process is documented within the individual model reports. It is important to note that treatment of ACMs within the individual model reports may differ significantly to be consistent with available data and current scientific understanding. For instance, some ACMs may be assessed qualitatively with the conclusion that the ACM is captured by the selected conceptual model abstraction recommended for use in the TSPA-LA Model. Whereas, in another case, a more detailed computational analysis may be needed to assess the ACM, resulting in additional uncertainty or other modification to the selected conceptual model abstraction used in the TSPA-LA Model. ACMs that were identified and evaluated in model components, submodels, process models, and model reports supporting the TSPA-LA Model are summarized in Table 6.2-1 and Sections 6.3, 6.4, 6.5, 6.6, and 6.7. Each model component and submodel discussion includes a summary evaluation of ACMs.

An important reason for considering ACMs at the subsystem level is to help build confidence that plausible changes in modeling assumptions or simplifications will not change conclusions regarding the subsystem and subsequently the total system performance. Consideration and treatment of ACMs used to support the TSPA-LA Model is demonstrated through a stepwise process including subsystem-level impact evaluations and analyses presented in the process level model reports. Important differences demonstrated at the subsystem level are evaluated through TSPA-LA Model sensitivity and regression analyses. Section 6.3 summarizes the general consideration and treatment of ACMs used to support the TSPA-LA Model in each submodel area.

Table 6.2-1. Table of Alternative Conceptual Models

Alternative Conceptual Models	Key Assumptions	Assessment and Basis
Unsaturated Zone Flow Model Component (Section 6.3.1 and Section 6.3.3)		
UZ Flow: Lateral flow in the PTn	The ACM employs a different hydrogeologic property set for the PTn unit that does not favor large-scale lateral diversion of flow in the PTn (BSC 2004 [DIRS 169861], Section 6.5.2.2).	Modeling results show that the base-case model generally provides slightly more conservative transport time estimates than the ACM (BSC 2004 [DIRS 169861], Section 6.9.2). Comparative studies of chloride distributions within the UZ, simulated using the base case and ACM flow fields, indicate consistently that the base-case flow fields provide an overall better match with the observed chloride data (BSC 2004 [DIRS 169861], Section 6.5.2.2). Note that this study was performed with flow models based on the original infiltration model, but the implications of the study are not expected to change.
UZ Flow: Transient infiltration pulse	The ACM assumes that episodic variations in surface infiltration rates may not be effectively dampened by the PTn and may still affect radionuclide transport initialized at the repository level.	Modeling studies show that episodic variations in infiltration in areas where the PTn is thick are largely dampened by the time they reach the repository level. In addition, since the episodic variations at the repository level for thin PTn sections are small relative to other uncertainties in percolation fluxes, the assumption of steady-state flow, as used in the TSPA-LA Model, is considered to be valid (SNL 2008 [DIRS 184614], Section 6.9).
UZ Flow: Film Flow	Film flow may occur between cavities and fractures (SNL 2008 [DIRS 184614], Section 7.8.3.3). Film flow may also be a process by which fast flow occurs in the fractures (BSC 2004 [170035] Section 7.3).	Film flow may occur between cavities and fractures as indicated by coatings and water release tests. Not considering the explicit influence of cavities is a conservative approach since the cavities would retard the transport of water (SNL 2008 [DIRS 184614], Section 7.8.3.3). Although the importance of film flow in the fractures is a matter of debate (BSC 2004 [170035] and Preuss 1999 [DIRS 104250]), a comparison between the AFM and a film-flow model has been performed (BSC 2004 [DIRS 170035] Section 7.3). The analysis, comparing the AFM and the film-flow model, showed that the AFM would capture the fast flow behavior of water film if film flow was the major fracture flow mechanism (BSC 2004 [170035] Section 7.3.1 and Section 8.2).

Table 6.2-1. Table of Alternative Conceptual Models (Continued)

Alternative Conceptual Models	Key Assumptions	Assessment and Basis
UZ Flow: Discrete Fracture Flow	The discrete-fracture or "weeps" type model is an alternative model that explicitly defines the fractures in a fracture-flow system.	The discrete-fracture or "weeps" type model is subject to extremely high uncertainties with respect to the fracture data needed to describe the system. In addition, the computational burden associated with this type model is beyond present or near future resources. Therefore, this type model is not considered (SNL 2008 [DIRS 184614], Section 6.1.2).
UZ Flow: Inclusion of TH, THC, and Thermal-Hydrologic-Mechanical Effects on UZ Flow	Vaporization due to repository heat will keep the drift dry for several hundred to a few thousand years. Thermal (TH), Thermal Hydrologic Chemical (THC), and thermal-hydrologic-mechanical (THM) effects may influence the flow fields used to describe flow in the UZ.	TH, THC, and thermal-hydrologic-mechanical effects are insignificant after the change to glacial-transition climate, the period when most radionuclide transport would take place (SNL 2008 [DIRS 184748], Section 6.7). Additional conclusions with respect to TH, THC, and thermal-hydrologic-mechanical effects on UZ Flow and Transport presented in *Mountain-Scale Coupled Processes (TH/THC/THM)* include: (1) mountain-scale TH will have a large impact on fluid flow near the repository at early times but insignificant impact on UZ flow fields (BSC 2005 [DIRS 174101], Section 8.1); (2) changes in water chemistry, mineralogy, and hydrologic properties in the ambient temperature regions are minimal over the 7,000 years the THC model was simulated (BSC 2005 [DIRS 174101], Section 8.2); and (3) thermal-hydrologic-mechanical induced changes in mountain-scale hydrologic properties have no significant impact on vertical percolation through the repository horizon (BSC 2005 [DIRS 174101], Section 8.3).
Drift Seepage: Flow Through Discrete Fractures	ACM that simulates flow through discrete fractures rather than through a stochastic continuum (SNL 2007 [DIRS 181244], Section 6.4).	It was concluded that conceptual model uncertainty is small compared to other sources of uncertainty that are explicitly accounted for by the base case conceptual model, its numerical implementation, and the associated uncertainty estimates that are propagated through the TSPA-LA Model (SNL 2007 [DIRS 181244], Section 6.4.1.2).

Table 6.2-1. Table of Alternative Conceptual Models (Continued)

Alternative Conceptual Models	Key Assumptions	Assessment and Basis
Drift Seepage: Episodic-Preferential Flow in Superheated Rock	The effectiveness of the vaporization barrier was examined with an ACM representing water flow into a superheated rock environment (SNL 2007 [DIRS 181244], Section 6.4.3.2). In this ACM, the thermally perturbed downward flux from the condensation zone toward the superheated rock zone is conceptualized to form episodic preferential-flow patterns.	It was concluded that results of the ACM are reasonably consistent with the thermal seepage process-model results used for the seepage abstraction used for TSPA-LA (SNL 2007 [DIRS 181244], Section 6.4.3.2).
Drift Seepage: Flow-focusing factor based on a coarser resolution of scale	This ACM flow-focusing factor was based on a coarser resolution of scale at which the flow-focusing factors were averaged over 5-meter long sections along the bottom of the model (SNL 2007 [DIRS 181244], Section 6.6.5.2.2).	Since no quantitative observation of flow focusing is available for a direct comparison of conceptual models model (SNL 2007 [DIRS 181244], Section 6.6.5.2.3), since this ACM would give less conservative (much lower seepage rates with only a slight increase in seepage fraction) results the base conceptual model should be used.
Drift Seepage: Igneous seepage model that considers a capillary barrier and flow diversion	The two ACMs for evaluating drift seepage after an igneous event are based on a conceptual model where thermal contraction gives rise to numerous fractures and joints in the cooling process filling the drift with fractured magma of relatively high permeability and low capillary strength (SNL 2007 [DIRS 181244], Section 6.5.1.7). This conceptualization gives rise to a capillary barrier and flow diversion. The two ACMs are based on whether the non-collapsed seepage lookup table or the collapsed seepage lookup table is used.	Since information on which one of the possible in-drift conditions after an igneous event is not available (SNL 2007 [DIRS 181244], Section 6.5.1.7), the conceptual model with the greatest seepage rates was chosen.
Drift-Wall Condensation: Thermal Conductivity/Heat Transfer	In the Thermal Conductivity/Heat Transfer ACM, the air phase is treated as a solid material (SNL 2007 [DIRS 181648], Section 6.1.4).	This ACM is essentially accounted for in the MSTHM Abstraction (SNL 2007 [DIRS 181648] Sections 6.1.4 and 6.4).
Drift-Wall Condensation: CFD Simulation for Drift Condensation Processes	ACM simulates the drift with a CFD code and the surrounding rock with porous media code. The CFD code FLUENT (Software Code: FLUENT. V6.0.12 (Fluent, Inc. [DIRS 164315]), contains limited porous media capabilities that only considers single-phase flow (SNL 2007 [DIRS 181648], Section 6.1.4).	Conduction-only heat transfer in the surrounding rock and the invert is acceptable, and this ACM is not considered further (SNL 2007 [DIRS 181648], Section 6.1.4).

Table 6.2-1. Table of Alternative Conceptual Models (Continued)

Alternative Conceptual Models	Key Assumptions	Assessment and Basis
EBS Environment Model Component (Section 6.3.2 and 6.3.4)		
EBS TH Environment: Mountain-Scale TH Model	An ACM to the MSTHM Process Model is a Mountain-Scale Thermal Hydrologic model developed by Lawrence Berkeley National Laboratory (Haukwa et al. 1998 [DIRS 117826]). The Lawrence Berkeley National Laboratory model is a monolithic TH model. The Mountain-Scale TH Model used: (1) coarser grid discretization at the drift scale than the MSTHM Process Model; (2) a line-averaged approximation of the heat-generation-rate-versus-time table (whereas the MSTHM Process Model represented the WPs as discrete heat sources); and (3) a lumped heat source that filled the entire cross section of the emplacement drift (SNL 2007 [DIRS 181383], Section 6.4)	Given the differences between the MSTHM Process Model and the east-west cross-sectional Lawrence Berkeley National Laboratory Mountain-Scale TH Model, the agreement between the two models is adequate (SNL 2007 [DIRS 181383], Section 6.4). Moreover, the differences in predicted temperatures between the MSTHM Process Model and the east-west cross-sectional Lawrence Berkeley National Laboratory Mountain-Scale TH Model are within the range of temperature differences resulting from parametric uncertainty (SNL 2007 [DIRS 181383], Tables 6.3-30 and 6.3-31).
EBS Chemical Environment: PTn Pore Water	The EBS Physical and Chemical Environment Model uses pore water compositions from the TSw to represent ambient conditions for the four starting waters (SNL 2007 [DIRS 177412], Section 6.6). The ACM selects ambient pore water from the overlying formation, the PTn, and then allows this water to seep up the geothermal gradient (from 23 to 96°C) [which is downward] through the TSw to the repository horizon (SNL 2007 [DIRS 177412], Section 6.11).	This ACM was not selected for use in the TSPA-LA Model because an analysis showed that using the TSw pore water adequately captures the chemistry of representative PTn pore waters. The use of PTn starting compositions does not significantly impact the key chemical components (pH, Pco_2, Ca, K, Si) of seepage (SNL 2007 [DIRS 177412], Section 6.11.1).
EBS Chemical Environment: Treatment of Alkali Fedspar by the Near Field Chemistry Model	Within the EBS Physical and Chemical Environment Model, the mixed feldspar phase adopted to represent the volcanic feldspar observed in the Topopah Spring Tuff is treated kinetically, i.e., this phase is always undersaturated with respect to clays, zeolites, and its own end-members (SNL 2007 [DIRS 177412], Section 6.11.2). An alternate approach would be to assume that the volcanic feldspar has reached equilibrium or near equilibrium, and thus thermodynamic controls of feldspar dissolution (e.g. saturation indices) must be considered when calculating seepage water compositions.	This equilibrium ACM was not chosen because at or near ambient temperatures, the volcanic waters are usually undersaturated with respect to feldspars and the kinetic treatment of the alkali feldspar is the appropriate approach (SNL 2007 [DIRS 177412], Section 6.11.2).

Table 6.2-1. Table of Alternative Conceptual Models (Continued)

Alternative Conceptual Models	Key Assumptions	Assessment and Basis
EBS Chemical Environment: Closed System with Respect to CO_2	The IDPS Model (SNL 2007 [DIRS 177411], Section 6.5), which is a process model implemented by the EBS P&CE suite of models (SNL 2007 [DIRS 177412]) describes an ACM that assumes a closed drift system with respect to CO_2. In a closed system, there is little or no exchange of CO_2 between the solution and the atmosphere; that is, the solution is modeled as essentially isolated from the atmosphere and H_2CO_3 is treated as a non-volatile acid. What little exchange might occur in a natural system approximating a closed system would alter the fugacity of CO_2 in the atmosphere. A closed system model might be appropriate for a wetter climate; however, relative humidity would be approximately 100 percent and little or no evaporation would occur.	A closed system with respect to CO_2 is not implemented in TSPA because the expected volume ratio of air to water in the drift is so large that CO_2 degassing from, or dissolving into, seepage water in the drift will negligibly affect CO_2 fugacity compared to the uncertainty in the input value for CO_2 fugacity. However, the EBS P&CE Model incorporates the uncertainty of an open or closed system by using the maximum and minimum Pco_2 values in the abstraction for the TSPA-LA (SNL 2007 [DIRS 177412], Section 6.3.2.8 and Section 6.15.1). The minimum value assumes a completely open system and the maximum value assumes a closed system. The actual system behaves in a manner between these two end-member assumptions.
WP and DS Degradation Model Component (Section 6.3.5)		
WP and DS Degradation: Parabolic General Corrosion Rate Law for DS Degradation (SNL 2007 [DIRS 180778], Section 6.5.6)	Assumes that the increasing oxide layer thickness on diffusion of oxidizing species to the underlying metal will have an inhibiting effect on corrosion.	Model is less conservative than the primary model.
WP and DS Degradation: Decreasing Rate Law for WP Degradation (SNL 2007 [DIRS 178519], Section 6.4.3.5.1)	General Corrosion rates of metals and alloys tend to decrease with time (SNL 2007 [DIRS 178519], Section 6.4.3.5.1).	The time-dependent general corrosion behavior of the WP was not included in the TSPA-LA because the constant (time-independent) rate model (for a given temperature) is more conservative and bounds the general corrosion behavior of the WP outer shell over the repository time period.
WP and DS Degradation: General Corrosion Rate Law based on Weight-loss samples only (SNL 2007 [DIRS 178519], Section 6.4.3.5.2)	The ACM discussion for a general corrosion rate law for WP degradation based on plain weight-loss samples (rather than crevice samples) and is found in the analysis model report (SNL 2007 [DIRS 178519], Section 6.4.3.5.2). The weight-loss data were fit to a Weibull distribution using maximum likelihood estimators (i.e., using the same methods applied to the crevice sample data).	A comparison of the general corrosion rate distribution resulting from fitting the 5-year exposed weight-loss sample to the Weibull distributions based on the crevice sample data shows that this alternative conceptual model is less conservative relative to the base case general corrosion model (SNL 2007 [DIRS 178519], Figures 6-28 and 6-23).

Table 6.2-1. Table of Alternative Conceptual Models (Continued)

Alternative Conceptual Models	Key Assumptions	Assessment and Basis
Localized Corrosion Initiation: Critical Temperature-Based Localized Corrosion Initiation Model (SNL 2007 [DIRS 178519], Section 6.4.4.8.1)	The evolution of WP temperature with time, coupled with knowledge of the critical temperature for the initiation of localized corrosion, (pitting/crevice corrosion) can be used to determine when localized corrosion initiates.	Test conditions at which the required critical temperatures have been measured are not directly relevant to the potential environments on the WP surface. The model does not account for the effects of electrochemical characteristics of the solution contacting the metal.
WP and DS Degradation: Coupled Environment Fracture Model for SCC Growth Rate (SNL 2007 [DIRS 181953], Section 6.4.6)	The model, based on charge conservation, incorporates the effects of oxygen concentration, flow rate, and the conductivity of the external environment, as well as accounting for the effect of stress on crack growth.	Model underestimates the crack growth rate, as compared to the slip dissolution/film rupture model, when both models were applied to predict the crack growth rate.
Localized Corrosion Initiation: Localized Corrosion Penetration as a Time-Dependent Growth Law (SNL 2007 [DIRS 178519], Section 6.4.4.8.2)	The overall rate of localized corrosion is controlled by the rate of surface complexation reactions. Once initiated, the crevice corrosion penetration rate would decrease with increasing depth.	Data needed to apply the model can only be estimated approximately from open literature. The time-independent constant penetration rate model is more conservative.
Localized Corrosion Initiation: Passive Film Breakdown Potential for Determination of Critical Potential (SNL 2007 [DIRS 178519], Section 6.4.4.1)	An alternative technique for the determination of critical potential would be to use the passive film breakdown potential (obtained from the forward scan of the cyclic potentiodynamic polarization tests).	This criterion would not account for the (often slow) kinetics of localized corrosion initiation and may not be appropriate for modeling the long time periods involved in repository environments. Furthermore, the breakdown potential is likely to be much higher when the passive film has been formed over long time periods, allowing for a decrease in the film defect density.
Localized Corrosion Initiation: WP Surface Area Subject to Localized Corrosion (SNL 2007 [DIRS 178519], Section 6.4.4.8.3)	A distribution for the minimum area affected by localized corrosion was developed (minimum of 0.05 percent and maximum of the percent of area wetted by seepage) (SNL 2007 [DIRS 178519], Section 6.4.4.8.3).	No information is available regarding local environments on the WP; therefore, the area affected by localized corrosion due to seepage is based on the fraction of the WP surface exposed to seepage. TSPA has conservatively taken the area affected by localized corrosion to be the area wetted by seepage. Therefore, the entire surface area can potentially undergo localized corrosion.

Table 6.2-1. Table of Alternative Conceptual Models (Continued)

Alternative Conceptual Models	Key Assumptions	Assessment and Basis
Waste Form Degradation and Mobilization Model Component (Section 6.3.7)		
In-Package Chemistry: ACMs (SNL 2007 [DIRS 180506], Table 6-14).	Three ACMs were considered as alternatives to the In-Package Chemistry Abstraction (SNL 2007 [DIRS 180506], Section 6.4). The first ACM was a one-dimensional column composed of *n* cells, where the reactants in each cell represent the WP components in a vertical cross section of a WP (SNL 2007 [DIRS 180506], Section 6.4.1). The second ACM considered variable-composition seepage entering a failed WP as a function of time, changing with time-varying changes in the physical and chemical environment in the drifts and the EBS (SNL 2007 [DIRS 180506], Section 6.4.2). A third ACM considers the alternate methodologies for determining the vapor flux rate through the stress corrosion cracks in a failed WP (SNL 2007 [DIRS 180506], Section 6.4.3).	The first two ACMs and the associated screening arguments for in-package chemistry are summarized in Table 6.3.7-67. The third ACM was excluded because the abstracted relationship for the vapor flux rate into a stress corrosion cracked-failed WP provided for the TSPA-LA Model is simpler and spans the expected range by this ACM.
Cladding Degradation: ACMs (SNL 2007 [DIRS 180616], Table 6-5)	Addresses various causes of fuel failure including initial cladding failures, stainless steel clad fuels, and splitting due to dry oxidation (SNL 2007 [DIRS 180616], Table 6-5).	In the TSPA-LA compliance model, no cladding credit is taken for CSNF (SNL 2007 [DIRS 180616], Section 6.2.1.2[a]). In other words, the cladding of all CSNF is assumed to be failed upon arrival at the repository. Cladding credit for CSNF was evaluated in the PMA (Appendix C).
Waste Form Degradation: CSNF Waste Form Degradation ACMs (BSC 2004 [DIRS 169987], Section 6.4.2)	1) Electrochemical - The anodic Tafel lines can be extrapolated to the corrosion potential. The long-term corrosion behavior of spent nuclear fuel is similar to that of unirradiated UO_2. Differences between the corrosion behavior of spent nuclear fuel and unirradiated UO_2 are due to water radiolysis (BSC 2004 [DIRS 169987]).	Do not incorporate into the TSPA-LA Model; data needed to apply the model can only be estimated. Use for Nominal Scenario Class model validation-particularly for validation of long-term extrapolation (BSC 2004 [DIRS 169987]).
	Surface Complexation Model - The overall rate of CSNF corrosion is controlled by the rate of surface complexation reactions. The long-term corrosion behavior of spent nuclear fuel is similar to that of unirradiated UO_2 (BSC 2004 [DIRS 169987]).	Do not incorporate into TSPA-LA Model; data needed to apply the model can only be estimated from open literature. Use for Nominal Scenario Class model validation-particularly for validation of long-term extrapolation (BSC 2004 [DIRS 169987]).

Table 6.2-1. Table of Alternative Conceptual Models (Continued)

Alternative Conceptual Models	Key Assumptions	Assessment and Basis
Waste Form Degradation: DSNF Waste Form Degradation ACM (BSC 2004 [DIRS 172453], Section 6.3)	An ACM for DSNF waste form degradation was based on the best-estimates dissolution models presented in *DSNF and Other Waste Form Degradation Abstraction* (BSC 2004 [DIRS 172453], Section 6.3). The application of this ACM would require that the dissolution rate expression be multiplied by the "actual" effective surface area of the SNF.	This ACM was screened out of the DSNF Waste Form Degradation Submodel (Section 6.3.7.4.2) because insufficient qualified data on the corrosion rates and the surface areas of the fuel in each group are available. In addition, the upper-limit degradation model that is implemented as a surrogate for all the DSNF, other than naval SNF, is a bounding model with respect to the degradation rate.
Waste Form Degradation: HLW Glass Degradation ACMs (BSC 2004 [DIRS 169988], Section 6.4)	Diffusion-Controlled Release—Release rate of radionuclides determined by solid-state diffusion rates (BSC 2004 [DIRS 169988], Table 6-2).	Not incorporated into TSPA-LA Model, since it doesn't have a sufficient basis using the available data for waste glasses (BSC 2004 [DIRS 169988], Table 6-2).
	Composition-Independent Effective Rate Constant—Intrinsic rate constants vary over a small interval for different compositions and the very low flow rates in the repository compared to those used in the laboratory mean that the affinity term will be low (BSC 2004 [DIRS 169988], Table 6-2).	Not incorporated into TSPA-LA Model. Current approach provides a much more robust range of values for use in the TSPA-LA (BSC 2004 [DIRS 169988], Table 6-2).
Dissolved Concentration Limits: ACMs (SNL 2007 [DIRS 177418], Table 6.23-1)	Plutonium—The theoretical fO_2 model. fO_2 = 0.2 bars (SNL 2007 [DIRS 177418], Table 6.23-1).	The results of this model differ significantly from experimental measurements (SNL 2007 [DIRS 177418]).
	Plutonium—The empirical Eh model. Eh = 1.04 – 0.0592*pH (SNL 2007 [DIRS 177418], Table 6.23-1).	The results of this model are lower than experimental results (SNL 2007 [DIRS 177418]).
	Neptunium—Neptunium incorporation into uranyl secondary phases. Neptunium concentration controlled by solid solution rather than by pure phases (SNL 2007 [DIRS 177418], Table 6.23-1).	Experimental studies on whether schoepite, the critical secondary uranyl phase, can incorporate sufficient neptunium and immobilize it during spent nuclear fuel corrosion do not provide a solid basis for recommending this model for use in the TSPA-LA (SNL 2007 [DIRS 177418], Table 6.23-1).
	Thorium—Solubility control by other thorium phases included in thermodynamic modeling database including ThO_2 (thorianite), $Th_{0.75}PO_4$, $Th(SO_4)_2$, ThF_4, $ThF_4 \cdot 2H_2O$. Solubility of thermodynamically most-stable phase controls concentrations (SNL 2007 [DIRS 177418], Table 6.23-1).	Solubilities calculated with ThO_2(am) are most consistent with measured thorium solubility in pure water. Other phases may be less soluble only under certain conditions or may be based on questionable data. More soluble ThO_2(am) was chosen for (SNL 2007 [DIRS 177418], Table 6.23-1).
	Americium—Solubility control by phase with properties between $Am(OH)_3$(am) to $Am(OH)_3$. Initially formed $Am(OH)_3$(am) will invert to more stable $Am(OH)_3$ with time. $Am(OH)_3$ stability decreases with time from self irradiation (SNL 2007 [DIRS 177418], Table 6.23-1).	$AmOHCO_3$ is formed in americium solubility experiments under Yucca Mountain conditions. Under some conditions, $Am(OH)_3$ may be less soluble, but generally choosing $AmOHCO_3$ is conservative (SNL 2007 [DIRS 177418], Table 6.23-1).

Table 6.2-1. Table of Alternative Conceptual Models (Continued)

Alternative Conceptual Models	Key Assumptions	Assessment and Basis
Dissolved Concentration Limits: ACMs (SNL 2007 [DIRS 177418], Table 6.23-1) (continued)	Protactinium—Solubility is same as that of ThO_2(am). Thorium is also a good analogue to protactinium and was modeled in this report (SNL 2007 [DIRS 177418], Table 6.23-1).	Solubility of Np_2O_5 was chosen because it is higher than that of ThO_2(am) under conditions modeled, so its choice is conservative (SNL 2007 [DIRS 177418], Table 6.23-1).
	Radium—Solid solution (Ra, Ba, Sr, Ca)SO_4 (SNL 2007 [DIRS 177418], Table 6.23-1).	Chemistry of in-package and invert waters are not so far outside the normal range of natural waters to cause different radium solubilities (SNL 2007 [DIRS 177418], Table 6.23-1).
	Technetium—Technetium incorporation into epsilon or "5 metal" phases during CSNF corrosion (SNL 2007 [DIRS 177418], Table 6.23-1).	Studies on fuel corrosion indicate the formation of Epsilon particles ("5 metal particles"). Technetium in these particles may not be released when the fuel corrodes. Sparse data on this phenomenon, however, do not provide a solid basis for recommending this as a Technetium model. Therefore, no solubility was defined, and inventory release should be in control (SNL 2007 [DIRS 177418], Table 6.23-1).
	Strontium—Solubility controlled by $SrCO_3$ or $SrSO_4$ (SNL 2007 [DIRS 177418], Table 6.23-1).	No solubility was defined, and inventory release should be in control. This is a conservative approach (SNL 2007 [DIRS 177418], Table 6.23-1).
	Tin—Solubility controlled by very insoluble crystalline phase cassiterite (SnO_2) (SNL 2007 [DIRS 177418], Table 6.23-1).	Solubilities calculated with SnO_2(am) are consistent with measured Sn solubility in pure water. Other phases may form only under certain conditions (SNL 2007 [DIRS 177418], Table 6.23-1).
EBS Colloids: ACMs (SNL 2007 [DIRS 177423], Section 6.4)	Kinetic Sorption—This model provides a method for predicting sorption behavior beyond laboratory time scales. Allows interpretation of data from different time scales. Based on model developed by Painter et al. (2002 [DIRS 174071]) and extended two- and three-site model developed by Wittman et al. 2005 [DIRS 174895].	This ACM is not supported by the available data (SNL 2007 [DIRS 177423]).
	Rate of Colloid Generation (Argonne National Laboratory) (SNL 2007 [DIRS 177423], Section 6.4.2,Table 6-19)—Rate of colloid spallation depends upon the rate of waste degradation. The rate of waste degradation may be defined by the rate of release to the boron content in the alteration fluid (for DHLWG) and technetium (for CSNF).	The ACM is tailored closely to the specific experimental configuration from which the supporting data were acquired. The position of this analysis is that, while promising, the ACM is currently not sufficiently developed for application to more generalized conditions.

Table 6.2-1. Table of Alternative Conceptual Models (Continued)

Alternative Conceptual Models	Key Assumptions	Assessment and Basis
	Mechanisms of Colloid Generation in CSNF (Pacific Northwest National Laboratory) (SNL 2007 [DIRS 177423], Table 6-10)-Colloid generation at, and mobilization from, the surface of degrading waste is primarily related to flow rate at the waste surface.	The supporting concepts and data from the peer-reviewed literature were developed in the context of deposition and remobilization of existing colloids under conditions of significant groundwater flow. These conditions likely will not apply to conditions anticipated in the repository. Mechanisms of colloid generation at the surface of corroding fuel may be different from mechanisms of mobilization of a discrete deposited colloid.
EBS Flow and Transport Model Component (Sections 6.3.6 and 6.3.8)		
EBS Transport: Dual-Continuum Invert Model	Crushed tuff invert ballast is modeled as a dual-continuum material consisting of intergranular pore space and intragranular pore space. All seepage flow into the drift flows through the intergranular pore space and into the UZ fractures. Imbibition from UZ host rock into the invert flows through the intragranular pore space. Diffusion of radionuclides also occurs in both the intergranular and intragranular pore spaces, from the WP corrosion products into UZ fractures and matrix, as well as between the two invert continua (SNL 2007 [DIRS 177407], Section 6.6.3).	Insufficient data to validate diffusion coefficients in individual continua. Insufficient data to confirm whether this is a bounding approach with respect to chemical conditions in the invert for calculating solubility and colloid stability.
EBS Flow: Bathtub Flow Model	Seepage water flowing into breached WP accumulates until void volume is filled before water containing dissolved radionuclides flows out. Various cases, such as changing inflow rates and effect of solubility and dissolution rate limits are evaluated (SNL 2007 [DIRS 177407], Section 6.6.1).	For several of the most pertinent cases, the flow-through model is conservative with respect to releases of radionuclides.
EBS Transport: Constrained Water Vapor and Oxygen Diffusion Model	The rate of steel component corrosion inside a WP is compared with the rate of diffusion of water vapor and oxygen through SCCs into a WP. A continuous film of absorbed water cannot form if the consumption rate is higher, which could delay the diffusive releases until all steel is fully corroded (SNL 2007 [DIRS 177407], Section 6.6.2).	Insufficient data to validate.

Table 6.2-1. Table of Alternative Conceptual Models (Continued)

Alternative Conceptual Models	Key Assumptions	Assessment and Basis
EBS Transport: Invert Diffusion Coefficient Model with Lower Limit on Water Content	As the water content of the crushed tuff ballast decreases, the water films that connect pore spaces become disconnected, and the effective diffusion coefficient drops more rapidly than predicted by Archie's law. Below some critical water content, the diffusion coefficient becomes zero, based on models of diffusion in soils (SNL 2007 [DIRS 177407], Section 6.6.4).	Insufficient data to validate diffusive behavior at very low water contents. Nonbounding; does not provide upper bounds on diffusion coefficients.
EBS Transport: Reversible Sorption of Radionuclides onto WP Corrosion	Iron oxyhydroxide corrosion products sorb many radionuclide species. Sorption is assumed to be reversible and will not compete with other radionuclides nor compete for irreversible sorption sites (SNL 2007 [DIRS 177407}, Section 6.6.5).	Does not account for limitations on total number of sorption sites. Does not account for competition with other radionuclides for sorption sites.
EBS Transport: Plutonium Sorption from Stationary Corrosion Products and Colloids	Plutonium sorbs strongly to iron oxyhydroxide corrosion product colloids and stationary corrosion products. Sorption may be considered slowly reversible (and modeled by computing the forward and reverse rate constants for the two-site model) (SNL 2007 [DIRS 177407], Section 6.6.6).	Experiment durations are short (hours to weeks) compared to the repository time scale. The mechanisms of plutonium sorption are not well enough understood to extrapolate the results outside the experimental design.
Unsaturated Zone Transport Model Component (Section 6.3.9)		
UZ Transport: Discretization of the UZ Matrix (DFM and MINC Models)	In the dual permeability model every fracture node has a parallel rock matrix node with the gradient between the two nodes defining the matrix diffusion process. A more accurate method of representing matrix diffusion would be to further discretize the rock matrix to more accurately define the concentration gradient at the matrix-fracture interface and within the matrix. Two models that include a finely discretized matrix the Discrete Fracture Model (DFM) and MINC Model are shown to predict longer breakthrough times than the implemented dual permeability model (SNL 2008 [DIRS 184748], Section 7.2.2 and Section 7.2.2[a]). The DFM uses flow fields based on the dual permeability flow simulations and the MINC model derives its flow fields based on the finer discretization of the rock matrix. A comparison of (DFM and MINC Model results showed that the MINC Model predicts longer breakthrough times than the Discrete Fracture Model (SNL 2008 [DIRS 184748], Section 7.2.2 and Section 7.2.2[a]).	The dual porosity model used for the TSPA-LA is conservative. The DFM is readily implementable in the UZ Transport Abstraction by replacing the transfer functions. The MINC Model is not practical because of its larger computational burden (SNL 2008 [DIRS 184748], Table 6-30).

Table 6.2-1. Table of Alternative Conceptual Models (Continued)

Alternative Conceptual Models	Key Assumptions	Assessment and Basis
UZ Transport: Alternative Finite Difference Numerical Models	An alternate method of approximating radionuclide transport in groundwater based on approximating the governing equations using finite difference equations (SNL 2008 [DIRS 184748], Table 6-30) was evaluated as an ACM for the FEHM Particle Tracking model.	The FEHM Particle Tracking Transport Abstraction Model matched the results predicted by the finite difference numerical methods (SNL 2008 [DIRS 184748], Sections 7.2.2[a] and 7.2.3.1[a]). Therefore the ACM supports the results using the particle tracking method.
UZ Transport: Lateral Flow Diversion In UZ Above the Repository	Lateral flow in the PTn will divert percolating water to the faults and reduce the percolation flux at the repository (BSC 2004 [DIRS 169861], Section 6.9.2).	Generally more conservative with respect to radionuclide transport (BSC 2004 [DIRS 169861], Section 6.9.2). Note that analyses used for this conclusion are based on the original infiltration model, but the conclusions are still valid. The updated model predicts significant diversion and redistribution into faults for the PTn (SNL 2007 [DIRS 184614], Section 8.6).
UZ Transport: No Radionuclide Release into Faults	The fault zones are defined as high-permeability zones subject to fast advective transport to the the top of the TSw and to the water table (SNL 2007 [DIRS 177396], Section 6.20.2).	The effects of not allowing direct release of radionuclides into the fault zones, on the overall transport to the water table, are not significant because lateral diversion directs the radionuclides into the fault zones (SNL 2007 [DIRS 177396], Section 6.20.2).
UZ Transport: Inclusion of Drift Shadow Effects	Inclusion of drift shadow effects would approximate the influence of capillary diversion, which may cause low fracture saturation below the drift (SNL 2008 [DIRS 184748], Section 6.7).	There is insufficient data to support this effect. It is considered conservative to ignore drift shadow effects. Additionally, the increased infiltration associated with future climate states may decrease the effects (SNL 2008 [DIRS 184748], Section 6.7).
UZ Transport: Inclusion of TH, THC, and THM Effects on UZ Flow	Vaporization due to repository heat will keep the drift dry for several hundred to a few thousand years. THC and THM effects may alter transport properties of the UZ rocks (SNL 2008 [DIRS 184748], Section 6.7).	TH, THC, and THM effects are insignificant after the change to glacial-transition climate (SNL 2008 [DIRS 184748], Section 6.7).

Table 6.2-1. Table of Alternative Conceptual Models (Continued)

Alternative Conceptual Models	Key Assumptions	Assessment and Basis
UZ Transport: Alternative Fracture-Matrix Interaction Model	The TSPA-LA Model utilizes the Active Fracture Model (AFM) (Liu et al. 1998 [DIRS 105729]), which assumes that only a fraction of connected fractures are active in conducting water. The AFM is implemented by applying a fracture-matrix effective interface area reduction term or a fracture-matrix interface area adjustment factor and a fracture spacing adjustment factor. The ACM assumes that all connected fractures are active in conducting water and represents a standard methodology with no fracture-matrix effective interface area reduction term applied. The active fracture model, with its reduced effective area of diffusion between fracture and matrix, is used in the TSPA-LA Model because of its more conservative nature and its ability to explain travel times associated with ^{14}C data (SNL 2008 [DIRS 184748], Section 5, Assumption 1) and (BSC 2004 [DIRS 170035], Section 7.4.1).	Using the standard methodology would enhance diffusion between the fracture and matrix. Because the active fracture model is more conservative and has better reflected field test results, the standard methodology was not recommended for inclusion in the TSPA-LA Model.
Saturated Zone Flow and Transport Model Component (Section 6.3.10)		
SZ Transport: Minimal Matrix Diffusion	Diffusion of radionuclides into the pore space of the rock matrix in the fractured volcanic units is extremely limited due to highly channelized groundwater flow, fracture coatings, or other factors (SNL 2008 [DIRS 183750], Section 6.4).	This ACM is implicitly included in the SZ Flow and Transport Model Abstraction and the 1-D SZ Flow and Transport Submodel through the range of uncertainty in key input parameters. The uncertain input parameters influencing matrix diffusion include DCVO, FISVO, and FPVO (SNL 2008 [DIRS 183750], Table 6.3.10-1).
SZ Transport: Horizontal Anisotropy in Permeability	Alternative interpretations of pump test results in the fractured volcanic units indicate preferential permeability along structural features oriented in the NNE-SSW direction, or in the WNW-ESE direction (SNL 2008 [DIRS 183750], Section 6.4).	This ACM is implicitly included in the 3-D SZ Flow and Transport Model Abstraction and the 1-D SZ Flow and Transport Abstraction through the range of uncertainty in an input parameter. The uncertain input parameter influencing horizontal anisotropy in permeability in the volcanic units near Yucca Mountain is the ratio of N-S to E-W permeability (SNL 2008 [DIRS 183750], HAVO; Table 6.3.10-2). This continuously distributed parameter varies from less than one to greater than one with most of the realizations greater than one.
Biosphere Model Component (Section 6.3.11)		
Biosphere: Radon Release from Soil (Air Submodel)	This ACM considers radon transport in the soil and the atmosphere, which requires more input data. The ERMYN conceptual model does not include these processes and uses a simple release factor.	This ACM is from the Biosphere Model Component based on an analysis (SNL 2007 [DIRS 177399], Section 7.4.3.1) showing that the ACM and the ERMYN model produce comparable results.

Table 6.2-1. Table of Alternative Conceptual Models (Continued)

Alternative Conceptual Models	Key Assumptions	Assessment and Basis
Biosphere: Evaporative Cooler (Air Submodel)	This ACM considers an inhalation dose from aerosols generated from evaporative coolers and is based on calculating radionuclide concentrations in the air due to an increase in humidity. The ERMYN conceptual model uses a submodel based on the amount of water evaporated rather than an increase in humidity.	This ACM is from the Biosphere Model Component based on an analysis (SNL 2007 [DIRS 177399], Section 7.4.3.2) showing that this ACM and the ERMYN model produce equivalent results.
Biosphere: Direct Deposition of Irrigated Water (Plant Submodel)	This ACM considers two processes, one where the deposited radionuclide moves from external plant surfaces into the plant tissues, and then from plant tissues into the edible portion of the crop. Weathering is applied only to contaminants that remain on external plant surfaces. Food processing loss is also considered in the ACM. The ERMYN conceptual model considers the radionuclides in irrigation water to be directly translocated to the edible parts of plants with weathering and accumulation during the growing period but without food preparation loss.	This ACM is from the Biosphere Model Component based on an analysis (SNL 2007 [DIRS 177399], Section 7.4.4.1) showing that this ACM and the ERMYN model produce comparable results.
Biosphere: Direct Deposition of Airborne Particulates (Plant Submodel)	This ACM is based on the crop external contamination. This contamination factor is very similar to a soil-to-plant transfer factor. The ERMYN conceptual model considers the deposited airborne particles on crop leaves acting the same way as the intercepted irrigation water.	This ACM is from the Biosphere Model Component based on an analysis (SNL 2007 [DIRS 177399], Section 7.4.4.3) showing that this ACM and the ERMYN model produce comparable results for reasonable input values.
Biosphere: Animal Product Contamination (Animal Submodel)	Two pathways are considered in this ACM. They are animal inhalation of contaminated air and animal soil ingestion. The ERMYN conceptual model excludes the inhalation of contaminated air, but it includes animal soil ingestion.	This ACM is from the Biosphere Model Component based on an analysis (SNL 2007 [DIRS 177399], Section 7.4.5) showing that soil ingestion is important but that inhalation of contaminated air is not.
Biosphere: ^{14}C Special Submodel	This ACM considered alternate ^{14}C pathways for plant uptake. This ACM considered uptake into plants only from roots and used a very low removal rate of carbon from soil because the model did not account for gaseous release of $^{14}CO_2$.	The method used by the biosphere model was chosen because it more realistically considered uptake of $^{14}CO_2$ gas into plants, resulting in higher plant concentrations (SNL 2007 [DIRS 177399], Sections 6.3.3, 7.3.6, and 7.4.7).
Biosphere: Environment-Specific Inhalation Submodel (Inhalation Submodel)	This ACM uses average values of input parameters for inhalation exposure. The ERMYN conceptual model considers inhalation exposure as a function of the environment because many model parameters, such as mass loading, breathing rate, and exposure time, differ among environments and activities.	This ACM is from the Biosphere Model Component based on an analysis (SNL 2007 [DIRS 177399], Section 7.4.9) showing that the ACM and the ERMYN model produce comparable results. In addition, it is easier to address uncertainty in the input parameters using environment-specific values.

Table 6.2-1. Table of Alternative Conceptual Models (Continued)

Alternative Conceptual Models	Key Assumptions	Assessment and Basis
Igneous Scenario Class (Section 6.5)		
Estimating the Igneous Event Rates in the Probabilistic Volcanic Hazard Analysis	The PVHA model uses the number of identified post-Miocene era volcanic events observable at the surface plus some buried in the Yucca Mountain region. *Characterize Framework for Igneous Activity at Yucca Mountain, Nevada* (BSC 2004 [DIRS 169989], Sections 6.3.1.6 through 6.3.1.7 and Table 6-4) identifies an ACM for the PVHA in which a significant number of buried (i.e., unidentified) volcanic centers would be included in the estimation of the igneous event rates. The basis for the ACM is that aeromagnetic anomalies suggest that a significant number of unidentified volcanic events were unaccounted for in the PVHA, thus underestimating the volcanic hazard.	This ACM was not propagated into the TSPA Model because its effects on the probability of an igneous event could not be quantified without further data collection. A drilling and sampling program is underway to determine whether any of these anomalies represent Quaternary buried volcanic centers. In addition, an update to the PVHA is underway to reassess the probability of intersection and the probability of a volcanic center being located on Yucca Mountain.
Estimating the Intersection Annual Probability in the Probabilistic Volcanic Hazard Analysis	*Characterize Framework for Igneous Activity at Yucca Mountain, Nevada* (BSC 2004 [DIRS 169989], Section 6.3.1.8 and Table 6-5) identifies several ACMs for estimating the intersection probability (i.e., the annual probability of a volcanic event intersecting the repository footprint).	The ACM probabilities are captured by the probability used in the PVHA.
Dike Propagation	*Dike/Drift Interactions* (SNL 2007 [DIRS 177430], Section 6.3.8) identifies ACMs for dike propagation that use hydraulic-fracture models.	*Dike/Drift Interactions* (SNL2007 [DIRS 177430], Section 6.3.8) concluded that none of these models were appropriate for the dike propagation in the vicinity of an underground repository as none of the models has a free surface that can model the changing behavior of the dike as the surface is approached.
Effusive Magma Flow Into Drifts	*Dike/Drift Interactions* (SNL 2007 [DIRS 177430], Section 6.3.3.5) identifies ACMs for effusive or pyroclastic flow from a dike into a drift.	Simulation of these flows and their interactions with WPs is computationally intensive and, therefore, not practical for implementation within the TSPA-LA Model. Instead, the abstractions included in Waste Packages Hit accounts for the effects of these flows within the TSPA framework.
Thermal Hydrologic Effects on Zones 1 and 2 Drifts	*Dike/Drift Interactions* (SNL 2007 [DIRS 177430], Section 6.4.7) identifies ACMs for the thermal hydrologic behavior of magma-filled drifts and its effects on neighboring drifts. These ACMs involve an evaluation of additional physics, including latent heat of crystallization, host-rock saturation, and enhanced vapor diffusion, and an alternative model for heat conduction from Zone 1 to Zone 2 emplacement drifts.	Inclusion of the latent heat of crystallization and host-rock saturation in the heat transfer analyses was evaluated and is shown to have a negligible effect on the results, producing elevated temperature histories (i.e., above boiling) no more than 2 to 5 years longer than without these ACMs included in the analysis (SNL 2007 [DIRS 177430], Section 7.3.2.1).

Table 6.2-1. Table of Alternative Conceptual Models (Continued)

Alternative Conceptual Models	Key Assumptions	Assessment and Basis
Volcanic Eruption Phase Dose	An ACM for the calculation of the radiation dose received by a receptor that does not leave the region during a volcanic eruption is detailed in Section 6.5.2.4. The eruption phase of a volcanic event refers to the conditions that exist during the volcanic eruption before the deposition of volcanic ash on the ground is completed The result of this calculation is used as the basis for excluding the potential eruption phase dose in the TSPA-LA Model.	Because a high concentration of airborne radioactive particulates is expected during this phase, inhalation of airborne-contaminated ash particles is the only pathway considered (SNL 2007 [DIRS 177399], Section 6.15.2). The receptor has the same inhalation characteristics as those for the RMEI discussed in Section 6.3.11.
Seismic Scenario Class (Section 6.6)		
Alternative Modeling Approaches Evaluated for Conceptual and Computational Models of Lithophysal and Nonlithophysal Rock (SNL 2007 [DIRS 166107], Section 7.4)	A standard approach for solving excavation stability problems is the use of numerical models based on continuum mechanics. Continuum models use constitutive relations to describe the mechanical behavior of a material. The use of a constitutive model requires that the mechanical effects of fractures be lumped into the constitutive relationships.	Continuum models are unable to predict instabilities, such as fracture and rockfall (SNL 2007 [DIRS 166107], Section 7.4.1). The discontinuum approach is more suitable for representing fracture of the rock mass and separation of the intact rock mass into blocks and was therefore adopted for modeling the drift degradation processes that occur after a seismic event (SNL 2007 [DIRS 166107], Section 7.4.2).
Alternative Conceptual Model for Crack Area Density Presented in Section 6.7.4 (SNL 2007 [DIRS 181953])	The alternative model considered a circular geometry circumscribed by a single through-wall crack. The base case model combines two conceptual models based on hexagonal geometry (SNL 2007 [DIRS 181953], Section 6.7.3).	The hexagonal geometry represents a high effective density of individual cracks and the two hexagonal geometry conceptual models are considered conservative representations. The ACM analysis, which uses circular geometry, is considered a limiting realistic case (SNL 2007 [DIRS 181953], Section 6.7.2).

Table 6.2-1. Table of Alternative Conceptual Models (Continued)

Alternative Conceptual Models	Key Assumptions	Assessment and Basis
Alternative Conceptual Models for Conditional Probability Distributions Representing Damaged Areas on WP, Damaged Areas on DS, and Volume of Rockfall from Seismic Event Considered	These alternate distributions included the gamma, normal, log-normal, Weibull, and triangular distributions, as presented in Sections 6.5.1.4, 6.5.2.4, 6.6.1.4, 6.6.2.4, 6.7.1.3, 6.7.2.4, 6.9.4, and 6.10.2.8 of *Seismic Consequence Abstraction* (SNL 2007 [DIRS 176828]).	Gamma distributions generally provided simpler and more accurate representations of the statistical observations than normal, log-normal, log-triangular, and Weibull distributions. The exception to the use of gamma distributions is that the fragility analyses (for drip shield plates and framework) have used log-normal representations to simplify manipulation of products and quotients of random variables.
Alternative Damage Abstraction for Fault Displacement Damage (SNL 2007 [DIRS 176828], Section 6.11.6)	The ACM considered the probability-weighted number of waste package failures from fault displacement and the number of fault intersections with emplacement drifts. The ACM was based on the use of historical data for fault displacement in the western United States.	The results provided by the ACM are consistent with the base-case model for both the probability-weighted number of WP failures and the number of fault intersections with the emplacement drifts (SNL 2007 [DIRS 176828], Section 6.11.6).

NOTES: ANL = Argonne National Laboratory; DHLWG = defense high-level waste glass; 1-D = one-dimensional; DCVO = effective diffusion coefficient in volcanic units; FISVO = flowing interval spacing in volcanic units; FPVC = flowing interval porosity; HAVO = ratio of horizontal anisotropy (north-south over east-west) in permeability; ERMYN = Environmental Radiation Model for Yucca Mountain, Nevada; DFM = discrete fracture model; MINC = multiple interacting continua.

INTENTIONALLY LEFT BLANK

6.3 TSPA-LA MODEL FOR THE NOMINAL SCENARIO CLASS

Section 6.3 presents a description of the Nominal Scenario Class for the Total System Performance Assessment for the License Application (TSPA-LA) Model. Sections 6.3.1 to 6.3.11 describe the conceptual models, the model abstractions, and implementation of these abstractions in the TSPA-LA Model. Each subsection of Section 6.3, namely Sections 6.3.1 to 6.3.11, will be introduced by two figures that have a consistent format and type of content. The first figure in each Section 6.3 subsection will illustrate how the submodels discussed in the subsection relate to other TSPA-LA submodels. The second figure in each subsection will illustrate important information about individual submodels. In particular, the figures illustrate the principal feeds, or inputs, to the submodels, the principal outputs from the submodels, highlights of the theoretical foundation and important characteristics of the submodels, and an indication of the sources of confidence, including field and laboratory data and auxiliary modeling in the submodels, and will vary according to the contents of the individual subsections. Detailed information describing the information feeds between the submodels of the TSPA-LA Model is included on wiring diagrams presented in Appendix G. Further information regarding the areas singled out on these figures can be found in the accompanying text of the individual Section 6.3 subsections and in the supporting analysis and/or model reports that are referenced in the Section 6.3 subsections.

The TSPA-LA Model of the Yucca Mountain repository system is a combination of integrated processes that have been conceptualized and modeled as a collection of coupled model components. For the TSPA-LA Model, eight principal model components are combined to evaluate repository system performance for the Nominal Scenario Class. The model components are:

- Unsaturated Zone (UZ) Flow
- Engineered Barrier System (EBS) Environment
- Waste Package (WP) and Drip Shield (DS) Degradation
- Waste Form Degradation and Mobilization
- EBS Flow and Transport
- Unsaturated Zone (UZ) Transport
- Saturated Zone (SZ) Flow and Transport
- Biosphere.

Section 6.3 provides detailed descriptions of the TSPA-LA submodels that comprise the model components. Table 6-1 can be considered a guide that links the principal TSPA-LA Model components shown on Figure 6-1 to the TSPA-LA submodels. Each submodel description in Section 6.3 includes:

- A discussion of how the submodel is connected to other submodels and model components in the TSPA-LA Model.
- A description of the conceptual model on which the submodel is based.
- A description of the submodel abstraction.

- A description of how the abstraction is implemented in the TSPA-LA Model.
- An evaluation of the consistency and conservatism in assumptions and parameters used in the TSPA-LA Model. Assumptions and parameter values that are different among submodels in the TSPA-LA Model are documented in each section.
- A summary of alternative conceptual models (ACMs) that were considered in the development of the conceptual model.

The focus of Section 6.3 is on the TSPA-LA Model components and submodels and their implementation for the Nominal Scenario Class.

6.3.1 Mountain-Scale Unsaturated Zone Flow

UZ flow in the TSPA-LA Model refers to the percolation of groundwater through the unsaturated rocks between the land surface and the water table. The Site-Scale UZ Flow Model (SNL 2007 [DIRS 184614]) provides the flow fields for the Multiscale Thermohydrologic Model (MSTHM) and the UZ Transport Submodel (Section 6.3.9). Figure 6.3.1-1 illustrates the connections between the Site-Scale UZ Flow Model and the submodels of the TSPA-LA Model. Figure 6.3.1-1 shows that the Climate Analysis, as described in *Future Climate Analysis* (BSC 2004 [DIRS 170002]) and *Data Analysis for Infiltration Modeling: Extracted Weather Station Data Used to Represent Present-Day and Potential Future Climate Conditions in the Vicinity of Yucca Mountain* (SNL 2007 [DIRS 177081]), and the Infiltration Model, as described in *Simulation of Net Infiltration for Present-Day and Potential Future Climates* (SNL 2007 [DIRS 182145]), contribute to the Site-Scale UZ Flow Model. *Future Climate Analysis* (BSC 2004 [DIRS 170002]) provides climate analogues to be used for assessing the future mean annual temperature and precipitation in the region, including Yucca Mountain. Future climate conditions at Yucca Mountain must be predicted to determine the hydrological conditions at and near Yucca Mountain. *Data Analysis for Infiltration Modeling: Extracted Weather Station Data Used to Represent Present-Day and Potential Future Climate Conditions in the Vicinity of Yucca Mountain* (SNL 2007 [DIRS 177081]) provides climatological data based on present-day conditions in the Yucca Mountain vicinity and the climate analogues presented in *Future Climate Analysis* (BSC 2004 [DIRS 170002]). Figure 6.3.1-2 illustrates the outputs provided by the Climate Analysis to the Infiltration Model and TSPA-LA Model. *Future Climate Analysis* (BSC 2004 [DIRS 170002]) provides three climate states for use in the TSPA-LA Model: present-day, monsoon, and glacial-transition. The outputs from the *Future Climate Analysis* (BSC 2004 [DIRS 170002]) include duration (Table 6.3.1-1), climate analogues for precipitation rates, and air temperatures for each climate state. *Data Analysis for Infiltration Modeling: Extracted Weather Station Data Used to Represent Present-Day and Potential Future Climate Conditions in the Vicinity of Yucca Mountain* (SNL 2007 [DIRS 177081]) provides climatological data, such as precipitation rates and air temperatures, to the infiltration model.

Figure 6.3.1-3 illustrates and describes the main differences among the three climate states used in the TSPA-LA Model. The future climate states (i.e., monsoon and glacial-transition) were based on analogue sites with representative conditions for those periods. Figure 6.3.1-3 lists the analogue sites used to define the conditions for these future climate states. The present-day climate is based on climatic data available for the Yucca Mountain site. The monsoon climate state will have a higher precipitation rate and higher temperature than the present-day climate (BSC 2004 [DIRS 170002], Section 7.1). The glacial-transition climate state will have a higher precipitation rate but lower temperature than the present-day climate (BSC 2004 [DIRS 170002], Section 7.1). A fourth climate state is also implemented as per regulations found in *Implementation of a Dose Standard After 10,000 Years* (70 FR 53313 [DIRS 178394]). The fourth climate state (post-10,000-year climate state) extends the simulations from 10,000 years to 1,000,000 years. The implementation of the fourth climate state is based on the NRC Proposed Rule 10 CFR 63.342 (c) (2) [DIRS 178394]:

> "DOE must assess the effects of climate change. The climate change analysis may be limited to the effects of increased water flow through the repository as a

> result of climate change, and the resulting transport and release of radionuclides to the accessible environment. The nature and degree of climate change may be represented by constant climate conditions. The analysis may commence at 10,000 years after disposal and shall extend to the period of geologic stability. The constant value to be used to represent climate change is to be based on a log-uniform probability distribution for deep percolation rates from 13 to 64 mm/year (0.5 to 2.5 inches/year)."

The implementation of the fourth climate state in the Site-Scale UZ Flow Model is described in *UZ Flow Models and Submodels* (SNL 2007 [DIRS 184614]).

Net infiltration is the flux across the depth where it can no longer be withdrawn by evaporation or transpiration by plants. The Infiltration Model provides net infiltration rates of meteoric water, which are used as inputs for the upper boundary condition for the Site-Scale UZ Flow Model. Figure 6.3.1-4 schematically shows the connection between the Infiltration Model and the Site-Scale UZ Flow Model, as well as inputs to and outputs from the Infiltration Model. Figure 6.3.1-5 is a schematic illustration showing the variation of precipitation and consequent net infiltration with respect to elevation and landforms at Yucca Mountain. Net infiltration will be influenced by a number of factors (BSC 2004 [DIRS 169734], Section 7.1.3). Precipitation in the Yucca Mountain region is spatially variable and dependent on meteorological conditions, as well as elevation and surface geology (BSC 2004 [DIRS 169734], Section 7.1.3.3). There is a correlation between surface elevations and local precipitation. In the higher elevations, there are likely to be thinner surface soils and shallower fractured bedrock. In the lower elevations, especially in washes, the surface tends to be alluvium and the bedrock tends to be at a greater depth. Some of the factors that have an influence on how precipitation becomes net infiltration are the amount and rate of precipitation, evaporation, transpiration, topography, thickness of surface soils, run-on and runoff of surface water, redistribution of moisture, permeability and sorptive capacity of the soils, and the amount of vegetation, as well as fractured bedrock characteristics. In addition, these factors may change through time due to long-term climatic and geomorphologic changes.

Figure 6.3.1-6 displays principal input and output interfaces between the Site-Scale UZ Flow Model, the MSTHM (Section 6.3.2), and the UZ Transport Submodel (Section 6.3.9). As shown on Figure 6.3.1-6, outputs of the Site-Scale UZ Flow Model are passed to the MSTHM to specify the percolation flux, consisting of liquid flux in both the fracture and matrix continua, at the base of the Paintbrush nonwelded hydrogeologic (PTn) unit. The percolation flux at the base of the PTn unit, above the repository horizon, is used as an upper boundary condition, as described in *Multiscale Thermohydrologic Model* (SNL 2007 [DIRS 181383], Section 6.2.6.6). UZ hydrologic properties, such as permeability, porosity, residual saturation, van Genuchten parameters, and Active Fracture Model parameters, are also passed to the MSTHM (SNL 2007 [DIRS 181383], Table 4.1-1, Sections 6.2.6 and 6.2.6.5). These parameter values are used to generate the EBS thermal-hydrologic (TH) conditions for implementation in the TSPA-LA Model. The above parameter values are also used to generate the drift-seepage conditions, as described in *Abstraction of Drift Seepage* (SNL 2007 [DIRS 181244], Section 6.7.1.2), for implementation in the TSPA-LA Model. In addition, flow fields are passed to the UZ Transport Submodel (Section 6.3.9). The UZ flow fields provide input of fracture and matrix liquid flux

and liquid flux between fracture and matrix continua, along with liquid saturation and pressure values.

6.3.1.1 Conceptual Model

The Site-Scale UZ Flow Model uses a dual-permeability conceptual model that captures the effects of fast-flow paths and allows for fracture-matrix coupling. Flow is modeled in both fracture and matrix continua and these continua interact with one another. Both fracture and matrix continua are assigned their own hydrologic properties, such as permeability and porosity. Hydrologic properties are, in general, uniform layer-wise. Generally, fractures are modeled as part of a highly permeable continuum having low porosity, whereas the matrix is modeled as a much less permeable continuum having higher porosity than the fracture continuum. Fracture-matrix interaction is represented with an active fracture model, in which only some fractures are actively conducting water under unsaturated conditions (SNL 2007 [DIRS 184614], Section 6.1.2). Major faults are explicitly included in the Site-Scale UZ Flow Model. When compared to the same hydrologic units outside the fault zone, the fault zone fracture permeabilities are generally much higher than in the rest of the Site-Scale UZ Flow Model, enabling preferential flow paths in portions of the Site-Scale UZ Flow Model (SNL 2007 [DIRS 179545], Section 6.3.4 and Tables B1 to B4). In addition to the fault zone properties differing from the surrounding units, each hydrogeologic unit (TCw, PTn, TSw, and CHn) has a different hydrologic property set. Either the ground surface at Yucca Mountain or the tuff-alluvium contact in areas of significant alluvial cover is taken as the top model boundary and the water table is taken as the bottom model boundary of the Site-Scale UZ Flow Model. For flow simulations, the top boundary is modeled as a Dirichlet-type condition and the water flux is specified as a source term to the fracture grid blocks in the second grid layer from the top and the water table is used as the bottom boundary that is assigned a single-valued fixed water pressure, which is equivalent to specifying a constant liquid saturation (SNL 2007 [DIRS 184614], Section 6.1.3). Changes in the water table elevation at the bottom boundary because of climate-related changes in recharge are not included in the Site-Scale UZ Flow Model simulations. The basis for this implementation is that water flow through the unsaturated rock within Yucca Mountain is predominantly downward and dominated by gravity. Therefore, the elevation of the water table has little influence on the fluxes calculated for the UZ flow fields.

To approximate the effects of a rising water table on a radionuclide transport simulated by the finite element heat and mass (FEHM) transfer code (FEHM V2.24-01, STN: 10086-2.24-01-00 [DIRS 179419]), the external monsoon climate, glacial-transition, and post-10,000-year climate flow field files used in the transport model are post-processed. In the UZ flow model area, the present-day water table varies from less than 730 m to greater than 980 m above mean sea level (BSC 2004 [DIRS 169855] Figure 6.2). Within the repository footprint, the present-day water table varies from around 730 m to 850 m above mean sea level (BSC 2004 [DIRS 169855] Figure 6.2). Note that the bottom boundary for the flow models of all climate states is the present day water table. For use in conjunction with FEHM's multi-species particle tracking model, the flow-field files for the monsoon, glacial-transition, and post-10,000-year climate flow fields from the UZ Flow Model Abstraction are post-processed to approximate the affects of a rising water table. The rising water table is approximated by constraining it to a minimum elevation of 850 m above mean sea level (SNL 2008 [DIRS 184748], Section 6.4.8). For future climates, at any locations where the present-day water table is below 850 m the water table is set

to 850 m, and at any locations where the present-day water table is above 850 m, the water table is not adjusted from the present day level (BSC 2004 [DIRS 169855]). The updating of the water table is implemented in the future climate flow-field files by changing saturations to 1.0 and replacing nodal fluxes with extremely large flux values for nodes located at or below 850 m mean sea level in areas where the water-table is truncated. In the UZ Transport Submodel's FEHM multi-species particle tracking analysis, the particle exit nodes, for future climate states, become the nodes at the elevation of the new water table that have been assigned the large water flux values by FEHM. At the time of the first updating of the flow field (at the time of change to the monsoon climate), all radionuclide particles below the new water table level are instantaneously made available to the SZ. The water table then remains constant for the rest of the simulation; the monsoon, glacial-transition, and post-10,000-year climates are assumed to have a similar water table elevation. Additional information concerning the water table interface between the UZ Transport Submodel and SZ Flow and Transport Submodels, as well as the effects of water table rise on flow and the transport of radionuclides, is discussed in the subsequent sections on UZ Transport (Section 6.3.9) and SZ Flow and Transport (Section 6.3.10).

Figure 6.3.1-7 shows how the distribution of mountain-scale UZ percolation flux changes as it moves downward through the mountain due to the hydrogeologic processes and conditions within the mountain. A detailed discussion of the Site-Scale UZ Flow Model is contained in *UZ Flow Models and Submodels* (SNL 2007 [DIRS 184614]), and a summary of the processes affecting the percolation flux through the mountain is in the following discussions. Figure 6.3.1-8 shows the stratigraphic column present at a central location within the Yucca Mountain site and is useful for this discussion to visualize the thickness and order of the stratigraphic formations as they are discussed. Water flows through the densely fractured Tiva Canyon welded (TCw) unit mainly through the fractures. The high density of interconnected fractures and low matrix permeabilities in the TCw unit (SNL 2007 [DIRS 179545], Tables 6-6 through 6-9 and Section 6.3.2) are considered to give rise to significant water flow in fractures and limited matrix imbibition (water flow from fractures to the matrix). Thus, episodic infiltration pulses are expected to move rapidly through the TCw fracture networks with little attenuation by the matrix. The relatively high matrix permeabilities and porosities and low fracture densities of the PTn unit (SNL 2007 [DIRS 179545], Tables 6-6 through 6-9 and Section 6.3.2) convert the predominant fracture flow in the TCw to dominant matrix flow within the PTn. The dominance of matrix flow in the PTn and the relatively large storage capacity of the matrix, resulting from its high porosity and low saturation (under the ambient conditions), give the PTn significant capacity to attenuate infiltration pulses. Faults (or geologic structures) may cut through the entire PTn unit at some locations, leading to fast flow paths if the local PTn tuff matrix is not able to convert all of the fault flow into matrix flow. In addition, some lateral diversion of water occurs in the PTn unit owing to the capillary barrier effects (SNL 2007 [DIRS 184614], Sections 6.1.2 and 6.2.2). Unsaturated flow in the Topopah Spring welded (TSw) hydrologic unit occurs primarily through fractures. The TSw hydrologic units are the host-rock units for the entire repository footprint (Figure 6.3.2-4).

The main hydrogeologic units below the repository are the Topopah Springs welded, Calico Hills (CHn) nonwelded, and Crater Flat undifferentiated units. All of these units have vitric and zeolitic components that differ in their degree of hydrothermal alteration and subsequent hydrologic properties. The zeolitic rocks have low matrix permeability and some fracture

permeability. On the other hand, similar to the PTn unit, the vitric units in the CHn have relatively high matrix porosity and permeability. Therefore, matrix flow dominates in the vitric units. One distinctive feature below the repository is the existence of perched-water zones (SNL 2007 [DIRS 184614], Section 6.2.2.2). The occurrence of perched water suggests that certain portions of the lower TSw (e.g., the basal vitrophyre) and the upper CHn (zeolitic portion) impede vertical flow (SNL 2007 [DIRS 184614], Section 6.2.2.2). These hydrogeologic units of lower permeability act to divert the downward progression of contaminant transport by forcing path changes and increases in lateral flow components (SNL 2007 [DIRS 184614], Section 6.2.2.2).

6.3.1.2 Model Abstraction

The UZ Flow Model Abstraction is comprised of 16 steady-state flow fields generated by the three-dimensional Site-Scale UZ Flow Model (SNL 2007 [DIRS 184614], Section 6.6). The sixteen flow fields consist of four flow fields representing uncertainty for each of four climate states. The flow fields provide spatial distributions of fracture-fracture, matrix-matrix, and fracture-matrix water flow rates and moisture contents in the unsaturated zone for use in the Multiscale Thermohydrologic Model (MSTHM) Abstraction (Section 6.3.2) and the UZ Transport Submodel Abstraction (Section 6.3.9). The MSTHM utilizes the flow rates at the base of the PTn, from the 16 flow fields, to generate invert DS and WP temperature, relative humidity, drift-wall temperature, percolation flux, and saturations used by other models and submodels in the TSPA model. The UZ Transport Model Abstraction is based on FEHM's multi-species particle tracking option that uses the 16 flow fields to evaluate the movement of radionuclides from the repository to the water table. During TSPA-LA Model simulations, temporal changes in climate are approximated by changes from one steady-state flow field to another. For example, at the onset of the monsoon climate stage, a present-day climate stage flow field is replaced with a monsoon climate stage flow field.

The four climate states used in the TSPA-LA Model are the present-day climate, monsoon climate state, glacial transition climate state, and a post-10,000-year climate state. A range of durations of the first three climate states, as given in *Future Climate Analysis* (BSC 2004 [DIRS 170002], Table 6-1), are 400 to 600 years for the present-day climate, and 900 to 1,400 years for the monsoon climate. The glacial-transition climate is then predicted to last until 10,000 years after postclosure or 8,000 to 8,700 years. These durations are based on a reconstruction of climate history for the last long earth-orbital cycle from the microfossil record of cores drilled at Owens Lake (BSC 2004 [DIRS 170002], Sections 6.5.1 and 6.6.1). The range of possible durations is developed from the evaluation of the durations using alternative sedimentation rates. The minimum durations of 400 years for the present-day climate and 900 years for the monsoon climate are based on a sediment accumulation rate of 63 cm per 1000 years (BSC 2004 [DIRS 170002], Section 6.6.1 and Litwin et al. [DIRS 109440]). The maximum durations of 600 years for the present-day climate and 1,400 years for the monsoon for the glacial-transition climate are based on a sediment accumulation rate of approximately 40 cm per thousand years (BSC 2004 [DIRS 170002], Section 6.6.1 and Smith and Bishoff (1997 [DIRS 109480]). The glacial-transition climate is then based on the remaining years needed to complete the 10,000 years for the future climate analog.

The Climate Submodel is implemented in the TSPA-LA Model, using the maximum present-day and monsoon durations (i.e., the present-day climate duration is modeled as 600 years, the monsoon climate duration is 1,400 years, and the glacial-transition climate is used until 10,000 years after postclosure). The maximum present-day and monsoon climate durations were chosen based on an evaluation of the sedimentation rates used to derive the climate durations which indicated that the rate of 40 cm per thousand years is the most representative sediment-accumulation rate (BSC 2004 ([DIRS 170002], 6.6.1). As discussed in BSC 2004 ([DIRS 170002], 6.6.1), in addition to their evaluation of the 6 m to 304 m interval of borehole OL-92 on which the 40 cm per thousand years rate is based, Smith and Bishoff (1997 [DIRS 109480]) also present a sediment-accumulation rate for the upper 6 to 24 m section of borehole OL-92 of 79 cm per thousand years. Correcting for differences in porosity and density in the upper 6 to 24 m of borehole OL-92, the mass accumulation rates for the upper 6 to 24 m of borehole OL-92 and the 6 m – 304 m interval, had nearly identical mass-accumulation rates of 52.4 and 51.4 g/cm^2 per thousand years. In addition, other work by Litwin et al. (1999 [DIRS 109440]) showed that although a Holocene age silt from the borehole OL-92 had a sediment-accumulation rate of 64.2 cm per thousand years, the mass accumulation rate was 42.6 g/cm^2 per thousand years, less than the 51.4 g/cm^2 average mass-accumulation rate associated with the 40 cm per thousand years sediment-accumulation rate (Smith and Bishoff 1997 [DIRS 109480]). This shows that to be comparative, sedimentation-accumulation rates need to be corrected for the impact of compaction. This also indicates that the rates of 60 to 66 cm per thousand years (the source of 63 cm per thousand years rate used to derive the minimum duration values) presented by Litwin et al. (1999 [DIRS 109440]) may need to be adjusted. In contrast, the sediment-accumulation rate of 40.1 cm per thousand years (Smith and Bishoff 1997 [DIRS 109480]), used to derive the maximum durations, does not need to be adjusted because the 6 m to 304 m borehole interval used to develop the sediment-accumulation rate accounts for much of the impact of compaction by nature of its length. Note that the present-day climate is simulated for 550 years after closure since the simulations start at closure.

The four uncertainty cases used in the UZ Flow Model were selected from an initial set of 40 infiltration uncertainty maps for each of the first three climate states. These were generated by MASSIF, based on the LHS sampling (2 replicates of 20 realizations each) of parameters as part of the Infiltration Model Abstraction (SNL 2007 [DIRS 182145], Section 6.5.7). Parameters sampled for the Present-Day Climate State LHS simulations include the annual average of the natural logarithm of the amount of daily rainfall on days with precipitation, plant height, maximum rooting depth, soil depth for soil depth class 4, bulk saturated hydraulic conductivities of bedrock IHUs 405 and 406, holding capacity of soil group 5/7/9, readily evaporable water, minimum transport coefficient, evaporation layer depth, and the slope of the normalized difference vegetation index-basal transpiration coefficient function (SNL 2007 [DIRS 182145], Table 6.5.1.1-1, Section 6.5.1, and SNL 2007 [DIRS 184077], Section 3). Parameters sampled for the Monsoon Climate State simulations include the annual average of the probability of zero precipitation given that the previous day was dry, annual average of the natural logarithm of the amount of daily rainfall on days with precipitation, amplitude of the annual variation in the median amount of daily rainfall on days with precipitation, annual average maximum daily temperature on days with precipitation, plant height, maximum rooting depth, slope of the relationship between duration of daily precipitation and amount of daily rainfall, soil depth for soil depth class 4, bulk saturated hydraulic conductivities of bedrock IHUs 405 and 406, holding capacity of soil group 5/7/9, readily evaporable water, minimum transport coefficient,

evaporation layer depth and the slope of the normalized difference vegetation index-basal transpiration coefficient function (SNL 2007 [DIRS 182145], Section 6.5.5.2, and SNL 2007 [DIRS 184077], Section 3). Parameters sampled for the Glacial-Transition Climate State LHS simulations include the annual average of the probability of zero precipitation given that the previous day was dry, annual average of the natural logarithm of the amount of daily rainfall on days with precipitation, phase of the annual variation of the mean daily rainfall on days with precipitation, slope of the relationship between duration of daily precipitation and amount of daily rainfall, plant height, maximum rooting depth, soil depth for soil depth class 4, bulk saturated hydraulic conductivities of bedrock IHUs 405 and 406, holding capacity of soil group 5/7/9, readily evaporable water, minimum transport coefficient, evaporation layer depth, slope of the normalized difference vegetation index-basal transpiration coefficient function, and minimum precipitation duration (SNL 2007 [DIRS 182145], Section 6.5.5.3, and SNL 2007 [DIRS 184077], Section 3). The four representative infiltration maps for each climate used in the development of the associated UZ Flow Model flow fields are the 10th, 30th, 50th, and 90th percentile realization outputs of the LHS analysis. The percentile position is based on the spatially averaged mean annual net infiltration for each realization (SNL 2007 [DIRS 182145], Sections 6.5.7.1, 6.5.7.2, and 6.5.7.3).

In the development of the infiltration maps, only climate and shallow soil layer information were considered. Data from the deep UZ can provide additional information with respect to infiltration/percolation processes that can be used to indicate which scenario is closer to reality (SNL 2007 [DIRS 184614], Section 6.8.2) and derive more appropriate weighting factors. Chloride and temperature data from the Yucca Mountain site UZ are especially amenable for use in conjunction with a generalized likelihood uncertainty estimate (GLUE) methodology to determine meaningful weighting factors for the selected infiltrations maps (SNL 2007 [DIRS 184614], Section 6.8.2). Temperature profiles of the Yucca Mountain UZ are controlled by several factors including formation thermal conductivity, net infiltration rates, and surface temperatures. The temperature profiles at Yucca Mountain were used to help constrain infiltration maps because of the sensitivity to infiltration rates. Simulated temperature distributions at five boreholes, for which qualified temperature data were available, were generated using the four present-day infiltration maps to help determine weighting factors (SNL 2007 [DIRS 184614], Section 6.8.3). Results were compared to measured borehole temperature data at 50 points (40 meters or more below the ground surface) to help determine the appropriateness of the four infiltration maps. Simulated temperature distributions and comparisons to measured data are presented in *UZ Flow Models and Submodels* (SNL 2007 [DIRS 184614], Section 6.3). Chloride, which is a natural tracer for studying water movement in geologic systems, provided a second parameter that was used to constrain the infiltration maps and help generate appropriate weighting factors (SNL 2007 [DIRS 184614], Section 6.8.3). Chloride data from two horizontal tunnels and twelve vertical boreholes provided a means to compare the fit of outputs from UZ chloride submodel simulations based on the four present-day infiltration rates (SNL 2007 [DIRS 184614], Section 6.8.3). Results of the chloride simulations are presented in *UZ Flow Models and Submodels* (SNL 2007 [DIRS 184614], Section 6.5). Based on the probability of the infiltration maps from the infiltration model and the relative agreement between model simulations and the temperature and chloride data, the GLUE methodology was applied to determine the most appropriate weighting factors to be used in the TSPA-LA Model. Note that because the GLUE methodology relies on field observations for present-day conditions, the weighting factors are determined using simulations based on present-

day climate infiltration maps. The steps used in the GLUE methodology can be summarized as follows: (1) determine the prior probability values (weighting factors) for each infiltration map; (2) perform UZ flow and transport calculations for each selected infiltration map and, based on model results and observations for temperature and chloride concentrations, calculate likelihood values; and (3) determine weighting factors based on the prior weights and the likelihood values (SNL 2007 [DIRS 184614], Section 6.8.5.1). The final weighting factors presented in *UZ Flow Models and Submodels* (SNL 2007 [DIRS 184614], Section 6.8.5.3) are an average of weighting factors based on combining different likelihood functions (SNL 2007 [DIRS 184614], Section 6.8.5.1) and averaging techniques. The average weighting factors that are used in the TSPA-LA Model are presented in Table 6.3.1-2 (see also SNL 2007 [DIRS 184614], Table 6.8-1).

For the post-10,000-year period, proposed 10 CFR 63.342(c)(2) [DIRS 178394] specifies that the average percolation flux through the repository follows a log-uniform probability distribution from 13 to 64 mm/yr. Therefore, independent infiltration maps are not generated from the Infiltration Model for the post-10,000-year period. The preamble to the proposed rule (70 FR 53316 [DIRS 178394]) also states that DOE should "continue such calculations of spatial variation, subject to the constraint that, across the repository footprint, the ''average'' overall percolation rate would remain within the range and distribution specified by NRC." As for the first three climate states, four uncertainty infiltration maps are developed to be used with the UZ Flow Model. The UZ Flow Model results indicate that average infiltration at the ground surface within the projection of the repository footprint is close to the average flux through the repository at depth (SNL 2007 [DIRS 184614], Section 6.1.4). The target average infiltration values are selected from the log-uniform probability distribution of deep percolation rates from 13 to 64 mm/year. The points on the cumulative distribution are (SNL 2007 [DIRS 184614], Table 6.1-3) in cumulative form, 31 percent, 70 percent, 86 percent, and 97 percent (SNL 2007 [DIRS 184614], Figure 6.1-6), which corresponds to the cumulative probabilities derived using the GLUE methodology for the first three climate states. The average infiltration rates corresponding to these cumulative probability values are 21.29, 39.52, 51.05, and 61.03 mm/yr (SNL 2007 [DIRS 184614], Table 6.1-3). The 12 infiltration maps generated for the Present-Day, Monsoon, and Glacial Transition Climate states are used as a basis for the spatial variability for the post-10,000-year climate state (SNL 2007 [DIRS 184614], Section 6.1.4). For the 12 infiltration maps, the average infiltration through the repository footprint was calculated. The four infiltration maps with average infiltration rates that most closely matched chosen average target infiltration rates were then used as a basis for generating the flow-fields. The closest infiltration rate maps for the post-10,000-year climate state determined by the analysis were the present-day 90th percentile, the 50th percentile Glacial Transition, the 90th percentile glacial transition, and the 90th percentile monsoon for the target values of 21.29, 39.52, 51.05, and 61.03 mm/yr, respectively. The four infiltration maps were then scaled so that the average infiltration through the repository footprint would match the target values.

Implementation of uncertainty in the infiltration map for the UZ Flow Model Abstraction is then based on sampling from the set of four flow fields for each climate that was developed using the 10th, 30th, 50th, and 90th percentile infiltration maps for the respective climates. For each TSPA-LA Model epistemic realization, the infiltration scenario (10th, 30th, 50th, or 90th percentile for the present-day, monsoon, and glacial transition climates and scaled versions of the present-day 90th percentile, the 50th percentile Glacial Transition, the 90th percentile glacial

transition, and the 90th percentile monsoon) is chosen based on sampling the weighting factors presented in Table 6.3.1-2. Note that the same weighting factors are used for the present-day, monsoon and glacial transition climates. The assumption that the same weighting factors can be used for the three climate states is based the similarity in modeling methods used for infiltration and UZ Flow (SNL 2007 [DIRS 184614], Section 6.8.8). Infiltration estimates for future climates are produced using the same hydrologic parameter ranges, the same methods for modeling weather patterns and the same infiltration model as used for the present-day climate. Additionally, UZ flow estimates are generated for future climates using the same parameter sets, the same modeling assumptions and the same UZ Flow Model as for the present-day climate. Due to the similarity of modeling methods across climate states, it is expected that any deviations between UZ Flow model results for temperature and chloride, based on infiltration model results for infiltration rates under the present-day climate, are comparable for future climates and the same weighting factors can be used for present-day, monsoon and glacial transition climates (SNL 2007 [DIRS 184614], Section 6.8.8). The probabilities associated with the weighting factors are also used to select the target cases for average percolation flux through the repository footprint. This produces weighting factors consistent with the probability distribution for the post-10,000-year period, proposed in 10 CFR 63.342(c)(2) [DIRS 178394].

The UZ flow fields were abstracted using the three-dimensional Site-Scale UZ Flow Model (SNL 2007 [DIRS 184614], Section 6.2). The four present-day cases (based on 10th, 30th, 50th, or 90th percentile infiltration maps) were used for model calibration and calibrated parameters from the four calibrated cases used in conjunction with the other 12 infiltration maps to generate 12 flow fields for the future climate states (SNL 2007 [DIRS 184614], Section 6.2.5 and Table 6.2.6). The three-dimensional model calibration started with four sets of calibrated parameters generated from one-dimensional calibration analyses (DTNs: LB0611MTSCHP10.001_R0 [DIRS 178586]; LB0611MTSCHP30.001_R0 [DIRS 180293]; LB0612MTSCHP50.001_R0 [DIRS 180294]; LB0612MTSCHP90.001_R0 [DIRS 180295]); and two-dimensional site-scale calibrated fault properties (DTN: LB0612MTSCHPFT.001_R0 [DIRS 180296]) documented in *Calibrated Unsaturated Zone Properties* (SNL 2007 [DIRS 179545], Section 6.3). The four present-day cases (based on the 10th, 30th, 50th, or 90th percentile infiltration maps) were calibrated against field measured liquid saturation, water potential, perched water occurrences, and pneumatic data (SNL 2007 [DIRS 184614], Section 6.2). The calibrated parameters included the van Genuchten α parameter of tsw31, and in the perched-water zones, intrinsic permeabilities of the fracture and matrix systems and van Genuchten α and m parameters for describing the saturation-capillary pressure relationships in the fracture and matrix systems. The final calibrated three-dimensional properties for the perched-water conceptual model, which are used to generate the 16 flow fields, are documented in *UZ Flow Models and Submodels* (SNL 2007 [DIRS 184614], Appendix B, Tables B1 to B4).

Figure 6.3.1-7 shows the surface infiltration map for the 10th percentile infiltration scenario during the glacial-transition climate along with the corresponding estimated vertical percolation flux at the repository horizon level and the water table level. Comparisons of the map of the calculated repository percolation flux with that of the surface infiltration map indicate that the spatial distributions of percolation flux at the repository horizon differ significantly in the northwest from the patterns of the net infiltration rate. The surface infiltration rates and distributions are independent of faults. The major differences in the percolation flux distribution at the repository level compared to the surface infiltration patterns are: (1) flow occurs mainly

through faults in the very northern part of the model domain, north of the 237,000-m northing coordinate (see Figure 6.3.1-7 for coordinates); (2) flow is diverted into or near faults located in the model domain; and (3) a west to east shift of high infiltration zones away from the Yucca Mountain crest (SNL 2007 [DIRS 184614], Section 6.6.2.1). Overall, percolation at the repository horizon displays a very different pattern than the distribution of surface infiltration in the northern part of the modeling domain. One reason for this difference is the substantial amount of large-scale lateral flow within the PTn unit. In addition, there is a flow redistribution in the very northern part of the model domain (beyond the repository block) caused by the repository grid layer horizon laterally intersecting the CHn zeolitic and perched-water zones locally, with major flow diverted to faults. The lateral flow within the PTn unit and flow focusing into faults in the north have a large influence on percolation flux distribution at the repository horizon (SNL 2007 [DIRS 184614], Section 6.6.2.1); however, there is significantly less lateral flow and flow focusing within the repository footprint. Computations have shown that the average flux flowing to the repository is within three percent of the average flux specified at the ground surface over the projected repository area (SNL 2007 [DIRS 184614], Section 6.1.4). Hence, percolation flux patterns at the repository are similar to the patterns of infiltration flux within the repository footprint. Figure 6.3.1-7 also shows that the distribution of percolation flux at the water table level, when compared to the distribution of net infiltration rates shown at the infiltration boundary, indicates the percolation fluxes corresponding to high infiltration rate zones reduced still further from what is shown at the repository horizon level.

6.3.1.3 TSPA-LA Model Implementation

Climate Submodel Abstraction—The durations of the climate states are 600 years (550 years postclosure) for the present-day climate; 1,400 years for the monsoon climate; 8,050 years for the glacial-transition climate; and the remainder of the simulation period is simulated as a post-10,000-year climate (Table 6.3.1-1). Climate change is specified within the TSPA-LA Model by assuming climate-specific boundary conditions for UZ flow and accessing the flow field that corresponds to the selected infiltration case and climate state of the simulation period.

Infiltration Submodel—The four different infiltration cases represent epistemic uncertainty in the net infiltration rates. These scenarios are sampled in the TSPA-LA Model once per realization, based on the probability-weighting factors 61.91 percent, 15.68 percent, 16.45 percent, and 5.96 percent for the 10th percentile, 30th percentile, 50th percentile, and 90th percentile, respectively (Table 6.3.1-2) (DTN: LB0701PAWFINFM.001_R0 [DIRS 179283]). Note that the classification of 10th, 30th, 50th, and 90th percentile weighting factors is based on the infiltration maps used for the first three climates. For the post-10,000-year climate, the 10th, 30th, 50th, and 90th percentile weighting factors are associated with flow fields generated using the scaled 90th percentile present-day, 50th percentile glacial transition, 90th percentile glacial transition, and the 90th percentile monsoon infiltration maps, respectively. Because of the once per realization sampling, the infiltration cases are completely correlated across the four climate states modeled during the simulation period (e.g., during a realization in which the 10th percentile infiltration case is sampled, the 10th percentile infiltration scenario of all four climate states will be used to select the appropriate UZ flow fields). This correlation of the infiltration uncertainty across the climate transitions ensures that the full effects of the infiltration uncertainty are not dampened out of the TSPA-LA Model performance results.

UZ Flow Fields Abstraction—The 16 base-case UZ flow fields and associated information generated by the Site-Scale UZ Flow Model (Output 1 in Section 6.1.4.1) are reformatted for use by the UZ Transport Submodel to simulate the transport of radionuclides in the UZ (note that information from Output 1 is provided to the MSTHM Model, as described in Section 6.3.2).

In the UZ Transport Submodel (Section 6.3.9), changes in climate states are approximated by changes from one steady-state flow field to another and by associated changes in water-table elevation (SNL 2008 [DIRS 184748], Section 5). An instantaneous change from one steady-state flow field to another is a reasonable approximation, given the uncertainties and the inability to observe climate changes directly (SNL 2008 [DIRS 184748], Section 6.4.8). With a change to wetter conditions in the future, flow velocities will immediately be greater, and the flow path length to the water table will be shorter due to the higher water table. By applying these conditions instantaneously, there will be no model implementation-caused delay imparted to climate transition-induced changes of UZ flow and radionuclide transport conditions (SNL 2008 [DIRS 184748], Section 6.4.8).

Prior to implementation, the reformatted UZ flow fields are placed in a library of files that are read by the UZ Transport Submodel during run time. There are 16 UZ flow field files for use by the UZ Transport Submodel, one for each of the combinations of the four climate states and four possible infiltration scenarios. These files include:

- Three-dimensional, steady-state flow fields defined at each node in the FEHM UZ grid below the repository, which contain the following information used in the particle-tracking model:

  - Fracture continuum liquid flux
  - Matrix continuum liquid flux
  - Fracture continuum liquid saturation values
  - Matrix continuum liquid saturation values
  - Liquid flux between matrix and fracture continua.

  Note that the files also contain dummy pressure values (pressures are not used in the particle tracking model) and large liquid flux values of 10^{10} kg/s to indicate to FEHM which nodes are watertable release nodes.

6.3.1.4 Model Component Consistency and Conservatism in Assumptions and Parameters

To enhance understanding of the complex interactions within the TSPA-LA Model, this section presents a discussion of consistency among model components and submodels and identification of conservative assumptions in abstractions, models, and parameter sets supporting the Mountain-Scale UZ Flow Submodel.

6.3.1.4.1 Consistency of Assumptions

UZ Transport Properties—Because of the sensitivity of the matrix-diffusion process implemented in the UZ Transport Submodel to various physical parameters that are also used to define the UZ flow fields, there is an inconsistency between the Mountain-Scale UZ Flow

Submodel and the UZ Transport Model. In defining the matrix diffusion process, parameters such as the AFM values, fracture frequency and fracture porosity are sampled from stochastic distributions. However, in developing the 16 different UZ flow fields that are used in the UZ transport calculations, the parameters were held constant. A discussion of this inconsistency between Mountain-Scale UZ Flow Submodel and the UZ Transport Model parameters can be found in Section 6.3.9.4.1.

6.3.1.4.2 Identification of Conservatisms in Submodels and Abstractions

Dual-Permeability Conceptual Model—The dual-permeability conceptual model and its dual-continuum grid system are used by the Site-Scale UZ Flow Model rather than a more refined-gridding method for fracture-matrix interaction, such as the Multiple Interacting Continua method. Dual-continuum models are needed in order to model the large domain and highly fractured rock at Yucca Mountain (SNL 2007 [DIRS 184614], Section 6.1.2). For mass applied initially to the fracture domain, the dual-permeability model generates faster breakthroughs for tracer transport, as compared with Multiple Interacting Continua method, because fracture-matrix interaction is less with a dual-permeability grid (SNL 2008 [DIRS 184748], Section 7.2.2, and SNL 2007 [DIRS 177396], Section 6.19.1). In addition, the dual-permeability (dual-continuum) representation of fractures as a continuum conservatively assumes the complete interconnectivity of the fracture system (i.e., the model does not account for discontinuous fractures) (SNL 2007 [DIRS 177396], Section 6.7.8). The effects of this conservatism tend to increase flow velocity and radionuclide transport rate in the fractures, resulting in shorter radionuclide transport times to the water table.

High-Permeability Fault Pathways—Faults are modeled as high-permeability pathways from the repository to the water table. Uncertainty in fault characteristics has led to the bounding consideration that these faults are high-permeability features that extend from the ground surface to the water table (SNL 2007 [DIRS 184614], Section 5, and SNL 2007 [DIRS 177396], Section 6.7.8). High-permeability fault pathways lead to flow in faults, providing localized high-flow pathways between the ground surface and the repository as well as between the repository and the water table. High-permeability fault pathways, therefore, result in shorter radionuclide transport times to the water table.

6.3.1.5 Alternative Conceptual Model(s) for the Mountain-Scale Unsaturated Zone Flow

Section 6.2 outlines the general consideration and treatment of ACMs used to support the TSPA-LA Model. A brief description of the Mountain-Scale UZ Flow ACMs summarized in Table 6.3.1-3 is presented below. Note that the first ACM is evaluated based on analyses performed with the original infiltration model and thus references a historical model report (BSC 2004 [DIRS 169861]). The analysis is considered valid because although the infiltration model has changed, the model spatial structures including heterogeneities have not radically changed.

Lateral Flow in the PTn—Uncertainties associated with UZ conceptual flow models were analyzed using two conceptual models of the water flow in the PTn unit (i.e., the base-case UZ Flow Model and an ACM (BSC 2004 [DIRS 169861], Section 6.9). The base-case UZ Flow Model has a hydrogeologic property set for the PTn unit that favors the lateral diversion of flow

(BSC 2004 [DIRS 169861], Section 6.5.2). The ACM employs a different hydrogeologic property set for the PTn unit that does not favor large-scale lateral diversion (BSC 2004 [DIRS 169861], Section 6.5.2.2). Each of the conceptual models uses three different parameter sets that were calibrated for the lower-bound, mean, and upper-bound infiltration rates that were used in order to address uncertainties in the infiltration (DTN: SN0308T0503100.008_R0 [DIRS 165640]). Steady-state UZ flow fields were produced for each of the three infiltration cases (lower-bound, mean, and upper-bound) at each of the three climate states (present-day, monsoon, and glacial-transition). This results in nine base-case and nine alternative three-dimensional UZ flow fields. In general, the nine base-case flow fields show more lateral flow occurring within the PTn than those estimated with the ACM. Additional analyses have been performed to estimate the impact of the flow model on tracer or radionuclide transport for the nine base-case and nine alternative flow fields. A total of 40 tracer transport simulations were conducted to evaluate the impacts of infiltration rates, perched-water, PTn conceptual models, and retardations on tracer migration from the repository to the water table (BSC 2004 [DIRS 169861], Section 6.7, Tables 6.7-2 and 6.7-3). The results of the 40 three-dimensional tracer-transport simulations show a wide range of tracer-transport times from the repository to the water table. The results show that the base-case model generally provides slightly more conservative transport time estimates (BSC 2004 [DIRS 169861], Section 6.9.2). Comparative studies of chloride distributions within the UZ, simulated using the base-case and alternative flow fields, indicate consistently that the base-case flow fields provide an overall better match with the observed chloride data (BSC 2004 [DIRS 169861], Section 6.5.2.2).

Transient Infiltration Pulse—The second ACM considered in the UZ is a flow model with a transient pulse infiltration boundary condition. The appropriateness of assuming a steady-state or quasi-steady-state infiltration boundary condition, as opposed to a transient pulse infiltration boundary condition, is a key modeling issue. This assumption relies on the effect of spatial and temporal damping of transient infiltration pulses when flowing through the PTn unit. The PTn consists mainly of non- to partially-welded tuffs. Over the UZ model domain, the thickness of the PTn ranges from 150 m in the north to 30 m or less in the south. The unit can even be missing in certain areas in the south. The PTn is present over the entire repository area where it ranges from 30 m to 60 m in the repository area (SNL 2007 [DIRS 184614], Section 6.2.2). In contrast to the units above it (TCw) and below it (TSw), the PTn has high porosity and low fracture intensity, thus having a large capacity for groundwater storage. The effectiveness of the PTn unit to damp episodic flow was examined using episodic infiltration pulses on the top boundary of the model (SNL 2007 [DIRS 184614], Section 6.9). The analyses presented (SNL 2007 [DIRS 184614], Section 6.9) indicate that the steady-state flow approximation used in the UZ flow model is reasonable due to existence of the PTn unit. The impact of the thickness of the PTn unit was examined in a one–dimensional column study discussed in *UZ Flow Models and Submodels* (SNL 2007 [DIRS 184614], Section 6.9). In the column study, two model columns located at the center and south of the model, with PTn thicknesses of 81 m and 21 m respectively, were considered. Pulses of 10,080 mm/yr and a duration of 1 week were applied to the top of the model every 50 years with an ambient rate of 28.1 mm/yr over the rest of the time. The average yearly rate for the entire simulation was 32 mm/yr. Results showed strong damping effects for both columns. The 81 m column test showed only minor variations in the fluxes over time (SNL 2007 [DIRS 184614], Figure 6.9-2). The thinner (21 m) thickness column model showed relatively large fluctuations over time compared to the 81 m column model, with a maximum variance over time of 17 mm/yr and a dynamic equilibrium variation after 500 years

of 10 mm/yr (SNL 2007 [DIRS 184614], Figure 6.9-3). This is still a large dampening effect when considering the magnitude of the pulses (10,080 mm/yr). In addition, the ratio of the maximum variation in flux (17 mm/yr) to the mean infiltration rate of 32 mm/yr is 0.5, and the ratio of equilibrium variation in flux (10 mm/yr) to the mean infiltration rate of 32 mm/yr is 0.3 (SNL 2007 [DIRS 184614], Section 6.9). These ratios are small when compared to the uncertainty in surface water flux where the ratio of the range (90th percentile flux minus the 10th percentile flux) to the mean surface water flux is 1.1 for the model column associated with the 21 m PTn thickness (SNL 2007 [DIRS 184614], Section 6.9). Since the episodic variations for the 21 m thickness model are small relative to other uncertainties, the assumption of steady-state flow is considered to be valid for even the thinner column model (SNL 2007 [DIRS 184614], Section 6.9). Manepally et al. (2007 [182155]) also examined the damping influence of the PTn on episodic flow. Transient simulations were performed at three locations representative of low, medium, and high PTn and TCw thicknesses to evaluate the importance of PTn and TCw thicknesses on the assumption of steady state flow at the repository horizon. Long term transients that span up to thousands of years were included in the study. The long term transients are expected to be reflected at the repository level due to the finite storage capacity of the PTn (SNL 2007 [DIRS 184614], Section 6.9). The percolation fluxes in the study were found to fall within ± 20 percent of the long term average infiltration rate 80 percent of the time with the range in the percolation rates being 50 percent of the long term average (SNL 2007 [DIRS 182155], Section 5). When compared with the uncertainty in the fluxes implemented in the UZ Flow Model where the standard deviation in the flux implemented for the post-10,000-year climate is about 60 percent of the mean flux and the range is 127 percent of the mean flux over the repository footprint (SNL 2007 [DIRS 184614], Section 6.9), the transient fluctuations in the Manepally et al. (2007 [DIRS 182155]) study are small. Higher infiltration rate scenarios in a study by Zhang et al. (2006 [DIRS 180273]) show that the damping effect will not be weakened by high rate infiltration pulses (SNL 2007 [DIRS 184614], Section 6.9), indicating that uncertainty in infiltration magnitude for short-term transients will not affect the validity of the steady-state assumption.

Film Flow—Although cavities connected to fractures are expected to act as capillary barriers under unsaturated conditions, there is evidence at the Yucca Mountain site suggesting that film flow from fractures to cavities may occur (SNL 2007 [DIRS 184614], Section 7.8.3.3). The evidence is in the form of water release tests performed at the Yucca Mountain site and field observations of coatings in many cavities (SNL 2007 [DIRS 184614], Section 7.8.3.3). Not considering the explicit influence of cavities is a conservative approach since the cavities would retard the transport of water. Film flow on fracture surfaces as an important mechanism for fast flow in unsaturated rocks has also been examined (BSC 2004 [170035] Section 7.3 and Tokunuga and Wan 1997 [DIRS 139195]). Although the importance of film flow in the fractures is a matter of debate (BSC 2004 [170035] and Pruess 1999 [DIRS 104250]), a comparison between the AFM and a film-flow model has been performed (BSC 2004 [170035] Section 7.3). The analysis, comparing the AFM and the film-flow model, showed that the AFM could capture the fast flow behavior of water film if film flow was the major fracture flow mechanism (BSC 2004 [170035] Section 7.3.1 and Section 8.2).

Discrete Fracture Flow—An alternative modeling approach, the discrete-fracture or "weeps" type model is subject to extremely high uncertainties with respect to the fracture data needed to describe the system. In addition, the computational burden associated with this type model is

beyond present or near future resources. Therefore, this type model is not considered (SNL 2007 [DIRS 184614], Section 6.1.2).

Inclusion of TH, THC, and Thermal-Hydrologic-Mechanical Effects on UZ Flow—Vaporization due to repository heat will keep the drift dry for several hundred to a few thousand years. TH, THC and thermal-hydrologic-mechanical effects may alter flow and properties of the UZ rocks. TH, THC, and thermal-hydrologic-mechanical effects are insignificant after the change to glacial-transition climate, the period when most radionuclide transport would take place (SNL 2008 [DIRS 184748], Section 6.7). Additional conclusions with respect to TH, THC, and thermal-hydrologic-mechanical effects on UZ Flow and Transport presented in *Mountain-Scale Coupled Processes (TH/THC/THM)* include: (1) mountain-scale TH will have a large impact on fluid flow near the repository at early times but insignificant impact on UZ flow fields (BSC 2005 [DIRS 174101], Section 8.1); (2) changes in water chemistry, mineralogy, and hydrologic properties in the ambient temperature regions are minimal over the 7,000 years the THC model was simulated (BSC 2005 [DIRS 174101], Section 8.2); and (3) thermal-hydrologic-mechanical induced changes in mountain-scale hydrologic properties have no significant impact on vertical percolation through the repository horizon (BSC 2005 [DIRS 174101], Section 8.3).

INTENTIONALLY LEFT BLANK

Table 6.3.1-1. Durations of Climate States in First 10,000 Years

Climate State	Duration
Present-Day	600 years
Monsoon	1,400 years
Glacial-Transition	Remainder of 10,000 Years

Source: DTN: GS000308315121.003_R0 [DIRS 151139]
10 CFR Part 63. Energy: Disposal of High-Level Radioactive Wastes in a Geologic Repository at Yucca Mountain, Nevada [DIRS 180319].

NOTE: The TSPA-LA Model assumes that the present-day climate period begins at first emplacement and that preclosure will be the first 50 years of the present-day climate period.

Table 6.3.1-2. Net Infiltration Rates Averaged over the Unsaturated Zone Model Domain and Probability-Weighting Factors for the Infiltration Scenarios

Infiltration Case	Present-Day Climate (mm/yr)	Monsoon Climate (mm/yr)	Glacial-Transition Climate (mm/yr)	Post-10k Years (mm/yr) [a]	Probability-Weighting Factors (All Climate States)
10th Percentile	3.03	6.74	11.03	16.89	0.6191
30th Percentile	7.96	12.89	20.45	28.99	0.1568
50th Percentile	12.28	15.37	25.99	34.67	0.1645
90th Percentile	26.78	73.26	46.68	48.84	0.0596

Sources: SNL 2007 [DIRS 184614], Tables 6.1-2, 6.1-3, and LB0701PAWFINFM.001_R0 [DIRS 179283].

[a] Note that for the Post 10,000 Years data the Infiltration cases differ and represent scaled versions of the present-day 90th percentile, the 50th percentile Glacial Transition, the 90th percentile glacial transition, and the 90th percentile monsoon maps, respectively.

Table 6.3.1-3. Alternative Conceptual Models Considered for the Mountain-Scale Unsaturated Zone Flow

Alternative Conceptual Models	Key Assumptions	Screening Assessment and Basis
Lateral Flow in the PTn	Uncertainties associated with UZ conceptual flow models were analyzed using two conceptual models of the water flow in the PTn unit (i.e., the base-case UZ Flow Model and an ACM (BSC 2004 [DIRS 169861], Section 6.9)). The base-case UZ Flow Model has a hydrogeologic property set for the PTn unit that favors lateral diversion of flow (BSC 2004 [DIRS 169861], Section 6.5.2). The ACM employs a different hydrogeologic property set for the PTn unit that does not favor large-scale lateral diversion (BSC 2004 [DIRS 169861], Section 6.5.2.2).	Model best fitting the field data chosen. For the original infiltration model, the base-case UZ Flow Model description of flow in the PTn was selected because it provides better estimates of chloride concentrations and moisture content. Each of the conceptual models used three different parameter sets that were calibrated for the lower-bound, mean, and upper-bound infiltration rates that were used in order to address uncertainties in the infiltration process (DTN: SN0308T0503100.008_R0 [DIRS 165640]).
Transient Infiltration Pulse	The appropriateness of assuming a steady-state or quasi-steady-state infiltration boundary condition was examined by analyzing the effects of using a model with a transient pulse infiltration boundary condition. Effectiveness of the PTn unit to damp episodic flow was examined using episodic infiltration pulses on the top boundary of the model (SNL 2007 [DIRS 184614], Section 6.9 and Figure 6.9-3[a]).	Screened out (FEP 2.2.07.05.0A). The analyses presented (SNL 2007 [DIRS 184614], Section 6.9 and Figure 6.9-3[a]) indicate that the steady-state flow approximation used in the UZ flow model is reasonable due to existence of the PTn unit.
Film Flow	Film flow may occur between cavities and fractures (SNL 2007 [DIRS 184614], Section 7.8.3.3). Film flow may also be a process by which fast flow occurs in the fractures (BSC 2004 [170035] Section 7.3).	Film flow may occur between cavities and fractures as indicated by coatings and water release tests. Not considering the explicit influence of cavities is a conservative approach since the cavities would retard the transport of water (SNL 2007 [DIRS 184614], Section 7.8.3.3). Although the importance of film flow in the fractures is a matter of debate (BSC 2004 [170035] and Preuss 1999 [DIRS 104250]), a comparison between the AFM and a film-flow model has been performed (BSC 2004 [170035] Section 7.3). The analysis, comparing the AFM and the film-flow model, showed that the AFM would capture the fast flow behavior of water film if film flow was the major fracture flow mechanism (BSC 2004 [170035] Section 7.3.1 and Section 8.2).

Table 6.3.1-3. Alternative Conceptual Models Considered for the Mountain-Scale Unsaturated Zone Flow (Continued)

Alternative Conceptual Models	Key Assumptions	Screening Assessment and Basis
Discrete Fracture Flow	The discrete-fracture or "weeps" type model is an alternative model that explicitly defines the fractures in a fracture-flow system.	The discrete-fracture or "weeps" type model is subject to extremely high uncertainties with respect to the fracture data needed to describe the system. In addition, the computational burden associated with this type model is beyond present or near future resources. Therefore, this type model is not considered (SNL 2007 [DIRS 184614], Section 6.1.2).
Inclusion of TH, THC, and Thermal-Hydrologic-Mechanical Effects on UZ Flow	Vaporization due to repository heat will keep the drift dry for several hundred to a few thousand years. Thermal (TH), Thermal Hydrologic Chemical (THC), and thermal-hydrologic-mechanical (THM) effects may influence the flow fields used to describe flow in the UZ.	TH, THC, and thermal-hydrologic-mechanical effects are insignificant after the change to glacial-transition climate, the period when most radionuclide transport would take place (SNL 2008 [DIRS 184748], Section 6.7). Additional conclusions with respect to TH, THC, and thermal-hydrologic-mechanical effects on UZ Flow and Transport presented in *Mountain-Scale Coupled Processes (TH/THC/THM)* include: (1) mountain-scale TH will have a large impact on fluid flow near the repository at early times but insignificant impact on UZ flow fields (BSC 2005 [DIRS 174101], Section 8.1); (2) changes in water chemistry, mineralogy, and hydrologic properties in the ambient temperature regions are minimal over the 7,000 years the THC model was simulated (BSC 2005 [DIRS 174101], Section 8.2); and (3) thermal-hydrologic-mechanical induced changes in mountain-scale hydrologic properties have no significant impact on vertical percolation through the repository horizon (BSC 2005 [DIRS 174101], Section 8.3).

INTENTIONALLY LEFT BLANK

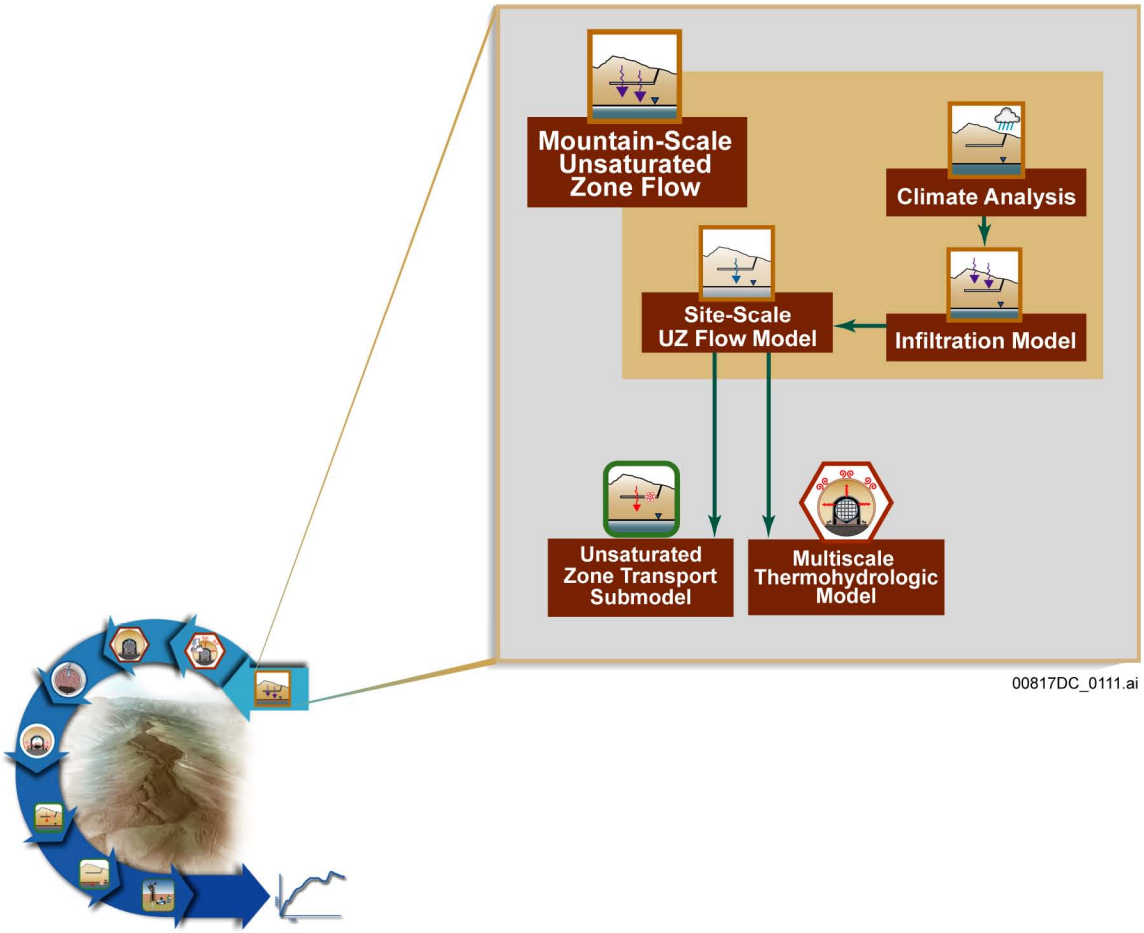

Figure 6.3.1-1. Information Flow Diagram for the Mountain-Scale Unsaturated Zone Flow

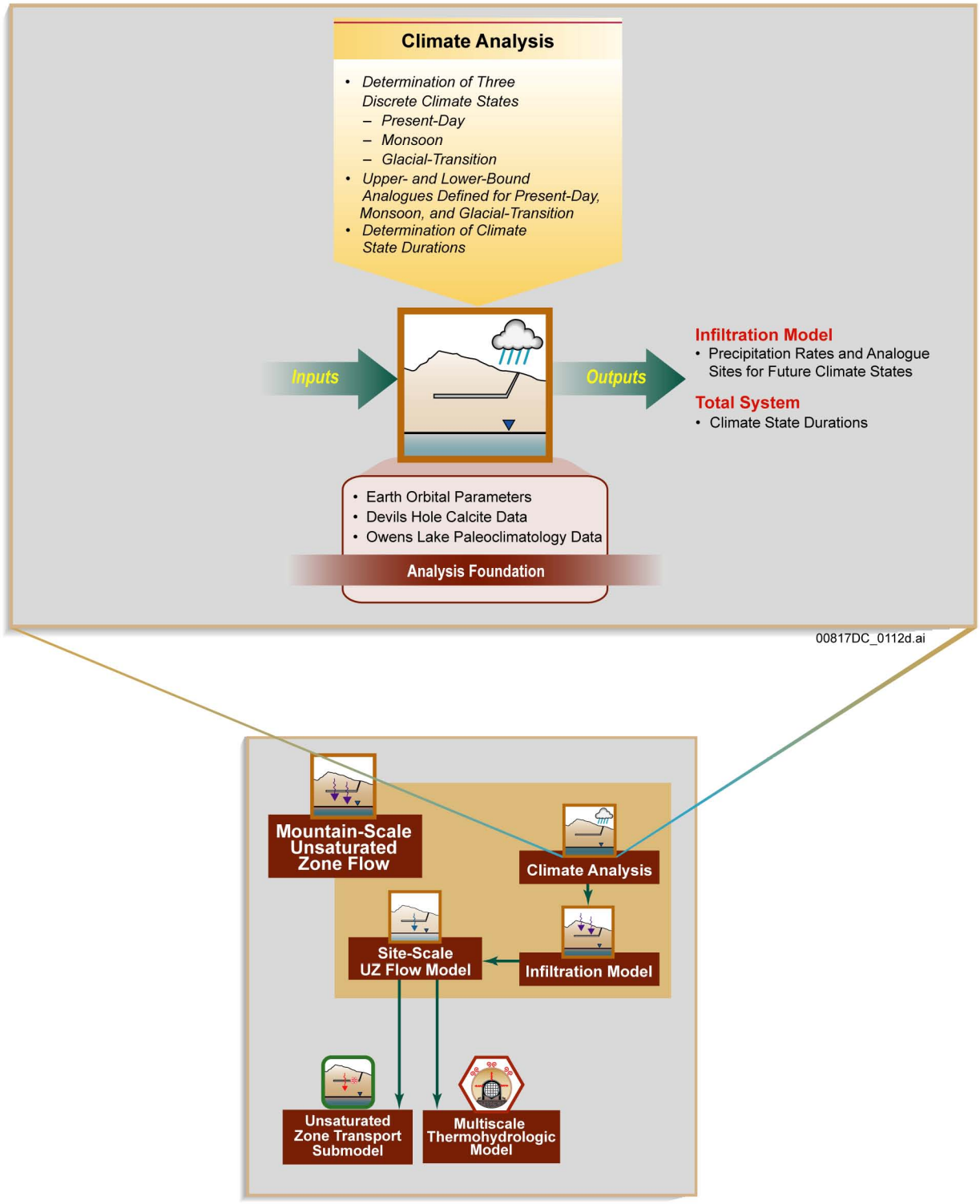

Figure 6.3.1-2. Inputs, Outputs, and Basis for Model Confidence for the Climate Analysis

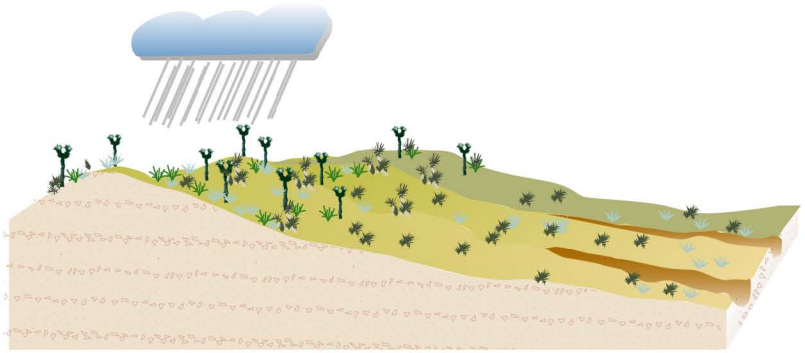

Present-Day Climate

Yucca Mountain:
Regional Meteorological Stations

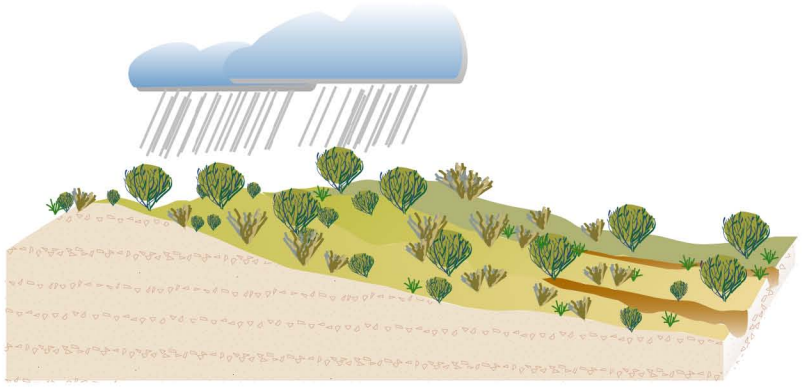

Monsoon Climate

Lower-bound analogue: Yucca Mountain
Upper-bound analogue: Nogales, AZ
Higher precipitation and temperature than present-day climate

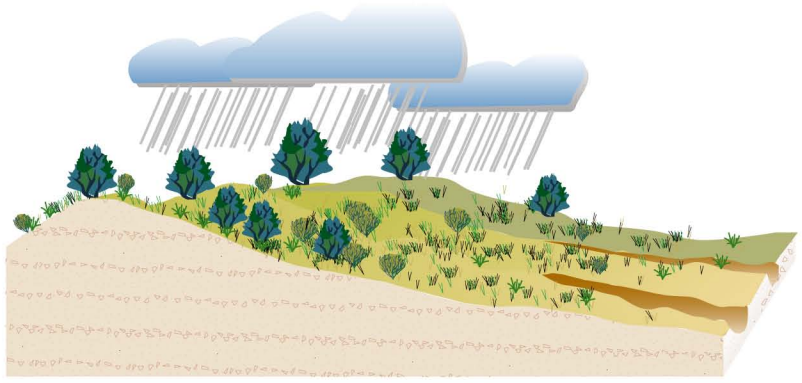

Glacial-Transition Climate

Lower-bound analogue: Delta, UT
Upper-bound analogue: Spokane, WA
Higher precipitation and lower temperature than present-day climate

00817DC_0113.ai

Figure 6.3.1-3. Illustration of the First Three Climate States Used in the TSPA-LA Model and the Analogues for the Monsoon and Glacial-Transition Climates

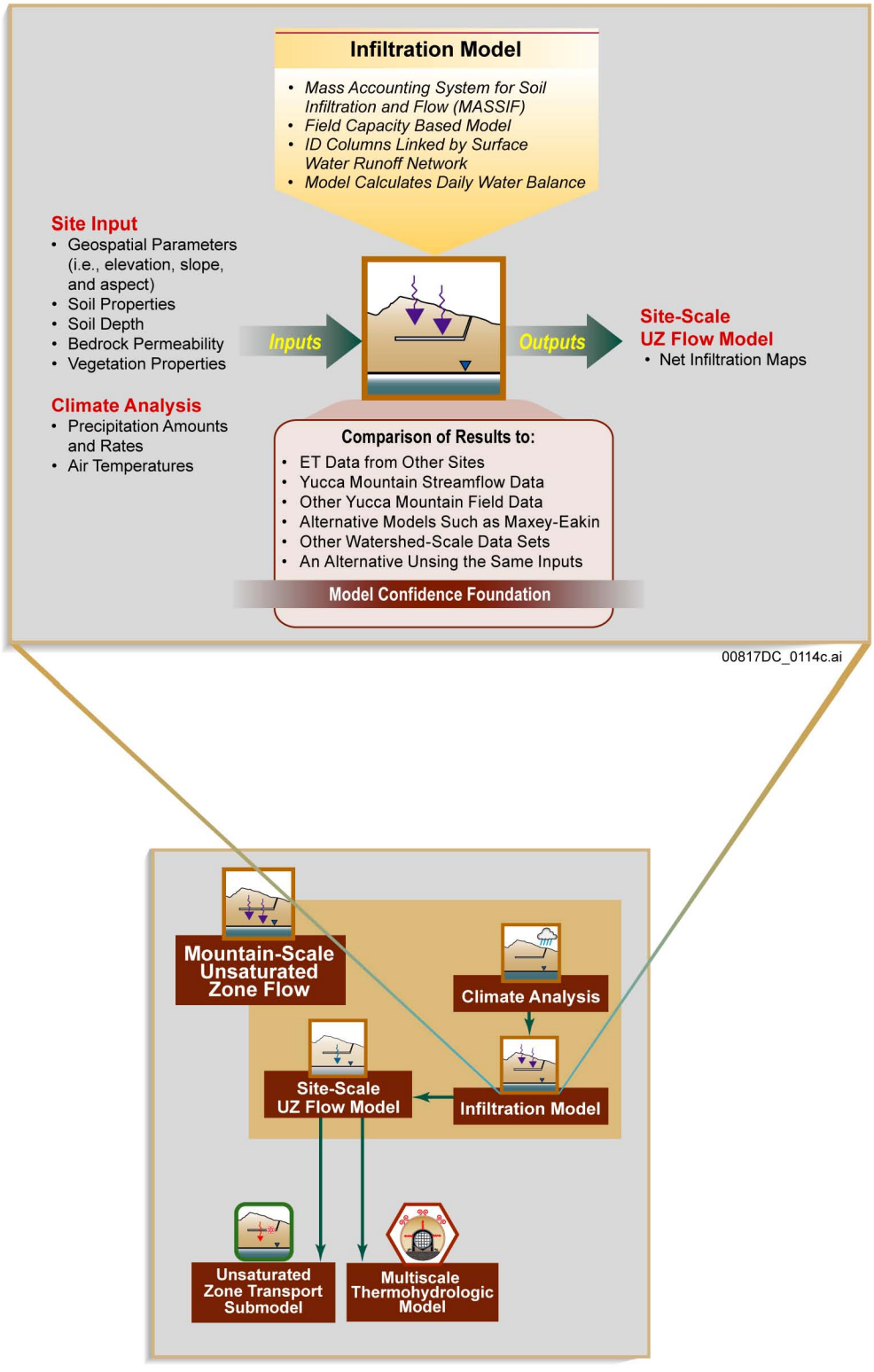

Figure 6.3.1-4. Inputs, Outputs, and Basis for Model Confidence for the Infiltration Model

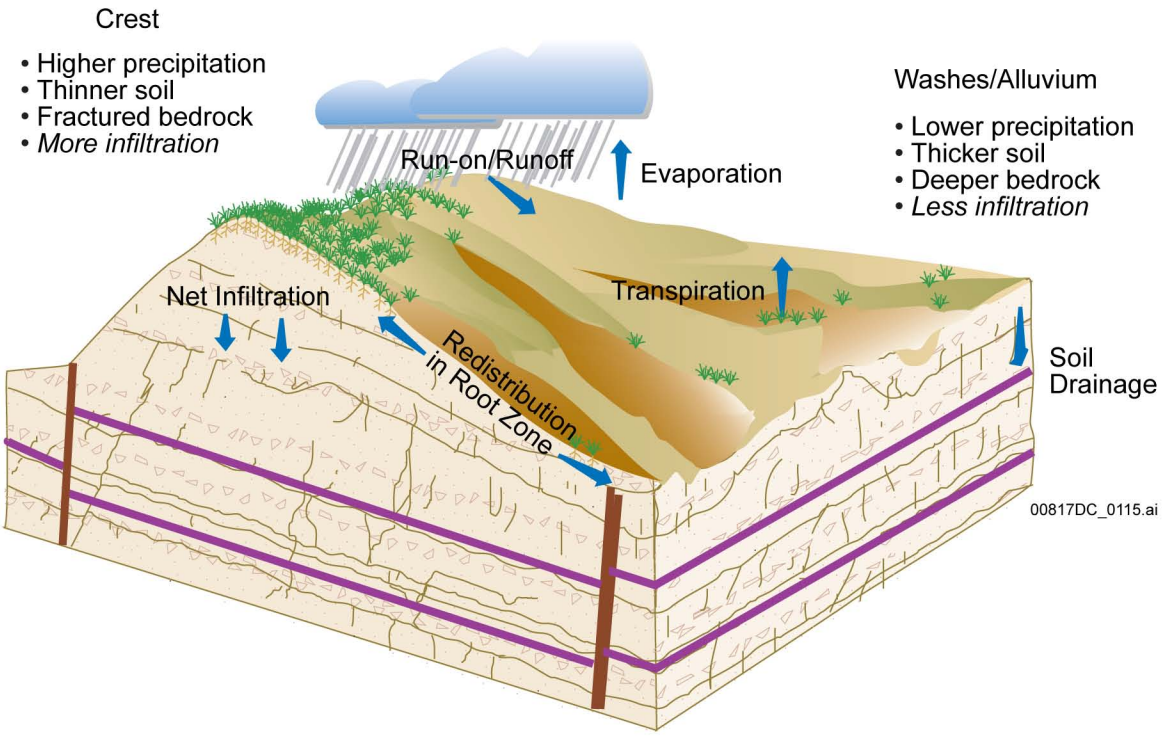

Figure 6.3.1-5. Schematic Illustration Showing the Variation of Precipitation and Consequent Infiltration with Respect to Elevation at Yucca Mountain

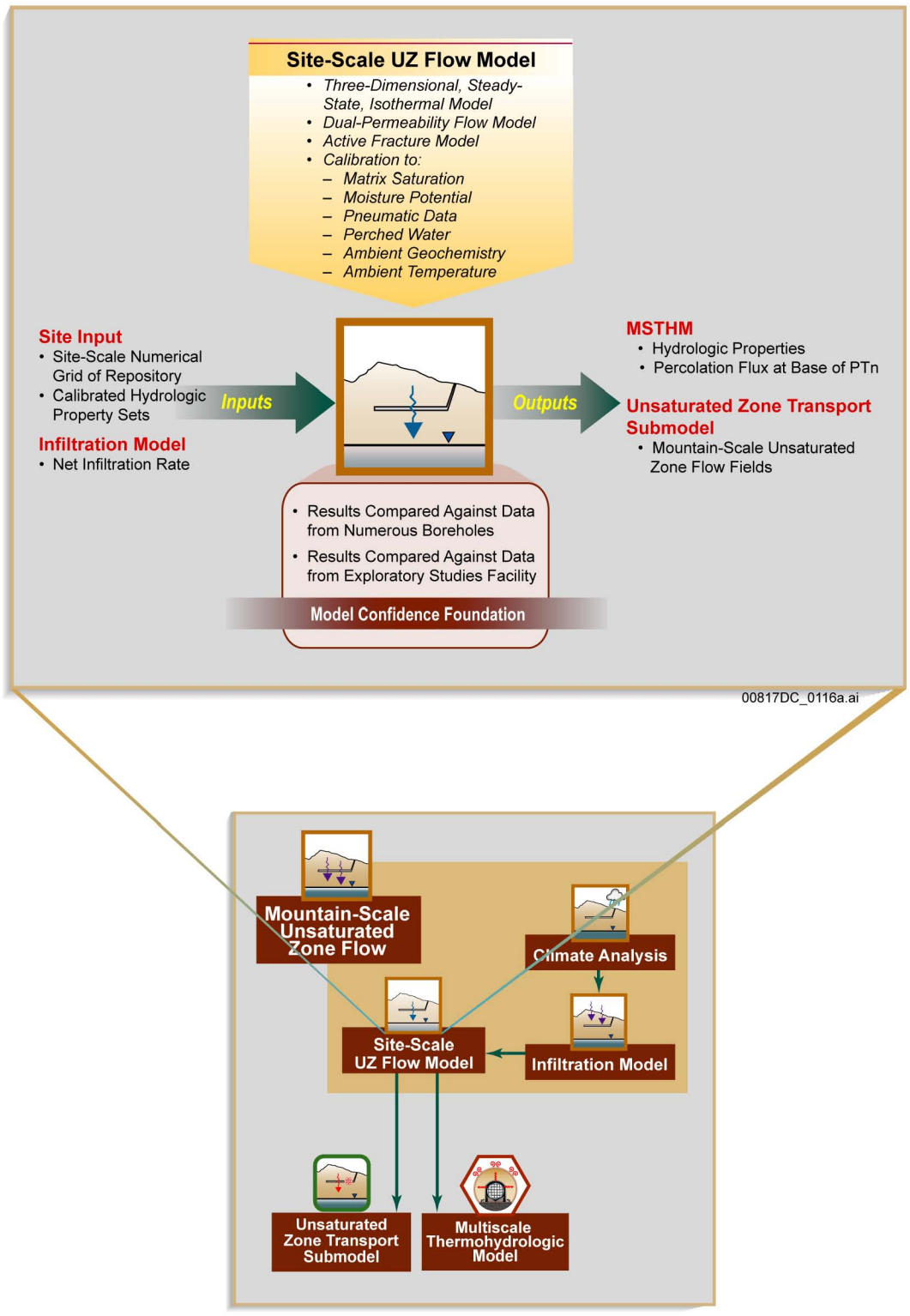

Figure 6.3.1-6. Inputs, Outputs, and Basis for Model Confidence for the Site-Scale Unsaturated Zone Flow Process Model

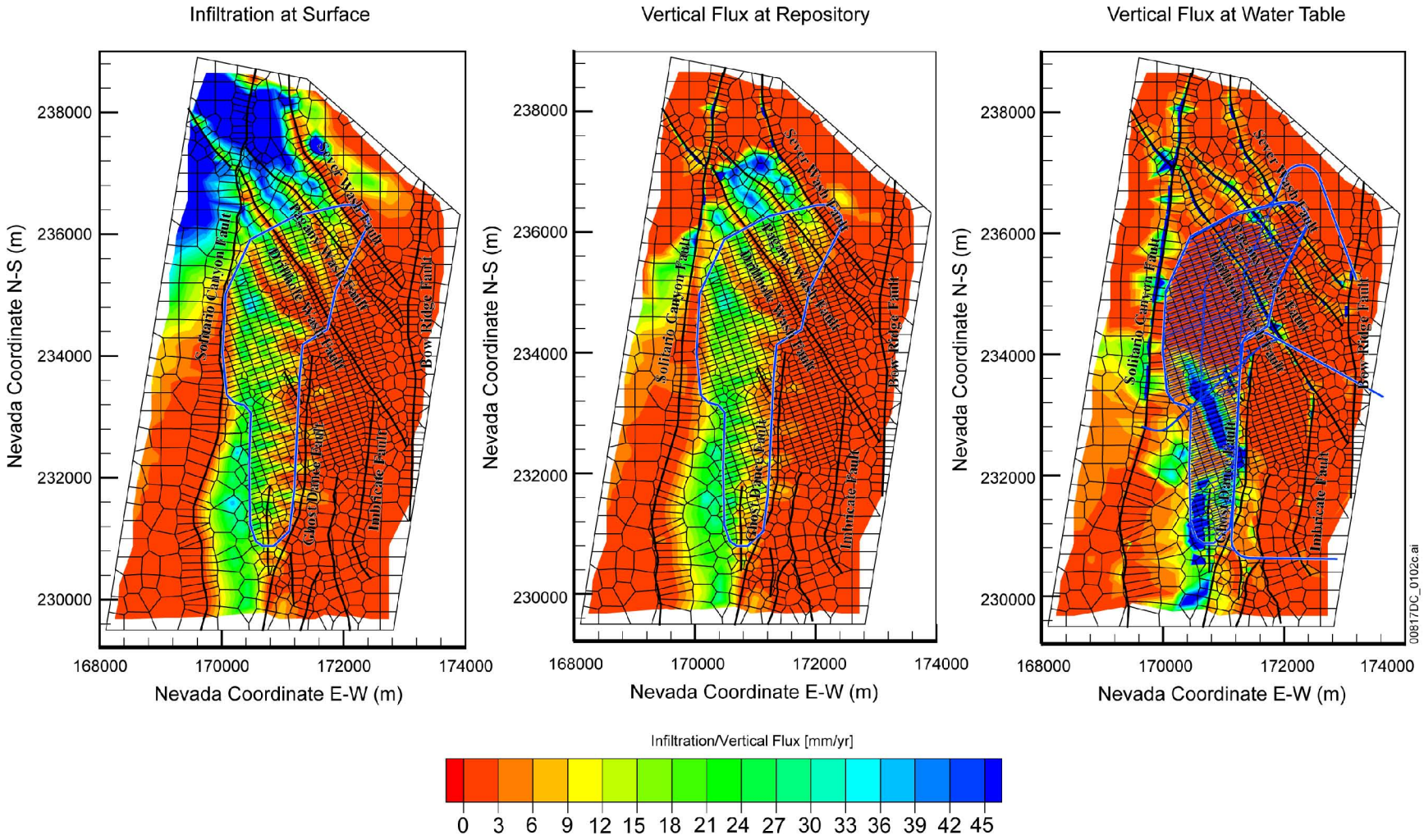

Source: Modified from SNL 2007 [DIRS 184614], Figures 6.1-4, 6.6-3, and 6.6-7

NOTE: The net infiltration boundary and water table are at varying elevations, while the repository horizon is approximated by a constant elevation of 1,080 m.

Figure 6.3.1-7. Comparison of Net Infiltration, Percolation Flux at the Repository Horizon, and Percolation Flux at the Water Table in the Tenth Percentile Infiltration Scenario During the Glacial-Transition Climate State

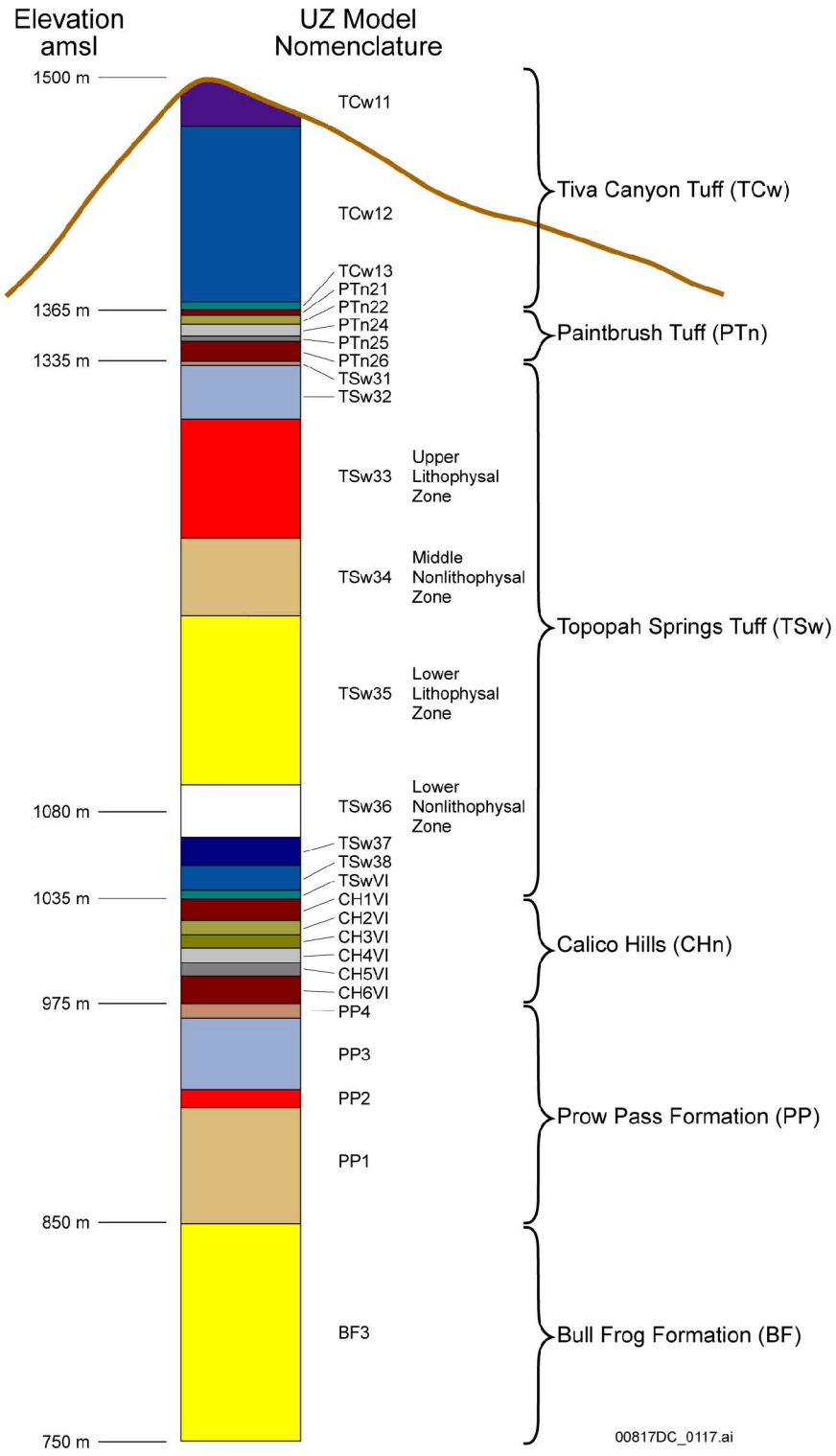

Source: DTN: LB03033DSSFF9I.001_R0 [DIRS 163047], SD-6 Borehole.

NOTE: Median elevation of the repository footprint is 1,080 m above mean sea level (amsl).

Figure 6.3.1-8. General Stratigraphy at the Yucca Mountain Site Observed at Borehole SD-6

6.3.2 Engineered Barrier System Thermal-Hydrologic Environment

After permanent closure of the repository, the heat produced by radioactive decay of the waste will influence the thermal and hydrologic conditions in the geologic formations surrounding the repository drifts, the seepage into the repository drifts, local temperature and relative humidity conditions around the WPs, and moisture movement within the drifts. For TSPA-LA Model simulations, the EBS TH Environment Model Component results are computed using results from *Multiscale Thermohydrologic Model* (SNL 2007 [DIRS 181383], Section 1 and Section 1[a]). These MSTHM Process Model results, in the form of the MSTHM Abstraction, are provided as input to the EBS TH Environment Submodel. Figure 6.3.2-1 illustrates the information flow between the Mountain-Scale UZ Flow Submodel (Section 6.3.1), the EBS TH Environment Submodel, and other TSPA-LA Model submodels.

The EBS TH Environment Model Component parameters consist primarily of time-dependent temperature and relative humidity values at various locations within the repository drifts. Other EBS TH Environment Model Component variables include percolation flux above the repository, thermally perturbed liquid saturations, and liquid-flow rates in the invert. Figure 6.3.2-1 shows these TH outputs are used by the Drift Seepage Submodel (Section 6.3.3.1), Drift Wall Condensation Submodel (Section 6.3.3.2), EBS Chemical Environment Submodel (Section 6.3.4), WP and DS Degradation Model Component (Section 6.3.5), Waste Form Degradation and Mobilization Model Component (Section 6.3.7), and the EBS Flow and Transport Model Component. The EBS Flow and Transport Model Component is composed of the EBS Flow Submodel (Section 6.3.6) and the EBS Transport Submodel (Section 6.3.8). Figure 6.3.2-2 summarizes the inputs provided to the MSTHM Process Model and the EBS TH Environment Submodel results provided by the MSTHM Abstraction (SNL 2007 [DIRS 181383], Section 8.3[a]). Figure 6.3.2-3 shows the information that the EBS TH Environment Submodel provides to other TSPA-LA submodels.

6.3.2.1 Conceptual Model

Nuclear waste emplaced in the Yucca Mountain repository will emit heat from radioactive decay. The MSTHM Process Model is used to model the effects of this decay heat on the evolution of the TH environment in the emplacement drifts. The MSTHM Process Model estimates TH conditions within the emplacement drifts and the surrounding rock as functions of time, WP type, and locations in the repository, as described in *Multiscale Thermohydrologic Model*, (SNL 2007 [DIRS 181383], Section 1). The MSTHM Process Model simulates the evolution of temperature and relative humidity for the components of the EBS. The results are abstracted for the TSPA-LA Model to provide the evolution of temperature and relative humidity on the surfaces of the DSs and WPs, temperature in the invert, temperature on the drift wall, and liquid saturation and liquid flow in the invert.

The heat output from the spent nuclear fuel (SNF) and high-level radioactive waste (HLW) will decline continuously due to the decrease in radioactive decay activity over time. After 50 years of ventilation, the repository enters its postclosure stage where ventilation will cease and the drift-wall rock temperature will be well below boiling but will increase sharply within a few years (SNL 2007 [DIRS 181383], Figure 6.2-4(c)). The maximum postclosure temperature of a WP at any location will be determined by the history of heat output, the resistance to dissipation

of heat in the host rock, heat transfer from the WP to the drift wall, and the relationship to other nearby heat sources. Peak WP temperature considered in the TSPA-LA Model for nominal performance ranges from 107.5°C to 211.0°C (SNL 2007 [DIRS 181383], Table 6.3-49[a]).

Heating of the host rock will produce movement of vapor and liquid water after permanent closure. Much of the heat will be transported away from the drifts by thermal conduction through the rock. A portion of the heat will be transported as latent heat by water that vaporizes near the drift and condenses in cooler rock farther away. Given the projected heat output of the waste and the host-rock characteristics, the near-field host rock, characterized by the drift wall temperature, will be heated to above-boiling temperatures (i.e., greater than 96°C at the repository elevation) for several centuries (SNL 2007 [DIRS 181383], Table 6.3-50[a]). Where temperature exceeds boiling, most of the water will be evaporated from the rock. The duration and extent of dry out will depend on the history of local heat generation, the percolation flux in the host rock, and host-rock properties, notably the thermal conductivity. The variability and uncertainty in host-rock hydrologic properties have an insignificant influence on host-rock dryout (SNL 2007 [DIRS 181383], Section 6.3.9). The maximum lateral extent of the dry-out zone surrounding the emplacement drifts will vary from location to location, ranging from several meters to 11.12 m, but is always expected to be much smaller than the half-drift spacing between emplacement drifts (i.e., 40.5 m) (SNL 2007 [DIRS 181383], Table 6.3-51[a]). Thermal evolution of a particular WP will also depend on its location in the repository layout (i.e., whether it is near the center or the edge of the repository). As the waste heat output decreases with time, the dry-out zone will eventually shrink back to the drift wall, cooling to below-boiling temperatures. The temperatures of the WPs will follow the evolution of the local drift-wall temperature but will be much warmer because of EBS heat transfer mechanisms between the WPs and the local drift wall. This temperature difference will approach zero at later times as the heat output declines.

The influence of heat-generation variability on WP relative humidity variability is similar to the influence on host-rock dry out (SNL 2007 [DIRS 181383], Section 6.3.9, and Section 6.3.13). Because the relative humidity at the drift wall strongly depends on the liquid-phase saturation (as well as on temperature) at the drift wall, the variability of drift-wall relative humidity is similar to that of drift-wall liquid-phase saturation. Relative humidity on a given WP depends on two factors: the drift-wall relative humidity adjacent to the WP, and the temperature difference between the WP and adjacent drift-wall surface. The relative humidity on a given WP is calculated using the relative humidity at the adjacent drift-wall surface and the temperature difference between the WP and the drift-wall surface (SNL 2007 [DIRS 181383], Section 6.1.4 and Section 6.2.4, Stage 6). WPs with higher heat-generation rates result in a greater relative humidity reduction than those with lower heat-generation rates. The differences in heat-generation rates between the eight different WP types result in differences in relative humidity histories.

6.3.2.2 Model Abstraction

The EBS TH Environment Abstraction is based on two-dimensional, drift-scale, dual-permeability TH models combined with one-, two-, and three-dimensional, thermal-conduction-only models of drift- and mountain-scale. The MSTHM Process Model combines these TH and thermal-conduction-only models in a methodology that incorporates

thermal interactions between WPs, other EBS components, and between the EBS and the surrounding hydrogeologic environment at the repository-scale, as described in *Multiscale Thermohydrologic Model* (SNL 2007 [DIRS 181383], Sections 1 and 6.2). The MSTHM Abstraction results describe heat-related responses within and among the component parts of the emplacement drifts, including the effects of repository-scale heat transfer to the surrounding environment.

The MSTHM Process Model simulates two categories of WPs: a commercial spent nuclear fuel (CSNF) WP, which includes CSNF from pressurized-water reactors (PWRs) and boiling-water reactors (BWRs), and a WP that contains both defense high-level (radioactive) waste (DHLW) and U.S. Department of Energy (DOE) owned SNF (DSNF) (SNL 2007 [DIRS 181383], Table6.2-6[a]). WPs that contain both DHLW and DSNF are referred to as DHLW/DOE SNF WPs in the *Multiscale Thermohydrologic Model* (SNL 2007 [DIRS 181383], Tables 4-1[a] and 6.2-6[a]). The TSPA-LA Model, however, refers to these DHLW/DOE SNF WPs as co-disposed (CDSP) WPs. Each waste fuel type has a different rate of heat generation over time. To develop the time histories of heat generated by the waste in the repository, the MSTHM Process Model considers a nominal WP sequence consisting of six CSNF WPs and two CDSP WPs producing results for eight distinct, local heating conditions for each repository subdomain, as described in *Multiscale Thermohydrologic Model* (SNL 2007 [DIRS 181383], Section 6.2.17[a], Table 6.2-6[a]).

The MSTHM Process Model accounts for the following natural and engineered system features:

- Repository-scale variability of percolation flux
- Temporal variability of percolation flux, as influenced by climate change
- Uncertainty in percolation flux addressed by the 10th, 30th, 50th, and 90th percentile infiltration scenarios.
- Uncertainty in thermal properties of the repository host rock using mean, high, and low values of thermal conductivity
- Variation in thermal properties between stratigraphic units in and around the repository
- Repository-scale variability of overburden thickness
- Edge-cooling effect relative to the repository footprint
- Repository design features including WPs, DSs, invert dimensions, invert material properties, drift spacing, WP spacing, and duration of preclosure ventilation
- WP-to-WP variability in heat generation rate
- Time- and distance-dependent heat removal efficiency of preclosure drift ventilation.

The effects of climate change and the resulting infiltration due to precipitation are included by changing the percolation flux boundary condition at the base of the PTn at prescribed times

during the simulations. At the beginning of the preclosure period, the climate is initially set to the present-day climate, which changes to the monsoonal climate after 600 years (of which 550 years are postclosure with present-day climate), followed by 1,400 years of a monsoonal climate, a glacial-transition climate at 2,000 years, and then a post-10,000-year climate (Section 6.3.1.2). A 50-year preclosure period with drift ventilation is included at the beginning of the MSTHM Process Model analyses and is accounted for in the input to the TSPA-LA Model (SNL 2007 [DIRS 181383], Sections 5.2.3 and 6.1.4, Table 4.1-1). However, because the TSPA-LA Model analyzes postclosure performance, the TSPA-LA Model uses the abstraction results starting at the time of closure (at the end of the ventilation period). Climate-induced changes to water table elevation are not included in the TH submodels of the TSPA-LA Model because the elevation of the water table is not expected to have a significant impact on the computed in-drift environments (SNL 2007 [DIRS 181383], Section 5.1.5).

Processes not included in the MSTHM Process Model are:

- Water vapor mixing or transport within the drifts along the drift axis caused by natural convection. See Section 6.3.3.2 for a description of how in-drift natural convection and condensation is included in the Drift Wall Condensation Submodel.

- The effects of drift degradation or collapse, due to reasons other than a seismic event, on the EBS TH responses are not included in the nominal TH abstractions. The Seismic Scenario Class includes a collapsed drift EBS TH adjustment that is limited to only a few EBS TH parameters, as described in Section 6.6.

- Changes in rock properties because of coupled thermal-hydrologic-chemical or thermal-hydrologic-mechanical processes (SNL 2007 [DIRS 181383], Section 6.2.1). The variability and uncertainty in host-rock hydrologic properties have an insignificant influence on host-rock dryout (SNL 2007 [DIRS 181383], Section 6.3.9). The influence of mechanical and chemical coupling on the TH response is demonstrated to be insignificant compared to parametric uncertainties addressed in the MSTHM Process Model (SNL 2007 [DIRS 181383], Section 8.4.1[a]).

- Changes in the TH properties of water because of dissolved solutes (SNL 2007 [DIRS 181383], Section 6.2.1).

- Flow focusing over distinct sections of emplacement drifts, though a sensitivity study was performed to analyze this exclusion (SNL 2007 [DIRS 181383], Section 6.3.2.1). See Section 6.3.3.1.2 for a description of how flow focusing is included in the Drift Seepage Submodel.

The results computed by the MSTHM Process Model are used directly in the MSTHM Abstraction for the TSPA-LA Model. The abstraction process is described below. Figure 6.3.2-4 shows the distribution of the four primary host-rock units that intersect the repository layout considered in the MSTHM Abstraction. Figures 6.3.2-5 and 6.3.2-6 show examples of the output from the MSTHM Abstraction, as described in *Multiscale Thermohydrologic Model* (SNL 2007 [DIRS 181383], Section 6.3[a]). Peak temperatures occur near the center of the repository and decreases near the edges. This spatial variability in

temperature is caused by increased lateral heat loss at the edges of the repository (i.e., the edge-cooling effect), and a reduction in heat removal efficiency due to ventilation exhaust shafts being located at the center of the repository. The location of the ventilation exhaust shafts at the center of the repository affects the spatial variability of heat in the repository because heat removal efficiency decreases with distance from the ventilation inlet (SNL 2007 [DIRS 181383], Section 6.3.1.1). Figure 6.3.2-5 shows estimated TH conditions for mean host-rock thermal conductivity and the 10th, 30th, 50th, and 90th percentile percolation flux cases, and Figure 6.3.2-6 shows estimated TH conditions for the 50th percentile percolation flux scenario combined with low, mean, and high estimates of host-rock thermal conductivity at the same location. Figures 6.3.2-5 and 6.3.2-6 show that TH conditions depend, to a moderate degree, on both the infiltration scenario and thermal conductivity of the host rock. Spatial variability of percolation flux at the repository horizon and heat transfer processes within and between drifts are two TH factors that are simulated by the MSTHM Process Model.

The MSTHM Process Model accounts for the impact of percolation-flux and host-rock thermal conductivity uncertainty on the TH environment conditions, using simulations conducted for the 10th, 30th, 50th, and 90th percentiles of percolation flux with the mean host-rock thermal conductivity values for the host-rock units. Three additional cases are used in conjunction with the four mean host-rock thermal conductivity cases to capture the impact of host-rock thermal conductivity uncertainty: 10th percentile percolation flux with low- and high-thermal conductivity, and 90th percentile percolation flux with high-thermal conductivity. The TH data sets associated with the remaining five of the 12 possible combinations of percolation flux and host-rock thermal conductivity are provided to the TSPA-LA Model as surrogates from the previously identified seven cases. These five cases use their associated values of percolation flux, but refer to one of the other seven cases for the TH data (SNL 2007 [DIRS 181383], Section 6.3.15[a]). The three thermal conductivities analyzed were assigned probability-weighting factors of 0.29, 0.37, and 0.34 for the low, mean, and high host-rock thermal conductivities, respectively (shown in Table 6.3.2-1 as a discrete distribution). The Infiltration Submodel (Section 6.3.1.2) uses weightings of 0.6191, 0.1568, 0.1645, and 0.0596 for the 10th, 30th, 50th, and 90th percentile percolation fluxes, respectively (shown in Table 6.3.1-2). Table 6.3.2-3 describes how the four probability weightings for percolation flux uncertainty and the three probability weightings for host-rock thermal conductivity uncertainty are used to determine the aggregate probability weightings for the 12 MSTHM Process Model data sets provided as input to the TSPA-LA Model. For further discussion of how the 12 combinations of host-rock thermal conductivity uncertainty and infiltration scenario uncertainties are addressed with the provided MSTHM Abstraction results, see *Multiscale Thermohydrologic Model* (SNL 2007 [DIRS 181383], Section 6.3.15[a]).

To characterize the variability in repository TH conditions, the MSTHM Process Model grid subdivides the drifts in the repository footprint into 3,264 equal-area subdomains corresponding to 20-m repository drift segments (SNL 2007 [DIRS 181383], Section 6.2.5.1 and Section 6.2.12[a]). For each of the 12 infiltration/host-rock thermal conductivity cases (Table 6.3.2-3) the MSTHM Abstraction includes the time-dependent TH variables, temperature, and relative humidity, for six different possible CSNF WPs and two different possible CDSP WPs at each of the 3,264 repository subdomains (SNL 2007 [DIRS 181383], Tables 6.2-6[a] and Section 6.2.17[a]). In addition, the MSTHM Abstraction includes time-dependent values for DS temperature and relative humidity; average drift-wall temperature, the duration of boiling at the

drift wall, the average invert temperature, the average invert saturation, and the average invert flux for each of the 3,264 repository subdomains. For the abstraction of the MSTHM Process Model data for downstream model components and submodels, two sets of output parameter analyses and organizations are performed. First, TH values and their associated repository subdomains are grouped into one of five repository percolation subregions based on the magnitude of the percolation flux at the base of the PTn. The second analysis involves determining a single 'representative' CSNF WP and a single 'representative' CDSP WP for each percolation subregion given the complete set of TH parameters at each of the repository subdomains in that percolation subregion. These output parameter analyses are summarized as follows.

6.3.2.2.1 Determination of Repository Percolation Subregions

The process used to assign each of the 3,264 MSTHM Process Model subdomains to each of the five repository percolation subregions is described in DTN: LA0702PANS02BR.001_R0 [DIRS 180322] and *Particle Tracking Model and Abstraction of Transport Processes* (SNL 2008 [DIRS 184748], Section 6.5.15[a]). Note that only the first three climate states were considered in the analysis used to find a single zone file with five sets of source nodes which best represents all the infiltration/climate combinations. The subdomains comprising each of the five repository percolation subregions were chosen based on the cumulative probability of percolation for the 12 flow fields (three different climate periods: present-day, monsoon and glacial-transition; each climate period is categorized with 4 infiltration scenarios: 10 percent, 30 percent, 50 percent and 90 percent). A 4-step binning process was applied to each of the twelve flow fields, resulting in a list of repository subdomains divided into 5 percolation subregions that share common infiltration ranges, based on the cumulative probability intervals for these subregions (SNL 2008 [DIRS 184748], Section 6.5.15[a]). The cumulative probability intervals for these five subregions of percolation rates sorted in ascending order are 0.0-0.05, 0.05-0.30, 0.30-0.70, 0.70-0.95, and 0.95-1.00 (SNL 2008 [DIRS 184748], Section 6.5.15[a]). The quantiles are shown in Table 6.3.2-2. An analysis, of the degree of similarity or difference of the results of the binning process depending on which flow field is considered, was performed. The results indicated that the bins for the 12 flow fields are quite similar to one another. As noted in SNL 2008 [DIRS 184748], Section 6.5.15[a], if a subregion is identified for a particular subdomain in the glacial-transition, 10th percentile flow field, it is very often identified as the same subregion for the other flow fields. When they are different, they almost always differ by only one subregion, that is, a 3 in one flow field becomes a 4 in another flow field, or a 2 becomes a 1. Based upon this result it was considered acceptable to use subregions from one flow field to approximate all infiltration scenarios and climate states. Therefore, the 10th percentile infiltration scenario for the glacial transition climate was used to define the five percolation subregions for all simulations including the post-10,000-year climate. The five repository percolation subregions are shown graphically on Figure 6.3.2-7. Because each of the 3,264 MSTHM Process Model subdomains are equally sized in area, 81 meters in width by 20 meters in length (SNL 2007 [DIRS 181383], Section 6.2.12[a]), the probability of an event (e.g., early failed WP) occurring in any of the five percolation subregions is the same as the quantile distribution used to define the percolation subregions (i.e., 5 percent, 25 percent, 40 percent, 25 percent, and 5 percent). The MSTHM Abstraction inputs to the TSPA-LA Model are provided in two output file sets. Both TH output file sets are indexed by subregion and waste fuel type categories.

The first file set contains WP surface temperature and relative humidity; DS surface temperature and relative humidity; and average drift-wall temperature for each of the eight WP at each repository subdomain within each percolation subregion. Because this data set from the MSTHM Abstraction is so extensive, covering eight different possible TH drift environments at each of the 3,264 repository subdomains, it is referred to as the comprehensive TH response data set. The parameter values provided in the comprehensive TH response data set are indexed by their percolation subregion and the percolation flux at each of the repository subdomains is included. Included with the comprehensive TH response data set at each of the 3,264 repository subdomains is the percolation flux experienced by that location during the simulation period. Also, included with each of the 3,264 repository subdomains are the fraction of each subdomain in lithophysal rock; the fraction of lithophysal unit value specifies whether each repository subdomain is in a lithophysal host-rock unit or not. These repository subdomain-specific TH data values and parameters are input to the WP and DS Degradation Model Component (Section 6.3.5), the Drift Seepage Submodel (Section 6.3.3.1), and the Drift Wall Condensation Submodel (Section 6.3.3.2).

A second MSTHM Abstraction file set for the TSPA-LA Model contains TH response histories for each of the five repository subregions based on a single, representative WP for each fuel type. The determination of the representative WP for each bin is described in Section 6.3.2.2.2. This data set from the MSTHM Abstraction is referred to as the representative TH response data set (Section 6.3.2.2.2). The TH information from a single representative CSNF WP and a representative CDSP WP for each repository subregion provides the following inputs: WP surface temperature and relative humidity; DS temperature and relative humidity; drift-wall temperature; invert temperature; invert saturation; and invert flux. Table 6.3.2-4 summarizes the variables estimated by the MSTHM Abstraction for the representative TH conditions at each of the five repository percolation subregions in the TSPA-LA Model. Parameter values from the representative TH response data set are used for input to the EBS Flow and Transport Model Component (Sections 6.3.6 and 6.3.8), the Waste Form Degradation and Mobilization Model Component (Section 6.3.7), the EBS Chemical Environment Submodel (Section 6.3.4), and the Drift Wall Condensation Submodel (Section 6.3.3.2).

In summary, Figure 6.3.2-1 shows the flow of MSTHM Abstraction results for the comprehensive and representative TH data sets provided to the TSPA-LA Model, consisting of TH abstractions at each of the 3,264 repository subdomains and TH abstractions at the representative WPs for each subregion. When a submodel or model component of the TSPA-LA Model requires input of TH response conditions associated with the representative CSNF or CDSP WP in a selected repository subregion, then the TH response conditions for that representative CSNF or CDSP WP are used as the TH response conditions for all CSNF or CDSP WPs in that subregion. For example, the time-dependent TH response conditions for the representative CSNF WP in a selected percolation subregion are used as the TH conditions for both the CSNF WPs in the dripping environment and the CSNF WPs in the non-dripping environment of that percolation subregion. The TH inputs to the TSPA-LA Model do not make a distinction between dripping and non-dripping environments because the TH conditions in the emplacement drifts are more strongly influenced by percolation flux and saturation in the host rock surrounding the drifts than by the flow-focusing effects associated with a dripping environment (SNL 2007 [DIRS 181383], Section 6.3.2.1). The influence of percolation flux on TH conditions is included in the MSTHM Process Model methodology. *Multiscale*

Thermohydrologic Model (SNL 2007 [DIRS 181383], Section 6.2.1) outlines the MSTHM Process Model approach and the TH processes accounted for by the model.

6.3.2.2.2 Determination of Representative Waste Packages

The representative CSNF and CDSP WPs are selected by compiling the peak WP temperature and the duration of boiling at the drift wall for each WP type in each repository percolation subregion. For each repository percolation subregion, these values are sorted from low to high, and a percentile is assigned to each WP location. For each repository percolation subregion, two representative WPs are selected, one for each WP type. Each representative WP is the one whose simulated peak WP temperature and drift-wall boiling period is closest to the calculated median value for peak WP temperature and the median boiling period duration in the selected percolation subregion, as described in *Multiscale Thermohydrologic Model* (SNL 2007 [DIRS 181383], Appendix VIII[a]). The two criteria, peak WP temperature and duration of boiling at the drift wall, that were used to select the representative CSNF and CDSP WP TH response curves were chosen because of their correlation to how dry the emplacement drifts will get and how quickly water or water vapor will return. After the process of selecting the representative WPs is completed for each waste fuel type in each percolation subregion, the TH response parameters of temperature and relative humidity values for each representative WP and associated DS, the average drift-wall temperature, the average invert temperature, the average invert saturation, and the average invert flux at each representative WP location are assembled in a representative TH response data file set. These data are accessed by the EBS TH Environment Submodel and provided as input to the Waste Form Degradation and Mobilization Model Component (Section 6.3.7), the EBS Flow and Transport Model Component (Sections 6.3.6 and 6.3.8), the EBS Chemical Environment Submodel (Section 6.3.4), and the Drift Wall Condensation Submodel (Section 6.3.3.2).

6.3.2.3 TSPA-LA Model Implementation

EBS TH Environment Submodel—Results from the MSTHM Abstraction serve as inputs to TSPA-LA Model components and submodels, as described in Section 6.3.2.2 and as follows. The TH parameters from the MSTHM Abstraction in the EBS TH Environment Submodel are time histories of:

- WP temperature
- DS Temperature
- Drift-wall temperature
- WP relative humidity
- Invert relative humidity
- Invert liquid flux (vertical component)
- Invert saturation.

An additional parameter, relative humidity of the invert, is calculated within the EBS TH Environment Submodel using the material and VanGenuchten properties of the invert (DTNs: MO0505SPAROCKM.000_R0 [DIRS 173893] and LB0610UZDSCP30.001_R0 [DIRS 179180]), the properties of water (DTN: MO0505SPAROCKM.000_R0 [DIRS 173893]), relative humidity caps (DTN: SN0706PAEBSPCE.016_R0 [DIRS 181837]),

and the methodology described in the MSTHM Process Model (SNL 2007 [DIRS 181383], Appendix XV[a]).

Two sets of TH parameter files are provided by the MSTHM Abstraction, a comprehensive set and a representative set (Section 6.3.2.2.1). The comprehensive TH response files have the TH parameter time histories (listed above) for each of the eight possible WPs at each of the 3,264 MSTHM Process Model repository subdomains, and are categorized by percolation subregion and fuel type (Figure 6.3.2-8). Included with the comprehensive TH response data set at each of the 3,264 repository subdomains is the percolation flux experienced by that location during the simulation period. Also, included for each of the 3,264 repository subdomains is a note specifying whether that repository subdomain is in a lithophysal host-rock unit or not. These comprehensive TH data values and parameters are input to the WP and DS Degradation Model Component (Section 6.3.5) and the Drift Seepage Submodel (Section 6.3.3.1). In addition, the comprehensive TH data set is used to calculate other TSPA-LA Model inputs including the average percolation flux for the drift used in the Drift Wall Condensation Submodel (Section 6.3.3.2).

The representative TH response file set has the TH parameter time histories for a single representative WP for a given fuel type in each percolation flux subregion. Each of the two sets of TH parameters is provided for the 12 infiltration/host-rock thermal-conductivity uncertainty combinations (Table 6.3.2-3). The TH parameter set containing the representative WPs is implemented into the TSPA-LA Model as a set of two-dimensional tables. Each two-dimensional table contains the TH parameter time histories for one of the 120 combinations of infiltration/thermal-conductivity uncertainty (twelve each), fuel type (two each), and percolation subregion (five each). The TH parameters from the representative WPs are used as inputs to the Waste Form Degradation and Mobilization Model Component (Section 6.3.7), EBS Flow and Transport Model Component (Sections 6.3.6 and 6.3.8), the EBS Chemical Environment Submodel (Section 6.3.4), and Drift Wall Condensation Submodel (Section 6.3.3.2). The comprehensive TH parameter set that includes each WP for a given fuel type (six CSNF WPs, two CDSP WPs) at each of the MSTHM Process Model repository subdomains (3,264 each) in a given percolation subregion (five each) is implemented as a set of externally carried model input files (DTN: MO0707PREWAPMS.000_R0 [DIRS 183002]) (see output DTN the discussion of PREWAP (PREWAP_LA V1.1, STN: 10939-1.1-00 [DIRS 181053]) output files in Appendix F-2.8), which are used by the seepage dynamically linked library (DLL) (SEEPAGEDLL_LA V.1.2.2005. Windows 2000 STN: 11076-1.2-00 [DIRS 173435]), the WP Degradation Model (WAPDEG) DLL (WAPDEG V.4.07.2003 Windows 2000. STN: 10000-4.07-00 [DIRS 181774]), and the Waste Package Localized Corrosion Initiation Analysis. In addition the representative TH data set is used to calculate the duration of boiling (e.g. time needed of drift cooling to 96°C) for each of the representative WPs which is used in the EBS Chemical Environment Submodel (Section 6.2.4).

6.3.2.4 Model Component Consistency and Conservatism in Assumptions and Parameters

To enhance understanding of the complex interactions within the TSPA-LA Model, a discussion of consistency among model components and submodels, and identification of conservative assumptions in abstractions, process models, and parameter sets supporting the EBS TH Environment Submodel are discussed below.

6.3.2.4.1 Consistency of Assumptions

In-Drift Axial Fluid Flow—The MSTHM Process Model, which provides the basis for the in-drift temperature and relative humidity abstraction of the TSPA-LA Model, does not consider the longitudinal transport of water vapor along the length of the emplacement drifts. Thus, the influence of evaporation, transport, and condensation in the heated and unheated regions of the drifts, which result in a cold-trap effect, is not fully accounted for. On the other hand, the influence of the longitudinal transport of water vapor and associated condensation on the drift walls is approximated in the In-Drift Natural Convection and Condensation Process Model (SNL 2007 [DIRS 181648], Section 6.3). Therefore, there is a conceptual difference between the MSTHM Process Model and the In-Drift Natural Convection and Condensation Process Model.

Effect on the TSPA-LA Model—Although drift-wall condensation effects have been included in the TSPA-LA Model (Section 6.3.3.2), the difference in the modeling assumptions regarding the axial transport of moisture between the MSTHM Process Model and the Drift Wall Condensation Abstraction are possibly contradictory. If longitudinal vapor transport were included in the MSTHM Process Model, condensation in the unheated regions of the repository would affect the longitudinal variation of predicted in-drift temperature and relative humidity, with the effects on relative humidity having the greater potential impact, with vapor transport resulting in drier conditions than those predicted by the MSTHM (SNL 2007 [DIRS 181383], Section 7.8[a]). The thermal effects associated with the evaporation and condensation tend to dampen longitudinal temperature and relative humidity variations because heat would more effectively move from the hotter regions in a drift where the water evaporates, and then move to the cooler regions of the drift where the water vapor condenses. Thus, the WP-to-WP variation in temperature and relative humidity could be affected. However, both model reports, *Multiscale Thermohydrologic Model* (SNL 2007 [DIRS 181383], Section 7.5.3) and *In-Drift Natural Convection and Condensation* (SNL 2007 [DIRS 181648], Section 6.3.7.2.4), indicate that these longitudinal mass/energy transfer processes have an insignificant effect on the primary MSTHM Model predictions of temperature and relative humidity.

6.3.2.4.2 Identification of Conservatisms in Submodels and Abstractions

Repository Edge Effect—Although the heat loss into the host rock due to the repository edge effect is captured in the MSTHM Process Model via thermal conduction, the thermal convection component of the heat loss into the host rock expected at the edges of the repository is not included (SNL 2007 [DIRS 181383], Section 5.2.1). The bulk permeability of the repository host rock makes thermal conductivity the dominant heat flow mechanism because mass movement, via convection, from the drifts into the host rock is impeded by the limited permeability (SNL 2007 [DIRS 181383], Section 5.2.1).

6.3.2.5 Alternative Conceptual Model(s) for Engineered Barrier System Thermal-Hydrologic Environment

An important reason for considering ACMs is to help build confidence that plausible changes in modeling assumptions or simplifications will not change conclusions regarding subsystem and total system performance. Section 6.2 outlines the general consideration and treatment of ACMs used to support the TSPA-LA Model. Conservatism at the subsystem level has been used to

select the best ACM to use rather than quantitatively propagate multiple ACMs to the TSPA-LA Model. Generally, additional uncertainty is incorporated into the selected conceptual model if more than one ACM is deemed appropriate for use rather than considering multiple ACMs in the TSPA-LA Model. If an ACM appears to be significant at the subsystem level, then an appropriate abstraction is developed for that ACM for consideration within the TSPA-LA Model. The result of the process is documented within the individual analysis and/or model reports. It is important to note that treatment of ACMs within the individual model reports may differ significantly to be consistent with available data and current scientific understanding. Therefore, a brief description of the EBS TH Environment ACM summarized in Table 6.3.2-5 is presented below.

Mountain-Scale TH Model ACM—An ACM to the MSTHM Process Model is the Mountain-Scale TH Model [DIRS 174101]. The Mountain-Scale TH Model is a monolithic TH model which used: (1) coarser grid discretization at the drift scale than the MSTHM Process Model; (2) a line-averaged approximation of the heat-generation-rate-versus-time table (whereas, the MSTHM Process Model represented the WPs as discrete heat sources); and (3) a lumped heat source that filled the entire cross section of the emplacement drift (SNL 2007 [DIRS 181383], Section 6.4).

The temperature predicted by the MSTHM Process Model is the perimeter-averaged drift-wall temperature adjacent to an "average" 21-PWR medium-heat CSNF WP. The MSTHM Process Model discretely represents the decay-heat source from individual WPs. The drift-wall gridblocks over which the drift-wall temperature is averaged extend 0.2 m to 0.5 m into the host rock surrounding the emplacement drifts (SNL 2007 [DIRS 181383], Section 6.4). The temperature prediction in the east-west cross-sectional Mountain-Scale TH Model is for a gridblock that occupies the entire cross section of a drift; therefore, it is a lumped representation of the drift temperature (SNL 2007 [DIRS 181383], Section 6.4). Moreover, because the east-west cross-sectional Mountain-Scale TH Model uses a line-averaged heat source, it axially smears out the differences between 'hot' and 'cold' WP locations along the drift (SNL 2007 [DIRS 181383], Section 6.4).

During the post-boiling period, the temperatures predicted by both the MSTHM Process Model and the ACM modeling approach are in good agreement (SNL 2007 [DIRS 181383], Section 6.4). During the early-time heat-up period, the coarse (lateral and axial) grid-block spacing in the east-west cross-sectional Mountain-Scale TH Model does not capture the rapid drift-wall temperature rise that the more finely gridded MSTHM Process Model predicts. Because of the coarse lateral grid block spacing in the east-west model, it smears out the lateral temperature gradient between the drift and the mid-pillar location. Therefore, it tends to overpredict the temperature at the mid-pillar location, thereby preventing condensate from shedding between drifts (SNL 2007 [DIRS 181383], Section 6.4). The fine lateral grid-block spacing in the MSTHM Process Model captures the influence that the lateral temperature gradient has on allowing condensate to shed between drifts. The tendency for the east-west cross-sectional Mountain-Scale TH Model to under represent condensate shedding results in a more substantial condensate buildup above the repository horizon (SNL 2007 [DIRS 181383], Section 6.4). Also, the line-averaged heat-source approximation smears out differences in temperature between otherwise 'hot' and 'cold' WP locations, thereby preventing condensate from breaking through 'cold' WP locations along the emplacement drifts (SNL 2007

[DIRS 181383], Section 6.4). Altogether, the under prediction of condensate shedding between drifts and condensate breakthrough at 'cold' WP locations causes the east-west cross-sectional Mountain-Scale TH Model to build up more condensate above the repository horizon that leads to episodic heat-pipe behavior.

The MSTHM Process Model and the east-west cross-sectional Mountain-Scale TH Model are in agreement (SNL 2007 [DIRS 181383], Section 6.4). Moreover, the differences in predicted temperatures between the MSTHM Process Model and the east-west cross-sectional Mountain-Scale TH Model are within the range of temperature differences resulting from parametric uncertainty (SNL 2007 [DIRS 181383], Tables 6.3-30 and 6.3-31).

No ACMs related to the EBS TH Environment Submodel were recommended for inclusion in the TSPA-LA Model.

Table 6.3.2-1. Parameter Distribution for Host-Rock Thermal-Conductivity Uncertainty

Parameter Name in TSPA-LA Model	Description	Distribution
Thermal_Conductivity_Uncert_a	Uncertainty between the three host-rock thermal-conductivity scenarios (1=low, 2=mean, and 3=high).	Discrete (p, v) [(0.29, 1), (0.37, 2), (0.34, 3)]

Sources: *Multiscale Thermohydrologic Model* (SNL 2007 [DIRS 181383], Table 6.3-47[a]); and DTN: LL0703PA026MST.013_R0 [DIRS 179981].

Table 6.3.2-2. Percolation-Based Probability Subregion Quantile Ranges

Subregion Index	Quantile Range
1	$p < 0.05$
2	$0.05 \leq p < 0.30$
3	$0.30 \leq p < 0.70$
4	$0.70 \leq p < 0.95$
5	$p \geq 0.95$

Source: DTN: MO0505SPAROCKM.000_R0 [DIRS 173893].

Table 6.3.2-3. Probability Weighting for the 12 Percolation Flux and Host-Rock Thermal-Conductivity Combinations

Percolation Flux Case	Probability			
	Host-Rock Thermal-Conductivity			
	All	Low	Mean	High
All	1.0000	0.29	0.37	0.34
10%	0.6191	0.1795	0.2291	0.2105
30%	0.1568	0.0455	0.0580	0.0533
50%	0.1645	0.0477	0.0609	0.0559
90%	0.0596	0.0173	0.0220	0.0203

Source: *Multiscale Thermohydrologic Model* (SNL 2007 [DIRS 181383], Table 6.3-47[a]).

Table 6.3.2-4. List of Thermal-Hydrologic Variables Predicted by the MSTHM Process Model and Used in the TSPA-LA Model

Thermal-Hydrologic Variable	Drift-Scale Location
Temperature	Drift wall (perimeter average)
	Drip shield (upper surface)
	Waste package (surface average)
	Invert (average)
Relative humidity	Waste package (surface average)
	Drip Shield (average)
Liquid-phase saturation (intragranular)	Invert (average)
Liquid-phase flux	Invert (average)

Table 6.3.2-5. Alternative Conceptual Model Considered for the Engineered Barrier System Thermal-Hydrologic Environment

Alternative Conceptual Models	Key Assumptions	Screening Assessment and Basis
Mountain-Scale TH Model	An ACM to the MSTHM Process Model is a mountain-scale TH model developed by Lawrence Berkeley National Laboratory (DIRS 174101)). The Lawrence Berkeley National Laboratory model is a monolithic TH model. The Lawrence Berkeley National Laboratory TH model used: (1) coarser grid discretization at the drift scale than the MSTHM Process Model; (2) a line-averaged approximation of the heat-generation-rate-versus-time table (whereas the MSTHM Process Model represented the WPs as discrete heat sources); and (3) a lumped heat source that filled the entire cross section of the emplacement drift (SNL 2007 [DIRS 181383], Section 6.4).	Screened out. Given the differences between the MSTHM Process Model and the east-west cross-sectional Lawrence Berkeley National Laboratory Mountain-Scale Model, the agreement between the two models is adequate (SNL 2007 [DIRS 181383], Section 6.4). Moreover, the differences in predicted temperatures between the MSTHM Process Model and the east-west cross-sectional Lawrence Berkeley National Laboratory Mountain-Scale Model are within the range of temperature differences resulting from parametric uncertainty (SNL 2007 [DIRS 181383], Tables 6.3-30 and 6.3-31).

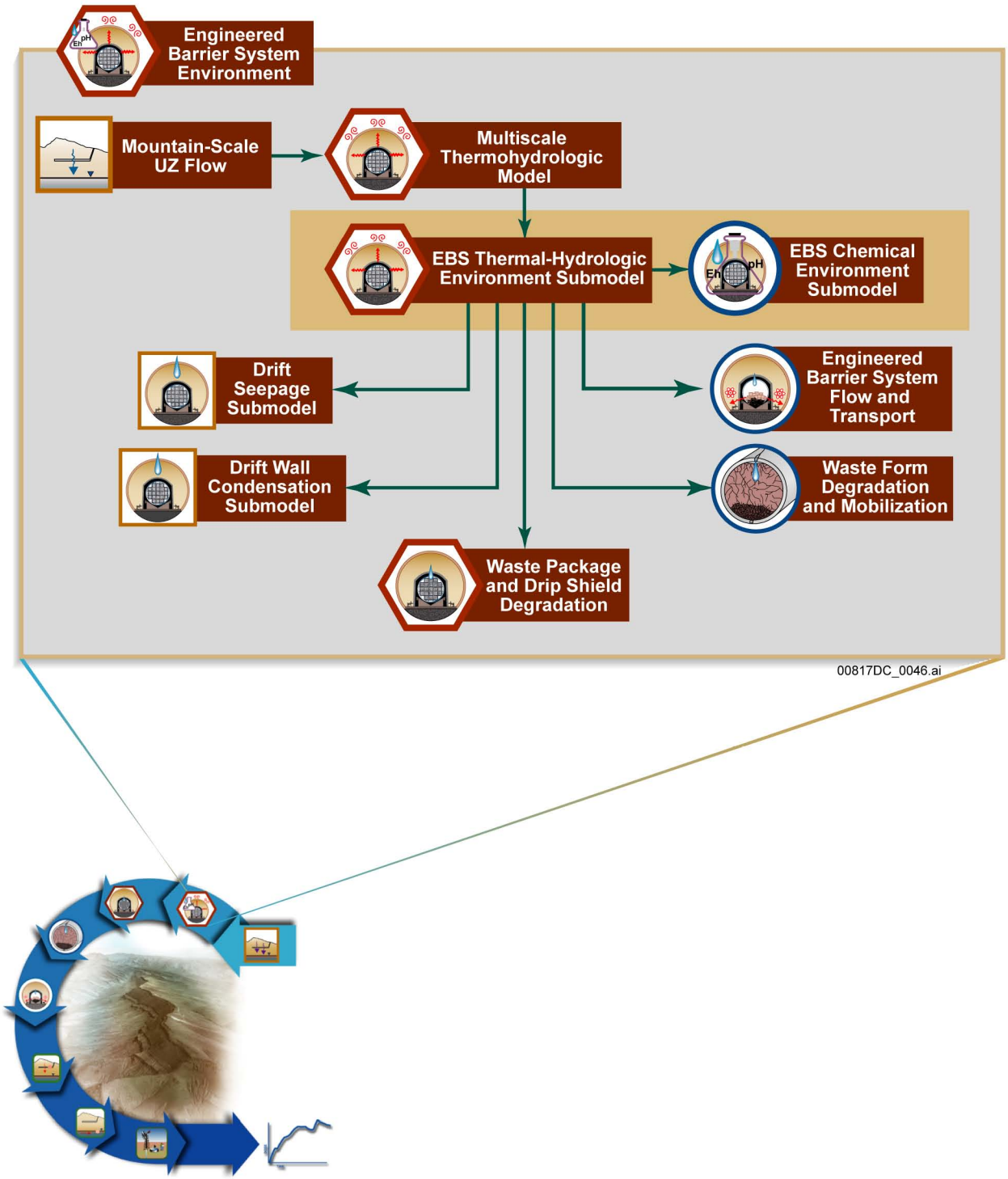

Figure 6.3.2-1. Information Flow Diagram for the EBS Thermal-Hydrologic Environment Submodel

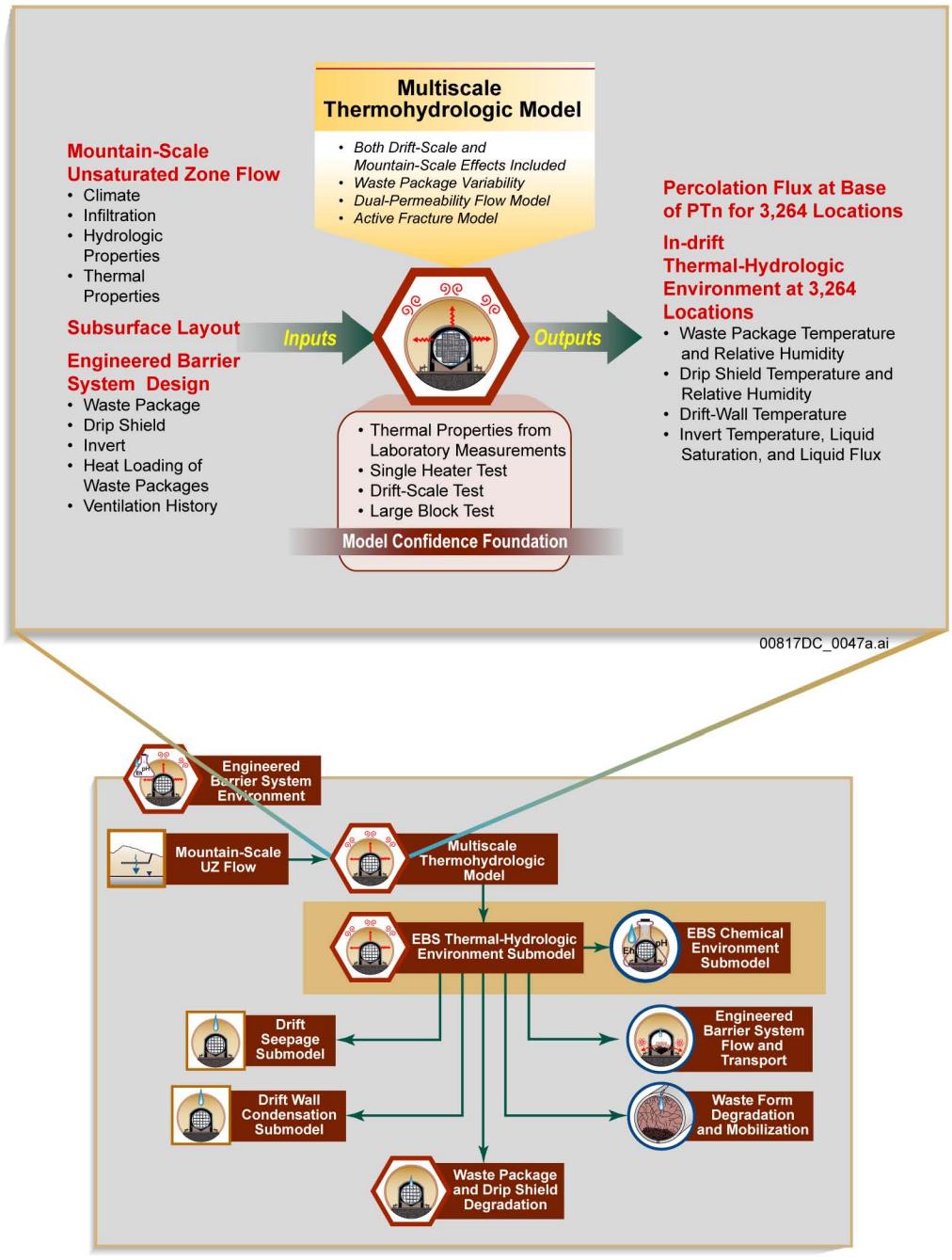

Figure 6.3.2-2. Inputs, Outputs, and Basis for Model Confidence for the Multiscale Thermohydrologic Process Model

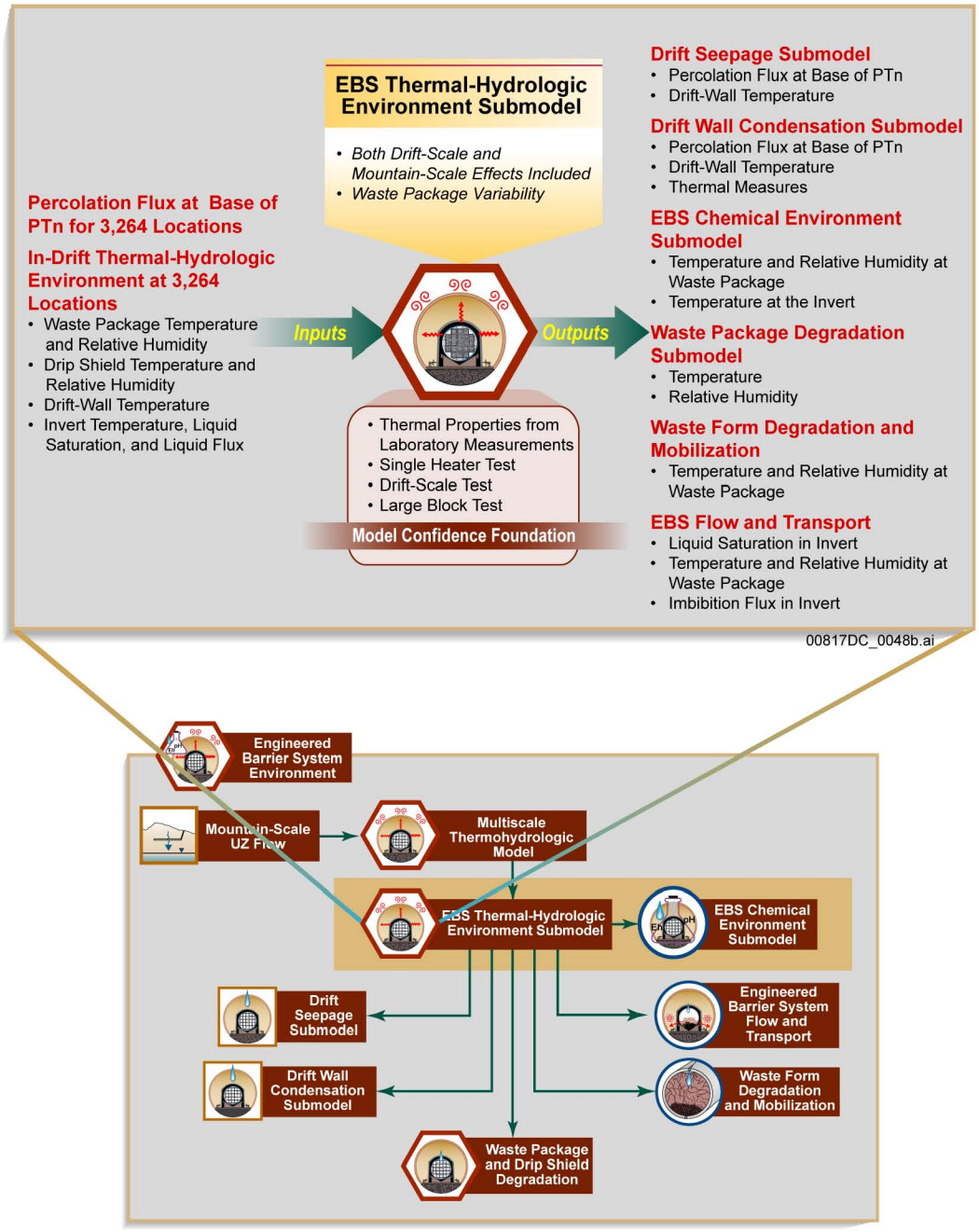

Figure 6.3.2-3. Inputs, Outputs, and Basis for Model Confidence for the EBS Thermal-Hydrologic Environment Submodel

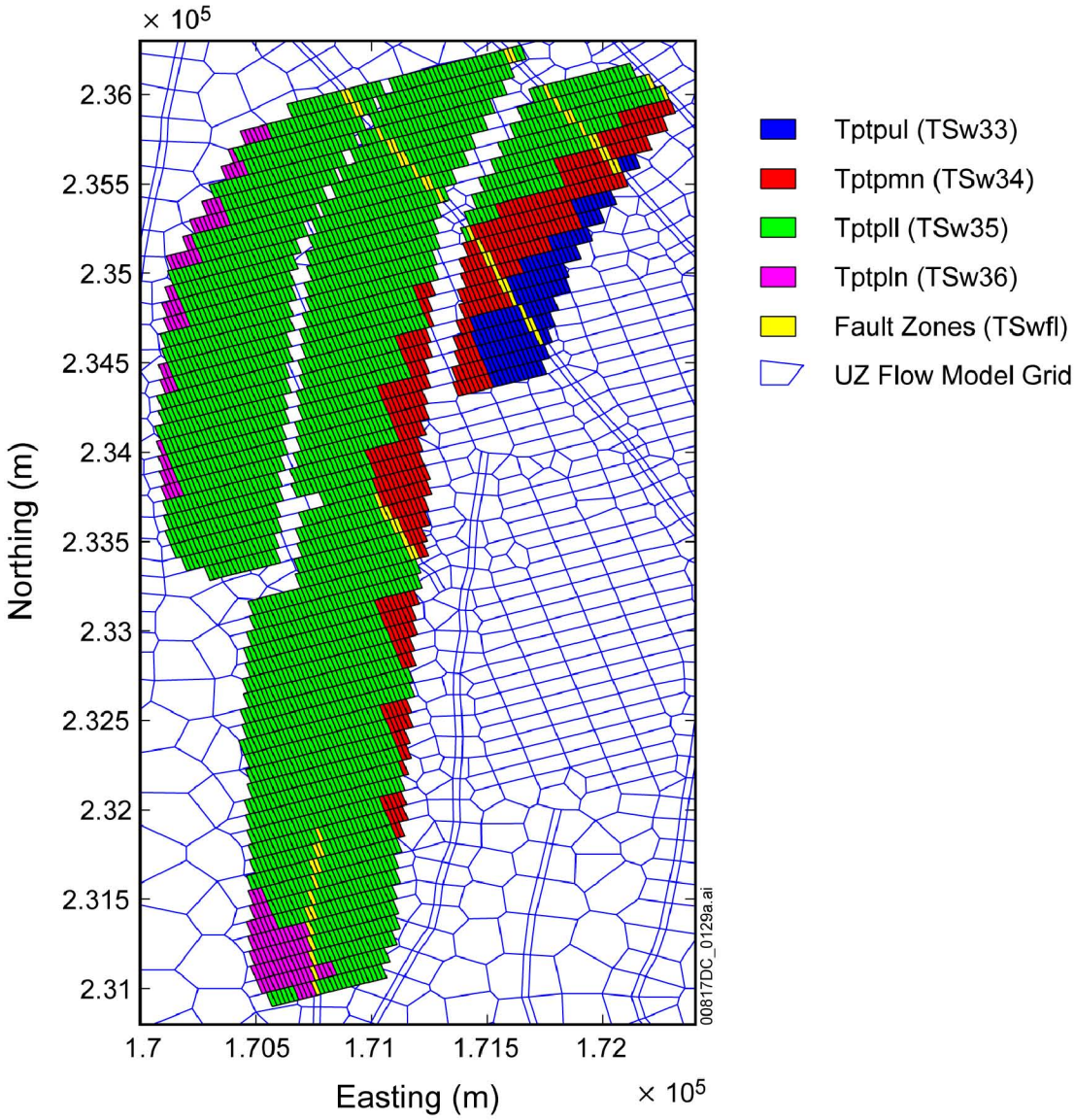

Source: SNL 2007 [DIRS 181383], Figure 6.2-18[a].

NOTES: Also shown are the five representative locations (indicated by circles) that were selected to examine thermal-hydrologic conditions in the four primary host-rock units.

Tptpul = Topopah Spring Tuff crystal-poor upper lithophysal zone; Tptpmn = Topopah Spring Tuff middle nonlithophysal zone; Tptpll = Topopah Spring Tuff crystal-poor lower lithophysal zone; Tptpln = Topopah Spring Tuff lower nonlithophysal zone.

Figure 6.3.2-4. The Distribution of the Four Primary Host-Rock Units is Shown for the Repository Layout Considered in the Multiscale Thermohydrologic Model Calculations for the TSPA-LA Model

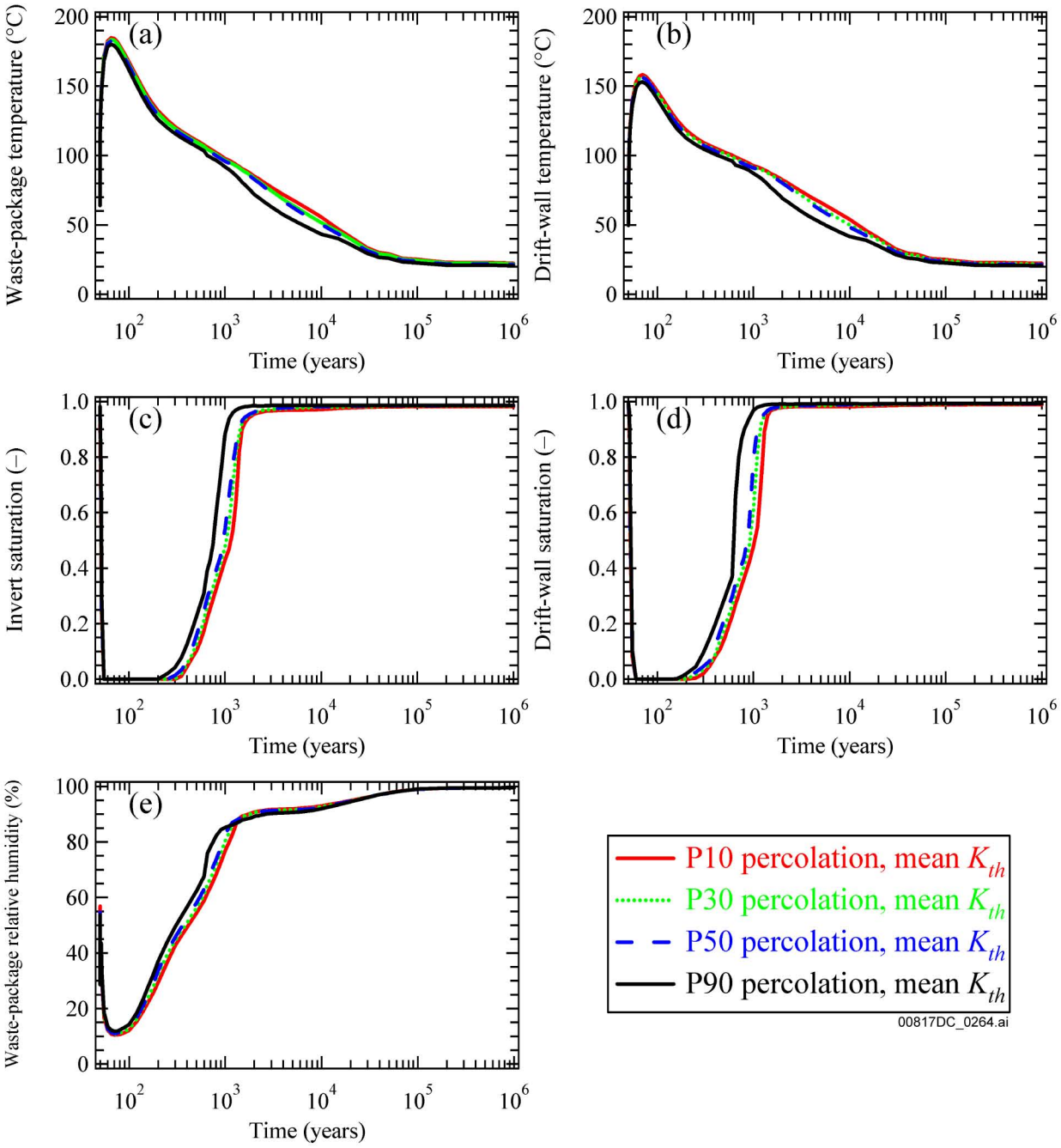

Source: DTNs: LL0703PA011MST.006_R0 [DIRS 179853]; LL0703PA012MST.007_R0 [DIRS 179854]; LL0703PA013MST.008_R0 [179855]; and LL0703PA014MST.009_R0 [DIRS 179856].

NOTE: Plotted thermal-hydrologic variables are: (a) waste-package temperature; (b) drift-wall temperature; (c) invert liquid-phase saturation; (d) drift-wall liquid-phase saturation; and (e) waste-package relative humidity.

Figure 6.3.2-5. Thermal-Hydrologic Conditions for the PWR1-2 Waste Package Plotted for 10th, 30th, 50th and 90th Percentile Percolation-Flux Cases at a Location near the Center of the Repository

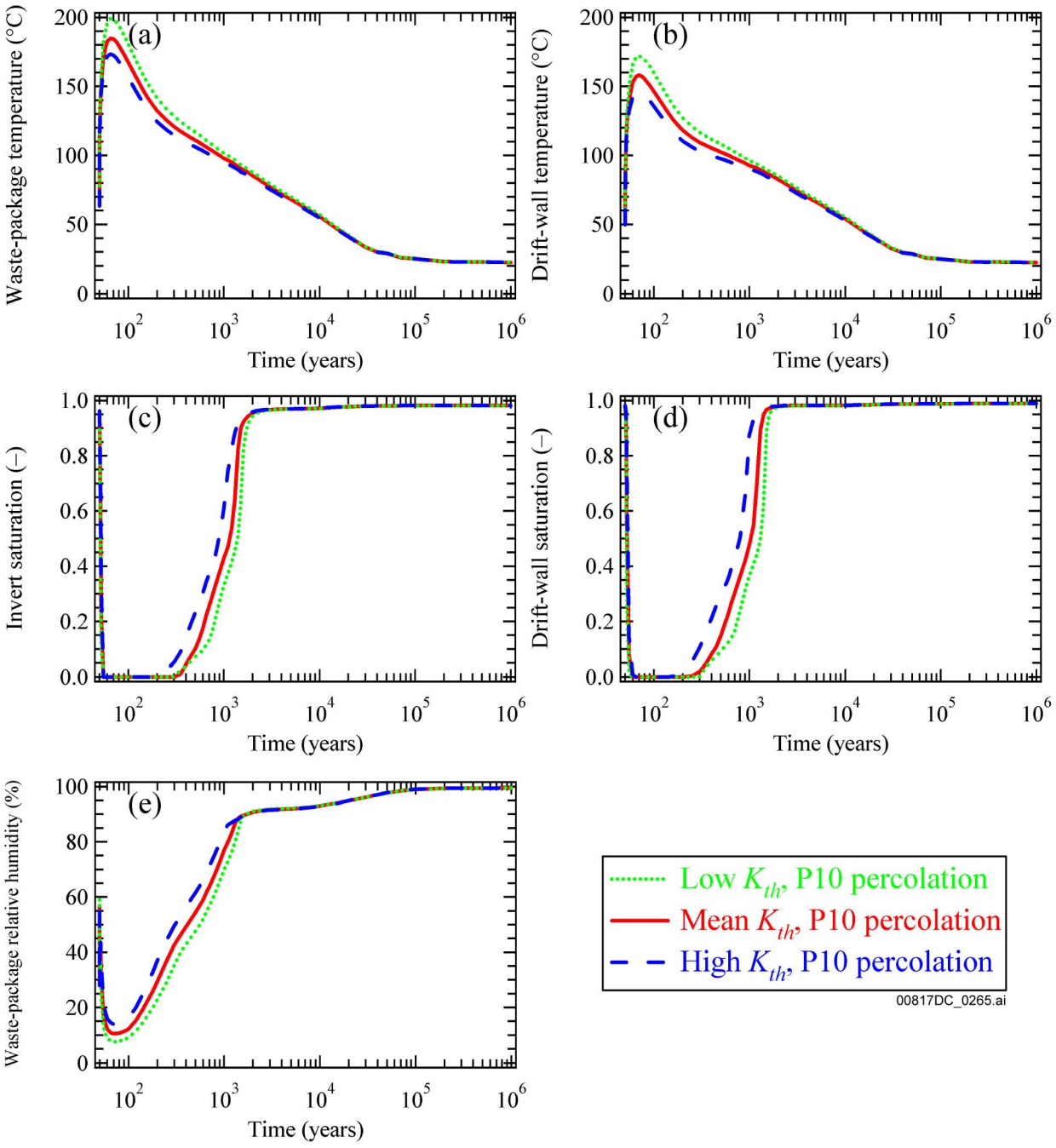

Source: DTNS: LL0703PA011MST.006 _R0 [DIRS 179853]; LL0703PA015MST.010_R0, [DIRS 179857]; and LL0703PA017MST.012_R0 [DIRS 179859].

NOTE: The plotted thermal-hydrologic variables are: (a) waste-package temperature; (b) drift-wall temperature; (c) invert liquid-phase saturation; (d) drift-wall liquid-phase saturation; and (e) waste-package relative humidity.

Figure 6.3.2-6. Thermal-Hydrologic Conditions for the PWR1-2 Waste Packages Plotted for 10th Percentile Percolation Flux Case at a Location Near the Center of the Repository

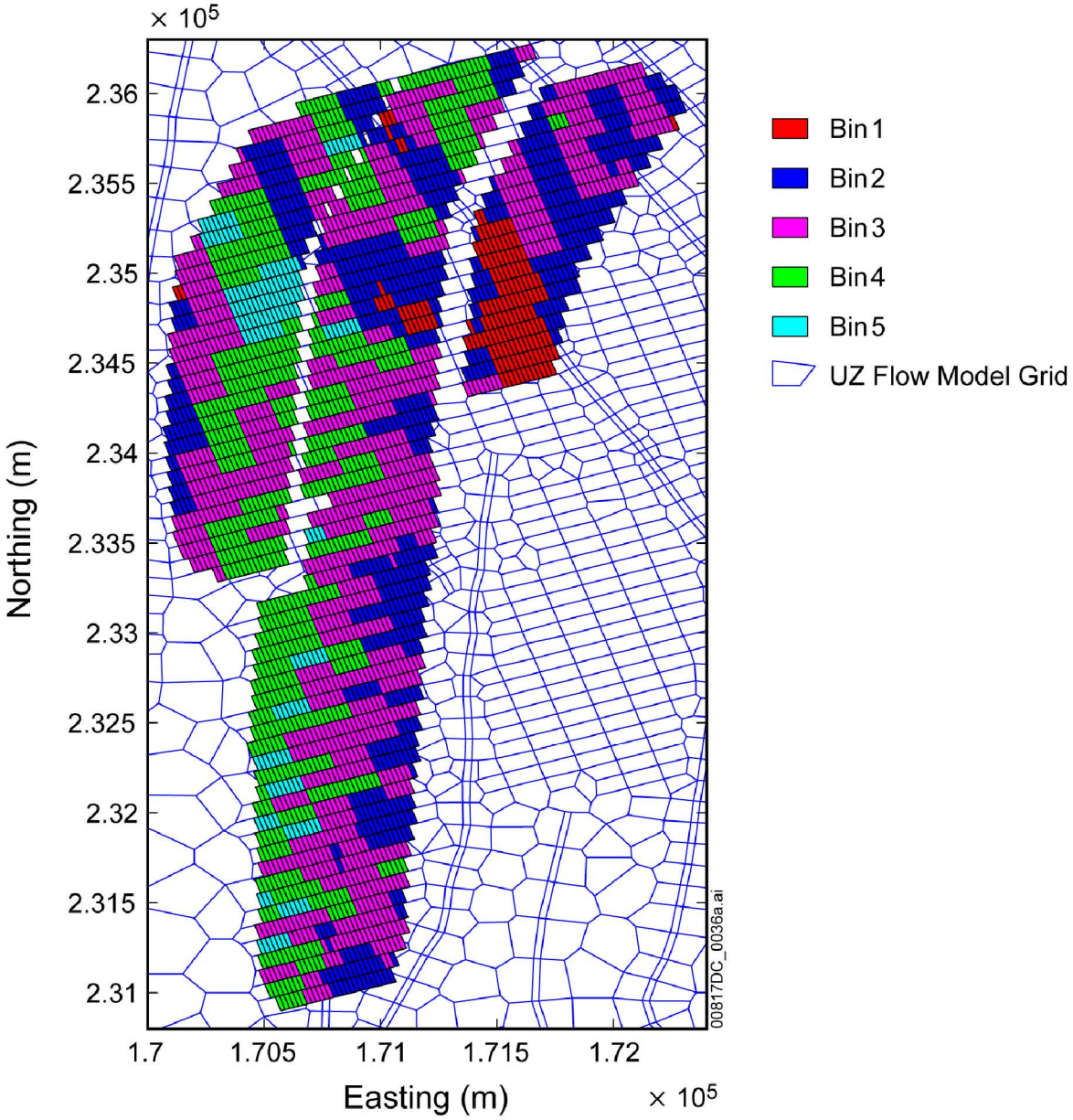

Sources: SNL 2007 [DIRS 181383], Figure VIII-1[a].

Figure 6.3.2-7. Repository Percolation Subregions Used in the TSPA-LA Model (based upon the 30th percentile infiltration case, glacial-transition period)

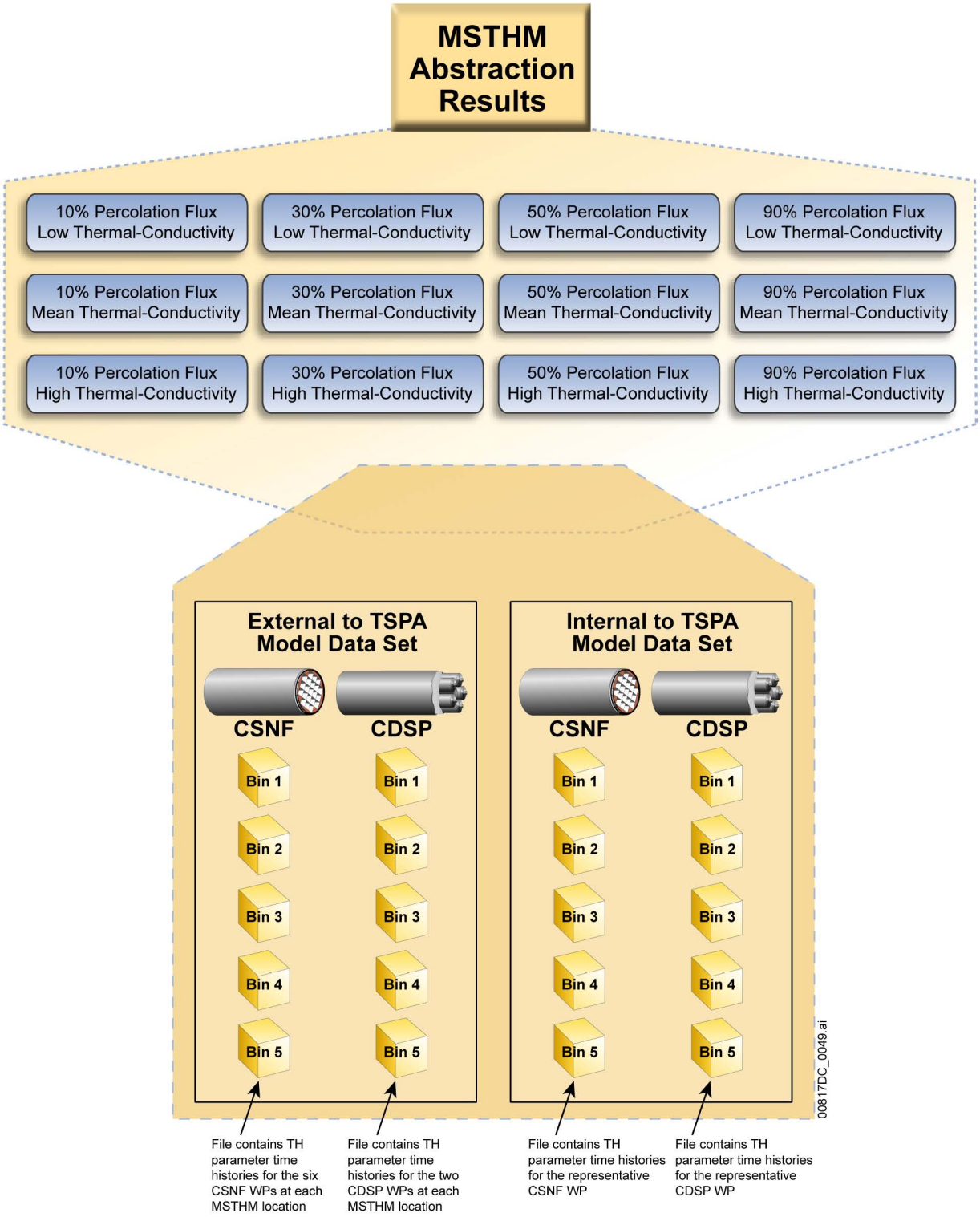

Figure 6.3.2-8. Thermal-Hydrologic Time History Parameter Inputs to the TSPA-LA Model

6.3.3 Drift-Scale Unsaturated Zone Flow

Water contacting DSs and WPs is expected to originate from two sources: (1) seepage of groundwater from the UZ above the repository into the emplacement drifts (SNL 2007 [DIRS 181244], Section 1) and (2) water-vapor condensate dripping from the walls of the drifts (SNL 2007 [DIRS 181648] Sections 6.3, 8.3, 6[a], and 8[a]). Percolation flux at the base of the PTn is used as the source of water for both drift seepage and drift-wall condensation. However, in this analysis no water balance is applied between the percolation flux, drift seepage, and drift-wall condensation. Note that even though the drift seepage and drift–wall condensation could possibly add up to more than the percolation flux, the approach chosen of not applying a water balance is considered conservative. The TSPA-LA Model calculates drift seepage and drift-wall condensation flow rates using the Drift Seepage Submodel (Section 6.3.3.1) and the Drift Wall Condensation Submodel (Section 6.3.3.2), respectively. These two flow rates are combined in the EBS Flow Submodel (Section 6.3.6) to yield a total dripping rate. Section 6.3.3.1 discusses the Drift Seepage Submodel (SNL 2007 [DIRS 181244], Section 6 and Section 6[a]), and Section 6.3.3.2 presents the Drift Wall Condensation Submodel (SNL 2007 [DIRS 181648], Section 6 and Section 6[a]).

6.3.3.1 Drift Seepage

Drift seepage refers to the flow of liquid water from the UZ above the repository into waste emplacement drifts. The Drift Seepage Submodel calculates two quantities: (1) the fraction of WP locations that experience seepage and (2) the average seepage flow rate for WP locations that have seepage (Section 6.3.3.1.3). The calculations are performed for each WP type in each percolation flux subregion (MSTHM Abstraction, Section 6.3.2.2.1). Figure 6.3.3-1 illustrates the flow of information for the Drift Seepage (SNL 2007 [DIRS 181244], Section 6) and Drift Wall Condensation Submodels (SNL 2007 [DIRS 181648], Section 6). Figure 6.3.3-2 shows the connections between the Drift Seepage Submodel and the EBS Flow Submodel (Section 6.3.6). Figure 6.3.3-2 shows inputs to and outputs from the Drift Seepage Submodel and indicates the principal features of the Drift Seepage Submodel and the foundation for confidence in the model.

6.3.3.1.1 Conceptual Model

Numerical modeling, natural analogues, and field tests summarized in (SNL 2007 [DIRS 181244], Sections 6.4.1, 6.4.2, 6.4.3, 7.3.1, and 7.3.2) indicate that seepage flux into emplacement drifts will be less than the local percolation flux. This difference results from two main processes: (1) the formation of capillary barriers at drift walls that are active during the thermal and ambient postclosure periods, and (2) the formation of dry-out zones helping to prevent percolation from reaching the repository during the thermal period. The effectiveness of these processes depends on the strength of the capillary pressure in the fractures close to the drift, the host rock's permeability close to the drift, the local percolation flux above the drift, the temperature of the rock near the drift wall, and the shape of the drift opening.

Figure 6.3.3-3 shows TH effects and the dry-out zone in the vicinity of the emplacement drifts due to repository heating. As water approaches a waste emplacement drift, conditions near the drift wall affect the amount of water that eventually seeps into the drifts. For preclosure conditions, the water may first encounter a dry-out zone caused by drift ventilation. During the

first several hundreds of years of the postclosure period, the dry-out zone may also develop from an increase in temperature due to decay heat from the emplaced waste, and where temperatures are high enough, may reach several meters from the drift wall due to boiling of rock water in the drift vicinity. Under boiling conditions, water will not enter the emplacement drifts (BSC 2005 [DIRS 172232], Section 6.1.2). The dry-out zone, indicated by the red shading around the drifts, is shown on Figure 6.3.3-3. The zone around the emplacement drift affected by TH processes is characterized by boiling, vapor transport, condensation, and migration of water back toward the heat source, either by capillary forces or gravity drainage (SNL 2007 [DIRS 181244], Section 6.3.2, p. 6-12). If liquid water approaches the immediate vicinity of the drift wall after the repository cools, a zone of increased saturation is expected to develop as a result of the capillary-barrier effect of the drift opening (Figure 6.3.3-4). Most of this water cannot seep into the drift because of capillary suction, which retains water in the pore space of the rock. If the permeability and capillarity of the fracture network are sufficiently high, some or all of the water is diverted around the drift under partially saturated conditions. Locally, however, the water potential in the formation could become great enough to allow seepage from the formation into the drifts, as described in *Seepage Model for PA Including Drift Collapse* (BSC 2004 [DIRS 167652], Section 6.2.1).

Emplacement drifts may degrade with time as a result of thermal stress, seismic ground motion, and time-dependent degradation of rock strength. These effects may lead to partial or complete drift collapse, with rock material filling the enlarged drifts and changing their shape and size. Depending upon the intensity of these effects, damage to drifts may be small, with local rockfall at the ceiling of otherwise intact drift openings, or in extreme cases, may result in partial or complete drift collapse, with rubble rock material filling the enlarged drifts. These changes alter the potential for drift seepage (SNL 2007 [DIRS 181244], Sections 6.2[a], 6.3.1 and 6.3.2). Local breakouts in the drift ceiling may also lead to geometry changes that may reduce or prevent flow diversion around the drifts and thus increase the seepage into drifts. The larger size and potentially altered shape of collapsed drifts can also bring about reduction in flow diversion. In addition, the larger footprint of collapsed drifts causes an increase in the percolation flux arriving at the drifts, which increases seepage into the drifts. Further, drift degradation may lead to fracture dilation that would promote flow diversion around the drifts, but at the same time decrease fracture capillary strength and cause less flow diversion around the drifts. Thus, the seepage into a collapsed drift may be different from that into an intact drift.

6.3.3.1.2 TSPA-LA Model Abstraction

As described in Section 6.1.4.3, water seepage into emplacement drift segments on the scale of a WP is a process that is modeled outside of the TSPA-LA Model, and the results are then abstracted (SNL 2007 [DIRS 181244]) for use in the TSPA-LA Model simulations. The abstracted results are based on drift-seepage simulations conducted for both ambient (BSC 2004 [DIRS 167652]) and thermal periods (BSC 2005 [DIRS 172232]).

The Drift Seepage Abstraction calculations differ for collapsed and noncollapsed drifts, as explained below. Drift collapse is not considered in Nominal or Early Failure Modeling Cases. In the 1,000,000 year Seismic GM Modeling Case, drift collapse can occur in both lithophysal and nonlithophysal units. Partial collapse is considered in the lithophysal units, by comparing the cumulative rubble volume generated by seismic events to a lower and an upper threshold to

determine whether to: (1) use the intact seepage model, (2) interpolate between intact-drift seepage model and collapsed drift seepage model, or (3) use the collapsed-drift seepage model (SNL 2007 [DIRS 181244], Section 6.2.2[a]). In the nonlithophysal units, once a specified degree of drift collapse has occurred, the intact-drift seepage model is no longer appropriate. The cumulative rubble volume generated by seismic events is compared to a threshold rubble volume to determine whether: (1) the intact-drift seepage model is used or (2) the percolation fluxes are used (SNL 2007 [DIRS 181244], Sections 6.2.3[a]). For the Seismic FD Modeling Case drift collapse in lithophysal units and drift degradation in the nonlithophysal units always occurs at the same time as an event. After an event, seepage rates in lithophysal units are estimated using the collapsed-drift seepage model (SNL 2007 [DIRS 181244], Section 6.2.2[a]). In nonlithophysal units, seepage rates per unit area are set equal to percolation fluxes after an event (SNL 2007 [DIRS 181244]). Drift collapse is not considered for the Igneous Scenario Class, as the drifts are filled with basalt by the intrusive event. For a detailed understanding of the rationale for the abstraction decisions, refer to *Abstraction of Drift Seepage* (SNL 2007 [DIRS 181244], Sections 6.5.1.5 and 6.5.1.7).

Ambient seepage process model simulations were conducted for a range of representative local percolation fluxes ($q_{perc,ff}$), ranges of local permeability (k) and capillary strength ($1/\alpha$), nondegraded and degraded drift profiles and multiple realizations of the small-scale heterogeneous fracture-permeability field (BSC 2004 [DIRS 167652], Sections 6.3, 6.4, and 6.6). The local percolation fluxes ($q_{perc,ff}$) are derived from the fluxes at the base of the PTn from the MSTHM Abstraction (q_{perc}) (Section 6.3.2) by multiplication with flow-focusing factors (f_{ff}). The flow-focusing factors account for intermediate-resolution heterogeneity (SNL 2007 [DIRS 181244], Section 6.6.5.2) (on the spatial resolution of a few drift diameters) that is not accounted for in the MSTHM Process Model. In addition, it is possible that the initially circular-shaped emplacement drifts degrade with time principally as a result of seismic ground motion. These changes affect the potential for drift seepage (SNL 2007 [DIRS 181244], Sections 6.2[a], 6.3.1 and 6.3.2). The Seepage Model for Performance Assessment simulations (SNL 2007 [DIRS 181244], Section 6.4.2) produce, for both nondegraded and degraded drifts, response surfaces in the form of look-up tables for a seepage rate into a 5.1-m long drift section and a seepage rate standard deviation (SD) that are functions of $q_{perc,ff}$, $\log(k)$, and $1/\alpha$ (DTN: LB0702PASEEP01.001_R0 [DIRS 179511]). Note that the output from *Seepage Model for PA Including Drift Collapse* (BSC 2004 [DIRS 167652]) is extended in *Abstraction of Drift Seepage* (SNL 2007 [DIRS 181244], Section 6.1[a]) and its output DTN: LB0702PASEEP01.001 [DIRS 179511].

Probability distributions were developed to represent the spatial variability in flow-focusing factor (f_{ff}), $\log(k)$, and $1/\alpha$, and the uncertainty in $\log(k)$ and $1/\alpha$ (SNL 2007 [DIRS 181244], Section 6.3[a] and Section 6.7.1.1).

Four different methods were identified to derive statistical parameters that describe spatial variability and uncertainty in $1/\alpha$ with respect to the geologic units present around the drifts (SNL 2007 [DIRS 181244], Sections 6.3[a] and 6.6.2.2). However, as discussed in *Abstraction of Drift Seepage*, the overall seepage results do not significantly differ between methods (SNL 2007 [DIRS 181244], Section 6.8.2). Therefore, the probability distributions for spatial variability and uncertainty in $1/\alpha$, defined in Table 6.3.3-1, are used (DTN: LB0407AMRU0120.001_R0 [DIRS 173280]). Spatial variability and uncertainty for

log(k) are dependent on the geologic units present around the drifts. The distributions for spatial variability and uncertainty in log(k) in the nonlithophysal and lithophysal repository units are defined in Table 6.3.3-2. Local percolation flux values in the vicinity of the drifts are determined from percolation fluxes at the base of the PTn. These are provided at each repository subdomain, r, by the MSTHM Abstraction which obtains the information from the Site-Scale UZ Flow Process Model (Figure 6.3.1-1), as described in Section 6.3.2. The percolation fluxes in the UZ are time dependent (represented by four different climate periods), spatially variable (because of nonuniform infiltration and nonuniform flow in the UZ), and uncertain (as represented by four different infiltration cases) as discussed in Section 6.3.1. As discussed in (SNL 2007 [DIRS 181244], Section 6.5.1.1), these percolation fluxes, q_{perc}, are adjusted for intermediate-scale heterogeneity, which is not represented in the distributions of fluxes provided by the MSTHM Abstraction. This adjustment uses a spatial distribution of flow-focusing factors (f_{ff}). Multiplication of the q_{perc} from the MSTHM Abstraction by the f_{ff} gives the local percolation flux, $q_{perc,ff}$, to be used in the TSPA-LA Model calculations. The spatial variability distribution for the flow-focusing factor is defined as a cumulative probability distribution in the following form (SNL 2007 [DIRS 181244], Section 6.7.1.1 and DTN: LB0407AMRU0120.001_R0 [DIRS 173280]).

The equation can be written as:

$$Y = -0.3137 f_{ff}^4 + 5.4998 f_{ff}^3 - 35.66 f_{ff}^2 + 102.3 f_{ff} - 11.434 \qquad \text{(Eq. 6.3.3-1)}$$

where Y is the cumulative probability in percent (SNL 2007 [DIRS 181244], Section 6.7.1.1).

The values of local percolation flux ($q_{perc,ff}$), the sampled values of local permeability (log(k)), and capillary strength parameters ($1/\alpha$) are used to interpolate from the look-up tables for the mean seepage rate into a 5.1-m-long drift section and the seepage rate SD. The value of SD is used to account for uncertainty in the estimation of seepage rates.

The estimation uncertainty in the calculated seepage rates is accounted for by a uniform distribution with a mean of zero and a range defined by the seepage rate SD (–1.7321 SD, 1.7321 SD) (SNL 2007 [DIRS 181244], Section 6.7.1.1 and DTN: LB0407AMRU0120.001_R0 [DIRS 173280]).

For noncollapsed drifts, the ambient seepage is increased by 20 percent to account for additional uncertainty due to partial drift degradation, such as breakouts in the drift ceiling that do not lead to complete drift collapse. However, for collapsed drifts, this increase is not implemented because this extreme degree of damage and its impact on seepage is represented by the seepage response surface for a collapsed drift, which includes sufficient conservatism (SNL 2007 [DIRS 181244], Section 6.7.2).

Analyses performed with the TH Seepage Process Model for noncollapsed drifts have shown that thermal seepage (seepage that is influenced by heat generated by the WP) will always be less than ambient seepage and that thermal seepage never occurs when there is boiling in the rock close to the emplacement drifts (BSC 2005 [DIRS 172232], Section 6.2.4). The recommended abstraction sets the thermal seepage equal to zero during the period of above-boiling temperatures at the crown of the drift. The threshold temperature that defines when seepage can

occur is set to 100°C (SNL 2007 [DIRS 181244], Sections 6.5.2.2 and 6.7.1.2). After the temperature falls below 100°C, thermal seepage is set equal to the estimated ambient seepage.

For collapsed drifts, the thermal seepage abstraction conservatively sets the seepage equal to the estimated ambient seepage at all times in the TSPA period. This is based on the results of analyses that found that with the expanded drift opening, the rock temperature at the crown, is always below 100°C, or nearly so (SNL 2007 [DIRS 181244], Section 6.4.3.4). Thus there is no vaporization barrier in the intact rock to prevent water flow into a rubble-filled drift (SNL 2007 [DIRS 181244], Section 6.5.3).

For the Igneous Intrusion Modeling Case, the abstraction considers setting the seepage percentage to 100 percent, where the seepage rate is equal to the local percolation rate (L/t) at the base of the PTn multiplied by the footprint area (L^2) of the considered drift segment. It is applied from the time at which the igneous event occurs.

6.3.3.1.3 TSPA-LA Model Implementation

The TSPA-LA Model implementation of drift seepage is primarily accomplished through the use of an external DLL. When drift-seepage submodel calculations are required by the TSPA-LA Model, the Seepage DLL (STN: 11076-1.3-00 [DIRS 181058]) is called, and a total of 35 inputs are passed by the TSPA-LA Model to the Seepage DLL (refer to Table 6.3.3-3 for a list of these inputs).

The output of the Seepage DLL is a set of tables of seepage flow rate versus time. Each table corresponds to a WP type and percolation flux subregion (e.g., CSNF subregion 1; see Section 6.3.2.2.1 for a description of how the subregions are defined). The timesteps in the tables are related to the climate periods and to the timesteps used in the MSTHM. These tables are then interpolated to determine the seepage flow rate at each TSPA-LA Model timestep. Note, the tables were developed for two units only, the Tptpll and Tptpmn units (BSC 2004 [DIRS 167652], Section 1). Based on current repository design, a small fraction of the emplacement drifts would also be located in the Tptpul and Tptpln units at Yucca Mountain. As noted in *Abstraction of Drift Seepage* (SNL 2007 [DIRS 181244], Sections 6.3.1 and 6.6.4), the Tptpul unit makes up about 4.5 percent and the Tptpln unit makes up about 2.6 percent of the repository area. In the TSPA-LA analysis the tables developed for the Tptpll and Tptpmn units are also applied to the Tptpul and Tptpln units. In addition, because of a paucity of data for the Tptpul and Tptpln units, capillary strength and permeability parameter distributions from the Tptpll and Tptpmn units are used for the Tptpul and Tptpln units, respectively.

In addition to these inputs passed directly from TSPA-LA Model to the Seepage DLL, the Seepage DLL reads a set of PREWAP (STN: 10939-1.1-00 [DIRS 181053]) output files and a set of seepage look-up tables. The PREWAP output files (DTN: MO0707PREWAPMS.000_R0 [DIRS 183002]) contain the output results from the MSTHM in a format that can be used by both the WP and DS Degradation Submodels (Section 6.3.5) for WP and DS failure calculations and by the Seepage DLL. There are 120 PREWAP files, one for each of the five percolation subregions, two WP types, four infiltration scenarios, and three TH uncertainty cases. The inputs that the Seepage DLL reads from these files are the percolation flux at the base of the PTn at each MSTHM subdomain location, the drift-wall temperature for each WP at that subdomain

location, and the fraction of lithophysal rock at that location. Two files containing seepage look-up tables, one for noncollapsed drifts and one for collapsed drifts, are provided by DTN: LB0702PASEEP01.001_R0 [DIRS 179511]. These files contain three-dimensional tables of mean seepage rate and seepage rate SD as functions of percolation flux, capillary strength, and fracture permeability.

The Seepage DLL uses these inputs to implement the calculations outlined in *Abstraction of Drift Seepage* (SNL 2007 [DIRS 181244], Section 6.7.1) to obtain the fraction of WPs that is expected to experience seepage and the seepage rate (m^3/yr per WP) onto those WPs that experience seepage. The DLL also adjusts the calculated ambient seepage rates for thermal and drift degradation effects, as necessary, as follows: (1) the ambient seepage rates are increased by 20 percent to account for drift degradation for the noncollapsed drift locations, and (2) seepage is set to zero for noncollapsed drift locations if the drift-wall temperature exceeds 100°C. The results of the Seepage DLL's seepage rate calculations (seepage rate versus time) are passed to the TSPA-LA Model in the form of 10 one-dimensional tables, one table for each WP type in each percolation subregion. The DLL also passes to GoldSim the fraction of WPs that experience seepage for each percolation subregion and WP type, and the fraction of each percolation subregion that is in nonlithophysal rock. The EBS Flow Submodel (Section 6.3.6) uses the results for seepage rate, the fraction of WPs that experiences seepage, and the fraction of each percolation subregion that is in nonlithosphysal rock. The Waste Package Localized Corrosion Submodel uses the results for the fraction of WPs that experiences seepage. The Drift Wall Condensation Submodel (Section 6.3.3.2) uses the results for the fraction of each percolation subregion that is in nonlithophysal rock.

The remainder of this section describes the drift-seepage implementation in more detail. Figure 6.3.3-5 illustrates the procedure for the probabilistic calculation of seepage in the TSPA-LA Model. The seepage DLL is applied for each WP (i.e., six CSNF or two CDSP WPs; Section 6.3.2.3) at each of the 3,264 repository subdomains, *r*, identified by the MSTHM Abstraction comprehensive data set (Engineered Barrier System Thermal-Hydrologic Environment, Section 6.3.2). For each WP at each repository subdomain, *r*, the calculation of drift seepage involves two main steps: (1) evaluate ambient seepage rate from seepage look-up tables, and (2) adjust ambient seepage rate for thermal and drift degradation effects. As shown on Figure 6.3.3-5, these two steps are implemented for each probabilistic TSPA-LA Model realization and repository location.

Step 1: Ambient Seepage—Step 1 involves three main activities. The first activity deals with random sampling of spatial variability and uncertainty distributions, and the application of spatial variability and uncertainty to arrive at values for the capillary-strength parameter ($1/\alpha$), fracture permeability ($\log(k)$), and local percolation flux ($q_{perc,ff}$). The sampling and calculations are performed as follows:

- The uncertainty distributions specified in Tables 6.3.3-1 and 6.3.3-2 are sampled once per TSPA-LA Model realization, *R*, to determine $\Delta\log(k)$ and $\Delta 1/\alpha$. The seepage rate uncertainty is sampled from a uniform distribution. At each subdomain, *r*, the following steps are completed:

- The spatial variability distributions specified in Tables 6.3.3-1 and 6.3.3-2 and Equation 6.3.3-1 are sampled randomly for $\log(k)$, $1/\alpha$, and f_{ff} at the subdomain, r, for each WP (six CSNF and two CDSP WPs).

- The $\log(k)$ and $1/\alpha$ values are adjusted, using the values for $\Delta\log(k)$ and $\Delta 1/\alpha$ that are sampled in each realization, R, to arrive at the values of $\log(k)$ and $1/\alpha$ that account for both spatial variability and uncertainty.

- The mountain-scale percolation flux at each subdomain, r, for each WP (six CSNF and two CDSP WPs) (from the MSTHM Abstraction as obtained from the Site-Scale UZ Flow Process Model), provided by the PREWAP_LA files, is adjusted by multiplying it by f_{ff} to yield a local percolation flux, $q_{perc,ff}$.

It is possible, but unlikely, that the parameter ranges for $1/\alpha$, $\log(k)$, and $q_{perc,ff}$ covered by the seepage look-up tables are exceeded for parameter values sampled from the unbounded distributions of permeability and percolation flux. To avoid sampling values outside the parameter's ranges, the following constraints on $1/\alpha$, $\log(k)$, and $q_{perc,ff}$ (based on the range limits presented in *Abstraction of Drift Seepage* (SNL 2007 [DIRS 181244], Section 6.1[a]), are imposed:

- If $1/\alpha$ is larger than 1,000 Pa, set it to 1,000 Pa.
- If local percolation flux is less than 0.01 mm/yr, set it to 0.01 mm/yr.
- If local percolation flux is more than 5,000 mm/yr, set it to 5,000 mm/yr.
- If $\log(k)$ is less than -14, set it to -14.
- If $\log(k)$ is larger than -10, set it to -10.

The second activity in Step 1 is to extract (by linear interpolation between the three independent input parameters) at each subdomain, r, the ambient mean seepage rate and SD of ambient seepage rate from the appropriate seepage look-up tables originally from the *Seepage Model for Performance Assessment Including Drift Collapse* (BSC 2004 [DIRS 167652], Section 6.6.1) but extended as noted in *Abstraction of Drift Seepage* [DIRS 181244], Section 6.1[a]. The lookup tables are contained in the files *ResponseSurfaceSMPA_Collapsed_ExtendedFlux.dat* and *ResponseSurfaceSMPA_ExtendedFlux.dat* (DTN: LB0702PASEEP01.001_R0 [DIRS 179511]). The TSPA-LA Model selects the appropriate look-up tables, depending on the host geologic unit and the selected Scenario Class. For the Nominal Scenario Class, look-up tables for noncollapsed drifts are selected because extensive roof collapse is not expected. The selection of the appropriate table for the Seismic Scenario Class depends on the character of the host-rock unit (SNL 2007 [DIRS 181244], Sections 6.2.2[a] and 6.2.3[a]). In the lithophysal zone, the appropriate tables correspond to the choice of noncollapsed or collapsed drift look-up tables. In the nonlithophysal zone, the appropriate tables correspond to the choice of the noncollapsed table or percolation rates (100 percent seepage). In the Seismic Scenario Class, multiple implementations of the Seepage DLL are utilized to simulate the effects of drift collapse (see Step 4).

The third activity in Step 1 is to calculate the local seepage rate; that is, the volumetric flow rate. Note that for this calculation, the density of water is assumed to be 960 kg/m^3 for water at 100°C and 1 atm (Incropera and DeWitt 2002 [DIRS 163337], Appendix A.6). The calculation

considers a footprint of 5.1 m × 5.5 m, representing a WP length of 5.1 m (SNL 2007 [DIRS 181244], Sections 6.7.1 and 4.1[a] and (BSC 2004 [DIRS 167652], Section 6.3.1)), and a drift diameter of 5.5 m (SNL 2007 [DIRS 181244], Section 6.4.2.1 and (BSC 2004 [DIRS 167652], Section 6.3.1)). The results, obtained from DTN: LB0310AMRU0120.002_R0 [DIRS 166116], are the mean seepage values and SDs. The SDs represent the estimation of uncertainty in the seepage results and are different for each sampled set of parameters. The mean seepage rates are, therefore, adjusted by applying a uniform distribution, with a mean of zero and upper and lower bounds, respectively, of +/-1.7321 times the seepage rate SD (SNL 2007 [DIRS 181244], Section 6.5.1.3). The sampled value from this uniform distribution is then added to the mean seepage value to obtain the ambient seepage rate. Note that the WP length of 5.1 m is based upon an average WP length of 5.0 m, which was the rounded length of the 44-BWR and 21-PWR WPs considered in previous designs (SNL 2007 [DIRS 181244], 4.1[a]). The additional 0.1 m represents 0.1-m spacings between packages. The 5.1 m length was the basis for the model domain length used in the Seepage Model for Performance Assessment seepage simulations and the resultant seepage look-up tables. The addition of the transportation, aging, and disposal (TAD) canisters for CSNF increased the average length of all WPs to 5.614 m (DTN: MO0702PASTREAM.001_R0 [DIRS 179925]). This longer average length increases the probability that an individual WP may encounter seepage (SNL 2007 [DIRS 181244], 4.1[a]). The increased WP length will have a direct influence on seepage rates since the seepage rates are per WP (m^3/yr/WP) and a function of the WP length. The influence on seepage fraction is not straightforward, since the increase in rate will not affect the locations that are already considered (in seepage calculations) to be seepage locations for the shorter WP. In addition, since some areas are prone to seepage and some not, increasing the WP length in areas not prone to seepage may have little effect on seepage fraction. The TSPA-LA Model does not account for this updating of the WP length in its seepage calculations. The impact on model results is quantified in an analysis in Appendix P (see P13).

Before Step 1 is completed, the results are checked for consistency. If the resulting seepage rates are less than zero, they are set to zero. If the resulting seepage rates correspond to a value higher than the local percolation flux applied to the footprint of 5.1 m × 5.5 m, the seepage rates are set to a rate corresponding to the local percolation flux.

For each TSPA-LA realization, *R*, the result from Step 1 of the seepage calculation is an ambient seepage rate for the four climate states in the TSPA-LA Model simulation for each WP (six CSNF and two CDSP WPs) at 3,264 MSTHM Abstraction locations (MSTHM Abstraction comprehensive data set as discussed in Section 6.3.2). Note that temporal changes in percolation flux through the UZ and, therefore, ambient seepage rate occur instantaneously when the climate state changes (Assumption 5.1.1). During a climate state, percolation flux and ambient seepage rate are at steady state.

Step 2: Seepage Adjusted for Thermal Effects and Drift Degradation Uncertainty—The ambient seepage rates calculated in Step 1 are adjusted to account for additional uncertainty due to the effects of some partial degradation (roof breakouts) of noncollapsed drifts and for thermal perturbations where the drift-wall temperature is at or above 100°C (determined for each repository location). The following adjustments are implemented:

- For all collapsed drift cases, uncertainty is already accounted for by using the look-up tables for fully collapsed drifts and taking into consideration uncertainty in the estimation of rubble volumes in the Seismic Submodel (see Step 4). For noncollapsed cases, the ambient seepage rates are increased by 20 percent to account for uncertainty associated with the seepage evaluation for these cases. This uncertainty stems in part from the limited number of simulation cases studied for moderately degraded drifts, but is mainly related to the large estimation differences between the stochastic realizations conducted for those cases (SNL 2007 [DIRS 181244], Section 6.7.1.2).

- Two abstraction approaches for thermal seepage are implemented: (1) for collapsed drifts, thermal seepage is set equal to the adjusted ambient seepage, and (2) for noncollapsed drifts, thermal seepage is set to zero for the period of above-boiling temperature, using a 100°C threshold temperature at the drift wall (SNL 2007 [DIRS 181244], Section 6.7.1.2).

Seepage in the Igneous Intrusion Modeling Case is discussed in Section 6.5.

Step 3: Determination of Seepage Fraction—The seepage fraction is calculated as the ratio of WPs experiencing seepage to all WPs in a percolation subregion by WP type for a given realization. WPs with seepage at any time during the 20,000-year simulation period are counted as WPs in a location with drift seepage (for 20,000-year simulations) and any time during the 1,000,000-year simulation period (for 1,000,000-year simulations). The seepage fraction is calculated using a threshold seepage rate of 0.1 kg/yr per WP. WP locations with less than this threshold rate are counted as locations where seepage does not occur because such small values are considered to be the result of the interpolation procedure (SNL 2007 [DIRS 181244], Section 6.8). WPs with seepage at any time are in a seep environment, and those without seepage are in a non-seep environment.

Step 4: Seismic Scenario Class—Separate implementations for collapsed and noncollapsed conditions are used. In addition, separate collapsed condition implementations are utilized for lithophysal and nonlithophysal rock. Composite tables are then generated within GoldSim to account for the change from noncollapsed to collapsed conditions. For lithophysal rock (SNL 2007 [DIRS 181244], Section 6.2.2[a]) if rockfall volumes into the drift are less than or equal to 5 m^3/m of drift length, the intact-drift look-up table is utilized. If rockfall volumes into drifts are greater than 60 m^3/m of drift length, the collapsed-drift look-up table is utilized. If rockfall volumes (per unit drift length) into the drift are between 5 m^3/m and 60 m^3/m, seepage values are linearly interpolated between a Seepage DLL analysis based on the intact-drift look-up table and a Seepage DLL analysis based on the collapsed-drift look-up table. In the nonlithophysal zone (SNL 2007 [DIRS 181244], Section 6.2.3[a]), if rockfall volumes into the drift are less than or equal to 0.5 m^3/m, the intact-drift look-up table is utilized; if not, the percolation rates are utilized. The above criteria based on rockfall volumes are described in

Abstraction of Drift Seepage [DIRS 181244], Section 6.1[a] and DTN: LB0702PASEEP02.001_R0 [DIRS 181635]. Note that since both collapsed and noncollapsed seepage analyses are used for the Seismic Scenario Class, the seismic threshold data and seismic event frequencies are now used only as control parameters for controlling the multiple calls to the Seepage DLL (Table 6.3.3-3).

6.3.3.2 Drift-Wall Condensation

Condensate dripping from drift walls affects TSPA-LA Model calculations by adding additional water to the drift seepage volumetric flow rate (which may be zero in the non-seep environments). This combined condensate and seepage flows through the invert and, in some scenarios, through the DSs, WPs, and the waste forms. The Drift Wall Condensation Submodel calculates a probability of condensation on the drift walls at any location and, if condensation occurs, the rate of condensation. The source of condensation water is evaporated water from the invert and evaporated seepage water from the drift wall. Water vapor is transported axially by convective mixing from hotter drift regions to cooler drift regions where it can then condense. The axial movement of the water vapor, the saturated vapor pressure at the drift wall and in the invert, and temperature differences along the drifts are important factors that drive the occurrence of condensation (SNL 2007 [DIRS 181648], Section 6.3.1.1). The probability of drift-wall condensation occurrence and the condensation rate are abstracted as functions of the percolation flux at the base of the PTn (Section 6.3.3.1.2) and simulation time, as described in *In-Drift Natural Convection and Condensation* (SNL 2007 [DIRS 181648], Section 8.1[a]).

Information flow and connections between the EBS TH Environment Submodel (Section 6.3.2) and the Drift Seepage Submodel (Section 6.3.3.1), Drift Wall Condensation Submodel (Section 6.3.3.2.1), and EBS Flow Submodel (Section 6.3.6) are shown on Figure 6.3.3-1. Figure 6.3.3-6 shows the inputs and outputs to the Drift Wall Condensation Submodel and indicates the principal features of the submodel and the bases for confidence in the submodel.

6.3.3.2.1 Conceptual Model

The Drift Wall Condensation Process Model (SNL 2007 [DIRS 181648], Section 6.3) is used to calculate the occurrence and quantity of water vapor condensation at WP locations along the entire lengths of seven drifts selected to characterize the expected range of axial temperature gradients (see discussion below). The Drift Wall Condensation Process Model includes heat transfer from WPs through EBS components to the drift walls, evaporation of water vapor at the drift walls, radial vapor flux from drift walls, axial water vapor movement along the drift by convection, and condensation on the drift walls where the wall temperature is less than the condensation temperature. Probabilities of condensation at any location are calculated as the ratio of the drift length over which condensation occurs to total drift length.

Temperature at drift locations where water evaporation or condensation may occur is based on heat transfer calculations. Heat transfer between surfaces (WPs and DSs, WPs and inverts, DSs and drift walls, drift walls and inverts, and DSs and inverts) is based on literature references for correlations of natural convection heat and mass transfer for representative geometry. Thermal radiation is calculated from surface-to-surface radiation with appropriate radiation view factors. Only heat transferred in the radial direction is considered. The effects of axial heat transfer are

assumed to be minimal, as described in *In-Drift Natural Convection and Condensation* (SNL 2007 [DIRS 181648], Sections 5.3, 6.3.3.2.6, and Executive Summary).

Evaporative water vapor sources include the drift wall and the invert at each WP location (Figure 6.3.3-7). The local water vapor partial pressure is the saturation pressure at the calculated temperature. The rate at which water evaporates from a surface depends on the local difference between the saturation vapor pressure at the evaporating surface and the local gas-phase partial pressure, using the corresponding mass-transfer correlation. The condensation rate is limited by the available water vapor, which, in turn, is limited by the rate of water transfer to the drift by capillary wicking and percolation through the host rock.

Condensation is modeled with a lumped parameter approach using standard heat and mass transfer processes within the drift. The Drift Wall Condensation Process Model considers the entire length of each of seven drifts. The seven drifts are chosen to represent the range of thermal conditions in the repository (SNL 2007 [DIRS 181648], Section 6.3.5.1). Figure 6.3.3-8 illustrates the locations of the seven drifts. Drift-wall temperature boundary conditions are derived from analytical heat line-source solutions. The amount and location of water vapor depend on the availability of water and the axial transport properties. Axial and radial mass transport equations and radial heat transport equations are solved to estimate the water vapor distribution and condensation on various surfaces along each of the seven selected drifts at six selected times of 1,000; 3,000; 10,000; 30,000; 100,000; and 300,000 years. The selection of the first three analysis times is based on when the wall temperature drops below the saturation temperature (boiling temperature—approximately 96°C at the repository elevation) and the rate at which the waste-form decay heat declines during the first 10,000 years after repository closure. The remaining three analysis times span the remainder of the TSPA modeling period. Note here that the Drift Wall Condensation Model uses 96°C as the boiling temperature of water at the repository elevation and the Seepage Abstraction sets a threshold of 100°C as the temperature for thermal seepage in the TSPA-LA Model (Section 6.3.3.3.1).

The calculated results for the seven drifts at the selected times are used to estimate the location and rate of condensation on the drift walls, under the DSs, and on individual WPs. The TSPA-LA Model uses only the condensation abstraction for condensation on drift walls. Condensation under DSs and on WPs is calculated by the model, but is not significant and is not recommended for inclusion in the TSPA-LA (SNL 2007 [DIRS 181648], Section 8.1[a] and DTN: MO0706SPAFEPLA.001_R0 [DIRS 181613], FEP Number 2.1.08.14.0A)). The condensation model defines three stages for the occurrence of condensation. Stage 1 is when the drift wall temperature is above the boiling temperature of water at all locations in the drift. No condensation occurs during Stage 1. Stage 2 is for times between when the first location in a drift drops below the boiling temperature and the last location drops below the boiling temperature. A separate part of the Drift Wall Condensation Abstraction (SNL 2007 [DIRS 181648], Section 6.2[a]) describes the Stage 2 condensation occurrence and rate. Stage 3 occurs after all WPs (and thus the drift wall) drop below the boiling temperature. The abstraction for Stage 2 uses a reasonable-bound approach for the occurrence and rate of condensation.

6.3.3.2.2 TSPA-LA Model Abstraction

The Drift Wall Condensation Abstraction (SNL 2007 [DIRS 181648], Section 8.1[a]) calculates a probability of condensation occurrence on the drift walls at a WP location and, if condensation occurs, a rate of condensation for all locations in the drift that are below the boiling temperature. Lower- and upper-bounding cases for axial dispersion coefficients are provided. Lower-bound values for the axial dispersion coefficients are computed without any axial gradients in the process model boundary temperatures, whereas the upper bound on the axial dispersion coefficients is computed using an axial gradient in the boundary temperature (SNL 2007 [DIRS 181648], Section 6.3.7.1). Additionally, high- and low-invert transport cases are computed, but only low-invert cases are recommended for use in the TSPA-LA (SNL 2007 [DIRS 181648], Section 6.1.2[a]). The low-invert transport case assumes that the partial pressure at the bottom of the invert surface is the saturation vapor pressure at the drift-wall temperature. The high-invert transport case assumes that the partial pressure at the invert surface underneath the DS is the saturation vapor pressure for the invert surface temperature (SNL 2007 [DIRS 181648], Section 6.3). Finally, ventilated and unventilated (alternatively, mixed and unmixed) DS cases are provided (SNL 2007 [DIRS 181648], Section 8.1[a]). This gives eight possible cases for drift-wall condensation. After further analysis, the high-invert transport case is determined to be unrealistic, so it is not included in the TSPA abstraction (SNL 2007 [DIRS 181648], Section 6.1.2[a]).

The Drift Wall Condensation Abstraction results are determined through 144 different steady-state simulations, with results for each of the seven drifts being produced for each of the 144 runs ((two axial dispersion coefficients) × (two invert transport properties) × (two DS ventilation cases) × (three infiltration cases) × (six simulation times)) (SNL 2007 [DIRS 181648], Section 6.1.1[a] and Section 6.1.2[a]). These three infiltration cases were chosen to cover the range of infiltration. Specifically, the 10th, 30th, and 90th percentiles were used to produce the regressions for the TSPA-LA Model abstraction. The actual infiltration values used between the upper and lower bounds are not as important as the range of values used to produce the regression (SNL 2007 [DIRS 181648], Section 6.1.1[a]). These results are reduced to four distinct cases because the three different infiltration case results for each of these 48 cases are combined and used to create functional relationships in which condensation flux and condensation fraction are dependent upon percolation flux. That is, the four cases are composed of eight simulations at each of the six output times of 1,000, 3,000, 10,000, 30,000, 100,000, and 300,000 years. The eight simulations include the possible combinations of two values of dispersion coefficient (low and high), two values of invert transport properties (low and high), and two values for DS ventilation (ventilated and unventilated). By performing linear regressions between the probability of condensation on the drift wall and the mean percolation fluxes for the chosen drifts at the given time as $\ln[1-P_w]$ and $\ln(\overline{p})$, and between the condensation rate and the percolation flux, as CW and $\overline{p}$ (time-dependent percolation rate), functional relationships are developed in which condensation flux and condensation fraction are dependent on average percolation flux. These functional relationships are developed for each of the 48 simulation cases. The following mathematical relationship was developed (SNL 2007 [DIRS 181648], Section 8.3.1.1, Equation 8.3.1.1-3) from the linear regression analysis to approximate the probability of condensation on the drift walls:

$$\hat{P}_w = 1 - e^{a\ln(\overline{p})+b} \quad \text{(Eq. 6.3.3-2)}$$

where the parameters a and b are the slope and y-intercept of the linear regressions. As mentioned previously, the high invert transport case is not included in the abstraction for TSPA. Also, the analysis showed that condensation only occurs at 1,000 years. The parameters for the regressions for 1,000 years are found in DTN: MO0702PALOVERT.000_R2 [DIRS 180377] and DTN: MO0702PALV010K.000_R2 [DIRS 180376]. There are four non-zero values for a and four non-zero values for b.

Uncertainty in $\hat{P}_w$ is captured using the standard error on the linear regression coefficients. They are found in DTN: MO0702PALOVERT.000_R2 [DIRS 180377]. Plus/minus one standard error is used as uncertainty ranges around the slope and intercept parameters. Uncertainty in the slope and intercept parameters are modeled as normally distributed about the computed value for each parameter, with the SD equal to the standard error. The parameter values are sampled independently (SNL 2007 [DIRS 181648], Section 8.3.1.1, Equation 8.3.1.1-4).

The equation:

$$CW = c\overline{p} + d \quad \text{(Eq. 6.3.3-3)}$$

approximates the rate of condensation on the wall, CW, where the parameters c and d are the slope and y-intercept of the linear regression and are found in DTN: MO0702PALOVERT.000_R2 [DIRS 180377] and DTN: MO0702PALV010K.000_R2 [DIRS 180376]. There are four non-zero values for c and four non-zero values for d.

Uncertainty in CW is captured using the standard error on the linear regression coefficients, which are also found in DTN: MO0702PALOVERT.000_R2 [DIRS 180377] and DTN: MO0702PALV010K.000_R2 [DIRS 180376]. The standard errors are used as uncertainty ranges around the slope and intercept parameters. Uncertainty in the slope and intercept parameters are modeled as normally distributed about the computed value for each parameter, with SD equal to the standard error. The parameter values are sampled independently (SNL 2007 [DIRS 181648], Section 8.3.1.1).

Table 6.3.3-4 (DTN: MO0702PALOVERT.000_R2 [DIRS 180377]) shows one of the four tables containing values and standard errors for coefficients a, b, c, and d used in Equations 6.3.3-2 and 6.3.3-3. The R-squared values for each regression are also provided to indicate how well each linear regression model fits the results. Table 6.3.3-5 shows the values for the parameter distributions, which are sampled independently in the TSPA-LA Model for each TSPA-LA realization.

For condensation rate correlations at 1,000 years and for high axial dispersion, the correlation models have a larger standard error. The correlation uncertainty is applied by sampling a normal distribution with the SD equal to the standard error (SNL 2007 [DIRS 181648], Section 8.3 and Appendix H). Applying the uncertainty to the correlation coefficients produces a range of possible values covering, and in some cases exceeding, the Drift Wall Condensation Abstraction

output that was used to develop the correlation model. The TSPA-LA Model uses zero as the lower bound on the condensation rate and condensation probability.

The Drift Wall Condensation Abstraction (SNL 2007 [DIRS 181648]), Section 6.2.2[a]) describes a reasonable-bound approach for the condensation rate during Stage 2. Ultimately, the Stage 2 condensation rate is a single reasonably bounding value with rate in kg/m/yr. Only CDSP WPs have non-zero Stage 2 condensation. Stage 2 begins at a particular WP location when the drift wall cools to the boiling temperature of water. The Stage 2 CDSP WP condensation rate is in DTN: MO0703PAEVSIIC.000_R2 [DIRS 181990]. No probability is given for Stage 2 condensation. In other words, the Stage 2 condensation rate is applied to all CDSP WPs during Stage 2.

TSPA-LA Model Implementation

The TSPA-LA Model implementation of the Drift Wall Condensation Submodel uses the abstracted probability of condensation on the drift wall (Equation 6.3.3-2) and an abstracted rate of condensation (Equation 6.3.3-3) whenever condensation occurs for Stage 3 condensation. The four cases corresponding to the four combinations of the two values for axial dispersion coefficient and two values of DS ventilation are treated as four equally likely cases and are sampled with equal frequency in the TSPA-LA Model (SNL 2007 [DIRS 181648], Section 8.1[a]). The CSNF and CDSP WPs are treated equally in terms of drift-wall condensation. The abstraction for the fraction of WPs that experience condensation and the corresponding condensation flow volume, apply equally to CSNF and CDSP WPs. In the Drift Wall Condensation Abstraction, the average percolation flux $\overline{p}$, represents the average of the MSTHM Abstraction percolation fluxes along the length of each of the seven simulated drifts. In the TSPA-LA Model, $\overline{q}_{perc}$ represents the average of the percolation flux over a TSPA-LA Model percolation subregion (EBS TH Environment, Section 6.3.2). This average characterizes the percolation flux for that subregion (SNL 2007 [DIRS 181648], Section 8.3.1.1). In the TSPA-LA Model, $\overline{q}_{perc}$ is used for $\overline{p}$ in the Drift Wall Condensation Submodel. The TSPA-LA Model implementation does not include condensation under the DSs (SNL 2007 [DIRS 181648], Section 6.1.2[a]).

Inputs to the Drift Wall Condensation Submodel include slope, intercept, and standard error values for the slope and intercept. These inputs are provided for each combination of the invert transport properties, axial dispersion coefficient, and time. In addition, the average percolation rate is for each percolation subregion. For the Seismic Scenario Class, drift collapse is not expected in the nonlithophysal units, so condensation can only occur on drift walls above DSs in the nonlithophysal units. In contrast, there is no condensation in the lithophysal units after drift collapse (SNL 2007 [DIRS 181648], Section 8.1[a]). Consequently, the fraction of WPs in the nonlithophysal region is used in the implementation of the Drift Wall Condensation Submodel for the Seismic Scenario Class in the TSPA-LA Model.

The Drift Wall Condensation Abstraction provides correlations to calculate the condensation rate and probability of condensation as a function of time and percolation rate (SNL 2007 [DIRS 181648], Section 8[a], Appendix A[a], and Appendix B[a]). The Drift Wall Condensation Abstraction is divided into three stages: Stage 1 is the initial stage when all WPs

in the drift are above boiling; Stage 2 is the middle stage after the first WP in the drift cools to below boiling, but before the last WP in the drift cools to below boiling; and Stage 3 is the final stage after all WPs in the drift are below boiling. During Stage 1, before the first WP location in the drift drops below boiling, the condensation rate everywhere in the drift is zero because all WPs are boiling. Recall that the TSPA-LA Model uses a "representative WP" to represent the thermal and flow properties for the percolation subregion. (See Section 6.1.5 for a discussion of the percolation subregions). The temperature of the representative WP drops below boiling some time during Stage 2, after the first location in the drift drops below boiling, but before the last location drops below boiling. The Stage 2 condensation rate is used until the time when Stage 3 starts, which is the time when the last location in the drift drops below boiling. For Stage 3, the 1,000-year condensation rate and probability are used until 2,000 years. After 2,000 years, the 3,000-year rate and probability would be used, but because they are zero, the Stage 3 condensation rate is zero. The condensation rate remains zero for the remainder of the simulation up to 1,000,000 years because the process model gives a condensation rate equal to zero for times beyond 2,000 years.

The TSPA-LA drift-wall condensation implementation also requires a stochastic parameter, Seepage_Condensation_Prob_a, a U[1,0] that is used to determine whether the first failed WP in a percolation subregion is in a location with condensation or not. Seepage_Condensation_Prob_a is an epistemic parameter sampled once per realization. The TSPA-LA treats WPs with seepage separately from WPs with no seepage. Drift-wall condensation is added to the seepage flux, or becomes the only advective flux in a non-seep environment. The drift-wall condensation fraction for Stage 3 is independent of the seepage fraction, so some of the WPs in both the seep and non-seep environments will potentially have condensation and some will not. Thus, the very first WP to fail in a percolation subregion can potentially have condensation or not. If Seepage_Condensation_Prob_a is less than or equal to the drift-wall condensation fraction, the first failed WP is assumed to be in an environment that can potentially have condensation. After more than one WP has failed in a percolation subregion, the drift-wall condensation flux is multiplied by the drift-wall condensation fraction to give an average condensation rate for the percolation subregion. This technique preserves the mass balance of condensing water and properly treats the percolation subregion as an average of WPs. It also properly applies the full condensation flux to a single failed WP in a percolation subregion during Stage 3. During Stage 2, no seepage fraction is applied and every CDSP WP receives the full condensation flux.

The output of the Drift Wall Condensation Submodel is the fraction of WPs exposed to condensation and the condensation rate as functions of percolation flux for each WP type (SNL 2007 [DIRS 181648], Section 8[a], Appendix A[a], and Appendix B[a]). These outputs are used in the EBS Flow Submodel to determine the average flow rate in the drift above a DS and WP and also below the WP in the invert. The EBS Flow Submodel calculations include effects of both drift seepage and drift-wall condensation. Specifically, the EBS Flow Submodel directly adds the drift seepage rate and the drift-wall condensation rate to obtain the total flow rate into the drift.

6.3.3.3 Model Component Consistency and Conservatism in Assumptions and Parameters

To enhance understanding of the complex interactions within the TSPA-LA Model, a discussion of consistency among model components and among submodels, and identification of conservative assumptions in abstractions, process models, and parameter sets supporting seepage and drift-wall condensation are discussed below.

6.3.3.3.1 Consistency of Assumptions

In-Drift Evaporation—In-drift evaporation of seepage flow is not included in the Drift Seepage Submodel in any of the scenario classes at temperatures less than 100°C, even though below-boiling evaporation is a process that is modeled in the MSTHM Process Model (Section 6.3.2), Drift Wall Condensation Submodel (Section 6.3.3.2), and the EBS Chemical Environment Submodel (Section 6.3.4).

Effect on TSPA—Not including evaporation of seepage flux (Section 5.1.4) leads to an overestimate in TSPA-LA Model of: (1) the water present at any point in time; (2) the amount of water flux through the invert and/or WP; and, therefore, (3) the radionuclide mass released.

Repository Boiling Temperature—The thermal seepage model conservatively uses 100°C for the boiling temperature of water while the drift wall condensation model uses 96°C, which is the actual boiling temperature at the repository horizon.

Effect on TSPA—The 100°C threshold for thermal seepage means that seepage starts sooner and water is available for transport sooner. This approach is conservative and can lead to earlier doses to the RMEI.

Water Balance—There is no water balance (liquid or vapor) between the MSTHM, drift seepage, and drift-wall condensation models.

Effect on TSPA—It is assumed for each model that there is sufficient water to support the predicted flow rates. This results in an over-prediction of flow rates, as well as an over-prediction of the number of WPs that are in an advective environment. This results in higher rates of radionuclide transport, which lead to higher doses to the RMEI. Therefore, this approach is conservative.

Thermal-Hydrologic Behavior of the Rock Mass—The condensation model does not explicitly consider the thermal-hydrologic behavior of the rock mass. The inclusion of rock characteristics in the condensation model is expected to affect the predicted condensation distributions. For example, the presence of the capillary behavior of the rock would tend to reduce the evaporation rate and increase the imbibition rate, both of which would decrease the net condensation rate.

Effect on TSPA—The different responses arising from these differing model assumptions tend to decrease with time as the repository cools. This difference in assumptions does not affect the thermal-hydrologic response following an igneous intrusion event or seismic event, which are the dominant contributors of dose to the RMEI. Therefore, the approach is conservative and would have little effect on dose.

6.3.3.3.2 Identification of Conservatisms in Submodels and Abstractions

Ambient Seepage—For drift-wall temperatures less than 100°C, the thermal seepage model implemented into the TSPA-LA Model conservatively uses ambient drift seepage instead of taking credit for thermal effects (SNL 2007 [DIRS 181244], Section 6.7.1.2). Ambient seepage, which does not account for thermal effects, is always greater than the thermal seepage as shown in *Abstraction of Drift Seepage* (SNL 2007 [DIRS 181244], Figure 6.4-15). In the TSPA-LA Model, rather than the seepage rate, the presence or absence of flowing water in the drift is the more dominant factor controlling radionuclide releases when the DSs are intact. Reducing the seepage slightly to account for thermal effects may have a slight impact on the radionuclide release from the EBS for WPs with breached DSs.

Flow Focusing—Two models for flow focusing have been developed for the Drift Seepage Model. The model implemented in the TSPA-LA Model is based on a fine grid resolution and the flow focusing factor distribution for the base model is described by a polynomial regression curve with a maximum factor of between five and six (SNL 2007 [DIRS 181244], Section 6.6.5.2). The model was selected because it is expected to be more conservative and generate considerably larger average seepage rates with only a small decrease in seepage fraction when compared to the ACM (SNL 2007 [DIRS 181244], Section 6.6.5.2.3).

Igneous Seepage Model—The base-case igneous seepage model is based on a conceptualization that after the event the waste may be encapsulated by solidified magma with few cooling joints, and water contact with the waste being limited by the small permeability of the solidified magma (SNL 2007 [DIRS 181244], Section 6.5.1.7). This conceptual model assumes that the solidified magma has the same hydrologic properties as the surrounding rock. To represent this conceptual model, the seepage flux is set equal to the percolation flux (SNL 2007 [DIRS 181244], Section 6.5.1.7).

6.3.3.4 Alternative Conceptual Model(s) for Drift Seepage and Drift-Wall Condensation

Section 6.2 outlines the general consideration and treatment of ACMs used to support the TSPA-LA Model. A brief description of the ACMs for the Drift Seepage and Drift Wall Condensation Submodels summarized in Table 6.3.3-6 is presented below.

Drift Seepage ACMs—Five ACMs for drift seepage were considered: (1) flow through discrete fractures; (2) episodic-preferential flow in superheated rock; (3) an alternative flow-focusing model and (4, 5) two alternative igneous seepage models.

The most important ACM for ambient seepage is one that simulates flow through discrete fractures rather than through a stochastic porous continuum. It was concluded that conceptual model uncertainty is small compared to other sources of uncertainty that are explicitly accounted for by the base-case conceptual model, its numerical implementation, and the associated uncertainty estimates, which are propagated through the TSPA-LA Model (SNL 2007 [DIRS 181244], Section 6.4.1.2).

The effectiveness of the vaporization barrier was examined with an ACM representing episodic-preferential flow into a superheated rock environment (SNL 2007 [DIRS 181244],

Section 6.4.3.2). In this ACM, the thermally perturbed downward flux from the condensation zone toward the superheated rock zone is conceptualized to form episodic preferential-flow patterns. The effectiveness of the vaporization barrier was then tested for these extreme conditions where downward flux is fast and large in magnitude compared to average flow. A semi-analytical solution was employed to simulate the complex flow processes of episodic fingerflow in a superheated fracture. With this solution, the maximum penetration distance into the superheated rock was determined for specific episodic flow events and thermal conditions. In addition, the amount of water arriving at the drift crown and the impact of capillary diversion were calculated. It was concluded that the thermal seepage process model results are reasonably consistent with the ACM (SNL 2007 [DIRS 181244], Section 6.4.3.2).

Two flow-focusing models were developed for the Drift Seepage Model. The base-case model was based on a fine grid resolution of < 1 m. The ACM was based on a coarser resolution of scale at which the flow-focusing factors were averaged over 5-meter long sections at the bottom of the model (SNL 2007 [DIRS 181244], Section 6.6.5.2). The flow-focusing factor distribution for the base model is described by a polynomial regression curve with a maximum factor of between five and six. The ACM flow-focusing factor distribution is described by a normal distribution with a maximum of 2.4. The base model is expected to be more conservative because it generates large increase in average seepage rates and only a small decrease in seepage fraction when compared to the ACM (SNL 2007 [DIRS 181244], Section 6.6.5.2.3).

The two ACMs for evaluating drift seepage after an igneous event are based on a conceptual model where thermal contraction gives rise to numerous fractures and joints in the cooling process filling the drift with fractured magma of relatively high permeability and low capillary strength (SNL 2007 [DIRS 181244], Section 6.5.1.7). If the capillary strength of the solidified magmas is much lower than the capillary strength of the surrounding rock, the capillary barrier and flow diversion at the interface would be preserved (SNL 2007 [DIRS 181244], Section 6.5.1.7). It is also possible for the magma to drain out of the drift, leaving an air space which would generate a capillary barrier (SNL 2007 [DIRS 181244], Section 6.5.1.7). The two ACMs that consider this conceptual model are based on the use of (1) the nondegraded drift seepage table which would provide a reasonable estimate of seepage rates or (2) the degraded drift seepage table which would account for the considerable uncertainty in in-drift conditions by providing higher seepage rates (SNL 2007 [DIRS 181244], Section 6.5.1.7).

Drift-Wall Condensation ACMs—Two ACMs for drift-wall condensation were considered: (1) a thermal conductivity/heat transfer ACM and (2) a computational fluid dynamics simulation for drift condensation processes ACM.

In the Thermal Conductivity/Heat Transfer ACM, the air phase is treated as a solid material. To account for the higher heat transfer between surfaces due to convection, the effective thermal conductivity of the solid (air) can be increased so that the same amount of heat can transfer from one surface to another for the same temperature difference. This ACM is essentially accounted for in the MSTHM Abstraction. This ACM is not considered further because it is implemented in the MSTHM Abstraction (SNL 2007 [DIRS 181648], Sections 6.1.4 and 6.4).

Another ACM simulates the drift with a computational fluid dynamics code and the surrounding rock with a porous media code. The computational fluid dynamics code FLUENT

(Fluent, Inc. 2003 [DIRS 164315]) contains limited porous media capabilities that only consider single-phase flow. To more rigorously simulate physical processes of the rock, the software would need to be able to simulate partially saturated flow as well as phase change in the porous media. Conduction-only heat transfer in the surrounding rock and the invert is acceptable, and this ACM is not considered further (SNL 2007 [DIRS 181648], Section 6.1.4).

No ACMs were recommended for inclusion in the TSPA-LA Model.

Table 6.3.3-1. Spatial Variability and Uncertainty Distributions for *1*/α for Method A as Defined in the Abstraction of Drift Seepage

***1*/α (Lithophysal Units)**		***1*/α (Nonlithophysal Units)**	
Spatial Variability Distribution	**Uncertainty Distribution**	**Spatial Variability Distribution**	**Uncertainty Distribution**
Uniform Distribution with Mean 591 Pa Lower Bound is 402 Pa. Upper Bound is 780 Pa.	Triangular Distribution with Mean 0 Lower Bound is – 105 Pa. Upper Bound is + 105 Pa.	Uniform Distribution with Mean 591 Pa Lower Bound is 402 Pa. Upper Bound is 780 Pa.	Triangular Distribution with Mean 0 Lower Bound is – 105 Pa. Upper Bound is + 105 Pa.

Sources: SNL 2007 [DIRS 181244], Section 6.3[a] and DTN: LB0407AMRU0120.001_R0 [DIRS 173280].

NOTE: Only one method, Method A, is used in the TSPA-LA model (SNL 2007 [DIRS 181244], Section 6.3[a]).

Table 6.3.3-2. Spatial Variability and Uncertainty Distributions for Fracture Permeability (log (k [m^2]))

Fracture log (k [m^2]) (Lithophysal Units)		**Fracture log(k [m^2]) (Nonlithophysal Units)**	
Spatial Variability Distribution	**Uncertainty Distribution**	**Spatial Variability Distribution**	**Uncertainty Distribution**
Log Normal Distribution with Mean – 11.5	Triangular Distribution with Mean 0	Log Normal Distribution with Mean – 12.2	Triangular Distribution with Mean 0
Standard Deviation 0.47	Lower Bound is – 0.92.	Standard Deviation 0.34	Lower Bound is – 0.68.
	Upper Bound is + 0.92.		Upper Bound is + 0.68.

Sources: SNL 2007 [DIRS 181244], Section 6.6.3, Figures 6.6-7 and 6.6-8 and DTN: LB0407AMRU0120.001_R0 [DIRS 173280].

Table 6.3.3-3. Inputs Passed by the TSPA-LA Model to the Seepage Dynamically Linked Library

Input #	Input Parameter Name	Description	Value	Source
1	Infiltration_Scenario_a	Provides the infiltration scenario for the current realization to the seepage DLL.	1= 10th percentile 2= 30th percentile 3= 50th percentile 4= 90th percentile	NA, not data
2	Random_Seed_1	The first of two random number seeds provided to the Seepage DLL for its internal random number generator. This allows the sampling sequence in the Seepage DLL to be repeated, consistent with the Latin hypercube sampling on uncertain parameters in the GoldSim model file.	Uniform ($1, 2^{31}–1$)	NA, not data
3	Random_Seed_2	The second of two random number seeds provided to the Seepage DLL for its internal random number generator (see above).	Uniform ($1, 2^{31}–1$)	NA, not data
4	Alpha_Uncert_Lith_a	Sampled value from uncertainty distribution for capillary strength parameter. The distribution minimum, most likely, and maximum are defined by which method is chosen.	Triangular; see Table 6.3.3-1.	[a]Section 6.7.1.1
5	Alpha_Uncert_NonLith_a	Sampled value from uncertainty distribution for capillary strength parameter. The distribution minimum, most likely, and maximum are defined by which method is chosen.	Triangular; see Table 6.3.3-1.	[a]Section 6.7.1.1
6	LogK_Uncert_NonLith_a	Sampled value from Log(k) uncertainty for the nonlithophysal rock units.	Triangular (-0.68, 0, 0.68)	[a]Section 6.7.1.1
7	LogK_Uncert_Lith_a	Sampled value from Log(k) uncertainty for the lithophysal rock units.	Triangular (-0.92, 0, 0.92)	[a]Section 6.7.1.1
8	Density_H2O	Density of seeping water.	960 kg/m^3	[b]This is an assumed input parameter.
9	Drift_Diameter	Drift diameter.	5.5 m	[a]Section 6.7.1.2
10	WP_Length_Seepage	WP length.	5.1 m	[a]Section 6.7.1
11	Seepage_Multiplier	A seepage multiplier for noncollapsed conditions that accounts for additional uncertainty due to drift degradation.	1.2	[a]Section 6.7.1.2
12	LogK_SV_Mean_NonLith	The mean of the log of permeability [log(k)] spatial variability for nonlithophysal rock units.	-12.2	[a]Section 6.7.1.1
13	LogK_SV_SD_NonLith	The standard deviation of the log of permeability [log(k)]) spatial variability for nonlithophysal rock units.	0.34	[a]Section 6.7.1.1
14	LogK_SV_Mean_Lith	The mean of the log of permeability [log(k)] spatial variability for lithophysal rock units.	-11.5	[a]Section 6.7.1.1
15	LogK_SV_SD_Lith	The standard deviation of the log of permeability [log(k)]) spatial variability for lithophysal rock units.	0.47	[a]Section 6.7.1.1

Table 6.3.3-3. The Inputs Passed by the TSPA-LA Model to the Seepage Dynamically Linked Library (Continued)

Input #	Input Parameter Name	Description	Value	Source
16	Alpha_SV_LB_Lith	The lower bound for the $1/\alpha$ spatial variability distributions for lithophysal rock. The value is selected based on which of the four ACMs (i.e., methods) is selected during a particular realization for the distribution.	Table 6.3.3-1.	[a]Section 6.7.1.1
17	Alpha_SV_UB_Lith	The upper bound for the $1/\alpha$ spatial variability distributions for lithophysal rock. The value is selected based on which of the four ACMs (i.e., methods) is selected during a particular realization for the distribution.	See Table 6.3.3-1	[a]Section 6.7.1.1
18	Alpha_SV_LB_NonLith	The lower bound for the $1/\alpha$ spatial variability distributions for nonlithophysal rock. The value is selected based on which of the four ACMs (i.e., methods) is selected during a particular realization for the distribution.	See Table 6.3.3-1	[a]Section 6.7.1.1
19	Alpha_SV_UB_NonLith	The upper bound for the $1/\alpha$ spatial variability distributions for nonlithophysal rock. The value is selected based on which of the four ACMs (i.e., methods) is selected during a particular realization for the distribution.	See Table 6.3.3-1	[a]Section 6.7.1.1
20	DE_Event_Time	Selects the appropriate disruptive event time (igneous or seismic) based on the scenario class for the simulation.	0 yr for both igneous and seismic, 20,000 yr or 1,000,000 yr if nominal case	NA, not data
21	Scenario_Flag_Feed _Seep	Determines which scenario class (e.g., nominal, igneous, or seismic) is being simulated.	1 = nominal 2 = igneous 3 = seismic	NA, not data
22	Seismic_Event_Freq _Seep_Feed	Annual exceedance frequency of the seismic event.	0.5 yr^{-1}	Section 6.3.3.1.3
23	Seismic_Thresh_Lith	Seismic event frequency at or below which collapse occurs for lithophysal rock.	1 yr^{-1} = collapsed condition 0 yr^{-1} = noncollapsed condition	Section 6.3.3.1.3
24	Seismic_Thresh_NonLith	Seismic event frequency at or below which collapse occurs for nonlithophysal rock.	1 yr^{-1} = collapsed condition 0 yr^{-1} = noncollapsed condition	Section 6.3.3.1.3
25	Rock_Str_Reduction_Lith	Placeholder for Lithophysal Rock Strength Reduction Function.	0	NA, not data

Table 6.3.3-3. The Inputs Passed by the TSPA-LA Model to the Seepage Dynamically Linked Library (Continued)

Input #	Input Parameter Name	Description	Value	Source
26	Rock_Str_Reduction_ NonLith	Placeholder for Nonlithophysal Rock Strength Reduction Function.	0	NA, not data
27	DE_Seepage_Model	Selects appropriate disruptive event seepage model flag based on the scenario class for the simulation.	Igneous or Seismic	NA, not data
28	Rock_Str_Thresh_Lith	Loss of rock strength, which will result in drift collapse in lithophysal rock units.	40%	[a]Section 6.4.2.4.1
29	Rock_Str_Thresh_ NonLith	Loss of rock strength, which will result in drift collapse in nonlithophysal rock units.	40%	[a]Section 6.4.2.4.1
30	Print_Flag	Controls the amount of information that is written to output files (e.g., none, seepage output only, all possible output, debug information only).	NA	NA, not data
31	Thermal_Seep_Temp _Limit	Drift crown temperature above which seepage will not occur.	96°C	[a]Section 6.3.2
32	Flow_Focusing_Flag	Specifies whether to use the flow-focusing factor built into the Seepage DLL or to use a value of 1.0 for flow focusing.	0 = use abstraction, 1 = use 1.0	NA, not data
33	End_Time	Specifies the time to which the Seepage DLL runs (TSPA-LA Model simulation time) and returns seepage time histories.	20,000 yr or 1,000,000 yr	NA, not data
34	Seepage_Uncertainty	Provides a value that is used to sample the seepage distribution in the Seepage DLL.	Uniform (0,1)	[a]Section 6.7.1.1
35	Climate4_FF_Index	Index for post 10-k climate state. Used to allow for flexibility in choosing percolation fluxed for the post 10-k climate state.	1	NA, not presently used

NOTE: [a] SNL 2007 [DIRS 181244].
[b] A low density (960 kg/m^3, associated with water at 100°C) is used to maximize the volumetric flow.

Table 6.3.3-4. Drift-Wall Condensation: 1,000 Years; High Dispersion Coefficient, Low Invert Transport Properties, Well-Ventilated Drip Shield

	Slope (c)	Y-intercept (d)
Rate (CW)	-1.33E+00	1.08E+02
Standard Error	1.42E+00	1.45E+02
Rate R-Squared	4.67E-01	—
	Slope (a)	**Y-intercept (b)**
Probability (P_w)	-2.59E-02	5.71E-02
Standard Error	9.35E-03	2.93E-02
Probability R-Squared	2.87E-01	—

Source: DTN: MO0702PALOVERT.000_R2 [DIRS 180377]
NOTE: An example of 1 of the 4 tables that provide values of regression slopes, intercepts, and statistical parameters for $\hat{P}_w$ and CW.

Table 6.3.3-5. Parameter Distributions for Drift Wall Condensation Abstraction

Parameter Name in TSPA-LA Model	Description	Distribution
DWC_Dispersivity_Cond_a	A random variable specifying whether the high dispersivity or low dispersivity modeling case is used (0 = low; 1 = high).	Discrete (p, v) [(0.5, 0), (0.5, 1)]
DWC_Invert_Properties_Cond_a	A random variable specifying whether the high invert transport or low invert transport modeling case is used (0 = low; 1 = high). Note that for TSPA-LA, the high invert transport case was determined to be an unrealistic upper bound (DTN: MO0706SPAFEPLA.001_R0 [DIRS 181613], FEP 2.1.08.14.0A). Only the value of zero is used.	Discrete (p, v) [(1.0, 0), (0.0, 1)]
DWC_Ventilated_Cond_a	A random variable specifying whether the ventilated or unventilated drip shield modeling case is used (0 = unventilated; 1 = ventilated).	Discrete (p, v) [(0.5, 0), (0.5, 1)]
Seepage_Condensation_Prob_a[a]	Random variable U[0,1] to determine the seepage/condensation regime for the first failed waste package in a seepage environment.	Uniform (0,1)
DWC_Std_Error_a_a	An uncertainty multiplier for the standard deviation on the slope coefficient for determining probability of condensation from the percolation rate.	Normal: mean = 0, standard deviation = 1
DWC_Std_Error_b_a	An uncertainty multiplier for the standard deviation on the y-intercept coefficient for determining probability of condensation from the percolation rate.	Normal: mean = 0, standard deviation = 1
DWC_Std_Error_c_a	An uncertainty multiplier for the standard deviation on the slope coefficient for determining condensation rate from the percolation rate.	Normal: mean = 0, standard deviation = 1
DWC_Std_Error_d_a	An uncertainty multiplier for the standard deviation on the y-intercept coefficient for determining condensation rate from the percolation rate.	Normal: mean = 0, standard deviation = 1

Source: SNL 2007 [DIRS 181648], Table A-3.

[a] Seepage_Condensation_Prob_a is a TSPA parameter developed in this report.

Table 6.3.3-6. Alternative Conceptual Models Considered for the Drift Seepage and Drift-Wall Condensation Submodels

Alternative Conceptual Models	Key Assumptions	Screening Assessment and Basis
Drift Seepage: Flow through discrete fractures	ACM that simulates flow through discrete fractures rather than through a stochastic continuum.	Screened out. It was concluded that conceptual model uncertainty is small compared to other sources of uncertainty that are explicitly accounted for by the base case conceptual model, its numerical implementation, and the associated uncertainty estimates that are propagated through the TSPA-LA Model.
Drift Seepage: Episodic-Preferential Flow in Superheated Rock	The effectiveness of the vaporization barrier was examined with an ACM representing water flow into a superheated rock environment (SNL 2007 [DIRS 181244], Section 6.4.3.2). In this ACM, the thermally perturbed downward flux from the condensation zone toward the superheated rock zone is conceptualized to form episodic preferential-flow patterns.	Screened out. It was concluded that results of the ACM are reasonably consistent with the thermal seepage process-model results used for this abstraction (SNL 2007 [DIRS 181244], Section 6.4.3).
Drift Seepage: Flow-focusing factor based on a coarser resolution of scale	The ACM flow-focusing factor was based on a coarser resolution of scale at which the flow-focusing factors were averaged over 5-meter long sections along the bottom of the model (SNL 2007 [DIRS 181244], Section 6.6.5.2.2).	Screened out. It was concluded that the flow focusing model based on the finer grid resolution gave more conservative results and therefore the appropriate model to use (SNL 2007 [DIRS 181244], Section 6.6.5.2.3).
Drift Seepage: Igneous seepage model that considers a capillary barrier and flow diversion	The two ACMs for evaluating drift seepage after an igneous event are based on a conceptual model where thermal contraction gives rise to numerous fractures and joints in the cooling process filling the drift with fractured magma of relatively high permeability and low capillary strength (SNL 2007 [DIRS 181244], Section 6.5.1.7). This conceptualization gives rise to a capillary barrier and flow diversion. The two ACMs are based on whether the non-collapsed seepage lookup table or the collapsed seepage lookup table is used.	Screened out. The model for igneous seepage used in the TSPA-LA model was chosen on the basis that it would be conservative to use percolation flux as the seepage flux.
Drift-Wall Condensation: Thermal Conductivity/Heat Transfer	In the Thermal Conductivity/Heat Transfer ACM, the air phase is treated as a solid material (SNL 2007 DIRS [181648], Section 6.1.4).	Screened out. This ACM is essentially accounted for in the MSTHM Abstraction (SNL 2007 [DIRS 181648], Sections 6.1.4 and 6.4).
Drift-Wall Condensation: CFD simulation for drift condensation processes	ACM simulates the drift with a CFD code and the surrounding rock with porous media code. The CFD code FLUENT (Fluent, Inc. [DIRS 164315]) contains limited porous media capabilities that only consider single-phase flow (SNL 2007 DIRS [181648], Section 6.1.4).	Screened out. The CFD code was determined to have insufficient advantages over the selected model (SNL 2007 [DIRS 181648], Section 6.1.4).

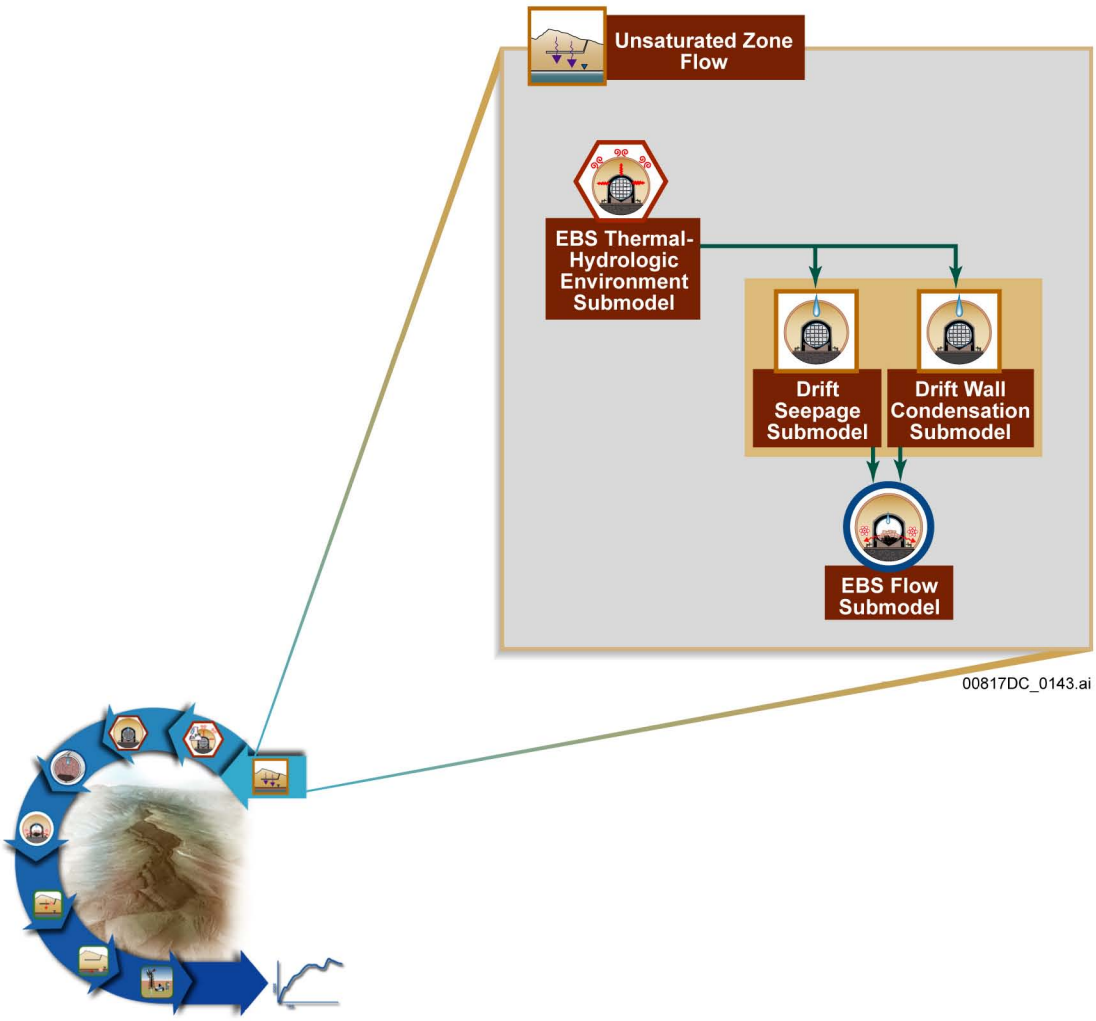

Figure 6.3.3-1. Information Flow Diagram for the Drift Seepage and Drift Wall Condensation Submodels

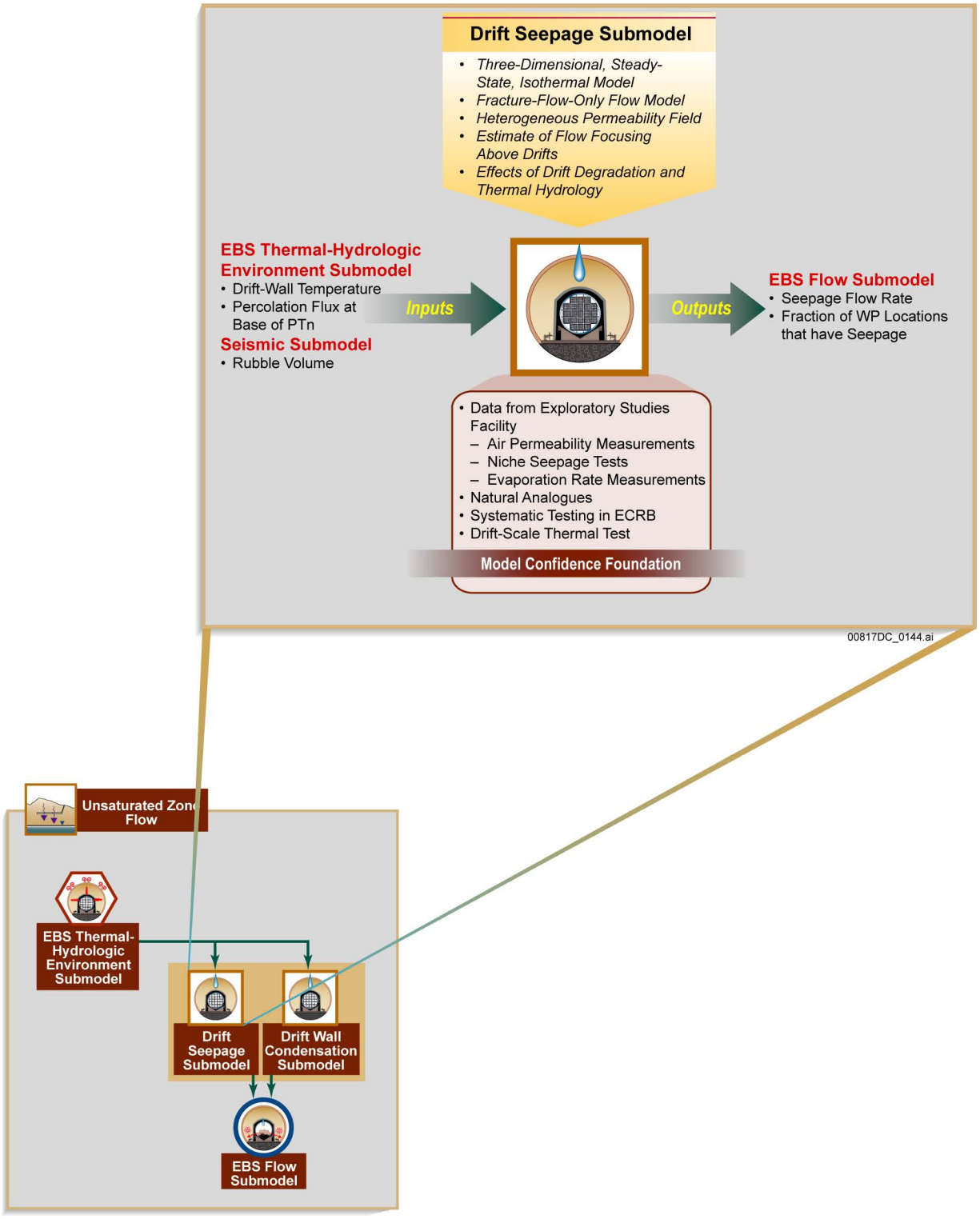

Figure 6.3.3-2. Inputs, Outputs, and Basis for Model Confidence for the Drift Seepage Submodel

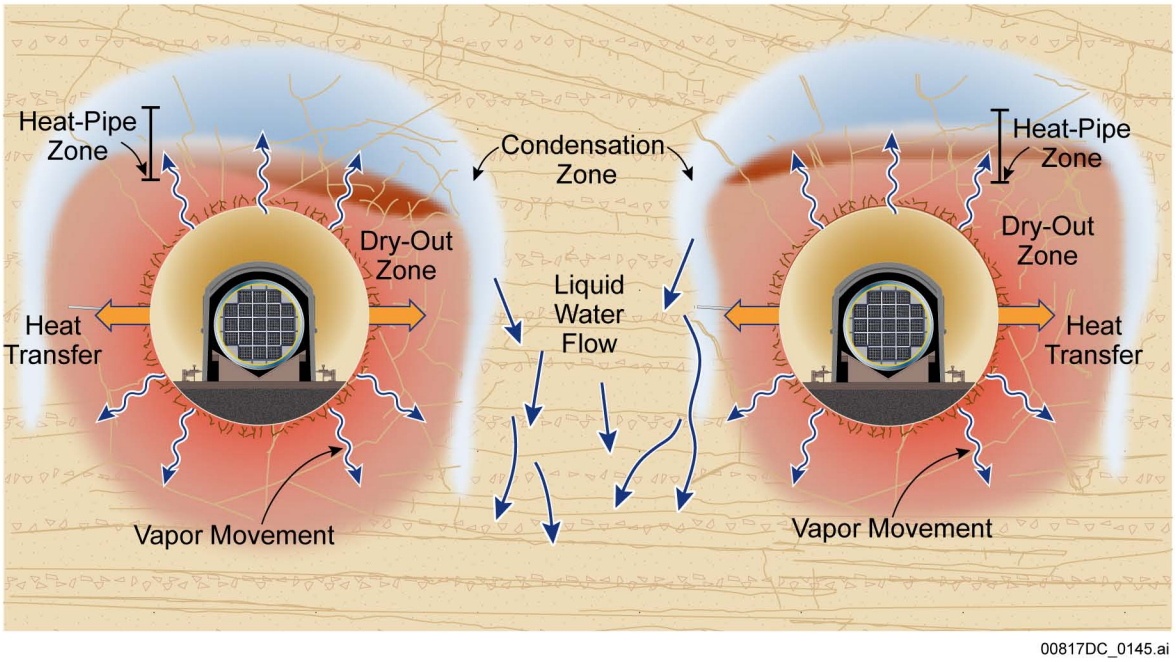

Source: Modified from BSC 2004 [DIRS 169734], Figure 5-81.

Figure 6.3.3-3. Schematic Illustration (not to scale) of Thermal-Hydrologic Processes in the Vicinity of the Emplacement Drifts Due to Repository Heating

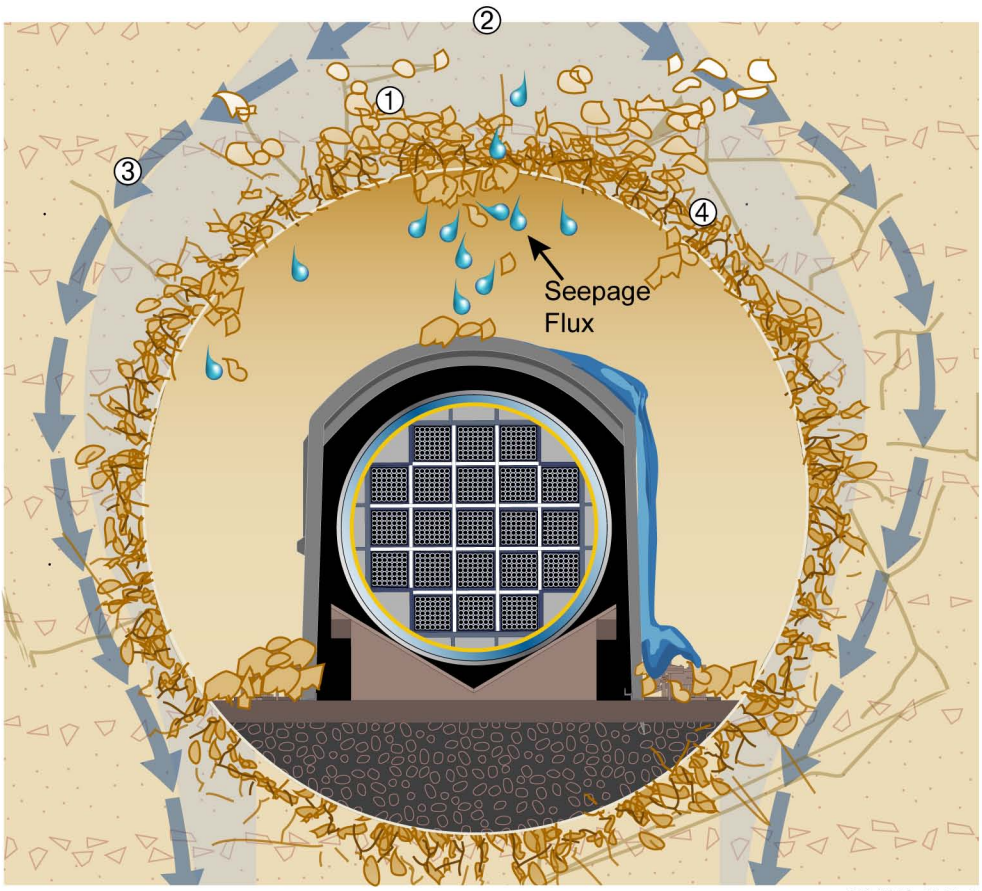

Figure 6.3.3-4. Schematic Illustration of the Processes Affecting Ambient Drift Seepage

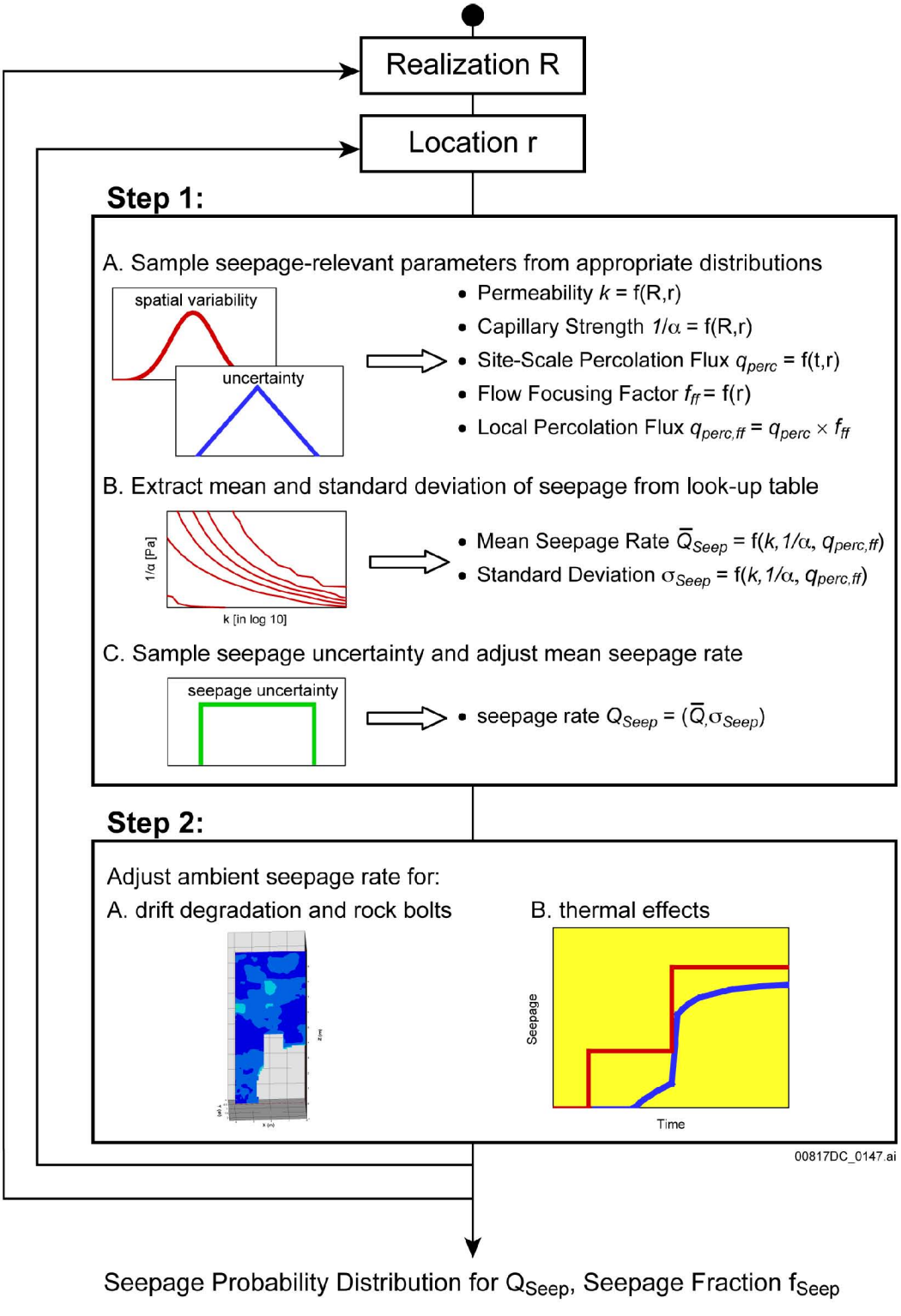

Source: SNL 2007 [DIRS 181244], Figure 6-1[a].

Figure 6.3.3-5. Procedure for Probabilistic Calculation of Seepage at Selected Timesteps in the TSPA-LA Model

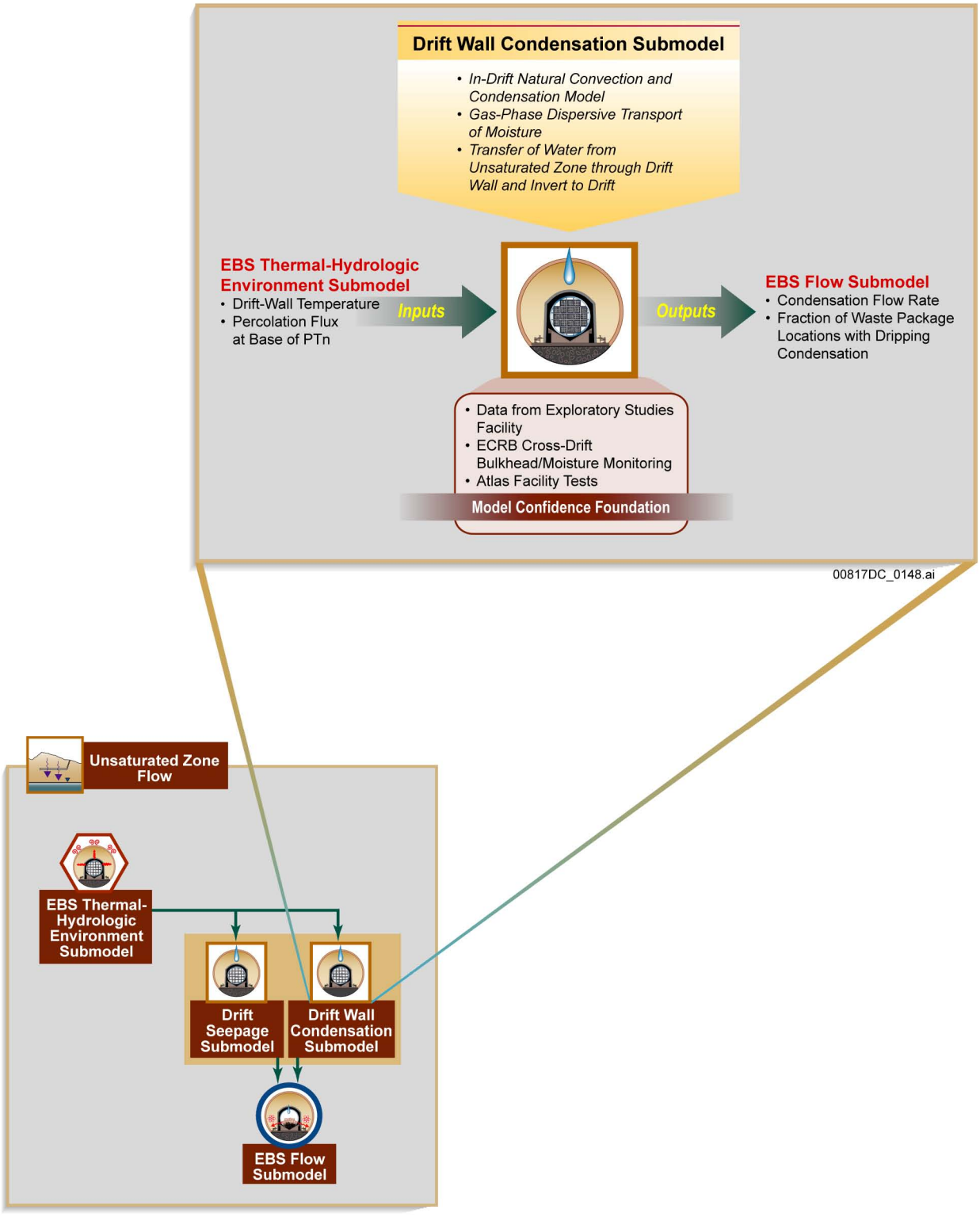

Figure 6.3.3-6. Inputs, Outputs, and Basis for Model Confidence for the Drift Wall Condensation Submodel

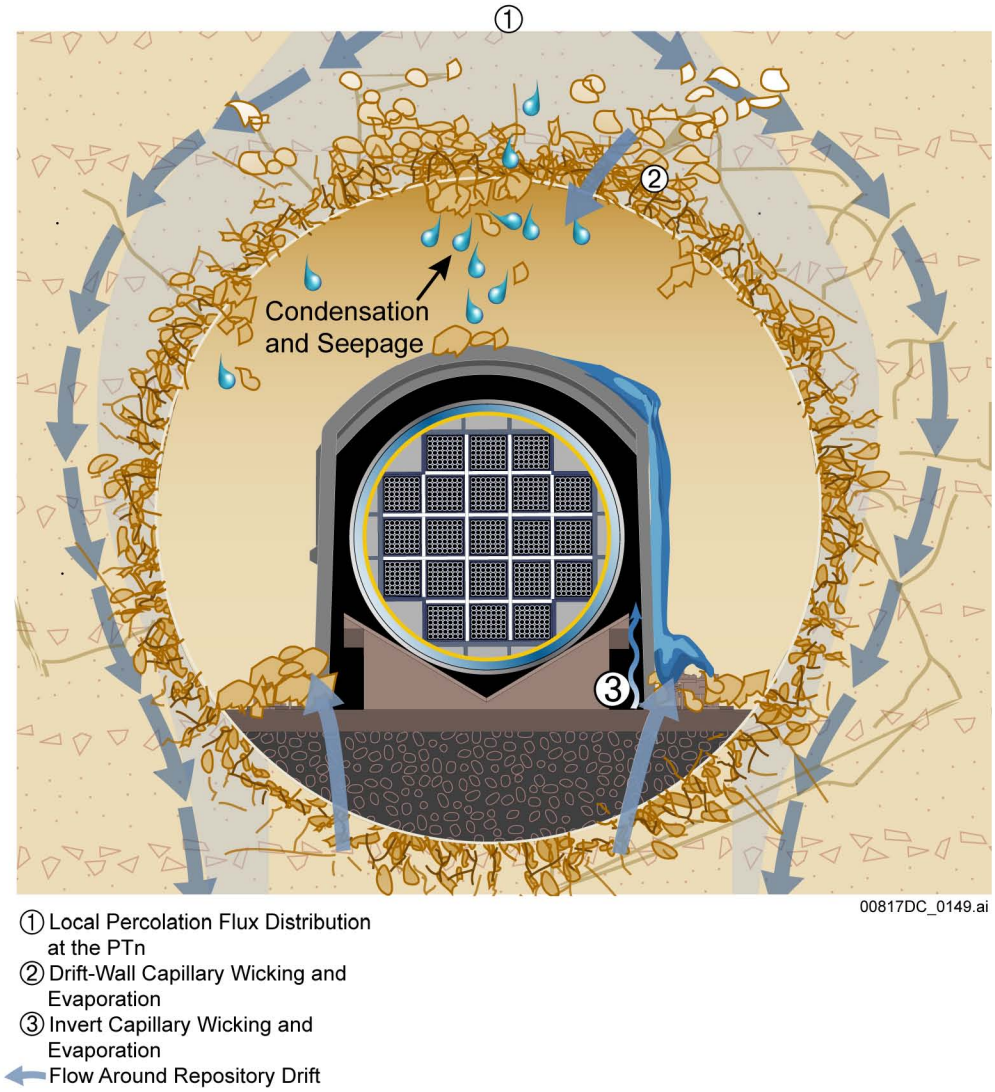

Figure 6.3.3-7. Schematic Illustration of the Processes Affecting Drift-Wall Condensation

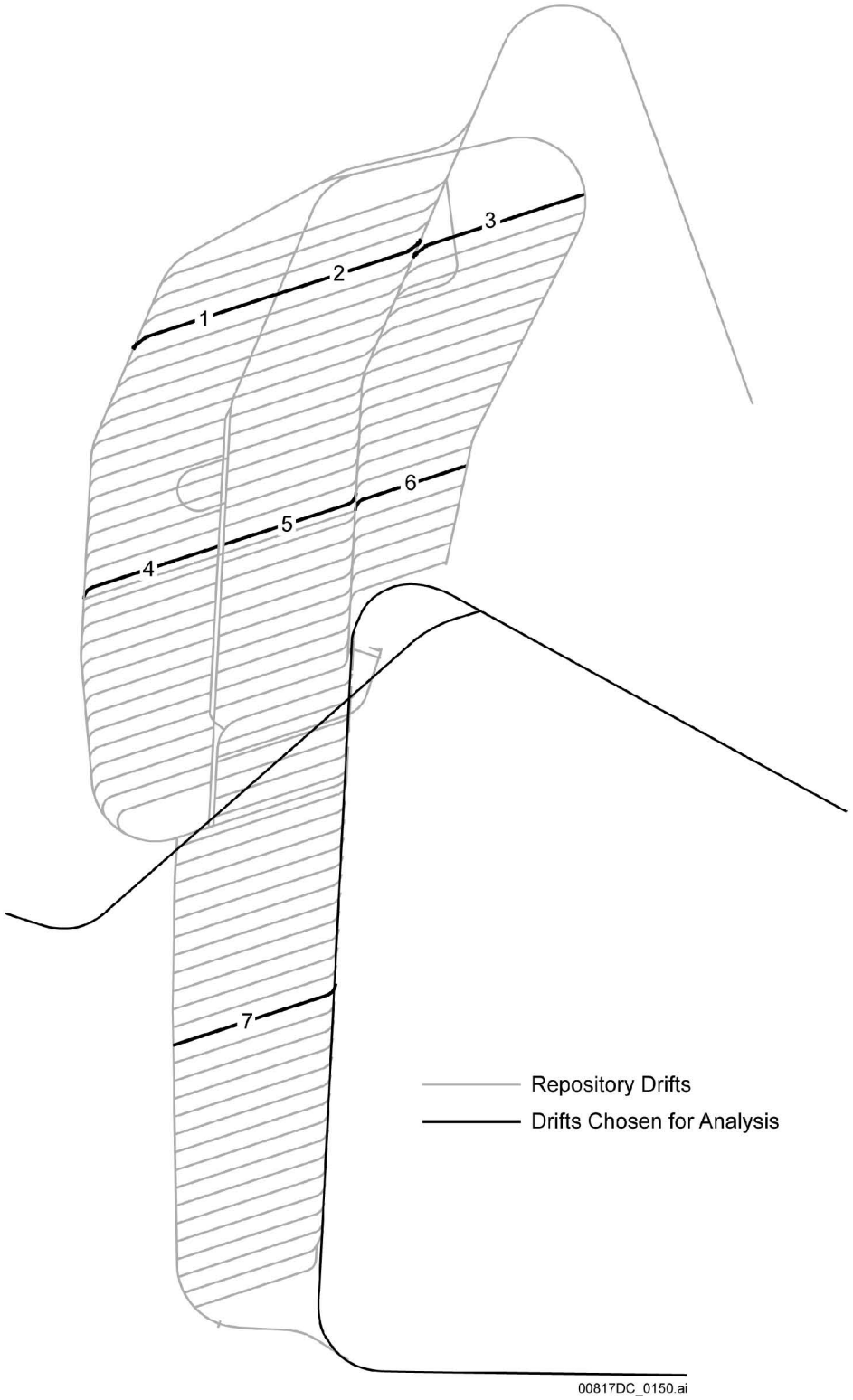

Source: Modified from SNL 2007 [DIRS 181648], Figures 6-1[a] and 6-2[a].

Figure 6.3.3-8. Schematic Depicting Approximate Locations of Disposal Drifts Chosen for Condensation Analysis

6.3.4 Engineered Barrier System Chemical Environment

Engineered Barrier System: Physical and Chemical Environment (*EBS P&CE*) (SNL 2007 [DIRS 177412]) suite of models is implemented in both the TSPA-LA Model and for calculations external to the TSPA-LA Model. The EBS P&CE Abstractions are implemented by the EBS Chemical Environment Submodel. This submodel consists of an algorithm to calculate the time-dependent partial pressure of CO_2 (Pco_2) and look-up tables to determine the values of the time-dependent parameters pH, ionic strength, aqueous chloride concentration [Cl^-], and aqueous nitrate concentration [NO_3^-]. These chemical-environment variables determine whether localized corrosion of the WP outer barrier occurs in the TSPA-LA Localized Corrosion Initiation Analysis, and they determine radionuclide mobility in the invert (i.e., radionuclide solubility and colloid stability) in the TSPA-LA Model. Within the TSPA-LA Model, outputs of the EBS Chemical Environment Submodel primarily serve as inputs used to calculate radionuclide solubility (Section 6.3.7.5.3) and colloid stability (Section 6.3.7.6.3) in the invert. Other than the Pco_2 in the drift, the EBS Chemical Environment Submodel does not provide input to in-package chemistry because *In-Package Chemistry Abstraction* (SNL 2007 [DIRS 180506], Section 6.6.2[a]), shows that the chemistry inside a failed WP is insensitive to incoming water composition.

The EBS Chemical Environment Submodel, as implemented in both the TSPA-LA Model and the Localized Corrosion Initiation Analysis, simulates the temporal changes of Pco_2, pH, ionic strength, [Cl^-], and [NO_3^-] by using models developed in *EBS P&CE* (SNL 2007 [DIRS 177412], Section 6.15). The algorithm for Pco_2 calculates the Pco_2 as a function of time and incoming seepage water composition. The response surfaces for pH, ionic strength, [Cl^-], and [NO_3^-] are calculated as functions of incoming seepage water composition, water-rock interaction parameter (WRIP), temperature, and Pco_2. The relative humidity is the independent variable in using the response surfaces. The Pco_2 is used as an input to the Dissolved Concentration Limits Submodel (Section 6.3.7.5) and the In-Package Chemistry Submodel (Section 6.3.7.2), as applied to the interior of a failed WP. In addition, Pco_2, pH, and ionic strength are used as inputs to the Dissolved Concentration Limits Submodel (Section 6.3.7.5) and the EBS Colloids Submodel (Section 6.3.7.6), as applied in the invert. The pH, [Cl^-], and [NO_3^-] are used to assess the potential to initiate localized corrosion on the WP outer barrier (Section 6.3.5.2). The EBS TH Environment Submodel described in Section 6.3.2 provides the comprehensive time histories of temperature and relative humidity to the EBS Chemical Environment Submodel crown seepage chemistry calculations and provides the representative time histories to the EBS Chemical Environment Submodel invert chemistry calculations. Information flow and connections between the EBS Chemical Environment Submodel and other TSPA-LA Model components and submodels are shown on Figure 6.3.4-1. Figure 6.3.4-2 presents an overview of the important in-drift processes that impact the results, inputs, outputs, and level of confidence in the EBS Chemical Environment Submodel. Figure 6.3.4-3 illustrates the locations of in-drift EBS structures and materials, including WPs, DSs, and the invert.

6.3.4.1 Conceptual Model

The EBS Chemical Environment Submodel quantifies Pco_2 in the drift and invert; pH and ionic strength in the invert water; and pH, [Cl^-], and [NO_3^-] in the crown seepage water. The *EBS P&CE* (SNL 2007 [DIRS 177412]) applies the same Pco_2 to the drift, the invert, and the inside of the WP. Various physical and chemical processes in the WPs and geochemical processes in the invert depend on the output from the EBS Chemical Environment Submodel. The Pco_2 inside the WPs influences the degradation of the waste forms and the solubility of the radionuclides inside failed WPs. The Pco_2 in the invert influences the solubility of the radionuclides in the invert. Brines that form by evaporative concentration from seepage which enters the invert by dripping, can influence radionuclide mobility (i.e., radionuclide solubility and colloid stability) in the invert. Acidic or alkaline water in the invert could enhance the solubility of radionuclides. The ionic strength of water in the invert will control the stability of colloidal material transporting sorbed radionuclides and could also influence the solubility of radionuclides in the invert. The pH, [Cl^-], and [NO_3^-] of the crown seepage water dripping onto a WP are parameters used to assess the initiation of localized corrosion of the WP outer barrier.

The *EBS P&CE* (SNL 2007 [DIRS 177412]) performed an analysis of the evolution of the physical and chemical environment in the EBS, including an evaluation of likely changes to the compositions of gas, water, and solids within the emplacement drifts under repository conditions. The following influences were evaluated for their potential to cause compositional changes in water in the EBS:

- The compositions of water and gas that enter the drifts from the host rock
- Changing thermal conditions in the drifts
- The interactions of seepage water and gas with introduced engineered materials
- The compositions of evaporating or condensing waters within the drifts.

The overall conceptual model is as follows. As infiltrating water moves downward toward the repository, it moves up a thermal gradient. The thermal gradient extends from the land surface to the repository level and is assumed to vary linearly with depth. The water interacts with minerals in the rock, maintaining equilibrium with calcite and amorphous silica, present in excess, and dissolving alkali feldspar, while precipitating out one or more secondary phases. The degree of feldspar dissolution is a function of the temperature at any location along the percolation path, and is calculated using a temperature-dependent dissolution rate. The dissolution rate was estimated for ambient conditions from the degree of alteration that the tuff has undergone since it erupted, 12.8 million years ago, and adjusted for temperature using literature data for the activation energy for feldspar dissolution (SNL 2007 [DIRS 177412], Section 6.3.2.1). Little evaporation or degassing occurs as the water moves up the thermal gradient, until it reaches a lower-saturation zone around which steam and gas can readily escape into the drift, where steam is transported axially to cooler zones and condenses. The low saturation zone is the drift and areas in the surrounding rock, including fractures connecting to the drift, which are readily accessed by the in-drift atmosphere. Evaporation occurs at the boundary between the higher saturation area surrounding the drift and the lower saturation area, which will, hereafter, be referred to as the evaporation front. During the boiling period, this boundary corresponds to the boiling zone around the drift. At later times, it corresponds to the drift wall and fractures extending outward from the drift, close enough to be in gas-phase

equilibrium with the drift wall. The Pco_2 in the drift is controlled by equilibrium with the water at the evaporation front, with dilution by water vapor, generated by evaporation at the front.

As seepage waters enter drifts their chemical compositions may change due to evaporation, mineral precipitation, or both. Throughout the thermal period (depending on the relative humidity in the drifts), evaporative concentration of seepage can occur in the EBS. Evaporation increases aqueous species concentrations, mineral precipitation, and the concentration of the most soluble components in brines. In accordance with the geochemical divide theory, the composition of the seepage water changes according to the sequence of minerals that precipitate from that solution as a function of initial water composition, thermal conditions, relative humidity, and gas composition where the evaporation occurs (SNL 2007 [DIRS 177412], Section 6.3.3.1).

Figure 6.3.4-4 depicts several representative locations along a vertical flow path from the crown of the drifts to the base of the invert. The chemical compositions of the water and the gas at each of these representative locations could directly affect the degradation rates of the EBS, the quantities and species of mobilized radionuclides, and/or the transport rates of radionuclides and fluids flowing through the drifts into the UZ.

The following describes conditions shown on Figure 6.3.4-4, Locations 1 through 5 (adapted from (SNL 2007 [DIRS 177407], Figure 6.6-4) and SNL 2007 [DIRS 177412], Section 6.5).

Location 1 (Drift Wall and Air Gap)—Possible seepage water and gas chemistries at Location 1 could be modified by interactions with engineered materials, such as rock bolts and stainless steel sheets and their corrosion products, or directly drip into the drifts and onto surfaces of the DSs (Location 2). Generally, potential seepage water interactions with engineered materials and their corrosion products will not alter the major ion composition in water entering the drifts (SNL 2007 [DIRS 177412], Section 6.8 and Tables 6.8-3 through 6.8-6). Given the limited longevity of the low-alloy steels that comprise some of the ground support and all of the invert materials such as gantry rails, support beams, and other engineered materials, this effect would be on the order of hundreds of years for most materials placed within the drifts (SNL 2007 [DIRS 177412], Section 6.5.2). A sensitivity analysis investigating the potential impacts on water chemistry revealed the impacts are negligible (SNL 2007 [DIRS 177412], Section 6.8). For the longer-lasting materials, such as the 316L stainless steel that comprises the wire mesh ground support component, sensitivity analyses also show that corrosion processes have a negligible effect on the composition of seepage waters (SNL 2007 [DIRS 177412], Section 6.8). Any potential impact of emplaced materials is indirectly considered in the TSPA-LA Model through the output of the EBS P&CE suite of models.

Location 2 (Surface of the DS)—Some portion of the water from Location 1 may be diverted directly to the invert (Location 5) by the DSs, or may undergo evaporative processes, and/or react with debris sitting on the DSs. If the DSs are breached, these fluids could flow onto the surface of the WPs (Location 3) but could only flow into the WPs (Location 4) through an available pathway. Corrosion products associated with the DSs are not expected to adversely affect the compositions of any waters flowing off or through DSs, due to the very slow corrosion rates for titanium and the insoluble nature of titanium oxides (SNL 2007 [DIRS 177412], Section 6.5.1.1). For the same reasons, the removal or addition of trace elements by sorption or

dissolution processes associated with active corrosion of the DSs' titanium alloy is not considered.

Location 3 (Outer Surface of WPs)—Alloy 22, the alloy of the WP outer barrier, like the titanium used for DSs, is also highly corrosion resistant (SNL 2007 [DIRS 177412], Section 6.5.1.2). The processes occurring at Location 2 also apply to Location 3. The potential for localized corrosion on the WP outer barrier depends on whether or not seepage-derived water contacting the WPs is capable of initiating localized corrosion.

Location 4 (Inside the WP)—This portion of the conceptual process is reported in other modeling reports, such as *In-Package Chemistry Abstraction* (SNL 2007 [DIRS 180506]) and in Section 6.3.7.2 of this report.

Location 5 (Invert)—The chemical environment in the invert affects radionuclide solubility and colloid stability. Both radionuclide solubility and colloid stability could affect the radionuclide mobilization from the source term for transport from the EBS to the UZ. Implementation of the P&CE integrated invert chemistry abstraction model is discussed in *EBS P&CE* (SNL 2007 [DIRS 177412], Section 6.13.4, Section 6.15.2, and Table 6.15-1).

6.3.4.2 TSPA Abstraction

Within the TSPA-LA Model, the EBS Chemical Environment Submodel calculates time-dependent Pco_2 in the gas phase in the drift above the invert and pH and ionic strength conditions in the invert. Within the Localized Corrosion Initiation Analysis (Section 6.3.5.2), the EBS Chemical Environment Submodel calculates time-dependent Pco_2 in the gas phase in the drift above the invert and the pH, $[Cl^-]$, and $[NO_3^-]$ in the crown seepage water. The same time-dependent Pco_2 in the gas phase in the drift above the invert is used for the drift Pco_2, the in-package Pco_2, and the invert Pco_2.

The EBS Chemical Environment Submodel is based on the Near Field Chemistry model developed in *Engineered Barrier System: Physical and Chemical Environment* (SNL 2007 [DIRS 177412]). The Near Field Chemistry model provides potential seepage water compositions at the drift wall, the water-rock interaction parameter, and the range of in-drift Pco_2. The evolution of pH, ionic strength, $[Cl^-]$, and $[NO_3^-]$ are also modeled using response surfaces in the form of look-up tables. Each look-up table is a function of initial water type, water-rock interaction parameter, temperature, and Pco_2 with relative humidity as the independent variable. The interaction between seepage water and engineered materials is not included in the analysis because the EBS P&CE Abstraction determined that this interaction has a negligible impact on the composition of seepage water and in-drift gas phases (SNL 2007 [DIRS 177412], Sections 6.5, 6.7, and 6.8). The following processes, represented by the EBS Chemical Environment Submodel, are abstracted below:

- Temporal evolution of incoming seepage water composition, where seepage includes dripping from the drift crown
- Changing Pco_2 in the drifts and the invert

- Evaporative evolution of seepage water composition from the drift crown and in the invert.

Evolution of Incoming Seepage Composition—The Near Field Chemistry model defines four starting waters as representative of the potential range of the Topopah Spring Tuff pore water compositions (SNL 2007 [DIRS 177412], Sections 6.3.2 and 6.6). As pore water percolates downward, it interacts with minerals in the rock. The water-rock interactions modify the water composition. During the thermal pulse, the degree of modification due to water-rock interactions is increased, relative to ambient conditions, as the water percolates down through the heated rock above the repository. Ultimately, this thermally altered water is what enters the drift and controls the chemical conditions in the drift.

The degree of alteration is determined by the amount of water-rock interaction, quantified by the parameter called the water-rock interaction parameter. The water-rock interaction parameter is affected by the percolation rate through the rock and the thermal field through which the water passes. Ambient conditions are characterized as having zero water-rock interaction. Large water-rock interactions can be caused by high temperatures and slow percolation fluxes through the TSw. Lower temperatures and/or faster water movement will cause less water-rock interaction. The model follows a packet of water from the surface as it passes through the time-dependent thermal field to the repository taking into account the climate changes that change the velocity of the infiltrating water.

The EBS physical and chemical environment defines water-rock interaction parameter as a time-dependent function of the glacial transition percolation flux and the thermal measure. The thermal measure is defined as the sum of peak WP temperature (in degrees C) and the duration of boiling (in years). Obviously, this parameter is not really physical because it is in mixed dimensional units. However, the summed value captures the effects of variations in the thermal history of a given WP due to the location in the repository, assumed rock properties (i.e., thermal conductivity), and WP specific heat generation rate. Therefore, it provides a useful metric for discriminating between thermal histories at different repository locations. The percolation rate also can influence the thermal measure of the WP because high percolation tends to cool the repository more quickly. The water-rock interaction parameter is parametrically evaluated at each location (i.e., thermal measure) using twenty different sets of four percolation fluxes representing the three climate states and the post-10,000 year percolation state. The glacial transition flux is used to represent each of the twenty sets of flux values. Thermal measures and glacial-transition percolation fluxes have been extracted from the MSTHM results for the representative WPs used in TSPA-LA. Once the thermal measure and glacial transition flux is specified, the time-dependent value of water-rock interaction parameter can be found from the water-rock interaction parameter look-up table.

Multiscale Thermohydrologic Model (SNL 2007 [DIRS 181383], Section 6.3.15[a]) provides the data for calculating the thermal measure. These MSTHM files contain the thermal histories for each representative package. The maximum temperature and the duration of boiling are manually extracted from the files and then added together. Note that the duration of boiling is defined as the time from WP emplacement until the WP cools below 96° C. These calculated thermal measures are then used to create two look-up tables in the TSPA-LA Model, one for CSNF WPs and one for CDSP WPs.

Uncertainty in input parameters for calculating the water-rock interaction parameter values is propagated through the Near Field Chemistry model as described in *EBS P&CE* (SNL 2007 [DIRS 177412], Section 6.12.2.5). These water-rock interaction parameter values are passed to TSPA as a beta distribution, the mean value of which is extracted from the water-rock interaction parameter look-up table. The maximum value of the beta distribution is specified to be 2.838 times the mean, the minimum is 0.2039 times the mean, and the standard deviation is 0.4251 times the mean. This uncertainty is primarily due to uncertainty in the feldspar dissolution rate (SNL 2007 [DIRS 177412], Section 6.12.2.5). In each realization, the TSPA-LA Model extracts the water-rock interaction parameter value from the look-up table and generates a new distribution at each timestep. The TSPA-LA Model correlates the water-rock interaction parameter beta distribution to a stochastic parameter, WRIP_beta_rand_a, which is uniform stochastic between 0 and 1. This correlation insures that even though the shape of the beta distribution changes at each timestep, the distribution is sampled at the same probability level at each timestep for the entire realization (SNL 2007 [DIRS 177412], Section 6.15.1).

The water-rock interaction parameter and the WP temperature form the basis for calculating the Pco_2 in the drift. Relevant CO_2 concentrations in the gas phase within the rock are difficult to determine (SNL 2007 [DIRS 177412], Section 6.3.2.5). As water percolates downward through the thermal field and heats up, CO_2 is partitioned into the gas phase. This is offset by the effects of feldspar dissolution, which raises the alkalinity and reduces the degree of partitioning into the gas phase. The relative rates of these two processes are important because the degree to which the gas phase acts as an open system—the amount of CO_2 that would be lost or gained by gas phase advection and mixing—is unknown. Given that matrix saturations are high and fracture porosity is low, it is assumed for the Near Field Chemistry model that gas phase transport is limited, except for the area immediately around the drift, where loss into the drift can occur; therefore, the gas phase composition at any location in the rock column is determined by assuming equilibrium with the aqueous composition, rather than being controlled by gas phase advection and mixing.

***Pco₂* as a Function of Time**—Calculating the Pco_2 in the drift is difficult because it is the result of competing processes such as evaporation, degassing, precipitation, diffusion, and advection of gas in the fractures, and scavenging of CO_2 by condensation in the cooler drift ends. Two bounding cases are considered (SNL 2007 [DIRS 177412], Section 6.3.2.8):

- *Minimum CO_2 concentration in the drift*. In this bounding case, gas movement into and out of the drift, and through the mountain, is assumed to occur readily through fractures. The CO_2 concentration in the air fraction entering the drift is equal to the ambient CO_2 concentration in the mountain at the repository level (10^{-3} bars). The contribution of this to the total CO_2 in the drift atmosphere is equal to this concentration times the mole fraction of air in the drift. Added to this is the CO_2 that is released by evaporating water at the dryout front. This yields a minimum concentration for CO_2 in the drift.

- *Maximum CO_2 concentration in the drift*. Behind the evaporation front, the gas phase is assumed to be in equilibrium with the aqueous phase at the temperature of the evaporation interface, assuming that the water moved up the temperature gradient to the interface without degassing. Treating the drift as a closed system, the in-drift Pco_2 would equal this value, which can be taken as a maximum for the in-drift atmosphere. If

the model predicts large amounts of feldspar dissolution, but relatively low temperatures (e.g., for extremely slow percolation flux rates, water percolated through hot rocks, but did not reach the drift wall until it had cooled), then it is possible for the predicted maximum Pco_2 to actually be below 10^{-3} bars. This is because the alkalinity increases as feldspar dissolves, increasing the amount of CO_2 dissolved into the water. If this occurs, it is assumed that the maximum Pco_2 value is 10^{-3} bars.

Thus, combining the lower and upper bounds for the in-drift Pco_2 yields the possible range of CO_2 concentrations in the drift and also in the invert.

Evaporative Evolution of Seepage at the Drift Crown and in the Invert—Equilibrium compositions of aqueous solutions and mineral precipitates that may form from seepage water within the emplacement drifts were calculated using the model developed in Section 6 and summarized in Section 8 of *In-Drift Precipitates/Salts Model* (IDPS) (SNL 2007 [DIRS 177411]), hereafter referred to as the IDPS Process Model. Calculations of water compositions at chemical equilibrium were performed using the geochemical equilibrium code, EQ3/6 Version 8.0 (*Software Code: EQ3/6*. V8.0 (BSC 2003 [DIRS 162228])), and a Pitzer thermodynamic database developed specifically for that purpose (SNL 2007 [DIRS 177412], Table 4.1-1 and Section 6.2.6). The IDPS Process Model simulates the evolution of water in the drifts as it evaporates from its initial composition into concentrated brine. The *EBS P&CE* applies the IDPS Process Model to each of the four starting waters (SNL 2007 [DIRS 177412] Section 6.6) to produce chemical composition look-up tables (SNL 2007 [DIRS 177412] Sections 6.15 and 8.2). Within the TSPA-LA Model, the EBS Chemical Environment Submodel evaluates the EBS P&CE Abstraction to determine the chemistry of two drift waters. One type of water is seepage water dripping from the drift crown and the second type of water is the invert water that originated as water dripping from the drift crown. Seepage water dripping from the drift crown may flow onto the DS and, in the event of a failed DS, may subsequently contact the WP surface. Invert water that originated as water dripping from the drift crown may flow directly into the invert or may contact the DS and/or WP before it reaches the invert.

The implementation instructions for evaluating the EBS P&CE, with uncertainties, are given in the *EBS P&CE* (SNL 2007 [DIRS 177412], Sections 6.12 and 6.15). The look-up tables for pH, ionic strength, $[Cl^-]$, and $[NO_3^-]$ are calculated as functions of incoming seepage water composition, water-rock interaction parameter (WRIP), temperature, and Pco_2. The relative humidity is the independent variable in using the look-up tables. These chemical composition look-up tables will be referred to as IDPS look-up tables, because they are generated with the IDPS Process Model, and to distinguish them from other look-up tables (such as water-rock interaction parameter look-up tables illustrated in Table 6.3.4-1) that are generated by the EBS P&CE suite of models (SNL 2007 [DIRS 177412], Section 6.15).

As described below, there are 396 IDPS look-up tables for seepage and invert water composition spanning combinations of Pco_2 and temperature for each of the four starting water types, 11 water-rock interaction parameter levels, and nine combinations of three Pco_2 values and three temperatures. Each table lists values for chemical composition, including pH, ionic strength, $[Cl^-]$, and $[NO_3^-]$ with relative humidity as the independent variable. Each IDPS look-up table is defined for a specific starting water type, temperature, and Pco_2. The tables are defined for Pco_2 values of 10^{-2}, 10^{-3}, and 10^{-4} bar; and temperature values of 30°C, 70°C, and 100°C. There are

99 tables for all possible combinations for each of the four starting waters. The IDPS tables for the TSPA-LA are part of DTN: SN0701PAEBSPCE.001_R1 [DIRS 180523] and guidance for using these inputs is provided in *EBS P&CE* (SNL 2007 [DIRS 177412], Sections 6.12 and 6.15).

An example of an IDPS look-up table is shown in Table 6.3.4-2.

Model Uncertainties, Variabilities, and Discretization Errors—Model confidence for incoming seepage water, Pco_2, pH, ionic strength, [Cl^-], and [NO_3^-] is discussed in the following paragraphs.

Incoming Seepage Water—The Near Field Chemistry process model (SNL 2007 [DIRS 177412]) provides potential seepage water compositions and the water-rock interaction parameter values for use in the P&CE abstraction models. Uncertainties in the inputs are treated as follows. The four input waters (Groups 1 through 4) were chosen statistically to represent the variability in 34 TSw waters upon evaporation. The uncertainty in the starting water composition is represented by randomly selecting one of the four water types for each realization. Because representative waters are used, it is also necessary to sample the range of Cl:N in the 34 TSw waters from a discrete CDF to capture the uncertainty associated with these key chemical parameters. Output seepage water compositions are presumed to span the natural variability of the pore water compositions in the repository units (SNL 2007 [DIRS 177412], Section 6.12.3).

Partial Pressure of Carbon Dioxide Gas—The range of uncertainty and variability is included in the abstractions of Pco_2 by using minimum and maximum Pco_2 bounding cases and then scaling between ambient and the bounding values. These two bounding cases provide the range of Pco_2. The TSPA-LA Model uses a uniform stochastic variable, PCE_Delta_pCO2_a, between -1 and 1, to choose which of the bounding cases to use in each realization (SNL 2007 [DIRS 177412], Section 6.15.1). A negative value of the variable implies using the minimum Pco_2 case and a positive value implies the maximum Pco_2 case. The actual Pco_2 in the drift is calculated by linearly scaling between ambient (0.001 bars) and the minimum or maximum, using the absolute value of PCE_Delta_pCO2_a as the scaling factor. This scaling accounts for the uncertainty in the in-drift Pco_2.

pH, Ionic Strength, [Cl^-], and [NO_3^-]—IDPS uncertainty factors for the [Cl^-], [NO_3^-], [Cl^-]/[NO_3^-], and ionic strength of in-drift water are used directly by the P&CE abstraction models. The uncertainty associated with [Cl^-] + [NO_3^-] is calculated assuming linear combinations of the individual uncertainties for [Cl^-] and [NO_3^-] provided by the IDPS Model (SNL 2007 [DIRS 177412], Table 6.12-1). These uncertainties apply between 20°C and 140°C and are defined as triangular distributions with the most likely uncertainty equal to 0.0 and the maximum and minimum uncertainties shown in Table 6.3.4-3 (SNL 2007 [DIRS 177412], Table 6.12-1).

The IDPS uncertainty for pH was developed by comparison of modeled data with pH values measured in several evaporation and mineral solubility experiments, and the process of measuring pH has significant error. The pH uncertainty value is taken directly from the look-up tables and is adjusted by the uncertainties reported in Table 6.3.4-3 (SNL 2007 [DIRS 177412],

Table 6.12-2), using a triangular distribution for relative humidity values below 75 percent. Between 100 percent and 75 percent relative humidity, pH uncertainties are sampled from a discrete CDF archived in DTN: SN0703PAEBSPCE.007_R2 [DIRS 184141] (see SNL 2007 [DIRS 177412], Section 6.12.3.1 for a discussion of how and why the pH uncertainty was reduced in the *EBS P&CE*).

No uncertainty is associated with the ionic strength below 85 percent relative humidity from the look-up tables because the ionic strength is not used by the TSPA-LA Model at these concentrations. Between 85 percent and 100 percent relative humidity, the ionic strength is adjusted for uncertainty by applying a triangular distribution and the value in Table 6.12-1 of *EBS P&CE* (SNL 2007 [DIRS 177412]). The guidance for applying these uncertainty distributions is provided in *EBS P&CE* (SNL 2007 [DIRS 177412], Section 6.12.3) and the input distributions are captured in DTN: SN0703PAEBSPCE.007_R2 [DIRS 184141].

6.3.4.3 TSPA-LA Model Implementation

The EBS Chemical Environment Submodel is implemented in the TSPA-LA Model to calculate the chemistry (pH and ionic strength) of the water in the invert (discussed in Section 6.3.4.3.1). The EBS Chemical Environment Submodel is also implemented in the Localized Corrosion Initiation Analysis (Section 6.3.5.2) to calculate the chemistry (pH, $[Cl^-]$, and $[NO_3^-]$) of the seepage water from the crown of the drift (discussed in Section 6.3.4.3.2). Although performed in two separate GoldSim files for three different applications, the submodel implementations are similar.

6.3.4.3.1 Invert Chemistry

The EBS Chemical Environment Submodel calculations for the invert are performed in two main levels of the TSPA-LA Model: global and local. Global calculations can be applied to all WPs and local calculations pertain only to those WPs in the local percolation subregion or percolation subregion environment. To reduce redundancy, the EBS Chemical Environment Submodel calculations that can be applied equally to all percolation subregions and both WP types are performed at a higher (global) level. For example, the selection of one of the four starting water compositions is performed at the global level. In the TSPA-LA Model, the selection of one of these four initial water compositions is randomly sampled with equal probability. The probability of selecting any one of the four source waters is 25 percent (SNL 2007 [DIRS 177412], Section 6.15.1). Once selected, the initial water composition determines which total carbon tables and maximum Pco_2 tables are used to calculate the Pco_2. Pco_2 in the drift and in the invert must also match the selected starting water. Therefore, Pco_2 in the drift and Pco_2 in the invert are determined at the global level and the resulting Pco_2 values are applied to the entire repository. The EBS Chemical Environment Submodel calculations for the pH and ionic strength of the invert water require invert temperature and invert relative humidity, which are percolation subregion specific feeds from the EBS TH Environment Submodel (Section 6.3.2), and must be performed separately (locally) within each percolation subregion.

Inputs—Sections 6.9.3 and 6.15 of *EBS P&CE* (SNL 2007 [DIRS 177412]) provide the guidance for applying the 396 IDPS look-up tables for seepage composition captured in SN0701PAEBSPCE.001 [DIRS180523]. The IDPS look-up tables are used to determine the pH

and ionic strength in the invert as a function of starting water type, water-rock interaction parameter, temperature and Pco_2. In the TSPA-LA Model implementation, the independent variable in each of the IDPS look-up tables is the applicable relative humidity. For the dependent variables, column 1 contains the pH, column 2 contains the ionic strength, column 3 contains [Cl^-], and column 4 contains [NO_3^-]. Only the pH and ionic strength values are used in the invert chemistry calculations. The [Cl^-] and [NO_3^-] values are only used in the crown seepage chemistry calculations (Section 6.3.4.3.2). Each set of look-up tables was developed for each temperature combination of 30°C, 70°C, and 100°C; and Pco_2 values of 10^{-2}, 10^{-3}, and 10^{-4} bar; and 11 water-rock interaction parameter levels for a total of 99 look-up tables for each of the 4 starting water types. The PCE_Chemistry_Tables container in the TSPA-LA Model's GoldSim model file provides more information regarding these look-up tables and their applications. The methodology for applying uncertainty to the calculated pH and ionic strength is described in Section 6.12.3 of EBS P&CE (SNL 2007 [DIRS 177412]), and the applied uncertainty values are captured in DTN: SN0703PAEBSPCE.007_R2 [DIRS 184141], Estimated IDPS Uncertainties.xls. Additional calculation details are provided below and in the TSPA-LA Model GoldSim file.

The following describes the determination of the seepage water composition, invert temperature, invert relative humidity, and Pco_2 and their use in selecting the appropriate IDPS look-up tables for chemical composition for the interpolation of the appropriate pH and ionic strength values.

Global Calculations—Global level calculations begin with selecting one of the four initial starting waters, the representative WP and its thermal measure, and then calculating the water-rock interaction parameter for each TSPA percolation subregion (SNL 2007 [DIRS 177412], Section 6.15). Each TSPA-LA Model realization randomly selects one of the four starting percolating water compositions used for all percolation subregions. All the starting percolating water compositions are equally probable and, therefore, the probability of any given water being selected is 25 percent.

The water-rock interaction parameter is the one time-dependent independent parameter in the EBS Chemical Environment Submodel calculated at the global level. The water-rock interaction parameter describes the evolution of the water and specifies, along with the temperature and Pco_2, which of the IDPS look-up tables (0-L) to use for pH, ionic strength, [Cl^-], and [NO_3^-]. As described earlier, the water-rock interaction parameter requires sampling from a beta distribution at every timestep. This resampling, as well as the separation of aleatory and epistemic uncertainty, requires that the water-rock interaction parameter for every percolation subregion and WP type be calculated as a time-series at the global level before the main calculation. Then the water-rock interaction parameter is passed to the local level calculations for use along with the temperature and Pco_2 in selecting the appropriate IDPS look-up table for pH, ionic strength, [Cl^-], and [NO_3^-].

Local Calculations—After the starting water is selected and the water-rock interaction parameter is calculated at the global level, the appropriate Pco_2 for the drift and the invert can be calculated. Pco_2 values are determined at each timestep. The drift Pco_2 is used to calculate radionuclide solubilities in the WPs (Section 6.3.7.5) and total carbonate concentration in the failed WPs (Section 6.3.7.2). The same Pco_2 applies in the invert and is used to calculate

radionuclide solubilities in the invert (Section 6.3.7.5) and the pH and ionic strength of the invert water.

The Pco_2 values in the invert are determined at each simulation timestep. The TSPA-LA Model then uses the invert Pco_2 value, the selected starting water composition, and water-rock interaction parameter value (0-L), along with the invert temperature and relative humidity feeds from the EBS TH Environment Submodel (Section 6.3.2), to determine pH and ionic strength in the invert water using the IDPS look-up tables. The EBS TH Environment Submodel (Section 6.3.2) feeds for the representative invert temperature and relative humidity are percolation subregion-specific values, so the remaining calculations in the EBS Chemical Environment Submodel are performed locally (i.e., separately for each percolation subregion or percolation subregion environment).

WPs occupying representative emplacement drift locations, shown on Figure 6.1.4-2, are characterized by representative time histories of TH (temperature and relative humidity) and average drift-seepage rates that are provided by the EBS TH Environment Submodel (Section 6.3.2) and the Drift Seepage Submodel (Section 6.3.3.1), respectively. The EBS Chemical Environment Submodel uses these conditions and Pco_2 to calculate time-dependent pH and ionic strength conditions in the invert for the representative WP location in each percolation subregion.

The determination of pH and ionic strength in the invert water is performed locally within each percolation subregion in the TSPA-LA Model. The actual chemistry used in the invert is determined by the scenario class, the dripping or non-dripping environment, whether the WP and/or DS is intact, whether drift wall condensation occurs, and the seepage flux, as specified in Table 6.3.4-4. The EBS TH Environment Submodel (Section 6.3.2) provides the EBS Chemical Environment Submodel the representative temperature and relative humidity for each percolation subregion at each timestep.

The discussion presented below describes how the IDPS look-up tables are applied in the TSPA-LA Model to determine the chemical parameters in the invert. Although presented as the calculation of invert chemistry in the TSPA-LA Model, the following discussion is meant to be a robust discussion of the EBS Chemical Environment Submodel covering the submodel applications in both the TSPA-LA Model and the Localized Corrosion Initiation Analysis (Section 6.3.5.2). In evaluating the EBS Chemical Environment Submodel for crown seepage chemistry in the Localized CorrosionInitiation Analysis (Section 6.3.5.2), the tables are still applicable and a discussion of these tables is still warranted.

At each timestep, the EBS Chemical Environment Submodel accesses eight of the 396 IDPS look-up tables (see example in Table 6.3.4-2) and uses the current starting water, water-rock interaction parameter value, Pco_2, temperature, and relative humidity to determine the corresponding pH and ionic strength in the invert. The eight most appropriate IDPS look-up tables for the local environment calculations in the invert are determined by eliminating tables that are not appropriate for current invert conditions, as described below. The starting water (1, 2, 3, or 4) reduces the applicability of the 396 IDPS look-up tables to 99. The applicability of the 99 IDPS look-up tables are reduced at each timestep to 18 by choosing only those tables that are associated with the water-rock interaction parameter value at the timestep. The actual

chemical conditions are determined by interpolation of values between eight of the 18 IDPS tables. The water-rock interaction parameter value is a decimal number between 0 and 10 that determines which of 11 sets of nine IDPS look-up table to use. These 11 sets of nine IDPS tables can be thought of as arranged in layers. The floor function can be used to calculate the integer below the water-rock interaction parameter value of interest and the ceil function can give the integer above the water-rock interaction parameter value. Thus, the actual water-rock interaction parameter value is somewhere between two layers of IDPS look-up tables. These 18 tables in two layers are further reduced to eight by selecting those tables that represent the eight nearest neighbors to the desired temperature and Pco_2. For example, if the invert temperature is below 70°C, the IDPS look-up tables corresponding to 30°C and 70°C will be used and the 100°C tables can be excluded. Otherwise, the IDPS look-up tables corresponding to 70°C and 100°C will be used and the 30°C tables can be excluded. Similarly, if the invert Pco_2 is below 10^{-3} bar, the IDPS look-up tables corresponding to 10^{-2} bar can be excluded, and if the invert Pco_2 is above 10^{-3} bar, the IDPS look-up tables corresponding to 10^{-4} bar can be excluded. The eight remaining IDPS look-up tables, four in each water-rock interaction parameter value layer, are the resulting look-up tables consistent with the current value of the water-rock interaction parameter, invert temperature, and invert Pco_2.

To select the pH and ionic strength corresponding to the specific invert relative humidity desired from each of the eight IDPS look-up tables, the EBS Chemical Environment Submodel applies linear interpolation in three directions between the eight tables. When selecting pH and ionic strength values for temperature and Pco_2 values that fall between the pre-defined values of the IDPS look-up tables, the parameters are estimated from the eight look-up table results using linear interpolation for temperature and water-rock interaction parameter layer, and log-linear interpolation for Pco_2. Chemistry values are extrapolated for pH and ionic strength if Pco_2 is outside the range of 10^{-4} to 10^{-2} bar. Extrapolation of Pco_2 is valid over the range 10^{-5} to 2×10^{-2} bar (SNL 2007 [DIRS 177412], Section 7.2.2). For temperatures greater than 100°C and less than 30°C, values are taken from the 100°C or 30°C IDPS look-up tables, respectively (SNL 2007 [DIRS 177412], Section 6.15.1). If the relative humidity is greater than the highest relative humidity value in the IDPS look-up tables, the TSPA-LA Model uses those pH and ionic strength values that are associated with the highest relative humidity in the applicable IDPS look-up table. If relative humidity is lower than the lowest relative humidity value in the IDPS look-up tables, the TSPA-LA Model uses the pH and ionic strength that are associated with the lowest relative humidity in the applicable look-up table (SNL 2007 [DIRS 177412], Section 6.15.1).

After the pH and ionic strength parameters are calculated, these quantities are adjusted for epistemic uncertainty and discretization error in accordance with the specific instructions provided in Section 6.12.3 of *EBS P&CE* (SNL 2007 [DIRS 177412]). The uncertainty for pH, ionic strength, $[Cl^-]$, $[NO_3^-]$, and $[Cl^-]/[NO_3^-]$ is specified as a function of the relative humidity. Except for the pH in the highest relative humidity range, the distributions are triangular distributions (DTN: SN0703PAEBSPCE.007_R2 [DIRS 184141]). The IDPS uncertainty for pH was developed by comparison of modeled data with pH values measured in several evaporation and mineral solubility experiments, and the process of measuring pH has significant error. In the *EBS P&CE* (SNL 2007 [DIRS 177412], Section 6.12.3.1), the uncertainty in pH, for the range from 100 percent to 75 percent relative humidity is determined indirectly, by

comparison of measured and predicted concentrations of pH-sensitive aqueous species. For this relative humidity range, the pH uncertainties are sampled from a discrete distribution archived in DTN: SN0703PAEBSPCE.007_R2 [DIRS 184141]. At relative humidities below 75 percent, the IDPS pH uncertainty value is used.

Additional detail on the application of uncertainty to the calculated pH and ionic strength in the invert is provided in the PEFs associated with the uncertain parameters. Additional details on the EBS Chemical Environment Submodel calculations, including the application of uncertainty, are provided in the TSPA-LA Model's GoldSim model file.

The EBS Chemical Environment Submodel provides the following outputs for each percolation subregion and each representative WP and early-failed WP group in dripping and non-dripping environments:

- Time-dependent Pco_2 in the invert
- Time-dependent pH in the invert
- Time-dependent ionic strength in the invert.

6.3.4.3.2 Crown Seepage Chemistry

The EBS Chemical Environment Submodel is also used to calculate the time-dependent $[Cl^-]$, $[NO_3^-]$, $[Cl^-]/[NO_3^-]$, and pH of the seepage water contacting the WP surface in the event that a DS fails to divert flow around a WP. These chemical-environment variables are used to calculate localized corrosion on the WP outer surface. These determinations are made outside of the main TSPA-LA Model in an analysis developed exclusively for determining the potential for localized corrosion occurrence (identified as the Localized Corrosion Initiation Analysis (Section 6.3.5.2)).

The EBS Chemical Environment Submodel is used to calculate pH, $[Cl^-]$, and $[NO_3^-]$ in the crown seepage water in the Localized Corrosion Initiation Analysis. The inputs and calculations discussed in Section 6.3.4.3.1 for the invert chemistry calculations are equally suitable for determinations of the crown seepage chemistry used in the Localized Corrosion Initiation Analysis. However, the feeds for Pco_2, relative humidity, and temperature differ from the invert application. The crown seepage water application of the EBS Chemical Environment Submodel performs the same submodel calculations as the invert calculations using the same 396 IDPS look-up tables, but it includes different feeds for the applicable Pco_2, temperature, and relative humidity. In the invert application of the EBS Chemical Environment Submodel, the applicable temperature and relative humidity is the representative invert temperature and invert relative humidity from the EBS TH Environment Submodel (Section 6.3.2). The representative data set is defined in Section 6.3.2.2.1 as the TH response histories for each of the five repository subregions based on a single, representative WP for each fuel type. The Localized Corrosion Initiation Analysis (Section 6.3.5.2) uses the WP surface temperature and relative humidity along with the drift Pco_2 to evaluate conditions on the WP surface from the 396 IDPS look-up tables. Similar to the seepage model, the Localized Corrosion Initiation Analysis evaluates WPs at each of the 3,264 subdomain locations from the MSTHM Process Model (SNL 2007 [DIRS 181383], Section 6.2.12[a]) as opposed to using representative packages for each subregion. When the IDPS look-up tables are used, instead of accessing columns 1 and 2 for pH and ionic strength,

the crown seepage calculations use the same look-up tables but they extract chemical information from column 1 for pH, column 3 for [Cl^-], and column 4 for [NO_3^-].

Global Calculations—The global calculations for the evaluation of crown seepage chemistry using the EBS Chemical Environment Submodel determine the applicable starting water and the water-rock interaction parameter time history. The implementation is identical to the previous discussion regarding invert calculations and is not being repeated.

Local Calculations—The local calculations of the EBS Chemical Environment Submodel determine the Pco_2 pH, [Cl^-], and [NO_3^-] of the crown seepage water. The extraction of chemical parameters from the 396 IDPS look-up tables is similar to that described for the invert water pH and ionic strength; however, WP surface values for temperature, Pco_2, and relative humidity are fed into the look-up table selections and subsequent calculations.

Section 6.12.3 in *EBS P&CE* (SNL 2007 [DIRS 177412]) discusses the addition of uncertainty to the EBS Chemical Environment Submodel calculations. The application of uncertainty for pH is analogous to the invert implementation. The treatment of [Cl^-] and [NO_3^-] uncertainty is significantly different from that previously discussed and requires further discussion.

The following steps should be taken to calculate the [Cl^-], [NO_3^-], [Cl^-+NO_3^-] concentrations and [Cl^-]/[NO_3^-] ratios. The EBS P&CE abstraction models (SNL 2007 [DIRS 177412], Section 6.12.3) use the molal concentrations of Cl and N to represent [Cl^-] and [NO_3^-] concentrations.

1. TSPA chooses a P&CE potential seepage water chemistry look-up table from among the 396 look-up tables using a randomly selected group water type (1 through 4); a water-rock interaction parameter value (0, 1, 2,…10); a Pco_2 value of either 10^{-2}, 10^{-3}, 10^{-4}, bar; and a T_{wp} = 30°C, 70°C, or 100°C. The T_{wp}, and the independent variable, RH_{wp}, are provided by the MSTHM (SNL 2007 [DIRS 181383], Appendix VIII[a]). The data used to make the look-up table selection are archived in DTNs: SN0701PAEBSPCE.001_R1 [DIRS 180523]; SN0701PAEBSPCE.002_R0 [DIRS 179425]; and SN0703PAEBSPCE.006_R2 [DIRS 181571].

2. TSPA evaluates potential salt separation by comparing the relative humidity from the look-up table selected in Step 1 with the salt separation relative humidity found in the group water salt separation tables (e.g., Gp1_Salt_separation_table.xls) in DTN: SN0703PAEBSPCE.006_R2 [DIRS 181571]. The relative humidity of salt separation is used directly from the salt separation look-up tables for all group waters.

   2.A. In the event of no salt separation:

      a. Use the [Cl+N] concentrations from the look-up tables archived in DTN: SN0701PAEBSPCE.001_R1 [DIRS 180523].

      b. Sample uncertainty in [Cl+N] by using the appropriate relative humidity range from IDPS uncertainty table and archived in DTN: SN0703PAEBSPCE.007_R2 [DIRS 184141] by applying a triangular distribution.

c. Calculate ([C+N] + uncertainty) (= x) obtained in Steps 2a and 2b.

d. Sample ($[Cl^-]/[NO_3^-]$) (= y) from discrete CDFs in DTN: SN0703PAEBSPCE.007_R2 [DIRS 184141]. Uncertainty due to the use of a single pore water to represent a group of waters (e.g., the effect of binning potential starting pore waters chemically) is incorporated into the model by sampling the $[Cl^-]/[NO_3^-]$ ratio (represented by Cl:N) for each starting water group from a discrete CDF for the starting water values.

e. Using x = ([Cl+N] + uncertainty) and y = (Cl:N) sampled from the CDFs to solve for $[Cl^-]$ and $[NO_3^-]$, the calculated values will include uncertainty.

2.B. In the event of salt separation:

a. Once salt has separated, the Cl:N CDFs no longer apply and $[Cl^-]$, $[NO_3^-]$, $[Cl^-]/[NO_3^-]$, and pH are taken directly from the look-up tables selected in Step 1 above. These values are valid at any relative humidity below that for salt separation.

b. The model assumes that $[Cl^-]$ is proportional to [Cl:N], and thus the uncertainties will also be correlated. Once TSPA samples the uncertainty on $[Cl^-]$ using a triangular distribution with the end-points as shown in the IDPS uncertainty table, an offset of the same sign (either positive or negative) is applied to the [Cl:N].

c. The look-up tables remain valid until the relative humidity in the drift exceeds the salt separation threshold. At that point, the look-up tables no longer apply and TSPA is instructed to assume that a Cl-rich brine can form. Because the process of salt-brine separation cannot be explicitly modeled, the P&CE report (SNL 2007 [DIRS 177412], Section 6.12.3) abstraction models do not attempt to provide the chemistry for the Cl-rich brines.

The crown seepage water pH, $[Cl^-]$, and $[NO_3^-]$ are used to assess the potential for localized corrosion on the WP outer barrier in the Localized Corrosion Initiation Analysis (Section 6.3.5.2).

6.3.4.4 Model Component Consistency and Conservatism in Assumptions and Parameters

To enhance understanding of the complex interactions within the TSPA-LA Model, a discussion of consistency among model components and submodels, and identification of conservative assumptions in abstractions, process models, and parameter sets supporting the EBS Chemical Environment Submodel is provided below.

6.3.4.4.1 Consistency of Assumptions

Seepage Water Compositions—The In-Package Chemistry Abstraction does not use the EBS Chemical Environment crown seepage (EBS P&CE suite of models) as its starting waters (Section 6.3.7.2.1). In the In-Package Chemistry Abstraction, a liquid influx (dripping case or seepage dripping) model where water from the drift, simulated as typical groundwater, enters a

WP at a rate determined by the seepage flow through the openings in the breached WP (SNL 2007 [DIRS 180506], Section 6.3).

Effect on the TSPA-LA Model—Using a typical groundwater as the starting water for the in-package chemistry model will have little effect on the TSPA-LA results. As discussed in the *In-Package Chemistry Abstraction* (SNL 2007 [DIRS 180506], Section 6.6.2[a]), the composition of the liquid influx has little effect on the in-package chemistry because the degradation reactions and the secondary minerals that precipitate have a large influence on the water composition inside the WP.

Partial Pressure of CO_2—The In-Package Chemistry Abstraction uses the in-drift EBS Chemical Environment Submodel (Section 6.3.7.2.1) for Pco_2 in the WP rather than calculating the Pco_2 inside the WP. The Near Field Chemistry process model developed in *EBS P&CE* (SNL 2007 [DIRS 177412]) provides potential seepage water compositions, which are then used to generate look-up tables for Pco_2 maximum and for total dissolved carbon used to calculate Pco_2 minimum.

Effect on the TSPA-LA Model—Using a single Pco_2 for the drift, invert, and WP conditions is the best way to have a consistent gas phase composition throughout the drift and is actually a good approximation because gas transport in and out the waste package is relatively fast. In addition, while in-package pH does depend on Pco_2, in-package ionic strength does not depend on the value of Pco_2 (SNL 2007 [DIRS 180506], Section 6.6.3[a]).

6.3.4.4.2 Identification of Conservatisms in Submodels and Abstractions

Mixing In the Invert—Water passing through a breached WP (i.e., reacting with the waste form and corrosion products) would be expected to enter the invert and mix with water that had been diverted around the DS and WP, as well as with waters already present in the invert that have equilibrated with the relative humidity in the drift. The TSPA-LA Model uses the in-package chemistry in the WP and the invert for a WP that exhibits advective releases. Mixing of waters would change buffer capacities of the EBS Chemical Environment.

pH buffering—The In-Package Chemistry Abstraction (Section 6.3.7.2.1) conceptual model is a batch reactor model that consists of water, oxygen, carbon dioxide, waste forms, and metal alloys. The In-Package Chemistry Abstraction considers the potential for mineral precipitation and WP internal materials to act as pH buffers (SNL 2007 [DIRS 180506], Section 6.3). However, neither the In-Package Chemistry Abstraction nor the P&CE model consider the potential for surface complexation reactions to buffer pH, despite the presence of abundant EBS components in the drift.

6.3.4.5 Alternative Conceptual Model(s) for Engineered Barrier System Chemical Environment

Section 6.2 outlines the general consideration and treatment of ACMs used to support the TSPA-LA Model. A brief description of ACMs for the EBS Physical and Chemical Environment is presented below and summarized in Table 6.3.4-5.

PTn Pore Water ACM—The EBS Physical and Chemical Environment Model uses pore water compositions from the TSw to represent ambient conditions for the four starting waters (SNL 2007 [DIRS 177412], Section 6.6). The ACM selects ambient pore water from the overlying formation, the PTn, and then allows this water to seep up the geothermal gradient (from 23 to 96°C) which is downward, through the TSw to the repository horizon (SNL 2007 [DIRS 177412], Section 6.11).

This ACM was not selected for use in the TSPA-LA Model because an analysis showed that using the TSw pore water adequately captures the chemistry of representative PTn pore waters. The use of PTn starting compositions does not significantly impact the key chemical components (pH, Pco_2, Ca, K, Si) of seepage (SNL 2007 [DIRS 177412], Section 6.11).

Treatment of Alkali Feldspar by the Near Field Chemistry Model: Kinetics versus Equilibrium—Within the EBS Physical and Chemical Environment Model, the mixed feldspar phase adopted to represent the volcanic feldspar observed in the Topopah Spring Tuff, is treated kinetically, i.e., this phase is always undersaturated with respect to clays, zeolites, and its own end-members (SNL 2007 [DIRS 177412], Section 6.11.2). An alternate approach would be to assume that the volcanic feldspar has reached equilibrium or near equilibrium, and thus thermodynamic controls of feldspar dissolution (e.g. saturation indices) must be considered when calculating seepage water compositions.

This equilibrium ACM was not chosen because at or near ambient temperatures, the volcanic waters are usually undersaturated with respect to feldspars and the kinetic treatment of the alkali feldspar is the appropriate approach (SNL 2007 [DIRS 177412], Section 6.11.2).

Closed System Model with Respect to CO_2—The IDPS Model (SNL 2007 [DIRS 177411], Section 6.5), which is a process model implemented by the EBS P&CE suite of models (SNL 2007 [DIRS 177412]), describes an ACM that assumes a closed drift system with respect to CO_2. In a closed system, there is little or no exchange of CO_2 between the solution and the atmosphere; that is, the solution is modeled as essentially isolated from the atmosphere and H_2CO_3 is treated as a non-volatile acid. What little exchange might occur in a natural system approximating a closed system would alter the fugacity of CO_2 in the atmosphere. A closed system model might be appropriate for a wetter climate; however, relative humidity would be approximately 100 percent and little or no evaporation would occur.

A closed system with respect to CO_2 is not implemented in the TSPA-LA because the expected volume ratio of air to water in the drift is so large that CO_2 degassing from, or dissolving into, seepage water in the drift will negligibly affect CO_2 fugacity compared to the uncertainty in the input value for CO_2 fugacity. However, the EBS P&CE Model incorporates the uncertainty of an open or closed system by using the maximum and minimum Pco_2 values in the abstraction for the TSPA-LA (SNL 2007 [DIRS 177412], Section 6.3.2.8 and Section 6.15.1). The minimum value assumes a completely open system and the maximum value assumes a closed system. The actual system behaves in a manner between these two end-member assumptions.

INTENTIONALLY LEFT BLANK

Table 6.3.4-1. Illustration of the Form of the Mean Water-Rock Interaction Parameter Table

Thermal Measure	Year	Percolation Flux (mm/yr)	Percolation Flux (mm/yr)
		0.05231146	0.495274154
37.7552	50.1	3.77E-09	3.77E-09
37.7552	51	3.77E-08	3.77E-08
37.7552	52	7.55E-08	7.55E-08
37.7552	55	1.89E-07	1.89E-07
37.7552	60	3.79E-07	3.79E-07
37.7552	65	5.71E-07	5.71E-07
37.7552	70	7.64E-07	7.64E-07
37.7552	75	9.61E-07	9.61E-07
37.7552	80	1.16E-06	1.16E-06
37.7552	90	1.58E-06	1.58E-06
37.7552	100	2.01E-06	2.01E-06
37.7552	120	2.96E-06	2.96E-06
37.7552	140	3.98E-06	3.98E-06
37.7552	160	5.09E-06	5.09E-06
37.7552	180	6.27E-06	6.26E-06
37.7552	200	7.51E-06	7.50E-06
37.7552	220	8.80E-06	8.79E-06
37.7552	240	1.01E-05	1.01E-05
37.7552	260	1.15E-05	1.15E-05
37.7552	280	1.29E-05	1.29E-05
37.7552	300	1.44E-05	1.44E-05
37.7552	320	1.59E-05	1.59E-05
37.7552	340	1.74E-05	1.74E-05
37.7552	360	1.89E-05	1.89E-05
37.7552	380	2.05E-05	2.05E-05
37.7552	400	2.21E-05	2.21E-05
37.7552	420	2.37E-05	2.37E-05
37.7552	440	2.54E-05	2.54E-05
37.7552	460	2.70E-05	2.70E-05
37.7552	480	2.87E-05	2.87E-05
37.7552	500	3.04E-05	3.04E-05
37.7552	520	3.21E-05	3.21E-05

Source: DTN: SN0703PAEBSPCE.006_R2 [DIRS 181571], *WRIP_Lookup_Table.xls*.

Table 6.3.4-2. Illustration of the Form of an In-Drift Precipitated Salts Look-up Table for Each Unique Set of Values of Carbon Dioxide Partial Pressure, Pco_2, and Temperature

Relative Humidity	pH $-\log([H^+])$	Ionic Strength molality	$[Cl^-]$ molality	$[NO_3^-]$ molality
0.999995	6.45	6.45	0.000041	0.000006
0.999994	6.64	6.64	0.000065	0.000010
0.999992	6.84	6.84	0.000102	0.000016
0.999989	7.04	7.04	0.000162	0.000026
0.999984	7.23	7.23	0.000256	0.000041
0.999977	7.42	7.42	0.000406	0.000065
0.999966	7.61	7.61	0.000643	0.000103
0.999948	7.79	7.79	0.001017	0.000163
0.999921	7.97	7.97	0.001607	0.000258
0.999898	8.06	8.06	0.002108	0.000340
0.999881	8.09	8.09	0.002368	0.000409
0.999822	8.18	8.18	0.003312	0.000649
0.99982	8.18	8.18	0.003361	0.000661
0.999816	8.18	8.18	0.003412	0.000673
0.999814	8.19	8.19	0.003455	0.000683
0.999813	8.19	8.19	0.003464	0.000686
0.9998111	8.19	8.19	0.003505	0.000696
0.999811	8.19	8.19	0.003515	0.000699
0.999809	8.20	8.20	0.003568	0.000713
0.999807	8.20	8.20	0.003622	0.000727
0.999805	8.21	8.21	0.003680	0.000742
0.999803	8.21	8.21	0.003740	0.000758
0.999801	8.22	8.22	0.003802	0.000774
0.999799	8.23	8.23	0.003868	0.000791
0.999796	8.23	8.23	0.003938	0.000809
0.999794	8.24	8.24	0.004011	0.000828
0.999792	8.25	8.25	0.004087	0.000847
0.999789	8.25	8.25	0.004168	0.000868
0.999786	8.26	8.26	0.004253	0.000889
0.999784	8.27	8.27	0.004329	0.000908
0.99978	8.28	0.004439	0.000935	0.000372
0.999777	8.29	0.004540	0.000960	0.000382
0.999773	8.29	0.004647	0.000986	0.000392
0.99977	8.30	0.004760	0.001014	0.000403
0.999766	8.31	0.004881	0.001044	0.000415

Table 6.3.4-2. Illustration of the Form of an In-Drift Precipitated Salts Look-up Table for Each Unique Set of Values of Carbon Dioxide Partial Pressure, Pco_2, and Temperature (Continued)

Relative Humidity	pH $-\log([H^+])$	Ionic Strength molality	$[Cl^-]$ molality	$[NO_3^-]$ molality
0.999762	8.32	0.005010	0.001075	0.000427
0.999757	8.33	0.005147	0.001108	0.000441
0.999753	8.34	0.005294	0.001143	0.000455
0.999748	8.35	0.005451	0.001180	0.000469
0.999742	8.37	0.005620	0.001220	0.000485
0.999737	8.38	0.005801	0.001263	0.000502
0.999731	8.39	0.005997	0.001309	0.000521
0.999724	8.40	0.006208	0.001358	0.000540
0.999717	8.42	0.006437	0.001412	0.000562
0.999709	8.43	0.006685	0.001469	0.000584
0.999701	8.45	0.006956	0.001532	0.000609
0.999692	8.46	0.007252	0.001600	0.000636
0.999682	8.48	0.007577	0.001674	0.000666
0.999671	8.50	0.007935	0.001756	0.000698
0.999659	8.52	0.008332	0.001846	0.000734
0.999646	8.53	0.008772	0.001946	0.000774
0.999631	8.56	0.009265	0.002057	0.000818
0.999614	8.58	0.009820	0.002181	0.000868
0.999595	8.60	0.010449	0.002322	0.000924
0.999574	8.63	0.011166	0.002482	0.000987
0.99955	8.65	0.011993	0.002666	0.001060
0.999522	8.68	0.012956	0.002879	0.001145

Source: This table is an example modified from DTN: SN0701PAEBSPCE.001_R1 [DIRS 180523].

NOTE: The table entries for relative humidity, $[Cl^-]$, $[NO_3^-]$, pH, and ionic strength have been rounded for display purposes and are based upon the seepage evaporation look-up table for Starting Water 1, $Pco_2 = 0.01$ bar, and T = 70°C.

For TSPA-LA Model use, the tabulated values displayed here are not used; the values are taken directly from DTN: SN0701PAEBSPCE.001_R1 [DIRS 180523]. Also, the table in the DTN has more lines than shown here, ending at an RH value of 0.500002.

Table 6.3.4-3. Illustration of Estimated Model Uncertainty Ranges for In-Drift Precipitated Salts Submodel Outputs of pH and Ionic Strength

Parameter	Units	Relative Humidity				
		Range 100% - 85%	**Range 85% - 65%**	**Range 65% - 40%**	**Range 40% - 20%**	**Range 20% - 0%**
I	log molal	+/- 0.1	0	0	0	0
Cl	log molal	0.0	+/- 0.1	+/- 0.4	+/- 0.5	+/- 0.7
N	log molal	0.0	+/- 0.2	+/- 0.4	+/- 0.5	+/- 0.9
$Cl:NO_3$	log mole ratio (unit less)	0.0	+/- 0.2	+/- 0.5	+/- 0.5	+/- 1.4
Cl+N	log molal	0.0	+/- 0.22	+/- 0.57	NA	NA
		Range 100% - 75%	**Range 75% - 65%**	**Range 65% - 0%**		
pH	pH units	[a]See table	+/- 1	+/-2		

Sources: Modified from DTN: SN0703PAEBSPCE.007_R2 [DIRS 184141], *PCE_IDPS-Uncertainties.xls*.

Ionic strength uncertainty below 85 percent relative humidity is zero (SNL 2007 [DIRS 177412], Table 6.12-1).

NOTE: These uncertainties are defined as triangular distributions.

[a]Table in the pH row refers to a table of pH uncertainty values contained within the source DTN.

Table 6.3.4-4. Summary of Chemistry for Seepage and Condensation in the TSPA-LA Model

	Seepage		No Seepage	
	Drift-Wall Condensation	**No Drift-Wall Condensation**	**Drift-Wall Condensation**	**No Drift-Wall Condensation**
Seismic/Nominal				
WP Outer Barrier; DS Intact	Dry air or humidity environment only.	Dry air or humidity environment only.	Dry air or humidity environment only.	Dry air or humidity environment only.
WP Outer Barrier; DS Failed	Use seepage composition equilibrated to T, RH, Pco_2 of WP outer barrier.	Use seepage composition equilibrated to T, RH, Pco_2 of WP outer barrier.	Use seepage composition equilibrated to T, RH, Pco_2 of WP outer barrier.	Dry air or humidity environment only.
IPC; DS Intact (WP Failed)	$[F^-]=0$; use chemistry for non-dripping case.	$[F^-]=0$; use chemistry for non-dripping case.	$[F^-]=0$; use chemistry for non-dripping case.	$[F^-]=0$; use chemistry for non-dripping case.
IPC; DS Failed (WP Failed)	$[F^-] \leq Fmax$; use chemistry for seepage case if $Q_4 \geq 0.1$ L/yr; otherwise non-dripping chemistry.	$[F^-] \leq Fmax$; use chemistry for seepage case if $Q_4 \geq 0.1$ L/yr; otherwise non-dripping chemistry.	$F^-=0$; use chemistry for seepage case if $Q_4 \geq 0.1$ L/yr; otherwise non-dripping chemistry.	$[F^-]=0$; use chemistry for non-dripping case.
Invert; DS Intact (WP Failed)	Use seepage composition equilibrated to T, RH, Pco_2 of invert.	Use seepage composition equilibrated to T, RH, Pco_2 of invert.	Use seepage composition equilibrated to T, RH, Pco_2 of invert.	Use seepage composition equilibrated to T, RH, Pco_2 of invert.
Invert; DS Failed (WP Failed)	Use in-package chemistry (seepage-based) to represent advective transport.	Use in-package chemistry (seepage-based) to represent advective transport.	Use in-package chemistry (seepage-based) to represent advective transport.	Use seepage composition equilibrated to T, RH, Pco_2 of invert.
Igneous Intrusion				
IPC; DS Failed (WP Failed)		Use basalt water without modification for environment; choose from alternatives in in-package chemistry documentation.		
Invert; DS Failed (WP Failed)		Use in-package chemistry selected above.		

Source: SNL 2007 [DIRS 177412], Table 6.15-1.

Table 6.3.4-5. Alternative Conceptual Models Considered for EBS Physical and Chemical Environment

Alternative Conceptual Models	Key Assumptions	Assessment and Basis
PTn Pore Water ACM	PTn pore water is used for the starting composition for the water that travels up the geothermal gradient downward through the TSw to the repository horizon (SNL 2007 [DIRS 177412], Section 6.11).	Not recommended for TSPA. Using PTn starting water compositions does not significantly impact the key chemical components (pH, Pco_2, Ca, K, Si) of seepage (SNL 2007 [DIRS 177412], Section 6.11). Using TSw starting waters adequately captures the behavior and uncertainty of the PTn pore water.
Treatment of Alkali Feldspar by the Near Field Chemistry Model: Kinetics versus Equilibrium	Volcanic feldspar has reached equilibrium or near equilibrium, and thus thermodynamic controls of feldspar dissolution (e.g. saturation indices) must be considered when calculating seepage water compositions (SNL 2007 [DIRS 177412], Section 6.11.2).	Not recommended for TSPA. At or near ambient temperatures, the volcanic waters are usually undersaturated with respect to feldspars and the kinetic treatment of the alkali feldspar is the appropriate approach (SNL 2007 [DIRS 177412], Section 6.11.2).
Closed System Model with Respect to CO_2	Carbonate exchange with the gas phase via CO_2 degassing or dissolution results in a corresponding increase or decrease of CO_2 in the gas phase (SNL 2007 [DIRS 177411], Section 6.5).	Not recommended for TSPA. A closed system with respect to CO_2 is not implemented in the IDPS model because the expected volume ratio of air to water in the drift is so large that CO_2 degassing from, or dissolving into, seepage water in the drift will negligibly affect the CO_2 fugacity compared to the uncertainty in the input value for CO_2 fugacity. A closed system might be appropriate in a wetter climate; however, RH would be ~100% and little or no evaporation would occur. To address this issue further, the IDPS model is used to quantify the output uncertainty resulting from the uncertainty in CO_2 fugacity in the P&CE Model (SNL 2007 [DIRS 177412], Section 6.3.2.8 and Section 6.15.1).

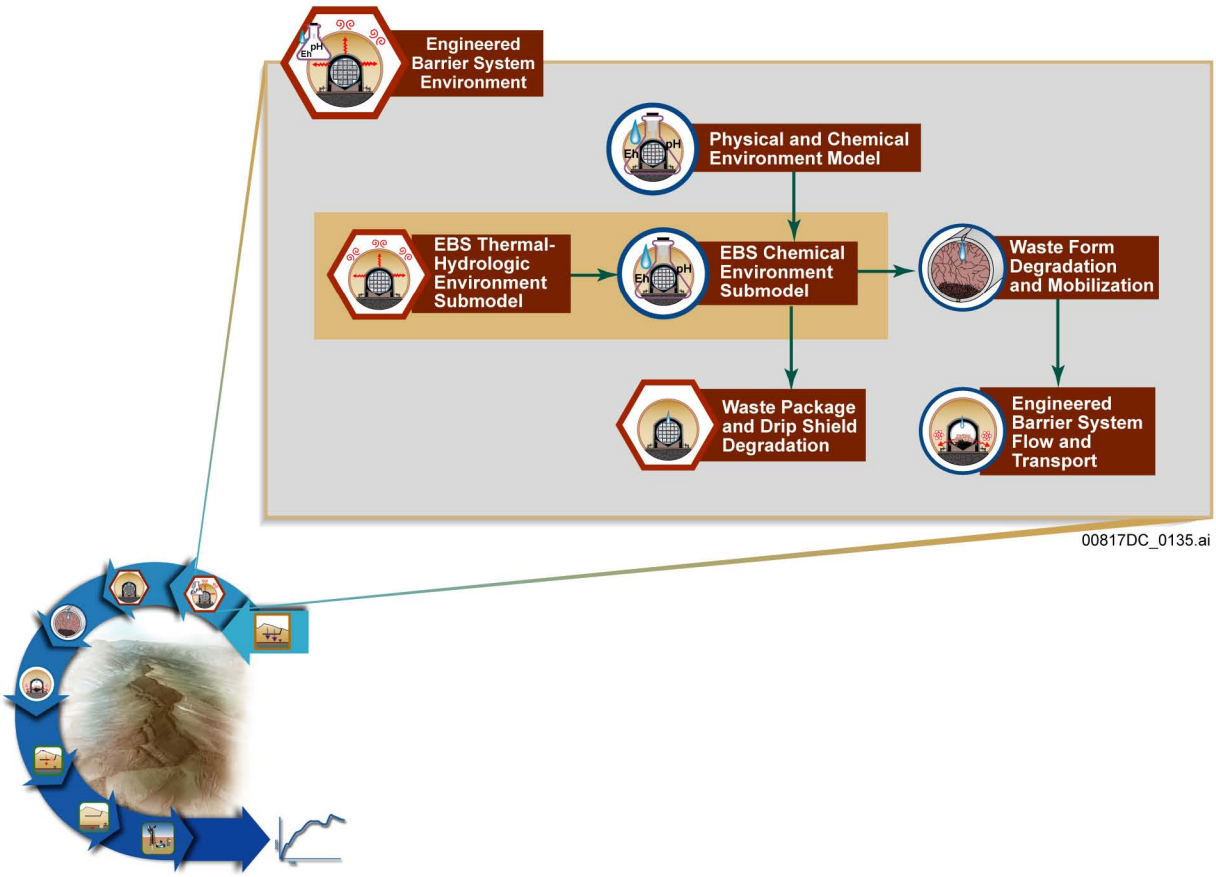

Figure 6.3.4-1. Information Flow Diagram for the EBS Chemical Environment Submodel

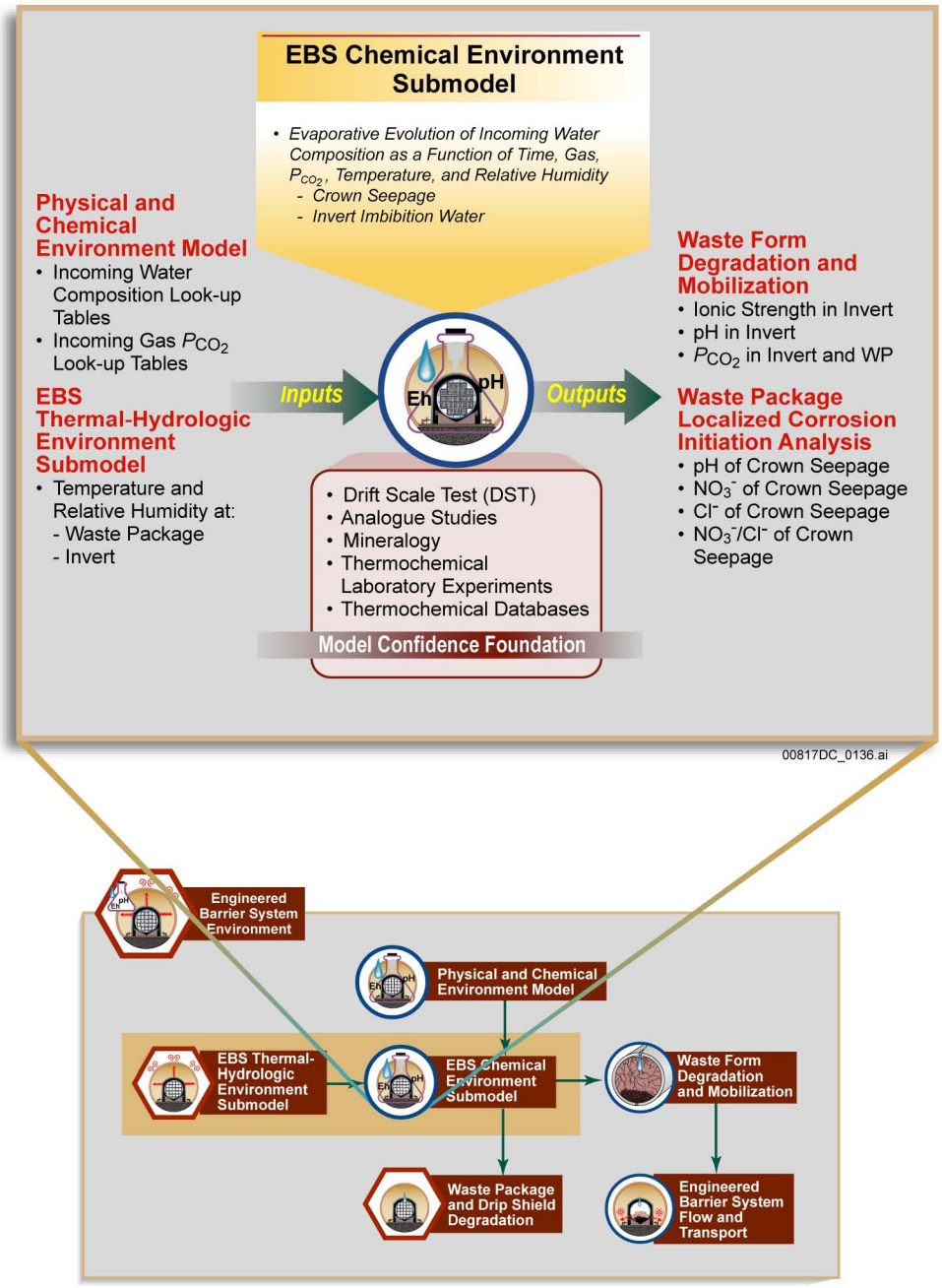

Figure 6.3.4-2. Inputs, Outputs, and Basis for Model Confidence for the EBS Chemical Environment Submodel

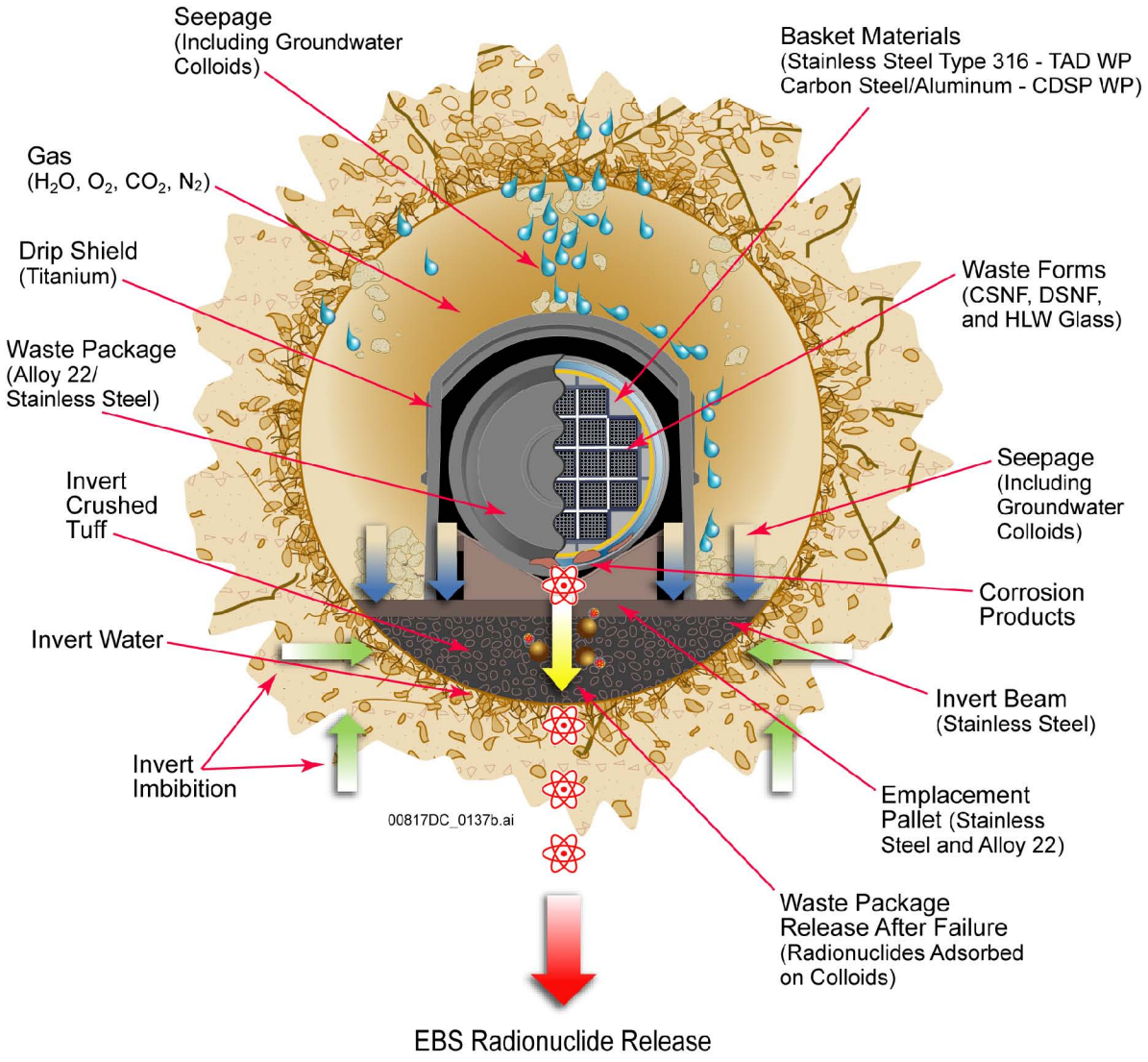

Figure 6.3.4-3. General EBS Design Features and Materials, Water Movement, and Drift Degradation

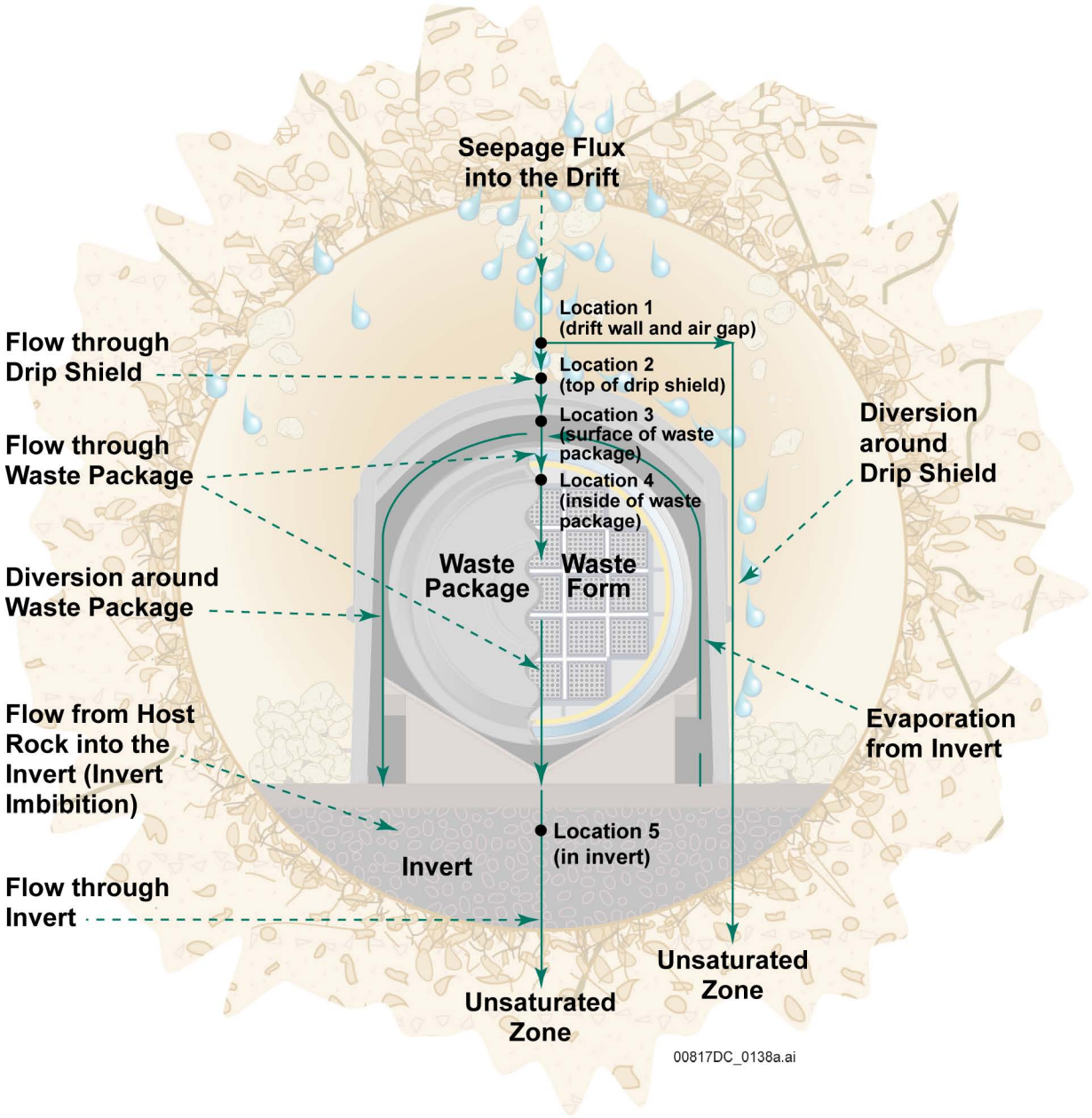

Figure 6.3.4-4. Schematic Diagram of EBS Flow Pathways (arrows) and Critical Locations (labels)

6.3.5 Waste Package and Drip Shield Degradation

The WPs and DSs are important components of the EBS. Figure 6.3.5-1 is a schematic illustration of the design features of the WPs and DSs. The two primary design functions of the DSs are to prevent seepage water from dripping directly on the WPs and to provide protection from rockfall damage to the WPs. The primary design functions of the WPs are to isolate the waste from the repository environment until the WPs fail and, after WP failure, to limit and delay the release of radionuclides to the EBS. The TSPA-LA Model for WP degradation includes five degradation mechanisms: general corrosion, microbially influenced corrosion (MIC), stress corrosion cracking (SCC), localized corrosion, and early failure of WPs. The TSPA-LA Model for DS degradation includes two degradation mechanisms: general corrosion and early failure of DSs. The DS and WP degradation mechanisms and their disposition for implementation in the TSPA-LA Model are documented in Table 6.3.5-1. The degradation mechanisms and their abstraction models are described in *General Corrosion and Localized Corrosion of the Drip Shield* (SNL 2007 [DIRS 180778], Section 6.1[a]); *General Corrosion and Localized Corrosion of Waste Package Outer Barrier* (SNL 2007 [DIRS 178519], Sections 6.4.3, 6.4.4, and 6.4.5); *Stress Corrosion Cracking of Waste Package Outer Barrier and Drip Shield Materials* (SNL 2007 [DIRS 181953], Section 6); and *Analysis of Mechanisms for Early Waste Package/Drip Shield Failure* (SNL 2007 [DIRS 178765], Section 6). The early failure of WPs and DSs is documented in two places. WP early failure resulting from weld flaws is documented in Section 6.3.5. All other WP and DS early failure degradation modes are documented in Section 6.4. The implementation of the localized corrosion degradation mechanism for the outer surface of WPs is summarized in the next paragraph. The relationships between the WP and DS Degradation Model Component and other TSPA-LA Model components and submodels are illustrated on Figure 6.3.5-2. The primary submodel supplying input to the WP and DS Degradation Model Component is the EBS TH Environment Submodel (Section 6.3.2), which provides exposure conditions (i.e., temperature and relative humidity) on WP outer surfaces. Output from the WP and DS Degradation Model Component is provided to the Waste Form Degradation and Mobilization Model Component and the EBS Flow and EBS Transport Submodels in the form of time-dependent tabulations of the fraction of WPs and DSs failed and the average breached area per failed WP and DS. Figure 6.3.5-3 summarizes the issues considered in the formulation of the WP and DS Degradation Model Component and its inputs and outputs.

The TSPA-LA Model implementation of localized corrosion of the outer surfaces of WPs is accomplished by exercising several interfaced TSPA-LA Model components and submodels in combination with the Localized Corrosion Initiation Abstraction in a probabilistic framework external to the TSPA-LA Model. A stand-alone analysis is used to compute time-dependent brine chemical composition and corrosion potential on WP outer surfaces. Outputs of the stand-alone analysis are time-dependent tabulations that specify the fraction of WPs that fail due to localized corrosion as a function of time. These WP fractional failure histories are imported into the TSPA-LA Model and used in the determination of WP degradation. The TSPA-LA implementation of localized corrosion is described in detail in Section 6.3.5.2.3.

The remainder of Section 6.3.5 is summarized as follows: Section 6.3.5.1 describes the WP and DS degradation conceptual models. The inclusion or exclusion of potentially important degradation mechanisms is outlined in Section 6.3.5.1.1. These include general corrosion, MIC,

and SCC. Manufacturing and material defects that result in WP early failures are also included. Section 6.3.5.1.2 contains the abstraction models corresponding to these conceptual models. Section 6.3.5.1.3 describes their implementation in the TSPA-LA Model. Section 6.3.5.2 focuses on the localized corrosion abstraction for the WP outer surface. This section describes how localized corrosion initiation is evaluated on the WP outer surface and how the results of this analysis are incorporated into the TSPA-LA Model. Section 6.3.5.3 discusses differences in assumptions and parameter sets that have arisen in the development of the supporting information for the TSPA-LA Model. Section 6.3.5.4 and Table 6.3.5-2 outline ACMs used to build confidence in the base-case model and ensure that the base-case model adequately captures the range of conceptual model uncertainty.

6.3.5.1 Waste Package and Drip Shield Degradation

DSs will be installed over the WPs just prior to repository closure. DSs will be made of Titanium Grade 7 plates with Titanium Grade 29 stiffeners and support beams to provide both corrosion resistance and structural strength. The DS plates will be at least 15 mm thick (SNL 2007 [DIRS179354], Table 4-2). As long as they remain substantially intact, the DSs will divert water that seeps into the drift away from the WPs and preclude damage to WPs resulting from rockfall. Because titanium is highly corrosion resistant, initial breaches of the DSs will not occur under nominal conditions until approximately 230,000 years postclosure (Section 6.3.5.1.3). The probability of DS plate failure before 10,000 years due to seismic ground motion and the resulting rockfall is estimated to be less than 3.4×10^{-4} (Section 7.3.2.6.1.3.2). WPs will prevent contact between water and waste as long as they are not breached and will limit water flow and radionuclide migration even after the WPs are breached. The WPs have a dual-metal design consisting of an inner vessel and a WP outer barrier. The inner vessel is composed of a 50-mm-thick layer of modified Stainless Steel Type 316. The WP outer barrier is a 25-mm-thick layer of Alloy 22, a corrosion-resistant nickel-based alloy (SNL 2007 [DIRS179394], Table 4-1). Alloy 22 protects the modified 316 stainless steel inner vessel from corrosion, and the modified 316 stainless steel inner vessel provides additional structural support for the thinner Alloy 22 WP outer barrier. The potential corrosion performance of the modified 316 stainless steel inner vessel is far less than that of the more corrosion-resistant Alloy 22 WP outer barrier. For this reason, the corrosion performance of the WP inner vessel is conservatively not included in this analysis. The WP outer barrier has a single Alloy 22 closure lid. The WP closure lid is welded to the WP outer barrier after the waste form (SNF or HLW glass, or both) is loaded.

6.3.5.1.1 Conceptual Model

The DSs and WPs are expected to be subject to many potential degradation mechanisms during the first 10,000 years after repository closure. Several of these degradation mechanisms were determined as ineffective under repository-relevant exposure conditions. The inclusion or exclusion of potentially important degradation mechanisms in the TSPA-LA Model is summarized in Table 6.3.5-1 and described as follows:

- General corrosion is a relatively uniform thinning of materials that occurs at all times. This degradation process is included in the TSPA-LA Model as a degradation mechanism for both the DSs and WPs (DTN: MO0706SPAFEPLA.001_R0

[DIRS 181613], FEP Numbers 2.1.03.01.0B and 2.1.03.01.0A). The conceptual models and abstractions are discussed in *General Corrosion and Localized Corrosion of the Drip Shield* (SNL 2007 [DIRS 180778], Section 6.1[a]) and *General Corrosion and Localized Corrosion of Waste Package Outer Barrier* (SNL 2007 [DIRS 178519], Section 6.4.3).

- Localized corrosion (pitting, crevice corrosion) is a phenomenon in which corrosion progresses at discrete sites or in a non-uniform manner.
  - Localized corrosion is excluded from the TSPA-LA Model as a DS degradation mechanism (DTN: MO0706SPAFEPLA.001_R0 [DIRS 181613], FEP Number 2.1.03.03.0B).
  - Localized corrosion is included as a WP degradation mechanism (DTN: MO0706SPAFEPLA.001_R0 [DIRS 181613], FEP Number 2.1.03.03.0A). Crevice corrosion is used to represent localized corrosion for the WP under the exposure conditions expected in the repository environment. This is a conservative and bounding assumption, as the initiation threshold for crevice corrosion in terms of exposure conditions is lower than for pitting corrosion (SNL 2007 [DIRS 178519], Section 6.4.4).
- SCC is a crack propagation process caused by the combined interaction of mechanical stress and corrosion reactions acting on a susceptible material. Possible sources of mechanical stress include weld-induced-residual stresses, plasticity-induced-residual stresses caused by seismic events, residual stresses produced by rockfall, and sustained rock rubble loading.
  - SCC is excluded in the TSPA-LA Model as a DS degradation mechanism (DTN: MO0706SPAFEPLA.001_R0 [DIRS 181613], FEP Number 2.1.03.02.0B).
  - SCC is included as a WP degradation mechanism (DTN: MO0706SPAFEPLA.001_R0 [DIRS 181613], FEP Number 2.1.03.02.0A). Because the waste container is fully annealed prior to being loaded with the waste form, the majority of the WP will not have appreciable residual tensile stresses upon emplacement. The outer barrier closure lid weld region cannot be fully annealed and is stress mitigated (by low plasticity burnishing) to produce a layer of compressive stress (SNL 2007 [DIRS 179394], Section 4.1.2.3; and SNL 2007 [DIRS 179567], Section 4.1.1.3) that prevents SCC initiation until general corrosion removes this layer (SNL 2007 [DIRS 181953], Section 8.4.2.1). Because fully annealed WPs will not contain tensile stresses, they will not be subject to SCC from nominal degradation processes. The WP outer surface is protected from rockfall by the presence of the DSs. Therefore, in the Nominal Scenario Class, SCC is considered only for the closure-lid welds. The number and size of weld flaws due to manufacturing defects is calculated in *Analysis of Mechanisms for Early Waste Package/Drip Shield Failure* (SNL 2007 [DIRS 178765], Section 6.3.1). Distributions for weld flaw number and size are incorporated into the WP SCC Abstraction. Weld flaws are not part of the Waste Package EF Modeling Case discussed in Section 6.4. *Stress Corrosion*

Cracking of Waste Package Outer Barrier and Drip Shield Materials discusses the modeling approach used to assess the degradation of the WP outer barrier due to SCC (SNL 2007 [DIRS 181953], Sections 6.4 and 6.5). SCC of the WP outer surface due to seismic degradation processes is discussed in Section 6.6.

- MIC is caused by the activity of microorganisms. Microorganisms can affect the corrosion of an alloy either by acting directly on the metal or through their metabolic products. MIC is documented in *General Corrosion and Localized Corrosion of the Drip Shield* (SNL 2007 [DIRS 180778], Sections 6.7.2 and 6.4[a]) and in *General Corrosion and Localized Corrosion of Waste Package Outer Barrier* (SNL 2007 [DIRS 178519], Section 8.2).
  - MIC is excluded from the TSPA-LA Model as a DS degradation mechanism (DTN: MO0706SPAFEPLA.001_R0 [DIRS 181613], FEP Number 2.1.03.05.0B).
  - MIC is included as a WP degradation mechanism as a multiplier to the general corrosion rate (DTN: MO0706SPAFEPLA.001_R0 [DIRS 181613], FEP Number 2.1.03.05.0A).
- Thermal aging and phase instability caused by prolonged exposure to elevated temperature environments can lead to microstructural changes of WP and DS materials, which could change their corrosion behavior. This process is excluded from the TSPA-LA Model as a DS degradation mechanism and as a WP degradation mechanism (DTN: MO0706SPAFEPLA.001_R0 [DIRS 181613], FEP Numbers 2.1.11.06.0B and 2.1.11.06.0A).
- Hydrogen-induced cracking is caused by the migration of atomic hydrogen into the metal and subsequent formation of metal hydrides. This process can cause metals to be more brittle and susceptible to cracking. This process is excluded from the TSPA-LA Model as a DS degradation mechanism and as a WP degradation mechanism (DTN: MO0706SPAFEPLA.001_R0 [DIRS 181613], FEP Numbers 2.1.03.04.0B and 2.1.03.04.0A).
- Mechanical damage due to dynamic loading conditions can damage WPs and DSs.
  - Mechanical damage is excluded as either a DS or WP degradation mechanism in the Nominal Scenario Class (DTN: MO0706SPAFEPLA.001_R0 [DIRS 181613], FEP Numbers 2.1.03.07.0B, 2.1.03.07.0A, and 2.1.06.07.0B).
  - Seismic-induced rockfall is included as a degradation mechanism for both DSs and WPs in the Seismic Scenario Class (DTN: MO0706SPAFEPLA.001_R0 [DIRS 181613], FEP Numbers 1.2.03.02.0C and 1.2.03.02.0B). The Seismic Scenario Class conceptual model and TSPA-LA Model implementation are discussed in Section 6.6.
- Radiolysis can result in the generation of hydrogen peroxide and changes in chemical conditions leading to enhanced corrosion. This process is excluded as a degradation

mechanism for both DSs and WPs (DTN: MO0706SPAFEPLA.001_R0 [DIRS 181613], FEP Number 2.1.13.01.0A).

Igneous-induced DS and WP degradation is discussed in *Number of Waste Packages Hit by Igneous Events* (SNL 2007 [DIRS 177432], Section 6.3). The impact of igneous events on DS and WP performance is summarized in Section 6.5 of this report.

Seismic-induced DS and WP degradation is described in *Seismic Consequence Abstraction* (SNL 2007 [DIRS 176828]) and summarized in Section 6.6 of this report.

6.3.5.1.2 Abstraction of Waste Package and Drip Shield Degradation

The WP and DS degradation processes included in the TSPA-LA Model are incorporated into the WP and DS Degradation Model Submodel, as documented in this section. The direct output from the WP and DS Degradation Submodel is a set of histories for WP and DS failure and the subsequent number of breaches in failed WPs and DSs, as a function of time. The WP and DS Degradation Submodel includes the DS General Corrosion Abstraction for DS degradation, the WP General Corrosion Abstraction, the WP MIC Abstraction, and the WP SCC Abstraction for WP degradation. The WP and DS Degradation Submodel also includes the abstraction for closure-lid weld flaws due to manufacturing defects. The primary submodel supplying input to the WP and DS Degradation Model Component is the EBS TH Environment Submodel (Section 6.3.2). The EBS TH Environment Submodel provides temperature and relative humidity histories. The WP degradation mechanisms modeled by the WP and DS Degradation Submodel (general corrosion, SCC, and MIC) are not chemistry-dependent. The DS general corrosion is chemistry dependent, and the development of two different abstractions for the outer and inner DS surfaces reflects this dependence. The WP general corrosion rate is a function of the temperature on the WP surface, while DS corrosion rates are independent of temperature.

DS Performance—General corrosion is the only DS degradation mechanism modeled in the WP and DS Degradation Submodel. This process is modeled as being independent of temperature and relative humidity and is initiated at the time of repository closure. General corrosion is modeled separately for the outer and inner surfaces of the DSs, each with a different general corrosion rate. The major difference between the inner and outer surfaces of the DSs is that the outer surfaces may be exposed to a more complex chemical environment because dust and/or seepage may reside on or contact the outer surfaces of the DSs. The inner surfaces are not expected to be exposed to seepage water.

The general corrosion models for the topside and underside surfaces of the DSs were developed based on corrosion rates determined from the weight-loss measurements of the Titanium Grade 7 coupons after a 2.5-year exposure to at the Long-Term Corrosion Testing Facility at Lawrence Livermore National Laboratory. The resulting weight-loss data set was divided into three groups with distinctively different rate distributions; namely, Aggressive Condition, Intermediate Condition, and Benign Condition. These groups span the range of expected conditions in the repository environment. The data subsets for two bounding conditions (Aggressive Condition and Benign Condition) were used for the model development and analysis (SNL 2007 [DIRS 180778], Section 6.1[a]). The data points termed aggressive were obtained from solutions

of simulated concentrated water considered to be representative of the evolution of groundwater compositions relevant to the repository environment.

The topsides of DSs in seeping environments in the repository are considered to be subject to the potentially aggressive conditions represented by the simulated concentrated water data. Because of the small number of data points available, the corrosion model for aggressive conditions is considered uncertain. The Student's t-distribution was used to characterize the uncertainty in the mean of the aggressive condition data (SNL 2007 [DIRS 180778], Section 6.1.6.2[a]). The undersides of all DSs are considered to be subject to benign conditions at all times. The uncertainty of the general corrosion model for benign conditions was developed by assuming the mean of the probability model is uncertain and the variance constant. A normal probability distribution was developed to characterize this uncertainty (SNL 2007 [DIRS 180778], Section 6.1.7.1[a]).

Although there is acknowledged variability in the DS general corrosion processes (SNL 2007 [DIRS 180778], Sections 6.1.6.1[a] and 6.1.7.2[a]), it is not considered in the TSPA-LA Model implementation. For TSPA-LA Model purposes, only the global aspect of DS degradation (DS thinning) is considered to be important. For the Seismic GM Modeling Case calculations the structural response is based on a discrete set of DS thicknesses (Section 6.6.1.2.2.1). Therefore, the uncertain Student's t-distribution for aggressive conditions and the uncertain normal distribution for benign conditions are used to model general corrosion on the topsides and undersides, respectively, of the DSs.

The general corrosion abstraction for the Titanium 29 DS framework in repository environments was developed in terms of the comparative behavior of Titanium Grade 29 versus Titanium Grade 7 (SNL 2007 [DIRS 180778], Section 6.2[a]). A cumulative distribution function (CDF) for the general corrosion rate ratio of Titanium Grade 29 to Titanium Grade 7 was developed. This CDF is to be sampled independently for every realization of the TSPA-LA Model. This parameter is used in the abstraction for DS damage in the Seismic Scenario Class (Section 6.6).

WP Performance—WP performance is modeled in the TSPA-LA Model by the WP and DS Degradation Model Component using two submodels. The first submodel, the WP and DS Degradation Submodel, includes general corrosion, MIC, and SCC. The second submodel, the WP Localized Corrosion Initiation Submodel, models the initiation and propagation of localized corrosion.

Two WP configurations are analyzed in the TSPA-LA Model file. The first WP configuration is referred to as the CSNF WP configuration for which the TAD canister configuration parameters are used. The second WP configuration analyzed is the CDSP WP configuration for which the 5 HLW/1 DOE SNF Long WP configuration parameters are used.

The WP surfaces are analyzed as being composed of sub-areas referred to as patches in order to represent spatial variation in degradation processes across the WP surfaces. The general corrosion, MIC, and SCC degradation mechanisms are modeled at the patch level on WPs, as shown on Figure 6.3.5-4, with each patch having, in general, a different general corrosion rate or SCC response. Figure 6.3.5-5 illustrates general corrosion processes for both dripping and non-dripping environments and degradation on the surfaces of both the DSs and the WPs. The

patches located in the last annulus shown on the WP on Figure 6.3.5-4 represent the closure-lid weld region, and SCC is modeled only on these closure-lid patches for nominal degradation processes. In contrast, SCC is modeled on the whole WP surface for seismic degradation processes (Section 6.6).

The general corrosion model used for the WP is based on weight-loss measurements for samples exposed in the Long-Term Corrosion Testing Facility (SNL 2007 [DIRS 178519], Section 6.4.3). For the WP outer barrier, samples with the crevice geometry were used to generate the general corrosion rate distribution (applied at 60°C). The crevice geometry samples have nominal dimensions of 2 in. × 2 in. × 1/8 in. and a 0.312-in. diameter hole in the center for sample mounting (SNL 2007 [DIRS 178519], Section 6.4.3). Therefore, the exposed surface area, A, for a crevice geometry sample is calculated as follows:

$$A = 2ab + 2bc + 2ac - \left(\frac{\pi d^2}{2}\right) + \pi dc \qquad \text{(Eq. 6.3.5-1)}$$

where a is the length of the specimen, b is the width of the specimen, c is the thickness of the specimen, and d is the diameter of hole. Using the dimensions above, the exposed surface area for a crevice sample (converted to mm^2) is 5,787 mm^2. The general corrosion analysis performed by the WAPDEG 4.07 software (STN: 10000-4.07-00 [DIRS 181774]; and STN: 10000-4.07-01 [DIRS 181064]) is limited to a maximum of 1,500 patches. Therefore, the TSPA-LA Model analysis uses a patch size of about four times that of the crevice coupon area of 23,150 mm^2 (output DTN: MO0707WPDRIPSD.000 [DIRS 183005]).

The surface areas of the CSNF and CDSP WPs are taken to be the values used in the EBS Radionuclide Transport Abstraction for the maximum diffusive area of corrosion products for the path through the outer barrier. These are defined in the file *SN0703PAEBSRTA.001-RTA.Input.Tables.doc* (DTN: SN0703PAEBSRTA.001_R3 [DIRS 183217], Table 8.2-6, parameters Diff_Area_CSNF_2_Max and Diff_Area_CDSP_2_Max). The number of patches used for calculation purposes can be derived by dividing the CSNF and CDSP surface areas by the patch area giving 1,430 patches for CSNF WPs and 1,408 patches for CDSP WP. The general corrosion rate distribution applied to the WP outer barrier is modified to reflect this change in scale between the smaller crevice geometry sample size and the patch size. This calculation is documented in output DTN: MO0707WPDRIPSD.000 [DIRS 183005].

For modeling purposes, the WP outer barrier is composed of two different regions; the closure-lid weld region and the shell region. The closure-lid weld region is represented as an annulus, one-patch side wide and with the same radius as the WP (Figure 6.3.5-1). Making the reasonable analysis assumption that the patches are square, the length of one side of a patch is then about 152 mm. The fraction of area represented by the closure-lid weld region for CSNF WPs is given by:

$$\frac{\text{Closure–Lid Weld Region Area}}{\text{WP Surface Area}} = \frac{\pi(diameter)(152)mm^2}{\pi(diameter)(5691)mm^2} \approx 0.0267 \qquad \text{(Eq. 6.3.5-2)}$$

or about 38 patches. For CDSP WPs, the fraction of area represented by the closure weld region is:

$$\frac{\text{Closure–Lid Weld Region Area}}{\text{WP Surface Area}} = \frac{\pi(diameter)(152)mm^2}{\pi(diameter)(5145)mm^2} \approx 0.0295 \quad \text{(Eq. 6.3.5-3)}$$

or about 42 patches.

The CSNF and CDSP WP lengths are 5,691 mm and 5,145 mm, respectively. These are defined in the file *SN0703PAEBSRTA.00-RTA Input Tables.doc* (DTN: SN0703PAEBSRTA.001_R3, [DIRS 183217], Table 8.2-6).

Note that the surface area of the closure lids themselves was not considered to be part of the WP surface area. Because the WP surface area is used primarily to determine the fraction of WP surface area subjected to SCC, it is conservative and appropriate to ignore the closure lid surface area in determining the total WP surface area.

Analyses presented in *Stress Corrosion Cracking of Waste Package Outer Barrier and Drip Shield Materials* (SNL 2007 [DIRS 181953], Section 6.6.1) indicate that the distance between two neighboring cracks must be greater than the plate thickness for the stress (and stress intensity factor) profile to be of sufficient magnitude to propagate a crack through-wall. Therefore, for the WP outer barrier outer closure-lid (which is 25 mm thick) and again making the analysis assumption that the patches are square (side length about 152 mm), about six cracks per patch are able to propagate through-wall.

Modeling degradation mechanisms at the patch level permits a representation of spatial variability in the degradation on the WP surfaces. Every WP patch is assigned a different corrosion rate and every WP is assigned different exposure conditions (WP temperature and relative humidity) and will, therefore, corrode at a different rate and fail at a different time. This variation represents WP-to-WP variability.

The WP and DS Degradation Submodel also considers general corrosion degradation of the WP inner surfaces, or inside-out corrosion. Inside-out general corrosion can only begin after WP failure. Note that inside-out SCC is not modeled because it would be of negligible consequence to WP performance, either because the WP would have already been breached by the much larger patch penetrations due to general corrosion or because the patches susceptible to SCC would have already been breached by SCC, thus reducing or eliminating the state of stress.

General Corrosion and MIC—The WP General Corrosion Abstraction for the outer surface of the WP is documented in *General Corrosion and Localized Corrosion of Waste Package Outer Barrier* (SNL 2007 [DIRS 178519], Section 8.2). The Alloy 22 general corrosion rate is considered to be a function of exposure temperature. The temperature-dependent general corrosion rate follows an Arrhenius relationship (SNL 2007 [DIRS 178519], Equation 6-28):

$$R = R_o \exp\left[C_1 \left(\frac{1}{333.15\ \text{K}} - \frac{1}{T} \right) \right]$$
$$= \exp\left[\ln(R_o) + C_1 \left(\frac{1}{333.15\ \text{K}} - \frac{1}{T} \right) \right] \quad \text{(Eq. 6.3.5-4)}$$

where

T = temperature in Kelvin.

C_1 = a slope term (in Kelvin) determined from short-term polarization resistance measurements for Alloy 22 specimens, tested for a range of sample configurations, metallurgical conditions, and exposure conditions. It is given by a truncated (-3 SD and +2 SD) normal distribution with a mean of 4,905 K and a SD of 1,413 K. The variation in C_1 is due entirely to epistemic uncertainty.

R_o = a rate (in mm/yr) sampled from one of three distributions for the corrosion rate of the WP outer surface at 60°C (333.15 K), developed from weight-loss data obtained from the five-year crevice geometry samples exposed in the Long-Term Corrosion Testing Facility.

For R_o, three Weibull distributions were developed from the five-year corrosion rate results for low, medium, and high uncertainty levels in the general corrosion rate (R_o) (SNL 2007 [DIRS 178519], Section 8.2). The distributions are randomly selected in such a way that the low and high general corrosion rate distributions are each used for 5 percent of epistemic realizations and the medium general corrosion rate distribution is used for the remaining 90 percent of epistemic realizations.

As noted above, the patch area used to analyze the WPs is four times the area of the crevice geometry sample size used to determine the three R_o distributions. Therefore, the general corrosion rates derived from the data analysis are adjusted to account for the effects of this change of scale (Aziz 1956 [DIRS 159379]; Shibata 1996 [DIRS 119589]). The method employed to accomplish this change in scale corresponds to using the highest of four sampled corrosion rates (from the two-parameter Weibull distribution) to analyze general corrosion of the WP patch. The approach is conservative because it is probable that not all four samples from the Weibull distribution will have the highest rate. A more realistic representation of the overall general corrosion rate would be the average of the four sampled corrosion rates. However, this approach would not account for the fact that one fourth of the patch has the maximum of the four sampled corrosion rates. On this basis, the proposed approach is conservative and appropriate for this application. Scaling the corrosion rates shifts the median general corrosion rate to higher values and decreases the probability of sampling lower general corrosion rates. This effect is shown on Figure 6.3.5-6 where the original distributions for R_o are plotted, along with the distributions resulting from a change of scale (or size factor) of four. The analysis for the change of scale is developed in the MathCad sheet, *WDlnRGC-ESC-hml.xmcd,* documented in TSPA output DTN: MO0707WPDRIPSD.000 [DIRS 183005].

The WP outer barrier is assumed to be subject to MIC when the relative humidity at the WP outer barrier surface is above a relative humidity threshold, which is uniformly distributed between 75 and 90 percent (SNL 2007 [DIRS 178519], Section 8.2). The entire variance of this

distribution is due to uncertainty. The effect of MIC on general corrosion of the WP outer barrier is represented by a multiplication factor (or MIC factor) to the general corrosion rate in the absence of MIC, such that:

$$CR_{MIC} = CR_{st} \times f_{MIC} \quad \text{(Eq. 6.3.5-5)}$$

where CR_{st} is the general corrosion rate in the absence of MIC, f_{MIC} is the MIC enhancement factor, and CR_{MIC} is the general corrosion rate in the presence of MIC. The MIC enhancement factor is assumed to be uniformly distributed between 1 and 2, and the entire variance of the distribution is due to patch-to-patch variability (SNL 2007 [DIRS 178519], Section 8.2).

SCC—All regions of the WPs, except the outer-closure-lid weld region, are solution annealed before the WPs are loaded with waste. Thus, in the absence of seismic activity, they do not develop residual stress or stress-intensity factors high enough for SCC to occur from nominal degradation processes (SNL 2007 [DIRS 181953], Section 6.5.3). The outer barrier closure-lid is 25 mm thick, as shown on Figure 6.3.5-7. The outer barrier closure lid weld region cannot be fully annealed and is stress mitigated (by low plasticity burnishing) to produce a layer of compressive stress (SNL 2007 [DIRS 179394], Section 4.1.2.3; SNL 2007 [DIRS 179567], Section 4.1.1.3) that prevents SCC initiation until general corrosion removes this layer (SNL 2007 [DIRS 181953], Section 8.4.2.1). SCC can be initiated on a smooth surface (incipient cracks) or at an existing weld flaw (due to manufacturing defects).

The analysis in *Stress Corrosion Cracking of Waste Package Outer Barrier and Drip Shield Materials* (SNL 2007 [DIRS 181953], Section 8) summarizes the abstractions for the SCC initiation and propagation process, the stress and stress intensity thresholds, and the crack growth model based on the slip dissolution film rupture (SDFR) theory.

In *Stress Corrosion Cracking of Waste Package Outer Barrier and Drip Shield Materials* (SNL 2007 [DIRS 181953], Section 8.4.2.2), it is noted that the hoop stress, which promotes radially oriented crack growth, is the dominant component of stress in the WP outer barrier closure-lid weld regions. On this basis, only the hoop stress profiles are considered in the TSPA-LA Model SCC implementation. The hoop stress (σ in MPa) as a function of depth (x in mm) in the closure weld regions of the Alloy 22 WP outer barrier is given by a third order polynomial equation (SNL 2007 [DIRS 181953], Equation 64):

$$\sigma(x,0) = A_0 + A_1 \times x + A_2 \times x^2 + A_3 \times x^3 . \quad \text{(Eq. 6.3.5-6)}$$

The second argument in the stress function is used to represent angular variation (θ = 0 arbitrarily chosen) around the circumference of the Alloy 22 WP outer closure-lid weld region. The angular variation is included using the following functional form (SNL 2007 [DIRS 181953], Equation 65):

$$\sigma(x,\theta,z) = \left(\sigma(x,0) - \nabla\sigma \times (1-\cos\theta)\right)\left(\frac{\sigma(th,\theta)+z}{\sigma(th,\theta)}\right) \quad \text{(Eq. 6.3.5-7)}$$

where x is the distance from the weld surface, θ is the angle in degrees from the reference location $\theta=0$, $\sigma(x,0)$ is the calculated weld residual stress profile at an angle $\theta=0$, and distance x from the weld surface, th is the lid thickness, $\nabla\sigma$ is the angular variation of the mean stress, and z is the uncertain scaling factor discussed below. Because stress intensity factor (K_I) is a linear function of stress, the variability in stress intensity factor around the circumference can be calculated as (SNL 2007 [DIRS 181953], Equation 66):

$$K_I(x,\theta,z) = K_I(x)\times\left(\frac{\sigma(th,\theta)+z}{\sigma(th,0)}\right) \quad \text{(Eq. 6.3.5-8)}$$

where th is the thickness of the closure-lid weld, z is the uncertain scaling factor discussed below, and $K_I(x)$ is the stress intensity factor at the zero position. The variation of the stress and stress intensity factor profiles with angle is due to variability.

The uncertainty in the stress and stress intensity factor profiles is introduced through a scaling factor, z. The scaling factor, z, which is sampled from a truncated normal distribution with a mean of zero and an SD of 5 percent of the yield strength, YS, has an upper-bound of 15 percent of the yield strength and a lower-bound of -15 percent of the yield strength (SNL 2007 [DIRS 181953], Section 6.5.6.2).

Flaws in the closure-lid welds are possible sites for SCC initiation. Weld flaws are generally larger than other surface defects and are conservatively considered to maintain their depth relative to the advancing general corrosion front (i.e., they are not removed by general corrosion processes). As discussed above, only radially oriented weld flaws are potential sites for SCC initiation. Weld flaws are a result of manufacturing defects (flaws not detected by the inspection processes). The analysis of the nondetection of weld flaws is documented in Section 6.3.1 of *Analysis of Mechanisms for Early Waste Package/Drip Shield Failure* (SNL 2007 [DIRS 178765]). The analysis was performed using the results from the welding of Alloy 22 specimen rings that duplicate closely the outer lid weld of a WP. Sixteen specimen rings were welded, employing procedures, processes, and equipment similar to that expected to be used for the closure of the WP. Nondestructive examinations were performed to accumulate significant information on the weld flaws and included ultrasonic and radiographic testing, which was followed by metallographic examination. This information consisted of weld flaw location, size, and shape. Based on this information, distributions were developed to characterize the size of the flaws in the through-wall extent of the weld, their density (mean number of flaws per volume of weld), and their depth (distance between the outer surface of the weld and the onset of the flaw).

The probability of nondetection, P_{ND}, of weld flaws of length x using an ultrasonic testing inspection technique is given by (SNL 2007 [DIRS 178765], Equation 17):

$$P_{ND}(x) = \varepsilon + \frac{1}{2}(1-\varepsilon)erfc\left(\nu\times\ln\left(\frac{x}{b}\right)\right) \quad \text{(Eq. 6.3.5-9)}$$

where

x = size of the flaw (in mm)

ε = lower limit of P_{ND}

v = shape factor

b = characteristic flaw size, in mm, which is the flaw size at the median of the P_{ND} distribution

erfc = complementary error function.

Weld flaw sizes follow an exponential distribution of parameter λ_s normalized to the weld thickness (*th)* (SNL 2007 [DIRS 178765], Equation 8). The flaw size probability density function is:

$$f_s(x) = \frac{\lambda_s \exp(-\lambda_s \cdot x)}{1 - \exp(-\lambda_s th)} \qquad \text{(Eq. 6.3.5-10)}$$

The flaw size distribution parameter (representing uncertainty), λ_s, is gamma distributed with shape parameter n_f (the number of weld flaws), and scale parameter, $1/S_f$ (where S_f is the cumulative size of test weld flaws).

The fraction of nondetected defects remaining in the weld (of thickness *th*) after inspection is given by the convolution of the probability of nondetection and the flaw size probability density (SNL 2007 [DIRS 178765], Equation 19):

$$F_{nr}(th) = \int_0^{th} P_{ND}(u) f_s(u) du \, . \qquad \text{(Eq. 6.3.5-11)}$$

The distribution for the number of defects before any inspection or repair is characterized by a flaw count distribution parameter λ_c (SNL 2007 [DIRS 178765], Equation 11). The flaw count distribution parameter (representing epistemic uncertainty), λ_c, is gamma distributed with shape parameter, $(n_f + ½)$, and scale parameter, $1/V_f$, where V_f is the cumulative weld volume in the test welds (SNL 2007 [DIRS 178765], Section 6.3.1.3).

The distribution for the number of defects that remain after inspection can be defined in terms of the quantities derived above. It is Poisson distributed with parameter λ (count per closure weld). For a weld of volume V and thickness *th*, λ is given by the product (SNL 2007 [DIRS 178765], Equations 23 and 24):

$$\lambda = F_\theta \times F_\psi \times F_{nr}(th) \times (V \times \lambda_c) \qquad \text{(Eq. 6.3.5-12)}$$

where

F_θ = fraction of weld flaws that are radially oriented (SNL 2007 [DIRS 178765], Equation 16) (equal to 0.008)

F_ψ = fraction of embedded weld flaws able to propagate (SNL 2007 [DIRS 181953], Section 6.3.4.2) (equal to 0.25)

$F_{nr}(th)$= fraction of nondetected flaws.

Note that Equation 6.3.5-12 includes two factors that are not explicitly discussed in Section 6.3.1.8 of *Analysis of Mechanisms for Early Waste Package/Drip Shield Failure* (SNL 2007 [DIRS 178765]). The first, F_θ, accounts for the fact that not all weld flaws will be radially oriented, and the second, F_ψ , for the fact that not all embedded weld flaws will propagate.

The detection and repair analysis uses coefficients such that there is a 50 percent probability of detection and repair of a 1/16 inch weld flaw (SNL 2007 [DIRS 178765], Appendix A.5). This treatment is conservative because design uses a repair criterion to repair all flaws 1/16 in. or greater (SNL 2007 [DIRS 179394], Table 4-1).

The slip dissolution-film rupture model describes the propagation of cracks after the stress and stress intensity thresholds are met. The slip dissolution-film rupture model relates SCC initiation and subsequent crack advance to the metal oxidation that occurs when the protective film at the crack tip is ruptured. The slip dissolution model can be applied to assess the breach of the WP due to crack propagation for either manufacturing defects (weld flaws) or inherent defects such as grain boundary junctions, surface asperities, or roughnesses (incipient cracks), or both. Inputs to the slip dissolution mechanism include threshold stress, threshold stress-intensity factor, an incipient crack size, and crack-growth-rate parameters.

The threshold stress is defined as the minimum stress at which cracks initiate on a smooth surface. This analysis refers to these as incipient cracks (to distinguish them from weld flaws) and typically form at local surface defects such as grain boundary junctions and surface roughness. Incipient cracks are considered to be 0.05 mm in length at the time of their nucleation (SNL 2007 [DIRS 181953], Section 8.4.2.1). The threshold stress is defined as a uniform distribution between 90 and 105 percent of the yield strength (SNL 2007 [DIRS 181953], Section 8.4.2.1). Incipient cracks nucleate when general corrosion has penetrated to the depth at which the stress profile (Section 8.4.2.2) exceeds the threshold stress. Weld flaws are already nucleated and, thus, do not require a stress threshold to nucleate. However, most weld flaws are embedded within the material and, therefore, are not exposed to the environment. As general corrosion proceeds, some initially embedded weld flaws will be exposed to the environment. The distribution for the number of weld flaws capable of propagation by the slip dissolution mechanism was derived in Equation 6.3.5-12.

Stress corrosion crack growth can occur when the stress intensity factor at the tip of the incipient crack or weld flaw exceeds or is equal to a threshold stress intensity factor. The depth of the tip is the sum of the general corrosion depth and the crack or weld flaw depth. The stress intensity

factor at this depth is determined from the stress intensity factor profile (Equation 6.3.5-8). The threshold stress intensity factor, K_{ISCC}, is given as a function of the repassivation slope, n, and the mean general corrosion rate, V_{GC}:

$$K_{ISCC} = \left(\frac{V_{GC}}{\overline{A}} \right)^{1/4n} \quad \text{(Eq. 6.3.5-13)}$$

where $\overline{A}$ is a function of n (repassivation slope) and V_{GC} is 7.23E-6 mm/yr (SNL 2007 [DIRS 181953], Section 8.4.2.3).

Once crack growth initiates, the crack(s) grows at a velocity given by (SNL 2007 [DIRS 181953], Section 8.4.2.3):

$$V_t = \overline{A}\left(K_I(x,\theta)\right)^{4n} . \quad \text{(Eq. 6.3.5-14)}$$

The repassivation slope n should be sampled from a truncated (at ±2 SD) normal distribution with a mean of 1.165 and upper and lower bounds of 1.395 and 0.935, respectively. The variation in the repassivation slope, n, is entirely due to uncertainty.

Figure 6.3.5-8 provides a summary and illustration of the information flow between the DS and WP General Corrosion and SCC Abstractions.

Treatment of Uncertainty—The TSPA-LA modeling of WP degradation accounts for variability by simulating the performance of several hundred WPs. The effects of spatial and temporal variations in the exposure conditions across the repository are included by explicitly incorporating the relevant exposure condition histories into the TSPA-LA Model. The exposure condition parameters that are considered to vary over the repository are temperature and relative humidity on the WP outer surfaces. In addition, the TSPA-LA Model considers spatial variability in corrosion processes on a single WP due to variability in corrosion rates. This variability is represented by dividing the WP outer surface area into sub-areas called patches and stochastically sampling the degradation model parameter values for each patch. The use of patches explicitly represents the variability in degradation processes on a single WP at a given time. Every WP in a given simulation is assigned different exposure conditions, thus addressing WP-to-WP variability.

In the TSPA-LA Model, epistemic uncertainty in WP and DS degradation is analyzed with multiple realizations of the TSPA-LA Model. For each realization, values are sampled for the uncertain degradation parameters shown in Table 6.3.5-3, and these values are passed to the WP and DS Degradation Submodel. Each TSPA-LA Model realization includes a complete model simulation of WP and DS degradation, using explicit values of the uncertain degradation parameters, as described in the following paragraphs.

General corrosion rates for the inner and outer surfaces of the DSs are represented by two distributions, one for aggressive environmental conditions and one for benign environmental conditions. These distributions represent epistemic uncertainty in DS general corrosion rates. For each realization, two general corrosion rates are sampled and applied to all DSs. All DSs in

a given realization fail at the same time. The Titanium Grade 29 to Titanium Grade 7 general corrosion rate multiplier, used to model general corrosion of the DS framework components in the Seismic GM Modeling Case, represents epistemic uncertainty and is sampled once for each realization of the TSPA-LA Model.

The general corrosion rate of the WP outer surface is temperature-dependent and includes epistemic uncertainty and spatial variability components. Epistemic uncertainty in the general corrosion rate is contained in its temperature-dependent slope term, C_1 (Equation 6.3.5-4). For each realization, a single general corrosion rate slope term is sampled and applied to all WPs, to represent epistemic uncertainty in the general corrosion rate with exposure temperature. The Alloy 22 general corrosion rate (R_o), which is represented by one of three CDFs determined from the five-year crevice geometry samples (Equation 6.3.5-4), has both variability and uncertainty components. Each individual CDF represents variability; the choice of which CDF to use for a particular realization represents the epistemic uncertainty in the fitting process. For every realization, each patch of each WP will have a different sampled value of R_o. In addition, spatial and temporal variability of the exposure temperature in the repository lead to spatial and temporal variability in the general corrosion rates used to model general corrosion of Alloy 22, due to the dependence of the general corrosion rate on temperature. A different exposure history file is assigned to each WP, resulting in a different WP surface temperature at each timestep. The net result is that every patch on each WP will have a different general corrosion rate, determined by the temperature read from the thermal history files at each timestep.

MIC is represented by an enhancement factor applied to the general corrosion rate of the WP outer surface, when the relative humidity threshold is exceeded. The value for the threshold relative humidity above which MIC takes place sampled from a uniform distribution, which represents epistemic uncertainty in the threshold. This distribution is sampled once per realization. The enhancement factor is also sampled from a uniform distribution, which represents spatial variability of the corrosion rate among various areas or patches on the WP outer surface. The MIC enhancement factor is sampled for each WP patch and applied if the threshold relative humidity is exceeded. The MIC enhancement factor has an additional WP-to-WP variability component due to the imposition of the relative humidity threshold, since the relative humidity on the WP surface varies from package to package.

The evaluation of weld flaw sizes and numbers of weld flaws includes epistemic uncertainty and variability. The variation in weld flaw sizes is expressed as variability at the WP level, given by a probability density function dependent on an uncertain flaw size parameter that is sampled for each realization (Equation 6.3.5-10). The variation in the number of weld defects is expressed as variability at the WP level given by a Poisson distribution with an uncertain parameter (count per closure weld) (Equation 6.3.5-12). This parameter is a function of the flaw size and count parameters that are sampled as uncertain for each realization (SNL 2007 [DIRS 178765], Table 7-1). The number and size of the weld flaws are randomly distributed to WP patches subject to SCC degradation. Thus, each SCC patch on every WP will have different initial values for the number and size of the weld flaws.

The evaluation of SCC initiation and propagation for the outer closure lid includes epistemic uncertainty and variability. Variability is represented by the variation of the stress and stress-intensity factor profiles with angle and depth. The epistemic uncertainty in the stress and

stress-intensity factor profiles is introduced through a scaling factor, *z*. The variations in the threshold stress and stress-intensity factor distributions are entirely due to epistemic uncertainty. The thresholds are sampled once per realization. The sampled threshold values are applied to all WP patches. The epistemic uncertainty in crack growth rate is a function of the repassivation slope. The variation in the repassivation slope is entirely due to epistemic uncertainty. The repassivation slope is sampled once per realization. The sampled repassivation slope value applies to all WP patches.

6.3.5.1.3 Implementation in the TSPA-LA Model

Overview—The TSPA-LA WP and DS Degradation Submodel makes use of several related software packages. The WAPDEG V4.07 software is a DLL that is responsible for simulating the spatial variability in WP degradation. The GoldSim V9.60.100 software (STN: 10344-9.60-01 [DIRS 181903]) is used to pass values to the WAPDEG V4.07 software and is responsible for treating the epistemic uncertainty in the WAPDEG V4.07 inputs. The GoldSim V9.60.100 software also calls several other DLLs that are used to incorporate uncertainty and variability in the inputs to the WAPDEG V4.07 software. These include the SCCD V2.01 software (STN: 10343-2.01-00 [DIRS 181157]; STN: 10343-2.01-01 [DIRS 181054]) for the treatment of variability in stress and stress-intensity factor profiles, and the CWD V2.0 software (STN: 10363-2.0-00 [DIRS 162809]; STN: 10363-2.0-01 [DIRS 181037]) for the treatment of uncertainty in the number and size of closure-lid weld manufacturing defects. The MkTable_LA V1.0 software (STN: 11217-1.0-00 [DIRS 181047]; STN: 11217-1.0-01 [DIRS 181048]) is used to randomly select a specified number of environment-history tables from the total set of environment-history tables. Each WP within a percolation subregion is assigned a different environment-history table. The environment-history tables are an output of the PREWAP_LA V1.0 software (STN: 10939-1.1-00 [DIRS 181053]), which processes the results from the comprehensive MSTHM Abstraction (Section 6.3.2.3). The PREWAP_LA V1.0 software reads these input files and writes corresponding environment-history output files, containing a subset of the data read from the MSTHM Abstraction files. These output files are created in a format that is compatible with the input files required by the WAPDEG V4.07 software program.

In the TSPA-LA Model, some of the parameters for the DS and WP degradation modes are sampled at the global level but the calculations, which use these parameters, are done at the second level of discretization (Section 6.1.5.3) in the percolation subregions associated with each WP type (CSNF WP or CDSP WP). The number of WPs to be emplaced in the repository is 11,629 (Table 6.3.7-1). The repository is divided into five spatially defined percolation subregions or bins (Section 6.3.2.2.1). Each percolation subregion contains a different number of WPs and is subject to different environmental conditions.

WP and DS Degradation Submodel—GoldSim Interface—The TSPA-LA Model file will typically call the WAPDEG V4.07 software program several times per GoldSim realization. The exact number of calls will depend on the modeling case being run. In the Nominal Modeling Case, 10 WAPDEG simulations are required: one for each CDSP WP and CSNF WP in each of the five repository percolation subregions. The main input to the WAPDEG V4.07 software program is a vector data element of real numbers. The values in the vector data element specify degradation models and degradation model parameters. The WAPDEG V4.07 software program

also requires distributions and tables stored in text files that cannot be passed by GoldSim. GoldSim instead passes line numbers that point to entries in a text file (WD4DLL.WAP) containing a list of the file names required by the WAPDEG V4.07 software. The vector data element and the contents of the files identified in the text file are the only inputs to the WAPDEG V4.07 software. The development of the WAPDEG input vector and associated files is documented in detail in TSPA output DTN: MO0707WPDRIPSD.000 [DIRS 183005].

Global Parameters and Calculations—The general corrosion of DSs has been specified with epistemic uncertainty in Section 8.1[a] of *General Corrosion and Localized Corrosion of the Drip Shield* (SNL 2007 [DIRS 180778]). Two uncertain mean corrosion rates are sampled independently per realization and are used for the general corrosion calculations for the DS. For this purpose, TSPA uses the parameters WDDSAggrGC_Mean_a and WDDSBenignGC_Mean_a (Table 6.3.5-3) for the Titanium Grade 7 corrosion rates. In addition, the DS general corrosion rate for aggressive conditions is used on the top side of all DSs, whether or not they encounter seeping conditions. The use of the aggressive rate for DSs that are not seeped on has no impact on dose calculations in the Nominal Modeling Case. The impact of the use of the aggressive rate for the top sides of DSs that are not seeped on in the Seismic GM Modeling Case is discussed in Appendix C (Section C6.3.1).

The earliest possible DS failure time can be calculated by combining the most severe degradation rates from the aggressive and benign distributions. Using the distributions given in the first two rows of Table 6.3.5-3 and using values at the 0.9999 probability level gives an aggressive rate of 5.75×10^{-5} mm/year and a benign rate of 0.824×10^{-5} mm/year. Combining these gives a rate of 6.57×10^{-5} mm/year, which corresponds to a DS failure time of about 230,000 years.

Some of the parameters defining the general corrosion rate for the WP are sampled globally, but the actual calculation of the WP general corrosion rate is done at the percolation subregion level, because the WP general corrosion rate is a function of exposure temperature. The first input to the calculation of the WP general corrosion rate is the slope term for the general corrosion rate, given by a truncated (-3 SD and +2 SD) normal distribution with a mean of 4,905 K and an SD of 1,413 K (DTN: MO0703PAGENCOR.001_R4 [DIRS 182029]). This parameter represents epistemic uncertainty and is sampled once per realization. The second parameter is a rate distribution (in mm/yr) for the WP outer surface at 60°C. One of three rate distributions is chosen randomly in such a way that the low and high general corrosion rate distributions are each used for 5 percent of realizations and the medium general corrosion rate distribution is used for the remaining 90 percent of realizations (DTN: MO0703PAGENCOR.001_R4 [DIRS 182029]). This distribution is sampled by the WAPDEG V4.07 software for every patch on each WP. Because the temperature of the WP surface is different for every WP simulated in a given percolation subregion, the result is a different general corrosion rate for every patch on every WP. General corrosion of Alloy 22 is implemented in WAPDEG using the general linear functional form (BSC 2002 [DIRS 162606], Section 4.2.6.5). The WP thickness is taken to be 25 mm, the minimum value specified for design purposes (SNL 2007 [DIRS 179394], Table 4-1).

The relative humidity threshold for MIC is an epistemically uncertain parameter, sampled once per realization. The relative humidity threshold is uniformly distributed between 75 percent and 95 percent. The MIC factor is uniformly distributed between one and two

(DTN: MO0703PAGENCOR.001_R4 [DIRS 182029]). However, the calculation is done at the percolation subregion level because the initiation of MIC occurs when a threshold relative humidity is exceeded. A unique relative humidity is read, as a function of time, from the environment-history tables generated by the MkTable_LA V1.0 software for each WP surface. The CWD V2.0 software implements the abstraction for the number and size of weld flaws documented above (Equations 6.3.5-9 to 6.3.5-12). The CWD V2.0 software is executed two times per realization: once for the outer-closure lid of the CSNF WPs and once for the outer-closure lid of the CDSP WPs. The CWD V2.0 software computes the cumulative probability of a manufacturing defect based on the probability for the nondetection of weld defects. The inputs to this calculation are weld thickness, weld volume (weld length × weld cross-section), the defect fraction considered, a detection threshold, a characteristic defect size, a shape factor, a defect count parameter, and a defect-size parameter. All of these inputs are taken from DTN: MO0701PASHIELD.000_R2 [DIRS 180508], except the weld length, which is calculated as the product of π and the outside diameter of the WP outer corrosion barrier (SNL 2007 [DIRS 179567], Table 4-8). The output of each invocation of the CWD V2.0 software consists of two tables and the probability of occurrence of at least one defect per WP. These output tables contain distributions for the density and size of defect flaws on the outer-closure lid. The CWD outputs are direct inputs to the WAPDEG V4.07 software.

The SCCD V2.01 software implements the abstraction for the stress and stress intensity factor profiles documented above (Equations 6.3.5-6 to 6.3.5-8). The SCCD V2.01 software is executed once per realization for the outer-closure lid. The SCC calculation is the same for both CDSP WPs and CSNF WPs. The SCCD V2.01 software calculates the variation in stress and stress intensity factor versus depth and angle. The inputs to this calculation are four regression coefficients from the model abstraction for stress as a function of depth, the sine of the fracture angle, the number of angles to be calculated, the expected yield strength, the yield-strength scaling factor, the angular amplitude of the stress variation, the uncertainty model, and an uncertain deviation from median yield-strength range. All of these inputs are taken from DTN: MO0702PASTRESS.002_R2 [DIRS 180514], except the sine of the fracture angle (SNL 2007 [DIRS 181953], Section 6.5.3.3.1 and Figure 6-18) and the uncertainty model (output DTN: MO0707WPDRIPSD.000_R0 [DIRS 183005], AB-TSPA-DOC (PEF 93)). Also required is the stress intensity factor versus depth profile for the zero reference angle. The outputs of the SCCD V2.01 software are stress and stress intensity factor tables, as a function of depth, calculated at a number of angles (equally spaced and in the range 0 to π radians, inclusive) (DTN: MO0702PASTRESS.002_R2 [DIRS 180514]). The SCCD V2.01 software outputs are direct inputs to the WAPDEG V4.07 software.

Percolation Subregion Parameters and Calculations—The total number of WPs modeled is 11,629 (8,213 CSNF WPs and 3,416 CDSP WPs) (DTN: MO0702PASTREAM.001_R0 [DIRS 179925], Item 4 of worksheet UNIT CELL in spreadsheet *DTN-Inventory-Rev00.xls*.). These WPs are partitioned among the five percolation subregions according to the percolation-flux distributions. The resulting partitioning is described in Section 6.3.2.2.1 and shown in Table 6.3.2-2. In the Nominal Modeling Case, the WAPDEG V4.07 software runs twice for each of the five percolation subregions: once for the CSNF WPs in that subregion and once for CDSP WPs. A sensitivity analysis (documented in output DTN: MO0709TSPAWPDS.000 [DIRS 183170]) was executed with 250, 500, 1,000, 1,500, and 3,000 DS and WP pairs. Comparison of the mean and 95th percentile WP first failure curves

showed that the analysis results were not very sensitive to the number of DS and WP pairs simulated over the range investigated. Therefore, in the TSPA-LA Model, if the percolation subregion contains fewer than 500 DS/WP pairs, the number of CSNF and CDSP DS and WP pairs simulated by the WAPDEG V4.07 software is equal to the number of pairs in the subregion. If the subregion contains more than 500 DS/WP pairs, then only 500 CSNF and 500 CDSP DS/WP pairs are simulated by the WAPDEG V4.07 software.

The primary submodel supplying input to the WP and DS Degradation Model Component is the EBS TH Environment Submodel (Section 6.3.2). The EBS TH Environment Submodel provides temperature and relative humidity histories for eight DS/WP pairs, composed of six CSNF WPs and two CDSP WPs at each of the 3,264 repository subdomain locations (Section 6.3.2.2). These 3,264 repository subdomain locations are partitioned among the five percolation subregions according to the percolation-flux distributions (Section 6.3.2.2.1). The resulting partitioning is shown in Table 6.3.2-2.

Each WAPDEG simulation requires a unique exposure history for each of the DS/WP pairs being simulated. The MkTable_LA V1.0 software samples these exposure histories from those available for the percolation subregion. The set of exposure histories that is available for sampling is determined by the WP type (CSNF WP or CDSP WP), the percolation subregion, the infiltration scenario, and the thermal conductivity. An external text file, *WDHist.inp*, contains a list of file names corresponding to exposure histories. The external file, *WDHist.inp*, is a generic file pointing to one of twelve possible files. These files correspond to combinations of the four possible infiltration scenarios (corresponding to the four climate states) and high, medium, and low thermal conductivity. The choice of which three files to use is controlled by the MFCP_LA V1.0 software (STN: 11071-1.0-00 [DIRS 167884], STN: 11071-1.0-01 [DIRS 181045]) on the basis of the sampled values for infiltration scenario and thermal-conductivity uncertainty.

WAPDEG V4.07 Software Overview—The WAPDEG V4.07 software simulates corrosion degradation of WPs by three penetration modes: patch penetration (due to general corrosion), crack penetration (due to crack tip growth or SCC), and pit penetration (due to pitting corrosion or crevice corrosion) (BSC 2002 [DIRS 162606], Section 3.3). Only the first two of these modes are invoked in the TSPA-LA Model. The WAPDEG V4.07 software structure specifies corrosion-affecting events that affect specific degradation processes. Each event is identified by a unique integer in the WAPDEG input vector. Each event has both event-specific data and generic data. The event-specific data triggers effects that are unique to that event. The data that describes the generic event effects has the same input structure for each event and is read at the end of the event-specific data. There are four possible generic effects of any event. These are to immediately fail the patches affected by the event, and/or to initiate localized corrosion modes, and/or to accelerate a corrosion mode or modes, and/or to reduce thresholds (BSC 2002 [DIRS 162606], Section 3).

General corrosion of Alloy 22 is implemented in the WAPDEG V4.07 software using the general linear functional form (BSC 2002 [DIRS 162606], Section 4.2.6.5). The form used for the TSPA-LA implementation of the Alloy 22 corrosion rate is:

$$D = \exp\left(\ln(R_o) + \frac{C_1}{333.15} + \varepsilon\right)\exp\left(-\frac{C_1}{T}\right)\ t^n \qquad \text{(Eq. 6.3.5-15)}$$

where D is corrosion depth (mm), t is time (yr), and T is exposure temperature (K). The parameter ε is not used in the TSPA-LA implementation. It is set to zero. The time exponent, n, has the value 1.0. The effect of MIC on the general corrosion of the WP is analyzed by the use of a MIC event (BSC 2002 [DIRS 162606], Section 4.2.7.10).

In the WAPDEG V4.07 software, the weld flaws are defined by a manufacturing defects event (BSC 2002 [DIRS 162606], Sections 3.3.2.1 and 4.2.7.2). The manufacturing defects event has only one specific effect, to introduce manufacturing defects onto patches. SCC is implemented in WAPDEG by the use of a slip dissolution event (BSC 2002 [DIRS 162606], Sections 3.3.2.1.1 and 4.2.7.5). Incipient cracks are automatically included in the event, but weld flaws must be specifically included via a manufacturing defects event. The slip dissolution event models the rate of crack growth and defines the time of crack penetration. The slip dissolution event implements the abstraction for crack growth presented in Equations 6.3.5-13 and 6.3.5-14.

The development of the WAPDEG input vector and associated files is documented in output DTN: MO0707WPDRIPSD.000 [DIRS 183005].

WP and DS Degradation Submodel Output—There is a one-dimensional table and a two-dimensional table output for each implementation of the WAPDEG V4.07 software. The one-dimensional table contains WP first-failure times versus the fraction of WPs failed. The WP first-failure time is defined as the first penetration by any mechanism (general corrosion or SCC) of the WP. The format of both of these tables is as follows; the first column contains the WP first-failure times in years (sorted in increasing order) and the second column contains the cumulative fraction WPs failed. The two-dimensional table contains 12 columns. The number of rows is controlled by the parameter NumBin (output DTN: MO0707WPDRIPSD.000 [DIRS 183005]) defined in the TSPA-LA Model and passed to the WAPDEG V4.07 software. The column contents are explained in *User's Manual for WAPDEG 4.07* (BSC 2003 [DIRS 162606], Table 19).

The outputs generated by the WP and DS Model Component and used by the EBS Flow and Transport Model Component (Sections 6.3.6 and 6.3.8) for each percolation subregion and each fuel type (CSNF and CDSP WPs) are:

- The average fraction of WP surface failed by general corrosion (patches), per failed WP, and the average fraction of WP surface failed by cracks, per failed WP, as a function of time
- The fraction of all the WPs and DSs in the subregion that were breached, as a function of time.

Note that the average fraction of WP surfaces failed by general corrosion or by cracks are values that apply to all WPs and DSs in a given percolation subregion and for a given fuel type. These values are calculated by the WAPDEG V4.07 software as an average over failed WPs.

6.3.5.2 Localized Corrosion on the Waste Package Outer Surface

The WP Localized Corrosion Initiation Submodel for the WP outer surface is based on the Localized Corrosion Initiation Abstraction developed in *General Corrosion and Localized Corrosion of Waste Package Outer Barrier* (SNL 2007 [DIRS 178519], Section 8.3.1). The temperature, pH, chloride-ion concentration, and nitrate-ion concentrations in aqueous solutions on the WP outer surface are the primary factors that determine the potential for initiating localized corrosion. These are obtained from the EBS TH Environment Submodel and the EBS Chemical Environment Submodel. Localized corrosion requires the presence of a liquid water film on the WP surface. Two types of aqueous solutions may lead to environmental conditions conducive to localized corrosion initiation on the WP outer surface: (1) dripping crown seepage water that contacts the WP outer surface, and (2) salt deliquescence in dust particles that may reside on the WP outer surface. Localized corrosion resulting from salt deliquescence in dust particles was screened out (SNL 2007 [DIRS 181267]). Also discussed in this section is the localized corrosion growth model, which applies to the WP during the time period when localized corrosion is indicated by the Localized Corrosion Initiation Abstraction. Appendix N discusses the details of the implementation of localized corrosion in the TSPA-LA Model.

6.3.5.2.1 Conceptual Model

Initiation of Localized Corrosion (Crevice Corrosion)—The Localized Corrosion Initiation Abstraction stipulates that localized corrosion of the WP outer surface occurs when the open-circuit potential, or corrosion potential (E_{corr}), is equal to or greater than the critical threshold potential ($E_{critical}$); that is, $\Delta E = E_{critical} - E_{corr} \leq 0$ (SNL 2007 [DIRS 178519], Section 8.3.1).

The open-circuit corrosion potential is the potential measured across a metal sample when it is immersed in a liquid. The corrosion potential can change with time, eventually approaching a steady state. Therefore, the long-term steady-state corrosion potential was used for the corrosion potential model of Alloy 22 (SNL 2007 [DIRS 178519], Section 4.1.1.5).

The long-term corrosion potential abstraction for the WP outer surface was developed using a regression model fit to the long-term corrosion potential data as a function of the major exposure-environment variables: temperature, pH, chloride ion concentration, and nitrate ion concentration. Only data with an immersion time of 250 days or higher were used (SNL 2007 [DIRS 178519], Section 6.4.4.5). The WP outer surface is potentially susceptible to crevice corrosion if an acidic chloride-containing solution with relatively lower concentrations of inhibitive ions contacts the WP outer surface while it is at elevated temperature.

The crevice repassivation potential from cyclic potentiodynamic polarization tests was selected as a conservative measure of $E_{critical}$, as described in *General Corrosion and Localized Corrosion of Waste Package Outer Barrier* (SNL 2007 [DIRS 178519], Section 6.4.4.1). The crevice repassivation potential (E_{rcrev}) is the potential at which the reverse scan of a cyclic potentiodynamic polarization curve using a creviced sample crosses the forward scan.

Corrosion Penetration Rate—Because of the relatively high corrosion resistance of Alloy 22, there are limited experimental results regarding localized corrosion under the conditions expected in the repository. The Localized Corrosion Penetration Rate Abstraction for the WP

outer surface was based on results that bound the extreme penetration rates found in the literature for Alloy 22. This distribution is considered to be a highly conservative representation of the localized corrosion rates of Alloy 22 for the exposure conditions anticipated in the repository environment (SNL 2007 [DIRS 178519], Section 8.3.2).

The Localized Corrosion Initiation Submodel uses a constant (time-independent) penetration rate after localized corrosion is initiated (SNL 2007 [DIRS 178519], Assumption 5.4). This constant penetration rate is sampled from the epistemic uncertainty distribution for the localized corrosion rate and differs from realization to realization. Although the localized corrosion rate is modeled as time invariant, the crevice corrosion propagation rate would be expected to decrease with increasing depth of the crevices and time under realistic conditions. The use of constant penetration rate versus time is a highly conservative assumption because localized corrosion rates generally decrease with time and this decrease is even more likely under the thin water film environment that is expected to form on the WP outer surface in the postclosure repository period, as described in *General Corrosion and Localized Corrosion of Waste Package Outer Barrier* (SNL 2007 [DIRS 178519], Section 8.3.2) and *Waste Package Degradation Expert Elicitation Project* (CRWMS M&O 1998 [DIRS 100349], Table 3-2).

In the absence of specific information regarding local environments on the WP, the area of the Alloy 22 WP outer barrier that is contacted by seepage is considered to be potentially subject to localized corrosion (SNL 2007 [DIRS 178519], Section 8.3.1).

6.3.5.2.2 Model Abstraction

For the TSPA-LA Model, the Localized Corrosion Initiation Abstraction uses the crevice repassivation potential (E_{rcrev}) as the critical potential. The crevice repassivation potential for crevice corrosion on the WP outer surface is defined in terms of WP surface temperature and chemical conditions as follows:

$$E_{rcrev} = a_o + a_1 T + a_2 \ln\left[Cl^-\right] + a_3 \frac{\left[NO_3^-\right]}{\left[Cl^-\right]} + a_4 T\left[Cl^-\right] + \varepsilon_{rcrev} \qquad \text{(Eq. 6.3.5-16)}$$

where a_o, a_1, a_2, a_3, and a_4 are regression constants, T is the WP outer surface temperature (°C), pH is the negative log of the hydrogen ion activity, [NO_3^-] is the nitrate ion molality (moles/kg water), and [Cl^-] is the chloride ion molality (moles/kg water), as presented in DTN: MO0703PAGENCOR.001_R4 ([DIRS 182029], file: *LC_Initiation.pdf*). The coefficient values and their epistemic uncertainty (±1 SD) are a_o= 190.242 ± 18.373, a_1= -3.008 ± 0.225, a_2= -46.800 ± 3.126, a_3= 535.625 ± 26.140, and a_4= 0.061 ± 0.010. The error term, ε_{rcrev}, is a term representing data variance not explained by the fitting procedure and has a normal distribution with a mean of zero mV versus the saturated silver chloride electrode and an SD of 45.055 mV versus saturated silver chloride. The units of the coefficients should be consistent with E_{rcrev} having units of mV. The covariation of the coefficients (due entirely to epistemic uncertainty) was represented through the use of a covariance matrix derived in *General Corrosion and Localized Corrosion of Waste Package Outer Barrier* (SNL 2007 [DIRS 178519], Section 8.3.1; DTN: MO0703PAGENCOR.001_R4 [DIRS 182029]). The Localized Corrosion Initiation Abstraction stipulates that the calculated value of E_{rcrev} be

compared to the ±2 SD prediction intervals of the unconstrained model and be truncated at these values. These coefficients are sampled in the TSPA-LA Model using a Cholesky factorization method to induce correlation (output DTN: MO0707WPDRIPSD.000 [DIRS 183005]).

The long-term steady-state corrosion potential, E_{corr}, for the WP outer surface is expressed as:

$$E_{corr} = c_o + c_1 T + c_2 pH + c_3 \frac{[NO_3^-]}{[Cl^-]} + c_4 T \frac{[NO_3^-]}{[Cl^-]} + c_5 pH \frac{[NO_3^-]}{[Cl^-]} + c_6 pH \ln[Cl^-] + \varepsilon_{corr}$$

(Eq. 6.3.5-17)

where c_o, c_1, c_2, c_3, c_4, c_5, and c_6 are coefficients of the parameters, and the other parameters are as previously defined. The regression coefficients and their epistemic uncertainty (± 1 SD) are: c_0 = 1,051.219 ± 119.774, c_1= -3.024 ± 0.977, c_2= -155.976 ± 11.495, c3 = -1,352.040 ± 252.224, c4 = 10.875 ± 1.890, c5 = 137.856 ± 23.158, and c_6 = -8.498 ± 0.801 (DTN: MO0703PAGENCOR.001_R4 [DIRS 182029], file: *LC_Initiation.pdf*). The error term, ε_{corr}, is a term representing data variance not explained by the fitting procedure and has a normal distribution with a mean of zero mV versus SSC and an SD of 85.265 mV versus SSC. The units of the coefficients should be consistent with E_{corr} having units of mV.

The covariation of the coefficients (due entirely to epistemic uncertainty) was represented through the use of a covariance matrix derived in DTN: MO0703PAGENCOR.001_R4 [DIRS 182029]. As with the crevice repassivation potential, E_{rcrev}, the uncertainty of the parameter coefficients of the corrosion potential, E_{corr}, should be limited to ±2 SDs. These coefficients are sampled in the TSPA-LA Model using a Cholesky factorization method to induce correlation (output DTN: MO0707WPDRIPSD.000 [DIRS 183005]).

The WP Localized Corrosion Penetration Rate Abstraction propagates corrosion in the WP outer surface at a constant rate (SNL 2007 [DIRS 178519], Assumption 5.4). The extreme penetration rates found in the literature were used to bound localized corrosion rates for Alloy 22 under expected repository conditions. Based on these published rates, the localized corrosion propagation rates for the WP outer surface were estimated to be log uniformly distributed with a range from 12.7 to 1,270 μm/year (DTN: MO0703PAGENCOR.001_R4 [DIRS 182029]).

Localized corrosion initiation requires the presence of liquid brine on the WP outer surface. This brine may be formed by aqueous solutions dripping onto the WP surface. For intact or moderately degraded drifts, there is no seepage water contacting the WP surface if the drift-wall exposure temperature is greater than 100°C (SNL 2007 [DIRS 181244], Section 6.5.3) or if the WP surface temperature is greater than 120°C. The 120°C limit is inferred from examination of peak drift-wall and WP temperatures for the seven modeled uncertainty cases presented in *Multiscale Thermohydrologic Model* (SNL 2000 [DIRS 181383], Table 6.3-49[a]). For collapsed drifts, boiling conditions persist later into the repository lifetime (SNL 2007 [DIRS 181383], Figure 6.3-79[a]). Therefore, the thermal seepage limit for intact or moderately degraded drifts can be considered bounding. Thus, the only relevant chemistries to consider for localized corrosion initiation, for WP surface temperatures greater than 120°C, are those that result from dust deliquescence. However, localized corrosion resulting from salt deliquescence

in dust particles was screened out of the TSPA-LA Model, based on geochemical analyses (DTN: MO0706SPAFEPLA.001_R0 [DIRS 181613], FEP Number 2.1.09.28.0A). Therefore, localized corrosion initiation at WP temperatures greater than 120°C need not be considered.

The limits of applicability and the procedures for the implementation of the Localized Corrosion Initiation Abstraction in the TSPA-LA Model are defined in *General Corrosion and Localized Corrosion of Waste Package Outer Barrier* (SNL 2007 [DIRS 178519], Section 8.3.1). The following initiation criteria apply:

1. Crown seepage localized corrosion does not occur if the drift-wall temperature is greater than 100°C (WP surface temperature greater than 120°C).

2. If it has been determined that localized corrosion can occur and the WP exposure temperature is at least 20°C but does not exceed 120°C, then the empirical correlations for the long-term corrosion potential (E_{corr}) and crevice repassivation potential (E_{rcrev}) are evaluated with the following implementation rules:

   a. If the nitrate-to-chloride ion ratio in the environment exceeds one then evaluate Ercrev and Ecorr at a nitrate-to-chloride ion ratio of one. If the molality of chloride ion is less than 0.0005 molal, evaluate the nitrate-to-chloride ion ratio with a chloride ion concentration of 0.0005 molal.

   b. If the molality of the chloride ion in the environment exceeds 20 molal, then evaluate E_{rcrev} and E_{corr} at a chloride ion molality of 20 molal. If the chloride ion molality is less than 0.0005 molal, then evaluate E_{rcrev} and E_{corr} at a chloride ion molality of 0.0005 molal.c.

   c. If the pH in the environment exceeds 10, then evaluate E_{rcrev} and E_{corr} at a pH of 10. If the pH in the environment is less than 1.9, then initiate localized corrosion.

3. If the WP relative humidity is below the threshold at which halite precipitates and the WP is below a failed DS, then when re-wetting occurs the in-package chemistry lookup tables no longer apply and TSPA is instructed to assume that Cl-rich brine can form (SNL 2007 [DIRS 177412], Sections 6.12.3 and 6.15.1.3). The relative humidity of salt separation for all modeled waters is archived in DTN: SN0703PAEBSPCE.006_R2, files: *Gp1_Salt_Separation_table.xls, Gp2_Salt_Separation_table.xls, Gp3_Salt_Separation_table.xls, Gp4_Salt_Separation_table.xls* [DIRS 181571]. Because the process of salt-brine separation cannot be explicitly modeled, the P&CE report (SNL 2007 [DIRS 177412]) abstraction models do not attempt to provide the chemistry for the Cl-rich brines. In this situation it is conservatively assumed that localized corrosion initiates when re-wetting occurs.

4. If crown seepage localized corrosion is determined to initiate, then allow localized corrosion to continue to occur at the sampled propagation rate, regardless of changes in the chemical environment.

5. The area of the Alloy 22 WP outer barrier that is contacted by seepage is potentially subject to localized corrosion (SNL 2007 [DIRS 178519], Section 8.3.1).

6.3.5.2.3 Implementation in the TSPA-LA Model

The Localized Corrosion Initiation Abstraction, described in Sections 6.3.5.2.1 and 6.3.5.2.2, provides input to the localized corrosion implementation in the TSPA-LA Model file by determining if environmental conditions on the WP outer surface will initiate localized corrosion and lead to WP failure. The Localized Corrosion Initiation Submodel is implemented in a modified version of the TSPA-LA Model, referred to as the Localized Corrosion Stand-Alone Model (output DTN: MO0709TSPALOCO [DIRS 182994]). Only the TSPA-LA submodels that are required to produce feeds to the Localized Corrosion Initiation Submodel are retained. The implementation of the thermal histories and the implementation of the seepage abstraction in the Localized Corrosion Stand-Alone Model differ from the corresponding implementations in the TSPA-LA Model. These differences are discussed below.

Implementation of the Localized Corrosion Initiation Submodel

Localized Corrosion Initiation Submodel calculations result from the interfacing of several TSPA-LA Model submodels and abstractions, as illustrated on Figure 6.3.5-9, to determine whether or not environmental conditions on the WP outer surface will initiate localized corrosion and lead to failure. These submodels include:

- EBS Chemical Environment Submodel look-up tables for Pco_2 in the emplacement drifts and abstraction bin history maps for incoming seepage composition history (Section 6.3.4.2). These abstractions are used to define Pco_2 in the emplacement drift as a function of time, and to define the chemical composition of seepage water entering the drifts as a function of time. Pco_2 is an input to the chemical evolution of crown seepage water.

- EBS Chemical Environment Submodel look-up tables for the chemical evolution of crown seepage water on the WP outer surface (Section 6.3.4.3.2) and distributions for the nitrate to chloride ratio (sampled once per realization). The EBS P&CE Abstraction is used to calculate the chloride concentration, nitrate concentration, and pH in crown seepage water as functions of relative humidity. These quantities are then used to evaluate localized corrosion initiation.

- Drift Seepage Submodel (Section 6.3.3.1). The calculations outlined in *Abstraction of Drift Seepage* (SNL 2007 [DIRS 181244], Section 6.7.1) and the seepage response surfaces for nondegraded and degraded drifts are used to determine if seepage occurs at each repository subdomain location.

- EBS TH Environment Submodel (Section 6.3.2). The EBS MSTHM Abstraction (Section 6.3.2.3) provides time-dependent values for temperature and relative humidity on WP surfaces and the drift-wall temperature. The EBS MSTHM Abstraction also provides time-dependent adjusted values that are used to correct temperature and relative humidity values for the insulating effect of rubble caused by drift degradation induced

by seismic ground motion in the lithophysal units. Drift-wall temperatures are used to calculate thermal seepage in the nonlithophysal units. WP temperatures, with adjusted values for rubble, are used to calculate thermal seepage in the lithophysal units.

- Localized Corrosion Initiation Abstraction (Section 6.3.5.2.2). The Localized Corrosion Initiation Abstraction derives the criteria for localized corrosion initiation.

- Seismic Ground Motion Damage Submodel (Section 6.6). The volume of rubble accumulated in the lithophysal and nonlithophysal zones are inputs to the Drift Seepage Submodel, as described above. The time of first DS plate failure due to seismic damage is used to determine the time of initiation of localized corrosion.

- WP and DS Degradation Submodel (Section 6.3.5). The time of first DS failure due to general corrosion is used to determine the time of initiation of localized corrosion. The general corrosion rate parameters and the MIC factor are used to determine a general corrosion rate, which is added to the localized corrosion rate to determine the WP failure fraction histories.

Figure 6.3.5-9 also illustrates the WP failure fraction histories that are the primary outputs produced by the Localized Corrosion Initiation Submodel. Figure 6.3.5-10 illustrates the steps taken to implement localized corrosion initiation in the Localized Corrosion Initiation Submodel. The Localized Corrosion Initiation Submodel, includes two computational loops: an outer epistemic uncertainty loop, and an inner spatial and temporal variability loop. In the outer loop, epistemic uncertainties associated with localized corrosion initiation, chemical environment on the WP outer surface, drift seepage, and rubble (natural backfill caused by a strong seismic ground motion event) are sampled using LHS for each localized corrosion realization. These epistemic uncertainties include the following (Table 6.3.5-4).

- Fifteen uncertain parameters from the Localized Corrosion Initiation Abstraction (Section 6.3.5.2.2); 14 coefficients that correspond to the linear regression fitting parameters (a_0, a_1, a_2, a_3, a_4, ε_{rcrev}, c_0, c_1, c_2, c_3, c_4, c_5, c_6, and ε_{corr}) associated with the crevice repassivation potential and the long-term steady-state corrosion potential, respectively; one uncertain parameter that represents the epistemic uncertainty in the localized corrosion propagation rate.

- Six parameters that quantify the evolution of the chemical environment on the WP outer surface; one parameter is used to select crown seepage starting water type (Section 6.3.4.3.1); one uncertain parameter represents uncertainty in partial pressure of CO_2; four parameters represent epistemic uncertainty (Table 6.3.4-3, Section 6.3.4.3.2) in calculated chloride concentration, the nitrate-to-chloride ratio, the combined chloride and nitrate concentration, and pH (each of these four is represented by one of several possible distributions, depending on relative humidity). Five parameters that represent uncertainty in drift-seepage, including the seepage uncertainty scale factor and the uncertainty in fracture permeability and capillary strength for both the lithophysal and nonlithophysal units (Tables 6.3.3-1 and 6.3.3-2, and Section 6.3.3.1.2).

- One parameter that represents epistemic uncertainty in thermal conductivity of the rubble deposited on the DSs and WPs due to drift degradation in the lithophysal unit (Section 6.6.1.3).

- Two uncertain parameters used to select exposure histories; one that represents epistemic uncertainty in infiltration scenario; one that represents epistemic uncertainty in thermal conductivity of the host rock.

- Two parameters that represent the uncertainty in the maximum rubble volume for the lithophysal and nonlithophysal units.

- Two uncertain parameters that represent the epistemic uncertainty in the Titanium Grade 7 general corrosion rate for aggressive and benign conditions; one uncertain parameter that represents the epistemic uncertainty in the temperature dependence of the Alloy 22 general corrosion rate; one uncertain parameter that represents the relative humidity threshold for the application of the MIC factor.

- Four parameters that represent uncertainty in the general corrosion rate of Alloy 22.

The MSTHM Abstraction subdivides the repository footprint into 3,264 equal-area subdomains and supplies temperature and relative humidity time histories for six CSNF WPs and two CDSP DS/WP pairs at each subdomain-center location. Time-dependent values for average drift-wall temperature are also supplied at each location. The TH variables and their associated locations are grouped into one of five repository subregions based on percolation flux at the base of the PTn (Section 6.3.2.2.1). Localized corrosion initiation analyses are implemented for each of the 12 cases considered by the MSTHM Abstraction. These 12 cases represent the combinations of epistemic uncertainty in infiltration and host-rock thermal conductivity (Section 6.3.2.2).

The implementation of the thermal histories and the implementation of the seepage abstraction in the Localized Corrosion Stand-Alone Model differ from the corresponding implementation in the TSPA-LA Model. In the TSPA-LA Model, EBS Chemical Environment Submodel calculations for representative temperature and relative humidity histories, are used for all subdomain locations in a particular percolation subregion (Section 6.3.2.3). In the TSPA-LA Model, the implementation of drift seepage is accomplished through the use of an external DLL (STN: 11076-1.3-00 [DIRS 181058]), which implements the same calculations but whose output is the fraction of WPs that experience seepage, averaged over all MSTHM subdomains in a percolation subregion (Section 6.3.3.1.3).

After the epistemic parameters are sampled, the percolation subregion and the TH case from the set of 12 are selected. Next, for each outer-loop realization, an inner loop over the TH locations in the percolation subregion is executed. The inner loop represents spatial and temporal variability in the parameters. It includes:

- Two sets of temperature and relative humidity time histories (associated with one of six CSNF WP time histories or one of two CDSP WP time histories): the first set represents values to be used under conditions of no drift collapse (or minor drift

collapse); the second set is adjusted for the presence of rubble by adding an increment in temperature and relative humidity (Section.3.2).

- Drift-seepage parameters for flow focusing factor, spatial variability of fracture permeability, and capillary strength (Equation 6.3.3-1, Tables 6.3.3-1 and 6.3.3-2, and Section 6.3.3.1.2.).

The following steps are performed at each WP location within this loop for each percolation subregion and at each timestep:

1. The chemical environment on the WP outer surface due to crown seepage is determined. A calculation is first made to determine if seepage into the drift occurs.

   This calculation is implemented for each WP location, as described in the Drift Seepage Abstraction (Section 6.3.3.1), using the sampled drift-seepage parameters representing epistemic uncertainty and variability, the percolation flux, and the drift-wall temperature to account for thermal seepage effects. In addition, if seepage occurs and a WP is located in the lithophysal unit, the adjusted (for the presence of rubble) WP temperature history is used to determine whether or not incoming seepage contacts the WP. If seepage does not contact the WP at the current location and time, localized corrosion initiation due to crown seepage is not evaluated. If drift seepage occurs, the following two evaluations are implemented.

2. The chemical environment on the WP outer surface, in terms of nitrate concentration, chloride concentration, nitrate-to-chloride ratio, and pH due to evolution of crown seepage, is calculated through time, as described in Section 6.3.4.3.2, using temperature and relative humidity time histories for the WP. If the WP is located in the lithophysal unit, the WP temperature and relative humidity values are adjusted for the presence of rubble from drift degradation in the Seismic Scenario Class using the thermal adjustment histories.

3. The values of temperature, relative humidity, pH, chloride concentration, and nitrate concentration are checked against the criteria listed in Section 6.3.5.2.2. If these parameters are outside the ranges specified, the appropriate bounding values are used. Otherwise, localized corrosion is initiated if $\Delta E \leq 0$ on a WP.

4. If localized corrosion initiates, the localized corrosion penetration continues at a constant rate through the regulatory period or until the WP is penetrated. The localized corrosion penetration rate is sampled from a uniform distribution from 0.0127 mm/yr to 1.27 mm/yr. A WP is considered failed by localized corrosion if the WP outer surface thickness is fully penetrated by the combined localized corrosion, general corrosion, and MIC penetration depths.

For each repository subregion and WP type, a corresponding fractional failure history is obtained by adding the failed WPs of that type and dividing by the total number of either CSNF WPs or CDSP WPs in the subregion. This evaluation is carried out for each TH timestep until simulation end time.

The evaluation of penetration time includes general corrosion and MIC enhancement of general corrosion. Because general corrosion is much slower than localized corrosion, a simplified general corrosion abstraction is incorporated into the Localized Corrosion Initiation Submodel. This simplified general corrosion abstraction uses the CDF for R_0, which was developed from the average corrosion rate with a scale factor of four and corresponds to the medium uncertainty level. MIC enhancement of general corrosion is activated only when relative humidity exceeds the MIC threshold.

The primary output from the Localized Corrosion Initiation Submodel is the fraction of CSNF WPs and CDSP WPs that fail by localized corrosion due to crown seepage, as a function of time, in each percolation subregion. These fractions are used to define the number of WPs that fail by localized corrosion during the simulation time and their average breach areas as a function of time.

TSPA-LA Modeling Cases

Localized corrosion is included in the two Seismic Scenario Class modeling cases discussed in Section 6.6, the Seismic GM Modeling Case and Seismic FD Modeling Case; and in the Nominal Modeling Case. In the Igneous Scenario Class, the affected WPs and DSs are immediately destroyed at the time of the intrusion event. Only dripping crown seepage water contacting the WP outer surface is considered, in the TSPA-LA Model, to lead to environmental conditions conducive to localized corrosion on the WP outer surface. The Localized Corrosion Stand-Alone Model was run five times (once for each percolation subregion) for 300 realizations with unified sampling for each of the three modeling cases considered. The model computes time-dependent chemical conditions of brine formation and corrosion potential.

Evaluation of the Localized Corrosion Stand-Alone Model results revealed that conditions for localized corrosion initiation occurred only in the first 12,000 years after closure (Section O1). Beyond this time, the chemistry of the seepage water is benign and localized corrosion no longer initiates. These analyses are documented in output DTN: MO0709TSPALOCO.000 [DIRS 182994]. In addition, localized corrosion can only occur if crown seepage water contacts the WP outer surface (i.e., if the DS is failed).

For the Nominal Modeling Case, the first DS failure occurs at about 230,000 years (Section 6.3.5.1.3), so localized corrosion does not impact this modeling case. In the Seismic GM Modeling Case, there is a low probability (Figure 7.3.2-16) of DS plate failure occurring before 12,000 years. Section 7.3.2.6.1.3.2 discusses the justification for not considering these early DS failures in the context of the Seismic GM (10,000-year) Modeling Case. The same arguments apply to the Seismic GM (1,000,000-year) Modeling Case, when considering localized corrosion, since only the first 12,000 years after closure are relevant. In the Seismic FD Modeling Case, there is a low probability of a fault event (and, therefore, DS failure) in the first 12,000 years after closure. However, localized corrosion does not impact the Seismic FD

Modeling Case even though DSs may be failed during the period of time that seepage water could initiate localized corrosion. The argument for this assertion is based on the observation that, when the DS is failed and the WP damage area is larger than 1/3 of the WP cross-sectional area, the releases cease to change significantly as more damage is applied (Section 7.3.2.7 and Figure 7.3.2-25). Since the dose result is insensitive to the damage area when more than 1/3 of the lid area is damaged, it is not expected that additional localized corrosion damage will affect the dose result.

Since localized corrosion is not expected to impact any of the three TSPA-LA modeling cases where its effects are modeled, the 30 input files (10 for each modeling case) containing the time histories for the fraction of WPs failed by localized corrosion will contain only zero entries. These input files were created using GoldSim v9.60.100 software, as described in output DTN: MO0708TSPAGENT.000 [DIRS 183000].

6.3.5.3 Model Component Consistency and Conservatism in Assumptions and Parameters

To enhance understanding of the complex interactions within the TSPA-LA Model, a discussion of consistency among model components and submodels and identification of conservative assumptions in abstractions, process models, and parameter sets supporting the WP and DS Degradation Model Submodel and the Localized Corrosion Initiation Submodel are discussed below.

6.3.5.3.1 Consistency of Assumptions

Salt Separation on the WP Surface—The current TSPA-LA Model includes a relative humidity threshold switch to account for a potential salt separation process during seepage water evaporation (Section 6.3.5.2.2). In principle, water evaporation on the Alloy 22 WP surface will first cause the precipitation of halite (NaCl) and then the remaining water will flow away from early precipitated salts, leaving the solids behind rich in Cl^-. In this case, the chemistry look-up tables no longer apply form (SNL 2007 [DIRS 177412], Sections 6.12.3 and 6.15.1.3). For implementation purposes, the TSPA-LA Model assumes that localized corrosion always initiates upon re-wetting of the salt film. The implementation for the WP Localized Corrosion Initiation Submodel represents potential differences between several submodels: Drift Seepage, EBS Flow, EBS Chemical Environment, and the localized corrosion aspect of WP degradation. The EBS Chemical Environment Submodel assumes well-mixed equilibrium conditions for chemistry in the drift (Section 5.1.2). Therefore, salt separation is not included in that submodel. In addition, evaporation and flow on a small scale of the possible salt separation phenomenon is overwhelmed by uncertainties at the larger scale of the Drift Seepage Submodel or the EBS Flow Submodel. Evaporation is integral, however, to the equilibrium chemistry response surfaces that are the output of the EBS Chemical Environment Submodel. In order to handle this difference, a conservative assumption is implemented in the TSPA-LA Model, using the NaCl deliquescence relative humidity threshold (Section 6.3.5.2.2; note that concentrated salt solutions are referred to as brines in Section 6.3.5.2.2).

Effect on TSPA—Based on a water volume argument, this separation is unlikely to occur, and if it were to occur, it would be limited in spatial extent. The approach taken in the TSPA-LA results in a greater likelihood that those conditions conducive to localized corrosion might exist

over the entire surface of the WP and is, therefore, conservative. The TSPA-LA Model assumes that there will always be a sufficient volume of brine available for WP degradation regardless of the types of the resulting brines (Section 6.3.5.2.2). In actual repository environments, however, brines formed from evaporation are expected to be limited in volume. For example, obtaining a saturated NaCl brine may require the seepage water to concentrate significantly. That is, 1 L of seepage water would result in only a small volume of NaCl solution. The assumption of sufficient brine volume may lead to a conservative overestimation of the potential for initiating localized corrosion if the brine volumes are too small to cause a continuous water film over the WP surface.

6.3.5.3.2 Identification of Conservatisms in Submodels and Abstractions

Threshold Relative Humidity for General Corrosion Initiation on WPs—There is no threshold relative humidity for the initiation of general corrosion of the WPs. A relative humidity threshold for the initiation of general corrosion clearly exists (ASM International 1987 [DIRS 133378], p. 82). However, there is insufficient information/data to quantify the general corrosion initiation threshold relative humidity for varying water chemistry conditions (SNL 2007 [DIRS 178519], Assumption 5.1). The assumption that no relative humidity threshold for the initiation of corrosion processes exists is conservative because use of a relative humidity threshold would delay the corrosion initiation start time.

Representation of the Critical Threshold Potential—The critical threshold potential ($E_{critical}$) is conservatively represented by the crevice repassivation potential (E_{rcrev}). The crevice repassivation potential (E_{rcrev}) determined from cyclic potentiodynamic polarization tests was selected as a conservative measure for the critical threshold potential ($E_{critical}$). Other less conservative choices for $E_{critical}$ are possible (e.g., the breakdown potential or potentials based on current density thresholds) (SNL 2007 [DIRS 178519], Section 6.4.4.1). The chemical exposure conditions in creviced regions can be more severe than those in noncreviced regions (SNL 2007 [DIRS 178519], Section 1.2). This leads to the measurement of lower repassivation (critical) potentials in creviced versus noncreviced regions.

Stainless Steel Inner Vessel—No corrosion credit is taken for the use of a stainless-steel inner vessel. The 50 mm inner vessel will provide structural support to the thinner outer barrier, and the outer barrier will protect the inner vessel from significant corrosion degradation while it remains intact. The inner vessel could provide some delay of radionuclide release before it fails and also could retard the release rate of radionuclides from the WP (SNL 2007 [DIRS 178519], Section 6.3.3).

General Corrosion Rate of WP Outer Surface—The general corrosion rate of the WP outer surface at a given temperature is time-independent. General corrosion rates of the WP outer surface decrease with time (SNL 2007 [DIRS 178519], Section 6.4.3.5.1). However, there is insufficient information/data to quantify the time dependence. This conservatism is expected to result in the overestimation of WP general corrosion rate (SNL 2007 [DIRS 178519], Figure 7-1).

General Corrosion Rate Distribution for WP Outer Surface—Two coupon (specimen) types are used for general corrosion weight-loss measurements. These are identified as weight-loss

coupons and crevice coupons. The general corrosion rate distribution for the WP outer surface is based on the weight-loss of crevice coupons (specimens). The creviced specimens exhibited generally higher general corrosion rates than the noncreviced specimens. This is attributed to the difference in the surface-polishing treatments between the two groups of specimens (SNL 2007 [DIRS 178519], Section 6.4.3.2). This conservatism is expected to overestimate the general corrosion rates on the WP outer surface. The evaluation of the general corrosion rate using crevice samples was included in the Performance Margin Analysis (PMA) (Appendix C).

General Corrosion Rate Distribution Adjustment for Patch Size—The general corrosion rate distribution is conservatively adjusted for patch size. The patch size used in the TSPA-LA Model is a factor of four larger than the size of the crevice samples in the experiments that generated the data from which the general corrosion rate was derived. The adjustment method is to effectively use the highest of four sampled values for the patch general corrosion rate (Section 6.3.5.1.2). The approach is conservative because it is probable that not all four samples from the Weibull distribution will have the highest rate.

Crevice Corrosion—The dominant form of localized corrosion is assumed to be crevice corrosion as opposed to pitting corrosion, which occurs on boldly exposed surfaces. Additionally, crevice corrosion is applied to the entire WP surface, though it is unlikely that crevice attack would occur over the entire surface area (SNL 2007 [DIRS 178519], Assumption 5.3). The initiation threshold for crevice corrosion, in terms of exposure conditions, is lower than that for pitting corrosion (SNL 2007 [DIRS 178519], Section 6.4.4). This conservatism is expected to result in the overestimation of the number of WPs that experience localized corrosion.

Effects of Inhibitive Anions—No credit is taken in the Localized Corrosion Initiation Abstraction for the effects of inhibitive anions other than nitrate. Nitrate ions inhibit localized corrosion initiation. Carbonate and sulfate ions may also have an inhibitive effect on localized corrosion. However, there is insufficient information and/or data to quantify the effect of other inhibitive anions on localized corrosion initiation (SNL 2007 [DIRS 178519], Section 8.3.1). Results for solutions with significant amounts of other potentially inhibitive ions are conservative (SNL 2007 [DIRS 178519], Section 8.3.1).

Localized Corrosion Rate of WP Outer Surface—The localized corrosion propagation rate for the WP outer surface is assumed to propagate at a (time-independent) constant rate (SNL 2007 [DIRS 178519], Assumption 5.4). The localized corrosion propagation rate is known to decrease with increasing time (SNL 2007 [DIRS 178519], Section 6.4.4.8.2); however, there is insufficient information and/or data to quantify the time dependence. This conservatism is expected to result in the overestimation of the number of WPs that fail due to localized corrosion.

Effect of Changing Chemical Environment on Localized Corrosion Propagation—Once localized corrosion is initiated, it continues to propagate regardless of any changes in the bulk chemical exposure environment. This is a conservative modeling assumption because no detailed chemistry evolution model of the crevice solution is available (SNL 2007 [DIRS 178519], Section 8.3.1). This conservatism is expected to result in the overestimation of the number of WPs that fail due to localized corrosion.

6.3.5.4 Alternative Conceptual Model(s) for Waste Package and Drip Shield Degradation

An important reason for considering ACMs is to help build confidence that plausible changes in modeling assumptions or simplifications will not change conclusions regarding subsystem and total system performance. Section 6.2.1 outlines the general consideration and treatment of ACMs used to support the TSPA-LA Model. Conservatism at the subsystem level was used to select the best ACM to use rather than quantitatively propagate multiple ACMs to the TSPA-LA Model. Generally, additional uncertainty is incorporated into the selected conceptual model if more than one ACM is deemed appropriate for use rather than considering multiple ACMs in the TSPA-LA Model. If an ACM appears to be significant at the subsystem level, then an appropriate abstraction is developed for that ACM for consideration within the TSPA-LA Model. The result of the process is documented within the individual analysis model reports. It is important to note that treatment of ACMs within the individual analysis model reports may differ significantly to be consistent with available data and current scientific understanding. Therefore, a brief description of the WP and DS Degradation Submodel ACMs and the Localized Corrosion Initiation Submodel ACMs are presented below and summarized in Table 6.3.5-2.

Parabolic General Corrosion Rate Law for DS—The parabolic general corrosion rate law for DS degradation (SNL 2007 [DIRS 180778], Section 6.5.6) assumes that the increasing oxide layer thickness on the diffusion of oxidizing species to the underlying metal will have an inhibiting effect on corrosion. This model is less conservative than the primary model and was not recommended for inclusion in the evaluation of DS degradation for the TSPA-LA Model.

Decreasing Rate Law for WP—The corrosion rates of metals and alloys tend to decrease with time (SNL 2007 [DIRS 178519], Section 6.4.3.5.1). The time-dependent general corrosion behavior of the WP was not included in the TSPA-LA because the constant (time-independent) rate model (for a given temperature) is more conservative and bounds the general corrosion behavior of the WP outer surface over the repository time period.

General Corrosion Rate Law Based on Weight-Loss Samples Only—The ACM discussion for a general corrosion rate law for WP degradation based on plain weight-loss samples (rather than crevice samples) and is found in the analysis model report (SNL 2007 [DIRS 178519], Section 6.4.3.5.2). The weight-loss data was fit to a Weibull distribution using maximum likelihood estimators (i.e., using the same methods applied to the crevice sample data). A comparison of the general corrosion rate distribution resulting from fitting the 5-year exposed weight-loss sample to the Weibull distributions based on the crevice sample data shows that this conceptual model is less conservative relative to the base case general corrosion model (SNL 2007 [DIRS 178519], Figures 6-28 and 6-23).

Critical Temperature-Based Localized Corrosion Initiation—The evolution of the WP temperature with time, coupled with the knowledge of the critical temperature for the initiation of localized corrosion (pitting/crevice corrosion), can be used to determine when localized corrosion initiates (SNL 2007 [DIRS 178519], Section 6.4.4.8.1). However, the test conditions at which the required critical temperatures were measured are not directly relevant to the potential environments on the WP surface. In addition, the critical temperature-based model does not account for the effects of electrochemical characteristics of the solution contacting the metal. Therefore, the critical temperature-based model is not considered in the TSPA.

Coupled Environmental Fracture Model—The coupled environment fracture model for stress corrosion crack growth rate was evaluated as an ACM for SCC (SNL 2007 [DIRS 181953], Section 6.4.6). The model, based on charge conservation, incorporates the effects of oxygen concentration, flow rate, and the conductivity of the external environment, as well as accounting for the effect of stress on crack growth. The model underestimated the crack growth rate, as compared to the slip dissolution-film rupture (SDFM) model, when both models were applied to predict the crack growth rate.

Time-Dependent Localized Corrosion Rate—An ACM for localized corrosion penetration is a time-dependent growth law of the form (SNL 2007 [DIRS 178519], Section 6.4.4.8.2):

$$D = k \times t^n \qquad \text{(Eq. 6.3.5-18)}$$

where D is the depth of penetration, t is time, and k is a growth constant. However, insufficient penetration rate data are available, especially for relatively new materials such as Alloy 22, to determine the values of k and n for the exposure conditions relevant to the repository. This ACM was not recommended for incorporation into the TSPA-LA Model because the data needed to apply the model can only be estimated approximately from open literature. The time-independent constant penetration rate model used in the TSPA-LA Model is more conservative.

Passive Film Breakdown Potential for the Determination of Critical Potential—An alternative technique for the determination of critical potential could be to use the passive film breakdown potential obtained from the forward scan of cyclic potentiodynamic polarization tests (SNL 2007 [DIRS 178519], Section 6.4.4.1). This technique would not account for the (often slow) kinetics of localized corrosion initiation and may not be appropriate for modeling the long time periods involved in repository environments. Furthermore, the breakdown potential is likely to be much higher when the passive film has been formed over long time periods, allowing for a decrease in the film defect density.

WP Surface Area Subjected to Localized Corrosion—No information is available regarding local environments on the WP; therefore, the area affected by localized corrosion due to seepage is based on the fraction of the WP surface exposed to seepage. TSPA has conservatively taken the area affected by localized corrosion to be the area wetted by seepage. Therefore, the entire surface area can potentially undergo localized corrosion. A distribution for the minimum area affected by localized corrosion was developed (minimum of 0.05 percent and maximum of the percent of area wetted by seepage) (SNL 2007 [DIRS 178519], Section 6.4.4.8.3). The ACM has not been implemented in the TSPA-LA Model. Sensitivity analyses have shown that dose results are insensitive to the magnitude of the failed area on the WP once the failed area has reached about 5 percent of the WP surface area (Section 7.3.2.7).

No ACMs were recommended for inclusion in the TSPA-LA Model.

Table 6.3.5-1. Drip Shield and Waste Package Degradation Mechanisms and Their Disposition for Implementation in the TSPA-LA Model

Failure Mechanism	Drip Shield Postclosure Assessment		Waste Package Postclosure Assessment	
	Included in TSPA-LA Model	Screened Out[a]	Included in TSPA-LA Model	Screened Out[a]
General Corrosion	X	—	X	—
Localized Corrosion	—	X	X	—
Stress Corrosion Cracking	—	X	X	—
Microbially Influenced Corrosion	—	X	X	—
Early Failure	X	—	X	—
Aging and Phase Instability	—	X	—	X
Hydrogen Induced Cracking	—	X	—	X
Mechanical Impacts	—	X[b]	—	X[b]
Radiolysis	—	X	—	X

NOTE: [a] Excluded FEPs, as shown in DTN: MO0706SPAFEPLA.001_R0 [DIRS 181613], Table 7.1.

[b] Screened out for the Nominal Scenario Class; included for both modeling cases of the Seismic Scenario Class.

Table 6.3.5-2. Alternative Conceptual Models Considered for Drip Shield and Waste Package Degradation

Alternative Conceptual Models	Key Assumptions	Screening Assessment and Basis
Parabolic general corrosion rate law for DS degradation (SNL 2007 [DIRS 180778], Section 6.5.6).	Assumes that the increasing oxide layer thickness on diffusion of oxidizing species to the underlying metal will have an inhibiting effect on corrosion.	Model is less conservative than the primary model.
Decreasing general corrosion rate law for WP degradation (SNL 2007 [DIRS 178519], Section 6.4.3.5.1).	General corrosion rates of metals and alloys tend to decrease with time.	The time-dependent general corrosion behavior of the WP was not included in the TSPA-LA because the constant (time-independent) rate model (for a given temperature) is more conservative and bounds the general corrosion behavior of the WP outer surface over the repository time period.
General Corrosion Rate Based on Weight-Loss Samples Only (SNL 2007 [DIRS 178519], Section 6.4.3.5.2).	A general corrosion rate law for WP degradation based on plain weight-loss samples (rather than crevice samples) was developed. The weight-loss data were fit to a Weibull distribution using maximum likelihood estimators (i.e., using the same methods applied to the crevice sample data).	A comparison of the general corrosion rate distribution resulting from fitting the 5-yr exposed weight-loss samples to the Weibull distribution based on the crevice sample data shows that this conceptual model is less conservative relative to the base case general corrosion model (SNL 2007 [DIRS 178519], Figures 6-28 and 6-23).

Table 6.3.5-2. Alternative Conceptual Models Considered for Drip Shield and Waste Package Degradation (Continued)

Alternative Conceptual Models	Key Assumptions	Screening Assessment and Basis
Critical Temperature-Based Localized Corrosion Initiation Model (SNL 2007 [DIRS 178519], Section 6.4.4.8.1).	The evolution of WP temperature with time, coupled with knowledge of the critical temperature for the initiation of localized corrosion (pitting/crevice corrosion), can be used to determine when localized corrosion initiates.	Test conditions at which the required critical temperatures were measured are not directly relevant to the potential environments on the WP surface. The model does not account for the effects of electrochemical characteristics of the solution contacting the metal. The model is not used in the TSPA-LA.
Coupled environment fracture model for stress corrosion crack growth rate (SNL 2007 [DIRS 181953], Section 6.4.6).	The model, based on charge conservation, incorporates the effects of oxygen concentration, flow rate, and the conductivity of the external environment, as well as accounting for the effect of stress on crack growth.	Model underestimates the crack growth rate, as compared to the slip dissolution/film rupture model, when both models were applied to predict the crack growth rate.
Localized corrosion penetration as a time-dependent growth law (SNL 2007 [DIRS 178519], Sections 6.4.4.8.2 and 7.2.5).	Once initiated, the localized corrosion penetration rate decreases with increasing time.	Data needed to apply the model can only be estimated approximately from open literature. The time-independent constant penetration rate model is more conservative.
Passive film breakdown potential for determination of critical potential (SNL 2007 [DIRS 178519], Section 6.4.4.1).	An alternative technique for the determination of critical potential would be to use the passive film breakdown potential (obtained from the forward scan of the cyclic potentiodynamic polarization tests).	This technique would not account for the (often slow) kinetics of localized corrosion initiation and may not be appropriate for modeling the long time periods involved in repository environments. Furthermore, the breakdown potential is likely to be much higher when the passive film forms over long time periods allowing for a decrease in the film defect density.
No information is available regarding local environments on the WP; therefore, the area affected by localized corrosion due to seepage is based on the fraction of the WP surface exposed to seepage. TSPA has conservatively taken the area affected by localized corrosion to be the area wetted by seepage. Therefore, the entire surface area can potentially undergo localized corrosion.	A distribution for the minimum area affected by localized corrosion was developed (minimum of 0.05 percent and maximum of the percent of area wetted by seepage) (SNL 2007 [DIRS 178519], Section 6.4.4.8.3).	The ACM has not been implemented in the TSPA-LA Model. Sensitivity analyses have shown that dose results are insensitive to the magnitude of the failed area on the WP once the failed area has reached about 5% of the WP surface area (Section 7.3.2.7).

Table 6.3.5-3. Uncertain Inputs to the TSPA-LA Model for Generalized Corrosion of the Drip Shield and Waste Package and Stress Corrosion Cracking of the Waste Package

TSPA_LA Parameter Name	Mathematical Model Symbol	Description	Units	Distribution Specification	Remarks
WDDSBenignGC_Mean_a	None	DS-underside general corrosion rate (epistemic uncertainty)	nm/yr	Normal Mean = 5.15 SD = 0.831	DTN: SN0704PADSGCMT.001_R2, [DIRS 182122], file: TSPA Implementation_DS GC Models.pdf
WDDSAggrGC_Mean_a	None	DS-topside general corrosion rate (epistemic uncertainty)	nm/yr	Student's-t Mean = 46.1 SD = 1.19 Degrees of Freedom: 5	DTN: SN0704PADSGCMT.001_R2, [DIRS 182122], file: TSPA Implementation_DS GC Models.pdf
WDlnR_ESC_L_cdf WDlnR_ESC_M_cdf WDlnR_ESC_H_cdf	ln R_o	Natural logarithm of general corrosion rate: 60°C: WP (spatial variability)	None	Three CDFs corresponding to low, medium, and high levels of epistemic uncertainty in the GC_shape and GC_scale parameters (fourth and fifth rows of this table)	Developed by TSPA from GC_scale and GC_shape parameters Output DTN: MO0707WPDRIPSD.000 [DIRS183005]
GC_shape	None	Shape parameter for Weibull distribution (WP general corrosion)	None	1.380 (low): 5% realizations 1.476 (medium): 90% realizations 1.578 (high): 5% realizations Different values are epistemic uncertainty. Overall distribution is spatial variability.	DTN: MO0703PAGENCOR.001_R4, [DIRS 182029], file: BaseCase GC CDFs.xls
GC_scale	None	Scale parameter for Weibull distribution (WP general corrosion)	None	6.628 (low): 5% realizations 8.134 (medium): 90% realizations 9.774 (high): 5% realizations Different values are epistemic uncertainty. Overall distribution is spatial variability.	DTN: MO0703PAGENCOR.001_R4, [DIRS 182029], file: BaseCase GC CDFs.xls

Table 6.3.5-3. Uncertain Inputs to the TSPA-LA Model for Generalized Corrosion of the Drip Shield and Waste Package and Stress Corrosion Cracking of the Waste Package (Continued)

TSPA_LA Parameter Name	Mathematical Model Symbol	Description	Units	Distribution Specification	Remarks
GC_ULevel_A22_a	None	Distribution for selecting the general corrosion rate CDF, based on a low, medium, or high level of epistemic uncertainty in the Weibull shape and scale parameters (GC_shape and GC_scale)	None	Discrete Distribution [0.05,1][0.9,2][0.05,3]	DTN: MO0703PAGENCOR.001_R4, [DIRS 182029], file: BaseCase GC CDFs.xls
C1_GenCorr_A22_a	C1	Temperature dependence-slope term of WP general corrosion rate (epistemic uncertainty)	K	Normal (truncated at +2 SD and -3 SD) Mean = 4,905 SD = 1,413	DTN: MO0703PAGENCOR.001_R4, file: BaseCase GC CDFs.xls [DIRS 182029]
Defect_Size_a	λ_s	Flaw size distribution parameter (epistemic uncertainty)	mm^{-1}	Gamma Mean = n_f / S_f SD = sqrt (n_f)/S_f	DTN: MO0701PASHIELD.000_R2, file: Tables for DTN Readme.doc [DIRS 180508]
Defect_Count_a	λ_c	Flaw count distribution parameter (epistemic uncertainty)	flaws/m^3	Gamma Mean = (n_f + ½)/V_f SD = sqrt (n_f + ½)/V_f	DTN: MO0701PASHIELD.000_R2, file: Tables for DTN Readme.doc [DIRS 180508]
Z_OL_a	z	Uncertainty variation in the yield strength of the outer WP closure lid (epistemic uncertainty)	None	Normal (truncated at ±3 SD) Mean = 0 SD = 1	DTN: MO0702PASTRESS.002_R2, file: Model Output DTN.doc, Table 8-15 [DIRS 180514]
n_SCC_a	n	Stress corrosion cracking growth rate exponent (repassivation rate) (epistemic uncertainty)	None	Normal (truncated at ±2 SD) Mean = 1.165 SD = 0.115	DTN: MO0702PASTRESS.002_R2, file: Model Output DTN.doc, Table 8-15 [DIRS 180514]

Table 6.3.5-3. Uncertain Inputs to the TSPA-LA Model for Generalized Corrosion of the Drip Shield and Waste Package and Stress Corrosion Cracking of the Waste Package (Continued)

TSPA_LA Parameter Name	Mathematical Model Symbol	Description	Units	Distribution Specification	Remarks
Stress_Thresh_SCC_a	None	Stress threshold for SCC nucleation (epistemic uncertainty)	MPa	Uniform distribution from 315.9 to 368.55.	DTN: MO0702PASTRESS.002_R2, file: Model Output DTN.doc, Table 8-15 [DIRS 180514] This parameter combines the definition for Stress_Thresh_A22 with Yield_Strength_A22 defined in Table 8-15.
MIC_A22_a	f_{MIC}	MIC general corrosion enhancement factor (spatial variability)	None	Uniform Lower bound = 1 Upper bound = 2	DTN: MO0703PAGENCOR.001_R4, file: MIC Summary.pdf [DIRS 182029]
MIC_RHThresh_a	None	Relative humidity threshold for MIC (epistemic uncertainty)	None	Uniform distribution between 75% to 90%	DTN: MO0703PAGENCOR.001_R4, file: MIC Summary.pdf [DIRS 182029]

Table 6.3.5-4. Uncertain Inputs to Localized Corrosion Initiation Stand-Alone Model

TSPA_LA Parameter Name	Model Symbol	Description	Units	Distribution Specification	Remarks
Two_StDev_a0_a	None	Stochastic used to develop the coefficients in crevice repassivation potential functional form (epistemic uncertainty)	None	Normal Distribution Mean = 0 SD = 1	None
Two_StDev_a1_a					
Two_StDev_a2_a					
Two_StDev_a3_a					
Two_StDev_a4_a					
LC_eps_rcrev_a	None	Error term of crevice repassivation potential (epistemic uncertainty)	mV SSC	Normal distribution with a mean of zero and a standard deviation of 45.055	DTN: MO0703PAGENCOR.001_R4, file: Mathcad – Ercrev_Ecorr3.pdf, p. 5 [DIRS 182029]
Two_StDev_c0_a	None	Stochastic used to develop the coefficients in corrosion potential functional form (epistemic uncertainty)	None	Normal Distribution Mean = 0 SD = 1	None
Two_StDev_c1_a					
Two_StDev_c2_a					
Two_StDev_c3_a					
Two_StDev_c4_a					
Two_StDev_c5_a					
Two_StDev_c6_a					
LC_eps_corr_a	None	Error term of long-term corrosion potential model (epistemic uncertainty)	mV SSC	Normal distribution with a mean of zero and a standard deviation of 85.265	DTN: MO0703PAGENCOR.001_R4, file: Mathcad – Ercrev_Ecorr3.pdf, p. 8 [DIRS 182029]
LC_rate_a	None	Localized corrosion penetration rate (epistemic uncertainty)	mm/yr	Log uniform 0 percentile = 0.0127 50th percentile = 0.127 100th percentile = 1.27	DTN: MO0703PAGENCOR.001_R4, file: LC_Propagation.pdf [DIRS 182029]
Seepage_Water_Type_a	None	Seepage water type (epistemic uncertainty)	None	Discrete Uniform [0.25,1][0.25,2][0.25,3][0.25,4]	SNL 2007 [DIRS 177412], Section 6.15.1

Table 6.3.5-4. Uncertain Inputs to Localized Corrosion Initiation Stand-Alone Model (Continued)

TSPA_LA Parameter Name	Model Symbol	Description	Units	Distribution Specification	Remarks
PCE_Delta_PCO2_a	None	Uncertainty in the partial pressure of CO_2 (epistemic uncertainty)	None	Uniform distribution from -1 to 1.	SNL 2007 [DIRS 177412], Section 6.15.1
PCE_Cl_MU_RH_0_20_a	None	Uncertainty in log chloride ion concentration (epistemic uncertainty)	None	Triangular Distribution Minimum: -0.7 Most Likely: 0.0 Maximum: 0.7	DTN: SN0703PAEBSPCE.007_R2, file: PCE_IDPS_uncertainties.xls [DIRS 184141]
PCE_Cl_MU_RH_20_40_a	None	Uncertainty in log chloride ion concentration (epistemic uncertainty)	None	Triangular Distribution Minimum: -0.5 Most Likely: 0.0 Maximum: 0.5	DTN: SN0703PAEBSPCE.007_R2, file: PCE_IDPS_uncertainties.xls [DIRS 184141]
PCE_Cl_MU_RH_40_65_a	None	Uncertainty in log chloride ion concentration (epistemic uncertainty)	None	Triangular Distribution Minimum: -0.4 Most Likely: 0.0 Maximum: 0.4	DTN: SN0703PAEBSPCE.007_R2, file: PCE_IDPS_uncertainties.xls [DIRS 184141]
PCE_Cl_MU_RH_65_85_a	None	Uncertainty in log chloride ion concentration (epistemic uncertainty)	None	Triangular Distribution Minimum: -0.1 Most Likely: 0.0 Maximum: 0.1	DTN: SN0703PAEBSPCE.007_R2, file: PCE_IDPS_uncertainties.xls [DIRS 184141]
PCE_Cl_MU_RH_85_100_a	None	Uncertainty in log chloride ion concentration (epistemic uncertainty)	None	Triangular Distribution Minimum: -0.0 Most Likely: 0.0 Maximum: 0.0	DTN: SN0703PAEBSPCE.007_R2, file: PCE_IDPS_uncertainties.xls [DIRS 184141]
PCE_Cl_N_MU_RH_40_65_a	None	Uncertainty in log chloride plus nitrate ion concentration (epistemic uncertainty)	None	Triangular Distribution Minimum: -0.57 Most Likely: 0.0 Maximum: 0.57	DTN: SN0703PAEBSPCE.007_R2, file: PCE_IDPS_uncertainties.xls [DIRS 184141]

Table 6.3.5-4. Uncertain Inputs to Localized Corrosion Initiation Stand-Alone Model (Continued)

TSPA_LA Parameter Name	Model Symbol	Description	Units	Distribution Specification	Remarks
PCE_Cl_N_MU_RH_65_85_a	None	Uncertainty in log chloride plus nitrate ion concentration (epistemic uncertainty)	None	Triangular Distribution Minimum: -0.22 Most Likely: 0.0 Maximum: 0.22	DTN: SN0703PAEBSPCE.007_R2, file: PCE_IDPS_uncertainties.xls [DIRS 184141]
PCE_Cl_N_MU_RH_85_100_a	None	Uncertainty in log chloride plus nitrate ion concentration (epistemic uncertainty)	None	Triangular Distribution Minimum: -0.0 Most Likely: 0.0 Maximum: 0.0	DTN: SN0703PAEBSPCE.007_R2, file: PCE_IDPS_uncertainties.xls [DIRS 184141]
PCE_Cl_NO3_MU_RH_0_20_a	None	Uncertainty in log chloride-to-nitrate ion concentration (epistemic uncertainty)	None	Triangular Distribution Minimum: -1.4 Most Likely: 0.0 Maximum: 1.4	DTN: SN0703PAEBSPCE.007_R2, file: PCE_IDPS_uncertainties.xls [DIRS 184141]
PCE_Cl_NO3_MU_RH_20_65_a	None	Uncertainty in log chloride-to-nitrate ion concentration (epistemic uncertainty)	None	Triangular Distribution Minimum: -0.5 Most Likely: 0.0 Maximum: 0.5	DTN: SN0703PAEBSPCE.007_R2, file: PCE_IDPS_uncertainties.xls [DIRS 184141]
PCE_Cl_NO3_MU_RH_65_85_a	None	Uncertainty in log chloride-to-nitrate ion concentration (epistemic uncertainty)	None	Triangular Distribution Minimum: -0.2 Most Likely: 0.0 Maximum: 0.2	DTN: SN0703PAEBSPCE.007_R2, file: PCE_IDPS_uncertainties.xls [DIRS184141]
PCE_Cl_NO3_MU_RH_85_100_a	None	Uncertainty in log chloride-to-nitrate ion concentration (epistemic uncertainty)	None	Triangular Distribution Minimum: -0.0 Most Likely: 0.0 Maximum: 0.0	DTN: SN0703PAEBSPCE.007_R2, file: PCE_IDPS_uncertainties.xls [DIRS184141]
PCE_pH_Uncert_RH_0_65_a	v	Uncertainty in pH (epistemic uncertainty).	None	Triangular Distribution Minimum: -2.0 Most Likely: 0.0 Maximum: 2.0	DTN: SN0703PAEBSPCE.007_R2, file: PCE_IDPS_uncertainties.xls [DIRS 184141]

Table 6.3.5-4. Uncertain Inputs to Localized Corrosion Initiation Stand-Alone Model (Continued)

TSPA_LA Parameter Name	Model Symbol	Description	Units	Distribution Specification	Remarks
PCE_pH_Uncert_RH_65_75_a	None	Uncertainty in pH (epistemic uncertainty)	None	Triangular Distribution Minimum: -1.0 Most Likely: 0.0 Maximum: 1.0	DTN: SN0703PAEBSPCE.007_R2, file: PCE_IDPS_uncertainties.xls [DIRS184141]
PCE_pH_Uncert_RH_75_100_a	None	Uncertainty in pH (epistemic uncertainty)	None	Discrete Distribution	DTN: SN0703PAEBSPCE.007_R2, file: Re-evaluation of pH uncertainty.xls, Tab: CDF of pH uncertainty (5 decimal digits) [DIRS184141]
Seepage_Uncertainty_a	None	Epistemic uncertainty in seepage scale factor	None	Uniform (0,1) Note that the sampled value from the distribution is converted to a uniform distribution between -1.7321 and 1.7321 in the SEEPAGEDLL_LA V1.3 software (STN: 11076-1.3-00 [DIRS 180318]; STN: 11076-1.3-01 [DIRS 181058]).	DTN: LB0407AMRU0120.001_R0, file: Summary_seepage_abstraction .doc [DIRS 173280]
Alpha_Uncert_Lith_a	$1/\alpha$	Epistemic uncertainty in capillary strength in lithophysal units	Pa	Triangular Mode = 0 Min = −105 Max = 105	DTN: LB0407AMRU0120.001_R0, file Summary_seepage_abstraction .doc [DIRS 173280]
Alpha_Uncert_NonLith_a	$1/\alpha$	Epistemic uncertainty in capillary strength in non-lithophysal units	Pa	Triangular Mode = 0 Min. = −105 Max. = 105	DTN: LB0407AMRU0120.001_R0, file: Summary_seepage_abstraction .doc [DIRS 173280]

Table 6.3.5-4. Uncertain Inputs to Localized Corrosion Initiation Stand-Alone Model (Continued)

TSPA_LA Parameter Name	Model Symbol	Description	Units	Distribution Specification	Remarks
LogK_Uncert_Lith_a	*log k*	Epistemic uncertainty in fracture permeability in lithophysal units	log m^2	Triangular Mode = 0 Min. = −0.92 Max. = 0.92	DTN: LB0407AMRU0120.001_R0, file: Summary_seepage_abstraction .doc [DIRS 173280]
LogK_Uncert_NonLith_a	*log k*	Epistemic uncertainty in fracture permeability in non-lithophysal units	log m^2	Triangular Mode = 0 Min. = −0.68 Max. = 0.68	DTN: LB0407AMRU0120.001_R0, file: Summary_seepage_abstraction .doc [DIRS 173280]
dt_dRh_uncertainty	None	Epistemic uncertainty in the thermal conductivity of the rubble resulting from a seismic event	None	Discrete [0.5,1][0.5, 2]	DTN: MO0505SPAROCKM.000_R0 [DIRS 173893]
Infiltration_Scenario_a	None	Uncertainty in infiltration scenario (10th, 30th, 50th, and 90th percentile) (epistemic uncertainty)	None	Discrete [0.6191,1][0.1568,2][0.1645, 3][0.0596,4]	DTN: LB0701PAWFINFM.001_R0, file: factors.doc [DIRS 179283]
Thermal_Conductivity_Uncert_a	None	Uncertainty in thermal conductivity (low, medium, or high) (epistemic uncertainty)	None	Discrete (p. v) [0.29,1], [0.37,2], [0.34,3]	SNL 2007 [DIRS 181383], Table 6.3-47[a]
Vol_Rubble_Max_Lith_a	$V_{rubble_\max}^{Lith}$	Volume of lithophysal rock that must fall to fill the drift (epistemic uncertainty)	m^3/m	Uniform (30,120)	DTN: MO0703PASEISDA.002_R4, Table 1-16 [DIRS 183156]
Vol_Rubble_Max_NonLith_a	$V_{rubble_\max}^{NonLith}$	Volume of nonlithophysal rock that must fall to fill the drift (epistemic uncertainty)	m^3/m	Uniform (30,120)	DTN: MO0703PASEISDA.002_R4, Table 1-16 [DIRS 183156]

Table 6.3.5-4. Uncertain Inputs to Localized Corrosion Initiation Stand-Alone Model (Continued)

TSPA_LA Parameter Name	Model Symbol	Description	Units	Distribution Specification	Remarks
WDDSBenignGC_Mean_a	None	DS-underside general corrosion rate(epistemic uncertainty)	nm/yr	Normal Mean = 5.15 SD = 0.831	DTN: SN0704PADSGCMT.001_R2, file: TSPA Implementation_DS GC Models.pdf [DIRS 182122]
WDDSAggrGC_Mean_a	None	DS-topside general corrosion rate (epistemic uncertainty)	nm/yr	Normal Mean = 46.1 SD = 1.19	DTN: SN0704PADSGCMT.001_R2, file: TSPA Implementation_DS GC Models.pdf [DIRS 182122]
C1_GenCorr_A22_a	C_1	Temperature dependent-slope term for general corrosion rate (epistemic uncertainty)	K	Normal (truncated at -3 SD and +2 SD) Mean = 4,905 SD = 1,413	DTN: MO0703PAGENCOR.001_R4, file: BaseCase GC CDFs.xls [DIRS 182029]
MIC_A22_a	f_{MIC}	MIC general corrosion enhancement factor (spatial variability)	None	Uniform(1,2)	DTN: MO0703PAGENCOR.001_R4, file: MIC Summary.pdf [DIRS 182029]
MIC_RHThresh_a	None	Relative humidity threshold for MIC (epistemic uncertainty)	None	Uniform(75%,90%)	DTN: MO0703PAGENCOR.001_R4, file: MIC Summary.pdf [DIRS 182029]
lnR0_a	ln R_o	Rate used to calculate the first general corrosion penetration for the calculations in the Localized Corrosion Stand-Alone Model, based on the medium distribution for uncertainty in the Weibull scale and shape parameters (spatial variability)	nm/yr	Weibull scale = 8.134 nm/yr shape = 1.476 Scaled by the average coupon rate with a size factor of 4	Developed by TSPA from GC_scale and GC_Shape parameters in DTN: MO0703PAGENCOR.001_R4 , file: BaseCase GC CDFs.xls [DIRS 182029] Output DTN: MO0707WPDRIPSD.000 [DIRS 183005]

INTENTIONALLY LEFT BLANK

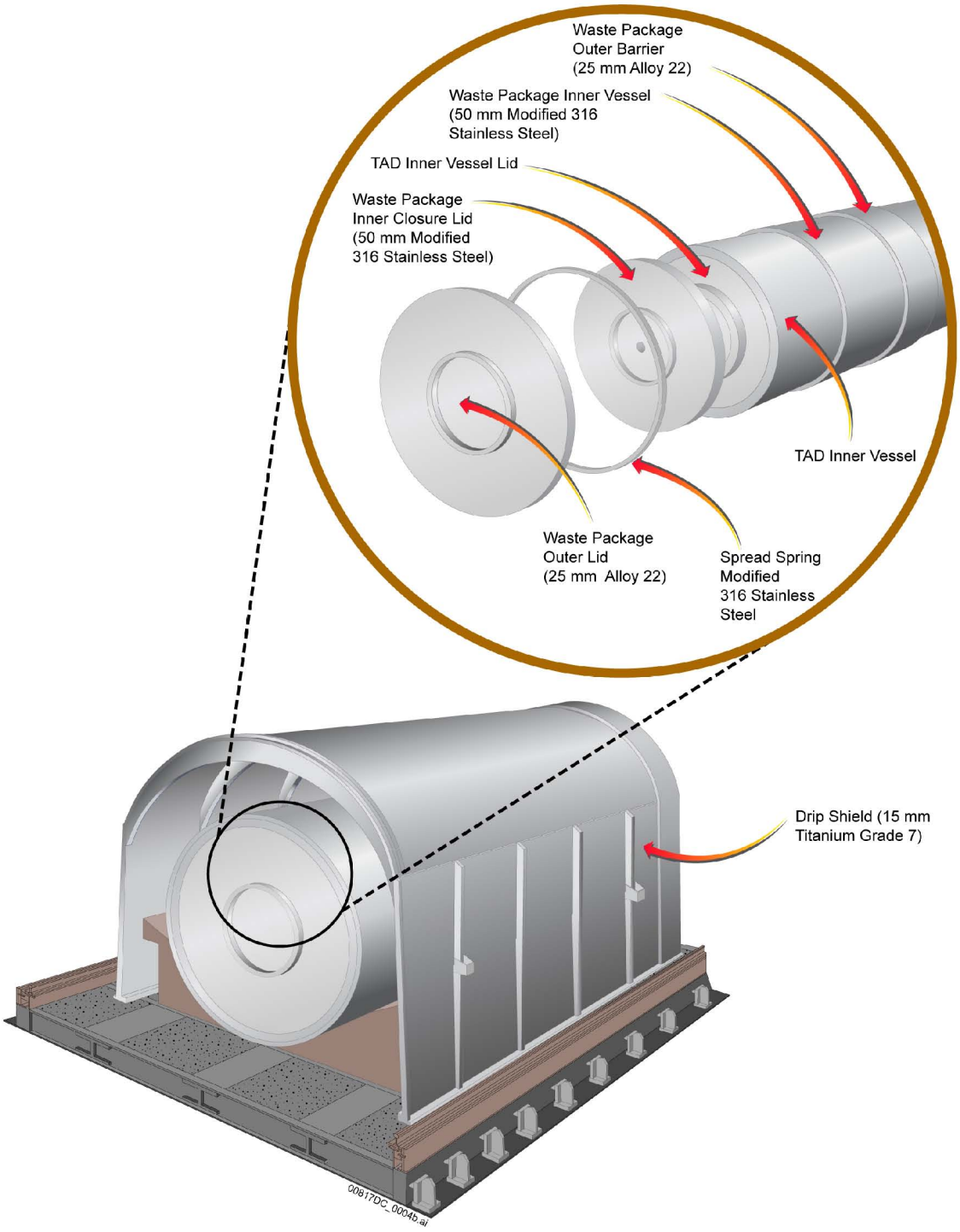

Sources: SNL 2007 [DIRS 179394] and [DIRS 179354].

Figure 6.3.5-1. Schematic Design of the Drip Shield and Waste Package

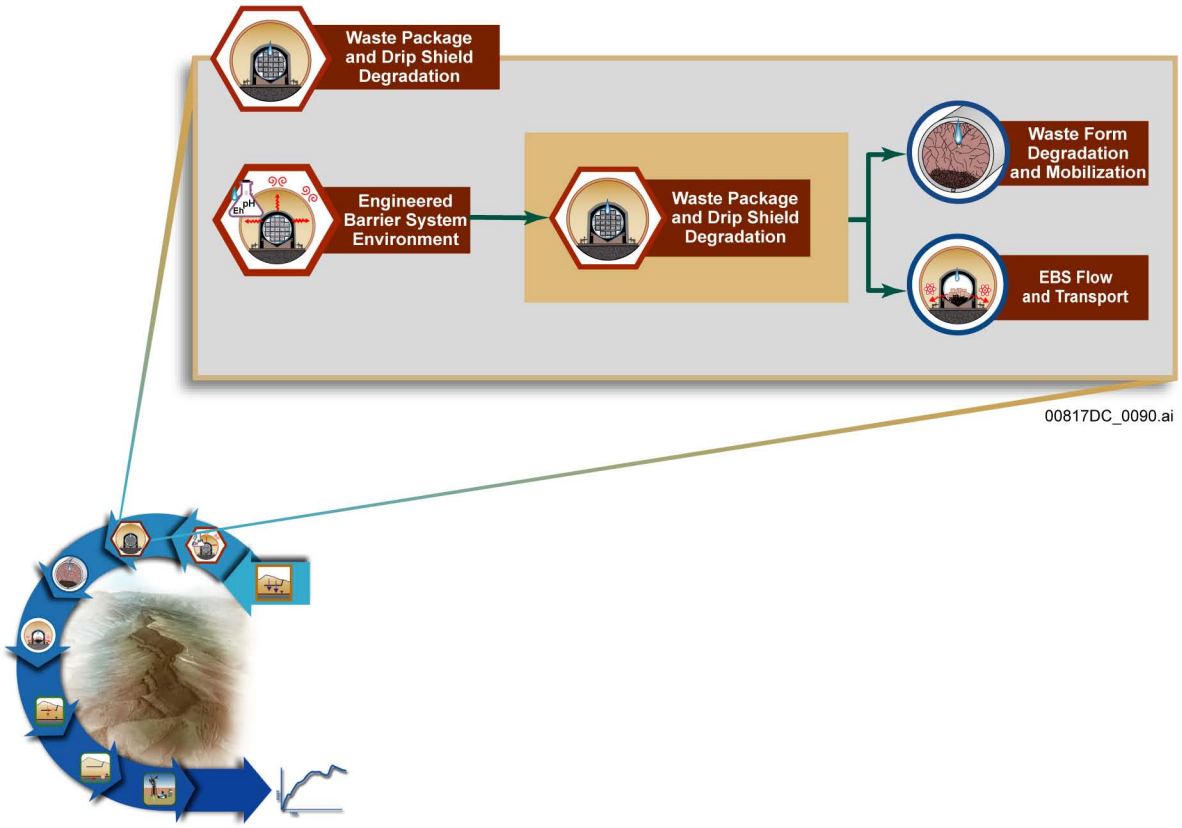

Figure 6.3.5-2. Information Flow Diagram for Waste Package and Drip Shield Degradation

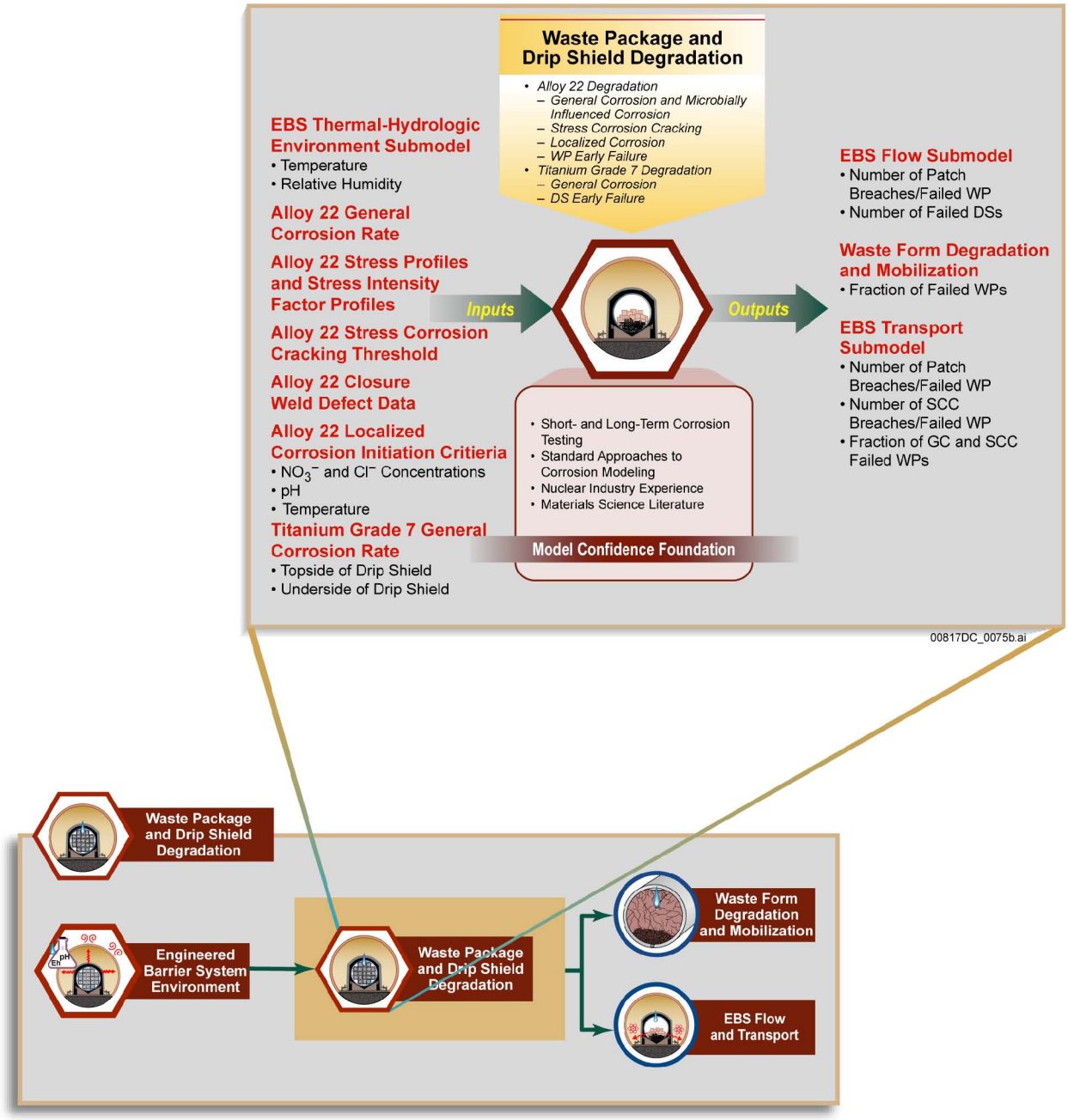

Figure 6.3.5-3. Inputs, Outputs, and Basis for Model Confidence for the Waste Package and Drip Shield Degradation Submodel

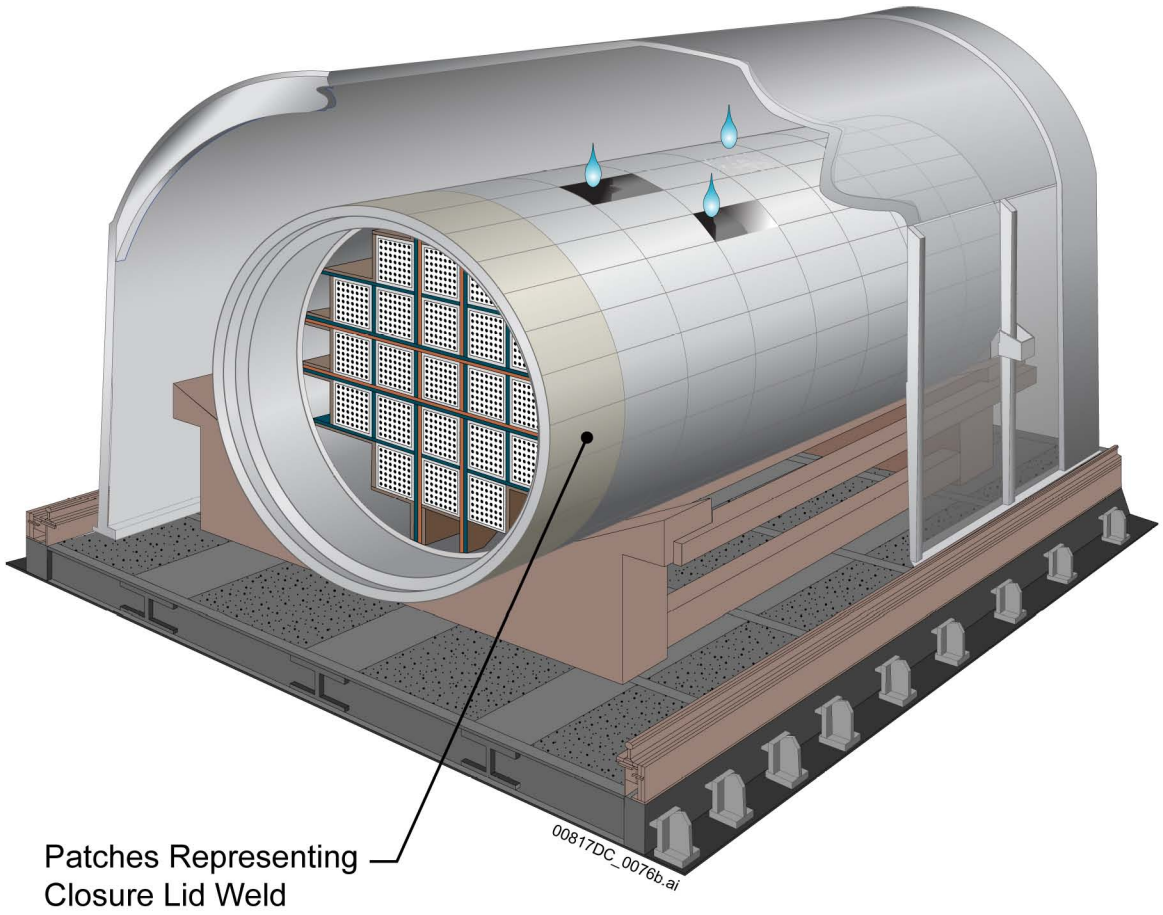

NOTE: Figure is for illustration purposes only and is not representative of repository postclosure performance.

Figure 6.3.5-4. Schematic of Waste Package Implementation in the Waste Package Degradation Model Showing a Waste Package in a Dripping Environment After a Drip Shield Failure and Patches Degrading from General Corrosion on the Surface of the Waste Package

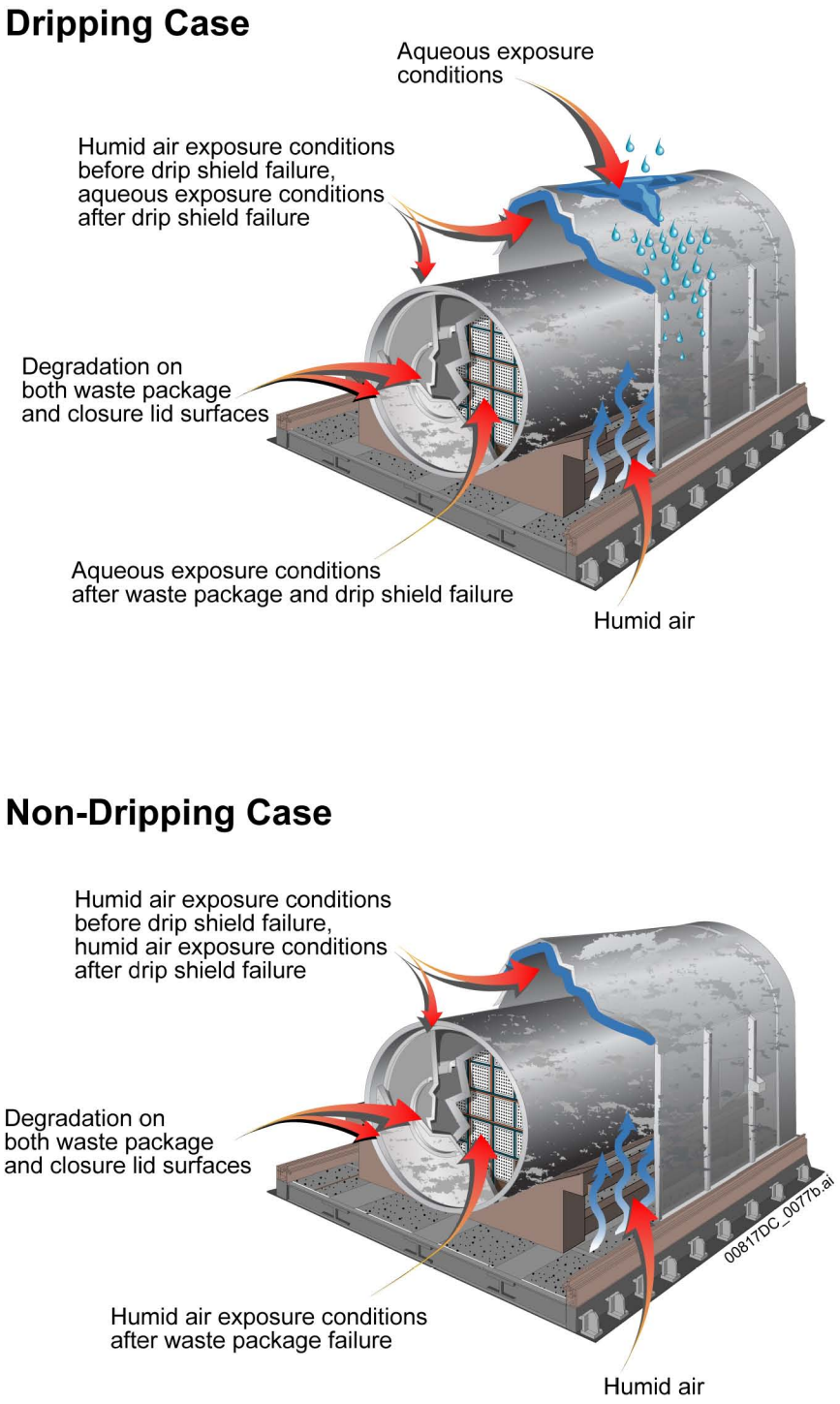

Figure 6.3.5-5. Exposure Conditions and Degradation Processes for the Drip Shield and Waste Package

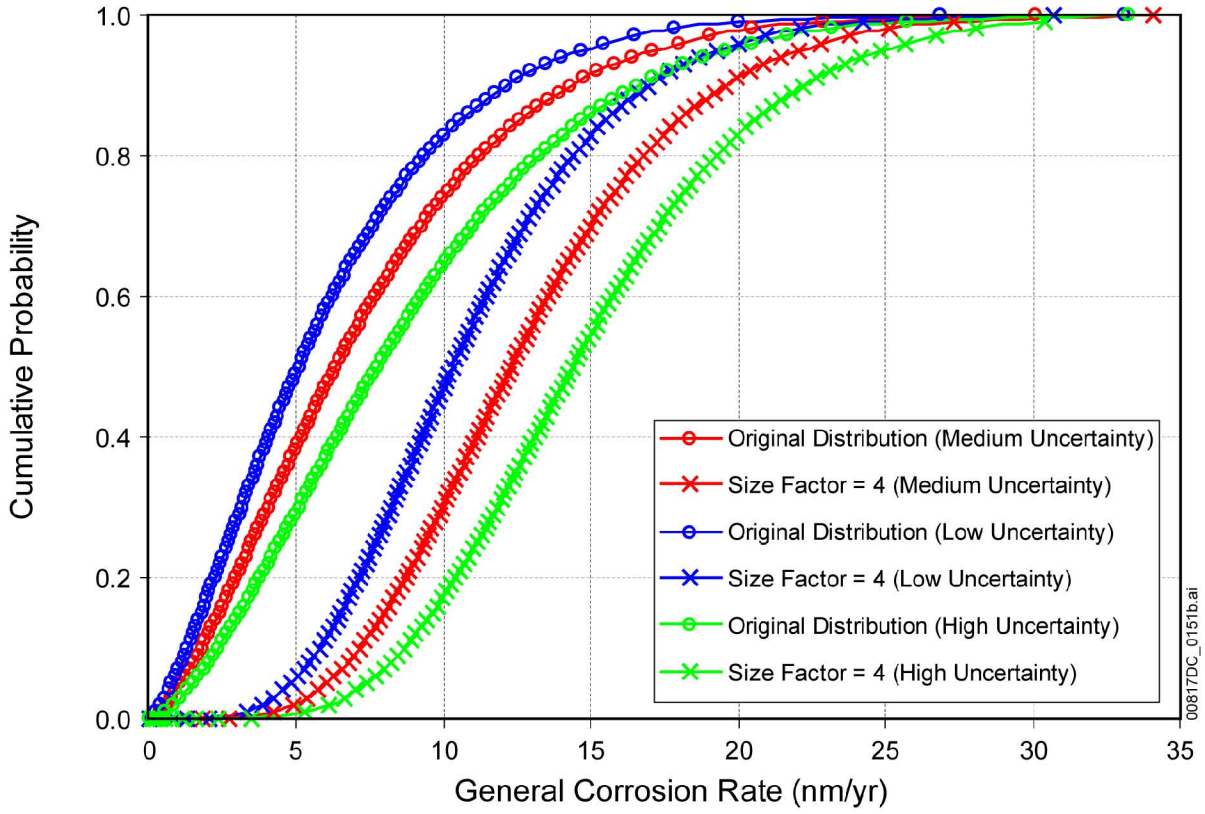

Source: Output DTN: MO0707WPDRIPSD.000 [DIRS 183005].

Figure 6.3.5-6. Effect of Scaling the General Corrosion Distribution by a Size Factor of Four

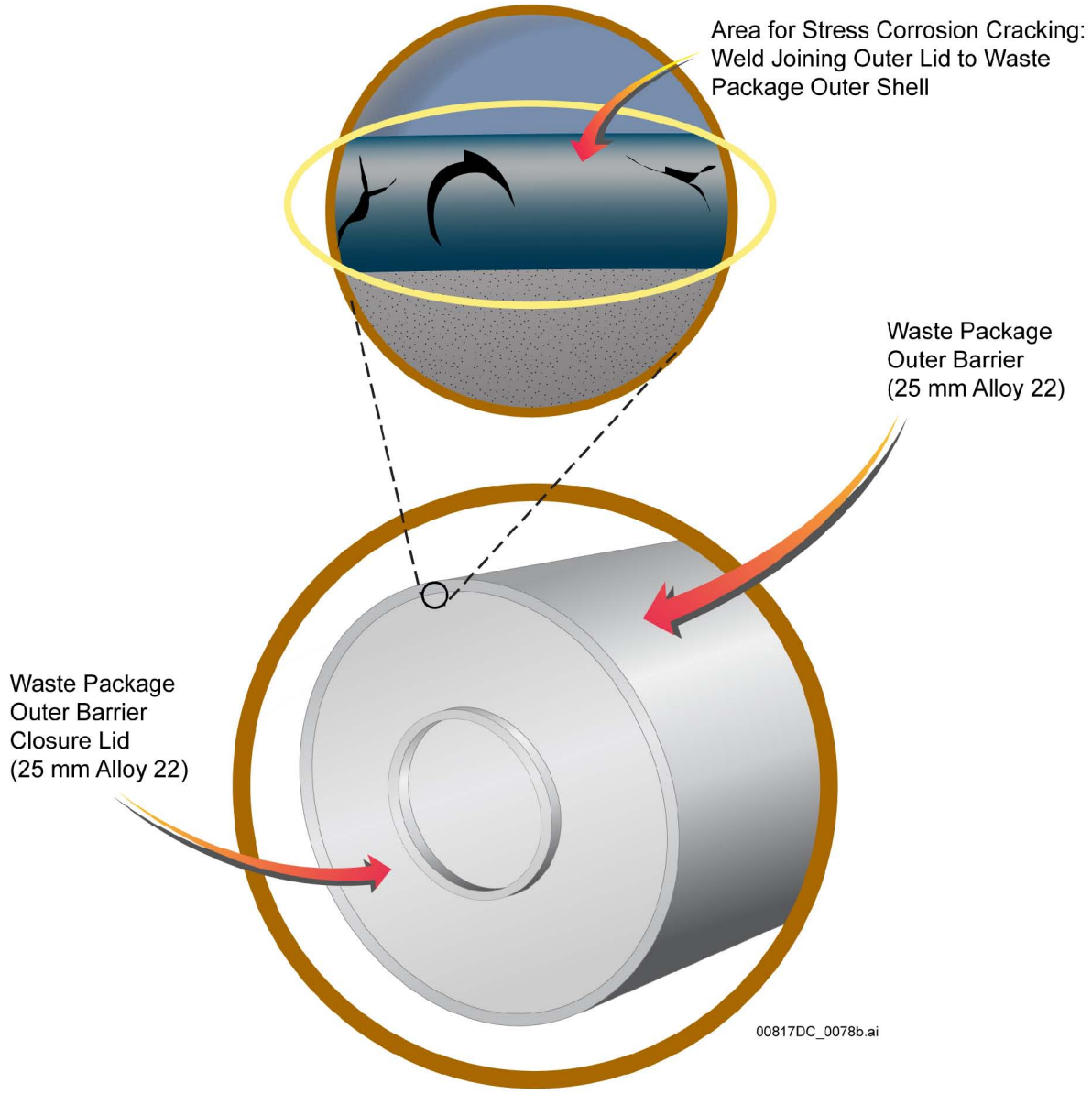

Figure 6.3.5-7. Schematic of Waste Package Closure Lid Design

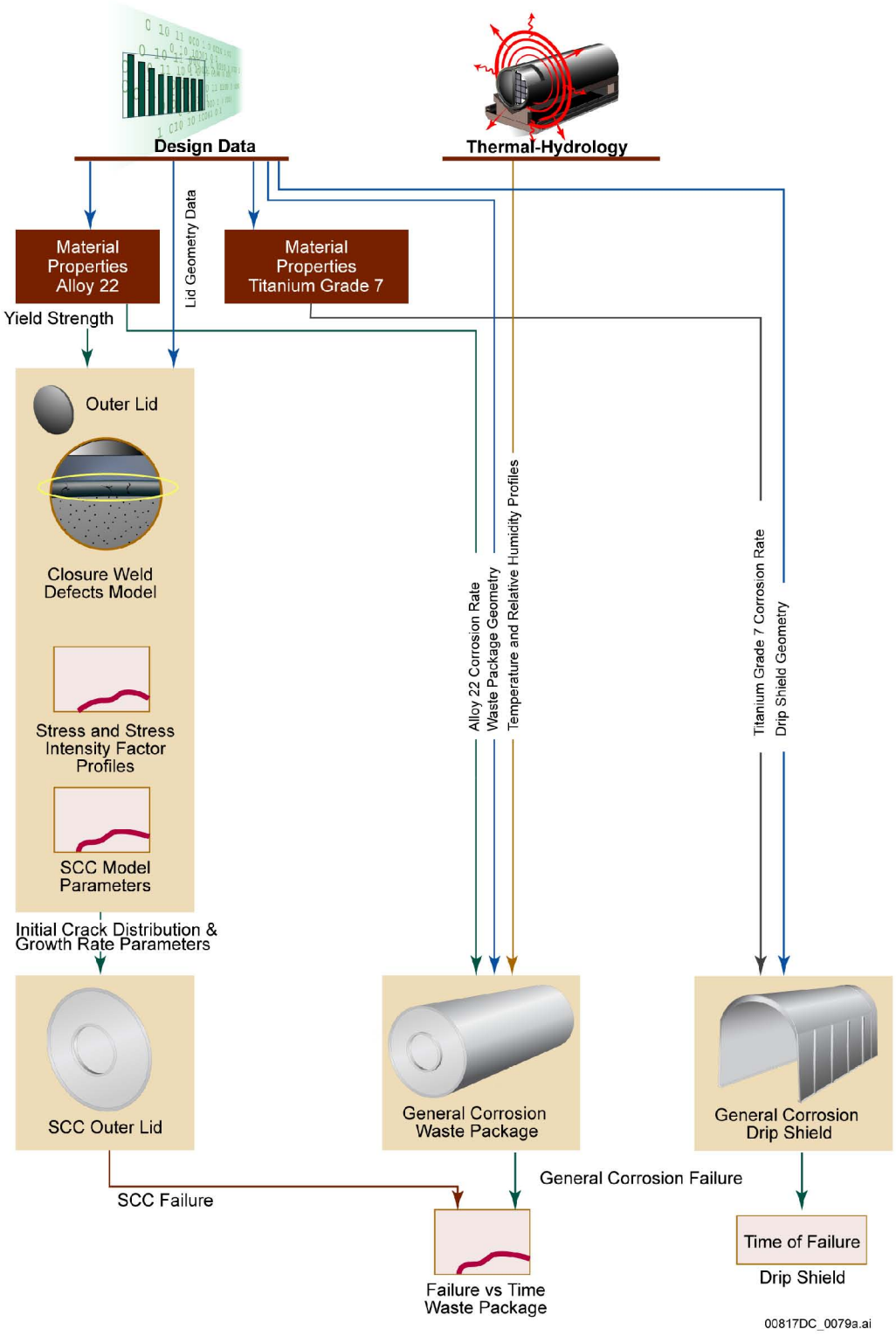

Figure 6.3.5-8. Process and Data Flow for the Waste Package and Drip Shield Degradation Model Component

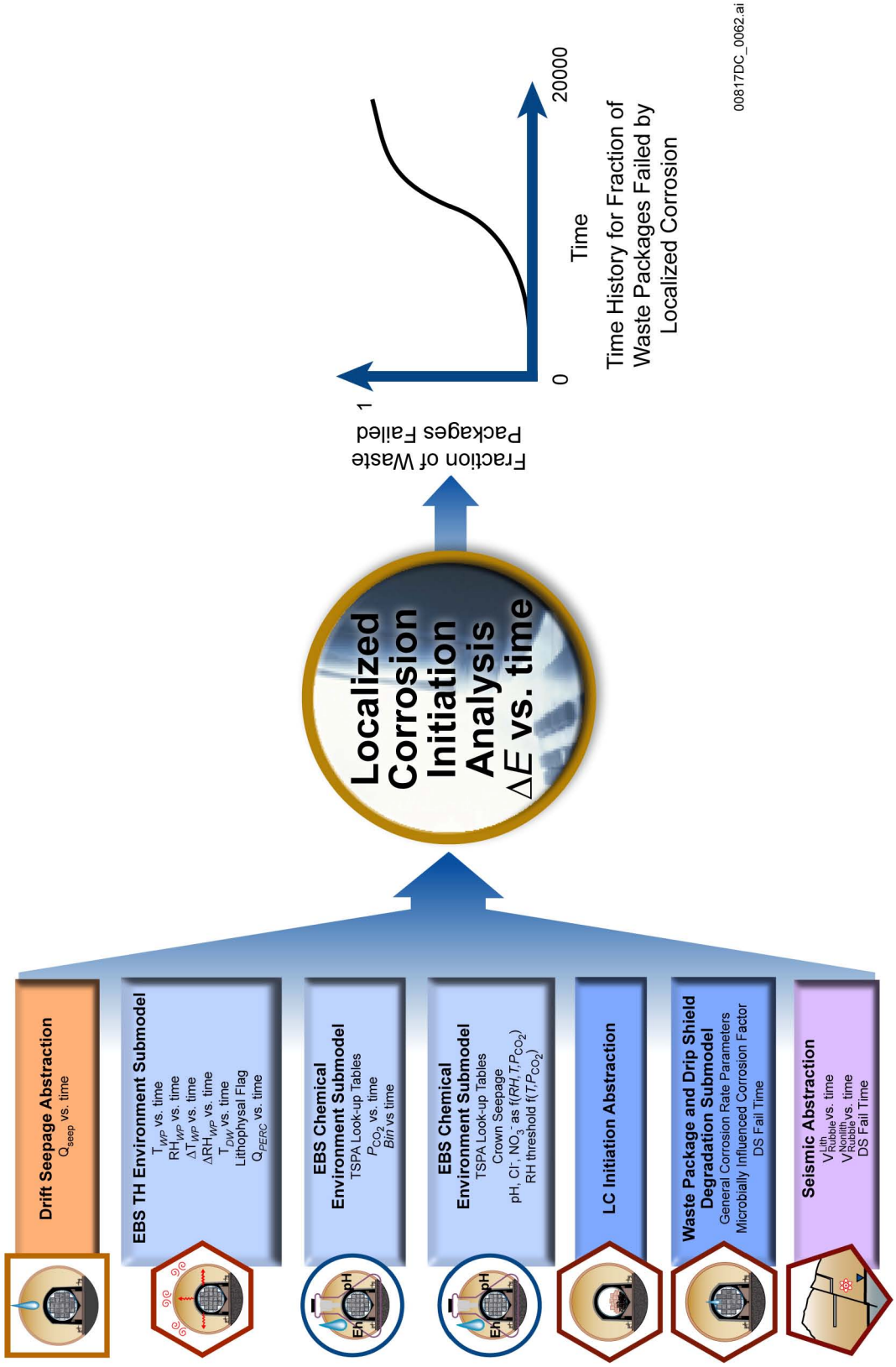

Figure 6.3.5-9. Integration of Submodels for Localized Corrosion Initiation Analysis

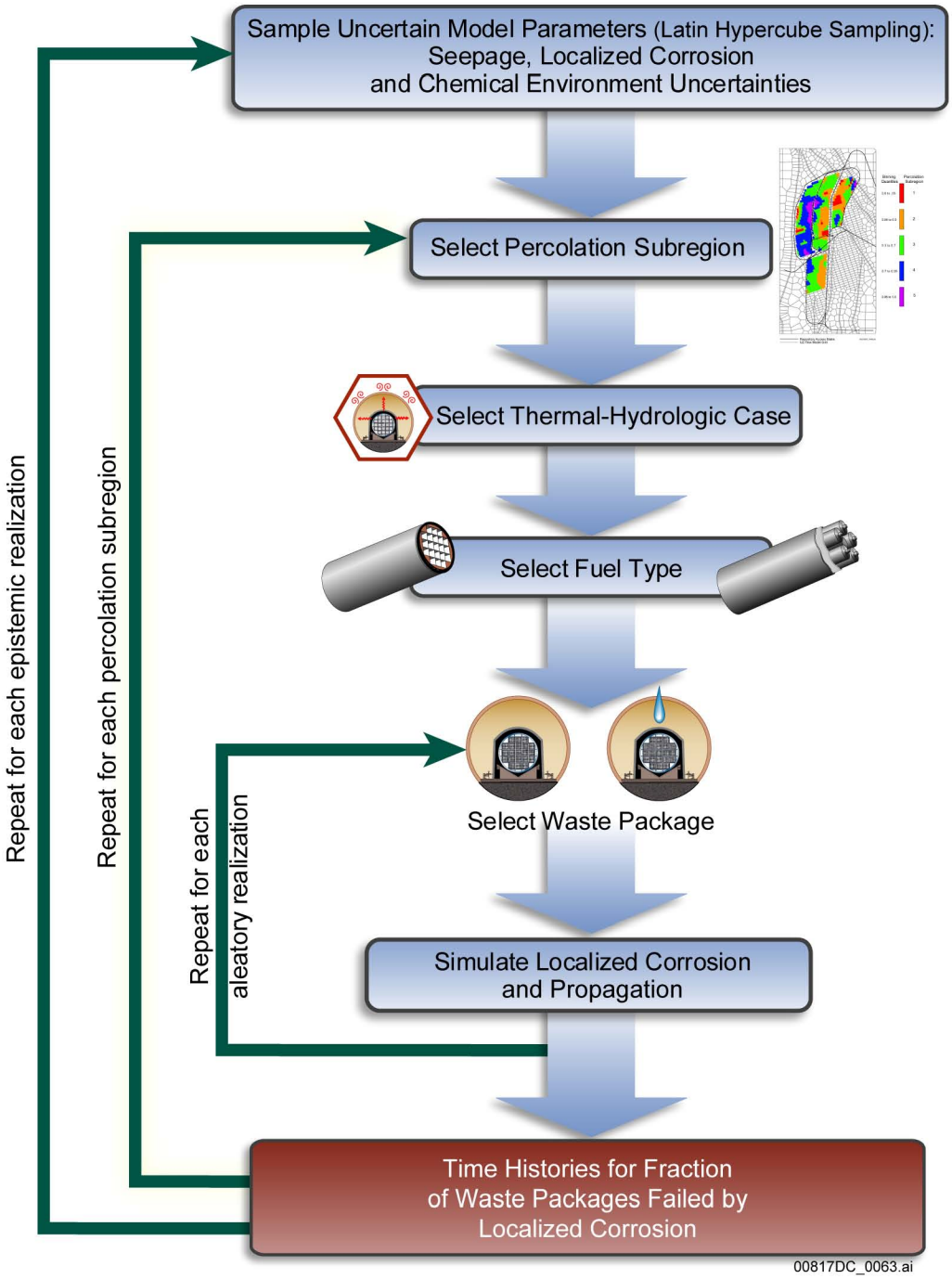

Figure 6.3.5-10. Computational Organization of Localized Corrosion Initiation Analysis for Crown Seepage

6.3.6 Engineered Barrier System Flow

The EBS Flow Submodel implemented in the TSPA-LA Model is described in *EBS Radionuclide Transport Abstraction* (SNL 2007 [DIRS 177407]). The EBS Flow Submodel defines the pathways for water flow in the EBS and specifies how the volumetric flow rate is computed for each pathway. Pathway flow rates are used as inputs to the TSPA-LA EBS Transport Submodel. The primary water inputs are the drift-seepage flow rate (SNL 2007 [DIRS 181244], Section 8.2[a]) and the drift wall condensation flow rate (SNL 2007 [DIRS 181648], Sections 8.1[a] and 8.2[a]). Drift seepage and drift wall condensation are further described in Sections 6.3.3.1 and 6.3.3.2, respectively. These two flow rates are combined in the EBS Flow Submodel to yield a total dripping flow rate. The type, number, and timing of breaches in the WPs and DSs are also inputs to the EBS Flow Submodel and are provided by the WP and DS Degradation Model Component (Section 6.3.5). An additional source of inflow to the EBS is imbibition into the invert crushed tuff from the surrounding UZ rock matrix (SNL 2007 [DIRS 177407], Section 6.3.1.1). The EBS TH Environment Submodel provides this input and calls it the liquid flow in the invert. Information flow between the EBS Flow Submodel and other TSPA-LA Model components and submodels is shown on Figure 6.3.6-1. Figure 6.3.6-2 presents an overview of the inputs, outputs, and foundation for confidence in the EBS Flow Submodel as implemented in the TSPA-LA Model.

6.3.6.1 Conceptual Model

Water is the principal medium for transport of radionuclides through the EBS (SNL 2007 [DIRS 177407], Section 6.1.1). Water, whether present as thin films or bulk stationary or flowing liquid, is necessary for radionuclides to be transported out of the WPs and through the invert to the UZ. Water flow through the EBS will be dependent on a series of processes in the repository. After the WPs are emplaced, radioactive decay of the waste will heat the drifts and locally perturb the normal percolation of water through the mountain. As the drifts cool, some of the water percolating through the mountain may drip into the drifts and subsequently contact some of the DSs. In addition, water that evaporates within the emplacement drifts may condense in cooler regions of the emplacement drifts and drip on DSs in these regions. Over time, the DSs, WPs, and other components of the EBS may degrade, allowing water as dripping or as liquid films to contact the waste forms, resulting in the mobilization and transport of radionuclides through the EBS to the UZ.

The design configuration of the EBS is shown on Figure 6.3.6-3. The drifts will be 5.5 m in diameter (SNL 2007 [DIRS 179354], Section 4.1.1 and Table 4-1). The lower portion of the drifts, commonly referred to as the invert, will be filled with crushed tuff (SNL 2007 [DIRS 179354], Table 4-1). The WPs will be placed on emplacement pallets set on the invert. Titanium DSs will be placed over the WPs and set on the invert.

The primary water input to the EBS will be the total flow rate from two sources: (1) seepage volumetric flow rate into the drifts provided by the Drift Seepage Submodel (Section 6.3.3.1), and (2) condensation volumetric flow rate on the drift walls provided by the Drift Wall Condensation Submodel (Section 6.3.3.2). A secondary source of inflow to the EBS is imbibition into the invert from the surrounding UZ rock matrix. Water from these sources flows

through the EBS along eight pathways, shown on Figure 6.3.6-4 and listed below (SNL 2007 [DIRS 177407], Sections 6.3.2 and 6.3.3).

1. **Seepage and Drift-Wall Condensation**—This is the dripping water flow from the crown (roof) of the drift. Drift seepage and any condensation that may occur on the wall of the drift on the section above the DS are included in the term dripping.

2. **Flow through the DSs**—The flow rate through the DSs is dependent on whether the DS is present. DS failure occurs due to general corrosion (SNL 2007 [DIRS 180778]), which is modeled as occurring uniformly on the DS surface. Stress corrosion cracks may occur, but advection of liquid water through stress corrosion cracks is excluded due to plugging (SNL 2007 [DIRS 181953], Sections 6.8.6 and 8.1.6, and DTN: MO0706SPAFEPLA.001_R0 [DIRS 181613], FEP 2.1.03.10.0B).

3. **Diversion around the DSs**—The dripping flows through the invert that bypasses the WP due to an intact DS.

4. **Flow through the WPs**—Three general types of openings can exist in the WPs due to corrosion: (1) stress corrosion cracks resulting from residual stress or seismic ground motion, (2) breaches resulting from general corrosion, and (3) breaches resulting from localized corrosion. The flow rate through the WPs is based on the presence of breaches due to general corrosion patches and localized corrosion. Localized corrosion is further discussed in Section 6.3.5. Stress corrosion cracks may occur, but advection of liquid water through stress corrosion cracks in the WPs is excluded for the following reasons (DTN: MO0706SPAFEPLA.001_R0 [DIRS 181613], FEP Number 2.1.03.10.0A): (1) capillary behavior allows water to reside indefinitely within the crack without flow, (2) surface tension opposes hydraulic pressure that may be present at the outlet, and (3) stress corrosion cracks are tight, rough, and tortuous, which limits the transient response to dripping water. Flow through the WPs is based on the presence of continuous flow paths through the patches that penetrate the WPs. In addition, vertical flow of dripping into the WPs, through the waste form, and out of the WPs is modeled as not affected by the location of patches on the surface of the WPs. Evaporation from the WP is ignored, as discussed further in Section 6.3.6.4.1.

5. **Diversion around the WPs**—The portion of the dripping water that does not flow into the WPs bypasses the waste forms and flows directly to the invert.

6. **Flow into the Invert**—All water flow from the WPs is modeled as flowing into the invert. All flow from the WPs flows to the invert, independent of breach location on the WPs. In addition, the dripping water that is diverted around the WPs and DSs flows into the invert. The presence of the emplacement pallets is ignored in the abstraction of EBS flow, and the WPs are modeled as being in intimate contact with the invert (SNL 2007 [DIRS 177407], Section 6.3.1.1). Thus, the flow leaving the WPs flows directly into the invert, with no resistance offered by the pallets.

7. **Imbibition Flow to the Invert**—Water can be imbibed from the host-rock matrix into the invert. The EBS TH Environment Submodel provides the rate of water imbibition into the invert from the host rock, which it calls the liquid flow in the invert.

8. **Flow from the Invert to the UZ**—The flow from the invert to the UZ is split so that a portion goes into the UZ fractures and a portion goes into the UZ matrix. The portion of the advective flow from the invert equal to the total dripping flow (F_1) flows directly into the UZ fractures. The portion of the advective flow from the invert equal to the imbibition flow to the invert (F_7) flows into the UZ matrix.

These pathways are time-dependent in the sense that total dripping flow, DS failures, and WP breaches will vary with time and percolation subregions. These pathways are further described in Section 6.3.6.2.

6.3.6.2 Abstraction

Figure 6.3.6-4 and Table 6.3.6-1 show that the flow through the EBS can be described by quantifying the flow rates at various flow pathways within the TSPA-LA Model. The EBS flow calculations are repeated in every percolation subregion for each WP type (CSNF WPs and CDSP WPs). Using F to indicate the flow rate at the numbered points on Figure 6.3.6-4, observe that

F_1 = seepage from the drift crown and drift-wall condensation dripping onto the DS (i.e., dripping flow)

F_2 = flow through the DS

F_3 = dripping flow diverted around the DS to the invert

F_4 = flow through the WP

F_5 = dripping flow diverted around the WP to the invert

F_6 = flow into the invert from flow through the WPs and dripping flow diverted around WP and DS

F_7 = imbibition flow between the host rock and the invert

F_8 = flow from the invert to the UZ.

The flow rates within the EBS are calculated based on pseudo steady state flow conditions. The primary input to the EBS Flow Submodel is the total dripping flow, F_1, and imbibition from host rock to the invert, F_7. Drift seepage and any condensation that may occur on the wall of the drift are included in this total quantity of dripping water, F_1. Effects of evaporation are ignored in order to maximize drift seepage, drift wall condensation and, consequently, advective releases of radionuclides. The calculation for various flow pathways in the EBS is described as follows:

The dripping flow diverted around the DS is

$$F_3 = F_1 - F_2 \quad \text{(Eq. 6.3.6-1)}$$

The dripping flow diverted around the WP is

$$F_5 = F_2 - F_4 \quad \text{(Eq. 6.3.6-2)}$$

The flow entering the invert due to seepage and condensation is

$$F_6 = F_1 = F_3 + F_4 + F_5 \quad \text{(Eq. 6.3.6-3)}$$

The flow exiting the invert is

$$F_8 = F_6 + F_7 = F_1 + F_7 \quad \text{(Eq. 6.3.6-4)}$$

The result of flow splitting of the dripping flow at the DS, F_2, and at the WP, F_4, determines all flow within the EBS. The flow through the DSs is a result of the DS flow splitting logic presented in *EBS Radionuclide Transport Abstraction* (SNL 2007 [DIRS 177407], Section 6.3.2.4) as

$$F_2 = \min\left[F_1 \frac{N_{pDS}\, l_{DS}}{L_{DS}} f'_{DS}, F_1\right] \quad \text{(Eq. 6.3.6-5)}$$

where

F_1 = seepage + condensation

N_{pDS} = number of DS general corrosion patches (Note that in the TSPA-LA Model, when the DS fails by general corrosion, the entire DS is modeled as having failed at once, and N_{pDS} = 1.)

l_{DS} = axial half-length of DS general corrosion patch

L_{DS} = axial length of DS

f'_{DS} = uncertainty factor (Table 6.3.6-2).

Flow through the WPs is a result of the WP flow splitting logic presented in *EBS Radionuclide Transport Abstraction* (SNL 2007 [DIRS 177407], Section 6.3.3.2), and is described as follows:

$$F_4 = \min\left[F_2 \frac{N_{pWP}\, l_{WP}}{L_{WP}} f'_{WP}, F_2\right] \quad \text{(Eq. 6.3.6-6)}$$

where

F_2 = flow through a DS

N_{pWP} = number of general corrosion patches on failed WP

l_{WP} = axial half-length of general corrosion patch on failed WP

L_{WP} = axial length of WP

f'_{WP} = WP uncertainty factor (Table 6.3.6-2).

The number of general corrosion patches on a failed WP, N_{pWP}, is the time-dependent parameter that controls the fraction of impinging flow that can enter and flow through the WPs. N_{pWP} can vary from zero to the maximum number of patches, depending on the modeling case. N_{pWP} increases with time due to general corrosion in the Seismic GM and Nominal Modeling Cases. N_{pWP} is set to the maximum value in the Igneous Intrusion, Waste Package EF, and Drip Shield EF Modeling Cases. In the Seismic FD Modeling Case, N_{pWP} is based on the number of patches equivalent to the WP damaged area caused by faulting. N_{pWP} is set to a value corresponding to a single drill hole in the Human Intrusion Modeling Case. Because the flow splitting model described by Equation 6.3.6-6 is based on the fractional opening length along the crown of the WP, rather than the fractional opening area over the entire WP, the flow splitting fraction reaches 1 (i.e., all the impinging flow can enter a WP) well before N_{pWP} reaches its maximum. For the mean value of the WP flux uncertainty term, f'_{WP}, equal to 1.2, only about 62 general corrosion patches are required on a CSNF WP to allow 100 percent of the impinging flow to enter a WP. This is about 4 percent of the area of the WP (excluding the lids). The EBS Flow Submodel in the TSPA-LA Model is summarized in Table 6.3.6-1.

Uncertainty in the EBS Flow Submodel—The EBS Flow Submodel uses one uncertain (epistemic) flow splitting parameter to characterize the fraction of flow that enters breaches in the DSs and one uncertain (epistemic) flow splitting parameter to characterize the fraction of flow that enters breaches in the WPs. Each parameter is sampled once per realization and applied to all representative WP locations in a dripping environment. Table 6.3.6-2 provides the distribution type and ranges for these two parameters.

6.3.6.3 TSPA-LA Implementation

The EBS flow calculation consists of two parts in the TSPA-LA Model. The first part of the EBS flow calculation combines the drift seepage and drift-wall condensation flows to determine the total dripping rate onto the DS and into the invert. The second part calculates the flow through the failed WPs and DSs using the flow splitting logic presented in Equation 6.3.6-5 and Equation 6.3.6-6.

Dripping Flow Calculations—The EBS Flow Submodel calculates the dripping flow into the drift. The EBS Flow Submodel receives feeds (inputs) (Figure 6.3.6-2) from the Drift Seepage

Submodel and the Drift Wall Condensation Submodel. The seepage fraction and seepage rate from the Drift Seepage Submodel is passed to the EBS Flow Model. The seepage fraction determines the number of WPs placed in seep and non-seep environments in each percolation subregion. A single element in the model then adds the seepage rate and the drift-wall condensation rate to produce the total dripping rate onto the DS and into the invert for WPs in a seep environment. For a non-seep environment, only the drift-wall condensation rate is used.

Flow Splitting Calculations—The flow splitting calculations determine the volumetric flow rate of water at different locations within the EBS as water moves through breached DSs, breached WPs, and the invert as shown on Figure 6.3.6-4. The volumetric flow rate of water through each breached DS or WP is proportional to the damage fraction on each DS or WP represented by N_{pDS} and N_{pWP} in Equations 6.3.6-5 and 6.3.6-6, respectively. The EBS Flow Submodel introduces two uncertain (epistemic) flow splitting parameters to characterize the fraction of flow that enters breaches on the DSs and WPs. These two parameters are sampled once per realization and applied to all representative DSs and WPs.

Inputs to the EBS Flow Submodel for each WP type and repository subregion include:

- Seepage and condensation rates from the Drift Seepage and Drift Wall Condensation Submodels (Section 6.3.3)
- Damage fraction per failed DS from the WP and DS Degradation Model Component (Section 6.3.5)
- Damage fraction per failed DS from Early DS Failure Abstraction (Drip Shield EF Modeling Case only) (Section 6.4)
- Damage fraction per failed DS from the Seismic Consequences Abstraction (Seismic Scenario Class only) (Section 6.6)
- Damage fraction per failed WP from the WP and DS Degradation Model Component (Nominal Scenario Class only) (Section 6.3.5)
- Damage fraction per failed WP from the Seismic Consequences Abstraction (Seismic Scenario Class only) (Section 6.6).

The EBS Flow Submodel does not use the average number of crack penetrations per failed WP because stress corrosion cracks are too small to allow water flow through these cracks (DTN: MO0706SPAFEPLA.001_R0 [DIRS 181613], FEP Number 2.1.03.10.0A).

The flow splitting model for water flow through a damaged DS is computed by multiplying the dripping flow falling on the DS by the ratio of patch opening length on the DS to the total length of the DS. Similarly, the flow entering each WP is computed by multiplying the flow falling on the WP (i.e., the flow of water through the DS) by the ratio of patch opening length on the WP to the total length of the WP. Both calculations are multiplied by a separate uncertainty factor to account for the variation in location of the patches with respect to the drip location (Table 6.3.6-2). However, the DS corrosion model does not include spatial variation between

DSs or between patches on individual DSs (Section 6.3.5.1.3). Therefore, for the TSPA-LA Model, all the DS patches fail when DS failure occurs. Additionally, when N_{pDS} is equal to the maximum number of DS patches, the DS flow splitting algorithm is not used and $F_2 = F_1$ (Eq. 6.3.6-5).

Outputs from the EBS Flow Submodel are used by: (1) the Waste Form Degradation and Mobilization Model Component (volumetric flow rate through a failed WP) to calculate pH and ionic strength in the WP, and (2) the EBS Transport Submodel (volumetric flow rate through a failed WP and volumetric flow rate through the invert) to calculate advective transport of radionuclides through a failed WP and the invert to the host rock.

6.3.6.4 Consistency and Conservatism in Assumptions and Parameters

To enhance understanding of the complex interactions within the TSPA-LA Model, a discussion of consistency among model components and submodels and identification of conservative assumptions in abstractions, process models, and parameter sets supporting the EBS Flow Submodel is presented below.

6.3.6.4.1 Consistency of Assumptions

Effects of Evaporation on EBS Flow—Less water may be available for transport if evaporation on the DSs or WPs were taken into account. Generally, the heat output from the WPs will cause the DSs to be hotter than the drift wall from which water is dripping. Some water that drips onto the DSs may be evaporated, thereby reducing the flow of water through the DSs. A reduction in the quantity of water flow through the DSs reduces the potential for advective transfer and subsequent release and transport of radionuclides from the WPs (SNL 2007 [DIRS 177407], Section 5.2).

Heat generated by the waste forms also has the potential to evaporate water within the WPs. In this situation, water cannot collect inside the WPs and cannot support the advective transport of radionuclides. However, complexities in the internal geometry of the WPs, particularly the response of any water pooled at the bottom of the WPs and the presence of small conduits for water vapor to escape through stress corrosion cracks, make it difficult to assess evaporation quantitatively. The potential for evaporation in the WPs is ignored in the TSPA-LA Model (SNL 2007 [DIRS 177407], Section 6.3.3.2).

Effect on the TSPA-LA Model—As further discussed in Section 6.3.8, neglecting the evaporation of water on the DSs and WPs means there is more water available for dissolution and advection of radionuclides. Also, neglecting evaporation leads to higher saturation and more diffusion of radionuclides. Evaporation and consumption of water and water vapor entering a WP is evaluated in Appendix C.

6.3.6.4.2 Identification of Conservatisms in Submodels and Abstractions

No DS Shadow in the Invert—For dripping locations, water will tend to shed around the DSs and not flow through the region of the invert directly under the DSs. However, because of limited information regarding the flow paths and mixing of waters, this effect is not accounted for (SNL 2007 [DIRS 177407], Section 6.5.2.6). For model scenarios without DS failures, a DS shadow would prevent advective transport for some distance beneath the WP, certainly within the invert and for some distance in the UZ fractures and matrix. However, the TSPA-LA Model assumes advection within the invert in the dripping locations. The effect of this assumption is to increase the release of radionuclides from the invert and increase the diffusive concentration gradient from the waste form to the invert and UZ, thereby conservatively increasing the diffusive mass flux.

All Dripping into Drifts is Assumed to Fall on the DSs—All dripping into drifts is assumed to fall on the DSs, not just dripping above the DSs. The approach taken is to simplify the model since uncertainty in dripping locations is difficult to quantify and seepage into a circular opening is more likely to occur near the crown (SNL 2007 [DIRS 177407], Section 5.1). While all dripping into the drift is assumed to fall on the DSs, the DS flow splitting uncertainty term in Equation 6.3.6-5 is applied. While this uncertainty term may reduce the flow through the DSs to account for the spatial variability of the location of DS patch openings, it does not account for spatial distribution of dripping. The conservative treatment tends to increase the dripping flow contacting the DSs, resulting in an increase in the dripping flow passing through a failed DS and an increase in the dripping flow diverted around the DSs (e.g., passing through the invert) within the dripping locations.

All the Dripping Penetrating a DS Falls on the Crown of the WP—A conservative approach is taken to simplify the modeling approach because uncertainty in dripping locations is difficult to quantify (SNL 2007 [DIRS 177407], Section 5.1). Any increase in the advective flow through the WPs as a result of assuming the entire flow penetrating the DSs falls on the WPs would be negligible with the result of a slight increase in the dripping flow through the breached WPs.

6.3.6.5 Alternative Conceptual Model(s) for Engineered Barrier System Flow

Section 6.2 outlines the general consideration and treatment of ACMs used to support the TSPA-LA Model. Brief descriptions of the EBS Flow Submodel ACMs are summarized in Table 6.3.6-3.

Bathtub Flow Model ACM—This ACM assumes that dripping water collects within the WP before being released to the EBS (SNL 2007 [DIRS 177407], Section 6.6.1). The bathtub effect would be most important during the period when only a few patches or cracks have penetrated the DSs and WPs. In this situation, there may be penetrations through the top of the WP while the bottom surface remains intact, leading to retention of liquid. At later times, the presence of multiple penetrations makes a flow-through geometry the more likely configuration. The response of the bathtub geometry was evaluated for a primary case, with constant boundary conditions and material properties, and for three secondary cases. The three secondary cases considered a step change in inflow rate, such as would occur from a climatic change, a step change in water chemistry, or a step change in flow geometry, as would occur if a patch

suddenly appeared beneath the waterline. All cases included the consideration of two limiting conditions on radionuclide releases: dissolution rate limited and solubility limited.

This ACM was not used for the TSPA-LA EBS Transport Model because analyses indicate that the base-case flow-through model is bounding for use in the TSPA-LA Model with respect to the release of radionuclides (SNL 2007 [DIRS 177407], Section 6.6.1).

Dual-Continuum Invert Model ACM—The dual-continuum invert model is an alternative conceptual EBS transport model in which crushed tuff invert ballast is modeled as a dual-continuum material consisting of intergranular pore space and intragranular pore space (SNL 2007 [DIRS 177407], Sections 6.6.3 and 6.6.4.2). All water dripping into the drift is modeled as flowing through the intergranular pore space and UZ fractures. Imbibition from UZ host rock into the invert is modeled as flowing through the intragranular pore space and into the UZ matrix under gravity. Diffusion of radionuclides also occurs in both the intergranular and intragranular pore spaces, from the WP corrosion products into UZ fractures and matrix, as well as between the two invert continua.

This ACM was not used for the TSPA-LA EBS Transport Model due to insufficient data to validate diffusion coefficients in individual continua and insufficient data to confirm whether this is a bounding approach with respect to chemical behavior in the invert (SNL 2007 [DIRS 177407], Section 6.6.3.5).

INTENTIONALLY LEFT BLANK

Table 6.3.6-1. The EBS Flow Abstraction within the TSPA-LA Model

Flow Pathway	Flow Parameters	Notes
1. Total dripping flow (seepage + wall condensation), F_1	Total dripping flow is a function of seepage flow and drift-wall condensation flow.	Drift Seepage Submodel (Section 6.3.3.1) provides time- and location-dependent values of seepage flow. Drift Wall Condensation Submodel (Section 6.3.3.2) provides time and location-dependent values of drift-wall condensation flow.
2. Flow through the DS, F_2	N_{pDS} is the number of DS general corrosion patches l_{DS} is the axial half-length of patches due to general corrosion of titanium. L_{DS} is the axial length of the DS. f'_{DS} is the sampled uncertain parameter, DS_Flux_Uncertainty_a.	WP and DS Degradation Model Component (Section 6.3.5) provides the number of general corrosion patches and stress corrosion cracks on the DS. No flow through stress corrosion cracks due to plugging (SNL 2007 [DIRS 181953], Sections 6.8.6 and 8.1.6, and DTN: MO0706SPAFEPLA.001_R0 [DIRS 181613], FEP 2.1.03.10.0B).
3. Diversion around DS, F_3	$F_3 = F_1 - F_2$.	Continuity of liquid flow.
4. Flow into the WP, F_4	N_{pWP} is the number of WP general corrosion patches l_{WP} is the axial half-length of all patches due to general corrosion of Alloy 22 (UNS N06022). L_{WP} is the axial length of the WP. f'_{WP} is the sampled uncertain parameter, WP_Flux_Uncertainty_a.	WP and DS Degradation Model Component (Section 6.3.5) provides the number of general corrosion patches on the WP. No flow through stress corrosion cracks (DTN: MO0706SPAFEPLA.001_R0 [DIRS 181613], FEP 2.1.03.10.0A). Pseudo steady state flow through WP (outflow = inflow in steady state; that is bounding for release).
5. Diversion around the WP, F_5	$F_5 = F_2 - F_4$.	Continuity of liquid flow.
6. Flow to the invert, F_6	$F_6 = F_5 + F_4 + F_3$ $= F_1$.	Note that only F_4 can transport radionuclides into the invert.
7. Imbibition flow from the host rock matrix into the invert, F_7	F_7 is an input to the EBS Flow Submodel.	EBS TH Environment Submodel (Section 6.3.2) provides the imbibition flow.
8. Flow from the invert into the UZ, F_8	$F_8 = F_6 + F_7$ $= F_1 + F_7$.	Total dripping flow portion ($F_1 = F_6$) of advective flow from the invert flows into the UZ fractures; imbibition flow (F_7) flows into the UZ matrix.

Source: Developed from SNL 2007 [DIRS 177407], Table 8.1-1.

NOTE: See Figure 6.3.6-4.

Table 6.3.6-2. Drip Shield and Waste Package Flow Splitting Parameters

TSPA-LA Model Name	Mathematical Symbol	Description	Units	Distribution Type	Distribution Specification
DS_Flux_Uncertainty_a	f'_{DS}	DS flow splitting uncertainty factor	None	Uniform	Min = 0 Max = 0.85
WP_Flux_Uncertainty_a	f'_{WP}	WP flow splitting uncertainty factor	None	Uniform	Min = 0 Max = 2.41

Sources: SNL 2007 [DIRS 177407], Table 8.2-4, and DTN: SN0703PAEBSRTA.001_R3 [DIRS 183217].

Table 6.3.6-3. Alternative Conceptual Models Considered for the EBS Flow

Alternative Conceptual Models	Key Assumptions	Assessment and Basis
Dual-continuum invert model	Crushed tuff invert ballast is modeled as a dual-continuum material consisting of intergranular and intragranular pore spaces. All seepage flow into the drift flows through the intergranular pore space and into the UZ fractures. Imbibition from UZ host rock into the invert flows through the intragranular pore space. Diffusion of radionuclides also occurs in both the intergranular and intragranular pore spaces, from the WP corrosion products into UZ fractures and matrix, as well as between the two invert continua (SNL 2007 [DIRS 177407], Section 6.6.4).	Insufficient data to validate diffusion coefficients in individual continua. Insufficient data to confirm whether this is a bounding approach with respect to chemical conditions in the invert for calculating solubility and colloid stability.
Bathtub flow model (alternative to flow-through model)	Seepage water flowing into breached WP accumulates until void volume is filled before water containing dissolved radionuclides flows out. Various cases, such as changing inflow rates and effect of solubility and dissolution rate limits, are evaluated (SNL 2007 [DIRS 177407], Section 6.6.1).	The flow-through model is determined to be conservative with respect to releases of radionuclides for use in the TSPA-LA Model (SNL 2007 [DIRS 177407], Section 6.6.1).

Source: Developed from SNL 2007 [DIRS 177407], Table 6.4-1.

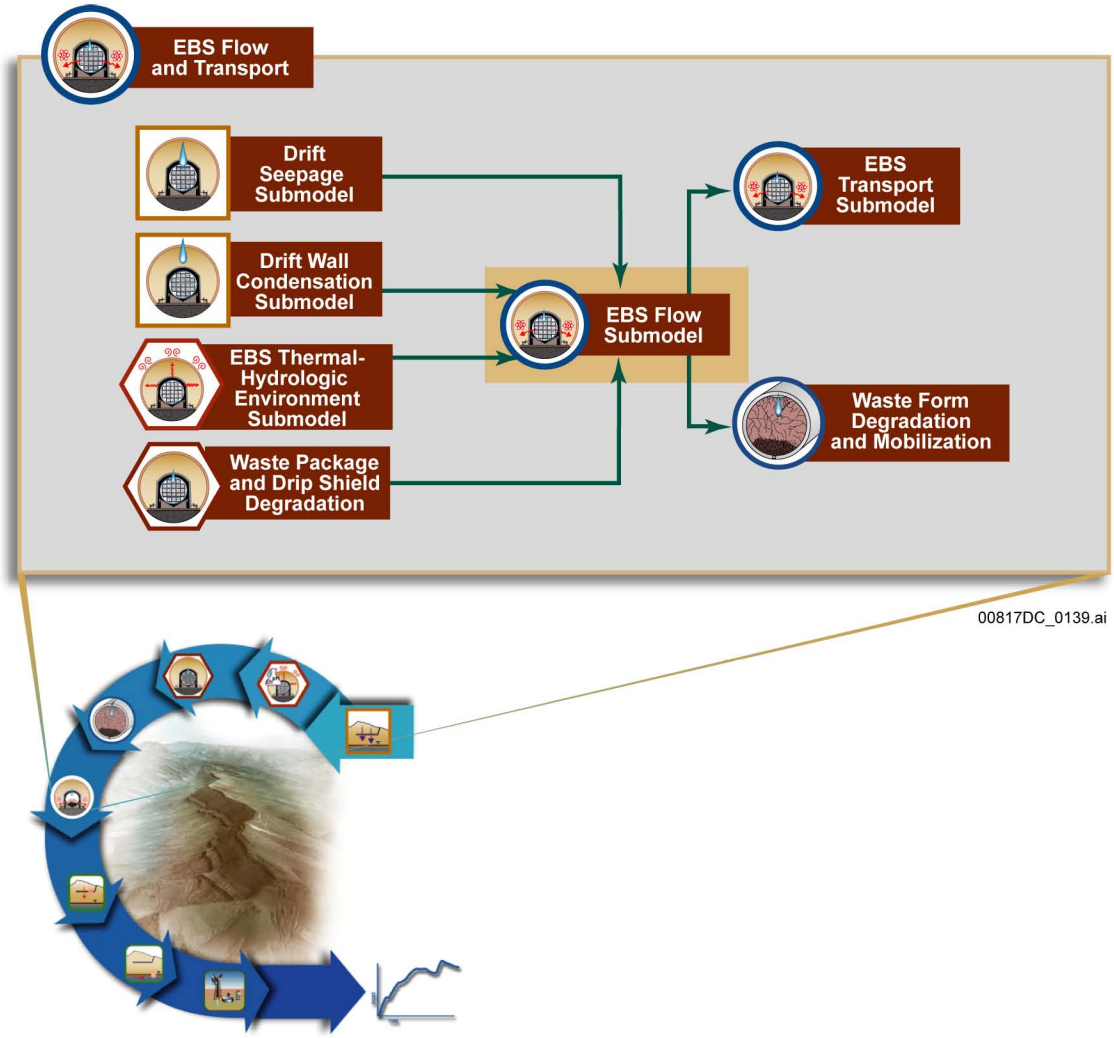

Figure 6.3.6-1. Information Flow Diagram for the EBS Flow Submodel

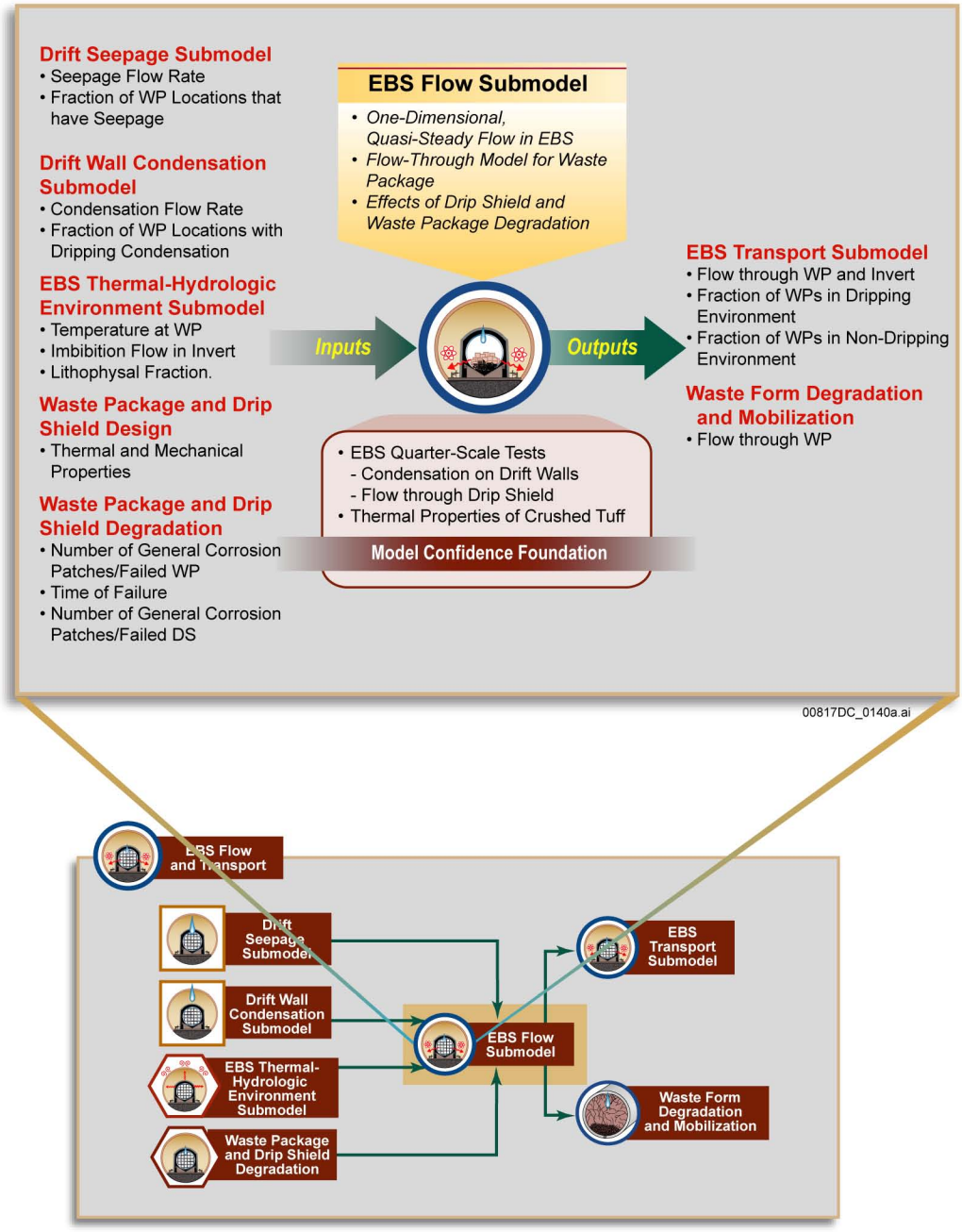

Figure 6.3.6-2. Inputs, Outputs, and Basis for Model Confidence for the EBS Flow Submodel

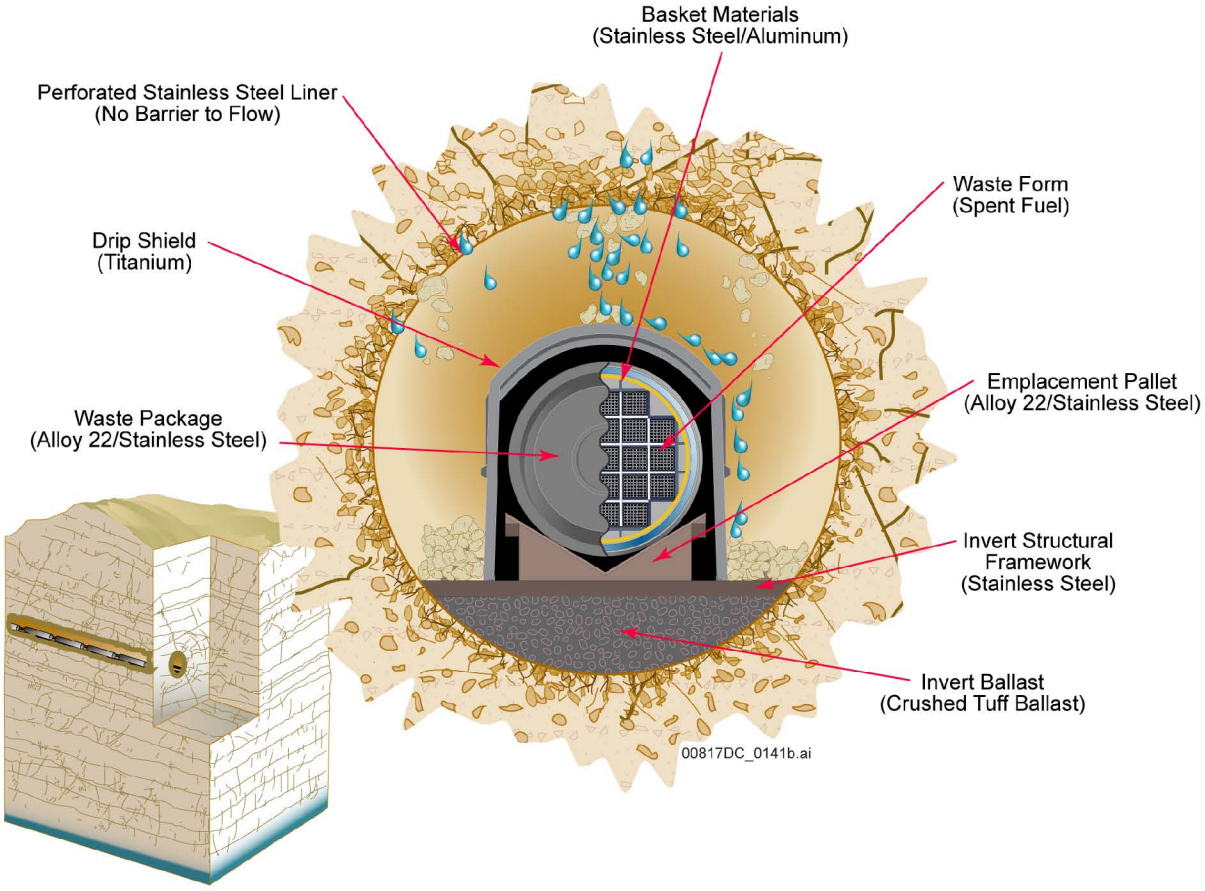

Figure 6.3.6-3. Cross Section of Typical Emplacement Drift

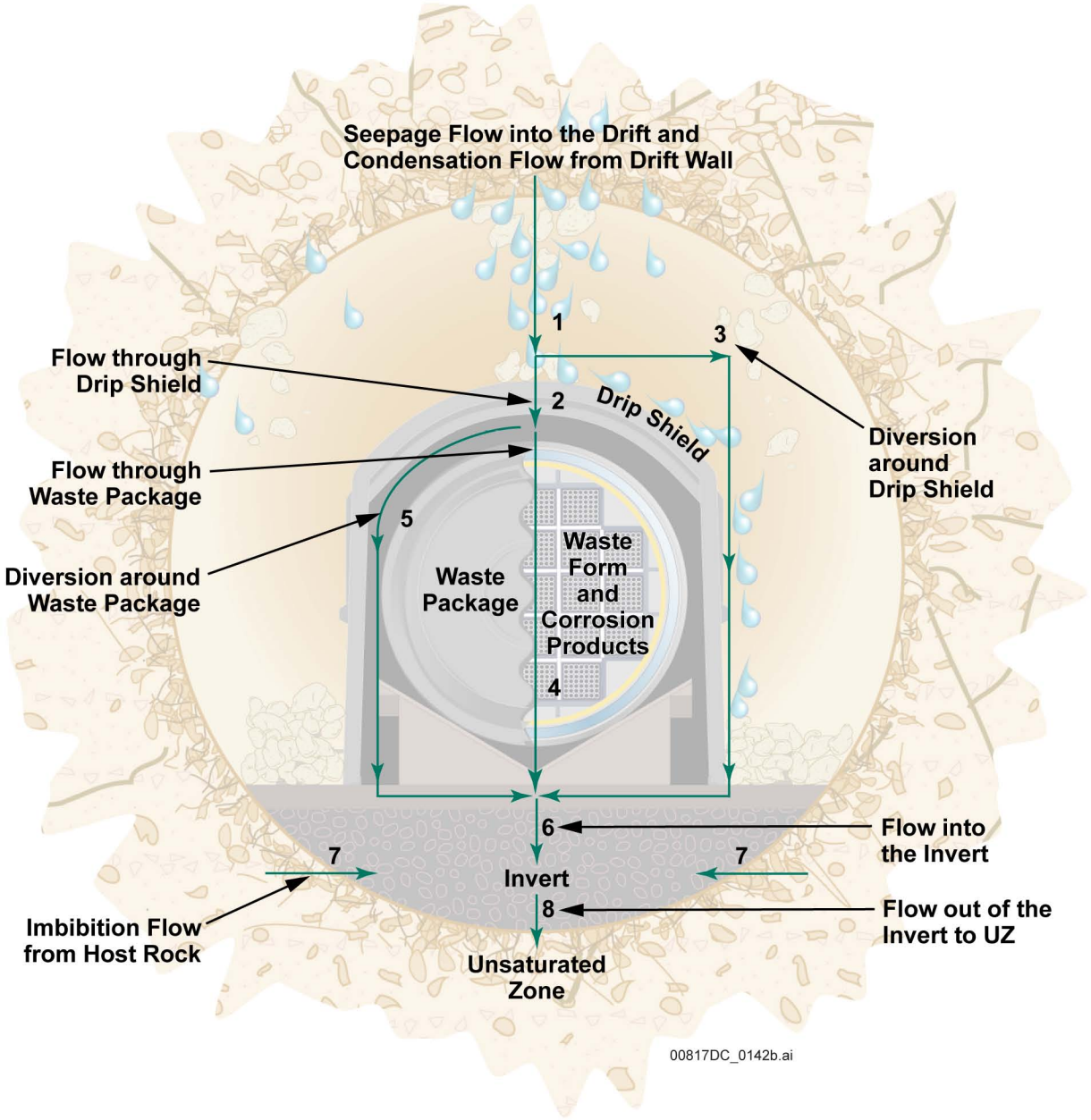

Figure 6.3.6-4. Schematic Diagram of Water Flow Pathways in the EBS

6.3.7 Waste Form Degradation and Mobilization

The Waste Form Degradation and Mobilization Model Component consists of five submodels: (1) Initial Radionuclide Inventory Submodel, which defines the radionuclide inventory and radionuclides of importance for the TSPA-LA; (2) In-Package Chemistry Submodel, which evaluates in-package chemical conditions; (3) Waste Form Degradation Rate Submodel, which calculates the degradation rates of CSNF, DSNF, and HLW waste forms; (4) Solubility (or Dissolved Concentration Limits) Submodel, which calculates solubilities (i.e., dissolved concentration limits) of radioactive elements in a failed WP and in the invert; and (5) EBS Colloids Submodel, which calculates colloidal concentrations of radionuclides in a failed WP and in the invert. Solubilities and colloidal concentration of radionuclides serve as inputs to the EBS Transport Submodel (Section 6.3.8), which calculates radionuclide transport within the WPs from the waste form to the EBS and through the EBS to the UZ below the repository.

The TSPA-LA Waste Form Degradation and Mobilization Model Component receives inputs from the following analyses and/or model reports:

- *Initial Radionuclide Inventories* (SNL 2007 [DIRS 180472]) and *Radionuclide Screening* (SNL 2007 [DIRS 177424])
- *In-Package Chemistry Abstraction* (SNL 2007 [DIRS 180506])
- *CSNF Waste Form Degradation: Summary Abstraction* (BSC 2004 [DIRS 169987]), *DSNF and Other Waste Form Degradation Abstraction* (BSC 2004 [DIRS 172453]), and *Defense HLW Glass Degradation Model* (BSC 2004 [DIRS 169988])
- *Dissolved Concentration Limits of Elements with Radioactive Isotopes* (SNL 2007 [DIRS 177418])
- *Waste Form and In-Drift Colloids-Associated Radionuclide Concentrations: Abstraction and Summary* (SNL 2007 [DIRS 177423]).

The three categories of waste form (CSNF, DSNF, and HLW glass) are contained and disposed in two types of WPs: CSNF WPs and CDSP WPs. The CDSP WPs will contain both DSNF and HLW glass. As was done in the TSPA for the Site Recommendation, WPs containing naval SNF waste forms are conservatively represented as containing CSNF. An evaluation of this conservatism is presented in Section 7.5.

Key inputs to the submodels for the Waste Form Degradation and Mobilization Model Component include: (1) a set of initial materials within the WP and the materials' major elemental compositions and physical and chemical properties; (2) time-dependent water flux into a failed WP provided by the EBS Flow Submodel (Section 6.3.6); (3) temperature and relative humidity in the WP provided by the EBS TH Environment Submodel (Section 6.3.2); and (4) partial pressure of CO_2 in the gas phase (Pco_2) or negative log of partial pressure of CO_2 (pCO_2) provided by the EBS Chemical Environment Submodel (Section 6.3.4).

Many of the abstractions that support the submodels in the Waste Form Degradation and Mobilization Model Component are implemented to describe single representative CSNF and CDSP WPs. The determination of what comprises a representative WP is discussed in Section 6.3.2.2.2. The EBS Transport Submodel is implemented in the TSPA-LA Model at the scale of a single WP (Section 6.3.8). The pertinent EBS Transport Submodel properties (including the Waste Form Degradation and Mobilization Model Component) for a single representative WP are scaled to the total number of WPs that have failed in each percolation subregion. These properties include the mass of available inventory, pore water volumes, mass of solid materials, advective flow rates, and diffusion areas. See the GoldSim user's guide for source-term element details (GoldSim Technology Group 2007 [DIRS 181727]).

The five submodels discussed in this section deal with processes that govern the mobility of radionuclides inside a failed WP. This section presents the principles and submodel implementation for radionuclide availability in a failed WP but does not discuss the specifics regarding transport in the EBS. This discussion is reserved for Section 6.3.8, which explains radionuclide transport as available inventory moves from the waste form into the waste form alteration products, then into the WP corrosion products, then out of the WP opening into the invert.

In general, the radionuclide inventory of each WP may be immediately available for transport upon WP failure or bound in a matrix that must first degrade before the inventory is available for transport inside the WP (Section 6.3.7.1). As discussed in Section 6.3.7.3, no credit is taken for CSNF and DSNF cladding for the TSPA-LA compliance model. After WP failure, the waste form begins to degrade at the calculated rate (Section 6.3.7.4). As the waste form degrades, waste form alteration products are formed (Section 6.3.7.4). The available inventory, from both the degraded waste form and that which was immediately available upon WP failure, is released into the pore water of the alteration product. The available inventory is dissolved in this pore water solution up to its solubility (Section 6.3.7.5). As the waste form degrades, waste form colloids are also formed, and these colloids may facilitate the release of the radionuclides from the breached WPs to the environment. Colloid formation and stability in the EBS are discussed in Section 6.3.7.6. Although the processes described below are closely related to the release of radionuclides from a failed WP into the environment, the topics covered in this section pertain to the availability of the radionuclides for transport. The transport of available radionuclides, by diffusion and advection, is covered in detail in Section 6.3.8.

The chemistry inside a failed WP is calculated by the In-Package Submodel using the abstracted relationships, and then the outputs are fed to other submodels that govern radionuclide availability (Waste Form Degradation Submodel (Section 6.3.7.4), Dissolved Concentration Limits Submodel (Section 6.3.7.5), and EBS Colloids Submodel (Section 6.3.7.6)).

The interaction between the five submodels in the Waste Form Degradation and Mobilization Model Component is common but is limited to the form of the abstractions presented. For example, the waste form degradation rate for a failed CSNF WP was an input to the In-Package Chemistry Process Model. However, the final abstraction, as presented for the TSPA-LA Model, was independent of the waste form degradation rate. This model abstraction is intended to span the range of waste form degradation rates anticipated in the TSPA-LA Model. Therefore, the In-Package Chemistry Submodel (Section 6.3.7.2) does not receive input from the CSNF Waste

Form Degradation Submodel (Section 6.3.7.4.1). The abstracted rate model from the degradation of the CSNF is a function of the pH inside a failed WP. Therefore, in the TSPA-LA Model, the In-Package Chemistry Submodel feeds the pH to the CSNF Waste Form Degradation Submodel (Section 6.3.7.4.1). Other submodel interactions are discussed in greater detail in the subsections below.

The five submodels discussed below are presented sequentially in the sections that follow, but in general, they are evaluated in every timestep of the TSPA-LA Model. Two of the five Waste Form Degradation and Mobilization Model Component Submodels described below may receive feeds from other model components, but they do not receive feeds from the other three submodels in the Waste Form Degradation and Mobilization Model Component. These two submodels are presented first and are the Radionuclide Inventory Submodel (Section 6.3.7.1) and the In-Package Chemistry Submodel (Section 6.3.7.2). The next three submodels discussed are the Waste Form Degradation Submodel (Section 6.3.7.4), the Dissolved Concentration Limits Submodel (Section 6.3.7.5), and the EBS Colloids Submodel (Section 6.3.7.6). These submodels are functions of other submodels of the Waste Form Degradation and Mobilization Model Components, as well as other model components in the TSPA-LA Model. For example, the Waste Form Degradation Submodel, including the calculations of the mass and volume of the alteration products as the waste forms degrade, are functions of the EBS TH Environment Submodel (Section 6.3.2) and the In-Package Chemistry Submodel (Section 6.3.7.2), and receive input feeds directly from these submodels at each TSPA-LA Model timestep. For the purposes of the rate model calculations, the TSPA-LA Model first computes the feed values at each timestep and then evaluates the degradation rate expression for those feed conditions. The simulation software maintains an element hierarchy for evaluating calculations that are dependent on other model calculations at the same simulation time.

Figures 6.3.7-1 and 6.3.7-2 are schematic illustrations showing the submodels of the Waste Form Degradation and Mobilization Model Component, the inputs and outputs of the model component, and the basis for confidence in the model component.

6.3.7.1 Radionuclide Inventory

The *Initial Radionuclide Inventories* analysis (SNL 2007 [DIRS 180472]), hereafter referred to as the Initial Radionuclide Inventory Abstraction for the TSPA-LA, considers four categories of wastes for disposal in the repository: DOE-owned HLW glass (including HLW glass from the Savannah River Site, Idaho National Laboratory, and Hanford, as well as commercial HLW glass from the West Valley Demonstration Project), CSNF, DSNF, and naval SNF. The radionuclides of importance to the TSPA-LA Model dose calculations were assessed in the Initial Radionuclide Inventory Screening Analysis in *Radionuclide Screening* (SNL 2007 [DIRS 177424]). Figure 6.3.7-3 shows how the waste types are to be placed in CSNF and CDSP WPs. The Initial Radionuclide Inventory Abstraction and Initial Radionuclide Inventory Screening Analysis together define the source terms for the CSNF and CDSP WPs in terms of both the quantity of WPs and the radionuclide inventory per WP. These two analyses indicate that 32 radionuclides are used to represent the inventory in the TSPA-LA Model. Note that ^{210}Pb, which is specified to be included in the inventory by the Initial Radionuclide Inventory Screening Analysis, is assumed to be in secular equilibrium with ^{226}Ra and is not explicitly modeled in the TSPA-LA Model. The TSPA-LA Model does account for the dose effects of ^{210}Pb by combining its

biosphere dose conversion factor with its parent, ^{226}Ra. Because the TSPA-LA Model accounts for the degradation and failure of individual WPs, the inventories of these 31 radionuclides are provided on a grams-per-WP basis.

6.3.7.1.1 Conceptual Model

The number of WPs projected to be emplaced in the repository is 11,629 (Table 6.3.7-1). This number of WPs is approximately 4 percent higher than necessary to emplace 70,000 metric tons heavy metal in the repository. This is to completely fill all of the available drifts (DTN: MO0702PASTREAM.001_R0 [DIRS 179925], Assumption 14). Eight WP configurations were designed to accommodate the CSNF, HLW, DSNF, and naval waste forms (Table 6.3.7-1). The CSNF configurations contain the commercial fuel assemblies from PWRs and BWRs. The CDSP WP configurations hold both DSNF and HLW in various-sized canisters within the WP. Naval fuel will be packaged in either short- or long-canister configurations. Even though the naval fuel is not considered a commercial fuel in the TSPA-LA Model, the 417 naval SNF WPs are treated as if they were CSNF WPs (SNL 2007 [DIRS 180472]), Table 7-3[a]). This number of naval SNF WPs is 4 percent higher than the originally specified 400 naval WPs. WPs containing naval SNF waste forms are conservatively represented in the TSPA-LA Model as containing CSNF. This modeling approximation is justified because the fuel degradation characteristics more closely resemble CSNF than DSNF, there is no HLW in a naval fuel WP, and surrogate analyses indicate that the dose due to releases from a CSNF WP bounds the dose due to releases from a naval WP (Section 7.5.3). The mixed oxide fuel (MOX) (Section 6.3.7.1.2.2) inventory is included as CSNF inventory in the TSPA-LA Model for release purposes. In contrast to the naval SNF that is treated as additional packages, the MOX inventory is averaged over the total number of CSNF WPs and then added to the per package CSNF inventory. For release purposes, the lanthanide borosilicate (LaBS) inventory (Section 6.3.7.1.2.2) is included as HLW inventory in the TSPA-LA Model. The LaBS inventory is averaged over the total number of CDSP WPs and then added to the HLW glass per package inventory.

The Initial Radionuclide Inventory Screening Analysis explicitly considered both 10,000-year and 1,000,000-year modeling periods for the repository at Yucca Mountain. Four scenario classes are considered: (1) Nominal Scenario Class, (2) Igneous Scenario Class, (3) Seismic Scenario Class, and (4) Human Intrusion Scenario. The radionuclide screening for each scenario class is based on the premise that the products of activity inventories and screening factors indicate the relative importance of each radionuclide with respect to the radiation dose that a person near the repository might receive (SNL 2007 [DIRS 177424], Section 6.2.1). The Initial Radionuclide Inventory Screening Analysis takes into account such factors as radionuclide decay rates, soil accumulation, uptake by plants, and exposure to contaminated groundwater. This screening analysis also accounts for differences in WPs and waste forms, radionuclide sorption, and radionuclide solubility. Results of the screening analysis are provided in Table 6.3.7-2. This table lists 32 radionuclides that may contribute the majority of the dose for the different scenario classes (Section 6.1.2) implemented in the TSPA-LA Model.

The radionuclide inventory for the CSNF and CDSP WPs, including uncertainty, is provided by the Initial Radionuclide Inventory Abstraction (SNL 2007 [DIRS 180472]) and is a direct input to the TSPA-LA Model. The CSNF, HLW, and DSNF radionuclide inventories are provided on

a grams-per-WP basis. The radionuclide inventories provided by the Initial Radionuclide Inventory Abstraction are calculated at year 2067 for CSNF WPs (DTN: MO0702PASTREAM.001_R0 [DIRS 179925], Assumption 13) and year 2030 for HLW and DSNF (DTN: MO0702PASTREAM.001_R0 [DIRS 179925]). Table 6.3.7-3 shows the expected average inventory in grams per WP for 31 radionuclides at year 2067 for CSNF and year 2030 for DSNF and HLW. For inventory purposes, all waste is assumed to be emplaced in year 2067 and then ventilated for 50 years before closure of the repository. The TSPA-LA Model simulation begins at post-closure and therefore requires an inventory calculated at the time of repository closure, currently estimated to be the year 2117 (DTN: MO0702PASTREAM.001_R0 [DIRS 179925]). Section 6.3.7.1.2.1 describes the radionuclide inventory decay and ingrowth calculations performed for 50 years and 87 years for CSNF and HLW/DSNF, respectively. The additional inventory decay is necessary to account for the preclosure period prior to the start time for the TSPA-LA Model simulations. Table 6.3.7-4a shows the per-package inventories aged to year 2117 and used as input to the TSPA-LA Model. In addition to the initial inventories presented in the Initial Radionuclide Inventory Abstraction discussed above, the TSPA-LA Model also includes MOX SNF and LaBS glass HLW. The contributions of MOX and LaBS glass HLW inventory are discussed in Section 6.3.7.1.2.2. Table 6.3.7-4b shows the per package inventories aged to year 2117 for MOX and LaBS glass HLW. Table 6.3.7-5 shows the specific activity for each radionuclide as well as the curies per package inventories for each WP type in the TSPA-LA Model.

6.3.7.1.2 TSPA-LA Model Abstraction

The Initial Radionuclide Inventory Abstraction specifies the initial quantity (grams/WP) of radionuclides for the CSNF, DSNF, and HLW WPs (Table 6.3.7-3). The initial inventories in each WP are decayed as a function of time. The decay chains and radionuclide half-lives are provided on Figure 6.3.7-4, where the radionuclides used for dose calculations are indicated. The following radionuclides are not members of chains: ^{14}C ($t_{1/2}$ = 5,720 yr) and fission products ^{36}Cl ($t_{1/2} = 3.01 \times 10^5$ yr), ^{135}Cs ($t_{1/2} = 2.30 \times 10^6$ yr), ^{137}Cs ($t_{1/2}$ = 30.1 yr), ^{129}I ($t_{1/2} = 15.7 \times 10^6$ yr), ^{79}Se ($t_{1/2} = 2.90 \times 10^5$ yr), ^{126}Sn ($t_{1/2} = 2.30 \times 10^5$ yr), ^{90}Sr ($t_{1/2}$ = 28.8 yr), and ^{99}Tc ($t_{1/2} = 2.13 \times 10^5$ yr) (DTN: MO0702PASTREAM.001_R0 [DIRS 179925]), and are not produced by decay of other radionuclides in the waste forms, therefore, they are not included on Figure 6.3.7-4.

Table 6.3.7-6 summarizes the treatment of each radionuclide within the EBS Transport Submodel (Section 6.3.8), the UZ Transport Submodel (Section 6.3.9), the SZ Transport Submodel (Section 6.3.10), and the Biosphere Submodel (Section 6.3.11) for the groundwater release modeling cases. Table 6.3.7-2, Column 3, lists the radionuclides transported in the atmosphere for the Volcanic Eruption Modeling Case. Among the 32 important radionuclides listed in Table 6.3.7-6, 27 are tracked and transported by the EBS Transport, the UZ Transport, and the SZ Transport Submodels. The five radionuclides that are not tracked and transported by the EBS, UZ, and SZ Submodels are ^{245}Cm, ^{241}Pu, ^{227}Ac, ^{228}Ra, and ^{210}Pb. In the Biosphere Submodel, doses from ^{227}Ac, ^{228}Ra, and ^{210}Pb are calculated by assuming they are in secular equilibrium with ^{231}Pa, ^{232}Th, and ^{226}Ra, respectively, because their half-lives are short. Doses from ^{245}Cm and ^{241}Pu are not calculated in the Biosphere Submodel because they are only important for their decay effects on the inventory of ^{241}Am and ^{237}Np, as stated in Table 7-1 of the *Radionuclide Screening* (SNL 2007 [DIRS 177424]). The different transport mechanisms for

each radionuclide listed in Table 6.3.7-6 are based upon: (1) the solubility of the radionuclide element within the WP; (2) the subsequent transportability beyond the EBS (based largely on the radionuclide's potential to remain in solution or sorb onto colloids, rather than being sorbed onto the host rock along the transport path from the WP to the biosphere); and (3) the persistence of the radionuclide during the transport period from the WP to the biosphere based on its half-life.

The discussion of uncertainty in the following two paragraphs is taken from information found in DTN: SN0310T0505503.004_R0 [DIRS 168761]. There are a number of sources contributing to the uncertainty in radionuclide inventories. Three sources of uncertainty are common in all waste types. The first is due to the computational method and nuclear characteristics used in predicting future radionuclide inventories (e.g., isotopic neutron cross section or decay half-life). The second source of uncertainty is the completeness of the records that are kept for the SNF and HLW materials (e.g., burn-up history or HLW batch compositions). The third source, and most difficult to quantify, is the uncertainty about future decisions that will influence the creation, packaging, or shipment of waste. These decisions influence the selection of waste types destined for emplacement into the repository directed by the Nuclear Waste Policy Act of 1982, as amended (42 U.S.C. 10101-10133, 1988 [DIRS 131951]) and implemented under NRC Proposed Rule 10 CFR Part 63 ([DIRS 178394] and [DIRS 180319]). Record keeping is important because, given that the wastes are heterogeneous, the selection process can significantly change the average waste characteristics.

For CSNF, an uncertainty multiplier with a uniform distribution between 0.85 and 1.4 was chosen for the TSPA-LA (SNL 2007 [DIRS 180472], Table 7-2). The sampled multiplier is applied to the nominal CSNF values, provided in Table 6.3.7-3, for all radionuclides except ^{238}U. For DSNF, an uncertainty multiplier is defined to capture the uncertainty for all radionuclides except ^{238}U. The inventory of ^{238}U has much less relative uncertainty than the other radionuclides because it is present in the initial fuel and generally changes little during reactor operation. The DSNF multiplier is defined as a triangular distribution, with a minimum of 0.45, a most likely value of 0.62, and a maximum value of 2.9. This multiplier is applied to the nominal values for DSNF grams per WP in Table 6.3.7-3 for all radionuclides except ^{238}U. For HLW, a triangular distribution is chosen for the HLW uncertainty multiplier, and this multiplier is applied to the nominal HLW inventories shown in Table 6.3.7-3 for all radionuclides, including ^{238}U. The uncertainty multiplier for HLW has a triangular distribution, with a minimum of 0.7, a most likely value of 1, and a maximum value of 1.5. Table 6.3.7-7 summarizes the uncertainty multipliers for each waste type.

6.3.7.1.2.1 Preclosure Radionuclide Decay and Ingrowth

The initial radionuclide inventory is provided as input to the TSPA-LA Model by DTN: MO0702PASTREAM.001_R0 [DIRS 179925]. There are three categories of waste provided in this per-package format: CSNF, HLW glass, and DSNF. Because the sum total of all waste received at the repository in each fuel type category is used to provide the per-package average source term used in the TSPA-LA Model, the inventory has an age associated with the expected year of the last WP emplacement (DTN: MO0702PASTREAM.001_R0 [DIRS 179925]). Based on previous schedules and repository designs, the CSNF inventory was expected to take 24 years to emplace in the repository, with waste emplacement beginning in the year 2010; the year when the last CSNF WP would have gone into the repository was 2033. The

initial radionuclide inventory input to the TSPA-LA Model is provided as it would appear in the year 2033. The HLW and DSNF inventories are each provided to the TSPA-LA Model as they would appear in the year 2030. Table 6.3.7-3 shows the expected average inventory in grams per package for the 31 radionuclides used in the TSPA-LA Model, categorized by waste type, for 2030 and 2033. The current estimate is for emplacement in 2067 (DTN: MO0702PASTREAM.001_R0 [DIRS 179925]). The CSNF waste stream is still being produced; therefore, the inventory abstraction assumes that CSNF waste, similar to what would have been emplaced in the year 2033, will be emplaced in 2067.

Because the TSPA-LA Model begins each simulation at repository closure, currently estimated in the year 2117, there will be 50 (CSNF) or 87 (for HLW and DSNF) years of radionuclide inventory decay and ingrowth before the inventory is first used by the TSPA-LA Model. In order to synchronize the radionuclide inventory age with the starting point of the TSPA-LA Model, an external calculation described below was performed to update the radionuclide inventory before entering them into the TSPA-LA Model.

GoldSim Version 9.60 (SP1) was used to perform the radionuclide aging calculation using the species element and the radionuclide half-lives from the TSPA-LA Model. Figure 6.3.7-4 shows the four radionuclide chains modeled in the TSPA-LA Model (note that ^{14}C and the fission products tracked in the TSPA-LA Model are not shown on this figure). Three inventory elements were created, one for each fuel type category, and the radionuclide inventory provided by the Initial Radionuclide Inventory Abstraction. A GoldSim source element for each fuel type performs the calculation, and a collector cell gathers the aged inventory at the closure year.

The updated CSNF inventory was extracted from a 50-year simulation, and the updated HLW and DSNF inventories were extracted from an 87-year simulation. Table 6.3.7-4a shows the inventories provided by the Initial Radionuclide Inventory Abstraction and the updated inventories, which account for the decay and ingrowth experienced during the preclosure period.

Table 6.3.7-4a shows that the majority of included radionuclides experience little to no decay or ingrowth, with the few exceptions of ^{241}Am, ^{137}Cs, ^{237}Np, ^{238}Pu, ^{241}Pu, ^{90}Sr, and ^{234}U. The fission products ^{137}Cs and ^{90}Sr have half-lives of 30.1 years and 28.8 years, respectively, and have decay but no ingrowth because they do not have parent radionuclides. The inventory changes observed with ^{241}Am, ^{237}Np, and ^{241}Pu are related because they are part of the same decay chain (Figure 6.3.7-4). The half-life of ^{241}Pu is 14.4 years and the half-life of ^{241}Am is 432.7 years. The inventory changes observed with ^{238}Pu and ^{234}U occur because of the relatively short ^{238}Pu half-life of 87.7 years, and the fact that the ^{238}Pu inventory decays into the ^{234}U inventory. The inventory changes observed with ^{227}Ac, more than doubling the initial inventory, occur because of the large initial inventories of ^{235}U and ^{231}Pa, compared to the much smaller initial inventories of ^{227}Ac.

6.3.7.1.2.2 Mixed Oxide Spent Nuclear Fuel and Lanthanide Borosilicate Glass Inclusion

The inclusion of MOX SNF and LaBS glass HLW in the TSPA-LA Model is accomplished by adding radionuclide-specific inventories to the inventories provided by DTN: MO0702PASTREAM.001_R0 [DIRS 179925]. More specifically, the LaBS glass inventory is added to the HLW portion of the initial radionuclide inventory and is then subject to

the same uncertainty sampling applied to the HLW radionuclide inventory. In addition, the MOX SNF is added to the CSNF portion of the initial radionuclide inventory and is also subject to the uncertainty sampling applied to that inventory. The MOX and LaBS inventories are described in the analysis *MOX Spent Nuclear Fuel and LaBS Glass for TSPA-LA* (SNL 2007 [DIRS 177422]).

Because the ages of the MOX and LaBS waste forms are provided at times that are before the closure of the repository, their inventories were decayed, as described in Section 6.3.7.1.2.1, before addition to the TSPA-LA Model. The MOX inventory is provided at the year 2035, so decay and ingrowth are performed for 82 years before entry into the TSPA-LA Model. The LaBS inventory was provided at the year 2003, so decay and ingrowth is performed for 114 years before entry into the TSPA-LA Model. Table 6.3.7-4b shows the additional radionuclide inventories due to MOX and LaBS waste that are used as input to the TSPA-LA Model; only the inventory that was aged to closure (i.e., after 82 and 114 years, respectively) is used in the TSPA-LA Model.

6.3.7.1.3 TSPA-LA Model Implementation

The initial mass of each radionuclide, provided by the Initial Radionuclide Inventory Abstraction in grams per WP and supplemented by the MOX and LaBS glass inventory, is adjusted to reflect the inventory distribution at repository closure and then is used to initialize source terms during each TSPA-LA Model realization (Table 6.3.7-5). The initial masses are then adjusted to account for uncertainty by applying the multipliers shown in Table 6.3.7-7. That is, at the beginning of each realization, the uncertainty multiplier for each waste form is sampled, and the inventories are adjusted by multiplying the uncertainty multiplier by the masses present at repository closure. The inventory is adjusted for radionuclide decay and ingrowth at each timestep by the simulation software using the first order decay rates shown on Figure 6.3.7-4. The CSNF WPs that are modeled in the TSPA-LA Model use the CSNF inventory values only, while the CDSP WPs contain both the DSNF and HLW inventories. The TSPA-LA Model calculates the specific activities for each radionuclide using the half-lives provided by DTN: MO0702PASTREAM.001_R0 [DIRS 179925].

Additional details regarding the placement of CSNF inventories into a GoldSim source element are provided in the discussion of the CSNF Waste Form Degradation Submodel (Section 6.3.7.4.1.3). The CSNF inventory discussion is presented in Section 6.3.7.4.1.3 because the TSPA-LA Model implementation specifically addresses inventory allocation based on the state of the CSNF waste form. Additional details regarding the placement of DSNF and HLW glass inventories into a GoldSim source element are provided in the discussion of the DSNF and HLW glass Waste Form Degradation Submodels (Sections 6.3.7.4.2.3 and 6.3.7.4.3.3). These inventory discussions are presented in Sections 6.3.7.4.2.3 and 6.3.7.4.3.3 because the TSPA-LA Model implementation specifically addresses inventory allocation based on the state of the DSNF waste form and HLW glass waste form.

6.3.7.2 In-Package Chemistry

The abstractions for determining the chemical parameters inside a failed WP are described in *In-Package Chemistry Abstraction* (SNL 2007 [DIRS 180506]), hereafter referred to as the

In-Package Chemistry Abstraction. As to be discussed in Section 6.3.7.2.1, in the TSPA-LA Model, CSNF WPs are discretized into two domains (Cell 1 and Cell 2) and CDSP WPs are discretized into three domains (Cell 1A, Cell 1B, and Cell 2). The In-Package Chemistry Abstraction discussed in this section, deals only with CSNF Cell 1, CDSP Cell 1A, and CDSP Cell 1B (they are collectively called waste form cells, as waste forms are located in those domains). Within the TSPA-LA Model, the In-Package Chemistry Submodel implements the In-Package Chemistry Abstraction to simulate the evolution of the water chemistry inside a failed WP as a function of the relative humidity provided by the EBS TH Environment Submodel (Section 6.3.2), Pco_2 provided by the EBS Chemical Environment Submodel (Section 6.3.4), and the water inflow rate provided by the EBS Flow Submodel (Section 6.3.6). Primary outputs from the In-Package Chemistry Submodel that are directly used in the TSPA-LA Model include pH, ionic strength, and total carbonate concentration (ΣCO_3) inside a failed WP.

The water chemistry determined by the In-Package Chemistry Submodel is used by four other Waste Form Degradation and Mobilization submodels. Specifically, the waste form matrix degradation rate for CSNF requires pH and ΣCO_3; the waste form matrix degradation rate for HLW requires pH; the dissolved concentration limits of radioactive elements require pH and ionic strength; and the stability of colloids requires pH and ionic strength. It is through the influences on other Waste Form Degradation and Mobilization Submodels that the In-Package Chemistry Submodel affects radionuclide availability for transport. Figure 6.3.7-5 is a schematic illustration of the inputs and outputs to and from the In-Package Chemistry Submodel.

6.3.7.2.1 Conceptual Model

The In-Package Chemistry Abstraction calculates the chemistry of water that has reacted with the WP components, including waste forms and basket materials, inside a failed WP. The In-Package Chemistry Submodel implements the abstraction in the TSPA-LA Model. The In-Package Chemistry Abstraction evaluates two different water ingress conceptual models:

- A vapor influx (non-dripping) model where the condensation of vapor onto the WP internals is simulated as pure water, and the resulting solution is in equilibrium with the relative humidity conditions in the drift (SNL 2007 [DIRS 180506], Section 6.3[a]).

- A liquid influx (dripping case or seepage dripping) model where water from the drift, simulated as typical groundwater or drift wall condensate, enters a WP at a rate determined by the liquid influx rate through the openings in the breached WP (SNL 2007 [DIRS 180506], Section 6.3[a]).

Two types of WPs are considered by the In-Package Chemistry Abstraction: CSNF WPs and the CDSP WPs. Furthermore, CSNF WPs are discretized into two domains:

1. CSNF Cell 1 (CSNF Waste Form Domain). This cell contains all materials within and including the baskets inside the CSNF WP, excluding the guides. This includes the fuel basket assembly of neutron moderator material and thermal shunts, fuel basket tubes, and CSNF assemblies.

2. CSNF Cell 2 (CSNF WP Corrosion Products Domain). This cell contains the TAD canister, and guide assembly.

Similarly, the CDSP WPs are discretized into three domains:

1. CDSP Cell 1A (or 2DHLW Cell). This cell comprises two containers of DHLW glass and their canisters, as designed for the two Multi Canister Overpack 2MCO/2DHLW WP.

2. CDSP Cell 1B (or 2MCO Cell). This cell comprises two containers of N reactor fuel and their canisters, as designed for the 2MCO/2DHLW WP.

3. CDSP Cell 2 (CDSP WP Corrosion Products Domain). This cell contains the divider plate, outer brackets, support tube, and inner vessel.

The In-Package Chemistry Abstraction discussed in this section deals only with CSNF Cell 1, CDSP Cell 1A, and CDSP Cell 1B. The chemistry of Cell 2 of CSNF and CDSP WPs are discussed in Section 6.3.8.

The In-Package Chemistry process model considers the 2MCO/2DHLW WPs, although the most numerous CDSP WPs are the 5DHLW/1DSNF Long. The reasons and justifications for doing that are given in Section 6.6.6[a] of *In-Package Chemistry Abstraction* (SNL 2007 [DIRS 180506]).

The In-Package Chemistry Abstraction conceptual model is discussed in Section 6.3[a] of *In-Package Chemistry Abstraction* (SNL 2007 [DIRS 180506]), and is briefly described in the paragraphs below.

The In-Package Chemistry Abstraction conceptual model is a batch reactor model that consists of water, oxygen, carbon dioxide, waste forms, and metal alloys. The batch reactor system is in equilibrium with atmospheric conditions, and the reactants degrade in the presence of water according to a rate determined by the physical properties and the exposed surface area of each reactant. For each solid reactant, a degradation rate is selected based on experimental measurements, and the surface area available to react is calculated based on the dimensions of the WP internals. During reaction progress, waste forms and metal alloys are consumed, secondary mineral phases and metal (hydr) oxide corrosion products precipitate from solution, and water changes in its composition and mass due to these reactions.

Inputs for the In-Package Chemistry Abstraction models include thermodynamic properties, parameters such as waste form reaction rates and incoming water compositions, gas phase Pco_2, and compositions and degradation rates of WP components (SNL 2007 [DIRS 180506], Sections 6.3[a]).

Physical-chemical processes considered by the In-Package Chemistry Abstraction model include kinetic dissolution of waste forms and WP internal components, equilibrium precipitation and dissolution of secondary minerals and metal corrosion products, equilibrium oxidation and reduction reactions among gases, secondary minerals, and aqueous species, incoming water compositions, and thermal effects on aqueous phase chemistry (SNL 2007 [DIRS 180506], Section 6.3[a]).

Additional sensitivity cases were run to evaluate the system response to changes in the base-case model. These sensitivity cases evaluated different quantities of water inside the failed WP, different seepage compositions, the oxidation state of chromium, different temperatures, P_{CO_2} and P_{O_2}, different water fluxes into the failed WP, different WP and waste form configurations and inventories, different corrosion rates of the WP internals, different predominant iron minerals (goethite versus hematite), and different degradation rates of the waste forms inside the failed WP (SNL 2007 [DIRS 180506], Sections 6.6[a]). These sensitivity studies were used to develop an uncertainty range around the base-case model results.

6.3.7.2.2 Model Abstraction

The In-Package Chemistry Abstractions are derived from the output of the In-Package Chemistry Process Models (SNL 2007 [DIRS 180506]) and provide either parameter distributions or response surfaces for the TSPA-LA Model. Both the vapor influx model and the liquid influx model have separate process and abstraction models, which allow the TSPA-LA Model to implement non-dripping and dripping conditions. In the *In-Package Chemistry Abstraction* (SNL 2007 [DIRS 180506]), the process model output is discussed in Section 6.5[a] and the abstraction model output, combining the base-case results presented in Section 6.5[a] with the sensitivity studies presented in Section 6.6[a], is discussed in Section 6.10[a]. In this section, the in-package ionic strength and pH abstractions are presented for CSNF Cell 1, CDSP Cell 1A, and CDSP Cell 1B under liquid influx and vapor influx conditions. There are total 12 abstractions (six for ionic strength and another 6 for pH) for the three types of cells under two different water influx conditions. The ΣCO_3 abstraction is developed from equilibrium mass action equations and is presented as a single equation for both liquid influx and vapor influx conditions for CSNF Cell 1 only because HLW glass and DSNF degradation rate calculations do not require this parameter.

The geochemical modeling codes, EQ3NR (Software Code: EQ3/6 V7.2b (CRWMS M&O 1999 [DIRS 153964])) and EQ6 (STN: 10075-7.2bLV-02 [DIRS 159731]), were used to simulate the in-package chemical environment (SNL 2007 [DIRS 180506], Section 1[a]). The In-Package Chemistry Abstraction simplifies the outputs into a form compatible with implementation in the TSPA-LA Model, as to be discussed below.

The abstractions of in-package chemistry are applicable for oxidizing conditions ($f_{O2} = 10^{-0.7}$ bars), a P_{CO_2} range of 10^{-4} to $10^{-1.5}$ bars, a temperature range from 25°C to 100°C, a relative humidity for vapor influx equal or higher than 95 percent, and a water volumetric flux (hereafter referred to as "flux") for liquid influx equal or higher than 0.1 L/yr (SNL 2007 [DIRS 180506], Section 8.1[a], Table 8-1[a]). Spatially, the applicability of the In-Package Chemistry Abstraction is limited to the waste form cells (i.e., Cell 1 of CSNF WPs, Cell 1a and Cell 1b of CDSP WPs).

The abstraction for the In-Package Chemistry Submodel consists of five parts:

Part I. Determination of whether In-Package Chemistry needs to be calculated

Part II. Determination of which abstraction to be used

Part III. Calculation of ionic strength

Part IV. Calculation of pH

Part V. Calculation of the total concentration of aqueous carbonate (for CSNF Cell 1 only).

These parts are discussed in detail below and summarized in Table 6.3.7-8.

Part I. Determine if In-Package Chemistry needs to be calculated—Whenever the water inflow rate is less than 0.1 L/yr and relative humidity is lower than 95 percent, no in-package chemistry calculation is conducted. The reason is, as stated in *In-Package Chemistry Abstraction* (SNL 2007 [DIRS 180506], Section 6.10.9.1[a]), a relative humidity of 95 percent is the minimum threshold value required to predict a meaningful pH and ionic strength from the vapor influx model. "Given the ultimately small volume of water film being considered at these relative humidity conditions (Relative Humidity < 95 percent), virtually all of the waste form materials degraded under these conditions will be precipitated in place and not be available for transport. The small mass of radionuclides that remains dissolved in this minuscule water volume would also not be available for transport because the water film is not expected to be interconnected under these conditions" (SNL 2007 [DIRS 180506], Section 6.10.9.1[a]). In other words, under such conditions, the in-package chemistry becomes undefined, and the in-package chemistry submodel is turned off. The solubilities for all radionuclides, including colloidal species, are set to zero so that no transport is allowed.

However, degradation of waste forms is not considered as ceased below the 95 percent relative humidity threshold because the non-interconnected water film does not prevent waste form from degrading. There are no measurements or methods to calculate waste form degradation rates under vapor flux conditions below 95 percent relative humidity. *In-Package Chemistry Abstraction* (SNL 2007 [DIRS 180506], Section 6.10.9.1[a]) gives the following estimated values for the HLW glass and CSNF waste forms:

1. For HLW glass, its degradation rate under such conditions is assumed to be equal to the degradation rate at pH of 10 under aqueous corrosion conditions, as is done in the TSPA for temperatures greater than 100°C (Assumption 5.5[a]).

2. For CSNF waste form, its degradation rate under such conditions is assumed to be equal to the degradation rate between pH of 6 and 7 under aqueous corrosion conditions. In the TSPA-LA Model, the pH value that is only used to calculate the CSNF degradation rate is uniformly sampled between 6 and 7.

Part II. Determine which abstraction to be used—Whenever the relative humidity is greater than 95 percent or the water inflow rate is greater or equal to 0.1 L/yr, the In-Package Chemistry Submodel is activated, and a decision is to be made to select one of the two abstractions (the vapor influx versus the liquid influx) to generate outputs for ionic strength and pH. The choice depends on the relative humidity, the water flux rate, and the abstraction that predicts lower ionic strength, as shown in Table 6.3.7-8.

As indicated in Table 6.3.7-8, ionic strength is calculated using the vapor influx abstraction whenever the liquid influx rate is less than 0.1 L/yr (and the relative humidity is equal or greater than 95 percent). At or above 0.1 L/yr, ionic strength is calculated using the liquid influx abstraction. There is an exception that if the vapor influx abstraction predicts a lower ionic strength than that predicted by the liquid influx abstraction, then the vapor influx result should be used. In other words, the vapor influx abstraction is used to set a reasonable upper limit for ionic strength. Its justification is provided in *In-Package Chemistry Abstraction* (SNL 2007 [DIRS 180506], Section 6.10.9.1[a]).

Part III. Calculate Ionic Strength—Ionic strength abstractions for the vapor influx case are given as functions of relative humidity with uncertainty added. The mean value is a piecewise linear function of relative humidity:

$$I = a + b * RH \qquad \text{(Eq. 6.3.7-1)}$$

The intercept (a) and the slope (b) in the above equation have different values under different relative humidities. Table 6.3.7-9 gives those values for CSNF Cell 1, CDSP Cell 1A, and CDSP Cell 1B. The uncertainty range is between the mean value times the lower uncertainty factor (fmin) and the mean value times the upper uncertainty factor (fmax) (i.e., I×fmin, I×fmax). A triangular distribution is assigned for the uncertainty range, with the mean value as the most likely value. The uncertainty factors are also shown in Table 6.3.7-9.

Ionic strength abstractions for the liquid influx case are presented in the logarithm space and are functions of water inflow rate through the breached WPs and time since the representative WP breached. The mean values of logarithm of ionic strength are presented as two-dimensional look-up tables, which are given in Tables 6.3.7-10 through 6.3.7-12 for CSNF Cell 1, CDSP Cell 1A, and CDSP Cell 1B, respectively.

Uncertainties are also included in the logarithm of ionic strength abstractions for the liquid influx case and are presented as a deviation from the mean value. Triangular distributions are assigned to the logarithm of ionic strength for the liquid influx case. That is, the minimum, most likely, and the maximum values are mean-deviation, mean, and mean+deviation, respectively. The deviations are also functions of water inflow rate through the breached WPs and time since breached, presented as two-dimensional look-up tables, which are given in Tables 6.3.7-13 through 6.3.7-15.

Part IV. Calculate pH—When the water influx rate is greater or equal to 0.1 L/yr, the liquid influx pH abstraction will be used to determine in-package pH ranges. The maximum and minimum pHs are functions of pCO_2 (the negative logarithm of P_{CO2}) and log ionic strength as shown in Tables 6.3.7-16 through 6.3.7-21 for those three different cells under the liquid influx conditions.

When the water influx rate is less than 0.1 L/yr, the vapor influx pH abstraction will be used to determine in-package pH ranges. The maximum and minimum pHs are functions of pCO_2 and log ionic strength, as shown in Tables 6.3.7-22 through 6.3.7-27 for those three different cells under the vapor influx conditions.

For a given pCO_2, the pHs have a uniform distribution between the minimum and maximum pH values defined in the look-up tables in *In-Package Chemistry Abstraction* (SNL 2007 [DIRS 180506], Section 6.10.9.1[a]).

Part V Total Carbonate Concentration Abstraction—ΣCO_3 is used in the degradation rate law for the CSNF waste form. An expression for ΣCO_3 (mol/kg) as a function of temperature, pH, and P_{CO_2} is based on equilibrium mass action expressions, as discussed in *In-Package Chemistry Abstraction* (SNL 2007 [DIRS 180506], Section 6.10.5). The ΣCO_3 abstraction is captured in *In-Package Chemistry Calculations and Abstractions* (DTN: SN0702PAIPC1CA.001_R2, [DIRS 180451], worksheet *Total Carbonate Validation* in *Total Carbonate and Eh Abstractions.xls*) as:

$$\sum CO_3 = P_{CO_2}\left(10^{K_1} + 10^{pH+K_1+K_2} + 10^{2\,pH+K_1+K_2+K_3}\right) \qquad \text{(Eq. 6.3.7-2)}$$

where P_{CO_2} is the carbon dioxide partial pressure in the gas phase. The in-drift P_{CO_2} (in units of bars) is provided by the EBS Chemical Environment Submodel (Section 6.3.4).

The K_i values in Equation 6.3.7-2 are temperature dependent. Table 6.3.7-28 provides the temperature-dependent K values. The ΣCO_3 abstraction is valid for temperatures ranging from 0°C to 100°C (SNL 2007 [DIRS 180506], Section 6.10.5).

The In-Package Chemistry Abstraction (SNL 2007 [DIRS 180506], Section 1[a]) lists several other limitations of the model, including: (1) limited availability of data on thin film chemistry; (2) limited availability of long-term metal alloy corrosion information such as the identities of the long-term corrosion products and the evolution of the surface area of the metal WP components as a function of time; (3) simplifications used to define the important processes in the waste form cells; (4) an assumption involving the pH under low water conditions and (5) the approach used to simulate the effects of evaporation.

6.3.7.2.3 TSPA-LA Model Implementation

The abstracted results from the In-Package Chemistry Abstraction are implemented in the TSPA-LA Model to quantify the temporal evolution of values of the aqueous chemistry variables pH, ionic strength, and ΣCO_3. In the TSPA-LA Model, the In-Package Chemistry Submodel is implemented for four different abstraction conditions representing CSNF and CDSP WPs that have water flow through them and CSNF and CDSP WPs that do not have water flow through them. A WP can have water flow through it only if it is in a dripping environment and its DS has failed and the WP failure is not a crack (e.g., cracks cannot support liquid influx (Section 6.3.6.1)). If WPs in a dripping environment are not dripped upon because the DSs remain intact, or the only failure is a crack, the In-Package Chemistry Submodel for non-dripping conditions (i.e., no water flow through the WPs) is evaluated for the WPs.

For the In-Package Chemistry Submodel, the time reference is to the elapsed time that a WP has been failed. Because the TSPA-LA Model models groups of failed WPs with each member of a group having the same in-package chemical compositions, it is possible that WPs within a group are failed for different periods of time. To account for this, the TSPA-LA Model calculates an average WP failure time for each group of WPs and uses this average time to evaluate the time

dependence for the In-Package Chemistry Submodel. The algorithm for determining the average failed duration in a group of failed WPs is determined by weighting the elapsed duration of failure for the WPs failed in the previous timestep (including the current timestep length) with the new failures in this timestep:

$$\bar{t} = \frac{(N_{WPFailed}^{New} \times \frac{1}{2} TimeStepLength) + (N_{WPFailed}^{Prev} \times (\bar{t}^{prev} + TimeStepLength))}{N_{WPFailed}^{New} + N_{WPFailed}^{Prev}} \quad \text{(Eq. 6.3.7-3)}$$

where

$\bar{t}$ = the average failure time

$N_{WPFailed}^{New}$ = the number of new failures in the current timestep

$N_{WPFailed}^{Prev}$ = the number of failures in the previous timestep

$\bar{t}^{prev}$ = the previous value of the average failure time

TimeStepLength = the timestep length.

Note that this implementation assigns one-half of a timestep length for newly failed WPs (i.e., on average, the new failures occur halfway through the current timestep). In the TSPA-LA Model, for the purposes of evaluating in-package chemistry, the average WP failure time for the current timestep is set to zero years if the WP temperature exceeds the boiling point of water (i.e., dry conditions prevail in the WP).

The In-Package Chemistry Submodel is implemented by accessing abstractions corresponding to the WP type and dripping condition. These abstractions include distributions representing epistemic uncertainties. For pH, uniform distributions are specified for a given pCO2, and for ionic strength, triangular distributions are specified for a given relative humidity for the vapor influx case or log-triangular distributions are specified for a given time and a given water inflow rate for the liquid influx case. Since pCO2, relative humidity, and water inflow rate all are time-dependent variables in the TSPA-LA Model, the recommended distributions for pH and ionic strength are also time dependent. In other words, the recommended distributions change with time and depend on the outputs of other submodels. Therefore, the pH and ionic strength values for each realization cannot be predetermined by simple sampling prior to the beginning of the realization. To properly account for this time-dependent nature of the In-Package Chemistry Abstraction, dynamic sampling techniques have been implemented in the TSPA-LA Model.

The dynamic sampling technique samples a distribution representing the CDF percentile defined by the specified distributions (for pH it is uniform, for ionic strength it is either triangular or log triangular) for each realization. This percentile remains constant for each realization for the whole duration of the simulation. The distributions are then determined at each timestep after the values of the time-varying variables become known. After that, this percentile is applied to the distributions to obtain a pH or an ionic strength values for the current timestep.

For example, for realization *i*, the sampled percentile for pH is 85 percent. At time *t*, the value of pCO2 is 2 and ionic strength is 1 for the CSNF Cell 1 of the liquid influx case. According to Tables 6.3.7-16 and 6.3.7-19, the maximum and minimum of pH are 7.19 and 4.99, respectively. Thus, the pH value at the current timestep is 4.99 + 0.85×[7.19-4.99] = 6.86. The ionic strength values at each timestep are obtained dynamically by a similar scheme, although it is a little bit more complicated than pH because it has a triangular or a log-triangular distribution.

The ΣCO_3 is calculated at each timestep using Equation 6.3.7-2 and the relationships provided in Table 6.3.7-28. The variables in the calculation include: (1) the calculated pH from the In-Package Chemistry Submodel (discussed above), (2) the WP temperature provided by the EBS TH Environment Submodel (Section 6.3.2), and (3) the P_{CO_2} provided by the EBS Chemical Environment Submodel (Section 6.3.4).

At each timestep, the outputs from the In-Package Chemistry Submodel are provided to four other Waste Form Degradation and Mobilization submodels. The pH and ΣCO_3 are provided to calculate the waste form matrix degradation rate for CSNF and the pH is also provided to calculate the degradation of HLW. The pH and ionic strength are provided to calculate solubility limits of radionuclides and to calculate the stability of colloids.

The outputs from the In-Package Chemistry Submodel are provided for each representative CSNF and CDSP cell (Section 6.1.4.7) in dripping and non-dripping environments in each percolation subregion. These outputs are:

- pH as a function of time
- Ionic strength as a function of time
- ΣCO3 as a function of time.

6.3.7.3 Cladding Degradation

Most CSNF is encased in zirconium-alloy cladding, and a small percentage is encased in stainless steel cladding. In the TSPA-LA compliance model, no cladding credit is taken for CSNF (SNL 2007 [DIRS 180616], Section 6.2.1.2[a] and Table 7-2[a]). In addition, DSNF cladding has been excluded from consideration in the TSPA-LA Model (DTN: MO0706SPAFEPLA.001_R0 [DIRS 181613], FEP Number 2.1.02.25.0A).

Naval SNF, as discussed in Section 6.3.7.1.1, is conservatively treated as CSNF in the TSPA-LA. Section 7.5.3 demonstrates that the dose resulting from a commercial WP is higher than the dose resulting from a naval WP (Section 7.5.3); thus, representing naval WPs as commercial WPs is conservative. Removing the CSNF cladding credit from the TSPA-LA calculations will not alter that conclusion.

6.3.7.3.1 Conceptual Model

The cladding of all CSNF and DSNF is assumed to be failed upon arrival at the repository (Section 5.1.3).

6.3.7.3.2 TSPA-LA Model Implementation

The TSPA-LA Model contains only two cladding related parameters: a cladding failure parameter and a cladding splitting parameter. In the TSPA-LA compliance model no credit is taken for CSNF cladding, therefore, it is assumed that the initial fraction of failed cladding (Initial_Rod_Failures), and the fraction of fuel available for corrosion (Fuel_Split_Fraction), is one.

6.3.7.4 Waste Form Degradation

The CSNF Waste Form Degradation Abstraction for the TSPA-LA Model is described in *CSNF Waste Form Degradation: Summary Abstraction* (BSC 2004 [DIRS 169987]). The DSNF Waste Form Degradation Abstraction for the TSPA-LA Model is described in *DSNF and Other Waste Form Degradation Abstraction* (BSC 2004 [DIRS 172453]). The HLW Glass Degradation Abstraction for the TSPA-LA Model is described in *Defense HLW Glass Degradation Model* (BSC 2004 [DIRS 169988]). The abstraction models for the waste form matrix estimate the rates at which the CSNF and HLW waste forms degrade as a function of chemical conditions in failed WPs. For DSNF waste forms, an instant degradation rate is implemented, and will be discussed in detail in Section 6.3.7.4.2.

In the TSPA-LA Model, radionuclide inventory added to a GoldSim source element and bound by a matrix (i.e., UO_2 or borosilicate glass) is not available for transport from a failed WP until the binding matrix degrades. The waste form degradation rates, calculated using the submodels discussed below, are applied by GoldSim source elements. Within each source element, the per-package inventory subject to waste form degradation prior to release from the source element is specified by defining an inventory and then specifying that the inventory is "bound in matrix" in the GoldSim source element. The source element requires a fractional degradation rate, and in the TSPA-LA Model, the applicable rate is the output of the Waste Form Degradation submodels, discussed below. Additional details on the use of GoldSim source elements are provided in Section 6.3.8 and in *User's Guide, GoldSim Probabilistic Simulation Environment* Version 9.60 (GoldSim Technology Group 2007 [DIRS 181727]). The source element applies the degradation rate to the bound inventory, releasing the inventory into the cell network where it then becomes available for transport. Transport of available inventory added to the cell network is discussed in Section 6.3.8.2.1.

Section 6.3.7.4.1 discusses the availability of CSNF inventory from the CSNF source elements in the TSPA-LA Model. Section 6.3.7.4.2 discusses the availability of DSNF inventory in the TSPA-LA Model. Section 6.3.7.4.3 discusses the availability of HLW glass inventory in the CDSP WP source elements of the TSPA-LA Model.

6.3.7.4.1 Commercial Spent Nuclear Fuel Waste Form Degradation

In the TSPA-LA Model, the CSNF Waste Form Degradation Submodel implements the CSNF Waste Form Degradation Abstraction described in *CSNF Waste Form Degradation: Summary Abstraction* (BSC 2004 [DIRS 169987]). Internal inputs to the CSNF Waste Form Degradation Submodel include representative WP temperature provided by the EBS TH Environment Submodel (Section 6.3.2) and pH and ΣCO_3 provided by the In-Package Chemistry Submodel

(Section 6.3.7.2). In addition to the temperature, pH, and total carbonate concentration inputs, the CSNF Waste Form Degradation Submodel is also dependent on the partial pressure of oxygen in the failed WP. The output of the CSNF Waste Form Degradation Submodel is the CSNF fractional degradation rate.

6.3.7.4.1.1 Conceptual Model

CSNF pellets and radionuclides in fuel rods with failed cladding will be isolated from the external repository environment until the CSNF WPs are breached. After a CSNF WP is breached, the CSNF may be exposed to dripping water or humid air. Upon exposure to moisture, radionuclides may be released by: (1) instantaneous release of the gap and grain boundary inventories of cesium, iodine, technetium, and strontium; (2) dissolution of the fuel matrix inventory under alkaline and acidic conditions; and (3) instantaneous release of carbon in the WP hardware, external to the cladding. The gap and grain boundary inventory denotes the fission gasses and more mobile radionuclides such as cesium, iodine, and technetium that migrated out of the fuel matrix during reactor operations and accumulated between the fuel pellets and cladding and the fuel matrix grain boundaries. In the TSPA-LA Model, because radionuclides in the gap and grain boundary may be released rapidly, CSNF fuel rods are modeled as two heterogeneous fractions: the matrix inventory and the combined gap and grain boundary inventory. The radionuclide inventory in the fuel matrix is referred to as the bound inventory. The inventory in the gap and grain boundary regions is referred to as the unbound inventory and is modeled as being available for instantaneous release from fuel rods. Additionally, a third CSNF inventory, the carbon inventory in the WP hardware region, is modeled as being available for instantaneous release from the failed WP.

The scope of the CSNF Waste Form Degradation Submodel does not address processes that control the extent to which the radionuclides available for dissolution are mobilized as dissolved and colloidal species. Those features, events, and processes (FEPs) are addressed as follows: Dissolved Concentration Limits Submodel, Section 6.3.7.5; EBS Colloids Submodel, Section 6.3.7.6; and EBS Transport Submodel, Section 6.3.8 illustrates the dependence of CSNF fuel degradation on the In-Package Chemistry Submodel (Section 6.3.7.2) and temperature. Figure 6.3.7-6 provides a schematic drawing of the CSNF fuel rods and CSNF waste form degradation processes.

6.3.7.4.1.2 TSPA-LA Model Abstraction

The CSNF Waste Form Degradation Abstraction developed in *CSNF Waste Form Degradation: Summary Abstraction* (BSC 2004 [DIRS 169987]) provides two abstractions: the instantaneous release fraction of CSNF inventory and the mathematical model for the rate of degradation for the CSNF matrix.

The instantaneous release fraction is computed as the fraction of cesium, iodine, technetium, and strontium in the total inventory in CSNF fuel that is instantly available for release once cladding is degraded, as discussed in Sections 6.3.1 and 6.3.2 of *CSNF Waste Form Degradation: Summary Abstraction* (BSC 2004 [DIRS 169987]). The release fractions implemented in the TSPA-LA Model are captured in *CSNF Radionuclide Release Model* (DTN: MO0404ANLSF001.001_R0 [DIRS 169007]). The fraction of CSNF inventory that

makes up this instantaneous release inventory is specified by four triangular distributions, as defined in Table 6.3.7-29.

CSNF Waste Form Degradation: Summary Abstraction (BSC 2004 [DIRS 169987]) provides the discussion and mathematical forms for alkaline conditions (Section 6.4.1.2), for acidic conditions (Section 6.4.1.3), and for calculating the specific or absolute dissolution rate, subject to a range of pH conditions, temperature conditions, total carbonate concentrations, and oxygen partial pressures (Section 8.2). The mathematical forms, including coefficient values, implemented in the TSPA-LA Model are captured in *CSNF Radionuclide Release Model* (DTN: MO0404ANLSF001.001_R0 [DIRS 169007]). The specific or absolute dissolution rate is a function of four independent variables, which vary spatially in the repository: WP temperature in degrees Kelvin, aqueous pH, ΣCO_3, and oxygen fugacity according to the rate law:

$$\log_{10}(F) = \log_{10}(A) + a_0 + a_1 \times IT + a_2 \times pCO_3 + a_3 \times pO_2 + a_4 \times pH \qquad \text{(Eq. 6.3.7-4)}$$

where dependent variable

$\log_{10}(F)$ = log base 10 of the fractional dissolution rate of the CSNF in unit of [1/d] (d stands for days)

and independent variables

IT = inverse temperature of the WP [K^{-1}] (i.e., IT = 1/T)

pCO_3 = negative base 10 log of ΣCO_3 [molar] (i.e., $pCO_3 = -\log_{10}([HCO_3^-]+[CO_3^{2-}])$)

pO_2 = negative base 10 log of the oxygen partial pressure (atmospheres)

pH = in-package pH

and parameters

$\log(A)$ = log base 10 of the fuel specific surface area (m^2/mg)

a_0, a_1, a_2, a_3, a_4 are regression parameters for the dissolution rate per unit area.

Under dripping conditions, the pH inside a failed WP is a function of the liquid flow rate through the failed WPs (Section 6.3.7.2). The flow rate through the failed WPs depends on the damage state of the WP outer shell and the dripping rate (Section 6.3.6), which may vary in the different percolation subregion environments in the TSPA-LA Model. Therefore, pH and pCO_3 are spatially dependent outputs of the In-Package Chemistry Submodel (Section 6.3.7.2) and in the TSPA-LA Model are calculated within each percolation subregion environment. The partial pressure of O_2 in the WP is a constant value of 0.2 bar and is equated to the partial pressure of O_2 in the drift environment, which is equal to atmospheric O_2 (See Section 5.1.3). The representative temperature of the WPs is a spatially dependent output of the EBS TH Environment Submodel (Section 6.3.2), and in the TSPA-LA Model it is calculated for each percolation subregion.

The dissolution rate is modeled for an alkaline state with a pH $\geq$ 6.8 and an acidic state with a pH < 6.8. The equation used for the alkaline state does not include pH dependence ($a_4 = 0$) and is:

$$\log_{10}(F) = \log_{10}(A) + a_0 + a_1 \times IT + a_2 \times pCO_3 + a_3 \times pO_2 \qquad \text{(Eq. 6.3.7-5)}$$

The distribution for the log base 10 of the specific surface area and values for the coefficients are presented in Table 6.3.7-30.

The equation used for the acidic state is

$$\log_{10}(F) = \log_{10}(A) + a_0 + a_1 \times IT + a_3 \times pO_2 + a_4 \times pH \qquad \text{(Eq. 6.3.7-6)}$$

For the acidic state, the dissolution rate does not depend on the ΣCO_3 ($a_2 = 0$). The distribution for the log of specific surface area and the coefficient values is shown in Table 6.3.7-31.

6.3.7.4.1.3 TSPA-LA Model Implementation

After a WP is breached, the entire CSNF is exposed to moisture. Radionuclides are then released by: (1) instantaneous release of the gap fraction inventory and (2) matrix dissolution under alkaline or acidic conditions. Cesium, iodine, technetium, and strontium are in the instantaneous release inventory. The fraction of emplaced inventory that makes up the instantaneous release inventory for cesium, iodine, technetium, and strontium is determined by sampling four triangular distributions representing epistemic uncertainty. These distributions are sampled once per realization. The instantaneous release inventory, the product of the instantaneous release fraction, and the per-package inventory (accounting for decay and ingrowth) are treated as unbound inventory within the inner barrier function of the GoldSim source element (GoldSim Technology Group 2007 [DIRS 181727]).

Similarly, the ^{14}C hardware inventory, the product of the hardware inventory fraction, and the per-package inventory (accounting for decay and ingrowth), are treated as unbound inventory between the inner and outer barrier functions of the GoldSim source element. The hardware inventory fraction originates from neutron activation of stainless-steel hardware outside the fuel rods and is specified to be 18 percent of the ^{14}C inventory in a CSNF WP (SNL 2007 [DIRS 180472], Section 6.7 and Table 7-1[a]).

The TSPA-LA Model considers three CSNF inventories in each CSNF WP of a GoldSim source element (e.g., group of WPs). The first inventory in the CSNF WP is the ^{14}C hardware inventory. At the global level, the hardware inventory is calculated as the fraction of per-package inventory that is associated with the WP hardware and the per-package inventory, discussed in Section 6.3.7.1. This inventory is calculated at the global level but is added to each GoldSim source element within each percolation subregion environment. Within the GoldSim source element, this inventory is immediately released when the WP fails.

The second inventory in the CSNF source term is the instantaneous release inventory. At the global level, the instantaneous release inventory is calculated as the fraction of the per-package inventory that is in the gap and grain boundaries (BSC 2004 [DIRS 169987], Sections 6.3.1

and 6.3.2) and the per-package inventory, discussed in Section 6.3.7.1. The gap and grain boundary inventory fractions are presented in Table 6.3.7-29. If a radionuclide in the CSNF WP is not included in Table 6.3.7-29, the radionuclides' instantaneous release inventory is zero grams per WP. This inventory is calculated at the global level but is added to each GoldSim source element within each percolation subregion environment. Within the GoldSim source element, this inventory is immediately released when the WP fails.

The third inventory in the CSNF source term is the inventory bound in the CSNF matrix. At the global level, the bound inventory is calculated as the total per package inventory minus the other hardware and instantaneous release inventories. This inventory is calculated at the global level but is added to each GoldSim source element within each percolation subregion environment. Within the GoldSim source element, this inventory is bound in a matrix and is only available for transport after the matrix is degraded. In the CSNF WP, the matrix degrades at the calculated degradation rate, discussed in Section 6.3.7.4.1.2. Within an intact CSNF WP, the waste form does not degrade. In a failed CSNF WP, the waste form is allowed to degrade and make radionuclides available for transport.

The fractional degradation rate is calculated using the rate formulas (Equations 6.3.7-5 and 6.3.7-6 described in Section 6.3.7.4.1.2) for conditions with a pH greater than or equal to 6.8 and for conditions with a pH less than 6.8. Degradation rates under both alkaline and acidic conditions are a function of the specific surface areas of exposed fuel, the representative WP temperature provided at each TSPA-LA Model timestep by the EBS TH Environment Submodel (Section 6.3.2), ΣCO_3 provided at each TSPA-LA Model timestep by the In-Package Chemistry Submodel (Section 6.3.7.2), the in-package pH provided by the In-Package Chemistry Submodel (Section 6.3.7.2), and the partial pressure of oxygen inside the failed WP. A triangular distribution is used to represent epistemic uncertainty in a specific surface area of exposed fuel (Tables 6.3.7-30 and 6.3.7-31). This distribution is sampled once per realization and the sampled value is applied in all of the percolation subregion environment degradation rate calculations. The values for the uncertain coefficients in the rate expressions are correlated. The covariance matrix capturing the uncertainties in the rate coefficients was converted to a lower triangular matrix using the Cholesky Factorization method (DTN: MO0404ANLSF001.001_R0 [DIRS 169007]). In the TSPA-LA Model, the uncertainties in the rate model coefficients are sampled with correlation using a Cholesky factorization method to induce correlation using standard normal distributions, as described in Section 6.1.3.

At temperatures greater than 100°C, the In-Package Chemistry Submodel (Section 6.3.7.2) pH and ΣCO_3 are not valid, nor is the CSNF degradation rate equation. Within the TSPA-LA Model, when a breached CSNF WP is exposed to temperatures exceeding 100°C, the calculated CSNF degradation rate is replaced with a rate that instantaneously degrades the exposed waste form, as recommended in the CSNF Waste Form Abstraction (BSC 2004 [DIRS 169987], Section 8.1) and CSNF Radionuclide Release Model (DTN: MO0404ANLSF001.001_R0 [DIRS 169007]). A rate of 1×10^6 per year (i.e., 0.032 per second) is used in the TSPA-LA Model to implement this recommendation because it results in complete CSNF degradation within one year.

The calculated fractional degradation rate is input to the GoldSim source element located in each percolation subregion environment. The GoldSim source element applies the fractional

degradation rate to degrade the CSNF waste form within a failed WP. The fraction of failed WPs is discussed in Section 6.3.5. After the waste form is degraded, the GoldSim source element releases the mass associated with the degraded fuel into the volume occupied by the waste form alteration products, the schoepite rind, and the inventory becomes available for transport. In addition, the GoldSim source element releases the hardware inventory and the instantaneous release inventory into this same volume. For modeling purposes, a default volume is applied before waste form degradation is initiated. Section 6.3.8.2.1 provides the discussion for calculating the volume of rind formed as the CSNF waste form degrades and the subsequent transport of the available inventory to other areas of the failed WP.

A supplemental calculation is provided in the TSPA-LA Model to evaluate the average fraction of the CSNF that is degraded inside each failed WP. This supplemental calculation is provided as an analysis tool for evaluating the performance of the waste form and also provides a desirable result used to determine the volume of rind formed in the waste form (Section 6.3.8.2.1). This calculation is the average fraction of the CSNF waste form that is degraded in the failed CSNF WPs. Equation 6.3.7-7 is the evaluation of F_{cor} in the TSPA-LA Model:

$$F_{cor}(t) = \frac{M_i^{released}(t)}{M_i(t=0)} = 1 - \frac{M_i^{retained}(t)}{M_i(t=0)} \qquad \text{(Eq. 6.3.7-7)}$$

where

$M_i^{released}$ = the cumulative mass of radionuclide ‘i’ released from the degraded waste form in the failed CSNF WPs

$M_i^{retained}$ = the total mass of radionuclide ‘i’ retained by an undegraded waste form in the failed CSNF WPs

and

$M_i(t=0)$ = the initial inventory (in grams) of radionuclide ‘i’ associated with the failed CSNF WPs.

This calculation uses the knowledge of the internal functions and properties of a GoldSim source element (GoldSim Technology Group 2007 [DIRS 181727]) to evaluate the degradation state of the CSNF matrix inside each failed CSNF WP. The GoldSim source element internally tracks the value of $M_i^{released}$ used in the evaluation of Equation 6.3.7-7. $M_i^{retained}$ can be computed by performing a mass balance on the failed WPs, using the released inventory, $M_i^{released}$, and the initial inventory for the failed WPs, accounting for decay and ingrowth as necessary. As discussed below, the species considered in the TSPA-LA Model calculation of F_{cor} is a non-radioactive species that does not participate in the transport and dose calculations, and is added as supplemental inventory to each CSNF WP specifically to calculate F_{cor}.

The TSPA-LA Model includes 10 grams of an additional species ‘Col’ per CSNF WP. In the TSPA-LA Model ‘Col’ is an unreacting species that is added as a fully bound species in the CSNF waste form. ‘Col’ does not participate in radionuclide decay chains or contribute to the

total dose. As a noncompeting species in the transport calculations ('Col' does not influence the solubility of other elements), 'Col' can be used as a 'tracer' to evaluate the waste form performance. Within each GoldSim source element, the amount of inventory accounting for decay and ingrowth, and number of WPs (both failed and not failed), are internally tracked. In addition, the cumulative amount of each bound and unbound radionuclide, both retained by and released from the waste form, is also tracked. By performing a mass balance on the amount of 'Col' remaining in the waste form, the average fraction of the CSNF waste form that has degraded can be evaluated at each timestep. Within each percolation subregion environment, the total amount of 'Col' associated with the GoldSim source element for that percolation subregion environment is the product of the 'Col' inventory per WP and the number of WPs. The total amount of 'Col' retained by each GoldSim source element is an output of the GoldSim source element and is internally tracked by GoldSim. However, the internally tracked value includes both failed and not failed WPs and is not the value discussed in Equation 6.3.7-7, unless all of the WPs in the source term are failed. The total amount of 'Col' released by the failed WPs associated with each GoldSim source element, $M_i^{released}$ in Equation 6.3.7-7, is also an output of the GoldSim source element and is internally tracked by GoldSim, but it can also be computed by subtracting the amount retained from the total inventory of 'Col.' The total amount of 'Col' released by the GoldSim source element, divided by the number of failed WPs associated with the GoldSim source element, is the average amount of 'Col' released from each of the failed WPs. This result divided by the initial per-package inventory for those failed WPs yields the average fraction of 'Col' released from each failed WP represented by the source element. With the knowledge that the GoldSim source element congruently releases each bound species as the waste form degrades (i.e., if 10 percent of species X is released in one timestep, then 10 percent of all other bound species are also released in that timestep), the average fraction of the waste form degraded in each WP can be equated to the average fraction of 'Col' that is released from each failed WP. This result is used to determine the volume of fuel that is degraded in the CSNF water volume calculations (Sections 6.3.8.2.1) and assess the performance of the CSNF waste form and WP.

6.3.7.4.2 U.S. Department of Energy Spent Nuclear Fuel Waste Form Degradation

The DSNF Waste Form Degradation Abstraction for the TSPA-LA Model is described in *DSNF and Other Waste Form Degradation Abstraction* (BSC 2004 [DIRS 172453]). The DSNF Waste Form Degradation Submodel implements this abstraction and does not require inputs from other TSPA-LA Model submodels. The output of the DSNF Waste Form Degradation Submodel is the instantaneous release of the DSNF inventory from a breached CDSP WP.

6.3.7.4.2.1 Conceptual Model

Several hundred distinct types of DSNF may eventually be emplaced in the Yucca Mountain repository. It is not practical to attempt to determine the impact of each individual fuel type on dose. Instead, the DSNF Waste Form Degradation Abstraction categorized the DSNF in 11 groups (BSC 2004 [DIRS 172453], Sections 1.2, 6.1, and Table 6-2) to represent the entire DSNF inventory for the TSPA-LA Model. These DSNF groups are:

- Group 1 – Naval SNF

- Group 2 – Plutonium/uranium alloy (Fermi 1 SNF)
- Group 3 – Plutonium/uranium carbide (Fast Flux Test Facility -Test Fuel Assembly SNF)
- Group 4 – Mixed oxide and plutonium oxide (Fast Flux Test Facility -Demonstration Fuel Assembly / Fast Flux Test Facility -Test Demonstration Fuel Assembly SNF)
- Group 5 – Thorium/uranium carbide (Fort St. Vrain SNF)
- Group 6 – Thorium/uranium oxide (Shippingport light water breeder reactor SNF)
- Group 7 – Uranium metal (N-Reactor SNF)
- Group 8 – Uranium oxide (Three Mile Island-2 core debris)
- Group 9 – Aluminum-based SNF (Foreign Research Reactor SNF)
- Group 10 – Other (Miscellaneous Fuel)
- Group 11 – Uranium-zirconium hydride (Training Research Isotopes–General Atomics SNF).

For the TSPA-LA Model, an upper-limit degradation model is used for all the DSNF other than naval SNF. In this upper-limit degradation model, the DSNF inventory is immediately available for mobilization, subject to solubility constraints, after the outer surface of the CDSP WP is breached. The release rate of radionuclides from exposed naval SNF is less than that from exposed CSNF. To provide a conservative simplification, the TSPA-LA Model represents naval WPs with an equivalent number of commercial WPs, as discussed in Section 6.3.7.1 and in *Initial Radionuclide Inventories* (SNL 2007 [DIRS 180472], Section 6.2). Thus, naval SNF will not be discussed below as a specific type of DSNF. Figure 6.3.7-7 is a schematic illustration of DSNF waste form degradation within the CDSP WP as part of the model for waste form degradation.

6.3.7.4.2.2 TSPA-LA Model Abstraction

The DSNF Waste Form Degradation Submodel releases the entire per package DSNF inventory for solubilization and mobilization from the CDSP WPs when the WPs are breached. Because of this simplification, the DSNF inventory is treated as unbound inventory in the TSPA-LA Model, and no TSPA parameters are necessary to implement a degradation rate calculation in the TSPA-LA Model.

The volume of water associated with the degraded DSNF is a product of the DSNF rind porosity, rind saturation, and rind volume. Within the representative CDSP WP, the volume occupied by DSNF is 1.0 m^3/WP (BSC 2004 [DIRS 172453], Section 8.1, Table 8-1). The porosity of the powdered form of the corrosion product occupying the volume of the DSNF is 0.20 and is fully saturated (SNL 2007 [DIRS 177407], Table 8.2-1).

6.3.7.4.2.3 TSPA-LA Model Implementation

In the TSPA-LA Model, the DSNF degradation rate is based on an instantaneous release of the radionuclide inventory and does not use any input parameters or rate equations. In addition, the DSNF inventory is not placed into a GoldSim source element with the HLW glass inventory. Instead, each time a CDSP WP fails, the DSNF inventory associated with the failed WP (accounting for decay and ingrowth) is placed into the volume of water associated with the volume occupied by the DSNF. Once released, radionuclides are available for transport to the WP corrosion products and through to the EBS, subject to solubility constraints.

In the TSPA-LA Model, the initial DSNF inventory, with the uncertainty described in Section 6.3.7.1 accounted for, changes through time as a result of radionuclide decay. The DSNF inventory for a single package is fed into a GoldSim source element at the global level of the TSPA-LA Model. This source element is used strictly for decay and ingrowth calculations for DSNF inventory and has been specified such that it is not allowed to fail and is, therefore, not a DSNF source for radionuclide releases. This implementation is a calculation to account for radionuclide decay. For each representative inventory (i.e., CSNF, DSNF, or HLW glass), a GoldSim source element internally tracks all of the radionuclide decay calculations for the specified decay chains. By utilizing a source element with the DSNF inventory, the TSPA-LA Model simplifies the implementation of the radionuclide decay and ingrowth calculations for DSNF inventory and is consistent with the decay rates specified for the HLW glass and CSNF inventories. Each time a CDSP WP fails, this DSNF source element is queried for the DSNF inventory, adjusted for decay and ingrowth, and the TSPA-LA Model subsequently adds a discrete amount of mass, equivalent to the current amount of "unexposed" mass in the DSNF source element, into the CDSP WP EBS cell network (Section 6.3.8) for each failed CDSP WP.

The volume of water associated with the fully saturated DSNF corrosion product is a product of the DSNF rind porosity, rind saturation, and DSNF volume.

6.3.7.4.3 High-Level Radioactive Waste Glass Waste Form Degradation

The HLW Glass Waste Form Degradation Submodel for the TSPA-LA Model is described in the HLW Glass Degradation Abstraction (BSC 2004 [DIRS 169988]). Internal inputs to the HLW Glass Degradation Submodel of the TSPA-LA Model include representative WP temperature and relative humidity provided by the EBS TH Environment Submodel (Section 6.3.2), and pH provided by the In-Package Chemistry Submodel (Section 6.3.7.2). The output from the HLW Glass Waste Form Degradation Submodel is the HLW radionuclide fractional degradation rate and the average fraction of the HLW glass that is degraded in each failed WP.

6.3.7.4.3.1 Conceptual Model

The HLW Glass Degradation Abstraction provides a rate equation that describes the degradation rate of HLW glass when the HLW glass is contacted by water or humid air. The radionuclide release rate is calculated as the product of the surface area of HLW glass contacted by water, the degradation rate of the HLW glass, and the mass fractions of the radionuclides in the HLW glass. Degradation of the HLW glass does not occur in the TSPA-LA Model when the relative humidity is less than 44 percent. Mathematical expressions and parameter values for the HLW

glass surface area and degradation rate are described in the following section. The mass fractions of radionuclides in the HLW glass are obtained from the Initial Radionuclide Inventory Abstraction described in Section 6.3.7.1. The HLW Glass Degradation Abstraction also provides functional relationships for the volume of water in the HLW glass degradation products (the rind) and the rind thickness. These parameters are used to model in-package radionuclide transport (Section 6.3.8.2.2) and calculate the diffusive release of radionuclides from the HLW rind. Although the HLW Glass Degradation Abstraction provides the conceptual model for both the glass degradation rate and the subsequent mass and volume of the rind formed from the degradation process, the discussion of the conceptual model for rind formation is deferred to Section 6.3.8.2.2. The rind layer affects the transport of the radionuclides after they become available. The discussions presented in Section 6.3.7, pertain to radionuclide availability, and the discussions presented in Section 6.3.8, pertain to the transport of available radionuclides.

6.3.7.4.3.2 TSPA-LA Model Abstraction

The HLW glass fractional degradation rate is the main quantity calculated in the TSPA-LA Model by the HLW Glass Waste Form Degradation Submodel.

Glass Degradation and Radionuclide Release—The same rate expression is used to calculate the degradation rate of HLW glass exposed to humid air, exposed to dripping water, or immersed in water, as discussed in Section 8.1 of *Defense HLW Glass Degradation Model* (BSC 2004 [DIRS 169988]). The resulting simplified HLW glass dissolution rate expression for the TSPA-LA Model is captured in HLW Glass Degradation Model (DTN: MO0502ANLGAMR1.016_R0 [DIRS 172830]):

$$rate_G = k_E 10^{\eta \bullet pH} \exp(-E_a / RT) \qquad \text{(Eq. 6.3.7-8)}$$

where

$rate_G$ = absolute HLW glass dissolution rate ($g/m^2/d$)

k_E = rate coefficient ($g/m^2/d$)

η = pH dependence coefficient (dimensionless)

E_a = effective activation energy (kJ/mol)

R = universal gas constant (8.14E-03 kJ/mol/K)

T = temperature (K).

The rate equation requires the specification of three parameter values: k_E, η, and E_a, and the two model variables, temperature and pH. HLW glass degradation does not occur if relative humidity is less than 44 percent (BSC 2004 [DIRS 169988], Section 8.1). If the relative humidity is greater than or equal to 44 percent, the same rate expression is used to calculate the degradation rate when HLW glass is exposed to humid air or dripping water, or is immersed in water. However, separate sets of parameter values are used for degradation in acidic and alkaline solutions. Values for η, E_a, and distributions for k_E for acidic and alkaline solutions are provided in Table 6.3.7-32. In accordance with the guidance provided in Section 8.1 of *Defense*

HLW Glass Degradation Model (BSC 2004 [DIRS 169988]), the degradation rate that is applied in the TSPA-LA Model is the greater of the acidic and alkaline condition degradation rates, regardless of modeled pH. At temperatures greater than 100°C, the In-Package Chemistry Submodel (Section 6.3.7.2) pH calculation is not valid. Therefore, the abstracted rate model, Equation 6.3.7-8, cannot be applied when the representative WP temperature is greater than 100°C. Within the TSPA-LA Model, when a breached CDSP WP is exposed to temperature exceeding 100°C, the abstracted HLW degradation rate model becomes independent of the pH. The developed rate equation is equivalent in form to Equation 6.3.7-8, replacing the pH term with a constant value (= 10) (BSC 2004 [DIRS 169988], Section 8.1). In addition, the alkaline side model coefficients are used to evaluate the modified rate equation. Furthermore, as stated in Section 8.1 of *Defense HLW Glass Degradation Model* (BSC 2004 [DIRS 169988]), glass degradation does not occur when relative humidity is below 44 percent (equivalent to a temperature of 125°C). Under such conditions, the degradation rate of HLW glass is set to zero.

However, if the temperature exceeds the melting point of the glass, as may occur in the Igneous Intrusion Modeling Case, volatile radionuclides may be released. As the glass cools, new crystalline and glass phases may form, which have different radionuclide-retaining properties from the original glass. In order to bound the uncertainty in the release fraction of the volatile radionuclides and in the degradation rates of radionuclide-containing phases, it is assumed that the glass will degrade instantaneously during an igneous intrusion.

The HLW glass mass dissolution rate, presented in *Defense HLW Glass Degradation Model* (BSC 2004 [DIRS 169988], Section 8.1) and captured in HLW Glass Degradation Model (DTN: MO0502ANLGAMR1.016_R0 [DIRS 172830]), is the specific rate, $rate_G$, multiplied by the surface area available for dissolution over a timestep. The surface area that remains as the HLW glass degrades is the product of the specific surface area, the exposure factor, and the mass of HLW glass that remains. The expression used to calculate the HLW glass surface area (m^2) as HLW glass dissolves in a timestep is:

$$S = f_{\text{exposure}} S_{sp} (M_0 - \Sigma M_t) \qquad \text{(Eq. 6.3.7-9)}$$

where

S_{sp} = the geometric specific surface area available for reaction (m^2/kg)

f_{exposure} = the exposure factor (accounting for the higher effective surface area of the glass log resulting from cracking of the HLW glass after it is poured into the canister)

M_0 = the initial mass of HLW glass (kg)

$\sum M_t$ = the total mass of HLW glass degraded in all previous timesteps (kg).

The mass of HLW glass degraded in a timestep is calculated as the product of the HLW glass degradation rate for that realization and the duration of the timestep. Table 6.3.7-32 provides the value for the specific surface area. The initial mass of HLW glass is 2,710 kg (DTN: MO0502ANLGAMR1.016_R0 [DIRS 172830]).

The expression used to calculate the surface area for the next timestep is:

$$S = 2.70 \times 10^{-3} f_{\text{exposure}} (2710 - \Sigma M_t) \quad \text{(Eq. 6.3.7-10)}$$

The exposure factor is an uncertain parameter with sampling shown in Table 6.3.7-32. The initial timestep is conducted with $\sum M_t = 0$. The value of $\sum M_t$ is revised after each timestep by adding the mass of HLW glass degraded over the current TSPA-LA Model timestep, as shown below:

$$M_t = rate_G \times \Delta t \times S \quad \text{(Eq. 6.3.7-11)}$$

The release rate of radionuclides due to HLW glass degradation is the product of the HLW glass mass dissolution rate and the mass fraction of a radionuclide in the HLW glass:

$$R_{RN} = S \times rate_G \times I_{RN} \quad \text{(Eq. 6.3.7-12)}$$

where

R_{RN} = radionuclide release rate (Ci/d)

I_{RN} = mass fraction of a radionuclide in the HLW glass (Ci/g).

The radionuclide release rate determines the rate of radionuclide release from degraded HLW glass to the volume of water in the rind of altered HLW glass.

6.3.7.4.3.3 TSPA-LA Model Implementation

The HLW glass source term within each percolation subregion environment of the TSPA-LA Model contains two HLW glass inventories: a bound inventory and an unbound inventory. In the TSPA-LA Model, the HLW glass inventory is fully bound in the glass; therefore, the unbound inventory becomes zero grams for each radionuclide in the glass inventory (Section 6.3.7.1). The unbound inventory is included in the TSPA-LA Model to facilitate the development of sensitivity runs. Both inventories are added to each GoldSim source term, but the package inventory is bound in the glass matrix. At the global level, the bound inventory is calculated as the total per-package inventory, including uncertainty, and the unbound inventory is set to zero grams. These inventories are calculated at the global level but are added to each GoldSim source element within each percolation subregion environment. Within the GoldSim source element, the bound inventory is bound in a matrix and is only available for transport after the matrix is degraded. In the CDSP WP, the HLW glass matrix degrades at the calculated degradation rate, discussed in Section 6.3.7.4.3.2. Within an intact CDSP WP, the waste form does not degrade. In a failed CDSP WP, the waste form degrades at the calculated rate, and radionuclides become available for transport.

Degradation of HLW glass starts when the CDSP WPs are breached and if relative humidity is greater than or equal to 44 percent. The rate of degradation used in the TSPA-LA Model is the fractional form of the dissolution rate. This degradation rate is the product of the absolute glass

dissolution rate (Section 6.3.7.4.3.2), the specific surface area of the glass, and the waste form exposure factor. The coefficients in the rate equation are dependent on pH conditions: one set for acidic conditions and one set for alkaline conditions (Table 6.3.7-32). The values for the coefficients are captured in the HLW Glass Degradation Model (DTN: MO0502ANLGAMR1.016_R0 [DIRS 172830]). The rate expression is simultaneously evaluated with both acidic and alkaline condition coefficients with the current inputs, regardless of the applied pH, and the greater of the two calculated rates is applied to degrade the HLW glass. At temperatures greater than 100°C and less than 125°C, the rate expression is evaluated using the alkaline-side coefficients, with the pH term taking on a constant alkaline value (=10). The rate equation is a function of an affinity term, temperature, pH, and HLW glass surface area. The affinity term is treated as an epistemic uncertainty and is represented by two triangular distributions (k_{E_acid}, $k_{E_alkaline}$) used for acidic and alkaline conditions. These distributions are sampled once per realization. The exposure factor, $f_{exposure}$, is treated as an epistemic uncertainty represented by a triangular distribution. This distribution is sampled once per realization, and the same exposure factor is used for alkaline and acidic conditions.

The calculated fractional degradation rate is input to the GoldSim source element located in each percolation subregion environment. The GoldSim source element applies the fractional degradation rate to degrade the HLW glass waste form inside a failed CDSP WP. The fraction of failed WPs is discussed in Section 6.3.5. After the glass degrades, the GoldSim source element releases the mass associated with the degraded waste form into the volume occupied by the waste form alteration products, the rind, and the inventory becomes available for transport. Section 6.3.8.2.2 provides the discussion for calculating the volume of rind formed as the HLW glass waste form degrades and the subsequent transport of the available inventory to other areas of the failed WP.

A supplemental calculation is provided in the TSPA-LA Model to evaluate the average fraction of the HLW glass waste form that is degraded inside each failed WP. This supplemental calculation is provided as an analysis tool for evaluating the performance of the waste form and also provides a desirable result used to determine the volume of rind formed in the waste form (Section 6.3.8.2.2). This calculation is the average fraction of the HLW glass waste form that is degraded in the failed CDSP WPs, and for the purposes of the CDSP rind volume calculation, is called variable F_{cor} to be consistent with the CSNF discussion. Equation 6.3.7-7, and the supplemental discussion provided in Section 6.3.7.4.1.3, is the evaluation of F_{cor} in the TSPA-LA Model and is applicable to both CSNF and CDSP WPs. Within the TSPA-LA Model, the calculation of F_{cor} is the same for both CSNF and CDSP source terms, so the discussion is not repeated.

Although presented in Section 6.3.7.4.3.2, Equations 6.3.7-9 through 6.3.7-12 are not directly incorporated into the TSPA-LA Model. These equations adjust the specific degradation rate to compensate for differences in the amount of glass degraded as a function of time. Using a fractional degradation rate, the type required by GoldSim source elements, the TSPA-LA Model does not need to compensate for depleting the glass as degradation processes occur. Similarly, because the TSPA-LA Model calculates the fraction of the HLW glass that is degraded, F_{cor} for analysis purposes, this result is used to determine the rind volume (Section 6.3.8.2.2) and assess the performance of the HLW glass waste form.

6.3.7.5 Dissolved Concentration Limits

The Dissolved Concentration Limits Abstraction for the TSPA-LA Model is described in *Dissolved Concentration Limits of Elements with Radioactive Isotopes* (SNL 2007 [DIRS 177418]). Within the TSPA-LA Model, the Dissolved Concentrations Limits (i.e., solubility) Submodel implements the Dissolved Concentrations Limits Abstraction to calculate solubilities for 8 elements, including plutonium (Pu), neptunium (Np), uranium (U), thorium (Th), americium (Am), protactinium (Pa), tin (Sn), and radium (Ra). As pointed out in Table 6.3.7-33, for technetium (Tc), carbon (C), iodine (I), cesium (Cs), strontium (Sr), selenium (Se), and chlorine (Cl), no solubility-controlling solids are expected to form under the repository conditions, therefore, their solubilities are not evaluated. As stated in Table 6.3.7-6, actinium (Ac) and curium (Cm) are not transported within the TSPA-LA Model. Thus, their solubilities are not needed and are not evaluated in the solubility abstraction. The output of the Dissolved Concentration Limits Submodel is used in the TSPA-LA Model to constrain the dissolved concentrations of radioactive elements in the WPs and in the invert.

6.3.7.5.1 Conceptual Model

The Dissolved Concentration Limits Abstraction is based on calculations using geochemical modeling tools and thermodynamic databases. Inputs to the Dissolved Concentration Limits Abstraction include solution chemistry, thermodynamic properties, and associated uncertainties of pertinent species (SNL 2007 [DIRS 177418], Table 4-1). Laboratory and field observations and measurements were used in the selection of solubility controlling phases and model validation. The Dissolved Concentration Limits Abstraction details the treatment of solubilities for 8 elements that are included in the TSPA-LA Model. The resulting outputs from the Dissolved Concentration Limits Abstraction are, with exceptions, functions of pH and f_{CO2} and can be applied for a wide range of environmental conditions in both the WPs and the invert. Figure 6.3.7-8 is a schematic illustration showing the relations of the Dissolved Concentration Limits (Solubility) Submodel with the other submodels of the Waste Form Degradation and Mobilization Model Component.

The selection of solubility controlling phase(s) has a direct impact on the outcome of the Dissolved Concentration Limits Abstraction calculations. Based on the laboratory and field observations, or conservative assumptions, solubility-controlling phases for the 8 elements considered in the TSPA-LA Model were selected, as summarized in Table 6.3.7-33. The justification for using each solid phase is discussed in *Dissolved Concentration Limits of Elements with Radioactive Isotopes* (SNL 2007 [DIRS 177418], Section 6).

The environmental conditions expected in the repository are considered for the solubility calculations. Ligands that can form aqueous complexes with radioactive elements and are common in Yucca Mountain waters, such as OH^-, CO_3^{2-}, F^-, HPO_4^{2-}, Cl^-, SO_4^{2-}, and NO_3^-, are included in solubility calculations in *Dissolved Concentration Limits of Elements with Radioactive Isotopes* (SNL 2007 [DIRS 177418], Section 6). The sensitivity analysis shows that, among the environmental conditions considered by the Dissolved Concentration Limits Abstraction, pH and f_{CO2} have the primary impact on actinide solubilities. Therefore, those two variables are chosen as the independent variables for solubility calculations. Solubility limits were calculated for a wide range of pH and f_{CO2} values. Other environmental variables that have

a significant impact on actinide solubilities are accounted for by assigning them as a charge balance species in the Dissolved Concentration Limits Abstraction calculations (e.g., SO_4^{2-}) or through an added uncertainty term to the Dissolved Concentration Limits Submodel (e.g., F^-).

Four types of uncertainties -(1) uncertainties in the K values of solubility controlling solids and aqueous species, (2) uncertainties of activity coefficients, (3) uncertainties in water chemistry, and (4) uncertainties in temperature - have been evaluated in *Dissolved Concentration Limits of Elements with Radioactive Isotopes* (SNL 2007 [DIRS 177418] Section 6.3.3.). In the outputs of the Dissolved Concentration Limits Abstraction, the first two types of uncertainties are combined together by the mean-square-root approach and are collectively called thermodynamic uncertainties. The third type of uncertainty is presented as the uncertainty associated with fluoride concentrations. The last type of uncertainty (i.e., uncertainty in temperature) was treated using a bounding approach. In other words, the solubility calculations are conducted at a temperature of 25°C and are applied for all temperatures greater than 25°C (up to 100°C). The use of solubility values calculated at 25°C for higher temperatures is bounding because there is evidence showing that the solubility of actinides decreases with increased temperature, which is called retrograde solubility in *Dissolved Concentration Limits of Elements with Radioactive Isotopes* (SNL 2007 [DIRS 177418], Section 6.3.3.3).

6.3.7.5.2 TSPA-LA Model Abstraction

Outputs from the Dissolved Concentration Limits Abstraction can be divided into three groups: (1) elements whose solubility is a function of pH and $\log f\mathrm{CO}_2$; (2) radium solubility that is a function of pH only; and (3) elements for which no solubility limits are defined (SNL 2007 [DIRS 177418], Section 8.1).

The first group includes americium, neptunium, plutonium, protactinium, thorium, tin, and uranium. The abstracted solubility models for these elements are in the form of look-up tables with pH and $\log f\mathrm{CO}_2$ as the independent variables. Two uncertainty terms accounting for uncertainties associated with thermodynamic properties and variations in water chemistry are also included for this group of elements. The exception to this treatment is protactinium, where the thermodynamic uncertainty is replaced by uncertainty in the choice of an analogue element. For tin, the uncertainty term associated with variations in fluoride concentrations is not given because the calculated tin solubility is not sensitive to fluoride concentrations (SNL 2007 [DIRS 177418], Section 6.19). For radium, solubility values are given as a step function of pH, uncertainties were not included.

The remaining elements (technetium, carbon, iodine, cesium, chlorine, selenium, and strontium) are considered highly soluble and no solubility-controlling solids are expected to form under repository conditions. Thus, their solubilities are not given. Consequently, their release is controlled by the dissolution rate of the waste form and waste inventories. Each of these three groups is discussed below.

pH and $\log f\mathrm{CO}_2$ Dependent Solubility—The pH and $\log f\mathrm{CO}_2$ dependent solubility for americium, neptunium, plutonium, protactinium, thorium, tin, and uranium can be summarized by the following relationship (SNL 2007 [DIRS 177418], Section 8.1):

$$[\text{Pu, Np, U, Am, Th, and Sn}] = 10^{s} \bullet 10^{\varepsilon_1} + \varepsilon_2 \bullet N \qquad \text{(Eq. 6.3.7-13a)}$$

and

$$[\text{Pa}] = 10^{s} \bullet 10^{\varepsilon_1} + \varepsilon_2 \qquad \text{(Eq. 6.3.7-13b)}$$

where

$[E]$ = the logarithm of the predicted solubility for a given element, E

$S(pH, \log f_{CO_2})$ = the logarithm of the base solubility value from a look-up table for that element, E, which is a function of pH and log f_{CO2}

ε_1 = a term accounting for uncertainty in thermodynamic properties for americium, neptunium, plutonium, thorium, and tin (for protactinium, uncertainty is accounted for using the analogue phase Np_2O_5)

ε_2 = the uncertainty term associated with variations in fluoride concentration. This uncertainty term is perfectly correlated among the Pu, Np, U, Th, Am, and Pa solubility models during sampling. This term has a right-sided triangular distribution with the minimum (indicated by "a"), most probable values (indicated by "b") equal to one another (i.e., a = b) and the maximum value (indicated by "c") corresponding to the maximum uncertainty.

$N(pH)$ = multiplication factor used to make the second uncertainty term a function of pH, with the exception of protactinium for which no multiplication factor is used.

While the calculation of uranium solubility uses Equation 6.3.7-13, its implementation is more complex and is discussed separately below. For the other elements listed above, the Dissolved Concentration Limits Abstraction provides a two-dimensional look-up table giving a calculated value of solubility as a function pH and log f_{CO2}. The look-up tables for americium, neptunium (Np_2O_5 and NpO_2), plutonium, protactinium, thorium, and tin can be found in Tables 6.3.7-34 through 6.3.7-40, respectively. A base solubility value, $S(pH, \log fco_2)$, for each element is obtained for a given pH and log fco_2 value by linear interpolation of the nearest pH and log fco_2 values in the table. After the base solubility value is determined, the uncertainty terms are added to it in the manner shown in Equation 6.3.7-13.

In general, two types of uncertainty terms are included to describe the pH and log fco_2 dependent solubility. The first term, ε_1, is used to account for uncertainty in the thermodynamic properties used to calculate the solubility look-up tables. These uncertainties are represented by truncated normal distributions with mean values of 0.0 and SDs specific to each element (Tables 6.3.7-41 through 6.3.7-47). The solubility calculations were conducted using the B-dot equation, which is only rigorously applicable up to ionic strength values of 1 molal. In order to extend the applicable range of the solubility model to 3 molal, extra uncertainty is added to the ε_1 uncertainty term (SNL 2007 [DIRS 177418], Section 8.1). For solutions with an ionic strength between 1 molal and 3 molal, a modified SD is used for the ε_1 uncertainty term. This

modification requires that 0.3 be added to the 1 molal SD using the root-mean-square method (SNL 2007 [DIRS 177418], Section 6.3.3.4, Equation 6.3-7). The resulting SDs are also shown in Tables 6.3.7-41 through 6.3.7-47. The ε_1 normal distributions are truncated at the 2σ level for all elements except protactinium (SNL 2007 [DIRS 177418], Section 8.2). The exception to the above discussion of ε_1 is protactinium. For protactinium, ε_1 represents uncertainty in the choice of analogue used to determine the base protactinium solubility, which has a uniform distribution over the range of (-4.42, -0.05) (SNL 2007, [DIRS 177418], Table 6.11-4).

The second uncertainty term, $\varepsilon_2 \bullet N$, is used to account for variations in the base solubility value due to variable fluoride concentration in the fluid. Because the vapor influx mode does not contribute fluoride to the fluid, this uncertainty term is zero for vapor influx mode (SNL 2007 [DIRS 177418], Section 8.1). For the liquid influx mode, this uncertainty term depends on the WP types and ionic strength. Thus, three groups of abstractions for this term were given. Group 1 is for CSNF WPs when ionic strength is less that 0.2 molal, and for CDSP WPs when ionic strength is less than 0.004 molal. Group 2 is for CSNF WPs when ionic strength is greater or equal to 0.2 molal, and for invert under CSNF WPs. Group 3 is for CDSP WPs when ionic strength is greater than or equal to 0.004 molal and for invert under CDSP WPs (SNL 2007 [DIRS 177418], Section 6.19.4.2.2 and Table 6.3-3).

The uncertainty parameters ε_2 are in the form of triangular distributions with minimum and most likely values of zero and maximum values specified for each element (SNL 2007 [DIRS 177418], Section 8.1). These parameters are perfectly correlated with each other during sampling (i.e., with a correlation coefficient of 1.0) (SNL 2007 [DIRS 177418], Section 8.1).

Because the impact of fluoride concentration on the actinide solubilities varies strongly with pH, as described in *Dissolved Concentration Limits of Elements with Radioactive Isotopes* (SNL 2007 [DIRS 177418], Section 6), the second part of the uncertainty term associated with fluoride concentrations, the multiplication factor, N, that is a function of pH, is introduced to present the pH dependency. The multiplication factor, N(pH), is an element-specific parameter that varies from zero to one as a function of pH. It is calculated by normalizing the differences in solubility values between the elevated F^- cases and the base case for each element by the maximum observed difference in solubility values (in *Dissolved Concentration Limits of Elements with Radioactive Isotopes* (SNL 2007 [DIRS 177418], Tables 6.6-4 and 6.6-6). This modification requires that the ε_2 uncertainty terms for each element be fixed at the values sampled for each realization. The sampled value of ε_2 is then multiplied by N(pH) at each timestep to produce a modified ε_2^i. Tables 6.3.7-48 through 6.3.7-52 give the multiplication factors for americium, Np_2O_5, NpO_2, plutonium, and thorium. For protactinium, no multiplication factor is used in conjunction with ε_2^i.

Neptunium Solubility—Neptunium solubility is calculated using Equation 6.3.7-13 and the uncertainty terms discussed above. However, two different solubility models are presented for neptunium in *Dissolved Concentration Limits of Elements with Radioactive Isotopes* (SNL 2007 [DIRS 177418], Section 6.6). These two models are based on different solubility-controlling solid phases, Np_2O_5 and NpO_2. The NpO_2 solubility model is used within WPs when reductants (CSNF fuels or stainless steels) remain. After reductants within WPs are consumed, Np_2O_5 will

be applied. For the invert, the Np_2O_5 solubility model is always applied (SNL 2007 [DIRS 177418], Section 6.6).

Uranium Solubility—There are two methods used to calculate uranium solubility based on different chemistries of in-package fluids (SNL 2007 [DIRS 177418], Section 6.7). In the first method, the amount of silica and alkaline elements in the fluid are far less than the amount of available uranium, which precludes the ubiquitous formation of uranyl silicates (e.g., Na-boltwoodite) and their use as solubility controlling phases. In the second method, the amount of silica and alkaline elements are comparable to the amount of available uranium and uranyl silicates can readily precipitate. These two methods apply as follows:

Method 1. CSNF WPs that are breached in the Nominal or Seismic Scenario Classes

Method 2. CDSP WPs breached under all scenario classes, CSNF WPs breached in the course of the igneous intrusion, and for all evaluations in the invert.

Using the first method, uranium solubility is controlled by schoepite under all pH and fco_2 conditions. This method is used because the source of the degrading water in a CSNF WP in the Nominal, Early Failure, or Seismic Scenario Classes is water vapor entering the WPs, which has low or no initial dissolved sodium or silica (SNL 2007 [DIRS 177418], Section 6.7.3). A single look-up table is used for calculating the base solubility value, $S(pH, log\ fco_2)$ (Table 6.3.7-53). The uncertainty terms are handled using the same method discussed above with a multiplication factor for ε_2^i. Values of the uncertainty terms and $N^i(pH)$ for the CSNF WPs (Nominal, Early Failure, and Seismic Scenario Classes) are given in Tables 6.3.7-54 and 6.3.7-55. There are two sets of ε_2 and N(pH): one for low ionic strength conditions (< 0.2 molal) and the other for high ionic strength conditions (greater than or equal to 0.2 molal).

Using the second method, uranium solubility is controlled by schoepite, Na-Boltwoodite, or $Na_4UO_2(CO_3)_3$, depending on the pH and fco_2. In this environment, silica is available to the degrading waste from the CDSP glass, surrounding igneous material, and invert construction material, so Na-boltwoodite is included as a uranium solubility-controlling phase (SNL 2007 [DIRS 177418], Section 6.7.3). As a result, two additional base solubility look-up tables are defined. The solubility limits in Table 6.3.7-56 represent schoepite solubility and extend over lower pH values, where this mineral is the least soluble of the three mineral phases considered. Table 6.3.7-57 represents solubilities of Na-Boltwoodite and $Na_4UO_2(CO_3)_3$ and covers the higher pH ranges. Uncertainties in thermodynamic properties lead to a range of pH and log fco_2 values in which either schoepite or Na-Boltwoodite could control the uranium solubility. The shading in Table 6.3.7-56 and the upper shaded area in Table 6.3.7-57 indicate these ranges. For environmental conditions within these ranges, the uranium solubility should be sampled from a uniform distribution with bounds based on the values in Tables 6.3.7-56 and 6.3.7-57. After the base solubility value is determined from one or both of the look-up tables, uncertainties are added as discussed above. Values for the uncertainties are shown in Table 6.3.7-58. The exception is that six sets of ε_2 and different N(pH) tables are now defined, as there are two sets for each of the three groups discussed previously, each set is for one solubility look-up table (SNL 2007 [DIRS 177418], Section 6.7.5). Table 6.3.7-59 gives the values of multiplication factors for this solubility model.

Radium Solubility—Radium solubility is based on calculated Ba solubility at 100°C using $BaSO_4$ as the solubility controlling phase, which is a good analog for modeling radium solubility (SNL 2007 [DIRS 177418], Section 6.12). Since the solubility data of $RaSO_4$ in the thermodynamic database (data0.ymp.R4) used in the solubility calculations do not have a temperature-dependent relationship, and the solubility data of $BaSO_4$ indicate that $BaSO_4$ solubility increases with temperatures up to 100°C, calculated $RaSO_4$ solubility could be not conservative. To be prudent, radium solubility is based on the conservative analog of $RaSO_4$ (i.e., $BaSO_4$ solubility calculated at 100°C (SNL 2007 [DIRS 177418], Section 6.12)).

Radium solubility is presented as a simple step function of pH. For pH values from 3.0 to 7.75, the logarithm of radium solubility is fixed at –1.16 mg/L; and at pH values between 7.75 and 9.75, it is fixed at 1.68 mg/L (log value) (SNL 2007 [DIRS 177418], Table 6.12-1). At pH values greater than 9.75, radium solubility is undefined, and its concentration is controlled by release from the waste form (DTN: MO0702PADISCON.001_R0 [DIRS 179358], Table 10).

Undefined Solubility—Under repository environmental conditions, no solubility-controlling solids are expected to form for carbon, cesium, chlorine, iodine, selenium, and technetium (SNL 2007 [DIRS 177418], Section 8.1); therefore, no solubilities are defined for these elements. Although strontium (Sr) may precipitate in carbonates and sulfates under repository conditions, for the purpose of simplicity, its solubility is also assumed to be undefined. In the TSPA-LA Model, the release of these elements is controlled by the waste inventory and dissolution rates of the waste forms.

Although actinium is not transported in the TSPA-LA Model (Table 6.3.7-60), it is included as a species in the TSPA-LA Model. This is because certain impact analyses consider the transport of actinium in the EBS. For this reason, it is necessary to specify an actinium solubility value in the TSPA-LA Model. However, no thermodynamic data exist for calculating actinium solubility (SNL 2007 [DIRS 177418], Section 6.10). Thus, in the TSPA-LA Model, no solubility is calculated for actinium.

Restrictions on the Dissolved Concentration Limits Abstraction—The solubility models developed for this abstraction are valid for a wide range of environmental conditions and can be applied both inside and outside the WPs. However, these models are subject to the following restrictions (SNL 2007 [DIRS 177418], Table 8-3):

1. The valid temperature range for the solubility models is from 25°C to 100°C.

2. The solubility models are also restricted to pH values between 3.0 and 11.0 and log fco_2 values from –1.5 to –5.0, with f_{CO2} in the unit of bar.

3. The solubility models are restricted to ionic strength less than or equal to 3 molal.

Treatments of Solubility Model Out-Of-Bounds—Under certain circumstances, the solubility of one or more elements cannot be calculated. This is called Out-of-Bounds solubility model. According to the cause, out-of-bounds can be categorized into three types.

Type I Out-of-Bounds: As shown on Figure 6.3.7-9, Type I out-of-bounds occur when the given pH-f_{CO2} conditions fall into the gray areas where the solubility look-up table has three valid values (A, B, and C) but with one flagged as invalid (i.e., 500) at D. Since GoldSim two-dimensional look-up tables use rectangular interpolation scheme, a meaningful solubility cannot be calculated using the standard interpolation scheme by the two-dimensional look-up table element. However, in general, solubility can be calculated using EQ3 for these conditions. This type of out-of-bounds is caused by the limited resolutions of solubility look-up tables. A triangular interpolation scheme that produces valid results for the gray shaded areas has been implemented for the uranium solubility models at CSNF Cell 1 to obtain solubility values when this type of out-of-bounds occurs.

Type II Out-of-Bounds: Type II out-of-bounds occurs when the given pH-f_{CO2} conditions are outside the valid ranges of the solubility look-up table and they cannot be removed by a triangular interpolation scheme. The unshaded area, of the rectangle ABCD on Figure 6.3.7-9 indicates the area where Type II out-of-bounds (in the plutonium solubility model) could occur. However, since the pH-f_{CO2} conditions given by the In-Package Chemistry Submodel may be narrower than the whole unshaded area, the ranges of pH-f_{CO2} conditions where Type II out-of-bounds can actually occur can be narrower than as shown on the figure. For the uranium solubility model at CSNF Cell 1, Type II out-of-bounds occurs only for a very narrow range. A base uranium solubility of 1,000 mg/L is assigned for this narrow range (SNL 2007 [DIRS 177418], Table 8-1). This value is justifiable, because the maximum uranium solubility calculated by EQ3 calculations for conditions very close to where Type II out-of-bounds occurs is 500 mg/L. Type II out-of-bounds can also occur for the uranium solubility model at CDSP Cell 1a. Uranium concentrations are capped at 71,400 mg/L (SNL 2007 [DIRS 177418], Table 8-1).

Type III Out-of-Bounds: Type III out-of-bounds occur when ionic strength is greater than 3 molal, and the concentrations of actinides are then capped at the values shown in Tables 6.3.7-60 and 6.3.7-61, for CSNF Cell 1 and CDSP Cell 1b, respectively (SNL 2007 [DIRS 177418], Tables 6.22-2 and 6.22-3).

An empirical approach that addresses Type III out-of-bounds in the plutonium solubility model has been developed and documented below.

The approach relies on the evaluation of the solubility-limited dissolved concentrations model for plutonium (including uncertainties for ionic strength above 1 molal (SNL 2007 [DIRS 177418], Table 6.5-1), against a data set for measured PuO_2(am) solubility at high ionic strengths (Rai et al., 2001 [DIRS 168392]). This evaluation is a direct comparison (Figure 6.3.7-10) of the look-up table model values to the data sets collected in 0.4 and 4 Molar $NaClO_4$ and NaCl solutions (i.e., 0.408 and 4.92 molal $NaClO_4$, respectively), and 0.4 and 4 Molar NaCl solutions (i.e., 0.403 and 4.36 molal NaCl, respectively).

Examination of Figure 6.3.7-10 indicates that the measured concentrations of plutonium in perchlorate (an oxyanion) solutions decrease at higher ionic strengths and are closely represented by the solubility-limited dissolved concentrations model for plutonium. The measured concentrations of plutonium in NaCl (salt) solutions increase at higher ionic strength and can be seen to exceed the 2-sigma upper uncertainty band shown on Figure 6.3.7-10 for the model

results. It is noted here that the data shown in the plot (Rai et al., 2001 [DIRS 168392]) are for the longest equilibration times reported by the authors. Because the observed increase for the 4.36 m NaCl solutions is seen for the longer equilibration times, this increase is attributed by Rai et al. (2001 [DIRS 168392]) as probably reflecting alpha radiolysis of the electrolyte to NaOCl with concurrent increase in the solution redox state. However, the measured data for plutonium in the 0.403 m NaCl solutions, show a slight decrease over approximately the same time. In a spectroscopic study of actinide solubilities in highly concentrated chloride solutions (Runde et al., 1997 [DIRS 182190]), it was shown that at increased chloride concentrations, chloride complexes were forming for plutonium (and other actinides), and it was concluded that the higher dissolved actinide concentrations were attributable to this process. Regardless of which of these two possibilities occurred in the experimental work, they are both relevant to potential increased solubility-limited concentrations of plutonium in concentrated chloride solutions above 3 molal, and therefore the data from Rai et al. (2001 [DIRS 168392]) can be used in an empirical approach to define a high ionic strength cap value that is for plutonium in about 4.3 molal chloride solutions. Given the behavior in perchlorate solutions, such a cap value would be bounding for concentrated solutions that are dominated by oxyanions because either mechanism discussed above involved the chloride in the electrolyte directly to account for the increased solubility at higher ionic strength.

Based on the values shown on Figure 6.3.7-10, the solubility cap can be generated to cover the pH range from 4 to 10 and provides an upper bounding value for the dissolved concentration of plutonium that is applicable in concentrated chloride solutions up to ionic strengths of about 4.3 molal. This empirically derived concentration cap is 100 mg/L based on the data set and would be applicable without any further uncertainty treatment because of its bounding nature. For the TSPA-LA Model, this application (TSPA parameter name: Pu_TSPA_DS_Cap) would take place above the 3.0 molal ionic strength limit of the plutonium model. Given the data sets from Rai et al. (2001 [DIRS 168392]), the applicable pH range is from 4 to 10 (the higher end considers the trend of the 4.36 molal NaCl data set, as well as the higher pH behavior of the other data). When pH condition is outside this applicable range, then, the Type III Pu Cap described previously in Tables 6.3.7-60 and 6.3.7-61 is invoked.

As the ionic strength of these solution increases, the equilibrium between the gas phase CO_2 and the aqueous solution will result in a lower solubility of CO_2 due to the "salting-out effect". The activity coefficient of certain neutral species increases with the increased ionic strength creating a corresponding concentration decrease (Langmuir, 1997 [DIRS 100051], Sec. 4.4). This is particularly true for NaCl solutions where the coefficient in the Setchenow equation is 0.231 for aqueous carbonate (Langmuir, 1997 [DIRS 100051], Section 4.4, page 144, and Table 4.5). This corresponds to lower CO_2 solubility and therefore should result in less effective carbonate complexation of actinides at these higher ionic strengths at any given CO_2 fugacity.

6.3.7.5.3 TSPA-LA Model Implementation

The Dissolved Concentration Limits Abstraction is implemented in the TSPA-LA Model to calculate elemental solubility values for both the in-package (CDSP WP and CSNF WP) and invert environments. The Dissolved Concentration Limits Submodel is implemented at two locations in the TSPA-LA Model. The stochastic elements describing the uncertainty

distributions are defined in the Epistemic_Params submodel. Solubility values are calculated within the EBS_Submodel container, which sits inside the percolation subregion loop.

In the Epistemic_Params Submodel, the stochastic elements describing solubility-related uncertainties are sampled once for each realization. These sampled values are then passed to the EBS_Submodel.

Within the EBS_Submodel, the environmental parameters, pH, log fco_2, and ionic strength pertaining to the current percolation subregion are provided to the Dissolved Concentration Limits Submodel by the In-Package Chemistry and EBS Chemical Environment Submodels (Sections 6.3.7.2 and 6.3.4, respectively). These parameter values are then used to obtain a local base solubility value from the look-up tables.

The sampled values of the uncertainty parameters are then added to the local base solubility according to Equation 6.3.7-13 to obtain the final solubility values at each timestep and for each realization. The same value sampled for a given uncertainty parameter is used in all percolation subregions at all times for a particular realization.

The Dissolved Concentration Limits Submodel provides elemental solubilities. The GoldSim software (GoldSim V9.60.100, STN: 10344-9.60-01 [DIRS 181903]), automatically partitions the elemental solubility among the isotopes of an element according to the isotopic ratios (GoldSim Technology Group 2007 [DIRS 181727]) so that the sum of the concentrations of all the element's isotopes will not exceed its solubility.

The GoldSim software requires that all the element's isotopes have the same solubility value. If isotopes of the same element are assigned different solubility values, GoldSim will force all of the isotopes to have the solubility values of the first isotope in the species list. When this is done, a warning message is generated in the GoldSim run log for every timestep and each isotope that had its solubility redefined. In the TSPA-LA Model, solubility values are calculated in units of mg/L. In its internal calculations, GoldSim converts all units to the International System of Units, which for solubility is mol/L. Therefore, each isotope of an element will have a slightly different solubility value after the conversion to the International System of Units. This results in as many as 100,000 warning messages being written to the GoldSim run log. In order to suppress these messages, a slight modification, as described below, is made to the calculated solubility values in the TSPA-LA Model.

The calculated solubility value for an element is converted from mg/L to mol/L by dividing it by the molecular weight of the lightest isotope for that element. For each isotope of an element, this mole-based solubility value is then reconverted to mg/L based on the molecular weight of the isotope in this calculation. As a result, all isotopes of an element will have equivalent solubility values in terms of mol/L but will have slightly differing values in terms of mg/L. This modification introduces a slight discrepancy between calculated solubility values and the estimated concentrations at which the solubility limit is reached in the TSPA-LA Model. Calculated element concentrations can be as much as 0.6 percent higher than the calculated solubility value.

6.3.7.6 Engineered Barrier System Colloids

The Waste Form and In-Drift Colloid Concentration Abstraction for the TSPA-LA Model is described in *Waste Form and In-Drift Colloids-Associated Radionuclide Concentrations: Abstraction and Summary* (SNL 2007 [DIRS 177423]). Within the TSPA-LA Model, the EBS Colloids Submodel implements the Waste Form and In-Drift Colloid Concentration Abstraction to address the formation, stability, and concentration of radionuclide-bearing colloids in the waste form and WP, as well as sorption of dissolved radionuclides. Colloids are fine particles ranging in size from 1 nm to 1 μm in maximum dimension that have the potential to remain in suspension. Colloids are of concern because radionuclides attached to colloids may move faster and farther than dissolved radionuclides; however, colloids may only significantly facilitate radionuclide transport when their suspensions are stable and when they carry significant amounts of radionuclides.

The processes included in the EBS Colloids Submodel are described in this section. Some processes that slow or limit colloid migration were not incorporated into the model, including colloid filtration, colloid sorption at the air-water interface, microbial effects, and the effects of elevated temperature (SNL 2007 [DIRS 177423], Sections 5 and 6.3.1).

6.3.7.6.1 Conceptual Model

Colloids—Three types of colloids were considered in the Waste Form and In-Drift Colloid Concentration Abstraction and are accounted for in the EBS Colloids Submodel implemented in the TSPA-LA Model: (1) Waste form degradation colloids: (a) colloids generated from degradation of the glass waste forms, (b) residue colloids generated from degradation of the CSNF waste forms, and (c) uranium mineral colloids generated from degradation of the SNF waste forms; (2) colloids produced from the steel components of the WPs; and (3) colloids present in natural seepage water entering the EBS.

1. Waste Form Degradation Colloids—(a) Glass Waste Form Colloids—Experimental work at Argonne National Laboratory has shown that quantities of colloids containing plutonium are generated from glass waste during the degradation process. These colloids are a mixture of clays, zeolites, and oxides but are predominantly clays. For further description of these colloids, see *Waste Form and In-Drift Colloids-Associated Radionuclide Concentrations: Abstraction and Summary* (SNL 2007 [DIRS 177423], Section 6.3.3). (b) Residue CSNF Waste Form Colloids—A layer of plutonium and zirconium-rich oxides forms at the reaction front of degrading CSNF waste forms, particles of which may become suspended (SNL 2007 [DIRS 177423], Section 6.3.4). (c) Uranium Mineral SNF Waste Form Colloids—Colloidal-sized particles of uranium minerals such as uranophane have been observed in solutions in contact with degrading CSNF. Degrading uranium metal DSNF has been shown to release colloid-sized particles of UO_2 (SNL 2007 [DIRS 177423], Sections 6.3.5 and 6.3.6).

2. Corrosion Product Colloids—The occurrence of iron oxyhydroxide colloids from the corrosion of the WP materials is included in the Waste Form and In-Drift Colloid Concentration Abstraction described in *Waste Form and In-Drift Colloids-Associated Radionuclide Concentrations: Abstraction and Summary* (SNL 2007 [DIRS 177423], Section 6.3.8). Iron oxyhydroxides derived from the corrosion of steel components in the

repository will occur in two forms: (1) large-sized corrosion products consisting of immobile materials and large particles; and (2) colloid-sized particles that could potentially transport sorbed radionuclides.

3. Seepage Water Colloids—Colloid concentrations in SZ groundwater were used in the Waste Form and In-Drift Colloid Concentration Abstraction to estimate the colloid concentrations in seepage water that could enter a failed WP. There is a wide range in natural groundwater colloid concentrations in the Yucca Mountain vicinity over a relatively narrow range of groundwater ionic strength. The Yucca Mountain colloid concentration data were collected from nine different sources.

Colloid Stability—The stability of a colloidal suspension is controlled by electrostatic and chemical processes at colloid surfaces and by the attractive and repulsive forces between colloids. The attractive force is inversely proportional to both the distance between the colloids and colloid size. That is, the closer the colloids are to each other and the smaller they are, the higher the strength of the attractive force, and the more likely the colloid suspensions are to become unstable and coagulate. Higher ionic strength and higher temperature lead to weaker repulsive forces between colloids, causing colloidal suspensions to become unstable and the colloids to coagulate.

Another factor in colloid stability is pH. Colloids become unstable and flocculate near a pH value (zero point of charge) that is characteristic for a particular colloid mineralogy because of reduced repulsive forces between the colloids. The result is an ionic strength threshold that is dependent on pH, above which, the colloid suspensions are unstable. Examples of the pH dependent ionic strength thresholds are shown on Figure 6.3.7-11 for the idealized minerals that represent the colloid types: montmorillonite for glass degradation and local groundwater clay colloids, ZrO_2 for CSNF degradation colloids with irreversibly attached radionuclides, meta-autunite ($Ca(UO_2)_2(PO_4)_2 \cdot 6\text{-}8H_2O$) for SNF degradation colloids with reversibly attached radionuclides, and hematite (Fe_2O_3) for steel degradation colloids (SNL 2007 [DIRS 177423], Section 6.3).

Radionuclide Attachment—Radionuclides may be attached to colloids in many ways. In some cases the attachment and detachment is relatively fast compared to the residence time (in a given transport domain) and can be described as an equilibrium sorption process and modeled via a K_d value. In other cases attachment may be fast but detachment very slow relative to the residence time (in a given transport domain), as in co-precipitation where the radionuclide becomes embedded in the host colloid. This type of attachment is more complex to model and is referred to here as irreversible sorption and modeled via kinetic attachment. Sorption of radionuclides on various types of colloids is approximated as follows:

1. Waste form degradation colloids

    a. HLW glass degradation colloids – reversible and irreversible
    b. CSNF degradation rind colloids – irreversible
    c. SNF uranium mineral colloids – reversible

2. Iron oxyhydroxide colloids – reversible and irreversible

3. Groundwater colloids – reversible.

Nine elements are modeled as reversibly sorbed to waste form and groundwater colloids using a linear isotherm model (K_d): plutonium, americium, cesium, protactinium, thorium, tin, radium, uranium, and neptunium. This list represents the isotopes most likely to exhibit dose-significant colloidal transport (SNL 2007 [DIRS 177423], Section 6.3.12.1). Only plutonium and americium are modeled as irreversibly attached to colloids.

A mechanistic, surface complexation-based competitive sorption model, is developed for sorption of actinides on the steel degradation products that account for the uncertainty in the available sorption sites and for competition among various aqueous complexes for the finite number of sorption sites under a given P_{CO_2} (SNL 2007 [DIRS 177407], Section 6.3.4.2.3 and Section 6.5.2.4). This model is applied for sorption onto both the stationary corrosion products and to the iron oxyhydroxide colloids derived from degradation of steel. Competition among six elements was considered: plutonium, americium, thorium, uranium, neptunium, and nickel. Sorption of thorium, uranium, and neptunium on the iron oxyhydroxide colloids is modeled as reversible (equilibrium) sorption, by computing an effective K_d (based on surface complexation modeling results) while the sorption of plutonium and americium on iron oxyhydroxide colloids is modeled as an irreversible sorption process, by kinetic attachment (with no detachment). Nickel transport is not considered in the TSPA Model however, the effect of nickel is accounted for, in the competitive sorption model.

6.3.7.6.2 TSPA-LA Model Abstraction

The TSPA-LA EBS Colloids Submodel addresses the formation and stability of three types of colloids in the waste forms and WPs and calculates colloid concentrations and reversible sorption of nine radionuclides to colloids. The EBS Colloids Submodel also calculates irreversible attachment of plutonium and americium to HLW and CSNF waste form colloids and iron oxyhydroxide colloids. These features are summarized in Section 6.3.7.6.1 and described in detail in *Waste Form and In-Drift Colloids-Associated Radionuclide Concentrations: Abstraction and Summary* (SNL 2007 [DIRS 177423]).

This section describes the abstraction of these processes for use in the TSPA-LA Model.

Colloid Stability—The following equations and pH bounds describe quantitatively the schematic ionic strength threshold model results on Figure 6.3.7-11. The pH bounds and equation coefficients are provided in Tables 6.3.7-62 through 6.3.7-66.

Groundwater and Glass Degradation Colloids:

$$I_{threshold} = (-0.008 \times pH^2) + (0.12 \times pH) - 0.03 \qquad \text{(Eq. 6.3.7-14)}$$

If $pH_{wp,inv}$ is greater than 9, then the $I_{threshold}$ value calculated at pH 9 is used, and if $pH_{wp,inv}$ is less than 1.5, then colloids are assumed to be unstable (DTN: MO0701PAGROUND.000_R0 [DIRS 179310]).

CSNF Residue (ZrO_2) Colloids:

Between pH 7 and 9.3, the irreversible CSNF colloids are unstable irrespective of the ionic strength.

When the pH is between 4 and 7, the following relationship is used:

$$I_{threshold} = (0.0089 \times pH^3) - (0.1466 \times pH^2) + (0.7462 \times pH) - 1.092 \quad \text{(Eq. 6.3.7-15)}$$

When the pH is greater than 9.3, equation 2-7b is used:

$$I_{threshold} = (0.087362 \times pH^3) - (2.4078 \times pH^2) + (22.126 \times pH) - 67.791 \quad \text{(Eq. 6.3.7-16)}$$

If the pH is less than 4.0, the $I_{threshold}$ value that was calculated at pH 4.0 is used, and if the pH is greater than 10.6, the $I_{threshold}$ value calculated at pH 10.6 is used. (DTN: MO0701PACSNFCP.000_R1 [DIRS 180439]).

SNF Uranium Mineral Colloids:

$$I_{threshold} = -(0.008 \times pH^2) + (0.14 \times pH) - 0.4 \quad \text{(Eq. 6.3.7-17)}$$

If the pH is less than 4.0, the $I_{threshold} = 0$; if the pH is greater than 9, the $I_{threshold}$ value calculated at pH 9 is used (DTN: MO0701PACSNFCP.000_R1 [DIRS 180439]).

Steel Degradation Colloids:

When the pH is between 4.5 and 8.4, the following relationship is used:

$$I_{threshold} = -0.013 \times pH + 0.11 \quad \text{(Eq. 6.3.7-18)}$$

In contrast, when the pH is between 9.4 and 10.4, the following equation is used:

$$I_{threshold} = (0.0017 \times pH^2) - (0.0327 \times pH) + 0.158 \quad \text{(Eq. 6.3.7-19)}$$

If the pH is less than 4.5, the $I_{threshold}$ value calculated at pH 4.5 is used; and if the pH is greater than 10.4, the $I_{threshold}$ value calculated at pH 10.4 is used (DTN: MO0701PAIRONCO.000 _R1 [DIRS 180440]).

Sorption Capacity—Reversible sorption on waste form and groundwater colloids is modeled by adjusting the sampled K_d value such that the sorption capacity of the colloids is not exceeded (SNL 2007 [DIRS 177423], Section 6.3.12.3). In this approach, the available sorption sites are first partitioned linearly amongst the radionuclides based on their sampled K_d values and their concentrations in solution. From this the theoretical maximum K_d value of the radionuclide is calculated (under given concentrations) and compared to the sampled value. The lower of the two values is then taken. This model is necessarily a recursive model as implemented in GoldSim; i.e., there will be a one timestep delay, as shown below, in the sorption capacity calculation.

By partitioning the total molar density of sorption sites, $\overline{c}_{\max_T}$, into an allowable molar density of sorption sites for each species, $\overline{c}^{n}_{\max_i}$, according to the following equation, the model assumes that all sites are available for reversible sorption:

$$\overline{c}^{n-1}_{\max_i} = \overline{c}_{\max_T} \left(\frac{\overline{K}_{d,i} \dfrac{c_i^{n-1}}{M_{W_i}}}{\sum_j \overline{K}_{d,j} \dfrac{c_j^{n-1}}{M_{W_j}}} \right) \qquad \text{(Eq. 6.3.7-20a)}$$

where:

$\overline{K}_{d,i}$ = sampled K_d for the ith species (different for each realization), [=] m^3 solution per kg smectite or uranophane colloids

$\overline{c}^{n}_{\max_i}$ = molar density of sites for the ith species at the $(n-1)$th timestep, [=] kg-moles sorbed of ith species per kg colloid mass

$\overline{c}_{\max_T}$ = molar density of sites, [=] kg-moles of sites per kg colloid mass

c_i^{n-1} = aqueous concentration of the ith species at the $(n-1)$th timestep, [=] kg ith species per m^3 solution

M_{W_i} = molecular weight of ith species, [=] kg of ith species per kg-mole.

Next, each side of Equation 6.3.7-20a is divided by $\dfrac{c_i^{n-1}}{M_{w_i}}$:

$$\frac{\overline{c}^{n-1}_{\max_i}}{c_i^{n-1} / M_{W_i}} = \overline{c}_{\max_T} \left(\frac{\overline{K}_{d,i}}{\sum_j \overline{K}_{d,j} \dfrac{c_j^{n-1}}{M_{W_j}}} \right) \qquad \text{(Eq. 6.3.7-20b)}$$

The left-hand side of the equation is defined to be the maximum allowable partition coefficient, $K_{d,i}^{\max,n}$, for the *i*th species at the *n*th timestep:

$$K_{d,i}^{\max,n} \equiv \frac{\overline{c}_{\max_i}^{n-1}}{c_i^{n-1}/M_{W_i}} = \overline{c}_{\max_T} \left(\frac{\overline{K}_{d,i}}{\sum_j \overline{K}_{d,j} \frac{c_j^{n-1}}{M_{W_j}}} \right) \quad \text{(Eq. 6.3.7-20c)}$$

At the *n*th timestep, the partition coefficient, $K_{d,i}^{n}$, that is used for the *i*th species is given by the following (i.e., it is the minimum of the competitive K_d computed in Equation 6.3.7-20c and the sampled K_d):

$$K_{d,i}^{n} = \min\left(\overline{K}_{d,i}, K_{d,i}^{\max,n}\right) \quad \text{(Eq. 6.3.7-20d)}$$

This sorption capacity model is not needed for sorption calculations on the iron oxyhydroxide colloids, as a mechanistic competitive sorption model has been developed, where the effective K_d is calculated from multiple regression model that accounts for the sorption sites and competition among various elements for the finite number of sorption sites (SNL 2007 [DIRS 177407], Section 6.5.2.4).

Irreversible sorption is modeled for plutonium and americium on iron oxyhydroxide, HLW, and CSNF colloids. This is achieved through the kinetic process by applying only a forward rate constant and zero backward rate constant. The forward rate constant for iron oxyhydroxide colloids is based on experimental values while that for the HLW glass and CSNF colloids is based on matching the predicted concentration of plutonium and americium associated irreversibly with colloids in solution.

6.3.7.6.3 TSPA-LA Model Implementation

All the elements of the EBS Colloids Submodel described in Sections 6.3.7.6.1 and 6.3.7.6.2 are combined in the TSPA-LA Model. The TSPA-LA Model takes the fluid characteristics, pH, and ionic strength and the concentrations of dissolved radionuclides and calculates the mass concentrations of each colloid type.

Reversible sorption of nine elements (plutonium, americium, cesium, protactinium, thorium, tin, radium, uranium, and neptunium) is considered on all colloids, except iron oxyhydroxide colloids, by sampling from an empirically derived K_d range. The sorption capacity is checked at each timestep, and if it is exceeded, the K_d values are adjusted downwards. Irreversible sorption of plutonium and americium is also modeled on HLW glass and CSNF colloids as an 'embedded' mass that is not in equilibrium with the solution. For iron oxyhydroxide colloids, the sorption calculations are based on a mechanistic surface complexation-based competitive sorption model: sorption of thorium, uranium, and neptunium is modeled as reversible by computing an effective K_d while the sorption of plutonium and americium on iron oxyhydroxide

colloids is modeled as an irreversible sorption process by kinetic attachment (with no detachment).

The plutonium concentration associated irreversibly with the HLW glass and CSNF colloids, is sampled from a range first (see range for CPu_Col_WF_Embed_Sampled_a and CPu_Col_CSNF_Sampled_a in Tables 6.3.7-62 and 6.3.7-63) and then based on the ionic strength and pH. The stability of the colloid suspension is determined from the stability field (Figure 6.3.7-11). If found stable then the sampled value is chosen, else the minimum value (CPu_Col_Glass_Embed_Min and CPu_Col_CSNF_Min) is selected. In addition, the concentration range of plutonium associated with a unit colloid concentration is also sampled (see range for CPu_Per_WF_Embed_Col_a and CPu_Per_CSNF_Embed_Col_a in Tables 6.3.7-62 and 6.3.7-63). The ratio of these two values provides the colloid concentration. Based on the mass flux of these colloids (mass of colloids transported in a given timestep), the plutonium mass irreversibly associated with the HLW glass and CSNF colloids is implemented by applying a linear rate constant through solving the mass balance equation (SNL 2007 [DIRS 177407], Section 6.5.2.5) . Similar calculation is performed for americium.

Figure 6.3.7-12 provides an overview of the implementation of the EBS Colloids Submodel in the TSPA-LA Model for the WP environment. All uncertain parameters are sampled once for each realization. At each timestep and for each representative WP in each percolation subregion environment in the TSPA-LA Model calculations, the EBS Colloids Submodel uses in-package ionic strength, pH, and dissolved radionuclide concentrations to calculate the formation and stability of colloids and the attachment of radionuclides to stationary corrosion products and to the waste form, iron oxyhydroxide, and seepage water colloids.

The colloid and radionuclide concentration values in the WPs, along with the ionic strength and pH of the solution and dissolved radionuclide concentrations in the solution, serve as source terms for the invert. The EBS Chemical Environment Submodel (Section 6.3.4) calculates the ionic strength and pH of the invert water. Based on the values of ionic strength and pH in the invert, the EBS Colloids Submodel determines colloid stabilities and concentrations for the invert conditions. For all colloid types, the colloid concentration is set to the minimum value when the invert colloid suspensions are unstable. But when the colloid suspensions are stable, the colloid concentrations are calculated differently for the colloid types. For groundwater colloids the sampled value is used, because groundwater colloids may enter the invert directly without going through the WP. For steel degradation colloids and reversible SNF mineral colloids, the concentration of colloids from the upstream corrosion products domain is used because that domain is the source for these colloids in the invert. (Note the steel in the invert is ignored.) For irreversible glass and CSNF residue waste form colloids, the colloid concentration is calculated within GoldSim by the transport of the species "Col" from the waste form domain. The EBS Colloids Submodel redistributes the reversibly sorbed radionuclides and dissolved radionuclides based on the distribution coefficients and the total mass of each type of colloid. For the steel degradation colloids, the distribution coefficients calculated in the corrosion products domain using the competitive sorption model are used in the invert. These colloids and associated radionuclides are then subject to transport through the invert and into the UZ.

The stability of colloids is calculated using the values of ionic strength and pH, with separate relationships for each colloid type. At each timestep and for each representative WP in each

percolation subregion environment, the values of ionic strength and pH of the solutions in the WPs are used as input to determine colloid stability. For all types of colloids, a low, nonzero colloid concentration limit is used under unstable conditions.

6.3.7.7 Model Component Consistency and Conservatism in Assumptions and Parameters

To enhance understanding of the complex interactions within the TSPA-LA Model, a discussion of consistency among model components and submodels and identification of conservative assumptions in abstractions, process models, and parameter sets supporting the Waste Form Degradation and Mobilization Submodel are discussed below.

6.3.7.7.1 Consistency of Assumptions

Waste Form Temperature versus WP Surface Temperature—In the absence of waste form temperatures, the TSPA-LA Model treats waste form temperature as if it were the same as the WP surface temperature. It is expected that waste form temperatures would be higher than WP surface temperatures, and the effect of hotter temperatures is not included in the waste form submodels.

Effect on TSPA—The submodels of the TSPA-LA Model that are directly dependent on the waste form temperature are the In-Package Chemistry Submodel for CSNF WPs (Section 6.3.7.2), the CSNF Waste Form Degradation Rate Submodel (Section 6.3.7.4.1), the HLW Glass Degradation Submodel (Section 6.3.7.4.3), and the EBS Transport Submodel (Section 6.3.8). The influences are discussed below. Both the CSNF Waste Form Degradation Submodel (Section 6.3.7.4.1) and HLW Glass Degradation Submodel (Section 6.3.7.4.3) are direct functions of temperature, with the rate increasing as temperatures increase. The temperature dependence for the In-Package Chemistry Submodel (Section 6.3.7.2) is in the total carbonate abstraction, which only impacts the CSNF Waste Form Degradation Submodel (Section 6.3.7.4.1) calculations. The temperature dependence in the EBS Transport Submodel (Section 6.3.8) pertains to the presence of water inside the waste form. At temperatures greater than 100°C, the TSPA-LA Model assumes that water in the WP evaporates and the system is dry and does not support radionuclide transport.

For all waste forms, the transport of the radionuclides released by any failure mechanism is driven by the amount of water available to entrain and transport the radionuclides past the WP boundary. In the TSPA-LA Model, water will not accumulate in the WP if the temperature is greater than 100°C. Because the waste form temperature is greater than the WP surface temperature, any transport calculations using the lower WP surface temperature would be conservative because water would be accumulating at higher temperatures than physically possible in the waste form.

In-Package Chemistry and the Instantaneous Degradation of CSNF—The In-Package Chemistry Abstraction (SNL 2007 [DIRS 180506]) does not consider the instantaneous degradation of CSNF in the process model and subsequent abstraction. However, within the TSPA-LA Model, the chemistry inside the failed CSNF WP following the instantaneous degradation of the CSNF is determined using the abstractions developed in *In-Package Chemistry Abstraction* (SNL 2007 [DIRS 180506]). Instantaneous degradation of the CSNF

occurs in the Waste Package EF Modeling Case, the Igneous Intrusion Modeling Case, and the Seismic GM and Seismic FD Modeling Cases when CSNF WPs are damaged and the CSNF is exposed to temperatures exceeding 100°C.

Effect on the TSPA—The instantaneous degradation of the CSNF waste form is the recommended waste form treatment when the waste form in a failed CSNF WP is exposed to temperatures exceeding 100°C (Section 6.3.7.4.1.3). The in-package chemistry process models presented in the In-Package Chemistry Abstraction (SNL 2007 [DIRS 180506]) considered very fast degradation rates but did not consider the instantaneous degradation of the CSNF.

Because the in-package pH conditions are controlled by the buffering capacity of the degradation products of CSNF (SNL 2007 [DIRS 180506], Section 6.3.4.1[a]), the instantaneous degradation of CSNF means that the maximum pH buffering capacity will be achieved after the CSNF experiences instantaneous degradation. Thus, the pH conditions within CSNF WPs after instantaneous degradation of CSNF will be well constrained.

Therefore, it is concluded that following the instantaneous degradation of CSNF inside a failed WP, the implemented pH abstraction is sufficient to cover this condition, although the consequence had not explicitly been included in the abstraction process.

The ionic strength abstraction for CSNF WPs under vapor influx conditions is based on Pitzer model calculations for simple salt solutions (SNL 2007 [DIRS 180506], Section 6.10.2.2[a]). Since the Pitzer model calculations are independent of the CSNF degradation rate, assuming instantaneous CSNF degradation would not impact the ionic strength abstraction for CSNF WPs under vapor influx conditions.

A sensitivity analysis has been conducted to evaluate the impact of degradation rates on ionic strength for CSNF WPs under liquid influx conditions (SNL 2007 [DIRS 180506], Section 6.6.5[a]). It reveals that although the CSNF degradation rate does impact the calculated ionic strength in the CSNF simulations, the variation is generally less pronounced than that in the 2DHLW and 2MCO simulations. The variation due to uncertainty in the degradation rates of CSNF and other WP materials has been incorporated in the ionic strength abstraction for CSNF WPs under liquid influx conditions. Moreover, additional uncertainty has been introduced into the ionic strength abstraction by extrapolations (SNL 2007 [DIRS 180506], Section 8.2.2[a]). Thus, the impact of instantaneous degradation of CSNF on the ionic strength for CSNF WPs under liquid influx conditions is captured in the abstraction.

Therefore, it is concluded that following the instantaneous degradation of CSNF inside a failed WP, the implemented ionic strength abstractions for vapor influx and liquid influx modes are sufficient to cover this condition, although the consequence had not explicitly been included in the abstraction process.

Representation of Co-Disposed Fuel—The most numerous CDSP WP in the design for the repository is the 5DHLW/1DSNF Long configuration (Tables 6.3.7-1 and 7.5-3). This WP contains five HLW glass canisters identical to the glass canisters in the 2MCO/2DHLW WP. Although this 5DHLW/1DSNF long WP is the most numerous of the CDSP WPs the total mass of uranium in all of the 2MCO/2DHLW WPs exceeds the total uranium mass in all of the

5DHLW/1DSNF long WPs (Table 7.5-1). That is the reason the In-Package Chemistry Model simulates the 2MCO/2DHLW WP. However, for radionuclide transport calculations (e.g., for mass of degradation products), the TSPA-LA Model simulates the 5DHLW/1DSNF long WP containing Three Mile Island SNF canisters (SNL 2007 [DIRS 177407], Section 6.3.4.6). The major differences between this WP and the 2MCO/2DHLW WP are: (1) the HLW glass waste form domain in the TSPA-LA EBS Transport Submodel contains five HLW glass canisters instead of two, and (2) the DSNF waste-form domain contains UO_2 instead of uranium metal.

Effect on the TSPA-LA Model—The parameters that could potentially be impacted by this difference between the EBS Transport Submodel and the In-Package Chemistry Submodel are pH, ionic strength, and fluoride. The main difference in the conceptual models for the HLW glass waste-form domain would be the total volumes of materials and water, which would be 2.5 times larger in the EBS Transport Submodel (5 canisters instead of 2). This is important only with respect to the turnover rate, which affects ionic strength. For a given liquid influx rate, the turnover rate would be 40 percent (2/5) of the turnover rate of the 2MCO/2DHLW WP. A lower turnover rate increases the effects of degradation rates, which in turn affect ionic strength. However, a reduction of 60 percent in the turnover rate is well within the order-of-magnitude uncertainty of the ionic strength abstraction (SNL 2007 [DIRS 180506], Section 6.10.8.2[a]). The fluoride abstraction, which is only a function of ionic strength (SNL 2007 [DIRS 180506], Section 6.10.3[a]), is therefore, also negligibly affected. The pH abstraction is not affected at all because it is not a function of turnover rate.

In the DSNF waste form domain, the Three Mile Island fuel will quickly degrade to schoepite in the presence of water, similarly to the behavior of both N-Reactor fuel and CSNF. Schoepite will be the dominant alkalinity buffer in the DSNF waste form cell in the EBS Transport Submodel for either co-disposal configuration, 2MCO/2DHLW, or 5DHLW/1 Three Mile Island long. Equilibrium dissolution of schoepite prevents pH from rising much above seven at high carbon dioxide fugacity and much above nine at low carbon dioxide fugacity (SNL 2007 [DIRS 180506], Sections 6.3.4[a] and 6.10.1[a]). On the acid side, degradation of the stainless steel structural materials, which are present regardless of the SNF type, produces oxides that define the pH minimum. Thus, the pH abstractions for N-Reactor fuel (2MCO) can be used for Three Mile Island fuel in the DSNF waste-form domain. Ionic strength and fluoride abstractions of the 5DHLW/1 Three Mile Island long WP can also be approximated by the 2MCO abstractions in the DSNF waste-form domain because the degradation products are similar and because other potential effects are small compared to the order of magnitude uncertainty of the ionic strength abstraction.

Other important DSNF fuel types are mixed-oxide, carbide, and aluminum-based fuels (Table 7.5-3). The justification for using the 2MCO fuel chemistry (pH, ionic strength, and fluoride) to represent them is contained in *In-Package Chemistry Abstraction* (SNL 2007) [DIRS 180506], Section 6.6.6[a].

6.3.7.7.2 Identification of Conservatisms in Submodels and Abstractions

Secondary Phases of Uranium—The TSPA-LA Model does not consider the incorporation of any elements into secondary phases of uranium. Neptunium would likely be incorporated into secondary phases; however, additional quantitative information required to develop a reliable predictive numerical model is not currently available. Using a neptunium-bearing uranyl

compound instead of a pure neptunium phase as the solubility-controlling solid would lead to lower solubilities. The details of this conservatism are discussed in *Dissolved Concentration Limits of Elements with Radioactive Isotopes* (SNL 2007 [DIRS 177418], Section 6.6.4).

Controlling Solid for Radium—Pure $RaSO_4$ is used as the controlling solid for radium instead of solid solutions. Field studies have shown that radium concentrations in some natural waters are orders of magnitude below levels corresponding to $RaSO_4$ saturation. Radium concentrations likely correspond to the solubilities of radium in solid solutions in more common sulfate solids such as $SrSO_4$ or $BaSO_4$ (SNL 2007 [DIRS 177418], Section 6.12). This results in the overestimation of aqueous radium concentrations.

Solubility versus Temperature—The solubility of radioactive elements at 25°C is used for all temperatures. Actinide solubility values tend to decrease with increasing temperature; however, this conservatism simplifies the model approach (SNL 2007 [DIRS 177418], Sections 6.3.3.3 and 6.4.2.2). This conservatism may result in the overestimation of aqueous radioactive element concentrations.

CSNF Radionuclide Release Rate—In developing the models for the rate of fractional radionuclide release from the CSNF matrix, it is assumed that the fractional degradation rate of the CSNF matrix conservatively bounds the rate of the fractional release of radionuclides located in the fuel matrix. The fission product and actinide elements embedded in the fuel matrix are made available for mobilization and behave (dissolve) as individual elements as the fuel matrix degrades. The fission-product technetium is known to be partly in the form of noble five-metal alloy particles. The properties of the five-metal alloy particles are likely to control the technetium release rate at a level much lower than the CSNF matrix degradation rate. Assuming that technetium release from the CSNF matrix is limited only by the matrix degradation rate, is therefore conservative, as demonstrated in *CSNF Waste Form Degradation* (BSC 2004 [DIRS 169987], Section 5.1).

Specific Surface Area of Corroding CSNF—In assessing the effective specific surface area of corroding CSNF in fuel rods following breaching of the cladding, it is conservatively assumed that the configuration of the fuel is represented by fuel pellet fragments and short fuel rod segments. There is insufficient information to discriminate between the scenarios proposed for the progression of the degradation of fuel rods after the cladding is breached. Thus, the conservative assumption is made that the degradation progresses rapidly, leaving the fuel in the form of fuel pellet fragments or short rod segments (BSC 2004 [DIRS 169987], Sections 5.2 and 6.2.2.1). This is a conservative assumption imposed by the cited source.

All CSNF Cladding Failed at Arrival—The TSPA-LA compliance model assumes all CSNF cladding failed at arrival. The impact of this conservatism is evaluated in the PMA (Appendix C).

Failed Cladding—After cladding failure, no credit is taken for the failed cladding limiting the amount of water or moist air that can contact the fuel pellets. The failed cladding still limits the interaction of the fuel pellets and the environment; however, no credit is taken for this in the TSPA-LA Model. In the TSPA-LA Model, after cladding failure, the fuel pellets corrode as if they were bare fuel pellets (SNL 2007 [DIRS 180616], Section 6.1.4). Credit is taken for the

reduction in the release rate of the radionuclides through the failed cladding. The diffusion of radionuclides across the split opening is modeled in *Cladding Degradation Summary for LA* (SNL 2007 [DIRS 180616], Section 6.2.4).

DSNF Cladding—No credit is taken for DSNF cladding. This simplified modeling approach is used because there is no technical basis for giving credit for DSNF cladding, and the recommended DSNF release model is an upper limit model invoking the complete release of DSNF upon exposure to groundwater (BSC 2004 [DIRS 172453], Section 8.1). Furthermore, a significant fraction of the Uranium Metal SNF (DSNF Group 7), the representative DSNF used in the TSPA-LA Model, is visibly damaged and much of the rest could have small pinholes/cracks in the cladding (BSC 2004 [DIRS 172453], Sections 6.1.7 and 6.1.12).

Note that this conservatism is not applied to naval SNF. Unlike some DSNF, naval SNF is completely characterized, and the degradation of naval SNF was modeled using the same environmental conditions used for the degradation of CSNF.

Degradation Of Metallic Uranium N-Reactor Fuel—A constant degradation rate is used that conservatively bounds degradation of metallic uranium present in N-Reactor fuel; upon WP breach, degradation of DSNF occurs in one timestep of TSPA. Little quality assurance data exists on DSNF fuel, so a conservative approach is used to bound uncertainty in the characteristics of the DSNF fuel (BSC 2004 [DIRS 172453], Section 8.1).

HLW Inventory—The number of canisters of HLW glass is overestimated by about 67 percent because of the assumption to emplace full CDSP WPs in the repository (SNL 2007 [DIRS 180472], Assumption 5.10[a]). The calculation for the number of CDSP WPs (DTN: MO0702PASTREAM.001_R0 [DIRS 179925], Non-commercial, Item 4) indicates that the DSNF waste fills 3,279 WPs with one canister of DSNF per package. However, emplacing HLW canisters in all of the available slots in these packages requires approximately 67 percent more HLW canisters than are actually predicted to be sent to the repository given the HLW allocation of two-thirds of 10 percent of 70,000 metric tons of heavy metal (SNL 2007 [DIRS 180472], Assumption 5.10[a]). This conservatism adds additional HLW glass waste to the inventory in the repository but does not add additional WPs to the repository.

Total Number of Waste Packages—The number of CSNF and CDSP WPs is overestimated by about four percent because TSPA assumes that all of the 108 drifts (including contingency drifts) in the repository design will be filled with WPs (SNL 2007 [DIRS 180472], Assumption 5.14[a]). This additional four percent of both types of WPs is in addition to the 67 percent extra HLW previously discussed. Filling all the drifts with WPs, results in the 'qualification' of all 108 drifts for emplacement, but increases the total metric tons of heavy metal in the footprint to 76,223 (including the extra HLW discussed above). The inclusion of more than 70,000 metric tons of heavy metal in the TSPA-LA Model is conservative for dose (SNL 2007 [DIRS 180472], Assumption 5.14[a]).

Degradation of CSNF Waste Greater Than 100°C—If the breached CSNF WP temperature exceeds 100°C, CSNF will undergo 'dry air oxidation' (BSC 2004 [DIRS 169987], Section 6.2.2.2). The major effect of dry air oxidation is the very large increase in the specific area of CSNF. As a result, the fractional dissolution rate increases accordingly. Therefore, it is

assumed that the degradation of the CSNF waste form would be instantaneous (BSC 2004 [DIRS 169987], Section 8.1). This treatment is conservative when considering that the estimation for the increase in specific surface area of CSNF undergoing dry air oxidation has a large uncertainty.

6.3.7.8 Alternative Conceptual Model(s) for Waste Form Degradation and Mobilization

Section 6.2 outlines the general consideration and treatment of ACMs used to support the TSPA-LA Model. A brief description of the Waste Form Degradation and Mobilization Submodel ACMs that are summarized in Tables 6.3.7-67 through 6.3.7-71 are presented below.

In-Package Chemistry ACMs—Three ACMs were considered as alternatives to the In-Package Chemistry Abstraction (BSC 2007 [DIRS 180506], Section 6.4). The first ACM was a one-dimensional column composed of *n* cells, where the reactants in each cell represent the WP components in a vertical cross section of a WP (BSC 2007 [DIRS 180506], Section 6.4.1). This model would eliminate the constraint of the solid-centered flow through mode of a well-mixed batch reactor used in the EQ6 (*Software Code: EQ6.* 7.2bLV (BSC 2002 [DIRS 159731]) calculations in the In-Package Chemistry Abstraction and provide a water stream with a variable composition along its flow path. This ACM was excluded from the In-Package Chemistry Abstraction on the basis that, in comparisons between the vapor influx model and the spatially heterogeneous model, the vapor influx model is much simpler and yielded comparable results (BSC 2007 [DIRS 180506], Section 6.4.1). Inclusion of this ACM in the TSPA-LA Model would not likely have an effect on dose because the implemented abstraction yields comparable results.

The second ACM considered variable-composition seepage entering a failed WP as a function of time, changing with time-varying changes in the physical and chemical environment in the drifts and the EBS (BSC 2007 [DIRS 180506], Section 6.4.2). Section 6.5.2 of *In-Package Chemistry Abstraction* (BSC 2007 [DIRS 180506]) demonstrates that the EQ6 STN: 10075–7.2bLV-02 (BSC 2002 [DIRS 159731]) calculations were largely insensitive to initial seepage water compositions because the WP materials have a stronger influence on the resulting chemistry. Inclusion of this ACM in the TSPA-LA Model would not likely have an effect because the implemented abstraction yields comparable results.

A third ACM considers the alternate methodologies for determining the vapor flux rate through the stress corrosion cracks in a failed WP (BSC 2007 [DIRS 180506], Section 6.4.3). In this ACM, Fick's Law and Stefan Tube Diffusion Calculations are used to develop a relationship between the vapor flux rate through SCC and relative humidity. Calculated results demonstrate that the abstracted relationship presented for the TSPA-LA Model is appropriate, and no change to dose is expected if this ACM were included in the TSPA-LA Model.

The first two ACMs and the associated screening arguments for in-package chemistry are summarized in Table 6.3.7-67. The third ACM was excluded because the abstracted relationship for the vapor flux rate into a stress corrosion cracked-failed WP provided for the TSPA-LA Model is simpler and spans the expected range by this ACM.

CSNF Waste Form Degradation ACMs—Two ACMs for CSNF waste form degradation were considered in the abstraction to TSPA: (1) an electrochemical model based on modeling the rates of redox reactions involved in fuel oxidation and dissolution and (2) a surface complexation model based on a three-step bicarbonate-promoted oxidative dissolution mechanism (BSC 2004 [DIRS 169987], Section 6.4.2).

Using estimates for the unknown parameters in the developed ACMs, an analysis was performed comparing the base-case abstraction with the ACMs. The degradation rates from the electrochemical model were three times greater than the base-case model implemented in the TSPA-LA Model (BSC 2004 [DIRS 169987], Section 7.2). However, it was later concluded that this model was overly conservative because it does not consider slower surface complexation, dissolution, and/or mass transfer limitations. Inclusion of this ACM in the TSPA-LA Model would only have an impact on the TSPA-LA Model dose in the Seismic Scenario when WP failures occur after the WP temperature is less than 100°C. In the Waste Package EF and Igneous Intrusion Modeling Cases, the WP temperature exceeds 100°C after the WP is failed and instantly degrades the CSNF waste form. Using estimates for the unknown parameters, the surface complexation ACM analysis yielded a CSNF degradation rate that was 40 percent lower than the base-case model implemented in the TSPA-LA Model. In the TSPA-LA Model, the inclusion of this ACM would only have a dose impact in the Seismic Scenario when WP failures occur after the WP temperature is less than 100°C. The expected result is a slower degradation rate for the CSNF. Both of these ACMs were screened out of the CSNF Waste Form Degradation Abstraction, and the basis for this assessment is summarized in Table 6.3.7-68.

DSNF Waste Form Degradation ACM—An ACM for DSNF waste form degradation was based on the best-estimates dissolution models presented in *DSNF and Other Waste Form Degradation Abstraction* (BSC 2004 [DIRS 172453], Section 6.3). The application of this ACM would require that the dissolution rate expression be multiplied by the 'actual' effective surface area of the SNF. This ACM was screened out of the DSNF Waste Form Degradation Submodel (Section 6.3.7.4.2) because insufficient qualified data on the corrosion rates and the surface areas of the fuel in each group are available. In addition, the upper-limit degradation model that is implemented as a surrogate for all the DSNF, other than naval SNF, is a bounding model with respect to the degradation rate.

HLW Glass Degradation ACM—The HLW Glass Degradation Abstraction (BSC 2004 [DIRS 169988], Section 6.4), screened ACMs to simplify the base-case mechanistic model for HLW glass degradation to a form that could be used in the TSPA-LA Model (Table 6.3.7-69). The screening eliminated parts of the mechanistic model that were deemed unnecessary for describing HLW glass degradation over the range of anticipated physical and chemical conditions in the repository. Most nuclear waste HLW glass degradation models were developed to predict a changing dissolution rate over long times. In contrast, the HLW Glass Degradation Abstraction was developed to provide a constant HLW glass degradation rate under a specific set of exposure conditions that could change for every realization in the simulation because time is not a parameter in the HLW Glass Degradation Abstraction. Instead, the exposure conditions, consisting of the amount of water contacting the HLW glass, the solution pH, and the waste form and in-package temperature, change with time.

ACMs for HLW glass degradation under near-saturation conditions are based on: (1) solid-state diffusion-controlled release; and (2) the composition-independent effective rate constant, which was screened out of the HLW Glass Degradation Abstraction for the TSPA-LA Model analysis. The first ACM was screened out as being unconvincing. Using estimates for unknown fitting parameters, a negligible impact on the calculated rates using this ACM was observed (BSC 2004 [DIRS 169988], Section 6.4.1).

The second ACM considered the effects of different compositions on the intrinsic dissolution rate and affinity term, which in the base-case model implemented in the TSPA-LA Model, have been combined into a single effective rate constant. An analysis of available literature data reveals that combining the two terms into one effective parameter has little effect on the overall reaction rate and that the base-case implementation is more robust for use in the TSPA-LA Model.

The screening arguments are described in detail in *Defense HLW Glass Degradation Model* (BSC 2004 [DIRS 169988], Section 6.4) and are summarized in Table 6.3.7-69. In addition, the *Defense HLW Glass Degradation Model* (BSC 2004 [DIRS 169988], Section 7) indicates that the base-case HLW Glass Degradation Abstraction is validated for HLW borosilicate glass waste forms. Thus, the HLW Glass Degradation Abstraction is applicable to both commercial HLW and DOE-owned HLW glass waste forms.

Dissolved Concentration Limits ACMs—Several ACMs were considered in developing the submodels for the solubility limits of radioactive elements for the TSPA-LA Model (SNL 2007 [DIRS 177418]), and these are summarized in Table 6.3.7-70. Two ACMs are considered for plutonium solubility: (1) the Theoretical fO_2 Model; and (2) the Empirical Eh Model. In the Theoretical fO_2 Model, calculations are carried out with the solution redox condition controlled by theoretical equilibrium between the solution and the atmosphere (with fO_2 equal to 0.2 bars). This ACM is screened out because the results differ significantly from experimental measurements. The Empirical Eh Model uses an empirical (instead of theoretical) equation to set the redox conditions. This ACM is not used because the plutonium solubility results for this model are lower than the experimental values. For the remaining elements (neptunium, thorium, americium, and strontium), the ACMs involved the use of other solubility-controlling solids. These ACMs are screened out because either there is not enough thermodynamic data available to justify their use or a more soluble solid was chosen for conservatism (Table 6.3.7-70).

EBS Colloids ACMs—Three conceptual models were considered as alternatives to the current TSPA-LA EBS Colloids Submodel (SNL 2007 [DIRS 177423], Section 6.4). These ACMs are listed in Table 6.3.7-71, along with the principal bases and screening criteria. The first ACM considers two-site and three-site sorption kinetic models as an alternative to the assumption of irreversible sorption used in the base-case model. The kinetic model represents a useful tool for examining sorption data and examining the evidence for slow reversible sorption of plutonium on colloids. The model clearly demonstrates that the data from Lu et al. (2000 [DIRS 166315]) can be fit with reversible components. The kinetic model has not been adopted because it is immature and the base model is conservative and bounding. A second ACM considers the rate of colloid generation as a function of the waste form degradation rate. In this ACM, the rate of colloid spallation would depend upon the rate of waste degradation. The rate of HLW glass degradation may be defined by the rate of boron release to the alteration fluid, and likewise, the

rate of technetium release could be correlated to the degradation rate of CSNF. However, this ACM is currently not sufficiently developed for application to more generalized conditions. A third ACM considers colloid generation as primarily a function of the rate of advective water flow penetrating the degrading waste forms. This ACM addresses the possibility that colloids can form from both DSNF and CSNF, but their release from the waste weathering rind is governed by the energy of flowing water. The supporting concepts for this ACM were developed in the context of deposition and remobilization of existing colloids under conditions of significant groundwater flow. These conditions likely will not apply to conditions anticipated in the repository.

Table 6.3.7-1. Waste Package Configurations

Waste Package Type	Number of Waste Packages[a]	Spent Nuclear Fuel Unit	Max # of Units per Package	# of Glass Canisters per Package	Glass Unit	Shorthand
CSNF	4,586	PWR assembly	21	0	None	21P-TAD
CSNF	173	PWR assembly	12	0	None	12-Long-TAD
CSNF	3,037	BWR assembly	44	0	None	44B-TAD
CDSP WP	1,940	Short canister	1	5	Short	CDSP-Short
CDSP WP	1,257	Long canister	1	5	Long	CDSP-Long
CDSP WP	219	MCO	2	2	Long	CDSP-MCO
Naval	323	Canister	1	0	None	SNF-Long
Naval	94	Canister	1	0	None	SNF-Short
Total CDSP	3,416					
Total in CSNF+Naval	8,213					
Grand Total	11,629					

Sources: DTN: MO0702PASTREAM.001_R0 [DIRS 179925]; Item 6 of worksheet 'COMMERCIAL,' Item 4 of worksheet 'NON-COMMERCIAL' (waste package configuration), and rows 49 and 59 of worksheet 'UNIT CELL' (numbers of waste packages) *in spreadsheet DTN-Inventory-Rev00.xls*.

NOTE: MCO = multicanister overpack, TAD = transportation, aging, and disposal (canister).

[a] These numbers of WPs are 4% higher than would be necessary for 70,000 metric tons heavy metal waste. Assumption 14 in MO0702PASTREAM.001_R0 [DIRS 179925] indicates this is to completely fill all of the available drifts with waste. This assumption implies a total of 417 naval WPs instead of the originally specified 400.

Table 6.3.7-2. Radionuclides Included in TSPA-LA

Radionuclide	Screened-in for Groundwater Modeling Cases: Nominal, Human Intrusion, Igneous Intrusion, and Seismic	Volcanic Eruption Modeling Case
^{227}Ac	^{227}Ac	^{227}Ac
^{241}Am	^{241}Am	^{241}Am
^{243}Am	^{243}Am	^{243}Am
^{14}C	^{14}C	None
^{36}Cl	^{36}Cl	None
^{245}Cm	Added to ensure that the effect of its decay on the inventory of ^{241}Am are included	
^{135}Cs	^{135}Cs	None
^{137}Cs	^{137}Cs	^{137}Cs
^{129}I	^{129}I	^{129}I
^{237}Np	^{237}Np	^{237}Np
^{231}Pa	^{231}Pa	^{231}Pa
^{210}Pb	Assumed to be in secular equilibrium with ^{226}Ra. Not explicitly modeled, but dose effects included with ^{226}Ra.	
^{238}Pu	^{238}Pu	^{238}Pu
^{239}Pu	^{239}Pu	^{239}Pu
^{240}Pu	^{240}Pu	^{240}Pu
^{241}Pu	Added to ensure that the effect of its decay on the inventory of ^{241}Am and ^{237}Np are included	
^{242}Pu	^{242}Pu	^{242}Pu
^{226}Ra	^{226}Ra	^{226}Ra
^{228}Ra	^{228}Ra	^{228}Ra
^{79}Se	^{79}Se	None
^{126}Sn	^{126}Sn	^{126}Sn
^{90}Sr	^{90}Sr	^{90}Sr
^{99}Tc	^{99}Tc	^{99}Tc
^{229}Th	^{229}Th	^{229}Th
^{230}Th	^{230}Th	^{230}Th
^{232}Th	^{232}Th	^{232}Th
^{232}U	^{232}U	None
^{233}U	^{233}U	^{233}U
^{234}U	^{234}U	^{234}U
^{235}U	^{235}U	None
^{236}U	^{236}U	None
^{238}U	^{238}U	^{238}U
Count	29	22

Sources: Developed from Table 7-1 in *Radionuclide Screening* (SNL 2007 [DIRS 177424]) and DTN: MO0701RLTSCRNA.000_R0 [DIRS 179334].

NOTE: The count in the last row does not include ^{245}Cm, ^{210}Pb and ^{241}Pu.

Table 6.3.7-3. Nominal Grams of Radionuclides per Waste Package for Each Type of Waste

Year of Projection: CSNF = Year 2067, DSNF = Year 2030, and HLW = Year 2030 Total Number of Waste Packages is 11,629 (8,213 CSNF and 3,416 CDSP WP)			
	Grams per Waste Package		
Radionuclide	CSNF	DSNF	HLW
^{227}Ac	2.47E-06	1.22E-03	1.91E-04
^{241}Am	8.18E+03	2.18E+02	3.75E+01
^{243}Am	1.24E+03	6.73E+00	5.75E-01
^{14}C [a]	1.35E+00	1.81E+00	0.00E+00[b]
^{36}Cl	3.23E+00	4.23E+00	0.00E+00[b]
^{245}Cm	1.75E+01	9.25E-02	5.43E-02
^{135}Cs	4.36E+03	9.74E+01	1.27E+02
^{137}Cs	5.90E+03	9.72E+01	3.02E+02
^{129}I	1.73E+03	3.56E+01	7.27E+01
^{237}Np	4.57E+03	8.14E+01	9.95E+01
^{231}Pa	9.17E-03	2.14E+00	1.53E+00
^{238}Pu	1.52E+03	1.25E+01	3.91E+01
^{239}Pu	4.32E+04	2.21E+03	5.58E+02
^{240}Pu	2.05E+04	4.35E+02	4.61E+01
^{241}Pu	2.66E+03	2.92E+01	1.22E+00
^{242}Pu	5.28E+03	3.02E+01	3.89E+00
^{226}Ra	0.00E+00[b]	4.57E-05	2.42E-05
^{228}Ra	0.00E+00[b]	1.51E-05	6.00E-06
^{79}Se	4.19E+01	6.82E+00	7.01E+00
^{126}Sn	4.63E+02	9.40E+00	1.70E+01
^{90}Sr	2.49E+03	5.22E+01	1.74E+02
^{99}Tc	7.55E+03	1.58E+02	1.01E+03
^{229}Th	0.00E+00[b]	3.24E-01	3.30E-03
^{230}Th	1.52E-01	1.18E-01	8.12E-04
^{232}Th	0.00E+00[b]	2.17E+04	2.98E+04
^{232}U	1.02E-02	1.28E+00	4.08E-04
^{233}U	5.76E-02	5.38E+02	1.94E+01
^{234}U	1.75E+03	4.73E+02	2.33E+01
^{235}U	6.26E+04	2.51E+04	1.41E+03
^{236}U	3.84E+04	1.25E+03	5.99E+01
^{238}U	7.82E+06	6.84E+05	2.37E+05

Source: DTN: MO0702PASTREAM.001_R0 [DIRS 179925],'worksheet 'RN INVENTORY' *in spreadsheet DTN-Inventory-Rev00.xls*.

NOTE: ^{210}Pb is not listed in this table because it is considered to be in secular equilibrium with ^{226}Ra.

[a] 18 percent of ^{14}C for CSNF resides in the hardware outside of the cladding (DTN: SN0310T0505503.004_R0 [DIRS 168761]).

[b] Grams listed as 0.00E+00 is the value presented in the data input source.

Table 6.3.7-4a. Radionuclide Inventory Per Waste Package Showing the Amount of Decay and Ingrowth Experienced During the Preclosure Period

Grams Per Waste Package Inventory, g/pkg						
Radionuclide	CSNF at 2067[a]	CSNF after 50 Years[b]	DSNF at 2030[a]	DSNF after 87 Years[b]	HLW at 2030[a]	HLW after 87 Years[b]
^{227}Ac	2.47E-06	6.27E-06	1.22E-03	1.39E-03	1.91E-04	9.47E-04
^{241}Am	8.18E+03	9.84E+03	2.18E+02	2.15E+02	3.75E+01	3.37E+01
^{243}Am	1.24E+03	1.23E+03	6.73E+00	6.68E+00	5.75E-01	5.70E-01
^{14}C	1.35E+00	1.34E+00	1.81E+00	1.79E+00	0.00E+00	0.00E+00
^{36}Cl	3.23E+00	3.23E+00	4.23E+00	4.23E+00	0.00E+00	0.00E+00
^{245}Cm	1.75E+01	1.74E+01	9.25E-02	9.18E-02	5.43E-02	5.39E-02
^{135}Cs	4.36E+03	4.36E+03	9.74E+01	9.74E+01	1.27E+02	1.27E+02
^{137}Cs	5.90E+03	1.86E+03	9.72E+01	1.31E+01	3.02E+02	4.07E+01
^{129}I	1.73E+03	1.73E+03	3.56E+01	3.56E+01	7.27E+01	7.27E+01
^{237}Np	4.57E+03	5.32E+03	8.14E+01	1.12E+02	9.95E+01	1.04E+02
^{231}Pa	9.17E-03	1.22E-02	2.14E+00	2.14E+00	1.53E+00	1.53E+00
^{238}Pu	1.52E+03	1.02E+03	1.25E+01	6.28E+00	3.91E+01	1.96E+01
^{239}Pu	4.32E+04	4.31E+04	2.21E+03	2.20E+03	5.58E+02	5.57E+02
^{240}Pu	2.05E+04	2.04E+04	4.35E+02	4.31E+02	4.61E+01	4.57E+01
^{241}Pu	2.66E+03	2.40E+02	2.92E+01	4.49E-01	1.22E+00	1.89E-02
^{242}Pu	5.28E+03	5.28E+03	3.02E+01	3.02E+01	3.89E+00	3.89E+00
^{226}Ra	0.00E+00	1.29E-04	4.57E-05	1.80E-04	2.42E-05	2.68E-05
^{228}Ra	0.00E+00	1.90E-11	1.51E-05	8.77E-06	6.00E-06	1.20E-05
^{79}Se	4.19E+01	4.19E+01	6.82E+00	6.82E+00	7.01E+00	7.01E+00
^{126}Sn	4.63E+02	4.63E+02	9.40E+00	9.40E+00	1.70E+01	1.70E+01
^{90}Sr	2.49E+03	7.46E+02	5.22E+01	6.43E+00	1.74E+02	2.14E+01
^{99}Tc	7.55E+03	7.55E+03	1.58E+02	1.58E+02	1.01E+03	1.01E+03
^{229}Th	0.00E+00	2.07E-05	3.24E-01	5.22E-01	3.30E-03	1.05E-02
^{230}Th	1.52E-01	4.32E-01	1.18E-01	2.33E-01	8.12E-04	9.02E-03
^{232}Th	0.00E+00	5.63E-02	2.17E+04	2.17E+04	2.98E+04	2.98E+04
^{232}U	1.02E-02	6.20E-03	1.28E+00	5.39E-01	4.08E-04	1.72E-04
^{233}U	5.76E-02	1.37E-01	5.38E+02	5.38E+02	1.94E+01	1.94E+01
^{234}U	1.75E+03	2.24E+03	4.73E+02	4.79E+02	2.33E+01	4.24E+01
^{235}U	6.26E+04	6.27E+04	2.51E+04	2.51E+04	1.41E+03	1.41E+03
^{236}U	3.84E+04	3.85E+04	1.25E+03	1.25E+03	5.99E+01	6.03E+01
^{238}U	7.82E+06	7.82E+06	6.84E+05	6.84E+05	2.37E+05	2.37E+05

[a] DTN: MO0702PASTREAM.001_R0 [DIRS 179925].

[b] Output DTN: MO0707EMPDECAY.000 [DIRS 182995].

Table 6.3.7-4b. Supplemental Radionuclide Inventory Per Waste Package due to Mixed Oxide Fuel and Lanthanide Borosilicate Waste Showing the Amount of Decay and Ingrowth Experienced During the Preclosure Period

Grams Per Waste Package MOX and LaBS Specific Additional Inventory, g/pkg				
Radionuclide	MOX at 2035[a]	MOX after 82 Years[b]	LaBS at 2003[a]	LaBS after 114 Years[b]
^{227}Ac	1.11E-10	4.29E-09	0.00E+00	1.40E-08
^{241}Am	1.90E+01	3.89E+02	2.78E+01	3.40E+01
^{243}Am	4.82E+01	4.78E+01	0.00E+00	0.00E+00
^{14}C	2.52E-02	2.50E-02	0.00E+00	0.00E+00
^{36}Cl	2.42E-07	2.42E-07	0.00E+00	0.00E+00
^{245}Cm	1.36E+00	1.35E+00	0.00E+00	0.00E+00
^{135}Cs	7.00E+01	7.00E+01	0.00E+00	0.00E+00
^{137}Cs	1.64E+02	2.48E+01	0.00E+00	0.00E+00
^{129}I	3.02E+01	3.02E+01	0.00E+00	0.00E+00
^{237}Np	1.44E+01	5.55E+01	4.77E-01	6.76E+00
^{231}Pa	3.99E-06	8.43E-06	0.00E+00	2.94E-05
^{238}Pu	1.46E+01	7.63E+00	3.43E+00	1.39E+00
^{239}Pu	1.00E+03	9.98E+02	3.48E+03	3.47E+03
^{240}Pu	7.09E+02	7.03E+02	3.10E+02	3.06E+02
^{241}Pu	4.20E+02	8.21E+00	1.26E+01	5.33E-02
^{242}Pu	1.79E+02	1.79E+02	6.09E+00	6.09E+00
^{226}Ra	8.79E-11	3.03E-07	0.00E+00	8.15E-07
^{228}Ra	5.89E-17	2.18E-14	0.00E+00	6.31E-09
^{79}Se	5.30E-01	5.30E-01	0.00E+00	0.00E+00
^{126}Sn	1.13E+01	1.13E+01	0.00E+00	0.00E+00
^{90}Sr	3.57E+01	4.96E+00	0.00E+00	0.00E+00
^{99}Tc	9.75E+01	9.75E+01	0.00E+00	0.00E+00
^{229}Th	2.68E-09	1.24E-07	0.00E+00	2.25E-08
^{230}Th	4.29E-06	1.07E-03	0.00E+00	1.71E-03
^{232}Th	1.15E-06	6.06E-05	1.56E+01	1.56E+01
^{232}U	9.85E-06	4.36E-06	0.00E+00	0.00E+00
^{233}U	2.28E-05	8.58E-04	0.00E+00	1.31E-04
^{234}U	8.91E-01	7.75E+00	4.24E+00	6.24E+00
^{235}U	5.48E+01	5.71E+01	2.61E+02	2.72E+02
^{236}U	2.18E+01	2.78E+01	0.00E+00	3.66E+00
^{238}U	7.99E+04	7.99E+04	8.58E+02	8.58E+02

[a] DTN: MO0702PASTREAM.001_R0 [DIRS 179925].

[b] Output DTN: MO0707EMPDECAY.000 [DIRS 182995].

Table 6.3.7-5. Initial Radionuclide Inventories and Initial Radionuclide Activities Per Waste Package Type in the TSPA-LA Model

Per Waste Package Inventory and Activity at Closure, 2117							
Radionuclide	Specific Activity[a] Ci/g	CSNF w/MOX added[b], g/pkg	CSNF w/MOX added, Ci/pkg	DSNF[b], g/pkg	DSNF, Ci/pkg	HLW w/LaBS added[b], g/pkg	HLW w/LaBS added, Ci/pkg
^{227}Ac	7.22E+01	6.27E-06	4.53E-04	1.39E-03	1.00E-01	9.47E-04	6.84E-02
^{241}Am	3.43E+00	1.02E+04	3.51E+04	2.15E+02	7.37E+02	6.77E+01	2.32E+02
^{243}Am	2.00E-01	1.28E+03	2.56E+02	6.68E+00	1.34E+00	5.70E-01	1.14E-01
^{14}C	4.46E+00	1.37E+00	6.09E+00	1.79E+00	7.98E+00	0.00E+00	0.00E+00
^{36}Cl	3.30E-02	3.23E+00	1.07E-01	4.23E+00	1.40E-01	0.00E+00	0.00E+00
^{245}Cm	1.72E-01	1.88E+01	3.23E+00	9.18E-02	1.58E-02	5.39E-02	9.27E-03
^{135}Cs	1.15E-03	4.43E+03	5.09E+00	9.74E+01	1.12E-01	1.27E+02	1.46E-01
^{137}Cs	8.67E+01	1.88E+03	1.63E+05	1.31E+01	1.14E+03	4.07E+01	3.53E+03
^{129}I	1.77E-04	1.76E+03	3.12E-01	3.56E+01	6.30E-03	7.27E+01	1.29E-02
^{237}Np	7.05E-04	5.38E+03	3.79E+00	1.12E+02	7.90E-02	1.11E+02	7.81E-02
^{231}Pa	4.72E-02	1.22E-02	5.76E-04	2.14E+00	1.01E-01	1.53E+00	7.22E-02
^{238}Pu	1.71E+01	1.03E+03	1.76E+04	6.28E+00	1.07E+02	2.10E+01	3.59E+02
^{239}Pu	6.21E-02	4.41E+04	2.74E+03	2.20E+03	1.37E+02	4.03E+03	2.50E+02
^{240}Pu	2.27E-01	2.11E+04	4.79E+03	4.31E+02	9.78E+01	3.52E+02	7.98E+01
^{241}Pu	1.03E+02	2.48E+02	2.56E+04	4.49E-01	4.62E+01	7.22E-02	7.44E+00
^{242}Pu	3.94E-03	5.46E+03	2.15E+01	3.02E+01	1.19E-01	9.98E+00	3.93E-02
^{226}Ra	9.89E-01	1.29E-04	1.28E-04	1.80E-04	1.78E-04	2.76E-05	2.73E-05
^{228}Ra	2.72E+02	1.90E-11	5.17E-09	8.77E-06	2.39E-03	1.20E-05	3.27E-03
^{79}Se	1.53E-02	4.24E+01	6.49E-01	6.82E+00	1.04E-01	7.01E+00	1.07E-01
^{126}Sn	1.13E-02	4.74E+02	5.36E+00	9.40E+00	1.06E-01	1.70E+01	1.92E-01
^{90}Sr	1.38E+02	7.51E+02	1.04E+05	6.43E+00	8.87E+02	2.14E+01	2.95E+03
^{99}Tc	1.70E-02	7.65E+03	1.30E+02	1.58E+02	2.69E+00	1.01E+03	1.72E+01
^{229}Th	2.14E-01	2.08E-05	4.46E-06	5.22E-01	1.12E-01	1.05E-02	2.25E-03
^{230}Th	2.06E-02	4.33E-01	8.92E-03	2.33E-01	4.80E-03	1.07E-02	2.21E-04
^{232}Th	1.10E-07	5.64E-02	6.20E-09	2.17E+04	2.39E-03	2.98E+04	3.28E-03
^{232}U	2.21E+01	06.20E-03	1.37E-01	5.39E-01	1.19E+01	1.72E-04	3.80E-03
^{233}U	9.65E-03	01.38E-01	1.33E-03	5.38E+02	5.19E+00	1.94E+01	1.87E-01
^{234}U	6.21E-03	2.25E+03	1.40E+01	4.79E+02	2.97E+00	4.86E+01	3.02E-01
^{235}U	2.16E-06	6.28E+04	1.36E-01	2.51E+04	5.42E-02	1.68E+03	3.63E-03
^{236}U	6.47E-05	3.85E+04	2.49E+00	1.25E+03	8.09E-02	6.40E+01	4.14E-03
^{238}U	3.36E-07	7.90E+06	2.65E+00	6.84E+05	2.30E-01	2.38E+05	7.99E-02

[a] DTN: MO0702PASTREAM.001_R0 [DIRS 179925].

[b] Output DTN: MO0707EMPDECAY.000 [DIRS 182995].

Table 6.3.7-6. Disposition of Radionuclides for Groundwater Release Modeling Cases: Nominal, Igneous Intrusion, and Seismic

Radionuclide (Table 6.3.7-2)	Disposition in WF, EBS, and UZ TSPA-LA Model Components (Section 6.3.7)	Disposition in 3-D UZ FEHM Submodel[a] (Section 6.3.9)	Disposition in SZ Submodels (3-D SZ_Convolute and 1-D Pipe)[b] (Section 6.3.10)	Disposition in Biosphere (Section 6.3.11)
^{227}Ac	Not transported	Not transported	Not transported	Dose from 1-D[g], assuming secular equilibrium with ^{231}Pa
^{241}Am	Transport embedded colloid $^{241}Am_{emb}$ (decay to ^{237}Np) Transport irreversible FeO colloid $^{241}Am_{FeO}$ (decay to ^{237}Np) Transport reversible colloid and solute (decay to ^{237}Np)	Transport slow irreversible colloid $^{241}Am_{irs}$ (decay to ^{237}Np) Transport fast irreversible colloid $^{241}Am_{irf}$ (decay to ^{237}Np) Transport reversible colloid and solute (decay to ^{237}Np)	3-D transport of americium/plutonium slow irreversible colloid [SZ BTC 6] 3-D transport of americium/plutonium fast irreversible colloid [SZ BTC 10] 3-D transport of americium/thorium/protactinium reversible colloid [SZ BTC 2]	Dose from 3-D
^{243}Am	Transport embedded colloid $^{243}Am_{emb}$ (decay to $^{239}Pu_{emb}$) Transport irreversible FeO colloid $^{243}Am_{FeO}$ (decay to $^{239}Pu_{FeO}$) Transport reversible colloid and solute (decay to ^{239}Pu)	Transport slow irreversible colloid $^{243}Am_{irs}$ (decay to $^{239}Pu_{irs}$) Transport fast irreversible colloid $^{243}Am_{irf}$ (decay to $^{239}Pu_{irf}$) Transport reversible colloid and solute (decay to ^{239}Pu)	3-D transport of americium/plutonium slow irreversible colloid [SZ BTC 6] 3-D transport of americium/plutonium fast irreversible colloid [SZ BTC 10] 3-D transport of americium/thorium/protactinium	Dose from 3-D
^{14}C	Transport solute	Transport solute	3-D transport of nonsorbing solute [SZ BTC 1]	Dose from 3-D
^{36}Cl	Transport solute	Transport solute	3-D transport of nonsorbing solute [SZ BTC 1]	Dose from 3-D
^{245}Cm[e]	Not transported (decay to ^{241}Pu)	Not transported	Not transported	Dose not computed
^{135}Cs	Transport reversible colloid and solute	Transport reversible colloid and solute	3-D transport of cesium colloid [SZ BTC3]	Dose from 3-D
^{137}Cs	Transport reversible colloid and solute	Transport reversible colloid and solute	3-D transport of cesium colloid [SZ BTC 3]	Dose from 3-D
^{129}I	Transport solute	Transport solute	3-D transport of nonsorbing solute [SZ BTC 1]	Dose from 3-D

Table 6.3.7-6. Disposition of Radionuclides for Groundwater Release Modeling Cases: Nominal, Igneous Intrusion, and Seismic (Continued)

Radionuclide (Table 6.3.7-2)	Disposition in WF, EBS, and UZ TSPA-LA Model Components (Section 6.3.7)	Disposition in 3-D UZ FEHM Submodel[a] (Section 6.3.9)	Disposition in SZ Submodels (3-D SZ_Convolute and 1-D Pipe)[b] (Section 6.3.10)	Disposition in Biosphere (Section 6.3.11)
^{237}Np	Transport solute (decay to ^{233}U)	Transport solute (decay to ^{233}U)	3-D transport of neptunium solute [SZ BTC 5], boosted[c] by $^{241}Am_{irs}$, $^{241}Am_{irf}$, and $^{241}Am_{rev/sol}$	Dose from 3-D
^{231}Pa	Transport reversible colloid and solute (decay to ^{227}Ac)	Transport reversible colloid and solute (simple decay)	1-D transport reversible colloid and solute (decay to ^{227}Ac) [SZ BTC 2]	Dose from 1-D
^{210}Pb[f]	Not explicitly included	Not explicitly included	Not explicitly included	Dose included with ^{226}Ra BDCF[f]
^{238}Pu	Transport embedded colloid $^{238}Pu_{emb}$ (decay to ^{234}U) Transport irreversible FeO colloid $^{238}Pu_{FeO}$ (decay to ^{234}U) Transport reversible colloid and solute (decay to ^{234}U)	Transport slow irreversible colloid $^{238}Pu_{irs}$ (decay to ^{234}U) Transport fast irreversible colloid $^{238}Pu_{irf}$ (decay to ^{234}U) Transport reversible colloid and solute (decay to ^{234}U)	3-D transport of americium/plutonium slow irreversible colloid [SZ BTC 6] 3-D transport of americium/plutonium fast irreversible colloid [SZ BTC 10] 3-D transport of plutonium reversible colloid [SZ-BTC 4]	Dose from 3-D
^{239}Pu	Transport embedded colloid $^{239}Pu_{emb}$ (decay to ^{235}U) Transport irreversible FeO colloid $^{239}Pu_{FeO}$ (decay to ^{235}U) Transport reversible colloid and solute (decay to ^{235}U)	Transport slow irreversible colloid $^{239}Pu_{irs}$ (decay to ^{235}U) Transport fast irreversible colloid $^{239}Pu_{irf}$ (decay to ^{235}U) Transport reversible colloid and solute (decay to ^{235}U)	3-D transport of americium/plutonium slow irreversible colloid [SZ BTC 6], boosted[c] by $^{243}Am_{irs}$ 3-D transport of americium/plutonium fast irreversible colloid [SZ BTC 10], boosted[c] by $^{243}Am_{irf}$ 3-D transport of plutonium reversible colloid [SZ BTC 4], boosted[c] by $^{243}Am_{rev/sol}$	Dose from 3-D
^{240}Pu	Transport embedded colloid Pu_{emb} (decay to ^{236}U) Transport irreversible FeO colloid $^{240}Pu_{FeO}$ (decay to ^{236}U) Transport reversible colloid and solute (decay to ^{236}U)	Transport slow irreversible colloid $^{240}Pu_{irs}$ (decay to ^{236}U) Transport fast irreversible colloid $^{240}Pu_{irf}$ (decay to ^{236}U) Transport reversible colloid and solute (decay to ^{236}U)	3-D transport of americium/plutonium slow irreversible colloid [SZ BTC 6] 3-D transport of americium/plutonium fast irreversible colloid [SZ BTC 10] 3-D transport of plutonium reversible colloid [SZ BTC 4]	Dose from 3-D
^{241}Pu[e]	Not transported (decay to ^{241}Am)	Not transported	Not transported	Dose not computed

Table 6.3.7-6. Disposition of Radionuclides for Groundwater Release Modeling Cases: Nominal, Igneous Intrusion, and Seismic (Continued)

Radionuclide (Table 6.3.7-2)	Disposition in WF, EBS, and UZ TSPA-LA Model Components (Section 6.3.7)	Disposition in 3-D UZ FEHM Submodel[a] (Section 6.3.9)	Disposition in SZ Submodels (3-D SZ_Convolute and 1-D Pipe)[b] (Section 6.3.10)	Disposition in Biosphere (Section 6.3.11)
^{242}Pu	Transport embedded colloid $^{242}Pu_{emb}$ (decay to ^{238}U) Transport irreversible FeO colloid $^{242}Pu_{FeO}$ (decay to ^{238}U) Transport reversible colloid and solute (decay to ^{238}U)	Transport slow irreversible colloid $^{242}Pu_{irs}$ (decay to ^{238}U) Transport fast irreversible colloid $^{242}Pu_{irf}$ (decay to ^{238}U) Transport reversible colloid and solute (decay to ^{238}U)	3-D transport[d] of americium/plutonium slow irreversible colloid [SZ BTC 6] 3-D transport[d] of americium/plutonium fast irreversible colloid [SZ BTC 10] 3-D transport[d] of plutonium reversible colloid [SZ BTC 4]	Dose from 3-D[g]
^{226}Ra	Transport solute (simple decay)	Transport solute (simple decay)	1-D transport of solute (simple decay) [SZ BTC 7]	Dose from 1-D[g]; concentration from 1-D[f]
^{228}Ra	Not transported	Not transported	Not transported	Dose from 1-D[g]; concentration from 1-D, both assuming secular equilibrium with ^{232}Th
^{79}Se	Transport solute	Transport solute	3-D transport of nonsorbing solute [SZ BTC 11]	Dose from 3-D
^{126}Sn	Transport solute	Transport reversible colloid and solute	3-D transport of tin colloid [SZ BTC 12]	Dose from 3-D
^{90}Sr	Transport solute	Transport solute	3-D transport of strontium solute [SZ BTC 8]	Dose from 3-D
^{99}Tc	Transport solute	Transport solute	3-D transport of nonsorbing solute [SZ BTC 1]	Dose from 3-D
^{229}Th	Transport reversible colloid and solute (simple decay)	Transport reversible colloid and solute (simple decay)	1-D transport of reversible colloid and solute (simple decay) [SZ BTC 2]	Dose from 1-D
^{230}Th	Transport reversible colloid and solute (decay to ^{226}Ra)	Transport reversible colloid and solute (decay to ^{226}Ra)	1-D transport of reversible colloid and solute (decay to ^{226}Ra) [SZ BTC 2]	Dose from 1-D[g]; concentration from 1-D
^{232}Th	Transport reversible colloid and solute (decay to ^{228}Ra)	Transport reversible colloid and solute (simple decay)	1-D transport of reversible colloid and solute (decay to ^{228}Ra) [SZ BTC 2]	Dose from 1-D[g]; concentration from 1-D
^{232}U	Transport solute	Transport solute	3-D transport of ^{232}U solute [SZ BTC 9]	Dose from 3-D
^{233}U	Transport solute (decay to ^{229}Th)	Transport solute (decay to ^{229}Th)	1-D transport of solute (decay to thorium) [SZ BTC 9]	Dose from 1-D

Table 6.3.7-6. Disposition of Radionuclides for Groundwater Release Modeling Cases: Nominal, Igneous Intrusion, and Seismic (Continued)

Radionuclide (Table 6.3.7-2)	Disposition in WF, EBS, and UZ TSPA-LA Model Components (Section 6.3.7)	Disposition in 3-D UZ FEHM Submodel[a] (Section 6.3.9)	Disposition in SZ Submodels (3-D SZ_Convolute and 1-D Pipe)[b] (Section 6.3.10)	Disposition in Biosphere (Section 6.3.11)
^{234}U	Transport solute (decay to ^{230}Th)	Transport solute (decay to ^{230}Th)	3-D transport of ^{234}U solute [SZ BTC 9], boosted[c] by ^{238}U, $^{238}Pu_{irs}$, $^{238}Pu_{irf}$, and $^{238}Pu_{rev/sol}$	Dose from 3-D
^{235}U	Transport solute (decay to ^{231}Pa)	Transport solute (decay to ^{231}Pa)	1-D transport of solute (decay to ^{231}Pa) [SZ BTC 9]	Dose from 1-D[g]
^{236}U	Transport solute (decay to ^{232}Th)	Transport solute (decay to ^{232}Th)	3-D transport[d] of ^{236}U solute [SZ BTC 9], boosted[c] by $^{240}Pu_{irs}$, $^{240}Pu_{irf}$, and $^{240}Pu_{rev/sol}$	Dose from 3-D
^{238}U	Transport solute (decay to ^{234}U)	Transport solute (decay to ^{234}U)	3-D transport of ^{238}U solute [SZ BTC 9], boosted[c] by $^{242}Pu_{irs}$, $^{242}Pu_{irf}$, and $^{242}Pu_{rev/sol}$	Dose from 3-D

NOTE: [a] Plutonium and americium isotopes are transported irreversibly on two different colloid types (minerals) in the EBS: FeO_x colloids (e.g., see $^{239}Pu_{FeO}$ in the above table) and waste form colloids (e.g., see $^{239}Pu_{emb}$ in the above table). However, at the EBS-UZ interface, the plutonium or americium mass associated with these two types of colloids is combined (effectively losing or ignoring the mineral specificity) and then resplit into slow-Transport and fast-Transport irreversible colloids in the natural system (e.g., see $^{239}Pu_{irs}$ and $^{239}Pu_{irf}$ in the above table). Thus, the specific radionuclides in GoldSim designated "Ic" and "If" are used differently in the EBS versus the natural system—in the EBS "Ic" stands for plutonium and americium mass transported in "embedded" colloids (i.e., the plutonium and americium mass is embedded in the mineral matrix of these colloid particles), and "If" stands for plutonium and americium mass sorbed irreversibly onto FeOx colloids, whereas in the UZ (Section 6.3.9) and SZ (Section 6.3.10), "Ic" stands for plutonium and americium mass transported irreversibly on slow colloids, and "If" stands for plutonium or americium mass transported irreversibly on fast colloids.

[b] Saturated Zone Breakthrough Curve and the associated number refers to the "Radionuclide Group Number" listed in the first column of Table 6.3.10-3 (see Section 6.3.10).

[c] Boosting of a daughter (e.g., ^{239}Pu) means that the injected mass of the daughter over any timestep at the UZ-SZ interface is increased by the maximum decay (over the remaining simulation time) of the designated parent (e.g., ^{243}Am).

[d] This nuclide could have been deleted from the 3-D SZ model (Section 6.3.10), because only the 1-D SZ transport results are used for the ingrowth of its daughter.

[e] ^{245}Cm and ^{241}Pu were recommended for inclusion in TSPA-LA in *Radionuclide Screening* (SNL 2007 [DIRS 177424], Section 6.6.2 and Table 7-1) only to ensure that the effect of their decay on the inventories of ^{241}Am and ^{237}Np are included in the model. They are not recommended for transport or dose consequences.

[f] Though ^{210}Pb is not tracked, it is assumed to be in secular equilibrium with ^{226}Ra; that is, the BDCF used for ^{226}Ra is the summation of the BDCFs provided for ^{226}Ra and ^{210}Pb.

[g] Doses only calculated for million-year simulations (SNL 2007 [DIRS 177424], Table 7-1).

WF = waste form; SZ BTC = Saturated Zone Breakthrough Curve.

Table 6.3.7-7. Uncertainty Multipliers for Grams per Waste Package of Radionuclides for Each Waste Type

TSPA Parameter Name	CSNF CSNF_Mass_Uncert_a	DSNF DSNF_Mass_Uncert_a	HLW HLW_Mass_Uncert_a
Isotopes	All except ^{238}U	All except ^{238}U	All
Distribution	Uniform	Triangular	Triangular
Minimum	0.85	0.45	0.70
Most Likely	None	0.62	1
Maximum	1.4	2.9	1.5

Sources: DTN: SN0310T0505503.004_R0 [DIRS 168761]
Initial Radionuclide Inventories (SNL 2007 [DIRS 180472], Table 7-2).

Table 6.3.7-8. Summary of In-Package Chemistry Abstraction (Vapor or Liquid Influx)

	RH			
	<95%		≥95%	
Q (L/yr)	< 0.1	≥0.1	< 0.1	≥0.1
I (V) < I(L)	In-Package Chemistry Submodel Off	I(L)	I (V)	I (V), pH(L)
I (V) ≥ I(L)		pH(L)	pH(V)	I (L), pH(L)

Source: Modified from *In-Package Chemistry Abstraction* (SNL 2007 [DIRS 180506]) Table 6-23[a].

NOTE: Q is the water inflow rate; I(V) and I(L) are ionic strength given by the vapor influx abstraction and that given by the liquid influx abstraction, respectively; pH(V) and pH(L) are pH given by the vapor influx abstraction and that given by the liquid influx abstraction, respectively.

Table 6.3.7-9. In-Package Ionic Strength Abstraction for Vapor Influx Case

Cell	RH Range	A	B	Lower Uncertainty Factor (fmin)	Upper Uncertainty Factor (fmax)
CSNF Cell 1	95%≤ RH < 98.3%	45.846	-45.525	0.5	1.5
	98.3%≤ RH <99.9%	64.0629	-64.0602		
	99.9%≤ RH ≤– 100%	66.4312	-66.4308		
CDSP Cell 1A	95%≤ RH <97.2%	42.992	-42.654	0.5	1.5
	97.2%≤ RH ≤100%	54.7803	-54.7776		
CDSP Cell 1B	95%≤ RH <98.33%	42.992	-42.654	0.5	1.5
	98.33%≤ RH ≤100%	62.4136	-62.4112		

Source: DTN: SN0702PAIPC1CA.001_R2 [DIRS 180451], *Abstr CSNF No Drip Ion Str.xls*; *Abstr 2DHLW No Drip Ion Str.xls*; and *Abstr 2MCO No Drip Ion Str.xls*.

Table 6.3.7-10. In-Package Ionic Strength Abstraction for CSNF Cell 1 of Liquid Influx Case (log I (molal))

Log Time Since WP Breach (year)	Log Liquid Influx Rate (L/yr)					
	3	2	1	0	-0.3	-1
-1.75	-2.451	-2.433	-2.452	-2.454	-2.454	-2.455
-1.25	-2.501	-2.494	-2.501	-2.502	-2.502	-2.502
-0.75	-2.503	-2.506	-2.503	-2.502	-2.502	-2.502
-0.25	-2.466	-2.477	-2.456	-2.453	-2.453	-2.453
0.25	-2.390	-2.365	-2.320	-2.339	-2.311	-2.247
0.75	-2.317	-2.107	-2.004	-2.032	-1.982	-1.866
1.25	-2.306	-1.803	-1.608	-1.586	-1.585	-1.582
1.75	-2.305	-1.586	-1.178	-1.163	-1.160	-1.154
2.25	-2.305	-1.530	-0.786	-0.686	-0.677	-0.657
2.75	-2.305	-1.945	-1.106	-0.371	-0.320	-0.202
3.25	-2.305	-2.091	-1.634	-0.411	-0.178	0.366
3.75	-2.305	-2.091	-1.929	-0.987	-0.426	0.881
4.25	-2.305	-2.091	-2.095	-2.072	-1.540	-0.299
4.75	-2.305	-2.091	-2.095	-2.134	-2.131	-2.124
5.25	-2.305	-2.091	-2.095	-2.134	-2.134	-2.134
5.75	-2.305	-2.091	-2.095	-2.134	-2.134	-2.134
6.00	-2.305	-2.091	-2.095	-2.134	-2.134	-2.134

Source: DTN: SN0702PAIPC1CA.001_R2 [DIRS 180451], *Abstr CSNF Seepage Ion Str 2.xls*.

Table 6.3.7-11. In-Package Ionic Strength Abstraction for CDSP Cell 1A of Liquid Influx Case (log I (molal))

Log Time Since WP Breach (year)	Log Liquid Influx Rate (L/yr)				
	3	2	1	0	-1
-1.75	-2.391	-2.391	-2.391	-2.391	-2.391
-1.25	-2.391	-2.391	-2.391	-2.391	-2.391
-0.75	-2.391	-2.391	-2.391	-2.390	-2.390
-0.25	-2.391	-2.389	-2.389	-2.388	-2.388
0.25	-2.391	-2.386	-2.384	-2.380	-2.381
0.75	-2.391	-2.384	-2.369	-2.358	-2.360
1.25	-2.391	-2.384	-2.342	-2.296	-2.298
1.75	-2.391	-2.384	-2.319	-2.179	-2.162
2.25	-2.391	-2.384	-2.315	-2.021	-1.878
2.75	-2.391	-2.384	-2.315	-1.928	-1.551
3.25	-2.391	-2.384	-2.315	-1.917	-1.239
3.75	-2.391	-2.384	-2.315	-1.917	-1.088
4.25	-2.391	-2.384	-2.315	-1.917	-1.070
4.75	-2.391	-2.384	-2.315	-1.917	-1.070
5.25	-2.391	-2.384	-2.315	-1.917	-1.070
5.75	-2.391	-2.384	-2.315	-1.917	-1.070
6.00	-2.391	-2.384	-2.315	-1.917	-1.070

Source: DTN: SN0702PAIPC1CA.001_R2 [DIRS 180451], *Abstr 2DHLW Seepage Ion Str 2.xls*.

Table 6.3.7-12. In-Package Ionic Strength Abstraction for CDSP Cell 1B of Liquid Influx Case (log I (molal))

Log Time Since WP Breach (year)	Log Liquid Influx Rate (L/yr)					
	3	2	1	0	-0.5	-1
-1.75	-2.511	-2.512	-2.514	-2.514	-2.493	-2.472
-1.25	-2.505	-2.509	-2.515	-2.515	-2.515	-2.515
-0.75	-2.489	-2.495	-2.514	-2.516	-2.516	-2.517
-0.25	-2.462	-2.448	-2.508	-2.514	-2.514	-2.515
0.25	-2.448	-2.315	-2.493	-2.512	-2.513	-2.515
0.75	-2.447	-2.087	-2.446	-2.506	-2.510	-2.515
1.25	-2.491	-1.912	-2.309	-2.486	-2.501	-2.515
1.75	-2.514	-2.477	-2.019	-2.444	-2.491	-2.538
2.25	-2.514	-2.512	-1.702	-2.208	-2.286	-2.364
2.75	-2.514	-2.513	-2.467	-1.374	-1.688	-2.003
3.25	-2.514	-2.513	-2.505	-1.242	-1.088	-0.935
3.75	-2.514	-2.513	-2.505	-2.144	-0.690	0.763
4.25	-2.514	-2.513	-2.505	-2.157	-1.663	-1.169
4.75	-2.514	-2.513	-2.505	-2.157	-1.675	-1.194
5.25	-2.514	-2.513	-2.505	-2.157	-1.675	-1.192
5.75	-2.514	-2.513	-2.505	-2.157	-1.675	-1.192
6.00	-2.514	-2.513	-2.505	-2.157	-1.675	-1.675

Source: DTN: SN0702PAIPC1CA.001_R2 [DIRS 180451*], Abstr 2MCO Seepage Ion Str 2.xls.*

Table 6.3.7-13. In-Package Ionic Strength Deviation for CSNF Cell 1 of Liquid Influx Case (log I (molal))

Log Time Since WP Breach (year)	Log Liquid Influx Rate (L/yr)					
	3	2	1	0	-0.3	-1
-1.75	1.00	1.00	1.00	1.00	1.00	1.00
-1.25	1.00	1.00	1.00	1.00	1.00	1.00
-0.75	1.00	1.00	1.00	1.00	1.00	1.00
-0.25	1.00	1.00	1.00	1.00	1.00	1.00
0.25	1.00	1.00	1.00	1.00	1.00	1.05
0.75	1.00	1.00	1.00	1.00	1.00	1.08
1.25	1.00	1.00	1.00	1.00	1.00	1.00
1.75	1.00	1.00	1.00	1.00	1.00	1.00
2.25	1.00	1.00	1.00	1.00	1.00	1.01
2.75	1.00	1.00	1.00	1.00	1.00	1.08
3.25	1.00	1.00	1.00	1.00	1.00	1.39
3.75	1.00	1.00	1.00	1.00	1.00	1.93
4.25	1.00	1.00	1.00	1.00	1.00	1.89
4.75	1.00	1.00	1.00	1.00	1.00	1.01
5.25	1.00	1.00	1.00	1.00	1.00	1.00
5.75	1.00	1.00	1.00	1.00	1.00	1.00
6.00	1.00	1.00	1.00	1.00	1.00	1.00

Source: DTN: SN0702PAIPC1CA.001_R2 [DIRS 180451], *Abstr CSNF Seepage Ion Str 2.xls*.

Table 6.3.7-14. In-Package Ionic Strength Deviation for CDSP Cell 1A of Liquid Influx Case (log I (molal))

Log Time Since WP Breach (year)	Log Liquid Influx Rate (L/yr)				
	3	2	1	0	-1
-1.75	1.0	1.0	1.0	1.0	1.0
-1.25	1.0	1.0	1.0	1.0	1.0
-0.75	1.0	1.0	1.0	1.0	1.0
-0.25	1.0	1.0	1.0	1.0	1.0
0.25	1.0	1.0	1.0	1.0	1.0
0.75	1.0	1.0	1.0	1.0	1.0
1.25	1.0	1.0	1.0	1.0	1.0
1.75	1.0	1.0	1.0	1.0	1.0
2.25	1.0	1.0	1.0	1.0	1.0
2.75	1.0	1.0	1.0	1.0	1.0
3.25	1.0	1.0	1.0	1.0	1.0
3.75	1.0	1.0	1.0	1.0	1.0
4.25	1.0	1.0	1.0	1.0	1.0
4.75	1.0	1.0	1.0	1.0	1.0
5.25	1.0	1.0	1.0	1.0	1.0
5.75	1.0	1.0	1.0	1.0	1.0
6.00	1.0	1.0	1.0	1.0	1.0

Source: DTN: SN0702PAIPC1CA.001_R2 [DIRS 180451], *Abstr 2DHLW Seepage Ion Str 2.xls*.

Table 6.3.7-15. In-Package Ionic Strength Deviation for CDSP Cell 1B of Liquid Influx Case (log I (molal))

Log Time Since WP Breach (year)	Log Liquid Influx Rate (L/yr)					
	3	2	1	0	-0.5	-1
-1.75	1.00	1.00	1.00	1.00	1.00	1.02
-1.25	1.00	1.00	1.00	1.00	1.00	1.00
-0.75	1.00	1.00	1.00	1.00	1.00	1.00
-0.25	1.00	1.00	1.00	1.00	1.00	1.00
0.25	1.00	1.00	1.00	1.00	1.00	1.00
0.75	1.00	1.00	1.00	1.00	1.00	1.00
1.25	1.00	1.00	1.00	1.00	1.00	1.01
1.75	1.00	1.00	1.00	1.00	1.00	1.05
2.25	1.00	1.00	1.00	1.00	1.00	1.08
2.75	1.00	1.00	1.00	1.00	1.00	1.31
3.25	1.00	1.00	1.00	1.00	1.00	1.15
3.75	1.00	1.00	1.00	1.00	1.00	2.45
4.25	1.00	1.00	1.00	1.00	1.00	1.49
4.75	1.00	1.00	1.00	1.00	1.00	1.48
5.25	1.00	1.00	1.00	1.00	1.00	1.48
5.75	1.00	1.00	1.00	1.00	1.00	1.48
6.00	1.00	1.00	1.00	1.00	1.00	1.24

Source: DTN: SN0702PAIPC1CA.001_R2 [DIRS 180451], *Abstr 2MCO Seepage Ion Str 2.xls.*

Table 6.3.7-16. Maximum pH for CSNF Cell 1 of Liquid Influx

pCO2 (bar)	Log Ionic Strength (molal)						
	-1.411	-0.162	-0.135	-0.059	0	0.5	1
4	9.07	8.90	8.90	8.90	8.90	8.90	8.90
3	8.32	8.14	8.13	8.13	8.13	8.13	8.13
2	7.55	7.22	7.21	7.19	7.19	7.19	7.19
1.5	7.17	6.82	6.81	6.79	6.79	6.79	6.79

Source: DTN: SN0702PAIPC1CA.001_R2 [DIRS 180451], *Abstr CSNF Seepage pH.xls.*

Table 6.3.7-17. Maximum pH for CDSP Cell 1A of Liquid Influx

pCO2 (bar)	Log Ionic Strength (molal)									
	-2.283	-1.516	-1.486	-1.418	-0.474	-0.406	-0.369	0	0.5	1
4	9.37	9.81	9.83	9.87	10.23	10.25	10.27	10.41	10.60	10.79
3	8.46	9.09	9.13	9.17	9.67	9.71	9.73	9.92	10.19	10.45
2	7.48	8.21	8.23	8.29	9.02	9.07	9.10	9.38	9.77	10.16
1.5	7.02	7.84	7.87	7.92	8.73	8.79	8.82	9.14	9.56	9.99

Source: DTN: SN0702PAIPC1CA.001_R2 [DIRS 180451], *Abstr 2DHLW Seepage pH.xls.*

Table 6.3.7-18. Maximum pH for CDSP Cell 1B of Liquid Influx

pCO2 (bar)	Log Ionic Strength (molal)									
	-2.409	-1.192	-1.166	-1.150	-0.128	-0.106	-0.014	0	0.5	1
4	8.99	9.06	9.06	9.06	8.89	8.89	8.89	8.89	8.89	8.89
3	8.15	8.30	8.31	8.31	8.12	8.11	8.11	8.11	8.11	8.11
2	7.21	7.55	7.54	7.53	7.21	7.20	7.17	7.17	7.17	7.17
1.5	6.78	7.17	7.16	7.15	6.81	6.80	6.77	6.77	6.77	6.77

Source: DTN: SN0702PAIPC1CA.001_R2 [DIRS 180451], *Abstr 2MCO Seepage pH.xls.*

Table 6.3.7-19. Minimum pH for CSNF Cell 1 of Liquid Influx

pCO2 (bar)	Log Ionic Strength (molal)				
	-1.531	-0.349	0	0.5	1
4	5.51	5.11	4.99	4.82	4.65
3	5.51	5.11	4.99	4.82	4.65
2	5.51	5.11	4.99	4.82	4.65
1.5	5.51	5.11	4.99	4.82	4.65

Source: DTN: SN0702PAIPC1CA.001_R2 [DIRS 180451], *Abstr CSNF Seepage pH.xls.*

Table 6.3.7-20. Minimum pH for CDSP Cell 1A of Liquid Influx

pCO2 (bar)	Log Ionic Strength (molal)					
	-2.259	-1.416	-0.422	0	0.5	1
4	5.88	5.54	5.20	5.04	4.87	4.68
3	5.87	5.54	5.20	5.04	4.87	4.69
2	5.87	5.54	5.20	5.04	4.87	4.69
1.5	5.87	5.54	5.20	5.04	4.87	4.69

Source: DTN: SN0702PAIPC1CA.001_R2 [DIRS 180451], *Abstr 2DHLW Seepage pH.xls.*

Table 6.3.7-21. Minimum pH for CDSP Cell 1B of Liquid Influx

pCO2 (bar)	Log Ionic Strength (molal)					
	-2.448	-1.399	-0.396	0	0.5	1
4	6.02	5.59	5.23	5.07	4.89	4.69
3	6.01	5.59	5.23	5.07	4.89	4.70
2	5.97	5.59	5.23	5.08	4.90	4.72
1.5	5.96	5.59	5.23	5.09	4.91	4.73

Source: DTN: SN0702PAIPC1CA.001_R2 [DIRS 180451], *Abstr 2MCO Seepage pH.xls.*

Table 6.3.7-22. Maximum pH for CSNF Cell 1 of Vapor Influx

pCO2 (bar)	Log Ionic Strength (molal)						
	-1.198	-0.164	-0.138	-0.066	0	0.5	1
4	9.06	8.90	8.90	8.90	8.90	8.90	8.90
3	8.31	8.12	8.12	8.12	8.12	8.12	8.12
2	7.54	7.22	7.21	7.19	7.19	7.19	7.19
1.5	7.17	6.82	6.81	6.79	6.79	6.79	6.79

Source: DTN: SN0702PAIPC1CA.001_R2 [DIRS 180451], *Abstr CSNF No Drip pH.xls.*

Table 6.3.7-23. Maximum pH for CDSP Cell 1A of Vapor Influx

pCO2 (bar)	Log Ionic Strength (molal)									
	-2.287	-1.517	-1.486	-1.419	-0.474	-0.406	-0.369	0	0.5	1.5
4	9.37	9.81	9.83	9.87	10.23	10.26	10.27	10.41	10.60	10.98
3	8.46	9.09	9.13	9.17	9.67	9.71	9.73	9.92	10.19	10.72
2	7.47	8.21	8.23	8.29	9.02	9.07	9.10	9.38	9.77	10.54
1.5	7.02	7.84	7.87	7.92	8.73	8.79	8.82	9.14	9.56	10.42

Source: DTN: SN0702PAIPC1CA.001_R2 [DIRS 180451], *Abstr 2DHLW No Drip pH.xls.*

Table 6.3.7-24. Maximum pH for CDSP Cell 1B of Vapor Influx

pCO2 (bar)	Log Ionic Strength (molal)									
	-2.127	-1.193	-1.166	-1.150	-0.129	-0.107	-0.015	0	0.5	1
4	9.04	9.06	9.06	9.06	8.89	8.89	8.89	8.89	8.89	8.89
3	8.25	8.31	8.31	8.31	8.12	8.11	8.11	8.11	8.11	8.11
2	7.38	7.55	7.54	7.53	7.21	7.20	7.17	7.17	7.17	7.17
1.5	6.94	7.17	7.15	7.15	6.75	6.74	6.70	6.70	6.70	6.70

Source: DTN: SN0702PAIPC1CA.001_R2 [DIRS 180451], *Abstr 2MCO No Drip pH.xls.*

Table 6.3.7-25. Minimum pH for CSNF Cell 1 of Vapor Influx

pCO2 (bar)	Log Ionic Strength (molal)				
	-1.344	-0.350	0	0.5	1
4	5.44	5.11	4.99	4.82	4.65
3	5.44	5.11	4.99	4.82	4.65
2	5.44	5.11	4.99	4.82	4.65
1.5	5.44	5.11	4.99	4.82	4.65

Source: DTN: SN0702PAIPC1CA.001_R2 [DIRS 180451], *Abstr CSNF No Drip pH.xls.*

Table 6.3.7-26. Minimum pH for CDSP Cell 1A of Vapor Influx

pCO2 (bar)	Log Ionic Strength (molal)					
	-2.318	**-1.372**	**-0.365**	**0**	**0.5**	**1.5**
4	5.84	5.46	5.12	4.98	4.81	4.45
3	5.84	5.46	5.12	4.98	4.81	4.45
2	5.83	5.46	5.12	4.98	4.81	4.45
1.5	5.83	5.46	5.12	4.98	4.81	4.45

Source: DTN: SN0702PAIPC1CA.001_R2 [DIRS 180451*], Abstr 2DHLW No Drip pH.xls.*

Table 6.3.7-27. Minimum pH for CDSP Cell 1B of Vapor Influx

pCO2 (bar)	Log Ionic Strength (molal)					
	-2.456	**-1.351**	**-0.352**	**0**	**0.5**	**1**
4	5.91	5.46	5.13	4.98	4.82	4.63
3	5.91	5.46	5.13	4.98	4.82	4.63
2	5.90	5.46	5.13	4.98	4.82	4.63
1.5	5.90	5.46	5.13	4.99	4.82	4.63

Source: DTN: SN0702PAIPC1CA.001_R2 [DIRS 180451], *Abstr 2MCO No Drip pH.xls.*

Table 6.3.7-28. Log K Temperature Interpolation Functions for Use in the Total Carbonate Concentration Abstraction

Log K Function of Temperature (°C)
$\mathrm{Log}(K_1) = 7.0 \times 10^{-5} T^2 - 0.0159T - 1.1023$
$\mathrm{Log}(K_2) = 5.0 \times 10^{-7} T^3 - 0.0002T^2 + 0.0132T - 6.5804$
$\mathrm{Log}(K_3) = -8.0 \times 10^{-5} T^2 + 0.0128T - 10.618$

Source: DTN: SN0702PAIPC1CA.001_R2 [DIRS 180451], worksheet *Total Carbonate Validation" in Total Carbonate and Eh Abstractions.xls* .

Table 6.3.7-29. Initial Release Fraction Percentage Distributions

TSPA-LA Parameter Name	Model Abstraction Symbol	Description	Units	Distribution Type	Distribution Specification
Initial_Release_Frac_Cs_a	None	Cesium release fraction %	None	Triangular	Min = 0.39 Max = 11.06 Most likely = 3.63
Initial_Release_Frac_I_a	None	Iodine release fraction %	None	Triangular	Min = 2.04 Max = 26.75 Most likely = 11.24
Initial_Release_Frac_Tc_a	None	Technetium release fraction %	None	Triangular	Min = 0.01 Max = 0.26 Most likely = 0.10
Initial_Release_Frac_Sr_a	None	Strontium release fraction %	None	Triangular	Min = 0.02 Max = 0.25 Most likely = 0.09

Source: DTN: MO0404ANLSF001.001_R0 [DIRS 169007].

Table 6.3.7-30. Linear Regression Model Alkaline Case (pH ≥ 6.8)

TSPA-LA Parameter Name	Model Abstraction Symbol	Description	Units	Distribution Type	Distribution Specification
Log_Specific_SA_CSNF_a	$Log_{10}(A)$	Log of fuel specific surface area	None	Triangular	Min = –7.3 Max = –5.4 Most likely = –6.7
DR_CSNF_Alk_a0_mean	a_0	Constant coefficient in dissolution rate model	None	None (Uncertainty based on covariance matrix)	μ = 4.705
DR_CSNF_Alk_a1_mean	a_1	Coefficient of inverse temperature in dissolution rate model	None	None (Uncertainty based on covariance matrix)	μ = –1093.826
DR_CSNF_Alk_a2_mean	a_2	Coefficient of $log_{10}TCC$ in dissolution rate model	None	None (Uncertainty based on covariance matrix)	μ = –0.102
DR_CSNF_Alk_a3_mean	a_3	Coefficient of pO_2 in dissolution rate model	None	None (Uncertainty based on covariance matrix)	μ = –0.338

Source: DTN: MO0404ANLSF001.001_R0 [DIRS 169007].

NOTE: Parameter a_4 = 0 under alkaline conditions.

Table 6.3.7-31. Linear Regression Model for Acid Case (pH < 6.8)

TSPA-LA Parameter Name	Model Abstraction Symbol	Description	Units	Distribution Type	Distribution Specification
Log_Specific_SA_CSNF_a	$Log_{10}(A)$	Log of fuel specific surface area	None	Triangular	Min = –7.3 Max = –5.4 Most likely = –6.7
DR_CSNF_Acid_a0_mean	a_0	Constant coefficient in dissolution rate model	None	None (Uncertainty based on covariance matrix)	μ = 6.60
DR_CSNF_Acid_a1_mean	a_1	Coefficient of inverse temperature in dissolution rate model	None	None	μ = –1093.826
DR_CSNF_Acid_a3_mean	a_3	Coefficient of pO_2 in dissolution rate model	None	None	μ = –0.338
DR_CSNF_Acid_a4_mean	a_4	Coefficient of pH in dissolution rate model	None	None (Uncertainty based on covariance matrix)	μ = –0.340

Source: DTN: MO0404ANLSF001.001_R0 [DIRS 169007].

NOTE: Parameter a_2 = 0 under acidic conditions.

Table 6.3.7-32. Dissolution Rate Parameters for High-Level Radioactive Waste Glass

TSPA-LA Parameter Name	Model Abstraction Symbol	Description	Units	Distribution Type/Uncertainty Type	Distribution Specification
Specific_Surface_Area_Glass	S_{sp}	Specific surface area for glass	m^2/kg	Single Value	2.70×10^{-3}
Rind_Porosity_CDSP	ϕ	Porosity of rind (alteration layer)	%	Single Value	17
HLW_Diss_Eta_Acidic	η_{acidic}	pH dependence coefficient acidic condition	None	Single Value	–0.49
HLW_Diss_Ea_Acidic	E_{a_acidic}	Effective activation energy acidic condition	kJ/mol	Single Value	31
HLW_Diss_kE_Acidic_a	k_{E_acid}	glass degradation rate coefficient for acidic solutions	$g/m^2/d$	Triangular	Min = 8.41×10^3 Max = 1.15×10^7 Most likely = 8.41×10^3
HLW_Diss_Eta_Alkaline	$\eta_{alkaline}$	pH dependence coefficient alkaline condition	None	Single Value	0.49
HLW_Diss_Ea_Alkaline	$E_{a_alkaline}$	Effective activation energy alkaline condition	kJ/mol	Single Value	69
HLW_Diss_kE_Alkaline_a	$k_{E_alkaline}$	glass degradation rate coefficient for alkaline solutions	$g/m^2/d$	Triangular	Min = 2.82×10^1 Max = 3.47×10^4 Most likely = 2.82×10^1
Exposure_Factor_a	$f_{exposure}$	Glass exposure factor	None	Triangular - Epistemic[a]	Min = 4 Max = 17 Most likely = 4
Glass_Log_Length_CDSP	L_o	Weighted average length of HLW glass	m	Single Value	3.9

Source: DTN: MO0502ANLGAMR1.016_R0 [DIRS 172830].

[a] The DTN lists this parameter as an aleatory uncertain parameter, but it is treated as an epistemic uncertain parameter in the TSPA-LA Model.

Table 6.3.7-33. Solubility-Controlling Solid Phases Used in the Dissolved Concentration Limits Model Abstraction

Radionuclide	Solubility-Controlling Solid	Comments
Americium	$AmOHCO_3$	None
Carbon	None	No solubility-controlling solid is expected to form under repository conditions.
Cesium	None	No solubility-controlling solid is expected to form under repository conditions.
Chlorine	None	No solubility-controlling solid is expected to form under repository conditions.
Iodine	None	No solubility-controlling solid is expected to form under repository conditions.
Neptunium	NpO_2 Np_2O_5 $NaNpO_2CO_3$	NpO_2 used within WPs while reductants remain. Np_2O_5 used within WPs after reductants are consumed and for Invert. $NaNpO_2CO_3$ used for high pH values.
Protactinium	No thermodynamic data available for Pa phases	Used calculated Np_2O_5 solubility values as analogue for Pa.
Plutonium	PuO_2 (hydrous, aged)	None
Radium	$BaSO_4$	Radium solubility is based on calculated Ba solubility at 100°C using $BaSO_4$ as the solubility controlling phase, which is a good analog for modeling radium solubility (SNL 2007 [DIRS 177418], Section 6.12). Since the solubility data of $RaSO_4$ in the thermodynamic database (data0.ymp.R4) used in the solubility calculations does not have a temperature-dependent relationship, and the solubility data of $BaSO_4$ indicates that $BaSO_4$ solubility increases with temperature up to 100°C, calculated $RaSO_4$ solubility could be no conservative. To be prudent, radium solubility is based on the conservative analog of $RaSO_4$; i.e., $BaSO_4$ solubility calculated at 100°C (SNL 2007 [DIRS 177418], Section 6.12).
Selenium	None	No solubility-controlling solid is expected to form under repository conditions.
Strontium	None	No solubility-controlling solid is expected to form under repository conditions.
Technetium	None	No solubility-controlling solid is expected to form under repository conditions.
Thorium	ThO_2 (amorphous)	None
Tin	SnO2(amorphous)	None
Uranium	Schoepite	Schoepite used for CSNF WPs in the Nominal and Seismic Scenario Classes.
Uranium	Schoepite Na-Boltwoodite $Na_4UO_2(CO_3)_3$	Schoepite used for lower pH values. Na-Boltwoodite used for higher pH values. $Na_4UO_2(CO_3)_3$ used only at high pH and log fco_2 values. This set of solubility-controlling solids is used for CSNF WPs in the Igneous Scenario Class, CDSP WPs in all scenarios and in all invert locations.

Source: *Dissolved Concentration Limits of Elements with Radioactive Isotopes* (SNL 2007 [DIRS 177418]).

Table 6.3.7-34. Base Americium Solubility Look-Up Table (log[Am], mg/L)

	log fco_2 (bars)							
pH	**-1.50**	**-2.00**	**-2.50**	**-3.00**	**-3.50**	**-4.00**	**-4.50**	**-5.00**
5.50	2.40E+00	3.27E+00	500	500	500	500	500	500
5.75	1.53E+00	2.10E+00	2.80E+00	500	500	500	500	500
6.00	7.99E-01	1.30E+00	1.83E+00	2.43E+00	3.30E+00	500	500	500
6.25	1.60E-01	5.93E-01	1.07E+00	1.58E+00	2.14E+00	2.84E+00	500	500
6.50	–3.33E-01	–2.76E-02	3.88E-01	8.60E-01	1.36E+00	1.89E+00	2.50E+00	3.37E+00
6.75	–6.62E-01	–5.20E-01	–2.16E-01	1.98E-01	6.69E-01	1.16E+00	1.68E+00	2.25E+00
7.00	–9.13E-01	–8.85E-01	–7.05E-01	–3.84E-01	3.99E-02	5.14E-01	1.01E+00	1.52E+00
7.25	–1.11E+00	–1.16E+00	–1.08E+00	–8.65E-01	–5.11E-01	–6.96E-02	4.11E-01	9.07E-01
7.50	–1.20E+00	–1.36E+00	–1.38E+00	–1.25E+00	–9.73E-01	–5.76E-01	–1.14E-01	3.74E-01
7.75	–1.12E+00	–1.46E+00	–1.60E+00	–1.56E+00	–1.35E+00	–1.01E+00	–5.65E-01	–8.59E-02
8.00	–7.46E-01	–1.39E+00	–1.71E+00	–1.80E+00	–1.67E+00	–1.37E+00	–9.51E-01	–4.80E-01
8.25	–3.64E-02	–1.07E+00	–1.66E+00	–1.93E+00	–1.93E+00	–1.68E+00	–1.29E+00	–8.22E-01
8.50	8.95E-01	–4.41E-01	–1.38E+00	–1.90E+00	–2.10E+00	–1.95E+00	–1.58E+00	–1.13E+00
8.75	1.93E+00	4.47E-01	–8.11E-01	–1.66E+00	–2.12E+00	–2.16E+00	–1.86E+00	–1.41E+00
9.00	500	1.48E+00	3.02E-02	–1.15E+00	–1.92E+00	–2.26E+00	–2.09E+00	–1.68E+00
9.25	500	2.63E+00	1.06E+00	–3.53E-01	–1.46E+00	–2.14E+00	–2.27E+00	–1.93E+00
9.50	500	500	2.24E+00	6.65E-01	–7.01E-01	–1.74E+00	–2.28E+00	–2.15E+00
9.75	500	500	500	1.88E+00	3.08E-01	–1.02E+00	–1.98E+00	–2.28E+00
10.00	500	500	500	500	1.56E+00	–1.70E-02	–1.31E+00	–2.15E+00
10.25	500	500	500	500	500	1.25E+00	–3.16E-01	–1.57E+00
10.50	500	500	500	500	500	500	9.70E-01	–5.94E-01
10.75	500	500	500	500	500	500	500	7.01E-01

Source: DTN: MO0702PADISCON.001_R0 [DIRS 179358], Table 8.

NOTE: This look-up table is implemented in the TSPA-LA Model as parameter Sol_Am_LUT. Entries reported as “500” in the table indicate conditions for which a valid solubility value does not exist.

Table 6.3.7-35. Base Neptunium (Np_2O_5) Solubility Look-Up Table (log[Np], mg/L)

	log fco_2 (bars)							
pH	**-1.5**	**-2.0**	**-2.5**	**-3.0**	**-3.5**	**-4.0**	**-4.5**	**-5.0**
3.00	4.38E+00	4.38E+00	4.38E+00	4.38E+00	4.38E+00	4.38E+00	4.38E+00	4.38E+00
3.25	4.10E+00	4.10E+00	4.10E+00	4.10E+00	4.10E+00	4.10E+00	4.10E+00	4.10E+00
3.50	3.82E+00	3.82E+00	3.82E+00	3.82E+00	3.82E+00	3.82E+00	3.82E+00	3.82E+00
3.75	3.55E+00	3.55E+00	3.55E+00	3.55E+00	3.55E+00	3.55E+00	3.55E+00	3.55E+00
4.00	3.29E+00	3.29E+00	3.29E+00	3.29E+00	3.29E+00	3.29E+00	3.29E+00	3.29E+00
4.25	3.03E+00	3.03E+00	3.03E+00	3.03E+00	3.03E+00	3.03E+00	3.03E+00	3.03E+00
4.50	2.77E+00	2.77E+00	2.77E+00	2.77E+00	2.77E+00	2.77E+00	2.77E+00	2.77E+00
4.75	2.52E+00	2.52E+00	2.52E+00	2.52E+00	2.52E+00	2.52E+00	2.52E+00	2.52E+00
5.00	2.26E+00	2.26E+00	2.26E+00	2.26E+00	2.26E+00	2.26E+00	2.26E+00	2.26E+00
5.25	2.01E+00	2.01E+00	2.01E+00	2.01E+00	2.01E+00	2.01E+00	2.01E+00	2.01E+00
5.50	1.76E+00	1.76E+00	1.76E+00	1.76E+00	1.76E+00	1.76E+00	1.76E+00	1.76E+00
5.75	1.51E+00	1.51E+00	1.51E+00	1.51E+00	1.51E+00	1.51E+00	1.51E+00	1.51E+00
6.00	1.26E+00	1.26E+00	1.26E+00	1.26E+00	1.26E+00	1.26E+00	1.26E+00	1.26E+00
6.25	1.01E+00	1.01E+00	1.01E+00	1.01E+00	1.01E+00	1.01E+00	1.01E+00	1.01E+00
6.50	7.66E-01	7.62E-01	7.61E-01	7.60E-01	7.60E-01	7.60E-01	7.60E-01	7.60E-01
6.75	5.35E-01	5.17E-01	5.12E-01	5.11E-01	5.10E-01	5.10E-01	5.10E-01	5.10E-01
7.00	3.46E-01	2.84E-01	2.68E-01	2.63E-01	2.61E-01	2.60E-01	2.60E-01	2.60E-01
7.25	2.41E-01	8.83E-02	3.52E-02	1.83E-02	1.28E-02	1.11E-02	1.05E-02	1.03E-02
7.50	2.76E-01	–1.94E-02	–1.63E-01	–2.14E-01	–2.31E-01	–2.37E-01	–2.39E-01	–2.39E-01
7.75	4.56E-01	8.77E-03	–2.77E-01	–4.12E-01	–4.64E-01	–4.81E-01	–4.87E-01	–4.89E-01
8.00	5.33E-01	1.71E-01	–2.53E-01	–5.29E-01	–6.61E-01	–7.13E-01	–7.31E-01	–7.37E-01
8.25	5.98E-01	4.49E-01	–9.89E-02	–5.11E-01	–7.78E-01	–9.11E-01	–9.63E-01	–9.81E-01
8.50	1.42E+00	1.00E+00	1.47E-01	–3.62E-01	–7.64E-01	–1.03E+00	–1.16E+00	–1.21E+00
8.75	500	1.06E+00	5.38E-01	–1.30E-01	–6.20E-01	–1.01E+00	–1.28E+00	–1.41E+00
9.00	500	500	7.93E-01	1.89E-01	–3.95E-01	–8.75E-01	–1.26E+00	–1.53E+00
9.25	500	500	500	8.19E-01	–1.08E-01	–6.54E-01	–1.12E+00	–1.51E+00
9.50	500	500	500	1.36E+00	3.72E-01	–3.81E-01	–9.10E-01	–1.37E+00
9.75	500	500	500	500	1.12E+00	2.16E-02	–6.44E-01	–1.16E+00
10.00	500	500	500	500	500	9.56E-01	–2.78E-01	–9.00E-01
10.25	500	500	500	500	500	1.96E+00	5.24E-01	–5.52E-01
10.50	500	500	500	500	500	500	1.76E+00	1.72E-01

Source: DTN: MO0702PADISCON.001_R0 [DIRS 179358], Table 3.

NOTE: This look-up table is implemented in the TSPA-LA Model as parameter Sol_Np2O5_LUT. Entries reported as "500" in the table indicate conditions for which a valid solubility value does not exist.

Table 6.3.7-36. Base Neptunium (NpO_2) Solubility Look-Up Table (log[Np], mg/L)

	log fco_2 (bars)							
pH	**-1.5**	**-2.0**	**-2.5**	**-3.0**	**-3.5**	**-4.0**	**-4.5**	**-5.0**
3.00	3.09E+00	3.09E+00	3.09E+00	3.09E+00	3.09E+00	3.09E+00	3.09E+00	3.09E+00
3.25	2.82E+00	2.82E+00	2.82E+00	2.82E+00	2.82E+00	2.82E+00	2.82E+00	2.82E+00
3.50	2.56E+00	2.56E+00	2.56E+00	2.56E+00	2.56E+00	2.56E+00	2.56E+00	2.56E+00
3.75	2.30E+00	2.30E+00	2.30E+00	2.30E+00	2.30E+00	2.30E+00	2.30E+00	2.30E+00
4.00	2.05E+00	2.05E+00	2.05E+00	2.05E+00	2.05E+00	2.05E+00	2.05E+00	2.05E+00
4.25	1.80E+00	1.80E+00	1.80E+00	1.80E+00	1.80E+00	1.80E+00	1.80E+00	1.80E+00
4.50	1.55E+00	1.55E+00	1.55E+00	1.55E+00	1.55E+00	1.55E+00	1.55E+00	1.55E+00
4.75	1.29E+00	1.29E+00	1.29E+00	1.29E+00	1.29E+00	1.29E+00	1.29E+00	1.29E+00
5.00	1.04E+00	1.04E+00	1.04E+00	1.04E+00	1.04E+00	1.04E+00	1.04E+00	1.04E+00
5.25	7.94E-01	7.94E-01	7.94E-01	7.94E-01	7.94E-01	7.94E-01	7.94E-01	7.94E-01
5.50	5.44E-01	5.44E-01	5.44E-01	5.44E-01	5.44E-01	5.44E-01	5.44E-01	5.44E-01
5.75	2.93E-01	2.94E-01	2.94E-01	2.94E-01	2.94E-01	2.94E-01	2.94E-01	2.94E-01
6.00	4.37E-02	4.36E-02	4.36E-02	4.36E-02	4.36E-02	4.36E-02	4.36E-02	4.36E-02
6.25	–2.05E-01	–2.06E-01	–2.06E-01	–2.06E-01	–2.06E-01	–2.06E-01	–2.06E-01	–2.06E-01
6.50	–4.48E-01	–4.54E-01	–4.56E-01	–4.56E-01	–4.56E-01	–4.56E-01	–4.56E-01	–4.56E-01
6.75	–6.65E-01	–6.98E-01	–7.04E-01	–7.06E-01	–7.06E-01	–7.06E-01	–7.06E-01	–7.06E-01
7.00	–8.00E-01	–9.24E-01	–9.48E-01	–9.54E-01	–9.56E-01	–9.56E-01	–9.56E-01	–9.56E-01
7.25	–7.26E-01	–1.09E+00	–1.18E+00	–1.20E+00	–1.20E+00	–1.21E+00	–1.21E+00	–1.21E+00
7.50	–3.77E-01	–1.09E+00	-1.36E+00	–1.43E+00	–1.45E+00	–1.45E+00	–1.46E+00	–1.46E+00
7.75	2.05E-01	–8.33E-01	–1.41E+00	–1.62E+00	–1.68E+00	–1.70E+00	–1.70E+00	–1.71E+00
8.00	2.70E-01	–3.51E-01	–1.23E+00	–1.70E+00	–1.87E+00	–1.93E+00	–1.95E+00	–1.95E+00
8.25	5.98E-01	3.96E-01	–8.43E-01	–1.59E+00	–1.97E+00	–2.12E+00	–2.18E+00	–2.20E+00
8.50	1.42E+00	4.41E-01	–2.14E-01	–1.27E+00	–1.90E+00	–2.23E+00	–2.37E+00	–2.43E+00
8.75	500	1.06E+00	4.57E-01	–7.55E-01	–1.65E+00	–2.18E+00	–2.48E+00	–2.63E+00
9.00	500	500	7.93E-01	9.62E-02	–1.22E+00	–1.98E+00	–2.45E+00	–2.74E+00
9.25	500	500	500	1.33E+00	–5.02E-01	–1.63E+00	–2.27E+00	–2.71E+00
9.50	500	500	500	1.36E+00	6.43E-01	–1.03E+00	–1.98E+00	–2.55E+00
9.75	500	500	500	500	1.12E+00	2.13E-02	–1.48E+00	–2.29E+00
10.00	500	500	500	500	500	9.54E-01	–5.42E-01	–1.88E+00
10.25	500	500	500	500	500	1.96E+00	8.53E-01	–1.05E+00
10.50	500	500	500	500	500	500	1.76E+00	3.90E-01
10.75	500	500	500	500	500	500	500	1.61E+00

Source: DTN: MO0702PADISCON.001_R0 [DIRS 179358], Table 2.

NOTE: This look-up table is implemented in the TSPA-LA Model as parameter Sol_NpO2_LUT. Entries reported as "500" in the table indicate conditions for which a valid solubility value does not exist.

Table 6.3.7-37. Base-Case Plutonium Solubility Look-Up Table (log[Pu], mg/L)

	log fco_2 (bars)							
pH	**-1.50**	**-2.00**	**-2.50**	**-3.00**	**-3.50**	**-4.00**	**-4.50**	**-5.00**
2.00	4.53E+00	4.53E+00	4.53E+00	4.53E+00	4.53E+00	4.53E+00	4.53E+00	4.53E+00
2.25	3.84E+00	3.84E+00	3.84E+00	3.84E+00	3.84E+00	3.84E+00	3.84E+00	3.84E+00
2.50	3.19E+00	3.19E+00	3.19E+00	3.19E+00	3.19E+00	3.19E+00	3.19E+00	3.19E+00
2.75	2.62E+00	2.62E+00	2.62E+00	2.62E+00	2.62E+00	2.62E+00	2.62E+00	2.62E+00
3.00	2.14E+00	2.14E+00	2.14E+00	2.14E+00	2.14E+00	2.14E+00	2.14E+00	2.14E+00
3.25	1.74E+00	1.74E+00	1.74E+00	1.74E+00	1.74E+00	1.74E+00	1.74E+00	1.74E+00
3.50	1.38E+00	1.38E+00	1.38E+00	1.38E+00	1.38E+00	1.38E+00	1.38E+00	1.38E+00
3.75	1.04E+00	1.03E+00	1.03E+00	1.03E+00	1.03E+00	1.03E+00	1.03E+00	1.03E+00
4.00	7.22E-01	7.12E-01	7.09E-01	7.08E-01	7.07E-01	7.07E-01	7.07E-01	7.07E-01
4.25	4.32E-01	4.12E-01	4.06E-01	4.04E-01	4.03E-01	4.03E-01	4.03E-01	4.03E-01
4.50	1.72E-01	1.35E-01	1.23E-01	1.19E-01	1.18E-01	1.17E-01	1.17E-01	1.17E-01
4.75	−5.78E-02	–1.22E-01	−1.45E-01	–1.52E-01	–1.54E-01	–1.55E-01	–1.55E-01	–1.55E-01
5.00	−2.54E-01	–3.60E-01	−3.99E-01	–4.12E-01	–4.17E-01	–4.18E-01	–4.19E-01	–4.19E-01
5.25	−4.13E-01	–5.75E-01	–6.42E-01	–6.65E-01	–6.73E-01	–6.75E-01	–6.76E-01	–6.76E-01
5.50	−5.33E-01	–7.62E-01	–8.70E-01	–9.11E-01	–9.25E-01	–9.29E-01	–9.30E-01	–9.31E-01
5.75	−6.17E-01	–9.17E-01	–1.08E+00	–1.15E+00	–1.17E+00	–1.18E+00	–1.18E+00	–1.18E+00
6.00	−6.73E-01	–1.03E+00	–1.27E+00	–1.37E+00	–1.41E+00	–1.43E+00	–1.43E+00	–1.43E+00
6.25	−7.07E-01	–1.12E+00	–1.42E+00	–1.58E+00	–1.65E+00	–1.67E+00	–1.68E+00	–1.69E+00
6.50	−7.28E-01	–1.17E+00	–1.54E+00	–1.77E+00	–1.88E+00	–1.92E+00	–1.93E+00	–1.93E+00
6.75	−7.39E-01	–1.21E+00	–1.62E+00	–1.92E+00	–2.08E+00	–2.15E+00	–2.18E+00	–2.18E+00
7.00	−7.44E-01	–1.23E+00	–1.67E+00	–2.04E+00	–2.27E+00	–2.38E+00	–2.42E+00	–2.43E+00
7.25	−7.44E-01	–1.24E+00	–1.70E+00	–2.12E+00	–2.42E+00	–2.58E+00	–2.65E+00	–2.67E+00
7.50	−7.32E-01	–1.24E+00	–1.72E+00	–2.17E+00	–2.53E+00	–2.76E+00	–2.87E+00	–2.91E+00
7.75	–6.64E-01	–1.23E+00	–1.72E+00	–2.20E+00	–2.61E+00	–2.91E+00	–3.08E+00	–3.15E+00
8.00	–2.26E-01	–1.17E+00	–1.71E+00	–2.20E+00	–2.65E+00	–3.02E+00	–3.25E+00	–3.37E+00
8.25	9.33E-01	–8.71E-01	–1.66E+00	–2.19E+00	–2.67E+00	–3.08E+00	–3.39E+00	–3.56E+00
8.50	2.39E+00	1.11E-01	–1.44E+00	–2.14E+00	–2.65E+00	–3.11E+00	–3.48E+00	–3.73E+00
8.75	500	1.50E+00	–6.37E-01	–1.96E+00	–2.59E+00	–3.09E+00	–3.51E+00	–3.84E+00
9.00	500	3.20E+00	6.73E-01	–1.31E+00	–2.43E+00	–3.01E+00	–3.49E+00	–3.88E+00
9.25	500	500	2.25E+00	–8.16E-02	–1.90E+00	–2.85E+00	–3.40E+00	–3.84E+00
9.50	500	500	500	1.46E+00	–7.69E-01	–2.41E+00	–3.22E+00	–3.74E+00
9.75	500	500	500	3.65E+00	7.62E-01	–1.39E+00	–2.86E+00	–3.56E+00
10.00	500	500	500	500	2.74E+00	1.24E-01	–1.96E+00	–3.24E+00

Table 6.3.7-37. Base-Case Plutonium Solubility Look-Up Table (log[Pu], mg/L)(Continued)

pH	log fco_2 (bars)							
	-1.50	**-2.00**	**-2.50**	**-3.00**	**-3.50**	**-4.00**	**-4.50**	**-5.00**
10.25	500	500	500	500	500	2.10E+00	–4.65E-01	–2.47E+00
10.50	500	500	500	500	500	500	1.52E+00	–1.02E+00
10.75	500	500	500	500	500	500	500	9.86E-01

Source: DTN: MO0702PADISCON.001_R0 [DIRS 179358], Table 1.

NOTE: This look-up table is implemented in the TSPA-LA Model as parameter Sol_Pu_LUT. Entries reported as "500" in the table indicate conditions for which a valid solubility value does not exist.

Table 6.3.7-38. Base Protactinium Solubility Look-Up Table (log[Pa], mg/L)

	log fco_2 (bars)							
pH	**-1.50**	**-2.00**	**-2.50**	**-3.00**	**-3.50**	**-4.00**	**-4.50**	**-5.00**
3.00	4.38E+00	4.38E+00	4.38E+00	4.38E+00	4.38E+00	4.38E+00	4.38E+00	4.38E+00
3.25	4.10E+00	4.10E+00	4.10E+00	4.10E+00	4.10E+00	4.10E+00	4.10E+00	4.10E+00
3.50	3.82E+00	3.82E+00	3.82E+00	3.82E+00	3.82E+00	3.82E+00	3.82E+00	3.82E+00
3.75	3.55E+00	3.55E+00	3.55E+00	3.55E+00	3.55E+00	3.55E+00	3.55E+00	3.55E+00
4.00	3.29E+00	3.29E+00	3.29E+00	3.29E+00	3.29E+00	3.29E+00	3.29E+00	3.29E+00
4.25	3.03E+00	3.03E+00	3.03E+00	3.03E+00	3.03E+00	3.03E+00	3.03E+00	3.03E+00
4.50	2.77E+00	2.77E+00	2.77E+00	2.77E+00	2.77E+00	2.77E+00	2.77E+00	2.77E+00
4.75	2.52E+00	2.52E+00	2.52E+00	2.52E+00	2.52E+00	2.52E+00	2.52E+00	2.52E+00
5.00	2.26E+00	2.26E+00	2.26E+00	2.26E+00	2.26E+00	2.26E+00	2.26E+00	2.26E+00
5.25	2.01E+00	2.01E+00	2.01E+00	2.01E+00	2.01E+00	2.01E+00	2.01E+00	2.01E+00
5.50	1.76E+00	1.76E+00	1.76E+00	1.76E+00	1.76E+00	1.76E+00	1.76E+00	1.76E+00
5.75	1.51E+00	1.51E+00	1.51E+00	1.51E+00	1.51E+00	1.51E+00	1.51E+00	1.51E+00
6.00	1.26E+00	1.26E+00	1.26E+00	1.26E+00	1.26E+00	1.26E+00	1.26E+00	1.26E+00
6.25	1.01E+00	1.01E+00	1.01E+00	1.01E+00	1.01E+00	1.01E+00	1.01E+00	1.01E+00
6.50	7.66E-01	7.62E-01	7.61E-01	7.60E-01	7.60E-01	7.60E-01	7.60E-01	7.60E-01
6.75	5.35E-01	5.17E-01	5.12E-01	5.11E-01	5.10E-01	5.10E-01	5.10E-01	5.10E-01
7.00	3.46E-01	2.84E-01	2.68E-01	2.63E-01	2.61E-01	2.60E-01	2.60E-01	2.60E-01
7.25	2.41E-01	8.83E-02	3.52E-02	1.83E-02	1.28E-02	1.11E-02	1.05E-02	1.03E-02
7.50	2.76E-01	–1.94E-02	–1.63E-01	–2.14E-01	–2.31E-01	–2.37E-01	–2.39E-01	–2.39E-01
7.75	4.56E-01	8.77E-03	–2.77E-01	–4.12E-01	–4.64E-01	–4.81E-01	–4.87E-01	–4.89E-01
8.00	5.33E-01	1.71E-01	–2.53E-01	–5.29E-01	–6.61E-01	–7.13E-01	–7.31E-01	–7.37E-01
8.25	5.98E-01	4.49E-01	–9.89E-02	–5.11E-01	–7.78E-01	–9.11E-01	–9.63E-01	–9.81E-01
8.50	1.42E+00	1.00E+00	1.47E-01	–3.62E-01	–7.64E-01	–1.03E+00	–1.16E+00	–1.21E+00
8.75	500	1.06E+00	5.38E-01	–1.30E-01	–6.20E-01	–1.01E+00	–1.28E+00	–1.41E+00
9.00	500	500	7.93E-01	1.89E-01	–3.95E-01	–8.75E-01	–1.26E+00	–1.53E+00
9.25	500	500	500	8.19E-01	–1.08E-01	–6.54E-01	–1.12E+00	–1.51E+00
9.50	500	500	500	1.36E+00	3.72E-01	–3.81E-01	–9.10E-01	–1.37E+00
9.75	500	500	500	500	1.12E+00	2.16E-02	–6.44E-01	–1.16E+00
10.00	500	500	500	500	500	9.56E-01	–2.78E-01	–9.00E-01
10.25	500	500	500	500	500	1.96E+00	5.24E-01	–5.52E-01
10.50	500	500	500	500	500	500	1.76E+00	1.72E-01

Source: DTN: MO0702PADISCON.001_R0 [DIRS 179358], Table 9.

NOTE: This look-up table is implemented in the TSPA-LA Model as parameter Sol_Pa_LUT. Entries reported as "500" in the table indicate conditions for which a valid solubility value does not exist.

Table 6.3.7-39. Base Thorium Solubility Look-Up Table (log[Th], mg/L)

	log fco_2 (bars)							
pH	**-1.50**	**-2.00**	**-2.50**	**-3.00**	**-3.50**	**-4.00**	**-4.50**	**-5.00**
3.25	3.84E+00	3.84E+00	3.84E+00	3.84E+00	3.84E+00	3.84E+00	3.84E+00	3.84E+00
3.50	2.54E+00	2.54E+00	2.54E+00	2.54E+00	2.54E+00	2.54E+00	2.54E+00	2.54E+00
3.75	1.61E+00	1.61E+00	1.62E+00	1.62E+00	1.62E+00	1.62E+00	1.62E+00	1.62E+00
4.00	1.14E+00	1.14E+00	1.14E+00	1.14E+00	1.14E+00	1.14E+00	1.14E+00	1.14E+00
4.25	9.41E-01	9.41E-01	9.41E-01	9.41E-01	9.41E-01	9.41E-01	9.41E-01	9.41E-01
4.50	7.42E-01	7.42E-01	7.42E-01	7.42E-01	7.42E-01	7.42E-01	7.42E-01	7.42E-01
4.75	3.82E-01	3.82E-01	3.82E-01	3.82E-01	3.82E-01	3.82E-01	3.82E-01	3.82E-01
5.00	–2.92E-01	–2.94E-01	–2.95E-01	–2.95E-01	–2.95E-01	–2.95E-01	–2.95E-01	–2.95E-01
5.25	–1.17E+00	–1.20E+00	–1.21E+00	–1.21E+00	–1.22E+00	–1.22E+00	–1.22E+00	–1.22E+00
5.50	–1.75E+00	–1.99E+00	–2.10E+00	–2.14E+00	–2.16E+00	–2.16E+00	–2.16E+00	–2.16E+00
5.75	–1.69E+00	–2.13E+00	–2.50E+00	–2.73E+00	–2.84E+00	–2.88E+00	–2.89E+00	–2.90E+00
6.00	–1.46E+00	–1.94E+00	–2.39E+00	–2.75E+00	–2.99E+00	–3.10E+00	–3.14E+00	–3.16E+00
6.25	–1.22E+00	–1.70E+00	–2.17E+00	–2.60E+00	–2.91E+00	–3.09E+00	–3.17E+00	–3.20E+00
6.50	–9.69E-01	–1.46E+00	–1.94E+00	–2.40E+00	–2.77E+00	–3.02E+00	–3.15E+00	–3.19E+00
6.75	–7.16E-01	–1.22E+00	–1.70E+00	–2.18E+00	–2.60E+00	–2.92E+00	–3.10E+00	–3.18E+00
7.00	–4.60E-01	–9.69E-01	–1.46E+00	–1.94E+00	–2.40E+00	–2.78E+00	–3.03E+00	–3.15E+00
7.25	–2.02E-01	–7.16E-01	–1.22E+00	–1.70E+00	–2.18E+00	–2.60E+00	–2.92E+00	–3.10E+00
7.50	5.88E-02	–4.60E-01	–9.69E-01	–1.46E+00	–1.94E+00	–2.40E+00	–2.78E+00	–3.03E+00
7.75	3.22E-01	–2.02E-01	–7.15E-01	–1.22E+00	–1.70E+00	–2.18E+00	–2.60E+00	–2.92E+00
8.00	5.90E-01	5.91E-02	–4.60E-01	–9.69E-01	–1.46E+00	–1.94E+00	–2.40E+00	–2.78E+00
8.25	1.04E+00	3.23E-01	–2.01E-01	–7.15E-01	–1.22E+00	–1.70E+00	–2.18E+00	–2.60E+00
8.50	500	5.96E-01	6.01E-02	–4.59E-01	–9.68E-01	–1.46E+00	–1.94E+00	–2.40E+00
8.75	500	1.41E+00	3.25E-01	–2.00E-01	–7.14E-01	–1.22E+00	–1.70E+00	–2.18E+00
9.00	500	500	6.29E-01	6.31E-02	–4.57E-01	–9.67E-01	–1.47E+00	–1.94E+00
9.25	500	500	2.62E+00	3.33E-01	–1.96E-01	–7.12E-01	–1.22E+00	–1.70E+00
9.50	500	500	500	9.49E-01	7.17E-02	–4.53E-01	–9.65E-01	–1.47E+00
9.75	500	500	500	500	3.81E-01	–1.86E-01	–7.07E-01	–1.21E+00
10.00	500	500	500	500	500	9.60E-02	–4.41E-01	–9.58E-01
10.25	500	500	500	500	500	1.67E+00	–1.61E-01	–6.93E-01
10.50	500	500	500	500	500	500	6.41E-01	–4.13E-01
10.75	500	500	500	500	500	500	500	4.71E-03

Source: DTN: MO0702PADISCON.001_R0 [DIRS 179358], Table 7.

NOTE: This look-up table is implemented in the TSPA-LA Model as parameter Sol_Pa_LUT. Entries reported as “500” in the table indicate conditions for which a valid solubility value does not exist.

Table 6.3.7-40. Base Tin Solubility Look-Up Table (log[Sn], mg/L)

pH	log fCO2 (bars)							
	-1.5	-2.0	-2.5	-3.0	-3.5	-4.0	-4.5	-5.0
2.00	-2.38E+00	-2.38E+00	-2.38E+00	-2.38E+00	-2.38E+00	-2.38E+00	-2.38E+00	-2.38E+00
2.25	-2.38E+00	-2.38E+00	-2.38E+00	-2.38E+00	-2.38E+00	-2.38E+00	-2.38E+00	-2.38E+00
2.50	-2.39E+00	-2.39E+00	-2.39E+00	-2.39E+00	-2.39E+00	-2.39E+00	-2.39E+00	-2.39E+00
2.75	-2.39E+00	-2.39E+00	-2.39E+00	-2.39E+00	-2.39E+00	-2.39E+00	-2.39E+00	-2.39E+00
3.00	-2.39E+00	-2.39E+00	-2.39E+00	-2.39E+00	-2.39E+00	-2.39E+00	-2.39E+00	-2.39E+00
3.25	-2.39E+00	-2.39E+00	-2.39E+00	-2.39E+00	-2.39E+00	-2.39E+00	-2.39E+00	-2.39E+00
3.50	-2.39E+00	-2.39E+00	-2.39E+00	-2.39E+00	-2.39E+00	-2.39E+00	-2.39E+00	-2.39E+00
3.75	-2.39E+00	-2.39E+00	-2.39E+00	-2.39E+00	-2.39E+00	-2.39E+00	-2.39E+00	-2.39E+00
4.00	-2.39E+00	-2.39E+00	-2.39E+00	-2.39E+00	-2.39E+00	-2.39E+00	-2.39E+00	-2.39E+00
4.25	-2.39E+00	-2.39E+00	-2.39E+00	-2.39E+00	-2.39E+00	-2.39E+00	-2.39E+00	-2.39E+00
4.50	-2.39E+00	-2.39E+00	-2.39E+00	-2.39E+00	-2.39E+00	-2.39E+00	-2.39E+00	-2.39E+00
4.75	-2.39E+00	-2.39E+00	-2.39E+00	-2.39E+00	-2.39E+00	-2.39E+00	-2.39E+00	-2.39E+00
5.00	-2.38E+00	-2.38E+00	-2.38E+00	-2.38E+00	-2.38E+00	-2.38E+00	-2.38E+00	-2.38E+00
5.25	-2.38E+00	-2.38E+00	-2.38E+00	-2.38E+00	-2.38E+00	-2.38E+00	-2.38E+00	-2.38E+00
5.50	-2.38E+00	-2.38E+00	-2.38E+00	-2.38E+00	-2.38E+00	-2.38E+00	-2.38E+00	-2.38E+00
5.75	-2.38E+00	-2.38E+00	-2.38E+00	-2.38E+00	-2.38E+00	-2.38E+00	-2.38E+00	-2.38E+00
6.00	-2.37E+00	-2.37E+00	-2.37E+00	-2.37E+00	-2.37E+00	-2.37E+00	-2.37E+00	-2.37E+00
6.25	-2.37E+00	-2.37E+00	-2.37E+00	-2.37E+00	-2.37E+00	-2.37E+00	-2.37E+00	-2.37E+00
6.50	-2.35E+00	-2.35E+00	-2.35E+00	-2.35E+00	-2.35E+00	-2.35E+00	-2.35E+00	-2.35E+00
6.75	-2.33E+00	-2.33E+00	-2.33E+00	-2.33E+00	-2.33E+00	-2.33E+00	-2.33E+00	-2.33E+00
7.00	-2.29E+00	-2.29E+00	-2.29E+00	-2.29E+00	-2.29E+00	-2.29E+00	-2.29E+00	-2.29E+00
7.25	-2.22E+00	-2.22E+00	-2.22E+00	-2.22E+00	-2.22E+00	-2.22E+00	-2.22E+00	-2.22E+00
7.50	-2.12E+00	-2.12E+00	-2.13E+00	-2.13E+00	-2.13E+00	-2.13E+00	-2.13E+00	-2.13E+00
7.75	-1.98E+00	-1.99E+00	-1.99E+00	-1.99E+00	-2.00E+00	-2.00E+00	-2.00E+00	-2.00E+00
8.00	-1.81E+00	-1.82E+00	-1.83E+00	-1.83E+00	-1.83E+00	-1.83E+00	-1.83E+00	-1.83E+00
8.25	-1.60E+00	-1.62E+00	-1.63E+00	-1.63E+00	-1.63E+00	-1.64E+00	-1.64E+00	-1.64E+00
8.50	-1.37E+00	-1.39E+00	-1.41E+00	-1.41E+00	-1.42E+00	-1.42E+00	-1.42E+00	-1.42E+00
8.75	-1.12E+00	-1.14E+00	-1.16E+00	-1.18E+00	-1.18E+00	-1.19E+00	-1.19E+00	-1.19E+00
9.00	500	-8.70E-01	-9.03E-01	-9.26E-01	-9.36E-01	-9.40E-01	-9.42E-01	-9.42E-01
9.25	500	-5.82E-01	-6.18E-01	-6.55E-01	-6.76E-01	-6.84E-01	-6.87E-01	-6.88E-01
9.50	500	500	-2.98E-01	-3.55E-01	-3.94E-01	-4.13E-01	-4.20E-01	-4.22E-01
9.75	500	500	500	2.60E-03	-7.35E-02	-1.16E-01	-1.34E-01	-1.40E-01
10.00	500	500	500	500	3.29E-01	2.28E-01	1.85E-01	1.67E-01

Table 6.3.7-40. Base Tin Solubility Look-Up Table (log[Sn], mg/L) (Continued)

pH	log fCO2 (bars)							
	-1.5	-2.0	-2.5	-3.0	-3.5	-4.0	-4.5	-5.0
10.25	500	500	500	500	500	6.89E-01	5.71E-01	5.17E-01
10.50	500	500	500	500	500	500	1.08E+00	9.45E-01
10.75	500	500	500	500	500	500	500	1.51E+00

Source: DTN: MO0702PADISCON.001_R0 [DIRS 179358], Table 16.

NOTE: This look-up table is implemented in the TSPA-LA Model as parameter Sol_Sn_LUT. Entries reported as "500" in the table indicate conditions for which a valid solubility value does not exist.

Table 6.3.7-41. Uncertainty in Americium Solubility Model

TSPA-LA Model Name	Model Abstraction Symbol	Description	Units	Distribution Type	Distribution Specification
Am_Eps_1_low_a	ε_1	Uncertainties in log K below 1 molal ionic strength.	None	Truncated normal	$\mu = 0$ $\sigma = 1.0$ $2\sigma = \pm 2.0$
Am_Eps_1_high_a	ε_1	Uncertainties in log K at 1 to 3 molal ionic strength.	None	Truncated normal	$\mu = 0$ $\sigma = 1.04$ $2\sigma = \pm 2.08$
Am_Eps_2_Glass_Low_a	$\varepsilon_2^{\text{CSNF-low}}$ $\varepsilon_2^{\text{CDSP-Glass}}$ $\varepsilon_2^{\text{CDSP-F-low}}$	Fluoride Uncertainty, CSNF waste packages when I < 0.2m. CDSP packages, Cell 1b when I < 0.004m and Cell 1a.	None	Triangular	Min = 0 Max = 4.42 Most likely = 0
Am_Eps_2_CSNF_High_a	$\varepsilon_2^{\text{CSNF-high}}$ $\varepsilon_2^{\text{CSNF-invert}}$	Fluoride Uncertainty, CSNF waste packages when I ≥ 0.2m and invert below CSNF waste packages.	None	Triangular	Min = 0 Max = 109.03 Most likely = 0
Am_Eps_2_CDSP_High_a	$\varepsilon_2^{\text{CDSP-F-high}}$ $\varepsilon_2^{\text{CDSP-invert}}$	Fluoride Uncertainty, CDSP waste packages when I ≥ 0.004m and invert below CDSP waste packages.	None	Triangular	Min = 0 Max = 688.6 Most likely = 0

Source: DTN: MO0702PADISCON.001_R0 [DIRS 179358], Table 19; DTN: MO0702PAFLUORI.000_R1 [DIRS 181219], Table 13.

Table 6.3.7-42. Uncertainty in Neptunium (Np_2O_5) Solubility Model

TSPA-LA Model Name	Model Abstraction Symbol	Description	Units	Distribution Type	Distribution Specification
Np2O5_Eps_1_low_a	ε_1	Uncertainties in log K below 1 molal ionic strength.	None	Truncated normal	$\mu = 0$ $\sigma = 0.8$ $2\sigma = \pm 1.6$
Np2O5_Eps_1_high_a	ε_1	Uncertainties in log K at 1 to 3 molal ionic strength.	None	Truncated normal	$\mu = 0$ $\sigma = 0.85$ $2\sigma = \pm 1.7$
Np2O5_Eps_2_ Glass_Low CSNF_High_a	$\varepsilon_2^{\text{CSNF-low}}$ $\varepsilon_2^{\text{CDSP-Glass}}$ $\varepsilon_2^{\text{CDSP-F-low}}$	Fluoride Uncertainty, CSNF waste packages when I < 0.2m. CDSP packages, Cell 1b when I < 0.004m and Cell 1a.	None	Triangular	Min = 0 Max = 11 Most likely = 0
Np2O5_Eps_2_CSNF_High_a	$\varepsilon_2^{\text{CSNF-high}}$ $\varepsilon_2^{\text{CSNF-invert}}$	Fluoride Uncertainty, CSNF waste packages when I ≥ 0.2m and invert below CSNF waste packages.	None	Triangular	Min = 0 Max = 197 Most likely = 0
Np2O5_Eps_2_CDSP_High_a	$\varepsilon_2^{\text{CDSP-F-high}}$ $\varepsilon_2^{\text{CDSP-invert}}$	Fluoride Uncertainty, CDSP waste packages when I ≥ 0.004m and invert below CDSP waste packages.	None	Triangular	Min = 0 Max = 853 Most likely = 0

Source: DTN: MO0702PADISCON.001_R0 [DIRS 179358], Table 19; DTN: MO0702PAFLUORI.000_R1 [DIRS 181219], Table 5.

Table 6.3.7-43. Uncertainty in Neptunium (NpO_2) Solubility Model

TSPA-LA Model Name	Model Abstraction Symbol	Description	Units	Distribution Type	Distribution Specification
NpO2_Eps_1_low_a	ε_1	Uncertainties in log K below 1 molal ionic strength.	None	Truncated normal	$\mu = 0$ $\sigma = 0.6$ $2\sigma = \pm 1.2$
NpO2_Eps_1_high_a	ε_1	Uncertainties in log K at 1 to 3 molal ionic strength.	None	Truncated normal	$\mu = 0$ $\sigma = 0.67$ $2\sigma = \pm 1.34$
NpO2_Eps_2_Glass_Low_a	$\varepsilon_2^{CSNF\text{-}low}$ $\varepsilon_2^{CDSP\text{-}Glass}$ $\varepsilon_2^{CDSP\text{-}F\text{-}low}$	Fluoride Uncertainty, CSNF waste packages when I < 0.2m. CDSP packages, Cell 1b when I < 0.004m and Cell 1a.	None	Triangular	Min = 0 Max = 14.1 Most likely =0
NpO2_Eps_2_CSNF_High_a	$\varepsilon_2^{CSNF\text{-}high}$ $\varepsilon_2^{CSNF\text{-}invert}$	Fluoride Uncertainty, CSNF waste packages when I ≥ 0.2m and invert below CSNF waste packages.	None	Triangular	Min = 0 Max = 255.8 Most likely =0
NpO2_Eps_2_CDSP_High_a	$\varepsilon_2^{CDSP\text{-}F\text{-}high}$ $\varepsilon_2^{CDSP\text{-}invert}$	Fluoride Uncertainty, CDSP waste packages when I ≥ 0.004m and invert below CDSP waste packages.	None	Triangular	Min = 0 Max = 1093.5 Most likely =0

Source: DTN: MO0702PADISCON.001_R0 [DIRS 179358], Table 19; DTN: MO0702PAFLUORI.000_R1 [DIRS 181219], Table 3.

Table 6.3.7-44. Uncertainty in Plutonium Solubility Model

TSPA-LA Model Name	Model Abstraction Symbol	Description	Units	Distribution Type	Distribution Specification
Pu_Eps_1_low_a	ε_1	Uncertainties in log K below 1 molal ionic strength.	None	Truncated normal	$\mu = 0$ $\sigma = 0.7$ $2\sigma = 1.4$
Pu_Eps_1_high_a	ε_1	Uncertainties in log K at 1 to 3 molal ionic strength.	None	Truncated normal	$\mu = 0$ $\sigma = 0.76$ $2\sigma = 1.52$
Pu_Eps_2_Glass_Low_a	$\varepsilon_2^{\text{CSNF-low}}$ $\varepsilon_2^{\text{CDSP-Glass}}$ $\varepsilon_2^{\text{CDSP-F-low}}$	Fluoride Uncertainty, CSNF waste packages when I < 0.2m. CDSP packages, Cell 1b when I < 0.004m and Cell 1a.	None	Triangular	Min = 0 Max = 79 Most likely = 0
Pu_Eps_2_CSNF_High_a	$\varepsilon_2^{\text{CSNF-high}}$ $\varepsilon_2^{\text{CSNF-invert}}$	Fluoride Uncertainty, CSNF waste packages when I ≥ 0.2m and invert below CSNF waste packages.	None	Triangular	Min = 0 Max = 1374 Most likely = 0
Pu_Eps_2_CDSP_High_a	$\varepsilon_2^{\text{CDSP-F-high}}$ $\varepsilon_2^{\text{CDSP-invert}}$	Fluoride Uncertainty, CDSP waste packages when I ≥ 0.004m and invert below CDSP waste packages.	None	Triangular	Min = 0 Max = 5460 Most likely = 0

Source: DTN: MO0702PADISCON.001_R0 [DIRS 179358], Table 19; DTN: MO0702PAFLUORI.000_R1 [DIRS 181219], Table 1.

Table 6.3.7-45. Uncertainty in Protactinium Solubility Model

TSPA-LA Model Name	Model Abstraction Symbol	Description	Units	Distribution Type	Distribution Specification
Pa_Eps_1_a	ε_1	Uncertainties in analogue	None	Uniform	Min = –4.42 Max = –0.05
Pa_Eps_2_Glass_Low_a	$\varepsilon_2^{\text{CSNF-low}}$ $\varepsilon_2^{\text{CDSP-Glass}}$ $\varepsilon_2^{\text{CDSP-F-low}}$	Fluoride Uncertainty, CSNF waste packages when I < 0.2m. CDSP packages, Cell 1b when I < 0.004m and Cell 1a.	None	Triangular	Min = 0 Max = 11 Most likely = 0
Pa_Eps_2_CSNF_High_a	$\varepsilon_2^{\text{CSNF-high}}$ $\varepsilon_2^{\text{CSNF-invert}}$	Fluoride Uncertainty, CSNF waste packages when I ≥ 0.2m and invert below CSNF waste packages.	None	Triangular	Min = 0 Max = 197 Most likely = 0
Pa_Eps_2_CDSP_High_a	$\varepsilon_2^{\text{CDSP-F-high}}$ $\varepsilon_2^{\text{CDSP-invert}}$	Fluoride Uncertainty, CDSP waste packages when I ≥ 0.004m and invert below CDSP waste packages.	None	Triangular	Min = 0 Max =853 Most likely = 0

Source: DTN: MO0702PADISCON.001_R0 [DIRS 179358], Table 19; DTN: MO0702PAFLUORI.000_R1 [DIRS 181219], Table 15.

Table 6.3.7-46. Uncertainty in Thorium Solubility Model

TSPA-LA Model Name	Model Abstraction Symbol	Description	Units	Distribution Type	Distribution Specification
Th_Eps_1_low_a	$\mathcal{E}_1$	Uncertainties in log K below 1 molal ionic strength.	None	Truncated normal	$\mu = 0$ $\sigma = 0.7$ $2\sigma = \pm 1.4$
Th_Eps_1_high_a	$\mathcal{E}_1$	Uncertainties in log K at 1 to 3 molal ionic strength.	None	Truncated normal	$\mu = 0$ $\sigma = 0.76$ $2\sigma = \pm 1.52$
Th_Eps_2_Glass_Low_a	$\varepsilon_2^{\text{CSNF-low}}$ $\varepsilon_2^{\text{CDSP-Glass}}$ $\varepsilon_2^{\text{CDSP-F-low}}$	Fluoride Uncertainty, CSNF waste packages when I < 0.2m. CDSP packages, Cell 1b when I < 0.004m and Cell 1a.	None	Triangular	Min = 0 Max = 626.2 Most likely = 0
Th_Eps_2_CSNF_High_a	$\varepsilon_2^{\text{CSNF-high}}$ $\varepsilon_2^{\text{CSNF-invert}}$	Fluoride Uncertainty, CSNF waste packages when I ≥ 0.2m and invert below CSNF waste packages.	None	Triangular	Min = 0 Max = 7848.3 Most likely = 0
Th_Eps_2_CDSP_High_a	$\varepsilon_2^{\text{CDSP-F-high}}$ $\varepsilon_2^{\text{CDSP-invert}}$	Fluoride Uncertainty, CDSP waste packages when I ≥ 0.004m and invert below CDSP waste packages.	None	Triangular	Min = 0 Max = 23723.3 Most likely = 0

Source: DTN: MO0702PADISCON.001_R0 [DIRS 179358], Table 19; DTN: MO0702PAFLUORI.000_R1 [DIRS 181219], Table 11.

Table 6.3.7-47. Uncertainty in Tin Solubility Model

TSPA-LA Model Name	Model Abstraction Symbol	Description	Units	Distribution Type	Distribution Specification
Sn_Eps_low_a	$\mathcal{E}_1$	Uncertainties in log K below 1 molal ionic strength.	None	Truncated normal	$\mu = 0$ $\sigma = 0.45$ $2\ \sigma = 0.90$
Sn_Eps_high_a	$\mathcal{E}_1$	Uncertainties in log K at 1 to 3 molal ionic strength.	None	Truncated normal	$\mu = 0$ $\sigma = 0.54$ $2\ \sigma = 1.08$

Source: DTN: MO0702PADISCON.001_R0 [DIRS 179358], Table 19.

Table 6.3.7-48. Multiplication Factor, N(pH), Used to Modify Fluoride Concentration Uncertainty Terms (ε2) for Americium

pH	Multiplication Factor for Fluoride Uncertainty		
	Glass, CSNF low, and CDSP low	CSNF high and CSNF invert	CDSP high and CDSP invert
6.00	1.00E+00	1.00E+00	1.00E+00
6.25	8.91E-02	1.45E-01	3.20E-01
6.50	1.30E-02	2.92E-02	7.24E-02
6.75	2.13E-03	5.61E-03	1.36E-02
7.00	3.44E-04	1.04E-03	2.47E-03
7.25	4.98E-05	1.98E-04	4.50E-04
7.50	3.39E-06	4.08E-05	8.39E-05
7.75	0.00E-00	1.04E-05	1.68E-05
8.00	0.00E-00	4.41E-06	4.13E-06
8.25	3.62E-06	2.41E-06	1.52E-06
8.50	3.39E-06	2.34E-06	1.36E-06
8.75	8.82E-06	6.00E-06	3.67E-06
9.00	3.69E-05	2.59E-05	1.65E-05
9.25	1.92E-04	1.36E-04	8.82E-05
9.50	1.13E-03	8.02E-04	5.23E-04
9.75	7.24E-03	5.10E-03	3.33E-03

Source: DTN: MO0702PAFLUORI.000_R1 [DIRS 181219], Table 14.

NOTE: These multiplication factors are implemented in the TSPA-LA Model as parameters Am_Eps_2_Glass_Low, Am_Eps_2_CSNF_High, Am_Eps_2_CDSP_High.

Table 6.3.7-49. Multiplication Factor, N(pH), Used to Modify Fluoride Concentration Uncertainty Terms (ε2) for Neptunium (Np_2O_5)

pH	Multiplication Factor for Fluoride Uncertainty		
	Glass, CSNF low, and CDSP low	CSNF high and CSNF invert	CDSP high and CDSP invert
3.00	1.00E+00	1.00E+00	1.00E+00
3.25	7.27E-01	7.36E-01	7.63E-01
3.50	4.91E-01	5.09E-01	5.47E-01
3.75	3.18E-01	3.30E-01	3.60E-01
4.00	1.91E-01	2.01E-01	2.17E-01
4.25	1.09E-01	1.17E-01	1.41E-01
4.50	6.64E-02	6.66E-02	9.31E-02
4.75	3.82E-02	3.74E-02	5.70E-02
5.00	2.09E-02	2.08E-02	3.36E-02
5.25	1.18E-02	1.16E-02	1.94E-02
5.50	6.64E-03	6.51E-03	1.11E-02
5.75	3.73E-03	3.68E-03	6.28E-03
6.00	2.09E-03	2.15E-03	3.55E-03
6.25	1.18E-03	1.24E-03	2.00E-03
6.50	6.64E-04	7.13E-04	1.13E-03
6.75	3.73E-04	4.12E-04	6.37E-04
7.00	2.09E-04	2.41E-04	3.60E-04
7.25	1.18E-04	1.44E-04	2.04E-04
7.50	6.45E-05	8.96E-05	1.17E-04
7.75	3.45E-05	6.01E-05	6.97E-05
8.00	1.55E-05	4.81E-05	4.52E-05
8.25	4.64E-05	4.15E-05	3.37E-05
8.50	4.09E-05	3.80E-05	3.11E-05
8.75	5.45E-05	5.13E-05	4.43E-05
9.00	1.55E-04	1.55E-04	1.47E-04
9.25	1.34E-03	1.32E-03	1.29E-03

Source: DTN: MO0702PAFLUORI.000_R1 [DIRS 181219], Table 6.

NOTE: These multiplication factors are implemented in the TSPA-LA Model as parameters Np2O5_Eps_2_Glass_Low_N, Np2O5_CSNF_High_N, Np2O5_CDSP_High_N .

Table 6.3.7-50. Multiplication Factor, N(pH), Used to Modify Fluoride Concentration Uncertainty Terms (ε2) for Neptunium (NpO2)

pH	Multiplication Factor for Fluoride Uncertainty		
	Glass, CSNF low, and CDSP low	CSNF high and CSNF invert	CDSP high and CDSP invert
3.00	1.00E+00	1.00E+00	1.00E+00
3.25	5.77E-01	6.74E-01	7.77E-01
3.50	2.86E-01	4.12E-01	5.75E-01
3.75	1.23E-01	2.16E-01	3.77E-01
4.00	4.96E-02	9.57E-02	2.04E-01
4.25	1.92E-02	3.78E-02	9.00E-02
4.50	7.66E-03	1.42E-02	3.50E-02
4.75	3.26E-03	5.53E-03	1.31E-02
5.00	1.49E-03	2.26E-03	4.98E-03
5.25	7.09E-04	9.96E-04	2.01E-03
5.50	3.62E-04	4.71E-04	8.74E-04
5.75	1.91E-04	2.37E-04	4.10E-04
6.00	1.06E-04	1.24E-04	2.04E-04
6.25	5.74E-05	6.74E-05	1.07E-04
6.50	3.12E-05	3.74E-05	5.74E-05
6.75	1.84E-05	2.11E-05	3.15E-05
7.00	9.93E-06	1.22E-05	1.75E-05
7.25	5.53E-06	7.21E-06	9.88E-06
7.50	3.05E-06	4.45E-06	5.68E-06
7.75	1.49E-06	3.01E-06	3.46E-06
8.00	4.26E-07	2.82E-06	2.61E-06
8.25	4.40E-06	3.92E-06	3.22E-06
8.50	1.00E-05	9.27E-06	8.17E-06
8.75	4.75E-05	4.55E-05	4.40E-05
9.00	4.18E-04	4.07E-04	4.07E-04
9.25	5.53E-03	5.47E-03	5.48E-03

Source: DTN: MO0702PAFLUORI.000_R1 [DIRS 181219], Table 4.

NOTE: These multiplication factors are implemented in the TSPA-LA Model as parameters NpO2_Glass_low_N, NpO2_CSNF_High_N, NpO2_CDSP_High_N.

Table 6.3.7-51. Multiplication Factor, N(pH), Used to Modify Fluoride Concentration Uncertainty Terms (ε2) for Plutonium

pH	Multiplication Factor for Fluoride Uncertainty		
	Glass, CSNF low, and CDSP low	CSNF high and CSNF invert	CDSP high and CDSP invert
2.00	1.00E+00	1.00E+00	1.00E+00
2.25	7.67E-01	7.58E-01	7.42E-01
2.50	5.08E-01	4.98E-01	4.83E-01
2.75	3.50E-01	3.42E-01	3.33E-01
3.00	2.41E-01	2.40E-01	2.44E-01
3.25	1.48E-01	1.60E-01	1.81E-01
3.50	7.51E-02	9.41E-02	1.27E-01
3.75	3.18E-02	4.69E-02	7.81E-02
4.00	1.18E-02	1.96E-02	3.95E-02
4.25	4.06E-03	7.20E-03	1.64E-02
4.50	1.34E-03	2.45E-03	5.90E-03
4.75	4.32E-04	8.03E-04	1.98E-03
5.00	1.37E-04	2.58E-04	6.44E-04
5.25	4.32E-05	8.19E-05	2.07E-04
5.50	1.34E-05	2.58E-05	6.61E-05
5.75	4.08E-06	8.04E-06	2.12E-05
6.00	1.19E-06	2.47E-06	6.81E-06
6.25	3.29E-07	7.39E-07	2.22E-06
6.50	6.33E-08	2.12E-07	7.38E-07
6.75	0.00E+00	5.60E-08	2.54E-07
7.00	0.00E+00	1.34E-08	9.23E-08
7.25	0.00E+00	3.20E-09	3.64E-08
7.50	0.00E+00	2.04E-09	1.62E-08
7.75	0.00E+00	3.35E-09	9.16E-09
8.00	0.00E+00	7.71E-09	8.44E-09
8.25	1.90E-08	1.68E-08	1.43E-08
8.50	4.94E-08	4.79E-08	4.62E-08
8.75	2.91E-07	2.90E-07	3.07E-07
9.00	2.85E-06	2.91E-06	3.15E-06
9.25	3.85E-05	3.94E-05	4.24E-05
9.50	7.34E-04	7.44E-04	7.90E-04
9.75	6.33E-02	6.43E-02	6.90E-02

Source: DTN: MO0702PAFLUORI.000_R1 [DIRS 181219], Table 2.

NOTE: These multiplication factors are implemented in the TSPA-LA Model as parameters Pu_Glass_low_N, Pu_CSNF_High_N, Pu_CDSP_High_N.

Table 6.3.7-52. Multiplication Factor, N(pH), Used to Modify Fluoride Concentration Uncertainty Terms (ε2) for Thorium

pH	Multiplication Factor for Fluoride Uncertainty		
	Glass, CSNF low, and CDSP low	CSNF high and CSNF invert	CDSP high and CDSP invert
3.25	1.00E+00	1.00E+00	1.00E+00
3.50	7.51E-02	1.01E-01	1.48E-01
3.75	2.70E-02	3.53E-02	4.75E-02
4.00	2.08E-02	2.74E-02	3.60E-02
4.25	1.76E-02	2.41E-02	3.19E-02
4.50	1.45E-02	2.15E-02	2.91E-02
4.75	1.05E-02	1.90E-02	2.67E-02
5.00	4.73E-03	1.59E-02	2.44E-02
5.25	8.99E-04	1.19E-02	2.17E-02
5.50	1.02E-04	6.88E-03	1.82E-02
5.75	1.04E-05	2.26E-03	1.32E-02
6.00	1.04E-06	3.40E-04	6.85E-03
6.25	1.03E-07	3.62E-05	1.77E-03
6.50	7.98E-09	3.65E-06	2.26E-04
6.75	0.00E-00	3.62E-07	2.34E-05
7.00	0.00E-00	3.25E-08	2.36E-06
7.25	0.00E-00	0.00E-00	2.63E-07
7.50	0.00E-00	4.33E-09	7.86E-08
7.75	0.00E-00	4.00E-08	1.08E-07
8.00	0.00E-00	1.73E-07	2.14E-07
8.25	2.87E-07	3.57E-07	3.72E-07
8.50	3.83E-07	5.08E-07	5.61E-07
8.75	5.11E-07	6.79E-07	7.91E-07
9.00	4.79E-07	8.28E-07	1.02E-06
9.25	7.98E-07	1.07E-06	1.42E-06
9.50	3.61E-05	5.21E-05	7.81E-05

Source: DTN: MO0702PAFLUORI.000_R1 [DIRS 181219], Table 12.

NOTE: These multiplication factors are implemented in the TSPA-LA Model as parameters Th_Glass_low_N, Th_CSNF_High_N, Th_CDSP_High_N.

Table 6.3.7-53. Uranium Solubility Look-Up Table (log[U], mg/L) for CSNF WPs Breached under Nominal Conditions or by Seismic Activity

pH	log fCO_2 (bars)							
	-1.5	-2.0	-2.5	-3.0	-3.5	-4.0	-4.5	-5.0
3.50	4.41E+00	4.41E+00	4.41E+00	4.41E+00	4.41E+00	4.41E+00	4.41E+00	4.41E+00
3.75	3.55E+00	3.55E+00	3.55E+00	3.55E+00	3.55E+00	3.55E+00	3.55E+00	3.55E+00
4.00	2.87E+00	2.87E+00	2.87E+00	2.87E+00	2.87E+00	2.87E+00	2.87E+00	2.87E+00
4.25	2.33E+00	2.33E+00	2.33E+00	2.33E+00	2.33E+00	2.33E+00	2.33E+00	2.33E+00
4.50	1.93E+00	1.92E+00	1.92E+00	1.92E+00	1.92E+00	1.92E+00	1.92E+00	1.92E+00
4.75	1.62E+00	1.60E+00	1.60E+00	1.59E+00	1.59E+00	1.59E+00	1.59E+00	1.59E+00
5.00	1.35E+00	1.32E+00	1.31E+00	1.31E+00	1.30E+00	1.30E+00	1.30E+00	1.30E+00
5.25	1.10E+00	1.03E+00	1.00E+00	9.95E-01	9.93E-01	9.92E-01	9.92E-01	9.91E-01
5.50	9.31E-01	7.65E-01	6.97E-01	6.74E-01	6.66E-01	6.63E-01	6.63E-01	6.62E-01
5.75	9.05E-01	6.19E-01	4.67E-01	4.07E-01	3.86E-01	3.79E-01	3.77E-01	3.76E-01
6.00	1.03E+00	6.26E-01	3.76E-01	2.51E-01	2.03E-01	1.87E-01	1.82E-01	1.80E-01
6.25	1.25E+00	7.58E-01	4.13E-01	2.07E-01	1.17E-01	8.36E-02	7.27E-02	6.92E-02
6.50	1.52E+00	9.60E-01	5.30E-01	2.48E-01	9.90E-02	3.93E-02	1.87E-02	1.19E-02
6.75	1.86E+00	1.21E+00	7.12E-01	3.53E-01	1.32E-01	3.21E-02	-4.74E-03	-1.71E-02
7.00	2.33E+00	1.51E+00	9.38E-01	5.01E-01	2.11E-01	5.47E-02	-8.42E-03	-3.04E-02
7.25	500	1.89E+00	1.20E+00	6.98E-01	3.34E-01	1.09E-01	6.00E-03	-3.21E-02
7.50	500	2.54E+00	1.52E+00	9.32E-01	4.92E-01	2.00E-01	4.29E-02	-2.10E-02
7.55	500	2.90E+00	1.60E+00	9.95E-01	5.39E-01	2.24E-01	5.35E-02	-1.69E-02
7.75	500	500	1.98E+00	1.21E+00	6.96E-01	3.26E-01	1.09E-01	7.58E-03
7.90	500	500	2.51E+00	1.42E+00	8.48E-01	4.32E-01	1.66E-01	3.59E-02
8.00	500	500	500	1.58E+00	9.38E-01	4.97E-01	2.12E-01	6.04E-02
8.25	500	500	500	2.27E+00	1.24E+00	7.07E-01	3.47E-01	1.45E-01
8.30	500	500	500	2.58E+00	1.33E+00	7.66E-01	3.88E-01	1.66E-01
8.50	500	500	500	500	1.73E+00	9.65E-01	5.26E-01	2.59E-01
8.65	500	500	500	500	2.31E+00	1.19E+00	6.64E-01	3.56E-01
8.75	500	500	500	500	500	1.34E+00	7.47E-01	4.16E-01
9.00	500	500	500	500	500	2.11E+00	1.04E+00	6.11E-01
9.07	500	500	500	500	500	2.67E+00	1.18E+00	6.84E-01
9.25	500	500	500	500	500	500	1.58E+00	8.56E-01
9.50	500	500	500	500	500	500	500	1.24E+00
9.75	500	500	500	500	500	500	500	2.08E+00

Source: DTN: MO0702PADISCON.001_R0 [DIRS 179358], Table 4.

NOTE: This look-up table is implemented in the TSPA-LA Model as parameter Sol_U_LUT_Schoepite_CSNF. Entries reported as '500' in the table indicate conditions for which a valid solubility value does not exist.

Table 6.3.7-54. Uncertainty in Log K Values for Base-Case Uranium Solubility Model (CSNF WP Nominal and Seismic Scenario Classes)

TSPA-LA Model Name	Model Abstraction Symbol	Description	Units	Distribution Type	Distribution Specification
U_Eps_1_low_Nominal_a	ε_1	Uncertainties in log K (schoepite) below 1 molal ionic strength	None	Truncated normal	$\mu = 0$ $\sigma = 0.5$ $2\sigma = \pm 1.0$
U_Eps_1_high_Nominal_a	ε_1	Uncertainties in log K (schoepite) at 1 to 3 molal ionic strength	None	Truncated normal	$\mu = 0$ $\sigma = 0.6$ $2\sigma = \pm 1.2$
U_Eps_2_CSNF_Low_Nomina_a	$\varepsilon_2^{\text{CSNF-low}}$	Fluoride Uncertainty, CSNF waste packages when I < 0.2m.	None	Triangular	Min = 0 Max = 78 Most likely = 0
U_Eps_2_CSNF_High_Nominal_a	$\varepsilon_2^{\text{CSNF-high}}$ $\varepsilon_2^{\text{CSNF-invert}}$	Fluoride Uncertainty, CSNF waste packages when I ≥ 0.2m	None	Triangular	Min = 0 Max = 1361 Most likely = 0

Source: DTN: MO0702PADISCON.001_R0 [DIRS 179358], Table 19;
DTN: MO0702PAFLUORI.000_R1 [DIRS 181219], Table 7.

Table 6.3.7-55. Multiplication Factor, N(pH), Used to Modify Fluoride Concentration Uncertainty Terms (ε_2) for Uranium (CSNF WP, Nominal and Seismic Scenario Classes)

pH	Multiplication Factor for Fluoride Uncertainty	
	CSNF low	CSNF high
3.50	1.00E+00	1.00E+00
3.75	7.24E-01	7.03E-01
4.00	5.17E-01	4.85E-01
4.25	4.18E-01	3.73E-01
4.50	3.48E-01	2.99E-01
4.75	2.70E-01	2.41E-01
5.00	1.85E-01	1.92E-01
5.25	1.06E-01	1.45E-01
5.50	4.86E-02	9.86E-02
5.75	1.83E-02	5.67E-02
6.00	6.17E-03	2.63E-02
6.25	1.99E-03	1.01E-02
6.50	6.31E-04	3.42E-03
6.75	1.94E-04	1.11E-03
7.00	5.00E-05	3.49E-04
7.25	0.00E-00	1.07E-04
7.50	0.00E-00	4.64E-05
7.75	0.00E-00	1.67E-04
8.00	0.00E-00	2.01E-03
8.25	2.44E-02	2.51E-02

Source: DTN: MO0702PAFLUORI.000_R1 [DIRS 181219], Table 8.

NOTE: This multiplication factor is implemented in the TSPA-LA Model as parameters U_CSNF_Low_Nominal_N and U_CSNF_High_Nominal_N.

Table 6.3.7-56. Schoepite Controlled Uranium Solubility Look-Up Table (log[U], mg/L) for CDSP WPs Breached Under any Scenario, CSNF WPs Breached in by an Igneous Intrusion, and in the Invert (all locations and scenarios)

	log fco_2 (bars)							
pH	**-1.50**	**-2.00**	**-2.50**	**-3.00**	**-3.50**	**-4.00**	**-4.50**	**-5.00**
3.50	4.41E+00	4.41E+00	4.41E+00	4.41E+00	4.41E+00	4.41E+00	4.41E+00	4.41E+00
3.75	3.55E+00	3.55E+00	3.55E+00	3.55E+00	3.55E+00	3.55E+00	3.55E+00	3.55E+00
4.00	2.86E+00	2.86E+00	2.86E+00	2.86E+00	2.86E+00	2.86E+00	2.86E+00	2.86E+00
4.25	2.33E+00	2.33E+00	2.33E+00	2.33E+00	2.33E+00	2.33E+00	2.33E+00	2.33E+00
4.50	1.92E+00	1.91E+00	1.91E+00	1.91E+00	1.91E+00	1.91E+00	1.91E+00	1.91E+00
4.75	1.61E+00	1.59E+00	1.59E+00	1.59E+00	1.59E+00	1.59E+00	1.59E+00	1.59E+00
5.00	1.34E+00	1.31E+00	1.30E+00	1.30E+00	1.30E+00	1.30E+00	1.30E+00	1.30E+00
5.25	1.10E+00	1.02E+00	9.94E-01	9.85E-01	9.83E-01	9.82E-01	9.81E-01	9.81E-01
5.50	9.24E-01	7.55E-01	6.86E-01	6.62E-01	6.54E-01	6.51E-01	6.51E-01	6.50E-01
5.75	9.10E-01	6.11E-01	4.57E-01	3.94E-01	3.73E-01	3.66E-01	3.64E-01	3.63E-01
6.00	1.04E+00	6.30E-01	3.68E-01	2.41E-01	1.92E-01	1.75E-01	1.70E-01	1.68E-01
6.25	1.25E+00	7.66E-01	4.09E-01	2.01E-01	1.09E-01	7.55E-02	6.43E-02	6.08E-02
6.50	1.52E+00	9.70E-01	5.37E-01	2.45E-01	9.45E-02	3.42E-02	1.33E-02	6.55E-03
6.75	1.86E+00	1.22E+00	7.22E-01	3.52E-01	1.30E-01	2.93E-02	–7.88E-03	–2.03E-02
7.00	2.33E+00	1.51E+00	9.48E-01	5.09E-01	2.10E-01	5.32E-02	–1.02E-02	–3.22E-02
7.25		1.89E+00	1.21E+00	7.08E-01	3.34E-01	1.08E-01	5.05E-03	–3.31E-02
7.50		2.54E+00	1.53E+00	9.44E-01	5.01E-01	2.00E-01	4.24E-02	–2.16E-02
7.75			1.98E+00	1.22E+00	7.07E-01	3.33E-01	1.09E-01	7.28E-03
8.00				1.57E+00	9.51E-01	5.06E-01	2.12E-01	6.02E-02

Source: DTN: MO0702PADISCON.001_R0 [DIRS 179358], Table 5.

NOTE: This look-up table is implemented in the TSPA-LA Model as parameter Sol_U_LUT_Schoepite. This solubility corresponds to schoepite saturation. The shaded area indicates the region where it is uncertain if uranium solubility is controlled by schoepite or Na-Boltwoodite.

Table 6.3.7-57. Na-Boltwoodite and $Na_4UO_2(CO_3)_3$ Controlled Uranium Solubility Look-Up Table (log[U], mg/L) for CDSP WPs Breached under Any Scenario, CSNF WPs Breached by an Igneous Intrusion, and in the Invert (all locations and scenarios)

	log fco_2 (bars)							
pH	**-1.50**	**-2.00**	**-2.50**	**-3.00**	**-3.50**	**-4.00**	**-4.50**	**-5.00**
6.50	2.56E+00							
6.75	2.16E+00	2.00E+00	1.51E+00	1.07E+00	7.46E-01	5.56E-01	4.73E-01	4.43E-01
7.00	1.94E+00	1.82E+00	1.28E+00	8.21E-01	4.79E-01	2.77E-01	1.88E-01	1.56E-01
7.25	2.14E+00	1.51E+00	1.09E+00	5.88E-01	2.28E-01	2.04E-02	–7.08E-02	–1.04E-01
7.50	2.79E+00	1.55E+00	1.03E+00	3.97E-01	–9.31E-03	–2.29E-01	–3.23E-01	–3.56E-01
7.75	4.78E+00	1.98E+00	1.03E+00	3.18E-01	–2.14E-01	–4.68E-01	–5.67E-01	–6.01E-01
8.00	4.78E+00	2.76E+00	1.34E+00	4.67E-01	–3.27E-01	–6.84E-01	–8.00E-01	–8.35E-01
8.25	4.78E+00	4.78E+00	1.92E+00	7.59E-01	–2.27E-01	–8.41E-01	–1.01E+00	–1.05E+00
8.50	4.78E+00	4.78E+00	2.75E+00	1.25E+00	1.67E-01	–8.36E-01	–1.19E+00	–1.25E+00
8.75	4.78E+00	4.78E+00	4.77E+00	1.89E+00	6.32E-01	–5.27E-01	–1.27E+00	–1.41E+00
9.00	4.78E+00	4.78E+00	4.77E+00	2.75E+00	1.20E+00	3.81E-02	–1.13E+00	–1.51E+00
9.25	4.78E+00	4.78E+00	4.77E+00	4.76E+00	1.88E+00	5.47E-01	–6.60E-01	–1.51E+00
9.50	4.78E+00	4.78E+00	4.77E+00	4.76E+00	2.78E+00	1.15E+00	–9.89E-02	–1.26E+00
9.75	4.78E+00	4.78E+00	4.77E+00	4.76E+00	4.73E+00	1.89E+00	4.56E-01	–7.58E-01
10.00	4.78E+00	4.78E+00	4.77E+00	4.76E+00	4.73E+00	2.92E+00	1.13E+00	–2.57E-01
10.25	500	500	500	500	500	500	2.02E+00	3.92E-01

Source: DTN: MO0702PADISCON.001_R0 [DIRS 179358] Table 6.

NOTE: This look-up table is implemented in the TSPA-LA Model as parameter Sol_U_LUT_Boltwoodite. The upper shaded area indicates the region where it is uncertain if uranium solubility is controlled by schoepite or Na-Boltwoodite saturation. The lower shaded area is where solubility is controlled by $Na_4UO_2(CO_3)_3$. Entries reported as '500' indicate conditions for which a valid solubility value does not exist.

Table 6.3.7-58. Uncertainty in Uranium Solubility Model in CDSP WPs Breached Under Any Scenario, CSNF WPs Breached by an Igneous Intrusion, and in the Invert (all locations and scenarios)

TSPA-LA Model Name	Model Abstraction Symbol	Description	Units	Distribution Type	Distribution Specification
U_Eps_1_low_other_a	ε_1	Uncertainties in solubility (schoepite and Na-Boltwoodite) below 1 molal ionic strength; to be used in the colorless and shaded regions in Table 6.3.7-37 and upper shaded region in Table 6.3.7-38	None	Truncated normal	$\mu = 0$ $\sigma = 0.5$ $2\sigma = \pm 1.0$
U_Eps_1_high_other_a	ε_1	Uncertainties in solubility (schoepite and Na-Boltwoodite) at 1 to 3 molal ionic strength; uncertainties in log K ($Na_4UO_2(CO_3)_3$) below 3 molal ionic strength (blue regions in Table 6.3.7-38)	None	Truncated normal	$\mu = 0$ $\sigma = 0.6$ $2\sigma = \pm 1.2$
U_Eps_2_Schoepite_Glass_Low_a	$\varepsilon_2^{\text{CSNF-low}}$ $\varepsilon_2^{\text{CDSP-Glass}}$ $\varepsilon_2^{\text{CDSP-F-low}}$	Fluoride uncertainty, CSNF waste packages when I < 0.2m. CDSP packages, Cell 1b when I < 0.004m and Cell 1a.	None	Triangular	Min = 0 Max = 78 Most likely = 0
U_Eps_2_Schoepite_CSNF_High_a	$\varepsilon_2^{\text{CSNF-high}}$ $\varepsilon_2^{\text{CSNF-invert}}$	Fluoride uncertainty, CSNF waste packages when I ≥ 0.2m and invert below CSNF waste packages	None	Triangular	Min = 0 Max = 1361 Most likely = 0
U_Eps_2_Schoepite_CDSP_High_a	$\varepsilon_2^{\text{CDSP-F-high}}$ $\varepsilon_2^{\text{CDSP-invert}}$	Fluoride uncertainty, CDSP waste packages when I ≥ 0.004m and invert below CDSP waste packages	None	Triangular	Min = 0 Max = 5385 Most likely = 0
U_Eps_2_Boltwoodite_Glass_Lo_a	$\varepsilon_2^{\text{CSNF-high}}$ $\varepsilon_2^{\text{CSNF-invert}}$	Fluoride uncertainty, CSNF waste packages when I < 0.2m. CDSP packages, Cell 1b when I < 0.004m and Cell 1a	None	Triangular	Min = 0 Max = 6.13 Most likely = 0
U_Eps_2_Boltwoodite_CSNF_Hig_a	$\varepsilon_2^{\text{CSNF-high}}$ $\varepsilon_2^{\text{CSNF-invert}}$	Fluoride uncertainty, CSNF waste packages when I ≥ 0.2m and invert below CSNF waste packages	None	Triangular	Min = 0 Max = 57.01 Most likely = 0
U_Eps_2_Boltwoodite_CDSP_Hig_a	$\varepsilon_2^{\text{CDSP-F-high}}$ $\varepsilon_2^{\text{CDSP-invert}}$	Fluoride uncertainty, CDSP waste packages when I ≥ 0.004m and invert below CDSP waste packages	None	Triangular	Min = 0 Max = 272.3 Most likely = 0
Schoepite_Boltwoodite_Interp_a	None	Used in the TSPA-LA Model to determine the fractional value that is used to interpolate between schoepite and Na-Boltwoodite look-up tables	None	Uniform	Min. = 0 Max = 1

Source: DTN: MO0702PADISCON.001_R0 [DIRS 179358], Table 19; DTN: MO0702PAFLUORI.000_R1 [DIRS 181219], Table 9.

NOTE: The parameter Schoepite_Boltwoodite_Interp_a was developed by TSPA based on information given in notes to Table 6 of DTN: MO0702PADISCON.001_R0 [DIRS 179358].

Table 6.3.7-59. Multiplication Factor, N(pH), Used to Modify Fluoride Concentration Uncertainty Terms (ε_2) for Uranium in CDSP WPs Breached under Any Scenario, CSNF Waste Packages Breached by an Igneous Intrusion and in the Invert (all locations and scenarios)

Glass, CSNF low, and CDSP low		
pH	**Schoepite**	**Boltwoodite-Na**
3.50	1.00E+00	None
3.75	7.24E-01	None
4.00	5.17E-01	None
4.25	4.18E-01	None
4.50	3.48E-01	None
4.75	2.70E-01	None
5.00	1.85E-01	None
5.25	1.06E-01	None
5.50	4.86E-02	None
5.75	1.83E-02	None
6.00	6.17E-03	None
6.25	1.99E-03	None
6.50	6.32E-04	6.36E-02
6.75	1.95E-04	1.89E-02
7.00	4.87E-05	7.98E-03
7.25	0.00E-00	4.36E-03
7.50	0.00E-00	3.13E-03
7.75	0.00E-00	3.82E-03
8.00	0.00E-00	9.87E-03
8.25	2.44E-02	4.89E-02
8.50	None	9.10E-02
8.75	None	2.40E-01
9.00	None	1.00E+00

CSNF high and CSNF invert		
pH	**Schoepite**	**Boltwoodite-Na**
3.50	1.00E+00	None
3.75	7.03E-01	None
4.00	4.85E-01	None
4.25	3.73E-01	None
4.50	2.99E-01	None
4.75	2.41E-01	None
5.00	1.92E-01	None
5.25	1.45E-01	None
5.50	9.86E-02	None
5.75	5.67E-02	None
6.00	2.63E-02	None
6.25	1.01E-02	None
6.50	3.42E-03	3.62E-01
6.75	1.11E-03	7.86E-02
7.00	3.48E-04	1.79E-02
7.25	1.07E-04	5.52E-03
7.50	4.58E-05	2.88E-03
7.75	1.64E-04	3.25E-03
8.00	1.98E-03	8.60E-03
8.25	2.50E-02	2.56E-02
8.50	None	6.80E-02
8.75	None	2.17E-01
9.00	None	1.00E+00

CDSP high and CDSP invert		
pH	**Schoepite**	**Boltwoodite-Na**
3.50	1.00E+00	None
3.75	6.68E-01	None
4.00	4.44E-01	None
4.25	3.34E-01	None
4.50	2.73E-01	None
4.75	2.31E-01	None
5.00	1.98E-01	None
5.25	1.68E-01	None
5.50	1.36E-01	None
5.75	1.03E-01	None
6.00	6.91E-02	None
6.25	3.93E-02	None
6.50	1.81E-02	1.00E+00
6.75	6.90E-03	3.30E-01
7.00	2.36E-03	7.49E-02
7.25	7.96E-04	1.55E-02
7.50	3.34E-04	4.08E-03
7.75	4.02E-04	2.75E-03
8.00	2.13E-03	6.92E-03
8.25	2.90E-02	1.93E-02
8.50	None	5.55E-02
8.75	None	1.82E-01
9.00	None	8.43E-01

Source: DTN: MO0702PAFLUORI.001_R1 [DIRS 181219], Table 10.

NOTE: These multiplication factors are implemented in the TSPA-LA Model as parameters: U_Schoepite_Glass_low_N, U_Schoepite_CSNF_High_N, U_Schoepite_CDSP_High_N, U_Boltwoodite_Glass_low_N, U_Boltwoodite_CSNF_High_N, and U_Boltwoodite_CDSP_High_N.

Table 6.3.7-60. Actinide Caps (mg/L) Between an Ionic Strength of 3 and 10 Molal for CSNF Packages

Controlling solid	Element	IS = 3	IS = 7	IS= 10
PuO_2 (hyd,aged)	Pu	39487	92135	131622
NpO_2	Np	981	2289	3270
Np_2O_5	Np	1417	3306	4723
Schoepite	U	29698	69294	98992
ThO_2 (am)	Th	1400	3266	4666
$AmOHCO_3$	Am	1285	2999	4285
Np_2O_5 (by analog)	Pa	1417	3306	4723

Source: DTN: MO0704PASOLCAP.000_R0 [DIRS 180389], Table 2.

NOTE: These caps are implemented in the TSPA-LA Model as parameters: CSNF_Pu_TypeIII_Cap, CSNF_NpO2_TypeIII_Cap, CSNF_Np2O5_TypeIII_Cap, CSNF_U_Scheopite_TypeIII_Cap, CSNF_Th_TypeIII_Cap, CSNF_Am_TypeIII_Cap, CSNF_Pa_TypeIII_Cap

IS = ionic strength in units of molal

Table 6.3.7-61. Actinide Caps (mg/L) Between an Ionic Strength of 3 and 10 Molal for CDSP Packages, Cell 1b

Controlling solid	Element	IS = 3	IS = 7	IS= 10
PuO_2 (hyd,aged)	Pu	39487	92135	131622
NpO_2	Np	981	2289	3270
Np_2O_5	Np	1417	3306	4723
Schoepite*	U	29698	69294	98992
Na-Boltwoodite*	U	33636	61967	88524
ThO_2 (am)	Th	1400	3266	4666
$AmOHCO_3$	Am	1285	2999	4285
Np_2O_5 (by analog)	Pa	1417	3306	4723

Source: DTN: MO0704PASOLCAP.000_R0 [DIRS 180389], Table 2.

NOTE: These caps are implemented in the TSPA-LA Model as parameters: CDSP_Pu_TypeIII_Cap, CDSP_NpO2_TypeIII_Cap, CDSP_Np2O5_TypeIII_Cap, CDSP_U_Scheopite_TypeIII_Cap, CDSP_U_Boltwoodite_TypeIII_Cap, CDSP_Th_TypeIII_Cap, CDSP_Am_TypeIII_Cap, CDSP_Pa_TypeIII_Cap.

When sampling between the schoepite and boltwoodite LUTs, use the schoepite values.

IS = ionic strength (molal).

Table 6.3.7-62. Parameters for TSPA-LA Glass Waste Form Colloid Abstraction

TSPA-LA Parameter Name	Model Abstraction Symbol	Description	Units	Distribution Type	Distribution Specification
DTN: MO0701PAGLASWF.000_R1 [DIRS 180393]					
CPu_Col_Wf_Embed_Sampled_a	$C_{RN,coll,DHLWG,embed,sampled}$	Concentration of irreversibly attached plutonium, associated with DHLWG colloids.	mol/L	Uniform	1.E-11 to 1.E-8
CPu_Col_Glass_Embed_Min	$C_{Rn,coll,DHLWG,embed,min}$	Lowest observed or expected concentration of irreversibly attached plutonium associated with DHLWG colloids.	mol/L	Single Value	1.E-13
CPu_Per_WF_Embed_Col_a	$C_{coll,DHLWG,sampled}$	Concentration of irreversibly attached plutonium per concentration of colloids.	(mol/L) /(mg/L)	Triangular Distribution	min 5×10^{-9} Mode 2×10^{-8} Max 2.5×10^{-8}
Smectite_ZPC	None	Smectite zero point of charge, pH below which the smectite does not sorb.	None	Single Value	1.5
Smectite_pH_hi	None	High pH for smectite ionic strength threshold fit.	None	Single Value	9
Coeff_pH_Sq_Smectite	None	Coefficient of pH squared term for fit of ionic strength threshold for smectite colloid stability.	None	Single Value	-0.008
Coeff_pH_Smectite	None	Coefficient of pH term for fit of ionic strength threshold for smectite colloid stability.	None	Single Value	0.12
Coeff_inter_Smectite	None	Intercept term for fit of ionic strength threshold for smectite colloid stability.	None	Single Value	0.03
Specific_SA_Smectite_Col_a	SA, Smectite, coll	Specific surface area for DHLWG (smectite) colloid.	M2/g	Uniform	10 to 100

Table 6.3.7-62. Parameters for TSPA-LA Glass Waste Form Colloid Abstraction (Continued)

TSPA-LA Parameter Name	Model Abstraction Symbol	Description	Units	Distribution Type	Distribution Specification	
Smectite_Site_Density	NS, Smectite, coll	Site density for DHLWG (smectite) colloid.	Sites/ nm^2	Single Value	2.3	
DTN: MO0701PASORPTN.000_R1 [DIRS 180391]						
Kd_Pu_Rev_Smectite_a	$K_{d,Pu,coll,wf}$	Distribution coefficient for reversible sorption of plutonium to smectite colloids.	mL/g	Cumulative Distribution Function	Prob Level	Value
					0	1×10^3
					0.45	5×10^3
					0.80	1×10^4
					0.95	5×10^4
					1	1×10^5
Kd_Am_Rev_Smectite_a Kd_Th_Rev_Smectite_a Kd_Pa_Rev_Smectite_a	$K_{d,Am,coll,wf}$ $K_{d,Th,coll,wf}$ $K_{d,Pa,coll,wf}$	Distribution coefficient for reversible sorption of americium, thorium, and protactinium to smectite colloids. Each distribution sampled independently.	mL/g	Cumulative Distribution Function	Prob Level	Value
					0	1×10^4
					0.07	5×10^4
					0.17	1×10^5
					0.4	5×10^5
					0.6	1×10^6
					0.92	5×10^6
					1	1×10^7
Kd_Cs_Rev_Smectite_a	$K_{d,Cs,coll,wf}$	Distribution coefficient for reversible sorption of cesium to smectite colloids.	mL/g	Cumulative Distribution Function	Prob Level	Value
					0	5×10^1
					0.05	1×10^2
					0.4	5×10^2
					0.7	1×10^3
					1	5×10^3
DTN: MO0701PAKDSUNP.000_R1 [DIRS 180392]						
Kd_Np_Rev_Smectite_a	$K_{d,Np,coll,Smecti}$	Distribution coefficient for reversible sorption of neptunium to smectite colloids.	mL/g	Log Uniform	1×10^1 to 5×10^2	
Kd_U_Rev_Smectite_a	$K_{d,U,coll,Smectit}$	Distribution coefficient for reversible sorption of tin to smectite colloids.	mL/g	Log Uniform	5×10^2 to 5×10^4	

Table 6.3.7-62. Parameters for TSPA-LA Glass Waste Form Colloid Abstraction (Continued)

TSPA-LA Parameter Name	Model Abstraction Symbol	Description	Units	Distribution Type	Distribution Specification
Kd_Sn_Rev_Smectite_a	$K_{d,Sn,coll,Smecti}$	Distribution coefficient for reversible sorption of uranium to smectite colloids.	mL/g	Log Uniform	1×10^{5} to 1×10^{6}
Kd_Ra_Rev_Smectite_a	$K_{d,Ra,coll,Smecti}$	Distribution coefficient for reversible sorption of radium to smectite colloids.	mL/g	Log Uniform	1×10^{2} to 5×10^{3}

Sources: DTN: MO0701PAGLASWF.000_R1 [DIRS 180393]; DTN: MO0701PASORPTN.000_R1 [DIRS 180391]; DTN: MO0701PAKDSUNP.000_R1 [DIRS 180392].

NOTE: Condition report 11424 describes the errata in the source documents.

Table 6.3.7-63. Parameters for TSPA-LA CSNF Waste Form Irreversible Colloid Abstraction

TSPA-LA Parameter Name	Model Abstraction Symbol	Description	Units	Distribution Type	Distribution Specification	
CPu_Col_CSNF_Sampled_a	$C_{RNcoll,SNF,embed,}$	Concentration of irreversibly attached radionuclide element RN (plutonium, americium) associated with SNF colloids.	mol/L	Cumulative Distribution Function	Prob Level	Value
					0	1×10^{-10}
					0.05	5×10^{-10}
					0.1	1×10^{-9}
					0.15	5×10^{-9}
					0.2	1×10^{-8}
					0.3	5×10^{-8}
					0.5	1×10^{-7}
					0.7	5×10^{-7}
					0.9	1×10^{-6}
					1	5×10^{-6}
CPu_Col_CSNF_Min	$C_{RNcoll,SNF,\min}$	Lowest observed or expected concentration of irreversibly attached plutonium associated with DHLWG colloids.	Mol/L	Single Value	1.E-13	
CPu_Per_CSNF_Embed_Col_a	$C_{coll,SNF,uniform}$	Concentration of Irreversibly attached plutonium per concentration of CSNF colloids.	(mol/L) /(mg/L)	Uniform Distribution	Min 5×10^{-7} Max 1×10^{-6}	
CSNF_pH_lo	None	Lower limit of pH range for CSNF colloid stability data	None	Single Value	4	
CSNF_ZPC_lo	None	Lower limit of pH range for zero point of charge for CSNF colloid stability data.	None	Single Value	7	
CSNF_ZPC_hi	None	Upper limit of pH range for zero point of charge for CSNF colloid stability data.	None	Single Value	9.3	
CSNF_pH_hi	None	Upper limit of pH range for CSNF colloid stability data.	None	Single Value	10.6	
Coeff_pH_Cube_lo_CSNF	None	Coefficient of pH cubed term for fit of ionic strength threshold for CSNF colloid stability at low pH.	None	Single Value	0.0089	

Table 6.3.7-63. Parameters for TSPA-LA CSNF Waste Form Irreversible Colloid Abstraction (Continued)

TSPA-LA Parameter Name	Model Abstraction Symbol	Description	Units	Distribution Type	Distribution Specification
Coeff_pH_Sq_lo_CSNF	None	Coefficient of pH squared term for fit of ionic strength threshold for CSNF colloid stability at low pH.	None	Single Value	−0.1466
Coeff_pH_lo_CSNF	None	Coefficient of pH term for fit of ionic strength threshold for CSNF colloid stability at low pH.	None	Single value	0.7462
Coeff_inter_pH_lo_CSNF	None	Coefficient of intercept term for fit of ionic strength threshold for CSNF colloid stability at low pH.	None	Single value	−1.092
Coeff_pH_Cube_hi_CSNF	None	Coefficient of pH cubed term for fit of ionic strength threshold for CSNF colloid stability at high pH.	None	Single value	0.087362
Coeff_pH_Sq_hi_CSNF	None	Coefficient of pH squared term for fit of ionic strength threshold for CSNF colloid stability at high pH.	None	Single value	−2.4078
Coeff_pH_hi_CSNF	None	Coefficient of pH term for fit of ionic strength threshold for CSNF colloid stability at high pH.	None	Single value	22.126
Coeff_inter_pH_hi_CSNF	None	Coefficient of intercept term for fit of ionic strength threshold for CSNF colloid stability at high pH.	None	Single value	−67.791

Source: DTN: MO0701PACSNF.000_R1 [DIRS 180439].

NOTE: Condition report 11424 describes the errata in the source documents.

Table 6.3.7-64. Parameters for TSPA-LA SNF Waste Form Reversible Colloid Abstraction

TSPA-LA Parameter Name	Model Abstraction Symbol	Description	Units	Distribution Type	Distribution Specification	
Conc_Col_U_Sampled_a	$m_{coll,Uranophane,sampled}$	Expected mass of uranophane colloids per unit volume or mass of water.	mg/L	Cumulative Distribution Function	Prob Level	Value
					0	1×10^{-3}
					0.5	1×10^{-1}
					0.75	1×10^{0}
					0.90	1×10^{1}
					0.98	5×10^{1}
					1	2×10^{2}
Conc_Col_U_Min	$m_{coll,Uranophane,min}$	Lowest observed or expected mass of uranophane colloids per unit volume or mass of water.	mg/L	Single value	1×10^{-6}	
U_pH_lo	None	Lower limit of pH range for U colloid stability data.	None	Single value	4	
U_pH_hi	None	Upper limit of pH range for U colloid stability data.	None	Single value	9	
Coeff_pH_Sq_U	None	Coefficient of pH squared term for fit of ionic strength threshold for U colloid stability.	None	Single value	−0.008	
Coeff_pH_U	None	Coefficient of pH term for fit of ionic strength threshold for U colloid stability.	None	Single value	0.14	
Coeff_inter_U	None	Coefficient of intercept term for fit of ionic strength threshold for U colloid stability.	None	Single value	0.4	
Kd_Pu_Rev_U_Col_a	$K_{d,Pucoll,uranophane}$	Distribution coefficient for reversible sorption of plutonium onto uranophane colloids.	mL/g	Log Uniform	5×10^{0} to 1×10^{4}	
Kd_Am_Rev_U_Col_a	$K_{d,Amcoll,uranophane}$	Distribution coefficient for reversible sorption of americium onto uranophane colloids.	mL/g	Log Uniform	5×10^{0} to 1×10^{4}	
Kd_Th_Rev_U_Col_a	$K_{d,Thcoll,uranophane}$	Distribution coefficient for reversible sorption of thorium onto uranophane colloids.	mL/g	Log Uniform	5×10^{0} to 1×10^{4}	

Table 6.3.7-64. Parameters for TSPA-LA SNF Waste Form Reversible Colloid Abstraction (Continued)

TSPA-LA Parameter Name	Model Abstraction Symbol	Description	Units	Distribution Type	Distribution Specification
Kd_Pa_Rev_U_Col_a	$K_{d,Pacoll,uranophane}$	Distribution coefficient for reversible sorption of Pa onto uranophane colloids.	mL/g	Log Uniform	5×10^{0} to 1×10^{4}
Kd_Cs_Rev_U_Col_a	$K_{d,Cscoll,uranophane}$	Distribution coefficient for reversible sorption of cesium onto uranophane colloids.	mL/g	Log Uniform	1×10^{1} to 1×10^{3}
Kd_Np_Rev_U_Col_a	$K_{d,Npcoll,uranophane}$	Distribution coefficient for reversible sorption of neptunium onto uranophane colloids.	mL/g	Log Uniform	1×10^{1} to 5×10^{2} Note: incorrectly implemented as 1 to 5×10^{2}; see Appendix P Table P-6
Kd_Ra_Rev_U_Col_a	$K_{d,Racoll,uranophane}$	Distribution coefficient for reversible sorption of radium onto uranophane colloids.	mL/g	Log Uniform	1×10^{1} to 1×10^{3}
Kd_Sn_Rev_U_Col_a	$K_{d,Sncoll,uranophane}$	Distribution coefficient for reversible sorption of tin onto uranophane colloids.	mL/g	Log Uniform	1×10^{0} to 1×10^{2}
Specific_SA_U_Col	$S_{A,\ uranophane,coll}$	Specific surface area for uranophane.	m^2/g	Single value	30
U_Site_Density	$N_{S,uranophane,coll}$	Site density for uranophane particle colloid.	Sites/ nm^2	Single value	2

Source: DTN: MO0701PACSNF.000_R1 [DIRS 180439].

NOTE: Condition report 11424 describes the errata in the source documents.

Table 6.3.7-65. Parameters for TSPA-LA Iron Oxyhydroxide Colloid Abstraction

TSPA-LA Parameter Name	Model Abstraction Symbol	Description	Units	Distribution Type	Distribution Specification
Conc_Col_FeOx_Min	$m_{coll,FeOx,\min}$	Minimum concentration of FeOx colloids.	mg/L	Single value	1×10^{-6}
Conc_Col_FeOx_CS_Sampled_a		Sampled FeOX colloid concentration when carbon steel is degrading.	mg/L	Truncated Log Normal	Mean = 03.69 Standard deviation = 2.79 Minimum 0.3 Maximum 30
Conc_Col_FeOx_SS_Sampled_a	$m_{coll,FeOx,sampled}$	Sampled FeOX colloid concentration for locations containing degraded stainless steel.	mg/L	Cumulative Distribution Function	Prob Level / Value 0 / 1×10^{-3} 0.6 / 1×10^{-1} 0.90 / 1×10^{0} 0.95 / 1×10^{1} 1 / 3×10^{1}
FeOx_pH_lo	None	Low pH for FeOx colloid ionic strength threshold fit.	None	Single value	4.5
FeOx_ZPC_lo	None	Low end of zero point of charge range.	None	Single value	8.4
FeOx_ZPC_hi	None	Low end of zero point of charge range.	None	Single value	9.4
FeOx_pH_hi	None	Low pH for FeOx colloid ionic strength threshold fit.	None	Single value	10.4
Coeff_pH_lo_FeOx	None	Coefficient of pH term for fit of ionic strength threshold for FeOx colloid stability at low pH.	None	Single value	−0.013
Coeff_Inter_pH_lo_FeOx	None	Intercept term for fit of ionic strength threshold for FeOx colloid stability at low pH.	None	Single value	0.11
Coeff_pH_sq_hi_FeOx	None	Coefficient of pH squared term for fit of ionic strength threshold for FeOx colloid stability at high pH.	None	Single value	0.0017
Coeff_pH_hi_FeOx	None	Coefficient of pH term for fit of ionic strength threshold for FeOx colloid stability at high pH.	None	Single value	−0.0327

Table 6.3.7-65. Parameters for TSPA-LA Iron Oxyhydroxide Colloid Abstraction (Continued)

TSPA-LA Parameter Name	Model Abstraction Symbol	Description	Units	Distribution Type	Distribution Specification
Coeff_inter_pH_hi_FeOx	None	Intercept term for fit of ionic strength threshold for FeOx colloid stability at high pH.	None	Single value	0.158
Min_Default_Fwd_Rate_Const	k	Minimum value for the log uniform default forward rate constant.	$m^3/m^2/yr$	Single value	0.002
Max_Default_Fwd_Rate_Const	k	Maximum value for the log uniform default forward rate constant.	$m^3/m^2/yr$	Single value	0.05
Default_Fwd_Rate_Const_a	k	Default forward rate constant	$m^3/m^2/yr$	Log-uniform	Min = Min_Default_Fwd_Rate_Const (0.002) Max = Max_Default_Fwd_Rate_Const (0.05)
Target_Flux_Out_Ratio_a	F_{RN}	Target flux-out ratio: ratio of radionuclide mass associated with colloids (reversible and irreversible) to radionuclide mass associated with colloids and dissolved radionuclide mass.	None	Uniform	Min = 0.9 Max = 0.99

Source: DTN: MO0701PAIRONCO.000_R1 [DIRS 180440].

NOTE: Condition report 11424 describes the errata in the source documents.

Table 6.3.7-66. Parameters for TSPA-LA Groundwater Colloid Abstraction

TSPA-LA Parameter Name	Model Abstraction Symbol	Description	Units	Distribution Type	Distribution Specification	
Conc_Col_GW_Min	$m_{coll,gw,\min}$	Minimum GW colloid concentration.	mg/L	Single value	1×10^{-6}	
Conc_Col_GW_Sampled_a	$m_{coll,gw,sampled}$	Sampled GW colloid concentration.	mg/L	Cumulative Distribution Function	Prob Level	Value
					0	0.001
					0.5	0.1
					0.75	1
					0.9	10
					0.98	50
					1	200
Kd_Pu_Rev_Smectite_a Kd_Am_Rev_Smectite_a Kd_Th_Rev_Smectite_a Kd_Pa_Rev_Smectite_a Kd_Cs_Rev_Smectite_a Kd_Np_Rev_Smectite_a Kd_U_Rev_Smectite_a Kd_Sn_Rev_Smectite_a Kd_Ra_Rev_Smectite_a	Table 6.3.7-62	Table 6.3.7-62	mL/g	Table 6.3.7-62	Table 6.3.7-62	
Smectite_ZPC Smectite_ph_hi Coeff_pH_Sq_Smectite Coeff_pH_Smectite Coeff_Inter_Smectite	None	Table 6.3.7-62	None	Single value	Table 6.3.7-62	

Source: DTN: MO0701PAGROUND.000_R0 [DIRS 179310].

Table 6.3.7-67. Alternative Conceptual Models Considered for In-Package Chemistry

Alternative Conceptual Model	Key Assumptions	Screening Assessment and Basis
Alternative Conceptual Model I	The WP is compositionally discrete.	The WVC model showed that the resulting chemical effects of individual WP components were comparable to that of their ensembles. See Section 6.5.1 in *In-Package Chemistry Abstraction* (SNL 2007 [DIRS 180506]).
Alternative Conceptual Model II	The composition of seepage entering a WP is likely to vary as a function of changing conditions in the UZ and drift environments.	The SDM showed that wide compositional ranges in the seepage composition had very little influence on the resulting in-package chemistry. See Section 6.5.2 in *In-Package Chemistry Abstraction* (SNL 2007 [DIRS 180506]).

Source: *In-Package Chemistry Abstraction* (SNL 2007 [DIRS 180506], Table 6-14).

Table 6.3.7-68. Alternative Conceptual Models Considered for CSNF Waste Form Degradation

Alternative Conceptual Model	Key Assumptions	Screening Assessment and Basis
Electrochemical	The anodic Tafel lines can be extrapolated to the corrosion potential. The long-term corrosion behavior of commercial spent nuclear fuel is similar to that of unirradiated UO_2. Differences between the corrosion behavior of commercial spent nuclear fuel and unirradiated UO_2 are due to water radiolysis.	Do not incorporate into the TSPA-LA Model; data needed to apply the model can only be estimated. Use for Nominal Scenario Class model validation–particularly for validation of long-term extrapolation.
Surface Complexation Model	The overall rate of CSNF corrosion is controlled by the rate of surface complexation reactions. The long-term corrosion behavior of commercial spent nuclear fuel is similar to that of unirradiated UO_2.	Do not incorporate into TSPA-LA Model; data needed to apply the model can only be estimated from open literature. Use for Nominal Scenario Class model validation–particularly for validation of long-term extrapolation.

Source: Table 6-13 in *CSNF Waste Form Degradation: Summary Abstraction* (BSC 2004 [DIRS 169987]).

Table 6.3.7-69. Alternative Conceptual Models Considered for High-Level Radioactive Waste Glass Degradation

Alternative Conceptual Model	Key Concepts	Screening Assessment and Basis
Diffusion-Controlled Release	Release rate of radionuclides determined by solid-state diffusion rates.	Not incorporated into TSPA-LA Model. Not supported by data for waste glasses.
Composition-Independent Effective Rate Constant	Intrinsic rate constants vary over a small interval for different compositions and the very low flow rates in the repository compared to those used in the laboratory mean that the affinity term will be low.	Not incorporated into TSPA-LA Model. Current approach provides a much more robust range of values for use in the TSPA-LA.

Source: *Defense HLW Glass Degradation Model* (BSC 2004 [DIRS 169988], Table 6-2).

Table 6.3.7-70. Alternative Conceptual Models Considered for Dissolved Concentration Limits

Element	Alternative Conceptual Model	Model Basis	Screening Assessment and Basis
Plutonium	The theoretical fO_2 model	fO_2 = 0.2 bars.	The results of this model differ significantly from experimental measurements.
	The empirical Eh model	Eh = 1.04 – 0.0592*pH.	The results of this model are lower than experimental results.
Neptunium	Neptunium incorporation into uranyl secondary phases	Neptunium concentration controlled by solid solution rather than by pure phases.	Experimental studies on whether secondary uranyl phase can incorporate neptunium and immobilize it during spent nuclear fuel corrosion do not provide a solid basis for recommending this model to be used in the TSPA-LA model.
Thorium	Solubility control by other thorium phases including ThO_2 (thorianite), $Th_{0.75}PO_4$, $Th(SO_4)_2$, ThF_4, $ThF_4 \cdot 2H_2O$	Solubility of thermodynamically most-stable phase controls concentrations.	Solubilities calculated with ThO_2(am) are consistent with measured thorium solubility in pure water. Other phases may be less soluble only under certain conditions or may be based on questionable data.
Americium	Solubility control by phase with properties between $Am(OH)_3$(am) to $Am(OH)_3$	Initially formed $Am(OH)_3$(am) will convert to more stable $Am(OH)_3$ with time. $Am(OH)_3$ stability decreases with time from self irradiation.	$AmOHCO_3$ is formed in americium solubility experiments under Yucca Mountain conditions. Under some conditions, $Am(OH)_3$ may be less soluble, but choosing $AmOHCO_3$ is, generally, conservative.
Radium	Solid solution (Ra, Ba, Sr, Ca)SO_4	None	Chemistry of in-package and invert waters are not so far outside the normal range of natural waters to cause different radium solubilities.
Technetium	Tc incorporation into epsilon or "5 metal" phases during CSNF corrosion	Tc in the epsilon particles may not be released when the fuel matrix corrodes.	Studies on fuel corrosion indicate the formation of Epsilon particles ("5 metal particles"). Tc in these particles may not be released when the fuel corrodes. Sparse data on this phenomenon, however, do not provide a solid basis for recommending this as a Tc model. Therefore, no solubility was defined, and inventory release should be in control.
Strontium	Solubility controlled by $SrCO_3$ or $SrSO_4$ or solid solution (Ra, Ba, Sr, Ca,)SO_4	None	No solubility was defined, and inventory release should be in control. This is a conservative approach.
Tin	Solubility controlled by very insoluble crystalline phase cassiterite (SnO_2)	Solubility of thermodynamically most-stable phase controls concentrations	Solubilities calculated with SnO_2(am) are consistent with measured Sn solubility in pure water. Other phases may form only under certain conditions.

Source: Modified from Table 6.23-1 in *Dissolved Concentration Limits of Radioactive Elements* (SNL 2007 [DIRS 177418]).

Table 6.3.7-71. Alternative Conceptual Models Considered for Colloids

Alternative Conceptual Model	Basis for Model	Screening Assessment
Kinetic Sorption	This model provides a method for predicting sorption behavior beyond laboratory time scales. Allows interpretation of data from different time scales. Based on the model developed by Painter et al. (2002 [DIRS 174071]) and extended two- and three-site model developed by Wittman et al. (2005 [DIRS 174895]).	This ACM is screened out for the following reasons: – Slow kinetic sorption rates are difficult to determine in laboratory tests that have been run for less than 150 days. – The lack of sufficient sorption data on colloids for sufficient time periods causes uncertainty in the extrapolation beyond the experimental times.
Rate of Colloid Generation	Method for using markers for waste form corrosion for estimating colloid production.	This ACM is screened out for the following reasons: – The model may overestimate colloid formation by not accounting for significant retention of actinides to the immobilized phase as has been observed in waste form corrosion experiments. – The model does not include colloids from CSNF and DSNF.
Mechanisms of Colloid Generation	Mobile colloid generation will require large perturbations to the system that may not occur within the waste package. Furthermore, attachment of particles to air-water interfaces may limit mobile colloid generation.	This ACM is screened out for the following reasons: – Data for Yucca Mountain related conditions are unavailable. – The process of attachment to air-water interfaces will depend on the degree of particle hydrophobicity. Smectite clays and iron oxyhydroxides in general will not attach to air-water interfaces but various oxides and U(VI) oxides phases may. – For flow rates similar to those anticipated in the repository waste package environment, there is no literature evidence to indicate mobile colloid generation.

Source: *Waste Form and In-Drift Colloids-Associated Radionuclide Concentrations: Abstraction and Summary* (SNL 2007 [DIRS 177423], Table 6-19).

NOTE: DHLWG = defense high-level waste glass.

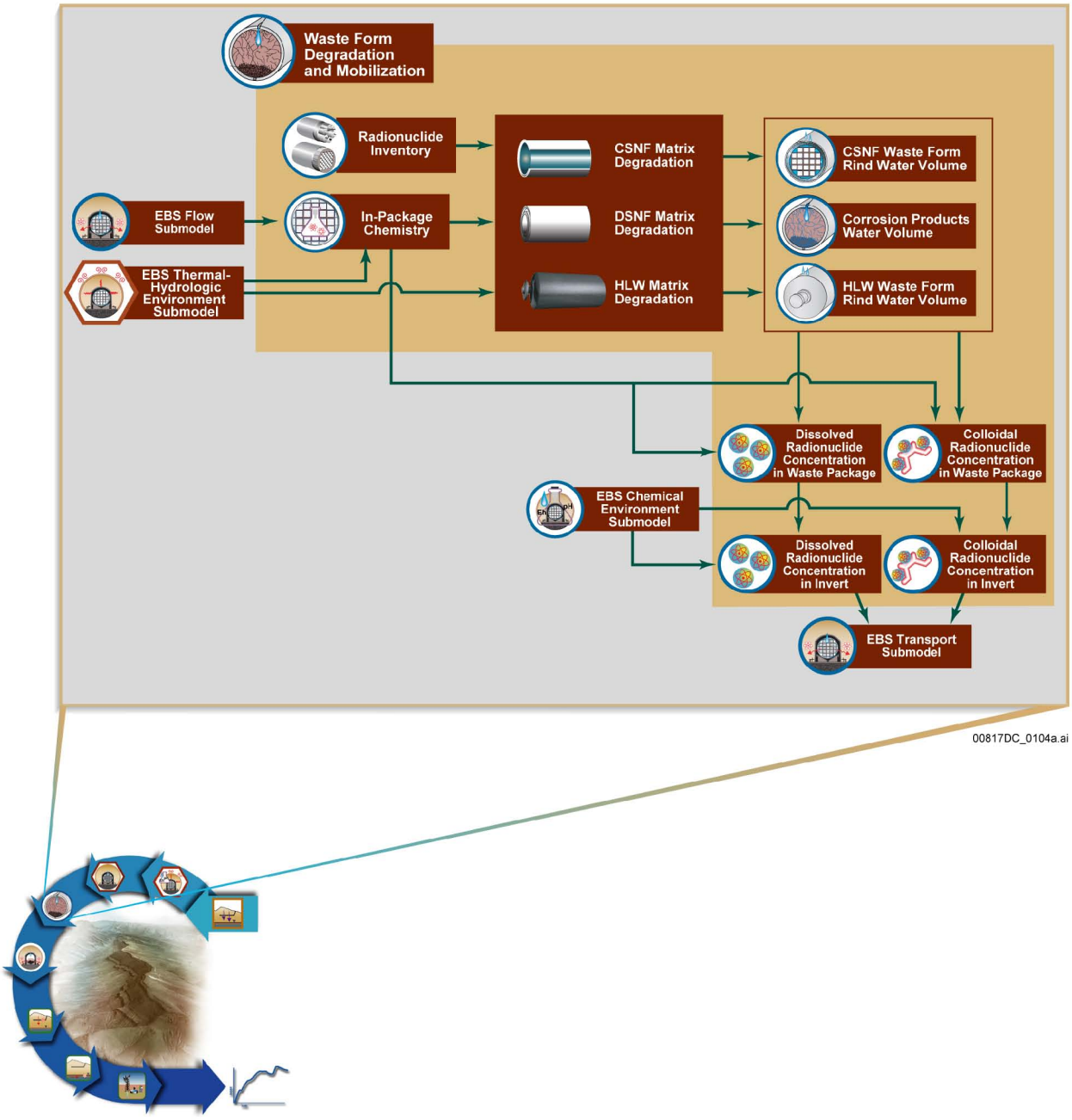

Figure 6.3.7-1. Information Flow Diagram for Waste Form Degradation and Mobilization

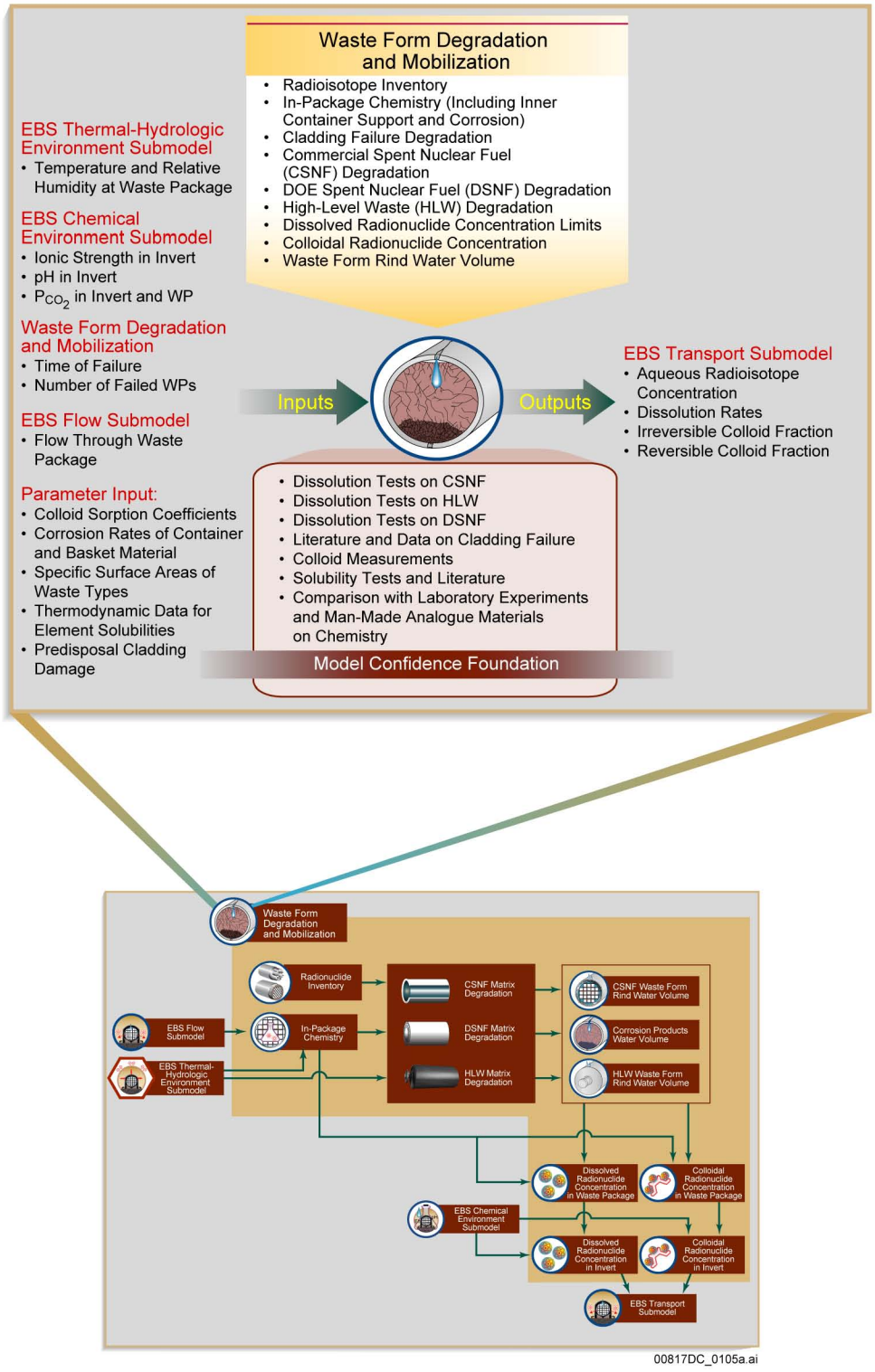

Figure 6.3.7-2. Inputs, Outputs, and Basis for Model Confidence for Waste Form Degradation and Mobilization

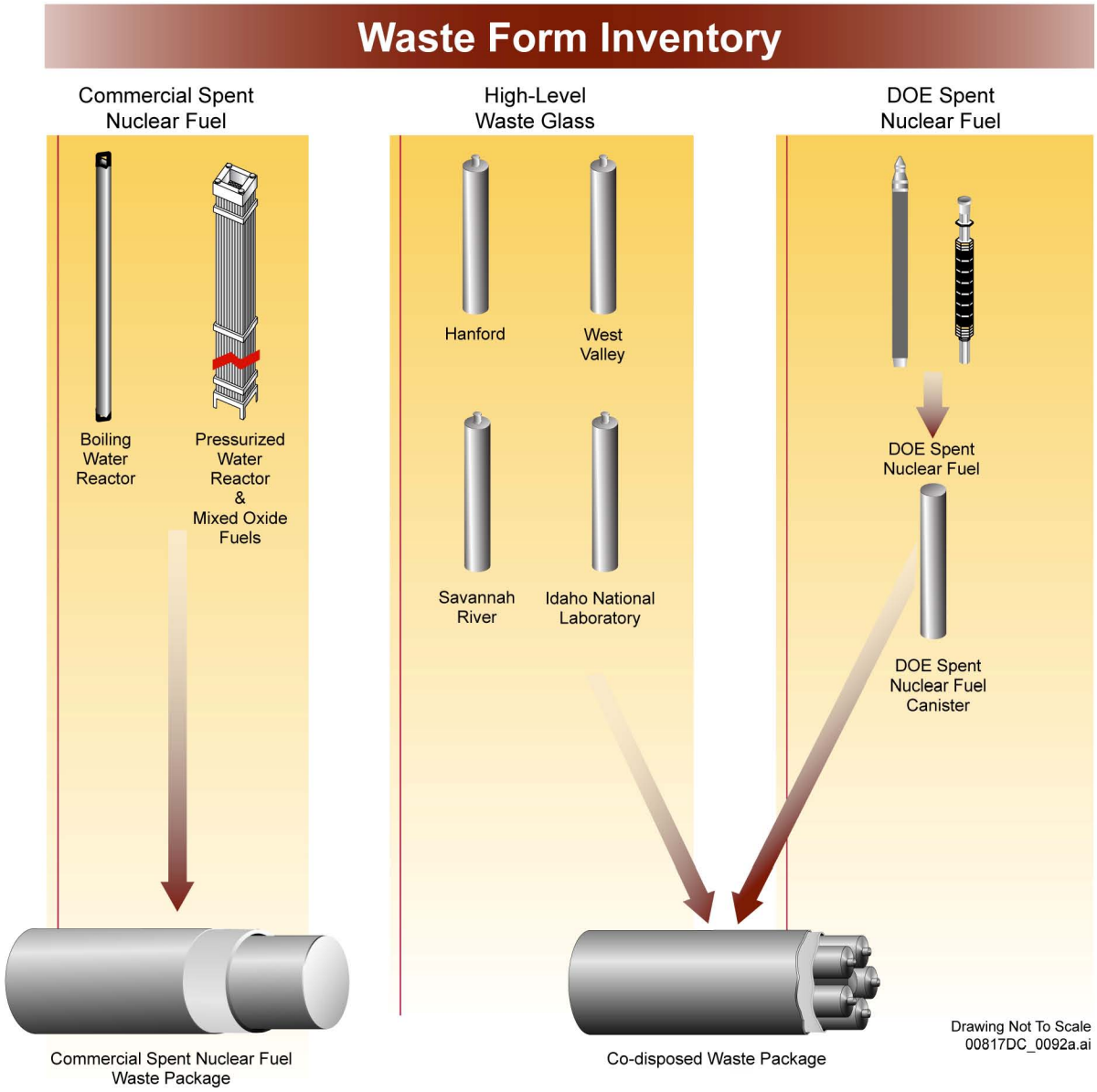

Source: Modified SNL 2007 [DIRS 180472], Figure 6-1.

NOTE: For modeling purposes, the naval waste packages are modeled as commercial waste packages.

Figure 6.3.7-3. Three Waste Types Grouped into Two Representative Waste Packages: CSNF and CDSP WPs

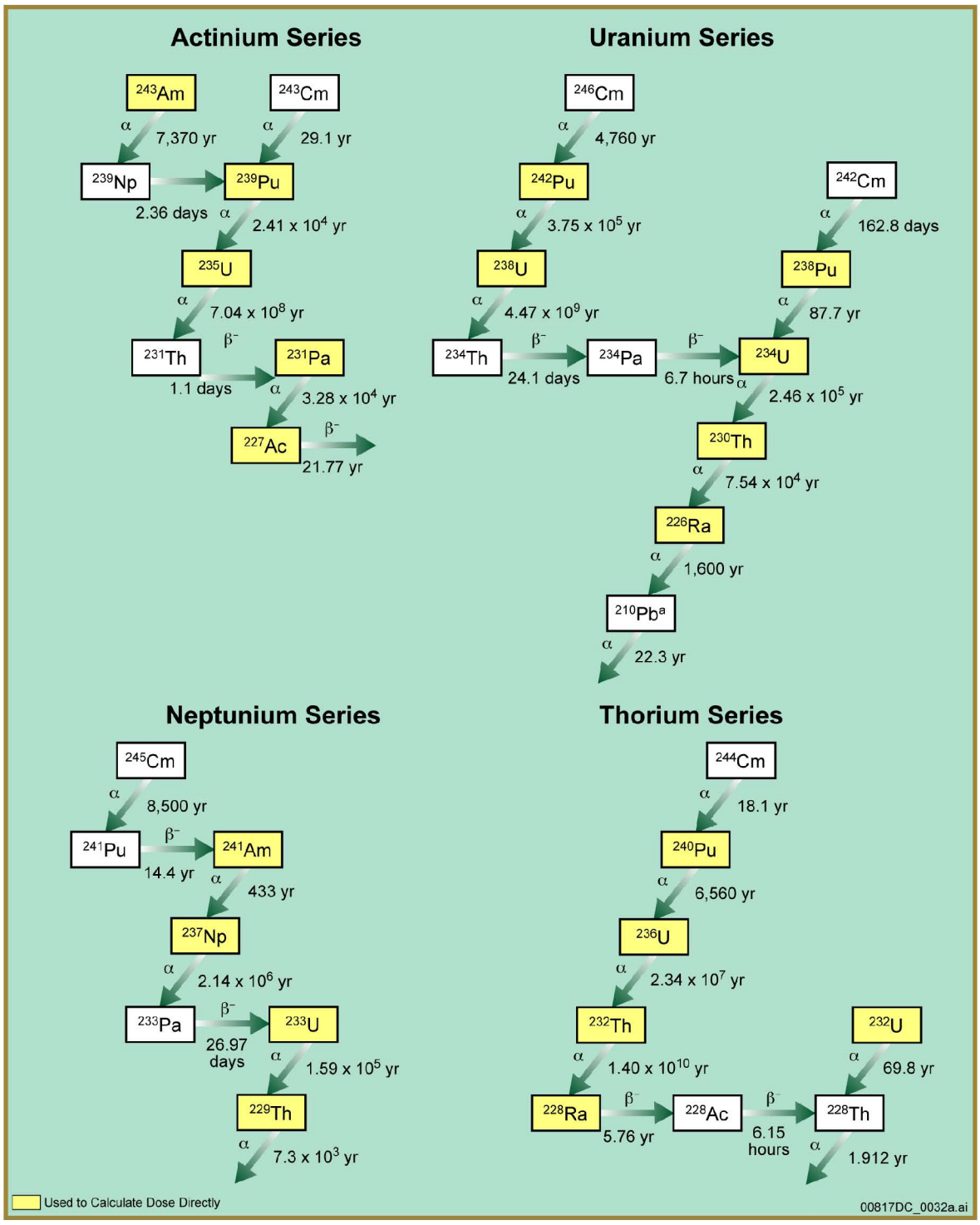

Source: Modified from Rechard 1993 [DIRS 147343], Volume 2 Appendices; and DTN: MO0702PASTREAM.001_R0 [DIRS 179925].

NOTE: Value listed under each radionuclide is the decay half-life for the radionuclide.

[a] A series of short-lived daughters is between ^{226}Ra and ^{210}Pb. Also, ^{210}Pb is not used to calculate dose directly, but its biosphere dose conversion factor is included with that of ^{226}Ra.

Figure 6.3.7-4. Decay Chains of the Actinide Elements

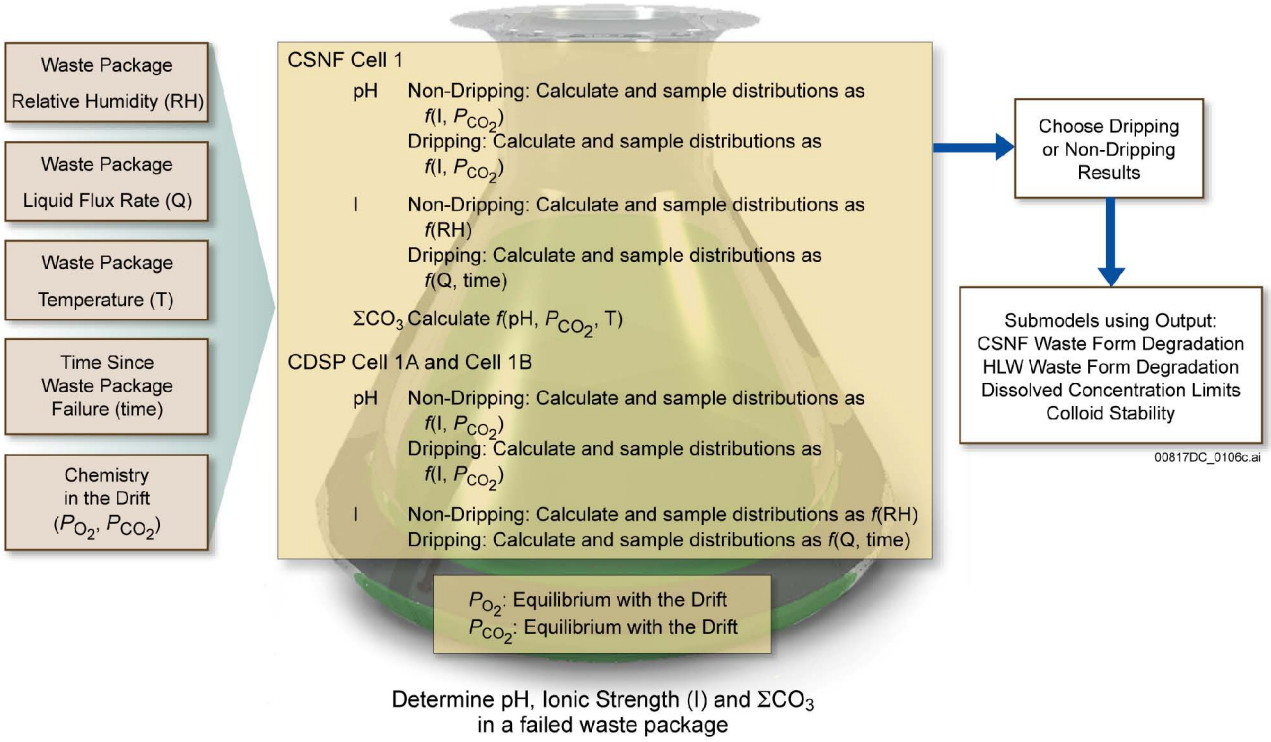

Figure 6.3.7-5. Implementation of the In-Package Chemistry Submodel

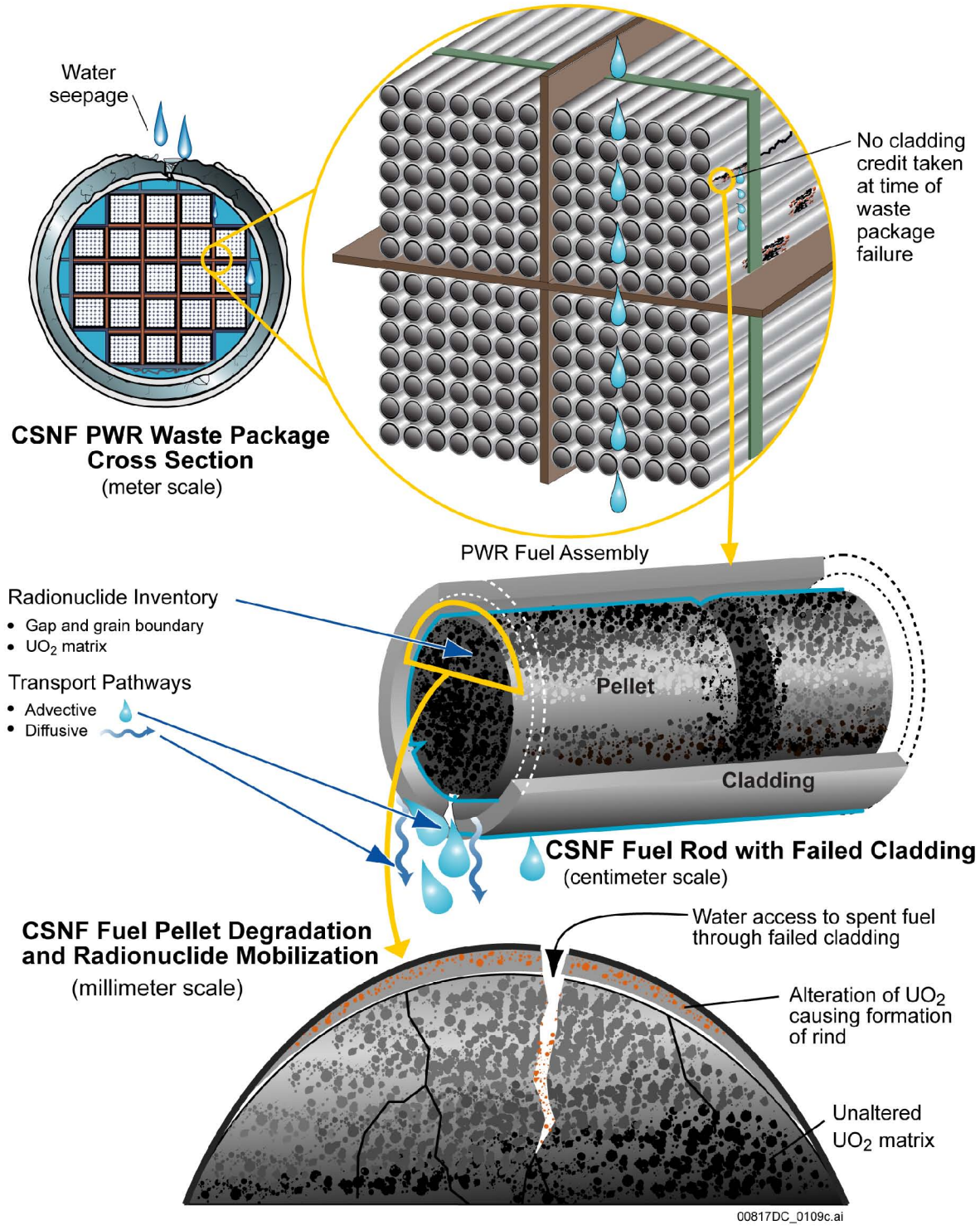

Figure 6.3.7-6. Schematic of CSNF Fuel Waste Form Degradation Mechanisms at Various Scales

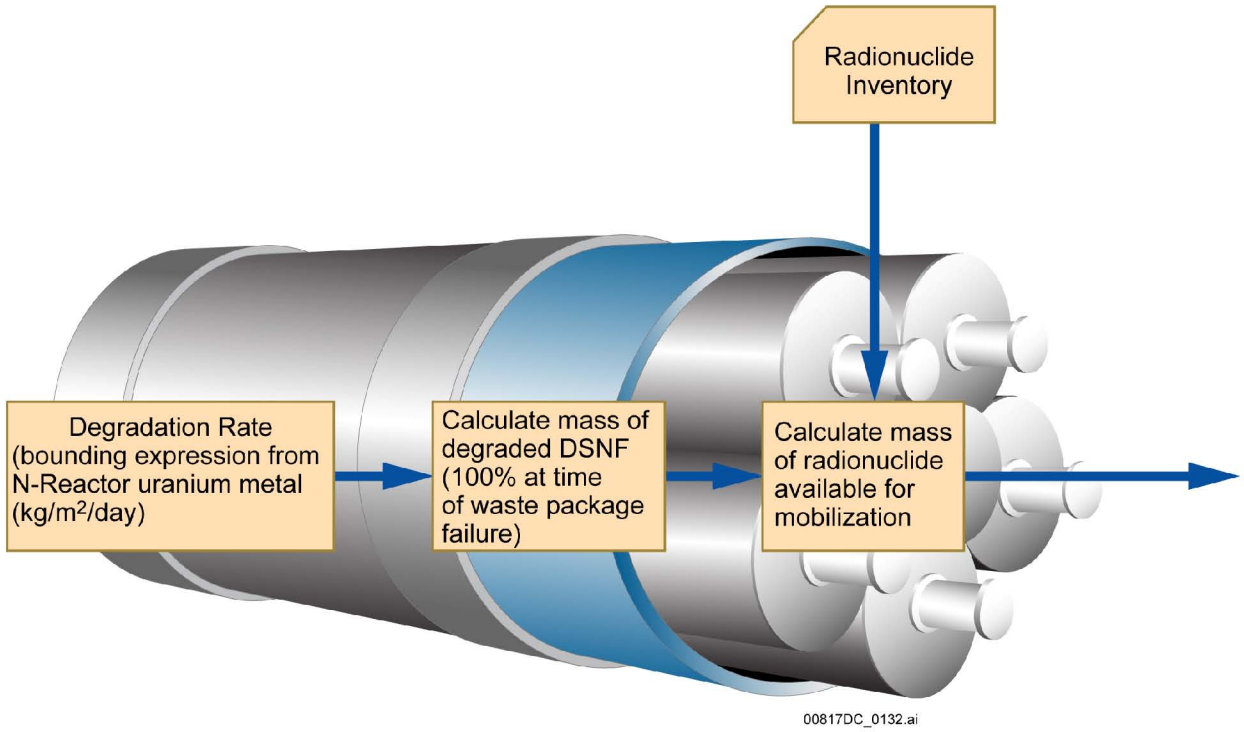

Figure 6.3.7-7. Implementation of the DSNF Degradation Submodel

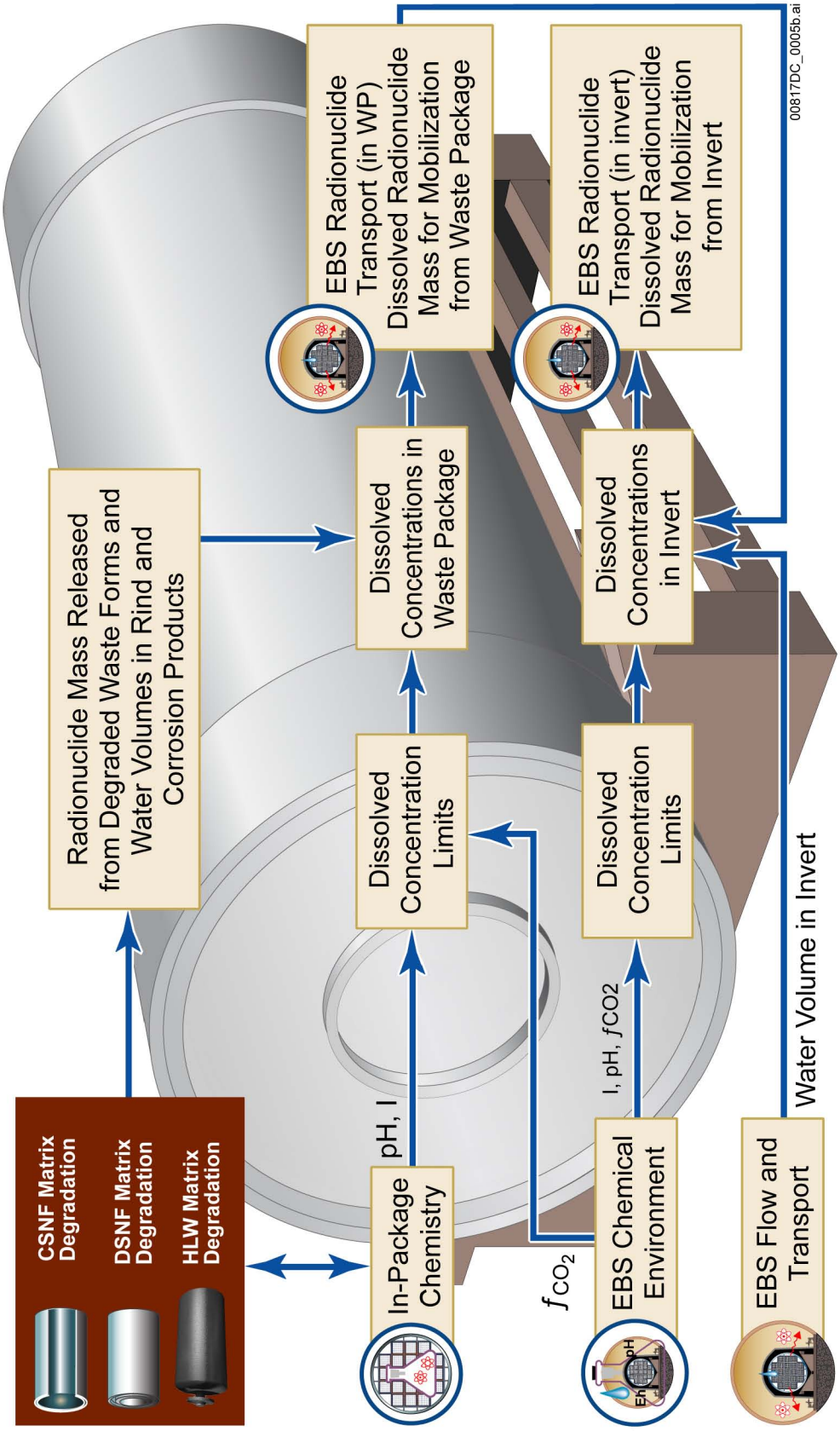

Figure 6.3.7-8. Connections between the Dissolved Concentrations Limits Submodel and Other TSPA-LA Submodels

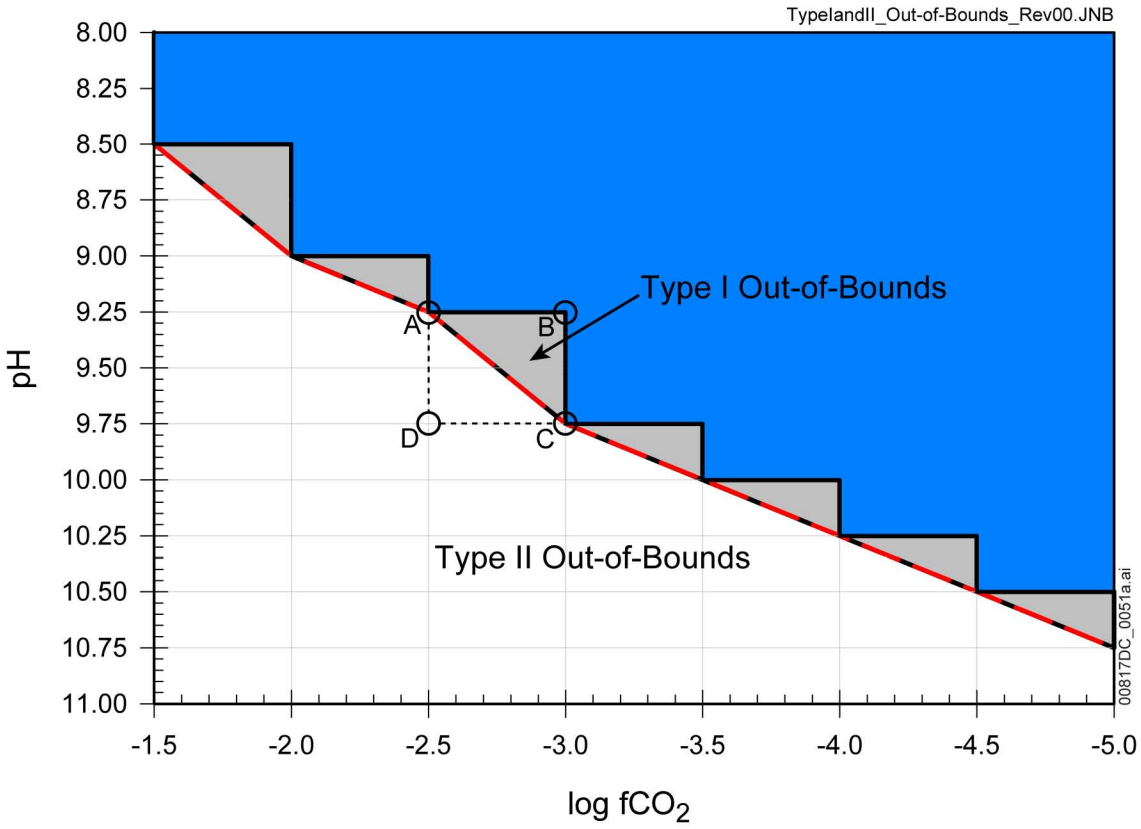

NOTE: Type I out-of-bounds can be removed by implementing a triangular interpolation scheme and a dynamic sampling approach for pH.

Figure 6.3.7-9. Illustration of Type I and Type II Out-of-Bound Conditions Using the Plutonium Solubility Model as an Example

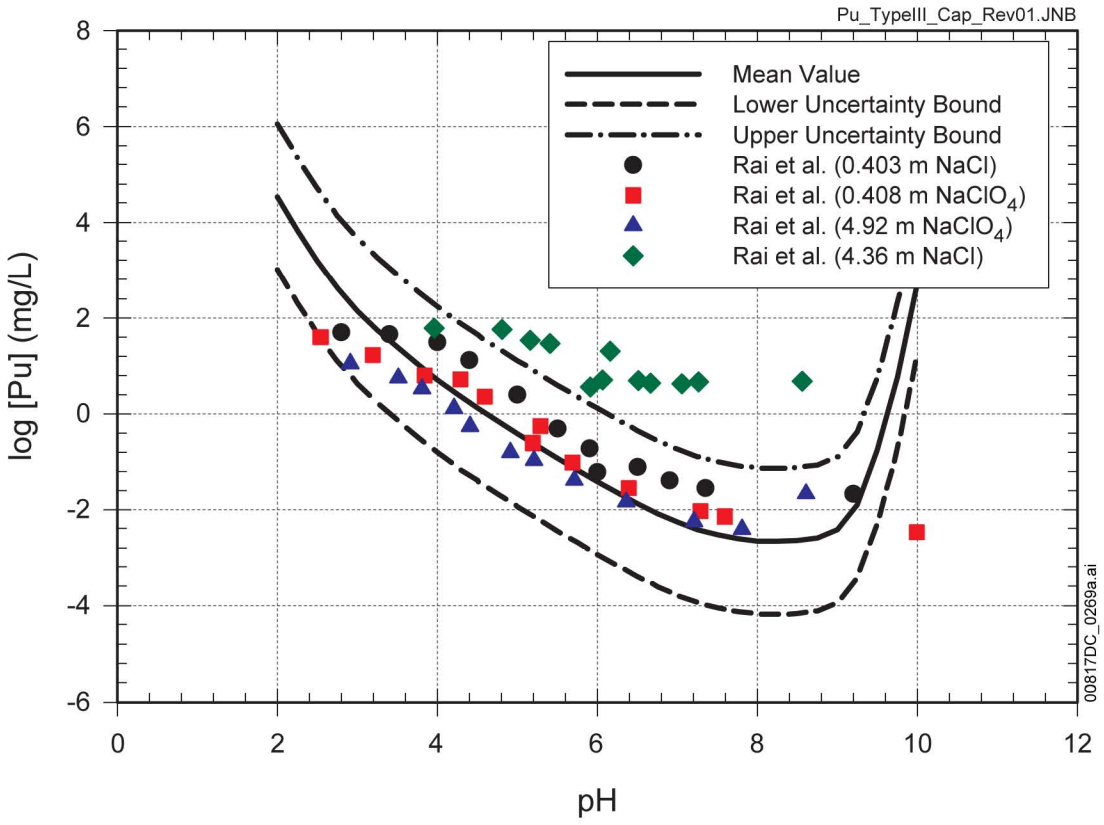

Sources: SNL 2007 [DIRS 177418], Table 6.5-1; and Rai et al. 2001 [DIRS 168392], Tables A.1 and A.2.

Figure 6.3.7-10. Comparison of the Solubility-Limited Dissolved Concentration Model for Plutonium

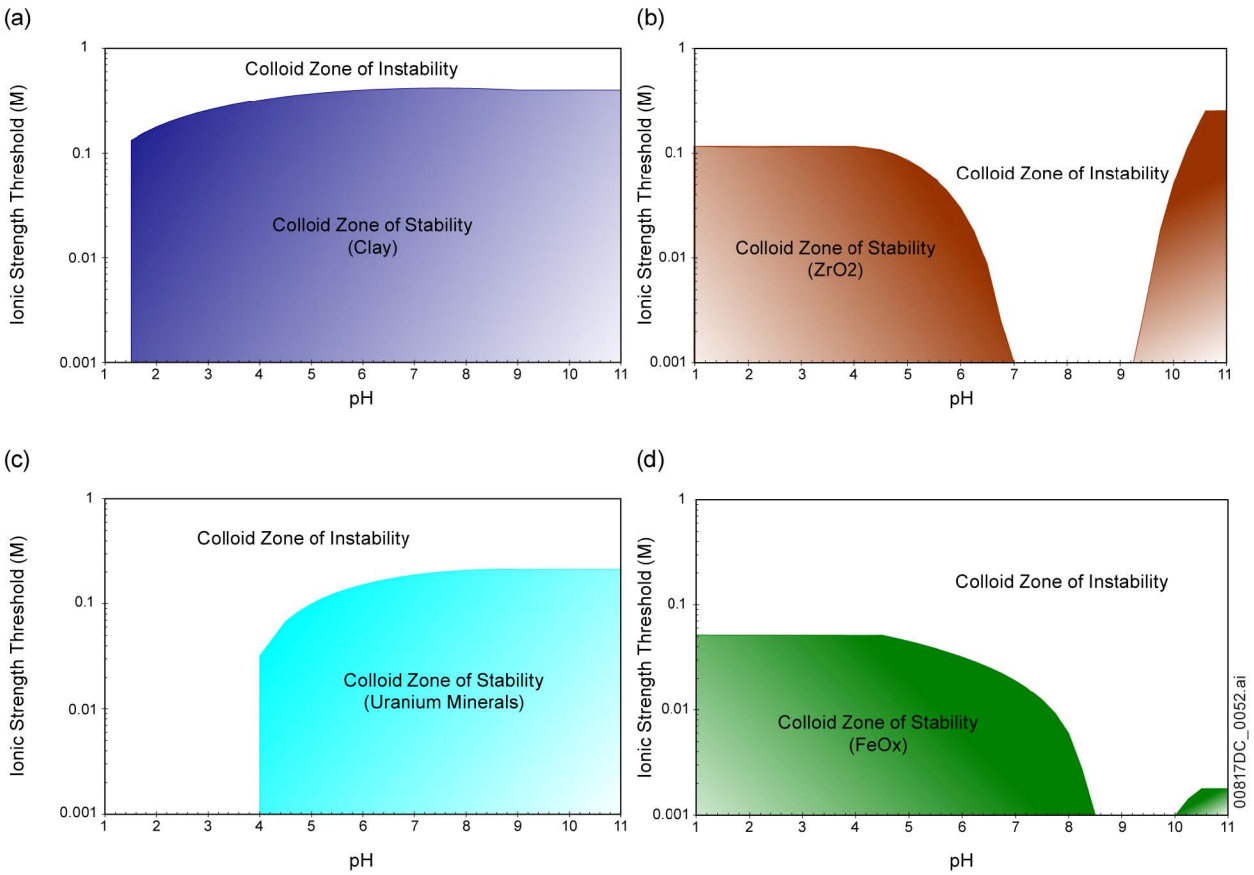

Source: Modified from SNL 2007 [DIRS 177423], Figures 6-9, 6-12, 6-14, and 6-5.

Figure 6.3.7-11. Schematic Representation of Colloid Suspension Stability as a Function of pH and Ionic Strength for (a) Groundwater and Glass Degradation Colloids (montmorillonite), (b) CSNF Residue Colloids (ZrO_2), (c) Uranium Mineral Colloids (meta-autunite), and (d) Steel Degradation Colloids (hematite)

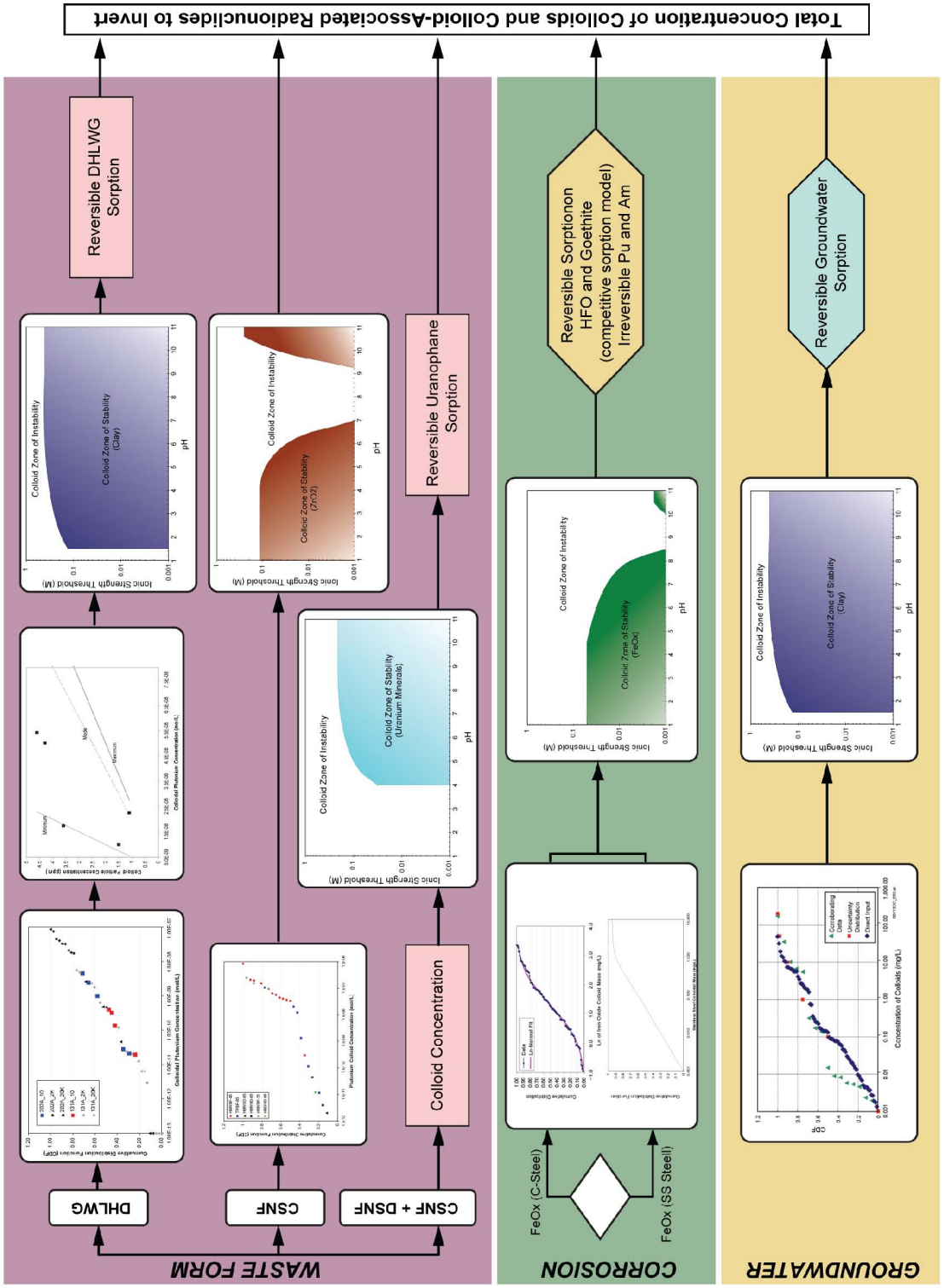

Source: Modified from SNL 2007 [DIRS 177423], Figure 6-17.

Figure 6.3.7-12. Logic Diagram for Computing the Concentration and Stability of All Colloids in the Waste Package

6.3.8 Engineered Barrier System Transport

The EBS Transport Submodel calculates the time-dependent mass flux of radionuclides from failed WPs through the EBS to the UZ Transport Submodel. The EBS Transport Submodel implemented in the TSPA-LA Model is described in *EBS Radionuclide Transport Abstraction* (SNL 2007 [DIRS 177407]). The EBS Transport Submodel considers the transport of radionuclides through the EBS after the radionuclides are mobilized. The mass of radionuclides available for transport through the EBS is provided by the Waste Form Degradation Submodel for the various waste forms (Section 6.3.7.4). Additional inputs and boundary conditions for the EBS Transport Submodel are provided by the EBS Flow Submodel (Section 6.3.6), the EBS TH Environment Submodel (Section 6.3.2), the Dissolved Concentration Limits Submodel (Section 6.3.7.5), and the EBS Colloids Submodel (Section 6.3.7.6). Information flow between the EBS Transport Submodel and other TSPA-LA Model components and submodels is shown on Figure 6.3.8-1. Figure 6.3.8-2 presents an overview of the inputs, outputs, and foundation for confidence in the EBS Transport Submodel as implemented in the TSPA-LA Model. In summary, the inputs include:

- Water flow through failed WPs and the underlying invert provided by the EBS Flow Submodel (Section 6.3.6)
- Temperature, relative humidity, saturation in the invert, and imbibition flux from the host rock exiting the invert under gravity provided by the EBS TH Environment Submodel (Section 6.3.2)
- The waste form dissolution rates provided by the Waste Form Degradation Submodel for the various waste forms (Section 6.3.7.4)
- Solubility limits provided by the Dissolved Concentration Limits Submodel (Section 6.3.7.5)
- Colloidal concentrations and sorption coefficients required to define the mobilized concentration of colloid-associated radionuclides provided by the EBS Colloids Submodel (Section 6.3.7.6).

The EBS Transport Submodel and many of the above supporting submodels that provide feeds were abstracted to describe single representative CSNF and CDSP WPs for each percolation subregion. The determination of what comprises a representative WP is discussed in Section 6.3.2.2.2. The EBS Transport Submodel is implemented in the TSPA-LA Model in terms of a single WP. The pertinent EBS Transport Submodel properties (including the Waste Form Degradation and Mobilization Model Components) for a single representative WP are integrated over the total number of WPs that have failed in each percolation subregion. These properties include the mass of available inventory, pore water volumes, mass of solid materials, advective flow rates, and diffusion areas.

6.3.8.1 Conceptual Model

The EBS consists of the DS, the WP on an emplacement pallet, and an invert constructed with steel supports and filled with crushed tuff between the steel framework. The conceptual model of radionuclide transport through the EBS (Figure 6.3.8-3) discretizes the system into three primary domains: (1) the waste form domain, (2) the WP corrosion products domain, and (3) the invert domain composed of crushed tuff. An additional domain, the EBS-UZ Interface, is included beneath the invert domain to establish a boundary condition for calculating the diffusive flux from the invert to the UZ and to compute the mass flux fraction going into the UZ fracture and matrix continua. The waste form and corrosion products domains are more specifically described below by the WP type (CSNF or CDSP) (SNL 2007 [DIRS 177407], Section 6.5.2.5):

Commercial spent nuclear fuel (CSNF) WP	
CSNF waste form domain	Waste form (CSNF rods), basket tubes (Stainless Steel Type 316), absorber plates (Stainless Steel Type 304B4)
Corrosion products domain	TAD canister (Stainless Steel Type 316), guide assembly (Stainless Steel Type 316), inner vessel (Stainless Steel Type 316)
Co-disposed (CDSP) WP	
High-level (radioactive) waste (HLW) glass waste form subdomain	HLW glass, HLW glass canisters (Stainless Steel Type 316)
DOE spent nuclear fuel (DSNF) waste form subdomain	DSNF (SNF and Stainless Steel Type 304), DSNF canister (Carbon Steel Type A 516, Stainless Steel Type 304, and Stainless Steel Type 316)
Corrosion products domain	Divider plate (Carbon Steel Type A 516), inner brackets (Carbon Steel Type A 516), outer brackets (Carbon Steel Type A 516), support tube (Carbon Steel Type A 516), inner vessel (Stainless Steel Type 316)

In the EBS Transport Submodel, the transport along the surface of the emplacement pallet is conservatively ignored and the WPs are modeled as being in intimate contact with the invert, (SNL 2007 [DIRS 177407], Sections 5.6 and 6.3.1.1). Thus, the mass flux leaving the WPs flows directly into the invert, with no resistance offered by the pallets. A schematic representation and discretization of various domains for the CSNF WP is shown on Figure 6.3.8-4. The implementation details are described in Section 6.3.8.3.

Radionuclide transport through each domain occurs by advection and diffusion. After the WP fails (breached by either general or localized corrosion, seismic damage, igneous intrusion or early failure mechanisms), a portion of the water that may flow through the DS could enter the WP, mobilizing radionuclides from the degraded waste form, and transporting these radionuclides into the UZ. Diffusion is the primary transport mechanism when the water flux into the WP is negligibly small or zero. Advective transport becomes important when there is

appreciable flow through the WP. When stress corrosion cracks are the only penetrations through the DS and WP, no advective transport can occur through them (SNL 2007 [DIRS 177407], Section 6.3.3.1.2.1, Table 8.1-2). Advective transport can only occur when there are corrosion patch failures or when the DS and WP are damaged by igneous intrusion or ruptured by a seismic event. Species-dependent free-water diffusion coefficients are applied that are corrected for tortuosity and temperature. The diffusion coefficient for the colloids is separately computed based on the sampled size of the colloids (SNL 2007 [DIRS 177407], Section 6.3.4.4).

Conceptually, the waste form domain represents that portion of the fuel that has degraded to rind (alteration product), along with the associated corrosion products from degradation of the steel that are present in the domain. Within the waste form domain, a number of processes occur. The waste form degradation processes include dissolution of SNF and HLW glass (Section 6.3.7.4), rapid degradation of DSNF, and formation of waste form colloids from the alteration of HLW glass and SNF (Section 6.3.7.6). Radionuclides may be reversibly sorbed or embedded irreversibly in the waste form colloids. The amount of each radionuclide mobilized from a waste form is limited by the solubility of the radionuclide in water (Section 6.3.7.5) and the amount of the radionuclide associated with suspended colloids (Section 6.3.7.6). Colloids may be important to the total system performance because they can increase the mass release of radionuclides from the WP. Both dissolved and colloid-associated radionuclide mass are transported by advection and/or diffusion to the WP corrosion products domain.

The CDSP WP has two fuel types (HLW and DSNF) and thus the CDSP waste form domain is divided into two subdomains, one for the HLW and the other for DSNF. This is required because a CDSP WP consists of five cylindrical canisters containing HLW glass logs surrounding a central canister of DSNF. After the WP is breached, the HLW glass degrades at a specified rate to a clay-like alteration product. However, the DSNF degrades almost instantaneously to oxides and hydrated oxides of uranium. In addition to the ongoing fuel degradation, the steel support framework inside the inner vessel of the WP will corrode gradually, allowing the HLW glass logs to collapse slowly within the inner vessel, such that the general cylindrical shape of the glass logs is retained. On the other hand, because DSNF degrades almost instantaneously, and with no credit taken for the canister, it is expected that DSNF will not retain its cylindrical geometry, and may settle to the bottom of the interior of the inner vessel. With this assumption of the internal configuration of a degraded CDSP WP, two separate waste form subdomains are conceptualized, one for HLW and the other for DSNF. The transport characteristics are expected to be different in each waste form subdomain. Because the EBS Transport Submodel is a one-dimensional model, the two waste form subdomains are modeled sequentially, such that the HLW domain is upstream of the DSNF domain. The mass released from the degradation of HLW glass moves to the DSNF domain by advection and/or diffusion and then is transported to the corrosion products domain. Because of the one-dimensional assumption, each waste form subdomain and the corrosion products domain have the same seepage flux.

Conceptually, the corrosion products domain is composed of corroded internal components of the WP, predominantly from the inner vessel and TAD canister. The internal components of a breached WP will degrade slowly over tens of thousands of years, forming corrosion products (assumed to be iron oxyhydroxides) that can sorb and delay the release of radionuclides from the

WP (SNL 2007 [DIRS 177407], Sections 6.3.4.2 and 6.5.1.2). Degradation of the internal WP components results in two types of materials: (1) stationary iron oxyhydroxide corrosion products that are assumed to remain in the WP, and (2) iron oxyhydroxide colloids that are mobile and can move out of the WP. The primary interactions with the corrosion products are equilibrium and kinetic sorption of dissolved radionuclide species onto the stationary corrosion products and iron oxyhydroxide colloids. The sorption parameters are developed from a mechanistic surface-complexation-based competitive sorption model that is applicable over the range of pH and P_{CO_2} expected in the repository over the simulation timescales. Dissolved species also undergo reversible sorption onto groundwater (seepage-water) colloids and waste form colloids that are passing through the corrosion products domain. Radionuclides are transported by advection and diffusion from the corrosion products domain to the invert domain.

In the invert domain of the EBS Transport Submodel, radionuclide transport occurs by both advection and diffusion and the mass flux of radionuclides (in both the dissolved state and associated with colloids) is passed to the UZ. Reversible sorption of radionuclides on the crushed tuff is also considered. The EBS-UZ Interface domain is conceptualized to apply an effective semi-infinite zero-concentration boundary condition for computing the diffusive flux from the invert to the UZ. It is also used to calculate the mass fraction going into the UZ fracture and matrix continua.

In all of the EBS domains, there are additional parameters that influence the release of radionuclide mass from each domain. For example, the water volume, porosity, water saturation, cross-sectional area for diffusion, diffusive path length, temperature, relative humidity, and chemistry affect the rate of advective and diffusive transport of radionuclides through the EBS domains. The concentration of dissolved species may also be solubility limited, which could result in precipitation of radionuclide mass if the solubility limit is reached. Radionuclide transport is assumed not to occur when the temperatures are greater than 100°C (the boiling point of water) due to a lack of bulk water and a continuous film of water. However, below this temperature, a continuous thin film of adsorbed water is assumed to behave as bulk liquid in order to allow radionuclides to dissolve and diffuse through it (SNL 2007 [DIRS 177407], Section 5.5).

6.3.8.2 Abstraction

The EBS Transport Submodel calculates the time-dependent rate of radionuclide releases from the EBS to the UZ. The mass of each radionuclide at any particular location is dependent on the transport characteristics of the radionuclide, the quantity of the radionuclide remaining at its source, the extent of radioactive decay or ingrowth associated with a particular radionuclide, and the diffusive area and diffusive length in a given domain. The continuum mass balance equations for the EBS Transport Submodel are described and developed in *EBS Radionuclide Transport Abstraction* (SNL 2007 [DIRS 177407], Section 6.5.1.2). These equations represent one-dimensional mass balance for:

- Transport of dissolved radionuclide species and radionuclide species that are reversibly sorbed onto three types of colloids: iron oxyhydroxide, waste form, and groundwater

- Transport of kinetically (and irreversibly) sorbed radionuclide species on iron oxyhydroxide colloids
- Kinetic sorption of radionuclide species onto stationary corrosion products in the WP
- Transport of embedded (irreversibly sorbed) radionuclide species in waste form colloids
- Decay and ingrowth for a given radionuclide.

Implementation of the three-domain EBS Abstraction requires that the following properties be specified for each domain: the domain water volume, volumetric flow rate, water saturation, porosity, diffusive area, diffusive path length, and diffusion coefficient. Note that species-dependent free water diffusion coefficients are used in each domain for dissolved radionuclides while a separate diffusion coefficient is computed for transport of radionuclides associated with colloids based on the sampled size of the colloids (SNL 2007 [DIRS 177407], Section 6.3.4.4). In addition, the diffusion coefficients are corrected for tortuosity and temperature. The preceding properties may vary among the dripping and non-dripping environments for each fuel type and WP (CSNF and CDSP WPs), the invert, and the EBS-UZ Interface. The advective or diffusive transport pathways and transport processes included in the EBS Transport Submodel of the TSPA-LA Model are summarized in Table 6.3.8-1. The parameters that define the transport of radionuclides through the waste form and the corrosion products domains, as discussed in the following sections, are summarized in Table 6.3.8-2. Table 6.3.8-3 and Table 6.3.8-4 summarize various sampled parameters used in the EBS Transport Submodel, with the ranges and distributions for each parameter provided. Table 6.3.8-5 provides the UZ fracture and matrix saturation and flux inputs for the four glacial transition climates (gt10, gt30, gt50, and gt90) and four post-10,000-year climates (pk10, pk30, pk50, and pk90) used in the EBS-UZ Interface model in each of the five percolation subregions (PS1, PS2, PS3, PS4, and PS5). Table 6.3.8-6 summarizes the parameters used in the rind volume calculation from the degradation of CSNF. The general modeling approach and properties used to calculate radionuclide transport in each of the domains are detailed in the following sections.

6.3.8.2.1 Commercial Spent Nuclear Fuel Waste Form Domain

The CSNF waste form domain represents material inside the TAD canister, which includes fuel rods, basket tubes, and absorbed plates, which may degrade once the WP is breached (Figure 6.3.8-5).

Transport out of the waste form domain can occur by advection, when there is liquid flow through the WPs, and by diffusion, through continuous thin water films assumed to be present in the WPs when temperatures are less than 100°C. Diffusion can occur in both dripping and non-dripping environments. In addition to being transported in the dissolved state, radionuclides in the CSNF waste form domain can be transported via waste form colloids and groundwater colloids. Two different waste form colloids are generated by the degradation and alteration of CSNF and have different stability fields and concentrations. One is modeled to only include embedded plutonium and americium, which are considered as intrinsic parts of the colloids and, thus, not in equilibrium with the aqueous system. These embedded radionuclides are modeled as

irreversibly attached to the host colloids. The second waste form colloid type is modeled to undergo only reversible sorption similar to groundwater colloids.

Solving the mass transport equations requires that the following properties be defined at the beginning of the timestep: (1) the volume of water in the domain, (2) the diffusive area of the domain, (3) the diffusive length of the domain, (4) diffusion coefficients, and (5) advective flow rates.

CSNF Waste Form Water Volume—The cladding degradation abstraction (SNL 2007 [DIRS 180616], Section 6.2.4) estimates the rind water volume for both dripping and non-dripping cases. The volume of water in the rind as a function of time is given by:

$$V_w(t) = \phi_{CSNF} S_{CSNF} V_{rr}(t) N_f(t) \quad \text{(Eq. 6.3.8-1)}$$

where

$V_w(t)$ = time-dependent volume of water in rind (m^3)

ϕ_{CSNF} = porosity of the CSNF rind material (schoepite)

S_{CSNF} = saturation of the CSNF rind material (schoepite)

$V_{rr}(t)$ = time-dependent volume of rind in a fuel rod (m^3)

$N_f(t)$ = number of failed rods as a function of time.

The porosity of the waste form rind is an epistemic uncertain parameter, sampled from a uniform distribution between 0.05 and 0.3 (Table 6.3.8-6). The time-dependent number of failed fuel rods, $N_f(t)$, is not needed as all the rods are assumed to be failed, as there is no credit taken for the cladding in the base-case calculations (Section 6.3.7.3).

The volume of rind in a rod, $V_{rr}(t)$, is (SNL 2007 [DIRS 180616], Table 6-4, Equation 6-7):

$$V_{rr}(t) = \frac{V_{init} F_{cor}(t) V_{rm}}{N_f(t)} \quad \text{(Eq. 6.3.8-2)}$$

where

V_{init} = initial volume of fuel in a WP (m^3)

$F_{cor}(t)$ = time-dependent fraction of total corroded waste form inventory

V_{rm} = rind volume multiplier.

The initial volume of fuel in a CSNF WP is calculated as the product of the number of fuel rods in a CSNF WP and the volume of a single undegraded fuel rod (SNL 2007 [DIRS 180616], Table 6-4, Equation 6-4). The time-dependent fraction of total corroded (degraded) waste form inventory, F_{cor}, is calculated within the TSPA-LA Model using Equation 6.3.7-7 (Section 6.3.7.4.1.3).

For the purposes of modeling the rind formation, the CSNF matrix and schoepite inside a failed cladding rod are abstracted as concentric cylinders, with the fuel matrix modeled as a receding inner cylinder and with the schoepite modeled as an expanding outer cylinder, constrained by a split cladding rod (Figure 6.3.8-5). The rind volume multiplier, V_{rm}, accounts for the increase in volume associated with rind development due to density change between fuel matrix (UO_2) and schoepite. This multiplier is proportional to the differences in density and molecular weight of the intact fuel and schoepite (SNL 2007 [DIRS 180616], Table 6-4, Equation 6-3):

$$V_{rm} = \left(\frac{MW_{sch}}{MW_{UO2}} \right) \frac{\rho_{UO2}}{(1-\phi_{sch})\rho_{sch}} \qquad \text{(Eq. 6.3.8-3)}$$

where

MW_{sch} = molecular weight of schoepite (g/mol)

MW_{UO2} = molecular weight of UO_2 (g/mol)

ρ_{UO2} = density of UO_2 (g/cm^3)

ρ_{sch} = density of schoepite (g/cm^3).

The parameters used in the TSPA-LA Model abstraction for CSNF rind volume are given in Table 6.3.8-6. The total bulk volume of the CSNF domain is the sum of the rind volume and the volume of basket tube and absorber plate steel corrosion products, which also increase over time:

$$V_{CSNF}(t) = V_{rind,CSNF}(t) + V_{CP,CSNF}(t). \qquad \text{(Eq. 6.3.8-4)}$$

The rind volume in a CSNF WP ($V_{rind,CSNF}$) is calculated by multiplying the volume of rind in a rod (V_{rr}) by the number of failed rods. The bulk volume of CSNF domain corrosion products is (SNL 2007 [DIRS 177407], Equation 6.5.2.2.2.1-4):

$$V_{CP,CSNF}(t) = \left(\frac{1}{1-\phi_{CP}} \right) \sum_{CPm} \left[\frac{\left[m_{CPm,CS,CSNF}(t) + m_{CPm,SS,CSNF}(t) \right]}{\rho_{CPm}} \right]. \qquad \text{(Eq. 6.3.8-5)}$$

where ϕ_{CP} is the steel corrosion products porosity (a constant value of 0.4), $m_{CPm,CS,CSNF}$ is the mass of corrosion products from degradation of carbon steel (zero for CSNF), $m_{CPm,SS,CSNF}$ is the mass of corrosion products from degradation of stainless steel, ρ_{CPm} is the grain density of corrosion products, and subscript m refers to the metal type (iron or nickel or chromium) in the steel from which the type of corrosion products is formed (goethite, ferrihydrite, NiO, Cr_2O_3).

The pore volume in the CSNF waste form domain is the sum of CSNF rind pore volume and steel corrosion products pore volume:

$$V_{\phi,CSNF}(t) = \phi_{CSNF} V_{rind,CSNF}(t) + \phi_{CP} V_{CP,CSNF}(t), \quad \text{(Eq. 6.3.8-6)}$$

where the CSNF rind porosity, ϕ_{CSNF}, is a sampled parameter.

The effective porosity of the CSNF waste form domain, which is needed for computing the diffusion coefficient using Archie's law, is time dependent because the pore volume and bulk volume of the domain are time dependent:

$$\phi_{CSNF}(t) = \frac{V_{\phi,CSNF}(t)}{V_{CSNF}(t)}. \quad \text{(Eq. 6.3.8-7)}$$

The water volume in the CSNF waste form domain is the sum of CSNF rind water volume and steel corrosion products water volume:

$$V_{w,CSNF}(t) = \phi_{CSNF} S_{w,rind,CSNF} V_{rind,CSNF}(t) + \phi_{CP} S_{w,CP,CSNF} V_{CP,CSNF}(t). \quad \text{(Eq. 6.3.8-8)}$$

The saturation of the rind and corrosion products is determined separately, when there is no flow through the WP, using separate water vapor adsorption isotherms that are functions of relative humidity and specific surface areas, among other parameters. The calculations are described in Section 6.5.2.2 of the *EBS Radionuclide Transport Abstraction* (SNL 2007 [DIRS 177407]). Since the adsorption isotherm functions are unbounded as relative humidity (*RH)* approaches 1.0, the saturation is limited to a value of 1.0. Under flowing conditions through the WP, complete saturation of the pore space is assumed. The effective water saturation for the CSNF waste form domain is given by:

$$S_{w,CSNF}(RH) = \min\left[\frac{V_{w,CSNF}(RH,t)}{V_{\phi,CSNF}(t)}, 1.0\right]. \quad \text{(Eq. 6.3.8-9)}$$

CSNF Waste Form Diffusive Area and Length—The area through which radionuclides may diffuse after being released from fuel rods depends on the state of the waste form. No credit is taken for the fuel rod cladding, so once a WP is breached, all of the SNF is modeled as exposed to the environment inside the WP. As a result, the diffusive area for the waste form domain is based on the radial geometry inside the WP that is bounded by the TAD canister. Since the diffusive area increases with increasing distance from the origin point in the radial geometry, the area of the CSNF waste form domain is taken at half the radius of the TAD canister (Figure 6.3.8-5) and set at a constant value of 12.5 m^2 (Table 6.3.8-2). The diffusive path length is set to be the inside radius of the TAD canister (= 0.819 m) (Table 6.3.8-2). In calculating the diffusive conductance across the interface between the CSNF waste form domain and the downstream corrosion products domain the harmonic average of the diffusive areas and diffusive lengths of the two domains is considered. The radial transport is modeled in the Cartesian coordinates in a one-dimensional model by specifying the diffusive areas and lengths consistent with the radial geometry (SNL 2007 [DIRS 177407], Appendix L).

Calculation of Diffusion Coefficients in the CSNF Waste Form Domain—Diffusion coefficients for dissolved radionuclides in the CSNF waste form domain are calculated using Archie's law. This approach implicitly includes the effects of porosity, saturation, and tortuosity in calculating an effective diffusion coefficient for a porous medium. For the CSNF waste form domain, Archie's law is expressed as (SNL 2007 [DIRS 177407], Equation 6.3.4.3.5-2):

$$\phi_{CSNF} S_{w,CSNF} D_{WF} = D_{wi} \phi_{CSNF}^{1.3} S_{w,CSNF}^{2} \quad \text{(Eq. 6.3.8-10a)}$$

where

D_{WF} = effective diffusion coefficient that includes the effect of tortuosity in a porous medium (cm^2/s)

D_{wi} = species dependent free water diffusion coefficient (cm^2/s)

ϕ_{CSNF} = porosity of domain

$S_{w,CSNF}$ = liquid saturation of the domain (fraction).

After the effective diffusion coefficient has been calculated using Equation 6.3.8-10a, it is modified to account for temperature effects. The diffusion coefficient at a given temperature is given as (SNL 2007 [DIRS 177407], Equation 6.3.4.1.2-4):

$$D_T = D_{T_0} \frac{T}{T_0} 10^{\left[\frac{1.3272(293.15-T_0)-0.001053(T_0-293.15)^2}{T_0-168.15}\right]-\left[\frac{1.3272(293.15-T)-0.001053(T-293.15)^2}{T-168.15}\right]} \quad \text{(Eq. 6.3.8-10b)}$$

where

D_T = effective diffusion coefficient at temperature T (cm^2/s)

D_{T_0} = diffusion coefficient at temperature T_0 (as calculated by Equation 6.3.8-10a) (cm^2/s)

T = invert temperature (K)

T_0 = reference temperature (298.15 K).

Advective Transport in the CSNF Waste Form Domain—Advective transport out of the waste form domain and into the corrosion products domain can only occur when there is liquid flow through the WPs. The EBS Flow Submodel determines the flux through the WP (flow pathway 4 on Figure 6.3.6-4) based on the flux through the DS, the damage fraction on a WP, and a WP flux-splitting logic (Section 6.3.6). Advective flux to the WPs is only possible when the DSs are breached. Details regarding the calculation of the flow through the WP are given in the EBS Flow Submodel (Section 6.3.6.2). If the only breaches in a WP are stress corrosion cracks, advective transport through the WP does not occur, but diffusion of radionuclides out of the WP could still take place.

6.3.8.2.2 Co-Disposed Waste Form Domain

As conceptualized in Section 6.3.8.1, the CDSP waste form domain is divided into two subdomains, one for the HLW glass and another for the DSNF. The two waste form subdomains are modeled sequentially, such that the HLW subdomain is upstream of the DSNF subdomain as described in Section 6.3.8.1. The mass released from the degradation of HLW glass moves to the DSNF domain by advection and/or diffusion and is then transported to the corrosion products domain. Radionuclide concentrations are subject to the solubility constraints defined by the Dissolved Concentration Limits Submodel (Section 6.3.7.5).

In addition to being transported in the dissolved state, radionuclides in the HLW subdomain can be transported via waste form colloids. These colloids are generated by the degradation and alteration of HLW glass and include embedded plutonium and americium, which are considered as intrinsic parts of the colloids and, thus, not in equilibrium with the aqueous system. These embedded radionuclides are modeled as irreversibly attached to the host colloids. Reversible sorption onto waste form colloids is also considered for various radionuclides. Details of the waste form colloid generation, stability, and sorption capability are given in Section 6.3.7.6.2.

Transport out of the CDSP waste form subdomains can occur by advection, when there is liquid flow through the WPs, and by diffusion, through continuous thin water films assumed to be present in the WPs. Diffusion can occur in both dripping and non-dripping environments. Solving the mass transport equation requires that the following properties be defined: (1) the volume of water in the degraded fuel, (2) the diffusive areas of the domains, (3) the diffusive length of the domains, (4) diffusion coefficients; (5) sorbent mass, and (6) advective flow rates. The diffusive areas through various subdomains are shown on Figure 6.3.8-6.

HLW Waste Form Water Volume—The HLW glass degradation abstraction (BSC 2004 [DIRS 169988]) estimates the rind water volume for both dripping and non-dripping cases. The rind volume in the altered rind is provided by the expression (BSC 2004 [DIRS 169988], Section D.1, Equation D-3b):

$$V_{rind,HLWG}(t) = \frac{1}{\rho_G} \sum M_t \qquad \text{(Eq. 6.3.8-11)}$$

where

$V_{rind,HLWG}$ = bulk rind volume (m^3)

ρ_G = the bulk HLW glass density (kg/m^3)

$\sum M_t$ = total mass of degraded HLW glass up to time t (kg).

Because the properties of the HLW glass and the clay making up the rind layer are similar, Equation 6.3.8-11 assumes that a degraded volume of glass generates an equal volume of clay as the rind layer (BSC 2004 [DIRS 169988], Section D.2). Therefore, the glass density (2,700 kg/m^3) is the same for the unreacted glass and the clay alteration products (DTN: MO0502ANLGAMR1.016_R0 [DIRS 172830], Table 8-1). The total mass of glass degraded over a timestep of size Δt is provided by the HLW Glass Waste Form Degradation Submodel (Section 6.3.7.4.3).

The total bulk volume of the HLW subdomain is the sum of the rind bulk volume and the bulk volume of corrosion products from degradation of steel canisters encasing the fuel, which also increase over time:

$$V_{HLWG}(t) = V_{rind,HLWG}(t) + V_{CP,HLWG}(t). \qquad \text{(Eq. 6.3.8-12)}$$

The bulk volume of HLW domain corrosion products is (SNL 2007 [DIRS 177407], Section 6.5.2.2):

$$V_{CP,HLWG}(t) = \left(\frac{1}{1-\phi_{CP}}\right)\sum_{CPm}\left[\frac{\left[m_{CPm,CS,HLWG}(t) + m_{CPm,SS,HLWG}(t)\right]}{\rho_{CPm}}\right]. \qquad \text{(Eq. 6.3.8-13)}$$

where ϕ_{CP} is the steel corrosion products porosity (a constant value of 0.4), $m_{CPm,CS,HLWG}$ is the mass of corrosion products from degradation of carbon steel, $m_{CPm,SS,HLWG}$ is the mass of corrosion products from degradation of stainless steel, ρ_{CPm} is the grain density of corrosion products, and subscript *m* refers to the type of corrosion products formed (goethite, ferrihydrite, NiO, Cr_2O_3).

The pore volume in the HLW waste form domain is the sum of HLW rind pore volume and steel corrosion products pore volume:

$$V_{\phi,HLWG}(t) = \phi_{rind} V_{rind,HLWG}(t) + \phi_{CP} V_{CP,HLWG}(t), \qquad \text{(Eq. 6.3.8-14)}$$

where ϕ_{rind} is the rind porosity given by a constant value of 0.17 (DTN: SN0703PAEBSRTA.001_R3 [DIRS 183217], Table 8.2-6).

The effective porosity of the HLW waste form domain, which is needed for computing the diffusion coefficient using Archie's law, is time dependent because the pore volume and bulk volume of the domain are time dependent:

$$\phi_{HLWG}(t) = \frac{V_{\phi,HLWG}(t)}{V_{HLWG}(t)}. \qquad \text{(Eq. 6.3.8-15)}$$

The water volume in the HLW waste form domain is the sum of HLW rind water volume and steel corrosion products water volume:

$$V_{w,HLWG}(t) = \phi_{rind} S_{w,rind,HLWG} V_{rind,HLWG}(t) + \phi_{CP} S_{w,CP,HLWG} V_{CP,HLWG}(t) \quad \text{(Eq. 6.3.8-16)}$$

The saturation of the rind and corrosion products is determined separately, when there is no flow through the WP, using separate water vapor adsorption isotherms that are functions of relative humidity and specific surface areas, among other parameters. The calculations are described in *EBS Radionuclide Transport Abstraction* (SNL 2007 [DIRS 177407], Section 6.5.2.2). Since the adsorption isotherm functions are unbounded as the relative humidity approaches one, the saturation is limited to a value of one. Under flowing conditions through the WP, complete saturation of the pore space is assumed.

The effective water saturation for the HLW waste form domain is given by:

$$S_{w,HLWG}(RH) = \min\left[\frac{V_{w,HLWG}(RH,t)}{V_{\phi,HLWG}(t)}, 1.0\right]. \quad \text{(Eq. 6.3.8-17)}$$

DSNF Waste Form Water Volume—The water volume of the DSNF waste form is computed by multiplying the initial volume of DSNF in a CDSP WP, which is equal to 1 m^3 (BSC 2004 [DIRS 172453], Section 8.1), by its porosity and saturation. The porosity of DSNF rind is assumed to be 0.2, as degraded DSNF is conceptualized to be a porous medium (SNL 2007 [DIRS 177407], Section 6.5.2.1.2). The total bulk volume of the DSNF waste form subdomain is the sum of the rind volume and the volume of corrosion products from degradation of associated steel (Section 6.3.8.1), which also increases with time. The equations used for calculating the bulk volume, pore volume, effective porosity, water volume, and effective saturation are the same as those shown for CSNF.

HLW Waste Form Diffusive Area and Length—Consistent with the treatment for the CSNF waste form domain, radionuclides will tend to diffuse radially outward from the HLWG waste form subdomain. Since the diffusive area increases with increasing distance from the origin point in the radial geometry, the area of the HLW waste form domain is taken at half the radius of the inner vessel cavity (Figure 6.3.8-6) and set at a constant value of 13.7 m^2 (Table 6.3.8-2). The diffusive path length is set to be the inside radius of inner vessel of a CDSP WP (= 0.941 m) (Table 6.3.8-2). In calculating the diffusive conductance across the interface between the HLW waste form subdomain, and the downstream DSNF waste form subdomain the harmonic average of the diffusive areas and diffusive lengths of the two domains is used.

DSNF Waste Form Diffusive Area and Length—DSNF is modeled as degrading instantaneously upon WP breach. Since the carbon steel support tube, divider plates, and brackets that support the HLWG canisters surrounding the DSNF also degrade rapidly (compared to the degradation rates of HLWG and stainless steel inner vessel), the DSNF is not expected to retain its initial cylindrical shape, but rather will settle to the bottom of the interior of the inner vessel. In the 1-D EBS Transport Model, this implies that the DSNF diffusive area is the same as for the HLWG waste form subdomain (= 13.7 m^2) (Table 6.3.8-2). The effective diffusive path length is calculated by dividing the initial volume of DSNF 1 m^3 by the diffusive area leading to a total diffusive length of 0.0730 m (Table 6.3.8-2).

Calculation of Diffusion Coefficients in the CDSP Waste Form Domain—The effective diffusion coefficient for dissolved radionuclides in the HLW and DSNF subdomain is computed using Archie's law (Equation 6.3.8-10a and b). Both subdomains are considered to be fully saturated when there is flow through the WP. The diffusion coefficient for the colloids is separately computed based on the sampled size of the colloids (SNL 2007 [DIRS 177407], Section 6.3.4.4).

Advective Transport in the CDSP Waste Form Domain—The HLW and DSNF waste form subdomains are modeled sequentially, such that the HLW subdomain is upstream of the DSNF subdomain. Because of the one-dimensional model geometry, the DSNF waste form subdomain sees the same water flux as the HLW waste form subdomain. The advective transport out of the HLW waste form subdomain and into the DSNF waste form subdomain can only occur when there is liquid flow through the WPs. The EBS Flow Submodel determines the flux through the WP (Section 6.3.6).

6.3.8.2.3 Corrosion Products Domain

The corrosion products domain represents that portion of the internal components of a WP that has degraded after the WP is breached (Section 6.3.8.1 for the steel components included in this domain). Degradation of the internal WP components results in two types of materials: (1) stationary iron oxyhydroxide corrosion products that are assumed to remain in the WP, and (2) iron oxyhydroxide colloids that are mobile and can move out of the WP. Although only iron oxyhydroxide colloids are generated in this domain, waste form colloids (generated from HLW degradation) and groundwater colloids (from seepage waters) can also be present.

A surface complexation-based competitive sorption model is developed for modeling sorption of dominant actinides in the inventory (uranium, neptunium, plutonium, americium, and thorium) to the iron oxyhydroxide surfaces. It is a mechanistic model based on a single-site diffuse-layer surface complexation model that couples the pH in the corrosion products domain with the type of surface complexes formed under varying chemical conditions and sorption site densities. The model is applicable to a wide range of concentrations and accounts for competition among various actinides for the finite number of sorption sites. The composition of the steel corrosion products is difficult to predict as it will vary over time but it is expected to be dominantly a mixture of iron oxyhydroxides (such as goethite, ferrihydrite, and hematite), chromium oxides, and nickel oxides. For the purposes of modeling radionuclide sorption on steel degradation products (stationary corrosion products and mobile colloids), only the iron oxyhydroxides are considered, which are assumed to be a mixture of goethite and ferrihydrite, the proportion of which is treated as uncertain. It should be noted that the pure iron oxide surface properties are used to model sorption onto what will in reality be a solid solution of Fe(III), Cr(III), and Ni(II). The details of the model development are described in *EBS Radionuclide Transport Abstraction* (SNL 2007 [DIRS 177407], Section 6.5.2.4).

The mass of corrosion products in a breached WP varies over time, from zero when the WP is first breached to a maximum amount (SNL 2007 [DIRS 177407], Table 6.3-8) when all of the steel in the domain is corroded. The mass, at any given time, is computed by linearly interpolating over the lifetime of each of the two major types of steel comprising the internal components of a WP—carbon steel and stainless steel. The equations used to calculate the

time-dependent mass of corrosion products, present in the corrosion products domain, are developed in *EBS Radionuclide Transport Abstraction* (SNL 2007 [DIRS 177407], Section 6.5.2.2.1). Note that only the mass of corrosion products contributed by goethite and ferrihydrite is used in competitive sorption calculations of radionuclides, while for water vapor adsorption calculations the entire mass of corrosion products is used, including nickel oxides and chromium oxides. The corrosion products mass from degradation of steel shield plug in the TAD canister is not considered in the TSPA as the mass is localized at one end of the WP and will not appreciably affect transport throughout the rest of the WP. A minimum initial mass of 10 kg of stationary corrosion products is assumed, as it is required to initiate the water volume and sorption calculations after the WP failure.

Corrosion Products Domain within a CSNF WP—Both advective and diffusive transport can occur from the corrosion products domain to the invert domain. Solving the mass transport equations requires that the following properties be defined: (1) mass of corrosion products, (2) volume of water in the corrosion products, (3) diffusive area of the domain, (4) diffusive length of the domain, and (5) advective flow rate.

CSNF Corrosion Products Water Volume—The volume of water in the CSNF corrosion products domain is calculated as the product of the pore volume and water saturation of the corrosion product mass. The pore volume of the corrosion products is calculated by the expression (SNL 2007 [DIRS 177407], Section 6.5.2.2.1)

$$V_{\phi,CP}(t) = \left(\frac{\phi_{CP}}{1-\phi_{CP}}\right)\sum_{CPm}\left[\frac{\left[m_{CPm,CS}(t)+m_{CPm,SS}(t)\right]}{\rho_{CPm}}\right] \qquad \text{(Eq. 6.3.8-18)}$$

where, ϕ_{CP} is the steel corrosion products porosity (a constant value of 0.4), $m_{CPm,CS}$ is the mass of corrosion products from degradation of carbon steel, $m_{CPm,SS}$ is the mass of corrosion products from degradation of stainless steel, ρ_{CPm} is the grain density of corrosion products, and subscript 'm' refers to the type of corrosion products formed (goethite, ferrihydrite, NiO, and Cr_2O_3).

When there is flow through the WP, the water saturation is assigned a value of 1.0 (SNL 2007 [DIRS 177407], Section 6.5.2.2). In conditions when there is no flow through the WP, the only water present is adsorbed water and the water saturation in the domain for each type of corrosion product (goethite, ferrihydrite, NiO, and Cr_2O_3) is computed separately as given by (SNL 2007 [DIRS 177407], Section 6.5.2.2.1):

$$S_{w,CPm}(RH) = \min\left[t_f \rho_{CPm} \bar{s}_{CPm}\left(\frac{1-\phi_{CP}}{\phi_{CP}}\right)\theta_{CP}(RH), 1.0\right] \qquad \text{(Eq. 6.3.8-19)}$$

where

$S_{w,CPm}$ = effective water saturation of corrosion products (fraction)

$\bar{s}_{CPm}$ = specific surface area of corrosion products (m^2/kg)

ρ_{CPm} = corrosion products grain density (kg/m^3)

θ_{CP} = number of monolayers of water adsorbed on the surface of corrosion products; a function of relative humidity

t_f = thickness of a monolayer of water (m)

RH = relative humidity (fraction).

A single adsorption isotherm is used for all corrosion products, so a single relative humidity-dependent value of $\theta_{CP}(RH)$ is used for all corrosion products in this domain. The water volume for the entire domain is calculated as:

$$V_{w,CP}(RH,t) = \sum_m V_{\phi,CPm}(t) S_{w,CPm}(RH) \qquad \text{(Eq. 6.3.8-20)}$$

The water saturation for the entire domain is calculated as:

$$S_{we,CP}(RH) = \min\left[\frac{V_{w,CP}(RH,t)}{V_{\phi,CP}(t)}, 1.0\right] \qquad \text{(Eq. 6.3.8-21)}$$

CSNF Corrosion Products Diffusive Area and Length—Since the WP outer barrier undergoes variable damage specified by the scenario classes and modeling cases, the corrosion products domain is divided into two regions: (a) the region that only includes the outer barrier and (b) the region that includes the TAD canister and inner vessel but excludes the outer barrier. The diffusive area for the path excluding the outer barrier is given by the surface area of a cylinder halfway between the inside surface of the TAD canister and the outside surface of the inner vessel (= 29.9 m^2) (Table 6.3.8-2), while the diffusive path length is given by the distance from the inside of the TAD canister to the outside of the inner vessel (= 0.0914 m) (Table 6.3.8-2). The diffusive area for the path through the outer barrier of the WP is taken to be the smaller of either: (a) the WP breached area (scenario class dependent) or (b) the surface area of a cylinder at the midpoint between the inner vessel outer surface and the outer surface of the CSNF WP outer barrier (= 33.1 m^2) (Table 6.3.8-2). The diffusive path length through the outer barrier is the radial distance from the outside of the inner vessel to the outside of the outer barrier (= 0.0302 m) (Table 6.3.8-2).

Calculation of Diffusion Coefficients in the CSNF Corrosion Products Domain—The diffusion coefficient of the corrosion products is computed using Archie's law (Equation 6.3.8-10a, b) with the porosity of the corrosion products (0.4) and an assigned water saturation as discussed earlier.

Advective Transport in the CSNF Corrosion Products Domain—Advective transport through the CSNF corrosion products domain can only occur when there is liquid flow through the WPs. The EBS Flow Submodel determines the flux through the WP (Section 6.3.6).

Corrosion Products Domain within a CDSP WP—The CDSP corrosion products domain consists of corroded internal WP components (Section 6.3.8.1 for the steel components included

in this domain). Both advective and diffusive transport can occur in the corrosion products domain. Solving the mass transport equations requires that the following properties be defined for each domain: (1) mass of corrosion products, (2) volume of water in the corrosion products, (3) diffusive area of the corrosion products domain, (4) diffusive length, and (5) advective flow rates.

The discussion presented for the corrosion products domain within a CSNF WP is applicable to CDSP WP except for parameter values such as mass of steel, diffusive lengths, and diffusive areas. Since the WP outer barrier undergoes variable damage specified by the scenario classes and modeling cases, the corrosion products domain, just like for CSNF, is divided into the region that only includes the outer barrier and the one that is inside the WP but excludes the outer barrier. The diffusive area for the path excluding the outer barrier is given by the surface area of a cylinder halfway between the inside surface and the outside surface of the inner vessel (= 29.7 m^2) and diffusive path length is given by the thickness of the inner vessel (= 0.0508 m). The diffusive area for the path through the outer barrier of the WP is taken to be the smaller of either (a) the WP breached area (scenario class dependent) or (b) the surface area of a cylinder at the midpoint between the inner vessel outer surface and the outer surface of the CDSP WP outer barrier (= 32.6 m^2). The diffusive path length through the outer barrier is the radial distance from the outside of the inner vessel to the outside of the outer barrier (= 0.0301 m).

6.3.8.2.4 Invert Domain

The invert domain is conceptualized as a single continuum rather than as a dual continuum for modeling radionuclide transport. Both advective and diffusive transport can occur from the invert domain to the UZ. Sorption of radionuclides may occur on the crushed tuff in the invert and is modeled by the linear sorption isotherm approach using the distribution coefficient (K_d). The ranges and distributions of radionuclide sorption coefficients for sorption on crushed tuff in the invert are the same as those for devitrified tuff implemented in the UZ Transport Submodel (Table 6.3.9-2). [Note: Since K_d for Se is set to zero for the TSw unit in the UZ Transport Submodel, the K_d for Se in the invert is also set to zero as most of the repository host rock is composed of TSw unit.] Solving the mass transport equations requires that the following properties be defined: (1) the volume of water in the invert, (2) the diffusive area of the invert domain, (3) the diffusive length, and (4) advective flow rates.

Invert Domain Water Volume—The water volume of the invert domain is calculated as the product of the bulk volume and the water content of the invert (SNL 2007 [DIRS 177407], Section 6.5.2.3). The total bulk invert volume is equal to the cross-section area of the invert times the length of a WP (CDSP or CSNF). The water content of the invert cell is calculated according to the following relationship (SNL 2007 [DIRS 177407], Equation 6.5.2.3-11):

$$\theta_{inv} = \theta_{inter} + (1 - \phi_{inter})\theta_{intra} \qquad \text{(Eq. 6.3.8-22)}$$

where

θ_{inv} = invert water content

θ_{inter} = water content of the intergranular invert

ϕ_{inter} = porosity of the intergranular invert

θ_{intra} = water content of the intragranular invert.

Because the crushed tuff invert has both intergranular and intragranular porosity, the bulk water content of the invert is calculated by combining the water contents of both pore types as shown in Equation 6.3.8-22. The intragranular water content is calculated by multiplying the intragranular water saturation with the intragranular porosity. The intragranular water saturation is provided by the MSTHM Abstraction from the EBS TH Environment Submodel (Section 6.3.2). The intergranular water saturation is calculated based on the seepage flux per cross-sectional area of the drift over the length of a WP (BSC 2004 [DIRS 167652], Section 6.3.1) by using the van Genuchten moisture retention relationship for the crushed tuff, as described in *EBS Radionuclide Transport Abstraction* (SNL 2007 [DIRS 177407], Section 6.5.2.3). The porosity of the intragranular continuum is 0.111 and that of the intergranular continuum is 0.224 (DTN: SN0703PAEBSRTA.001_R3 [DIRS 183217], Table 8.2-6) and the residual water content of the intergranular continuum is 0.00224 (DTN: MO0703PAHYTHRM.000_R1 [DIRS 182093]). The bulk density of the invert material is estimated to be 1842 kg/m^3 (DTN: MO0703PAHYTHRM.000_R1 [DIRS 182093]).

Invert Diffusive Length—The true geometry of the invert is that of a segment of a circle where the top of the invert is flat and the bottom is formed by the arc of the drift. However, for the purposes of modeling flow and diffusion through the invert, the invert is regarded as having a rectangular cross section with the top being the actual top surface of the invert (Figure 6.3.8-7). The bulk volume of the invert is conserved by calculating an average thickness of the invert using the following equation (SNL 2007 [DIRS 177407], Equation 6.5.2.3-5):

$$\bar{t}_I = \frac{A_I}{w_I} = 0.934 \text{ m} \qquad \text{(Eq. 6.3.8-23)}$$

where

$\bar{t}_I$ = average invert thickness (m)

A_I = actual invert vertical cross-sectional area (4.39 m^2) (SNL 2007 [DIRS 177407], Section 6.5.2.3)

w_I = actual width of invert top surface (4.70 m) (SNL 2007 [DIRS 177407], Section 6.5.2.3).

The diffusive path length from the WP outer barrier to the mid-point of the invert is a sampled value between 0.3 m and 1.24 m to represent uncertainty in the location of the breach on the WP and the average thickness from the invert (Table 6.3.8-4). The diffusive length from the mid-

point of the invert to the interface with the host rock (part of EBS-UZ Interface domain) is taken to be half of the average invert thickness.

Invert Diffusive Area—The diffusive area implemented for the invert cell is the plan area of the rectangular invert. It is equal to the width of the invert top surface times the length of a WP (CDSP or CSNF).

Calculation of Diffusion Coefficients in the Invert Domain—The diffusion coefficient for dissolved radionuclides in the invert is computed using the following formulation of Archie's law (SNL 2007 [DIRS 177407], Equation 6.3.4.1.1-22):

$$\phi_{inv} S_w D = D_{wi} \theta_{inv}^{1.863} 10^{ND(\mu=0.033,\sigma=0.218)} \quad \text{(Eq. 6.3.8-24)}$$

where

D = invert diffusion coefficient (cm^2/s)

D_{wi} = species dependent free water diffusion coefficient (cm^2/s)

S_w = invert water saturation

ϕ_{inv} = bulk invert porosity

ND = truncated normal distribution (±3 SDs from the mean)

μ = mean

σ = SD.

After the invert diffusion coefficient has been calculated using Equation 6.3.8-24, it is modified to account for temperature effects. The diffusion coefficient at a given temperature is given by (SNL 2007 [DIRS 177407], Equation 6.3.4.1.2-4)

$$D_T = D_{T_0} \frac{T}{T_0} 10^{\left[\frac{1.3272(293.15-T_0)-0.001053(T_0-293.15)^2}{T_0-168.15}\right]-\left[\frac{1.3272(293.15-T)-0.001053(T-293.15)^2}{T-168.15}\right]} \quad \text{(Eq. 6.3.8-25)}$$

where

D_T = invert diffusion coefficient at temperature T (cm^2/s)

D_{T_0} = invert diffusion coefficient at temperature T_0 (as calculated by Equation 6.3.8-24) (cm^2/s)

T = invert temperature (K)

T_0 = reference temperature (298.15 K).

Advective Transport in the Invert Domain—There are two sources of advective water flux into the invert domain. The first is the advective flux that comes from the overlying corrosion

products domain. This flux is defined by Flow Pathway F_6 (flux into the invert) of the EBS Flow Submodel (Section 6.3.6.2). The other advective flux source is due to possible imbibition from the host rock that enters the invert and flows out under gravity. This imbibition flux is defined by Flow Pathway F_7 (Section 6.3.6.2 and Figure 6.3.6-4). The EBS TH Environment Submodel (Section 6.3.2) provides the rate of water imbibition from the host rock that enters the invert and flows out under gravity.

EBS-UZ Interface Domain—The EBS-UZ Interface domain is included beneath the invert domain to establish a boundary condition for calculating the diffusive flux from the invert to the UZ and to compute the radionuclide mass flux fraction going into each of the UZ fracture and matrix continua. The EBS Transport Abstraction applies a semi-infinite zero-concentration boundary condition near the base of the drift (SNL 2007 [DIRS 177407], Section 6.5.2.6). This boundary condition is approximated by applying an effective zero-concentration boundary in the UZ at approximately three drift diameters below the invert-UZ boundary. In the EBS-UZ Interface domain, the near-field UZ is modeled as a dual continuum consisting of overlapping UZ-matrix and UZ-fracture continua. This approach is consistent with the dual-permeability modeling approach used by the UZ Transport Submodel, as described in *Particle Tracking Model and Abstraction of Transport Processes* (SNL 2008 [DIRS 184748], Section 1). The ranges and distributions of radionuclide sorption coefficients for sorption on the UZ matrix are the same as those for devitrified tuff implemented in the UZ Transport Submodel (Table 6.3.9-2). [Note: Since K_d for Se is set to zero for the TSw unit in the UZ Transport Submodel, the K_d for Se in the UZ matrix of the EBS-UZ Interface domain is also set to zero as most rock near the drift is composed of TSw unit.] Advective fluid flux defined by Flow Pathway F_6 (combined seepage and condensation) is passed to the UZ fracture from the invert, while the advective flux due to imbibition from the host rock, defined by Flow Pathway F_7, is passed from the invert to the UZ matrix. Details of the implementation of the EBS-UZ Interface boundary condition are given in Section 6.3.8.3.

The radionuclide mass flux fractions going into the near-field UZ-matrix and UZ-fracture continua is calculated from the EBS-UZ Interface domain for each radionuclide species and passed to the UZ model along with the mass flux from the invert. The mass flux fraction varies as a function of time and may differ for each radionuclide species based on its transport characteristics. A detailed description of how the mass fractions are calculated is given in the next section.

6.3.8.3 TSPA-LA Model Implementation

The transport of radionuclides through the EBS is modeled in the TSPA-LA Model by spatially discretizing the EBS components into transport domains, as described in Section 6.3.8.1. In each domain, the four EBS transport one-dimensional continuum-form mass balance equations described at the beginning of Section 6.3.8.2 are approximated and solved using a finite-difference approach. The implementation and numerical solution of the EBS Transport Submodel's equations are performed using the GoldSim software cell pathway capability, available in the *GoldSim Contaminant Transport Module* (GoldSim Technology Group 2007 [DIRS 183214]). The number of cell pathways in the finite-difference network and the discretization of the cells are chosen in such a way as to capture the physical and chemical properties of the EBS components with respect to radionuclide transport. The cell pathway acts

as a batch reactor, where radionuclide mass is modeled as instantaneously and completely mixed and partitioned among all media, fluid or solid, within the cell. Both advective and diffusive transport mechanisms can be explicitly represented using the cell pathways. When multiple cells are linked together via advective and diffusive connections, the performance of the cell network is mathematically described using a coupled system of differential equations, and is mathematically equivalent to a finite-difference network. The GoldSim software numerically solves the coupled system of equations to compute the radionuclide mass present in each cell and the mass fluxes between cells as a function of time. Both initial and boundary conditions for a cell can be defined explicitly, and systems of varying geometry can be modeled.

This finite-difference approach used to solve the mass balance equations requires the discretization of the time derivative (or mass accumulation term) and the advective and diffusive terms for both dissolved and colloidal transport. The spatially dependent derivative terms, which include advective and diffusive transport, are discretized using implicit difference approximations. Using an implicit difference approximation, if the solution is known at timestep, n, and is to be computed at the next timestep, n+1, the advective/diffusive flux difference approximations use the concentrations at timestep n+1. Further, the source terms, such as radionuclide decay/ingrowth and reactions due to reversible sorption, are also represented implicitly. Therefore, the difference equations are fully implicit in the unknown cell concentrations. The difference equations have variable coefficients (e.g., water content), which can be both time and space dependent. These coefficients are evaluated at the start of the timestep. The resulting system of difference equations is a linear algebraic system in the unknown cell concentrations. A complete description of the discretized transport equations is provided by *EBS Radionuclide Transport Abstraction* (SNL 2007 [DIRS 177407], Section 6.5.2.5). Another consideration is the computational time requirement. An implicit solution technique is used because it provides an unconditionally stable solution (i.e., a solution is obtainable for any size timestep). A study of sensitivity to timestep selection is provided in Section 7.3.3. In addition, the GoldSim equation-solver software tests solution accuracy by applying several mass balance and convergence tests based on a GoldSim model file precision setting of high, medium, or low. All simulations for the TSPA-LA are run using the high-precision setting. If a solution in a given cell pathway fails to meet the mass balance and convergence criteria in the user-specified timestep, the software will dynamically reduce the computational timestep until the required precision is obtained (for details see *GoldSim Contaminant Transport Module* (GoldSim Technology Group 2007 [DIRS 183214])).

Figure 6.3.8-4 shows a schematic representation of the GoldSim cell pathway network used to implement the EBS Transport Submodel for CSNF WPs. For the waste form domain, a single waste form cell (Cell 1) is used to represent the entire volume of the degraded waste form and the associated mass transport processes. Similarly, for CDSP WPs (figure not shown), two cell pathways representing each waste form subdomain are used: one for HLW fuel (Cell 1a) and another for DSNF fuel (Cell 1b). The mass transport processes in the corrosion products domain are modeled by the corrosion product cell (Cell 2), where sorption reactions are modeled. Similarly, the processes in the invert domain are modeled by the invert cell (Invert Cell). The EBS-UZ domain is modeled by an array of near-field UZ cells (UZ Fracture Cell and UZ Matrix Cell). The interface cell, namely, Invert-UZ Interface cell, shown on Figure 6.3.8-4, is used for computing the concentrations at the interface boundaries for maintaining diffusive flux

continuity between a single continuum domain and a dual continuum domain as described in (SNL 2007 [DIRS 177407], Section 6.5.2.5).

Within the GoldSim cell network, diffusive and advective flux connections are defined for each cell. The advective and diffusive flux connections between the various cells in the EBS Transport Submodel are indicated on Figure 6.3.8-4. The flow through various cells is based on the continuity equations and conservation of mass, as described in *EBS Radionuclide Transport Abstraction* (SNL 2007 [DIRS 177407], Section 6.3.1.1). Each computational cell is provided with parameters describing water volumes, diffusive properties, and advective and diffusive flux links to other cells. Between any two cells, the diffusive flux can be bidirectional, depending on the concentration gradient, while the advective flux is unidirectional. The output of a cell is given in terms of the advective and diffusive mass fluxes for each radionuclide species and its concentration at the cell center. Species-dependent free water diffusion coefficients are used in each domain for dissolved radionuclides while a separate diffusion coefficient is computed for transport of radionuclides associated with colloids based on the sampled size of the colloids (SNL 2007 [DIRS 177407], Section 6.3.4.4). In addition, the diffusion coefficients are corrected for tortuosity and temperature. The mass transport equations in a cell network are solved on a per package basis and then scaled by GoldSim to the number of failed WPs.

Implementation of the EBS Transport Submodel for the TSPA-LA Model uses the output of the Waste Form Degradation Submodel (Section 6.3.7.4), the EBS Flow Submodel (Section 6.3.6), the EBS TH Environment Submodel (Section 6.3.2), the Dissolved Concentration Limits Submodel (Section 6.3.7.5), and the EBS Colloids Submodel (Section 6.3.7.6). An overview of the computational model for the TSPA-LA Model, as implemented using the GoldSim software, is provided below.

Waste Form Cells—The waste form cell receives radionuclide mass from a specialized GoldSim Source element, which models the WP failure, degradation of the waste form, and release of the radionuclide inventory for possible transport through the EBS. The Source element provides the specified flux boundary condition for solving the mass transport equations. There is no advective or diffusive transport of dissolved radionuclides or radionuclides sorbed onto colloids when the temperature is greater than the boiling point of water in the TSPA-LA Model (Section 5.1.4). This is achieved by setting the radionuclide solubilities to zero at temperatures greater than 100°C (the boiling point of water).

CSNF Waste Form—The setup of a waste form cell for CSNF WPs and its relationship to other cells for modeling transport through the WP are illustrated on Figure 6.3.8-5. Both advective and diffusive transport can occur from the waste form cell (Cell 1) to the corrosion products cell (Cell 2). Radionuclides are transported from this cell to the downstream cell in the dissolved state and reversibly sorbed on waste form and groundwater colloids. Plutonium and americium can also be transported as irreversibly sorbed on the specified waste form colloids. Solving the mass transport equation requires that the following properties be defined: (1) the volume of water in the rind, (2) the diffusive area, (3) the diffusive length, and (4) advective flow rates.

CDSP Waste Form—The implementation of the waste form cells for CDSP WPs differs from the approach used for CSNF WPs, in that degraded fuel is represented by two cell pathways. The setup of the waste form cell pathways for both CDSP WP fuel types and their relationship to actual waste forms are illustrated on Figure 6.3.8-6. One cell pathway (Cell 1a) represents the degraded HLW glass logs, while the other cell pathway is for the degraded DSNF waste form (waste form Cell 1b). Solving the mass transport equations for these cells requires that the similar properties be defined as for the CSNF waste form.

Although presented in Section 6.3.8.2.2, Equation 6.3.8-11 is not directly implemented into the TSPA-LA Model. The TSPA-LA Model calculates the fraction of the HLW glass that is degraded at each timestep (Section 6.3.7.4.3.3) and the result is used to determine the rind volume at each timestep. For the CDSP WP rind volume, the TSPA-LA Model implements a modification to the relationship provided in Equation 6.3.8-11, which utilizes the fraction of mass degraded instead of the total mass degraded:

$$V_{rind,HLWG}(t) = \phi_{rind} V_{total} F_{cor} \qquad \text{(Eq. 6.3.8-26)}$$

where

$V_{rind,HLWG}(t)$ = the time-dependent rind volume (m^3)

ϕ_{rind} = rind porosity

V_{total} = the initial total volume of HLW glass in a CDSP WP (m^3)

F_{cor} = fraction of mass degraded into rind.

The rind porosity and initial total volume of HLW glass are based on values shown in Table 8-1 of DTN: MO0502ANLGAMR1.016_R0 [DIRS 172830]. The fraction of mass degraded is calculated by Equation 6.3.7-8.

In addition to being transported in the dissolved state, radionuclides in the CDSP WP waste form cell can be transported via waste form colloids and groundwater colloids. The waste form colloids form from the degradation of HLW glass and can reversibly sorb radionuclide. They also include embedded plutonium and americium, which are considered as intrinsic parts of the colloids and, thus, not in equilibrium with the aqueous system. These embedded radionuclides are modeled as attached irreversibly to the host colloids. Details of the waste form colloid generation, stability, and sorption capability are given in Section 6.3.7.6.2. Waste form colloids are also produced in the DSNF waste form subdomain (Waste Form Cell 1b). The waste form colloids generated from the HLW waste form subdomain, as well as groundwater colloids from the seepage water, pass through the DSNF waste form cell.

Corrosion Products Cell—Conceptually, the corrosion products cell (Cell 2) is the part of the corrosion products domain (described in Section 6.3.8.1) that represents the degraded steel components of the WP, which is modeled as iron oxyhydroxides. However, it does not include the corrosion products from the degradation of the outer barrier, which is treated as a separate cell (see discussion below). The corrosion products cell includes both stationary corrosion

products and iron oxyhydroxide colloids, which both participate in equilibrium and kinetic sorption of radionuclide mass. A surface complexation-based competitive sorption model is used to calculate sorption of uranium, neptunium, plutonium, thorium, and americium onto stationary corrosion products and iron oxyhydroxide colloids as a function of available sorption sites, P_{CO_2}, and dissolved concentration of the radionuclides. For a detailed discussion of this mechanistic model, see *EBS Radionuclide Transport Abstraction* (SNL 2007 [DIRS 177407], Section 6.3.4.2.3 and Section 6.5.2.4). A multiple regression model for computing the sorbed mass is developed based on the dissolved concentration of the radionuclides computed at the end of the previous timestep. The effective K_d value, which is needed by the GoldSim solver, is calculated by dividing the sorbed mass by the dissolved concentration. The computed effective K_d value is directly used in the transport equation for uranium, neptunium, and thorium, which are modeled to undergo equilibrium sorption. Plutonium and americium are modeled to undergo kinetic sorption-desorption reactions where the desorption rate is calculated by dividing the forward reaction rate by the K_d for plutonium and americium (from the surface complexation based regression equation).

Table 6.3.8-3 summarizes the distributions used to determine the available sites for competitive sorption on the stationary corrosion products and iron oxyhydroxide colloids. The pH in the cell is also computed based on the results of surface complexation modeling by the following equation (SNL 2007 [DIRS 177407], Equation 6.5.2.4.6-2):

$$\mathrm{pH} = 4.5342 + 0.6132(\mathrm{pCO2}) - 0.3805\log_{10}[\mathrm{U}] - 0.0254(\log_{10}[\mathrm{U}])^2 + E \qquad \text{(Eq. 6.3.8-27)}$$

where, pCO_2 is the negative log of the in-drift CO_2 partial pressure (bars), [U] is the dissolved concentration of U in mol L^{-1}, and E is the error term (pH_Cell_2_Regression_Error) defined by a normal distribution with mean of zero and SD of 0.32 truncated at ± 2 SDs.

As with the waste form cells there is no advective or diffusive transport of dissolved radionuclides or radionuclides sorbed onto colloids in the corrosion products cell when the WP temperature is greater than 100°C in the TSPA-LA Model. This is achieved by setting the radionuclide solubilities to zero at temperatures greater than 100°C.

Outer Barrier Cell—An additional cell pathway is added at the base of the corrosion products domain to represent transport through the outer barrier. The WP outer barrier is composed of Alloy 22 (UNS N06022) and undergoes general corrosion at a different rate than the stainless steel inside the WP and the corrosion products formed from the degradation of Alloy 22 are different from those formed from the degradation of stainless steel. The breach area of the outer barrier varies by the individual scenario class modeling cases and exerts strong control on the advective and diffusive releases out of the WP: (1) for the Nominal Scenario Class, the outer barrier degradation from general corrosion and stress corrosion is determined by WAPDEG code (Section 6.3.5.1.3); (2) for the Seismic Scenario Class, the outer barrier damage from the ground motion and fault displacement is variable and determined probabilistically by the seismic damage abstraction (Section 6.6); (3) for the Igneous Intrusion Modeling Case, the entire surface area of the outer barrier is assumed to be breached at the time of the igneous event (Section 6.5); (4) for the Waste Package EF and Drip Shield EF Modeling Cases, the entire surface of the outer barrier is assumed to be breached at the start of simulation (Section 6.4); and (5) for the Human

Intrusion Modeling Case, the breach area is considered to be the same as the cross-sectional area of the borehole (Section 6.7.3). No radionuclide sorption is modeled in the outer barrier cell even though the tortuosity computed for Cell 2 is applied to the outer barrier cell.

Invert Cells—In the TSPA-LA Model, the invert domain is represented by the invert cell pathway. For radionuclide transport, the invert is modeled as a single-continuum porous medium composed of crushed tuff (SNL 2007 [DIRS 177407], Section 6.5.2.3). The invert cell receives advective and diffusive mass flux from the outer barrier cell. The setup of the invert cell pathway is illustrated on Figure 6.3.8-7. Both advective and diffusive mass transport can occur from the invert cell to the near-field UZ cells.

Invert-UZ Interface Cell—This cell pathway is added between the invert cell and EBS-UZ Interface cells to model diffusive transport between a single-continuum invert (represented by one cell) and the dual-continuum UZ (represented by two cells). The diffusive flux needs to be bifurcated correctly between the two UZ continua while preserving the flux continuity condition at the interface. This is achieved by introducing the Invert-UZ Interface cell, which is conceptualized as a very thin slice of the invert cell (Figure 6.3.8-4). The purpose of this interface cell is to provide an approximate concentration boundary at the interface for diffusive flux calculation. All the properties of the interface cell are the same as the invert cell, except for the diffusive length, mass, and volume, which are computed by multiplying the equivalent invert cell properties by a scale factor of 10^{-6}. The diffusive area is the same as that of the overlying invert cell. For more details, see *EBS Radionuclide Transport Abstraction* (SNL 2007 [DIRS 177407], Section 6.5.2.5).

EBS-UZ Interface Cells—The TSPA-LA Model uses an array of cells to model part of the near-field UZ below the invert. Modeling the near-field UZ serves to establish a far-field zero-concentration boundary for computing the flux from the invert to the UZ. The dual-continuum approach for modeling the near-field UZ is implemented by creating an overlapping continua of UZ matrix and fracture cells. Figure 6.3.8-8 illustrates how the conceptual model of the near-field UZ domain is implemented into the EBS Transport Submodel. The invert interface cell is connected with the UZ matrix and fracture cells directly below it in the UZ cell array.

The overlapping matrix and fracture continua are represented by a two-dimensional vertical array of cells oriented parallel to a cross section of a drift and located immediately beneath a drift. The entire cell array, consisting of three sets of two columns or vertical zones, with each zone containing both a fracture cell and a matrix cell, is shown on Figure 6.3.8-9. The invert is directly connected with the middle zone of UZ matrix/fracture cells. Each zone is four layers deep in the vertical direction. Thus, the array consists of 12 pairs of matrix and fracture cells within the UZ (Figure 6.3.8-9). Laterally, each zone is one drift diameter wide, with the middle zone centered beneath the drift, so that each layer of the array extends one drift diameter on either side of the drift. In the longitudinal direction of a drift, the length of the array is equal to the length of the WP being modeled.

As described in *EBS Radionuclide Transport Abstraction* (SNL 2007 [DIRS 177407], Section 6.5.2.6), the thickness of the first (top) layer of cells is 1.0274 m, or 10 percent greater than the 0.934 m average invert thickness beneath a WP. The thickness of the second layer is

double that of the first layer, or 2.05481 m. The third and fourth layers are given a thickness of 5 m and 10 m, respectively (Figure 6.3.8-9). Grid sizes are more refined near the base of the invert to accurately capture the higher concentration gradient in the region. A collector cell is placed beneath the fourth layer and is given a very large, numerically infinite water volume (10^{10} m^3) to simulate an effective zero-concentration boundary. This collector cell acts as a sink for all the mass flux from the UZ cells.

A description of the mass flux between the invert and UZ fracture and matrix cells is provided in *EBS Radionuclide Transport Abstraction* (SNL 2007 [DIRS 177407], Section 6.5.2.6). Each fracture cell interacts, via a diffusive connection only, with the matrix cell of the same zone (Figure 6.3.8-9). The fracture cell also interacts vertically via a diffusive connection with the fracture cell of overlying and underlying layers. The matrix cell interacts via a diffusive connection laterally with adjacent matrix cells in the same layer and vertically with the matrix cells of overlying and underlying layers. Radionuclides diffuse based on the concentration gradient between cells. Advection occurs vertically downward only, from the fracture cell of one layer to the fracture cell of the underlying layer and from the matrix cell of one layer to the matrix cell of the underlying layer in the same zone. Lateral advection is not considered. Figure 6.3.8-9 illustrates the diffusive and advective flux connections between the various cells in the network.

The pore volume of each continuum is computed by multiplying the bulk volume for each discretized zone (based on the geometry) by either the fracture continuum porosity or the matrix continuum porosity. Similarly, the water volume is calculated by multiplying the pore volume of each continuum by its respective saturation. Reversible sorption of radionuclides to the matrix is modeled by using the K_d values for the devitrified tuff sampled by the UZ Transport Submodel (Table 6.3.9-2). The mass of the UZ matrix is computed by multiplying the matrix volume (bulk volume × (1- fracture porosity)) of the cell by the dry bulk density of the UZ matrix.

Advective fluid flux due to seepage flows from the invert into the top middle UZ fracture cell, while the advective flux due to imbibition from the host rock, which enters the invert and flows under gravity, goes from the invert into the top middle UZ matrix cell. This partitioning of fracture and matrix advective flux is based on the actual source of the two components. That is, seepage comes from the host-rock fractures and imbibition from the host-rock matrix. An additional component of flow from the invert to the UZ is flux due to condensation on the drift walls. The condensation flux is treated in the same manner as seepage flux and is combined with the seepage flux. In the dripping environment, the advective flux flowing through the UZ fracture cells in the middle zone is the larger of the advective flux out of the invert or the steady-state UZ fracture flux. The advective flux in the two outer zones is the steady-state UZ flux in each continuum at the repository horizon.

Diffusive mass flux from the invert can go into both fracture and matrix UZ continua based on the concentration gradient and effective diffusion coefficient. All three types of colloids in the TSPA-LA Model are transported from the invert to the UZ cells. Groundwater colloids are present in all four layers. Because the UZ Transport Submodel only models groundwater colloids (with reversibly sorbed radionuclide mass), in order to be consistent, the iron oxyhydroxide and waste form colloids with reversibly sorbed radionuclides are modeled as present in only the first two layers of the middle column, making the groundwater colloids the

only types of colloids available for far-field transport. As a result, the mass reversibly associated with the iron oxyhydroxide and waste form colloids is transferred into the solution where it is repartitioned onto the groundwater colloids based on the sorption coefficient. Americium and plutonium mass that is irreversibly sorbed on iron oxyhydroxide colloids or embedded in waste form colloids is transported from the invert to the UZ cells, as long as these colloids are stable in the invert. If the chemical conditions in the invert are such that the iron oxyhydroxide or waste form colloids become unstable, they are not transported from the invert to the UZ. However, if the colloids are stable in the invert, then they also remain stable in the UZ and SZ. Solubility constraints are not imposed on any species in the UZ cells. Additional details regarding the hydrologic parameters used in the EBS-UZ interface cells are provided in *EBS Radionuclide Transport Abstraction* (SNL 2007 [DIRS 177407], Section 6.5.2.6).

EBS Transport Submodel Outputs—The output from the EBS Transport Submodel consists of the total radionuclide mass flux out of the single-continuum invert. The mass flux from the single-continuum invert to the dual-continuum UZ, computed by the EBS-UZ Interface cells, is passed to the UZ Transport Submodel for TSPA-LA Model calculations. It is used as the mass flux boundary condition for the UZ Transport Submodel, as described in Section 6.3.9. Three different types of mass fluxes are passed to the UZ Transport Submodel. The first type of mass flux is applicable for all radionuclides transported in the TSPA-LA Model. This flux includes all of the radionuclide mass that exists in the dissolved state or is reversibly sorbed onto the three different colloid types: groundwater, waste form, and iron oxyhydroxide. After it is input into the UZ Transport Submodel, this mass is repartitioned onto the groundwater colloids in the UZ based on the sampled colloid concentration and sorption coefficients defined for the UZ Transport Submodel (Section 6.3.9.2). Radionuclides that are irreversibly sorbed onto waste form and iron oxyhydroxide colloids form the basis for the next two mass flux types. These masses are defined in the EBS Transport Submodel as distinct species ("Ic" species for mass irreversibly sorbed onto waste form colloids and "If" species for mass irreversibly sorbed onto iron oxyhydroxide species). After exiting the EBS, and before being passed to the UZ Transport Submodel, the "Ic" and "If" masses are added together for each irreversibly sorbed radionuclide. The total irreversibly sorbed mass, for a given radionuclide, is then repartitioned onto a fast and a slow colloid fraction through the UZ and SZ. The fraction of colloids that travel unretarded through the UZ and SZ are called the fast fraction, while the remaining colloids that undergo some degree of retardation are called the slow fraction. A value of 0.00168 is used in the TSPA to represent the fast fraction of colloids (GoldSim parameter: Fast_Fraction) based on the cumulative probability distribution of unretarded fraction of colloids presented in the output DTN: LA0303HV831352.003_R0 [DIRS 165624] and by choosing the value corresponding to the combined travel time of 100 years in the UZ and SZ (BSC 2004 [DIRS 170006], Section 6.6 and Table 6-4). The partitioning of irreversible mass associated with the fast fraction is calculated by multiplying the total irreversibly sorbed mass for a radionuclide by 0.00168, while that for the slow fraction is done by multiplying total irreversibly sorbed mass by (1–0.00168). The mass associated with the fast fraction is assigned to the "If" species, while the mass associated with the slow fraction is assigned to the "Ic" species in the UZ and SZ transport submodels. In effect, for the EBS Transport calculations, the terms "Ic" and "If" represent irreversibly sorbed mass on the waste form colloids and iron oxyhydroxide colloids, respectively, but for the UZ and SZ transport (and for the dose calculations) the "Ic" means irreversibly sorbed mass traveling on the slow colloid fraction while the "If" means irreversibly sorbed mass traveling on the fast colloid fraction.

In addition to the total mass flux, the relative fraction of the mass going into each of the fracture and matrix cells at the EBS-UZ boundary is required by the UZ Transport Submodel. This fracture-matrix partitioning of mass is calculated on the basis of the mass fraction going into the fracture continuum, as compared to the total going into the fracture and matrix continua, from the invert. This partitioning is time-dependent and captures the temporal processes active in the EBS, such as varying radionuclide concentrations in the WP and invert and changing water flow through various components of the EBS. Furthermore, this partitioning is computed by solving the mass transport equations for the EBS and part of the UZ as a coupled system with appropriate boundary conditions.

Modification of Diffusive Lengths in GoldSim—When two cells with different diffusive areas are connected, an adjustment is required in the GoldSim setup to properly compute the diffusive conductance. Figure 6.3.8-10 is a simplified depiction of a cell-to-cell connection in which two cells have different diffusive areas. Such differences in diffusive area between connected cells occur due to varying domain dimensions, for example, the diffusive area at the node of the waste form cell (Cell 1) is different from the diffusive area at the node of the corrosion products cell (Cell 2).

The diffusive conductance (C_{12}) from the node in Cell 1 to the node in Cell 2 controls the diffusive mass flux to Cell 2. This conductance is properly calculated as the harmonic sum of two diffusive conductance links (SNL 2007 [DIRS 177407], Section 6.5.2.5, simplified from Equation 6.5.2.5-7):

$$C_{12} = \frac{1}{\frac{(L_1/2)}{D_1 A_1} + \frac{(L_2/2)}{D_2 A_2}} \qquad \text{(Eq. 6.3.8-28)}$$

where

L_1 = diffusive length of Cell 1 (m)

D_1 = effective diffusion coefficient of Cell 1 (includes effects of porosity, saturation, and tortuosity) (m^2/s)

A_1 = diffusive area of Cell 1 (m^2)

L_2 = diffusive length of Cell 2 (m)

D_2 = effective diffusion coefficient of Cell 2 (includes effects of porosity, saturation, and tortuosity) (m^2/s)

A_2 = diffusive area of Cell 2 (m^2).

That is, each conductance link is properly defined using the effective diffusion coefficient, length, and area of that link. However, in the GoldSim cell pathway only a single diffusive area can be defined, which is the area of the upstream cell (in this case A_1). In order to conform to the GoldSim formulation, the assigned diffusive area is set equal to a unit area of 1.0 m^2 (the numerator in the following equation) and the cell areas are implicitly included in the

diffusive length terms by dividing the diffusive lengths by their respective areas, as shown below:

$$C_{12} = \frac{1}{\frac{(L_1/2)/A_1}{D_1} + \frac{(L_2/2)/A_2}{D_2}} . \quad \text{(Eq. 6.3.8-29)}$$

In the TSPA-LA Model, the approach illustrated by Equation 6.3.8-29 is applied to all diffusive connections between cells in the EBS Transport Submodel. Within each GoldSim cell pathway the diffusive areas are set equal to 1.0 m^2 and the calculated diffusive half-length is divided by the appropriate diffusive area to compute an effective diffusive half-length. This modification results in the proper diffusive conductance being calculated in the solution of the EBS Transport mass balance equations.

6.3.8.4 Model Component Consistency and Conservatism in Assumptions and Parameters

To enhance understanding of the complex interactions within the TSPA-LA Model, a discussion of consistency among model components and submodels, and identification of conservative assumptions in abstractions, process models, and parameter sets supporting the EBS Transport Submodel are discussed below.

6.3.8.4.1 Consistency of Assumptions

Water Balance in the TSPA-LA Model Within the EBS—The conceptual, mathematical, and abstraction models for estimating how much water can enter, accumulate, and move through various EBS components are discussed in Sections 6.3.6 and 6.3.8.2. The water balance discussion can be divided into two categories, one related to water flow and the other to water volumes.

There are two potential inconsistencies with respect to water flow through various EBS components in the TSPA-LA Model: (1) the reduction in water flow due to evaporation and consumption by chemical reactions is conservatively ignored, and (2) the condensation flux calculations are performed separate from the MSTHM calculations that are used to define the temperature and relative humidity conditions in the EBS.

With respect to inconsistencies or differences related to water volume in the EBS, it should first be stated that these calculations in the TSPA-LA are primarily based on phenomenological laws for fluid retention in porous media. For example, the saturation and water volume in the invert are calculated based on the soil moisture retention relationships of crushed tuff, while the saturation of the corrosion products and waste form rind under no flow conditions are computed as a function of relative humidity based on measured adsorption isotherms. Although most calculations for the saturations (and water volumes) are based on phenomenological laws, some assumptions must be made under certain conditions. These include the assumption of 100 percent saturation of corrosion products and waste form rind under water flowing conditions. In addition, some inconsistencies in water volumes exist among process-level models mainly due to the limitation of the models used in the calculations. For example, a minimum water volume

is required for in-package chemistry calculations in order to keep the ionic strengths less than 4 molal, the effective limit of the B-dot activity coefficient equation used in the EQ3/6 computer code. This minimum water volume is independent of the relative humidity and temperature histories as predicted in the MSTHM abstraction and is likely larger than is realistic at low relative humidity conditions.

Chemical processes in the EBS will consume and, possibly, produce water. Conversion of CSNF to schoepite (UO_3:$2H_2O$) and steel to goethite (FeOOH) and other hydrated corrosion products will likely remove large quantities of water from incoming fluids and the vapor phase. Over time, hydrated phases will alter to less hydrated phases and release water to the breached waste package in the process. While water uptake by waste form degradation should be relatively fast, the release of water from dehydration reactions should be slower. The overall uptake and release of water over time is certainly a complex function of water availability, temperature, and time and is difficult to predict accurately. The assumption of no water uptake or release is a simplification of a complex process that will tend to over-predict the water saturation in a breached WP.

For diffusion-dominated modeling cases after breach of the outer Alloy 22 WP barrier, the following assumptions are made in the TSPA-LA Model with respect to the water balance inside the WP: (1) sufficient condensate water is available for waste form degradation and metal alloy (e.g., steel) degradation, and (2) sufficient water vapor is present to establish a continuous film of liquid water on fuel and corroded-metal surfaces under no flow conditions when relative humidity is greater than 95 percent, which is thick enough to permit diffusive transport of radionuclides from the WP either as dissolved species or bound to colloids.

Effect on the TSPA—Within the EBS, water balance issues have more of an effect in diffusion-dominated modeling cases, where the limited water availability may control the degree of liquid saturation inside the WP and, therefore, the radionuclide transport rates through the WP. In the advection-dominated modeling cases, the water balance related issues are not as important because sufficient water flows through the WP to result in a rapid turnover rate with respect to pore volume in the WP and, thus, the assumption of complete saturation is a reasonable one. The overall effect of the previous assumptions regarding the complete saturation inside the WP under flowing conditions is a conservative over estimate of the release of radionuclides and timing of the release.

With respect to diffusion-dominated cases, the assumption that there is a high enough vapor flux to instantly saturate the WP internals to local equilibrium conditions (which is the assumption underlying the use of an adsorption isotherm) would tend to over estimate the timing and amount of EBS releases, by providing for no kinetic constraints on waste form degradation with respect to water availability for reactions and by assuming bulk chemical and bulk diffusion transport conditions (also a continuous liquid pathway to the outside of the WPs). All of these assumptions should be conservative with respect to release and dose.

6.3.8.4.2 Identification of Conservatisms in Submodels and Abstractions

All Seepage Falls on DSs—All seepage into the drifts is assumed to fall on the DSs, not just seepage above the DSs. This conservative approach is taken to simplify the modeling approach

and because the uncertainty in the seepage locations is difficult to quantify (SNL 2007 [DIRS 177407], Section 5.1). This approach will increase the seepage flux contacting the DS and thereby increase the radionuclide release in the scenarios where there is advective flux in the waste form cell.

Seepage on the WP—All the seepage penetrating a DS falls on the crown of the WP. This conservative approach is taken to simplify the modeling approach and because the uncertainty in the seepage locations is difficult to quantify (SNL 2007 [DIRS 177407], Section 5.1). This conservatism will increase the flux through the breached DSs and WPs and thereby increase the radionuclide release in the scenarios where there is advective flux in the waste form cell.

No Evaporation of the Seepage Water from the Surfaces of the DSs—A reduction in the quantity of water flux through the DS reduces the potential for advective transfer and subsequent release and transport of radionuclides from the WPs (SNL 2007 [DIRS 177407], Section 5.2). Ignoring evaporation from the DS surface tends to increase the seepage flux falling on the WPs.

No Evaporation of the Seepage Water from the WPs—Transport within the WP is not possible if evaporation eliminates liquid fluxes and effective water saturation (SNL 2007 [DIRS 177407], Section 5.3). Ignoring evaporation on the WP surface tends to increase the potential for advective and diffusive transport of radionuclides.

Emplacement Pallets—The presence of emplacement pallets for WPs is conservatively ignored to allow water and radionuclides to pass directly from the WP to the invert without increasing the transport distance (SNL 2007 [DIRS 177407], Section 6.3.1.1). This conservatism leads to a shortened advective flow path and increases the concentration gradient for diffusion.

Consumption of Water—There is no consumption of water by chemical reactions. The consumption of water by the corrosion of iron inside a WP and by hygroscopic salts deposited on the DS and WP surfaces would reduce the amount of water for dissolution and transport of radionuclides (SNL 2007 [DIRS 177407], Section 5.4). The assumption that there is no consumption of water is a bounding assumption, which increases the amount of water available for advective transport.

Thin Water Films—It is conservatively assumed that continuous thin water films exist on the internal components of the breached WPs and on the breached areas at temperatures less than the boiling point of water. Multiple water layers are needed in order for radionuclides to dissolve in and diffuse. Ignoring the thickness of the water film will overestimate the release of radionuclides. Assuming the presence of continuous water film allows radionuclides to diffuse from the degraded waste form to the outside of the breached WP (SNL 2007 [DIRS 177407], Section 5.5). Diffusive transport occurs continuously after the WP is breached and the waste form is degraded, irrespective of the path length.

One-Dimensional Advective and Diffusive Transport through the EBS—A one-dimensional vertical advective and diffusive transport from the WPs to the invert occurs irrespective of the breach location on the WP surface (SNL 2007 [DIRS 177407], Section 6.3.1.2) even though breaches in the WP are expected to occur randomly over the WP surface area. In other words,

assuming diffusion can occur through all breaches, regardless of location, maximizes the diffusive area thereby giving a conservative estimate of releases from the WP.

Invert Corrosion Products—No corrosion products exist in the invert. By assuming that there are no corrosion products in the invert, there will be no sorption or delay of radionuclides by corrosion products (SNL 2007 [DIRS 177407], Section 5.6). Not taking credit for the sorption of radionuclides onto the corrosion products will tend to increase the mass flux of radionuclides through the invert.

No DS Shadow in the Invert—Water will tend to divert around the DS and not flow through the region of the invert directly under the DS. However, because of the limited information regarding the flow paths and mixing of waters, this effect is not accounted for (SNL 2007 [DIRS 177407], Sections 6.3.3.4 and 6.5). The flux diverted by the DSs to the invert is assumed to mix with the water carrying the radionuclides from the WPs to the invert, which tends to increase the advective transport.

No Physical Filtration or Gravitational Settling of Colloids—Stable colloids once formed do not undergo physical filtration or gravitation settling in the CSNF and CDSP WPs and in the invert (SNL 2007 [DIRS 177407], Section 5.7). By assuming that there is no physical filtration or gravitational settling of colloids, the model will tend to overestimate the colloid mass flux and the colloid-facilitated radionuclide transport in the EBS.

Colloid Retardation—Colloid retardation due to sorption at the air-water interface and interaction with microbes and organic components is not modeled. Not including colloid retardation tends to increase the colloid mass flux and the colloid-facilitated radionuclide transport in the EBS (SNL 2007 [DIRS 177423], Section 5.9).

6.3.8.5 Alternative Conceptual Model(s) for Engineered Barrier System Transport

Section 6.2 outlines the general consideration and treatment of ACMs used to support the TSPA-LA Model. A brief description of the EBS Transport Submodel ACMs summarized in Table 6.3.8-7 is presented below.

Bathtub Flow Model ACM—This ACM assumes that seepage collects within the WP before being released to the EBS (SNL 2007 [DIRS 177407], Section 6.6.1). The bathtub effect would be most important during the period when only a few patches or cracks have penetrated the DS and WP. In this situation, there may be penetrations through the top of the WP while the bottom surface remains intact, leading to retention of liquid. At later times, the presence of multiple penetrations makes a flow-through geometry the more likely configuration. The response of the bathtub geometry was evaluated for a primary case, with constant boundary conditions and material properties, and for three secondary cases. The three secondary cases considered a step change in inflow rate, such as would occur from a climatic change, a step change in water chemistry, or a step change in flow geometry, as would occur if a patch suddenly appeared beneath the waterline. All cases included consideration of two limiting conditions on radionuclide releases: dissolution rate limited and solubility limited.

This ACM was not used for the TSPA-LA EBS Transport Model because, for most of the pertinent cases, the basecase flow-through model is bounding with respect to the release of radionuclides.

Constrained Water Vapor and Oxygen Diffusion through SCC ACM—This ACM compares the rate of water vapor and oxygen diffusion through stress corrosion cracks with the rate of corrosion of steel components inside a WP (SNL 2007 [DIRS 177407], Section 6.6.2). If the consumption rate is greater than the diffusion rate then a film of adsorbed water cannot form, which could delay diffusive releases until all steel is fully corroded. The water vapor concentration inside a WP is assumed to be zero to maximize the concentration gradient. Alternative cases consider the effects of stress corrosion cracks that are assumed to be: (1) fully open, and (2) filled with corrosion products but still permeable. This ACM could potentially delay releases for hundreds to thousands of years. However, the assumption that no water is physically adsorbed until all steel is corroded is questionable, because adsorption is typically a fast process. On the other hand, if water consumption by corrosion keeps the relative humidity inside the WP low, the effective water saturation will be so low that the bulk liquid phase behavior allowing dissolution and diffusion of dissolved radionuclides will not exist until the corrosion is complete.

This ACM was not used for the TSPA-LA EBS Transport Submodel because it is potentially nonconservative and there are insufficient data to validate this ACM.

Dual-Continuum Invert Model ACM—The dual-continuum invert model is an alternative conceptual EBS Transport Model in which crushed tuff invert ballast is modeled as a dual-continuum material consisting of intergranular pore space and intragranular pore space (SNL 2007 [DIRS 177407], Section 6.6.3). All seepage into the drift flows through the intergranular pore space and into the UZ fractures. Imbibition from the UZ host rock into the invert flows through the intragranular pore space and into the UZ matrix under gravity. Diffusion of radionuclides also occurs in both the intergranular and intragranular pore spaces, from the WP corrosion products into UZ fractures and matrix, as well as between the two invert continua.

This ACM was not used for the TSPA-LA EBS Transport Model. It was screened out due to insufficient data to validate diffusion coefficients in individual continua and insufficient data to confirm whether this is a bounding approach with respect to chemical behavior in the invert.

Alternative Invert Diffusion Coefficient ACM—The invert diffusion coefficient model with a lower limit on water content is an alternative conceptual EBS Transport Model in which, as the water content of the crushed tuff decreases, the water films that connect pore spaces become disconnected, and the effective diffusion coefficient drops more rapidly than predicted by Archie's law (SNL 2007 [DIRS 177407], Section 6.6.4). Below some critical water content, the diffusion coefficient becomes zero, based on models of diffusion in soils.

This ACM was not used for the TSPA-LA EBS Transport Model because there is insufficient data to validate diffusive behavior at very low water contents.

Reversible Sorption of Radionuclides onto WP Corrosion Products ACM—In this ACM, an empirical approach based on sampling a partition coefficient (K_d value) for reversible sorption of radionuclides onto stationary corrosion products is considered (SNL 2007 [DIRS 177407], Section 6.6.5). Iron oxyhydroxides are generated through corrosion of mild steel and stainless steels within the WP. The iron oxyhydroxides are known to be excellent sorbers (as indicated by their high K_d values) of many radionuclide species. In this ACM, sorption is modeled as being completely reversible for all radionuclides and represented by linear adsorption isotherms in the form of K_d values. The K_d values allow retardation factors to be computed for transport through the EBS.

This ACM was not used for the TSPA-LA EBS Transport Submodel because it does not account for limitations on the total number of sorption sites. Also, this ACM does not account for competition with other radionuclides.

Plutonium Sorption from Stationary Corrosion Products and Colloids ACM—This ACM accounts for the slow desorption of plutonium observed in experiments investigating sorption and desorption of plutonium from iron oxyhydroxide (SNL 2007 [DIRS 177407], Section 6.6.6). Postulated mechanisms of plutonium sorption are described and the experimentally observed desorption is interpreted in the context of these mechanisms. K_d values are calculated for application to plutonium transport in the EBS.

This ACM is not incorporated into the basecase EBS Transport Submodel because the fitting parameters are specific to the experiment design and cannot be extrapolated to other transport conditions as would be expected in the TSPA-LA Model. Furthermore, the developed parameters do not take into account the competition with other radionuclides.

INTENTIONALLY LEFT BLANK

Table 6.3.8-1. Summary of EBS Transport Abstraction

Transport Pathway	Transport Modes	Transport Parameters and Data Sources
1. Waste form and corrosion products domains	Waste form domain: Diffusion and advection (when possible) through the waste form rind. Corrosion products domain: Diffusion through SCC (no advective transport through stress corrosion cracks). Diffusion and advection through corrosion patches.	No lateral or longitudinal dispersion. Colloidal particles will transport radionuclides. Diffusive area for stress corrosion cracks is obtained. Diffusion coefficient (all radionuclides): • Species-dependent free-water diffusion coefficients given in DTN: LB0702PAUZMTDF.001_R1 [DIRS 180776], file *Readme.doc*, Table 8 • Modified for temperature, porosity, and saturation • Colloid diffusion coefficient computed as a function of waste form and corrosion product temperatures and sampled colloid particle diameter (SNL 2007 [DIRS 177407], Section 6.3.4.4). Competitive sorption of radionuclides onto corrosion products; time-dependent mass of corrosion products available for sorption is calculated based on corrosion rates of carbon and stainless steels. The breach area of the WP outer barrier for radionuclide transport is dependent on the scenario class modeled.
2. Invert domain	Diffusion and advection from corrosion products domain into the invert domain.	Liquid flux for advection (sum of drift seepage flux, drift condensation flux, and invert imbibition flux). Diffusion coefficient (all radionuclides): • Species-dependent free-water diffusion coefficients given in DTN: LB0702PAUZMTDF.001_R1 [DIRS 180776], file *Readme.doc*, Table 8. • Modified for temperature, porosity, and saturation • Colloid diffusion coefficient computed as a function of invert temperature and sampled colloid particle diameter. The diffusive area for radionuclide transport is the width of the invert times the waste package length. Transport of radionuclides is retarded by sorption onto crushed tuff in invert.
3. Invert-UZ interface domain	Advection from the invert to UZ fractures and matrix. Diffusion from the invert to UZ fractures and matrix.	The invert diffusion calculation uses radionuclide concentrations in the WP corrosion products domain as the boundary condition at the top of the invert and a series of UZ computational cells below the invert that provide a gradient to a zero radionuclide concentration at some distance from the bottom of the invert. For additional details, see SNL 2007 [DIRS 177407], Section 6.5.2.6.

Sources: Modified from DTN: SN0703PAEBSRTA.001_R3 [DIRS 183217] from *EBS Radionuclide Transport Abstraction* (SNL 2007 [DIRS 177407], Table 8.1-2).

Table 6.3.8-2. Parameters for EBS Transport Abstraction

Waste Type	Transport Properties	Seeping Case	Non-Seeping Case
Waste Form Domains			
CSNF	Domain bulk volume, pore volume, and water volume	Waste Form Domain consists of degradation products in fuel rods (SNF rind), fuel basket tubes (steel corrosion products), absorber plates (steel corrosion products): • SNF rind volume (V_{rind}, function of time) and porosity (ϕ_{rind}) provided by *Cladding Degradation Summary for LA* (SNL 2007 [DIRS 180616], Tables 6-3 and 6-4) • Steel corrosion products (CP) mass from Equation 8-4, pore volume ($V_{\phi,CP}$) from Equation 8-7, bulk volume from Equation 8-8 of *EBS Radionuclide Transport Abstraction* (SNL 2007 [DIRS 177407]) • Total pore volume of CSNF Waste Form Domain, $V_{\phi,CSNF}$, given by Equation 8-13 of *EBS Radionuclide Transport Abstraction* (SNL 2007 [DIRS 177407]) • S_w = water saturation in domain = 1.0 • Domain water volume = total pore volume.	• Domain characteristics (rind volume, corrosion products mass and volume, total pore volume) same as for Seeping Case • $S_{w,rind}$ function of relative humidity and sampled density and specific surface area of rind (SNL 2007 [DIRS 177407], Equation 8-12) • Rind water volume: $V_{w,rind} = S_{w,rind}\ \phi_{rind}\ V_{rind}$ • $S_{w,CP}$ function of relative humidity, density, and sampled specific surface area of corrosion products (SNL 2007 [DIRS 177407], Equation 8-5) • Corrosion products water volume: $V_{w,CP} = S_{w,CP}\ V_{\phi,CP}$ • Domain water volume = $V_{w,CSNF} = V_{w,rind} + V_{w,CP}$.
	Advection and Diffusion	Advective flow = volumetric flow rate through the waste package Diffusive area of Waste Form Domain: • Set equal to surface area of a cylinder at half the radius of the TAD canister excluding ends (= 12.5 m^2). Diffusive path length: • Set equal to TAD inside radius (= 0.819 m). Diffusion coefficient in Waste Form Domain, D_{WF}: • $\phi S_w D_{WF} = \phi^{1.3} S_w^2 D_{wi}$ • ϕ = effective porosity of CSNF Waste Form Domain given by Equation 8-14 of *EBS Radionuclide Transport Abstraction* (SNL 2007 [DIRS 177407]) • S_w = water saturation in domain = 1.0 • D_{wi} = species dependent free water diffusion coefficient. (D_{WF} is an effective value that implicitly includes the effect of tortuosity in a porous medium).	• No advective flux • Diffusive area same as for Seeping Case • Diffusive path length same as for Seeping Case Diffusion coefficient in Waste Form Domain, D_{WF}: • $\phi S_w D_{WF} = \phi^{1.3} S_w^2 D_{wi}$ • Effective porosity ϕ of CSNF Waste Form Domain given by Equation 8-14 of *EBS Radionuclide Transport Abstraction* (SNL 2007 [DIRS 177407]), same as for Seeping Case • Water saturation in Waste Form Domain is based on water vapor adsorption isotherms: $S_w = \min[(V_{w,CSNF} / V_{\phi,CSNF}), 1.0]$ • D_{wi} = species dependent free water diffusion coefficient • Modified for temperature. (D_{WF} is an effective value that implicitly includes the effect of tortuosity in a porous medium).

Table 6.3.8-2. Parameters for EBS Transport Abstraction (Continued)

Waste Type	Transport Properties	Seeping Case	Non-Seeping Case
Waste Form Domains			
CDSP	Domain bulk volume, pore volume, and water volume	Waste Form Domain is divided into two subdomains: HLWG and DSNF Subdomains HLWG Subdomain: • Consists of degradation products of five stainless steel canisters and HLW glass contained therein • Volume of HLWG degradation rind provided as function of time by *Defense HLW Glass Degradation Model* (BSC 2004 [DIRS 169988], Section 8.1, Eq. 54) • Porosity of HLWG rind provided by *Defense HLW Glass Degradation Model* (BSC 2004 [DIRS 169988], Table 8-1) • Steel corrosion products (CP) mass from Equation 8-4, pore volume ($V_{\phi CP}$) from Equation 8-7, bulk volume from Equation 8-8 of *EBS Radionuclide Transport Abstraction* (SNL 2007 [DIRS 177407]) • Total pore volume of HLWG Waste Form Subdomain, $V_{\phi HLWG}$, given by Equation 8-13 of *EBS Radionuclide Transport Abstraction* (SNL 2007 [DIRS 177407]) • S_w = water saturation in HLWG Waste Form Subdomain = 1.0. DSNF Subdomain: • Consists of degradation products of standard stainless steel DSNF canister containing degraded DSNF (rind) • Volume of DSNF rind, V_{DSNF} = 1.0 m^3 (BSC 2004 [DIRS 172453], Section 8.1) • Porosity of DSNF rind, ϕ_{DSNF} = 0.2 • Steel corrosion products (CP) mass from Equation 8-4 , pore volume ($V_{\phi CP}$) from Equation 8-7, bulk volume from Equation 8-8 of *EBS Radionuclide Transport Abstraction* (SNL 2007 [DIRS 177407]) • Total pore volume of DSNF Waste Form Subdomain, $V_{\phi DSNF}$, given by Equation 8-13 of *EBS Radionuclide Transport Abstraction* (SNL 2007 [DIRS 177407]) • S_w = water saturation in DSNF = 1.0.	HLWG Subdomain: Diffusion coefficient in HLWG Waste Form Subdomain, D_{WF}: • $\phi S_w D_{WF} = \phi^{1.3} S_w^2 D_{wi}$ • Effective porosity ϕ of HLWG Waste Form Subdomain given by Equation 8-14 of *EBS Radionuclide Transport Abstraction* (SNL 2007 [DIRS 177407]), same as for Seeping Case • Water saturation in HLWG Waste Form Subdomain is based on water vapor adsorption isotherm: S_w = min[($V_{w,HLWG}/V_{\phi,HLWG}$),1.0] • Modified for temperature • D_{wi} = species dependent free water diffusion coefficient. DSNF Subdomain: Diffusion coefficient in DSNF Waste Form Subdomain, D_{WF}: • $\phi S_w D_{WF} = \phi^{1.3} S_w^2 D_{wi}$ • Effective porosity ϕ of DSNF Waste Form Subdomain given by Equation 8-14 of *EBS Radionuclide Transport Abstraction* (SNL 2007 [DIRS 177407]), same as for Seeping Case • Water saturation in DSNF Waste Form Subdomain is based on water vapor adsorption isotherm: S_w = min[($V_{w,DSNF}/V_{\phi,DSNF}$),1.0] • Modified for temperature • D_{wi} = species dependent free water diffusion coefficient. (D_{WF} is an effective value that implicitly includes the effect of tortuosity in a porous medium).

Table 6.3.8-2. Parameters for EBS Transport Abstraction (Continued)

Waste Type	Transport Properties	Seeping Case	Non-Seeping Case
Waste Form Domains			
CDSP (continued)	Advection and Diffusion	Advective flow = volumetric flow rate through the waste package. HLWG Subdomain: Diffusive area: • Diffusive area equal to surface area of cylinder with radius equal to half the radius of inner vessel cavity of five DHLW/DOE SNF Long waste package, excluding ends (= 13.7 m^2). Diffusive path length: • Set equal to the radius of inner vessel of 5 DHLW/DOE SNF Long waste package (= 0.941 m). Diffusion coefficient in HLWG Waste Form Subdomain, D_{WF}: • $\phi S_w D_{WF} = \phi^{1.3} S_w^2 D_{wi}$ • ϕ = effective porosity of HLWG Waste Form Subdomain given by Equation 8-14 of *EBS Radionuclide Transport Abstraction* (SNL 2007 [DIRS 177407]) • S_w = water saturation = 1.0 • D_{wi} = species dependent free water diffusion coefficient. (D_{WF} is an effective value that implicitly includes the effect of tortuosity in a porous medium).	• No advective flux • Diffusive area same as for Seeping Case • Diffusive path length same as for Seeping Case
		DSNF Subdomain: Diffusive area: • Diffusive area set equal to the geometric surface area of HLWG subdomain (= 13.7 m^2). Diffusive path length: • The effective diffusive path length is calculated by dividing the initial volume of DSNF (1 m^3) by the diffusive area leading to total diffusive length of 0.0730 m. Diffusion coefficient in Waste Form Subdomain, D_{WF}: • $\phi S_w D_{WF} = \phi^{1.3} S_w^2 D_{wi}$ • ϕ = effective porosity of DSNF Waste Form Subdomain given by Equation 8-14 of *EBS Radionuclide Transport Abstraction* (SNL 2007 [DIRS 177407]) • S_w = water saturation = 1.0 • D_{wi} = species dependent free water diffusion coefficient.	• No advective flux • Diffusive area same as for Seeping Case • Diffusive path length same as for Seeping Case

Table 6.3.8-2. Parameters for EBS Transport Abstraction (Continued)

Waste Type	Transport Properties	Seeping Case	Non-Seeping Case
Corrosion Products Domain			
CSNF	Bulk volume and water volume	Pore volume of Corrosion Products Domain, $V_{\phi CP}$: • Mass of corrosion products, m_{CP}, is function of time, Equation 8-4 of *EBS Radionuclide Transport Abstraction* (SNL 2007 [DIRS 177407]) • Porosity ϕ_{CP} = 0.4 • $V_{\phi CP}$ from Equation 8-7 of *EBS Radionuclide Transport Abstraction* (SNL 2007 [DIRS 177407]).	• Same as Seeping Case.
		Volume of water: • S_w = water saturation in corrosion products = 1.0 • Water volume: $V_{w,CP} = S_w V_{\phi CP}$.	Volume of water: • $S_{we,CP}$ = effective water saturation in Corrosion Products Domain from Equation 8-11 of *EBS Radionuclide Transport Abstraction* (SNL 2007 [DIRS 177407]) • Water volume = $S_{we,CP} V_{\phi CP}$.
	Advection and Diffusion	Advective flow = volumetric flow rate through the waste package	• No advective flux.
		Diffusive area: • Diffusive area, for the path excluding the outer barrier, is the surface area of a cylinder halfway between the inside surface of the TAD canister and the outside surface of the inner vessel (= 29.9 m^2) • Diffusive area for the path through the outer barrier of the waste package is taken to be the minimum of total area of all waste package breaches (scenario class dependent) and surface area of CSNF waste package (= 33.1 m^2).	• Same as Seeping Case.
		Diffusive path length: • Diffusive path excluding the outer barrier is given by the combined thickness of TAD canister and inner vessel, constant parameter (= 0.0914 m) • Diffusive path through the outer barrier is the radial distance from the outside of the inner vessel to the outside of the outer barrier (= 0.0302 m).	• Same as Seeping Case.

Table 6.3.8-2. Parameters for EBS Transport Abstraction (Continued)

Waste Type	Transport Properties	Seeping Case	Non-Seeping Case
		Diffusion coefficient in Corrosion Products Domain, D_{CP}: • $\phi_{CP} S_w D_{CP} = \phi_{CP}^{1.3} S_w^2 D_{wi}$ • ϕ_{CP} = porosity of corrosion products = 0.4 • S_w = water saturation in corrosion products = 1.0 • D_{wi} = species dependent free water diffusion coefficient. (D_{CP} is an effective value that implicitly includes the effect of tortuosity in a porous medium).	Diffusion coefficient in Corrosion Products Domain, D_{CP}: • $\phi_{CP} S_{we,CP} D_{CP} = \phi_{CP}^{1.3} S_{we,CP}^2 D_{wi}$ • $S_{we,CP}$ = effective water saturation in corrosion products, Equation 8-11 of *EBS Radionuclide Transport Abstraction* (SNL 2007 [DIRS 177407]) • ϕ_{CP} = porosity of corrosion products = 0.4 • Modified for temperature • D_{wi} = species dependent free water diffusion coefficient. (D_{CP} is an effective value that implicitly includes the effect of tortuosity in a porous medium).
Corrosion Products Domain			
CDSP	Bulk volume and water volume	Pore volume of Corrosion Products Domain, $V_{\phi,CP}$: • Same as for CSNF Seeping Case • ϕ_{CP} = porosity of corrosion products = 0.4.	• Same as Seeping Case
		Volume of water: • S_w = water saturation in corrosion products = 1.0 • Water volume = S_w $V_{\phi,CP}$.	• $S_{we,CP}$ = effective water saturation in corrosion products, Equation 8-11 of *EBS Radionuclide Transport Abstraction* (SNL 2007 [DIRS 177407]) • Water volume = $S_{we,CP}$ $V_{\phi,CP}$.

Table 6.3.8-2. Parameters for EBS Transport Abstraction (Continued)

Waste Type	Transport Properties	Seeping Case	Non-Seeping Case
	Advection and Diffusion	Advective flow = volumetric flow rate through the waste package Diffusive area: • Diffusive area, for the path excluding the outer barrier, is given by the surface area of a cylinder halfway between the inside surface and the outside surface of the inner vessel (= 29.7 m^2) • Diffusive area for the path through the outer barrier of the waste package is taken to be the minimum of total area of all waste package breaches (scenario class dependent) and surface area of CDSP waste package given by the constant parameter (= 32.6 m^2). Diffusive path length: • Diffusive path excluding the outer barrier is given by the thickness of the inner vessel, constant parameter (= 0.0508 m) • Diffusive path through the outer barrier is the radial distance from the outside of the inner vessel to the outside of the outer barrier (= 0.0301 m). Diffusion coefficient in Corrosion Products Domain, D_{CP}: • $\phi_{CP} S_w D_{CP} = \phi_{CP}^{1.3} S_w^2 D_{wi}$ • ϕ_{CP} = porosity of corrosion products = 0.4 • S_w = water saturation = 1.0 • D_{wi} = species dependent free water diffusion coefficient. (D_{CP} is an effective value that implicitly includes the effect of tortuosity in a porous medium).	• No advective flux • Diffusive area same as for Seeping Case • Diffusive path length same as for Seeping Case. Diffusion coefficient in Corrosion Products Domain, D_{CP}: • $\phi_{CP} S_{we,CP} D_{CP} = \phi_{CP}^{1.3} S_{we,CP}^2 D_{wi}$ • $S_{we,CP}$ = effective water saturation in corrosion products, Equation 8-11 of *EBS Radionuclide Transport Abstraction* (SNL 2007 [DIRS 177407]) • ϕ_{CP} = porosity of corrosion products = 0.4 • D_{wi} = species dependent free water diffusion coefficient. (D_{CP} is an effective value that implicitly includes the effect of tortuosity in a porous medium).

Sources: Modified from DTN: SN0703PAEBSRTA.001_R3 [DIRS 183217] from *EBS Radionuclide Transport Abstraction* (SNL 2007 [DIRS 177407], Table 8.2-1).

Table 6.3.8-3. Sampled Parameter Ranges and Distributions Used for Kinetic Sorption on Stationary Corrosion Products

Input Name	Input Description	Range	Distribution
Goethite_Site_Density_a	Goethite site density; discrete distribution	Density (sites nm^{-2})	Probability Level
		1.02	0.01786
		1.21	0.01786
		1.32	0.03571
		1.46	0.01786
		1.50	0.01786
		1.66	0.01786
		1.68	0.03571
		1.70	0.01786
		1.80	0.01786
		1.87	0.01786
		1.93	0.01786
		1.95	0.01786
		1.97	0.01786
		2.20	0.01786
		2.30	0.07143
		2.31	0.01786
		2.32	0.01786
		2.55	0.01786
		2.60	0.03571
		2.70	0.01786
		2.89	0.01786
		2.90	0.03571
		3.00	0.01786
		3.12	0.01786
		3.13	0.01786
		3.30	0.03571
		3.40	0.01786
		4.00	0.01786
		4.20	0.01786
		4.60	0.01786
		4.84	0.01786
		4.90	0.01786

Table 6.3.8-3. Sampled Parameter Ranges and Distributions Used for Kinetic Sorption on Stationary Corrosion Products (Continued)

Input Name	Input Description	Range	Distribution
Goethite_Site_Density_a (continued)	Goethite site density; discrete distribution (continued)	5.00	0.01786
		5.53	0.01786
		6.15	0.01786
		6.30	0.01786
		6.31	0.03571
		6.60	0.01786
		7.00	0.05357
		7.20	0.01786
		7.40	0.01786
		8.00	0.01786
		8.16	0.01786
		8.38	0.01786
		8.59	0.01778
HFO_Site_Density_a	HFO site density; discrete distribution	Density (sites nm^{-2})	Probability Level
		0.56	0.05263
		1.13	0.10526
		1.47	0.05263
		1.58	0.05263
		1.69	0.10526
		1.81	0.05263
		2.03	0.10526
		2.26	0.26316
		2.60	0.05263
		2.71	0.05263
		4.00	0.05263
		5.65	0.05265

Sources: Modified from DTN: SN0703PAEBSRTA.001_R3 [DIRS 183217] from *EBS Radionuclide Transport Abstraction* (SNL 2007 [DIRS 177407], Table 8.2-2).

Table 6.3.8-4. Sampled Model Inputs Used in the EBS Radionuclide Transport Abstraction

Input Name	Input Description	Range	Distribution
Invert_Diff_Coeff_Uncert_a	Invert diffusion coefficient uncertainty	Range: $10^{\mu \pm 3\sigma}$ (dimensionless) Mean: $\mu = 0.033$; Std. Dev. $\sigma = 0.218$	10ND
SS_Corrosion_Rate_a	Stainless steel corrosion rate	0.01 – 0.51 μm yr-1 Mean = 0.267 μm yr-1 Std. Dev. = 0.209 μm yr-1	Truncated Lognormal
CS_Corrosion_Rate_a	Carbon steel corrosion rate	25 – 135 μm yr^{-1} Mean = 78.5 μm yr^{-1} Std. Dev. = 25.0 μm yr^{-1}	Truncated Lognormal
DS_Flux_Uncertainty_a	Drip shield flux-splitting uncertainty factor	0 – 0.85 (dimensionless)	Uniform
WP_Flux_Uncertainty_a	Waste package flux-splitting uncertainty factor	0 – 2.41 (dimensionless)	Uniform
Diameter_Colloid_a	Diameter of colloid particle	50 – 300 nm	Uniform
Goethite_SA_a	Specific surface area of goethite (FeOOH)	14.7 – 110 $m^2\ g^{-1}$ Mean = 51.42 $m^2\ g^{-1}$ Std. Dev. = 30.09 $m^2\ g^{-1}$	Log-Normal (Truncated)
HFO_SA_a	Specific surface area of HFO	68 – 600 $m^2\ g^{-1}$ Mean = 275.6 $m^2\ g^{-1}$ Std. Dev. = 113.4 $m^2\ g^{-1}$	Log-Normal (Truncated)
NiO_SA_a	Specific surface area of NiO	1 – 30 $m^2\ g^{-1}$	Uniform
Cr2O3_SA_a	Specific surface area of Cr_2O_3	1 – 20 $m^2\ g^{-1}$	Uniform
Relative_Abundance_Goethite_a	Mass fraction of iron oxides (goethite and HFO) that is goethite	0.45 – 0.80 (fraction)	Uniform
FHH_Isotherm_k_CP_a	FHH adsorption isotherm parameter *k* for corrosion products	1.048 – 1.370 (dimensionless)	Uniform
FHH_Isotherm_s_CP_a	FHH adsorption isotherm parameter *s* for corrosion products	1.525 – 1.852 (dimensionless)	Uniform
CSNF_Rind_SA_a	Specific surface area of CSNF rind	0.5 – 60 $m^2\ g^{-1}$	Uniform
Density_CSNF_Rind_a	Density of CSNF rind	5,600 – 11,500 kg m^{-3}	Uniform
Porosity_Rind_CSNF_a	Porosity of CSNF rind	0.05 – 0.3 (fraction)	Uniform
FHH_Isotherm_k_CSNF_Rind_a	FHH adsorption isotherm parameter *k* for CSNF rind	1.606 – 8.215 (dimensionless)	Uniform
FHH_Isotherm_s_CSNF_Rind_a	FHH adsorption isotherm parameter *s* for CSNF rind	1.656 – 3.038 (dimensionless)	Uniform
HLWG_Rind_SA_a	Specific surface area of HLWG rind	10 – 38 $m^2\ g^{-1}$	Uniform
Diameter_Colloid_a	Colloid particle diameter	50 – 300 nm	Uniform
Gamma_AFM_a	Active fracture model gamma parameter DTN: LA0701PANS02BR.003_R2 [DIRS 180497]	0.2 – 0.6	Uniform

Table 6.3.8-4. Sampled Model Inputs Used in the EBS Radionuclide Transport Abstraction (Continued)

Input Name	Input Description	Range	Distribution
EBS_UZ_Flux_Sat_PS1 EBS_UZ_Flux_Sat_PS2 EBS_UZ_Flux_Sat_PS3 EBS_UZ_Flux_Sat_PS4 EBS_UZ_Flux_Sat_PS5	Unsaturated zone fracture saturation DTN: LA0701PANS02BR.003_R2 [DIRS 180497] This includes the average fracture and matrix percolation fluxes and saturations for both glacial transition and post-10,000-year periods. There are a total of five percolation subregions.	Average values for the five percolation subregions based on the average of repository nodes in each percolation subregion.	2-D Table; see Table 6.3.8-5
pH_Cell_2_Regression_Error	Error term added to the surface complexation based pH calculation in the corrosion products domain.	Mean: $\mu = 0$; Std. Dev. $\sigma = 0.32$ Truncated at ± 2 Std. Dev.	Truncated Normal
Diff_Path_Length_Invert_Top_a	Diffusive path length from waste package outer corrosion barrier to mid-point of invert.	0.30 – 1.24 m	Uniform

Sources: Modified from DTN: SN0703PAEBSRTA.001_R3 [DIRS 183217] from *EBS Radionuclide Transport Abstraction* (SNL 2007 [DIRS 177407], Table 8.2-4).

NOTES: ND = Truncated normal distribution

Table 6.3.8-5. Unsaturated Zone Saturation and Flux Inputs Used in the EBS Radionuclide Transport Abstraction

Parameter: EBS_UZ_Flux_Sat_PS1				
	Fracture Saturation	**Matrix Saturation**	**Fracture Flux**	**Matrix Flux**
gt10	1.29E-02	9.14E-01	3.44E-01	3.32E-01
gt30	1.65E-02	9.34E-01	1.82E+00	4.81E-01
gt50	1.41E-02	9.00E-01	1.94E+00	4.25E-01
gt90	1.43E-02	8.85E-01	4.77E+00	5.86E-01
pk10	1.57E-02	9.66E-01	1.55E+00	7.14E-01
pk30	1.65E-02	9.32E-01	1.99E+00	4.66E-01
pk50	1.52E-02	9.23E-01	3.55E+00	5.39E-01
pk90	1.52E-02	9.02E-01	7.10E+00	7.01E-01
Parameter: EBS_UZ_Flux_Sat_PS2				
	Fracture Saturation	**Matrix Saturation**	**Fracture Flux**	**Matrix Flux**
gt10	1.69E-02	9.75E-01	2.81E+00	5.12E-01
gt30	2.17E-02	9.83E-01	1.11E+01	6.21E-01
gt50	1.61E-02	9.68E-01	1.21E+01	6.45E-01
gt90	1.82E-02	9.39E-01	3.29E+01	7.77E-01
pk10	2.23E-02	9.87E-01	1.27E+01	7.23E-01
pk30	2.25E-02	9.84E-01	1.35E+01	6.55E-01
pk50	1.79E-02	9.73E-01	2.41E+01	7.37E-01
pk90	1.87E-02	9.41E-01	3.81E+01	8.16E-01
Parameter: EBS_UZ_Flux_Sat_PS3				
	Fracture Saturation	**Matrix Saturation**	**Fracture Flux**	**Matrix Flux**
gt10	2.06E-02	9.86E-01	9.10E+00	6.69E-01
gt30	2.50E-02	9.88E-01	2.43E+01	7.64E-01
gt50	1.86E-02	9.75E-01	3.28E+01	7.92E-01
gt90	2.09E-02	9.31E-01	6.96E+01	9.21E-01
pk10	2.51E-02	9.88E-01	2.18E+01	7.28E-01
pk30	2.76E-02	9.89E-01	3.67E+01	7.89E-01
pk50	2.03E-02	9.76E-01	5.15E+01	8.11E-01
pk90	2.06E-02	9.30E-01	6.34E+01	8.99E-01
Parameter: EBS_UZ_Flux_Sat_PS4				
	Fracture Saturation	**Matrix Saturation**	**Fracture Flux**	**Matrix Flux**
gt10	2.36E-02	9.87E-01	1.92E+01	7.25E-01
gt30	2.72E-02	9.88E-01	3.72E+01	7.99E-01
gt50	1.95E-02	9.70E-01	5.36E+01	8.14E-01
gt90	2.14E-02	9.14E-01	9.32E+01	9.77E-01
pk10	2.53E-02	9.87E-01	2.62E+01	7.34E-01
pk30	3.07E-02	9.88E-01	6.00E+01	8.12E-01
pk50	2.04E-02	9.70E-01	6.93E+01	8.24E-01
pk90	2.06E-02	9.11E-01	7.62E+01	9.20E-01

Table 6.3.8-5. Unsaturated Zone Saturation and Flux Inputs Used in the EBS Radionuclide Transport Abstraction (Continued)

Parameter: EBS_UZ_Flux_Sat_PS5				
	Fracture Saturation	**Matrix Saturation**	**Fracture Flux**	**Matrix Flux**
gt10	2.52E-02	9.88E-01	2.81E+01	7.34E-01
gt30	2.82E-02	9.89E-01	4.51E+01	8.04E-01
gt50	1.95E-02	9.73E-01	6.68E+01	8.15E-01
gt90	2.16E-02	9.30E-01	1.09E+02	1.02E+00
pk10	2.55E-02	9.88E-01	2.95E+01	7.36E-01
pk30	3.21E-02	9.90E-01	7.48E+01	8.20E-01
pk50	2.03E-02	9.74E-01	8.11E+01	8.18E-01
pk90	2.05E-02	9.26E-01	8.49E+01	9.42E-01

Sources: Modified from DTN: SN0703PAEBSRTA.001_R3 [DIRS 183217] from *EBS Radionuclide Transport Abstraction* (SNL 2007 [DIRS 177407], Table 8.2-5).

NOTE: Flux values are given in mm/yr but are entered as dimensionless in database. The units are added later in the model.

Table 6.3.8-6. Summary of CSNF Rind Volume Calculation Parameters for TSPA-LA

TSPA-LA Parameter Name	Model Abstraction Symbol	Description	Units	Distribution Type	Distribution Specification
Initial_Rod_Failures_a	None	Initial fraction of failed cladding, as received	None	Constant	100%
Fuel_Split_Fraction	None	Fraction of fuel available for corrosion at any timestep	None	Deterministic	1.0
Density_UO2	ρ_{UO_2}	Density of UO_2	g/cm^3	Deterministic	10.97
Density_Schoepite	ρ_{sch}	Density of schoepite	g/cm^3	Deterministic	4.83
MW_UO2	MW_{UO_2}	Molecular weight of UO_2	g/mole	Deterministic	270
MW_Schoepite	MW_{sch}	Molecular weight of schoepite	g/mole	Deterministic	322.1
Rind_Porosity_CSNF_a	ϕ_{sch}	Porosity in rind	None	Uniform	Min = 0.05 Max = 0.3
Rod_Length_CSNF	L_r	Active fuel rod length	cm	Deterministic	366
Num_Rods_WP_CSNF	N_r	Number of rods per WP	None	Deterministic	5,544
Pellet_Diameter_CSNF	D_{init}	Initial pellet diameter	cm	Deterministic	0.819

Source: SNL 2007 [DIRS 180616], Tables 7-1[a] and 7-2[a]

Table 6.3.8-7. Alternative Conceptual Models Considered for EBS Transport

Alternative Conceptual Models	Key Assumptions	Assessment and Basis
Bathtub flow model	Seepage water flowing into breached waste package accumulates until void volume is filled before water containing dissolved radionuclides flows out. Various cases, such as changing inflow rates and effect of solubility and dissolution rate limits, are evaluated (SNL 2007 [DIRS 177407], Section 6.6.1).	For several of the most pertinent cases, the flow-through model is bounding with respect to releases of radionuclides.
Constrained water vapor and oxygen diffusion model	The rate of steel component corrosion inside a WP is compared with the rate of diffusion of water vapor and oxygen through stress corrosion cracks into a WP. A continuous film of adsorbed water cannot form if the consumption rate is higher, which could delay the diffusive releases until all steel is fully corroded (SNL 2007 [DIRS 177407], Section 6.6.2).	Insufficient data to validate.
Dual-continuum invert model	Crushed tuff invert ballast is modeled as a dual-continuum material consisting of intergranular pore space and intragranular pore space. All seepage flow into the drift flows through the intergranular pore space and into the UZ fractures. Imbibition from UZ host rock into the invert flows through the intragranular pore space. Diffusion of radionuclides also occurs in both the intergranular and intragranular pore spaces, from the WP corrosion products into UZ fractures and matrix, as well as between the two invert continua (SNL 2007 [DIRS 177407], Section 6.6.3).	Insufficient data to validate diffusion coefficients in individual continua. Insufficient data to confirm whether this is a bounding approach with respect to chemical conditions in the invert for calculating solubility and colloid stability.
Invert diffusion coefficient model with lower limit on water content	As the water content of the crushed tuff ballast decreases, the water films that connect pore spaces become disconnected, and the effective diffusion coefficient drops more rapidly than predicted by Archie's law. Below some critical water content, the diffusion coefficient becomes zero, based on models of diffusion in soils (SNL 2007 [DIRS 177407], Section 6.6.4).	Insufficient data to validate diffusive behavior at very low water contents.
Reversible sorption of radionuclides onto WP corrosion products (empirical K_d sorption model)	Iron oxyhydroxide corrosion products sorb many radionuclide species. Sorption is assumed to be reversible and will not compete with other radionuclides nor compete for irreversible sorption sites (SNL 2007 [DIRS 177407], Section 6.6.5).	Does not account for limitations on total number of sorption sites. Does not account for competition with other radionuclides for sorption sites.
Plutonium sorption from stationary corrosion products and colloids	Plutonium sorbs strongly to iron oxyhydroxide corrosion product colloids and stationary corrosion products. Sorption may be considered slowly reversible (and modeled by computing the forward and reverse rate constants for the two-site model) (SNL 2007 [DIRS 177407], Section 6.6.6).	Experiment durations are short (hours to weeks) compared to the repository time scale. The mechanisms of plutonium sorption are not understood well enough to extrapolate the results outside the experiment design. Plutonium sorption and desorption data are not available for the highest pH ranges expected in the repository environment.

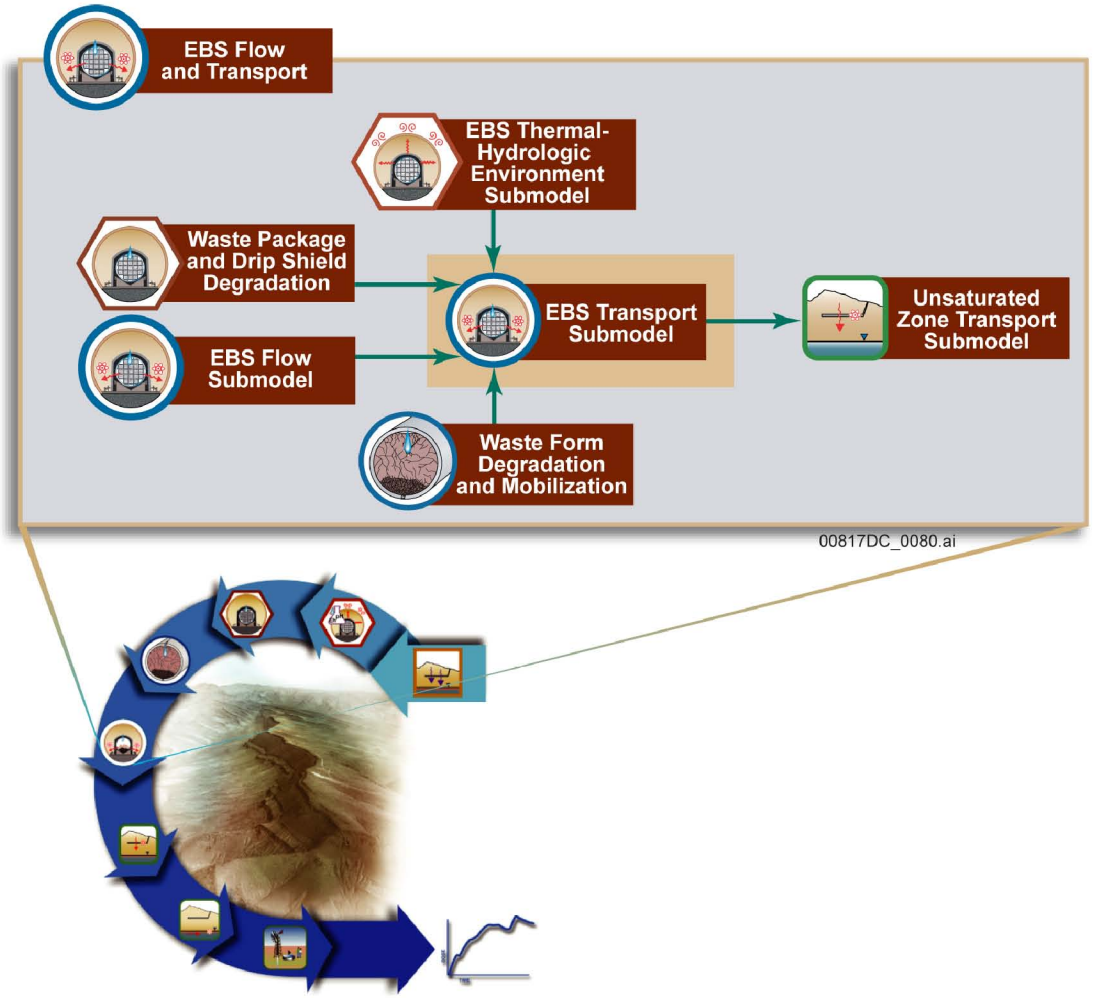

Figure 6.3.8-1. Information Flow Diagram for the EBS Transport Submodel

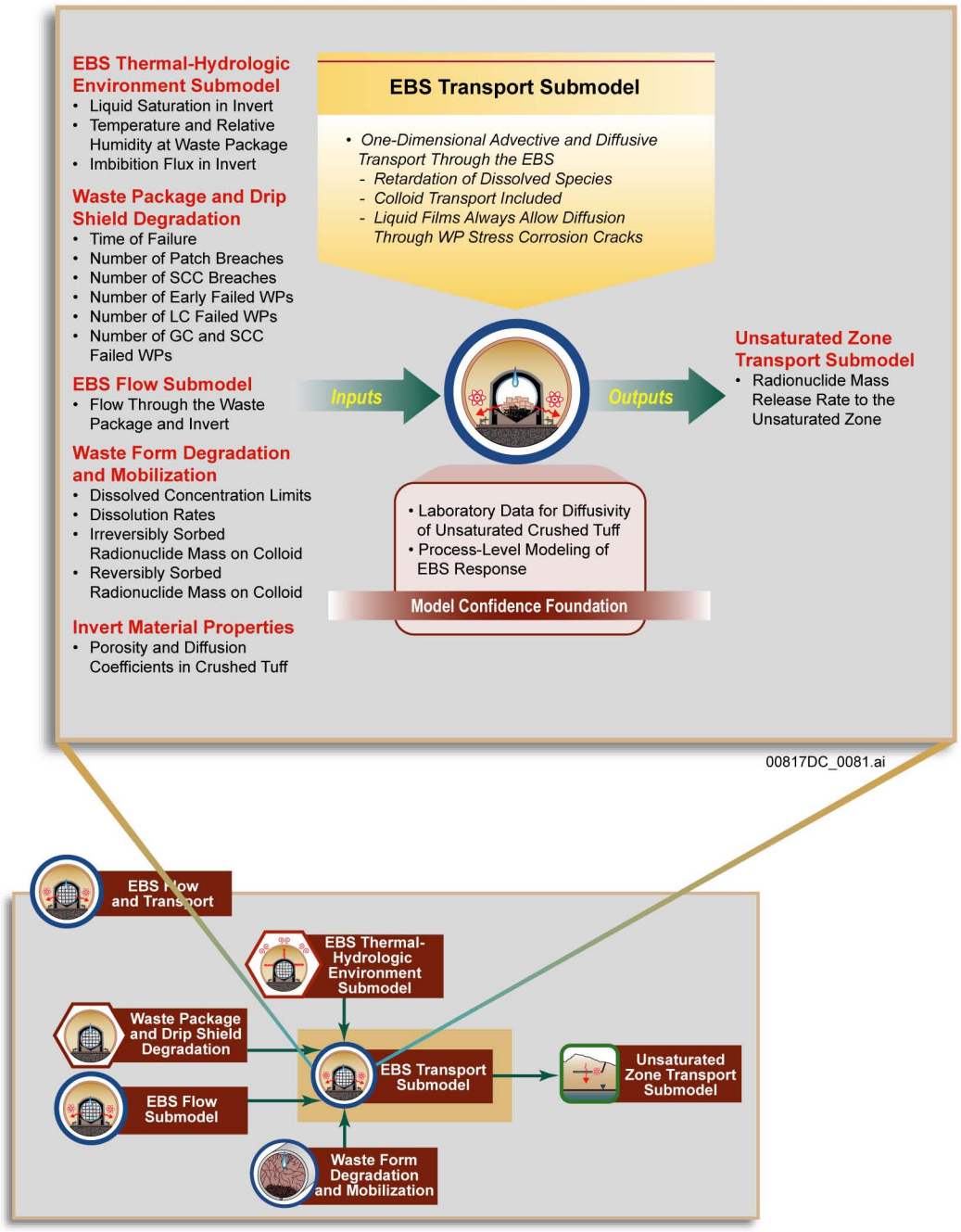

Figure 6.3.8-2. Inputs, Outputs, and Basis for Model Confidence for the EBS Transport Submodel

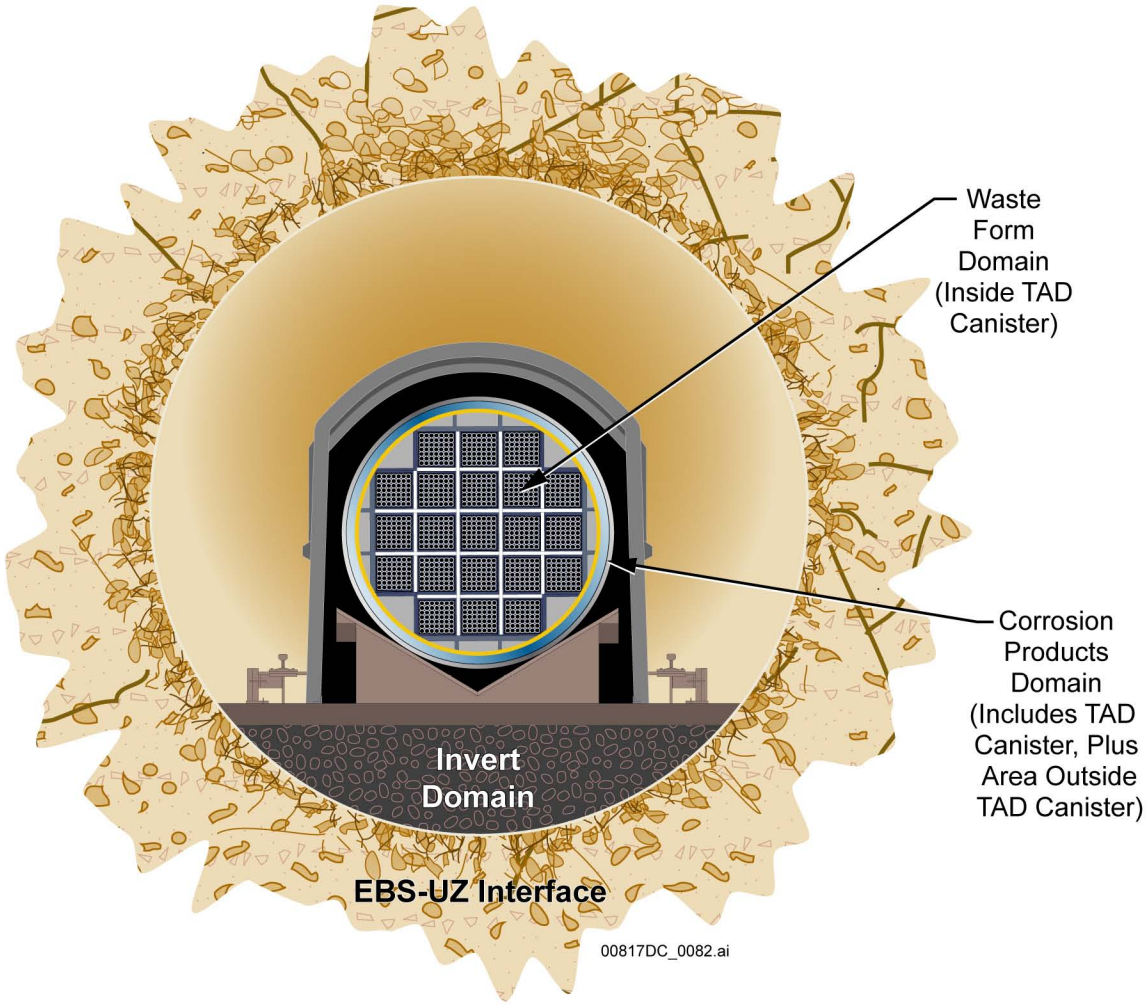

Figure 6.3.8-3. Cross Section of Idealized Drift Showing EBS Transport Submodel Domains for a CSNF Waste Package

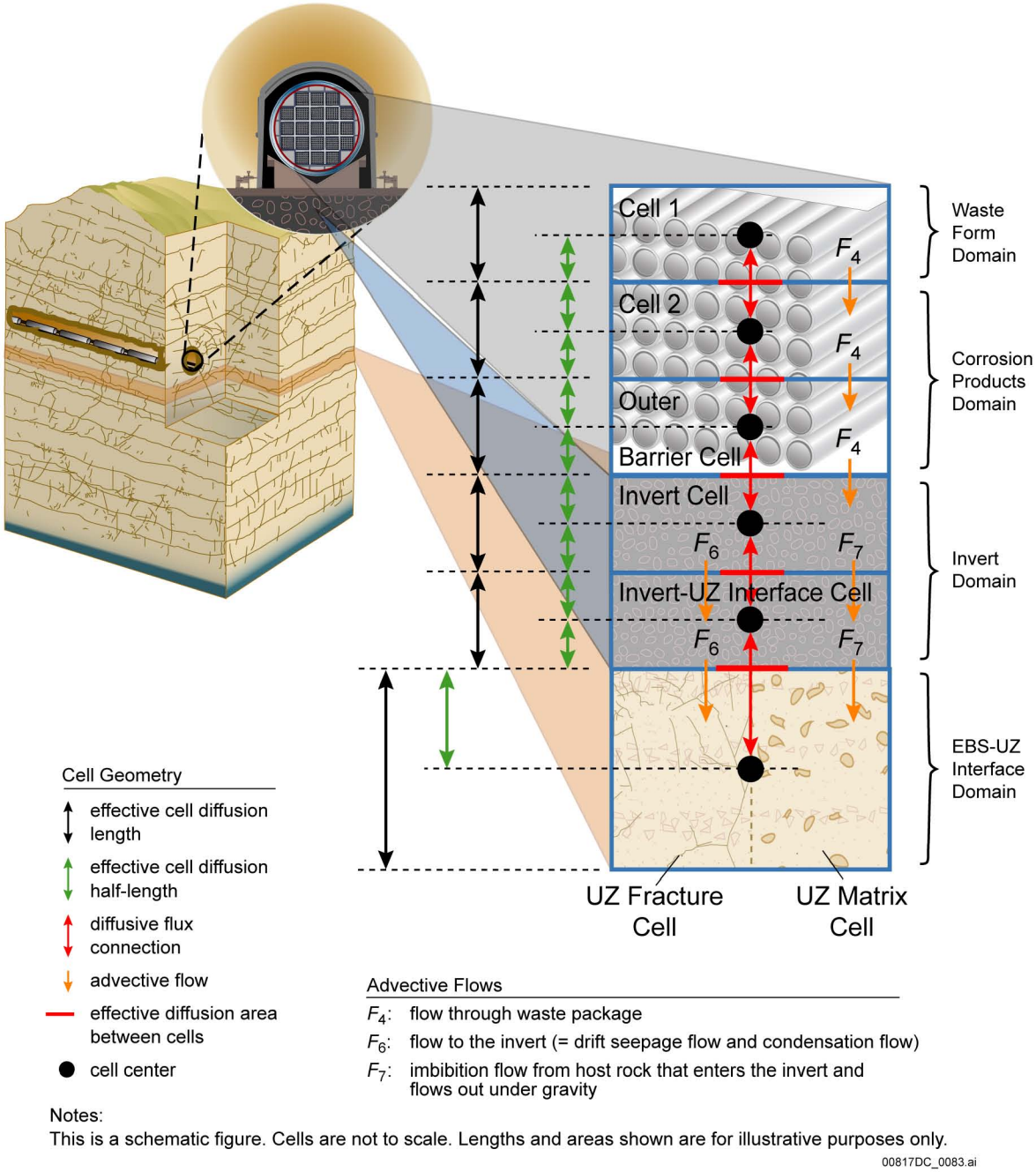

Figure 6.3.8-4. Schematic Representation of CSNF Waste Package Showing its Relationship to the Cell Pathway Network Used to Implement the EBS Transport Submodel

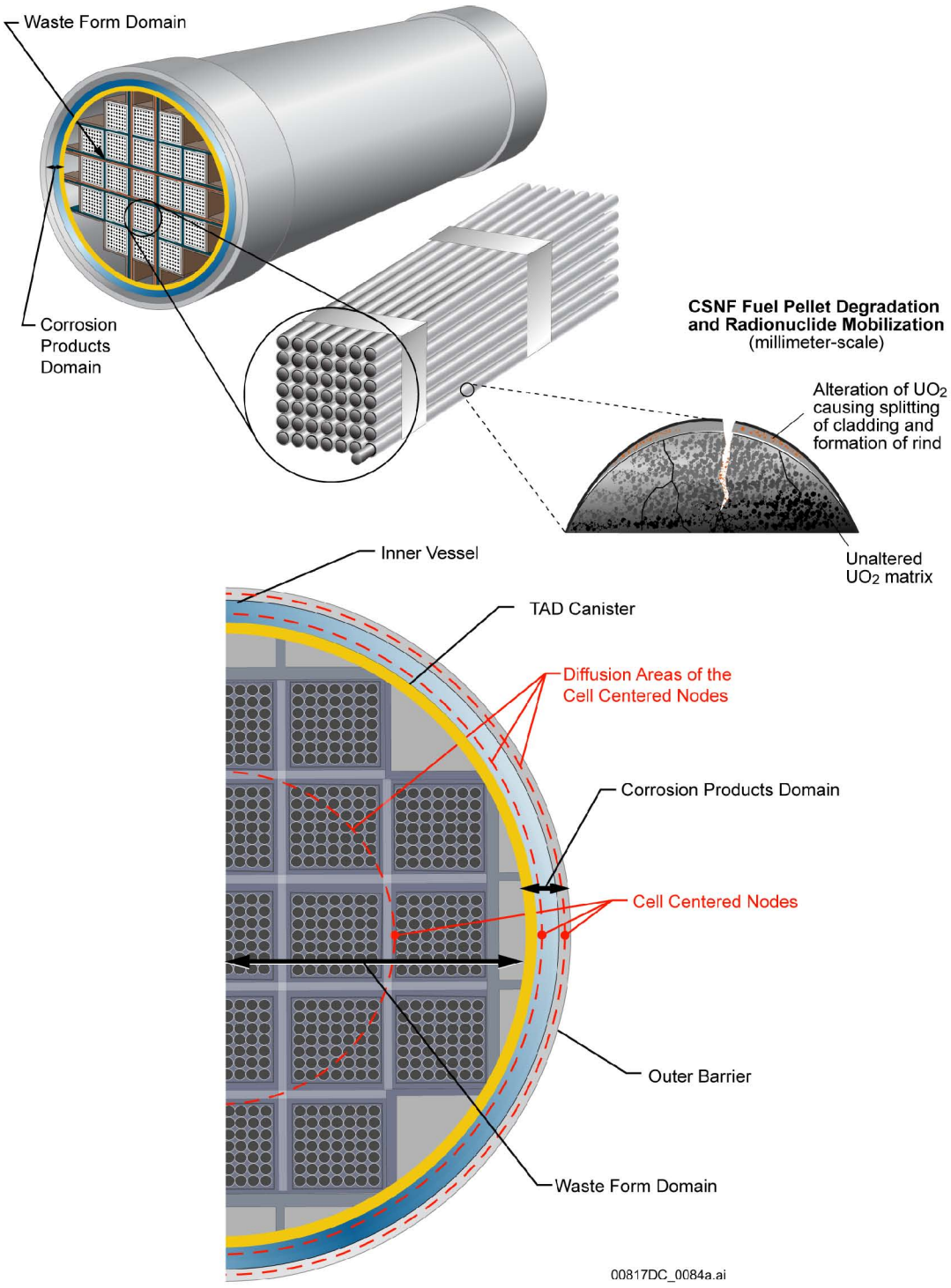

Figure 6.3.8-5. Setup of Cell Pathways for a CSNF Waste Package Used in the EBS Transport Submodel

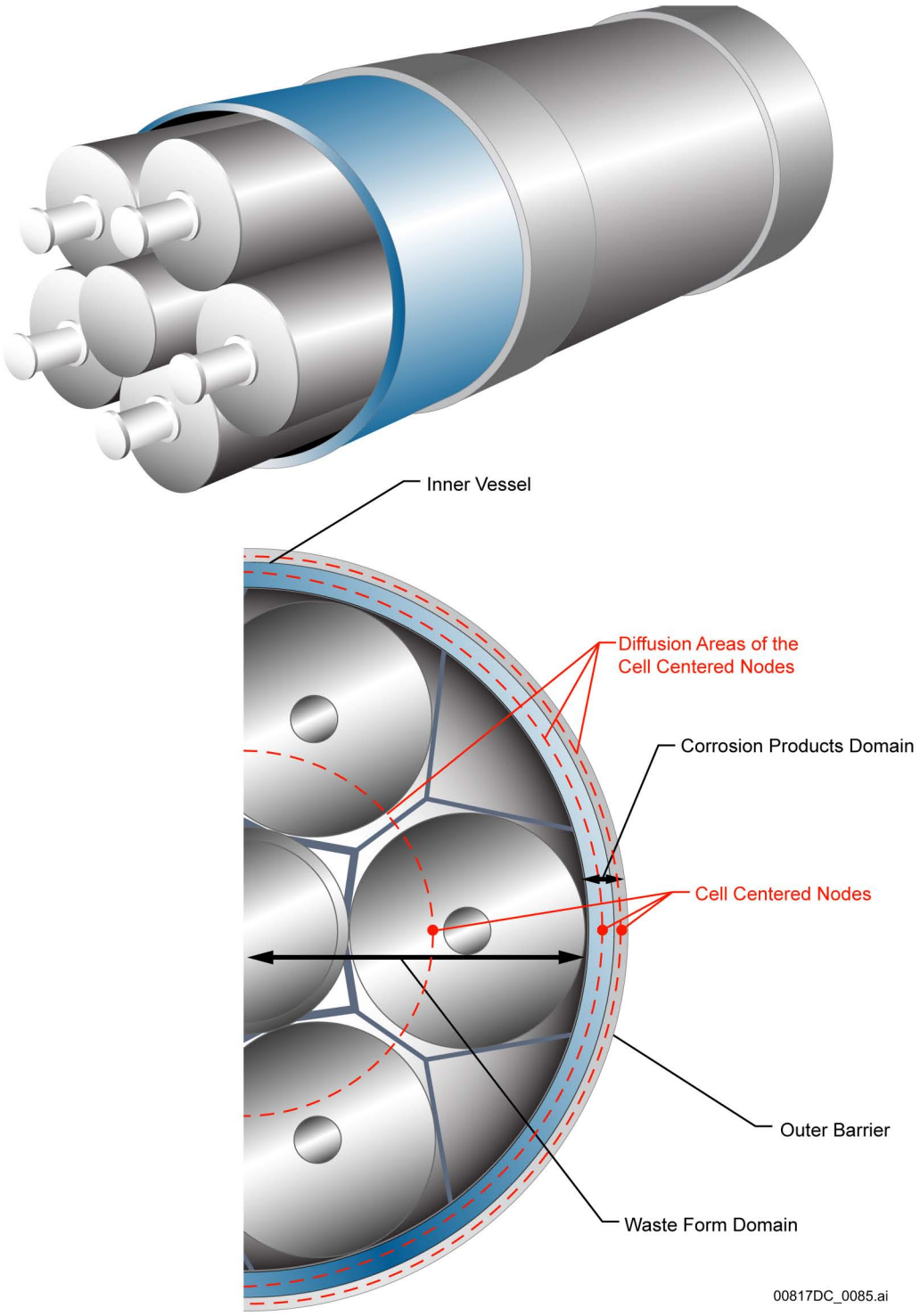

Figure 6.3.8-6. Setup of Cell Pathways for a CDSP Waste Package Used in the EBS Transport Submodel

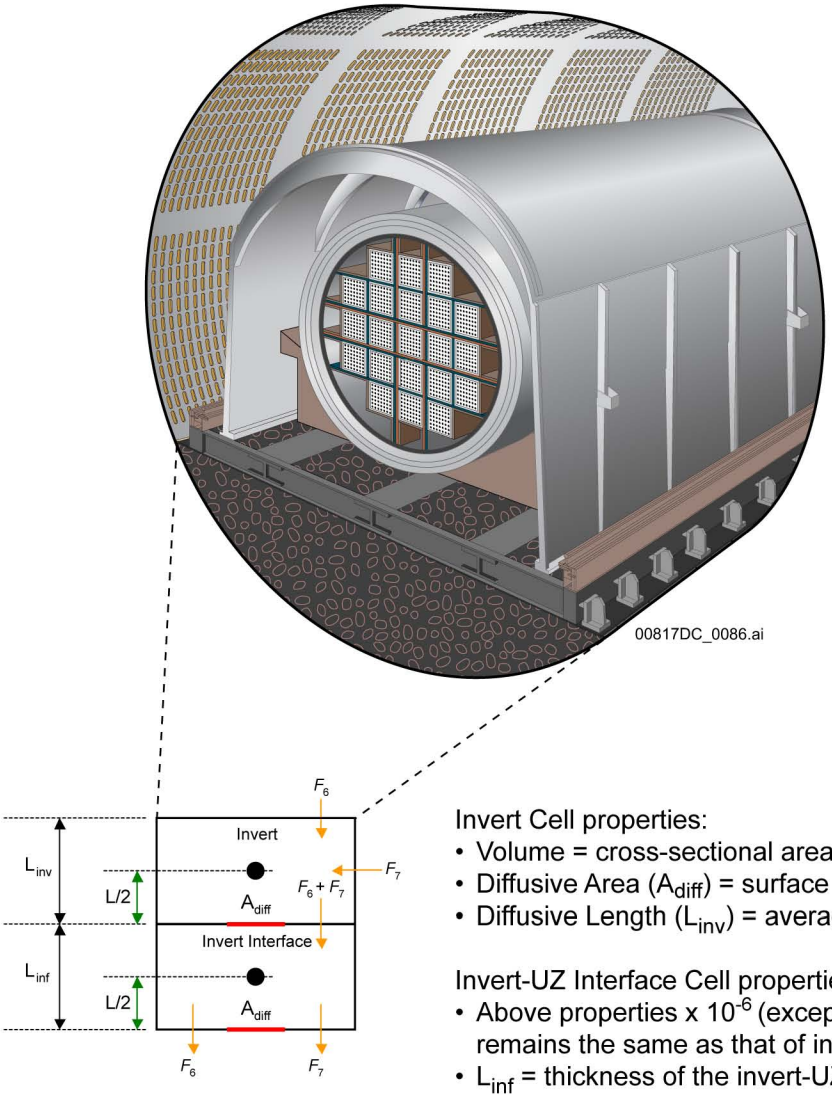

NOTE: The flow pathways (F_6 and F_7) are discussed in Section 6.3.6.1 and on Figure 6.3.6-4.

Figure 6.3.8-7. Setup of Invert Cell Pathways Used in the EBS Transport Submodel and their Relationship to the Actual Invert Geometry

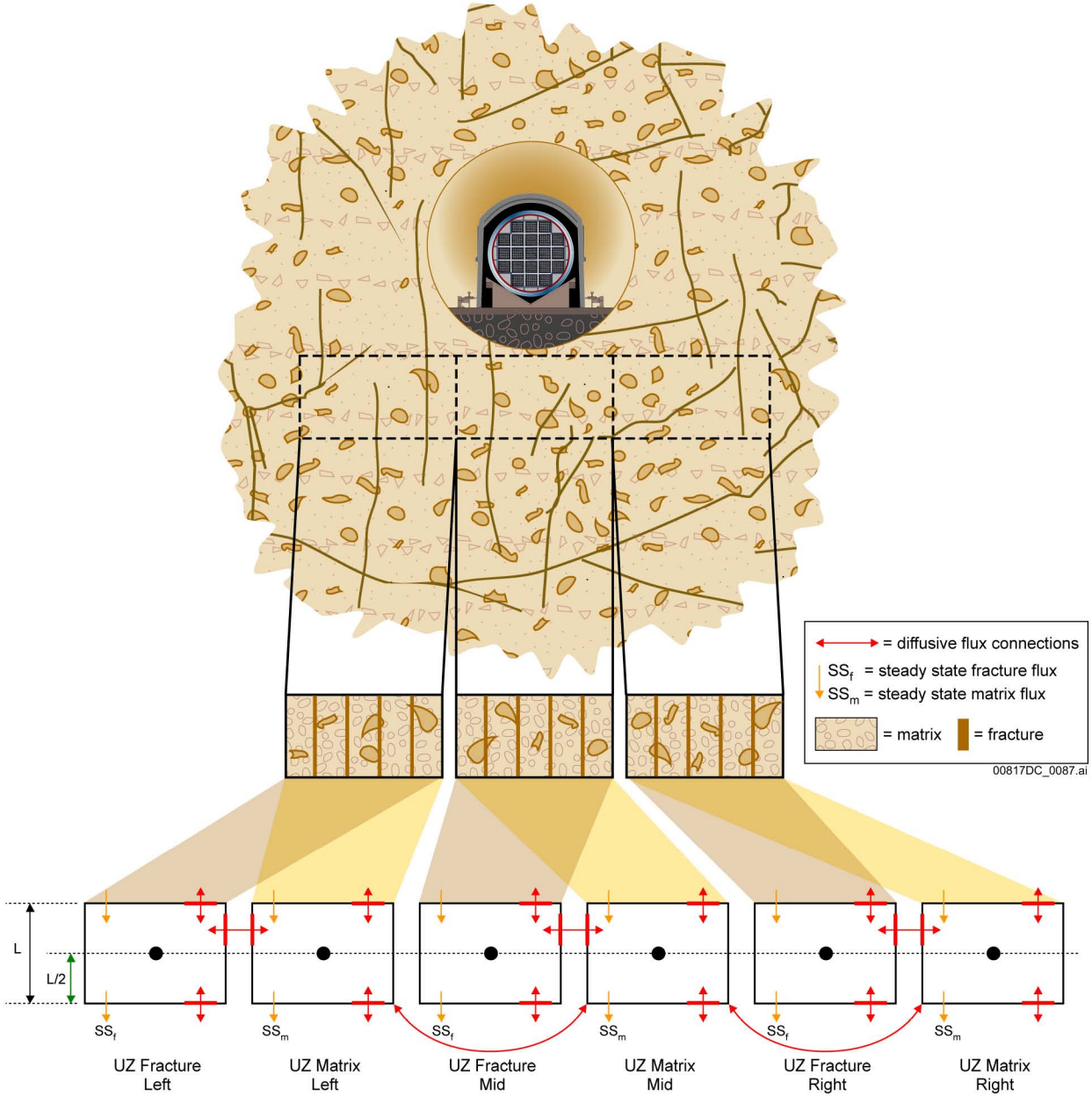

EBS-UZ Cell Properties:

- Bulk Volume = Drift Diameter × Cell Height × Waste Package Length
- Pore Volume (Matrix) = Bulk Volume × Matrix Porosity × (1-Fracture Fraction)
- Pore Volume (Fracture) = Bulk Volume × Fracture Fraction
- Diffusive length and area are based on geometry

Figure 6.3.8-8. Setup of Dual-Continuum EBS-UZ Interface Cell Pathway Network and its Relationship to the Near-Field Unsaturated Zone

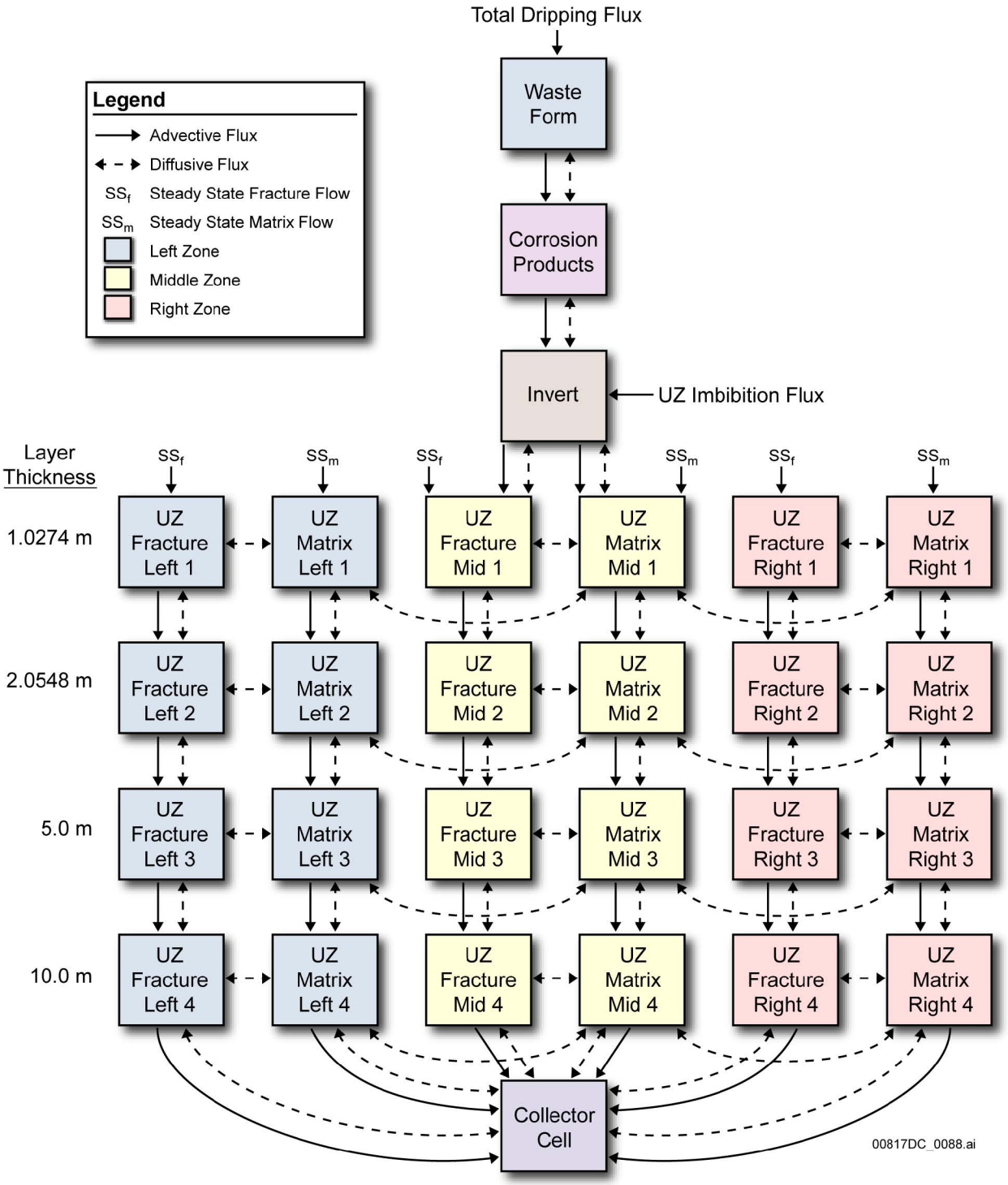

Source: SNL 2007 [DIRS 177407], Figure 6.5-4.

Figure 6.3.8-9. Schematic Representation of the Computational Grid for the EBS-UZ Interface Model

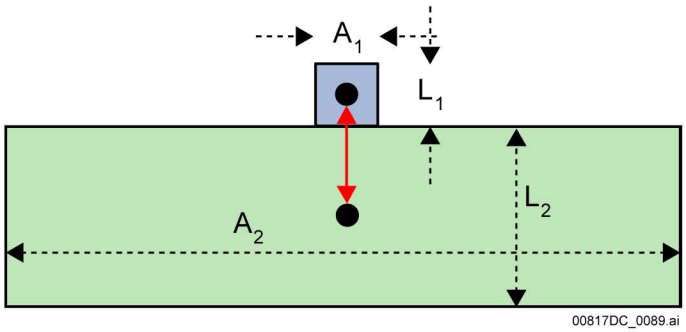

Figure 6.3.8-10. Simple Model Setup Using Cell Pathways with Different Diffusive Areas

6.3.9 Unsaturated Zone Transport

The UZ Radionuclide Transport Submodel of the TSPA-LA Model calculates the transport of radionuclides from the EBS of the Yucca Mountain repository, through the UZ to the SZ. UZ transport will depend on the flow fields from the *UZ Flow Models and Submodels* (SNL 2007 [DIRS 184614]) and on the rates of radionuclide mass releases from the waste emplacement drifts, as well as uncertainties associated with transport parameters. The UZ Transport Submodel provides, as output, the rate and spatial distribution of radionuclide releases to the SZ Flow and Transport Model Component. Information flow between the UZ Transport Submodel and other TSPA-LA Model components and submodels is shown on Figure 6.3.9-1. Figure 6.3.9-2 shows the connections between the UZ Transport Submodels and indicates elements of the foundation for confidence in the UZ Transport Submodel, the characteristics of radionuclide transport in the UZ, and the inputs and outputs associated with the UZ Transport Submodel. Note to differentiate between the first Addendum or the revision to that Addendum, and the base version, all references to the Addendums for *Particle Tracking Model and Abstraction of Transport Processes* (SNL 2008 [DIRS 184748], will be denoted by "[a]" or "[b]" after Section, Table and Figure numbers. References to the base version will have no bracketed index.

Note that for the UZ Transport Submodel, the basic parameters used in the model are input from the external input files from the FEHM DLL (FEHM V2.24-01, STN: 10086-2.24-01-00 [DIRS 179419]). These basic FEHM DLL input parameters and their sources are described in this section. Input variable names presented in the tables of this section are of two origins. For deterministic values of parameters, the names provided in the tables are consistent with the input variable names defined in the FEHM user guide (LANL 2003 [DIRS 167579]; DOE 2007 [DIRS 181096]). For stochastic input parameters, found in FEHM external files, the variable names reference the GoldSim elements that are used to generate the sampled values. These sampled values are downloaded from a supplemental GoldSim TSPA-LA Model simulation, performed at any stage in the model development or utilization, when any parameter stochastic distribution changes. The sampled values are downloaded from GoldSim into the FEHM stochastic parameter external files (Appendix F2.1.13). Using the updated FEHM stochastic parameter external files, simulations are then performed using these files until there is any change in any stochastic parameter. The names of the external input files, used by the FEHM DLL in the TSPA-LA Model, are listed in Table F-2 of Appendix F. A description of the contents of these external files can be found in Appendix F2.1.

Also, note that all references to FEHM in this section (Section 6.3.9) refer to FEHM Version 2.24-01 [DIRS 179419], which is the version used in the TSPA-LA Compliance Model and it will not be repeated every time FEHM is mentioned.

6.3.9.1 Conceptual Model

Transport of dissolved and colloid-bound radionuclides through the UZ below the repository will occur in both the fractures and the rock matrix, as shown on the conceptual drawing of UZ transport processes on Figure 6.3.9-3. Flow pathways will be determined by the hydrogeologic characteristics of the rock units, the presence or absence of faults, and whether or not there is perched water present along individual flow pathways. These characteristics will control the

extent of downward versus lateral flow, advective transport between the fractures and matrix, matrix diffusion, and the partitioning of flow between the fractures and rock matrix. Fractures and faults can provide fast flow paths. Additionally, diffusion into the rock matrix and/or sorption onto the rock/mineral surfaces are important retardation processes for radionuclide transport (BSC 2004 [DIRS 170035], Sections 6.2.2 and 6.2.3).

Five basic processes will affect the transport of radionuclides:

- **Advection**—Advection is the movement of dissolved in conjunction with the bulk flow of water containing radionuclides. Advection tends to enhance radionuclide transport.

- **Matrix Diffusion**—Diffusion of radionuclides from fluid flowing in fractures into rock-matrix pores will be a potential retardation mechanism because matrix transport is typically slower than fracture transport. Conversely, diffusion from the matrix to the fractures would tend to decrease transport times. Figure 6.3.9-4 is a conceptual drawing of diffusion into and out of matrix pores. Diffusion within the matrix is also considered in the fracture matrix interaction model (SNL 2008 [DIRS 184748], Section C1).

- **Sorption**—Sorption onto the rock/mineral surfaces will slow or retard the transport of certain dissolved radionuclides through the UZ. Sorption also results in radionuclide attachment to colloids, which can enhance radionuclide transport.

- **Hydrodynamic Dispersion**—Hydrodynamic dispersion, which is the spreading of a plume of dissolved constituents, such as radionuclides released from the repository as they are transported, is caused by localized variations in the flow field. Hydrodynamic dispersion tends to smear sharp concentration gradients and reduce the concentration at the leading edge of a breakthrough curve of radionuclides at the water table. Hydrodynamic dispersion is an approximate way of accounting for flow system heterogeneities of various scales that are not captured in the simulated flow fields. The UZ Transport Submodel only considers longitudinal hydrodynamic dispersion and does not consider transverse dispersion (SNL 2008 [DIRS 184748], Section 5.0, Assumption 3).

- **Radioactive Decay and Ingrowth**—Radioactive decay reduces the concentration of radionuclides in a predictable way, but it also produces decay products that typically have sorption characteristics different from those of the source radionuclides.

- **Colloid Transport**—In addition to being transported in a dissolved state, radionuclides can be transported while attached to colloids which are subject to advective-dispersive transport in the fractures and rock matrix. The colloid attachment can be effectively irreversible or reversible as described by an equilibrium sorption constant between the colloid and groundwater (SNL 2008 [DIRS 184748], Section 6.4.5). Colloids in turn may be subject to retardation within the fractures and other processes including size exclusion between the fractures and rock matrix and permanent filtration in the rock matrix, especially when entering units of differing pore size. A more complete discussion of colloid transport and the processes that control it follows below.

Colloid transport in the UZ is primarily in the fractures because colloids are limited in their capacity to diffuse into rock matrix as reflected in the low estimated values for diffusion coefficients (SNL 2007 [DIRS 177396], Section 6.18.2). Colloid transport into the rock matrix is also limited by size exclusion. Colloids can also be transported between the fractures and rock matrix and through the rock matrix by advection as long as the colloids are smaller than the matrix pores. In the UZ Transport Submodel, diffusion of colloids between the fractures and rock matrix is assumed to be negligible, while advective transport between the fractures and rock matrix is modeled explicitly. Figure 6.3.9-5 is a conceptual drawing showing some of the elements related to colloid-facilitated transport. Two principal types of colloid attachment can exist: reversible attachment where the radionuclides are temporarily attached to the surface of colloids and irreversible attachment where the radionuclides are permanently imbedded in the colloid structure. Advection of colloids through fractures is expected to dominate colloid transport in welded and zeolitic tuffs because permeability in the welded and zeolitic tuff matrix is much lower than that in the fractures. The rock matrix pores are typically smaller than the fracture apertures and the colloids themselves in many instances. Colloid filtration can occur in the matrix during transport from one hydrogeologic unit to another. That is, when the size of the colloids is larger than the matrix pores in the downgradient unit, the colloids are stopped at the unit interface. This filtration effect results in permanent immobilization of radionuclides irreversibly attached to the colloids but not of radionuclides reversibly attached to colloids. In the latter instance, the radionuclides could desorb from the colloids and continue to migrate. For this reason only irreversible colloids are filtered at unit interfaces in the TSPA-LA Model. In addition, colloid exclusion from the matrix can occur when there is a component of flow from the fractures into the matrix, and some colloids that would otherwise migrate from the fracture continuum to the matrix continuum are excluded due to their size relative to the matrix pore size. Filtration of colloids during transport within fractures is implicitly considered in the colloidal retardation factor.

A change to wetter climates may also impact the transport of radionuclides through the UZ by increasing net infiltration at the ground surface and, subsequently, the percolation flux through the UZ. Along with increased transport rates through the UZ, wetter climates would also lead to an increase in water table elevation. A higher water table shortens transport distances from the EBS to the water table. In the TSPA-LA Model, a rise in the water table is accompanied by an instantaneous release, to the SZ, of the radionuclides that are presently in the geologic units impacted by the water table rise.

6.3.9.2 TSPA-LA Model Abstraction

Consistent with the Mountain-Scale UZ Flow Submodel, the UZ Transport Submodel is a dual-continuum model. In the UZ Transport Submodel, fracture and matrix transport are coupled and calculated using the FEHM [DIRS 179419] residence-time transfer-function particle-tracking technique, as described in *Particle Tracking Model and Abstraction of Transport Processes* (SNL 2008 [DIRS 184748], Section 6.4). This technique is a cell-based approach in which particles move from cell to cell in the FEHM numerical grid. Particle movement from cell to cell is computed probabilistically based on flow balance, dispersivity, and matrix diffusion. The fracture matrix interactions are evaluated using transfer functions when diffusive transport between fracture and matrix (i.e., dual-permeability or discrete fracture models) is simulated. The transfer functions used in the TSPA-LA Model are a set of

breakthrough curves defined using dual-permeability numerical solutions of the transport equations for parallel flow in a fracture and adjacent rock matrix and diffusion normal to the flow direction (SNL 2008 [DIRS 184748], Appendix C). After a particle enters a cell, the adjacent cell it will travel to next (or whether it will switch media in the same cell) is probabilistically determined using random sampling based on the water flow balance. Note that only outflows from cells are included in the calculations; particles are not moved to a cell if water flows from that cell to the current cell. For the dissolved species and reversible colloids simulated in the TSPA-LA Model, the transfer functions are used to randomly decide if a particle will change medium (go from fracture to matrix or from matrix to fracture) and to determine the cell residence times for each particle. For the irreversible colloids, which are not subject to matrix diffusion, the residence times for each particle are a function of the cell pore volumes, the flux out of the cells, and the colloid retardations (for the retarded or Ic species only). To simulate the effects of longitudinal dispersivity in dissolved species, reversible colloids, and irreversible colloids, the residence times are updated with a random factor based on the Peclet number between cells, where the Peclet number is a function of the dispersivity and the distance between cells.

The dual-continuum UZ Transport Submodel includes a numerical grid of fracture cells representing the fracture continuum and a grid of matrix cells representing the matrix continuum, with each fracture cell connected to a corresponding matrix cell. Twenty-seven radionuclides are transported through the UZ. The radionuclide half-lives and decay products used in the TSPA-LA Model are listed in Table 6.3.9-1. The following processes are simulated in the TSPA-LA Model:

- Advective-dispersive transport of dissolved radionuclides in the fracture and matrix continua and between continua
- Fracture-matrix interaction and matrix diffusion
- Sorption of dissolved radionuclides in the matrix continuum
- Advective-dispersive transport of colloids with radionuclides attached (transport of colloids is explicitly simulated when radionuclides are considered to be irreversibly attached and implicitly simulated in conjunction with the transport storage term when radionuclides are considered to be reversibly sorbed)
- Retardation in the fracture continuum of colloids, on which radionuclides are reversibly and irreversibly sorbed
- Colloid filtration at interfaces between rock-matrix units
- Colloid size exclusion at fracture-matrix continua interfaces
- Radioactive decay and ingrowth

- Climate change and its effect on fluid flow rates in the UZ
- Rise in water-table elevation and its effect on radionuclide release to the SZ.

Uncertainty is included in the UZ Transport Submodel by defining statistical distributions for a number of input parameters. Thus, each realization of the total system has a unique set of input parameters. In addition, each realization is considered to be equally likely. Some of the uncertainty in UZ transport results from uncertainties passed to the UZ Transport Submodel from other submodels. For example, there may be uncertainty in infiltration and UZ flow from the Site-Scale UZ Flow Process Model; uncertainty in the number of failed WPs from the WP and DS Degradation Model Component; and uncertainty in numerous EBS parameters and processes used to define the radionuclide source term received from the EBS Transport Submodel. These uncertainties from upstream submodels are passed to the UZ Transport Submodel either implicitly through the passing of the radionuclide fluxes and ratios of fluxes applied to the fractures versus total fluxes (fluxes applied to fractures and rock matrix) from GoldSim to FEHM, or explicitly through the passing of data, such as the number of WPs failed in each percolation subregion (source bin) or indices denoting which infiltration rate scenario should be applied (10th percentile, 30th percentile, 50th percentile, or 90th percentile rate scenario). For the sampled infiltration rate scenario, a set (10th percentile, 30th percentile, 50th percentile, or 90th percentile) of four flow fields representing the three climates of present day, monsoon, and, glacial-transition, is read in by the FEHM DLL for that realization. Note that the classification of 10th, 30th, 50th, and 90th percentile infiltration scenarios is based on the infiltration maps used to develop the flow fields for the first three climates. For the post-10,000-year climate, the four equivalent flow fields are generated using the scaled 90th percentile present-day, 50th percentile Glacial Transition, 90th percentile glacial transition, and the 90th percentile monsoon infiltration maps, respectively (see Section 6.3.1). The uncertainty distributions sampled to derive parameters for the FEHM DLL are summarized in Tables 6.3.9-2 through 6.3.9-12. The uncertainty distribution for the infiltration scenarios is presented in Table 6.3.1-2. Note that some of the parameters derived for the UZ Transport Submodel, such as matrix sorption and matrix diffusion coefficients, are also used in the EBS Submodel for sections of cell networks representing the UZ directly below the repository.

The UZ Transport Model Abstraction is based on FEHM's multi-species particle tracking option that uses the 16 flow fields from the UZ Flow Model Abstraction to evaluate the movement of radionuclides from the repository to the water table. The UZ Flow Model Abstraction is comprised of 16 steady-state flow fields generated by the three-dimensional Site-Scale UZ Flow Model (Section 6.3.1.2). The 16 flow fields consist of four flow fields representing uncertainty for each of four climate states, including present-day, monsoon, glacial transition, and post-10,000-year (Section 6.3.1.2). The flow fields provide spatial distributions of fracture-fracture, matrix-matrix, and fracture-matrix water flow rates and moisture contents in the UZ. During TSPA-LA Model simulations, temporal changes in climate are approximated by changes from one steady-state flow field to another. For example, at the onset of the monsoon climate stage, a present-day climate stage flow field is replaced with a monsoon climate stage flow field. Uncertainty in the UZ Flow Model Abstraction is implemented through probabilistic sampling of the four flow fields that correspond to the infiltration uncertainty maps generated for each climate state (Section 6.3.1.2). The sampling of four infiltration cases is based on a set of weighting factors (Table 6.3.1-2) developed using a generalized likelihood uncertainty estimate

methodology to determine meaningful weighting factors for the selected infiltration maps (Section 6.3.1.2). To approximate the effects of a rising water table on a radionuclide transport simulated by the FEHM multi-species particle tracking option, the monsoon climate, glacial-transition, and post-10,000-year climate flow-field files used in the transport model have been post-processed (see Section 6.3.1.1). In the updated files, the water table elevations for the monsoon, glacial-transition, and post-10,000-year climate flow fields have been constrained to a minimum level of 850 m above mean sea level. For the future climates, any locations where the present-day water table is below 850 m, it is set to 850 m and any locations where the present-day water table is above 850 m, the water table is not adjusted from the present day level (see BSC 2004 [DIRS 169855]). Note that the bottom boundary for the flow models of all climate states is the present day water table. Within the repository footprint, the present-day water table varies from around 730 m to 850 m above mean sea level (BSC 2004 [DIRS 169855] Figure 6.2). The changes to the monsoon, glacial-transition, and post-10,000-year climate flow fields, represent a water table rise of up to 120 m within the repository fingerprint (Section 6.3.1.1), effectively shortening the transport path through the UZ. After the instantaneous change in water table levels following the onset of the monsoon climate, all radionuclide mass associated with particles residing between the original and updated water tables are instantaneously added to the SZ source term.

In the TSPA-LA Model, radionuclide sorption on the rock matrix is approximated using a linear, equilibrium sorption model characterized by a single parameter, the sorption coefficient K_d. A set of three probability distributions for the K_ds used in the model have been developed for each radioelement. Each set of K_ds describes the radioelement's sorptive behavior in each of three major rock types (vitric, devitrified, and zeolitic tuffs) in the UZ (SNL 2007 [DIRS 177396], Appendices A[a] and B[a] for selenium and tin, and Appendices A and B for all other species). These effective sorption coefficients are a function of many factors, including mineralogy, groundwater aqueous chemistry, and heterogeneity, at scales smaller than those considered in the numerical model. Furthermore, in developing the sorption coefficients, the kinetics of sorption reactions and nonlinear sorption effects that would lead to lower K_ds were considered. The above factors were considered when establishing the parameter uncertainty distributions for the K_d values. In addition, sorption coefficients may be affected by temperature. With elevated temperatures, the sorption coefficient generally increases for cationic species, thereby causing longer transport times (SNL 2007 [DIRS 177396], Section 6.1.2.9). The linear equilibrium sorption coefficients used in the TSPA-LA Model do not account for elevated temperatures and, therefore, are conservative with respect to transport times for cationic species through the UZ (SNL 2007 [DIRS 177396], Section 6.1.5.2). Note that shorter travel times are considered to be conservative. The parameter distributions used in the UZ Transport Submodel for matrix sorption coefficients are provided in Table 6.3.9-2.

For the TSPA-LA Model, unsaturated matrix diffusion coefficients are generated as the product of the matrix tortuosities for specified rock groups and the free-water diffusion coefficients for the elements considered. The tortuosities are based on a correlation between matrix diffusion, matrix porosity, and matrix saturated permeability developed from diffusion data in saturated samples by Reimus et al. (2007 [DIRS 179246]). To adapt the relationship for the UZ, porosity is replaced by water content, and saturated permeability is replaced by effective permeability. The methodology used in the derivation of the distributions for tortuosities is described in *Particle Tracking Model and Abstraction of Transport Processes* (SNL 2008 [DIRS 184748],

Section 6.5.5[a] and Appendix A[a]). The resultant tortuosity distributions are found in DTN: LB0702PAUZMTDF.001_R1 [DIRS 180776]. The derivation of the constant values for element specific free-water matrix diffusion coefficients is also described in *Particle Tracking Model and Abstraction of Transport Processes* (SNL 2008 [DIRS 184748], Section 6.5.5[a] and Appendix A[a]). The free-water matrix diffusion coefficients used in the UZ Transport Submodel of the TSPA-LA Model are found in DTN: LB0702PAUZMTDF.001_R1 [DIRS 180776].

The equation describing the correlation between matrix diffusion (or matrix tortuosity), porosity (or water content for the UZ), and saturated permeability (or effective permeability for the UZ) used for calculating the matrix diffusion coefficient, is (SNL 2008 [DIRS 184748], Eq. A-1[a]):

$$\log_{10}\left(D_m / D^*\right) = 1.42 + 1.91\theta_m + 0.19\log_{10}\left(k_m\right) \qquad \text{(Eq. 6.3.9-1)}$$

where

D_m/D^* = the matrix tortuosity

D_m = the matrix diffusion coefficient in m^2/s

D^* = the free water diffusion coefficient in m^2/s

θ_m = the matrix water content

k_m = the effective permeability to water in m^2.

Note that Equation 6.3.9-1 is an adaptation of the original equation for the UZ with water content replacing matrix porosity and effective permeability replacing permeability. The element-specific values for free-water diffusion coefficients are presented in Table 6.3.9-3. The $\log_{10}$ values of the mean tortuosities for the three rock groups that are assembled based on similar attributes are presented in Table 6.3.9-4. The SDs of the $\log_{10}$ tortuosities, based on the standard error of the regression curves defined by Equation 6.3.9-1, are also presented in Table 6.3.9-4 (also SNL 2008 [DIRS 184748], Table 6.5.5-1[a] and Section 6.5.5.4 [a]). The uncertainty is implemented in the TSPA-LA Model for each rock group by selecting a standard normal random number and adding the product of the standard normal random number and SD (in $\log_{10}$ space) to the $\log_{10}$ value of the mean tortuosity, taking the antilog of the value to derive the tortuosity for the present realization and multiplying each element-specific free-water diffusion coefficient by the tortuosity to derive 15 element-specific effective diffusion coefficients (SNL 2008 [DIRS 184748], A-3 [a]).

As previously noted for TSPA-LA simulations, the diffusion of colloids from the fracture to the matrix is not simulated. This treatment is considered conservative with respect to reducing colloid transport times to the SZ (SNL 2008 [DIRS 184748], Section 6.5.5).

In the UZ Transport Submodel, the fracture dispersivity is set to 10 m. According to *Particle Tracking Model and Abstraction of Transport Processes* (SNL 2008 [DIRS 184748], Section 4.1.6[a] and Section 6.5.2), the value of 10 m represents a conservative value chosen from the lower end of the field studies. A higher dispersivity tends to spread the plume and reduce the peak concentrations. In addition, in comparison with the effects of matrix diffusion

and the large-scale heterogeneities in the UZ, dispersivity effects are expected to have a small influence on the breakthrough curves (SNL 2008 [DIRS 184748], Section 6.5.2). Note that FEHM's multi-species particle tracking model limits the Peclet number between adjacent nodes to ≥ 1, where the Peclet number is the ratio of path length to dispersivity (SNL 2008 [DIRS 184748], Section 6.4.2). This means that for nodal distances ≤ 10.0 m, the dispersivity will be set equal to the path length. For most of the TSPA-LA Model, the dispersivity will be 10 m; just below the repository, for some of the links between cells, the dispersivities may be as low as 5 m.

Part of the conceptual model upon which the UZ Transport Submodel is based, is the Active Fracture Model (AFM) of Liu et al. (1998 [DIRS 105729]). The AFM takes into consideration the fact that due to the nonlinearities associated with unsaturated flow, only a portion of fractures in the UZ fracture network are subject to water flow and the others are bypassed. The AFM assumes that since only a portion of the fractures in a network have water flowing through them, there is an effect on the spacing of flow and transport pathways in the fracture network, the fracture/matrix interface area, and the number of active fractures in a grid block. In the TSPA-LA Model, the spacing between flowing fractures is calculated as a function of the geometric fracture spacing, fracture saturation, fracture residual saturation, and the active AFM parameter (γ) (Liu et al. 1998 [DIRS 105729]). In the TSPA-LA Model, a constant fracture residual saturation of 0.01 is used for all layers (SNL 2008 [DIRS 184748], Section 6.5.6).

In addition to adjusting the spacing between flowing fractures, the active fracture conceptualization calls for an adjustment to the interface area across which matrix diffusion occurs. The effective area reduction factor (R) described by Liu et al. (1998 [DIRS 105729]) can be written in the form:

$$R = S_e^{1+\gamma} \qquad \text{(Eq. 6.3.9-2)}$$

where S_e is the effective water saturation. As implemented in FEHM, the effective area reduction factor can be broken down into the product of the S_e and S_e^{γ}, where the first term represents the area adjustment factor and the second term represents the fracture spacing adjustment factor (SNL 2008 [DIRS 184748], Section C5). The interface adjustment accounts for the reduction of the wetted area within an individual fracture and for the reduction in area caused by the smaller number of active fractures. This adjustment to the interface area is a reduction by a factor of the effective saturation (SNL 2008 [DIRS 184748], Appendix C, Section C-5). Note that the effective interface area (Equation 6.3.9.2) between the fracture and matrix is reduced by a factor of the effective saturation even when all fractures are considered active ($\gamma = 0$). The area reduction associated with the active fracture model is a conservative representation for situations in which radionuclide mass is introduced into the fracture continuum. An underestimation of the diffusive area would slow the movement of mass applied to the rock matrix and increase the rate of movement of mass through the fractures. For mass applied to the rock matrix, there would be a decrease in mass diffusing out of the matrix slowing its movement through the system. As implemented, the active fracture conceptualization is consistent with the assumptions of the fracture-matrix interaction, as validated in *Particle Tracking Model and Abstraction of Transport Processes* (SNL 2008 [DIRS 184748], Section 7.2.3.3). Note that the UZ Transport Submodel uses different active fracture model parameter values than the UZ Flow Field Abstraction. In the

UZ Flow Model, the active fracture model parameter values are calibrated. To be rigorous, the AFM parameters should be consistent between the flow and transport model because the AFM parameters affect both flow and transport processes (SNL 2008 [DIRS 184748], Section 6.6.4). However, since process flow model studies (SNL 2007 [DIRS 184614]) have shown that the AFM parameter values have little influence on the fluid saturations and steady-state fracture to fracture and matrix to matrix flow, the use of the base case flow fields is justified (SNL 2008 [DIRS 184748], Section 6.6.4). Sensitivity studies presented in *Particle Tracking Model and Abstraction of Transport Processes* (SNL 2008 [DIRS 184748], Section 6.6.4, Figures 33 and 35) show the sensitivity of transport to the variance in the AFM γ, indicating that consideration of uncertainty is important for the transport process. Uncertainty in the active fracture parameter γ is applied to the TSPA-LA Model by sampling the parameter uniformly over a range between 0.2 and 0.6 as noted in Table 6.3.9-5 (SNL 2008 [DIRS 184748], Section 6.5.6[a]). This range of γ values spans the values considered appropriate for tsw32-tsw38, based on ^{14}C data (SNL 2008 [DIRS 184748], Section 6.5.6[a]) and the values based on the flow model calibration.

Fracture spacing and aperture values are used to estimate the effect of matrix diffusion on radionuclide transport. In the TSPA-LA Model, the fracture spacing is the inverse of fracture frequency. Fracture apertures are calculated from randomly sampled fracture porosity and frequency values using the following relationship (SNL 2008 [DIRS 184748], Section 6.5.7, Equation 6-26):

$$2b = \phi_f / f \qquad \text{(Eq. 6.3.9-3)}$$

where

$2b$ = the fracture aperture (m)

ϕ_f = the fracture porosity (dimensionless)

f = the fracture frequency (m^{-1}).

The distributions used by the TSPA-LA Model for fracture porosity values (ϕ_f) and fracture frequency values (f, unit 1/m) are presented in Tables 6.3.9-6 and 6.3.9-7, respectively. The fracture porosity estimates determined from air permeability testing in TSw34 are considered fairly reliable (BSC 2004 [DIRS 170038], Section 6.1.3.3), even though several factors are not explicitly accounted for, including gas compressibility, heterogeneity, anisotropy, cavity occurrence, and dispersion (note that adjustments are made to account for matrix diffusion effects). . The fracture porosities for other units are derived from 1-D borehole and 2-D mapping data which are used in conjunction with the average aperture widths to provide relative ratios of fracture porosity for different stratigraphic units. These relative ratios are used in conjunction with the TSw34 air permeability testing estimates to provide unit-specific estimates. Note that there is a large amount of uncertainty in the estimates of fracture porosity for the other units (BSC 2004 [DIRS 170038], Section 6.1.3). This uncertainty stems from two areas: (1) the estimated apertures are hydraulic apertures that may be quite different from average geometric apertures, and (2) the estimates for other units are based on 1-D borehole data and 2-D mapping data used to approximate 3-D fracture networks (BSC 2004 [DIRS 170038], Section 6.1.3.1).

The uncertainty in the fracture porosities is addressed by the sampling of the parameter to derive the apertures.

Retardation of dissolved radionuclides associated with sorption onto fracture surfaces is not simulated in the TSPA-LA Model. Therefore, fracture retardation factors are set to 1.0 to conservatively minimize travel times to the SZ (SNL 2008 [DIRS 184748], Section 6.5.8).

For irreversible colloids, colloid sizes and matrix pore sizes are used in FEHM to determine filtration of irreversible colloids at interfaces between rock matrix units. At the start of each FEHM simulation, each potential particle is assigned a size based on sampling from a colloid size distribution. The uncertainty in colloid size is represented by a CDF, shown in Table 6.3.9-8 (SNL 2008 [DIRS 184748], Section 6.5.11). During particle tracking, when a particle in the rock matrix moves to the matrix of another unit, the size of each particle is compared to a randomly sampled value from a CDF for colloid transport at a matrix interface, which reflects the distribution of pore sizes of the matrix rock unit(s) (SNL 2008 [DIRS 184748], Section 6.5.9). If the particle size is larger than the sampled pore size, then the colloid does not enter the underlying rock matrix unit and is removed from the simulation or permanently filtered out. Table 6.3.9-9 lists the cumulative probability distributions for colloid transport at matrix interfaces for UZ transport in the various UZ rock units.

For the case in which colloids travel from fractures to the matrix via advection, an exclusion process may occur based on the matrix pore size. This colloid-exclusion process is implemented for irreversible colloids in the TSPA-LA Model through the use of an exclusion factor, f_c, based on the percentage of pores that are greater than the expected colloid size of 100 nm (SNL 2008 [DIRS 184748], Section 6.5.10). Each colloid particle has a chance of being excluded from entering the matrix based on a probability, equal to the fraction of matrix pores that are smaller than the expected colloid size. The colloid exclusion factors used in the TSPA-LA Model are presented in Table 6.3.9-10.

The sorption of radionuclides onto colloids may be either a reversible or an irreversible process. When the sorption process is irreversible, a very large number (10^{20}) is assigned to the colloid equilibrium sorption coefficient, K_c (SNL 2008 [DIRS 184748], Section 6.5.12). For reversible radionuclide sorption on the colloids, the K_c values are calculated by multiplying a radionuclide's sorption coefficient for a species onto a colloid, K_d, by the colloid concentrations in the water. Table 6.3.9-8 provides the CDF for colloid concentration (SNL 2008 [DIRS 184748], Section 6.5.12[a]).

Uncertainties associated with colloid sorption coefficients for various radionuclides are represented by a set of CDFs, as shown in Table 6.3.9-11. These colloid sorption coefficient distributions are consistent with those used in the EBS Transport Submodel and SZ Flow and Transport Submodel although sampled independently for each submodel (SNL 2008 [DIRS 184748], Section 6.5.12[a]). The colloid sorption coefficient distributions for americium, protactinium, and thorium are the same and are considered to be 100 percent correlated (sampled as one) in the UZ. Note that only the CDFs for smectite colloids are presented in Table 6.3.9-11. The use of smectite colloids in the UZ is consistent with the guidance presented in *Waste Form and In-Drift Colloids-Associated Radionuclide Concentrations: Abstraction and Summary* (SNL 2007 [DIRS 177423], Section 6.5.3).

A colloid retardation factor, R_{coll}, is used in the TSPA-LA Model to simulate the impact of reversible filtration of both the reversible and irreversible colloids in fractures. Because there is no information regarding colloid retardation factors in the UZ, the TSPA-LA Model uses the SZ output, which is deemed appropriate for use in the UZ (SNL 2008 [DIRS 184748], Section 6.5.13). Table 6.3.9-12 shows the CDF for colloid retardation factors used in the UZ Submodel. The CDF for colloid retardation factors, presented in Table 6.3.9-12, is consistent with the CDF for the colloidal retardation factor in volcanic units for the SZ, as presented in Table 6.3.10-2. There is also a fraction of colloids escaping retardation due to physical and chemical processes. In the TSPA-LA Model, this fraction is defined as a function of the residence time of the colloid. In this relationship, progressively fewer colloids migrate unretarded with time. Based on a combined UZ/SZ travel time of 100 years, the model uses a value of 0.00168 for the fraction of colloids migrating unretarded, as recommended in *Particle Tracking Model and Abstraction of Transport Processes* (SNL 2008 [DIRS 184748], Section 6.5.13). Colloids traveling unretarded are given a retardation factor of 1.0.

6.3.9.3 TSPA-LA Model Implementation

The TSPA-LA Model implementation of UZ transport calculations is primarily achieved through the use of the FEHM DLL. The UZ Transport Submodel is directly coupled (i.e., dynamically linked) with the TSPA-LA Model using an external pathway element within the GoldSim software (STN: 10344-9.60.100.00 [DIRS 181903]) to link with the UZ transport code, FEHM. The FEHM external pathway element is used to call the FEHM DLL, pass it a set of inputs, define the set of inflows from the EBS that the DLL will receive, and define the outflow cells to which the FEHM results will be sent.

The FEHM DLL receives inputs at run time both directly from GoldSim and from a set of external files. At run time, GoldSim passes direct inputs to FEHM, such as the flow field index (used to select the desired UZ flow field abstraction based on climate state and infiltration scenario), the number of radionuclides, and the number of source zones (i.e., percolation subregions). In addition, for each realization, a randomly selected initial random seed is passed from GoldSim to FEHM for use in FEHM's particle migration logic. Similarly, a second random seed is passed to FEHM for use in the logic that locates the release points associated with each failed WP. GoldSim also passes inputs from the EBS, such as the combined EBS releases for both WP types (from each of the five percolation subregions), the ratio of the EBS release applied to fractures to the total EBS release (which is used to apportion the released radionuclides between fracture and matrix nodes), and the total number of failed CSNF WPs and CDSP WPs in each repository subregion. The FEHM DLL receives new sets of inputs from GoldSim every realization and for time-dependent inputs every timestep in each realization.

FEHM must also read in a set of external files that provides many inputs including the control parameters, deterministic transport parameters, and values for all the stochastic transport parameters (see Appendix F for a detailed accounting of the files and their contents). Data provided from the external input files include: (1) the numerical grid structure; (2) rock properties, such as porosity and bulk density; (3) solute transport parameters, such as fracture apertures, matrix diffusion coefficients, matrix K_d values, colloid distribution parameters, colloid retardation factors, and AFM γs; and (4) the UZ flow fields. A complete list of these files can be found in Table F-2 of Appendix F of this report. One line of input comprised of fracture

apertures, AFM γ, matrix diffusion coefficients, matrix K_d values, colloid distribution parameters, and colloid retardation factors is read from an external file for each realization. Each TSPA-LA realization also uses one of four sets of UZ flow fields based on four infiltration scenarios (Sections 6.1.4.1 and 6.3.1). Each set has four flow fields: one each for present-day, monsoon, glacial-transition, and post-10,000-year climates (Section 6.3.1). The input flow fields for the present-day climate can be found in DTN: LB0612PDFEHMFF.001_R0 [DIRS 179296]. The input flow fields with raised water tables for the monsoon, glacial-transition, and post-10,000-year climates can be found in DTNs: LB0701MOFEHMFF.001_R0 [DIRS 179297]; LB0701GTFEHMFF.001 [DIRS 179160]; and LB0702PAFEM10K.002_R0 [DIRS 179507], respectively. When a climate change occurs, a new flow field is read in and the particles instantly travel with the updated water fluxes. In addition, when transition occurs from present-day to monsoon climate with a raised water table, mass associated with all particles located between the previous water table, and the new water table is released to the SZ Submodel during the timestep when the flow field change takes place.

The set of uncertain transport properties, consisting of matrix sorption coefficients, matrix diffusion coefficients, fracture apertures, AFM γs, colloid sorption coefficients, and colloid retardation factors (SNL 2008 [DIRS 184748], Sections 6.5.4, 6.5.5[a], 6.5.6[a], 6.5.7, 6.5.9, 6.5.10, 6.5.11, and 6.5.12[a]), is statistically sampled or generated from a set of statistically sampled parameters using GoldSim. During a supplemental simulation, the TSPA-LA Model is used to generate a set of external files containing these sampled parameters for FEHM. The set contains files sampled for 300 and 1,000 realizations. The TSPA-LA Model can then be run for simulations of 300 or 1,000 realizations. These files are used until there is a change in a parameter distribution or sampling seed, in which case a new set of files is generated. To use these files, the multiple species particle-tracking files contain placeholder indices identifying which of the variables in the external FEHM stochastic sample file belongs at the locations of the placeholder indices (Appendix F and Sections F.2.1.11 and F.2.1.13). Additionally, to ensure compatibility between the UZ and EBS Transport Submodels, matrix K_d values generated by the sampling elements in the TSPA-LA GoldSim Model are fed from these elements to the EBS for use in cell-networks representing the UZ immediately beneath the repository.

The matrix K_d values as generated in the process described above take their distributions from *Radionuclide Transport Models Under Ambient Conditions* (SNL 2007 [DIRS 177396], Table 6-1[a]). The K_d values are also correlated based on the similarities in the chemical dependencies of the sorption coefficients for the various radionuclides as discussed in *Radionuclide Transport Models Under Ambient Conditions* (SNL 2007 [DIRS 177396], Appendix B[a]). Starting with the correlation matrix defined by the similarities in the chemical dependencies of the sorption coefficients for the various radionuclide (DTN: LB0701PAKDSESN.001_R0 [DIRS 179299], *Sorption Correlation Table.xls*), a subset containing only a single representative (basis) species for each subset of 100 percent correlated species is developed. Such a subset or non-singular correlation matrix is presented in *Radionuclide Transport Models Under Ambient Conditions* (SNL 2007 [DIRS 177396], Appendix B[a], Table B-2[a]). Note that in the TSPA-LA analysis, the correlation matrix presented in *Radionuclide Transport Models Under Ambient Conditions* (SNL 2007 [DIRS 177396], Appendix B[a], Table B-2[a]) is redefined as two separate non-singular correlation matrices. The use of two matrices is based on the non-correlation of uranium and selenium to any of the other species. Therefore, the TSPA-LA model utilizes a 10 by 10

non-singular correlation matrix for all species except uranium and selenium, and a 2 by 2 non-singular correlation matrix for uranium and selenium. The method used in the TSPA-LA Model to induce correlations is the Cholesky factorization method (SNL 2007 [DIRS 177396], Appendix B[a]).

The basic correlation procedure used is as follows. The *m* (rows) by *m* (columns) matrix, **C**, is the target rank correlation to be imposed. Note that in the TSPA-LA model, two **C** matrices, one 10 by 10 and one 2 by 2, are evaluated. For each non-singular correlation matrix and associated species, which is 100 percent correlated with any of the basis species, the procedure used in the TSPA-LA model is as follows:

1. Compute by Cholesky factorization (Press et al. 1992 [DIRS 103316], Section 2.9), the m by *m* lower triangular matrix, **P**, such that $\mathbf{P}\mathbf{P}^{T} = \mathbf{C}$ (Tables 6.3.9-13 and 6.3.9-14, respectively)

2. Create **z**, a vector of length, *m*, consisting of independent standard normal values

3. Compute the vector, **x**, of length, *m*, such that **x** = **Pz**. Note $\mathbf{x} \sim N(0,\mathbf{C})$

4. Compute the result sample vector, **u**, such that $\mathbf{u}_i = \mathbf{F}_i^{-1}(\mathbf{\Phi}(x_i))$, for the *m* different variables, i = 1,…, *m*,. where $\mathbf{F}_i(x)$ are the marginal CDFs for each of the *m* variables and $\mathbf{\Phi}(x)$ is the standard normal CDF.

The resultant vector, **u**, has a rank correlation structure that approximates **C**. The sample vector **w** for the species not chosen as basis species can then be generated as $\mathbf{w}_{ij} = \mathbf{F}_i^{-1}(\mathbf{\Phi}(x_j))$, where j is the index denoting the basis species with which the species i is 100 percent correlated. The two lower triangular matrices used in the TSPA-LA Model can be found in (Output DTN: MO0707UZKDCORR.000 [DIRS 183003], radio_020807a.xmcd, and radio_020807a_SE_U.xmcd).

Within FEHM, the matrix K_d values are used in conjunction with bulk density, matrix porosity, and matrix saturation values to derive the retardation factor used to determine the effective transport rate for sorbing species. The retardation factor, *R*, can be defined as

$$R = 1 + \frac{\rho_{bulk} K_d}{\phi_{matrix} S_{matrix}} \qquad \text{(Eq. 6.3.9-4)}$$

where

ρ_{bulk} = the bulk density (g/mL)

K_d = the rock matrix sorption coefficient (mL/g)

ϕ_{matrix} = the rock matrix porosity (-)

S_{matrix} = the rock matrix saturation (-).

The values of bulk density and matrix porosity used in the TSPA-LA Model are presented in *Particle Tracking Model and Abstraction of Transport Processes* (SNL 2008 [DIRS 184748],

Section 6.5.3[a]). The rock matrix saturations, used by FEHM to derive the matrix retardation factors, are read from the appropriate input flow-field files (based on the sampled infiltration scenario) and are updated during the simulation to account for present-day, monsoon, glacial-transition, and post-10,000-year climates (DTNs: LB0612PDFEHMFF.001_R0 [DIRS 179296]; LB0701MOFEHMFF.001_R0 [DIRS 179297]; LB0701GTFEHMFF.001_R0 [DIRS 179160]; and LB0702PAFEM10K.002_R0 [DIRS 179507]).

Radionuclide mobilization and transport through the EBS are calculated during each TSPA-LA Model simulation, and the radionuclide mass flux at the EBS boundary at each timestep is provided as the boundary condition for UZ transport (Section 6.3.8). The UZ Transport Submodel then provides radionuclide mass fluxes at the water table, for each timestep, as the boundary condition for SZ transport (Section 6.3.10). The elevation of the water table changes instantaneously when a climate change occurs. Any change in the water table level redefines the release points for mass leaving the UZ. In addition, as previously noted, any radionuclides between the old water table and the updated water table at the time the water table elevation changes are immediately removed from the UZ Transport Submodel and are provided as input to the SZ Flow and Transport Model Component (SNL 2008 [DIRS 184748], Section 6.4.8).

Releases from the EBS are computed for each environmental group: dripping and non-dripping CSNF WPs, dripping and non-dripping CDSP WPs, and each selected early-failed WP group, including CSNF-Zircaloy, CSNF-stainless steel, and CDSP WPs, in each repository percolation subregion. As described in Section 6.3.8 of the EBS Transport Submodel, radionuclide releases from the EBS enter both the fracture and matrix continua of the UZ Transport Submodel. Radionuclide releases from each of the five repository percolation subregions are modeled using a random release model that accounts for early failed WPs and temporally and spatially variable radionuclide releases (SNL 2008 [DIRS 184748], Section 6.4.7). This random release model avoids spreading out radionuclide releases artificially by taking into account the number of WPs that have failed within each of the five subregions. If only one WP has failed in a subregion, the releases for that subregion are put into a single numerical grid node that is randomly sampled from the nodes in that subregion. If two WPs have failed, releases are put into two randomly selected nodes. This process continues for additional WPs until the number of failed WPs is equal to the number of nodes in the subregion. The nodes are randomly selected without replacement. After the number of failed WPs exceeds the number of nodes in a subregion, later releases are evenly spread over all nodes in the subregion, and additional WP failures cause no change to the release locations (SNL 2008 [DIRS 184748], Section 6.4.7).

The process used to assign repository radionuclide release nodes to each of the five repository percolation subregions accounted for in the FEHM zone2 file is described in DTN: LA0702PANS02BR.001_R1 [DIRS 180322] and *Particle Tracking Model and Abstraction of Transport Processes* (SNL 2008 [DIRS 184748], Section 6.5.15[a]). Note that only the first three climate states were considered in the analysis used to find a single zone file with five sets of source nodes that best represent all the infiltration/climate combinations. The repository-release nodes comprising each of the five repository percolation subregions were chosen based on the cumulative probability of percolation for the 12 flow fields (three different climate periods: present-day, monsoon, and glacial-transition; each climate period is categorized with 4 infiltration scenarios: 10 percent, 30 percent, 50 percent, and 90 percent). A 4-step binning process was applied to each of the twelve flow fields, resulting in a list of repository

release nodes divided into 5 percolation subregions (bins) that share common infiltration ranges, based on the cumulative probability intervals for these bins (SNL 2008 [DIRS 184748], Section 6.5.15[a]). The cumulative probability intervals for these five bins of percolation rates sorted in ascending order are 0.0-0.05, 0.05-0.30, 0.30-0.70, 0.70-0.95, and 0.95-1.00 (SNL 2008 [DIRS 184748], Section 6.5.15a). An analysis of the degree of similarity or difference of the results of the binning process, depending on which flow field is considered, was performed. The results indicated that the bins for the 12 flow fields are quite similar to one another. As noted in *Particle Tracking Model and Abstraction of Transport Processes* (SNL (2008 [DIRS 184748], Section 6.5.15[a]), if a bin is identified for a particular node in the glacial-transition, 10th percentile flow field, it is very often identified as the same bin for the other flow fields. When they are different, they almost always differ by only one bin; that is, a 3 in one flow field becomes a 4 in another flow field or a 2 becomes a 1. Based upon this result, it was considered acceptable to use bins from one flow field to approximate all infiltration scenarios and climate states. Therefore, for the compliance model, the file fehmn.zone2_GT10% (based on the 10th percentile infiltration scenario for the glacial transition climate) from the DTN is used to define the bins for all simulations, including the post-10,000-year climate. Figure 6.3.9-6 shows the locations of the FEHM repository release nodes, colored by percolation bin for the glacial-transition, 10th-percentile flow field.

The fraction of irreversible colloids traveling through the UZ unretarded is determined before releasing colloids from the EBS (Section 6.3.8). After they are released into the UZ, the fraction of unretarded colloids remains unchanged. Based on a conservative estimate for transport time in the natural system (UZ and SZ) of 100 years (SNL 2008 [DIRS 184748], Section 6.5.13 and Table 6-23), the fraction of unretarded colloids leaving the EBS is estimated to be 0.00168. This value is used in all TSPA-LA Model realizations and is referred to as the fast fraction in the implementation of the EBS Colloids Transport Submodel. Since the transport time through the UZ and SZ of the fast fraction of colloids is uncertain, and the fast fraction model is also uncertain, a conservative approach is taken for implementing the fast fraction of colloids (BSC 2004 [DIRS 170006], Section 6.6). The approach is conservative because it is highly unlikely that any TSPA-LA Model realization will have a combined UZ-SZ transport time of less than 100 years (BSC 2004 [DIRS 170006], Section 6.6).

To account for arrival locations and reduce artificial spreading in releases to the SZ, all nodes at or below the water table of the UZ Transport Submodel are grouped into four collecting bins (equivalent to SZ source regions), as shown on Figure 6.3.10-6. Radionuclide mass reaching the water table in one location may have a different SZ travel path and transport time than mass arriving at some other location. To reduce the effects of artificial dilution at the interfaces between TSPA-LA Model submodels, the total radionuclide mass flow rate in each of these four source regions is focused at a random point within each of the four source regions in the SZ Flow and Transport Model Component.

The random release point in each of the four UZ Transport Submodel (Figure 6.3.10-6) collecting bins is a function of sampling during each realization. The four UZ collecting bins are named 701, 702, 703, and 704 in FEHM, corresponding to the SZ source inflow regions 1, 2, 3, and 4, respectively (SNL 2008 [DIRS 184748], Section 6.5.16).

The four FEHM UZ collecting bins (Figure 6.3.10-6) are as follows (SNL 2008 [DIRS 184748], Section 6.5.16):

- Collecting bin 701 contains all nodes with a Universal Transverse Mercator (UTM) grid easting coordinate less than 548500 m (Nevada State Plane [NSP]: 171189.79 m) and a UTM northing coordinate greater than 4078630 m (NSP: 233459.87 m).

- Collecting bin 702 contains all nodes with a UTM easting coordinate greater than 548500 m (NSP: 171189.79 m) and a UTM northing coordinate greater than 4078630 m (NSP: 233459.87 m).

- Collecting bin 703 contains all nodes with a UTM easting coordinate less than 548500 m (NSP: 171189.79 m) and a UTM northing coordinate less than 4078630 m (NSP: 233459.87 m).

- Collecting bin 704 contains all nodes with a UTM easting coordinate greater than 548500 m (NSP: 171189.79 m) and a UTM northing coordinate less than 4078630 m (NSP: 233459.87 m).

The radionuclide mass release from FEHM is applied to four UZ collecting bins modeled using four GoldSim mixing cells. The mass outflows of the four cells are then fed to the SZ convolution integral model, SZ_Convolute (SZ_Convolute V3.10, STN: 10207-3.10-10 [DIRS 181060]), at each TSPA-LA Model timestep. The release rates are also integrated over time using GoldSim integrator elements for use as input to the alternative SZ one-dimensional pipe element model (SNL 2008 [DIRS 183750], Section 6.5.1.2).

6.3.9.4 Model Component Consistency and Conservatism in Assumptions and Parameters

To enhance understanding of the complex interactions within the TSPA-LA Model, a discussion of consistency among model components and submodels and the identification of conservative assumptions in abstractions, process models, and parameter sets supporting the UZ Transport Submodel is presented below.

6.3.9.4.1 Consistency of Assumptions

UZ Transport Properties—The UZ Transport Submodel uses different material properties than those used to develop the UZ flow fields. In the UZ Transport Submodel, fracture frequency and fracture porosity, which are used to derive fracture apertures, are sampled for every realization for nine different rock groups (SNL 2008 [DIRS 184748], Table 6-13). However, in developing the 16 different UZ flow fields that are used in the UZ transport calculations, fracture frequency and fracture porosity were held constant. The AFM γ values are calibrated values in the UZ Flow Submodel calculations. Although calibrated, the flow model is relatively insensitive to this parameter. To the contrary, during transport modeling when subject to matrix diffusion γ represents a parameter to which the system is sensitive. For this reason, γ is sampled from a distribution that is based both on the flow model calibrated values and field test-based values. Thus, fracture frequency, fracture porosity, and AFM γ values used to derive UZ transport

processes may differ between the UZ Transport Submodel and the UZ Flow Fields Abstraction (Section 6.3.1).

Effect on TSPA-LA Results—Pairs of randomly sampled fracture porosity and fracture frequency values are used to generate fracture apertures for the fracture-matrix interface submodel of the UZ Transport Submodel. By using the sampled values, uncertainty in the fracture-matrix diffusion process in the model is considered. Note that the fracture porosity values used to define the advective transport process in the particle tracking are the same values used in the flow model. Random sampling of the AFM γ in the UZ Transport Submodel also allows for consideration of uncertainty in the fracture-matrix diffusion process. This is important because the fracture-matrix diffusion process is sensitive to AFM γ. Since the sampled values range between 0.2 and 0.6 (SNL 2008 [DIRS 184748], Section 6.5.6[a]) and the calibrated flow values are 0.4 or less (SNL 2007 [DIRS 184614], Appendix B), the TSPA-LA Model will allow for faster transport in some realizations while better representing the uncertainty in the parameter. These and other transport parameters, along with their uncertainties as used in the UZ Transport Submodel, are discussed and justified in *Particle Tracking Model and Abstraction of Transport Processes* (SNL 2008 [DIRS 184748], Sections 6.5 and 6.5[a]). Therefore, even though the material properties may be different among respective submodels, separate sampling is necessary to adequately propagate uncertainty in mass transport under steady-state flow conditions.

UZ Mass Release to the SZ—The particles leaving the UZ at the water table are assigned to one of four collecting bins that are defined by four quadrants (NE, NW, SE, SW) (see Sections 6.3.9.3 and Figure 6.3.10-6). For a specific zone and water-table configuration, when a particle reaches a node that is considered an exit node, it becomes inactive in the UZ model, and its assigned mass is added to the spatially appropriate collecting bin. The four source terms defined by the collecting bins are then used as source terms for the four SZ source regions (NE, NW, SE, SW). The breakthrough curves used in the SZ-Convolute algorithm are based on a randomly sampled release location within each source region. The release zone assignment process is described in *Particle Tracking Model and Abstraction of Transport Processes* (SNL 2008 [DIRS 184748], Section 6.5.16).

Effect on TSPA-LA Results—Release of the mass for each SZ source region to a randomly selected location within the region during a single realization will focus the mass release. A point source of radionuclides is appropriate for release from a single WP or for considering the influence of groundwater flow focusing along a fault or single fracture. A more diffuse release of radionuclides at the water table may be more physically appropriate for later times when more numerous WPs are leaking and flow focusing does not occur. The use of a point source will overestimate the concentration of the radionuclides near the source (SNL 2008 [DIRS 183750], Section 6.5.2.13).

6.3.9.4.2 Identification of Conservatisms in Submodels and Abstractions

Climate Change—Climate changes can be considered in an approximate way by imparting an instantaneous jump from one steady-state flow field to another with a corresponding instantaneous rise in the water table (SNL 2008 [DIRS 184748], Section 6.4.8). This approximation is considered conservative because it instantaneously shortens the time it takes for

mass to reach the SZ. The method instantaneously increases the flow velocities due to the change in climate and shortens the pathway to the SZ due to the rising of the water table. In addition, all mass between the original water table and the updated water table is immediately applied to the SZ (SNL 2008 [DIRS 184748], Section 5, Assumption 6). This conservatism is a logical approach, given the uncertainties associated with temporal delays in reaching the more rapid transport conditions and the inability to observe the process directly (SNL 2008 [DIRS 184748], Section 5, Assumption 6).

This conservatism tends to shorten radionuclide transport times (SNL 2008 [DIRS 184748], Section 6.4.8).

Fixed Water Table Rise—To approximate the effects of a rising water table on a radionuclide transport simulated by the finite element heat and mass (FEHM) transfer code (FEHM V2.24-01, STN: 10086-2.24-01-00 [DIRS 179419]), the external monsoon climate, glacial-transition, and post-10,000-year climate flow field files used in the transport model are post-processed. In the UZ flow model area, the present-day water table varies from less than 730 m to greater than 980 m above mean sea level (BSC 2004 [DIRS 169855] Figure 6.2). Within the repository footprint, the present-day water table varies from around 730 m to 850 m above mean sea level (BSC 2004 [DIRS 169855] Figure 6.2). Note that the bottom boundary for the flow models of all climate states is the present day water table. For use in conjunction with FEHM's multi-species particle tracking model the flow-field files for the monsoon, glacial-transition, and post-10,000-year climate flow fields from the UZ Flow Model Abstraction are post-processed to approximate the affects of a rising water table. The rising water table is approximated by constraining the water table to a minimum elevation of 850 m above mean sea level (SNL 2008 [DIRS 184748] Section 6.4.8). That is for future climates, at any locations where the present-day water table is below 850 m the water table is set to 850 m and at any locations where the present-day water table is above 850 m, the water table is not adjusted from the present day level (see BSC 2004 [DIRS 169855]). The rise in the water table of up to 120 m is assumed to occur immediately following the change from present-day to monsoon climate, instantly reducing the flow path of radionuclides in the UZ by up to 120 m. However, there could be a significant period of water table adjustment associated with transition to a wetter climate. After the water table is raised to a minimum of 850 m above sea level, it is assumed to remain at that level for the duration of the simulation period; there is no change to the water table elevation assumed between the monsoon and glacial-transition climates. This conservatism is evaluated as part of the PMA documented in Appendix C.

Sorption on Fractures—Sorption of radionuclides on fracture surfaces is neglected in the UZ Transport Submodel because sufficient data are not available to consider the process (SNL 2008 [DIRS 184748], Section 6.5.8). This assumption eliminates retardation of radionuclides within the fractures and results in shorter radionuclide transport times (SNL 2008 [DIRS 184748], Section 6.5.8).

Unretarded Colloid Fraction—Unretarded fraction of irreversible colloids used in the UZ model is based on a 100-year transport time. Travel time is uncertain through both the UZ and SZ, but it is unlikely that any TSPA realization will have a combined UZ-SZ travel time of less than 100 years (BSC 2004 [DIRS 170006], Section 6.6).

This assumption results in an increase in the unretarded colloidal fraction, rapidly increasing the mass that reaches the SZ (BSC 2004 [DIRS 170006], Section 6.6; and SNL 2008 [DIRS 184748], Section 6.5.13).

Isothermal Transport Conditions in the UZ—UZ transport occurs at isothermal 25°C conditions. Increased temperature would result in increased diffusion from the fractures into the matrix (SNL 2007 [DIRS 177396], Section 6.1.2.9). However, to simplify the modeling approach, higher temperatures from decay heat and the geothermal gradient are conservatively ignored. Additionally, increased temperature leads to increased sorption of cationic species and decreased sorption of anionic species (SNL 2007 [DIRS 177396], Section 6.1.2.9). Conclusions of the K_d temperature dependence study presented in *Radionuclide Transport Models under Ambient Conditions* (SNL 2007 [DIRS 177396], Section I) indicate that for various radionuclides a small positive increase in K_d with temperature is seen. Therefore, neglecting temperature dependence as suggested in *Radionuclide Transport Models under Ambient Conditions* (SNL 2007 [DIRS 177396]) would conservatively decrease travel time to the SZ.

This assumption results in a reduction of matrix diffusion at early times and a shortening of radionuclide transport times (SNL 2007 [DIRS 177396], Section 6.1.2.9).

No Drift Shadow Effects—No drift shadow effects from flow diversion around the waste emplacement drift are included in the UZ Transport Model Component. Capillary diversion, even under ambient conditions, may result in low fracture saturation below the drift. Reductions in fracture saturations below the drift would delay diffusive radionuclide transport from the EBS.

Ignoring drift shadow effects is a conservative assumption that will result in faster mass release to the UZ (SNL 2008 [DIRS 184748], Section 6.7).

Effects of Perched Water Zones—Effects of perched water low permeability zones are implicit to the UZ flow fields used in the UZ Transport Submodel. Although perched water indicates areas of lower permeability, which can delay and dilute radionuclide concentration and result in a reduced advective transport of radionuclides from the UZ (DTN: MO0706SPAFEPLA.001 [DIRS 181613]), another impact of the perched (and zeolitic) zone in the TSPA-LA Model is to create a lateral diversion of water into the faults and downward to the water table (SNL 2007 [DIRS 184614], Section 8.6).

The lateral diversion of water around perched zones and into faults may result in shorter transport times to the UZ.

6.3.9.5 Alternative Conceptual Model(s) for Unsaturated Zone Transport

Section 6.2 outlines the general consideration and treatment of ACMs used to support the TSPA-LA Model. A brief description of the UZ Transport Submodel ACMs is summarized in Table 6.3.9-15. A detailed discussion of these ACMs can be found in *Particle Tracking Model and Abstraction of Transport Processes* (SNL 2008 [DIRS 184748], Section 6.7).

Discretization of the UZ Matrix (DFM and MINC Models)—Discrete Fracture Models and Multiple Interacting Continua (MINC) models of UZ fracture/matrix interaction represent ACMs. A set of transfer functions obtained using a Discrete Fracture Model with fine

discretization in the matrix has been developed to allow FEHM's multi-species particle-tracking model to capture sharp concentration gradients. In this Discrete Fracture Model abstraction of the fracture/matrix interaction, the more accurate depiction of the concentration gradients between the fracture and the matrix represents an ACM, which is also more consistent with a MINC formulation (SNL 2008 [DIRS 184748], Section 7.2.2 and Section 7.2.2[a]). Note that the FEHM multi-species particle-tracking model using the Discrete Fracture Model transfer functions still uses the dual-permeability (dual-k) flow fields, while the MINC formulation, as described in *Particle Tracking Model and Abstraction of Transport Processes* (SNL 2008 [DIRS 184748]), differs in the flow regimes. Simulations performed using Discrete Fracture Model and MINC models are shown to result in later breakthrough times than the Dual-k Model (SNL 2008 [DIRS 184748], Section 7.2.2 and Section 7.2.2[a]). A comparison of Discrete Fracture Model and MINC model results showed that the MINC model predicts even later breakthrough times than the Discrete Fracture Model (SNL 2008 [DIRS 184748], Section 7.2.2 and Section 7.2.2[a]). Presently, a Multiple Interacting Continua formulation is not directly used in the TSPA because of its large computational burden.

To evaluate the impact on the dose calculations associated with the use of the Discrete Fracture Model ACM, the sensitivity of the model simulations to the choice of matrix diffusion models was examined in a simulation using the Discrete Fracture Model transfer functions described in *Particle Tracking Model and Abstraction of Transport Processes* (SNL 2008 [DIRS 184748], Section 6.8.2[a]). The ACM impact evaluation is described in *Particle Tracking Model and Abstraction of Transport Processes* (SNL 2008 [DIRS 184748], Section 7.2.3.2[a]).

Alternate Finite Difference Numerical Models—The UZ Transport Submodel used FEHM particle tracking. Alternate finite difference numerical models include EOS9nT, T2R3D, and DCPT particle tracking. Two of these models provide a basis for modeling coupled flow and transport of single (T2R3D) or multiple radionuclides (EOS9nT). They were used primarily to provide validated models of UZ transport processes that form the basis for the abstraction models used in the TSPA-LA Model. The computationally intensive nature of these models limits the finite difference ACMs use for multiple realizations that can provide uncertainty estimates. The FEHM Particle Tracking Transport Abstraction Model can reproduce the results predicted by dual-k models by using transfer functions developed using a dual-k formulation (SNL 2008 [DIRS 184748], Sections 7.2.2[a] and 7.2.3.1[a]).

Lateral Flow Diversion in UZ above the Repository—Lateral flow in the PTn will divert percolating water to the faults and reduce the percolation flux at the repository. The original base case model, which shows more lateral flow occurring within the PTn than the ACM, was chosen due to better predictions of chloride and moisture data (SNL 2007 [DIRS 184614], Section 6.9.2). It was also generally more conservative with respect to reducing radionuclide transport times to the SZ (SNL 2007 [DIRS 184614], Section 6.9.2). The updated base case model predicts significant diversion and redistribution into faults for the PTn (SNL 2007 [DIRS 184614], Section 8.6).

No Radionuclide Release into Faults—The fault zones are defined as high permeability zones subject to fast advective transport to the top of the TSw and to the water table. The effects of not allowing direct release of radionuclides into the fault zones on the overall transport to the water

table are not significant because lateral diversion directs the radionuclides into the fault zones (SNL 2007 [DIRS 177396], Section 6.20.2).

Inclusion of Drift Shadow Effects—Inclusion of drift shadow effects would approximate the influence of capillary diversion that may cause low fracture saturation below the drift. It is considered conservative to ignore drift shadow effects and associated faster mass release to the UZ (SNL 2008 [DIRS 184748], Section 6.7). Additionally, the increase of infiltration associated with later climate states may decrease the effects (SNL 2008 [DIRS 184748], Section 6.7).

Inclusion of TH, THC, and Thermal-Hydrologic-Mechanical Effects on UZ Flow and Transport—Vaporization due to repository heat will keep the drift dry for several hundred to a few thousand years. TH, THC, and thermal-hydrologic-mechanical effects may alter flow and transport properties of the UZ rocks. TH, THC, and thermal-hydrologic-mechanical effects are insignificant after the change to glacial-transition climate, the period when most radionuclide transport would take place (SNL 2008 [DIRS 184748], Section 6.7). Additional conclusions with respect to TH, THC, and thermal-hydrologic-mechanical effects on UZ Flow and Transport presented in *Mountain-Scale Coupled Processes (TH/THC/THM)* include: (1) mountain-scale TH will have a large impact on fluid flow near the repository at early times but insignificant impact on UZ flow fields (BSC 2005 [DIRS 174101], Section 8.1); (2) changes in water chemistry, mineralogy, and hydrologic properties in the ambient temperature regions are minimal over the 7,000 years the THC model was simulated (BSC 2005 [DIRS 174101], Section 8.2); and (3) thermal-hydrologic-mechanical induced changes in mountain-scale hydrologic properties have no significant impact on vertical percolation through the repository horizon (BSC 2005 [DIRS 174101], Section 8.3).

Alternative Fracture Model—The TSPA-LA Model utilizes the active fracture model (Liu et al. 1998 [DIRS 105729]), which takes into consideration flow focusing and the associated reduction in fracture/matrix interaction. The active fracture model, with its reduced effective area of diffusion between fracture and matrix, is used in the TSPA-LA Model because of its more conservative nature in reducing fracture to matrix diffusion, which retards radionuclide transport and its ability to explain travel times associated with ^{14}C test data (SNL 2008 [DIRS 184748], Section 5, Assumption 1, and BSC 2004 [DIRS 170035], Section 7.4.1). An alternative fracture model would use the standard methodology, which does not consider a reduced fracture-matrix interface area. Using the standard methodology would enhance diffusion between the fracture and matrix. Because the active fracture model is more conservative and has better reflected field test results, the standard methodology was not recommended for inclusion in the TSPA-LA Model.

No ACMs were recommended for inclusion in the TSPA-LA Model.

INTENTIONALLY LEFT BLANK

Table 6.3.9-1. Radionuclide Half-Life and Daughter Products Used in the TSPA-LA Model

No.	Species	Half Life (years)	Daughter Index
1	^{14}C	5.715×10^{3}	NA
2	^{135}Cs (rev)	2.3×10^{6}	NA
3	^{137}Cs (rev)	3.007×10^{1}	NA
4	^{129}I	1.57×10^{7}	NA
5	^{90}Sr	2.878×10^{1}	NA
6	^{99}Tc	2.13×10^{5}	NA
7	^{243}Am (rev)	7.37×10^{3}	10
8	^{243}Am (Ic)	7.37×10^{3}	11
9	^{243}Am (If)	7.37×10^{3}	12
10	^{239}Pu (rev)	2.410×10^{4}	13
11	^{239}Pu (Ic)	2.410×10^{4}	13
12	^{239}Pu (If)	2.410×10^{4}	13
13	^{235}U	7.04×10^{8}	14
14	^{231}Pa (rev)	3.28×10^{4}	NA
15	^{241}Am (rev)	4.327×10^{2}	18
16	^{241}Am (Ic)	4.327×10^{2}	18
17	^{241}Am (If)	4.327×10^{2}	18
18	^{237}Np	2.14×10^{6}	19
19	^{233}U	1.592×10^{5}	20
20	^{229}Th (rev)	7.3×10^{3}	NA
21	^{240}Pu (rev)	6.56×10^{3}	24
22	^{240}Pu (Ic)	6.56×10^{3}	24
23	^{240}Pu (If)	6.56×10^{3}	24
24	^{236}U	2.342×10^{7}	25
25	^{232}Th (rev)	1.40×10^{10}	NA
26	^{232}U	6.98×10^{1}	NA
27	^{242}Pu (rev)	3.75×10^{5}	33
28	^{242}Pu(Ic)	3.75×10^{5}	33
29	^{242}Pu (If)	3.75×10^{5}	33
30	^{238}Pu (rev)	8.77×10^{1}	34
31	^{238}Pu(Ic)	8.77×10^{1}	34
32	^{238}Pu (If)	8.77×10^{1}	34
33	^{238}U	4.47×10^{9}	34
34	^{234}U	2.46×10^{5}	35
35	^{230}Th (rev)	7.54×10^{4}	36

Table 6.3.9-1. Radionuclide Half-Life and Daughter Products Used in the TSPA-LA Model (Continued)

No.	Species	Half Life (years)	Daughter Index
36	^{226}Ra	$1.599x10^{3}$	NA
37	^{36}Cl	$3.01x10^{5}$	NA
38	^{79}Se	$2.95x10^{5}$	NA
39	^{126}Sn (rev)	$2.50x10^{5}$	NA

Sources: SNL 2008 [DIRS 184748], Table 6-25 [a].

Reference for Half-Lives: Parrington et al. 1996 [DIRS 103896] for all radionuclides except ^{79}Se, which comes from Singh 2002 [DIRS 164741].

Table 6.3.9-2. Matrix Sorption Coefficient Distributions for Unsaturated Zone Units in the Unsaturated Zone Transport Submodel

Parameter Name in TSPA-LA Model	Description	Distribution Type	Coefficients Describing Distribution (K_d: mL/g)
KdU_Zeo_a	K_d of Uranium in Zeolitic Tuff	Cumulative	(K_d value, probability) (0, 0) (0.5, 0.5) (30, 1.0)
KdU_Devit_a	K_d of Uranium in Devitrified Tuff	Cumulative	(K_d value, probability) (0, 0) (0.2, 0.5) (4, 1.0)
KdU_Vit_a	K_d of Uranium in Vitric Tuff	Cumulative	(K_d value, probability) (0, 0) (0.2, 0.5) (3, 1.0)
KdNp_Zeo_a	K_d of Neptunium in Zeolitic Tuff	Cumulative	(K_d value, probability) (0, 0) (0.5, 0.5) (6, 1.0)
KdNp_Devit_a	K_d of Neptunium in Devitrified Tuff	Cumulative	(K_d value, probability) (0, 0) (0.5, 0.5) (6, 1.0)
KdNp_Vit_a	K_d of Neptunium in Vitric Tuff	Cumulative	(K_d value, probability) (0, 0) (1.0, 0.5) (3, 1.0)
KdPu_Zeo_a	K_d of Plutonium in Zeolitic Tuff	Cumulative	(K_d value, probability) (10, 0) (100, 0.5) (200, 1.0)
KdPu_Devit_a	K_d of Plutonium in Devitrified Tuff	Cumulative	(K_d value, probability) (10, 0) (70, 0.5) (200, 1.0)
KdPu_Vit_a	K_d of Plutonium in Vitric Tuff	Cumulative	(K_d value, probability) (10, 0) (100, 0.5) (200, 1.0)
KdAm_Zeo_a	K_d of Americium in Zeolitic Tuff	Truncated Normal	Range = 1,000 – 10,000; μ = 5,500, σ = 1,500
KdAm_Devit_a	K_d of Americium in Devitrified Tuff	Truncated Normal	Range = 1,000 – 10,000; μ = 5,500, σ = 1,500
KdAm_Vit_a	K_d of Americium in Vitric Tuff	Cumulative	(K_d value, probability) (100, 0) (400, 0.5) (1,000, 1.0)
KdPa_Zeo_a	K_d of Protactinium in Zeolitic Tuff	Truncated Normal	Range = 1,000 – 10,000; μ = 5,500, σ = 1,500
KdPa_Devit_a	K_d of Protactinium in Devitrified Tuff	Truncated Normal	Range = 1,000 – 10,000; μ = 5,500, σ = 1,500
KdPa_Vit_a	K_d of Protactinium in Vitric Tuff	Truncated Normal	Range = 1,000 – 10,000; μ = 5,500, σ = 1,500
KdCs_Zeo_a	K_d of Cesium in Zeolitic Tuff	Cumulative	(K_d value, probability) (425, 0) (5,000, 0.5) (20,000, 1.0)
KdCs_Devit_a	K_d of Cesium in Devitrified Tuff	Uniform	Minimum = 1 Maximum = 15
KdCs_Vit_a	K_d of Cesium in Vitric Tuff	Cumulative	(K_d value, probability) (0, 0) (2, 0.5) (100, 1.0)
KdSr_Zeo_a	K_d of Strontium in Zeolitic Tuff	Uniform	Minimum = 50 Maximum = 2,000
KdSr_Devit_a	K_d of Strontium in Devitrified Tuff	Uniform	Minimum = 10 Maximum = 70
KdSr_Vit_a	K_d of Strontium in Vitric Tuff	Uniform	Minimum = 0 Maximum = 50
KdRa_Zeo_a	K_d of Radium in Zeolitic Tuff	Uniform	Minimum = 1,000 Maximum = 5,000
KdRa_Devit_a	K_d of Radium in Devitrified Tuff	Uniform	Minimum = 100 Maximum = 1,000
KdRa_Vit_a	K_d of Radium in Vitric Tuff	Uniform	Minimum = 50 Maximum = 600
KdTh_Zeo_a	K_d of Thorium in Zeolitic Tuff	Uniform	Minimum = 1,000 Maximum = 30,000
KdTh_Devit_a	K_d of Thorium in Devitrified Tuff	Uniform	Minimum = 1,000 Maximum = 10,000

Table 6.3.9-2. Matrix Sorption Coefficient Distributions for Unsaturated Zone Units in the Unsaturated Zone Transport Submodel (Continued)

Parameter Name in TSPA-LA Model	Description	Distribution Type	Coefficients Describing Distribution (K_d: mL/g)
KdTh_Vit_a	K_d of Thorium in Vitric Tuff	Uniform	Minimum = 1,000 Maximum = 10,000
KdSe_Zeo_a	K_d of Selenium in Zeolitic Tuff	Truncated Log-Normal	Mean = 14.3 Standard deviation = 7.9 Minimum = 1.0 Maximum = 35.0
KdSe_Devit_a	K_d of Selenium in Devitrified Tuff	Truncated Log-Normal	Mean = 14.0 Standard deviation = 11.2 Minimum = 1.0 Maximum = 50.0
KdSe_Vit_a	K_d of Selenium in Vitric Tuff	Truncated Log-Normal	Mean = 8.6 Standard deviation = 7.9 Minimum = 0.0 Maximum = 25.0
KdSn_Zeo_a	K_d of Tin in Zeolitic Tuff	Log-Uniform	Minimum = 100.0 Maximum = 5,000.0
KdSn_Devit_a	K_d of Tin in Devitrified Tuff	Log-Uniform	Minimum = 100.0 Maximum = 100,000.0
KdSn_Vit_a	K_d of Tin in Vitric Tuff	Log-Uniform	Minimum = 100.0 Maximum = 5,000.0

Sources: DTN: LA0408AM831341.001_R0 [DIRS 171584]

DTN: LB0701PAKDSESN.001_R0 [DIRS 179299], *Readme.pdf*, Table 3-1.

NOTES: Se is set to zero for rock in the TSw.

All non-sorbing species utilize a Kd of 0.0 mL/g in the TSPA-LA Model (SNL 2007 [DIRS 184748], Table 8.2).

The parameter names given here are those from the TSPA-LA Model and more detail on these source inputs can be found in Table K3-3.

Table 6.3.9-3. Species Dependent Free Water Diffusivities Used to Calculate the Effective Matrix Diffusion Coefficients for Unsaturated Zone Transport

Parameter Name in TSPA-LA Model	Description	Distribution Type	Coefficients Describing Distribution
Am_Dfw	Americium free water diffusivity (m^2/s)	Constant	9.49E-10
C_Dfw	Carbon free water diffusivity (m^2/s)	Constant	1.18E-09
Cl_Dfw	Chlorine free water diffusivity (m^2/s)	Constant	2.03E-09
Cs_Dfw	Cesium free water diffusivity (m^2/s)	Constant	2.06E-09
I_Dfw	Iodine free water diffusivity (m^2/s)	Constant	2.05E-09
Np_Dfw	Neptunium free water diffusivity (m^2/s)	Constant	6.18E-10
Pa_Dfw	Protactium free water diffusivity (m^2/s)	Constant	6.04E-10
Pu_Dfw	Plutonium free water diffusivity (m^2/s)	Constant	1.30E-09
Ra_Dfw	Radium free water diffusivity (m^2/s)	Constant	8.89E-10
Se_Dfw	Selenium free water diffusivity (m^2/s)	Constant	1.04E-09
Sn_Dfw	Tin free water diffusivity (m^2/s)	Constant	1.55E-09
Sr_Dfw	Strontium free water diffusivity (m^2/s)	Constant	7.91E-10
Tc_Dfw	Technicium free water diffusivity (m^2/s)	Constant	1.95E-09
Th_Dfw	Thorium free water diffusivity (m^2/s)	Constant	5.97E-10
U_Dfw	Uranium free water diffusivity (m^2/s)	Constant	6.64E-10

Source: DTN: LB0702PAUZMTDF.001_R1 [DIRS 180776], *Free-Water Diffusion Coefficients.xls*

Table 6.3.9-4. Parameter Distributions for Tortuosities Used to Calculate the Effective Matrix Diffusion Coefficients for Unsaturated Zone Transport

Parameter Name in TSPA-LA Model	Description	Parameters (in Log10) Describing Distribution
UZDC_Mean_RG1	Log mean tortuosity for rock units: ch1z, ch6v, pp3, pp2, bf2/tr2	-1.15
UZDC_SD_RG1	Log standard deviation of tortuosity for rock units: ch1z, ch6v, pp3, pp2, bf2/tr2	0.29
UZDC_Mean_RG2	Log mean tortuosity for rock units: tsw33, tsw39z, tsw39v, ch1v, ch[2-5]z, ch[2-5]v, ch6z, pp4, bf3/tr3, pcM1z, pcM[2,5]z, pcM6z, M	-1.57
UZDC_SD_RG2	Log standard deviation of tortuosity for rock units: tsw33, tsw39z, tsw39v, ch1v, ch[2-5]z, ch[2-5]v, ch6z, pp4, bf3/tr3, pcM1z, pcM2,5]z, pcM6z, pcM4p	0.29
UZDC_Mean_RG3	Log mean tortuosity for rock units: tsw34, tsw35, tsw3[6,7], tsw38, pp1, pcM38, pcM39	-1.84
UZDC_SD_RG3	Log standard deviation of tortuosity for rock units: : tsw34, tsw35, tsw3[6,7], tsw38, pp1, pcM38, pcM39	0.29

Source: DTN: LB0702PAUZMTDF.001_R1 [DIRS 180776], *Readme.pdf*, Table 2-5.
See also SNL 2008 [DIRS 184748], Tables 6.5.5-1 and Section 6.5.5.4.

NOTE: The Log10 values are rounded off to two decimal places that could give slightly different mean values than the antilogs.

Table 6.3.9-5. Fracture γ Parameter Distribution for all Rock in the Unsaturated Zone Transport

Parameter Name in TSPA-LA Model	Description	Distribution Type	Lower-Bound Infiltration	Upper-Bound Infiltration
GAMMA_AFM_a	Fracture γ for all rock units	Uniform	0.2	0.6

Source: DTN: LA0701PANS02BR.003_R2 [DIRS 180497], *Readme.doc*.

NOTE : A detailed description for this input can be found in Table K3-3.

Table 6.3.9-6. Parameter Distributions for Fracture Porosity for Unsaturated Zone Transport

Parameter Name in TSPA-LA Model	Description	Distribution Type	Coefficients Describing Distribution
Por_group1_a	Porosity for chnFf rock unit	Beta	Mean = 1.0E-03 Standard deviation = 3.09E-04 Minimum = 0 Maximum = 1
Por_group2_a	Porosity for tswFf rock unit	Beta	Mean = 2.5E-02 Standard deviation = 7.25E-03 Minimum = 0 Maximum = 1
Por_group3_a	Porosity for rock units: ch[2, 5]Fz/ pcF[2,5]z, ch[3,4]Fz, pp4Fz/pcf4p, pp1Fz, bf2Fz, tr2Fz	Beta	Mean = 3.7E-04 Standard deviation = 1.09E-04 Minimum = 0 Maximum = 1
Por_group4_a	Porosity for rock units: pp3Fd, pp2Fd, bf3Fd, tr3Fd	Beta	Mean = 9.7E-04 Standard deviation = 2.85E-04 Minimum = 0 Maximum = 1
Por_group5_a	Porosity for rock units: ch1Fz/pcF1z, ch6Fz/pcF6z	Beta	Mean = 1.6E-04 Standard deviation = 4.71E-05 Minimum = 0 Maximum = 1
Por_group6_a	Porosity for rock units: ch[1,2,3,4,5,6]Fv	Beta	Mean = 6.9E-04 Standard deviation = 2.03E-04 Minimum = 0 Maximum = 1
Por_group7_a	Porosity for rock units: tswFv, tswFz/pcF39 (tswF9)	Beta	Mean = 4.3E-03 Standard deviation = 1.26E-03 Minimum = 0 Maximum = 1
Por_group8_a	Porosity for rock units: tswF[4,5], tswF[6,7], tswF8/pcF38	Beta	Mean = 1.05E-02 Standard deviation = 3.10E-03 Minimum = 0 Maximum = 1
Por_group9_a	Porosity for tswF3 rock unit	Beta	Mean = 5.8E-03 Standard deviation = 1.71E-03 Minimum = 0 Maximum = 1

Source: DTN: LA0701PANS02BR.003_R2 [DIRS 180497], *Table 1.doc*.

Table 6.3.9-7. Parameter Distributions for Fracture Frequency for Unsaturated Zone Transport

Parameter Name in TSPA-LA Model	Description	Distribution Type	Coefficients Describing Distribution
ff_group1_a	Fracture frequency [1/m] for chnFf rock unit	Log normal	Mean ln *f* = -2.33E00 Standard deviation ln *f* = 7.24E-01
ff_group2_a	Fracture frequency [1/m] for tswFf rock unit	Log normal	Mean ln *f* = 2.96E-01 Standard deviation ln *f* = 7.24E-01
ff_group3_a	Fracture frequency [1/m] for rock units: ch[2, 5]Fz/ pcF[2,5]z, ch[3,4]Fz, pp4Fz/pcf4p, pp1Fz, bf2Fz, tr2Fz	Log normal	Mean ln *f* = -2.23E00 Standard deviation ln *f* = 7.24E-01
ff_group4_a	Fracture frequency [1/m] for rock units: pp3Fd, pp2Fd, bf3Fd, tr3Fd	Log normal	Mean ln *f* = -1.87E00 Standard deviation ln *f* = 7.24E-01
ff_group5_a	Fracture frequency [1/m] for rock units: ch1Fz/pcF1z, ch6Fz/pcF6z	Log normal	Mean ln *f* = -3.48E00 Standard deviation ln *f* = 7.24E-01
ff_group6_a	Fracture frequency [1/m] for rock units: ch[1,2,3,4,5,6]Fv	Log normal	Mean ln *f* = -2.38E00 Standard deviation ln *f* = 7.24E-01
ff_group7_a	Fracture frequency [1/m] for rock units:tswFv, tswFz/pcF39 (tswF9)	Log normal	Mean ln *f* = -3.03E-01 Standard deviation log *f* = 7.24E-01
ff_group8_a	Fracture frequency [1/m] for rock units: tswF[4,5], tswF[6,7], tswF8/pcF38	Log normal	Mean ln *f* = 1.12E00 Standard deviation ln *f* = 7.24E-01
ff_group9_a	Fracture frequency [1/m] for tswF3 rock unit	Log normal	Mean ln *f* = -6.92E-01 Standard deviation ln *f* = 9.81E-01

Source: DTN: LA0701PANS02BR.003_R2 [DIRS 180497], *Table 1.doc*.

Table 6.3.9-8. Colloid Size and Concentration Distributions for Unsaturated Zone Transport

Parameter Name in TSPA-LA Model	Description	Distribution Type	Coefficients Describing Distribution
PART_SIZE[a, b]	Colloid size [nm] distribution data for use in simulating colloid filtration effect at matrix interface	Cumulative	(Colloid size, probability): (450, 1.0) (200, 0.8) (100, 0.6) (50, 0.4) (6, 0.2) (1, 0)
Colloidal_Concentration_uz_a[c]	Colloid concentration [mg/L] when ionic strength is less than 0.05	Cumulative	(Colloid concentration, probability): (200, 1.0) (50, 0.98) (10, 0.9) (1.0, 0.75) (0.1, 0.5), (0.001, 0.0)

[a] This parameter has no formal name in the TSPA-LA Model because it is implemented directly in the FEHM UZ Particle Tracking Submodel.
[b] DTN: LA0701PANS02BR.003_R2 [DIRS 180497], *Table 4.doc* .
[c] DTN: LA0701PANS02BR.003_R2 [DIRS 180497], *Table 7.doc* .

Table 6.3.9-9. Cumulative Probability Distributions for Colloid Transport at Matrix Interfaces for Unsaturated Zone Transport

Parameter Name in TSPA-LA Model[a]	Description	Distribution Type	Coefficients Describing Distribution
ITFCPORSIZE	Effective pore size [nm] for rock units: TMN/TSW4	Cumulative	(Effective pore size, probability): (2,000, 1.0) (1,000, 0.92) (450, 0.87) (200, 0.81) (100, 0.71) (50, 0.55) (6, 0.31)
ITFCPORSIZE	Effective pore size [nm] for rock units: TLL/TSW5	Cumulative	(Effective pore size, probability): (2,000, 1.0) (1,000, 0.8) (450, 0.79) (200, 0.70) (100, 0.61) (50, 0.51) (6, 0.19)
ITFCPORSIZE	Effective pore size [nm] for rock units: TM2/TSW6	Cumulative	(Effective pore size, probability): (2,000, 1.0) (1,000, 0.94) (450, 0.9) (200, 0.82) (100, 0.65) (50, 0.51) (6, 0.21)
ITFCPORSIZE	Effective pore size [nm] for rock units: TM1/TSW7	Cumulative	(Effective pore size, probability): (2,000, 1.0) (1,000, 0.99) (450, 0.99) (200, 0.99) (100, 0.93) (50, 0.68) (6, 0.36)
ITFCPORSIZE	Effective pore size [nm] for rock units: PV3/TSW8	Cumulative	(Effective pore size, probability): (2,000, 1.0) (1,000, 0.98) (450, 0.96) (200, 0.94) (100, 0.90) (50, 0.89) (6, 0.68)
ITFCPORSIZE	Effective pore size [nm] for rock units: PV2/TSW9	Cumulative	(Effective pore size, probability): (2,000, 1.0) (1,000, 0.72) (450, 0.57) (200, 0.47) (100, 0.39) (50, 0.35) (6, 0.22)
ITFCPORSIZE	Effective pore size [nm] for rock units: BT1a/CH1	Cumulative	(Effective pore size, probability): (2,000, 1.0) (1,000, 0.91) (450, 0.89) (200, 0.87) (100, 0.85) (50, 0.83) (6, 0.53)
ITFCPORSIZE	Effective pore size [nm] for rock units: CHV	Cumulative	(Effective pore size, probability): (2,000, 1.0) (1,000, 0.58) (450, 0.49) (200, 0.43) (100, 0.39) (50, 0.36) (6, 0.07)
ITFCPORSIZE	Effective pore size [nm] for rock units: CHZ	Cumulative	(Effective pore size, probability): (2,000, 1.0) (1,000, 0.79) (450, 0.76) (200, 0.73) (100, 0.68) (50, 0.56) (6, 0.3)
ITFCPORSIZE	Effective pore size [nm] for rock units: BT/CH6	Cumulative	(Effective pore size, probability): (2,000, 1.0) (1,000, 0.95) (450, 0.94) (200, 0.92) (100, 0.92) (50, 0.85) (6, 0.40)
ITFCPORSIZE	Effective pore size [nm] for rock units: PP1	Cumulative	(Effective pore size, probability): (2,000, 1.0) (1,000, 0.79) (450, 0.68) (200, 0.63) (100, 0.57) (50, 0.48) (6, 0.21)
ITFCPORSIZE	Effective pore size [nm] for rock units: PP2	Cumulative	(Effective pore size, probability): (2,000, 1.0) (1,000, 0.91) (450, 0.86) (200, 0.81) (100, 0.65) (50, 0.53) (6, 0.22)
ITFCPORSIZE	Effective pore size [nm] for rock units: PP3	Cumulative	(Effective pore size, probability): (2,000, 1.0) (1,000, 0.49) (450, 0.34) (200, 0.26) (100, 0.21) (50, 0.16) (6, 0.07)
ITFCPORSIZE	Effective pore size [nm] for rock units: PP4	Cumulative	(Effective pore size, probability): (2,000, 1.0) (1,000, 0.99) (450, 0.99) (200, 0.98) (100, 0.98) (50, 0.96) (6, 0.32)
ITFCPORSIZE	Effective pore size [nm] for rock units: BF2	Cumulative	(Effective pore size, probability): (2,000, 1.0) (1,000, 0.98) (450, 0.97) (200, 0.96) (100, 0.96) (50, 0.83) (6, 0.25)
ITFCPORSIZE	Effective pore size [nm] for rock units: BF3	Cumulative	(Effective pore size, probability): (2,000, 1.0) (1,000, 0.97) (450, 0.94) (200, 0.83) (100, 0.74) (50, 0.66) (6, 0.14)

Source: DTN: LA0701PANS02BR.003_R2 [DIRS 180497], *Table 2.doc*.

[a] These parameters are listed with one name in the TSPA-LA Model because they are implemented directly in the FEHM UZ Particle Tracking Submodel.

Table 6.3.9-10. Colloid Size Exclusion Factor Used in the Compliance Model

HGU (Group Numbers)	UZ Model Units (Entry Layer)	Size Exclusion Factor
TMN / TSW4	tswF4	0.29
TLL / TSW5	tswF5	0.39
TM2 / TSW6	tswF6	0.35
TM1 / TSW7	tswF7	0.07
PV3 / TSW8	tswF8/pcF38	0.10
PV2 / TSW9	tswFz, tswFv (tswF9) / pcF39	0.61
BT1a / CH1	ch1Fv, ch1Fz/pcF1z	0.15
CHV	ch[2,3,4,5]Fv	0.61
CHZ	ch[3,4]Fz, ch[2,5,6]Fz/pcF[2,5,6]z	0.27
BT / CH6	ch6Fv	0.08
PP4	pp4Fz/pcF4p	0.02
PP3	pp3Fd	0.79
PP2	pp2Fd	0.35
PP1	pp1Fz	0.43
BF3	bf3Fd, tr3Fd	0.26
BF2	bf2Fz, tr2Fz	0.04
	tswFf	0.29
	chnFf	0.27

Source: DTN: LA0701PANS02BR.003_R2 [DIRS 180497], *Table 3.doc*.

FEHM = finite element heat and mass (model)

HGU = Hydrogeologic Units or layers (SNL 2007 [DIRS 184614], Section 6.1); Correlation of HGU units and list of all UZ Model layers (FEHM zones) (SNL 2008 [DIRS 184748], Table 6-3).

Table 6.3.9-11. Radionuclide Sorption Coefficients onto Colloids for Unsaturated Zone Transport (revised groundwater colloid mass concentration parameters for TSPA-LA Model)

Parameter Name in TSPA-LA Model	Description	Distribution Type	K_d Value Intervals	K_d Value Interval Probability of Occurrence
Colloidal_Kd_Pu_uz_a	K_d [mL/g] of Plutonium on Smectite Colloid	Cumulative	1×10^3 to 5×10^3	0.45
			5×10^3 to 1×10^4	0.8
			1×10^4 to 5×10^4	0.95
			5×10^4 to 1×10^5	1.00
Colloidal_Kd_Am_uz_a	K_d [mL/g] of Americium on Smectite Colloid	Cumulative	1×10^4 to 5×10^4	0.07
			5×10^4 to 1×10^5	0.17
Colloidal_Kd_Th_uz_a	K_d [mL/g] of Thorium on Smectite Colloid		1×10^5 to 5×10^5	0.40
			5×10^5 to 1×10^6	0.60
Colloidal_Kd_Pa_uz_a	K_d [mL/g] of Protactinium on Smectite Colloid		1×10^6 to 5×10^6	0.92
			5×10^6 to 1×10^7	1.00
Colloidal_Kd_Cs_uz_a	K_d [mL/g] of Cesium on Smectite Colloid	Cumulative	5×10^1 to 1×10^2	0.05
			1×10^2 to 5×10^2	0.40
			5×10^2 to 1×10^3	0.70
			1×10^3 to 5×10^3	1.00
Colloidal_Kd_Sn_uz_a	K_d [mL/g] of Tin on Smectite Colloid	Log Uniform	1×10^5 to 1×10^6	NA

Source: SNL 2008 [DIRS 184748], Table 6-22[a].

Table 6.3.9-12. Colloid Retardation Factors (Colloidal_Retard_Factor_dist) for Unsaturated Zone Transport

Colloid Retardation Factor	Cumulative Probability	Input Description
6.00	0	The colloid retardation factor is used by FEHM in simulating the effects of colloid retardation in fractured rock on colloid-facilitated radionuclide transport.
6.00[a]	0.15	
10.23	0.25	
26.00	0.5	
59.98	0.8	
799.83[b]	1	

Source: DTN: LA0701PANS02BR.003_R2 [DIRS 180497], *Table 5.doc*.

[a] The value used in the TSPA-LA Model is 6.00000001. This change was implemented to coincide with the GoldSim requirement that cumulative probability functions are defined by monotonically increasing values.

[b] The source DTN: LA0303HV831352.002_R0 (for the TSPA-LA feed DTN [DIRS 180497]) presents the colloid retardation factor as 799.83 for a cumulative probability of 1.00 rather than rounded to 800 as presented in Table 5 [DIRS 180497].

Table 6.3.9-13. Lower Triangular Matrix for all Species Except Uranium and Selenium as Generated from the Correlation (Covariance) Matrix by Cholesky Factorization Using MathCad

Basic Species	Am_ devit	Cs_ devit	Cs_ zeo	Np_ devit	Pa_ devit	Pu_ devit	Ra_ zeo	Sn_ devit	Sr_ devit	Th_ devit
Am_devit	1	0	0	0	0	0	0	0	0	0
Cs_devit	0	1	0	0	0	0	0	0	0	0
Cs_zeo	0	0.1	0.995	0	0	0	0	0	0	0
Np_devit	0.25	0	0	0.968	0	0	0	0	0	0
Pa_devit	0.75	0	0	-0.194	0.632	0	0	0	0	0
Pu_devit	0.1	0	0.754	0.077	-0.095	0.638	0	0	0	0
Ra_zeo	0	0.1	0.492	0	0	0.202	0.841	0	0	0
Sn_devit	0.75	0	0	-0.09	0.269	0.09	-0.022	0.59	0	0
Sr_devit	0	0.25	0.075	0.516	0.158	-0.128	0.076	0.029	0.786	0
Th_devit	0	0	0	0.516	0.158	-0.039	0.009414	0.013	0.576	0.612

Source: Output DTN: MO0707UZKDCORR.000 [DIRS 183003], *radio_020807a.xmcd*.

Table 6.3.9-14. Lower Triangular Matrix for Uranium and Selenium as Generated from the Correlation (Covariance) Matrix by Cholesky Factorization Using MathCad

Basic Species	Se_devit	U_devit
Se_devit	1	0
U_devit	0.75	0.661

Source: Output DTN: MO0707UZKDCORR.000 [DIRS 183003], radio_020807a_SE_U.xmcd.

Table 6.3.9-15. Alternative Conceptual Models Considered for the Unsaturated Zone Transport Model

Alternative Conceptual Model	Key Assumptions	Screening Assessment and Basis
Discretization of the UZ Matrix (MINC Model)	The matrix is discretized to allow for a more accurate approximation of the concentration gradient at the matrix-fracture interface and within the matrix. Use of the Discrete Fracture Model or Multiple Interacting Continua (MINC) Model results in later breakthrough times than generated using the dual-k model. The breakthrough times of the Multiple Interacting Continua Model are later than those generated using the Discrete Fracture Model.	The dual-k model is conservative. The Multiple Interacting Continua Model is not used because of its large computational burden.
Alternative Finite Difference Numerical Models	An alternate method of approximating radionuclide transport in groundwater based upon approximating the governing equations using finite difference equations.	Although used for validation of the UZ Abstraction, large computational burden limits the utility of models such as T2R3D and EOS9nT.
Lateral Flow Diversion In UZ Above The Repository	Lateral flow in the PTn will divert percolating water to the faults and reduce the percolation flux at the repository.	The original base case model, which shows more lateral flow occurring within the PTn than the ACM, was chosen due to better predictions of chloride and moisture data (SNL 2007 [DIRS 184614], Section 6.9.2). It was also generally more conservative with respect to radionuclide transport. The updated base case model predicts significant diversion and redistribution into faults for the PTn (SNL 2007 [DIRS 177396], Section 6.20.2).
No Radionuclide Release Into Faults	The fault zones are defined as high permeability zones subject to fast advective transport to the top of the TSw and to the water table.	The effects of not allowing direct release of radionuclides into the fault zones, on the overall transport to the water table, are not significant because lateral diversion directs the radionuclides into the fault zones (SNL 2007 [DIRS 177396], Section 6.20.2).

Table 6.3.9-15. Alternative Conceptual Models Considered for the Unsaturated Zone Transport Model (Continued)

Alternative Conceptual Model	Key Assumptions	Screening Assessment and Basis
Inclusion of Drift Shadow Effects	Inclusion of drift shadow effects would approximate the influence of capillary diversion which may cause low fracture saturation below the drift.	It is considered conservative to ignore drift shadow effects. Additionally, the increased infiltration associated with later climate states may decrease the effects.
Perched Water Permeability Zones	Perched water may delay and dilute radionuclide concentration and reduce advective transport. Large scale lateral flow of water can also occur in perched water zones which can divert and redistribute flow into faults. Continuous well-connected fractures are used to model transport processes in the particle tracking method and the flow fields from the UZ Flow Submodel account for perched water effects.	Perched water may only be present in the northern part of the repository. Treating perched water in a manner such that well connected pathways exist is a conservative treatment.
Inclusion of TH, THC, and THM Effects on UZ Flow and Transport	Vaporization due to repository heat will keep the drift dry for several hundred to a few thousand years. THC and THM effects may alter flow and transport properties of the UZ rocks.	TH, THC, and THM effects are insignificant after the change to glacial-transition climate.
Alternative Fracture-Matrix Interaction Model	The TSPA-LA Model utilizes the Active Fracture Model (AFM) (Liu et al. 1998 [DIRS 105729]), which assumes that only a fraction of connected fractures are active in conducting water. The AFM is implemented by applying a fracture-matrix effective interface area reduction term or a fracture-matrix interface area adjustment factor and a fracture spacing adjustment factor. The ACM assumes that all connected fractures are active in conducting water and represents a standard methodology with no fracture-matrix effective interface area reduction term applied. The active fracture model, with its reduced effective area of diffusion between fracture and matrix, is used in the TSPA-LA Model because of its more conservative nature and its ability to explain travel times associated with ^{14}C data (SNL 2008 [DIRS 184748], Section 5, Assumption 1) and (BSC 2004 [DIRS 170035], Section 7.4.1).	Using the standard methodology would enhance diffusion between the fracture and matrix. Because the active fracture model is more conservative and has better reflected field test results, the standard methodology was not recommended for inclusion in the TSPA-LA Model.

Source: SNL 2008 [DIRS 184748], Table 6-30. Additional sources are noted within the text.

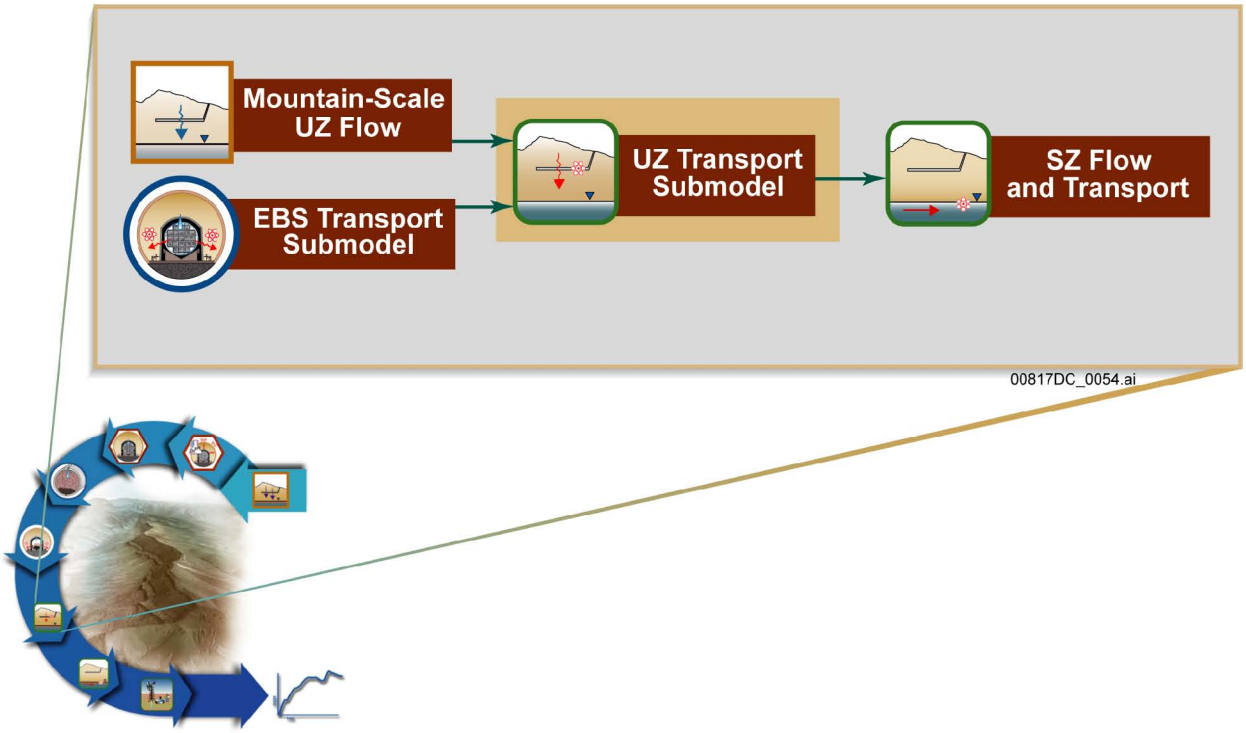

Figure 6.3.9-1. Information Flow Diagram for Unsaturated Zone Transport

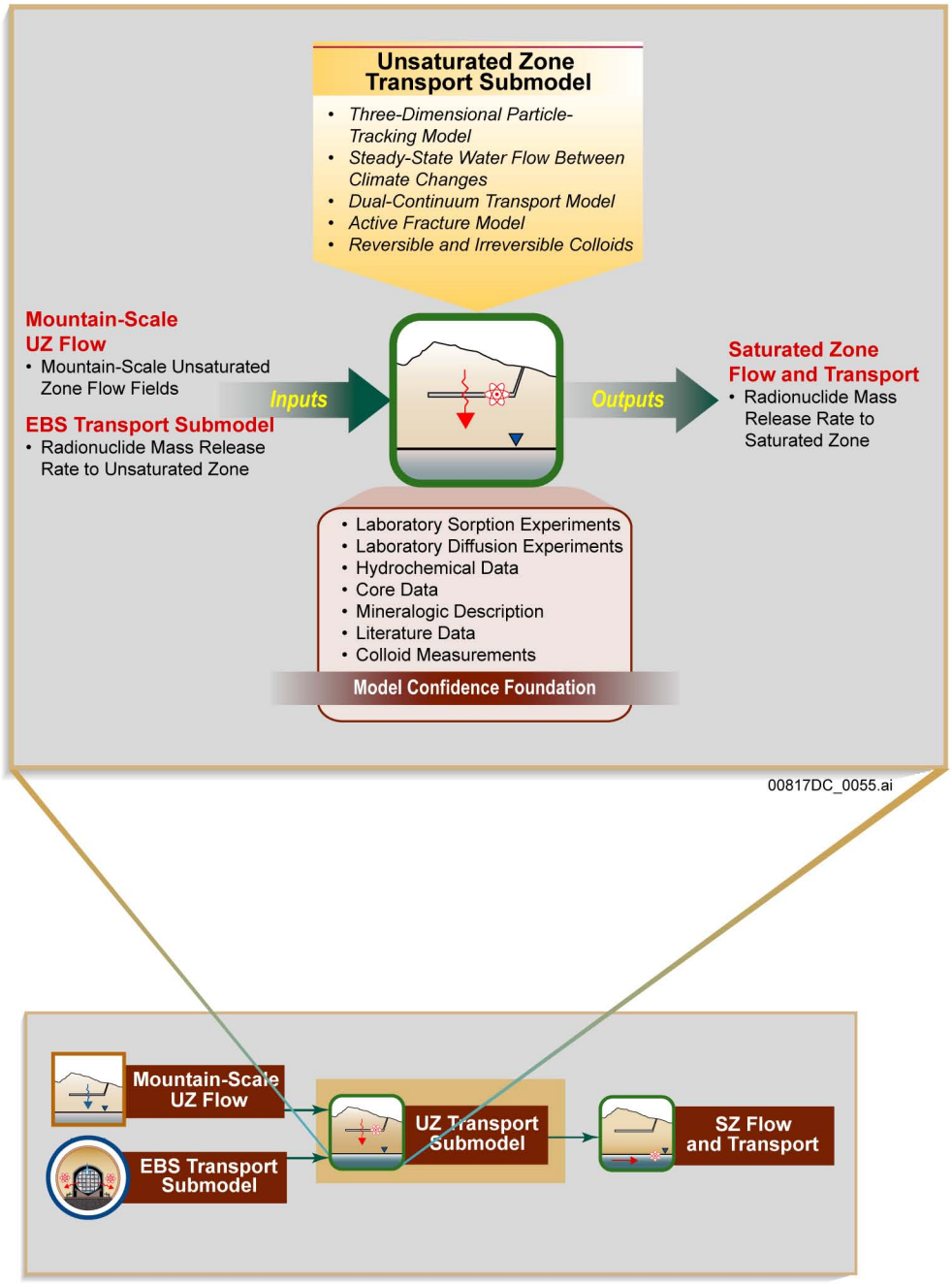

Figure 6.3.9-2. Inputs, Outputs, and Basis for Model Confidence for the Unsaturated Zone Transport Submodel

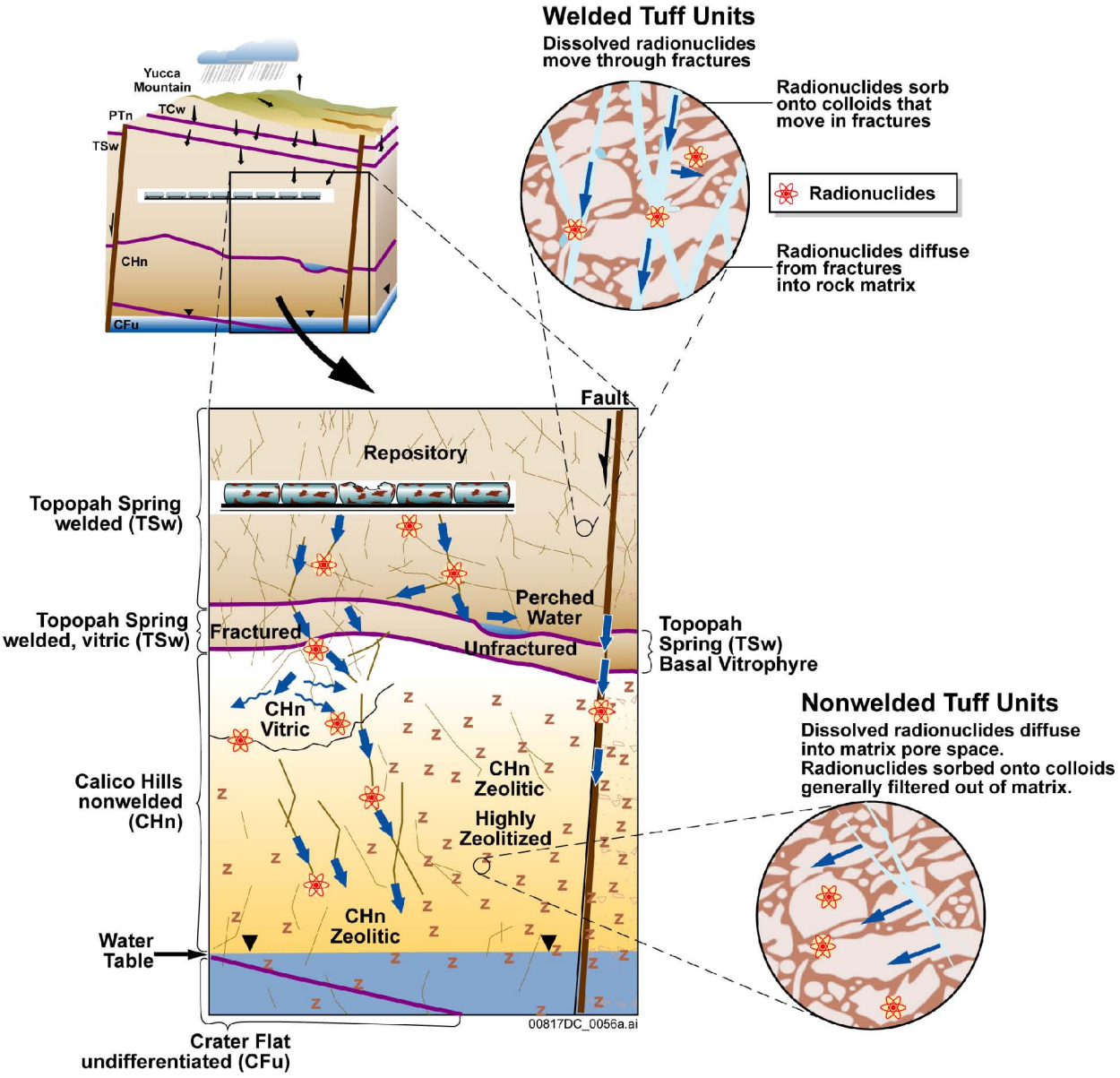

Figure 6.3.9-3. Conceptualization of Unsaturated Zone Transport Processes

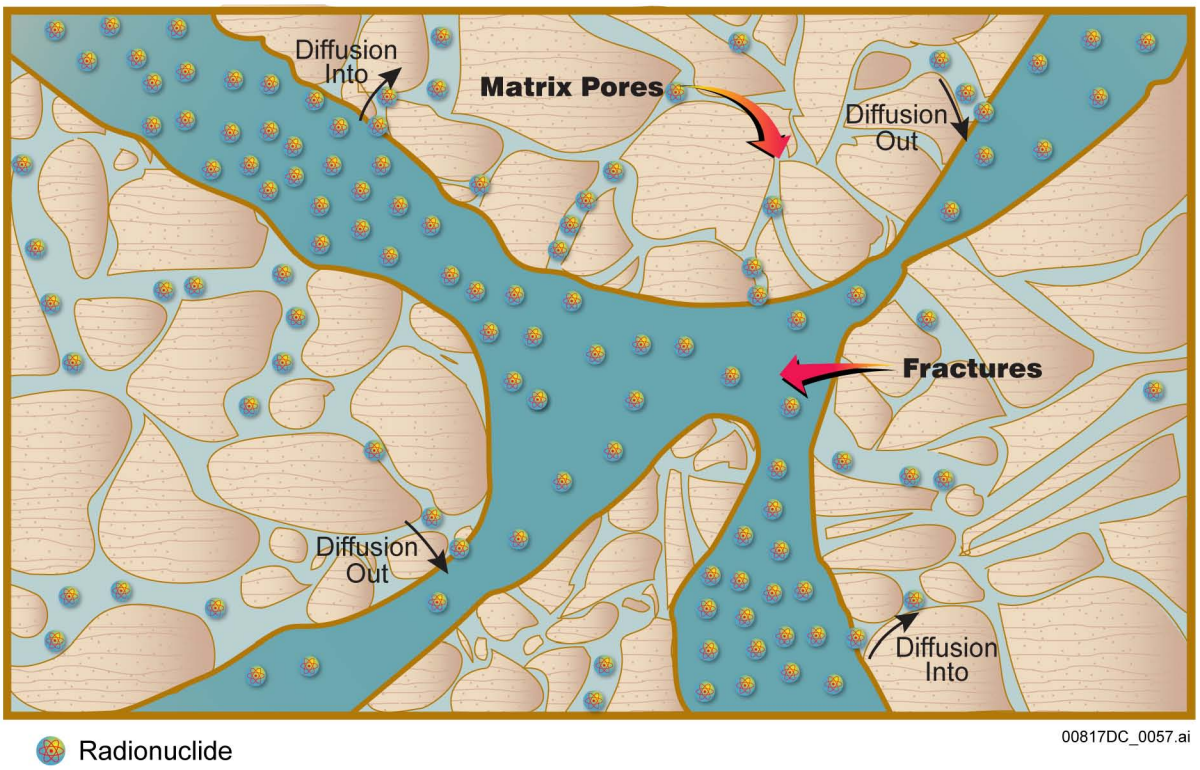

Figure 6.3.9-4. Illustration of Radionuclide Diffusion Into and Out of Matrix Pores

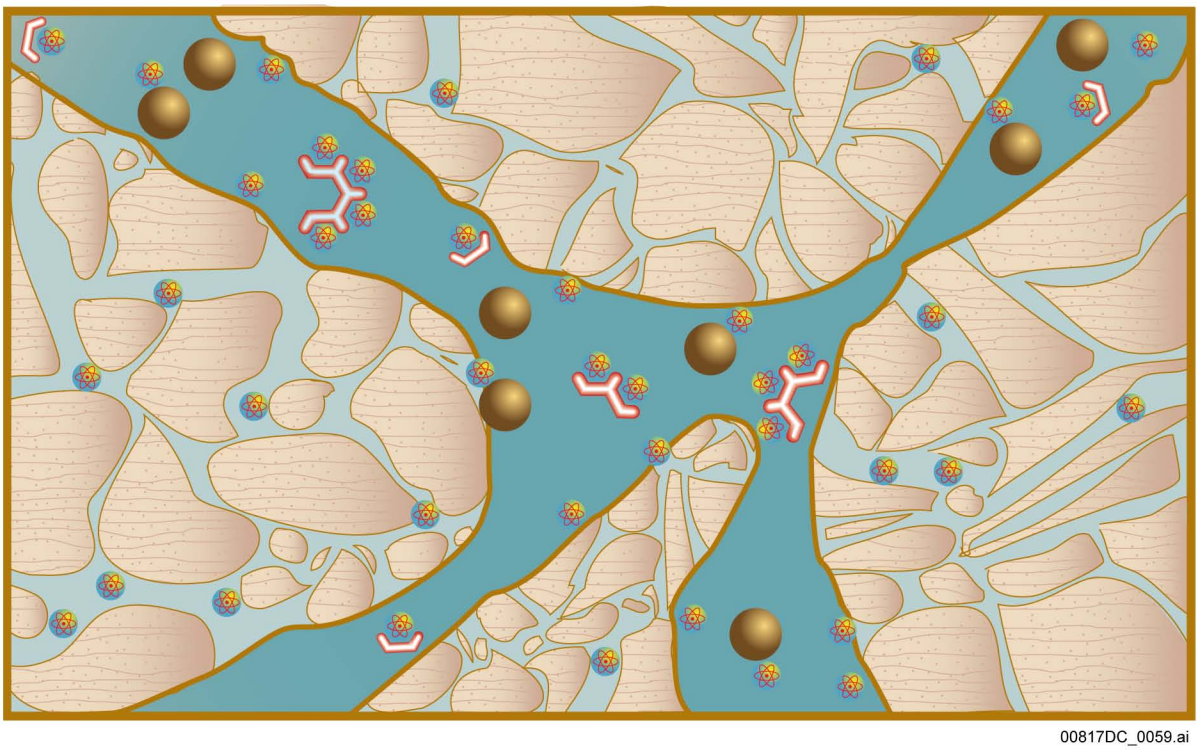

Figure 6.3.9-5. Illustration of Colloid-Facilitated Transport Processes

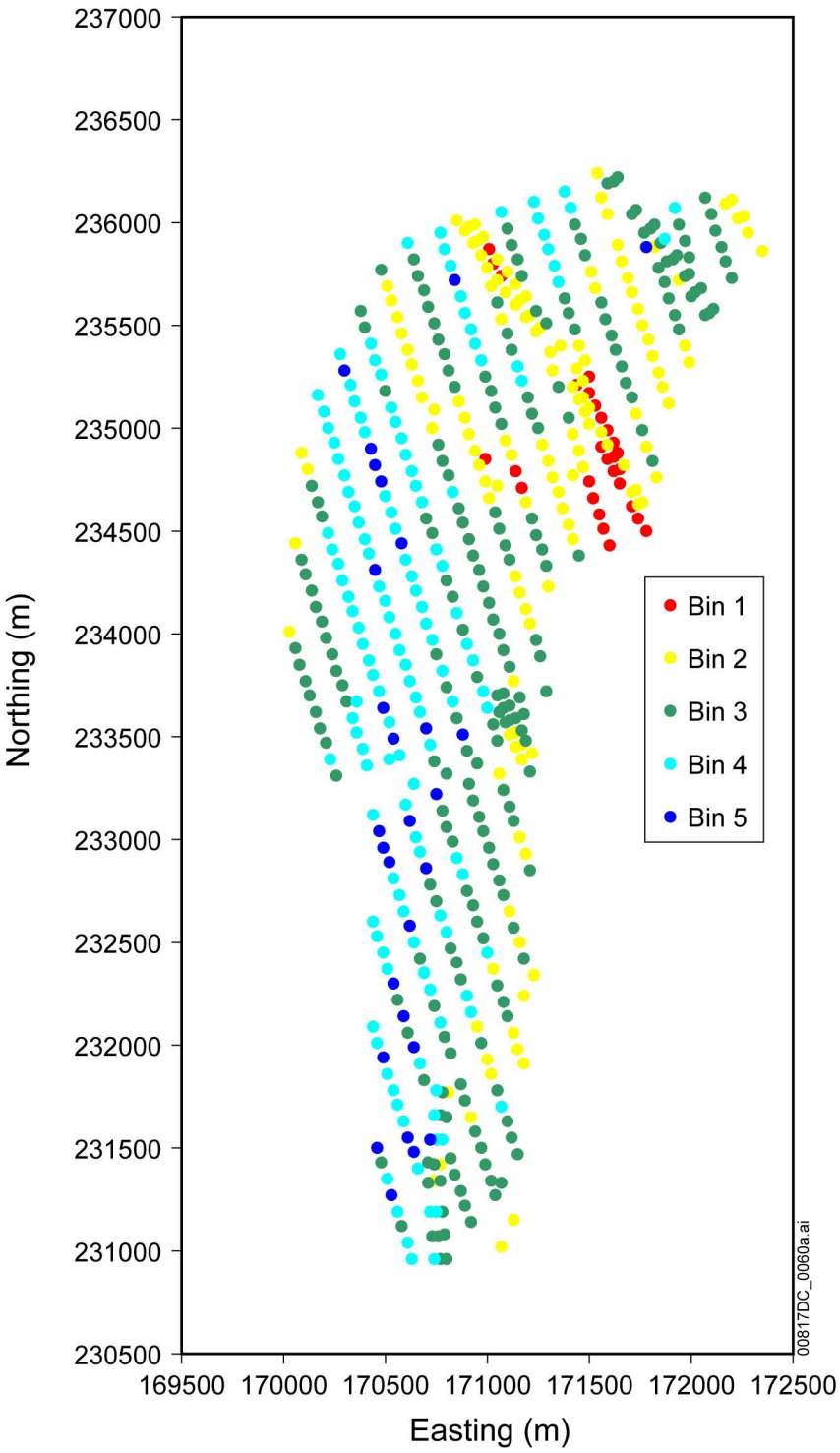

Source: DTN: LA0702PANS02BR.001_R1 [DIRS 180322], *fehm_repo_nodes_PD10%.xls*.

Figure 6.3.9-6. Location of Repository Release Nodes for Five Percolation Subregions

6.3.10 Saturated Zone Flow and Transport Model Component

The SZ Flow and Transport Model Component of the TSPA-LA Model (Table 6-1 and Figure 6-1) is used to evaluate the transport of radionuclides from their introduction at the water table to the accessible environment that is approximately 18 km downgradient from the repository. Figure 6.3.10-1 shows the relationship between the SZ Flow and Transport Model Component and other model components and submodels of the TSPA-LA Model. The UZ Transport Submodel provides the magnitude and distribution of radionuclide mass release rates to the SZ. Figure 6.3.10-2 summarizes the principal inputs and outputs, model features, and the foundations for confidence in the SZ Flow and Transport Model Component. The SZ Flow and Transport Model Component is linked to the Biosphere Model Component through the simulated time histories of radionuclide concentrations in groundwater at the boundary to the accessible environment. In the TSPA-LA Model analyses for different scenario classes and groundwater protection per 10 CFR 63.331 [DIRS 180319], radionuclide concentrations are calculated by including the mass of all radionuclides that reaches the accessible environment in any given annual period into 3,000 acre-feet of water, as specified in 10 CFR 63.312(c) [DIRS 180319].

6.3.10.1 Conceptual Model

Figure 6.3.10-3 provides a conceptual illustration of SZ flow and transport between Yucca Mountain and the biosphere, showing the relevant processes and geologic media in the SZ. The conceptual model of SZ flow includes southerly groundwater flow from recharge areas at higher elevations north of Yucca Mountain, through the Tertiary age volcanic rocks, and into the alluvium and other valley-fill deposits. For the SZ flow and transport abstraction used in the TSPA-LA Model (SNL 2008 [DIRS 183750]), groundwater flow between the repository and the biosphere is modeled using three-dimensional steady-state flow conditions. A continuum representation is used for the fracture network in the volcanic rocks beneath the repository, and the alluvium and valley-fill deposits are modeled as porous media. The model of the SZ flow system includes higher groundwater flux during potential wetter and cooler monsoon and glacial-transition climate states that are likely to occur within the 20,000-year and one-million-year modeling time periods.

Several processes are involved in the transport of radionuclides through the SZ. Advection in groundwater, dispersion, matrix diffusion in fractured media, sorption of radionuclides, colloid-facilitated transport, radioactive decay, and radioactive ingrowth are explicitly included in the TSPA-LA Model simulations. The processes are represented in the TSPA-LA Model as follows:

- **Advective transport**—This process occurs only within the fracture network of the volcanic hydrogeologic units due to the very high contrast in permeability between the fractures and the rock matrix but is widely distributed within the alluvium, except in low-permeability materials. This mode of transport is the primary mechanism for the transport of radionuclides from the SZ to the accessible environment. Climate change affects radionuclide transport by changing the rates of groundwater advection, which results from increased hydraulic gradient associated with the rise in the water table.

- **Dispersion of radionuclide mass**—This process, which includes hydrodynamic dispersion and molecular diffusion, occurs in both the fractured volcanic units and in the alluvium, with longitudinal dispersion typically much greater than transverse dispersion.

- **Matrix diffusion in fractured volcanic units**—This process determines the transfer of dissolved radionuclide mass from the flowing groundwater within fractures to the relatively stagnant groundwater contained in the pores of the rock matrix. The mass transfer, which could be in either direction, is a function of the concentration of the radionuclide in the fractures and matrix. The process of matrix diffusion of colloids is considered to be small and thus is not accounted for. The diffusion of colloids from fractures into the rock matrix is not included in the TSPA-LA Model.

- **Radionuclide sorption**—Sorption in fractured media occurs in the rock matrix only. In the alluvium, sorption occurs only in the effective porosity of the alluvium.

- **Colloid-facilitated transport**—This process can occur by two modes: (1) when radionuclides are reversibly sorbed onto colloids and (2) when radionuclides are irreversibly sorbed onto colloids. A large fraction of the colloids with irreversibly sorbed radionuclides undergoes reversible filtration during transport. Figure 6.3.10-4 illustrates the mechanisms involved in colloid-facilitated transport. Reversible filtration of irreversible colloids is represented by a retardation factor in the SZ Flow and Transport Model Component.

- **Radioactive decay and ingrowth**—Radioactive decay occurs for all radionuclides. Radionuclide ingrowth is represented for the daughter radionuclides in four principal decay chains.

Section 6.3.9.2 describes transport processes in the UZ. Two ACMs regarding groundwater flow and radionuclide transport in the SZ were considered in the development of the SZ Flow and Transport Model Component. These ACMs are discussed in Section 6.3.10.5.

6.3.10.2 TSPA-LA Model Abstraction

Two abstractions of the SZ Flow and Transport Model Component were implemented for the TSPA-LA Model:

- The 3-D SZ Flow and Transport Abstraction Model was developed outside of the TSPA-LA Model to calculate the flow and transport through the SZ to the accessible environment for individual radionuclides important to dose. The output from the 3-D SZ Flow and Transport Abstraction Model is developed in the form of unit-source radionuclide breakthrough curves (DTN: SN0702PASZFTMA.001_R0 [DIRS 179504]). Within the TSPA-LA Model, a convolution integral technique combines these radionuclide breakthrough curves with the time-varying radionuclide sources from the UZ to quantify radionuclide transport to the accessible environment. The convolution technique inherently assumes the system being simulated exhibits a linear response to the input function and a steady-state flow condition in the SZ. This approach was validated for the 3-D SZ Flow and Transport Abstraction, as documented

in *Saturated Zone Flow and Transport Model Abstraction* (SNL 2008 [DIRS 183750], Section 7.1.1[a]).

- The 1-D SZ Flow and Transport Abstraction is implemented directly in the TSPA-LA Model to calculate the radioactive decay, ingrowth, and transport for four decay chains. Although the decay products from these chains are not significant contributors to total dose, regulations for groundwater protection (contained in 10 CFR 63.331 [DIRS 180319]) require explicit analysis of their concentrations in the water supply of the critical group.

A brief summary of these two submodels is presented below.

3-D SZ Flow and Transport Abstraction—The three-dimensional SZ flow and transport process modeling, described in *Saturated Zone Site-Scale Flow Model* (SNL 2007 [DIRS 177391]) and *Site-Scale Saturated Zone Transport* (SNL 2007 [DIRS 177392]) forms the technical bases for the 3-D SZ Flow and Transport Abstraction, as implemented in the TSPA-LA Model. Figure 6.3.10-5 is a regional map showing the area of the SZ flow system, the direction of SZ flow, and an outline of the 3-D SZ Flow and Transport Process Model domain. The 3-D SZ Flow and Transport Abstraction is based on the 3-D SZ Flow and Transport Abstraction Model that uses a control-volume, finite-element method to model groundwater flow and a particle-tracking method to model SZ radionuclide transport. These methods, as implemented in FEHM V2.24-01 (FEHM V2.24-01, STN: 10086-2.24-01-00 [DIRS 179419]), simulate groundwater flow in fractured and porous media, as well as advection along groundwater streamlines, dispersion, retardation due to sorption, matrix diffusion, and colloid-facilitated transport. The groundwater flow boundary conditions for the 3-D SZ Flow and Transport Abstraction Model are specified heads at the lateral boundaries, a no-flow condition on the lower model boundary, and specified groundwater flux for recharge at the upper model boundary. These boundary conditions are described in detail in *Saturated Zone Site-Scale Flow Model* (SNL 2007 [DIRS 177391], Sections 6.3.1.6 and 6.3.1.7). The new percolation fluxes used in the UZ Flow Model were derived from the updated infiltration flux estimates documented in *Simulation of Net Infiltration for Present-Day and Potential Future Climates* (SNL 2007 [DIRS 182145]). However, the fluxes derived from the UZ Flow Model that are used in SZ Flow and Transport Model Abstraction (SNL 2008 [DIRS 183750]) are those of the previous UZ Flow Model. As discussed in *Saturated Zone Site-Scale Flow Model* (SNL 2007 [DIRS 177391], Section 6.4.3.9), the change in net infiltration through the UZ footprint is very small compared to the entire flow budget through the lateral boundaries.

The specified flux for recharge at the upper model boundary is scaled in proportion to an uncertainty in groundwater specific discharge that is represented by an uncertainty distribution (SNL 2008 [DIRS 183750], Table 6.7[a]). This parameter (groundwater specific discharge scaling factor) is a multiplier that is applied to all values of permeability, and values of specified recharge fluxes, in the 3-D SZ Flow and Transport Abstraction Model to effectively scale the simulated specific discharge in the model. Scaling the recharge flux and the values of permeability in proportion to the uncertainty in groundwater specific discharge maintains the calibration of the 3-D SZ Flow and Transport Abstraction Model with regard to water-level measurements (SNL 2008 [DIRS 183750], Section 6.5[a]). The uncertainty in groundwater specific discharge is applied to all of the climate states.

The sources of radionuclides entering the SZ are specified as point sources within each of the four source regions beneath the repository, as described in Section 6.3.9 (UZ Radionuclide Transport). Figure 6.3.10-6 shows the repository outline and the four SZ source regions used in the TSPA-LA Model. The horizontal location of the point source in each of the four source regions varies randomly from simulation to simulation. Source Regions 1 and 3 and part of Source Region 2 are primarily located directly below the repository to capture radionuclides transported vertically downward in the UZ Transport Submodel. Portions of Source Regions 2 and 4 are located to the east of the repository to capture radionuclides transported by the lateral diversion of groundwater to the east along dipping volcanic strata in the UZ. In addition, the northern part of Source Region 2 underlies a northeasterly extension of the repository. The random locations of the radionuclide source terms for each realization are defined by eight stochastic parameters (input names listed in the first column, last row of Table 6.3.10-2) that determine the areal model coordinates for the source locations within Source Regions 1 to 4, respectively. These parameter values are drawn from independent, uniform distributions from 0.0 to 1.0 and result in randomly located point sources within each of the four source regions for each realization of the SZ Flow and Transport Submodel.

In addition to the transport of radionuclides as solutes in groundwater, radionuclides may also be sorbed onto colloids and travel through the SZ to the accessible environment (BSC 2004 [DIRS 170006], Section 6.3). The radionuclides may be reversibly or irreversibly sorbed onto colloids. A retardation factor is established for radionuclides that are irreversibly sorbed onto colloids. Implied in the use of a retardation factor to describe colloid transport is that colloid filtration and detachment rates are fast relative to groundwater transport times through the system (BSC 2004 [DIRS 170006], Section 7.1). In addition, a small fraction of colloids, also called the fast fraction, is transported unretarded through the SZ, based on groundwater transport times (BSC 2004 [DIRS 170006], Section 6.6). As discussed in *Saturated Zone Colloid Transport* (BSC 2004 [DIRS 170006], Section 6.6), field experimental work has shown that a small percentage of colloids transport in groundwater with no retardation. Experimental results show that the attachment rate constant can be used to determine the fraction of colloids that are transported with no retardation. Specifically, colloids for which the reciprocal of the attachment rate constant is smaller than the transport time through the system will transport with no retardation. Radionuclides that are reversibly sorbed onto colloids are in equilibrium with the aqueous phase and the geologic medium. In this mode of transport, the effective retardation of these radionuclides during transport in the SZ depends on the sorption of radionuclides to colloids, the concentration of colloids in the groundwater, and the sorption coefficient of the radionuclide onto the geologic medium. Because the effective sorptive capacity of the porous medium is reduced when groundwater colloids carry a significant fraction of radionuclide mass in the system, an adjusted sorption coefficient is calculated for the alluvium and undifferentiated valley fill hydrologic units (SNL 2008 [DIRS 183750], Section 6.5.1.1, Equation 6-5). For transport in fractured media, the effective diffusion coefficient into the rock matrix is reduced due to the affinity of radionuclides for sorption onto colloids in the fractures (SNL 2008 [DIRS 183750], Section 6.5.1.1, Equation 6-9).

As discussed in Section 6.3.7.1.2, 27 of the 31 important radionuclides are tracked and transported by the SZ Transport Submodel. The 4 radionuclides that are not tracked and transported are ^{245}Cm, ^{241}Pu, ^{227}Ac, and ^{228}Ra. Details on the 4 radionuclides can be found in Section 6.3.7.1.2. The radionuclides tracked by the SZ Flow and Transport Model Component

are divided into 12 groups, based on their transport characteristics. These 12 groups and their modes of transport are summarized in Table 6.3.10-1. The first group contains the nonsorbing radionuclides technetium, iodine, carbon, and chlorine; they are grouped together in the TSPA-LA Model because their solute migration is identical. Carbon is considered nonsorbing and is transported without chemical reactions or ionic exchange with the host rocks, thus providing a conservative bound on transport in the absence of a detailed model for reactive transport. The second group contains americium, thorium, and protactinium, representing colloid-facilitated transport of the radionuclides reversibly sorbed onto colloids. The third group contains cesium, representing colloid-facilitated transport of the radionuclide reversibly sorbed onto colloids. The fourth group contains plutonium, representing colloid-facilitated transport of the radionuclide reversibly sorbed onto colloids. The fifth group contains neptunium, being transported as a solute. The sixth group contains plutonium and americium, representing colloid-facilitated transport of the radionuclides irreversibly sorbed onto colloids. The seventh, eighth, and ninth groups contain radium, strontium, and uranium, respectively, all transported as a solute. The tenth group contains plutonium and americium, representing the fast fraction of colloid-facilitated transport of the radionuclides irreversibly sorbed onto colloids. The eleventh group contains selenium, transported as a solute. Lastly, the twelfth group contains tin, representing colloid-facilitated transport of the radionuclide reversibly attached to colloids.

The 3-D SZ Flow and Transport Abstraction breakthrough curves are calculated outside of the TSPA-LA Model, as shown on Figure 6.1.4-1. The epistemic uncertain parameters shown in Table 6.3.10-2 are sampled 200 times to produce 200 sets of input parameters to the 3-D SZ Flow and Transport Abstraction Model (DTN: SN0702PASZFTMA.001_R0 [DIRS 179504]). The 3-D SZ Flow and Transport Abstraction Model then uses these 200 input parameter sets to perform a series of probabilistic transport simulations for a unit mass flux source. The simulated transport particle paths from the Site-Scale Saturated Zone Transport Model (SNL 2007 [DIRS 177392]) are illustrated on Figure 6.3.10-7. The output of these simulations is a set of 200 breakthrough curves for each of the four source regions and 12 radionuclide groups (DTN: SN0702PASZFTMA.001_R0 [DIRS 179504]). The resulting 9,600 breakthrough curves describe the (unit-source) mass of radionuclides that cross the 18-km boundary as a function of time. These breakthrough curves, the SZ_Convolute DLL (SZ_Convolute V3.10.01, STN: 10207-3.10.01-00 [DIRS 181060]) and control files for SZ_Convolute (described in DTN: SN0702PASZFTMA.001_R0 [DIRS 179504]), are the principal parts of the 3-D SZ Flow and Transport Abstraction. The convolution integral method employed in SZ_Convolute exhibits a linear response to the input function. In the case of solute transport in the SZ, this approach implies, for example, that a doubling of the input mass flux results in a doubling of the output mass flux. This approach is valid for the SZ Flow and Transport Submodel because the underlying transport processes (e.g., advection and sorption) are described by linear partial differential equations with respect to solute mass (SNL 2007 [DIRS 177392], Section 6.4.2.1, Equation 1 and Section 6.4.2.5, Equation 42).

The processes of colloid filtration and sorption are both represented as equilibrium retardation processes. Simple retardation affects the timing of the release of radionuclides from the SZ but still constitutes a linear relationship between mass input and mass output for the SZ. Future monsoonal and glacial-transition climate states with potentially wetter and cooler climate conditions would increase groundwater recharge, which in turn would increase the specific discharge. When climate change occurs, the convolution technique accounts for the change in

specific discharge explicitly (*Design Document for: SZ_Convolute Version 3.0* (DOE 2003 [DIRS 167588], Section 3.1). The climate state groundwater flow scaling factors presented in Table 6.3.10-3 (i.e., parameters Flow_Rate_Fact_Vclim_CS1, Flow_Rate_Fact_Vclim_CS2, and Flow_Rate_Fact_Vclim_CS3) are based on mean case conditions and do not include uncertainty in groundwater flux estimates within a given climate state. The uncertainty is captured by the stochastic parameter groundwater specific discharge multiplier (Table 6.3.10-2). The uncertainty in groundwater specific discharge multiplier is applied to all of the climate states. It is assumed that the instantaneous change from one climate steady-state flow condition to another steady-state condition in the SZ can be described as a linear function (SNL 2008 [DIRS 183750], Section 6.5, p. 6-18). For post-10,000-year (climate state 4) calculations, the scaling factor Flow_Rate_Fact_Vclim_CS3, which represents the glacial transition climate conditions, is applicable.

As discussed in *Saturated Zone Flow and Transport Model Abstraction* (SNL 2008 [DIRS 183750], Section 6.5.3[a]), the glacial-transition climate state is appropriate for use in the post-10,000-year simulations of SZ flow and transport because hydrologic conditions for this state are consistent with proposed regulations (10 CFR 63.342 [DIRS 178394]). The proposed regulation (10 CFR 63.342 [DIRS 178394]) specifies that the constant value for climate change in the post-10,000-year period be based on a distribution of deep percolation ranging from 13 to 64 mm/yr. As shown in *Saturated Zone Flow and Transport Model Abstraction* (SNL 2008 [DIRS 183750], Table 6-1[a]), the range of simulated average glacial-transition infiltration from the MASSIF model (SNL 2007 [DIRS 182145]) (16.0 mm/yr at the 10th percentile to 46.2 mm/yr at the 90th percentile) approximately covers the range of deep percolation specified in 10 CFR 63.342 [DIRS 178394]. Therefore, the glacial-transition climate, as defined in the MASSIF infiltration model (SNL 2007 [DIRS 182145]) and in the SZ Flow and Transport Abstraction Model, is the appropriate constant representation of climate change for use in the post-10,000-year simulations of radionuclide transport.

1-D SZ Flow and Transport Abstraction—Because the ingrowth of radionuclides is not explicitly included in the 3-D SZ Flow and Transport Abstraction, a 1-D SZ Flow and Transport Abstraction is used to account for the decay and ingrowth of radionuclide daughter products for the four decay chains shown on Figure 6.3.10-8. The representation of the radionuclide decay chains is simplified in a manner that overestimates the concentration of daughter radionuclides by calculating the secular equilibrium between the final daughter products and their parents in two decay chains (SNL 2008 [DIRS 183750], Section 6.5.1.2). ^{227}Ac is in secular equilibrium with ^{231}Pa in the actinium chain at the downstream end of the one-dimensional SZ flow pathway, and ^{228}Ra is in secular equilibrium with ^{232}Th in the thorium series.

A conceptualization of the 1-D SZ Flow and Transport Abstraction is shown on Figure 6.3.10-9. The 1-D SZ Flow and Transport Abstraction is implemented directly in the TSPA-LA Model as a series of one-dimensional GoldSim model elements (called pipes). The one-dimensional pipes are able to simulate advection, longitudinal dispersion, retardation, decay and ingrowth, and matrix diffusion. Thus, the same radionuclide transport processes that are simulated in the 3-D SZ Flow and Transport Abstraction are included in the one-dimensional pipes, with the exception of transverse dispersion, which cannot be included in a one-dimensional model. Groundwater specific discharge in each pipe segment and pipe segment lengths in the 1-D SZ transport model are based on estimates derived from the 3-D SZ Flow and Transport Abstraction

Model (SNL 2008 [DIRS 183750], Section 6.5.1.2[a]). The 1-D SZ Flow and Transport Abstraction includes the same uncertain input parameters as the 3-D SZ Flow and Transport Abstraction (DTN: SN0702PASZFTMA.001_R0 [DIRS 179504]), shown in Table 6.3.10-2. The two abstractions are coupled so that, for a given realization, the same set of sampled input parameters is used. In addition, the 1-D SZ abstraction uses the constant parameters given in Table 6.3.10-3. Flow rates in the one-dimensional pipe segments are modified for the transitions in climate state, using the same climate state scaling factors listed in Table 6.3.10-3 that are used to modify the flow rates in the 3-D SZ Flow and Transport Abstraction. However, note that limitations in the Laplace transform solution implemented in the pipe module of GoldSim (GoldSim V9.60.100, STN: 10344-9.60-01 [DIRS 181903]; *User's Guide, GoldSim Probabilistic Simulation Environment* (GoldSim Technology Group 2007 [DIRS 181727])) preclude a change to the migration velocity of radionuclides that have entered the pipe segments. The values of longitudinal dispersivity in the SZ one-dimensional transport model have also been increased by one order of magnitude from the sampled values. This adjustment results in a better agreement between the SZ one-dimensional transport model and the SZ Site-Scale Transport Model as documented in *Saturated Zone Flow and Transport Model Abstraction* (SNL 2008 [DIRS 183750], Section 7.3.2[a]). This adjustment to the values of dispersivity are made because of the higher contrasts in permeability among the hydrogeologic units in the three-dimensional SZ site-scale transport model and the resulting enhancement to the dispersion in the random walk particle tracking algorithm (SNL 2008 [DIRS 183750], Section 6.5.1.2[a]). However, the adjustment and the use of unbounded log-normal distribution for longitudinal dispersivity resulted in large values for some sampled points. The impact of these large longitudinal dispersivity values is addressed in Appendix P, Section P15.2.

Radionuclide mass already within a given pipe segment of the 1-D SZ Flow and Transport Abstraction does not increase in velocity in response to increased specific discharge resulting from climate change. Radionuclide mass introduced after the change in specific discharge is transported at the proper, correspondingly faster rate. Therefore, a potential discrepancy exists between the rate at which the radionuclides are transported using the 3-D SZ Flow and Transport Abstraction Model and the 1-D SZ Flow and Transport Abstraction. The impacts of this limitation to calculations in the TSPA-LA Model are not large due to the following considerations. First, the 1-D SZ Flow and Transport Abstraction results are used only for the daughter products of the decay chains in the TSPA-LA Model calculations. Second, this limitation applies only to radionuclide mass that enters a given pipe segment prior to 2,000 years, after which glacial-transition climatic conditions continue unchanged. The radionuclide mass that enters the 1-D SZ Flow and Transport Abstraction prior to 600 years, at the time of change from present to monsoon conditions, would experience this limitation to the largest extent because it would be subject to two climate changes. Section 6.3.10.3 describes the implementation of this process in greater detail.

In the 1-D SZ Flow and Transport Abstraction, the flow path from the repository to the accessible environment is subdivided into three concentric zones centered on the repository that are nominally: (1) 0 km to 5 km from the repository, (2) 5 km to 13 km from the repository, and (3) 13 km to 18 km from the repository. The actual flow path length (Table 6.3.10-4) of each pipe segment in zones 2 and 3 varies as a function of: (1) the northwestern boundary of the alluvial uncertainty zone (FPLANW in Table 6.3.10-2), (2) the value of horizontal anisotropy (HAVO in Table 6.3.10-2), and (3) the source region from which the radionuclide source

originates beneath the repository. The value of the parameter defining the location of the northwestern boundary of the alluvial uncertainty zone varies from zero to one and is used to establish the location of the contact between tuff and alluvium below the water table. The length of the first pipe segment is fixed at 5 km for all realizations. The second pipe segment represents that portion of the flow path from a 5-km distance to contact between the volcanic aquifer and the alluvial aquifer in the SZ. The third pipe segment represents the portion of the flow path from the contact between the volcanic units and the alluvium out to the accessible environment. The lengths of the second and third pipe segments are estimated from the particle-tracking results of the 3-D SZ Flow and Transport Abstraction Model, as summarized in Table 6.3.10-4. It is important to note that the total length of the three pipe segments for a given source region can be greater than 18 km due to the effects of the horizontal anisotropy on the simulated flow paths (Figure 6.3.10-10). Estimated pipe segment lengths are shown for differing values of the horizontal anisotropy and for the four source regions. Each entry in the table contains a range of values in pipe length, where the minimum value shown for the second pipe (5- to 13-km zone) is used when the parameter defining the location of the northwestern boundary of the alluvial uncertainty zone is equal to 1.0, and the maximum value is used when the northwestern boundary parameter is equal to 0.0. By contrast, the minimum value of length for the third (13-to 18-km zone) pipe segment is used when the parameter defining the location of the northwestern boundary of the alluvial uncertainty zone is equal to 0.0, and the maximum value corresponds to a northwestern boundary parameter equal to 1.0. In other words, the maximum length of the flow path in the alluvial aquifer corresponds to the maximum northwesterly extent of the alluvial uncertainty zone, and the minimum length of the flow path in the alluvial aquifer corresponds to the minimum northwesterly extent of the alluvial uncertainty zone. The values in Table 6.3.10-4 are input into the SZ One-Dimensional Transport Model as a look-up table.

The average specific discharge along each pipe segment of the 1-D SZ Flow and Transport Abstraction varies as a function of the horizontal anisotropy. The resulting values of average specific discharge, as used in the 1-D SZ Flow and Transport Abstraction, are shown in Table 6.3.10-5. Figure 6.3.10-10 shows the simulated flow paths from Source Region 1 for the different values of horizontal anisotropy listed in Table 6.3.10-5.

The values of specific discharge are also scaled linearly using the groundwater specific discharge multiplier (Table 6.3.10-2) to represent the uncertainty in specific discharge. The values of specific discharge within the three pipe segments are calculated within the 1-D SZ Flow and Transport Abstraction by interpolating between the values of horizontal anisotropy, shown in Table 6.3.10-5, and through scaling by the value of the groundwater specific discharge multiplier (Table 6.3.10-2). The volumetric flow rate is the same for all segments in the 1-D SZ Flow and Transport Abstraction, and variations in specific discharge along the flow path are incorporated into the model by varying the cross-sectional areas of the pipe segments.

A summary of alpha concentration results in Amargosa Valley groundwater is given in Table 6.3.10-6 (DTN: SN0702PASZFTMA.002_R1 [DIRS 183471]). The best estimate for the mean gross alpha concentration in groundwater is 0.50 pCi/L with a 95 percent confidence that the concentration will not exceed 0.71 pCi/L. In the absence of data on the combined concentrations of ^{226}Ra and ^{228}Ra, it should be conservatively assumed for these radionuclides that they are responsible for all gross alpha activity. For ^{226}Ra and ^{228}Ra, the mean concentration is 0.50 pCi/L with a 95 percent confidence that the concentration will not exceed 0.71 pCi/L. To

allow for sampling, the values found in output DTN: MO0708TSPAGENT.000 ([DIRS 183000], file BL-TSPA-DTN-5, PEF #89) are those of mean, standard deviation, and upper limit, where the standard deviation is derived from the mean and 95th percentile values and the upper limit represents three standard deviations above the mean. The standard deviation can be derived using the fact that, by definition in a normal distribution, the 95th percentile is 1.645 standard deviations above the mean. For both mean gross alpha concentration and background ^{226}Ra and ^{228}Ra, the 95th percentile is 0.21 pCi/L above the mean of 0.50 pCi/L. The standard deviation is therefore (0.21 pCi/L)/1.645 or 0.128 pCi/L. Details can be found in *Saturated Zone Flow and Transport Model Abstraction* (SNL 2008 [DIRS 183750], Section 6.8.6). These parameters are used in the biosphere model component of the TSPA-LA Model (Section 6.3.11).

6.3.10.3 TSPA-LA Model Implementation

Figure 6.3.10-11 presents a flow chart that shows the implementation of the SZ Flow and Transport Submodel.

The 3-D SZ Flow and Transport Submodel calculations are performed by an external DLL, SZ_Convolute V3.10.01, which is directly coupled to the TSPA-LA Model. The input files for SZ_Convolute are described in Appendix F, Section F2.5. At the beginning of each realization, an integer variable (SZ index) with a range of 1 to 200 is randomly sampled in the TSPA-LA Model and is used to select the radionuclide breakthrough curve to be used for that realization. The same breakthrough curve is selected for each radionuclide group based on the sampled SZ index value. This maintains consistency among the different radionuclide groups because the breakthrough curves for each value of the SZ index were produced using the same set of input parameters. For each timestep, the SZ_Convolute DLL takes the radionuclide source mass from the nodes at the water table of the UZ Transport Submodel (Section 6.3.9.1) and combines it with the selected breakthrough curve for that radionuclide and source region.

Because the 3-D SZ Flow and Transport Abstraction does not account for ingrowth of daughter products in the chain decay, adjustments are necessary to properly account for these radionuclides (Figure 6.3.10-8). The TSPA-LA Model adjustments increase the inventory of the first-generation daughters (namely: ^{239}Pu, ^{237}Np, ^{236}U, ^{238}U, and ^{234}U) before they are released into the 3-D SZ Flow and Transport Abstraction. This adjustment is performed using a method termed inventory boosting in the TSPA-LA Model's GoldSim model file. For each timestep, the inventory of each of these first-generation daughters is increased or boosted by the amount that their respective parent radionuclides would decay during the remaining simulation time.

The 1-D SZ Flow and Transport Abstraction is used to account for the ingrowth of the second-generation daughters: ^{235}U, ^{231}Pa, ^{227}Ac, ^{233}U, ^{229}Th, ^{232}Th, ^{228}Ra, ^{230}Th, and ^{226}Ra. The 1-D SZ Flow and Transport Abstraction is incorporated directly into the TSPA-LA Model as four sets of three pipe elements (one set for each SZ source region). The radionuclide mass input to the 1-D SZ Flow and Transport Abstraction also comes from the UZ Transport Submodel. The same integer value used by the 3-D SZ Flow and Transport Abstraction to select a set of breakthrough curves is used in the 1-D SZ Flow and Transport Abstraction to choose additional input parameter values from look-up tables in the TSPA-LA Model. This method ensures

consistency between the 1-D and 3-D SZ Flow and Transport Abstractions on a realization-by-realization basis.

Even though they are accounted for in the 3-D SZ Flow and Transport Abstraction, the parents of the second-generation daughters are also transported in the 1-D SZ Flow and Transport Abstraction. The parents are included in the 1-D SZ Flow and Transport Abstraction to account for the ingrowth of the second-generation daughters. The first-generation daughter products are not boosted for the 1-D SZ Flow and Transport Abstraction because the GoldSim software correctly calculates the decay and ingrowth of radionuclides.

The radionuclide mass for all species is tracked in both the 1-D and 3-D SZ Flow and Transport Abstractions. However, the radionuclide mass exiting each submodel is then screened, such that only the mass for second-generation daughter species is taken from the 1-D SZ Flow and Transport Abstraction. All the other radionuclide results are taken from the 3-D SZ Flow and Transport Abstraction.

Radionuclides are released from the SZ to the accessible environment approximately 18 km from the repository (66 FR 55732 [DIRS 156671], III Public Comments and Responses, 3.5, p. 55753). The 18-km regulatory boundary represents the location where a RMEI resides (66 FR 55732 [DIRS 156671], III Public Comments and Responses, 3.2, p. 55750). All of the radionuclide mass that crosses this regulatory boundary in the SZ is assumed to be homogeneously distributed in a 3,000 acre-ft volume per annum (10 CFR 63.332(3) [DIRS 180319]). The resulting release of radionuclide mass to the biosphere is then used to calculate dose to the RMEI (Section 6.3.11).

6.3.10.4 Model Component Consistency and Conservatism in Assumptions and Parameters

To enhance understanding of the complex interactions within the TSPA-LA Model, a discussion of consistency among model components and submodels and identification of conservative assumptions in abstractions, process models, and parameter sets supporting SZ flow and transport are discussed below.

6.3.10.4.1 Consistency of Assumptions

SZ Release Location—The 3-D SZ Flow and Transport Abstraction, which is used to transport all parent radionuclides and first-generation daughters, is based on three-dimensional simulations that use a random release location beneath the repository for each of the four SZ source regions (Section 6.3.10.2). However, the 1-D SZ Flow and Transport Abstraction, used for most granddaughters, is based on a central release location for each of the four source regions. This can result in different transport behavior for isotopes of the same chemical element in a given realization. For example, ^{234}U (a daughter of ^{238}Pu, but a granddaughter of ^{242}Pu) is transported with the three-dimensional model, whereas ^{233}U is transported with the one-dimensional model. Thus, for certain realizations, where the three-dimensional random-release model produces a significantly different transport pathway than the one-dimensional central-location model, the transport times through the SZ for the two radionuclides can be different by thousands of years,

even though they would be expected to behave similarly because they have similar transport properties.

Effect on TSPA—The effect of this difference is minimal because the central release location used in the 1-D SZ Flow and Transport Abstraction is representative of the average behavior taken over multiple realizations.

6.3.10.4.2 Identification of Conservatisms in Submodels and Abstractions

Radionuclide Mass Release from the UZ Matrix to the SZ—The transfer of radionuclide mass reaching the water table from the matrix of the UZ directly to the fractures of the SZ tends to maximize the simulated concentrations of radionuclides at the outlet to the accessible environment. This approximation results in less dispersion of the radionuclide transport times through the SZ and, thus, to less attenuation of peaks in radionuclide discharge. This conservatism is used because it simplifies the modeling approach (SNL 2008 [DIRS 183750], Sections 6.3.3 and 6.5.2.13). Appendix C contains an analysis in which the mass from the UZ matrix is transferred to new cells that model matrix diffusion before reaching the SZ.

Instantaneous Change in SZ Groundwater Flow at Climate State Changes—The increase in groundwater flux will be gradual during the transition period going from drier conditions to wetter conditions. However, in the TSPA-LA Model, groundwater flux is assumed to increase instantaneously at climate state changes. This conservatism is applied because it simplifies the modeling approach (SNL 2008 [DIRS 183750], Section 6.5, p. 6-18). This approach tends to overestimate the rate of radionuclide transport in the SZ. Appendix C contains an analysis on the effect of climate changes in UZ transport, which directly affects the SZ.

Colloids are Retarded by Filtration—The conceptual model of filtration for colloids with irreversibly sorbed radionuclides assumes that colloids are retarded by filtration. Permanent removal of colloids by mechanical filtration in the SZ is not considered in the TSPA-LA Model, although it is likely to occur (SNL 2008 [DIRS 183750], Sections 6.3.1, 6.3.2, 6.5.1[a], and 6.5.2.11). The exclusion of permanent colloid filtration tends to overestimate the quantity of colloids that are transported through the SZ. In the compliance model (SNL 2008 [DIRS 183750], Section 6.5.2.11), transport of retarded irreversible colloids in both the volcanic units and the alluvium is calculated using single retardation factors (one for the volcanic units and another for the alluvium). Analysis of experimental data shows that use of a single retardation factor does not fit experimental observations (output DTN: LA0705PR150304.001 [DIRS: 181744]). Appendix C contains an analysis of the colloid diversity model, in which colloids are assigned a wide range of retardation factors that are based on experimental data.

No Solubility Limits or Enhanced Sorption Applied to Radionuclide Concentrations in the SZ—No solubility limits are applied to radionuclide concentrations in the SZ. Dissolved radionuclide concentrations in the far field are assumed to be the same as in the near field regardless of the chemical conditions. The application of solubility limits in the SZ is screened out as part of FEP 2.2.08.07.0A (DTN: MO0706SPAFEPLA.001_R0 [DIRS 181613]). In addition, significantly greater sorption could occur for some redox-sensitive radionuclides if chemically reducing conditions occur locally in the SZ. Changes due to redox conditions in the SZ could have a potential impact on solubility, sorption, and radionuclide transport through the

SZ. Enhanced sorption due to the presence of reducing zones in the SZ could increase retardation, resulting in longer travel times in the SZ. The potential impact of redox conditions in the SZ is discussed in Appendix C.

Implementation of Ingrowth of radionuclides in the SZ Model—Ingrowth of radionuclides is not explicitly included in the SZ transport model component of the TSPA-LA model for some radionuclides. A simplified approach, inventory boosting, accounts for this process for some of the radionuclides that have parent radionuclides as described in *Saturated Zone Flow and Transport Model Abstraction* (SNL 2008 [DIRS 183750], Sections 6.3.1). The TSPA-LA 1-D SZ Transport Model adds the pre-decayed daughter products to transported inventory in the SZ and also transports the full inventory of the parents by applying inventory boosting. The parent radionuclides of these boosted decay products are not diminished, resulting in an overestimation of the mass of radionuclides transported in the SZ.

6.3.10.5 Alternative Conceptual Model(s) for Saturated Zone Flow and Transport

Section 6.2 outlines the general consideration and treatment of ACMs used to support the TSPA-LA Model. A brief description of the SZ flow and transport ACMs summarized in Table 6.3.10-7 is presented below.

Minimal Matrix Diffusion ACM—Diffusion of radionuclides into the pore space of the rock matrix in the fractured volcanic units is potentially extremely limited due to highly channelized groundwater flow, fracture coatings, or other factors. The uncertain input parameters influencing matrix diffusion in the SZ Flow and Transport Submodel include effective diffusion coefficient, flowing interval spacing, and flowing interval porosity. Minimal matrix diffusion in the SZ Flow and Transport Submodel would tend to increase the rate of radionuclide transport. However, this ACM is implicitly included in the 3-D SZ Flow and Transport Abstraction and in the 1-D SZ Flow and Transport Abstraction through the range of uncertainty in the key input parameters mentioned above (SNL 2008 [DIRS 183750], Section 6.4).

This ACM was shown to be captured within the range of uncertainty already in the SZ Flow and Transport Submodel and, therefore, is not recommended for inclusion in the TSPA-LA Model.

Horizontal Anisotropy in Permeability ACM—Alternative interpretations of pump test results in the fractured volcanic units indicate preferential permeability along structural features oriented in the NNE-SSW direction or in the WNW-ESE direction. This ACM is implicitly included in the 3-D SZ Flow and Transport Abstraction and in the 1-D SZ Flow and Transport Abstraction through the range of uncertainty in the input parameter HAVO. The uncertain input parameter influencing horizontal anisotropy in permeability in the volcanic units near Yucca Mountain is the ratio of N-S to E-W permeability (SNL 2008 [DIRS 183750], Section 6.5.2.10). This continuously distributed parameter varies from less than one to greater than one with most of the realizations greater than one.

This ACM was also shown to be captured within the range of uncertainty already in the SZ Flow and Transport Submodel and, therefore, is not recommended for inclusion in the TSPA-LA Model.

Table 6.3.10-1. Radionuclides Transported in the Saturated Zone Flow and Transport Submodel

Radionuclide Group Number	Transport Mode	Radionuclides
1	Solute	Carbon, Technetium, Iodine, Chlorine
2	Colloid-facilitated (Reversible)	Americium, Thorium, Protactinium
3	Colloid-facilitated (Reversible)	Cesium
4	Colloid-facilitated (Reversible)	Plutonium
5	Solute	Neptunium
6	Colloid-facilitated (Irreversible)	Plutonium, Americium
7	Solute	Radium
8	Solute	Strontium
9	Solute	Uranium
10	Colloid-facilitated (Fast fraction of Irreversible)	Plutonium, Americium
11	Solute	Selenium
12	Colloid-facilitated (Reversible)	Tin

Source: *Saturated Zone Flow and Transport Model Abstraction* (SNL 2008 [DIRS 183750], Table 6-9[a]).

Table 6.3.10-2. Uncertain Model Inputs Used in the 3-D Saturated Zone Flow and Transport Process Model and 1-D Saturated Zone Flow and Transport Abstraction

Input Name	Input Description	Value or Distribution	Units	Type of Uncertainty
Kd_Np_Vo	Neptunium sorption coefficient in volcanic units	CDF: Probability / Value 0.0 / 0.0 0.05 / 0.99 0.90 / 1.83 1.0 / 6.0	mL/g	Epistemic
Kd_Np_Al	Neptunium sorption coefficient in alluvium	CDF: Probability / Value 0.0 / 1.8 0.05 / 4.0 0.95 / 8.7 1.0 / 13.0	mL/g	Epistemic
Kd_Sr_Vo	Strontium sorption coefficient in volcanic units	Uniform: Minimum 20.0 Maximum 400.0	mL/g	Epistemic
Kd_Sr_Al	Strontium sorption coefficient in alluvium	Uniform: Minimum 20.0 Maximum 400.0	mL/g	Epistemic
Kd_U_Vo	Uranium sorption coefficient in volcanic units	CDF: Probability / Value 0.0 / 0.0 0.05 / 5.39 0.95 / 8.16 1.0 / 20.0	mL/g	Epistemic
Kd_U_Al	Uranium sorption coefficient in alluvium	CDF: Probability / Value 0.0 / 1.7 0.05 / 2.9 0.95 / 6.3 1.0 / 8.9	mL/g	Epistemic
Kd_Ra_Vo	Radium sorption coefficient in volcanic units	Uniform: Minimum 100.0 Maximum 1,000.0	mL/g	Epistemic
Kd_Ra_Al	Radium sorption coefficient in alluvium	Uniform: Minimum 100.0 Maximum 1,000.0	mL/g	Epistemic
Kd_Pu_Vo	Plutonium sorption coefficient in volcanic units	CDF: Probability / Value 0.0 / 10.0 0.25 / 89.9 0.95 / 129.87 1.0 / 300.0	mL/g	Epistemic
Kd_Pu_Al	Plutonium sorption coefficient in alluvium	Beta: Mean 100 Standard Deviation 15 Minimum 50 Maximum 300	mL/g	Epistemic

Table 6.3.10-2. Uncertain Model Inputs Used in the 3-D Saturated Zone Flow and Transport Process Model and 1-D Saturated Zone Flow and Transport Abstraction (Continued)

Input Name	Input Description	Value or Distribution	Units	Type of Uncertainty
Kd_Am_Vo	Americium sorption coefficient in volcanic units	Truncated Normal: Mean 5,500 Standard Deviation 1,500 Minimum 1,000 Maximum 10,000	mL/g	Epistemic
Kd_Am_Al	Americium sorption coefficient in alluvium	Truncated Normal: Mean 5,500 Standard Deviation 1,500 Minimum 1,000 Maximum 10,000	mL/g	Epistemic
Kd_Cs_Vo	Cesium sorption coefficient in volcanic units	CDF: Probability Value 0.0 100.0 0.05 3,000.59 1.0 6,782.92	mL/g	Epistemic
Kd_Cs_Al	Cesium sorption coefficient in alluvium	Truncated Normal: Mean 728 Standard Deviation 464 Minimum 100 Maximum 1,000	mL/g	Epistemic
Kd_Se_Vo	Selenium sorption coefficient in volcanic units	Truncated Log_Normal: Mean 14.0 Standard Deviation 11.2 Minimum 1.0 Maximum 50.0	mL/g	Epistemic
Kd_Se_Al	Selenium sorption coefficient in alluvium	Truncated Log_Normal: Mean 14.0 Standard Deviation 11.2 Minimum 1.0 Maximum 50.0	mL/g	Epistemic
Kd_Sn_Vo	Tin sorption coefficient in volcanic units	Log-Uniform: Minimum 1.e2 Maximum 1.e5	mL/g	Epistemic
Kd_Sn_Al	Tin sorption coefficient in alluvium	Log-Uniform: Minimum 1.e2 Maximum 1.e5	mL/g	Epistemic
Correlation matrix for K_d sampling in the SZ	Correlation coefficient values among radionuclides and between volcanic units and alluvium	DTN: LA0702AM150304.001 [DIRS 184763]	None	Matrix of Single Values

Table 6.3.10-2. Uncertain Model Inputs Used in the 3-D Saturated Zone Flow and Transport Process Model and 1-D Saturated Zone Flow and Transport Abstraction (Continued)

Input Name	Input Description	Value or Distribution	Units	Type of Uncertainty
FISVO	Flowing interval spacing in volcanic units	CDF: Probability / Value 0.0 / 1.860 0.01 / 2.925 0.20 / 12.036 0.50 / 25.773 0.80 / 39.965 0.90 / 45.797 0.92 / 47.207 0.94 / 49.115 0.96 / 51.710 0.98 / 55.249 0.99 / 58.439 1.0 / 80.0	M	Epistemic
CORAL	Colloid retardation factor in alluvium	CDF: (Log_{10}-transformed) Probability / Value 0.0 / 0.903 0.331 / 0.904 0.50 / 1.531 1.0 / 3.715	None	Epistemic
CORVO	Colloid retardation factor in volcanic units	CDF: (Log_{10}-transformed) Probability / Value 0.0 / 0.778 0.15 / 0.779 0.25 / 1.010 0.50 / 1.415 0.80 / 1.778 1.0 / 2.903	None	Epistemic
HAVO	Ratio of horizontal anisotropy (north-south over east–west) in permeability	CDF: Probability / Value 0.0 / 0.05 0.0042 / 0.2 0.0168 / 0.4 0.0379 / 0.6 0.0674 / 0.8 0.10 / 1.0 0.60 / 5.0 0.744 / 8.0 0.856 / 11.0 0.936 / 14.0 0.984 / 17.0 1.0 / 20.0	None	Epistemic
LDISP	Longitudinal dispersivity	Normal: (Log_{10}-transformed) Mean 2.0 Standard Deviation 0.75	m	Epistemic

Table 6.3.10-2. Uncertain Model Inputs Used in the 3-D Saturated Zone Flow and Transport Process Model and 1-D Saturated Zone Flow and Transport Abstraction (Continued)

Input Name	Input Description	Value or Distribution	Units	Type of Uncertainty
Kd_Pu_Col	Plutonium sorption coefficient onto colloids	CDF: Probability — Value 0.0 — 1.e3 0.45 — 5.e3 0.80 — 1.e4 0.95 — 5.e4 1.0 — 1.e5	mL/g	Epistemic
Kd_Am_Col	Americium sorption coefficient onto colloids	CDF: Probability — Value 0.0 — 1×10^4 0.07 — 5×10^4 0.17 — 1×10^5 0.40 — 5×10^5 0.60 — 1×10^6 0.92 — 5×10^6 1.0 — 1×10^7	mL/g	Epistemic
Kd_Cs_Col	Cesium sorption coefficient onto colloids	CDF: Probability — Value 0.0 — 5.e1 0.05 — 1.e2 0.40 — 5.e2 0.70 — 1.e3 1.0 — 5.e3	mL/g	Epistemic
Kd_Sn_Col	Tin sorption coefficient onto colloids	Log-Uniform: Minimum 1.e5 Maximum 1.e6	mL/g	Epistemic
Conc_Col*	Groundwater concentration of colloids	CDF: (Log_{10}-transformed) Probability — Value 0.0 — -9.0 0.50 — -7.0 0.75 — -6.0 0.90 — -5.0 0.98 — -4.3 1.0 — -3.6	g/mL	Epistemic
FPLANW	Northwestern boundary of alluvial uncertainty zone	Uniform: Minimum 0.0 Maximum 1.0	None	Epistemic
NVF26	Effective porosity in shallow alluvium	Truncated Normal: Mean 0.18 Standard Deviation 0.051 Minimum 0.00 Maximum 0.30	None	Epistemic
NVF11	Effective porosity in undifferentiated valley fill	Truncated Normal: Mean 0.18 Standard Deviation 0.051 Minimum 0.00 Maximum 0.30	None	Epistemic

Table 6.3.10-2. Uncertain Model Inputs Used in the 3-D Saturated Zone Flow and Transport Process Model and 1-D Saturated Zone Flow and Transport Abstraction (Continued)

Input Name	Input Description	Value or Distribution	Units	Type of Uncertainty
FPVO	Fracture porosity in volcanic units	CDF: (Log_{10}-transformed) Probability / Value 0.0 / –5.0 0.05 / –4.0 0.50 / –3.0 0.80 / –2.0 1.0 / –1.0	None	Epistemic
DCVO	Effective diffusion coefficient in volcanic units	CDF: (Log_{10}-transformed) Probability / Value 0.0 / –11.3 0.08 / –10.7 0.50 / –10.3 0.83 / –9.9 1.0 / –9.3	m^2/s	Epistemic
GWSPD	Groundwater specific discharge multiplier	CDF: (Log_{10}-transformed) Probability / Value 0.0 / -0.951 0.05 / -0.506 0.10 / -0.394 0.25 / -0.208 0.5 / 0.000 0.75 / 0.208 0.90 / 0.394 0.95 / 0.506 1.0 / 0.951	None	Epistemic
Alluvium_Density	Bulk density of alluvium	Normal: Mean 1,910 Standard Deviation 78	kg/m^3	Epistemic
SRC1X SRC1Y SRC2X SRC2Y SRC3X SRC3Y SRC4X SRC4Y	Source regions beneath the repository	Uniform: Minimum 0.0 Maximum 1.0	None	Epistemic and Aleatory

Sources: Modified from Saturated Zone Flow and Transport Model Abstraction (SNL 2008 [DIRS 183750], Tables 6-7[a] and 6-8). The following updated or new parameters are from Table 6-7[a]: GWSPD, FISVO, FPLANW, Kd_Pu_Col, Kd_Cs_Col, Kd_Sn_Col, Kd_Sn_Vo, Kd_Sn_Al, Kd_Se_Vo, Kd_Sn_Al, and Correlation matrix for Kd sampling in the SZ. Parameters NVF26 and NVF11 are new names for Parameters NVF19 and NVF7 in Table 6-8. Only the names are changed. The rest of the parameters are from Table 6-8.

NOTES: Only those parameters in the source that are uncertain were included in this table; Log10-transformed values are given in Log10. They are transformed to actual values when used.

* Please refer Saturated Zone Flow and Transport Model Abstraction (SNL 2008 [DIRS 183750], Section 6.5.3[b]) for a discussion on the distribution of parameter Conc_Col.

Table 6.3.10-3. Constant TSPA Parameters for Saturated Zone Flow One-Dimensional Transport Model

Parameter Name	Input Description	Input Value	Units
Coating Porosity	Porosity of the fracture coating	0.01	None
Coating Thickness	Fracture coating thickness	0.00001	m
Flow_Rate_fact_Vclim_CS1	SZ_1D, Discharge flowrate multiplier for climate state 1 (present day)	1	None
Flow_Rate_fact_Vclim_CS2	SZ_1D, Discharge flowrate multiplier for climate state 2 (monsoonal)	1.9	None
Flow_Rate_fact_Vclim_CS3	SZ_1D, Discharge flowrate multiplier for climate state 3 (glacial)	3.9	None
Pipe_Length_Pipe_a	Pipe length for pipe segment a	5,000	m
Volcanic_Fracture_Perimeter	Volcanic fracture perimeter for the determination of fracture surface area	2	m
Alluvium_Porosity	Effective porosity of the alluvium	0.30	None
Volcanic_Matrix_Porosity	Porosity of the volcanic matrix	0.22	None
Volcanic_Density	Bulk density of the volcanic matrix material	1,880	kg/m^3
Fracture_Porosity	Average fracture porosity of the volcanic units	0.001	None

Source: DTN: SN0702PASZFTMA.002 R1 [DIRS 183471].

Table 6.3.10-4. Flow Path Lengths of Pipe Segments

Horizontal Anisotropy	Minimum and Maximum Flow Path Lengths of Pipe Segments (km)							
	Source Region 1		Source Region 2		Source Region 3		Source Region 4	
	5 - 13 km	13 - 18 km	5 - 13 km	13 - 18 km	5 - 13 km	13 - 18 km	5 - 13 km	13 - 18 km
0.05	15.9 - 16.4	7.7 – 8.2	15.2 - 15.5	7.7 - 8.0	13.6 - 14.4	6.9 - 7.7	14.1 - 15.0	6.7 - 7.6
1.00	11.3 - 12.3	6.7 - 7.7	10.3 - 11.0	7.2 - 7.9	7.7 - 8.6	6.5 - 7.4	7.3 - 8.3	6.8 - 7.8
5.00	11.3 - 12.3	6.7 - 7.7	10.0 - 10.6	7.3 - 7.9	7.7 - 8.6	6.5 - 7.4	7.3 - 8.3	6.8 - 7.8
20.00	11.3 - 12.3	6.7 - 7.7	10.0 - 10.7	7.2 - 7.9	7.7 - 8.6	6.5 - 7.4	7.3 - 8.3	6.8 - 7.8

Source: DTN: SN0702PASZFTMA.002 R1 [DIRS 183471]. (Located in file DTN_TDIP_SZFT-2.doc).

Table 6.3.10-5. Average Specific Discharge in Flow Path Segments

Horizontal Anisotropy	Average Specific Discharge (m/yr)		
	0 - 5 km	5 - 13 km	13 - 18 km
0.05	0.354	0.408	2.56
1.00	0.459	0.486	0.769
5.00	0.409	0.544	5.98
20.00	0.555	0.500	5.93

Source: DTN: SN0702PASZFTMA.002 [DIRS 183471].
(Located in file DTN_TDIP_SZFT-2.doc).

Table 6.3.10-6. Summary of Alpha Concentration Results in Amargosa Valley Groundwater

Input	Expected Value (mean) pCi/L	Upper (95%) Limit pCi/L
Gross Alpha Concentration	0.50	0.71
Combined Concentration of 226Ra and 228Ra	0.50	0.71

Source: DTN: SN0702PASZFTMA.002 R1 [DIRS 183471]. (Located in file DTN_TDIP_SZFT-2.doc).

Table 6.3.10-7. Alternative Conceptual Models Considered for Saturated Zone Flow and Radionuclide Transport

Alternative Conceptual Model	Key Assumptions	Screening Assessment and Basis
Minimal Matrix Diffusion	Diffusion of radionuclides into the pore space of the rock matrix in the fractured volcanic units is extremely limited due to highly channelized groundwater flow, fracture coatings, or other factors.	This ACM is implicitly included in the 3-D SZ Flow and Transport Abstraction and in the 1-D SZ Flow and Transport Abstraction through the range of uncertainty in key input parameters. The uncertain input parameters influencing matrix diffusion include DCVO, FISVO, and FPVO (Table 6.3.10-2).
Horizontal Anisotropy in Permeability	Alternative interpretations of pump test results in the fractured volcanic units indicate preferential permeability along structural features oriented in the NNE-SSW direction or in the WNW-ESE direction.	This ACM is implicitly included in the 3-D SZ Flow and Transport Model Abstraction and in the 1-D SZ Flow and Transport Abstraction through the range of uncertainty in an input parameter. The uncertain input parameter influencing horizontal anisotropy in permeability in the volcanic units near Yucca Mountain is the ratio of N-S to E-W permeability (HAVO; Table 6.3.10-2). This continuously distributed parameter varies from less than one to greater than one, with most of the realizations greater than one.

Source: *Saturated Zone Flow and Transport Model Abstraction* (SNL 2008 [DIRS 183750], Section 6.4).

NOTES: 1-D = one-dimensional; DCVO = effective diffusion coefficient in volcanic units; FISVO = flowing interval spacing in volcanic units; FPVC = flowing interval porosity; HAVO = ratio of horizontal anisotropy (north-south over east-west) in permeability.

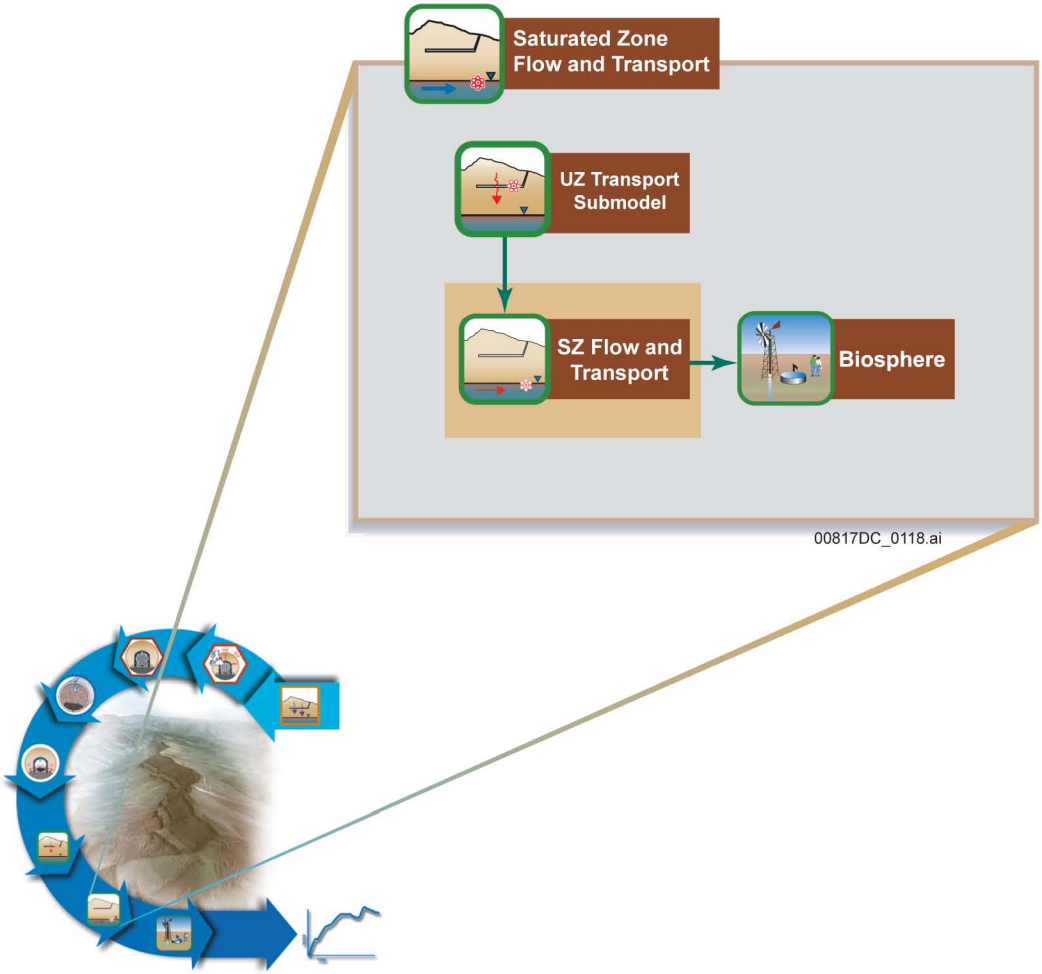

Figure 6.3.10-1. Information Flow Diagram for Saturated Zone Flow and Transport

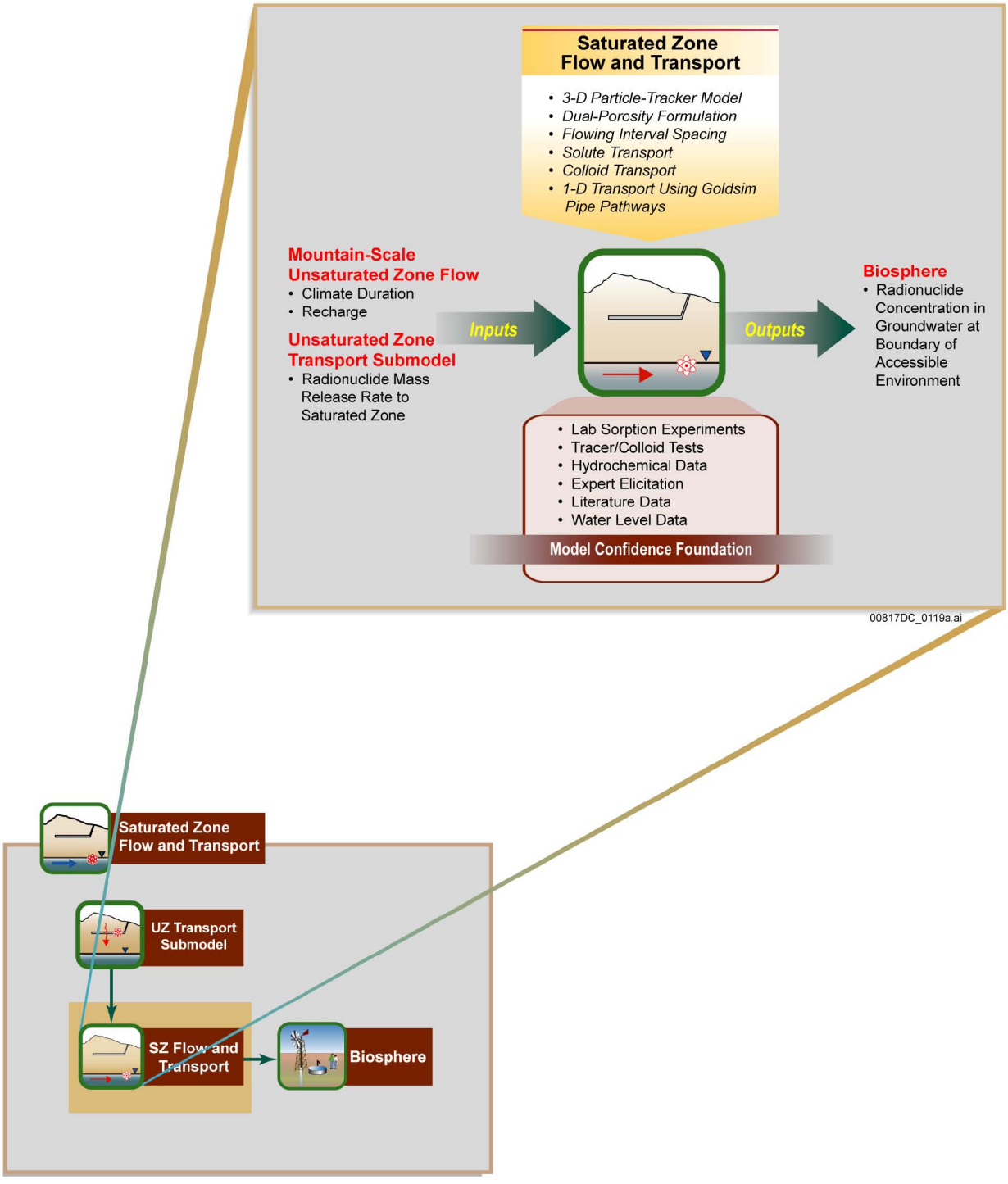

Figure 6.3.10-2. Inputs, Outputs, and Basis for Model Confidence for the Saturated Zone Flow and Transport Model Component

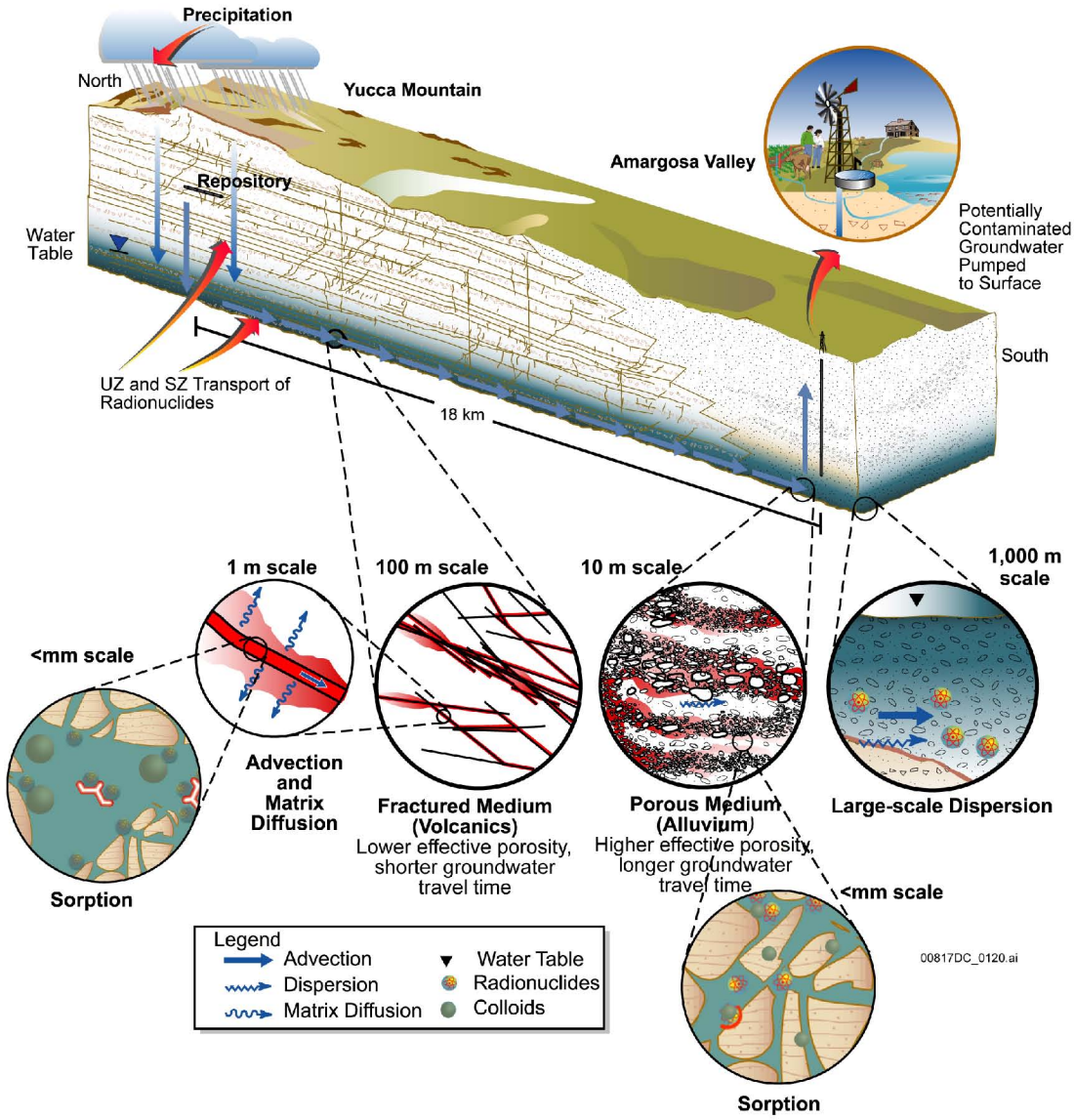

Figure 6.3.10-3. Conceptualization of Features and Processes Important to Saturated Zone Transport

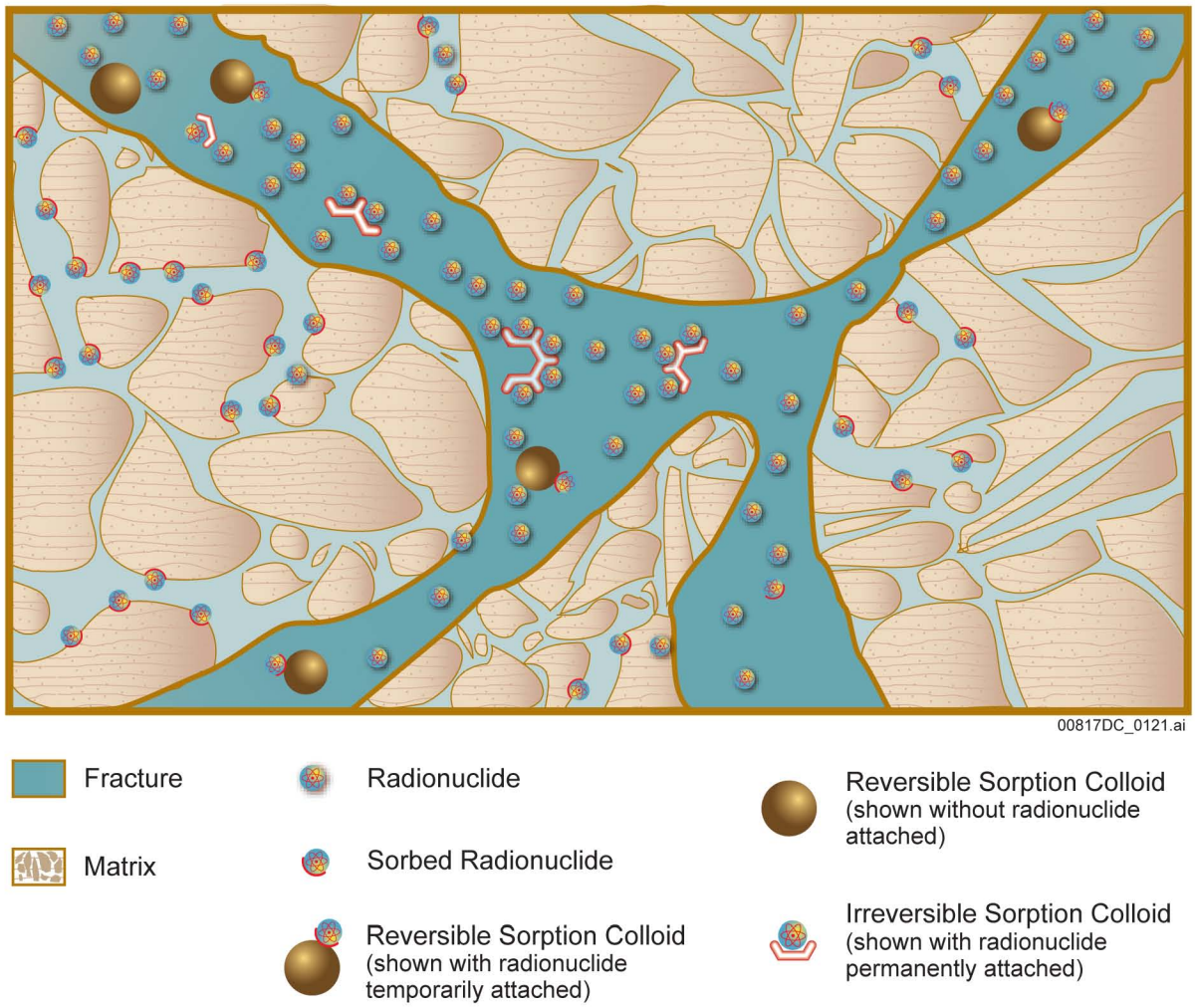

Figure 6.3.10-4. Illustration of Colloid-Facilitated Transport Processes

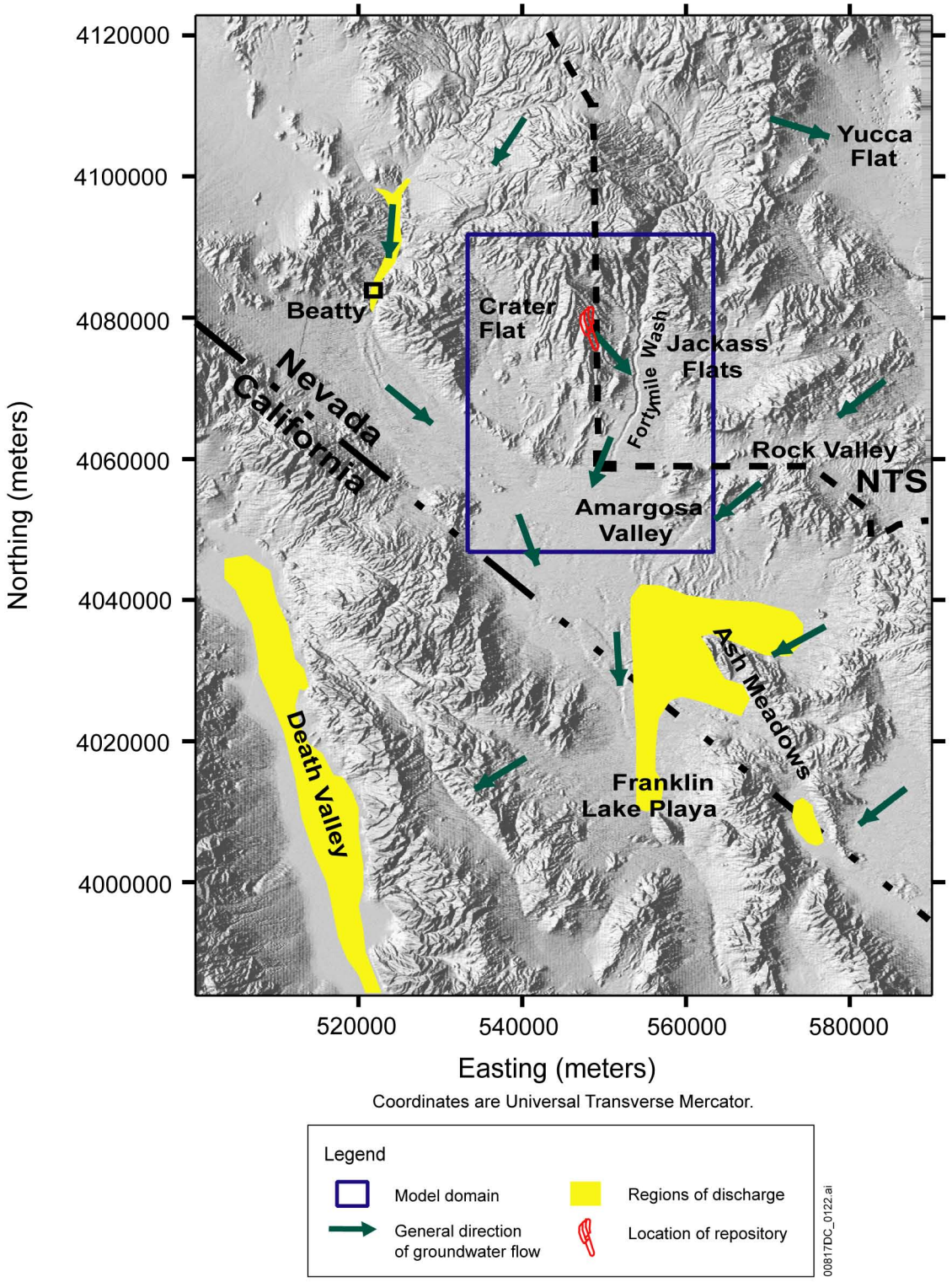

Source: Compiled from BSC 2004 [DIRS 169734], Figures 8-2, 8-5, and 8-6.

Figure 6.3.10-5. Regional Map of the Saturated Zone Flow System Showing Direction of Flow and Outline of the 3-D Saturated Zone Site-Scale Flow Model Domain

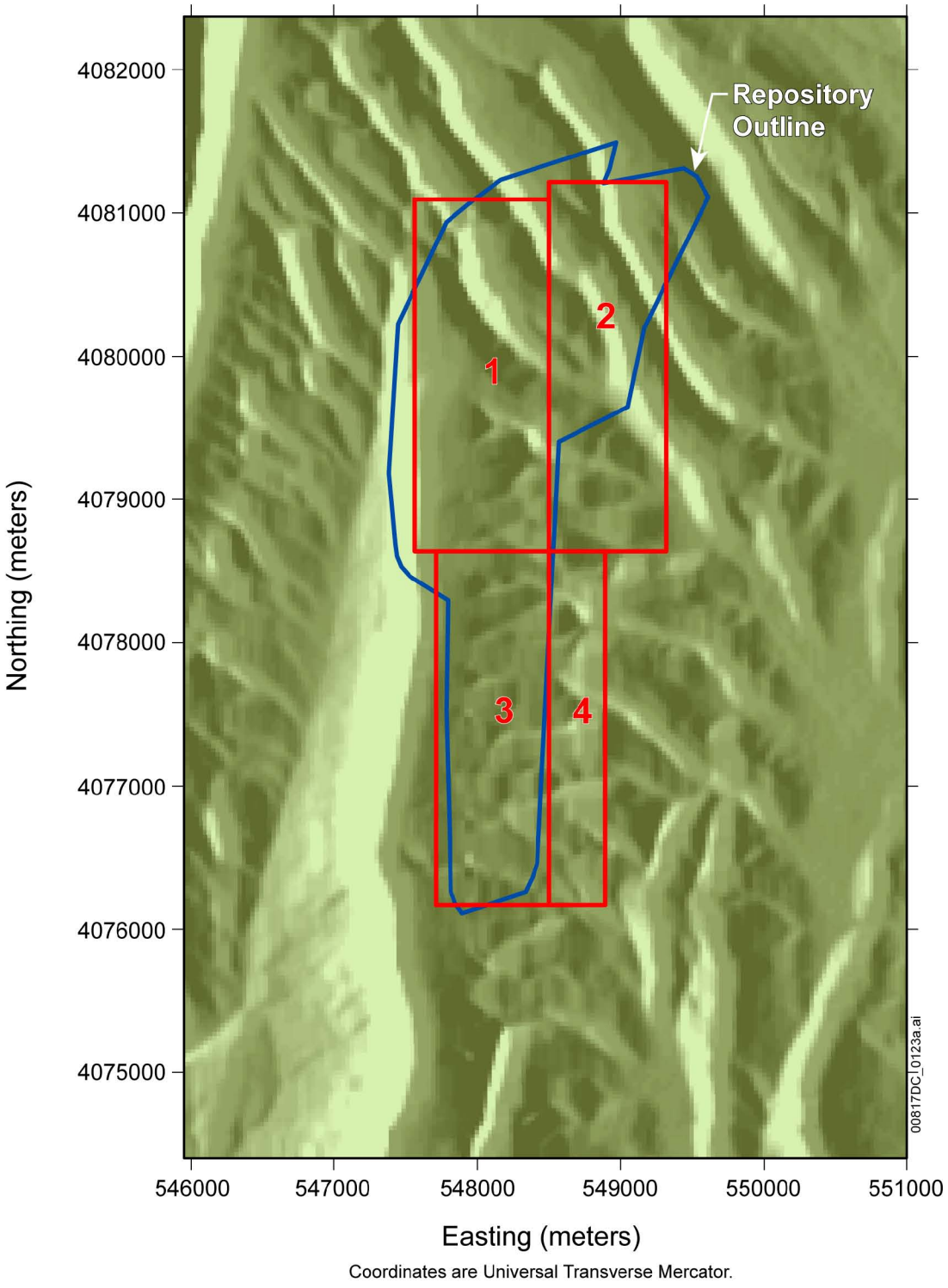

Source: Modified from SNL 2008 [DIRS 183750], Figure 6-27.

NOTE: The solid blue line shows repository outline and the solid red lines show the four source regions.

Figure 6.3.10-6. Source Regions for Radionuclide Release in the Saturated Zone Flow and Transport Abstraction Model

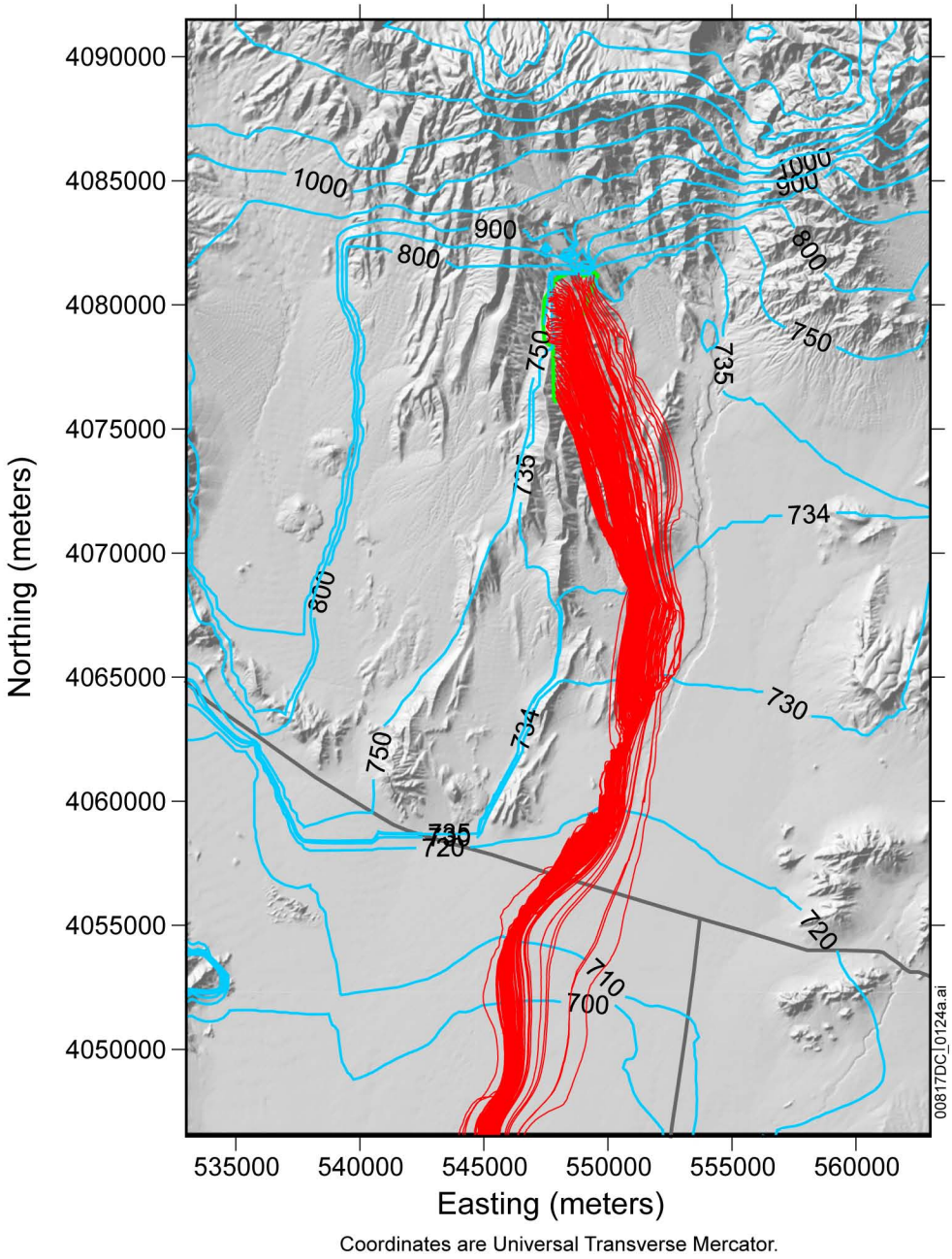

Source: Modified from SNL 2007 [DIRS 177391], Figure 6-43.

NOTE: Blue lines refer to simulated head contours at the water table in meters; red lines refer to simulated particle paths; direction of flow is from the repository to the accessible environment (bottom of figure).

Figure 6.3.10-7. Map of the 3-D Saturated Zone Model Domain Showing Simulated Particle Paths

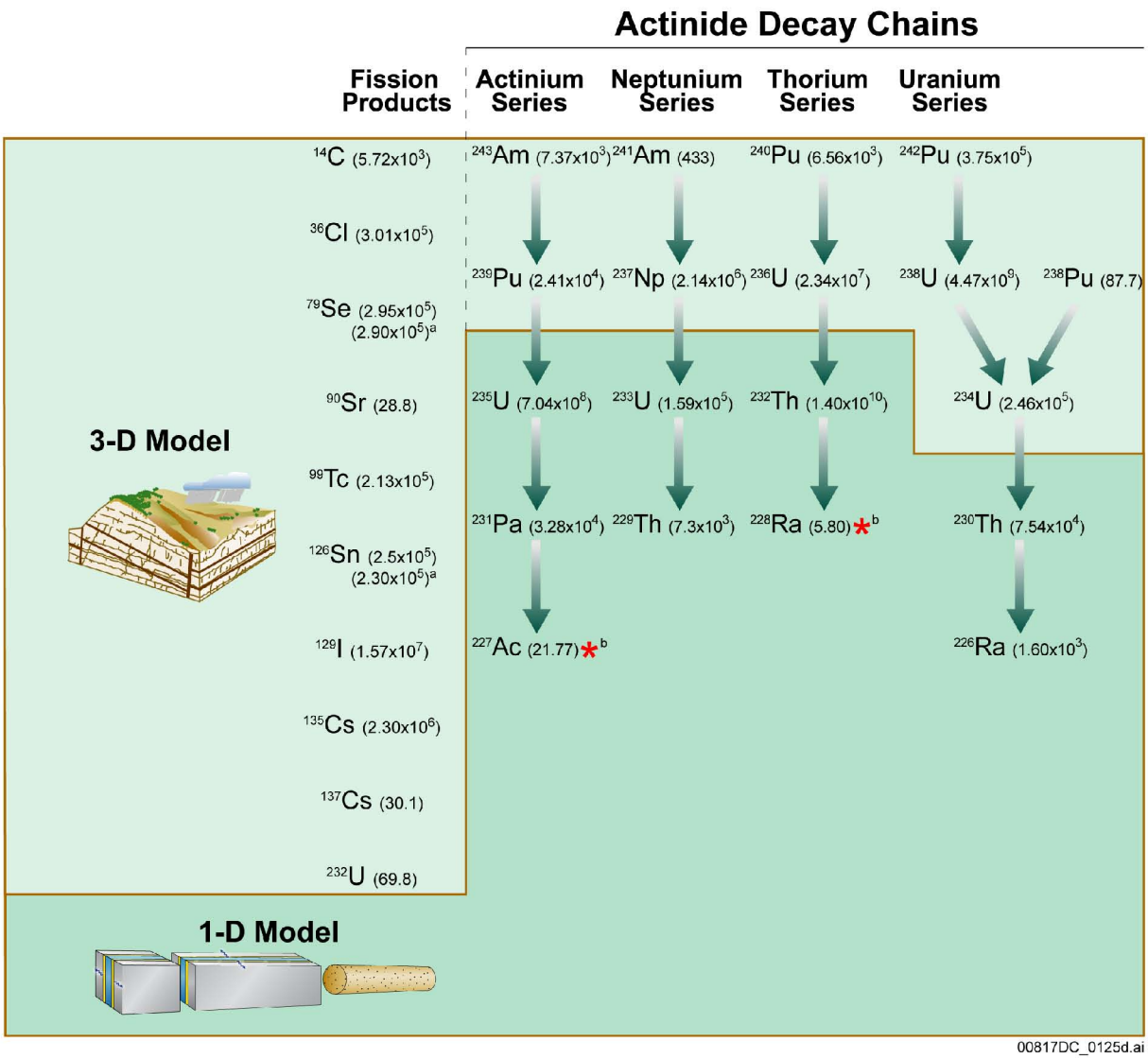

* Mass of RN calculated by assuming secular equilibrium with parent RN

(2.3x10^6) Half-life of RN indicated in parentheses (years)

Sources: DTNs: SN0702PASZFTMA.002_R1 [DIRS 183471]; MO0702PASTREAM.001_R0 [DIRS 179925].

NOTE: (a) Half-life values used in the 1-D Transport Model and (b) Half-life values used in secular equilibrium calculations.

Figure 6.3.10-8. Radionuclide Decay Chains Considered in Saturated Zone Transport Calculations

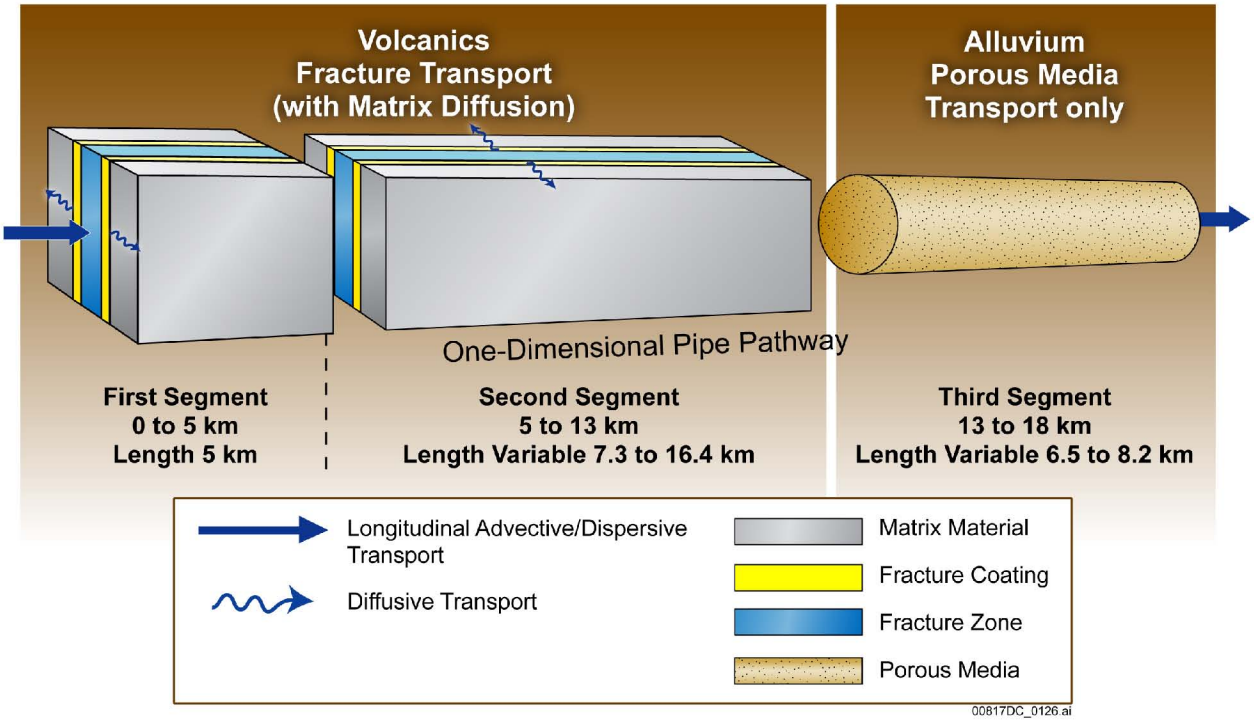

Figure 6.3.10-9. Conceptualization of the 1-D Saturated Zone Flow and Transport Abstraction

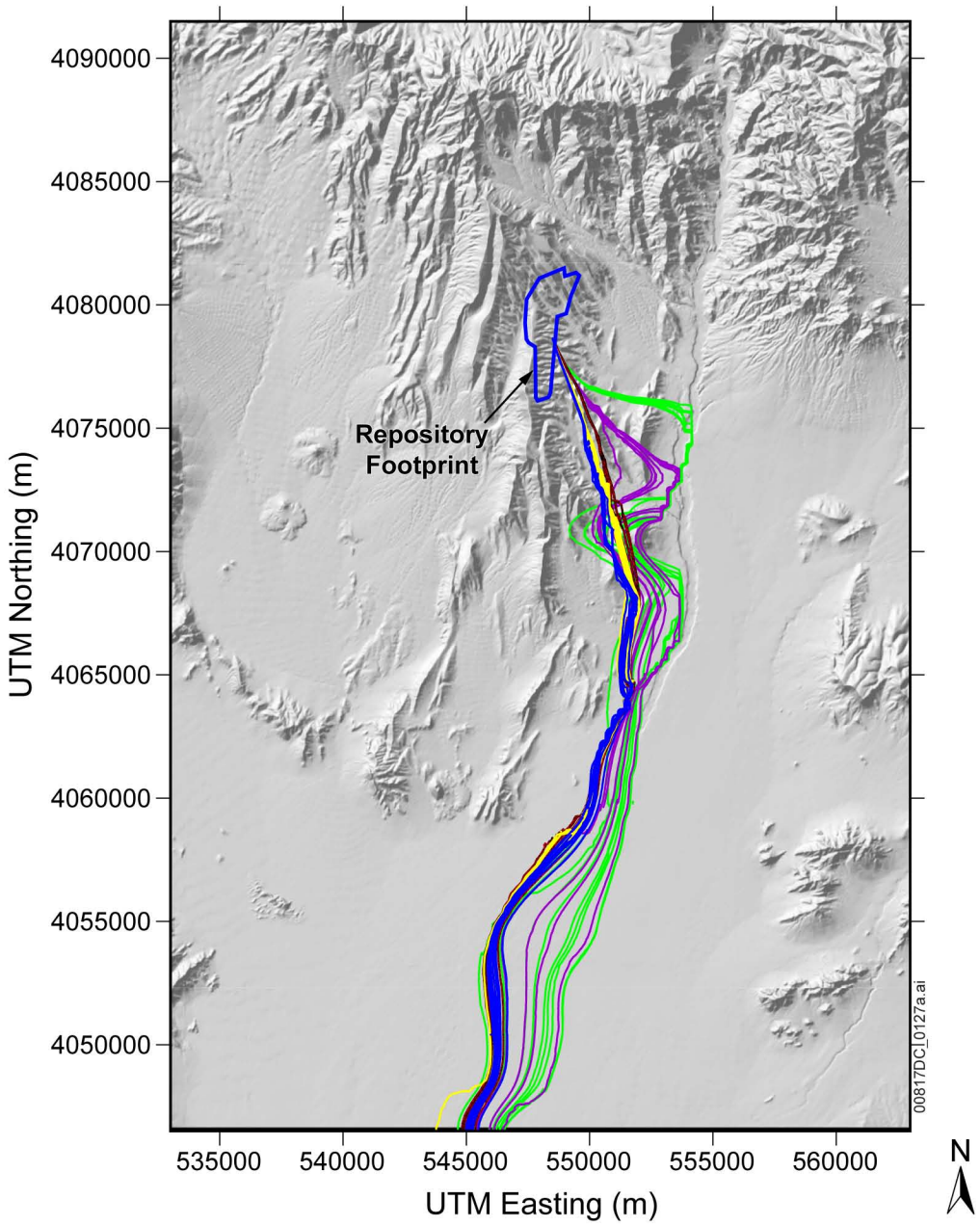

Source: Modified from SNL 2008 [DIRS 183750], Figure 6-1 [a].

NOTE: Green, purple, blue, yellow, and red lines show simulated particle paths for particles released from Source Region 1 for horizontal anisotropy values of 0.05, 0.20, 1.0, 5.0, and 20.0, respectively.

Figure 6.3.10-10. Simulated Particle Paths for Different Values of Horizontal Anisotropy in Permeability

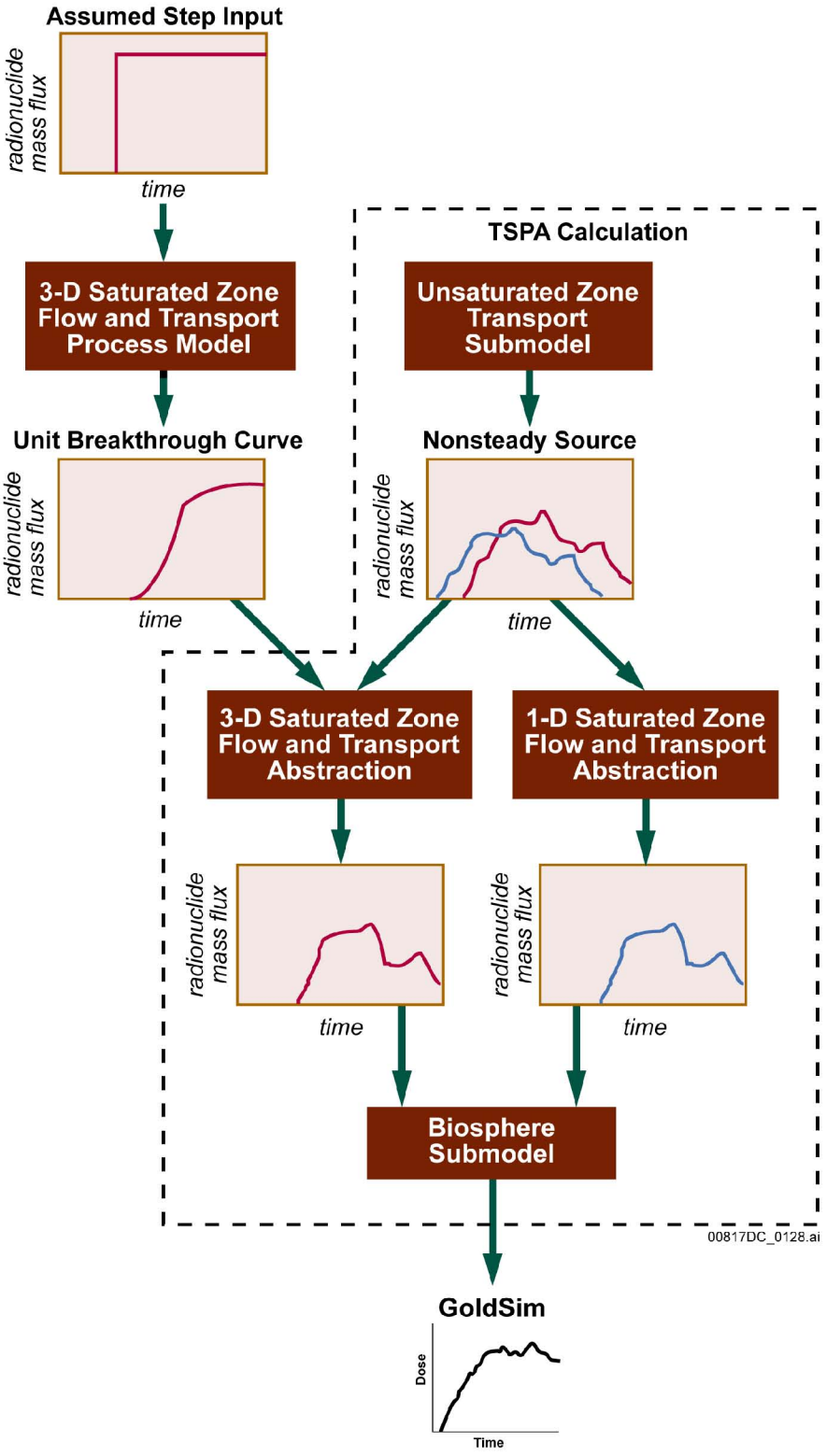

Figure 6.3.10-11. Flowchart of the Implementation of the Saturated Zone Flow and Transport Submodel in the TSPA-LA Model

INTENTIONALLY LEFT BLANK

6.3.11 Biosphere

The Biosphere Model Component of the TSPA-LA Model estimates the annual radiation dose to the RMEI that is expected to result if radionuclides are released to the accessible environment from the repository after closure. For the set of scenario classes considered in the TSPA-LA Model, there are two possible radionuclide release pathways from the repository to the accessible environment: one through groundwater and one through the atmosphere with volcanic ejections (tephra). These two radionuclide release pathways result in the two exposure scenarios developed in the biosphere. To eliminate possible confusion with the TSPA scenario classes, these two exposure scenarios, which are developed in the biosphere documents, are called the exposure cases in this TSPA-LA document. The groundwater exposure case applies to those TSPA-LA Model modeling cases that consider the groundwater transport of radionuclides from the repository at Yucca Mountain to the accessible environment. These modeling cases are included in the Nominal Scenario Class, the Early Failure Scenario Class, the Seismic Scenario Class, the Igneous Intrusion Modeling Case of the Igneous Scenario Class, and the Human Intrusion Scenario. The volcanic ash exposure case applies to the Volcanic Eruption Modeling Case of the Igneous Scenario Class, which considers a volcanic release of radionuclides from the repository at Yucca Mountain.

The Biosphere Process Model documented in *Biosphere Model Report* (SNL 2007 [DIRS 177399]) is implemented external to the TSPA-LA Model and is used to develop the capabilities for calculating annual radiation dose to the RMEI using the TSPA-LA Model. The analyses and abstractions of the two exposure cases in the Biosphere Process Model and reported in *Biosphere Model Report* (SNL 2007 [DIRS 177399]) resulted in the following two data sets giving biosphere dose conversion factors (BDCFs) for the groundwater and volcanic exposure cases as inputs to the TSPA-LA Model:

- Groundwater Biosphere Dose Conversion Factors (DTN: MO0702PAGBDCFS.001_R0 [DIRS 179327])
- Volcanic Biosphere Dose Conversion Factors (DTN: MO0702PAVBPDCF.000_R0 [DIRS 179330]).

An additional set of data was provided in *Inhalation Dose Factors* DTN: MO0702PAINHALA.001_R0 [DIRS 179329] to estimate the inhalation dose to the RMEI accrued during a tephra deposition.

These BDCFs are used in the Biosphere Model Component of the TSPA-LA Model to calculate the annual dose to the RMEI, which is required to assess compliance with the postclosure individual protection standard in 10 CFR 63.311 [DIRS 178394] and 10 CFR 63.321 for the individual protection standard for human intrusion [DIRS 178394]. In addition to the BDCFs, the data used in TSPA to demonstrate compliance with the groundwater protection standards in 10 CFR 63.331 [DIRS 180319] are titled *Groundwater Protection Standards Conversion Factors* (DTN: MO0702PAGWPROS.001_R0 [DIRS 179328]) and are included in two calculations: the estimation of annual dose (whole body and individual organs) from beta and photon emitting radionuclides from consuming two liters of well water daily, and the contribution to the gross

alpha activity concentration in groundwater, as defined in 10 CFR 63.331 ([DIRS 180319], Table 1) from radionuclides released from the repository.

Figure 6.3.11-1 uses the example of the groundwater exposure case to show the relationships between the Biosphere Model Component, the SZ Flow and Transport Model Component, and the calculation of annual dose for evaluation of compliance with the individual protection standard and with the groundwater protection standards. Figure 6.3.11-2 summarizes the TSPA-LA Biosphere Model Component, its inputs and outputs, and the technical basis for confidence in the Biosphere Model Component. The inputs for the Biosphere Model Component from the first two and last DTN cited above (the two BDCF sets for the groundwater and volcanic cases and the groundwater protection standards data set) are used in TSPA-LA GoldSim. The other DTN (inhalation dose factors for the period during the volcanic eruption) is used outside the TSPA-LA Model and this use is documented in Section 6.5.2.4.

6.3.11.1 Conceptual Models

The two exposure cases considered in the TSPA-LA Model are illustrated on Figures 6.3.11-3 and 6.3.11-4. For the groundwater exposure case, radionuclides enter the biosphere from one or more wells that extract contaminated groundwater from an aquifer. Human exposure arises from using the contaminated water for domestic and agricultural purposes. Groundwater BDCFs apply to all modeling cases except the Volcanic Eruption Modeling Case of the Igneous Scenario Class. In the volcanic ash exposure case, human exposure arises from contaminated tephra deposited on surface soil and the subsequent radionuclide transport from surface soil to other environmental media (e.g., air and plants). Volcanic ash BDCFs apply only to the Volcanic Eruption Modeling Case of the Igneous Scenario Class.

The radionuclides of interest for the Biosphere Process Model, also referred to as the primary radionuclides as tracked in the TSPA-LA Model, depend on the exposure case and are developed in *Radionuclide Screening* (SNL 2007 [DIRS 177424]) and defined in DTN: MO0701RLTSCRNA.000_R0 [DIRS 179334]. The treatment of radionuclide transport in the Biosphere Process Model is the same for most radionuclides in both exposure cases. However, two radionuclides, ^{14}C and ^{222}Rn (a short-lived decay product of ^{226}Ra), are modeled differently because of the large amount of stable carbon (^{12}C) in the environment and the gaseous release from soils of ^{222}Rn and $^{14}CO_2$.

To facilitate modeling for dose calculations, the reference biosphere is developed in the *Biosphere Model Report* (SNL 2007 [DIRS 177399], Section 6.1.1). The reference biosphere has to represent the environment inhabited by the RMEI along with associated human exposure pathways and parameters (10 CFR 63.102(i) [DIRS 180319]). Required characteristics of the reference biosphere are the following:

- Features, events, and processes that describe the reference biosphere must be consistent with present knowledge of the conditions in the region surrounding the Yucca Mountain site (10 CFR 63.305(a) [DIRS 180319]).

- DOE should not project changes in society, the biosphere (other than climate), human biology, or increases or decreases of human knowledge or technology. In all analyses

done to demonstrate compliance with this part, DOE must assume that all of those factors remain constant as they are at the time of submission of the license application (10 CFR 63.305(b) [DIRS 180319]).

- DOE must vary factors related to the geology, hydrology, and climate based upon cautious but reasonable assumptions consistent with present knowledge of factors that could affect the Yucca Mountain Repository system during the period of geologic stability (10 CFR 63.302 [DIRS 178394]) and consistent with the requirements for performance assessments specified in 10 CFR 63.342 [DIRS 178394] (10 CFR 63.305(c), [DIRS 178394]).

- Biosphere pathways must be consistent with arid or semi-arid conditions (10 CFR 63.305(d) [DIRS 180319]).

The RMEI is a hypothetical person who meets the following criteria (10 CFR 63.312 [DIRS 180319]):

a. Lives in the accessible environment above the highest concentration of radionuclides in the plume of contamination.

b. Has a diet and living style representative of the people who now reside in the Town of the Amargosa Valley, Nevada, based on surveys that determine current diets and living styles, and for whom the mean values of these factors are used in the assessments conducted for the Individual Protection Standard in 10 CFR 63.311 [DIRS 178394] and the Individual Protection Standard for Human Intrusion in 10 CFR 63.321 [DIRS 178394].

c. Uses well water with average concentrations of radionuclides based on annual water demand of 3,000 acre-feet.

d. Drinks two liters of water per day from wells drilled into the groundwater from a point above the highest concentration of radionuclides in the plume of contamination.

e. Is an adult with metabolic and physiological considerations consistent with present knowledge of adults.

To meet the requirement in 10 CFR 63.312(b) [DIRS 180319], the dietary and living style characteristics of the RMEI were determined based on surveys of people living in the Amargosa Valley, combined with the 2000 census data (Bureau of the Census 2002 [DIRS 159728]) as well as regional and national information on behavioral patterns and food intake (USDA 2000 [DIRS 154158], EPA 1997 [DIRS 116135], and ICRP 1994 [DIRS 153705]). Characteristics of the RMEI were developed, using these data, in a separate analysis (BSC 2005 [DIRS 172827]).

Groundwater Exposure Case—In the groundwater exposure case, radionuclides are introduced into the biosphere with groundwater pumped from wells for agricultural and domestic purposes. Once in the biosphere, the radionuclides migrate through various environmental components. During this migration, some of the radionuclides give rise to a dose to the RMEI through one of

three exposure pathways: inhalation, ingestion, or external exposure. Each of the exposure pathways is modeled using the diet, living style, and other characteristics of the RMEI. The biosphere model for the groundwater exposure case considered five environmental components (or submodels): soil, air, plant, animal, and fish. The radionuclides in each of these components can result in exposure to the RMEI. Figure 6.3.11-5 illustrates the relationships among the biosphere submodels indicating the migration of radionuclides in the biosphere between the various biosphere submodels starting with the introduction of contaminated groundwater into the biosphere and resulting in a dose to the RMEI. On Figure 6.3.11-5, arrows point in the direction of radionuclide transfer between biosphere components in the Biosphere Process Model. For example, groundwater is used for human drinking water (to ingestion submodel), animal drinking water (to animal submodel), irrigation water (to soil and plant uptake submodels), fish pond water (to fish submodel), and evaporative cooler water (to air submodel).

The submodels described above are the same for all primary radionuclides with the sole exception of ^{14}C. Special submodels are used to calculate ^{14}C concentrations in the surface soil, air, crops, and animal products because the transfer mechanisms for this radionuclide are different from the others in the model by virtue of the presence of the stable carbon (^{12}C) in the biosphere. The transfer of ^{14}C between submodels follows that for other radionuclides as shown on Figure 6.3.11-5.

The following environmental transport processes are explicitly included in the Biosphere Process Model (SNL 2007 [DIRS 177399], Section 6.3.1.3)

- Radionuclide accumulation in surface soil layers as a result of continuous long-term cultivation using contaminated water
- Resuspension of contaminated soil
- Radionuclide deposition on crop surfaces by dry processes (resuspension of contaminated soil and subsequent adhesion of soil particles onto vegetation surfaces)
- Radionuclide deposition on crop surfaces by interception of contaminated irrigation water
- Removal of surface contamination by weathering processes
- Translocation and retention of contaminants from the deposition site to the edible tissues of vegetation
- Radionuclide uptake from soil by plants through the roots
- Release of radionuclides in gaseous phases, ^{222}Rn and $^{14}CO_2$, from the soil into the air with subsequent inhalation
- Photosynthesis by crops of $^{14}CO_2$ from the atmosphere

- Radionuclide intake by animals through consumption of contaminated feed, water, and soil, followed by transfer to animal products
- Radionuclide transfer from water to air through use of evaporative coolers
- Radionuclide transfer from water to fish.

Exposure to radionuclides in the environment arises when the RMEI's diet and living style give rise to intake of, and external exposure to, radionuclides in environmental media. The Biosphere Process Model then calculates the annual dose from ingestion, inhalation, and external exposure pathways resulting from those intakes and exposures. Table 6.3.11-1 provides a summary of human-exposure pathways for the groundwater exposure case considered in the Biosphere Process Model, including the contributing submodels of the environmental media and the examples of typical activities that may potentially lead to radiation exposure (SNL 2007 [DIRS 177399], Section 6.3.1.1).

The TSPA-LA only considers the release and transport of the primary radionuclides. To avoid underestimating annual dose to the RMEI, the Biosphere Process Model accounts for the decay products of the primary radionuclides after they are introduced into the biosphere. The short-lived decay products with half-lives of less than 180 days are considered to be in secular equilibrium with the parent radionuclide, and their radiation dose contributions are included in the BDCF for the primary radionuclide or a long-lived decay product of the primary radionuclide (SNL 2007 [DIRS 177399] Sections 6.3.1.4 and 6.3.5). The Biosphere Process Model also accounts for the build-up of the primary radionuclides in soil as well as the decay and ingrowth of long-lived decay products in the soil as a result of long-term irrigation (from 25 years up to one thousand years) (SNL 2007 [DIRS 177399] Sections 6.4.1.1 and 6.4.1.2). In this case, the BDCF contributions of the long-lived decay products created in the soil are added to that of the parent primary radionuclides (SNL 2007 [DIRS 177399], Section 6.4.1.2 and Table 6.4-3). The output of the Biosphere Process Model for the groundwater exposure case is the *Groundwater Biosphere Dose Conversion Factors* (DTN: MO0702PAGBDCFS.001_R0 [DIRS 179327]). This DTN provides the groundwater case BDCFs for all primary radionuclides and the following combination of radionuclides where the effects of longer term decay products are included with the BDCF of the initial primary radionuclide (^{226}Ra and ^{210}Pb; ^{232}Th, ^{228}Ra, and ^{228}Th; and ^{232}U and ^{228}Th). This summation approach allows a realistic assessment of dose to be made if TSPA does not directly consider (i.e., track) all radionuclides.

To support climate change modeling for the TSPA-LA Model, BDCFs for the groundwater exposure case were initially developed for the three climate states (SNL 2007 [DIRS 177399], Sections 6.1.1.2 and 6.11.1.2.2) but were further analyzed for consistency with the regulatory requirements. Future climate forecasts (BSC 2004 [DIRS 170002], Section 6.1) indicate that the climate at Yucca Mountain is reasonably expected to evolve to the cooler, wetter conditions of a glacial transition climate within the first 10,000 years after disposal. Monsoon and glacial-transition (intermediate) climate states are predicted to last until 38,000 years A.P. (after present) (Sharpe 2003 [DIRS 161591], p. 57). Over the period of geologic stability, it is expected that there will be more than one climate cycle. 10 CFR 63.305(c) [DIRS 178394] requires that the DOE vary factors related to climate based on cautious, but reasonable assumptions. At the same time, changes in society, the biosphere (other than climate), human

biology, or increases or decreases of human knowledge or technology should not be projected (10 CFR 63.305(b) [DIRS 180319]). The climate change in the Biosphere Process Model was thus evaluated and addressed from the perspective of natural processes and from the perspective of the factors that are related to human activity.

In the Biosphere Process Model (SNL 2007 [DIRS 177399], Section 6.11.1.2), the effect of climate change on the BDCFs for the groundwater exposure scenario was evaluated from the perspective of the factors that are related to the human society, which 10 CFR 63.305(b) [DIRS 180319] directs DOE not to vary in its performance assessments, and those factors that are independent of human activities, which 10 CFR 63.305(c) [DIRS 178394] directs DOE to vary over the period of geologic stability. The climate-related factors that have the largest effect on the BDCFs depend on human activities and the BDCFs are relatively insensitive to the effects of climate changes in the other factors. Furthermore, the BDCFs for the future climate, which is predicted to be cooler and wetter than the present-day climate, are lower than the corresponding present-day climate BDCFs and would result in lower doses to the RMEI. Therefore, using the present-day climate BDCFs represents a conservative choice, meets the requirements in 10 CFR 63.305(a) and (b) [DIRS 180319], and is appropriate for the assessment of doses to the RMEI for the entire period of the geologic stability (SNL 2007 [DIRS 177399], Sections 6.11.1.2). Thus, for all TSPA-LA dose calculations, the BDCFs for the present day climate are used.

Volcanic Ash Exposure Case—The biosphere conceptual model for the volcanic ash exposure case uses a similar reference biosphere and human receptor as the groundwater exposure case. The major difference between the exposure cases is that in this case the radionuclide source consists of contaminated tephra deposited on the ground surface and mixed with soil, rather than the multiple uses of contaminated groundwater. Figure 6.3.11-6 illustrates the relationships among the biosphere submodels indicating the migration of radionuclides in the reference biosphere between the various biosphere submodels starting with the introduction of contaminated tephra into the reference biosphere and resulting in a dose to the RMEI. On Figure 6.3.11-6, arrows point in the direction of radionuclide transfer between components in the Biosphere Process Model.

The following environmental transport processes are explicitly included in the Biosphere Process Model for the ash exposure case (SNL 2007 [DIRS 177399], Sections 6.3.2.1 and 6.3.2.6):

- Resuspension of contaminated soil and tephra from soils both undisturbed and from activities that disturb the soil surface
- Dry deposition of radionuclides on crop surfaces, including resuspension of contaminated soil and subsequent adhesion of soil particles on crop surfaces
- Removal of surface contamination by weathering processes
- Translocation and retention of contaminants from the site of deposition to the edible portions of crops
- Radionuclide uptake by crops through the roots

- Radionuclide intake by animals through consuming contaminated feed and soil, and subsequent transfer to animal products

- Release of radon (^{222}Rn) from the soil.

Because the groundwater is contamination free in the volcanic ash exposure case, fewer exposure pathways are considered, as shown in Table 6.3.11-2, than for the groundwater exposure case. As described in *Biosphere Model Report* (SNL 2007 [DIRS 177399], Section 6.3.2.1), the volcanic ash exposure case does not include a contribution to annual dose from ingestion of drinking water, ingestion of locally produced fish, and inhalation of indoor aerosols generated by evaporative coolers. In addition, the dose contribution from ^{14}C in solid or gaseous forms is not considered because ^{14}C was assessed to be a negligible contributor to dose in the volcanic ash exposure case in *Radionuclide Screening* (SNL 2007 [DIRS 177424], Tables 6-7 and 6-8). The consideration of short-lived non-primary radionuclide decay products in the volcanic ash exposure case is the same as discussed above for the groundwater exposure case (i.e., their contributions to dose are included in the BDCFs of the parent radionuclide).

The analysis of BDCFs for the volcanic ash exposure case (SNL 2007 [DIRS 177399], Section 6.12.1.2) indicates that the results of the Biosphere Process Model for the volcanic ash exposure case are relatively insensitive to climate change (BDCF changes over climate are less than 1 percent). Therefore, one set of BDCFs, applies to all climate states considered in the TSPA-LA Model.

6.3.11.2 TSPA-LA Model Abstraction

The objectives of the Biosphere Process Model and analyses are to develop the capabilities and associated data sets to allow TSPA to evaluate compliance with the postclosure individual protection standard in 10 CFR 63.311 [DIRS 178394], the groundwater protection standards in 10 CFR 63.331 [DIRS 180319], and the individual protection standard for human intrusion in 10 CFR 63.321 [DIRS 178394]. In the case of the individual protection standard, this information is identified in *Biosphere Model Report* (SNL 2007 [DIRS 177399], Section 8.1.1). The mathematical abstraction and the required BDCFs for the two exposure cases needed to calculate annual dose to the RMEI from radionuclide concentrations in groundwater or soil at the accessible environment are presented in *Groundwater Biosphere Dose Conversion Factors* (DTN: MO0702PAGBDCFS.001_R0 [DIRS 179327]) and *Volcanic Biosphere Dose Conversion Factors* (DTN: MO0702PAVBPDCF.000_R0 [DIRS 179330]). In addition, dose factors to calculate inhalation exposure during the volcanic eruption from predictions of atmospheric concentrations of radionuclides are provided in *Inhalation Dose Factors* (DTN: MO0702PAINHALA.001_R0 [DIRS 179329]). The dose factors are used outside of the TSPA model to calculate inhalation dose during a volcanic eruption (Section 6.5.2.4).

The information required to demonstrate compliance with the groundwater protection standards is given in *Biosphere Model Report* (SNL 2007 [DIRS 177399], Section 8.1.1), which presents the equations and data that allows the TSPA to use radionuclide concentrations in groundwater to evaluate the whole body and individual organ doses from consumption of two liters of water per day and to calculate alpha particle activity in groundwater as per 10 CFR 63.331 [DIRS 180319].

These data are provided in *Groundwater Protection Standards Conversion Factors* DTN: MO0702PAGWPROS.001_R0 [DIRS 179328].

To incorporate uncertainty into the TSPA-LA model input, BDCFs were calculated in a manner to propagate the uncertainties of the biosphere input parameters. This was accomplished by conducting a series of 1,000 stochastic model realizations. Uncertain input parameters to the Biosphere Process Model were sampled using Latin hypercube sampling for consistency with the sampling technique used for the TSPA-LA Model as discussed in this report. The resulting set of BDCFs incorporates the uncertainty from those input parameters. The sampling was structured such that for a given iteration the sampled value for each non-radionuclide specific parameter was the same for every radionuclide. This approach ensured that the correlation between BDCFs arising from the commonality of receptor and environmental characteristics was retained. The full set of BDCFs consists of a BDCF for each primary radionuclide for each Biosphere Process Model realization. As listed in Table 6.3.7-2, there are 29 radionuclides for the groundwater exposure case and 22 radionuclides for the volcanic ash exposure case. Table 6.3.11-3 lists the TSPA-LA parameters used to represent groundwater BDCF uncertainty in the TSPA-LA Model. In addition to the BDCFs for the primary radionuclides, the BDCF data set also contains composite values for a few cases where a radionuclide that is individually tracked in the Biosphere Process Model is combined with the BDCF for the much longer-lived parent radionuclide (e.g., ^{226}Ra + ^{210}Pb and ^{232}Th + ^{228}Ra + ^{228}Th). This approach allows the TSPA the option to only track the parent without systematic underestimation of dose.

Summaries of the parameters and their distributions used to develop BDCFs for the groundwater and volcanic eruption cases are provided in *Biosphere Model Report* (SNL 2007 [DIRS 177399], Tables 6.6-2 and 6.6-3).

Calculation of Annual Dose to the RMEI for the Groundwater Exposure Case—The TSPA-LA Model calculates the total annual dose to the RMEI at a given time using the set of BDCFs and radionuclide concentrations in the groundwater used by the RMEI. The total annual dose is the sum of the annual doses from all radionuclides tracked in the TSPA-LA Model as is given in *Biosphere Model Report* (SNL 2007 [DIRS 177399], Sections 6.4.10.4 and 6.11.3):

$$D_{total}(t) = \sum_i BDCF_i \times Cw_i(t) \qquad \text{(Eq. 6.3.11-1)}$$

where

$D_{total}(t)$ = time-dependent total annual dose from groundwater to the RMEI resulting from the release of radionuclides from the repository. This includes contributions from all radionuclides considered in the TSPA-LA Model (Sv/yr).

$BDCF_i$ = groundwater biosphere dose conversion factor for radionuclide i (Sv/yr per Bq/m^3).

$Cw_i(t)$ = time-dependent activity concentration of radionuclide i in groundwater at the RMEI location (Bq/m^3).

Calculation of Alpha Activity Concentration in Groundwater—The methods and the conversion factor values described in *Biosphere Model Report* (SNL 2007 [DIRS 177399], Section 6.15.1.1) are used to calculate the gross alpha activity concentration in groundwater for evaluation of compliance with the groundwater protection standards in 10 CFR 63.331 [DIRS 180319]. Natural background activity concentrations (DTN: SN0702PASZFTMA.002_R1 [DIRS 183471]) are added to calculated values for comparison with the limit for combined ^{226}Ra and ^{228}Ra activity concentration in groundwater and with the limit for gross alpha activity concentration. The alpha particle activity concentration in the groundwater is calculated in the TSPA-LA Model using the number of alpha particles per decay of each primary radionuclide (DTN: MO0702PAGWPROS.001_R0 [DIRS 179328]) and using the following equation (SNL 2007 [DIRS 177399], Equation 6.15-1 and Table 6.15-3):

$$C_{\alpha}(t) = \sum_{i} Cw_{i}(t)\, N\alpha_{i} \qquad \text{(Eq. 6.3.11-2)}$$

where $Cw_i(t)$ (Bq/m^3 or pCi/L) is defined above and

$C_{\alpha}(t)$ = the time-dependent total alpha particle activity concentration in groundwater (Bq/m^3 or pCi/L)

$N\alpha_i$ = number of alpha particles emitted per one decay of a primary radionuclide i.

Contributions from radon and uranium are excluded when calculating $N\alpha_i$, as directed in 10 CFR 63.331 [DIRS 180319].

Calculation of Beta-Photon Dose from Drinking Two Liters of Water per Day—The beta-photon doses to the whole body and individual organs are calculated using conversion factors from *Biosphere Model Report* (SNL 2007 [DIRS 177399], Table 6.15-6); DTN: MO0702PAGWPROS.001_R0 [DIRS 179328]) and the following equation (SNL 2007 [DIRS 177399], Equation 6.15-4):

$$D(t) = \sum_{i} Cw_{i}(t)\, CF_{i} \qquad \text{(Eq. 6.3.11-3)}$$

where $Cw_i(t)$ (Bq/m^3) is defined above and

$D(t)$ = time-dependent total annual dose for an individual organ or for the whole body from beta-gamma emitters in the groundwater from daily consumption of 2 liters of water (Sv/yr)

CF_i = conversion factor for calculating beta-photon annual dose for an individual organ or for the whole body from radionuclide i from daily consumption of 2 liters of water (Sv/yr per Bq/m^3).

The conversion factors are provided for the following organs (23) and for the whole body:

Adrenals	Muscle
Bone Surface	Ovaries
Brain	Pancreas
Breast	Red Bone Marrow
Stomach Wall	Skin
Small Intestine Wall	Spleen
Upper Large Intestine Wall	Testes
Lower Large Intestine Wall	Thymus
Kidneys	Thyroid
Liver	Uterus
Extrathoracic Airways	Urinary Bladder Wall
Lung	Whole Body

Calculation of Annual Dose to the RMEI for the Volcanic Ash Exposure Case—The TSPA-LA Model calculates the total annual dose for the volcanic ash exposure case using the following equations (SNL 2007 [DIRS 177399], Section 6.12.3 and Equation 6.12-1):

$$D_{total}(t,T) = \sum_i D_{all\ pathway,i}(t,T)$$

and

$$D_{all\ pathway,i}(t,T) = BDCF_{ext,ing,Rn,i}\ Cs_i(t) + \left(BDCF_{inh,v,i} f(t-T) + BDCF_{inh,p,i}\right) Cs_{mc,i}(t)$$

(Eq. 6.3.11-4)

where

$D_{total}(t,T)$ = total annual dose from all radionuclides at time t-T after a volcanic release of radionuclides from the repository at time t after repository closure (Sv/yr)

$D_{all\ pathway,i}(t,T)$ = all-pathway annual dose for primary radionuclide i at time t-T after a volcanic release of radionuclides from the repository at time t after repository closure (Sv/yr)

$BDCF_{ext,ing,Rn,i}$ = BDCF component for external exposure, ingestion, and inhalation of radon decay products for primary radionuclide i (Sv/yr per Bq/m^2)

$Cs_i(t)$ = areal radionuclide concentration in a specified depth of surface soil at time t (year) after the repository closure (Bq/m^2) calculated in TSPA-LA model

$BDCF_{inh,v,i}$ = BDCF component representing average early-time increase in inhalation exposure in the first year after a volcanic eruption; used in

calculation of short-term inhalation exposure at post-eruption level of mass loading in excess of nominal mass loading for primary radionuclide *i* (Sv/yr per Bq/kg)

$BDCF_{inh,p,i}$ = BDCF component for long-term inhalation at nominal level of mass loading for primary radionuclide *i* (Sv/yr per Bq/kg)

$f(t\text{-}T)$ = decay function describing reduction of the annual average mass loading with time at time $t\text{-}T$ following a volcanic

$Cs_{mc,i}(t)$ = activity concentration of radionuclide *i* per unit mass of soil in the resuspendable layer of surface soil (critical thickness) at time t (year) after the repository closure (Bq/kg).

The time function, $f(t)$, accounts for the reduction of mass loading in the years immediately following a volcanic eruption. The mass loading decreases exponentially with time as (SNL 2007 [DIRS 177399], Equation 6.12-3):

$$f(t-T) = e^{-\lambda(t-T)} \qquad \text{(Eq. 6.3.11-5)}$$

where

λ = fractional mass loading decrease rate constant (1/yr)

$t\text{-}T$ = time after a volcanic eruption at T (years); $t\text{-}T = 0$ is the first year after a volcanic eruption.

The mass loading decrease rate is provided by the Biosphere Process Model as an input parameter implemented in the TSPA-LA Model.

Both source terms used in the calculation of doses (Equation 6.3.11-4) (i.e., the areal radionuclide concentration in surface soil, $Cs_i(t)$, and the mass radionuclide concentration in the resuspendable soil layer, $Cs_{mc,i}(t)$), are calculated in the TSPA by weighting the appropriate radionuclide concentrations by the respective expected areas of the distributary channels and the interchannel divides at the location of the RMEI. The radioactive waste mass concentrations in the resuspendable layer of soil, $Cs_{mc,i}(t)$, and in the surface soil, $Csi(t)$, are determined from the results of the ASHPLUME and FAR models as discussed in Section 6.5.2.2.

These models produce the results in terms of waste volumetric concentration. The waste volumetric concentration can be converted to waste mass concentration in the soil by dividing it by the density of the resuspendable layer, ρ_c. In the interchannel divides, the density of the resuspendable layer, ρ_c, can be calculated from the known tephra thickness, d_a, and density, ρ_a, and surface soil density, ρ_s, (SNL 2007 [DIRS 177399], Equation 6.12-2) as:

$$\rho_c = \frac{d_a\,\rho_a + (d_c - d_a)\,\rho_s}{d_c} \qquad \text{when } d_a < d_c \text{ and}$$

$$\rho_c = \rho_a \qquad \text{when } d_a \geq d_c \qquad \text{(Eq. 6.3.11-6)}$$

where

ρ_c = bulk density of resuspendable layer of surface soil, including tephra (kg/m^3)

d_c = thickness of resuspendable soil layer (i.e., the critical thickness (m))

d_a = thickness of initial tephra layer (m)

ρ_a = bulk density of tephra (kg/m^3)

ρ_s = bulk density of the original surface soil (i.e., without tephra) (kg/m^3).

The TSPA model keeps track of the radionuclide activity concentration per unit mass of waste and apportions the correct activity of each radionuclide to the known waste concentration in the surface soil.

The sampling results of bulk density and tillage depth of the surface soil for individual biosphere model realizations are included in DTN: MO0702PAVBPDCF.000_R0 [DIRS 179330]. In the channels, where the tephra is mixed with soil and diluted, the density of resuspendable layer, ρ_c, can be approximated by the density of soil, ρ_s (SNL 2007 [DIRS 177399], Section 6.12.3).

Calculation of Inhalation Dose Accrued During the Volcanic Eruption—To calculate the inhalation dose to the RMEI during the eruption phase of a volcanic event (usually lasting less than a year), dose factors for the inhalation exposure pathway are used instead of the all pathway BDCFs. The daily dose from inhaling a specific radionuclide during the tephra fall from a volcanic eruption was calculated external to the TSPA-LA Model. The total daily inhalation dose, D_{inh}, from concentrations of primary radionuclides in the air was calculated as (SNL 2007 [DIRS 177399], Section 6.15.2.2, Equation 6.15-9):

$$D_{inh} = \sum_i D_{inh,i} = \sum_i DF_i \times Ca_{i,outdoor} \quad \text{(Eq. 6.3.11-7)}$$

where

$D_{inh,i}$ = daily inhalation dose (i.e., committed dose from one day's inhalation intake) for a primary radionuclide i (Sv/d)

DF_i = inhalation dose factor for a primary radionuclide i (Sv/d per Bq/m^3)

$Ca_{i,outdoor}$ = one day average activity concentration of a primary radionuclide i in outdoor air (Bq/m^3).

The inhalation of airborne radionuclides in tephra once they are deposited on the ground and subsequently resuspended is included in the BDCFs. The calculation results show that the expected annual dose (i.e., the probability-weighted annual dose) from inhalation of airborne radionuclides in tephra during the deposition phase is lower by several orders of magnitude than the expected annual dose (as presented in Section 6.1.2) caused by tephra deposited on the ground. Therefore, the contribution of an eruptive phase dose is neglected in the TSPA-LA

Model. See Section 6.5.2.4 for details of this calculation and comparison with the TSPA-LA Model results.

6.3.11.3 TSPA-LA Model Implementation

The Biosphere Process Model provides stochastic BDCFs for the calculation of the annual dose to the RMEI. In addition, deterministic conversion factors for beta and photon dose from drinking two liters of water per day, and the number of alpha particles emitted per decay of primary radionuclides, are provided as inputs to the TSPA-LA Model. The BDCFs are transferred into the TSPA-LA Model in the form of one-dimensional tables, one for each radionuclide, that consist of 1,000 rows, which represent individual model realizations. The conversion factors used to calculate beta-photon dose are in a two-dimensional look-up table consisting of 19 columns representing each of the relevant (i.e., beta-photon emitting), primary radionuclides and three additional columns for the combination of long- and short-lived radionuclide combinations. The table has 24 rows that correspond to individual organs and the whole body. In the case of alpha activity calculations, a look-up table is provided that gives the total number of alpha particles attributable to one radioactive decay of each of the (16) primary radionuclides that include alpha emitters in their short-lived decay chains.

The annual dose to the RMEI is calculated in the TSPA-LA Biosphere Model Component using the BDCFs that convert radionuclide concentrations in groundwater or soil-tephra mixture to an annual all-pathway dose (based on Equations 6.3.11-1 and 6.3.11-4). A discrete distribution, Bio_Index is sampled in TSPA to represents the epistemic model uncertainty from the Biosphere Model. Bio_Index, an equally probable integer from 1 to 1,000 inclusive, is used to randomly select a particular sequence of realizations from the BDCF tables. For the groundwater exposure case, one set of BDCFs, the set corresponding to the present-day climate, is used throughout the modeling time period of the TSPA-LA Model (Section 6.3.11.1). The selected BDCFs are then multiplied by the radionuclide concentrations provided by the SZ Flow and Transport Model Component (or by concentrations in tephra as calculated by the FAR Model [Section 6.5.2.1.3]) to compute the annual dose (Equations 6.3.11-1 and 6.3.11-4). Probability weighting of dose is calculated in the Biosphere Model Component for the Nominal Early Failure (Section 6.4) and Igneous Intrusion Modeling Cases (Section 6.5.1) and the Seismic Scenario Class (Section 6.6). The probability weighting for the Volcanic Eruption Modeling Case is handled in the source term calculation (Section 6.5.2).

The calculations for the groundwater protection standards are based on the activity concentration of each primary radionuclide in groundwater, as calculated from radionuclide concentrations provided by the SZ Flow and Transport Model Component. The alpha particle activity concentration in water and the beta-photon dose from drinking two liters of water per day are then calculated using Equations 6.3.11-2 and 6.3.11-3, respectively. Equations 6.3.11-5 and 6.3.11-6 are implemented in the Volcanic Ash Exposure Submodel under the Volcanic Eruption Modeling Case (Section 6.5.2.2). As noted previously, the inhalation dose during a volcanic eruption period (Equation 6.3.11-7) was not implemented in the TSPA-LA Model because, as a result of external evaluation, it was determined that the contribution from this pathway to the probability-weighted annual dose was insignificant.

6.3.11.4 Model Component Consistency and Conservatism in Assumptions and Parameters

To enhance understanding of the complex interactions within the TSPA-LA Model, a discussion of consistency among model components and submodels and identification of conservative assumptions in abstractions, process models, and parameter sets supporting the biosphere are discussed as follows.

6.3.11.4.1 Consistency of Assumptions

It is important to ensure that the parameters and assumptions in each model component or submodel of the TSPA-LA Model are consistent. The first discussion concerns tephra particle sizes during eruptive atmospheric transport and when they are used for the inhalation dose calculation. The second applies to the groundwater release case and concerns the elemental partition coefficients used for transport calculations in the UZ and SZ and those employed in the soil submodel of the Biosphere Process Model.

Volcanic Tephra Particle Size—In the Biosphere Process Model, the reference biosphere describes the environment around the location of the RMEI (10 CFR 63.312 [DIRS 180319]), which is located about 18 km south of the repository, (66 FR 55732 [DIRS 156671] III Public Comments and Responses 3.2, p. 55750), as specified in the definition of the *Controlled Area* found in 10 CFR 63.302 [DIRS 180319]. The size of resuspended particles used to calculate the inhalation component of the dose to the RMEI is smaller than the particle size in the ASHPLUME code used to predict atmospheric transport (advection and diffusion) and surface deposition (gravitational settling) of the tephra from a volcanic eruption. After the eruption, fluvial processes redistribute the tephra from the immediate vicinity of the eruption down Fortymile Wash to the location of the RMEI. This Tephra Redistribution Submodel (Section 6.5.2.1.3) does not explicitly consider mechanical processes that generate smaller tephra particles nor is any account taken of subsequent weathering processes. However, the redistribution model does account for the diffusion of radionuclides into the adjacent soil or soil-tephra mixture. This diffusion process is calibrated from measured ^{137}Cs profiles on channels and inter-channel divides of the upper Fortymile Wash alluvial fan and models the migration of the contaminants in the tephra to the local soil, thereby providing a source of resuspendable contaminated particles. The inhalation dose is calculated in the Biosphere Process Model by using inhalation dose coefficients for 1-μm particles, while the ASHPLUME code predictions concern particles greater than 15 to 30 μm. This is because of ASHPLUME's inability to accurately represent the transport of tephra particles of mean diameter less than approximately 15 μm (Jarzemba et al. 1997 [DIRS 100987], Section 2.1; and SNL 2007 [DIRS 177431], Section 1.3.1). Because the typical mean diameter of tephra particles after an eruption is generally much larger than 15 μm, the model is applicable for calculating the distribution of the majority of the mass of potential tephra and radionuclide releases from a possible future eruption at Yucca Mountain (SNL 2007 [DIRS 177431], Section 1.3.1). However, it does not address well the particles in the respirable (less than 4 μm) and thoracic (less than 10 μm) size range, which are more important for the evaluation of inhalation doses (BSC 2005 [DIRS 172827], Section 6.5.5.1). This apparent difference in the particle size distribution of tephra deposited at the location of the RMEI and the particle size distribution used to calculate inhalation dose to the RMEI becomes less significant with time as tephra particles

weather and radionuclides diffuse and attach to small soil particles. The processes that cause redistribution of the contaminated tephra after the volcanic eruption, as well as other natural processes and human activities at the location of the RMEI, may change the initial particle size distribution of deposited tephra.

Effect of Volcanic Tephra Particle Size on TSPA—A study was completed in *Characteristics of the Receptor for the Biosphere Model* (BSC 2005 [DIRS 172827], Section 6.5.5.2) regarding the effect of differences in particle size on predicted inhalation dose. It was concluded that "…the application of dose coefficients for particles with activity median aerodynamic diameter of 1 μm will not underestimate the doses from inhalation of resuspended material and that these dose coefficients are adequate for use in the biosphere model."

6.3.11.4.2 Identification of Conservatisms in Submodels and Abstractions

Dose Coefficients for Internal Exposure—The dose coefficients for internal exposure (inhalation and ingestion) used to calculate the BDCFs are the most conservative of the values provided in the source reference (EPA 2002 [DIRS 175544]) for a given radionuclide. Different dose coefficient choices correspond to different gastrointestinal absorption fractions for ingestion and, in the case of inhalation, differing transfer fractions from the lung to blood stream for different chemical compounds of a given radionuclide. The conservative values were used because of uncertainty in the final chemical/physical form of the radionuclides supplied to the biosphere from groundwater and the uncertainty in the subsequent evolution of the chemical/physical form in the biosphere (SNL 2007 [DIRS 177399], Sections 6.4.8.5 and 6.4.9.6). This conservatism results in either a realistic estimate of dose or an overestimation of dose.

Dose Coefficients for External Exposure to Contaminated Soil—For calculating the external dose from exposure to contaminated soil for the groundwater case, the dose coefficients for an infinite depth of contamination were used. This approach allowed the time evolution of soil build-up to be considered only in the tillage depth while accounting for the external exposure to radionuclides that could have been leached from the surface soil into the deep soil. Use of these dose coefficients is reasonable yet conservative as dose coefficients for an infinite depth and those for a 15-cm depth (note that tillage depths extend up to 30 cm) differ by less than 10 percent for most primary radionuclides (EPA 2002 [DIRS 175544]). Only for radionuclides with strong gamma emissions, such as ^{226}Ra and ^{137}Cs, do dose coefficients exhibit a larger difference for these two depths. The use of dose coefficients for an infinite depth cannot underestimate dose.

Roots in Surface Soil—All crop roots are considered to be in the surface soil layer (i.e., the soil layer extending down to the tilling depth). For many crops, the root systems can extend to below the tillage depth. This approach effectively assumes (conservatively) that all roots, the source of radionuclide uptake for plants, are exposed to a radionuclide concentration as calculated for the tillage region.

Resuspended Volcanic Ash—Radionuclide concentrations in the air were calculated separately for cultivated and uncultivated lands. The concentration of radionuclides in cultivated (i.e., tilled) soil was used to calculate concentrations of radionuclides in crops and animal

products. The concentration of radionuclides in uncultivated soil was used to calculate inhalation and external exposure to the RMEI. This was done because for most of the land area the soil in the reference biosphere would not be cultivated. Using radionuclide mass concentrations of uncultivated soil to calculate inhalation and external exposure is a conservative approach because the concentrations in uncultivated soil would be higher than in cultivated soil where tilling causes additional dilution. Because uncultivated lands would not be disturbed by agricultural activities, tephra would not mix quickly with surface soil and tephra would remain on or near the soil surface where it is available for resuspension (SNL 2007 [DIRS 177399], Section 6.3.2.6). This conservatism results in the overestimation of dose.

External Exposure from Tephra on the Ground Surface—Unlike the groundwater exposure scenario, where soil contamination could be deep, tephra and associated radionuclides could be distributed on or near the soil surface and the source for external exposure could be a thin layer of uncultivated soil on the ground surface. Thus, external exposure was evaluated using the dose coefficients for exposure to contaminated ground surface (EPA 2002 [DIRS 175544]) rather than volumetric concentrations. This modeling approximation was reasonable because there is considerably more uncultivated land than cultivated land in Amargosa Valley (BSC 2004 [DIRS 177101], Section 6.2), and the mixing of tephra on uncultivated lands would be limited. The effects of radiation attenuation in the soil and tephra were conservatively minimized (SNL 2007 [DIRS 177399], Section 6.3.2.4). This conservative assumption results in the overestimation of dose in cases where radionuclides are distributed throughout the soil where their radiations are attenuated by the soil layer between the point of emission and the RMEI. For radionuclides with a significant dose contribution from external exposure, such as ^{137}Cs and ^{126}Sn this conservatism could overestimate annual dose predictions.

6.3.11.5 Alternative Conceptual Model(s) for Biosphere

Section 6.2 outlines the general consideration and treatment of ACMs used to support the TSPA-LA Model. Brief descriptions of the biosphere ACMs as discussed in *Biosphere Model Report* (SNL 2007 [DIRS 177399], Section 6.3.3) and summarized in Table 6.3.11-4 are presented below.

ACM for Radon Release from Soil—The conceptual model for radon used in the Biosphere Process Model is based on a radon release factor from radium-contaminated soil. The ACM relies on modeling radon transport in the soil and the atmosphere (Yu et al. 2001 [DIRS 159465], Appendix C). A numerical comparison between the selected model and the ACM shows that the resulting ^{222}Rn concentrations in air are comparable (SNL 2007 [DIRS 177399], Section 7.4.3.1). The method used in the Biosphere Process Model was selected because it required fewer parameters. The more complex ACM did not produce results different enough to warrant its implementation (SNL 2007 [DIRS 177399], Section 7.3.2.2).

ACM for Evaporative Cooler—The conceptual model for evaporative coolers used in the Biosphere Process Model was based on the mechanical operation of evaporative coolers and considered the generation of aerosols as air is forced through a wet, porous surface. An ACM would be to calculate radionuclide concentrations based on differences in absolute humidity between indoor and outdoor air caused by the operation of evaporative coolers. An evaluation of

these two methods showed that they produced results of air activity concentrations that were deemed to be acceptably equivalent (SNL 2007 [DIRS 177399], Section 7.4.3.2).

ACM for Direct Deposition of Irrigation Water on Plant Surfaces—The Biosphere Process Model considers a fraction of radionuclides in irrigation water to be directly translocated into edible plant parts with accumulation and weathering occurring during the growing period. An ACM developed in BIOMASS ERB2A (BIOMASS 2003 [DIRS 168563]) considers this process in two sequential steps: (1) movement of deposited radionuclides from external plant surfaces into the plant tissues, and (2) movement of radionuclides from plant tissues into edible parts of the crop. This ACM applies weathering to contaminants that remain on external plant surfaces and also considers food-processing losses (BIOMASS 2003 [DIRS 168563], Section C3). The two models were evaluated using the same input values or using default data from BIOMASS ERB2A (BIOMASS 2003 [DIRS 168563]). The ACM and the selected model produced comparable results with reasonable input values (SNL 2007 [DIRS 177399], Section 7.4.4.1). The ACM was not chosen because it requires parameters that are not commonly used in environmental transport modeling and are, thus, difficult to quantify. In addition, the ACM was developed for a temperate climate and implies infrequent irrigation episodes, which may be inappropriate for the arid or semiarid conditions at Yucca Mountain (SNL 2007 [DIRS 177399], Section 7.3.3.2).

ACM for Direct Deposition of Airborne Particulates on Plant Surfaces—In the Biosphere Process Model, resuspended soil deposited on crop leaves is treated in the same manner as intercepted irrigation water. The ACM takes a different approach based on a contamination factor for the external contamination of crops, which is similar to a soil-to-plant transfer factor. Differences between the selected model and the ACM were evaluated using the same input values when the parameters are comparable or by using default data from the published ACM. The evaluation showed that the approach used in the Biosphere Process Model and that used in the ACM produce comparable results for reasonable input values (SNL 2007 [DIRS 177399], Section 7.4.4.3).

ACM for Animal Product Contamination—The Biosphere Process Model considers animal contamination resulting from the ingestion of contaminated water, soil, and feed. The GENII Model (Napier et al. 1988 [DIRS 157927]; Leigh et al. 1993 [DIRS 100464]) only includes the consumption of water and feed; however, GENII Version 2 (Napier et al. 2006 [DIRS 177331]) includes soil ingestion, and the BIOMASS ERB2A model (BIOMASS 2003 [DIRS 168563]) includes an additional pathway: inhalation of contaminated air by animals. These animal transport pathways are compared to determine their relative importance (SNL 2007 [DIRS 177399], Section 7.4.5). For this comparison, meat (i.e., beef, pork, and game) was used as an example animal product with ^{239}Pu as the test radionuclide. Soil ingestion is an important contributor to the total activity concentration in meat and, therefore, is included in the Biosphere Process Model. The inhalation of contaminated dust contributes little to concentrations in meat and, therefore, is not included.

ACM for ^{14}C Special Submodel—The methods used in the Biosphere Process Model to calculate ^{14}C concentrations in environmental media were different from those used for the other primary radionuclides. Concentrations of ^{14}C in crops were based on experimental results of the release of $^{14}CO_2$ gas from soil (Sheppard et al. 1991 [DIRS 159545]; Yu et al. 2001

[DIRS 159465], Section L.3). The Biosphere Process Model included two transport pathways of ^{14}C to plants: direct root uptake and intake of $^{14}CO_2$ gas by plants during photosynthesis. Six RMEI exposure pathways were considered: external exposure to and ingestion of ^{14}C in soil, inhalation of $^{14}CO_2$ gas and airborne particulate matter containing ^{14}C, and ingestion of ^{14}C in crops and animal products. An ACM (Napier et al. 1988 [DIRS 157927], p. 4.89) used different methods to calculate ^{14}C concentrations. That model considered uptake into plants only from roots and used a very low removal rate of carbon from soil because the model did not account for gaseous release of $^{14}CO_2$. The method used by the biosphere model was chosen because it more realistically considered uptake of $^{14}CO_2$ gas into plants, resulting in higher plant concentrations (SNL 2007 [DIRS 177399], Sections 6.3.3, 7.3.6, and 7.4.7). An additional alternative model for calculating concentrations of ^{14}C in plant and animal products has also been proposed (BIOMASS 2000 [DIRS 154522], Appendix A) but was not considered because the default parameter values necessary to run the model have not been developed by the authors of the model (SNL 2007 [DIRS 177399], Section 7.3.6 and Table 7.3-21).

ACM for Environment-Specific Inhalation Submodel—In the Biosphere Process Model, inhalation exposure was treated as a function of environment and human activity because many of the input parameters (mass loading, breathing rate, exposure time, and enhancement factors) would be influenced by human activities. Similar models, called microenvironmental models, were used to assess exposure to particulate matter and other contaminants (Duan 1982 [DIRS 162466]; Mage 1985 [DIRS 162465]; and Klepeis 1999 [DIRS 160094]). An alternative but simpler method that is commonly used in risk assessments is to use one or two environments that are representative of the entire range of people, conditions, and times being modeled. These methods produce the same results if average values used in the biosphere model for each environment are used for the alternative method. The method used in the Biosphere Process Model better incorporates variation and uncertainty in each of the input parameters and provides more transparency for the expected RMEI exposure changes between the groundwater (localized contamination) and volcanic release cases (widespread contamination) (SNL 2007 [DIRS 177399], Sections 6.3.3, 7.3.7, 7.3.8, and 7.4.9).

All seven ACMs are numerically compared with those selected in the Biosphere Process Model. The results indicate that most of the ACMs are numerically similar to those selected, and some ACMs are not chosen because those selected match better conceptually with site-specific conditions. Therefore, none of the ACMs were used in the calculations of BDCFs that support the TSPA-LA Model.

No ACMs were recommended for inclusion in the TSPA-LA Model.

Table 6.3.11-1. Pathways for the Groundwater Exposure Case

Environmental Medium	Exposure Mode	Exposure Pathways	Examples
Water	Ingestion	Water intake	Drinking water and water-based beverages.
Soil	Ingestion	Inadvertent soil ingestion	Recreational activities, occupational activities, gardening, and consumption of fresh fruits and vegetables with attached soil.
Soil	External	External radiation exposure	Activities on or near contaminated soils.
Air	Inhalation	Breathing resuspended particles, gases (^{222}Rn and progeny, plus $^{14}CO_2$), and aerosols from evaporative coolers	Outdoor activities, including soil-disturbing activities related to work and recreation; domestic activities including sleeping.
Plants	Ingestion	Consumption of locally produced crops: vegetables, fruits, and grains	Eating contaminated crops.
Animals	Ingestion	Consumption of locally produced animal products: meat, poultry, milk, and eggs	Eating contaminated animal products.
Fish	Ingestion	Consumption of locally produced freshwater fish	Eating contaminated fish.

Source: Modified from Table 6.3-1 in *Biosphere Model Report* (SNL 2007 [DIRS 177399])

Table 6.3.11-2. Pathways for the Volcanic Ash Exposure Case

Environmental Medium	Exposure Mode	Exposure Pathways	Examples
Soil	Ingestion	Inadvertent soil ingestion	Recreational activities, occupational activities, gardening, and consumption of fresh fruit and vegetables with attached soil.
Soil	External	External radiation exposure	Activities on or near contaminated soils.
Air	Inhalation	Breathing resuspended particles; ^{222}Rn and progeny	Outdoor activities, including soil-disturbing activities related to work and recreation; domestic activities, including sleeping.
Plants	Ingestion	Consumption of locally produced crops: vegetables, fruits, and grains	Eating contaminated crops.
Animals	Ingestion	Consumption of locally produced animal products: meat, poultry, milk, and eggs	Eating contaminated animal products.

Source: Modified from Table 6.3-3 in *Biosphere Model Report* (SNL 2007 [DIRS 177399])

Table 6.3.11-3. Groundwater BDCF Uncertainty Representation in the TSPA-LA Model, GoldSim Model File for the Present-Day Climate

TSPA-LA Parameter Name[a,b]	Description
Bio_Index	Uniform random integer (1, 1000) generated in TSPA to select a BDCF vector from the data provided
GW_BDCF_MIC_Ac227	^{227}Ac - Modern Interglacial Climate BDCF
GW_BDCF_MIC_Am241	^{241}Am - Modern Interglacial Climate BDCF
GW_BDCF_MIC_Am243	^{243}Am - Modern Interglacial Climate BDCF
GW_BDCF_MIC_C14	^{14}C - Modern Interglacial Climate BDCF
GW_BDCF_MIC_Cl36	^{36}Cl - Modern Interglacial Climate BDCF
GW_BDCF_MIC_Cs135	^{135}Cs - Modern Interglacial Climate BDCF
GW_BDCF_MIC_Cs137	^{137}Cs - Modern Interglacial Climate BDCF
GW_BDCF_MIC_I129	^{129}I - Modern Interglacial Climate BDCF
GW_BDCF_MIC_Np237	^{237}Np - Modern Interglacial Climate BDCF
GW_BDCF_MIC_Pa231	^{231}Pa - Modern Interglacial Climate BDCF
GW_BDCF_MIC_Pb210	^{210}Pb - Modern Interglacial Climate BDCF
GW_BDCF_MIC_Pu238	^{238}Pu - Modern Interglacial Climate BDCF
GW_BDCF_MIC_Pu239	^{239}Pu - Modern Interglacial Climate BDCF
GW_BDCF_MIC_Pu240	^{240}Pu - Modern Interglacial Climate BDCF
GW_BDCF_MIC_Pu242	^{242}Pu - Modern Interglacial Climate BDCF
GW_BDCF_MIC_Ra226	^{226}Ra - Modern Interglacial Climate BDCF
GW_BDCF_MIC_Ra226_Pb210[c]	^{226}Ra & ^{210}Pb - Modern Interglacial Climate BDCF
GW_BDCF_MIC_Ra228	^{228}Ra - Modern Interglacial Climate BDCF
GW_BDCF_MIC_Se79	^{79}Se - Modern Interglacial Climate BDCF
GW_BDCF_MIC_Sn126	^{126}Sn - Modern Interglacial Climate BDCF
GW_BDCF_MIC_Sr90	^{90}Sr - Modern Interglacial Climate BDCF
GW_BDCF_MIC_Tc99	^{99}Tc - Modern Interglacial Climate BDCF
GW_BDCF_MIC_Th228	^{228}Th - Modern Interglacial Climate BDCF
GW_BDCF_MIC_Th229	^{229}Th - Modern Interglacial Climate BDCF
GW_BDCF_MIC_Th230	^{230}Th - Modern Interglacial Climate BDCF
GW_BDCF_MIC_Th232	^{232}Th - Modern Interglacial Climate BDCF
GW_BDCF_MIC_Th232_Ra228_Th_228[c]	^{232}Th & ^{228}Ra & ^{228}Th - Modern Interglacial Climate BDCF
GW_BDCF_MIC_U232	^{232}U - Modern Interglacial Climate BDCF
GW_BDCF_MIC_U232_Th228	^{232}U & ^{228}Th - Modern Interglacial Climate BDCF
GW_BDCF_MIC_U233	^{233}U - Modern Interglacial Climate BDCF
GW_BDCF_MIC_U234	^{234}U - Modern Interglacial Climate BDCF

Table 6.3.11-3. Groundwater BDCF Uncertainty Representation in the TSPA-LA Model, GoldSim Model File for the Present-Day Climate (Continued)

TSPA-LA Parameter Name[a,b]	Description
GW_BDCF_MIC_U235	^{235}U - Modern Interglacial Climate BDCF
GW_BDCF_MIC_U236	^{236}U - Modern Interglacial Climate BDCF
GW_BDCF_MIC_U238	^{238}U - Modern Interglacial Climate BDCF

Source: DTN: MO0705GOLDSIMB.000_R0 [DIRS 181281] for BDCF data

[a] There are three one-dimensional tables, one for each of the three climate states (MIC = modern interglacial climate, MC = monsoonal climate, and GTC = glacial-transitional climate) modeled for each radionuclide; only the MIC is shown here. Using ^{227}Ac as an example, the TSPA-LA Model contains the following one-dimensional BDCF tables for the groundwater exposure scenarios: GW_BDCF_MIC_Ac227, GW_BDCF_MC_Ac227, and GW_BDCF_GTC_Ac227.

[b] To incorporate uncertainty into the model input, the biosphere model component ran a series of 1,000 model realizations to define a set of BDCFs for each radionuclide modeled. The resulting probability distribution represents uncertainty in the BDCFs. This set of BDCFs is given in a one-dimensional table for each radionuclide.

[c] These composite BDCF data were defined to provide the opportunity to only consider the release and transport of the long-lived parent radionuclide while retaining the dose consequences of the short-lived progeny.

Table 6.3.11-4. Alternative Conceptual Models Considered for the Biosphere

Alternative Conceptual Model	Overview	Screening Assessment and Basis
Radon release from soil (Air Submodel)	This ACM considers radon transport in the soil and the atmosphere, which requires more input data. The ERMYN conceptual model does not include these processes and uses a simple release factor.	This ACM is screened from the Biosphere Model Component based on an analysis showing that the ACM and the ERMYN Model produce comparable results (SNL 2007 [DIRS 177399], Section 7.4.3.1).
Evaporative cooler (Air Submodel)	This ACM considers an inhalation dose from aerosols generated from evaporative coolers and is based on calculating radionuclide concentrations in the air due to an increase in humidity. The ERMYN conceptual model uses a submodel based on the amount of water evaporated rather than an increase in humidity.	This ACM is screened from the Biosphere Model Component based on an analysis showing that this ACM and the ERMYN Model produce equivalent results (SNL 2007 [DIRS 177399], Section 7.4.3.2).
Direct deposition of irrigated water (Plant Submodel)	This ACM considers two processes: one where the deposited radionuclide moves from external plant surfaces into the plant tissues and the other from plant tissues into the edible portion of the crop. Weathering is applied only to contaminants that remain on external plant surfaces. Food processing loss is also considered in the ACM. The ERMYN conceptual model considers the radionuclides in irrigation water to be directly translocated to the edible parts of plants with weathering and accumulation during the growing period, but without food preparation loss.	This ACM is screened from the Biosphere Model Component based on an analysis showing that this ACM and the ERMYN Model produce comparable results (SNL 2007 [DIRS 177399], Section 7.4.4.1).
Direct deposition of airborne particulates on crops (Plant Submodel)	This ACM is based on the crop external contamination. This contamination factor is very similar to a soil-to-plant transfer factor. The ERMYN conceptual model considers the deposited airborne particles on crop leaves acting the same way as the intercepted irrigation water.	This ACM is screened from the Biosphere Model Component based on an analysis showing that this ACM and the ERMYN Model produce comparable results for reasonable input values (SNL 2007 [DIRS 177399], Section 7.4.4.3).
Animal product contamination (Animal Submodel)	This ACM considers animal inhalation of contaminated air. The ERMYN conceptual model excludes the inhalation of contaminated air as a negligible pathway.	This ACM is screened from the Biosphere Model Component based on an analysis showing that inhalation of contaminated air is not an important contributor to the animal product contamination (SNL 2007 [DIRS 177399], Section 7.4.5).
^{14}C Special Submodel (^{14}C Special Submodel)	This ACM considers root uptake as the only mechanism of ^{14}C transfer to crops. ERMYN also includes ^{14}C uptake from air during photosynthesis. In addition to ingestion, ERMYN also includes other pathways that result in human exposure to ^{14}C: external exposure, inhalation of ^{14}C as gas and in soil, as well as soil ingestion.	This ACM is screened from the Biosphere Model Component based on an analysis showing that the selected ^{14}C special submodel considers more processes of ^{14}C transfer to plants than this ACM, which results in a higher ^{14}C concentration in plants (SNL 2007 [DIRS 177399], Section 7.4.7).
Environment-Specific Inhalation Submodel (Inhalation Submodel)	This ACM uses average values of input parameters for inhalation exposure. The ERMYN conceptual model considers inhalation exposure as a function of the environment because many model parameters, such as mass loading, breathing rate, and exposure time, differ among environments and activities.	This ACM is screened from the Biosphere Model Component based on an analysis showing that the ACM and the ERMYN model produce comparable results (SNL 2007 [DIRS 177399], Section 7.4.9). In addition, it is easier to address uncertainty in the input parameters using environment-specific values.

Source: Table 6.3-5 in *Biosphere Model Report* (SNL 2007 [DIRS 177399])

NOTE: ERMYN = Environmental Radiation Model for Yucca Mountain, Nevada.

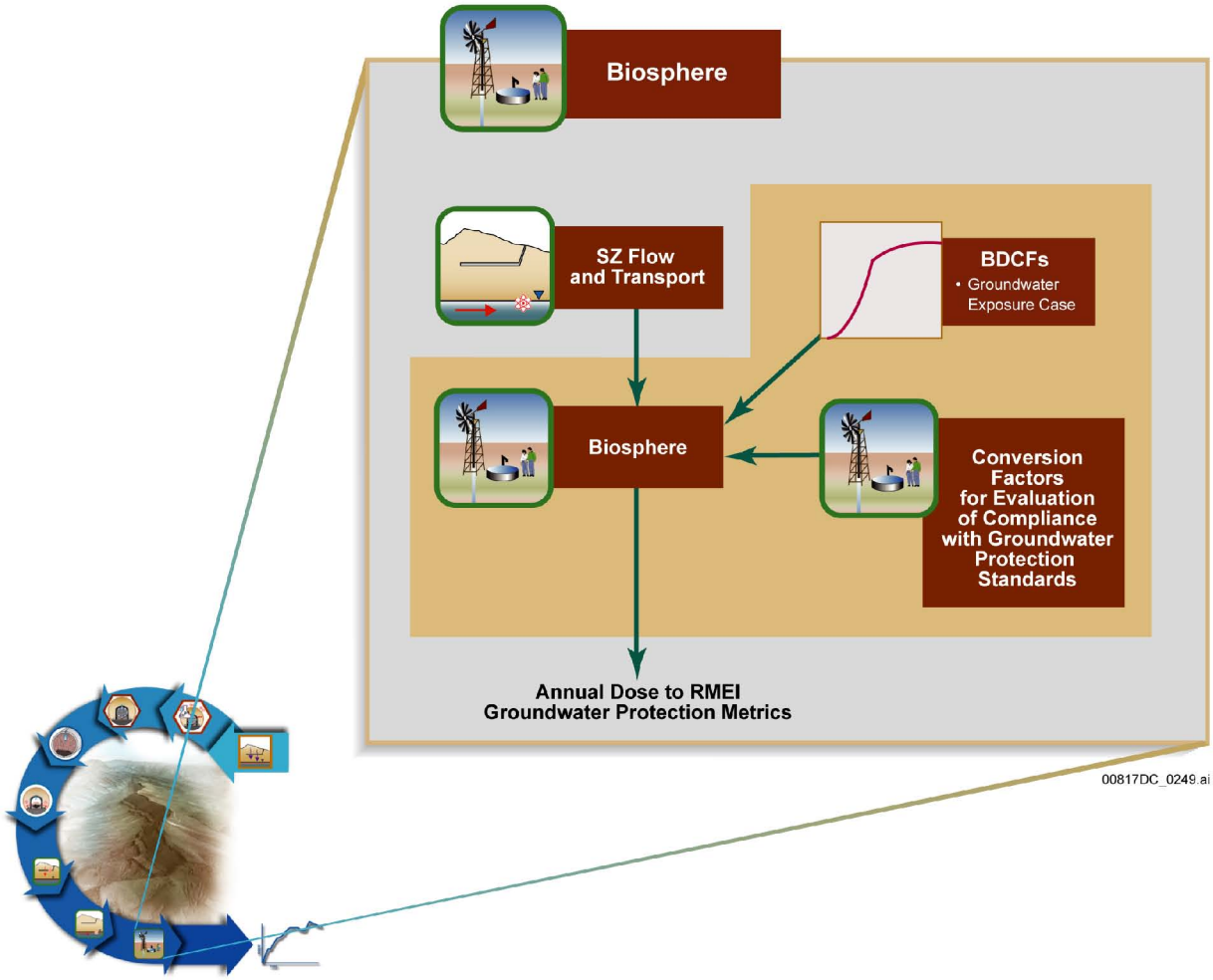

Figure 6.3.11-1. Information Flow Diagram for the Biosphere Model Component of the TSPA-LA Model

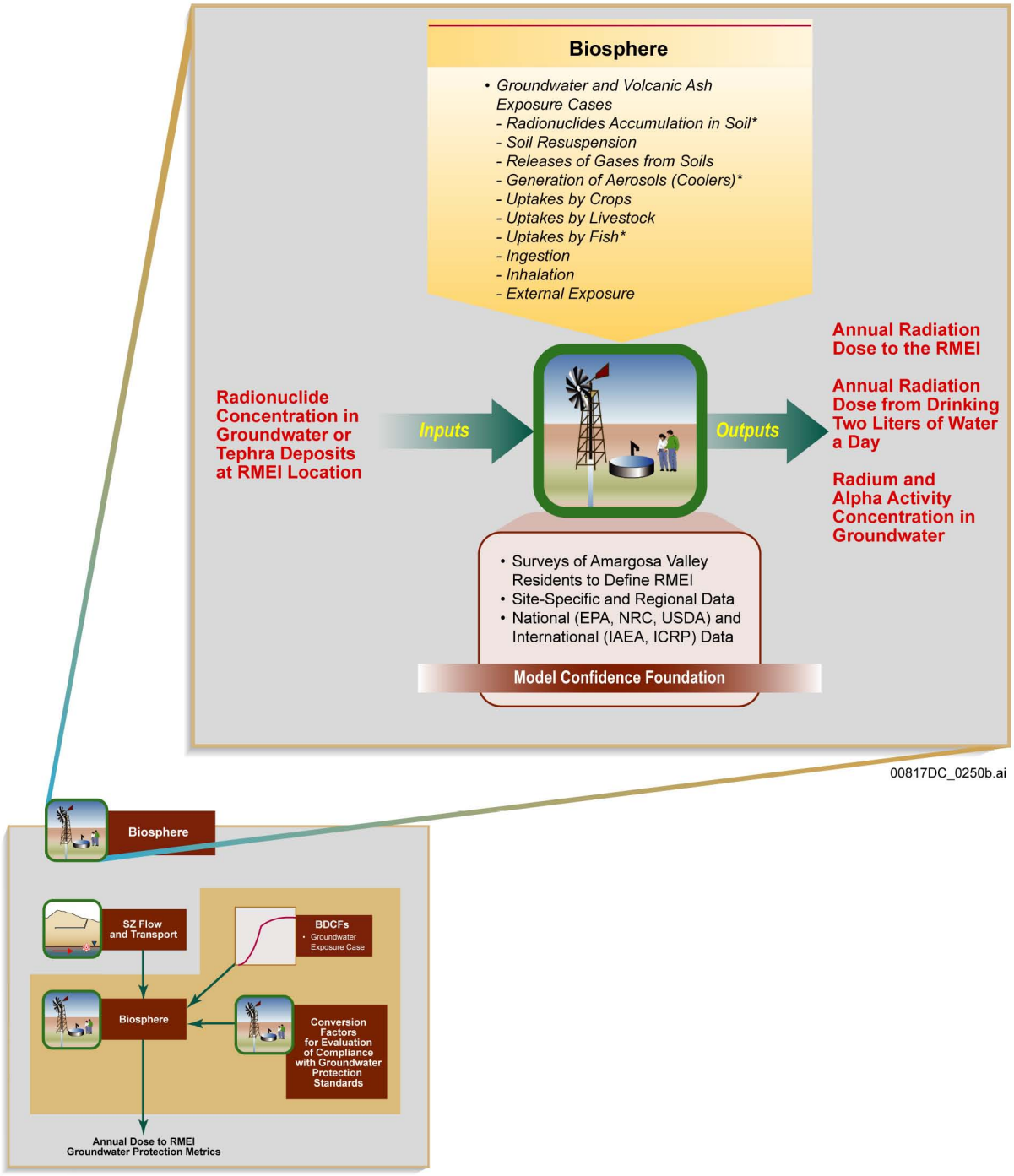

NOTE: The flow diagram in the lower part of this figure only depicts the Groundwater Exposure Case. The flow diagram for the Biosphere Volcanic Ash Exposure Case is shown in Figure 6.5-8. The asterisks in the figure identify those environmental transport pathways that are only included in the Groundwater Exposure Case. ICRP = International Commission on Radiological Protection.

Figure 6.3.11-2. Inputs, Outputs, and Basis for Model Confidence for the Biosphere Model Component of the TSPA-LA Model

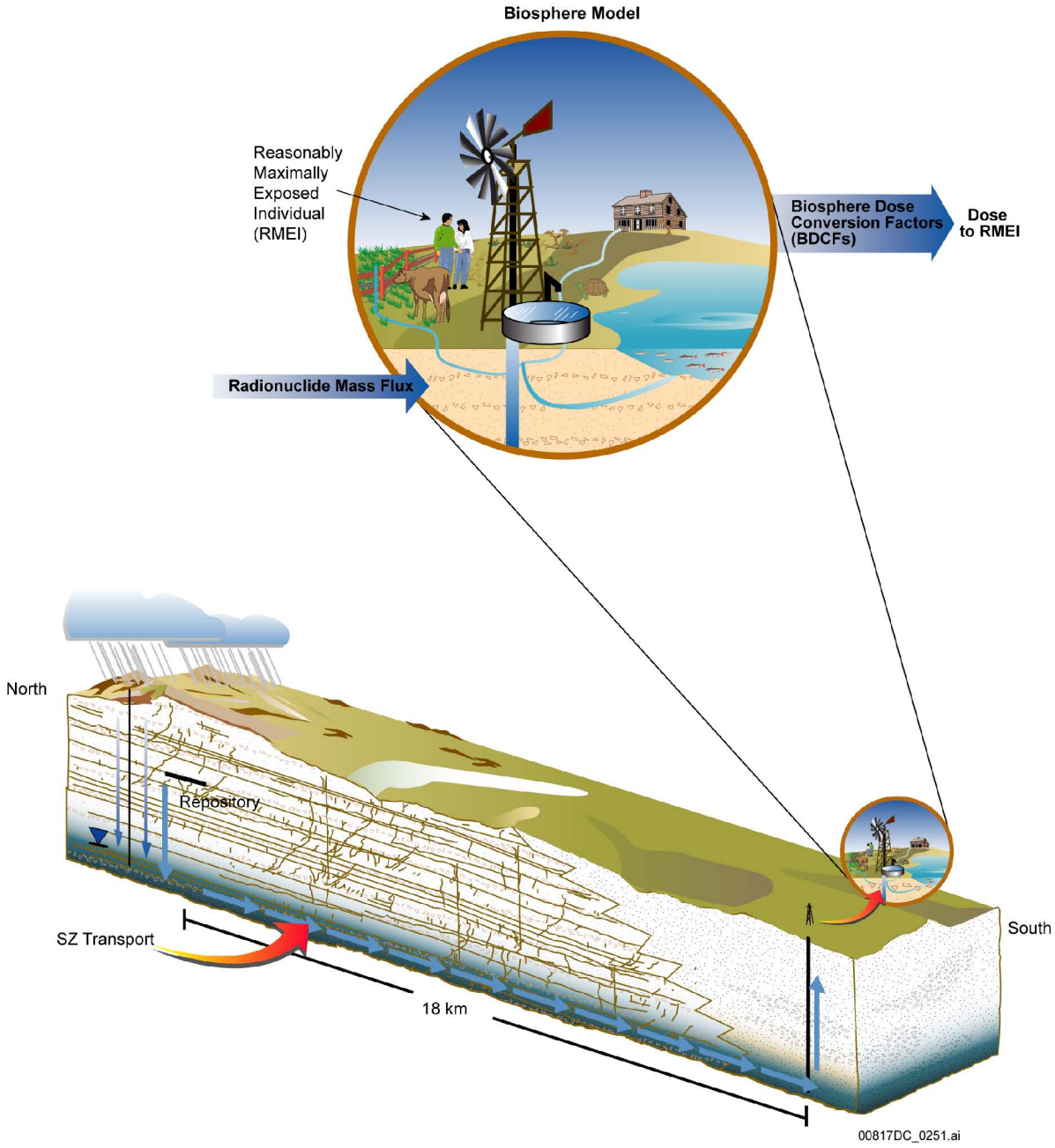

Figure 6.3.11-3. Overview of the Biosphere Groundwater Exposure Case Showing Groundwater Transport of Radionuclides and Exposure to the Reasonably Maximally Exposed Individual

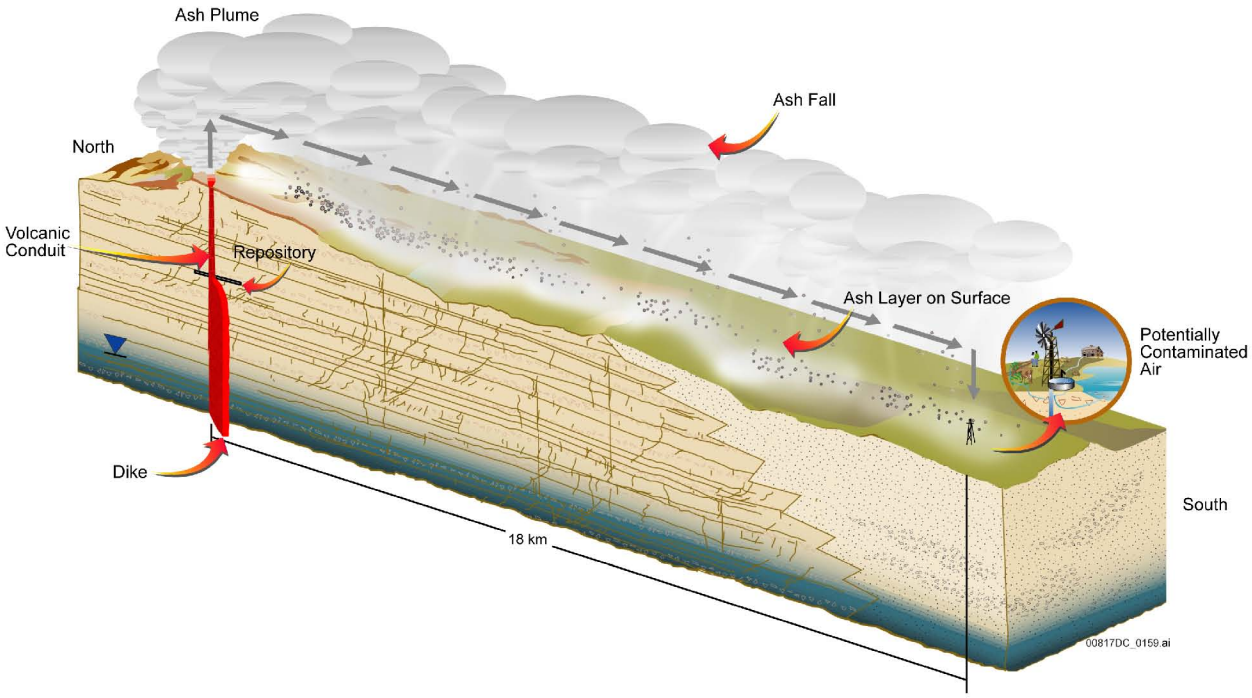

Figure 6.3.11-4. Schematic Representation of the Transport of Radioactive Waste in the Volcanic Ash Exposure Case

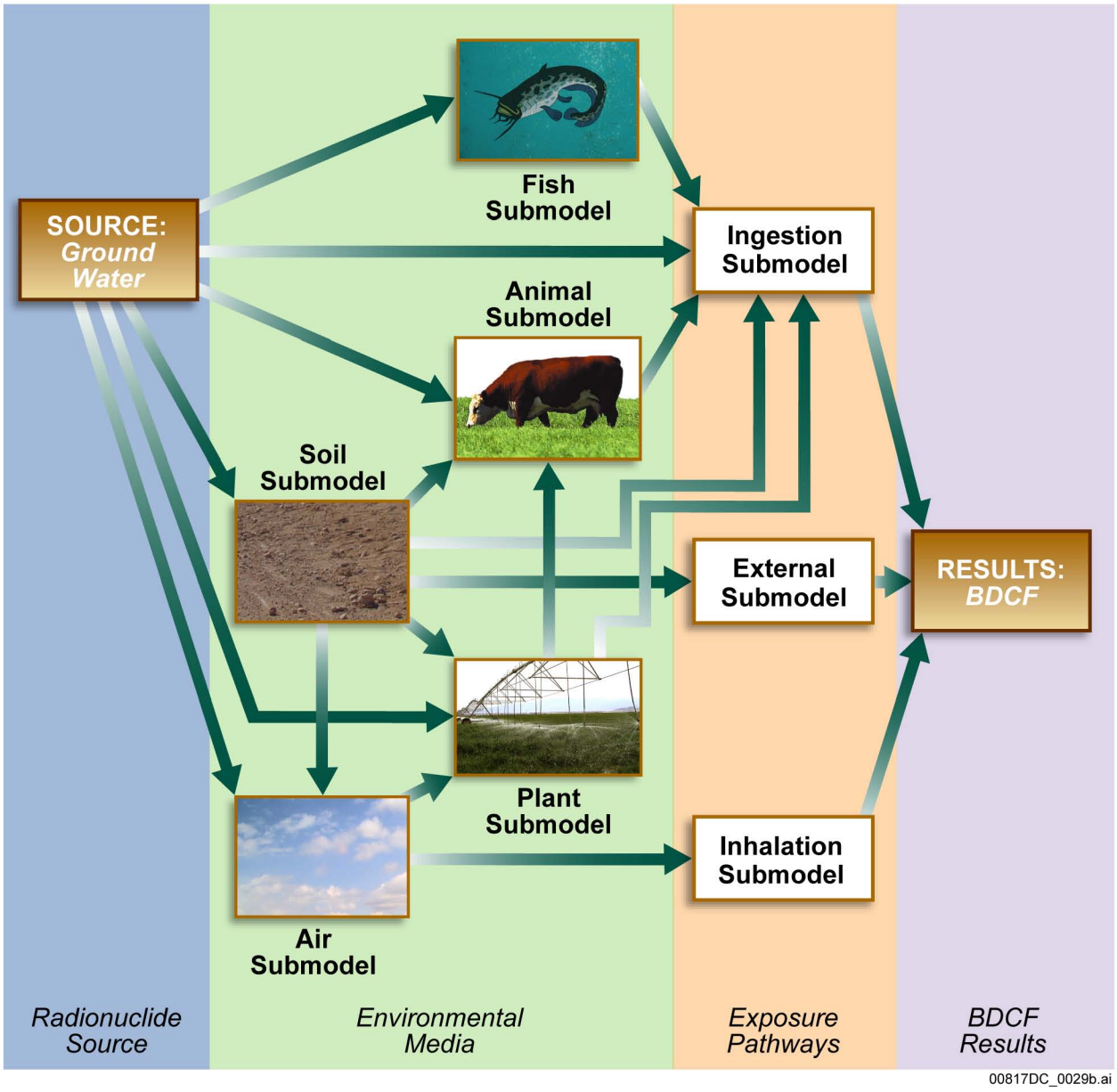

Source: Modified from SNL 2007 [DIRS 177399], Figure 6.3-2.

Figure 6.3.11-5. Relationship among Biosphere Submodels for the Groundwater Exposure Case

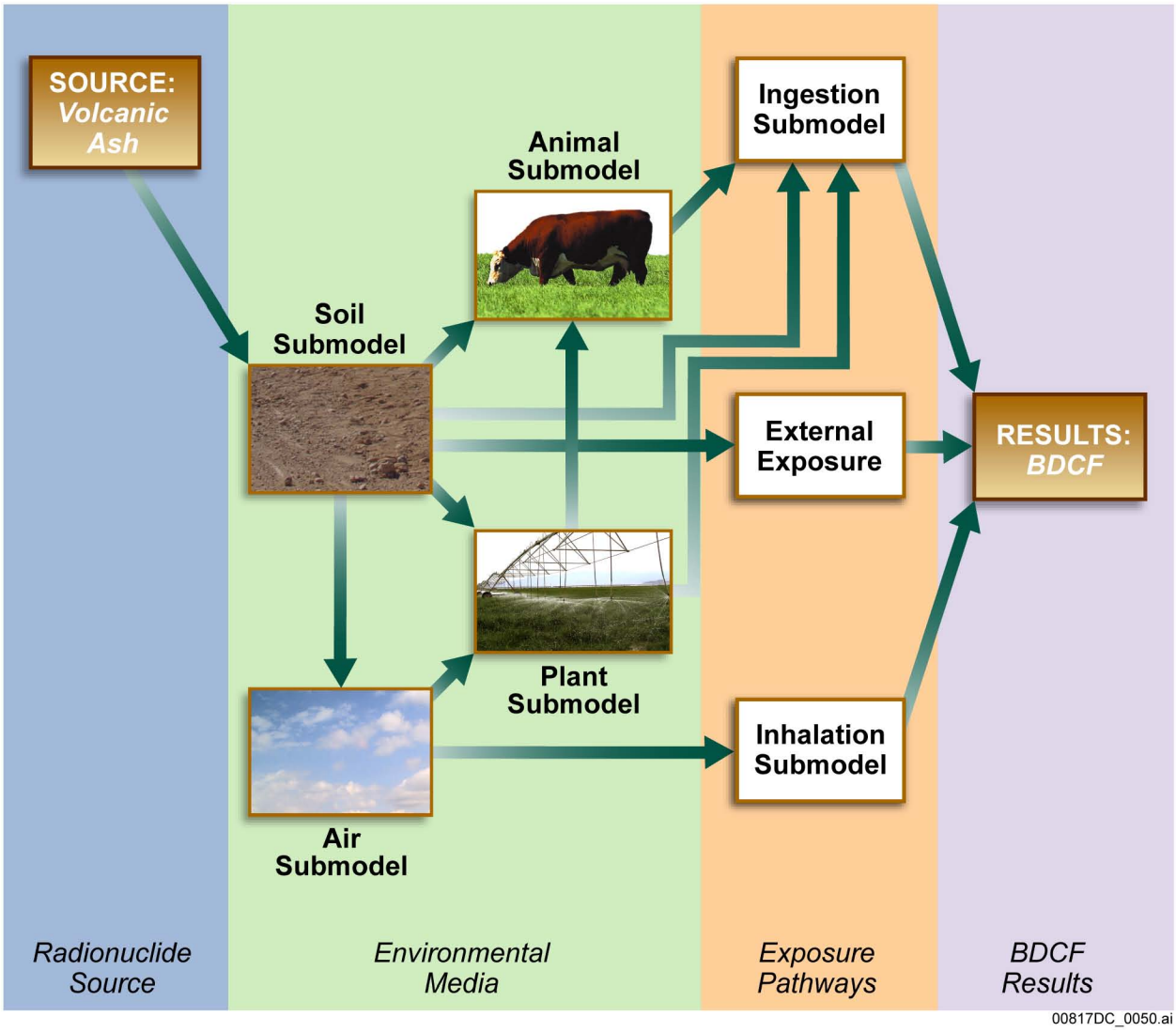

Source: SNL 2007 [DIRS 177399], Figure 6.3-4.

Figure 6.3.11-6. Relationship among Biosphere Submodels for the Volcanic Ash Exposure Case

6.4 TSPA-LA MODEL FOR THE EARLY FAILURE SCENARIO CLASS

The Early Failure Scenario Class describes future performance of the repository system in the event of early failure of waste packages (WPs) and drip shields (DSs). An early failure is defined as the through wall penetration of a WP or DS due to manufacturing or handling-induced defects at a time earlier than would be predicted by mechanistic degradation models for a defect-free WP or DS. The conceptual models and abstractions for probability of WP and DS early failure are documented in *Analysis of Mechanisms for Early Waste Package/Drip Shield Failure* (SNL 2007 [DIRS 178765], Sections 6.1 through 6.5).

The Early Failure Scenario Class contains two modeling cases: the Drip Shield EF Modeling Case and the Waste Package EF Modeling Case. In the Drip Shield EF Modeling Case, complete failure of the DS is assumed to occur. A WP under an early failed DS is assumed to experience localized corrosion as soon as seepage contacts the WP, since the area of the Alloy 22 WP outer barrier that is contacted by seepage is potentially subject to localized corrosion (Section 6.3.5.2.3). In the Waste Package EF Modeling Case, an early failed WP is considered breached from the beginning of the simulation, and its entire surface area is considered degraded. General corrosion of the DSs due to nominal corrosion processes (Section 6.3.5.1.2) is included in the Waste Package EF Modeling Case.

The two modeling cases in the Early Failure Scenario Class have the same framework as the Nominal Scenario Class Modeling Case. The two modeling cases invoke the same modeling components and submodels as are invoked in the Nominal Scenario Class. That is, the framework includes the TSPA-LA Model components to evaluate the mobilization of radionuclides exposed to seeping water, release from the EBS, transport in the unsaturated zone (UZ) down to the saturated zone (SZ), and transport in the SZ to the location of the reasonably maximally exposed individual (RMEI). In the WP and DS Degradation Model Component, the Nominal Scenario Class WP and DS degradation modes are replaced with the early failure DS and early failure WP degradation modes. The relationships between the TSPA-LA Model components and submodels for the Early Failure Scenario Class are illustrated on Figure 6.4-1. Figure 6.4-2 shows the information flow within the TSPA-LA Model associated with the Early Failure Scenario Class. Figure 6.4-3 indicates the major inputs and outputs of the model components and submodels of the Early Failure Scenario Class, features included in the TSPA-LA Model, and foundation for confidence in the TSPA-LA Model.

The statistical distribution of annual dose is estimated in a Monte Carlo approach in which a set of realizations of repository system characteristics is used to represent the range of uncertainty and variability in the parameters of the TSPA-LA Model components. The mean annual dose is estimated as described in Equation 6.1.2-13 for the Waste Package EF Modeling Case and Equation 6.1.2-14 for the Drip Shield EF Modeling Case.

Section 6.4 can be summarized as follows: Section 6.4.1 describes the conceptual and abstraction models for the Drip Shield EF Modeling Case. Section 6.4.1.1 outlines the DS early failure conceptual model. Section 6.4.1.2 contains the abstraction model corresponding to this conceptual model. Section 6.4.1.3 describes the implementation in the TSPA-LA Model. Section 6.4.2 describes the conceptual and abstraction models for the Waste Package EF Modeling Case. Sections 6.4.2.1, 6.4.2.2, and 6.4.2.3 describe the WP early failure conceptual

model, corresponding abstraction model, and implementation in the TSPA-LA Model. Section 6.4.3 discusses the treatment of uncertainty. Section 6.4.4 discusses consistency of assumptions between TSPA submodels and model components. It also discusses conservatisms in model abstractions.

6.4.1 Drip Shield Early Failure Modeling Case

6.4.1.1 Drip Shield Early Failure Modeling Case Conceptual Model

Thirteen potential mechanisms that could cause manufacturing defects in welded metallic containers were identified in Section 6.1.6 of *Analysis of Mechanisms for Early Waste Package/Drip Shield Failure* (SNL 2007 [DIRS 178765]). Of these thirteen flaws or processes, four were identified as potentially significant for mechanisms leading to early DS failure. Four processes were retained for further analysis:

- Improper heat treatment
- Base metal selection flaws
- Improper weld filler material
- Emplacement errors.

For the applicable DS defects, the probability of occurrence and consequences for postclosure performance were assessed. The four processes were analyzed using an event tree/fault tree approach (SNL 2007 [DIRS 178765], Section 6.4). The probabilities of occurrence for the four DS early failure mechanisms were combined to yield a probability distribution for the rate of occurrence of undetected defects in DSs. The occurrence of an undetected defect is assumed to result in complete failure of the DS as a barrier to seepage at the time of repository closure (SNL 2007 [DIRS 178765], Section 6.5.2); hence, the probability distribution for the rate of occurrence of undetected defects is equivalent to a probability distribution for the rate of DS early failures. The occurrence of undetected defects is assumed to be independent between DSs; hence, DS early failure is also independent between DSs.

6.4.1.2 Abstraction of Drip Shield Early Failure

The uncertain rate of DS early failures was abstracted to a log-normal distribution (SNL 2007 [DIRS 178765], Table 7-1). Because DS early failure is independent between DSs, the number of DS early failures can be represented by a Poisson distribution for any particular value of the rate of DS early failures, λ. Appendix B of GoldSim Technology Group 2007 ([DIRS 181727], p. 670) contains a summary of the properties of a Poisson distribution. The Poisson distribution for the number of DS early failures was developed (output DTN: MO0707WPDRIPSD.000 [DIRS 183005], folder: AB-TSPA-DTN-3 (PEF 118)) by integrating the Poisson probability density function for each rate of early failure with the probability density function for the rate of early failure, $f(\lambda)$, given by the log-normal distribution. The integral was numerically evaluated over its domain from zero to a truncated upper-bound λ_m, and set at the 0.999999 quantile value for the given log-normal distribution. The log-normal probability density function $f(\lambda)$ was also adjusted to its truncated upper-bound representation so that the probability density function integrates to one over the specified range. The integral is shown in

Equation 6.4-1, where $f(\lambda)$ and $F(\lambda)$ are the probability density function and cumulative distribution function (CDF) of the log-normal distribution, N is the population of DSs considered, $n = 0, 1, 2, 3, \ldots$ is the count of early failures, and $p(n)$ is the probability of n DS early failures.

$$p(n) = \int_0^{\lambda_m} (\lambda N)^n \times \frac{e^{(-\lambda N)}}{n!} \times \frac{f(\lambda)}{F(\lambda_m)} \times d\lambda \qquad \text{(Eq. 6.4-1)}$$

Table 6.4-1 shows the results of evaluating Equation 6.4-1. The probability of no DS early failures is 0.9834. The probability of only one DS early failure is 0.0155, and the probability of two or more DS early failures is 0.0011. The expected number of DS early failures is given by the sum:

$$\sum_{n=0}^{n_m} p(n) \times n = 0.018 \qquad \text{(Eq. 6.4-2)}$$

where n_m is the number of terms in the distribution for the number of DS early failures, chosen so that including more terms in the summation is not significant.

Analyses in *Analysis of Mechanisms for Early Waste Package/Drip Shield Failure* (SNL 2007 [DIRS 178765], Table 7-1) predicted rates for the introduction of defects into DS fabrication but did not predict the impact on repository performance. The report acknowledged that failure of the DS will only occur after degradation processes take place, which may happen hundreds or even thousands of years after emplacement. However, a realistic estimate of the time at which components with defects will fail was considered difficult to develop. Therefore, the report recommended the assumption of complete failure of the DS, with respect to its seepage diversion function, at the time of repository closure for implementation in the TSPA-LA Model (SNL 2007 [DIRS 178765], Section 6.5.2). This assumption will overestimate the potential for radionuclide release early in the life of the repository.

6.4.1.3 Implementation of Drip Shield Early Failure in the TSPA-LA Model

The rate of DS early failure is sampled from a log-normal distribution with a median of 4.30×10^{-7} and an error factor of 14 (Table 6.4-2). These inputs need to be adjusted to conform to the input requirements of GoldSim (GoldSim Technology Group 2007 [DIRS 181727], Appendix B, p. 668) for log-normal distributions, which require either the geometric mean and geometric standard deviation (SD) or the true mean and true SD as parameters. First, note that the median is equal to the geometric mean for log-normal distributions (Evans et al. 1993 [DIRS 112115], Chapter 25). Second, the shape parameter, σ_l, is related to the error factor by:

$$\sigma_l = \frac{\ln(errorfactor)}{1.645} = \ln\left(errorfactor^{1/1.645}\right). \qquad \text{(Eq. 6.4-3)}$$

The shape parameter is the SD of the log transformed variates (Evans et al. 1993 [DIRS 112115], Chapter 25). Therefore, the geometric SD of the log-normal distribution is given by Equation 6.4-4 (GoldSim Technology Group 2007 [DIRS 181727], Appendix B, p. 668):

$$\sigma_g = \exp(\sigma_l) = errorfactor^{1/1.645}. \quad \text{(Eq. 6.4-4)}$$

For the DS early failure implementation, the DSs are associated with the two WP fuel type groups (commercial spent nuclear fuel [CSNF] and co-disposed [CDSP]). The TSPA-LA model makes the simplifying assumption that each DS early failure affects a single WP. The length of a DS is approximately 228 inches (SNL 2007 [DIRS 179354], Table 4-2); the length of a WP varies between 146 and 230 inches (SNL 2007 [DIRS 179567], Table 4-5) and (SNL 2007 [DIRS 179394], Table 4-3)). Thus, the assumption that a DS early failure affects one WP is reasonable.

The TSPA-LA models a DS early failure by removing the DS as a barrier to seepage at the time of repository closure and allowing the full volume of seepage to contact the WP (Section 6.4.1.2).

The TSPA-LA model conservatively assumes that a WP underneath an early failed DS experiences localized corrosion, which completely compromises the outer barrier of the WP at the time of repository closure, allowing both the advective and diffusive transport of radionuclides. Analysis of the Localized Corrosion Initiation Abstraction shows that localized corrosion initiation conditions can be present in the repository for the first few hundred years in a minority of epistemic realizations. Rather than incurring significant computational expense to account for the epistemic uncertainty and the temporal and spatial variation in the initiation of localized corrosion, this simplifying assumption of immediate initiation of localized corrosion is made. Similarly, the TSPA-LA model assumes that localized corrosion rapidly compromises the entire outer barrier of the affected WP, rather than modeling the progression and extent of localized corrosion, to simplify the calculation of expected dose.

DS early failures that occur in locations but that do not experience seepage are assumed to contribute negligibly to the expected dose. In a location without seepage, localized corrosion does not occur because the WP surface is not wetted. Since localized corrosion does not occur, and the Drip Shield EF Modeling Case does not address other events (i.e., seismic events) that could compromise the WP integrity, there are no mechanisms in the Drip Shield EF Modeling Case that would lead to releases from a WP in a location without seepage. Therefore, the assumption of negligible dose impact is justified.

The GoldSim component of the TSPA-LA Model computes the dose resulting from a single DS early failure occurring in each of the 5 percolation subregions (Section 6.3.2.2.1), in a seeping environment, and affecting each type of WP (CSNF or CDSP), for a total of 10 dose histories for each epistemic realization. The GoldSim results are used in Equation 6.1.2-14 with the sampled rate of DS early failure, the distribution of the numbers of WPs of each type, and the seepage fraction for each percolation bin, to calculate the expected dose for each epistemic realization. The mean and median dose is estimated from the ensemble of expected dose results at each point in time.

6.4.2 Waste Package Early Failure Modeling Case

6.4.2.1 Waste Package Early Failure Modeling Case Conceptual Model

Thirteen potential mechanisms that could result in early failed WPs were identified in Section 6.1.6 of *Analysis of Mechanisms for Early Waste Package/Drip Shield Failure* (SNL 2007 [DIRS 178765]). Of these thirteen flaws or processes, seven were identified as potentially significant for the waste package outer corrosion barrier (OCB). The seven processes retained for further analyses were (SNL 2007 [DIRS 178765], Section 6.3):

- Weld flaws
- Improper heat treatment of OCB
- Improper heat treatment of OCB lid
- Improper stress relief of OCB lid (low plasticity burnishing)
- WP mishandling damage
- Improper base metal selection
- Improper weld filler material.

The processes were assessed for probability of occurrence and consequences for postclosure performance of the WPs.

A more detailed analysis was done for WP weld flaws (SNL 2007 [DIRS 178765], Section 6.3.1) than for the other six processes. This analysis resulted in distributions for the size and number of undetected weld flaws. The characteristics of weld flaws that remain in the WP closure welds can be calculated from these distributions by knowing the per-WP closure weld volume and weld thickness. The TSPA-LA Model utilizes these results, with the critical flaw orientation probability and an applicable depth factor to model where undetected flaws might remain and might result in stress corrosion cracking that could penetrate the WP closure weld. The implementation of the weld flaw analysis requires inputs that are supplied by the TSPA-LA Model file (Section 6.3.5.1.2). Therefore, the implementation of the weld flaw analysis is not part of the Waste Package EF Modeling Case but is part of the Nominal Modeling Case WP and DS degradation analysis (Section 6.3.5.1.2).

The remaining six processes were analyzed using an event tree/fault tree approach (SNL 2007 [DIRS 178765], Section 6.3). Improper base metal selection was rejected as a potential mechanism (SNL 2007 [DIRS 178765], Section 6.3.2), based on the probability of selecting improper base metal material in the fabrication of the OCB of the WP and the probability that the error is not detected.

Results from the event tree analyses of WP event sequences for the remaining five processes were collected into event tree end states and probability distributions for the presence of undetected defects were developed by running 90,000 realizations for these end states (SNL 2007 [DIRS 178765], Section 6.5.1). The occurrence of an undetected defect is assumed to result in early failure of the WP; hence, the probability distribution for the rate of occurrence of undetected defects is equivalent to a probability distribution for the rate of WP early failures. The occurrence of undetected defects is assumed to be independent between WPs; hence, WP

early failure is also independent between WPs. No distinction is made between the different types of WP (i.e., DSNF-Short and DSNF-Long).

6.4.2.2 Abstraction of Waste Package Early Failure

The uncertain rate of WP early failures was abstracted to a log-normal distribution (SNL 2007 [DIRS 178765], Table 7-1). Because WP early failure is independent between WPs, the number of WP early failures can be represented by a Poisson distribution. The distribution for the number of early failure WPs was developed in an analagous manner to the development described in Section 6.4.1.2 for early failure DSs (output DTN: MO0707WPDRIPSD.000 [DIRS 183005], folder: AB-TSPA-DTN-3 (PEF 118)). Table 6.4-1 shows the results of evaluating Equation 6.4-1 for WP early failures. The probability of no WP early failures is 0.558. The probability of only one WP early failure is 0.224, the probability of exactly two WP early failures is 0.096, and the probability of three or more WP early failures is 0.123. The expected number of early-failed WPs is 1.09, evaluated using Equation 6.4-2, and the probability of WP early failures.

Analyses in *Analysis of Mechanisms for Early Waste Package/Drip Shield Failure* (SNL 2007 [DIRS 178765], Table 7-1) predicted rates for the introduction of defects into WP fabrication but did not predict the impact on the WP performance. The report acknowledged that failure of the WP will only occur after degradation processes take place, which may happen hundreds or even thousands of years after emplacement. However, a realistic estimate of the time at which components with defects will fail was considered difficult to develop. Therefore, the report recommended, for implementation in the TSPA-LA Model, the assumption of complete failure of the WP, with respect to radionuclide containment, at the time of repository closure (SNL 2007 [DIRS 178765], Section 6.5.2). This assumption will overestimate the potential for radionuclide release early in the life of the repository.

6.4.2.3 Implementation of Waste Package Early Failure in the TSPA-LA Model

The rate of WP early failure is sampled from a log-normal distribution with a median of 4.14×10^{-5} and an error factor of 8.17 (Table 6.4-2). These inputs are adjusted as described in Section 6.4.1.3 to conform to the input requirements of GoldSim.

For WP early failure implementation, the WPs are divided into two fuel type groups denoted by CSNF early failed WPs and CDSP early failed WPs. The GoldSim component of the TSPA-LA Model computes the dose resulting from early failure of a single WP of each type, occurring in each of the five percolation subregions (Section 6.3.2.2.1), with and without seepage in each percolation subregion, for a total of 20 dose histories for each epistemic realization. The GoldSim results are used in Equation 6.1.2-13 with the sampled rate of WP early failure, the distribution of the numbers of WPs of each type, and the seepage fraction for each percolation bin, to calculate the expected dose for each epistemic realization. The mean and median dose is estimated from the ensemble of expected dose results at each point in time.

The WAPDEG V4.07 software (STN: 10000-4.07 [DIRS 181744 and 181064]) is used to cause each early failed WP to fail at the beginning of the simulation (i.e., at the end of the first timestep). A simplified WAPDEG V4.07 input vector is used for this purpose (output

DTN: MO0707WPDRIPSD.000 [DIRS 183005], folder: AB-TSPA-DTN-4 (PEF 88)). The input vector contains a single corrosion-affecting event that uses the power law functional form (BSC 2002 [DIRS 162606], Section 4.2.6.6) to impose an arbitrarily chosen large corrosion rate that causes breach of all WPs in the first time step. In addition, all WPs completely fail at the end of the first timestep. The use of the WAPDEG software allows a relative humidity threshold to be imposed for the initiation of WP failure. General corrosion of DSs over early failed WPs occurs according to the nominal corrosion processes discussed in Section 6.3.5.1.2.

6.4.3 Treatment of Uncertainty

The TSPA-LA Model includes input parameter uncertainty in the Early Failure Scenario Class. See Table 6.4-2 for a list of uncertain parameters specific to the Early Failure Scenario Class. The Early Failure Scenario Class also includes other uncertain parameters associated with the model components and submodels shown on Figure 6.4-1 and described in Section 6.3. The treatment of aleatory uncertainty in the Early Failure Scenario Class is described in Section 6.1.2.4.2.

6.4.4 Model Component Consistency and Conservatisms in Assumptions and Parameters

To enhance understanding of the complex interactions within the TSPA-LA Model, a discussion of consistency among model components and submodels and identification of conservative assumptions in abstractions, process models, and parameter sets supporting the DS Early Failure Submodel and the WP Early Failure Submodel are discussed below.

6.4.4.1 Consistency of Assumptions

The Early Failure Scenario Class does not include potential inconsistencies between model components or submodels since its effect on the TSPA-LA Model is limited to replacing the Nominal Scenario Class conceptual models for DS and WP degradation with the early failure conceptual models. These models are simpler, in the sense that failure mechanisms are not treated in detail and failure is assumed to occur at the beginning of the simulation. No inconsistencies have been identified between the DS and WP Early Failure Submodels and other Submodels of the TSPA-LA Model.

6.4.4.2 Identification of Conservatisms in Submodels and Abstractions

Consequences of Defects—Section 6.5.2 of *Analysis of Mechanisms for Early Waste Package/Drip Shield Failure* (SNL 2007 [DIRS 178765]) notes that even if a WP or DS is affected by a type of defect that may lead to its early failure, it does not mean that this WP or DS is due to fail at emplacement in the repository. Failure of the WP will only occur after degradation processes take place, which may happen hundreds or even thousands of years after emplacement. Even if a WP or DS were to fail soon after emplacement because of a defect, its radionuclide inventory might not necessarily be available for transport. This is because most through-wall penetrations, especially cracks from SCC, are usually tight, highly tortuous, and limited in length. A realistic estimate of when components with defects will fail would be difficult to develop and justify given the nature of the problem:

- Physical failure of highly corrosion resistant metallic structures with very small loads under nominal conditions
- The time frames involved—centuries to millennia or longer
- The lack of experience with such engineered systems in standard industrial or engineering practice.

Because of such considerations, an approach to the assumption of complete failure of the components with respect to radionuclide containment or seepage diversion function at the time of repository closure was recommended for implementation in the TSPA-LA Model. This approach will overestimate the potential for radionuclide release early in the life of the repository.

Table 6.4-1. Early Failure Unconditional Probability Values

n (Number of Early Failures)	p(n), Waste Packages	p(n), Drip Shields
0	0.5580	0.9834
1	0.2237	0.0155
2	0.0955	0.0009
≥ 3	0.1228	0.0002

Source: Output DTN: MO0707WPDRIPSD.000 [DIRS 183005], folder: AB-TSPA-DTN-3 (PEF 118)

Table 6.4-2. Uncertain Inputs Used in the Early Failure Scenario Class

TSPA-LA Parameter Name	Description	Units	Distribution	Remarks
UNC_WP_EF	Parameters for probability distribution for undetected defects in WPs. For TSPA purposes, this distribution is the probability that a WP will experience early failure after emplacement.	per WP	Log-normal distribution with a median of 4.14×10^{-5} and an error factor of 8.17. (epistemic uncertainty)	DTN: MO0701PASHIELD.000_R2 [DIRS 180508], file: Tables for DTN Readme.doc
UNC_DS_EF	Parameters for probability distribution for undetected defects in DSs. For TSPA purposes, this distribution is the probability that a DS will experience early failure after emplacement.	per WP	Log-normal distribution with a median of 4.30×10^{-7} and an error factor of 14. (epistemic uncertainty)	DTN: MO0701PASHIELD.000_R2 [DIRS 180508], file: Tables for DTN Readme.doc

INTENTIONALLY LEFT BLANK

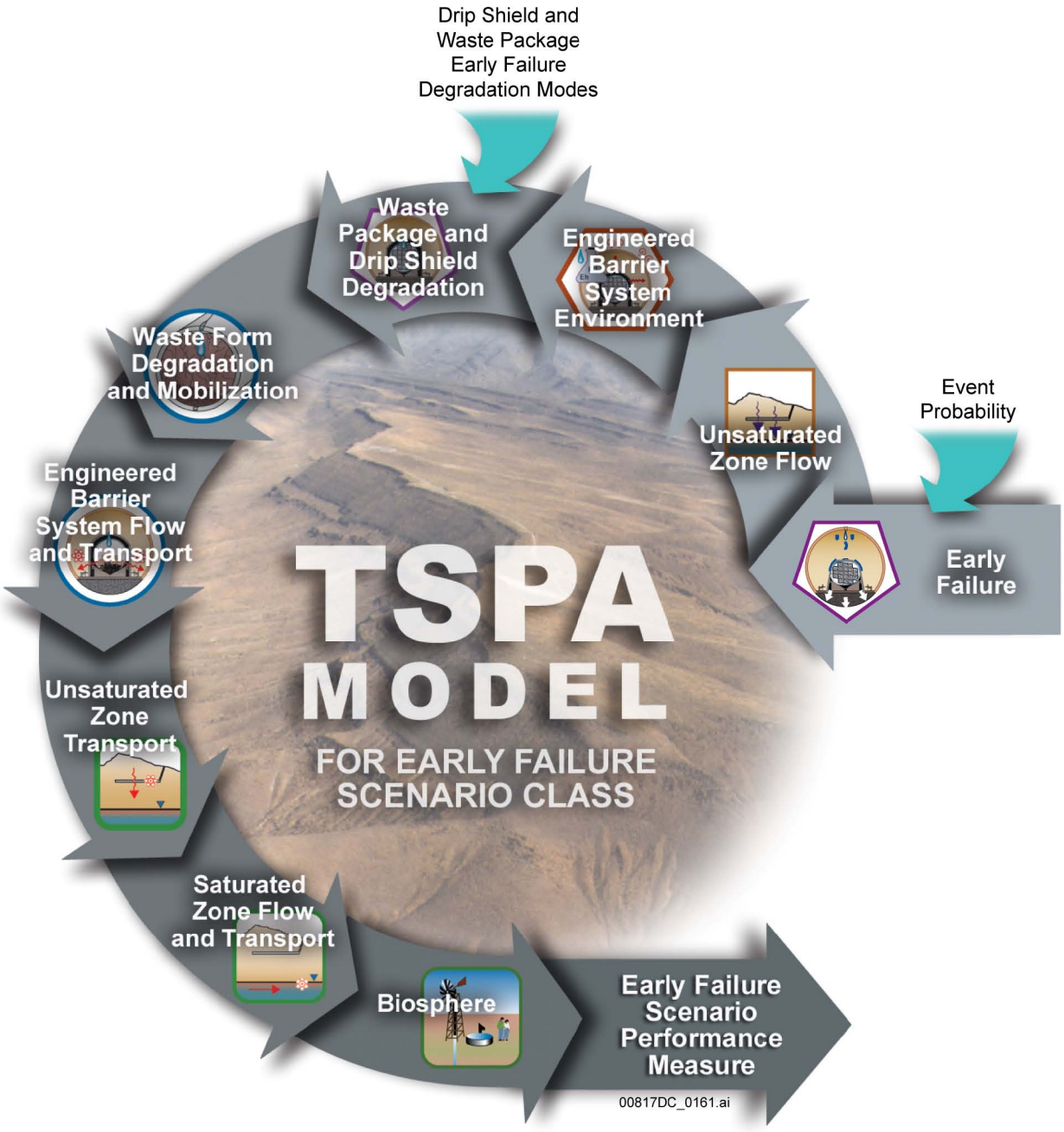

Figure 6.4-1. Schematic Representation of the TSPA-LA Model Components for the Early Failure Scenario Class

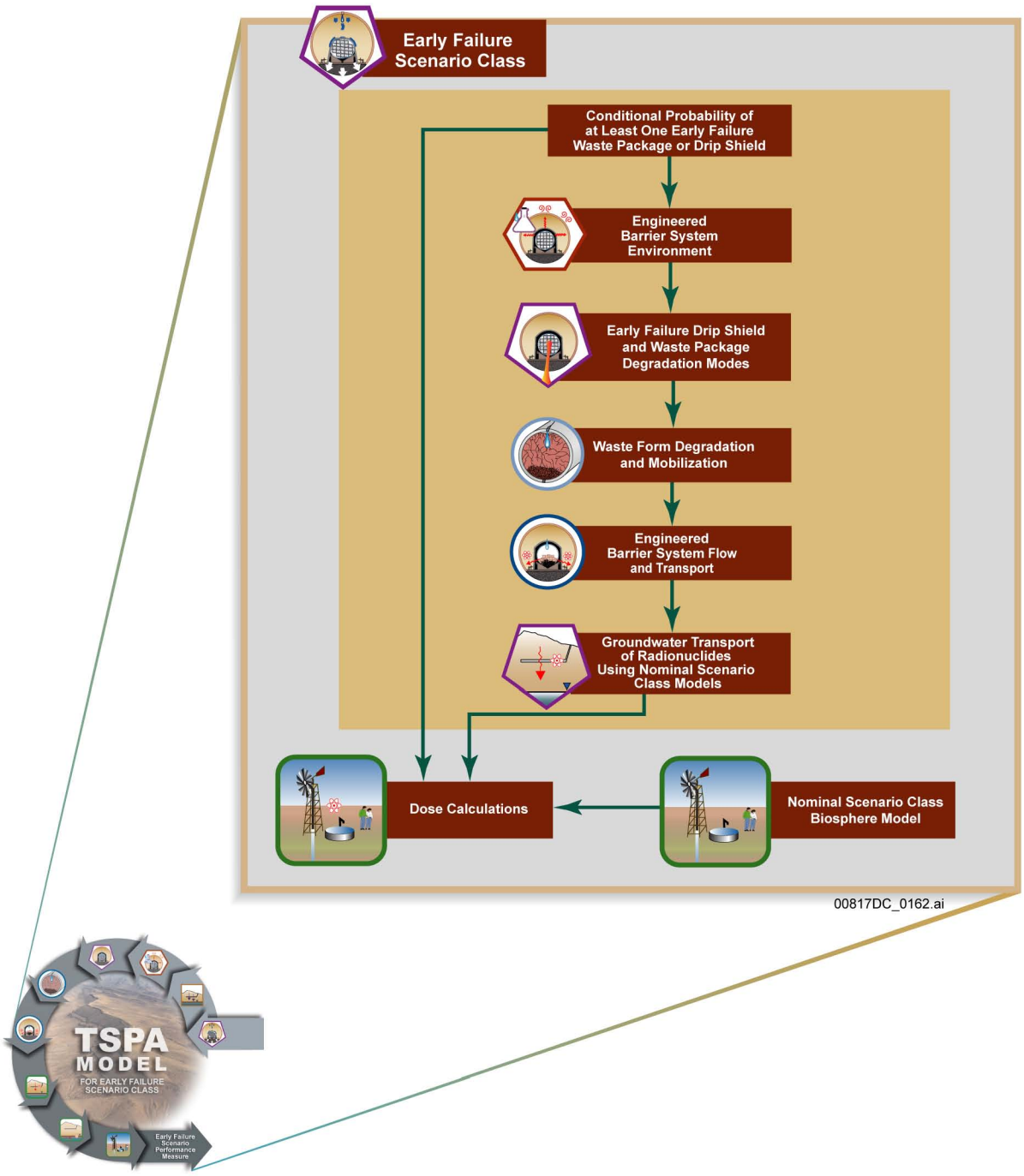

Figure 6.4-2. Information Flow Diagram for the Early Failure Scenario Class in the TSPA-LA Model

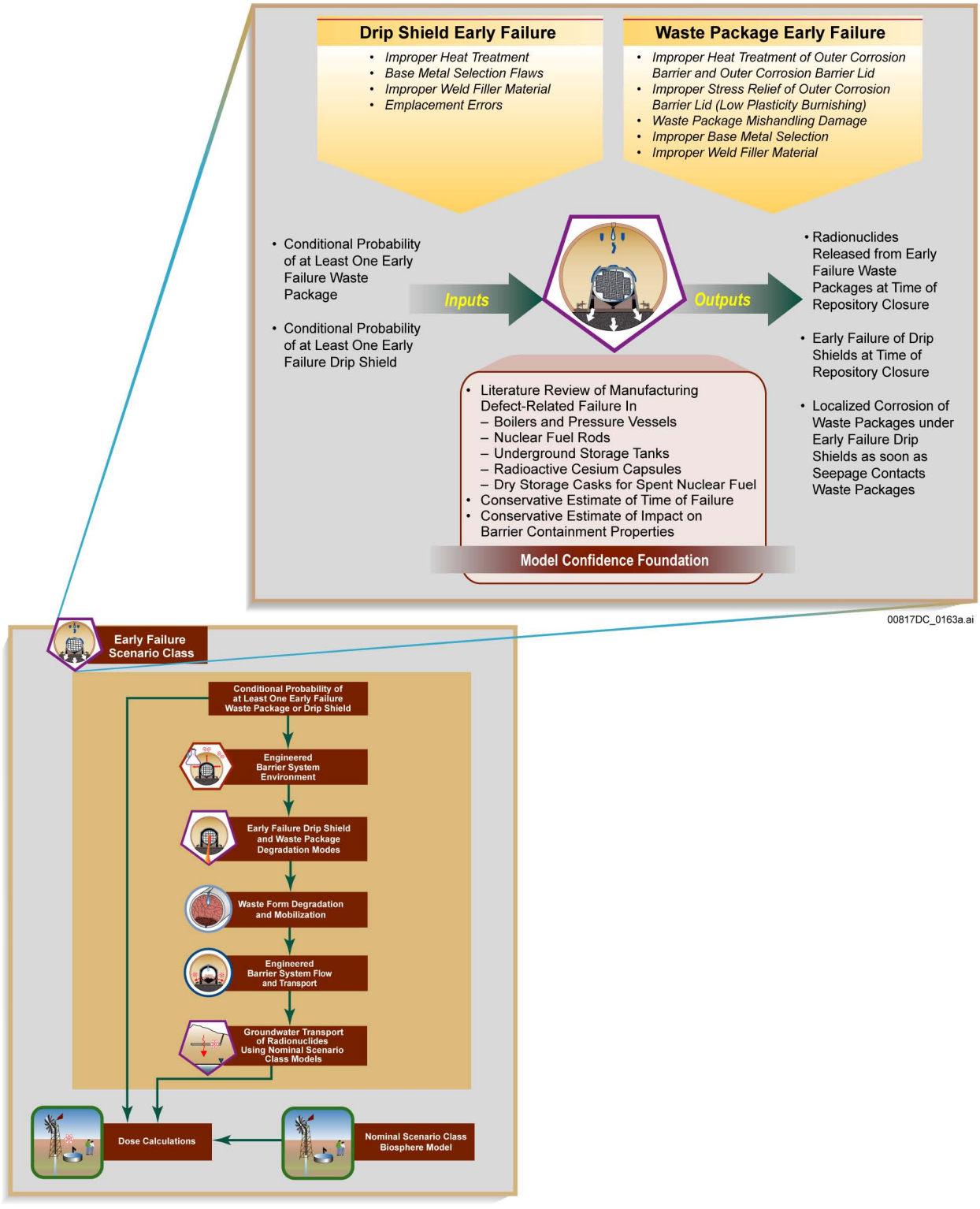

Figure 6.4-3. Inputs, Outputs, and Basis for Model Confidence for the Early Failure Scenario Class

INTENTIONALLY LEFT BLANK

6.5 TSPA-LA MODEL FOR THE IGNEOUS SCENARIO CLASS

Igneous activity can lead to disruptive events that can affect the long-term performance of the Yucca Mountain repository. Yucca Mountain is in a region that has had volcanic activity in the geologic past, and, although there is a very low probability of recurrence of igneous activity affecting the repository, the mean probability is greater than 1 in 10,000 in 10,000 years (BSC 2004 [DIRS 169989], Table 7-1). Accordingly, igneous activity is examined with the TSPA-LA Model because it is not excluded under the probability criterion at 10 CFR 63.642 (a) [DIRS 178394]). The framework for this examination is the Igneous Scenario Class. The Igneous Scenario Class includes all screened-in features, events, and processes (FEPs) related to igneous activity (SNL 2007 [DIRS 179476]). Analysis of igneous activity in the Yucca Mountain region has led to a focus on post-Miocene activity as a basis for the TSPA-LA Model (BSC 2004 [DIRS 169989], Section 6.1.1.1). Figure 6.5-1 is a Yucca Mountain region map that shows the locations and ages of post-Miocene (less than 5.3 million years) igneous activity, represented by multiple volcanic centers.

A probabilistic volcanic hazard analysis (PVHA) was performed to assess the volcanic hazard at Yucca Mountain. For the PVHA, an expert panel was convened in the year 1995 to review pertinent data relating to volcanism at Yucca Mountain and, based on these data, to quantify both the annual probability and associated uncertainty of a volcanic event intersecting a proposed repository sited at Yucca Mountain (BSC 2004 [DIRS 169989], Section 6.1).

Disruption of the repository in the Igneous Scenario Class is addressed by two modeling cases: the Igneous Intrusion Modeling Case and the Volcanic Eruption Modeling Case. Figure 6.5-2 shows the theoretical relationship between an igneous intrusion and volcanic eruption at Yucca Mountain. Information about natural volcanic systems and parameters used to model their behavior is provided in *Characterize Eruptive Processes at Yucca Mountain, Nevada* (SNL 2007 [DIRS 174260]. In both modeling cases, magma propagates upward through the Earth's crust in fluid-driven cracks (dikes). The Igneous Intrusion Modeling Case considers only the intersection of repository drifts by one or more dikes. The Igneous Eruption Modeling Case considers an eruptive conduit that forms when a portion of the erupting dike begins to widen, creating a conduit to focus magma flow to the surface.

In the Igneous Intrusion Modeling Case, magma from dikes that intersect the repository footprint engulfs all DSs and WPs in the repository, rendering them incapable of protecting their contents. The CDSP WP and CSNF WP inner and outer barriers, the cladding in the case of CSNF, and the waste form itself including high-level radioactive waste (HLW) (Section 5.3.1) are instantly degraded during an igneous intrusion. The magnitude of radionuclide transport to the unsaturated zone (UZ) is controlled by the amount of seepage and the radionuclide solubilities. The radionuclides may be transported by groundwater downward through the UZ to the water table, then to the accessible environment by the water that flows in the SZ.

In the Volcanic Eruption Modeling Case, magma erupts at the Earth's surface. The eruptive conduit(s) intersects the repository and damages the WPs located within the conduit cross-sectional area. The rising magma entrains radionuclide waste particles and a portion of the erupting stream becomes a buoyant, convecting column that is ejected into the atmosphere. The contaminated tephra plume is transported downwind and the particles in the plume are dispersed

and eventually deposited on the land surface. The contaminated tephra is then subject to redistribution by hillslope and fluvial processes. The conceptual and mathematical model of contaminated tephra transport implemented by the TSPA-LA Model is described in *Atmospheric Dispersal and Deposition of Tephra from a Potential Volcanic Eruption at Yucca Mountain, Nevada* (SNL 2007 [177431]). The conceptual and mathematical model of redistribution processes implemented by the TSPA-LA Model is described in *Redistribution of Tephra and Waste by Geomorphic Processes Following a Potential Volcanic Eruption at Yucca Mountain, Nevada* (SNL 2007 [DIRS 179347]).

Both of these modeling cases are represented separately in the TSPA-LA Model analyses. Section 6.5.1 discusses the Igneous Intrusion Modeling Case and Section 6.5.2 discusses the Volcanic Eruption Modeling Case.

6.5.1 Igneous Intrusion Modeling Case

The implementation of the Igneous Intrusion Modeling Case includes the definition of submodels for the processes affecting release of radionuclides associated with igneous intrusion, and the implementation of submodels in the integrated TSPA-LA Model for the calculation of mean annual dose. The following sections address these two different aspects of the implementation.

6.5.1.1 TSPA-LA Submodels for the Igneous Intrusion Modeling Case

The Igneous Intrusion Modeling Case considers an igneous event in which a dike intersects the repository, and magma flows into and fills the drifts. This modeling case accounts for the effects of an intrusion on the subsurface characteristics and performance of the repository, and may or may not be accompanied by an eruptive conduit that intersects an emplacement drift and ejects material onto the surface or into the atmosphere. The flow characteristics of the intruding magma cause it to fill every drift within the repository. Contact with magma damages all WPs, DSs, and fuel cladding so that they no longer have waste isolation capability (DTN: LA0702PADE01EG.002_R0 [DIRS 179496], parmameters Fraction_DS_Failed_Ign_Input and Fraction_WP_Failed_Ign_Input). Magma intrusion, however, does not damage the invert. Because an intruded drift will fill with magma within 15 to 25 minutes (depending on the size of the aperture) (SNL 2007 [DIRS 177430], Sections 6.3.3.5.6), the igneous event is treated as an instantaneous event in the TSPA-LA Model. The magma then cools and solidifies in the emplacement drifts. Radionuclides dissolved in water moving through the basalt may be transported by the groundwater downward through the invert and into the UZ to the water table, and then to the accessible environment by flow and transport processes in the SZ, just as is simulated by the Nominal Modeling Case.

The TSPA-LA Model selects parameter values from the appropriate distributions for each of the model components and submodels for each realization of the Igneous Intrusion Modeling Case. The radionuclides in the CSNF and U.S. Department of Energy spent nuclear fuel (DSNF), including the HLW, are considered immediately available for dissolution and transport. Using these inputs, the fate of the radionuclides mobilized by the igneous intrusion is evaluated using the Nominal Scenario Class TSPA-LA Model components and submodels for flow and transport of the released radionuclides in the invert of the EBS, UZ, and SZ. The TSPA-LA Model

components needed to estimate mean annual dose in the Igneous Intrusion Modeling Case are shown on Figure 6.5-3. Modifications to the Nominal Scenario Class are indicated by the bulleted items on the figure.

- The probability of an igneous event is the annual frequency, expressed as a cumulative distribution function (CDF), of an intersection of the repository by a volcanic dike. The CDF is calculated in *Characterize Framework for Igneous Activity at Yucca Mountain, Nevada* (BSC 2004 [DIRS 169989], Section 6.5 and Table 7-1; DTN: LA0307BY831811.001_R0 [DIRS 164713], file PVHA-4PA.DST). The annual frequency of an intersection by an igneous event ranges from approximately 7.4×10^{-10} to 5.5×10^{-8} for the 5th and 95th percentiles, respectively, with a mean annual frequency of 1.7×10^{-8}. This mean annual frequency, which is independent of the characteristics of the event (i.e., size, duration, power) is applied to both the Igneous Intrusion and Volcanic Eruption Modeling Cases to determine mean annual dose.

- Because nominal processes do not progress sufficiently in 20,000 years to result in the release of any radionuclides, the Igneous Intrusion Modeling Case for 20,000 years does not evaluate any pre-intrusion degradation of the WPs, DSs, or CSNF cladding. Degradation of these EBS components is accounted for in the Nominal Scenario Class for 20,000 years (Section 6.1.3). However, for the 1,000,000-year Igneous Intrusion Modeling Case, the nominal processes of degradation of the WPs, DSs, and CSNF cladding do occur up until the time of the igneous intrusion. The inclusion of nominal processes before the igneous intrusion prevents over counting of any radionuclides released by nominal processes prior to the igneous intrusion.

- The intruded drifts have a seepage flux equal to the local percolation flux (SNL 2007 [DIRS 181244], Section 6.7.1.1) (i.e., capillary effects at the drift wall are neglected). The volumetric seepage rate is, therefore, obtained by applying the percolation flux at the base of the Paintbrush nonwelded hydrologic unit (PTn), provided by the EBS Thermal-Hydrologic (TH) Environment Submodel for the appropriate percolation flux subregion, to the projected area of the emplacement drift. In particular, the volumetric seepage rate for a single WP is set equal to that obtained by applying the flux at the base of the PTn to the 5.1-m-long by 5.5-m-wide drift segment representing one WP footprint.

- The DSs and WPs provide no hindrance to flow because they were damaged at the time of the igneous intrusion. Likewise, the basalt that has filled the drift is considered to be fractured so as to not hinder the flow of seepage (SNL 2007 [DIRS 177430], Section 8.1.2).

- No credit is taken for the CSNF cladding because it is considered entirely degraded at the time of the igneous intrusion (SNL 2007 [DIRS 177430], Section 8.1.2).

- All EBS and in-package chemistry-related submodels and parameters are the same as in the Nominal Scenario Class Modeling Case, with the exception of the uranium solubility submodel. As indicated in Section 6.3.7.5.2, Method 2 for uranium solubility is used for the Igneous Intrusion Modeling Case. Method 2 is based on the presence of silica in the

aqueous environment. In particular, the presence of basalt in the drifts implies that Na-boltwoodite needs to be included as a uranium solubility-controlling phase (SNL 2007 [DIRS 177418], Section 6.7.3). More specifically, two additional base solubility look-up tables are defined for this case, which include schoepite, Na-boltwoodite, and $Na_4UO_2(CO_3)_3$, depending on the pH and Pco_2.

Figure 6.5-4 shows information flow within the TSPA-LA Model for the Igneous Intrusion Modeling Case. Figure 6.5-5 indicates major inputs and outputs for each TSPA-LA Model realization, and describes the basis for confidence in the TSPA-LA Model analysis. Figures 6.5-3 and 6.5-4 indicate that the TSPA-LA Model framework for the Igneous Intrusion Modeling Case is similar to that of the Nominal Scenario Class. The principal model components and submodels used in the Igneous Intrusion Modeling Case are the same as those included in the Nominal Scenario Class. They are described in Sections 6.3.1 to 6.3.11. However, Sections 6.5.1.1.1 and 6.5.1.1.2 describe some model components and submodels that are modified to account for igneous intrusion. The following describes other changes to the Nominal Scenario Class that apply to the Igneous Intrusion Modeling Case.

6.5.1.1.1 Igneous Intrusion Engineered Barrier System Damage Submodel

Conceptual Model—The Igneous Intrusion Modeling Case describes the consequences of magma that intrudes into repository emplacement drifts, damages CSNF WPs and CDSP WPs in the intruded drifts, and solidifies. Since the flow characteristics of the magma cause it to intrude into every drift within the repository, every WP (and CSNF cladding) and DS is rendered incapable of protecting its contents. Conceptually, the CDSP and CSNF WP inner and outer barriers, the cladding in the case of CSNF, and the waste form itself are instantly degraded, leaving radionuclides available for transport through normal dissolution processes when seepage re-enters the drift. While the entire inventory is available for transport following an igneous intrusion, the magnitude of radionuclide transport to the UZ is controlled by the amount of seepage and the radionuclide solubilities. WP and DS degradation processes associated with normal conditions are considered in the Igneous Intrusion Modeling Case for 1,000,000 years up until the time of the event, but are not considered in the Igneous Intrusion Modeling Case for 20,000 years.

The geologic feature associated with an igneous intrusion entering the repository is a dike. Dikes are subvertical, elongated, tabular bodies of magma that can extend for many kilometers from a magma source. In the Yucca Mountain region, and for the Igneous Intrusion Modeling Case, the dikes are generally vertically oriented (SNL 2007 [DIRS 177432], Section 6.3.1). A grouping of more than one dike related to the same source of magma is a dike swarm. It is possible for one or more dikes in a swarm to intersect the repository and damage WPs. Figure 6.5-6 is a schematic diagram of the intersection of an igneous dike and a repository drift containing WPs.

TSPA-LA Model Abstraction—The TSPA-LA Model analysis of the Igneous Intrusion Modeling Case considers the assessment of the consequences of an igneous intrusion intersecting the repository. *Number of Waste Packages Hit by Igneous Events* (SNL 2007 [DIRS 177432]) describes the analysis conducted to estimate the number of WPs that would be damaged by an igneous intrusion.

6.5.1.1.2 Engineered Barrier System Environment Submodels in the Igneous Intrusion Modeling Case

The EBS TH Environment Submodel for the Igneous Intrusion Modeling Case differs from that used for the Nominal Scenario Class Modeling Case (Sections 6.3.2), in that it accounts for the temperature increase within and around the drift due to the intrusion of magma that fills the drift.

Conceptual Model—The heat from magma intruding into repository emplacement drifts will affect the EBS TH environment. Temperatures of the WPs, DSs, and the invert, spike to a maximum temperature at the time of the intrusion, and then cool back to ambient conditions (i.e., pre-igneous intrusion) over a 100-year time period. The associated temperature increases are described in *Dike/Drift Interactions* (SNL 2007 [DIRS 177430], Section 6.4.6 and Table 6-13). The in-drift relative humidity, invert liquid saturation, and invert liquid flux are similarly affected. The EBS chemical environment conditions are simulated just as they are for the Nominal Modeling Case since the ranges of pH and ionic strength of seepage water that has interacted with basalt is bounded by the ranges used by the Nominal Modeling Case (SNL 2007 [DIRS 177430], Section 6.7.6). EBS flow and transport processes are also simulated just as they are for the Nominal Modeling Case. Relevant EBS chemical, and flow and transport processes are turned "off" while boiling conditions exist within the drift.

TSPA-LA Model Abstraction—The EBS TH Environment Submodel (Sections 6.3.2) for the Igneous Intrusion Modeling Case accounts for the temperature of the intrusive body and its effect on the EBS temperatures at the time of intrusion. This temperature is derived as described in *Dike/Drift Interactions* (SNL 2007 [DIRS 177430], Section 6.4.6 and DTN: LA0702PADE01EG.001_R0 [DIRS 179495]). The Igneous Intrusion Modeling Case uses an initial temperature of the intrusive body of 1,150°C, and uses a cylindrical one-dimensional, transient heat conduction model to describe the cooling of the intrusive body and the surrounding rock mass. The effects of latent heat were considered and were found to have no impact on the results provided to the TSPA (SNL 2007 [DIRS 177430], Section 7.3.2.1.1.2). Temperatures return to ambient conditions (i.e., temperatures just before the event occurred) in approximately 100 years. Temperatures resulting from this abstraction are shown in Table 6.5-1. The five main columns of the table, labeled "For an Intrusion into a Repository at 25, 50, 100, 150, or 200°C," represent different 100-year temperature history shifts on the WP and drift wall depending on the temperatures of the WP and the drift wall at the time of the event.

The relative humidity within the intruded drifts is modeled as equal to zero when the magma temperature is at or greater than 100°C. Water saturation in the waste form and in corrosion product cells is set to zero for temperatures greater than 100°C, and set to one for temperatures less than 100°C.

All EBS and in-package chemistry-related submodels and parameters are the same as in the Nominal Scenario Class Modeling Case, with the exception of the uranium solubility submodel. As indicated in Section 6.3.7.5.2, Method two for uranium solubility is used for the Igneous Intrusion Modeling Case. Method two is based on the presence of silica in the aqueous environment. In particular, the presence of basalt in the drifts implies that Na-boltwoodite needs to be included as a uranium solubility-controlling phase (SNL 2007 [DIRS 177418],

Section 6.7.3). More specifically, two additional base solubility look up tables are defined for this case, which include schoepite, Na-boltwoodite, and $Na_4UO_2(CO_3)_3$, depending on the pH and Pco_2.

6.5.1.2 Mean Annual Dose Submodel for the Igneous Intrusion Modeling Case (Integration of Submodels)

The TSPA-LA Model calculates the mean annual dose for the Igneous Intrusion Modeling Case using a three-step process. First, a latin hypercube sample (LHS) of uncertain TSPA-LA Model parameters is generated. Each element of the LHS is a vector, specifying a value for each uncertain parameter. For each element in the LHS, a number of annual dose histories are computed using GoldSim. Each annual dose history is associated with a single igneous intrusion occurring at a specified time. For the 20,000-year intrusion case, the LHS size is 300 with event times at 10, 100, 600, 1000, 2000, 4000, 6000, 10,000, 14,000, and 18,000 years. For the 1,000,000-year intrusion case, the LHS sample size is 300 with event times at 250, 600, 1000, 4000, 10,000, 40,000, 100,000, 200,000, 400,000, and 800,000 years. The adequacy of the LHS sample size and the number of event times is discussed in Section 7.3.1 and 7.3.2.4, respectively. The in-package chemistry and temperature specific to the Igneous Intrusion Modeling Case are used to calculate radionuclide mobilization. Using these inputs, the fate of the mobilized radionuclides is evaluated using the Nominal Scenario Class submodels for radionuclide transport in the EBS, UZ, and SZ.

Second, for each element in the LHS, the expected annual dose history is calculated by Equation 6.1.2-16, using the annual dose histories computed for that realization. The integral in Equation 6.1.2-16 accounts for the uncertainty in the time of an igneous intrusion, and for the uncertainty in the frequency of igneous events, and is evaluated numerically by EXDOC (Section 6.1.5). The frequency of igneous events is sampled from the probability distribution described by Table 6.5-2. Finally, the mean annual dose history is calculated as the average of the expected annual dose histories from the set of realizations. Therefore, the analysis performed in the TSPA-LA Model for the Igneous Intrusion Modeling Case relies on: (1) inputs to assess consequences of an igneous intrusion within the repository and (2) inputs associated with the probability of the intrusive event.

6.5.1.3 Implementation in the TSPA-LA Model

Several inputs and feeds to the Igneous Intrusion Modeling Case originate from other TSPA-LA Models and are used in Igneous Intrusion Modeling Case calculations. Feeds from other model components and submodels to the Igneous Intrusion Modeling Case include the number of CSNF WPs and CDSP WPs in the intruded drifts and the log of the carbon dioxide fugacity. The Igneous Intrusion Modeling Case inputs are: (1) time-dependent temperature look-up tables and (2) parameters for the timing and probability of an igneous intrusion. Igneous Intrusion Modeling Case inputs are described in more detail in the following paragraphs.

For the temperature perturbation associated with an igneous intrusion, a two-dimensional look-up table based on Table 6.5-1 is implemented, which defines the shift in WP temperature for times up to 100 years after magma intrusion into the drift(s). A similar two-dimensional look-up table is implemented for drift-wall and invert temperatures as magma enters the drift(s).

Temperature values are interpolated from the tables based on: (1) the temperatures of the WP, drift wall, and invert when the igneous intrusion occurs and (2) the elapsed time since the igneous intrusive event occurred (SNL 2007 [DIRS 177430], Table 8-2), where $T_{r=0m}$ and $T_{r=3m}$ refer to the temperatures at a radius of 0 m (i.e., centerline of the WP) and 3 m (i.e., drift wall and invert) from the drift center, respectively.

Inputs also include: (1) the mean annual frequency of a dike intersecting the repository (BSC 2004 [DIRS 169989]), Section 6.5.3); and (2) the minimum and maximum times during the simulation at which the igneous intrusion can occur.

6.5.1.4 Model Component Consistency and Conservatism in Assumptions and Parameters

There are differences in assumptions and parameter sets used in the TSPA-LA Model that have arisen in the development of the abstractions and process models. Most of these differences are due to the use of conservative assumptions in the process model or analysis when uncertainty is difficult to quantify. Understanding and evaluating potential impacts from these assumptions with respect to the mean annual dose is conducted through a series of processes described in Section 7.4 (Uncertainty Characterization Reviews), Section 7.7 (Corroboration of Results with Auxiliary Analyses), and Section 8.4 (Validity and Defensibility of Performance Demonstration). To enhance understanding of the complex interactions within the TSPA-LA Model, a discussion of consistency among model components and submodels and identification of conservative assumptions in abstractions, process models, and parameter sets supporting the Igneous Intrusion Modeling Case are discussed below.

6.5.1.4.1 Consistency of Assumptions

In-Package Chemistry and the Instantaneous Degradation of CSNF—The In-Package Chemistry Abstraction (SNL 2007 [DIRS 180506]) does not consider instantaneous degradation of CSNF in the range of conditions analyzed with the process model and in the development of the subsequent abstraction. Very fast degradation rates were considered but did not approach instantaneous degradation of CSNF. However, within the TSPA-LA Model, instantaneous degradation of the CSNF occurs in the Igneous Intrusion Modeling Case.

Effect on the TSPA-LA Model—The instantaneous degradation of the CSNF waste form is recommended during an igneous intrusion. Because the in-package pH conditions are controlled by the buffering capacity of the degradation products of CSNF (SNL 2007 [DIRS 180506], Section 6.3.4.1[a]), instantaneous degradation of CSNF means that the maximum pH buffering capacity will be achieved almost immediately, at which time the pH conditions will be well constrained. Well-buffered chemical solutions are part of the in-package chemistry abstraction, therefore, the implemented pH abstraction is sufficient to cover this instantaneous CSNF degradation condition. Similarly, the ionic strength abstraction is sufficient to cover the condition following the instantaneous degradation of CSNF inside a failed WP.

6.5.1.4.2 Identification of Conservatisms in Submodels and Abstractions

WPs and DSs are Completely Damaged— Because there will be no backfill in the drifts, there are no credible mechanisms to block or mitigate the resulting effects from a dike intrusion into a

drift or the effects of the magma on the WPs and DSs (SNL 2007 [DIRS 177432], Section 5.1). Hence, in the Igneous Intrusion Modeling Case, all WPs and DSs located in magma-intruded drifts are assumed to be sufficiently damaged that they provide no hindrance to flow, or protection of their radionuclide inventories to dissolution processes. In addition, no credit is taken for entombment of the waste by the solidified magma. Rather, when in-drift conditions are favorable for the re-entry of seepage, the mobilization of the CDSP and CSNF inventories is controlled only by the radionuclide solubilities.

In addition, since the waste form is conservatively assumed to be entirely degraded during an igneous intrusion, any contribution to its degradation that could have occurred by seepage through fracturing of the basalt is already accounted for. This conservative assumption increases the release of radionuclides from the EBS above the release that would occur if some credit were taken for WPs, DSs, and the solidified magma, all of which would provide some hindrance to flow through the waste form.

Drift Seepage Equal to Percolation after Intrusion—In the Igneous Intrusion Modeling Case, the seepage is set equal to 100 percent of the local percolation flux at the base of the PTn (Section 6.3.3) for magma-intruded drifts. The intruded basalt in the drift is assumed to provide no resistance to water flow. Because all of the WPs and DSs are failed, the entire seepage flux enters the WP and is available for advective transport of radionuclides from the EBS (SNL 2007 [DIRS 181244], Section 6.7.1.1).

This is a conservative abstraction for implementation in the TSPA-LA Model that results in an increase in the release of radionuclides from the EBS over that which would occur if some credit were taken for the cooled magma diverting some of the seepage away from the waste form.

Drift and Dike Interactions—Several conservative assumptions are made for the dike and drift interactions as follows:

1. The filling of the drifts with magma does not consider the presence of the EBS component (e.g., DSs), rubble filled drift, or other features, nor the effects of cooling and temperature-dependent viscosity during magma flow, that could impede the flow of magma and therefore contact fewer WPs than the total inventory (SNL 2007 [DIRS 177430], Section 5.2).

2. WPs engulfed by magma are instantaneously failed and provide no further protection of their contents (SNL 2007 [DIRS 177430], Section 8.1.2).

3. Upon cooling, the basalt is highly fractured and does not provide any hindrance to seepage. The thermal properties of the basalt-filled drift are assumed to be the same as the surrounding host rock (SNL 2007 [DIRS 177430], Section 5.3.1).

These conservative assumptions result in an overestimation of the amount and mobilization of radionuclide inventory for transport through the EBS, UZ and SZ, and hence contribute to higher than expected doses.

6.5.1.5 Alternative Conceptual Model(s) for Igneous Intrusion Modeling Case

An important reason for considering alternative conceptual models (ACMs) is to help build confidence that plausible changes in modeling assumptions or simplifications will not change conclusions regarding subsystem and total system performance. Section 6.2 outlines the general consideration and treatment of ACMs used to support the TSPA-LA Model. Conservatism at the subsystem level has been used to select the best ACM to use rather than quantitatively propagate multiple ACMs to the TSPA-LA Model. Generally, additional uncertainty is incorporated into the selected conceptual model if more than one ACM is deemed appropriate for use rather than considering multiple ACMs in the TSPA-LA Model. If an ACM appears to be significant at the subsystem level, then an appropriate abstraction is developed for that ACM for consideration within the TSPA-LA Model. The result of the process is documented within the individual analysis model reports. It is important to note that treatment of ACMs within the individual analysis model reports may differ significantly to be consistent with available data and current scientific understanding. Therefore, the Igneous Intrusion Modeling Case ACMs are summarized below.

ACM for Estimating the Igneous Event Rates in the Probabilistic Volcanic Hazard Analysis—The PVHA model uses the number of identified post-Miocene era volcanic events observable at the surface plus some buried in the Yucca Mountain region. *Characterize Framework for Igneous Activity at Yucca Mountain, Nevada* (BSC 2004 [DIRS 169989], Sections 6.3.1.6 through 6.3.1.7 and Table 6-4) identifies an ACM for the PVHA in which a significant number of buried (i.e., unidentified) volcanic centers would be included in the estimation of the igneous event rates. The basis for the ACM is that aeromagnetic anomalies suggest that a significant number of unidentified volcanic events were unaccounted for in the PVHA, thus underestimating the volcanic hazard. However, this ACM was not considered because its effects on the probability of an igneous event could not be quantified without further data collection. A drilling and sampling program is underway to determine if any of these anomalies represent Quaternary buried volcanic centers. In addition, an update to the PVHA is underway to reassess the probability of intersection and the probability of a volcanic center being located on Yucca Mountain. Total mean annual dose from the Igneous Scenario Class can reasonably be expected to vary linearly with frequency.

ACMs for Estimating the Intersection Annual Probability in the Probabilistic Volcanic Hazard Analysis—*Characterize Framework for Igneous Activity at Yucca Mountain, Nevada* (BSC 2004 [DIRS 169989], Section 6.3.1.8 and Table 6-5) identifies several ACMs for estimating the intersection probability (i.e., the annual probability of a volcanic event intersecting the repository footprint). The ACM probabilities are captured by the probability used in the PVHA, which indicates that any impacts on the TSPA-LA from using one of these ACMs would be negligible.

ACMs for Dike Propagation—*Dike/Drift Interactions* (SNL 2007 [DIRS 177430], Section 6.3.3.5), identifies ACMs for dike propagation that use hydraulic-fracture models. The *Dike/Drift Interactions* report (SNL 2007 [DIRS 177430], Section 6.3.8) concluded that none of these models were appropriate for the dike propagation in the vicinity of an underground repository, as none of the models has a free surface that can model the changing behavior of the

dike as the surface is approached. Thus, the ACMs were used for validation comparisons only and were not appropriate for use in the TSPA-LA.

ACMs for Effusive Magma Flow into Drifts—*Dike/Drift Interactions* (SNL 2007 [DIRS 177430], Section 6.3.3.5) identifies ACMs for effusive or pyroclastic flow from a dike into a drift. Simulation of these flows and their interactions with WPs is computationally intensive and, therefore, not practical for implementation within the TSPA-LA Model. Instead, the abstractions included in *Number of Waste Packages Hit by Igneous Events* (SNL 2007 [DIRS 177432]), accounts for the effects of these flows within the TSPA framework.

ACMs for TH Effects on Magma Filled and Neighboring Non-Magma Filled Drifts Drifts—*Dike/Drift Interaction* (SNL 2007 [DIRS 177430], Section 6.4.7) identifies ACMs for the TH behavior of magma-filled drifts and its effects on neighboring drifts when an igneous intrusion into the repository affects a limited number of drifts rather than all the drifts. These ACMs involve an evaluation of additional physics, including latent heat of crystallization, host-rock saturation, and enhanced vapor diffusion, and an alternative model for heat conduction around affected emplacement drifts. Inclusion of the latent heat of crystallization and host-rock saturation in the heat transfer analyses was evaluated and is shown to have a negligible effect on the results, producing elevated temperature histories (i.e., above boiling) no more than two to five years longer than without these ACMs included in the analysis (SNL 2007 [DIRS 177430], Section 6.4.7).

With respect to the TH implementation of igneous intrusion in the TSPA-LA, these ACMs do not produce elevated temperature histories (i.e., above boiling) significantly longer than those already in use. Hence, the impact to the TSPA-LA of using any of these TH ACMs is negligible.

No ACMs were recommended for inclusion in the TSPA-LA Model.

6.5.2 Volcanic Eruption Modeling Case

The Volcanic Eruption Modeling Case in the TSPA-LA Model considers the possibility of a volcanic eruptive conduit intersecting the repository footprint resulting in the dispersal of waste-contaminated tephra in the atmosphere with eventual deposition on the ground surface. This modeling case evaluates only the post-eruption consequences due to waste deposited at the location of the reasonably maximally exposed individual (RMEI) directly or redistributed from upstream in the Fortymile Wash watershed. It does not include an evaluation of annual dose received during the active volcanic eruption phase when the waste is transported and dispersed in the atmosphere. The active eruption phase is evaluated separately in Section 6.5.2.4 to show that the mean annual dose during the active eruption phase is small compared to the mean annual dose during the post-eruption time period.

Implementation of the Volcanic Eruption Modeling Case for the TSPA-LA Model includes the determination of both the probability of the event and its consequences. The probability of an eruptive event is determined by two factors. The first is the probability of an eruption penetrating the repository sampled from the probability distribution for the annual frequency of an intersection of the repository by a dike, as provided in *Characterize Framework for Igneous Activity at Yucca Mountain, Nevad*a (BSC 2004 [DIRS 169989], Table 6-8, Section 6.5.3.1;

DTN: LA0307BY831811.001_R0 [DIRS 164713]) and shown in Table 6.5-2. The second factor is the probability of an eruption that intersects the repository footprint, given that a dike intersection of the repository occurs; this value is 0.28 (parameter Eruptive_Center_Probability_a in *Number of Waste Packages Hit by Igneous Events* (SNL 2007 [DIRS 177432], Section 7.2). Note that all igneous events with dikes that intersect the repository are assumed to also have eruptive conduits, but only a fraction of these conduits intersect the repository footprint (other conduits might form along a dike where it extends outside the repository footprint). The annual frequency of an eruption through the repository is estimated by multiplying the two probability factors described above.

The Volcanic Eruption Modeling Case in the TSPA-LA Model includes submodels for the processes affecting the release, transport, and redistribution of radionuclides associated with the volcanic eruption, and implements the submodels for the calculation of mean annual dose. The following sections (Sections 6.5.2.1 to 6.5.2.2) address these submodels and their implementation for the Volcanic Eruption Modeling Case. In addition, the model evaluation, model conservatism, and ACMs are discussed in Sections 6.5.2.3 and 6.5.2.4.

6.5.2.1 TSPA-LA Submodels for the Volcanic Eruption Modeling Case

The submodels for evaluating the consequences of the Volcanic Eruption Modeling Case are shown on Figure 6.5-7, which does not contain as many model components and submodels as the Igneous Intrusion Modeling Case (Figure 6.5-3). Figure 6.5-8 illustrates the flow of information in the TSPA-LA Volcanic Eruption Modeling Case and the relationship between the submodels for the Volcanic Eruption Modeling Case. Figure 6.5-9 indicates the major inputs and outputs of the Volcanic Eruption Modeling Case, the features included in the TSPA-LA Model, and the foundation for confidence in the Volcanic Eruption Modeling Case.

Four submodels are considered in the Volcanic Eruption Modeling Case. Volcanic Interaction with the Repository Submodel (Section 6.5.2.1.1) describes the number of WPs that may be destroyed by, and entrained in, a volcanic eruption and the amount of waste available for atmospheric transport. The Atmospheric Transport Submodel (Section 6.5.2.1.2) describes the atmospheric transport of this erupted tephra/waste mixture and eventual deposition on the land surface. The Tephra Redistribution Submodel (Section 6.5.2.1.3) describes the redistribution of the contaminated tephra to the location of the RMEI. The Volcanic Ash Exposure Submodel (Section 6.5.2.1.4) uses the volcanic ash biosphere dose conversion factors (BDCFs) to estimate mean annual dose to the RMEI, which was previously presented in the Biosphere Model Component (Section 6.3.11.2). The following subsections describe these four components of the Volcanic Eruption Modeling Case.

6.5.2.1.1 Volcanic Interaction with the Repository Submodel

Conceptual Model—Eruptive events involving the intersection of an eruptive conduit with the repository could result in the atmospheric release of volcanic tephra and mobilized waste from the repository and subsequent deposition on the ground surface. Figure 6.5-10 is a schematic diagram of the intersection of an igneous dike and eruptive conduit with the repository. The quantity of waste erupted into the atmosphere is conceptualized in the Volcanic Eruption Modeling Case as depending on the distribution of WPs in the emplacement drifts, the number

and size of eruptive conduits intersecting the drifts, the degree of damage to those WPs, the amount of waste from the WPs that is entrained into the erupting material, and the fraction of magma that is erupted into the ash cloud (tephra). The size and number of dikes associated with an eruptive event considered credible for the Yucca Mountain region are described in *Characterize Eruptive Processes at Yucca Mountain, Nevada* (SNL 2007 [DIRS 174260], Table 7-1). The conduit diameter is given as a normal distribution with a mean diameter of 15 m. Data and output from *Characterize Eruptive Processes at Yucca Mountain, Nevada* (SNL 2007 [DIRS 174260], Table 7-1) allow for up to three conduits to form along the thickest dike (referred to as the master dike) in a dike swarm. The number of WPs intersected by conduits is a function of conduit area, the number of conduits, and the conduit location within the repository. Only WPs located partially or entirely within a conduit are assumed to be destroyed, making all of the waste in these WPs available for entrainment in the erupting pyroclastic material. The potential for WPs located outside the conduit diameter to be mobilized by magma and moved toward the conduit is analyzed in *Dike/Drift Interactions* (SNL 2007 [DIRS 177430], Section 6.4.8.3.2). The analysis concludes that WP movement outside of a conduit profile is not expected considering expected magma velocities, pressures, and viscosities, as well as WP dimensions and densities. Estimates of the number of WPs that might be intersected during an eruptive sequence are based on the probability distribution described in *Number of Waste Packages Hit by Igneous Events* (SNL 2007 [DIRS 177432], Section 7.1).

TSPA-LA Model Abstraction—The mass of waste incorporated in the tephra plume from an eruptive event depends on the waste inventory, the number of WPs intersected, and the fraction of waste-containing magma that is erupted in a tephra plume instead of lava flows and scoria cone. The CDF for the number of WPs intersected by conduits is shown in Table 6.5-3. Figure 6.5-11 graphically illustrates the CDF and probability for the number of WPs that could be potentially intersected by an eruptive conduit(s) from igneous activity culminating in a volcanic eruption within the repository footprint (SNL 2007 [DIRS 177432], Section 7.1). As seen on the figure, the Waste Packages Hit analysis indicates that there is approximately a 70 percent probability that no WPs will be hit by a volcanic eruption intersecting the repository. The small conduit diameters relative to drift spacing mean that 70 percent of the conduits intersecting the repository footprint would form between drifts and therefore not intersect any WPs. In the 30 percent of cases in which one or more packages are hit, the most likely number hit is four and the maximum number hit is seven.

The Volcanic Eruption Modeling Case includes the mass of waste in both the CSNF WPs and CDSP WPs that are hit, and the proportions of each kind of waste released from the repository in the erupting material. The mass of waste hit is multiplied by the magma partitioning factor to account for the partitioning of magma into surface lava flows, scoria cone, and tephra plume (SNL 2007 [DIRS 177431], Section 6.5.2.9). The magma partitioning factor is specified as a uniform distribution from 0.1 to 0.5 and represents the fraction of magma that is erupted into the tephra plume to be considered in the Volcanic Eruption Modeling Case. Waste potentially deposited with surface lava flows and scoria cone is not part of the contaminated tephra that is ejected into the atmosphere, and is therefore, not considered in the TSPA-LA analysis which models only aerial dispersal and subsequent redistribution of contaminated tephra.

6.5.2.1.2 Atmospheric Transport Submodel

Conceptual Model—The conceptual model for the Atmospheric Transport Submodel is a vertical column of heated tephra and waste particles, resulting in a buoyant plume that reaches neutral buoyancy at some level in the atmosphere. The plume is then transported downwind and, because of dispersive processes, spreads out laterally as it is transported. Solids fall from the plume as it travels depending on the wind speed, particle density, and settling velocity. The pyroclastic material ejected into the atmosphere from a volcanic eruption eventually falls to the ground surface and forms a contaminated tephra sheet of varying thickness extending and thinning, generally, downwind from the volcanic vent (SNL 2007 [DIRS 177431], Section 6.3).

Figure 6.5-12 is a schematic illustration of a volcanic eruption intersecting the repository at Yucca Mountain. The figure shows the transport of radioactive waste in the tephra plume from the repository to the location of the RMEI under the condition of a southerly directed wind.

TSPA-LA Model Abstraction—Atmospheric transport and deposition of erupted waste is evaluated using the ASHPLUME code (ASHPLUME_DLL_LA V2.1, STN: 11117-2.1-00 [DIRS 181035]) described in *Atmospheric Dispersal and Deposition of Tephra from a Potential Volcanic Eruption at Yucca Mountain, Nevada* (SNL 2007 [DIRS 177431], Section 6.5). The ASHPLUME code is implemented directly in the TSPA-LA Volcanic Eruption Model, using the ASHPLUME computer code as a dynamically linked library (DLL).

The ASHPLUME code simulates a violent Strombolian eruption with entrainment of radioactive waste in the erupted plume as waste particles attached to the pyroclastic fragments in the plume. The waste-contaminated tephra particles ejected into the atmosphere form a contaminated deposit on the land surface. The parameter "incorporation ratio" is a cutoff ratio for the minimum size of a tephra particle that can carry a waste particle of a given size. Expressed as the Log_{10} of the ratio, an incorporation ratio of 0 is used in the TSPA implementation, meaning the maximum waste particle size is equal to the tephra particle size. The mathematical formulation of this incorporation ratio and the approach to determining the mass fraction of waste that is incorporated in an eruption is discussed in *Atmospheric Dispersal and Deposition of Tephra from a Potential Volcanic Eruption at Yucca Mountain, Nevada* (SNL 2007 [DIRS 177431], Section 6.5.2.6). The wind speed and direction that result in atmospheric transport of the erupted material are represented in the ASHPLUME code in terms of CDFs (DTN: MO0408SPADRWSD.002_R0 [DIRS 171751]). These CDFs are specified for 1-km height increments between 0 km and 13 km above the mountain. Wind speed and direction for a given model realization are selected from the height bin appropriate to the eruption column height for that realization. Once selected, the wind speed and direction are assumed to be constant throughout the eruption duration in the ASHPLUME model. The impact of this simplification is considered to be negligible based on the analysis in *Atmospheric Dispersal and Deposition of Tephra from a Potential Volcanic Eruption at Yucca Mountain, Nevada* (SNL 2007 [DIRS 177431], Section 7.6). The ASHPLUME mathematical model for atmospheric dispersion and deposition of the particles in the plume is based on the theoretical model by Suzuki in "A Theoretical Model for Dispersion of Tephra" (Suzuki 1983 [DIRS 100489], pp. 95 to 113). The movement of air mass in the atmosphere is random within the scale of eddy motions in wind currents. Therefore, the dispersion of the contaminated tephra particles in the atmosphere is also random. Particles disperse in the atmosphere in both vertical

and horizontal directions. The scale of horizontal turbulence is much greater than the scale of vertical turbulence. Therefore, particle diffusion is considered to be two-dimensional in the horizontal "x-y" plane. Particle movement in the vertical "z" direction is accounted for by the particle settling velocity. The ASHPLUME mathematical model and its solution are described in *Atmospheric Dispersal and Deposition of Tephra from a Potential Volcanic Eruption at Yucca Mountain, Nevada* (SNL 2007 [DIRS 177431], Section 6.5). The Atmospheric Transport Submodel predicts the ground-level concentrations (areal density, g/cm^2) of tephra and waste directly deposited at the location of the RMEI and the spatial distribution of tephra and waste in the Fortymile Wash watershed for a simulated volcanic event. The tephra concentration in the Fortymile Wash watershed is converted into volcanic ash thickness by the Tephra Redistribution Submodel and redistributed to the RMEI location along with incorporated waste.

The uncertain ASHPLUME code input parameters that may significantly affect the outcome of TSPA-LA Model calculations are expressed as probability distributions to be used in the TSPA-LA Model. Table 6.5-4 shows key ASHPLUME code input parameters, and indicates those that are represented by probability distributions and those that use fixed values.

6.5.2.1.3 Tephra Redistribution Submodel

Conceptual Model—Waste-contaminated tephra deposited on the ground surface in Fortymile Wash by the Atmospheric Transport Submodel could be redistributed to the RMEI location due to hillslope and fluvial processes. Therefore, the waste concentration used in the Biosphere Submodel to determine dose consists of contributions from both waste-contaminated tephra at the RMEI location deposited directly when atmospheric conditions move the eruptive plume toward that location, and any waste-contaminated tephra redistributed from upstream that may have been deposited in the Fortymile Wash Watershed. Three major processes are considered in the tephra redistribution conceptual model: (1) mobilization from hillslopes; (2) mixing and dilution with uncontaminated sediments during channel transport; and (3) diffusion into the soil column at the RMEI location. A detailed description of the tephra redistribution conceptual model can be found in *Redistribution of Tephra and Waste by Geomorphic Processes Following a Potential Volcanic Eruption at Yucca Mountain, Nevada* (SNL 2007 [DIRS 179347], Section 6.2).

The conceptual tephra redistribution model divides the Fortymile Wash drainage area into two domains: the drainage basin and the alluvial fan. The drainage basin includes the vent location and the tephra and waste deposited on the landscape in the event of a volcanic eruption through the repository (Figure 6.5-13). The RMEI location is considered to be on the Fortymile Wash alluvial fan south of the fan apex. The drainage basin and the alluvial fan are divided at the fan apex. The location of the RMEI is specified in the same area for the igneous eruption case as for all other modeling cases so that estimates of the dose are calculated at a consistent location for the nominal, intrusive, and eruptive modeling cases. This means that model realizations with wind blowing away from this location and away from the Fortymile Wash do not contribute to dose calculations.

The tephra redistribution model uses a spatially distributed analysis of hillslopes and channels in the drainage basin upstream of the fan apex to provide an estimate of the mass of tephra and waste that could be transported from the upper drainage basin to the RMEI location by hillslope

and fluvial processes. The model mobilizes and transports tephra and waste deposited on the landscape toward the RMEI location if it falls on steep slopes or on active channels. Before the mobilized tephra and waste are deposited at the RMEI location, they are transported through the alluvial channel system where mixing with uncontaminated channel sediments leads to dilution. Mixing occurs during flood events as sediment and tephra are entrained from the bed, mixed by turbulent flow, and redeposited on the bed. The depth to which tephra and channel sediment are mixed is the scour depth. The ratio of the tephra thickness to the scour depth at the fan apex, just upstream from the RMEI location, is used as the fraction of channel-bed material composed of tephra when the redistributed tephra and waste reach the RMEI location.

The tephra and waste transported from the upper drainage basin, and primary tephra and waste deposited at the RMEI location, provide the initial conditions for redistribution of radionuclides into the soil column at the RMEI location. The Tephra Redistribution Submodel considers the migration of radionuclides within the soil as a diffusion process due to suspension and redeposition of fine particles by infiltration, and physical mixing of soil particles by freeze-thaw cycles and bioturbation. The diffusion coefficients used in the model were calibrated using measured ^{137}Cs profiles on channels and inter-channel divides of the upper Fortymile Wash alluvial fan and therefore incorporate all of the potential diffusion processes (SNL 2007 [DIRS 179347], Sections 6.3.3 and 6.5.9). The time-dependent concentration resulting from the diffusion process is used by the Volcanic Ash Exposure Submodel to calculate dose to the RMEI.

TSPA-LA Model Abstraction–The Tephra Redistribution Submodel is implemented in the TSPA-LA Volcanic Eruption Model using the computer code FAR V1.2 (STN: 11190-1.2-00 [DIRS 182225]). The FAR V1.2 code is implemented as a DLL and is incorporated directly within the TSPA-LA Volcanic Eruption Model. The mathematical description of the FAR V1.2 code is provided in *Redistribution of Tephra and Waste by Geomorphic Processes Following a Potential Volcanic Eruption at Yucca Mountain, Nevada* (SNL 2007 [DIRS 179347], Section 6.3).

Gridded values of tephra and waste concentration computed by the ASHPLUME code are passed to the FAR code for redistribution calculations. FAR V1.2 maps the tephra and waste concentration to a 30-m resolution digital elevation model grid covering the Fortymile Wash drainage basin. The calculation of time-dependent waste concentration at the RMEI location proceeds in six steps (SNL 2007 [DIRS 179347], Section 6.3.3).

Step 1: Because ASHPLUME calculations are carried out on a relatively coarse polar grid, a bilinear interpolation is performed on the ASHPLUME-generated grid values of tephra and waste concentration to rectify the concentration values to the much higher resolution digital elevation model grid.

Step 2: The digital elevation model file is processed to fill any artificial "holes" in topography due to imperfections in the digital elevation model data. The file is scanned recursively to slightly raise any "pits" or "flats" where the downstream direction is not well defined.

Step 3: A set of spatial analyses are performed on the input digital elevation model to determine slopes, contributing area, and scour depths for the drainage basin. The waste-contaminated tephra is mobilized from slopes greater than a specified critical slope.

Step 4: The mobilized tephra is routed through the channel system to model the dilution effect. Routing of mobilized tephra and uncontaminated channel-bed sediments is performed using a bifurcation routing algorithm. The resulting grid of tephra thickness routed through each digital elevation model pixel is divided by the grid of scour depth routed through each pixel to yield a dilution factor at each channel grid cell in the basin. The dilution factor at the apex of the alluvial fan (one particular cell in the grid) is used in subsequent steps.

Step 5: Initial concentrations of waste in channels and on interchannel divides at the RMEI location are determined. This step represents the transfer of waste from the upper drainage basin to the RMEI location on the alluvial fan. In channels, the mass of waste is the sum of the direct deposition of waste and waste transported from the upper basin by fluvial processes. On interchannel divides, the concentration of waste is determined solely from direct deposition of waste-contaminated tephra.

Step 6: Time-dependent diffusion of radionuclides within a finite depth of permeable soil is calculated using the initial concentrations determined in **Step 5**. Inputs to this step include the permeable depths on divides, L_d, and in channels, L_c, and diffusivity values for divides, D_d, and channels, D_c.

The mixing/dilution processes implemented in Steps 1 to 5 are assumed to occur instantaneously after the potentially contaminated tephra is deposited on the ground surface after a volcanic eruption. To simplify the model conceptualization, the diffusion process in Step 6 is the only process considered to be time-dependent in the Tephra Redistribution Submodel. This is a reasonable simplification, given the expected relatively short time scale of the mixing processes.

Descriptions of the key input parameters to the Tephra Redistribution Submodel are shown in Table 6.5-5. The results of the Tephra Redistribution Submodel calculations are passed to the Volcanic Ash Exposure Submodel for dose calculations. The results consist of four time series of mass concentration: (1) concentration on divides averaged over the tillage depth; (2) concentration on divides averaged over the resuspendable surface layer; (3) concentration in channels averaged over the tillage depth; and (4) concentration in channels averaged over the resuspendable surface layer. The concentrations on divides and channels are combined using the weighting factor, F, for the fraction of the alluvial fan composed of channels (and 1-F for the fraction of the alluvial fan composed of divides) to yield one concentration for the resuspendable surface layer and one concentration for the tillage depth for use by the Volcanic Ash Exposure Submodel in dose calculations.

6.5.2.1.4 Volcanic Ash Exposure Submodel

The Volcanic Ash Exposure Submodel provides the calculation of annual dose for the Volcanic Eruption Modeling Case. Details of the dose calculation are provided with the Biosphere Model

Component description in Section 6.3.11. Implementation of the Volcanic Eruption Modeling Case for the TSPA-LA Model includes the determination of both the probability of the event and its consequences.

During the atmospheric transport and redistribution on the ground surface, radionuclide concentrations in the waste are proportional to those in the waste inventory that combine each type of WP hit, with consideration of radionuclide decay. The calculated radionuclide concentrations in volcanic tephra or in a soil/tephra mixture using the redistribution submodel provide the radioactive source term for calculating annual dose to the RMEI. A set of the BDCFs appropriate to the Volcanic Eruption Modeling Case is developed according to the Biosphere Model Component described in Section 6.3.11. The annual dose associated with the radioactive source is calculated by multiplying radionuclide concentrations by the volcanic ash BDCFs.

6.5.2.2 Implementation in the TSPA-LA Model

This subsection describes the inputs, feeds, software, and model calculations required for the Volcanic Eruption Modeling Case. The Volcanic Eruption component of the TSPA-LA Model is implemented as a separate, stand-alone GoldSim model file.

The determination of atmospheric dispersal and deposition of ash and waste fuel particles from a hypothetical volcanic eruption that intersects the repository is accomplished using the ASHPLUME_DLL_LA V.2.1 code, which is dynamically coupled to the TSPA-LA Model. The ASHPLUME DLL requires input parameters that define the characteristics of the eruptive event, the environmental conditions, and the mass of the waste to be included in the event. The key ASHPLUME input parameters are shown in Table 6.5-4. The mass of waste to be included in the eruptive event is calculated based on the proportion of CSNF WPs to CDSP WPs in the repository, a sampled parameter that selects the number of WPs affected by the eruptive event, and a factor that accounts for the proportion of waste-contaminated magma that is erupted into the tephra column. Note that this is the total mass of waste that the ASHPLUME code uses, and not a mass vector by radionuclide species. These inputs to the ASHPLUME code are located in the ASHPLUME_DLL input container in the TSPA-LA Model. GoldSim (GoldSim V.9.60.100, STN: 10344-9.60-01 [DIRS 181903]) first samples the input parameters that are probability distributions, and then passes all parameters to the ASHPLUME code. The ASHPLUME code then calculates the waste and ash deposition results (g/cm^2) at the RMEI location, followed by an additional calculation (using the same input parameters) at many grid points covering the Fortymile Wash watershed.

The TSPA-LA Model then performs calculations for the Tephra Redistribution Submodel. The consequences of a volcanic eruption include the potential increase in dose at the location of the RMEI from the transport of radioactive waste-contaminated ash through hillslope and fluvial transport mechanisms. The Tephra Redistribution Submodel accounts for this effect at the location of the RMEI for both interchannel divides and distributary channels. The volcanic ash redistribution calculations are performed using the computer code FAR V1.2 (STN: 11190-1.2-00 [DIRS 182225]). Inputs to this DLL define such parameters as directly deposited ash and waste concentrations at the RMEI location and at grid points covering the Fortymile Wash watershed; critical gradient and drainage density for tephra mobilization; scour

depth; diffusion parameters; and Biosphere Model Component inputs. GoldSim samples those inputs that are probability distributions and then passes all inputs to FAR V1.2, which uses these inputs to calculate the time-dependent waste concentration on interchannel divides and distributary channels. The TSPA-LA Model takes these ash redistribution results and, using the areal weighting factor, F (Table 6.5-5), for interchannel divides and distributary channels, determines the source terms for:

- Ingestion and radon exposure for the interchannel divides and distributary channels
- Long-term inhalation exposure for interchannel divides and distributary channels
- Short-term inhalation exposure for interchannel divides and distributary channels.

The TSPA-LA Model then converts the source terms back into the masses of the individual radionuclide species based on total repository inventory and accounts for radioactive decay. As described in Section 6.3.11, these source terms are then multiplied by the corresponding BDCFs to determine dose.

Section 6.1.2.4.3 describes the calculation of annual dose histories for the TSPA-LA Model for the Volcanic Eruption Modeling Case. The TSPA-LA Model calculates the mean annual dose for the Volcanic Eruption Modeling Case using a three-step process. First, an LHS of epistemically uncertain TSPA-LA Model parameters is generated. Each element $\mathbf{e}_i$ in the LHS defines values for the epistemic parameters listed in Table 6.5-4. For each element in the LHS, a number of annual dose histories are computed using GoldSim. The characteristics of each eruption (e.g., eruptive power and eruptive height) and the wind conditions at the time of the eruption are specified by elements of a separate LHS, $\mathbf{u}$, for the aleatory parameters listed in Table 6.5-4. Using these inputs, the amount of waste entrained in the eruptive plume, its deposition and redistribution are evaluated using the models described above, to produce a single annual dose history, $D_{IE}(\tau \mid [1, t, 1, \mathbf{u}_l], \mathbf{e}_i)$. Each annual dose history D_{IE} is associated with a single volcanic eruption occurring at a specified time t, which affects one WP, and with specified eruptive characteristics and specified wind conditions.

Second, for each element of the LHS of epistemic parameters, the expected annual dose history is calculated by Equation 6.1.2-18 (Section 6.1.2.4.3), using the annual dose histories computed for that realization. The integral in Equation 6.1.2-18 (Section 6.1.2.4.3) accounts for the aleatory uncertainty in the time and characteristics of the eruption and the wind conditions, as well as the uncertainty in the frequency of igneous events, and is evaluated numerically by EXDOC (Section 6.1.5). The frequency of igneous events is sampled from the probability distribution described in Table 6.5-2. Finally, the mean annual dose history is calculated as the average of the expected annual dose histories from the set of realizations.

The total expected annual dose result for the Volcanic Eruptive Modeling Case presented in Section 8.2.3.2 was calculated using GoldSim to implement the dose histories, and EXDOC to implement Equation 6.1.2-18 (Section 6.1.2.4.3). To implement the calculation of the contribution of individual radionuclides to the mean annual dose histories presented in Section 8.2.3.2, an alternative technique was used. In addition to implementing the single annual dose history calculation, the GoldSim model file for the Volcanic Eruption Modeling Case also implements a calculation of the mean dose history for individual radionuclides by considering a "blended" sampling of all epistemic and aleatory parameters as follows:

$$\overline{\overline{D_i}}(\tau) = \frac{pE}{M}\sum_{j=1}^{M}\lambda_{I,j}N_{IE,j}F_j\int_0^{\tau} D_{IE,i}(\tau \mid t,1,\mathbf{u}_j,\mathbf{e}_j)dt \qquad \text{Eq. 6.5.2-1}$$

where

$\overline{\overline{D_i}}(\tau)$ = mean annual dose history for radionuclide i

M = the number of samples of "blended" aleatory **u** and epistemic **e** parameters used to compute the mean

λ_I = frequency of igneous events (Table 6.5-2) **e**

pE = probability that an igneous event includes a conduit that intersects waste, or 0.083 (This is the probability that one or more waste packages are intersected by a conduit (i.e. 1.0 minus 0.703 from Table 6.5-3) times the probability that a conduit forms inside the repository footprint on a dike that intersects the repository (0.28 from SNL 2007 [DIRS 177432], Section 7.2))

N_{IE} = the number of WPs affected by an eruptive conduit (sampled from the non-zero portion of Table 6.5-3) **u**

F = the fraction of WP contents ejected into the atmosphere (Magma_Partitioning_a in Table 6.5-4) **u**, and

$D_{IE,i}(\tau|t,1,\mathbf{u}_j,\mathbf{e}_j)$ = annual dose history for radionuclide i conditional on an eruption at time t, which affects one repository average WP for "blended" sample j of all aleatory and epistemic parameters.

The total mean annual dose for the Volcanic Eruption Modeling Case is the sum of the contributions from the individual radionuclides. Equation 6.5.2-1 was used to calculate the contribution of individual radionuclides to the mean annual dose histories presented in Section 8.2.3.2. It should be noted that the mean of the expected dose calculated using EXDOC as presented in Section 6.1.2.4.3, and the mean calculated with Equation 6.5.2-1 are mathematically equivalent, however, slight numerical differences will be observed in the results of the two methods due to different parameter sampling and the different numerical solution techniques employed by the two methods. Equation 6.5.2-1 was used to produce the individual radionuclide contribution results for the Volcanic Eruption Modeling Case because it is less computationally intensive when only the mean value is required.

6.5.2.3 Model Component Consistency and Conservatism in Assumptions and Parameters

To enhance understanding of the complex interactions within the TSPA-LA Model, a discussion of consistency among model components and submodels, and identification of TSPA-LA Model conservatisms in submodels and abstractions specific to the Volcanic Eruption Modeling Case, are discussed below.

6.5.2.3.1 Consistency of Assumptions

Volcanic Ash Particle Size—The size distribution of ash particles transported by the ASHPLUME code is generally much larger than the particle size used to calculate the inhalation BDCFs. The ASHPLUME model is appropriate for particles of mean diameter greater than 15 to 30 µm (Jarzemba et al. 1997 [DIRS 100987], p. 2-2). The dose coefficients for inhalation are for particles with activity median aerodynamic diameter of 1 µm (BSC 2005 [DIRS 172827], Section 6.5.3.1).

Effect on the TSPA-LA Model—An analysis was conducted in *Characteristics of the Receptor for the Biosphere Model* (BSC 2005 [DIRS 172827], Section 6.5.5.2) regarding the effects of the size distribution of ash particles transported by the ASHPLUME code being generally much larger than the particle size used to calculate the inhalation BDCFs. It was concluded from that analysis that the application of dose coefficients for particles with activity median aerodynamic diameter of 1 µm will not underestimate the doses from inhalation of resuspended material and that the dose coefficients are adequate for use in the biosphere model.

6.5.2.3.2 Identification of Conservatisms in Submodels and Abstractions

Radionuclide Waste Form Completely Destroyed—As described in *Atmospheric Dispersal and Deposition of Tephra from a Potential Volcanic Eruption at Yucca Mountain, Nevada*, (SNL 2007 [DIRS 177431], Section 5.1.2), WP failure and entrainment of fragmented waste within rising magma is assumed to occur due to the intersection of an eruptive conduit with WPs. In the TSPA-LA Model implementation, the WPs hit are assumed to be completely destroyed and all of the waste contained in the WPs is available to be erupted. This conservative assumption tends to maximize the release of radionuclides from the EBS.

6.5.2.4 Alternative Conceptual Model(s) for the Volcanic Eruption Modeling Case

Secondary Dike Propagation ACM—Woods et al. (2002 [DIRS 163662]) describe an eruptive ACM in which magma could potentially flow horizontally in a drift to a secondary vent opening at some point along the drift, sometimes referred to as the "dogleg" scenario. In this ACM, after an intersected dike fills with magma, the pressurization generates a new opening at some distance down the drift that becomes the main vent to the surface. This ACM could potentially affect a larger number of waste packages than is considered in the Volcanic Eruption Modeling Case in which the eruptive conduit propagates vertically through a drift. However, modeling of magma flow in drifts described in *Dike/Drift Interactions* (SNL 2007 [DIRS 177430], Sections 6.3.3.5.6, 6.5, and 8.1.3), indicates that this secondary breakout condition is not expected to occur because of heat loss and stoppage due to solidification of the magma in the secondary fracture. Based on the results of this analysis (SNL 2007 [DIRS 177430]), the Secondary Dike Propagation ACM was not included in the Volcanic Eruption Modeling Case in the TSPA-LA Model.

Volcanic Eruption Phase Dose ACM—This subsection describes an ACM for the volcanic eruption phase dose received by a receptor that does not leave the region during a volcanic eruption. The result of this calculation, showing that the mean eruption phase dose is insignificant compared to the mean post eruption phase dose, is used as the basis for excluding

this ACM from the Volcanic Eruption Modeling Case in the TSPA-LA Model. Because a high concentration of airborne radioactive particulates is expected during this phase, inhalation of airborne-contaminated ash particles is the only pathway considered, as described in *Biosphere Model Report* (SNL 2007 [DIRS 177399], Section 6.15.2). The receptor has the same inhalation characteristics as those for the RMEI discussed in Section 6.3.11.

The eruption phase of a volcanic event refers to the conditions that exist during the volcanic eruption before the deposition of volcanic ash on the ground is completed. The dose factors for determining inhalation dose during a volcanic eruption are different from the BDCFs used for the time period after the deposition of volcanic ash on the ground. These dose factors are provided for use in the TSPA-LA Model in DTN: MO0702PAINHALA.001_R0 [DIRS 179329]. To calculate the daily dose from inhaling a specific radionuclide during a volcanic eruption, the activity concentration of that radionuclide in air is multiplied by the appropriate dose factor. The total inhalation dose from concentrations of primary radionuclides in air is then calculated as (SNL 2007 [DIRS 177399], Section 6.15.2.2, Equation 6.15-9):

$$D_{inh} = \sum_i D_{inh,i} = \sum_i DF_i \times Ca_i \qquad \text{(Eq. 6.5.2-2)}$$

where

D_{inh} = total inhalation dose rate for all radionuclides (Sv/day)

$D_{inh,\,i}$ = inhalation dose rate for a primary radionuclide i (Sv/day)

DF_i = dose factor for a primary radionuclide i (Sv/day per Bq/m^3)

Ca_i = activity concentration of a primary radionuclide i in air (Bq/m^3) (Equation 6.5.2-5).

The total inhalation dose during a volcanic eruption can then be calculated by multiplying the inhalation dose rate by the duration of the volcanic eruption:

$$D = D_{inh} \times t_{vol} \qquad \text{(Eq. 6.5.2-3)}$$

where

D = total inhalation dose during volcanic eruption (Sv)

t_{vol} = duration of volcanic eruption, or volcanic eruption time (day).

The activity concentration of a radionuclide in air, Ca_i, is proportional to the volcanic ash concentration in air, which can vary with time during the eruption phase. To estimate the activity concentration in air, it is assumed that the ratio of waste to ash in volcanic ash does not change between the time it was in the air and the time it was deposited on the ground:

$$Ca_{waste_air} = Ca_{ash_air} \times \frac{C_{waste_dep}}{C_{ash_dep}} \qquad \text{(Eq. 6.5.2-4)}$$

where

Ca_{waste_air} = mass concentration of waste in air (g/m^3)

Ca_{ash_air} = mass concentration of volcanic ash in air (g/m^3) (Equation 6.5.2-7)

C_{waste_dep} = mass concentration of waste deposited on the ground (g/m^2)

C_{ash_dep} = mass concentration of volcanic ash deposited on the ground (g/m^2).

Both mass concentrations of waste and volcanic ash deposited at the location of the RMEI on the ground can be obtained from the results of the TSPA-LA Model for the Igneous Scenario Class. By using the mass concentration of waste in air, activity concentrations of individual radionuclides can be calculated as:

$$Ca_i = Ca_{waste_air} \times f_i \times SA_i \quad \text{(Eq. 6.5.2-5)}$$

where

f_i = fraction of an individual radionuclide, i, among the total waste mass, dimensionless (Equation 6.5.2-6)

SA_i = specific activity for the individual radionuclide, i, (pCi/g).

The fraction of an individual radionuclide should be weighted by the number of CSNF and CDSP WPs hit, as follows:

$$f_i = \frac{N_{CSNF} \times m_{CSNF,i} + N_{CDSP} \times (m_{HLW,i} + m_{DSNF,i})}{\sum_i [N_{CSNF} \times m_{CSNF,i} + N_{CDSP} \times (m_{HLW,i} + m_{DSNF,i})]} \quad \text{(Eq. 6.5.2-6)}$$

where

N_{CSNF} = number of CSNF WPs hit by volcanic eruption

N_{CDSP} = number of CDSP WPs hit by volcanic eruption

$m_{CSNF,\,i}$ = mass of radionuclide, i, per CSNF WP (g)

$m_{HLW,\,i}$ = mass of radionuclide, i, for HLW per CDSP WP (g)

$m_{DSNF,\,i}$ = mass of radionuclide, i, for DSNF per CDSP WP (g).

As mentioned before, the mass concentration of volcanic ash may vary with time during the eruption phase. However, the average mass concentration of volcanic ash in air, Ca_{ash_air}, can be calculated using the amount of ash deposited on the ground, ash settling velocity, and volcanic eruption time:

$$Ca_{ash_air} = \frac{C_{ash_dep}}{0.01 \times V_0 \times 86{,}400 \times t_{vol}} \quad \text{(Eq. 6.5.2-7)}$$

where

V_0 = settling velocity for volcanic ash (cm/sec) (Equation 6.5.2-8)

t_{vol} = eruption duration (days)

0.01 = unit conversion (m/cm)

86,400 = unit conversion (sec/day).

The settling velocity of volcanic ash can be calculated, and its equation and inputs are given in *Atmospheric Dispersal and Deposition of Tephra from a Potential Volcanic Eruption at Yucca Mountain, Nevada,* (SNL 2007 [DIRS 177431], Section 6.5.1 Equation 6-4 and Table 8-2):

$$V_0 = \frac{\psi_p g d^2}{9\eta_a F^{-0.32} + \sqrt{81\eta_a^2 F^{-0.64} + \frac{3}{2}\psi_p \psi_a g d^3 \sqrt{1.07 - F}}} \quad \text{(Eq. 6.5.2-8)}$$

where

Ψ_a = density of air (0.001734 g/cm^3 used in TSPA-LA Model)

Ψ_p = density of particles, dependent on particle size (g/cm^3) (Equation 6.5.2-9)

g = gravitational acceleration constant (980 cm/s^2)

η_a = viscosity of air (0.000185 g/cm-s used in TSPA-LA Model)

F = shape factor for particles (0.5 used in TSPA-LA Model)

d = mean particle diameter (cm).

The particle density, Ψ_p, depends on the particle size, and larger particles are less dense because of the incorporation of more gas bubbles. Particle density is a function of the particle log-diameter, ρ_a in cm, as follows (SNL 2007 [DIRS 177431], Section 6.5.1, Equation 6-5):

$$\begin{aligned} &\Psi_p = \Psi_p^{high} && \text{for } \rho_a < \rho_a^{low} \\ &\Psi_p = \Psi_p^{low} + (\Psi_p^{high} - \Psi_p^{low})(\rho_a^{high} - \rho_a)/(\rho_a^{high} - \rho_a^{low}) && \text{for } \rho_a^{low} < \rho_a < \rho_a^{high} \quad \text{(Eq. 6.5.2-9)} \\ &\Psi_p = \Psi_p^{low} && \text{for } \rho_a > \rho_a^{high} \end{aligned}$$

where

Ψ_p^{high} = ash particle density at minimum particle size (2.08 g/cm^3 used in TSPA-LA Model)

Ψ_p^{low} = ash particle density at maximum particle size (1.04 g/cm^3 used in TSPA Model)

ρ_a^{low} = log ash particle size in cm at maximum ash density (-3 used in TSPA-LA Model)

ρ_a^{high} = log ash particle size in cm at minimum ash density (0 used in TSPA-LA Model)

ρ_a = log(d), log particle diameter in cm.

The mass of radionuclides in CSNF, DSNF, and HLW ($m_{CSNF,\,i}$, $m_{DSNF,\,i}$ and $m_{DSNF,\,i}$), changes with time due to decay and ingrowth in the radioactive waste. This causes the annual dose during the eruption phase to decrease with time if a volcano occurs at a later time, T. Because some parameters that define an eruptive event are uncertain as shown in Table 6.5-4, the calculation of Equations 6.5.2-2 to 6.5.2-9 was carried out using the GoldSim software. The input values for these equations were taken directly from the Volcanic Eruption Modeling Case of the Igneous Scenario Class in the TSPA-LA Model. The mean annual dose for eruptions that occur at times $T = \tau$ due to M realizations of the volcanic eruption phase parameters are calculated with GoldSim as

$$\overline{\overline{D}}(\tau) \cong \frac{pE}{M}\sum_{j=1}^{M} D(\tau, \mathbf{a}_j, \mathbf{e}_j)\,\lambda_{I,j} \qquad \text{Eq. 6.5.2-10}$$

where

$\overline{\overline{D}}(\tau)$ = mean total annual eruption phase inhalation dose at time τ due to volcanic eruptions that occur at times $T = \tau$ (Sv/yr)

$D(\tau,\mathbf{a}_j,\mathbf{e}_j)$ = total annual eruption phase inhalation dose (Eq. 6.5.2-3) for eruptions that occur at times $T = \tau$ and with aleatory parameters $\mathbf{a}_j$ and epistemic parameters $\mathbf{e}_j$ (Table 6.5-4) (Sv)

$\lambda_{I,j}$ = annual frequency of intersection of the repository by a volcanic dike (1/yr)

pE = probability of one or more eruptive centers intersecting the repository given the intersection of a dike (0.28).

The detailed calculations and the output of eruption phase dose are in output DTN: MO0708TSPAGENT.000 [DIRS 183000]. The calculation results of 1,000 realizations of Equation 6.5.2-10 using the GoldSim software are shown on Figure 6.5-14, which includes a comparison between the mean annual doses to the RMEI during the volcanic eruptive phase and post-eruption processes (Volcanic Eruption Modeling Case, Equation 6.5.2-1). The mean annual dose from the volcanic eruption phase is small compared to the mean annual dose caused by volcanic ash deposited on the ground calculated in the TSPA-LA Model. Because of its relative insignificance to the annual dose, the contribution from this eruptive phase dose ACM is not included in the TSPA-LA Model.

Table 6.5-1. Waste Form Temperatures Inside Intrusive Body

Time Since Igneous Event	For an Intrusion into a Repository at 25°C		For an Intrusion into a Repository at 50°C		For an Intrusion into a Repository at 100°C		For an Intrusion into a Repository at 150°C		For an Intrusion into a Repository at 200°C	
Years	WP	Drift Wall	WP	Drift Wall	WP	Drift Wall	WP	Drift Wall	WP	Drift Wall
0	1,150	1,150	1,150	1,150	1,150	1,150	1,150	1,150	1,150	1,150
0.1	977	592	1,006	620	1,012	644	1,019	668	1,026	692
0.2	702	462	749	494	768	524	786	553	804	583
0.3	530	382	577	416	603	449	629	483	655	516
0.4	422	326	467	360	498	396	529	432	560	468
0.5	351	284	394	318	428	356	462	394	497	431
0.6	301	252	341	286	378	325	415	364	452	403
0.7	264	226	303	260	341	300	380	341	418	381
0.8	236	206	273	239	313	281	353	322	392	363
0.9	213	189	249	222	290	264	331	306	372	349
1	195	175	230	208	272	251	314	293	356	336
2	111	106	142	136	187	182	233	228	279	274
3	82.8	80.4	111	109	158	156	206	203	253	251
4	68.4	67.0	96.0	94.5	144	142	192	190	240	238
5	59.7	58.9	86.8	85.8	135	134	183	183	232	231
6	54.0	53.4	80.7	80.0	129	129	178	177	227	226
7	49.8	49.4	76.3	75.8	125	125	174	173	223	222
8	46.7	46.4	73.0	72.6	122	122	171	171	220	220
9	44.3	44.0	70.5	70.2	120	119	169	168	218	217
10	42.4	42.2	68.4	68.2	118	117	167	167	216	216
20	33.7	33.6	59.2	59.2	109	109	158	158	208	208
30	30.8	30.8	56.1	56.1	106	106	156	156	205	205
40	29.3	29.3	54.6	54.6	104	104	154	154	204	204
50	28.5	28.5	53.7	53.7	104	104	153	153	203	203
60	27.9	27.9	53.1	53.1	103	103	153	153	203	203
70	27.5	27.5	52.6	52.6	103	103	152	152	202	202
80	27.2	27.2	52.3	52.3	102	102	152	152	202	202
90	26.9	26.9	52.0	52.0	102	102	152	153	202	202
100	26.7	26.7	51.8	51.8	102	102	152	152	202	202

Sources: DTN: LA0702PADE01EG.001_R0 [DIRS 179495].
Modified from Table 6-13 in *Dike/Drift Interactions* (SNL 2007 [DIRS 177430], Section 6.4.6).

Table 6.5-2. Annual Frequencies of Intersection of Repository by a Dike for the License Application Footprint

Hazard Level (%)	Annual Frequency of Intersection of Repository by a Dike
Mean	1.69×10^{-8}
5	7.41×10^{-10}
10	1.48×10^{-9}
15	2.29×10^{-9}
20	3.02×10^{-9}
30	4.57×10^{-9}
40	6.92×10^{-9}
50	1.00×10^{-8}
60	1.45×10^{-8}
70	2.04×10^{-8}
80	2.69×10^{-8}
85	3.31×10^{-8}
90	4.07×10^{-8}
95	5.50×10^{-8}

Sources: DTN: LA0307BY831811.001_R0 [DIRS 164713].
Composite frequency results from full enumeration of the expert elicitation, excerpted from Table 6-8 in *Characterize Framework for Igneous Activity at Yucca Mountain, Nevada* (BSC 2004 [DIRS 169989], Section 6.5.3.1).

Table 6.5-3. Cumulative Distribution Function for the Number of Waste Packages Hit by Conduits

Number of WPs Hit	CDF Value
0	0.703
1	0.710
2	0.748
3	0.806
4	0.942
5	0.981
6	0.994
7	1.000

Source: DTN: SN0701PAWPHIT1.001_R2 [DIRS 182961].

Table 6.5-4. Key Parameters for the ASHPLUME Code

TSPA-LA Model Parameter Name	Description	Distribution Type	Uncertainty Type	Value(s)
C	Constant relating eddy diffusivity and particle fall time ($cm^2/s^{5/2}$)	Point value	Fixed value	400
Erupt_Power_a	Eruptive power (W)	Log uniform	Aleatory	Min = 1.0×10^9 Max = 1.0×10^{12}
Beta_Dist_a	Column diffusion constant	Uniform	Epistemic	Min = 0.01 Max = 0.5
Erupt_Velocity_a	Initial rise velocity (cm/s)	Uniform	Aleatory	Min = 1 Max = 1.0×10^4
AirDen	Density of air (g/cm^3)	Point value	Fixed value	0.001734
AirVis	Viscosity of air (g/cm-s)	Point value	Fixed value	0.000185
Fshape	Ash particle shape factor	Point value	Fixed value	0.5
Dash_Mean_a	Mean ash particle diameter (cm)	Log triangular	Epistemic	Min = 0.001 Mode = 0.01 Max = 0.1
Dash_sigma_a	Ash particle diameter standard deviation (log cm)	Uniform	Epistemic	Min = 0.301 Max = 0.903
Dmax_trans	Maximum particle diameter for transport (cm)	Point value	Fixed value	10
AshDen_maxD	Ash particle density at minimum particle size (g/cm^3)	Point value	Fixed value	2.08
AshDen_MinD	Ash particle density at maximum particle size (g/cm^3)	Point value	Fixed value	1.04
LogD_minDen	Log ash particle size at minimum ash density (log(cm))	Point value	Fixed value	0
LogD_maxDen	Log ash particle size at maximum ash density (log(cm))	Point value	Fixed value	–3
D_min	Minimum waste particle diameter (cm)	Point value	Fixed value	0.0001
D_mode	Mode of waste particle diameter (cm)	Point value	Fixed value	0.0013
D_max	Maximum waste particle diameter (cm)	Point value	Fixed value	0.2

Table 6.5-4. Key Parameters for the ASHPLUME Code (Continued)

TSPA-LA Model Parameter Name	Description	Distribution Type	Uncertainty Type	Value(s)
Rhocut	Waste incorporation ratio	Point value	Fixed value	0.0
Erupt_Time_a	Eruption duration (seconds)	Log uniform	Aleatory	DTN: LA0702PADE03GK.002_R1 [DIRS 179980]
Wind_Direction	Wind direction (degrees)	Empirical	Aleatory	DTN: MO0408SPADRWSD.002_R0 [DIRS 171751]
Wind_Speed	Wind speed (cm/s)	Empirical	Aleatory	DTN: MO0408SPADRWSD.002_R0 [DIRS 171751]
A_cutoff	Threshold limit on ash accumulation (g/cm^2)	Point value	Fixed value	1×10^{-10}
Magma_Partitioning_a	Fractional multiplier on waste mass to account for waste-containing magma erupted in scoria cone and lava flows	Uniform	Aleatory	Min = 0.1 Max = 0.5

Source: DTN: LA0702PADE03GK.002_R1 [DIRS 179980].

Table 6.5-5. Key Input Parameters to the Tephra Redistribution Submodel

TSPA Parameter Name	Parameter Description	Distribution type	Uncertainty Type	Value (s)
Critical_Slope_a	Critical gradient for tephra mobilization from hillslopes	Uniform	Epistemic	0.21 – 0.47
Drainage_Density_a	Average drainage density for the Fortymile Wash drainage basin	Uniform	Epistemic	20 – 33 km^{-1}
Scour_Depth_a	Scour depth in Fortymile Wash at the fan apex	Uniform	Epistemic	73 – 122 cm
RMEI_Area	Area of the Fortymile Wash fan	Constant	fixed value	33 km^2
Fraction_Channel_a	Fraction, *F*, of the Fortymile Wash fan subject to fluvial activity	Uniform	Epistemic	0.09 – 0.54
L_Channels_a	Depth of permeable soil on channels, L_c, of the Fortymile Wash fan (RMEI location)	Constant	fixed value	200 cm
L_Divides_a	Depth of permeable soil on divides, L_d. of the Fortymile Wash fan (RMEI location)	Uniform	Epistemic	102 – 140 cm
D_Channels_a	Diffusivity of waste in channels, D_c, of the Fortymile Wash fan (RMEI location)	Uniform	Epistemic	0.035 – 0.266 cm^2/yr
D_Divides_a	Diffusivity of waste in divides, D_d, of the Fortymile Wash fan (RMEI location)	Uniform	Epistemic	0.001 – 0.095 cm^2/yr
Ash_Density_a	Tephra settled density	Truncated normal	Epistemic	300 – 1,500 kg/m^3 mean = 1,000 kg/m^3 std. dev. = 100 kg/m^3
b_Tillage	Tillage depth	Uniform	Epistemic	0.05 – 0.30 m

Source: DTNs: MO0702PAFARDAT.001_R3 [DIRS 182578];
LA0612DK831811.001_R1 [DIRS 179987] (Tephra density);
MO0702PAVBPDCF.000_R0 [DIRS 179330] (Tillage depth);
MO0704PASCOURD.000_R1 [DIRS 182149] (Scour depth).

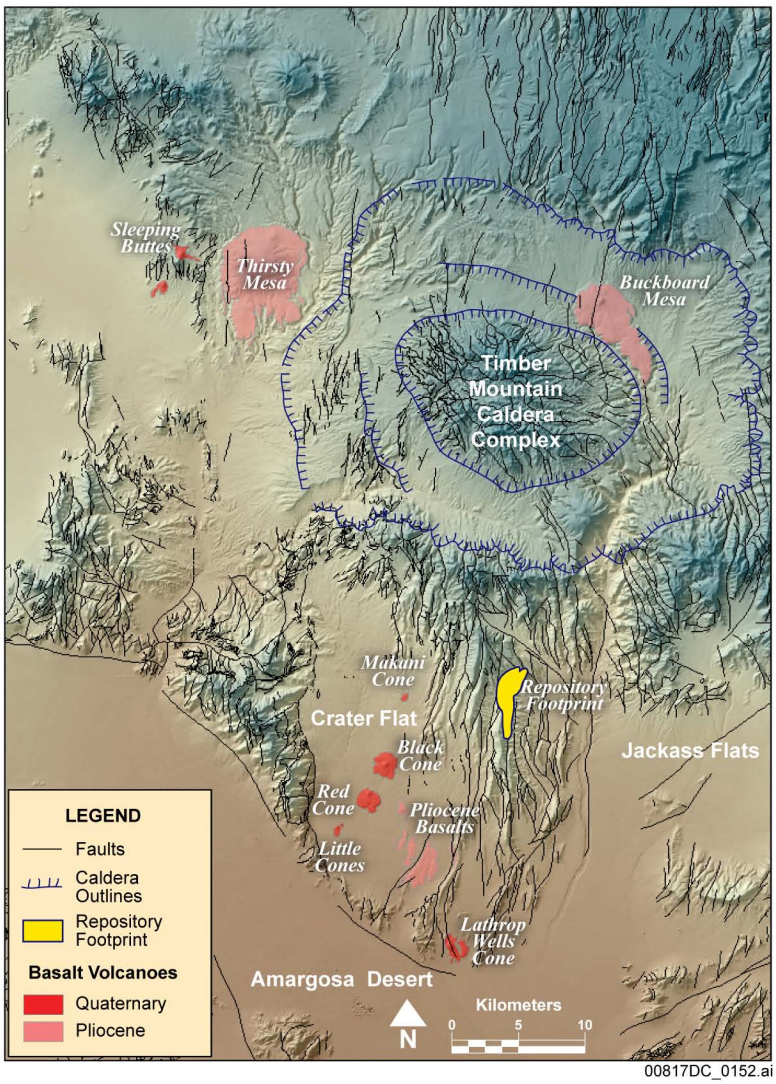

Source: Modified from CRWMS M&O 1998 [DIRS 123196], Figure 2.1.

NOTE: Only volcanoes exposed on the surface are shown.

Figure 6.5-1. Location and Age of Post-Miocene (less than 5.3 million years) Volcanoes (or clusters where multiple volcanoes have indistinguishable ages) in the Yucca Mountain Region

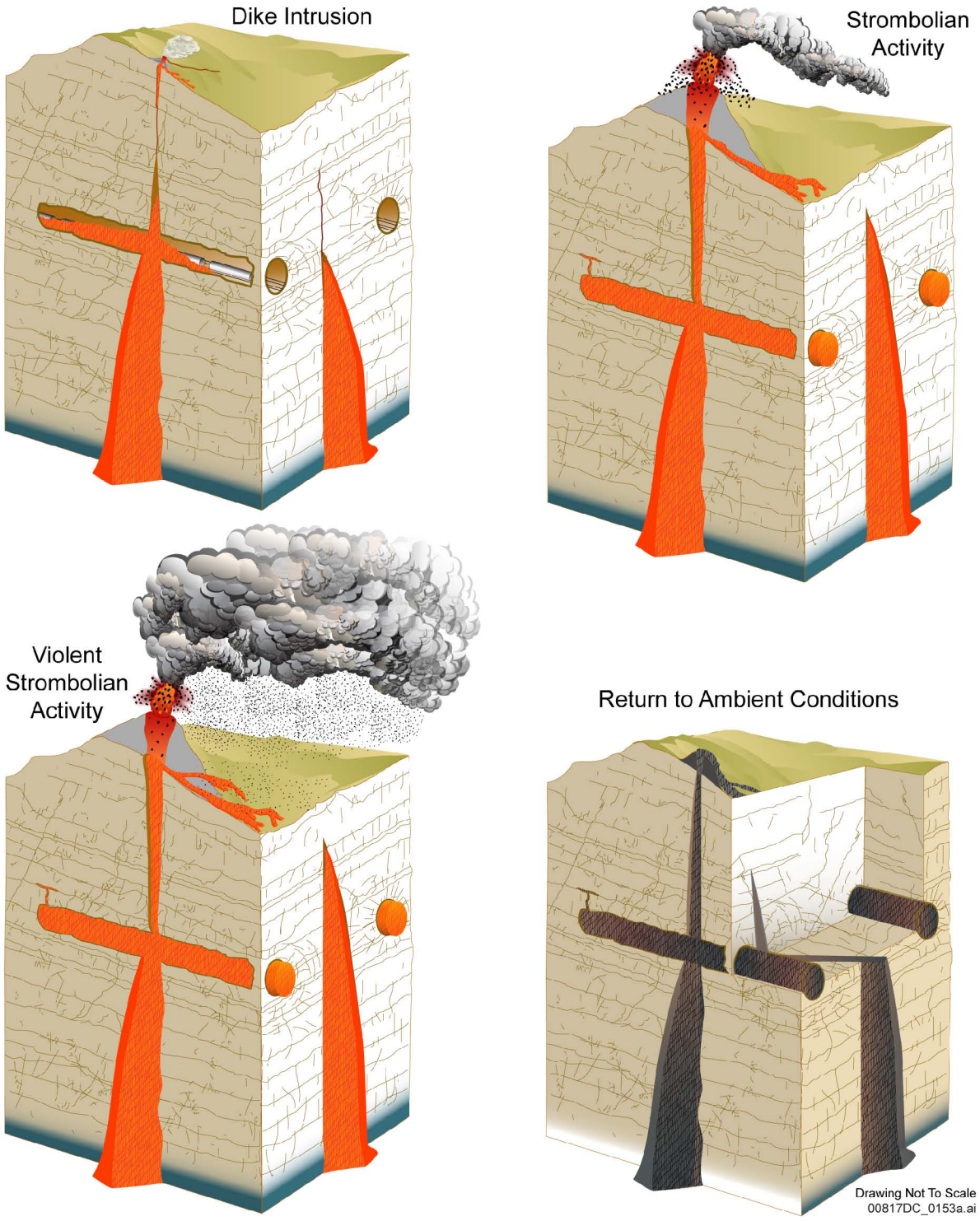

Source: Modified from SNL 2007 [DIRS 177430], Figure 1-1.

Figure 6.5-2. Schematic Drawing of the Processes Associated with a Dike Intrusion or Eruption through the Repository

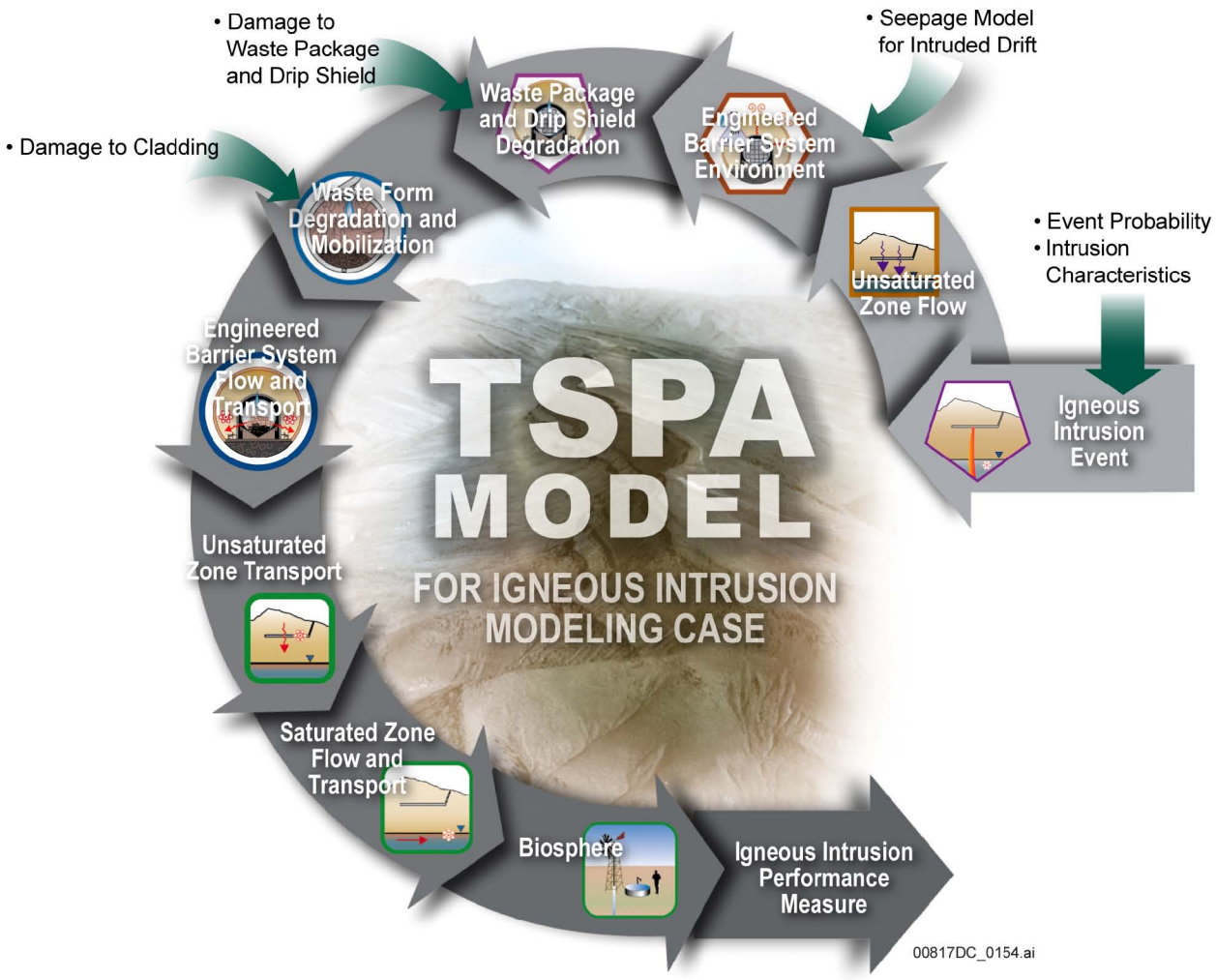

Figure 6.5-3. TSPA-LA Model Components for the Igneous Intrusion Modeling Case

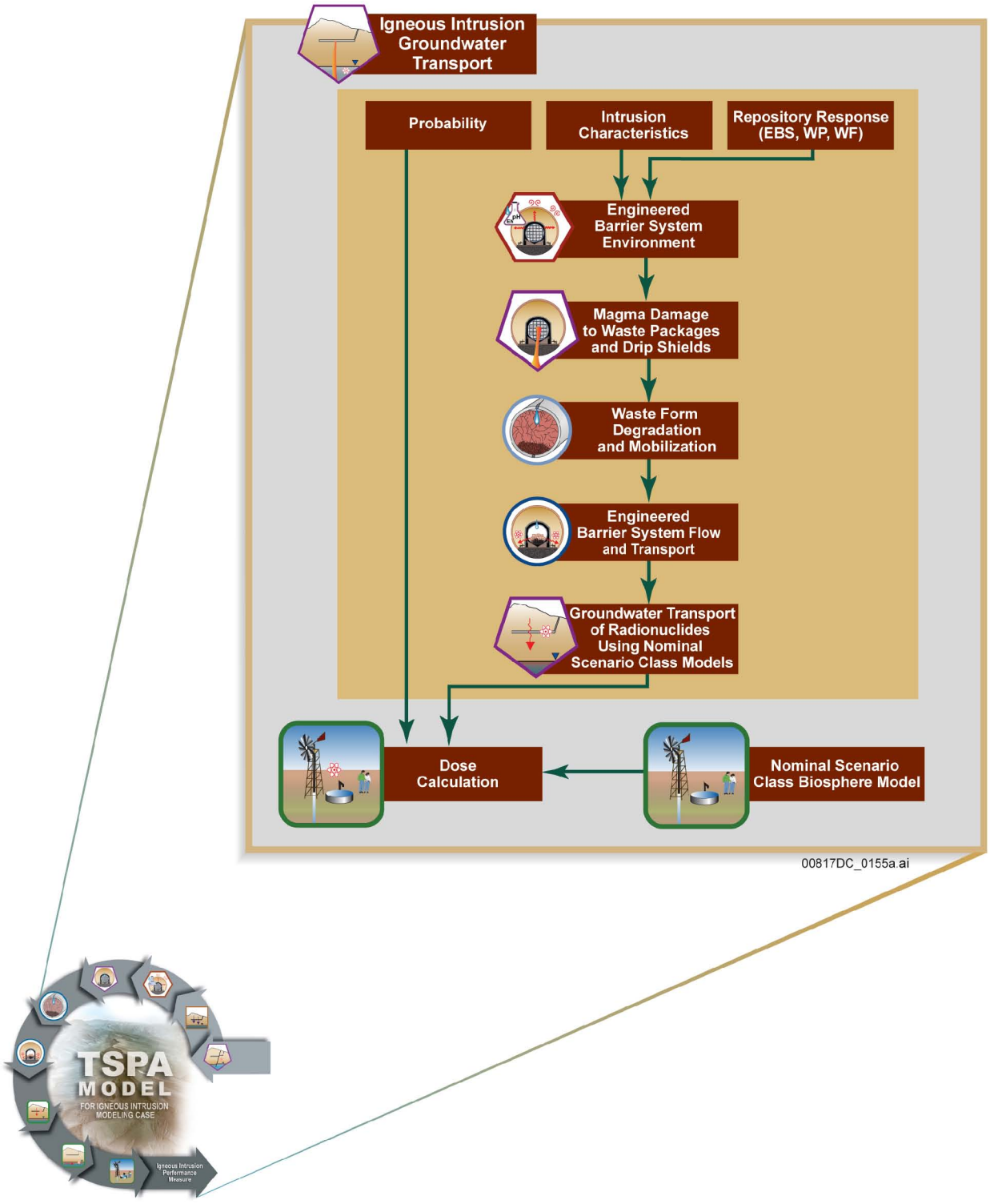

Figure 6.5-4. Information Flow Diagram for the TSPA-LA Igneous Intrusion Modeling Case

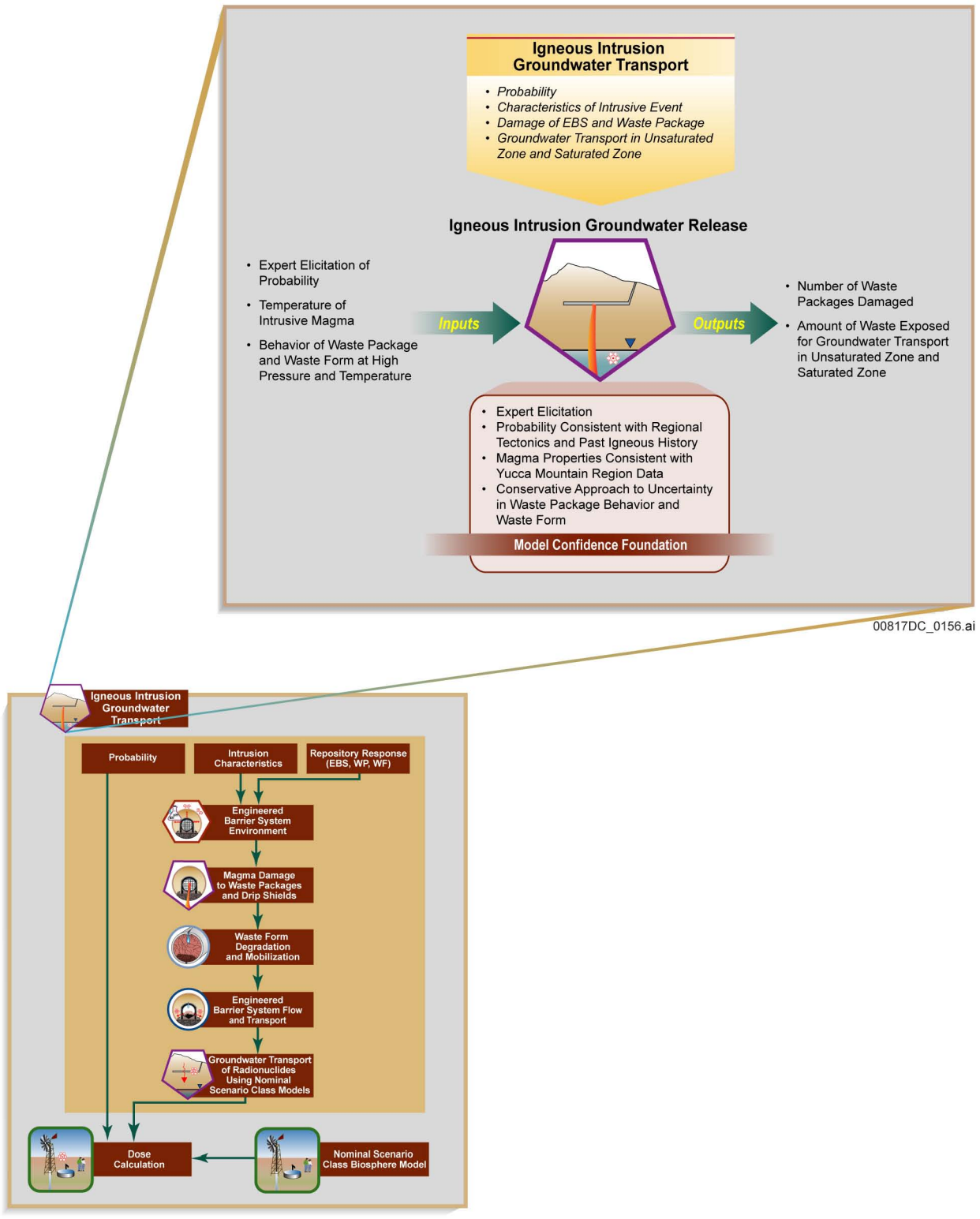

Figure 6.5-5. Inputs, Outputs, and Basis for Model Confidence for the TSPA-LA Igneous Intrusion Modeling Case

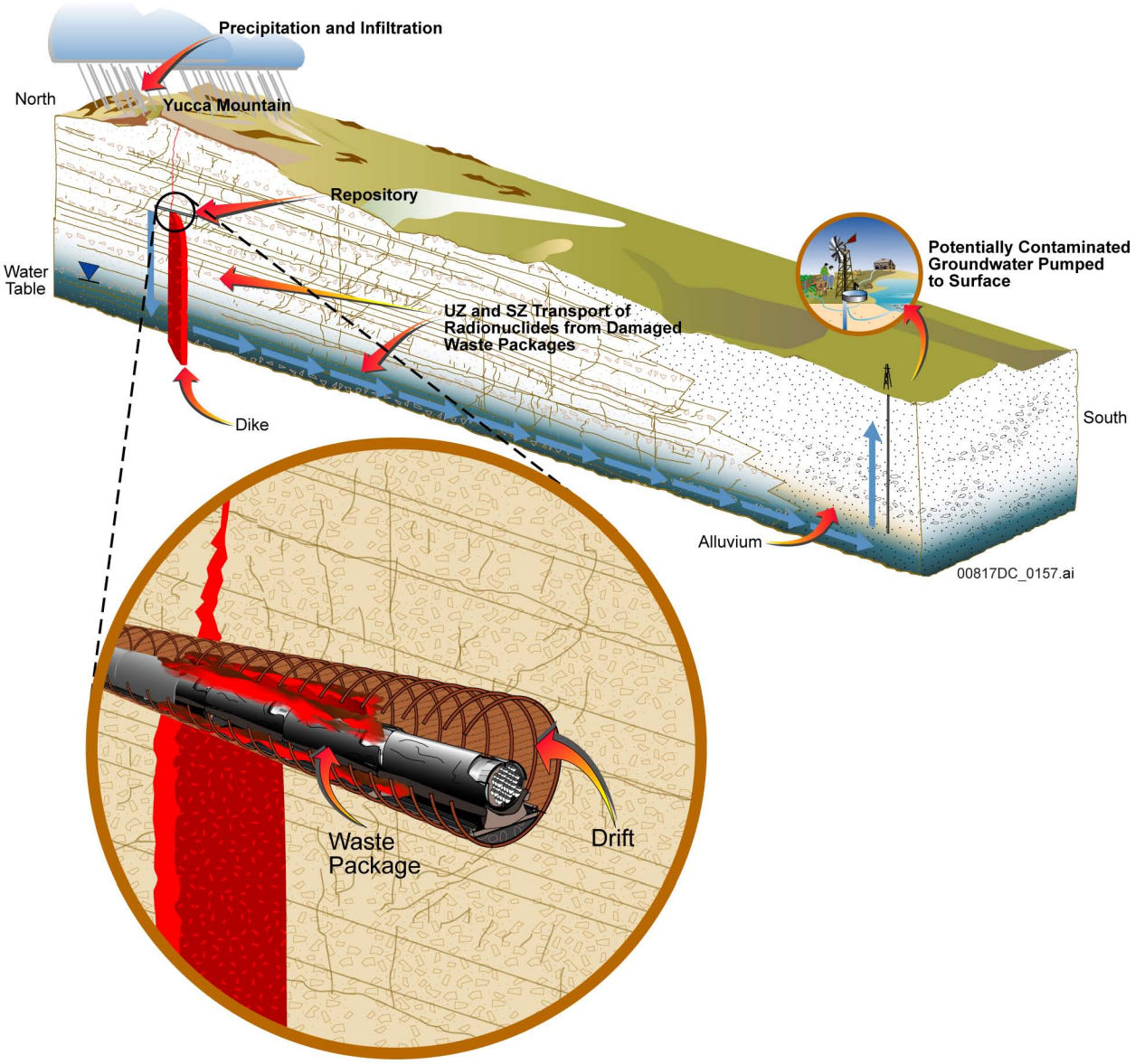

Figure 6.5-6. Schematic Diagram of the Intersection of an Igneous Dike with the Repository and Waste Packages

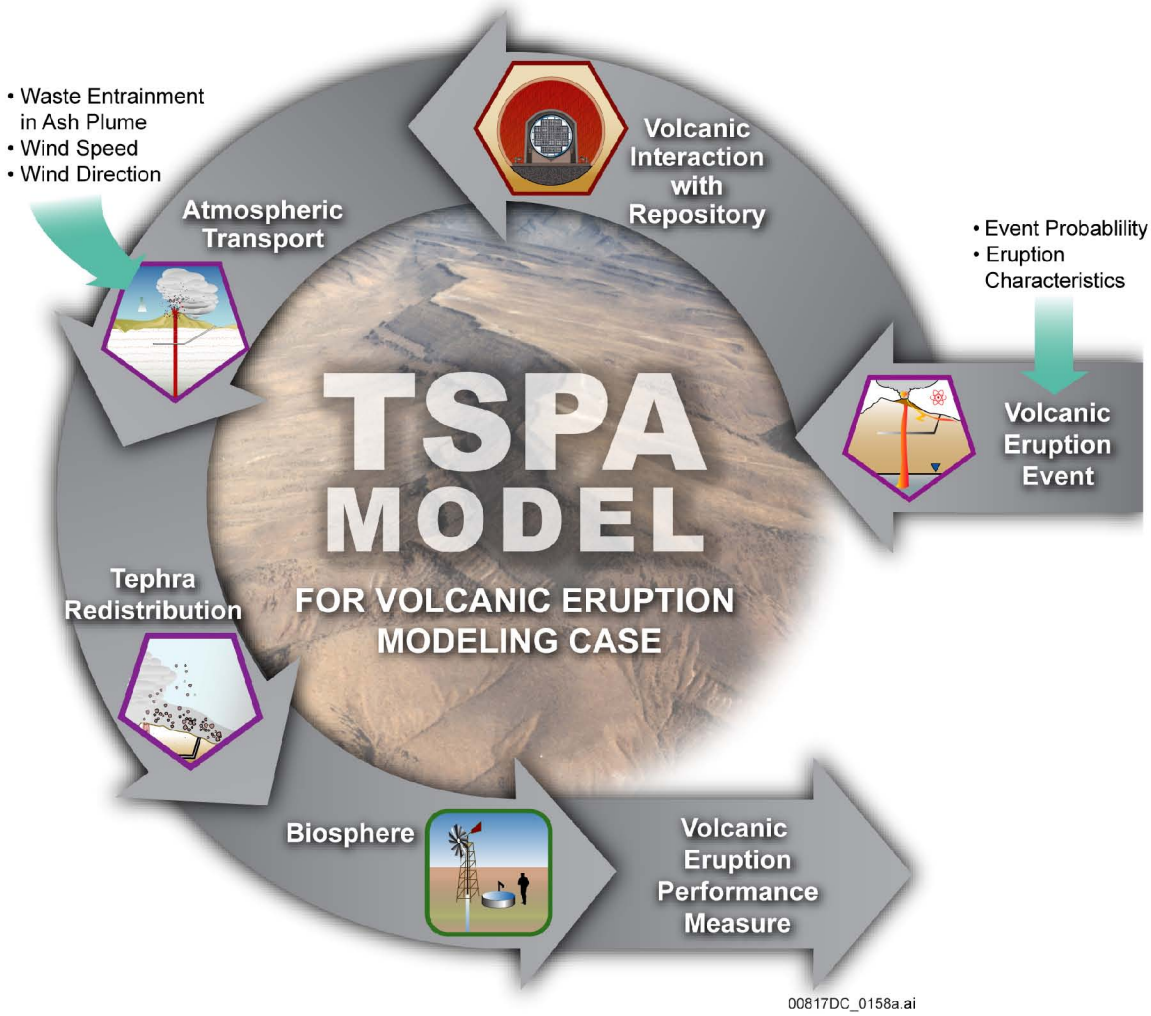

Figure 6.5-7. TSPA-LA Model Components for the Volcanic Eruption Modeling Case

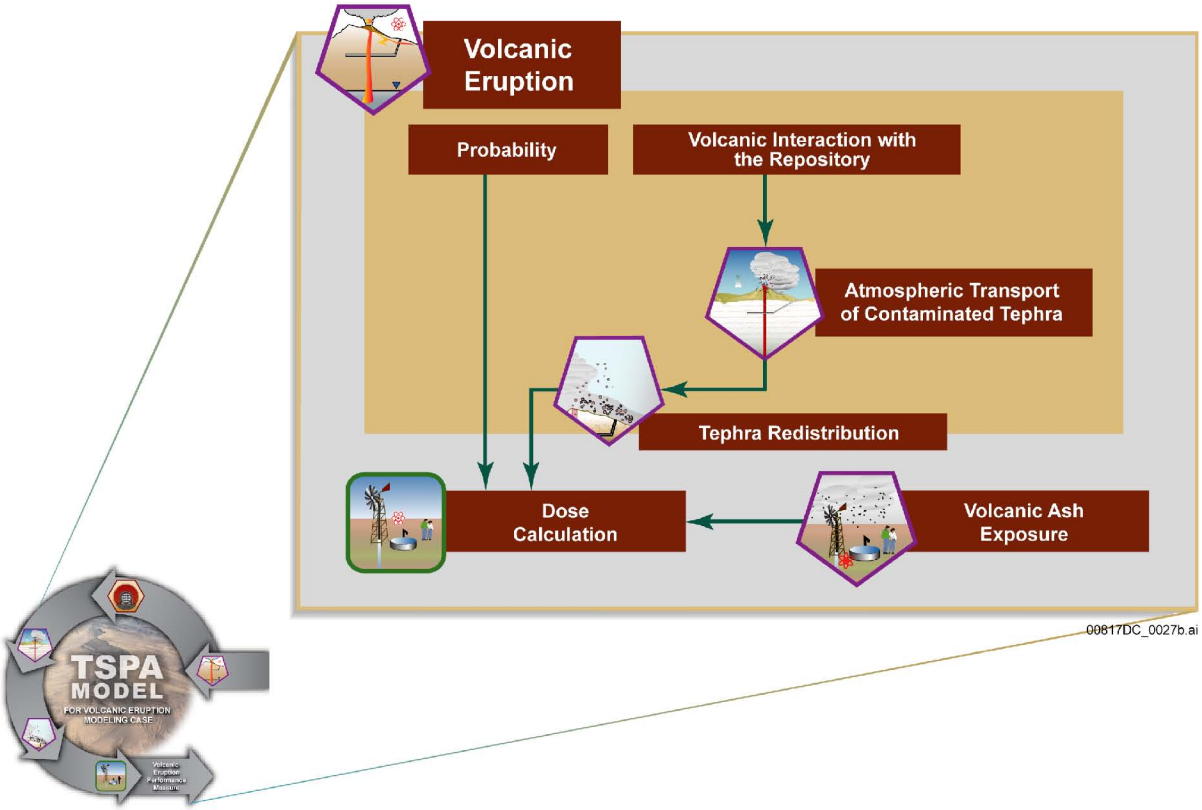

Figure 6.5-8. Information Flow Diagram for the TSPA-LA Volcanic Eruption Modeling Case

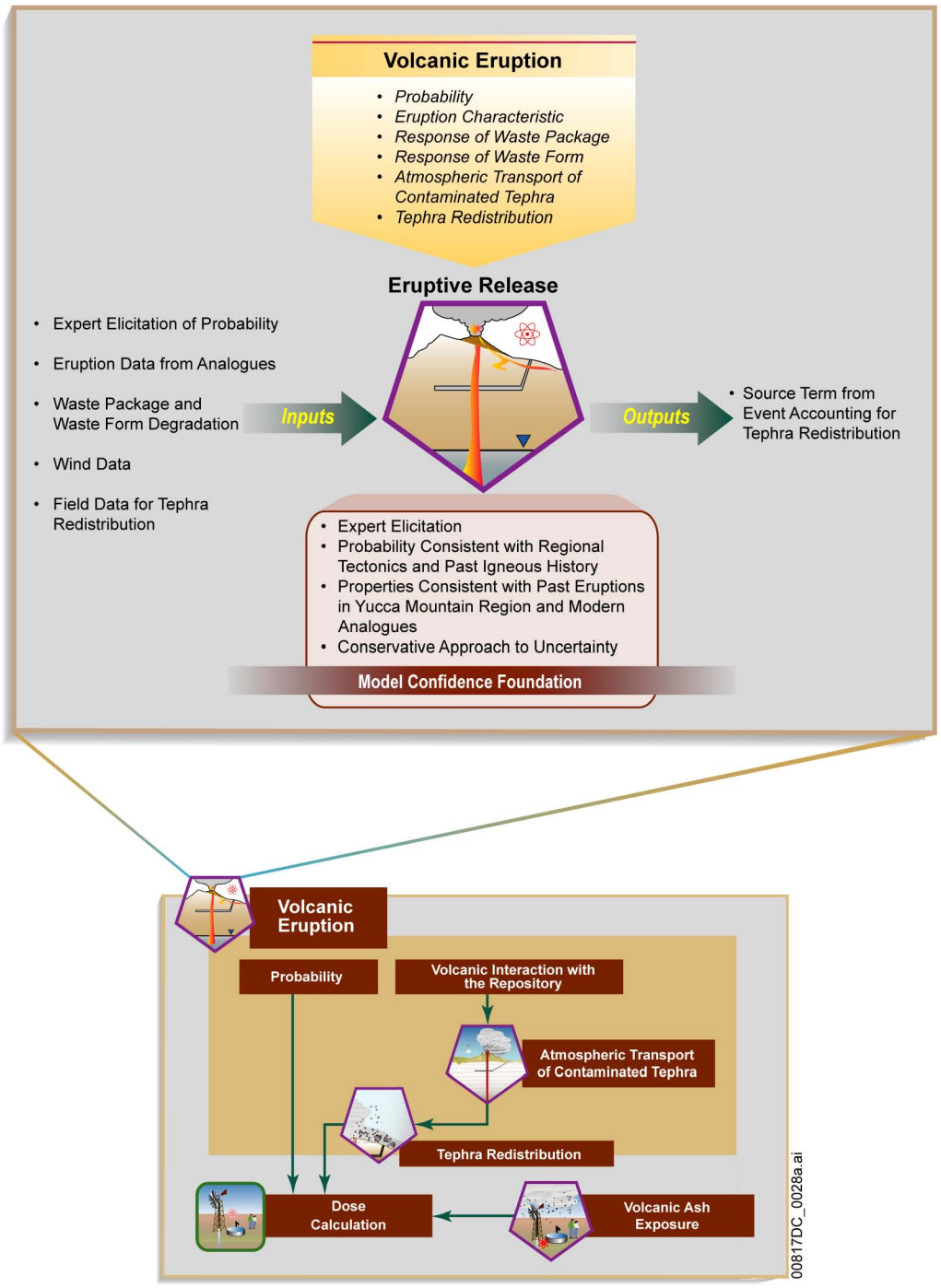

Figure 6.5-9. Inputs, Outputs, and Basis for Model Confidence for the TSPA-LA Volcanic Eruption Modeling Case

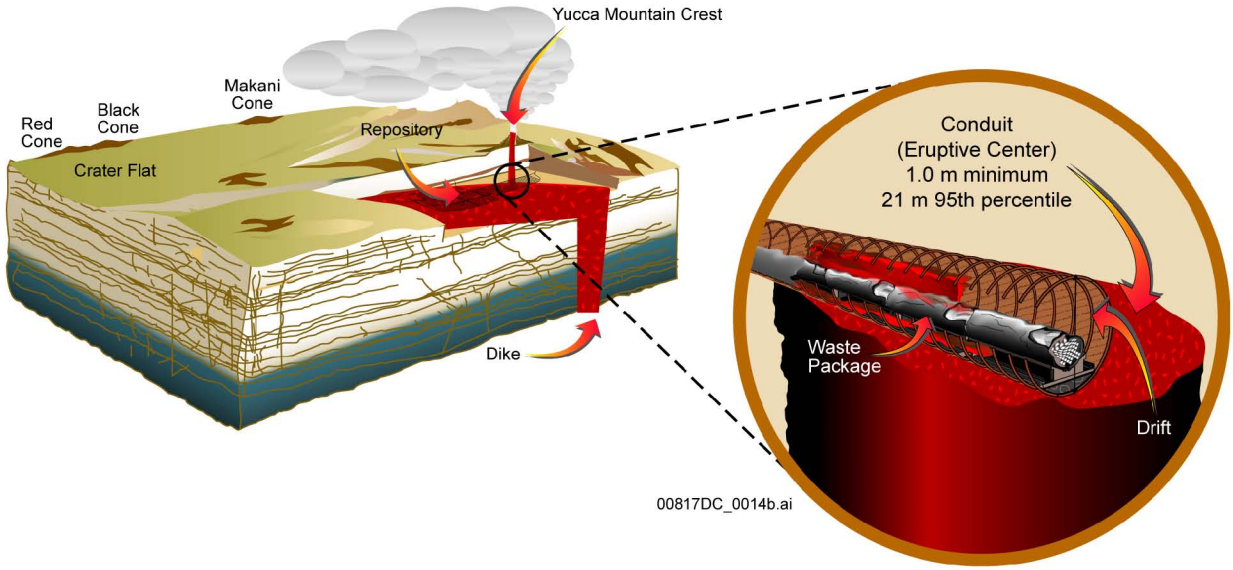

Figure 6.5-10. Schematic Diagram of the Intersection of an Igneous Dike and Eruptive Conduit with the Repository

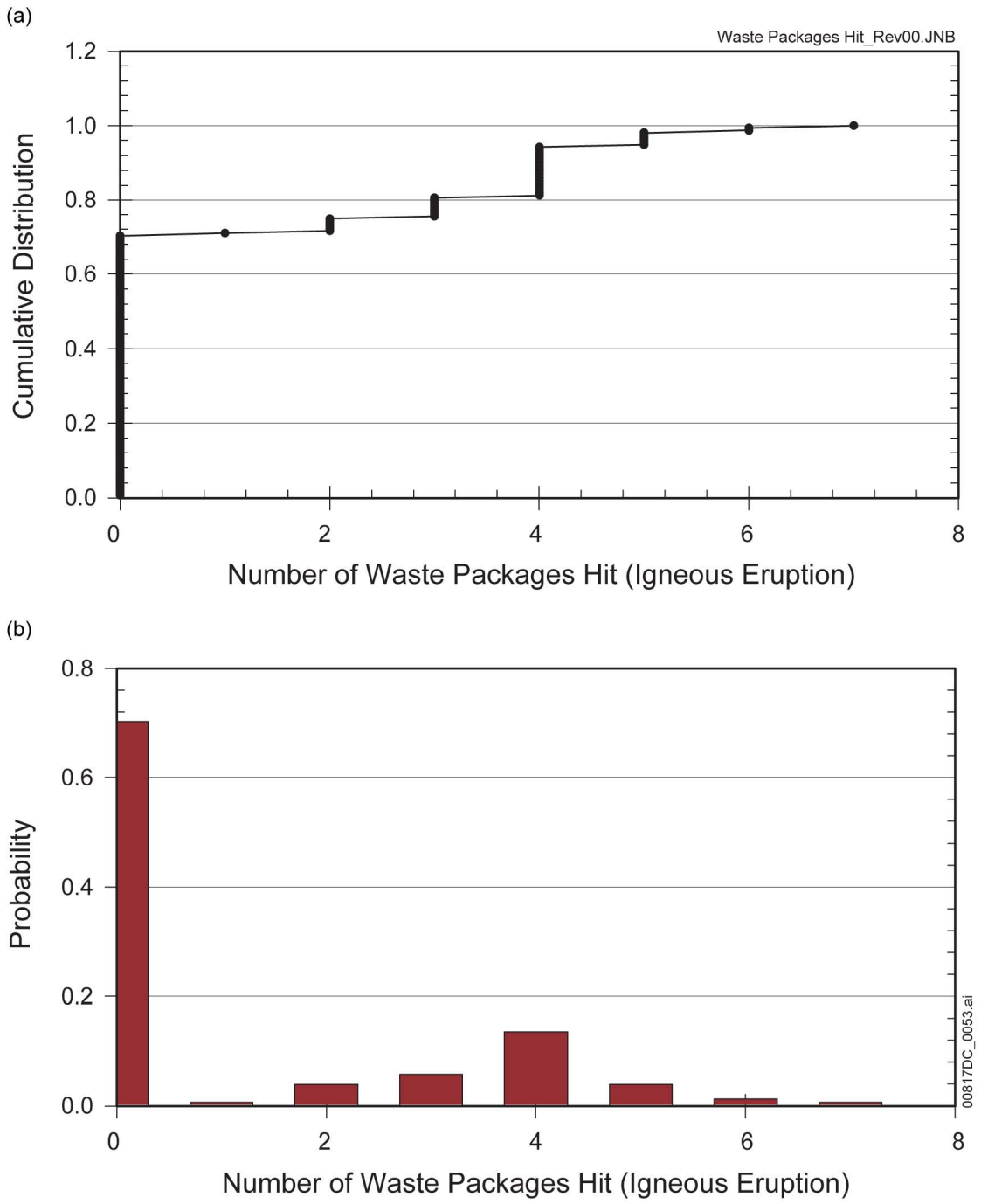

Source: DTN: SN0701PAWPHIT1.001_R2 [DIRS 182961].

Figure 6.5-11. Number of Waste Packages Hit by Conduits from a Volcanic Eruption

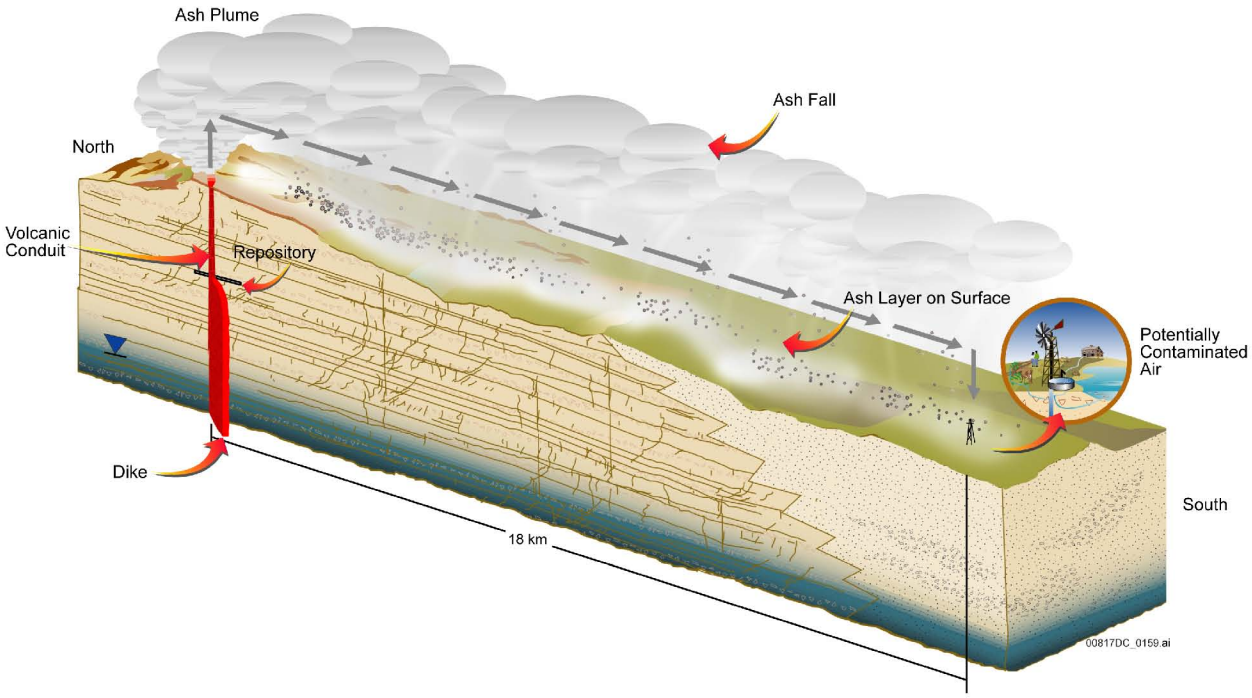

Figure 6.5-12. Schematic Representation of a Volcanic Eruption at Yucca Mountain, Showing Transport of Radioactive Waste in a Tephra Plume

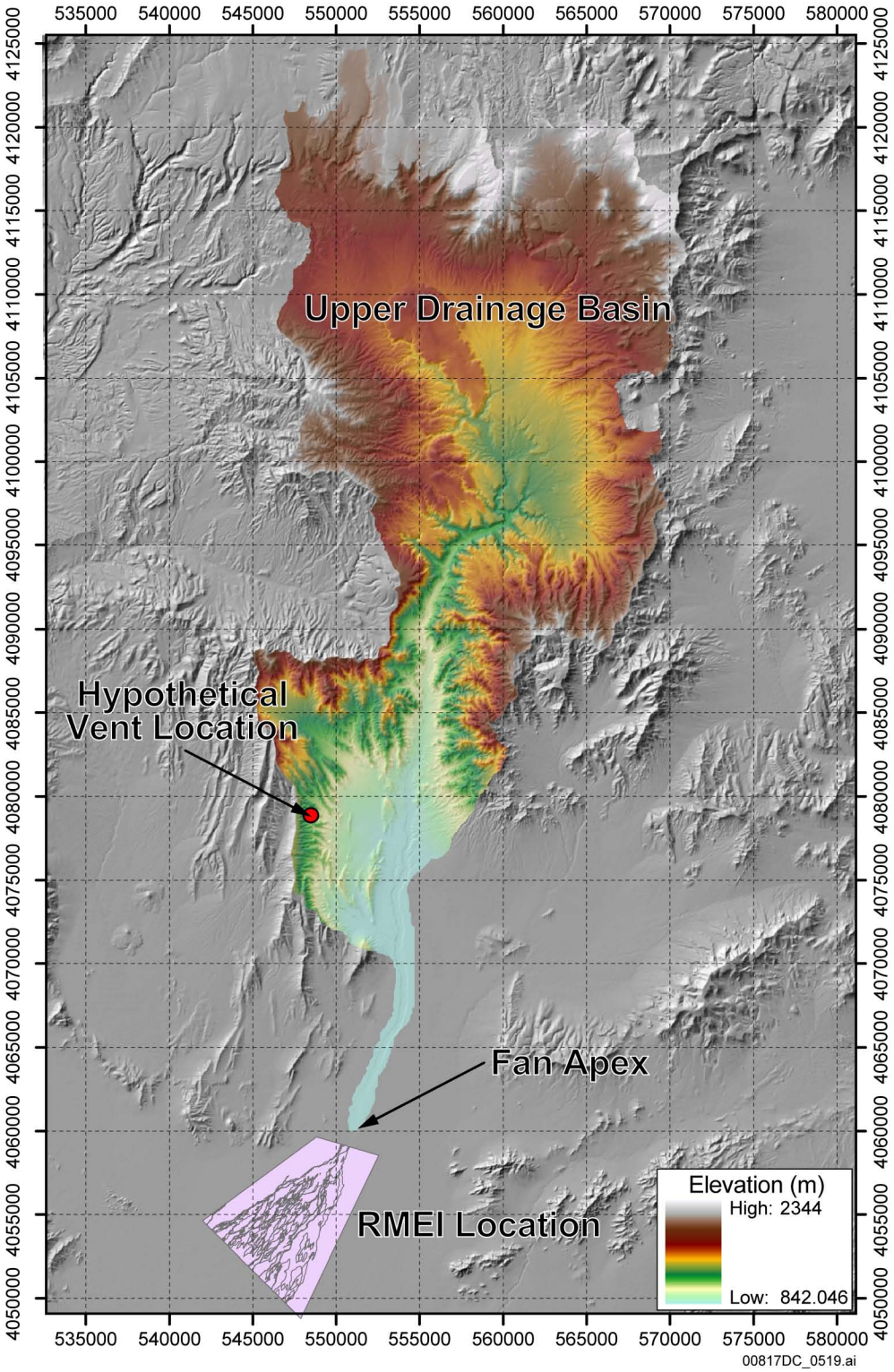

Source: SNL 2007 [DIRS 179347], Figure 1-2,

Figure 6.5-13. Schematic Diagram of Tephra Redistribution Model

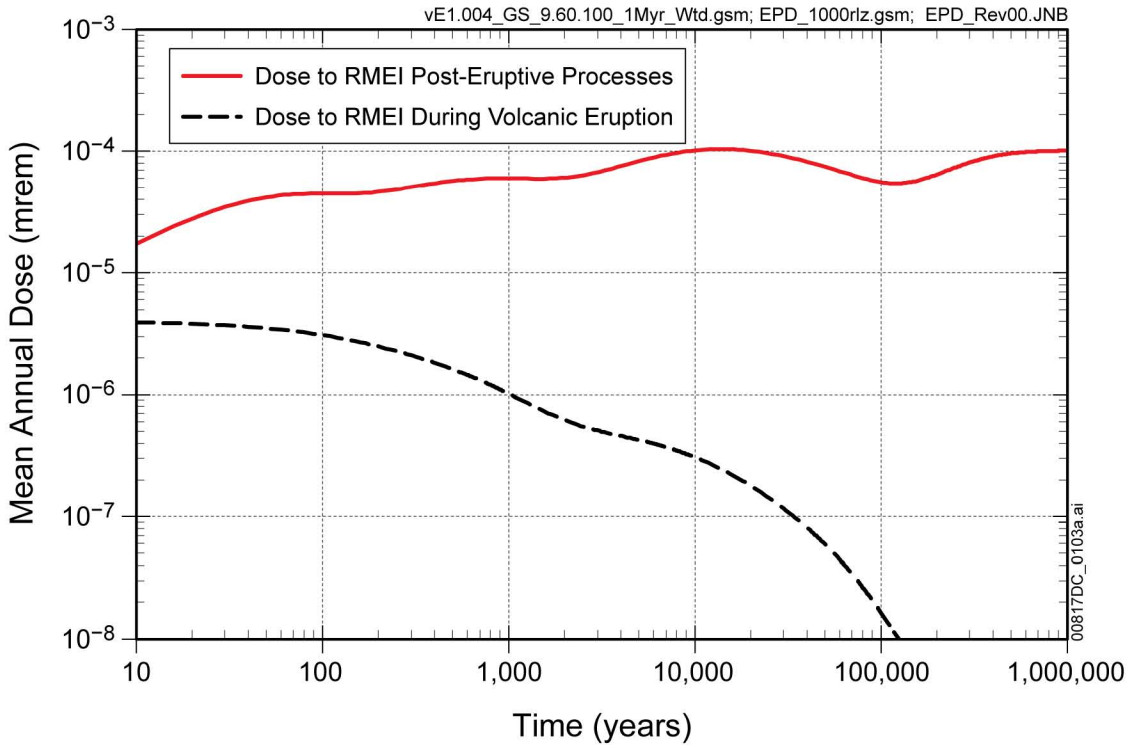

Source: Output DTN: MO0709TSPAREGS.000 [DIRS 182976].

Figure 6.5-14. Comparison of Dose to the RMEI for Post-Eruptive Processes and Dose to the RMEI During a Volcanic Eruption

6.6 TSPA-LA MODEL FOR THE SEISMIC SCENARIO CLASS

The Seismic Scenario Class describes future performance of the repository system in the event of seismic activity that could disrupt the repository system. The Seismic Scenario Class represents the direct effects of vibratory ground motion and fault displacement associated with seismic activity. Indirect effects of drift collapse and rockfall induced by vibratory ground motion are also considered in this scenario class. The Seismic Scenario Class considers the effects of the seismic hazards on DSs and WPs because damage to or failure of these components has the potential to initiate or increase releases of radionuclides by forming new diffusive or advective transport pathways. The Seismic Scenario Class also takes into account changes in seepage and drift wall condensation, WP and DS degradation, and in-drift thermal environment that might be associated with a seismic event. The conceptual models and abstractions for the mechanical response of EBS components to seismic hazards at a geologic repository are documented in *Seismic Consequence Abstraction* (SNL 2007 [DIRS 176828]). The structural response calculations and rockfall calculations that provide the basis for the seismic damage abstractions are documented in *Mechanical Assessment of Degraded Waste Packages and Drip Shields Subject to Vibratory Ground Motion* (SNL 2007 [DIRS 178851]).

The Seismic Scenario Class estimates the annual dose due to seismic activity by accounting for the probability of occurrence of activity, expressed in terms of its mean annual exceedance frequency (SNL 2007 [DIRS 176828], Section 6.1.7), and the associated consequences to EBS components. The estimate of annual dose takes into account the relevant processes that affect system performance. The Seismic Scenario Class is represented by two modeling cases. The first modeling case includes those WPs that fail solely due to the ground motion damage associated with the seismic event and it is denoted as the Seismic GM Modeling Case. Because nominal corrosion processes have the potential to alter the repository's susceptibility to damage during a seismic ground motion event, the Seismic GM Modeling Case includes these nominal processes when calculating consequences. The second modeling case includes only those WPs that fail due to fault displacement damage and it is denoted as the Seismic FD Modeling Case. Nominal corrosion processes are not included in the Seismic FD Modeling Case because the damage abstraction for fault displacement is based on a comparison of clearances between EBS components with fault displacements, independent of the thickness of EBS components. The mean annual dose calculated by the two modeling cases (Section 6.6.1.3.1) will be compared to the regulatory standard within 10,000 years after disposal, as required by the NRC Proposed Rule 10 CFR 63.303(a) [DIRS 178394], and the median annual dose will be compared to the regulatory standard for the period after 10,000 years of disposal and through the period of geologic stability, as required by the NRC Proposed Rule 10 CFR 63.303(b) [DIRS 178394]. The Individual Protection Standards for two periods are provided in 10 CFR 63.311 [DIRS 178394].

The two modeling cases in the Seismic Scenario Class have the same framework as the Nominal Scenario Class Modeling Case. This framework includes the TSPA-LA Model components that evaluate the mobilization and transport of radionuclides from the repository to the location of the RMEI. In other words, the mobilization of radionuclides in seeping water, the release of these radionuclides from the EBS, and the transport of these radionuclides through the UZ and SZ to the RMEI are based on the same model components for the Nominal Scenario Class as described in Section 6.3. The effects of the seismic event are taken into account in the changing

state of the EBS components, as required by the NRC proposed rule, 10 CFR 63.342(c)(1)(i) [DIRS 178394] and 10 CFR 63.102(j) [DIRS 180319], but not in the natural system components, which have been screened out by the FEPs screening process.

The calculational approach for the two Seismic Scenario Class modeling cases is discussed in Section 6.1.2.4.4.

Section 6.6 is organized as follows. Section 6.6.1 summarizes the model components and submodels of the Seismic Scenario Class. Sections 6.6.1.1 through 6.6.1.3 describe the ground motion damage and fault displacement damage conceptual models, the corresponding abstraction models, and their implementation in the TSPA-LA Model. Section 6.6.2 discusses the changes to other TSPA-LA Submodels that occur as a result of a seismic event. These include changes to the Drift Seepage Submodel and Drift Wall Condensation Submodel (Section 6.6.2.1), changes to the EBS TH Environment Submodel (Section 6.6.2.2), changes to the WP and DS Degradation Submodel (Section 6.6.2.3), and the potential effect of crown-seepage induced localized corrosion (Section 6.6.2.4). Model component consistency and conservatisms in assumptions and parameters are discussed in Section 6.6.3. In Section 6.6.4, alternative conceptual models (ACMs) are considered.

6.6.1 TSPA-LA Model Components and Submodels for the Seismic Scenario Class

The Seismic Scenario Class considers seismic events in the mean annual exceedance frequency range of 4.287×10^{-4} to 10^{-8} per year. The upper bound on the mean annual exceedance frequency is based on the minimum peak ground velocity (PGV) threshold for the onset of kinematic damage (SNL 2007 [DIRS 176828]), Section 6.4.3) and the lower bound is dictated by regulation (NRC proposed rule 10 CFR 63.342(b) [DIRS 178394]). If a seismic event breaches the WPs, radionuclides are mobilized and transported from the EBS into the repository host rock. The mobilized radionuclides can then be transported by water percolating through the UZ to the water table, and then to the accessible environment by flow and transport processes in the SZ.

The model components and submodels of the TSPA-LA Model for the Seismic Scenario Class are shown on Figure 6.6-1. Figure 6.6-2 shows the information flow within the TSPA-LA Model associated with the Seismic Scenario Class. Figure 6.6-3 indicates the major inputs and outputs of the model components and submodels of the Seismic Scenario Class, the processes included in the Seismic Scenario Class, and the foundation for confidence in the TSPA-LA Model. These figures indicate that the TSPA-LA Model framework for the Seismic Scenario Class is similar to that of the Nominal Scenario Class. However, some of the model components and submodels differ from those described in Section 6.3. These include the following:

- WP and DS Degradation Model Component
- Drift Seepage Submodel and Drift Wall Condensation Submodel of the UZ Flow Model Component
- EBS TH Environment Submodel of the EBS Environment Model Component.

Figure 6.6-4 provides a schematic illustration of the various elements of the Seismic Scenario Class. The figure shows the likely seismic effects within an emplacement drift of the repository, the subsequent radionuclide releases to the SZ, and their transport to the accessible environment.

In order to provide a complete description of the model components and submodels needed for the Seismic Scenario Class modeling cases, the model components and submodels that differ from those described in Section 6.3 are described in the following sections, according to their effects on repository performance.

6.6.1.1 Conceptual Model for Seismic Response of the Engineered Barrier System

The conceptual model for mechanical damage to the EBS associated with seismic activity is documented in *Seismic Consequence Abstraction* (SNL 2007 [DIRS 176828], Sections 6.1.1 to 6.1.3). The conceptual model for the mechanical response of the EBS components is summarized in the following sections.

6.6.1.1.1 Conceptual Model for Rockfall from Ground Motion

Rockfall induced by vibratory ground motion has the potential to fill the emplacement drifts during the period of geologic stability for dose assessment as defined in NRC proposed rule 10 CFR 63.302 [DIRS 178394]. Rockfall refers to the large rock blocks that may be ejected from the nonlithophysal units of the repository during vibratory ground motion. Rockfall also refers to the fractured and rubblized material that may surround the DS and fill the drifts during partial or complete collapse of drifts in lithophysal units of the repository. Detailed rockfall analyses have been performed for both lithophysal and nonlithophysal rock, under vibratory ground motion.

In the lithophysal zones, the rock mass has very low compressive strength and is permeated with void spaces of varying size (SNL 2007 [DIRS 176828], Section 6.7.1). The drifts in the lithophysal zone are predicted to collapse into small fragments with particle sizes of centimeters to decimeters under the loads imposed by vibratory ground motion. In the nonlithophysal zones, large rock blocks may be shaken loose from the drift walls and fall onto DSs in response to vibratory ground motion.

Drift collapse impacts the temperature and relative humidity of the outer surface of a WP in lithophysal regions of the repository because rubble fills the collapsed drift, essentially forming a thermal blanket covering the DSs and possibly the WPs if the DSs have failed as a barrier to rockfall. Drift collapse also impacts seepage flux and drift-wall condensation in the emplacement drifts in the lithophysal zones. The abstraction and implementation of the effect of drift collapse on seepage and temperature are discussed in more detail in Sections 6.6.2.1 and 6.6.2.2.

6.6.1.1.2 Conceptual Model for Drip Shield and Waste Package Failure from Ground Motion

The components of the EBS are illustrated on Figure 1-11. Mechanical processes that occur during a significant seismic event (i.e., an event with the capacity to degrade or rupture WPs and/or DSs) have the potential to compromise the functionality of the DSs as barriers to seepage

and rockfall and of the WPs as barriers to radionuclide release. For significant vibratory ground motions, impacts can occur between adjacent WPs and between a WP and its emplacement pallet, the surrounding DS, and the invert. Impacts can also occur between DSs and emplacement pallets, the invert, and the drift wall. Rockfall induced by vibratory ground motions can result in impacts on DSs in the postclosure period. Lithophysal rockfall induced by vibratory ground motion can result in static loads on DSs from the surrounding mass of fractured rock. Finally, mechanical loads may be generated by fault displacement within the repository block. In this case, EBS components may become sheared if fault displacement is greater than the available clearances between or around components.

DS Failure Mechanisms—The mechanical response of DSs to vibratory ground motion, which could adversely affect the ability of a DS to prevent flow from reaching a WP, was examined in *Seismic Consequence Abstraction* (SNL 2007 [DIRS 176828], Sections 6.8 and 6.10) and is described as follows:

- The static load from rockfall combined with the dynamic load during a seismic event may rupture DS plates or buckle the DS framework. Rupture or buckling compromises the capacity of a DS to deflect seepage and rockfall away from a WP (SNL 2007 [DIRS 176828], Sections 6.8.2 and 6.8.3).

- The static load from rockfall combined with the dynamic load during a seismic event may deform the plates on the crown of a DS. High levels of residual tensile stress may lead to accelerated degradation processes like SCC. The damaged or deformed area that exceeds a residual stress threshold (RST) is conceptualized to result in a tightly spaced network of stress corrosion cracks, providing a potential pathway for radionuclide transport and release (SNL 2007 [DIRS 176828], Sections 6.3 and 6.10).

- Impacts by large rock blocks in unfilled or partly filled drifts in nonlithophysal units may deform DSs or fail plates and axial stiffeners on the crown of a DS. Failed DS plates provide a potential pathway for seepage to contact the WPs (SNL 2007 [DIRS 176828] Section 6.10.2).

WP Failure Mechanisms—The potential failure mechanisms for the response of WPs to vibratory ground motion were examined in *Seismic Consequence Abstraction* (SNL 2007 [DIRS 176828], Sections 6.5, 6.6, and 6.9) and were described as follows.

- Dynamic loads may dent WPs, resulting in permanent structural deformation with residual tensile stress. The damaged or deformed area that exceeds a residual tensile stress threshold is conceptualized to result in a tightly spaced network of stress corrosion cracks. WP structural response was evaluated for three values of the residual tensile stress threshold for Alloy 22: 90 percent, 100 percent, and 105 percent of the yield strength of Alloy 22.The network of stress corrosion cracks is considered to immediately form once the residual tensile stress threshold is exceeded, providing potential pathways for radionuclide transport and release (SNL 2007 [DIRS 181953], Section 6.7). For WPs subject to SCC damage, the effective transport area for a damaged WP is much smaller than the total damaged area because transport occurs through a network of stress corrosion cracks, rather than through the total damaged area that exceeds the RST. The

effective area for flow and transport is based on the crack density model and associated scaling factor for Alloy 22 developed in *Stress Corrosion Cracking of Waste Package Outer Barrier and Drip Shield Materials* (SNL 2007 [DIRS 181953], Section 6.7). The distribution representing the scaling factor has a mean value of 0.00819 (Section 6.6.1.3.7).

- Dynamic loads on WPs free to move during a seismic event have the potential to result in a rupture (tear) of a WP if the local strain exceeds the ultimate tensile strain. Dynamic loading from a single impact may not produce tensile strains in the Alloy 22 outer corrosion barrier (OCB) that exceed the ultimate tensile strain. However, the extreme deformation from a major seismic event could weaken the OCB, potentially resulting in a ruptured OCB from a subsequent extreme seismic event (SNL 2007 [DIRS 176828], Section 6.1.2). WPs that have been ruptured provide potential pathways for seepage and for radionuclide transport and release. An abstraction for WP rupture from kinematic impacts has been included in the Seismic Scenario Class (Section 6.6.1.2.2.2). WP rupture occurs only for WPs free to move under intact DSs.

- The probability of rupture for WPs with degraded internals surrounded by rubble is zero because the strain on the OCB is always below the ultimate tensile strain for Alloy 22 (SNL 2007 [DIRS 178851], Section 6.5.1.4.1). However, a severely deformed OCB may be punctured by the sharp edges of fractured or partly degraded internal components. The WP internals are assumed to degrade as structural elements after the OCB is first breached. Extreme deformation of the cylindrical OCB can eliminate the free volume within the OCB, allowing the sharp corners or sharp edges from degraded internal elements to puncture the OCB when it is surrounded by lithophysal rubble (SNL 2007 [DIRS 176828], Section 6.1.2). The punctured area is conceptualized to be a small patch on the surface of the OCB (SNL 2007 [DIRS 176828], Section 6.9.1). WPs that have been punctured provide potential pathways for seepage and for radionuclide transport and release. An abstraction for puncture of WPs surrounded by rubble has been included in the Seismic Scenario Class (Section 6.6.1.2.2.2). WP puncture occurs only for WPs with degraded internals, surrounded by lithophysal rubble.

6.6.1.1.3 Fault Displacement Conceptual Model

The conceptual model for fault displacement was developed using data from known and hypothetical faults in the repository. The expected number of WP failures that could occur due to fault displacement is a small fraction of the total number of WPs in the repository. The number of failed WPs is estimated based on an understanding of the displacements that could occur on these faults and geometrical considerations, as described in *Seismic Consequence Abstraction* (SNL 2007 [DIRS 176828], Section 6.11). A fault displacement that occurs in an emplacement drift may cause a sudden discontinuity in the profile of the drift. This could result in one portion of the drift being displaced vertically relative to the adjacent section. Such a discontinuity in the drift could cause shearing of the WP and DS located over the fault if the fault displacement exceeds the available clearance in the EBS. The comparison of fault displacements with available clearances defines the potential for damage to EBS components from fault displacement.

Two distinct cases were considered in analyzing the clearances between EBS components: (1) an intact DS, and (2) a failed DS. The first case represents the as-emplaced configuration of the EBS, shortly after repository closure, and is expected to be applicable to the first 10,000 years after repository closure. The second case represents the late time response of the EBS after DS framework and DS plates have failed and rockfall has partly filled the emplacement drifts and surrounded WPs with rubble. The results of the analyses representing failed DSs with WPs surrounded by rubble were deemed appropriate for use in the TSPA-LA Model, since they are conservative relative to unfailed DS results (SNL 2007 [DIRS 176828], Section 6.11.1.3).

Given the complexity of the response of EBS components and the invert to a fault displacement, a simplified failure criterion was applied to determine shear failure in a collapsed drift. If the fault displacement exceeds one-quarter of the outer diameter of the OCB (about 0.4 meters to 0.5 meters), the WP fails from shear (SNL 2007 [DIRS 176828], Section 6.11.1.2). This simple failure criterion is appropriate because shear failure from fault displacement only occurs from extremely low-frequency, high-amplitude fault displacements, corresponding to a mean annual exceedance frequency of less than or equal to 2.5×10^{-7} per year (SNL 2007 [DIRS 176828], Table 6-67). Fault displacement in excess of these values is conservatively considered to fail WPs and the overlying DSs through direct shearing, allowing advective flow through the sheared components. The cladding within the affected WPs would also be failed, but cladding failure is not analyzed because the compliance case for TSPA-LA Model not taking credit for the cladding. The damage abstraction for cladding is included in the Performance Margin Analysis found in Appendix C.

6.6.1.2 Abstraction Model for Seismic Response of the Engineered Barrier System

The mechanical response of EBS components to a seismic event will be highly dependent on the in-drift configuration of EBS components and on the structural integrity of the EBS components at the time of the seismic event. The future configuration of the EBS components has been represented by three idealized configurations, as shown on Figure 6.6-5. Figure 6.6-5 (a) represents the as-emplaced EBS configuration, with an intact DS and minimal rockfall in the drifts. In this configuration, WPs can move freely beneath DSs. Figure 6.6-5 (b) represents an intermediate state of the system where the legs of a DS have buckled under combined rockfall/seismic load (i.e., DS framework failed), but DS plates remain intact. In this configuration, a DS may collapse onto a WP, inhibiting free movement of the WP and emplacement pallet during the seismic event. Figure 6.6-5 (c) represents the end state of the system, in which rubble surrounds WPs after failure of DS plates. The transition between these configurations is determined by fragility curves for DS framework and plates, based on the intensity of the seismic event and on the thickness of DS components and accumulated rockfall load at the time of the seismic event. The structural integrity of the DS is determined by structural response calculations (SNL 2007 [DIRS 178851], Sections 6.4.3 and 6.4.4).

This potential for DS failure leads to three distinct damage mechanisms for WPs. The first mechanism, referred to as kinematic damage, exists when WPs are free to move beneath DSs (Figure 6.6-5(a)). The second and third damage mechanisms occur when the motion of WPs is restricted and are shown on Figure 6.6-5(b) and Figure 6.6-5(c). These mechanisms are referred

to as damage for a WP beneath (loaded by) a buckled DS and damage for a WP surrounded by rubble, respectively.

The future state of the internal structures within WPs is also important for the damage mechanisms. This internal structure includes a 2-inch thick inner vessel of stainless steel, a TAD canister (for CSNF), and the basket structure that supports the fuel rod assemblies within the WPs. The internal structures add structural strength to the WPs. These internal structures may degrade much faster than Alloy 22, depending on the in-package chemical environment, the residual stress near welds in the inner vessel, and the potential for galvanic contact between the Alloy 22 OCB and the stainless steel inner vessel. Given the uncertainties related to these long-term degradation processes, the future state of the internals is represented as either intact or degraded. The internals remain intact structurally until the first breach of the OCB, after which time they are treated as a degraded material with minimal strength and minimal cohesion. Breach refers to any penetration of the OCB. First breach will usually occur from SCC in the lid welds or in response to seismic events (SNL 2007 [DIRS 176828], Section 6.1.3).

The timing of the first seismic event that breaches a WP is a function of the type of WP. The CSNF WP has two independent stainless steel vessels, the inner vessel and its lids, and the TAD canister. The CDSP WP has only the inner vessel and its lids. The CSNF WP is demonstrably more robust based on a comparison of the probabilities of damage to WPs with intact internals (Section 6.6.1.2.2.2).

The assumption (SNL 2007 [DIRS 176828], Assumption 5.4) that the internal structures degrade by the time of the next seismic event after the OCB is first breached adds conservatism to the seismic WP damage abstraction. Since the Poisson frequency of seismic events is 4.287×10^{-4} per year (Section 6.6.1.3.2), the typical time interval between seismic events is about 2,300 years. However, stainless steel internal structures may remain structurally intact for much more than 2,300 years if in-package chemical conditions remain similar to a fresh water environment, which is the expected condition until after DS failure (SNL 2007 [DIRS 176828], Section 6.1.3). Because seismic damage to a WP is much greater when the internals are degraded, due to the much lower structural strength, this nearly instantaneous degradation of the internals maximizes seismic-related damage to the WP.

A probabilistic seismic hazard analysis (PSHA) was performed to assess the seismic hazards of vibratory ground motion and fault displacement at Yucca Mountain. The PSHA (CRWMS M&O 1998 [DIRS 103731]) provides quantitative hazard results to support an assessment of the repository's long-term performance and to form the basis for developing seismic design criteria. The PSHA methodology for vibratory ground motions is standard practice for deriving vibratory ground motion hazards for design purposes. In addition, probabilistic fault displacement analyses were conducted to provide quantitative assessments of the location and amount of differential ground displacement that might occur. Both analyses provide hazard curves, which express the annual frequency of exceeding various amounts of ground motion (or fault displacement) (SNL 2007 [DIRS 176828], Section 6.4.1). The Seismic Scenario Class for the TSPA-LA Model uses the mean hazard curves for PGV and fault displacement. Each mean hazard curve is defined as the mean estimate or average of a distribution of hazard curves. For annual frequencies of exceedance less than about 10^{-5} to 10^{-6}, the mean curve typically lies above the 80th percentile of the distribution because the average is

dominated by the larger values of the distribution. The use of mean hazard curves is conservative relative to median hazard curves, and provides an accurate representation for the mean dose. The mean hazard curve for ground motion defines the relationship between the estimate of mean annual exceedance frequency, and the amplitude of the vibratory ground motion, measured by the PGV of the first horizontal component of the ground motion(SNL 2007 [DIRS 176828], Section 1.1, footnote 1, p. 1-2). Analysis of the limits for maximum shear strain in the lithophysal rock typical of geologic conditions at Yucca Mountain led to a determination of a mean bounded hazard curve for horizontal PGV at the repository emplacement level. Figure 6.6-6 (DTN: MO0501BPVELEMP.001_R0 [DIRS 172682], file: *Bounded Horizontal Peak Ground Velocity Hazard at the Repository Waste Emplacement Level.xls*) shows the mean bounded hazard curve. The effect of fault displacement on the EBS is evaluated in terms of mean fault displacement hazard curves developed for faulting conditions mapped within the immediate vicinity of Yucca Mountain (SNL 2007 [DIRS 176828], Section 6.11.3).

6.6.1.2.1 Abstraction for Rockfall Volume from Ground Motion

The probability of lithophysal rockfall from a seismic event was abstracted, based on computational results for 15 ground motions at the 0.4 m/s, 1.05 m/s, and 2.44 m/s PGV levels and five rock mass categories (SNL 2007 [DIRS 176828], Section 6.7.1.1, Table 6-28). The probability of rockfall was calculated based on a weighted average of the results for each rock mass category, since the rock mass categories are not equally probable. The resulting piecewise linear definition for the probability of rockfall is given in *Seismic Consequence Abstraction* (SNL 2007 [DIRS 176828], Equation 6.7-1):

$$P_{rockfall} = Min(1.0, Max(0.0, (1.288)PGV - 0.353)) \quad \text{(Eq. 6.6-1)}$$

When rockfall occurs, the volume of lithophysal rock that collapses per meter of drift length is represented by a gamma distribution with mean and standard deviations (SDs) that are quadratic functions of PGV (Figure 6.6-7).

The lithophysal rock volume from multiple seismic events is defined as the sum of the volumes from the individual seismic events. Examination of the mean volume on Figure 6.6-7 shows that rock volume in the lithophysal units will accumulate fairly rapidly. The total rock volume from multiple seismic events is an important parameter because it defines the static load of rubble based on the fraction of the drift filled by rubble. This fraction is defined as the total rubble volume (from multiple seismic events) divided by the rubble volume needed to fill a drift (the effective drift volume after collapse). The effective drift volume after collapse is estimated to be 30 m^3/m to 120 m^3/m for both lithophysal and nonlithophysal zones (SNL 2007 [DIRS 176828], Section 6.7.1.5).

Calculations for the nonlithophysal zones evaluated the response of a 21.74-meter-long section of drift in nonlithophysal rock for the 1.05 m/s, 2.44 m/s, and 5.35 m/s PGV levels. The volume of nonlithophysal rock that collapses per meter of drift length was represented by a gamma distribution with mean and SD that are quadratic functions of PGV. The mean and SD are shown on Figure 6.6-7. Examination of the mean curves shows that the mean rockfall volume in the lithophysal rock is a factor of 32 to 188 greater than the mean rockfall volume in the

nonlithophysal rock for the 1.05 m/s and 2.44 m/s PGV levels, respectively (SNL 2007 [DIRS 176828], Section 6.7.2.1).

The results for nonlithophysal rockfall show probabilities of rockfall that are similar to those for rockfall in the lithophysal zones, except at the 0.4 m/s level, where the calculations could not be compared (SNL 2007 [DIRS 176828], Section 6.7.2.2). Therefore, the probability of rockfall in the nonlithophysal zones is set to be the same as the probability of rockfall in the lithophysal zones, based on the comparison at higher PGV levels than 0.4 m/s.

6.6.1.2.2 Abstraction for Drip Shield and Waste Package Degradation from Ground Motion

Three types of calculations form the basis of the seismic damage abstractions for the WP and DS. The three types of calculations are: (1) three-dimensional kinematic calculations for EBS damage due to vibratory ground motion, appropriate for the early postclosure period, when the DSs are intact and the WPs can move freely beneath the DSs; (2) calculations for deformation and damage of a DS under static and dynamic conditions with intact and degraded EBS components; and (3) calculations for a WP surrounded by rubble that estimate damage after the DS plates have failed (SNL 2007 [DIRS 178851], Section 7.2.1).

Three-dimensional kinematic calculations are used to examine the motion and impact of multiple WPs, pallets, and DSs in an emplacement drift. The objective of these analyses is to define the history of impact parameters for collisions of the WPs, pallets, and DSs as a function of the applied ground motion time histories, and to determine the associated probability of rupture and damaged areas on a WP. Seventeen separate ground motion time histories are used at each of four different PGV levels. A separate kinematic calculation is performed for each ground motion time history at each PGV level, and separate kinematic models are used for CSNF WPs and CDSP WPs.

The kinematic calculations are appropriate when the DS is intact and the WP can move freely beneath the DS. At late times, when the degraded DS plates may fail from rockfall and seismic loads, the WP will be surrounded by rubble. The direct loads from this rubble may cause damage to the WP in response to vibratory ground motion. Rubble in the lithophysal zone is most relevant here because the small particle size of the lithophysal rubble means it can more easily slip or fall through gaps or tears in the plates of the DS and because the lithophysal zones encompass approximately 80 to 85 percent of the emplacement drifts in the repository. The damage induced by the rubble surrounding the WP is based on the two-dimensional coupled rockfall/structural response of the Alloy 22 outer barrier during vibratory ground motion. Damage is determined directly from the finite-difference output for the stress and strain state of the outer barrier. The input data for the calculations of a single WP surrounded by rubble include 17 ground motion time histories at four PGV levels, elastic and plastic properties of the outer barrier, and the bulk properties of degraded WP internals (SNL 2007 [DIRS 178851], Section 6.5.1.1).

6.6.1.2.2.1 Drip Shield Fragility Abstraction

The fragility analysis for DSs defines the probability of failure as a function of the thickness and plastic load capacity of DS components, the static rockfall load on DSs, and the vertical component of peak ground acceleration (PGA) for the seismic event (SNL 2007 [DIRS 176828], Section 6.8). Fragility curves were developed for two modes of failure: (1) rupture or tearing of DS plates, and (2) buckling or collapse of the sidewalls and/or crown of a DS. A third failure mode, from lateral WP impacts to the DS or from longitudinal impacts of the WP on the bulkhead support beams, was considered but not incorporated into the TSPA-LA Model. This third failure mode is not represented in the TSPA-LA Model for two reasons. First, lateral impact of the WP on the DS does not cause catastrophic failure of the DS. Second, high velocity longitudinal impacts of the WP on the bulkhead support beams exposed on the underside of the crown of the DS occur infrequently, even at the 4.07 m/s PGV level (SNL 2007 [DIRS 176828], Section 6.8.5).

The fragility analysis is based on the vertical component of PGA because the average loads on the crown are significantly greater than the average loads on the sidewalls of a DS, indicating that vertical loads are likely to be the critical loads for failure. The vertical component of PGA is defined by a probability distribution that is conditional on the PGV level for a seismic event. The static load from rockfall was based on lithophysal rubble. Rockfall in lithophysal rock has significantly greater volume (SNL 2007 [DIRS 176828], Section 6.7.2.1) than rockfall in nonlithophysal rock, resulting in greater static loads from lithophysal rubble than from nonlithophysal rubble. The load from lithophysal rubble was treated as uniform on the crown on a DS because the typical particulate sizes in the lithophysal rubble are less than the typical dimensions of DS plates.

Plate Failure

Finite-element calculations were performed to define the plastic (nonlinear) load-bearing capacity of the curved plates on the crown of a DS (SNL 2007 [DIRS 176828], Section 6.8.2.1). These calculations defined the magnitude of the uniform load that causes an element of the plate to exceed the failure criteria for Titanium Grade 7, which are based on both accumulated plastic strain and maximum stress (SNL 2007 [DIRS 178851], Section 6.4.3.1.3). For these calculations, the ultimate plastic load capacity of a DS was determined as a function of plate thickness, the static load from rubble in the drifts, and the vertical PGA. Calculations to represent degraded states of the system were performed for 15-mm-, 10-mm-, and 5-mm-thick plates. The plate thicknesses correspond to 0-mm, 5-mm, 10-mm and 13-mm thickness reductions from the initial plate thickness of 15-mm. The probability of DS plate failure as a function of PGV is illustrated on Figure 6.6-8, for 10 percent, 50 percent, and 100 percent rockfall load (i.e., for drifts that are 10 percent, 50 percent, and 100 percent filled with rubble).

If DS plates fail from a seismic event, then all DSs fail as a barrier to seepage (no spatial variability) and this failure is a permanent change for the rest of the realization. See Section 6.6.3.2 for a discussion of spatial variability.

After DS plate failure, the mechanical response of WPs to seismic events is determined by the abstraction, discussed below, for a WP surrounded by rubble.

Framework Failure

A series of dynamic calculations was performed, using selected ground motions for the 2.44 m/s and 4.07 m/s PGV levels, to determine the failure modes of DS framework. Based on these results, the failure mode for the fragility analysis for DS framework was determined to be buckling or collapse of the sidewalls of a DS. Finite-element calculations were carried out to define the plastic (nonlinear) load-bearing capacity of DS framework with intact plates. These calculations defined the magnitude of the load on the crown that caused the side or leg of a DS to buckle. The thickness of all DS components, including the plates and the individual structural members in the framework, was reduced by a constant value of 0-mm, 5-mm, or 10-mm for these calculations. The thickness reduction was taken in the smaller dimension for each structural member in the framework (SNL 2007 [DIRS 176828], Section 6.8.3.2).

The probability of DS framework failure as a function of PGV is illustrated on Figure 6.6-9, for 10 percent, 50 percent and 100 percent rockfall load. Comparison with Figure 6.6-8 shows that the probability of framework failure is always higher than the probability of plate failure, for a given rockfall load and PGV. The framework is expected to collapse before the plates rupture (SNL 2007 [DIRS 176828], Section 6.12.2, Step 13(c)).

If DS framework fails for a seismic event, then DSs do not fail as a barrier to seepage. Plate failure must subsequently occur for seepage to pass through the DS. There is no spatial variability (Section 6.6.3.2) for DS collapse (all DSs collapse), and the framework remains collapsed for the rest of the realization. After DS failure, the mechanical response of WPs to seismic events is a function of the state of the internals. If the internals are intact, the abstraction for a WP surrounded by rubble applies as given below. If the internals are degraded, the kinematic damage abstraction for a WP, under an intact DS but with degraded internals, applies.

Abstraction for Drip Shield Damage from Rockfall Loading

Before DS plates fail, DSs accumulate damage from vibratory ground motion and from rockfall induced by vibratory ground motion. In the lithophysal units, the accumulation of rubble from multiple seismic events and the dynamic motion during a seismic event can generate SCC damaged areas on DSs. These damaged areas are regions that exceed the residual (tensile) stress threshold for DS plates, potentially leading to a network of stress corrosion cracks. The damaged area occurs on the crown of a DS; damage to the sides was not abstracted because any seepage through the sides is considered unlikely to drip onto a WP. The damaged areas in the lithophysal zones were analyzed as a function of the thickness of DS plates, the rockfall load on DSs, and the vertical component of PGA for the seismic event. The abstraction for damaged area on DSs in the lithophysal zones is discussed in Section 6.10.1 of *Seismic Consequence Abstraction* (SNL 2007 [DIRS 176828]). Because DS damage in lithophysal zones is in the form of a network of stress corrosion cracks and because advective flow through stress corrosion cracks in DSs has been screened out (DTN: MO0706SPAFEPLA.001_R0 [DIRS 181613], FEP 2.1.03.10.0B), the abstraction for DS damage due to rockfall loading in the lithophysal units has not been included in the TSPA-LA Model file.

Abstraction for Drip Shield Damage from Rock Block Impacts

Before DSs fail in the nonlithophysal units, rock blocks can impact DSs in an unfilled or partially filled drift. Rock block impacts may result in damaged areas on DS plates and, in more extreme cases, may result in tearing or rupture of the plates and failure of the axial stiffeners beneath the crown of a DS. Section 6.10.2 of *Seismic Consequence Abstraction* (SNL 2007 [DIRS 176828]) develops abstractions for damaged area and plate failures for DSs in unfilled or partly filled drifts in the nonlithophysal units of the repository. The abstractions developed there support the screening arguments for excluding DS damage due to rock block impacts in the nonlithophysal units. The screening analysis is documented in DTN: MO0706SPAFEPLA.001_R0 [DIRS 181613], FEP 1.2.03.02.0B. As a result, DS damage due to rock block impacts in nonlithophysal units is excluded from the TSPA-LA Model.

6.6.1.2.2.2 Waste Package Damage Abstraction

Throughout this section reference is made to damage estimates for WPs based on calculations for an OCB at two thicknesses, 23 mm and 17 mm. The 23-mm thick OCB provides representation of an intact or almost intact WP. The 17-mm thick OCB provides a representation for a degraded WP at late times after repository closure. If the OCB thickness is between 17 mm and 23 mm, linear interpolation is used to define the damaged area (i.e., the area that exceeds the RST) within the damage abstractions. If the OCB thickness is greater than 23 mm, damage estimates at 23 mm are used. If the OCB thickness is less than 17 mm, damage estimates at 17 mm are used.

A 17-mm-thick OCB is appropriate for late times after repository closure. The median corrosion rate of Alloy 22 at 60°C is less than 7 nm/yr, based on a medium uncertainty level in the distributions for general corrosion rate (SNL 2007 [DIRS 178519] Figure 6-23). The value of 60°C is appropriate because it is an upper bound on OCB temperature beyond 10,000 years after repository closure (SNL 2007 [DIRS 178851], Figure 1-3), and because it is consistent with the structural response calculations for the seismic scenario (SNL 2007 [DIRS 178851], Assumption 5.7, Section 5). The 17-mm-thick OCB, which corresponds to an 8.4-mm ≈ 8-mm thickness reduction, will occur at a time of $(8 \times 10^{-3}\ \text{m})/(7 \times 10^{-9}\ \text{m/yr}) \approx 1{,}100{,}000$ years. More detailed corrosion calculations require a probabilistic analysis, but this estimate indicates that the 17-mm-thick OCB provides a reasonable representation for seismic response at the end of the period for assessment of repository performance.

The adequacy of the 17-mm thick OCB to represent the degraded states that may occur up to one million years after repository closure has been confirmed by a stand-alone probabilistic analysis of WP degradation. The stand-alone analysis model is a modified version of the TSPA-LA Model. The model components not pertaining to WP and DS degradation have been removed, to allow increased computational speed and to allow more detailed results to be saved. All epistemically uncertain parameters have been retained and all aleatory parameters related to WP and DS degradation have been retained. The sampling sequence is identical to the TSPA-LA Model 300-realization unified sampling Seismic GM Modeling Case (Section 6.6.1.3.1). The stand-alone model is documented in output DTN: MO0709TSPAWPDS [DIRS 183170].

Stress Corrosion Cracking Damage to CSNF and CDSP Waste Packages under Intact Drip Shields

Kinematic and structural response calculations were performed to develop damage estimates for the failed WP surface area for CSNF and CDSP WPs under intact DSs (SNL 2007 [DIRS 176828], Sections 6.5.1 through 6.5.4 and 6.6.1 through 6.6.4). As described in *Seismic Consequence Abstraction* (SNL 2007 [DIRS 176828], Sections 6.5 and 6.6), kinematic damage abstractions were developed for three future states of CSNF and CDSP WPs:

- 23-mm-thick OCB with intact internals
- 23-mm-thick OCB with degraded internals
- 17-mm-thick OCB with degraded internals.

The probability of damage to CSNF or CDSP WPs for the jth seismic event is defined as a function of (1) the state of the internals (intact or degraded), (2) the PGV for the jth seismic event, (3) the value of RST for the ith realization, and (4) the OCB thickness (SNL 2007 [DIRS 176828] Sections 6.5.1.2, 6.5.2.2, 6.6.1.2, and 6.6.2.2). Figures 6.6-10 and 6.6-11 illustrate these probabilities, for the three states of the WP (23-mm, intact; 23-mm, degraded; and 17-mm, degraded). When the WP internals are intact the probability of damage is much lower for CSNF WPs, than for CDSP WPs.

If CSNF or CDSP WPs are damaged by the jth seismic event, then their conditional damaged area is represented by a gamma distribution. Separate gamma distributions were defined for three states of WPs: (1) 23-mm-thick OCB with intact internals, (2) 23-mm-thick OCB with degraded internals, and (3) 17-mm-thick OCB with degraded internals. The values for the mean and SD of these gamma distributions are derived in Sections 6.5.1.3, 6.5.2.3, 6.6.1.3, and 6.6.2.3 of Seismic Consequence Abstraction (SNL 2007 [DIRS 176828]). Figures 6.6-12 and 6.6-13 illustrate the quadratic fits for mean damaged area for the CSNF and CDSP WPs, respectively. The means are a function of PGV and there is a separate gamma distribution for the three values of RST (90 percent, 100 percent, and 105 percent of yield strength). For CSNF and CDSP WPs with degraded internals, the damage abstractions show consistently higher SCC damage for the CSNF WPs, compared to the CDSP WPs.

Note that for the CSNF WP with intact internals damage occurs only at the 4.07 m/s PGV level (the probability is zero for all other PGVs – Figure 6.6-10). In this particular case, the single point results are conservative for all values of PGV less than 4.07 m/s and all values of the RST greater than 90 percent. In addition, the magnitude of the conditional damaged area is less than 0.006 which is a very small fraction of the cylindrical surface area of the CSNF WP of 33.64 m^2 (SNL 2007 [DIRS 176828], Sections 6.5.1.3). Therefore, the conditional damage at 4.07 m/s and 90 percent RST is considered to represent the damage at all values of PGV and RST in the TSPA-LA Model (SNL 2007 [DIRS 176828], Section 6.5.1.3).

For either intact or degraded internals, there is no WP-to-WP spatial variability for the conditional damaged area (Section 6.6.3.2). For a single package, the damaged area is randomly located on the cylindrical surface of the OCB. The total damaged area increases with each seismic event that causes damage to the WP OCB. Damaged area cannot exceed the total surface area of a CSNF or CDSP WP.

Rupture of CSNF and CDSP Waste Packages under Intact Drip Shields

CSNF or CDSP WPs that can move freely beneath a DS can rupture from the accumulation of severe deformation due to multiple impacts, which can accumulate in either one seismic event or multiple seismic events. The probability of rupture for the 23-mm-thick OCB with intact internals was determined to be zero (SNL 2007 [DIRS 176828], Sections 6.5.1.1 and 6.6.1.1). However, for CSNF or CDSP WPs with degraded internals, the effect of multiple WP-to-pallet impacts was assessed by evaluating the severity of accumulated deformation. The degree of deformation was used to define the probability of rupture. A minor degree of deformation indicated that no rupture occurred, consistent with the observation that the strain in the OCB is below the ultimate tensile strain for Alloy 22 for individual impacts. A significant degree of deformation was interpreted as causing an incipient rupture, in the sense that a second severe impact, during a subsequent seismic event, would have the potential to cause rupture. Finally, if two severe impacts occurred during the same seismic event, then the accumulation of severe deformation was interpreted as causing immediate rupture in the OCB. The probability of incipient rupture and the probability of immediate rupture for CSNF or CDSP WPs with degraded internals are abstracted as power laws in Sections 6.5.2.1 and 6.6.2.1 of *Seismic Consequence Abstraction* (SNL 2007 [DIRS 176828]). Figure 6.6-14 compares the probability for incipient and immediate rupture of the CSNF and CDSP WPs. For a given PGV, CSNF WPs have a higher rupture probability.

When a WP is ruptured, the failed area is determined by sampling a uniform distribution for failed area, with a lower bound of 0 m^2 and an upper bound equal to the cross-sectional area of the WP OCB. This failed area allows advective flow through and advective and diffusive transport out of ruptured CSNF or CDSP WPs. Once the WP is ruptured, there is no further damage from rupture in successive events, and the WPs remain ruptured for the remainder of the realization.

Stress Corrosion Cracking Damage to CSNF and CDSP Waste Packages Surrounded by Rubble

Structural response calculations were performed to develop damage estimates for the failed WP surface area of a CSNF WP surrounded by rubble (SNL 2007 [DIRS 176828], Sections 6.9.1 through 6.9.9). Two damage abstractions were developed for a WP with degraded internals that is surrounded by lithophysal rubble:

- 23-mm-thick OCB with degraded internals
- 17-mm-thick OCB with degraded internals.

Damage for WPs with intact internals was not calculated for WPs surrounded by rubble. A WP becomes surrounded by rubble after DS framework and DS plates have failed during a seismic event. This is expected to occur at late times after repository closure. For CDSP WPs the OCB is likely to be breached by SCC at these times, resulting in degraded internals. In contrast, the probability of SCC damage to CSNF WPs with intact internals under intact DSs is zero except at 4.07 m/s PGV levels. Therefore, CSNF WPs are not likely to have degraded internals at the time of DS failure. Regardless of the time scale, the damage abstractions for degraded internals will result in greater damaged area relative to the response with intact internals, so this approach is

conservative. Separate abstractions were not developed for CSNF and CDSP WPs surrounded by rubble because it was considered that the results for the CSNF WPs provide a reasonable estimate of damage to the CDSP WP (SNL 2007 [DIRS 176828], Sections 6.9.10).

Lithophysal rubble was selected for the dynamic load on WPs. The analysis acknowledges that large rock blocks would tend to have point loading contacts in localized areas on a WP, but the cumulative loading from the lithophysal rubble is expected to be significantly greater because the volume of lithophysal rubble is much greater than the volume of nonlithophysal rockfall (SNL 2007 [DIRS 176828], Table 6-32 and Figure 6-58).

The probability of damage for the jth seismic event was abstracted as a function of the value of PGV for the jth seismic event, the value of RST for the ith realization, and of the OCB thickness (SNL 2007 [DIRS 176828], Section 6.9.2). Figure 6.6-15 illustrates these probabilities, for the two states of the WP (23-mm degraded and 17-mm degraded).

If WPs are damaged by the jth seismic event, then the conditional damaged area is represented by a gamma distribution. Separate gamma distributions were defined for two states of WPs: (1) 23-mm-thick OCB with degraded internals, and (2) 17-mm-thick OCB with degraded internals. The mean and SD of the gamma functions are quadratic equations in RST (SNL 2007 [DIRS 176828], Section 6.9.3). For the 23-mm thick and the 17-mm thick OCB, relatively few data points showed SCC damage (SNL 2007 [DIRS 176828], Sections 6.9.3 and 6.9.5). Therefore, the abstraction for damage was done at a single PGV level (4.07 m/s). It was considered to be conservative to use the conditional damage at the 4.07 m/s PGV level for all values of PGV (SNL 2007 [DIRS 176828], Section 6.9.3). Figure 6.6-16 shows the quadratic fit for the mean damage area as a percent of the total surface area, for the 23-mm and 17-mm thick OCB.

There is no WP-to-WP spatial variability for the conditional damaged area (SNL 2007 [DIRS 176828], Section 6.9.9). Spatial variability is also discussed in Section 6.6.3.2. For a single package, the damaged area is randomly located on the cylindrical surface of the OCB. The total damaged area increases with each seismic event that causes damage to the OCB. The damaged area cannot exceed the total surface area of a CSNF or CDSP WP.

Puncture of CSNF and CDSP Waste Packages Surrounded by Rubble

For a WP surrounded by rubble, loss of WP integrity is conceptualized to occur from puncture by sharp internal fragments, rather than rupture of the OCB due to impact with other EBS components. The probability of puncture for the 23-mm-thick and 17-mm-thick OCBs is abstracted as a power law in PGV (SNL 2007 [DIRS 176828], Section 6.9.1). Figure 6.6-17 shows the probability of puncture for 23-mm and 17-mm OCBs. Comparison with Figure 6.6-14 shows that puncture can be more likely than rupture, particularly for 17-mm OCBs and at lower PGVs.

When WPs are punctured, the failed area is determined by sampling a uniform distribution, with a lower bound of 0 m^2 and an upper bound of 0.10 m^2. The upper bound of the uniform distribution is based on two estimates for the area of a hypothetical puncture. If the puncture occurs from a sharp fragment of a fuel rod, the corresponding hole is likely to be quite small. In

the second estimate, one of the fuel basket plates is conceptualized to form a lengthwise slice through the OCB (SNL 2007 [DIRS 176828], Section 6.9.1). The upper bound of 0.10 m^2 represents the maximum estimated area from either mechanism.

This failed area allows advective flow through punctured WPs and advective and diffusive transport out of the punctured WPs. Once a WP is penetrated, there is no further damage from penetrations in successive events and the WPs remain punctured for the remainder of the realization.

6.6.1.2.3 Fault Displacement Abstraction

In addition to the damage from vibratory ground motion, it is possible that WP and DS failures may occur due to fault displacement. Damage to WPs by fault displacement occurs when the fault displacement exceeds the available clearances between or around EBS components. Two distinct cases were considered in analyzing the clearances between EBS components (Section 6.6.1.1.3). The maximum allowable displacement, for six different WP types (SNL 2007 [DIRS 176828], Tables 6-58 and 6-59), was determined for the two cases, one with an intact DS and a second with a failed DS. The values corresponding to the second case (failed DSs) are used for the TSPA-LA Model because these values result in more failures than for the first case, with an intact DS.

Fault displacement hazard curves for 15 faulting conditions mapped within the immediate vicinity of Yucca Mountain were used to provide displacement values as a function of the mean annual exceedance frequency (SNL 2007 [DIRS 176828], Section 6.11.3). The inventory of WP types was split into two groups (CSNF and CDSP WP). WPs of similar design and similar waste type were grouped together. The WP designs with the smallest diameter in the group are chosen to represent the clearance for all packages in that group. The clearance is given by one-quarter of the outer diameter of the OCB, so the smallest diameter results in the least clearance for all WPs in the group. The probability of finding a WP in each group on a fault was calculated based on the total length of the WP types in the group versus the total length of all emplaced WPs (rather than the number of each type of WP divided by the total number of WPs). The hazard curve data is combined with the clearance data and the probability of finding a WP from each group on a fault to give the expected number of WP failures as a function of mean annual exceedance frequency. The expected number of WPs that could fail from fault displacement was found to be a small fraction of the total number of WPs in the repository. If a WP fails from fault displacement, then the surrounding DS also fails from fault displacement (if it hasn't already failed in a previous seismic event). The results are summarized in Table 6.6-1. The table indicates that damage to WPs and DSs from fault displacement is not expected if the mean annual frequency of occurrence is greater than 2.5×10^{-7} per year (DTN: MO0703PASEISDA.002_R4 [DIRS 183156], Table 1-14).

Shearing of the WP and DS over the fault can occur if the fault exceeds the available clearance in the EBS (SNL 2007 [DIRS 176828], Section 6.11). When a WP fails by fault displacement, the failed area is determined by sampling a uniform distribution with a lower bound of zero and an upper bound equal to the area of a WP lid. The lower bound is appropriate for mean annual exceedance frequencies near 10^{-7} per year because a WP that is minimally pinned from fault displacement is expected to have only minor crimping and is unlikely to rupture. The upper

bound is appropriate for a large fault displacement that shears a WP near its lid. In this case, the lid welds have the potential to fracture, separating the lid from the package and potentially exposing the entire waste form to seepage and release (SNL 2007 [DIRS 176828], Section 6.11.5). The use of a uniform distribution is appropriate because reasonable upper and lower bounds can be defined and because the use of this type of distribution maintains the uncertainty in the damaged area for this abstraction.

In the TSPA model the failed area is conceptualized to be a shear that lies in a plane normal to the central axis of a WP. The failed area can be represented as a circumferential band around a WP for transport calculations in the TSPA. Once WPs fail in shear, there is no further damage on successive events and WPs remain failed for the remainder of the realization. The resulting damage is assumed to allow flow into WPs (if seepage is present) and allow advective and diffusive transport out of WPs. When a WP fails from fault displacement, the associated DS is also presumed to fail, causing damage to the total surface area of the DS. A sheared DS will allow all seepage to pass through no flux splitting (SNL 2007 [DIRS 176828], Section 6.11.5). A damage abstraction for the cladding in a fault-failed WP was not developed because the TSPA-LA Model does not take credit for cladding as a barrier to radionuclide releases (SNL 2007 [DIRS 180616], Section 6.2.1.2[a]).

6.6.1.2.4 Treatment of Uncertainty

The TSPA-LA Model includes parameter uncertainty in the Seismic Scenario Class at two levels: in the implementation of the abstraction in the TSPA-LA Model, and in the underlying process models used in the development of the Seismic Consequences Abstraction. The term parameter uncertainty encompasses uncertainty in input parameters for process level models (like ground motions) and uncertainty in random variables for seismic damage, such as the damaged areas.

Uncertainty can be characterized as epistemic (representing limited data and knowledge) or aleatory (representing variability or natural randomness in a process). Uncertainty in the Seismic Scenario Class is directly represented in the TSPA-LA Model by defining uncertain parameters that are sampled either once per realization (epistemic parameters) or multiple times per realization (i.e., at the occurrence of each seismic event (aleatory parameters)). Table 6.6-2 lists the parameters that represent uncertainty in the Seismic Scenario Class. In this table the parameters are categorized according to whether they represent epistemic or aleatory uncertainty.

The uncertainty in the input parameters to the underlying process models, and its propagation in the TSPA-LA Model, is discussed in Section 8.2 of Seismic Consequence Abstraction (SNL 2007 [DIRS 176828]), and summarized as follows:

- The structural response calculations for the responses of WPs that are affected by vibratory ground motion include three principal sources of uncertainty: (1) the ground motion time histories (aleatory uncertainty); (2) the metal-to-metal friction coefficient (epistemic uncertainty); and (3) the metal-to-rock friction coefficient (epistemic uncertainty) (SNL 2007 [DIRS 176828], Section 8.2, Acceptance Criterion 3). The variations of these uncertain input parameters are simultaneously included in the 17 structural response calculations at each seismic hazard level. This is accomplished by a

Latin Hypercube Sampling (LHS) procedure that ensures robust sampling of the uncertain parameters over their full ranges (SNL 2007 [DIRS 178851], Sections 6.3.1, 6.4.4.5, and 6.5.1.1).

- All rockfall analyses include the ground motion time histories as a major source of aleatory uncertainty. Fifteen ground motions represent the uncertainty in the seismic forcing functions. Note that the rockfall calculations predate the WP calculations and for these earlier calculations only 15 of the 17 ground motion histories were used (SNL 2007 [DIRS 176828], Section 6.1.3). In the lithophysal units, the rock compressive strength is an uncertain input parameter that is represented as five discrete levels of rock strength. The computational results for probability of lithophysal rockfall are based on 15 realizations with LHS for the ground motion histories and the rock strengths. In the nonlithophysal units, the synthetic fracture pattern that defines the fracture geometry is an uncertain input parameter that is used in the rockfall analyses for the nonlithophysal units. The nonlithophysal analysis evaluated the response of a 25-meter long section of drift in nonlithophysal rock with randomly selected fracture patterns paired with randomly selected ground motion time histories (BSC 2004 [DIRS 166107], Section 6.3.1).

- The calculations of damaged areas on WPs that are due to vibratory ground motion exhibit substantial variability (primarily aleatory uncertainty) induced by the uncertainties in seismic ground motions and other input parameters. This variability in damaged area is represented as conditional probability distributions that are provided to and sampled in the TSPA-LA Model.

6.6.1.3 Implementation in the TSPA-LA Model

The potential for deformation and rupture/puncture of EBS components from multiple seismic events within a given realization of the TSPA-LA Model, is described in the following sections. These sections are aligned with the separate elements of the seismic damage abstractions. A realization of the TSPA-LA Model represents one of many future potential histories of the repository. Each realization generally has a unique value for each random variable that represents epistemic (knowledge) uncertainty, such the RST for initiation of potential stress corrosion cracking. Each realization also has a unique sequence of seismic events whose timing and intensity capture the aleatory uncertainty (i.e., the randomness) in the seismic process.

6.6.1.3.1 TSPA-LA Modeling Cases

The implementation of the Seismic Damage Abstraction involves two modeling cases, the Seismic GM Modeling Case and the Seismic FD Modeling Case.

Seismic GM Modeling Case

The Seismic GM Modeling Case calculates mean annual dose due to damage to WPs resulting from vibratory ground motion. This modeling case also accounts for fragility of the DSs under the combined loads from vibratory ground motion and accumulated rockfall around the DS. In addition, corrosion processes are included in the Seismic GM Modeling Case calculation for

1,000,000 years, and the dose due to corrosion processes is calculated as part of the Seismic GM Modeling Case for 1,000,000 years. The Seismic GM Modeling Case does not include damaged areas (due to SCC) on the DS because advective flow through the DS has been screened out by FEP 2.1.03.10.0B, *Advection of Liquids and Solids Through Cracks in the Drip Shield* (DTN: MO0706SPAFEPLA.001_R0 [DIRS 181613]). This modeling case also does not include failure of the DSs from large rock block impacts in nonlithophysal units because these processes have been screened out by FEP 1.2.03.02.0B, *Seismic-Induced Rockfall Damages EBS Components* (DTN: MO0706SPAFEPLA.001_R0 [DIRS 181613]).

The Seismic GM Modeling Case for 10,000 years and the Seismic GM Modeling Case for 1,000,000 years use different numerical techniques to calculate mean annual dose. These are described in the following paragraphs.

The TSPA-LA Model calculates the mean annual dose for the Seismic GM Modeling Case for 10,000 years using a three-step process. First, a LHS of uncertain TSPA-LA Model parameters is generated. Each element of the LHS is a vector, specifying a value for each epistemically uncertain parameter. For each element in the LHS, a number of annual dose histories are computed using GoldSim. Each annual dose history represents a single seismic ground motion event, which occurs at a specified time, and results in a specified damage area to each WP simulated. The mobilization and transport of radionuclides is evaluated using the Nominal Scenario Class submodels for radionuclide transport in the EBS, UZ, and SZ.

Second, for each element in the LHS, the expected annual dose history is calculated by Equation 6.1.2-22, using the annual dose histories computed for each element of the LHS. The integral in Equation 6.1.2-22 accounts for the uncertainty in the number of seismic events, the time of each event, and the damaged area. The integral is evaluated numerically by EXDOC software (Section 6.1.5). The mean annual dose history is calculated as the average of the expected annual dose histories from the set of realizations.

Because relatively few seismic events (approximately 5) occur within 10,000 years, and the probability of damage to CDSP WPs is much greater than that of damage to the CSNF WPs, the expected dose for the Seismic GM Modeling Case for 10,000 years relies on a number of simplifying approximations:

- Corrosion of WP and DS materials is bounded by a 2 mm thickness reduction to the WP and a 2 mm thickness reduction to the DS
- Only CDSP WPs are considered because the probability of damaging the CSNF WP is very low during the first 10,000 years
- Rupture and puncture events are not considered
- The DS remains intact and functional
- Seepage and temperature are not altered due to rockfall.

Section 7.3.2 provides justification for these approximations. Calculation of the mean annual dose for the Seismic GM Modeling Case for 1,000,000 years also begins by generating an LHS of uncertain TSPA-LA Model parameters. For each element in the LHS, a number of annual dose histories are computed using GoldSim. Each annual dose history is associated with a sequence of seismic events generated by GoldSim. The effects of corrosion on EBS components are included, and rockfall and damage to EBS components are accumulated as seismic events occur. The mobilization and transport of radionuclides is evaluated using the Nominal Scenario Class submodels for radionuclide transport in the EBS, UZ, and SZ.

The expected annual dose history is calculated by Equation 6.1.2-24, using the annual dose histories computed for each element of the LHS. The mean annual dose history is calculated as the average of the expected annual dose histories from the set of realizations.

Seismic FD Modeling Case

The Seismic FD Modeling Case calculates mean annual dose due to damage caused by fault displacements. This modeling case accounts for damage to WPs and DSs through direct shearing which allows advective flow through the sheared components. Corrosion processes are not included in the Seismic FD Modeling Case. The modeling case considers a single seismic event. This modeling case does not consider rockfall accumulation in the drifts, however, after the seismic event occurs drifts are considered to be filled with rockfall.

Calculation of the mean annual dose for the Seismic FD Modeling Case for either 10,000 years or 1,000,000 years also begins by generating an LHS of uncertain TSPA-LA Model parameters, and, for each element of the LHS, computing a number of annual dose histories using GoldSim. Each annual dose history is associated with a single seismic fault displacement event occurring at a specified time, and resulting in a specified damage area to each WP represented. The effects of the fault displacement are applied to the DS and to the drift, and the mobilization and transport of radionuclides is evaluated using the Nominal Scenario Class submodels for radionuclide transport in the EBS, UZ, and SZ.

The expected annual dose history is calculated by Equation 6.1.2-25, using the annual dose histories computed for each element of the LHS. The integral in Equation 6.1.2-25 accounts for the uncertainty in the time of the seismic fault displacement event, the uncertainty in the damaged area caused by the seismic event, and the number of WPs affected; this equation is evaluated numerically by EXDOC (Section 6.1.5). The mean annual dose history is calculated as the average of the expected annual dose histories from the set of realizations. Table 6.6-3 summarizes the calculations for the two modeling cases.

The computational approach used in GoldSim in the implementation of the Seismic Scenario Class is described in DTN: MO0703PASEISDA.002_R4 ([DIRS 183156], Section 1.1). The input parameters required by the Seismic Scenario Class model components are taken from the TSPA Input Database.

6.6.1.3.2 Seismic Event Time and Magnitude Calculations for the 1,000,000-Year Ground Motion Case

For the Seismic GM Modeling Case 1,000,000-year simulation, each realization includes multiple seismic events. In the discussions that follow, a particular seismic event, the jth event, will be considered representative of all seismic events in a particular Monte Carlo realization. The time of the jth event is determined by GoldSim's random time internal (Poisson) event generator (GoldSim Technology Group 2007 [DIRS 181727], Appendix B) using a Poisson frequency of ($\lambda_{max} - \lambda_{min}$). The values of λ_{min} and λ_{max} are set to 1×10^{-8} per year and 4.287×10^{-4} per year, respectively (DTN: MO0703PASEISDA.002_R4 [DIRS 183156], Table 1-15). The Poisson frequency is then given by (4.287×10^{-4} per year $- 1 \times 10^{-8}$ per year) = 4.287×10^{-4} per year.

The mean annual exceedance frequency for the jth event is sampled from a uniform distribution between λ_{min} and λ_{max}. The bounds are chosen to encompass all mean annual exceedance frequencies with the potential to result in significant damage to DSs or WPs. The range of mean annual exceedance frequencies, spans the response of the system from no damage to the regulatory probability limit at 10^{-8} per year (DTN: MO0703PASEISDA.002_R4 [DIRS 183156], Table 1-15).

After the value of the mean annual exceedance frequency has been determined for the jth event, the corresponding value of the PGV is calculated. The relationship between the PGV and the mean annual exceedance frequency (bounded hazard curve) is represented in the model by a one-dimensional table (DTN: MO0703PASEISDA.002_R4 [DIRS 183156], Table 1-15). Interpolation between points on the hazard curve is based on a piecewise linear interpolation with the values of log(λ) and log (PGV) at the individual points.

6.6.1.3.3 Methodology for Damage Abstraction Implementation

The seismic damage abstractions are generally based on a three-part approach:

1. The probabilities of incipient rupture (which may lead to rupture during a subsequent timestep), immediate rupture, or puncture are defined as a function of horizontal PGV and the thickness of the OCB. If rupture or puncture occurs, the resulting rupture area or puncture area is defined using a bounding, uniform distribution. The probabilities of incipient rupture, immediate rupture, or puncture are represented as a power-law function of PGV. The rationale for two types of rupture, incipient and immediate, is explained in Section 6.6.1.2.2.2.

2. The probability of damage is defined as a function of PGV, RST, and the thickness of the WP. Damaged area is defined as the area that exceeds the RST and is thereby susceptible to potential SCC. Damaged area represents the physical area of a dented region with high residual stress. Damaged area is significantly greater than the effective area for transport through a network of stress corrosion cracks, as explained in Section 6.6.1.1.2.

   The probability of nonzero damaged area, or more simply the probability of damage, is usually represented as a lookup table that uses PGV and RST as the independent variables.

The typical lookup table for probability of damage at a given OCB thickness has 12 entries defined by four values of PGV (0.4 m/s, 1.05 m/s, 2.44 m/s, and 4.07 m/s) and by three values of RST (90 percent, 100 percent, and 105 percent of the yield strength of Alloy 22). A piecewise linear interpolation scheme is used between the points in the lookup table, avoiding the need for a functional fit to a probability surface.

3. When nonzero damaged area occurs, a conditional probability distribution for the magnitude of the conditional damaged area is defined as a function of PGV, RST, and the thickness of the OCB. The conditional damaged areas are always nonzero areas, by definition.

This approach is useful because it eliminates zero values from the conditional probability distributions in Step 3. A similar approach is applied for rockfall induced by a seismic event, based on Steps 2 and 3, as described in the next section.

6.6.1.3.4 Implementation of Rockfall for the 1,000,000-Year Ground Motion Case

Lithophysal Rockfall Calculation

The probability of rockfall was abstracted as a linear function of PGV (Equation 6.6-1). The occurrence of rockfall is determined by comparing the calculated probability of rockfall for the jth seismic event, $P_{rockfall}$, to a random number between 0 and 1, R_j , corresponding to the jth seismic event

$$If \quad R_j \le P_{rockfall} \quad \text{then } RV_{LITH,j} > 0 \qquad \text{(Eq. 6.6-2)}$$

$$else \quad RV_{LITH,j} = 0$$

where $RV_{LITH,,j}$ is the volume of lithophysal rockfall. The random number is resampled for each seismic event because the uncertainty in the probability of rockfall is related to the aleatory uncertainty in 17 ground motion time histories.

For each seismic event where rockfall occurs, the volume of lithophysal rock that collapses per meter of drift length is represented by a gamma distribution with mean (μ) and SD (σ) that are quadratic functions of PGV (DTN: MO0703PASEISDA.002_R4 [DIRS 183156], Section 1.1, Step 5c and Table 1-16). If the PGV determined from the bounded hazard curve is less than 0.4 m/s, then the values at 0.4 m/s are used in the volume calculations (DTN: MO0703PASEISDA.002_R4 [DIRS 183156], Table 1-16), since Equations 6.6-4 and 6.6-5 may produce negative values of the mean and/or SD for PGVs less than 0.4 m/s.

$$PGV_{rf} = MAX(PGV, 0.4 m/s), \qquad \text{(Eq. 6.6-3)}$$

$$\mu = (20.307)\left(PGV_{rf}\right)^2 - (18.023)PGV_{rf} + 4.0102, \qquad \text{(Eq. 6.6-4)}$$

$$\sigma = -(3.5613)\left(PGV_{rf}\right)^2 + (18.018)PGV_{rf} - 6.6202. \qquad \text{(Eq. 6.6-5)}$$

The total volume of lithophysal rock that collapses per meter of drift length after the jth seismic event, $TV_{LITH,j}$, is the sum of the volumes for the first j seismic events.

$$TV_{LITH,j} = \sum_{k=1}^{j} RV_{LITH,k} \quad \text{(Eq. 6.6-6)}$$

The volume of lithophysal rock that must collapse to fill the drift ($V_{L,i}$) is defined as a uniform distribution between 30 m^3 per meter to 120 m^3 per meter of drift length. This parameter is sampled once per realization (DTN: MO0703PASEISDA.002_R4 [DIRS 183156], Section 1.1, Step 5e).

The fraction of the drift that is filled after the jth seismic event, FD_j, is defined as the ratio of the total volume of collapsed lithophysal rock after the jth seismic event to the volume that is required to fill the drift ($V_{L,i}$), for the ith realization (DTN: MO0703PASEISDA.002_R4 [DIRS 183156], Equation 1-11).

$$FD_{LITH,j} = MIN\left(\frac{TV_{LITH,j}}{V_{L,i}}, 1.0\right) \quad \text{(Eq. 6.6-7)}$$

The fraction of drift filled by lithophysal rubble ($FD_{LITH,j}$) is a parameter used in DS fragility calculations.

Nonlithophysal Rockfall Calculation

The probability of nonlithophysal rockfall has been abstracted to be the same as the probability of lithophysal rockfall (Section 6.6.1.2.1). Thus the probability of occurrence of nonlithophysal rockfall is given in Equation 6.6-2.

For each seismic event where rockfall occurs, the volume of nonlithophysal rock that collapses per meter of drift length is represented by a gamma distribution with mean (μ) and SD (σ) that are quadratic functions of PGV (DTN: MO0703PASEISDA.002_R4 [DIRS 183156], Table 1-16):

$$\mu = (-0.0142)(PGV)^2 + (0.2064)PGV + 0.0387 \quad \text{(Eq. 6.6-8)}$$

$$\sigma = (-0.037)(PGV)^2 + (0.3057)PGV + 0.0696. \quad \text{(Eq. 6.6-9)}$$

The total volume of nonlithophysal rock that collapses per meter of drift length after the jth seismic event, the volume of nonlithophysal rock that must collapse to fill a drift, and the fraction of the drift that is filled after the jth seismic event are all defined in an analogous fashion to the definitions for lithophysal rockfall.

The fraction of a drift filled by nonlithophysal rubble is a parameter used by the drift seepage abstraction (Section 6.6.2.1) for the Seismic GM Modeling Case for 1,000,000 years.

6.6.1.3.5 Implementation of Drip Shield Plate and Framework Damage from Ground Motion

Plate Fragility

DS plate fragility is defined as the probability of rupturing a plate during a seismic event. Plate fragility is a function of *PGV* for the jth seismic event, of the thickness of DS plates, and of the static load on plates from rockfall. The thickness of DS plates is a feed from WP and DS Degradation Model Component (Section 6.3.5) of the TSPA-LA Model, based on the time of the event, the top-side (upper surface of the DS) and bottom-side (lower surface of the DS) corrosion rates for Titanium Grade 7, and the initial plate thickness. The static load is defined by the fraction of the drift that is filled with lithophysal rubble ($FD_{LITH,j}$), as discussed in Section 6.6.1.3.4 and the resulting failure probability is applied to all zones of the repository.

Four two-dimensional look-up tables represent the probability of failure of DS plates at 0 percent, 10 percent, 50 percent, and 100 percent rockfall load (Figure 6.6-8 and DTN: MO0703PASEISDA.002_R4 [DIRS 183156], Table 1-2). Each of these tables is a function of PGV and DS plate thickness. A two-stage linear interpolation process is used to determine the probability. The first step in this interpolation is to linearly interpolate within each of the four sections of Table 1-2 (DTN: MO0703PASEISDA.002_R4 [DIRS 183156]) using the values of PGV for the jth event and of the plate thickness at the time of the jth event. This first interpolation produces four failure probabilities for drifts that are 0 percent, 10 percent, 50 percent, and 100 percent filled with rubble. A second linear interpolation using the value of $FD_{LITH,j}$ (Equation 6.6-7) for the jth event versus the failure probabilities at these four points determines the probability of DS plate failure. Plate failure is determined by comparing the calculated probability of failure for the jth seismic event to a random number, R_j, between 0 and 1, corresponding to the jth seismic event (DTN: MO0703PASEISDA.002_R4 [DIRS 183156], Section 1.1, Step 7c)

$$If \quad R_j \le P_{plate\ failure} \quad then \quad Plate\ Failure = true$$

$$else \quad Plate\ Failure = false\ .$$

For the jth seismic event, the random number, R_j , used above is the same random number as was used in Section 6.6.1.3.4 for the determination of the occurrence of rockfall. This random number is also used for the determination of DS framework failure and WP damage. The reason for this is that a more intense ground motion is likely to simultaneously cause rockfall, WP damage, and DS failure because the intensity of the ground motion for a given PGV level is the major driver of system response. The probabilities of rockfall, WP damage, and DS failure are therefore expected to be highly correlated, rather than independent random variables (DTN: MO0703PASEISDA.002_R4 [DIRS 183156], Section 1.1, Step 5b). This random number is resampled for each event because the uncertainty in these probabilities is primarily caused by the aleatory uncertainty in the ground motions (DTN: MO0703PASEISDA.002_R4 [DIRS 183156], Section 1.1, Step 9c).

The consequence of plate failure is that all DSs fail as a barrier to seepage for the remainder of the simulation (DTN: MO0703PASEISDA.002_R4 [DIRS 183156], Section 1.1, Step 9d). In

addition, the damage abstraction for WPs under failed DSs (Section 6.6.1.2.2.2) will be applied to all WPs for the remainder of the simulation.

Framework Fragility

DS framework fragility is defined as the probability of collapsing the sides of a DS during a seismic event. Framework fragility is a function of PGV for the jth seismic event, of the reduction in thickness of DS framework, and of the static load on the crown of a DS from rockfall. The reduction in thickness of DS plates is a feed from the WP and DS Degradation Model Component (Section 6.3.5) of the TSPA-LA Model, based on the time of the event, the external (upper surface of the DS) corrosion rate for Titanium Grade 7, and the corrosion rate multiplier that converts the Titanium Grade 7 corrosion rate to a corrosion rate appropriate for Titanium Grade 29 (DTN: SN0704PADSGCMT.002_R1 [DIRS 182188]). The external (upper surface) corrosion rate is appropriate because the predicted failure mode for the DS framework is collapse of the legs, and the supporting bulkheads on the sides of the DS are located on the exterior side of the DS plates. The external (upper surface) corrosion rate is applied to both sides of the framework components (double-sided corrosion). Double-sided corrosion is considered appropriate since the width of the bulkheads and stiffeners in the axial direction of the DS is usually less than the depth of the bulkheads and stiffeners normal to the plates. In this geometry, the thickness reduction of the width is the important parameter for buckling of the legs. Both sides of the bulkhead or stiffener that are perpendicular to the width will be exposed to the in-drift environment and experience general corrosion (DTN: MO0703PASEISDA.002_R4 [DIRS 183156], Section 1.1, Step 8; and SNL 2007 [DIRS 176828], Section 6.8.3.3). The static load is defined by the fraction of the drift that is filled with lithophysal rubble.

The calculation of probability of framework failure (i.e., buckling of the sidewalls) is analogous to that for plate failure. The probability is represented by four look-up tables, each a function of PGV and framework thickness reduction (Figure 6.6-9) and DTN: MO0703PASEISDA.002_R4 ([DIRS 183156], Table 1-3). A two-stage linear interpolation process is used to determine the probability of framework failure. The first step in this interpolation is to linearly interpolate within each of the four sections of Table 1-3 (DTN: MO0703PASEISDA.002_R4 [DIRS 183156]) using the values of PGV for the jth event and of the reduction in framework thickness at the time of the jth event. This first interpolation produces four conditional failure probabilities, for drifts that are 0 percent, 10 percent, 50 percent, and 100 percent filled with rubble. A second linear interpolation using the value of $FD_{LITH,j}$ for the jth event versus the failure probabilities at these four points determines the probability of collapse. Framework failure is determined by comparing the calculated probability for the jth seismic event to the same random number used to determine DS plate failure for the jth seismic event (DTN: MO0703PASEISDA.002_R4 [DIRS 183156], Section 1.1, Step 8c).

If DS framework fails, DSs are considered collapsed but are not considered failed as a barrier to seepage. Two calculations were done to represent the response of CSNF (TAD-bearing) WPs, one with intact internals and one with degraded internals (SNL 2007 [DIRS 176828], Section 6.8.4). The expected damage for a CSNF WP surrounded by rubble was found to provide an upper bound for the damage to a CSNF WP with intact internals loaded by a collapsed DS. The results for degraded internals showed a higher level of damage which was consistent with the kinematic damage abstractions for CSNF WPs with degraded internals.

Separate calculations were not performed for CDSP WPs loaded by collapsed DSs. Since the calculations for the CSNF WPs were performed quasi-statically, it was anticipated that the response of the CDSP WPs would be very similar (SNL 2007 [DIRS 176828], Section 6.8.4). Therefore, after DS framework failure, but before DS plate failure, the damage abstractions for WPs surrounded by rubble are applied, if the WP internals are still intact. When the WP internals become degraded (after the first damage-causing event), the damage abstractions for WPs under intact DSs, but with degraded internals, apply until the DS plates also fail (DTN: MO0703PASEISDA.002_R4 [DIRS 183156], Section 1.1, Step 8e).

6.6.1.3.6 Implementation of WP Rupture and Puncture from Ground Motion

The rupture of a CSNF or CDSP WP that can move freely beneath a DS can occur only up until the time of DS plate failure. After DS plate failure, WPs are surrounded by rubble and the failure mechanism is abstracted to be WP puncture.

Ruptured Waste Packages

The probability of rupture for CSNF or CDSP WPs with intact internals is zero. For WPs with degraded internals, two rupture probabilities are calculated; one for incipient rupture, one for immediate rupture. For both CSNF and CDSP WPs, they are given by power laws in PGV (DTN: MO0703PASEISDA.002_R4 [DIRS 183156], Eq. 1-12, Eq. 1-13, Eq. 1-17, Eq. 1-18, and Table 1-17). There are three possible rupture states: immediate rupture, PR_{immed}; incipient rupture, PR_{incip}; and no rupture, PR_{none} (given by one minus the sum of the two rupture probabilities). The appropriate state is determined using a random number R_{ruptue}, and a counter, C, with the following logic:

$$\begin{array}{llll} \textit{If} & R_{rupture} < PR_{none} & \textit{then} & C = 0 \\ \textit{else if} & R_{rupture} < PR_{none} + PR_{incip} & \textit{then} & C = 1 \\ \textit{else} & & & C = 2 . \end{array}$$

A counter value of 1 indicates an incipient condition for rupture after a single severe impact. A counter value of 2 indicates immediate rupture. The value of the counter is retained, so if an event is deemed to be incipient (C=1) and a subsequent seismic event is also deemed to be incipient, then a rupture will occur during the subsequent seismic event. Independent random numbers (not correlated) are used for the determination of rupture for CSNF and CDSP WPs.

When a WP is ruptured, the failed area is determined by sampling a uniform distribution with a lower bound of 0 m^2 and an upper bound equal to the cross-sectional area, 2.78 m^2 and 3.28 m^2 for CSNF and CDSP WPs, respectively (DTN: MO0703PASEISDA.002_R4 [DIRS 183156], Table 1-20). This failed area allows advective flow into and advective and diffusive transport out of ruptured CSNF or CDSP WPs.

Punctured Waste Packages

The probability of rupture for a WP surrounded by rubble is represented by two power laws in PGV (DTN: MO0703PASEISDA.002_R4 [DIRS 183156], Equations 1-22 and 1-23 and Table 1-17), one that applies to WPs with 23-mm-thick OCBs and one that applies to WPs with

17-mm-thick OCBs. For thicknesses greater than 23 mm or less than 17 mm, the 23-mm power law and 17-mm power law are used, respectively, for the probabilities of puncture. For intermediate thicknesses, linear interpolation is used.

The determination of the occurrence of puncture is done by comparing the calculated probability of puncture to a random number between 0 and 1. This random number is not correlated with any of the other random numbers used either for assessing the probability of rockfall, WP crack damage, or rupture (Section 6.6.1.3.4). If the random number is less than or equal to the calculated probability of puncture, then all CSNF or CDSP WPs are punctured by this seismic event. Note that the evaluation of puncture is done separately for CSNF and CDSP WPs because the probability depends on WP OCB thickness, which in turn depends on general corrosion rate.

When WPs are punctured, the failed area is determined by sampling a uniform distribution with a lower bound of 0 m^2 and an upper bound of 0.1 m^2 (DTN: MO0703PASEISDA.002_R4 [DIRS 183156], Section 1.1, Step 15c and Table 1-17). This failed area allows advective flow through the punctured WP and advective and diffusive transport out of the punctured WP.

6.6.1.3.7 Implementation of Waste Package Stress Corrosion Cracking Damage from Ground Motion

The damage to WP OCB surface has been abstracted to occur as a dense network of stress corrosion cracks (Sections 6.6.1.2.3 and 6.6.1.2.4). Both the probability of WP damage and the conditional probability distributions for the amount of damage have been abstracted to be functions of the PGV level for the seismic event and of the RST threshold for Alloy 22. Residual stress threshold (RST) for Alloy 22 is a random variable that is sampled once per realization from a uniform distribution between 90 and 105 percent of the yield strength of Alloy 22 (DTN: MO0703PASEISDA.002_R4 [DIRS 183156], Table 1-15). The random variable is sampled once per realization because it represents the epistemic uncertainty in the RST.

The abstractions for probability of WP damage and for the conditional damaged area are functions of whether or not the WP internals are degraded. The internals are considered intact until the first event that causes damage, or breach by nominal general corrosion processes, if this occurs first. After this time, WPs are considered to have degraded internals and the probability and damage abstractions for degraded internals are used.

Probability of WP Damage

The probability of WP damage is represented as a look-up table that uses PGV and RST as the independent variables. The typical look-up table for probability of damage at a given WP OCB thickness has up to six values of PGV (forming the rows of the table) and three values of RST (90 percent, 100 percent, and 105 percent of the yield strength of Alloy 22). A piecewise linear interpolation scheme is used between the points in each look-up table, avoiding the need for a functional fit to a probability surface. Figures 6.6-10, 6.6-11, and 6.6-15 illustrate these probabilities.

The determination of damage is done by comparing the calculated probability of damage to a random number between 0 and 1. The random number (R_j) is the same random number used for the determination of rockfall and DS fragility for the jth seismic event (Sections 6-6.1.3.4

and 6.6.1.3.5). If the random number is less than or equal to the calculated probability of damage, then all CSNF or CDSP WPs are damaged by the jth seismic event and the internals of CSNF or CDSP WPs are considered degraded for all subsequent seismic events.

Probability of Damage to CSNF and CDSP Waste Packages under Intact Drip Shields

For WPs under an intact DS, with intact internals, two look-up tables represent the probability of damage to a WP with OCB thickness 23 mm. One table represents the CSNF WPs and one represents the CDSP WPs. A single table look-up is done in each table to obtain the probability of damage.

For WPs under an intact DS, with degraded internals, there are four look-up tables that represent the probability of damage to WPs, two representing CSNF and CDSP WPs at OCB thickness 23 mm and two representing CSNF and CDSP WPs at OCB thickness 17 mm. The current WP thickness is used to interpolate between the values from the look-up tables at 23 mm and 17 mm. The probability of damage is set equal to the value at 23 mm if the average OCB thickness is greater than 23 mm. The probability is set equal to the value at 17 mm if the average OCB thickness is less than 17 mm.

Probability of Damage to CSNF and CDSP Waste Packages Surrounded by Rubble

For WPs surrounded by rubble, four look-up tables represent the probability of damage to CSNF and CDSP WPs of thickness 23 mm and 17 mm with degraded internals. Two tables represent the probability of CSNF WP failure at 23 mm and 17 mm OCB thicknesses and two tables represent the probabilities of CDSP WP failure at 23 mm and 17 mm OCB thicknesses. The current WP thickness is used to interpolate between the values from the look-up tables at 23 mm and 17 mm. If the current WP thickness lies outside this range, the 23 mm or 17 mm table values are used.

Calculation of WP Damage Area

The conditional (nonzero) damaged areas are represented by gamma distributions. The parameters for the gamma distributions are their mean and SDs. All gamma distributions are resampled for each event.

The damage abstractions for WPs with degraded internals are derived for two different thicknesses of the WP OCB, 23 mm and 17 mm. These are both represented by gamma distributions that must be sampled at the same level of probability (i.e., in a correlated manner) to allow interpolation between the two thicknesses. Three independent random numbers are used to maintain this correlation, one for damage to CSNF WPs under intact DSs, one for CDSP WPs under intact DSs, and one for damage to WPs surrounded by rubble. These random numbers are resampled for each event to represent the aleatory uncertainty in the ground motions.

If the OCB thickness is greater than 23 mm, the damaged area is conservatively set equal to the value at 23 mm. The damaged area is set equal to the value at 17 mm if the average OCB thickness is less than 17 mm.

The total damaged area increases with each seismic event that causes damage to the OCB. Total damaged area for CSNF or the CDSP WPs is the sum of the damaged areas for the first through j^{th} seismic events. Total damaged area cannot exceed the total surface area of a CSNF or CDSP WP, respectively.

Seismically damaged areas are represented as a dense network of stress corrosion cracks. The effective area for transport through the crack network is determined by the product of the total damaged area and the crack density per unit surface area. The crack density model developed for Alloy 22 was abstracted as a uniform distribution between 0.00327 and 0.0131 (DTN: MO0702PASTRESS.002_R2 [DIRS 180514], file: Model Output.doc, Table 8-15). This parameter represents epistemic uncertainty and is sampled once per realization.

Damage Area for CSNF and CDSP Waste Packages under Intact Drip Shields

The mean and SDs of the gamma distribution for damaged area for CDSP WPs with intact internals under intact DSs are quadratic functions in PGV and have coefficients that are linear in RST (DTN: MO0703PASEISDA.002_R4 [DIRS 183156], Tables 1-5 and 1-17). The parameters for CSNF WPs with intact internals under intact DSs are based on computational results at PGV = 4.07 m/s and RST = 90 percent, which will have the maximum damaged area and apply to all values of PGV and RST (DTN: MO0703PASEISDA.002_R4 [DIRS 183156], Section 1.1, Table 1-7, Step 14a, and Table 1-17). In spite of this conservatism, damage will still be zero at most values of PGV and RST because the damage is conditional on the probability of damage, and this probability is 0 except for a single point in the first five lines of Table 1-6 in Step 13(a) (DTN: MO0703PASEISDA.002_R4 [DIRS 183156]). There are two pairs of gamma distributions representing the damaged area for CSNF and CDSP WPs with degraded internals under intact DSs. One pair represents CSNF WPs and one pair represents CDSP WPs. Their means and SDs are quadratic functions in PGV and have coefficients that are linear in RST (Figure 6.6-13 and DTN: MO0703PASEISDA.002_R4 [DIRS 183156], Tables 1-7, 1-5, and 1-17).

Damage Area for CSNF and CDSP Waste Packages Surrounded by Rubble

There are two gamma distributions representing the conditional damaged area for CSNF WPs with 23-mm and 17-mm thick OCBs surrounded by rubble (degraded DSs). Their means and SDs are quadratic functions of RST, with no PGV dependence (Section 6.6.1.2.3) (Figure 6.6-16 and DTN: MO0703PASEISDA.002_R4 [DIRS 183156], Tables 1-9 and 1-17). The damage to CDSP WPs is represented by the same gamma distributions as those used for CSNF WPs, although the thicknesses of the OCBs for the CDSP and CSNF WPs may be different at the time of the jth seismic event.

6.6.1.3.8 Waste Package Thickness Calculations

WPs and overlying DSs are partitioned among the five percolation subregions according to the partitioning described in Section 6.3.2.2.1. In the Seismic GM Modeling Case, the calculations for the probability and damaged area are a function of WP OCB thickness, which depends on the general corrosion rate of Alloy 22. The general corrosion calculation depends on temperature, and other parameters that vary at the percolation subregion level and with fuel type

(Section 6.3.5.1.2). Therefore, the time-dependent WP OCB thickness will be different for each of the five percolation subregions and for each of the two fuel types.

The general corrosion rate of the Titanium Grade 7 DSs is given by a distribution that is independent of percolation subregion parameters and will be the same for all DSs (Section 6.3.5.1.2).

The abstractions for WP degradation used in the Seismic GM Modeling Case require the spatially-averaged thickness of the WP OCB as a function of time. This calculation is done as part of the WP and DS Degradation Submodel calculations. The WAPDEG V4.07 software is run 10 times, once for each percolation subregion and fuel type, to produce a time history of WP thickness. This calculation is done separately from the calculation of WP breach used to feed the EBS Flow and Transport Model Component (Sections 6.3.6 and 6.3.8) for nominal corrosion processes. The general corrosion rate used for the feed to the Seismic GM Modeling Cases is done with an average rate rather than an extreme patch approximation to the general corrosion rate discussed in Section 6.3.5.1.2. The method discussed in Section 6.3.5.1.2 used the highest of four sampled corrosion rates (from the two-parameter Weibull distribution) to analyze general corrosion of the WP patch. For the purposes of the seismic abstractions, the average of the four sampled corrosion rates was used to generate the general corrosion rate fed to the WAPDEG v4.07 software (output DTN: MO0707WPDRIPSD.000 [DIRS 183005]). The GetThk_LA v1.0 (STN: 11229-1.0-00 [DIRS 181040]) software was used to post-process the thickness file output by the WAPDEG v4.07 software and generate a one-dimensional table of mean WP OCB thickness versus time. This mean thickness is a spatially-averaged WP OCB thickness over all the WPs in a particular percolation subregion for each fuel type.

Since the nominal corrosion processes calculated by the WAPDEG V4.07 software calculations are included in the Seismic GM Modeling Case, the inside-out corrosion that occurs after a seismic event has damaged a WP must be accounted for. The mean time of the first seismic event that causes WP damage must be passed as an input to the WAPDEG V4.07 calculations. However, the WAPDEG 4.07 calculations are done at the beginning of the simulation, before any seismic calculations are done. Therefore, a separate *a priori* calculation of the time that WPs are first damaged by a seismic event is carried out.

CSNF and CDSP WPs are considered to have intact internals before the first seismic damage event and the probability of damage for WPs with intact internals under intact DSs is not a function of WP thickness (Figures 6.6-10 and 6.6-11; and DTN: MO0703PASEISDA.002_R4 [DIRS 183156], Tables 1-4 and 1-6). However, for CSNF WPs, damage is not likely to occur before DS failure. In this case, the abstraction for the probability of damage for WPs surrounded by rubble with a 17 mm thickness is used as a conservative estimate of the probability of first failure time (Figure 6.6-15; and DTN: MO0703PASEISDA.002_R4 [DIRS 183156], Table 1-8). This estimate is conservative because it gives the highest possible probability of failure for a WP surrounded by rubble. The same approximation is used for CDSP WPs if the WP damage does not occur before DS failure. However, in the case of CDSP WPs, the probability of WP damage under intact DSs is higher (Figures 6.6-11).

6.6.1.3.9 Implementation of Fault Displacement Damage

The two simulations for Seismic FD Modeling Case are both run using pre-specified parameters (Table 6.6-3). The fraction of damage is set at 0.028, 0.056, or 0.084, for CSNF WPs, and at 0.0335, 0.067, or 0.101, for CDSP WPs. These values represent 1/3, 2/3, 3/3 of the ratio of lid area to WP surface area, for CSNF and CDSP WPs respectively.

The time of the seismic event is set to be 1,000 years, 20,000 years, 80,000 years, 200,000 years, 400,000 years, or 800,000 years, for the 1,000,000-year Seismic FD Modeling Case. For the 10,000-year Seismic FD Modeling Case, the time of the seismic event is set to be either 200 years, 800 years, 2,000 years, 4,000 years, 8,000 years, or 18,000 years.

The time at which the drifts fill with rubble is set to be the time of the seismic event. The DS damage fraction is set to 1.0.

The number of failed WPs is set to 100. This number is chosen so that there will be failed WPs in each percolation subregion. The dose calculation is then scaled by the ratio of the expected number of WP failures divided by 100 (Section 6.1.2.4.3, Equation 6.1.2-24).

For model development purposed, a unified sampling Seismic FD Modeling Case is also run. In the unified sampling case a single seismic event is modeled. The time of the seismic event is determined by sampling a log uniform distribution that spans the simulation duration. The mean annual exceedance frequency is sampled from a log uniform distribution with an upper bound of 2.5×10^{-7} per year, the largest frequency for for which fault displacement damage will occur (Section 6.6.1.2.3) and the same lower bound as for the Seimsic GM Modeling Case (10^{-8} per year). The expected number of WP failures due to fault displacement is extracted from a table over a series of mean annual exceedance frequency intervals for each of two WP groups (DTN: MO0703PASEISDA.002_R4 [DIRS 183156], Tables 1-14 and 1-20) and is rounded to the nearest integer. Note that inspection of the failure numbers shows that the maximum number of failures for the CSNF and CDSP WP groups is approximately 159 and 53, respectively. The failed area is determined by sampling a uniform distribution with a lower bound zero and upper bound equal to the area of the CSNF or CDSP WP lid (Section 6.6.1.2.3).

The amount of rubble in a drift following a seismic fault displacement event is 112 m^3/m in the lithophysal zones and 2.9 m^3/3 in the nonlithophysal zones output (SNL 2007 [DIRS 176828], Figure 6-63).

The DSs and cladding corresponding to fault-failed WPs are also considered to be completely failed (DTN: MO0703PASEISDA.002_R4 [DIRS 183156], Section 1.1, Step 21)

6.6.2 Interaction of Seismic Scenario Class Submodels with other TSPA-LA Submodels

The rockfall accumulation calculations described in Section 6.6.1.3.4 have consequences with respect to other TSPA-LA submodels.

6.6.2.1 Drift Seepage Submodel and Drift Wall Condensation Submodel Modifications for Seismic Disruption

The Drift Seepage Submodel's (Section 6.3.3.1) drift seepage simulations produce response surfaces in the form of look-up tables for the seepage flux into the degraded drifts. The values of the independent variables in the look-up tables are local percolation flux, permeability, and capillary strength. For the Seismic Scenario Class, drift collapse occurs in both lithophysal and nonlithophysal zones. Partial collapse, followed by full collapse, can occur in the lithophysal units. The switch from noncollapsed to collapsed conditions depends on rockfall volume in the drifts. For lithophysal rock, if rockfall volumes in the drifts are less than or equal to 5 m^3/m of drift length, the intact drift seepage response surface table is utilized in the analysis. If rockfall volumes in the drifts are greater than 60 m^3/m of drift length, the collapsed drift seepage response surface is utilized in the analysis. If rockfall volumes (per unit drift length) in the drifts are between 5 m^3/m and 60 m^3/m, seepage values are linearly interpolated between the two response surfaces (Section 6.3.3.1.3). In the nonlithophysal units, once a specified degree of drift collapse has occurred, the intact-drift seepage model is no longer appropriate. Therefore, in the nonlithophysal zone, if rockfall volumes in the drifts are less than or equal to 0.5 m^3/m, the intact drift seepage response surface is utilized; if not, the percolation rates are utilized instead of seepage rates (Section 6.3.3.1.3).

The rockfall volume in the drifts is a feed from the seismic rockfall calculations to the drift seepage calculations. The rockfall volumes in the lithophysal and nonlithophysal zones are calculated as described in Section 6.6.1.3.4, for the Seismic GM Modeling Case 1,000,000–year simulation, which uses GoldSim-sampled event sequences. For the 1,000,000-year Seismic FD Modeling Case and the 10,000-year Seismic FD Modeling Case simulations, rockfall volumes are pre-specified (Table 6.6-3). The Drift Wall Condensation Abstraction (Section 6.3.3.2.2) calculates a probability of condensation occurrence on the drift walls at a WP location and, if condensation occurs, a rate of condensation. For the Seismic Scenario Class, drift collapse is expected in the lithophysal regions but is not expected in the nonlithophysal units. Condensation occurs on drift walls above DSs in the nonlithophysal units at all times. In contrast, there is no condensation in the lithophysal units after drift collapse. The Seismic Scenario Class modeling cases calculate the time of drift collapse in terms of the time at which rubble fills the lithophysal drifts. For the Seismic GM Modeling Case 1,000,000-year simulation, this calculation is described in Section 6.6.1.3.4. For the 1,000,000-year Seismic FD Modeling Case and the 10,000-year Seismic FD Modeling Case simulations, drift collapse times are pre-specified (Section 6.6-4) and are set to either the time of the first seismic event or are set to be non-collapsed.

6.6.2.2 Engineered Barrier System Thermal-Hydrologic Environment Submodel Modifications for Seismic Disruption

Seismically induced ground motion can cause drift collapse in the lithophysal zones, requiring an adjustment to the temperature and relative humidity histories to account for the presence of rubble on WPs. The adjusted temperature and relative humidity histories for the Seismic Scenario Class modeling cases are provided by a supplemental analysis performed on the EBS TH Environment Submodel thermal-hydrology data (DTN: LL0702PA027MST.082_R0 [DIRS 179590]). The data tracking number provides eight files containing time-dependent

temperature adjustments and eight files containing time-dependent relative humidity adjustments: one file for each of the six representative CSNF and two representative CDSP WP/DS pairs (Section 6.3.2.2). Each file contains two types of temperature/relative humidity adjustments, one associated with a collapsed drift with low thermal-conductivity rubble and one associated with a collapsed drift with high thermal-conductivity rubble. The assignment of a low or high thermal-conductivity adjustment is based on sampling a discrete distribution with equal probability for high or low (SNL 2007 [DIRS 181383], Section 6.2.10.3).

The Seismic GM and FD Modeling Cases calculate the time required to fill the drift with rockfall, after which the adjustments apply. For the Seismic GM Modeling Case 1,000,000-year simulation, this time is based on the calculations described in Section 6.6.1.3.4. For the 1,000,000-year Seismic FD Modeling Case and the 10,000-year Seismic FD Modeling Case simulations, drift fill times are pre-specified (Section 6.6.1.3.9) and are set to either the time of the first seismic event or the end of the simulation. The adjusted temperature and relative humidity values are used for both lithophysal and nonlithophysal zones in the TSPA-LA Model because the TSPA-LA Model does not distinguish between the lithophysal and nonlithophysal components of a percolation subregion.

6.6.2.3 Waste Package and Drip Shield Degradation Submodel Modifications for Seismic Disruption

Nominal corrosion processes are included in the Seismic GM Modeling Case when calculating consequences after 10,000 years. When WPs are first damaged by a seismic event, the resulting cracks will impact the nominal corrosion processes. In particular, corrosion on the inner surface of a WP OCB (inside-out corrosion) will be initiated. An *a priori* calculation is done to determine the time of the first seismic event that causes WP damage and this time is fed to the input vector for the WAPDEG V4.07 software. This time will be different for CSNF and CDSP WPs. The WAPDEG V4.07 software will initiate an inside-out corrosion event at that time, thus accelerating the corrosion processes that ultimately lead to WP breach. This effect is also included in the separate WAPDEG V4.07 calculations that determine mean WP thickness for each percolation subregion. These calculations are used by the Seismic GM Modeling Case as input to the WP damage calculations (Section 6.6.1.3.8).

6.6.2.4 Waste Package Localized Corrosion Initiation Submodel for Seismic Disruption

The Seismic Scenario Class does not include the potential effect of crown-seepage initiated localized corrosion on the WP outer surface. Although crown-seepage induced localized corrosion is possible for both the Seismic GM and FD Modeling Cases, a stand-alone localized corrosion initiation analysis has been carried out to determine that the environmental conditions required for localized corrosion initiation are present only for the first 4,000 years after repository closure. Beyond this time, the chemistry of the seepage water is benign, and localized corrosion no longer occurs. This stand-alone analysis is documented in Section 6.3.5.2. The temperature, pH, chloride-ion concentration, and nitrate-ion concentrations in aqueous solutions on the WP outer surface are the primary factors that determine the potential for initiating localized corrosion. In addition, localized corrosion can only occur if crown seepage water contacts the WP outer surface, i.e., if the DS is failed.

In the Seismic GM Modeling Case simulations, there is a low probability (Figure 7.3.2-16) of DS plate failure occurring before 4,000 years. Section 7.3.2.6.1.3.2 discusses the justification for not considering localized corrosion due to these early DS failures. In the Seismic FD Modeling Case simulations, DS can be failed at early times, where environmental conditions are suitable for localized corrosion initiation. However, it is assumed that the advective damage due to the fault displacement is sufficient to account for the effects of localized corrosion. This assumption has been verified by simulation runs which show that the dose is insensitive to increasing the fraction of damaged area beyond 1/3 of the WP cross-sectional area (Section 7.3.2.7 and Figure 7.3.2-25).

A description of localized corrosion of the WP outer surface is provided in Section 6.3.5.2. Section 6.3.5.2 describes the Localized Corrosion Initiation Analysis and Localized Corrosion Penetration Rate Abstraction that form the components of the Localized Corrosion Initiation Submodel. Section 6.3.5.2.1 provides the conceptual models for these localized corrosion processes, and Section 6.3.5.2.2 describes the model abstractions.

For the localized corrosion initiation analysis, a temperature constraint is applied to the seepage flux after drift collapse in the lithophysal zones. Specifically, seepage onto WPs is set to zero for the period of above-boiling temperatures by using a 100°C threshold temperature at a WP surface. This constraint implies that seepage can enter the drift and be diverted through the rubble to the invert beneath a WP, but it cannot contact a WP surface until the surface temperature drops to less than 100°C. This threshold temperature is based on a sensitivity study of seepage arrival times at a DS crown for a collapsed drift that is filled with rubble (SNL 2007 [DIRS 181383], Section 6.3.7.3 and Table 6.3-44). This study considers rubble with high and low values of thermal conductivity and seepage magnitudes that vary between 10 liter/yr/WP and 1,000 liter/yr/WP. The temperature threshold of 100°C is a reasonable upper bound to the ranges of WP temperatures that significantly delay the arrival of seepage at a DS crown. A 100°C temperature is, therefore, an appropriate threshold to limit the presence of liquid seepage in a rubble-filled drift. This temperature constraint on seepage flux after drift collapse is applied only in the Localized Corrosion Initiation and Propagation Analysis. The constraint is not applied to the calculation of seepage flux in the Drift Seepage Submodel (Section 6.3.3.1).

The Localized Corrosion Initiation Analysis also accounts for changes in temperature and relative humidity due to the presence of rubble after a seismic event. The Localized Corrosion Initiation Analysis uses the same eight WP emplacement configurations to calculate temperature and relative humidity adjustments discussed in Section 6.6.2.2, for the purposes of localized corrosion initiation. The rubble fill time is based on the calculations described in Section 6.6.1.3.4 for the lithophysal zones. In addition, the Localized Corrosion Initiation Analysis does distinguish between lithophysal and nonlithophysal regions and, therefore, the temperature and relative humidity adjustments are applied only when a WP location lies in the lithophysal zone. For the nonlithophysal zones, examination of Tables 6-30 and 6-31 in *Seismic Consequence Abstraction* (SNL 2007 [DIRS 176828]) shows that all of the calculated rockfall volumes are significantly less than those in the lithophysal zones at the same PGV level. Therefore, the temperature and relative humidity adjustments are not applied in the nonlithophysal zones.

6.6.3 Model Component Consistency and Conservatisms in Assumptions and Parameters

To enhance understanding of the complex interactions within the TSPA-LA Model, a discussion of consistency among model components and submodels and identification of conservative assumptions in abstractions, process models, and parameter sets supporting the Seismic Scenario Class are discussed below.

6.6.3.1 Consistency of Assumptions

Degradation of the Internal Structures After Breach of Outer Corrosion Barrier—In the Seismic GM Modeling Case calculations once the OCB is breached due to seismic damage it is assumed that the internal structure of the WP would degrade as a structural element, quickly leading to an overall loss of WP structural strength by the time of next seismic event. As a result the damage abstractions for the fully degraded internals are applied after the WP is breached for the first time. This is a conservative assumption and inconsistent with the slow degradation of steel internals modeled in the EBS Transport model, where the stainless steel is expected to last for tens of thousands of years on average thus maintaining the integrity of the WP for much longer duration than the time to the next seismic event.

Effect on the TSPA-LA Model—Using the WP damage abstraction for the fully degraded internals subsequent to the seismic event that leads to the first breach is conservative as it would lead to larger damage area on the WP due to lower structural strength of the WP. This would likely result in a greater diffusive release rate out of the WP.

6.6.3.2 Identification of Conservatisms in Submodels and Abstractions

Conservatism in Ground Motion Calculations—The use of a bounded hazard curve for PGV does not mean that all three components of a ground motion are bounded. Only one horizontal component of the ground motion is scaled to a given PGV value on the bounded hazard curve (SNL 2007 [DIRS 176828], Section 6.4.3). In developing the time histories used in the kinematic and structural response calculations, the second horizontal component and the vertical component are not directly scaled, but rather are allowed to vary to maintain the inter-component variability of the original accelerogram. This means that these components can vary substantially even when the PGV for the first horizontal component is at a fixed value. This inter-component variability reflects the aleatory uncertainty inherent in vibratory ground motions. In some cases, this results in PGV values for these components that exceed the maximum scaled value for the first horizontal component. Thus, the damage abstractions, although parameterized using one horizontal component, in some cases represent damage associated with larger PGVs on the other components. Thus, although the hazard curve for horizontal PGV is bounded, the damage abstractions include larger, unbounded PGVs on the other components as given in Acceptance Criterion 3, Propagation of Uncertainty into TSPA (SNL 2007 [DIRS 176828], Section 8.2). Alternate ground motions with bounded components are not available to quantify this conservatism.

Seismic Failure Criteria—The seismic abstractions for WPs and DSs make use of two failure criteria: a RST and the ultimate tensile strain. If the residual stress from mechanical damage exceeds the stress threshold for the barrier, then the affected area(s) are represented as a network

of stress corrosion cracks. The RST for WPs is based on a uniform distribution between 90 percent and 105 percent of the yield strength for Alloy 22. The RST for Titanium Grade 7 is conservatively set to a constant value of 80 percent of its yield strength (and for Titanium Grade 29 at 50 percent of its yield strength). These thresholds are conservative estimates for the initiation of SCC (SNL 2007 [DIRS 181953], Sections 6.2.2 (Alloy 22), 6.8.3.1.3 (Titanium Grade 7), and 6.8.3.2.3 (Titanium Grades 25 and 29)). The potential for tearing or rupture of EBS components is based on the ultimate tensile strain for Alloy 22 and Titanium Grade 7, with a conservative knockdown factor of 2 (the maximum value), which adjusts the uniaxial data for ultimate tensile strain in a multidimensional stress field .

Spatial Variability—Spatial variability in the mechanical response of EBS components to vibratory ground motion has not been represented in the TSPA-LA Model. Damage to the WP and DS from vibratory ground motion is constant throughout the repository for each seismic event. Although spatial variability is not included within the TSPA-LA Model, it has been included in the kinematic calculations through the variability of friction factors on a package-by-package basis and in the abstraction of damaged areas for the two or three central WPs in the kinematic calculations. Lack of spatial variability is not important for estimating the mean annual dose from the Seismic Scenario Class. The mean dose is accurately estimated because the sum of the mean doses from groups of WPs with different damage levels is equal to the mean of the sum of the doses from the individual groups. Using a constant mean value for the damage is an accurate approach for calculating the mean annual dose from the repository (SNL 2007 [DIRS 176828], Section 1.2).

Conservatism in Hazard Curve—The development of hazard curves for vibratory ground motion and fault displacement included an expert elicitation—(*Probabilistic Seismic Hazard Analyses for Fault Displacement and Vibratory Ground Motion at Yucca Mountain, Nevada,* Milestone SP32IM3, September 23, 1998 (CRWMS M&O 1998 [DIRS 103731]). Evaluations by multiple experts were made within a structured process designed to minimize uncertainty due to uneven or incomplete knowledge and understanding (Budnitz et al. 1997 [DIRS 103635]). The weighted alternative interpretations were expressed by the use of logic trees. Each pathway through the logic tree represented a weighted interpretation of the seismotectonic environment of the site for which a seismic hazard curve was computed. The result of computing the hazard for all relevant pathways was a distribution of hazard curves representing the full variability and uncertainty in the hazard at Yucca Mountain. The Seismic Scenario Class for the TSPA-LA Model uses the mean hazard curves for PGV and for fault displacement. Each mean hazard curve is defined as an average of the distribution of hazard curves and each typically lies above the 80th percentile of the distribution for high intensity ground motions (i.e., at low annual exceedance frequencies) because the average is dominated by the larger values of the distribution (SNL 2007 [DIRS 176828], Section 6.4.1). The use of the mean hazard curves ensures a conservative representation of the seismic hazard in the TSPA-LA Model. An analysis that includes a suite of hazard curves to represent epistemic uncertainty was done as part of the PMA (Appendix C).

Conservatism in Initiation of Inside-Out Corrosion Processes—Corrosion on the inner surface of a WP OCB (inside-out corrosion) is initiated at the time of the first seismic event that causes WP damage. An *a priori* calculation is done to determine the time of the first seismic event that causes WP damage. The probability that a CSNF WP with intact internals under intact

DSs will be damaged by a seismic event is small (Figure 6.6-10). Therefore, DS failure is likely to occur before a damaging seismic event occurs. If such a WP has not been damaged, its internals will still be intact even though it is under a failed DS and surrounded by rubble. However, there is no abstraction for probability of damage for a CSNF WP with intact internals under a failed DS. Such a WP is also likely to have a reduced shell thickness. Therefore the probability of damage to a CSNF WP with degraded internals and an OCB thickness of 17 mm is used as a surrogate to the damage on a CSNF WP with intact internals under a failed DS. This is a conservative assumption, as can be seen from an examination of Figure 6.6-15.

6.6.4 Alternative Conceptual Model(s) for Seismic Scenario Modeling Cases

A brief description of the Seismic Scenario Class ACMs is presented below. The Seismic Scenario Class ACMs are also summarized in Table 6.6-4.

Lithophysal and Nonlithophysal Rock—Alternative modeling approaches were evaluated for the conceptual and computational models of lithophysal and nonlithophysal rockfall (BSC 2004 [DIRS 166107], Section 7.4). A standard approach for solving excavation stability problems is the use of numerical models based on continuum mechanics. Continuum models use constitutive relations to describe the mechanical behavior of a material. The use of a continuum model requires that the mechanical effects of fractures be lumped into the constitutive relationships. Continuum models are unable to predict instabilities such as fracture and rockfall (BSC 2004 [DIRS 166107], Section 7.4.1).

The ACM based on continuum mechanics (BSC 2004 [DIRS 166107], Section 7.4.1) was not used to represent rockfall. The estimation of rockfall requires that the modeling technique and mechanical material model be capable of representing fracture of the rock mass and separation of the intact rock mass into blocks. The discontinuum approach is more suitable for these purposes and was therefore adopted for modeling the drift degradation processes that occur after a seismic event (BSC 2004 [DIRS 166107], Section 7.4.2).

Fault Displacement WP Damage Abstraction—The damage abstraction for fault displacement was compared to an ACM proposed by Waiting et al. (SNL 2003 [DIRS 164449], described in *Seismic Consequence Abstraction* (SNL 2007 [DIRS 176828], Section 6.11.6). The ACM considered the probability-weighted number of WP failures from fault displacement and the number of fault intersections with emplacement drifts. The ACM, based on the use of historical data for fault displacement in the western United States, provided results that are consistent with the base case model for both the probability weighted number of WP failures and the number of fault intersections with the emplacement drifts (SNL 2007 [DIRS 176828], Section 6.11.6).

The ACM based on historical western United States data was not used in the TSPA-LA Model. The damage abstraction used in the TSPA-LA Model is based on hazard curves specific to Yucca Mountain. Nevertheless, the agreement between the two models is very good and this adds confidence to the TSPA-LA Model damage abstraction.

Effective Cross-sectional Area for Transport—The effective cross-sectional area for transport out of Alloy 22 WPs through a network of stress corrosion cracks is given by a crack area density based on two conceptual models (SNL 2007 [DIRS 181953], Section 6.7.3). The first

conceptual model is based on a hexagonal array of randomly oriented cracks, while the second conceptual model is based on a hexagonal array of cracks in parallel rows. The distribution for crack area density used in the TSPA-LA Model is based on both conceptual models. An alternative conceptual model for crack area density is presented in *Stress Corrosion Cracking of Waste Package outer barrier and Drip Shield Materials* (SNL 2007 [DIRS 181953] Section 6.7.4). The alternative model considers a circular geometry circumscribed by a single through-wall crack.

The ACM was not used for the TSPA-LA Model implementation of seismic crack density. The hexagonal geometry represents a high effective density of individual cracks and the two hexagonal geometry conceptual models are considered conservative representations. The ACM analysis which uses circular geometry is considered a limiting realistic case (SNL 2007 [DIRS 181953], Section 6.7.2).

Conditional Probability Distributions for Damaged Areas—The seismic consequence abstractions have considered ACMs for the conditional probability distributions representing damaged areas on the WP, damaged areas on the DS, and the volume of rockfall from a seismic event. These alternate distributions include the gamma, normal, log-normal, Weibull and triangular distributions, as presented in Sections 6.5.1.4, 6.5.2.4, 6.6.1.4, 6.6.2.4, 6.7.1.3, 6.7.2.4, 6.9.4, and 6.10.2.8 of *Seismic Consequence Abstraction* (SNL 2007 [DIRS 176828]). Gamma distributions generally provided simpler and more accurate representations of the statistical observations than normal, log-normal, log-triangular, and Weibull distributions. The exception to the use of gamma distributions is that the fragility analyses (for DS plates and framework) have used log-normal representations to simplify manipulation of products and quotients of random variables.

The alternative conditional probability distributions for WP damaged areas were investigated, in the sections noted above, but not used since gamma distributions provided the simplest and most accurate representation of the data.

Table 6.6-1. Expected Waste Package Failure Due to Fault Displacement

Annual Exceedance Frequency (1/yr)	Expected Number of Failures – CSNF (TAD) Group	Annual Exceedance Frequency (1/yr)	Expected Number of Failures – CDSP Group
$> 2.2 \times 10^{-7}$	0	$> 2.5 \times 10^{-7}$	0
1.4×10^{-7} to 2.2×10^{-7}	19.5	1.6×10^{-7} to 2.5×10^{-7}	6.5
7.8×10^{-8} to 1.4×10^{-7}	27.7	8.6×10^{-8} to 1.6×10^{-7}	9.3
2.6×10^{-8} to 7.8×10^{-8}	30.7	2.9×10^{-8} to 8.6×10^{-8}	10.3
1×10^{-8} to 2.6×10^{-8}	158.8	1×10^{-8} to 2.9×10^{-8}	53.2

Source: DTN: MO0703PASEISDA.002_R4 [DIRS 183156], Table 1-14. See NOTES: for an explanation of the values in rows 4 and 5 of columns 2 and 4.

NOTE: TAD = transportation, aging, and disposal (canister); CSNF = commercial spent nuclear fuel; CDSP = co-disposed (waste package).

Table 6.6-2. Uncertain Inputs Used in the Seismic Scenario Class

TSPA-LA Parameter Name	Description	Units	Distribution	Remarks
Epistemic Parameters				
Stress_Thresh_A22_a (RST)	Residual stress threshold of Alloy 22.	None	Uniform(90,105)	DTN: MO0703PASEISDA.002_R4 [DIRS 183156], Table 1-15
Vol_Rubble_Max_Lith_a (MAX_RUBBLE_VOLUME)	Volume of lithophysal rock that must fall to fill the drift.	m^3/m	Uniform(30,120)	DTN: MO0703PASEISDA.002_R4 [DIRS 183156], Table 1-16
Vol_Rubble_Max_NonLith_a (MAX_BLOCK_VOLUME)	Volume of nonlithophysal rock that must fall to fill the drift.	m^3/m	Uniform(30,120)	DTN: MO0703PASEISDA.002_R4 [DIRS 183156], Table 1-16
DS_Crack_Area_Density_a	Crack area per unit of seismic DS damage.	None	Uniform(0.00467, 0.01875)	MO0702PASTRESS.002_R2 [DIRS 180514], file: Model Output DTN.doc, Table 8-15
WP_Crack_Area_Density_a	Crack area per unit area of seismic WP damage.	None	Uniform(0.00327, 0.0131)	MO0702PASTRESS.002_R2 [DIRS 180514], file: Model Output DTN.doc, Table 8-15
Aleatory Parameters				
Exceedance_Frequency_a (LAMBDA)	Annual exceedance frequency for the seismic hazard.	1/yr	Uniform(Seismic_Lambda_Min, Seismic_Lambda_Max) Seismic_Lambda_Min=$1x10^{-8}$ (LAMBDA_MIN) Seismic_Lambda_Max=$4.287x10^{-4}$ (LAMBDA_MAX)	DTN: MO0703PASEISDA.002_R4 [DIRS 183156], Table 1-15
Rubble_Vol_Lith_a (LITH_VOL)	Distribution used to calculate the rubble area deposited around the DS / WP in the last seismic event.	m^3/m	Gamma Distribution Mean: LITH_MU SD: LITH_SIGMA	DTN: MO0703PASEISDA.002_R4 [DIRS 183156], Table 1-16
Rubble_Vol_NonLith_a (NONLITH_VOL)	Distribution used to calculate the rubble volume deposited around the DS / WP in the last seismic event (nonlithophysal zones).	m^3/m	Gamma Distribution Mean: NONLITH_MU SD: NONLITH_SIGMA	DTN: MO0703PASEISDA.002_R4 [DIRS 183156], Table 1-16
Ln_Dyn_Load_DS (DS_LOAD_LN)	Dynamic load on the DS due to a seismic event.	None	Normal Distribution Mean: DSLOAD_LAMBDA SD: 0.536 (DSLOAD_BETA_	DTN: MO0703PASEISDA.002_R4 [DIRS 183156], Table 1-18

Table 6.6-2. Uncertain Inputs Used in the Seismic Scenario Class (Continued)

TSPA-LA Parameter Name	Description	Units	Distribution	Remarks
Aleatory Parameters (continued)				
Corr_TAD_Dam_DS_Intact_a	Random number for maintaining correlation while sampling the TAD-bearing WP damage gamma distributions for intact DSs.	None	Uniform(0,1)	DTN: MO0708TSPAGENT.000, file: AB-TSPA-DTN-5 (PEF 132)
Corr_CDSP_Dam_DS_Intact_a	Random number for maintaining correlation while sampling the CDSP WP damage gamma distributions for intact DSs.	None	Uniform(0,1)	DTN: MO0708TSPAGENT.000, file: AB-TSPA-DTN-5 (PEF 132)
Corr_WP_Dam_DS_Failed_a	Random number for maintaining correlation while sampling the WP (CDSP and TAD) damage gamma distributions for failed DSs.	None	Uniform(0,1)	DTN: MO0708TSPAGENT.000, file: AB-TSPA-DTN-5 (PEF 132)
Gamma_A_Intact_TAD (DA_TADi23_GAMMA)	Damage to a TAD-bearing WP of thickness 23 mm with intact internals under an intact DS.	m^2	Gamma Distribution Mean: 0.00408 (DA_TADi23_MU) SD: 0.0013 (DA_TADi23_SIGMA)	DTN: MO0703PASEISDA.002_R4 [DIRS 183156], Table 1-17
Gamma_A_Degrdd_TAD (DA_TADd23_GAMMA)	Damage to a TAD-bearing WP of thickness 23 mm with degraded internals under an intact DS.	m^2	Gamma Distribution Mean: DA_TADd23_MU SD: DA_TADd23_SIGMA	DTN: MO0703PASEISDA.002_R4 [DIRS 183156], Table 1-17
Gamma_B_Degrdd_TAD (DA_TADd17_GAMMA)	Damage to a TAD-bearing WP of thickness 17 mm with degraded internals under an intact DS.	m^2	Gamma Distribution Mean: DA_TADd17_MU SD: A_TADd17_SIGMA	DTN: MO0703PASEISDA.002_R4 [DIRS 183156], Table 1-17
Gamma_A_Intact_CDSP (DA_CDSPi23_GAMMA)	Damage to a CDSP WP of thickness 23 mm with degraded internals under an intact DS.	m^2	Gamma Distribution Mean: DA_CDSPi23_MU SD: DA_CDSPi23_SIGMA	DTN: MO0703PASEISDA.002_R4 [DIRS 183156], Table 1-17
Gamma_A_Degrdd_CDSP (DA_CDSPd23_GAMMA)	Damage to a CDSP WP of thickness 23 mm with degraded internals under an intact DS.	m^2	Gamma Distribution Mean: DA_CDSPd23_MU SD: DA_CDSPd23_SIGMA	DTN: MO0703PASEISDA.002_R4 [DIRS 183156], Table 1-17
Gamma_B_Degrdd_CDSP (DA_CDSPd17_GAMMA)	Damage to a CDSP WP of thickness 17 mm with degraded internals under an intact DS.	m^2	Gamma Distribution Mean: DA_CDSPd17_MU SD: DA_CDSPd17_SIGMA	DTN: MO0703PASEISDA.002_R4 [DIRS 183156], Table 1-17

Table 6.6-2. Uncertain Inputs Used in the Seismic Scenario Class (Continued)

TSPA-LA Parameter Name	Description	Units	Distribution	Remarks
Aleatory Parameters (continued)				
Gamma_A_Degrdd_WP_NoDS (DA_23_GAMMA)	Damage to a CDSP WP of thickness 23 mm with degraded internals under a degraded DS.	m^2	Gamma Distribution Mean: DA_23_MU SD: DA_23_SIGMA	DTN: MO0703PASEISDA.002_R4 [DIRS 183156], Table 1-17
Gamma_B_Degrdd_WP_NoDS (DA_17_GAMMA)	Damage to a CDSP WP of thickness 17 mm with degraded internals under a degraded DS.	m^2	Gamma Distribution Mean: DA_17_MU SD: DA_17_SIGMA	DTN: MO0703PASEISDA.002_R4 [DIRS 183156], Table 1-17
RN_DSF_a (RN_DSF)	Random number to determine rockfall damage, WP damage, and drip shield plate and/or framework failure.	None	Uniform(0,1)	DTN: MO0703PASEISDA.002_R4 [DIRS 183156], Table 1-15
RN _Rupture_TAD_a	Random number used to determine rupture TAD of WPs under intact DSs, due to multiple impacts.	None	Uniform(0,1)	DTN: MO0708TSPAGENT.000, file: AB-TSPA-DTN-5 (PEF 132)
RN_Rupture_CDSP_a	Random number used to determine rupture of CDSP WPs under intact DSs, due to multiple impacts.	None	Uniform(0,1)	DTN: MO0708TSPAGENT.000, file: AB-TSPA-DTN-5 (PEF 132)
RN_Puncture_a (RN_PUNC)	Random number used to determine puncture of WPs under failed DSs, due to multiple impacts.	None	Uniform(0,1)	DTN: MO0703PASEISDA.002_R4 [DIRS 183156], Table 1-17
TAD_Rupture_Area_a (FAILED_AREA_TAD)	Failed area of the TAD-bearing WP due to WP rupture damage.	m^2	Uniform(0, 2.78)	DTN: MO0703PASEISDA.002_R4 [DIRS 183156], Table 1-20
CDSP_Rupture_Area_a (FAILED_AREA_CDSP)	Failed area of the CDSP WP due to WP rupture damage.	m^2	Uniform(0, 3.28)	DTN: MO0703PASEISDA.002_R4 [DIRS 183156], Table 1-20
Puncture_Area_a (PP_AREA)	Failed area when WPs surrounded by rubble are punctured.	m^2	Uniform(0, 0.1)	DTN: MO0703PASEISDA.002_R4 [DIRS 183156], Table 1-17
TAD_Failed_Area_a (FAILED_AREA_TAD)	Failed area of the TAD WP due to fault displacement damage.	m^2	Uniform(0,2.78)	DTN: MO0703PASEISDA.002_R4 [DIRS 183156], Table 1-20
CDSP_Failed_Area_a (FAILED_AREA_CDSP)	Failed area of the CDSP WP due to fault displacement damage.	m^2	Uniform(0,3.28)	DTN: MO0703PASEISDA.002_R4 [DIRS 183156], Table 1-20

NOTE 1: CDSP (WP) = co-disposed; TAD (WP) = transportation, aging, and disposal (canister); PGV = peak ground velocity; SD = standard deviation.

NOTE 2: In some cases the TSPA parameter name is different than the parameter name in the DTN. In these cases the parameter name in the DTN is noted in brackets.

Table 6.6-3. Seismic Ground Motion and Fault Displacement Modeling Cases Using Pre-Specified Parameters

Modeling Case	Seismic Event Time (yr)	CSNF WP Damage Fraction (fraction of WP surface area)	CDSP WP Damage Fraction (fraction of WP surface area)	Number of Failed CSNF WPs	Number of Failed CDSP WPs	Rubble Volume Accumulated (m^3/m)	Rubble Fill Time (yr)	DS Damage Fraction (fraction of WP surface area)
Seismic 1M yr FD Case[a]	1,000 20,000 80,000 200,000 400,000 800,000	0.028 0.056 0.084	0.0335 0.067 0.101	0 100	100 0	120	Seismic Event Time	1.0
Seismic 10k yr FD Case[b]	200 800 2,000 4,000 8,000 18,000	0.028 0.056 0.084	0.0335 0.067 0.101	0 100	100 0	120	Seismic Event Time	1.0
Seismic 10k yr GM Case[c]	100 1,000 3,000 6,000 12,000 18,000	0	1.00×10^{-7} 1.00×10^{-6} 0.00001 0.001	0	3416	0	2,000,000	0.0
Seismic 1M yr GM Case	Section 6.6.1.3.1	Section 6.6.1.3.4	Section 6.6.1.3.4	Section 6.6.1.3.4	Section 6.6.1.3.4	Section 6.6.1.3.2	Section 6.6.1.3.2	Section 6.6.1.3.3

Sources: [a]Output DTN: MO0708TSPAGENT.000 [DIRS 183000], folders: PL-TSPA-DTN-9. (PEF 126)
[b]Output DTN: MO0708TSPAGENT.000 [DIRS 183000], folder: PL-TSPA-DTN-8 (PEF 125)
[c]Output DTN: MO0708TSPAGENT.000 [DIRS 183000], folder: PL-TSPA-DTN-7 (PEF 124)

NOTES: For each modeling case run defined above, the model cycles through all possible combinations of the aleatory parameters one realization at time, holding the epistemic sample number constant. For the Seismic one-million year FD Modeling Case and the Seismic 10,000 year FD Modeling Case, there are 108 possible combinations of aleatory parameters. For the Seismic 10,000 year GM Modeling Case there are 24 possible combinations of aleatory parameters.

Table 6.6-4. Alternative Conceptual Models Considered for the Seismic Scenario Class

Alternative Conceptual Models	Key Assumptions	Assessment and Basis
Alternative modeling approaches were evaluated for the conceptual and computational models of lithophysal and nonlithophysal rock (BSC 2004 [DIRS 166107], Section 7.4).	A standard approach for solving excavation stability problems is the use of numerical models based on continuum mechanics. Continuum models use constitutive relations to describe the mechanical behavior of a material. The use of a constitutive model requires that the mechanical effects of fractures be lumped into the constitutive relationships.	Continuum models are unable to predict instabilities, such as fracture and rockfall (BSC 2004 [DIRS 166107], Section 7.4.1). The discontinuum approach is more suitable for representing fracture of the rock mass and separation of the intact rock mass into blocks and was therefore adopted for modeling the drift degradation processes that occur after a seismic event (BSC 2004 [DIRS 166107], Section 7.4.2).
An alternative damage abstraction for fault displacement damage was proposed by Waiting et al., described in Seismic Consequence Abstraction (SNL 2007 [DIRS 176828], Section 6.11.6).	The ACM considered the probability-weighted number of waste package failures from fault displacement and the number of fault intersections with emplacement drifts. The ACM, based on the use of historical data for fault displacement in the western United States.	The results provided by the ACM are consistent with the base-case model for both the probability-weighted number of WP failures and the number of fault intersections with the emplacement drifts (SNL 2007 [DIRS 176828], Section 6.11.6).
An alternative conceptual model for crack area density was presented in Section 6.7.4 (SNL 2007 [DIRS 181953]).	The alternative model considered a circular geometry circumscribed by a single through-wall crack. The base case model combines two conceptual models based on hexagonal geometry (SNL 2007 [DIRS 181953], Section 6.7.3).	The hexagonal geometry represents a high effective density of individual cracks and the two hexagonal geometry conceptual models are considered conservative representations. The ACM analysis which uses circular geometry is considered a limiting realistic case (SNL 2007 [DIRS 181953], Section 6.7.2).
Alternative conceptual models for the conditional probability distributions representing damaged areas on the waste package, damaged areas on the drip shield, and the volume of rockfall from a seismic event were considered.	These alternate distributions included the gamma, normal, log-normal, Weibull and triangular distributions, as presented in Sections 6.5.1.4; 6.5.2.4; 6.6.1.4; 6.6.2.4; 6.7.1.3; 6.7.2.4; 6.9.4; and 6.10.2.8 of Seismic Consequence Abstraction (SNL 2007 [DIRS 176828]).	Gamma distributions generally provided simpler and more accurate representations of the statistical observations than normal, log-normal, log-triangular, and Weibull distributions. The exception to the use of gamma distributions is that the fragility analyses (for drip shield plates and framework) have used log-normal representations to simplify manipulation of products and quotients of random variables.

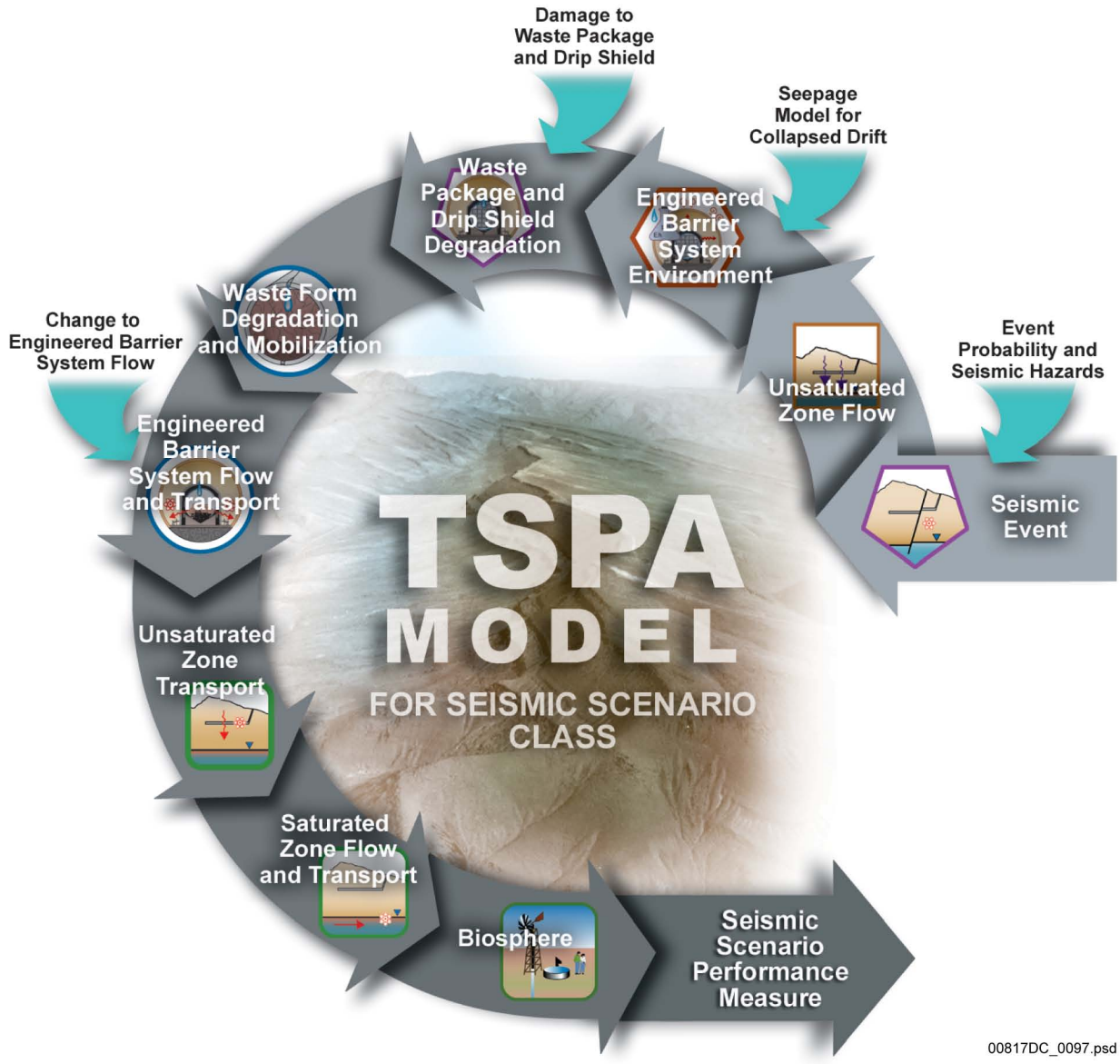

Figure 6.6-1. Schematic Representation of the TSPA-LA Model Components for the Seismic Scenario Class

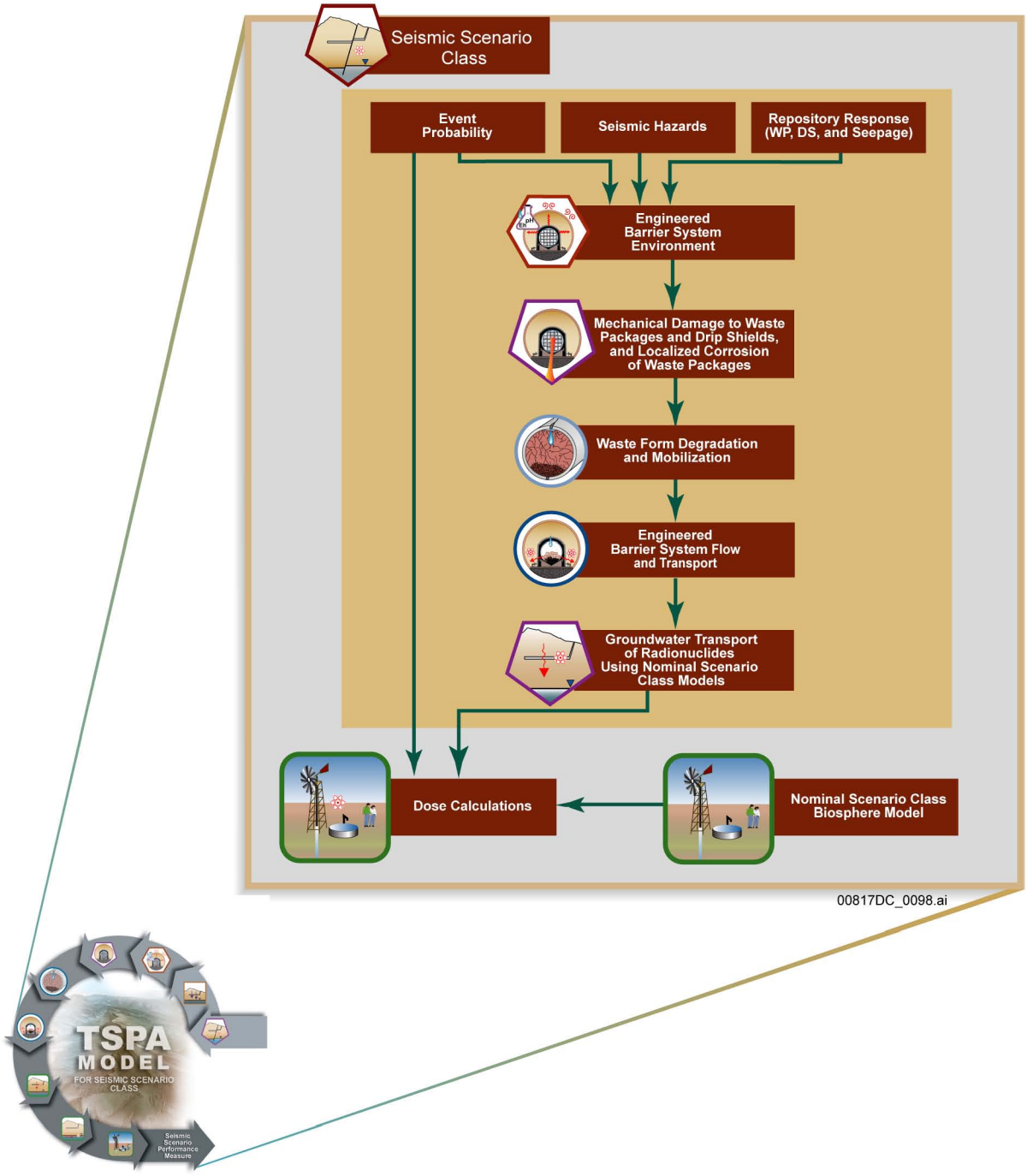

Figure 6.6-2. Information Flow Diagram for the Seismic Scenario Class in the TSPA-LA Model

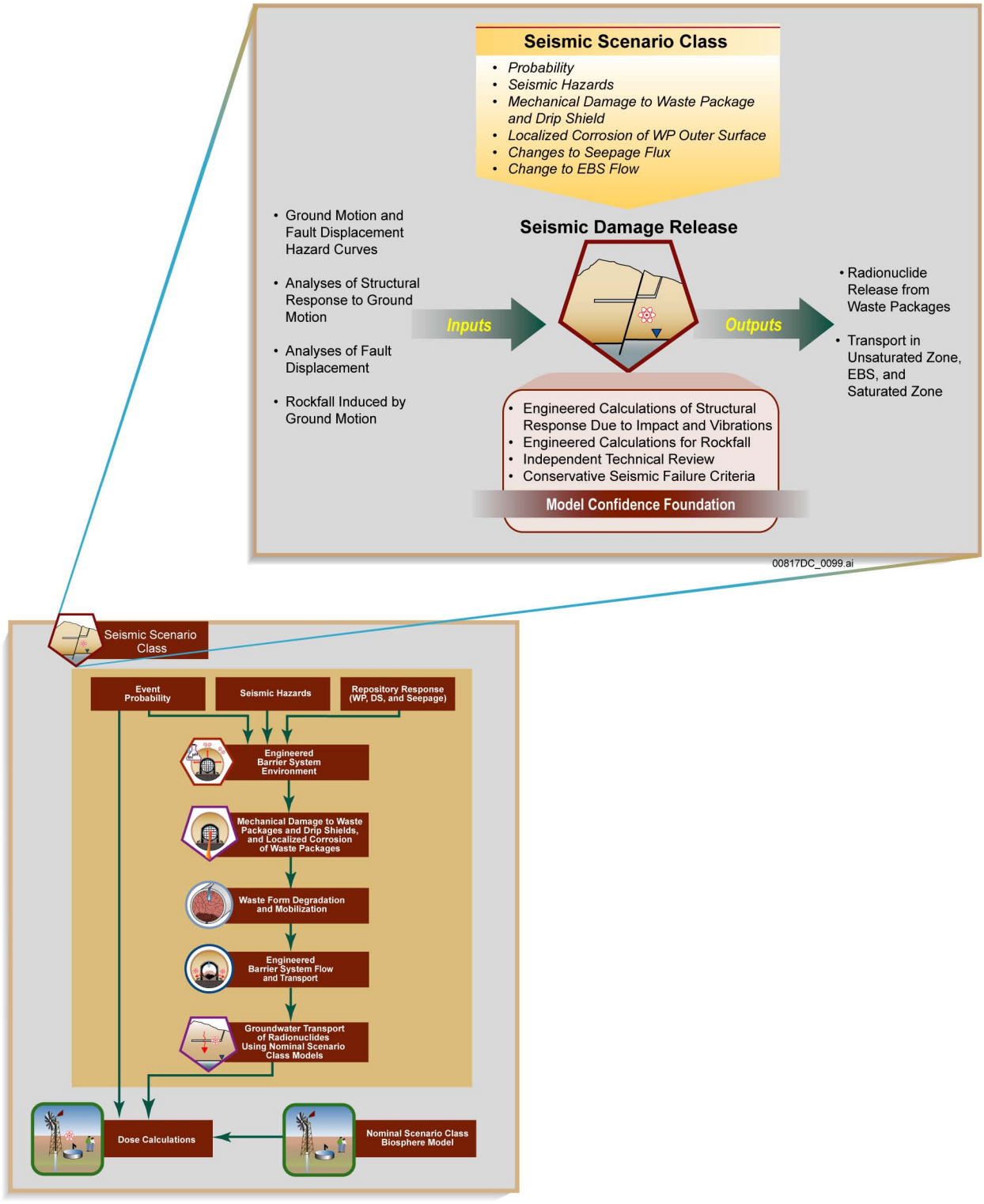

Figure 6.6-3. Inputs, Outputs, and Basis for Model Confidence for the Seismic Scenario Class

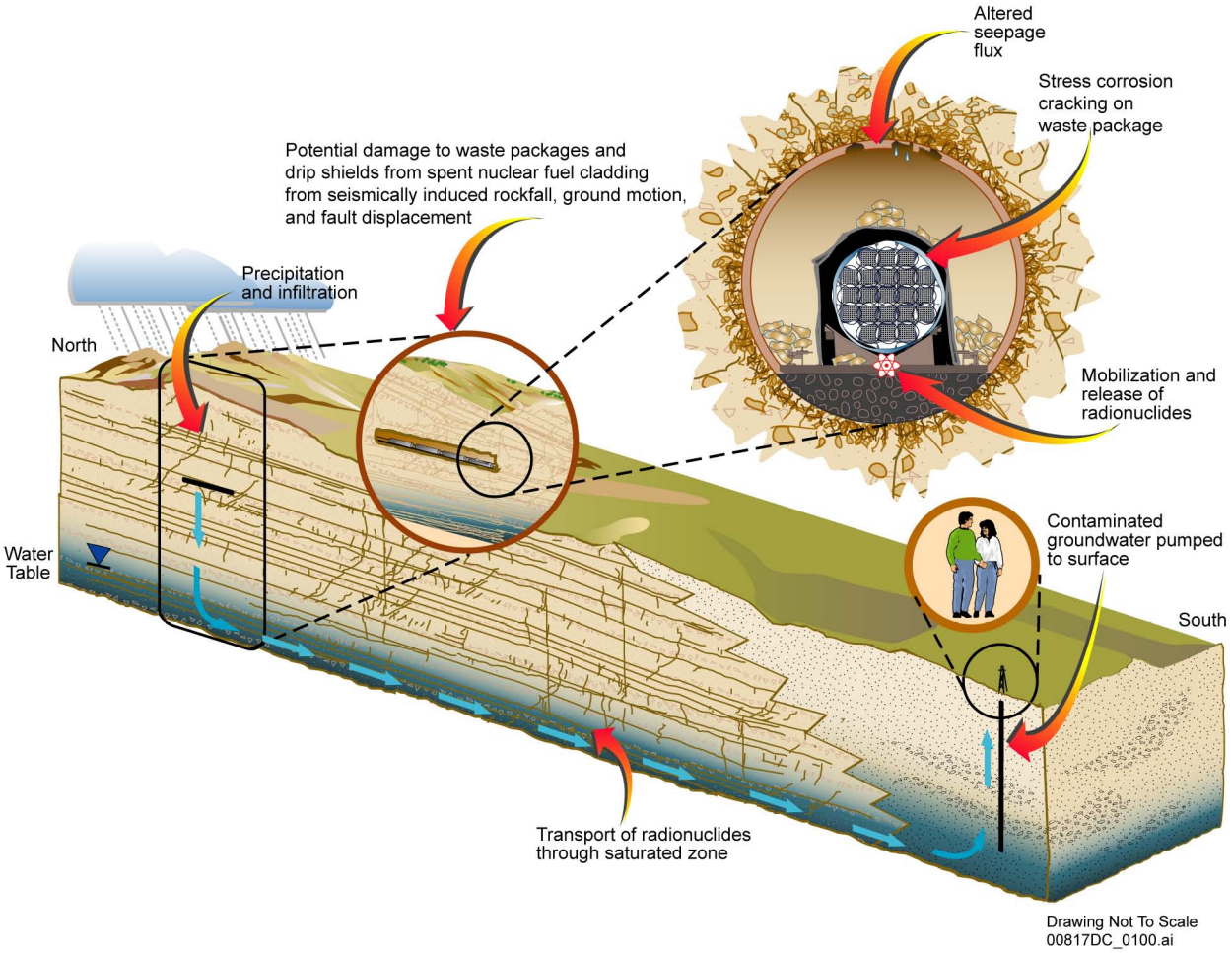

Figure 6.6-4. Schematic Illustration of the Seismic Scenario Class, the Seismic Effects within a Drift, and Subsequent Radionuclide Releases to the Accessible Environment

Figure 6.6-5. Schematic Representation of Future Configurations of EBS Components for Seismic Damage Abstraction

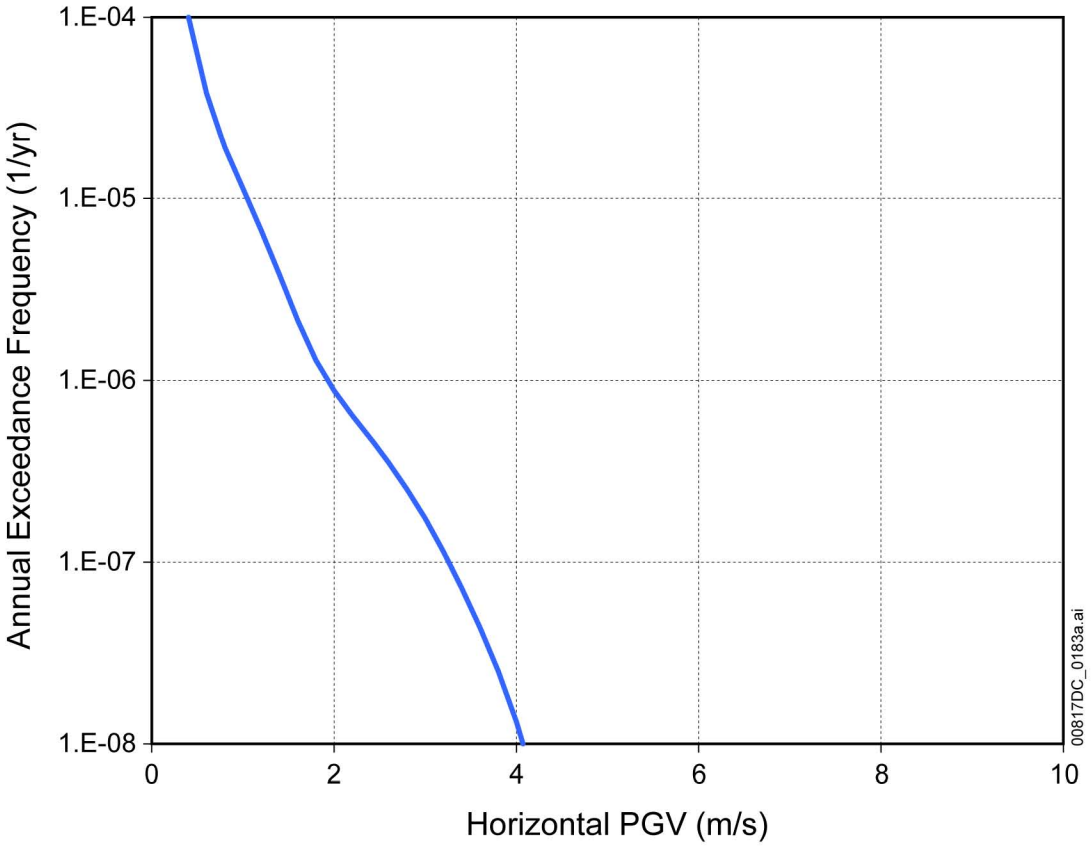

Source: DTN: MO0501BPVELEMP.001_R0 [DIRS 172682], *Bounded Horizontal Peak Ground Velocity Hazard at the Repository Waste Emplacement Level.xls*.

NOTE: Data is plotted on a linear scale for the Horizontal PGV.

Figure 6.6-6. Hazard Curve for Seismic Scenario Class

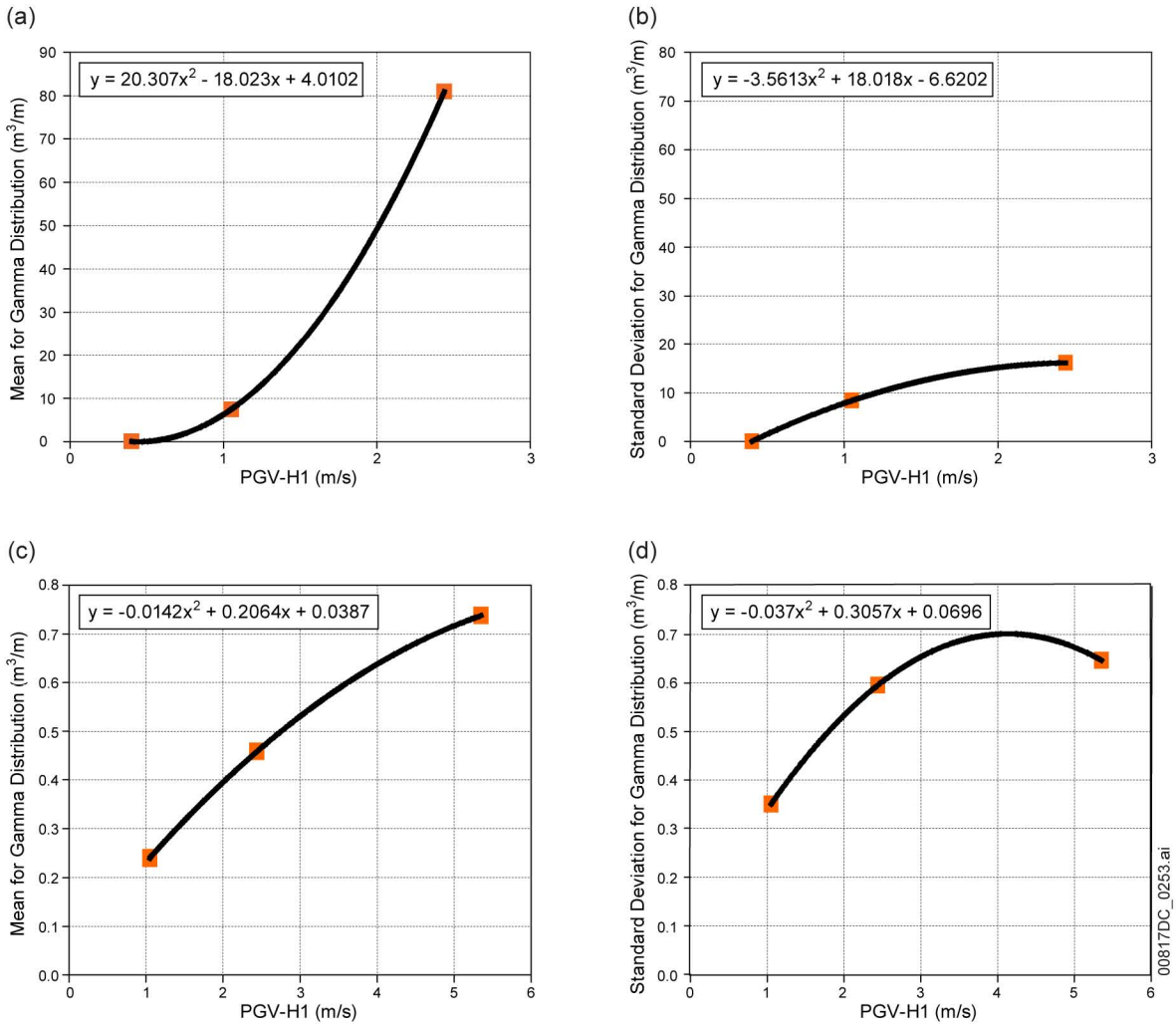

Source: DTN: MO0703PASDSTAT.001_R3 [DIRS 183148], *Lith Rubble Abstraction.xls* (a and b) and *Nonlith Rockfall Abstraction.xls* (c and d).

NOTE: The scales in plots (a) and (b) are different from those in plots (c) and (d).

Figure 6.6-7. Comparison of Mean Rockfall Volumes for Lithophysal (a and b) and Nonlithophysal (c and d) Zones

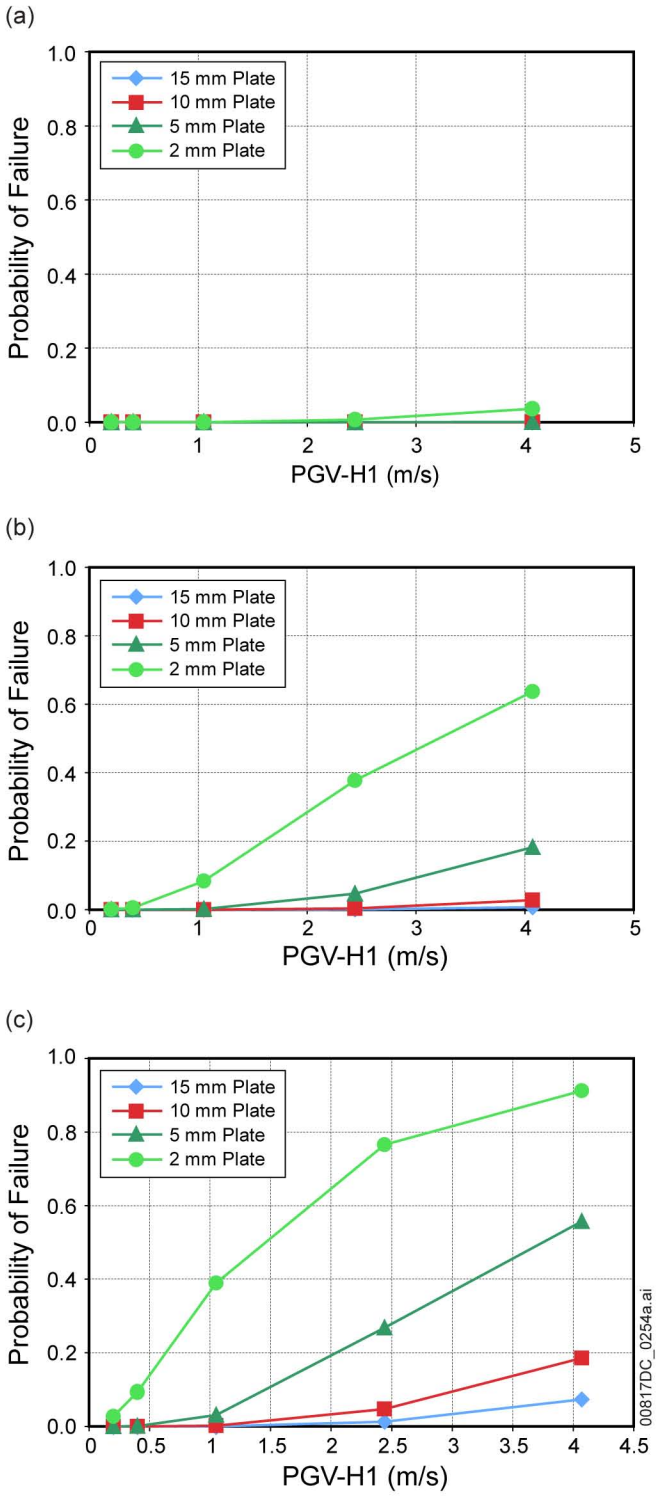

Source: DTN: MO0703PASDSTAT.001_R3 [DIRS 183148], *Plate Fragility Analysis.xls*.

Figure 6.6-8. Drip Shield Plate Fragility as a Function of Rockfall Load: (a) 10 Percent, (b) 50 Percent, and (c) 100 Percent

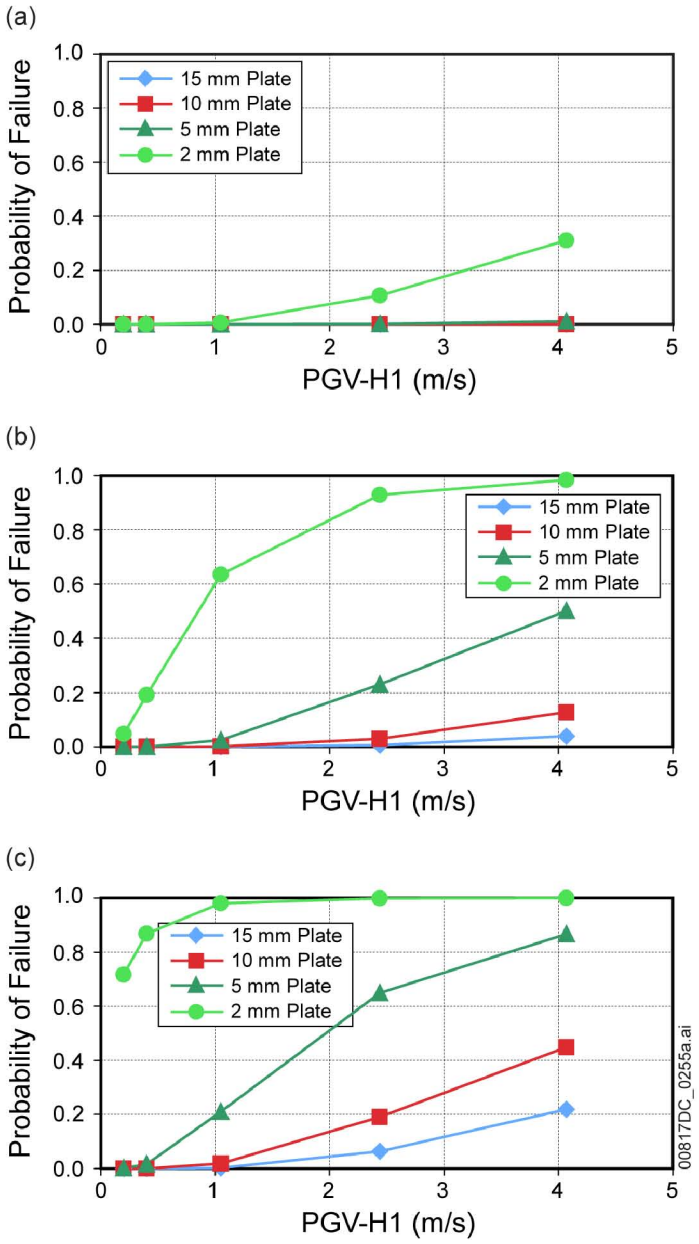

Source: DTN: MO0703PASDSTAT.001_R3 [DIRS 183148], *Frame Fragility Analysis.xls*.

Figure 6.6-9. Drip Shield Framework Fragility as a Function of Rockfall Load: (a) 10 Percent, (b) 50 Percent, and (c) 100 Percent

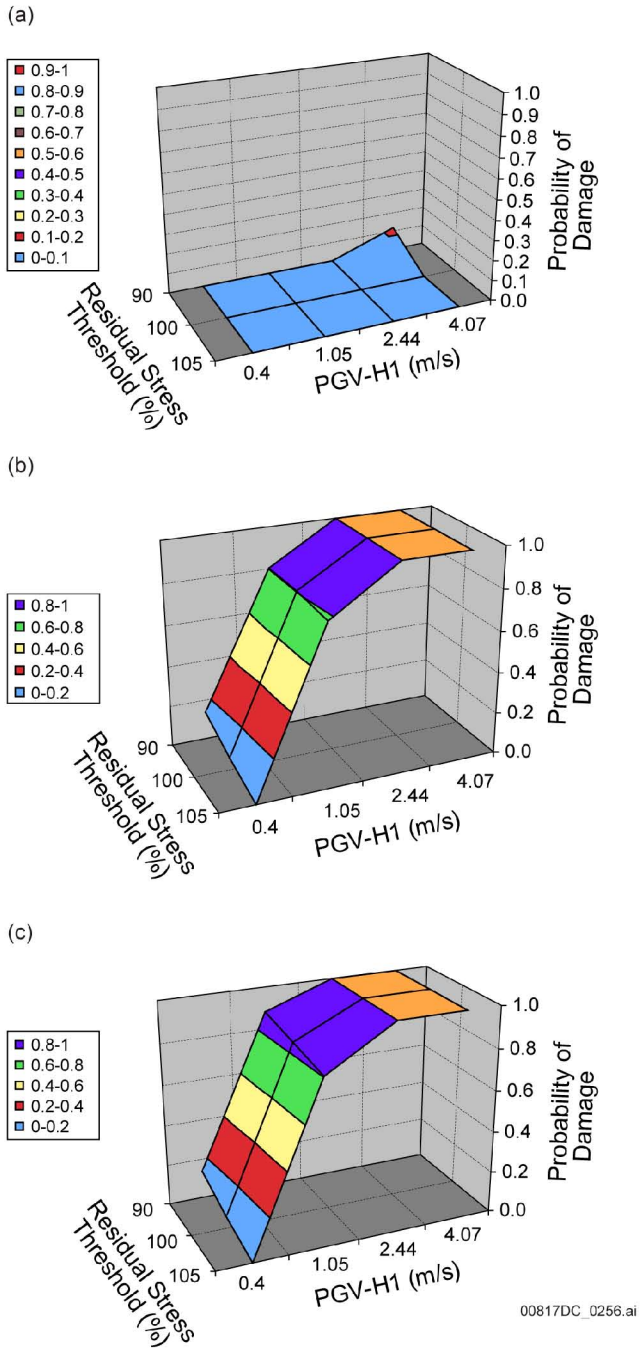

Source: DTN: MO0703PASDSTAT.001_R3 [DIRS 183148], *Kinematic Damage Abstraction 23-mm Intact.xls, Kinematic Damage Abstraction 23-mm Degraded.xls, and Kinematic Damage Abstraction 17-mm Degraded.xls*.

NOTE: Orange represents a probability of 1.0.

Figure 6.6-10. Probability of Damage for a CSNF WP under and Intact Drip Shield: (a) 23 mm OCB with Intact Internals, (b) 23 mm OCB with Degraded Internals, and (c) 17 mm OCB with Degraded Internals

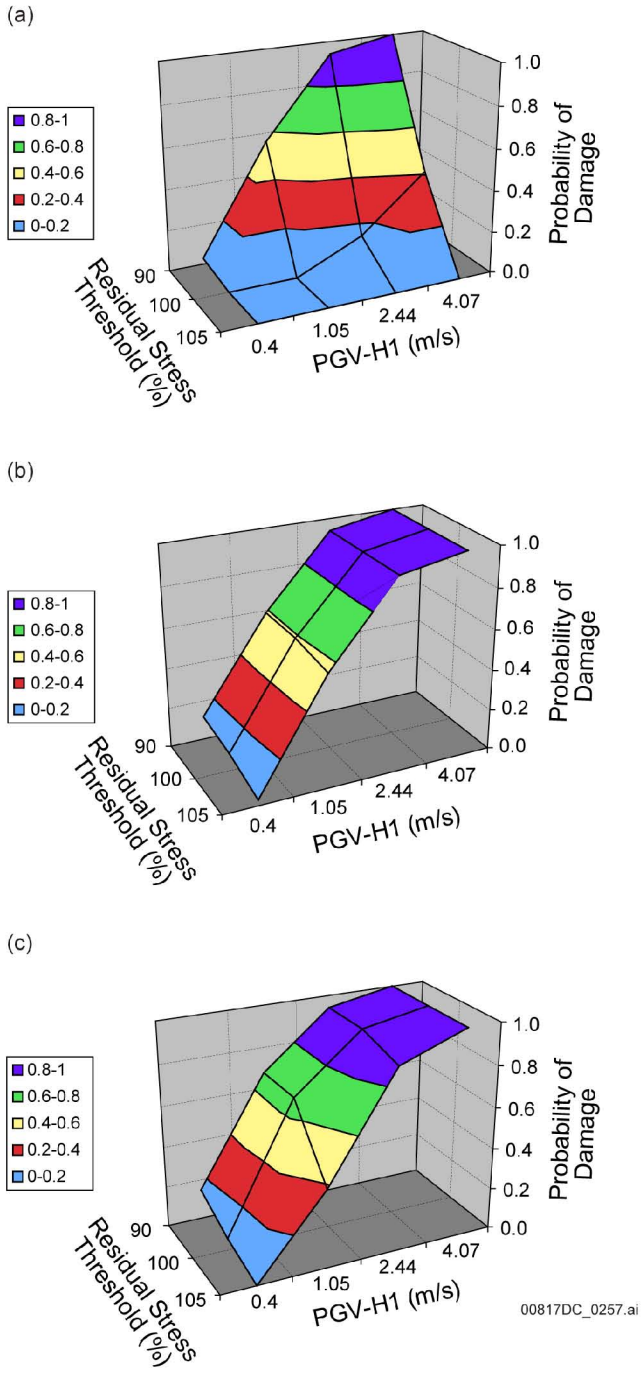

Source: DTN: MO0703PASDSTAT.001_R3 [DIRS 183148], *CDSP Kinematic Damage Abstraction 23-mm Intact.xls, CDSP Kinematic Damage Abstraction 23-mm Degraded.xls, and CDSP Kinematic Damage Abstraction 17-mm Degraded.xls.*

Figure 6.6-11. Probability of Damage for a CDSP WP under an Intact Drip Shield: (a) 23-mm OCB with Intact Internals, (b) 23-mm OCB with Degraded Internals, and (c) 17-mm OCB with Degraded Internals

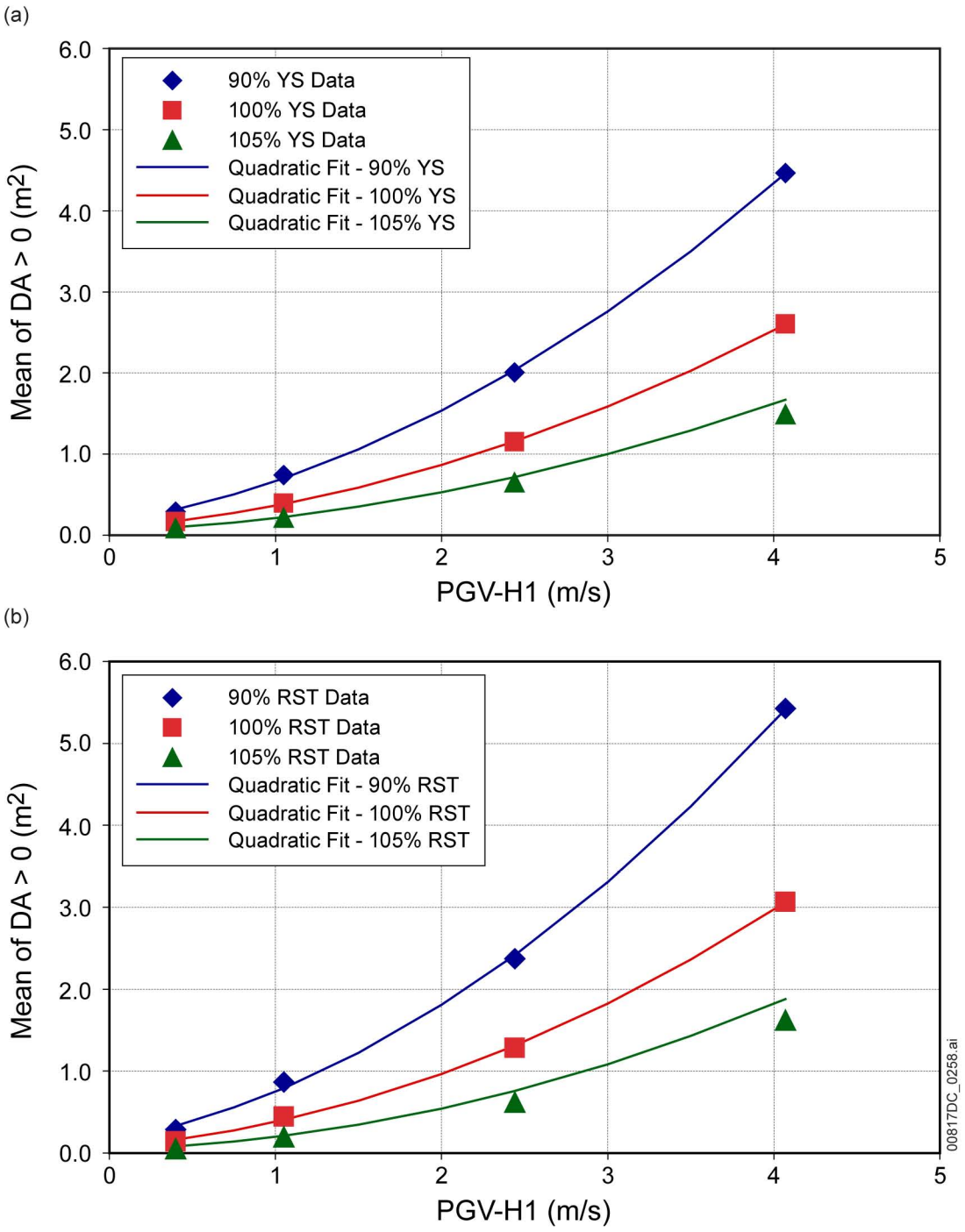

Source: DTN: MO0703PASDSTAT.001_R3 [DIRS 183148], *Kinematic Damage Abstraction 23-mm Degraded.xls* and *Kinematic Damage Abstraction 17-mm Degraded.xls*.

Figure 6.6-12. Quadratic Fit for Mean Damaged Area on a CSNF WP with Degraded Internals under an Intact Drip Shield: (a) 23-mm OCB and (b) 17-mm OCB

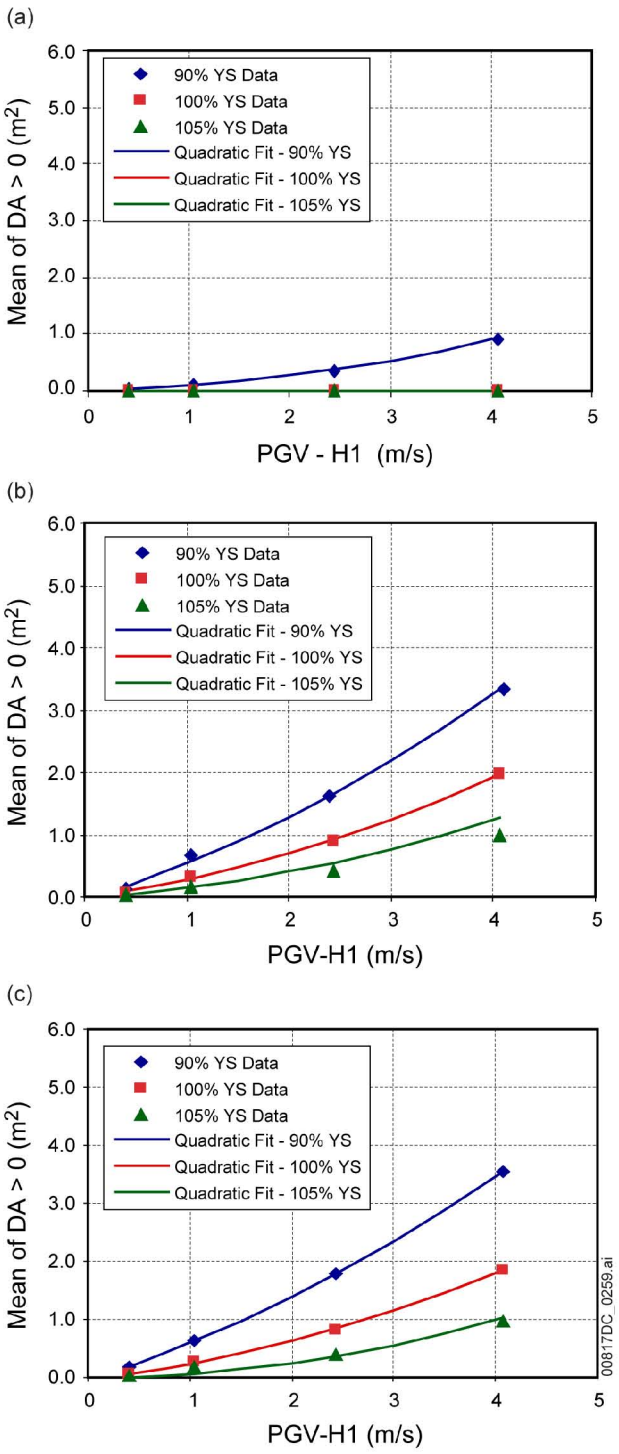

Source: DTN: MO0703PASDSTAT.001_R3 [DIRS 183148], CDSP *Kinematic Damage Abstraction 23-mm Intact.xls, CDSP Kinematic Damage Abstraction 23-mm Degraded.xls*, and *CDSP Kinematic Damage Abstraction 17-mm Degraded.xls*.

Figure 6.6-13. Quadratic Fit for Mean Damaged Area on a CDSP WP under an Intact Drip Shield: (a) 17-mm OCB with Degraded Internals, (b) 23-mm OCB with Degraded Internals, and (c) 23-mm OCB with Intact Internals

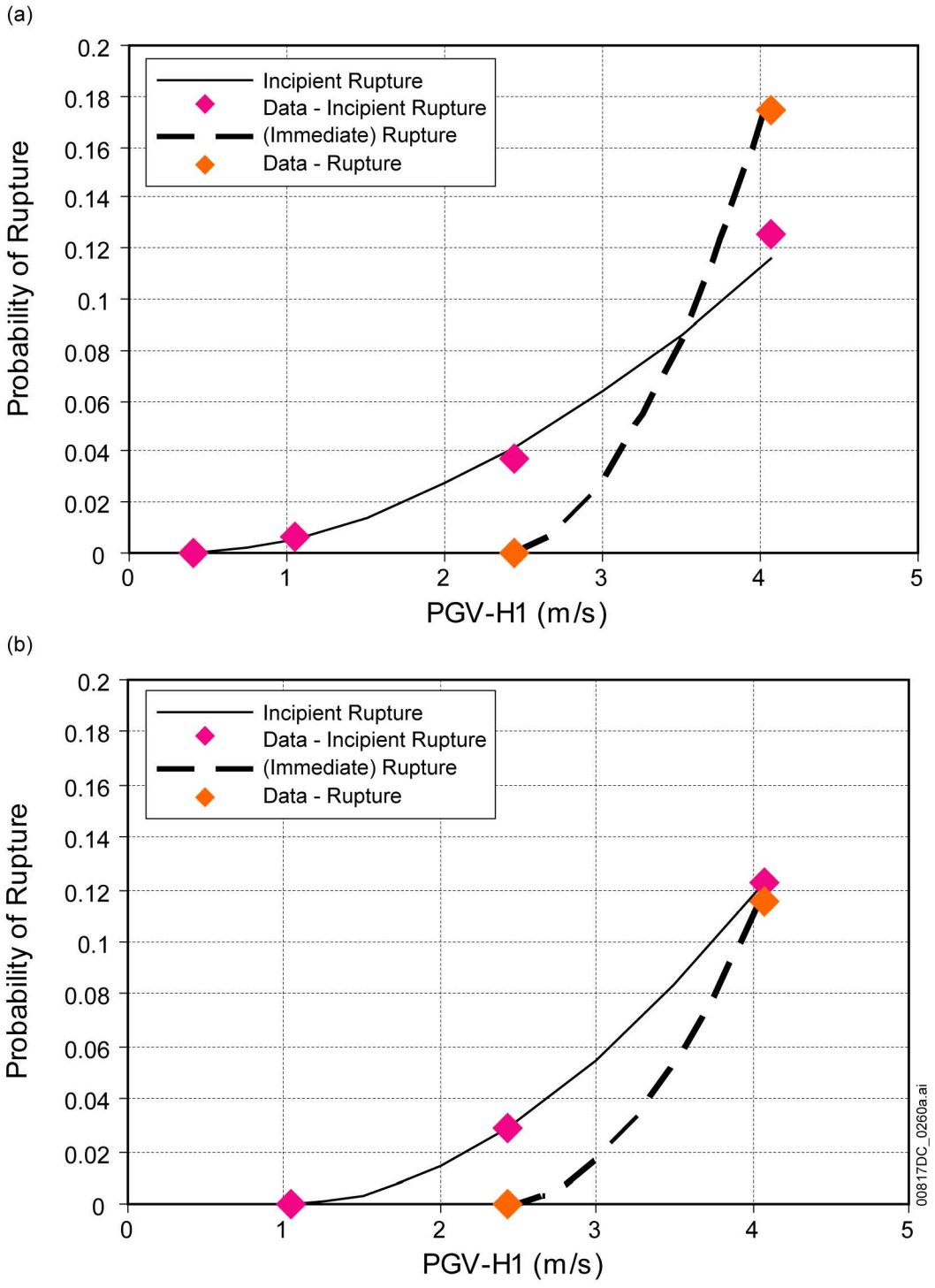

Source: DTN: MO0703PASDSTAT.001_R3 [DIRS 183148], *Rupture and Puncture Abstractions.xls*.

Figure 6.6-14. Probability of Incipient and Immediate Rupture for (a) CSNF and (b) CDSP WPs under Intact Drip Shields

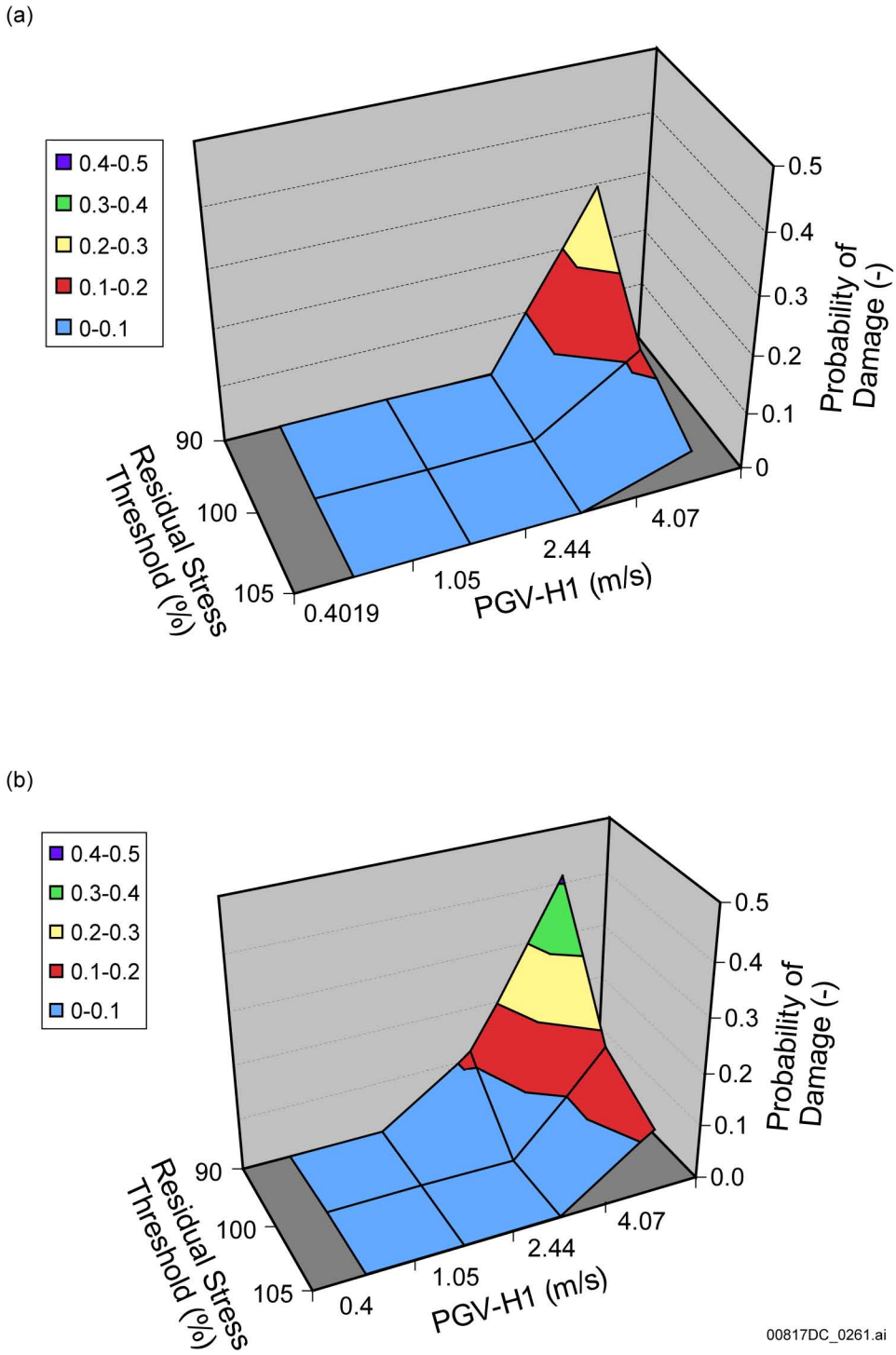

Source: DTN: MO0703PASDSTAT.001_R3 [DIRS 183148], *WP-Rubble Damage Abstraction 23-mm Degraded.xls* and *WP-Rubble Damage Abstraction 17-mm Degraded.xls*.

Figure 6.6-15. Probability of Damage for a CSNF WP Surrounded by Rubble: (a) 23-mm and (b) 17-mm

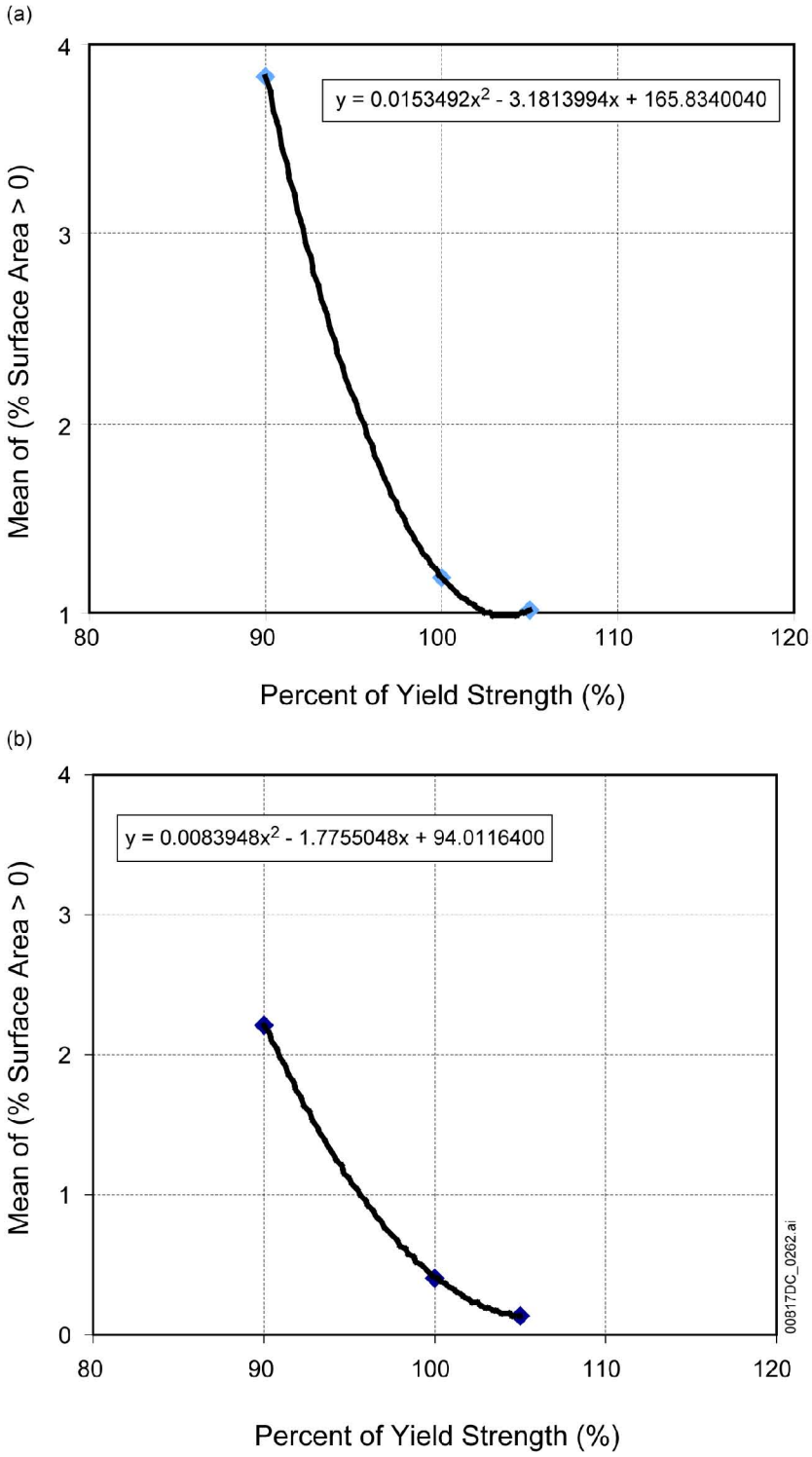

Source: DTN: MO0703PASDSTAT.001_R3 [DIRS 183148], *WP-Rubble Damage Abstraction 23-mm Degraded.xls* and *WP-Rubble Damage Abstraction 17-mm Degraded.xls*.

Figure 6.6-16. Quadratic Fit for Mean Damage Area on a CSNF WP with Degraded Internals Surrounded by Rubble: (a) 23-mm and (b) 17-mm

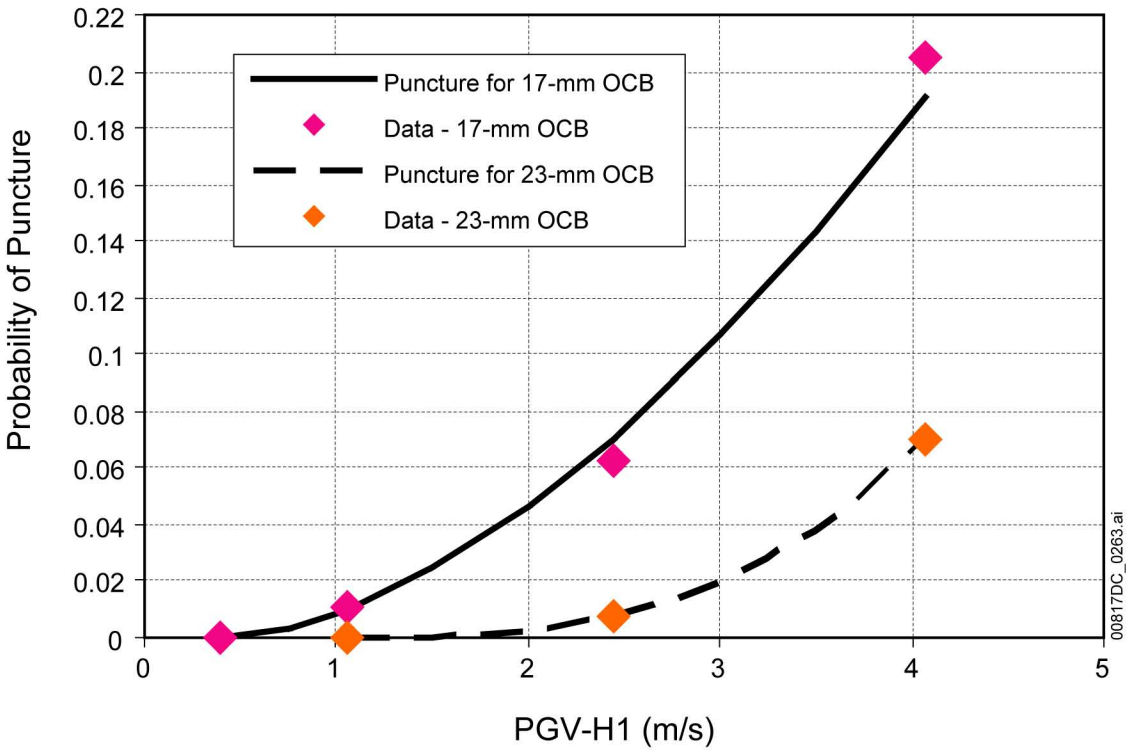

Source: DTN: MO0703PASDSTAT.001_R3 [DIRS 183148], *Rupture and Puncture Abstractions.xls*.

Figure 6.6-17. Probability of Puncture for a CSNF WP Surrounded by Rubble

INTENTIONALLY LEFT BLANK

6.7 TSPA-LA MODEL FOR THE HUMAN INTRUSION SCENARIO

The Human Intrusion Modeling Case is based on the stylized Human Intrusion Scenario as specified in NRC rule 10 CFR 63.322 [DIRS 180319], and the individual protection standard for a human intrusion of the repository in the NRC Proposed Rule 10 CFR 63.321 [DIRS 178394]. The TSPA-LA stylized Human Intrusion Scenario is based on NRC rule in 10 CFR 63.322 [DIRS 180319] as follows:

"For the purposes of the analysis of human intrusion, DOE must make the following assumptions:

(a) There is a single human intrusion as a result of exploratory drilling for ground water;

(b) The intruders drill a borehole directly through a degraded waste package into the uppermost aquifer underlying the Yucca Mountain repository;

(c) The drillers use the common techniques and practices that are currently employed in exploratory drilling for ground water in the region surrounding Yucca Mountain;

(d) Careful sealing of the borehole does not occur, instead natural degradation processes gradually modify the borehole;

(e) No particulate waste material falls into the borehole;

(f) The exposure scenario includes only those radionuclides transported to the saturated zone by water (e.g., water enters the waste package, releases radionuclides, and transports radionuclides by way of the borehole to the saturated zone); and

(g) No releases are included which are caused by unlikely natural processes and events."

In addition, NRC Proposed Rule in 10 CFR 63.321 [DIRS 178394] specifies the individual protection standard for human intrusion as follows:

"(a) DOE must determine the earliest time after disposal that the waste package would degrade sufficiently that a human intrusion (see § 63.322) could occur without recognition by the drillers.

(b) DOE must demonstrate that there is a reasonable expectation that the reasonably maximally exposed individual receives, as a result of human intrusion, no more than the following annual dose:

(1) 0.15 mSv (15 mrem) for 10,000 years following disposal; and

(2) 3.5 mSv (350 mrem) after 10,000 years, but within the period of geologic stability.

(c) DOE's analysis must include all potential environmental pathways of radionuclide transport and exposure, subject to the requirements at § 63.322."

Section 6.7 is organized as follows. Section 6.7.1 summarizes the model components and submodels of the Human Intrusion Scenario. The earliest time at which a waste package (WP) is expected to be breached by an inadvertent drilling event is discussed in Section 6.7.2. Section 6.7.2.1 describes the TSPA-LA analysis for drip shield (DS) and WP degradation. Section 6.7.2.2 discusses the unlikely events-related damage mechanisms. Section 6.7.2.3 describes the potential for WP penetration by a drilling event. Section 6.7.2.4 summarizes the findings from the analysis discussed in Sections 6.7.2.1 through 6.7.2.3. Section 6.7.2.5 discusses the treatment of likely DS and WP degradation processes considered in the Human Intrusion TSPA. Implementation and the process for estimating the mean and median annual dose for the Human Intrusion Scenario is discussed in Section 6.7.3. This section is divided into four subsections based on the treatment of radionuclide transport through the following TSPA submodels, the EBS (Section 6.7.3.1), the UZ (Section 6.7.3.2), the SZ (Section 6.7.3.3), and the Biosphere Submodel, which calculates dose (Section 6.7.3.4). The model component and submodel integration points, as well as conservatisms in submodels and abstraction models, are discussed in Section 6.7.4. The consistency of model assumptions in the Human Intrusion TSPA is discussed in Section 6.7.4.1, while Section 6.7.4.2 includes the discussion on model conservatisms. In Section 6.7.5, alternative conceptual models (ACMs) are considered.

6.7.1 TSPA-LA Model Components and Submodels for the Human Intrusion Scenario

The Human Intrusion Scenario describes performance of the repository system in the event that exploratory drilling disrupts the repository. Human intrusion disruption of the repository is addressed by a single modeling case.

The Human Intrusion Modeling Case, based upon NRC rule 10 CFR 63.322 [DIRS 180319], assumes that exploratory drilling activities intersect the repository and destroy a single DS and WP without recognition by the drillers. After penetrating a degraded DS and WP, the drillers continue to bore a conduit through to the SZ. The drillers penetrate a DS and WP with an opening the size of the drill bit and water enters the WP, mobilizing radionuclides. The released radionuclides may then be transported out of the repository (bypassing the EBS Invert Environment), moving down through the borehole to the SZ, to be transported through the SZ to the accessible environment. The TSPA-LA Model components and submodels needed to calculate total system performance for the Human Intrusion Modeling Case include the following, given that a single WP is destroyed by the intrusion:

- UZ Flow
- EBS Environment
- Waste Form Degradation and Mobilization
- EBS Flow and Transport
- SZ Flow and Transport
- Biosphere.

The model components and submodels of the TSPA-LA Model for the Human Intrusion Scenario are shown on Figure 6.7-1. Figure 6.7-2 shows the information flow within the model for the Human Intrusion Scenario in the TSPA-LA. Figure 6.7-3 indicates the major inputs and outputs of the model components and submodels included in the Human Intrusion Scenario and the foundation for confidence in the TSPA-LA Model. The TSPA-LA Model framework for the

Human Intrusion Scenario is similar to that of the Nominal Scenario Class. However, some of the submodels differ from those described in Section 6.3. These include the following:

- Mechanical damage to WPs and DSs
- Drift seepage for the Human Intrusion Scenario
- UZ Transport for the Human Intrusion Scenario
- EBS flow for the Human Intrusion Scenario.

The WP and DS Degradation Submodel is not used to calculate the corrosion failure of WPs prior to penetration time in the Human Intrusion Modeling Case. It is conservatively assumed that the WP could be penetrated without detection by the drillers. Nominal corrosion damage (either cracks or patches) subsequent to the drilling intrusion penetration releases and their dose are already included in the overall TSPA. Also, they could only serve to lower the dose attributable to release down the borehole pathway, since they would provide an avenue of escape into the UZ at spatial locations different than the borehole location (i.e., the occurrence of seismic crack damage and nominal corrosion patches and cracks would generally occur on a part of the WP surface not in contact with the borehole pathway). Thus, nominal WP breaches would not contribute in any way to increasing the possible concentration of radionuclides in the water flowing down the borehole and would rather reduce the resulting peak dose.

6.7.2 Evaluation of the Earliest Time of Waste Package Penetration by Human Intrusion

The Human Intrusion Scenario considers the effects of a single well drilled from the land surface above the repository, which penetrates the repository and passes through a single DS and WP, and into the underlying SZ. For the stylized Human Intrusion Scenario, the WP corrosion is conservatively ignored and the assumed DS failure at 200,000 years is considered to be the earliest time a driller could penetrate a WP without recognition. To determine the earliest time after disposal that a WP would degrade sufficiently that a human intrusion could occur without recognition by the drillers, the degradation mechanisms for DSs and WPs were evaluated and the earliest time at which a WP could be breached without recognition by the drillers was conservatively selected. The following discussion considers all the degradation states for a WP and DS considered for the TSPA-LA. Because degradation of WPs and DSs occurs gradually with time, the probability that a human intrusion could occur without recognition by the drillers increases with time.

6.7.2.1 General Corrosion of the Waste Package and Drip Shield

The EBS design includes Titanium Grade 7 DS supported by a Titanium Grade 29 framework, which is placed over the WPs (SNL 2007 [DIRS 179354], Section 4.1.2). As long as they remain substantially intact, the DS will divert an inadvertent drilling event (Section 6.7.2.3) away from the WP and preclude damage to a WP. The TSPA-LA Model for general corrosion is the only DS corrosion mechanism modeled. This degradation mode and abstraction model is described in Section 6.3.5. This process is modeled as being independent of temperature and relative humidity and is initiated at the time of repository closure. Because of the low corrosion rate of titanium alloy used for the DSs, the initial breaches of the DSs are not expected to occur until well after 10,000 years; more specifically, analyses predict that initial breaches of the DSs will not occur under nominal conditions until after approximately 230,000 years postclosure

(Section 6.3.5.1.3). General corrosion is modeled separately for the topside and underside surfaces of the DSs. The mean Titanium DS corrosion rates are the sum of the topside surface corrosion rate plus the underside surface corrosion rate. The corrosion rates are found in DTN: SN0704PADSGCMT.001_R2 [DIRS 182122], where the spreadsheet DS_GC_Model_Analysis_Benign Condition.xls contains the data for the underside surface, and the spreadsheet DS_GC_Model_Analysis_Agressive Condition.xls contains the data for the topside surface (used only for DSs that are exposed to dripping). The benign chemistry DS corrosion rates are applied to both the topside and underside of the DS for DSs that are not exposed to dripping water. Applying a conservative 0.9999 quantile for the DS (topside and underside) general corrosion rates over a 10,000-year period (Section 6.3.5.1.3) would reduce the original DS thickness of 15 mm (SNL 2007 [DIRS 179354], Table 4-2, Parameter Number 07-04A) by approximately 0.66 mm, to a thickness of 14.34 mm. Even applying the 0.9999 quantile titanium corrosion rate (for the topside and underside), the first DS failures due to general corrosion are not likely to occur until approximately 230,000 years after repository closure under nominal conditions.

The TSPA-LA Model for WP degradation includes four degradation modes: general corrosion, microbially influenced corrosion (MIC), stress corrosion cracking (SCC), and localized corrosion. These degradation modes and their abstractions are described in Section 6.3.5. The WPs have a dual-metal design consisting of an inner vessel and outer barrier. The inner vessel is composed of a 50.8-mm-thick layer of Stainless Steel Type 316 (material type SA-240 (UNS S31600) SNL 2007 [DIRS 179394], Table 4-3). The outer shell (i.e., outer corrosion barrier [OCB]) is a 25-mm-thick layer of Alloy 22 (material type SB-575 (UNS N06022)), a corrosion-resistant, nickel-based alloy surrounding transportation, aging, and disposal (TAD) canister made of a 300-series stainless steel such as Stainless Steel Type 316 (SNL 2007 [DIRS 179567], Tables 4-6 through 4-10). Alloy 22 protects the Stainless Steel Type 316 inner vessel from corrosion, and the Stainless Steel Type 316 inner vessel provides structural support for the thinner Alloy 22 outer shell. Because the WP outer shell is highly corrosion resistant, WPs will not be breached by corrosion processes during the 10,000-year modeling period in the absence of localized corrosion (SNL 2007 [DIRS 178519], Section 8.1). WP degradation models under nominal conditions indicate that it is unlikely that the time to initial breaching of the WPs will occur before 230,000 years postclosure (Section 6.3.5).

The WP Localized Corrosion Initiation and Propagation Analysis for the WP outer surface is based on the Localized Corrosion Initiation Abstraction developed in *General Corrosion and Localized Corrosion of Waste Package Outer Barrier* (SNL 2007 [178519], Section 6.4.4). The primary factors that determine the potential for initiating localized corrosion are sample configuration, metallurgical conditions, and exposure conditions including temperature, pH, chloride-ion concentration, and nitrate-ion concentration, which are obtained from the EBS TH Environment Submodel (Section 6.3.2) and the EBS Chemical Environment Submodel (Section 6.3.4). Localized corrosion requires the presence of seepage water on the WP surface. The potential effects of localized corrosion on the WPs during the initial 10,000-year period are, therefore, conditional on a DS failure (Section 6.3.5.2). Until a breach of the DS occurs, the WP itself is not susceptible to localized corrosion. Therefore, under nominal conditions, localized corrosion of WPs will not occur because DS failures are not expected until well after the chemical environment necessary for localized corrosion initiation has subsided (Section 6.3.5.2).

General corrosion of DSs and WPs occurs gradually over time. The general corrosion process is a surface phenomenon and the underlying metal retains its integrity and resistance to drilling until a significant amount of material has been corroded and the remaining DS or WP thickness is insufficient to prevent penetration by a drill bit. Nominal WP and DS degradation processes are insufficient to significantly degrade the titanium DS in 10,000 years. Given the slower relative degradation rates of the WPs and barring disruptive events of large magnitude, until there is a DS failure, the structural integrity of a WP is maintained and provides an additional barrier to borehole drill penetration.

6.7.2.2 Occurrence of Unlikely Events

In NRC Proposed Rule 10 CFR 63.342(b) [DIRS 178394], the NRC specifies that the human intrusion standards "…shall exclude the unlikely features, events, and processes, or sequences of events and processes, i.e., those that are estimated to have less than one chance in 10 and at least one chance in 10,000 of occurring within 10,000 years…" (i.e., an annual frequency of 10^{-5} (yr^{-1}) to 10^{-8} (yr^{-1})). Therefore, FEPs that have at least one chance in 10 of occurring within 10,000 years (i.e., a probability of occurrence greater than or equal to 1×10^{-5} per year) need to be considered for the human intrusion calculations. The following FEPs are discussed below in terms of their probability of occurrence: early failure of DSs, igneous events, and seismic events.

Early Failed Drip Shield

Although the TSPA-LA Model results show some DS failures at an early time, these failures are the result of manufacturing defects that increase susceptibility to SCC (SNL 2007 [DIRS 178765], Section 6.4). The probability of DS early failure (i.e., having an undetected defect that could cause an early failure) is determined from the DS cumulative uncertainty distribution for undetected DS defects (SNL 2007 [DIRS 178765], Table 6-10). This cumulative distribution function (CDF) gives the probability of having an undetected defect for a given DS. Considering that only a single WP and DS are penetrated during a human intrusion event, the probability of a human intrusion event intersecting a WP location that has an early failed DS can be determined by the probability of a DS defect occurring at that location. To evaluate the likelihood of this scenario, a conservative DS defect probability was chosen at the 0.95 quantile value of 6.968×10^{-6} from the DS cumulative uncertainty distribution for undetected DS defects (SNL 2007 [DIRS 178765], Table 6-10). There is no time dependency on this probability. However, it can be excluded from consideration as an unlikely event as it is an event with less than one chance in 10 in 10,000 years as defined by the NRC rule in 10 CFR 63.342 (b) [DIRS 178394]; and 10 CFR 63.322 (g) [DIRS 180319]. Even in the unlikely event that the human intrusion event were to intersect a location with an early failed DS, the likelihood of the WP being failed at the same location as a DS is even smaller. The joint probability (using the 0.9999 quantiles for DS and WP defects) for DS and WP early failure occurring at the same location is approximately 4.2×10^{-7} (SNL 2007 [DIRS 178765], Section 6.5.1, Table 6-11).

Similarly, potential effects of localized corrosion on the WPs during the initial 10,000-year period are conditional on a DS failure (Section 6.3.5.2). Given the probability of a human intrusion event at a location with an early failed DS (at a 0.95 quantile value) is 6.968×10^{-6}; a human intrusion event intersecting a WP failed by localized corrosion can be excluded as an

unlikely event (events with less than one chance in 10) per NRC rule in 10 CFR 63.342 (b) [DIRS 178394]; and 10 CFR 63.322 (g) [DIRS 180319].

Igneous Disruptive Events

Igneous disruptive events capable of causing significant damage are unlikely (i.e., igneous intrusion of the repository footprint has an annual probability of exceedance of less than 10^{-5} but greater than 10^{-8}). Therefore, further consideration of an igneous event in consort with a human intrusion stylized analysis is excluded from consideration. The exclusion is consistent with requirements of the NRC rule at 10 CFR 63.342 (b) [DIRS 178394] and 10 CFR 63.322 (g) [DIRS 180319], which exclude consideration of unlikely events (events with less than one chance in 10 in 10,000 years (i.e., an annual frequency of 10^{-5} yr^{-1}) in consort with a human intrusion event.

Seismic Disruptive Events

The analyses for seismic damage to DSs and WPs are documented in *Seismic Consequence Abstraction* (SNL 2007 [DIRS 176828]). The analyses provide a description of the damage that may occur to DSs and WPs from the mechanical response of EBS components to seismic hazards at the proposed repository horizon. The seismic induced damage to WPs and DSs includes the effects from fault displacement along faults that intersect the repository, seismic ground motion induced mechanical damage, or by rock fall, via imposed residual stresses in DSs and WPs (Section 6.6). The effect of fault displacement on the EBS is evaluated in terms of mean fault displacement hazard curves developed for faulting conditions mapped within the immediate vicinity of Yucca Mountain (SNL 2007 [DIRS 176828], Section 6.11 and Table 6-61). The Seismic FD Modeling Case includes disruption of the DSs and breach of the WPs affected by the displacement of faults, as well as nominal failures of DSs and WPs (Section 6.6.1.3). The expected number of WPs and DSs that fail from fault displacement is small because the number of WPs lying on known and generic faults is estimated to be 214, which is a small fraction of the approximately 11,000 WPs in the repository (SNL 2007 [DIRS 176828], Section 6.12.2, p. 6-255). Seismic events capable of causing significant damage from fault displacement are unlikely (i.e., WP failure due to fault displacement along faults intersecting the repository footprint has an annual probability of exceedance less than 2.2×10^{-7} [yr^{-1}] for TAD canisters and less than 2.5×10^{-7} [yr^{-1}] for co-disposed WPs (CDSP WPs) (SNL 2007 [DIRS 176828], Table 6-65). Therefore, further consideration of a seismic fault displacement event in combination with a human intrusion stylized analysis is excluded from consideration. The exclusion is consistent with requirements of the NRC rule in 10 CFR 63.342 (b) [DIRS 178394] and 10 CFR 63.322 (g) [DIRS 180319], which exclude consideration of unlikely events.

The effect of strong seismic ground motion is evaluated in terms of mean bounded ground motion hazard curve developed for Yucca Mountain (SNL 2007 [DIRS 176828], Section 6.4.3 and Table 6-3). For the seismic ground motion analysis, the threshold for considering the potential for damage to WPs and DSs is reached if the residual stress from mechanical damage exceeds the residual stress threshold (RST) for the barrier. The presence of residual stress induced by seismic events and/or related rock fall may result in local barrier degradation from accelerated SCC or rupture of the WPs and/or DSs (SNL 2007 [DIRS 176828], Sections 6.1.3

and 6.1.4). While SCC is appropriate for consideration of EBS flow and transport, it does not necessarily reflect changes to the effective material properties and may not constitute failure with respect to recognition of a change in conditions while drilling. Even with an imposed residual stress and minor amounts of corrosion and cracking, a rotating drill bit that encounters a metallic object will behave significantly different than when encountering naturally occurring geologic materials (Section 6.7.2.3). However, DS rupture, or plate fragility, is defined as the probability of rupturing or puncturing the DS plate during a seismic event (Section 6.6.1.2.2). For the evaluation of a human intrusion event, the DS rupture (plate fragility abstraction) is evaluated with respect to the earliest time a WP could be penetrated without recognition by the drillers.

The plate fragility abstraction is a function of peak ground velocity (PGV), the thickness of the DS plate, and the static load on the plates from rock fall (Section 6.6.1.2.2) (SNL 2007 [DIRS 176828], Section 6.8 and Table 6-36). Applying the maximum DS general corrosion rates over a 10,000-year period would reduce the original DS thickness of 15 mm by approximately 0.67 mm (using the 0.9999 quantiles for the underside and topside of the DS as discussed in Section 6.5.3.2.1). Given this conservative DS thickness (14.34 mm), there is a very small probability ($p<0.001$) for DS rupture to occur in a seismic event with a PGV of 1.05 (m/s). This evaluation assumes the probability of DS plate failure for a drift 100 percent filled with rubble (i.e., maximum static loading) linearly interpolated between a 10 mm and a 15 mm DS thickness (SNL 2007 [DIRS 176828], Table 6-36). A PGV of 1.05 m/s corresponds to an annual probability of exceedance of 9.955×10^{-6} (yr^{-1}) (SNL 2007 [DIRS 176828], Table 6-3). Given an annual probability of exceedance of 9.955×10^{-6} (yr^{-1}), seismic disruptive events capable of causing DS rupture are unlikely.

The other mechanism for rupture of a DS is from large rock block impacts in the nonlithophysal zones. These probabilities are given in the *Seismic Consequence Abstraction* (SNL 2007) [DIRS 176828], Table 6-54). The frequency of seismic events that result in a rupture of one or more DSs from large rock block impacts is evaluated to be 1.17×10^{-6} (yr^{-1}) (DTN: MO0712PBANLNWP.000_R0 [DIRS 184664], Nonlith LC Calculation Rev03.mxd). This again is less than the likely event cutoff of 0.1 in 10,000 years.

Consequently, with regard to the human intrusion stylized analysis in combination with a seismic event, it is concluded that seismic ground motion events are insufficient to significantly alter material properties of the DS to a sufficient degree that it would not be noticed by a driller in 10,000 years.

Finally, it should be mentioned that even in the unlikely event that a DS is damaged by a seismic event in 10,000 years, the chance of a WP being damaged by seismicity in the same time frame, in a way that it would not be recognized by the driller, is very low and below the likely/unlikely FEPs cutoff. In particular, stress corrosion cracks due to seismically-induced residual stresses in the Alloy 22 would not compromise the structural integrity of the WP; however, rupture (from the outside) or puncture (from the inside) of a WP could compromise its structural integrity. But, as demonstrated in Sections 7.3.2.6.1.3.5 and 7.3.2.6.1.3.6, both of these probabilities are less than 0.1 in 10,000 years. Thus, they are excluded from the Human Intrusion Scenario.

6.7.2.3 Potential for Waste Package Penetration by Drilling

The NRC, in the discussion regarding the timing and frequency of human intrusion (66 FR 55732 [DIRS 156671], p. 55761), states that "some evaluations of resource potential of the site suggest that Yucca Mountain (and the area immediately around it) does not represent an attractive candidate for either random or systematic exploratory drilling at this time...". A list of citations for those studies is available in the regulation. Furthermore, the elevation of the mountain, with the resultant greater depth to water compared to shallower groundwater wells that would be drilled to the south of the mountain, decreases the likelihood of groundwater exploration through the repository footprint. Regardless, the regulations specify evaluation of the timing of a human intrusion event and consideration of a stylized human intrusion assuming exploratory drilling for groundwater in the region surrounding Yucca Mountain (10 CFR 63.322(c) [DIRS 180319]). The following discussion presents several lines of evidence relevant to estimating the time when a human intrusion could occur, based upon the earliest time that current technology and practices used for groundwater exploration could lead to WP penetration without recognition by a driller.

There are a number of operational parameters that would indicate to a driller that a change in down-hole conditions would merit additional investigation, including a bit run (the removal of the bit from the hole for review and grading). These down-hole conditions could include loss of circulation, decreased penetration rate, increased drill string and bit instability, and increased drill string torque caused by differing material properties.

6.7.2.3.1 Initial Bit Selection and Drilling Principles

The bases for the following discussions are focused on typical practices used in drilling water wells in the southwestern United States. Generally speaking, the drill string assembly consists of the drill bit, drill collar, drill pipe, and in some instances, the use of stabilizers.

As described in Driscoll (1986 [DIRS 116801], pp. 278 to 286) and Bourgoyne et al. (1986 [DIRS 155233], Section 5.1), roller bits are typically used in drilling water wells due to their low cost and wide range of operational flexibility. Polycrystalline diamond cutter and diamond cutter drag bits typically are not used in water well drilling because of the high costs of these drill bits. Direct circulation down-hole hammer drills are sometimes used to drill brittle competent rock, such as welded volcanic tuff, but they typically are inefficient in unconsolidated alluvium or incompetent rock formations. This limitation reduces the use of these drills in typical water well drilling. The discussions provided herein are generally applicable to roller or hammer bits.

The initial selection of bit type is typically based on what is known about the formation characteristics. The terms usually used by drilling engineers to describe the formation characteristics are drillability and abrasiveness. The drillability of the formation is a measure of how easy the rock formation is to drill. It is inversely related to the compressive strength of the rock, although other factors are also important. The abrasiveness of the formation is a measure of how rapidly the cutting surface of a bit will wear when drilling the formation. Although there are some exceptions, the abrasiveness tends to increase as the drillability decreases (Bourgoyne et al. 1986 [DIRS 155233], Chapter 5).

The International Association of Drilling Contractors (IADC 1992 [DIRS 155232]) has developed a classification chart for selection of roller bits. Using this classification chart, roller bits with characteristics of 7-1 or 7-2 (hard semi-abrasive and abrasive formations) would be selected for drilling through the welded geologic units at Yucca Mountain, based on geomechanical properties. Roller bits are designed to take advantage of brittle failure of the rock matrix to crush, break, and remove the rock in an efficient manner. The volume of rock that is newly fractured by a tooth depends on the geometry, rock properties, and tooth penetration depth below the rock surface. The force applied to the tooth is supplied by the drill string torque and weight on the bit. The force applied to a particular situation determines the tooth penetration depth. The bit tooth penetrates into the rock until the resistant force offered back by the rock equals the force applied to the tooth. As a load is applied to a bit tooth, the pressure beneath the tooth increases until it exceeds the crushing strength of the rock and a wedge of finely powdered rock is formed beneath the tooth.

As the force of the tooth increases, the material in the wedge compresses and exerts high lateral forces on the solid rock surrounding the wedge until the shear stress exceeds the shear strength of the solid rock and the rock fractures. The rock may also exhibit ductility such that a greater tooth penetration is required to cause sufficient strain for chipping to occur (Warren 1987 [DIRS 155234]). The tooth will penetrate until the shear stress on the tooth is balanced by the shear strength of the rock.

These forces generate fractures that propagate along a maximum shear surface. As the force of the tooth increases above the threshold value, subsequent fracturing occurs in the region above the initial fracture, forming a zone of broken rock. The bit tooth moves forward until it reaches the margins of the wedge and/or fracture zone, and the process repeats (Bourgoyne et al. 1986 [DIRS 155233], Chapter 5). The crushed and broken material is then removed from the boring using circulated drilling fluids (air, water, or admixtures thereof) that also provide cooling and cleaning for the drill bit.

The drill collar is a heavy-walled length of drill pipe with a diameter less than the borehole diameter. If too much force is applied at the top of the drill stem, the drill pipe will bow and tend to cause the bit to cut off-center and, thereby, cause deviations in the borehole alignment. To compensate, drill collars are used to add weight to the lower part of the drill string assembly. This concentration of weight and the increased rigidity of the collars helps to keep the lower part of the drill assembly in alignment and provide weight to the bit to maintain appropriate penetration rate (Driscoll 1986 [DIRS 116801], p. 281). Drill collars may also be fitted with stabilizer devices that contact the borehole walls. The drill collars and stabilizers are used to maintain alignment of the drill string within the borehole and reduce vibration or wobble of the bit and drill pipe that transfers the torque from the surface to the drill bit.

6.7.2.3.2 Bit Operating Conditions and Change-in-Conditions

Bit operating conditions (i.e., drilling fluid properties and circulation rates, drill string stability, bit weight, and rotary speed) affect the rate of penetration and vibrations felt on the drill rig. These factors would be affected by the drilling assembly's entry into the emplacement drift, and the bit operating conditions would be significantly affected by the rounded geometry of the emplacement drift, DS, and WP.

The loss of drilling fluid circulation and sudden drop in weight on the bit when the drill bit breaks through the top of the emplacement drift would provide initial indications that conditions had changed significantly. The loss of circulation would occur because of the flow of drilling fluids from the borehole and into the emplacement drift which, at 5.5 m diameter and on the scale of a kilometer (km) in length, represents an essentially instantaneous increase in volume compared to the borehole volume. At that point, the driller would either try to continue drilling without compensating for the fluid loss in the hope of passing through the loss zone, would try various additives in the drilling fluid to try to seal the formation (Driscoll 1986 [DIRS 116801], p. 360), or would have to pull the drill assembly and either change drilling methods or install temporary or permanent casing to seal off the cavity. In the event of continued drilling, encountering of the DS or WP would prevent progress, and the lack of cooling from circulated fluids would eventually destroy the drilling bit and result in the drilling assembly being pulled from the hole (or otherwise cause the driller to consider alternative courses of action). Given the volume difference between the borehole and emplacement drift, it is implausible that any amount of additive would resolve the lost circulation problem, again leading the driller to some alternative course of action. Alternative courses of action, such as spot cementing through the loss zone or setting casing through the cavity, would involve pulling the drilling assembly from the borehole. In either scenario, the driller would then encounter continued volumetric problems or would encounter problems in trying to set casing due to the presence of the DS or WP within the emplacement drift.

In addition to loss of circulation, the space between the crown or sides of the emplacement drift (5.5 m) and the DS would cause the operating conditions to become unstable and would evidence themselves with a sudden increase in rotation speed as the weight on the drill bit was unloaded, followed by a sudden drop in the drill assembly (i.e., essentially free fall until the DS or invert of the drift was encountered), and/or a significant increase in the amount of vibration at the surface. Any of these conditions would cause the destabilization of the drill bit (i.e., tend to allow the bit to change direction from the original concentric alignment) and would trigger a response by the driller to address the change in conditions. This is particularly true as drilling conditions would noticeably change (due to the difference in rock and alloy material properties) if the drilling assembly came in contact with the DS material (Section 6.7.2.3.4).

The conditions described above assume that the drift has not collapsed. Rubble material in a collapsed drift could reduce the degree of these effects on drilling but would likely not eliminate them. The analysis of drift degradation (BSC 2004 [DIRS 166107]) indicates that during the regulatory period of 10,000 years, the ground support will completely lose its integrity, and drift degradation will occur due to strength decay of the rock mass within the lithophysal zone (BSC 2004 [DIRS 166107], Section 6.4.2.4). However, the collapse results in the bulking of, or increase in, the volume of the rock as the rock mass disintegrates into a number of pieces resulting in increased porosity and overall volume. The resulting bulk properties of the fill are different from that of the intact rock mass. Loss of drilling fluid circulation would still occur but perhaps could be accommodated by the driller. Additionally, the rubble pile of rocks would tend to move or shift under small loads, and the uneven loading on the drill bit would increase the lateral deviation forces (Bourgoyne et al. 1986 [DIRS 155233], Chapter 5). As such, even if the drifts collapse, the character of the rubble would be insufficient to stabilize the drill string. Severe wobbling bit action would result as the bit is rotated if the drill collars or stabilizers above the bit are not held in a concentric position in the borehole.

6.7.2.3.3 Penetration of the Drip Shield and Waste Package

To have any possibility of penetrating the DS or WP, the drilling assembly would have to contact the surfaces in an essentially perpendicular orientation. In general, deviation in alignment may be caused by the character of the subsurface material. This is because lateral deviation forces increase with relatively small changes in the contact angle between the bit and drilled material (Bourgoyne et al. 1986 [DIRS 155233], Chapter 5). Deviations may also be caused by too much or too little weight on the drill bit and differences in the pull-down force applied to the drill pipe during rotary drilling. Additionally, the varying hardness of different materials being penetrated deflects the bit from a consistent alignment.

Given that the top of the DS is curved and that most groundwater exploration holes are drilled in a near-vertical orientation (i.e., angle and directional drilling are possible but are not typically used for groundwater exploration purposes due to increased difficulty and cost), the drill bit would have to make contact at the relatively small areas that make up the apex of the DS or WP, where the surfaces are essentially perpendicular to the drill bit orientation. Only the apex of the DS or WP provides a perpendicular surface for which DS and WP geometry would not increase the lateral deviation forces.

If the drilling assembly contacts any location other than the relatively small areas that make up the apex of the DS or WP, then the relatively small drill bit diameter and high rotational speeds and the increased strength of material used for the DS and WP compared to the geologic materials (Section 6.7.2.3.4) would result in large lateral deviation forces and uneven loading on the bit. In turn, this would lead to drilling assembly instability and the bit would essentially bounce and slide on the top or side of the engineered barriers and potentially cause the drill bit to slip off of the DS or WP apex. Consequently, no penetration of the WP would occur. Furthermore, any non-slip contact with the DS or WP would be accompanied by a noticeable increase in drill string torque and reduced rate of penetration as the bit teeth contacted the metallic alloy. At the surface, the driller would recognize these conditions as a lack of drill bit penetration and excessive vibration. High levels of vibration and correspondingly low rates of penetration, such as these observed with poorly designed bits when crossing hard and abrasive formations would prompt the driller to adjust the rotary speed and weight on bit that eliminates shock. In some cases, this could include removing the drilling assembly from the borehole to inspect the bit condition (Putot et al. 2000 [DIRS 167791], p. 118), which would increase the chance for recognition of excessive bit wear and possible recognition that a metallic object had been encountered.

The ability of the drill string to penetrate a WP as a result of a sudden drop when the drill bit breaks through the top of the emplacement drift and the weight of the drill string-free falls, and potentially impacts the apex of the engineered barriers was considered. Impacts to a WP and resulting damaged area and rupture condition are determined for the OCB of the WP as documented in *Mechanical Assessment of Degraded Waste Packages and Drip Shields Subject to Vibratory Ground Motion* (SNL 2007 [DIRS 178851]).

The rupture condition of a WP is determined by comparing the maximum effective strain in the OCB (of a WP subjected to a single impact) to the ultimate tensile strain limit, which can be as low as 0.285, based on a triaxiality factor of 2.0 (SNL 2007 [DIRS 178851], Section 6.3.3, and

Appendix A). The procedure for determining the strain-based rupture condition is described in *Mechanical Assessment of Degraded Waste Packages and Drip Shields Subject to Vibratory Ground Motion* (SNL 2007 [DIRS 178851], Section 6.3.2.2.5, Figure 6-25). The maximum effective strain and rupture conditions for WP-to-pallet damage analyses, evaluated over a range of impact velocities up to 10m/s, a variety of impact locations, and a variety of impact angles, indicate that no rupture will occur for TAD-bearing and co-disposed WPs, whether intact or degraded to 17 mm with degraded internals (SNL 2007 [DIRS 178851], Tables 6-55 through 6-63 and 6-83 through 6-93).

Using Torricelli's equation (Equation 6.7-1), the upper bound estimate of impact velocity for the drill string at the WP outer barrier would be approximately 5.9 m/s for a TAD-bearing WP and 5.7 m/s for a co-disposed WP given a drop distance of 1.8 m and 1.6 m, respectively (Table 6.7-1).

$$v_f^2 = v_i^2 + 2a\Delta d \qquad \text{(Eq. 6.7-1)}$$

where

v_f = final velocity (or impact velocity of the drill string)

v_i = the initial velocity (0 m/s)

a = acceleration due to gravity (9.8 m/s)

Δd = distance from drift crown to the top of the WP (Table 6.7-1).

A 300-m long drill string assembly consisting of a drill bit, drill collar, and drill pipe, can be estimated to be approximately 14 metric tons (Table 6.7-2). Since the weight of the drill string (14 metric tons) is much less than the weight of a fully loaded WP (73.5 metric tons for a TAD-bearing WP, 58 metric tons for a co-disposed WP), and the upper bound of the impact velocity (5.9 m/s) of the lighter drill string is much less than the impact velocities used for the analyses cited above (10 m/s), no rupture of the WP will occur. The drill string velocity is an upper bound, since drilling mud and cuttings filling the borehole would create friction along the 300 m drop as well as, the likely presence of rockfall that would have accumulated in the drifts over the DSs and WPs would prevent the drill string from impacting the EBS components (i.e., a zero drop height). In addition the DS itself is another likely barrier to the drill string penetration which was not considered. The worst case location of drill string impact is at the DS crown and the DS is strongest at that point. A more probable scenario would be that the drill string would bend the DS into contact with the WP which would result in a very distributed load to the WP, further reducing the impact velocity. If the drill string could penetrate the DS, much of the impact energy to the WP would be reduced by the penetration (or crushing) of the DS.

6.7.2.3.4 Comparative Material Strength

Assuming that the drilling assembly does not slide off the apex of the DS, then a significant change in down-hole conditions would also be recognized because the failure mechanisms of brittle rock (such as that present at the repository host horizon) and ductile alloys (such as the materials used for the DS and WPs) differ significantly. These changes in failure mechanisms are so significant that specialized down-hole techniques and tools are used to drill through metal.

Milling (a technique used for drilling through metal) produces a different failure mechanism than brittle failure that roller bits and hammer bits typically produce. Bits designed for drilling rock would not be efficient for drilling through metal and would likely be seriously damaged, and the milling techniques needed to bore metals (Avallone 1987 [DIRS 103508], pp. 13-63 to 13-64) are not used in rock drilling unless required for specialized applications (i.e., Driscoll 1986 [DIRS 116801], pp. 316 to 319, Figure 10.10 and Figure 10.54).

Brittle materials are characterized by the fact that rupture occurs without any noticeable prior change in the rate of elongation. Thus, for brittle materials under tension, there is no difference between the ultimate strength and breaking strength. Also, under tension, the strain at the time of rupture is much smaller for brittle than for ductile materials (Beer and Johnston 1981 [DIRS 166708], p. 36). In general, brittle materials are weaker in tension than in shear (Beer and Johnston 1981 [DIRS 166708], p. 101), and brittle materials are significantly stronger in compression than in tension (i.e., the tensile strength of concrete is about 10 to 20 percent of its compressive strength; also see Table 6.7-3 for a comparison of rock strength in compression and tension). For brittle materials, strength is typically reported as compressive strength rather than tensile strength, while ductile material strengths are typically determined in tension.

The ductility of a material, such as the alloys used for the DSs and WPs, is usually measured as the percent reduction in area (or the elongation that occurs during a tensile test). Ductile materials, with a minimum elongation in tensile testing, will not fail in service through brittle fracture (Boyer and Gall 1984 [DIRS 155318]), which is the failure mode exhibited by the repository host horizon materials. Also, for ductile metals, the compression strength is generally assumed equal to the tensile strength (Beer and Johnson 1981 [DIRS 166708], p. 584). Generally speaking, values obtained for the yield strength and ultimate strength of a given material are only about half as large in shear as they are in tension, and the shear modulus is generally less than one-half, but more than one-third, of the modulus of elasticity of that material (Beer and Johnston 1981 [DIRS 166708], pp. 68 and 69).

Therefore, if the differences between milling and rotary drilling tools are ignored and rotary bits could be used to penetrate the engineered barriers, a measure for comparing strength properties between brittle and ductile materials is needed. One such parameter is a comparison of the modulus of elasticity of these differing materials. Because of the lack of elongation, the stress-strain diagram for brittle materials is generally linear, and the modulus of elasticity provides a convenient method for comparing material properties between brittle and ductile materials. This also suggests that comparison of tensile strength of brittle materials to yield strength of ductile materials may also be appropriate. Comparison of the compressive strength of rock materials and tensile strength of alloy is also appropriate. Furthermore, the reported shear modulus could be compared (if available) or a value of twice to three times the shear modulus could be compared to the modulus of elasticity.

Various rock properties for materials at Yucca Mountain are shown on Figure 6.7-4 and in Table 6.7-3, including uniaxial compressive strength, tensile strength, and modulus of elasticity (Young's modulus). Based on the design drawings and data tracking numbers (DTNs) cited, the yield strength, tensile strength, and modulus of elasticity for the DS and WP materials are shown in Table 6.7-4.

Studies that have been conducted to correlate operational parameters to the rate of penetration of the drill bit indicate that the rate of penetration may range from inversely proportional to the square of the strength of the material being drilled to inversely proportional to the strength of the material, all other factors being equal (Bourgoyne et al. 1986 [DIRS 155233], Equation 5-19; Kahraman 2000 [DIRS 167761], Equations 8, 12, and 14). Putot et al. 2000 [DIRS 167791], p. 123) suggests, at least for balling tendencies in shales and for a given weight on the bit, that drilling performance collapses upon a doubling of the rotary speed. Assuming that a change in the penetration rate by a factor of 1.5 or greater (increase) or 0.66 or less (decrease) (i.e., some condition occurring before performance collapse) would be sufficient to be noticed by a driller, a change in compressive strength of materials by a factor of 1.5 (or possibly less if one assumes the inverse square relationship presented by Bourgoyne et al. 1986 [DIRS 155233]) would cause a significant change in drilling conditions that would be recognized by the driller.

Table 6.7-3 indicates that the mean compressive strength of the rock material ranges from 19.3 MPa to 188.8 MPa. At room temperature, the tensile strength of the DS materials ranges from 345 MPa to 895 MPa (Table 6.7-4). Thus, the factor of compressive strengths ranges from about 1.8 (345/188.8) to as great as 46 (895/19.3). The tensile strength of the WP material at room temperature ranges from 550 MPa to 802 MPa (Table 6.7-4). This represents factors of 2.9 (550/188.8) to as great as 42 (802/19.3). If one conservatively assumes the yield strength of the engineered barrier materials is comparable to rock compressive strength, the factors decrease. For the DS material at room temperature, the factor ranges from 1.5 (275/188.8) to 23 (450/19.3). For the WP material at room temperature, the factors range from 1.3 (240/188.8) to as great as 21 (403/19.3). However, given that all WPs include Alloy 22 material in the outer barrier, the lower end of the range is bounded at a factor of 1.9 (358/188.8). Therefore, at room temperature, there is a minimum factor of 1.9 for the WPs and 1.5 for the DSs. If one assumes an inverse proportionality of rock strength to rate of penetration, the penetration rates would decrease to less than 67 percent of the rock penetration rate when intersecting a DS and to less than 53 percent of the rock penetration rate when intersecting a WP and, therefore, be recognizable, as previously discussed.

At elevated temperatures, such as those during the thermal period (i.e., 200°C), the strength properties of the DS material are reduced (DTN: MO0003RIB00073.000_R0 [DIRS 152926]) for Titanium Grades 7 and 16. The factor reduces in range from 1.1 (207/188.8) to as great as 12 (228/19.3), based on compressive strength. However, the properties of the Alloy 22 outer barrier are not as significantly reduced. The factor for compressive strengths for the elevated temperature ranges from 3.5 (662/188.8) to 36 (701/19.3). The minimum factor of 1.1 for the DS and rock strength comparison at elevated temperature would not by itself produce a sufficient change in penetration rate to be noticed by a driller. However, further penetration to a WP, with a larger compressive strength change, would produce a sufficiently reduced penetration rate.

Furthermore, the mean tensile strength of the brittle rock units is reported to range from 7.9 MPa to 10.9 MPa (or approximately 6 percent of the corresponding mean compressive strength). These rock tensile strengths are at least a factor of 19 less than those of the ductile engineered barrier materials, even at elevated temperatures. Even conservatively assuming an equivalence of the yield strength of a ductile material to tensile strength of brittle material generates a difference of a factor of 13.

Similarly, the mean modulus of elasticity for the rock materials is on the order of 6.9 to 33.6 GPa. By contrast, for the ductile alloys, the modulus of elasticity ranges from 107 to 206 GPa, representing a minimum factor of 3.2 different from the rock properties. These differences in tensile strength and modulus of elasticity between the brittle rock and ductile engineered barrier materials would further contribute to lack of drill bit penetration and excessive vibration.

Finally, the recognizable differences in penetration rate or vibrations are only applicable in the improbable situation of a rock drill bit hitting sufficiently near the engineered barrier apex to avoid bouncing or sliding (such as by impacting a metal crack) to initiate penetration into the engineered barrier. It is more likely that rotary bits for rock, which are not designed for drilling in metal, would simply bounce and slip off either the DS or WP.

The discussion provided above would be applicable even if the DS or one of the materials used in the WP were degraded to the point where structural integrity were lost or, in the case of the DS, the interlock mechanism were bent and penetrated by the drilling assembly.

Summary of Waste Package Penetration by Drilling Analysis

Selection of a bit for drilling involves knowledge of the characteristics of the rock. As indicated in Tables 6.7-1 and 6.7-2, there are significant differences between the tensile strengths and other material properties of the geologic units at Yucca Mountain and the materials for the DS and WP. Because the materials used in the DSs and WPs have high tensile strengths, yield strengths, and increased modulus of elasticity compared to the host rock properties, the tooth of a roller bit cannot penetrate enough to cause sufficient strain for chipping to occur. Rather, if contact with the DS occurs, the rotation of the bit would result in a tearing or shearing action with associated and recognizable high torque values. Consequently, the ductility of the metals makes them nearly impenetrable by techniques used in drilling rock. Boring in metals typically utilizes a milling technique. The down-hole milling tools needed to penetrate the DS and WP are not typically used in groundwater exploration, and use of such tools would be a clear indicator of recognition of penetration of some type of metallic, anthropogenic structure.

6.7.2.4 Earliest Time of Waste Package Penetration by Human Intrusion

Conclusions based on information presented above suggest that a human intrusion event, if it were to occur before the WPs and DSs had sufficiently degraded, would not happen without recognition by the drillers. General corrosion of the DS is not expected to thin the DS plates significantly before 230,000 years (Section 6.7.2.1) and seismic ground motion cracks are not expected to affect a rotating drill bit because the failure mode and drill bit interaction are significantly different for rock and metals, as discussed in Section 6.7.2.3. In general, until a breach of the DS occurs, the structural integrity of the WP is maintained, providing an additional barrier to drill-bit penetration. The analysis provided in this section indicates that an unrecognized intrusion will not occur prior to 10,000 years following closure of the repository and that several possible modes of DS and WP damage that might contribute to drilling penetration of the DS or WP can be screened out as unlikely (per 10 CFR 63.342(b) [DIRS 178394]), such as early failure and all damage modes related to seismicity. For the TSPA-LA Human Intrusion Scenario, the WP degradation is conservatively ignored and the human intrusion event time, based on DS corrosion and observable effect on the drilling system

is taken to be no less than 200,000 years. Although some uncertainty exists about the timing of when penetrating a WP would not be detected, an assumption of penetration at 200,000 years is appropriate. This is a conservative estimate since there is less than a 0.0001 chance of DS general corrosion failure prior to 230,000 years (based upon the 0.9999 percentile corrosion rates) and because WP degradation (formation of open breaches) takes significantly longer than this. Thus, until some time after 200,000 years, there is a double barrier to drilling penetration of the waste forms. Therefore, for the stylized Human Intrusion Scenario, 200,000 years is conservatively assumed to be the earliest time a driller could penetrate a WP without recognition. The dose results described below use this conservative intrusion time without uncertainty.

6.7.2.5 Treatment of Likely Waste Package Degradation Processes

Section 6.7.2.2 described the screening of unlikely DS degradation FEPs from the analysis of the occurrence time of the earliest unrecognizable drilling penetration, since this earliest time is conservatively based on DS degradation rather than actual WP penetration. It also indicated that seismic rupture or puncture damage of a WP, even in the unlikely event of a DS failure, is unlikely, too. However, 10 CFR 63.322(g) [DIRS 180319] does imply that all likely FEPs must be included. For DS degradation only, the general corrosion process is considered to be a likely FEP, while for WP degradation, both nominal corrosion processes and seismic degradation of co-disposal WPs are likely FEPs. However, the effects of these likely WP degradation FEPs are treated conservatively in this human intrusion analysis by effectively screening out their effects. In particular, as implied by 10 CFR 63.322 [DIRS 180319], it would appear that the main focus of the Human Intrusion Scenario is on the incremental dose possible due to drilling penetration. Dose to the RMEI arising from general corrosion or likely seismic degradation FEPs is already part of the overall TSPA. Therefore, the only reason for including these FEPs in the human intrusion TSPA would be if they could increase the dose due to a drilling penetration of a single WP. However, the opposite is true, as explained below.

It is highly probable, for example, based on the results of the Seismic Ground Motion Modeling Case (Section 6.6), that co-disposal packages will fail by seismically-induced stress corrosion cracks before the occurrence of the postulated human intrusion event at 200,000 years, even for smaller ground motions that occur at annual frequencies greater than 10^{-5} per year (the likely/unlikely FEP cutoff). For example, as described in Section 7.3.2.6.1.3.7, the maximum frequency of events that causes SCC damage to a co-disposal WP is estimated to be 2.181×10^{-5} per year. For a Poisson process at this occurrence frequency, this implies a 98.7% chance of one or more damaging seismic events within 200,000 years $[= 1 - \exp\{(-2.181 \times 10^{-5}\ \text{yr}^{-1})(2 \times 10^{-5}\ \text{yrs})\}]$. Ignoring diffusive radionuclide releases through these cracks prior to the time of the drilling intrusion is conservative; however, because accounting for these diffusive releases would reduce the radionuclide content of the WP for nuclides that are not solubility limited, such as ^{99}Tc and ^{129}I including minor, but conservative, effects on the actinide releases. The same logic applies to possible WP damage prior to 200,000 years due to nominal SCC processes.

Regarding likely seismic crack damage and nominal corrosion damage (either cracks or patches) subsequent to the drilling intrusion penetration, these releases and their dose are already included in the overall TSPA. Also, inclusion of these releases could only serve to lower the dose attributable to release down the borehole pathway, since the cracks and patches would provide an

avenue of escape into the UZ at spatial locations different than the borehole location (i.e., the occurrence of seismic crack damage and nominal corrosion patches and cracks would generally occur on a part of the WP surface not in contact with the borehole pathway). Thus, these seismic or nominal WP breaches would not contribute in any way to increasing the possible concentration of radionuclides in the water flowing down the borehole. In fact, if included, the releases associated with these patches and cracks would lower the concentration of radionuclides flowing down the borehole for nuclides that are not solubility limited, such as ^{99}Tc and ^{129}I.

In summary, general corrosion and likely seismic degradation of the WP can be conservatively omitted from the human intrusion TSPA.

6.7.3 TSPA-LA Model Implementation

The stylized Human Intrusion Scenario is based on the human intrusion scenario in NRC rule 10 CFR 63.322 [DIRS 180319], and the individual protection standard for a human intrusion of the repository in 10 CFR 63.321 [DIRS 178394].

6.7.3.1 EBS Transport for Human Intrusion

Conceptual Model—The human intrusion borehole is assumed to be drilled from the ground surface (at a random location within the footprint of the repository), through the DS and a single WP (top and bottom) to the water table. All cladding, either CSNF or DSNF, is assumed destroyed when drilling intersects a WP. The initial fraction of failed cladding and the fraction of fuel available for corrosion are set to one. The WP type is randomly selected, either CDSP WP or CSNF WP. The location of the intrusion is also unknown and is therefore randomly placed in one of the five repository percolation subregions. After penetration of the WP via a drilling event, water will flow into the WP and the waste form degradation and mobilization will occur. Nominal Scenario Class submodels for Waste Form Degradation and Mobilization (Section 6.3.7) and EBS TH Environment (Section 6.3.2) were applied in the Human Intrusion Scenario. Radionuclide mass is released from the intruded WP to the EBS Transport Submodel (described in Section 6.3.8). Nominal Scenario Class submodels for transport of mass from the UZ to the SZ (described in Section 6.3.9) were modified for the Human Intrusion Scenario calculation to simulate mass transport through a borehole pathway.

Implementation—For a human intrusion event, the WP type (CSNF or CDSP) and WP location within the repository footprint need to be characterized. These properties, WP type and WP location, are treated as aleatory uncertainties and randomly selected from assigned probability weights:

1. The probability of a human intrusion event impacting a CSNF type WP is set equal to the fraction of CSNF WPs relative to the total number of WPs in the repository (combined CSNF and CDSP WPs). The probability of impacting a CDSP WP is assigned the remaining percentage. The number of WPs projected to be emplaced in the repository is 11,629 (Section 6.3.7, Table 6.3.7-1). There are 8,213 CSNF WPs (including 417 Naval SNF WPs) and 3,416 CDSP WPs (Section 6.3.7, Table 6.3.7-1). Thus, there is about 70 percent probability the intruded WP is a CSNF WP and about 30 percent probability the intruded WP is a CDSP WP.

2. The location of the WP intersected by a Human Intrusion drilling event can be randomly selected based upon the areal distribution of the five percolation subregions that have been defined over the repository horizon as defined by the EBS TH Environment Model Component described in Section 6.3.1. The mean infiltration, glacial-transition climate percolation flux values at the base of the PTn for each of the 3,264 MSTHM Process Model subdomains are used to group each of the subdomains into one of five repository percolation subregions (Section 6.3.2). The probability of an event (i.e., Human Intrusion failed WP) occurring in any of the five percolation subregions is the same as the distribution used to define the percolation subregions (i.e., 5 percent, 25 percent, 40 percent, 25 percent, and 5 percent) (Section 6.3.2.2.1).

Once the WP type and percolation subregion are selected, the representative temperature and relative humidity time histories are applied for calculating the waste form degradation rate, in-package chemistry, and transport properties in the EBS. The seepage flux through the intruded WP is applied by taking the percolation flux at the base of the PTn (supplied by the MSTHM; Section 6.3.2) for the selected percolation subregion. The Seepage DLL, used to compute the drift-scale seepage, is exercised using the same method as the Igneous Intrusion Modeling Case to get the percolation flux without flow focusing effects at the drift boundary (Section 6.5.1).

The percolation flux (a Darcy flux) is converted into a volumetric flux by multiplying it with the borehole cross-sectional area, 0.0324 m^2, which is calculated using an 8 in. (20.3 cm) borehole diameter. The borehole diameter is a fixed value based on the range of outer drill pipe diameters used in direct rotary drilling, or 2 3/8 to 6 in. (0.60 to 15.2 cm) (Driscoll 1986 [DIRS 116801], p. 282). It is assumed that the diameter of the borehole would be slightly larger than the outer drill pipe diameter; therefore, 8 in. (20.3 cm) is adopted.

The entire calculated volumetric flux is used as the flow through the WP for the advective transport calculation through the WP. For the diffusive transport calculation through the WP, the diffusive area is set equal to the cross-sectional area of the borehole, and the downstream boundary concentration is effectively set to zero concentration to maximize diffusion out of the WP. This is done by giving the invert cell pathway a very large water volume. The borehole water flux is assumed to flow directly into the penetrated WP without any diversion of the water by the DS or WP. The advective and diffusive mass flux out of the WP is summed and then passed to the UZ borehole below the WP.

6.7.3.2 UZ Transport for Human Intrusion

Conceptual Model—The radionuclide mass (both dissolved and colloidal) released from the WP penetrated by the human intrusion borehole is assumed to be vertically transported down the borehole to the water table. The borehole transport pathway is conceptualized to be an originally uncased borehole that undergoes degradation shortly after it was drilled from wall collapse. For the purposes of modeling transport through this degraded borehole, the matrix and fracture properties of the UZ rock types comprising the repository horizon are utilized. The rubble fill in the borehole is considered to have properties similar to the undisturbed repository host rock matrix while any preferential pathways within the rubble fill are given fracture properties of the host rock. As a result, the collapsed matrix blocks are expected to occupy about 99 percent of

the borehole volume while about 1 percent of the borehole volume is occupied by the fracture (consistent with the fracture porosity of the undisturbed rock). Although the preferential pathways may be tortuous and may not remain continuous throughout the length of the borehole and over the simulated time periods, the assumption of a continuous vertical fracture pathway over the entire length of the borehole is considered to simplify the modeling. When a human intrusion occurs, the three-dimensional TSPA-LA UZ Transport Submodel (Section 6.3.9) is replaced with a one-dimensional Human Intrusion Borehole Transport Submodel. The three-dimensional submodel calculates UZ transport using FEHM (V2.24-01, STN: 10086-2.24-01-00 [DIRS 179419]), whereas the Human Intrusion one-dimensional submodel calculates mass transport from the base of the WP to the water table using a single GoldSim pipe element.

The mass released from the intruded WP is passed to the one-dimensional pipe that simulates the borehole effects in the UZ beneath the WP. The properties that define the borehole fill are chosen to be consistent with the near-drift rock properties used in the UZ Transport Submodel (described in Section 6.3.9). The transport path length through the borehole is determined to be the vertical path length between the repository and the future water table. Because the repository host rock and water table elevations change over the UZ and SZ transport domains, the shortest possible transport path length is conservatively chosen. The volumetric water flux that is passed through the WP for computing advective transport is maintained throughout the borehole – there are no additional sources or sinks for water in the borehole.

Implementation—A schematic cross-section of a borehole bisecting the repository system and intruding through the underlying UZ to the water table is shown on Figure 6.7-5. The borehole is conceptualized to be filled with the rubble of collapsed matrix blocks that have preferential pathways similar to the fractures in the undisturbed host rock near the drift (Figure 6.7-6). The volume fraction occupied by the preferential pathways is assumed to be the same as the fracture porosity of the undisturbed host rock. Figure 6.7-7 is a schematic illustration of the key parameters used to calculate flow and transport through the UZ borehole pipe to the saturated zone and on to the biosphere. The fracture properties such as fracture aperture, porosity, and frequency (Table 6.7-5) are assumed to be the same as that for the undisturbed rock type in the vicinity of the repository horizon (such as the TSw unit). To be consistent with the UZ Transport Submodel, the property sets grouped for rock units TSw34, 35, 36, 37, and 38 are used to define the borehole properties (see property set associated with Group 8 given in Table 1 of DTN: LA0701PANS02BR.003_R2 [DIRS 180497]). For model simplification, these values do not vary with depth, although the borehole may cut across other lithologic units. Table 6.7-6 shows the calculated fracture properties associated with the borehole pathway. The number of vertical fractures within the diameter of the borehole is determined by considering the fracture frequency (calculated to be about four fractures per meter) and comparing it to the diameter of the borehole (approximately 0.2 m) calculated from a borehole cross-sectional area of 0.0324 m^2. This results in less than one fracture per borehole diameter, which is rounded up to be one fracture for the borehole. Assumption of vertical orientation of the fractures is consistent with the conceptualization of fractures in the UZ Transport Submodel (Section 6.3.9). The vertical fracture geometry is assumed to be like parallel plates without any infill material throughout the length of the borehole. The rubble filling the borehole surrounds the fracture. The fracture aperture and fracture porosity (fraction of the borehole volume occupied by the fracture) are considered fixed at 0.00264 m and 0.0105, respectively, which are average values for Group 8 rock type of the UZ Transport Submodel (DTN: LA0701PANS02BR.003_R2 [DIRS 180497]).

No uncertainty is applied to these parameters as it is not currently known how the uncertainty range would be affected by a borehole that cuts across several lithologic units of varying thicknesses. In order to compute the plan area of the fracture, the fracture width is needed in addition to the fracture aperture. Since the width of the cross-cutting fracture could vary in the circular borehole based on the fracture orientation, the average width, calculated by dividing the borehole cross-sectional area by its diameter, giving a value of about 0.16 m, is used.

Both advective and diffusive transport of radionuclides in the borehole are modeled by using the pipe pathway in GoldSim. A dual-porosity approach is adopted by modeling a discrete fracture that is surrounded by the matrix. The cross-sectional area of the pipe pathway is defined to be equal to the plan area of the fracture (a discrete fracture with no infill) while the matrix diffusion zones in the pipe pathway are used to define the rubble material that fills up the borehole around the fracture. The radionuclide mass flux from the WP is passed into the fracture, where it advects vertically downwards and diffuses into the surrounding matrix normal to the flow. The maximum diffusive distance into the matrix is set equal to half the distance between two fractures (about 0.125 m), and the entire surface of the fracture wall within the borehole is assumed to be wetted for diffusive transfer to the matrix (Figure 6.7-6). The diffusion of radionuclides irreversibly associated with colloids is not modeled between fracture and matrix, consistent with the UZ Transport Submodel implemented using FEHM DLL. All of the water flowing through the borehole is passed through the vertical fracture, which is the most conductive zone in the borehole. The fractures are assumed to be free flowing with no infill or obstructions. No retardation of the radionuclides (dissolved or colloidal) is modeled on the fracture surface. A fracture longitudinal dispersivity value of 10 m is assumed in the fracture that is consistent with the values used in the UZ Transport Submodel (SNL 2008 [DIRS 184748], Section 4.1.6).

The saturation values for the fracture and matrix along with the matrix density and porosity are taken from the EBS-UZ Interface Model described in Section 6.3.8, while the matrix tortuosity for diffusion calculations are taken from DTN: LB0702PAUZMTDF.001_R1 [DIRS 180776], for Rock Group 3, which includes values for rock unit TSw. Within the matrix media, the radionuclides are assigned the sampled K_d values for devitrified units used in the UZ Transport Submodel, for the entire pathway.

A flat lying water table beneath the repository is estimated to be located at an elevation of about 850 m, based on the water table rise estimated to occur during the glacial-transition climate period (SNL 2008 [DIRS 184748], Section 6.4.8). For the repository elevation, a value of 1,040 m is assumed which is consistent with present design documents where all repository drifts are at elevations of 1,039 m or higher (SNL 2007 [DIRS 179466], parameter 01-02). Thus, the path length of the borehole from the repository to the SZ is set at 190 m.

6.7.3.3 SZ Transport for Human Intrusion

Conceptual Model— The transport of radionuclides through the SZ in the Human Intrusion Scenario is identical to the Nominal Scenario Modeling Case, with the exception of the selection of the mass entry point to the SZ Source Region. From the borehole, the radionuclides are passed to one of the four SZ source regions (SZ region). The SZ source region is selected in such a way that it spatially corresponds to the EBS percolation subregion intersected during the

human intrusion event. Additionally, mass irreversibly associated with colloids are partitioned to fast and slow fractions in the SZ.

Implementation—In order to apply spatial correlation between the EBS percolation subregions (where the radionuclides enter the borehole) and SZ source regions (where the radionuclides exit the borehole), the five EBS percolation subregions are mapped to the four SZ source regions. The relative areal fraction of the five EBS percolation subregions within the four SZ source regions is determined first and then converted into the probability of each SZ source region to accept the radionuclides released from a given EBS percolation subregion through the borehole. A more detailed description of the four SZ source regions (quadrants) can be found in *Particle Tracking Model and Abstraction of Transport Processes* (SNL 2008 [DIRS 184748], Section 6.5.16).

The spreadsheet *fehm_repo_nodes_GT10%.xls* (DTN: LA0702PANS02BR.001_R1 [DIRS 180322]) provides the mapping of the UZ nodes at the repository horizon with the five EBS percolation subregions. There are 560 UZ nodes included in the five percolation subregions, along with their geographic locations in UTM coordinates. The 560 UZ node locations sorted by percolation subregion are mapped to the SZ quadrants in the spreadsheet *PS_EBSmaptoSZ.x*ls (output DTN: MO0708TSPAGENT.000 [DIRS 183000]) and the fraction of each of the five percolation subregions to the four SZ regions is calculated (Table 6.7-7).

6.7.3.4 Mean Annual Dose Submodel for the Human Intrusion Scenario

The TSPA-LA Model calculates the mean or median annual dose for the Human Intrusion Scenario using a two-step process. First, the TSPA-LA Model generates a set of 9,000 realizations, i.e., 9,000 annual dose histories, by using a LHS sample of 30 over the three aleatory parameters (WP type, percolation subregion, and SZ source region) and an LHS sample of 300 over the epistemically uncertain parameters in all the submodels. For each realization, the single human intrusion time is fixed at 200,000 years after the closure of the repository. The resulting 9,000 annual dose histories are then averaged in groups of 30, corresponding to the 30 aleatory samples for each epistemic sample thus producing 300 expected dose histories (Equation 6.1.2-26). These 300 expected dose histories are then averaged at each time to produce the overall mean annual dose history or their 50th percentile values are computed at each time to produce the median annual dose history. Note that the 300 epistemic samples for this modeling case match the 300 epistemic samples used for the overall performance assessment calculations.

6.7.4 Model Component Consistency and Conservatism in Assumptions and Parameters

To enhance understanding of the complex interactions within the TSPA-LA Model, a discussion of consistency among model components and submodels and identification of conservative assumptions in abstractions, process models, and parameter sets supporting the Human Intrusion Scenario are discussed below. Many of the nominal abstractions, process models, and parameter sets are used in the Human Intrusion Scenario and, therefore, many of the discussions of the implementation provisions in Section 6.3 apply to the Human Intrusion Scenario.

6.7.4.1 Consistency of Assumptions

WP and DS Material Corrosion in the Human Intrusion Scenario—General corrosion and SCC of the WP and DS materials are not applied to the WP/DS pair penetrated by a human intrusion event. The WP/DS general corrosion and SCC submodels are turned off for the Human Intrusion Modeling Case.

Effect on the TSPA-LA Model—The early penetration time of a WP/DS pair of 200,000 years postclosure during a Human Intrusion Scenario event is a conservative assumption. After the WP is penetrated, the entire waste form is exposed to the water flux through the WP. Applying the general corrosion model would not result in an earlier failure time (as demonstrated in Section 6.7.2). The radionuclide releases will be predominately via advective transport. Additional SCC cracks or general corrosion patches would not increase the volumetric water flux or mass flux of radionuclides released from the WP. This assumption will have no effect on the results of the Human Intrusion Scenario.

6.7.4.2 Identification of Conservatisms in Submodels and Abstractions

Human Intrusion Event Time—The probability associated with a human intrusion event time of 200,000 years postclosure assumes a WP would be degraded sufficiently to be undetected by drillers using the common techniques and practices that are currently employed in exploratory drilling for ground water in the region surrounding Yucca Mountain (NRC Rule 10 CFR 63.322(c) [DIRS 180319]). Assuming an early event time is conservative in respect to the probability of WP failure.

UZ Borehole as a Fracture Pathway—This fracture is conceived to be a highly conductive zone with elevated flow velocities through the fracture void space. Matrix diffusion into the host rock occurs and depends on fracture frequency. Using the fracture frequency for the UZ host rock (~ 4 per meter) yields only one fracture, given the diameter of the borehole. Matrix diffusion over the length is calculated as half the distance from the nearest fracture. Therefore, a limited amount of matrix medium is used to define the matrix diffusion zone between fractures in the pipe pathway.

Fewer fractures result in less surface area in the pipe pathway. A smaller surface area results in less sorption into the UZ rock matrix as the radionuclides travel through the UZ pipe pathway.

UZ Borehole Pathway Length—The Human Intrusion Scenario assumes the shortest possible transport path length. The conservative estimate for future water table rise places a flat water table at an 850 m elevation, reached during the glacial transition climate period (SNL 2008 [DIRS 184748], Section 6.4.8). Based on elevations reported in *TSPA Data Input Package for Requirements Analysis for Subsurface Facilities* (SNL 2007 [DIRS 179466], parameter number 01-02), a value of 1,040 m is assumed for the repository drift elevation (all repository drifts are at elevations of 1,039 m or higher).

A conservative length of the borehole from the repository to the SZ is set at 190 m. This conservatism tends to shorten radionuclide transport times.

6.7.5 Alternative Conceptual Model(s) for the Human Intrusion Scenario for TSPA-LA

Section 6.2.1 outlines the general consideration and treatment of ACMs used to support the TSPA-LA Model. ACMs related to individual submodels used in the Human Intrusion Scenario calculations are discussed in relevant Section 6.3 sections. There are no ACMs specific to the stylized Human Intrusion Scenario.

INTENTIONALLY LEFT BLANK

Table 6.7-1. Waste Package Specification and Design Dimensions

Parameter		Source	Description
Drop Height (TAD-bearing)	1.80 m	SNL 2007 [DIRS 179354], Figure 4-1, *In-Drift Configuration*.	Distance from drift crown to top of DS plus the distance from the DS to the top of WP.
Drop Height (CDSP WP)	1.63 m		
Nominal loaded mass for TAD-bearing waste package	162,055 lbm (73.5 mT)	SNL 2007 [DIRS 179394], Table 4-3	NA

Table 6.7-2. Specifications of Drilling Components

Parameter		Source	Description
Length of Drill String	300 m	SNL 2007 [DIRS 179466], Table 4-1	Assumed depth from the surface to the repository horizon. Based upon design information for minimum standoff distance from repository to water table.
Weight of Drill Steel	20 lb/ft (29.8 kg/m)	American Petroleum Institute 1992. Specification for Drill Pipe. API Spec. 5D, 3rd Edition, Table 6-1, 4.5-in drill pipe.	Drill pipe weight for standard 4.5 inch OD well pipe.
Length of Drill Collar	30 ft (9.1 m)	Grant Prideco 2003 [DIRS 183165], p. 99, drill collar number NC 44-62	Typical drill collar length for 6.25 inch OD drill collar.
Number of Drill Collars	4	NA	Assumed 100 ft of drill collar (10% of depth), based on common drilling practices.
Weight of Drill Collar	90.52 lbs (41.0 kg)	Grant Prideco 2003 [DIRS 183165], p. 99, drill collar number NC 44-62	Typical weight for 6.5 inch OD drill collar.
Weight of Drill Bit	38 kg (83 lb)	Varel International 2006 [DIRS 183166], Bit Weights Table, p.27, 8.5 " bit	Assumed approximately 8" (20.3 cm) borehole diameter, based on current drilling practices for a typical water well with an outer pipe diameter less than 6 in (15.2 cm) (Driscoll 1986 [DIRS 116801], p.282).
Total Weight of Drill String Assembly	13.8 mT	NA	(Length of Drill Sting × Weight of Drill Steel) + (Length of Drill Collar × Number of Drill Collars × Weight of Drill Collar)+ Weight of Drill Bit

Table 6.7-3. Uniaxial Compressive Strength and Young's Moduli by Rock Unit

Rock Unit	Uniaxial Compressive Strength Mean (MPa)	Tensile Strength Mean; Range (MPa)	Shear Modulus (GPa)	Elasticity (Young's Modulus) Mean; Range (GPa)
Topopah Springs Tuff – upper lithophysal zone (Tptpul)	19.3	–	–	13.0; 5.0–21.5
Topopah Springs Tuff – lower lithophysal zone (Tptpll)	23.8	8.3; 3.2–14.3	0.80–8.21	6.9; 5.0–9.2
Topopah Springs Tuff – middle nonlithophysal zone (Tptpmn)	188.8	10.9; 4.3–16.8	–	33.6; 13.4–47.3
Topopah Springs Tuff – lower nonlithophysal zone (Tptpln)	129.9	7.9; 4.8–13.7	–	33.6; 13.4–47.3

Sources: Mean Uniaxial Compressive Strength data (also referred to as Ultimate Strength) for the Tptpul and Tptpll are calculated as the mean of the strength data from *Drift Degradation Analysis* (SNL 2007 [DIRS 166107], Table E-9). The Mean Uniaxial Compressive Strength of the Tptpmn unit is from *Drift Degradation Analysis* (SNL 2007 [DIRS 166107], Table E-14). The Mean Uniaxial Compressive Strength of the Tptpln is calculated as the mean of the strength data from DTN: MO0408MWDDDMIO.002 [DIRS 171483], *Calculation Files\Material property\rock mass strength v2.xls*, worksheet Intact Strength (using Ultimate Differential Strength data with a Confining Pressure of either 0 or 0.1 MPa).

Tensile Strength (SNL 2007 [DIRS 166107], Table E-70).

Shear Modulus estimated for rock mass qualities 1 through 5 (SNL 2007 [DIRS 166107], Table E-10).

Mean for Elastic Modulus (Young's Modulus) (SNL 2007 [DIRS 166107], Tables E-6 and E-9).

Table 6.7-4. Material Properties for Drip Shield and Waste Package Fabrication

Engineered Barrier Material	Use	Yield Strength at 0.2% Offset (MPa)	Tensile Strength (MPa)	Modulus of Elasticity (GPa)
Titanium Grade 7[a] and Grade 16 (at room temperature)	Drip Shield	275–450	345	106.87
Titanium Grade 7[a] and Grade 16 (at 400°F/204°C)	Drip Shield	138–152	207–228	–
Titanium Grade 24	Drip Shield	–	895[b]	113.8[c]
Alloy 22 (UNS N06022) (at room temperature)[d]	Waste Package	358–403	765–802	206
Alloy 22 (UNS N06022) (at 400°F/204°C)[d]	Waste Package	262–303	662–701	196
Type 316 N Grade Stainless Steel (minimum properties)[e]	Waste Package	240	550	196

[a]DTN: MO0003RIB00073.000_R0 [DIRS 152926] for Titanium Grades 7 and 16.
[b]Tensile strength for Titanium Grade 24 (ASME 1998 [DIRS 145103], Section II, Table 1).
[c]Modulus of Elasticity for Titanium Grade 24 (ASM International 1990 [DIRS 141615], p. 621).
[d]DTN: MO0003RIB00071.000_R0 [DIRS 148850] for Alloy 22 (UNS N06022).
[e]DTN: MO0003RIB00076.000_R0 [DIRS 153044] for Type 316N.

Table 6.7-5. Borehole Properties used in UZ Flow and Transport Calculations

Parameter Name	Description	Parameter Value	Reference
HI_UZ_Borehole_Length	Distance between the repository horizon elevation and the estimated maximum water table elevation during the Glacial-Transition Climate.	190 m	(SNL 2008 [DIRS 184748], Section 6.4.8) and (BSC 2003 [DIRS 161727])
HI_UZ_Borehole_Disp	UZ borehole fracture dispersivity.	10 m	(SNL 2008 [DIRS 184748], Section 4.1.6)
HI_UZ_Fracture_Aperture	Distance between fracture openings in UZ borehole. Aperture, 2b (m), is calculated using fracture porosity and frequency distribution for rock units closest to the repository horizon (Group 8 or tswF[4,5]).	0.00264 m	(SNL 2008 [DIRS 184748], Table 6-15)
HI_Drill_Patch_Area	Borehole cross-sectional (circular) area. Also referred to as the drill patch area which is the area assumed to be affected by the intruding drill bit. This value is calculated using an 8 in (20.3 cm) borehole diameter. The borehole diameter is assumed to be slightly larger than the commonly used 2 3/8 to 6 in (0.60 to 15.2 cm) outer drill pipe diameters used in current drilling practices.	0.0324 m^2 (based on 8 in (20.3 cm) borehole diameter)	(Driscoll 1986 [DIRS 116801], p. 282)
HI_UZ_Fracture_Porosity	Fraction of the borehole area occupied by the fracture	0.0105	(SNL 2008 [DIRS 184748], Table 6-15)

Table 6.7-6. Borehole Fracture Properties used in UZ Flow and Transport Calculations

Parameter Name	Description	Parameter Value
Hl_UZ_Frac_Freq	The number of fractures per meter in host rock. Value is used as estimate of fractures in borehole and is calculated as fracture porosity divided by fracture aperture.	~4 1/m
Diff_Distance_To_Matrix	The distance between the fracture and matrix set equal to half the distance between two fractures.	~0.125 m
Radius_Drill_Patch	Radius of the borehole equal to the square root of the circular borehole cross-sectional area (drill patch area) divided by pi.	~0.101 m
Avg_Width_Fracture	Assuming the fracture is vertical in orientation and is cross-cutting the borehole, the fracture width is a function of the bisecting location relative to borehole center (Figure 6.7-6). This width can vary from a minimum value approaching zero to a maximum value equal to the borehole diameter (~0.2 m). Therefore, an average width is calculated by dividing the drill patch area by the borehole diameter.	~ 0.160 m
Fracture_Plan_Area	Cross-sectional (rectangular) area of the fracture. Equal to the product of the fracture aperture and average fracture width.	~0.0004 m^2
Fracture_Perimeter	The length of all sides of the rectangle created by fracture aperture and fracture width.	~0.324 m

Source: UZ Transport model parameters used to calculate the values listed in the table taken from DTN: LA0701PANS02BR.003_R2 [DIRS 180497].

Table 6.7-7. Fraction of SZ Source Region Nodes in each Percolation Subregion Bin

Fraction of SZ Source Region Nodes in each Percolation Subregion Bin					
	B1	**B2**	**B3**	**B4**	**B5**
SZ1	0.1071	0.3786	0.3973	0.4929	0.6071
SZ2	0.8929	0.4571	0.2857	0.1000	0.0000
SZ3	0.0000	0.1357	0.3125	0.4071	0.3929
SZ4	0.0000	0.0286	0.0045	0.0000	0.0000
Total	1	1	1	1	1

Source: Output DTN: MO0708TSPAGENT.000 [DIRS 183000], file *PS_EBSmaptoSZ.xls* .

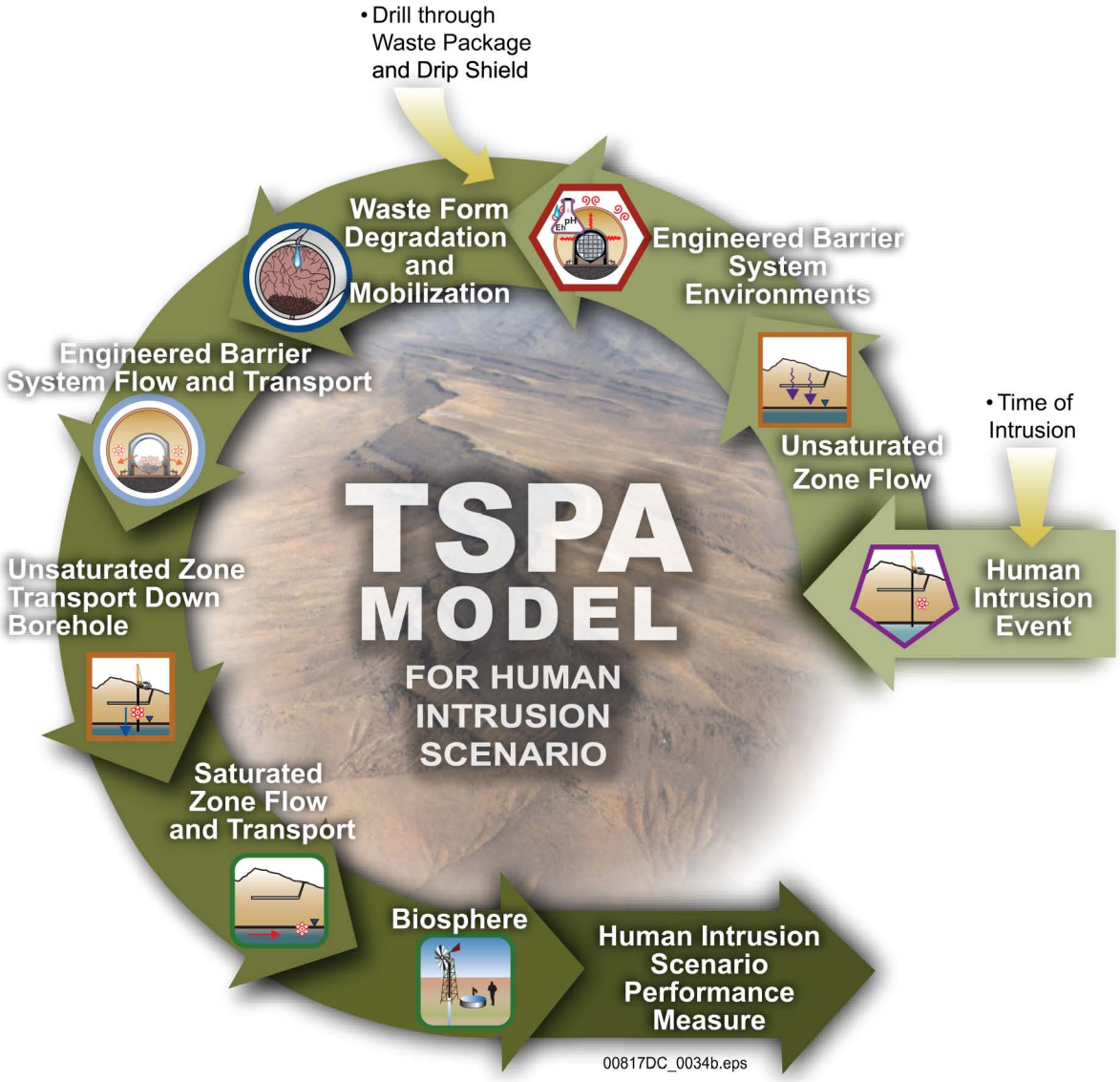

Figure 6.7-1. Schematic Representation of the TSPA-LA Model Components for the Human Intrusion Scenario

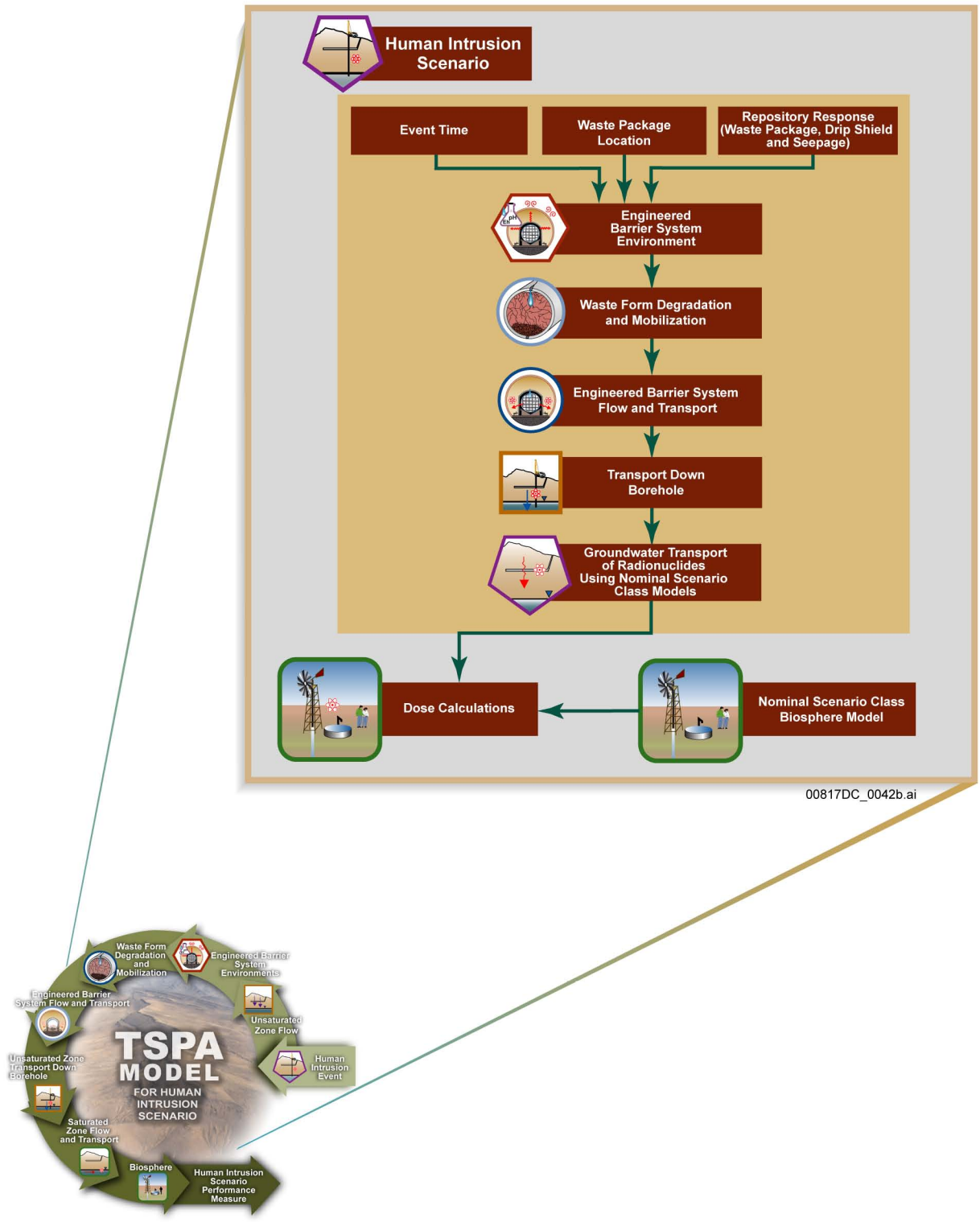

Figure 6.7-2. Information Flow Diagram for the Human Intrusion Scenario in the TSPA-LA Model

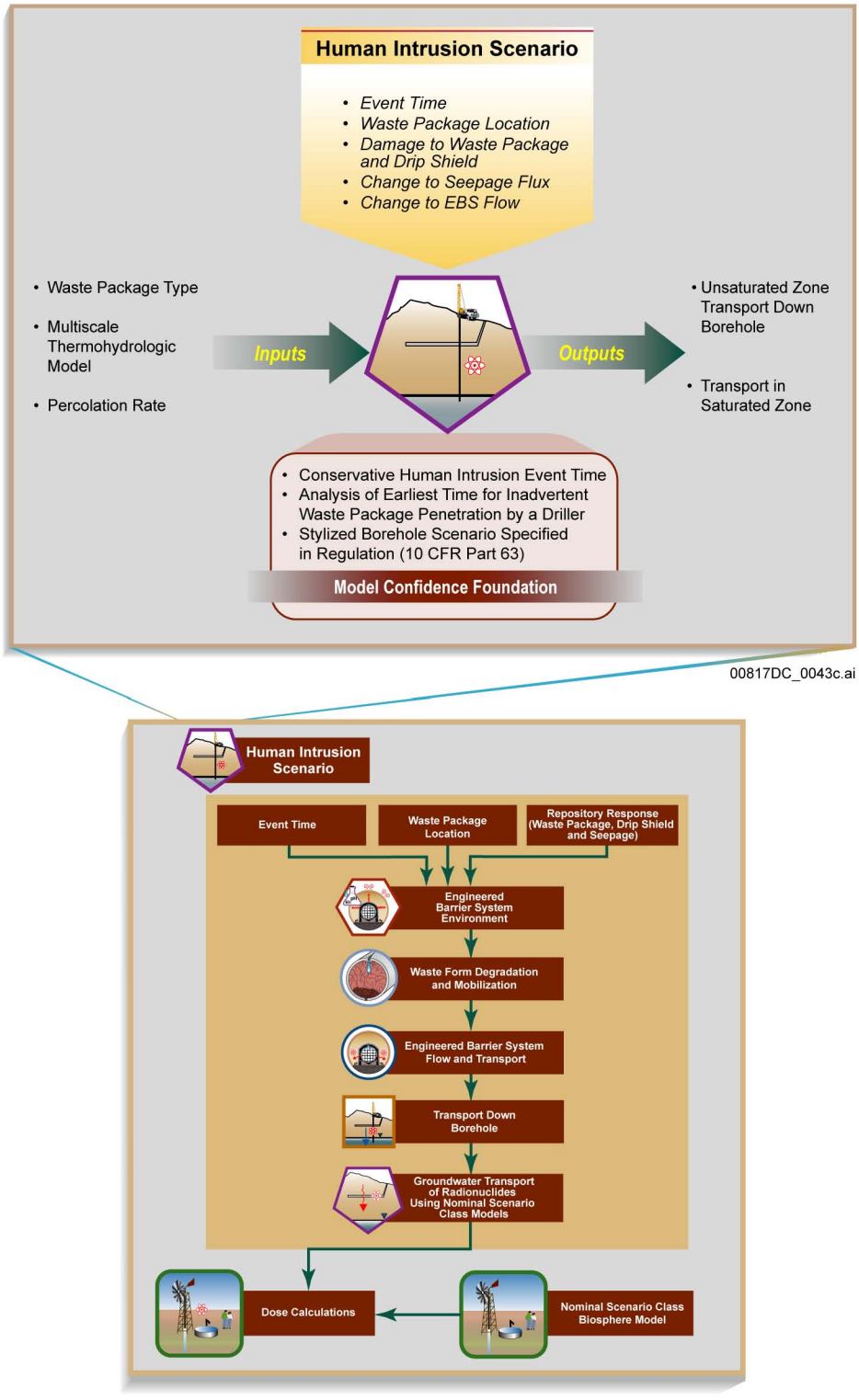

Figure 6.7-3. Inputs, Outputs, and Basis for Model Confidence for the Human Intrusion Scenario

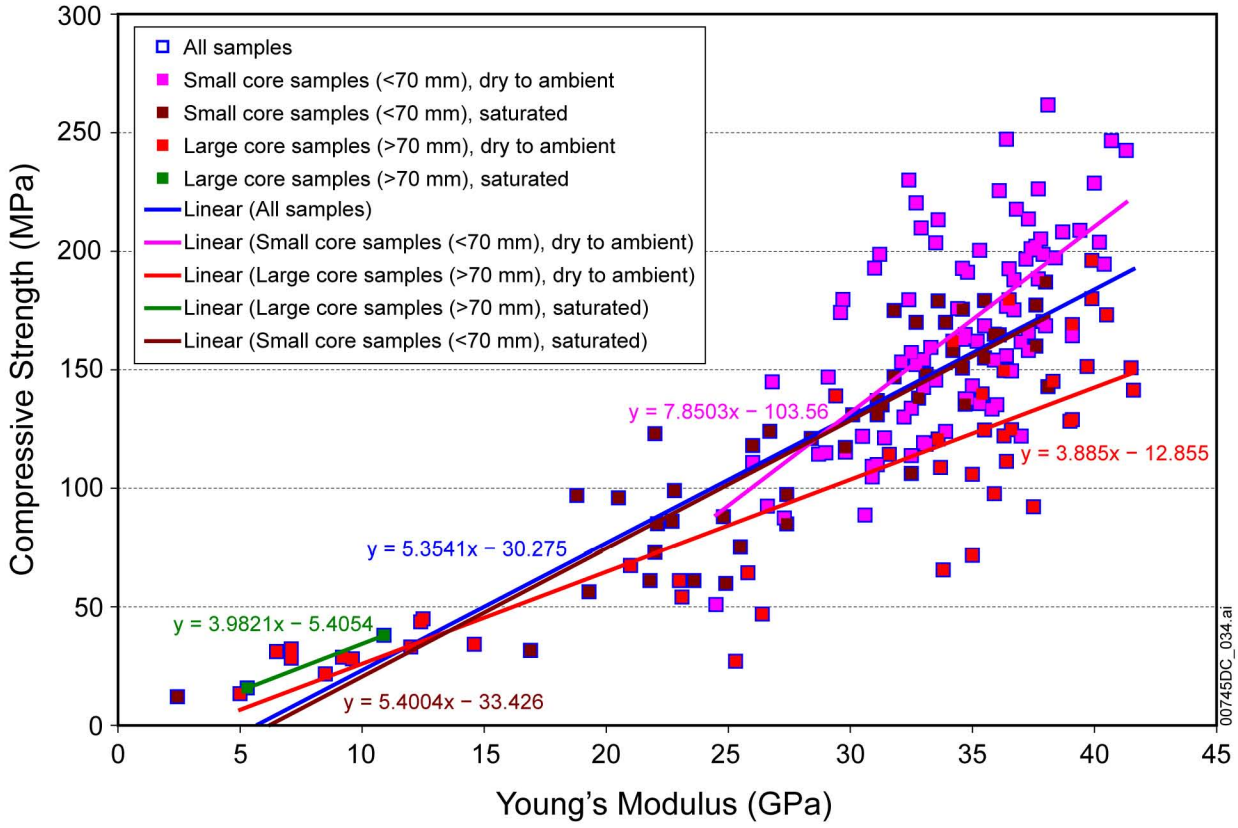

Source: BSC 2007 [DIRS 178693], Figure 6-37.

Figure 6.7-4. Unconfined Compressive Strength versus Young's Modulus in Tptpll Zone

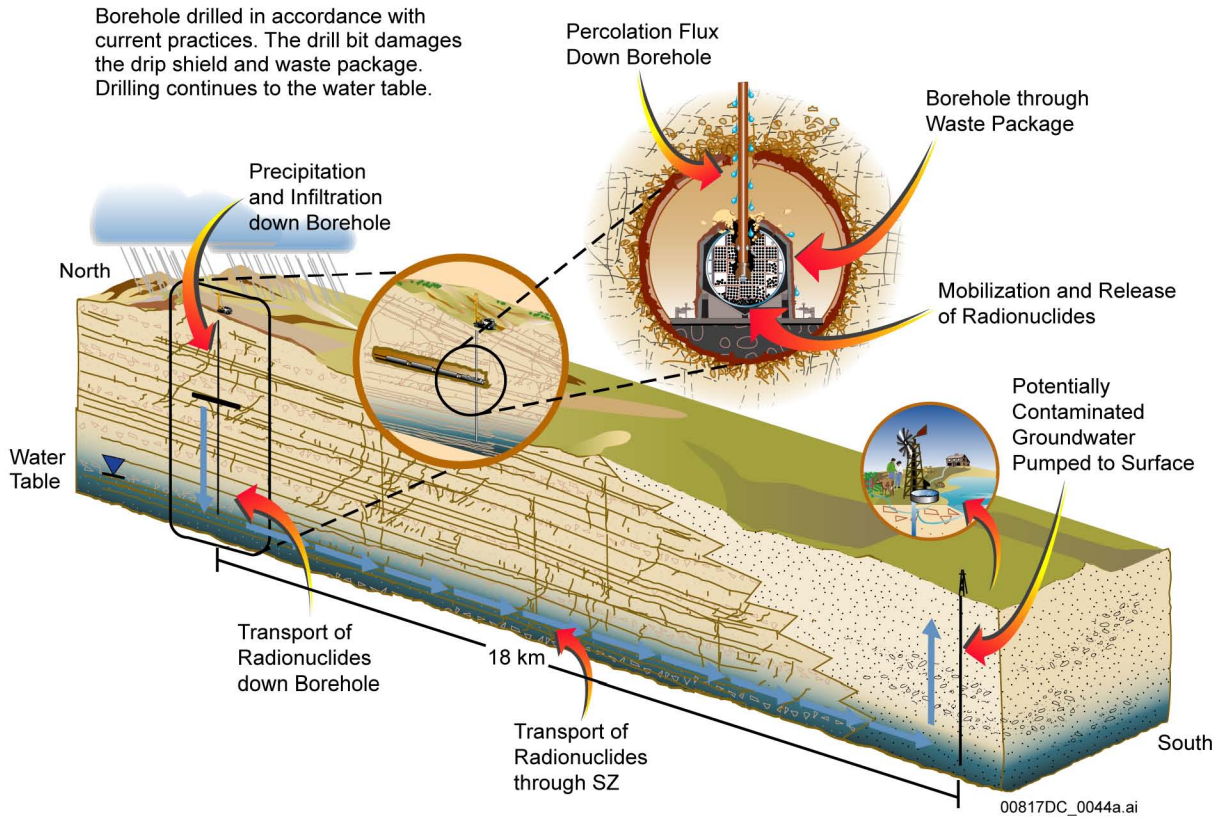

Figure 6.7-5. Conceptualization of the Human Intrusion Scenario for the TSPA-LA and Subsequent Radionuclide Releases to the Accessible Environment

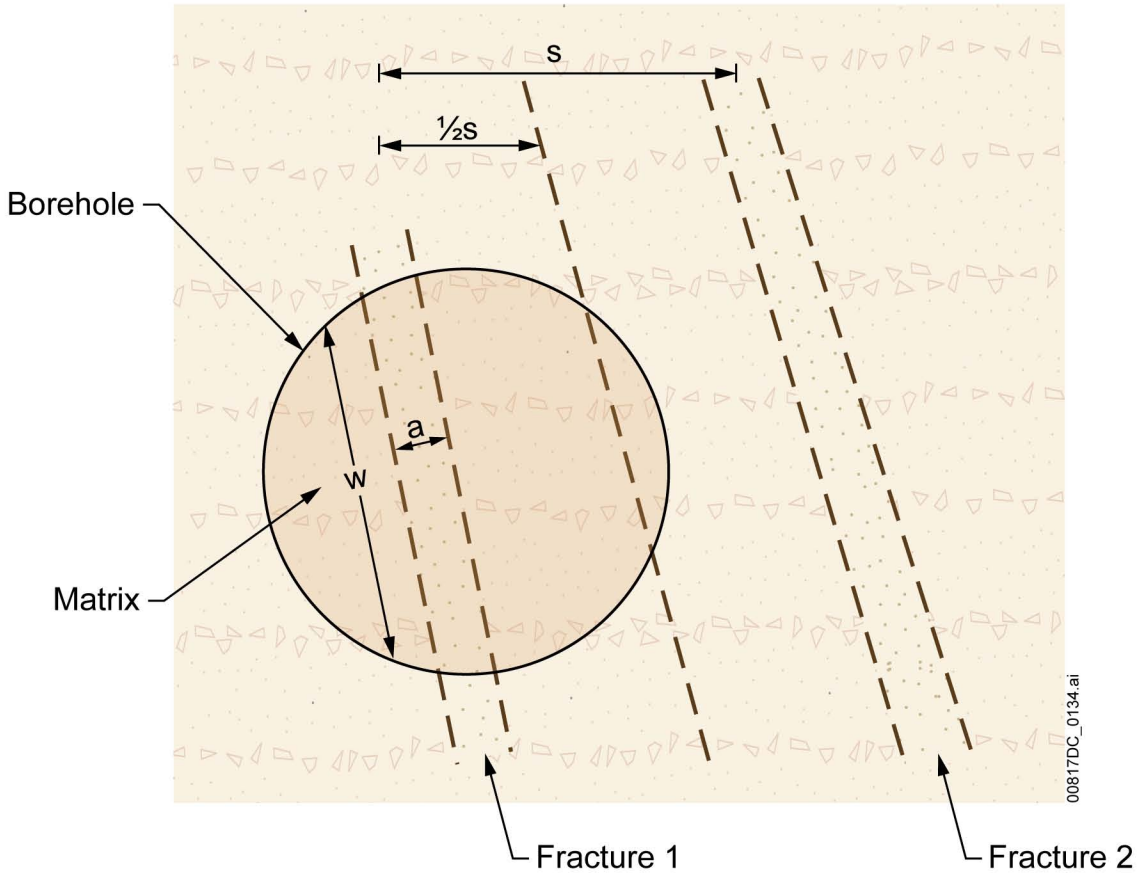

w = fracture width
s = fracture spacing
a = fracture aperture
½s = diffusion length between fracture and matrix
Borehole = Drill Patch Area = 0.0324 m^2

Figure 6.7-6. Schematic Depiction of Borehole (map view) with a Bisecting Fracture

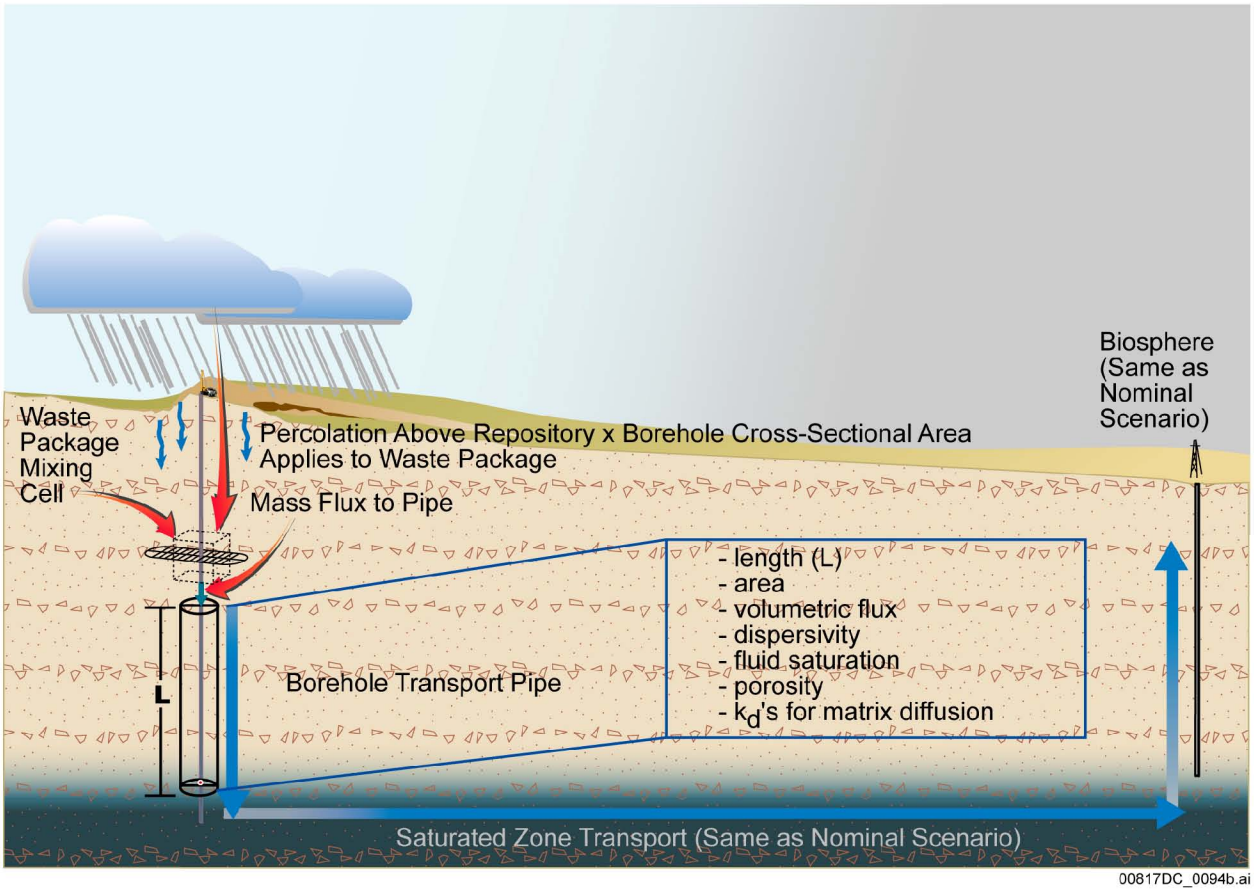

Figure 6.7-7. Schematic Illustration of the Implementation of Human Intrusion in TSPA-LA

INTENTIONALLY LEFT BLANK

QA: QA

MDL-WIS-PA-000005 REV00

January 2008

Total System Performance Assessment Model/Analysis for the License Application

Volume II

Prepared for:
U.S. Department of Energy
Office of Civilian Radioactive Waste Management
Office of Repository Development
1551 Hillshire Drive
Las Vegas, Nevada 89134-6321

Prepared by:
Sandia National Laboratories
OCRWM Lead Laboratory for Repository Systems
1180 Town Center Drive
Las Vegas, Nevada 89144

Under Contract Number
DE-AC04-94AL85000

DISCLAIMER

This report was prepared as an account of work sponsored by an agency of the United States Government. Neither the United States Government nor any agency thereof, nor any of their employees, nor any of their contractors, subcontractors or their employees, makes any warranty, express or implied, or assumes any legal liability or responsibility for the accuracy, completeness, or any third party's use or the results of such use of any information, apparatus, product, or process disclosed, or represents that its use would not infringe privately owned rights. Reference herein to any specific commercial product, process, or service by trade name, trademark, manufacturer, or otherwise, does not necessarily constitute or imply its endorsement, recommendation, or favoring by the United States Government or any agency thereof or its contractors or subcontractors. The views and opinions of authors expressed herein do not necessarily state or reflect those of the United States Government or any agency thereof.

Total System Performance Assessment Model/Analysis for the License Application

Volume II

MDL-WIS-PA-000005 REV00

January 2008

CONTENTS

Page

7. VALIDATION AND CONFIDENCE BUILDING 7-1
7.1 MODEL VALIDATION STRATEGY 7.1-1
7.1.1 Introduction 7.1-1
7.1.2 During-Development Model Validation Activities 7.1-3
7.1.3 Post-Development Model Validation Activities 7.1-9
7.2 COMPUTER CODE AND INPUT VERIFICATION 7.2-1
7.2.1 Selection and Verification of the Integrated System Software: GoldSim 7.2-1
7.2.2 Verification of Dynamically Linked Libraries in an Integrated System 7.2-3
7.2.3 Verification of Inputs in Total System Performance Assessment Database 7.2-3
7.2.4 Verification of Single Model Components 7.2-4
7.2.5 Verification of Coupling Among Submodels and Model Components 7.2-20
7.2.6 Verification of Range of Applicability of Submodels and Model Components 7.2-21
7.3 MODEL STABILITY 7.3-1
7.3.1 Statistical Stability 7.3.1-1
7.3.2 Numerical Accuracy of Expected Annual Dose 7.3.2-1
7.3.3 Temporal Stability 7.3.3-1
7.3.4 Analysis of Spatial Discretization 7.3.4-1
7.3.5 Stability of FEHM Particle Tracking Model 7.3.5-1
7.4 UNCERTAINTY AND VARIABILITY CHARACTERIZATION REVIEWS 7.4-1
7.4.1 Approach 7.4-1
7.4.2 Risk Informed Ranking of Scenario Classes and Modeling Cases 7.4-2
7.4.3 Risk Informed Identification of Stochastic Parameters Important to Dose 7.4-3
7.4.4 Review Team 7.4-7
7.4.5 Review Findings and Implementations 7.4-9
7.4.6 Summary of Sensitivity Analyses 7.4-18
7.5 SURROGATE WASTE FORM VALIDATION 7.5-1
7.5.1 Methodology 7.5-1
7.5.2 Spent Fuel Categories and Representation in Model 7.5-2
7.5.3 Naval Spent Fuel, Category 1 ..... 7.5-5
7.5.4 U.S. Department of Energy Spent Fuel, Categories 2 through 11 ..... 7.5-9
7.5.5 Selected Sensitivity Analyses 7.5-12
7.5.6 Summary of Results for U.S. Department of Energy Spent Fuel 7.5-14
7.6 CORROBORATION OF ABSTRACTION MODEL RESULTS WITH VALIDATED PROCESS MODELS 7.6-1
7.6.1 Introduction 7.6-1

CONTENTS (Continued)

Page

7.6.2 Requirement and Objective 7.6-2
7.6.3 Methods Used 7.6-3
7.6.4 Results of Corroboration 7.6-4
7.7 CORROBORATION OF RESULTS WITH AUXILIARY ANALYSES 7.7-1
7.7.1 Analysis of Single Realizations 7.7.1-1
7.7.2 Comparison with Simplified TSPA Analysis 7.7.2-1
7.7.3 Comparison with Electric Power Research Institute Analysis 7.7.3-1
7.7.4 Performance Margin Analysis 7.7.4-1
7.8 NATURAL ANALOGUES 7.8-1
7.8.1 Performance Assessment Comparison with Ash Fall at Cerro Negro 7.8-8
7.8.2 Nopal I Uranium Mine at Peña Blanca, Chihuahua, Mexico 7.8-10
7.9 TECHNICAL REVIEWS SUMMARY 7.9-1
7.9.1 TSPA-VA Review 7.9-4
7.9.2 International Review Team Peer Review 7.9-7
7.9.3 Independent Validation Review Team Review 7.9-9
7.10 SUMMARY OF MODEL CONFIDENCE BUILDING 7.10-1
7.10.1 Validation Strategy 7.10-3
7.10.2 Code and Input Verification 7.10-6
7.10.3 Model Stability Testing 7.10-8
7.10.4 Uncertainty Characterization Reviews and Sensitivity Analyses 7.10-11
7.10.5 Surrogate Waste Form Validation 7.10-13
7.10.6 Corroboration of Abstraction Results with Validated Process Models 7.10-13
7.10.7 Corroboration of Results with Auxiliary Analyses 7.10-14
7.10.8 Corroboration of Results with Natural Analogues 7.10-18
7.10.9 Technical Reviews Summary 7.10-19
7.10.10 Conclusions 7.10-21

FIGURES

Page

7.1-1. Generalized Performance Assessment Approach F7.1-1
7.1-2. Model Validation Approach F7.1-2

7.2-1. Comparison of EBS Physical and Chemical Environment pH Calculations between a Stand-Alone Verification Calculation and the TSPA-LA Model F7.2-1
7.2-2. Comparison of EBS Physical and Chemical Environment Ionic Strength Calculations between a Stand-Alone Verification Calculation and the TSPA-LA Model F7.2-2
7.2-3. Comparison of the Average Number of Waste Package Side Patch and Crack Failures between a Stand-Alone Verification Calculation and the TSPA-LA Model F7.2-3
7.2-4. Comparison of In-Package Chemistry Ionic Strength Calculations between a Stand-Alone Verification Calculation and the TSPA-LA Model F7.2-4
7.2-5. Comparison of In-Package Chemistry pH Calculations between a Stand-Alone Verification Calculation and the TSPA-LA Model F7.2-5
7.2-6. Comparison of In-Package Chemistry Total Carbonate Calculations between a Stand-Alone Verification Calculation and the TSPA-LA Model F7.2-6
7.2-7. Comparison of the Calculated Solubility of Americium (Am), Neptunium (Np), and Uranium (U) from the Verification of the Dissolved Concentrations Limits Submodel for the Nominal and Seismic Scenario Classes F7.2-7
7.2-8. Comparison of the Calculated Solubility of Uranium (U) from the Verification of the Dissolved Concentrations Limits Submodel for the Igneous Intrusion Modeling Case F7.2-8
7.2-9. Verification of the Dissolved and Colloidal Radionuclide Transport within the EBS Transport Submodel for the Case with Advection and Diffusion F7.2-9
7.2-10. Verification of the Dissolved and Colloidal Radionuclide Transport within the EBS Transport Submodel for the Case with Diffusion Only F7.2-10
7.2-11. Comparison of the ^{237}Np and ^{233}U Breakthrough Curves for the Verification of the Unsaturated Zone Transport Submodel F7.2-11
7.2-12. Comparison of the ^{237}Np Breakthrough Curve Using the SZ_Convolute DLL in the Verification of the 3-D Saturated Zone Flow and Transport Abstraction F7.2-12
7.2-13. Comparison of the Breakthrough Curves for ^{14}C and ^{237}Np from the Verification of the 1-D Saturated Zone Flow and Transport Abstraction F7.2-13
7.2-14. Comparison of Expected Annual Dose Calculations from the Verification of the Biosphere Submodel F7.2-14

FIGURES (Continued)

Page

7.2-15. Verification of the Impact on the EBS Thermal-Hydrologic Properties, as Represented by the CDSP WP Temperature, Resulting from an Igneous Intrusion Event F7.2-15

7.2-16. Comparison of the Diffusive Flux of ^{99}Tc across the EBS-UZ Interface for Different Placement Locations of an Effective Zero-Concentration Boundary below the Invert F7.2-16

7.3.1-1. Stability of Nominal Modeling Case: (a) Comparison of Expected Annual Dose for Three Replicates and (b) Confidence Interval around Mean Annual Dose F7.3.1-1

7.3.1-2. Stability of Waste Package Early Failure Modeling Case for 20,000 Years: (a) Comparison of Expected Annual Dose for Three Replicates and (b) Confidence Interval around Mean Annual Dose F7.3.1-2

7.3.1-3. Stability of Waste Package Early Failure Modeling Case for 1,000,000 Years: (a) Comparison of Expected Annual Dose for Three Replicates and (b) Confidence Interval around Mean Annual Dose F7.3.1-3

7.3.1-4. Stability of Drip Shield Early Failure Modeling Case for 20,000 Years: (a) Comparison of Expected Annual Dose for Three Replicates and (b) Confidence Interval around Mean Annual Dose F7.3.1-4

7.3.1-5. Stability of Drip Shield Early Failure Modeling Case for 1,000,000 Years: (a) Comparison of Expected Annual Dose for Three Replicates and (b) Confidence Interval around Mean Annual Dose F7.3.1-5

7.3.1-6. Stability of Igneous Intrusion Modeling Case for 20,000 Years: (a) Comparison of Expected Annual Dose for Three Replicates and (b) Confidence Interval around Mean Annual Dose F7.3.1-6

7.3.1-7. Stability of Igneous Intrusion Modeling Case for 1,000,000 Years: (a) Comparison of Expected Annual Dose for Three Replicates and (b) Confidence Interval around Mean Annual Dose F7.3.1-7

7.3.1-8. Stability of Volcanic Eruption Modeling Case for 20,000 Years: (a) Comparison of Expected Annual Dose for Three Replicates and (b) Confidence Interval around Mean Annual Dose F7.3.1-8

7.3.1-9. Stability of Volcanic Eruption Modeling Case for 1,000,000 Years: (a) Comparison of Expected Annual Dose for Three Replicates and (b) Confidence Interval around Mean Annual Dose F7.3.1-9

7.3.1-10. Stability of Seismic Ground Motion Modeling Case for 20,000 Years: (a) Comparison of Expected Annual Dose for Three Replicates and (b) Confidence Interval around Mean Annual Dose F7.3.1-10

7.3.1-11. Stability of Seismic Ground Motion Modeling Case for 1,000,000 Years: (a) Comparison of Expected Annual Dose for Three Replicates and (b) Confidence Interval around Mean Annual Dose F7.3.1-11

7.3.1-12. Stability of Seismic Fault Displacement Modeling Case for 20,000 Years: (a) Comparison of Expected Annual Dose for Three Replicates and (b) Confidence Interval around Mean Annual Dose F7.3.1-12

FIGURES (Continued)

Page

7.3.1-13. Stability of Seismic Fault Displacement Modeling Case for 1,000,000 Years: (a) Comparison of Expected Annual Dose for Three Replicates and (b) Confidence Interval around Mean Annual Dose F7.3.1-13

7.3.1-14. Stability of Human Intrusion Scenario: (a) Comparison of Expected Annual Dose for Three Replicates and (b) Confidence Interval around Mean Annual Dose F7.3.1-14

7.3.1-15. Stability of Total Mean Annual Dose 20,000 Years: (a) Comparison of Expected Annual Dose for Three Replicates and (b) Confidence Interval around Mean Annual Dose F7.3.1-15

7.3.1-16. Stability of Total Mean Annual Dose for 1,000,000 Years: (a) Comparison of Expected Annual Dose for Three Replicates and (b) Confidence Interval around Mean Annual Dose F7.3.1-16

7.3.2-1. Expected Annual Dose for the Nominal Modeling Case: (a) Latin Hypercube Sampling Size of 300 and (b) Latin Hypercube Sampling Size of 1,000 ..... F7.3.2-1

7.3.2-2. Uncertainty in Expected Annual Dose for the Nominal Modeling Case using Latin Hypercube Sampling Sizes of 300 and 1,000 ..... F7.3.2-2

7.3.2-3. Annual Dose Over 20,000 Years for the Igneous Intrusion Modeling Case Considering Additional Specified Event Times for Epistemic Realization 2 ..... F7.3.2-3

7.3.2-4. Expected Annual Dose Over 20,000 Years for the Igneous Intrusion Modeling Case Considering Additional Specified Event Times F7.3.2-4

7.3.2-5. Expected Annual Dose Over 1,000,000 Years for Igneous Intrusion Modeling Case Considering Additional Specified Event Times F7.3.2-5

7.3.2-6. Expected Annual Dose Over 1,000,000 Years for Volcanic Eruption Modeling Case Using Aleatory Latin Hypercube Sampling Sizes of 40 and 80 ..... F7.3.2-6

7.3.2-7. Expected Annual Dose for Volcanic Eruption Modeling Case Considering Additional Specified Event Times Over (a) 20,000 Years and (b) 1,000 Years F7.3.2-7

7.3.2-8. Annual Dose Over 20,000 Years for the Seismic Ground Motion Modeling Case Considering Additional Specified Event Times with Constant Damage Fraction 10^{-6} for Epistemic Realization 1 ..... F7.3.2-8

7.3.2-9. Annual Dose Over 20,000 Years for Seismic Ground Motion Modeling Case Considering Additional Specified Damage Fractions from a Seismic Event at 100 Years for Epistemic Realization 1 ..... F7.3.2-9

7.3.2-10. Annual Dose Over 20,000 Years for Seismic Ground Motion Modeling Case Considering Additional Specified Damage Fractions from a Seismic Event at 11,200 Years for Epistemic Realization 1 ..... F7.3.2-10

7.3.2-11. Expected Annual Dose Over 20,000 Years for Seismic Ground Motion Modeling Case Considering Additional Specified Event Times and Damage Fractions F7.3.2-11

FIGURES (Continued)

Page

7.3.2-12. Annual Dose vs. Damage Fraction for a Seismic Ground Motion Event at 100 Years for Epistemic Realization 1 ..... F7.3.2-12
7.3.2-13. Expected Annual Dose Over 20,000 Years from First Damaging Seismic Ground Motion Event F7.3.2-13
7.3.2-14. Expected Annual Dose Over 20,000 Years from All Damaging Seismic Ground Motion Events F7.3.2-14
7.3.2-15. Spatially-Averaged Waste Package Thickness for 1,000,000 Years for (a) CSNF WPs and (b) CDSP WPs F7.3.2-15
7.3.2-16. Bounding Probability of Drip Shield Plate Failure for (a) 250,000 Years and (b) 10,000 Years F7.3.2-16
7.3.2-17. Expected Annual Dose Over 10,000 Years from Seismic Ground Motion Events that Result in Drip Shield Plate Failure F7.3.2-17
7.3.2-18. Bounding Probability of Drip Shield Framework Failure for (a) 250,000 Years and (b) 10,000 Years F7.3.2-18
7.3.2-19. Volume of (a) Lithophysal and (b) Nonlithophysal Rockfall Over 20,000 Years F7.3.2-19
7.3.2-20. State Diagram for Waste Package Rupture in the Seismic Consequences Abstraction F7.3.2-20
7.3.2-21. Estimated Expected Annual Dose Over 10,000 Years from Seismic Ground Motion Events that Result in Rupture F7.3.2-21
7.3.2-22. Annual Dose from (a) One Early Failure CSNF WP and (b) One Early Failure CDSP WP Considering All Five Percolation Bins and 300 Epistemic Realizations F7.3.2-22
7.3.2-23. Expected Annual Dose for 1,000,000 Years from Seismic Ground Motion for Epistemic Realization 2 for Aleatory Sample Size of 30 and 90 ..... F7.3.2-23
7.3.2-24. Annual Dose Over 20,000 Years for Seismic Fault Displacement Modeling Case for (a) CDSP WPs and (b) CSNF WPs Considering Additional Specified Event Times with Constant Damage Area for Epistemic Realization 1 ..... F7.3.2-24
7.3.2-25. Annual Dose over 20,000 Years for a Fault Displacement Event at 200 Years Considering Additional Damage Areas for Epistemic Realization 1 for (a) CDSP WPs and (b) CSNF WPs F7.3.2-25
7.3.2-26. Expected Annual Dose Over 20,000 Years for Seismic Fault Displacement Modeling Case Considering Additional Specified Event Times and Damage Areas F7.3.2-26
7.3.2-27. Expected Annual Dose Over 1,000,000 Years for Human Intrusion Modeling Case Considering Increased Aleatory Sample Size F7.3.2-27

7.3.3-1. Annual Dose from One Early Failed Waste Package for (a) CSNF WP and (b) CDSP WP F7.3.3-1
7.3.3-2. Expected Annual Dose from Early Failed Waste Packages for Base Case and 20-Year Timestep Schemes F7.3.3-2

FIGURES (Continued)

Page

7.3.3-3. Annual Dose from an Igneous Intrusion at 400,000 Years for Three Timestep Schemes for Epistemic Realization 2 ..... F7.3.3-3
7.3.3-4. Detail of Annual Dose from an Igneous Intrusion at 400,000 Years for Three Timestep Schemes for Epistemic Realization 2 ..... F7.3.3-4
7.3.3-5. Expected Annual Dose from Igneous Intrusion for Base Case and Alternate Timestep Schemes for Five Epistemic Realizations F7.3.3-5
7.3.3-6. Annual Dose from an Igneous Intrusion at 1,000 Years for Three Timestep Schemes F7.3.3-6
7.3.3-7. Detail of Annual Dose from an Igneous Intrusion at 1,000 Years for Three Timestep Schemes F7.3.3-7
7.3.3-8. Annual Dose from a Seismic Ground Motion Event at 1,000 Years with Damage Fraction 10^{-6} for Three Timestep Schemes F7.3.3-8
7.3.3-9. Detail of Annual Dose from a Seismic Ground Motion Event at 1,000 Years with Damage Fraction 10^{-6} for Three Timestep Schemes F7.3.3-9
7.3.3-10. Expected Annual Dose from a Human Intrusion Event at 200,000 Years for Two Timestep Schemes F7.3.3-10
7.3.3-11. Detail of Expected Annual Dose from a Human Intrusion Event at 200,000 Years for Two Timestep Schemes F7.3.3-11

7.3.4-1. Comparison of the Representative and Comprehensive Thermal Hydrologic Data Sets for (a) EBS Releases of ^{99}Tc, ^{129}I, and ^{239}Pu, and (b) Time when the CSNF WP Temperature Drops Below Boiling for the Drip Shield Early Failure Modeling Case, 10th Percentile Infiltration Flux, Low Host-Rock Thermal Conductivity, Percolation Subregion 1 ..... F7.3.4-1
7.3.4-2. Comparison of the Representative and Comprehensive Thermal Hydrologic Data Sets for (a) EBS Releases of ^{99}Tc, ^{129}I, and ^{239}Pu, and (b) Time when the CSNF WP Temperature Drops Below Boiling for the Drip Shield Early Failure Modeling Case, 10th Percentile Infiltration Flux, Low Host-Rock Thermal Conductivity, Percolation Subregion 3 ..... F7.3.4-2
7.3.4-3. Comparison of the Representative and Comprehensive Thermal Hydrologic Data Sets for (a) EBS Releases of ^{99}Tc, ^{129}I, and ^{239}Pu, and (b) Time when the CSNF WP Temperature Drops Below Boiling for Drip Shield Early Failure Modeling Case, 50th Percentile Infiltration Flux, Mean Host-Rock Thermal Conductivity, Percolation Subregion 3 ..... F7.3.4-3
7.3.4-4. Comparison of the Representative and Comprehensive Thermal Hydrologic Data Sets for (a) EBS Releases of ^{99}Tc, ^{129}I, and ^{239}Pu, and (b) Time when the CSNF WP Temperature Drops Below Boiling for the Drip Shield Early Failure Modeling Case, 90th Percentile Infiltration Flux, High Host-Rock Thermal Conductivity, Percolation Subregion 3 ..... F7.3.4-4
7.3.4-5. Comparison of the Representative and Comprehensive Thermal Hydrologic Data Sets for (a) EBS Releases of ^{99}Tc, ^{129}I, and ^{239}Pu, and (b) Time when the CSNF WP Temperature Drops Below Boiling for the Drip Shield Early Failure Modeling Case, 90th Percentile Infiltration Flux, High Host-Rock Thermal Conductivity, Percolation Subregion 5 ..... F7.3.4-5

FIGURES (Continued)

Page

7.3.4-6. Comparison of the Representative and Comprehensive Thermal Hydrologic Data Sets for (a) EBS Releases of ^{99}Tc, ^{129}I, and ^{239}Pu, and (b) Time when the WP Relative Humidity is above 95 Percent for the Waste Package Early Failure Modeling Case, 10th Percentile Infiltration Flux, Low Host-Rock Thermal Conductivity, Percolation Subregion 1 ..... F7.3.4-6

7.3.4-7. Comparison of the Representative and Comprehensive Thermal Hydrologic Data Sets for (a) EBS Releases of ^{99}Tc, ^{129}I, and ^{239}Pu, and (b) Time when the WP Relative Humidity is above 95 Percent for the Waste Package Early Failure Modeling Case, 10th Percentile Infiltration Flux, Low Host-Rock Thermal Conductivity, Percolation Subregion 3 ..... F7.3.4-7

7.3.4-8. Comparison of the Representative and Comprehensive Thermal Hydrologic Data Sets for (a) EBS Releases of ^{99}Tc, ^{129}I, and ^{239}Pu, and (b) Time when the WP Relative Humidity is above 95 Percent for the Waste Package Early Failure Modeling Case, 50th Percentile Infiltration Flux, Mean Host-Rock Thermal Conductivity, Percolation Subregion 3..... F7.3.4-8

7.3.4-9. Comparison of the Representative and Comprehensive Thermal Hydrologic Data Sets for (a) EBS Releases of ^{99}Tc, ^{129}I, and ^{239}Pu, and (b) Time when the WP Relative Humidity is above 95 Percent for the Waste Package Early Failure Modeling Case, 90th Percentile Infiltration Flux, High Host-Rock Thermal Conductivity, Percolation Subregion 3..... F7.3.4-9

7.3.4-10. Comparison of the Representative and Comprehensive Thermal Hydrologic Data Sets for (a) EBS Releases of ^{99}Tc, ^{129}I, and ^{239}Pu, and (b) Time when the WP Relative Humidity is above 95 Percent for the Waste Package Early Failure Modeling Case, 90th Percentile Infiltration Flux, High Host-Rock Thermal Conductivity, Percolation Subregion 5..... F7.3.4-10

7.3.5-1. Annual Dose for the Drip Shield Early Failure Modeling Case Simulations using a Maximum of 500,000; 750,000; and 900,000 Particles in the Unsaturated Zone Transport Submodel F7.3.5-1

7.3.5-2. Annual Dose for the Igneous Intrusion Modeling Case Simulations Using a Maximum of 500,000; 750,000; and 900,000 Particles in the Unsaturated Zone Transport Submodel F7.3.5-2

7.3.5-3. Annual Dose for the Seismic Ground Motion Modeling Case Simulations Using a Maximum of 500,000; 750,000; and 900,000 Particles in the Unsaturated Zone Transport Submodel F7.3.5-3

7.3.5-4. Annual Dose Contribution from ^{237}Np for the Drip Shield Early Failure Modeling Case Simulations Using a Maximum of 500,000; 750,000; and 900,000 Particles in the Unsaturated Zone Transport Submodel F7.3.5-4

7.3.5-5. Annual Dose Contribution from ^{99}Tc for the Drip Shield Early Failure Modeling Case Simulations Using a Maximum of 500,000; 750,000; and 900,000 Particles in the Unsaturated Zone Transport Submodel F7.3.5-5

7.3.5-6. Annual Dose Contribution from ^{233}U for the Drip Shield Early Failure Modeling Case Simulations Using a Maximum of 500,000; 750,000; and 900,000 Particles in the Unsaturated Zone Transport Submodel F7.3.5-6

FIGURES (Continued)

Page

7.3.5-7. Annual Dose Contribution from ^{234}U for the Drip Shield Early Failure Modeling Case Simulations Using a Maximum of 500,000; 750,000; and 900,000 Particles in the Unsaturated Zone Transport Submodel F7.3.5-7

7.3.5-8. Annual Dose Contribution from (a) ^{239}Pu Total, (b) ^{239}Pu on Reversible Colloids, (c) ^{239}Pu on Retarded Irreversible Colloids, and (d) ^{239}Pu on Unretarded Irreversible Colloids for the Drip Shield Early Failure Modeling Case Simulations Using a Maximum of 500,000; 750,000; and 900,000 Particles in the Unsaturated Zone Transport Submodel F7.3.5-8

7.3.5-9. Annual Dose Contribution from ^{237}Np for the Igneous Intrusion Modeling Case Simulations Using a Maximum of 500,000; 750,000; and 900,000 Particles in the Unsaturated Zone Transport Submodel F7.3.5-10

7.3.5-10. Annual Dose Contribution from ^{99}Tc for the Igneous Intrusion Modeling Case Simulations Using a Maximum of 500,000; 750,000; and 900,000 Particles in the Unsaturated Zone Transport Submodel F7.3.5-11

7.3.5-11. Annual Dose Contribution from ^{233}U for the Igneous Intrusion Modeling Case Simulations Using a Maximum of 500,000; 750,000; and 900,000 Particles in the Unsaturated Zone Transport Submodel F7.3.5-12

7.3.5-12. Annual Dose Contribution from ^{234}U for the Igneous Intrusion Modeling Case Simulations Using a Maximum of 500,000; 750,000; and 900,000 Particles in the Unsaturated Zone Transport Submodel F7.3.5-13

7.3.5-13. Annual Dose Contribution from ^{239}Pu for the Igneous Intrusion Modeling Case Simulations Using a Maximum of 500,000; 750,000; and 900,000 Particles in the Unsaturated Zone Transport Submodel F7.3.5-14

7.3.5-14. Annual Dose Contribution from ^{237}Np for the Seismic Ground Motion Modeling Case Simulations Using a Maximum of 500,000; 750,000; and 900,000 Particles in the Unsaturated Zone Transport Submodel F7.3.5-15

7.3.5-15. Annual Dose Contribution from ^{99}Tc for the Seismic Ground Motion Modeling Case Simulations Using a Maximum of 500,000; 750,000; and 900,000 Particles in the Unsaturated Zone Transport Submodel F7.3.5-16

7.3.5-16. Annual Dose Contribution from ^{233}U for the Seismic Ground Motion Modeling Case Simulations Using a Maximum of 500,000; 750,000; and 900,000 Particles in the Unsaturated Zone Transport Submodel F7.3.5-17

7.3.5-17. Annual Dose Contribution from ^{234}U in for the Seismic Ground Motion Modeling Case Simulations Using a Maximum of 500,000; 750,000; and 900,000 Particles in the Unsaturated Zone Transport Submodel F7.3.5-18

7.3.5-18. Annual Dose Contribution from ^{239}Pu for the Seismic Ground Motion Modeling Case Simulations Using a Maximum of 500,000; 750,000; and 900,000 Particles in the Unsaturated Zone Transport Submodel F7.3.5-19

7.3.5-19. Annual Unsaturated Zone Mass Release of ^{237}Np for the Igneous Intrusion Modeling Case Simulations Using a Maximum of 500,000; 750,000; and 900,000 Particles in the Unsaturated Zone Transport Submodel F7.3.5-20

FIGURES (Continued)

Page

7.3.5-20. Annual Unsaturated Zone Mass Release of ^{99}Tc for the Igneous Intrusion Modeling Case Simulations Using a Maximum of 500,000; 750,000; and 900,000 Particles in the Unsaturated Zone Transport Submodel F7.3.5-21

7.3.5-21. Annual Unsaturated Zone Mass Release of ^{233}U for the Igneous Intrusion Modeling Case Simulations Using a Maximum of 500,000; 750,000; and 900,000 Particles in the Unsaturated Zone Transport Submodel F7.3.5-22

7.3.5-22. Annual Unsaturated Zone Mass Release of ^{234}U for the Igneous Intrusion Modeling Case Simulations Using a Maximum of 500,000; 750,000; and 900,000 Particles in the Unsaturated Zone Transport Submodel F7.3.5-23

7.3.5-23. Annual Unsaturated Zone Mass Release of ^{239}Pu for the Igneous Intrusion Modeling Case Simulations Using a Maximum of 500,000; 750,000; and 900,000 Particles in the Unsaturated Zone Transport Submodel F7.3.5-24

7.4-1. Uncertainty Characterization Review Process F7.4-1

7.5-1. Mean Annual Dose and Dose Contributors from DSNF Only Using Surrogate Inventory (One Waste Package Failure with no HLW) F7.5-1

7.5-2. Comparison of Radionuclide Activities on a per Waste Package Basis for the Nominal/Early Failure NSNF and CSNF Inventories F7.5-2

7.5-3. Comparison of Radionuclide Activities on a per Waste Package Basis for the Igneous Intrusion NSNF and CSNF Inventories F7.5-3

7.5-4. Comparison of Mean Annual Dose for a Single CSNF WP and a Single Waste Package with a Naval Source Term for the Drip Shield Early Failure Modeling Case F7.5-4

7.5-5. Comparison of Mean Annual Dose for a Single CSNF WP and Single Waste Package with a Naval Source Term for the Igneous Intrusion Modeling Case F7.5-5

7.5-6. Comparison of Radionuclide Activities on a per Waste Package Basis for the Igneous NSNF and CSNF Inventories for the Radionuclides that are Major Contributors to the Volcanic Eruption Mean Annual Dose F7.5-6

7.5-7. Comparison of Radionuclide Activities on a per Waste Package Basis for the Igneous NSNF and CSNF Inventories for the Radionuclides that are Major Contributors to the Human Intrusion Mean Annual Dose F7.5-7

7.5-8. Comparison of Radionuclide Activities on a per Waste Package Basis for the Igneous NSNF and CSNF Inventories for the Radionuclides that are Major Contributors to the Seismic Ground Motion Mean Annual Dose F7.5-8

7.5-9. Comparison of Mean Spent Fuel Degradation Rates for Categories 2 to 11, Air Alteration Rates for Categories 5 and 7, and Category 7 Bounding Surface Area of DSNF F7.5-9

FIGURES (Continued)

Page

7.5-10. Comparison of Mean Annual Dose from the Failure of One Waste Package of Plutonium/Uranium Alloy Spent Fuel (Category 2) with One Waste Package of DSNF Surrogate (with no HLW) F7.5-10

7.5-11. Comparison of Mean Annual Dose from the Failure of One Waste Package of Plutonium/Uranium-Carbide Spent Fuel (Category 3) with One Waste Package of DSNF Surrogate (with no HLW) F7.5-11

7.5-12. Comparison of Mean Annual Dose from the Failure of One Waste Package of Mixed Oxide Spent Fuel (Category 4) with One Waste Package of DSNF Surrogate (with no HLW) F7.5-12

7.5-13. Comparison of Mean Annual Dose from the Failure of One Waste Package of Uranium/Thorium-Carbide Spent Fuel (Category 5) with One Waste Package of DSNF Surrogate (with no HLW) F7.5-13

7.5-14. Comparison of Mean Annual Dose from the Failure of One Waste Package of Uranium/Thorium-Oxide Spent Fuel (Category 6) with One Waste Package of DSNF Surrogate (with no HLW) F7.5-14

7.5-15. Comparison of Mean Annual Dose from the Failure of One Waste Package of Uranium-Metal Spent Fuel (Category 7) with One Waste Package of DSNF Surrogate (with no HLW) F7.5-15

7.5-16. Comparison of Mean Annual Dose from the Failure of One Waste Package of Uranium-Oxide Spent Fuel (Category 8) with One Waste Package of DSNF Surrogate (with no HLW) F7.5-16

7.5-17. Comparison of Mean Annual Dose from the Failure of One Waste Package of Aluminum-Based Spent Fuel (Category 9) with One Waste Package of DSNF Surrogate (with no HLW) F7.5-17

7.5-18. Comparison of Mean Annual Dose from the Failure of One Waste Package of Miscellaneous Spent Fuel (Category 10) with One Waste Package of DSNF Surrogate (with no HLW) F7.5-18

7.5-19. Comparison of Mean Annual Dose from the Failure of One Waste Package of Uranium-Zirconium Hydride Spent Fuel (Category 11) with One Waste Package of DSNF Surrogate (with no HLW) F7.5-19

7.5-20. Comparison of the Weighted Sum (weighted by the number of packages per category) of the Mean Annual Dose from One Waste Package Failure of Categories 2 to 11 DSNF with One Waste Package Failure of DSNF Surrogate and Revision 1 DSNF Surrogate F7.5-20

7.5-21. Comparison of Mean Annual Dose from One Waste Package Failure of Uranium-Metal DSNF (Category 7) Using the Nominal Dissolution Model, Uranium-Metal Dissolution Model with Air Alteration, and Instantaneous Dissolution (with no HLW) F7.5-21

7.5-22. Comparison of Mean Annual Dose from One Waste Package Failure of Uranium/Thorium-Carbide DSNF (Category 5) Using the Nominal Dissolution Model, Uranium/Thorium-Carbide Dissolution Model with Air Alteration, and Instantaneous Dissolution (with no HLW) F7.5-22

FIGURES (Continued)

Page

7.5-23. Comparison of Mean Annual Dose from One Waste Package Failure of Uranium-Metal DSNF (Category 7) Using the Nominal Fuel Surface Area with the Bounding Fuel Surface Area (with no HLW) F7.5-23
7.5-24. Comparison of Mean Annual Dose from One Waste Package Failure of Uranium-Metal DSNF (Category 7) Using the Nominal Free Inventory with the Bounding Free Inventory (with no HLW) F7.5-24
7.5-25. Comparison of Mean Annual Dose from Aluminum-Based DSNF (Category 9) Minimum, Nominal, and Bounding Number of Waste Packages (with no HLW) F7.5-25
7.5-26. Comparison of Mean Annual Dose from One Waste Package Failure of Uranium-Metal DSNF (Category 7) Using the Nominal Inventory with the Bounding Inventory (with no HLW) F7.5-26
7.5-27. Plot of Key Radionuclides that Contribute to Mean Annual Dose from Five Canisters of HLW (with no DSNF) F7.5-27
7.5-28. Plot of Key Radionuclides that Contribute to Mean Annual Dose from One Waste Package Failure of Uranium-Metal Spent Fuel (Category 7) (with no HLW) F7.5-28
7.5-29. Plot of Key Radionuclides that Contribute to Mean Annual Dose from One Waste Package Failure of Uranium/Thorium-Carbide Spent Fuel (Category 5) (with no HLW) F7.5-29
7.5-30. Plot of Key Radionuclides that Contribute to Mean Annual Dose from One Waste Package Failure of Uranium/Thorium-Oxide Spent Fuel (Category 6) (with no HLW) F7.5-30

7.7.1-1. Expected Annual Dose for the Waste Package Early Failure Modeling Case for the 1,000,000-Year Simulation after Repository Closure: (a) Linear Time and (b) Log Time F7.7.1-1
7.7.1-2. Annual Dose from Realizations 5601 through 5620 of the Waste Package Early Failure Modeling Case for the 1,000,000-Year Simulation after Repository Closure F7.7.1-2
7.7.1-3. Major Radionuclide Contributors to Mean Annual Dose for the Waste Package Early Failure Modeling Case for the 1,000,000-Year Simulation after Repository Closure F7.7.1-3
7.7.1-4. Major Radionuclide Contributors to Mean Annual Dose for Realization 5608 of the Waste Package Early Failure Modeling Case for the 1,000,000-Year Simulation after Repository Closure F7.7.1-4
7.7.1-5. Release Rates of Technetium from the Waste Form, EBS, Unsaturated Zone, and Saturated Zone for Realization 5608 of the Waste Package Early Failure Modeling Case for the 1,000,000-Year Simulation after Repository Closure F7.7.1-5
7.7.1-6. (a) Release Rates and (b) Concentration of ^{239}Pu for Realization 5608 of the Waste Package Early Failure Modeling Case for the 1,000,000-Year Simulation after Repository Closure F7.7.1-6

FIGURES (Continued)

Page

7.7.1-7. (a) Dissolved Concentrations of Plutonium in the CSNF Waste Form Domain for Realization 5608 and (b) CSNF Waste Form Domain Chemistry for Realization 5608 of the Waste Package Early Failure Modeling Case for the 1,000,000-Year Simulation after Repository Closure.....F7.7.1-7

7.7.1-8. (a) Release Rates and (b) Concentration of ^{242}Pu for Realization 5608 of the Waste Package Early Failure Modeling Case for the 1,000,000-Year Simulation after Repository Closure.....F7.7.1-8

7.7.1-9. Major Radionuclide Contributors to Mean Annual Dose for Realization 5618 of the Waste Package Early Failure Modeling Case for the 1,000,000-Year Simulation after Repository Closure.....F7.7.1-9

7.7.1-10. Cumulative Release from HLW and DSNF Waste Forms for Realization 5618 of the Waste Package Early Failure Modeling Case for the 1,000,000-Year Simulation after Repository Closure.....F7.7.1-10

7.7.1-11. Release Rates of ^{99}Tc from the Waste Form, EBS, Unsaturated Zone, and Saturated Zone for Realization 5618 of the Waste Package Early Failure Modeling Case for the 1,000,000-Year Simulation after Repository Closure.....F7.7.1-11

7.7.1-12. (a) Release Rates and (b) Concentration of ^{239}Pu for Realization 5618 of the Waste Package Early Failure Modeling Case for the 1,000,000-Year Simulation after Repository Closure.....F7.7.1-12

7.7.1-13. DSNF Waste Form Domain Chemistry for Realization 5618 of the Waste Package Early Failure Modeling Case for the 1,000,000-Year Simulation after Repository Closure.....F7.7.1-13

7.7.1-14. (a) Release Rates and (b) Concentration of ^{242}Pu for Realization 5618 of the Waste Package Early Failure Modeling Case for the 1,000,000-Year Simulation after Repository Closure.....F7.7.1-14

7.7.1-15. Comparison of Expected Annual Dose for all Realizations along with that from Realization 228 (Epistemic Uncertainty Vector) of the Drip Shield Early Failure Modeling Case for the 1,000,000-Year Simulation after Repository Closure.....F7.7.1-15

7.7.1-16. Major Radionuclide Contributors to Mean Annual Dose for the Drip Shield Early Failure Modeling Case for the 1,000,000-Year Simulation after Repository Closure.....F7.7.1-16

7.7.1-17. Annual Dose for Ten Aleatory Uncertainty Realizations (vectors) for the Epistemic Uncertainty Realization 228 of the Drip Shield Early Failure Modeling Case for the 1,000,000-Year Simulation after Repository Closure.....F7.7.1-17

7.7.1-18. (a) Annual Dose along with Major Radionuclide Dose Contributors and (b) Contribution of Dissolved ^{239}Pu and ^{242}Pu and that Associated Irreversibly with Colloids (Denoted by Superscript Ic) for Realization 2278 of the Drip Shield Early Failure Modeling Case for the 1,000,000-Year Simulation after Repository Closure.....F7.7.1-18

FIGURES (Continued)

Page

7.7.1-19. EBS Release Rates of ^{99}Tc Along with Waste Package Temperatures for the Two Selected Realizations of Drip Shield Early Failure Modeling Case for the 1,000,000-Year Simulation after Repository Closure F7.7.1-19

7.7.1-20. Seepage Rate Incident on the Waste Package Showing the Effects of Drift Wall Condensation and Climate Change for the Two Selected Realizations of the Drip Shield Early Failure Modeling Case for the 1,000,000-Year Simulation after Repository Closure F7.7.1-20

7.7.1-21. Fraction of CSNF and CDSP Waste Form Degraded for the Two Selected Realizations of the Drip Shield Early Failure Modeling Case for the 1,000,000-Year Simulation after Repository Closure F7.7.1-21

7.7.1-22. Fraction of EBS Mass Flux Released into Unsaturated Zone Fractures for Selected Radionuclides for Realization 2278 of the Drip Shield Early Failure Modeling Case for the 1,000,000-Year Simulation after Repository Closure F7.7.1-22

7.7.1-23. Cumulative Mass Release of ^{99}Tc and ^{242}Pu from the EBS, Unsaturated Zone, and Saturated Zone for Realization 2278 of the Drip Shield Early Failure Modeling Case for the 1,000,000-Year Simulation after Repository Closure F7.7.1-23

7.7.1-24. Major Radionuclide Contributors to Mean Annual Dose for the Igneous Intrusion Modeling Case for the 1,000,000-Year Simulation after Repository Closure F7.7.1-24

7.7.1-25. Expected Annual Dose from the 300 Epistemic Vectors Along with their Quantiles and Expected Dose from Epistemic Uncertainty Vector #286 for the Igneous Intrusion Modeling Case for the 1,000,000-Year Simulation after Repository Closure F7.7.1-25

7.7.1-26. Annual Dose for Realizations 2851 through 2860 (representing Epistemic Uncertainty Vector 286) along with Selected Realization 2855 of the Igneous Intrusion Modeling Case for the 1,000,000-Year Simulation after Repository Closure F7.7.1-26

7.7.1-27. Annual Dose along with Major Radionuclide Dose Contributors for Realization 2855 of the Igneous Intrusion Modeling Case for the 1,000,000-Year Simulation after Repository Closure F7.7.1-27

7.7.1-28. Dissolved Concentrations and Solubility Limits of Neptunium, Plutonium, Uranium, and Radium in the CSNF Waste Form Domain for Percolation Subregion 3 Dripping Environment for Realization 2855 of the Igneous Intrusion Modeling Case for the 1,000,000-Year Simulation after Repository Closure F7.7.1-28

7.7.1-29. In-Package pH and P_{CO2} in the Waste Form Domain for Percolation Subregion 3 Dripping Environment for Realization 2855 of the Igneous Intrusion Modeling Case for the 1,000,000-Year Simulation after Repository Closure F7.7.1-29

7.7.1-30. Release Rate of Major Radionuclides from all WPs for Realization 2855 of the Igneous Intrusion Modeling Case for the 1,000,000-Year Simulation after Repository Closure F7.7.1-30

FIGURES (Continued)

Page

7.7.1-31. Advective and Diffusive Release Rates of Major Radionuclides from the CSNF WPs for Realization 2855 of the Igneous Intrusion Modeling Case for the 1,000,000-Year Simulation after Repository Closure F7.7.1-31

7.7.1-32. Total Dissolved Concentrations and Solubility Limits of Neptunium, Plutonium, Uranium, and Radium in the Corrosion Products Domain of CSNF WP Located in Percolation Subregion 3 Dripping Environment for Realization 2855 of the Igneous Intrusion Modeling Case for the 1,000,000-Year Simulation after Repository Closure..... F7.7.1-32

7.7.1-33. Cumulative Releases of: (a) ^{237}Np, (b) ^{234}U, (c) ^{242}Pu, and (d) ^{226}Ra from the EBS, Unsaturated Zone, and Saturated Zone for Realization 2,55 of the Igneous Intrusion Modeling Case for the 1,000,000-Year Simulation after Repository Closure..... F7.7.1-33

7.7.1-34. Concentrations of Major Radionuclides at the RMEI Location for Realization 2,855 of the Igneous Intrusion Modeling Case for the 1,000,000-Year Simulation after Repository Closure..... F7.7.1-35

7.7.1-35. Expected Annual Dose from the 300 Epistemic Uncertainty Realizations (Vectors) Along With their Quantiles and Expected Dose from Epistemic Uncertainty Vector #155 for the Seismic Ground Motion Modeling Case for the 1,000,000-Year Simulation after Repository Closure..... F7.7.1-36

7.7.1-36. Annual Dose from the Thirty Aleatory Vectors (Seismic Event Sequences) Associated with the Epistemic Vector 155 for the Seismic Ground Motion Modeling Case for the 1,000,000-Year Simulation after Repository Closure..... F7.7.1-37

7.7.1-37. Annual Dose along with Major Radionuclide Dose Contributors for Realization 4,641 of the Seismic Ground Motion Modeling Case for the 1,000,000-Year Simulation after Repository Closure..... F7.7.1-38

7.7.1-38. Number of Seismic Events and the Peak Ground Velocity Time History for Realization 4641 of the Seismic Ground Motion Modeling Case for the 1,000,000-Year Simulation after Repository Closure..... F7.7.1-39

7.7.1-39. Failure Fraction for the Drip Shield Plate and Framework and the Rubble Fill Fraction in the Drift (Lithophysal Zone) for Realization 4,641 of the Seismic Ground Motion Modeling Case for the 1,000,000-Year Simulation after Repository Closure..... F7.7.1-40

7.7.1-40. CDSP WP Failure History in all Five Percolation Subregions for Both Dripping and Non-Dripping Environments for Realization 4641 of the Seismic Ground Motion Modeling Case for the 1,000,000-Year Simulation after Repository Closure..... F7.7.1-41

7.7.1-41. CSNF WP Failure History for Each Percolation Subregion for Both Dripping and Non-Dripping Environments for Realization 4641 of the Seismic Ground Motion Modeling Case for the 1,000,000-Year Simulation after Repository Closure..... F7.7.1-42

7.7.1-42. CDSP WP Opening Area after Failure for Percolation Subregion 3 from Crack and Patches for Realization 4641 of the Seismic Ground

FIGURES (Continued)

Page

Motion Modeling Case for the 1,000,000-Year Simulation after Repository Closure F7.7.1-43
7.7.1-43. Diffusive Release Rates of: (a) ^{99}Tc and (b) ^{242}Pu from CDSP WPs from each Percolation Subregion for Realization 4641 of the Seismic Ground Motion Modeling Case for the 1,000,000-Year Simulation after Repository Closure F7.7.1-44
7.7.1-44. Dissolved Concentration of ^{242}Pu in the Corrosion Products Domain Compared to the Sorbed Concentration on Corrosion Products for CDSP Percolation Subregion 3 Dripping Environment for Realization 4641 of the Seismic Ground Motion Modeling Case for the 1,000,000-Year Simulation after Repository Closure F7.7.1-45
7.7.1-45. Diffusive Release Rates of: (a) ^{99}Tc and (b) ^{242}Pu from CSNF WPs from each Percolation Subregion for Realization 4641 of the Seismic Ground Motion Modeling Case for the 1,000,000-Year Simulation after Repository Closure F7.7.1-46
7.7.1-46. CSNF WP Opening Area after Failure for Percolation Subregion 3 from Cracks and Patches for Realization 4641 of the Seismic Ground Motion Modeling Case for the 1,000,000-Year Simulation after Repository Closure F7.7.1-47
7.7.1-47. Comparison of ^{242}Pu Cumulative Mass Released from the Inventory, Mass Sorbed on Corrosion Products, and the Dissolved Concentration in the Corrosion Products Domain for CSNF Percolation Subregion 3, Dripping Environment for Realization 4641 of the Seismic Ground Motion Modeling Case for the 1,000,000-Year Simulation after Repository Closure F7.7.1-48
7.7.1-48. pH and Ionic Strength Profile in the Corrosion Products Domain for CSNF Percolation Subregion 3, Dripping Environment for Realization 4641 of the Seismic Ground Motion Modeling Case for the 1,000,000-Year Simulation after Repository Closure F7.7.1-49
7.7.1-49. EBS Release Rates from CSNF and CDSP WPs (All Percolation Subregions) for Realization 4641 of the Seismic Ground Motion Modeling Case for the 1,000,000-Year Simulation after Repository Closure F7.7.1-50
7.7.1-50. Fraction of ^{242}Pu Mass Going to Unsaturated Zone Fractures as Compared to the Unsaturated Zone Matrix at the Repository Horizon for Realization 4641 of the Seismic Ground Motion Modeling Case for the 1,000,000-Year Simulation after Repository Closure F7.7.1-51
7.7.1-51. Cumulative Mass Release of ^{99}Tc and ^{242}Pu from the EBS, Unsaturated Zone, and Saturated Zone for Realization 4641 of the Seismic Ground Motion Modeling Case for the 1,000,000-Year Simulation after Repository Closure F7.7.1-52

FIGURES (Continued)

Page

7.7.1-52. Comparison of Saturated Zone Breakthrough Curves for ^{99}Tc and ^{242}Pu for All Four Saturated Zone Regions for Realization 4641 of the Seismic Ground Motion Modeling Case for the 1,000,000-Year Simulation after Repository Closure....F7.7.1-53

7.7.1-53. Saturated Zone Release to the Biosphere for ^{99}Tc and ^{242}Pu for Realization 4641 of the Seismic Ground Motion Modeling Case for the 1,000,000-Year Simulation after Repository Closure....F7.7.1-54

7.7.2-1. Mean Annual Dose and Annual Dose for Individual Radionuclides for the Simplified TSPA Analysis Waste Package Early Failure Modeling Case for 1,000,000 Years after Repository Closure....F7.7.2-1

7.7.2-2. Annual Dose for the Simplified TSPA Analysis Waste Package Early Failure Modeling Case for All Realizations for 1,000,000 Years after Repository Closure....F7.7.2-2

7.7.2-3. Time-Slice Comparison of the Simplified TSPA Analysis Results against the TSPA-LA Model Results for the Waste Package Early Failure Modeling Case....F7.7.2-3

7.7.2-4. Mean Annual Dose and Annual Dose for Individual Radionuclides for the Simplified TSPA Analysis Nominal Modeling Case....F7.7.2-4

7.7.2-5. Annual Dose for the Simplified TSPA Analysis Nominal Modeling Case....F7.7.2-5

7.7.2-6. Time-Slice Comparison of the Simplified TSPA Analysis Results against the TSPA-LA Model Results for the Nominal Modeling Case....F7.7.2-6

7.7.2-7. Mean Annual Dose and Annual Dose for Individual Radionuclides for the Simplified TSPA Analysis Seismic Ground Motion Modeling Case for 1,000,000 Years after Repository Closure....F7.7.2-7

7.7.2-8. Mean Annual Dose and Annual Dose for Individual Radionuclides for the Simplified TSPA Analysis Seismic Ground Motion Modeling Case for 1,000,000 Years after Repository Closure....F7.7.2-8

7.7.2-9. Time-Slice Comparison of the Simplified TSPA Analysis Results against the TSPA-LA Model Results for the Seismic Ground Motion Modeling Case....F7.7.2-9

7.7.2-10. Mean Annual Dose and Annual Dose for Individual Radionuclides for the Simplified TSPA Analysis Igneous Intrusion Modeling Case for 1,000,000 Years after Repository Closure....F7.7.2-10

7.7.2-11. Mean Annual Dose and Annual Dose for Individual Radionuclides for the Simplified TSPA Analysis Igneous Intrusion Modeling Case for 1,000,000 Years after Repository Closure....F7.7.2-11

7.7.2-12. Time-Slice Comparison of the Simplified TSPA Analysis Results against the TSPA-LA Model Results for the Igneous Intrusion Motion Modeling Case....F7.7.2-12

7.7.3-1. Comparisons of (a) Seepage Rate and (b) Seepage Fraction versus Infiltration Rates as Used in the EPRI Analysis and the TSPA-LA Model....F7.7.3-1

FIGURES (Continued)

Page

7.7.3-2. TSPA-LA Nominal Scenario Class Mean Failure Curves for the Drip Shield and Waste Package F7.7.3-2
7.7.3-3. TSPA-LA Mean Dose Histories for Major Radionuclides for the Combined Early Failure and Nominal Scenario Classes F7.7.3-3

7.7.4-1. Total Expected Annual Dose for the Performance Margin Analysis for 10,000 Years after Repository Closure F7.7.4-1
7.7.4-2. Comparison of the Total Mean Annual Dose for the TSPA-LA Model to the Performance Margin Analysis 10,000 Years after Repository Closure F7.7.4-2
7.7.4-3. Contributions of Individual Radionuclides to Total Mean Annual Dose for (a) the TSPA-LA Model and (b) the Performance Margin Analysis 10,000 Years after Repository Closure F7.7.4-3
7.7.4-4. Total Expected Annual Dose for the Performance Margin Analysis for 1,000,000 Years after Repository Closure F7.7.4-4
7.7.4-5. Comparison of the Total Mean Annual Dose for the TSPA-LA Model to the Performance Margin Analysis 1,000,000 Years after Repository Closure F7.7.4-5
7.7.4-6. Contributions of Individual Radionuclides to Total Mean Annual Dose for (a) the TSPA-LA Model and (b) the Performance Margin Analysis 1,000,000 Years after Repository Closure F7.7.4-6

7.8-1. Comparison of Ash Fall at Cerro Negro with ASHPLUME Simulated Results F7.8-1
7.8-2. TSPA-LA Model for the Igneous Scenario Class Volcanic Eruption Modeling Case F7.8-2
7.8-3. Location of Peña Blanca Study Area F7.8-3
7.8-4. Location of Peña Blanca Nopal I Ore Deposit F7.8-4
7.8-5. Peña Blanca Mine Shaft Schematic F7.8-5
7.8-6. Geologic Characterization of Nopal I Ore Body F7.8-6
7.8-7. Location of Observation Wells at the Nopal I Mine in the Peña Blanca Uranium District F7.8-7
7.8-8. Geophysical and Geologic Logs of Observation Well PB1 ..... F7.8-8
7.8-9. Schematic Northwest to Southeast Cross Section of the Sierra Peña Blanca Showing the Relative Position of the Water Table in the Encinillas Basin, the Nopal I District, and the El Cuervo Basin F7.8-9
7.8-10. Comparative Reaction Paragenetic Sequences for Uranium Alteration Phases F7.8-10
7.8-11. Uranium Concentration Determined in Groundwater Samples from Wells at and Near the Nopal I Ore Deposit F7.8-11

TABLES

Page

7.1-1. TSPA-LA Model Validation Analyses T7.1-1

7.2-1. Verification of TSPA-LA Model Dynamically Linked Libraries T7.2-1
7.2-2. Verification of Dynamically Linked Libraries and Model Abstractions Used in the TSPA-LA Model T7.2-2
7.2-3. Verification Summary of the Drift Seepage Dynamically Linked Library T7.2-5
7.2-4. Comparison of the Drift-Wall Condensation Rates Verification Calculations T7.2-6
7.2-5. Summary of the Verification Inputs and Outputs for Calculation of the Pco_2 Values in the EBS Physical and Chemical Environment Abstraction T7.2-7
7.2-6. Summary of Input Values Used in EBS Physical and Chemical Environment Verifications of pH and Ionic Strength T7.2-8
7.2-7. Values Used in the WAPDEG Dynamically Linked Library for Verifying the TSPA-LA Model T7.2-8
7.2-8. Summary of Input/Output Values and GoldSim Verification Checks for the CSNF Rind Volume and Mass Calculations T7.2-9
7.2-9. Summary of Input/Output Values and GoldSim Verification Checks for the CDSP WPs HLW Rind Thickness and Mass T7.2-10
7.2-10. Summary of Verification Checks for the CSNF Waste Form Degradation Submodel T7.2-11
7.2-11a. Summary of Verification Checks for the HLW Glass Degradation Submodel T7.2-12
7.2-11b. Summary of Verification Checks for the HLW Glass Degradation Submodel T7.2-13
7.2-12. Summary of Parameter Ranges Used in Developing the Input Data Sets for the In-Package Chemistry Submodel Verifications of Ionic Strength, pH, and Total Carbonate T7.2-14
7.2-13. Comparison of Results for the ASHPLUME Verification T7.2-14
7.2-14. Comparison of Results for the FAR Verification T7.2-14
7.2-15. Comparison of the Seismic Damage Abstraction Ground Motion Submodel Verification Calculations T7.2-15
7.2-16. Comparison of the Seismic Damage Abstraction Fault Displacement Submodel Verification Calculations T7.2-16

7.3.2-1. Times for Igneous Intrusions in the Base Case and the Expanded Case T7.3.2-1
7.3.2-2. Event Times in the Volcanic Eruption Modeling Case for 20,000 Years T7.3.2-2
7.3.2-3. Event Times and Damage Fractions in the Seismic Ground Motion Modeling Case for 20,000 Years T7.3.2-2
7.3.2-4. Event Times and Damage Areas in the Seismic Fault Displacement Modeling Case for 20,000 Years T7.3.2-2

7.3.3-1. Timestep Schemes Used in Temporal Stability Analysis T7.3.3-1

TABLES (Continued)

Page

7.3.4-1. Summary of the Thermal-Hydrologic Variability Cases Run to Validate the Use of Representative Thermal-Hydrologic Data Sets Over the Use of Computationally Expensive Comprehensive Thermal-Hydrologic Data Sets...T7.3.4-1

7.3.5-1. Peak Dose Values for Drip Shield Early Failure, Igneous, and Seismic Ground Motion Modeling Cases Evaluated for Particle Stability T7.3.5-1

7.4-1. Key TSPA Parameters for Seismic Scenario Class for the Ground Motion and Rockfall Abstractions.....T7.4-1

7.4-2. Key TSPA Parameters for Igneous Scenario Class T7.4-1

7.4-3. Key TSPA Parameter Sets for the Nominal Scenario Class by Model Abstraction.....T7.4-2

7.4-4. Summary of Selected Sensitivity Analysis Results T7.4-4

7.5-1. U.S. Department of Energy Spent Fuel Categories Analyzed for the TSPA-LA Model.....T7.5-1

7.5-2. Radionuclide Inventory for Each U.S. Department of Energy Spent Fuel Category and the U.S. Department of Energy Surrogate Spent Fuel (grams/waste package).....T7.5-2

7.5-3. Number of Canisters by Size of Canister and Total Number of Waste Packages for Each DSNF Category T7.5-4

7.5-4. Dissolution Models and Fuel Surface Areas for Each DSNF Category T7.5-5

7.5-5. Disposition of the Use of CSNF as a Surrogate for NSNF for the TSPA-LA Model.....T7.5-6

7.5-6. Air Alteration Rate for DSNF Category 5, Uranium/Thorium Carbide, and Category 7, Uranium Metal T7.5-6

7.5-7. Nominal and Bounding Inventories for Uranium-Metal Spent Fuel (Category 7) T7.5-7

7.6-1. Model Abstractions and Confidence in the Direct-Input TSPA-LA Parameters.....T7.6-1

7.7.1-1. Calculation of Dose Per Unit Concentration of Selected Radionuclides for the Igneous Intrusion Modeling Case (for Realization 2855).....T7.7.1-1

7.7.2-1. Summary of Modeling Approaches Used for TSPA-LA Model and the Simplified TSPA Analysis.....T7.7.2-1

7.7.3-1. Model Components and Processes Represented in the TSPA-LA Model and the EPRI TSPA Analysis T7.7.3-1

7.8-1. ASHPLUME Parameters Used for Cerro Negro Comparison.....T7.8-1

7.9-1. Summary of Responses to the Remaining IVRT Comments.....T7.9-1

7. VALIDATION AND CONFIDENCE BUILDING

The intended purpose of the Total System Performance for the License Application (TSPA-LA) Model, as defined in Section 1.1 of *Technical Work Plan for: Total System Performance Assessment FY 07-08 Activities* (SNL 2008 [DIRS 184920], Section 2.3.5), is to provide the TSPA-LA Model for use in evaluations of compliance with the quantitative postclosure requirements of U.S. Nuclear Regulatory Commission (NRC) Proposed Rule 10 CFR Part 63 (DIRS 178394] and [DIRS 180319]).

The TSPA-LA Model analyzes the complex system of features, events, and processes (FEPs), natural disruptive events, such as igneous intrusion, volcanic eruption, seismic ground motion and fault displacement, and a human-intrusion scenario that could occur at the Yucca Mountain Repository after closure of the repository during the first 10,000 years but within the period of geologic stability (i.e., to and at 1,000,000 years after disposal) (NRC Proposed Rule 10 CFR 63.302 [DIRS 178394]). The FEPs' screening and scenario development for the TSPA-LA Model are discussed in Section 6.1.1. The modeling cases to address the scenario classes are discussed in Section 6.1.2. The modeling cases include:

- Nominal Modeling Case
- Drip Shield Early Failure (EF) Modeling Case
- Waste Package Early Failure (EF) Modeling Case
- Igneous Intrusion Modeling Case
- Volcanic Eruption Modeling Case
- Seismic Ground Motion (GM) Modeling Case
- Seismic Fault Displacement (FD) Modeling Case
- Human Intrusion Scenario.

Validation of the TSPA-LA Model consists of a sequence of activities as described in the *Technical Work Plan for: Total System Performance Assessment FY 07-08 Activities* (SNL 2008 [DIRS 184920], Section 2.3.5). These activities are consistent with the requirements contained in *Quality Assurance Requirements and Description* (QARD) (DOE 2007[DIRS 182051], Supplement SIII.2.6), and Section 6.3 in SCI-PRO-006, *Models*, and are designed to build confidence in the results of the TSPA-LA Model. The activities include verification that consists of checking that the inputs are correct and the software is passing information correctly among its submodels and model components. Several computer software and associated electronic input files were used in developing the TSPA-LA Model. These software and input files are controlled by IM-PRO-003, *Software Management.* The procedural control of the model validation activities, and the software and input files used in developing the TSPA-LA Model, are necessary to ensure overall fidelity and confidence in the results of the TSPA-LA Model.

The verification activities were carried out during development of the TSPA-LA Model, where development follows the generalized approach shown on Figure 7.1-1. These verification activities and the activities conducted for validation of the TSPA-LA Model after its development are shown on Figure 7.1-2.

The during-development activities of model validation include the following:

- Verification of inputs and software (Section 7.2)
- Stability testing (Section 7.3)
- Uncertainty characterization reviews of the values of direct-input parameters and uncertainty and sensitivity analyses (Section 7.4) of the parameters
- Surrogate waste form analyses (Section 7.5) for U.S. Department of Energy (DOE)-owned spent nuclear fuel (DSNF) and naval spent nuclear fuel (NSNF).

Post-development model validation activities were conducted to provide confidence in the results of the TSPA-LA Model and include the following:

- Corroboration of abstraction results with the underlying validated process models (Section 7.6)
- Corroboration of the TSPA-LA Model results with auxiliary analyses (Section 7.7)
- Corroboration of the TSPA-LA Model results with relevant man-made and natural analogues (Section 7.8)
- Incorporation of the comments and recommendations from independent technical reviews (Section 7.9).

A summary of the analyses conducted for validation of the TSPA-LA Model is presented in Table 7.1-1.

The strategy for the model validation is discussed in Section 7.1, followed by discussions of the specific activities conducted to validate the TSPA-LA Model (Figure 7.1-2). Section 7.2 presents testing and input verification activities. Section 7.3 contains a discussion of the statistical, temporal, and spatial discretization tests which are necessary to evaluate model convergence to a stable mean value of the distribution of results. Section 7.3 also evaluates the accuracy of the computed results. Section 7.4 provides a review of the treatment of uncertainties associated with the TSPA-LA Model and parameter input values. Section 7.4 includes a description of the criteria used in the uncertainty review, the review findings, and the corrective actions taken for the situations where the review identified issues in uncertainty treatment of the values of the TSPA-LA direct-input parameters. This section also summarizes the parameter uncertainty and sensitivity analyses performed on the TSPA-LA Model parameters with the details of the analyses presented in Appendix K. Section 7.5 describes application of the TSPA modeling approach to the development of the surrogate waste forms used to represent DSNF and NSNF.

Sections 7.6 to 7.9 describe validation activities conducted for the TSPA-LA Model. Section 7.6 provides a corroborative evaluation of the results of the abstractions that serve as the basis for the TSPA-LA Model. Section 7.6 also evaluates the consistency of the results of model abstractions relative to those obtained with the underlying process models. Section 7.7 describes the results

of a number of auxiliary analyses that were performed in order to corroborate the results of the TSPA-LA Model; in particular, to add confidence by a set of performance margin analyses that the TSPA-LA Model results are indeed conservative without producing any significant risk-dilution, to demonstrate that the TSPA-LA Model is performing as expected and that the TSPA-LA Model results are not sensitive to changes in submodel representations. The various auxiliary analyses performed are of four distinct mutually complementing categories, which were identified to evaluate the reasonableness of the TSPA-LA Model results by applying techniques that are different from those used in the development of the TSPA-LA Model. These auxiliary analyses categories are (1) single realization analyses, (2) comparison of the results of the TSPA-LA Model with a Simplified TSPA Analysis that was developed using a separate numerical code, (3) comparison of the results of the TSPA-LA Model with the performance assessment model developed by the Electric Power Research Institute (EPRI), and (4) a performance margin analyses. Section 7.8 discusses the use of several man-made and natural analogues, which provide confidence in the results of the TSPA-LA Model. Section 7.8 contains quantitative modeling comparisons with the Cerro Negro volcanic eruption of 1995, an analogue for a future potential volcanic eruption at the Yucca Mountain site. In addition, Section 7.8 includes a qualitative comparison of the relevant components of the TSPA-LA Model with those of the Nopal I uranium deposit in the sierra Peña Blanca, Chihuahua, Mexico. Section 7.9 presents summaries of reviews of previous TSPA analyses of the Yucca Mountain Repository including a 1998 peer review of the Total System Performance Assessment for the Viability Assessment (TSPA-VA), a 2001 International Review Team (IRT) evaluation of the performance assessment model used for the Yucca Mountain site recommendation, and a 2006 Independent Validation Review Team (IVRT) evaluation of drafts of the TSPA-LA Model and its supporting process models and submodels. Section 7.9 includes a discussion of the findings and recommendations provided by the IVRT, and summarizes responses to the IVRT's findings and the implementation of the IVRT's recommendations. Section 7.10 provides a summary of the material presented in Sections 7.1 through 7.9.

In addition to the validation activities mentioned above, potential impact on the TSPA-LA Model results due to issues identified after the model runs were completed was evaluated as stated in *Technical Work Plan for: Total System Performance Assessment FY 07-08 Activities* (SNL 2008 [DIRS 184920], Section 2.3.5.3). Appendix P contains the results of this evaluation. No significant impact on the TSPA-LA results was noted.

INTENTIONALLY LEFT BLANK

7.1 MODEL VALIDATION STRATEGY

7.1.1 Introduction

Validation of a computer model for a physical system involves a series of activities designed to generate and enhance confidence in the model's conceptualization and results during and after model development. The modeling process starts with the modeler's understanding of the physical system. A conceptual model is then formulated based on available information, using assumptions, simplifications, and idealizations. The conceptual model is translated into a mathematical model and then implemented into a numerical model. An appropriate computer code/software suite is selected or developed to implement the numerical model. The input to the computer code is prepared, and the code is executed to obtain the model output. This process is illustrated on Figure 7.1-1.

Converting the numerical model to a set of computer code algorithms is a process that must be transparent and traceable. Model inputs are checked, controlled, and documented (Section 4). The process of checking both the development of the computer code and the associated inputs and documentation of decisions generates confidence in the validity of the model during model development (SCI-PRO-002, *Planning for Science Activities*, Attachment 3, Level I Validation). IM-PRO-005, *Software Independent Verification and Validation*, controls computer code verification and validation to ensure that the code implements the numerical model correctly. In conventional modeling practice, model validation is achieved by comparing model results with experimental measurements. However, such measurements are impossible to obtain at the temporal and spatial scales of interest for postclosure performance of the Yucca Mountain repository. From a strictly computational perspective, a well-designed, correctly implemented numerical model should produce results that are explainable and appropriate for its intended purpose. Validation of the TSPA-LA Model is a process to establish confidence that the model adequately represents with sufficient accuracy the postclosure performance of the repository and satisfies its intended purpose.

Preparation of a validated model for a complex system such as the Yucca Mountain repository is an iterative evolutionary process (Eisenberg et al. 1999 [DIRS 155354]). Model development proceeds as the FEPs that could affect the repository system are progressively better understood through testing, analyses, and refinement of the conceptual models, and improvements are made in the computer software needed to implement the numerical model. The TSPA-LA Model is a result of such an evolutionary process of progressive improvements in the database development, refining the process models used as inputs to the next iteration of the TSPA models and their internal as well as external peer reviews. The earlier versions of the performance assessment model, such as the TSPA-VA Model and the Total System Performance Assessment for the Site Recommendation (TSPA-SR) Model, as well as key process models that directly supported the performance assessment models, were subjected to independent reviews. The TSPA-SR Model is the direct precursor to the TSPA Final Environmental Impact Statement (FEIS) Model (Williams 2001 [DIRS 157307]) from which the TSPA-LA Model was developed. The DOE subjected the TSPA-SR Model to a peer review by the Organization for Economic Cooperation and Development (OECD), Nuclear Energy Agency (NEA), and International Atomic Energy Agency (IAEA) IRT (OECD and IAEA 2002 [DIRS 158098]). To quote from their findings:

> "…the TSPA-SR methodology is soundly based and has been implemented in a competent manner… Overall the IRT considers that the implemented performance assessment approach provides an adequate basis for supporting a statement on likely compliance within the regulatory period of 10,000 years."

The IRT also recommended a number of improvements and changes to result in more confidence in and robustness of the TSPA Model. Appendix E, Table E-1, provides a summary of the IRT's comments and identifies the work conducted to improve the TSPA Model as development progressed to the TSPA-FEIS Model and then to the TSPA-LA Model. Given that the TSPA-LA Model evolved directly from the TSPA-SR and TSPA-FEIS Model (Williams 2001 [DIRS 157307]) using the same methods and approach, IRT review and DOE's subsequent favorable response to recommendations provide confidence in the validity of the developmental approach for the TSPA-LA Model.

As a part of the continued effort for confidence building, in addition to the IRT review of the TSPA-SR Model, the TSPA-LA Model was the subject of an independent model validation review conducted on earlier iterations of the model by a team of experts who were independent of the TSPA-LA Model development. Section 7.9 presents additional information on the review by the IVRT. The IVRT review observed that the draft TSPA-LA Model was developed through a recognized iterative and evolutionary process. The recommendations and comments of the IVRT (Section 7.9.3) have been addressed in development of the supporting models and the TSPA-LA product. This provides an enhanced technical basis for the work, and increases confidence in the technical quality and defensibility of the TSPA-LA Model.

Confidence in the results of the TSPA-LA Model is partly based on the results of conducting the checking and documentation activities as required by SCI-PRO-006, *Models*. There are two main categories of procedural activities required for developing a model that is valid for its intended use: (1) those conducted during development of the model (described in SCI-PRO-002, Attachment 3, Validation Level I), and (2) those conducted after development of the model (described in Section 6.3.2. of SCI-PRO-006). Figure 7.1-2 is a flow diagram indicating how the activities identified in the two procedures were applied to the TSPA-LA Model. The basis for the activities conducted for verification and validation of the TSPA-LA Model is documented in *Technical Work Plan for: Total System Performance Assessment FY 07-08 Activities* (SNL 2008 [DIRS 184920], Section 2.3.5). The goal of these activities is to support the demonstration that the results of the procedurally validated TSPA-LA Model satisfy the applicable NRC's individual dose and groundwater protections requirements. The activities are also to address the applicable TSPA-LA Model acceptance criteria identified by the NRC in its Yucca Mountain Review Plan. Table H-1 in Appendix H provides a roadmap of the NRC requirements and the Yucca Mountain Review Plan acceptance criteria applicable to the TSPA-LA Model.

The analyses planned for the verification and validation in the technical work plan (SNL 2008 [DIRS 184920], Section 2.3.5) are described in Table 7.1-1, which generally corresponds to the organization of Section 7.

The technical work plan (SNL 2008 [DIRS 184920], Section 2.3.5.1) describes the activities conducted during development to verify the TSPA-LA Model, as required by SCI-PRO-002, Attachment 3, Validation Level I. Section 2.3.5.2 of the technical work plan (SNL 2008

[DIRS 184920]) describes the post-development activities conducted to validate the TSPA-LA Model to the required validation Level II (as required by SCI-PRO-006, Section 6.3.2). Section 7.1.2 summarizes the activities conducted during development, and Section7.1.3 summarizes the post-development activities. Figure 7.1-2 provides a conceptual flow of model-validation activities performed during and after the development of the TSPA-LA Model and maps these validation activities to the corresponding sections of SCI-PRO-006.

Table 7.1-1 shows the TSPA-LA Model analyses that support the various validation activities. Table 7.1-1 shows the category/subcategory of each model activity (analysis or set of analyses), the purpose of the activity, a brief description of the activity, and the section where the detailed discussions of the results are found. Section 7 and the output data tracking number (DTN) describe the results of each of the analyses in Table 7.1-1. The output DTN contains the run log for the analysis, raw results, and any transformations to produce the figures and tables used in the discussion of the analysis. A complete set of output DTNs is provided in Appendix B.

7.1.2 During-Development Model Validation Activities

The following during-development activities, listed in Section 2.3.5.1 of the technical work plan (SNL 2008 [DIRS 184920]), were performed to demonstrate the validation of the TSPA-LA Model in relationship to its intended use and required level of confidence, are as follows:

1. Selection of input parameters and/or input data and a discussion of how the selection process builds confidence in the model (SCI-PRO-002, Attachment 3, Level I, Validation 1).

2. Description of calibration activities, and/or initial boundary condition simulations, and/or simulation convergences, and a discussion of how the activity or activities build confidence in the model. Includes a discussion of impacts of any run non-convergences (SCI-PRO-002, Attachment 3, Level I, Validation 5).

3. Discussion of the impacts of uncertainties on the results (SCI-PRO-002, Attachment 3, Level I, Validation 4 and 6).

In addition, the TSPA-LA Model input parameter values and abstraction models, including their ranges of applicability, were reviewed and verified for accuracy (Section 7.2). Stability tests were conducted to identify the appropriate number of realizations, timestep size, and spatial discretization to ensure that the model was stable for each modeling case (Section 7.3).

In addition to the discussion on the uniform treatment of uncertainty throughout the model in Section 6.1.3, Section 7.4 presents uncertainty characterization reviews that were conducted to evaluate characterization of the uncertainty associated with the direct-input parameters of the key submodels that support the TSPA-LA Model. Section 7.4 includes a summary of the parameter uncertainty and sensitivity analyses performed on the TSPA-LA Model parameters, with the details of the analyses presented in Appendix K.

The technical work plan (SNL 2008 [DIRS 184920]) includes two additional considerations related to model development and validation:

1. Formulation of defensible assumptions and simplifications (SCI-PRO-002, Attachment 3, Level I, Validation 2).

2. Consistency with physical principles, such as conservation of mass, energy, and momentum (SCI-PRO-002, Attachment 3, Level I, Validation 3).

Formulation of defensible assumptions and simplifications: The TSPA-LA Model was developed by integrating assumptions, process models, abstractions, and the results of analysis or model reports. Section 5 presents the assumptions that support the TSPA-LA Model. These TSPA-LA Model assumptions reflect the relevant assumptions from the supporting analysis or model reports. Section 5 provides the assumptions, their bases for the individual scenario classes, and references to the source submodels where the assumptions were justified.

In addition to the assumptions described in Section 5, the subsections of Section 6.3 describe modeling decisions that describe the technical bases for the TSPA-LA Model and its submodels.

Section 6.1.3 describes how the uncertainties in the direct inputs to the TSPA-LA Model (Table 4-1) were addressed. The uncertainty treatments used in the individual abstraction models are presented in the source reports referenced in Table 4-1. Section 7.4 contains a review of the uncertainty characterizations of the inputs to the TSPA-LA Model, along with the implemented remedies for the uncertainty issues identified during the review.

Section 6.1.4 describes the mechanisms and reasoning used in integrating the process models and submodels from the supporting analysis or model reports into the TSPA-LA Model. The post-development model validation activities, especially the suite of auxiliary analyses, were designed to increase confidence that the TSPA-LA Model results are reasonable, given the complexity of the repository system.

Consistency with physical principles, such as conservation of mass, energy, and momentum: Section 6 describes the development of the TSPA-LA Model. Implicit in the model description is ensuring that the physical principles such as conservation of mass, energy, and momentum are strictly followed in development of mathematical relationships; for example, the particular flow and transport components used in modeling the performance of the engineered and natural barrier systems. The mathematical relationships describing the physical components of models or calculations were developed and presented in the direct-input parameters (Table 4-1) and in their underlying process models and calculations. The Parameter Uncertainty Team, which consisted of a team of subject matter experts (SMEs), evaluated the appropriateness of the input parameters and addressed the uncertainty issues associated with key parameter.

The input verification tests described in Section 7.2 ensure that the inputs, for example, equations describing the abstracted model, are functioning as expected. The calibration and stability testing described in Section 7.3 ensures that the TSPA-LA Model runs are statistically, temporally, and spatially stable and the model produces reliable results, identifies any residual issues, and implements remedial actions. All of these activities ensure that the physical principles on which the process models and calculations were developed were incorporated during the development of the TSPA-LA Model.

In addition to the validation activities mentioned above, potential impact on the TSPA-LA Model results due to issues identified after the model runs were completed was evaluated as stated in *Technical Work Plan for: Total System Performance Assessment FY 07-08 Activities* (SNL 2008 [DIRS 184920], Section 2.3.5.3). Appendix P contains the results of this evaluation. No significant impact on relevant TSPA-LA performance measures (i.e., mean dose) was noted. As a part of the continuing improvement effort by the Project, the impact on the results of this version of the TSPA-LA Model will be included in an addendum to this TSPA-LA Model report.

7.1.2.1 Input Selection and Verification

The TSPA-LA Model is composed of linked submodels. To permit checking of submodel implementation, Section 6.1.5 documents the links from the TSPA-LA Model documentation to submodels in the GoldSim model file (V. 9.60. STN: 10344-9.60-00 [DIRS 181903]). The supporting analysis or model reports for these submodels document the validation of the underlying process models or abstracted models. Each submodel was validated before being integrated into the TSPA-LA Model. Therefore, although the submodels of the TSPA-LA Model were individually validated, validation of the TSPA-LA Model is still necessary. The input verification described in the technical work plan (SNL 2008 [DIRS 184920], Section 2.3.5.1) (Figure 7.1-2), includes the comparison of TSPA-LA Model inputs with the source analyses and model reports from which they were derived. More specifically, this activity consists of checking the input information and models in the TSPA-LA Model against the source analysis or model report results, making certain that individual submodel results do not exceed the validity range of successive submodels, and confirming that the coupling from one submodel to the next is correct. Where submodels yield values that exceed the validity range of a successive submodel, an appropriate value within the valid range is selected. The documentation of the process of selecting submodel input parameters and/or data, including their uncertainties, is included in the relevant supporting document and not in this document. However, it is conceivable that the coupling of submodels in the TSPA-LA Model might generate conditions that cause one or more submodels to produce output that is beyond the validated range of input for the next successive submodel. Occurrence of out-of-valid-range samples for which a valid value is selected is documented in the source analysis or model abstraction report that provides the input in question to the TSPA-LA Model. Section 7.2 presents the results of the computer code and input verification.

Additional measures were added to the computer code verification and input selection activities required by SCI-PRO-002, Attachment 3, because of the critical role of the TSPA-LA Model in estimating repository performance, and because the TSPA-LA Model couples and integrates numerous computer codes and submodels. These measures are intended to verify that the suite of software codes and their associated input files are properly implemented in the integrated TSPA-LA Model. Computer code and input verification and selection consist of the following activities:

- **Selection and Verification of the Integrated System Software: GoldSim**—The integrated system code, GoldSim (V. 9.60. STN: 10344-9.60-00 [DIRS 181903]), is fully verified by the code vendor, GoldSim Technology, and has been qualified for use for TSPA in accordance with IM-PRO-004, *Qualification of Software*.

- **Verification of the Dynamically Linked Libraries as Single Modules and in an Integrated System**—Some of the submodels used within the TSPA-LA Model are implemented as dynamically linked libraries (DLLs) that are separately compiled as linked modules or subroutines that can be called by GoldSim. Examples of single module DLLs are the Waste Package Degradation DLL (WAPDEG V. 4.07, STN: 10000-4.07-00 [DIRS 161240]) and the unsaturated zone (UZ) transport module finite element, heat and mass transfer code (FEHM) (FEHM V. 2.24. STN: 10086-2.24-01-00 [DIRS 179419]). The DLLs for single modules have been validated as adequate representations of their underlying conceptual and mathematical models, and verified in terms of their mechanical operation as DLLs. Because the ability to properly call DLLs is a feature for which GoldSim has been validated, the DLLs are, by default, qualified when called from within the TSPA-LA Model. However, the input to and output from each DLL must be confirmed (Section 7.2.2).

  There are two aspects to confirmation of the DLLs within the integrated TSPA-LA Model. The first is the potential for two or more DLLs to conflict with each other in terms of memory requirements, duplicate input, or output file unit numbers. The second is the potential interaction between DLLs, such as when an output file generated by one DLL is used as an input file to another DLL. Appropriate test cases documented during model development ensure that these types of confirmation issues have been properly resolved (Section 7.2.2).

- **Verification of Inputs in the TSPA Database**—Input to the TSPA-LA Model is controlled by the TSPA Input Database described in Section 4. Input parameters are manually extracted from DTNs stored in the Technical Data Management System, analysis or model reports, and other sources. Table 4-1 summarizes the inputs to the TSPA-LA Model. Parameter Entry Forms, discussed in Section 4.1, provide traceability of the input to its source in the cited document or a DTN. Parameters entered into the TSPA Input Database were checked and confirmed against their sources (Section 7.2.3).

- **Validation and Verification of Single Model Components**—The submodels in the integrated TSPA-LA Model were validated before incorporation into the TSPA-LA Model as described in the analysis or model reports. Section 7.2.4 describes the verification of the proper implementation of submodels within the TSPA-LA Model.

- **Verification of Coupling among Submodels and Model Components**—Section 7.2.5 describes the verification of proper information transfer between connected submodels and software within the integrated TSPA-LA.

The parameter uncertainty and variability, along with model and scenario uncertainty, comprise the overall uncertainty in the TSPA-LA Model results. The parameter uncertainty and variability in the TSPA-LA Model causes a spread of results of the mean dose between the 5th and 95th percentile of about two to three orders of magnitude depending on the modeling case (Section 7.4). The criterion for verification of input parameters to the TSPA-LA Model DLLs and submodels is that the parameter values should be the exact same value as the inputs used in the DLL and/or submodel validation process presented in the respective analysis or model reports. The verification criterion for the results calculated within the TSPA-LA Model and

passed from one submodel to another and/or calculated by DLLs that use abstracted models is that they should agree, within five percent, with the validation results presented in the respective analysis or model reports. The five percent criterion was chosen arbitrarily. Differences between the results from the two calculations are derived from different solution techniques and/or differences in the numbers and durations of the model timesteps between the calculations. The calculation results from individual submodels presented in the respective analysis or model reports and those calculated with the TSPA-LA Model should agree within five percent. The choice of the acceptance criterion of a five percent difference in the results was arbitrary but is justified in view of the overall uncertainty in the TSPA-LA Model.

The tests outlined above are described in detail in Section 7.2. Completion of computer code and input verification is a necessary condition for model validation but, by itself, is insufficient to ensure confidence in the TSPA-LA Model without completion of additional activities, such as those described in the following sections.

7.1.2.2 Model Stability Testing

Model stability testing activities include three types of stability tests: statistical stability, temporal stability, and spatial stability or discretization. Collectively, these three tests are referred to as model stability testing.

Statistical stability (Section 7.3.1) testing involves a number of activities related to demonstrating that a sufficient number of stochastic realizations have been run to achieve a numerically stable mean dose, including: (1) determining confidence intervals (with 3 replicates and using t-test) around the total mean annual dose and mean annual dose for each modeling case (Section 7.3.1); (2) demonstrating numerical accuracy of mean annual dose for the Nominal Modeling Case by comparing the results of the base case 300 realizations with those using 1,000 realizations (Section 7.3.2); (3) demonstrating the numerical accuracy of the expected dose calculations for the Igneous and Seismic Scenario Classes and for the Human Intrusion Scenario (Section 7.3.2); (4) demonstrating for the Seismic GM Modeling Case for 10,000 years that the simplification from *Seismic Consequence Abstraction* (SNL 2007 [DIRS 176828]) used in the calculation of the expected dose is reasonable for: (a) omitting rupture and puncture mechanisms for breaching waste packages (WPs) and omission of rockfall effects on temperature and seepage entering the repository drifts (Section 7.3.2), and (b) assuming that drip shields (DSs) remain intact for 10,000 years (Section 7.3.2); and, (5) checking UZ transport modeling to: (a) ensure that the particle tracking conserves mass, and (b) obtain a sufficient number of particles for the Igneous Intrusion and Seismic GM Modeling Cases (7.3.5).

Temporal stability refers to the use of an appropriate timestep size necessary to achieve a stable solution. Section 7.3.3 describes timestep size evaluation for the Waste Package EF, Igneous Intrusion, Seismic GM and Human Intrusion Modeling Cases, which collectively encompass the range of events and processes that lead to radionuclide mobilization and transport. The degree of stability shown in the graphical comparisons of the results of the stability analysis, using timesteps as short as one year, indicated that a statistical comparison of timestep changes was not necessary.

Spatial stability/discretization in the TSPA-LA Model involves studying the scale at which the repository must be modeled. In particular, because of computational constraints, the TSPA-LA Model does not simulate the individual performance of each of the 11,629 WPs to be emplaced in the repository but groups the WPs into representative WP groups. Section 7.3.4 evaluates the effect of the WP groupings on TSPA-LA Model results.

7.1.2.3 Uncertainty Characterization Reviews and Uncertainty and Sensitivity Analyses

Uncertainty characterization reviews on the direct-input TSPA-LA parameters were undertaken to ensure that appropriate treatment of parameter uncertainty and variability was implemented in preparation of the TSPA-LA Model as required by the technical work plan (SNL 2008 [DIRS 184920], Section 2.3.5.1, Criterion 3). Uncertainty and sensitivity analyses were performed to ensure that the parameter uncertainty is appropriately propagated during the TSPA-LA Model development and the sensitivity of the dose calculations to the parameter uncertainty during and after the model development were identified and addressed.

Section 7.4 documents the results of the activities performed for the uncertainty characterization reviews, and the uncertainty and sensitivity analyses. The discussion presented in Section 7.4 include: (1) approach used for the reviews (Section 7.4.1); (2) risk-informed ranking of the TSPA-LA scenario classes and modeling cases so as to focus the reviews on those modeling cases that have a significant impact on dose (Section 7.4.2), which resulted in identification of three key modeling cases: Seismic GM Modeling Case; Igneous Intrusion Modeling Case; and Volcanic Eruption Modeling Case (Section 7.4.2); (3) performing risk-informed identification and prioritization of the key uncertain parameters that are important to dose in the Seismic, Igneous, and Nominal Scenario Classes (Section 7.4.3); (4) scope of the uncertainty reviews, including identifying the appropriate review team to cover the breadth and depth of the scope of the review, conducting the reviews, and documenting the results in appropriate analysis or model reports (Section 7.4.4); (5) corrective actions for the key uncertainty-related issues identified during the reviews; and, (6) summary of the results of the uncertainty and sensitivity analyses, the details of which are presented in Appendix K as mentioned in the paragraph below.

Appendix J describes the strategy for separating aleatory and epistemic uncertainty including the overall computational strategy, the derivation of the expected annual dose to the reasonably maximally exposed individual (RMEI) for each of the modeling case considered, and presents the results of expected dose calculations. Appendix K discusses uncertainty results for physical processes associated with the release, flow, and transport of radionuclides, and presents sensitivity analysis results for both physical processes and expected dose.

7.1.2.4 Surrogate Waste Form Analyses

Section 7.5 describes the application of the TSPA-LA modeling approach to develop the surrogate waste forms to represent DSNF and NSNF. Section 7.5 includes: (1) discussions on methodology as to how the surrogate waste form represents the DOE and naval waste forms and how the modeling was conducted; (2) a description of the spent fuel categories and how they are represented in the TSPA-LA Model; (3) a discussion of the naval spent fuel Category 1; (4) a representation of the DSNF Category 2 through Category 11; and (5) the results of the analyses that applying the surrogate waste forms.

7.1.3 Post-Development Model Validation Activities

This section discusses the post-development validation activities performed. Post-development model validation activities (SNL 2008 [DIRS 184920], Sections 2.3.5.2 and 2.3.5.3) include possible analyses and evaluations to build the level of confidence that is necessary to demonstrate that the TSPA-LA Model is valid for its intended use. The required validation level for the TSPA-LA Model falls into the Level II Validation category (SCI-PRO-002, *Planning for Science Activities,* Attachment 3) that requires use of at least two of the activities from Section 6.3.2 of SCI-PRO-006. Exceeding the procedural requirements, the technical work plan (SNL 2008 [DIRS 184920], Sections 2.3.5.2 and 2.3.5.3) identified several post-development model validation activities and a number of possible analyses and evaluations for the individual activities to ensure the model is validated.

These activities include the following:

- Corroborating the direct-input abstraction results to the results of the validated mathematical model or process model from which the abstraction was derived (Section 7.6; Figure 7.1-2).

- Performing auxiliary analyses to corroborate the results provided by the TSPA-LA Model or model abstractions and/or submodels used in the TSPA-LA Model (Section 7.7; Figure 7.1-2). The auxiliary analyses include comparison of the TSPA-LA Model results with: (1) those of analyses of single realizations that are significant contributors to dose (Section 7.7.1); (2) the results of a Simplified TSPA Analysis (Section 7.7.2); (3) results calculated by EPRI for the repository using its own performance assessment code (Section 7.7.3); and (4) results of performance margin analyses to provide objective evidence for assessing performance margin and degree of conservatism or non-conservatism in the TSPA-LA Model (Section 7.7.4; Figure 7.1-2).

- Comparing the relevant portions of the TSPA-LA Model with appropriate analogue information. The comparison included quantitative comparisons of the TSPA-LA Model components with: (1) an analogous volcanic eruption (Cerro Negro); and (2) a qualitative description of the groundwater flow and transport of radionuclides in a natural system (Peña Blanca) analogous to Yucca Mountain (Section 7.8; Figure 7.1-2).

- As an additional confidence building activity, the comments and recommendations by past technical reviews, including those by the IVRT review of earlier drafts of the TSPA-LA were addressed and implemented as appropriate (Section 7.9; Figure 7.1-2).

The technical work plan (SNL 2008 [DIRS 184920], Section 2.3.5.3) contains additional contingent activities planned to further build confidence in the TSPA-LA results and complementing the post-development confidence building activities described above. These activities include sensitivity analyses to ensure that the TSPA-LA results remain unchanged due to any essential future revision made in the parameter inputs or submodels. These analyses, if needed, will be conducted utilizing the updated information to evaluate the effect of the changes on the results or conclusions obtained using the TSPA-LA Model. Results of any such

supplemental sensitivity analyses will be documented and reviewed to ensure that the model validation was not adversely impacted through incorporation of the revised information.

Successful completion of the during- and post-development model verification and validation activities described above satisfies the Level II requirements in SCI-PRO-006, Section 6.3.2, for validation of the TSPA-LA Model for its intended purpose.

7.1.3.1 Corroboration of Abstraction Model Results with Validated Process Models

The TSPA-LA Model's abstraction models and their underlying process models were validated during their individual development and post-development validation phases following SCI-PRO-006 and performing the needed activities planned in the appropriate technical work plans. The details of the validation activities and the results of such activities for the process models that served as direct inputs (Table 4-1) to the TSPA-LA Model are documented in the respective analysis or model reports. Validation that the abstraction model results agree with the underlying process model results and quantitatively represent their respective process models before and after their implementation in the TSPA-LA Model is essential to the validation of the TSPA-LA Model. These submodels must function coherently when linked together as integral components of the TSPA-LA Model to provide results that are stable and properly represent the contributing abstraction models. This linkage of individually validated submodels is evaluated by performing input-verification and stability testing activities during the TSPA-LA Model development.

The integrity of the abstraction models during their implementation in the TSPA-LA Model is ensured by performing: (1) independent checks to confirm that the direct inputs are accurately applied in the TSPA-LA Model simulations; and (2) independent verification, for example, by model re-runs to confirm that the inputs produce the result that is expected. The checking and verification activities are documented controlled processes. The verification activities are summarized in Section 7.1.2.1, and a discussion of the verification analyses is provided in Section 7.2. The checking and verification activities ensure that the TSPA-LA Model is built on verified inputs and that the abstraction models accurately reflect the underlying process models. Section 7.1.2.2 summarizes model stability analyses. Section 7.3 provides a discussion of these analyses and the results obtained.

Once the integrity of the underlying process models are ensured through the abstraction and implementation processes used in the TSPA-LA Model, and it is clear that the individual abstraction models are functioning well when they are applied together as components during the computation of the TSPA-LA Model itself, certain post-development model validation and confidence building activities that are unrelated to the TSPA-LA Model development activities need to be performed in order to assess that the TSPA-LA Model, which is built on the abstraction models, is valid for its intended use.

Ensuring the integrity of the direct-input process models during abstraction and their successful application in the TSPA-LA Model is the first step toward defining and executing these follow-up post-development validation and confidence building activities and addressing the intent of the technical work plan goal for Corroboration of Abstraction Model Results with Validated Process Models [Section 7.6]. The technical work plan (SNL 2008 [DIRS 184920],

Section 2.3.5.2) identified corroboration of abstraction model results with those of the respective underlying validated process models as a TSPA-LA Model validation criterion to demonstrate that the actual results of the abstracted models do, in fact, corroborate with those of the respective underlying process models that were abstracted. To accomplish this confirmation, the abstraction models' results were compared with those of the respective process models. Details of the comparisons are presented in Section 7.6.

7.1.3.2 Corroboration of Results with Auxiliary Analyses

Auxiliary analyses are confidence building activities often based on the use of stylized inputs or test cases that help to demonstrate that the TSPA-LA Model and its submodels are functioning correctly. If the outputs from these stylized cases do not agree with scientific judgment and intuition, then an explanation of these counterintuitive results would have to be sought through additional analyses of the underlying processes. Conversely, if the stylized cases produce results that are logical, confidence in the model is enhanced. The auxiliary or stylized analyses for the TSPA-LA Model (Section 7.7) include analyses of selected realizations (e.g., upper-bound realizations at peak mean-dose times) from the full suite of probabilistic realizations (Section 7.7.1); comparison of the results of the TSPA-LA Model with a Simplified TSPA Analysis (Section 7.7.2); a comparison of the TSPA-LA Model results with those from an independent organization (Section 7.7.3); and analyses of performance margins (Section 7.7.4). The impact analyses examine alternative submodels as they relate to issues of conservatism and consistency that were identified by the IVRT. Performance margin analyses provide objective evidence for assessing performance margin and the degree of conservatism or non-conservatism present in the TSPA-LA Model. Specifically, the performance margin analyses will utilize revisions to selected component models in the TSPA-LA compliance model, including alternative conceptual models and/or alternative probability density functions for specific parameters, to assess the performance margin in the TSPA-LA Model (i.e., the degree to which repository system performance is underestimated by the TSPA-LA Model). The Performance Margin Analysis is specifically designed to address IVRT comments. The analyses were conducted both with individual model-component revisions as well as with a combined analysis that incorporates all of the selected component revisions.

7.1.3.3 Corroboration of Results with Analogues

In accordance with SCI-PRO-006, Section 6.3.2, comparisons with several analogues that are relevant to barrier performance of the Yucca Mountain repository were conducted for the TSPA-LA Model. Section 7.8 provides a summary of these comparisons. Specifically, a detailed quantitative comparison was conducted for the atmospheric dispersal and deposition of tephra from a potential volcanic eruption (SNL 2007 DIRS 177431] to ash fall at Cerro Negro, Nicaragua, using the code ASHPLUME [181035], an analogue for the Volcanic Eruption Modeling Case (Section 7.8.1). In addition, Section 7.8.2 provides a qualitative comparison of the Nopal I uranium mine, located in the Sierra Peña Blanca, Chihuahua, Mexico, to the performance of the Yucca Mountain repository. The Nopal I uranium deposit is a natural analogue for groundwater transport of radionuclides in the TSPA-LA modeling cases. These two natural analogues were selected because they incorporate significant components of the TSPA-LA Model. Cerro Negro enhances confidence in the ash distribution model, and Peña

Blanca enhances confidence in the groundwater transport models for the UZ and saturated zone (SZ) of the natural system of the Yucca Mountain repository.

7.1.3.4 Independent Technical Reviews

The TSPA methodology is iterative. The TSPA process adopted by the DOE is based generally on the methodology developed by Cranwell et al. (1990 [DIRS 101234], Sections 2 and 3). Over time, the methodology has been enhanced and applied to numerous projects by various international organizations involved in radioactive waste management. The TSPA-LA Model was developed initially to analyze the ability of the natural and engineered systems of the Yucca Mountain repository to isolate nuclear waste following repository closure. Performance Assessments and related supplemental analyses of the Yucca Mountain repository have been conducted following the publication of the Nuclear Waste Policy Act as Amended in 1987, Public Law No. 100-203 [DIRS 100016]. TSPAs of the Yucca Mountain repository have been iterative and periodically updated, each building on the previous TSPAs. The iterative assessments incorporate both an improved understanding of the processes affecting repository performance and, through additional field observations and laboratory analyses, better identification and quantification of the values of the parameters used in the TSPAs.

Early iterations of probabilistic TSPAs for the Yucca Mountain repository include TSPA-91 (Barnard et al. 1992 [DIRS 100309]), TSPA-93 (Wilson et al. 1994 [DIRS 100191]), TSPA-95 (CRWMS M&O 1995 [DIRS 100198]), and *Total System Performance Assessment – Viability Assessment of a Repository at Yucca Mountain (TSPA-VA)* (DOE 1998 [DIRS 100550], Volume 3). The more recent TSPA iterations include *Total System Performance Assessment for the Site Recommendation* (TSPA-SR) (CRWMS M&O 2000 [DIRS 153246]) and the application of the Total System Performance Assessment-Site Recommendation Model to the Final Environmental Impact Statement for the Yucca Mountain repository (Williams 2001 [DIRS 157307]).

Previous performance assessments of the Yucca Mountain repository have been evaluated and independently reviewed by technical staff and various external organizations, and reviewers generally make recommendations for improvements for consideration in future TSPA iterations. Examples of empanelled reviews include the TSPA Peer Review conducted by Budnitz et al. (1999 [DIRS 102726]) and an evaluation by an IRT that is summarized in *An International Peer Review of the Yucca Mountain Project TSPA-SR, Total System Performance Assessment for the Site Recommendation (TSPA-SR)* (OECD and IAEA 2002 [DIRS 158098]). These independent technical reviews for the TSPA-LA development process are summarized in Section 7.9.1. As mentioned earlier, the IVRT reviewed the earlier iterations of the TSPA-LA Model. A detailed discussion on the IVRT review is presented in Section 7.9.2.

Table 7.1-1. TSPA-LA Model Validation Analyses

Activity Category/Subcategory	Purpose	Activity Description	Document Section
During–Development Validation Activities (Technical Work Plan Validation (SNL 2008 [DIRS 184920], Section 2.3.5.1))			
Computer Code and Input Verification			
Model Testing and Verification	Testing of software that is the basis for the TSPA-LA Model.	Verify GoldSim software.	7.2.1
	Checking to determine whether the correct input parameters are used.	Verify input parameters.	7.2.3
	Test cases to determine whether the model is working correctly, saving appropriate results, interfacing with DLLs, feeding the correct information among model components, and not exceeding the applicable range of model components.	Includes verification of DLLs, submodels, model components, and coupling among submodels and model components; and comparison with other models (e.g., stand-alone models from analysis model reports). In addition, the verification of coupling among submodels and model components includes subsystem analyses of annual release across model interfaces, drift-wall condensation, and localized corrosion initiation.	7.2.2, 7.2.4, 7.2.5; Tables 7.2-1 and 7.2-2
Model Stability Testing			
Statistical Stability of Mean Annual Dose	Determine confidence interval around total mean annual dose and mean annual dose for each modeling case using three replicates.	Generate total mean annual dose and mean annual dose for each modeling case using three replicates with different random seeds. Determine a confidence interval around the estimate of the overall mean with a *t*-test.	7.3.1
Numerical Accuracy of Expected Annual Dose Calculation – Igneous Scenario Class	Demonstrate accuracy of calculation of expected annual dose for the modeling cases of the Igneous Scenario Class.	For the Igneous Intrusion Modeling Case, demonstrate accuracy of the quadrature integration technique by increasing the discretization used in the integral. Increase the number of specified event times from 10 to 50. Calculate expected annual dose for five epistemic realizations for both 10,000 and 1,000,000 years. For the Volcanic Eruption Modeling Case for 10,000 years, demonstrate accuracy of the combined Monte Carlo and quadrature integration techniques by increasing the sample size used in the Monte Carlo integration and the discretization used in the quadrature integration. Calculate expected annual dose for 10,000 years for five epistemic realizations, increasing the aleatory LHS sample size from 40 to 120, and the number of specified event times from 10 to 20. Conclusions for 10,000 years apply to the 1,000,000 year calculations.	7.3.2

Table 7.1-1. TSPA-LA Model Validation Analyses (Continued)

Activity Category/Subcategory	Purpose	Activity Description	Document Section
Model Stability Testing (Continued)			
Numerical Accuracy of Expected Annual Dose Calculation – Seismic Scenario Class	Demonstrate accuracy of calculation of expected annual dose for the modeling cases of the Seismic Scenario Class.	For the Seismic GM Modeling Case for 1,000,000 years, demonstrate the accuracy of the Monte Carlo integration technique by means of increased sample size. Repeat Replicate 1 (300 epistemic realizations) with a different aleatory seed to generate a second set of 9,000 dose histories (30 independent aleatory samples for each epistemic realization). Pool the two sets of 9,000 dose histories and generate expected annual dose based on the pooled set of 60 independent aleatory samples per epistemic realization, and compare to expected annual dose for the base case of 30 independent aleatory samples per epistemic realization. For the Seismic GM Modeling Case for 10,000 years, demonstrate accuracy of the quadrature integration technique by increasing the discretization used in each integral. Increase the number of specified event times from 6 to 12 and the number of specified damage levels from 4 to 8. Calculate expected annual dose for 5 epistemic realizations. For the Seismic FD Modeling Case, demonstrate accuracy of the quadrature integration technique by increasing the discretization used in each integral. Increase the number of specified event times from 6 to 12 and the number of specified damaged areas from 3 to 6. Calculate expected annual dose for 5 epistemic realizations for both 10,000 and 1,000,000 years.	7.3.2

Table 7.1-1. TSPA-LA Model Validation Analyses (Continued)

Activity Category/Subcategory	Purpose	Activity Description	Document Section
Model Stability Testing (Continued)			
Justification of Simplifications for the Seismic GM Modeling Case for 10,000 Years	For the Seismic GM Modeling Case for 10,000 years, demonstrate that simplifications of the Seismic Consequences Abstraction used in the calculation of expected annual dose are reasonable.	Justify omission of TAD waste packages for SCC damage by computing the probability of SCC damage to the TAD over 10,000 years. Justify omission of the rupture mechanism for breaching WPs by computing the probability of rupture for the CDSP and TAD WPs over 10,000 years. Justify omission of the puncture mechanism for breaching WPs by computing the probability of puncture for the CDSP and TAD WPs over 10,000 years. Justify assumption that the DS remains intact for 10,000 years by computing the probability of DS framework and plate failure over 10,000 years and estimating the consequent dose assuming plate failure before 10,000 years. Justify omission of rockfall effects on temperature and seepage entering the drift by computing the expected and 95th percentile volumes of rockfall over 10,000 years.	7.3.2
Temporal Stability	Demonstrate stability of expected annual dose for temporal discretization in GoldSim.	Comparison of expected annual dose histories for five epistemic vectors for the following modeling cases: Nominal; Seismic GM (10,000 years); Igneous Intrusion (10,000 and 1,000,000 years); and Drip Shield EF (10,000 years). Compare expected annual dose histories for three different temporal discretizations.	7.3.3
Spatial Discretization	Evaluate the impact due to the spatial discretizations inherited by the TSPA-LA Model from the supporting natural and engineered-barrier process models.	Evaluate the appropriateness of use of the inherited spatial discretization schemes of the process model abstractions that feed the TSPA-LA. These abstractions include the process models: Mountain-Scale UZ Flow, EBS TH Environment, UZ Transport, and SZ Flow and Transport abstractions.	7.3.4.1
	Evaluate the impact due to the spatial discretizations created within the TSPA-LA Model.	Describe the spatial discretization of the repository on the basis of percolation subregions and the binning of the percolation subregions by quantiles (0.0 to 0.05, 0.05 to 0.3, 0.3 to 0.7, 0.7 to 0.95, and 0.95 to 1.0).	7.3.4.2
		Demonstrate the appropriateness and validity of using the representative TH histories as inputs to the EBS Thermal-Hydrologic Environments Submodel of the TSPA-LA, as opposed to using the comprehensive data set available from the MSTHM.	7.3.4.3

Table 7.1-1. TSPA-LA Model Validation Analyses (Continued)

Activity Category/Subcategory	Purpose	Activity Description	Document Section
Model Stability Testing (Continued)			
Stability of UZ Transport Modeling for the Igneous Intrusion Modeling Case	Evaluate the stability of results in reference to the maximum number of particles allowed per species for the Igneous Intrusion Modeling Case for 1,000,000 years.	Analyze the differences in UZ releases of ^{99}Tc, ^{233}U, ^{234}U, ^{237}Np, and ^{239}Pu, and in cumulative dose for three cases (500,000; 750,000; and 900,000 particles).	7.3.5
Stability of UZ Transport Modeling for the Seismic GM Modeling Case	Evaluate the stability of results in reference to the maximum number of particles allowed per species for the Seismic GM Modeling Case for 10,000 years.	Analyze the differences in UZ releases of ^{99}Tc, ^{233}U, ^{234}U, ^{237}Np, and ^{239}Pu and in cumulative dose for three cases (500,000; 750,000; and 900,000 particles.).	7.3.5
Stability of UZ Transport Modeling for the Drip Shield EF Modeling Case	Evaluate the stability of results in reference to the maximum number of particles allowed per species for the Drip Shield EF Modeling Case for 1,000,000 years.	Analyze the differences in UZ releases of ^{99}Tc, ^{233}U, ^{234}U, ^{237}Np, and ^{239}Pu, and in cumulative dose for three cases (500,000; 750,000; and 900,000 particles).	7.3.5
Uncertainty Characterization Reviews			
Ranking of Scenario Classes	Prioritize scenario classes of higher significance to dose.	Develop a risk-based ranking of TSPA-LA scenario classes and modeling cases in order to focus the uncertainty characterization reviews of the most important component model abstractions.	7.4.2
Key Uncertain Parameters	Identify the key uncertain parameters that are important to dose.	Select the key uncertain parameters that are important to dose in the Seismic, Igneous, and Nominal Modeling Cases for characterization review based on both importance rankings from past TSPA scoping studies and recommendations provided by model abstraction developers and experienced TSPA analysts.	7.4.3
Uncertainty-Characterization Review Findings and their Implementation	Review uncertainty characterization and address findings.	Perform uncertainty characterization of the selected key parameters impacting dose for the Seismic, Igneous, and Nominal Modeling Cases and implement corrective actions for observed deficiencies.	7.4.4

Table 7.1-1. TSPA-LA Model Validation Analyses (Continued)

Activity Category/Subcategory	Purpose	Activity Description	Document Section
Surrogate Waste Form Validation			
Spent Fuel Categories	Comparison of naval surrogate fuel to naval fuel (Category 1).	Perform probabilistic runs to compare the naval surrogate (Zircaloy-clad commercial fuel) with naval fuel for Nominal, Igneous Intrusion, and Volcanic Eruption Modeling Cases.	7.5.3
	Comparison of the DOE surrogate fuel to each DOE spent fuel category (Category 2 through Category 11).	Perform probabilistic run using Drip Shield EF Modeling Case to compare the DOE surrogate with plutonium/uranium alloy spent fuel (Category 2), plutonium/uranium-carbide spent fuel (Category 3), mixed-oxide spent fuel (Category 4), uranium/thorium-carbide spent fuel (Category 5), uranium/thorium-oxide spent fuel (Category 6), uranium-metal spent fuel (Category 7), uranium-oxide spent fuel (Category 8), aluminum-based spent fuel (Category 9), miscellaneous spent fuel (Category 10) for two inventories, and uranium-zirconium hydride spent fuel (Category 11).	7.5.4
Selected Sensitivity Analyses	Justification of the DOE surrogate dissolution model.	Perform probabilistic comparison of fuel degradation models for Category 2 through Category 11 and air alteration rates for Category 5 and Category 7.	7.5.5
	Justification of the DOE surrogate dissolution model.	Perform comparison of uranium-metal dissolution model, uranium-metal dissolution model with air alteration, and instantaneous dissolution (Category 7). Perform similar comparison for the uranium/thorium-carbide dissolution model (Category 5).	7.5.5
	Effects of fuel surface area and free inventory and uncertainty of radionuclide inventory.	Perform probabilistic comparison of uranium-metal nominal surface area with bounding surface area and free inventory and comparison of nominal inventory with the bounding inventory (Category 7).	7.5.5
	Uncertainty in number of WPs.	Perform probabilistic comparison of aluminum-based spent fuel for nominal and bounding number of WPs (Category 9).	7.5.5
	Comparison of radionuclides that contribute to annual dose from surrogate DOE spent fuel, HLW, uranium-metal spent fuel (Category 7), uranium/thorium-carbide spent fuel (Category 5), and uranium/thorium-oxide spent fuel (Category 6).	Analyze plots of key radionuclides that contribute to total annual dose for the DOE surrogate spent fuel only, HLW only, Category 7 only, Category 5 only, and Category 6 only.	7.5.5
	Justification of the DOE surrogate fuel.	Compare of the weighted sum of Category 2 through Category 11 spent fuel with a single WP of the DOE surrogate spent fuel.	7.5.5

Table 7.1-1. TSPA-LA Model Validation Analyses (Continued)

Activity Category/Subcategory	Purpose	Activity Description	Document Section
Post–Development Validation Activities (Technical Work Plan Validation (SNL 2008 [DIRS 184920], Section 2.3.5.2))			
Corroboration of Direct Input Abstraction Results with Validated Process Models			
Corroboration of Abstraction Results with Underlying Process Models	Evaluate consistency of the abstraction results with the underlying validated key natural system environment models.	Perform quantitative and qualitative evaluation of how well the direct input abstraction results corroborate with the underlying validated key natural system environment models. Provide the evidence that builds confidence in the direct inputs.	7.6. 4.1
	Evaluate consistency of the abstraction results with the underlying validated key engineered barrier system models.	Perform quantitative and qualitative evaluation of how well direct input abstraction results corroborate the underlying validated key EBS models. Provide the evidence that builds confidence in the direct inputs.	7.6.4.2
	Evaluate consistency of the abstraction results with the underlying validated key DS, WP, and waste form degradation and mobilization models.	Perform quantitative and qualitative evaluation of how well the direct input abstraction results corroborate the underlying validated key DS, WP, and waste form degradation and mobilization models. Provide the evidence that builds confidence in the direct inputs.	7.6.4.3
	Evaluate consistency of the abstraction results with the underlying validated key disruptive events models.	Perform quantitative and qualitative evaluation of how well the direct input abstraction results corroborate the underlying validated key seismic and igneous disruptive events models. Provide the evidence that builds confidence in the direct inputs.	7.6.4.4
	Evaluate consistency of the abstraction results with the underlying validated biosphere model.	Provide the evidences that build confidence in the direct inputs from the biosphere model to the TSPA-LA Model.	7.6.4.5
Corroboration of Results with Auxiliary Analyses			
Analysis of Single Realizations	Evaluate the realization that contributes significantly to mean annual dose for the Early Failure Modeling Cases.	Select a realization each from the Waste Package EF Modeling Case and Drip Shield EF Modeling Case and analyze it to examine how the transport of key radionuclides is affected by coupling various components of the EBS, UZ, and SZ domains following the WP failure under varying physical-chemical-thermal-mechanical conditions.	7.7.1
	Evaluate the realization that contributes significantly to mean annual dose for the Igneous Intrusion Modeling Case.	Select a realization from the Igneous Intrusion Modeling Case and analyze it to examine how the transport of key radionuclides is affected by coupling various components of the EBS, UZ, and SZ domains following the waste package failure under varying physical-chemical-thermal-mechanical conditions	7.7.1
	Evaluate the realization that contributes significantly to mean annual dose for the Seismic GM Modeling Case.	Select a realization from the Seismic GM Modeling Case and analyze it to examine how the transport of key radionuclides is affected by coupling various components of the EBS, UZ, and SZ domains following the WP failure under varying physical-chemical-thermal-mechanical conditions.	7.7.1

Table 7.1-1. TSPA-LA Model Validation Analyses (Continued)

Activity Category/Subcategory	Purpose	Activity Description	Document Section
Corroboration of Results with Auxiliary Analyses (Continued)			
Comparison with Other Simple Models	Compare the TSPA-LA Model component results with a simplified analysis.	Perform an Simplified TSPA Analysis and compare the results with those of the TSPA-LA Model.	7.7.2
	Compare with the Energy and Power Research Institute (EPRI) TSPA Analysis.	Develop a comparison of the approach and results of the TSPA independently conducted by EPRI using its code IMARC for the postclosure performance of the Yucca Mountain repository.	7.7.3
Performance Margin Analyses	Provide objective evidence for assessing performance margin and degree of conservatism or non conservatism in the TSPA-LA Model.	Conduct several auxiliary analyses (see Section 7.7.4 for the list) utilizing revisions to selected component models in the TSPA-LA compliance model, including conceptual or uncertainty alternatives, to assess the performance margin in the compliance model and to evaluate whether the compliance model dose is underestimated. The analyses include both individual component revisions as well as a combined analysis that incorporates all of the selected component revisions.	7.7.4
Corroboration of Results with Natural Analogues			
Cerro Negro	Validation of ASHPLUME for the Volcanic Eruption Modeling Case.	Compare of Cerro Negro ash-fall measurements to the results from ASHPLUME.	7.8.1
Peña Blanca	Validation of the UZ and SZ Transport Model.	Compare of field data from Peña Blanca with the TSPA-LA Model results using a modified TSPA model.	7.8.2
Independent Technical Reviews Performed in Preparation of TSPA-LA Model			
TSPA-VA Peer Review	Evaluate the TSPA-VA methodology and prediction of the future behavior of the total system.	Performed peer review of the TSPA-VA and the supporting process models. The review was to be conducted by an independent group of external experts. 1997 -1999	7.9.1
TSPA-SR Peer Review	Evaluation of the TSPA-SR for methodology and ability to meet the needs for SR and future LA compliance.	Performed peer review of the TSPA-SR and selected supporting documents to evaluate the approach used in the performance assessment, and how well the TSPA-SR and the future TSPA-LA needs were addressed. The review was to be conducted by an international panel of experts managed by the OECD/NEA in 2002.	7.9.2
Draft TSPA-LA Technical Review	Evaluate the earlier draft iterations of the TSPA-LA Model as they were being drafted as to the degree of validation of the model for its intended purpose.	Perform technical review on the evaluation of the degree to which the draft TSPA-LA Model was valid for its intended purpose for the 10,000 years compliance period for which the model was prepared. The review was to be conducted by a team of experts during 2004, 2005, and early part of 2006.	7.9.3

INTENTIONALLY LEFT BLANK

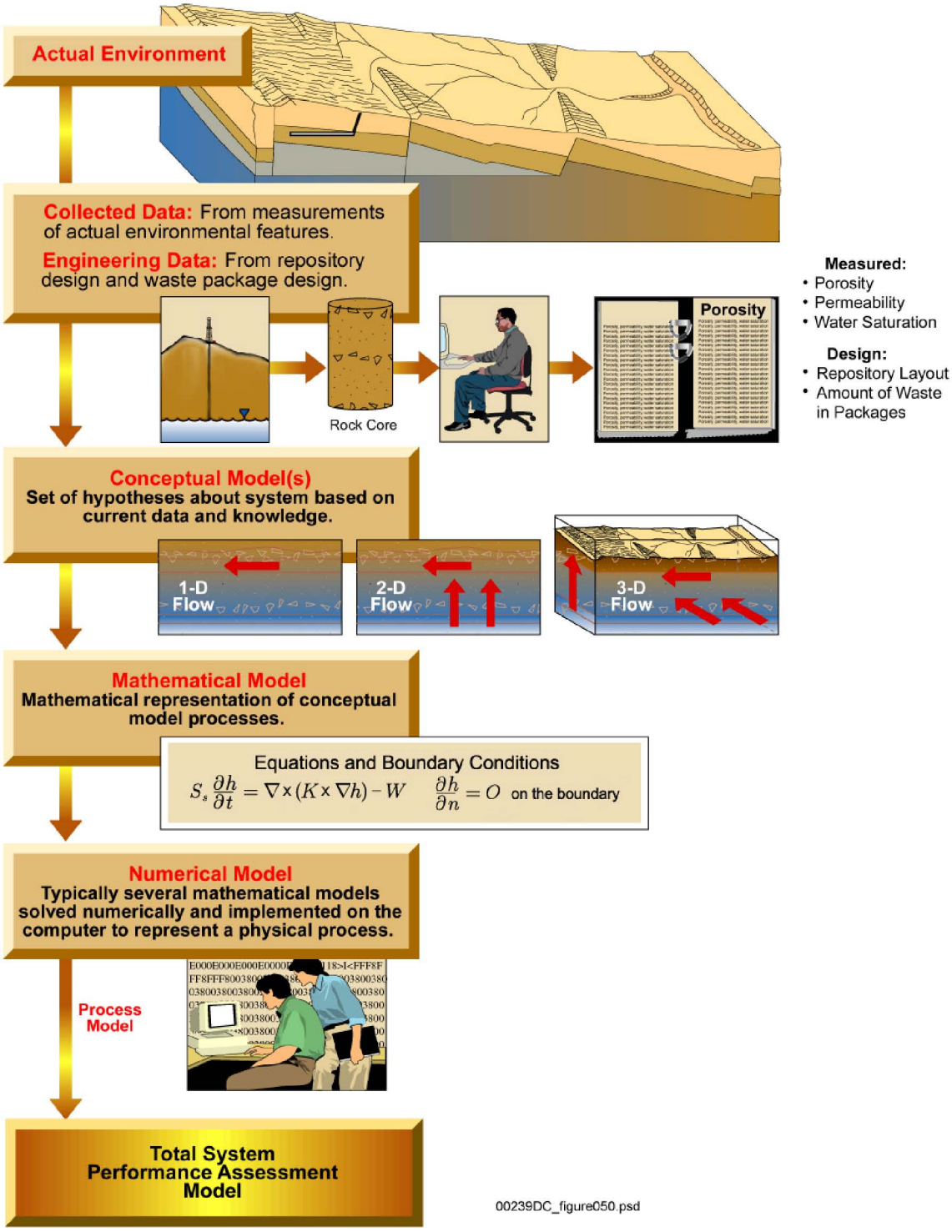

Figure 7.1-1. Generalized Performance Assessment Approach

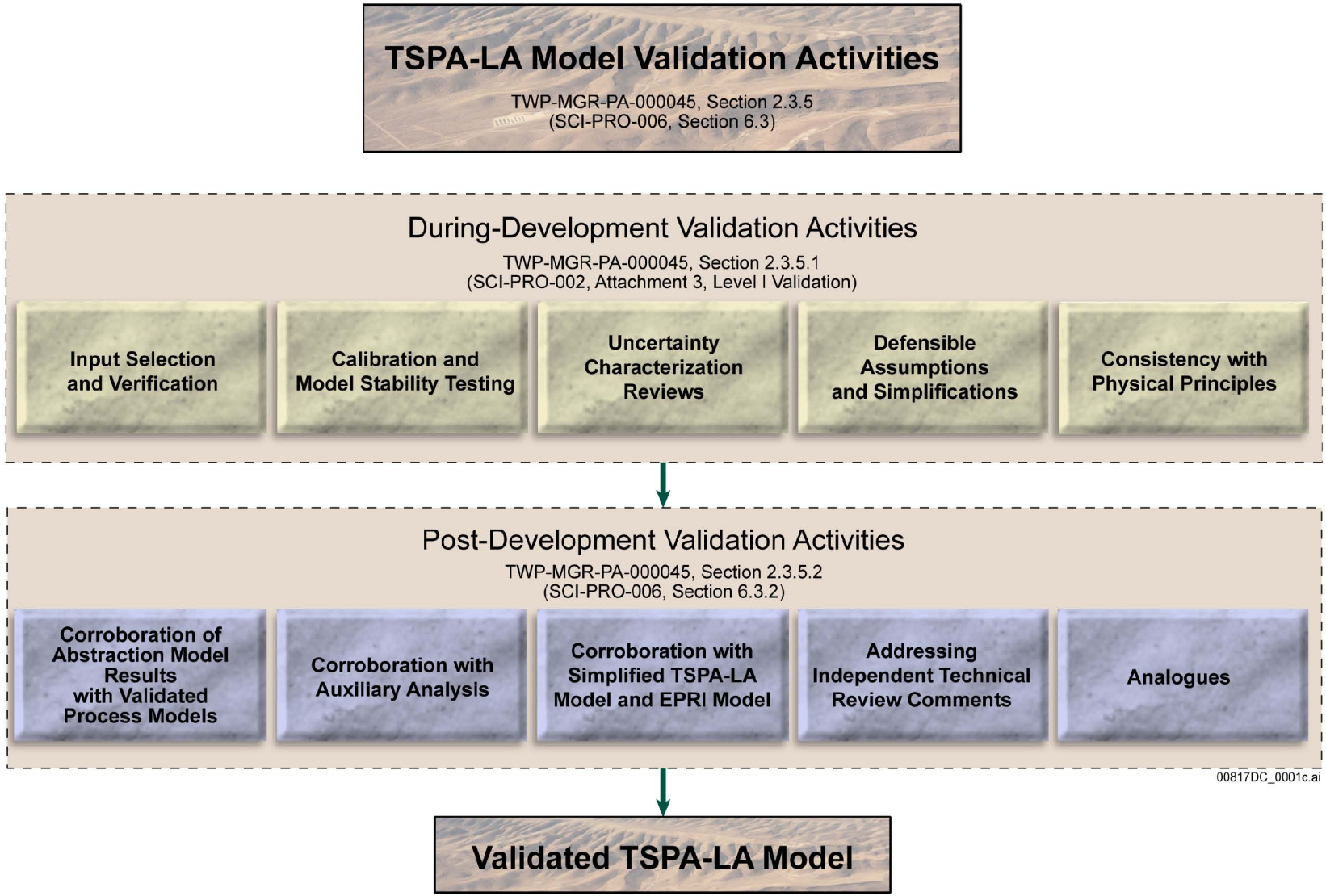

NOTE: The model validation activities, discussed in the TSPA TWP, are shown in the boxes. The corresponding procedural activities are in parenthesis.

Figure 7.1-2. Model Validation Approach

7.2 COMPUTER CODE AND INPUT VERIFICATION

The activities discussed in this section were conducted to comply with the requirements of SCI-PRO-006, *Models,* and Section 2.3.5.1 of *Technical Work Plan for: Total System Performance Assessment FY 07-08 Activities* (SNL 2008 [DIRS 184920]). They include verification of the integrated TSPA-LA Model software (GoldSim), verification of DLL implementations within the TSPA-LA Model, verification of model inputs entered into the TSPA Input Database, and verification of the implementation of the submodel abstractions within the TSPA-LA Model. Verification of the DLL/abstraction implementations was conducted by executing the TSPA-LA Model with a known set of input parameters and comparing the calculated results to those presented in the DLL/abstraction supporting documentation (Sections 7.2.2 and 7.2.4). Coupling between submodels within the TSPA-LA Model is examined by verifying that the information generated by one submodel is fed correctly to successive submodels, and the information does not exceed the applicable range of the successive submodel (Section 7.2.5). Additional information related to the use of the TSPA-LA software codes mentioned in the verification process is provided in Section 3.0.

7.2.1 Selection and Verification of the Integrated System Software: GoldSim

The GoldSim software (V9.60.100, STN: 10344-9.60-01 [DIRS 181903]) was selected as the TSPA Model's integration software based on its capabilities and use in similar applications. The TSPA-LA Model was developed within the GoldSim software framework. GoldSim provides the capability for the user to:

- address the inherent variability and uncertainty that is present in real-world systems by using Monte Carlo simulation
- superimpose the occurrence and consequences of discrete events onto continuously varying systems
- build top-down models using hierarchical containers that facilitate the simulation of large, complex systems while keeping them easy to understand and navigate
- dynamically link external programs or spreadsheets directly to the GoldSim software
- directly exchange information between any open connectivity-compliant database and
- simulate the release, transport, and ultimate fate of mass within the system with an included contaminant transport module.

The GoldSim software application was originally developed specifically for use in the evaluation of radioactive waste disposal facilities. In the past decade, the following are some examples of applications of GoldSim (GoldSim Technology Group 2007 [DIRS 184807]):

- Evaluation of the safety of the proposed high-level radioactive waste (HLW) repository at Yucca Mountain, including the SR

- Evaluation of potential host rocks as part of a program to select a disposal site for the Spanish Radioactive Waste Disposal Research efforts

- Evaluation of waste disposal sites in Los Alamos, New Mexico, to aid in risk characterization and to help identify monitoring requirements for low-level radioactive waste disposal areas

- Evaluation of alternative remediation and closure options for abandoned uranium mill tailings facilities and mine workings in Germany and Canada

- Sensitivity calculations for various applications to supplement the Performance Assessments of the Waste Isolation Pilot Plant in Carlsbad, New Mexico

- Evaluation of different conceptual models of the groundwater flow system on estimates of radionuclide migration at the Nevada Test Site.

Prior to release of each version of the software, the vendor, GoldSim Technology Group, executed tests in an internal verification plan that are included in *Design Document for: GoldSim v9.60* (DOE 2007 [DIRS 181107]). This plan exercises the graphical user interface, internal functions, stochastic processes, contaminant transport code, and result displays for the purpose of demonstrating that the software performs its numerical, logical, and input/output operations correctly.

The vendor's software verification plan consists of over 250 tests that cover the program's capabilities, including the user interface, user-defined expressions, internal functions, and distributed processing capabilities. These tests include:

- 93 Basic Functional Tests
- 23 Time and Monte Carlo Tests
- 130 Contaminant Transport Tests
- 17 Reliability Module Tests.

Specific tests from the vendor's verification plan are independently rerun as part of the Sandia National Labs (SNL) Quality Assurance (QA) procedure, IM-PRO-004, *Qualification of Software*, that demonstrates that the TSPA-identified functional requirements listed in *Requirements Document for: GoldSim v9.60* (DOE 2007 [DIRS 181106]) are satisfactorily implemented. For added confidence, key functions and capabilities of the simulation software are combined into four TSPA-developed tests and the results are compared to independently generated results. The independent tests are described in the *Design Document for: GoldSim v9.60* (DOE 2007 [DIRS 181107], Section 7.2.1) and the results are shown in *Software Validation Report for: GoldSim v9.60 on Windows 2000* (DOE 2007 [DIRS 181109], Sections 4.2.34 through 4.2.37).

The integrated system software (GoldSim) was qualified in accordance with IM-PRO-004. It was obtained from Software Configuration Management in accordance with IM-PRO-003, *Software Management*, and was installed in accordance with installation test instructions listed in Section 3.1 of *User Information Document for: GoldSim Version 9.60* (DOE 2007

[DIRS 181108]). GoldSim was used to develop the analyses for the TSPA-LA Model within the limitations and the range of verification guidance presented in Appendix G of the *User's Guide, GoldSim Probabilistic Simulation Environment* (GoldSim Technology Group 2007 [DIRS 181727]). Additional information regarding the GoldSim software is discussed in Section 3.8 and in the documents listed in Table 3-8.

7.2.2 Verification of Dynamically Linked Libraries in an Integrated System

This section describes the verification of DLLs in the integrated TSPA-LA Model. The DLLs that implement model abstractions are listed in Table 7.2-1 along with the section where the verification of these DLLs is discussed. The verification analyses for the implementation of the DLLs, the abstractions used from the analysis and/or model reports, and the coupling between TSPA-LA Model components are discussed in Sections 7.2.4.1 and 7.2.5. A roadmap of the verification analyses is provided in Table 7.2-2 along with the analysis description, the status of the verification, and the document section where the analysis is described.

The general approach to verifying the implementation of a DLL or other abstraction within an integrated model is described as follows. A validation test example reported in an analysis and/or model report, or a validation test report with known results, is first run on the stand-alone implementation of a DLL or other model abstraction to verify that the answer reported in the analysis and/or model report can be reproduced. The answer is then compared with the results of the implementation in the TSPA-LA Model. In some instances, small differences resulting from uncertainty and differences in calculation schemes between the two model implementations (e.g., discretization, timesteps, and numerical solutions as compared to analytical solutions) may be observed between the results reported in the analysis and/or model report and those calculated by the stand-alone implementation. Knowing these small variations were likely to occur, a screening criterion against which the importance of these variations could be evaluated was established. In many cases, the results calculated from the single realization of the TSPA-LA Model should be exactly equal to those calculated by the stand-alone implementation of the DLL.

7.2.3 Verification of Inputs in Total System Performance Assessment Database

Parameters used in the analyses for the TSPA-LA Model are documented in the TSPA Input Database described in Section 4.7. The TSPA Input Database supports the TSPA-LA Model by providing the parameter values and distributions necessary for performance assessment analysis of the repository. The TSPA Input Database categorizes, stores, and retrieves both fixed and distributed values of the TSPA-LA Model's parameters and allows qualified/authorized analysts to view and update values in the database.

Each TSPA-LA Model simulation accesses the database in order to obtain values for the model's parameters. Parameter values are obtained from the sources listed in Table 4-1 and manually entered into the database. Parameter values are maintained as originally entered. There is no transformation or post-processing of these parameter values. Parameter values are entered into the database using a number of forms. These forms include the Parameter Identification Form (PIF) that serves as the primary means to enter parameters into the TSPA Input Database. The PIF is linked by parameter identification to a Parameter Documentation Form (PDF) that

documents the source of the parameter information. The PDF is linked by value identification to a Parameter Value Entry Form that passes to the TSPA-LA Model the type of information to expect (i.e., distribution type, maximum, minimum, and parameter code). Figure 4-3 shows the structural framework of the database that is described in Section 4.8.

Before using parameter values in the TSPA-LA Model for the performance assessment analysis, each parameter undergoes a check of the PIF to verify that the information has been entered correctly. During development of the TSPA-LA Model, identified inconsistencies in parameter values were documented, revised values were entered into the TSPA-LA Model database, and the calculations affected by the inconsistencies were rerun. The parameter verification is documented on the Parameter Verification Form (Section 4.8). Only users with access to the TSPA-LA Model's controlled access input database can verify parameter values. The verification process includes recording the checker's name along with the date and time to identify the last user who changed any one of the parameter categories using a PIF, a PDF, a Parameter Value Entry Form, or a Parameter Verification Form. Strict control of access and the documentation trail increases the confidence in the security, integrity, and traceability of information entered into, or downloaded from, the TSPA Input Database.

7.2.4 Verification of Single Model Components

The TSPA-LA Model is composed primarily of submodels that are derived from abstraction models documented in various analysis and/or model reports. One technique used to improve confidence in a numerical model is to calibrate or compare model results with known results under a set of controlled conditions. Such confidence building activities may be divided into verification and validation activities. Validation activities test the applicability of the model to simulate an event or a process, and may be described as a process to establish model accuracy. On the other hand, verification activities are designed to establish model precision (i.e., they determine whether the model can calculate results with a satisfactory degree of confidence under a given set of controlled inputs). A discussion of verification activities of various submodels in the TSPA-LA Model is given in the following sections.

The approach used to verify the submodels implemented in the TSPA-LA Model was based on the type of information provided in the supporting analysis and/or model reports. In general, the information from the analysis and/or model reports used in verification of the submodels was in the following form:

- Look-up tables
- Abstraction equations with ranges of input values
- A qualified stand-alone implementation of the abstraction or DLL with a GoldSim-based model file.

When inputs or results used from an analysis and/or model report are in the form of a look-up table, a verification subroutine is implemented in the TSPA-LA Model file that is triggered by a verification switch. After the verification switch is triggered, input values corresponding to the independent variables in the look-up table are fed into the appropriate submodel in the TSPA-LA Model file. The verification switch is set so that the simulation can be run deterministically with no uncertain parameters. The verification results are values that have been retrieved from

look-up tables with appropriate interpolations. Because the results have no built-in uncertain parameters, these values should equal the values presented in the look-up tables or equal the linearly interpolated values exactly. The expected results for a given set of inputs are stored in a TSPA-LA Model file results element. Values that are calculated by the submodel implemented in the TSPA-LA Model file are also stored in a TSPA-LA Model file results element. The expected values and the estimated values in the TSPA-LA Model file are compared to determine the verification outcome.

The same approach is used when the analysis and/or model report presents results in the form of an abstraction equation. The verification subroutine calculates results for a range of input values under which the abstraction equation is valid. Results from the TSPA-LA Model file calculations are compared with values estimated from the equations presented in the analysis and/or model reports. A good match between the expected values and TSPA-LA Model file-calculated values indicates that the abstracted model has been verified. As with the earlier case of model verification using look-up tables, the TSPA-LA Model file calculations are run deterministically with no uncertainty.

In some instances, the feed to the TSPA-LA Model may not be in the form of a table or equation presented in an analysis and/or model report. Such TSPA-LA submodels or components may be receiving inputs from qualified DLLs or may be retrieving information from qualified external databases. Furthermore, under certain circumstances, the TSPA-LA Model may be using a simple equation with no values provided for verification testing in the associated analysis and/or model report. Under these conditions, the verification process involves checking to ensure that the TSPA-LA Model is correctly linked to the TSPA Input Database and the correct values are returned. In addition, checking also verifies that equations were implemented correctly.

Finally, in some instances where an external DLL is used to do calculations or when a simple implementation within a GoldSim-based model is available in the analysis and/or model report, the verification process involves conducting test runs presented in the analysis and/or model report or in DLL software qualification documents. Verification runs in the TSPA-LA Model are set to simulate the runs presented in the validation documentation (i.e., the TSPA-LA Model is run with the same set of inputs as those presented in the DLL validation). Outputs of the TSPA-LA Model are compared to results presented in the DLL validation.

As discussed earlier, the approach to verification is to compare TSPA-LA Model file results with results of stand-alone implementations reported in analysis and/or model reports or validation test reports, where applicable. Therefore, the input values for a validation run are taken from a validation test report or analysis and/or model report and used in the TSPA-LA Model. In some instances, the input values may be truncated for ease of reporting in a table. As an illustration, a value of 2.61364 may be truncated to 2.61. Therefore, in a verification realization, an error is introduced with the use of a truncated input value. Consequently, a small difference occurs between expected and calculated results. In some submodels, where the calculated values are strongly dependent upon inputs, such as the solubility submodels, the error can be potentially higher depending upon the input values used. In some cases, the supporting analysis and/or model report utilizes a separate GoldSim-based model file. A comparison is made whereby the separate model file is run deterministically for a set of inputs described in the analysis and/or

model report. Then, the TSPA-LA Model is run with the same set of inputs, and the results of the two runs are compared.

7.2.4.1 Verification Results

The variety of methods by which the various submodel abstractions were implemented within the TSPA-LA Model yielded some implementations that were of limited modeling complexity and thus were considered verified by checking activities conducted during the model development phase. Examples of these types of submodel abstractions would include the Infiltration Submodel, the Climate Submodel, the Radionuclide Inventory Submodel, and the Human Intrusion Submodel. For the Infiltration Submodel, the selection of the infiltration percentage was a simple probability selection. For the Climate Submodel, the change in the climate scenario was a function of time. The Radionuclide Inventory Submodel was verified by ensuring that the inventory elements in the TSPA-LA Model file were correctly linked to the database. The Human Intrusion Submodel included defined parameters and simple model implementation. Therefore, a verification description for each submodel listed in Table 6-1 is not presented.

Results for the submodel verifications that were conducted for the TSPA-LA Model are presented in the following sections. All submodel verifications were performed using GoldSim V9.60.100 [DIRS 181903]. The supporting documentation, which consists of electronic versions of the TSPA-LA Model output files and results, is provided in the supporting material (output DTN: MO0708TSPAPOST.000 [DIRS 182986]). The submodel verifications were performed during the TSPA-LA Model development for those submodels that were no longer subject to development changes. As a result, the verification simulations were, in many cases, performed with earlier versions of the TSPA-LA Model that are labeled by specific version numbers found in the relevant records package. A brief description of the analyses described below is presented in Table 7.2-2 along with the status of the verification and identification of the section that contains the discussion of the verification.

7.2.4.1.1 Drift Seepage

The Drift Seepage Submodel, as implemented in the TSPA-LA Model, is defined in *Abstraction of Drift Seepage* (SNL 2007 [DIRS 181244]). The verification of the Drift Seepage Submodel was conducted to ensure the proper implementation of the submodel within the TSPA-LA Model (v5.000) via the SEEPAGEDLL_LA V.1.3 [DIRS 181058] DLL. The verification focused on the flow of information into and the results out of the SEEPAGEDLL_LA DLL.

A stand-alone GoldSim-based model file that contained the implementation of the SEEPAGEDLL_LA validation test case TC-24 (*User Information Document for: SEEPAGEDLL_LA V1.3* (DOE 2006 [DIRS 181133])) was selected for use in the verification of the TSPA-LA Model implementation. This test case is identified as the stand-alone model file.

The verification process was initiated by running a single realization of the TSPA-LA Model (v5.000) and saving the values of the SEEPAGEDLL_LA input parameters. This input parameter set was then fed into the parameter elements of the stand-alone TC-24 implementation to develop a set of verification results. Table 7.2-3 lists the results from the outputs generated by

the SEEPAGEDLL_LA for both the TSPA-LA Model and the stand-alone model. The verification results shown in Table 7.2-3 are identical for the TSPA-LA Model single realization and the stand-alone model. Therefore, the implementation of the Drift Seepage Submodel, including the seepage DLL, is considered verified (output DTN: MO0708TSPAPOST.000 [DIRS 182986]).

7.2.4.1.2 Drift Wall Condensation Submodel Verification

The Drift Wall Condensation Submodel and Abstraction (Table 6-1) is defined in *In-Drift Natural Convection and Condensation* (SNL 2007 [DIRS 181648], Sections 8.3 and 8.0[a]). The abstraction calculates a probability of condensation occurrence on the drift walls at a WP location. If condensation occurs, its rate is calculated.

The implementation of the Drift Wall Condensation Submodel was verified using version 4.042 of the TSPA-LA Model. The model was modified to verify the implementation of the Drift Wall Condensation Submodel by comparing the simulated model results to a set of drift-wall condensation rates independently calculated in a Microsoft Excel spreadsheet. The Excel spreadsheet calculations were based on *In-Drift Natural Convection and Condensation* (SNL 2007 [DIRS 181648], Sections 8.3 and 8.0[a]). A set of known inputs were defined for both the TSPA-LA Model (v4.042) and the Excel spreadsheet (output DTN: MO0708TSPAPOST.000 [DIRS 182986]). Then simulation and calculated condensation rates were compared to verify the implementation of the abstraction in the TSPA-LA Model (output DTN: MO0708TSPAPOST.000 [DIRS 182986]).

The abstraction is implemented such that the independent variables of time, percolation rate, invert transport condition (high or low), dispersivity condition (high or low) for axial transport, and the ventilation condition of the DS (ventilated or unventilated) are sampled. Then, based on a set of correlation tables using these independent variables, the correlation of the fraction of locations where condensation occurs (probability) is determined. If the probability is such that condensation will occur, then another set of correlation tables is utilized to determine the actual condensation rate. For the verification task, the values for the independent variables were specified at each timestep for a simulation time of 3,000 years. The timestep length was set equal to 75 years, yielding a total of 40 parameter sets. The specified simulation duration of 3,000 years was due to no condensation occurring after a simulation time of 3,000 years as defined in the abstraction.

Table 7.2-4 shows the comparison of the drift-wall condensation rates simulated by the TSPA-LA Model (v4.042) and calculated by the Excel spreadsheet (output DTN: MO0708TSPAPOST.000 [DIRS 182986]). The percent differences in the condensation rates indicate that the values are identical and thus the implementation of the Drift Wall Condensation Submodel and Abstraction in the TSPA-LA Model is considered verified.

7.2.4.1.3 Engineered Barrier System Chemical Environment

Verification of the Engineered Barrier System (EBS) Chemical Environment Submodel (Table 6-1) was conducted in a version of the TSPA-LA Model that was modified to allow the use of a controlled set of input parameters. The goal of the verification process was to determine

the ability of the TSPA-LA Model file to satisfactorily estimate, under both evaporative and condensation conditions, the Pco_2, pH, and ionic strength for a set of controlled inputs. Verification consists of comparing expected Pco_2, pH, and ionic strength values against those calculated by the TSPA-LA Model file. The implementation of the EBS Chemical Environment Submodel is defined in *Engineered Barrier System: Physical and Chemical Environment* (SNL 2007 [DIRS 177412], Section 6.15.1).

The verification of the Pco_2 calculation was conducted separately from the pH and ionic strength calculations. The implementation of the Pco_2 calculation within the TSPA-LA Model was based on determining the bounding values for a range in Pco_2 from look-up tables as a function of seepage water type, water-rock interaction parameter, temperature, and relative humidity. Next a Pco_2 uncertainty parameter was sampled that defined the relative location of a single Pco_2 value within the determined range. The verification process developed a set of known input parameter combinations. This input set was used to calculate the Pco_2 values in the TSPA-LA Model (v4.043) and in an independent calculation within a Microsoft Excel worksheet (output DTN: MO0708TSPAPOST.000 [DIRS 182986]). A single realization of the TSPA-LA Model (v4.043) was simulated with a different set of input parameter values at each timestep, with a total of 44 input parameter combinations. Table 7.2-5 lists the values of the water-rock interaction parameter, temperature, and relative humidity input parameters and the calculated Pco_2 values. The calculation was conducted for seepage water type number 2, which was randomly chosen from the three seepage water types. The values presented in Table 7.2-5 indicate that the calculated Pco_2 values are essentially the same. Therefore, the implementation of the EBS Chemical Environment Submodel Pco_2 determination process in the TSPA-LA Model is considered verified.

The verification of the pH and ionic strength implementation within the TSPA-LA Model was conducted in a similar manner as the Pco_2 verification. The pH and ionic strength is obtained from a series of look-up tables as a function of seepage water type, Pco_2, temperature, and relative humidity at the WP surface, and the water-rock interaction parameter. A total of 396 combinations of constant-value input parameters were specified and the pH and ionic strength values calculated for each input set. Table 7.2-6 lists the range of the input parameters used in developing the input sets. A comparison of the pH and ionic strength values calculated in the TSPA-LA Model (v4.043) and in an independent Microsoft Excel worksheet (output DTN: MO0708TSPAPOST.000 [DIRS 182986]) were used for the verification. Figures 7.2-1 and 7.2-2 present the comparison plots for the pH and ionic strength values, respectively, calculated for each of the 396 input sets. An examination of the data indicates that the difference in the pH and ionic strength values between the two calculation methods is essentially zero. Therefore, the implementation of the pH and ionic strength calculation in the EBS Chemical Environment Submodel within the TSPA-LA Model is considered verified.

7.2.4.1.4 Waste Package and Drip Shield Degradation

An integrated WP and DS Degradation Submodel is implemented in the TSPA-LA Model and contains a set of external DLLs that operate in series. The DLLs are WAPDEG V 4.07 [DIRS 181064]; CWD V2.0 [DIRS 181037]; and SCCD V2.01 [DIRS 181054].

The verification process uses a previously defined stand-alone GoldSim-based model test case, documented in *WAPDEG Analysis of Waste Package and Drip Shield Degradation* (BSC 2004 [DIRS 169996], Section 7.1 and Appendix I), as the basis for comparison to the implementation within the TSPA-LA Model (v4.042). The original stand-alone model files are located in DTN: MO0310MWDWAPAN.002_R0 [DIRS 165800]. The stand-alone model configuration was updated in the current version of the GoldSim software (v9.60) for direct comparison to the TSPA-LA Model (v5.000) results (output DTN: MO0708TSPAPOST.000 [DIRS 182986]).

An identical set of constant input parameter values were specified for the stochastic parameters in both the stand-alone model file and the TSPA-LA Model (v5.000) (Table 7.2-7). Examination of the Failure_Opening output table values verify that the DS and WP breaches occur in the correct time bins consistent with the input (i.e., supplied general corrosion rates and microbially influenced corrosion factor) and that stress corrosion cracking (SCC) is taking place. Figure 7.2-3 presents a comparison of results for two parameters from the Failure_Opening output tables. These are the average number of patch failures and average number of crack failures on the side of a failed waste package. The results from the output table which are not presented in Figure 7.2-3 are identical for both cases. The comparison verifies implementation of the WP and DS Degradation Submodel in the TSPA-LA Model.

7.2.4.1.5 Waste Form Degradation and Mobilization

Verification of the Waste Form Degradation and Mobilization submodels (Table 6-1) involved testing of the rind volume and rind mass calculations for the co-disposed waste packages (CDSP WPs) and commercial spent nuclear fuel (CSNF) WPs, the waste form degradation calculations for the CSNF, the in-package chemistry, and the dissolved concentration limits. The following discusses the results of the Waste Form Degradation Submodel verifications (Table 6-1).

CSNF Rind Volume and Mass—The ability of the Waste Form Degradation and Mobilization Submodels (Table 6-1) to satisfactorily estimate the volume and mass of the CSNF WP rind was verified for the TSPA-LA Model. Inputs for verification were taken from values given in *Cladding Degradation Summary for LA* (SNL 2007 [DIRS 180616], Table 6-3). The values of rind porosity, fraction of failed rods, and the fraction of total WP inventory that was corroded were varied over a range of values for a total of 12 input sets. The degradation values to be used in the TSPA-LA Model are given in *Cladding Degradation Summary for LA* (SNL 2007 [DIRS 180616], Table 7-1) and were used to calculate the rind volume and mass in a CSNF WP using the parameters and equations in *Cladding Degradation Summary for LA* (SNL 2007 [DIRS 180616], Tables 6-3 and 6-4, Equations 6-3, 6-4, 6-5, and 6-12). The estimated values of the CSNF WP rind volume and mass were calculated using a Microsoft Excel spreadsheet (output DTN: MO0708TSPAPOST.000 [DIRS 182986]). Modification of the TSPA-LA Model (v4.041) was made to allow for the use of the same input values as in the spreadsheet calculations. Details of the verification module implementation are given in the supporting information (output DTN: MO0708TSPAPOST.000 [DIRS 182986]). The results of the rind volume and mass calculations from the TSPA-LA Model (v4.041) were compared against those calculated in the spreadsheet (Table 7.2-8). The percent difference between the calculation methods was found to be essentially zero. Therefore, the ability of the submodel implementation

within the TSPA-LA Model to estimate the rind volume and mass in the failed CSNF WPs has been verified.

CDSP Rind Volume and Mass—The ability of the Waste Form Degradation and Mobilization Submodels (Table 6-1) to satisfactorily estimate the HLW rind volume and mass in the CDSP WPs was verified for the TSPA-LA Model. In addition, the ability to estimate HLW rind thickness was also verified.

A Microsoft Excel spreadsheet was used to calculate the HLW rind properties using the equations given in *Defense HLW Glass Degradation Model* (BSC 2004 [DIRS 169988], Section 8.1). Input parameters, such as the initial radius and length of the glass log, were also obtained from *Defense HLW Glass Degradation Model* (BSC 2004 [DIRS 169988], Section 8.1). The fraction of the waste form degraded varied between 0.01 and 0.99, resulting in a total of 12 separate verification calculations.

The details of the verification module implementation in v4.041 of the TSPA-LA Model are given in the supporting document (output DTN: MO0708TSPAPOST.000 [DIRS 182986]). The main input change to the model was the specification of the 12 values of the fraction of waste form degraded. A single realization of the TSPA-LA Model (v4.041) was simulated with these input changes. The values of the HLW rind thickness, volume, and mass estimated in the Microsoft Excel spreadsheet (output DTN: MO0708TSPAPOST.000 [DIRS 182986]) were compared to the TSPA-LA Model file-estimated values (Table 7.2-9). The percent difference in the values was found to be essentially zero. Therefore, the ability of the submodel implementation within the TSPA-LA Model to estimate the HLW rind thickness, volume, and mass in the failed CDSP WPs has been verified.

CSNF Waste Form Degradation—The ability of the CSNF Waste Form Degradation Abstraction (Table 6-1) to satisfactorily estimate the waste form degradation rate was verified for the TSPA-LA Model. The variables controlling the waste form degradation rate under acidic and alkaline conditions are pH, temperature, pO_2, and pCO_3, as defined in *CSNF Waste Form Degradation: Summary Abstraction* (BSC 2004 [DIRS 169987], Sections 6.4.1.3 and 6.4.1.2). A Microsoft Excel spreadsheet was used to calculate values of the waste form degradation rate under both acidic and alkaline conditions (output DTN: MO0708TSPAPOST.000 [DIRS 182986). The Microsoft Excel-calculated values of the logarithm of the waste form degradation rate were compared with values estimated by implementation of the CSNF Waste Form Degradation Abstraction in the TSPA-LA Model (v4.041).

The results of the verification under both acidic and alkaline conditions are summarized in Table 7.2-10. These results indicate that the ability of the CSNF Waste Form Degradation Abstraction (Table 6-1) to calculate the waste form degradation rates under both acidic and alkaline conditions with a satisfactory degree of confidence (maximum percent difference of less than 0.1 percent).

HLW Glass Degradation—The ability of the HLW Glass Degradation Abstraction (Table 6-1) to satisfactorily estimate the waste form degradation rate was verified for the TSPA-LA Model. The variables controlling the HLW glass degradation rate are pH, temperature, and relative humidity, as defined in *Defense HLW Glass Degradation Model* (BSC 2004 [DIRS 169988],

Section 6.7). Microsoft Excel was used to calculate verification values of the glass degradation rate under both acidic and alkaline conditions (output DTN: MO0708TSPAPOST.000 [DIRS 182986]). The glass degradation rates were calculated for relative humidity conditions less than and greater than 0.44 even though *Defense HLW Glass Degradation Model* (BSC 2004 [DIRS 169988], Section 6.7) stipulates that no glass degradation occurs if relative humidity is less than 0.44. The Microsoft Excel-calculated verification values of the glass degradation rate were compared with values estimated by the implementation of the HLW Glass Degradation Abstraction in the TSPA-LA Model (v4.041) as shown in Table 7.2-11. The comparison indicates that the percent difference is essentially zero and that this verifies the ability of the HLW Glass Degradation Abstraction to satisfactorily calculate glass degradation rates under both acidic and alkaline conditions.

In-Package Chemistry—The ability of the In-Package Chemistry Submodel and Abstraction (Table 6-1), implemented in the TSPA-LA Model, to satisfactorily estimate values of pH, ionic strength, and total carbonate was verified. The submodel and abstraction are defined in *In-Package Chemistry Abstraction* (SNL 2007 [DIRS 180506]). The goal of verification was to determine the ability of the TSPA-LA Model file to satisfactorily estimate ionic strength, pH, and total carbonate values inside the WP based on a set of known inputs. The main inputs included temperature, relative humidity, Pco_2, seepage flow rate, and bin number. Verification consisted of comparing the values of pH and ionic strength calculated from the TSPA-LA Model to those calculated independently in a Microsoft Excel spreadsheet (output DTN: MO0708TSPAPOST.000 [DIRS 182986]).

The implementation within the TSPA-LA Model calculated the ionic strength and pH parameters under two seepage conditions and the total carbonate parameter. A series of look-up tables that define these parameters, based on a set of known inputs, are presented in DTN: SN0702PAIPC1CA.001_R2 [DIRS 180451] along with the steps required to implement the abstraction. Each parameter was calculated for the TSPA-LA Model cells that represent the CSNF WP, the HLW canister portion of the CDSP WP, and the multi canister over pack canister portion of the CDSP WP.

The ionic strength is determined inside a WP only if the relative humidity is greater than or equal to 95 percent. If the relative humidity is greater than or equal to 95 percent, the ionic strength is then determined from a series of look-up tables based on the seepage condition. If the seepage flow rate at the location of the WP is less than or equal to 0.1 L/yr, then the vapor influx abstraction tables are used, else the liquid influx abstraction tables are used (DTN: SN0702PAIPC1CA.001_R2 [DIRS 180451]). Once the appropriate table has been selected, the ionic strength value is determined for the liquid influx case as a function of seepage flow rate and time since the WP failure, or for the vapor influx case as a function of relative humidity. The implementation of the ionic strength calculation within the TSPA-LA Model (v4.043) was verified against an independent calculation in a Microsoft Excel spreadsheet (output DTN: MO0708TSPAPOST.000 [DIRS 182986]). The calculation developed in the spreadsheet was based on the identical abstraction and look-up tables as presented in DTN: SN0702PAIPC1CA.001_R2 [DIRS 180451].

Table 7.2-12 presents the range of values for the defined input parameters of time since WP failure and seepage flow rate, along with a random stochastic parameter used in incorporating

uncertainty into the final ionic strength value (Section 6.3.7). Figure 7.2-4 presents a comparison plot of the TSPA-LA Model (v4.043), and calculated verification ionic strength values for both the non-seeping and seeping cases. The percent differences between the two sets of calculations were essentially zero.

The pH is determined inside the CSNF and DHLW WPs for relative humidity values less than 95 percent. The CSNF pH is uniformly sampled between 6 and 7. The DHLW pH is set to 10. The implementation of these two pH calculations was not verified in this section. For relative humidity values greater than or equal to 95 percent, the pH is determined as function of the ionic strength and the Pco_2 using a series of look-up tables (DTN: SN0702PAIPC1CA.001_R2 [DIRS 180451]). The ionic strength selected is based on either the vapor influx or liquid influx conditions as defined previously. If the liquid influx case is determined, then the minimum of the liquid influx or the vapor influx ionic strength is selected. If the vapor influx case is determined, then the ionic strength is based on the vapor influx. The implementation of the pH calculation within the TSPA-LA Model (v4.043) was verified against an independent calculation in a Microsoft Excel spreadsheet (output DTN: MO0708TSPAPOST.000 [DIRS 182986]). The calculation developed in the spreadsheet was based on the identical abstraction and look-up tables as presented in DTN: SN0702PAIPC1CA.001_R2 [DIRS 180451]. Table 7.2-12 presents the range of values for the constant input parameters of ionic strength and Pco_2, along with a random stochastic parameter used in incorporating uncertainty into the pH calculation (Section 6.3.7). Figure 7.2-5 presents a comparison plot of the TSPA-LA Model (v4.043), and Excel calculated verification pH values for both the non-seeping and seeping cases. The percent differences between the two sets of calculations were essentially zero.

The total carbonate is determined as function of the Pco_2, pH, and temperature using an equation. The equation along with a set of calculated total carbonate values is given in DTN: SN0702PAIPC1CA.001_R2 [DIRS 180451]. These calculated values were used as the verification calculations with which the TSPA-LA Model (v4.043) was verified against (output DTN: MO0708TSPAPOST.000 [DIRS 182986]). Table 7.2-12 presents the range of values for the constant input parameters of P_{CO2}, pH, and temperature. Figure 7.2-6 presents a comparison plot of the TSPA-LA Model (v4.043) and DTN calculated total carbonate values. The percent differences between the two sets of calculations were essentially zero.

Based on these verification results, the In-Package Chemistry Submodel and Abstraction implementation within the TSPA-LA Model is considered verified.

Dissolved Concentration Limits: Nominal Scenario—Verification of the Dissolved Concentration Limits Submodel (Table 6-1), as implemented within the TSPA-LA Model based on *Dissolved Concentration Limits of Elements with Radioactive Isotopes* (SNL 2007 [DIRS 177418]), was divided into two segments. This section discusses that solubility of americium, neptunium, protactinium, plutonium, tin, thorium, and uranium were verified for the Nominal Scenario Class Modeling Case. The solubility model for uranium was independently verified for the Igneous Scenario Class (Igneous Intrusion Modeling Case only), as described below.

Modeling of dissolved concentration limits (also referred to as solubility limits) of elements with radioactive isotopes has been implemented within the TSPA-LA Model. These dissolved

concentration limits calculations are needed to determine radionuclide solubilities–an important component in calculating releases from the EBS. Three key parameters to the calculation of the dissolved concentration limits are pH, ionic strength, and the Pco_2. Values for these parameters are calculated elsewhere within the TSPA-LA Model but for this verification, a set of parameter ranges was defined. The ranges were a pH of 5.5 to 10.5, an ionic strength of 0.1 to 10 mol/kg, and a Pco_2 of 1×10^{-5} to 1×10^{-1} bars. Using the defined parameter ranges, a total of 471 data input sets were developed to use in the calculation of the dissolved concentration limits. With these data sets, a single realization of the TSPA-LA Model (v5.000) was conducted. The dissolved concentration limits results for americium, neptunium, protactinium, plutonium, tin, thorium, and uranium were extracted from this model simulation.

An independent calculation of the expected dissolved concentration limits was developed within a Microsoft Excel spreadsheet for use as verification data to the TSPA-LA Model results. This calculation was based on the methods provided by three DTNs and the *Dissolved Concentration Limits of Elements with Radioactive Isotopes* (SNL 2007 [DIRS 177418]). The three DTNs were MO0702PADISCON.001_R0 [DIRS 179358], MO0702PAFLUORI.000_R1 [DIRS 181219], and MO0704PASOLCAP.000_R0 [DIRS 180389]. The input parameters utilized in the verification calculation included the same parameter ranges for pH, ionic strength, and Pco_2. In addition, the epistemic sampled parameter values from the TSPA-LA Model single realization run were exported and utilized in the verification calculation.

The calculation of the dissolved concentration limits values by the TSPA-LA Model and the verification calculation for americium, neptunium, and uranium are presented on Figure 7.2-7. The remaining four elements were not presented on the figure for easier viewing of the comparison results. However, the percent differences between the stand-alone and the TSPA-LA Model calculations for all seven elements for each of the input parameter sets were essentially zero. Based on these results, the Dissolved Concentration Limits Submodel is considered to be verified as implemented within the TSPA-LA Model. The results of this verification are presented in output DTN: MO0708TSPAPOST.000 [DIRS 182986].

Dissolved Concentration Limits: Uranium in the Igneous Scenario—The calculation of uranium-dissolved concentration limits in the Igneous Intrusion Modeling Case for the Igneous Scenario Class, were performed using the same approach as presented above. The difference to the modeling approaches was not extensive and mainly required the sampling of variables from a larger number of tables, based on the calculated conditions.

These various tables provide for solubility control of uranium by three solids, whereas the solubilities of all other radionuclides were controlled by only one or two solids. The three solids controlling uranium solubilities are schoepite ($UO_3{\cdot}2H_2O$), Na-boltwoodite ($NaUO_2SiO_3OH{\cdot}1.5H_2O$), and the solid $Na_4UO_2(CO_3)_3$, as described within *Dissolved Concentration Limits of Elements with Radioactive Isotopes* (SNL 2007 [DIRS 177418]). Based on the variables and the conditions, values were either sampled from one table or interpolated between multiple tables.

The same approach to verification used for the other dissolved concentration limits calculations was used for verifying uranium in the Igneous Intrusion Modeling Case. The independent verification calculations were modified appropriately. The initial verification of the TSPA-LA

Model (v5.000) failed. The cause of the failure was found to be two TSPA-LA Model file elements being linked to incorrect tables. When the CSNF WPs were subjected to high ionic strength (greater than 3 mol/kg) and solubilities were controlled by the schoepite mineral phase, the model read the incorrect look-up tables for low ionic strength conditions, using Na-boltwoodite-controlled solubilities. The discrepancy was documented in the TSPA-LA Model file, and it's impact was assessed as described in Appendix P. The incorrect element links were corrected in the TSPA-LA Model (v5.000) for verification purposes only, and the verification analysis was conducted again. Using the revised values, the model results were within the acceptable verification range. The results of the updated verification are provided on Figure 7.2-8. The verification calculations are described in greater detail in the output DTN: MO0708TSPAPOST.000 [DIRS 182986]. Based on the results of this verification analysis, the dissolved concentration limits calculations for uranium in the Igneous Intrusion Modeling Case are considered to be not verified due to the noted incorrect element linkages. However, when these linkages are corrected, the verification results show that the remainder of the dissolved concentration limits calculations for uranium in the Igneous Intrusion Modeling Case, are properly implemented within the TSPA-LA compliance model.

7.2.4.1.6 Engineered Barrier System Transport

The EBS Flow Submodel and the EBS Transport Submodel are defined in *EBS Radionuclide Transport Abstraction* (SNL 2007 [DIRS 177407]). This section describes the verification of both the EBS Flow Submodel and the EBS Transport Submodel as implemented in the TSPA-LA Model.

The EBS Flow Submodel, as described in *EBS Radionuclide Transport Abstraction* (SNL 2007 [DIRS 177407]) and in Section 6.3.6 of this document, does not directly calculate the flow of water through the various components of the EBS (i.e., DS, WP, invert) but takes flow rates from the Drift Seepage and Drift Wall Condensation Submodels as inputs and applies a series of conditional statements to determine the amount and rate of water available for transport within and out of the EBS. Based on this method by which the EBS Flow Submodel was implemented within the TSPA-LA Model, it was considered that the checking conducted during the model development process, and documented in the relevant records package was sufficient for verification purposes.

The implementation of the EBS Transport Submodel within the TSPA-LA Model (v4.042) was verified by comparing the results of dissolved radionuclide transport and colloid-facilitated radionuclide transport within the EBS from the TSPA-LA Model and a finite-difference approximation of the governing mass balance equations implemented in a Microsoft Excel spreadsheet (*Transport_Calc_Appendix_B.xls* in output DTN: SN0703PAEBSRTA.001_R3 [DIRS 183217]). The mass balance equations describe the transport of radionuclides (^{239}Pu) and associated colloids with irreversible sorption onto iron oxyhydroxide colloids and the stationary corrosion products, as well as reversible sorption onto both waste form and groundwater colloids within the WP.

Two verification cases were conducted. The first includes both advective and diffusive transport and the second includes only diffusive transport. The input parameter values for both the TSPA-LA Model and the Excel spreadsheet implementation were set to the same values,

including a specified constant flow rate. Figure 7.2-9 is a comparison of the results for the case that includes both advection and diffusion. This case shows good agreement between the TSPA-LA Model (v4.042) results and those based on the finite-difference approximation of the sample calculation, except for the initial timesteps where the difference is approximately 10 percent based on examination of the numerical values. The comparison for the case with only diffusive transport is shown on Figure 7.2-10. This case shows good agreement for the dissolved ^{239}Pu and ^{239}Pu reversibly sorbed onto groundwater and waste form colloids as well as for the ^{239}Pu irreversibly sorbed onto the stationary corrosion products, with some slight deviation for the initial timesteps. The agreement is not as good for ^{239}Pu irreversibly sorbed to the FeOH colloids. In this case, the differences at the initial timesteps between the TSPA-LA Model (v4.042) results and those based on the finite-difference approximation range from 50 to 100 percent based on examination of the numerical values. The differences decrease rapidly with time and by the time the system reaches a steady state there is only a two percent difference in value. Given the different solution methods used in the TSPA-LA Model and in the Excel spreadsheet calculations, some differences in the simulation results were expected. If identical solution techniques with identical timesteps were used in the comparison, then the expectation would be that the results should be identical and thus would be held to a more stringent degree of comparison. Therefore, the agreement is still considered good and contributes to increasing the level of confidence in the model. The implementation of the EBS Transport Submodel in the TSPA-LA Model can be considered verified.

7.2.4.1.7 Unsaturated Zone Transport

The verification of the UZ Transport Submodel (Table 6-1), as implemented within the TSPA-LA Model, was conducted by verifying that the implementation of the FEHM_V2.24-01 DLL (STN: 10086-2.24-01 [DIRS 179419]) provided the expected results based on a set of known inputs. The implementation of the UZ Transport Submodel within the TSPA-LA Model was verified against a stand-alone test-case model developed with the glacial-transition climate with the 10th percentile flow field with the water table raised to 850 meters above mean sea level. The stand-alone test case was derived from the base-case UZ Transport model that utilized the FEHM (FEHM V2.24-01 [DIRS 179419]) numerical model as defined in *Particle Tracking Model and Abstraction of Transport Processes* (SNL 2008 [DIRS 184748]).

The verification activities simulated the decay chain of ^{241}Am→^{237}Np→^{233}U→^{229}Th in both the stand-alone model and in the TSPA-LA Model (v5.000). The source term consisted of prescribing 1.0 g/yr of ^{241}Am to the inflow connection for the UZ fractures. With ^{241}Am as the only source, the other radionuclides in the decay chain were produced only by in-growth. The files associated with both the stand-alone test case and the TSPA-LA Model (v5.000) are contained in output DTN: MO0708TSPAPOST.000 [DIRS 182986].

A comparison plot showing the mass breakthrough of ^{237}Np and ^{233}U at the base of the UZ is presented on Figure 7.2-11. The mass breakthrough for ^{229}Th was essentially zero so it was not included in Figure 7.2-11. The plot shows excellent agreement for the ^{237}Np mass breakthrough between the stand-alone model and the TSPA-LA Model (v5.000). For ^{233}U, both curves show oscillations in the breakthrough curves with a slight shift in the oscillations during the middle of the simulation timeframe. This shift is due to a different number of particles being tracked between the two FEHM simulations and thus differences in randomly generated seed numbers.

However, the overall match between the two simulation cases is considered valid. Therefore, the implementation of the UZ Transport Submodel within the TSPA-LA Model is considered verified.

7.2.4.1.8 Saturated Zone Flow and Transport

The SZ Flow and Transport Model, as implemented in the TSPA-LA Model, is defined in *Saturated Zone Flow and Transport Model Abstraction* (SNL 2008 [DIRS 183750]). Verification of the SZ Flow and Transport Submodel was conducted by verifying the implementations of both the 1-D and the 3-D SZ Flow and Transport Abstractions within the TSPA-LA Model.

The implementation of the 3-D SZ Flow and Transport Abstraction, including the SZ_Convolute V3.1 DLL (STN: 10207-3.10.01-00 [DIRS 181060]), in the TSPA-LA Model (v4.042) was verified. The result from a base-case transport simulation developed in *Site-Scale Saturated Zone Transport* (SNL 2007 [DIRS 177392]; DTN: LA0306SK831231.001_R0 [DIRS 164362]) was utilized for comparison to the TSPA-LA Model (v4.042) results. The input parameters that defined the realization 1 for the base-case transport simulation (DTN: LA0306SK831231.001_R0 [DIRS 164362]) were also implemented into the TSPA-LA Model (v4.042) with some modifications, as defined in the output DTN: MO0708TSPAPOST.000 [DIRS 182986]. The SZ source term was defined by assigning a unit mass flux (1.0 g/yr) for a sorbing radionuclide (^{237}Np) that includes radioactive decay (output DTN: MO0708TSPAPOST.000 [DIRS 182986). This source term was assigned to the UZ Transport Submodel output element that feeds mass out of the UZ and into the SZ at Source Region 1. The mass input into this region was then input into the SZ_Convolute DLL in the TSPA-LA Model (v4.042). The ^{237}Np mass flux output from the SZ_Convolute DLL was passed into the model elements, which sums all mass flux out of the 3-D SZ Transport Submodel. The results of the TSPA-LA Model (v4.042) simulation were then compared to the single-realization transport median case breakthrough curve provided by the SZ Site-Scale Transport Model (DTN: LA0306SK831231.001_R0 [DIRS 164362]). The mass fluxes from the two simulations are plotted on Figure 7.2-12 and indicate good overall agreement. There is a slight deviation at early times due to an increase in the timestep size for the TSPA-LA Model.

It should be noted that when the modifications to the TSPA-LA Model were conducted for the verification activities, a documented test case simulation which utilized the updated 3-D SZ Flow and Transport breakthrough curves within the SZ_Convolute DLL had not been developed and thus an older set of breakthrough curve files were utilized. The purpose of the verification activities was to ensure that the 3-D SZ Flow and Transport Abstraction had been implemented correctly and that the flow of information into and out of the submodel was correct. Therefore, the use of the older external breakthrough curve files is justified as long as the correct inputs are implemented and the flow of information through the submodel yields the expected results.

The 1-D SZ Flow and Transport Abstraction, as defined in *Saturated Zone Flow and Transport Model Abstraction* (SNL 2008 [DIRS 183750]), consists of a one-dimensional pathway model that is used to simulate the transport of daughter products through the SZ. The 1-D SZ Flow and Transport Abstraction was developed as a separate stand-alone GoldSim-based model file which was qualified prior to implementation within the TSPA-LA Model

(DTN: SN0702PASZFTMA.002_R1 [DIRS 183471]). The transport results from this stand-alone model were used as the verification data for comparison to the implementation of the 1-D SZ Flow and Transport Abstraction within the TSPA-LA Model. The verification of the abstraction in the TSPA-LA Model (v4.042) was performed by taking the fixed input parameters as defined in the stand-alone model and implementing them in the TSPA-LA Model. In addition, a unit mass flux (1.0 g/yr) was assigned for each radionuclide as cumulative input into each of the four SZ source zone regions, resulting in a total source mass flux of 4.0 g/yr. The calculated total SZ mass flux outflows for ^{14}C and ^{237}Np are shown on Figure 7.2-13 for both the stand-alone and the TSPA-LA Model. The curves indicate good agreement between the two model simulations.

The verification results for the implementation of both the 1-D SZ Flow and Transport Abstraction and the 3-D SZ Flow and Transport Abstraction indicate that both are considered verified and thus the overall implementation of the SZ Flow and Transport Model Component is verified. The verification of the 3-D SZ Flow and Transport Abstraction also demonstrates proper implementation of the UZ-SZ interface.

7.2.4.1.9 Biosphere

Verification of the Biosphere Model Component involved checking of the groundwater exposure case of the Biosphere Submodel (Table 6-1) in the TSPA-LA Model (v4.041). The main parameters controlling the annual dose calculation are the climate state, biosphere dose conversion factors (BDCF), and the concentration of the radionuclides from the SZ. A single realization of the TSPA-LA Model (v4.041) was simulated to calculate the SZ radionuclide concentrations and the corresponding annual dose. The SZ radionuclide concentrations were subsequently exported to provide for an independent calculation of the annual dose for verification purposes.

BDCFs based on three climate states (Present-Day, Monsoon, and Glacial Transition) were developed and documented in *Biosphere Model Report* (SNL 2007 [DIRS 177399], Section 6.4.10.4). The capabilities to utilize the BDCFs for multiple climates states were incorporated into the TSPA-LA Model. However, the TSPA-LA Model, currently only utilizes the Present-Day BDCFs, as discussed in Section 6.3.11.

The verification simulation of the TSPA-LA Model tested the groundwater source term to annual dose. The BDCF values, per radionuclide and climate state, were taken from data tables provided in DTN: MO0702PAGBDCFS.001_R0 [DIRS 179327]. The SZ radionuclide concentrations exported from the TSPA-LA Model (v4.041) (output DTN: MO0708TSPAPOST.000 [DIRS 182986]) were used along with the BDCFs as inputs to independently calculate the annual dose, as defined in the *Biosphere Model Report* (SNL 2007 [DIRS 177399], Section 6.4.10.4). The independent annual dose calculations were developed using a Microsoft Excel spreadsheet (output DTN: MO0708TSPAPOST.000 [DIRS 182986]).

The annual dose calculated by the TSPA-LA Model (v4.041) model file was compared to that calculated using Microsoft Excel (output DTN: MO0708TSPAPOST.000) [DIRS 182986]. This comparison is shown on Figure 7.2-14 along with the percent difference in the two calculations. The maximum percent difference between the calculated annual doses is approximately 0.043

percent with the differences in the dose calculations likely due to round-off in the calculation of the specific activities for each radionuclide. The verification results indicate a good match and thus the groundwater source term to dose submodel is considered verified. Similar verification results would be expected if the present-day BDCF's were used for the entire simulation duration, as is used in the current TSPA-LA Model.

7.2.4.1.10 Igneous Scenario Class Modeling Cases

Verification of the Igneous Scenario Class Modeling Cases includes verification of the ASHPLUME_DLL_LA V2.1 (STN: 11117-2.1-01 [DIRS 180147]) and the FAR V1.2 DLL (STN: 11190-1.2-00 [DIRS 182225]) for the Volcanic Eruption Modeling Case. In addition, the impact on the physical-chemical environment of the EBS, and the input parameters controlling the probability of an igneous intrusion event, are analyzed for the Igneous Intrusion Modeling Case.

Volcanic Eruption Modeling Case (ASHPLUME)—The ability of the Volcanic Eruption Modeling Case to estimate values of ash and fuel concentrations using ASHPLUME_DLL_LA V2.1 [DIRS 180147] was verified in the Volcanic Eruption TSPA-LA Model (vE1.003). The approach for the verification was to compare the results from the Volcanic Eruption TSPA-LA Model (vE1.003) to the results developed in stand-alone GoldSim-based model files used as installation tests for the ASHPLUME V2.1 DLL as in *User Information Document for: ASHPLUME_DLL_LA Version 2.1*, (DOE 2006 [DIRS 181076]), based on a consistent set of fixed input values as defined in the installation test files. The details and associated documentation in terms of the input files and the model files used in the verification are presented in output DTN: MO0708TSPAPOST.000 [DIRS 182986].

The comparison of results between the stand-alone file and the Volcanic Eruption TSPA-LA Model (vE1.003) file, as shown in Table 7.2-13, shows exactly the same values for the parameters X_ash and X_fuel. Because of the identical match in the results reported, the implementation of the ASHPLUME_DLL_LA V2.1 is considered verified in the Volcanic Eruption Modeling Case.

Volcanic Eruption Modeling Case (FAR)—A verification test for the implementation of the FAR 1.2 DLL in the Volcanic Eruption TSPA-LA Model (vE1.003) was performed. The approach for the verification was to compare the results from the Volcanic Eruption TSPA-LA Model (vE1.003) to the results developed in stand-alone GoldSim-based model files used as installation tests for the FAR 1.2 DLL as in *User Information Document for*: FAR Version 1.2 (DOE 2007 [DIRS 183116]), based on a consistent set of fixed input values as defined in the installation test files. The details of the input parameters, installation test case, and the output results are included in the output DTN: MO0708TSPAPOST.000 [DIRS 182986].

A single realization was conducted and a comparison of the output results at 10 years after a volcanic eruption was presented in Table 7.2-14. The results are identical for all four output parameters (Table 7.2-14). A comparison of the model results calculated at each timestep by each model file shows the same values for each parameter (output DTN: MO0708TSPAPOST.000 [DIRS 182986]) and thus the implementation of the FAR V1.2 DLL is considered verified in the Volcanic Eruption Modeling Case.

Igneous Intrusion Modeling Case—As defined in *Dike/Drift Interactions* (SNL 2007 [DIRS 177430], Table 8-2, Section 8.2.2) and DTN: LA0702PADE01EG.001_R0 [DIRS 179495], when an igneous intrusion event that intersects the repository is simulated within the TSPA-LA Model, the intrusion of magma into the repository causes a perturbation in the EBS thermal-hydrologic (TH) properties for approximately 100 years. The global timestep size in the TSPA-LA Model is set at 250 years and thus the perturbation in the EBS TH properties would not be accurately reflected. Therefore, conditional logic was incorporated into the TSPA-LA Model to force a five-year timestep for approximately 100 years following the initiation of a single igneous intrusion event to accurately calculate the change in the TH properties of the EBS TH Environment Submodel (Section 6.5.1.3).

The verification process for the Igneous Intrusion Modeling Case captured the temperature within the CDSP WPs at each of the forced five-year timesteps as simulated in the TSPA-LA Model (v4.042). For verification comparison, a stand-alone GoldSim-based model file was developed with a global timestep increment of five years and with the same pre-event thermal-hydrological properties as the TSPA-LA Model (v4.042) (output DTN: MO0708TSPAPOST.000 [DIRS 182986]). The comparison of the CDSP WP temperatures calculated for both model files are shown on Figure 7.2-15. A comparison of the actual temperature values indicates that the maximum difference in the temperatures was significantly less than one percent and a result of round off. This comparison verifies the ability of the model to accurately calculate the impact on the TH properties of the EBS TH Environment Submodel as a result of an igneous-intrusion event.

7.2.4.1.11 Seismic Scenario Class Modeling Cases

The Seismic Damage Abstraction implementation was verified against two separate stand-alone GoldSim-based models. One stand-alone model was used to verify the implementation of the Ground Motion Submodel, whereas the second verified the Fault Displacement Submodel. The Seismic Damage Abstraction as defined in *Seismic Consequence Abstraction* (SNL 2007 [DIRS 176828]) is implemented in the TSPA-LA Model and was also used to develop the two stand-alone verification models.

In the TSPA-LA Model (v4.046), modifications were made to force a set of input values to be used in the place of inputs and feeds associated with any uncertainty or variability. For example, the exceedance frequency, which controls the peak ground velocity (PGV) during a ground motion event, was set to 1×10^{-8} yr^{-1}. There were 29 variable inputs identified and changed. The same set of inputs was used in both verification stand-alone models (output DTN: MO0708TSPAPOST.000 [DIRS 182986]). For simplification, these inputs were set to static values (i.e., the values remain unchanged over time). Therefore, most of the results did not change over time.

A set of 13 outputs was created from the Seismic Damage Abstraction implemented in the TSPA-LA Model. These outputs were compared to those from the two stand-alone verifications model (output DTN: MO0708TSPAPOST.000 [DIRS 182986]). The comparison of the Seismic Ground Motion Submodel results is shown in Table 7.2-15. The comparison of the Fault Displacement Submodel results is shown in Table 7.2-16. Based on these results, the Seismic Damage Abstraction implementation within the TSPA-LA Model is considered verified.

7.2.5 Verification of Coupling Among Submodels and Model Components

Verification of the coupling of submodels and TSPA-LA Model components within the TSPA-LA Model was accomplished through checking the model implementation during development of the TSPA-LA Model. Verification of coupling among other model components includes verification of the DLLs and the single model components described in Section 7.2.4.

Coupling among TSPA-LA Model components includes flow and transport through the EBS, coupling at the EBS-UZ interface (Section 7.2.5.1), and coupling at the UZ-SZ interface (Section 7.2.4.1.8). Verification of the single components of the TSPA-LA Model, which is discussed in Section 7.2.4, is also important for verification of coupling across model interfaces. After development, the verification of coupling among TSPA-LA Model components is primarily accomplished through auxiliary analyses, discussed in Section 7.7, in order to demonstrate that the TSPA-LA Model yields results that would be expected.

7.2.5.1 Placement of an Effective Zero-Concentration Boundary in the Engineered Barrier System-Unsaturated Zone Interface Domain

The EBS-UZ Interface domain is included beneath the invert domain for modeling EBS radionuclide transport in the TSPA-LA Model. The primary purpose of the EBS-UZ Interface domain is to establish an effective zero-concentration boundary condition at some distance away from the base of the invert in order to compute the diffusive flux from the invert to the UZ and the fraction of total mass flux that goes into the UZ fracture and matrix continua (Section 6.3.8). For this purpose, the EBS-UZ Interface domain is discretized into four layers and the zero-concentration boundary is applied at the base of the fourth layer, approximately 17 m below the invert (Figure 6.3.8-9). The dual continuum of overlapping matrix and fracture continua is represented by cell pathways. The thickness of the first (top) layer of cells is chosen to be 0.6567 m, which is 10 percent greater than the average invert thickness (0.597 m). The thickness of the second layer is set to be double that of the first layer, or 1.3134 m. The third and fourth layers are given a thickness of 5 m and 10 m, respectively. Grid sizes are more refined near the base of the invert to accurately capture the higher concentration gradient in the region. A collector cell is placed beneath the fourth layer and is given a very large water volume to simulate an effective zero-concentration boundary. This collector cell acts as a sink for all the mass flux from the UZ cells. For more details on the implementation, refer to Section 6.3.8.3.

An analysis is performed to evaluate the appropriateness of the location of the effective zero-concentration boundary for the diffusive flux calculation from the invert. The TSPA-LA Model (v5.000) was used for the analysis. In this study, the effective zero-concentration boundary is applied at the base of the invert and then moved down one layer at a time. The effect of the placement of this boundary is evaluated in terms of the diffusive flux from the invert. It is expected that, as the distance to the zero-concentration boundary increases, the diffusive flux from the invert will decrease and converge to a true value. Because analytical solutions do not exist for a dual-continuum representation, the convergence of the invert diffusive flux with increasing distance to the zero-concentration boundary is deemed adequate for evaluating the appropriateness of the location of the effective zero-concentration boundary.

The study is performed for a nonsorbing radionuclide such as ^{99}Tc. The radionuclide mass is injected in the invert cell at 100 years, and the concentration is held constant in the invert at 100 mg/L. The simulation is performed for 20,000 years using the TSPA-LA Model optimal timesteps. The study is only performed for a non-dripping environment for Percolation Subregion 3 for CSNF WPs, where the release from the invert is primarily diffusive (a small advective component is also present due to imbibition flux from the host rock into the invert). A total number of 300 realizations is run in order to sample the epistemic uncertainty in the hydrologic properties of the invert and the UZ. The results of the study are shown on Figure 7.2-16 to compare the total mean diffusive mass flux of ^{99}Tc from the invert for varying placement of the zero-concentration boundary (output DTN: MO0708TSPAPOST.000 [DIRS 182986]). Almost all of the diffusive mass flux from the invert goes into the matrix continuum, as the effective diffusive area for the matrix continuum is much greater than that for the fracture continuum. As would be expected, the diffusive flux decreases as the zero-concentration boundary is moved farther down from the invert. The diffusive flux at 10,000 years for the case where the zero concentration is applied at the base of the invert is about 7.4 g/yr, but reduces to about 0.62 g/yr when the boundary is placed at the base of the first layer (a distance of about 0.66 m from the base of invert). The diffusive flux reduces further to about 0.55 g/yr when the zero-concentration boundary is placed at the base of the second layer (a total distance of about 1.97 m from the base of invert) and then to about 0.54 g/yr when the zero-concentration boundary is applied to the base of the third and fourth layers (at total respective distances of 6.97 m and 16.97 m).

This analysis shows that it is important to properly locate the zero-concentration boundary when the dominant flux from the invert is diffusive. The analysis further shows that the diffusive flux converges when the zero-concentration boundary is applied at the base of the third and fourth layers, indicating that placement of the zero-concentration boundary at further distances is not going to appreciably affect the diffusive mass flux from the invert. This analysis also shows that the discretization chosen for the EBS-UZ Interface domain is adequate for the purpose of computing the diffusive flux from the invert.

7.2.6 Verification of Range of Applicability of Submodels and Model Components

The verification of the range of applicability of submodels and model components is another important aspect of TSPA-LA Model confidence building. When provided by the supporting analysis and/or model reports, the range of applicability of inputs to submodels implemented in the TSPA-LA Model are verified as part of the checking of the TSPA-LA Model. The records that document the implementation and checking of the TSPA-LA Model are located in the relevant records package.

The type of verification performed to ensure that the range of applicability was properly defined within the TSPA-LA Model depends on the nature of the implementation. In some cases, logic has been built into the TSPA-LA Model to verify that the inputs are within the appropriate range. If an input is outside its valid range, a flag is set. In other cases, logic has been built into the TSPA-LA Model such that if a parameter value is selected outside the valid range, the value is reset to the bounding value depending on if the value is greater than or less than that of the range.

An example of this logic implemented within the TSPA-LA Model can be seen in the implementation of the Drift Seepage Submodel (Section 6.3.3.1). First, the drift-wall temperature must be below 100°C for seepage to occur into no-collapsed drifts. Logic is built into the model such that if the temperature is greater than or equal to 100°C, then a flag is set that turns off the presence of drift seepage (Section 6.3.3.1.3). Second, the range of percolation flux over which the Drift Seepage Submodel is valid is from 0.01 to 5,000 mm/yr. If a percolation flux that is input into the Drift Seepage Submodel is less than 0.01 mm/yr or greater than 5,000 mm/yr, the value is reset to the bounding value of 0.01 mm/yr or 5,000 mm/yr, respectively (Section 6.3.3.1.3).

Table 7.2-1. Verification of TSPA-LA Model Dynamically Linked Libraries

DLL (Version)	Type of Verification	Where Described
SEEPAGEDLL_LA (v1.3)	Verification analysis	Section 7.2.4.1.1
WAPDEG (v4.07)	Verification analysis	Section 7.2.4.1.4
CWD (v2.0)	Verification analysis	Section 7.2.4.1.4
SCCD (v2.01)	Verification analysis	Section 7.2.4.1.4
FEHM_V2_24-01 (v2.24)	Verification analysis	Section 7.2.4.1.7
SZ_CONV_3.10 (v3.1)	Verification analysis	Section 7.2.4.1.8
ASHPLUME_DLL_LA (v2.1)	Verification analysis	Section 7.2.4.1.10
FAR (v1.2)	Verification analysis	Section 7.2.4.1.10

NOTE: Comparison with Table 3-1 shows that the versions used for verification of the TSPA-LA Model DLLs match those used in the final version of the TSPA-LA Model.

Table 7.2-2. Verification of Dynamically Linked Libraries and Model Abstractions Used in the TSPA-LA Model

Model Component/Submodel	Analysis Description	Status	Section Described
Drift Seepage			
Drift Seepage Implementation	Verification of Seepage DLL by comparison of the TSPA-LA Model results with a stand-alone GoldSim-based implementation	Verified	Section 7.2.4.1.1
Drift Wall Condensation			
Verification of the Drift Wall Condensation Submodel	Comparison of drift-wall condensation rates and probability data to that supplied in supporting DTNs	Verified	Section 7.2.4.1.2
Engineered Barrier System Chemical Environment			
Physical and Chemical Environment Submodel	Verification of TSPA-LA Model file to accurately estimate (under both evaporative and condensation conditions) pH and ionic strength for a set of controlled inputs of temperature, relative humidity, Pco_2, and percolation bin number	Verified	Section 7.2.4.1.3
Waste Package and Drip Shield Degradation			
Integrated Waste Package and Drip Shield Degradation	Verification of the WAPDEG, CWD, and SCCD DLLs through comparison of the results of TSPA-LA Model implementation with the results of a stand-alone implementation	Verified	Section 7.2.4.1.4
Waste Form Degradation and Mobilization			
Verification of Waste Rind Degradation	Comparison of the rind volume and thickness in a CSNF WP using a Microsoft Excel spreadsheet and the TSPA-LA Model file	Verified	Section 7.2.4.1.5
	Comparison of the rind volume and thickness in a CDSP WP using a Microsoft Excel spreadsheet and the TSPA-LA Model file	Verified	Section 7.2.4.1.5
Verification of CSNF Waste Form Degradation	Comparison of waste form degradation rate in a CSNF WP using a Microsoft Excel spreadsheet and the TSPA-LA Model file	Verified	Section 7.2.4.1.5
Verification of HLW Glass Degradation	Comparison of TSPA-LA Model file results with a spreadsheet implementing the source analysis model report equations for acidic and alkaline conditions with relative humidity less and greater than 0.44	Verified	Section 7.2.4.1.5
Verification of Dissolved Concentration Limits	Nominal Scenario: Comparison of TSPA-LA Model file results with a spreadsheet implementing the calculation of radionuclide solubilities using look-up tables and applying epistemic uncertainty	Verified	Section 7.2.4.1.5
	Igneous Scenario (Igneous Intrusion Modeling Case): Comparison of TSPA-LA Model file results with a spreadsheet implementing the calculation of uranium solubilities using look-up tables and applying epistemic uncertainty	Impact Analysis Conducted using TSPA-LA Model	Section 7.2.4.1.5
Verification of the In-Package Chemistry Submodel	Comparison of pH, ionic strength, and total carbonate in the WPs using a Microsoft Excel spreadsheet and the TSPA-LA Model file	Verified	Section 7.2.4.1.5

Table 7.2-2. Verification of Dynamically Linked Libraries and Model Abstractions Used in the TSPA-LA Model (Continued)

Model Component/Submodel	Analysis Description	Status	Section Described
Engineered Barrier System Transport			
Verification of EBS Transport Submodel	Comparison of results of plutonium transport and colloidal transport for both reversible and irreversible sorption on iron oxyhydroxide colloids using a Microsoft Excel implemented finite-difference approximation and the TSPA-LA Model file transport submodel	Verified	Section 7.2.4.1.6
Unsaturated Zone Transport			
Verification of FEHM Particle Tracking for the UZ Transport Submodel	Comparison of results from the TSPA-LA Model (FEHM DLL) with that of a test case developed from the base case FEHM model	Verified	Section 7.2.4.1.7
Saturated Zone Flow and Transport			
Verification of SZ Flow and Transport	Comparison of TSPA-LA Model results with the site-scale SZ transport base case for ^{99}Tc	Verified	Section 7.2.4.1.8
	Comparison of a 1-D stand-alone model that was used for validation of the site-scale model with the TSPA-LA Model for ^{14}C	Verified	Section 7.2.4.1.8
Biosphere			
Verification of the Groundwater Source Term to Dose Submodel	Comparison of calculated dose using a Microsoft Excel spreadsheet and the TSPA-LA Model file	Verified	Section 7.2.4.1.9
Igneous Scenario Class Modeling Cases			
Volcanic Eruption Modeling Case	Comparison of TSPA-LA Model results with the stand-alone model used for validation of the ASHPLUME DLL	Verified	Section 7.2.4.1.10
	Comparison of TSPA-LA Model results with a Microsoft Excel spreadsheet based on the FAR model	Verified	Section 7.2.4.1.10
Igneous Intrusion Modeling Case	Comparison of TSPA-LA Model with a stand-alone GoldSim-based model file showing the impact of an igneous intrusion event on the EBS thermal-hydrologic properties	Verified	Section 7.2.4.1.10
Seismic Scenario Class Modeling Cases			
Verification of Seismic Damage Abstraction	Comparison of TSPA-LA Model calculated ground motion and fault displacement damage with that of stand-along GoldSim-based models developed based on the source analysis model report	Verified	Section 7.2.4.1.11

Table 7.2-2. Verification of Dynamically Linked Libraries and Model Abstractions Used in the TSPA-LA Model (Continued)

Model Component/Submodel	Analysis Description	Status	Section Described
Verification of Coupling Between Model Components			
EBS Transport and EBS-UZ Interface	Transport through the EBS-UZ interface to demonstrate proper placement of the Effective Zero-Concentration Boundary	Verified	Section 7.2.5.1
UZ-SZ Interface	Included in results presented for Verification of SZ Flow and Transport in which a radionuclide source term was specified at the base of the UZ Submodel domain and passed across the interface for use in the SZ Submodel.	Verified	Section and 7.2.4.1.8

Table 7.2-3. Verification Summary of the Drift Seepage Dynamically Linked Library

	Stand-Alone Verification Model			TSPA-LA Model (v5.000)		
Percolation Subregion	Seepage Rate (m^3/yr) at 10,000 years	Seepage Fraction	Non-Lithophysal Fraction	Seepage Rate (m^3/yr) at 10,000 years	Seepage Fraction	Non-Lithophysal Fraction
CDSP 1	0.030	0.021	0.319	0.030	0.021	0.319
CDSP 2	0.070	0.108	0.237	0.070	0.108	0.237
CDSP 3	0.103	0.163	0.173	0.103	0.163	0.173
CDSP 4	0.125	0.135	0.041	0.125	0.135	0.041
CDSP 5	0.140	0.171	0.110	0.140	0.171	0.110
CSNF 1	0.019	0.015	0.319	0.019	0.015	0.319
CSNF 2	0.076	0.103	0.237	0.076	0.103	0.237
CSNF 3	0.108	0.160	0.173	0.108	0.160	0.173
CSNF 4	0.120	0.154	0.041	0.120	0.154	0.041
CSNF 5	0.159	0.206	0.110	0.159	0.206	0.110

Source: Stand-alone and TSPA-LA Model results are contained in output DTN: MO0708TSPAPOST.000 [DIRS 182986].

Table 7.2-4. Comparison of the Drift-Wall Condensation Rates Verification Calculations

Time (yr)	Condensation Rate [m^3/yr], Verification	Condensation Rate [m^3/yr], TSPA-LA Model (v4.042)
0 to 600	0	0
675	0	0
750	0	0
825	5.92E-06	5.92E-06
900	0	0
975	1.25E-05	1.25E-05
1,050	0	0
1,125	1.79E-05	1.79E-05
1,200	0	0
1,275	2.76E-05	2.76E-05
1,350	0	0
1,425	6.32E-06	6.32E-06
1,500	0	0
1,575	1.08E-06	1.08E-06
1,650	0	0
1,725	6.07E-06	6.07E-06
1,800	0	0
1,875	4.53E-06	4.53E-06
1,950	0	0
2,025	0	0
2,100 to 3,000	0	0

Source: Output DTN: MO0708TSPAPOST.000 [DIRS 182986].

Table 7.2-5. Summary of the Verification Inputs and Outputs for Calculation of the P_{CO2} Values in the EBS Physical and Chemical Environment Abstraction

Input Set	Water:Rock Interaction Parameter	Temperature (°C)	Relative Humidity (%)	P_{CO2} (bar) Verification	P_{CO2} (bar) TSPA-LA Model(v4.043)
1	0.0002	0	0	1.000E-03	1.000E-03
2	0.1932	23	0	1.000E-03	1.000E-03
3	0.1046	40	0	1.000E-03	1.000E-03
4	0.0585	55	0	1.000E-03	1.000E-03
5	0.0378	70	0	1.000E-03	1.000E-03
6	0.0278	85	0	1.000E-03	1.000E-03
7	0.0222	96	0	1.000E-03	1.000E-03
8	0.0166	23	0.2	1.000E-03	1.000E-03
9	0.0111	40	0.2	1.000E-03	1.000E-03
10	0.0077	55	0.2	9.996E-04	9.996E-04
11	0.0077	70	0.2	9.955E-04	9.955E-04
12	0.0077	85	0.2	9.886E-04	9.886E-04
13	0.0077	96	0.2	9.807E-04	9.807E-04
14	0.0077	23	0.4	1.000E-03	1.000E-03
15	0.0077	40	0.4	9.998E-04	9.998E-04
16	0.0077	55	0.4	9.954E-04	9.954E-04
17	0.0077	70	0.4	9.874E-04	9.874E-04
18	0.0077	85	0.4	9.734E-04	9.734E-04
19	0.0077	96	0.4	9.577E-04	9.577E-04
20	0.0077	23	0.65	1.000E-03	1.000E-03
21	0.0077	40	0.65	9.974E-04	9.974E-04
22	0.0077	55	0.65	9.903E-04	9.903E-04
23	0.0072	70	0.65	9.772E-04	9.772E-04
24	0.0063	85	0.65	9.544E-04	9.544E-04
25	0.0054	96	0.65	9.289E-04	9.289E-04
26	0.0045	23	0.75	1.000E-03	1.000E-03
27	0.0036	40	0.75	9.964E-04	9.964E-04
28	0.0028	55	0.75	9.882E-04	9.882E-04
29	0.0019	70	0.75	9.731E-04	9.731E-04
30	0.0010	85	0.75	9.468E-04	9.468E-04
31	0.0001	96	0.75	9.174E-04	9.174E-04
32	10	23	0.85	1.000E-03	1.000E-03
33	10	40	0.85	9.955E-04	9.955E-04
34	10	55	0.85	9.862E-04	9.862E-04
35	10	70	0.85	9.690E-04	9.690E-04
36	10	85	0.85	9.393E-04	9.392E-04
37	10	96	0.85	9.059E-04	9.059E-04

Table 7.2-5. Summary of the Verification Inputs and Outputs for Calculation of the P_{CO2} Values in the EBS Physical and Chemical Environment Abstraction (Continued)

Input Set	Water:Rock Interaction Parameter	Temperature (°C)	Relative Humidity (%)	P_{CO2} (bar), Verification	P_{CO2} (bar), TSPA-LA Model (v4.043)
38	10	23	1	1.000E-03	1.000E-03
39	10	40	1	9.940E-04	9.940E-04
40	10	55	1	9.831E-04	9.831E-04
41	10	70	1	9.629E-04	9.628E-04
42	10	85	1	9.279E-04	9.278E-04
43	10	96	1	8.886E-04	8.886E-04
44	10	150	1	8.886E-04	8.886E-04

Source: Output DTN: MO0708TSPAPOST.000 [DIRS 182986].

Table 7.2-6. Summary of Input Values Used in EBS Physical and Chemical Environment Verifications of pH and Ionic Strength

Parameter	Range
Seepage Water Type	1, 2, 3, or 4
P_{CO2} (bar)	0.0001 to 0.01
Temperature on Waste-Package Surface (°C)	30, 70, or 100
Relative Humidity at Waste-Package Surface	0.99
WRIP	0 to 10

Source: Output DTN: MO0708TSPAPOST.000 [DIRS 182986].

Table 7.2-7. Values Used in the WAPDEG Dynamically Linked Library for Verifying the TSPA-LA Model

Element Name	Value	Comment
C1_GenCorr_A22	3,116.47	Slope term for the WP outer shell general corrosion temperature dependence (K^{-1})
WDDSAggrGC	2.0×10^{-3}	DS general corrosion rate under aggressive conditions (mm/yr)
WDDSBenignGC	2.0×10^{-3}	DS general corrosion rate under benign conditions (mm/yr)
MIC_RHThresh	0.825	Microbially influenced corrosion (MIC) relative humidity threshold
Stress_Thress_SCC	342.225	Stress threshold for SCC
n_SCC	1.165	SCC model parameter
WDSeed	123456789	WAPDEG random seed value
z_OL	0	Outer lid uncertainty
GC_ULevel_A22	2.0	Uncertainty level for Alloy 22 general corrosion
Defect Count	4.02997×10^{-7}	Defect count (mm^{-3})
Defect Size	0.220472	Defect size (mm^{-1})

Source: Output DTN: MO0506MWDTLMPI.001 [DIRS 174808].

Table 7.2-8. Summary of Input/Output Values and GoldSim Verification Checks for the CSNF Rind Volume and Mass Calculations

Input Set No.	Porosity	Fraction of Failed Rods	Fraction of Corroded WPs	CSNF Rind Volume (cm^3) Verification	CSNF Rind Volume (cm^3), TSPA-LA Model (v4.041)	CSNF Rind Mass (g) Verification	CSNF Rind Mass (g) TSPA-LA Model (v4.041)
1	0.05	0.01	0.005	15243.9	15243.9	69946.4	69946.4
2	0.3	0.01	0.005	20688.1	20688.1	69946.4	69946.4
3	0.05	0.01	0.01	30487.7	30487.7	139892.9	139892.9
4	0.3	0.01	0.01	41376.2	41376.2	139892.9	139892.9
5	0.05	0.05	0.005	15243.9	15243.9	69946.4	69946.4
6	0.3	0.05	0.005	20688.1	20688.1	69946.4	69946.4
7	0.05	0.05	0.05	152438.6	152438.6	699464.4	699464.4
8	0.3	0.05	0.05	206880.9	206880.9	699464.4	699464.4
9	0.05	0.1	0.005	15243.9	15243.9	69946.4	69946.4
10	0.3	0.1	0.005	20688.1	20688.1	69946.4	69946.4
11	0.05	0.1	0.1	304877.1	304877.1	1398928.7	1398928.7
12	0.3	0.1	0.1	413761.8	413761.8	1398928.7	1398928.7

Sources: Parameters in Table 6-3 and Equations 6-3, 6-4, 6-5, and 6-12 in Table 6-4 of *Cladding Degradation Summary for LA* (SNL 2007 [DIRS 180616]) were used to calculate the CSNF rind volume and mass.

Output DTN: MO0708TSPAPOST.000 [DIRS 182986].

Table 7.2-9. Summary of Input/Output Values and GoldSim Verification Checks for the CDSP WPs HLW Rind Thickness and Mass

Input Set No.	Fraction Degraded	HLW Rind Thickness (cm) Verification	HLW Rind Thickness (cm) TSPA-LA Model (v4.041)	HLW Rind Mass (g) Verification	HLW Rind Mass (g) TSPA-LA Model (v4.041)
1	0.01	0.15	0.15	123.6	123.6
2	0.02	0.30	0.30	247.1	247.1
3	0.05	0.76	0.76	617.8	617.8
4	0.1	1.54	1.54	1235.6	1235.6
5	0.2	3.17	3.17	2471.1	2471.1
6	0.3	4.90	4.90	3706.7	3706.7
7	0.4	6.76	6.76	4942.3	4942.3
8	0.5	8.79	8.79	6177.9	6177.9
9	0.6	11.03	11.03	7413.4	7413.4
10	0.8	16.58	16.58	9884.6	9884.6
11	0.9	20.51	20.51	11120.2	11120.2
12	0.99	27.00	27.00	12232.2	12232.2

Sources: Parameters and equations in Section 8-1 and Table 8-1 of *Defense HLW Glass Degradation Model* (BSC 2004 [DIRS 169988]) were used to calculate CDSP rind thickness and water volume.

Output DTN: MO0708TSPAPOST.000 [DIRS 182986].

Table 7.2-10. Summary of Verification Checks for the CSNF Waste Form Degradation Submodel

Acidic Verifications		
pH	Degradation Rate (yr^{-1}) Verification	Degradation Rate (yr^{-1}) TSPA-LA Model (v4.041)
2.00	1.448E-02	1.449E-02
3.00	6.619E-03	6.624E-03
4.00	3.026E-03	3.028E-03
5.00	1.383E-03	1.384E-03
6.00	6.321E-04	6.326E-04
6.50	4.274E-04	4.277E-04
Alkaline Verifications		
pco_3	Degradation Rate (yr^{-1}) Verification	Degradation Rate (yr^{-1}) TSPA-LA Model (v4.041)
0.0002	3.703E-04	3.705E-04
0.0005	4.065E-04	4.068E-04
0.001	4.363E-04	4.366E-04
0.005	5.142E-04	5.145E-04
0.01	5.518E-04	5.522E-04
0.02	5.923E-04	5.926E-04

Sources: *CSNF Waste Form Degradation: Summary Abstraction* (BSC 2004 [DIRS 169987], Sections 6.4.1.2 and 6.4.1.3).

Output DTN: MO0708TSPAPOST.000 [DIRS 182986].

Table 7.2-11a. Summary of Verification Checks for the HLW Glass Degradation Submodel

HLW Degradation Verification at Relative Humidity Conditions Less Than 0.44				
Temperature (°C)	pH	Relative Humidity	Degradation Rate (yr^{-1}) Verification	Degradation Rate (yr^{-1}) TSPA-LA Model (v4.041)
50	4	0.2	0	0
50	5	0.2	0	0
50	6	0.2	0	0
50	7	0.2	0	0
50	8	0.2	0	0
50	9	0.2	0	0
50	10	0.2	0	0
75	4	0.2	0	0
75	5	0.2	0	0
75	6	0.2	0	0
75	7	0.2	0	0
75	8	0.2	0	0
75	9	0.2	0	0
75	10	0.2	0	0
100	4	0.2	0	0
100	5	0.2	0	0
100	6	0.2	0	0
100	7	0.2	0	0
100	8	0.2	0	0
100	9	0.2	0	0
100	10	0.2	0	0
125	4	0.2	0	0
125	5	0.2	0	0
125	6	0.2	0	0
125	7	0.2	0	0
125	8	0.2	0	0
125	9	0.2	0	0
125	10	0.2	0	0
150	4	0.2	0	0
150	5	0.2	0	0
150	6	0.2	0	0
150	7	0.2	0	0
150	8	0.2	0	0
150	9	0.2	0	0
150	10	0.2	0	0

Source: Output DTN: MO0708TSPAPOST.000 [DIRS 182986].

Table 7.2-11b. Summary of Verification Checks for the HLW Glass Degradation Submodel

HLW Degradation Verification at Relative Humidity Conditions Greater Than 0.44				
Temperature (°C)	pH	Relative Humidity	Degradation Rate (yr^{-1}) Verification	Degradation Rate (yr^{-1}) TSPA-LA Model (v4.041)
50	4	0.8	1.17E-05	1.17E-05
50	5	0.8	3.80E-06	3.80E-06
50	6	0.8	1.23E-06	1.23E-06
50	7	0.8	3.98E-07	3.98E-07
50	8	0.8	1.29E-07	1.29E-07
50	9	0.8	6.65E-08	6.65E-08
50	10	0.8	2.05E-07	2.05E-07
75	4	0.8	2.69E-05	2.69E-05
75	5	0.8	8.70E-06	8.70E-06
75	6	0.8	2.81E-06	2.81E-06
75	7	0.8	9.11E-07	9.11E-07
75	8	0.8	2.95E-07	2.95E-07
75	9	0.8	4.20E-07	4.20E-07
75	10	0.8	1.30E-06	1.30E-06
100	4	0.8	5.51E-05	5.51E-05
100	5	0.8	1.78E-05	1.78E-05
100	6	0.8	5.77E-06	5.77E-06
100	7	0.8	1.87E-06	1.87E-06
100	8	0.8	6.72E-07	6.72E-07
100	9	0.8	2.08E-06	2.08E-06
100	10	0.8	6.42E-06	6.42E-06
125	4	0.8	2.59E-05	2.59E-05
125	5	0.8	2.59E-05	2.59E-05
125	6	0.8	2.59E-05	2.59E-05
125	7	0.8	2.59E-05	2.59E-05
125	8	0.8	2.59E-05	2.59E-05
125	9	0.8	2.59E-05	2.59E-05
125	10	0.8	2.59E-05	2.59E-05
150	4	0.8	8.88E-05	8.88E-05
150	5	0.8	8.88E-05	8.88E-05
150	6	0.8	8.88E-05	8.88E-05
150	7	0.8	8.88E-05	8.88E-05
150	8	0.8	8.88E-05	8.88E-05
150	9	0.8	8.88E-05	8.88E-05
150	10	0.8	8.88E-05	8.88E-05

Source: Output DTN: MO0708TSPAPOST.000 [DIRS 182986].

Table 7.2-12. Summary of Parameter Ranges Used in Developing the Input Data Sets for the In-Package Chemistry Submodel Verifications of Ionic Strength, pH, and Total Carbonate

Parameter	Range
Ionic Strength (Seepage)	
Time Since Waste Package Failure (years)	5,250 to 42,500
Seepage Flow Rate (L/yr)	0.1 to 1,000
Random Number	0.5
Ionic Strength (Non-Seepage)	
pH	0.95 to 1.0
Random Number	0, 0.3, and 1.0
pH (Seepage and Non-Seepage)	
Ionic Strength (molality)	0.003 to 10
P_{CO2} (bar)	1.5, 2, 3, and 4
Random Number	0.5
Total Carbonate (Seepage and Non-Seepage)	
Temperature (°C)	25, 40, and 100
pH	2, 4, 6, 8, and 10
P_{CO2} (bar)	0.001 and 0.01

Source: Output DTN: MO0708TSPAPOST.000 [DIRS 182986].

Table 7.2-13. Comparison of Results for the ASHPLUME Verification

TSPA-LA Model Output Element Name	Description	Value (g/cm^2) Verification	Value (g/cm^2) TSPA-LA Model (vE1.003)
X_Ash	Ash concentration on gridded area	0.126	0.126
X_Fuel	Fuel concentration on gridded area	2.03E-07	2.03E-07

Source: Output DTN: MO0708TSPAPOST.000 [DIRS 182986].

Table 7.2-14. Comparison of Results for the FAR Verification

Output Parameter Description	Verification Model	TSPA-LA Model (vE1.003)
Concentration at surface channels (g/cm^3)	3.05E-07	3.05E-07
Depth Integrated concentration in channels (g/cm^2)	6.10E-06	6.10E-06
Concentration at surface along divides (g/cm^3)	9.75E-07	9.75E-07
Depth Integrated concentration along divides (g/cm^2)	1.00E-06	1.00E-06

Source: Output DTN: MO0708TSPAPOST.000 [DIRS 182986].

Table 7.2-15. Comparison of the Seismic Damage Abstraction Ground Motion Submodel Verification Calculations

TSPA-LA Model Parameter Element Name	Parameter Description	Value Verification	Value TSPA-LA Model (v4.046)
Seismic_Rubble_Fill_time [years]	Time that the drift fills with rubble as a consequence of a seismic event	2.0×10^6	2.0×10^6
F_DS_Patch_Damage_Seismic	Fraction of the DS surface open to advective flow	1.0	1.0
Event_Time_Seismic_CDSP [years]	Initiation time of the seismic event for CDSP WPs	451.64	451.64
Event_Time_Seismic [years]	Initiation time of the seismic event	451.64	451.64
Event_Time_Seismic_TAD [years]	Initiation time of the seismic event for TAD WPs	451.64	451.64
F_WP_Crk_Damage_Seismic	Fraction of WP surface failed by ground motion	0.003977	0.003977
WP_Failure_Fraction_Seismic	Fraction of WPs failed following a seismic event	1.0	1.0
F_WP_Patch_Damage_Seismic	Fraction of WP surface failed by ruptures or fault displacement	0.002973	0.002973
Cum_Event_Occurs	Cumulative discrete change signals indicating a seismic event has been triggered	446	446
Rubble_Vol_Accum_Li_max [m^3/m]	Maximum lithophysal rubble volume required to fill drift, per length of drift	22.3(1)	0(1)
Rubble_Vol_Accum_NoLi_max [m^3/m]	Maximum non-lithophysal rubble volume required to fill drift, per length of drift	22.3(1)	0(1)
Rubble_Vol_Accum_Li [m^3/m]	Calculated lithophysal rubble volume required to fill drift, per length of drift	0	0
Rubble_Vol_Accum_NoLi [m^3/m]	Calculated non-lithophysal rubble volume required to fill drift, per length of drift	0	0

NOTE: (1) The TSPA-LA Model (v4.046) has a switch that does not allow the calculation of the maximum rubble volume parameters if no rock fall occurs. This switch was not included in the stand-alone verification model and thus a value was determined even though no rock fall occurred.

Source: Output DTN: MO0708TSPAPOST.000 [DIRS 182986].

Table 7.2-16. Comparison of the Seismic Damage Abstraction Fault Displacement Submodel Verification Calculations

TSPA-LA Model Parameter Element Name	Parameter Description	Value Verification	Value TSPA-LA Model (v4.046)
Seismic_Rubble_Fill_time [years]	Time that the drift fills with rubble as a consequence of a seismic event	250	250
F_DS_Patch_Damage_Seismic	Fraction of the DS surface open to advective flow	1	1
Event_Time_Seismic_CDSP [years]	Initiation time of the seismic event for CDSP WPs	250	250
Event_Time_Seismic [years]	Initiation time of the seismic event	250	250
Event_Time_Seismic_TAD [years]	Initiation time of the seismic event for TAD WPs	250	250
F_WP_Crk_Damage_Seismic	Fraction of WP surface failed by ground motion	0	0
WP_Failure_Fraction_Seismic	Fraction of WPs failed following a seismic event	1	1
F_WP_Patch_Damage_Seismic	Fraction of WP surface failed by ruptures or fault displacement	0.05	0.05
Cum_Event_Occurs	Cumulative discrete change signals indicating a seismic event has been triggered	0	0
Rubble_Vol_Accum_Li_max [m^3/m]	Maximum lithophysal rubble volume required to fill drift, per length of drift	112	112
Rubble_Vol_Accum_NoLi_max [m^3/m]	Maximum non-lithophysal rubble volume required to fill drift, per length of drift	2.9	2.9
Rubble_Vol_Accum_Li [m^3/m]	Calculated lithophysal rubble volume required to fill drift, per length of drift	112	112
Rubble_Vol_Accum_NoLi [m^3/m]	Calculated non-lithophysal rubble volume required to fill drift, per length of drift	2.9	2.9

Source: Output DTN: MO0708TSPAPOST.000 [DIRS 182986].

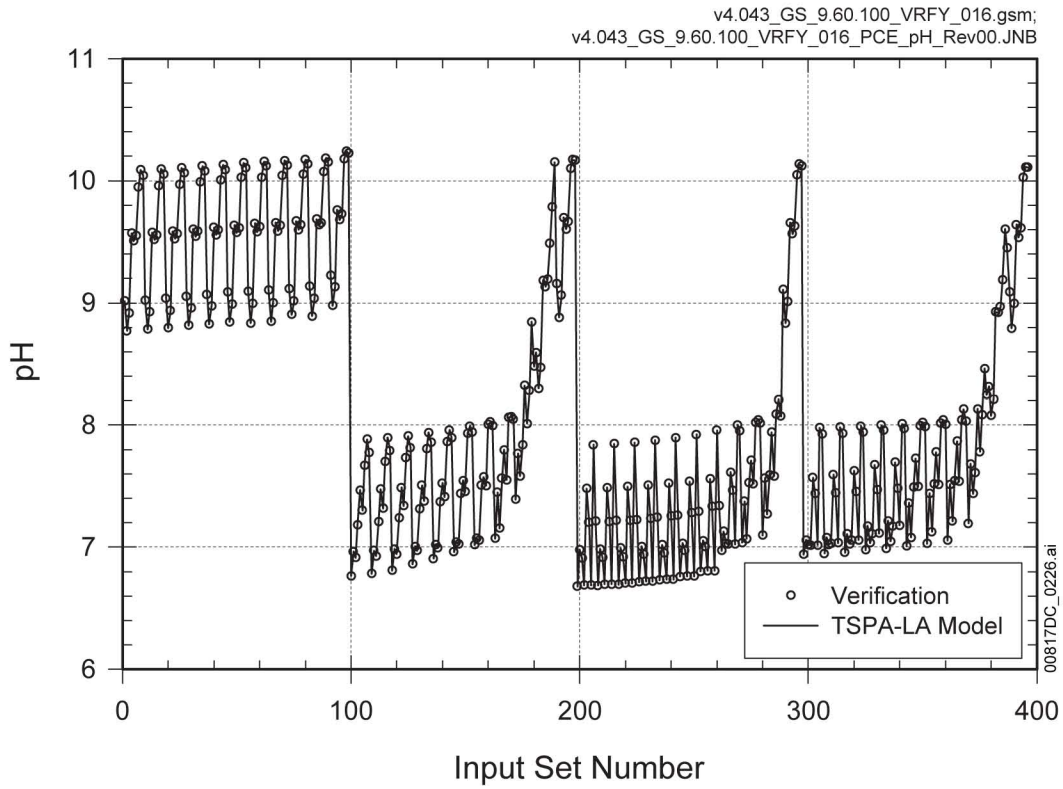

Source: Output DTN: MO0708TSPAPOST.000 [DIRS 182986].

Figure 7.2-1. Comparison of EBS Physical and Chemical Environment pH Calculations between a Stand-Alone Verification Calculation and the TSPA-LA Model

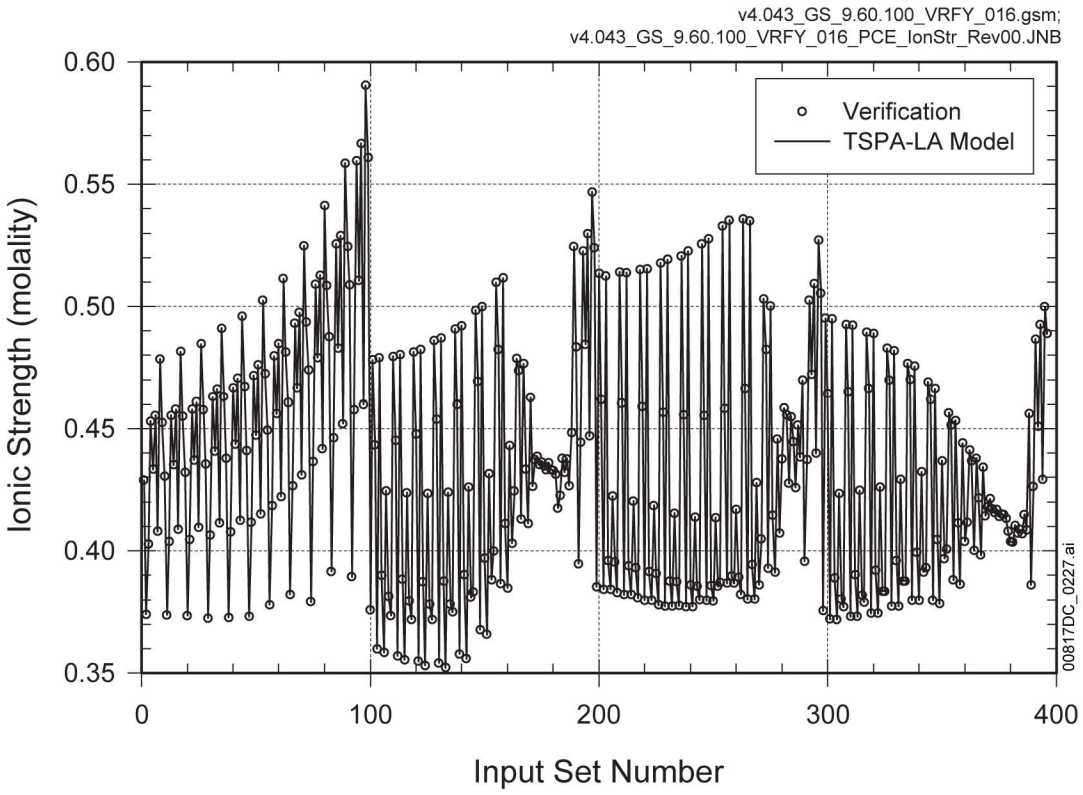

Source: Output DTN: MO0708TSPAPOST.000 [DIRS 182986].

Figure 7.2-2. Comparison of EBS Physical and Chemical Environment Ionic Strength Calculations between a Stand-Alone Verification Calculation and the TSPA-LA Model

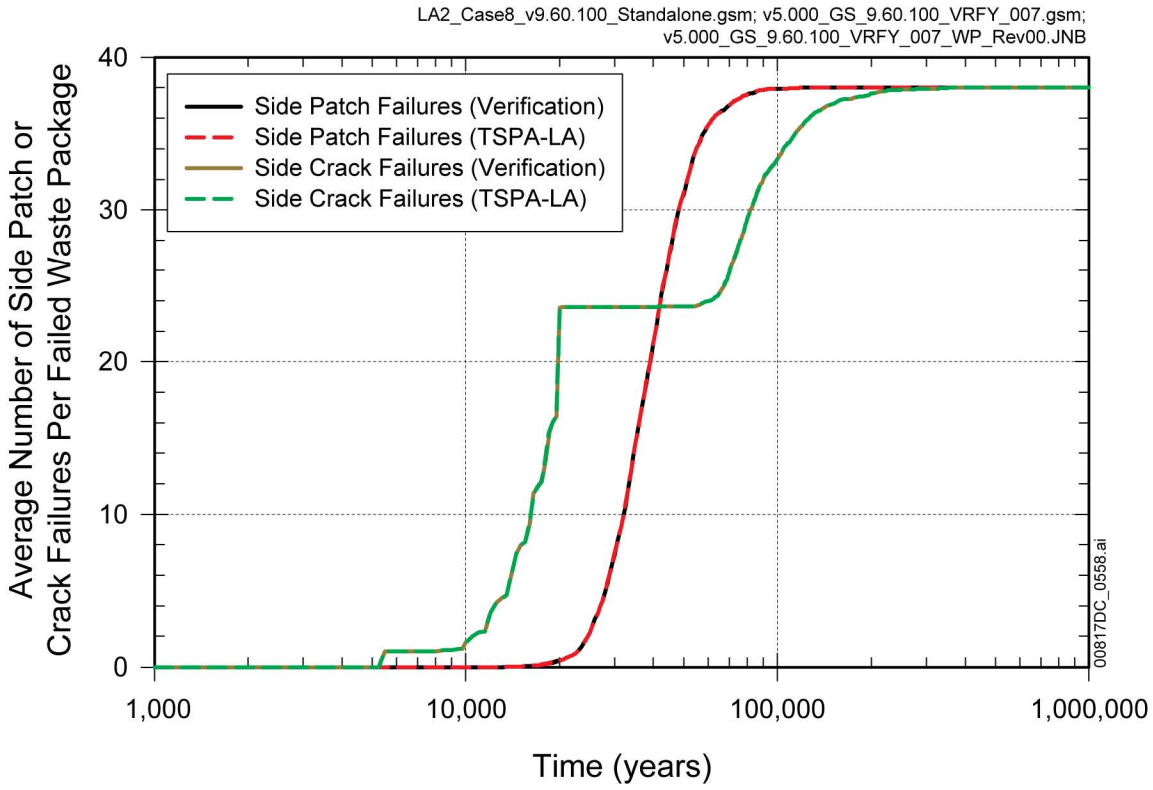

Source: Output DTN: MO0708TSPAPOST.000 [DIRS 182986].

Figure 7.2-3. Comparison of the Average Number of Waste Package Side Patch and Crack Failures between a Stand-Alone Verification Calculation and the TSPA-LA Model

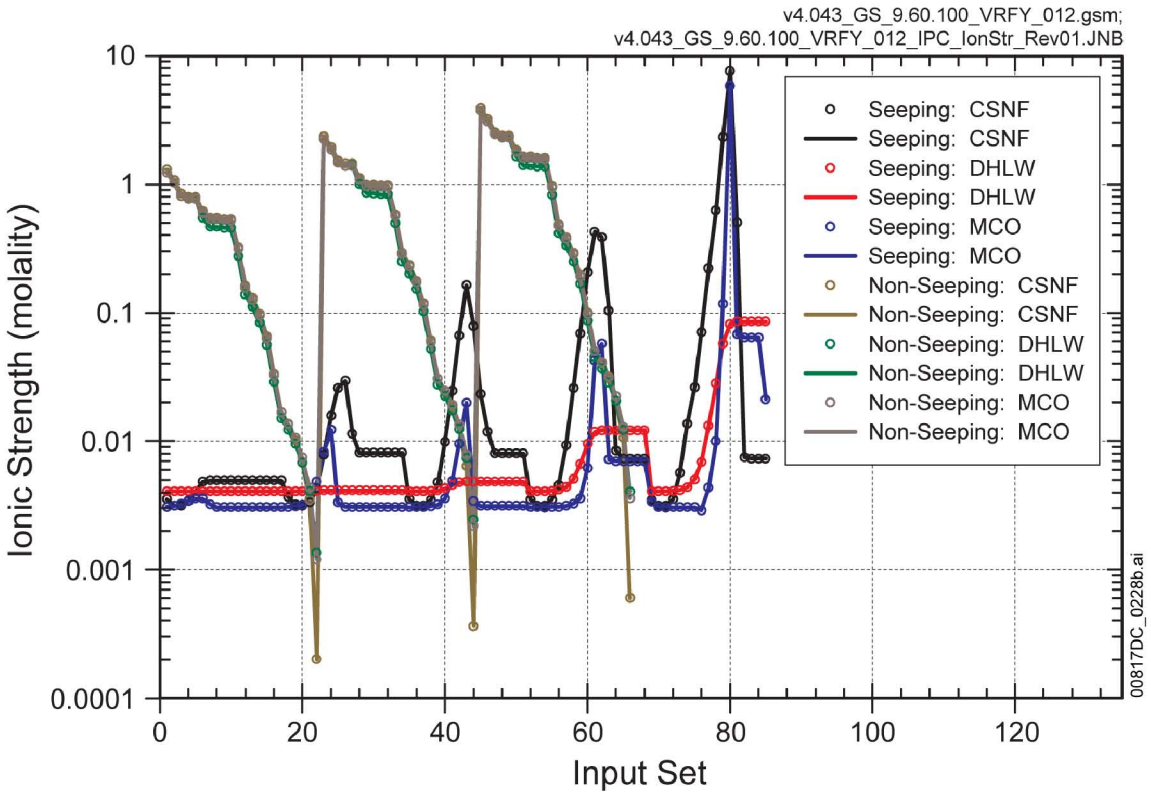

Source: Output DTN: MO0708TSPAPOST.000 [DIRS 182986].

NOTE: The verification data and the TSPA-LA Model results are represented by the open circles and solid lines, respectively. Some of the No Seepage data lines cannot be seen due to being obscured by other data lines.

Figure 7.2-4. Comparison of In-Package Chemistry Ionic Strength Calculations between a Stand-Alone Verification Calculation and the TSPA-LA Model

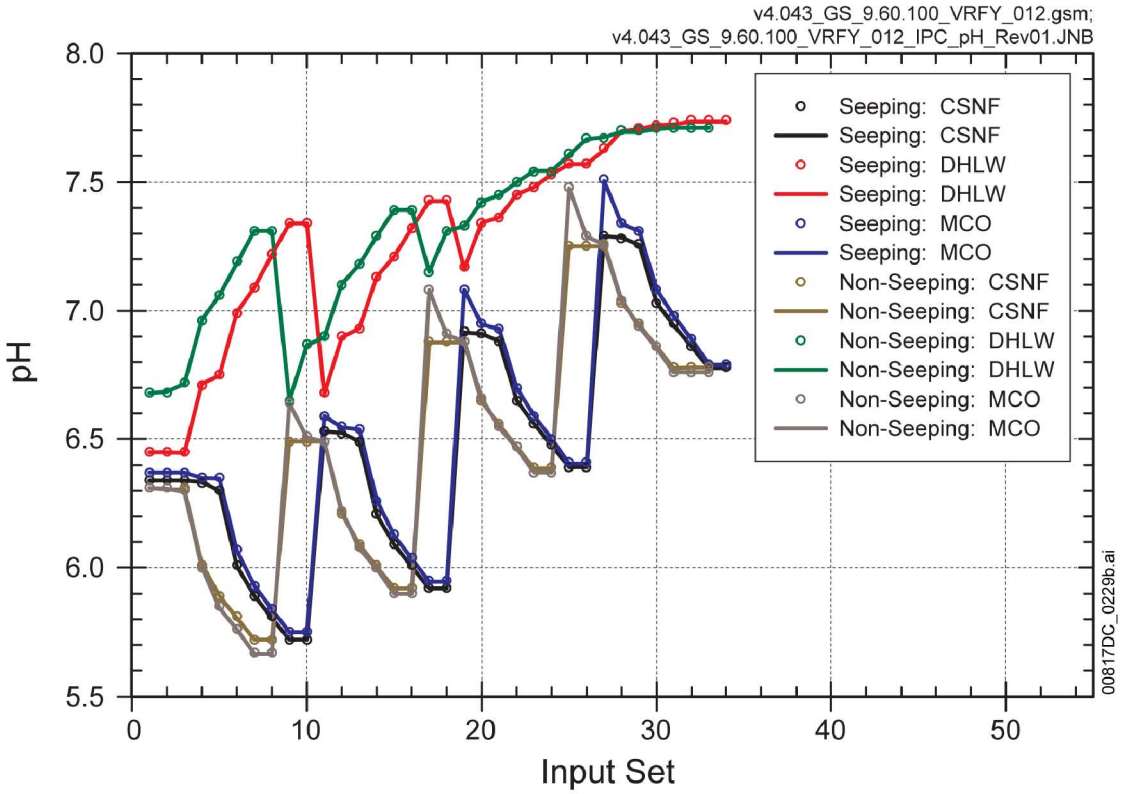

Source: Output DTN: MO0708TSPAPOST.000 [DIRS 182986].

NOTE: The verification data and the TSPA-LA Model results are represented by the open circles and solid lines, respectively. Some of the No Seepage data lines cannot be seen due to being obscured by other data lines.

Figure 7.2-5. Comparison of In-Package Chemistry pH Calculations between a Stand-Alone Verification Calculation and the TSPA-LA Model

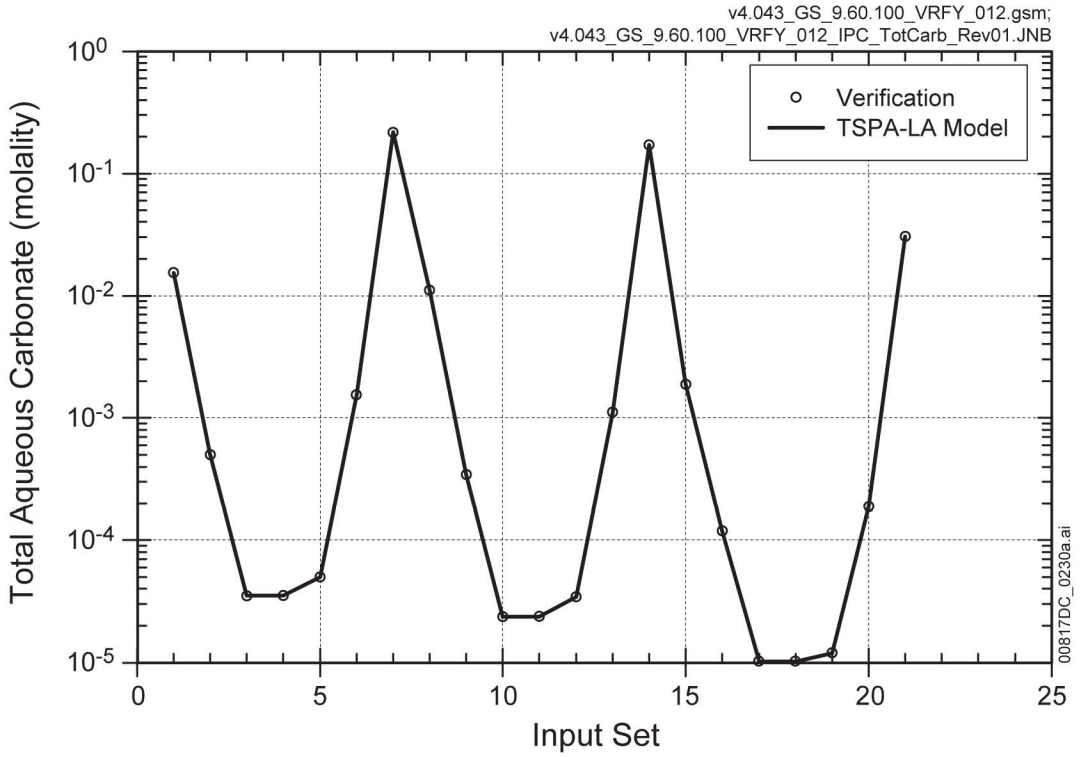

Source: Output DTN: MO0708TSPAPOST.000 [DIRS 182986].

Figure 7.2-6. Comparison of In-Package Chemistry Total Carbonate Calculations between a Stand-Alone Verification Calculation and the TSPA-LA Model

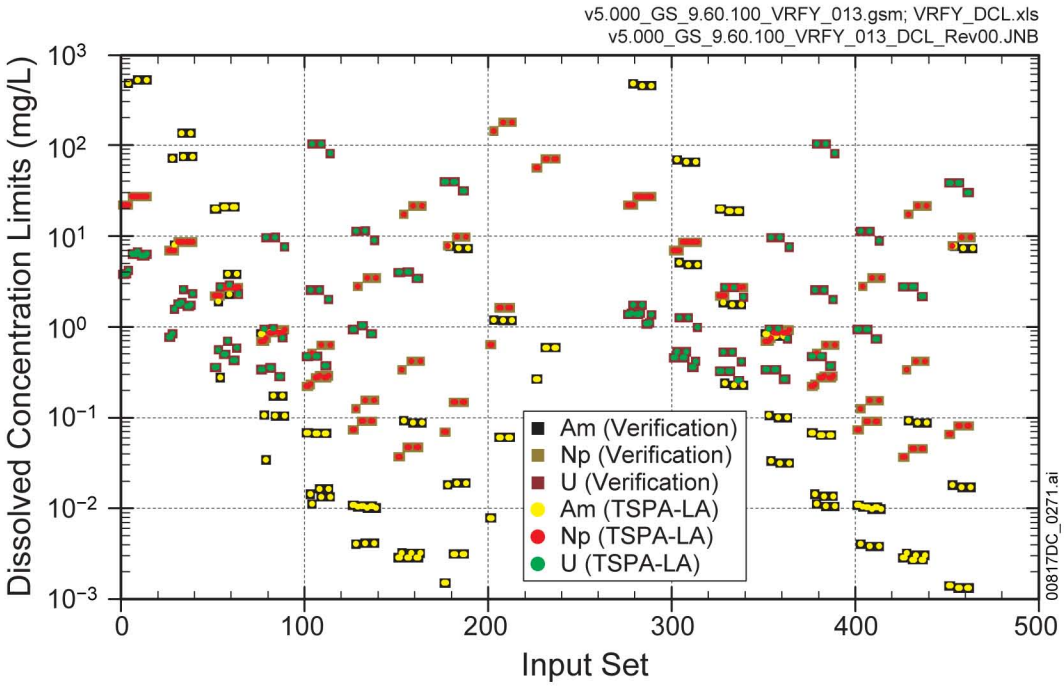

Source: Output DTN: MO0708TSPAPOST.000 [DIRS 182986].

Figure 7.2-7. Comparison of the Calculated Solubility of Americium (Am), Neptunium (Np), and Uranium (U) from the Verification of the Dissolved Concentrations Limits Submodel for the Nominal and Seismic Scenario Classes

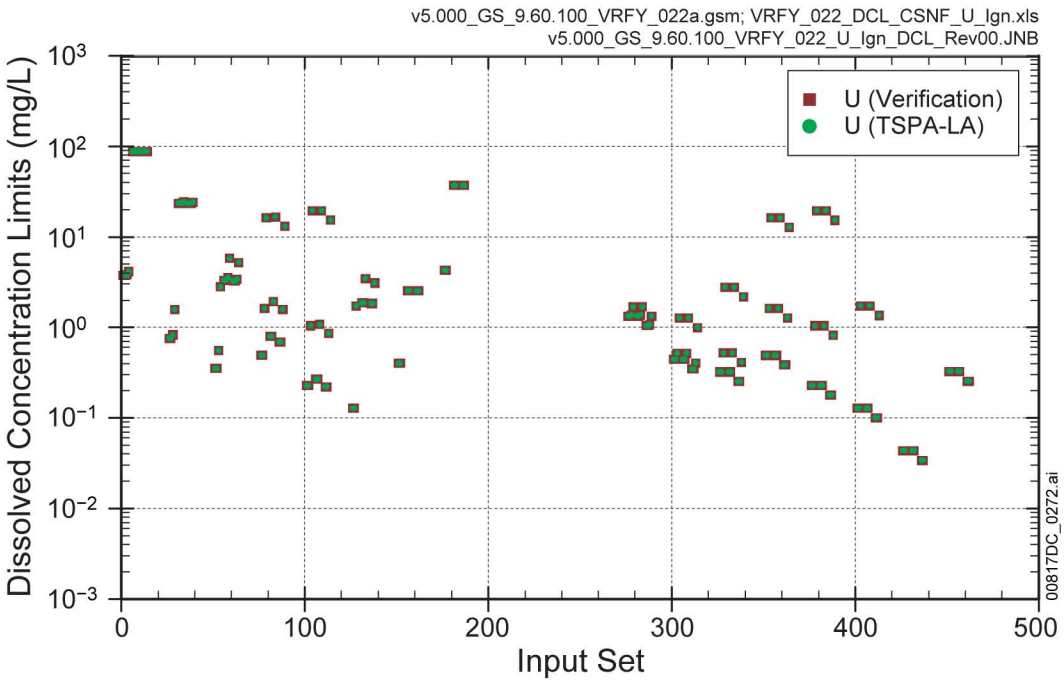

Source: Output DTN: MO0708TSPAPOST.000 [DIRS 182986].

Figure 7.2-8. Comparison of the Calculated Solubility of Uranium (U) from the Verification of the Dissolved Concentrations Limits Submodel for the Igneous Intrusion Modeling Case

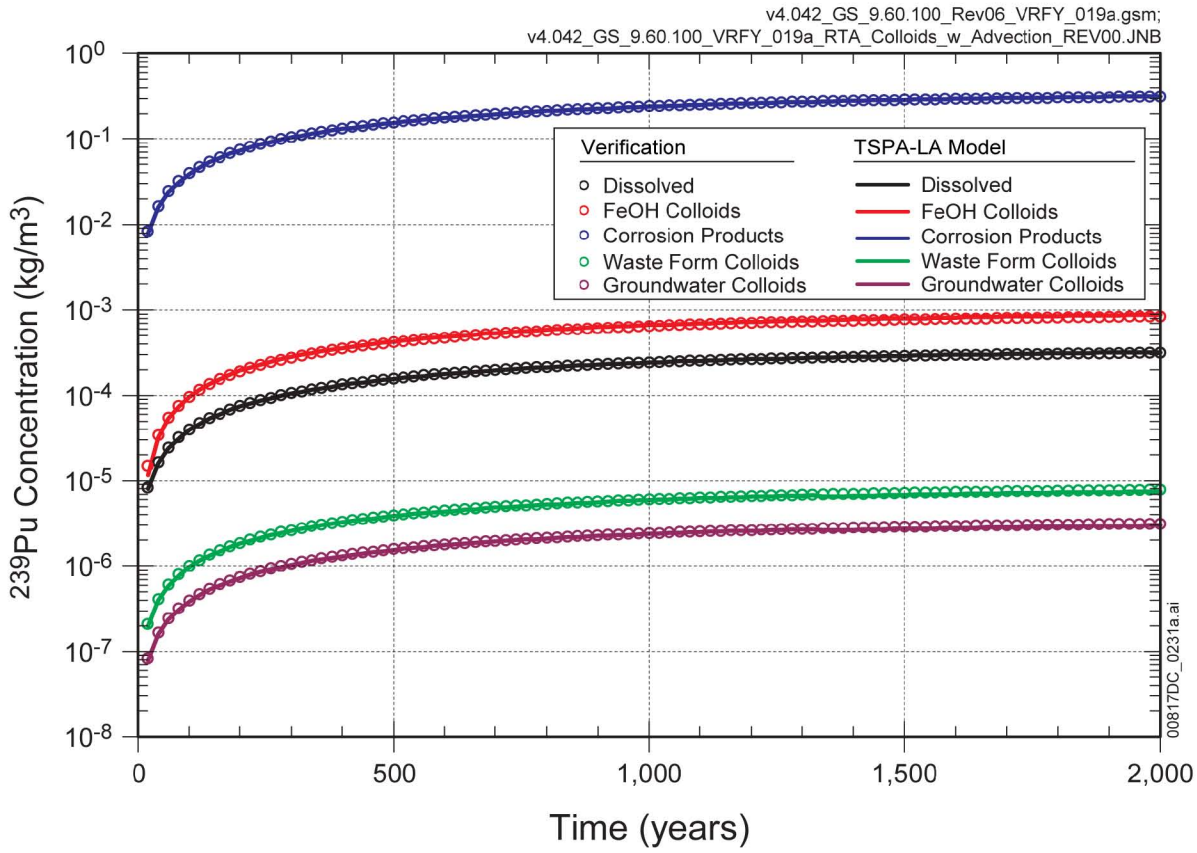

Source: Output DTN: MO0708TSPAPOST.000 [DIRS 182986].

NOTE: The verification data and the TSPA-LA Model results are represented by the open circles and solid lines, respectively.

Figure 7.2-9. Verification of the Dissolved and Colloidal Radionuclide Transport within the EBS Transport Submodel for the Case with Advection and Diffusion

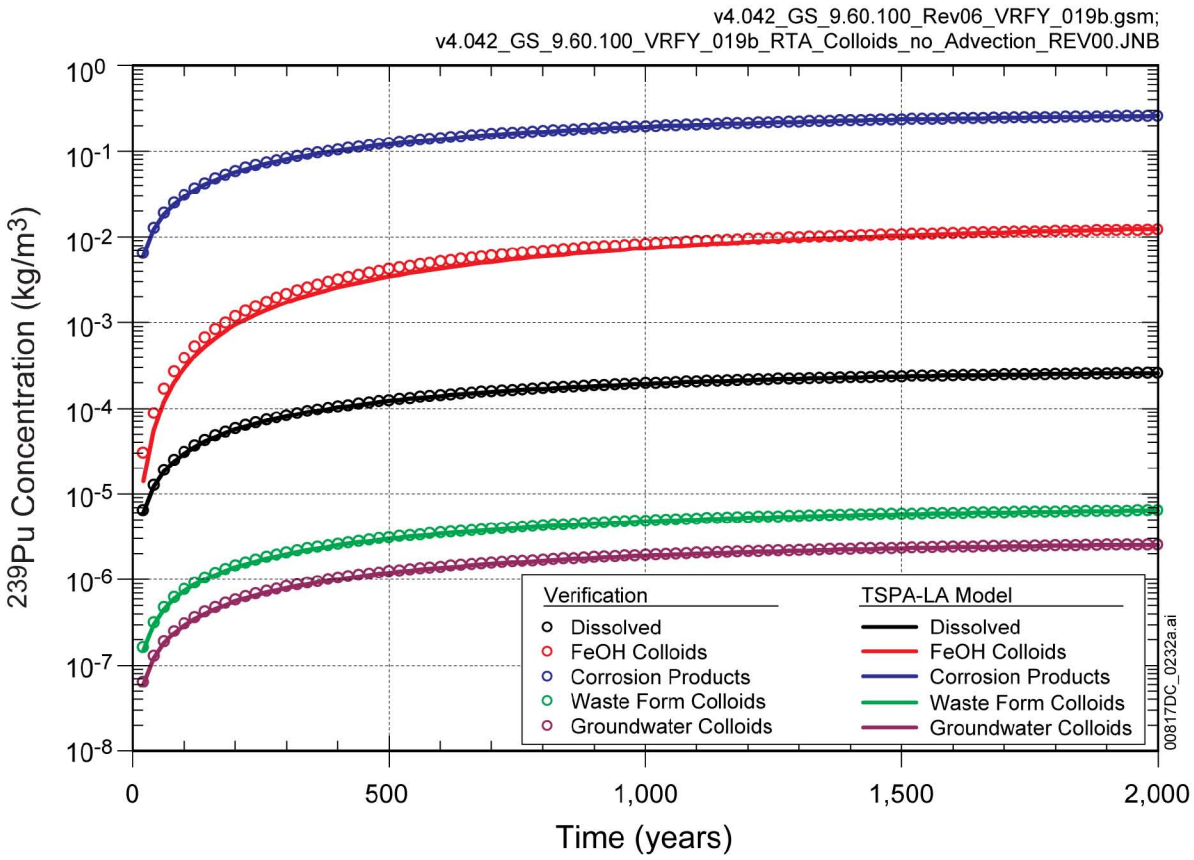

Source: Output DTN: MO0708TSPAPOST.000 [DIRS 182986].

NOTE: The verification data and the TSPA-LA Model results are represented by the open circles and solid lines, respectively.

Figure 7.2-10. Verification of the Dissolved and Colloidal Radionuclide Transport within the EBS Transport Submodel for the Case with Diffusion Only

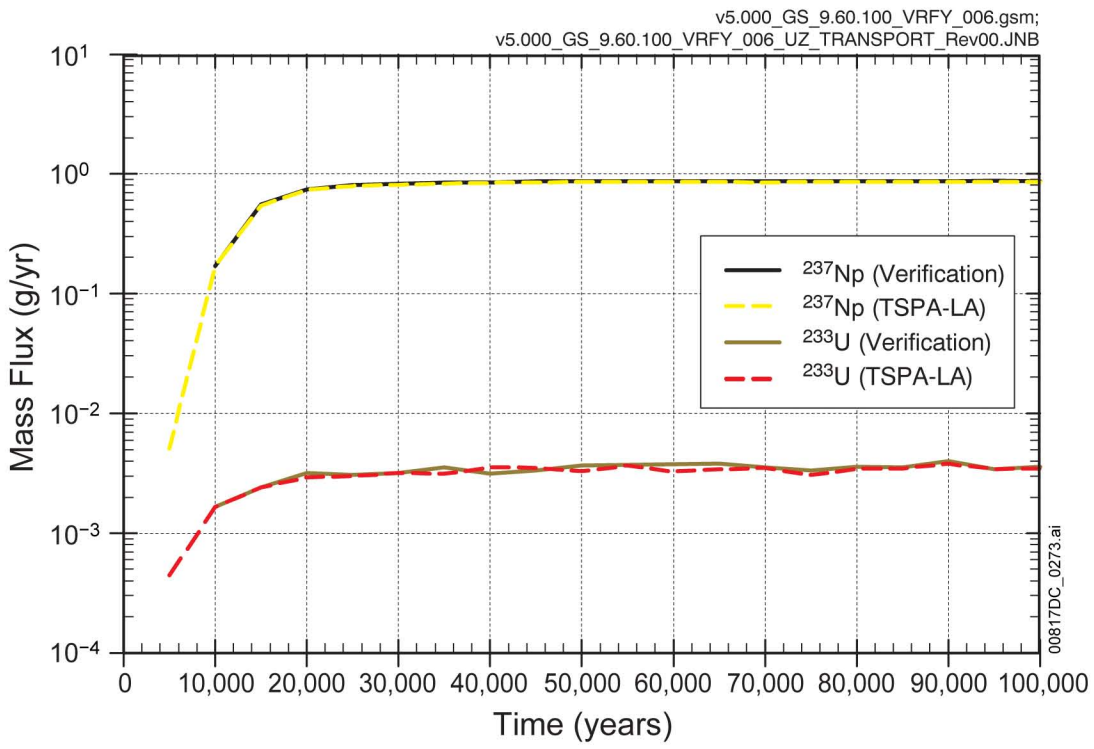

Source: Output DTN: MO0708TSPAPOST.000 [DIRS 182986].

Figure 7.2-11. Comparison of the ^{237}Np and ^{233}U Breakthrough Curves for the Verification of the Unsaturated Zone Transport Submodel

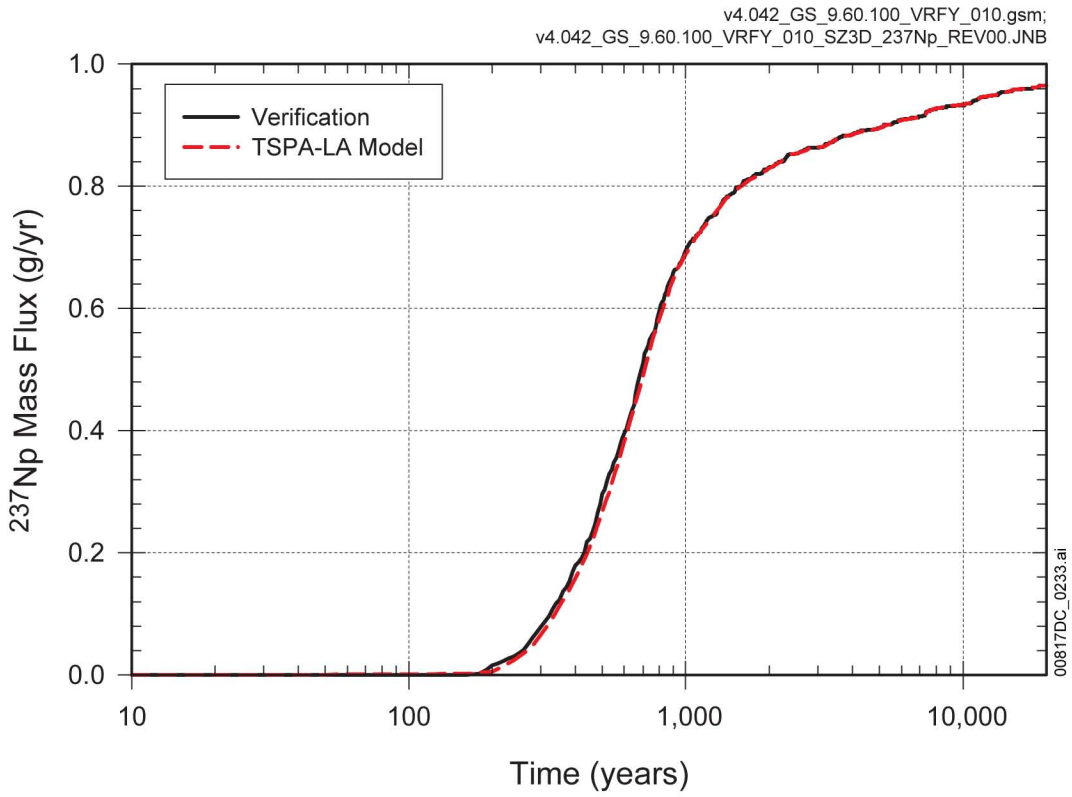

Source: Output DTN: MO0708TSPAPOST.000 [DIRS 182986].

Figure 7.2-12. Comparison of the ^{237}Np Breakthrough Curve Using the SZ_Convolute DLL in the Verification of the 3-D Saturated Zone Flow and Transport Abstraction

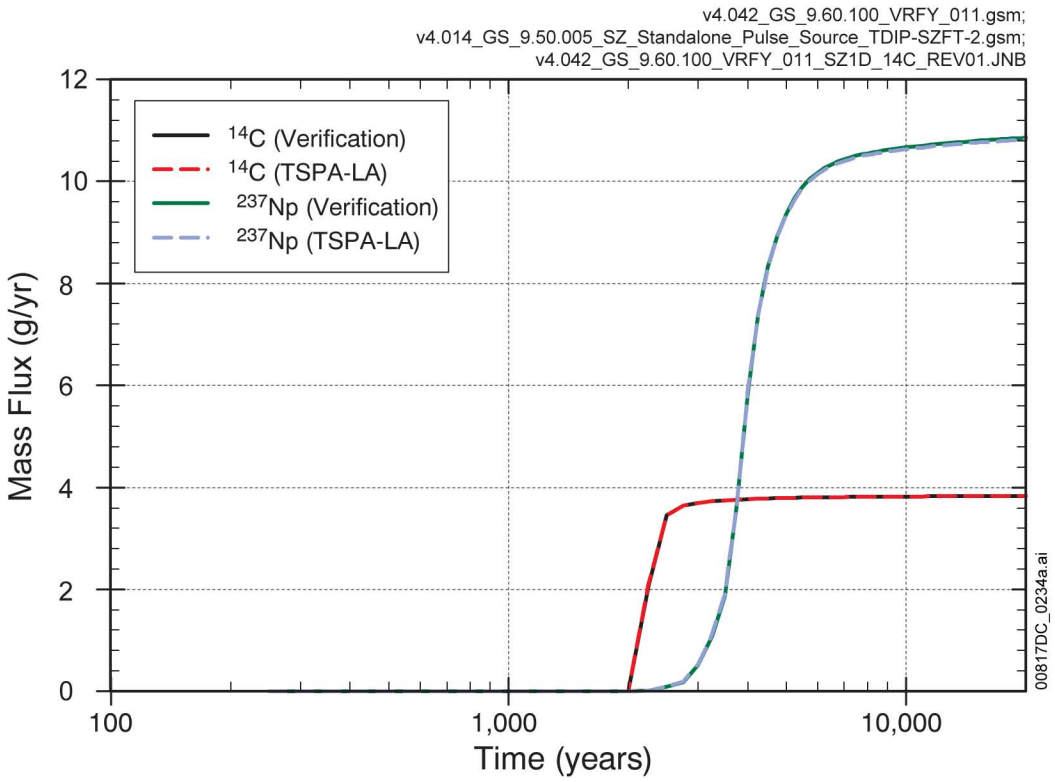

Source: Output DTN: MO0708TSPAPOST.000 [DIRS 182986].

Figure 7.2-13. Comparison of the Breakthrough Curves for ^{14}C and ^{237}Np from the Verification of the 1-D Saturated Zone Flow and Transport Abstraction

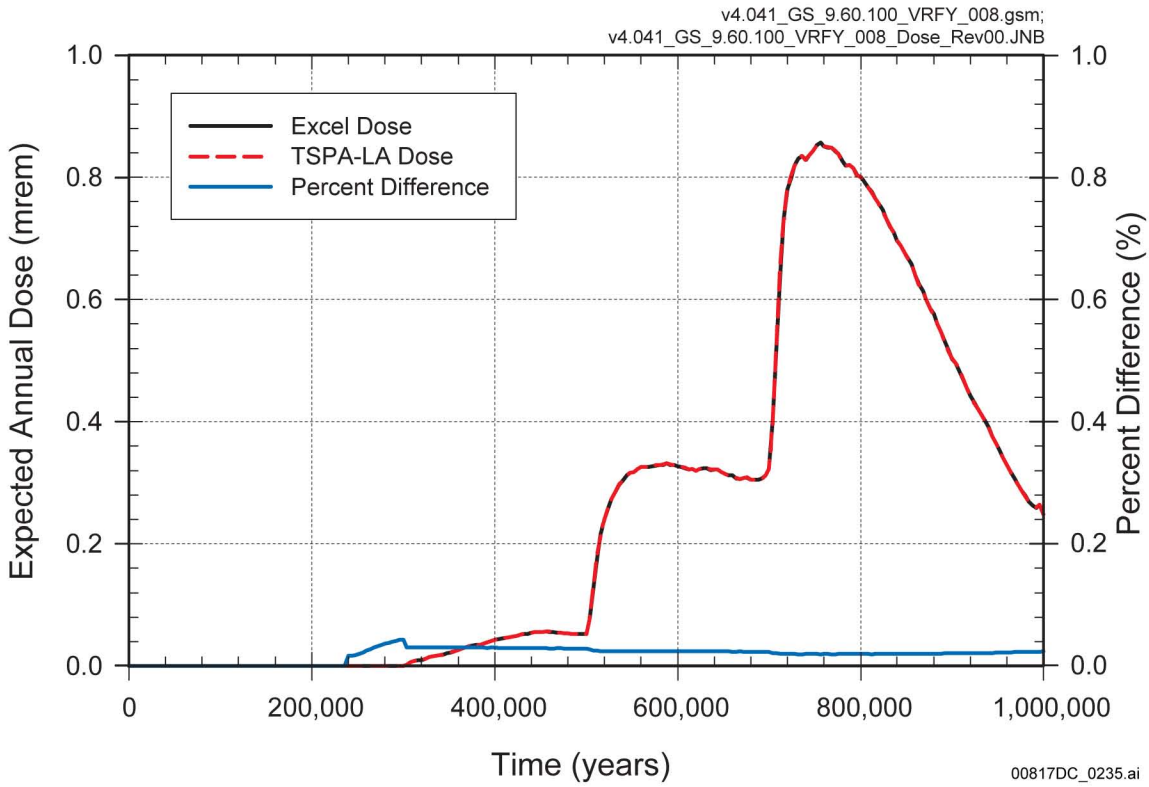

Source: Output DTN: MO0708TSPAPOST.000 [DIRS 182986].

Figure 7.2-14. Comparison of Expected Annual Dose Calculations from the Verification of the Biosphere Submodel

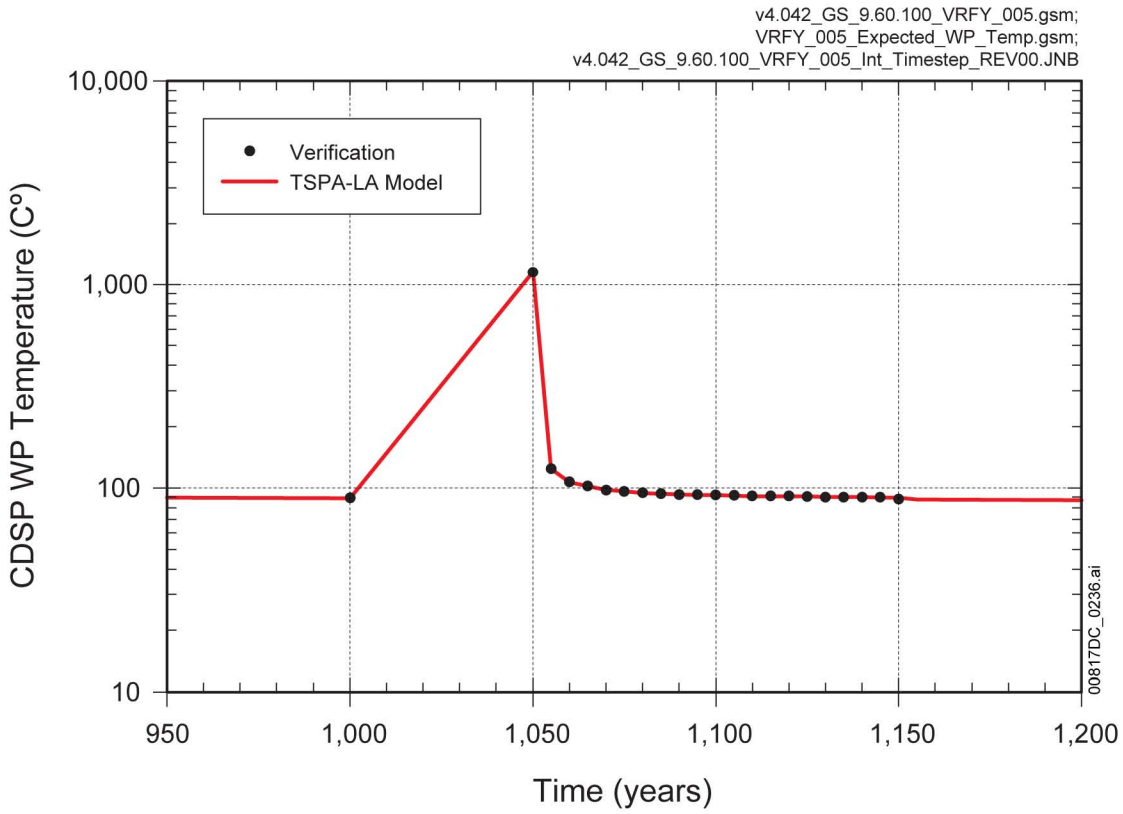

Source: Output DTN: MO0708TSPAPOST.000 [DIRS 182986].

Figure 7.2-15. Verification of the Impact on the EBS Thermal-Hydrologic Properties, as Represented by the CDSP WP Temperature, Resulting from an Igneous Intrusion Event

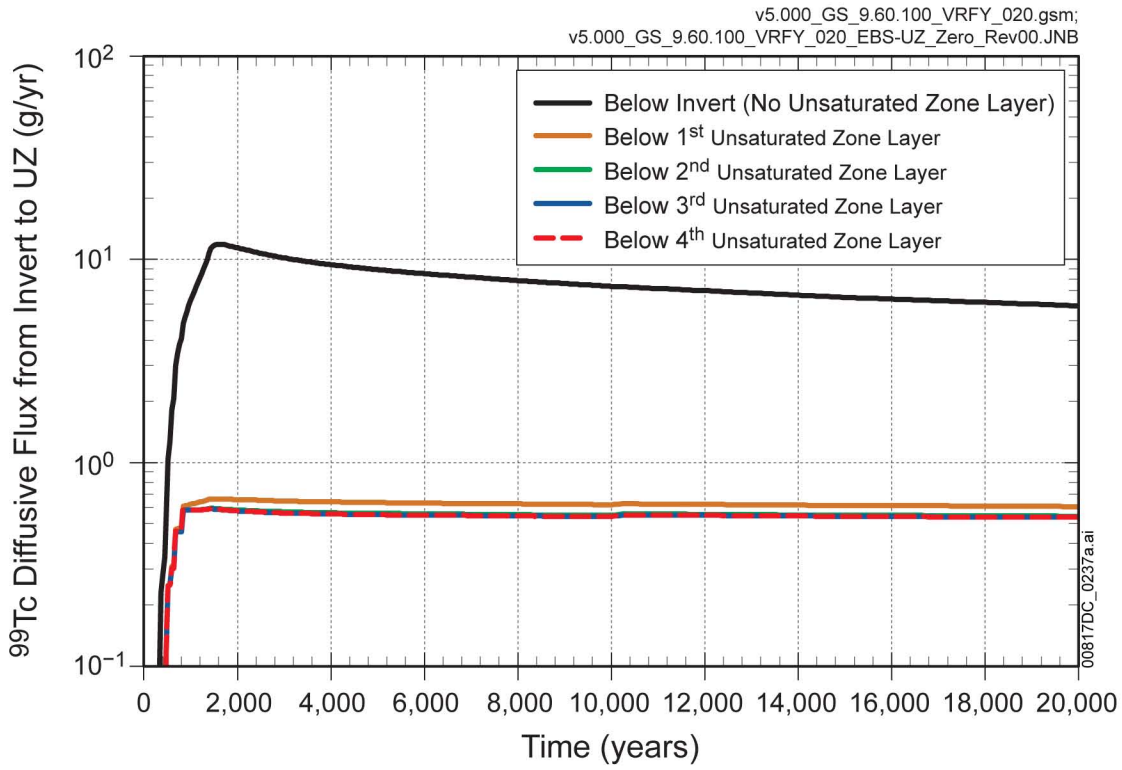

Source: Output DTN: MO0708TSPAPOST.000 [DIRS 182986].

Figure 7.2-16. Comparison of the Diffusive Flux of ^{99}Tc across the EBS-UZ Interface for Different Placement Locations of an Effective Zero-Concentration Boundary below the Invert

7.3 MODEL STABILITY

Yucca Mountain Review Plan, Final Report (NRC 2003 [DIRS 163274], Section 2.2.1.4.1.3) specifically mentions the stability of the TSPA-LA Model results as an acceptance criterion, stating:

> "A sufficient number of realizations has been obtained, for each scenario class, using the total system performance assessment code, to ensure that the results of the calculations are statistically stable."

The TSPA-LA Model is statistically stable if the mean annual dose computed by the model is stable. Demonstrating stability of the mean annual dose requires evaluation of the sufficiency of the sample size for uncertain parameters, the accuracy of numerical integration employed, and the stability of the models for physical processes with regards to discretizations of temporal and spatial variables. Stability is generally determined by demonstrating that the estimate of the mean annual dose does not depend on the sample size, the numerical integration, or on the discretizations in models for physical processes. The stability of the TSPA-LA Model results is discussed in this section.

The TSPA-LA Model computes total mean annual dose $\bar{\bar{D}}(\tau)$ at time τ by numerically evaluating

$$\begin{aligned}\bar{\bar{D}}(\tau) &= \int_{\mathcal{E}} \bar{D}(\tau|\mathbf{e})\, d_E(\mathbf{e})\, dE \\ &= \int_{\mathcal{E}} \left[\int_{\mathcal{A}} D(\tau|\mathbf{a},\mathbf{e})\, d_A(\mathbf{a})\, dA \right] d_E(\mathbf{e})\, dE\end{aligned} \qquad \text{(Eq. 7.3-1)}$$

where E is a probability space comprising the epistemic uncertain parameters, A is a probability space comprising the aleatory uncertainties that describe possible future states of the repository, and $D(\tau|\mathbf{a},\mathbf{e})$ is a function that computes the annual dose at time τ for a given element $\mathbf{e}$ in E, and $\mathbf{a}$ in A. The intermediate quantity $\bar{D}(\tau|\mathbf{e})$ is termed expected annual dose, and is more formally defined as the expectation of annual dose over aleatory uncertainty, conditional on epistemic uncertainty. Section 6.1.2 outlines the calculation of total mean annual dose, the scenario classes and modeling cases employed in this calculation, and the calculation methods used for each modeling case.

Numerical evaluation of Equation 7.3-1 involves four steps:

1. Selection of values for epistemic parameters $\mathbf{e}$ and aleatory uncertainties $\mathbf{a}$
2. Evaluation of the function $D(\tau|\mathbf{a},\mathbf{e})$ by numerically solving a complex, coupled system of differential equations describing radionuclide decay, flow, transport and other physical processes
3. Integration over aleatory uncertainty, carried out either by quadrature or Monte Carlo techniques, depending on the modeling case (see Section 6.1.2.4 for details)

4. Integration over epistemic uncertainty, conducted by a Monte Carlo technique due to the large number of epistemic parameters that define the probability space E.

These steps are carried out for each modeling case defined in Section 6.1. The results of the modeling cases are summed to compute total mean annual dose, which is the overall measure of repository compliance with the individual protection standard within 10,000 years of disposal as specified in the NRC Proposed Rule 10 CFR 63.303(a) [DIRS 178394]. The results are also used to calculate the median annual dose as the measure of compliance for the period 10,000 years after disposal through the period of geologic stability as required by NRC Proposed Rule 10 CFR 63.303(b) [DIRS 178394]. The individual protection standards for these measures of compliance are specified in 10 CFR 63.311 [DIRS 178394]. The stability of each of these three steps is examined in this section, in the reverse order listed above.

The integration over epistemic uncertainty employs Latin hypercube sampling (McKay et al. 1979 [DIRS 127905]) to sample the distributions of epistemic uncertain parameters. This sampling technique was selected, as in past TSPAs, because of the efficient manner in which it stratifies the sampling of values across the range of each uncertain variable, and the stability it provides for uncertainty and sensitivity analysis results in performance assessments of complex systems (McKay et al. 1979 [DIRS 127905]; Iman and Helton 1991 [DIRS 159039]; Helton 1999 [DIRS 159042]). Here, stability relates to how much variability takes place in the outcome of interest as model results are repeatedly calculated with different samples. Theoretical results indicate that, under certain conditions, Latin hypercube sampling does indeed exhibit better statistical convergence properties than random sampling (McKay et al. 1979 [DIRS 127905]; Stein 1987 [DIRS 159060]). However, due to the complexity of the TSPA-LA Model, it is not possible to prove that these conditions are respected. As a result, a practical method of assessing the stability of the results obtained with Latin hypercube sampling is used. Section 7.3.1 compares mean annual dose and uncertainty in the underlying distribution of expected annual dose for three independent LHSs, each of size 300. Using these three independent LHSs, confidence intervals are computed and shown. The analysis concludes that the sample size of 300 is adequate to estimate mean annual dose for each modeling case as well as to estimate total mean annual dose (summed over all modeling cases).

Section 7.3.2 discusses the numerical accuracy of the integration over aleatory uncertainty. These calculations evaluate the expected annual dose

$$\bar{D}(\tau|\mathbf{e}) = \int_{\mathcal{A}} D(\tau|\mathbf{a},\mathbf{e}) d_A(\mathbf{a}) dA \qquad \text{(Eq. 7.3-2)}$$

for each modeling case. Expected dose is computed either by quadrature techniques or by Monte Carlo techniques, depending on the modeling case. Quadrature integration is implemented in EXDOC_LA V2.0 (STN: 11193-2.0-00 [DIRS 182102]); Monte Carlo integration is done with GoldSim V9.60.100 (STN: 10344-9.60-01 [DIRS 181903]). Section 7.3.2 presents analyses that conclude that the discretization used for the quadrature techniques is adequate, and that the sample sizes used for the Monte Carlo techniques are sufficient.

The evaluation of annual dose, $D(\tau|\mathbf{a},\mathbf{e})$, involves numerical solution of a complex, couple systems of differential equations. Some of these equations are evaluated in model abstractions

provided as input to the TSPA-LA Model (as outlined in Section 6.3). The various analysis and/or model reports that document model abstractions also discuss the stability of these abstractions. Other equations are evaluated within the TSPA-LA Model, using techniques that discretize the temporal and spatial domains within which the equations are applied. Section 7.3.3 discusses the temporal discretization within the TSPA-LA Model and shows that temporal discretization is sufficient to adequately evaluate annual dose. Section 7.3.4 describes the spatial discretization employed in the TSPA-LA Model and its component abstractions and evaluates the adequacy of the percolation subregions to represent spatial variability in the TSPA-LA Model. Section 7.3.5 investigates the stability of the UZ Transport Model, which employs a particle tracking technique, by showing that a sufficient number of particles are used to obtain stable transport results.

INTENTIONALLY LEFT BLANK

7.3.1 Statistical Stability

As outlined in Section 7.3, mean annual dose is calculated as the expected value over epistemic uncertainty and aleatory uncertainty of the estimates of annual dose (Equation 7.3-1). The expectation of annual dose over aleatory uncertainty is evaluated first, the result of which is termed (for brevity) expected annual dose. The accuracy of the integral over aleatory uncertainty is discussed in Section 7.3.2. The integral of expected annual dose over epistemic uncertainty is referred to as the mean annual dose and is evaluated numerically using a Monte Carlo technique. The mean annual dose is statistically stable if the sample employed in the Monte Carlo technique produces an adequate estimate of the mean annual dose.

This section describes the replicated sampling procedure used to determine statistical stability and to compute the confidence intervals for the mean annual dose. Results are presented for each modeling case and for total mean annual dose (summed over all modeling cases). The analysis concludes that the sample size used in the Monte Carlo technique is adequate to estimate mean annual dose in each modeling case as well as to estimate the total mean annual dose. Moreover, the analysis demonstrates that the three independent replicates produce similar estimates of repository performance by comparing the mean annual dose and the distribution of uncertainty in expected annual dose among the three replicates. Therefore, the results of the TSPA-LA Model are statistically stable, and the repository performance can be evaluated by examining any one of the three generated replicates.

7.3.1.1 Replicated Sampling Procedure

As outlined in Section 6.1.3, values for epistemic parameters are selected using an LHS technique. In the TSPA-LA Model, the LHS includes 300 epistemic uncertain parameters in the groundwater model (comprising all modeling cases except the Volcanic Eruption Modeling Case) and 87 epistemic uncertain parameters in the model for the Volcanic Eruption Modeling Case. The parameters are listed in Table K.3-1. Section 7.4 describes review efforts undertaken to ensure that uncertainty in important parameters is appropriately characterized. The base sample size for the LHS is 300 for all modeling cases.

A replicated sampling procedure developed in the NRC HLW program at SNL provides an effective approach to estimating the potential sampling error in quantities derived from LHS (Iman 1982 [DIRS 146012]). With this procedure, the LHS is repeatedly generated with different random seeds. Each LHS is used to produce an estimate of the mean annual dose. The ensemble of estimates of the mean annual dose is used to compute an overall mean and standard error. Confidence intervals for the mean annual dose can then be estimated by means of the *t*-distribution. Appendix J, Section J.4.10, provides details on the replicated sampling procedure and the application of the *t*-distribution. The appropriate value for the number of replicates cannot be known with assurance before an analysis. In practice, a reasonable computational strategy is to start with a small number of replicates (e.g., three to five) and then add additional replicates if additional refinement of the confidence interval is desired.

7.3.1.2 Stability Analysis Results for Modeling Cases

The stability analysis was conducted by generating three replicates for each modeling case. The mean annual dose and statistics for the underlying distribution of uncertainty in the expected annual dose are compared for the three replicates. The three sample means are used to compute an overall mean and a 95 percent confidence interval about the overall mean. The confidence interval is displayed as an upper and lower bound. At each point in time, the true mean annual dose is less than the upper bound of the confidence interval (and greater than the lower bound) with probability 0.95.

Nominal Modeling Case—Figure 7.3.1-1(a) shows the mean annual dose for each of the three replicates of the Nominal Modeling Case, along with the median and the 5th and 95th percentiles of the distribution of uncertainty in the expected annual dose. The similarity of the median and the 5th and 95th percentiles indicates that the distributions of expected annual dose are similar in all three replicates. The means differ somewhat before 200,000 years because the mean is being determined by a very few realizations (less than 5 percent) that have corrosion failures before 200,000 years.

Figure 7.3.1-1(b) shows the mean annual dose for each of the three replicates, the overall mean, and the upper and lower bounds for the 95 percent confidence interval about the overall mean. The interval indicates that, with probability 0.975, there is no numerically significant dose from nominal processes before 100,000 years. Between 100,000 years and 300,000 years, when relatively few realizations have corrosion failures, the confidence intervals are wider than after 300,000 years, when corrosion failures are observed in many realizations. The confidence interval narrows at around 500,000 years because at that time most realizations have experienced SCC failures of WPs. Because the uncertainty in occurrence of SCC is reduced, the variability in expected dose between realizations decreases, resulting in more precise estimates of the mean and consequently narrow confidence interval about the mean. The confidence interval widens after 500,000 years because general corrosion failures begin to occur in some realizations. The uncertainty in the occurrence of general corrosion failures increases the variability in expected dose between realizations and contributes variability to the estimated mean and results in a wider confidence interval. The lower bound of the confidence interval is somewhat visually unappealing at early times because a logarithmic scale is used for display in keeping with the convention for displaying dose. However, for most of the 1,000,000-year period, the mean of each replicate is within an order of magnitude of the upper confidence interval, indicating that the true mean annual dose is estimated adequately by each of the three replicates. The similarity evident among the three replicates and the relatively small width of the confidence interval demonstrate that the sample size of 300 is adequate.

Early Failure Modeling Cases—Figure 7.3.1-2(a), shows the mean annual dose for each of the three replicates of the Waste Package EF Modeling Case for 20,000 years, along with the median and the 5th and 95th percentiles of the distribution of the expected annual dose. Figure 7.3.1-2(b) displays the confidence interval for the Waste Package EF Modeling Case for 20,000 years. Again, the lower bound of the confidence interval is visually distorted by the logarithmic scale used for dose. The similarity evident among the three replicates and the relatively small width of the confidence interval demonstrates that the mean annual dose is estimated with sufficient accuracy with the sample size of 300.

Figure 7.3.1-3(a) shows the mean annual dose for each of the three replicates of the Waste Package EF Modeling Case for 1,000,000 years, along with the median and the 5th and 95th percentiles of the distribution of uncertainty in the expected annual dose. Figure 7.3.1-3(b) displays the confidence interval for the Waste Package EF Modeling Case for 1,000,000 years. The figures indicate that the sample size for 300 is adequate to estimate the mean annual dose.

Figure 7.3.1-4(a), Figure 7.3.1-4(b), Figure 7.3.1-5(a) and Figure 7.3.1-5(b) display the mean annual dose along with the median and the 5th and 95th percentiles of expected annual dose, for each of the three replicates of the Drip Shield EF Modeling Case, and the confidence intervals for the Drip Shield EF Modeling Case, for both 20,000 years and 1,000,000 years. The figures indicate that the sample size for 300 is adequate for the Drip Shield EF Modeling Cases.

Igneous Modeling Cases—Figure 7.3.1-6(a) shows the mean annual dose for each of the three replicates of the Igneous Intrusion Modeling Case for 20,000 years, along with the median and the 5th and 95th percentiles of the distribution of the expected annual dose. Figure 7.3.1-6(b) displays the confidence interval for this modeling case. The high degree of similarity among replicates and the overall narrow confidence interval indicates that the mean annual dose for this modeling case is estimated accurately, and the sample size of 300 is adequate.

Figure 7.3.1-7(a) shows the mean annual dose for each of the three replicates of the Igneous Intrusion Modeling Case for 1,000,000 years, along with the median and the 5th and 95th percentiles of the distribution of the expected annual dose. Figure 7.3.1-7(b) displays the confidence interval for this modeling case. As in the 20,000-year calculation, the high degree of similarity among replicates and the overall narrow confidence interval indicates that the mean annual dose for this modeling case is estimated accurately, and the sample size of 300 is adequate. The confidence interval in Figure 7.3.1-7(b) narrows at 200,000 years because the means of Replicate 1 and Replicate 3 cross over, however, this narrowing of the confidence interval is an artifact of the intersection of the means, and may not represent an actual reduction in the uncertainty in the results at 200,000 years.

Figure 7.3.1-8(a), Figure 7.3.1-8(b), Figure 7.3.1-9(a), and Figure 7.3.1-9(b) display the mean annual dose along with the median and the 5th and 95th percentiles of expected annual dose, for each of the three replicates of the Volcanic Eruption Modeling Case, and the confidence intervals for this modeling case, for both 20,000 years and 1,000,000 years. The figures indicate that the sample size of 300 is adequate to estimate mean annual dose for the Volcanic Eruption Modeling Cases.

Seismic Modeling Cases—Figure 7.3.1-10(a) shows the mean annual dose for each of the three replicates of the Seismic GM Modeling Case for 20,000 years, along with the median and the 5th and 95th percentiles of the distribution of the expected annual dose. Figure 7.3.1-10(b) displays the confidence interval for this modeling case. The high degree of similarity among replicates and the very narrow confidence interval indicates that the mean annual dose for this modeling case is estimated accurately, and the sample size of 300 is adequate.

Figure 7.3.1-11(a) shows the mean annual dose for each of the three replicates of the Seismic GM Modeling Case for 1,000,000 years, along with the median and the 5th and 95th percentiles of the distribution of the expected annual dose. Figure 7.3.1-11(b) displays the confidence

interval for this modeling case. Because the Seismic GM Modeling Case employs a Monte Carlo technique for 1,000,000 years and a quadrature technique for 20,000 years (Section 6.1.2.4), the 1,000,000-year results are not as smooth as the 20,000 year results. However, the distribution of expected annual dose compares very well between the three replicates, and the confidence interval indicates that the mean annual dose is estimated well within an order of magnitude. Therefore, the sample size of 300 is adequate for estimating mean annual dose in this modeling case.

Figure 7.3.1-12(a) shows the mean annual dose for each of the three replicates of the Seismic FD Modeling Case for 20,000 years, along with the median and the 5th and 95th percentiles of the distribution of the expected annual dose. Figure 7.3.1-12(b) displays the confidence interval for this modeling case. The high degree of similarity among replicates and the very narrow confidence interval indicates that the mean annual dose for this modeling case is estimated accurately, and the sample size of 300 is adequate.

Figure 7.3.1-13(a) and Figure 7.3.1-13(b) display the distributions of expected annual dose and the confidence interval for the Seismic FD Modeling Case for 1,000,000 years. The figures indicate that the sample size of 300 is adequate to estimate mean annual dose for this modeling case.

Human Intrusion Modeling Case—Figure 7.3.1-14(a) shows the mean annual dose for each of the three replicates of the Human Intrusion Modeling Case, along with the median and the 5th and 95th percentiles of the distribution of the expected annual dose. Figure 7.3.1-14(b) displays the confidence interval for this modeling case. The high degree of similarity among replicates and the very narrow confidence interval indicates that the mean annual dose for this modeling case is estimated accurately, and the sample size of 300 is adequate.

7.3.1.3 Stability Analysis Results for Total Mean Annual Dose

Total mean annual dose is computed by summing the results of each modeling case, except for the Human Intrusion Modeling Case. The distribution of total expected annual dose is first obtained by summing the expected annual doses for each modeling case by epistemic sample element, resulting in one total expected annual dose history for each sample element. The mean of the distribution of total expected annual dose is the total mean annual dose.

Stability of the total mean annual dose is determined by computing the distribution of total expected annual dose for each of the three replicated LHS samples, and by computing the confidence interval using the total mean annual doses for the three replicates. Figure 7.3.1-15(a) shows the total mean annual dose for the three replicates for 20,000 years, along with the median and the 5th and 95th percentiles of the distribution of the total expected annual dose. Figure 7.3.1-15(a) indicates that the means from each replicate differ by approximately a factor of 2. These differences are attributable to the differences in the sampling of parameters for each replicate, and could be reduced if the sample size was increased. Figure 7.3.1-15(b) displays the confidence interval for total mean annual dose for 20,000 years, and shows that, with probability 0.975, the true mean is estimated to lie more than an order of magnitude below the regulatory standard specified in 10 CFR 63.311 [DIRS 178394]. Therefore, the high degree of similarity among replicates, the very narrow confidence interval, and the large separation between the

confidence interval and the regulatory limit relative to the width of the confidence interval indicates that total mean annual dose is estimated with sufficient accuracy, and the sample size of 300 is adequate. The stability evident in the total mean annual dose for 20,000 years is primarily due to the stability of the mean annual dose results for the Seismic GM Modeling Case for 20,000 years (Figure 7.3.1-10b) and for the Igneous Intrusion Modeling Case for 20,000 years (Figure 7.3.1-6b) because these two modeling cases constitute almost all of the total mean annual dose (Figure 8.1-3a).

Figure 7.3.1-16(a) and Figure 7.3.1-16(b) display the distributions of total expected annual dose and the confidence interval for total mean annual dose for 1,000,000 years. The figures indicate that the total mean annual dose is estimated with sufficient accuracy, and that the sample size of 300 is adequate. The stability evident in the total mean annual dose for 1,000,000 years is primarily due to the stability of the mean annual dose results for the Seismic GM Modeling Case for 1,000,000 years (Figure 7.3.1-11b) and for the Igneous Intrusion Modeling Case for 1,000,000 years (Figure 7.3.1-7b) because these two modeling cases constitute almost all of the total mean annual dose (Figure 8.1-3b).

7.3.1.4 Conclusion

Statistical stability of the total mean annual dose was evaluated by means of a replicated sampling procedure. Three independent LHSs of epistemic uncertain parameters were generated, and with these LHSs, three estimates of total mean annual dose were computed using the TSPA-LA Model. Comparison of these three estimates of total mean annual dose and the associated distributions of uncertainty in expected annual dose showed that the three independent LHSs produced statistically similar values of the total mean annual dose, as well as similar distributions of uncertainty in expected annual dose. The analysis concludes that the results of the TSPA-LA Model are statistically stable. Moreover, the similarity between replicates demonstrates that repository performance can be evaluated using any one of the three replicates. Consequently, Replicate 1 was selected for analysis and evaluation. The model results presented in this report are all taken from Replicate 1.

INTENTIONALLY LEFT BLANK

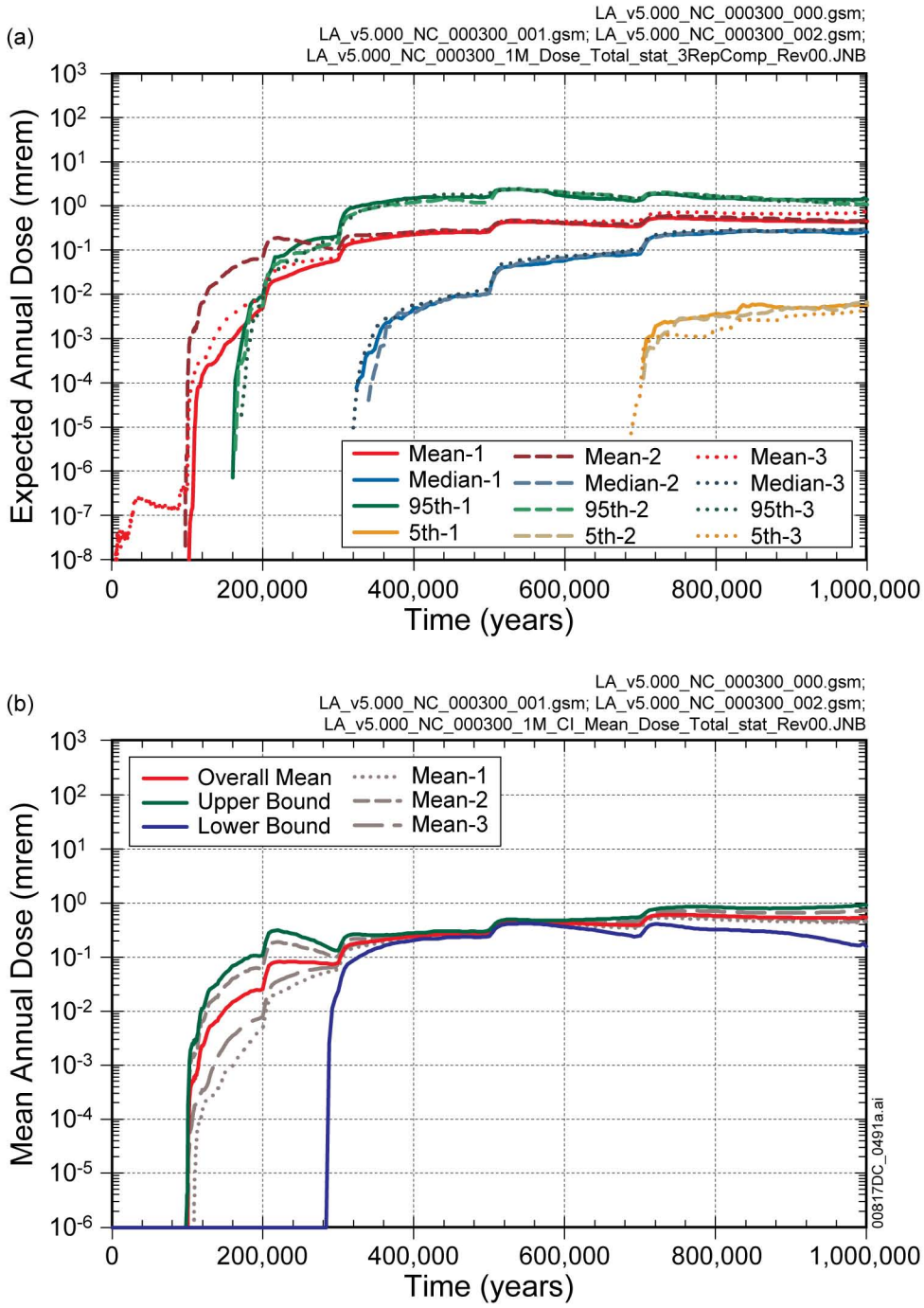

Source: Output DTNs: MO0709TSPASTAB.000 [DIRS 182983]; and MO0709TSPAREGS.000 [DIRS 182976].

Figure 7.3.1-1. Stability of Nominal Modeling Case: (a) Comparison of Expected Annual Dose for Three Replicates and (b) Confidence Interval around Mean Annual Dose

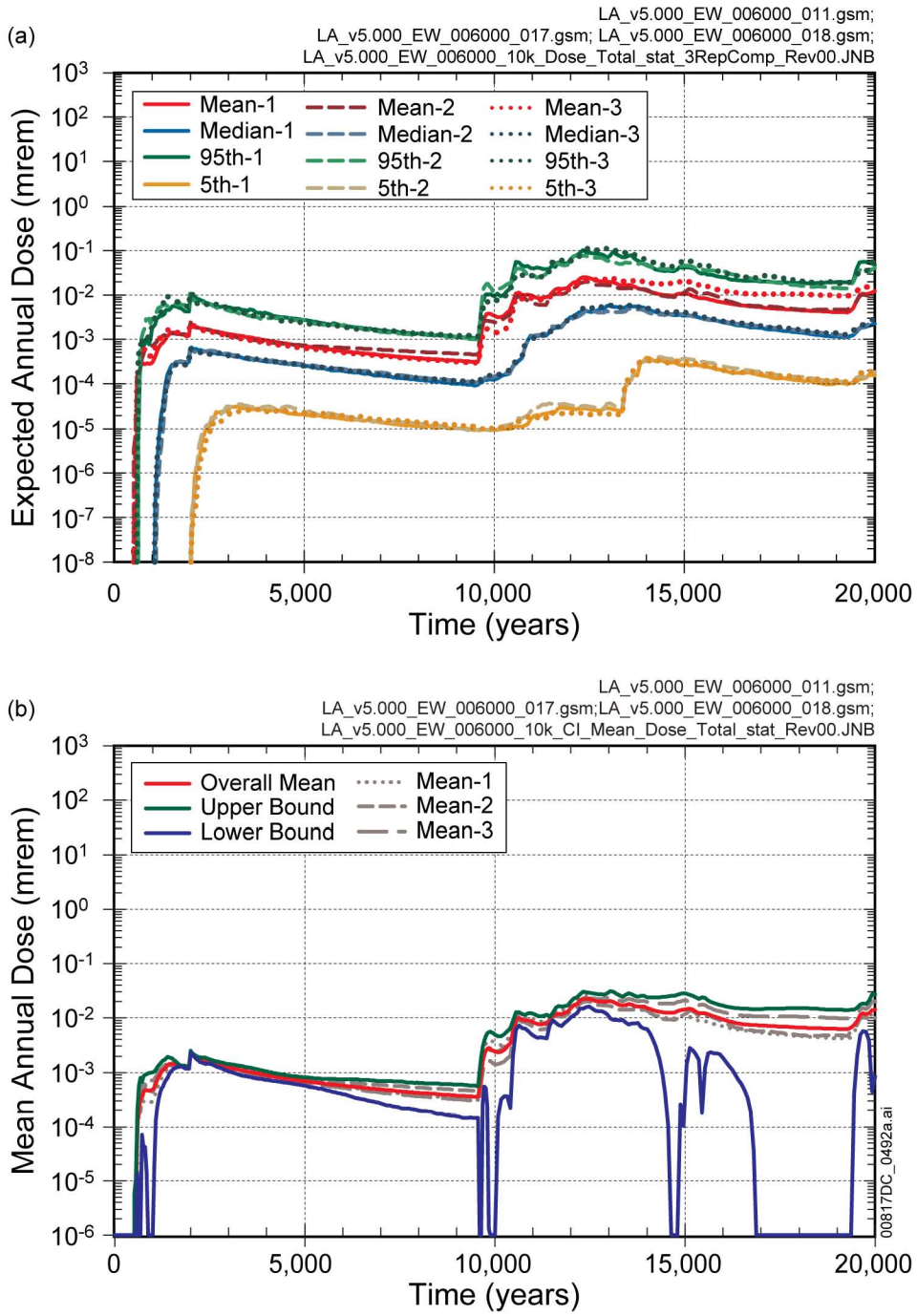

Source: Output DTNs: MO0709TSPASTAB.000 [DIRS 182983]; and MO0709TSPAREGS.000 [DIRS 182976].

Figure 7.3.1-2. Stability of Waste Package Early Failure Modeling Case for 20,000 Years: (a) Comparison of Expected Annual Dose for Three Replicates and (b) Confidence Interval around Mean Annual Dose

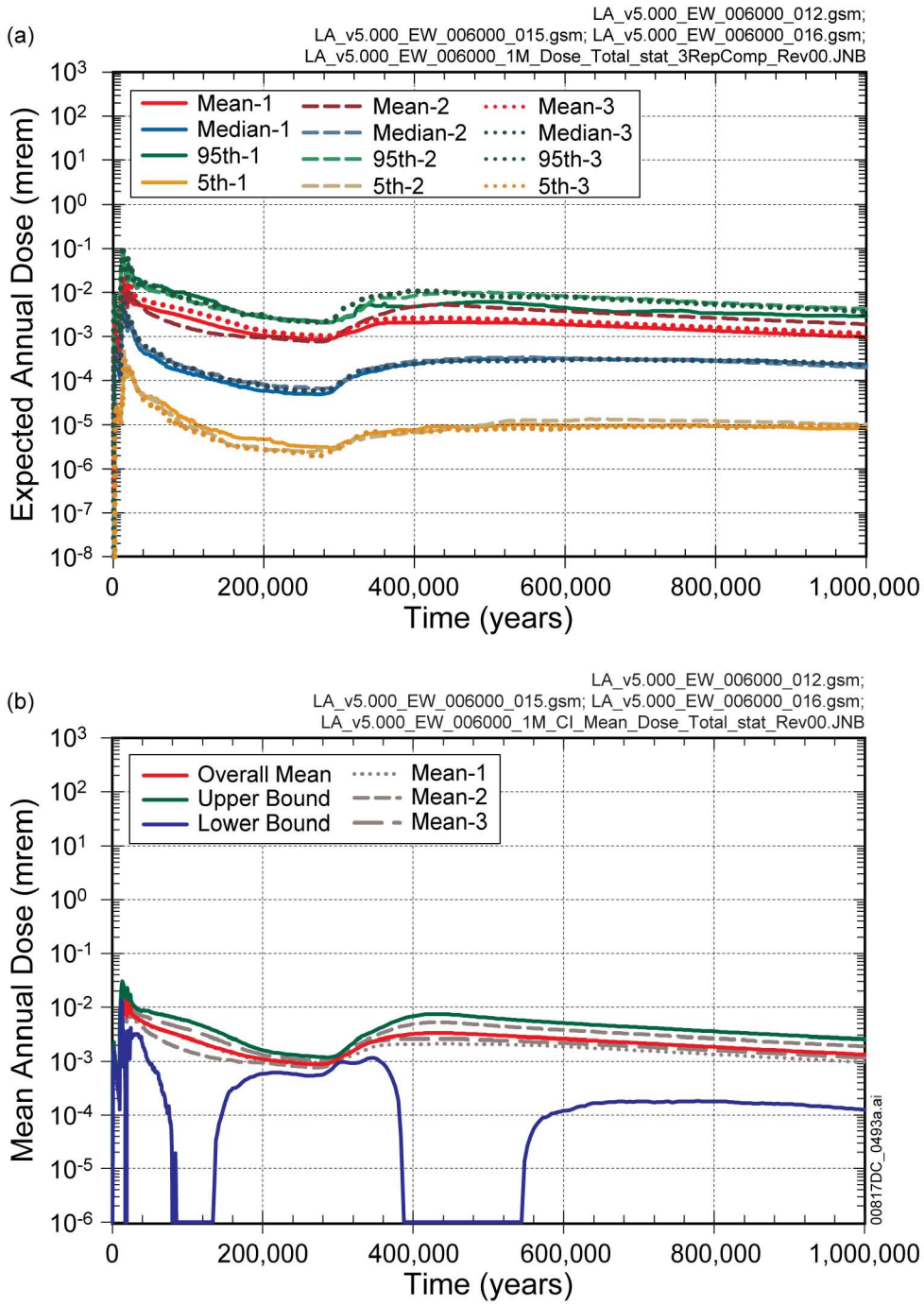

Source: Output DTNs: MO0709TSPASTAB.000 [DIRS 182983]; and MO0709TSPAREGS.000 [DIRS 182976].

Figure 7.3.1-3. Stability of Waste Package Early Failure Modeling Case for 1,000,000 Years: (a) Comparison of Expected Annual Dose for Three Replicates and (b) Confidence Interval around Mean Annual Dose

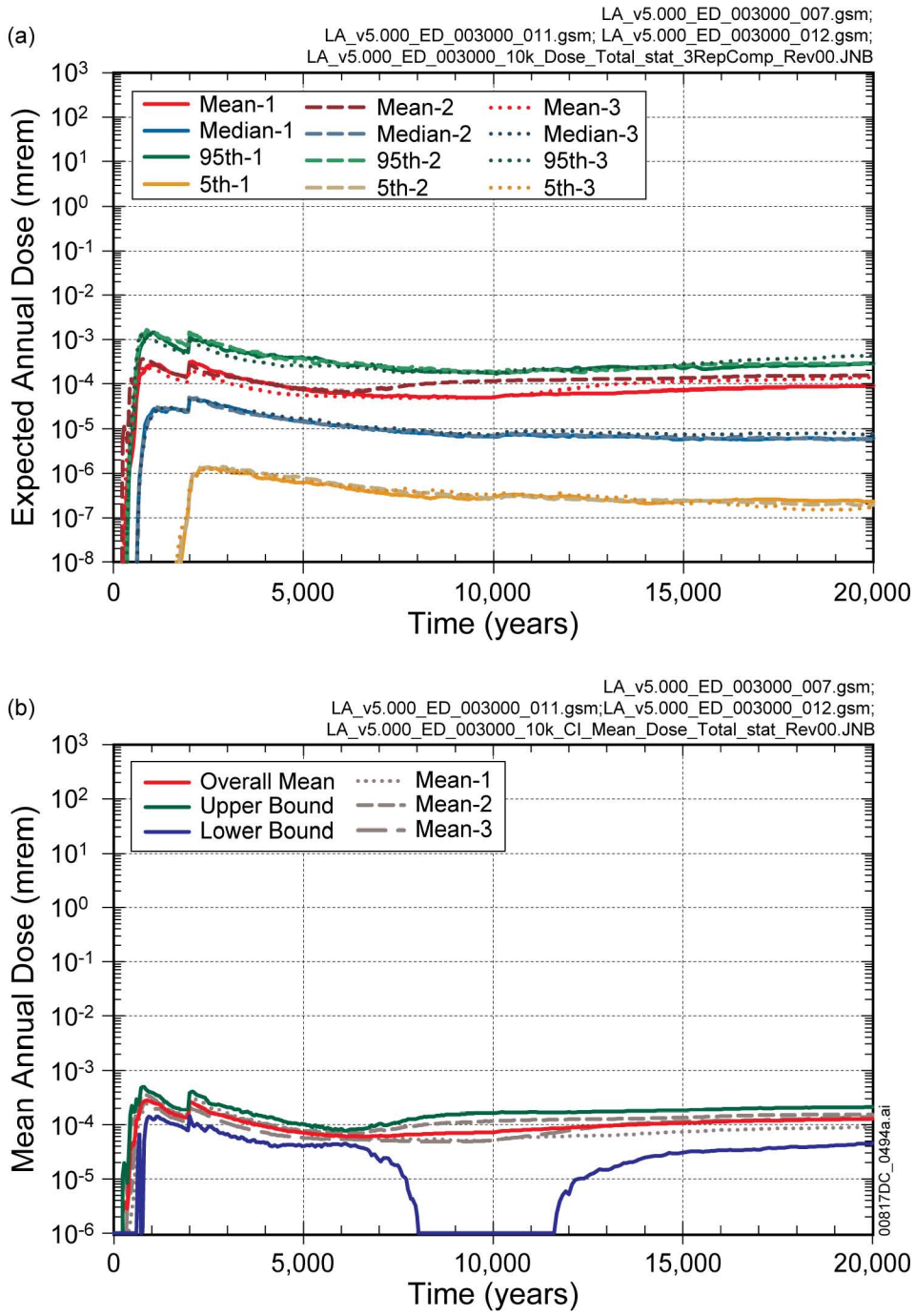

Source: Output DTNs: MO0709TSPASTAB.000 [DIRS 182983]; and MO0709TSPAREGS.000 [DIRS 182976].

Figure 7.3.1-4. Stability of Drip Shield Early Failure Modeling Case for 20,000 Years: (a) Comparison of Expected Annual Dose for Three Replicates and (b) Confidence Interval around Mean Annual Dose

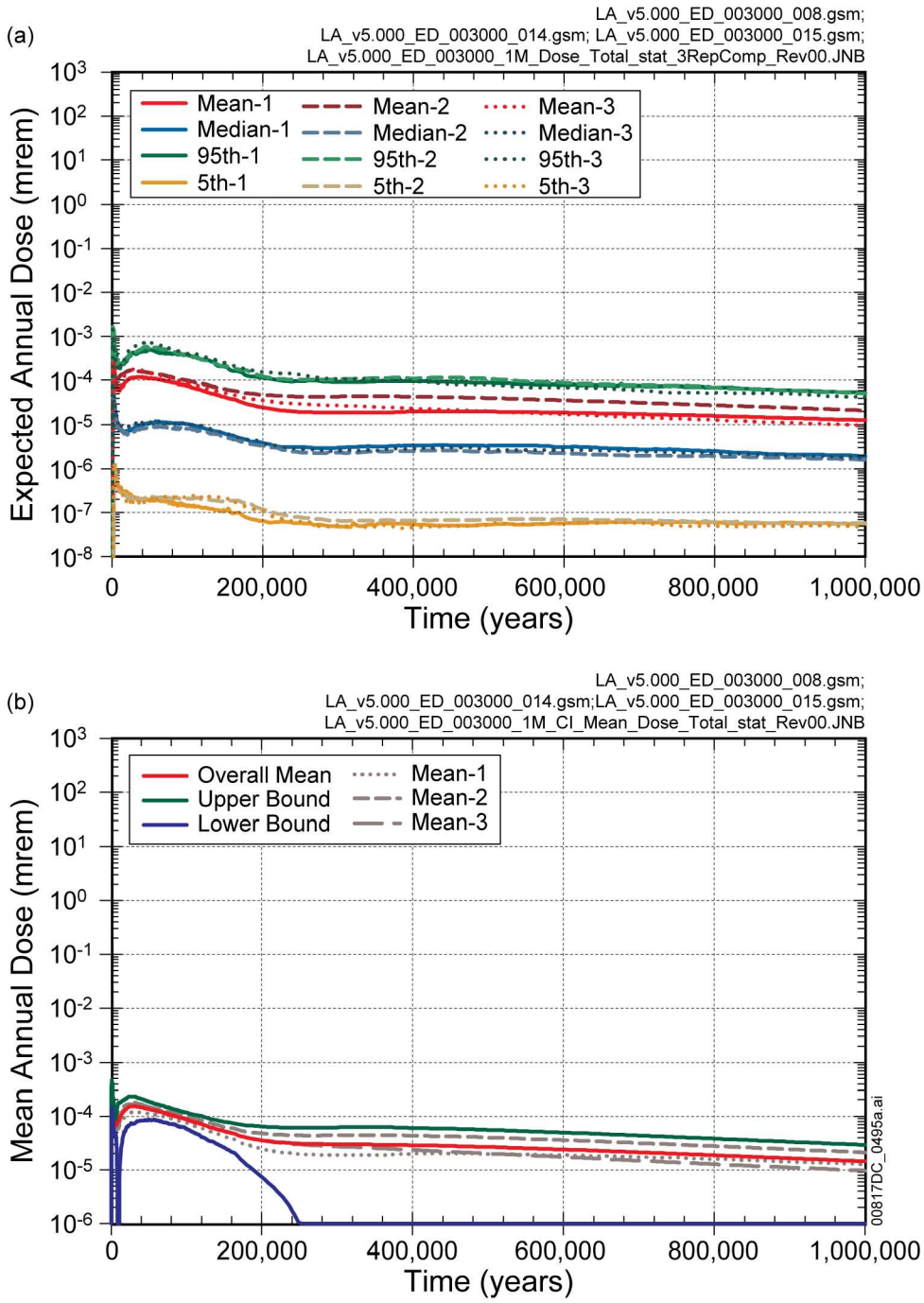

Source: Output DTNs: MO0709TSPASTAB.000 [DIRS 182983]; and MO0709TSPAREGS.000 [DIRS 182976].

Figure 7.3.1-5. Stability of Drip Shield Early Failure Modeling Case for 1,000,000 Years: (a) Comparison of Expected Annual Dose for Three Replicates and (b) Confidence Interval around Mean Annual Dose

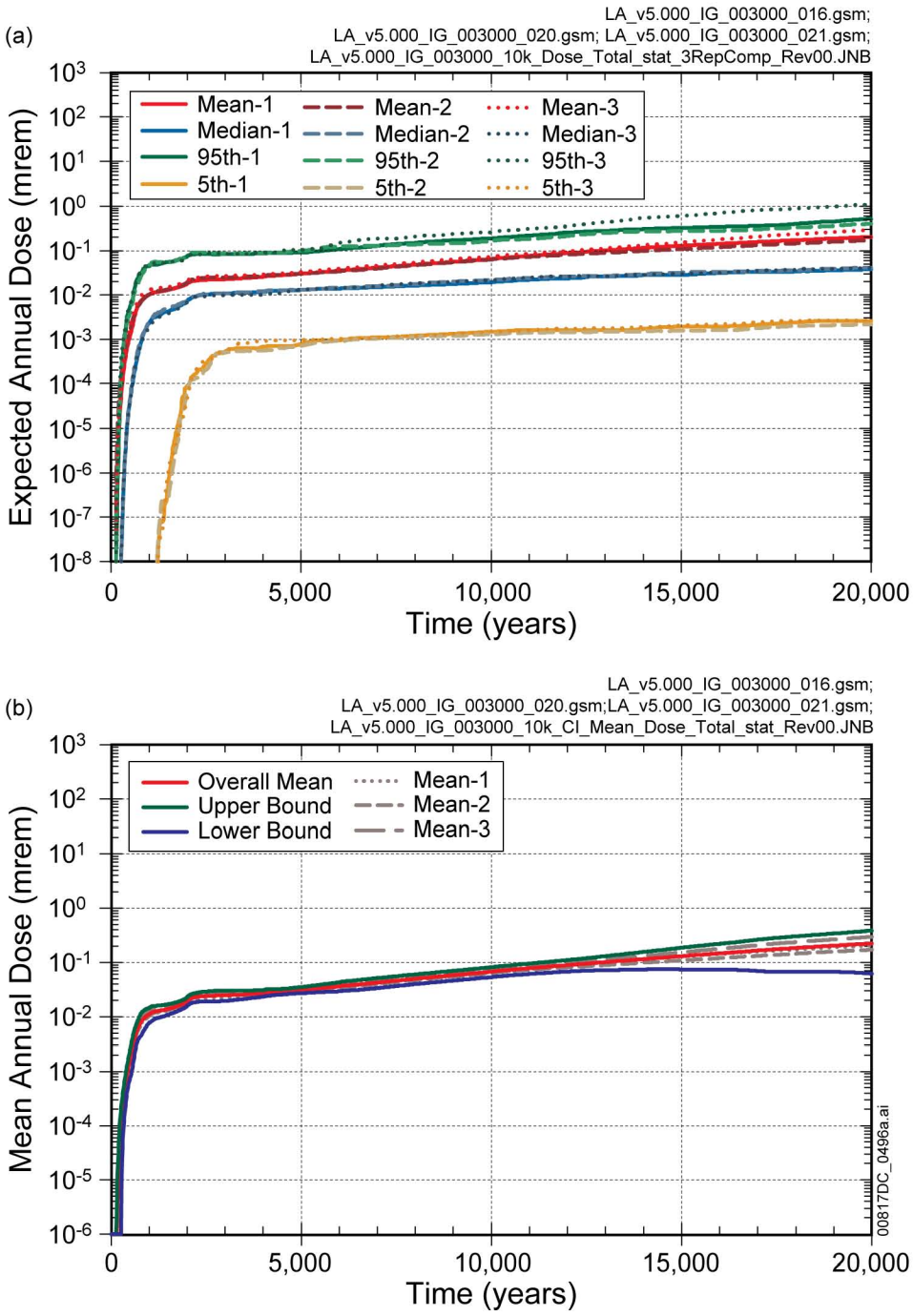

Source: Output DTNs: MO0709TSPASTAB.000 [DIRS 182983]; and MO0709TSPAREGS.000 [DIRS 182976].

Figure 7.3.1-6. Stability of Igneous Intrusion Modeling Case for 20,000 Years: (a) Comparison of Expected Annual Dose for Three Replicates and (b) Confidence Interval around Mean Annual Dose

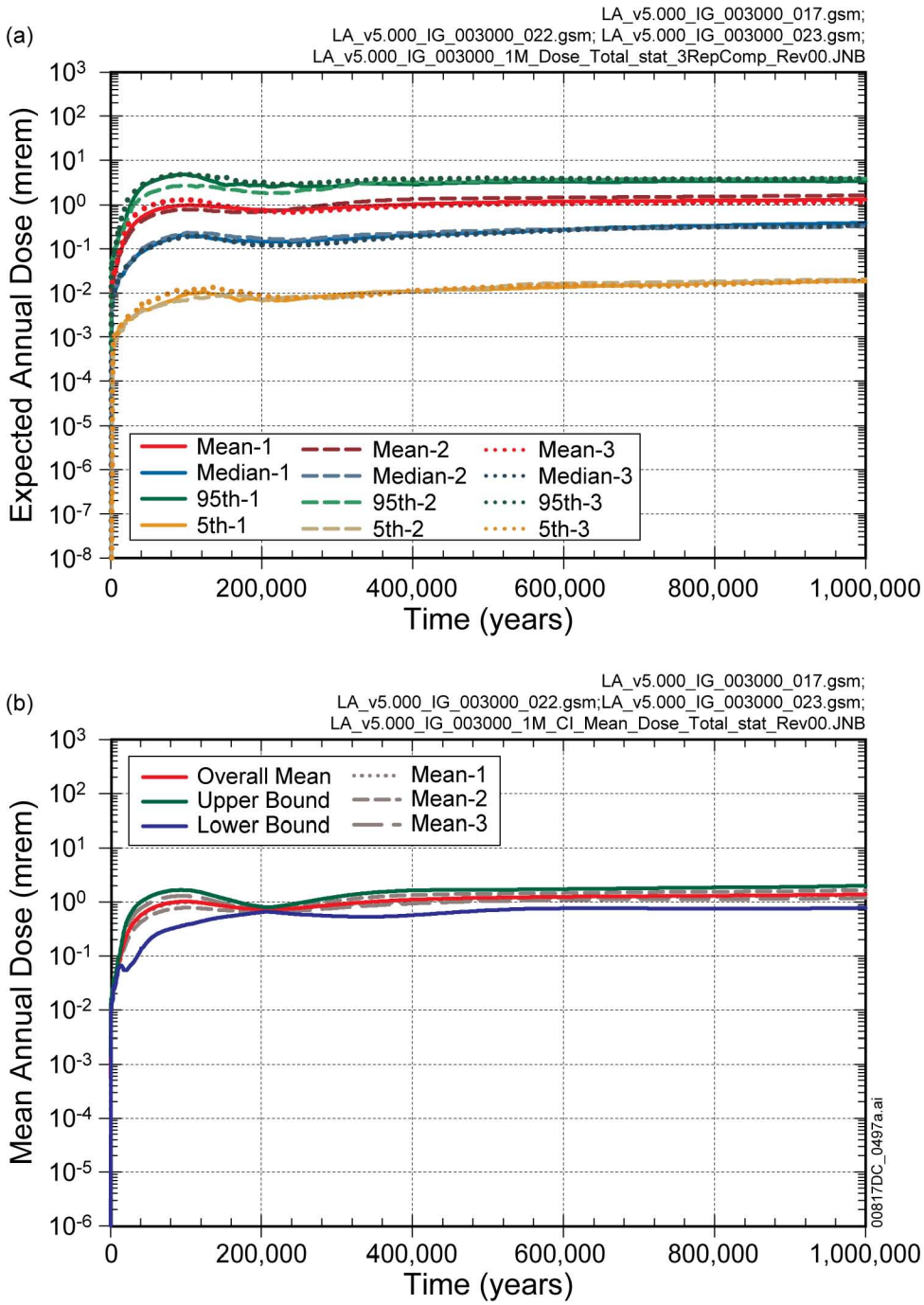

Source: Output DTNs: MO0709TSPASTAB.000 [DIRS 182983]; and MO0709TSPAREGS.000 [DIRS 182976].

Figure 7.3.1-7. Stability of Igneous Intrusion Modeling Case for 1,000,000 Years: (a) Comparison of Expected Annual Dose for Three Replicates and (b) Confidence Interval around Mean Annual Dose

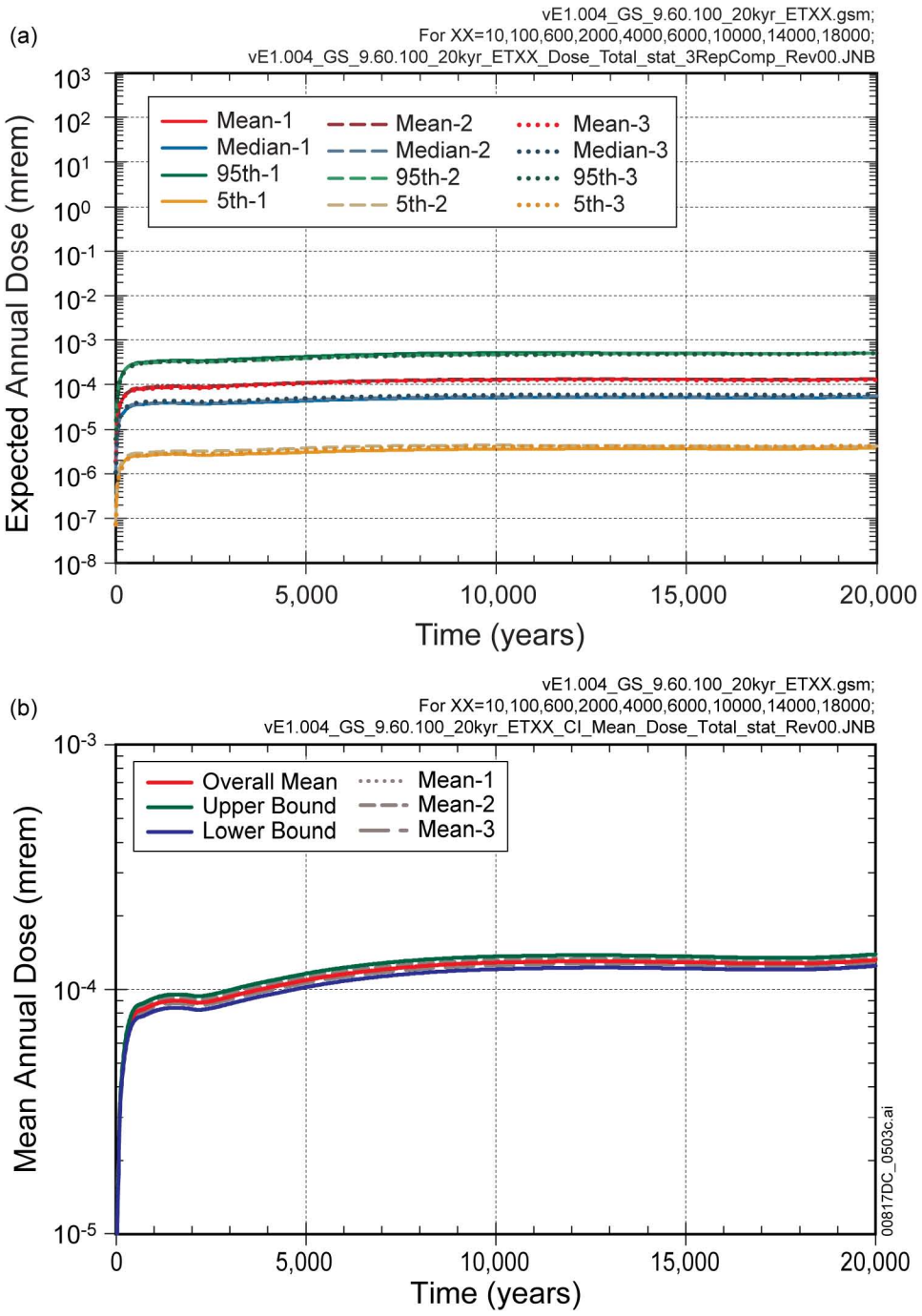

Source: Output DTN: MO0709TSPAREGS.000 [DIRS 182976].

Figure 7.3.1-8. Stability of Volcanic Eruption Modeling Case for 20,000 Years: (a) Comparison of Expected Annual Dose for Three Replicates and (b) Confidence Interval around Mean Annual Dose

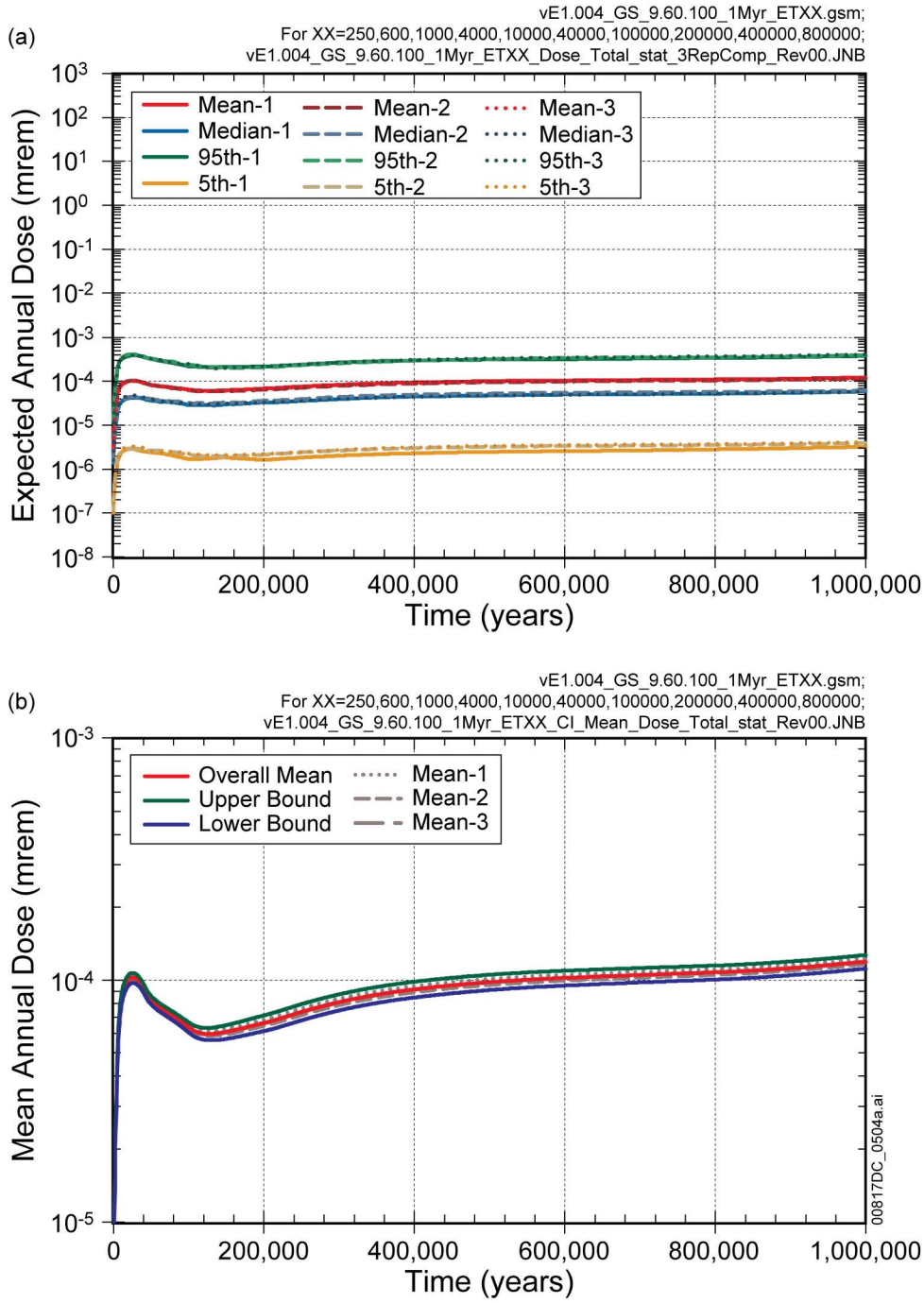

Source: Output DTN: MO0709TSPAREGS.000 [DIRS 182976].

Figure 7.3.1-9. Stability of Volcanic Eruption Modeling Case for 1,000,000 Years: (a) Comparison of Expected Annual Dose for Three Replicates and (b) Confidence Interval around Mean Annual Dose

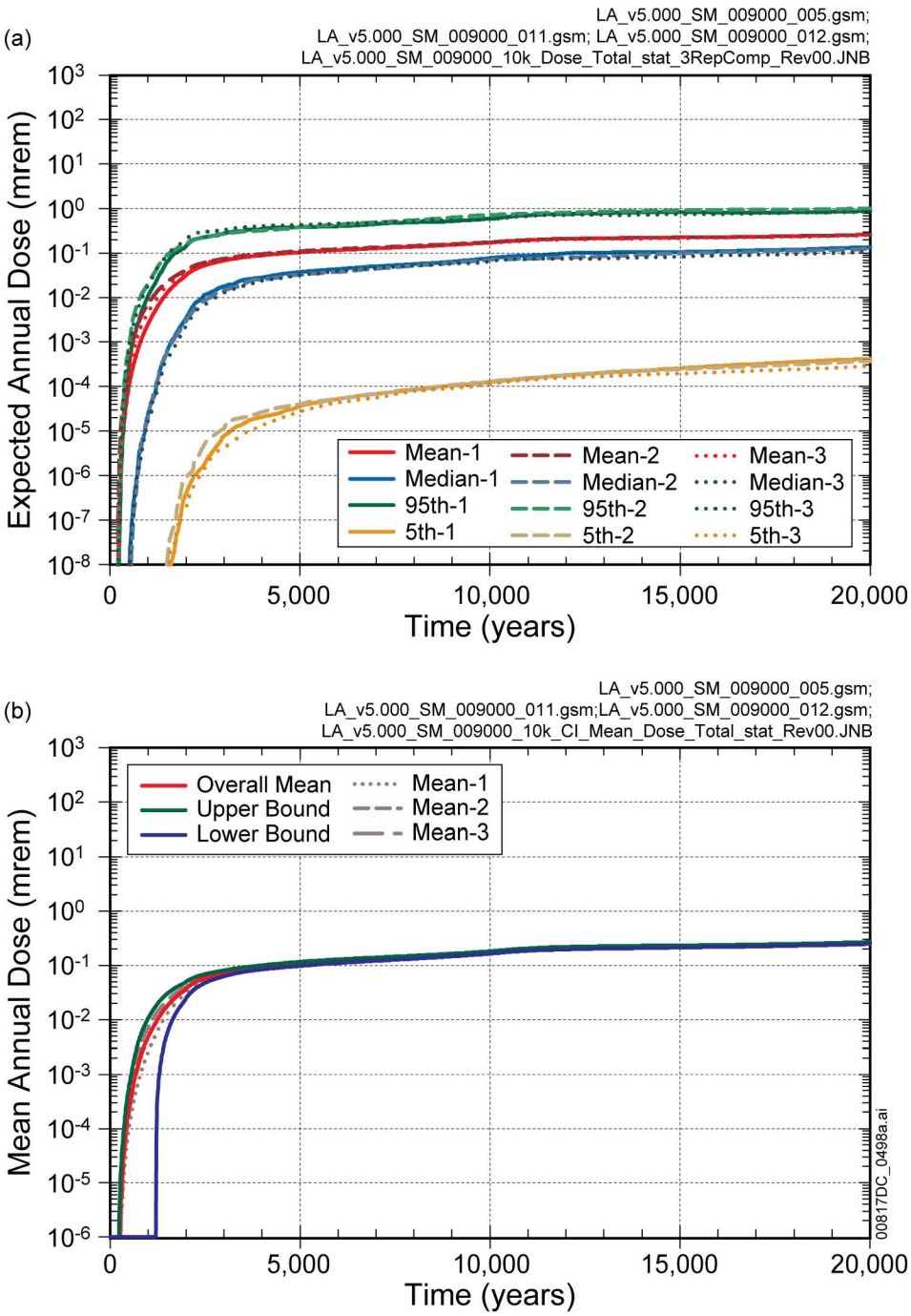

Source: Output DTNs: MO0709TSPASTAB.000 [DIRS 182983]; and MO0709TSPAREGS.000 [DIRS 182976].

Figure 7.3.1-10. Stability of Seismic Ground Motion Modeling Case for 20,000 Years: (a) Comparison of Expected Annual Dose for Three Replicates and (b) Confidence Interval around Mean Annual Dose

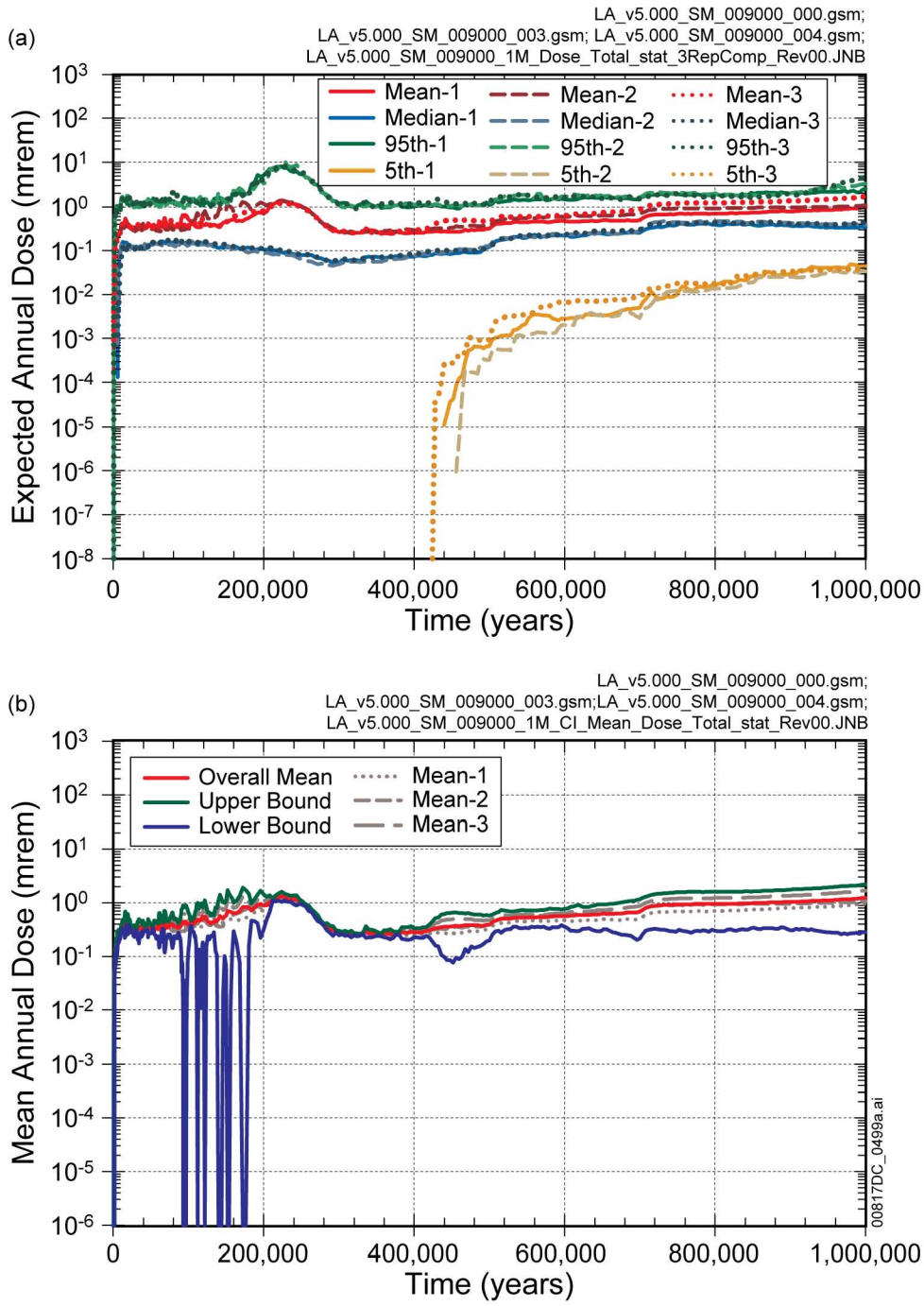

Source: Output DTNs: MO0709TSPASTAB.000 [DIRS 182983]; and MO0709TSPAREGS.000 [DIRS 182976].

Figure 7.3.1-11. Stability of Seismic Ground Motion Modeling Case for 1,000,000 Years: (a) Comparison of Expected Annual Dose for Three Replicates and (b) Confidence Interval around Mean Annual Dose

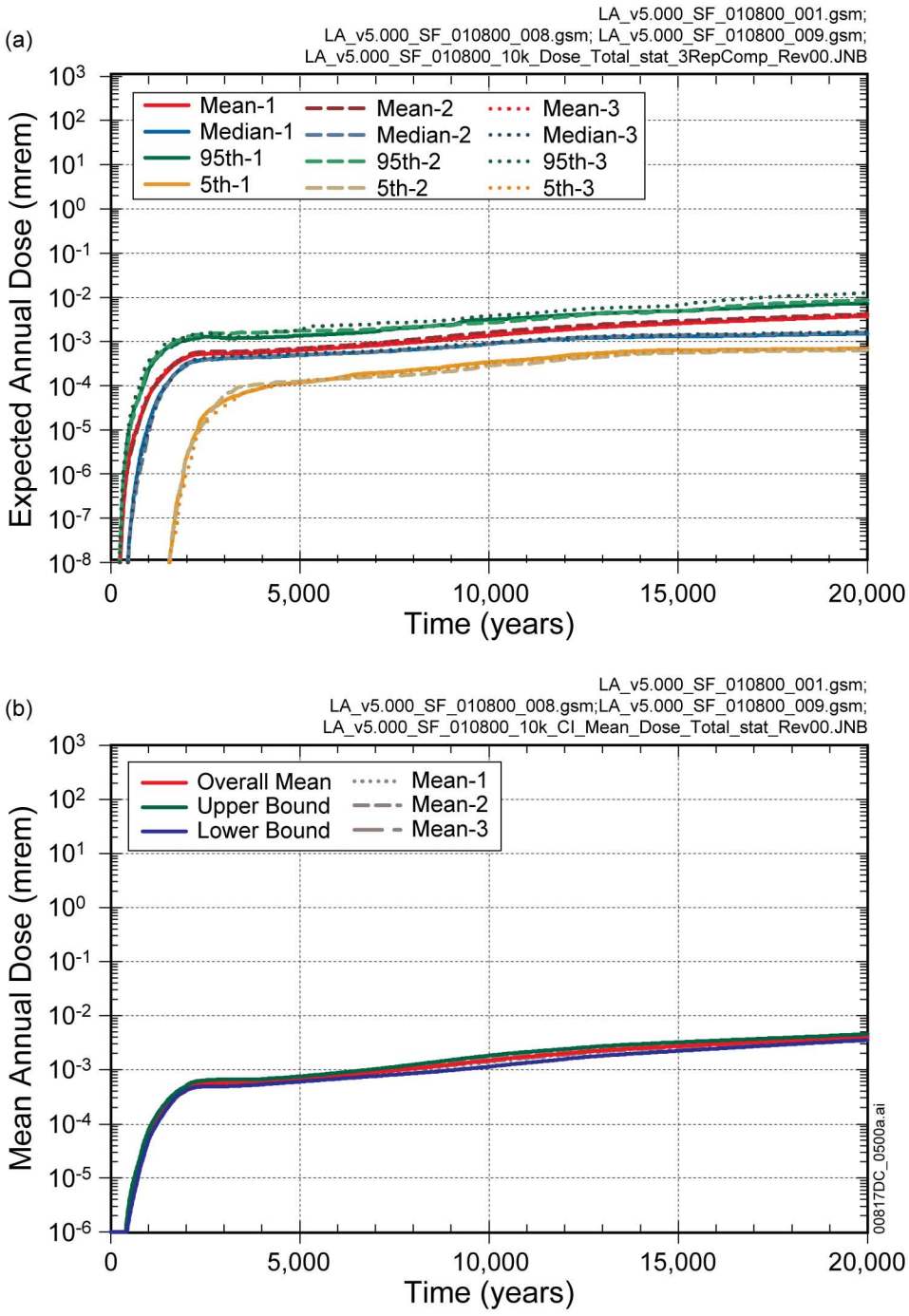

Source: Output DTNs: MO0709TSPASTAB.000 [DIRS 182983]; and MO0709TSPAREGS.000 [DIRS 182976].

Figure 7.3.1-12. Stability of Seismic Fault Displacement Modeling Case for 20,000 Years: (a) Comparison of Expected Annual Dose for Three Replicates and (b) Confidence Interval around Mean Annual Dose

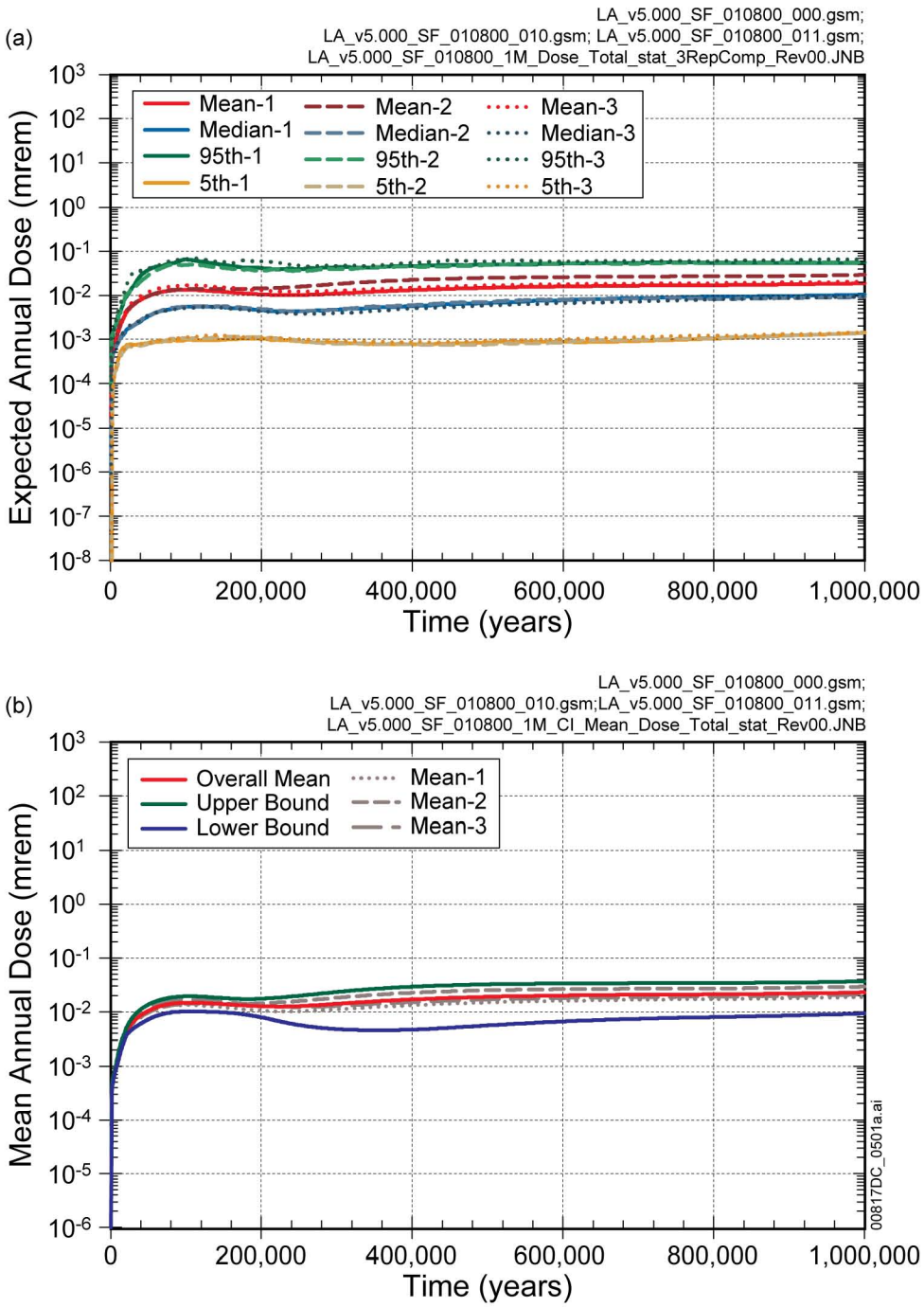

Source: Output DTNs: MO0709TSPASTAB.000 [DIRS 182983]; and MO0709TSPAREGS.000 [DIRS 182976].

Figure 7.3.1-13. Stability of Seismic Fault Displacement Modeling Case for 1,000,000 Years: (a) Comparison of Expected Annual Dose for Three Replicates and (b) Confidence Interval around Mean Annual Dose

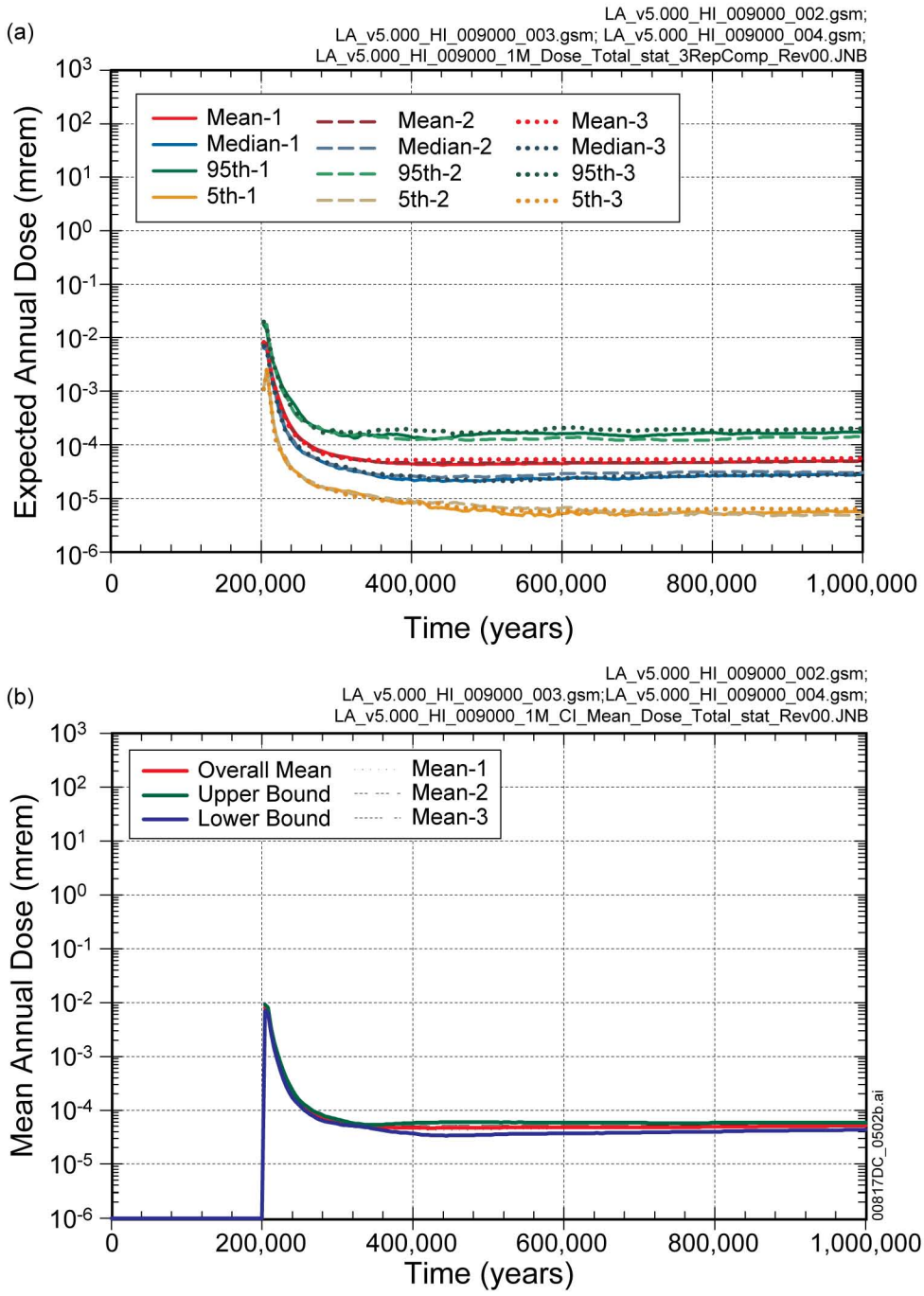

Source: Output DTNs: MO0709TSPASTAB.000 [DIRS 182983]; MO0709TSPAREGS.000 [DIRS 182976].

Figure 7.3.1-14. Stability of Human Intrusion Scenario: (a) Comparison of Expected Annual Dose for Three Replicates and (b) Confidence Interval around Mean Annual Dose

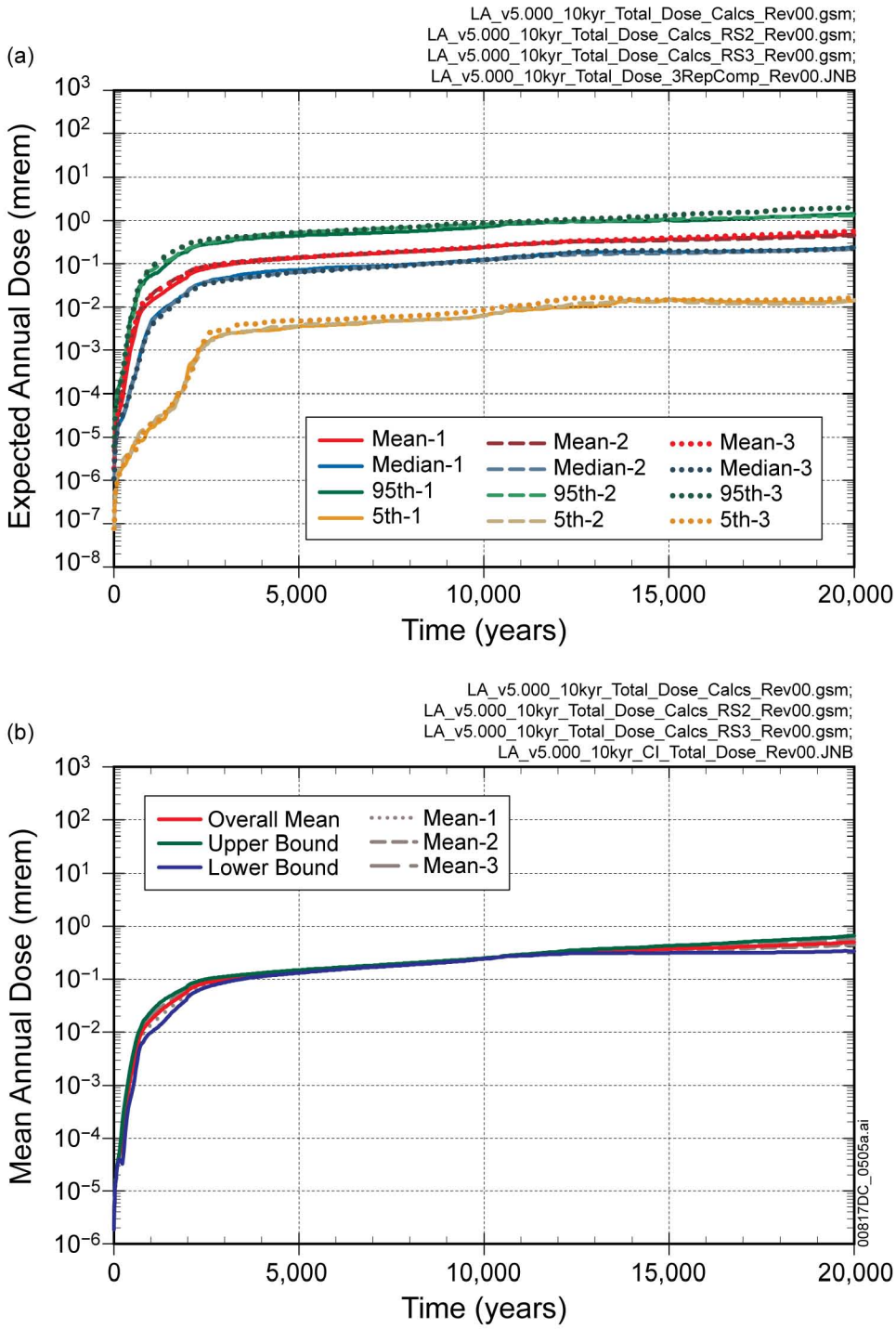

Source: Output DTN: MO0709TSPAPLOT.000 [DIRS 183010].

Figure 7.3.1-15. Stability of Total Mean Annual Dose 20,000 Years: (a) Comparison of Expected Annual Dose for Three Replicates and (b) Confidence Interval around Mean Annual Dose

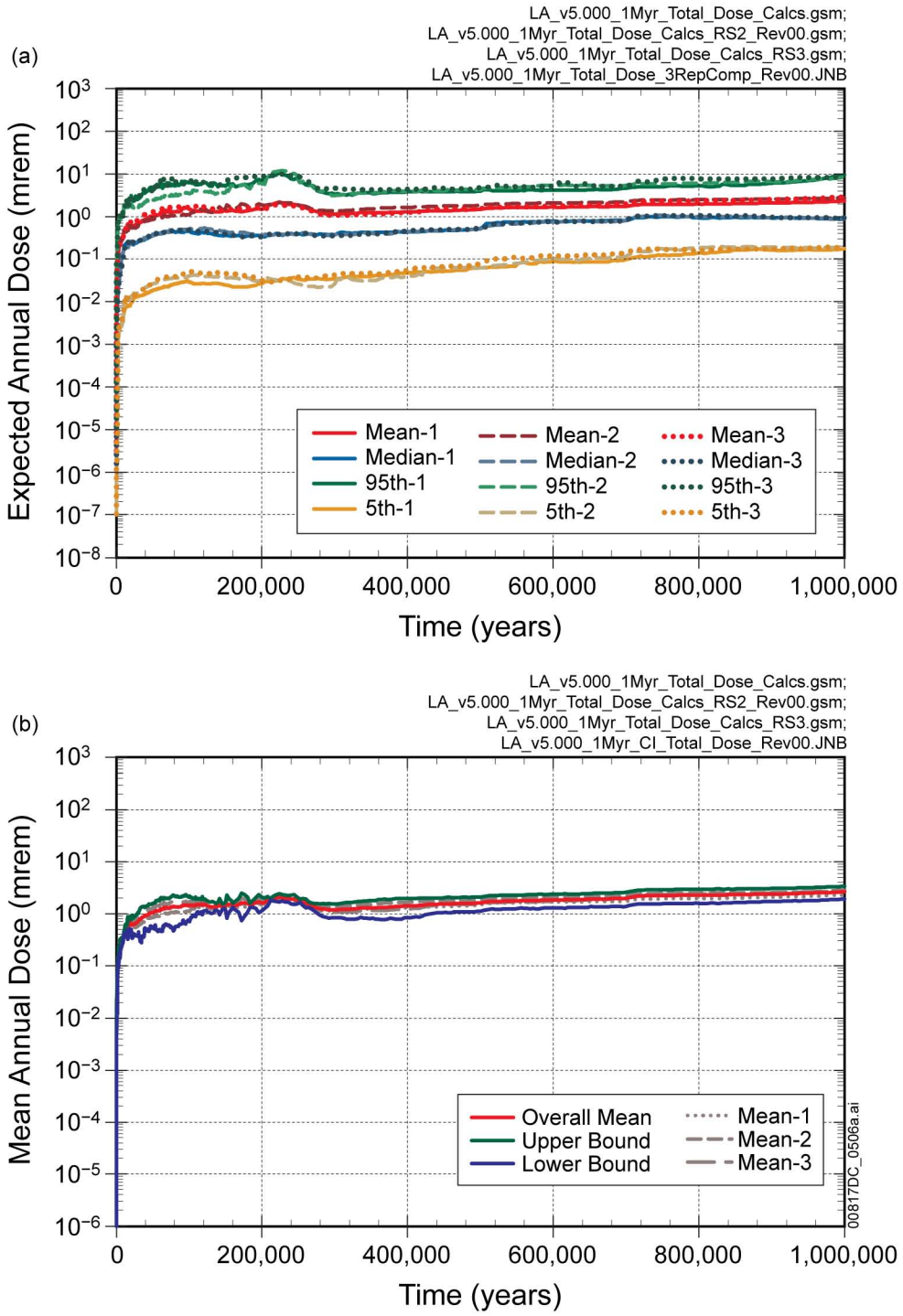

Source: Output DTN: MO0709TSPAPLOT.000 [DIRS 183010].

Figure 7.3.1-16. Stability of Total Mean Annual Dose for 1,000,000 Years: (a) Comparison of Expected Annual Dose for Three Replicates and (b) Confidence Interval around Mean Annual Dose

7.3.2 Numerical Accuracy of Expected Annual Dose

The TSPA-LA Model calculates expected annual dose $\overline{D}(\tau|\mathbf{e})$ for each epistemic realization. As a reminder, the term expected annual dose refers to the expectation of dose over aleatory uncertainty but conditional on epistemic uncertainty. Section 6.1.2.4 describes the calculation of expected annual dose for each modeling case. In general, the calculation involves numerical evaluation of one or more integrals. Because each modeling case addresses different aleatory uncertainties, the methods of calculating expected annual dose differ for each modeling case. This section examines the numerical accuracy of these calculations for each modeling case. In general, numerical accuracy is determined by refining the discretization employed in the numerical evaluation of each integral and showing that the results of the evaluation do not significantly change with improved discretization.

7.3.2.1 Nominal Modeling Case

Because the aleatory uncertain variables in the Nominal Modeling Case are sampled with the epistemic uncertain variables, the expected annual dose is the same as the annual dose calculated directly by GoldSim. For each element of the LHS of epistemic parameters, the GoldSim component of the TSPA-LA Model calculates the expected annual dose. The ensemble of expected annual doses is averaged to obtain the mean annual dose for the Nominal Modeling Case.

The numerical accuracy of the mean annual dose for the Nominal Modeling Case is confirmed by increasing the size of the LHS and comparing the mean annual doses. Figure 7.3.2-1 shows the expected annual dose for the Nominal Modeling Case for (a) an LHS of size 300 and (b) an LHS of size 1,000. Increasing the LHS size to 1,000 samples ensures that more extreme values for epistemic parameters are represented, and increases the probability that combinations of extreme values for different epistemic parameters are also represented. Increasing the LHS size to 1,000 resulted in corrosion failures before 100,000 years in six realizations, which did not occur in the smaller LHS size of 300. Additionally, increasing the LHS size resulted in a greater expected annual dose for the realizations with the largest expected annual dose after 800,000 years. Figure 7.3.2-2 shows the mean, median, 95th percentile, and 5th percentile of expected annual dose for both LHS sizes. The mean annual dose for LHS size of 1,000 is larger at very early times than the mean dose for LHS size of 300, due to the six realizations with very early corrosion failures. However, the magnitude of the mean dose at early times for either LHS size is small ($<10^{-5}$ mrem) compared to the long-term mean dose (~0.4 mrem), and the uncertainty in expected annual dose (as depicted by the median, 95th, and 5th percentiles) is nearly identical. Moreover, despite greater expected annual dose in some realizations after 800,000 years, the 95th percentile is essentially the same after 800,000 years, demonstrating that increasing the sample size only changes the extremes of the distribution of expected annual dose. Consequently, the mean annual dose computed using a LHS of size 300 is sufficiently accurate.

7.3.2.2 Waste Package Early Failure Modeling Case

Expected annual dose for the Waste Package EF Modeling Case is calculated as described by Equation 6.1.2-13. Because Equation 6.1.2-13 involves only sums rather than numeric integration, the calculation of expected annual dose is exact and does not require an estimate of

numerical accuracy. The EXDOC calculation of expected annual dose for the Waste Package EF Modeling Case was verified by reproducing the EXDOC results using Mathcad (output DTN: MO0708TSPAVALI.000 [DIRS 182985]).

7.3.2.3 Drip Shield Early Failure Modeling Case

Expected annual dose for the Drip Shield EF Modeling Case is calculated as described by Equation 6.1.2-14. Because Equation 6.1.2-14 involves only sums rather than numeric integration, the calculation of expected annual dose is exact and does not require an estimate of numerical accuracy. The EXDOC calculation of expected annual dose for the Drip Shield EF Modeling Case was verified by reproducing the EXDOC results using Mathcad (output DTN: MO0708TSPAVALI.000 [DIRS 182985]).

7.3.2.4 Igneous Intrusion Modeling Case

Expected annual dose for the Igneous Intrusion Modeling Case is calculated as described by Equation 6.1.2-16. Equation 6.1.2-16 is numerically evaluated as indicated in Equation 6.1.2-17 in two steps. First, for each of a sequence $[t_0, t_2, \ldots, t_N]$ of times for igneous intrusions, annual dose at time τ from an intrusion occurring at time, t_j, $D_{II}\left(\tau \middle| [1, t_j], \mathbf{e}_i\right)$, is calculated using the GoldSim component of the TSPA-LA Model. Second, the GoldSim results are used by the EXDOC component of the TSPA-LA Model to calculate expected annual dose.

The accuracy of the numerical evaluation of Equation 6.1.2-16 was examined by increasing the number of times of igneous intrusions for which GoldSim results are calculated from 10 to 50. Table 7.3.2-1 lists the 10 intrusion times considered in the base case for 20,000 years and for 1,000,000 years, and the 50 intrusion times considered in the stability analysis.

Figure 7.3.2-3 shows the annual dose resulting from each intrusion in the base case, and the annual dose resulting from the additional intrusions modeled in the stability analysis, for epistemic realization 2, for 20,000 years. In terms of Equation 6.1.2-16, Figure 7.3.2-3 shows the quantities $D_{II}\left(\tau \middle| [1, t_j], \mathbf{e}_2\right)$ for t_j as listed in Table 7.3.2-1. Each dose history's shape is similar for different times of intrusion within the same climate period, indicating that the interpolation techniques within the EXDOC software are justified. When the climate changes (at 2,000 and 10,000 years) the percolation rates increase in each percolation bin, resulting in more rapid transport of radionuclides through the UZ, and correspondingly, higher concentrations of radionuclides in the SZ and a larger maximum annual dose after the intrusion. Since UZ flow is modeled as steady (Section 6.3.1), when a climate change occurs, the UZ flow rates change instantaneously from one set of constant rates to another set, resulting in an abrupt change in the maximum annual dose.

Figure 7.3.2-4 compares the expected annual dose over 20,000 years for five epistemic realizations calculated using the 10 intrusion times and again using the 50 intrusion times listed in Table 7.3.2-1. The comparison shows that 10 intrusion times are sufficient to obtain a numerically accurate calculation of expected annual dose over 20,000 years. Using more intrusion times provides better resolution of the abrupt change in dose coincident with a climate

change. However, the abrupt change in dose is a result of modeling UZ flow as steady (Section 6.3.1) and the difference between the two cases is small enough that a better resolution of this change is not warranted. Figure 7.3.2-5 compares the expected annual dose over 1,000,000 years for five epistemic realizations calculated using the 10 intrusion times, and again using the 50 intrusion times listed in Table 7.3.2-1. Figure 7.3.2-5 shows that 10 intrusion times are sufficient to obtain a numerically accurate calculation of expected annual dose over 1,000,000 years.

7.3.2.5 Volcanic Eruption Modeling Case

Expected annual dose for the Volcanic Eruption Modeling Case is calculated as described by Equation 6.1.2-18. Equation 6.1.2-18 is numerically evaluated as indicated in Equation 6.1.2-19 in two steps. First, for each of a sequence $[t_1, t_2, \ldots, t_N]$ of times for eruption events and a LHS of uncertain aleatory parameters describing an eruption event $[\mathbf{u}_1, \mathbf{u}_2, \ldots, \mathbf{u}_M]$, annual dose at time τ from an eruption event occurring at time t_j and described by parameters $\mathbf{u}_k$ and affecting one WP, $D_{VE}\left(\tau \middle\| [1, t_j, 1, \mathbf{u}_k], \mathbf{e}_i\right)$, is calculated using the GoldSim component of the TSPA-LA Model. Second, the GoldSim results are used by the EXDOC component of the TSPA-LA Model to calculate expected annual dose.

Validation of the calculation of expected annual dose involved two steps: (1) demonstration that the size of the LHS of aleatory parameters is sufficient, and (2) demonstration that the integration over time of the eruption event is numerically accurate. Sufficiency of the size of the LHS for aleatory parameters is demonstrated by increasing the LHS size from 40 to 80. Numerical accuracy of the integration over time is demonstrated by increasing the number of specified times for volcanic eruption events. The aleatory parameters included in the LHS described by $[\mathbf{u}_1, \mathbf{u}_2, \ldots, \mathbf{u}_M]$ are eruptive power, eruptive velocity, eruptive duration, wind speed, and wind direction. Table 7.3.2-2 lists the times of eruption events considered in the base case and the additional times used to demonstrate numerical accuracy.

Figure 7.3.2-6 shows the expected annual dose resulting from the two different LHS sizes (40 vs. 80) for five realizations of epistemic parameters. The expected annual dose curves shown on Figure 7.3.2-6, use the eruption times for the base case. The expected annual dose is generally greater for the larger LHS, but the difference is no more than 10 percent, and is relatively constant throughout the 1,000,000-year period. Moreover, the mean annual dose from the Volcanic Eruption Modeling Case is very small relative to the compliance limits of 15 mrem and 300 mrem. Consequently, a difference of 10 percent due to numerical accuracy is acceptable, and the LHS size of 40 used in the base case is adequate to estimate expected annual dose.

Because the mean annual dose from volcanic eruption constitutes most of the total mean annual dose during the first 1,000 years (Figure 8.1-3(a)), the evaluation of the numerical accuracy of the expected annual dose from volcanic eruption focuses on this time period. Additional event times were added primarily during the first 1,000 years, as listed in Table 7.3.2-2. Figure 7.3.2-7(a) shows the expected annual dose for 20,000 years calculated using the specified eruption times for the base case and again using the additional times listed in Table 7.3.2-2, for the first five epistemic realizations. Figure 7.3.2-7(b) focuses on the expected annual dose for

the first 1,000 years. The expected annual dose curves shown on Figure 7.3.2-7 use the LHS of size 40 for aleatory parameters describing eruptive power, eruptive velocity, eruptive duration, wind speed, and wind direction. The expected annual dose does not change when more event times are used, either during the first 1,000 years or throughout the 20,000 year period. Consequently, the ten specified eruption times listed in Table 7.3.2-2 for the base case provide a sufficiently accurate calculation of expected annual dose. Because the expected annual dose is stable and relatively constant throughout the 20,000 year period, it is reasonable to presume that the expected annual dose calculation for 1,000,000 years is also numerically stable.

7.3.2.6 Seismic Ground Motion Modeling Case

Validation of the calculation of expected annual dose for the Seismic GM Modeling Case differs for the 10,000-year and 1,000,000-year time periods because of the different numerical techniques employed.

7.3.2.6.1 Seismic Ground Motion Modeling Case for 10,000 years

Expected annual dose for the Seismic GM Modeling Case is calculated as described by Equation 6.1.2-21. Equation 6.1.2-21 is numerically evaluated as indicated in Equation 6.1.2-22 in two steps. First, for each of a sequence $[t_1, t_2, \ldots, t_N]$ of times for seismic events and a set of damage fractions $[A_1, A_2, \ldots, A_M]$, annual dose at time τ from a seismic event occurring at time t_j and resulting in damage fraction A_k, $D_{SG}\left(\tau \middle\| [1, t_j, A_k], \mathbf{e}_i\right)$, is calculated using the GoldSim component of the TSPA-LA Model. Second, the GoldSim results are used by the EXDOC component of the TSPA-LA Model to calculate expected annual dose. The term "damage fraction" is used for brevity; this quantity is more precisely defined as the fraction of WP surface area that consists of open cracks.

For the 10,000-year period, validation of the calculation of expected annual dose involved three separate steps:

1. Demonstration that expected annual dose calculations are numerically accurate
2. Justification of assumption about linearity in damage fraction
3. Justification of simplifications to the Seismic Consequences Abstraction.

7.3.2.6.1.1 Accuracy of Expected Annual Dose Calculations

To demonstrate that the expected annual dose calculations conducted by EXDOC are numerically accurate, the number of times of seismic events was increased from 6 to 12, and the number of damage fractions was increased from 5 to 8. Table 7.3.2-3 lists the times of seismic events and the damage fractions considered in the base case and in the expanded case for numerical accuracy.

Figure 7.3.2-8 shows the annual dose resulting from each seismic event in the base case, and the annual dose resulting from the additional seismic events in the expanded case, for the damage fraction of 1.0×10^{-6}, for epistemic realization 1. In terms of Equation 6.1.2-21, Figure 7.3.2-8

shows the quantities $D_{SG}\left(\tau\middle|\left[1,t_j,1.0\times10^{-6}\right],\mathbf{e}_1\right)$ for t_j as listed in Table 7.3.2-3. Each dose history's shape is similar for different times of the seismic event. Since UZ flow is modeled as steady (Section 6.3.1) when a climate change occurs, the UZ flow rates change instantaneously from one set of constant rates to another set, resulting in a small change in the annual dose at 10,000 years. The dose histories for an event at 200 years (base case) and at 100 years (expanded case) coincide on Figure 7.3.2-8, as do the dose histories for events at 1,000 years (base case) and at 1,600 years (expanded case). These dose histories coincide because, before about 2,000 years, the time that radionuclides are released from the WP is determined by the time that diffusive transport begins rather than the time that the damage occurred. Diffusive transport begins when relative humidity inside the WP reaches 95 percent (Section 5.1.4). The TSPA-LA Model does not model the dynamics of water transport through cracks in the WP in computing relative humidity inside the waste package. When damage to the WP consists of cracks, as in the Seismic GM Modeling Case, the relative humidity inside the WP is assumed to be in equilibrium with the relative humidity in the drift (Section 6.3.7.2.1). Thus, the time that diffusion begins depends only on the environmental conditions external to the WP, and is not affected by the time that the damage occurred to the WP.

Figure 7.3.2-9 shows the annual dose resulting from a seismic event at 100 years for each of the different damage fractions for epistemic realization 1. In terms of Equation 6.1.2-21, Figure 7.3.2-9 shows the quantities $D_{SG}\left(\tau\middle|\left[1,100,A_k\right],\mathbf{e}_1\right)$ for A_k as listed in Table 7.3.2-3. Each dose history's shape is similar for different damage fractions. As discussed in detail in the next section, the magnitude of annual dose increases proportionally with increasing damage fraction up to damage fraction of 1.0×10^{-5}. The effect of the climate changes at 2,000 years and at 10,000 years can be observed. Figure 7.3.2-10 shows the annual dose resulting from a seismic event at 11,200 years for each of the different damage fractions, for epistemic realization 1, and shows that the shape of dose history does not significantly change for events occurring at later times. The curves for damage fractions of 1×10^{-3} and 5×10^{-3} coincide on Figure 7.3.2-9 and Figure 7.3.2-10.

EXDOC computes expected annual dose by interpolating between single dose histories for different event times and damage fractions, similar to those illustrated on Figure 7.3.2-8 and Figure 7.3.2-9, and performing numerical integration using the interpolated dose histories. Because the dose histories maintain similar shapes as the event time and damage fraction change, the interpolation scheme implemented in EXDOC is justified.

Figure 7.3.2-11 compares the expected annual dose over 20,000 years calculated for the base case and the expanded case for five epistemic realizations (identified as #1 through #5 on the figure), using the times of seismic events and damage fractions listed in Table 7.3.2-3 in the calculation of expected dose for each realization. Figure 7.3.2-11 shows that increasing the number of event times and the number of damage fractions does not change the expected annual dose calculation for any realization. Therefore, the discretization used to calculate expected annual dose is adequate and the calculation of expected annual dose is numerically accurate.

7.3.2.6.1.2 Linearity in Damage Fraction

As noted in Section 6.1.2.4.3, Equation 6.1.2-22 is based on the assumption that the annual dose from two or more events causing cumulative damage to WPs is reasonably approximated by the sum of the annual doses from the events modeled independently. Figure 7.3.2-12 illustrates the change in annual dose at 10,000 years due to changes in damage fraction, after an event at 100 years, for epistemic realization 1. The change in annual dose is proportional to changes in damage fraction, up to the damage fraction of about 10^{-5}. Beyond damage fraction of 10^{-5}, annual dose does not increase proportionally with increasing damage fraction. Thus, when two or more seismic events cause cumulative damage fraction exceeding 10^{-5}, the linearity assumption results in an overestimate of the annual dose resulting from seismic events. The dose resulting from a single event causing damage fraction exceeding 10^{-5} is not overestimated, since this quantity is computed by interpolation between the level curves shown on Figure 7.3.2-9.

To estimate the degree of conservatism incurred by this linearity assumption, expected annual dose from one seismic event was calculated, by evaluating the first integral term in Equation 6.1.2-22:

$$\bar{D}_{SG}\left(\tau\middle|1,\mathbf{e}_i\right)=\int_0^{\tau}\left(\lambda_1\left(\mathbf{e}_i\right)e^{-\lambda_1(\mathbf{e}_i)t}\left(\int_{A_{\min}}^{A_{\max}}D_{SG}\left(\tau\middle|[1,t,A],\mathbf{e}_i\right)d_{A1}\left(A\middle|\mathbf{e}_i\right)dA\right)\right)dt \quad \text{(Eq. 7.3.2-1)}$$

The integral displayed in Equation 7.3.2-1 computes the expected annual dose from the first seismic event that damages CDSP WPs. The second integral in Equation 6.1.2-22 computes the additional expected annual dose from the second and subsequent seismic events. Figure 7.3.2-13 shows the expected annual dose from the first damaging seismic event; Figure 7.3.2-14 shows the expected annual dose from all damaging seismic events for all 300 epistemic realizations. Comparison of the expected annual dose from the first damaging event to the expected annual dose from all damaging events shows that the second and subsequent damaging events add somewhat to the magnitude of the expected annual dose, but do not change the magnitude or range of uncertainty to any great extent. Consequently, the assumption that seismic consequences are linear in damage fraction, while conservative, does not result in a significant overestimate of the expected annual dose.

7.3.2.6.1.3 Simplifications to the Seismic Consequences Abstraction

For 10,000 years, the consequences of seismic ground motion events are approximated by examining only the occurrence of SCC damage to CDSP WPs with the DS intact and without significant rockfall, and without considering the effects of corrosion processes. Figure 7.3.2-14 shows expected annual dose for the Seismic GM Modeling Case for 10,000 years. Corrosion processes do not appreciably thin the WP in 10,000 years; hence, it is reasonable to omit these processes. The probability of DS plate or framework failure within 10,000 years is low enough that these failures are omitted from the calculation. The expected volume of rockfall within 10,000 years is small enough that it is reasonable to omit the changes in thermal and flow modeling caused by rockfall. Rupture and puncture of CDSP WPs are not considered because the probability that these events occur within 10,000 years is low enough that the expected annual dose from these events is also low. Finally, damage to CSNF WPs is omitted because the

low probability of seismic damage to the transportation, aging, and disposal (TAD)-bearing WPs results in low estimate of the expected annual dose from CSNF WPs. Each of these approximations is justified in the following discussion.

7.3.2.6.1.3.1 General Corrosion of Waste Package

General corrosion reduces the thickness of the WP outer corrosion barrier (OCB) and the DS, and this reduction in thickness alters the probability and extent of seismic damage to WPs and DSs. General corrosion of WP is modeled by time-dependent rates, calculated using several uncertain parameters, that vary spatially among WP locations and over a WP surface. The seismic consequences abstraction uses the spatially-averaged WP OCB thickness to calculate the probability and extent of seismic damage. The WP outer barrier initial thickness is 25 mm (SNL 2007 [DIRS 179394], Table 4-1). Seismic consequence calculations are performed for WP thickness of 23 mm and are used while WP thickness exceeds 23 mm. Figure 7.3.2-15 shows the spatially-averaged WP thickness for each realization for 1,000,000 years for (a) CSNF WPs and (b) CDSP WPs. No realization shows thickness reduced below 23 mm before about 200,000 years. Consequently, WP thicknesses below 23 mm are not considered in seismic calculations for 10,000 years.

7.3.2.6.1.3.2 Drip Shield Plate Failure

Section 6.6.1.3.3 outlines the mechanisms leading to DS plate failure. The probability of plate failure depends on the uncertainties describing DS corrosion and accumulated rockfall. DS corrosion is determined by two independent epistemic parameters: an aggressive corrosion rate for the upper surface, which is exposed to seepage, and a benign rate for the lower surface. One additional epistemic uncertainty describes the volume of intact lithophysal rock that must collapse to fill the drift.

Figure 7.3.2-16 shows the probability of DS plate failure for (a) 250,000 years and (b) 10,000 years, conditional on DS corrosion rates above the 99.99th percentile of the joint distribution for corrosion rate and the minimal value for the volume of intact lithophysal rock that must collapse to fill the drift (30 m^3/m). Because DS plate failure becomes less likely for lower rates of DS corrosion and for larger values of the volume of intact lithophysal rock that must collapse to fill the drift, the probability of DS plate failure shown on Figure 7.3.2-16 is bounding. The calculations included on Figure 7.3.2-16 are averaged over 100,000 sequences of seismic events and thus account for uncertainty in seismic event magnitude and amount of rockfall from each event. The probability of DS plate failure before 10,000 years is thus estimated to be less than 3.4×10^{-4} for all epistemic realizations.

If DS plate failure occurs, then all DSs fail as a barrier to seepage. After DS failure, radionuclide release depends on the condition of the WPs underneath failed DS. WP condition falls into one of three categories:

1. WPs are ruptured from seismic events. In this case, the consequence in terms of expected annual dose to the RMEI is discussed in Section 7.3.2.6.1.3.5 and is shown to be small.

2. WPs are damaged from seismic events and localized corrosion does not occur. In this case, the damage to WPs consists of cracks in the WP outer barrier. Failure of the DS does not alter the condition of the WP outer barrier. Dissolved radionuclides and radionuclides sorbed to colloids can diffuse out of the waste, through the cracks in the WP outer barrier, and into the invert. Transport of radionuclides out of the invert is not changed by DS failure because the volume of seepage flowing into the invert is unchanged. While the DS is intact, the seepage entering the drift diverts around the DS and flows into the invert. After the DS fails, the same volume of seepage flows through the DS, around the WP (since only cracks are present in the WP outer barrier), and into the invert. Because radionuclide transport through the WP outer barrier and the invert are not affected by the failure of the DS, the expected annual dose to the RMEI is unchanged in this case.

3. WPs are intact or damaged from seismic events and localized corrosion can occur. In this case, failure of the DS can lead to additional radionuclide releases because seepage that was diverted around the DS now falls onto the WP and localized corrosion breaches or enlarges existing breaches in WPs. The consequences of this case are analyzed below.

The expected annual dose to the RMEI at time τ, from seismic events that cause DS failure, and in circumstances in which localized corrosion causes WP failure, $\bar{D}_{DS}\left(\tau|\mathbf{e}_i\right)$, is estimated by:

$$\bar{D}_{DS}\left(\tau|\mathbf{e}_i\right)=\sum_{p=1}^{2}\sum_{b=1}^{5}E\left(n_{LC}\left(p,b,\mathbf{e}_i\right)\right)\times D_{ED}\left(\tau-t_{LC}\,|1,p,b,\mathbf{e}_i\right) \qquad \text{(Eq. 7.3.2-2)}$$

where

$E\left(n_{LC}\left(p,b,\mathbf{e}_i\right)\right)$ is the expected number of WPs of type p in bin b that fail due to DS failure and localized corrosion, in epistemic realization $\mathbf{e}_i$.

$D_{ED}\left(\tau|1,p,b,\mathbf{e}_i\right)$ is the annual dose at time τ from a failed DS co-located with a failed WP of type p, in dripping conditions in bin b, in epistemic realization $\mathbf{e}_i$.

$t_{LC}=t_{LC}\left(p,b,\mathbf{e}_i\right)$ is the earliest time that localized corrosion is possible on a WP of type p in bin b in epistemic realization $\mathbf{e}_i$.

The quantities $D_{ED}\left(\tau|1,p,b,\mathbf{e}_i\right)$ are computed by the Drip Shield EF Modeling Case. The Drip Shield EF Modeling Case computes the dose that results following complete failure of a DS and the outer barrier of the underlying WP. Use of the Drip Shield EF Modeling Case in this estimate is conservative, because the modeling case assumes that the entire outer barrier of a WP is compromised, and that all of the impinging seepage flows through the waste.

The term t_{LC} is included because localized corrosion requires seepage to be present, which may not occur until some time after repository closure. The inclusion of t_{LC} in

$D_{ED}\left(\tau - t_{LC} \middle| 1, p, b, \mathbf{e}_i\right)$ shifts the beginning of radionuclide transport to the earliest time that localized corrosion could result in WP failure.

The term $E\left(n_{LC}\left(p, b, \mathbf{e}_i\right)\right)$ is estimated by

$$E\left(n_{LC}\left(p, b, \mathbf{e}_i\right)\right) = \lambda_F \times T_{LC}\left(p, b, \mathbf{e}_i\right) \times \left(f_p \times f_b \times N\right) \times f_{LC}\left(p, b, \mathbf{e}_i\right) \quad \text{(Eq. 7.3.2-3)}$$

where

λ_F	is the frequency of DS failure due to seismic events
$T_{LC}\left(p, b, \mathbf{e}_i\right)$	is the latest time that localized corrosion could occur on a WP of type p in bin b, in epistemic realization $\mathbf{e}_i$
$\left(f_p \times f_b \times N\right)$	is the total number of WP of type p in percolation subregion b
f_p	is the fraction of WPs of type p (CDSP WP or CSNF WP)
f_b	is the fraction of WPs in percolation subregion b
N	is the total number of WP in the repository
$f_{LC}\left(p, b, \mathbf{e}_i\right)$	is the maximum fraction of WPs of type p in bin b, on which localized corrosion may occur, in epistemic realization $\mathbf{e}_i$.

The frequency of DS failure due to seismic events is not larger than $3.4\times10^{-4}/10^{4}$ yr $= 3.4\times10^{-8}$ yr^{-1} (Figure 7.3.2-16). Figure 7.3.2-17 displays the expected annual dose computed by Equation 7.3.2-2. The expected annual dose considering DS failure is substantially less than the expected annual dose calculated in the Seismic GM Modeling Case (compare Figures 7.3.2-17 and 7.3.2-14). Moreover, the mean annual dose considering DS failures is less than 5×10^{-3} mrem during 10,000 years, which is numerically insignificant compared to the mean annual dose in the Seismic GM Modeling Case. Thus, the omission of DS failure from the Seismic GM Modeling Case is justified.

The estimate of expected annual dose considering DS failure is very conservative. The frequency of DS failure (3.4×10^{-8} yr^{-1}) is computed using extreme values for DS corrosion and for the volume of lithophysal rockfall required to fill the drift. If the analysis was repeated to include the uncertainty in DS corrosion and rockfall, the frequency of DS failure would decrease, and lead to lower expected annual dose from DS failure. Additionally, the use of the Drip Shield EF Modeling Case as a surrogate for the dose resulting from DS failure from seismic events is very conservative. For simplicity, the Drip Shield EF Modeling Case assumes that DS early failure results in compromise of the entire outer barrier of the underlying WP. This assumption overestimates the extent of localized corrosion damage, and consequently overestimates the volume of seepage that flows through the waste, and the amount of radionuclides mobilized and transported from the WP.

7.3.2.6.1.3.3 Drip Shield Framework Failure

The omission of framework failure from the Seismic GM Modeling Case for 10,000 years conservatively overestimates the occurrence of seismic damage, as outlined in the following sections. If DS framework failure occurs, the DS continues to prevent seepage from contacting the WPs; however, framework failure alters the probability of damage to WP from seismic events (Section 6.6.1.2.2.1). In general, the probability for damage to CDSP WP is reduced but the probability for damage to CSNF WP is increased. This change in the probability of damage is not accounted for the in Seismic GM Modeling Case for 10,000 years. The modeling case calculates damage to WPs as if the DS framework was intact.

Figure 7.3.2-18 shows the probability of DS framework failure over (a) 250,000 years and (b) 20,000 years, conditional on DS corrosion rates above the 99.99th percentile of the joint distribution for corrosion rate and the minimal value for the volume of intact lithophysal rock that must collapse to fill the drift, per unit length of drift (30 m^3/m). DS framework corrosion rates are scaled from the sampled values for DS plate corrosion rates. Because DS framework failure becomes less likely for lower rates of DS corrosion and for larger values for the value for the volume of intact lithophysal rock that must collapse to fill the drift, the probability of DS framework failure shown on Figure 7.3.2-18 is bounding. From a simulation of 100,000 sequences of seismic events, the probability of DS framework failure before 10,000 years is approximately 3×10^{-3}. Consequently, the frequency of DS framework failure is less than 3×10^{-7} yr^{-1}.

After DS framework failure, the mechanical response of WPs to seismic events is a function of the state of the internals. If the internals are degraded (i.e., the WP has already been damaged), the kinematic damage abstraction for a WP under intact DS plates but with degraded internals applies. If the internals are intact, the abstraction for a WP surrounded by rubble applies (Section 6.6.1.2.2.2).

The Seismic GM Modeling Case accounts for the radionuclides released from CDSP WPs for all seismic events that damage the WP while DS plates are intact. The first damaging event is assumed to occur while the DS framework is intact. The effects of any subsequent damaging events are computed using the appropriate abstraction. Consequently, the omission of DS framework failure only affects the probability of occurrence for the first damaging event. For RST=90, the frequency of damage to CDSP WPs with intact internals and intact DS framework is 2.181×10^{-5} (output DTN: MO0708CDSPSEIS.000 [DIRS 183007], *FreqDamageCDSP_v5.pdf*). In contrast, the frequency of damage to CDSP WP with intact internals and failed DS framework (described by the abstraction for a WP surrounded by rubble) is 3.923×10^{-8} (output DTN: MO0708FREQCALC.000 [DIRS 183006], *Rubble_Damage.pdf*). Because the probability of first damage to CDSP WPs decreases significantly after DS framework failure, omitting DS framework failure is conservative. However, because DS framework failure is unlikely before 10,000 years, the conservatism has a small, if any, effect on the results of the modeling case.

The Seismic GM Modeling Case does not account for the radionuclides released from CSNF WPs because, as discussed in Section 7.3.2.6.1.3.7, the probability of damage to intact TAD-bearing WPs is less than 1.575×10^{-8} yr^{-1} and the expected annual dose considering

damage to CSNF WPs is less than 0.036 mrem. If the DS framework fails before the CSNF WPs are damaged, the frequency of damage to CSNF WPs with intact internals increases, from 1.575×10^{-8} yr^{-1} (for RST=90) to 3.923×10^{-8} (for RST=90), due to the switch from the abstraction for WPs under an intact DS to WPs surrounded by rubble. Although the frequency of damage to CSNF WPs increases by a factor of 2.5, the increase is offset by the low probability of DS framework failure. Expected annual dose considering DS framework failure is estimated by

$$\begin{aligned} &(\text{prob DS framework failure}) \times (\text{prob damage TAD}) \\ &\quad \times (\text{num TAD}) \times \max_t \left(\text{Dose}(t \mid 1 \text{ TAD})\right) \\ &\leq \left(3 \times 10^{-3}\right) \times \left(3.923 \times 10^{-4}\right) \times 8213 \times (0.028) \\ &= 2.7 \times 10^{-4} \text{ mrem/yr} \end{aligned} \qquad \text{(Eq. 7.3.2-4)}$$

Thus, expected annual dose from CSNF considering DS framework failure is numerically small, and consequently, omission of DS framework failure from the Seismic GM Modeling Case is justified.

7.3.2.6.1.3.4 Rockfall

Besides contributing to the possibility of DS failure, as discussed in Section 7.3.2.6.1.3.2, rockfall caused by seismic events also alters the seepage entering the drift. Section 6.6.1.2.1 describes the model for rockfall; Section 6.6.2.1 describes the changes to drift seepage that may occur as a consequence of rockfall.

Figure 7.3.2-19(a) shows the volume of lithophysal rockfall that may accumulate during 20,000 years, determined by simulating 10,000 possible sequences of seismic events. The threshold volume of lithophysal rockfall per meter of drift length, that causes a change to the seepage model, is 5 m^3/m. When rockfall exceeds this threshold, seepage increases, as described in Section 6.3.3.1.3. At 10,000 years, approximately 11 percent of realizations have lithophysal rockfall at or above the threshold of 5 m^3/m, and approximately 1 percent of the realizations have lithophysal rockfall exceeding the 60 m^3/m volume that identifies a fully collapsed drift. When rockfall exceeds the threshold of 5 m^3/m, the volume of seepage flowing into the drift is increased. However, as long as the DS remains intact, there is no change in the radionuclides released from a WP, because the diffusion of radionuclides through the WP outer barrier does not depend on the volume of seepage in the invert. Transport of radionuclides through the invert would be somewhat faster if seepage increases, resulting in an increase in the rate of mass entering the UZ, and possibly an increase the rate of mass arriving at the RMEI location through the SZ. However, because seepage does not increase by as much as a factor of 5 from intact to fully collapsed drift (SNL 2007 [DIRS 181244], Table 6-7[a]), it is reasonable to expect that any increase in dose would not be more than a factor of 5, and likely would be much smaller, as uncertainty and variability in travel time through the UZ and SZ would tend to ameliorate any increase in mass flux from the invert. Moreover, any increase in dose would be observed in only 11 percent of realizations, and thus would not significantly alter the mean annual dose to the RMEI.

Figure 7.3.2-19(b) shows the volume of nonlithophysal rockfall that may accumulate during 20,000 years, determined by simulating 10,000 possible sequences of seismic events. The threshold volume of nonlithophysal rockfall per unit length of drift for change to the seepage model is 0.5 m^3/m. When rockfall exceeds this threshold, seepage increases, as described in Section 6.3.3.1.3. At 10,000 years, less than 1 percent of realizations have nonlithophysal rockfall at or above the threshold. When nonlithophysal rockfall exceeds the threshold, the rate of percolation rather than seepage is used. Percolation rates tend to be approximately 10 times greater than seepage rates (SNL 2007 [DIRS 181244], Table 6-6[a]). However, only approximately 20 percent of WPs are located in nonlithophysal zones, and few realizations have nonlithophysal rockfall at or above the threshold of 0.5 m^3/m, so seepage changes due to nonlithophysal rockfall have little effect on mean annual dose. Thus, the omission of rockfall effects from the Seismic GM Modeling Case for 10,000 years is justified.

7.3.2.6.1.3.5 Rupture

Rupture is conceptualized to occur when extreme deformation of the WP outer barrier accumulates as a result of package-to-pallet impacts during seismic events (Section 6.6.1.2.2.2). Rupture can only occur after package internals are degraded and when the packages can move freely beneath the DS (Section 6.6.1.2.2.2). Hence, rupture requires that a damaging seismic event has already occurred, and that the DS plates are still intact. After the DS plates have failed, the WPs are surrounded by rubble from rockfall, and rupture is not considered possible.

A seismic event may result in immediate rupture of a WP. Alternatively, the event may cause an incipient rupture, meaning that the event caused damage that increases the probability of rupture from a subsequent event. After an incipient rupture occurs, any subsequent event that would cause either incipient rupture or immediate rupture causes a rupture. Figure 7.3.2-20 diagrams the transition from an intact WP to a ruptured WP. The probabilities of immediate rupture ($p_{imm}(v)$) and incipient rupture ($p_{inc}(v)$) are conditional on the occurrence of a seismic event after WP internals have degraded, and are functions of the PGV v of the seismic event (DTN: MO0703PASEISDA.002_R4 [DIRS 183156], Eq. 1-12, Eq. 1-13, Eq. 1-17, Eq. 1-18, and Table 1-17).

If rupture occurs, the rupture creates an opening in the WP OCB sampled uniformly between 0 m^2 and the cross-sectional area of the WP (Section 6.6.1.2.2.2), 2.78 m^2 and 3.28 m^2 for CSNF and CDSP WPs, respectively (DTN: MO0703PASEISDA.002_R4 [DIRS 183156], Table 1-17). The opening allows both advection and diffusion of radionuclides out of the WP. A fault displacement event creates a similar opening in the WP OCB (Section 6.6.1.2.3). The Seismic FD Modeling Case calculates the annual dose $D_{SFr}\left(\tau \middle| [1, t, 100, A_r], \mathbf{e}_i\right)$ at time τ resulting from a fault displacement occurring at time t, which damages 100 WPs of type r, causing an opening with an area equal to A_r on each WP, where $\mathbf{e}_i$ is a realization of epistemic parameters. Because a fault displacement causes damage similar to a WP rupture, the Seismic FD Modeling Case results can be used to approximate the dose resulting from a rupture event occurring at time t that affects $nWP(r)$ WPs of type r and causing a damage fraction equal to A_r on each WP. This dose from rupture is denoted by $D_R\left(\tau \middle| [1, t, nWP(r), A_r], \mathbf{e}_i\right)$, and the relationship between the dose from rupture and the results of the Seismic FD Modeling Case is

$$D_R\left(\tau\left|[1,t,nWP(r),A_r],\mathbf{e}_i\right.\right)\approx\frac{nWP(r)}{100}D_{SFr}\left(\tau\left|[1,t,100,A_r],\mathbf{e}_i\right.\right) \qquad \text{(Eq. 7.3.2-5)}$$

Divide the interval $[0,\tau]$ into n intervals of width Δt. The probability that the first damaging event occurs within an interval $[t_i,t_i+\Delta t]$ is $e^{-\lambda_D(\mathbf{e}_i)t_i}\lambda_D(\mathbf{e}_i)\Delta t$, where $\lambda_D(\mathbf{e}_i)$ is the frequency of events that cause damage to a WP with intact internals, calculated as

$$\lambda_D(\mathbf{e}_i)=\int_{\lambda_{\min}}^{\lambda_{\max}} pD\left(r,v(\lambda)\left|\mathbf{e}_i\right.\right)d\lambda \qquad \text{(Eq. 7.3.2-6)}$$

where

$\lambda_{\min}$ and $\lambda_{\max}$ are the minimum and maximum frequencies of seismic events included in the seismic hazard curve (10^{-8} and 4.287×10^{-4}, respectively) (DTN: MO0703PASEISDA.002_R4 [DIRS 183156], Table 1-15)

$pD\left(r,v(\lambda)\left|\mathbf{e}_i\right.\right)$ is the probability of damage occurring to a WP of type r with intact internals and residual stress threshold (RST) given by an element RST in $\mathbf{e}_i$, given that a seismic event with PGV v occurs (DTN: MO0703PASEISDA.002_R4 [DIRS 183156], Table 1-4 and Table 1-6).

The probability of one or more events that causes rupture occurring in the interval $[t_i+\Delta t,\tau]$ is $1-e^{-\lambda_R(\tau-t_i-\Delta t)}$, where λ_R is the frequency of events that cause rupture to packages with degraded internals, calculated as

$$\lambda_R(r)=\int_{\lambda_{\min}}^{\lambda_{\max}} p_R\left(r,v(\lambda)\right)d\lambda \qquad \text{(Eq. 7.3.2-7)}$$

where

$p_R\left(r,v(\lambda)\right)$ is the probability of immediate rupture occurring to a WP of type r with degraded internals given that a seismic event with PGV v occurs (DTN: MO0703PASEISDA.002_R4 [DIRS 183156], Eq. 1-12, Eq. 1-13, Eq. 1-17, Eq. 1-18, and Table 1-17).

Evaluation of Equation 7.3.2-7, yields frequencies of rupture of 8.327×10^{-9} yr^{-1}, for CDSP WP and 1.378×10^{-8} yr^{-1} for CSNF WP (output DTN: MO0708FREQCALC.000 [DIRS 183006], *FreqRupture.pdf*). Equation 7.3.2-7 is simplified by considering only events that cause immediate rupture. The frequency of events that cause immediate rupture can be expressed as $P\left(\text{Imm.}\left|\text{seismic event}\right.\right)\times\lambda_S$ where $P\left(\text{Imm.}\left|\text{seismic event}\right.\right)$ is the probability of immediate rupture conditional on a seismic event occurring, and λ_S is the frequency (yr^{-1}) of seismic events

(10^{-4} yr^{-1}). In contrast, the frequency of rupture occurring from the sequence of an incipient rupture followed by an incipient or immediate rupture can be expressed as

$$\left[P\left(\text{Imm.}\middle|\text{seismic event}\right)\times\lambda_S\right]\times\left[\left(P\left(\text{Inc.}\middle|\text{seismic event}\right)+P\left(\text{Imm.}\middle|\text{seismic event}\right)\right)\times\lambda_S\right]$$
$$=\left(P^2\left(\text{Inc.}\middle|\text{seismic event}\right)+P\left(\text{Inc.}\middle|\text{seismic event}\right)P\left(\text{Imm.}\middle|\text{seismic event}\right)\right)\times\lambda_S^2$$

where $P\left(\text{Inc.}\middle|\text{seismic event}\right)$ is the probability of an incipient rupture conditional on a seismic event occurring. Since $P\left(\text{Inc.}\middle|\text{seismic event}\right)$ is of the same order of magnitude as $P\left(\text{Imm.}\middle|\text{seismic event}\right)$, the frequency of rupture from the sequence of an incipient rupture followed by a second event is several orders of magnitude less than the frequency of immediate rupture.

The expected annual dose at time τ from events that cause rupture to WP of type r can be estimated by

$$\bar{D}_R\left(\tau\middle|r,\mathbf{e}_i\right)\approx\sum_{j=0}^{n}e^{-\lambda_D(\mathbf{e}_i)t_j}\lambda_D\left(\mathbf{e}_i\right)\Delta t\left(1-e^{-\lambda_R\left(\tau-t_j-\Delta t\right)}\right)\left\{\int_0^{A_{\max}}D_R\left(\tau\middle|\left[1,t_j,nWP(r),A\right],\mathbf{e}_i\right)dA\right\}$$
$$\cong\int_0^{\tau}e^{-\lambda_D(\mathbf{e}_i)t}\lambda_D\left(\mathbf{e}_i\right)\left(1-e^{-\lambda_R(\tau-t)}\right)\left\{\int_0^{A_{\max}}D_R\left(\tau\middle|\left[1,t,nWP(r),A\right],\mathbf{e}_i\right)dA\right\}dt$$

(Eq. 7.3.2-8)

Figure 7.3.2-21 displays the expected annual dose from events that cause rupture, estimated by Equation 7.3.2-8. Except for one realization, the expected annual dose at 10,000 years is less than 4×10^{-3} mrem/yr. In contrast, the expected annual dose at 10,000 years in the Seismic GM Modeling Case exceeds 4×10^{-3} mrem in approximately 70 percent of the realizations (Figure 7.3.2-14). Moreover, the mean annual dose at 10,000 years in the Seismic GM Modeling Case is approximately 0.2 mrem, whereas the mean dose at 10,000 years due to events that cause rupture is about 3×10^{-4} mrem. Thus, the expected annual dose from rupture events is small enough that its exclusion from the dose for the Seismic GM Modeling Case for 10,000 years is justified.

Moreover, using the Seismic FD Modeling Case results to estimate bounds on the dose due to rupture over-estimates the dose from rupture in two ways. First, the dose resulting from fault displacement assumes that DSs fail at the time of the fault displacement event, allowing advective transport through the affected WPs. In contrast, the probability of DS failure is not accounted for in Equation 7.3.2-8. If the DS plates remained intact after a rupture event, radionuclide transport from the underlying package would occur by diffusion, which tends to be slower than transport by advection, and would result in lower annual doses. Additionally, the Seismic FD Modeling Case considers only the effects of fault displacement events. Thus, using these results to estimate rupture neglects the effects of the damaging events that precede rupture,

and overcounts the released radionuclides because the content of the WPs is not reduced by any radionuclides that would be released prior to a rupture occurring.

7.3.2.6.1.3.6 Puncture

Puncture is conceptualized to be possible after the DS plates have failed, rubble from rockfall surrounds the WP, and the outer corrosion barrier collapses around the degraded internal contents of the WP. Although the internal components of the WP are conceptualized to degrade structurally after the OCB is breached, large fragments of the stainless steel inner vessel and parts of the waste assembly may persist for long periods of time. Puncture may result when a severely deformed outer corrosion barrier is loaded down by rubble from rockfall and thus impinges on the edges or corners of fragments of the degraded internal structure. Puncture can only occur after package internals are degraded and the rubble from rockfall surrounds the WP; hence, puncture requires that a damaging seismic event has already occurred and that the drift has fully degraded.

When puncture occurs, the resulting puncture area allows both advection and diffusion of radionuclides out of the WP. The puncture area for the TSPA-LA ranges between 0 m^2 and 0.1 m^2 (DTN: MO0703PASEISDA.002_R4 [DIRS 183156], Table 1-17), generally smaller than the area considered for rupture, which ranges between 0 m^2 and 2.78 m^2 (3.28 m^2) for CSNF (CDSP) WPs (DTN: MO0703PASEISDA.002_R4 [DIRS 183156], Table 1-17).

For 10,000 years, corrosion of the WP outer barrier does not reduce the spatially averaged outer barrier thickness below 23 mm. Thus, the calculation of the frequency of puncture does not consider the outer barrier thickness changing with time. The frequency of events that cause puncture to a WP with degraded internals and which is surrounded by rubble, λ_P, is calculated as

$$\lambda_P = \int_{\lambda_{min}}^{\lambda_{max}} p_P\left(v(\lambda)\right) d\lambda = 1.453 \times 10^{-8} \quad \text{(Eq. 7.3.2-9)}$$

where

$p_P\left(v(\lambda)\right)$ is the probability of puncture occurring to a WP with degraded internals, surrounded by rubble, with 23 mm thick OCB, given that a seismic event with PGV v occurs (DTN: MO0703PASEISDA.002_R4 [DIRS 183156], Eqs. 1-22 and 1-23 and Table 1-17)).

Equation 7.3.2-9 is evaluated and reported in output DTN: MO0708FREQCALC.000 [DIRS 183006], *FreqPuncture.pdf*. Figure 7.3.2-16 shows the bounding probability of DS plate failure as a function of time for each realization. Over all realizations, at 10,000 years, the probability of DS plate failure does not exceed 3.4×10^{-4}. Thus, the probability of rubble surrounding the WPs within 10,000 years is also less than 3.4×10^{-4}, and the frequency of events that cause puncture is less than

$$3.4\times10^{-4}\times\lambda_P=\left(3.4\times10^{-4}\right)\times\left(1.453\times10^{-8}\right)=5.2\times10^{-12}. \qquad \text{(Eq. 7.3.2-10)}$$

As expressed by Equation 7.3.2-10, the frequency of puncture is much less than the frequency of rupture (Equation 7.3.2-7). Since the area opened by a puncture is smaller than the area opened by rupture, the expected annual dose from seismic events that puncture WPs would not be larger than the expected annual dose from seismic events that rupture WPs. Hence, the expected annual dose from puncture would be much less, than the expected annual dose from rupture, and the exclusion of puncture from the expected annual dose for the Seismic GM Modeling Case for 10,000 years is also justified.

7.3.2.6.1.3.7 Damage to CSNF Waste Packages

The frequency of seismic events that cause SCC damage to a CSNF WP with intact internals and 23 mm thick OCB is estimated by Equation 7.3.2-6. The maximum frequency corresponds to RST=90 and is calculated to be 1.575×10^{-8} (output DTN: MO0708FREQCALC.000 [DIRS 183006], *FreqDamageTAD.pdf*). In contrast, the maximum frequency of events that cause SCC damage to a CDSP WP is estimated to be 2.181×10^{-5} (output DTN: MO0708CDSPSEIS.000 [DIRS 183007], *FreqDamageCDSP_v5.pdf*). The expected annual dose from seismic events that damage CSNF WPs is estimated by comparing the dose resulting from CSNF and CDSP WPs in the Waste Package EF Modeling Case. This modeling case calculates the annual dose from a single WP with a completely compromised WP outer barrier (Section 6.4). Figure 7.3.2-22 shows the mean annual dose resulting from (a) one CSNF WP and (b) one CDSP WP, as modeling in the Waste Package EF Modeling Case, considering all locations within the repository and all realizations of epistemic parameters. The maximum mean annual dose from CSNF WPs with SCC damage is estimated by

$$\begin{aligned}&\left(\text{prob damage CSNF in 10,000 yrs}\right)\times\left(\text{num CSNF}\right)\times\max_t\left(\text{Dose}(t\,|1\text{ CSNF})\right)\\&=\left(1.575\times10^{-4}\right)\times8213\times\left(0.028\right)\\&=0.036\text{ mrem}\end{aligned} \qquad \text{(Eq. 7.3.2-11)}$$

Because the quantity, $\max_t\left(\text{Dose}(t\,|1\text{ CSNF})\right)$, is estimated from the results of the Waste Package EF Modeling Case for CSNF WPs, in which the entire WP outer barrier is assumed to fail, the estimate of this quantity effectively assumes that the entire surface area of each CSNF WP consists of cracks. Consequently, the quantity 0.036 mrem estimated by Equation 7.3.2-11 should not be compared to the mean annual dose from CDSP WPs from the Seismic GM Modeling Case, but rather to the comparable quantity for CDSP WPs using the results of the Waste Package EF Modeling Case for CDSP WPs:

$$\begin{aligned}&(\text{prob damage CDSP in 10,000 yrs})\times(\text{num CDSP})\times\max_t\left(\text{Dose}(t\,|1\text{ CDSP})\right)\\&=\left(2.181\times10^{-1}\right)\times3416\times(0.008)\\&=5.96\text{ mrem/yr}\end{aligned}$$

(Eq. 7.3.2-12)

Comparison of the results of Equation 7.3.2-11 and Equation 7.3.2-12 shows that the maximum mean annual dose associated with seismic damage to CSNF WPs is expected to be less than 1 percent of the maximum mean annual dose associated with seismic damage to CDSP WPs. Thus, the omission of damage to TADs from the Seismic GM Modeling Case for 10,000 years is justified.

7.3.2.6.2 Seismic Ground Motion Modeling Case for 1,000,000 Years

Expected annual dose for the Seismic GM Modeling Case for 1,000,000 years is calculated as described by Equation 6.1.2-23, using a Monte Carlo technique. First, a LHS of size 300 is generated for epistemic parameters. Next, for each vector $\mathbf{e}_i$ in the epistemic LHS, an aleatory sample is randomly generated, consisting of 30 independent sequences $\{\mathbf{a}_{ij}\}_{j=1,30}$ of seismic events and corrosion failures, and annual dose at time τ from the combination of corrosion processes and seismic ground motion events, $D_{N+G}\left(\tau\left|\mathbf{a}_{ij},\mathbf{e}_i\right.\right)$, is calculated. For each vector $\mathbf{e}_i$ in the epistemic LHS, expected annual dose $\bar{D}_{SG}\left(\tau\left|\mathbf{e}_i\right.\right)$ is computed as

$$\bar{D}_{SG}\left(\tau\left|\mathbf{e}_i\right.\right)=\sum_{j=1}^{30}D_{N+G}\left(\tau\left|\mathbf{a}_{ij},\mathbf{e}_i\right.\right)\Big/30 \qquad \text{(Eq. 7.3.2-13)}$$

Mean annual dose $\bar{\bar{D}}_{GM}\left(\tau\right)$ is computed as

$$\begin{aligned}\bar{\bar{D}}_{SG}\left(\tau\right)&=\sum_{i=1}^{300}\bar{D}_{SG}\left(\tau\left|\mathbf{e}_i\right.\right)\Big/300\\&=\sum_{i=1}^{300}\left(\sum_{j=1}^{30}D_{N+G}\left(\tau\left|\mathbf{a}_{ij},\mathbf{e}_i\right.\right)\Big/30\right)\Big/300\end{aligned} \qquad \text{(Eq. 7.3.2-14)}$$

Because of the Monte Carlo technique used in the Seismic GM Modeling Case for 1,000,000 years, the relatively small size (30) of the aleatory sample, and the wide variability in the effects of a seismic event (Section 6.6), it is not reasonable to presume that the expected annual dose would be numerically stable for each individual epistemic vector $\mathbf{e}_i$. Moreover, due to the computational requirements of this modeling case, it is not practical to dramatically increase the aleatory sample size. Figure 7.3.2-23 compares expected annual dose for an aleatory sample size of 30 to expected annual dose for an aleatory sample size of 90, for epistemic realization 2, in which the sampled value of RST is low (93.5) and thus the frequency of seismic events that cause damage is relatively high. The similarity in the two expected annual dose results indicates

that increasing the aleatory sample size does not produce a qualitatively different expected annual dose, although at any particular time τ the expected annual dose may vary significantly.

Section 7.3.1.2 demonstrates that the mean annual dose calculated by Equation 7.3.2-14 is statistically stable by means of replicated sampling. Moreover, the quantiles of the distribution of expected annual dose are also reasonably stable. The mean annual dose is calculated for each of three independent epistemic LHSs, and the overall mean annual dose for the pooled set of 900 LHS elements is computed by averaging the three independent mean dose histories. Confidence intervals around the overall mean are computed by applying a *t*-test to the sample of three independent means. The overall mean, three independent means, and the confidence intervals are shown on Figure 7.3.1-11. The confidence intervals follow the overall mean quite closely, and the upper confidence interval is consistently about twice the magnitude of the overall mean, indicating that the overall mean annual dose is statistically stable.

7.3.2.7 Seismic Fault Displacement Modeling Case

Expected annual dose for the Seismic FD Modeling Case is calculated as described by Equation 6.1.2-25. Equation 6.1.2-25 is numerically evaluated in two steps. First, for each of a sequence $[t_1, t_2, \ldots, t_N]$ of times for fault displacement events, each WP type r, and each of a set of damage areas $[A_1, A_2, \ldots, A_M]$, annual dose at time τ from a fault displacement event occurring at time t_j resulting in damage area A_k to 100 WPs of type r, $D_{SFr}\left(\tau \middle\| \left[1, t_j, 100, A_k\right], \mathbf{e}_i\right)$, is calculated using the GoldSim component of the TSPA-LA Model. The 100 WPs are placed proportionally into each percolation bin, and within each bin, proportionally into dripping and non-dripping locations. Second, the GoldSim results are used by the EXDOC component of the TSPA-LA Model to calculate expected annual dose.

To determine if the expected annual dose calculations conducted by EXDOC are numerically accurate, the number of times of fault displacement events was increased from 6 to 12, and the number of damage areas was increased from 3 to 5. Table 7.3.2-4 lists the times of seismic events and the damage fractions considered in the base case and in the expanded case for numerical accuracy.

Figure 7.3.2-24 shows the annual dose resulting from each fault displacement event in the base case, and the annual dose resulting from the additional fault displacement events in the expanded case, for a damage area of 1/3 of the cross-sectional area, for both CDSP and CSNF WPs, for epistemic realization 1. In terms of Equation 6.1.2-25, Figure 7.3.2-24 shows the quantities $D_{SFr}\left(\tau \middle\| \left[1, t_j, 100, \frac{1}{3} A_r\right], \mathbf{e}_i\right)$ for t_j as listed in Table 7.3.2-4. For each type of WP, each dose history's shape is similar for different times of the fault displacement event, although the dose history has a different shape for the different WP types since the radionuclide inventory and the temperature of different WP types are different.

Figure 7.3.2-25 shows the annual dose resulting from a fault displacement event at 200 years for each of the different damage areas, for (a) CDSP and (b) CSNF WPs, for epistemic realization 1.

In terms of Equation 6.1.2-25, Figure 7.3.2-25 shows the quantities $D_{SFr}\left(\tau \middle| [1, 200, 100, A_k], \mathbf{e}_i\right)$ for A_k as listed in Table 7.3.2-4. For each type of WP, the shape of each dose history is similar for different damage areas, for all but the smallest damage areas on CDSP WPs. For most damage areas, the area is large enough that it does not limit the rate of radionuclide transport through the WP OCB. For CDSP WPs, Figure 7.3.2-25 indicates that dose is proportional to damage area when damage area is quite small. When the damage area increases to approximately 5 percent of the WP cylindrical surface area, essentially all of the seepage that contacts the WP is captured by the openings in the WP. In the Seismic FD Modeling Case, water flux into the WP is modeled with the EBS Flow Submodel described in Section 6.3.6. For this modeling case, the application of the EBS Flow Submodel obviates the need to explicitly consider the geometry of openings in the WP caused by fault displacement. As a consequence of this simplification, the maximum influx of water is achieved at relatively low damage areas from fault displacement events. The effect is observed for CDSP WPs because the annual dose from CDSP WPs between 10,000 and 20,000 years is largely due to ^{239}Pu sorbed to colloids, which transport primarily by advection. In contrast, the annual dose from CSNF WPs is primarily from ^{99}Tc and ^{129}I, which transport rapidly through very small openings in the WPs, as discussed in Section 7.3.2.6.1 for the Seismic GM Modeling Case for 10,000 years.

EXDOC computes expected annual dose by interpolating between single dose histories for different event times and damage areas, similar to those illustrated on Figure 7.3.2-24 and 7.3.2-25, and performing numerical integration using the interpolated dose histories. Because the dose histories maintain similar shapes as the event time and damage fraction change, the interpolation scheme implemented in EXDOC is justified.

Figure 7.3.2-26 compares the expected annual dose over 20,000 years for five epistemic realizations calculated for the base case and the expanded case, using the times of seismic events and damage fractions listed in Table 7.3.2-3. Using additional event times and damage areas increases the expected annual dose by approximately 30 percent in all 5 realizations. Because the dose histories are not different for different damage areas, the change in expected annual dose is due to the additional event times included in the numerical integration. Inclusion of these additional event times in the baseline expected annual dose calculation would improve the accuracy of the baseline results, by approximately 30 percent, as indicated by Figure 7.3.2-26. However, because the contribution to total mean annual dose from the Seismic FD Modeling Case is small compared to other modeling cases (for example, compare Figure 7.3.1-12 for the Seismic FD Modeling Case and Figure 7.3.1-10 for the Seismic GM Modeling Case), the improvement in the accuracy of this modeling case does not justify the additional computational burden imposed by the additional event times.

The analysis of the calculation of expected annual dose for the Seismic FD Modeling Case for 20,000 years showed that, although improvements are possible, the expected annual dose is estimated with sufficient accuracy for 20,000 years. In addition, because the computation of expected annual dose for the Seismic FD Modeling Case for 1,000,000 years is carried out using the same numerical technique, it is reasonable to presume that the expected annual dose for 1,000,000 years is also estimated with sufficient accuracy.

7.3.2.8 Human Intrusion Modeling Case

Expected annual dose for the Human Intrusion Modeling Case is calculated as described by Equation 6.1.2-26. Equation 6.1.2-26 is numerically evaluated using a Monte Carlo technique. One intrusion is modeled, and the time of intrusion is fixed at 200,000 years. For each epistemic realization $\mathbf{e}_i$, a sample of aleatory realizations $\{r_j, q_j, SR_j\}$ is generated, describing the type of WP r_j, the percolation rate q_j, and the SZ source region SR_j at the location of the intrusion. For each combination of epistemic and aleatory realization, annual dose at time τ from an intrusion, $D_{HI}\left(\tau \middle\| \left[1, r_j, q_j, SR_j\right], \mathbf{e}_i\right)$, is calculated using the GoldSim component of the TSPA-LA Model and is used in Equation 6.1.2-26 to compute expected annual dose.

To demonstrate that expected annual dose calculations are numerically stable, the size of the aleatory sample was increased from 30 to 90, and expected annual dose was calculated for the first five epistemic realizations. Figure 7.3.2-27 compares expected annual dose for the two aleatory sample sizes. Increasing aleatory sample size has no significant effect on the expected annual dose. Hence, an aleatory sample size of 30 is adequate to obtain a numerically stable estimate of expected annual dose.

Table 7.3.2-1. Times for Igneous Intrusions in the Base Case and the Expanded Case

Calculation Period	Base Case	Expanded Case
20,000 yr	10, 100, 600, 1000, 2000, 4000, 6000, 10000, 14000, 18000	10, 400, 800, 1200, 1600 2000, 2400, 2800, 3200, 3600 4000, 4400, 4800, 5200, 5600 6000, 6400, 6800, 7200, 7600 8000, 8400, 8800, 9200, 9600 10000, 10400, 10800, 11200, 11600 12000, 12400, 12800, 13200, 13600 14000, 14400, 14800, 15200, 15600 16000, 16400, 16800, 17200, 17600 18000, 18400, 18800, 19200, 19600
1,000,000 yr	250, 600, 1000, 4000, 10000, 40000, 100000, 200000, 400000, 800000	250, 20000, 40000, 60000, 80000 100000, 120000, 140000, 160000, 180000 200000, 220000, 240000, 260000, 280000 300000, 320000, 340000, 360000, 380000 400000, 420000, 440000, 460000, 480000 500000, 520000, 540000, 560000, 580000 600000, 620000, 640000, 660000, 680000 700000, 720000, 740000, 760000, 780000 800000, 820000, 840000, 860000, 880000 900000, 920000, 940000, 960000, 980000

Source: Output DTNs: MO0709TSPAREGS.000 [DIRS 182976] for Base Case and MO0708TSPAVALI_000 [DIRS 182985 for Expanded Case.

Table 7.3.2-2. Event Times in the Volcanic Eruption Modeling Case for 20,000 Years

Base Case	Expanded Case
0, 10, 100, 600, 2000, 4000 6000, 10000, 14000, 18000	0, 10, 40, 100, 240, 400, 600 800, 1000, 2000, 4000, 6000 10000, 14000, 18000

Source: Output DTN: MO0709TSPAREGS.000 [DIRS 182976] for Base Case and MO0708TSPAVALI_000 [DIRS 182985] for Expanded Case.

Table 7.3.2-3. Event Times and Damage Fractions in the Seismic Ground Motion Modeling Case for 20,000 Years

	Base Case	Expanded Case
Event Times (yrs)	200, 1000, 3000, 6000, 12000, 18000	100, 1600, 3200, 4800, 6400, 8000, 9600, 11200, 12800, 14400, 16000, 19200
Damage Fractions	10^{-7}, 10^{-6}, 10^{-5}, 10^{-4}, 10^{-3}	10^{-9}, 10^{-8}, 10^{-7}, 10^{-6}, 10^{-5}, 10^{-4}, 10^{-3}, $5x10^{-3}$

Source: Output DTN: MO0709TSPAREGS.000 [DIRS 182976] for Base Case and MO0708TSPAVALI_000 [DIRS 182985] for Expanded Case.

Table 7.3.2-4. Event Times and Damage Areas in the Seismic Fault Displacement Modeling Case for 20,000 Years

	Base Case	Expanded Case
Event Times (yrs)	200, 800, 2000, 4000, 8000, 18000	200, 1600, 3200, 4800 6400, 8000, 9600, 11200 12800, 14400, 16000, 19200
Damage Areas (fraction of cross section area)	1/3, 2/3, 1	1/12, 1/6, 1/3, 2/3, 1

Source: Output DTN: MO0709TSPAREGS.000 [DIRS 182976] for Base Case and MO0708TSPAVALI_000 [DIRS 182985] for Expanded Case

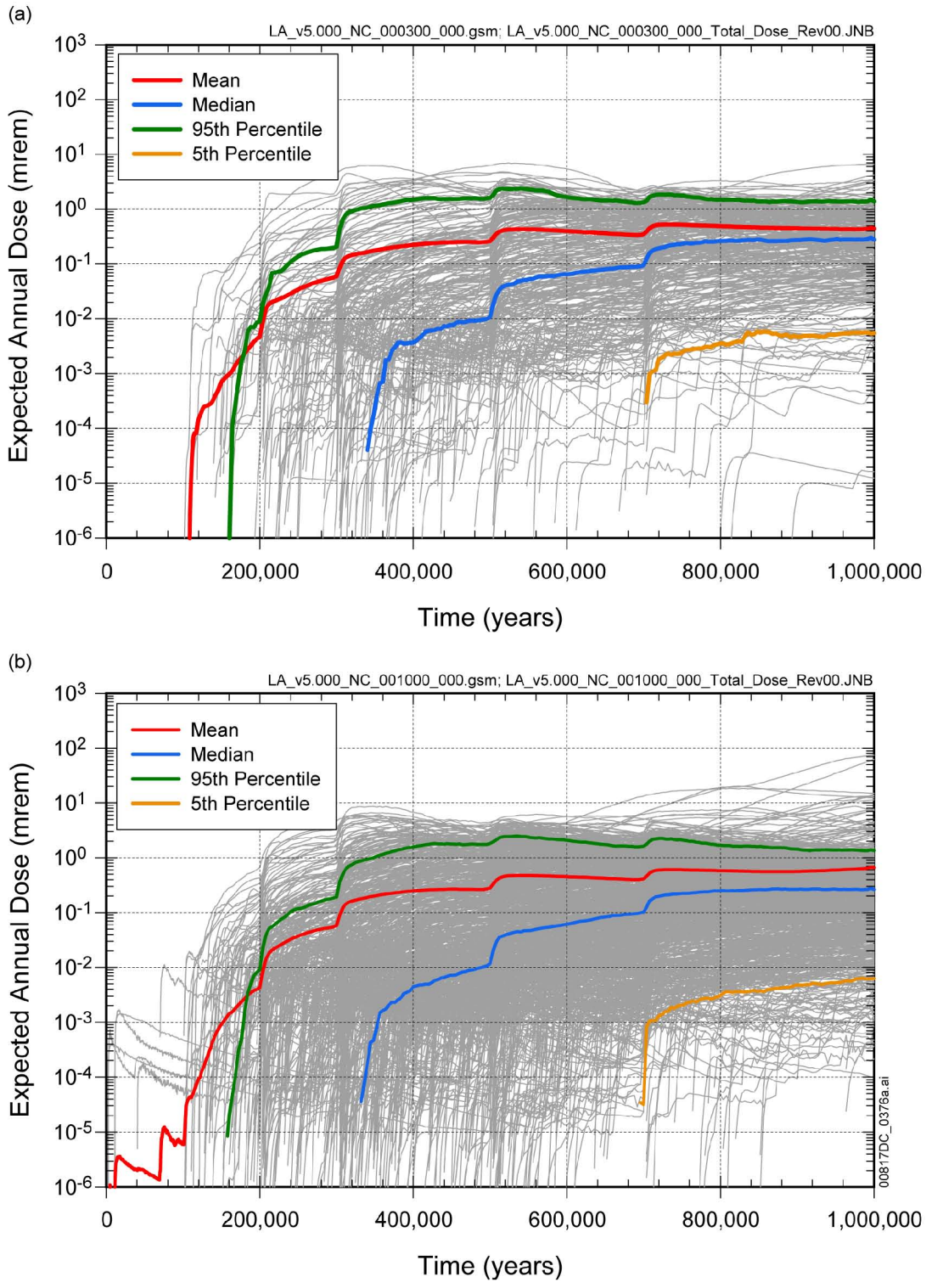

Source: Output DTNs: MO0709TSPASTAB.000 [DIRS 182983] and MO0709TSPAREGS.000 [DIRS 182976].

Figure 7.3.2-1. Expected Annual Dose for the Nominal Modeling Case: (a) Latin Hypercube Sampling Size of 300 and (b) Latin Hypercube Sampling Size of 1,000

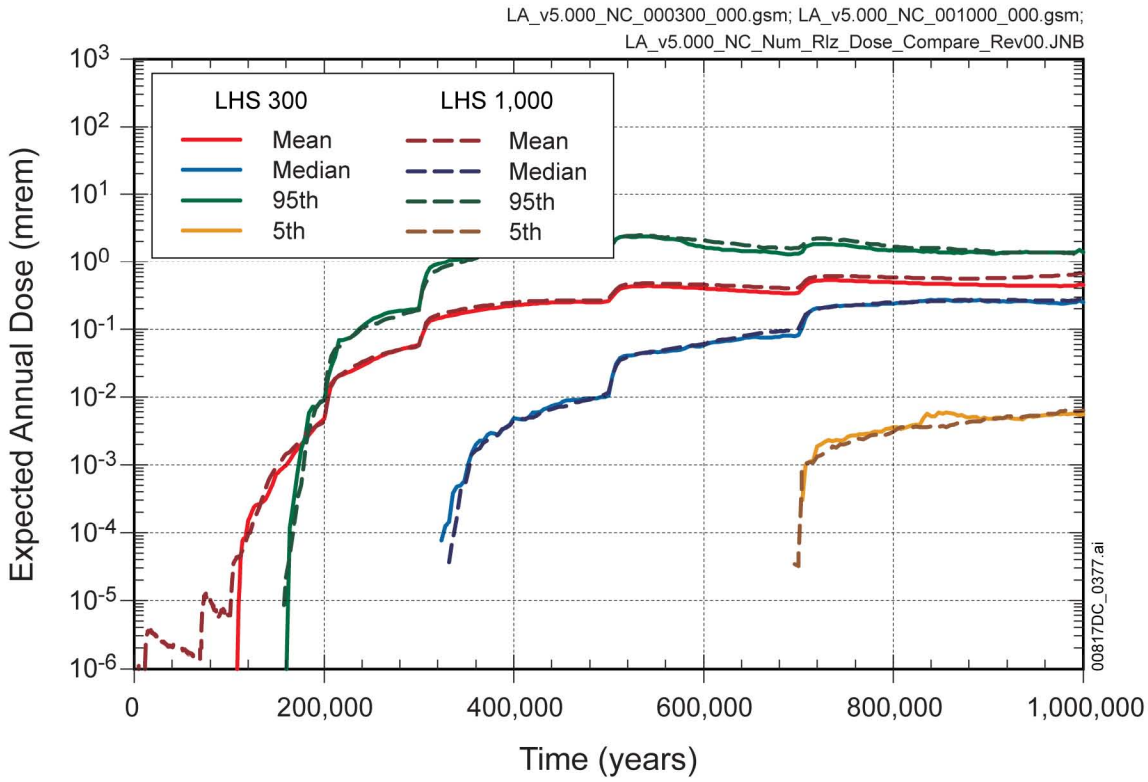

Source: Output DTNs: MO0709TSPASTAB.000 [DIRS 182983] and MO0709TSPAREGS.000 [DIRS 182976].

Figure 7.3.2-2. Uncertainty in Expected Annual Dose for the Nominal Modeling Case using Latin Hypercube Sampling Sizes of 300 and 1,000

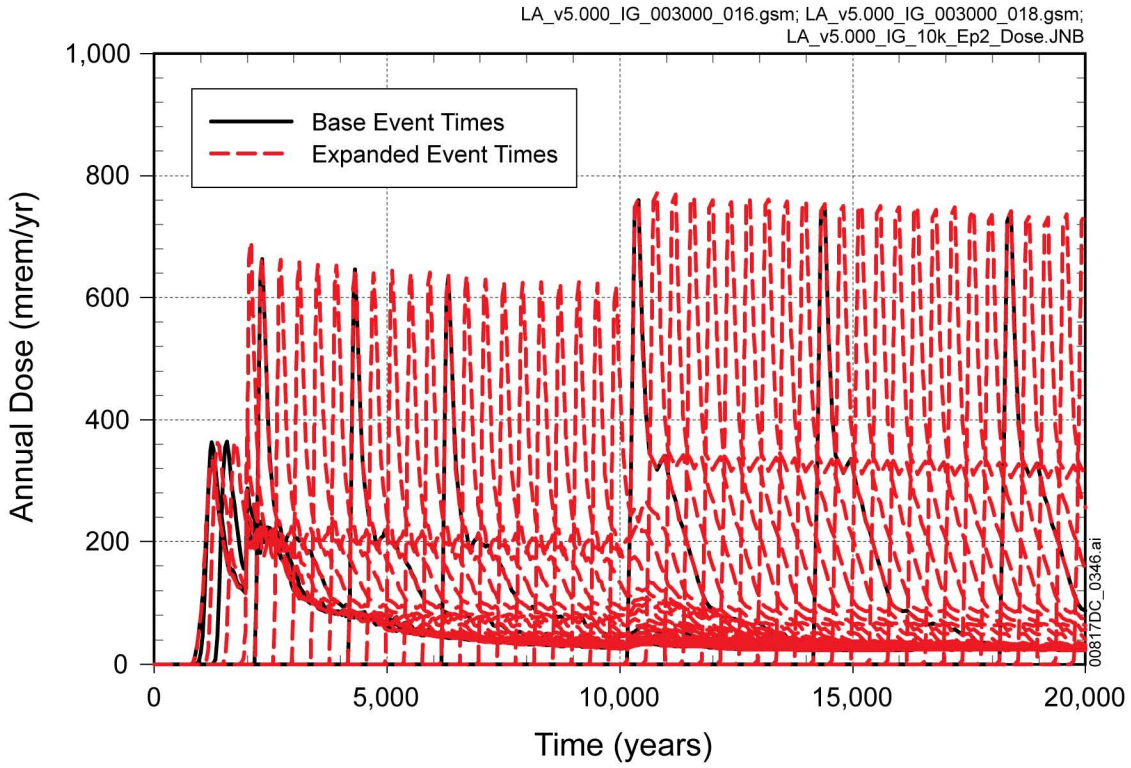

Source: Output DTNs: MO0709TSPASTAB.000 [DIRS 182983] and MO0709TSPAREGS.000 [DIRS 182976].

Figure 7.3.2-3. Annual Dose Over 20,000 Years for the Igneous Intrusion Modeling Case Considering Additional Specified Event Times for Epistemic Realization 2

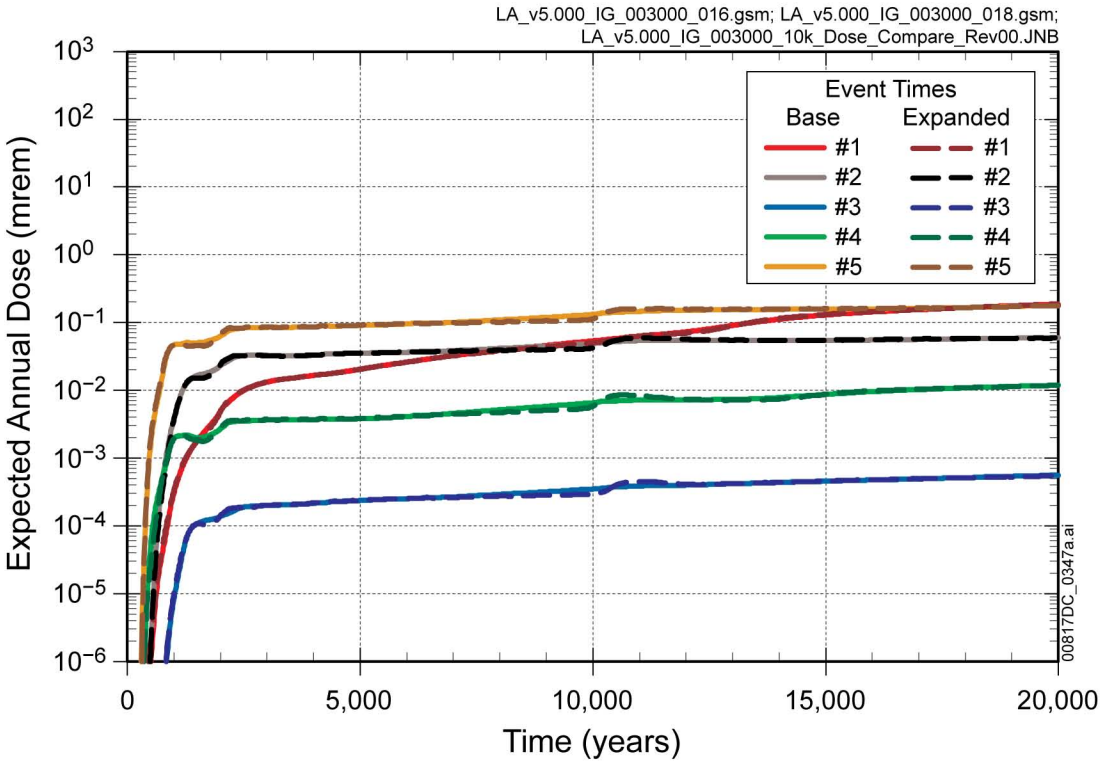

Source: Output DTNs: MO0709TSPASTAB.000 [DIRS 182983] and MO0709TSPAREGS.000 [DIRS 182976].

Figure 7.3.2-4. Expected Annual Dose Over 20,000 Years for the Igneous Intrusion Modeling Case Considering Additional Specified Event Times

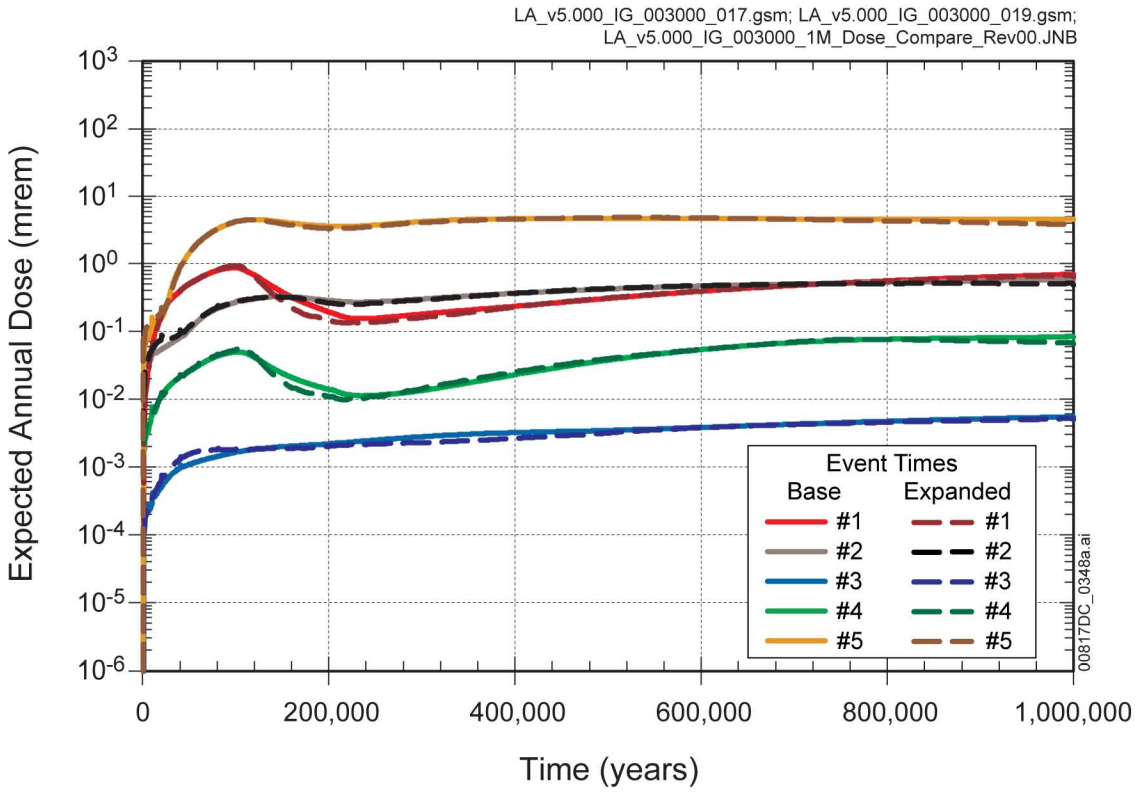

Source: Output DTNs: MO0709TSPASTAB.000 [DIRS 182983] and MO0709TSPAREGS.000 [DIRS 182976].

Figure 7.3.2-5. Expected Annual Dose Over 1,000,000 Years for Igneous Intrusion Modeling Case Considering Additional Specified Event Times

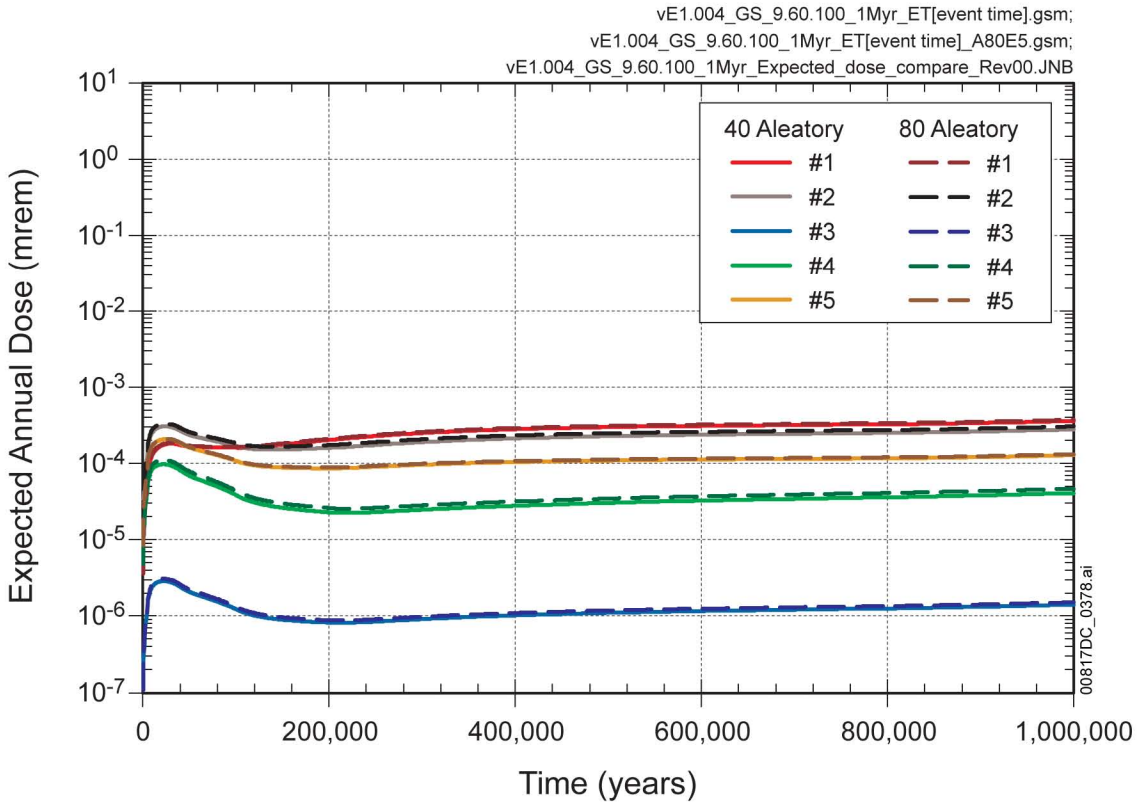

Source: Output DTNs: MO0709TSPASTAB.000 [DIRS 182983] and MO0709TSPAREGS.000 [DIRS 182976].

Figure 7.3.2-6. Expected Annual Dose Over 1,000,000 Years for Volcanic Eruption Modeling Case Using Aleatory Latin Hypercube Sampling Sizes of 40 and 80

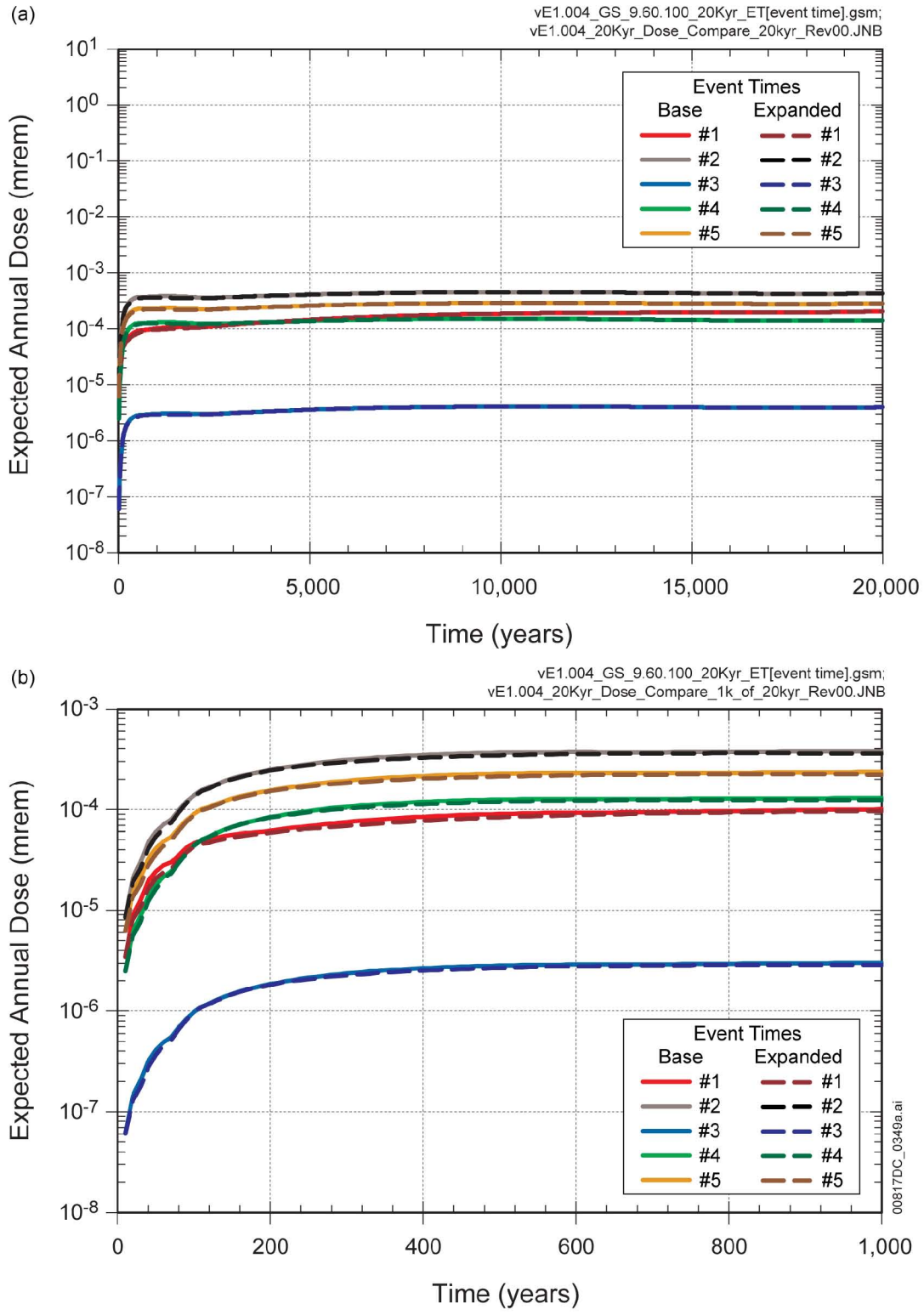

Source: Output DTNs: MO0709TSPASTAB.000 [DIRS 182983] and MO0709TSPAREGS.000 [DIRS 182976].

Figure 7.3.2-7. Expected Annual Dose for Volcanic Eruption Modeling Case Considering Additional Specified Event Times Over (a) 20,000 Years and (b) 1,000 Years

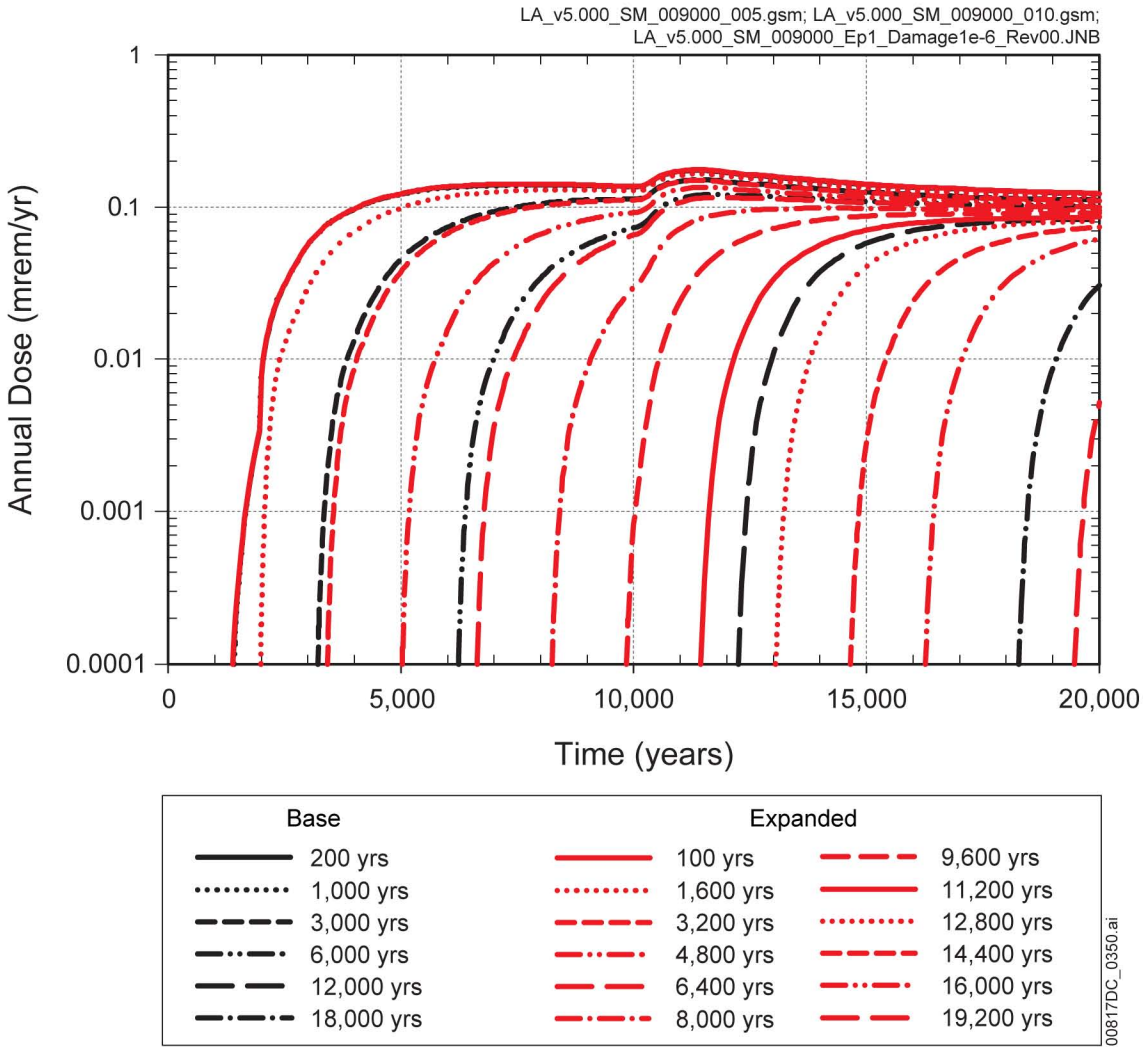

Source: Output DTNs: MO0709TSPASTAB.000 [DIRS 182983] and MO0709TSPAREGS.000 [DIRS 182976].

Figure 7.3.2-8. Annual Dose Over 20,000 Years for the Seismic Ground Motion Modeling Case Considering Additional Specified Event Times with Constant Damage Fraction 10^{-6} for Epistemic Realization 1

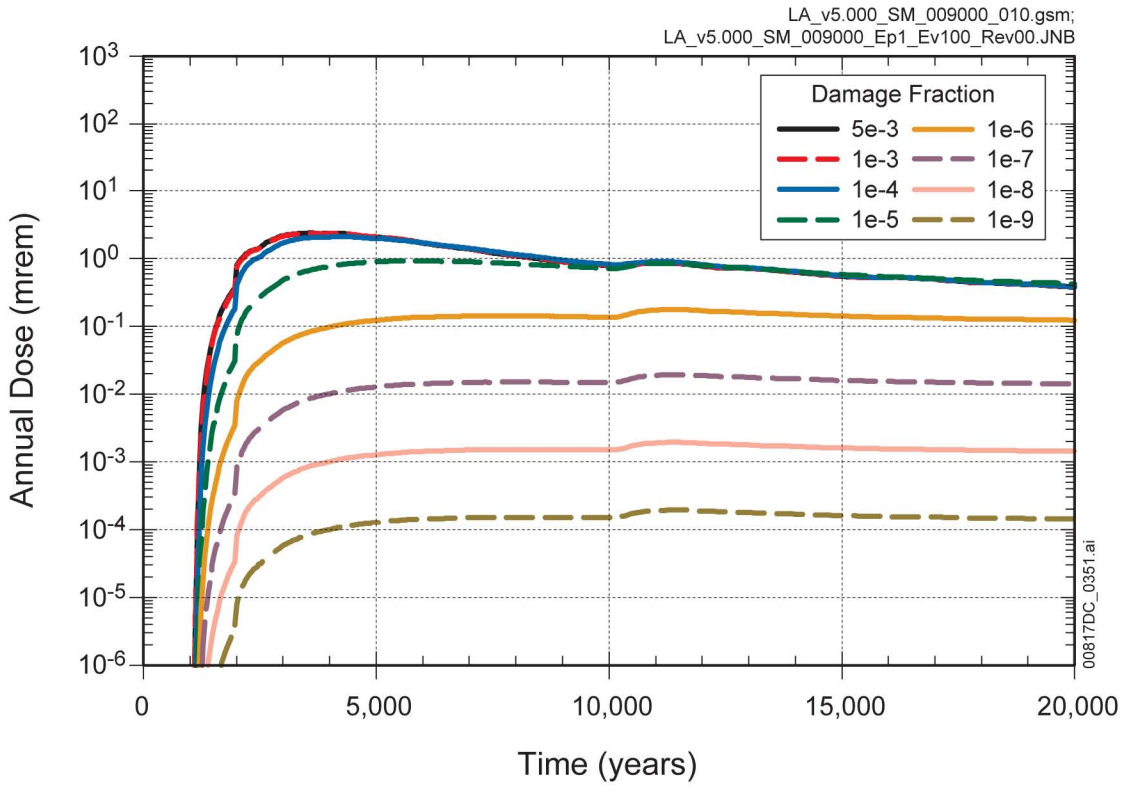

Source: Output DTN: MO0709TSPASTAB.000 [DIRS 182983].

Figure 7.3.2-9. Annual Dose Over 20,000 Years for Seismic Ground Motion Modeling Case Considering Additional Specified Damage Fractions from a Seismic Event at 100 Years for Epistemic Realization 1

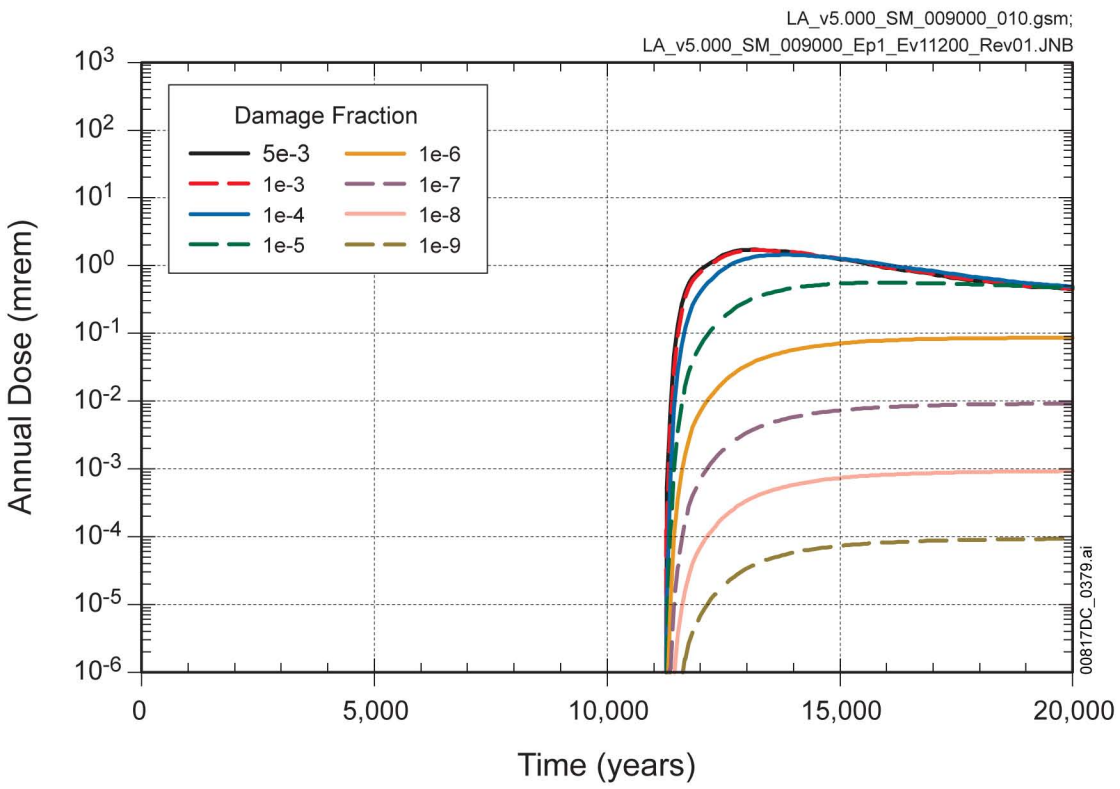

Source: Output DTN: MO0709TSPASTAB.000 [DIRS 182983].

Figure 7.3.2-10. Annual Dose Over 20,000 Years for Seismic Ground Motion Modeling Case Considering Additional Specified Damage Fractions from a Seismic Event at 11,200 Years for Epistemic Realization 1

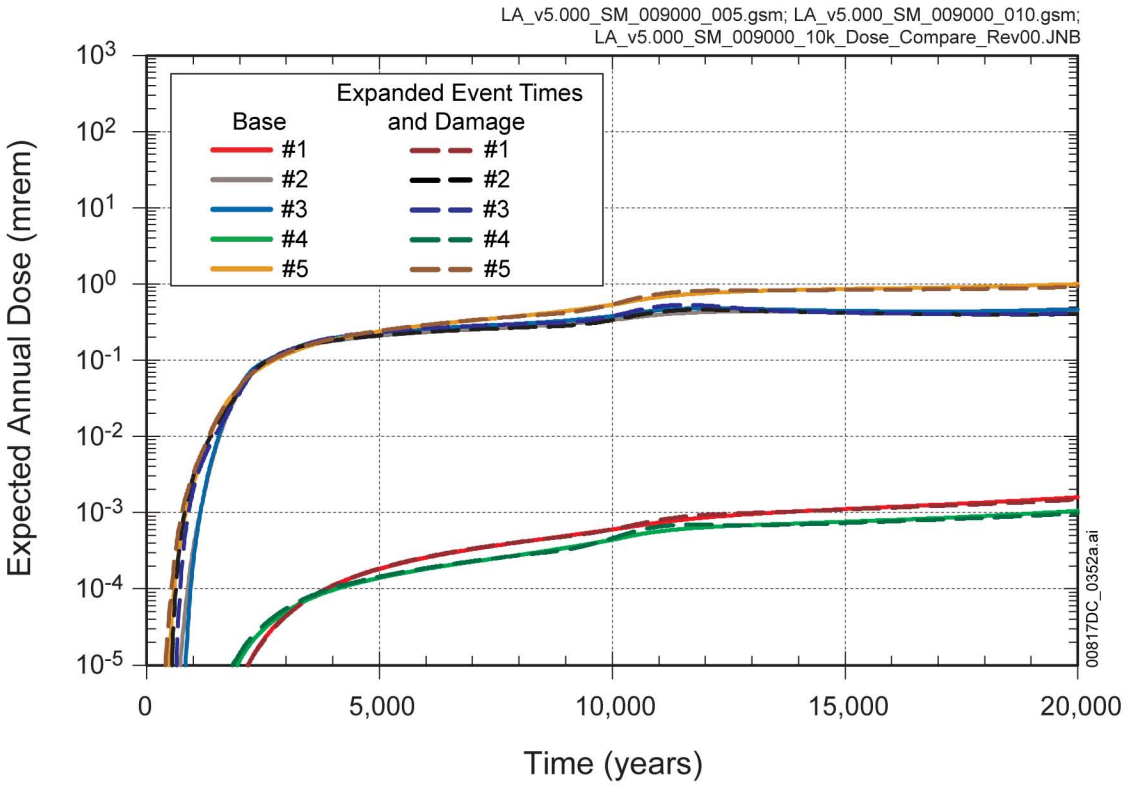

Source: Output DTNs: MO0709TSPASTAB.000 [DIRS 182983] and MO0709TSPAREGS.000 [DIRS 182976].

Figure 7.3.2-11. Expected Annual Dose Over 20,000 Years for Seismic Ground Motion Modeling Case Considering Additional Specified Event Times and Damage Fractions

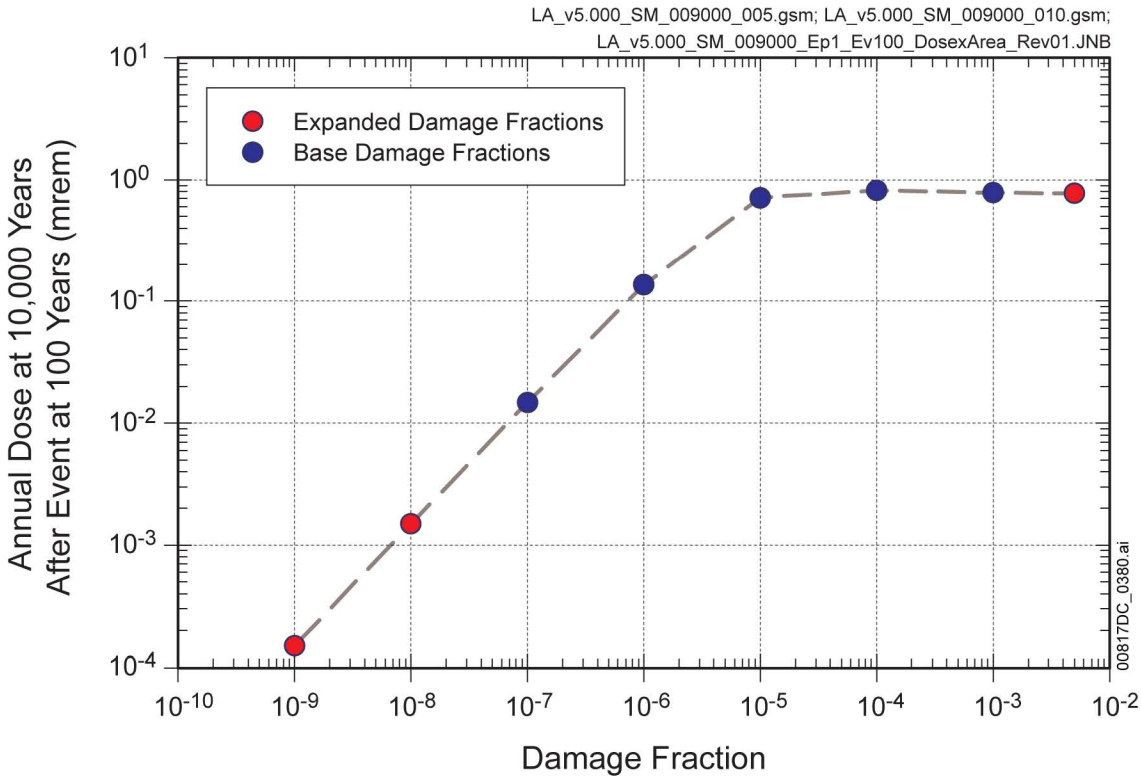

Source: Output DTNs: MO0709TSPASTAB.000 [DIRS 182983] and MO0709TSPAREGS.000 [DIRS 182976].

Figure 7.3.2-12. Annual Dose vs. Damage Fraction for a Seismic Ground Motion Event at 100 Years for Epistemic Realization 1

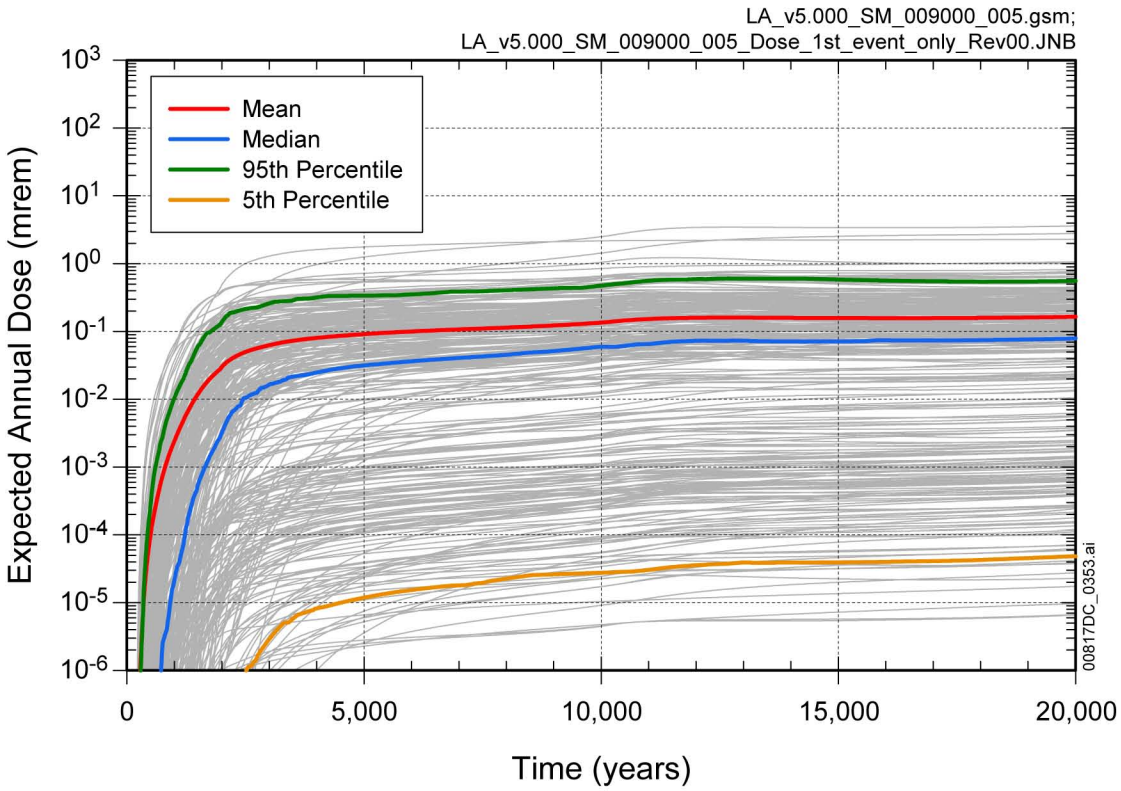

Source: Output DTN: MO0709TSPAREGS.000 [DIRS 182976].

Figure 7.3.2-13. Expected Annual Dose Over 20,000 Years from First Damaging Seismic Ground Motion Event

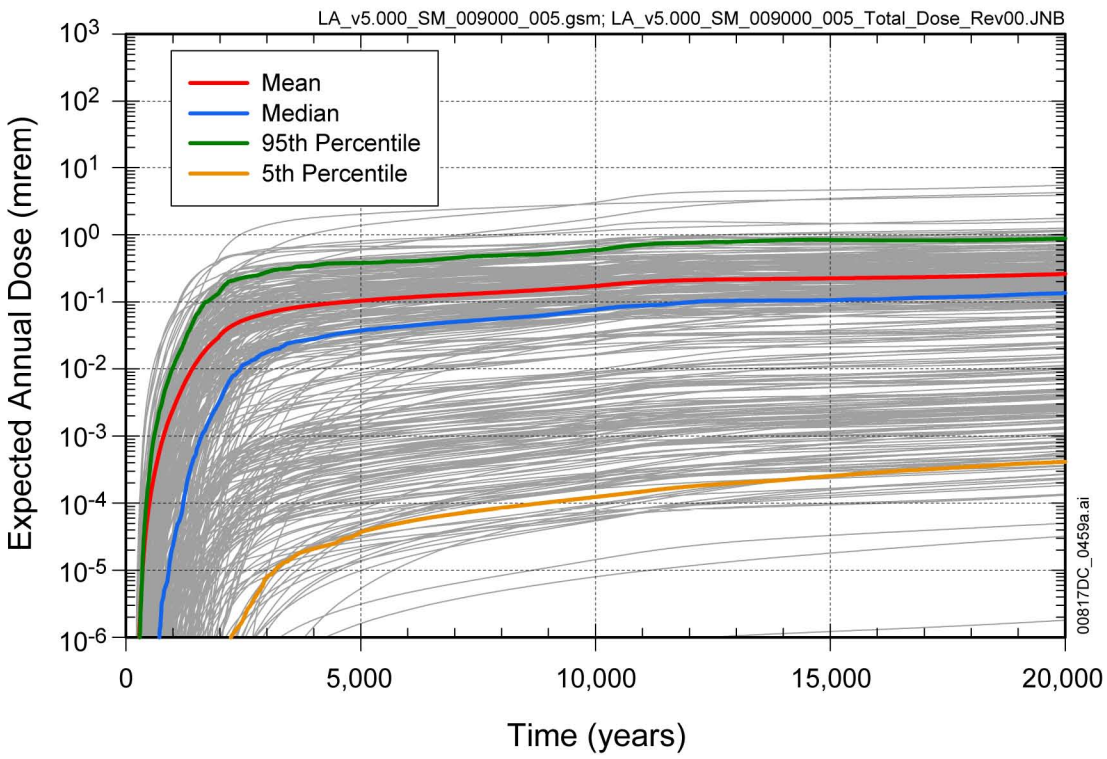

Source: Output DTN: MO0709TSPAREGS.000 [DIRS 182976].

Figure 7.3.2-14. Expected Annual Dose Over 20,000 Years from All Damaging Seismic Ground Motion Events

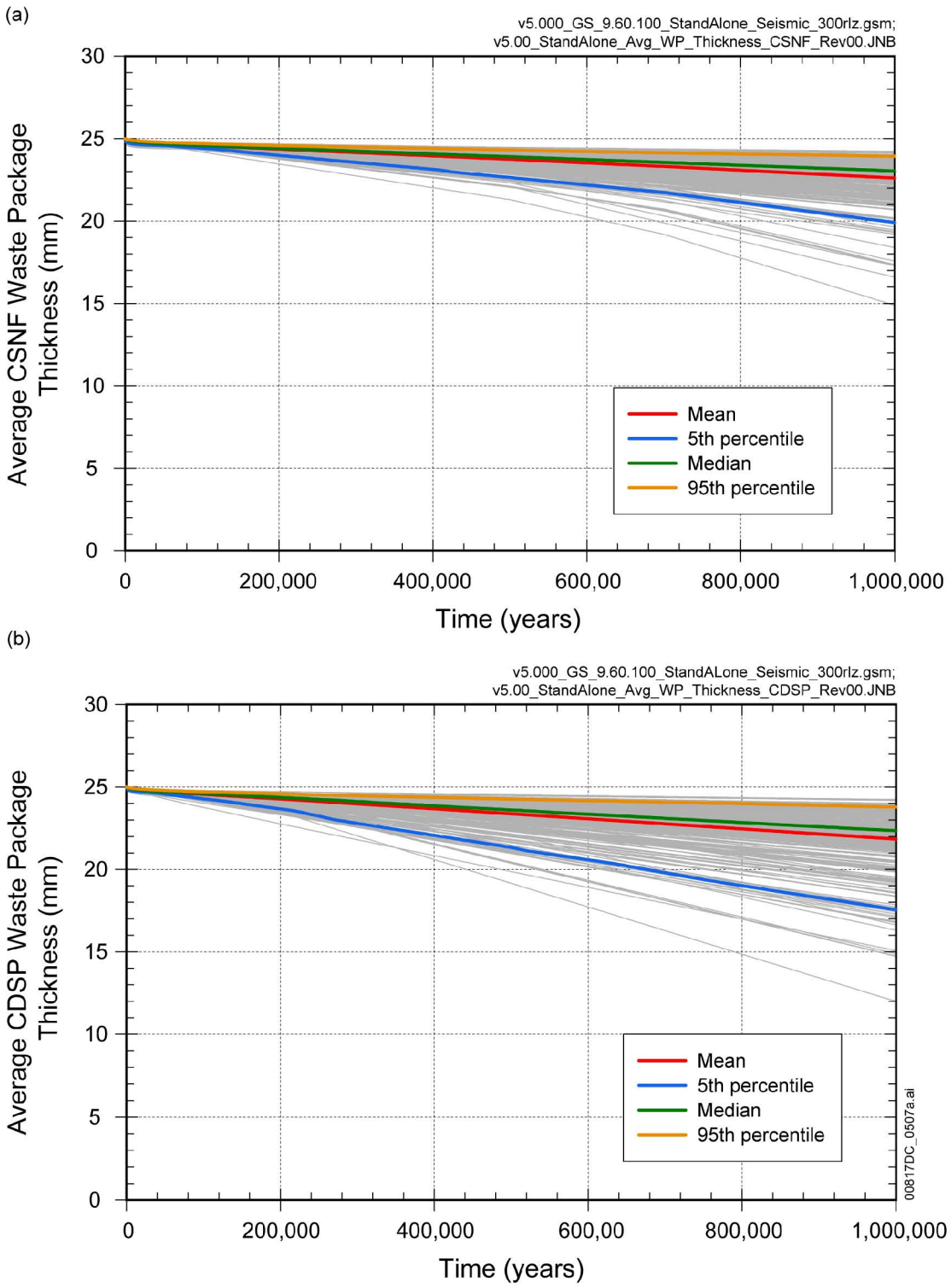

Source: Output DTN: MO0709TSPAWPDS.000 [DIRS 183170].

Figure 7.3.2-15. Spatially-Averaged Waste Package Thickness for 1,000,000 Years for (a) CSNF WPs and (b) CDSP WPs

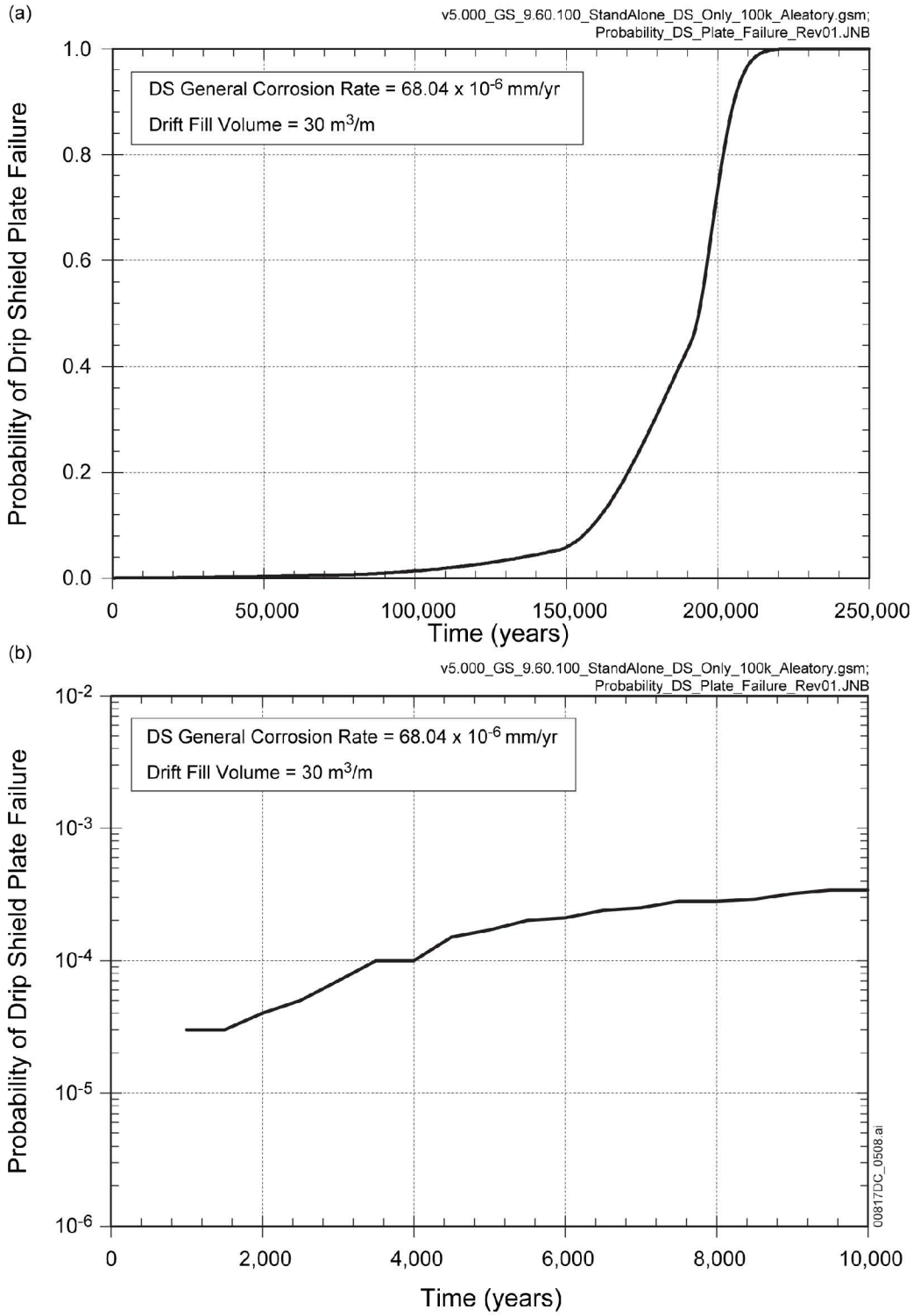

Source: Output DTN: MO0709TSPAWPDS.000 [DIRS 183170].

Figure 7.3.2-16. Bounding Probability of Drip Shield Plate Failure for (a) 250,000 Years and (b) 10,000 Years

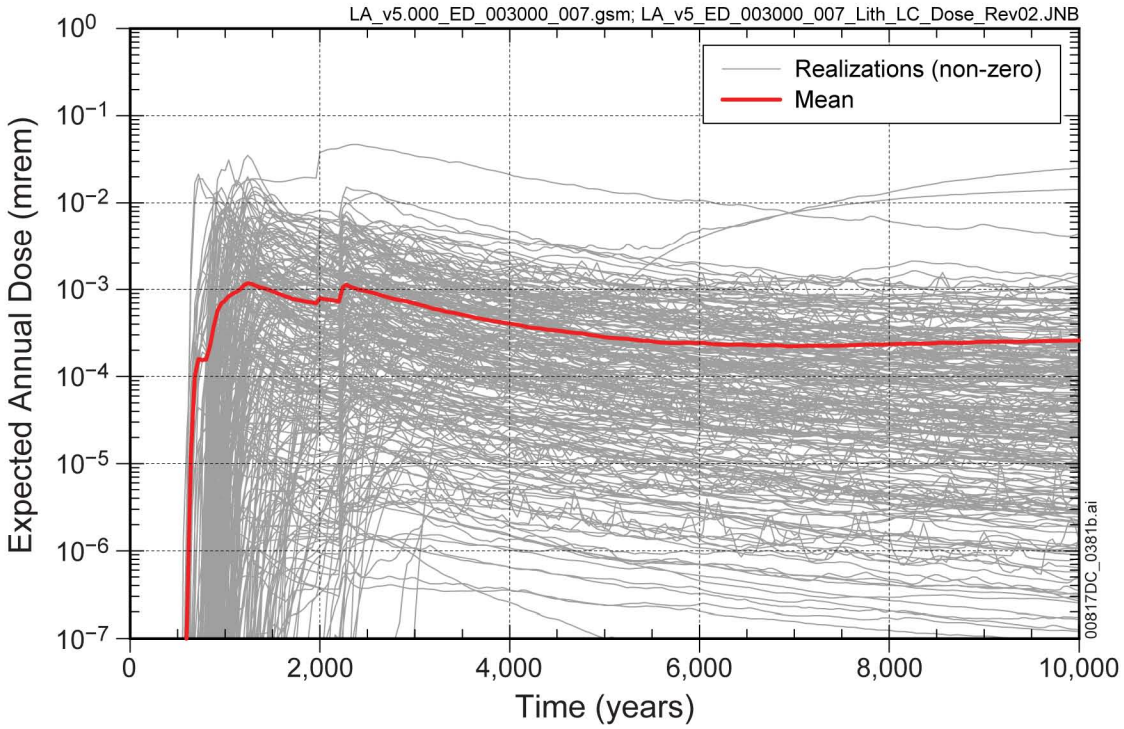

Source: Output DTNs: MO0709TSPAREGS.000 [DIRS 182976] and MO708FREQCALC.000 [DIRS 183006].

Figure 7.3.2-17. Expected Annual Dose Over 10,000 Years from Seismic Ground Motion Events that Result in Drip Shield Plate Failure

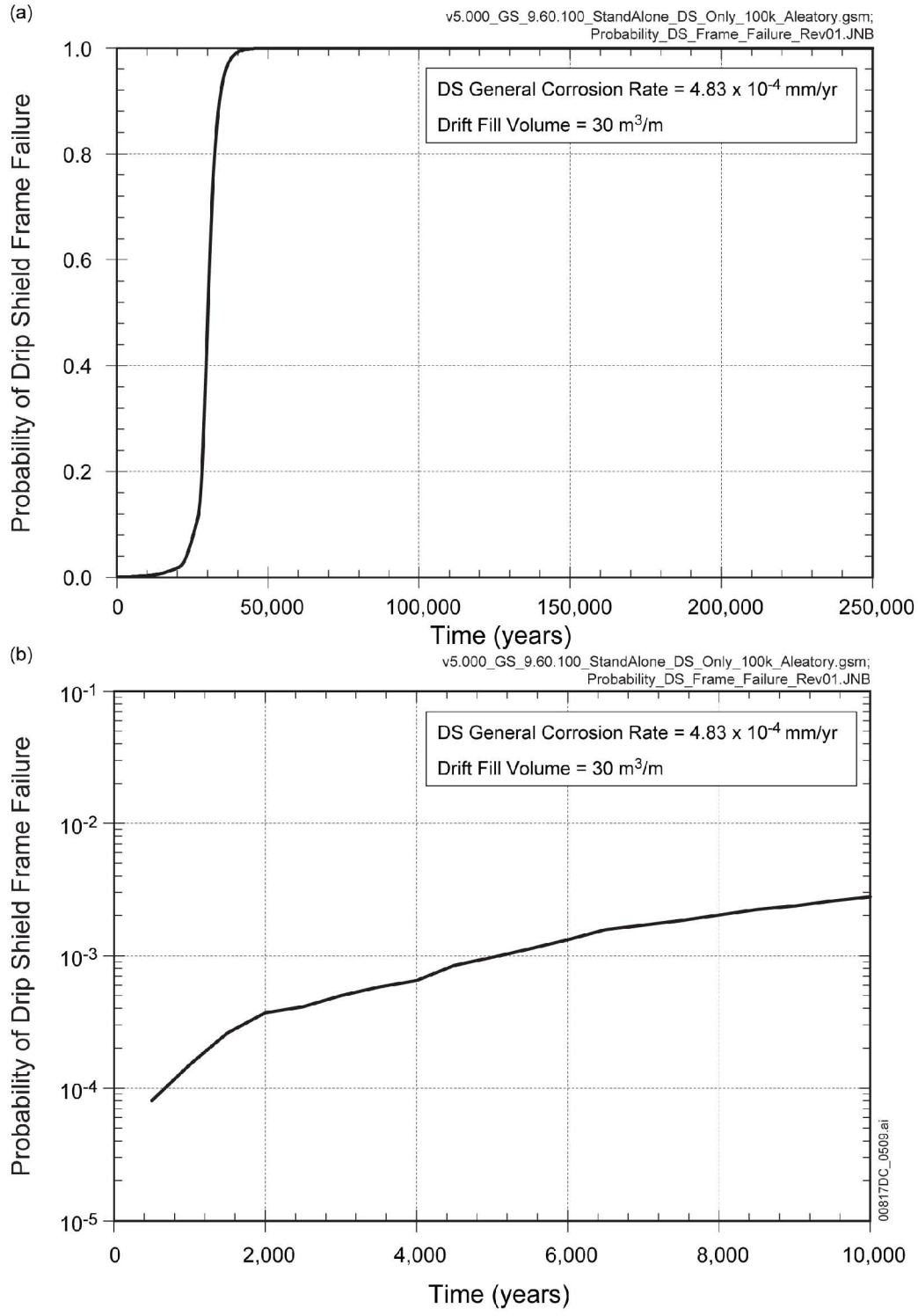

Source: Output DTN: MO0709TSPAWPDS.000 [DIRS 183170].

Figure 7.3.2-18. Bounding Probability of Drip Shield Framework Failure for (a) 250,000 Years and (b) 10,000 Years

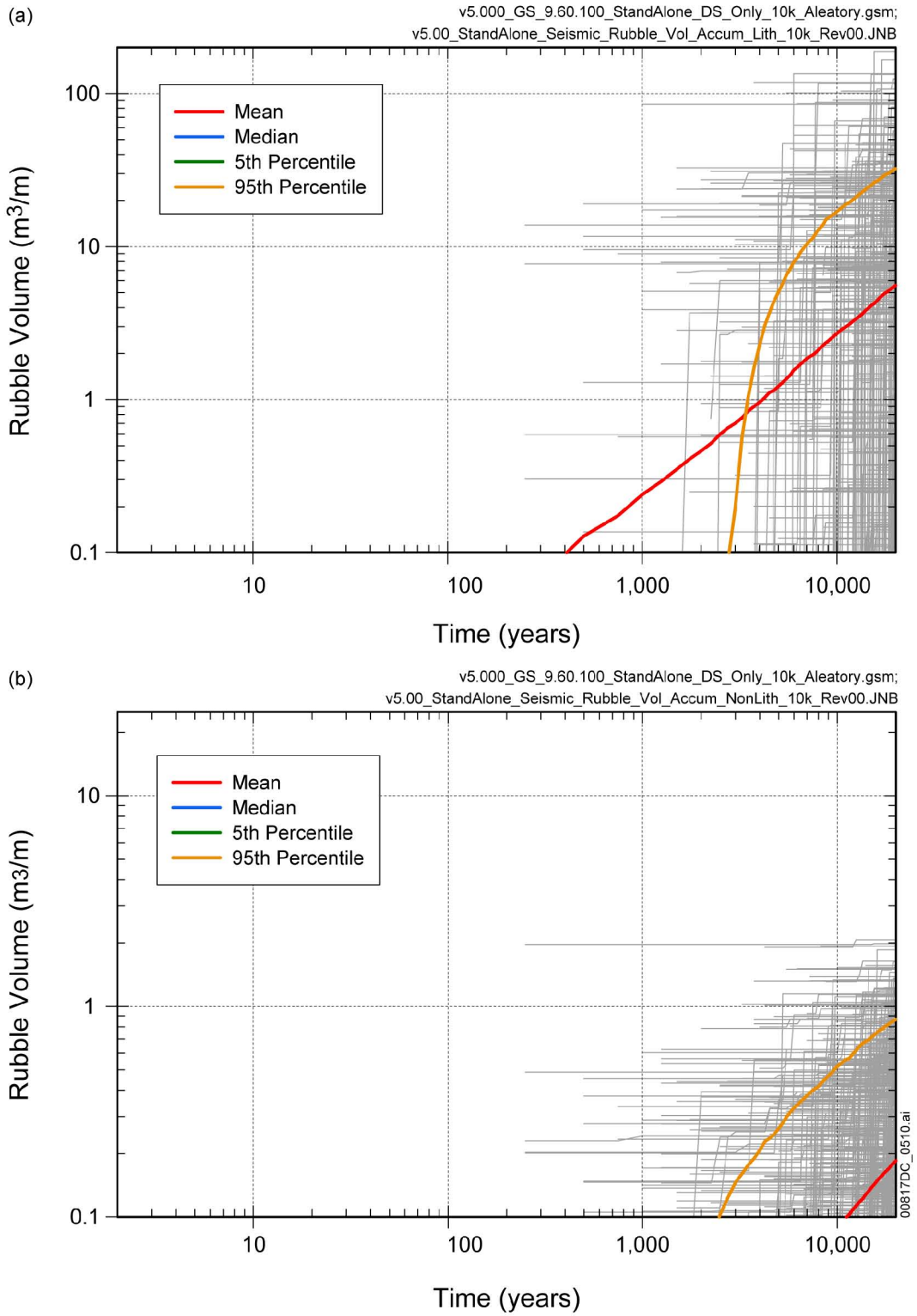

Source: Output DTN: MO0709TSPAWPDS.000 [DIRS 183170].

Figure 7.3.2-19. Volume of (a) Lithophysal and (b) Nonlithophysal Rockfall Over 20,000 Years

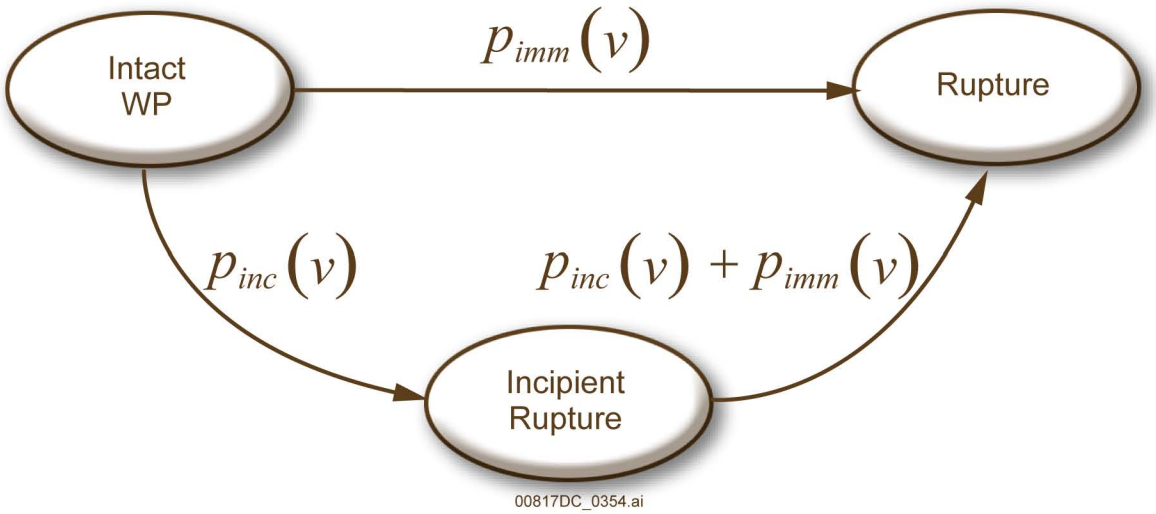

Figure 7.3.2-20. State Diagram for Waste Package Rupture in the Seismic Consequences Abstraction

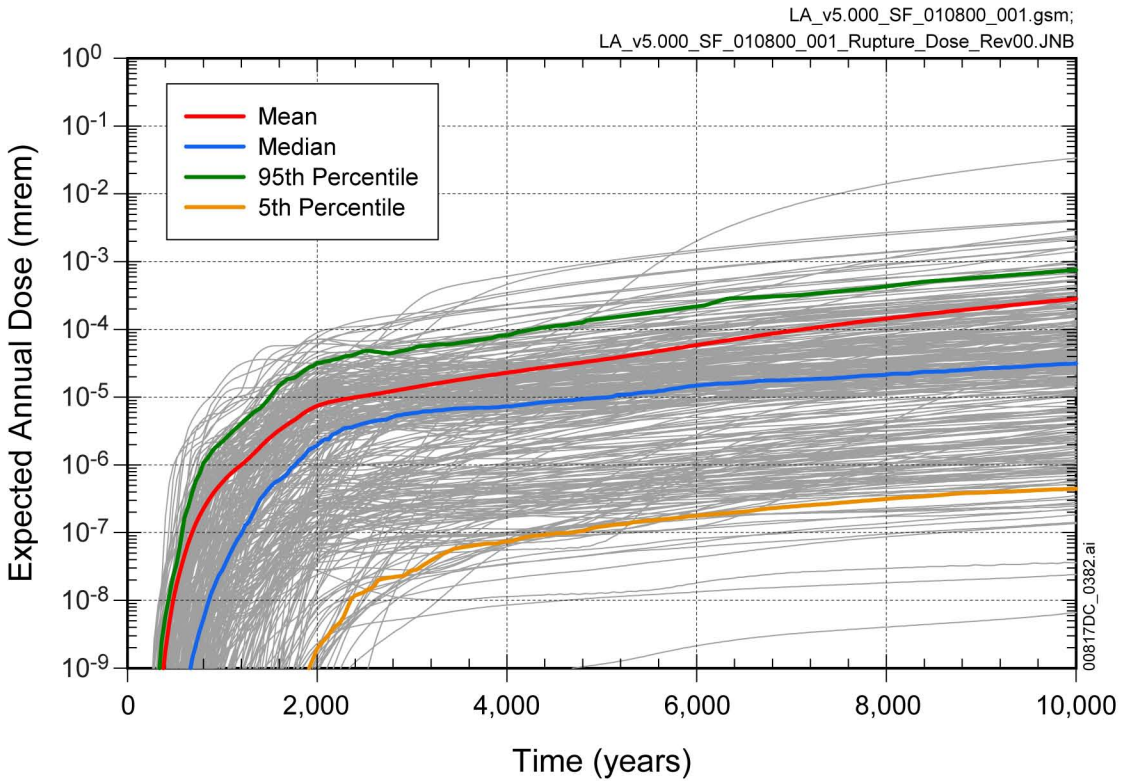

Source: Output DTN: MO0709TSPAREGS.000 [DIRS 182976].

Figure 7.3.2-21. Estimated Expected Annual Dose Over 10,000 Years from Seismic Ground Motion Events that Result in Rupture

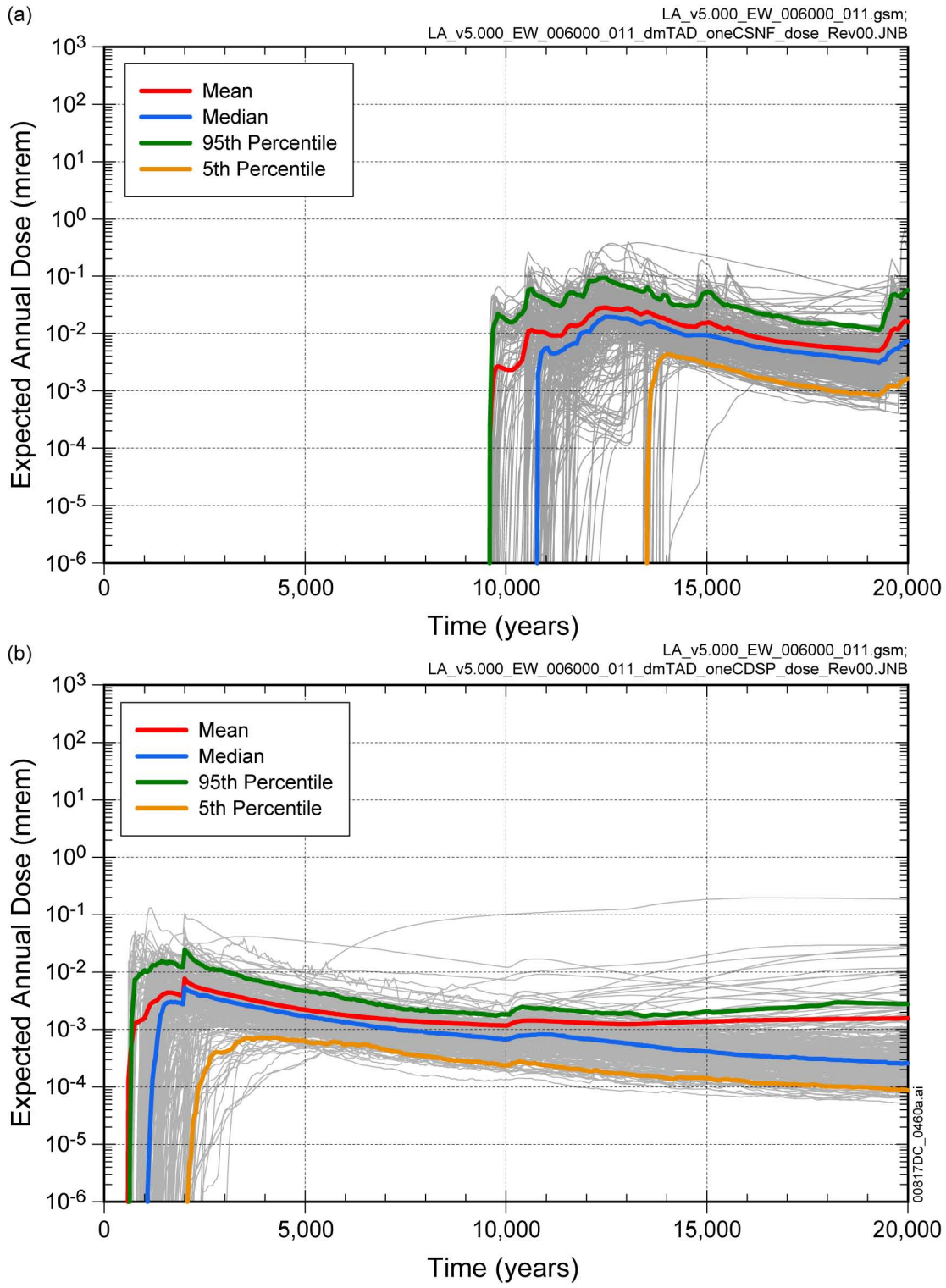

Source: Output DTN: MO0709TSPAREGS.000 [DIRS 182976].

Figure 7.3.2-22. Annual Dose from (a) One Early Failure CSNF WP and (b) One Early Failure CDSP WP Considering All Five Percolation Bins and 300 Epistemic Realizations

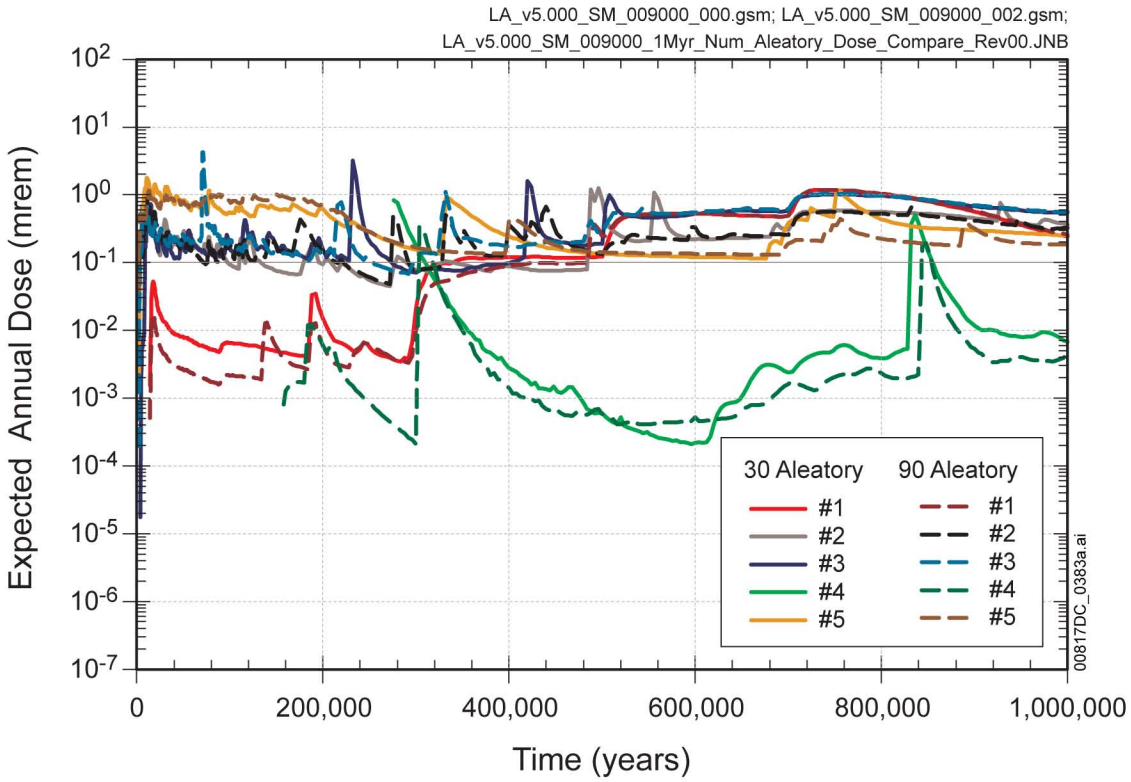

Source: Output DTNs: MO0709TSPASTAB.000 [DIRS 182983] and MO0709TSPAREGS.000 [DIRS 182976].

Figure 7.3.2-23. Expected Annual Dose for 1,000,000 Years from Seismic Ground Motion for Epistemic Realization 2 for Aleatory Sample Size of 30 and 90

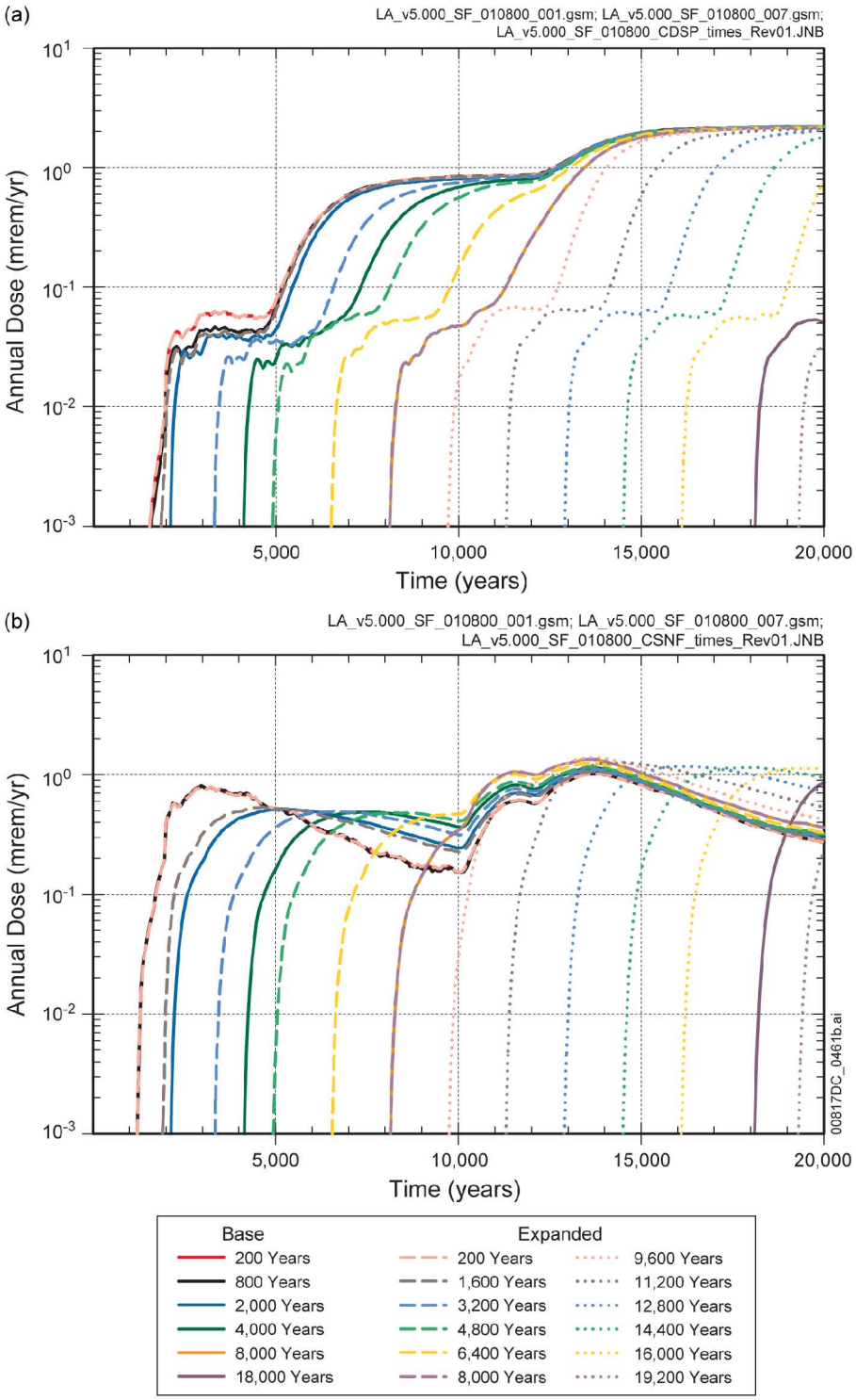

Source: Output DTNs: MO0709TSPASTAB.000 [DIRS 182983] and MO0709TSPAREGS.000 [DIRS 182976].

Figure 7.3.2-24. Annual Dose Over 20,000 Years for Seismic Fault Displacement Modeling Case for (a) CDSP WPs and (b) CSNF WPs Considering Additional Specified Event Times with Constant Damage Area for Epistemic Realization 1

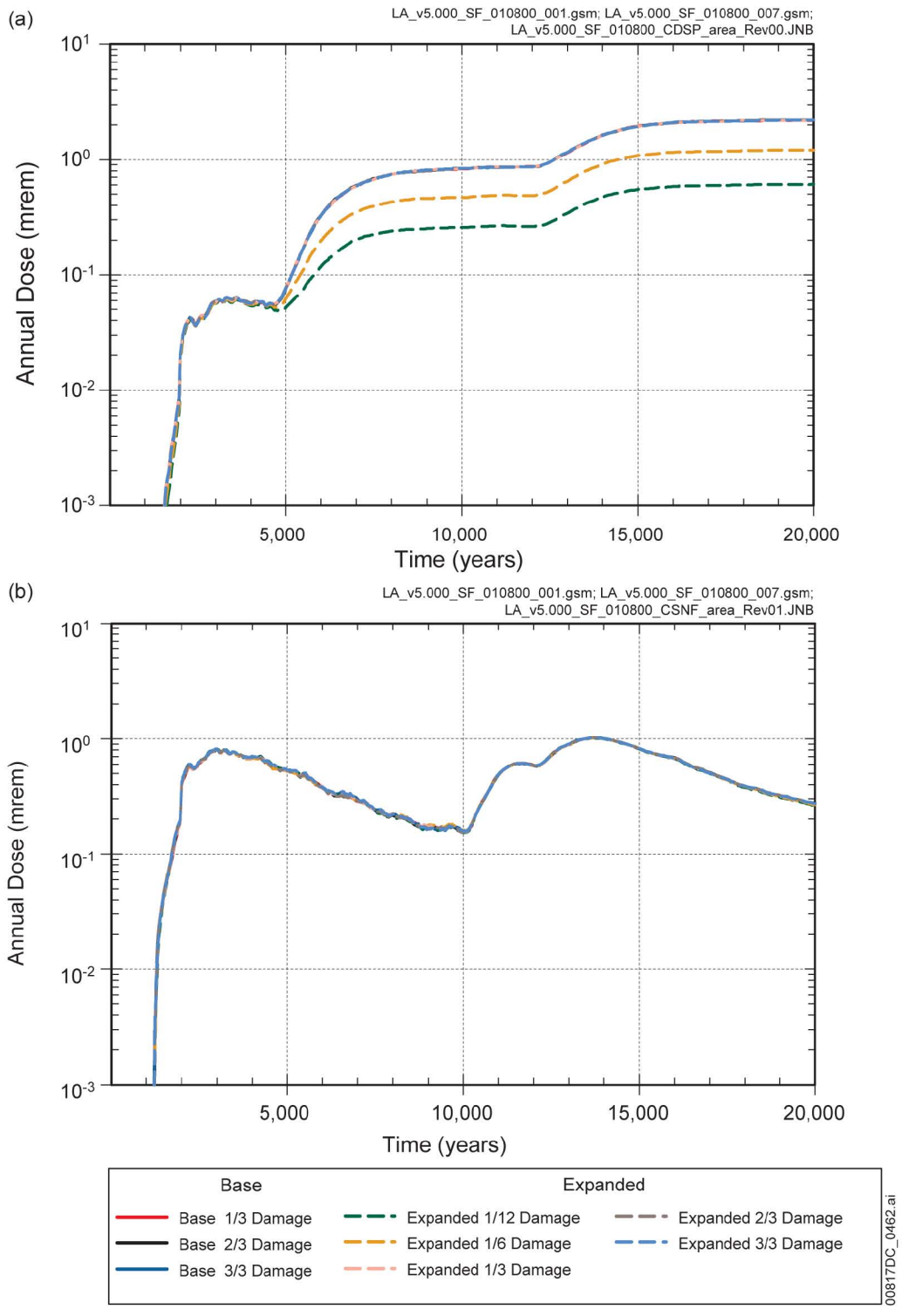

Source: Output DTNs: MO0709TSPASTAB.000 [DIRS 182983] and MO0709TSPAREGS.000 [DIRS 182976].

Figure 7.3.2-25. Annual Dose over 20,000 Years for a Fault Displacement Event at 200 Years Considering Additional Damage Areas for Epistemic Realization 1 for (a) CDSP WPs and (b) CSNF WPs

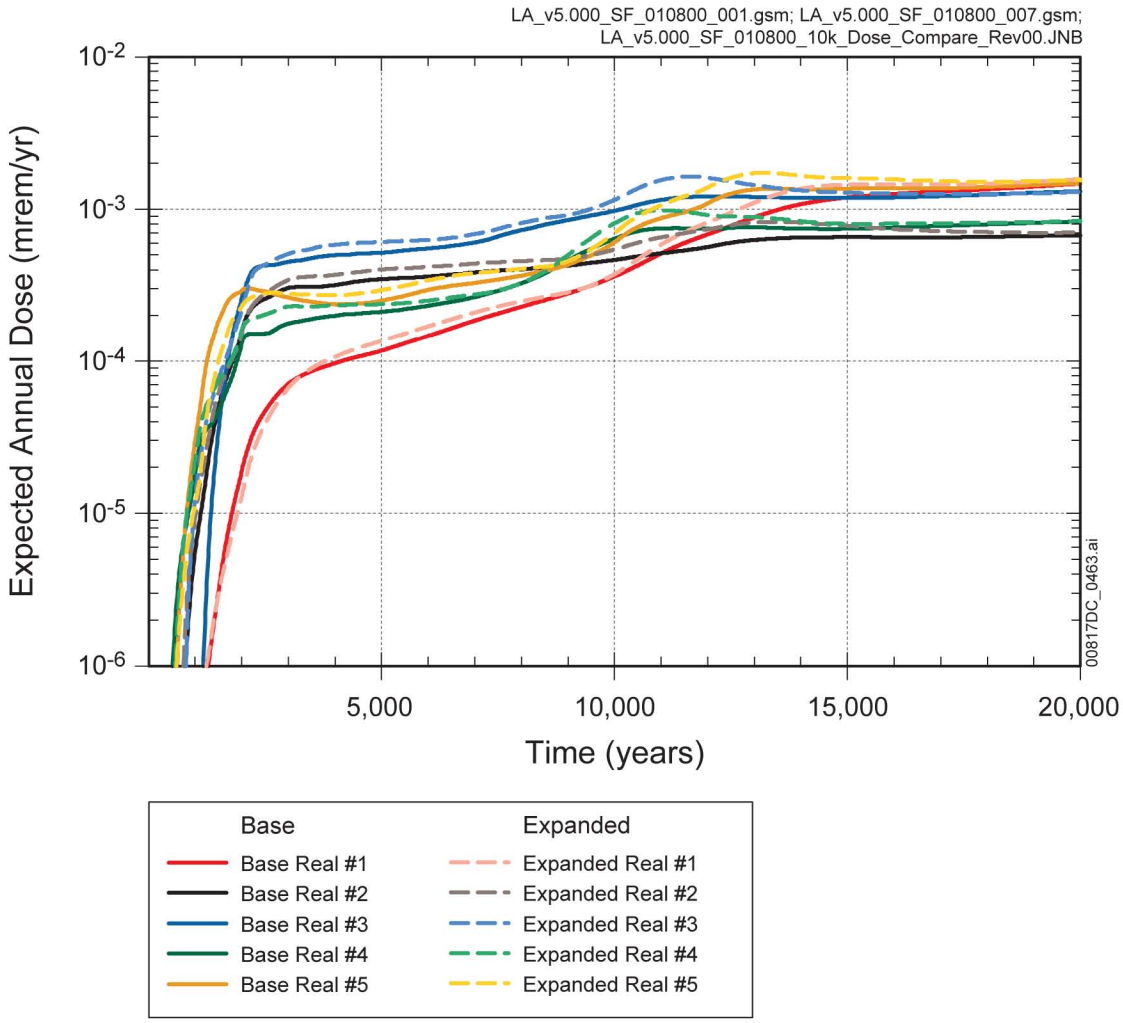

Source: Output DTNs: MO0709TSPASTAB.000 [DIRS 182983] and MO0709TSPAREGS.000 [DIRS 182976].

Figure 7.3.2-26. Expected Annual Dose Over 20,000 Years for Seismic Fault Displacement Modeling Case Considering Additional Specified Event Times and Damage Areas

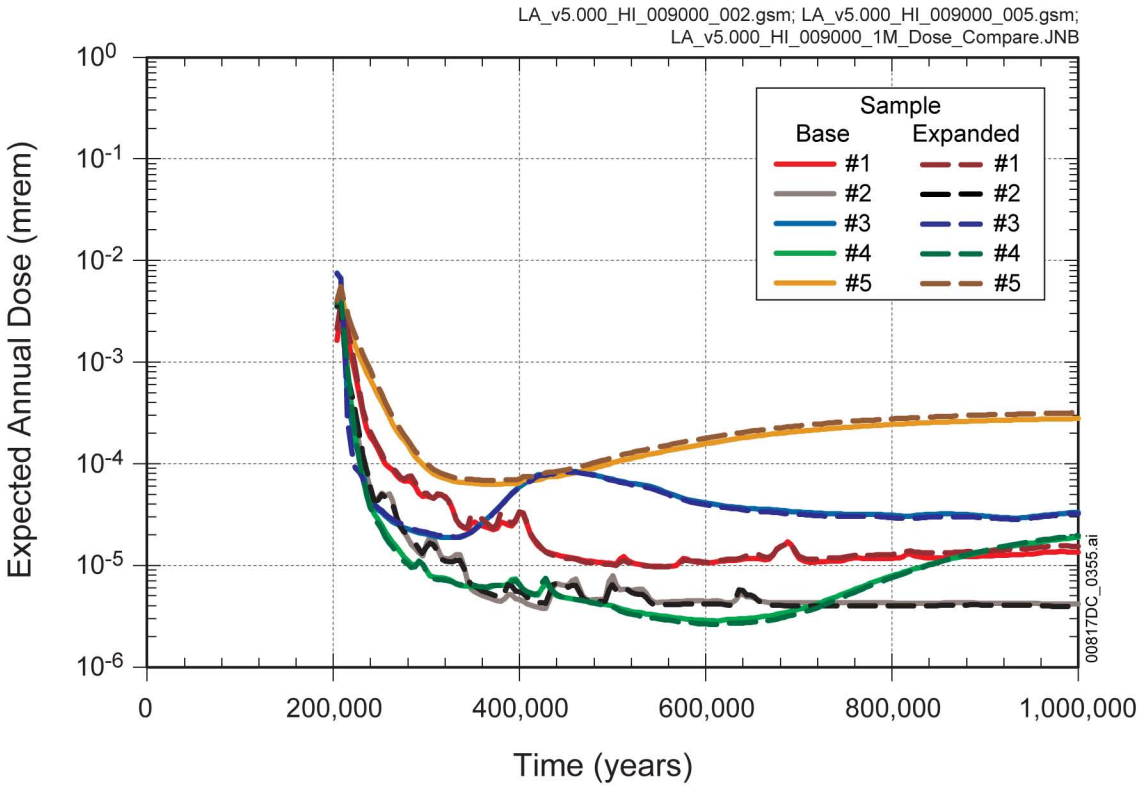

Source: Output DTNs: MO0709TSPAREGS.000 [DIRS 182976]; and MO0709TSPASTAB.000 [DIRS 182983].

Figure 7.3.2-27. Expected Annual Dose Over 1,000,000 Years for Human Intrusion Modeling Case Considering Increased Aleatory Sample Size

INTENTIONALLY LEFT BLANK

7.3.3 Temporal Stability

Another issue related to the stability of the TSPA-LA Model results is temporal discretization of the model. In order to estimate the movement of radionuclides, the TSPA-LA Model solves partial differential equations numerically in various submodels (e.g., FEHM for UZ transport) and model abstractions (e.g., EBS Chemical Environment Submodel). The numerical solution involves computations with discrete timesteps, referred to as temporal discretization. The temporal discretization may affect the accuracy of the solution to the differential equations, and thus affect the outputs of TSPA-LA Model. Several different TSPA-LA Model runs are performed to evaluate the potential for variability in model output due to timestep size. The analysis demonstrates that the output of the TSPA-LA Model is not significantly affected by refining the temporal discretization. Thus, the analysis concludes that the temporal discretization used in the TSPA-LA Model is adequate.

7.3.3.1 Selection of Modeling Cases

The TSPA-LA Model describes repository performance by analyzing the complex system of FEPs; natural disruptive events, such as igneous intrusion, volcanic eruption, seismic ground motion, and fault displacement; and a human-intrusion scenario that could occur at the Yucca Mountain repository after closure during the first 10,000 years and up to the period of geologic stability (1,000,000 years) (NRC Proposed Rule 10 CFR 63.342(c) [DIRS 178394]). The screening and scenario development of FEPs for the TSPA-LA Model are discussed in Section 6.1.1. The modeling cases to address the scenario classes are discussed in Section 6.1.2 and include:

- Nominal Modeling Case
- Drip Shield EF Modeling Case
- Waste Package EF Modeling Case
- Igneous Intrusion Modeling Case
- Volcanic Eruption Modeling Case
- Seismic GM Modeling Case
- Seismic FD Modeling Case
- Human Intrusion Modeling Case.

For each modeling case, separate calculations are performed for two time periods: up to 20,000 years and up to 1,000,000 years.

The Waste Package EF, Igneous Intrusion, Seismic GM, and Human Intrusion Modeling Cases were selected for the temporal stability analysis. These modeling cases are the most influential on repository system performance, and encompass the range of events and processes that result in radionuclide transport. Each modeling case describes repository performance subsequent to failure of parts of the engineered barrier, although the time and nature of the failures varies between modeling cases. When failure occurs, the initial mobilization of radionuclides out of the WP generates an impulse of mass into the models for transport, resolution of which may be dependent upon the timesteps used in the TSPA-LA GoldSim model file.

The Waste Package EF Modeling Case calculation for 20,000 years models the diffusive release of radionuclides from an initial WP failure under an intact DS. During the first 20,000 years, diffusive releases from the WP can vary greatly with time as temperature and relative humidity change (Section 7.7.1.3). The timestep analysis for this modeling case examines both types of WP (CDSP and TAD) in one of the 10 possible environments (percolation bin and dripping conditions). The effect of timesteps on diffusive releases across the environments is examined in the Seismic GM Modeling Case calculation for 20,000 years, which models the diffusive releases that result from seismic events that affect all CDSP WPs in all environments. The Igneous Intrusion Modeling Case for 20,000 years models the release of radionuclides primarily by advection and includes all WPs in all environments.

For the time period of 1,000,000 years, only the Igneous Intrusion Modeling Case is analyzed because this modeling case represents the extreme transient effect of an event that completely compromises the engineered barrier at a single time. In contrast, the Seismic GM Modeling Case describes degrees of degradation and failure of the components of the engineered barrier through time, resulting from corrosion processes and seismic events. The Seismic GM Modeling Case essentially models a series of less extreme events. If the timestep scheme for 1,000,000 years is adequate for the Igneous Intrusion Modeling Case, it is reasonable to expect that this same timestep scheme would be adequate for the Seismic GM Modeling Case.

The Human Intrusion Modeling Case was examined separately because this modeling case uses a different model for transport through the UZ.

The Nominal, Drip Shield EF, and Seismic FD Modeling Cases use the same timestep scheme as is used in the Waste Package EF, Seismic GM, and Igneous Intrusion Modeling Cases. The submodels included in the Nominal, Drip Shield EF, and Seismic FD Modeling Cases differ from the Waste Package EF, Seismic GM, and Igneous Intrusion Modeling Cases primarily in the characterization of failure of parts of the EBS. Radionuclide mobilization and transport are computed with a similar set of sub-models in all of these modeling cases. Therefore, if the timestep scheme is shown to be adequate for the Waste Package EF, Seismic GM, and Igneous Intrusion Modeling Cases, the temporal stability analysis need not be conducted for the remaining modeling cases.

The Igneous Eruption Modeling Case uses a different timestep scheme than the other modeling cases because of the highly-transient nature of the eruptive processes. This timestep scheme employs 1-year timesteps after an eruption. Because the quantity computed by the modeling case is the annual dose (i.e., dose averaged over a year), reducing the timestep below one year is not warranted. No temporal stability analysis was performed for the Igneous Eruption Modeling Case.

7.3.3.2 Methodology

Separate calculations are performed for each of two time periods: 20,000 years and 1,000,000 years following repository closure. For each time period, one base timestep scheme is used for all modeling cases. The base timestep scheme uses shorter timesteps during the period of time immediately following repository closure, when environmental variables such as

temperature and relative humidity are changing more rapidly. As repository environmental conditions become stable, longer timesteps are employed.

The temporal stability of the selected modeling cases was examined by introducing additional, shorter timesteps immediately following the events that fail components of the engineered barrier. For each modeling case, two additional simulations were constructed and run, varying the timestep scheme from the baseline TSPA-LA Model. The baseline TSPA-LA Model timestep scheme and the two alternative timestep schemes used in the modeling cases are presented in Table 7.3.3-1. Each simulation calculated repository performance for the first five of 300 epistemic realizations of the baseline TSPA-LA Model. The timestep analysis was conducted for five epistemic realizations rather than the full set of 300 to reduce the computational burden. It was anticipated that examining five realizations would be sufficient to expose any systematic effect on model results of varying the timesteps. TSPA-LA Model runs with different timestep sizes were compared graphically to determine the effect of refining the timesteps. Due to the high degree of stability evident in the graphical comparison of model results, statistical comparison of model results for different timesteps was not deemed necessary.

7.3.3.3 Waste Package EF Modeling Case

The TSPA-LA models early failures as occurring at repository closure. However, since the DS remains functional in this modeling case, seepage does not contact the early failed WPs, so radionuclides transport out of the WP by diffusion only. Diffusion does not begin until sufficient water is present inside the WP, and the rate of water accumulation depends on temperature and relative humidity within the drift. Consequently, diffusive transport begins at different times for different WPs.

The base-case timestep scheme uses 10-year timesteps until 120 years, followed by 40-year timesteps until 10,000 years, and then 80-year timesteps until 20,000 years. Temporal stability was tested by considering an alternate timestep scheme, which begins with the 10-year timesteps until 120 years and then switches to 20-year timesteps for the remaining duration of the simulation. Because the onset of transport can occur at different times, the alternate timestep scheme uses additional, shorter timesteps throughout the calculation year period.

The Waste Package EF Modeling Case considers a total of twenty possible combinations of aleatory variables: five different percolation subregions, two WP types, and either dripping or non-dripping conditions. Two aleatory combinations were chosen for analysis: CSNF and CDSP WPs, in percolation bin three, with dripping conditions. For each of five epistemic realizations and the timestep schemes listed in Table 7.3.3-1, the annual dose from one early failed WP was calculated. Figure 7.3.3-1 shows the results for both CSNF and CDSP WPs. In both cases, the annual dose is very similar for the two-timestep schemes.

Annual dose for the other eighteen aleatory combinations was computed for both timestep schemes, and the ensemble of twenty dose histories was used to compute expected annual dose as described by Equation 6.1.2-13. Figure 7.3.3-2 shows the expected annual dose for each of five epistemic realizations for the timestep schemes listed in Table 7.3.3-1. The similarity in expected annual dose for the two-timestep schemes confirms that the Waste Package EF Modeling Case is stable with respect to temporal discretization.

7.3.3.4 Igneous Intrusion Modeling Case

In the Igneous Intrusion Modeling Case, annual dose is computed by the GoldSim component of the TSPA-LA Model at each of a set of specified intrusion times (Table 7.3.2-1). For each epistemic realization, the ensemble of dose histories (one for each intrusion time) is used to compute expected annual dose, as described by Equation 6.1.2-16. At the time of an intrusion, the DS and WP cease to isolate the waste from seepage waters. Immediately after an intrusion, relatively large quantities of radionuclides enter the natural system over a few timesteps. Temporal stability was tested for the 1,000,000-year and 20,000-year calculations by considering the alternate timestep schemes listed in Table 7.3.3-1. The alternate timestep schemes add additional, shorter timesteps immediately after the modeled intrusions to provide better resolution of the effects of each intrusion.

For the 1,000,000 year calculation, the intrusion is fixed at 400,000 years. The base-case timesteps are used up to the time of the intrusion. After the intrusion, the first alternate timestep scheme uses 250-year timesteps until 640,000 years and then reverts back to the base-case timestep of 4,000 years until 1,000,000 years. The second alternate scheme uses 25-year timesteps until 424,000 years, then uses the base-case timestep of 4,000 years until 1,000,000 years. Figure 7.3.3-3 shows the annual dose for the second epistemic realization and the three-timestep schemes. The overall shape of the dose history for each epistemic realization is similar for all timestep schemes. Thus, better resolution of the short-term effects of an intrusion, provided by the alternate timestep schemes, does not alter the estimates of the long-term effects of the intrusion.

To examine the short-term effects, Figure 7.3.3-4 focuses on the period immediately after 400,000 years and shows that the alternate timestep schemes result in higher dose that occur earlier than in the base-case timestep scheme. Although radionuclides are released at the same intrusion time in all timestep schemes, the first dose cannot occur until the next time GoldSim timestep (404,000 years in the base case, compared to 400,250 years and 400,025 years in the alternate timestep schemes.)

The dose shown on Figure 7.3.3-4 is the annual dose conditional on the occurrence of an intrusion at 400,000 years. In contrast, the quantities compared to the individual protection standards specified in 10 CFR 63.311 [DIRS 178394] to determine compliance is the total mean annual dose, as defined in Section 6.1.2.2, for the first 10,000 years post closure (10 CFR 63.303(a) [DIRS 178394]); and the median of the projected doses for the period 10,000 years after disposal through the period of geologic stability (10 CFR 63.303(b) [DIRS 178394]). The median annual dose is calculated for each modeling case by first calculating expected annual dose (average over aleatory uncertainty) as described in Section 6.1.2.2 for each realization of epistemic parameters, and then by averaging over the ensemble of expected annual doses. Thus, if the differences shown on Figure 7.3.3-4 do not affect expected annual dose, they also would not affect mean annual dose, and thus would not be important.

To determine if the higher dose values for the alternate timestep schemes affect expected annual dose, expected annual dose was computed for each of five epistemic realizations using an increased timestep scheme similar to that illustrated on Figure 7.3.3-4. One dose history is computed for each epistemic realization and four of the ten specified igneous event times listed

for the base case in Table 7.3.2-1. However, to avoid having to create 10 unique GoldSim files, regardless of a dose history's specified igneous event time, one alternate timestep scheme was used. This alternate timestep scheme used 50-year timesteps for the 4,000-year period immediately following each of the ten specified event times.

Figure 7.3.3-5 shows the expected annual dose results for the five epistemic realizations. Although small variations can be observed for the two timestep schemes, each expected annual dose history's shape and magnitude are similar. Thus, the timestep scheme used in the Igneous Intrusion Modeling Case for 1,000,000 years is adequate. The similarity in expected annual dose occurs because expected annual dose at time τ involves averaging over the dose at time τ from all possible events that could occur prior to time τ. Because the dose that follows an event appears as a pulse, both the magnitude and duration of each pulse influence the expected annual dose. When the alternate scheme with shorter timesteps is used, the pulse of dose that immediately follows an event is larger in magnitude but shorter in duration. Consequently, with the alternate timesteps, the expected annual dose at time τ is determined by fewer, larger pulses of dose prior to τ. However, similar values of expected annual dose result in the base-case timestep scheme, which produces dose pulses of lower magnitude and longer duration. The similarity in expected annual dose shows that the timestep scheme provides sufficient resolution of the annual dose to obtain a stable value for the integral defining expected annual dose.

For the 20,000-year calculation, the intrusion is fixed at 1,000 years. The base-case timesteps are used up to the time of the intrusion. After the intrusion, the first alternate timestep scheme uses ten-year timesteps until 10,000 years and then reverts back to the base-case timesteps until 20,000 years. The second alternate scheme uses one-year timesteps for 1,000 years following the intrusion and then reverts back to the base-case timesteps until 20,000 years. Figure 7.3.3-6 shows the annual dose for each of five epistemic realizations and the three-timestep schemes. The overall shape of the dose history for each epistemic realization is very similar for all three timestep schemes. Figure 7.3.3-7 focuses on the period immediately following the intrusion and shows that, similar to the 1,000,000 year calculation, the finer timestep schemes result in a higher dose that occurs earlier. However, the analysis of the 1,000,000 year calculation showed that the earlier, higher dose observed in the finer timestep scheme did not affect the expected annual dose for 1,000,000 years. Because the differences in dose shown on Figure 7.3.3-7 due to finer timesteps in the 20,000-year calculation are qualitatively similar to those observed on Figure 7.3.3-4 for the 1,000,000-year calculation, the differences in annual dose shown on Figure 7.3.3-7 should not significantly affect the expected annual dose, and the timestep scheme used in the 20,000-year calculation is adequate.

7.3.3.5 Seismic Ground Motion Modeling Case

In the Seismic Ground Motion Modeling Case for 20,000 years, annual dose is computed by the GoldSim component of the TSPA-LA Model at each combination of a specified event time and specified damage fraction (Table 7.3.2-3). For each epistemic realization, the ensemble of dose histories (one for each combination of event time and damage fraction) is used to compute expected annual dose, as described by Equation 6.1.2-22. At the time of a seismic event, damage to the WP allows water to build inside the WP and, when sufficient water is present, radionuclides begin to diffuse out of the WP and into the natural system. The time required for diffusion to begin depends on the area of the WP that is damaged, as well as temperature and

relative humidity in the drift. It is possible that relatively large quantities of radionuclides would enter the natural system over a few timesteps following a seismic event. Temporal stability was tested for the 20,000-year calculation by considering the alternate timestep schemes listed in Table 7.3.3-1. The alternate timestep schemes add additional, shorter timesteps immediately after the modeled seismic event to provide better resolution of the effects of the event.

The event time was fixed at 1,000 years and the damage fraction at 10^{-6}. The base-case timesteps were used up to the time of the event. After the event, the first alternate timestep scheme uses 10-year timesteps until 10,000 years and then reverts to the base-case timestep for the remainder of the calculation. The second alternate scheme uses one-year timesteps until 2,000 years, followed by the base-case timesteps until 20,000 years. Although a fixed combination of event time and damage fraction are investigated in the analysis of timesteps, the results for other combinations of event times and damage fractions would be similar. Figure 7.3.2-9 and Figure 7.3.2-10 illustrate the annual dose resulting from seismic events at two different fixed times for varying damage fractions, and show that the doses resulting from the combinations of event times and damage fractions have different magnitudes but retain similar shape.

Figure 7.3.3-8 shows the annual dose for each of five epistemic realizations and the three timestep schemes. The overall shape of the dose history for each epistemic realization is similar for all timestep schemes. Figure 7.3.3-9 focuses on the annual dose immediately after the seismic event at 1,000 years and shows variations in dose between timestep schemes. The abrupt change in dose just before 2,000 years is due to the change in climate and is not an important feature in the computation of expected annual dose. The dose following the seismic event generally occurs sooner after the event when using the alternate timestep schemes. However, unlike the Igneous Intrusion Modeling Case, the dose does not exhibit a large peak followed by rapid decline but, rather, reaches and maintains a steady state. In the Igneous Intrusion Modeling Case, the engineered barrier does not restrict radionuclide transport after the intrusion; whereas in the Seismic GM Modeling Case, only a small fraction of WP surface is damaged, which in turn constrains the rate of radionuclide transport. The expected annual dose for the Seismic GM Modeling Case will be determined by the magnitude of the steady state dose after the seismic event. Because the magnitude of the steady state dose is similar for the base case and the alternate timestep schemes, the differences in annual dose shown on Figure 7.3.3-9 will have no significant effect on expected annual dose. Therefore, the timestep scheme used in the 20,000-year calculation is adequate.

7.3.3.6 Human Intrusion Modeling Case

In the Human Intrusion Modeling Case, a single stylized intrusion occurs at 200,000 years. Annual dose is computed by the GoldSim component of the TSPA-LA Model for each combination of a sampled intrusion location (characterized by percolation rate and entry point into the SZ) and epistemic realization. For each epistemic realization, the ensemble of dose histories is averaged to compute expected annual dose, as described by Equation 6.1.2-26. At the time of the intrusion, percolation waters begin to flow through the waste, entrain mobilized radionuclides, and transport the radionuclides down the borehole to the SZ. Thus, the dose following an intrusion has a large initial value that rapidly decreases as radionuclide inventory is depleted or decays.

Temporal stability was tested by considering the alternate timestep scheme listed in Table 7.3.3-1. The alternate timestep schemes add additional, shorter timesteps immediately after the drilling intrusion to provide better resolution of the effects of the event. Figure 7.3.3-10 compares the expected annual dose that results from the two timestep schemes and shows that both timestep schemes result in similar long-term doses. Figure 7.3.3-11 focuses on the expected annual dose immediately after the intrusion and shows that the alternate timestep scheme provides better resolution of the dose immediately following the intrusion. Because the expected annual doses are many orders of magnitude below the limit specified in NRC Proposed Rule 10 CFR 63.321 [DIRS 178394], the coarse resolution of expected annual dose provided by the base-case timestep is adequate.

INTENTIONALLY LEFT BLANK

Table 7.3.3-1. Timestep Schemes Used in Temporal Stability Analysis

Modeling Case	Base Case Timestep Scheme	First Alternate Timestep Scheme	Second Alternate Timestep Scheme
Waste Package Early Failure	10 yr from 0 yr to 120 yr 40 yr from 120 yr to 10k yr 80 yr from 10k yr to 20k yr	10 yr from 0 yr to 120 yr 20 yr from 120 yr to 20,000 yr	NA
Igneous Intrusion 1M yr (intrusion occurs at 400,000 yr)	250 yr from 0 to 10k yr 500 yr from 10k to 100k yr 1,000 yr from 100k to 120k yr 2,000 yr from 120k to 160k yr 4,000 yr from 160k to 1M yr	250 yr from 0 to 10k yr 500 yr from 10k to 100k yr 1,000 yr from 100k to 120k yr 2,000 yr from 120k to 160k yr 4,000 yr from 160k to 400k yr 250 yr from 400k to 640k yr 4,000 from 640k yr to 1M yr	250 yr from 0 to 10k yr 500 yr from 10k to 100k yr 1,000 yr from 100k to 120k yr 2,000 yr from 120k to 160k yr 4,000 yr from 160k to 400k yr 25 yr from 400k to 424k yr 4,000 from 424k yr to 1M yr
Igneous Intrusion 20k yr (intrusion occurs at 1,000 yr)	10 yr from 0 yr to 120 yr 40 yr from 120 yr to 10k yr 80 yr from 10k yr to 20k yr	10 yr from 0 yr to 120 yr 40 yr from 120 yr to 1k yr 10 yr from 1k yr to 10k yr 80 yr from 10k yr to 20k yr	10 yr from 0 yr to 120 yr 40 yr from 120 yr to 1k yr 1 yr from 1k yr to 2k yr 40 yr from 2k yr to 10k yr 80 yr from 10k yr to 20k yr
Seismic GM 20k yr (seismic event occurs at 1,000 yr)	10 yr from 0 yr to 120 yr 40 yr from 120 yr to 10k yr 80 yr from 10k yr to 20k yr	10 yr from 0 yr to 120 yr 40 yr from 120 yr to 1k yr 10 yr from 1k yr to 10k yr 80 yr from 10k yr to 20k yr	10 yr from 0 yr to 120 yr 40 yr from 120 yr to 1k yr 1 yr from 1k yr to 2k yr 40 yr from 2k yr to 10k yr 80 yr from 10k yr to 20k yr
Human Intrusion (intrusion occurs at 200,000 yr)	250 yr from 0 to 10k yr 500 yr from 10k to 100k yr 1,000 yr from 100k to 120k yr 2,000 yr from 120k to 160k yr 4,000 yr from 160k to 1M yr	250 yr from 0 to 10k yr 500 yr from 10k to 100k yr 1,000 yr from 100k to 120k yr 2,000 yr from 120k to 160k yr 4,000 yr from 160k to 200k yr 40 yr from 200k to 204k yr 400 yr from 204k to 212k yr 4,000 yr from 212k to 1M yr	NA

Source: Output DTN: MO0709TSPAREGS.000_R0 [DIRS 182976] (for Base Case); and MO0708TSPAVALI.000_R0 [DIRS 182985] (for Alternates).

INTENTIONALLY LEFT BLANK

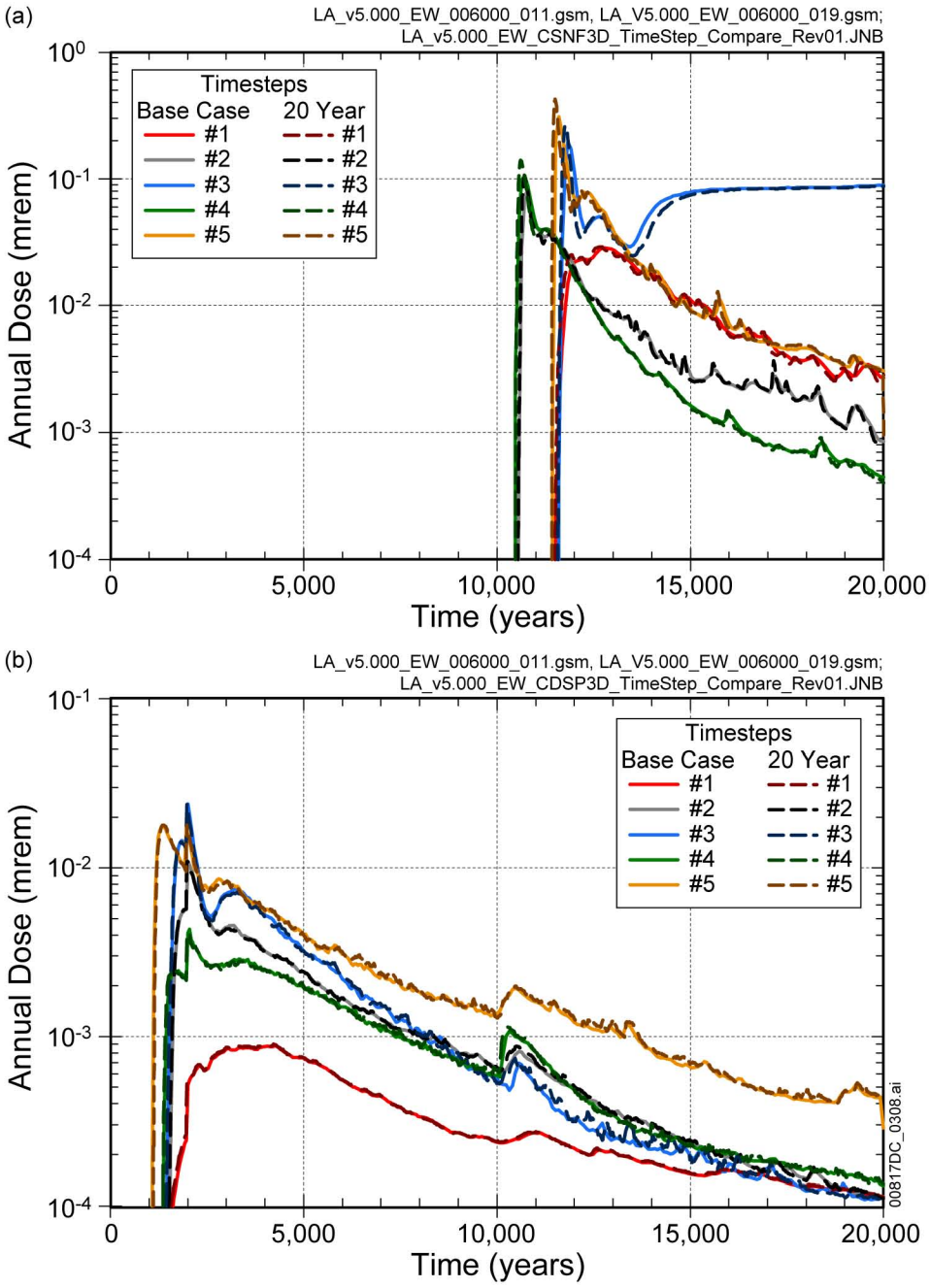

Source: Output DTNs: MO0708TSPAVALI.000 [DIRS 182985]; and MO0709TSPAREGS.000 [DIRS 182976].

Figure 7.3.3-1. Annual Dose from One Early Failed Waste Package for (a) CSNF WP and (b) CDSP WP

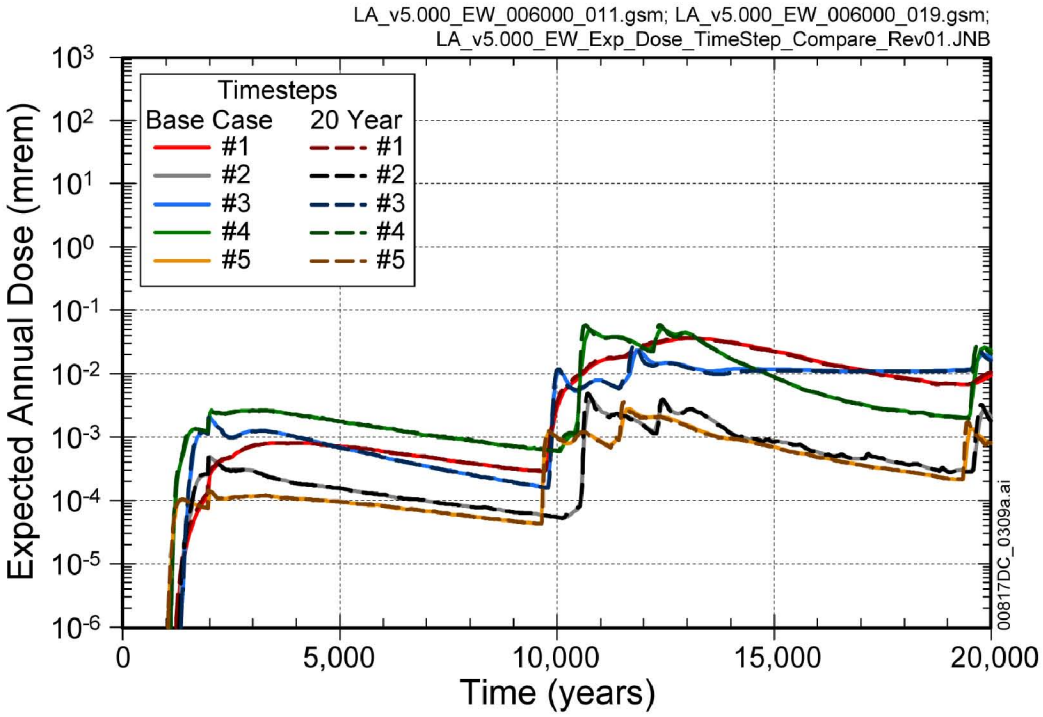

Source: Output DTNs: MO0708TSPAVALI.000 [DIRS 182985]; and MO0709TSPAREGS.000 [DIRS 182976].

Figure 7.3.3-2. Expected Annual Dose from Early Failed Waste Packages for Base Case and 20-Year Timestep Schemes

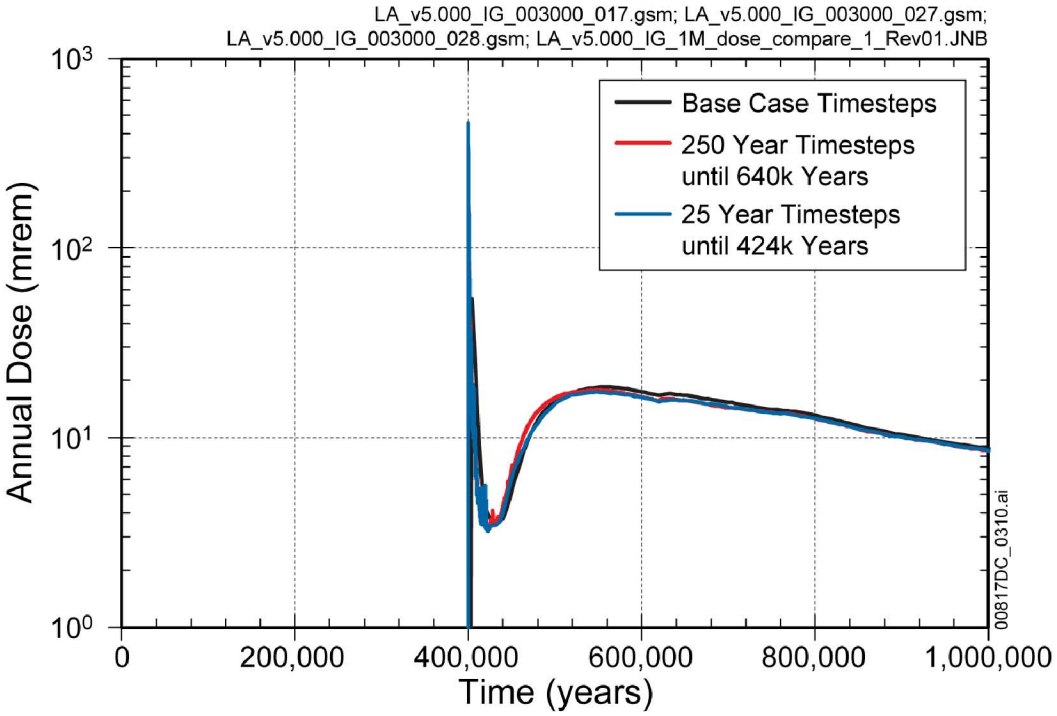

Source: Output DTNs: MO0708TSPAVALI.000 [DIRS 182985]; and MO0709TSPAREGS.000 [DIRS 182976].

Figure 7.3.3-3. Annual Dose from an Igneous Intrusion at 400,000 Years for Three Timestep Schemes for Epistemic Realization 2

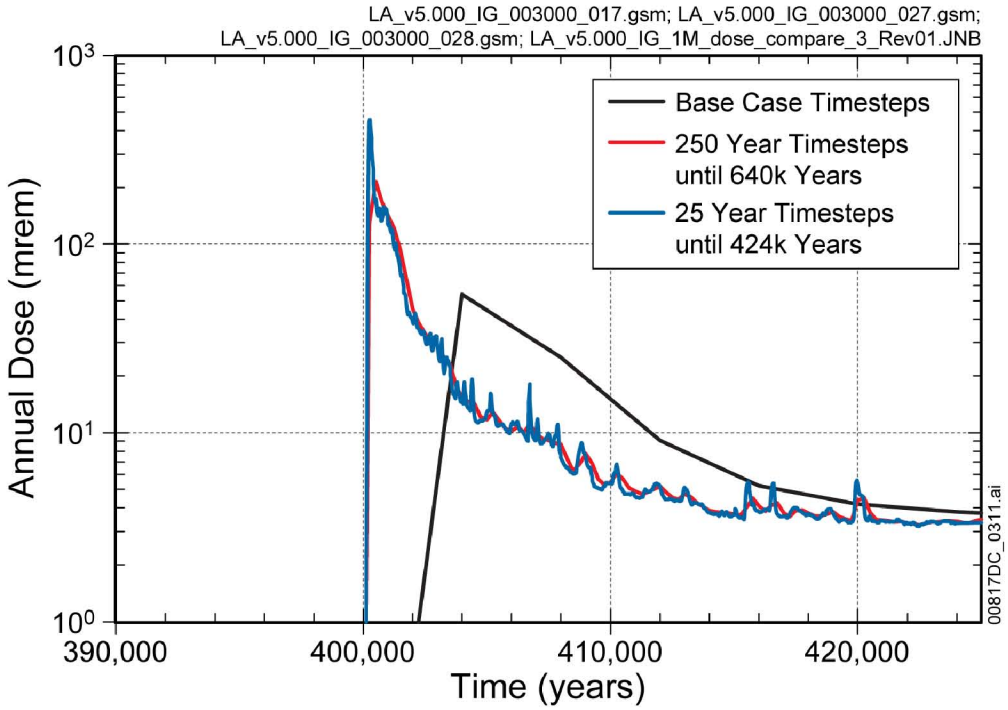

Source: Output DTNs: MO0708TSPAVALI.000 [DIRS 182985]; and MO0709TSPAREGS.000 [DIRS 182976].

Figure 7.3.3-4. Detail of Annual Dose from an Igneous Intrusion at 400,000 Years for Three Timestep Schemes for Epistemic Realization 2

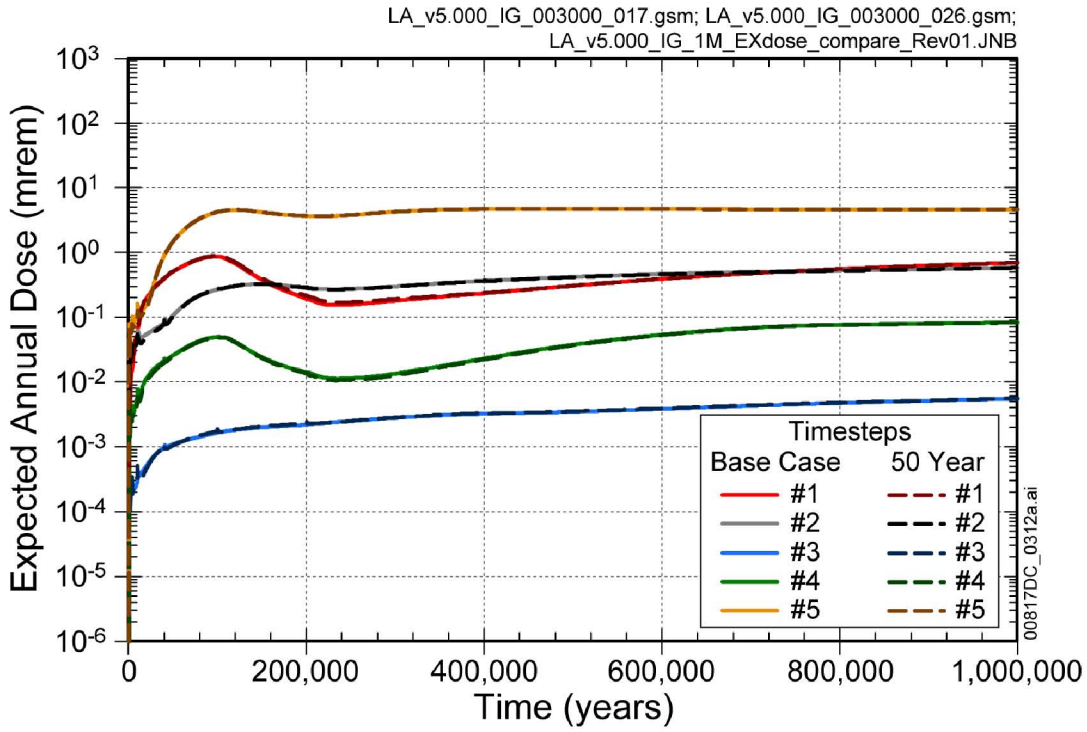

Source: Output DTNs: MO0708TSPAVALI.000 [DIRS 182985]; and MO0709TSPAREGS.000 [DIRS 182976].

Figure 7.3.3-5. Expected Annual Dose from Igneous Intrusion for Base Case and Alternate Timestep Schemes for Five Epistemic Realizations

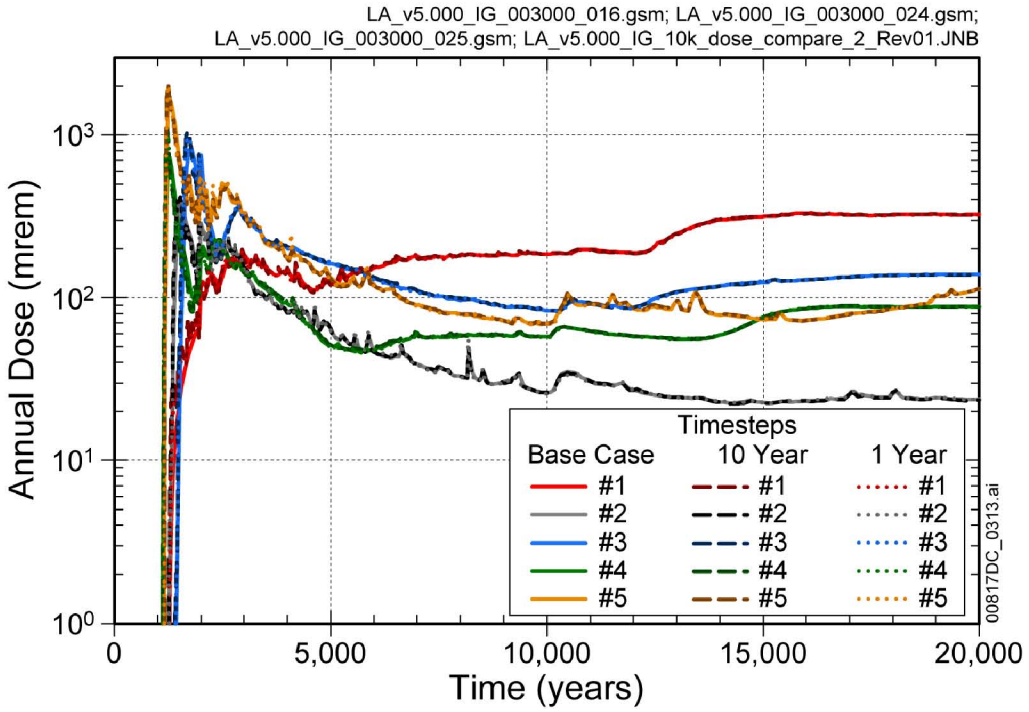

Source: Output DTNs: MO0708TSPAVALI.000 [DIRS 182985]; and MO0709TSPAREGS.000 [DIRS 182976].

Figure 7.3.3-6. Annual Dose from an Igneous Intrusion at 1,000 Years for Three Timestep Schemes

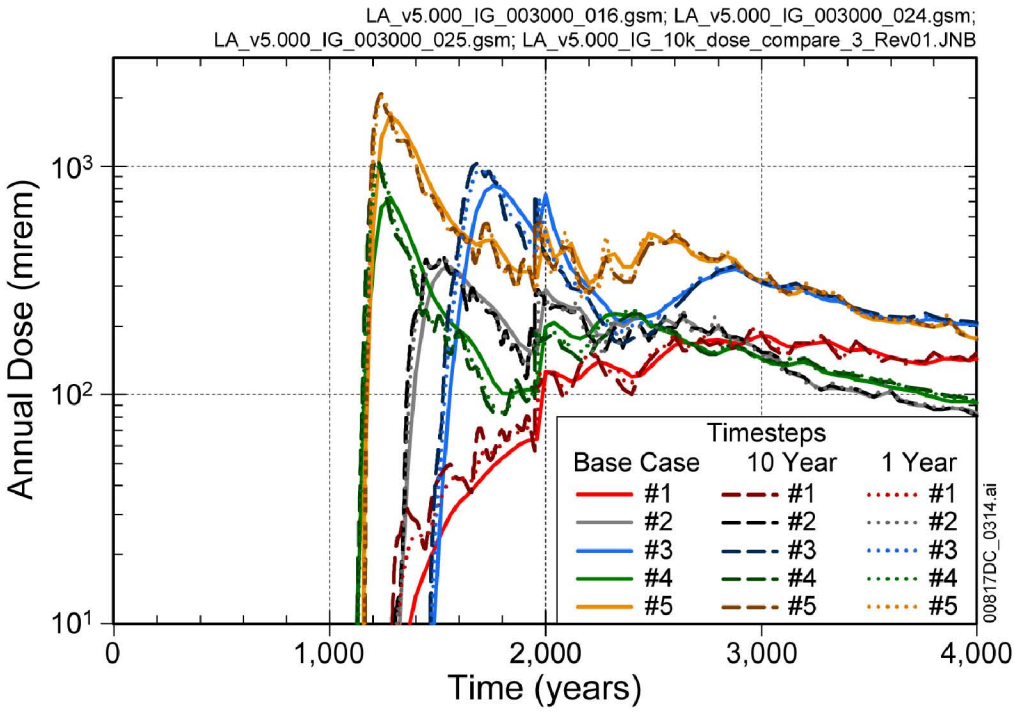

Source: Output DTNs: MO0708TSPAVALI.000 [DIRS 182985]; and MO0709TSPAREGS.000 [DIRS 182976].

Figure 7.3.3-7. Detail of Annual Dose from an Igneous Intrusion at 1,000 Years for Three Timestep Schemes

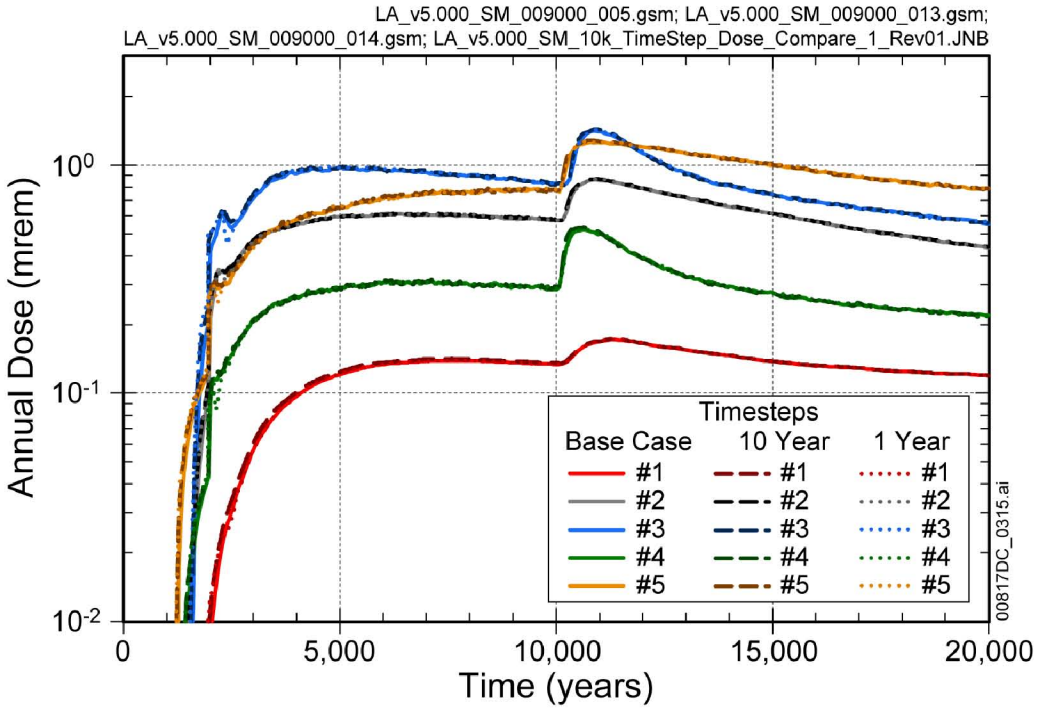

Source: Output DTNs: MO0708TSPAVALI.000 [DIRS 182985]; and MO0709TSPAREGS.000 [DIRS 182976].

Figure 7.3.3-8. Annual Dose from a Seismic Ground Motion Event at 1,000 Years with Damage Fraction 10^{-6} for Three Timestep Schemes

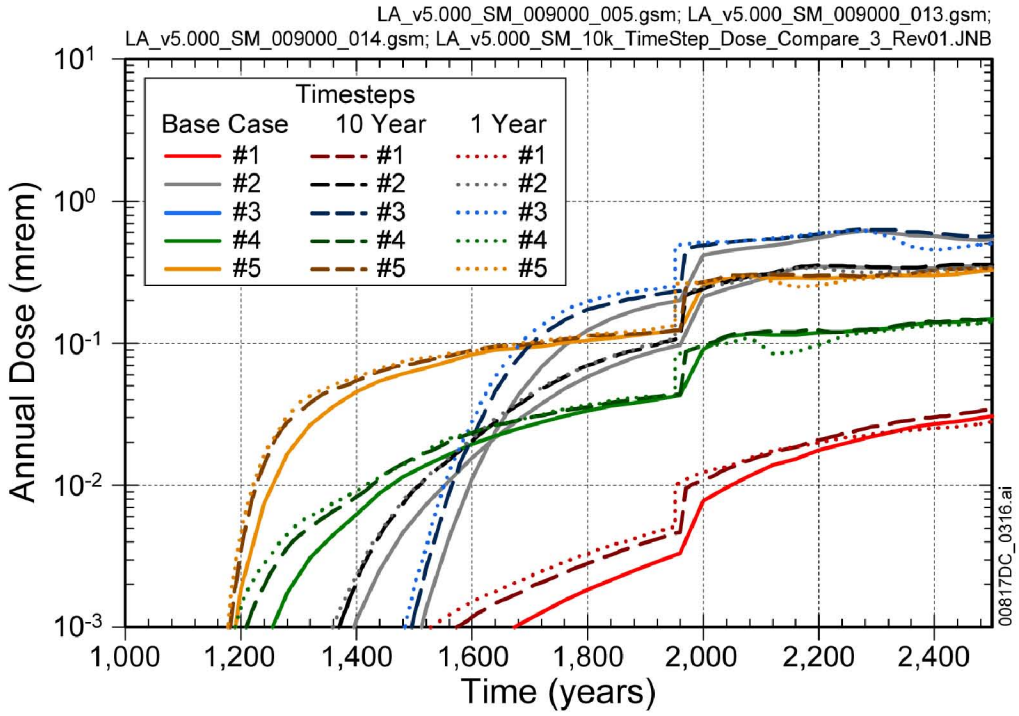

Source: Output DTNs: MO0708TSPAVALI.000 [DIRS 182985]; and MO0709TSPAREGS.000 [DIRS 182976].

Figure 7.3.3-9. Detail of Annual Dose from a Seismic Ground Motion Event at 1,000 Years with Damage Fraction 10^{-6} for Three Timestep Schemes

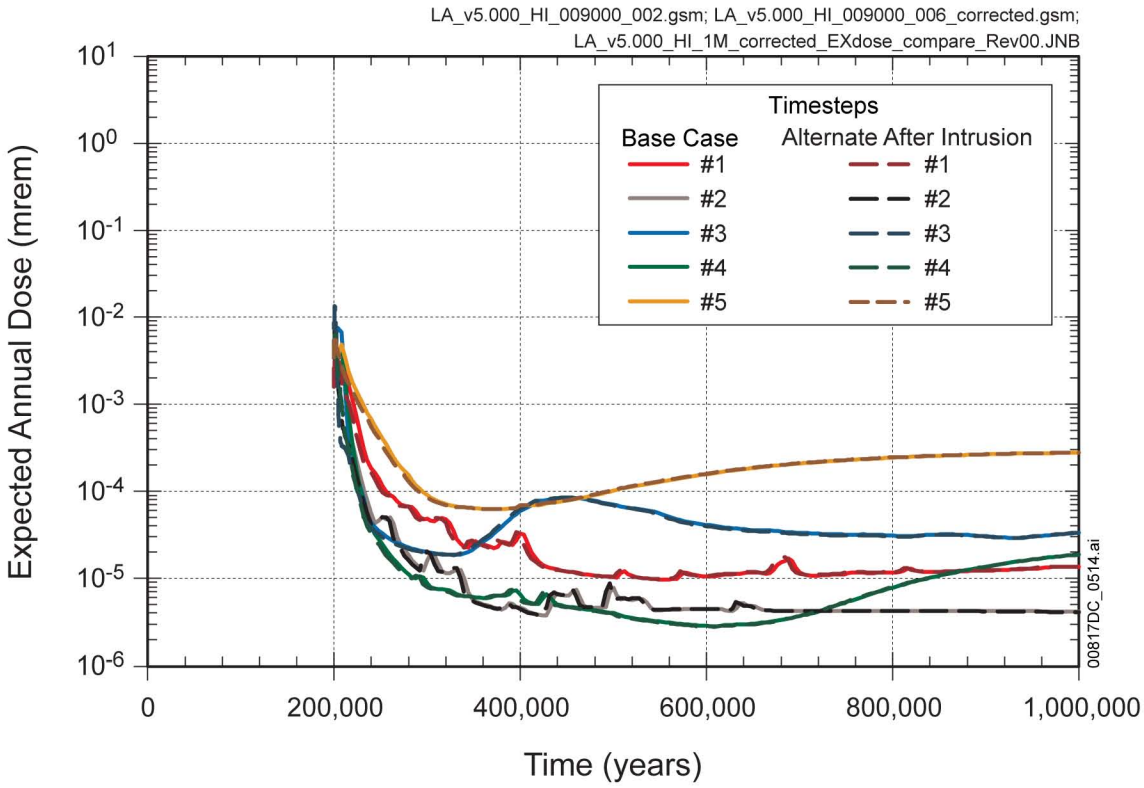

Source: Output DTNs: MO0708TSPAVALI.000 [DIRS 182985]; and MO0709TSPAREGS.000 [DIRS 182976].

Figure 7.3.3-10. Expected Annual Dose from a Human Intrusion Event at 200,000 Years for Two Timestep Schemes

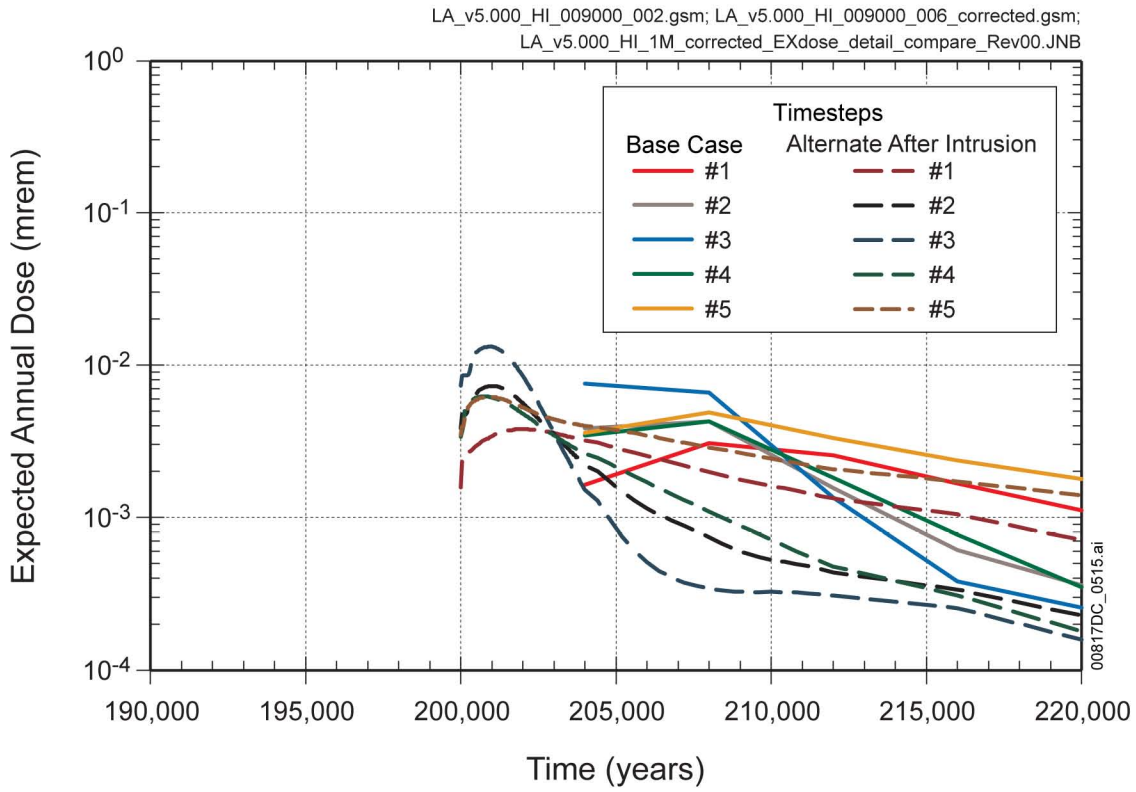

Source: Output DTNs: MO0708TSPAVALI.000 [DIRS 182985]; and MO0709TSPAREGS.000 [DIRS 182976].

Figure 7.3.3-11. Detail of Expected Annual Dose from a Human Intrusion Event at 200,000 Years for Two Timestep Schemes

INTENTIONALLY LEFT BLANK

7.3.4 Analysis of Spatial Discretization

Part of the uncertainty addressed by the TSPA-LA Model deals with the variability associated with spatial discretization of the various model domains. Different scales exist within the TSPA-LA Model relative to how spatially dependent information is used. Spatially discrete information used at one scale (e.g., the Mountain-Scale UZ Flow Submodel, Table 6-1 and Section 6.3.1) may be combined or averaged in order to be used at a different scale (e.g., the Drift Seepage Submodel, Table 6-1 and Section 6.3.3.1, and the Drift Wall Condensation Submodel, Table 6-1 and Section 6.3.3.2). The TSPA-LA Model inherits these different spatial scales from the process models that feed it, namely the Mountain-Scale UZ Flow, EBS TH Environment, UZ Transport, and SZ Flow and Transport abstractions. The spatial discretization and scales of these abstractions are investigated and validated for their intended use in the TSPA-LA within each abstraction's respective model report.

The TSPA-LA Model adds its own spatial domain by subdividing the repository into percolation subregions at the EBS Submodel level. Furthermore, the EBS thermal-hydrologic environment within a percolation subregion is characterized using a subset of the comprehensive TH dataset provided by the Multiscale Thermohydrologic Model (MSTHM) process model and is meant to be representative of the all different TH histories bounded by that particular percolation subregion. The purpose of this spatial discretization within the TSPA-LA is to reduce the model's computational overhead.

The primary purposes of this section are to: (1) summarize the inherited spatial discretization schemes of the process model abstractions that feed the TSPA-LA, (2) describe how the TSPA-LA discretizes the repository domain into percolation subregions, (3) describe and validate the use of representative TH histories within the percolation subregions in-lieu of using the comprehensive TH dataset, and (4) determine what impact, if any, this spatial discretization has on the results of the EBS releases that feed the UZ. The impacts to the TSPA-LA in terms of dose to the RMEI, if any, of the spatial discretization of the EBS releases to the nodes of the UZ within each percolation subregion, and the subsequent discretization of the UZ releases to the SZ, were not considered.

7.3.4.1 Inherited Spatial Discretization within the TSPA-LA

The areas within the TSPA-LA Model where the spatial discretization has been inherited from the upstream process model abstractions include the Mountain-Scale UZ Flow Submodel (Section 6.3.1), EBS TH Environment Submodel (Table 6-1 and Section 6.3.2), UZ Transport Submodel (Table 6-1 and Section 6.3.9), and SZ Flow and Transport Submodel (Section 6.3.10). The TSPA-LA Model implementation of the UZ transport calculations is achieved through the use of the FEHM DLL (Section 6.3.9). The UZ Transport Submodel is directly coupled (i.e., dynamically linked) with the TSPA-LA Model using an external pathway element within the GoldSim software (GoldSim V. 9.60.100 [DIRS 181903]) to link with the UZ transport code, FEHM. The FEHM particle-tracking code transports particles with the same dual-permeability spatial domain used in the Mountain-Scale UZ Flow Submodel (Section 6.3.1) and, therefore, the UZ Transport Submodel uses the same spatial discretization as the underlying Site-Scale UZ Flow Process Model and, hence, the variabilities associated with these spatial domains are coincident.

The SZ Flow and Transport Model Component of the TSPA-LA Model is used to evaluate the transport of radionuclides from their introduction, at the water table, to the accessible environment that is approximately 18 km downgradient from the repository (Section 6.3.10). A 3-D SZ Flow and Transport Process Model was developed to calculate the flow and transport of radionuclides through the SZ to the accessible environment. The output from the 3-D SZ Flow and Transport Process Model is provided to the TSPA-LA Model as 200 breakthrough curves for each of the four source saturated zone source regions and 12 radionuclide groups. This results in 9,600 spatially discretized unit-source radionuclide breakthrough curves (as discussed in Section 6.3.10.2). Within the TSPA-LA Model, a convolution integral technique combines these randomly sampled radionuclide breakthrough curves with the time-varying radionuclide sources from the UZ to quantify radionuclide transport to the accessible environment (as discussed in Section 6.3.10.3). This approach has been validated for the 3-D SZ Flow and Transport Abstraction, as documented in *Saturated Zone Flow and Transport Model Abstraction* (SNL 2008 [DIRS 183750], Section 7.1.1).

The EBS TH Environment Submodel implements the TH environment in and around an emplacement drift from the MSTHM Abstraction (Table 6-1 and Section 6.3.2). The MSTHM Process Model Abstraction results include the spatial discretization of TH conditions of the EBS and its components, as well as the variability of these results due to uncertainties with the percolation flux and the host-rock thermal conductivity inherited from the Site-Scale UZ Flow Process Model. These spatially discretized inputs to the TSPA-LA are provided by the MSTHM Process Model Abstraction at two scales, a fine-scale or comprehensive data set which is appropriate for determining WP failure histories due to general or localized corrosion, and a coarse-scale or representative data set, which is sufficient for capturing waste-form mobilization and transport processes. This scheme involves the discretization of the repository domain into a specified number of subregions based upon percolation flux, and each subregion's TH conditions are characterized by a subset of the comprehensive TH dataset that is meant to be representative of the TH conditions everywhere within that specific percolation subregion. This spatial discretization scheme, and the appropriateness of its use in the TSPA-LA to measure repository performance, is discussed in the following sections.

7.3.4.2 Spatial Discretization of the TSPA-LA into Percolation Subregions

Spatially discretizing the repository into subregions is a balance between a minimum number of subregions that would adequately capture the variability of the EBS TH environment across the footprint and the increased computational burden associated with each additional subregion. As described in Section 6.3.2, five percolation subregions were used. These five repository percolation subregions were selected in order to maximize the ability of the TSPA-LA Model to include spatial effects when sensitivity analyses and alternative scenarios were analyzed.

7.3.4.2.1 Percolation Flux as a Basis for Discretizing the Repository

Percolation flux at the base of the PTn has a primary role in determining the long-term in-drift TH environment (SNL 2007 [DIRS 181383], Section 6.3.2.1). Subregions in the repository footprint with similar percolation fluxes have similar long-term TH conditions, such as WP temperature or drift-wall temperature. However, using the percolation flux to determine the in-drift TH environment may not capture the short-term TH behavior like WP peak temperature,

which occurs within the first few decades after repository closure. Percolation flux, for use as a subregion selection parameter, has a temporal advantage over parameters, such as WP temperature or drift-wall temperature. Parameters such as WP or drift-wall temperature could have similar peaks from one subdomain location to another but have much different temperature histories over the course of time. TH environment variables, such as invert flux, that are used in EBS Transport Model Components (e.g., the EBS-UZ Interface Submodel, Table 6-1) have a short dry-out period at the beginning of the postclosure period (during the ramp up of heat in the repository), followed by long rewetting periods as the heat pulse decays (SNL 2007 [DIRS 181383], Section 6.3.3). The use of percolation flux as a parameter to define subregions in the repository footprint can be more predictive of the availability of liquid at a subdomain location than either the WP or drift-wall temperature because it remains constant during the duration of each climate period. In addition, percolation flux at the base of the PTn is used directly as input to the Drift Seepage Submodel and the Drift Wall Condensation Submodel and is abstracted from the UZ flow fields to be used as a direct input to the UZ Transport Submodel. In summary, percolation flux at the base of the PTn was selected as the primary parameter to discretize the repository into subdomains because:

- TH response in the emplacement drifts is sensitive to percolation flux (SNL 2007 [DIRS 181383], Section 6.3.2)
- Chemical environment for radionuclide mobility is driven by TH conditions (Section 6.3.4)
- Percolation flux is the boundary condition for the Drift Seepage Submodel (Table 6-1), and variability in drift seepage is the primary cause of variability in advective radionuclide releases from the EBS (Section 6.3.3).

7.3.4.2.2 Binning the Percolation Subregions by Quantiles

The process used to assign or bin each of the 3,264 MSTHM Process Model subdomains to each of the five repository percolation subregions is described in DTN: LA0702PANS02BR.001_R1 [DIRS 180322] and SNL 2008 [DIRS 184748], Section 6.5.15[a]. Note that only the first three climate states were considered in the analysis used to find a single zone file with five sets of source nodes that best represents all the infiltration/climate combinations. The subdomains comprising each of the five repository percolation subregions were chosen based on the cumulative probability of percolation for the 12 flow fields (three different climates: present-day, monsoon, and glacial-transition; each climate is categorized with 4 infiltration scenarios: 10th percentile, 30th percentile, 50th percentile, and 90th percentile). A four-step binning process was applied to each of the twelve flow fields, resulting in a list of repository subdomains divided into five percolation subregions that share common percolation fluxranges, based on the cumulative probability intervals for these subregions (SNL 2008 [DIRS 184748], Section 6.5.15[a]). The cumulative probability intervals for these five subregions of percolation rates sorted in ascending order are 0.0-0.05, 0.05-0.30, 0.30-0.70, 0.70-0.95, and 0.95-1.00 (SNL 2008 [DIRS 184748], Section 6.5.15[a]). The quantiles are shown in Table 6.3.2-2. An analysis of the degree of similarity or difference of the results of the binning process depending on which flow field is considered was performed. The results indicated that the bins for the 12 flow fields are quite similar to one another. As noted in *Particle Tracking Model and*

Abstraction of Transport Processes (SNL 2008 [DIRS 184748], Section 6.5.15[a]), if a subregion is identified for a particular subdomain in the glacial-transition, 10th percentile flow field, it is very often identified as the same subregion for the other flow fields. When they are different, they almost always differ by only one subregion; that is, a 3 in one flow field becomes a 4 in another flow field, or a 2 becomes a 1. Based upon this result, it was considered acceptable to use subregions from one flow field to approximate all infiltration scenarios and climate states. Therefore, the 10th percentile infiltration scenario for the glacial transition climate was used to define the five percolation subregions for all simulations including the post-10,000-year climate. The five percolation subregions are shown graphically on Figure 6.3.2-7. There are 163; 817; 1,300; 820; and 164 subdomains (i.e., different TH data sets) for Percolation Subregions 1, 2, 3, 4, and 5, respectively. The following points should be noted:

- The subregions are not completely contiguous in space but are located throughout the repository in different regions.
- Each subregion includes both edge and interior repository subdomain locations.
- The five selected subregions have a fixed set of repository subdomain locations for all realizations of the TSPA-LA Model, regardless of percolation flux, host-rock thermal conductivity, or climate state.
- The range of percolation flux values calculated for each percolation subregion will be different depending on the percolation flux and/or host-rock thermal conductivity scenario being considered and/or climate state.

7.3.4.3 Variability Analysis of the Engineered Barrier System Thermal-Hydrology within the TSPA-LA

To characterize the variability in repository TH conditions, the MSTHM Process Model subdivides the drifts in the repository footprint into 3,264 equal-area subdomains corresponding to 20-m repository drift segments (SNL 2007 [DIRS 181383], Section 6.2.12[a]). For each of the 12 percolation flux/host-rock thermal conductivity cases (Table 6.3.2-3), the MSTHM Abstraction includes the time-dependent TH variables, temperature, and relative humidity for six different possible CSNF WPs and two different possible CDSP WPs at each of the 3,264 repository subdomains (SNL 2007 [DIRS 181383], Tables 5.4-1 and 6.3-13, and Section 6.2.17[a]). In addition, the MSTHM Abstraction includes time-dependent values for DS temperature and relative humidity, average drift-wall temperature, the duration of boiling at the drift wall, the average invert temperature, the average invert saturation, and the average invert flux for each of the 3,264 repository subdomains. In all, that makes 19,584 different TH histories associated with CSNF WPs and 6,528 different TH histories associated with the CDSP WPs for each of the 12 infiltration/host-rock thermal conductivity cases. This comprehensive data set is used for the WAPDEG and seepage DLLs of the TSPA-LA. As for the TSPA-LA submodels that require TH inputs and feeds, the use of this comprehensive data set is not feasible with respect to computer simulation time and resources. Therefore, the MSHTM Process Model also provides an abstraction of the comprehensive TH data set by first grouping 3,264 repository subdomains into one of the five repository percolation subregions as described above. Next, the MSTHM Process Model determines a representative TH history associated with a single CSNF

WP and a single CDSP WP for each percolation subregion. These representative TH data are then used as input to the EBS Submodel and propagated throughout the rest of the TSPA-LA Model. The purpose of the TH variability analysis discussed in the following section is to demonstrate the appropriateness and validity of using the representative TH histories as inputs to the EBS Submodel of the TSPA-LA as opposed to using the comprehensive data set.

7.3.4.3.1 Use of Representative Thermal-Hydrology Histories Compared to the Comprehensive Thermal-Hydrology Histories

To conduct the analysis, the TSPA-LA Model was exercised over a range of percolation flux percentiles, host-rock thermal conductivities, and percolation subregions that represent the range of TH conditions from the driest and hottest, to the wettest and coolest, with appropriate conditions in between. Radionuclide releases from the EBS for a one million year compliance period were used as the benchmark for comparison between the two types of TH histories (i.e., representative versus comprehensive) invoked over the range of TH conditions described above. Since there is both a diffusive and an advective component to the release of radionuclides from the EBS, comparisons were made for both the Drip Shield EF (advection dominated transport) and the Waste Package EF (diffusion dominated transport) Modeling Cases.

For the runs using a representative TH data set, the TSPA-LA Model was run over a specified number of realizations corresponding to the number of subdomains for a specific percolation subregion but with the key epistemic and aleatory variables of infiltration and host-rock thermal conductivity fixed to be the same for each realization. By fixing these variables, the same representative TH history was used over the course of each respective run. For the Drip Shield EF Modeling Case, only a single DS over a CSNF WP and a single DS over a CDSP WP was allowed to fail during each realization. In similar manner, only a single CNSF WP and a single CDSP WP were allowed to fail for the Waste Package EF Modeling Cases.

For the runs using the comprehensive TH data set, a different implementation strategy was needed. This strategy involved the use of a single Monte Carlo realization coupled with the ability of the GoldSim software to loop over the number of subdomains associated with a specific percolation subregion. As was done for the runs using the representative TH data set, the key epistemic and aleatory variables of infiltration and host-rock thermal conductivity, and percolation subregion, were fixed for the single realization. In this case, however, the number of loops for that single realization, rather then the number of realizations, corresponded to the number of subdomains within the specified percolation subregion. To reduce the computational time of these runs to a more manageable quantity (days instead of weeks), only one of the six TH histories associated with the six CSNF WPs at each subdomain (or loop) was used, and only one of the two TH histories associated with the two CDSP WPs at each subdomain (or same loop) was used. These were chosen stochastically using discrete distributions each time the model looped to the next subdomain.

Table 7.3.4-1 outlines the TH variability cases that were run (output DTN: MO0708TSPAVALI.000 [DIRS 182985]). As an example, TH variability case LA_v5.000_ED_000300_002 represents the Drip Shield EF run where the representative TH was used that is associated with the 10th percentile infiltration, the low host-rock thermal conductivity value, and percolation subregion number one. This case was run for 163 Monte

Carlo realizations using the same set of representative TH data, where 163 represents the number of subdomains in percolation subregion one. For each realization, a single DS failure was forced to occur and, subsequently, a single WP was failed when conditions allowed. The TH variability comparison case, LA_v5.000_ED_000300_007, loops 163 times during a single Monte Carlo realization, failing a single DS and subsequent WP per loop. Each loop stochastically selects one of six CSNF TH histories and one of two CDSP TH histories for the subdomain associated with that loop, for a total of 163 different CSNF and CDSP TH histories. In the end, running 163 realizations with a single early failure is the same as running one realization with 163 early failures (one for each loop) but with the caveat that the single realization run uses 163 different TH histories per WP type versus one TH history per WP type for the multiple realization run.

7.3.4.3.2 Results of the Engineered Barrier System Thermal-Hydrology Variability Analysis

For each set of TH variability runs outlined in Table 7.3.4-1, a comparison of the means of the radionuclide cumulative releases of ^{99}Tc, ^{129}I, and ^{239}Pu from the EBS is the benchmark by which the appropriateness and validity of using a representative TH history over a comprehensive TH history is gauged. Figure 7.3.4-1(a) shows the EBS releases for the two cases described in the example above. That is, the case that used the representative TH data set compared to the case that used the comprehensive TH data for the Drip Shield EF Modeling Case, 10th percentile infiltration, low host-rock thermal conductivity, and Percolation Subregion 1. After about 1,000 years, the EBS cumulative release of these radionuclides is very similar for both the representative and comprehensive TH data sets. The same behavior is shown on Figures 7.3.4-2(a), 7.3.4-3(a), 7.3.4-4(a), and 7.3.4-5(a) for the other infiltration percentile, host-rock thermal conductivity, and percolation subregion cases.

The EBS releases that used the TH histories from the comprehensive data set generally begin earlier than the cases that used a representative TH history. The exception occurs for the cases that use the 90th percentile infiltration and high host-rock thermal conductivity where the releases from the EBS are initiated at about the same times. Figures 7.3.4-1(b) through 7.3.4-5(b) compare the CSNF WP temperature histories below 100°C for the representative and comprehensive TH data sets. The CSNF WP temperature histories for the representative TH data sets are similar to the means of the CSNF WP temperature histories associated with the comprehensive TH data set for each respective infiltration percentile, host-rock thermal conductivity, and percolation subregion case. This illustrates that the representative TH can be used as a surrogate for the comprehensive TH data set. The WP temperatures from the comprehensive TH data sets have lower and upper bounds. Since the TSPA-LA Model requires the WP temperature to drop below 100°C before transport from the EBS can be initiated, and since there is some spread between the lower bound and the mean CSNF WP temperatures from the comprehensive TH data set, the EBS releases from these cases start earlier than those that used the representative TH data.

Figures 7.3.4-6a through 7.3.4-10a show the EBS cumulative releases of ^{99}Tc, ^{129}I, and ^{239}Pu from the EBS for the Waste Package EF Modeling Case. The Waste Package EF Modeling Case is characterized by a relatively early EBS release from the CDSP WPs, followed later by an upward shift in cumulative release due to the failure of the CSNF WPs. The magnitudes of EBS releases from the cases that use the representative TH data is very similar to the releases from the

cases that use the comprehensive TH data sets after about 10,000 years. As was the situation with the Drip Shield EF Modeling case discussed previously, EBS releases from CDSP WPs occur sooner for the cases that use the comprehensive TH data set. This is again attributable to the times at which the WP temperatures drop below 100°C. EBS releases from the CSNF WPs also occur sooner for the cases that use the comprehensive TH data set. This is attributable to a 95 percent relative humidity threshold for EBS transport applied to CSNF WPs by the TSPA-LA Model for WP early failure cases. Figures 7.3.4-6b through 7.3.4-10b demonstrate this behavior by showing the representative relative humidity histories for CSNF WPs compared to the mean and lower and upper bounds of relative humidity histories from the comprehensive TH data sets.

In summary, in the Waste Package Early Failure Modeling Case, the EBS releases of ^{99}Tc, ^{129}I and ^{239}Pu tend to occur earlier in cases that use the comprehensive TH data sets than in cases that use the representative TH data, from either CDSP or CSNF WPs. However, the cumulative mass released from either type of WP is the same for both TH data sets. In particular, the equivalence in cumulative mass of these radionuclides released from CDSP WP can be observed in Figure 7.3.4-6(a) though Figure 7.3.4-10(a), for the time period before roughly 9,500 years. Before 9,500 years, radionuclides are diffusing only from CDSP WPs, because the relative humidity in CSNF WPs has not yet reached 95%, as shown in Figure 7.3.4-6(b) through Figure 7.3.4-10(b). The earlier release from CSNF WPs, and the equivalence in cumulative mass released from CSNF WPs, are also shown in Figure 7.3.4-6(a) though Figure 7.3.4-10(a), with the earlier release beginning at roughly 9,500 years and the equivalent cumulative releases being achieved at about 12,000 years.

The Drip Shield Early Failure Modeling Case, as modified for this analysis, demonstrates that the use of comprehensive or representative TH data results in equivalent cumulative releases from one WP. The Waste Package Early Failure Modeling Case, as modified for this analysis, demonstrates that the use of comprehensive or representative TH data results in equivalent cumulative releases from one WP, although the releases may occur earlier when using the comprehensive TH data. As demonstrated by Figure 8.1-3(a), total mean annual dose prior to 10,000 years is attributable primarily to radionuclides released due to igneous intrusion and seismic ground motion events. After an igneous intrusion, the EBS components (DS and WP) are destroyed, thus, radionuclide mobilization and transport is similar to that observed in the Drip Shield Early Failure Modeling Case. As demonstrated in Section 7.3.2.6, the mean annual dose from seismic ground motions events prior to 10,000 years is attributable to damage caused to CDSP WPs lying under functional drip shields. Because the damage consists of cracks, and the drip shield remains functional, radionuclide mobilization and transport in the Seismic Ground Motion Modeling Case is similar to that observed in the Waste Package Early Failure Modeling Case results for CDSP WPs. Because the mean annual dose at each time is determined by averaging over the dose resulting from all possible preceding events (as well as over uncertainty in input parameters), the mean annual dose is primarily determined by the cumulative release of radionculides, rather than the instantaneous release rates. Therefore, the use of either the comprehensive or representative TH data would produce equivalent estimates of mean annual dose, because the cumulative radionuclide releases from WPs are equivalent for the two data sets.

INTENTIONALLY LEFT BLANK

Table 7.3.4-1. Summary of the Thermal-Hydrologic Variability Cases Run to Validate the Use of Representative Thermal-Hydrologic Data Sets Over the Use of Computationally Expensive Comprehensive Thermal-Hydrologic Data Sets

Thermal –Hydrologic Variability Case ID	Modeling Case	Thermal-Hydrologic Data Set	Infiltration Percentile	Thermal Conductivity Case	Percolation Subregion	Number of Loops	Number of DS and/or WP Failures per Loop	Total Number of DS and/or WP Failures
LA_v5.000_ED_000300_002	DS EF	Representative	10th	Low	1	1	163	163
LA_v5.000_ED_000300_007	DS EF	Comprehensive	10th	Low	1	163	1	163
LA_v5.000_ED_000300_003	DS EF	Representative	10th	Low	3	1	1,300	1,300
LA_v5.000_ED_000300_008	DS EF	Comprehensive	10th	Low	3	1,300	1	1,300
LA_v5.000_ED_000300_004	DS EF	Representative	50th	Mean	3	1	1,300	1,300
LA_v5.000_ED_000300_009	DS EF	Comprehensive	50th	Mean	3	1,300	1	1,300
LA_v5.000_ED_000300_005	DS EF	Representative	90th	High	3	1	1,300	1,300
LA_v5.000_ED_000300_010	DS EF	Comprehensive	90th	High	3	1,300	1	1,300
LA_v5.000_ED_000300_006	DS EF	Representative	90th	High	5	1	164	164
LA_v5.000_ED_000300_011	DS EF	Comprehensive	90th	High	5	164	1	164
LA_v5.000_EW_000300_000	WP EF	Representative	10th	Low	1	1	163	163
LA_v5.000_EW_000300_005	WP EF	Comprehensive	10th	Low	1	163	1	163
LA_v5.000_EW_000300_001	WP EF	Representative	10th	Low	3	1	1,300	1,300
LA_v5.000_EW_000300_006	WP EF	Comprehensive	10th	Low	3	1,300	1	1,300
LA_v5.000_EW_000300_002	WP EF	Representative	50th	Mean	3	1	1,300	1,300
LA_v5.000_EW_000300_007	WP EF	Comprehensive	50th	Mean	3	1,300	1	1,300
LA_v5.000_EW_000300_010	WP EF	Representative	90th	High	3	1	1,300	1,300
LA_v5.000_EW_000300_008	WP EF	Comprehensive	90th	High	3	1,300	1	1,300
LA_v5.000_EW_000300_011	WP EF	Representative	90th	High	5	1	164	164
LA_v5.000_EW_000300_009	WP EF	Comprehensive	90th	High	5	164	1	164

Source: (Output DTN MO0708TSPAVALI.000 [DIRS 182985]).

INTENTIONALLY LEFT BLANK

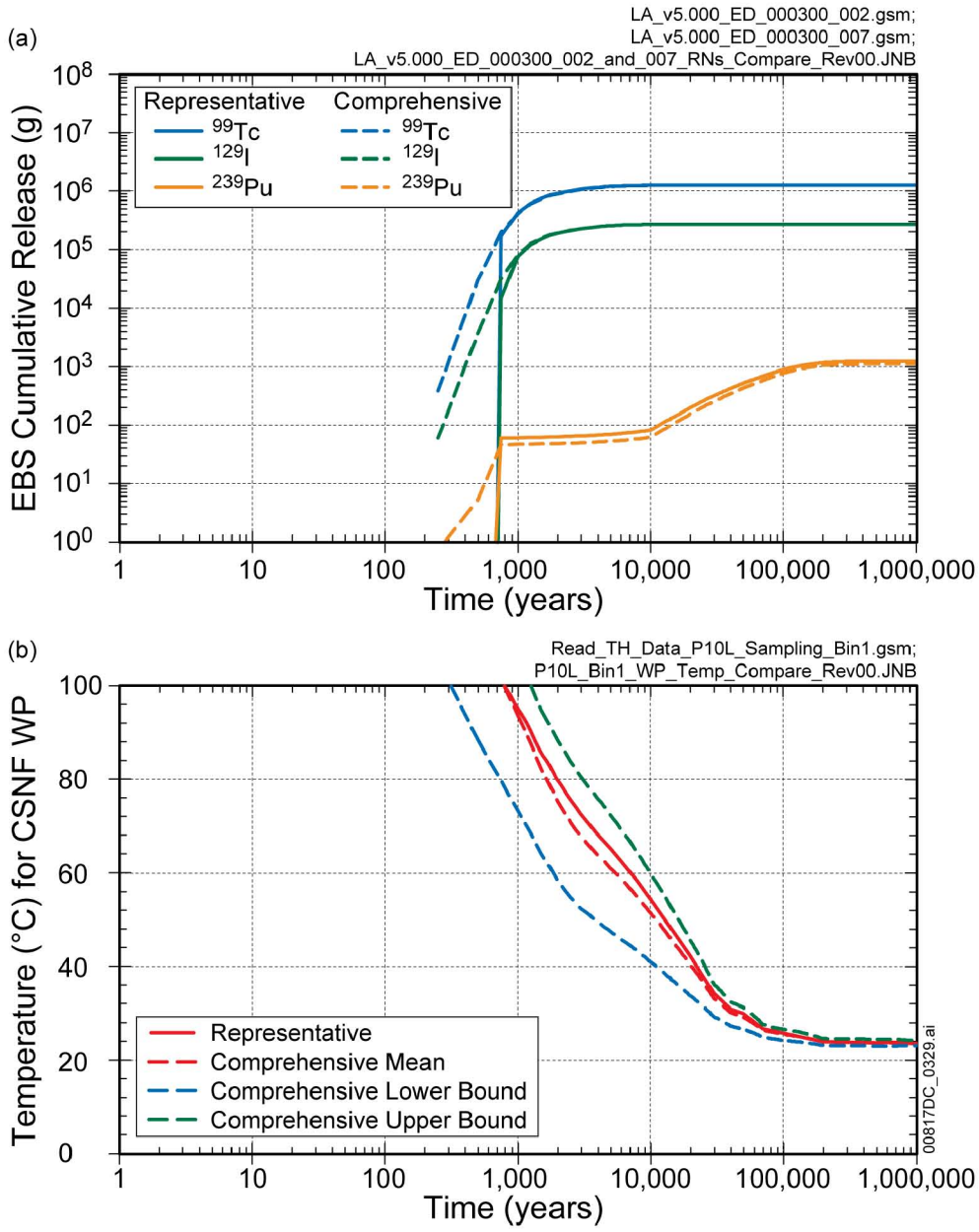

Source: Output DTN: MO0708TSPAVALI.000 [DIRS 182985].

Figure 7.3.4-1. Comparison of the Representative and Comprehensive Thermal Hydrologic Data Sets for (a) EBS Releases of ^{99}Tc, ^{129}I, and ^{239}Pu, and (b) Time when the CSNF WP Temperature Drops Below Boiling for the Drip Shield Early Failure Modeling Case, 10th Percentile Infiltration Flux, Low Host-Rock Thermal Conductivity, Percolation Subregion 1

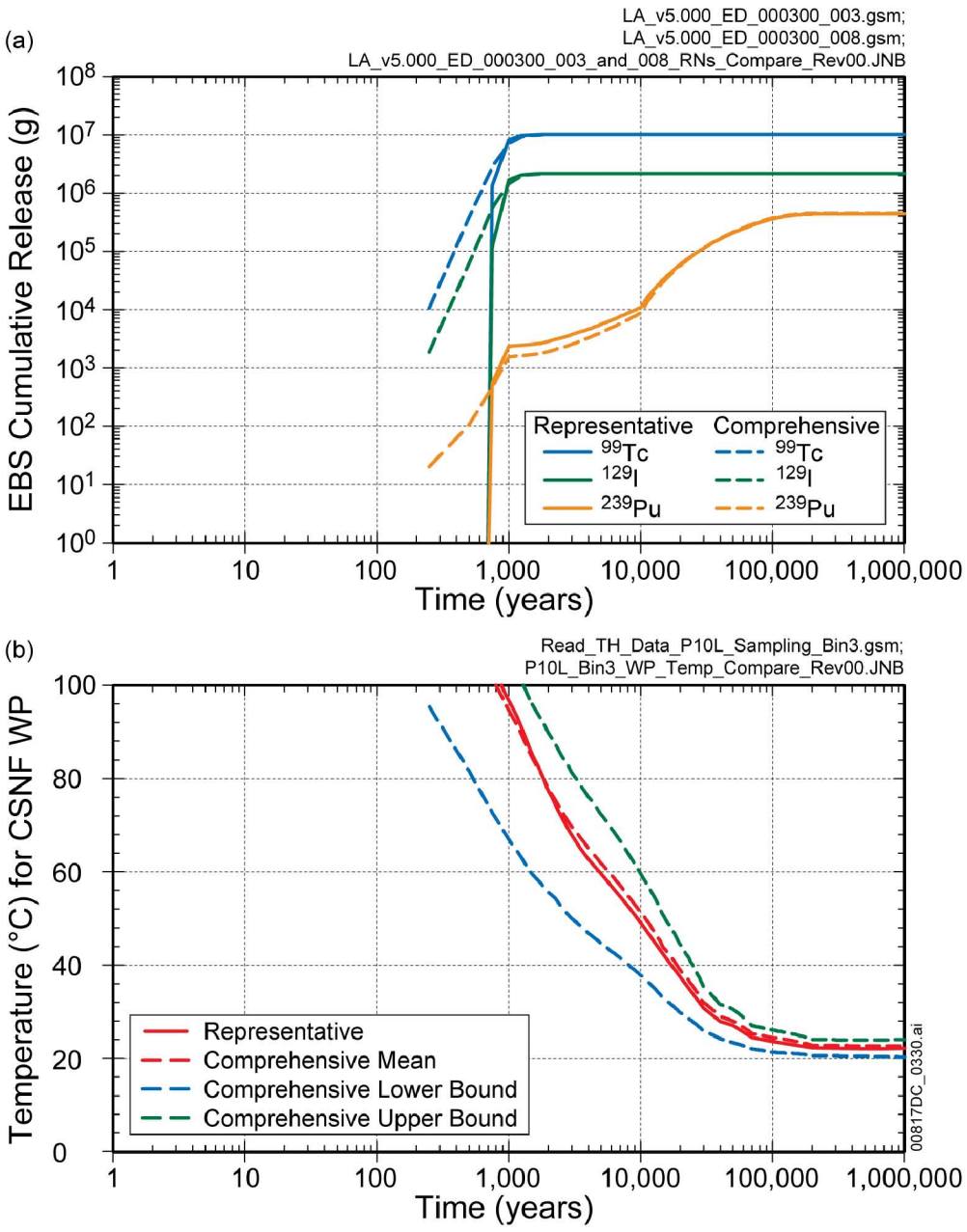

Source: Output DTN: MO0708TSPAVALI.000 [DIRS 182985].

Figure 7.3.4-2. Comparison of the Representative and Comprehensive Thermal Hydrologic Data Sets for (a) EBS Releases of ^{99}Tc, ^{129}I, and ^{239}Pu, and (b) Time when the CSNF WP Temperature Drops Below Boiling for the Drip Shield Early Failure Modeling Case, 10th Percentile Infiltration Flux, Low Host-Rock Thermal Conductivity, Percolation Subregion 3

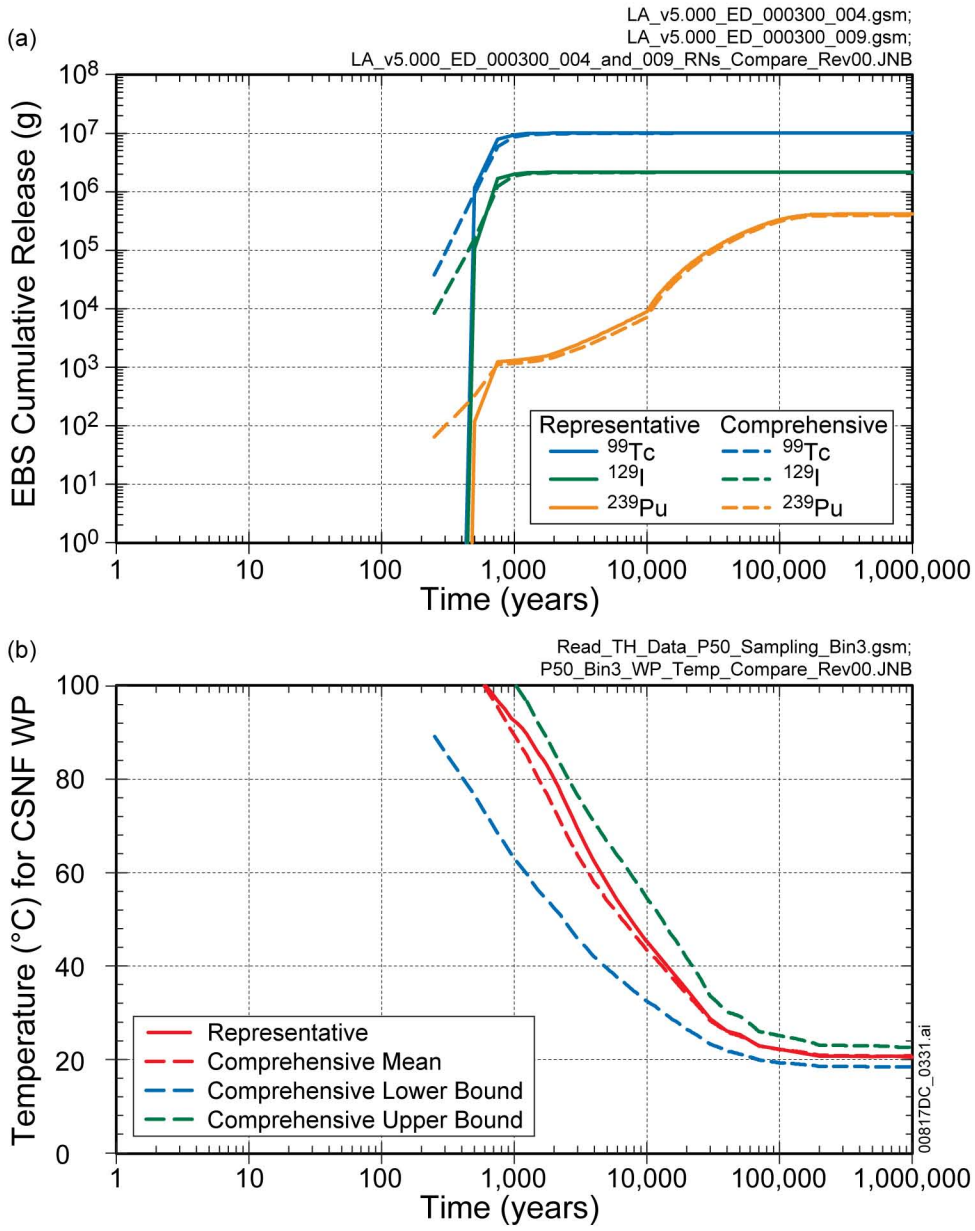

Source: Output DTN: MO0708TSPAVALI.000 [DIRS 182985].

Figure 7.3.4-3. Comparison of the Representative and Comprehensive Thermal Hydrologic Data Sets for (a) EBS Releases of ^{99}Tc, ^{129}I, and ^{239}Pu, and (b) Time when the CSNF WP Temperature Drops Below Boiling for Drip Shield Early Failure Modeling Case, 50th Percentile Infiltration Flux, Mean Host-Rock Thermal Conductivity, Percolation Subregion 3

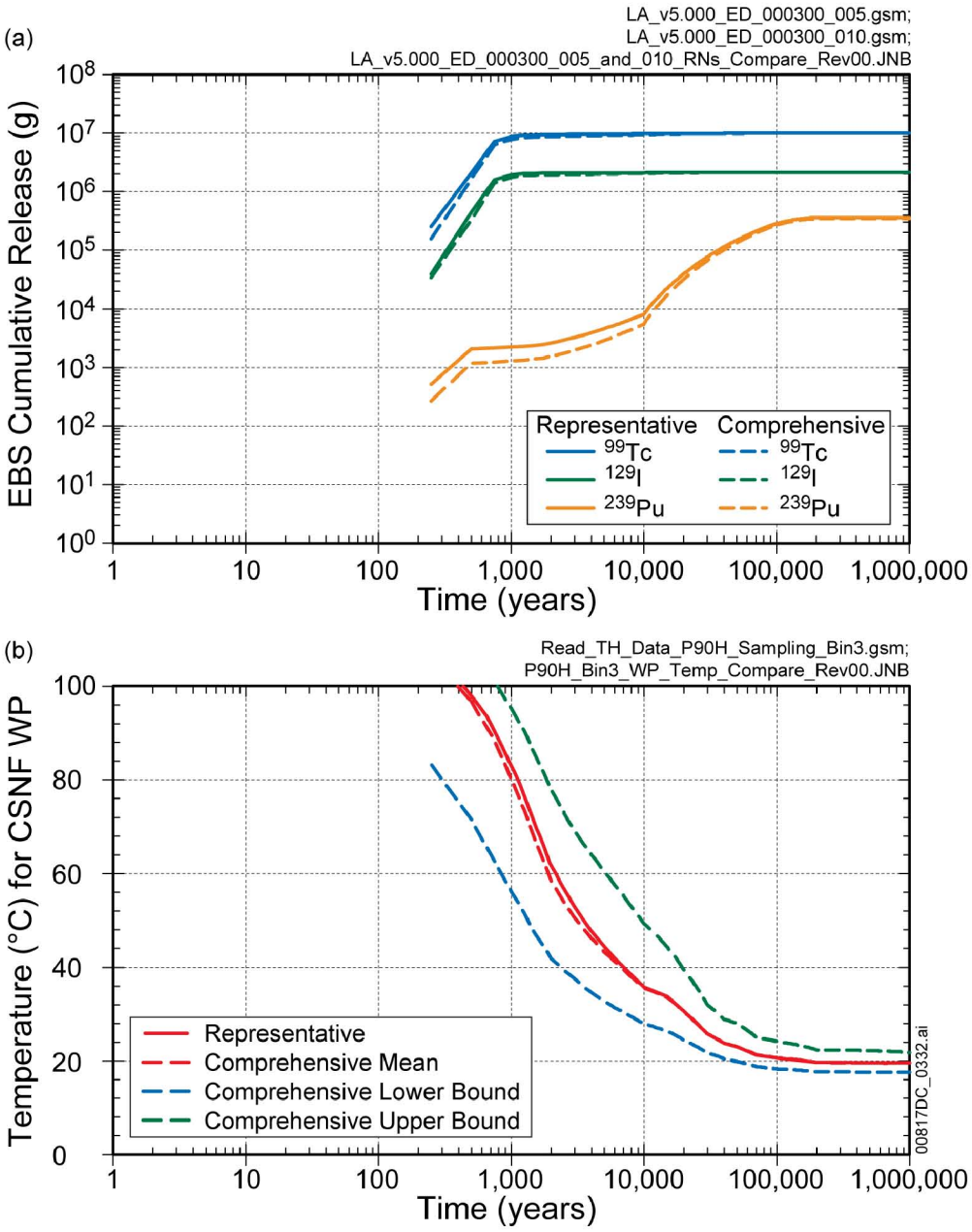

Source: Output DTN: MO0708TSPAVALI.000 [DIRS 182985].

Figure 7.3.4-4. Comparison of the Representative and Comprehensive Thermal Hydrologic Data Sets for (a) EBS Releases of ^{99}Tc, ^{129}I, and ^{239}Pu, and (b) Time when the CSNF WP Temperature Drops Below Boiling for the Drip Shield Early Failure Modeling Case, 90th Percentile Infiltration Flux, High Host-Rock Thermal Conductivity, Percolation Subregion 3

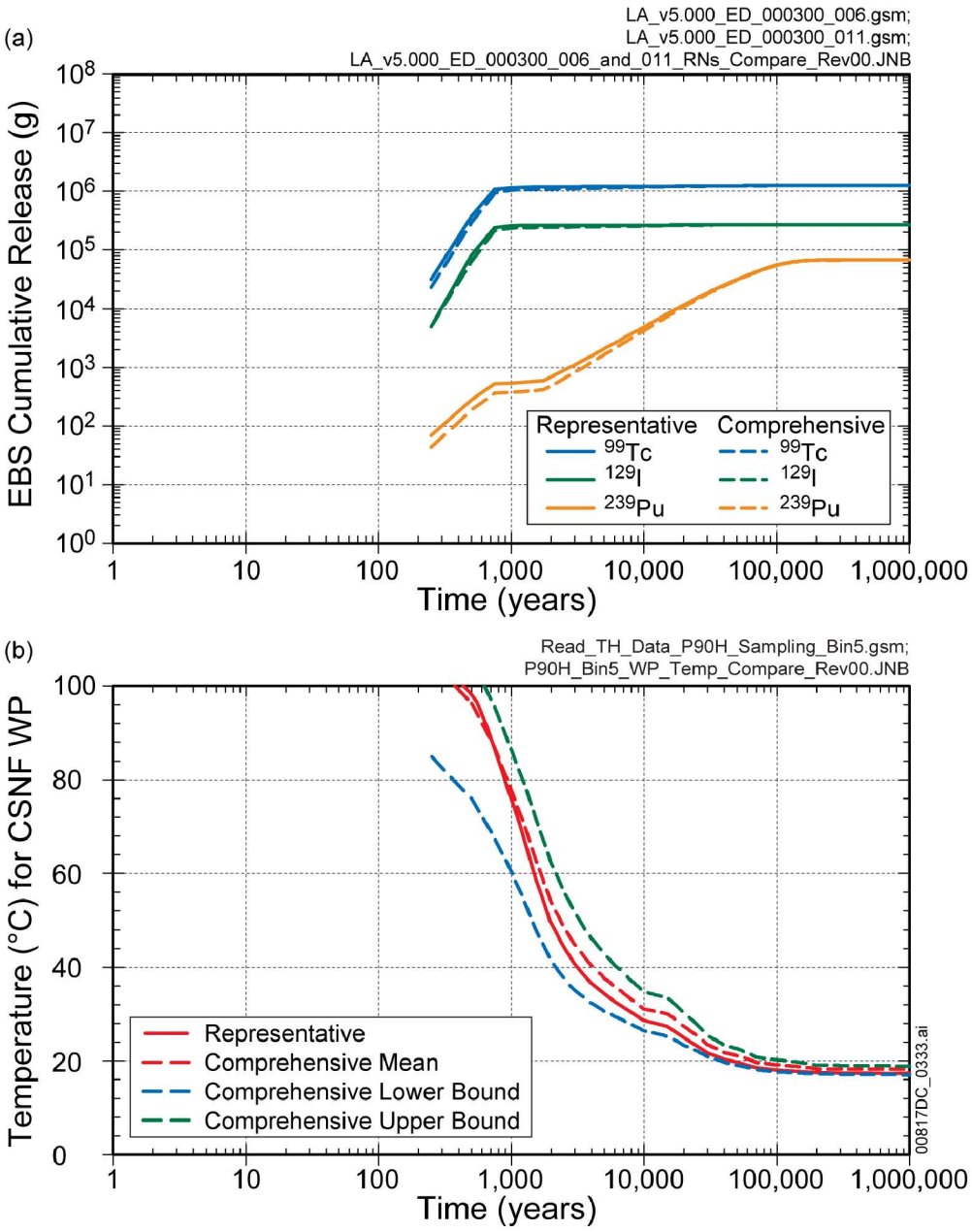

Source: Output DTN: MO0708TSPAVALI.000 [DIRS 182985].

Figure 7.3.4-5. Comparison of the Representative and Comprehensive Thermal Hydrologic Data Sets for (a) EBS Releases of ^{99}Tc, ^{129}I, and ^{239}Pu, and (b) Time when the CSNF WP Temperature Drops Below Boiling for the Drip Shield Early Failure Modeling Case, 90th Percentile Infiltration Flux, High Host-Rock Thermal Conductivity, Percolation Subregion 5

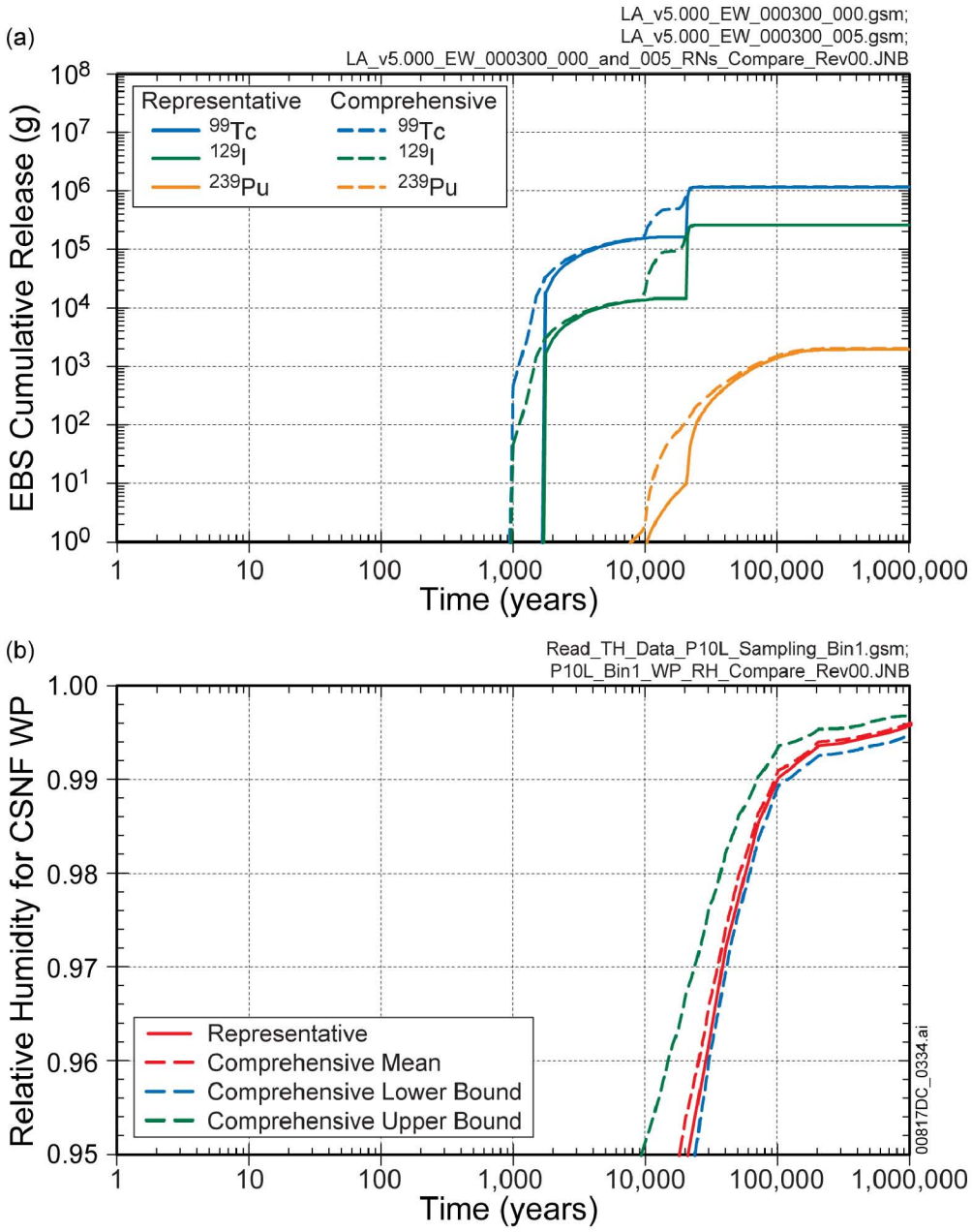

Source: Output DTN: MO0708TSPAVALI.000 [DIRS 182985].

Figure 7.3.4-6. Comparison of the Representative and Comprehensive Thermal Hydrologic Data Sets for (a) EBS Releases of ^{99}Tc, ^{129}I, and ^{239}Pu, and (b) Time when the WP Relative Humidity is above 95 Percent for the Waste Package Early Failure Modeling Case, 10th Percentile Infiltration Flux, Low Host-Rock Thermal Conductivity, Percolation Subregion 1

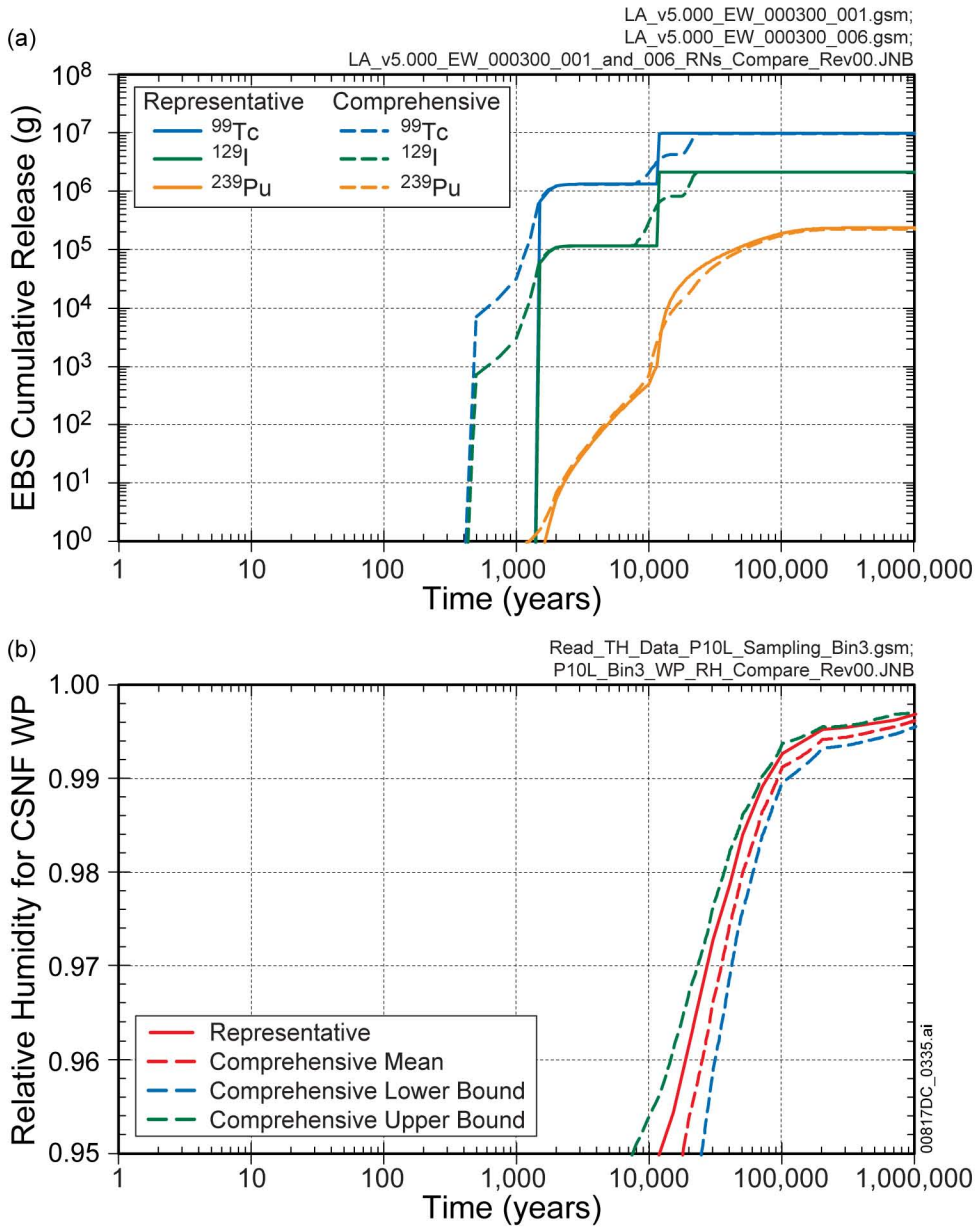

Source: Output DTN: MO0708TSPAVALI.000 [DIRS 182985].

Figure 7.3.4-7. Comparison of the Representative and Comprehensive Thermal Hydrologic Data Sets for (a) EBS Releases of ^{99}Tc, ^{129}I, and ^{239}Pu, and (b) Time when the WP Relative Humidity is above 95 Percent for the Waste Package Early Failure Modeling Case, 10th Percentile Infiltration Flux, Low Host-Rock Thermal Conductivity, Percolation Subregion 3

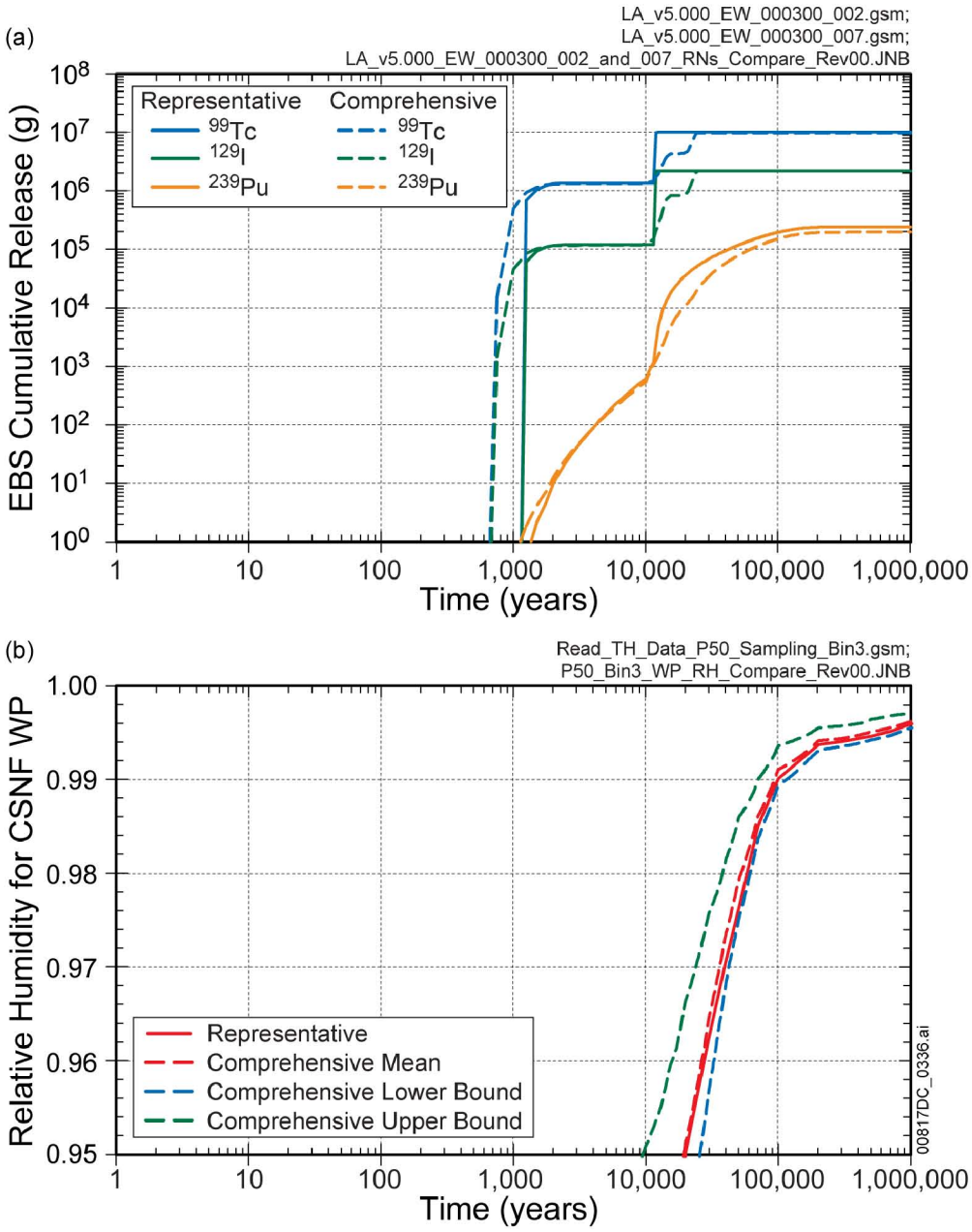

Source: Output DTN: MO0708TSPAVALI.000 [DIRS 182985].

Figure 7.3.4-8. Comparison of the Representative and Comprehensive Thermal Hydrologic Data Sets for (a) EBS Releases of ^{99}Tc, ^{129}I, and ^{239}Pu, and (b) Time when the WP Relative Humidity is above 95 Percent for the Waste Package Early Failure Modeling Case, 50th Percentile Infiltration Flux, Mean Host-Rock Thermal Conductivity, Percolation Subregion 3

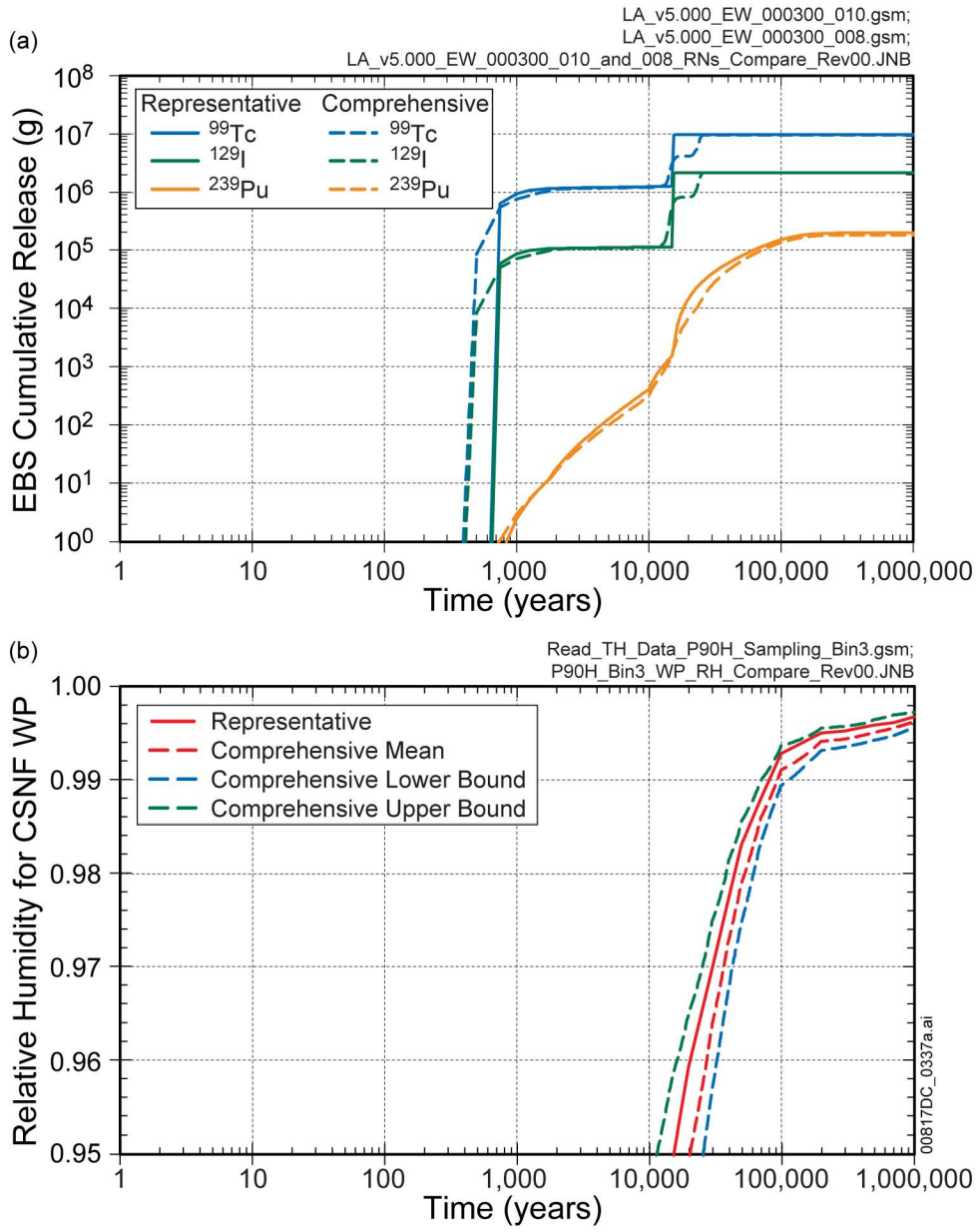

Source: Output DTN: MO0708TSPAVALI.000 [DIRS 182985].

Figure 7.3.4-9. Comparison of the Representative and Comprehensive Thermal Hydrologic Data Sets for (a) EBS Releases of ^{99}Tc, ^{129}I, and ^{239}Pu, and (b) Time when the WP Relative Humidity is above 95 Percent for the Waste Package Early Failure Modeling Case, 90th Percentile Infiltration Flux, High Host-Rock Thermal Conductivity, Percolation Subregion 3

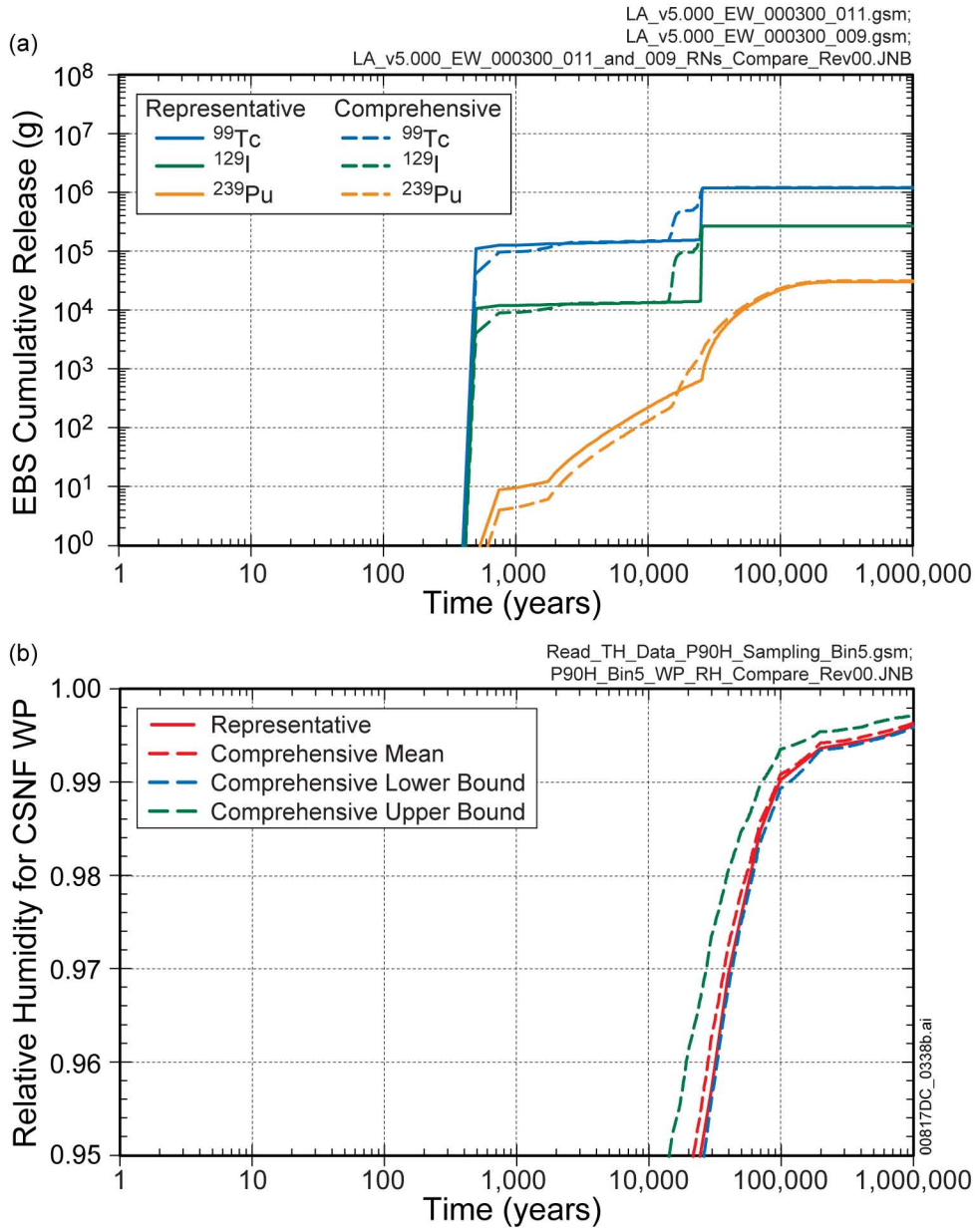

Source: Output DTN: MO0708TSPAVALI.000 [DIRS 182985].

Figure 7.3.4-10. Comparison of the Representative and Comprehensive Thermal Hydrologic Data Sets for (a) EBS Releases of ^{99}Tc, ^{129}I, and ^{239}Pu, and (b) Time when the WP Relative Humidity is above 95 Percent for the Waste Package Early Failure Modeling Case, 90th Percentile Infiltration Flux, High Host-Rock Thermal Conductivity, Percolation Subregion 5

7.3.5 Stability of FEHM Particle Tracking Model

In the TSPA-LA Model, radionuclide transport through the UZ is simulated using the FEHM (Zyvoloski et al. 1997 [DIRS 100615]) residence-time transfer-function particle-tracking technique, as described in *Particle Tracking Model and Abstraction of Transport Processes* (SNL 2008 [DIRS 184748], Section 6.4 and Appendix C). To have confidence in the results generated by the particle-tracking model, it is important to examine the stability of the TSPA-LA Model results relative to the number of particles being used. For particle-tracking models, the accuracy of the model is a function of the number of particles used to represent the source releases: the greater the number of particles, the greater the degree of stability (SNL 2008 [DIRS 184748], Section 6.6.2.1[a]) and accuracy. As the number of particles increases, a level will be reached where results stabilize and there will be little change in results associated with increasing the number of particles. In the TSPA-LA Model, the input for the maximum number of particles allowed in the TSPA-LA Model is 900,000 per species, which represents a near upper limit to the number of particles that can be used in conjunction with a three Gigabyte process limit on servers using the Windows 2000 and Windows Server 2003 operating systems. The memory needed for a FEHM multi-species particle-tracking simulation is a function of the number of particles used to represent the mass loading of each species, the number of species being tracked in the UZ (39 for the TSPA-LA Model), the number of timesteps simulated (the number of timesteps squared for daughter species), and the number of parents associated with daughter species. For each species, the maximum array length needed to store any timestep-dependent data, such as mass value of specific particles (this is a constant value for all particles of a specific species released at a specific timestep), is determined as follows:

$$ArrayLength_{\max} = \left[nts + \frac{nts}{2}(nts+1)\max_{dcl} \right] n_{bins} \qquad \text{(Eq. 7.3.5-1)}$$

where nts is the actual number of timesteps, max_{dcl} is the maximum number of parent species decaying into the specified species, and n is the number of source bins modeled (which is five for the TSPA-LA Model). Note that Equation 7.3.5-1 represents the maximum array length needed. There will be timesteps where no release of mass occurs and where no decay product is produced.

To test the stability of the results in reference to the number of particles used in the TSPA-LA Model, two supplemental simulations were performed with 500,000 and 750,000 particles as the maximum allowed. Note that the input to FEHM is the maximum number of particles allowed. The number of particles actually used by a specific species during a simulation is limited because FEHM saves part of the particle-based array length (a total length of 900,000 for the TSPA-LA Model) for any species that has mass introduced to the system from ingrowth. The saved space will be used to track particle-based data from particles that originally started as its parent species. The remainder of the particle-based array space is used to store data for particles representing mass released from the UZ. The maximum number of particles allowed per species covers both the particles representing releases from the EBS and the particles that will come from ingrowth.

To evaluate the particle-tracking model's stability, with reference to the number of particles used in the TSPA-LA Model, stability testing was performed using Version 5.000 of the TSPA-LA Model. LHS was utilized to generate TSPA-LA Model inputs for one aleatory realization of

base-case simulations that used 300 epistemic realizations. The base-case simulations considered in this study were the 3,000 realization (10 aleatory and 300 epistemic), 10,000-year duration Drip Shield EF Modeling Case; the 3,000 realization (10 aleatory and 300 epistemic), 1,000,000-year duration Igneous Intrusion Modeling Case; and the 9,000 realization (30 aleatory and 300 epistemic), 10,000-year duration Seismic GM Modeling Cases. The Drip Shield EF Modeling Case results used an aleatory realization comprised of percolation Bin 3 WPs and CSNF fuel type. The Igneous simulations used an aleatory realization with an event time of 250 years. The Seismic GM Modeling Case simulations used an aleatory realization comprised of a 10^{-6} damage fraction and an event time of 200 years. The base-case TSPA-LA Model simulations used for comparison in this analysis were LA_v5.000_ED_003000_007, LA_v5.000_IG_003000_017 output DTN: MO0709TSPAREGS.000 [DIRS 182976]), and LA_v5.000_SM_009000_008 (output DTN: MO0709TSPASENS.000 [DIRS 182982]). The simulations using a maximum of 500,000 particles to represent each species were LA_v5.000_ED_003000_018, LA_v5.000_IG_003000_029, and LA_v5.000_ SM_009000_006 (output DTN: MO0708TSPAVALI.000 [DIRS 182985]). The simulations using a maximum of 750,000 particles per species were LA_v5.000_ED_003000_019, LA_v5.000_IG_003000_030, and LA_v5.000_SM_009000_007 (output DTN: MO0708TSPAVALI.000 [DIRS 182985]). For each chosen modeling case, the results for five of the 300 epistemic realizations were examined closely to evaluate the effect of reducing the number of particles used in the simulations. Single realizations were examined because the averaging process would likely hide the differences. For igneous and seismic simulations, the choice of the single realizations is the first five epistemic realizations for the aleatory sample, making them random selections based on the epistemic sampling of the TSPA-LA Model. The choice of aleatory sample for the igneous and seismic simulations should have little influence on the results with the exception of allowing for the longest release time that would allow for the most complete evaluation. The DS early failure analysis uses a biased sampling of realizations chosen to allow for examination of how realizations with temporally oscillatory UZ ^{99}Tc releases are affected by the number of particles used to represent the releases. This choice of realizations was used to allow for an examination of the effect of the number of particles used on UZ releases that are not smooth over time and may be problematic because of it. As described later in this section, the results of simulations using 500,000 and 750,000 for the maximum number of particles were graphically compared to the TSPA-LA Compliance Model (900,000 particles) results in order to assess how much change in the annual doses occurs when the maximum number of particles is reduced. Although the doses are the output of concern in the TSPA-LA Model, the mass fluxes from the UZ for the Igneous Intrusion Modeling Case are also examined to show how the model is relatively insensitive to minor deviations in UZ transport results associated with the limit to the number of particles that are used.

7.3.5.1 Testing Procedure

As noted above, two supplemental simulations using different numbers of particles to represent the EBS releases were performed for each modeling case to test the stability of the TSPA-LA Model results relative to changes in the maximum number of particles (per species) used in the UZ particle-tracking analysis. These additional simulations used 500,000 and 750,000 as the maximum number of particles. For each chosen modeling case, the results for five of 300 epistemic realizations (for a chosen aleatory realization) were examined closely and compared to compliance model results to evaluate the effect of reducing the number of particles used in the

simulations. All parameters, except for the maximum number of particles allowed (900,000; 750,000; or 500,000) per species and, where applicable, the FEHM input parameter defining the number of particles assigned per mole, were the same for each set of simulations. In general, for the UZ submodel particle tracking analysis, particles are assigned on a per timestep basis. An exception has been made for the Igneous and Early Failure Modeling Cases where ^{99}Tc and ^{129}I particles are assigned on a particle per mole basis. The inputted ratio of particles allowed per mole is based on the maximum total release possible for the modeling case. This value is based on the inventories with all uncertainties included and the maximum possible WPs in the release (11,629 for igneous and one for the DS early failure analysis). This allows for a more accurate depiction of the spike-like portion of their EBS releases to the UZ. This technique more accurately simulates the portions of the release that are large contributors to dose. The major radionuclides considered in this analysis include ^{99}Tc, ^{233}U, ^{234}U, ^{237}Np, and Total ^{239}Pu (combined reversible and slow and fast irreversible colloids) (Section 6.3.7.1). The above species cover a range of transport behavior and are large contributors to dose. The Total ^{239}Pu includes the combined dissolved and reversibly sorbed colloidal phases and are summed with the (fast and slow fraction) irreversibly sorbed colloidal phases.

Note that the realization numbers for compliance runs and their associated stability analysis runs may differ because 300 realization subsets (based on the choice of a single aleatory event) of the full 3,000 and 9,000 realizations compliance runs (900,000 maximum particles) are utilized in the stability runs (500,000 and 750,000 maximum particles). The TSPA-LA Model allows for running subsets based on a single aleatory realization, but the realizations in the 300 realization subsets are numbered 1 to 300, where realizations in a compliance run with 3,000 realizations are numbered 1 to 3,000. To avoid confusion, realization references used in comparisons will be given in the form *a*/*b* where *a* is the realization number for a compliance run and *b* is a realization number for the stability run. The relationship between *a* and *b* is as follows:

$$a = N_{aleatory}(b-1) + I_{aleatory} \qquad \text{(Eq. 7.3.5-2)}$$

where, $N_{aleatory}$ is the number of aleatory realizations and $I_{aleatory}$ is the chosen aleatory realization. For cases where the compliance realization number is the same as the stability run realization, a subset run was performed for the compliance model, and the data from that subset was used in the comparison.

7.3.5.2 Simulation Results

7.3.5.2.1 Dose Calculations

The examination of the annual doses for the major radionuclides showed only minor differences between annual-dose results for simulations with different maximum particle allocations as depicted for each of the three chosen modeling cases (Drip Shield EF Modeling Case, Igneous Intrusion Modeling Case, and Seismic GM Modeling Case) on Figures 7.3.5-1, 7.3.5-2, and 7.3.5-3, respectively. The curves for the stability runs overlaid the curves for the compliance runs, indicating that the number of particles is unlikely to affect the timing and magnitude of peak dose values. Note that all figures referred to in this section can be found in output DTN: MO0709TSPAPLOT.000 [DIRS 183010]. To show the limited effects of reducing the number of particles on the TSPA-LA peak-dose analysis, the peak dose results for each

representative realization for each modeling case are presented in Table 7.3.5-1. The results presented in Table 7.3.5-1 indicate that peak doses for individual realizations are relatively insensitive to the reduction of maximum number of particles allowed to represent the mass of each radionuclide in the particle tracking analysis, from 900,000 to 750,000 or 500,000. Note that the oscillatory nature of the results for the Drip Shield EF Modeling Case presented on Figure 7.3.5-1 is a function of the release pattern of ^{99}Tc. Most of the large ^{99}Tc releases from the EBS is over a very short period of time. A large component of the mass following the most likely pathway reaches the water table relatively early. This mass release at the 18 km boundary is followed by smaller mass releases following other stochastically determined pathways.

7.3.5.2.2 Radionuclide Contributions to Dose

Because the annual dose results are summations of annual dose contributions from 39 different radionuclide species (or phases of species) with varied transport behavior in the UZ, a representative group of radionuclides (^{237}Np, ^{99}Tc, ^{233}U, ^{234}U, and Total ^{239}Pu) was chosen to evaluate how much influence the changes in maximum particle assignment has on the dose contributions from the different radionuclides.

For the Drip Shield EF Modeling Case analysis, annual dose plots were drawn for each of the radionuclides ^{237}Np, ^{99}Tc, ^{233}U, ^{234}U, and Total ^{239}Pu. Each plot contains the 900,000; 750,000; and 500,000 maximum particle simulation results for five realizations. As can be seen on Figure 7.3.5-4, the ^{237}Np annual dose results show negligible differences except for low values found in realization 1166/117. The ^{99}Tc results (Figure 7.3.5-5) show a little more difference associated with the changes in maximum particle assignments, but differences are still minor. Results for the ^{233}U (Figure 7.3.5-6) annual doses show minor differences for realization 266/27 and negligible differences for the other four realizations. Figure 7.3.5-7 shows negligible differences in annual doses for the ^{234}U results. Results for the Total ^{239}Pu (Figure 7.3.5-8a) annual doses also show only minor differences. Note that Total ^{239}Pu is the sum of ^{239}Pu on reversible colloids, ^{239}Pu on retarded irreversible colloids, and ^{239}Pu on unretarded colloids. Total ^{239}Pu represents the dose contribution due to ^{239}Pu release. For the Drip Shield EF Modeling Case, the dose contributions for the individual phases, ^{239}Pu on reversible colloids, ^{239}Pu on retarded irreversible colloids, and ^{239}Pu on unretarded colloids are also presented on Figure 7.3.5-8b, Figure 7.3.5-8c, and Figure 7.3.5-8d, respectively, so that the influence of particle number on the stability of the different phases can also be seen.

The Igneous Intrusion Modeling Case simulations also show only minor differences in results for different maximum particle allocations, with the exception of the ^{99}Tc annual doses. As can be seen on Figure 7.3.5-9, the ^{237}Np annual dose results show minor differences. The ^{99}Tc results (Figure 7.3.5-10a) show that the peak values that exert a strong influence on total dose show a negligible difference associated with the change in maximum particles allowed. Figure 7.3.5-10b, which portrays the time axis on a log scale, shows that at lower annual dose values a larger discrepancy between results can be found. This larger discrepancy is associated with the use of FEHM's mass based particle assignment, which more accurately describes larger releases over time at the price of less accurately simulating lower mass-flux releases. Results for

the ^{233}U (Figure 7.3.5-11) annual doses show some minor differences for realization 21/3 and negligible differences for the other four realizations. Figure 7.3.5-12 shows some early differences in annual doses for the ^{234}U results but negligible differences through most of the simulation. Note that FEHM's timestep based particle assignment logic, as used for ^{234}U, assigns a smaller number of particles per timestep during the smaller early timesteps. Results for the Total ^{239}Pu (Figure 7.3.5-13) annual doses also show some differences early on, which are reduced with time and are minimal at the larger annual dose values.

For the Seismic GM Modeling Case analysis, the annual dose plots showed very little difference between 900,000; 750,000; and 500,000 maximum particle simulation results. As can be seen on Figure 7.3.5-14, the ^{237}Np annual dose results show negligible differences for all five realizations. The ^{99}Tc results (Figure 7.3.5-15) showed minor differences. Results for the ^{233}U (Figure 7.3.5-16) annual doses show negligible differences in annual dose between 900,000; 750,000; and 500,000 maximum particle simulation results. Figure 7.3.5-17 shows very minor changes in annual dose contributions from ^{234}U when the maximum particle numbers are changed. Results for the Total ^{239}Pu (Figure 7.3.5-18) annual doses also show only minor differences.

7.3.5.2.3 Comparison of Radionuclide Contributions to Dose Results to Unsaturated Zone Release Results

For the Igneous Intrusion Modeling Case, the annual mass release from the UZ for individual radionuclides were examined and compared to the annual dose results. This analysis was performed to show that expected differences in UZ mass releases associated with the nature of particle tracking in a dual permeability system are not reflected in the annual dose results. For individual realizations, a change in the number of particles representing mass releases will have some effect on the mass releases from the system. This is especially true at times where there are a number of particles representing parts of larger masses released from the EBS that are slowly being released from storage in the rock matrix a few particles at a time. It is also common when particles are being assigned by mass at times when relatively small masses are being released from the EBS. The UZ mass releases represent boundary conditions in the SZ Flow and Transport Submodel. Differences in the smoothness of the mass of the time-dependent boundary conditions are offset by dispersive processes as the mass travels 18 km downgradient.

A comparison of the ^{237}Np releases from the UZ shown on Figure 7.3.5-19 to the annual dose plot for ^{237}Np presented on Figure 7.3.5-9 shows that the differences in the shapes of UZ mass release source terms associated with using 900,000; 750,000; or 500,000 as the maximum number of particles representing a radionuclides mass in the UZ do not matter once the mass has moved 18 km through the SZ. The ^{99}Tc UZ mass release results presented on Figure 7.3.5-20 show large differences at the lower release rates. As previously noted, these differences are associated with the decision to more accurately depict the large, relatively short-term releases from the EBS that control the peak doses at early time. By the time the mass has traveled 18 km, the differences caused by changing the maximum particles allowed has mainly dissipated except at values six orders of magnitude less than the peak values (Figure 7.3.5-10a). UZ mass release

results for ^{233}U (Figure 7.3.5-21), when compared to the annual dose curves for ^{233}U (Figure 7.3.5-11), again show that differences in UZ mass releases associated with using 900,000; 750,000; or 500,000 as the maximum number of particles representing a radionuclides mass in the UZ are small enough that negligible differences in annual doses occur. Comparisons of Figure 7.3.5-12 with Figure 7.3.5-22 for ^{234}U and Figure 7.3.5-13 with Figure 7.3.5-23 for Total ^{239}Pu show similar dissipation of source term differences with downgradient transport in the SZ.

7.3.5.3 Conclusions

This stability test indicates that the use of 900,000 particles in the TSPA-LA Model analyses provides a stable result with respect to the number of particles used in all three of the modeling cases (Drip Shield EF Modeling Case, Igneous Intrusion Modeling Case, and Seismic GM Modeling Case). A reduction of the maximum number of particles to 750,000 or 500,000 is shown to have little effect on the annual dose results. Likewise, peak dose results showed that the reductions in the maximum number of particles used to represent the EBS releases had little influence on the TSPA-LA Model results. A more detailed comparison of annual doses for representative radionuclide species and UZ mass flux releases showed that slight differences in particle tracking results associated with the reductions to the number of particles representing source releases (and ingrowth contributions) represent differences in the refinement of source terms to the SZ. This difference in the source terms is dampened by the time mass has been transported 18 km.

Table 7.3.5-1. Peak Dose Values for Drip Shield Early Failure, Igneous, and Seismic Ground Motion Modeling Cases Evaluated for Particle Stability

		Peak Dose in mrems for Stability Based on the Maximum Number of Particles Per Species		
	Realization	**900,000**	**750,000**	**500,000**
Igneous – 1 Million years	1/1	364.8	357.7	358.7
	11/2	320.7	328.0	317.1
	21/3	671.3	668.7	656.6
	31/4	552.1	534.9	535.6
	41/5	1,310	1,303	1,308
Drip Shield Early Failure – 10,000 years	266/27	0.04533	0.04437	0.04533
	686/69	0.1030	0.1052	0.1055
	756/76	0.03040	0.02960	0.03052
	956/96	0.07744	0.07434	0.07509
	1,166/117	0.009840	0.009535	0.009815
Seismic Ground Motion – 10,000 years	2/1	0.1749	0.1752	0.1726
	32/2	0.9198	0.9236	0.9032
	62/3	1.473	1.476	1.478
	92/4	0.5553	0.5595	0.5558
	122/5	1.351	1.355	1.346

From output DTN: MO0709TSPAPLOT.000 [DIRS 183010] Files:
LA_v5.000_ED_003000_007_Total_Dose_Wt_300rlza.txt
From output DTN: MO0709TSPAVALI.000 [DIRS 182985] Files:
LA_v5.000_ED_003000_018_Total_Dose_Wt.txt
LA_v5.000_ED_003000_019_Total_Dose_Wt.txt
LA_v5.000_IG_003000_029_Total_Dose_UnWt.txt
LA_v5.000_IG_003000_030_Total_Dose_UnWt.txt
LA_v5.000_SM_009000_006_Total_Dose_UnWt.txt
LA_v5.000_SM_009000_007_Total_Dose_UnWt.txt
From output DTN: MO0709TSPAREGS.000 [DIRS 182976] Files:
LA_v5.000_IG_003000_017_Total_Dose_UnWt.txt
LA_v5.000_SM_009000_005_Total_Dose_UnWt.txt

INTENTIONALLY LEFT BLANK

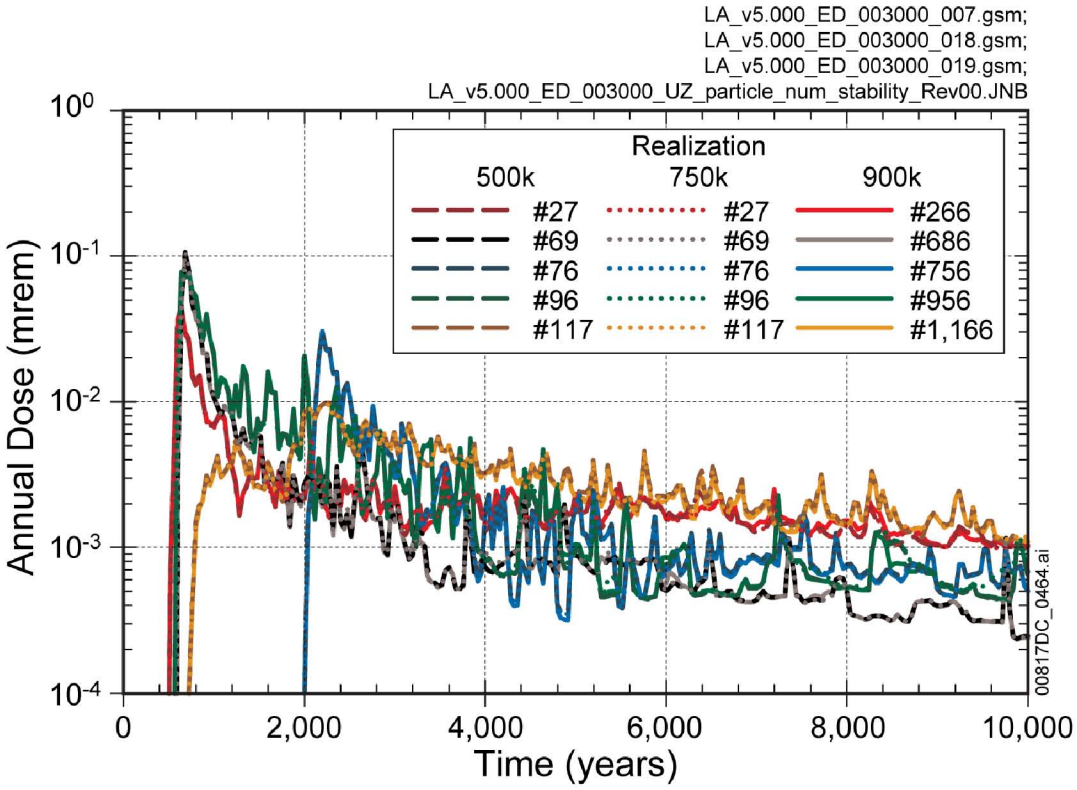

Source: Output DTNs: MO0708TSPAVALI.000 [DIRS 182985]; and MO0709TSPAREGS.000 [DIRS 182976].

Figure 7.3.5-1. Annual Dose for the Drip Shield Early Failure Modeling Case Simulations using a Maximum of 500,000; 750,000; and 900,000 Particles in the Unsaturated Zone Transport Submodel

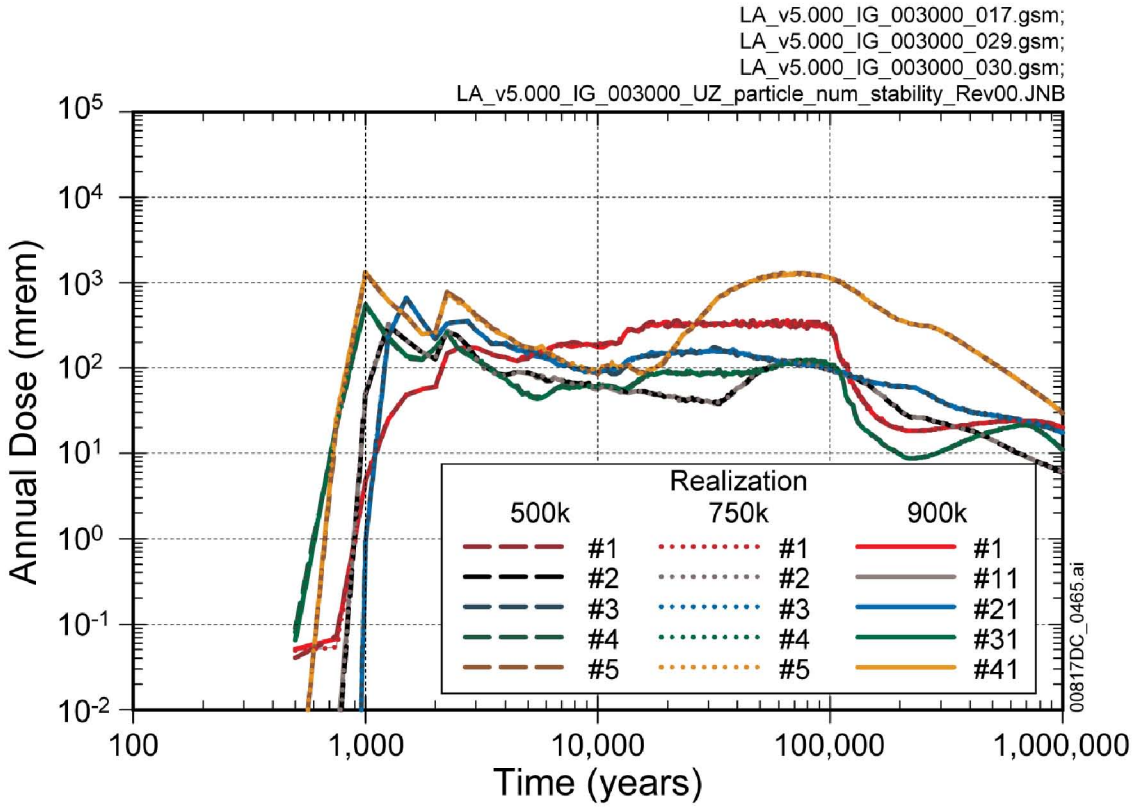

Source: Output DTNs: MO0708TSPAVALI.000 [DIRS 182985]; and MO0709TSPAREGS.000 [DIRS 182976].

Figure 7.3.5-2. Annual Dose for the Igneous Intrusion Modeling Case Simulations Using a Maximum of 500,000; 750,000; and 900,000 Particles in the Unsaturated Zone Transport Submodel

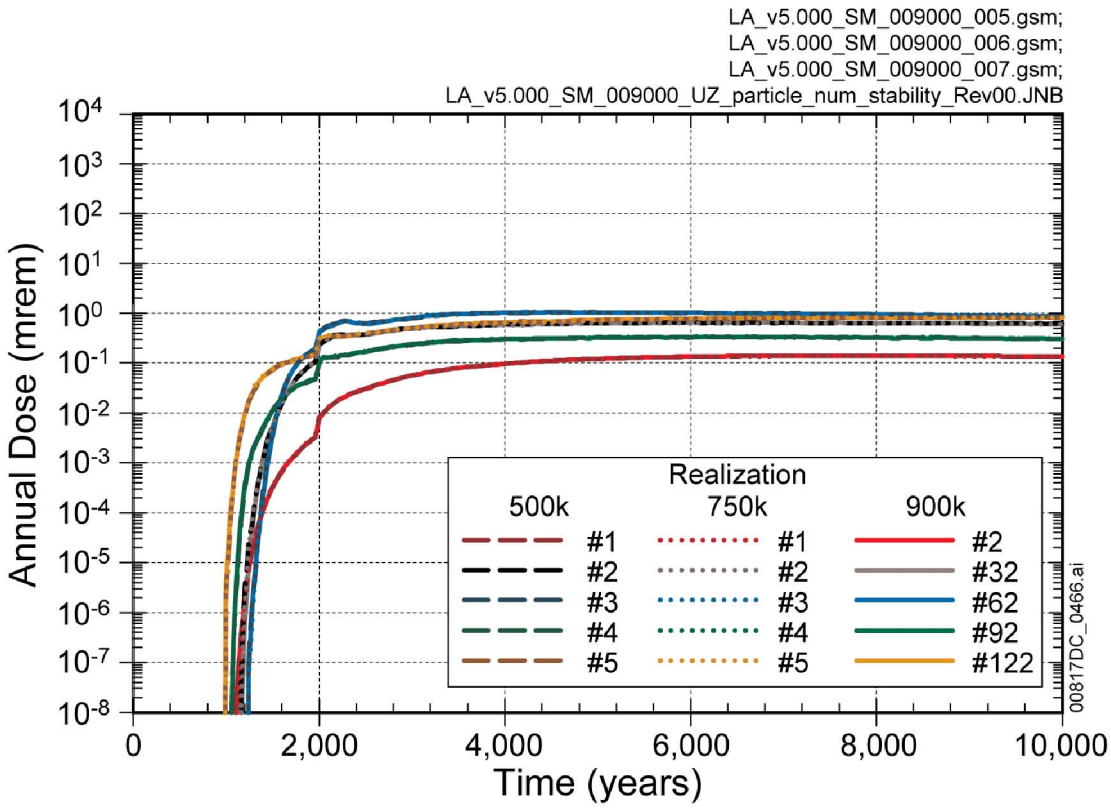

Source: Output DTNs: MO0708TSPAVALI.000 [DIRS 182985]; and MO0709TSPAREGS.000 [DIRS 182976].

Figure 7.3.5-3. Annual Dose for the Seismic Ground Motion Modeling Case Simulations Using a Maximum of 500,000; 750,000; and 900,000 Particles in the Unsaturated Zone Transport Submodel

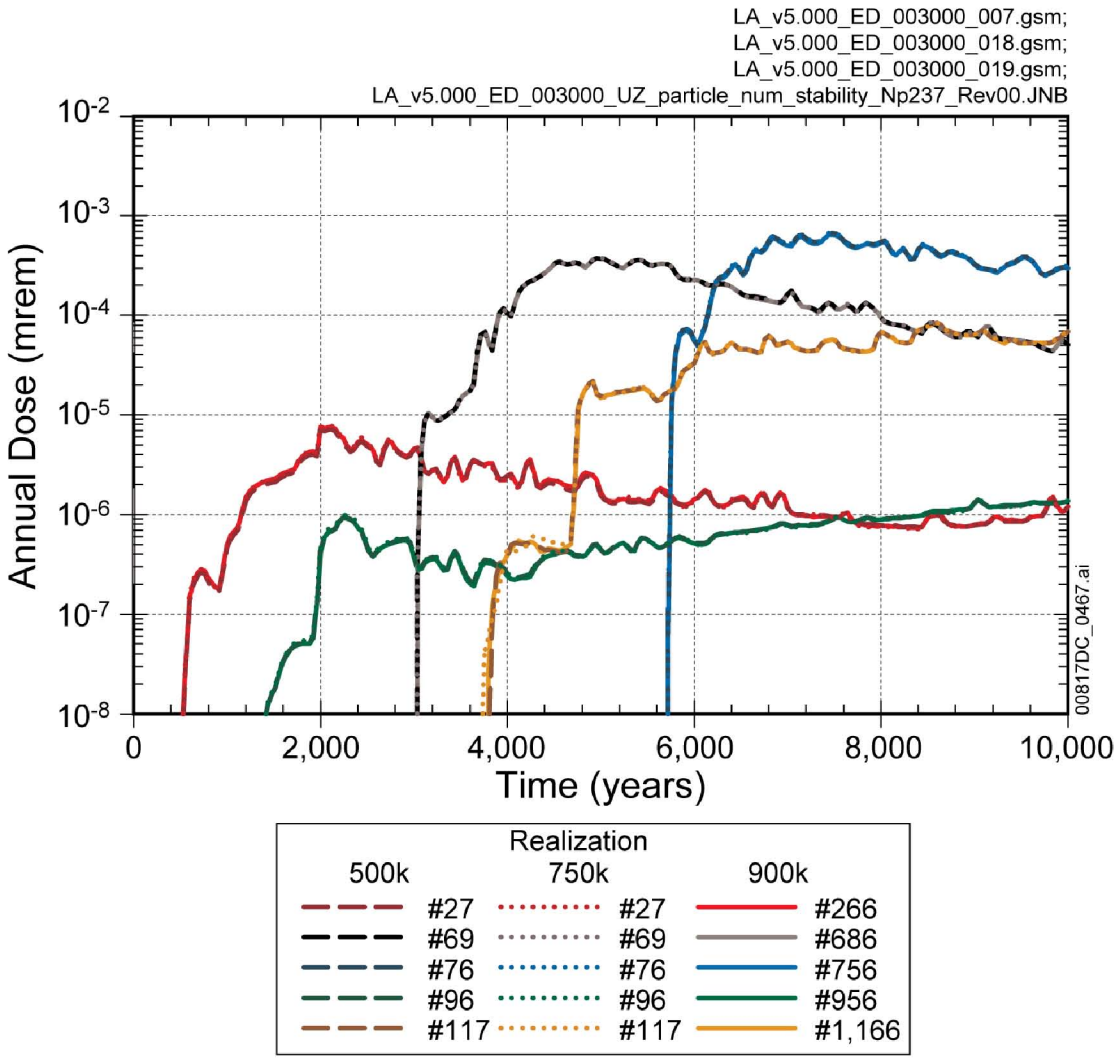

Source: Output DTNs: MO0708TSPAVALI.000 [DIRS 182985]; and MO0709TSPAREGS.000 [DIRS 182976].

Figure 7.3.5-4. Annual Dose Contribution from ^{237}Np for the Drip Shield Early Failure Modeling Case Simulations Using a Maximum of 500,000; 750,000; and 900,000 Particles in the Unsaturated Zone Transport Submodel

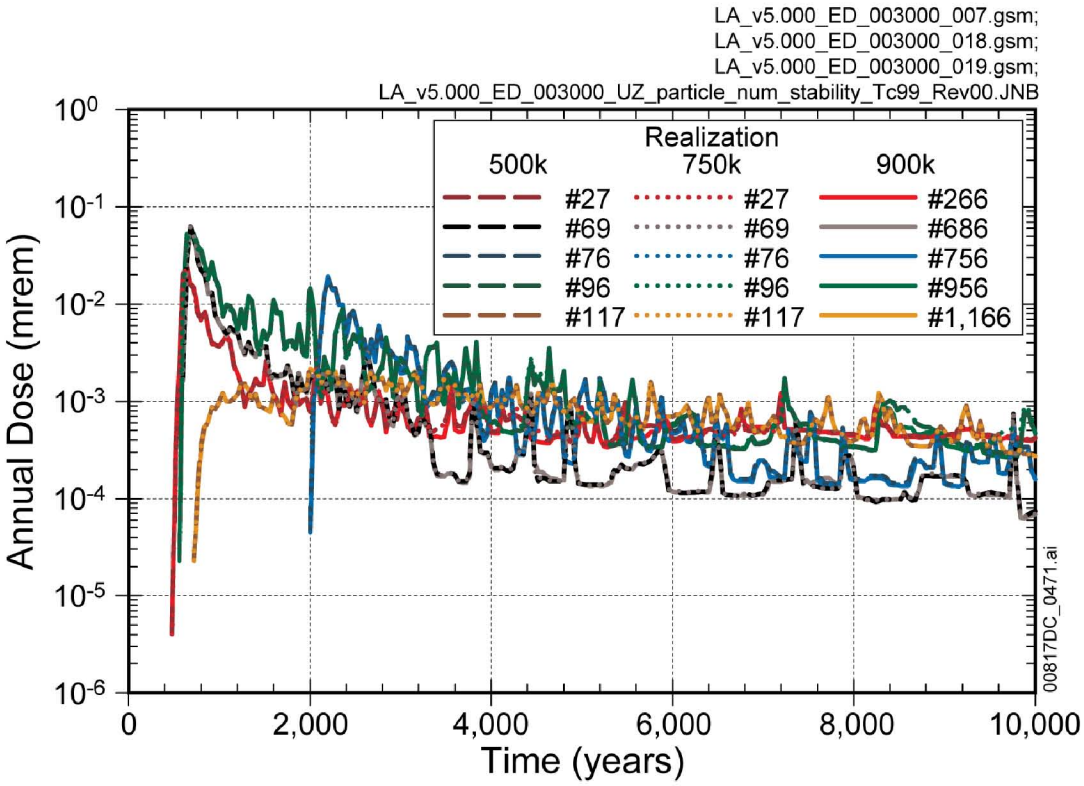

Source: Output DTNs: MO0708TSPAVALI.000 [DIRS 182985], and MO0709TSPAREGS.000 [DIRS 182976].

Figure 7.3.5-5. Annual Dose Contribution from ^{99}Tc for the Drip Shield Early Failure Modeling Case Simulations Using a Maximum of 500,000; 750,000; and 900,000 Particles in the Unsaturated Zone Transport Submodel

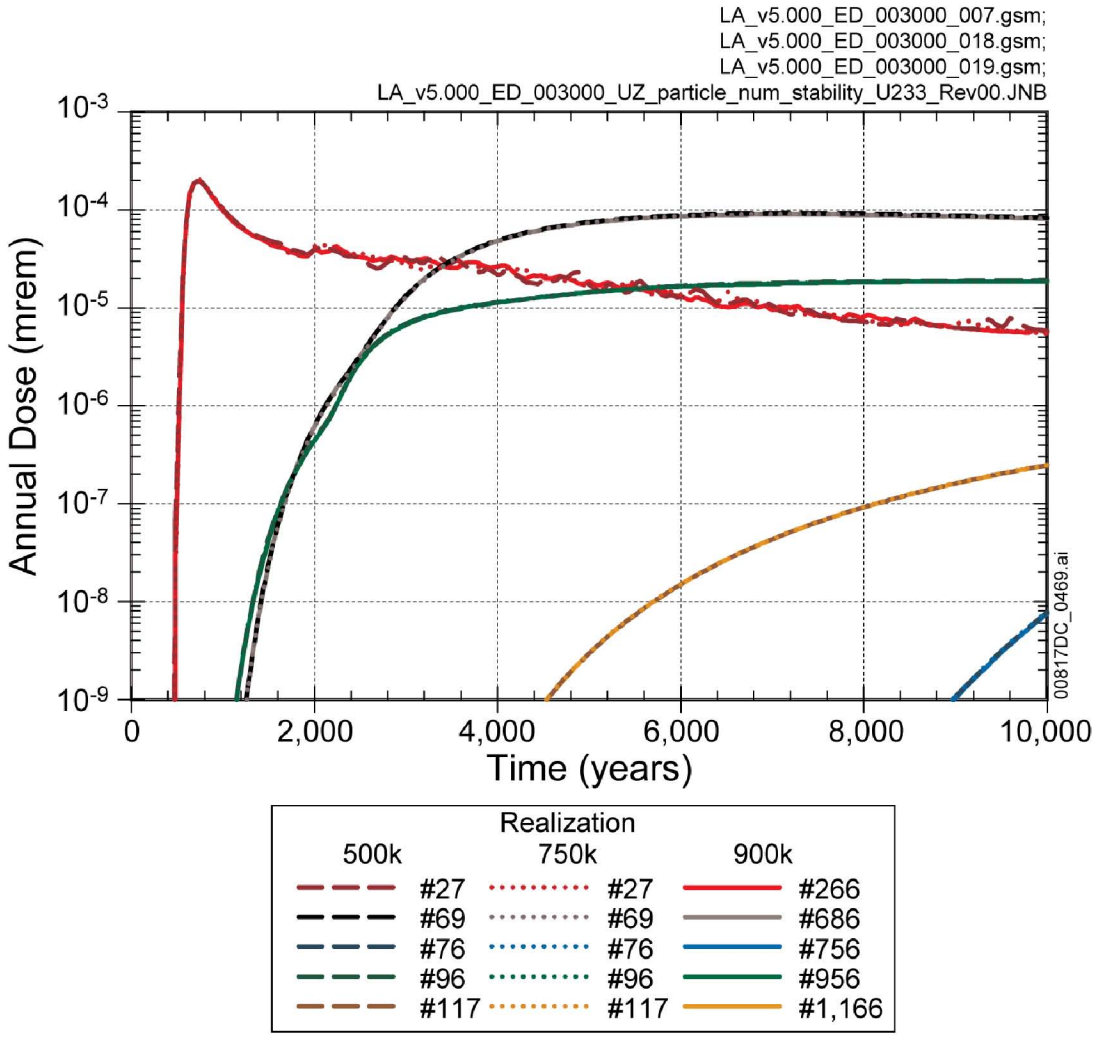

Source: Output DTNs: MO0708TSPAVALI.000 [DIRS 182985]; and MO0709TSPAREGS.000 [DIRS 182976].

Figure 7.3.5-6. Annual Dose Contribution from ^{233}U for the Drip Shield Early Failure Modeling Case Simulations Using a Maximum of 500,000; 750,000; and 900,000 Particles in the Unsaturated Zone Transport Submodel

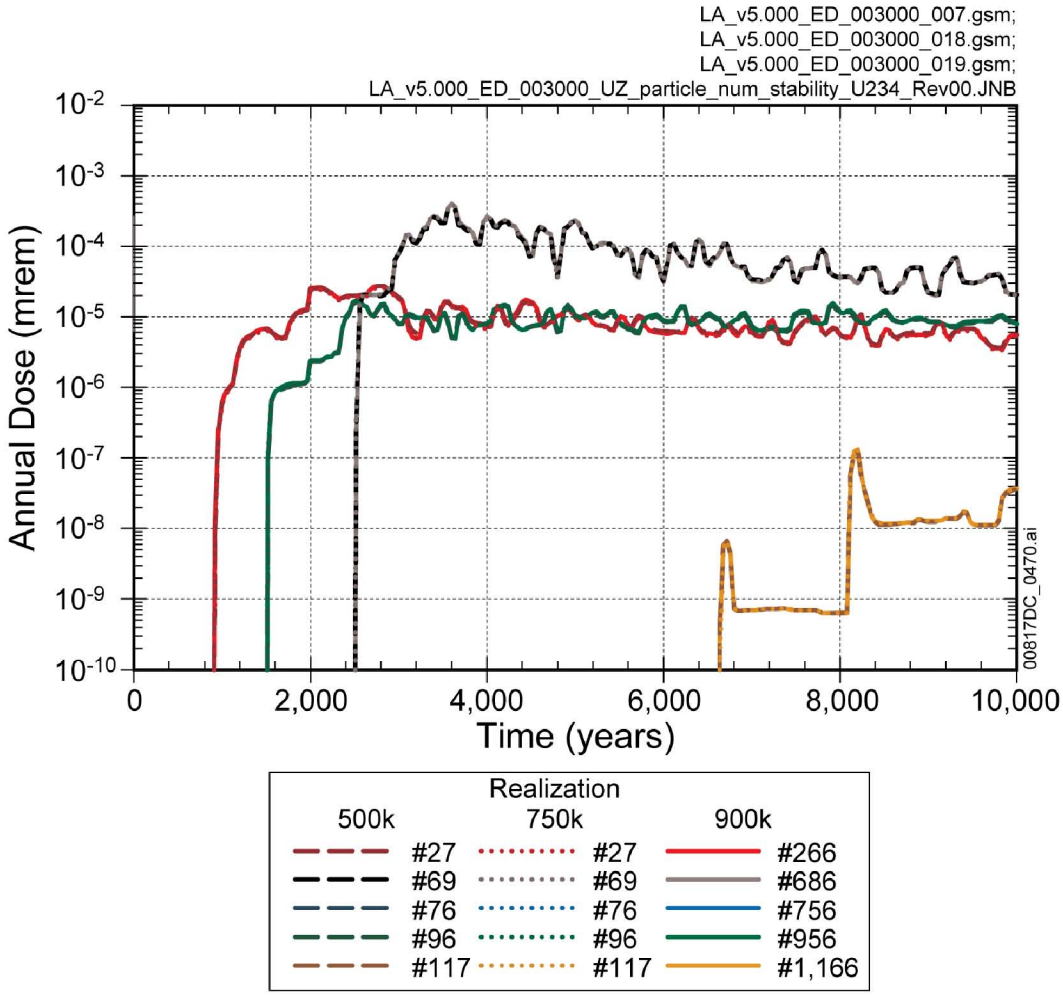

Source: Output DTNs: MO0708TSPAVALI.000 [DIRS 182985], MO0709TSPAREGS.000 [DIRS 182976].

Figure 7.3.5-7. Annual Dose Contribution from ^{234}U for the Drip Shield Early Failure Modeling Case Simulations Using a Maximum of 500,000; 750,000; and 900,000 Particles in the Unsaturated Zone Transport Submodel

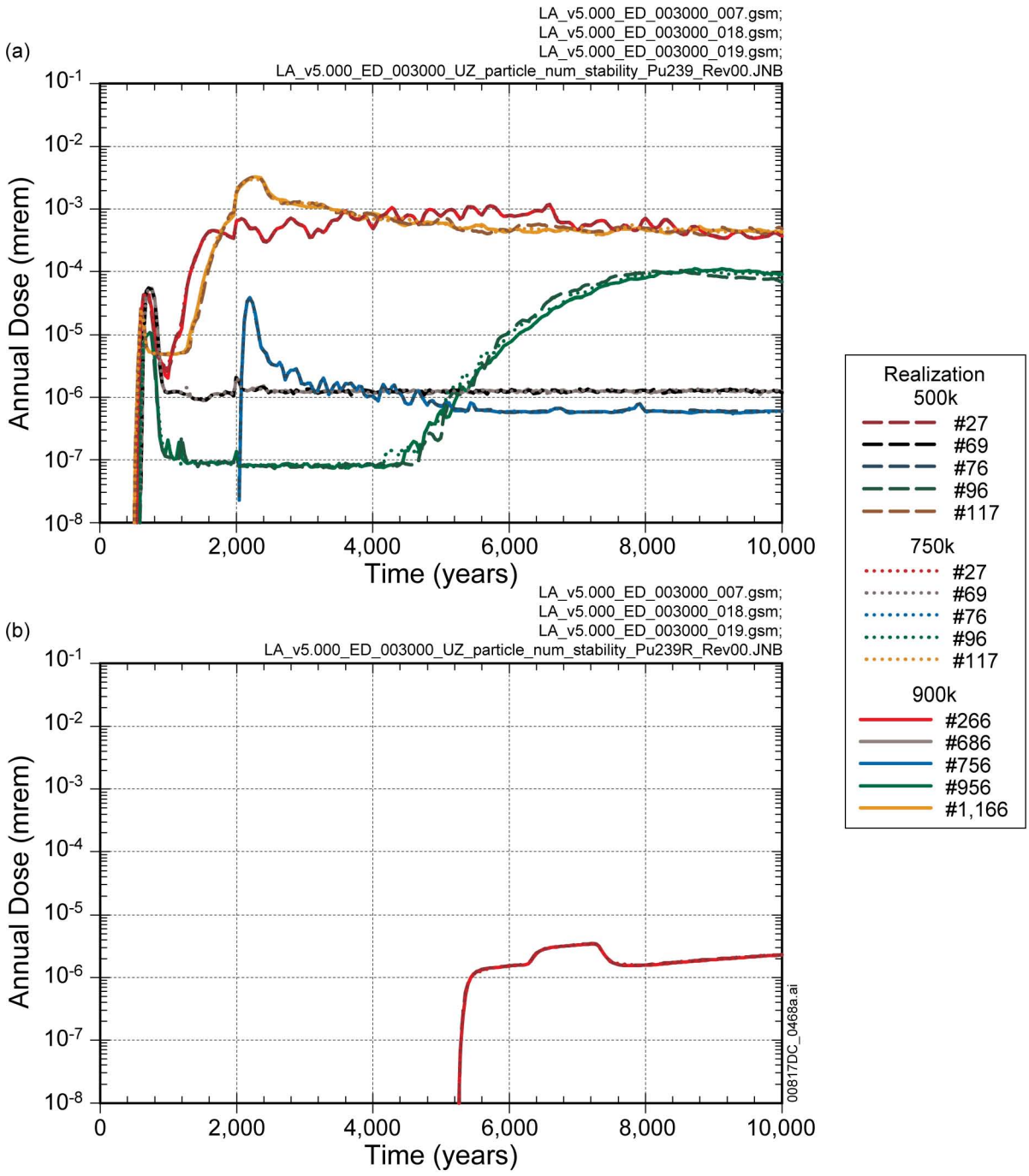

Source: Output DTNs: MO0708TSPAVALI.000 [DIRS 182985], MO0709TSPAREGS.000 [DIRS 182976].

Figure 7.3.5-8. Annual Dose Contribution from (a) ^{239}Pu Total, (b) ^{239}Pu on Reversible Colloids, (c) ^{239}Pu on Retarded Irreversible Colloids, and (d) ^{239}Pu on Unretarded Irreversible Colloids for the Drip Shield Early Failure Modeling Case Simulations Using a Maximum of 500,000, 750,000; and 900,000 Particles in the Unsaturated Zone Transport Submodel

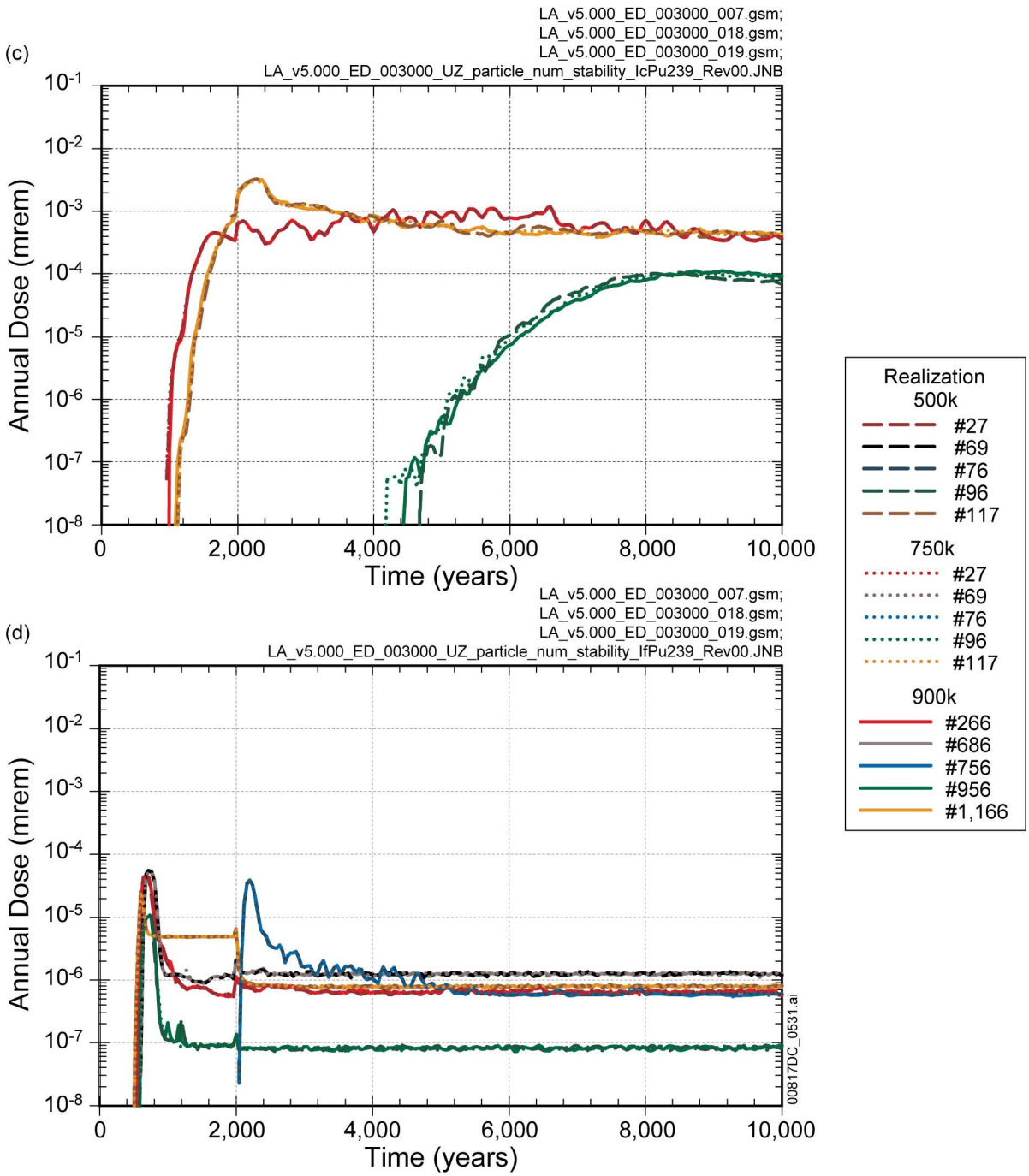

Source: Output DTNs: MO0708TSPAVALI.000 [DIRS 182985], and MO0709TSPAREGS.000 [DIRS 182976].

Figure 7.3.5-8. Annual Dose Contribution from (a) ^{239}Pu Total, (b) ^{239}Pu on Reversible Colloids, (c) ^{239}Pu on Retarded Irreversible Colloids, and (d) ^{239}Pu on Unretarded Irreversible Colloids for the Drip Shield Early Failure Modeling Case Simulations Using a Maximum of 500,000; 750,000; and 900,000 Particles in the Unsaturated Zone Transport Submodel (Continued)

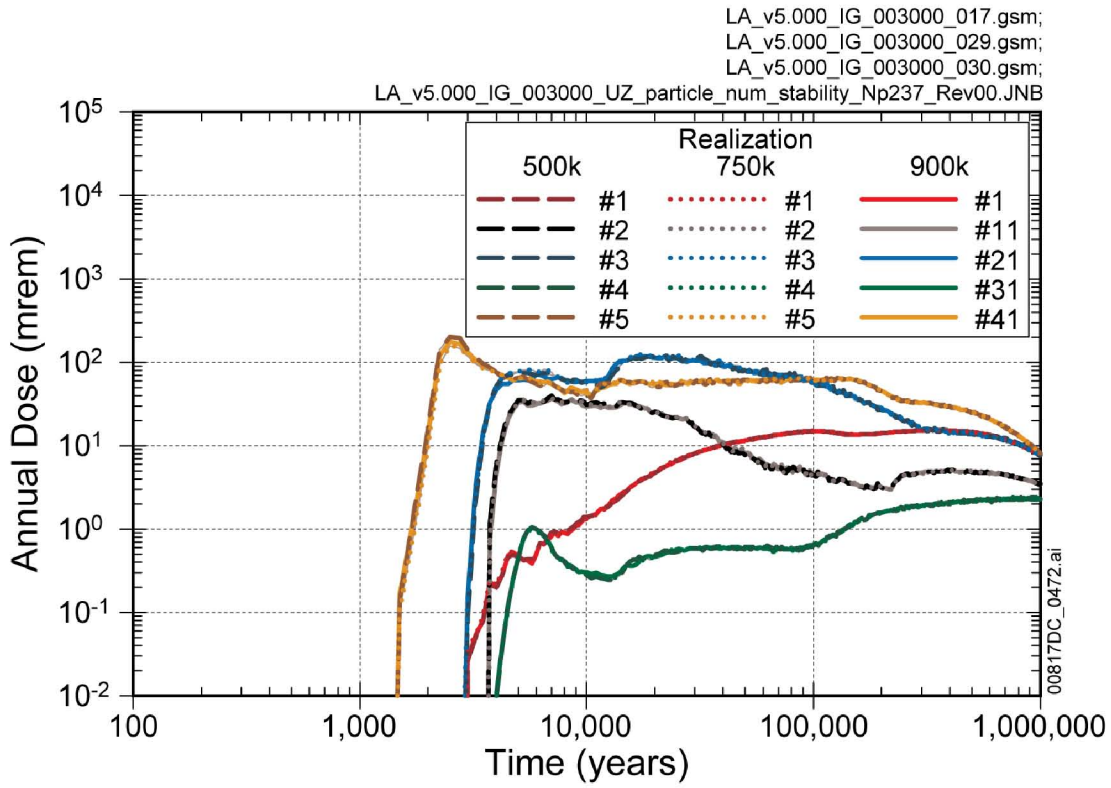

Source: Output DTNs: MO0708TSPAVALI.000 [DIRS 182985]; and MO0709TSPAREGS.000 [DIRS 182976].

Figure 7.3.5-9. Annual Dose Contribution from ^{237}Np for the Igneous Intrusion Modeling Case Simulations Using a Maximum of 500,000; 750,000; and 900,000 Particles in the Unsaturated Zone Transport Submodel

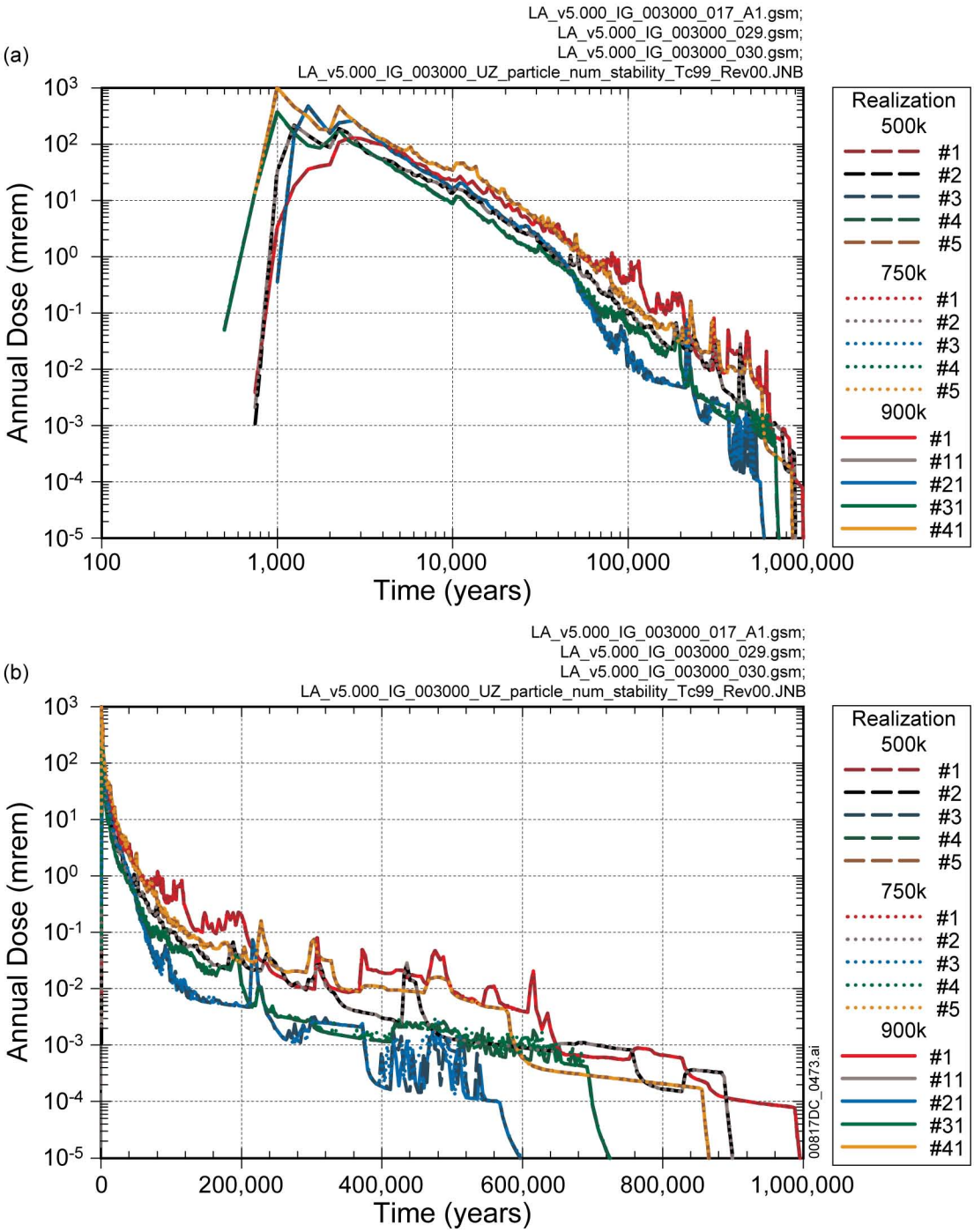

Source: Output DTNs: MO0708TSPAVALI.000 [DIRS 182985]; MO0709TSPAREGS.000 [DIRS 182976].

Figure 7.3.5-10. Annual Dose Contribution from ^{99}Tc for the Igneous Intrusion Modeling Case Simulations Using a Maximum of 500,000; 750,000; and 900,000 Particles in the Unsaturated Zone Transport Submodel

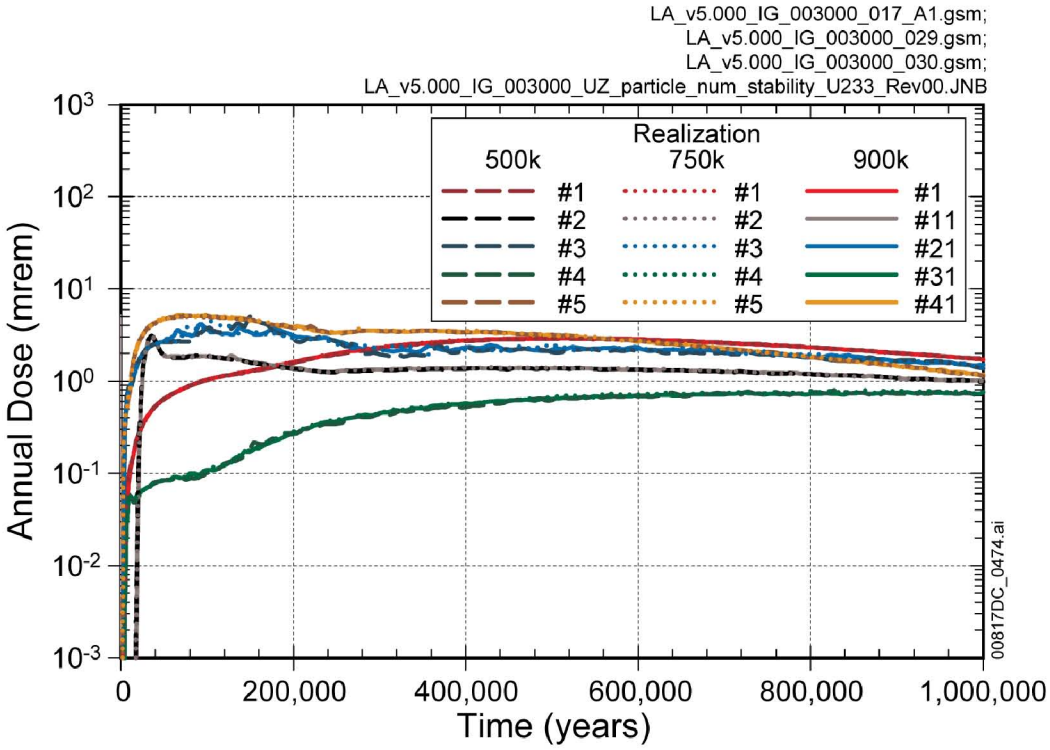

Source: Output DTNs: MO0708TSPAVALI.000 [DIRS 182985], MO0709TSPAREGS.000 [DIRS 182976].

Figure 7.3.5-11. Annual Dose Contribution from ^{233}U for the Igneous Intrusion Modeling Case Simulations Using a Maximum of 500,000; 750,000; and 900,000 Particles in the Unsaturated Zone Transport Submodel

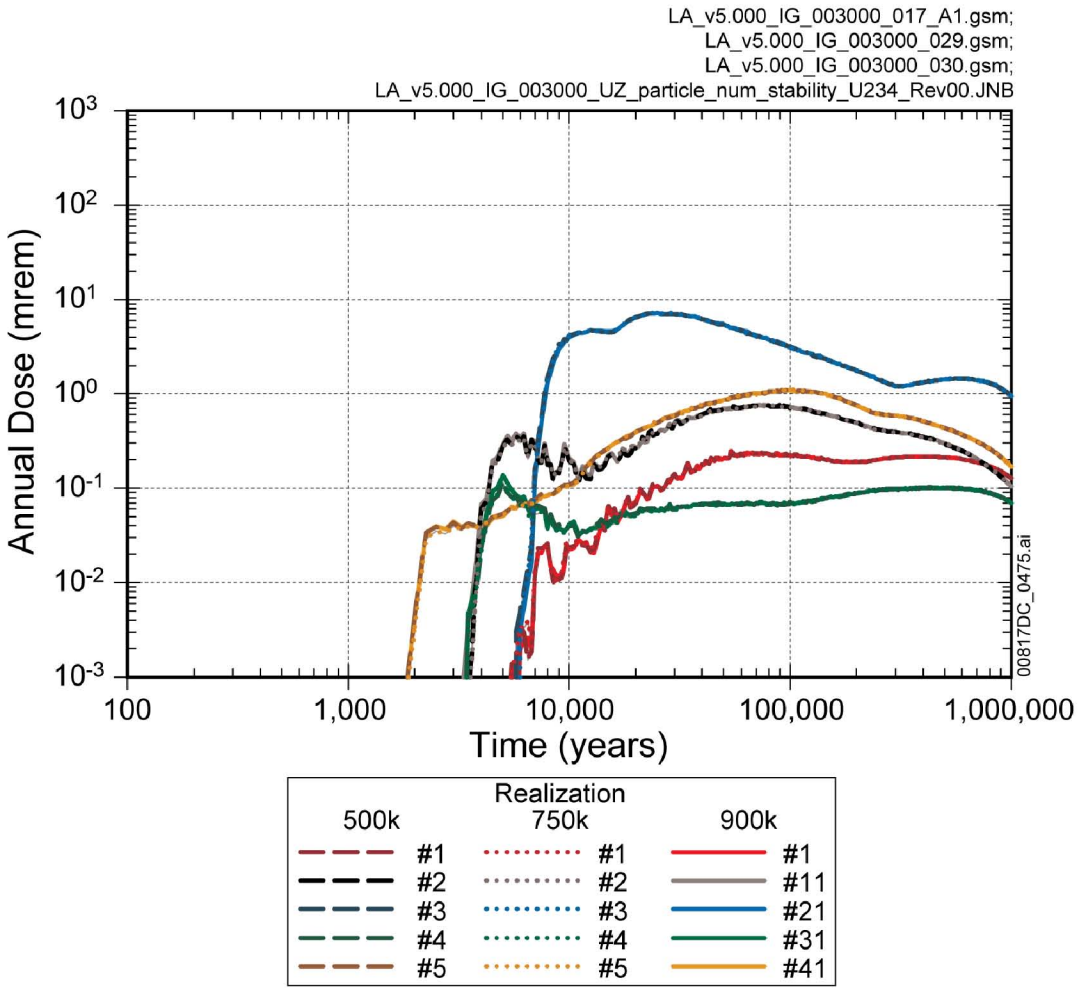

Source: Output DTNs: MO0708TSPAVALI.000 [DIRS 182985]; and MO0709TSPAREGS.000 [DIRS 182976].

Figure 7.3.5-12. Annual Dose Contribution from ^{234}U for the Igneous Intrusion Modeling Case Simulations Using a Maximum of 500,000; 750,000; and 900,000 Particles in the Unsaturated Zone Transport Submodel

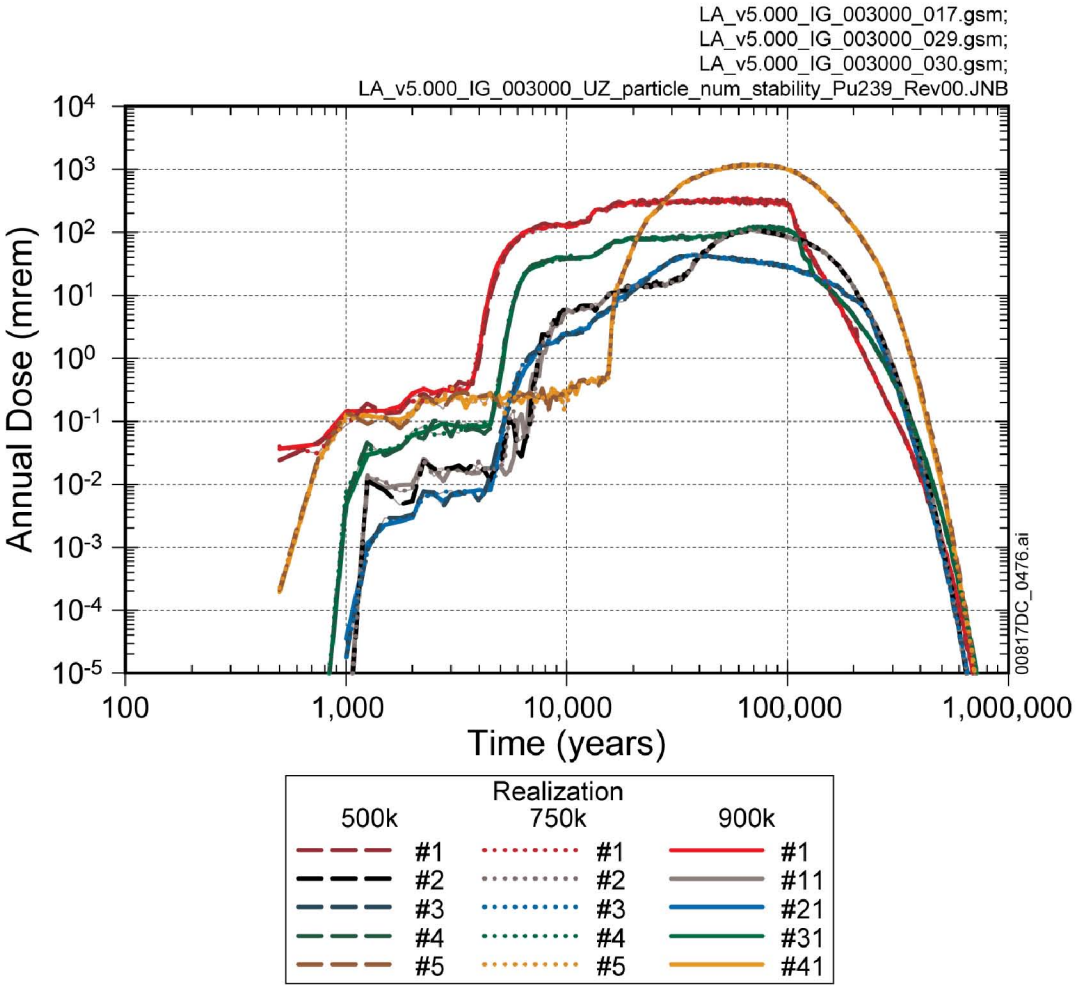

Source: Output DTNs: MO0708TSPAVALI.000 [DIRS 182985]; MO0709TSPAREGS.000 [DIRS 182976].

Figure 7.3.5-13. Annual Dose Contribution from ^{239}Pu for the Igneous Intrusion Modeling Case Simulations Using a Maximum of 500,000; 750,000; and 900,000 Particles in the Unsaturated Zone Transport Submodel

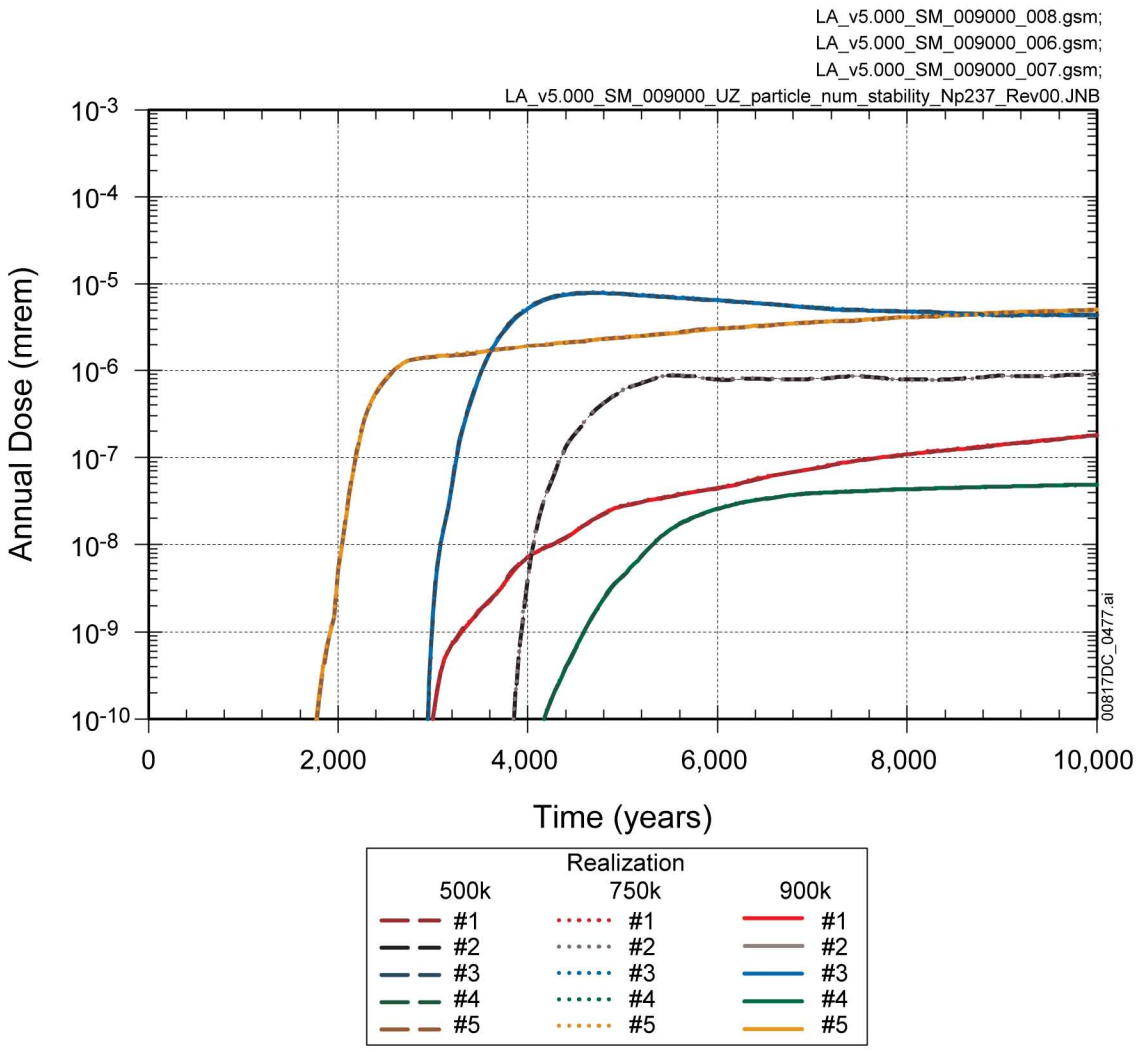

Source: Output DTNs: MO0708TSPAVALI.000 [DIRS 182985]; and MO0709TSPASENS.000 [DIRS 182982].

Figure 7.3.5-14. Annual Dose Contribution from ^{237}Np for the Seismic Ground Motion Modeling Case Simulations Using a Maximum of 500,000; 750,000; and 900,000 Particles in the Unsaturated Zone Transport Submodel

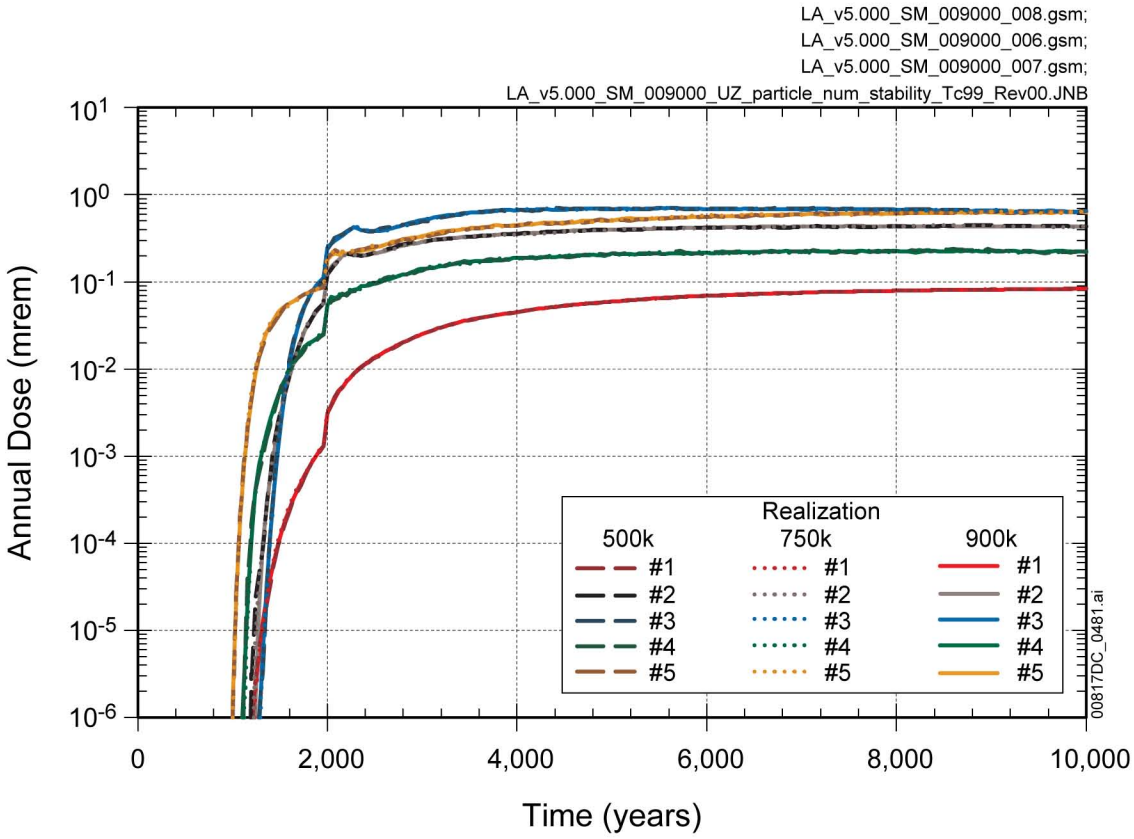

Source: Output DTNs: MO0708TSPAVALI.000 [DIRS 182985]; and MO0709TSPASENS.000 [DIRS 182982].

Figure 7.3.5-15. Annual Dose Contribution from ^{99}Tc for the Seismic Ground Motion Modeling Case Simulations Using a Maximum of 500,000; 750,000; and 900,000 Particles in the Unsaturated Zone Transport Submodel

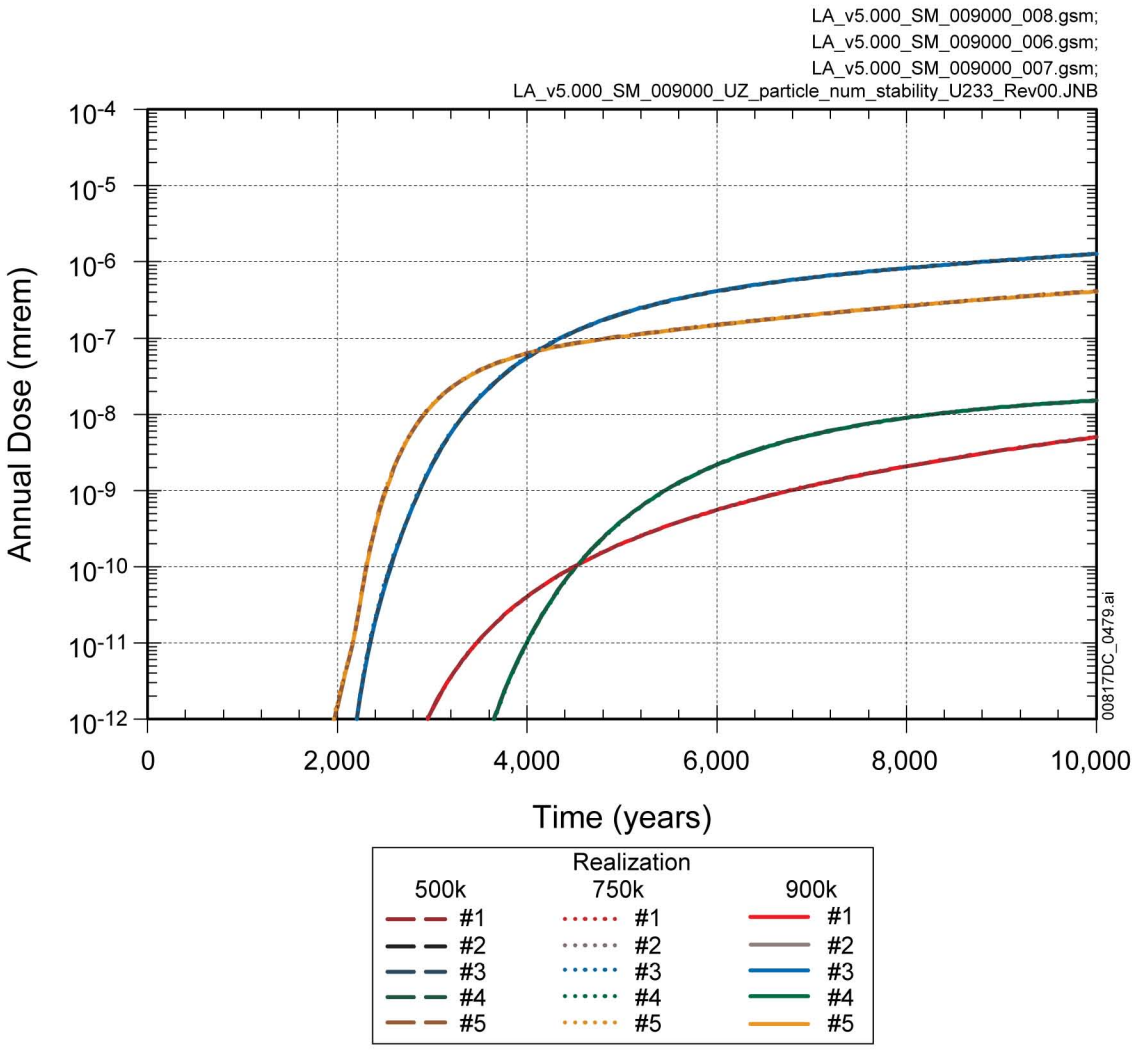

Source: Output DTNs: MO0708TSPAVALI.000 [DIRS 182985]; and MO0709TSPASENS.000 [DIRS 182982].

Figure 7.3.5-16. Annual Dose Contribution from ^{233}U for the Seismic Ground Motion Modeling Case Simulations Using a Maximum of 500,000; 750,000; and 900,000 Particles in the Unsaturated Zone Transport Submodel

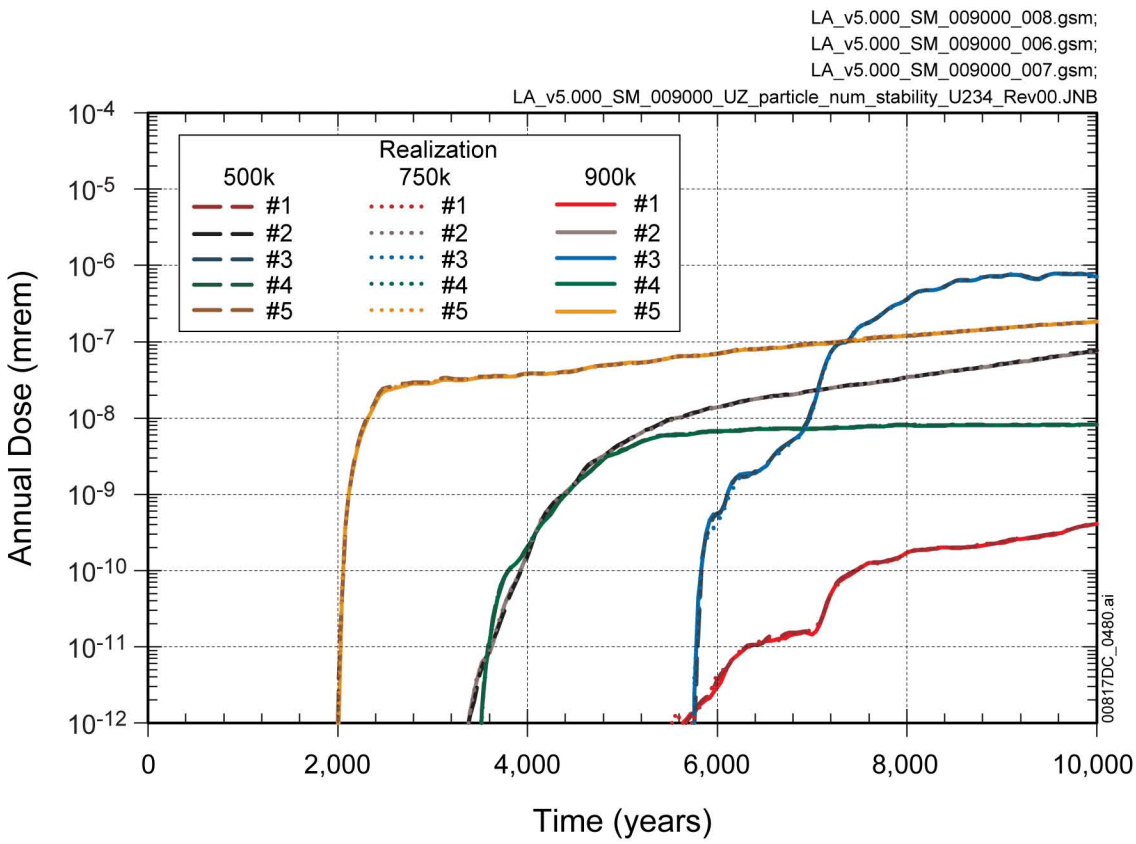

Source: Output DTNs: MO0708TSPAVALI.000 [DIRS 182985]; and MO0709TSPASENS.000 [DIRS 182982].

Figure 7.3.5-17. Annual Dose Contribution from ^{234}U in for the Seismic Ground Motion Modeling Case Simulations Using a Maximum of 500,000; 750,000; and 900,000 Particles in the Unsaturated Zone Transport Submodel

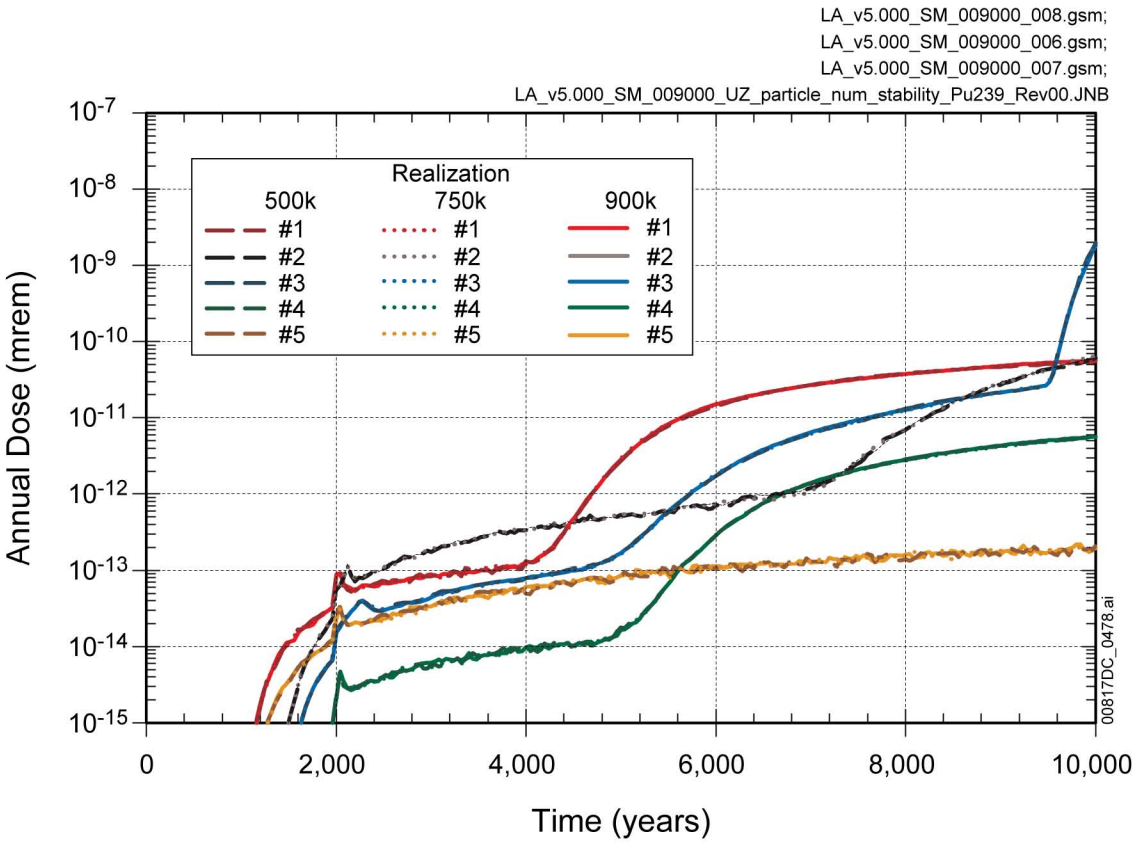

Source: Output DTNs: MO0708TSPAVALI.000 [DIRS 182985]; and MO0709TSPASENS.000 [DIRS 182982].

Figure 7.3.5-18. Annual Dose Contribution from ^{239}Pu for the Seismic Ground Motion Modeling Case Simulations Using a Maximum of 500,000; 750,000; and 900,000 Particles in the Unsaturated Zone Transport Submodel

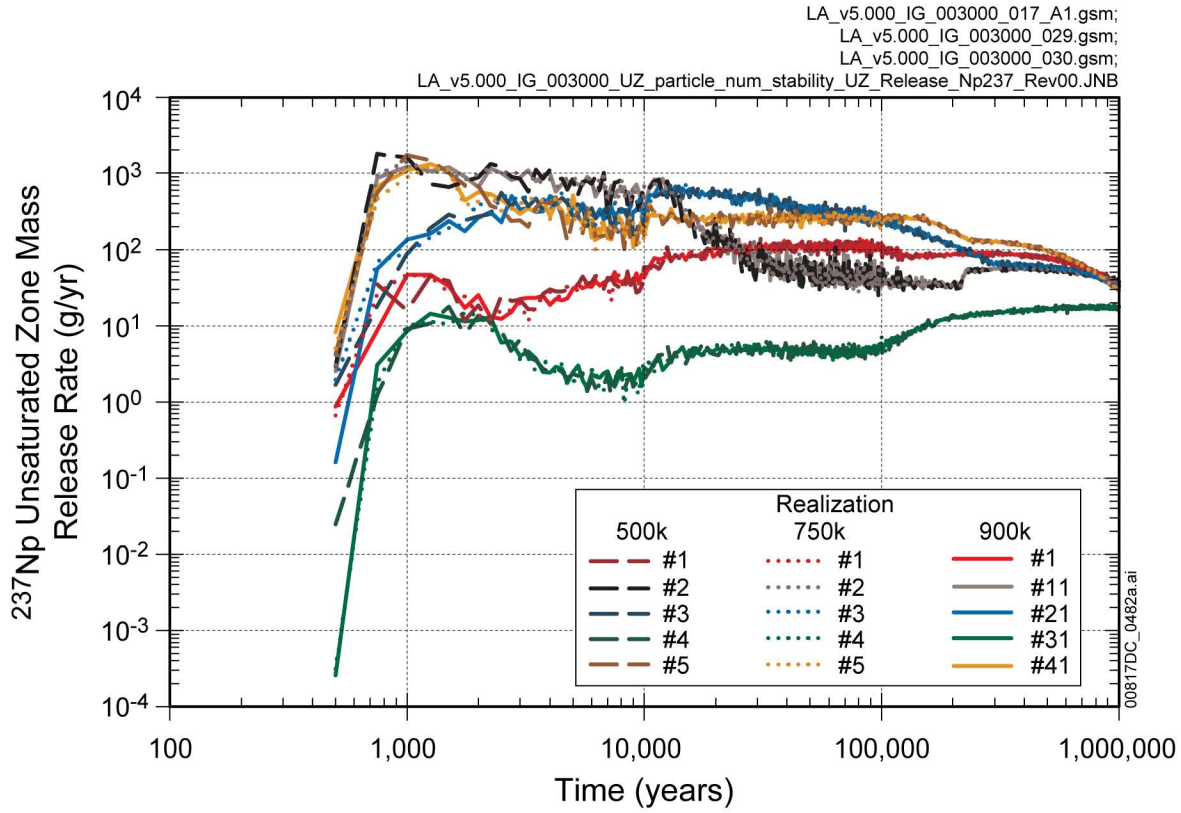

Source: Output DTNs: MO0708TSPAVALI.000 [DIRS 182985]; and MO0709TSPAREGS.000 [DIRS 182976].

Figure 7.3.5-19. Annual Unsaturated Zone Mass Release of ^{237}Np for the Igneous Intrusion Modeling Case Simulations Using a Maximum of 500,000; 750,000; and 900,000 Particles in the Unsaturated Zone Transport Submodel

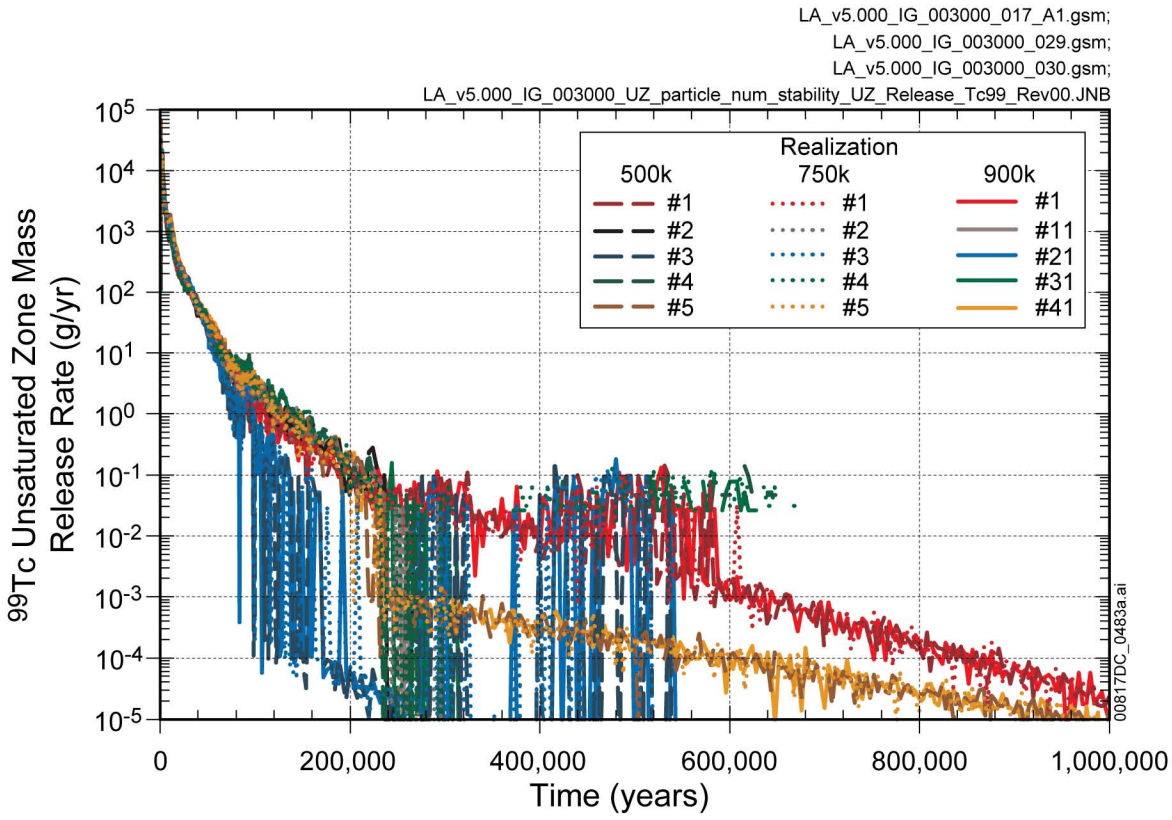

Source: Output DTNs: MO0708TSPAVALI.000 [DIRS 182985]; and MO0709TSPAREGS.000 [DIRS 182976].

Figure 7.3.5-20. Annual Unsaturated Zone Mass Release of ^{99}Tc for the Igneous Intrusion Modeling Case Simulations Using a Maximum of 500,000; 750,000; and 900,000 Particles in the Unsaturated Zone Transport Submodel

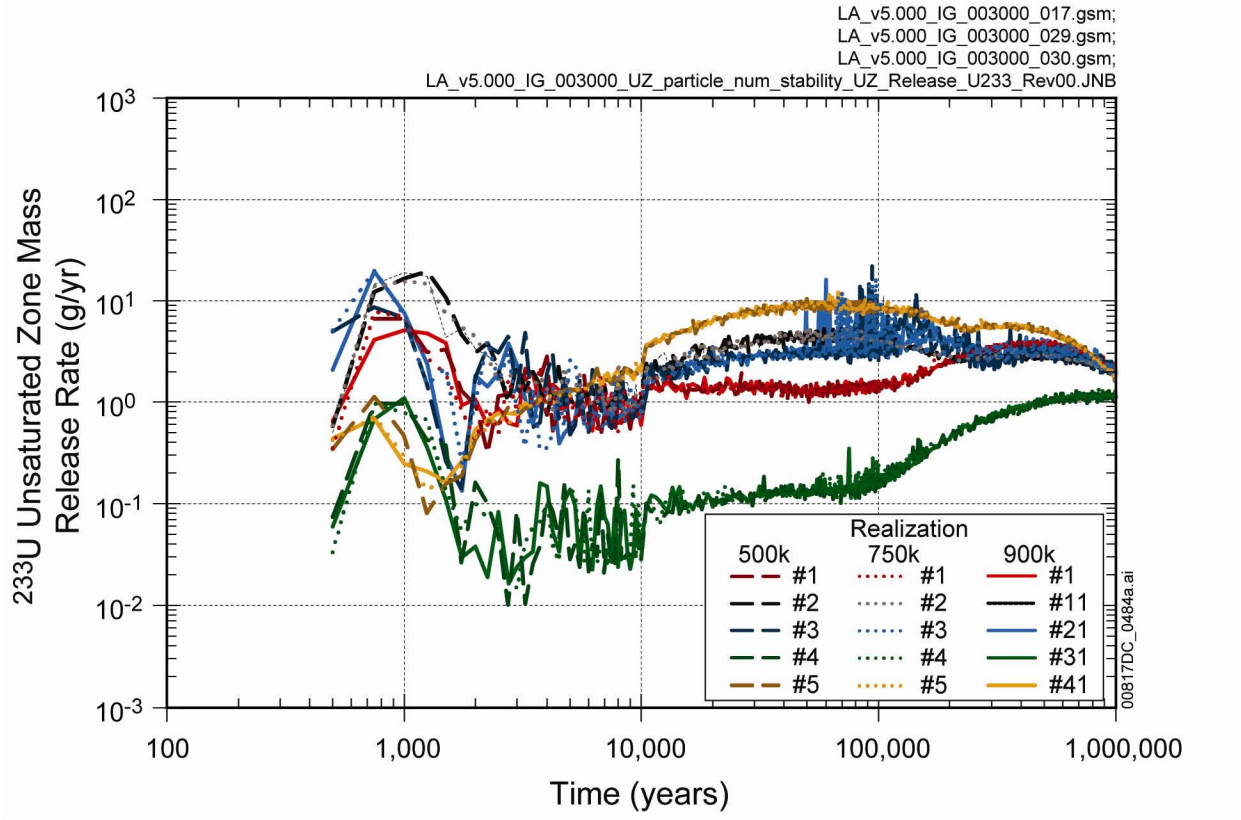

Source: Output DTNs: MO0708TSPAVALI.000 [DIRS 182985]; and MO0709TSPAREGS.000 [DIRS 182976].

Figure 7.3.5-21. Annual Unsaturated Zone Mass Release of ^{233}U for the Igneous Intrusion Modeling Case Simulations Using a Maximum of 500,000; 750,000; and 900,000 Particles in the Unsaturated Zone Transport Submodel

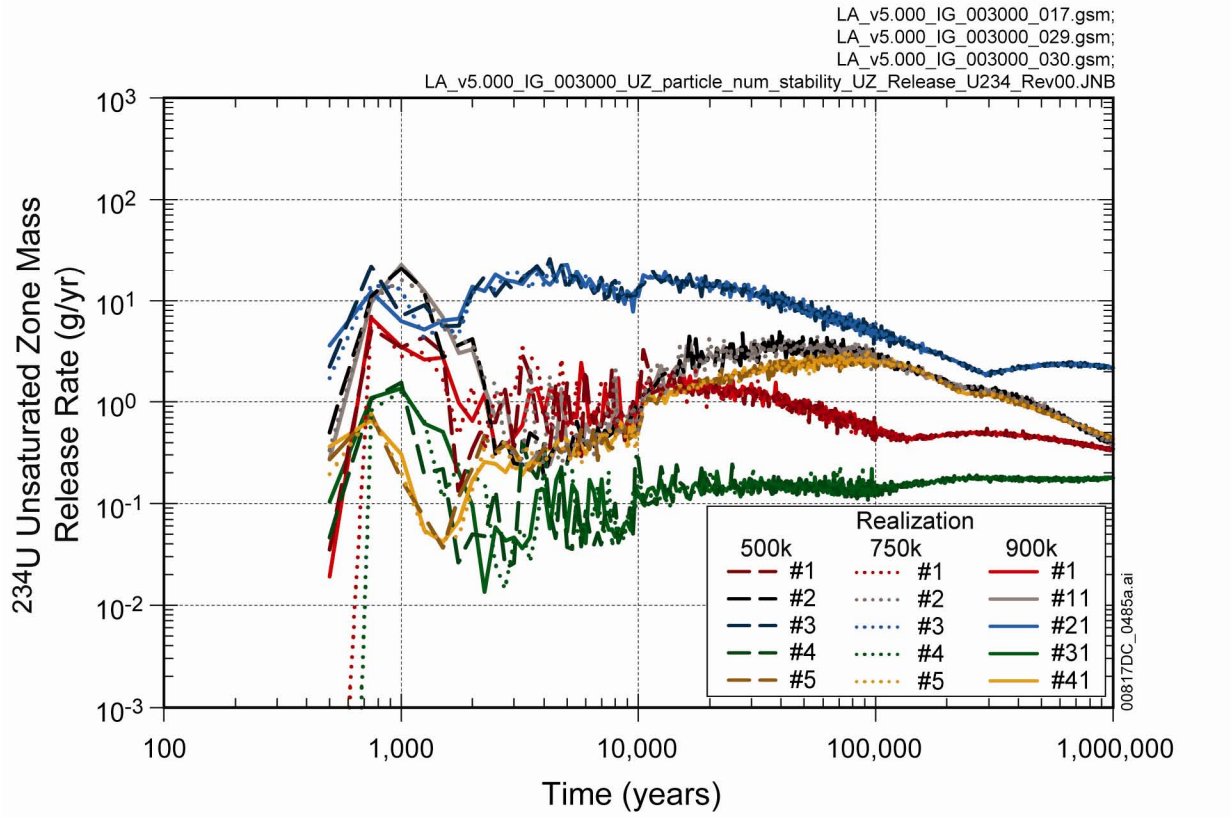

Source: Output DTNs: MO0708TSPAVALI.000 [DIRS 182985]; and MO0709TSPAREGS.000 [DIRS 182976].

Figure 7.3.5-22. Annual Unsaturated Zone Mass Release of ^{234}U for the Igneous Intrusion Modeling Case Simulations Using a Maximum of 500,000; 750,000; and 900,000 Particles in the Unsaturated Zone Transport Submodel

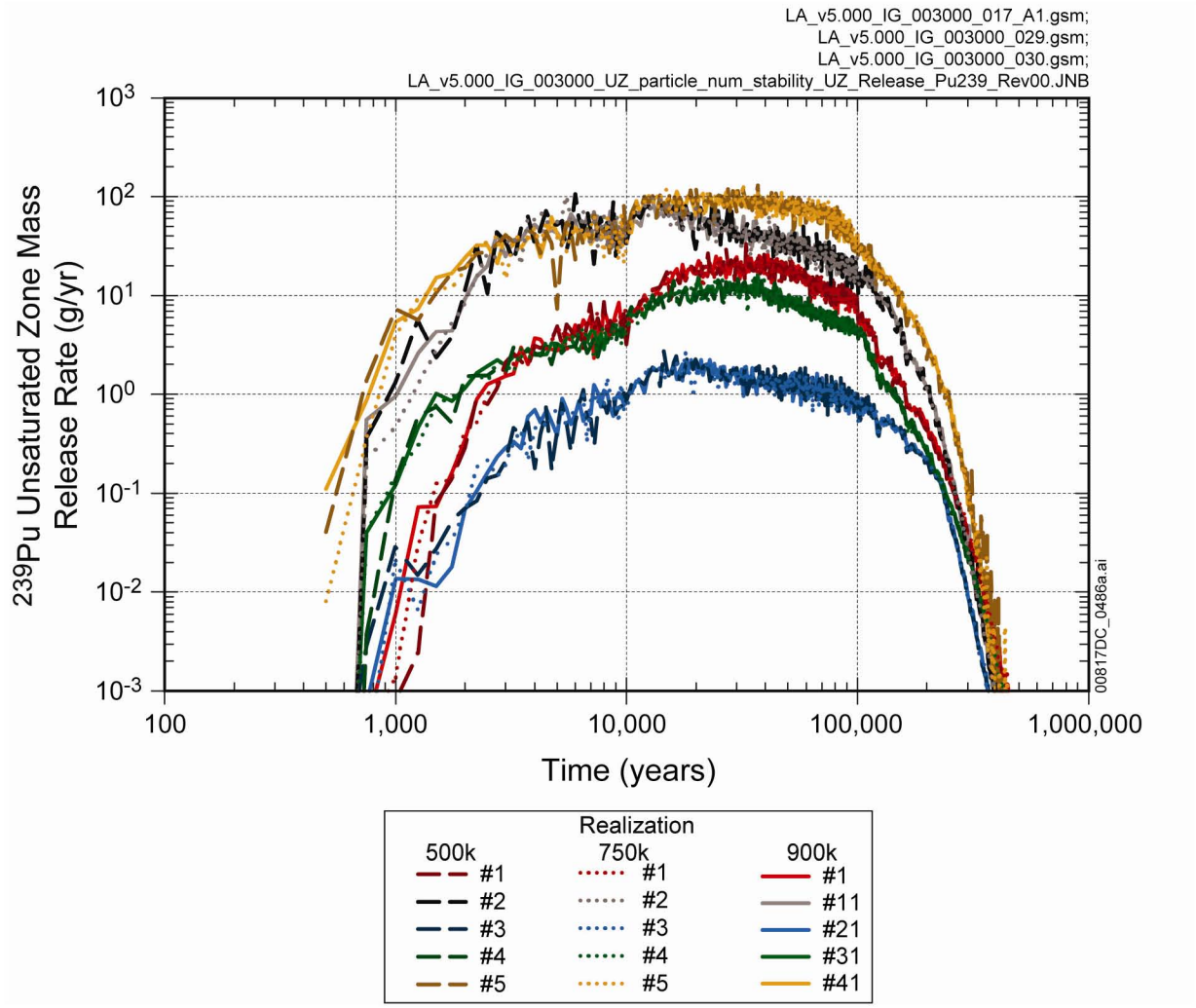

Source: Output DTNs: MO0708TSPAVALI.000 [DIRS 182985]; and MO0709TSPAREGS.000 [DIRS 182976].

Figure 7.3.5-23. Annual Unsaturated Zone Mass Release of ^{239}Pu for the Igneous Intrusion Modeling Case Simulations Using a Maximum of 500,000; 750,000; and 900,000 Particles in the Unsaturated Zone Transport Submodel

7.4 Uncertainty and Variability Characterization Reviews

One of the basic NRC requirements for a repository performance assessment is that it includes an appropriate treatment of parameter uncertainty and variability (10 CFR 63.114(a)(2) [DIRS 178394]). Specific details on how the NRC determines conformance with this requirement are given in *Yucca Mountain Review Plan, Final Report* (NRC 2003 [DIRS 163274], Section 2.2.1.3). To ensure compliance with this basic requirement and to build confidence in this aspect of the TSPA-LA Model, the Lead Laboratory conducted a risk informed review of the TSPA-LA uncertainty and variability characterizations for consistency, defensibility, and traceability of the direct-input parameters to the TSPA-LA Model. A special review team was formed to carefully examine stochastic parameter representations and correct or modify them as necessary. In addition, uncertainty and sensitivity analyses were performed during the development of the TSPA-LA Model based on the direct-input parameters in order to ensure that the parameter uncertainties are accurately propagated during the model development. After the model development, a final sensitivity analysis was conducted in order to identify the dominant sources of uncertainty in total expected dose to the RMEI and the errors that might have occurred during the TSPA-LA Model development. The results of the uncertainty characterization reviews on the direct-input parameters together with the uncertainty and sensitivity analyses performed during and after the TSPA-LA Model development built the foundation of confidence in the results of the model and ensured that supporting documentation was ready for regulatory review. The subsequent sections describe the overall review process, specific parameters and abstractions reviewed, and the actions taken to ensure that the treatment of parameter uncertainty and variability was of suitable quality for the LA, and summarizes the performed uncertainty and sensitivity analyses with the details of the analyses presented in Appendix K.

7.4.1 Approach

The technical reviews performed focused on: (1) confirming that the stochastic parameter representations appropriately reflect the major sources of uncertainty and/or variability, (2) verifying that the probability distributions were derived using sound statistical methods and interpretations, and (3) ensuring model parameter representations (i.e., probability distributions) are reasonable and defensible, as opposed to depicting extreme variations that could potentially introduce risk dilution (i.e., underestimation of dose risk). The reviews provided a risk informed or risk based evaluation of parameters important to dose in the TSPA-LA Model. A total of 15 formal reviews were performed to scrutinize the uncertainty characterizations of some 40 key TSPA input parameters (Table 7.4-1 through 7.4-3) and their associated abstractions.

A core team of several senior staff members of the Yucca Mountain Project (YMP) was formed with special expertise in probability and statistics, uncertainty analysis, TSPA modeling, and knowledge of the regulatory guidance regarding consistent treatment of uncertainty and variability. In addition, selected YMP subject matter experts (SMEs) provided support on an as-needed basis and facilitated the reviews of data, parameters, and model abstractions. This approach is based on, but not as formalized as the guidelines for uncertainty characterization and propagation presented in *Guidelines for Developing and Documenting Alternative Conceptual Models, Model Abstractions, and Parameter Uncertainty in the Total System Performance Assessment for the License Application* (BSC 2002 [DIRS 158794]).

The general work scope of the review team included:

- Familiarizing YMP SMEs with methodologies for analyzing data uncertainties and variabilities as well as use of statistical techniques to derive probability distributions, (i.e., probability density functions (pdfs) and cumulative density functions (CDFs))
- Performing independent statistical analyses and interpretations of laboratory and field data
- Checking the appropriateness of probability distributions chosen to fit data and ensuring consistency with respect to the quantity of available data
- Deriving probability distributions using advanced statistical techniques, including subjective methods such as Bayesian updating
- Ensuring parameter values are representative of component model scale (i.e., up-scaling data from small-scale samples and tests to the physical scale of the model)
- Examining subjective probability distributions to ensure that informal professional judgments were reasonable and consistent.

Potential inadequacies or problems in the uncertainty or variability treatment were generally resolved through review team collaborations with data collectors, TSPA data input package and analysis and model report authors, and TSPA component model leads. Inconsistencies or issues that could not be resolved through collegial interactions were presented to the Performance Assessment Systems Integration Management Team (a senior technical team) for resolution (Figure 7.4-1). Final resolution of parameter uncertainty team review comments were incorporated into the appropriate analysis and/or model reports.

7.4.2 Risk Informed Ranking of Scenario Classes and Modeling Cases

A risk-based ranking of TSPA-LA scenario classes and modeling cases was focused on the uncertainty/variability characterization reviews on the most important component model abstractions. Simulation results from past TSPA scoping studies were used to rank the major scenario classes and modeling cases according to their contribution to overall risk. It is important to note that past TSPA analyses have been largely limited to a 10,000-year time period. For simplicity, it was assumed that the ranking was also valid for post-10,000-year time periods.

There are four major scenario classes (Section 1.5) that are analyzed in demonstrating compliance with the individual protection standard (10 CFR 63.311(a) (1) and (2) [DIRS 178394]). Specific TSPA-LA scenario classes that are considered include:

- Nominal Scenario Class (i.e., expected evolution of the natural environment and degradation of the WPs and DSs, excluding early failures and disruptive processes and events)

- Early Failure Scenario Class (i.e., early failure of WPs and DSs due to material defects, process failures, and human errors)
- Igneous Scenario Class (includes Igneous Intrusion and Volcanic Eruption Modeling Cases)
- Seismic Scenario Class (includes Ground Motion and Fault Displacement Modeling Cases).

The Human Intrusion Scenario was excluded from the ranking because the relevant model parameters (for release, flow, and transport) are addressed in the Nominal Scenario.

Based on comparison of past TSPA dose projections (Gibson 2007 [DIRS 181099], Section 8.2), the following ranking (from highest to lowest) of the Scenario Classes and Modeling Cases were obtained:

1. Seismic Scenario Class, Seismic GM Modeling Case
2. Igneous Scenario Class, Igneous Intrusion Modeling Case
3. Igneous Scenario Class, Volcanic Eruption Modeling Case
4. Early Failure Scenario Class, Waste Package and Drip Shield EF Modeling Cases
5. Seismic Scenario Class, Seismic FD Modeling Case
6. Nominal Scenario Class, Nominal Modeling Case.

The magnitudes of the projected mean annual doses indicated that the first three modeling cases by far dominated the projected total mean annual dose for 10,000 years. As a result of this ranking and selection, the uncertainty/variability characterization reviews were focused on the top three modeling cases. However, because many component models of the Nominal Scenario Class are actually used in the Seismic and Igneous Modeling Cases, it was included in the selected set of modeling cases.

7.4.3 Risk Informed Identification of Stochastic Parameters Important to Dose

Because of the relatively large number of stochastic parameters used in the TSPA-LA simulation model (see Table K.3-2 in Appendix K for a detailed list), it was necessary to use a risk informed approach to prioritize the parameters associated with the Seismic, Igneous, and Nominal Modeling Cases. This approach builds confidence in the TSPA-LA Model, as it provides the review and consideration of the parameters that most impact the expected annual dose.

The risk informed selection of TSPA parameters was based on both importance rankings from preliminary TSPA scoping studies (Gibson 2007 [DIRS 181099], Appendix M) and recommendations provided by model abstraction developers and experienced TSPA analysts. The list of parameters was considered a candidate set appropriate for setting review priorities. The set of parameters was grouped into three of the four scenario classes. For each of the modeling cases selected, a cross-walk between the model abstractions and their associated key parameters was developed. The following sections briefly describe the relevant model abstractions and their associated key parameter sets.

7.4.3.1 Seismic Scenario Class—Key Abstractions and Parameters

The Seismic GM Modeling Case simulates the damage of WPs and DSs resulting from kinematic motion and rockfall for a range of seismic conditions. For the Seismic GM Modeling Case, seven major categories of parameters were identified as potentially having high importance. Within this parameter set, the seismic hazard curve was expected to dominate the importance ranking; this expectation is based on the previous TSPA scoping calculations (Gibson 2007 [DIRS 181099], Section 8.2.1.7), which indicated that the Seismic GM Modeling Case was an important contributor to the projected total mean annual dose. The seismic hazard curve defines the annualized probability of a given magnitude of PGV; WP damage abstractions are a function of PGV.

The set of key parameters identified for the Seismic GM Modeling Case, and the rationale for their selection, is presented in Table 7.4-1. The model abstractions for the Seismic GM Modeling Case are substantially more detailed than those used in past TSPA scoping calculations. The more detailed process and damage abstractions introduced several new parameters; the set of parameters considered to be important to simulation of repository system performance are included in Table 7.4-1. Detailed descriptions of these parameters and their uncertainty/variability characterizations are documented in *Seismic Consequence Abstraction* (SNL 2007 [DIRS 176828], Tables 6-88 through 6-93).

A number of Nominal Scenario parameters are also used in the Seismic Scenario Modeling Cases. For example, DS general corrosion rate is used in the damage seismic abstraction; this abstraction simulates the structural behavior of the DS as a function of plate thickness, which is a function of corrosion rate.

7.4.3.2 Igneous Scenario Class—Key Abstractions and Parameters

The Igneous Scenario Class consists of two modeling cases, Igneous Intrusion and Volcanic Eruption. Previous TSPA scoping calculations, performed for a 10,000-year time frame, have indicated that the annual frequency or occurrence rate is of high importance to both modeling cases. Similarly, the number of WPs hit parameter was also considered by the TSPA analysts to be important for both modeling cases. These and other key parameters for the Igneous Scenario Class are presented in Table 7.4-2.

For the Igneous Intrusion Modeling Case, it is important to clarify that at the time of the uncertainty/variability characterization reviews, the number of WPs hit was a stochastic parameter; subsequent to the review, however, it was decided to assign a constant value to the number of WPs hit. For the TSPA-LA compliance analysis (presented in Section 8), it was conservatively assumed that all the CDSP and CSNF WPs in the repository are damaged for any realization in which a main, drift, turnout, or other extension is intersected by an igneous intrusion (SNL 2007 [DIRS 177432], Section 5.1).

In the Volcanic Eruption Modeling Case, there are two basic and potentially important parameters, namely wind speed and direction. These stochastic parameters determine the characteristics of atmospheric dispersion and deposition of ash and contaminants produced by a hypothetical eruption through the repository. The scour depth parameter represents the depth to

which tephra and channel sediments are mixed and its tephra redistribution abstraction (i.e., simulates the transport of deposited ash to the location of the RMEI). Detailed descriptions of these parameters and their uncertainty/variability characterizations are documented in *Atmospheric Dispersal and Deposition of Tephra from a Potential Volcanic Eruption at Yucca Mountain, Nevada* (SNL 2007 [DIRS 177431], Tables 8-2 through 8-4) and in *Redistribution of Tephra and Waste by Geomorphic Processes Following a Potential Volcanic Eruption at Yucca Mountain, Nevada* (SNL 2007 [DIRS 179347], Table 6.4-1).

7.4.3.3 Nominal Scenario Class—Key Abstractions and Parameters

The Nominal Scenario Class represents the changes of the repository system that are expected to occur over a regulatory time frame. A total of eight component models have been developed to describe the isolation characteristics of the three primary barriers (i.e., upper natural barrier, engineered barrier, and lower natural barrier). As described in Section 6.3, the model components for the Nominal Modeling Case consist of: (1) UZ Flow, (2) EBS Environment, (3) WP and DS Degradation, (4) Waste Form Degradation and Mobilization, (5) EBS Flow and Transport, (6) UZ Transport, (7) SZ Flow and Transport, and (8) Biosphere.

Of the eight model components, five have abstractions that are likely to play a dominant role in the calculation of postclosure performance, even with the added effects of disruptive events. The model components are:

- UZ Flow (climate-induced infiltration, UZ flow fields, and drift seepage)
- WP and DS Degradation (general corrosion, localized corrosion, and SCC of WP outer barrier, and general corrosion of DS)
- Waste Form Degradation and Mobilization (radionuclide solubilities and waste form colloids)
- EBS Radionuclide Transport (corrosion products and colloids)
- SZ Flow and Transport (breakthrough curves and transport).

The key TSPA parameters for this scenario class are listed in Table 7.4-3. Based on sensitivity analyses carried out with preliminary TSPA scoping calculations (Gibson 2007 [DIRS 181099], Section 8.2), several of these probabilistic parameters have been shown to have a strong influence on the calculated distribution of expected annual dose.

In the UZ Flow Model Component, the parameter of fundamental importance is the net infiltration rate. This rate or flux is computed for pre-10,000-years from infiltration maps for the three climate states (i.e., present-day, monsoon, and glacial-transition) using a probabilistic approach that uses weighting factors. The uncertainty range for the post-10,000-years percolation rates has been specified in the NRC proposed regulation (10 CFR 63.342(c)(2) [DIRS 178394]). Two other important UZ parameters are the effective soil thickness of the soil cover and permeability of the lithophysal rock of the emplacement horizon. The effective soil

thickness is used in the process-level model for infiltration, while the permeability is used in the drift seepage abstraction.

The WP and DS degradation component models simulate the effects of various degradation processes and mechanisms as a function of the drip seepage, geochemical, and thermal conditions. The WP outer barrier, which is fabricated of Alloy 22 (UNS N06022), is degraded by general corrosion, localized corrosion, and SCC. The DSs are manufactured with Titanium Grade 7 metal plates and frame. The Titanium Grade 7 is relatively corrosion resistant and degrades only by general corrosion.

Of the six submodels that make up the Waste Form Degradation and Mobilization Model Component, the key parameters are the radionuclide solubility uncertainty factor in the Dissolved Concentration submodel (accounts for uncertainty in the thermodynamic coefficients) and the concentration of plutonium irreversibly attached to the waste form colloids in the EBS colloids submodel.

In the EBS Flow and Transport Model Component, the key parameters are corrosion rates for stainless and carbon steel, which determines the accumulation of corrosion products, and the specific surface and site density of the iron oxide mineral goethite. The importance of these parameters is associated with their influence on the sorption of dissolved and colloidal phase radionuclides and, thereby, affects the rate of release from the EBS.

In the SZ Flow and Transport Model Component, the two key parameters for groundwater flow are groundwater-specific discharge and the flowing interval spacing of the volcanic units. Parameters particularly important to dissolved and colloidal phase radionuclide transport are the radionuclide sorption coefficients and colloid retardation factor for the alluvium.

Detailed descriptions of these parameters and their statistical representations are documented in the following documents:

1. *Simulation of Net Infiltration for Present-Day and Potential Future Climates* (SNL 2007 [DIRS 182145], Section 6.5.5); *UZ Flow Models and Submodels* (SNL 2007 [DIRS 184614], Sections 6.10 and 6.8.5); and *Abstraction of Drift Seepage* (SNL 2007 [DIRS 181244], Section 6.6);

2. *General Corrosion and Localized Corrosion of the Drip Shield* (SNL 2007 [DIRS 180778], Section 8.1[a]); *General Corrosion and Localized Corrosion of Waste Package Outer Barrier* (SNL 2007 [DIRS 178519], Section 8.4); *Stress Corrosion Cracking of Waste Package Outer Barrier and Drip Shield Materials* (SNL 2007 [DIRS 181953], Section 8.4); *Analysis of Mechanisms for Early WP/DS Failure* (SNL 2007 [DIRS 178765], Section 7.1);

3. *Waste Form and In-Drift Colloids-Associated Radionuclide Concentrations: Abstraction and Summary* (SNL 2007 [DIRS 177423], Section 6); *Dissolved Concentration Limits of Elements with Radioactive Isotopes* (SNL 2007 [DIRS 177418], Section 8.1);

4. *EBS Radionuclide Transport Abstraction* (SNL 2007 [DIRS 177407], Section 8.2); and

5. *Saturated Zone Flow and Transport Abstraction* (SNL 2008 [DIRS 183750], Section 6.5.2).

7.4.4 Review Team

As noted above, a multi-disciplinary team of scientists and engineers was formed to conduct the parameter uncertainty/variability reviews. The skill composition of the review team was chosen to ensure a large breadth of expertise, experience, and knowledge. The review team selected brought together technical expertise spanning:

- Modeling of physical and chemical processes with inherent aleatory and epistemic uncertainty
- Statistical analysis and interpretation of data
- Analysis of probabilistic modeling results (via sensitivity and uncertainty analyses) to identify parameter importance ranking
- Conceptual and calculational structure of the TSPA-LA Model for the proposed Yucca Mountain repository system
- Encoding professional judgment to formulate subjective representations of uncertainty or variability.

In addition, the core members chosen were required to have an in-depth knowledge of the proposed NRC and U.S. Environmental Protection Agency (EPA) regulations for deep geologic repositories, regulatory guidance on consistent and adequate treatment of uncertainties, and the NRC review methods and guidance presented in *Yucca Mountain Review Plan, Final Report* (NRC 2003 [DIRS 163274]). The core review team that was formed consisted of five senior YMP staff members. The technical backgrounds of the core team members included: (1) TSPA modeling of deep geologic repositories, (2) statistical analysis of field and laboratory data, (3) application of probabilistic modeling and uncertainty propagation, (4) sensitivity and uncertainty analysis, and (5) seismic and volcanic hazard analysis.

A group of SMEs was also selected to provide support to the review activities. The SMEs were primarily used to perform independent evaluations of data, as well as facilitate in-depth reviews of the technical basis of model abstractions. These SMEs had specialized knowledge in: (1) hydrogeology and groundwater transport, (2) material science (e.g., WP and DS corrosion), (3) soil physics, soil chemistry, and groundwater geochemistry, and (4) reliability analysis and human factors engineering, and (5) elicitation methods for encoding professional judgment.

7.4.4.1 Review Scope, Process, and Criteria

For the most part, the scope of the uncertainty/variability characterization reviews was limited to a total of 15 formal reviews. Collectively, these reviews examined in detail the uncertainty/variability characterizations for the 40 plus TSPA input parameters listed in Tables 7.4-1 through 7.4-3. While the reviews primarily focused on scrutinizing the technical basis, they also included consistency aspects of the NRC Review Method for data uncertainty

described in *Yucca Mountain Review Plan, Final Report* (NRC 2003 [DIRS 163274]) for the 14 abstraction topics. In addition, the supporting documentation was reviewed and critiqued with respect to clarity and transparency. Verifying the traceability of data was outside the scope of these reviews; however, such reviews were performed separately in accordance with the YMP QA procedures for document review.

Each uncertainty/variability characterization review involved: (1) reviewing the relevant source documents (i.e., draft TSPA Data Input Packages and analysis and/or model reports); (2) meetings with the authors, data collectors, SMEs, and TSPA analysts to gain additional information and clarification; (3) developing recommendations and/or independent probabilistic representations; and (4) presenting the findings and recommendations to the authors and the Performance Assessment Systems Integration Team.

Parameter uncertainty/variability characterizations were judged appropriately, based on the criteria consistent with the NRC Acceptance Criterion for data uncertainty. More specifically, the criteria consisted of: (1) must be technically defensible and reasonably account for major sources of uncertainties and variabilities, and (2) will not introduce inappropriate risk dilution when propagated through the TSPA-LA Model. A review finding with respect to the first criterion was ascertained by addressing fundamental questions such as:

- What are the sources of uncertainty (i.e., aleatory and epistemic) and spatial variability?
- Is the parameter distribution consistent with the level of knowledge (i.e., maximum informational entropy) and/or quantity of data?
- Is there an underlying physical or mechanistic basis for the type of probability distribution used?
- Was the probability distribution evaluated for goodness-of-fit?
- Have potential correlations to other parameters been evaluated?

Similarly, the finding for the second criterion focused on questions such as:

- Are the bounds of the distribution reasonable and supported by data or other technical information?
- Have extreme conservatisms been embedded in the choice of location and scale parameters of the distribution (i.e., to skew the distribution)?
- What informal professional judgments have been made in uncertainty characterization and have they been peer reviewed?

The general review process is outlined in the flowchart shown on Figure 7.4-1. It is important to note the pivotal role of the Performance Assessment Systems Integration Team in this process, which was to evaluate the review team's findings and recommend an appropriate implementation, based on a risk-informed perspective.

7.4.5 Review Findings and Implementations

As explained in Section 7.4.2, a risk informed evaluation was conducted of the major scenario classes and their associated modeling cases to rank them according to their potential contribution to the overall dose-risk. This section gives highlights from selected reviews, principal findings, and recommended revisions to the uncertainty or variability characterizations.

7.4.5.1 Seismic Scenario Class—Ground Motion Modeling Case

The Seismic GM Modeling Case is one component of the seismic consequences model. The ground motion component evaluates the likelihood and consequences of both kinematic motion and rockfall on the WPs and DSs. The key probabilistic parameters for the Seismic GM Modeling Case can be grouped into the following three categories:

- Mean seismic hazard curve
- Fragility curves for the DSs
- Damage abstractions for kinematic motion and rockfall.

The model theory and stochastic parameter representations for the Seismic GM Modeling Case are documented in *Seismic Consequences Abstraction* (SNL 2007 [DIRS 176828], Section 6). The formal review of the Seismic GM Modeling Case examined six key parameter representations, which are listed in Table 7.4-1. Significant findings and recommendations are summarized below.

Seismic Hazard Curve—The ground motion component of the seismic consequences model uses the mean seismic hazard curve (Section 6.6.1.2) for the repository location, which is the product of several years of study conducted by the YMP under the *Probabilistic Seismic Hazards Analysis for Fault Displacement and Vibratory Ground Motion at Yucca Mountain, Nevada* (PSHA) (CRWMS M&O 1998 [DIRS 103731]). The mean hazard curve, which is defined as the mean estimate or average of the distribution of hazard curves derived by the PSHA expert elicitation (Budnitz et al. 1997 [DIRS 103635]), lies above the 80th percentile of the distribution for high intensity ground motions (i.e., at low annual exceedance frequencies) because the average is dominated by the larger PGV values of the distribution.

The review team noted that use of the mean hazard curve does not explicitly propagate the available distribution of epistemic uncertainty in the hazard curve to the estimate of the distribution of expected annual dose. Moreover, the use of a mean hazard curve is inconsistent with the probabilistic framework outlined in Section 6.1.3. Because the uncertainty distribution in the hazard curve could contribute significantly to the uncertainty distribution of the expected annual dose curves, the review team recommended projecting the annual dose for the Seismic GM Modeling Case using the distribution of hazard curves. The Performance Assessment Systems Integration Team elected not to adopt the review team recommendation because of a letter agreement between DOE and NRC on the approach to postclosure seismic analyses. That letter agreement states: "As the objective of the probabilistic risk assessment will be to determine mean risk, the mean ground motion hazard curve will be used" (Brocoum 2001 [DIRS 159576], enclosure, Section 3.2).

Fragility Curves and Damage Abstractions—Most of the key parameters for the Seismic GM Modeling Case are associated with the fragility curves and damage abstractions. Those curves and abstractions are based on detailed simulations of structural response to seismic histories. Two concerns were noted by the review team with regard to sources of uncertainty not included in the ground motion model:

1. The curves and abstractions are based on a relatively small number (i.e., 17) of representative ground motion histories.

2. The number of simulated structural response outcomes for these histories typically produced data sets with small sample sizes.

The first concern is that the number of histories used was arbitrary and not shown to adequately capture the spectrum of seismic conditions. The second and related concern is that the uncertainties in the functional fits (to the structural response data) were not quantified.

Bulking Factor for Rockfall—The bulking factor for rockfall (i.e., ratio of free volume in drift to volume of rock corresponding to complete drift collapse) is assumed as specified to range from 0.1 to 0.4. Correspondingly, given a value of 12 m^3 per meter as the value for the unfilled drift volume, the volume of rockfall per meter of rock is estimated to be between 30 (i.e., 12/0.4) and 120 (i.e., 12/0.1) m^3, and a uniform distribution is assigned to this range. This assumption implied that the PDF for the bulking factor (which is the primary uncertain variable) has to be a monotonically decreasing distribution, with its mode corresponding to the minimum value. The use of uniform distribution for both bulking factor and rock volume was found to be an inconsistent representation of uncertainty in the bulking factor (because of the reciprocal nature of the relationship). This inconsistency was corrected as a result of review comments.

7.4.5.2 Igneous Scenario Class—Igneous Intrusion and Volcanic Eruption Modeling Cases

The Igneous Intrusion and Volcanic Eruption Modeling Cases evaluate the likelihood and consequences of magma flow penetrating the repository footprint. Two types of penetrations are analyzed consisting of: (1) intrusive vertical tabular igneous dike, and (2) extrusive volcanic conduit. Component models for these modeling cases simulate the igneous penetrations in order to calculate the number of WPs damaged during hypothetical events. The total number of WPs damaged, in turn, provides a means to calculate the quantity of radionuclides released to the groundwater or atmosphere.

The key stochastic parameters for these two igneous modeling cases are:

- Annual frequency for an igneous event intersecting the repository footprint

- Number of WPs hit by an intrusive dike (resulting in release of radionuclides to the groundwater pathway)

- Number of WPs hit by an extrusive volcanic conduit (resulting in radionuclides dispersed into the atmosphere pathway)

- Eruptive center probability (i.e., percentage of intrusive penetrations with extrusive conduits).

The model theory and stochastic parameter representations for these igneous modeling cases are documented in *Number of Waste Packages Hit by Igneous Events* (SNL 2007 [DIRS 177432], Sections 6 and 7). The formal review of the Igneous Intrusion Modeling Case examined the key parameter representations, which are listed in Table 7.4-2. Significant findings and recommendations are summarized below.

Annual Frequency of Igneous Event—The probability distribution for the annual frequency of igneous event intersecting the repository footprint is the product of several years of work conducted under the YMP's ongoing *Probabilistic Volcanic Hazards Analysis* (CRWMS M&O 1996 [DIRS 100116]) study. The probability distribution accounts for both the aleatory and epistemic uncertainty in the occurrence of igneous events. The technical basis for this probability distribution has been extensively and independently peer reviewed. The review team concluded that the uncertainty representation of the annual frequency accounts for the major sources of aleatory and epistemic uncertainty and is suitable for its intended use.

Number of Waste Packages Hit—The probability distributions for the number of WPs hit are computed via computer simulations of igneous intrusive and extrusive events. As discussed in *Number of Waste Packages Hit By Igneous Events* (SNL 2007 [DIRS 177432]), the DIRECT code is used to simulate these processes using the distribution of annual frequency of igneous events, along with probability distributions for the dimensional, geometric, and spatial variability of the igneous events. The computed CDFs for WPs hit are provided as tabular data to the TSPA-LA Model.

Although the probabilistic inputs (e.g., dike spacing, dike length, and conduit diameter) to the DIRECT code are evidence supported, these inputs do not currently account for epistemic uncertainty. The review team concluded that the absence of these epistemic uncertainties is most likely to be offset by conservatism in the igneous component model. For example, subsequent to this review, the YMP opted to treat the number of WPs hit by intrusion events as a fixed conservative value. More specifically, any intrusive dike intersecting an emplacement drift is assumed to fail all the WPs.

Eruptive Center Probability—This parameter is represented by a point probability value (i.e., P = 0.28) and not by a probability distribution. Thus, there is no epistemic uncertainty included in the representation of this parameter. The review team concluded, however, that the eruptive center probability will most likely play a small role in the probabilistic outcomes of this modeling case because of the embedded conservatisms.

7.4.5.3 Igneous Scenario Class—Volcanic Eruption Modeling Case

This Volcanic Eruption Modeling Case is simulated using two coupled models, ASHPLUME and Fortymile Wash Ash Redistribution (FAR). These computer models simulate the atmospheric transport, deposition, and redistribution of ash through the Fortymile Wash watershed for a hypothetical volcanic eruption intersecting the repository footprint.

Two key probabilistic parameters and one abstraction were reviewed for the Volcanic Eruption Modeling Case, namely:

- Wind speed (functions of altitude)
- Wind direction (functions of altitude)
- Tephra redistribution abstraction.

The model theory and parameter representations for this modeling case are documented in *Atmospheric Dispersal and Deposition of Tephra from a Potential Volcanic Eruption at Yucca Mountain, Nevada* (SNL 2007 [DIRS 177431], Sections 5, 6, and 8, and Tables 8-2 through 8-4) and in *Redistribution of Tephra and Waste by Geomorphic Processes Following a Potential Volcanic Eruption at Yucca Mountain, Nevada* (SNL 2007 [DIRS 179347], Sections 5 and 6 and Table 6.4-1). Significant findings and recommendations are summarized below.

Wind Speed and Direction—The ASHPLUME model uses CDFs for wind speed and wind direction data for 13 altitude bins, ranging from 0 to 13 km. The CDFs for wind speed and wind direction are based on an analysis of a large data set for the Desert Rock weather station. The review team concluded that the uncertainty characterization for these parameters was appropriate. However, it noted that the parameters are treated as independent stochastic variables. Moreover, no statistical tests had been performed to evaluate potential correlation between wind speed and wind direction. A review of the literature on statistical analyses of wind data was performed to ascertain if statistical correlations were commonly observed; no such correlations were noted in the available literature, suggesting that assumption-independent random variables may be appropriate.

Tephra Redistribution Abstraction—The FAR model uses the spatial distribution of ash (computed by the ASHPLUME model) as input and then simulates the transport of tephra and waste from the Fortymile Wash drainage basin to the RMEI location. The FAR Model simulates mass transport by hill slope and fluvial processes and basically assumes that there is no significant redistribution by aeolian processes. The review team raised a concern regarding conceptual model uncertainty associated with the assumption of aeolian processes being unimportant.

The review team noted that the ASHPLUME calculations indicate tephra ranging from 0.0001-cm diameter particles (clay size) to about 0.2-cm diameter particles (coarse sand). The sampled particle size mode is 0.0013-cm diameter particles corresponding to fine silt-size class. Thus, the sand-sized tephra particles would be susceptible to redistribution by wind within the Fortymile Wash. The finer silt- and clay-sized particles could potentially be picked up and transported for miles from the source area by strong, sustained winds. Therefore, the FAR Model could be ignoring a relevant redistribution and/or removal process.

The review team concluded that this uncertainty in the conceptual model was most likely offset by the very conservative modeling assumption that the redistribution of ash and waste particles occurs instantaneously. In actuality, the time scale of the redistribution of material could take many thousands of years.

7.4.5.4 Nominal Scenario Class

The TSPA-LA Model is based on the Nominal Scenario Class, which incorporates all expected FEPs to describe the most likely fundamental processes that would persist under ambient conditions, as well as possible changes to those processes after repository closure. The Nominal Scenario Class includes a single modeling case that addresses FEPs that describe the natural degradation of the EBS (i.e., DSs and WPs).

7.4.5.4.1 Unsaturated Zone Flow

The UZ Flow Model Component consists of five submodels that collectively model water flow, beginning with climate-induced precipitation at the land surface, net infiltration into the soil cover, deep percolation through the geologic strata and to the repository horizon, seepage into the drifts, moisture condensation on drift walls, and subsequent flow into the underlying water table.

The uncertainty/variability characterization review examined key stochastic parameters of the Infiltration (SNL 2007 [DIRS 182145]), UZ Flow (SNL 2007 [DIRS 184614], Section 6.8) and Drift Seepage (SNL 2007 [DIRS 181244]) submodels. Three key parameters that were reviewed in depth were:

- Effective soil depth for surface infiltration
- Weighting factors for net infiltration
- Permeability of lithophysal rock units.

The importance of these parameters was identified from sensitivity analyses of preliminary TSPA scoping calculations. For brevity, only the review findings and recommendations for the effective soil depth and weighting factors for net infiltration are presented here.

Effective Soil Depth—While effective soil depth is not a parameter in the TSPA Model, it is an important parameter used in the analysis of infiltration in the surface soils. This parameter has a strong effect on the net infiltration into the UZ. The infiltration model considers a range of soils that were divided into five classes: (1) very deep, (2) moderately deep, (3) intermediate, (4) shallow soils, and (5) bedrock (no soil cover). Sensitivity analyses described in *Simulation of Net Infiltration for Present-Day and Potential Future Climates* (SNL 2007 [DIRS 182145]) showed that the effective thickness for soil class 4 was shown to be a very dominant parameter in the calculations of net infiltration.

The uncertainty/variability characterization reviews identified a concern with the method used to calculate upscaled effective soil depth (i.e., thickness). To address this concern, an analytic relationship was developed for properly upscaling the probability distribution for soil thickness that ensured that the average water flux was preserved. The new approach was implemented in the infiltration model and is documented in *Simulation of Net Infiltration for Present-Day and Potential Future Climates* (SNL 2007 [DIRS 182145]).

Weighting Factors—The UZ Flow Field weighting factors are used in the TSPA for stochastic sampling of the flow field uncertainty scenarios. These scenarios are characterized by the

10th percentile, 30th percentile, 50th percentile, and 90th percentile infiltration maps. For a given TSPA simulation, one of the four uncertainty scenarios is randomly selected based on the weighting factors and the selected flow field used through the climate states (present-day, monsoon, glacial-transition, and post-10,000-year) simulated.

The UZ Flow Field weighting factors were developed using the generalized likelihood uncertainty estimation (GLUE) method (Beven et al. 2000 [DIRS 179825] and SNL 2007 [DIRS 184614], Section 6.8.5.1). The GLUE approach takes into account prior information from the infiltration model for the probability of the infiltration maps, as well as the relative agreement between the flow model results corresponding to each infiltration map and corresponding field observations. The methodology uses a Bayesian framework to produce posterior probabilities (weighting factors) for the infiltration maps.

The review team questioned the appropriateness of the non-standard application of the GLUE methodology, as well as the lack of a rationale for the selection of likelihood functions. The review team questioned the use of a suite of likelihood functions and then averaging the results. In checking the GLUE calculations, the review team noted that the results from some of the likelihood functions lacked consistency. The review team proposed that likelihood functions be screened on the basis of consistency with the field data and only one be used in the GLUE method.

After several meetings, the review team and authors, with the concurrence from the Performance Assessment Systems Integration Team, decided to proceed forward with the original weighting factors. However, it was recommended that the documentation of the GLUE methodology show weighting factor calculations obtained by eliminating the likelihood functions that appeared to overweight or underweight selected model comparisons. The recommendation was implemented in *UZ Flow Models and Submodels* (SNL 2007 [DIRS 184614], Section 6.8.6.3).

7.4.5.4.2 Waste Package and Drip Shield

The WP and DS Degradation Model Component accounts for the following degradation processes: general corrosion of the DSs, general corrosion and localized corrosion of the outer surfaces of the WPs, and SCC of the WPs.

The uncertainty/variability characterization reviews examined the following key parameters of the DSs (SNL 2007 [DIRS 180778], Sections 6.1.5[a] through 6.1.7[a]) and WPs (SNL 2007 [DIRS 181031], Table 1-1; SNL 2007 [DIRS 181953], Table 1-1):

- DS (Titanium Grade 7) general corrosion rate
- WP outer barrier (Alloy 22) general corrosion rate and temperature dependence
- WP outer barrier SCC growth rate (repassivation rate)
- WP outer barrier material yield strength.

For brevity, only the review findings and recommendations for the review of DS general corrosion are presented here. The review team confirmed that the bases for the parameter uncertainty characterizations for the other parameters listed above were appropriate and defensible.

The original probabilistic model developed to simulate general corrosion of the DS was based on 1-year corrosion rate data for Titanium Grade 16 (SNL 2007 [DIRS 180778], Section 6.5.3.1). The YMP Corrosion team opted to develop a new probabilistic model using more relevant corrosion data (i.e., 2.5-year data for Titanium Grade 7). The review team provided direct assistance to the SMEs with performing statistical analyses of the laboratory data and development of a new probabilistic model that addressed both variability and epistemic uncertainty.

Weight-loss data for corrosion of Titanium Grade 7 consisted of tests in groundwater compositions for three groups: aggressive, intermediate, and benign conditions. The data subsets for aggressive and benign conditions were chosen to develop bounding models for general corrosion. A normal distribution was fit to the aggressive conditions data, while a gamma distribution was fit to the data set for the benign conditions. These probability distributions were used to describe variability in the DS general corrosion rate. Statistical relationships were also developed to estimate the uncertainty in the mean corrosion rates. The development of these statistical models included testing for normality, goodness-of-fit, and fitting with alternative distributions (SNL 2007 [DIRS 180778], Sections 6.1.5[a] through 6.1.7[a]).

7.4.5.4.3 Waste Form Degradation and Mobilization

The Waste Form Degradation and Mobilization Model Component consists of six submodels. Collectively, these submodels account for the following processes and conditions: in-package water chemistry; waste form cladding degradation; matrix degradation rates for CSNF, DSNF, and HLW waste forms; radionuclide solubilities; and the types and concentrations of waste form and in-drift colloids.

The uncertainty/variability characterization reviews focused on two key stochastic parameters used in the dissolved concentration (SNL 2007 [DIRS 177418], Tables 6.6-11) and EBS colloid transport (SNL 2007 [DIRS 177423], Table 6-24) submodels, namely:

- Radionuclide solubility uncertainty factor, low and high ionic strength
- Concentration of irreversibly attached plutonium on colloids.

For brevity, only the review findings and recommendations for the review of key colloids parameters for the colloids are presented here.

Concentration of Irreversibly Attached Plutonium on Colloids—The uncertainty/variability characterization review focused on examining the probability distributions for two colloid parameters: (1) $C_{RNcoll,DHLWG,embed,\ sampled}$ (concentration of irreversibly attached plutonium associated with defense HLW glass colloids), and (2) $C_{coll,DHLWG,\ triangular}$ (concentration of irreversibly attached plutonium per concentration of colloids). The draft documentation available for these parameters was initially found to be unclear or insufficient to lead to an unambiguous understanding of the technical basis.

Written comments were provided to the SMEs for improving the documentation, which were subsequently addressed and documented (SNL 2007 [DIRS 177423]). The review team

confirmed that the basis for the parameter uncertainty characterizations was appropriate and defensible.

7.4.5.4.4 Engineered Barrier System Radionuclide Transport

The Radionuclide Transport Abstraction, which is part of the EBS Flow and Transport Model Component, defines the water flow pathways in the EBS and simulates the advective and diffusive mass transport from a breached WP. The model considers radionuclide transport in both dissolved and colloidal phases. In addition, the model accounts for irreversible sorption of radionuclides onto corrosion products that builds up with time in the breached WP.

The uncertainty/variability characterization review of this component model focused on the stochastic parameters associated with the corrosion product generation and sorption. The relevant key parameters are:

- Stainless steel corrosion rate
- Carbon steel corrosion rate
- Specific surface area of Fe_2O_3 and FeOOH corrosion products
- Goethite site density.

Because of the important effect of corrosion products on radionuclide releases from the EBS, the formal review focused on the stainless steel and carbon steel corrosion rates, as documented in *EBS Radionuclide Transport Abstraction* (SNL 2007 [DIRS 177407], Section 6.3.4.3.4.3, and Appendix F, and Table 8.2-4). Review findings and recommendations for these parameters are summarized here.

Stainless Steel Corrosion Rate—The original uncertainty representation for Stainless Steel Type 316L corrosion rate consisted of an empirical CDF; that representation had been constructed from available short-term data from laboratory tests in a fresh water environment for temperatures ranging from 50°C to 100°C. With assistance from SMEs, the available laboratory measurements were reviewed to confirm their appropriateness. Some of the low values in the data were considered to be of questionable accuracy. As a result, the minimum value was set to a reasonable bound (i.e., set to the mean of the Alloy 22 corrosion rate, which has a much lower corrosion rate than stainless steel).

After review of the corrosion data, a rigorous statistical analysis was performed. A Bayesian updating procedure was then used to derive a truncated lognormal distribution. From the analytic probability curve, it was possible to also quantify the uncertainty in the median corrosion rate. A new CDF distribution was developed and used in place of the original empirical CDF. In addition to providing an excellent fit to the data, the new continuous distribution facilitated the implementation LHS in the TSPA-LA Model.

Carbon Steel Corrosion Rate—The original uncertainty representation for Carbon Steel Type A516 corrosion rate consisted of an empirical CDF. This CDF was based on data from short-term laboratory tests using simulated dilute J-13 well water (10 times the normal concentration of J-13 water) at 60°C and 90°C; the 10-times concentration in the simulated dilute J-13 well water was considered representative of the small potential degree of concentration that

might occur inside a breached WP. The corrosion rate data were obtained from laboratory tests of 0.5 year and 1.0 year in duration. The review team assisted the SME with development of the new carbon steel corrosion rate CDF.

A statistical analysis of the data was performed and a new probability distribution developed using a Bayesian updating method. A truncated lognormal distribution was derived and shown to provide an excellent fit to the data points. In addition, a statistical relationship was developed to quantify the uncertainty in the median corrosion rate.

7.4.5.4.5 Saturated Zone Flow and Transport

The SZ Flow and Transport Model Component simulates the transport of radionuclides from their introduction at the water table below the repository to the regulatory boundary at approximately 18 km. The uncertainty/variability characterization review of the SZ submodel (SNL 2008 [DIRS 183750], Table 6-8; SNL 2007 [DIRS 177392], Section 6.7.1) examined the following stochastic parameters:

- Groundwater-specific discharge multiplier
- Flowing interval spacing for volcanic units
- Radionuclide sorption coefficients.

For brevity, only the review findings and recommendations for groundwater-specific discharge and flowing interval spacing are presented here.

Groundwater Specific Discharge—Preliminary TSPA scoping studies have shown that the groundwater specific discharge multiplier is a dominant parameter for both Seismic GM and Igneous Intrusion Modeling Cases. Its high importance ranking is derived from the fact that groundwater specific discharge is a stochastic scale factor, which is applied to all values of permeability and boundary fluxes in the SZ Flow Model. The uncertainty characterization for groundwater specific discharge had been previously developed based on elicitation of expert judgment (CRWMS M&O 1998 [DIRS 100353]), and supplemented by tracer test results from the Alluvium Testing Complex (SNL 2007 [DIRS 177394]). The end points of the distribution and certain quantiles were subjectively selected, and a piecewise log uniform distribution was assumed between these point values.

The review team assisted the SME with revising the subjective probability distribution using a Bayesian updating procedure. Such a procedure provides a formal and systematic basis for combining prior information with new data to produce an updated distribution. Analytical expressions for Bayesian updating (SNL 2008 [DIRS 183750], Section 6.5.2.1[a]), appropriate for the specific distributional form (i.e., log-normal), were applied to characterize the uncertainty in groundwater specific discharge. The resulting new CDF for groundwater specific discharge is more defensible in that it is based on a formal statistical procedure for combining old information (i.e., expert elicitation) with new data (i.e., tracer test results), as opposed to a subjective integration of information.

Flowing Interval Spacing—The flowing interval spacing of volcanic units parameter is used in defining the effective flow in the fractured volcanic units. Previous TSPA scoping studies have

indicated that flowing interval spacing of volcanic units is one of the dominant SZ parameters. An empirical CDF (BSC 2004 [DIRS 170024], Section 6.3-6.4) for this parameter was originally developed from flow meter survey data obtained for various hydrogeologic units. The SZ SME requested that the review team perform an independent statistical analysis of the field data and derive the new CDF.

In examining the data, the review team noted that data had not been corrected for the dip angle of the fractures in the original analysis. After making this adjustment to the data, the review team used a Bayesian updating procedure (SNL 2008 [DIRS 183750], Section 6.5.2.3[a]) to develop a new CDF. Statistical tests indicated that the new distribution provided a very good fit to the field data. The new CDF for flowing interval spacing of volcanic units is more defensible in that it accounts for both variability in the data and epistemic uncertainty.

7.4.6 Summary of Sensitivity Analyses

Sensitivity analyses identify the contribution of uncertain model inputs to the uncertainty in model output. During development of the TSPA-LA Model, sensitivity analyses were performed using output from developmental versions of the TSPA-LA Model to investigate the propagation of uncertainty through the system model and to identify uncertain inputs that may be significant to the uncertainty in the results of the final TSPA-LA Model. These during-development analyses followed the analysis scheme presented in Appendix K, which documents results from the final sensitivity analysis completed after model development. The during-development sensitivity analyses generally confirmed that the uncertainty reviews had covered all key uncertain inputs. In addition, the during-development analyses provided a measure of confirmation that important uncertain inputs are propagated appropriately through the process models and that the effects of these uncertainties are consistent with physical principles underlying the models. The during-development sensitivity analyses also uncovered a number of implementation errors in developmental versions of the model, which were subsequently corrected before the TSPA-LA Model became final.

After model development, a final sensitivity analysis was conducted and is documented in Appendix K. This analysis identifies the dominant sources of uncertainty in total expected dose to the RMEI. For each modeling case, the analyses also investigate the sources of uncertainty in expected dose to the RMEI and in the movement of several key radionuclides (i.e., ^{239}Pu, both dissolved and sorbed to colloids, ^{237}Np, and ^{99}Tc). These radionuclides were chosen to illustrate a range of radionuclide behavior, including colloid-facilitated transport. In addition, for a few modeling cases, the analyses investigate uncertainty in other process model results such as the time of drip shield failure and the chemical environment in the drifts. Table 7.4-4 summarizes sensitivity analysis results for total expected annual dose and expected annual dose by modeling case by listing the key uncertain inputs identified by the analysis. The key uncertain inputs identified by the analyses that were also subjects of uncertainty reviews are indicated by **bold** font.

As presented in the discussion accompanying the sensitivity analysis results in Appendix K, the final sensitivity analysis confirms that the uncertainty in some high profile (or statistically significant) inputs are propagated through the TSPA-LA Model and that the effects of uncertainty in these inputs is consistent with physical principles. The confirmation is

demonstrated through causal explanations of the relationships between input and output variables. For example, where the analysis indicates a positive correlation between the input and output variables, the causal explanation illustrates the reasons why a positive correlation should be observed.

The final sensitivity analysis also identified a relatively small number of implementation errors present in the final version of the TSPA-LA Model (v5.000). These errors, along with others identified by check and review activities, are documented in Appendix P along with impact assessments investigating the effect of each error on the TSPA-LA Model v5.000 results. Although the errors do not significantly affect the output from the TSPA-LA Model, the errors influence the selection of uncertain input variables correlated to uncertainty in the transport of plutonium sorbed to certain colloids. As a consequence, the affected results were removed from the final version of Appendix K. These analyses were removed, rather than corrected, because the results of the analyses are not significant in determining the key uncertain inputs to the TSPA-LA Model.

INTENTIONALLY LEFT BLANK

Table 7.4-1. Key TSPA Parameters for Seismic Scenario Class for the Ground Motion and Rockfall Abstractions

Model Abstractions	Parameter Description	Basis for Selection
Ground Motion and Rockfall	Mean Seismic Hazard Curve	Identified in previous sensitivity and uncertainty analyses
	DS Plate and Frame fragility curves	Proposed by TSPA component model developer
	Damaged area of DS crown	Proposed by model abstraction developer
	Fraction of drift filled with lithophysal rock and accumulated volume of rock	Proposed by model abstraction developer
	Total damaged area for TAD and CDSP WPs	Proposed by model abstraction developer
	Probability of rupture for TAD and CDSP WPs	Proposed by model abstraction developer

Table 7.4-2. Key TSPA Parameters for Igneous Scenario Class

Model Abstractions	Parameter Description	Basis for Selection
Intrusion and Eruption	Annual frequency of a volcanic event intersecting the repository footprint	Identified in previous sensitivity and uncertainty analyses
	Number of WPS hit during a hypothetical igneous intrusion	Proposed by TSPA component model lead
	Number of WPs hit during a hypothetical volcanic eruption	Proposed by TSPA component model lead
	Wind speed and direction	Proposed by TSPA component model lead
	Scour depth at alluvial fan apex	Proposed by TSPA component model lead

Table 7.4-3. Key TSPA Parameter Sets for the Nominal Scenario Class by Model Abstraction

Model Abstraction	Parameter Description (TSPA-LA Model Name)	Basis for Selection
UZ Flow	Weighting factors for calculating net percolation over the repository (Infiltration_Scenario_a)	Identified in previous sensitivity and uncertainty analyses
	Effective soil depth over repository (used in infiltration process model) (Soil_Density_a)	Proposed by TSPA component model lead
	Uncertainty in permeability of lithophysal rock units (Alpha_Uncert_Lith_a)	Identified in previous sensitivity and uncertainty analyses
WP and DS	WP outer barrier (Alloy 22) general corrosion rate (GC_ULevel_A22_a)	Proposed by TSPA component model lead
	General corrosion rate (Alloy 22) temperature dependence (C1_GenCorr_A22_a)	Proposed by TSPA component model lead
	WP outer barrier SCC growth rate (repassivation rate) (n_SCC_a)	Proposed by TSPA component model lead
	Stress threshold for SCC nucleation (Stress_Thresh_A22_a, Stress_Thresh_SCC_a)	Proposed by TSPA component model lead
	DS (Titanium Grade 7) general corrosion rate (WDDSAggrGC_Mean_a, WDDSBenignGC_Mean_a)	Proposed by TSPA component model lead
Waste Form Degradation and Mobilization	Radionuclide Solubility (U, Np, Th, Pu, Am) ε_1, low ionic strength (See Tables 6.3.7-41 through 6.3.7-46)	Identified in previous sensitivity and uncertainty analyses
	Radionuclide Solubility (U, Np, Th, Pu, Am) ε_1, high ionic strength (See Tables 6.3.7-41 through 6.3.7-46)	Identified in previous sensitivity and uncertainty analyses
	Actinide Solubility, maximum limit (See Section 6.3.7.5.2, Treatments of Solubility Model Out-Of-Bounds)	Proposed by TSPA component model lead
	Concentration of irreversibly attached plutonium, associated with DHLWG colloids (CPu_Col_Wf_Embed_Sampled_a, CPu_Per_WF_Embed_Col_a)	Proposed by TSPA component model lead
EBS Radionuclide Transport Abstraction	Stainless Steel (316L) corrosion rate (SS_Corrosion_rate_a)	Proposed by TSPA component model lead
	Carbon Steel (A516) corrosion rate (SS_Corrosion_rate_a)	Proposed by TSPA component model lead
	Goethite site density (Goethite_Site_Density_a)	Identified in previous sensitivity and uncertainty analyses
	Specific surface area of Fe_2O_3 and FeOOH corrosion products (HFO_SA_a)	Identified in previous sensitivity and uncertainty analyses

Table 7.4-3. Key TSPA Parameter Sets for the Nominal Scenario Class by Model Abstraction (Continued)

Model Abstraction	Parameter Description (TSPA-LA Model Name)	Basis for Selection
SZ Flow and Transport	Groundwater specific discharge (GWSPD)	Identified in previous sensitivity and uncertainty analyses
	Flowing interval spacing in volcanic units (FISVO)	Identified in previous sensitivity and uncertainty analyses
	Colloidal retardation factor for alluvium (CORAL)	Identified in previous sensitivity and uncertainty analyses

Table 7.4-4. Summary of Selected Sensitivity Analysis Results

Modeling Case	TSPA-LA Model Output	Key Uncertain Inputs[a]
Total System	Total expected dose over 20,000 years	**Residual stress threshold for SCC (SCCTHRP)** Frequency of occurrence of igneous events (IGRATE) **Scale factor in ground water specific discharge (SZGWSPDM)**
	Total expected dose over 1,000,000 years	Frequency of occurrence of igneous events (IGRATE) **Residual stress threshold for SCC (SCCTHRP)** **General corrosion rate (Alloy 22) temperature dependence (WDGCA22)** **Scale factor in ground water specific discharge (SZGWSPDM)**
Nominal	Expected dose resulting from corrosion processes	**General corrosion rate (Alloy 22) temperature dependence (WDGCA22)** Deviation from median yield strength range for outer lid (WDZOLID)
Early Failure Waste Package	Expected dose resulting from early failure of waste packages over 20,000 years	Probability of early failure per waste package (PROBWPEF) **Pointer variable for infiltration scenario (INFIL)** Selector for host-rock thermal conductivity scenario (THERMCON)
Early Failure Drip Shield	Expected dose resulting from early failure of drip shields over 20,000 years	Probability of early failure per drip shield (PROBDSEF) Uncertainty factor accounting for small-scale heterogeneity in fracture permeability (SEEPUNC) Flowing interval porosity in volcanic units (SZFIPOVO)
Igneous Intrusion	Expected dose resulting from igneous intrusion over 1,000,000 years	Frequency of occurrence of igneous events (IGRATE) **Scale factor in ground water specific discharge (SZGWSPDM)** **Pointer variable for infiltration scenario (INFIL)**
Volcanic Eruption	Expected dose resulting from volcanic eruption over 1,000,000 years	**Frequency of occurrence of volcanic eruptions (IGERATE)** Depth of soil within which radionuclides affect the biosphere (BTILLAGE)

Table 7.4-4. Summary of Selected Sensitivity Analysis Results (Continued)

Modeling Case	TSPA-LA Model Output	Key Uncertain Inputs[a]
Seismic Ground Motion	Expected dose resulting from seismic ground motion over 20,000 years	**Residual stress threshold for SCC (SCCTHRP)**
	Expected dose resulting from combination of seismic ground motion and corrosion processes over 1,000,000 years	**Residual stress threshold (SCCTHRP)** **General corrosion rate (Alloy 22) temperature dependence (WDGCA22)**
Seismic Fault Displacement	Expected dose resulting from fault displacement over 20,000 years	**Groundwater biosphere dose conversion factor (MICTC99)** **Scale factor in ground water specific discharge (SZGWSPDM)**
	Expected dose resulting from fault displacement over 1,000,000 years	**Scale factor in ground water specific discharge (SZGWSPDM)** **Pointer variable for infiltration scenario (INFIL)**

[a] Bold font indicates uncertain parameters that were subject to uncertainty reviews. Name (in parentheses) is the variable name used in the sensitivity analyses (see Table K3-1).

INTENTIONALLY LEFT BLANK

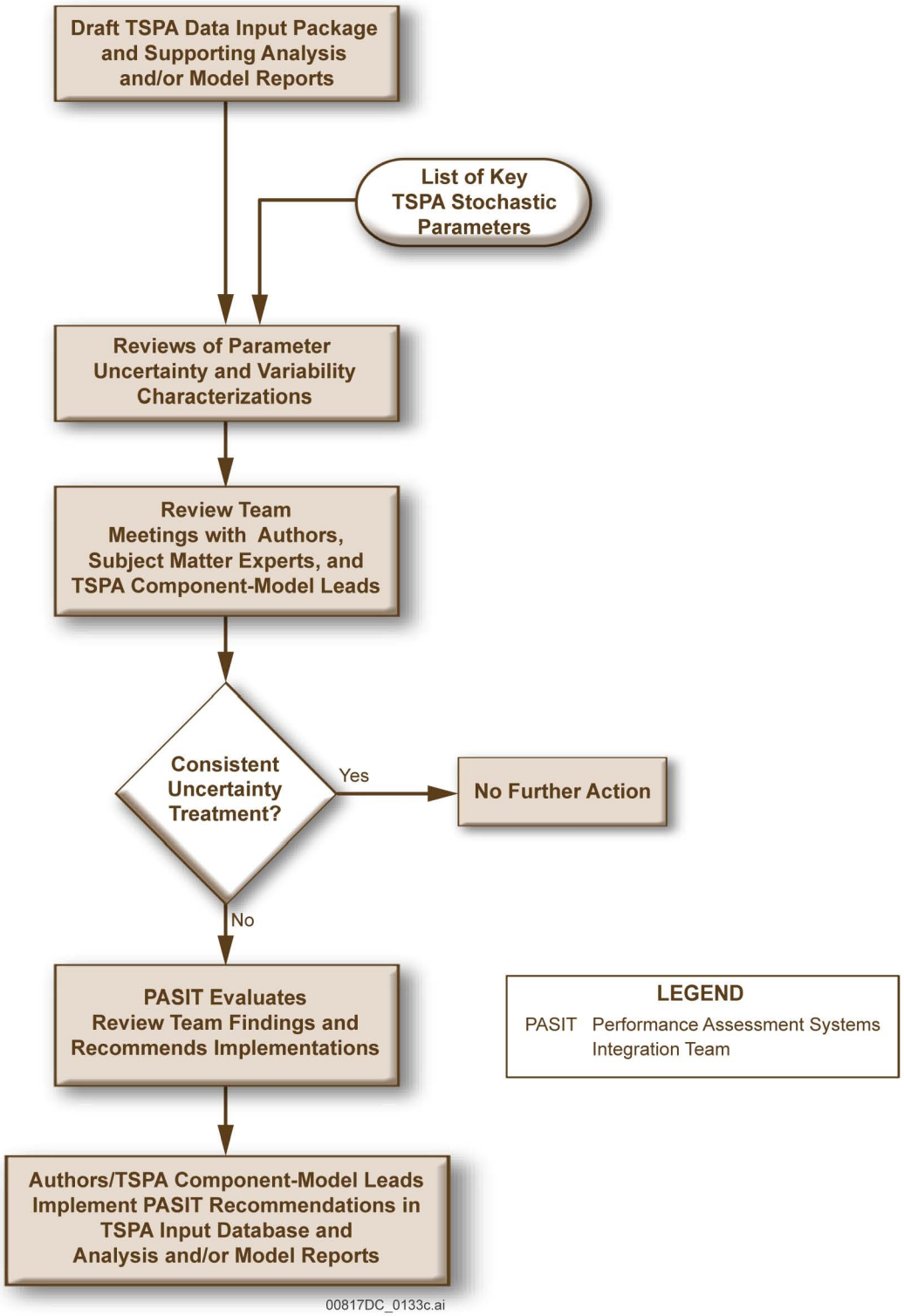

Figure 7.4-1. Uncertainty Characterization Review Process

INTENTIONALLY LEFT BLANK

7.5 SURROGATE WASTE FORM VALIDATION

The purpose of the analyses that follow is to show that the surrogate representation of naval spent fuel (Category 1 DSNF) and the DSNF surrogate, that is the average of DSNF Categories 2 through 11, are appropriate. The averaging of Categories 2 through 11 is related to the spatial averaging that is analyzed in Section 7.3.4.

The TSPA-LA Model represents Categories 2 through 11 of the DSNF using a surrogate fuel, as recommended by *DSNF and Other Waste Form Degradation Abstraction* (BSC 2004 [DIRS 172453], Sections 6.1.12 and 8.1). The abstraction represents each DSNF category with an instantaneous degradation and dissolution model. Therefore, for the analysis of DSNF, all of the radionuclides are available for release after WP failure (i.e., the instantaneous dissolution in the DSNF Waste Form Degradation Abstraction [Table 6-1]). The TSPA-LA Model uses the surrogate inventory for DSNF that is documented in *Initial Radionuclide Inventories* (SNL 2007 [DIRS 180472], Table 7-1[a]).

The analyses below confirm that it is appropriate to represent Categories 2 through 11 of the DSNF with a surrogate that has an average inventory and a bounding instantaneous degradation rate in the TSPA-LA Model. The analysis is conducted by using the TSPA-LA Model to simulate the performance of each of the individual DSNF categories and then comparing the results to the performance of the surrogate. The data used to model each of the individual fuel categories are from *Additional DOE Spent Nuclear Fuel Information in Support of TSPA-LA Analysis* (Loo et al. 2004 [DIRS 168999], Sections 6 and 7).

The analyses also confirm that Zircaloy-clad CSNF adequately represents Category 1 DSNF. Category 1 DSNF, naval spent fuel in the TSPA-LA Model, is represented as Zircaloy-clad CSNF. Section 7.5.3 discusses the analyses using the TSPA-LA Model where the naval source term replaced the CSNF source term for the Drip Shield EF and Igneous Intrusion Modeling Cases. The radionuclide release from naval spent fuel WPs would be expected to be lower than from CSNF WPs because of the robust nature of naval spent fuel, smaller inventory of key dose-producing radionuclides, and lower dissolution rate of naval spent fuel (Gisch 2004 [DIRS 171782]).

7.5.1 Methodology

In order to investigate the relative performance of the categories of DSNF versus the surrogate, the Drip Shield EF Modeling Case was chosen. This case fails one WP and DS at time zero and thus removes the variability of the engineered barrier. Only one DSNF inventory is needed per realization and a direct comparison between DSNF types is possible. This analysis tests whether the surrogate produces dose curves comparable to the sum of the doses from the individual DSNF types weighted by the fraction of WPs of each type.

The model file, v5.000_GS_9.60.100.gsm (output DTN: MO0707TSPADSNF.000 [DIRS 182992]), was modified to have no commercial or high-level waste glass inventory so that differences in dose due to DSNF would not be masked by the CSNF and HLW releases. To simplify the calculation and to focus on the variability due to DSNF, only the largest subregion, Subregion 3, was modeled. The dripping case was chosen because the doses from WPs with dripping are higher. Furthermore, the

aleatory uncertainty was removed because it should have little bearing on the relative performance of DSNF. The epistemic uncertainty was unmodified. The resulting analysis, LA_v5.000_ed_003300_002.gsm (output DTN: MO0707TSPADSNF.000 [DIRS 182992]), used 300 realizations for 11 inventories for one million years and thus required 3,300 simulations.

Figure 7.5-1 shows the results from a 300 realization run with the DSNF surrogate only, which serves as a base case for comparison. A series of analyses, based on the expected performance of each of the DSNF categories, provides confidence that the surrogate fuel used in the TSPA-LA Model is a reasonable representation of all of the DSNF that will be emplaced in the repository. The analyses include: (1) the comparison of the dose from the surrogate fuel with the weighted sum of the doses from the DSNF categories, (2) the comparison of the surrogate fuel with each DSNF fuel category, and (3) the evaluation of impacts from uncertainty parameters (e.g., degradation mechanisms, surface areas, number of WPs, radionuclide inventory, free inventory, and bounding radionuclide inventory). The analyses were conducted using the 300 realization DS early failure simulation (with DSNF inventories only) to compare the DSNF surrogate spent fuel and DSNF Categories 2 through 11 (output DTN: MO0707TSPADSNF.000 [DIRS 182992]).

For naval spent fuel, probabilistic analyses were conducted for the Drip Shield EF and Igneous Intrusion Modeling Cases. The results of failure for a single WP of CSNF were compared with the failure of a single WP of naval spent fuel. In addition, the Naval Nuclear Propulsion Project conducted seismic scenarios to evaluate the use of CSNF as a surrogate for navy spent fuel (Gisch 2004 [DIRS 171782]).

7.5.2 Spent Fuel Categories and Representation in Model

During the last four decades, the DOE and its predecessor agencies have generated approximately 250 varieties of spent fuel from weapons production, nuclear propulsion, and research missions. A method described by Fillmore (1998 [DIRS 104385], Section 2) allowed the grouping of these varieties of DSNF into 16 categories for the repository performance assessment. The 16 DSNF fuel categories were further reduced to 11 categories (DOE 2000 [DIRS 118968], Section 8). The reduction reflects a better understanding of the behavior of DOE fuels under expected repository conditions and allows the combining of some of the 16 DSNF categories. The reduced number of DSNF categories helps streamline repository analyses of the spent fuels. The grouping method used regulatory requirements to identify the parameters that affect the performance of DSNF in the repository and to meet analysis needs for the repository LA. Three fuel parameters (fuel matrix, fuel compound, and fuel-cladding condition) influence the performance of the DSNF in the repository. The grouping methodology categorizes the characteristics of a select number of fuel types by either a bound or by representing a particular characteristic of the whole category. Table 7.5-1 lists the DSNF categories and a typical fuel in the category that best fits the characteristics of the category.

A brief description of the fuel categories follows (DOE 2000 [DIRS 118968]):

Category 1—Classified Navy: NSNF was placed in its own category for several reasons: (1) the design of naval spent fuel is significantly different from other DSNF designs; (2) because of its robust design, naval spent fuel will remain virtually intact well beyond

10,000 years resulting in its impact on repository performance occurring much later than other DSNF designs; and (3) the design of naval spent fuels is classified.

Category 2—Plutonium/Uranium Alloy Fuel: The plutonium/uranium alloy fuels are grouped together because of the alloy microstructure and its effect on grain boundary attacks, stress fractures, and crazing (microcracking). For example, it is uncertain if there will be preferential attacks on the grain boundaries that could result in a large increase in the surface area of uranium-zirconium alloy fuel. However, the zirconium could also stabilize the uranium metal and, thus, this category could perform differently than the uranium-metal fuels. On the other hand, uranium alloyed with ten weight-percent molybdenum corrodes at only one percent of the rate of pure uranium. However, after corrosion starts, molybdenum causes stress fractures and crazing. This increases the matrix porosity and surface area and potentially increases the dissolution rate.

Category 3—Plutonium/Uranium-Carbide Fuel: This category consists primarily of fuels from the Fast Flux Test Facility. The Fast Flux Test Facility fuels are either UC_2 pellets or UC_2 spheres, with helium or sodium bonded between the fuels and cladding. The performance of the carbide particles is uncertain as compared to the Fort St. Vrain fuels (Category 5). Thus, this fuel was placed into its own category. The release rate of this category may be 100 times that from pure uranium-metal fuel. The effective enrichments (including the ^{239}Pu) vary from about 10 to 18 percent ^{235}U.

Category 4—Mixed Oxide Fuel (MOX): MOX fuels are composed of a mixture of uranium and plutonium oxides with various types of cladding. The uranium enrichment is low, but the plutonium content increases the effective enrichment above 15 percent ^{235}U. The Fast Flux Test Facility driver fuel assembly and test fuel assembly contributed to the large quantity of the fuel in this category. Because the fuels were fabricated using techniques similar to that of the commercial oxide fuels, performance of the MOX fuels should be very similar. Because of the high plutonium content, as compared to the uranium-oxide fuel, this fuel was placed into its own category.

Category 5—Uranium/Thorium-Carbide Fuel: This category primarily consists of fuel from the Fort St. Vrain Reactor and fuels from Core 1 and 2 of the Peach Bottom Reactor. Fuel from the General Atomic Gas-Cooled Reactor is also included in this category. The fuel in Category 5 is in the form of carbide particles coated with layers of pyrolytic carbon and it may also have a silicon carbide coating, bonded together by a carbonaceous matrix material. Two types of particles are used: fissile and fertile. The fissile particles contain thorium and approximately 93 percent enriched uranium. The fertile particles contain only thorium. One difference between the Fort St. Vrain and Peach Bottom fuels is that the Peach Bottom particles lack the silicon-carbide coating. The fuel particles in the Fort St. Vrain and Peach Bottom Core 2 fuel assemblies are in excellent condition; however, the fuel particles in the Peach Bottom Core 1 fuel assemblies are in poor condition. Some preliminary tests indicated that up to 60 percent of the particles may have been breached. Thus, the release rate of this category may be ten times the uranium-metal rate (Category 7) because of possible water or carbide reactions. The effective enrichment (including the ^{233}U) level at the end of life varies from about 78 to 83 percent ^{235}U.

Category 6—Uranium/Thorium-Oxide Fuel: Shippingport Light Water Breeder Reactor fuels make up the major inventory of the fuel in Category 6. The Shippingport Light Water Breeder Reactor fuel was used to demonstrate the production of fissile ^{233}U from thorium in a water-cooled reactor. The fuel is composed of uranium oxide, enriched up to 98 percent ^{233}U, mixed with thorium oxide in cylindrically-shaped ceramic pellets. These ceramic pellets are expected to dissolve at a different rate than the standard uranium-oxide fuel and, thus, this fuel was placed into its own category.

Category 7—Uranium-Metal Fuel: The majority of this category consists of zirconium-clad N-Reactor fuel with a small amount of aluminum-clad Single Pass Reactor fuel. Enrichments are less than 2 percent ^{235}U. The majority of the fuels have low burn up. Some uranium target materials are also included in this category.

Category 8—Uranium-Oxide Fuel: This category consists of the fuels removed from commercial reactors or test fuel with uranium-oxide matrices similar to CSNF. In addition, the fuels removed from commercial reactors or test fuels with uranium-oxide matrices that have failed cladding, or are declad, are also included in this category. This category is modeled as CSNF but with a potentially much higher fuel surface area due to the damage or the physical state (small pieces of disrupted fuel) of the fuel. Because enrichment should not alter the release rate for fuels with the same matrix, enrichments from about one to two percent (the commercial range, such as Three Mile Island Reactor fuels) to 93 percent ^{235}U fuel from the High Flux Isotope Reactor and Shippingport pressurized water reactor are included in this category.

Category 9—Aluminum-Based Fuel (Uranium-Aluminide Fuel, Uranium Silicide, and Uranium Oxide in Aluminum): This category consists of fuels with the: (1) uranium aluminide dispersed in a continuous aluminum phase, (2) uranium silicide dispersed in a continuous aluminum phase, and (3) uranium oxide dispersed in a continuous aluminum phase. This category should perform better than uranium-metal fuel (Category 7) depending upon the continuity of the primary aluminum phase and the release rate from each of the phases. Foreign Research Reactor fuels make up a large part of the aluminum-based fuel. The enrichment level varies from about 11 to 93 percent ^{235}U, with the majority of the silicide fuels having less than 20 percent ^{235}U.

Category 10—Miscellaneous Fuel: The DSNFs with unknown matrices are placed in this category. Because of the potential varying matrices, cladding, and condition of this category of fuel, the fuel properties need to be conservatively represented with a dissolution model that reasonably represents this category. Based on the category inventory, the uranium-metal dissolution model is most representative of the dissolution rate of DSNF in this category.

Category 11—Uranium-Zirconium Hydride Fuel: Category 11 contains fuel with the uranium/zirconium hydride matrix. Fuels from the Training Research Isotopes General Atomics reactors make up the majority of the fuel in this category. The uranium-zirconium hydride in this category provides the reactor with its built-in control and inherent safety. The fuel consists of uranium-metal particles dispersed in the zirconium hydride matrix, clad with aluminum, stainless steel, or Incoloy-800, with varying enrichment and weight percents of ^{235}U. Because of the unique uranium/zirconium hydride matrix, this fuel was placed in its own category. This fuel matrix is expected to perform better than the uranium-oxide fuel.

Table 7.5-2 shows the radionuclide inventory for each category (Categories 2 through 11) of DSNF (DOE 2004 [DIRS 169354], Appendix D). The inventory was developed from the total radionuclide inventory in each DSNF category divided by the number of WPs for that category. Table 7.5-2 also shows the DSNF surrogate inventory that is used in the TSPA-LA Model to represent Categories 2 through 11 DSNF.

The number of canisters by canister size for each DSNF category and the total number of WPs per category are presented in Table 7.5-3 (DOE 2004 [DIRS 169354], Appendix D). The primary canister lengths are 10 and 15 ft. The multicanister overpack is used for the N-Reactor DSNF. The multicanister overpack CDSP WP contains two multicanister overpacks and two canisters of HLW in a 15-ft WP. The other two CDSP WPs contain one DSNF canister and four or five canisters of HLW in 10- or 15-ft WPs. The CDSP WP with a 24-in. canister of DSNF contains four canisters of HLW (Table 7.5-3).

A degradation rate for each fuel category was developed and applied to the TSPA-LA Model in order to compare the results of individual categories of DSNF to the DSNF surrogate spent fuel from *Additional DOE Spent Nuclear Fuel Information in Support of TSPA-LA Analysis* (Loo et al. 2004 [DIRS 168999], Section 6). The degradation rate is the product of a dissolution rate times a fuel surface area. The dissolution rate equations and fuel surface areas for each DSNF category are shown in Table 7.5-4.

7.5.3 Naval Spent Fuel, Category 1

Analyses were performed to disposition the use of CSNF as a surrogate for NSNF. These analyses are outlined in Table 7.5-5 and in the following sections. They were performed out to 10,000 years, and a qualitative argument for the extension of the results beyond the 10,000-year compliance period is also presented. The TSPA-LA Model was exercised explicitly using NSNF inventories in place of the CSNF inventory for an early failure case and an igneous intrusion case. The dose results from these cases were compared to show that CSNF inventory bounds the NSNF inventory. Quantitative comparisons of NSNF and CSNF inventories for the major radionuclide contributors to dose for the Volcanic Eruption, Human Intrusion, and Seismic Modeling Cases were made to disposition the use of the CSNF as a surrogate for NSNF for these cases. The Nominal Modeling Case, as it relates to NSNF, is also discussed. The seismic modeling cases were also evaluated by the Naval Nuclear Propulsion Project (Gisch 2004 [DIRS 171782]), and confirmed to be valid as discussed in Section 7.5.3.7.

7.5.3.1 Comparison of the Naval Spent Nuclear Fuel and Commercial Spent Nuclear Fuel Inventories for 10,000 Years and 1,000,000 Years

Radionuclide release rates for an NSNF WP are provided for the first 10,000 years of the compliance period for the early failure case and out to 1,000,000 years for the igneous intrusion case. These release rates, in terms of activities, are plotted on Figures 7.5-2 and 7.5-3 for the radionuclides that are major contributors to the mean annual total dose. Figure 7.5-2 shows that for the early failure case, the activities of the NSNF inventory on a per WP basis are orders of magnitude lower than the activities of the CSNF inventory for the first 10,000 years. The only exception to this is for ^{229}Th for the first 200 years. An extrapolation of the NSNF activities out to 1,000,000 years would show the same behavior.

Figure 7.5-3 shows that for the Igneous Intrusion Modeling Case, the activities of the NSNF inventory on a per WP basis are again generally lower out to 1,000,000 years, although by not as much as was the case for the early failure source term. The activities for ^{229}Th and ^{233}U for the NSNF are higher for the first few thousand years but diverge below the CSNF source term over the majority (i.e. hundreds of thousands of years) of the compliance period. This is because initially the NSNF inventory, on a per WP basis, has more ^{229}Th and ^{233}U than the CSNF inventory (McKenzie 2007 [DIRS 182657]), but the ingrowth of ^{229}Th and ^{233}U from the decay of ^{237}Np is greater for the CSNF because there is more ^{237}Np in the CSNF inventory.

7.5.3.2 Disposition of Commercial Spent Nuclear Fuel as a Surrogate for Naval Spent Nuclear Fuel for the Early Failure Modeling Cases

NSNF was analyzed using inventories, or source terms, supplied by the Navy for radionuclides that are available for release from naval spent fuel. The source terms are based on a hypothetically failed WP of naval spent fuel for the Drip Shield EF and Igneous Intrusion Modeling Cases. These source terms were provided by the Naval Nuclear Provision Program (McKenzie 2007 [DIRS 182657]). The analyses of naval spent fuel are special cases developed to compare CSNF and naval spent fuel for the Drip Shield EF and Igneous Intrusion Modeling Cases. For these analyses, the NSNF source term (radionuclides available for release within a failed WP) was modeled in a failed CSNF WP, and the radionuclides were then subject to all of the transport processes that are applied to dissolved CSNF (e.g., solubility, sorption, and chemistry along the transport pathway from dissolved CSNF to the RMEI) in the TSPA-LA Model.

In the modeled repository, there are 8,213 WPs of CSNF, 417 of which represent naval spent fuel (SNL 2007 [DIRS 180472], Table 6-2[a]). The TSPA-LA Model does not explicitly include naval spent fuel, but bounds its behavior with 417 CSNF WPs that represent naval spent fuel. The special case analyses in this section were conducted to demonstrate that the annual dose from naval spent fuel is bounded by the annual dose from CSNF.

For the validation of CSNF as a surrogate for naval spent fuel for the nondisruptive event cases, the Drip Shield EF Modeling Case was chosen over the Waste Package EF Modeling Case because of the following considerations. First, the transport of radionuclides within the EBS for the Drip Shield EF Modeling Case is advection dominated with some diffusion. The transport of radionuclides within the EBS for the Waste Package EF Modeling Case is diffusion dominated since the DS stays intact. The Waste Package EF Modeling Case would produce lower radionuclide doses compared to the Drip Shield EF Modeling Case and, therefore, can be considered a subset of the Drip Shield EF Modeling Case for the NSNF analysis. In addition, in the TSPA-LA Model, the Waste Package EF Modeling Case applies not only a temperature threshold to transport, but a relative humidity threshold to transport radionuclides from the waste form to the WP outer barrier. Since the naval source term is a release from a failed WP, it is implemented in the TSPA-LA Model by applying the release to the WP transport cell and, therefore, bypasses the relative humidity threshold for transport from the waste form transport cell. The result of using the Waste Package EF Modeling Case for the analysis would be an early release of radionuclides to the accessible environment for the naval source term, which would be inconsistent with a later release of radionuclides for the CSNF source term. The delay in release from the waste form to the WP outer barrier due to the relative humidity threshold for

transport is not implemented in the Drip Shield EF Modeling Case. Therefore, for the Drip Shield EF Modeling Case, the timing of the release of radionuclides to the accessible environment from a failed WP with a CSNF source term is more consistent with the timing of the release from a failed WP where the naval source term has been substituted for the CSNF source term in the WP transport cell.

For the Drip Shield EF Modeling Case, a single DS failure was forced to occur at the first timestep of the simulation. Two simulations were run: one for a single CSNF WP and one for a single WP where the naval source term replaced the CSNF source term. The simulations were run for 10,000 years and used a unified sampling of epistemic and aleatory uncertainty over 300 model realizations. The results, in terms of a mean annual dose over the unified sampling of epistemic and aleatory uncertainty, are shown on Figure 7.5-4. The results show that over a 10,000-year period, the dose associated with the naval source term is less than that of the CSNF source term. At 10,000 years, the mean annual dose from a failed WP with a naval source term is about two orders of magnitude lower than the mean annual dose for a failed CSNF WP, justifying the use of a CSNF WP as a surrogate for a naval WP.

7.5.3.3 Disposition of Commercial Spent Nuclear Fuel as a Surrogate for Naval Spent Nuclear Fuel for the Igneous Intrusion Modeling Case

A similar analysis conducted for the Igneous Intrusion Modeling Case is used to disposition the use of CSNF as a surrogate for NSNF. For both the CSNF and naval source term scenarios, the time of the igneous intrusion was forced to occur at a specified timestep, and a single WP was failed. The simulations were run for 10,000 years and used a unified sampling of epistemic and aleatory uncertainty over 300 model realizations. The results, in terms of a mean annual dose over the unified sampling of epistemic and aleatory uncertainty, are shown on Figure 7.5-5. As was the case for the Drip Shield EF Modeling Case, the results for the Igneous Intrusion Modeling Case show that at over a 10,000-year period the dose associated with the naval source term is less than that of the CSNF source term, again justifying the use of a CSNF WP as a surrogate for a naval WP.

7.5.3.4 Disposition of Commercial Spent Nuclear Fuel as a Surrogate for Naval Spent Nuclear Fuel for the Volcanic Eruption Modeling Case

The disposition of CSNF as a surrogate for NSNF for the Volcanic Eruption Modeling Case is done by showing that the NSNF inventory for the radionuclides that are the major contributors to the mean annual dose is less than the CSNF inventory and by taking credit for the robustness of the naval WP. Figure 8.2-10 shows ^{239}Pu and ^{241}Am, early in time, and ^{226}Ra, ^{229}Th, ^{237}Np, ^{126}Sn, and ^{238}U, later in time, as the major contributors to the volcanic eruptive total mean annual dose. The inventory activities for these same radionuclides are plotted on Figure 7.5-6 using the igneous NSNF and CSNF source terms. With respect to when each of these radionuclides breakthrough in terms of the eruptive dose, each has a lower activity for the NSNF source term than for the CSNF. Therefore, the use of CSNF as a surrogate for NSNF for the Volcanic Eruption Modeling Case is justified.

7.5.3.5 Disposition of Commercial Spent Nuclear Fuel as a Surrogate for Naval Spent Nuclear Fuel for the Human Intrusion Modeling Case

The disposition of CSNF as a surrogate for NSNF for the Human Intrusion Modeling Case is done by showing that the NSNF inventory for the radionuclides that are the major contributors to the mean annual dose is lower than the CSNF inventory and by taking credit for the robustness of the naval WP. Figure 8.1-13 shows the ^{99}Tc; ^{129}I; ^{79}Se near the time of the event, and ^{242}Pu, ^{135}Cs, and ^{237}Np, later in time, as the major contributors to the human intrusive total mean annual dose. The inventory activities for these same radionuclides are plotted on Figure 7.5-7 using the igneous NSNF and CSNF source terms. With respect to when each of these radionuclides breaks through in terms of the human intrusion dose, each has a lower activity for the NSNF source term than for the CSNF. Therefore, in combination with the robustness of the naval WP, the use of CSNF as a surrogate for NSNF for the Human Intrusion Modeling Case is justified.

7.5.3.6 Disposition of Commercial Spent Nuclear Fuel as a Surrogate for Naval Spent Nuclear Fuel for the Nominal Modeling Case

The use of CSNF as a surrogate for NSNF for the first 10,000 years of the Nominal Modeling Case is justified because there are no WP failures during this time period, and because the naval WP is more robust than the commercial WP as discussed in the naval classified technical support document. The 1,000,000 year Nominal Modeling Case is a stylized case (see Section 8.2.1) where the WP fails by SCC and general corrosion sometime after the first 10,000 years. These effects are accounted for in the 1,000,000 year Seismic GM Modeling Case. The use of CSNF as a surrogate for NSNF for the 1,000,000 year Nominal Modeling Case is justified because of the NSNF is adequately represented by CSNF in the early failure cases, and again because the naval WP is more robust than the commercial WP.

7.5.3.7 Disposition of Commercial Spent Nuclear Fuel as a Surrogate for Naval Spent Nuclear Fuel for the Seismic Ground Motion Modeling Cases.

The disposition of CSNF as a surrogate for NSNF for the Seismic GM Modeling Case is done by showing that the NSNF inventory for the radionuclides that are the major contributors to the mean annual dose is lower than the CSNF inventory and by taking credit for the robustness of the naval WP. Figure 8.2-12 shows ^{129}I, ^{242}Pu, ^{237}Np, ^{226}Ra, and ^{135}Cs as the major contributors to the seismic ground motion total mean annual dose at 1,000,000 years. Figure 8.2-12 also shows ^{99}Tc, ^{129}I, and ^{79}Se as the major contributors to the seismic ground motion total peak mean annual dose around 225,000 years. The inventory activities for these same radionuclides are plotted on Figure 7.5-8 using the igneous NSNF and CSNF source terms. With respect to when each of these radionuclides breaks through in terms of the seismic ground motion dose, each has a lower activity for the NSNF source term than for the CSNF. Therefore, in combination with the robustness of the naval WP, the use of CSNF as a surrogate for NSNF for the Seismic GM Modeling Case is justified. In addition to the analyses presented here, three seismic scenario class cases were evaluated by the Naval Nuclear Propulsion Project (Gisch 2004 [DIRS 171782]). The three modeling cases are for a large seismic event: (1) without the formation of a rock blanket, (2) with the formation of a rock blanket, and (3) with faulting through a WP. For each modeling case, the release rate of the key isotopes from naval SNF is bounded by the release rate of the key isotopes from CSNF.

7.5.4 U.S. Department of Energy Spent Fuel, Categories 2 through 11

The analyses of DSNF are based on several 300 realization simulations of the Drip Shield EF Modeling Case. In these simulations, aleatory uncertainty is fixed on percolation Subregion 3 in a dripping environment, where a single CDSP WP and the overlying DS are failed, allowing advective and diffusive transport from the waste. One simulation is performed for each category of DSNF and for the DSNF surrogate, with each simulation including 300 realizations, one for each element of the LHS for epistemic parameters. The HLW in the CDSP WP is not included in the analyses, so the results show the annual dose from the DSNF only. The analysis computes a mean annual dose for each simulation, and compares the mean annual dose for each DSNF category to the mean annual dose for the DSNF surrogate. In these analyses, the term mean annual dose refers to the average dose at each time conditional on the fixed aleatory quantities; for brevity the term mean annual dose is used to describe this quantity.

The dose from each category is expected to differ from the surrogate because of differences in (1) the degradation rate of the matrix, (2) fraction of bound inventory, and (3) the inventory of key isotopes per WP. Some categories will yield lower doses and some will yield higher doses, but the weighted sum of the dose from all categories should be close to the dose from the surrogate. This analysis confirms that the dose from the surrogate adequately represents or bounds the weighted sum of the dose from all categories.

The degradation rate of the matrix for the surrogate is set to instantaneous, so early dose from the surrogate that is controlled by degradation rate should bound or be equal to the dose from individual categories. The effect of degradation rate is only expected to be seen for the categories that have degradation rates that are slow compared to the 250 year timestep. Figure 7.5-9 shows the degradation rates of the categories, and only categories 4 and 6 have rates slow enough to require multiple times steps to degrade all the fuel. These two categories are expected to have lower doses during early times before all the fuel has degraded. The fraction of bound inventory parameter is important only for the slowly degrading fuels.

There are three ways the inventory can influence dose: (1) for highly soluble, low sorbing isotopes, the early dose should be proportional to the inventory released per WP; (2) for solubility controlled elements, the isotopic abundance should determine the relative release of the isotope; and (3) for long-lived, low solubility isotopes, the inventory and flow rate will determine how long it takes to deplete the WP. Looking at the mean annual dose from surrogate DSNF (Figure 7.5-1), it can be seen that the low solubility, highly sorbing isotopes ^{239}Pu and ^{226}Ra dominate at late times. The peak mean dose comes from ^{239}Pu with only a minor contribution from ^{233}U. The late time ^{226}Ra comes from decay of ^{234}U and ^{230}Th. Doses from ^{233}U and ^{234}U do not go above 10^{-3} mrem because these isotopes share solubility with the abundant but long-lived ^{238}U. From this, we would expect that the fuel that is more highly burned than the surrogate would have higher doses because of increased inventory per WP of ^{99}Tc and ^{237}Np. Other fuels that are based on ^{239}Pu or ^{233}U instead of ^{235}U for fission are also expected to result in significantly different dose from these isotopes. Although it is difficult to see on a linear time scale, the highly soluble and low sorbing isotopes ^{14}C and ^{99}Tc dominate the early mean annual dose (less than 5,000 years), and the moderately soluble and sorbing ^{237}Np dominates at 10,000 years.

Figure 7.5-10 shows the comparison of one WP of Category 2 (plutonium/uranium alloy) DSNF with one WP of DSNF surrogate. The Category 2 DSNF has a higher mean annual dose curve because of a higher per WP inventory of ^{14}C and ^{99}Tc from higher burn-up. The mean annual dose at late times is higher because of the weight percent of ^{234}U (4 percent for Category 2, 0.06 percent for the surrogate, calculated from information in Table 7.5-2) results in higher release of ^{234}U and its daughters, ^{230}Th and ^{226}Ra.

Figure 7.5-11 shows the comparison of one WP of Category 3 (plutonium/uranium carbide) DSNF with one WP of DSNF surrogate. The Category 3 DSNF mean annual dose curve is slightly lower than the surrogate because of lower per WP inventories of key dose contributors. This is in part due to the small amount of Category 3 fuel per WP (1.5×10^4g versus 7.4×10^5g for the surrogate) (Table 7.5-2). Late time mean annual dose may also be lower than the surrogate because of lower ^{234}U weight percent (0.01 percent, calculated from information in Table 7.5-2) leading to lower ^{230}Th and ^{226}Ra release.

Figure 7.5-12 shows the comparison of one WP of Category 4 (mixed oxide) DSNF with one WP of DSNF surrogate. The Category 4 DSNF has a lower mean annual dose curve up to about 10,000 years because the calculated degradation rate for Category 4 is less than 1×10^{-4} per year compared to the instantaneous degradation rate of the DSNF surrogate. The Category 4 DSNF mean annual dose is slightly higher after 100,000 years because of higher per WP inventories of long-lived radionuclides such as ^{226}Ra, ^{237}Np, and ^{230}Th (Table 7.5-2). This is due in part to the higher percent of ^{234}U in the fuel (0.26% for Category 4, 0.06% for the surrogate, calculated from information in Table 7.5-2) leading to higher late time ^{230}Th and ^{226}Ra release.

Figure 7.5-13 shows the comparison of one WP of Category 5 (uranium/thorium carbide) DSNF with one WP of DSNF surrogate. The Category 5 DSNF has a lower mean annual dose curve after 20,000 years when compared to the DSNF surrogate. The mean annual dose curve is slightly higher for Category 5 DSNF between 3,000 years and 20,000 years because of ^{233}U. The per WP inventories of ^{234}U, ^{235}U, ^{236}U, and ^{238}U are lower in Category 5 than for the DSNF surrogate (Table 7.5-2). This allows much more ^{233}U to be dissolved and transported in the Category 5 case because all uranium species share the same solubility limit in proportion to their inventory.

Figure 7.5-14 shows the comparison of one WP of Category 6 (uranium/thorium oxide) DSNF with one WP of DSNF surrogate. The Category 6 DSNF has a higher mean annual dose curve because of a higher per WP inventory of ^{233}U. The inventory of ^{238}U is significantly lower (than the surrogate) for Category 6, allowing more of the other uranium species to be dissolved and transported. Category 6 DSNF has a significantly higher ^{233}U per WP inventory than the other nine categories of DSNF. Category 6 DSNF contains about 92 percent of the total ^{233}U for all 10 categories on a per-WP basis (calculated from information in Table 7.5-2). Thus, Category 6 DSNF has a significantly higher ^{233}U inventory than the DSNF surrogate. The initial inventory of ^{233}U for the DSNF surrogate is 538 g per WP. The initial inventory of ^{233}U for Category 6 DSNF is 31,600 g per WP (Table 7.5-2).

Figure 7.5-15 shows the comparison of one WP of Category 7 (uranium metal) DSNF with one WP of DSNF surrogate. The mean annual dose curve is higher for Category 7 DSNF after about 100,000 years because of higher per WP inventories of long-lived radionuclides such as ^{237}Np,

^{226}Ra, and ^{230}Th (which decays to ^{226}Ra). This per WP concentration is larger in part due to the much larger amount of Category 7 fuel in the WP than the other fuels. The total inventory of Category 7 is 9.7×10^{6}g per WP while the next largest amount is Category 6 with 9.5×10^{5}g per WP and the surrogate having 7.4×10^{5}g per WP (Table 7.5-2).

Figure 7.5-16 shows the comparison of one WP of Category 8 (uranium oxide) DSNF with one WP of DSNF surrogate. The Category 8 DSNF has a slightly lower mean annual dose curve than the surrogate, but it follows the surrogate very well.

Figure 7.5-17 shows the comparison of one WP of Category 9 (aluminum-based) DSNF with one WP of DSNF surrogate. The Category 9 DSNF has a lower mean annual dose curve than the surrogate during the first 10,000 years because of a lower per WP inventory of key contributors (i.e., ^{99}Tc, ^{129}I, and ^{14}C). The mean annual dose curve is lower for Category 9 DSNF after 10,000 years because of lower per WP inventories of long-lived radionuclides such as ^{226}Ra, ^{234}U, ^{237}Np, ^{239}Pu, ^{233}U, and ^{230}Th. Category 9 fuel has one of the lowest amounts of fuel per WP (1.6×10^{4}g) compared to the surrogate (7.4×10^{5}g) (Table 7.5-2).

Figure 7.5-18 shows the comparison of one WP of Category 10 (miscellaneous) DSNF with one WP of DSNF surrogate. The Category 10 DSNF has a slightly higher mean annual dose curve because of higher per WP inventories of key contributors (i.e., ^{99}Tc, ^{233}U, and ^{14}C).

Figure 7.5-19 shows the comparison of one WP of Category 11 (uranium-zirconium hydride) DSNF with one WP of DSNF surrogate. The Category 11 DSNF has a lower mean annual dose curve during the first 10,000 years because of lower per WP inventories of key contributors (i.e., ^{99}Tc, ^{129}I, and ^{14}C), and because the calculated degradation rate for Category 11 is less than 1.0 per year. The mean annual dose curve is lower than the surrogate after 10,000 years because of lower per WP inventories of ^{237}Np, ^{233}U, ^{234}U, ^{226}Ra, and ^{239}Pu. Category 11 fuel has a low amount of fuel per WP (2.2×10^{4}g) (Table 7.5-2).

The analyses of Categories 2 through 11 show that the DSNF surrogate is a reasonable representation of all categories except Categories 2, 6, and 7 where significant differences occur due to higher per WP inventories of key dose contributors. However, Category 2 DSNF only accounts for about 0.5 percent of the total WPs of DSNF, Category 6 DSNF fills only 1.6 percent of the WPs, and Category 7 DSNF fills 6.6 percent of the WPs (Table 7.5-3). When the weighted sum (based on the number of WPs) is taken of all the individual DSNF categories, the resulting weighted sum dose curve matches up reasonably well with the DSNF surrogate (Figure 7.5-20). The weighted sum dose curve is dominated by the contribution from the Category 7 fuel at early and late times, and by the contribution from the Category 6 fuel from about 2,500 to 268,000 years. The mean dose of the surrogate bounds that of the weighted sum from about 40,000 years to about 400,000 years. The peak mean dose from the surrogate has the same magnitude as the weighted sum, but occurs later in the simulation.

The results for DSNF have been shown for the Drip Shield EF Modeling Case because a direct comparison between releases from single WPs in the same thermohydrology subregion (bin) is possible. The relative performance of DSNF in other bins is expected to be similar because the factors limiting release, available per WP inventory and solubility, do not vary significantly within bins. In the other modeling cases, multiple WPs in several bins are breached at different

times (Section 6.1.2). However, in these modeling cases, an approximation is made that the mean annual dose history from *n* breached WPs in the same bin is equal to the mean annual dose history from one breached WP in that bin times *n*. Thus it would be expected that the mean annual dose history from a single DS early failure would be similar to 1/*n* times the mean annual dose history from either a seismic or igneous event that occurs at time 0. The relative performance of the DSNF surrogate versus the Categories 2 through 11 fuels in the igneous and seismic cases is thus expected to be similar to the Drip Shield EF Modeling Case.

7.5.5 Selected Sensitivity Analyses

Sensitivity analyses for selected DSNF categories were performed to further build confidence in the TSPA-LA Model and to investigate how changing uncertain parameters (e.g., degradation rate, fuel surface area, free inventory, bounding inventory, and number of WPs) would affect the results (output DTN: MO0707TSPADSNF.000 [DIRS 182992]). The categories selected include: (1) uranium-metal DSNF, because it consists of a majority of the fuel (about 87 percent by metric tons of heavy metal), it has a free inventory as the remaining cladding degrades, and it increases surface area as it degrades; (2) uranium/thorium-carbide DSNF because of its slow degradation rate; and (3) aluminum-based DSNF because of the uncertainty in the number of WPs needed for disposal. The major contributors to mean annual dose are also examined for three categories of DSNF.

Figure 7.5-9 shows a comparison of the mean degradation rates for Categories 2 through 11 DSNF (Table 7.5-4), for the air alteration rate for Categories 5 and 7, and for the bounding surface area for Category 7. Table 7.5-6 contains the air alteration rates for Category 5 DSNF (uranium/thorium-carbide DSNF) and Category 7 DSNF (uranium-metal DSNF). These were applied to the TSPA-LA Model to provide comparisons with the nominal dissolution models of the same categories (Figures 7.5-21 and 7.5-22). The air alteration rate refers to the air oxidation rate of the DSNF under the repository conditions from *Additional DOE Spent Nuclear Fuel Information in Support of TSPA-LA Analysis* (Loo et al. 2004 [DIRS 168999], Section 7.3). Here it is interesting to note that the air alteration rate of Category 5 DSNF is extremely low and would affect its release of ^{233}U. Sensitivity runs were conducted for Category 7 DSNF because it represents 87 percent of the total DSNF (by mass) and for Category 5 DSNF because of its low air alteration rate.

Two model runs were performed using the Category 7 DSNF inventory. One used the Category 7 air alteration dissolution rate and the other used instantaneous dissolution (Table 7.5-6). The results are shown on Figure 7.5-21. On Figure 7.5-21, the mean annual dose curves are stacked on top of one another. This occurs because the calculated nominal degradation rate for Category 7 starts out greater than 1.0 per year, which equates to instantaneous degradation. In addition, the calculated air alteration rate starts out at about 0.2 per year, which equates to instantaneous degradation when applied over the first 250-year timestep.

The same analysis was performed for Category 5 DSNF (Tables 7.5-4 and 7.5-6). On Figure 7.5-22, the nominal and instantaneous dissolution rates produce mean annual dose results that plot on top of each other. This occurs because the calculated nominal degradation rate for Category 5 starts out greater than 1.0 per year, which equates to instantaneous degradation. The mean annual dose curve for air alteration is much lower than the nominal degradation because

the calculated air alteration rate starts out at about 8×10^{-11} per year, causing the fuel to degrade slowly over time.

A bounding fuel surface area of 2.8×10^{-4} m^2/g for Category 7 DSNF (uranium-metal DSNF) was used to compare the degradation rate to results using the nominal fuel surface area, which is 7.0×10^{-5} m^2/g (Table 7.5-4). The results show that there is no effect from the uncertainty in the surface area of uranium-metal DSNF (Figure 7.5-23). This occurs because the calculated degradation rates for both the nominal and bounding surface areas for Category 7 start out greater than 1.0 per year, which equates to instantaneous degradation.

For Category 7 (uranium-metal DSNF), the nominal free inventory fraction is 0.001. This parameter was changed to a bounding value of 0.01 for comparison. The nominal free and bounding free inventories refer to the fraction of radionuclide inventory that may be available immediately for transport from the fuel when the WP is breached, as referenced from *Additional DOE Spent Nuclear Fuel Information in Support of TSPA-LA Analysis* (Loo et al. 2004 [DIRS 168999], Section 7.5). A comparison of the nominal and bounding free radionuclide inventory for Category 7 (uranium metal) DSNF is shown on Figure 7.5-24. The nominal and bounding curves plot on top of each other because the calculated degradation rate for Category 7 starts out greater than 1.0 per year.

A bounding number of WPs (i.e., 2,030) (DOE 2004 [DIRS 169354], Appendix F) for Category 9 DSNF (aluminum-based DSNF) was used in the TSPA-LA Model to compare results with the nominal number of WPs (i.e., 1,415) (Table 7.5-3). This sensitivity analysis was conducted due to the uncertain number of WPs for the aluminum-based DSNF. The results show that the mean annual dose decreases slightly as the number of WPs increases because the radionuclide inventory is spread over more WPs (Figure 7.5-25). A similar run was performed with the minimum number of WPs (i.e., 1,016) (DOE 2004 [DIRS 169354], Appendix F). The results show that the mean annual dose increases slightly as the number of WPs decreases because the radionuclide inventory is concentrated in fewer WPs.

A similar analysis was conducted for Category 7 DSNF due to the uncertainty in the radionuclide inventory. Table 7.5-7 contains the nominal and bounding radionuclide inventories for Category 7 DSNF (uranium-metal DSNF). A plot comparing the mean annual dose curves of these inventories is shown on Figure 7.5-26. The bounding inventory was developed with the intention of bounding the actual source term for Category 7 DSNF (DOE 2004 [DIRS 169354], Appendix D). The bounding mean annual dose curve increased slightly, reflecting an increase in radionuclide inventory.

Figure 7.5-27 shows a 1,000,000-year plot of the top dose producing radionuclides that contribute to mean annual dose from HLW only. Here it is seen that the five HLW canisters contribute about the same to the mean annual dose as one canister of DSNF surrogate (compare to Figure 7.5-1). The major contributor to mean annual dose during the first 3,000 years is ^{99}Tc, and then ^{239}Pu dominates the mean annual dose curve until about 300,000 years. After that, ^{226}Ra, ^{234}U, ^{237}Np, and ^{242}Pu dominate the mean annual dose. Note that ^{14}C does not contribute to mean annual dose because it has a zero inventory for HLW.

Figure 7.5-28 shows a 1,000,000-year plot of the top dose producing radionuclides that contribute to the mean annual dose from Category 7, uranium-metal DSNF. The key mean annual dose contributors from Category 7 DSNF are similar to the DSNF surrogate. The major contributor to mean annual dose is ^{14}C and ^{99}Tc until about 10,000 years, and then ^{237}Np, ^{239}Pu, and ^{226}Ra dominate the mean annual dose curve in the later years.

Figure 7.5-29 shows a 1,000,000-year plot of the top dose producing radionuclides that contribute to the mean annual dose from Category 5, uranium/thorium-carbide DSNF. The major contributors to mean annual dose during the first 1,000 years are ^{99}Tc and ^{129}I. After 1,000 years, ^{233}U and ^{226}Ra dominate the mean annual dose curve. As explained in Section 7.5.4, the mean annual dose for ^{233}U is much higher for Category 5 because the inventory of ^{238}U is about three orders of magnitude lower for Category 5 than it is for the surrogate. This allows much more ^{233}U to be dissolved and transported in the Category 5 case because all uranium species have the same solubility limit in proportion to their inventory.

Figure 7.5-30 shows a 1,000,000-year plot of the top dose producing radionuclides that contribute to mean annual dose from Category 6, uranium/thorium-oxide DSNF. The major contributors to mean annual dose during the first 1,000 years are ^{14}C and ^{99}Tc, and then ^{233}U dominates thereafter because of a much higher inventory of ^{233}U and a lower inventory of ^{238}U.

7.5.6 Summary of Results for U.S. Department of Energy Spent Fuel

The result for naval spent fuel in comparison to Zircaloy-clad CSNF shows that the CSNF bounds the results of naval spent fuel for both the nondisruptive and disruptive event modeling cases. Additional analyses performed by the Naval Nuclear Propulsion Project confirm the use of CSNF as a surrogate for naval spent fuel for the seismic scenarios (Gisch 2004 [DIRS 171782]). The representation of naval spent fuel by CSNF as its surrogate in the TSPA-LA Model adequately bounds the behavior of naval spent fuel (Section 7.5.3).

Figure 7.5-20 shows a comparison of a single WP of DSNF surrogate with the weighted sum of the mean annual dose from DSNF Categories 2 through 11. The weighting of the mean annual dose in each category is based on the number of WPs in the category (Table 7.5-3). The weighted-sum lines up well with the surrogate curve, and has about the same peak mean dose. The current DSNF surrogate radionuclide inventory is based on *Source Term Estimates for DOE Spent Nuclear Fuels* (DOE 2003 [DIRS 163377]). These inventories were updated in *Source Term Estimates for DOE Spent Nuclear Fuels* (DOE 2004 [DIRS 169354]). The DSNF surrogate based on Revision 1 inventories is also plotted on Figure 7.5-20 for comparison.

The weighted-sum of the mean annual dose curves from DSNF Categories 2 through 11 is slightly higher than the surrogate mean annual dose curve at about 10,000 years. This is primarily due to the influence of Category 6 DSNF (Figure 7.5-14) and to a lesser extent Category 5 DSNF (Figure 7.5-13) and their high contribution to mean annual dose from ^{233}U (Figures 7.5-30 and 7.5-29). However, it still results in a similar peak mean dose as the surrogate mean annual dose curve.

Although for some DSNF, such as Categories 2, 6, 7, and 10, where the mean annual dose history shows a higher mean annual dose as compared to the surrogate, the number of WPs in these categories is much lower than the total number of DSNF WPs. These categories make up about 9 percent of the total number of DSNF WPs (Table 7.5-3). Thus, the probability of a WP failure in one of these categories is lower when compared to the probability of WP failure in Categories 3, 4, 5, 8, 9, and 11, which make up about 91 percent of the total number of DSNF WPs. Overall, Figure 7.5-20 shows that the DSNF surrogate is a reasonable representation of the combination of the ten DSNF categories.

INTENTIONALLY LEFT BLANK

Table 7.5-1. U.S. Department of Energy Spent Fuel Categories Analyzed for the TSPA-LA Model[a,b]

Category	Fuel Category/Fuel Matrix	Typical Fuel in Category	Mass (MTHM)[c]	Percent of Total
1	Naval nuclear fuel	Naval Nuclear Fuel	70[b]	2.88
2	Plutonium/uranium alloy	Enrico Fermi Reactor (FERMI) Core 1 and 2 (standard fuel subassembly)	4.58	0.19
3	Plutonium/uranium carbide	Fast Flux Test Facility Test Fuel Assembly (FFTF-TFA-FC-1)	0.0765	0.003
4	Mixed oxide fuel (plutonium/ uranium oxide and plutonium oxide)	Fast Flux Test Facility Driver Fuel Assembly (FFTF-DFA/TDFA)	12.0	0.49
5	Uranium/thorium carbide	Fort St. Vrain Reactor	26.3	1.08
6	Uranium/thorium oxide	Shippingport Light Water Breeder Reactor (Reflect. IV)	50.2	2.06
7	Uranium metal	N-Reactor	2,110	86.77
8	Uranium oxide	Three Mile Island (TMI-2) Core Debris	134	5.51
9	Aluminum based (UAlx, U_3Si_2, uranium oxide in aluminum)	Foreign Research Reactor Pin Cluster (Canada)	22.3	0.92
10	Miscellaneous	Miscellaneous Radioactive Scrap Waste Facility Fuel	0.438	0.02
11	Uranium-zirconium hydride	Training Research Isotopes General Atomics (TRIGA)	1.95	0.08

[a] *Additional DOE Spent Nuclear Fuel Information in Support of TSPA-LA Analysis* (Loo et al. 2004 [DIRS 168999], Table 5-1).

[b] *DSNF and Other Waste Form Degradation Abstraction* (BSC 2004 [DIRS 172453], Section 6.2) states that naval spent fuel represents approximately one-tenth of one percent of the MTHM inventory in the repository. Based on *The Nuclear Waste Policy Act, as Amended, with Appropriations Acts Appended* (DOE 1995 [DIRS 122137], Section 114), the repository contains 70,000 MTHM and the approximate naval mass is 70 MTHM.

[c] MTHM from *Source Term Estimates for DOE Spent Nuclear Fuels* (DOE 2004 [DIRS 169354], Appendix D, pp. D-3 through D-567). Summed heavy metal mass end of life values from each worksheet for TSPA Categories 2 to 11, excluding bare fuel transfers.

NOTE: The total number of WPs is provided in Table 7.5-3.

Table 7.5-2. Radionuclide Inventory for Each U.S. Department of Energy Spent Fuel Category and the U.S. Department of Energy Surrogate Spent Fuel (grams/waste package)[a]

Radionuclide	Category 1 (g/WP)	Category 2 (g/WP)	Category 3 (g/WP)	Category 4 (g/WP)	Category 5 (g/WP)	Category 6 (g/WP)
^{227}Ac	NA	1.34E-05	1.47E-10	1.81E-05	8.94E-05	1.41E-02
^{241}Am	NA	2.42E+02	6.35E+01	1.60E+03	1.50E+00	4.28E+01
^{243}Am	NA	3.61E-01	9.02E-01	4.68E+01	3.73E-01	1.41E+00
^{14}C	NA	8.86E+00	9.78E-03	1.43E+01	8.37E-03	6.76E-01
^{36}Cl	NA	1.00E-02	1.74E-05	3.65E+01	5.23E-02	1.75E+00
^{245}Cm	NA	9.97E-05	1.72E-02	1.68E-01	3.78E-02	3.56E-03
^{135}Cs	NA	4.31E+02	6.95E+01	4.89E+02	3.47E+01	2.63E+02
^{137}Cs	NA	3.45E+02	2.67E+01	2.07E+02	2.23E+01	1.73E+02
^{129}I	NA	1.81E+02	1.22E+01	8.24E+01	9.25E+00	9.37E+01
^{237}Np	NA	3.12E+02	8.99E+00	1.59E+02	2.88E+01	5.64E+00
^{231}Pa	NA	3.34E-02	4.50E-07	3.20E-02	1.62E-01	2.63E+01
^{238}Pu	NA	1.04E+01	1.42E+00	5.08E+01	1.48E+01	3.22E+00
^{239}Pu	NA	1.21E+04	3.28E+03	1.90E+04	3.54E+00	1.19E+02
^{240}Pu	NA	1.29E+03	7.41E+02	3.87E+03	1.94E+00	2.27E+01
^{241}Pu	NA	1.18E+01	3.59E+01	3.10E+02	2.50E-01	8.20E+00
^{242}Pu	NA	1.82E+01	1.38E+01	2.60E+02	1.60E+00	1.07E+01
^{226}Ra	NA	1.05E-03	1.39E-08	5.38E-05	5.31E-06	2.36E-04
^{228}Ra	NA	1.54E-07	1.52E-15	1.16E-06	5.46E-06	1.75E-04
^{79}Se	NA	3.39E+01	1.11E+00	1.12E+01	2.22E+00	2.40E+01
^{126}Sn	NA	5.33E+01	6.49E+00	3.46E+01	3.16E+00	3.65E+01
^{90}Sr	NA	1.87E+02	6.00E+00	8.13E+01	1.33E+01	1.09E+02
^{99}Tc	NA	1.04E+03	3.90E+01	3.72E+02	3.18E+01	2.05E+02
^{229}Th	NA	1.14E-03	2.17E-08	5.37E-03	8.78E-02	3.23E+00
^{230}Th	NA	2.91E+00	8.71E-05	1.88E-01	1.59E-02	5.85E-01
^{232}Th	NA	3.82E+02	4.92E-06	2.88E+03	4.21E+04	9.07E+05
^{232}U	NA	1.51E-04	9.55E-05	5.41E-03	1.13E-01	1.73E+01
^{233}U	NA	3.34E+00	1.02E-04	1.97E+01	3.45E+02	3.16E+04
^{234}U	NA	1.33E+04	1.17E+00	1.09E+03	7.59E+01	1.39E+03
^{235}U	NA	5.20E+04	1.90E+01	1.42E+05	3.10E+03	4.88E+03
^{236}U	NA	1.54E+04	4.71E+00	1.93E+03	2.16E+02	8.31E+01
^{238}U	NA	2.20E+05	1.08E+04	2.37E+05	2.54E+02	6.03E+03
Totals:	NA	3.17E+05	1.51E+04	4.12E+05	4.63E+04	9.52E+05

Table 7.5-2. Radionuclide Inventory for Each U.S. Department of Energy Spent Fuel Category and the U.S. Department of Energy Surrogate Spent Fuel (grams/waste package)[a] (Continued)

Radionuclide	Category 7 (g/WP)	Category 8 (g/WP)	Category 9 (g/WP)	Category 10 (g/WP)	Category 11 (g/WP)	Surrogate[b] (g/WP)
^{227}Ac	6.71E-07	5.44E-07	5.72E-08	4.40E-05	8.57E-08	1.22E-03
^{241}Am	1.01E+03	1.29E+02	6.52E+00	2.01E+02	2.41E+00	2.18E+02
^{243}Am	8.72E+00	8.39E+00	1.36E-01	1.83E+01	6.16E-02	6.73E+00
^{14}C	3.17E+00	8.47E-01	2.42E-04	2.17E+00	3.81E-02	1.81E+00
^{36}Cl	5.17E+00	1.69E+00	3.13E-05	5.31E+00	1.09E-01	4.23E+00
^{245}Cm	3.50E-02	2.98E-01	6.05E-03	1.42E+00	8.90E-04	9.25E-02
^{135}Cs	3.12E+02	5.98E+01	1.31E+01	9.54E+02	3.51E+01	9.74E+01
^{137}Cs	3.46E+02	5.29E+01	8.76E+01	3.86E+02	2.86E+01	9.72E+01
^{129}I	1.73E+02	2.12E+01	1.60E+01	1.58E+02	5.83E+00	3.56E+01
^{237}Np	4.56E+02	5.36E+01	6.41E+01	1.34E+02	8.69E+00	8.14E+01
^{231}Pa	1.95E-03	1.32E-03	2.04E-04	1.16E-01	2.40E-04	2.14E+00
^{238}Pu	3.67E+01	1.13E+01	7.65E+00	9.87E+00	1.12E+00	1.25E+01
^{239}Pu	1.64E+04	8.16E+02	1.15E+02	8.37E+03	9.96E+01	2.21E+03
^{240}Pu	3.46E+03	2.12E+02	1.66E+01	2.10E+02	1.16E+01	4.35E+02
^{241}Pu	9.82E+01	1.65E+01	3.45E+00	1.40E+01	1.35E+00	2.92E+01
^{242}Pu	1.29E+02	4.49E+01	1.08E+00	4.54E+01	5.59E-01	3.02E+01
^{226}Ra	7.59E-05	2.27E-05	1.51E-06	1.28E-05	5.91E-09	4.57E-05
^{228}Ra	8.72E-09	9.33E-09	2.01E-11	2.86E-07	8.87E-10	1.51E-05
^{79}Se	2.61E+01	3.54E+00	3.20E+00	2.63E+01	1.19E+00	6.82E+00
^{126}Sn	3.70E+00	7.47E+00	3.84E+00	7.96E+01	1.51E+00	9.40E+00
^{90}Sr	1.55E+02	2.46E+01	5.19E+01	2.12E+02	1.68E+01	5.22E+01
^{99}Tc	7.81E+02	1.03E+02	9.48E+01	6.56E+02	3.58E+01	1.58E+02
^{229}Th	6.83E-05	6.11E-05	1.64E-07	3.59E-03	2.81E-06	3.24E-01
^{230}Th	2.29E-01	6.35E-02	7.82E-03	3.68E-02	2.98E-05	1.18E-01
^{232}Th	2.16E+01	2.31E+01	5.24E-02	6.21E+04	2.40E+00	2.17E+04
^{232}U	2.19E-05	8.08E-05	1.85E-05	1.07E-02	8.32E-06	1.28E+00
^{233}U	2.05E-01	1.80E-01	1.46E-03	2.24E+03	1.58E-02	5.38E+02
^{234}U	1.21E+03	2.96E+02	8.69E+01	1.77E+02	3.75E-01	4.73E+02
^{235}U	1.02E+05	5.84E+03	7.22E+03	2.42E+04	4.37E+03	2.51E+04
^{236}U	7.09E+03	8.14E+02	9.08E+02	4.86E+03	2.82E+02	1.25E+03
^{238}U	9.56E+06	1.69E+05	7.36E+03	6.40E+04	1.74E+04	6.84E+05
Totals:	9.69E+06	1.78E+05	1.61E+04	1.69E+05	2.23E+04	7.37E+05

[a] *Source Term Estimates for DOE Spent Nuclear Fuels* (DOE 2004 [DIRS 169354], Appendix D, pp. D-577 to D-586, excluding bare fuel transfers). The units of the radionuclide inventories in the document are in curies. The conversion from curies to grams required the half-life of each radionuclide from *Initial Radionuclide Inventories* (SNL 2007 [DIRS 180472], Table 4-12). Inventory values for ^{245}Cm are from *Radionuclide Inventory Calculation Checks, SFD Version 5.0.1* (DOE 2007 [DIRS 182943]).

[b] *Initial Radionuclide Inventories* (SNL 2007 [DIRS 180472]), Table 7-1[a]). The DSNF inventory from Table 7-1[a] is a surrogate inventory that represents the 10 categories of DSNF. In the analyses in Section 7.5, the entire DSNF inventory is referred to as DSNF surrogate to distinguish it from Categories 2 through 11 DSNF.

NOTE: N/A = not applicable; not available for public review.

Table 7.5-3. Number of Canisters by Size of Canister and Total Number of Waste Packages for Each DSNF Category[a]

Category, Group/Matrix	18-Inch × 10-Foot Canisters	18-Inch × 15-Foot Canisters[b]	24-Inch × 10-Foot Canisters	24-Inch × 15-Foot Canisters	Multicanister Overpack[c]	Total WPs[d]	Percent of Total WPs
1. Naval fuel	N/A	N/A	N/A	N/A	N/A	N/A	N/A
2. Plutonium/uranium alloy	10	8	0	0	0	18	0.5
3. Plutonium/uranium carbide	2	3	0	0	0	5	0.2
4. Mixed oxide	15	128	0	0	0	143	4.3
5. Uranium/thorium carbide	1	568	0	0	0	569	17.3
6. Uranium/thorium oxide	13	13	0	27	0	53	1.6
7. Uranium metal	15	2	0	0	401	218	6.6
8. Uranium oxide	277	489	0	0	18	775	23.6
9. Aluminum based	1,013	236	166	0	0	1,415	43.0
10. Miscellaneous	3	1	0	0	0	4	0.1
11. Uranium-zirconium hydride	89	0	0	0	0	89	2.7

[a] *Source Term Estimates for DOE Spent Nuclear Fuels* (DOE 2004 [DIRS 169354], Appendix F, Table F-1). The number of WPs is rounded up to a whole WP for this table. The number of WPs is used for the analysis of each category of DSNF.
[b] For the analysis of DSNF, the high-integrity cans are included in the 10-ft and 15-ft canisters.
[c] Two multicanister overpacks per WP.
[d] The total number of CDSP WPs (3,289) shown in this table is different than the total shown in Table 6.3.7-1 (3,416). This is due to the use of a multiplier in *Initial Radionuclide Inventories* (SNL 2007 [DIRS 180472]) used to fill the entire footprint of the repository. The sensitivity analysis in Section 7.5.5 (on the number of WPs) indicates that this difference does not have a significant effect on annual dose.

NOTE: N/A = not applicable to DSNF; Naval spent fuel does not use any of the DOE canisters.

Table 7.5-4. Dissolution Models and Fuel Surface Areas for Each DSNF Category[a]

Category, Group/Matrix	Dissolution Model[b]	Nominal Fuel Surface Area (m^2/g)
1. Naval fuel	N/A	N/A
2. Plutonium/uranium alloy	$k = 1.15\times10^{8}\exp\left[\frac{-66.5\,kJ/mol}{RT}\right] mg\,metal/cm^2h$	3.6E-4
3. Plutonium/uranium carbide	$k = 8.9\times10^{10}\exp\left[\frac{-17\,kJ/mol}{RT}\right] mg\,UC/m^2d$	2.6E-3
4. Mixed oxide	$k = 4.46\times10^{4}\exp\left[\frac{-39\,kJ/mol}{RT}\right] mg\,PuO_2/m^2d$	5.5E-4
5. Uranium/thorium carbide	$k = 5.37\times10^{11}\exp\left[\frac{-35\,kJ/mol}{RT}\right] mg\,UC_2/m^2d$	2.2E-2
6. Uranium/thorium oxide	$k_{alkaline} = 5\times10^{4}[CO_3]^{0.12}\times[O_2]^{0.32}\times\exp\left[\frac{-20.8\,kJ/mol}{RT}\right] mg\,UO_2/m^2d$ $k_{acidic} = 1.35\times10^{7}[H^+]^{0.41}\times[O_2]^{0.32}\times\exp\left[\frac{-20.8\,kJ/mol}{RT}\right] mg\,UO_2/m^2d$	3.6E-4
7. Uranium metal	$k = 5.03\times10^{9}\exp\left[\frac{-66.4\,kJ/mol}{RT}\right] mg\,U/cm^2h$	7.0E-5 (Bounding = 2.8E-4)
8. Uranium oxide	$k_{alkaline} = 5\times10^{4}[CO_3]^{0.12}\times[O_2]^{0.32}\times\exp\left[\frac{-20.8\,kJ/mol}{RT}\right] mg\,UO_2/m^2d$ $k_{acidic} = 1.35\times10^{7}[H^+]^{0.41}\times[O_2]^{0.32}\times\exp\left[\frac{-20.8\,kJ/mol}{RT}\right] mg\,UO_2/m^2d$	2.2E-2
9. Aluminum based	$k = 4.29\exp\left[\frac{-32.8\,kJ/mol}{RT}\right] mg\,metal/cm^2h$	6.5E-3
10. Miscellaneous	$k = 5.03\times10^{9}\exp\left[\frac{-66.4\,kJ/mol}{RT}\right] mg\,metal/cm^2h$	2.2E-2
11. Uranium-zirconium hydride	$k = 2\times10^{-6}\,g^2\,ZrH_2/cm^4h$	1.0E-4

[a] *Additional DOE Spent Nuclear Fuel Information in Support of TSPA-LA Analysis* (Loo et al. 2004 [DIRS 168999], Section 6 and Table 7-1).

[b] k is the dissolution rate, R is the universal gas constant (8.3145 J/K·mol); T is the temperature (K). In some cases, these dissolution models were used outside of their range of validity. This was done only to produce a comparison of a potential dissolution model for a specific spent fuel type to the dissolution model used in the TSPA-LA Model. It has no impact on the dose from the TSPA-LA Model that uses an instantaneous dissolution model as a reasonable surrogate.

NOTE: N/A = not applicable; not available for public review.

Table 7.5-5. Disposition of the Use of CSNF as a Surrogate for NSNF for the TSPA-LA Model

Modeling Case	Disposition	Documented
Early Failure	Advection + diffusion case (Drip Shield EF), and a subset with just diffusion (Waste Package EF). Modeled DS early failure explicitly with nominal naval source term replacing commercial source term. Qualitative arguments for WP early failure.	Section 7.5.3.2
Igneous Intrusion	Modeled explicitly with igneous naval source term replacing commercial source term.	Section 7.5.3.3
Volcanic Eruption	Quantitative comparison using igneous naval source term, naval WP percentage of the total inventory, and robustness of naval WP.	Section 7.5.3.4
Human Intrusion	Quantitative comparison using igneous naval source term, naval WP percentage of the total inventory, and robustness of naval WP.	Section 7.5.3.5
Nominal	Qualitative. Zero probability case. No WP failures in 10,000 years; generalized corrosion (i.e. patch) failures in 1,000,000 years. WP patch failures similar to an human intrusion WP failure.	Section 7.5.3.6
Seismic	Quantitative comparison using the naval source term and robustness of the naval WP.	Section 7.5.3.7

Table 7.5-6. Air Alteration Rate for DSNF Category 5, Uranium/Thorium Carbide, and Category 7, Uranium Metal[a]

Category, Group/Matrix	Air Alteration Dissolution Model[b]
5. Uranium/thorium carbide	$k = 3.12\times10^{9}\exp\left[\frac{-94.3\,kJ/mol}{RT}\right] mg^{2}\,SiC/m^{4}d$
7. Uranium metal	$k = 1.09\times10^{8}\exp\left[\frac{-71.3\,kJ/mol}{RT}\right] mgU/cm^{2}h$

[a] *Additional DOE Spent Nuclear Fuel Information in Support of TSPA-LA Analysis* (Loo et al. 2004 [DIRS 168999], Table 7-3).

[b] In some cases, these dissolution models were used outside of their range of validity. This was done only to produce a comparison of a potential dissolution model for a specific spent fuel type to the dissolution model used in the TSPA-LA Model. It has no impact on the dose from the TSPA-LA Model that uses an instantaneous dissolution model as a reasonable surrogate.

Table 7.5-7. Nominal and Bounding Inventories for Uranium-Metal Spent Fuel (Category 7)[a]

Radionuclide	Nominal Inventory (g/WP)	Bounding Inventory (g/WP)	Radionuclide	Nominal Inventory (g/WP)	Bounding Inventory (g/WP)
^{227}Ac	6.71E-07	1.07E-06	^{242}Pu	1.29E+02	2.56E+02
^{241}Am	1.01E+03	1.98E+03	^{226}Ra	7.59E-05	8.37E-05
^{243}Am	8.72E+00	1.73E+01	^{228}Ra	8.72E-09	8.73E-09
^{14}C	3.17E+00	3.85E+00	^{79}Se	2.61E+01	4.98E+01
^{36}Cl	5.17E+00	5.18E+00	^{126}Sn	3.70E+00	4.62E+00
^{245}Cm	3.50E-02	6.81E-02	^{90}Sr	1.55E+02	2.98E+02
^{135}Cs	3.12E+02	6.07E+02	^{99}Tc	7.81E+02	1.50E+03
^{137}Cs	3.46E+02	6.71E+02	^{229}Th	6.83E-05	6.90E-05
^{129}I	1.73E+02	3.36E+02	^{230}Th	2.29E-01	2.70E-01
^{237}Np	4.56E+02	8.84E+02	^{232}Th	2.16E+01	2.16E+01
^{231}Pa	1.95E-03	3.30E-03	^{232}U	2.19E-05	3.04E-05
^{238}Pu	3.67E+01	7.21E+01	^{233}U	2.05E-01	2.11E-01
^{239}Pu	1.64E+04	3.19E+04	^{234}U	1.21E+03	1.57E+03
^{240}Pu	3.46E+03	6.81E+03	^{235}U	1.02E+05	1.22E+05
^{241}Pu	9.82E+01	1.94E+02	^{236}U	7.09E+03	1.32E+04
			^{238}U	9.56E+06	9.59E+06

[a] *Source Term Estimates for DOE Spent Nuclear Fuels* (DOE 2004 [DIRS 169354], Appendix D, p. D-581, excluding bare fuel transfers). The units of the radionuclide inventories in the document (DOE 2004 [DIRS 169354]) are in curies. The conversion from curies to grams (presented above) required the half-life of each radionuclide from *Initial Radionuclide Inventories* (SNL 2007 [DIRS 180472], Table 4-12). Inventory values for ^{245}Cm are from *Inventory Values for Curium-245 for DOE SNF in the License Application* (DOE 2007 [DIRS 182943]).

INTENTIONALLY LEFT BLANK

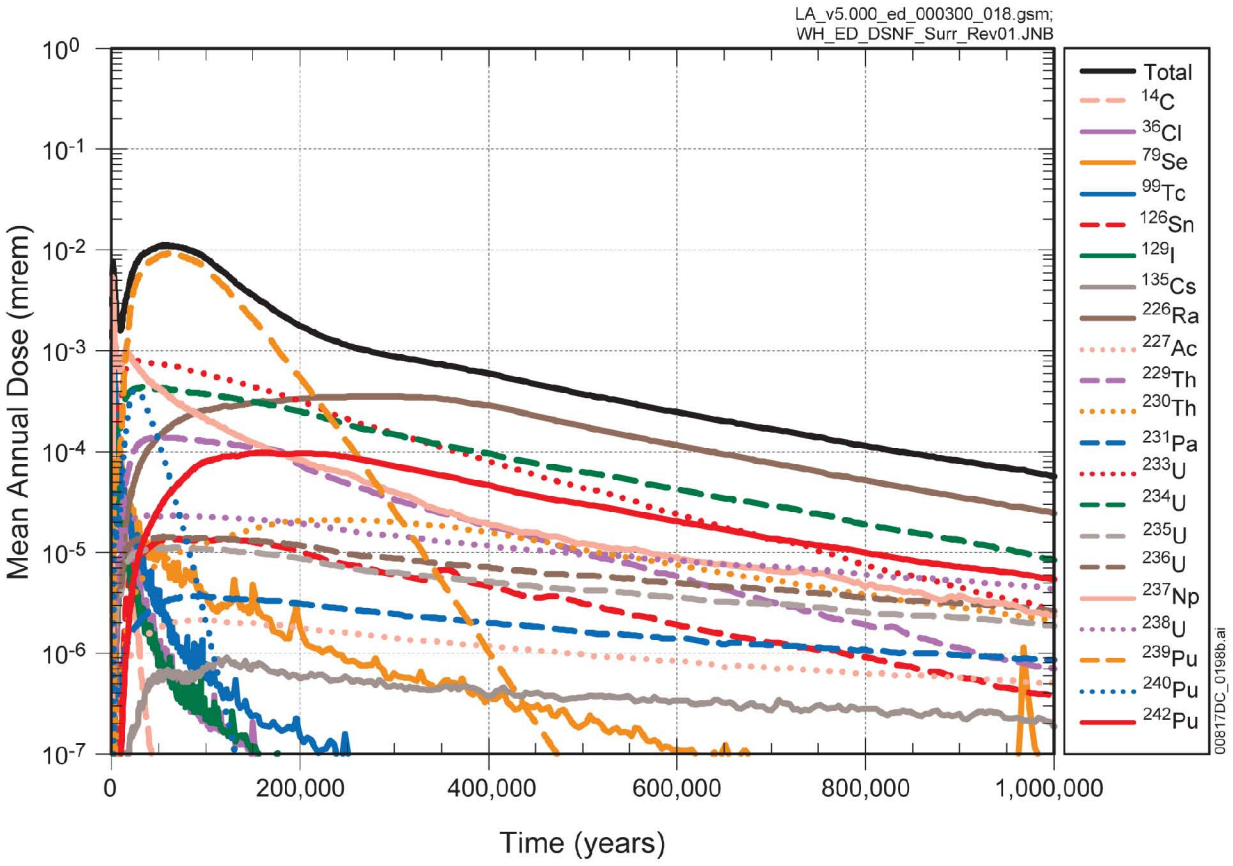

Source: Output DTN: MO0707TSPADSNF.000 [DIRS 182992].

NOTE: ^{226}Ra dose is the sum of ^{226}Ra and ^{210}Pb doses (secular equilibrium assumed).

Figure 7.5-1. Mean Annual Dose and Dose Contributors from DSNF Only Using Surrogate Inventory (One Waste Package Failure with no HLW)

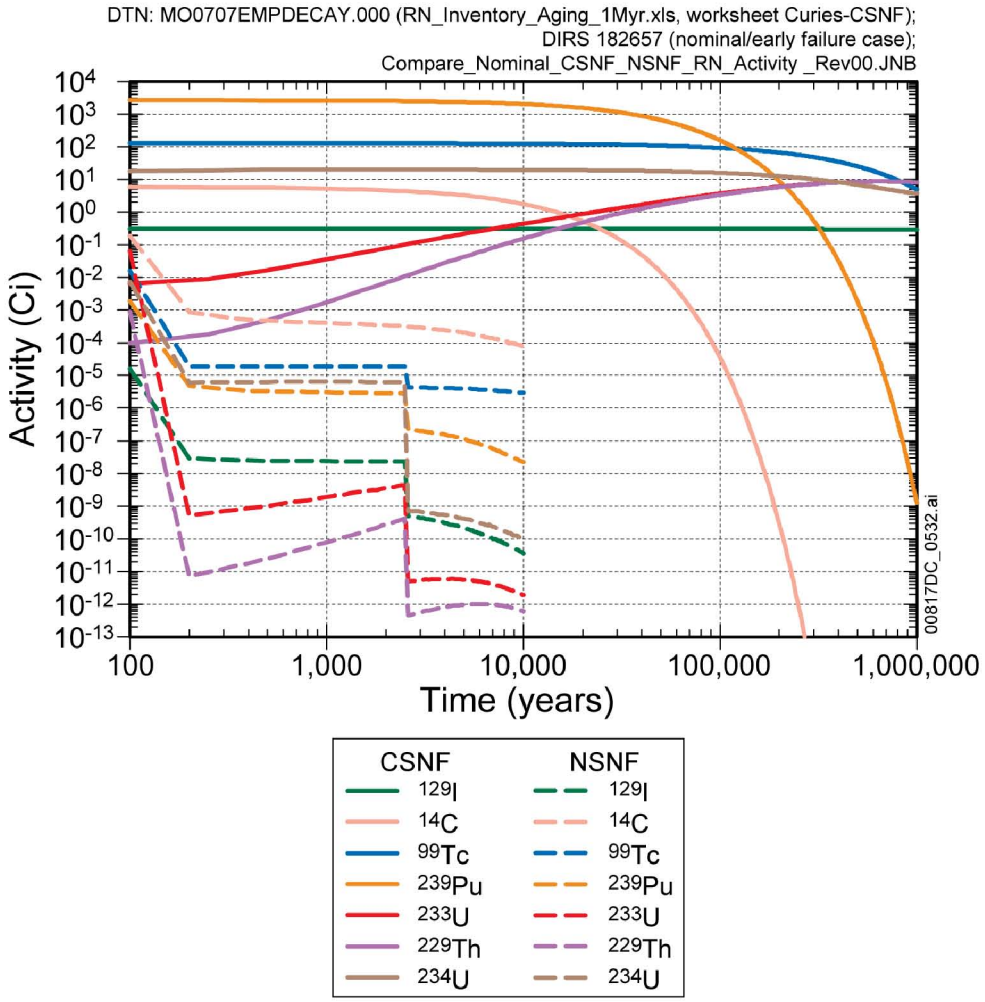

Sources: McKenzie 2007 [DIRS 182657] and Output DTN: MO0707EMPDECAY.000 [DIRS 183475], *FileRN_Inventory_Aging_1Myr.xls*, worksheet Curies-CSNF.

Figure 7.5-2. Comparison of Radionuclide Activities on a per Waste Package Basis for the Nominal/Early Failure NSNF and CSNF Inventories

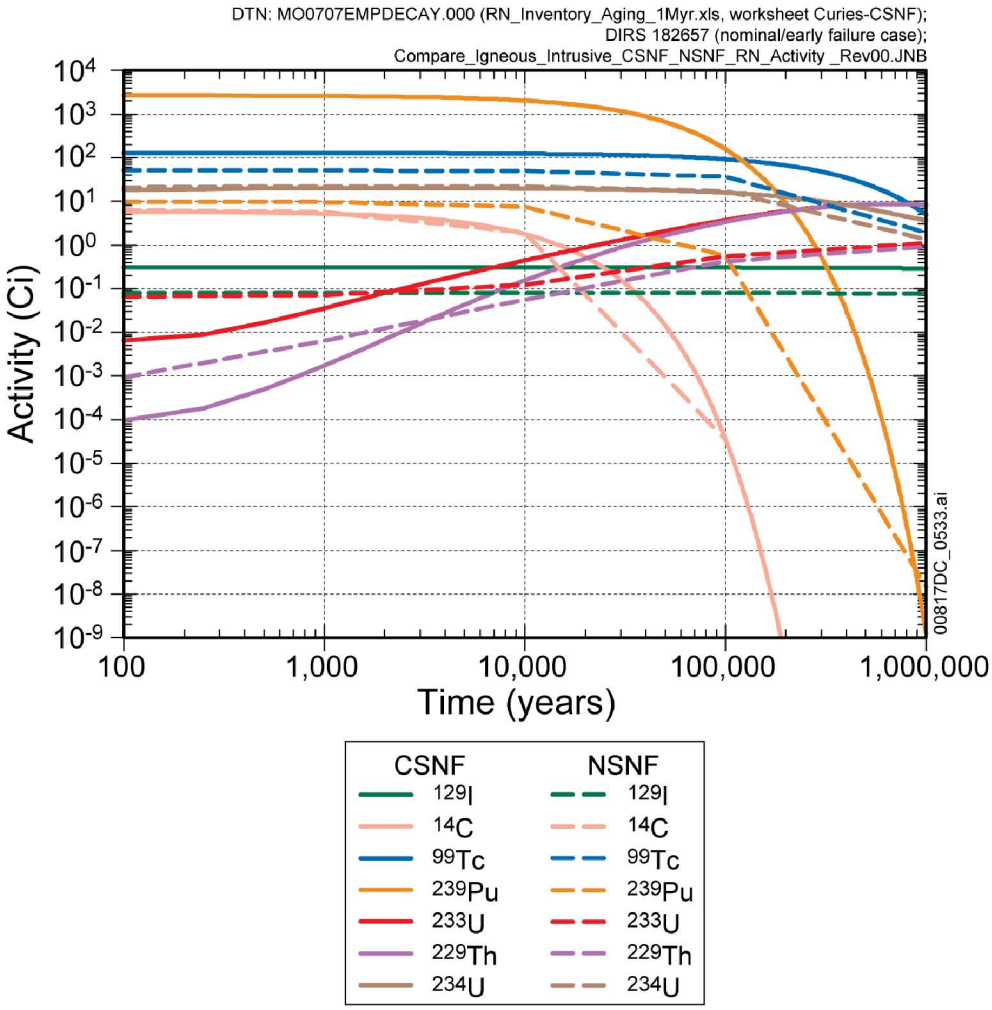

Sources: McKenzie 2007 [DIRS 182657] and Output DTN: MO0707EMPDECAY.000 [DIRS 183475], *FileRN_Inventory_Aging_1Myr.xls*, worksheet Curies-CSNF.

Figure 7.5-3. Comparison of Radionuclide Activities on a per Waste Package Basis for the Igneous Intrusion NSNF and CSNF Inventories

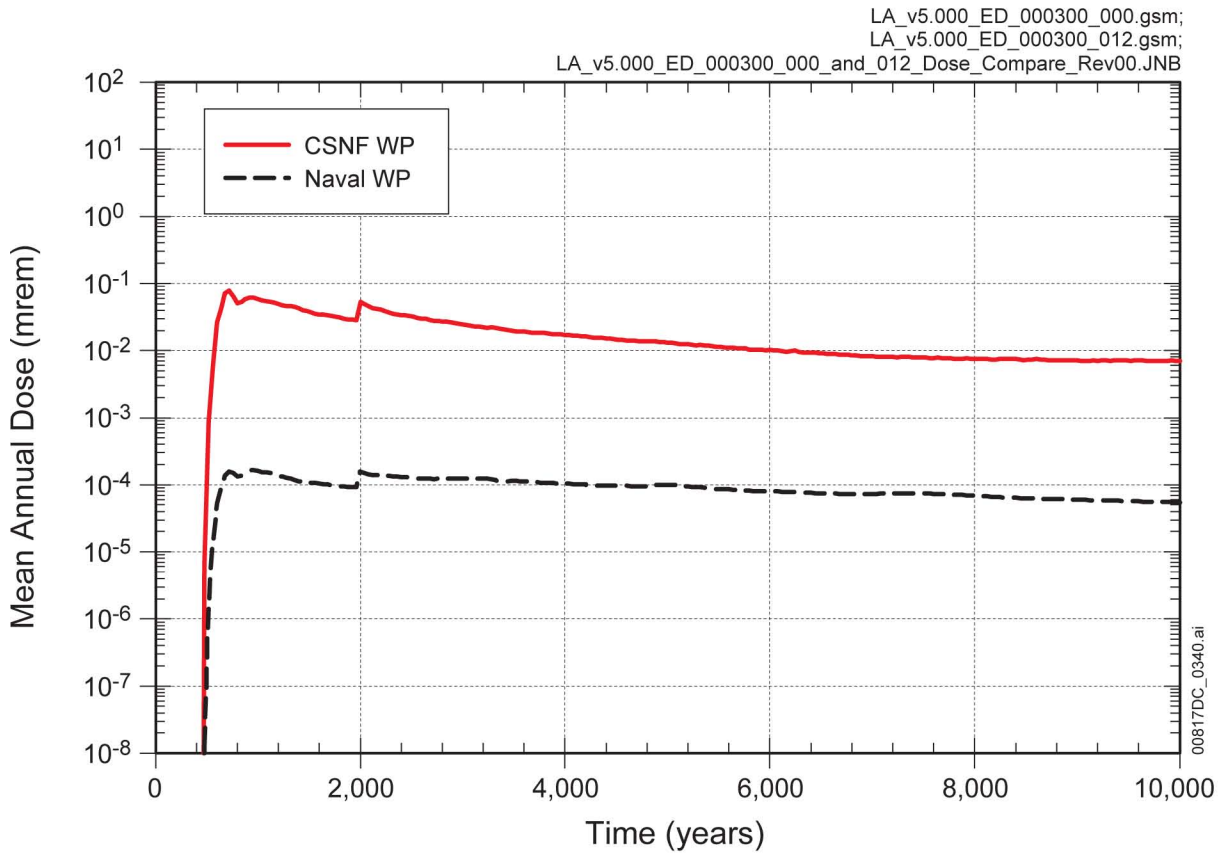

Source: Output DTN: MO0707NAVYFUEL.000 [DIRS 182991].

Figure 7.5-4. Comparison of Mean Annual Dose for a Single CSNF WP and a Single Waste Package with a Naval Source Term for the Drip Shield Early Failure Modeling Case

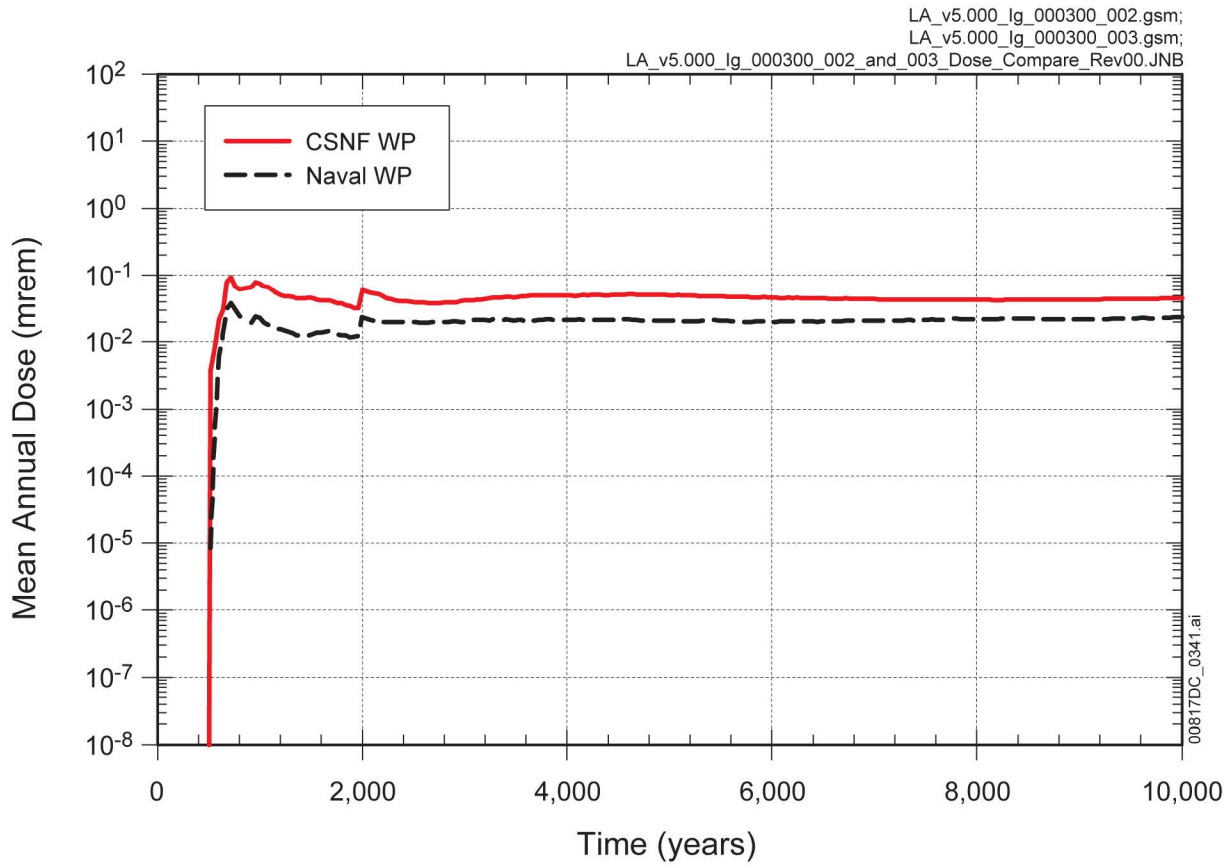

Source: Output DTN: MO0707NAVYFUEL.000 [DIRS 182991].

Figure 7.5-5. Comparison of Mean Annual Dose for a Single CSNF WP and Single Waste Package with a Naval Source Term for the Igneous Intrusion Modeling Case

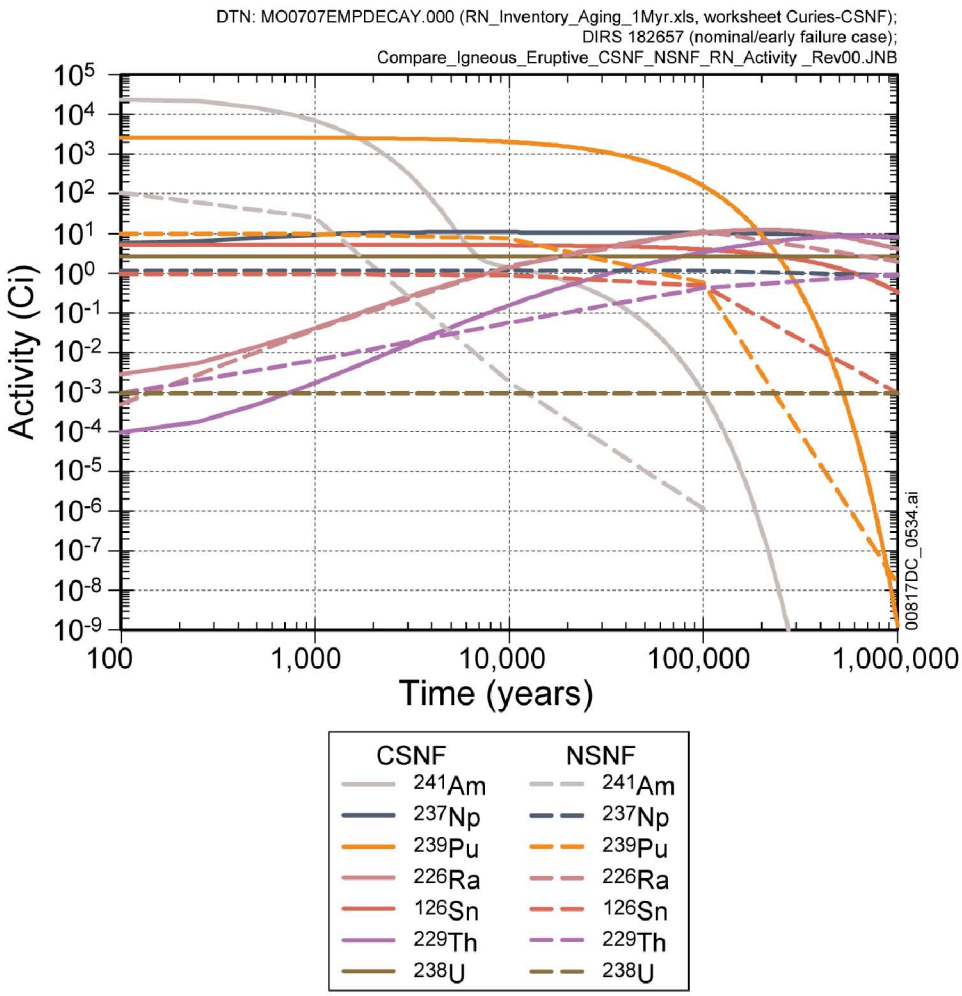

Sources: McKenzie 2007 [DIRS 182657] and Output DTN: MO0707EMPDECAY.000 [DIRS 183475], *FileRN_Inventory_Aging_1Myr.xls*, worksheet Curies-CSNF.

Figure 7.5-6. Comparison of Radionuclide Activities on a per Waste Package Basis for the Igneous NSNF and CSNF Inventories for the Radionuclides that are Major Contributors to the Volcanic Eruption Mean Annual Dose

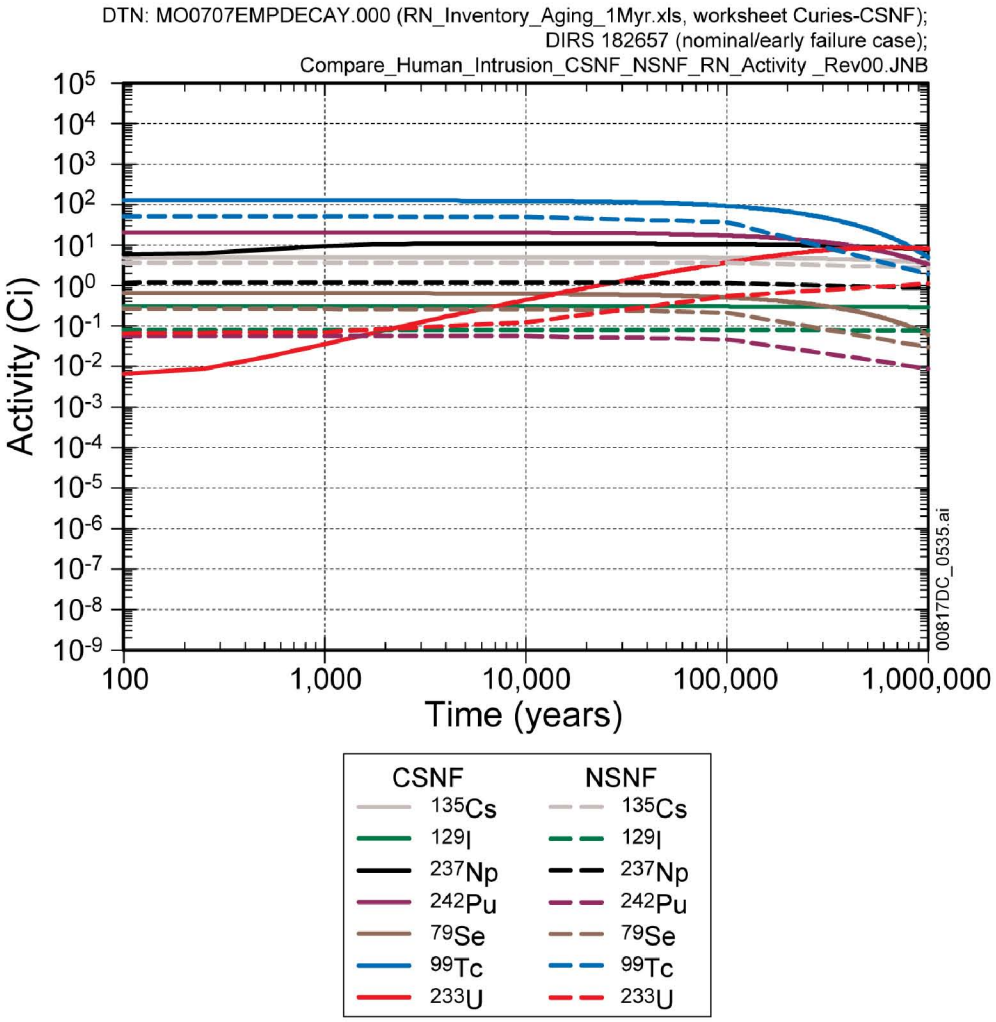

Sources: McKenzie 2007 [DIRS 182657] and Output DTN: MO0707EMPDECAY.000 [DIRS 183475], *FileRN_Inventory_Aging_1Myr.xls*, worksheet Curies-CSNF.

Figure 7.5-7. Comparison of Radionuclide Activities on a per Waste Package Basis for the Igneous NSNF and CSNF Inventories for the Radionuclides that are Major Contributors to the Human Intrusion Mean Annual Dose

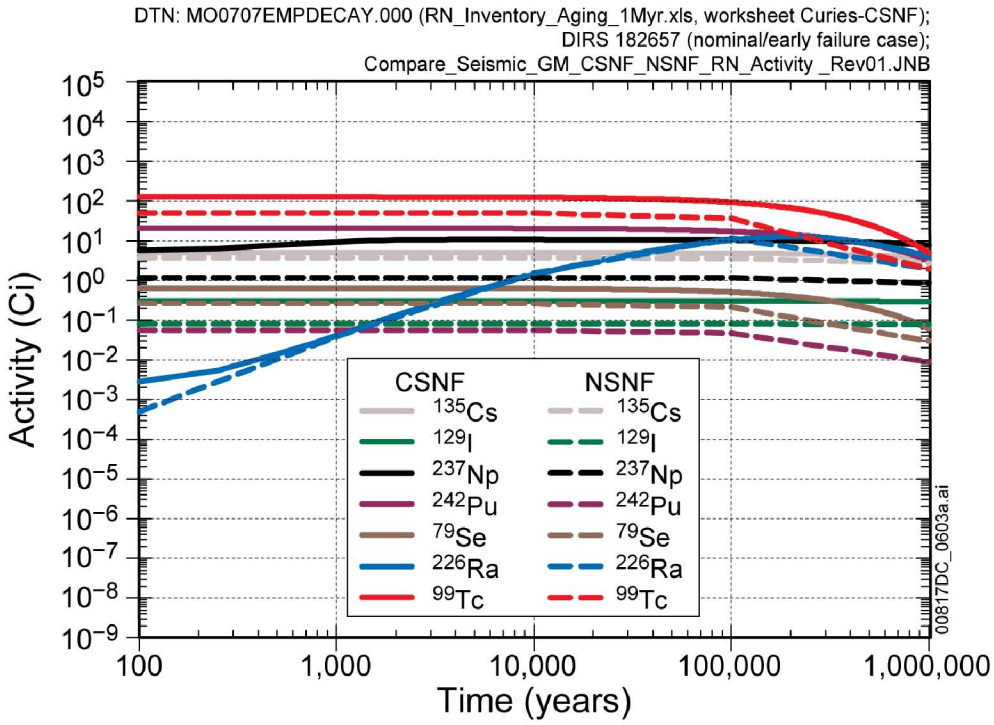

Sources: McKenzie 2007 [DIRS 182657] and Output DTN: MO0707EMPDECAY.000 [DIRS 183475], *FileRN_Inventory_Aging_1Myr.xls*, worksheet Curies-CSNF.

Figure 7.5-8. Comparison of Radionuclide Activities on a per Waste Package Basis for the Igneous NSNF and CSNF Inventories for the Radionuclides that are Major Contributors to the Seismic Ground Motion Mean Annual Dose

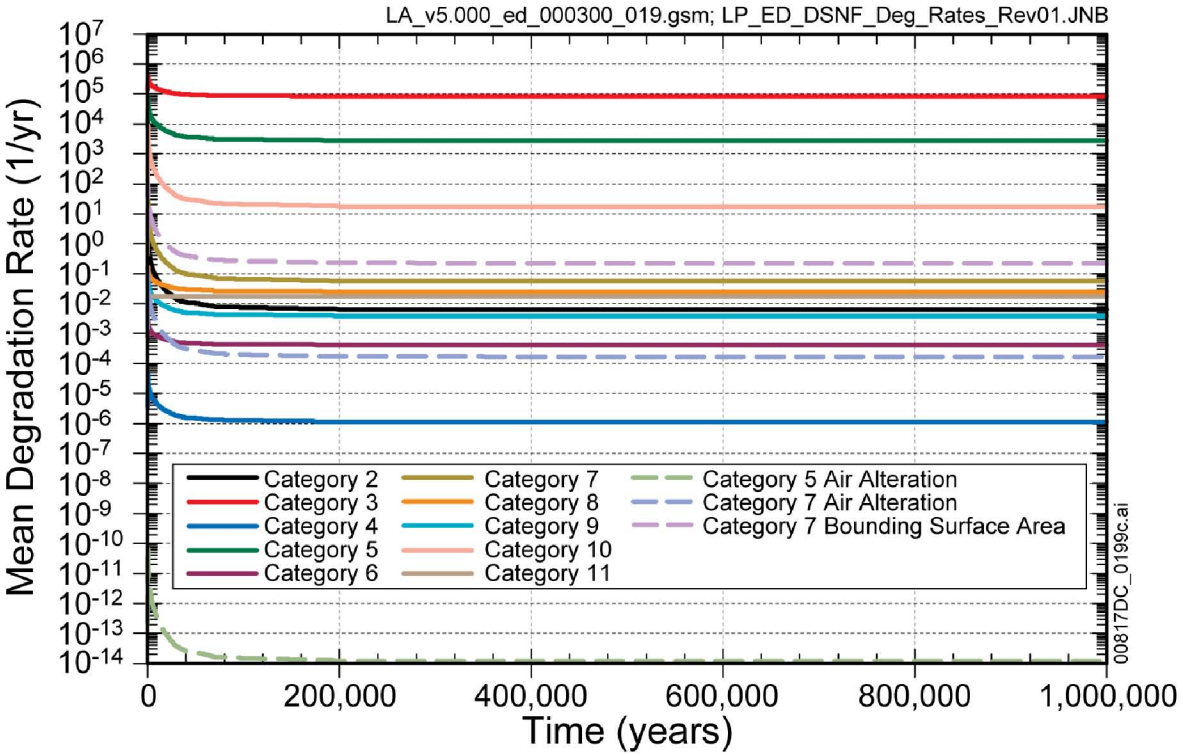

Source: Output DTN: MO0707TSPADSNF.000 [DIRS 182992].

Figure 7.5-9. Comparison of Mean Spent Fuel Degradation Rates for Categories 2 to 11, Air Alteration Rates for Categories 5 and 7, and Category 7 Bounding Surface Area of DSNF

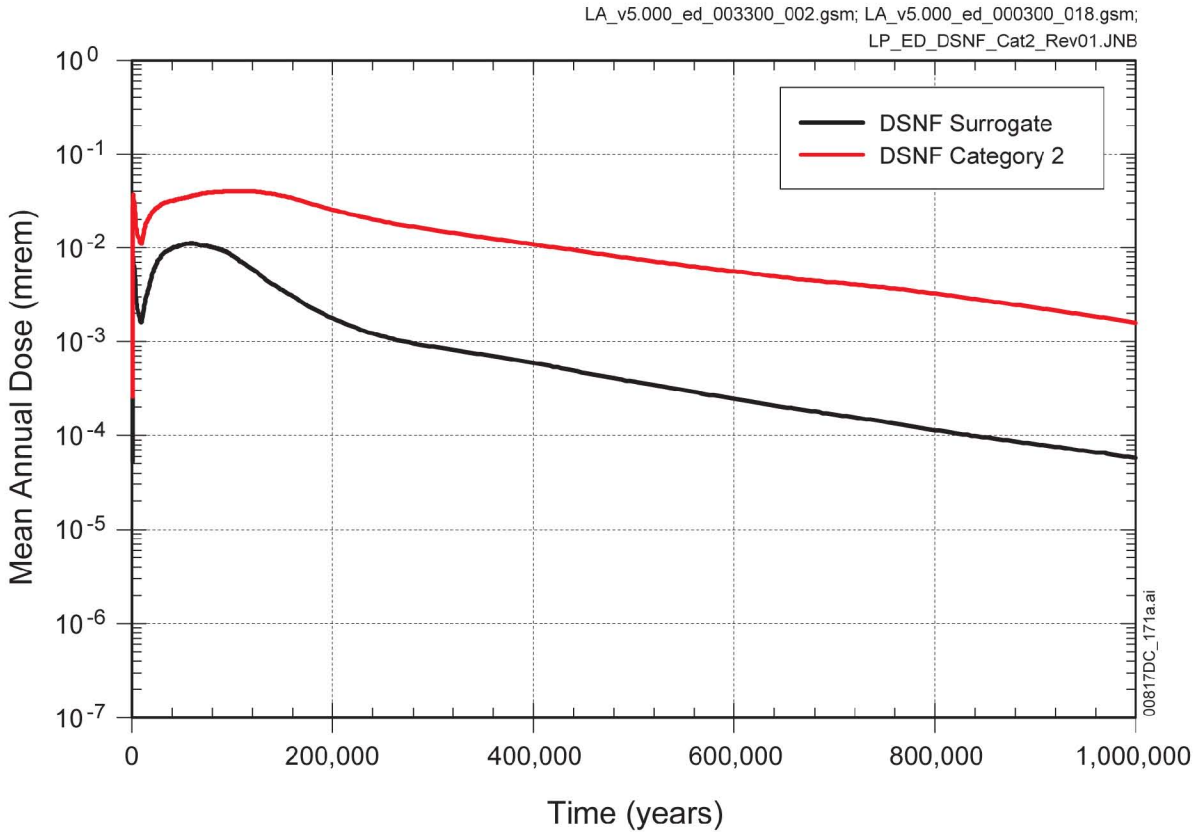

Source: Output DTN: MO0707TSPADSNF.000 [DIRS 182992].

Figure 7.5-10. Comparison of Mean Annual Dose from the Failure of One Waste Package of Plutonium/Uranium Alloy Spent Fuel (Category 2) with One Waste Package of DSNF Surrogate (with no HLW)

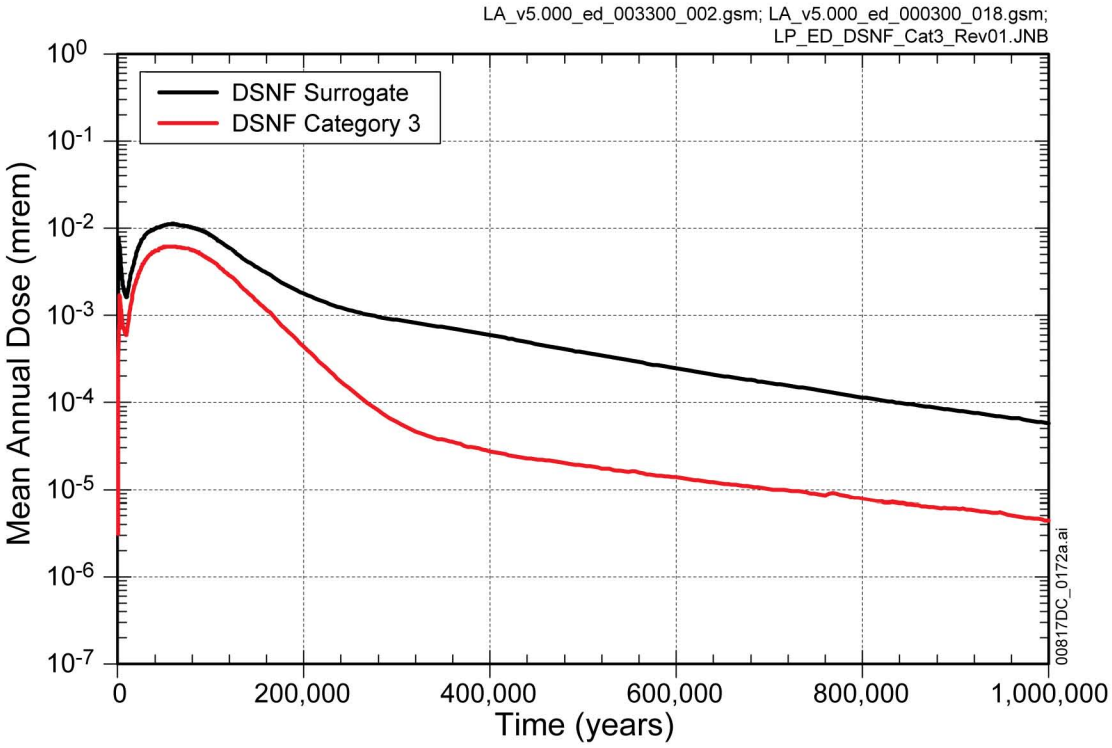

Source: Output DTN: MO0707TSPADSNF.000 [DIRS 182992].

Figure 7.5-11. Comparison of Mean Annual Dose from the Failure of One Waste Package of Plutonium/Uranium-Carbide Spent Fuel (Category 3) with One Waste Package of DSNF Surrogate (with no HLW)

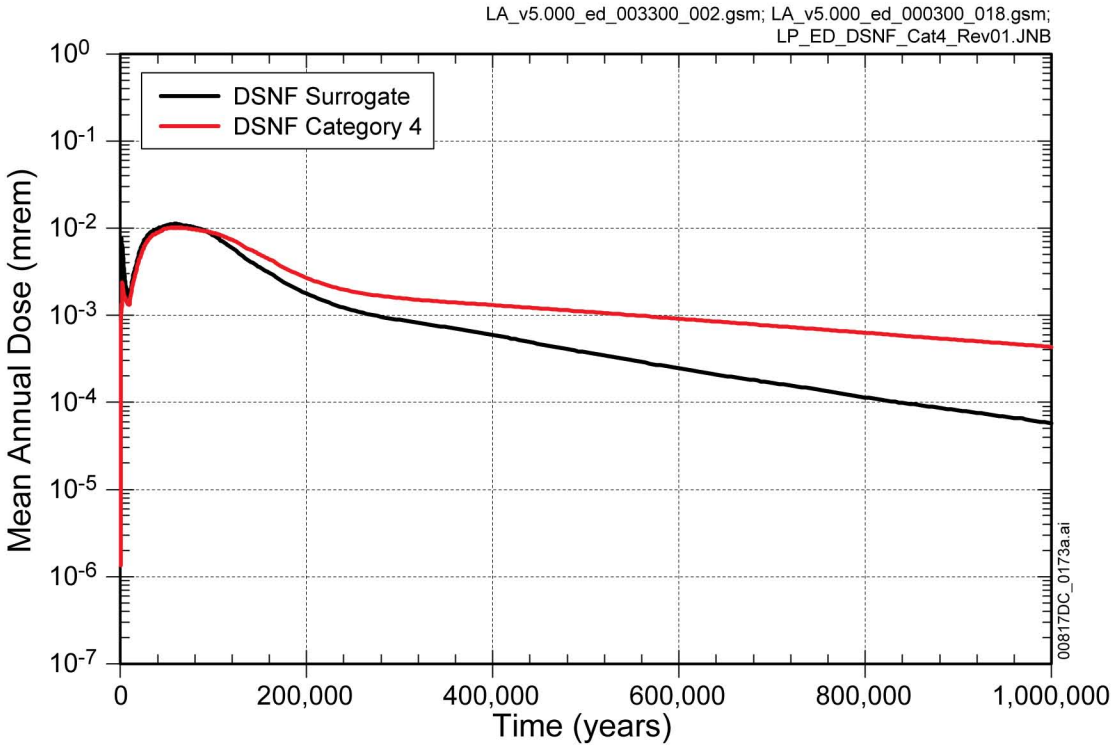

Source: Output DTN: MO0707TSPADSNF.000 [DIRS 182992].

Figure 7.5-12. Comparison of Mean Annual Dose from the Failure of One Waste Package of Mixed Oxide Spent Fuel (Category 4) with One Waste Package of DSNF Surrogate (with no HLW)

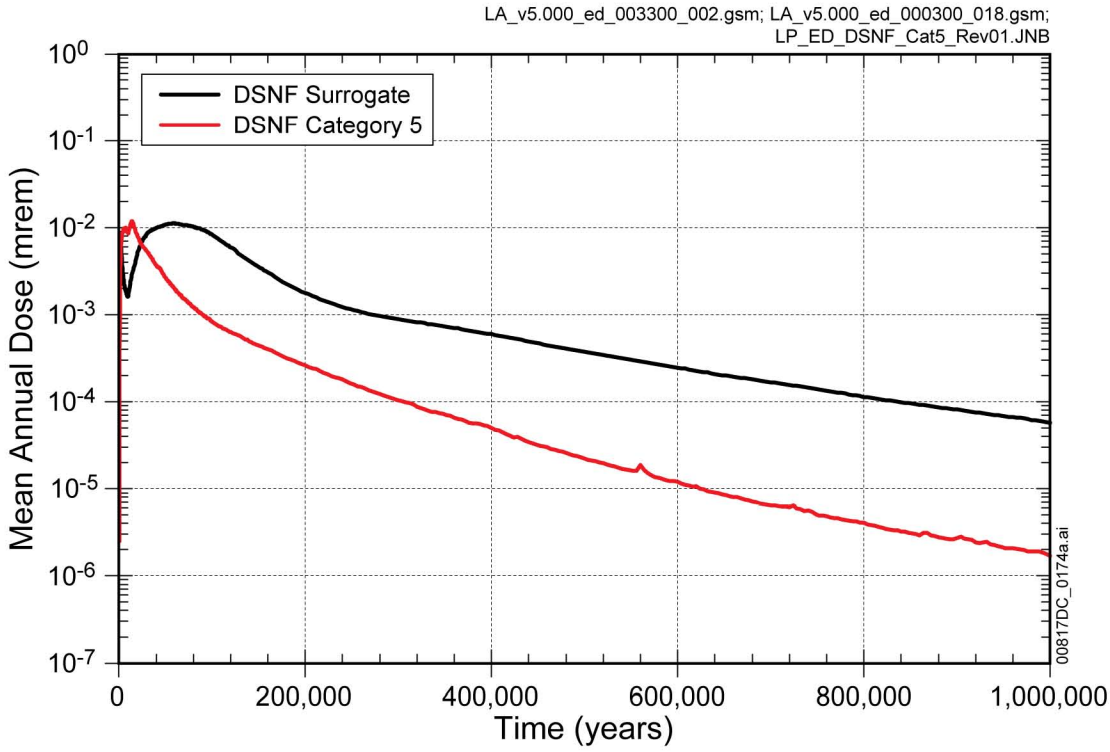

Source: Output DTN: MO0707TSPADSNF.000 [DIRS 182992].

Figure 7.5-13. Comparison of Mean Annual Dose from the Failure of One Waste Package of Uranium/Thorium-Carbide Spent Fuel (Category 5) with One Waste Package of DSNF Surrogate (with no HLW)

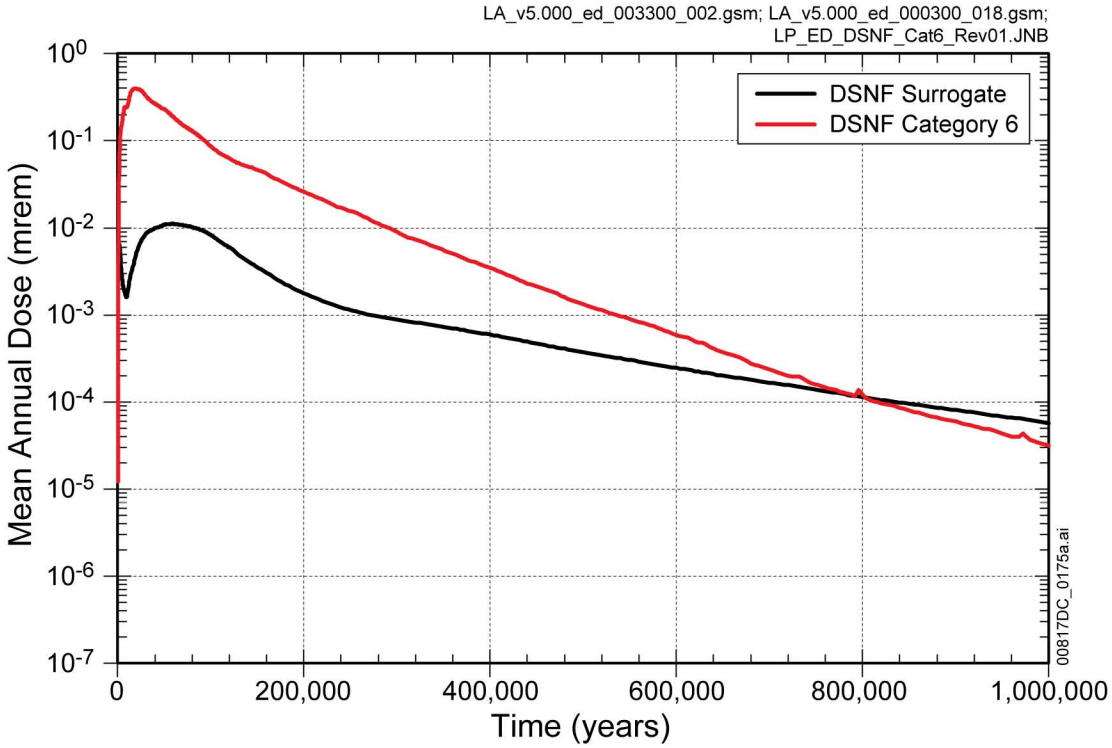

Source: Output DTN: MO0707TSPADSNF.000 [DIRS 182992].

Figure 7.5-14. Comparison of Mean Annual Dose from the Failure of One Waste Package of Uranium/Thorium-Oxide Spent Fuel (Category 6) with One Waste Package of DSNF Surrogate (with no HLW)

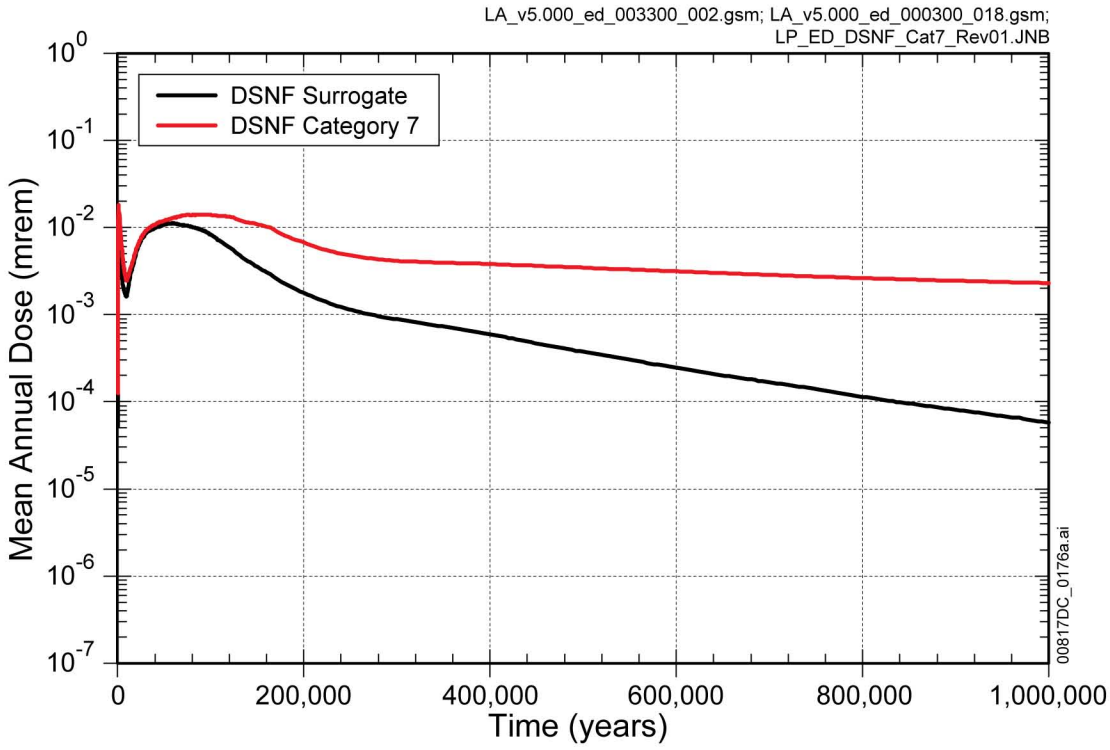

Source: Output DTN: MO0707TSPADSNF.000 [DIRS 182992].

Figure 7.5-15. Comparison of Mean Annual Dose from the Failure of One Waste Package of Uranium-Metal Spent Fuel (Category 7) with One Waste Package of DSNF Surrogate (with no HLW)

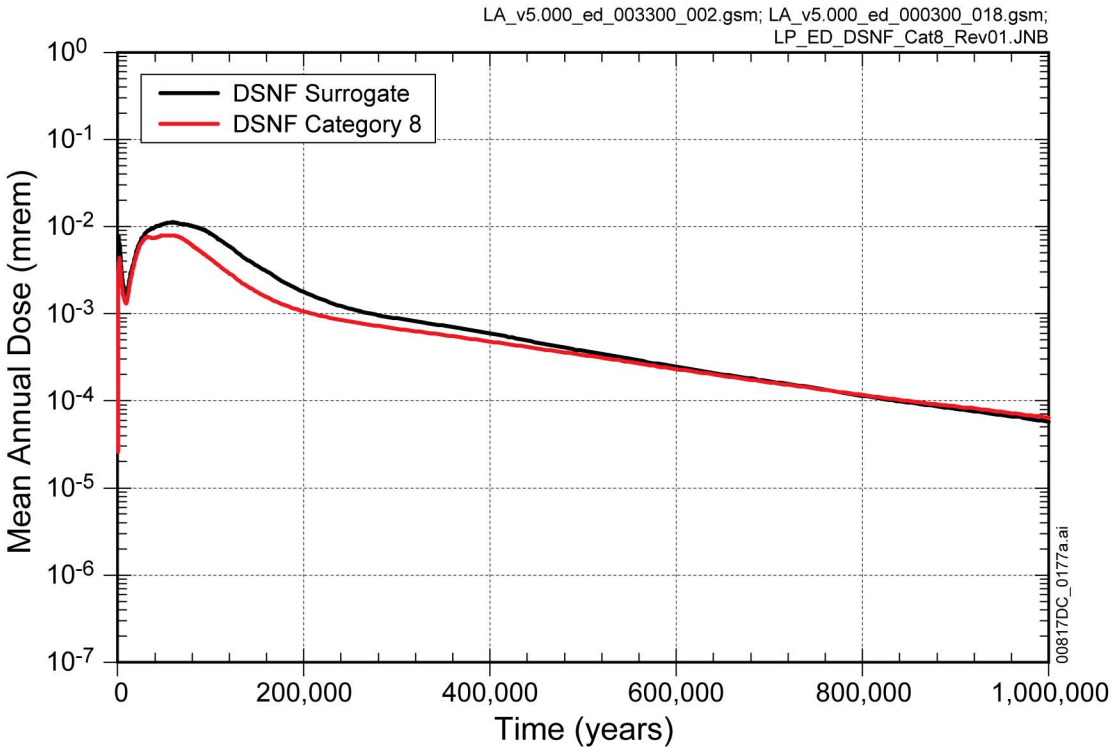

Source: Output DTN: MO0707TSPADSNF.000 [DIRS 182992].

Figure 7.5-16. Comparison of Mean Annual Dose from the Failure of One Waste Package of Uranium-Oxide Spent Fuel (Category 8) with One Waste Package of DSNF Surrogate (with no HLW)

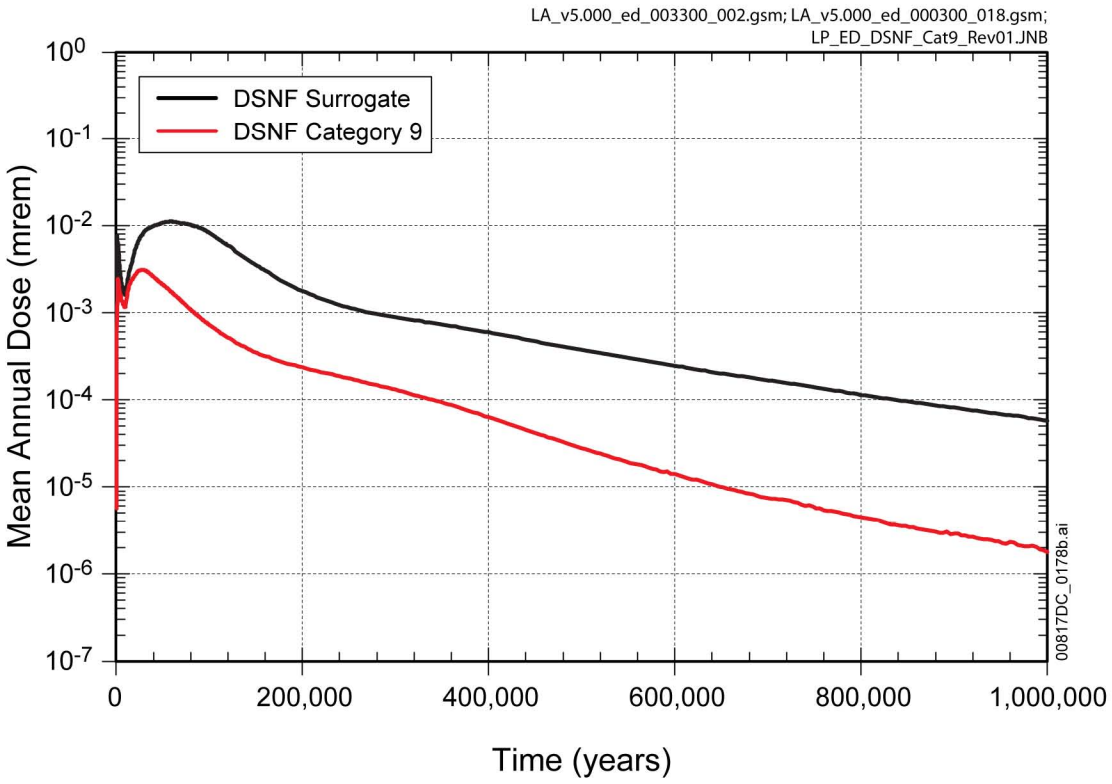

Source: Output DTN: MO0707TSPADSNF.000 [DIRS 182992].

Figure 7.5-17. Comparison of Mean Annual Dose from the Failure of One Waste Package of Aluminum-Based Spent Fuel (Category 9) with One Waste Package of DSNF Surrogate (with no HLW)

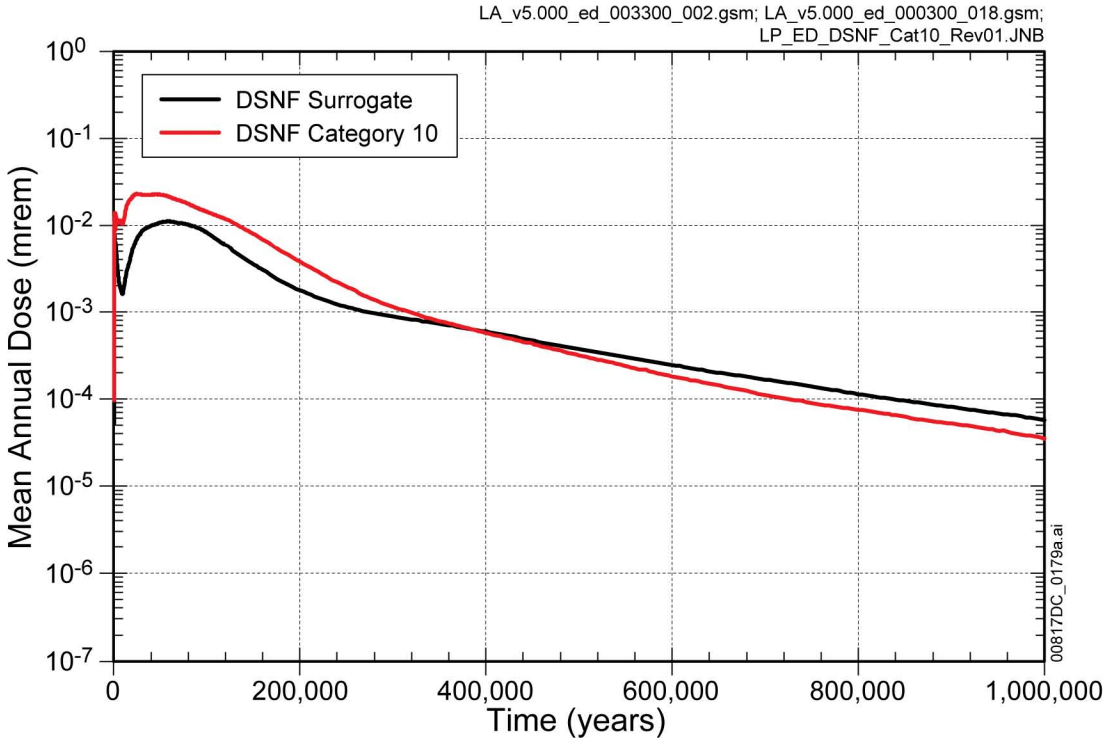

Source: Output DTN: MO0707TSPADSNF.000 [DIRS 182992].

Figure 7.5-18. Comparison of Mean Annual Dose from the Failure of One Waste Package of Miscellaneous Spent Fuel (Category 10) with One Waste Package of DSNF Surrogate (with no HLW)

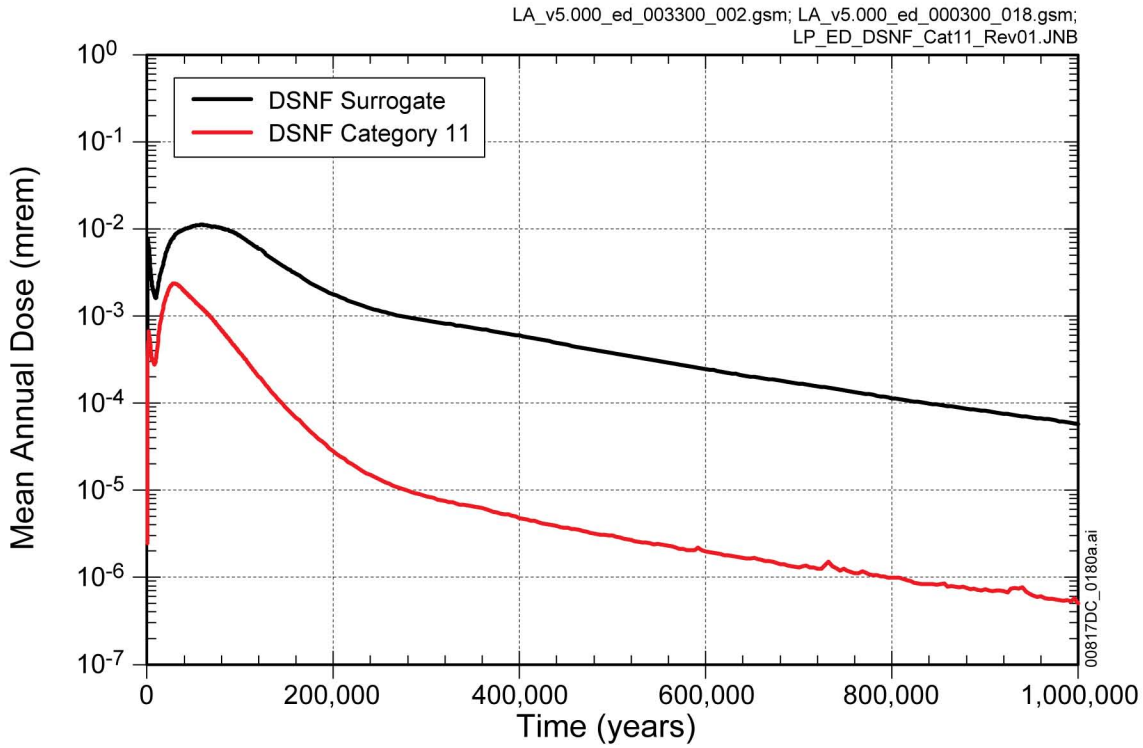

Source: Output DTN: MO0707TSPADSNF.000 [DIRS 182992].

Figure 7.5-19 Comparison of Mean Annual Dose from the Failure of One Waste Package of Uranium-Zirconium Hydride Spent Fuel (Category 11) with One Waste Package of DSNF Surrogate (with no HLW)

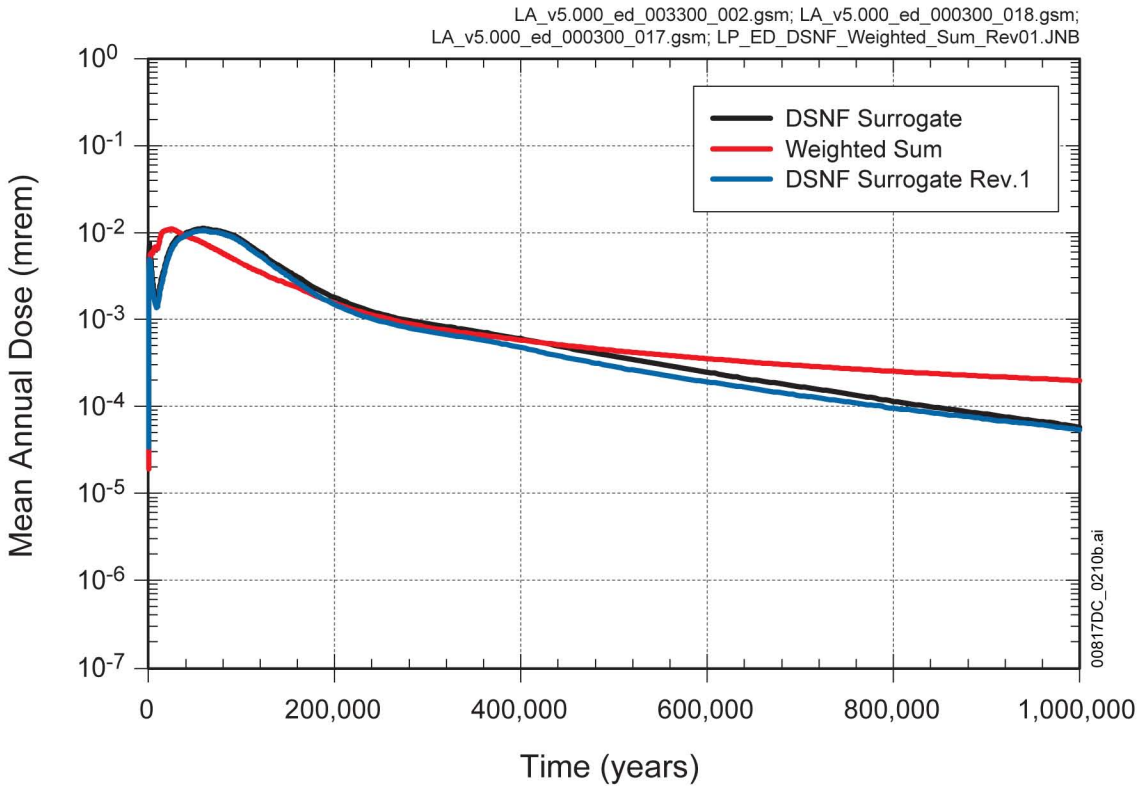

Source: Output DTN: MO0707TSPADSNF.000 [DIRS 182992].

Figure 7.5-20. Comparison of the Weighted Sum (weighted by the number of packages per category) of the Mean Annual Dose from One Waste Package Failure of Categories 2 to 11 DSNF with One Waste Package Failure of DSNF Surrogate and Revision 1 DSNF Surrogate

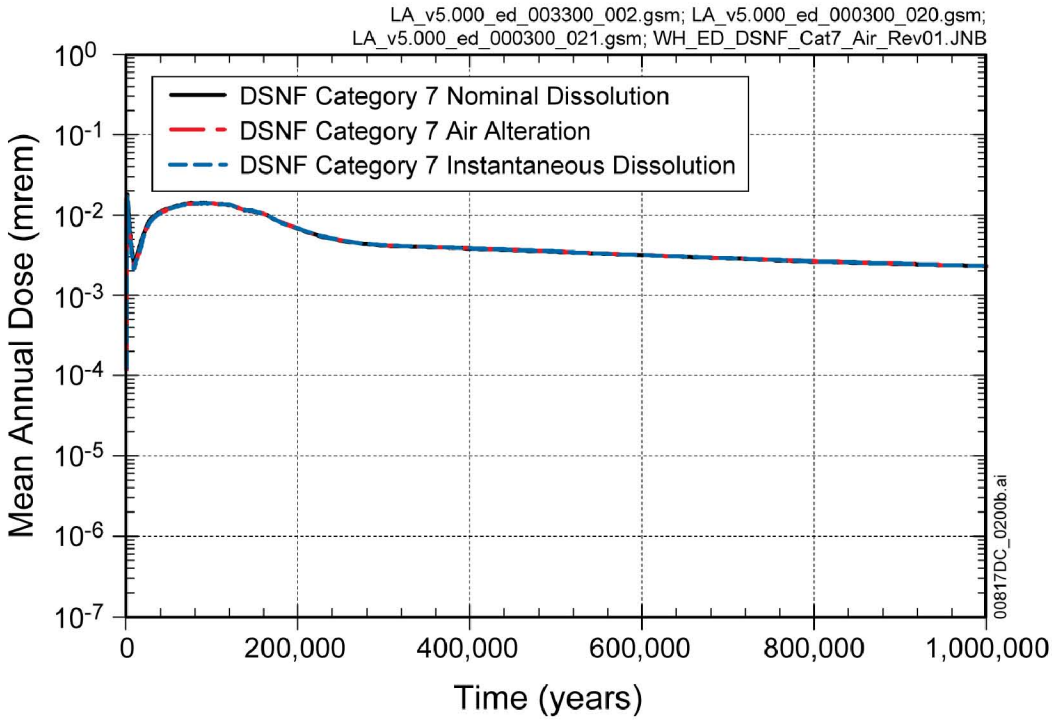

Source: Output DTN: MO0707TSPADSNF.000 [DIRS 182992].

NOTE: Lines plot on top of one another, making colors slightly indistinguishable.

Figure 7.5-21. Comparison of Mean Annual Dose from One Waste Package Failure of Uranium-Metal DSNF (Category 7) Using the Nominal Dissolution Model, Uranium-Metal Dissolution Model with Air Alteration, and Instantaneous Dissolution (with no HLW)

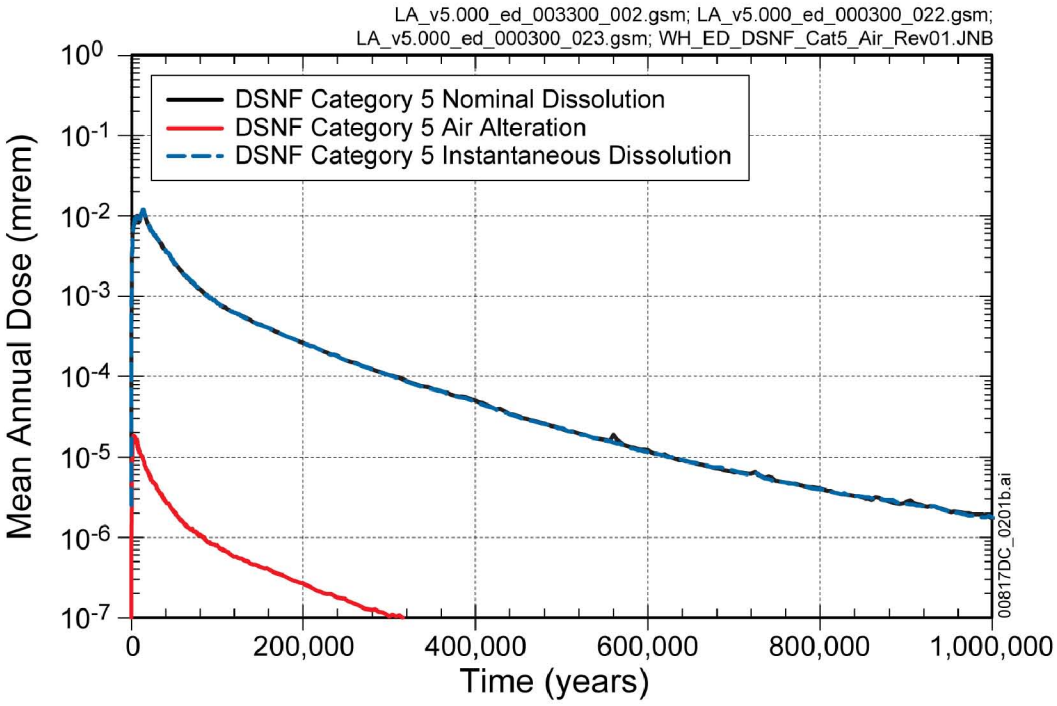

Source: Output DTN: MO0707TSPADSNF.000 [DIRS 182992].

NOTE: Lines plot on top of one another, making colors slightly indistinguishable.

Figure 7.5-22. Comparison of Mean Annual Dose from One Waste Package Failure of Uranium/Thorium-Carbide DSNF (Category 5) Using the Nominal Dissolution Model, Uranium/Thorium-Carbide Dissolution Model with Air Alteration, and Instantaneous Dissolution (with no HLW)

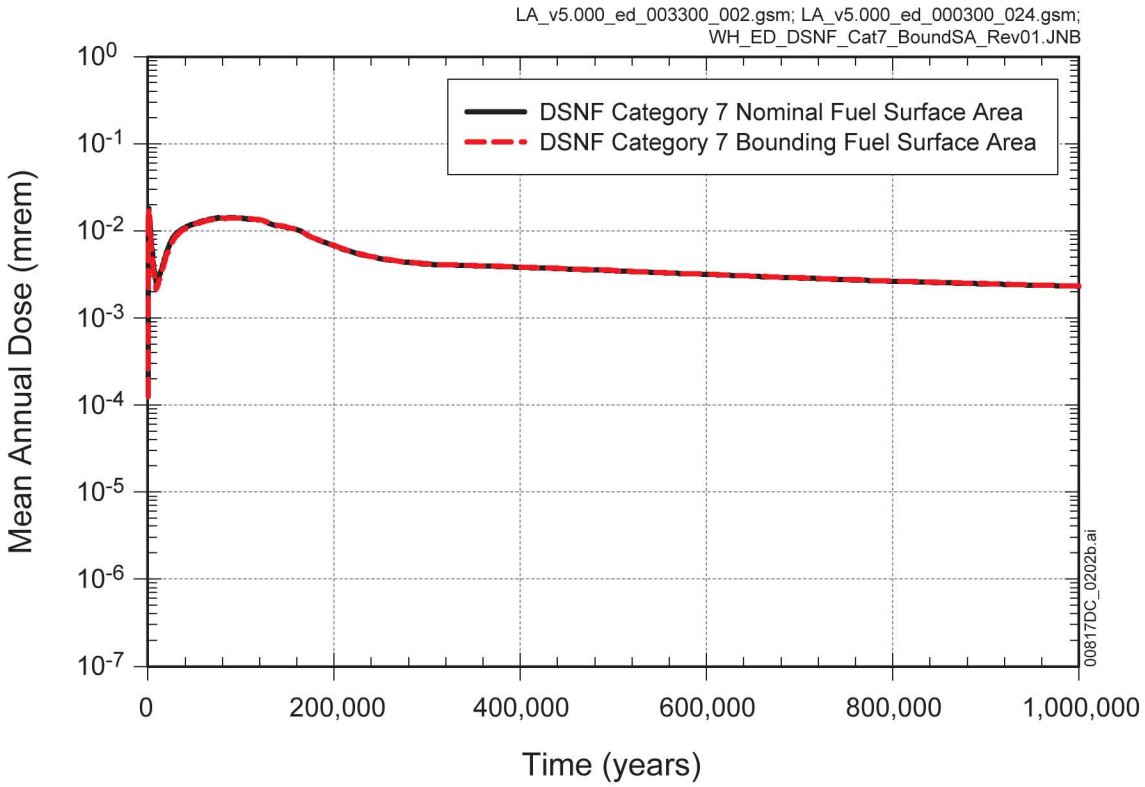

Source: Output DTN: MO0707TSPADSNF.000 [DIRS 182992].

NOTE: Lines plot on top of one another, making colors slightly indistinguishable.

Figure 7.5-23. Comparison of Mean Annual Dose from One Waste Package Failure of Uranium-Metal DSNF (Category 7) Using the Nominal Fuel Surface Area with the Bounding Fuel Surface Area (with no HLW)

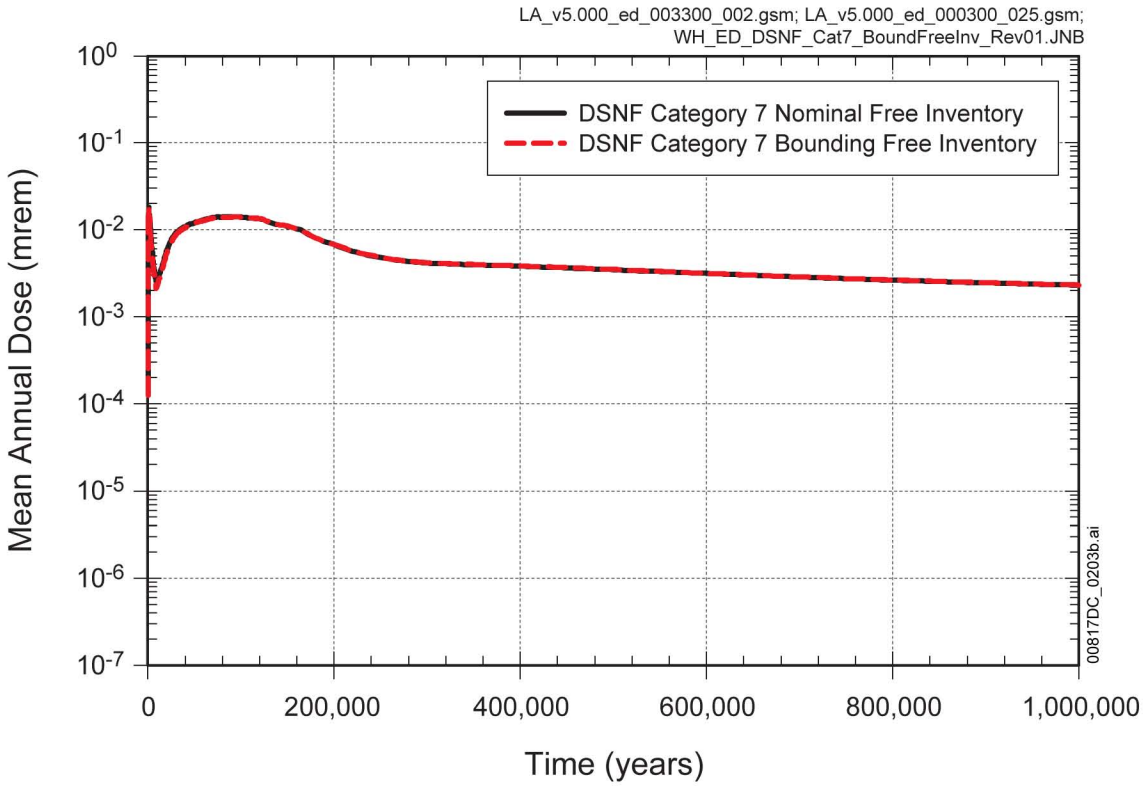

Source: Output DTN: MO0707TSPADSNF.000 [DIRS 182992].

NOTE: Lines plot on top of one another, making colors slightly indistinguishable.

Figure 7.5-24. Comparison of Mean Annual Dose from One Waste Package Failure of Uranium-Metal DSNF (Category 7) Using the Nominal Free Inventory with the Bounding Free Inventory (with no HLW)

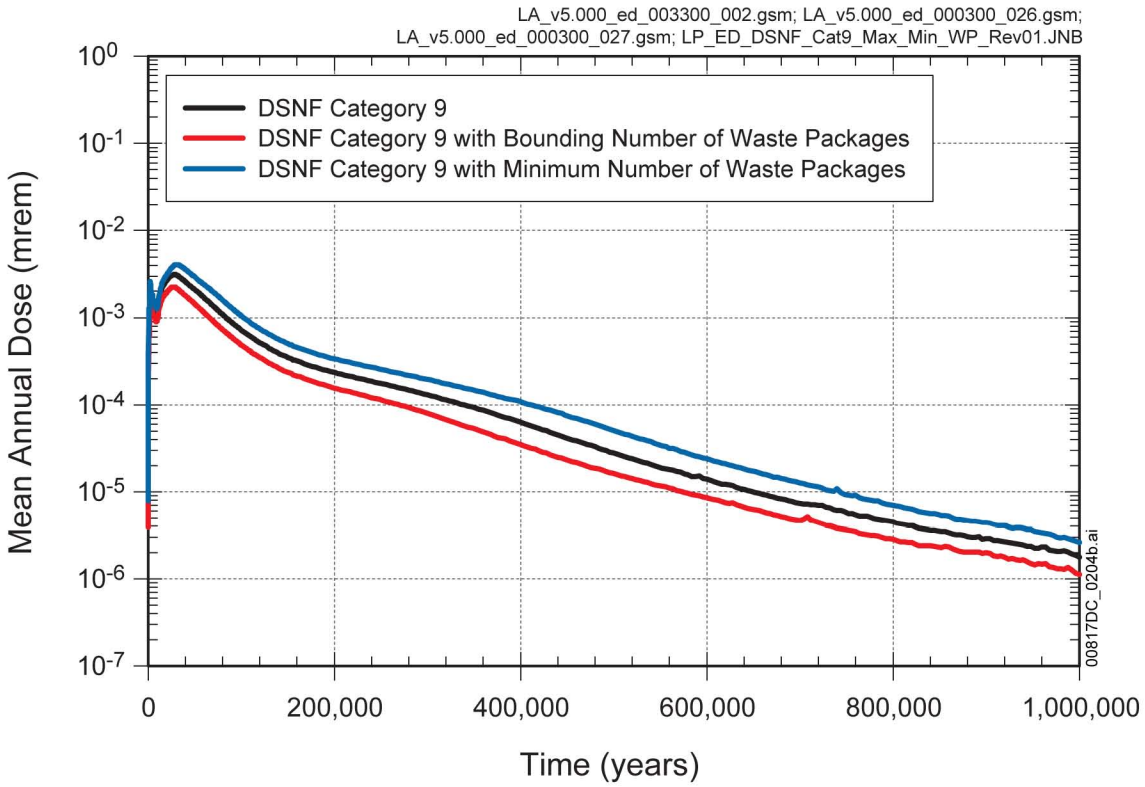

Source: Output DTN: MO0707TSPADSNF.000 [DIRS 182992].

Figure 7.5-25. Comparison of Mean Annual Dose from Aluminum-Based DSNF (Category 9) Minimum, Nominal, and Bounding Number of Waste Packages (with no HLW)

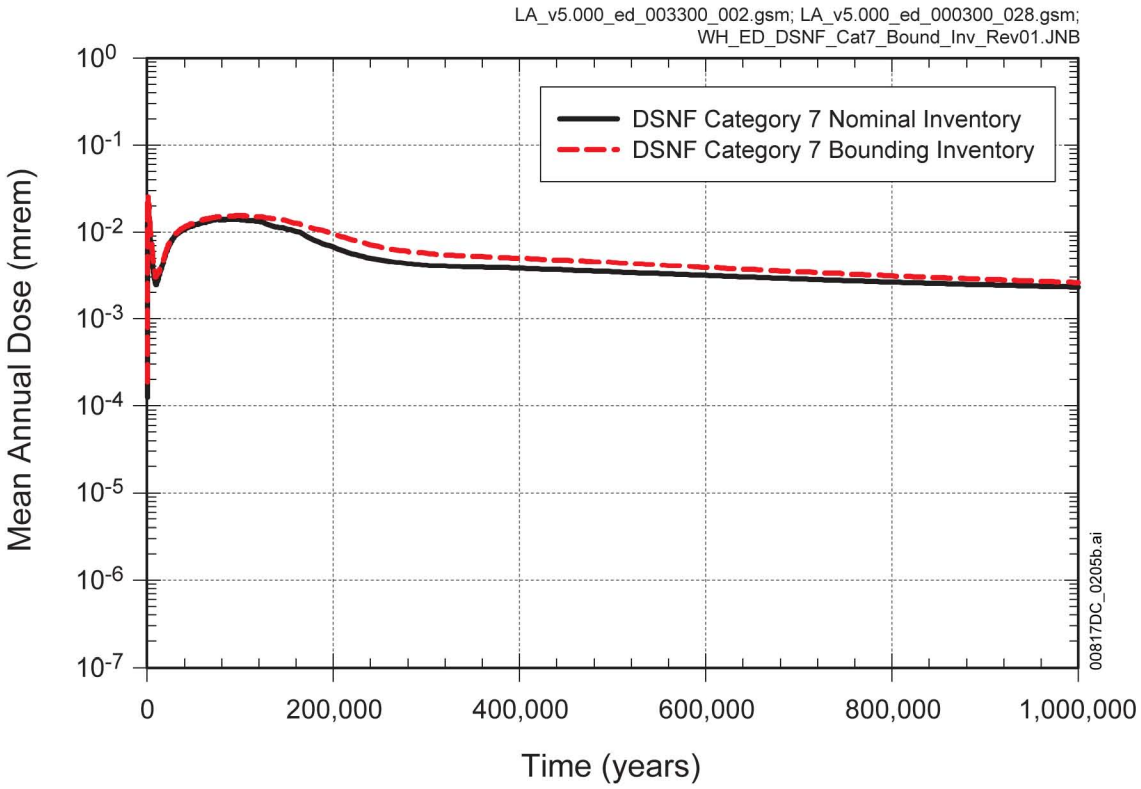

Source: Output DTN: MO0707TSPADSNF.000 [DIRS 182992].

Figure 7.5-26. Comparison of Mean Annual Dose from One Waste Package Failure of Uranium-Metal DSNF (Category 7) Using the Nominal Inventory with the Bounding Inventory (with no HLW)

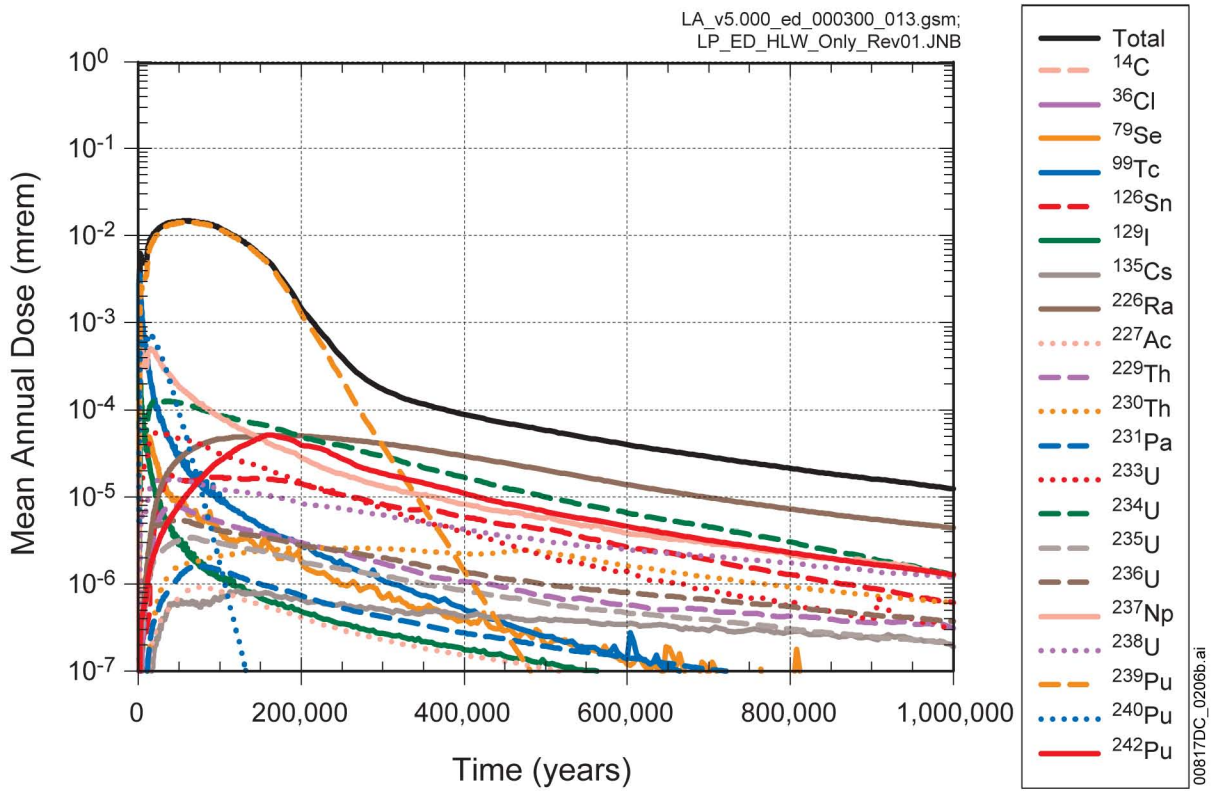

Source: Output DTN: MO0707TSPADSNF.000 [DIRS 182992].

NOTE: ^{226}Ra dose is the sum of ^{226}Ra and ^{210}Pb doses (secular equilibrium assumed).

Figure 7.5-27. Plot of Key Radionuclides that Contribute to Mean Annual Dose from Five Canisters of HLW (with no DSNF)

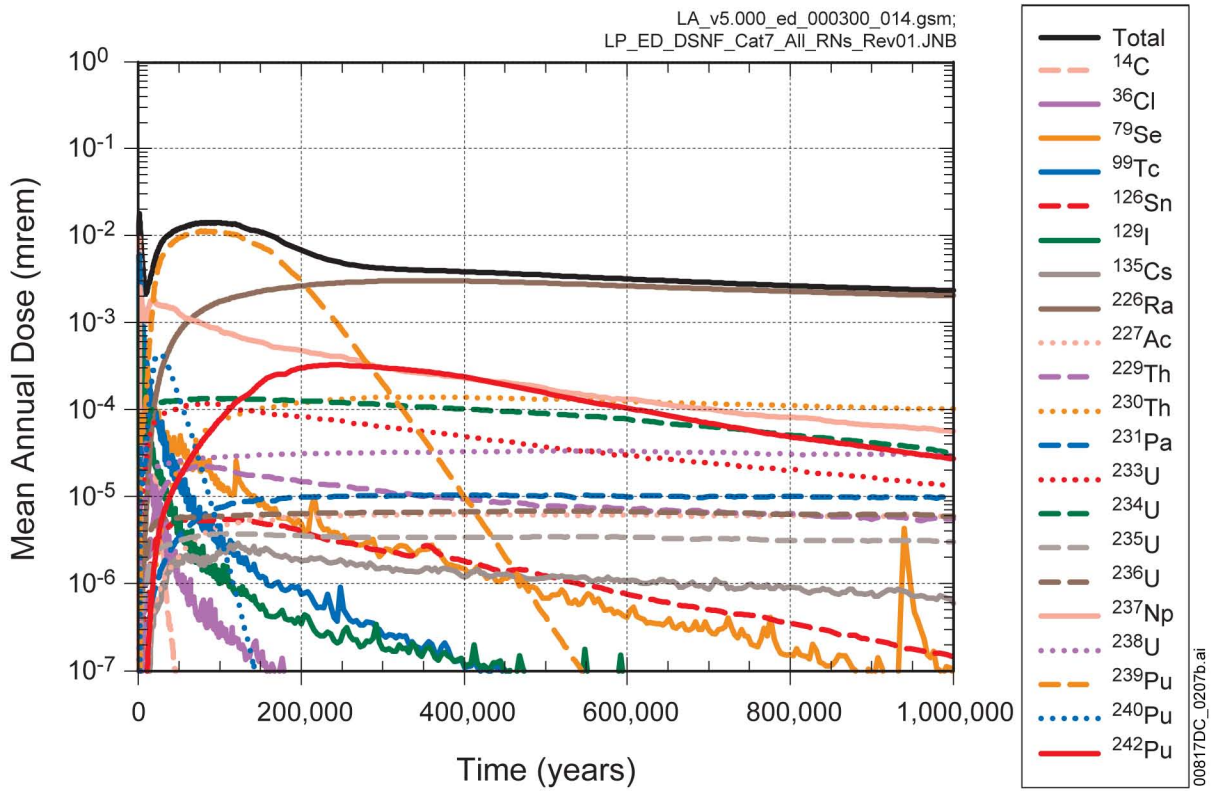

Source: Output DTN: MO0707TSPADSNF.000 [DIRS 182992].

NOTE: ^{226}Ra dose is the sum of ^{226}Ra and ^{210}Pb doses (secular equilibrium assumed).

Figure 7.5-28. Plot of Key Radionuclides that Contribute to Mean Annual Dose from One Waste Package Failure of Uranium-Metal Spent Fuel (Category 7) (with no HLW)

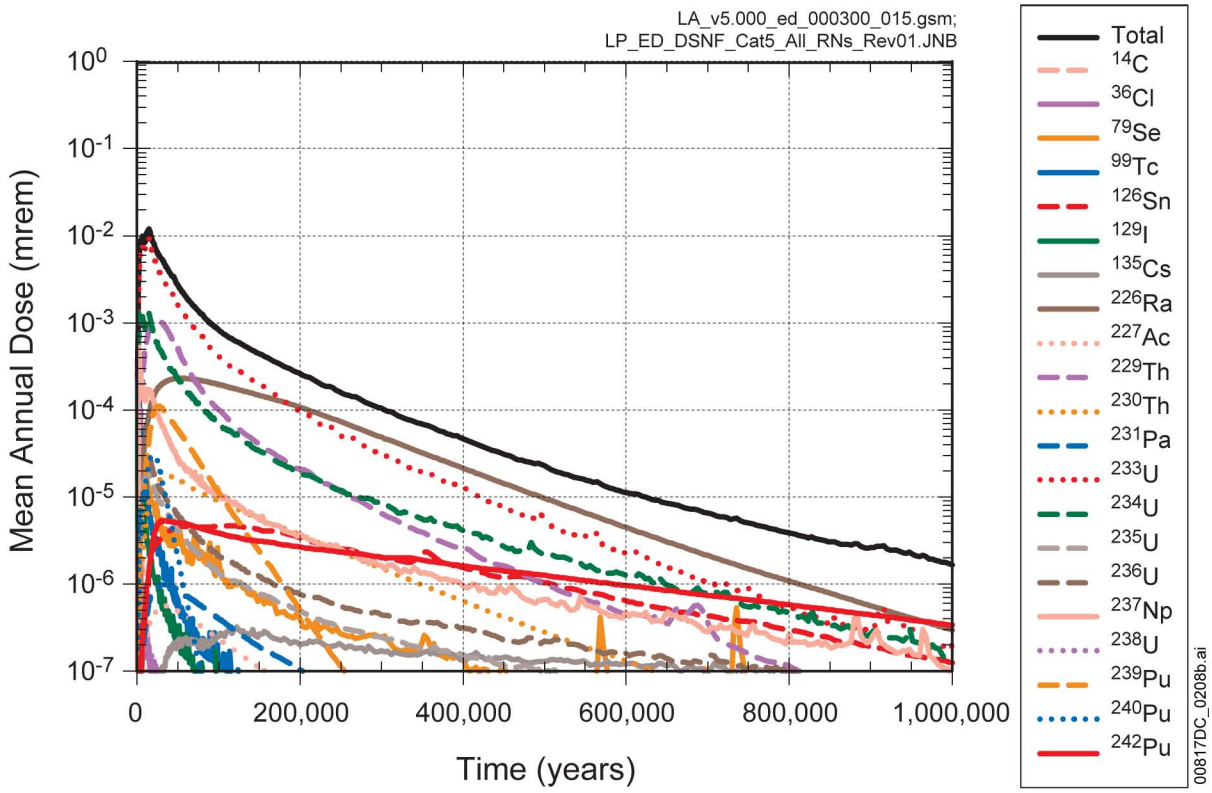

Source: Output DTN: MO0707TSPADSNF.000 [DIRS 182992].

NOTE: ^{226}Ra dose is the sum of ^{226}Ra and ^{210}Pb doses (secular equilibrium assumed).

Figure 7.5-29. Plot of Key Radionuclides that Contribute to Mean Annual Dose from One Waste Package Failure of Uranium/Thorium-Carbide Spent Fuel (Category 5) (with no HLW)

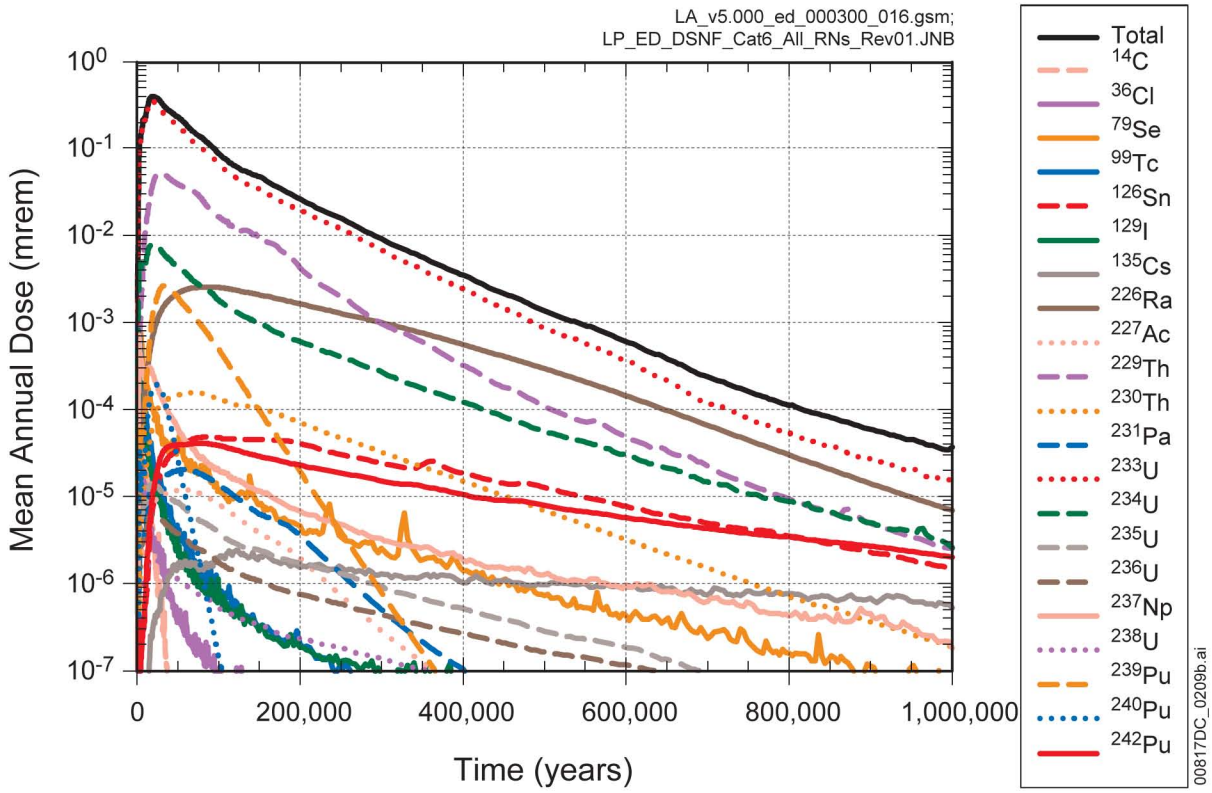

Source: Output DTN: MO0707TSPADSNF.000 [DIRS 182992].

NOTE: ^{226}Ra dose is the sum of ^{226}Ra and ^{210}Pb doses (secular equilibrium assumed).

Figure 7.5-30. Plot of Key Radionuclides that Contribute to Mean Annual Dose from One Waste Package Failure of Uranium/Thorium-Oxide Spent Fuel (Category 6) (with no HLW)

7.6 CORROBORATION OF ABSTRACTION MODEL RESULTS WITH VALIDATED PROCESS MODELS

Development of the TSPA-LA Model required abstraction of process models that serve as direct inputs and that provide parameter values as direct inputs to the TSPA-LA Model. SCI-PRO-006, *Models* lists corroboration of results of abstractions with their respective process models as one of nine post-development model validation criteria. For the TSPA-LA Model results to be valid, it is required that the abstractions are also accurately implemented in the TSPA-LA Model. Sections 7.2 (Computer Code and Input Verification) and 7.3 (Model Stability Testing) describe the implementation of the abstractions into the TSPA-LA Model. This section discusses the corroboration of the results of the abstractions with their respective process models and thus provides confidence that the TSPA-LA direct input parameters that were abstracted are technically sound for their intended purpose. The corroboration process provides the technical basis for the postclosure repository performance simulated by the TSPA-LA Model. Coupled with Table 7.6-1, this section summarizes the results of the corroboration, thus confirming that the TSPA-LA Model is based on technically defensible abstracted parameter values.

Section 7.6.1 provides a brief description of the processes used to develop the TSPA-LA Model. Section 7.6.2 describes the requirements and objectives for the verification of the model abstraction results. Section 7.6.3 explains the methods used in corroborating the abstraction model results, and the limitations associated with the results that are presented in Section 7.6.4.

7.6.1 Introduction

Figure 1-2 shows the key steps involved in the TSPA approach as four levels of a pyramid and the information flow and the feedback loops among the four levels. The foundation of the TSPA pyramid consists of a repository-system characterization involving the assimilation of the information collected in site characterization and engineering design activities. The repository system characterization entails data collection regarding waste properties and design of the repository facilities, as well as the regional geology, hydrology, and environmental characteristics of the Yucca Mountain site. The foundation of the pyramid represents more than a 20-year body of knowledge collected in the field, laboratory, and the design basis of the repository system.

The accumulated body of knowledge constitutes the technical database that was used to identify the set of possible FEPs that may affect the performance of the repository system after the repository closure and also provides the basis for the second stage of the TSPA pyramid; that is, development of conceptual models and process models (Figure 1-2). The TSPA-LA Model is built on the family of analyses of the identified FEPs, including analyses related to the exclusion of FEPs that are either very unlikely, are not required for regulatory reasons, or that have a low impact on performance. The second stage of the TSPA pyramid consists of the development and testing of models used to conceptually describe the retained probable FEPs and their outcomes regarding repository performance. The conceptual models consist of sets of hypotheses, assumptions, simplifications, and idealizations, which together describe the essential aspects of a system or subsystem of the repository relative to its performance. Model conceptualization identifies and selects FEPs that collectively comprise the scenarios (Section 1.5) considered in the conceptual models. The second stage of the TSPA pyramid (Figure 1-2) includes the

development of mathematical representations of the conceptual models of the FEPs or scenarios, or both, that contribute to overall repository performance.

The TSPA-LA Model includes a numerical representation of water flow through Yucca Mountain as an abstraction (Figure 7.1-1) consisting of a series of statistical or mathematical expressions, including look-up tables, equations representing response surfaces, probability distributions, linear transfer functions, or reductions of model dimensionality. Inputs developed by the abstraction process were either implemented directly into the TSPA-LA Model or through a series of simplifying steps, depending upon the relative complexity and/or importance of the FEPs being abstracted. This abstraction, or progressive simplification of the conceptual models to more compact and usable numerical models, is the essence of the third level of the TSPA pyramid. The models used to analyze the projected evolution through time of the various components of the repository system are abstracted models that capture the salient features of the process models, along with their associated uncertainties. The top level of the TSPA pyramid consists of the integrated total system model. The total system model is a numerical model used to simulate the behavior of the Yucca Mountain repository system. The TSPA-LA Model incorporates the abstracted process models and/or the results of analyses that describe the model components and their submodels from their development to their implementation.

7.6.2 Requirement and Objective

An abstraction is a quantitative simplification process required for the numerical implementation of the process models in the TSPA Model computation using a complex and integrated computer code such as GoldSim, which is used for computation of the TSPA-LA Model. It is essential, therefore, to ensure that the abstraction results corroborated by the underlying process model results. The abstractions quantitatively represent their respective process models before and after their implementation in the TSPA-LA Model. When the abstractions are applied together as the integral components of the TSPA-LA Model, they function coherently so that the TSPA-LA Model results are stable, and properly represent the contributing abstractions. This consistency is achieved by performing several steps: (1) ensuring that the individual abstractions are validated after abstraction for their intended use in the TSPA-LA Model, (2) performing input-verification activities during their implementation in the TSPA-LA Model, and (3) testing model stability during the model development process.

The abstractions and their underlying process models are validated during their individual development and post-development validation phases described in SCI-PRO-006. These validation activities and their results are documented in analysis and model reports. As a means of validating the abstractions, their results were corroborated with their underlying process models. Validated process models themselves feed the TSPA-LA Model when appropriate without further abstraction. The process models that served as the sources of the input parameters to the TSPA-LA Model are listed in Table 4-1. The input parameters are in the Parameter Entry Forms (PEFs) listed in Table 4-1. These inputs are referred to as direct input in Table 4-1 to reflect the fact that the process models that provide the inputs are supported by validated submodels. During implementation in the TSPA-LA Model development process, the integrity of the direct input models or analyses is ensured by performing: (1) independent checks to ensure that the direct inputs are accurately applied in the TSPA Model runs, and (2) independent verification, such as model re-runs, to confirm that the inputs produce the result

that is expected. These checking and verification activities are documented controlled processes. The verification activities are summarized in Section 7.1.2.1, and a detailed discussion of the verification analyses performed is provided in Section 7.2. The checking and verification activities ensure that the TSPA-LA Model is built with the inputs from the abstractions that have been accurately implemented. The development phase also involves determining whether or not the abstractions, when applied together as the integral components of the TSPA-LA Model, function coherently and provide stable TSPA-LA Model results. The TSPA-LA Model stability testing activities are summarized in Section 7.1.2.2 and discussed in Section 7.3.

Once the integrity of the implementation of the abstractions in the TSPA-LA Model is ensured through the verification process, and it is clear that the individual abstractions are functioning well when they are applied together as components of the TSPA-LA Model, certain post-development model validation and confidence building activities unrelated to the development of the TSPA-LA Model need to be performed in order to show that the TSPA-LA Model is valid for its intended use.

Ensuring the integrity of the direct-input models during abstraction and successful application of the abstractions to the TSPA-LA Model is the first step towards defining and executing these follow-up post-development validation and confidence building activities. The TSPA-LA Technical Work Plan (SNL 2008 [DIRS 184920], Section 2.3.5.2) identified corroboration of abstraction model results with validated process models as a TSPA-LA Model validation method in order to document in the TSPA-LA Model report that the results of the abstractions corroborate the results of the respective underlying process models. To accomplish this confirmation, corroboration of the abstraction results with those of the respective process models are evaluated in this section. The validation criterion, ensure that there is confidence in outputs from the models, and they are appropriate for their intended use in the TSPA-LA Model. The information on validation and the basis for confidence in the model outputs to the TSPA-LA Model are included in the discussion here and summarized in Table 7.6-1.

7.6.3 Methods Used

The model and analysis reports that were sources for the direct input parameters to the TSPA-LA Model are identified in Table 4-1. The functional relationships among these models and analyses as integral components of the TSPA-LA Model, and implementation of the parameters, are discussed in the individual subsections of Section 6 of the TSPA-LA Model report. The discussion here focuses on the corroboration of abstraction results with the underlying models and analyses that are referenced in Table 4-1 and Table 6-1. These references are cited in Table 7.6-1 as appropriate for transparency. As mentioned earlier, the direct input models are themselves usually based on a number of submodels and/or analyses. The submodels often need to be abstracted during their implementation in the models that serve as the direct input to the TSPA-LA Model. These submodels are not discussed here because their validation and confidence building activities and results are documented in the respective model or analysis reports. There are a few exceptions. For example, the UZ Site-Scale Process Model (SNL 2007 [DIRS 184614]), which is discussed here and shown in Table 7.6-1, is not a direct input. It is implemented in the TSPA-LA Model via the UZ Transport Model and MSTHM. However, the flow fields, rock properties, and percolation flux parameters from the UZ Site-Scale Process Model (SNL 2007 [DIRS 184614]) are parameters that form the basis for the predictions for

radionuclide transport in the UZ below the repository and the TH conditions in the repository. This relationship is shown on Figure 6.3.1-6. The validation and consistency of these models are presented in Section 7 of the respective model or analysis reports.

Table 7.6-1 shows the process models and analyses that served as direct input to the TSPA-LA Model computation are represented by the following groups: Natural System Environment, EBS Environment, Waste Form and Waste Package Degradation and Mobilization, Disruptive Events, and Biosphere.

The first column in Table 7.6-1 shows the general model area within individual groups. The second and the third columns identify the abstractions and the respective underlying process models or analyses. The column on the right in Table 7.6-1 provides the results. This column discusses the results of corroboration qualitatively, providing quantitative information when appropriate but mostly providing references to the figures and tables in the source model or analysis reports. A summary of the basis for the confidence in the output parameters used in the TSPA-LA Model preparation is also provided in the results column, again by largely deferring the detail to the cited respective source documents.

The results presented in the last column in Table 7.6-1 do not discuss the assumptions and uncertainties associated with the parameters from the abstractions and the underlying process models and analyses. The respective analysis reports describe the justifications of the assumptions and document the uncertainties of the output parameters. Assumptions used in the TSPA-LA Model are presented in Section 5. The treatment of uncertainty in the TSPA-LA Model is discussed in Section 6.1.3. The TSPA-LA parameter uncertainty characterization reviews and remedial actions on the findings are presented in Section 7.4. Appendix K discusses the uncertainty and sensitivity analyses conducted using the TSPA-LA Model. The auxiliary analyses presented in Section 7.7 provide confidence in the results of the TSPA-LA Model simulations based on the parameters from the direct input models and analyses discussed here.

7.6.4 Results of Corroboration

The following discussion focuses on the process models and the analyses that provide direct inputs to the TSPA-LA Model. The discussion follows the group sequence of Table 7.6-1: Natural System Environment, EBS Environment, Waste Form and Waste Package Degradation and Mobilization, Disruptive Events, and Biosphere.

7.6.4.1 Natural System Environment

This section presents results of corroboration of abstractions with the underlying validated process models of the natural system and provides information on the confidence built into the direct-input TSPA-LA Model parameters abstracted from these process models. The key models are on the UZ flow and SZ flow and transport processes.

7.6.4.1.1 UZ Flow Model

The model report that sources the input parameters on UZ flow to the TSPA-LA computation is *UZ Flow Models and Submodels* (SNL 2007 [DIRS 184614]).

Section 6.3.1 discusses implementation of the UZ flow model in the TSPA-LA Model. Figure 6.3.1-6 lists some activities on which the confidence in the output parameters from the UZ Site-Scale Flow Model is based. The details are provided in Section 7 of *UZ Flow Models and Submodels* (SNL 2007 [DIRS 184614]). The activities include corroborating the model-output parameters (hydrologic properties and percolation flux as inputs for the MSTHM and mountain-scale UZ flow fields as inputs for the UZ Transport Models). These parameters are shown in PEFs # 38, 39, 40, 42, and 43 in Table 4-1 with observations from numerous boreholes and the enhanced characterization of repository block (ECRB) and exploratory studies facility (ESF) tests and pretest predictions. For example, Figure 7.2-1 (SNL 2007 [DIRS 184614]) shows that the model prediction of water potential falls within the range observed in the ECRB, Figure 7.3-1 (SNL 2007 [DIRS 184614]) shows that the predicted water potential is consistent with the data observed in borehole WT-24, and Figures 7.5-1 and 7.5-2 (SNL 2007 [DIRS 184614]) demonstrate that the predicted groundwater ages in the UZ compare well with the measured 14C age in the samples from boreholes UZ-1 and SD-12. Similarly, Sections 7.6 to 7.8 (SNL 2007 [DIRS 184614]) demonstrate corroboration of predicted flow parameters with the fracture-flow infiltration and tracer test data from the Alcove 8/Niche 3 tests, Section 7.6 (SNL 2007 [DIRS 184614]) validates the flow model with the measured chloride data, and Section 7.7 (SNL 2007 [DIRS 184614]) corroborates fracture-flow percolation flux with the site-specific calcite deposition model. These numerous site-specific corroborative measurements and modeling activities serve to demonstrate that the UZ flow model parameters are technically sound.

In addition, the key flow and transport processes pertaining to the UZ at Yucca Mountain have been investigated through natural analogues (BSC 2004 [DIRS 169218]). These analogue studies contained both literature review and data analyses. One of the important case studies was the flow experiment and tracer infiltration test in fractured media at Box Canyon, Idaho. One of the desired confidence building activities is publication in a peer-reviewed journal. There have been numerous such publications on the UZ flow model by the YMP. These include the publications dealing with the following topics on the UZ flow model:

- A three-dimensional UZ numerical model was developed to simulate flow and distribution of moisture, gas, and heat at Yucca Mountain (Wu et al. 1999 [DIRS 117161]).
- Flow and transport processes within the UZ were characterized under current and future climates (Wu et al. 2002 [DIRS 160195]).
- Work on capillary barriers in the unsaturated rock of Yucca Mountain have been published (Wu et al. 2002 [DIRS 161058]).
- The perched-water phenomena in the UZ at Yucca Mountain have been investigated (Wu et al. 1999 [DIRS 117167]).

- Subsurface pressure variations have been used to determine the pneumatic diffusivity of important geological features (Ahlers et al. 1999 [DIRS 109715]).

- Subsurface borehole temperature data were used to estimate percolation flux (Bodvarsson et al. 2003 [DIRS 162477]).

- Chloride measurements were used to calculate infiltration rates along the ESF (Fabryka-Martin et al. 1998 [DIRS 146355]).

- Chloride data, in conjunction with hydrostructural and hydrogeological features, were used to constrain infiltration rates (Liu et al. 2003 [DIRS 162478]).

- Chloride and strontium geochemistry were investigated using three-dimensional modeling for insights into the hydrology of the UZ (Sonnenthal and Bodvarsson 1999 [DIRS 117127]).

The UZ Flow Model area in Table 7.6-1 shows two submodels: future climate analysis (BSC 2004 [DIRS 170002]) and infiltration (SNL 2007 [DIRS 182145]). These two submodels support the UZ Site-Scale Flow Model that provides the UZ flow fields, percolation flux, and rock properties parameters for the succeeding direct input models for the TSPA-LA Model: UZ radionuclides transport and MSTHM as shown on Figure 6.3.1-6. Figure 6.3.1-2 provides the flow of information and the basis for confidence in *Future Climate Analysis* (BSC 2004 [DIRS 170002]) outputs (PEF # 33) for use in the TSPA-LA Model, as described in Section 6.3.1. *Future Climate Analysis* (BSC 2004 [DIRS 170002], Section 7.1) presents an assessment of the confidence in the analysis results and concludes that the analysis is reasonable and defensible in that it is based on a consistent interpretation of available data, which include the earth orbital parameter and paleoclimate data. The defensibility is based on a body of data and a possibility rather than that the climate forecast by this analysis is much more likely to occur relative to other possible methods.

Figure 6.3.1-4 provides information on infiltration analysis (SNL 2007 [DIRS 182145]) and its output to the TSPA-LA as described in Section 6.3.1. The confidence building activities in the analysis results are described in Section 7 of *Simulation of Net Infiltration for Present-Day and Potential Future Climates* (SNL 2007 [DIRS 182145]). The report (SNL 2007 [DIRS 182145], Sections 7.1, 7.2, and 7.3]) also describes the activities performed on validation and confidence building in the infiltration parameters. The activities included: (1) comparison of MASSIF predictions of infiltration for present-day, monsoon, and glacial-transition climates for 40 realizations for each climate, with infiltration estimates from published models and data for the Yucca Mountain area, the southwestern United States, and the western United States, (2) comparison of MASSIF predictions of infiltration with seepage estimates observed in the South Ramp of the ESF in the winter of 2005; and (3) alternative model approach corroboration activity in which MASSIF results are compared to HYDRUS 1-D results for four different soil depths and using the same model inputs. Table 7.3-1 (SNL 2007 [DIRS 182145]) tabulates the output DTNs of the validation and confidence building activities. The results of these activities demonstrate that the infiltration parameters used in defining the UZ flow fields and percolation fluxes are technically sound and defensible.

7.6.4.1.2 UZ Radionuclide Transport Model

The model report that sources the input parameters on UZ radionuclide transport to the TSPA-LA computation is *Radionuclide Transport Models Under Ambient Conditions* (SNL 2007 [DIRS 177396]). The radionuclide transport computation utilizes the flow fields defined in *UZ Flow Models and Submodels* (SNL 2007 [DIRS 184614]) discussed in Section 7.6.4.1.1.

Figure 6.3.9-2 shows the model components and inputs for the TSPA-LA UZ transport computation. The UZ transport in the TSPA-LA Model is calculated using particle-tracking methodology as described in Section 6.3.9.2, and using the FEHM code (FEHM V2.24-01 [DIRS 179419]). The results of the Particle Tracking Model were compared, for the needed range of complexity, with the breakthrough curves developed from *Radionuclide Transport Models Under Ambient Conditions* (SNL 2007 [DIRS 177396]), which is a validated process model. Results show good comparisons. For example, Figure 7-11 of *Particle Tracking Model and Abstraction of Transport Processes* (SNL 2008 [DIRS 184748]) compares the FEHM results for several alternative conceptual models (ACMs) with the breakthrough curves from the process model using the code T2R3D. The dual-k results show the best match. The detail of the FEHM abstraction is presented in *Particle Tracking Model and Abstraction of Transport Processes* (SNL 2008 [DIRS 184748], Section 7).

7.6.4.1.3 SZ Flow and Transport Flow Models

The source of the SZ direct-inputs to the TSPA-LA computation are the breakthrough curves for the radionuclides of concern at the location of the RMEI. The breakthrough curves are developed using a three-dimensional transport model for the radionuclides without considering radioactive decay products. The effects of the decay products on the transport are accomplished separately through a one-dimensional transport model. Figure 6.3.10-2 summarizes the principal inputs and outputs, model features, and the foundations for confidence in the SZ Flow and Transport Model components as described in Section 6.3.10 of the TSPA-LA Model. These abstractions are described and validated in *Saturated Zone Flow and Transport Model Abstraction* (SNL 2008 [DIRS 183750]). The underlying validated process model is the SZ Site-Scale Transport Model (SNL 2007[DIRS 177392]).

For the three-dimensional simulations, breakthrough curves for a non-sorbing dissolved species (SNL 2008 [DIRS 183750], Figure 7-1 [a]) and moderately sorbing species of neptunium (SNL 2008 [DIRS 183750], Figure 7-2 [a]) of the 3-D SZ Transport Abstraction agree with those of the process model, based on visual inspection, within a few percent of relative mass of the respective species. For the non-sorbing case, one-million-year simulations were performed with an input condition of 1 g/yr for the first 1,000 years. The sum of the output mass was at 100.4 percent, 99.8 percent, and 101.6 percent of the median case, slow case, and fast case, respectively (SNL 2008 [183750], Figure 7-3 [a]). This demonstrates that the three-dimensional abstraction model represents the underlying process model with respect to total mass flux.

For the one-dimensional abstraction model, visual comparison of breakthrough curves for a non-sorbing dissolved species (SNL 2008 [DIRS 183750], Figure 7-4 [a]) and moderately sorbing species of neptunium (SNL 2008 [DIRS 183750], Figure 7-5 [a]) of the 1-D SZ

Transport Abstraction Model without radioactive decay and the 3-D SZ Transport Process Model indicate acceptable agreement. There is generally close agreement in the overall shapes of the breakthrough curves and generally good agreement at the mid-points of the breakthrough curves. The results of one-million-year simulations, expressed as the mean breakthrough curves of 200 realizations for a non-sorbing species and moderately sorbing species, indicate similar behavior for the two models, with somewhat less apparent dispersion exhibited by the 1-D SZ Transport Model relative to the three-dimensional process model. The validation testing indicates acceptable agreement of the one-dimensional transport model abstraction with the underlying 3-D process model.

7.6.4.2 Engineered Barrier System Environment

This section presents results of corroboration abstractions with the underlying validated models and analyses of the EBS environment. It provides information on the confidence built into the direct input TSPA-LA Model parameters that were abstracted from these process models and analyses. As shown on the first column in Table 7.6-1, the key models and analyses areas are seepage into drift, in-drift convection and condensation, repository thermo hydrology due to waste heat, and the EBS physical and chemical environment. The outputs from these TSPA-LA components are used in defining the WP and waste form degradation and release and transport of radionuclides through the EBS to the invert-UZ contact underlying the repository.

7.6.4.2.1 Seepage into Drift

The TSPA-LA seepage parameters were abstracted from the validated process models. The principal two process models that serve as direct inputs to the drift-seepage abstraction are: (1) Seepage Model for Performance Assessment (SNL 2007 [DIRS 181244], Section 6.4.2), and (2) TH Seepage Model (SNL 2007 [DIRS 181244], Section 6.4.3). Section 7.2 of *Abstraction of Drift Seepage* (SNL 2007 [DIRS 181244]) discusses the results of comparison of the abstracted seepage parameters with the underlying respective process models that were already validated for their intended use. The information flow for the drift-seepage abstraction for the TSPA-LA Model is shown on Figure 6.3.3-1. The TSPA-LA Model input parameters from *Abstraction of Drift Seepage* (SNL 2007 [DIRS 181244]) are shown in Table 4-1 (PEFs # 37, 44, and 45). The submodels of the Abstraction of Drift Seepage submodels are shown on Figure 6.3.3-2.

Abstraction of Drift Seepage (SNL 2007 [DIRS 181244], Section 7.2) provides evidence that the abstracted results of the drift seepage model satisfy the validation requirement (of Level 1 validation set by the technical workplan (BSC 2006 [DIRS 177465])) with agreement within 20 percent between the process models and abstracted results. Additional confidence in the abstracted TSPA-LA parameters was built by qualitative comparisons (SNL 2007 [DIRS 181244], Section 7.3) with: (a) the south ramp seepage predictions with actual observations, (b) Alcove 8-Niche 3 seepage tests results, and (c) observations with seepage in the Peña Blanca natural analogue. *Abstraction of Drift Seepage* (SNL 2007 [DIRS 181244, Section 7.3]) documents that the abstracted seepage value corroborates reasonably with the data from the above-mentioned analogues. The abstraction of Drift Seepage Model (SNL 2007 [DIRS 181244]) produces an upper-bound (i.e., a conservative) seepage value.

7.6.4.2.2 In-Drift Convection and Condensation

The information flow for the In-Drift Convection and Condensation Model (SNL 2007 [DIRS 181648]) in the TSPA-LA Model implementation is shown on Figure 6.3.3-1. The condensation model is based on the convection model and the average percolation flux derived from the MSTHM. The confidence in the MSTHM model outputs is described below. The convection model was validated by: (1) comparison of simulation results to small-scale (centimeter dimension) literature data for natural convection in horizontal concentric cylinders, (2) 44 percent of full-scale dimension tests, and (3) an independent technical review. The details of validation test and results are presented in *In-Drift Natural Convection and Condensation* (SNL 2007 [DIRS 181648], Sections 7.3, 7.4, and 7.5). The condensation model was validated by a technical review (AP-SIII.10Q, Section 5.3.2, c 5), the scope of which required affirmative answers by the reviewer to all six questions in its Technical Work Plan (BSC 2004 [DIRS 170950], Sections 2.3.3 and 2.3.4). The technical review also included in its scope a review of the convection model. The results are presented in *In-Drift Natural Convection and Condensation* (SNL 2007 [DIRS 181648], Section 7.6 and Appendix G).

7.6.4.2.3 Repository Thermohydrology Due to Waste Heat

The integrated MSTHM defines TH conditions in the drift due to waste-generated heat as a function of time and location. Figure 6.3.2-1 shows the integration of the component models for input to the TSPA-LA Model computation. Table 4-1 lists the parameters from the MSTHM that serve as the inputs to the TSPA-LA Model (PEFs # 79, 12, 15, 86, 16, 17, 18, 19, 20, 21, 22, 23, 24, 25, 26, 27, 28, 29, and 114). Section 6.3.2 discusses the implementation of the TH conditions in the drifts. The outputs from MSTHM (SNL 2007 [DIRS 181383]) produce percolation flux at the base of PTn at 3,264 locations and predict the in-drift thermohydrologic environment at these locations. The predictions consist of the following TSPA-LA parameters, which are implemented without further simplification: (1) temperature for drift-wall, DS, WP, and invert; (2) relative humidity of WP and invert; and (3) invert liquid-phase saturation. The MSTHM bases the predictions on application of its own methodology integrating its components (SNL 2007 [DIRS 181383]): (a) discrete-heat-source, drift-scale, thermal conduction; (b) smeared-heat-source, drift-scale, thermal conduction; and (c) smeared-heat-source, mountain-scale, thermal conduction, which are conduction-only calculations. The confidence in the predicted parameters was built by direct corroboration of test data (e.g., Large Block Test and Drift-Scale Test at the repository) and the results predicted by another model. The details are presented in Sections 7.3 through 7.6 of the MSTHM (SNL 2007 [DIRS 181383]). The results of these corroborative activities indicate that the parameters from MSTHM are technically sound for their intended use in the TSPA-LA Model.

The validation of the MSTHM involves the validation of both the MSTHM integrated prediction methodology as well as its supporting component submodels used in the integrated MSTHM. The MSTHM component, smeared-heat-source, drift-scale, thermal conduction, and smeared-heat-source, mountain-scale, thermal conduction are executed with the NUFT v3.0s code (Section 3.1.1). Because the smeared-heat-source, drift-scale, thermal conduction, smeared-heat-source, mountain-scale, thermal conduction, and discrete-heat-source, drift-scale, thermal conduction components are conduction-only calculations, which utilize standard scientific methods (e.g., Fourier's Law) to perform the calculations, they do not require separate

validation. Moreover, the smeared-heat-source, drift-scale, thermal conduction, smeared-heat-source, mountain-scale, thermal conduction, and discrete-heat-source, drift-scale, thermal conduction components are not applied as stand-alone models for analysis. Validation testing of the NUFT v3.0s code included conduction-only test problems (bmrk002 and verif02), which are described in the Validation Test Plan for NUFT 3.0s (LLNL 2002 [DIRS 170259]; LLNL 2000 [DIRS 170258]). These conduction-only test problems are sufficient to validate the usage of the conduction-only submodels in the MSTHM. Additional confidence building activity involving corroboration with results obtained from an alternate conduction-only mathematical model is described in *Multiscale Thermohydrologic Model* (SNL 2007 [DIRS 181383], Sections 6.2.5, 6.2.7, and 6.2.9), pertaining to the smeared-heat-source, mountain-scale, thermal conduction, smeared-heat-source, drift-scale, thermal conduction, and discrete-heat-source, drift-scale, thermal conduction components, respectively. This model-corroboration example is found in *Drift Degradation Analysis* (BSC 2004 [DIRS 166107], Section 6.2 and Figure 6-26).

The *Multiscale Thermohydrologic Model* (SNL 2007 [DIRS 181383], Section 7.4) documents the comparison of NUFT-predicted temperatures against those measured in the Drift Scale Test results and supports the ability of the MSTHM to predict a reasonable range of temperatures in the host rock. The confidence building activity for the ability of the MSTHM to predict a reasonable range of temperatures in the host rock is presented in *Multiscale Thermohydrologic Model* (SNL 2007 [DIRS 181383], Section 7.3), which documents the comparison of NUFT-predicted temperatures against those measured in the Large Block Test. The *Multiscale Thermohydrologic Model* (SNL 2007 [DIRS 181383], Section 7.6) also documents a comparison of the MSTHM-predicted in-drift temperature differences against those predicted by the FLUENT model, which supports the ability of the MSTHM to predict temperature differences between the drift wall and the DS and WP surfaces.

Section 7.4 of *Multiscale Thermohydrologic Model* (SNL 2007 [DIRS 181383]), which documents the comparison of NUFT-predicted liquid-phase saturations against those measured in the Drift Scale Test, also supports the ability of the MSTHM to predict a reasonable range of liquid-phase saturation in the invert. This ability of the MSTHM is supported by virtue of the relationship between liquid-phase flux and liquid-phase saturation, which is documented in Section 6.3.3 of *Multiscale Thermohydrologic Model* (SNL 2007 [DIRS 181383]). Note that for The TSPA-LA, the MSTHM-predicted liquid-phase flux is only applied to WPs that experience no seepage and no condensation. The ability of the MSTHM to predict a reasonable range of relative humidity on the drift wall and DS and liquid-phase saturation values is supported in *Multiscale Thermohydrologic Model* (SNL 2007 [DIRS 181383], Section 7.5) by virtue of a direct comparison between values predicted by the MSTHM and those predicted by a corresponding three-dimensional monolithic thermal-hydrologic model for a three-drift validation test case.

7.6.4.2.4 EBS Physical and Chemical Environment

The abstractions from the models in *Engineered Barrier System: Physical and Chemical Environment* (SNL 2007 [DIRS 177412]) are implemented by the EBS Chemical Environment Submodel. The inputs, outputs, and basis for model confidence for the EBS Chemical Environment Submodel are depicted on Figure 6.3.4-2. Table 4-1 lists the parameters inputs to

the TSPA-LA Model (PEFs # 75, 76, 77, and 78) from the Physical and Chemical Environment, and Section 6.3.4 discusses the TSPA-LA implementation.

The submodel provides seepage chemistry parameters (chloride ion concentration; nitrate ion concentration; and chloride to nitrate ion molar ratio, ionic strength, and pH) through the Seepage Dilution/Evaporation Abstraction Model (SNL 2007 [DIRS 177412]). It also provides the invert chemistry parameters (pH and I) via Seepage Dilution/Evaporation Abstraction Model (SNL 2007 [DIRS 177412]) and Integrated Invert Chemistry Abstraction Model (SNL 2007 [DIRS 177412]). The process models Near-Field Chemistry and In-Drift Precipitates Salts (IDPS) support the two abstraction models. The validation documentation for the abstraction models is presented in Section 7.2 of *Engineered Barrier System: Physical and Chemical Environment* (SNL 2007 [DIRS 177412]). Comparison of an interpolation of the look-up tables of the chemistry parameters with the underlying validated IDPS (SNL 2007 [DIRS 177412]) shows (Figure 7.2-2) that the difference is substantially less than the model uncertainty for the IDPS model for the model outputs from the same representative set of environmental conditions. In addition to these seepage and invert chemistry parameters, the validated Near-Field Chemistry model (SNL 2007 [DIRS 177412]) provides water rock interaction parameters and a range of in-drift partial pressure of carbon dioxide ($pCO2$) values for the TSPA-LA. These Integrated Invert Chemistry Abstraction parameters are validated by the same set of test cases as those used for the Seepage Dilution/Evaporation Abstraction parameters because both models utilize the same look-up tables in the same manner.

7.6.4.3 Drip Shield, Waste Package, and Waste Form Degradation and Mobilization

This section presents corroboration of abstraction results with the underlying validated models or analyses on the DS, WP, and waste form degradation and mobilization. It also provides information on the confidence built into the direct-input TSPA-LA Model parameters derived from these process models or analyses.

7.6.4.3.1 Drip Shield, Waste Package, and Waste Form Degradation

Waste Package and Drip Shield Degradation, Section 6.3.5, discusses implementation of the SCC information in the TSPA-LA Model as shown graphically on Figure 6.3.5-8, which provides a summary and illustration of the information flow between the DS and WP SCC Abstractions. SCC is not implemented in the TSPA-LA Model for DS as discussed in Section 6.3.5.1.1. The outputs from the Alloy 22 slip dissolution-film rupture and WP SCC models (BSC 2006 [DIRS 169996]) provide direct feeds (parameters in PEF # 4 in Table 4-1) to the TSPA-LA Model. The outputs from the Alloy 22 and DS seismic crack density model feed Seismic Consequence Abstraction (SNL 2007 [DIRS 176828]), which is described below. These three models and the two key input parameters (threshold stress intensity factor and threshold stress for SCC initiation) to the slip dissolution-film rupture model are validated for their intended use, and the details of the validation activities and results are described in Sections 7.1 through 7.5 of *Stress Corrosion Cracking of Waste Package Outer Barrier and Drip Shield Materials* (SNL 2007 [DIRS 181953]).

Comparison with the literature data shows that the SCC growth rate is within two to three orders of magnitude of the literature data (SNL 2007 [DIRS 181953], Figure 7-2), which is considered

reasonable and acceptable because of the large scatter in experimental and literature data. Additionally, as a defensible approach, the threshold stress intensity factor and the threshold stress for SCC initiation under environmental conditions were established (SNL 2007 [DIRS 181953]).

General Corrosion and Localized Corrosion of Waste Package Outer Barrier—Figure 6.3.5-3 shows information flow from SCC and other corrosion submodels to WP and DS degradation modeling as a part of the WAPDEG analysis of WP and DS Degradation and PEF # 5, 7, and 117 in Table 4-1.

General Corrosion and Localized Corrosion of Waste Package Outer Barrier (SNL 2007 [DIRS 178519], Sections 7.1 and 7.2) provides detailed discussions on the comparison of experimental and literature data on general corrosion and localized corrosion parameters with the model predictions and present the validation and confidence building for the general corrosion and localized corrosion models. Figure 7-1 and Table 7-1 in *General Corrosion and Localized Corrosion of Waste Package Outer Barrier* (SNL 2007 [DIRS 178519]) provide comparison of the Project experimental data with literature data on general corrosion rates as a function of time and Table 7-4 for comparison of model prediction of localized corrosion susceptibility with experimental data of Alloy 22 crevice samples. The conclusion is that the general and localized corrosion models for the WP outer barrier corroborates well with the experimental data and those reported in the scientific literature.

Drip Shield Corrosion—Section 6.3.5.1 and Figure 6.3.5-3 show information flow from DS Corrosion (Titanium Grade 29) (SNL 2007 [DIRS 180778]) and other corrosion submodels to WP and DS degradation modeling as a part of the WAPDEG analysis of WP and DS degradation models (Parameters in PEF # 3 and 105 in Table 4-1). As is the case for most of the supporting submodels for the TSPA-LA Model, the long time of application involved does not allow validating these models in the usual way (i.e., by comparison of model-predicted values with those observed experimentally for the whole range of time (ASTM 1998 [DIRS 105725], Sections 19.3 and 20.4). Consequently, these models were validated by a combination of validating the input parameter values used and comparing these parameters and model predictions to experimental data that were not used (SNL 2007 [DIRS 180778], Figures 24, 25, and 27) and the available peer-reviewed data (e.g., Ogden 1960 [DIRS 160556], Chapter 10, Figure 30.18; Mattsson and Olefjord 1990 [DIRS 111885]; Molecke et al. 1982 [DIRS 161678]; Schutz and Thomas 1987 [DIRS 112147], Table 23); and Hua et al. 2004 [DIRS 167022]). The peer-reviewed data represent varied experimental designs. The fact that the parameters generally agree with these data provides confidence that the model predictions are appropriate. Further, comparison with the experimental data shows that the model predictions conservatively provide the upper bounds. Detailed description of the validation activities and results are provided in Sections 7.3 (dry oxidation), 7.4 (general corrosion), and 7.5 (localized corrosion) of *General Corrosion and Localized Corrosion of the Drip Shield* (SNL 2007 [DIRS 180778]). As discussed in Section 6.3.5.1.1, localized corrosion for DS was excluded and therefore not implemented in the TSPA-LA Model.

Waste Form Degradation—Section 6.3.7.4 of the TSPA-LA Model describes the TSPA-LA implementation of the three types (CSNF, DSNF, and Defense HLW glass) of waste-degradation (Table 7.6-1 and the parameters in PEF # 31, 82, 32, and 83 listed in Table 4-1). Figure 6.3.7-2

shows the inputs, outputs and the basis for confidence in the waste-form degradation models. The output from the three analyses is the mass-release rates of radionuclides due to degradation of the respective waste forms.

The rates developed by the three analyses were validated as required for their intended purpose of the calculations. The details of the validation and confidence building activities are documented in Section 7 of the respective documents: *CSNF Waste Form Degradation: Summary Abstraction* (BSC 2004 [DIRS 169987]); *DSNF and Other Waste Form Degradation Abstraction* (BSC 2004 [DIRS 172453]); and *Defense HLW Glass Degradation Model* (BSC 2004 [DIRS 169988]). The calculated release rates for the CSNF were corroborated with: (1) experimental and literature data that show that CSNF model rates and the experimental and literature data are within the range of associated uncertainty (Section 7.1 tables); (2) results of two ACMs (surface-complexation model and electrochemical model), which indicate the model dissolution rates are reasonable; and (3) comparison of the oxidative alteration rate and phases of relevant natural analogues with those of laboratory experiments, which indicates that the model results are reasonable. The natural analogues included the uranium deposits at Peña Blanca, Mexico; Koongarra, Australia; Pecos de Caldas, Brazil; and Shinkolobwe mine in Congo and Krunkelbach mine in Germany.

For the DSNF, the model data from the analysis were validated by comparison with alternate mathematical models (BSC 2004 [DIRS 172453], Section 6.1, Table 6-9), which showed complete degradation in one year, thus supporting the instantaneous release model for DSNF.

The degradation rate derived for the Defense HLW Glass Degradation analysis was validated by comparison with laboratory test results and relevant observations in studies with simulated HLW and natural analog glasses that were not used to develop the model. The details are presented in *Defense HLW Glass Degradation Model* (BSC 2004 [DIRS 169988], Section 7 and Table 7-1).

Drip Shield and Waste Package Early Failure—Section 6.4 discusses early failure and Figure 6.4-3 shows the information flow of inputs (parameters in PEFs # 2 and 118 in Table 4-1), outputs, and basis for confidence for the Early Failure Scenario Class. No validation is required. The Early Failure Scenario Class parameters were developed by an analysis using standard scientific and engineering practice and require no post-development validation. Nonetheless, confidence in the Early Failure Scenario Class parameters is based on: (1) the fact that the calculations were performed using manufacturing-industry defect-related controlled failure data sets, (2) conservative probability estimate of occurrences of flaws per WP and DS that lead to early failure, and (3) conservative estimate of impact on barrier containment properties.

7.6.4.3.2 Mobilization

Radionuclide Inventory—Section 6.3.7.1 of the TSPA-LA Model discusses the implementation of the data from *Initial Radionuclide Inventories* (SNL 2007 [DIRS 180472]) and its addendum. Figure 6.3.7-1 shows the information (parameters in PEFs # 72, 74, and 113 in Table 4-1) flow as implemented in the TSPA-LA Model. Figure 6.3.7-3 shows the basis for defining the waste inventory. The inventory was developed based on the latest available qualified and controlled dataset as stated in the source document in *Initial Radionuclide Inventories* (SNL 2007

[DIRS 180472], Section 7 and Table 7.1-1). The inventory is an analysis that was performed applying standard scientific principles and practices, pursuing the requirements of SCI-PRO-005, and thus providing confidence in the inventory presented in Table 7.1-1.

In-Package Chemistry—Section 6.3.7 discusses and Figure 6.3.7-5 shows the TSPA-LA Model implementation of the output parameters (PEFs # 12 and 79 in Table 4-1) from *In-Package Chemistry Abstraction* (SNL 2007 [DIRS 180506]). The in-package chemistry model is made up of two main underlying process models: the batch reactor model and the surface complexation model. The batch reactor model is made up of two water-influx models, the liquid-influx and the vapor-influx models, and several other component submodels, including the fuel-degradation and the steel-degradation submodels. The primary output parameters of the in-package chemistry model abstraction to TSPA are ranges of pH and ionic strength. The abstraction pH and ionic strength values were compared with the process-model output on Figures 7-1 through 7-8 in *In-Package Chemistry Abstraction* (SNL 2007 [DIRS 180506]) for a fixed flux and a range of fluxes. The abstracted values are consistent with the model outputs, and their reasonableness is evaluated by corroborating the values with natural analogues as presented in *In-Package Chemistry Abstraction* (SNL 2007 [DIRS 180506], Section 7.4.5) with favorable results.

Dissolved Concentration Limits of Elements with Radioactive Isotopes—Section 6.3.7.5 of the TSPA-LA Model discusses how the outputs from *Dissolved Concentration Limits of Elements with Radioactive Isotopes* (Parameters in PEFs # 9, 10, and 11 in Table 4-1) are implemented in the TSPA-LA Model. Figure 6.3.7.10 shows how the dissolved concentration limits are integrated with the WP sources, EBS flow and chemical environment and the in-package chemistry model outputs, as well as the inputs to the downstream submodels of radionuclide transport through EBS and invert. The solubility models used in TSPA-LA are based on four key components: (1) a thermodynamic database and modeling tool, (2) the environmental conditions of concern, (3) the construction of the conceptual model, and (4) the calculation of solubility limits using a geochemical modeling tool based on the conceptual model. Because the thermodynamic database used in this report and the EQ3/6 code are controlled products and are used within their valid ranges, the first and fourth components need no validation. The second component is represented by inputs to the model and also needs no validation. Therefore, the model-validation need focuses on the third component, the conceptual model (e.g., the solubility-controlling mechanism). The during-development and post-development model validation activities for the conceptual model are described in detail in *Dissolved Concentration Limits of Elements with Radioactive Isotopes* (SNL 2007 [DIRS 177418], Section 7). The solubilities of the radionuclides of interest predicted by the solubility models were corroborated with experimental data, publications in peer-reviewed journals (SNL 2007 [DIRS 177418], Table 7-1), and an independent technical review. The results of these activities provide confidence that the model solubilities of the radionuclides used as input in the TSPA-LA Model computations are appropriate for the purpose. The validation and confidence building activities for the solubilities models are discussed in detail in *Dissolved Concentration Limits of Elements with Radioactive Isotopes* (SNL 2007 [DIRS 177418], Sections 7.2.1 through 7.2.9).

Waste Form and In-Drift Colloids-Associated Radionuclide Concentrations—Section 6.3.7.6 of the TSPA-LA Model discusses the colloidal radionuclide transport in the TSPA-LA Model. Figure 6.3.7-13 conceptually displays the information flow. The colloid

model abstraction (parameters in PEFs # 53, 54, 55, 56, 57, and 58 in Table 4-1) is used in TSPA-LA to estimate the stability and concentration of colloid suspensions, as well as concentrations of radionuclides associated with the colloids, based on in-package and in-drift fluid chemistry and in-package dissolved radionuclide concentrations. The component models of colloidal transport, namely the: (a) mathematical; (b) stability and colloids-concentration (of CNSF, U-oxide, DHLWG, or WP); and (c) sorption of radionuclides to the colloids, are validated by corroboration with laboratory, field, and literature data. The validation activities and the results are documented in *Waste Form and In-Drift Colloids-Associated Radionuclide Concentrations: Abstraction and Summary* (SNL 2007 [DIRS 177423], Section 7). Table 7-1 of the above-mentioned report (SNL 2007 [DIRS 177423]) lists the corroborative data used to validate the specific requirements for the colloids component models. The mathematical form of the colloid model consists of a stability criterion based on the DLVO theory (DLVO theory is designed to account for the interactions between charged colloidal particles) with inputs from ionic strength and pH. By comparison with the literature data (SNL 2007 [DIRS 177423], Table 7-1), it was shown that the ionic strength and pH dependence of colloids stability is valid and a reasonable colloids stability threshold could be defined (SNL 2007 [DIRS 177423], Figure 7-1). The stability of waste-form colloids (of CNSF, U-oxide, DHLWG, or WP) is documented further in *Waste Form and In-Drift Colloids-Associated Radionuclide Concentrations: Abstraction and Summary* (SNL 2007 [DIRS 177423], Sections 7.1.2 and 7.1.3), which also discusses the confidence in the concentrations of radionuclides associated with colloidal sorption-desorption processes.

Sections 7.1.4 and 7.1.5 (SNL 2007 [DIRS 177423]) document the basis for confidence in the distribution-coefficient of radionuclide and predicted colloidal concentrations of radionuclides (SNL 2007 [DIRS 177423], Figure 7-5).

EBS Radionuclide Transport—Section 6.3.8 of the TSPA-LA Model discusses the EBS transport abstraction and implementation in the TSPA-LA Model. Figure 6.3.8-2 displays the abstraction model components, and the input parameters (in PEF # 59 of Table 4-1) to the TSPA-LA Model. Figure 6.3.8-2 also lists the activities performed that form the basis for confidence in the TSPA-LA Model input parameters from the supporting model components. The outputs (*EBS Radionuclide Transport Abstraction* (SNL 2007 [DIRS 177407], Table 8.2-1) from the submodels—EBS Flow, EBS Transport, and EBS-UZ Interface—were integrated as the EBS Radionuclide Transport Abstraction model and implemented unchanged. The submodels were validated for their intended use as required by SCI-PRO-006 and the confidence building was accomplished by corroborating the model outputs with an independent critical review. The results of the critical review on the flow and transport and the EBS-UZ interface submodels are documented in *EBS Radionuclide Transport Abstraction* (SNL 2007 [DIRS 177407], Section 7.2.3 and 7.3.2).

In addition, Section 7.1.1 of *EBS Radionuclide Transport Abstraction* (SNL 2007 [DIRS 177407]) documents the results of further validation of the flux-splitting portion of the EBS flow submodel by corroboration with experimental data (SNL 2007 [DIRS 177407], Tables 7.1-7 and 7.1-12). The corroboration demonstrates that the DS and WP flux data used in the EBS flow are conservatively credible. The diffusion portion of the EBS transport model was further validated through corroboration with alternate models as documented in *EBS Radionuclide Transport Abstraction* (SNL 2007 [DIRS 177407], Section 7.2). The alternate

models are based on the data available in the literature (SNL 2007 [DIRS 177407], Figure 7.2-4) in the EPRI Phase 5 report (EPRI 2000 [DIRS 154149]) and as shown on Figure 7-8 (SNL 2007 [DIRS 177407]), and also that included in the model by Lee et al. (1996 [DIRS 100913]) for diffusive releases from WP containers with multiple perforations. The results of these corroboration activities demonstrate that the input to the TSPA-LA Model parameters are technically sound.

7.6.4.4 Disruptive Events

This section presents results of corroboration of the abstractions with the underlying validated process models and analyses for the seismic and igneous events and provides information on the basis for confidence in the direct input TSPA-LA Model parameters.

7.6.4.4.1 Seismic Event

Seismic Consequence—Figure 6.6-2 shows the inputs to and out from the seismic scenario class modeling and analyses cases, and shows the basis for confidence in the output parameters from these cases. Section 6.6.1 of the TSPA-LA Model report discusses the implementation of parameters from the vibratory Seismic GM Modeling Case, and Section 6.6.2 of the report discusses that for the Seismic FD Modeling Case. The abstractions for damage to the WP and DS in response to vibratory ground motion are treated as models because they rely on analyses of structural response over a range of ground motion that is wider than typically covered by seismic designs for buildings or nuclear power plants. The abstractions for kinematic response of the WP and for the response of a WP surrounded by rubble was validated by: (1) corroboration of abstraction model results with the results of the validated structural response model from which the abstraction model is derived, and (2) a technical review by an independent reviewer. For the DS damage abstractions, the fragility curves for the DS and/or its plates and the abstraction for rubble accumulation was validated by: (1) corroboration of the abstraction results with the results of the validated structural response model or rockfall model from which the abstractions are derived, and (2) a technical review by an independent reviewer. The damage abstraction for fault displacement is a scientific analysis because it is based on a standard engineering approach that bounds component response through an analysis of clearances around the different types of WPs. Consequently, this abstraction does not require further validation.

Table 7-1 (SNL 2007 [DIRS 176828]) lists the figures and tables that corroborate the abstraction results with the underlying data. In addition to these, as mentioned above, an independent technical review is included as Appendix C (SNL 2007 [DIRS 176828]). Table 7-1 (SNL 2007 [DIRS 176828]) summarizes the results of the corroboration, which show that the abstractions for kinematic damage to the WP, for the WP surrounded by rubble, for the DS fragility curves, and for the damage to the DS provide reliable input parameters to the TSPA-LA Model. The independent technical review findings agree with this observation.

7.6.4.4.2 Igneous Event

Annual Frequency of Intersection—Section 6.5.1.1 of the TSPA-LA Model report discusses the TSPA-LA implementation of the annual frequency (i.e., probability) information. Figure 6.5-4 shows how the parameter (PEF # 60 in Table 4-1) from the probability estimate

flows to the eventual dose calculation by the TSPA-LA Model computation. The inputs to this scientific analysis report are the repository design elements and the results of the expert elicitation, *Probabilistic Volcanic Hazard Analysis for Yucca Mountain, Nevada* (CRWMS M&O 1996 [DIRS 100116]), conducted in a manner consistent with the guidance in the NRC Technical Position on Expert Elicitation (Kotra et al. 1996 [DIRS 100909]). The output parameter developed for the revised repository footprint was verified by ACMs and estimates. The combined output parameter for TSPA-LA Model is the annual frequency of intersection of the repository footprint by a volcanic event. Confidence in this parameter was established as summarized in Section 7.1 and discussed in *Characterize Framework for Igneous Activity at Yucca Mountain, Nevada* (BSC 2004 [DIRS 169989], Sections 6.3, 6.4.1.5, and 6.5).

7.6.4.4.3 Dike/Drift Interactions

Section 6.5.1 of the TSPA-LA Model discusses the TSPA-LA implementation of the parameters (parameters in PEFs # 13 and 14 in Table 4-1) and Figure 6.5-5 shows the inputs, outputs, and the basis for the confidence in the modeling case. Table 7-2 (SNL 2007 [DIRS 177430]) documents the methods used to validate and build confidence in the two submodels: dike propagation during intrusion and basalt cooling and solidification. The discussions in the sections cited in Table 7-2 and the appendices attached (SNL 2007 [DIRS 177430]) provide confidence in the output parameters from these submodels that support the TSPA-LA Model.

Briefly, the extensive post-development confidence building activities summarized below demonstrate the technical soundness of the parameters. Post-model development confidence in the dike propagation during intrusion submodel was built by the following four activities: (1) application of analytical solutions for a vertical self-similar dike. The results are documented in *Dike/Drift Interactions* (SNL 2007 [DIRS 177430], Section 7.3.1.1.3); (2) corroboration with analogue studies was conducted for effect of underlying geologic structure component (SNL 2007 [DIRS 177430], Section 7.3.2.3); (3) corroboration by comparison with data from independent, peer-reviewed research conducted for the effect of topography component (SNL 2007 [DIRS 177430], Section 7.3.1.2); and (4) corroboration with analogue studies conducted for effect of underlying geologic structure component (SNL 2007 [DIRS 177430], Section 7.3.2.3).

The basalt cooling and solidification submodel was validated by comparison with: (1) alternative analytic solutions; (2) alternative numerical models described in Sections 7.3.2.2.1.1 and 7.3.2.2.1.2, respectively, in *Drift/Dike Interactions* (SNL 2007 [DIRS 177430]); (3) field observations and associated mathematical model (SNL 2007 [DIRS 177430], Section 7.3.2.2.2); and (4) uncertainty studies (SNL 2007 [DIRS 177430], Section 7.3.2.2.3).

Number of Waste Packages Hit by Igneous Intrusion—Section 6.5.1.1 of the TSPA-LA Model describes the TSPA-LA implementation of the *Number of Waste Packages Hit by Igneous Intrusion* (SNL 2007 [DIRS 177432] and parameter in PEFs # 30 and 61 in Table 4-1). Figure 6.5-5 provides a graphical presentation of the inputs, outputs, and the basis for model confidence for the Igneous Intrusion and Volcanic Eruption Modeling Cases included in this calculation. The outputs of the calculation are:

- Igneous Intrusion Modeling Case: Number of WPs damaged by intrusion is CDF representing step function with values of 0 (no intersection of the repository) or 11,629 (intersection of repository and all WPs assumed damaged).

- Volcanic Eruption Modeling Case: Number of WPs intersected by conduits. CDF with a range of 0 to 7 and eruptive center probability—fraction of intrusion cases in which eruption also occurs.

Confidence in the three parameters is built by performing the calculations by following the established scientific process, and a traceable documentation of the process. Information on confidence building activities and results on the CDFs that were derived from the calculations is reported in *Number of Waste Packages Hit by Igneous Events* (SNL 2007 [DIRS 177432], Section 6.3).

Atmospheric Dispersal and Deposition of Tephra from a Potential Volcanic Eruption—The radioactive-waste mass concentration in the resuspendable layer of soil is determined from the results of the ASHPLUME and FAR Models (the FAR Model is described below). The implementation of the ASHPLUME in the TSPA-LA Model is described in Section 6.5.2.1.2 of the TSPA-LA Model. These two models produce the results in terms of waste volumetric concentrations, and the Biosphere Model uses the results. Section 6.3.11 of the TSPA-LA Model discusses TSPA-LA Model implementation in the Biosphere Model (presented below).

Confidence was built in the ASHPLUME Model by a number of post-model development buildings, including corroboration of the model results with: (a) the data collected for three volcanoes representative of volcanic ash deposits in the Yucca Mountain region (Cerro Negro, Nicaragua; Lathrop Wells, Nevada; and Cinder Cone, California); (b) an independent technical review performed to assess the applicability of the ASHPLUME Model (SNL 2007 [DIRS 177431], Appendix F) and the ash redistribution conceptual model (SNL 2007 [DIRS 177431], Appendix G); (c) comparison of the ASHPLUME model with published results of the ASHFALL model (SNL 2007 [DIRS 177431]); and (d) sensitivity analyses of the key parameters (SNL 2007 [DIRS 177431], Figures C-1 through C-11; Tables C-10 and C-11).

Redistribution of Tephra and Waste by Geomorphic Processes Following a Potential Volcanic Eruption at Yucca Mountain, Nevada—As mentioned above, the radioactive waste mass concentration in the resuspendable layer of soil is determined from the results of the ASHPLUME and Fortymile Wash Ash Redistribution (FAR) models. The FAR Model implements the FAR conceptual model. The implementation of the FAR Model in the TSPA-LA Model is described in Section 6.5.2.1.3. The Biosphere Model receives ash redistribution input as dynamically linked to the FAR code and ASPLUME code. Section 6.3.11 of the TSPA-LA Model discusses the TSPA-LA Model implementation in the Biosphere Model as discussed below.

Confidence in the FAR Model was built by corroborating the results with: (a) testing against measurements of radionuclides in soil at sites in the Nevada Test Site, using geomorphological data from the Fortymile Wash drainage basin, and measurements on ash redistribution in the Fortymile Wash due to the 1995 flood event to enhance confidence in the FAR Model inputs and the FAR Model during its development (SNL 2007 [DIRS 179347], Sections 7.1 and 7.2);

(b) corroboration of model results with relevant information published in a peer-reviewed journal (SNL 2007 [DIRS 179347], Section 7.3.1); and (c) independent technical review (SNL 2007 [DIRS 179347], Section 7.3.2). Details are documented in *Redistribution of Tephra and Waste by Geomorphic Processes Following a Potential Volcanic Eruption at Yucca Mountain Nevada* (SNL 2007 [DIRS 179347]).

7.6.4.5 Biosphere

This section presents outcome of corroboration of the abstraction results for the Biosphere Model with the underlying validated process models and analyses and provides information on the confidence built into the output parameters from the Biosphere Model.

7.6.4.5.1 Biosphere Model for Effects on RMEI

Biosphere Model—Figure 6.3.11-2 describes the inputs, outputs, and basis for model confidence for the Biosphere Model component of the TSPA-LA Model. The Biosphere Model outputs to the TSPA-LA Model are documented in Table 4-1 (PEFs # 67, # 68, and # 69). The Biosphere Model provides TSPA with the following inputs for dose calculation: (a) BDCFs and methodology to use these data to generate dose applicable to all modeling cases involving release of radionuclides to the accessible environment by pumping groundwater from the SZ, BDCFs, and (b) methodology to use these data to generate dose for the Volcanic Eruption Modeling Case and dose coefficients to calculate inhalation dose during the volcanic ash fall. In addition, the model also provides the data sets required for the TSPA to evaluate compliance with the ground water protection standard (alpha activities and beta-gamma dose derived from radionuclide concentrations developed in TSPA).

The Biosphere Model code, ERMYN, is used to generate both sets of BDCFs. ERMYN is a stochastic GoldSim model of the biosphere and provides TSPA with 1,000 random BDCFs for each radionuclide deemed important and tracked by TSPA in the appropriate modeling case. ERMYN itself was validated by comparisons at the submodel level with national and international peer-reviewed Biosphere Models.

The ground water protection standard and inhalation data sets are deterministic and are generated from the base data contained in Federal Guidance Report 13 (and the included database). Data for individual radionuclides were concatenated to provide the inputs required for the radionuclides considered in the TSPA-LA. These and the BDCF data are qualified in the Biosphere Model Report per SCI-PRO-006.

INTENTIONALLY LEFT BLANK

Table 7.6-1. Model Abstractions and Confidence in the Direct-Input TSPA-LA Parameters

General Model Area	Model Abstraction (Name and DIRS Number)	Underlying Process Model (Name and DIRS Number)	Model Abstractions and Confidence in the Direct-Input TSPA-LA Parameters
Natural System Environment			
Unsaturated Zone Flow	*UZ Flow Models and Submodels* (SNL 2007 [DIRS 184614]) Reference 1 in Table 6-1.	*UZ Flow Models and Submodels* (SNL 2007 [DIRS 184614]) Reference 1 in Table 6-1.	The UZ Flow Model is the validated supporting model implemented in the TSPA-LA Model via the UZ Transport Submodel and MSTHM discussed below. Comparison of the flow parameters predicted by the UZ Flow Model with the on-site borehole, Exploratory Studies Facility, and enhanced characterization of repository block tests data show that the predicted parameter values are supported by the range of observed data. Confidence in the values of the model parameters is further enhanced by comparison with natural analogues, and especially with a number of publications in peer-reviewed journals (Section 7.6.4).
	Future Climate Analysis (BSC 2004 [DIRS 170002]) Reference 3 in Table 6-1.	*Future Climate Analysis* (BSC 2004 [DIRS 170002]) Reference 3 in Table 6-1.	*Future Climate Analysis* (BSC 2004 [DIRS 170002], Section 7.1) presents an assessment of the confidence in the analysis results and concludes that the analysis is reasonable and, based on a consistent interpretation of available data that includes the earth orbital parameter and paleoclimate data it is, defensible.
	Simulation of Net Infiltration for Present-day and Potential Future Climates (SNL 2007 [DIRS 182145]) Reference 2 in Table 6-1).	*Simulation of Net Infiltration for Present-day and Potential Future Climates* (SNL 2007 [DIRS 182145]) Reference 2 in Table 6-1.	Confidence in the model output parameters was provided by a number of activities as summarized in Section 7.6.4 and listed on Figure 6.3.1-4. The activities included: (1) comparison of MASSIF predictions of infiltration for present-day, monsoon, and glacial-transition climates for 40 realizations for each climate, with infiltration estimates from published models and data for the Yucca Mountain area, the southwestern United States, and the western United States, (2) comparison of MASSIF predictions of infiltration with seepage estimates observed in the South Ramp of the Exploratory Studies Facility in the winter of 2005, and (3) alternative model approach corroboration activity in which MASSIF results are compared to HYDRUS one-dimensional results for four different soil depths and using the same model inputs. The results of these validation activities show that the predicted infiltration parameters fall within the range supported by these activities.

Table 7.6-1. Model Abstractions and Confidence in Direct-Input TSPA-LA Parameters (Continued)

General Model Area	Model Abstraction (Name and DIRS Number)	Underlying Process Model (Name and DIRS Number)	Model Abstractions and Confidence in the Direct-Input TSPA-LA Parameters
Natural System Environment (Continued)			
Unsaturated Zone Radionuclide Transport	*Particle Tracking Model and Abstraction of Transport Processes* (SNL 2008 [DIRS 184748]) Reference 14 in Table 6-1.	UZ Transport Model is implemented by particle-tracking methodology using FEHM (FEHM V2.24-01 [DIRS 179419]) and documented in *Particle Tracking Model and Abstraction of Transport Processes* (SNL 2008 [DIRS 184748]) Reference 14 in Table 6-1.	The breakthrough curves from the validated UZ Transport Model were compared with those of the underlying process model and several ACMs using FEHM and the results demonstrated reasonably good comparison, especially for the dual-k approach. For example, *Particle Tracking Model and Abstraction of Transport Processes* (SNL 2008 [DIRS 184748], Figure 7-11) compares the FEHM results with the breakthrough curves from the process model using the code T2R3D.
Saturated Zone Flow and Transport	*Saturated Zone Flow and Transport Model Abstraction* (SNL 2008 [DIRS 183750]) Reference 16 in Table 6-1.	SZ Site-Scale Transport Model (SNL 2007 [DIRS 177392]) Reference 18 in Table 6-1.	As discussed in detail in Section 7.6.4, and demonstrated in *Saturated Zone Flow and Transport Model Abstraction* (SNL 2008 [DIRS 183750], Figures 7-1 through 7.5), results of the sorbing and non-sorbing radionuclides from both the 3-D and 1-D Abstraction Models compare reasonably well with those of the underlying process models.
Engineered Barrier System Environment			
Seepage into Drift	*Abstraction of Drift Seepage* (SNL 2007 [DIRS 181244]) Reference 4 in Table 6-1.	The key process models are: (1) Seepage Model for Performance Assessment Including Drift Collapse (SNL 2007 [DIRS 181244], Section 6.4.2), and (2) Thermal Seepage Model (SNL 2007 [DIRS 181244], Section 6.4.3) Reference 5 in Table 6-1.	The *Abstraction of Drift Seepage* provides evidence that the abstracted results of the Drift Seepage Model satisfies the validation requirement (Level 1 validation set by the technical work plan (BSC 2006 [DIRS 177465], Section 7.2) with agreement within 20 percent between the process models and abstracted results. Additional confidence (Section 7.3) in the TSPA-LA Parameters was built by qualitative comparison with (a) the South Ramp seepage predictions with actual observations, (b) Alcove 8-Niche 3 seepage tests results, and (c) observations with seepage in the Pena Blanca natural analogue. Section 7.3 of the Abstraction of Drift Seepage Model documents that the abstracted seepage value is corroborated by the data from these analogues. The upper-bound seepage (i.e., a conservative) value is produced by the *Abstraction of Drift Seepage* (SNL 2007 [DIRS181244)] for the TSPA-LA parameters.

Table 7.6-1. Model Abstractions and Confidence in Direct-Input TSPA-LA Parameters (Continued)

General Model Area	Model Abstraction (Name and DIRS Number)	Underlying Process Model (Name and DIRS Number)	Model Abstractions and Confidence in the Direct-Input TSPA-LA Parameters
Engineered Barrier System Environment (Continued)			
In-Drift Convection and Condensation	The TSPA-LA used directly the condensation predictions for boiling and sub-boiling drift temperatures developed using the *In-Drift Natural Convection and Condensation Model* (SNL 2007 [DIRS 181648]) Reference 7 in Table 6-1.	*In-Drift Natural Convection and Condensation Model* (SNL 2007 [DIRS 181648]) Reference 7 in Table 6-1.	The Condensation Model is based on the Convection Model and the average percolation flux derived from MSTHM. The Convection Model was validated by: (1) comparison of simulation results to small-scale (centimeter dimension) literature data for natural convection in horizontal concentric cylinders, (2) 44 percent of full-scale dimension tests, and (3) independent technical review. The details of validation test plans and results are presented in *In-Drift Natural Convection and Condensation* (SNL 2007 [DIRS 181648], Sections 7.3, 7.4, and 7.5). The Condensation Model was validated by an independent technical review that included the supporting Convection Model. The results are presented in *In-Drift Natural Convection and Condensation* (SNL 2007 [DIRS 181648], Section 7.6 and Appendix G).
Repository Thermohydrology Due to Waste Heat	*Multiscale Thermohydrologic Model* (SNL 2007 [DIRS 181383]. The MSTHM produces direct predictions on the following TSPA-LA Parameters: (1) Temperature for drift-wall, DS, WP, and invert; (2) relative humidity of WP and invert; and (3) invert liquid-phase saturation. The MSTHM bases the direct predictions on application of its own methodology integrating SDT, SMT, and DDT (SNL 2007 [DIRS 181383]).	*Multiscale Thermohydrologic Model* (SNL 2007 [DIRS 181383]) Reference 6 in Table 6-1.	See Section 7.6.4 for additional discussion on the results of corroboration of the MSTHM predictions with test data and alternate model predictions with reasonable agreement. The predictions consist of the following TSPA-LA parameters, which are implemented without further simplification: (1) temperature for drift-wall, DS, WP, and invert; (2) relative humidity of WP and invert; and (3) invert liquid-phase saturation. The MSTHM bases the predictions on application of its own methodology integrating SDT, SMT, and DDT (SNL 2007 [DIRS 181383]), which are conduction-only calculations. The confidence in the predicted parameters was built by direct comparison of test data (e.g., Large Block Test and Drift-Scale Test at the repository) and results predicted by another model. The details are presented in Sections 7.3 through 7.6 of the MSTHM (SNL 2007 [DIRS 181383]), which indicate that the abstracted parameters are appropriate for their intended use in the TSPA-LA Model.

Table 7.6-1. Model Abstractions and Confidence in Direct-Input TSPA-LA Parameters (Continued)

General Model Area	Model Abstraction (Name and DIRS Number)	Underlying Process Model (Name and DIRS Number)	Model Abstractions and Confidence in the Direct-Input TSPA-LA Parameters
Engineered Barrier System Environment (Continued)			
EBS Physical and Chemical Environment	*Engineered Barrier System: Physical and Chemical Environment* (SNL 2007 [DIRS 177412]) produced the following abstractions: (a) Seepage Dilution/Evaporation Abstraction Model (abstracted parameters: chloride ion concentration; nitrate ion concentration; and chloride to nitrate ion molar ratio, ionic strength, and pH); (b) Integrated Invert Chemistry Abstraction Model (for pH and I).	*Engineered Barrier System: Physical and Chemical Environment* (SNL 2007 [DIRS 177412]) Reference 8 in Table 6-1. The process models are: (a) Validated Near-Field Chemistry (NFC) Model (for seepage water compositions, water-rock interaction parameters, and a range of in-drift partial pressure of carbon dioxide (pCO_2) values, and (b) Validated In-Drift Precipitates/Salt (IDPS) Model (provides the estimated uncertainties on the chemical parameters (pH, I, [Cl], [N]) as a function of in-drift relative humidity).	Comparison of an interpolation of the lookup tables of the chemistry parameters with the underlying validated In-Drift Precipitates/Salt (IDPS) model outputs (with uncertainty) for the same representative set of environmental conditions, show (SNL 2007 [DIRS 177412], Figure 7.2-2) that the difference is less than the model uncertainty for the IDPS model. Section 7.6.4 provides more information. The detail of the corroboration results are presented in *Engineered Barrier System: Physical and Chemical Environment* (SNL 2007 [DIRS 177412], Section 7).

Table 7.6-1. Model Abstractions and Confidence in Direct-Input TSPA-LA Parameters (Continued)

General Model Area	Model Abstraction (Name and DIRS Number)	Underlying Process Model (Name and DIRS Number)	Model Abstractions and Confidence in the Direct-Input TSPA-LA Parameters
Waste Form and Waste-Package Degradation and Mobilization			
Drip Shield, Waste Package, and Waste Form Degradation	SCC growth rate of the DS and the WP Outer Barrier (SNL 2007 [DIRS 181953]) Reference 11 in Table 6-1.	Three component process models of SCC feed the TSPA-LA model. These component process models are: (1) Alloy 22 SDFR, (2) drip shield SCC model, and (3) Alloy 22 and drip shield seismic crack density model.	The models and the two key input parameters (threshold stress intensity factor and the threshold stress for SCC initiation) to the SDFR model are validated for their intended uses (SNL 2007 [DIRS 181953], Sections 7.1, 7.2, 7.3, 7.4, and 7.5). Comparison with literature data show the SCC growth rate is within two to three orders of magnitude of the literature data, which is considered reasonable and acceptable. Additionally, as a defensible approach the threshold stress intensity factor and the threshold stress for SCC initiation under the relevant environmental conditions were established (SNL 2007 [DIRS 181953], Section 7.3.4).
	General Corrosion and Localized Corrosion of Waste Package Outer Barrier (SNL 2007 [DIRS 178519]) Reference 10 in Table 6-1.	*General Corrosion and Localized Corrosion of Waste Package Outer Barrier* (SNL 2007 [DIRS 178519]) constitutes a part of the WAPDEG analysis of waste-package and drip shield degradation (Reference 10 in Table 6-1).	Comparison of the project experimental data with literature data on general corrosion rates as a function of time (SNL 2007 [DIRS 178519], Figure 7-1 and Table 7-1) and comparison of model prediction of localized corrosion susceptibility with experimental data of Alloy 22 crevice samples (SNL 2007 [DIRS 178519], Table 7-4) lead to the conclusion that the general and localized corrosion models for the WP outer barrier corroborate well with the experimental data and those reported in the scientific literature.
	General Corrosion and Localized Corrosion of the Drip Shield (Ti - 29) (SNL 2007 [DIRS 180778]). The three parameters developed by DS Corrosion (Ti - 29) are: DS inner and outer surface corrosion rates and general corrosion rate ratio of Titanium Grade 29/Titanium Grade 7.	Drip Shield Corrosion (Ti - 29) (SNL 2007 [DIRS 180778]) Process models that produced the three corrosion parameters for the TSPA-LA Model are: (a) dry oxidation, (b) the general corrosion, and (c) the localized corrosion models for drip shield.	Comparison shows that the parameters generally agree with the data in the peer reviewed literature representing a wide range of environments, providing confidence that the model predictions are appropriate. Comparison with the experimental data shows that the model predictions provide the upper bound values of the parameters used in the TSPA-LA. The predictions are thus conservative. Detailed results are provided in Sections 7.3 (dry oxidation), 7.4 (general corrosion), and 7.5 (localized corrosion) of *General Corrosion and Localized Corrosion of the Drip Shield* (SNL 2007 [DIRS 180778]).

Table 7.6-1. Model Abstractions and Confidence in Direct-Input TSPA-LA Parameters (Continued)

General Model Area	Model Abstraction (Name and DIRS Number)	Underlying Process Model (Name and DIRS Number)	Model Abstractions and Confidence in the Direct-Input TSPA-LA Parameters
Waste Form and Waste-Package Degradation and Mobilization (Continued)			
Drip Shield, Waste Package, and Waste Form Degradation (Continued)	*CSNF Waste Form Degradation: Summary Abstraction* (BSC 2004 [DIRS 169987]).	*CSNF Waste Form Degradation: Summary Abstraction* (BSC 2004 [DIRS 169987]).	The basis for confidence in the TSPA-LA parameters from the three waste form degradation models is discussed in Section 7.6.4. The calculated release rates for the CSNF were compared with experimental and literature data that show (BSC 2004 [DIRS 169987], Tables in Section 7.1) CSNF model rates and the experimental and literature data are within the range of associated uncertainty. Additional confidence was built by comparing the: (1) results of ACMs (Surface-Complexation Model and Electrochemical Model), which indicate the model dissolution rates are reasonable; (2) oxidative alteration rate and phases with those of laboratory experiments, which indicates that the model results are reasonable, and (3) natural analogues that included the uranium deposits at Peña Blanca, Mexico; Koongarra, Australia; Pecos de Caldas, Brazil; Shinkolobwe mine in Congo; and Krunkelbach mine in Germany, which indicate consistency with the degradation modes.
	DSNF and Other Waste Form Degradation Abstraction (BSC 2004 [DIRS 172453]).	*DSNF and Other Waste Form Degradation Abstraction* (BSC 2004 [DIRS 172453]).	For the DSNF, the model output from the analysis were validated by comparison with alternate mathematical models (Section 6.1, Table 6-9), which showed complete degradation in one year, thus providing confidence in the instantaneous release model for DSNF.
	Defense HLW Glass Degradation Model (BSC 2004 [DIRS 169988]).	*Defense HLW Glass Degradation Model* (BSC 2004 [DIRS 169988]).	Validation of the defense HLW glass degradation rate model (rate expression) was accomplished by comparison with laboratory test results and relevant observations in studies with simulated HLW and natural analog glasses that were not used to develop the model. The details are presented in *Defense HLW Glass Degradation Model* (BSC 2004 [DIRS 169988], Section 7 and Table 7-1).
	Analysis of Mechanisms for Early Waste Package/Drip Shield Failure (SNL 2007 [DIRS 178765]).	*Analysis of Mechanisms for Early Waste Package/Drip Shield Failure* (SNL 2007 [DIRS 178765]).	Confidence in the Early Failure Scenario Class parameters is based on (1) the fact that the calculations were performed using controlled manufacturing industry defect-related failure data sets; (2) conservative estimate for probability of occurrences of flaws per WP and DS that lead to early; and (3) conservative estimate of impact on barrier containment properties.

Table 7.6-1. Model Abstractions and Confidence in Direct-Input TSPA-LA Parameters (Continued)

General Model Area	Model Abstraction (Name and DIRS Number)	Underlying Process Model (Name and DIRS Number)	Model Abstractions and Confidence in the Direct-Input TSPA-LA Parameters
Waste-Form and Waste-Package Degradation and Mobilization (Continued)			
Transport of Radionuclides Out of the EBS	*Initial Radionuclides Inventory* (SNL 2007 [DIRS 180472]; and SNL 2007 [DIRS 177422]) References 20 and 35 in Table 6-1.	*Initial Radionuclides Inventory* (SNL 2007 [DIRS 180472]; SNL 2007 [DIRS 177422]) References 24 and 39 in Table 6-1.	The inventory was developed based on the latest available qualified and controlled dataset as stated in the source document in *Initial Radionuclide Inventory* (SNL 2007 [DIRS 180472], Section 7 and Table 7.1[a]). The inventory is an analysis that was performed applying standard scientific principles and practices pursuing the requirements of SCI-PRO-005, and thus providing confidence in the inventory presented in Table 7.1[a].
	In-Package Chemistry Abstraction (SNL 2007 [DIRS 180506]) Reference 21 in Table 6-1.	In-Package Chemistry Model (SNL 2007 [DIRS 180506]). The In-Package Chemistry Model is made up of two main underlying process models: the batch reactor model and the surface complexation model. The batch reactor model is made up of two water-influx models, the liquid-influx and the vapor-influx models, and several other component submodels, including the fuel-degradation and the steel-degradation submodels. The In-Package Chemistry Model is presented in *In-Package Chemistry Abstraction* (SNL 2007 [DIRS 180506], Section 6) Reference 25 in Table 6-1.	See Section 7.6.4 for more information. The abstraction pH and ionic strength values were compared with the process-model output in *In-Package Chemistry Abstraction* (SNL 2007 [DIRS 180506], Figures 7-1 to 7-8) for a fixed flux and a range of fluxes. The abstracted values are consistent with the model outputs. The reasonableness of the abstracted values, was evaluated also by comparing the values with natural analogs as presented in *In-Package Chemistry Abstraction* (SNL 2007 [DIRS 180506], Section 7.4.5.8) with favorable results.

Table 7.6-1. Model Abstractions and Confidence in Direct-Input TSPA-LA Parameters (Continued)

General Model Area	Model Abstraction (Name and DIRS Number)	Underlying Process Model (Name and DIRS Number)	Model Abstractions and Confidence in the Direct-Input TSPA-LA Parameters
Waste-Form and Waste-Package Degradation and Mobilization (Continued)			
Transport of Radionuclides Out of the EBS (Continued)	*Dissolved Concentration Limits of Elements with Radioactive Isotopes* (SNL 2007 [DIRS 177418]).	*Dissolved Concentration Limits of Elements with Radioactive Isotopes* (SNL 2007 [DIRS 177418]).	The solubilities of the radionuclides of interest predicted by the solubility models were corroborated with the experimental data, publications in refereed journals (SNL 2007 [DIRS 177418], Table 7-1), and an independent technical review. The results of the comparison provide confidence that the model solubilities of the radionuclides used as inputs to the TSPA-LA Model computations are appropriate for the purpose. The validation and confidence building activities for the solubilities models are discussed in detail in *Dissolved Concentration Limits of Elements with Radioactive Isotopes* (SNL 2007 [DIRS 177418], Sections 7.2.1 through 7.2.9).
	Waste Form and In-Drift Colloids-Associated Radionuclide Concentrations: Abstraction and Summary (SNL 2007 [DIRS 177423]) Reference 27 in Table 6-1.	The component models of colloidal transport are: (a) mathematical, (b) stability and concentration of colloids (of CNSF, U-oxide, DHLWG, or WP), and (c) sorption of radionuclides to the colloids. These models were developed, validated, and applied to TSPA directly and documented in *Waste Form and In-Drift Colloids-Associated Radionuclide Concentrations: Abstraction and Summary* (SNL 2007 [DIRS 177423]) Reference 31 in Table 6-1.	*Waste Form and In-Drift Colloids-Associated Radionuclide Concentrations: Abstraction and Summary* (SNL 2007 [DIRS 177423], Sections 7.1.1 through 7.1.5, and Table 7-1) provides the basis for confidence in the parameters used in the TSPA-LA Model, which were derived from the colloids stability model, colloids concentration, and colloids-associated concentrations of radionuclides. The mathematical form of the colloid model consists of a stability criterion based on the DLVO theory with inputs from ionic strength and pH. By comparison with the literature data (SNL 2007 [DIRS 177423], Table 7-1), it was shown that the ionic strength and pH dependence of colloids stability is valid and a reasonable colloids stability threshold could be defined (SNL 2007 [DIRS 177423], Figure 7-1). The stability of waste form colloids (of CSNF, U-oxide, DHLWG, WP) is documented further in *Waste Form and In-Drift Colloids-Associated Radionuclide Concentrations: Abstraction and Summary* (SNL 2007 [DIRS 177423], Sections 7.1.2 and 7.1.3), which also discuss the confidence in the concentrations of radionuclides associated with colloidal sorption-description processes. Finally, *Waste Form and In-Drift Colloids-Associated Radionuclide Concentrations: Abstraction and Summary* documents the basis for confidence in the distribution-coefficient of radionuclides and predicted colloidal concentrations of radionuclides (SNL 2007 [DIRS 177423], Sections 7.1.4 and 7.1.5, and Figure 7-5).

Table 7.6-1. Model Abstractions and Confidence in Direct-Input TSPA-LA Parameters (Continued)

General Model Area	Model Abstraction (Name and DIRS Number)	Underlying Process Model (Name and DIRS Number)	Model Abstractions and Confidence in the Direct-Input TSPA-LA Parameters
Waste-Form and Waste-Package Degradation and Mobilization (Continued)			
Transport of Radionuclides Out of the EBS (Continued)	*EBS Radionuclide Transport Abstraction* (SNL 2007 [DIRS 177407]). The integrated EBS Radionuclide Transport Abstraction and its submodels: EBS Flow, EBS Transport, and EBS-UZ Interface, were developed for direct implementation into TSPA-LA. No simplification was involved.	EBS Radionuclide Transport Abstraction (SNL 2007 [DIRS 177407]) includes the following submodels for the EBS Radionuclide Transport Abstraction: (a) EBS Flow Model (b) EBS Transport Model – Invert diffusion submodel – WP corrosion products diffusion submodel – Waste form degradation rind diffusion submodel – Temperature dependence of diffusion coefficient – Colloid transport – Radionuclide sorption onto stationary corrosion products and mobile colloids – Two-cell (waste form and corrosion products) EBS implementation in TSPA (c) EBS–UZ Interface Model – Advection/diffusion across interface – Boundary condition based on transport through portion of UZ	Section 7.6.4 provides more discussion on the basis for confidence in the EBS parameters used in the TSPA-LA Model computation. The confidence was based on corroborating the model outputs with: (1) an independent review of the EBS Flow, EBS Transport, and EBS-UZ Interface Submodels; and (2) alternate models based on literature data, including the EPRI model (EPRI 2000 [DIRS 154149]) and a model developed by Lee et al., (1996 [DIRS 100913]). The results of these corroboration activities demonstrate that the input the TSPA-LA Model parameters are technically sound.

Table 7.6-1. Model Abstractions and Confidence in Direct-Input TSPA-LA Parameters (Continued)

General Model Area	Model Abstraction (Name and DIRS Number)	Underlying Process Model (Name and DIRS Number)	Model Abstractions and Confidence in the Direct-Input TSPA-LA Parameters
Disruptive Events			
Seismic Event	*Seismic Consequence Abstraction* (SNL 2007 [DIRS 176828]).	The parameters abstracted are based on kinematic and structural response calculations that were developed using finite element models. Details are presented in *Mechanical Assessment of Degraded Waste Packages and Drip Shields Subject to Vibratory Ground Motion* (SNL 2007 [DIRS 178851]) and the *Seismic Consequence Abstraction* (SNL 2007 [DIIRS 176828]).	The *Seismic Consequence Abstraction* lists the figures and tables that corroborate the abstraction results with the underlying data and summarizes the results of the corroboration, which show that the abstractions for kinematic damage to the WP, for the WP surrounded by rubble, for the DS fragility curves, and for the damage to the DS, provide technically reasonable input parameters to the TSPA-LA Model (SNL 2007 [DIRS 176828], Table 7-1). In addition to these, the results were corroborated with the results of an independent technical review (SNL 2007 [DIRS 176828], Appendix C) where the findings agreed with the above observation.
Igneous Event	Annual Frequency of Interaction (*Characterize Framework for Igneous Activity at Yucca Mountain, Nevada* (BSC 2004 [DIRS 169989]) Reference 29 in Table 6-1.	Annual frequency of intersection is a scientific analysis.	Confidence in the output parameter from the analysis (i.e., annual frequency of repository intersection by an igneous intrusion) was established in *Characterize Framework for Igneous Activity at Yucca Mountain, Nevada* (BSC 2004 [DIRS 169989], Sections 6.3, 6.4.1.5, 6.5, and 7.1). The inputs to this scientific analysis (i.e., annual frequency of intersection) are repository design elements (which were verified by alternate conceptual models and estimates) and the results of the expert elicitation, *Probabilistic Volcanic Hazard Analysis for Yucca Mountain, Nevada* (CRWMS M&O 1996 [DIRS 100116]).

Table 7.6-1. Model Abstractions and Confidence in Direct-Input TSPA-LA Parameters (Continued)

General Model Area	Model Abstraction (Name and DIRS Number)	Underlying Process Model (Name and DIRS Number)	Model Abstractions and Confidence in the Direct-Input TSPA-LA Parameters
Disruptive Events (Continued)			
Igneous Event (continued)	The outputs of the component models of the *Dike/Drift Interactions* (SNL 2007 [DIRS 177430]) Reference 9 in Table 6-1.	(a) Dike propagation (b) Magma cooling and solidification (SNL 2007 [DIRS 177430]). In addition, inputs for water chemistry are provided by *In-Package Chemistry Abstraction* (SNL 2007 [DIRS 180506]). The input to TSPA is drift centerline and rib temps for various times following intrusion.	Confidence in the dike propagation during intrusion submodel was built by corroboration of the results with: (1) analytical solutions for a vertical self-similar dike (SNL 2007 [DIRS 177430], Section 7.3.1.1.3); (2) corroboration with analogue studies conducted for effect of underlying geologic structure component (SNL 2007 [DIRS 177430], Section 7.3.2.3); (3) corroboration by comparison with independent peer-reviewed research conducted for the effect of topography component (SNL 2007 [DIRS 177430], Section 7.3.1.2); and (4) corroboration with analogue studies conducted for effect of underlying geologic structure component (SNL 2007 [DIRS 177430], Section 7.3.2.3). The basaltic magma cooling and solidification submodel was validated by comparison with (1) Alternative Analytic Solutions and (2) Alternative Numerical Models (SNL 2007 [DIRS 177430], Sections 7.3.2.2.1.1 and 7.3.2.2.1.2); (3) Field observations and associated mathematical model (SNL 2007 [DIRS 177430], Section 7.3.2.2.2); and (4) uncertainty studies (SNL 2007 [DIRS 177430], Section 7.3.2.2.3).
	Number of Waste Packages Hit by Igneous Intrusion (SNL 2007 [DIRS 177432]). The outputs of the calculation are: (1) CDF representing step function with values of 0 (no intersection of the repository) or 11,629 (intersection of repository and all WPs assumed damaged); (2) Number of WPs intersected by conduits; CDF with range of 0-7; and, (3) Eruptive center probability—fraction of intrusion cases in which eruption also occurs.	*Number of Waste Packages Hit by Igneous Intrusion* (SNL 2007 [DIRS 177432]).	Confidence in the three parameters is built by performing the calculations following established scientific process and developing traceable documentation of the process. Information on confidence building activities and results on the CDFs that were derived from the calculations is reported in *Number of Waste Packages Hit by Igneous Events* (SNL 2007 [DIRS 177432], Sections 6 and 7).

Table 7.6-1. Model Abstractions and Confidence in Direct-Input TSPA-LA Parameters (Continued)

General Model Area	Model Abstraction (Name and DIRS Number)	Underlying Process Model (Name and DIRS Number)	Model Abstractions and Confidence in the Direct-Input TSPA-LA Parameters
Disruptive Events (Continued)			
Igneous Event (Continued)	*Atmospheric Dispersal and Deposition of Tephra from a Potential Volcanic Eruption at Yucca Mountain, Nevada* (SNL 2007 [DIRS 177431]).	The ASHPLUME_DLL_LA V.2.1 [DIRS 181035] implements the mathematical model of atmospheric dispersal and deposition of tephra of Suzuki (1983 [DIRS 100489]) for estimation of the aerial density of tephra deposits on the surface of the earth following a volcanic eruption and provides direct input to the TSPA-LA computation.	Confidence was built in the ASHPLUME Model by corroboration of results with: (a) data collected for three volcanoes representative of volcanic ash deposits in the Yucca Mountain region: Cerro Negro, Nicaragua; Lathrop Wells, Nevada; and Cinder Cone, California (SNL 2007 [DIRS 177431], Section 7.3); (b) independent technical review performed to assess the applicability of the ASHPLUME Model (SNL 2007 [DIRS 177431], Section 7.4 and Appendix E) and the Ash Redistribution Conceptual Model (SNL 2007 [DIRS 177431], Appendix G); (c) published results of the ASHFALL Model (SNL 2007 [DIRS 177431], Section 7.5); and, (d) sensitivity analyses of the key parameters (SNL 2007 [DIRS 177431], Section 7.6 and Figures C-1 through C-11).
	Redistribution of Tephra and Waste by Geomorphic Processes Following a Potential Volcanic Eruption at Yucca Mountain, Nevada (SNL 2007 [DIRS 179347]).	The Fortymile Wash Ash Redistribution (FAR) model was implemented by the computer code FAR, which is coupled with the ASHPLUME code providing direct inputs to the TSPA-LA Model computation. That is, the ASHPLUME DLL and FAR DLL are coupled within GoldSim.	The methods and results of confidence building in the FAR model are discussed in detail in *Redistribution of Tephra and Waste by Geomorphic Processes Following a Potential Volcanic Eruption at Yucca Mountain, Nevada* (SNL 2007 [DIRS 179347], Section 7). These include corroborating the results with: (a) testing against measurements of radionuclides in soil at sites in the NTS, using geomorphological data from the Fortymile Wash drainage basin, and measurements on ash redistribution in the Fortymile Wash due to the 1995 flood event to enhance confidence in the FAR model inputs and as well as for the FAR model conceptual development process (SNL 2007 DIRS [179347], Sections 7.1 and 7.2); (b) corroboration of model results with relevant information published in a refereed journal (SNL 2007 [DIRS 179347], Section 7.3.1), and (c) independent technical review (SNL 2007 [DIRS 179347], Section 7.3.2).

Table 7.6-1. Model Abstractions and Confidence in Direct-Input TSPA-LA Parameters (Continued)

General Model Area	Model Abstraction (Name and DIRS Number)	Underlying Process Model (Name and DIRS Number)	Model Abstractions and Confidence in the Direct-Input TSPA-LA Parameters
Biosphere			
Biosphere Model for Effects on RMEI	*Biosphere Model Report* (SNL 2007 [DIRS 177399]).	*Biosphere Model Report* (SNL 2007 [DIRS 177399]).	Section 7.6.4 of the TSPA-LA Model report provides additional information. ERMYN is a stochastic GoldSim model used in the biosphere modeling. ERMYN was validated by comparisons of results at the sub-model level with national and international peer-reviewed biosphere models. The groundwater protection standard and inhalation data sets are deterministic and are generated from the base data contained in Federal Guidance Report 13 (and the included database). Data for individual radionuclides were concatenated to provide the input required for the radionuclides considered in TSPA. These and the BDCF data are qualified in the biosphere model report per SCI-PRO-006.

INTENTIONALLY LEFT BLANK

7.7 CORROBORATION OF RESULTS WITH AUXILIARY ANALYSES

The auxiliary analyses, described in this section and listed in Table 7.1-1, play an important part in building confidence that the TSPA-LA Model results are reasonable for the model's intended purpose. To gain confidence in the TSPA-LA Model, auxiliary analyses include analyses of single realizations (Section 7.7.1), comparisons of the TSPA-LA Model results with a simplified TSPA analysis produced using a FORTRAN code (Section 7.7.2), and with the TSPA results independently produced by EPRI using its Integrated Multiple Assumptions and Release code (IMARC) (Section 7.7.3). In addition, performance margin analyses (PMA) were performed using the same modeling cases and dose computation methodology as was used for the compliance modeling cases of the TSPA-LA Model (Section 7.7.4). While the results of all four groups of these auxiliary analyses add confidence in making the determination as to whether the model results are reasonable and ensure achievement of the required validation status for the model's intended purpose, the PMA results were of special significance in this regard. As required by the technical work plan, the PMA utilized revisions to selected component models in the TSPA-LA compliance model, including conceptual or uncertainty alternatives, to assess the performance margin in the compliance model, and to evaluate the degree to which the compliance model results are conservative.

The analysis of single realizations examines coupling of the model components and processes that constitute the foundation for the nature of the TSPA-LA annual dose history plots and validate reasonableness of the calculated dose by the TSPA-LA Model. Single realizations are analyzed for the Waste Package and Drip Shield EF Modeling Cases, the Igneous Intrusion Modeling Case, and the Seismic GM Modeling Case. The Simplified TSPA Analysis results are compared with results of the TSPA-LA Model of repository performance to demonstrate that the more complex TSPA-LA Model yields results that would be expected. The Simplified TSPA Analysis conducted simulations of the Nominal Scenario Modeling Case, Waste Package EF Modeling Case, Seismic GM Modeling Case and Igneous Intrusion Modeling Case. For the EPRI comparison, the TSPA-LA Nominal Scenario Modeling Case and Waste Package EF Modeling Case results were compared with the EPRI PA results for the equivalent modeling cases. The differences between the two model results are found reflective of the modeling approach and input differences between them. The PMA analysis (Section 7.7.4) confirmed that the implicit and explicit conservatisms in the TSPA-LA model components are indeed conservative and do not introduce undue risk dilution in the TSPA-LA results. The analysis also revealed the presence of performance margins, which is especially large for the Seismic GM Modeling case. The PMA analysis was performed on the same set of modeling cases as the TSPA-LA Model.

INTENTIONALLY LEFT BLANK

7.7.1 Analysis of Single Realizations

Analysis of single realizations provides a unique insight into the coupling of various submodel processes within the TSPA-LA Model. A comprehensive explanation detailing how the transport of key radionuclides is affected by coupling various components of the EBS, UZ, and SZ domains following the WP failure under varying physical-chemical-thermal-mechanical conditions provides confidence that the various submodel processes are working as expected and in-turn helps in providing confidence in the TSPA-LA Model.

Four different modeling cases are chosen to cover the range of WP failure mechanisms considered in TSPA-LA and to highlight the various processes affecting and controlling the radionuclide releases under various thermal and chemical conditions. The four modeling cases are: (1) Waste Package EF Modeling Case (Section 7.7.1.1), (2) Drip Shield EF Modeling Case (Section 7.7.1.2), (3) Igneous Intrusion Modeling Case (Section 7.7.1.3), and (4) Seismic GM Modeling Case (Section 7.7.1.4).

The methodology for calculating the expected annual dose (expectation of annual dose over aleatory uncertainty) for the various modeling cases is described in Section 6.1.2, which discusses differentiating epistemic uncertainty from aleatory uncertainty in the TSPA-LA Model. Although the treatment of aleatory uncertainty varies by the modeling case, the general methodology for selecting a realization for detailed analysis is similar in all four modeling cases. First, an epistemic uncertainty vector is chosen from the set of epistemic uncertainty realizations. The criteria for selecting an epistemic uncertainty vector is such that the general behavior of the expected annual dose (from that vector) is similar to the mean annual dose (expectation over both aleatory and epistemic uncertainty) and the magnitude of the expected annual dose is somewhat higher than the mean annual dose over time periods of interest. This choice is intended to select epistemic realizations that highlight processes of interest in each modeling case. Since the expected annual dose for an epistemic vector is calculated by taking the expectation over aleatory uncertainty, each expected annual dose is further broken down to select the realization(s) representing individual aleatory uncertainty vectors. The aleatory vectors are chosen by comparing each realization's dose contribution to the dose from other aleatory vectors in the set and selecting aleatory realizations which best describe the behavior of the expected annual dose. For the Igneous Intrusion and Seismic GM Modeling Cases, one GoldSim realization representing a unique combination of epistemic and aleatory uncertainty is chosen for detailed analysis while in the Waste Package EF and Drip Shield EF Modeling Cases, two GoldSim realizations representing two aleatory uncertainty vectors (representing CSNF and CDSP WP locations) for a given epistemic uncertainty vector are selected, to best describe the expected annual dose for the chosen epistemic uncertainty vector. More details regarding the selection of a single realization for analysis are presented in each subsection. All single realization analyses discussed here are carried out by running the single realization using GoldSim software (GoldSim V9.60.100, STN: 10344-9.60-01 [DIRS 181903]). However, the expected annual dose results presented are based on calculations performed using EXDOC_LA software (EXDOC_LA V2.0 STN: 11193-2.0-00 [DIRS 182102]) with proper weighting of scenario specific probabilities and expectation over aleatory and epistemic uncertainties.

7.7.1.1 Waste Package Early Failure Modeling Case

This section presents analyses of two realizations selected from the 6,000-realization base case run performed for calculating the expected annual dose from the Waste Package EF Modeling Case (GoldSim filename: LA_v5.000_EW_006000_012.gsm; output DTN: MO0709TSPAREGS.000 [DIRS 182976]). The distribution of expected annual dose along with the mean and various quantiles is shown on Figure 7.7.1-1a on a linear time scale and on Figure 7.7.1-1b with a log time scale to show the variation in dose at early time more clearly. The 300 displayed expected annual dose histories correspond to the 300 epistemic uncertainty vectors. Each expected annual dose history is calculated as a weighted average of twenty aleatory uncertainty vectors (Eq. 6.1.2-13). The twenty aleatory uncertainties are derived by considering the five spatial percolation subregions, two environments (dripping and non-dripping environments) for each percolation subregion, and two WP types for each environment (Section 6.1.2.4). One early failed WP is modeled in each of the aleatory vectors. From the Figure 7.7.1-1, the epistemic vector 281 is chosen for detailed analysis as it has an expected annual dose curve similar to the mean. The twenty aleatory uncertainty vectors which correspond to epistemic vector 281 are GoldSim realizations 5601 through 5620 (Figure 7.7.1-2).

The mean annual dose from this modeling case has several peaks (Figure 7.7.1-1b). The first broad peak is between 1,000 and 2,000 years due to contribution from CDSP WPs predominantly, when the relative humidity in the CDSP packages in the various percolation subregions goes above 95 percent and diffusive transport starts (Section 5.1.4). The second set of peaks that occur between 10,000 and 30,000 years are due to contribution from CSNF WPs when the relative humidity of the CSNF packages in the various percolation bins go above 95 percent. The last broad peak occurs after the DSs fail (between around 250,000 and 300,000 years) and water flux through the WPs starts.

The radionuclides contributing to the mean annual dose are shown on Figure 7.7.1-3. ^{99}Tc and ^{129}I are the top contributors at the peak of the mean annual dose, which occurs around 12,500 years. Beyond about 30,000 years, ^{239}Pu and ^{242}Pu become major contributors, with additional contribution from ^{237}Np and ^{226}Ra. In the sections that follow, transport characteristics of ^{99}Tc will be discussed as an example of high-solubility, non-sorbing radionuclides, while ^{239}Pu and ^{242}Pu will be discussed as examples of low-solubility, high-sorbing radionuclides.

In order to investigate the peaks in the mean annual dose curve, it was necessary to inspect two GoldSim realizations (representing two aleatory uncertainty vectors for the same epistemic uncertainty vector), one with an early CSNF WP failure and one with an early CDSP WP failure, because they each affect the expected annual dose at different time periods. Realization 5,608 is chosen to represent the early failure of CSNF WP while realization 5618 is chosen to represent the early failure of CDSP WP. These realizations were chosen because they have early failure of CSNF and CDSP packages within percolation subregion 3, which represents 40 percent of the repository area, and the dripping environment where releases are typically greater than from the non-dripping environment. The annual dose from the two realizations, are highlighted on Figure 7.7.1-2 along with other 18 realizations representing aleatory uncertainty vectors. These two realizations are examined more closely in the sections that follow.

Early Failure CSNF Package—Realization 5608

Figure 7.7.1-4 shows the annual dose from the major radionuclides for realization 5608 (GoldSim filename: LA_v5.000_EW_006000_020.gsm; output DTN: MO0708TSPAVALI.000 [DIRS 182985]). ^{99}Tc and ^{129}I dominate the first sharp peak at 11,500 years. There is a broad peak due to ^{239}Pu between 20,000 and 100,000 years and a broad peak due to ^{242}Pu and ^{237}Np after the DS fails at 292,000 years. At no time do the irreversibly attached colloids significantly contribute to the dose.

The peak dose is due to the almost pulse-like release of ^{99}Tc and ^{129}I from CSNF packages that transport unretarded through EBS, UZ, and SZ. In the Waste Package EF Modeling case, the CSNF matrix is modeled to instantaneously degrade when the WP is breached and while the temperature is above 100°C. However, release of the radionuclides cannot occur until there is a continuous water film within the WP to support diffusion that is modeled to occur once the relative humidity rises above the threshold of 95 percent in the absence of flow. In realization 5608 this occurs at 11,500 years, causing the diffusive release to start. All of the highly soluble radionuclides such as technetium and iodine from the CSNF inventory dissolve into the available water volume establishing a large concentration gradient between the waste form domain and the invert that drives diffusion and rapidly depletes the mass. Figure 7.7.1-5 shows the technetium release rate from the WF, EBS, UZ, and SZ for realization 5608. The initial pulse-like release rate from the waste form is lowered and broadened only slightly by the transport through the WP corrosion products domain and the invert domain, and on this plot, the curves are virtually on top of each other. There is small but observable lowering and broadening of the release rate peak in the UZ and SZ due to hydrodynamic dispersion caused by fracture-matrix interaction in the volcanic units and transport through alluvium. The small but sharp increase in the SZ release rate around 164,000 years is due to a step-change in the SZ breakthrough curve from Source Region 2 that results from coarse time discretization.

Plutonium, in contrast, is a low-solubility and high-sorbing element so its behavior is quite different from technetium. Unlike technetium, which had a large pulse-like release, the plutonium release from the waste form rises to a lower value and stays constant for a long time (Figure 7.7.1-6a). This is because the plutonium concentration is solubility limited unlike unbounded technetium concentration. As a result, degraded plutonium mass precipitates within the waste form domain. Figure 7.7.1-7a shows the plutonium solubility and concentrations within the CSNF waste form domain. The isotopes share the element solubility in proportion to their mass in the waste form cell, so ^{239}Pu dominates the plutonium inventory at early times and ^{242}Pu dominates at late times as ^{239}Pu decays away. The plutonium remains precipitated in the waste form domain throughout the simulation period in realization 5608. The drop in solubility observed around 292,000 years is due to the change in in-package chemistry calculations (Figure 7.7.1-7b) that occur following the failure of DS and as flow through the WP starts resulting in the switch from vapor-influx chemistry calculations to flow-through chemistry calculations. Note that at no point during the transport calculations do the pH and ionic strength go outside the range of instability for CSNF colloids (Figure 6.3.7-11b).

Besides precipitation within the waste form domain, sorption onto WP corrosion products is very important to controlling plutonium release from the WP. The effect of sorption on the plutonium concentration within the WP corrosion products can be seen in Figure 7.7.1-6b, where after an

initial spike, the concentration is maintained below the solubility limit within that domain. The initial spike results from the initial calculation of low corrosion products K_ds, when the competitive sorption regression uses a minimum value for the radionuclide concentrations. Once the radionuclide concentrations rise above the minimum, the K_ds adjust to higher values. The low initial K_d allows a pulse of radionuclides, most notably ^{239}Pu and ^{243}Am, to be released through the WP corrosion products and sorbed onto the invert before significant K_ds are calculated in the corrosion products. This is a model limitation due to the explicit-in-time solution method for the competitive sorption calculations. However, the current implementation is adequate because it causes only a minor over-prediction of the ^{239}Pu release to the invert in a single time step and is conservative. Because of decay of ^{243}Am to ^{239}Pu, the dissolved concentration of ^{239}Pu in the WP corrosion products is calculated to exceed that in the waste form domain. In the subsequent time steps, the higher K_ds cause the WP corrosion products domain ^{239}Pu concentration to drop below that of the waste form domain and then below that of the invert. As a result, there is backward diffusion from the invert into the WP corrosion products (represented by a negative release rate in Figure 7.7.1-6a). Flow through the invert eventually drops the concentration in the invert below that in the WP corrosion products and positive release from the WP to the invert is reinstated. The diffusion gradient between the invert and the UZ remains positive, however, resulting in continuous downgradient releases (Figure 7.7.1-6a). The release rates decrease in the UZ and further in the SZ, due to dispersion, sorption, and radioactive decay during transport. The small concentration of ^{239}Pu irreversibly attached to CSNF colloids in the waste form domain (referred as Ic on Figure 7.7.1-6b) shows that colloidal transport is not important in CSNF WPs.

The release rates of ^{242}Pu (Figure 7.7.1-8a) correlates well with its concentrations (Figure 7.7.1-8b). The share of ^{242}Pu relative to the elemental solubility increases with time as mentioned earlier, so its concentration and release rate also increases. Release from the WP corrosion product domain is significantly reduced due to sorption onto the WP corrosion products. Unlike ^{239}Pu where the concentration in the WP corrosion products domain exceeded that in the waste form domain in the initial timestep (at 11,500 years), ^{242}Pu is not the daughter of a significant short-lived parent, and the concentration in the WP corrosion products domain remains below that of the waste form domain. At 292,000 years the DS breaches, so water flux through the WP starts increasing the release rate from the WP. Delay and lowering of the release rates can be seen from the EBS (at invert), UZ, and SZ.

Early Failure CDSP Package—Realization 5618

Figure 7.7.1-9 shows the annual dose from the major radionuclides for realization 5618 (GoldSim filename: LA_v5.000_EW_006000_021.gsm; output DTN: MO0708TSPAVALI.000 [DIRS 182985]). ^{14}C, ^{99}Tc, and ^{129}I dominate the first peak which starts at about 1,000 years when relative humidity of the CDSP package rises above 95 percent. Although the CDSP WP is failed at the start of the simulation, only the DSNF is assumed to degrade instantaneously; the HLW glass degrades more slowly based on its degradation rate. This process can be seen from the plot of the cumulative release of selected isotopes from the waste form domain (Figure 7.7.1-10). The DSNF release is seen at the end of the first timestep (250 year timestep), with a gradual rise in the cumulative release, as the HLW glass degrades. The line for ^{14}C is flat because there is no ^{14}C inventory in the HLW glass. The slow degradation of HLW leads to a gradual release of ^{99}Tc from the HLW waste form domain (Figure 7.7.1-11) compared to that

from the CSNF waste form (Figure 7.7.1-5). The lower inventory of ^{99}Tc within the DSNF compared to that within CSNF (on a per package basis) results in a lower initial release rate. Once again there is small but observable lowering and delay of the release rate peak in the UZ and SZ.

Figure 7.7.1-12a shows the release rates of ^{239}Pu from the different domains. Figure 7.7.1-12b shows the concentration of ^{239}Pu in each domain of the EBS transport model: the HLW glass, DSNF, WP corrosion products, and invert. Each domain has its own chemistry and plutonium solubility. The plutonium starts out precipitated in both the HLW glass domain and the DSNF domain, but is depleted first in the DSNF domain by about 4,000 years. After that time its concentration in DSNF domain is controlled by transport from the upstream HLW cell. Kinetic sorption and desorption processes that are modeled in the WP corrosion products domain control the concentration of plutonium and maintain it at the solubility limit. As diffusive release continues to the invert, the plutonium mass is depleted from the corrosion products domain. By 75,000 years, the dissolved concentrations cannot be maintained at the solubility limits leading to its gradual decline. This reduction in corrosion product domain concentrations increases the concentration gradient between the HLW and WP corrosion products domains and increases the release rate from the waste form domain (Figure 7.7.1-12a). After 176,000 years, the plutonium within the HLW glass waste form domain is depleted, so the total release from the waste form domain drops to zero. In addition to the dissolved concentrations, Figure 7.7.1-12b also shows the concentrations of ^{239}Pu irreversibly attached to glass waste form colloids. The ionic strength (Figure 7.7.1-13) remains above the threshold for glass waste form colloid stability (Figure 6.3.7-11a) until 50,000 years. After that time, the ^{239}Pu concentration irreversibly associated with the glass waste form colloids remain orders of magnitude below the dissolved concentration, so significant colloidal release of ^{239}Pu is not observed in realization 5,618.

The release rate curves of ^{242}Pu from CDSP packages (Figure 7.7.1-14a) are similar to the curves for ^{239}Pu (Figure 7.7.1-12a), except that ^{242}Pu does not decay away as quickly (half life is 375,000 years), leading to significant late time releases. Once again, the ^{242}Pu becomes depleted in the DSNF domain at 4,000 years, but the concentration in the WP corrosion products domain is held steady due to sorption-desorption processes. The concentration of ^{242}Pu in the HLW waste form domain is low at early times as the elemental solubility is dominated by the ^{239}Pu concentration. As ^{239}Pu concentration declines due to radioactive decay the concentration of ^{242}Pu increases to match the elemental solubility (Figure 7.7.1-14b), and reaches a maximum around 176,000 years when ^{239}Pu concentration drops. As a result, the diffusion gradient which was from the WP corrosion products domain to the upstream waste form domains reverses leading to increasing downgradient (positive) release and depletion of the mass in the waste form domain. Once the mass is depleted the concentration in the waste form domain decreases and the backward diffusion from the WP corrosion products domain resumes. Release of ^{242}Pu irreversibly attached to glass waste form colloids (referred as Ic) is low but increases after the DS fails due to advective release from the WP. This is the only significant release of colloidal radionuclides for this modeling case, with the release rate of irreversibly attached plutonium nearly equal to that of dissolved plutonium.

7.7.1.2 Drip Shield Early Failure Modeling Case

This section presents analysis of two realizations selected from the 3,000-realization base case run performed for calculating the expected annual dose from the Drip Shield EF Modeling Case (GoldSim filename: LA_v5.000_ED_003000_008.gsm; output DTN: MO0709TSPAREGS.000 [DIRS 182976]). The 3,000 realizations in GoldSim represent 300 epistemic uncertainty vectors where each epistemic vector is used for 10 aleatory uncertainty vectors.

In the stylized Drip Shield EF Modeling Case, a single CSNF or CDSP WP is modeled in a dripping environment under a DS that is assumed to be completely failed (breached) at the start of the simulation. Furthermore, the WP is assumed to fail completely from localized corrosion at the onset of drift seepage when the in-drift temperatures are still hot. This stylized analysis is used to calculate the dose from WP failure by localized corrosion conditional on the early failure of the DS.

The expected annual dose from all 300 epistemic vectors, along with the statistics on the distribution of expected annual dose, is shown on Figure 7.7.1-15. Figure 7.7.1-16 shows the major radionuclides that contribute to the mean annual dose. There is an early peak due to ^{99}Tc, later, ^{239}Pu, and ^{242}Pu are the top contributors. Based on Figure 7.7.1-15, epistemic vector 228 is chosen for further analysis because it has a shape similar to the mean annual dose curve but has higher dose near the early peak.

The expected annual dose from this epistemic vector is calculated as a weighted average of annual dose for ten aleatory vectors (Eq. 6.1.2-14). The ten annual dose histories for epistemic vector 228 are GoldSim realizations 2,271 to 2,280 (Figure 7.7.1-17). The ten aleatory vectors represent dripping environments in five percolation subregions for both CSNF and CDSP WP types. As outlined in Equation 6.1.2-14, the dose from each realization is then multiplied by the probability of early DS failure, the waste type fraction, the seepage fraction, and the percolation bin fraction, which is equal to the number of WPs in the percolation subregion divided by the total number of WPs in the repository. These weighted doses are then summed to get the expected annual dose for epistemic vector 228 on Figure 7.7.1-15. Two GoldSim realizations (2,273 and 2,278) are highlighted on Figure 7.7.1-17 to show the relative difference in unweighted dose behavior between a CSNF WP type (realization 2,273) and CDSP WP type (realization 2,278) located in the same percolation subregion (percolation subregion 3). Both realizations are considered for further analysis (GoldSim filenames: LA_v5.000_ED_003000_016.gsm and LA_v5.000_ED_003000_017.gsm; output DTN: MO0708TSPAVALI.000 [DIRS 182985]). The major dose contributors for realization 2,278 are shown on Figure 7.7.1-18a, and they are similar to the major dose contributors for the mean annual dose (Figure 7.7.1-16): the early part of the dose curve is controlled by ^{99}Tc, the middle part is controlled by ^{239}Pu, and the late time part is controlled by ^{242}Pu after the decay of ^{239}Pu. The major dose contributors for realization 2,273 are similar to the ones shown for realization 2,278. ^{79}Se is also important early on as there is no solubility controlling phase and it is retarded moderately during transport. It shows spiky behavior due to the particle tracking algorithm used in the UZ Transport Model to track mass.

In the first 5,000 years, annual dose is controlled by the unretarded species that have no solubility constraints, such as ^{99}Tc, ^{79}Se, and ^{14}C. After 5,000 years and until 250,000 years,

^{239}Pu is the dominant radionuclide. As shown on Figure 7.7.1-18b, the dose from ^{239}Pu is a combination of dissolved plutonium and plutonium irreversibly sorbed on colloids. The dose from ^{239}Pu mass irreversibly associated with slow traveling fraction of colloids (defined by symbol Ic) is comparable to the dose from dissolved ^{239}Pu. At late times (past 300,000 years), ^{242}Pu is the dominant contributor to dose, just like in the Waste Package EF Modeling Case previously discussed. Here again, the dose from ^{242}Pu is a combination of dissolved and irreversibly sorbed colloidal plutonium (Figure 7.7.1-18b). Note that the colloidal plutonium was not important in the Waste Package EF Modeling Case (7.7.1.1) until the DS failure because of only diffusive releases from the WP. In this Drip Shield EF Modeling Case, the releases from the WP are mainly advective and colloids become important.

This type of transport behavior is expected because ^{99}Tc, ^{79}Se, and ^{14}C are transported as solutes with little or no retardation in the engineered barrier and natural system. Despite their similar transport properties and travel times to the biosphere, these radionuclides exhibit variations in terms of dose due to differences in the initial inventory, decay rates, and BDCFs for each of the radionuclides. Unlike the above radionuclides, the transport characteristic of ^{239}Pu is affected by retardation in the EBS, UZ, and SZ. This retardation is due to reversible sorption on the WP corrosion products and invert material (crushed tuff) in the EBS and on the lithologic units in the UZ and SZ. Almost all of the ^{239}Pu that is associated irreversibly with colloids (embedded in HLW glass waste form colloids) is transported faster than the dissolved ^{239}Pu due to a lesser degree of fracture-matrix interaction in the UZ and SZ, so it is observed earlier than dissolved ^{239}Pu.

The first ^{99}Tc release out of the EBS occurs at approximately 500 years for the CDSP WP even though the WP failures occur at the start of the simulation (Figure 7.7.1-19). Temperature effects cause this delay as no transport (diffusive or advective) is modeled to occur while the temperatures are above the boiling point of water (100°C). Figure 7.7.1-19 shows that the temperature within a CDSP WP does not fall below 100°C until approximately 500 years and, for CSNF WPs, the temperature does not fall below 100°C until approximately 700 years.

Releases from Engineered Barrier System—A number of processes in both the WP and invert influence the release of radionuclides from the EBS. Figure 7.7.1-19 shows the mass flux of ^{99}Tc out of the EBS into the UZ from both CSNF and CDSP WPs (from realizations 2,273 and 2,278, respectively).

The ^{99}Tc release curve for the CDSP WP starts at 500 years and initially decreases as the drift wall condensation changes from Stage 2 to Stage 3, as discussed next. The change in climate state is marked by an instantaneous increase in seepage rates through the EBS (Figure 7.7.1-20). The climate changes are at 600 years, 2,000 years, and 10,000 years. The small spike in release rates at around 2,000 years is in response to the switch from monsoonal to glacial-transition climate state. Another spike occurs around 10,000 years in response to the change to the long-term average climate state with its higher infiltration and higher seepage rate.

Figure 7.7.1-20 shows the flow rate into the WP as a function of time for the CDSP and CSNF WPs. The initial high CDSP seepage rate is from Stage 2 drift wall condensation (Section 6.3.3.2). The flow into the WP becomes equal to the seepage rate after 500 years when Stage 2 ends. The CSNF package shows low initial seepage because there is no CSNF Stage 2

drift wall condensation. The figure shows the flow into the WP increases at each climate change because the percolation rate increases.

Figure 7.7.1-21 shows the fraction of the waste form degraded for CDSP and CSNF. The CSNF waste form is completely degraded when the WP fails at the start of simulation because the temperature exceeds 100°C. The CDSP waste form, however, degrades slowly with the degradation rate declining gradually as WP temperature decreases; the entire waste form is completely degraded by about 10,000 years.

Unsaturated Zone–After their releases from the EBS, the radionuclides enter the UZ and are partitioned among the UZ fractures and matrix. For the major contributors to dose (^{99}Tc, ^{129}I, ^{237}Np, ^{239}IcPu (irreversible mass associated with colloids ^{239}Pu, and ^{242}Pu), most of the radionuclide mass released from EBS is partitioned into the UZ fractures where there is very little delay in transport. The release is mainly into the fractures because most of the release is by advection because the DS is failed and the WP is in the seeping percolation subregion in this modeling case. Figure 7.7.1-22 shows the fraction of each radionuclide partitioned into the fractures for percolation subregion 3 (CDSP WP) releases. (The results for CSNF WP releases are similar.) Figure 7.7.1-22 shows that, at a minimum, 80 percent of the mass flux enters the UZ fractures, but generally more than 95 percent of the mass flux is partitioned into the UZ fractures. The spikes down to zero (near the end of the simulation) are due to numerical approximations in the partitioning algorithm when essentially all of the ^{239}IcPu and ^{239}Pu have decayed and the actual release is approximately zero. Because of the fast transport times in the UZ fractures there is very little delay of radionuclides within the UZ, as shown on Figure 7.7.1-23.

Saturated Zone—Transport of radionuclides through the SZ has the potential for significant retardation due to sorption in the SZ volcanics and alluvium for some radionuclides. Because there is no sorption of ^{99}Tc in the SZ, its transport is relatively fast (Figure 7.7.1-23). This realization does not show much retardation for plutonium in the SZ. The combined UZ and SZ, delays and reduces the cumulative release of ^{242}Pu, with the majority of the reduction in the UZ.

7.7.1.3 Igneous Intrusion Modeling Case

This section presents analyses of a single realization selected from the 3,000-realization base-case run performed for calculating the expected annual dose from the Igneous Intrusion Modeling Case for one-million year simulation duration (GoldSim filename: LA_v5.000_IG_003000_017.gsm; output DTN: MO0709TSPAREGS.000 [DIRS 182976]). The 3,000 realizations are the combination of 300 epistemic vectors that are sampled over all the epistemic uncertainties and 10 aleatory samples that specify the time of an igneous intrusion event. In other words, each realization of this modeling case has one igneous intrusion event occurring at a specified time with one given epistemic vector. The duration of simulation for this modeling case is 1,000,000 years. The reader is referred to Sections 6.1.2 and 6.1.3 for how aleatory uncertainties and epistemic uncertainties are treated and how expected annual dose is calculated for the Igneous Intrusion Modeling Case. Section 6.5.1 provides the details of the conceptual model, model abstraction, and TSPA-LA implementations for the Igneous Intrusion Modeling Case.

It should be noted that all WPs and DSs are assumed to completely fail from the igneous intrusion event and the barrier capability of WP and DS to water flow is conservatively ignored. In addition, before the intrusion time, the nominal corrosion processes are included in this modeling case such that the WPs could be breached by either SCC or general corrosion and could release the radionuclides.

The mean annual dose and contributing radionuclides for the base case are shown on Figure 7.7.1-24. This figure shows that the mean annual dose increases rapidly for the first 100,000 years to about 1 mrem, then decreases slowly until around 200,000 years to a low value of 0.76 mrem, and then increases gradually for the remaining time to a maximum of 1.3 mrem. ^{239}Pu is the dominant radionuclide early on (for the first 200,000 years) with decreasing contribution as it undergoes radioactive decay. While the contribution from ^{239}Pu decreases, the contributions from ^{226}Ra, ^{242}Pu, and ^{237}Np increases. Around 200,000 years, ^{226}Ra overtakes ^{239}Pu as the dominant radionuclide. After 250,000 years, ^{226}Ra, ^{242}Pu, and ^{237}Np are the major radionuclides.

The expected annual dose from all 300 epistemic vectors is shown on Figure 7.7.1-25. The expected annual dose of epistemic vector 286 is very similar to the mean annual dose and thus this epistemic vector was chosen for this analysis. Figure 7.7.1-26 presents the annual dose for the ten aleatory vectors paired with epistemic vector 286 (GoldSim realizations 2851 through 2860). Among these, realization 2,855, which has an igneous event occurring at 10,000 years, was chosen for the single realization analysis as its dose contribution starts early. The model for realization 2,855 was run twice to first save information for all the percolation subregions and then to specifically save EBS cell-pathway details related to percolation subregion 3 under dripping environment (GoldSim filenames: LA_v5.000_IG_003000_032.gsm and LA_v5.000_IG_003000_033.gsm; output DTN: MO0708TSPAVALI.000 [DIRS 182985]).

This analysis of realization 2,855 focuses on 5 major contributors to dose. They are ^{239}Pu; ^{226}Ra; ^{242}Pu; and ^{237}Np mentioned above; plus ^{234}U. ^{234}U is included in this analysis because ^{226}Ra is a decay product of ^{234}U and is largely controlled by the transport behavior of ^{234}U. Note that the annual dose from realization 2,855 slowly decreases, which is somewhat different from the late-time trend of the expected annual dose shown for epistemic vector 286, which also has contribution from other aleatory vectors with late igneous event times.

Figure 7.7.1-27 shows the time history of annual dose and the contributions to annual dose from the selected radionuclides for realization 2855. A spike in dose (1,000 mrem) is noticeable immediately after the igneous intrusion event. This spike is caused by mobile radionuclides such as ^{99}Tc, ^{129}I, and ^{14}C. Dose contributions from those mobile elements decrease very quickly. In about 6,000 years their doses decrease by more than two orders of magnitude from their peak and for this reason, these radionuclides are not analyzed in detail hereafter. While the contributions from these mobile radionuclides decrease, dose from ^{239}Pu, ^{237}Np, and ^{242}Pu increases and a plateau (400 to 700 mrem) forms between 36,000 and 126,000 years. The annual dose starts decreasing gradually after that.

Note in the Igneous Intrusion Modeling Case, there are differences in the EBS environment that affect the waste form degradation and radionuclide mobilization (discussed in Section 6.5.1.1.2) from that in the Nominal Scenario Class (discussed in Section 6.3.4).

Igneous Event—For realization 2,855, the igneous intrusion event occurs at 10,000 years. The event fails all CSNF and CDSP WPs (total number = 11,629) as well as the DSs. None of the WPs and DSs have failed by the nominal corrosion processes prior to this igneous event. The WPs and waste forms experience a high temperature (the peak temperature is 1,150°C) because of the heat of the magma. The high temperature converts the uranium in CSNF WPs to U_3O_8 that has a very high specific surface area (BSC 2004 [DIRS 169987], Section 6.2.2.2). The increased surface area of the U_3O_8 results in an essentially instantaneous degradation of CSNF. The high temperature also results in a very fast degradation of HLW glass. After 500 years (the following GoldSim specified timestep after the intrusive event), the WP temperature drops to 52°C.

EBS Releases—The high degradation rates of CSNF and HLW lead to quick release of the waste inventories into solution. Because of solubility constraints, some of the radionuclides precipitate within the waste form domain of the EBS transport model. As shown on Figure 7.7.1-28, following the igneous event, the dissolved concentrations of neptunium, plutonium, and uranium from CSNF waste form domain reach and maintain at their solubilities for variable time durations. The solution is saturated with neptunium for about 40,000 years after the intrusion event, while it is saturated with plutonium for about 200,000 years. The solution is always saturated with uranium due to its large inventory. However, Ra concentration is below its solubility in the CSNF waste form domain. The dissolved concentration of Ra increases first followed by gradual decrease, due to the decay chain ingrowth from ^{234}U and the decay of itself. The dissolved concentrations of neptunium and plutonium decrease rapidly once their precipitated mass is depleted. As a result, their releases at later time are not solubility controlled.

The gradual declines in uranium, neptunium, and plutonium solubilities between 10,000 and 170,000 years are caused by the slow shift of pH towards neutral and the decrease of P_{CO2} with time for that period of time, as shown on Figure 7.7.1-29. The sudden increase in neptunium solubility at 172,000 years (Figure 7.7.1-28) is because at this time the neptunium solubility controlling phase switches from NpO_2 to Np_2O_5 due to complete degradation of steel inside the waste form domain, which acts as a reductant (Section 6.3.7.5). The releases of plutonium, uranium, neptunium, and radium from CDSP waste form domain have similar characteristics.

As discussed in Section 6.5.1.1.1, in the Igneous Intrusion Modeling Case, every WP and DS is rendered incapable of protecting its contents after the igneous intrusion event. As a result, high seepage fluxes, which are set equal to the local percolation flux after igneous intrusion (Section 6.5.1) and range from 0.18 to 3.54 m^3/yr, flow through each WP. This in turn causes rapid release of radionuclides from the WPs once the temperature drops below the boiling point of water (Figure 7.7.1-30). Among the selected radionuclides, the highest peak release rate is observed for ^{237}Np (approximately 553 g/yr), and its release rate decreases gradually as its inventory is consumed. The releases of ^{242}Pu, ^{234}U, and ^{226}Ra have a similar trend, but the release of ^{239}Pu decreases rapidly because of its relatively short half-life (2.41×10^4 years). Figure 7.7.1-30 also shows that a large percentage (>90 percent) of ^{239}Pu is transported in the form of dissolved species with the rest in the form of colloidal species. In addition, the dissolved component of total ^{239}Pu increases with time. For ^{242}Pu, the dissolved species is more than 99 percent of its total. For this reason, only the dissolved component of plutonium will be analyzed hereafter.

Figure 7.7.1-31 shows the advective and diffusive release rates of major radionuclides from CSNF WPs. It shows that advection is the major transport mechanism for radionuclides released from WPs for the Igneous Intrusion Modeling Case. Diffusion contributes less than one percent of the total release from WPs except for ^{242}Pu at late time. Comparing Figure 7.7.1-31 with Figure 7.7.1-30 reveals that CSNF WPs are the dominant source for those major radionuclides.

Figure 7.7.1-32 presents the dissolved concentrations of neptunium, uranium, plutonium, and radium and their solubilities in the CSNF corrosion products domain for percolation subregion 3 under dripping environment. It shows that in the corrosion products domain, neptunium and plutonium concentrations maintain at their solubilities for a longer time than in the waste form domain (see Figure 7.7.1-28). However, unlike in the waste form domain, uranium concentration does not reach its solubility. Similar to the waste form domain, radium concentration does not reach its solubility. Moreover, the dissolved concentrations of neptunium and plutonium decrease at slower rates than in the waste form domain, because in the corrosion products domain, the corrosion products gradually release neptunium and plutonium that were once sorbed onto them. The solubility controlled releases of ^{237}Np and ^{239}Pu are responsible for the dose curve plateau between 36,000 and 126,000 years presented on Figure 7.7.1-27.

The changes in radium solubility at 57,500 and 340,000 years are due to pH changes that cause switches between the two values of the radium solubility (Section 6.3.7.5.2). The changes in uranium solubility at those times are also due to pH changes that cause switches between Na-boltwoodite controlled uranium solubility and schoepite controlled uranium solubility (Section 6.3.7.5.2 and Tables 6.3.7-56 and 6.3.7-57).

Natural System—The cumulative releases for ^{237}Np, ^{242}Pu, ^{234}U, and ^{226}Ra from the EBS, UZ, and SZ are presented on Figures 7.7.1-33 (a) through (d).

Figure 7.7.1-33(a) shows that there is a small delay for ^{237}Np in the UZ and SZ (500 years or one timestep for the UZ and another 500 years for the SZ). This small delay is due to predominance of fast transport along fracture pathway with limited diffusion into the matrix. At the end of the simulation (one-million years), 99 percent of neptunium that was released from the EBS has migrated through the UZ and 96 percent of that has migrated through the SZ. In other words, the UZ and SZ provide insignificant retardation for ^{237}Np in the Igneous Intrusion Modeling Case. This is attributed to the relatively small K_d values of neptunium. Similarly, ^{234}U is not retarded significantly by the UZ and SZ, as shown on Figure 7.7.1-33(b). The figure shows that the cumulative release of ^{234}U from the SZ after 330,000 years is higher than that from the EBS. This is not a numerical error but is caused by the inventory boosting performed at the UZ-SZ interface for transport through the SZ (Section 6.3.10.3).

The cumulative release curves for ^{242}Pu, presented on Figure 7.7.1-33(c), show that the UZ delays plutonium release for a few thousand years, while the SZ delays plutonium release for more than 10,000 years. At the end of the simulation, about 24 percent of ^{242}Pu that was released from the EBS was held in the UZ, and 29 percent of ^{242}Pu that was released from the UZ was held in the SZ. The UZ and SZ provide significant retardation for ^{242}Pu. This is attributed to sorption of plutonium in the SZ alluvium and the volcanic matrix as a result of fracture-matrix interaction.

The cumulative release history for ^{226}Ra is presented on Figure 7.7.1-33(d). It shows that a large amount of ^{226}Ra that was released from the EBS did not enter the biosphere. Without considering decay and decay chain ingrowth, at 1,000,000 years, only 25 percent of ^{226}Ra that was released from the EBS migrates through the UZ and less than 0.1 percent of ^{226}Ra that was released from the UZ migrates through the SZ. The significant reduction of ^{226}Ra mass at the UZ and SZ is caused by the high K_d values in the UZ and SZ (Tables 6.3.9-2 and 6.3.10-2). It not only retards the transport of ^{226}Ra through the UZ and SZ, but also causes a large percentage of ^{226}Ra to decay during the prolonged transport processes through the UZ and SZ due to the short half-life of ^{226}Ra (1,600 years; see Figure 6.3.7-4).

As pointed out previously, Figure 7.7.1-27 shows that the annual dose curve has a plateau that appears between 36,000 and 126,000 years. This plateau corresponds to the SZ groundwater concentration plateau of ^{237}Np and ^{239}Pu at the RMEI location for the same time period as shown on Figure 7.7.1-34. The concentration plateaus correspond to the solubility controlled releases of neptunium and plutonium from the corrosion products domain shown on Figure 7.7.1-32. Note that the SZ groundwater concentrations shown on Figure 7.7.1-34 are obtained by dividing the annual releases of radionuclides from the SZ by the 3,000 acre-ft/yr annual water usage, as required by federal regulations. Although the SZ groundwater concentration of ^{237}Np is higher than that of ^{239}Pu, the latter has a higher concentration-dose conversion factor, as shown in Table 7.7.1-1. As a result, ^{239}Pu dose is higher than ^{237}Np dose.

Table 7.7.1-1 gives the specific activities for major radionuclides and the sampled BDCF values for realization 2,855. The last column of the table lists the Concentration-Dose Conversion Factors for the individual radionuclides, which are obtained by multiplying specific activities by the sampled BDCF values. This table shows that ^{226}Ra has the highest concentration-dose conversion factor (2.90×10^{13} (mrem/yr)/(g/L)), while ^{237}Np has the lowest concentration-dose conversion factor (8.81×10^{8} (mrem/yr)/(g/L)). The annual doses for the major radionuclides, presented on Figure 7.7.1-27, are the products of the SZ groundwater concentrations (Figure 7.7.1-34) and the concentration-dose converting factor for realization 2,855.

Figure 7.7.1-34 shows that for the first 500,000 years, the ^{234}U concentration increases with time and then decreases, so does the ^{226}Ra concentrations. This suggests that ^{226}Ra concentration is largely controlled by ^{234}U concentration, since the former is a decay product of the latter.

This single realization analysis examined important aspects that control the release of radionuclides from WPs to the environment in the Igneous Intrusion Modeling Case. It demonstrated that submodels are connected properly and the model as a whole functions as constructed and designed, to the extent of single realization level. The objective of this confidence building activity has been achieved.

7.7.1.4 Seismic Ground Motion Modeling Case

This section presents an analysis of a single realization from the 9,000-realization base case run performed for calculating the expected dose from the Seismic GM Modeling Case (GoldSim filename: LA_v5.000_SM_009000_000.gsm; output DTN: MO0709TSPAREGS.000 [DIRS 182976]) for the million-year simulation duration. The expected annual dose is presented on Figure 7.7.1-35, where each of the 300 realizations represent expected annual dose for one

epistemic uncertainty vector. The expected annual dose for each epistemic uncertainty vector is generated by taking an expectation over a sample of 30 aleatory uncertainty vectors (for more details on the computational methodology, refer to Sections 6.1.2.4.4 and 7.3.2.6.2). A single epistemic vector is selected for further analysis in such a manner that the expected annual dose is broadly representative of the modeling case and similar in behavior to the mean annual dose curve (Figure 7.7.1-35).

The epistemic uncertainty vector 155 is selected. The thirty corresponding aleatory sampling sequences are GoldSim realizations 4,621 through 4,650 (Figure 7.7.1-36). Of these, GoldSim realization 4,641 is selected for further analysis (solid red curve). Note that realization 4,641 represents epistemic uncertainty vector 155 and aleatory uncertainty vector (sampling sequence) 21. The GoldSim file for realization 4,641 was run twice to first save information for all the percolation subregions and then to specifically save EBS cell-pathway details related to percolation subregion 3 for the dripping environment (GoldSim filenames: LA_v5.000_SM_009000_016.gsm and LA_v5.000_SM_009000_017.gsm; output DTN: MO0708TSPAVALI.000 [DIRS 182985]).

The annual dose from realization 4,641 is presented on Figure 7.7.1-37 along with the dose contribution from major radionuclides. In general, the annual dose profile shows four peaks, of which two of them occur before 100,000 years and the remaining two around 200,000 years. Before 300,000 years, the dominant radionuclides are ^{99}Tc, ^{129}I, ^{79}Se, ^{239}Pu, but afterwards the dose is predominantly from ^{242}Pu with minor contribution from ^{135}Cs and ^{237}Np. The dose increases gradually past 300,000 years and there is no dose prior to 24,500 years.

Seismic events are modeled as a Poisson process that are generated randomly with the specified rate of 4.287×10^{-4} yr^{-1} (equal to the difference between maximum annual exceedance frequency of 4.287×10^{-4} yr^{-1} and the minimum annual exceedance frequency of 1×10^{-8} yr^{-1}) (Section 6.6.1.3.2). Over the course of any simulation several seismic events can occur with an average value of 428 events (computed by multiplying the specified rate of the Poisson process, 4.287×10^{-4} yr^{-1}, by the simulation time-period of one-million years). For realization 4,641, as shown on Figure 7.7.1-38, a total of 460 seismic events occur over the simulated duration. The horizontal component of the PGV corresponding to each seismic event is also shown, which is calculated from the mean bounded seismic hazard curve (Figure 6.6-6) by uniformly sampling the annual exceedance frequency between the minimum and maximum values for each event and reading the corresponding PGV value.

The probability of damage from an event is calculated separately for the CDSP and CSNF packages due to the inclusion of TAD canister in the CSNF packages, which increases its structural strength. Though the response surface for the probability of damage is different among CDSP and CSNF packages they are both functions of the PGV and the residual stress threshold of Alloy 22. The PGV value varies by each seismic event (as shown on Figure 7.7.1-38) while the residual stress threshold of Alloy 22 is treated as an epistemic uncertainty with a sampled value of 91.92 percent of the yield strength which is held constant over the realization. The residual stress threshold can vary uniformly from 90 percent to 105 percent of the yield strength and thus the value of 91.92 percent indicates a sample from the lower end of the distribution. A lower residual stress threshold value typically results in a greater probability of damage to the WP during a given seismic event; however, the actual

damage depends on a number of other conditions, such as whether the WP has intact internals or degraded internals, whether the DS framework and plate are intact or not, or whether the WP is covered by rubble or not. These conditions are determined separately.

Based on the DS plate and framework fragility analysis (Section 6.6.1.3.5), which is a function of DS plate and framework thickness at the event time, the fraction of the drift filled by rubble (in lithophysal zones) at the event time, and the PGV of the event, it is calculated that the DS framework does not fail until after 90,485 years and the DS plate does not fail until 268,000 years (Figure 7.7.1-39). It should be noted that at the time of DS plate failure the fraction of drift filled by rubble is still less than half. The failure time of the DS from rubble fill due to seismic events is computed to be much earlier than the DS failure time from general corrosion processes, which is computed to occur around 307,000 years.

The first damage time from a seismic event for the WP (Section 6.6.1.3.8) is determined separately for CDSP and CSNF WP, and it is calculated as the earliest of (a) the first damage time to the WP surrounded by rubble (using degraded internals damage abstraction) after the DS (either framework or plate) is failed or (b) the first damage time to the intact WP moving freely beneath the intact DS (the probability of damage is a function of PGV and residual stress threshold, assuming a 23-mm thickness of the WP outer barrier).

For CDSP WP, the first damage is caused by the seismic event at about 24,100 years, which is much earlier than the DS failure time (DS framework fails at 90,485 years). The PGV of the seismic event is about 0.7 m/s and at the sampled residual stress threshold of 91.92 percent, based on results presented on Figure 6.6-11a, the probability of damage is computed to be about 0.22. This value is compared to a random number generated by sampling a uniform distribution between 0 and 1 for each seismic event, such that if the probability of damage exceeds the random number then the WP damage would occur. At the event time of about 24,100 years, the random number value is 0.15 and thus the CDSP WP damage occurs. All CDSP WPs fail at this time as there is no spatial variability from seismic damage. The number of CDSP WPs failing in each percolation subregion for both dripping and non-dripping environments is shown on Figure 7.7.1-40.

For CSNF WP, the first damage that could result from a seismic event is calculated to be around 850,000 years. This evaluation is based on the damage abstraction of WP surrounded by rubble (using the degraded internals damage abstraction) after the DS is failed. This is to be expected since the probability of the WP getting damaged directly from a seismic event is extremely small (Figure 6.6-10a). However, the breach times from stress corrosion cracking by nominal processes, as calculated by WAPDEG, are much earlier than the seismic damage time. The WAPDEG calculated breach times differ for each percolation subregion due to spatial variability in the corrosion processes and thermal profiles of the WP. The first breach on CSNF WPs in percolation subregion 1 occurs at around 192,000 years, at around 168,000 years in percolation subregion 2, and around 204,000 years in percolation subregions 3, 4, and 5. Once any WP in a given percolation subregion is breached by the nominal corrosion processes, then to evaluate the damage from the subsequent seismic events, the degraded internals abstraction is conservatively applied to all WPs in that percolation subregion. Since the DS plate has not failed yet (failure time is 268,000 years), the seismic damage abstraction for fully degraded internals under intact DS is used (Figures 6.6-10b and 10c). The total number of CSNF packages that fail in each

percolation subregion for both dripping and non-dripping environment is shown on Figure 7.7.1-41. Since the first CSNF WP breach in the percolation subregion 2 occurs the earliest, one of the seismic events that occurs within the next timestep leads to failure of all WPs in that percolation subregion. All other percolation subregions following their first breaches undergo gradual failures of CSNF WPs from nominal processes until around 224,000 years, when a seismic event occurs that causes failure of all the CSNF WPs in the given percolation subregion. Note that the WP outer barrier thickness is greater than 23 mm in all percolation subregions when the seismic damage occurs. This highlights that even when the outer barrier thickness is near its maximum value, there is high probability of WP failure from seismic event when fully degraded WP internals abstraction under intact DS is used.

Although all CDSP WPs fail around 24,100 years, the damaged area on a WP increases gradually from subsequent seismic events. At each seismic event the probability of damage is computed and if it exceeds the random number then the corresponding damage area is added to the previous damaged area. The probability of damage from seismic event is based on using the damage abstractions for CDSP WPs with degraded internals under intact DS as shown on Figures 6.6-11b and 11c. When the outer barrier thickness is between 23 mm and 17 mm, the probability of damage is linearly interpolated between these two end member damage abstractions based on the thickness. Similarly, the damaged areas are computed from sampling gamma distributions for 23 mm and 17 mm outer barrier thickness as a function of the PGV and residual stress threshold and linearly interpolated. The mean damaged area of a CDSP WP with degraded internals under intact DS is shown on Figure 6.6-13. The failure-area time history for percolation subregion 3 for dripping environment is shown on Figure 7.7.1-42. Before 600,000 years the predominant damage area is from stress corrosion cracks due to seismic events, while the breach area from general corrosion patches becomes dominant afterwards. The initial damage area increases sharply around 49,000 years followed by a few more increases from events that cause damage, but after the DS plate failure (around 268,000 years) the WP is assumed to be surrounded by rubble and the probability of damage becomes even smaller leading to no failure from subsequent seismic events until the seismic event that occurs about 850,000 years.

Since the general corrosion patches on the WP do not appear until much later (500,000 years or more), all of the release from the WP is diffusive through stress corrosion cracks (at least until 500,000 years). The comparison of diffusive mass flux of ^{99}Tc out of the WP, which is the major dose contributor in the first 280,000 years (Figure 7.7.1-37), for various percolation subregions for CDSP WPs, is shown on Figure 7.7.1-43a. The releases start when the WP is first damaged, then decrease with time as steady state conditions get established, but then increase again around 49,500 years due to increase in the damage area (Figure 7.7.1-42). Most of the ^{99}Tc mass in the inventory is released out of the WP in the following few timesteps as there is no solubility controlling mineral phase for ^{99}Tc. The small diffusive areas associated with the WP outer barrier exert a strong control on the diffusive release of ^{99}Tc out of the EBS. In contrast, the diffusive mass flux of ^{242}Pu out of the WP, which is the major dose contributor past 280,000 years (Figure 7.7.1-43b), follows the WP outer barrier area curve indicating that the diffusive release is proportional to the opening area. The release is maintained for the simulated time because of various factors, such as: (a) ^{242}Pu has a comparatively long half life (~ 375,000 years), (b) the dissolved concentration inside the waste form domain is controlled by the solubility controlling mineral phase and thus not all of the degraded mass is available for

release, (c) the sorption of ^{242}Pu in the corrosion products domain retards the transport and further reduces the concentration gradient for diffusive flux, and (d) the small diffusive areas associated with the WP outer barrier reduces the mass flux. Of these factors, the most important is the sorption onto the corrosion products. For example, in the percolation subregion 3 for dripping environment, 1,055 CDSP WPs fail around 24,100 years. The total initial ^{242}Pu mass in the inventory, combined for HLW and DSNF mass, is about 38.66 g/pkg (from Table 6.3.7-5 with adjustment based on the uncertainty in the inventory). Using the decay rate of 1.85×10^{-6} yr^{-1}, the maximum mass at breach time would be about 36.97 g/pkg and about 35.31 g/pkg at 49,000 years (the time when the breach area increases). Based on the results of the calculation, the sorbed mass on corrosion products at 49,000 years is about 35.3 g/pkg, which accounts for almost all of the available mass. The mass gets slowly released by desorption from corrosion products into the solution, thus controlling the dissolved concentration (Figure 7.7.1-44) and the diffusive flux. Note that a mechanistic competitive sorption model that considers kinetic sorption-desorption processes is implemented for plutonium in the corrosion products domain. As a result, the concentration variations in the corrosion products domain are moderated even though the upstream concentrations (in waste form domain) could vary over a larger range based on degradation rates and solubility.

The diffusive flux of ^{99}Tc and ^{242}Pu from all five percolation subregions for CSNF WPs is shown on Figures 7.7.1-45a and b. The release from percolation subregion 2 is earlier than others as expected since the WP failure in percolation subregions 2 occurs earlier as shown on Figure 7.7.1-41. Figure 7.7.1-46 shows the WP outer barrier opening area with time for CSNF WPs that belong to the percolation subregion 3 for dripping environment. As discussed for CDSP packages, the ^{99}Tc diffusive release starts at the time of first breach and increases as the WP area increases. The inventory is quickly depleted and the concentrations fall rapidly. In contrast, the ^{242}Pu release is gradual and follows the breach area curve. The breached area increases after about 800,000 years after the patch area becomes significant. Although all CSNF WPs in a given percolation subregion undergo failure from seismic event at the same time, the release of ^{242}Pu is gradual due to sorption on the corrosion products. Figure 7.7.1-47 shows the example for percolation subregion 3 for dripping environment, where most of the ^{242}Pu mass released is sorbed on the corrosion products and then is gradually released by desorption thereby controlling the dissolved concentration and diffusive release out of the WP.

The pH and ionic strength time history in the corrosion products domain is shown on Figure 7.7.1-48. The first sharp decline in ionic strength occurs around 380,000 years because that is the time when rubble fills the drift (a consequence of multiple seismic events). At that time, the differential temperature and relative humidity time histories for a high thermal conductivity rubble is imposed leading to a small increase in relative humidity from 0.9956 to 0.9984. Since this increase in relative humidity corresponds to an equivalent increase in activity of water, it causes an appreciable decrease in ionic strength, indicating its high degree of sensitivity to relative humidity under vapor influx conditions (see Section 6.3.7.2.2 for details on ionic strength abstraction). The second decline in ionic strength that occurs around 724,000 years is caused by water flowing through the WP after general corrosion patches have formed and exceeding a threshold of 0.1 L/yr, thereby leading to a change in the in-package chemistry abstraction from calculations based on vapor influx to calculations based on liquid influx. Despite the changes in ionic strength over the course of the simulation, pH in the corrosion

products domain remains nearly constant as a result of buffering by surface complexation reactions.

Most of the ^{242}Pu mass released from the WP is in the dissolved state and very little is associated with colloids. This is because (a) the groundwater colloids in the WP are not present until 600,000 years as there is no flow through the WP, (b) the iron oxyhydroxide colloids and CSNF waste form colloids are unstable under the given pH and ionic strength conditions throughout the simulated duration (see Figure 6.3.7-11 for colloid stability relationships), and (c) the uranium colloids, which become stable around 384,000 years when the ionic strength drops from about 0.3 mol/kg to about 0.1 mol/kg, have limited carrying capacity as both the colloid concentration (about 3.7 mg/L) and the K_d for plutonium (about 247 ml/g) is small.

The total EBS release (summed over all percolation subregions) of ^{99}Tc and ^{242}Pu from CSNF and CDSP WPs is shown on Figure 7.7.1-49. As expected, the mass release from CSNF WPs is higher than that for CDSP WPs due to greater number of WPs and larger inventory on a per package basis (Tables 6.3.7-1 and 6.3.7-5). The majority of the mass passed to the UZ from EBS at the repository horizon goes into the fracture nodes of the UZ as compared to the matrix nodes, as shown on Figure 7.7.1-50 for ^{242}Pu. This is because the majority of the WPs in a given percolation subregion are in the dripping environment where drift seepage that flows out through the invert carries the mass advectively through the fractures even though most of the mass is diffusing out of the WP. For percolation subregion 1, the fraction of mass going into the fracture is relatively small (around 0.4) and increases (to around 0.9) at 396,000 years. This behavior is due to the change in seepage flux, which remains relatively small (about 0.005 m^3/yr) until around 396,000 years and then increases to a value of about 0.08 m3/yr. This is because at this time, the nonlithophysal locations are considered to be collapsed from drift degradation based on the drift seepage model abstraction, resulting in the seepage flux for such locations to change from the non-collapsed drift seepage to the percolation flux (Section 6.3.3.1.2). The effect of this change is greatest for percolation subregion 1 because, compared to other percolation subregions, it has (a) the smallest ambient seepage rates prior to the drift collapse and (b) he highest fraction of nonlithophysal locations (about 32 percent).

The cumulative mass release from EBS, UZ, and SZ are compared on Figure 7.7.1-51 for ^{99}Tc and ^{242}Pu. The transport characteristics are quite different for ^{99}Tc and ^{242}Pu in the UZ and SZ domains as ^{99}Tc is transported as unretarded species while ^{242}Pu undergoes significant retardation due to sorption on the tuff matrix and alluvium. Almost all of the mass that is released from the EBS for ^{99}Tc is also released out of the SZ model boundary within a relatively short period compared to the simulation time. In contrast, the amount of ^{242}Pu mass released from the UZ and SZ model boundaries at the end of simulation (one-million years) is appreciably smaller than that released out of the EBS (about 67 percent in UZ and 34 percent in SZ), indicating significant retardation. Since most of the mass is passed to the fracture nodes of the UZ, the mass mostly diffuses from the fracture continuum into the matrix continuum due to fracture-matrix interaction in the UZ with some also advecting due to lateral flow. Even though the free water diffusion coefficient in the UZ (as in EBS) varies by species (Table 6.3.9.3), the difference is relatively small between ^{99}Tc and ^{242}Pu and can be ignored for all practical purposes. Thus, both are likely to equally diffuse (assuming equal concentrations) into the matrix continuum from the fracture continuum. Because of the sorption of ^{242}Pu in the UZ matrix, the concentration gradient from the fracture to matrix is higher for ^{242}Pu compared to

^{99}Tc leading to its greater diffusive flux into the matrix and lesser cumulative release at the UZ-SZ boundary. In the SZ domain, the mass release from each of the four UZ regions is passed to the corresponding SZ region. In each SZ region, a location is randomly selected as the starting point for transport, which is manifested through sampling one of the 200 pre-generated SZ breakthrough curves for a given species (Section 6.3.10.2). Separate sets of breakthrough curves are available for ^{99}Tc and ^{242}Pu due to their different transport characteristics through the volcanic units and alluvium. The breakthrough curves are pre-generated as an impulse response function to a unit pulse and are convolved with the incoming UZ mass flux using the convolution integral approach to produce the SZ mass flux at the location of the RMEI. In this realization, the SZ breakthrough curve 122 is selected and the breakthrough times for all four zones for ^{99}Tc and ^{242}Pu are compared on Figure 7.7.1-52. The breakthrough of ^{99}Tc from all four SZ regions is much earlier than that for ^{242}Pu, with almost half of the mass input recovered after a few hundred years of travel in the SZ for ^{99}Tc compared to almost 100,000 years of travel time required for ^{242}Pu. However, there is a long tail in the breakthrough curve for ^{99}Tc for the remaining half of the input mass that results from longitudinal and transverse dispersion in the volcanic units and alluvium are due to fracture-matrix diffusive interaction in the dual porosity volcanic domain of the SZ transport model. The ^{242}Pu breakthrough is further impacted by sorption in the volcanic matrix and by sorption to the alluvium. For SZ breakthrough curve 122, the initially sampled plutonium K_d for volcanic matrix units is around 120 ml/g and that for the alluvium is 107 ml/g, which are modified to calculate effective K_d values but nevertheless introduce significant retardation. Most of the transport of plutonium occurs in the dissolved phase with a small fraction (less than 0.001) being transported via reversible sorption on the groundwater colloids. This is because the groundwater colloid concentration sampled is about 0.11 mg/L and the K_d for plutonium on the colloid is sampled to be about 6,560 ml/g, which when multiplied together, provided the mass associated with colloids compared to mass in dissolved state per unit water volume.

The SZ release rates for ^{99}Tc and ^{242}Pu are shown on Figure 7.7.1-53 for realization 4,641. They more or less follow the release rates out of the EBS (Figure 7.7.1-49). The SZ releases are converted into annual dose by taking the annual releases out of the SZ for each radionuclide, dissolving them in the 3,000 acre-ft of water (annual usage at RMEI as defined by the regulation) to compute the mass concentrations, converting the mass concentration into concentration of radioactivity (in curies per liter of water), and then multiplying with the corresponding BDCFs computed for the modern-interglacial climate (present-day climate). The end result of this is Figure 7.7.1-37.

7.7.1.5 Summary

The single realization analyses, of the four modeling cases, provide a useful insight into the interaction of several submodels under varying thermal-mechanical-chemical-physical conditions in the repository. They help in understanding the coupling of the EBS, UZ, and SZ transport models for calculating the annual dose to RMEI in a given realization. Within each transport model domain, the interaction of various submodels (and their abstractions) under a given set of physicochemical conditions is described in detail, which provides confidence that the submodels are coupled as intended and their behavior can be explained in a logical manner leading to the dose calculations. Besides explaining the interaction of submodels, the transport behavior of major dose contributing radionuclides is also described and highlighted in the

various modeling cases. For example, the Waste Package EF and Drip Shield EF Modeling Cases highlight the controls on transport at early times when the repository is hot and show the effect of climate changes while the DS are still intact. In contrast, the Igneous Intrusion and Seismic GM Modeling Cases show the effects of various processes occurring late in time and when the DSs are breached. In all cases the early release following the WP breach is dominated by non-sorbing and non-solubility limited radionuclides such as ^{99}Tc and ^{129}I, while the late time release is dominated by longer-lasting solubility-limited radionuclides that undergo sorption such as ^{242}Pu, ^{237}Np, and ^{239}Pu.

INTENTIONALLY LEFT BLANK

Table 7.7.1-1. Calculation of Dose Per Unit Concentration of Selected Radionuclides for the Igneous Intrusion Modeling Case (for Realization 2855)

Radionuclide	Specific Activity (Ci/g)[a]	BDCF (mrem/yr)/(pCi/L)[b]	Concentration-Dose Converting Factor[c] (mrem/yr)/(g/L)
^{237}Np	7.05E-04	1.25E+00	8.81E+08
^{239}Pu	6.21E-02	3.57E+00	2.22E+11
^{242}Pu	3.94E-03	3.39E+00	1.34E+10
^{234}U	6.21E-03	4.03E-01	2.50E+09
^{226}Ra	9.89E-01	2.93E+01	2.90E+13

[a] Taken from the species element of GoldSim file: LA_v5.000_IG_003000_032.gsm (output DTN: MO0708TSPAVALI.000) [DIRS 182985]).
[b] Taken from BDCF_Nominal element of GoldSim file: LA_v5.000_IG_003000_032.gsm (output DTN: MO0708TSPAVALI.000 [DIRS 182985]).
[c] Dose per unit concentration (mrem/yr)/(g/L) = (Specific Activity)∗(BDCF)∗(1E+12 pCi/Ci).

INTENTIONALLY LEFT BLANK

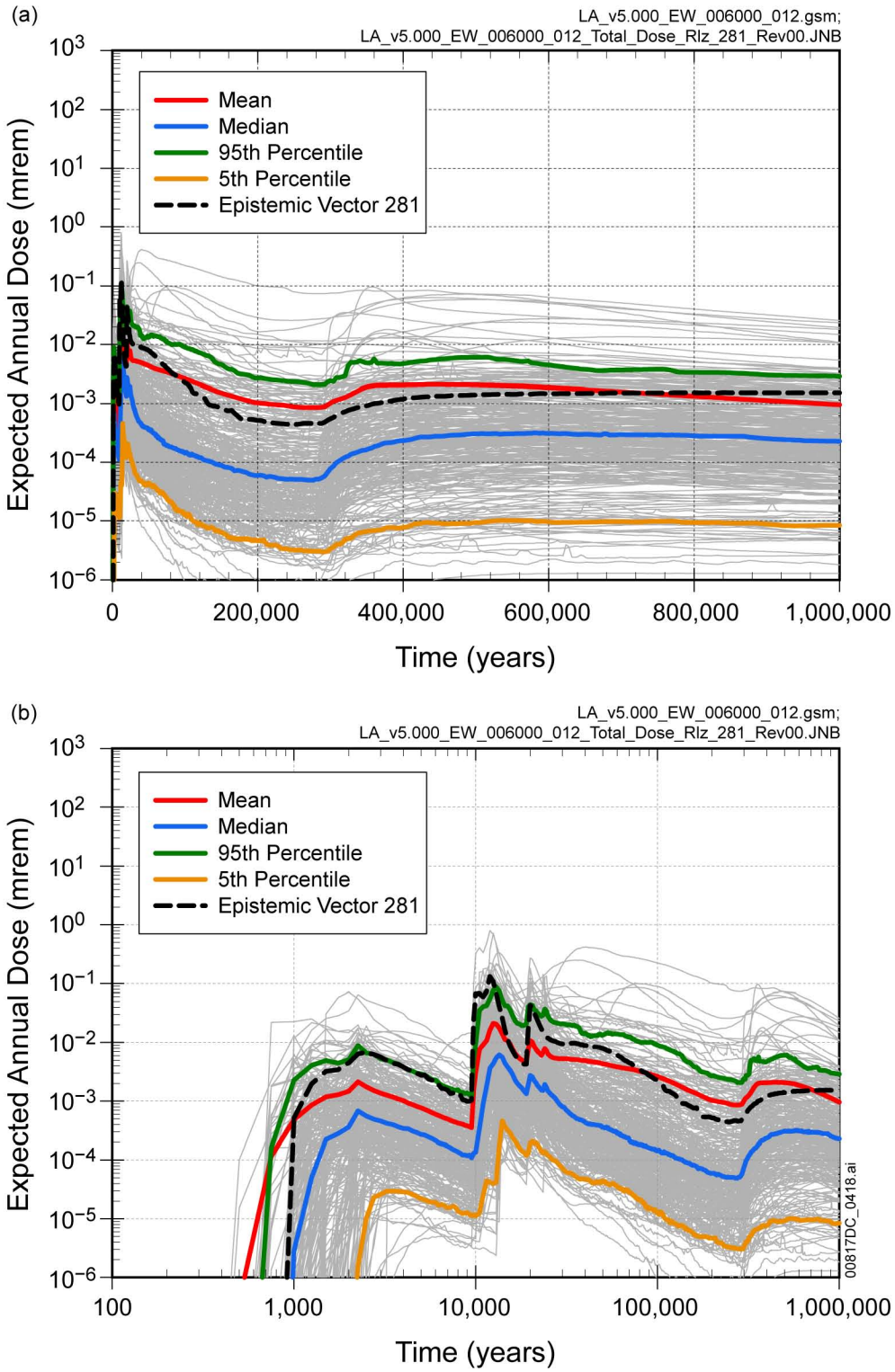

Source: Output DTN: MO0709TSPAREGS.000 [DIRS 182976].

Figure 7.7.1-1. Expected Annual Dose for the Waste Package Early Failure Modeling Case for the 1,000,000-Year Simulation after Repository Closure: (a) Linear Time and (b) Log Time

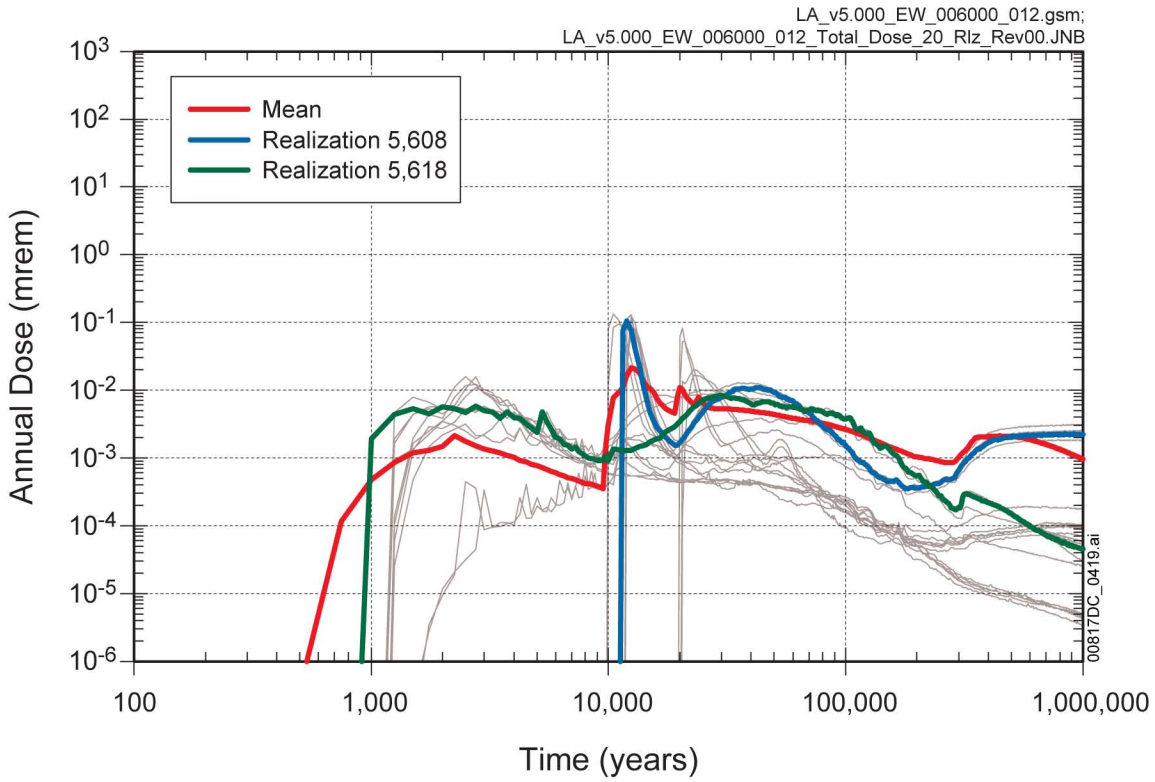

Source: Output DTN: MO0709TSPAREGS.000 [DIRS 182976].

Figure 7.7.1-2. Annual Dose from Realizations 5601 through 5620 of the Waste Package Early Failure Modeling Case for the 1,000,000-Year Simulation after Repository Closure

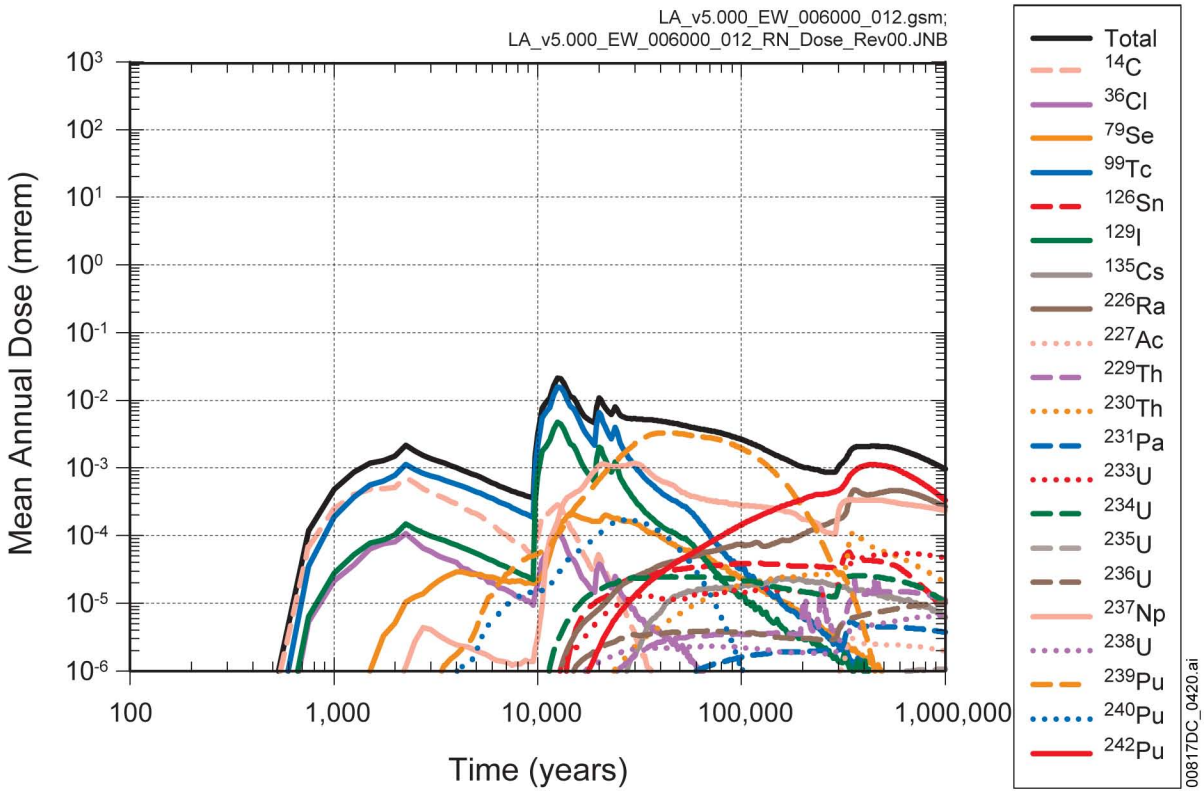

Source: Output DTN: MO0709TSPAREGS.000 [DIRS 182976].

NOTES: ^{226}Ra dose is the sum of ^{226}Ra and ^{210}Pb doses (secular equilibrium assumed).

Figure 7.7.1-3. Major Radionuclide Contributors to Mean Annual Dose for the Waste Package Early Failure Modeling Case for the 1,000,000-Year Simulation after Repository Closure

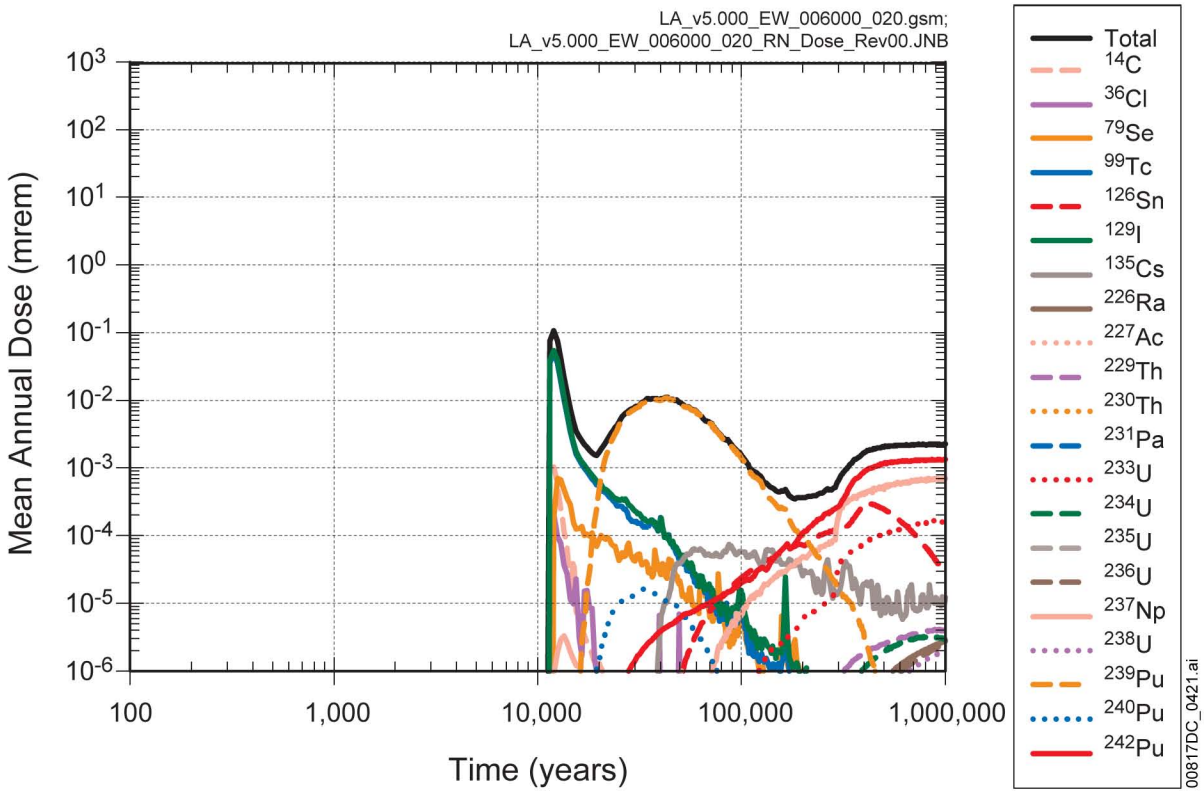

Source: Output DTN: MO0708TSPAVALI.000 [DIRS 182985].

NOTES: ^{226}Ra dose is the sum of ^{226}Ra and ^{210}Pb doses (secular equilibrium assumed).

Figure 7.7.1-4. Major Radionuclide Contributors to Mean Annual Dose for Realization 5608 of the Waste Package Early Failure Modeling Case for the 1,000,000-Year Simulation after Repository Closure

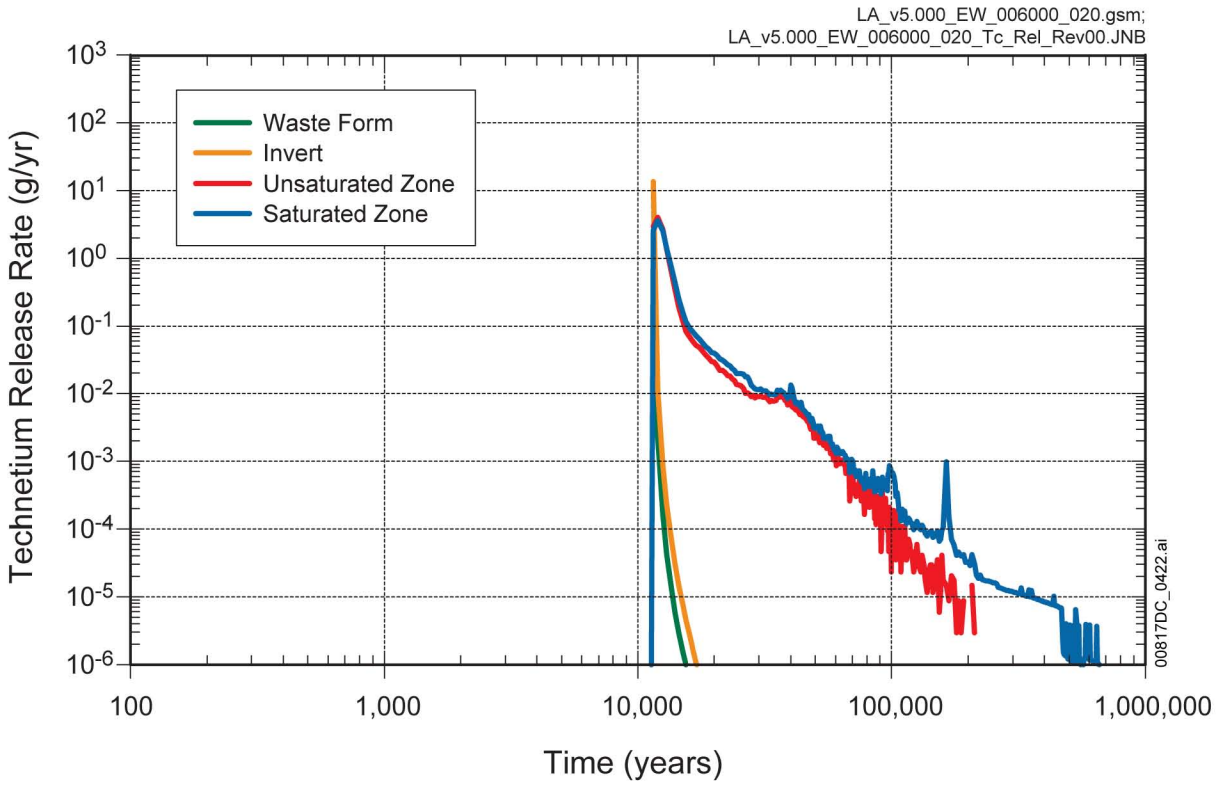

Source: Output DTN: MO0708TSPAVALI.000 [DIRS 182985].

Figure 7.7.1-5. Release Rates of Technetium from the Waste Form, EBS, Unsaturated Zone, and Saturated Zone for Realization 5608 of the Waste Package Early Failure Modeling Case for the 1,000,000-Year Simulation after Repository Closure

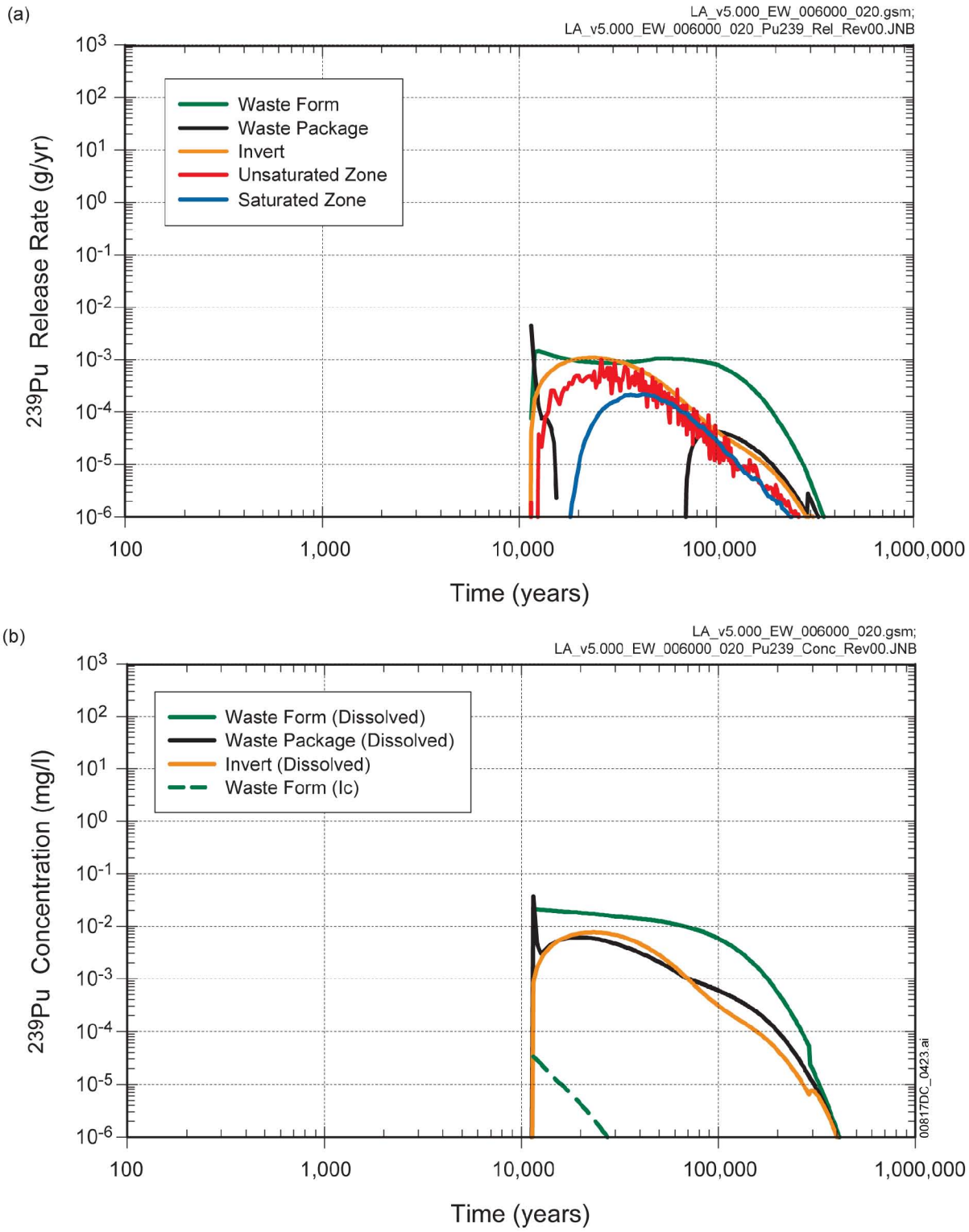

Source: Output DTN: MO0708TSPAVALI.000 [DIRS 182985].

Figure 7.7.1-6. (a) Release Rates and (b) Concentration of ^{239}Pu for Realization 5608 of the Waste Package Early Failure Modeling Case for the 1,000,000-Year Simulation after Repository Closure

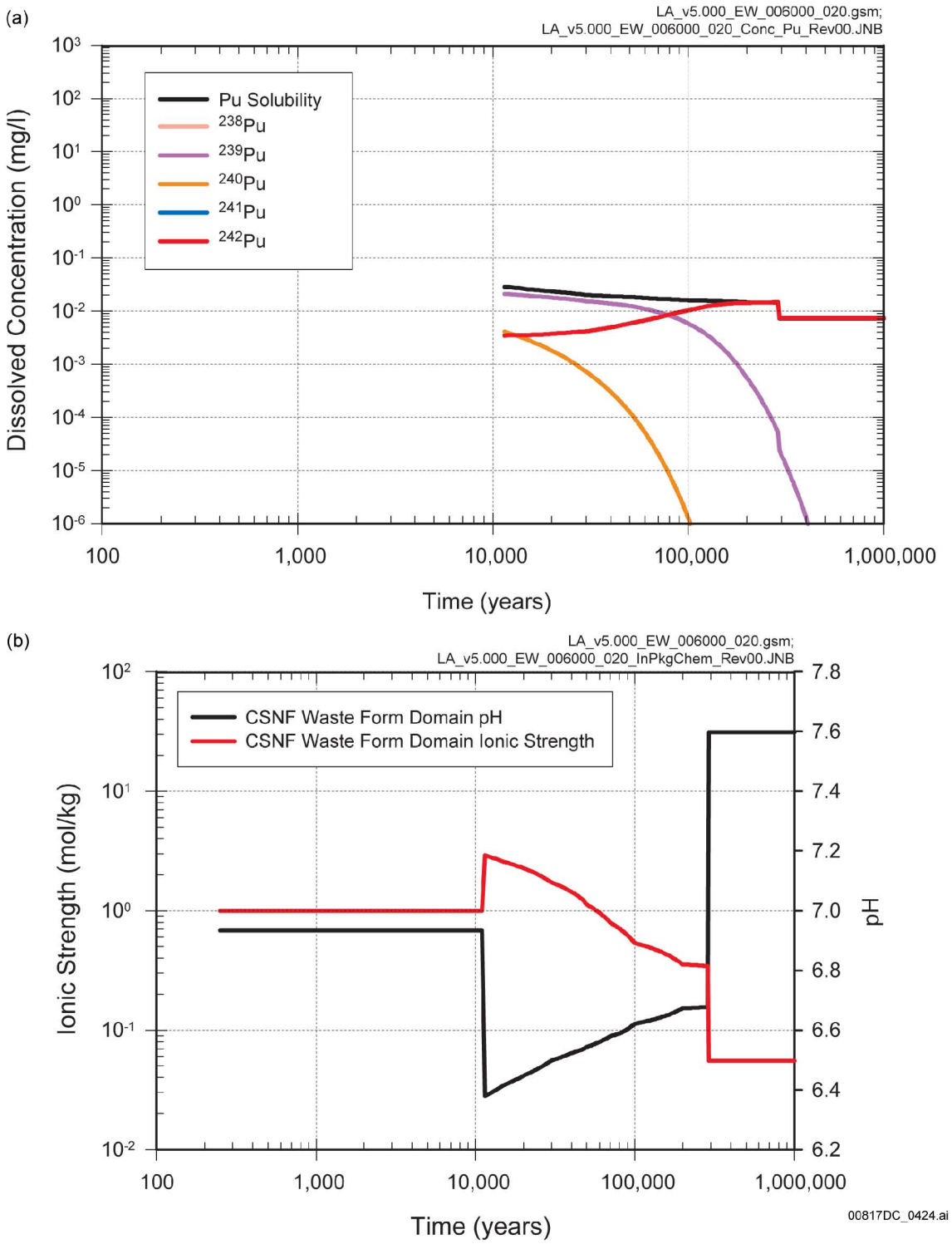

Source: Output DTN: MO0708TSPAVALI.000 [DIRS 182985].

Figure 7.7.1-7. (a) Dissolved Concentrations of Plutonium in the CSNF Waste Form Domain for Realization 5608 and (b) CSNF Waste Form Domain Chemistry for Realization 5608 of the Waste Package Early Failure Modeling Case for the 1,000,000-Year Simulation after Repository Closure

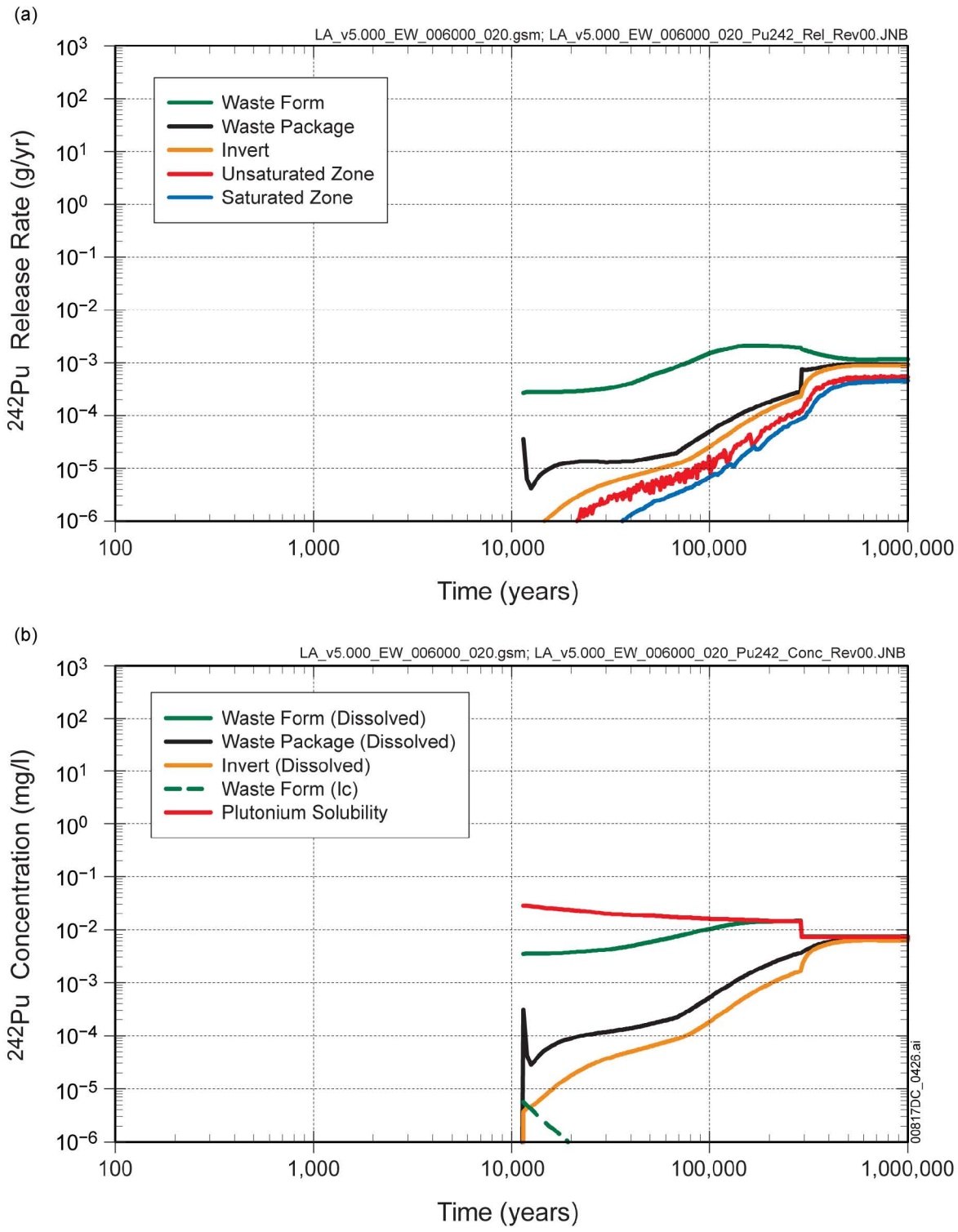

Source: Output DTN: MO0708TSPAVALI.000 [DIRS 182985].

Figure 7.7.1-8. (a) Release Rates and (b) Concentration of ^{242}Pu for Realization 5608 of the Waste Package Early Failure Modeling Case for the 1,000,000-Year Simulation after Repository Closure

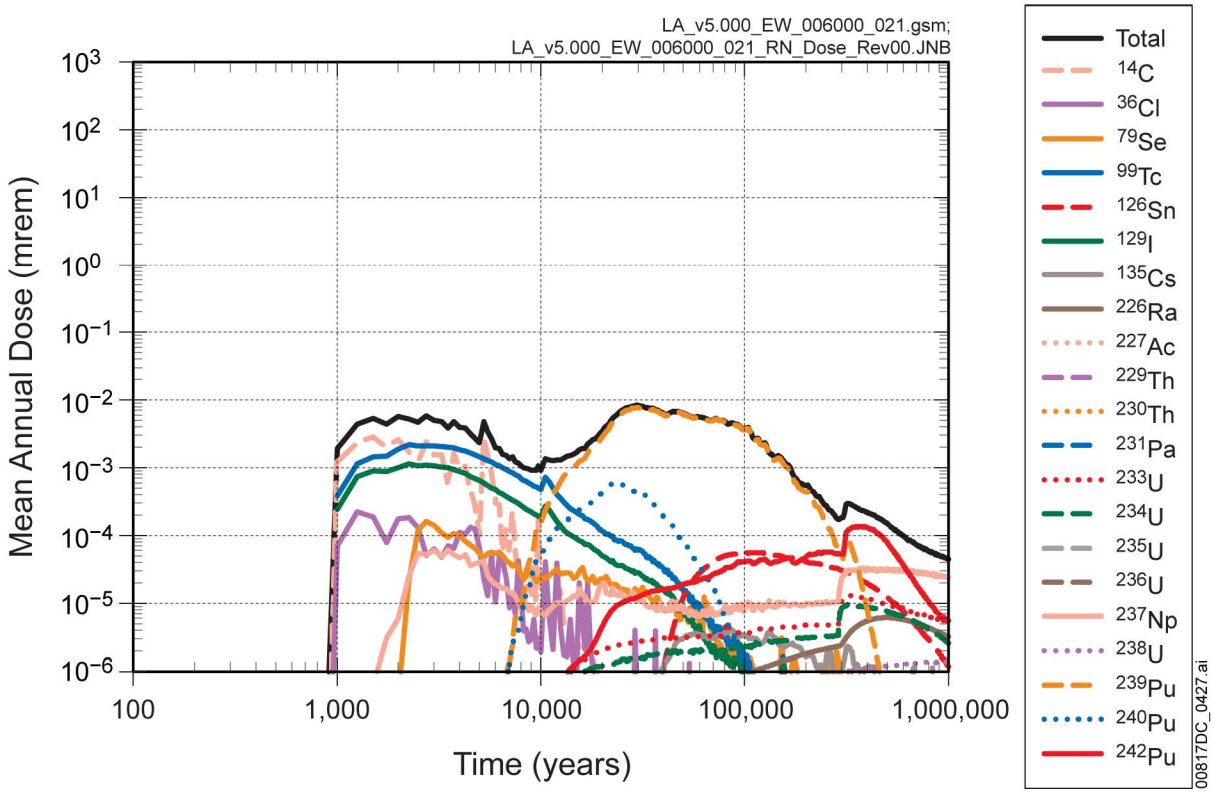

Source: Output DTN: MO0708TSPAVALI.000 [DIRS 182985].

NOTES: ^{226}Ra dose is the sum of ^{226}Ra and ^{210}Pb doses (secular equilibrium assumed).

Figure 7.7.1-9. Major Radionuclide Contributors to Mean Annual Dose for Realization 5618 of the Waste Package Early Failure Modeling Case for the 1,000,000-Year Simulation after Repository Closure

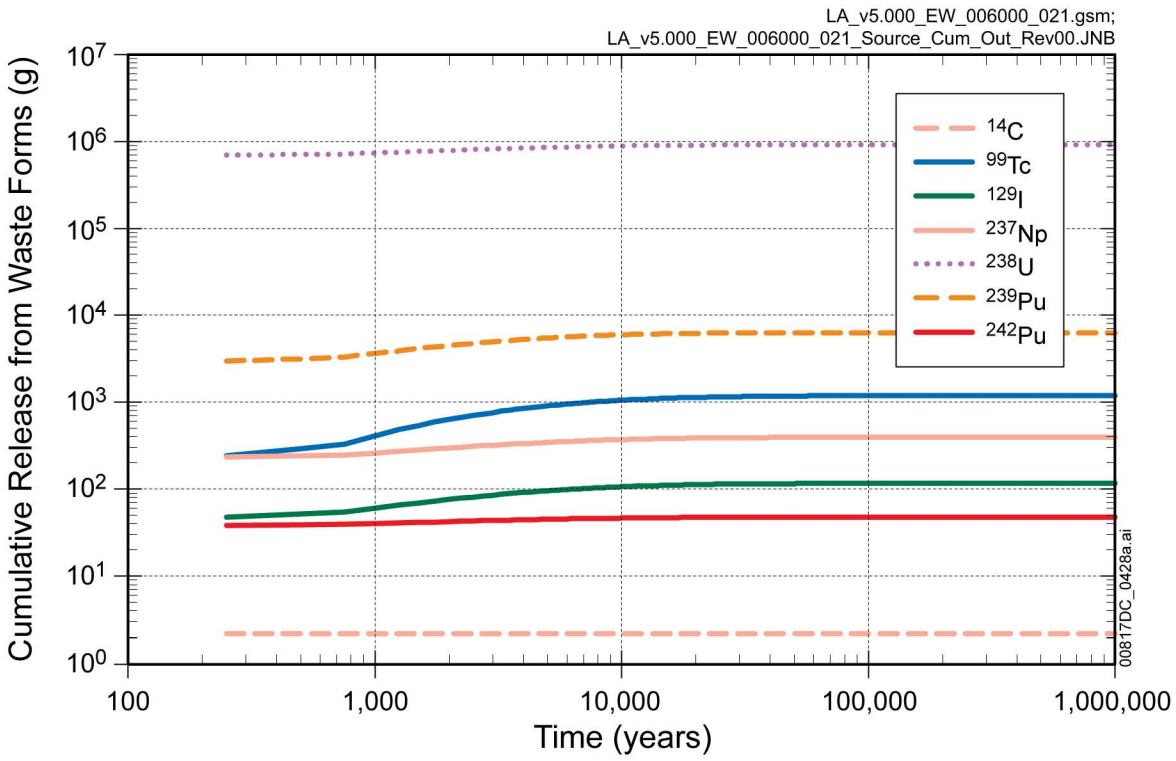

Source: Output DTN: MO0708TSPAVALI.000 [DIRS 182985].

Figure 7.7.1-10. Cumulative Release from HLW and DSNF Waste Forms for Realization 5618 of the Waste Package Early Failure Modeling Case for the 1,000,000-Year Simulation after Repository Closure

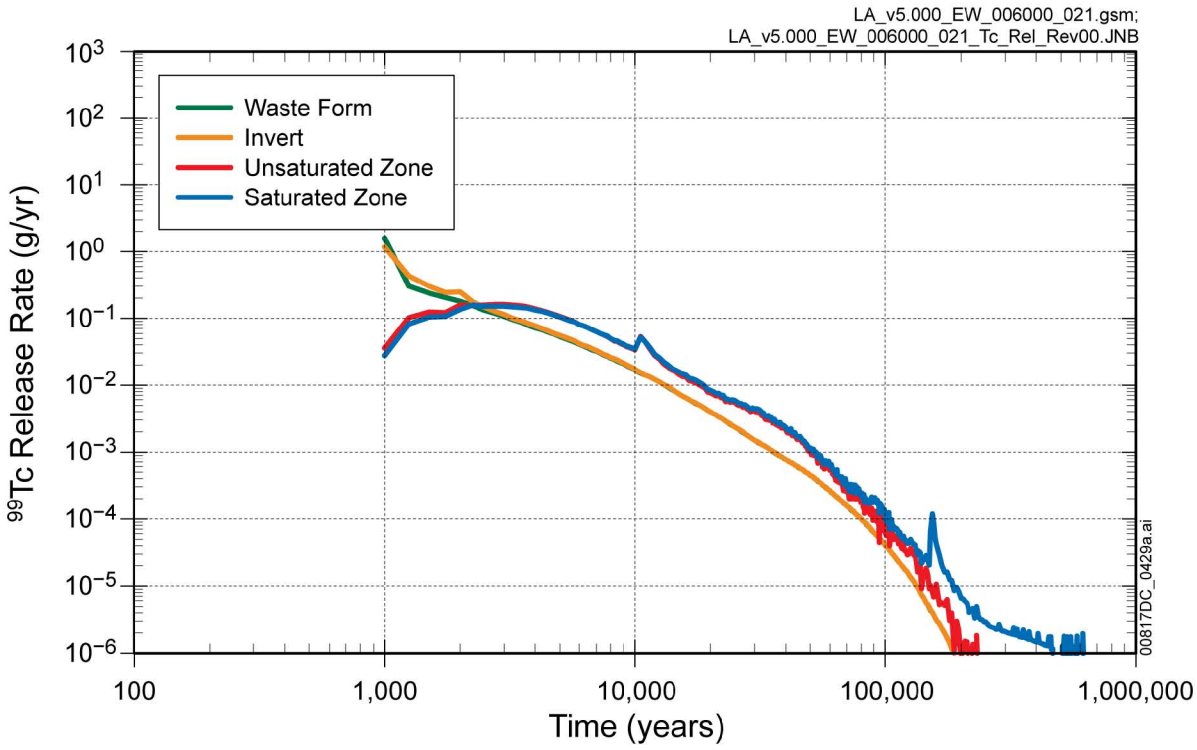

Source: Output DTN: MO0708TSPAVALI.000 [DIRS 182985].

Figure 7.7.1-11. Release Rates of ^{99}Tc from the Waste Form, EBS, Unsaturated Zone, and Saturated Zone for Realization 5618 of the Waste Package Early Failure Modeling Case for the 1,000,000-Year Simulation after Repository Closure

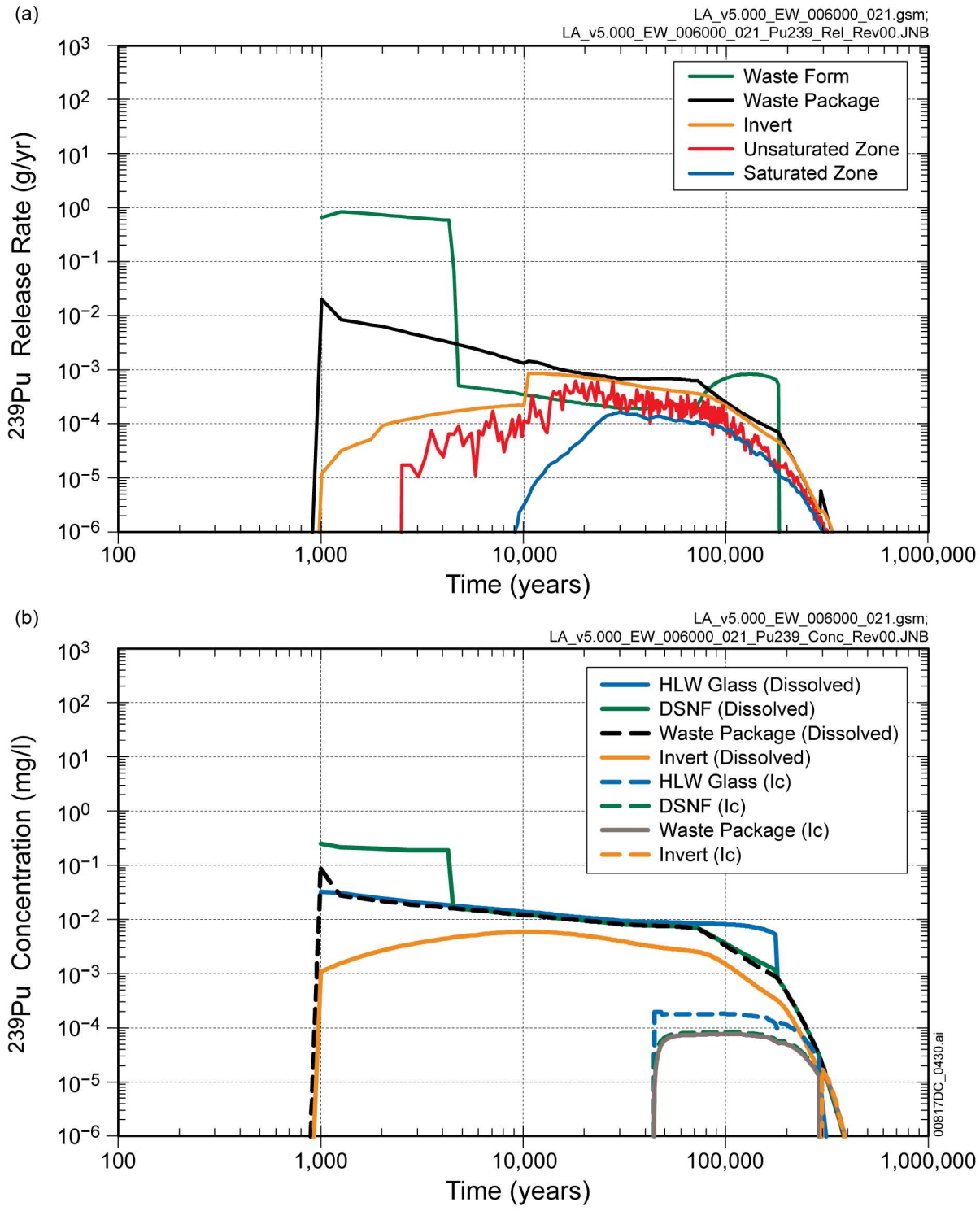

Source: Output DTN: MO0708TSPAVALI.000 [DIRS 182985].

Figure 7.7.1-12. (a) Release Rates and (b) Concentration of ^{239}Pu for Realization 5618 of the Waste Package Early Failure Modeling Case for the 1,000,000-Year Simulation after Repository Closure

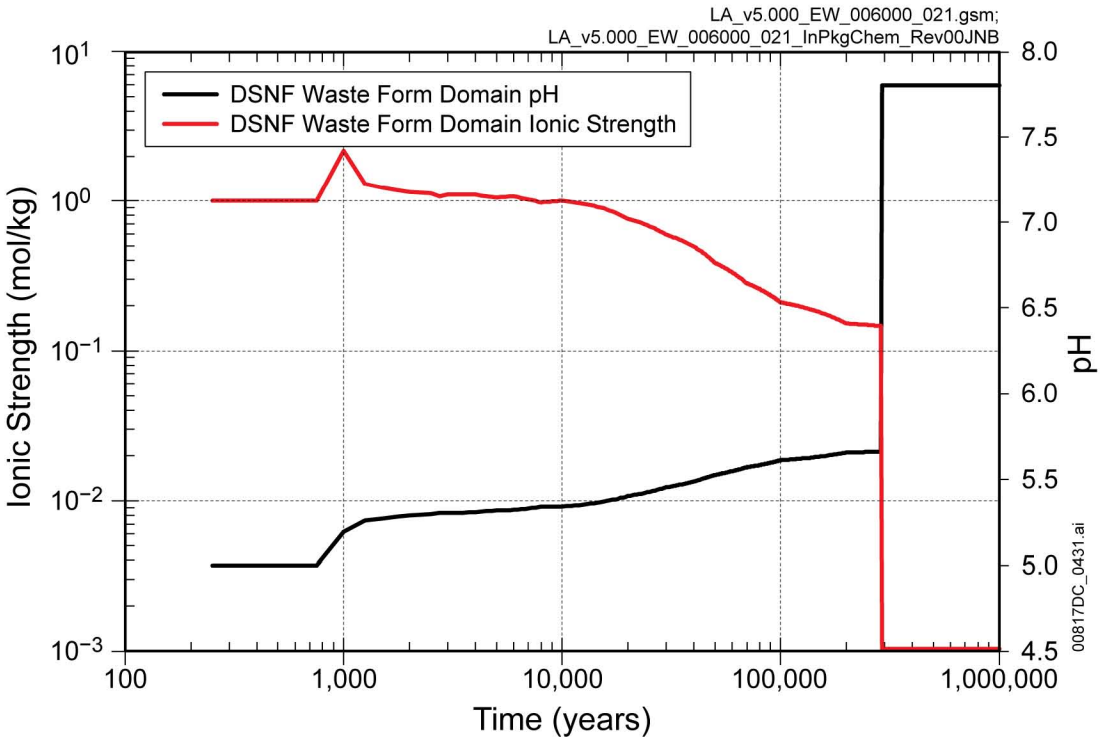

Source: Output DTN: MO0708TSPAVALI.000 [DIRS 182985].

Figure 7.7.1-13. DSNF Waste Form Domain Chemistry for Realization 5618 of the Waste Package Early Failure Modeling Case for the 1,000,000-Year Simulation after Repository Closure

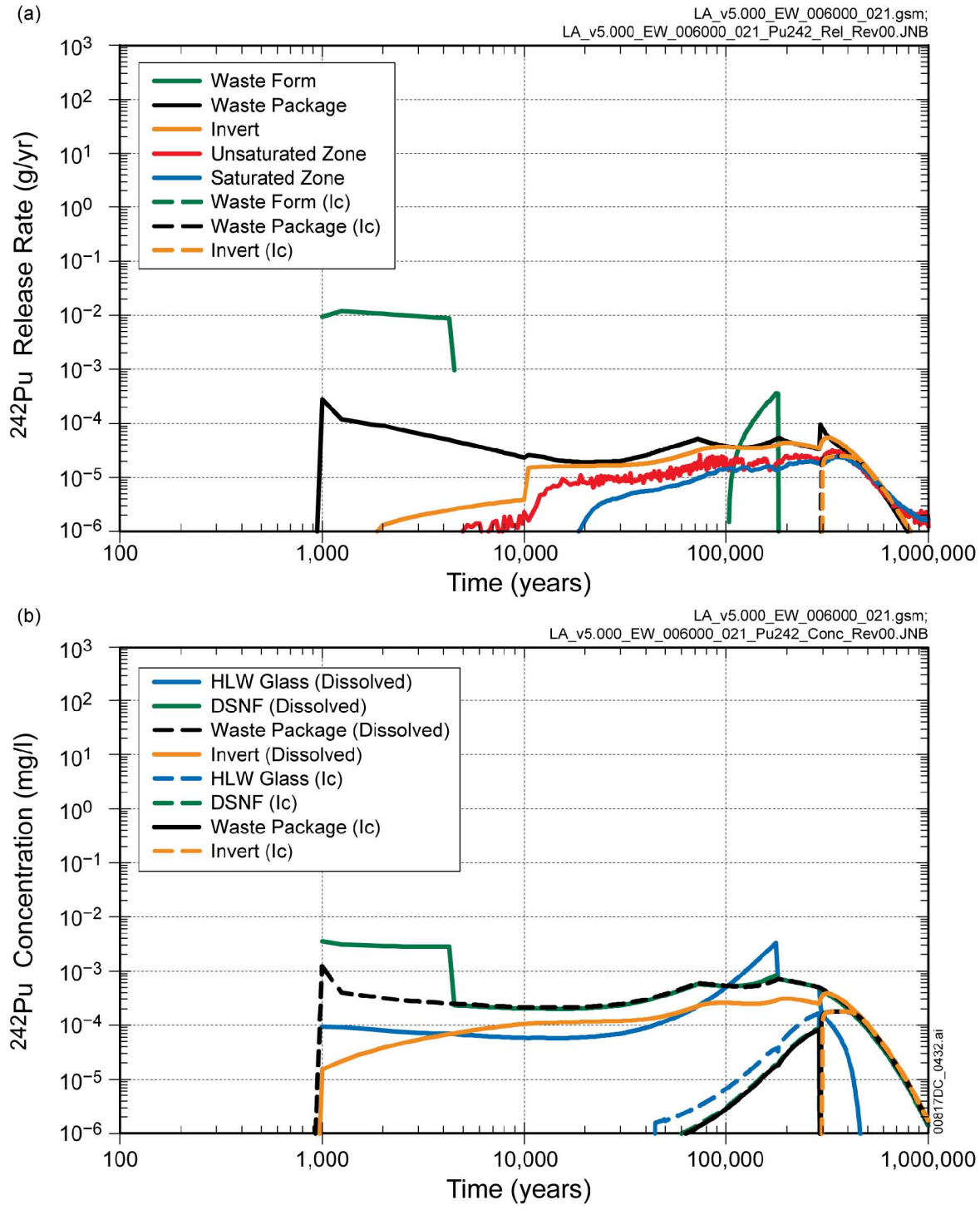

Source: Output DTN: MO0708TSPAVALI.000 [DIRS 182985].

Figure 7.7.1-14. (a) Release Rates and (b) Concentration of ^{242}Pu for Realization 5618 of the Waste Package Early Failure Modeling Case for the 1,000,000-Year Simulation after Repository Closure

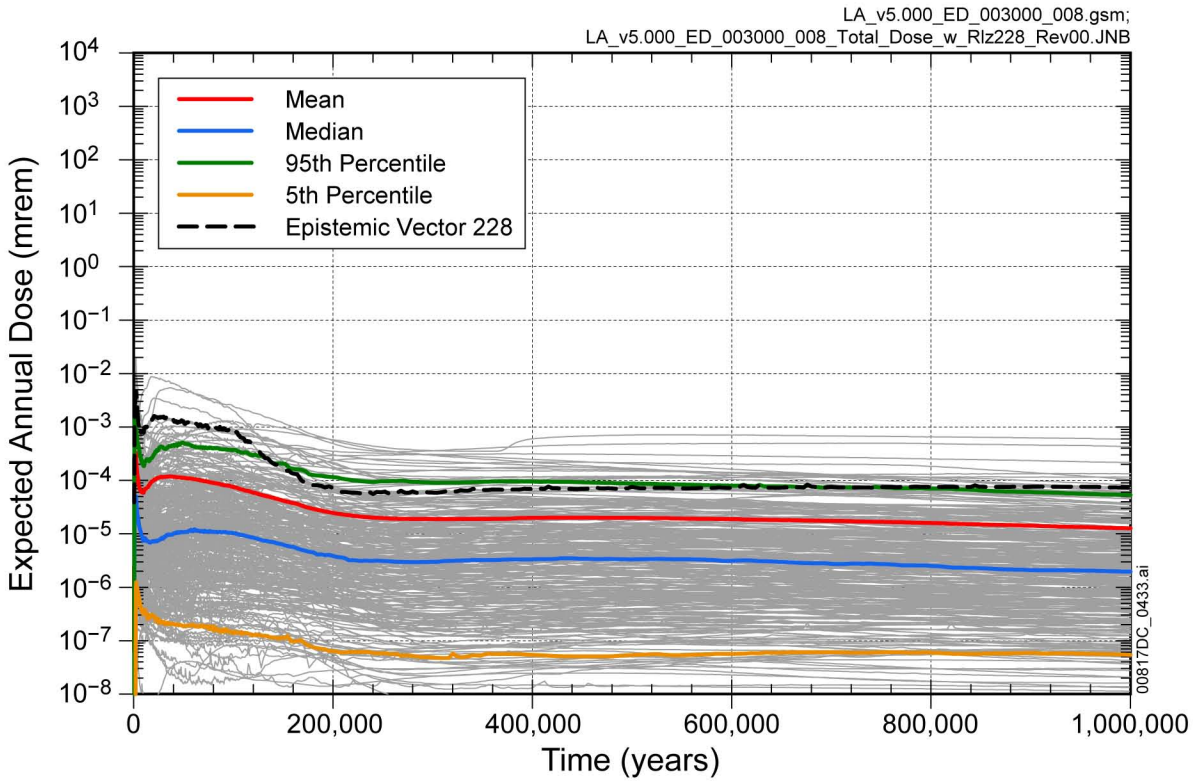

Source: Output DTN: MO0709TSPAREGS.000 [DIRS 182976].

NOTES: ^{226}Ra dose is the sum of ^{226}Ra and ^{210}Pb doses (secular equilibrium assumed).

Figure 7.7.1-15. Comparison of Expected Annual Dose for all Realizations along with that from Realization 228 (Epistemic Uncertainty Vector) of the Drip Shield Early Failure Modeling Case for the 1,000,000-Year Simulation after Repository Closure

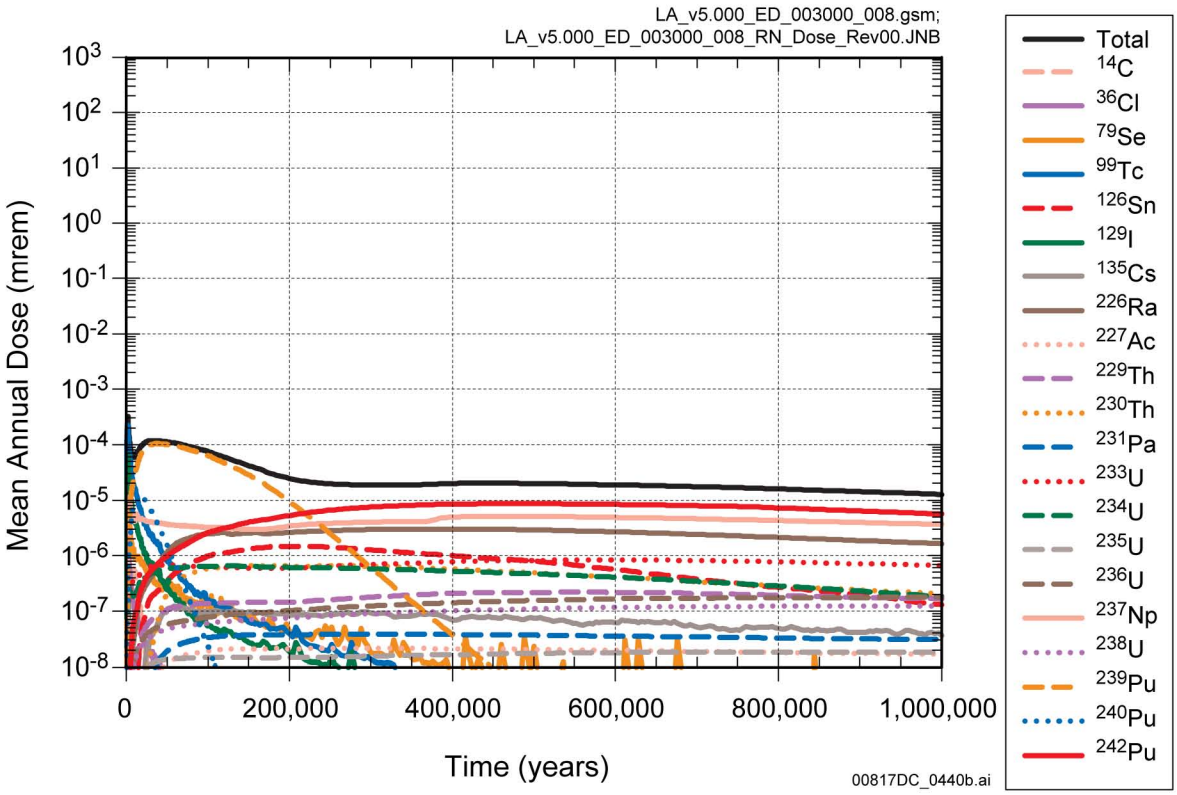

Source: Output DTN: MO0709TSPAREGS.000 [DIRS 182976].

NOTES: ^{226}Ra dose is the sum of ^{226}Ra and ^{210}Pb doses (secular equilibrium assumed).

Figure 7.7.1-16. Major Radionuclide Contributors to Mean Annual Dose for the Drip Shield Early Failure Modeling Case for the 1,000,000-Year Simulation after Repository Closure

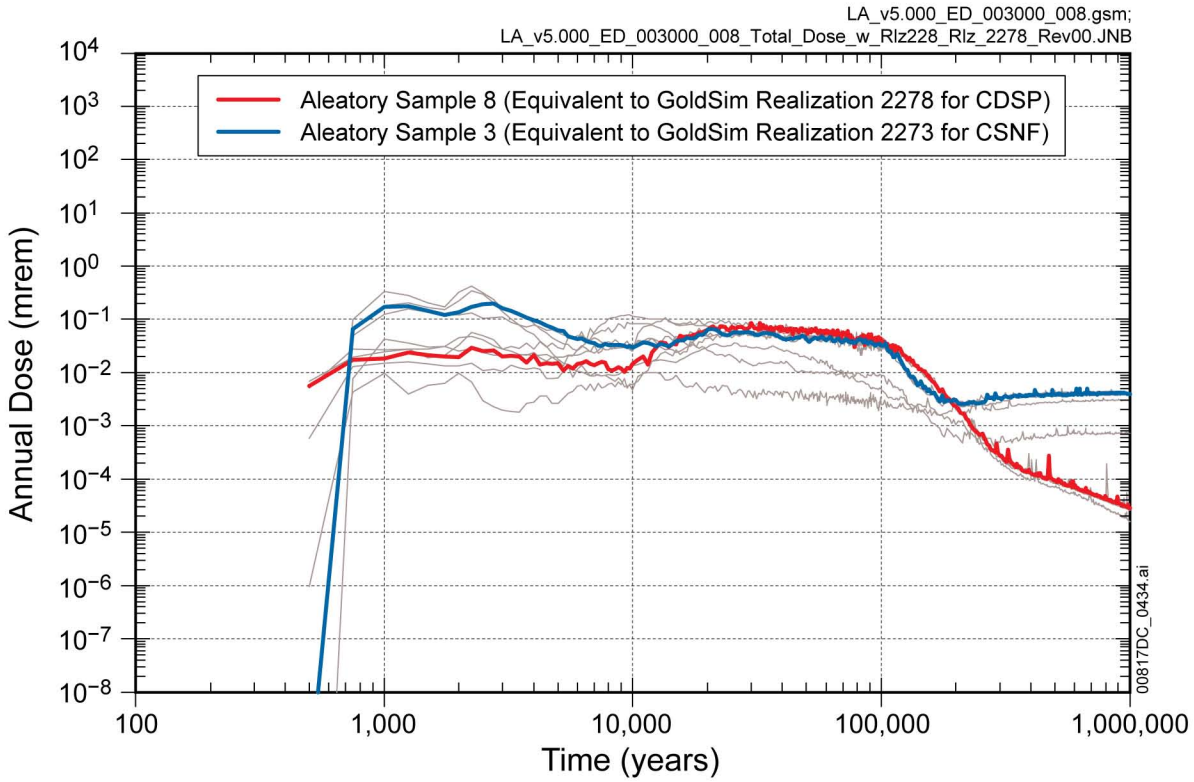

Source: Output DTN: MO0709TSPAREGS.000 [DIRS 182976].

Figure 7.7.1-17. Annual Dose for Ten Aleatory Uncertainty Realizations (vectors) for the Epistemic Uncertainty Realization 228 of the Drip Shield Early Failure Modeling Case for the 1,000,000-Year Simulation after Repository Closure

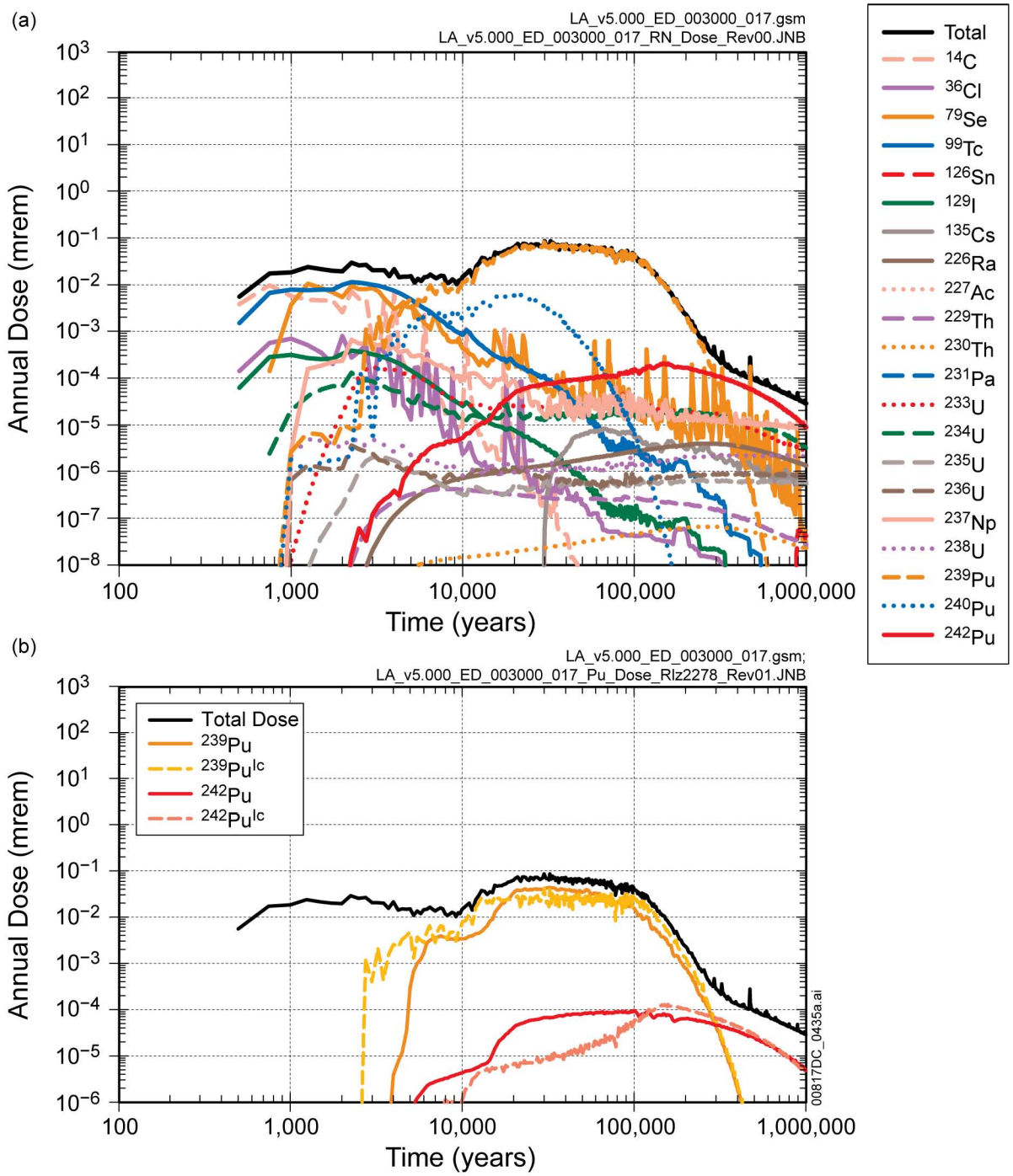

Source: Output DTN: MO0708TSPAVALI.000 [DIRS 182985].

NOTES: ^{226}Ra dose is the sum of ^{226}Ra and ^{210}Pb doses (secular equilibrium assumed).

Figure 7.7.1-18. (a) Annual Dose along with Major Radionuclide Dose Contributors and (b) Contribution of Dissolved ^{239}Pu and ^{242}Pu and that Associated Irreversibly with Colloids (Denoted by Superscript Ic) for Realization 2278 of the Drip Shield Early Failure Modeling Case for the 1,000,000-Year Simulation after Repository Closure

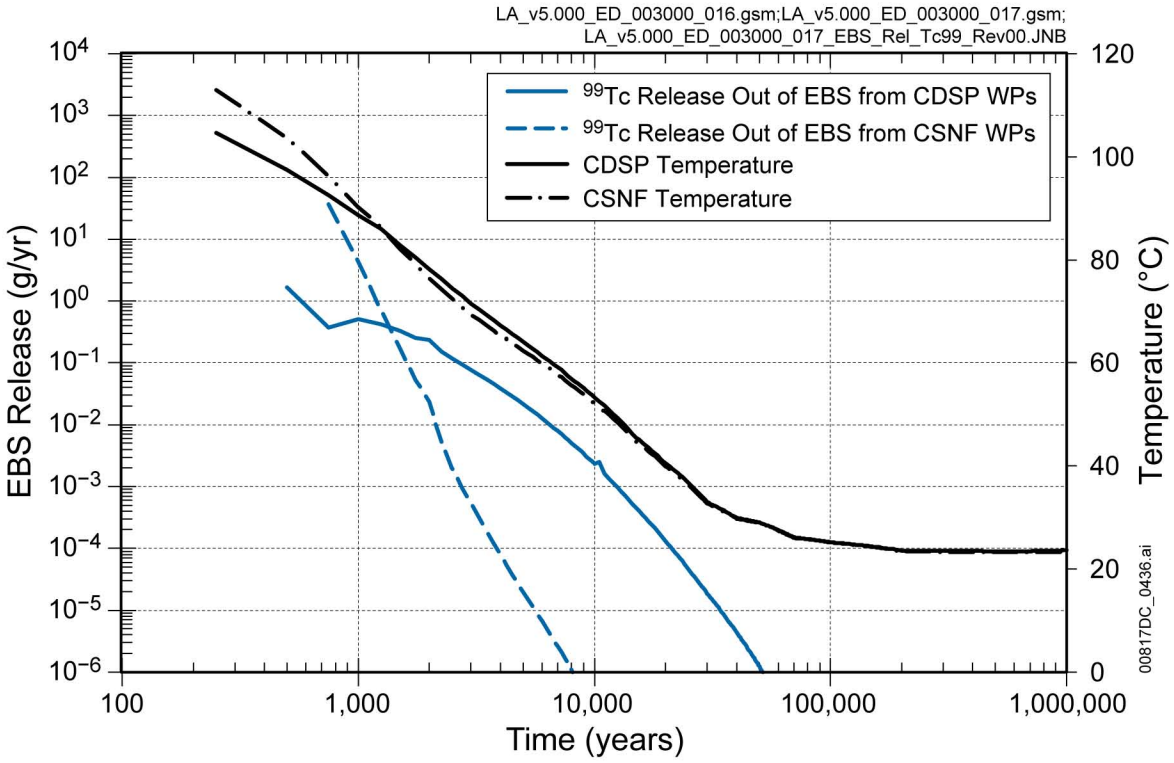

Source: Output DTN: MO0708TSPAVALI.000 [DIRS 182985].

Figure 7.7.1-19. EBS Release Rates of ^{99}Tc Along with Waste Package Temperatures for the Two Selected Realizations of Drip Shield Early Failure Modeling Case for the 1,000,000-Year Simulation after Repository Closure

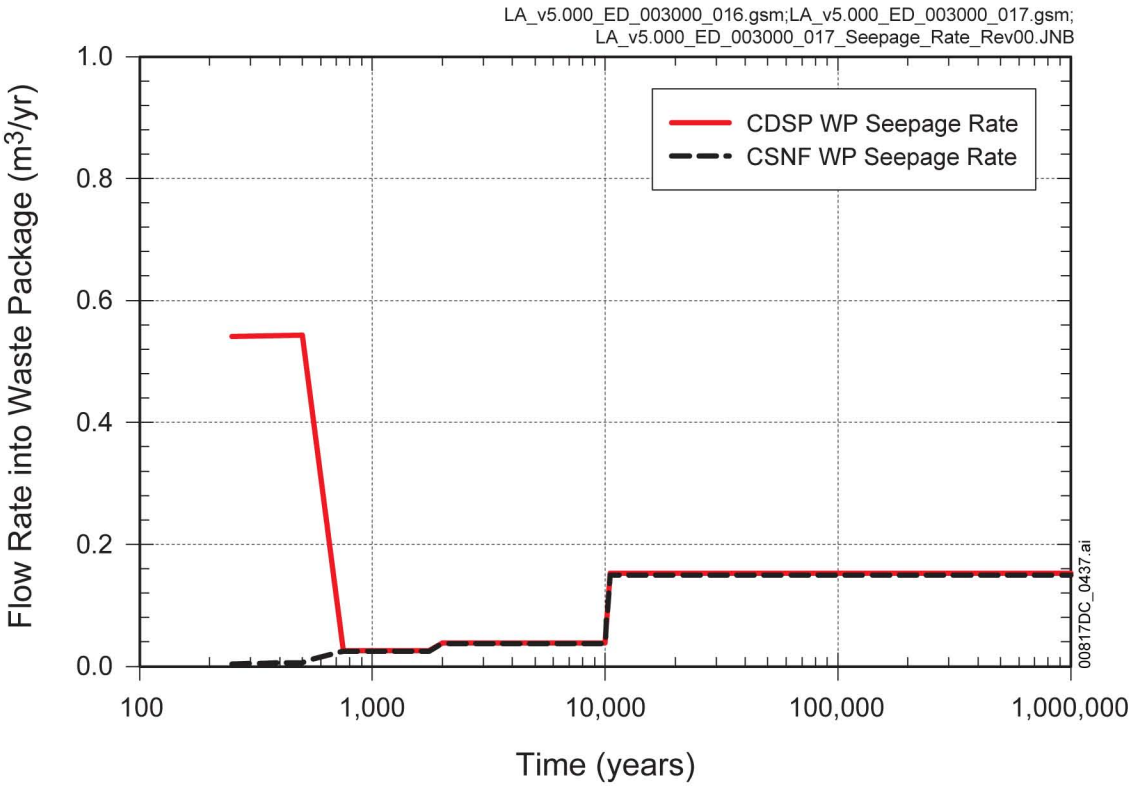

Source: Output DTN: MO0708TSPAVALI.000 [DIRS 182985].

Figure 7.7.1-20. Seepage Rate Incident on the Waste Package Showing the Effects of Drift Wall Condensation and Climate Change for the Two Selected Realizations of the Drip Shield Early Failure Modeling Case for the 1,000,000-Year Simulation after Repository Closure

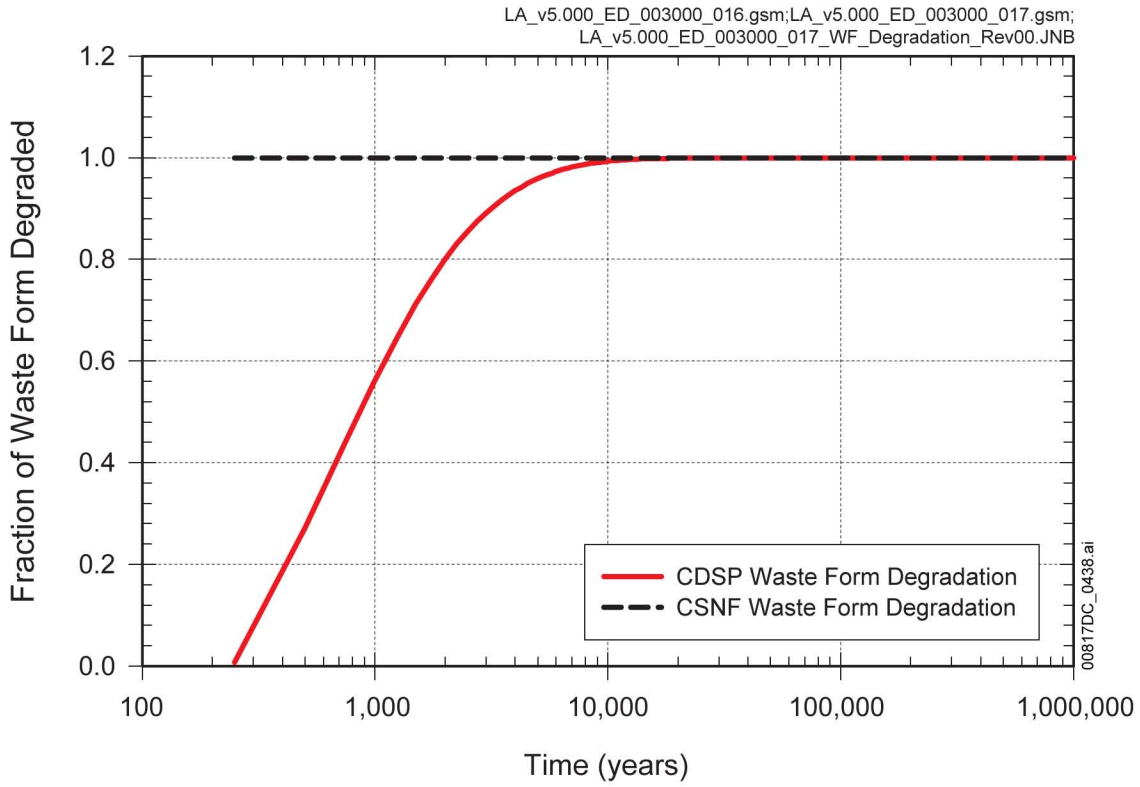

Source: Output DTN: MO0708TSPAVALI.000 [DIRS 182985].

Figure 7.7.1-21. Fraction of CSNF and CDSP Waste Form Degraded for the Two Selected Realizations of the Drip Shield Early Failure Modeling Case for the 1,000,000-Year Simulation after Repository Closure

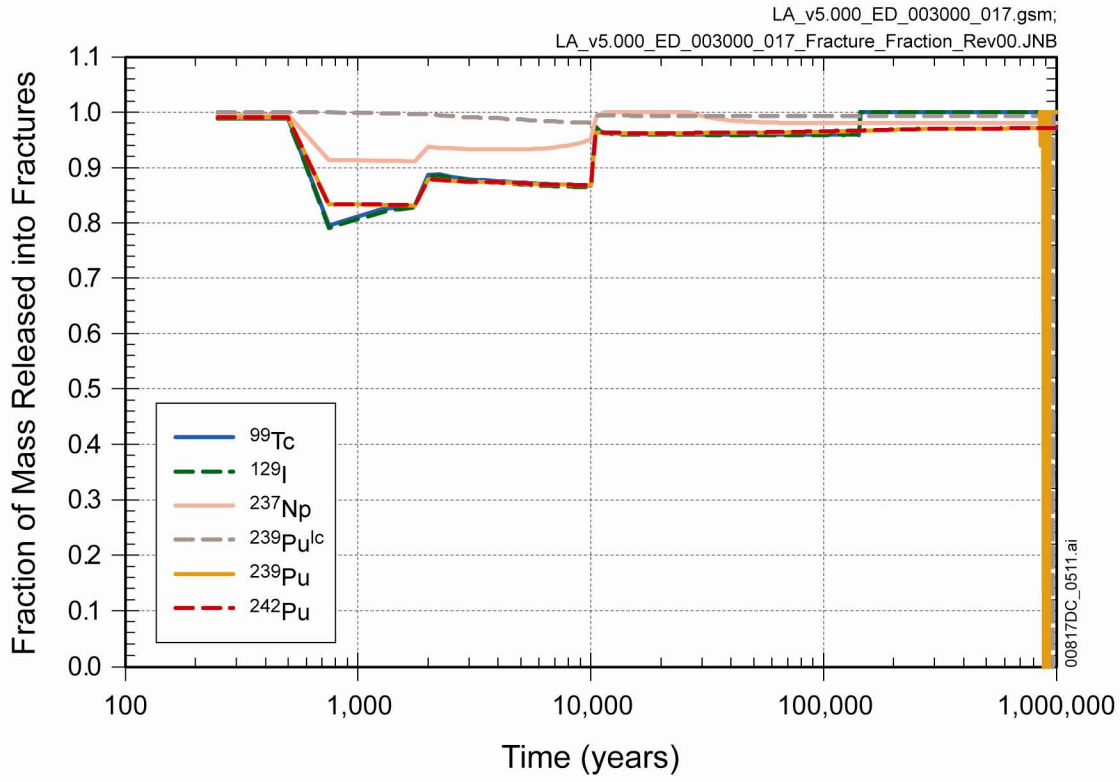

Source: Output DTN: MO0708TSPAVALI.000 [DIRS 182985].

NOTES: The GoldSim realization 2278 represents a CDSP WP in percolation subregion 3.

Figure 7.7.1-22. Fraction of EBS Mass Flux Released into Unsaturated Zone Fractures for Selected Radionuclides for Realization 2278 of the Drip Shield Early Failure Modeling Case for the 1,000,000-Year Simulation after Repository Closure

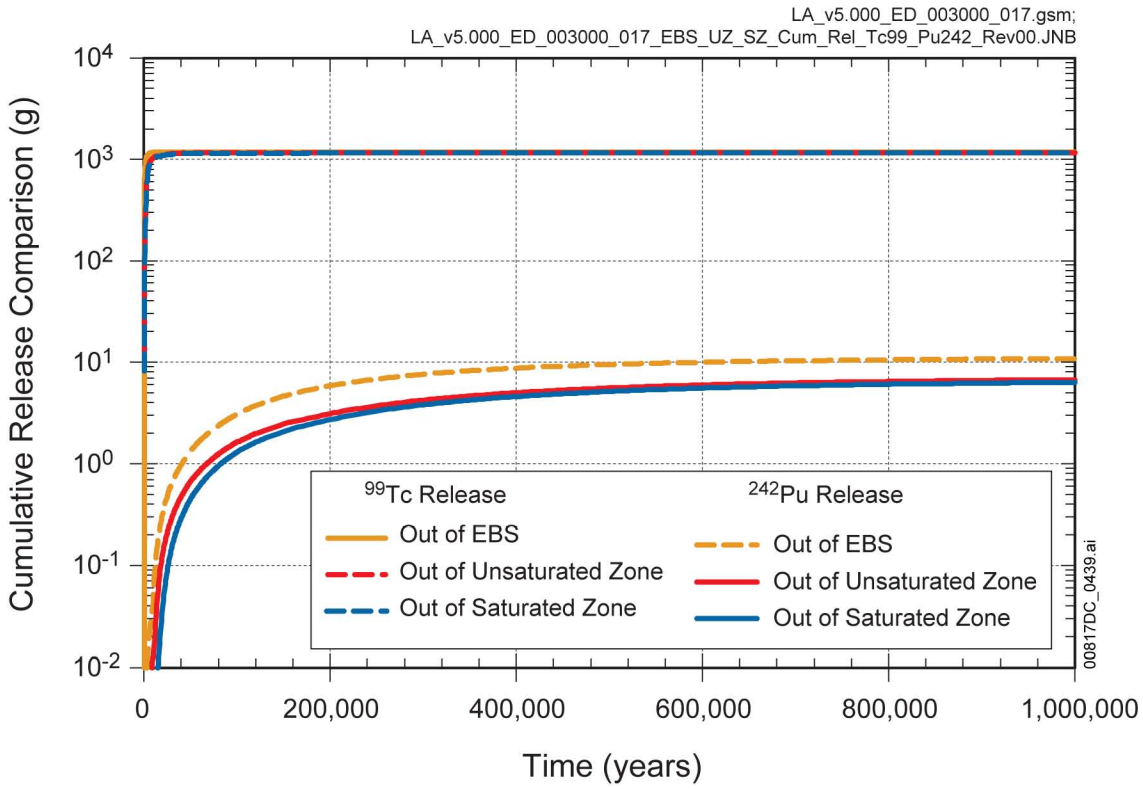

Source: Output DTN: MO0708TSPAVALI.000 [DIRS 182985].

Figure 7.7.1-23. Cumulative Mass Release of ^{99}Tc and ^{242}Pu from the EBS, Unsaturated Zone, and Saturated Zone for Realization 2278 of the Drip Shield Early Failure Modeling Case for the 1,000,000-Year Simulation after Repository Closure

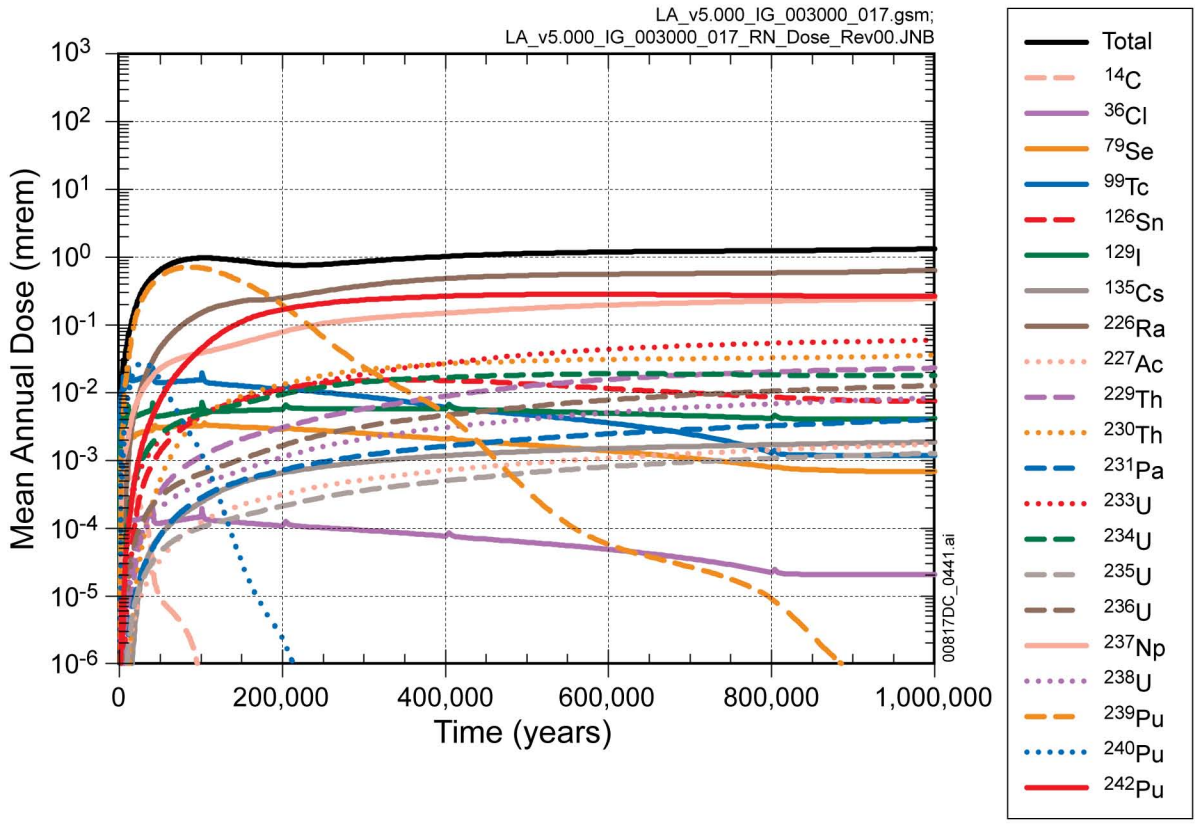

Source: Output DTN: MO0709TSPAREGS.000 [DIRS 182976].

NOTES: ^{226}Ra dose is the sum of ^{226}Ra and ^{210}Pb doses (secular equilibrium assumed).

Figure 7.7.1-24. Major Radionuclide Contributors to Mean Annual Dose for the Igneous Intrusion Modeling Case for the 1,000,000-Year Simulation after Repository Closure

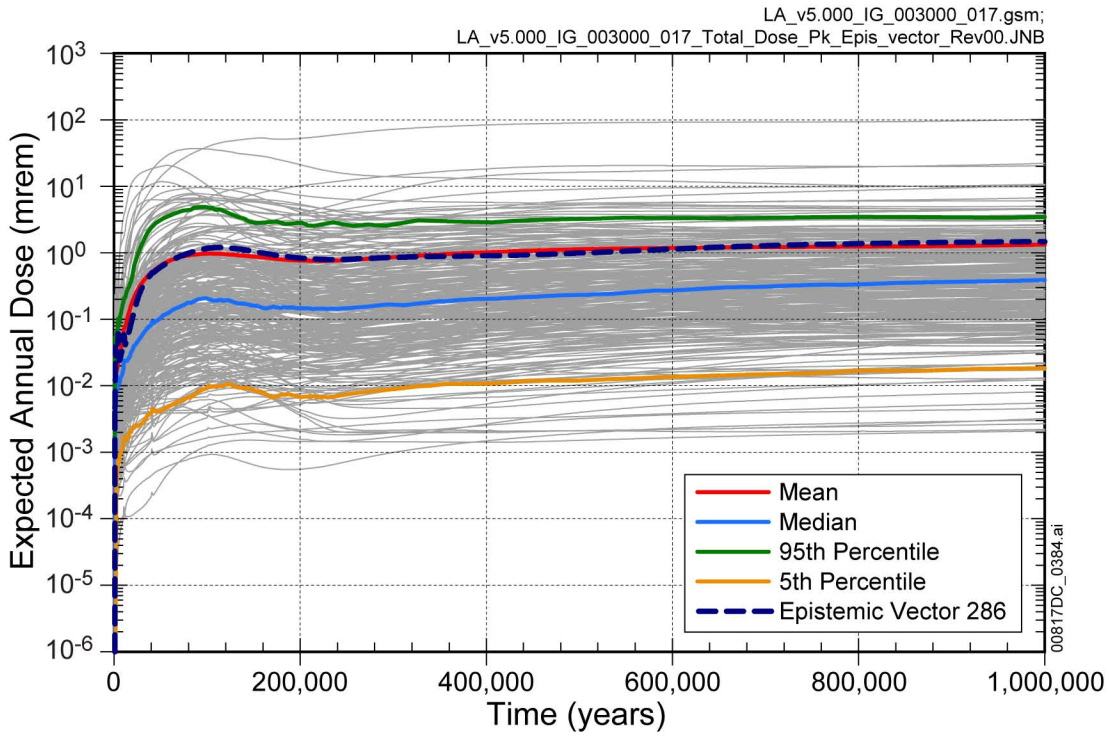

Source: Output DTN: MO0709TSPAREGS.000 [DIRS 182976].

NOTES: ^{226}Ra dose is the sum of ^{226}Ra and ^{210}Pb doses (secular equilibrium assumed).

Figure 7.7.1-25. Expected Annual Dose from the 300 Epistemic Vectors Along with their Quantiles and Expected Dose from Epistemic Uncertainty Vector #286 for the Igneous Intrusion Modeling Case for the 1,000,000-Year Simulation after Repository Closure

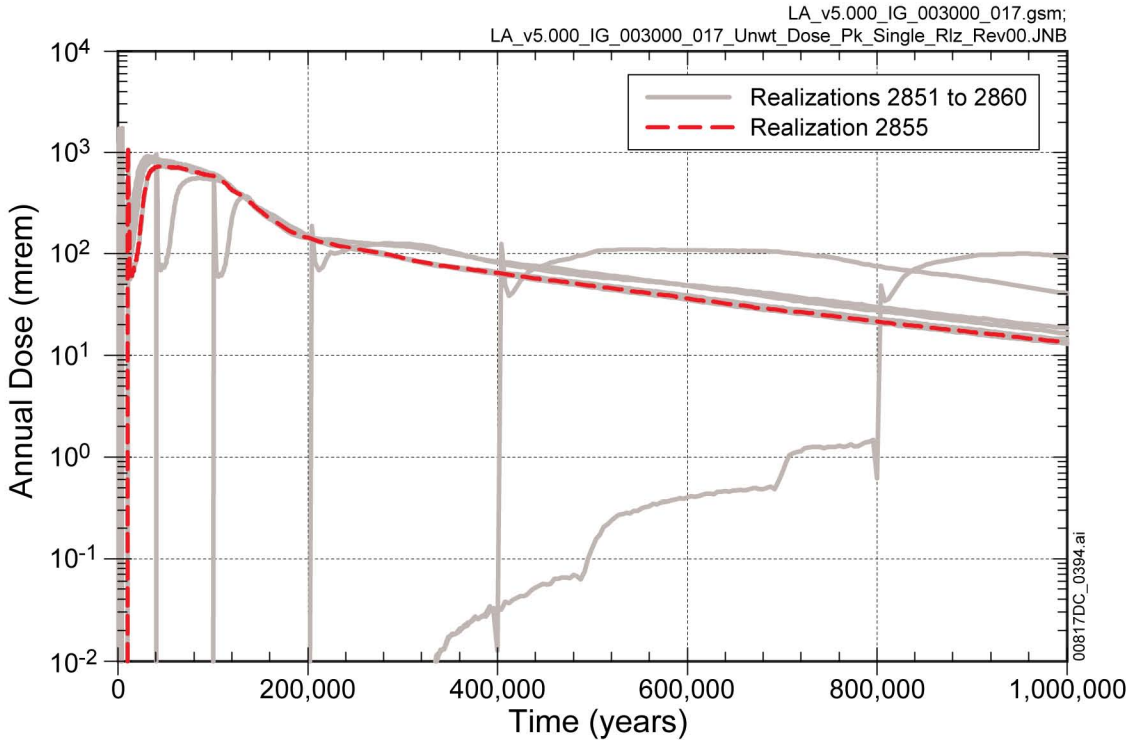

Source: Output DTN: MO0709TSPAREGS.000 [DIRS 182976].

Figure 7.7.1-26. Annual Dose for Realizations 2851 through 2860 (representing Epistemic Uncertainty Vector 286) along with Selected Realization 2855 of the Igneous Intrusion Modeling Case for the 1,000,000-Year Simulation after Repository Closure

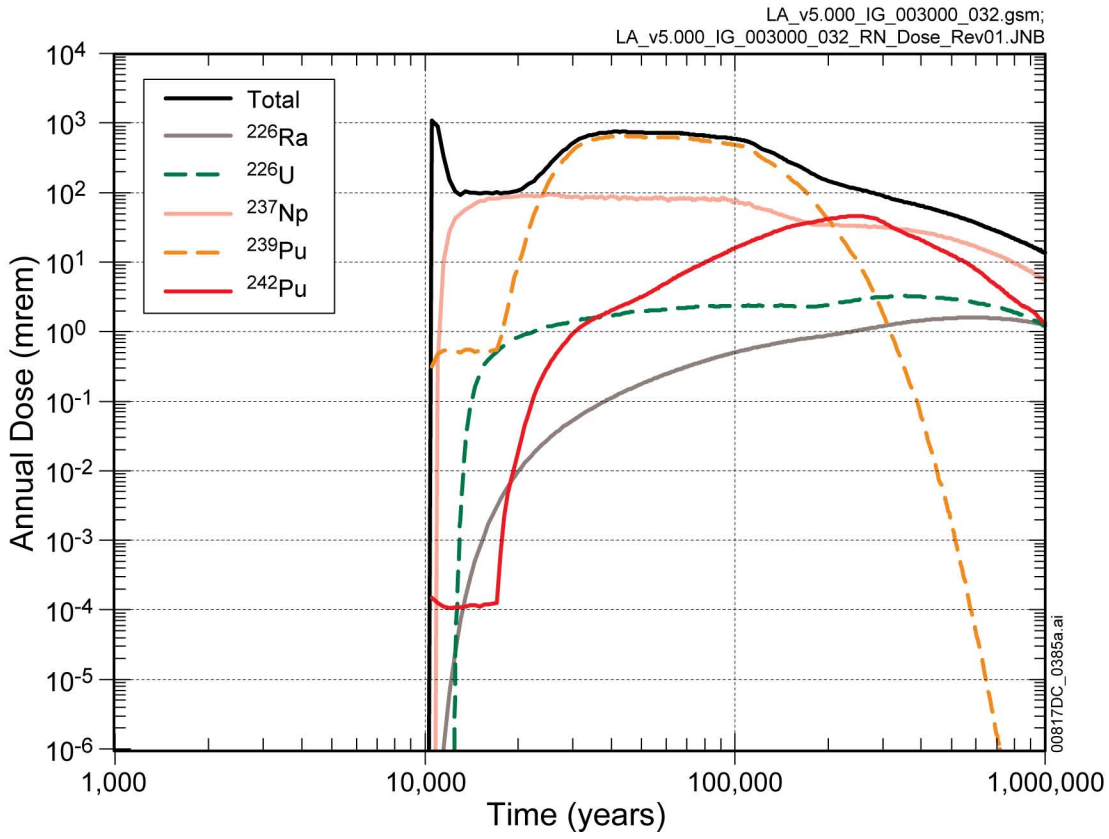

Source: Output DTN: MO0708TSPAVALI.000 [DIRS 182985].

NOTES: ^{226}Ra dose is the sum of ^{226}Ra and ^{210}Pb doses (secular equilibrium assumed).

Figure 7.7.1-27. Annual Dose along with Major Radionuclide Dose Contributors for Realization 2855 of the Igneous Intrusion Modeling Case for the 1,000,000-Year Simulation after Repository Closure

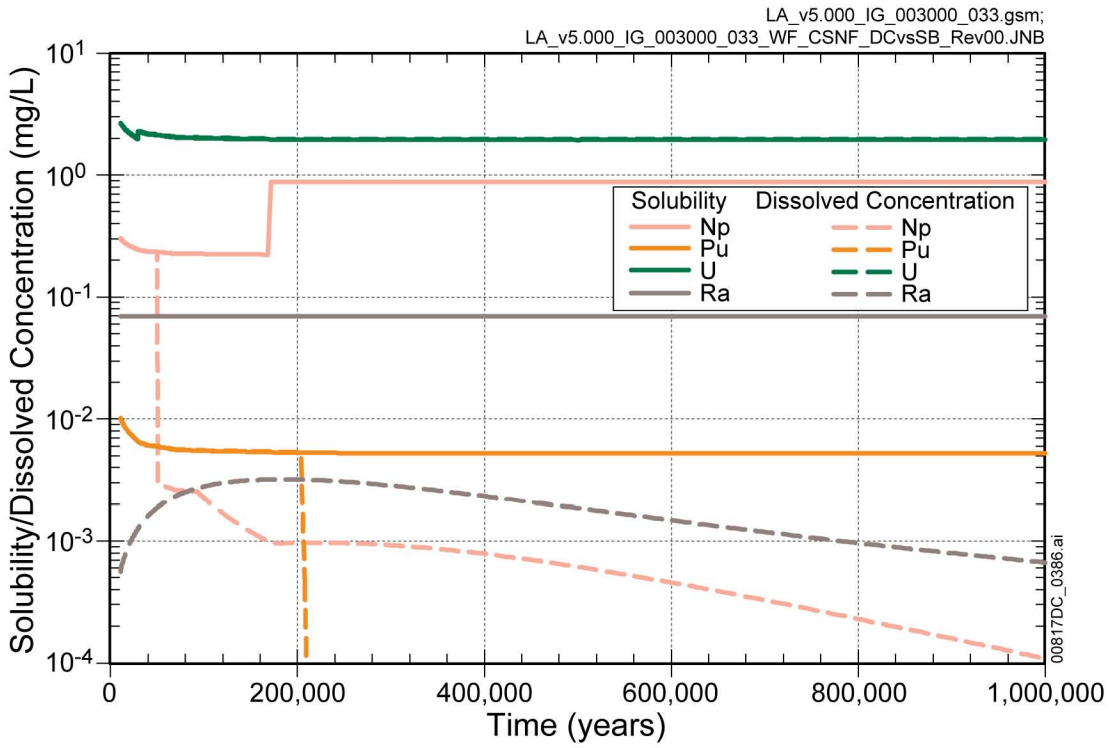

Source: Output DTN: MO0708TSPAVALI.000 [DIRS 182985].

Figure 7.7.1-28. Dissolved Concentrations and Solubility Limits of Neptunium, Plutonium, Uranium, and Radium in the CSNF Waste Form Domain for Percolation Subregion 3 Dripping Environment for Realization 2855 of the Igneous Intrusion Modeling Case for the 1,000,000-Year Simulation after Repository Closure

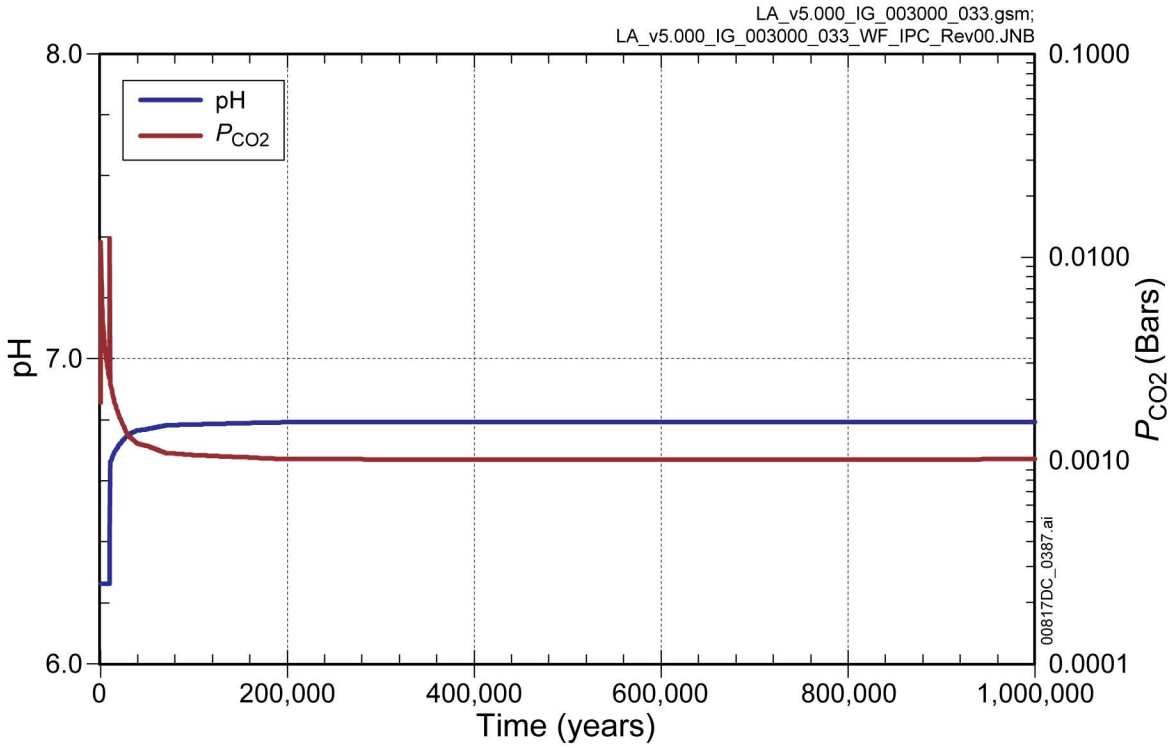

Source: Output DTN: MO0708TSPAVALI.000 [DIRS 182985].

Figure 7.7.1-29. In-Package pH and P_{CO2} in the Waste Form Domain for Percolation Subregion 3 Dripping Environment for Realization 2855 of the Igneous Intrusion Modeling Case for the 1,000,000-Year Simulation after Repository Closure

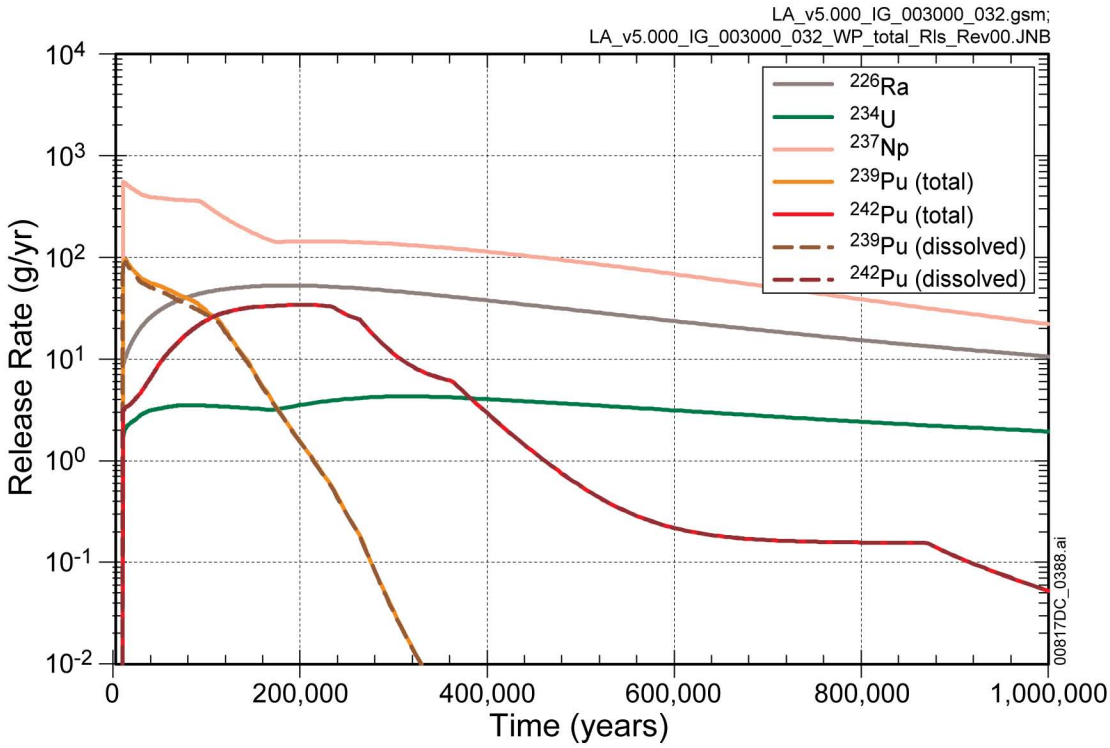

Source: Output DTN: MO0708TSPAVALI.000 [DIRS 182985].

Figure 7.7.1-30. Release Rate of Major Radionuclides from all WPs for Realization 2855 of the Igneous Intrusion Modeling Case for the 1,000,000-Year Simulation after Repository Closure

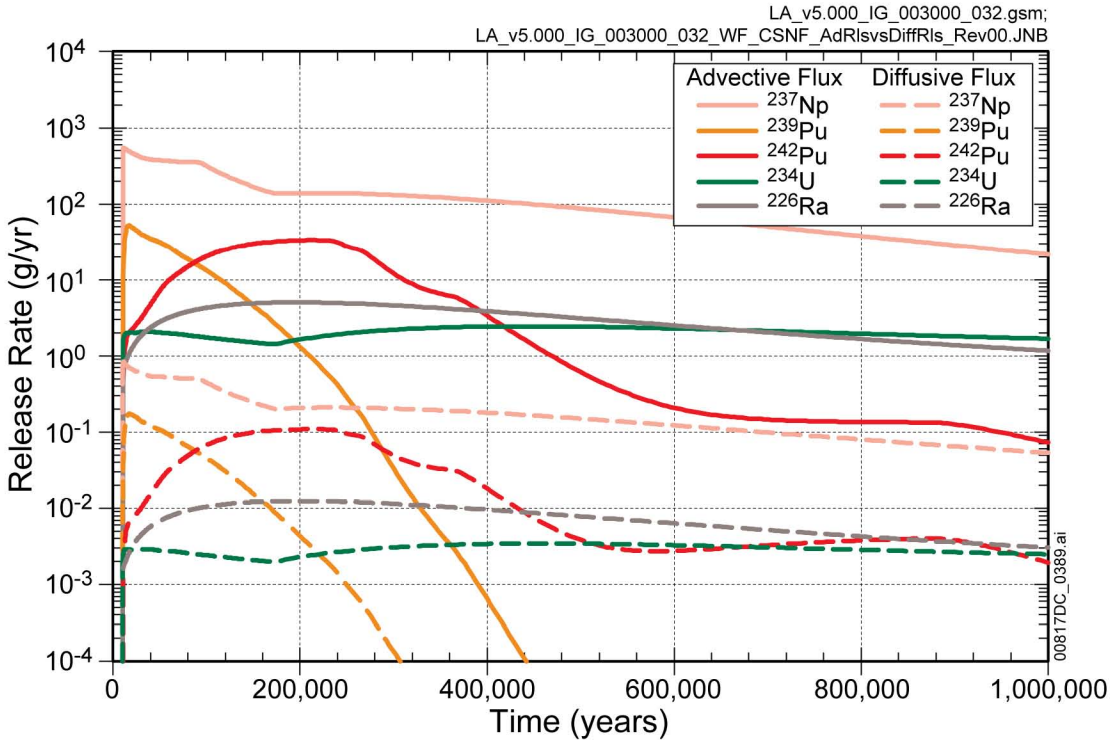

Source: Output DTN: MO0708TSPAVALI.000 [DIRS 182985].

Figure 7.7.1-31. Advective and Diffusive Release Rates of Major Radionuclides from the CSNF WPs for Realization 2855 of the Igneous Intrusion Modeling Case for the 1,000,000-Year Simulation after Repository Closure

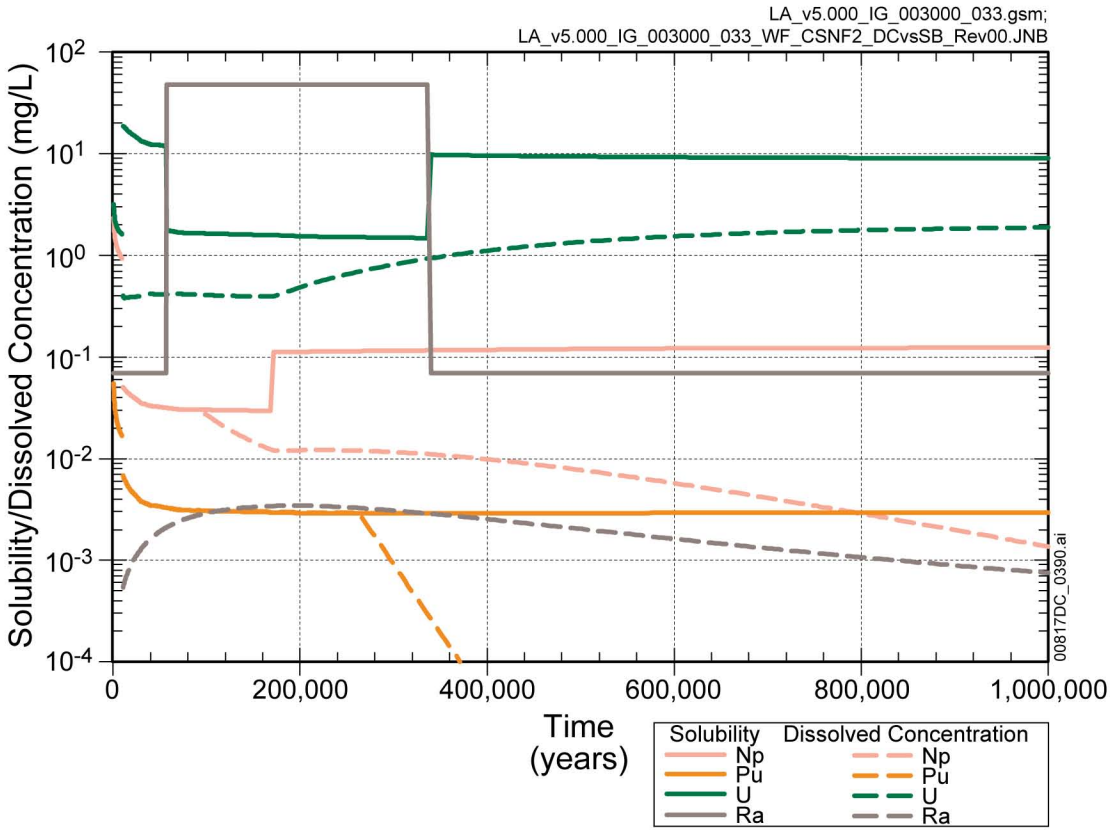

Source: Output DTN: MO0708TSPAVALI.000 [DIRS 182985].

Figure 7.7.1-32. Total Dissolved Concentrations and Solubility Limits of Neptunium, Plutonium, Uranium, and Radium in the Corrosion Products Domain of CSNF WP Located in Percolation Subregion 3 Dripping Environment for Realization 2855 of the Igneous Intrusion Modeling Case for the 1,000,000-Year Simulation after Repository Closure

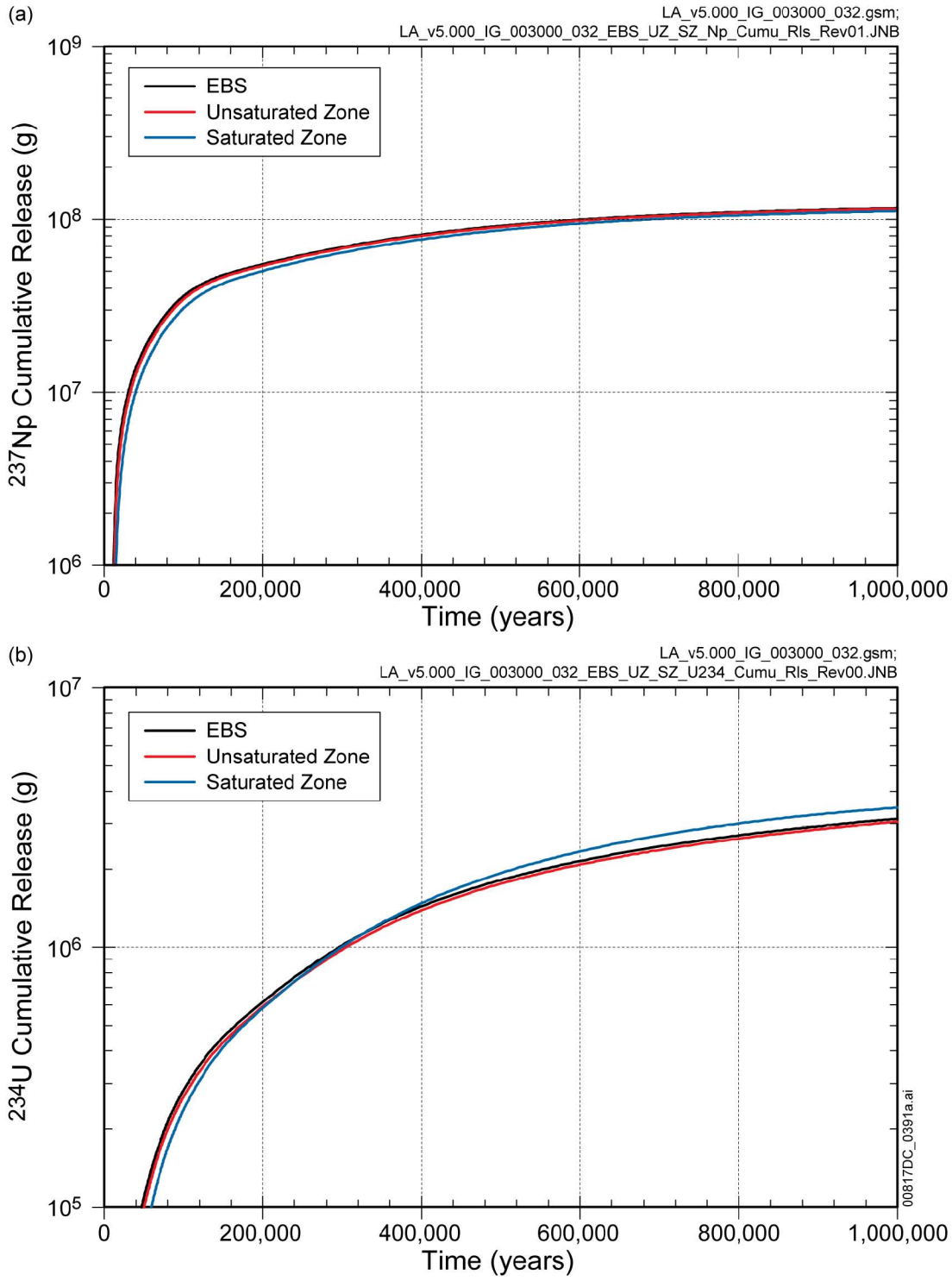

Source: Output DTN: MO0708TSPAVALI.000 [DIRS 182985].

Figure 7.7.1-33. Cumulative Releases of: (a) ^{237}Np, (b) ^{234}U, (c) ^{242}Pu, and (d) ^{226}Ra from the EBS, Unsaturated Zone, and Saturated Zone for Realization 2855 of the Igneous Intrusion Modeling Case for the 1,000,000-Year Simulation after Repository Closure

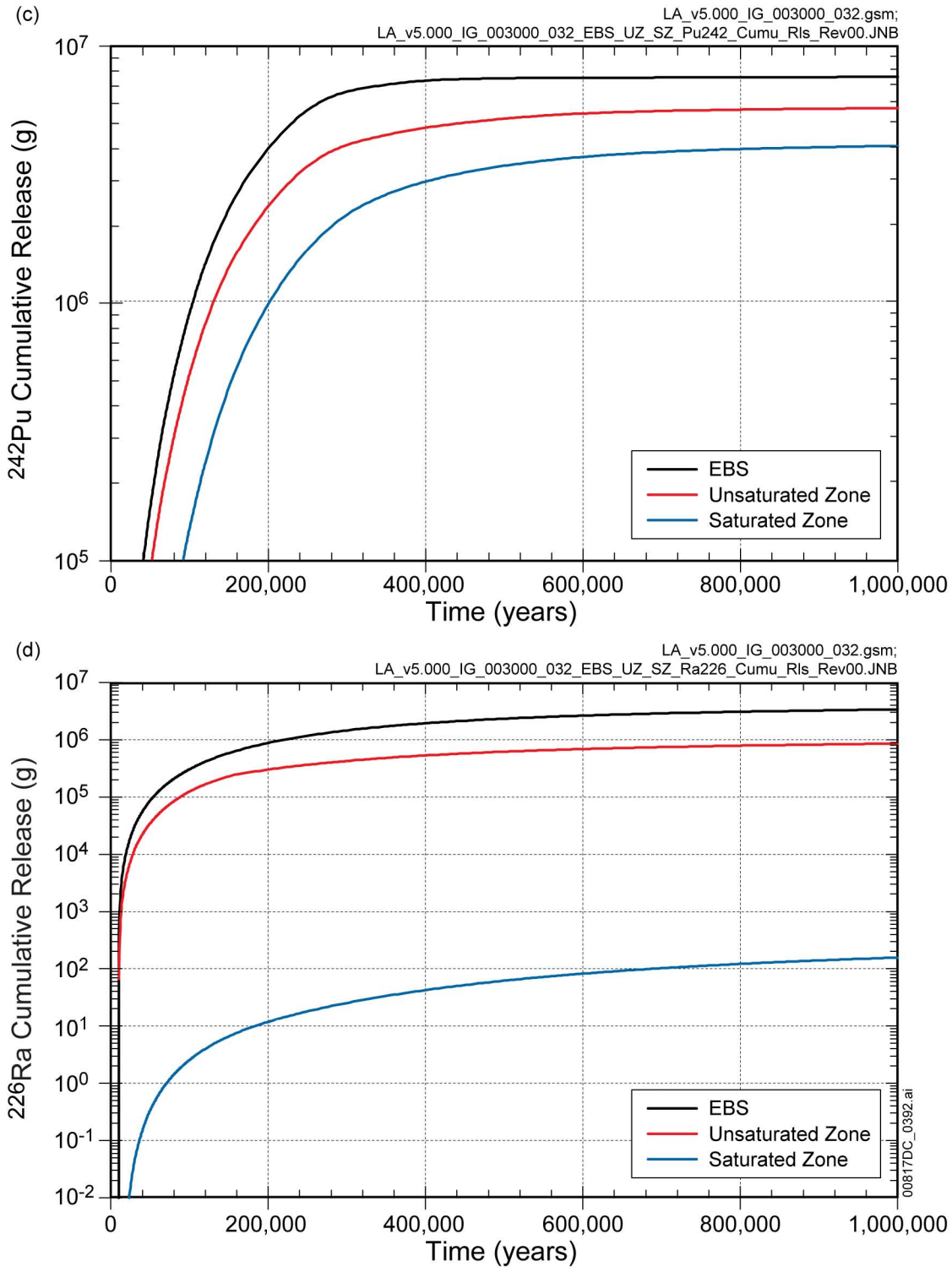

Source: Output DTN: MO0708TSPAVALI.000 [DIRS 182985].

Figure 7.7.1-33. Cumulative Releases of: (a) ^{237}Np, (b) ^{234}U, (c) ^{242}Pu, and (d) ^{226}Ra from the EBS, Unsaturated Zone, and Saturated Zone for Realization 2855 of the Igneous Intrusion Modeling Case for the 1,000,000-Year Simulation after Repository Closure (Continued)

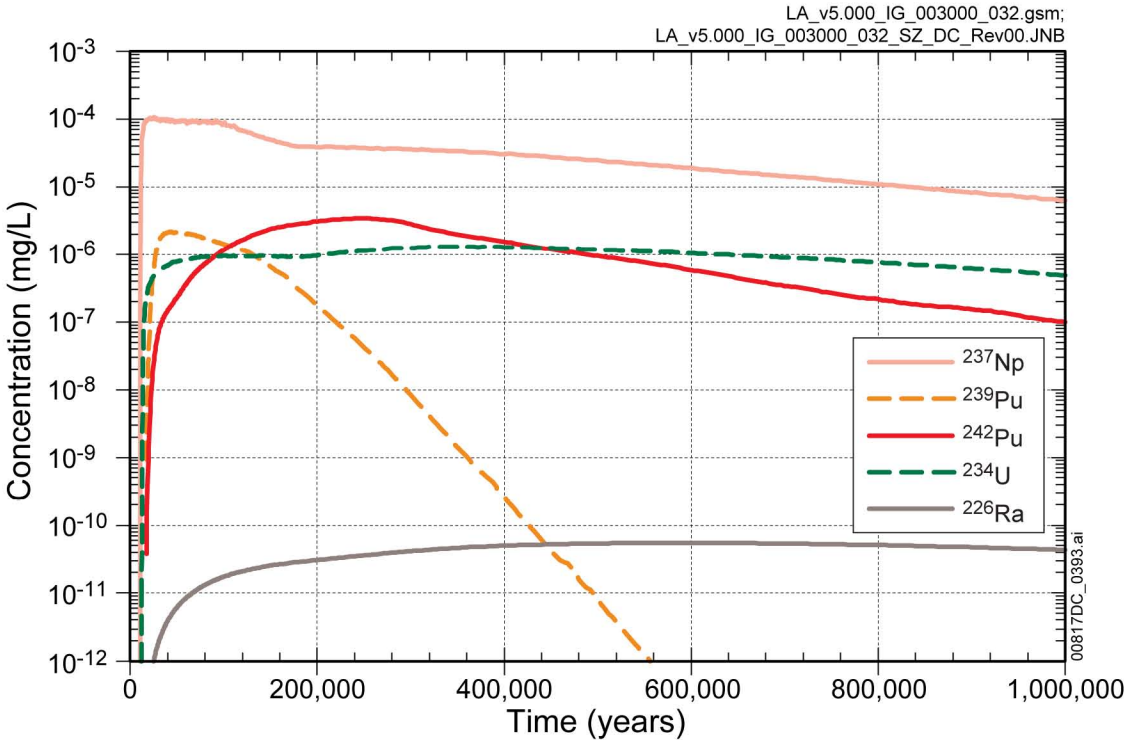

Source: Output DTN: MO0708TSPAVALI.000 [DIRS 182985].

NOTE: The saturated zone concentrations shown on this figure are obtained by dividing the annual releases of radionuclides from the saturated zone by the 3,000 acre-ft/yr annual water usage, as required by regulations.

Figure 7.7.1-34. Concentrations of Major Radionuclides at the RMEI Location for Realization 2855 of the Igneous Intrusion Modeling Case for the 1,000,000-Year Simulation after Repository Closure

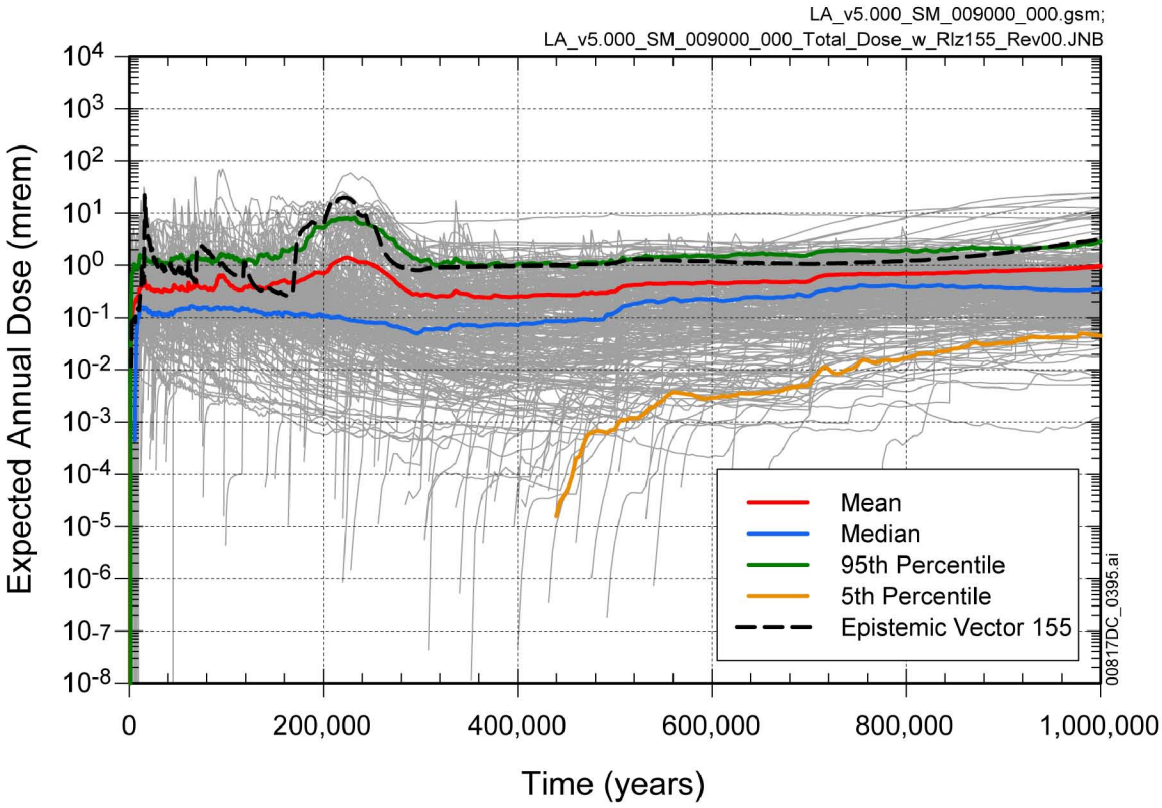

Source: Output DTN: MO0709TSPAREGS.000 [DIRS 182976].

NOTE: ^{226}Ra dose is the sum of ^{226}Ra and ^{210}Pb doses (secular equilibrium assumed).

Figure 7.7.1-35. Expected Annual Dose from the 300 Epistemic Uncertainty Realizations (Vectors) Along With their Quantiles and Expected Dose from Epistemic Uncertainty Vector #155 for the Seismic Ground Motion Modeling Case for the 1,000,000-Year Simulation after Repository Closure

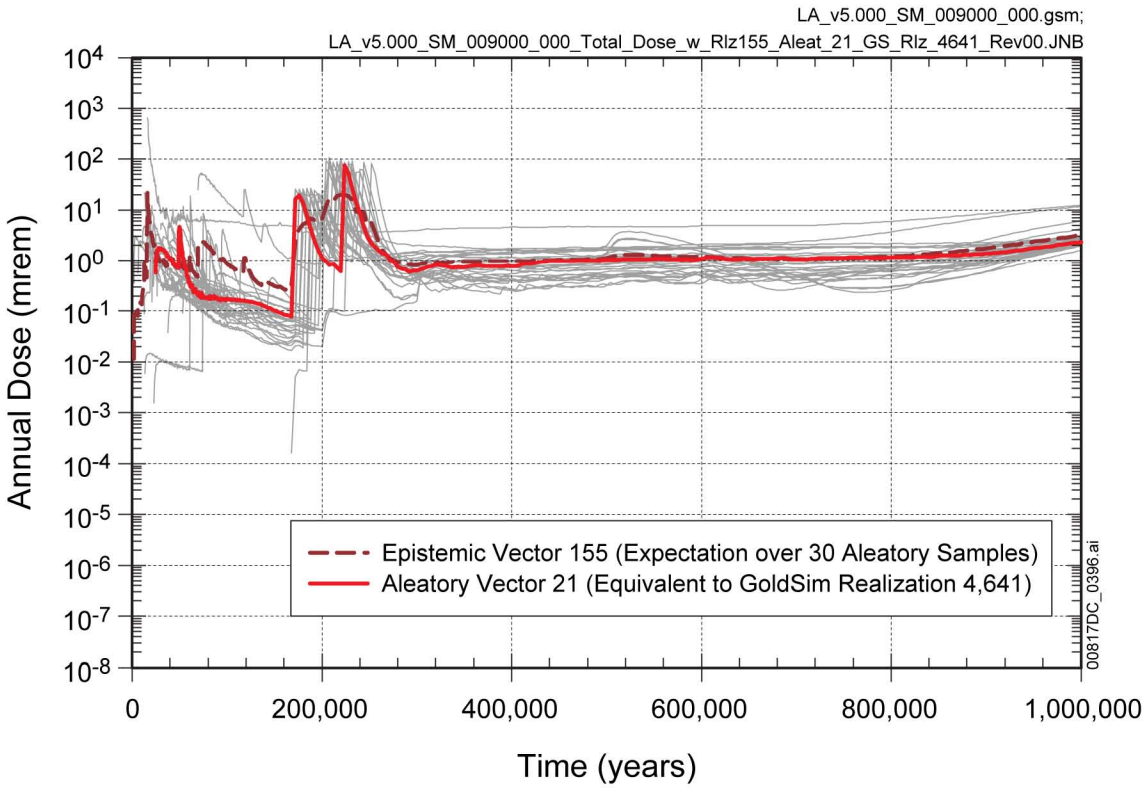

Source: Output DTN: MO0709TSPAREGS.000 [DIRS 182976].

NOTE: The dashed line is the expected annual dose for epistemic uncertainty vector 155 by taking expectation over the thirty aleatory vectors. The solid red line is the annual dose from aleatory vector 21, which is equivalent to GoldSim realization 4641.

Figure 7.7.1-36. Annual Dose from the Thirty Aleatory Vectors (Seismic Event Sequences) Associated with the Epistemic Vector 155 for the Seismic Ground Motion Modeling Case for the 1,000,000-Year Simulation after Repository Closure

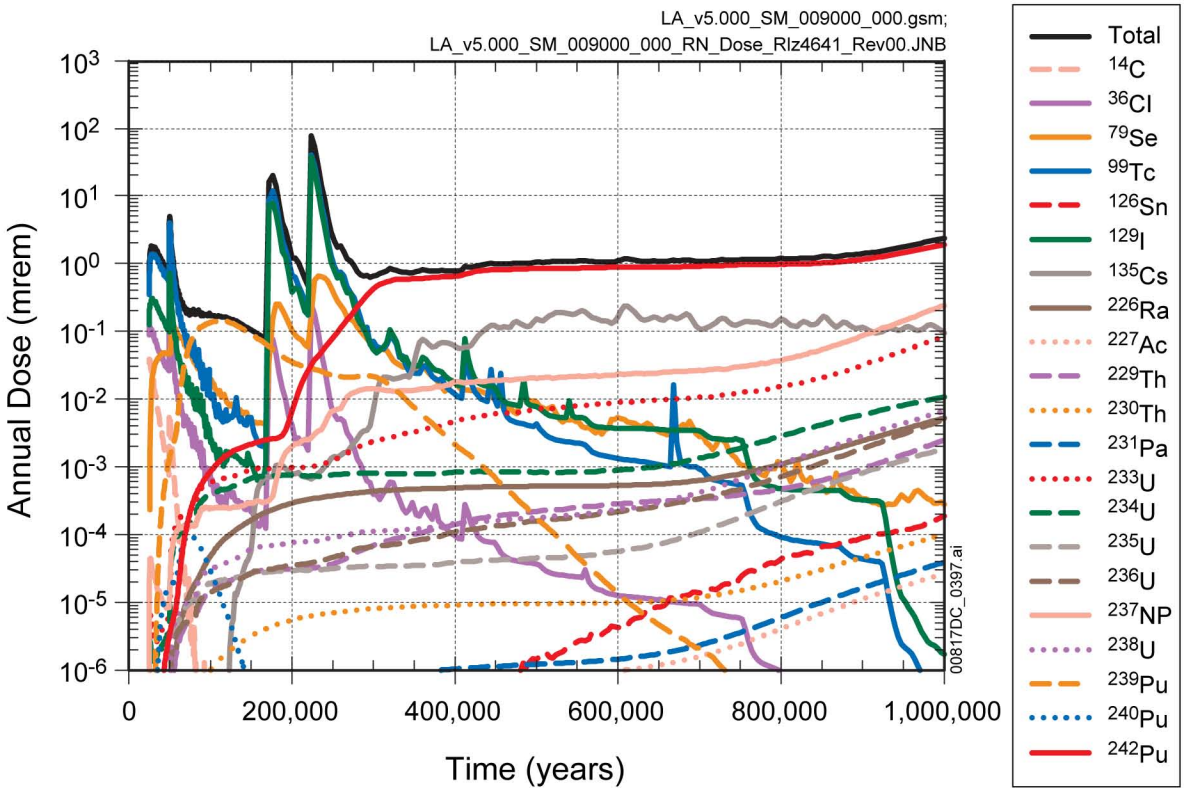

Source: Output DTN: MO0709TSPAREGS.000 [DIRS 182976].

NOTE: ^{226}Ra dose is the sum of ^{226}Ra and ^{210}Pb doses (secular equilibrium assumed).

Figure 7.7.1-37. Annual Dose along with Major Radionuclide Dose Contributors for Realization 4641 of the Seismic Ground Motion Modeling Case for the 1,000,000-Year Simulation after Repository Closure

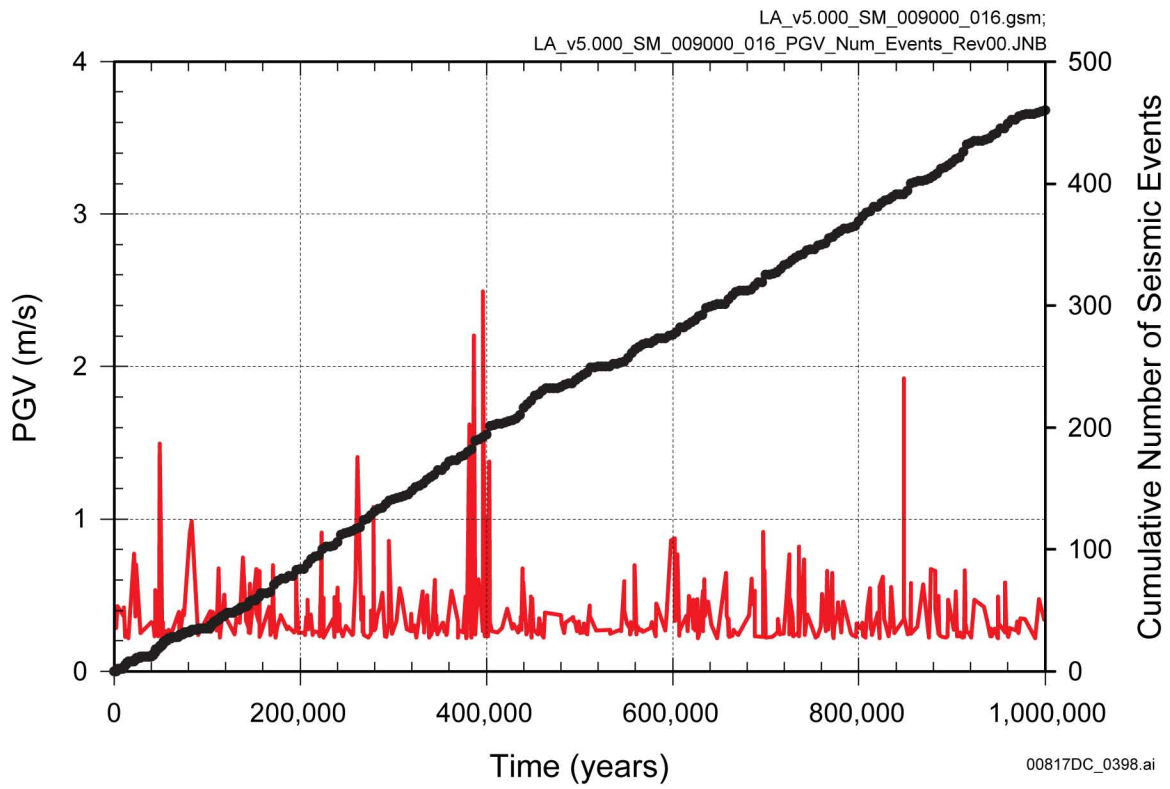

Source: Output DTN: MO0708TSPAVALI.000 [DIRS 182985].

Figure 7.7.1-38. Number of Seismic Events and the Peak Ground Velocity Time History for Realization 4641 of the Seismic Ground Motion Modeling Case for the 1,000,000-Year Simulation after Repository Closure

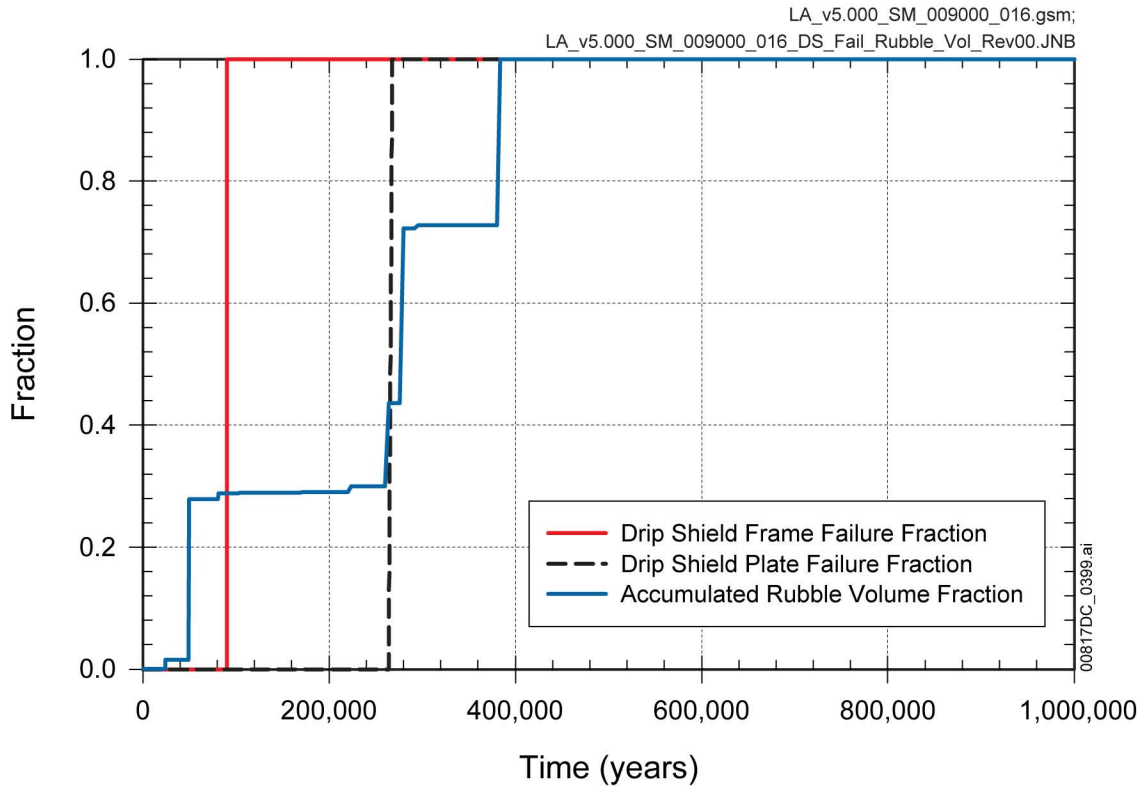

Source: Output DTN: MO0708TSPAVALI.000 [DIRS 182985].

Figure 7.7.1-39. Failure Fraction for the Drip Shield Plate and Framework and the Rubble Fill Fraction in the Drift (Lithophysal Zone) for Realization 4641 of the Seismic Ground Motion Modeling Case for the 1,000,000-Year Simulation after Repository Closure

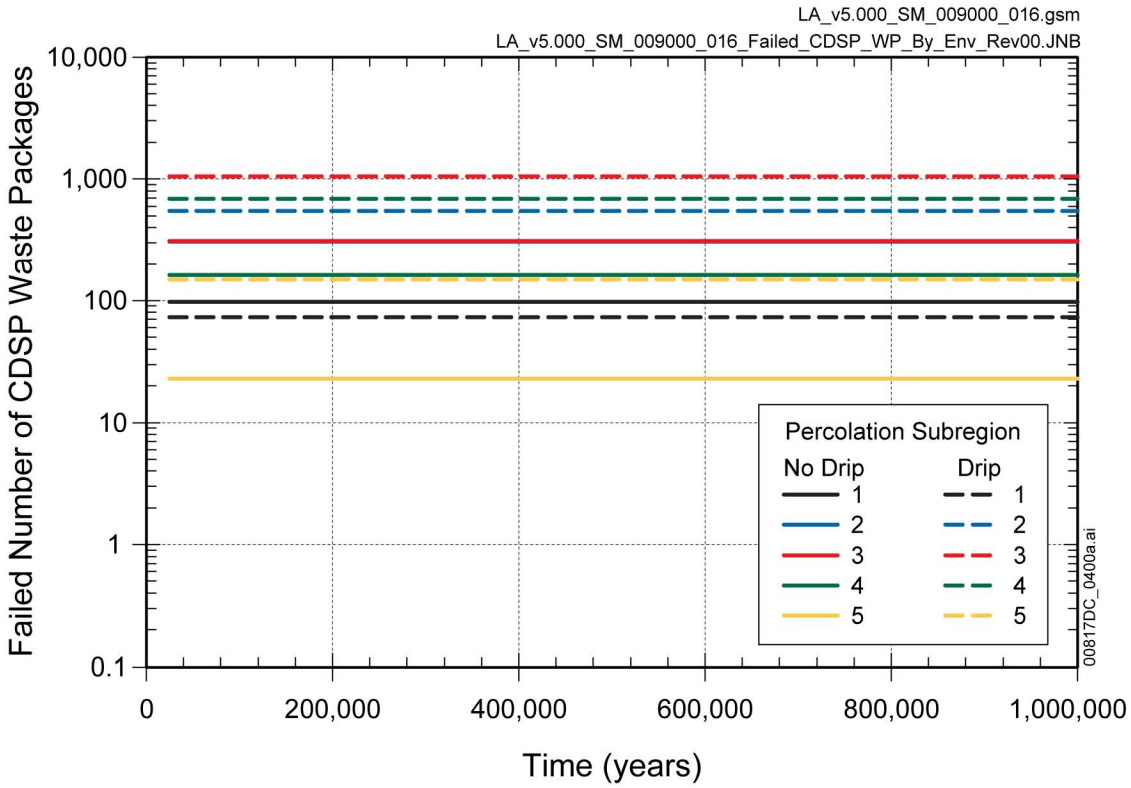

Source: Output DTN: MO0708TSPAVALI.000 [DIRS 182985].

Figure 7.7.1-40. CDSP WP Failure History in all Five Percolation Subregions for Both Dripping and Non-Dripping Environments for Realization 4641 of the Seismic Ground Motion Modeling Case for the 1,000,000-Year Simulation after Repository Closure

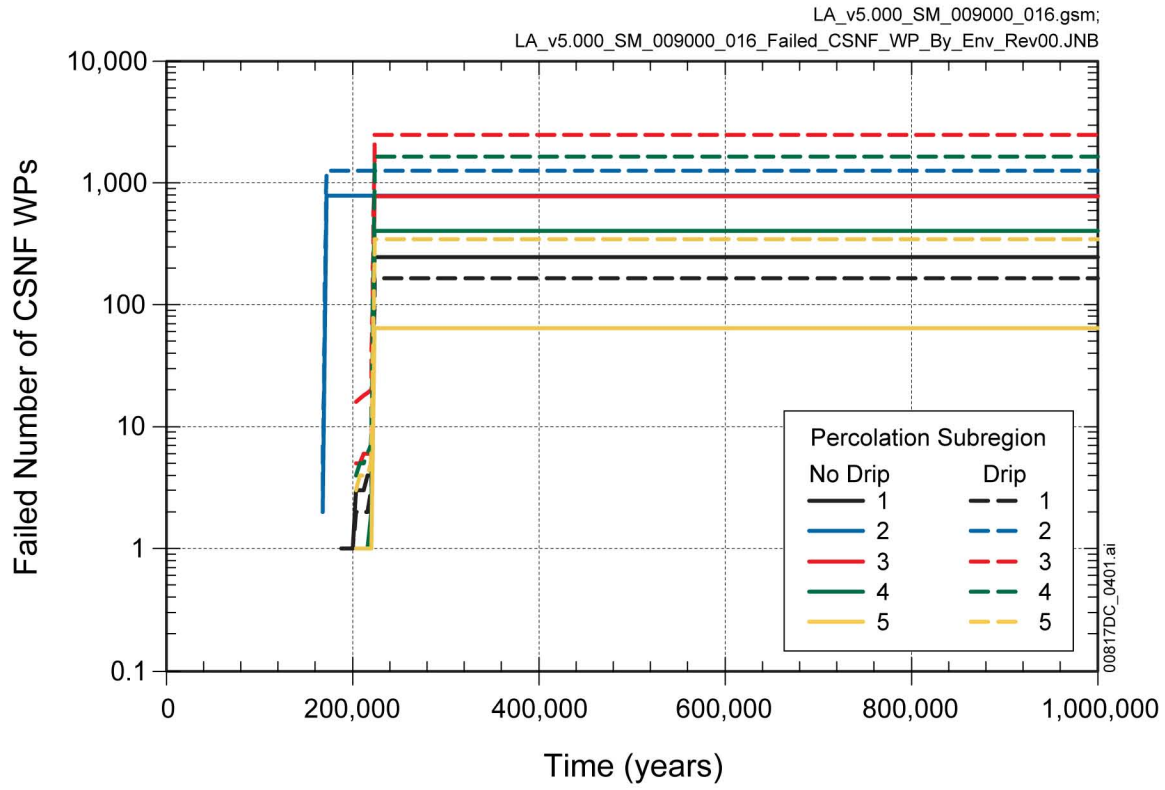

Source: Output DTN: MO0708TSPAVALI.000 [DIRS 182985].

Figure 7.7.1-41. CSNF WP Failure History for Each Percolation Subregion for Both Dripping and Non-Dripping Environments for Realization 4641 of the Seismic Ground Motion Modeling Case for the 1,000,000-Year Simulation after Repository Closure

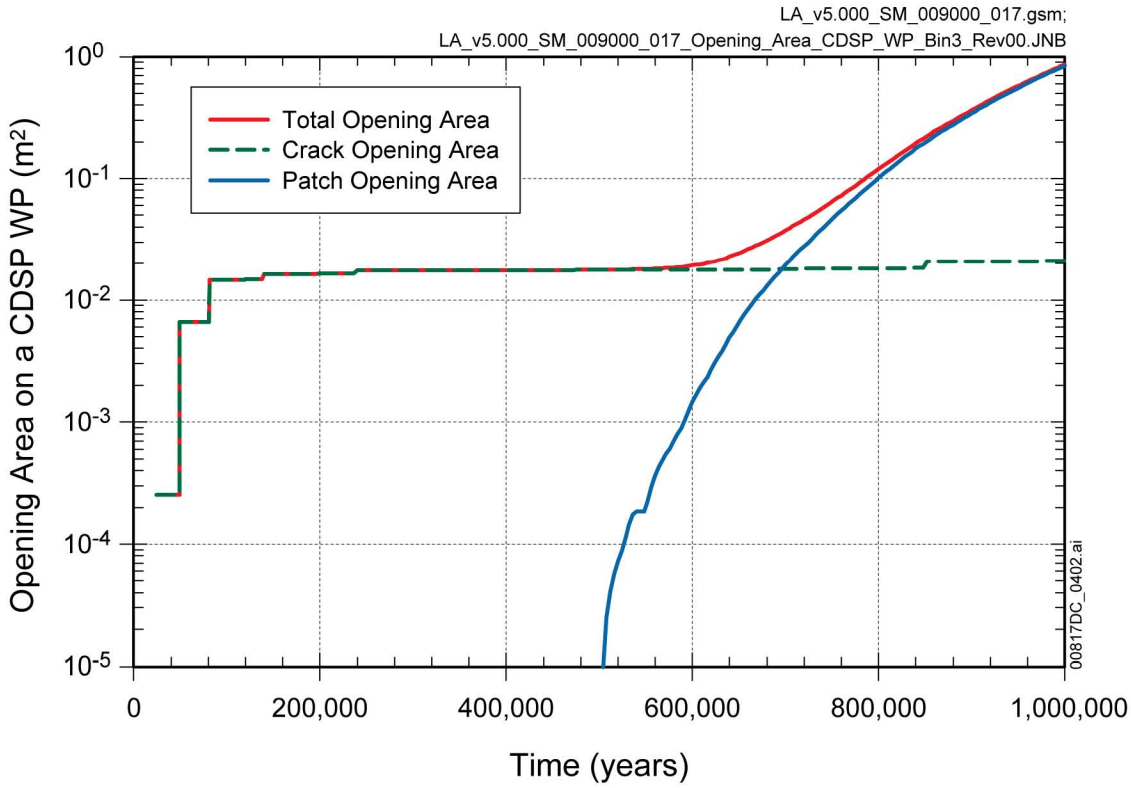

Source: Output DTN: MO0708TSPAVALI.000 [DIRS 182985].

Figure 7.7.1-42. CDSP WP Opening Area after Failure for Percolation Subregion 3 from Crack and Patches for Realization 4641 of the Seismic Ground Motion Modeling Case for the 1,000,000-Year Simulation after Repository Closure

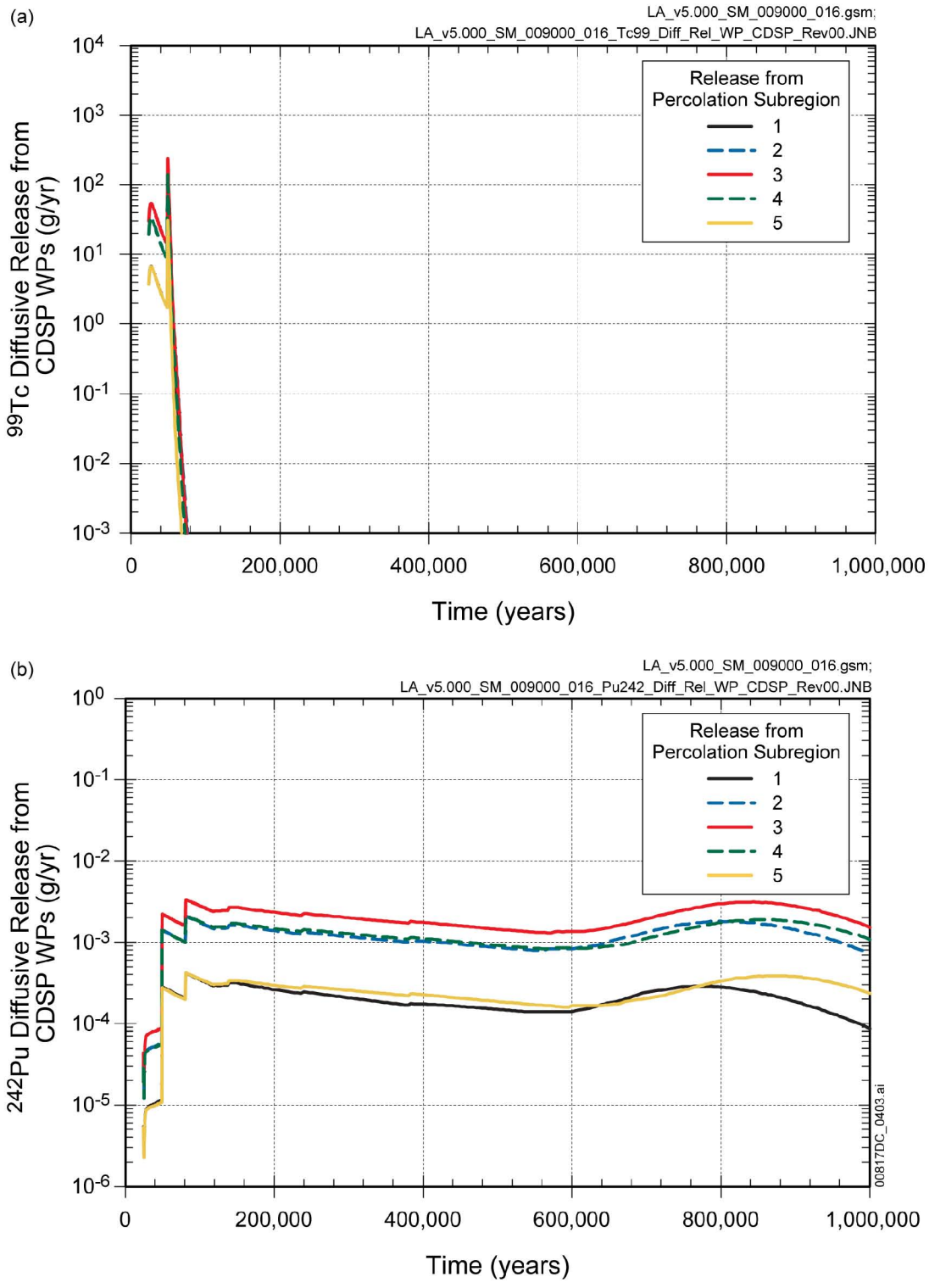

Source: Output DTN: MO0708TSPAVALI.000 [DIRS 182985].

Figure 7.7.1-43. Diffusive Release Rates of: (a) ^{99}Tc and (b) ^{242}Pu from CDSP WPs from each Percolation Subregion for Realization 4641 of the Seismic Ground Motion Modeling Case for the 1,000,000-Year Simulation after Repository Closure

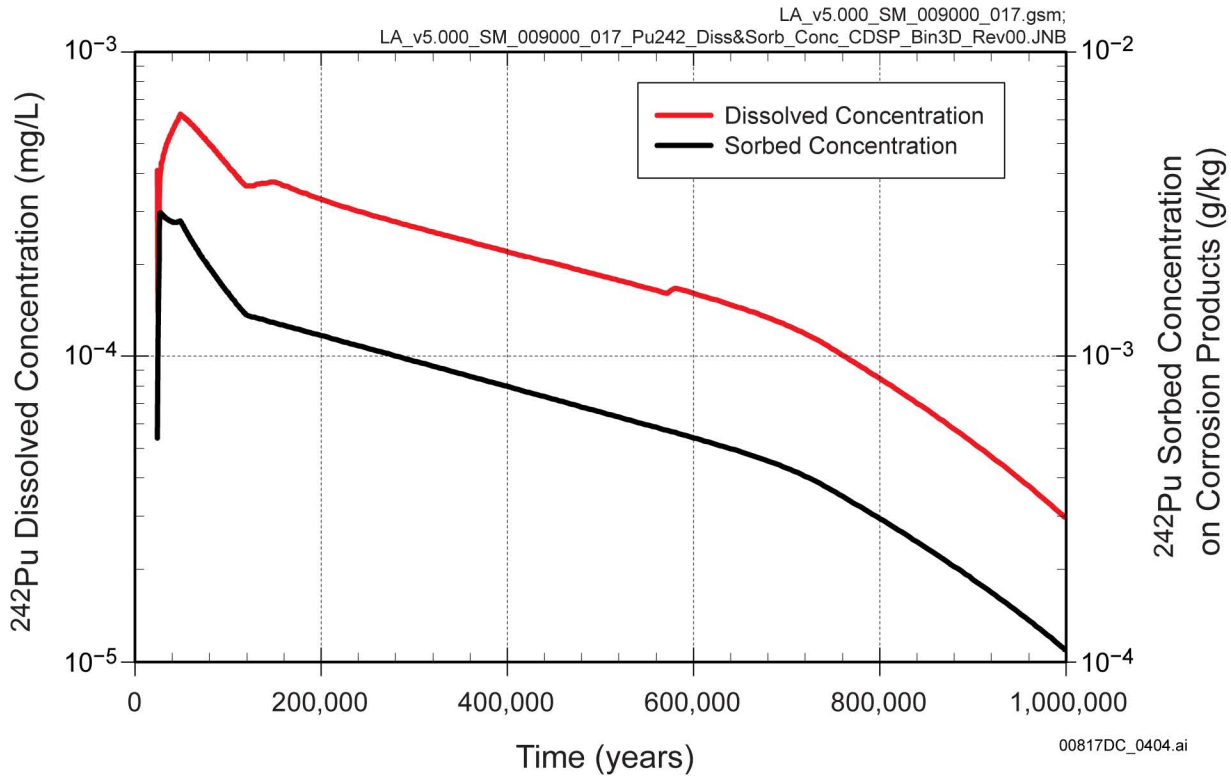

Source: Output DTN: MO0708TSPAVALI.000 [DIRS 182985].

Figure 7.7.1-44. Dissolved Concentration of ^{242}Pu in the Corrosion Products Domain Compared to the Sorbed Concentration on Corrosion Products for CDSP Percolation Subregion 3 Dripping Environment for Realization 4641 of the Seismic Ground Motion Modeling Case for the 1,000,000-Year Simulation after Repository Closure

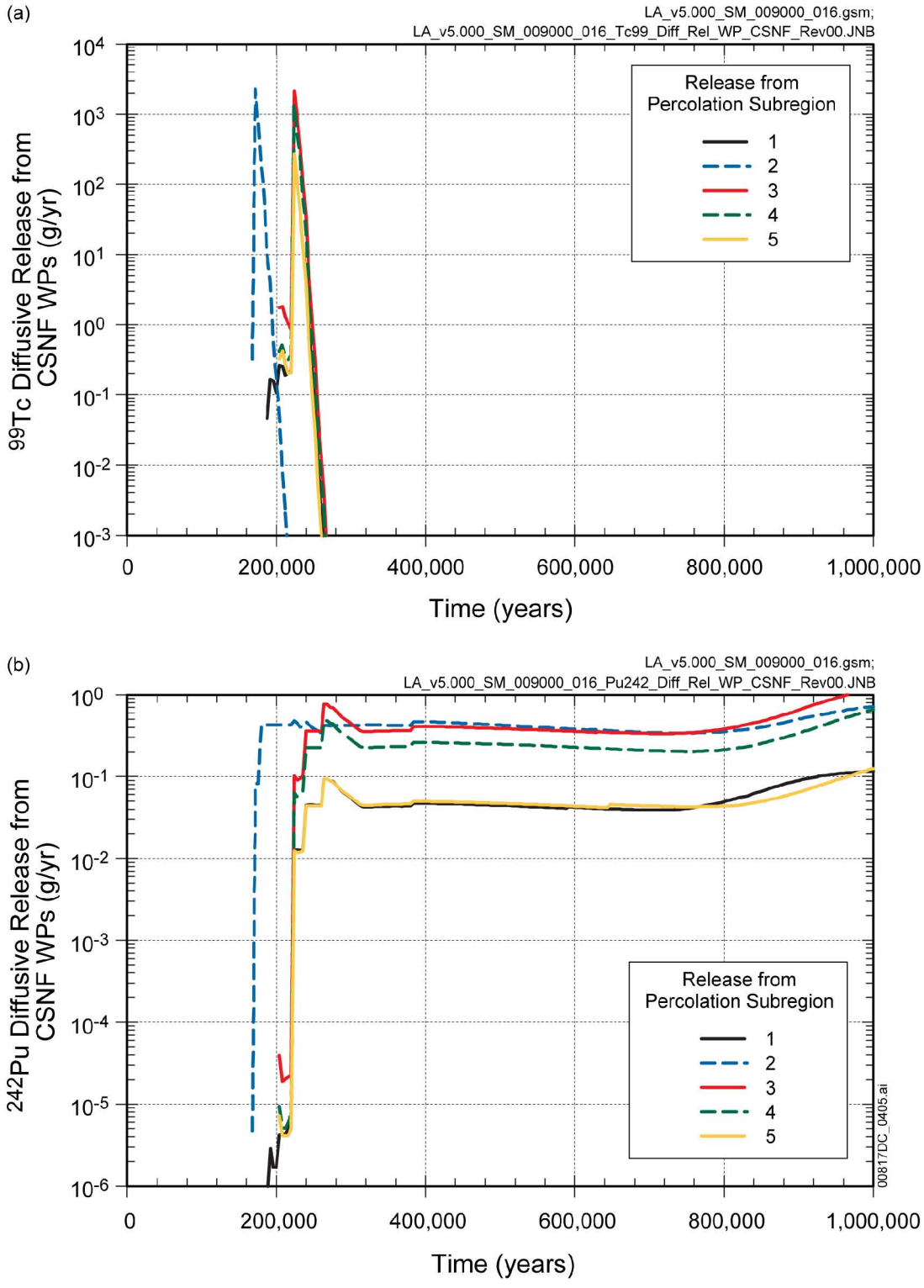

Source: Output DTN: MO0708TSPAVALI.000 [DIRS 182985].

Figure 7.7.1-45. Diffusive Release Rates of: (a) ^{99}Tc and (b) ^{242}Pu from CSNF WPs from each Percolation Subregion for Realization 4641 of the Seismic Ground Motion Modeling Case for the 1,000,000-Year Simulation after Repository Closure

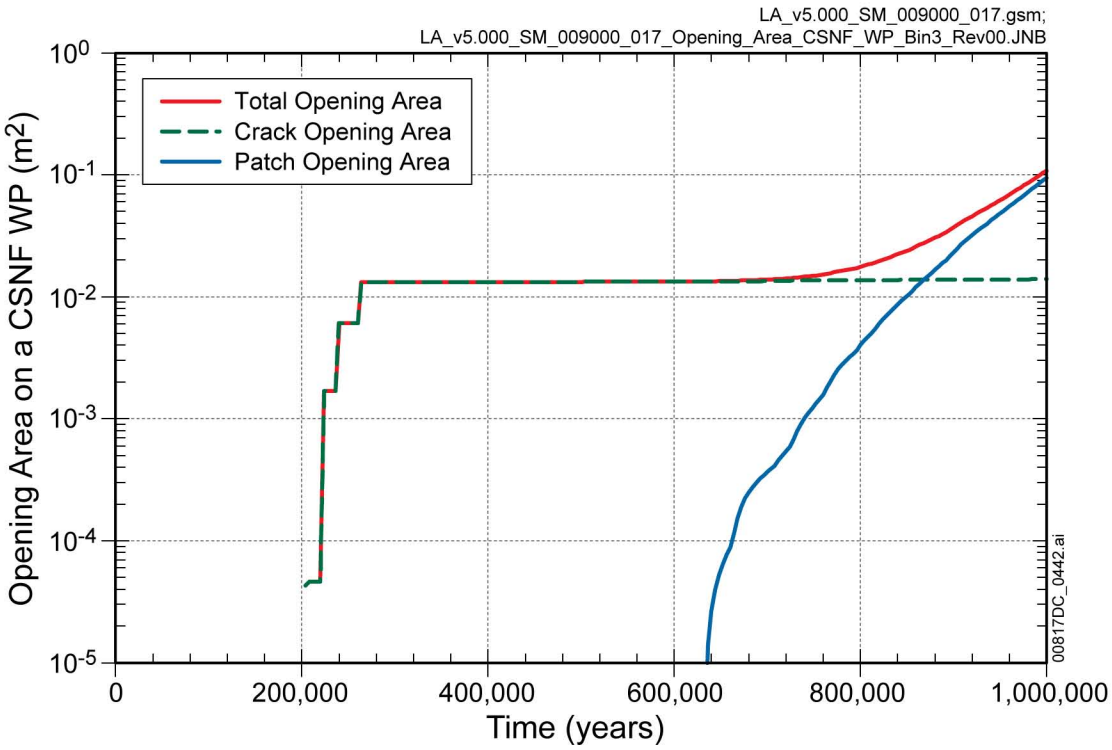

Source: Output DTN: MO0708TSPAVALI.000 [DIRS 182985].

Figure 7.7.1-46. CSNF WP Opening Area after Failure for Percolation Subregion 3 from Cracks and Patches for Realization 4641 of the Seismic Ground Motion Modeling Case for the 1,000,000-Year Simulation after Repository Closure

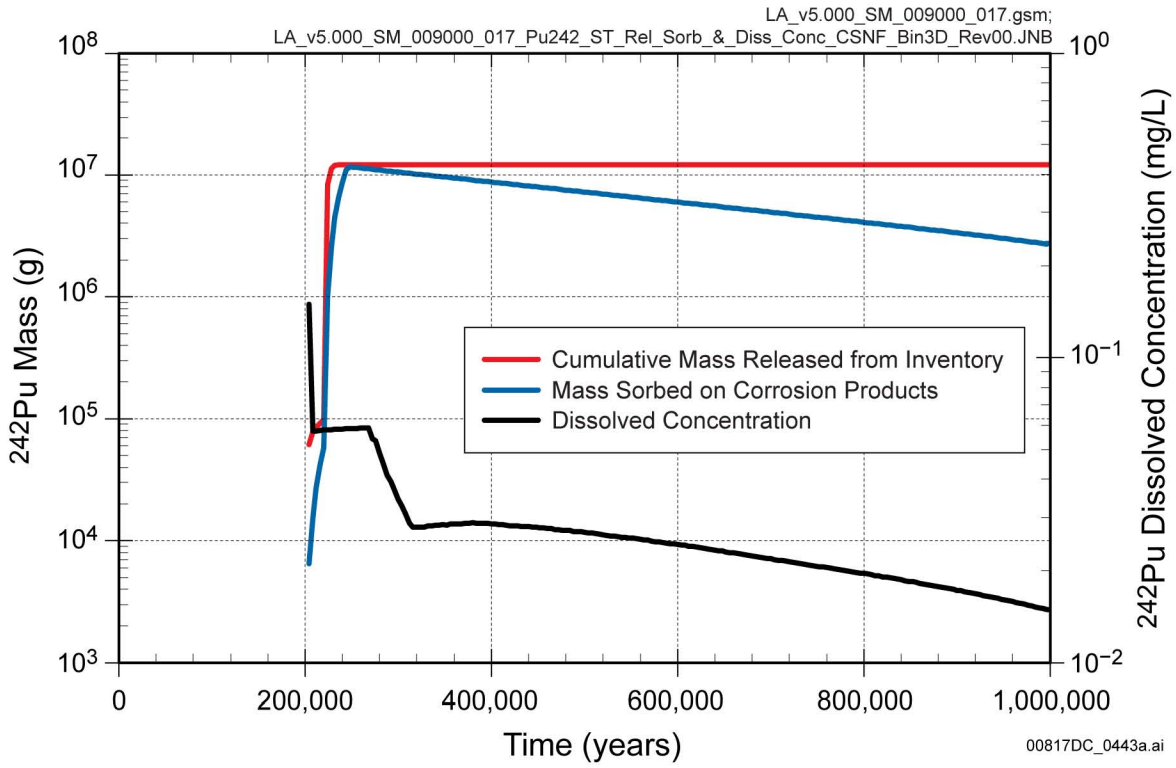

Source: Output DTN: MO0708TSPAVALI.000 [DIRS 182985].

Figure 7.7.1-47. Comparison of ^{242}Pu Cumulative Mass Released from the Inventory, Mass Sorbed on Corrosion Products, and the Dissolved Concentration in the Corrosion Products Domain for CSNF Percolation Subregion 3, Dripping Environment for Realization 4641 of the Seismic Ground Motion Modeling Case for the 1,000,000-Year Simulation after Repository Closure

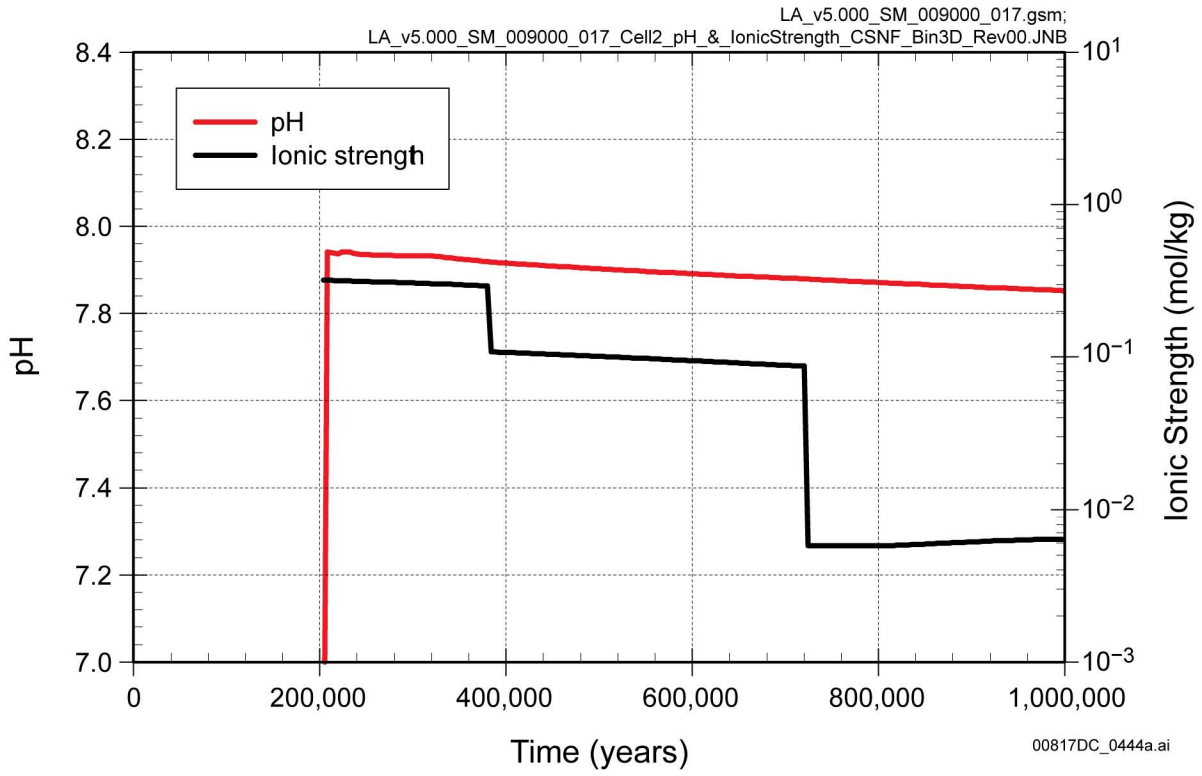

Source: Output DTN: MO0708TSPAVALI.000 [DIRS 182985].

Figure 7.7.1-48. pH and Ionic Strength Profile in the Corrosion Products Domain for CSNF Percolation Subregion 3, Dripping Environment for Realization 4641 of the Seismic Ground Motion Modeling Case for the 1,000,000-Year Simulation after Repository Closure

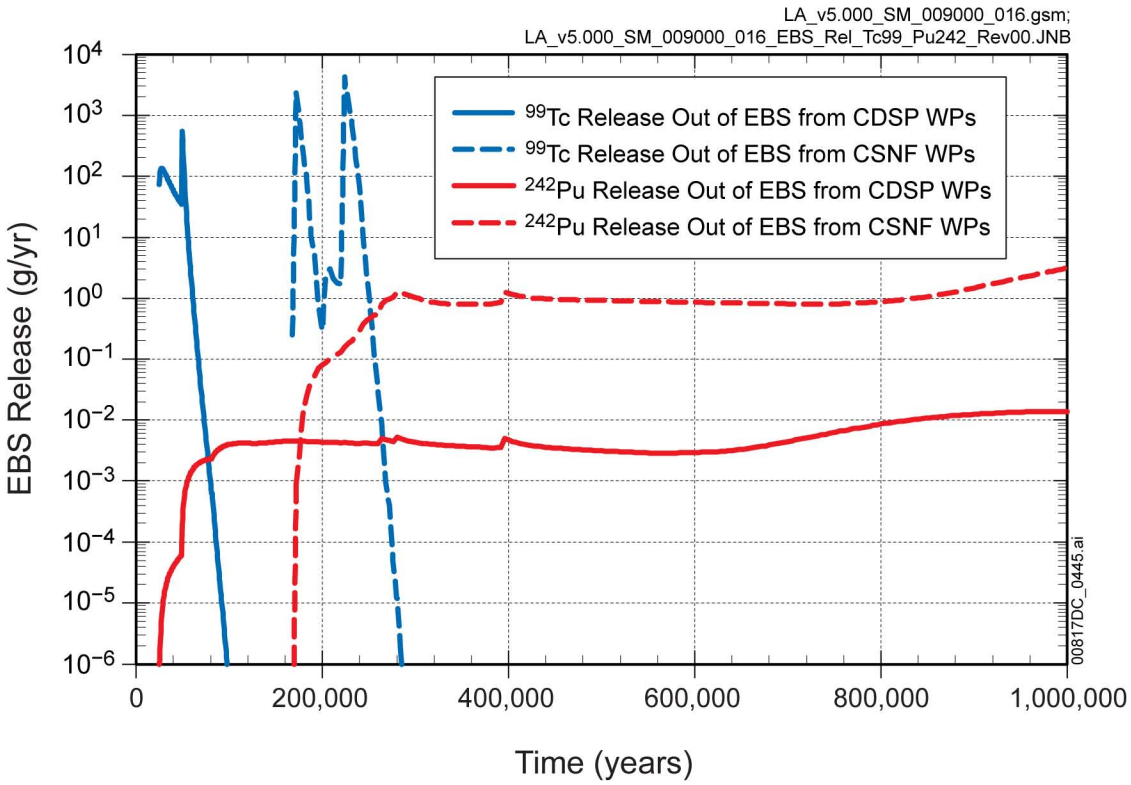

Source: Output DTN: MO0708TSPAVALI.000 [DIRS 182985].

Figure 7.7.1-49. EBS Release Rates from CSNF and CDSP WPs (All Percolation Subregions) for Realization 4641 of the Seismic Ground Motion Modeling Case for the 1,000,000-Year Simulation after Repository Closure

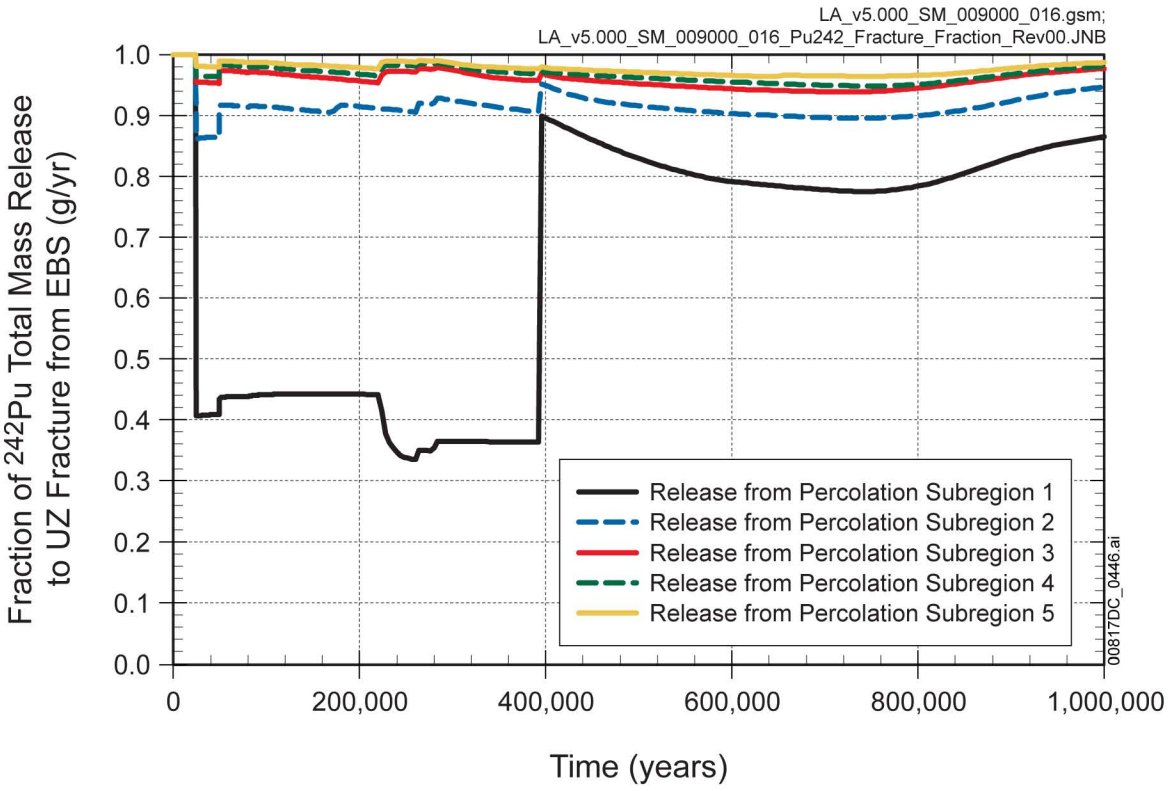

Source: Output DTN: MO0708TSPAVALI.000 [DIRS 182985].

Figure 7.7.1-50. Fraction of ^{242}Pu Mass Going to Unsaturated Zone Fractures as Compared to the Unsaturated Zone Matrix at the Repository Horizon for Realization 4641 of the Seismic Ground Motion Modeling Case for the 1,000,000-Year Simulation after Repository Closure

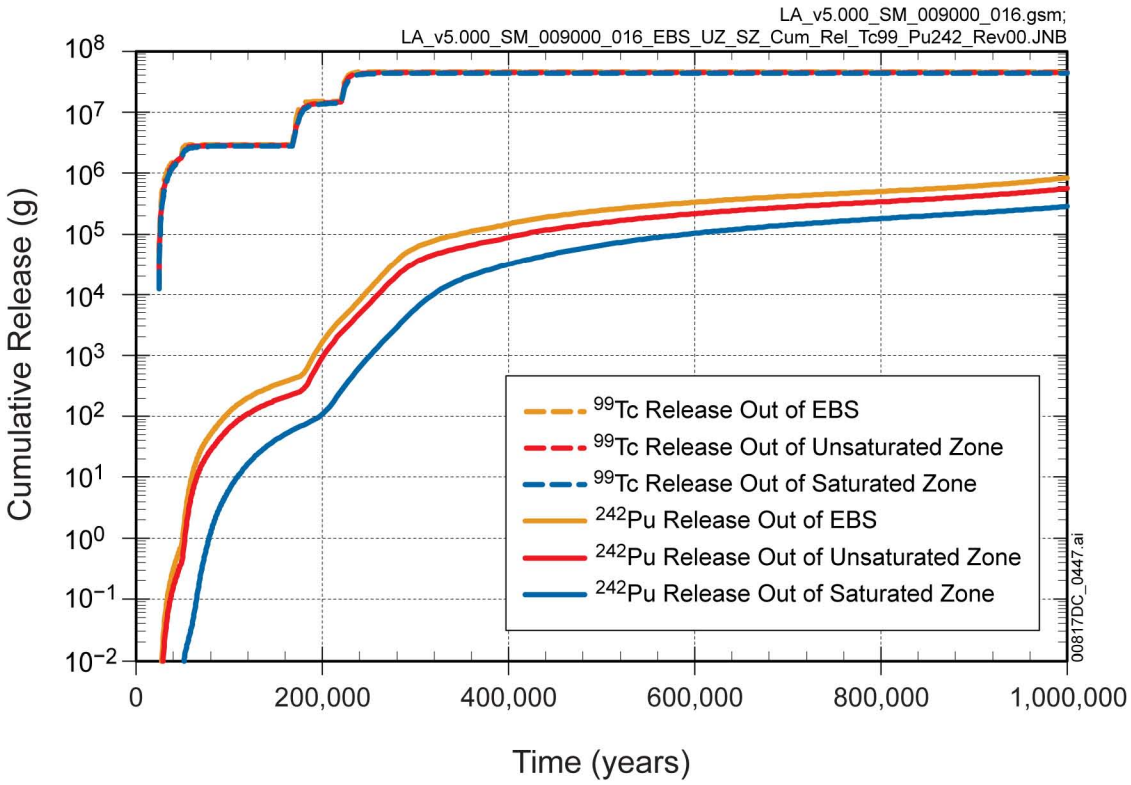

Source: Output DTN: MO0708TSPAVALI.000 [DIRS 182985].

Figure 7.7.1-51. Cumulative Mass Release of ^{99}Tc and ^{242}Pu from the EBS, Unsaturated Zone, and Saturated Zone for Realization 4641 of the Seismic Ground Motion Modeling Case for the 1,000,000-Year Simulation after Repository Closure

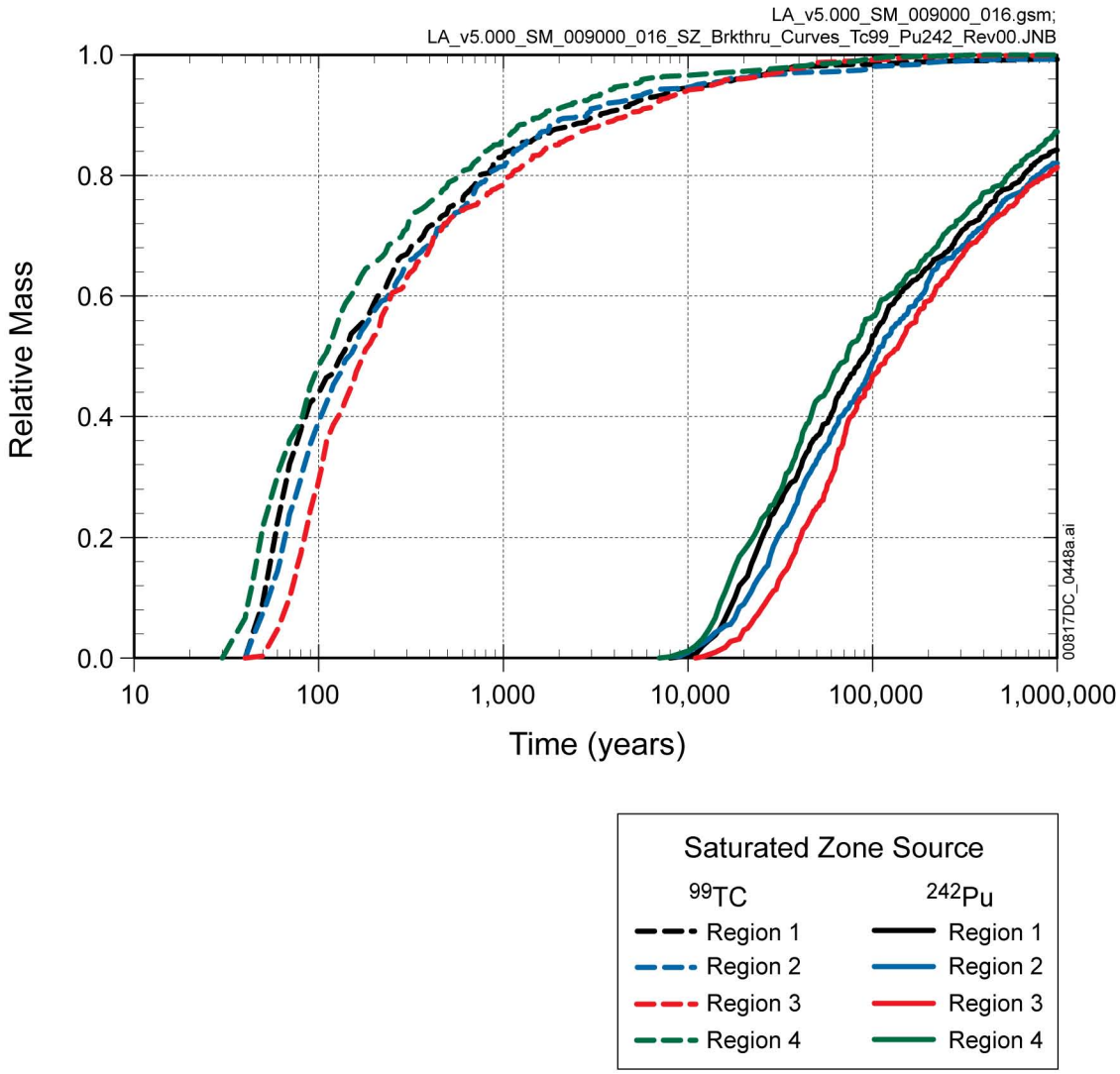

Source: Output DTN: MO0708TSPAVALI.000 [DIRS 182985].

NOTE: The SZ breakthrough curve #122 is used in Realization 4641.

Figure 7.7.1-52. Comparison of Saturated Zone Breakthrough Curves for ^{99}Tc and ^{242}Pu for All Four Saturated Zone Regions for Realization 4641 of the Seismic Ground Motion Modeling Case for the 1,000,000-Year Simulation after Repository Closure

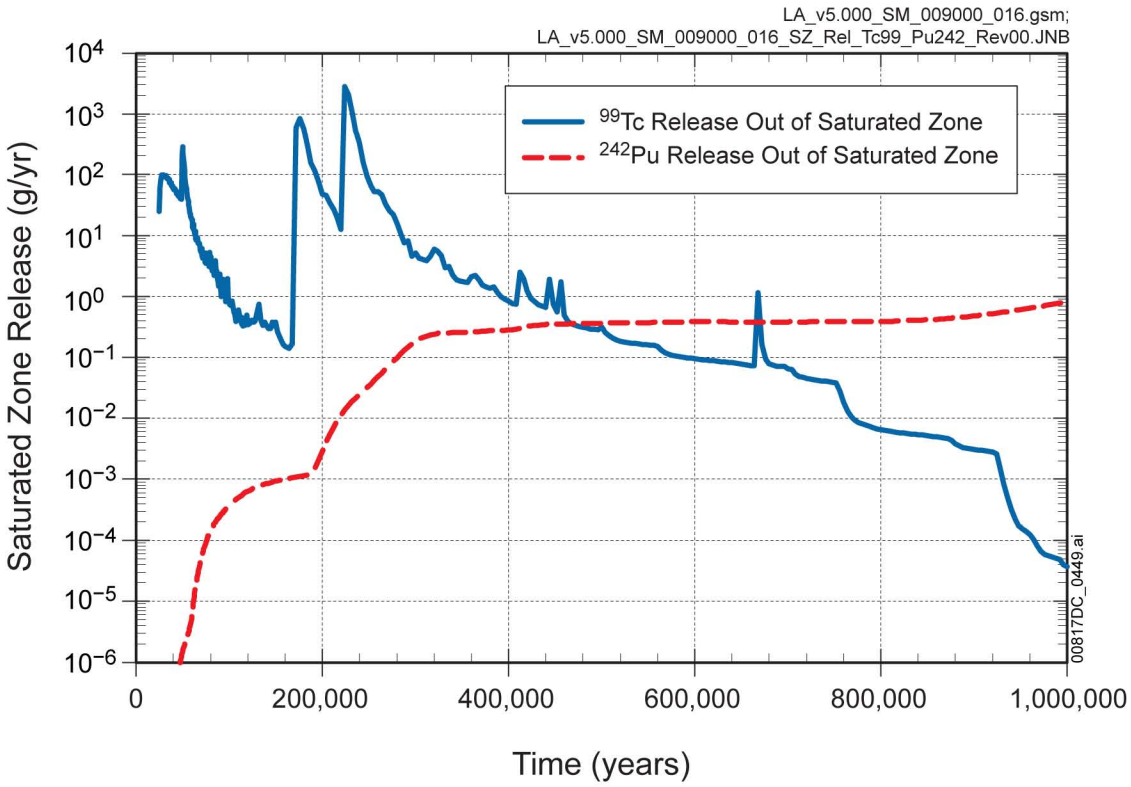

Source: Output DTN: MO0708TSPAVALI.000 [DIRS 182985].

Figure 7.7.1-53. Saturated Zone Release to the Biosphere for ^{99}Tc and ^{242}Pu for Realization 4641 of the Seismic Ground Motion Modeling Case for the 1,000,000-Year Simulation after Repository Closure

7.7.2 Comparison with Simplified TSPA Analysis

The TSPA-LA Model, presented in Chapter 6, describes the models and submodels used to calculate spatially varying radionuclide mass transfer rates from the EBS, the UZ, and the SZ. The mass flux exiting the SZ is then used to determine the annual dose to a RMEI. A complex numerical model is required to appropriately solve the coupled differential equations that describe repository performance while taking into account the spatial variability in properties and processes.

A Simplified Analysis has been developed to evaluate repository performance utilizing simplified representations of the mathematical equations that describe radionuclide mass transfer rates. This analysis, called Simplified TSPA Analysis (also referred herein as Simplified Analysis) is described in detail in Appendix L, and is being used to build confidence and corroborate the TSPA-LA Model presented in Chapter 6 and the results it generates that are shown in Chapter 8. The Simplified TSPA Analysis was developed as a stand-alone computer program written in FORTRAN 90 and compiled/linked using Compaq Visual Fortran as unqualified software. Unqualified software can be used to corroborate analysis or calculation results per Section 6.2.1 M of SCI-PRO-006, *Model.*

Overall, the Simplified TSPA Analysis is a higher-level abstraction than the TSPA-LA Model. In general, it includes the same FEPs that are considered in the TSPA, but the manner in which they are modeled is much simpler. Some FEPs have not been included in the Simplified TSPA Analysis based on a qualitative assessment of their importance in past TSPA models. For those FEPs that are included, the simplification primarily involves removing a considerable amount of detail included in the TSPA-LA to capture spatial and temporal variability and treating the repository system with a more "average" representation. In addition, many of the process level modeling results are further abstracted for inclusion in the Simplified TSPA Analysis.

The Simplified TSPA Analysis has its bases in the process- and abstraction-level modeling captured in the supporting Analysis and Model reports. Thus, it represents the same conceptualization of the repository system and its underlying technical bases are identical to those of the TSPA-LA Model. However, the Simplified TSPA Analysis is different than the TSPA-LA Model both in its structure and computational method. A summary of the key differences between the TSPA-LA Model and the Simplified TSPA Analysis is provided in Table 7.7.2-1, which summarizes those FEPs that were not included in the Simplified TSPA Analysis and the differences in the treatment of the FEPs between the Simplified TSPA Analysis and the TSPA-LA Model.

The largest degree of simplification was in the modeling of radionuclides within the UZ and SZ. A simple one-dimensional radionuclide transport model was developed using average properties for each hydrologic unit in the UZ and SZ. This simplified approach reflects the general behavior of the breakthrough curve, rather than the detailed behavior of ground water flow and radionuclide transport within the UZ and SZ.

A more complex, but still simplified, analysis was developed to model radionuclide transport within the EBS. The relative complexity of this portion of the Simplified TSPA Analysis, as compared to the UZ and SZ models, was necessary to appropriately model the rate that

radionuclides are released from the EBS, or the source term. This model included submodels that calculated the rate and manner that the WPs degrade, the rate the waste form degrades, and the rate radionuclides are transported through the engineered barriers.

The Simplified TSPA Analysis, as an auxiliary analysis of the overall repository system, is a different system-level mathematical model and its results can be used to build confidence in the TSPA-LA Model, its results, and the conclusions drawn from those results. Despite the differences in level of detail, the basic results of the two models (i.e. dose over time and contribution to dose of dominant radionuclides) can be compared for individual modeling cases. If the comparison between the Simplified TSPA Analysis and the TSPA-LA Model demonstrates that the two models produce results that are similar in magnitude with similar trends, then the comparison supports the verification that the TSPA-LA Model produces reasonable results.

Models of the degradation of the engineered barriers were developed for the nominal, seismic ground motion, and igneous intrusion conditions. This was done to allow for comparisons with the modeling cases evaluated with the TSPA-LA Model.

The Simplified TSPA Analysis described in Appendix L was used to simulate four modeling cases that were analyzed using the TSPA-LA Model over a 1,000,000 year period. These are:

- Waste Package EF Modeling Case: This case evaluated repository performance considering only those WPs that experience early failure. In this case, no failure of the WPs is considered to occur due to general corrosion, SCC, or seismic mechanical damage.

- Nominal Modeling Case: This scenario considered degradation of the WPs and DSs from corrosion processes only. Early WP failure was not considered in this scenario and mechanical damage of the DS and WP was not considered in this scenario. Seismic induced rockfall and its subsequent effects on seepage were also not considered.

- Seismic GM Modeling Case: This scenario considered degradation of the WPs and DS from corrosion processes. The effects of seismic ground motion were also considered including mechanical damage to the WPs and DS, and seismic induced rockfall. Aleatory and epistemic uncertainty were randomly sampled in each realization. Seismic events of varying magnitude were assumed to occur randomly following a Poisson process. The subsequent effects on rockfall, DS damage, and WP damage were then calculated.

- Igneous Intrusion Modeling Case: This scenario considered the degradation of the engineered barriers as a result of an intruding magma dike. Degradation of the WPs and DS due to corrosion processes, seismic mechanical damage, and early WP failure were not considered. Aleatory and epistemic uncertainty were randomly sampled in each realization. A single igneous intrusion was assumed to occur randomly over the simulation period resulting in the failure of all DS and WPs.

7.7.2.1 Waste Package Early Failure Modeling Case

A 500 realization simulation of the Waste Package EF Modeling Case was conducted over a 1,000,000 year period using the Simplified TSPA Analysis. Key aspects of this simulation case are:

- The number of early CSNF and CDSP WP failures was determined using the approach described in Section L.2.8.2. In summary, the number of CSNF and CDSP WPs that experience early failure, in a given realization, is sampled from a Poisson distribution. Several realizations do not result in any early WP failures.

- It is assumed that the entire surface of any of the WPs that experience early failure is degraded.

- DS degradation occurs only due to general corrosion following the approach presented in Section L.2.7.1. Radionuclide transport within and out of the WP is via diffusive processes until the DS fail due to general corrosion

- All WPs that experience early failure are assumed to be in a region of the repository that experiences seepage.

Figure 7.7.2-1 presents the annual dose histories for the Waste Package EF Modeling Case using the Simplified TSPA Analysis. This mean annual dose history takes into account the probability of early WP failure through the Poisson sampling discussed above and in Section L.2.8.2. Figure 7.7.2-1 also shows the contribution to mean annual dose from radionuclides that contribute most strongly to the mean annual dose for the Waste Package EF Modeling Case using the Simplified TSPA Analysis

The results shown on Figure 7.7.2-1 indicate that the mean annual dose and the individual radionuclide mean annual dose are similar in magnitude to those obtained for the WP Early Failure Modeling Case simulated over a 1,000,000 year period with the TSPA-LA Model shown on Figure 8.2-6. In addition, the most significant radionuclides are also similar with the mobile radionuclides ^{99}Tc and ^{129}I and moderately mobile radionuclide ^{237}Np initially dominating, then by ^{239}Pu until approximately 200,000 years after repository closure, then ^{242}Pu and ^{229}Th. The TSPA-LA results shown in Figure 8.2-6 also show that the mobile and soluble radionuclides (^{99}Tc, ^{129}I, and ^{14}C) dominating first with the solubility limited and less mobile radionuclides (^{239}Pu, ^{242}Pu, ^{237}Np, and ^{226}Ra), becoming important later.

The overall trends are very similar except for ^{229}Th being a key radionuclide at later times in the Simplified TSPA Analysis while the TSPA-LA Model shows ^{226}Ra being a key radionuclide. Two factors contribute to the increased importance of ^{229}Th in the Simplified TSPA Analysis relative to the TSPA-LA Model.

- Both models assume ^{226}Ra is in secular equilibrium with ^{230}Th at the receptor well. As discussed in Section L2.16, the Simplified TSPA Analysis uses a very rough approximation to handle chain decay in the UZ and SZ. The UZ is divided into three layers to represent the Topopah Spring, Calico Hills, and Prow Pass units while the SZ is

divided into two fractured-volcanic segments and one alluvial segment. The chain decay approach implemented in the Simplified TSPA Analysis calculates how much mass of a parent radionuclide breaks through a UZ layer or SZ segment both without and with decay. The difference is assumed to be the daughter radionuclide and is introduced at the beginning of the next UZ layer or SZ segment. This approach does not allow for decay of the daughter in the layer where it is formed. Because of this, the Simplified TSPA Analysis adds a bit more of a daughter to the top of layers than would be present with a more explicit method as is used in the TSPA-LA Model. Since ^{229}Th has roughly an order of magnitude shorter half-life than ^{230}Th, the Simplified TSPA Analysis effectively "adds more" ^{229}Th relative to ^{230}Th, artificially increasing its importance as compared to the TSPA-LA Model.

- ^{229}Th is a daughter product of ^{233}U and builds in both the engineered and natural systems. ^{229}Th that is released from the EBS is transported throughout the natural barrier system with the properties of thorium. However, when ^{229}Th is created in one of the components of the natural system (UZ layer or segment of the SZ) in the Simplified TSPA Analysis, it is assumed to transport through that component with the properties of uranium until it exits that component. Thorium travels much more slowly through the natural barriers than uranium because it has a higher sorption coefficient. Thus, the modeling approach for the natural barrier system in this simplified analysis leads to artificially high transport rates for thorium and results in higher annual doses as is seen for ^{229}Th in this modeling case.

An estimate of the uncertainty in the annual dose for the WP Early Failure Modeling case using the Simplified TSPA Analysis is shown on Figure 7.7.2-2. The estimates of annual dose shown on Figure 7.7.2-2 takes into account uncertainties in the various submodels of this modeling case in addition to sampling the number of CSNF and CDSP WPs that experience early failure. These uncertainties are addressed in terms of probability distributions for parameters of the submodels (i.e., adsorption coefficients for transport of radionuclides in the UZ, the uncertainty term added for actinide solubilities). These uncertainties along with uncertainty in the number of WPs that experience early failure are addressed in the estimate of mean annual dose by evaluating 500 realizations with each realization providing an annual dose that results from one set of values representing the uncertainty and the sampled number of WPs that experience early failure. The mean annual dose at a given time is the average for the 500 annual dose values. The range of uncertainty in the annual dose is represented by the 5th and 95th percentiles of the annual dose values for each of the 500 realizations.

These 5th, 50th, and 95th percentile annual dose histories are shown, along with the mean annual dose, on Figure 7.7.2-2. However, approximately 60 percent of the realizations sample no early WP failures, resulting in 5th and 50th percentile annual dose histories of zero. Comparing Figure 7.7.2-2 and Figure 8.2-5 shows that the Simplified TSPA Analysis yields higher mean annual total and individual radionuclide doses than does the TSPA-LA Model. The higher mean annual dose is due to higher mean individual radionuclide doses for ^{239}Pu and ^{242}Pu as a result of the simplified approach used for modeling radionuclide transport in the EBS.

A comparison of the Simplified TSPA Analysis results considering all realizations and the TSPA-LA Model results for this modeling case at 200,000 years, 400,000 years 600,000 years,

800,000 years, and 1,000,000 years following repository closure, is shown on Figure 7.7.2-3. This comparison shows that the Simplified TSPA Analysis results in annual doses that are similar in magnitude to, but higher, than those of the TSPA-LA.

7.7.2.2 Nominal Modeling Case

The Nominal Modeling Case accounts for the WPs that fail under nominally expected conditions because of general corrosion and SCC and for the DSs that fail under nominally expected conditions because of general corrosion.

Figure 7.7.2-4 presents the mean annual dose histories for the Nominal Modeling Case using the Simplified TSPA-LA Analysis. Figure 7.7.2-4 also shows the contribution to mean annual dose from the radionuclides that contribute most strongly to the mean annual dose for the Nominal Modeling Case using the Simplified TSPA-LA Analysis.

The results shown on Figure 7.7.2-4 indicate that the mean annual dose and the individual radionuclide mean annual dose are similar in magnitude to those obtained for the Nominal Modeling Case simulated over a 1,000,000 year period with the TSPA-LA Model, as shown on Figure-8.2-2. In addition, the most significant radionuclides are also similar with the soluble and mobile radionuclides ^{129}I and ^{99}Tc dominating, and the less mobile radionuclide ^{135}Cs to a lesser extent. The mean annual dose of solubility limited radionuclides (i.e., ^{237}Np and ^{242}Pu) is shown to be steadily increasing out to 1,000,000 years in both models. These trends are consistent with those of the TSPA-LA Model shown on Figure 8.2-2.

An estimate of the uncertainty in the annual dose for the Nominal Modeling Case using the Simplified TSPA Analysis is shown on Figure 7.7.2-5. The estimate of mean annual dose shown on Figure 7.7.2-5 takes into account uncertainties in the various submodels of this scenario. These uncertainties are addressed in terms of probability distributions for parameters of the submodels. These uncertainties are addressed in the estimate of mean annual dose by evaluating 500 realizations with each realization providing an annual dose that results from one set of values representing the uncertainty. The mean annual dose at a given time, is the average for the 500 annual dose values. The range of uncertainty in the annual dose is represented by the 5th and 95th percentiles of those annual dose values.

The annual dose results shown on Figure 7.7.2-5 for the Simplified TSPA Analysis are lower than those from the TSPA-LA Model shown in Figure 8.2-1. This is further illustrated on Figure 7.7.2-6 which shows a comparison of the Simplified TSPA Analysis results and the TSPA-LA Model results for this modeling case at 200,000 years, 400,000 years, 600,000 years, 800,000 years, and 1,000,000 years following repository closure. The Simplified TSPA Analysis results in mean annual doses that are around an order of magnitude lower than the TSPA-LA results until about 800,000 years following repository closure. The mean annual dose calculated by the Simplified TSPA Analysis is approximately a factor of two lower than that calculated by the TSPA-LA at 1,000,000 years. This difference is attributed to differences in the rate and manner that the WPs fail between the Simplified TSPA Analysis and the TSPA-LA Model.

The general corrosion rate of the WP outer barrier material is dependent on temperature in both the Simplified TSPA Analysis and the TSPA-LA Model. General corrosion failure of the WP

outer barrier occurs in three percent of the realizations in the Simplified TSPA Analysis, all occurring after 800,000 years following repository closure. As discussed in Section 8.2.1, by 1,000,000 years, approximately 10 percent of the WPs are projected to be failed by general corrosion breaches.

The Simplified TSPA Analysis results in SCC occurring in approximately 50 percent of the realizations. The earliest failures due to SCC occur around 300,000 years following repository closure in the Simplified TSPA Analysis, whereas the earliest failures due to SCC occur around 100,000 years in the TSPA-LA Model. Approximately 50 percent of the realizations of the Simplified TSPA Analysis result in no WP failure due to stress corrosion, and no resultant dose, within a 1,000,000 year period. Over 95 percent of the realizations of the TSPA-LA Model result in SCC of the WPs within a 1,000,000 year period. This difference is shown in Figure 7.7.2-6 in the comparison of the mean values of the annual dose between the two models. The difference in the time that SCC begins between the Simplified TSPA Analysis and the TSPA-LA Model results in the difference in the annual dose histories. In a sense, the annual dose from the Simplified TSPA Analysis are translated outward in time by a few hundred thousand years.

The general trend in the annual dose between the two models is very similar and the peak mean annual dose calculated using the Simplified TSPA Analysis is within approximately half of an order of magnitude as that calculated by the TSPA-LA Model.

7.7.2.3 Seismic Ground Motion Modeling Case

The Seismic Ground Motion Modeling Case evaluates repository performance for those WPs that fail due to the ground motion damage associated with the seismic event. This case begins with the Nominal Modeling Case discussed above and includes the effect of seismic events over a 1,000,000 year period. The occurrence of seismic events is modeled using the approach presented in Section L.2.1. The effects of seismic events on rockfall/drift degradation and seepage are modeled as presented in Sections L.2.2 and L.2.5 respectively. The effects of seismic ground motion on the performance of the DS and WP is modeled as presented in Sections L.2.7.2 and L.2.8.3 respectively.

Figure 7.7.2-7 presents the mean annual dose histories for the Seismic GM Modeling Case using the Simplified TSPA-LA Analysis. Figure 7.7.2-8 also shows the contribution to mean annual dose from the radionuclides that contribute most strongly to the mean annual dose for the Seismic GM Modeling Case using the Simplified TSPA-LA Analysis.

The results shown in Figure 7.7.2-7 indicate that the mean annual dose is similar in magnitude to that obtained for the Seismic GM Modeling Case simulated over a 1,000,000 year period with the TSPA-LA Model shown on Figure 8.2-12. The most significant radionuclides for the Simplified TSPA Analysis initially are ^{129}I and ^{99}Tc, followed by ^{239}Pu dominating until about 300,000 years following repository closure. After 300,000 years ^{242}Pu becomes the dominant radionuclide contributing to the mean annual dose with ^{129}I, ^{99}Tc, ^{237}Np, ^{135}Cs, and ^{229}Th also contributing.

Comparing the results from this Simplified TSPA Analysis shown on Figure 7.7.2-7 with those of the TSPA-LA Model shown on Figure 8.2-12 indicates that the trend in the mean annual dose for the key radionuclides are similar although the magnitude may be slightly different. For example, the TSPA-LA Model results show ^{129}I and ^{99}Tc as the primary contributors to the mean annual dose over a 1,000,000 year period with ^{79}Se, ^{239}Pu, ^{242}Pu, ^{226}Ra, and ^{237}Np contributing to a lesser degree. The Simplified TSPA Analysis results also show ^{129}I and ^{99}Tc as the primary contributors, but ^{229}Th, ^{239}Pu, ^{242}Pu, and ^{237}Np are shown to contribute more to the mean annual dose than is shown in the TSPA-LA Model results. The increased importance of the actinide radionuclides in the Simplified TSPA Analysis is attributed to the simplified treatment of radionuclide transport within the EBS, UZ, and SZ (e.g., neglecting matrix diffusion). In addition, the simplified treatment of radionuclide decay chains leads to an artificially high annual dose from ^{229}Th as discussed in Section 7.7.2.1. These simplifications result in somewhat higher transport of solubility limited and less mobile radionuclides through both the engineered and natural barrier systems and lead to slightly more rapid releases and slightly larger doses for this modeling case as compared to the TSPA-LA Model. However, in general the trends are similar with the mobile radionuclides (^{129}I and ^{99}Tc) being important over the entire 1,000,000 year period with the importance of the less mobile, solubility limited actinides becoming more important at later times.

An estimate of the uncertainty in the annual dose for the Seismic GM Modeling Case using the Simplified TSPA Analysis is shown on Figure 7.7.2-8. The estimate of mean annual dose shown on Figure 7.7.2-8 takes into account uncertainties in the various submodels of this scenario. These uncertainties are addressed in terms of probability distributions for parameters of the submodels. These uncertainties are addressed in the estimate of mean annual dose by evaluating 500 realizations with each realization providing an annual dose that results from one set of values representing the uncertainty. The mean annual dose at a given time is the average for the 500 annual dose values. The range of uncertainty in the annual dose is represented by the 5th and 95th percentiles of those annual dose values for each of 500 realizations.

The mean annual dose results shown on Figure 7.7.2-8 for the Simplified TSPA Analysis are similar to, but slightly higher than those from the TSPA-LA Model shown in Figure 8.2-11. This is further illustrated on Figure 7.7.2-9 which shows a comparison of the Simplified TSPA Analysis results and the TSPA-LA Model results for the Seismic GM Modeling Case at 200,000 years, 400,000 years, 600,000 years, 800,000 years, and 1,000,000 years following repository closure. This is again due to the simplifications applied in the Simplified TSPA Analysis that result in slightly larger EBS releases when WPs are breached, and subsequently higher dose rates.

The Simplified TSPA Analysis results show no annual dose at the 5th percentile whereas, the TSPA-LA Model results for the Seismic GM Modeling Case show doses occurring. In addition, the median annual dose from the Simplified TSPA Analysis shown on Figure 7.7.2-8 is significantly lower than that shown on Figure 8.2-11 for the TSPA-LA Model. This is due to differences in sampling between the two models.

The sampling technique used in the TSPA-LA Model effectively and efficiently takes into account both epistemic and aleatory uncertainty associated with characteristics of future seismic events. The Simplified TSPA Analysis combines aleatory and epistemic uncertainty within the

500 realizations sampled. Thus, the Simplified TSPA Analysis sample size of 500 realizations is not sufficiently large to resolve the 5th and 50th (median) percentiles. However, a sample size of 500 realizations is sufficient to estimate the mean annual dose for the purposes of comparison with that from the TSPA-LA.

In addition, as discussed in Section 7.7.2.2, the WP outer barrier general corrosion rate is lower in the Simplified TSPA Analysis as compared to the TSPA-LA Model. This results in WPs that tend to be more durable under seismic loadings. The predominant mechanism causing damage to the CDSP and CSNF WPs in both the Simplified TSPA Analysis and the TSPA-LA Model, consisted of small cracks that result in releases from the WPs by diffusion. Diffusive transport of dissolved radionuclides through the cracks is high enough to contribute significantly to the mean annual dose.

The sampling technique used in the Simplified TSPA Analysis and the lower rate of general corrosion results in 40 percent of the realizations having no WP failures over the 1,000,000 year simulation period. This is also further illustrated in Figure 7.7.2-9.

Both models demonstrate that the mean annual dose is strongly affected by realizations that cause higher annual doses. This is evident because the mean annual dose is within an order of magnitude of the 95th percentile annual dose.

7.7.2.4 Igneous Intrusion Modeling Case

The Igneous Intrusion Modeling evaluates repository performance for the disruptive event where a volcanic dike intersects the repository. A 1,000,000 year simulation was conducted where a single igneous intrusion event was assumed to randomly occur over the simulation period in each of 500 realizations. All WPs are assumed to be completely failed when the event occurs.

Figure 7.7.2-10 presents the mean annual dose for the Igneous Intrusion Modeling Case using the Simplified TSPA Analysis. Figure 7.7.2-10 also shows the contribution to mean annual dose associated with the radionuclides that contribute most strongly to the mean annual dose for the Igneous Intrusion Modeling Case using the Simplified TSPA-LA Analysis.

The results shown on Figures 7.7.2-10 indicate that the mean annual dose is similar in magnitude to that obtained for the Igneous Intrusion Modeling Case simulated over a 1,000,000 year period with the TSPA-LA Model shown on Figure 8.2-8. The most significant radionuclides for the Simplified TSPA Analysis are ^{129}I, ^{99}Tc, and ^{237}Np for approximately the first 10,000 years following repository closure, followed by ^{239}Pu dominating until about 200,000 years following repository closure, then ^{237}Np and ^{242}Pu, and ^{229}Th. The TSPA-LA Model shows the same trends, but has ^{229}Th being of lesser importance and ^{226}Ra being of greater importance after 200,000 years following repository closure. As discussed in Section 7.7.2.1 above, the increased importance of ^{229}Th is attributed to how its transport in the natural system is being modeled in the Simplified TSPA Analysis.

An estimate of the uncertainty in the distribution of the probability-weighted annual dose for the Igneous Intrusion Modeling Case using the Simplified TSPA Analysis is shown on Figure 7.7.2-11. The estimate of mean annual dose shown on Figure 7.7.2-11 takes into account uncertainties in the various submodels of this scenario in addition to the random sampling of the

time that the intrusion event occurs. These uncertainties are addressed in terms of probability distributions for parameters of the submodels. These uncertainties are addressed in the estimate of mean annual dose by evaluating 500 realizations with each realization providing an annual dose that results from one set of values representing the uncertainty and the sampled number of WPs that experience early failure. Each realization is then weighted by the overall probability of an igneous intrusion event occurring during the 1,000,000 year simulation period. The product of the probability of one igneous intrusion event and the annual dose is termed the probability-weighted annual dose. The mean annual dose at a given time is the average of the 500 probability-weighted annual dose values. The range of uncertainty in the distribution of the probability-weighted annual dose is represented by the 5th and 95th percentiles of those annual dose values for each of 500 realizations.

The results shown on Figure 7.7.2-11 are similar in magnitude as those generated by the TSPA-LA Model shown on Figure 8.2-7 with the Simplified TSPA Analysis yielding slightly higher mean and 95th percentile probability-weighted annual doses. The range of uncertainty is also very similar. The results of both models indicate that the mean annual dose is skewed towards the 95th percentile probability-weighted annual dose. The sampling technique used in the Simplified TSPA Analysis results in only two events being sampled in the 10,000 year period whereas the TSPA-LA approach has much greater resolution during this period. These differences are further illustrated on Figure 7.7.2-12 which shows a comparison of the Simplified TSPA results and the TSPA-LA Model results for this modeling case at 200,000 years, 400,000 years, 600,000 years, 800,000 years, and 1,000,000 years following repository closure.

INTENTIONALLY LEFT BLANK

Table 7.7.2-1. Summary of Modeling Approaches Used for TSPA-LA Model and the Simplified TSPA Analysis

Component Model	TSPA-LA Model		Simplified TSPA Analysis	
	Section	Approach	Section	Approach
Climate	6.3.1	Four climate states, present-day (600 year), monsoon (1,400 year duration), glacial-transition (8,000 year duration), post-10,000 years.	L2.3	Four climate states, present day (600 year), monsoon (1,400 year duration), glacial-transition (8,000 year duration), post-10,000 years.
Infiltration	6.3.1	Four infiltration cases for each climate state with each case weighted.	L2.4	Four infiltration cases for each climate state with each case weighted.
UZ Flow	6.3.1	Three-dimensional flow fields and percolation rate maps at the repository horizon for each infiltration rate and climate state.	L2.4 and L2.16.1	Percolation flux distribution and average percolation rates at the repository horizon.
Emplacement Drift Seepage	6.3.3	Calculates seepage at each of 3,264 repository subdomains. Uses percolation flux at those locations where percolation flux depends on climate state and infiltration rate case. Samples fracture permeability, capillary strength, and flow focusing factor for each subdomain. Uses results to determine seepage rate and seepage fraction for CSNF and CDSP WPs in each of five percolaton subregions. Considers intact and collapsed drift conditions and adjusts seepage rate for drift degradation.	L2.5	Calculates average seepage fraction and seepage rate over the entire repository horizon. Uses percolation flux distribution to determine localized flux at 100 'locations' over the repository horizon. Samples fracture permeability and capillary strength from distributions representing uncertainty and applies them over the entire repository horizon. Samples flow focusing factor at each of 100 'locations'. Considers intact and collapsed drift conditions and adjusts seepage rate for drift degradation.
Drift Wall Condensation	6.3.3	Calculates a probability of condensation occurrence on the drift walls at a WP location and, if condensation occurs, a rate of condensation after all locations in the drift are below the boiling temperature.		Not included.

Table 7.7.2-1. Summary of Modeling Approaches Used for TSPA-LA Model and Simplified TSPA Analysis (Continued)

Component Model	TSPA-LA Model		Simplified TSPA Analysis	
	Section	Approach	Section	Approach
EBS Thermal-Hydrologic Environment	6.3.2	Time histories of • WP temperature • Invert temperature • Drift wall temperature • WP relative humidity • Invert relative humidity • Invert liquid flux (vertical component) • Invert saturation at 3,264 repository subdomains for four different infiltration rate cases •Three levels of host rock thermal conductivity (low, medium, high) • CSNF and CDSP representative WPs. These are categorized into five percolation subregions.	L2.6.1	Considers only WP temperature, determined for one infiltration rate case. To account for spatial variability, the WP temperature time histories for each 3,264 subdomains were used to develop a distribution of WP temperature time history over the entire repository area for the CSNF and CDSP representative WPs and for three levels of host rock thermal conductivity. The average CSNF and CDSP WP temperature histories were also determined for each host rock thermal conductivity.
EBS Chemical Environment	6.3.4	Calculates the time-dependent pCO_2 in the gas phase in the drift above the invert and pH and ionic strength conditions in the invert for each of five percolation subregion. Calculates the chemistry (pH, $[Cl^-]$, and $[NO_3^-]$) of the seepage water from the crown of the drift for the localized corrosion initiation analysis.	L2.6.2	Assumes constant pCO_2 and a range of invert pH over the entire repository, neither change with time.
Drip Shield Degradation - General Corrosion	6.3.5	Calculates DS degradation rate by sampling general corrosion rates for the top- and under-side of the DS. Does not consider spatial variability across DS or on the surface of individual DSs.	L2.7.1	Calculates DS degradation rate by sampling general corrosion rates for the top- and under-side of the DS. Does not consider spatial variability across DS or on the surface of individual DSs.
Drip Shield Degradation - Drip Shield Early Failure	6.4	Samples rate of early DS failure and uses a Poisson distribution to determine the number of DSs that experience early failure. A DS early failure removes the DS as a barrier to seepage at the time of repository closure and allows the full volume of seepage to contact the WP.		Not included.

Table 7.7.2-1. Summary of Modeling Approaches Used for TSPA-LA Model and Simplified TSPA Analysis (Continued)

Component Model	TSPA-LA Model		Simplified TSPA Analysis	
	Section	Approach	Section	Approach
Waste Package Degradation - General Corrosion	6.3.5	Calculates general corrosion penetration on individual CSNF and CDSP WPs within each percolation subregion. The general corrosion rate is sampled and assumed to vary spatially over the surface of the WP. The general corrosion rate also is temperature dependent and a unique WP temperature history is applied to each WP. Samples MIC enhancement factor that increases the general corrosion rate after the relative humidity in the drift exceeds a threshold. A unique WP relative humidity history is applied to each WP. Determines the fraction of WPs that are initially breached as a function of time due to general corrosion and the average number of general corrosion breaches present on breached WPs in each percolation subregion.	L2.8.1.1	Calculates general corrosion penetration on CSNF and CDSP WPs at 100 'locations' over the entire repository area. The general corrosion rate is sampled and assumed to vary over the surface of the WP. The 100 'locations' cover the range of WP temperature histories and the WP temperature at each 'location' is used to determine the temperature dependent general corrosion rate. Samples MIC enhancement factor that increases general corrosion rate after the relative humidity in the drift exceeds a threshold. The relative humidity threshold is assumed to be exceeded at the same time over the entire repository and depends on the WP type (CSNF or CDSP). The host rock thermal conductivity determines the fraction of WPs that are initially breached as a function of time and the average number of general corrosion breaches present on each breached WP over the entire repository.

Table 7.7.2-1. Summary of Modeling Approaches Used for TSPA-LA Model and Simplified TSPA Analysis (Continued)

Component Model	TSPA-LA Model		Simplified TSPA Analysis	
	Section	Approach	Section	Approach
Waste Package Degradation - Stress Corrosion Cracking	6.3.5	Considers both incipient crack initiation and pre-existing (manufacturing defect) weld flaws, the stress conditions (that drive the crack initiation and propagation), the stress threshold (that defines the crack initiation), the threshold stress intensity factor (that defines propagation of both initiated incipient cracks and weld flaws), and the crack growth model (based on the slip dissolution-film rupture theory) that determines the crack growth rate. Calculates whether SCC will occur at individual locations over the circumference of the closure lid weld region for individual locations within each percolation subregion. Samples uncertain parameters associated with SCC (uncertainty in stress conditions and crack growth rate). Applies general corrosion rate model discussed above that accounts for spatial variability in the general corrosion rate over the circumference of the closure lid and spatial variability in the WP temperature. Calculates SCC penetrations that occur on individual WPs within each percolation flux subregion. Determines the fraction of WPs that are initially breached as a function of time due to SCC and the average number of SCC breaches present on breached WPs in each percolation sub-region.	L2.8.1.2	Considers incipient crack initiation, the stress conditions (that drive the crack initiation and propagation), the stress threshold (that defines the crack initiation), the threshold stress intensity factor (that defines propagation of both initiated incipient cracks and weld flaws), and the crack growth model (based on the slip dissolution-film rupture theory) that determines the crack growth rate. Calculates conditions where stress corrosion occurs for average conditions over the circumference of the closure lid weld region. Determines average depth that must be removed by general corrosion before SCC can initiate and propagate. Applies general corrosion model discussed above to determine when SCC occurs. Determines the fraction of WPs that are initially breached as a function of time due to SCC and the average number of SCC breaches present on breached WPs over the entire repository.
Waste Package Degradation - Localized Corrosion	6.3.5	Determines if environmental conditions on the WP outer surface will initiate localized corrosion and lead to WP failure for each repository percolation subregion and WP type.		Not included.
Waste Package Degradation - Waste Package Early Failure	6.4	The uncertain rate of WP early failures was abstracted to a log-normal distribution. For any particular value of the rate of WP early failures, the number of WP early failures is described by a Poisson distribution because WP early failure is independent between packages. Assumes complete failure of the WP, with respect to radionuclide containment, at the time of repository closure.	L2.8.2	The uncertain rate of WP early failures was abstracted to a log-normal distribution. For any particular value of the rate of WP early failures, the number of WP early failures is described by a Poisson distribution because WP early failure is independent between packages. Assumes complete failure of the WP, with respect to radionuclide containment, at the time of repository closure.

Table 7.7.2-1. Summary of Modeling Approaches Used for TSPA-LA Model and Simplified TSPA Analysis (Continued)

Component Model	TSPA-LA Model		Simplified TSPA Analysis	
	Section	Approach	Section	Approach
EBS Flow	6.3.6	Complete diversion of seepage around the WP until the DSs fail, then all seepage contacts the WP. Calculates the fraction of seepage that flows through breaches in WP as a function of the number of general corrosion breaches.	L2.13	Complete diversion of seepage around the WP until the DSs fail, then all seepage contacts the WP. All water flowing through the breached DS is assumed to be diverted around the WP until the first general corrosion breach occurs. Then all water flowing through the breached DS is assumed to flow through the breached WP.
In-Package Chemistry	6.3.7	Quantifes the temporal evolution of values of the aqueous chemistry variables pH, ionic strength, and ΣCO_3 for four different abstraction conditions representing CSNF and CDSP WPs that have water flow through them and CSNF and CDSP WPs that do not have water flow through them in each percolation sub-region.	L2.9	Does not include ionic strength. The in-package pH is sampled and assumed to be constant with time and applicable to both CSNF and CDSP WPs. Calculates ΣCO_3 as a function of time using a constant pCO_2, the sampled pH and the average CSNF WP temperature history.
Cladding Degradation	6.3.7	The cladding of all CSNF and DSNF is assumed to be failed upon arrival at the repository.	L2.11	The cladding of all CSNF and DSNF is assumed to be failed upon arrival at the repository.
CSNF Waste Form Degradation	6.3.7	The instantaneous release fraction is computed as the fraction of cesium, iodine, technetium, and strontium in the total inventory in CSNF fuel that is instantly available for release once cladding is degraded. Calculates the specific or absolute dissolution rate as a function of four independent variables, which vary spatially in the repository: WP temperature in degrees Kelvin, aqueous pH, ΣCO_3, and oxygen fugacity according to the rate law. The four independent variables are determined in each percolation subregion. This results in a time-dependent CSNF waste form degradation rate in each percolation sub-region.	L2.12.1	The instantaneous release fraction is computed as the fraction of cesium, iodine, technetium, and strontium in the total inventory in CSNF fuel that is instantly available for release once cladding is degraded.Calculates the specific or absolute dissolution rate as a function of four independent variables, which do not vary spatially in the repository: WP temperature in degrees Kelvin, aqueous pH, ΣCO_3, and oxygen fugacity according to the rate law. The four independent variables are determined for average repository conditions. This results in a time-dependent CSNF waste form degradation rate representative of repository average conditions.
DSNF Waste Form Degradation	6.3.7	Releases the entire per package DSNF inventory for solubilization and mobilization from the CDSP WPs when the WPs are breached.	L2.11	Releases the entire per package DSNF inventory for solubilization and mobilization from the CDSP WPs when the WPs are breached.

Table 7.7.2-1. Summary of Modeling Approaches Used for TSPA-LA Model and Simplified TSPA Analysis (Continued)

Component Model	TSPA-LA Model		Simplified TSPA Analysis	
	Section	Approach	Section	Approach
DHLW Waste Form Degradation	6.3.7	The rate equation requires the specification of three parameter values: k_E, η, and E_a, and the two model variables, temperature and pH. The parameters kE, h, and Ea are different for acidic and alkaline conditions. Temperature histories are determined in each percolation subregion and pH is determined for dripping and non-dripping conditions in each percolation subregion. The DHLW degradation rate is determined for both acidic and alkaline conditions as a function of time and the maximum of the two is taken as the DHLW degradation rate. This results in a time-dependent DHLW waste form degradation rate in each percolation subregion.	L2.12.2	The rate equation requires the specification of three parameter values: k_E, η, and E_a, and the two model variables, temperature and pH. The parameters k_E, h, and Ea are different for acidic and alkaline conditions. The average CDSP WP temperature history and the sampled pH is determined. The DHLW degradation rate is determined for both acidic and alkaline conditions as a function of time and the maximum of the two is taken as the DHLW degradation rate. This results in a time-dependent DHLW waste form degradation rate representative of repository average conditions.
Dissolved Concentration Limits	6.3.7	The solubility models for americium, neptunium, plutonium, protactinium, thorium, tin, and uranium are in the form of look-up tables with pH and log pCO_2 as the independent variables. Two uncertainty terms accounting for uncertainties associated with thermodynamic properties and variations in water chemistry are also included for this group of elements. Since pH and log pCO_2 vary both spatially and temporally, the dissolved concentration limits also vary spatially (each percolation subregion) and temporally.The remaining elements (technetium, carbon, iodine, cesium, chlorine, selenium, and strontium) are considered highly soluble and no solubility-controlling solids are expected to form under repository conditions.		The solubility models for americium, neptunium, plutonium, protactinium, thorium, tin, and uranium are in the form of look-up tables with pH as the independent variable assuming a constant log pCO_2. A single uncertainty terms accounting for uncertainties associated with thermodynamic properties is also included for this group of elements. Since pH and log pCO_2 are assumed to be constant both spatially and temporally, the dissolved concentration limits do not vary spatially (each percolation sub-region) and temporally.The remaining elements (technetium, carbon, iodine, cesium, chlorine, selenium, and strontium) are considered highly soluble and no solubility-controlling solids are expected to form under repository conditions.
Colloids	6.3.7	Calculates the formation, stability, and concentration of radionuclide bearing colloids in the waste form and WP, as well as sorption of dissolved radionuclides.	L2.15	Not included.

Table 7.7.2-1. Summary of Modeling Approaches Used for TSPA-LA Model and Simplified TSPA Analysis (Continued)

Component Model	TSPA-LA Model		Simplified TSPA Analysis	
	Section	Approach	Section	Approach
EBS Radionuclide Transport	6.3.8	The four EBS transport one-dimensional continuum form mass balance equations are approximated and solved using a finite difference approach: • Transport of dissolved radionuclide species and radionuclide species that are reversibly sorbed onto three types of colloids: iron oxyhydroxide, waste form, and groundwater. • Transport of kinetically (and irreversibly) sorbed radionuclide species on iron oxyhydroxide colloids. • Kinetic sorption of radionuclide species onto stationary corrosion products in the WP. • Transport of embedded (irreversibly sorbed) radionuclide species in waste form colloids. The domains considered are: • CSNF: CSNF Waste Form, CSNF Corrosion Product, Invert underlying CSNF WPs • CDSP: DHLW Waste Form, DSNF Waste Form, DHLW Corrosion Product, Invert underlying CDSP WPs. These domains are represented as cell networks in each percolation subregion for dripping and non-dripping conditions. The number of cell pathways in the finite difference network and the discretization of the cells are chosen to capture the physical and chemical properties of the EBS components with respect to radionuclide transport. Both advective and diffusive transport mechanisms are explicitly represented. Linking of cells results in a coupled system of differential equations that is mathematically equivalent to a finite difference network.	L2.15	The EBS transport one-dimensional continuum form mass balance equation for dissolved radionuclide species is approximated and solved using a simplified explicit-in-time approach for a each domain: • CSNF: CSNF Waste Form, CSNF Corrosion Product, Invert underlying CSNF WPs • CDSP: DHLW Waste Form (DSNF inventory assumed to be in DHLW), DHLW Corrosion Product, Invert underlying CDSP WPs. These domains are represented as cell networks in a single representation of repository average conditions for seeping and non-seeping conditions. Advective and diffusive transport mechanisms are approximately represented. Key differences between the TSPA-LA Model and the Simplified TSPA Analysis are: • No radionuclide sorption onto stationary corrosion products. • No relative humidity threshold for radionuclide transport within the CSNF waste form cells • All EBS media are assumed to be fully saturated.

Table 7.7.2-1. Summary of Modeling Approaches Used for TSPA-LA Model and Simplified TSPA Analysis (Continued)

Component Model	TSPA-LA Model		Simplified TSPA Analysis	
	Section	Approach	Section	Approach
UZ Transport	6.3.9	Utilizes a three-dimensional dual-continuum model that includes a numerical grid of fracture cells representing the fracture continuum and a grid of matrix cells representing the matrix continuum, with each fracture cell connected to a corresponding matrix cell. The following processes are simulated: • Advective transport of dissolved and colloidal-bound radionuclides in the fracture and matrix continua utilizing three-dimensional flow fields • Longitudinal dispersion • Sorption of dissolved radionuclides to the matrix continuum (linear, equilibrium sorption model) • Matrix diffusion • Retardation of irreversible and reversible colloids in the fracture continuum • Colloid filtration at interfaces between rock-matrix units • Colloid size exclusion at fracture matrix continua interfaces • Radioactive decay and ingrowth • Climate change and its effect on fluid flow rates in the UZ • Climate change and associated rise in water table elevation and its effect on radionuclide release to the SZ.	L2.16.1	Utilizes a simplified one-dimensional solution of the advective-dispersive transport for radionuclides transported in the rock matrix. Assumes rapid transport of radionuclides in the fracture continuum. Discretizes the UZ underneath the repository into three layers with average properties. Determines the fraction of radionuclides transported in the matrix and fractures using the average percolation flux over the repository horizon. Includes the following processes: • Advective transport of dissolved and colloidal-bound radionuclides in the fracture and matrix continua utilizing a simplified approach • Longitudinal dispersion in the matrix continuum • Sorption of dissolved radionuclides to the matrix continuum (linear, equilibrium sorption model) • Radionuclide decay and ingrowth Processes not included are: • Matrix diffusion • Colloids are not included • UZ fluid flow rates for post-10,000 year climate state only • Change in water table elevation
SZ Transport	6.3.10	Utilizes the results of three-dimensional SZ flow and transport modeling to calculate the flow and transport through the SZ to the accessible environment for individual radionuclides important to dose. The output from the three-dimensional SZ Flow and Transport Process Model is developed in the form of unit source radionuclide breakthrough curves that are combined with the time varying radionuclide sources from the UZ using a convolution integral technique to quantify radionuclide transport to the accessible environment.Utilizes a one-dimensional SZ Flow and Transport Model to calculate the radioactive decay, ingrowth, and transport for four decay chains.	L2.16.2	Utilizes a simplified one-dimensional solution of the advective-dispersive transport for radionuclides transported in the SZ. This approach is identical to that used to model UZ radionuclide transport.

Table 7.7.2-1. Summary of Modeling Approaches Used for TSPA-LA Model and Simplified TSPA Analysis (Continued)

Component Model	TSPA-LA Model		Simplified TSPA Analysis	
	Section	Approach	Section	Approach
Biosphere	6.3.11	Utilizes BDCF distributions for the present-day climate state.	L2.17	Utilizes BDCF distributions for the present day climate state.
Igneous Intrusion	6.5	Utilizes the nominal scenario model with the following modifications: • All DSs and WPs are failed when the igneous intrusion event occurs • Local seepage rate equals the local percolation flux.	L2.18	Utilizes the nominal scenario model with the following modifications: • All DSs and WPs are failed when the igneous intrusion event occurs • The seepage rate equals the average seepage rate for collapsed drift conditions.
Seismic Mechanical Damage	6.6	Utilizes the nominal scenario model with the following additional models included: • Rockfall - the amount of rock that falls into the emplacement drifts is determine as a function of the peak ground velocity for the seismic event • Seepage - the amount of rock that accumulates in the emplacement drifts determines whether intact or collapsed drift seepage conditions are used • DS damage - determines whether the DSs fail either due to failure of the DS plates or DS frame structure. Failure of the DS in response to a seismic event renders all DSs failed as a barrier to seepage DS damage - determines the state of damage to the WP outer barrier due to vibrational ground motion or due to rockfall (when the DS fails). Calculates the area of the WP outer barrier damaged due to SCC.	L2.1 L2.2 L2.7.2 L2.8.3	Utilizes the nominal scenario model with the following additional models included: •Rockfall - the amount of rock that falls into the emplacement drifts is determined as a function of the peak ground velocity for the seismic event •Seepage - the amount of rock that accumulates in the emplacement drifts determines whether intact or collapsed drift seepage conditions are used •DS damage - determines whether the DSs fail either due to failure of the DS plates or DS frame structure. Failure of the DS in response to a seismic event renders all DSs failed as a barrier to seepage DS damage - determines the state of damage to the WP outer barrier due to vibrational ground motion or due to rock fall (when the DS fails). Calculates the area of the WP outer barrier damaged due to SCC. Simpler approaches are used to determine seismic consequences as compared to the TSPA-LA

INTENTIONALLY LEFT BLANK

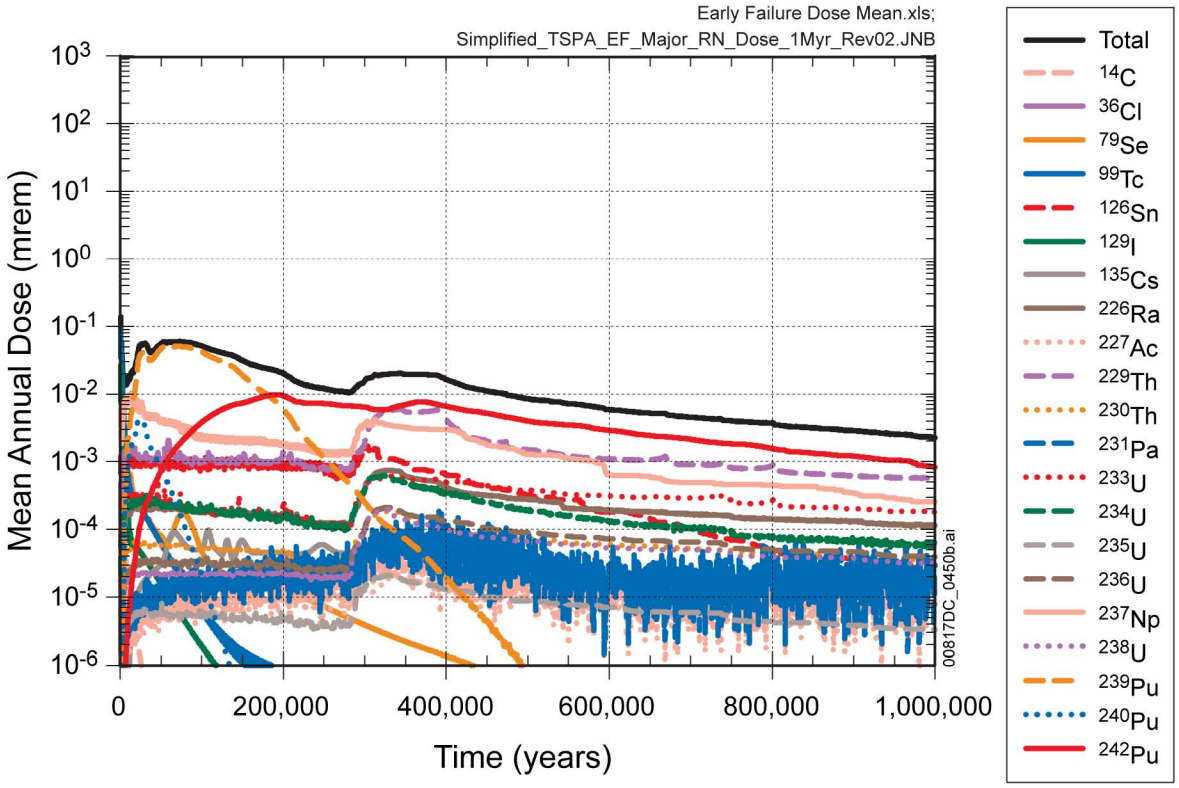

Source: Corroborative DTN: MO0708SIMPLIFI.000 [DIRS 182980].

Figure 7.7.2-1. Mean Annual Dose and Annual Dose for Individual Radionuclides for the Simplified TSPA Analysis Waste Package Early Failure Modeling Case for 1,000,000 Years after Repository Closure

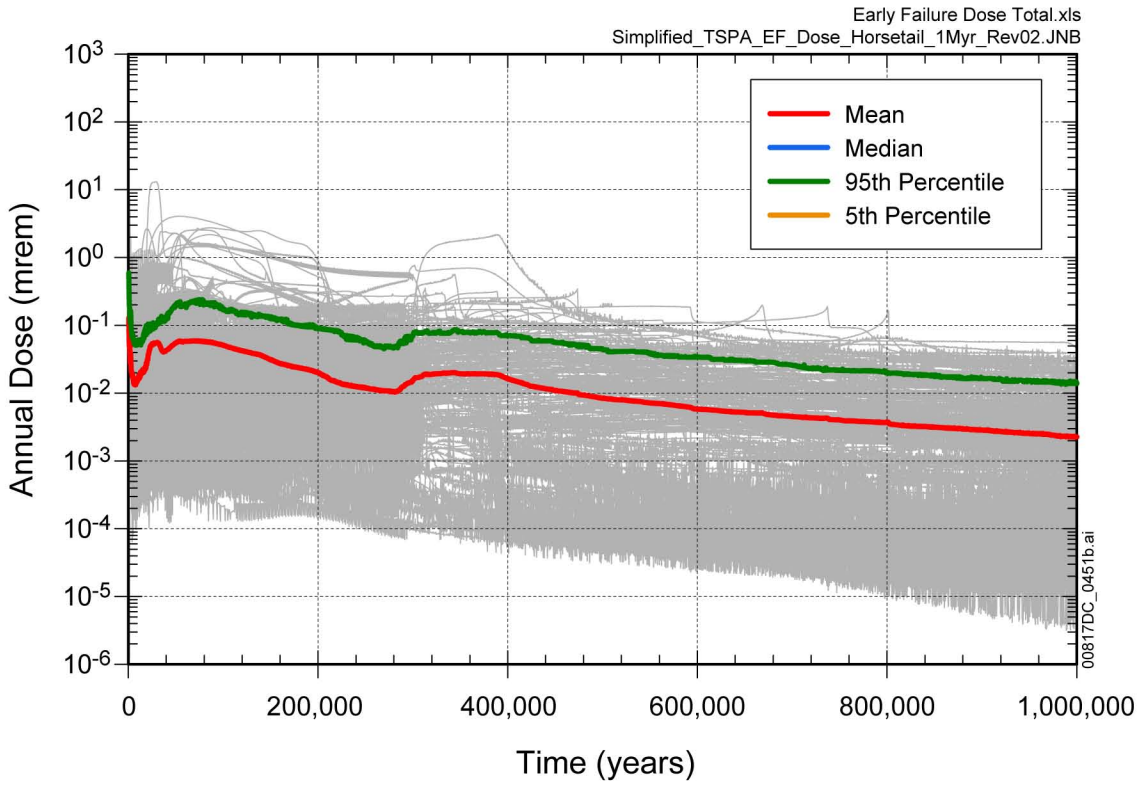

Source: Corroborative DTN: MO0708SIMPLIFI.000 [DIRS 182980].

Figure 7.7.2-2. Annual Dose for the Simplified TSPA Analysis Waste Package Early Failure Modeling Case for All Realizations for 1,000,000 Years after Repository Closure

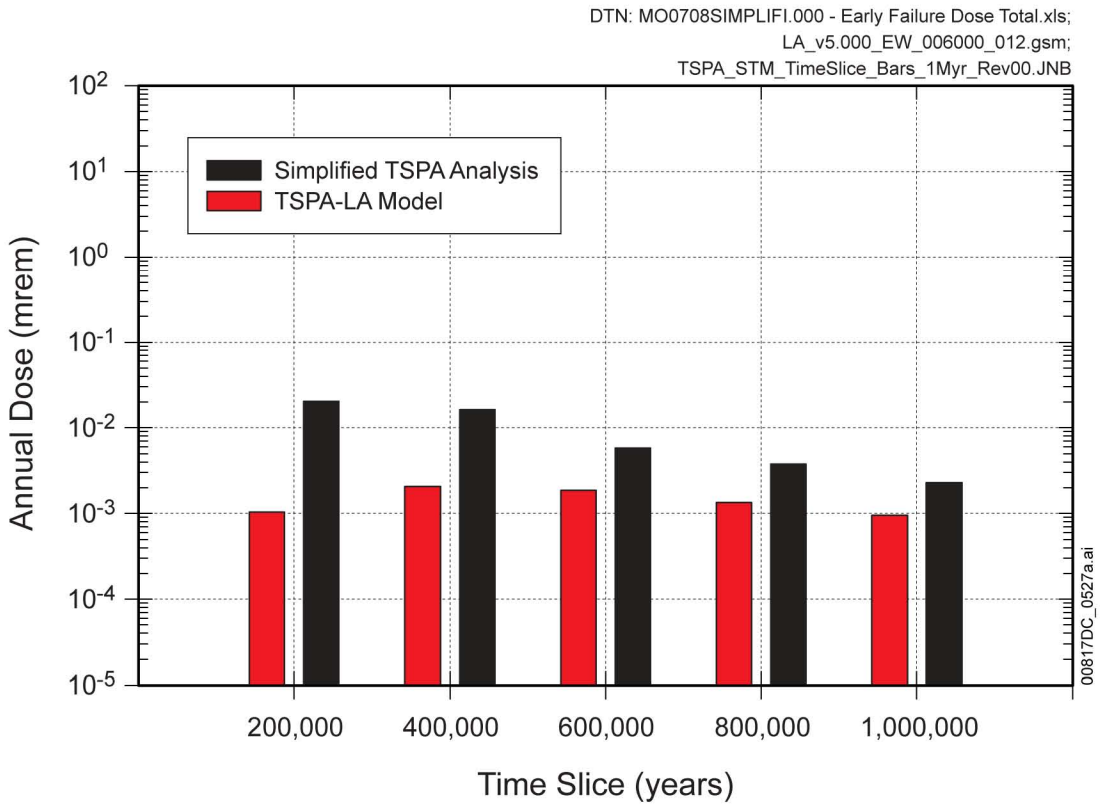

Source: Corroborative DTN: MO0708SIMPLIFI.000 [DIRS 182980]; and Output DTN: MO0709TSPAREGS.000 [DIRS 182976].

Figure 7.7.2-3. Time-Slice Comparison of the Simplified TSPA Analysis Results against the TSPA-LA Model Results for the Waste Package Early Failure Modeling Case

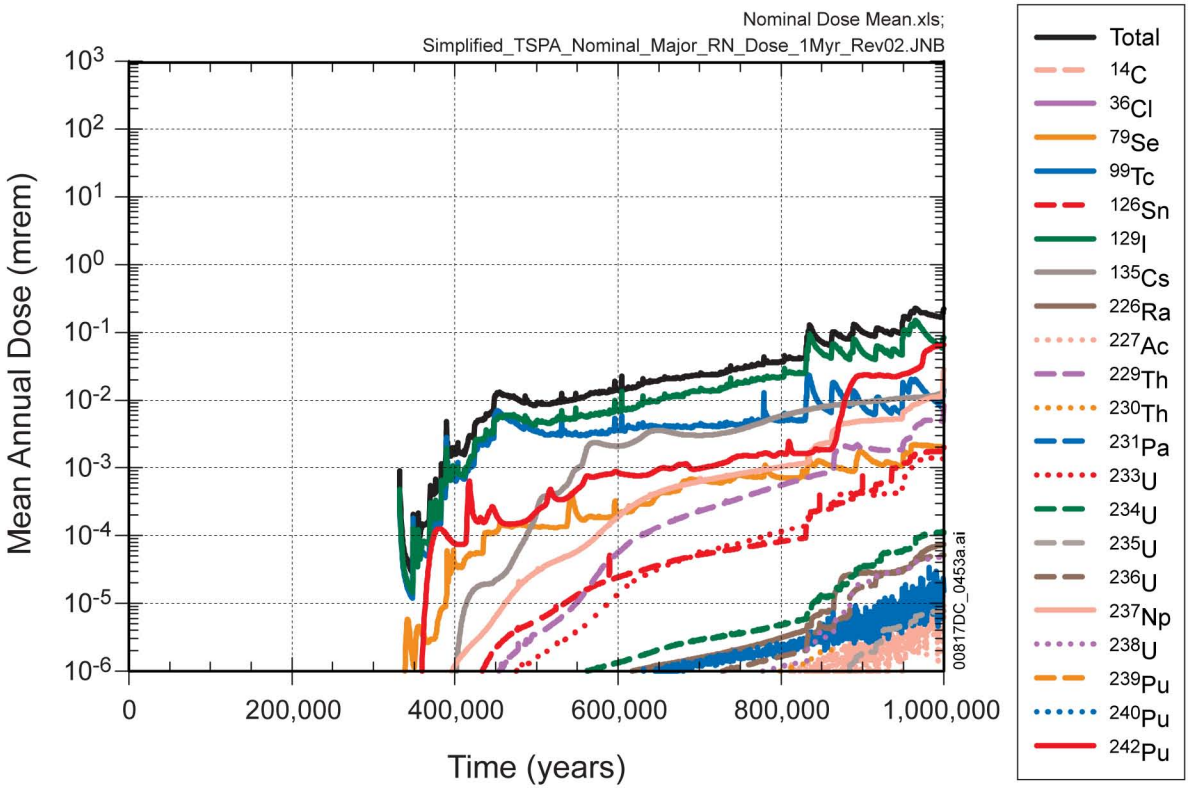

Source: Corroborative DTN: MO0708SIMPLIFI.000 [DIRS 182980].

Figure 7.7.2-4. Mean Annual Dose and Annual Dose for Individual Radionuclides for the Simplified TSPA Analysis Nominal Modeling Case

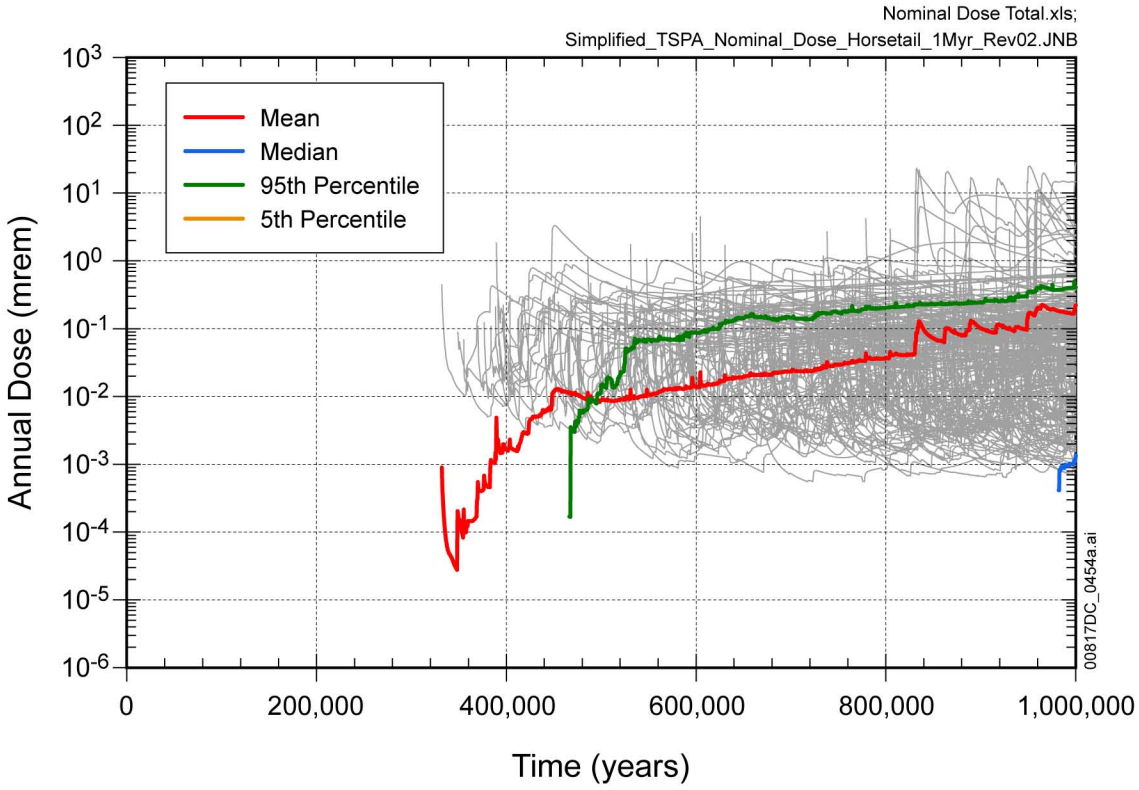

Source: Corroborative DTN: MO0708SIMPLIFI.000 [DIRS 182980].

Figure 7.7.2-5. Annual Dose for the Simplified TSPA Analysis Nominal Modeling Case

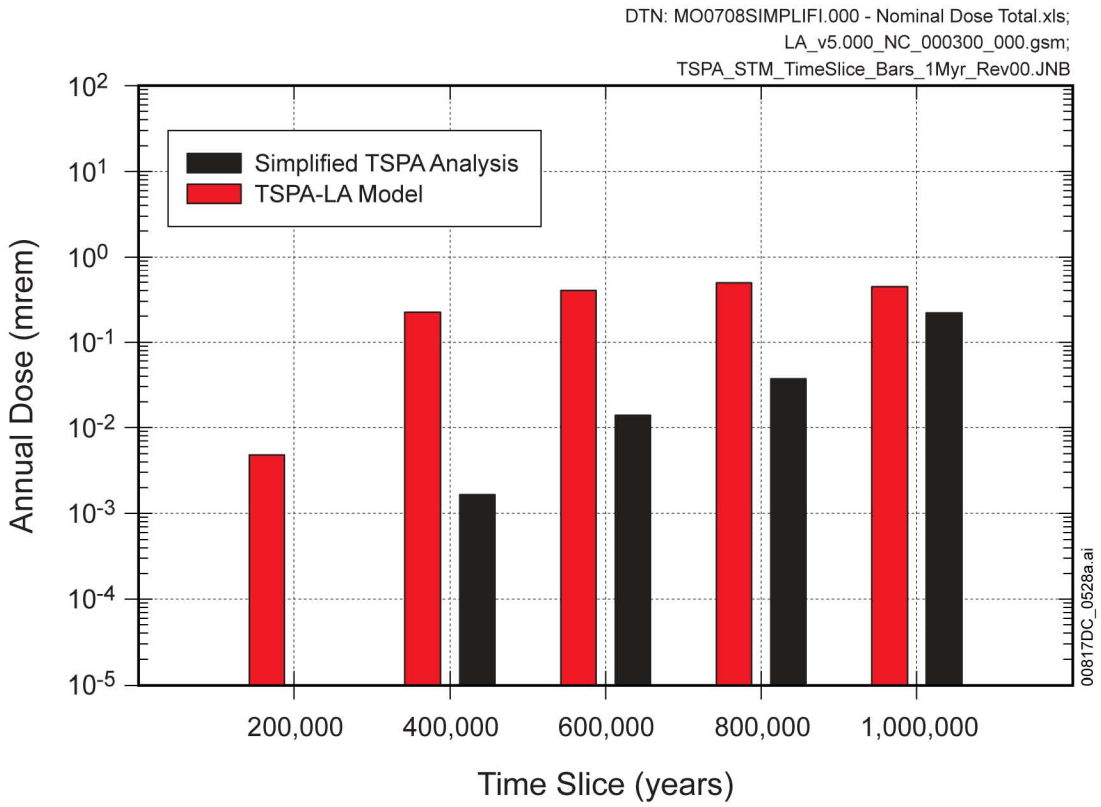

Source: Corroborative DTN: MO0708SIMPLIFI.000 [DIRS 182980]; and Output DTN: MO0709TSPAREGS.000 [DIRS 182976].

Figure 7.7.2-6. Time-Slice Comparison of the Simplified TSPA Analysis Results against the TSPA-LA Model Results for the Nominal Modeling Case

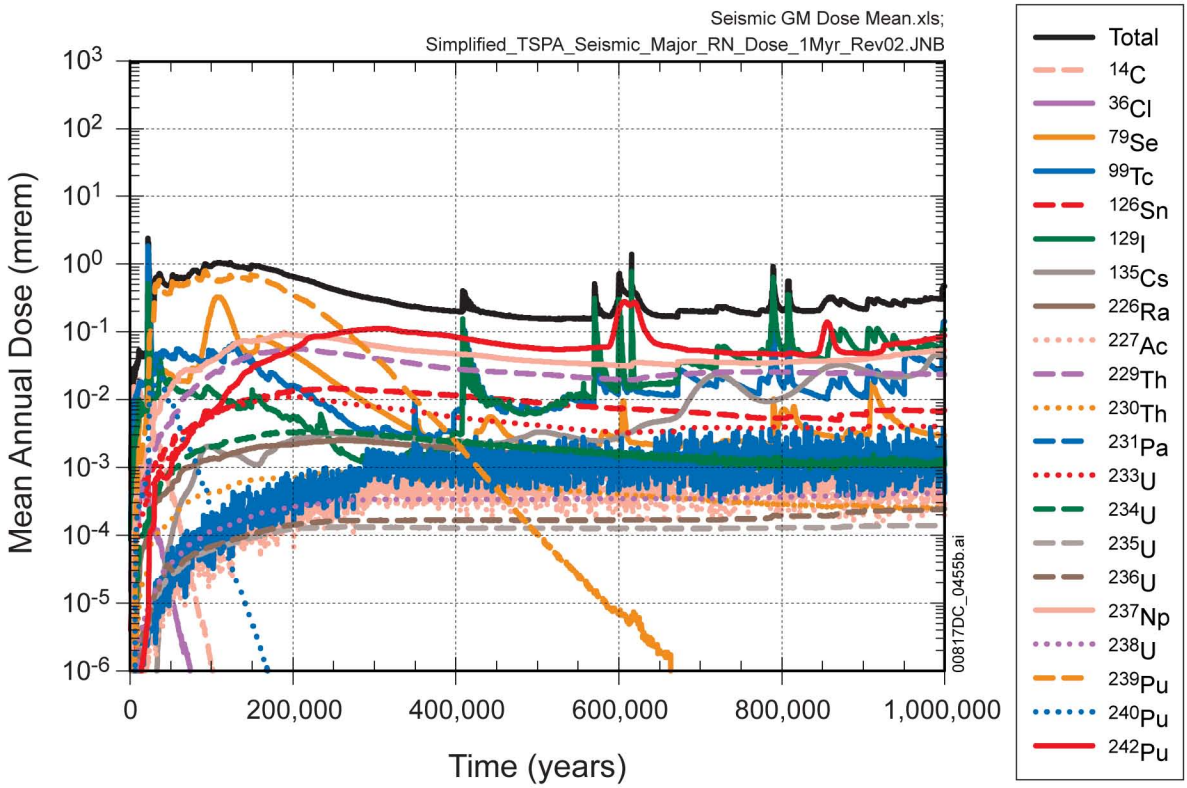

Source: Corroborative DTN: MO0708SIMPLIFI.000 [DIRS 182980].

Figure 7.7.2-7. Mean Annual Dose and Annual Dose for Individual Radionuclides for the Simplified TSPA Analysis Seismic Ground Motion Modeling Case for 1,000,000 Years after Repository Closure

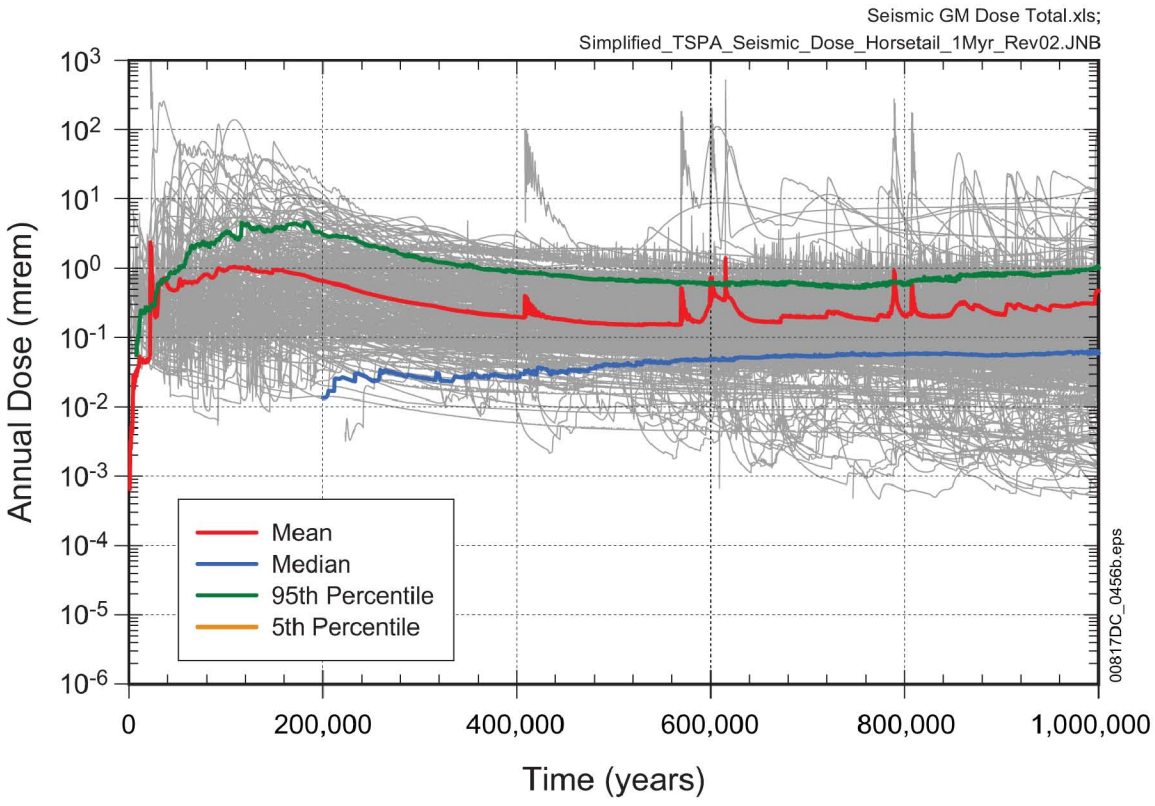

Source: Corroborative DTN: MO0708SIMPLIFI.000 [DIRS 182980].

Figure 7.7.2-8. Mean Annual Dose and Annual Dose for Individual Radionuclides for the Simplified TSPA Analysis Seismic Ground Motion Modeling Case for 1,000,000 Years after Repository Closure

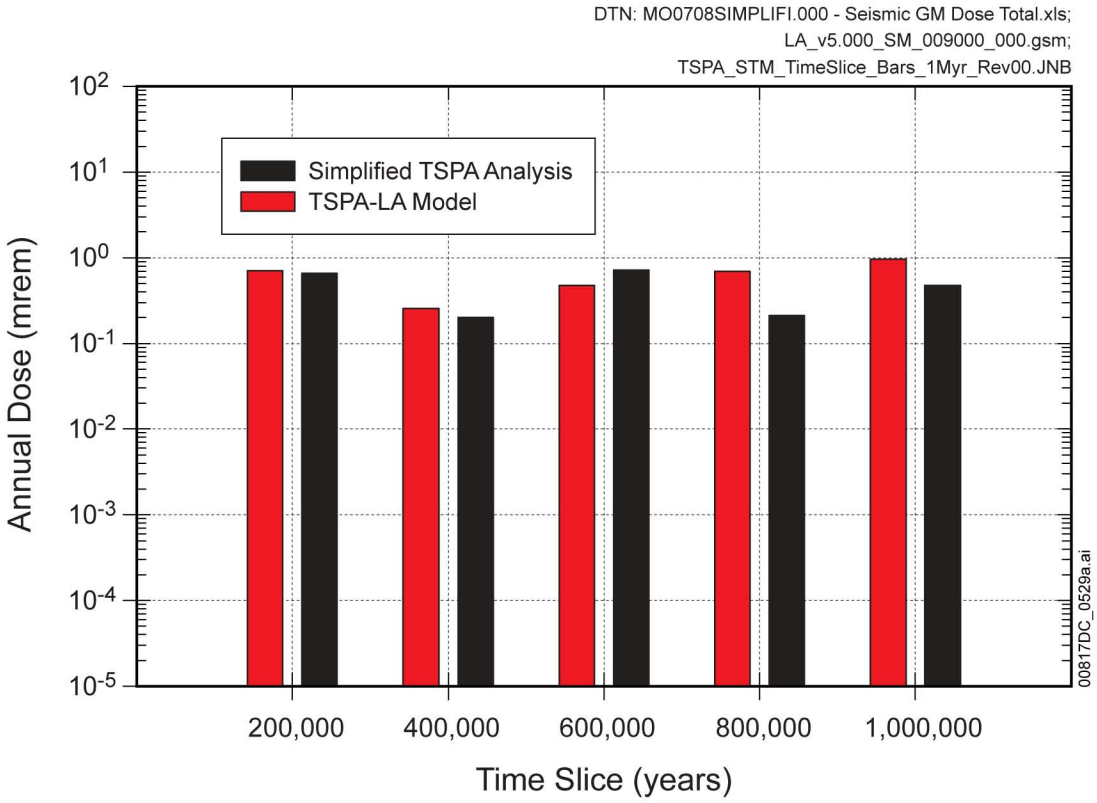

Source: Corroborative DTNs: MO0708SIMPLIFI.000 [DIRS 182980]; and Output DTN: MO0709TSPAREGS.000 [DIRS 182976].

Figure 7.7.2-9. Time-Slice Comparison of the Simplified TSPA Analysis Results against the TSPA-LA Model Results for the Seismic Ground Motion Modeling Case

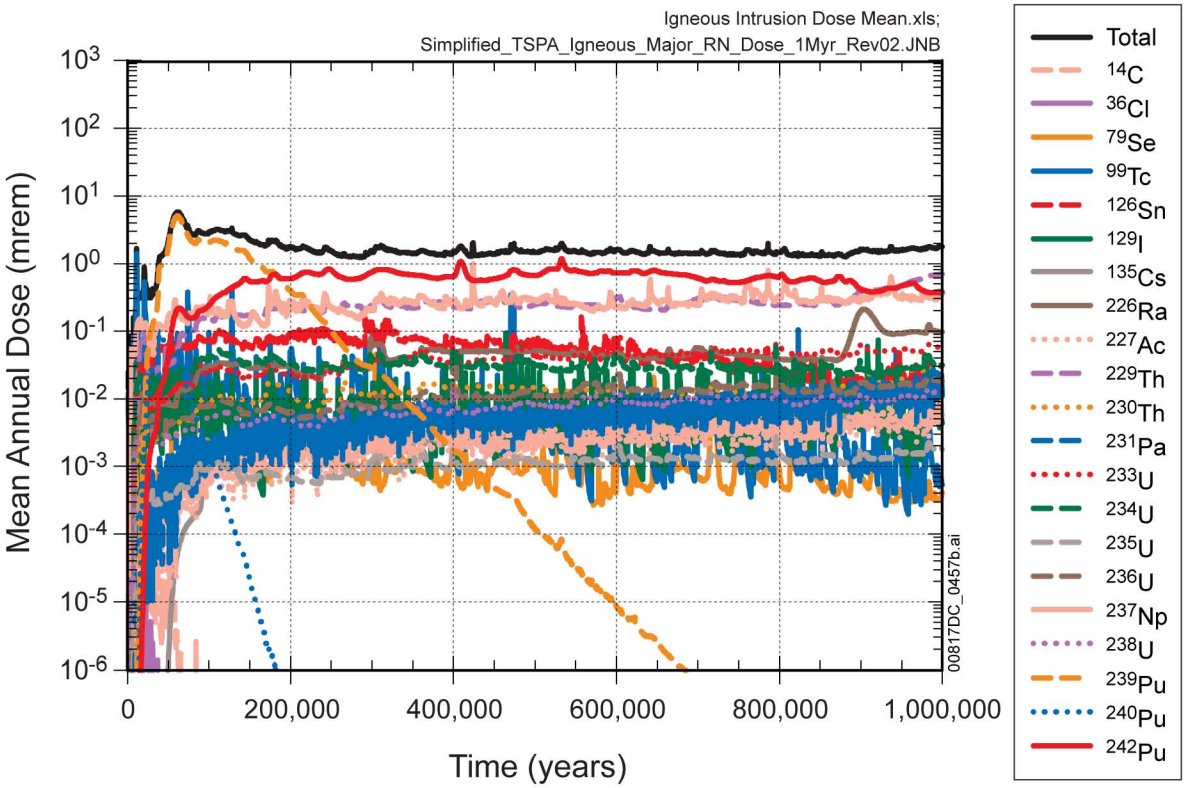

Source: Corroborative DTN: MO0708SIMPLIFI.000 [DIRS 182980].

Figure 7.7.2-10. Mean Annual Dose and Annual Dose for Individual Radionuclides for the Simplified TSPA Analysis Igneous Intrusion Modeling Case for 1,000,000 Years after Repository Closure

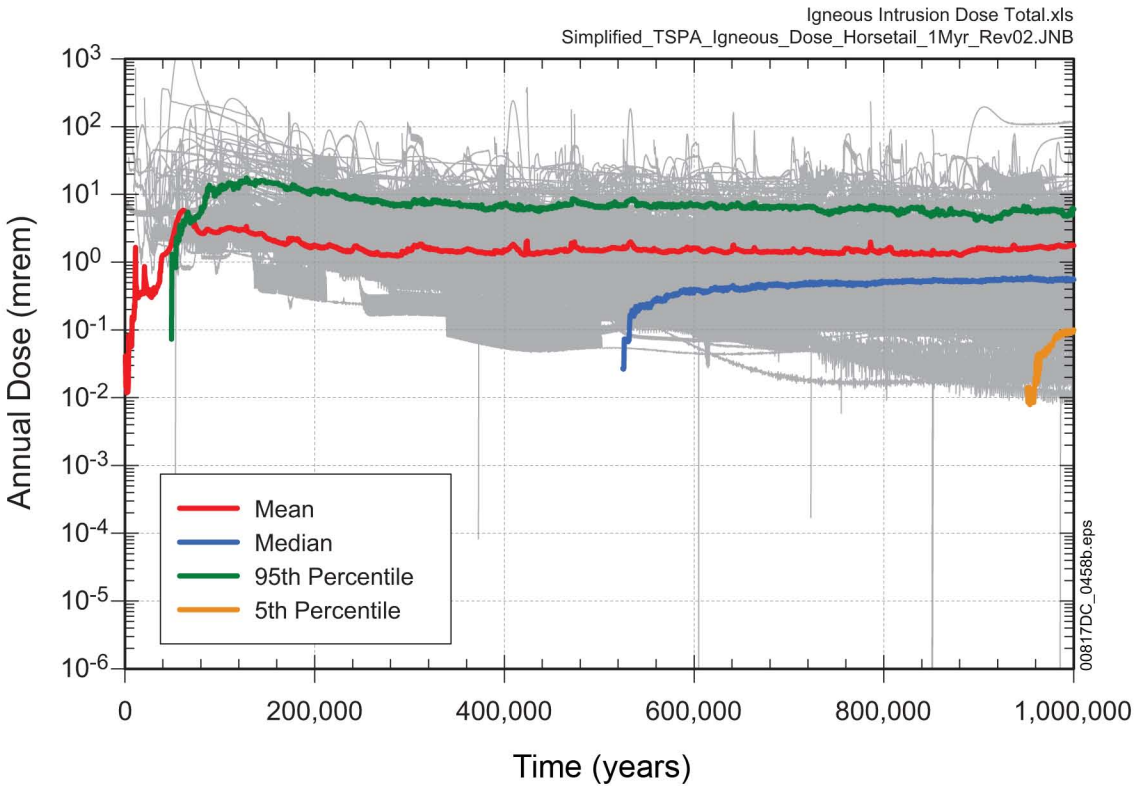

Source: Corroborative DTN: MO0708SIMPLIFI.000 [DIRS 182980].

Figure 7.7.2-11. Mean Annual Dose and Annual Dose for Individual Radionuclides for the Simplified TSPA Analysis Igneous Intrusion Modeling Case for 1,000,000 Years after Repository Closure

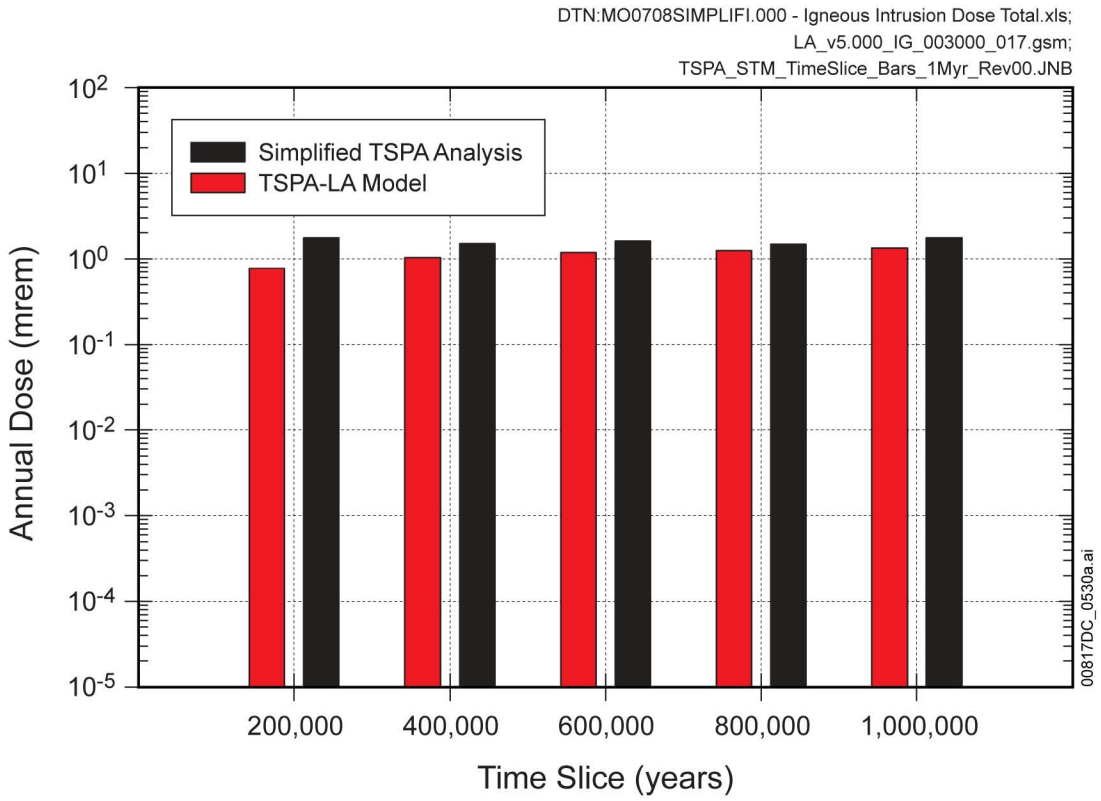

Source: Corroborative DTNs: MO0708SIMPLIFI.000 [DIRS 182980]; and Output DTN: MO0709TSPAREGS.000 [DIRS 182976].

Figure 7.7.2-12. Time-Slice Comparison of the Simplified TSPA Analysis Results against the TSPA-LA Model Results for the Igneous Intrusion Motion Modeling Case

7.7.3 Comparison with Electric Power Research Institute Analysis

7.7.3.1 Introduction and Purpose

The Electric Power Research Institute (EPRI) has been conducting assessments of the total system performance of the candidate radioactive waste repository at Yucca Mountain, Nevada (Apted and Ross 2005 [DIRS 182229]). The objective of the EPRI's TSPA Analysis is to provide an independent third-party assessment of key technical and scientific issues associated with the proposed geologic repository at Yucca Mountain. The EPRI TSPA Analysis was developed by an independent organization, based on independently developed methodology and its own total systems performance code, IMARC (Kozak and Kessler 2005 [DIRS 178580]).

This section gives a summary of the comparison between the EPRI TSPA Analysis and the TSPA-LA Model. The purpose of the comparison is to use the EPRI model as another auxiliary analysis to satisfy the post-development validation criterion related to auxiliary analyses. This section includes a general overview of the EPRI TSPA and briefly describes the main features of the different model components, which are presented in more detail in Appendix M. The main results in terms of dose history curves from the EPRI and TSPA-LA Model are compared and apparent differences are discussed. The main features of the computed dose release curves for the nominal scenario in the EPRI TSPA Analysis compare reasonably well with the TSPA-LA Model, and differences can be related to different treatment of seepage, inventory, and EBS failure characteristics.

These differences are mostly due to the fact that the EPRI TSPA does not incorporate the most recent updates of analysis and/or model reports which are included in the TSPA-LA Model. That is, most of the input to the EPRI TSPA Analysis corresponds to an earlier version of the TSPA Model. As a result, a direct comparison between the results from the EPRI TSPA Analysis and from the TSPA-LA Model is not possible. However, the overall features of the dose history curves can be compared and, together with evaluating the apparent differences, provides a validation of the general methodology and strategy used in the TSPA-LA Model.

7.7.3.2 Overview of the TSPA Models

The overall conceptual approach of the IMARC and the basic elements of the analysis method are similar to the TSPA-LA approach as depicted on Figure 6.1.5-9 in Section 6.1.5. The differences between IMARC and the TSPA-LA Model are in the details of the implementation and the specifics of the assumptions, models, parameters, and couplings used. The EPRI TSPA Analysis has evolved over the years updating to the Yucca Mountain regulations, the disposal system design, and conceptual understanding of the proposed repository. However, most of the input into the EPRI TSPA Analysis corresponds to that used in the earlier version of the TSPA-LA Model.

The EPRI TSPA Analysis represents a more simplified implementation of the various process models and associated uncertainties compared to the TSPA-LA Model. The EPRI TSPA Analysis implemented a logic-tree approach and the TSPA-LA approach uses a Monte-Carlo sampling approach, which represent two ends of a spectrum of TSPA analysis methods. The EPRI TSPA Analysis uses a logic-tree approach for quantifying the impacts of model and

parameter uncertainty in the TSPA calculations. Logic-tree analysis is used for uncertainty propagation of parameters, which are described using a limited number of probable states (e.g., high, medium, and low values), and their likelihoods (Kozak and Kessler 2005 [DIRS 178580], Figure 2-3). In addition, the Monte Carlo simulation method is used to generate cumulative probability distributions for WP and DS degradation and for BDCFs.

The TSPA-LA Model accounts for the epistemic uncertainty of parameters, model components, and/or assumptions by sampling uncertainty distributions of large numbers of parameters or model inputs using Monte Carlo simulations. Furthermore, the TSPA-LA Model accounts for aleatory uncertainty associated with spatial variability of infiltration and seepage and timing of igneous and seismic events. The spatial variability in infiltration and seepage is represented by different percolation subregions).

The EPRI TSPA Analysis does not consider aleatory uncertainty. The EPRI TSPA Analysis assumes fixed times for the occurrence of igneous and seismic events. The EPRI TSPA Analysis does not account for spatial variability of infiltration, but assumes spatially uniform infiltration and accounts for uncertainty in infiltration rates in the logic-tree analysis, using high, medium, and low infiltration rates, each having a different probability.

Similar to TSPA-LA Model, the EPRI TSPA Analysis considers different scenarios, which include nominal, igneous, a seismic scenario and a human intrusion scenario, although the human intrusion scenario has only been studied in a preliminary fashion. Both the EPRI TSPA Analysis and TSPA-LA Model account for corresponding model components, which are summarized in Table 7.7.3-1.

The focus of the comparison described here between the EPRI TSPA Analysis and TSPA-LA Model is on the Nominal Scenario Class. The following sections summarize the implementation of the different model components in the EPRI TSPA Analysis for comparison with the TSPA-LA Model, which is described in detail in Section 6. Given the differences in the TSPA approaches implemented in the EPRI TSPA Analysis and in the TSPA-LA, it builds confidence when the two approaches yield similar results, or if the differences in the results can be explained based on the different assumptions and models underlying the two TSPAs.

7.7.3.3 Unsaturated Zone Flow

In the EPRI TSPA Analysis, the UZ flow above the repository is not represented by a process model as in the TSPA-LA Model, but is represented via lumped parameters incorporating time history of infiltration accounting for different climate states, flow focusing factor accounting for focused flow along fractures, and seepage into the repository. Infiltration rates for the different climate states used in the EPRI TSPA Analysis (Table M-1) compare reasonably well with the weighted mean infiltration rates used in the TSPA-LA Model (Table M-2). The seepage rates used in the EPRI TSPA Analysis (Table M-3a) are based on computed seepage and fraction of the repository experiencing flowing water summarized in *Abstraction of Drift Seepage* (CRWMS M&O 2001 [DIRS 154291], Table 16). A comparison of the seepage rates given in Table M-3a with those given in the recent analysis and/or model report (Table M-3b) indicates that the seepage rates used in the EPRI TSPA Analysis are significantly lower than those in the TSPA-LA Model (Figure 7.7.3-1).

7.7.3.4 Engineered Barrier System Environment

The EPRI TSPA Analysis neglects thermal effects on water flow, release, and migration of radionuclides for the nominal scenario. It is assumed that there is little to no liquid water present to facilitate radionuclide mobilization and migration until temperatures have decreased to near the local boiling point of water. However, failure distributions generated for each of the three main engineering barrier system components, (i.e., DS, WP, and cladding) do take into account thermal history within the drift and drift stability due to thermal stresses.

7.7.3.5 Waste Package and Drip Shield Degradation

The EBS Corrosion Model is used in the EPRI TSPA Analysis to compute failure distributions for the different components of the EBS, which comprises three versions for the nominal, seismic, and igneous scenarios. The EBS Corrosion Model accounts for various failure mechanisms and uncertain parameters that are sampled using Monte Carlo simulations to produce mean failure distribution curves for the DS, WP, and cladding. These mean failure distribution curves are used as input in the near-field model, which is described in greater detail in Appendix M. The current TSPA-LA Model does not take credit for cladding; that is, radionuclides can be released as soon as the WP starts to fail. The EPRI TSPA Analysis accounts for cladding failure for dripping and non-dripping conditions following WP failure.

The computed failure distributions curves for the nominal scenario for the DS and WP are shown on Figure 4-5 in Apted and Ross (2005 [DIRS 182229]). In comparison, the mean WP and DS failure curves for the TSPA-LA Nominal Scenario Class (Figure 7.7.3-2) indicate a later failure onset but a steeper curve, where 6,256 WPs failed after one-million years. The EPRI TSPA Analysis only considers 8,160 CSNF WPs, of which about 5,304 WPs fail after one-million years.

The EPRI TSPA Analysis accounts for early failure whereby one WP and one DS are assumed to fail initially from a manufacturing defect. The probability of a joint failure of a WP and a DS at the same location is not considered, due to an extremely low probability.

7.7.3.6 Waste Form Degradation and Mobilization

Waste form degradation and mobilization is computed as part of the near-field radionuclide release and transport submodel COMPASS (Compartment Model for Partially Saturated Repository Source Terms) in IMARC, which is described in greater detail in Appendix M. Radionuclides dissolve into water congruently with waste form degradation rate subject to the cladding failure rate. Uncertainty in waste form degradation rates is accounted for in the logic-tree analysis; using alteration times of 1,000 years, 3,000 years, and 5,000 years and associated probabilities of 0.05, 0.9, and 0.05 respectively (Kozak and Kessler 2005 [DIRS 178580], Figure 2-3).

The EPRI TSPA Analysis accounts for gradual cladding failure whereby the fraction of radionuclides, in the gap and grain boundaries of the spent fuel, dissolve instantaneously into water. For specific radionuclides bound in the waste form, the release of radionuclides in water is constrained by solubility limits. The ranges in solubility limits used in TSPA-LA Model and in the EPRI TSPA Analysis are summarized in Table M-4. In the EPRI TSPA Analysis, the

uncertainty in the solubility limits represented by low, moderate, and high values is linked to the probabilities for the alteration times of the waste form degradation. Overall, the median solubility limits used in the EPRI TSPA Analysis fall within the range of those used in the TSPA-LA Model, except for neptunium which is slightly below the range given in TSPA-LA Model (Table M-4).

The EPRI TSPA Analysis only considers CSNF WPs and the associated inventory, whereby the inventory is based on that given in *Initial Radionuclide Inventories* (SNL 2007 [DIRS 180472], Table 7-1). Furthermore, the EPRI TSPA Analysis considers only 12 radionuclides which were identified to have a significant contribution to total dose. The inventory used in the EPRI TSPA Analysis in comparison with that used in the current TSPA-LA Model (Table M-5) indicates that the total inventory per WP compares well with that for CSNF in the TSPA-LA Model. The inventory for DSNF and HLW, which is not considered in the EPRI TSPA Analysis, amounts to about 12.5 percent of the inventory of a CSNF WP. The EPRI TSPA Analysis accounts for 8,160 CSNF WPs, whereas the TSPA-LA Model considered 8,203 CSNF WPs and 3,413 CDSP WPs containing DSNF and HLW.

7.7.3.7 Engineered Barrier System Flow and Transport

In the EPRI TSPA Analysis, radionuclides are transported by diffusion and advection through the near-field, which is comprised of a series of compartments including waste, corrosion products, a pallet or basalt layer, and invert, and the near-field rock matrix and fracture (Table 7.7.3-1). The radionuclide transport in the EBS is computed in the near-field radionuclide release and transport submodel. The computed radionuclide release rates from the near-field to the far-field UZ is then used as boundary conditions for the unsaturated-zone submodel simulating radionuclide transport in the UZ below the repository. The EBS flow and transport implemented in the TSPA-LA Model is described in detail in Section 6.3.6 and 6.3.8.

7.7.3.8 Unsaturated Zone Transport

The EPRI TSPA Analysis flow and transport of the UZ below the repository is simulated by the IMARC submodel 'UZ-code' which is represented by several one-dimensional vertical columns approximating spatial variations of repository releases and different lengths corresponding to spatial and temporal variations in the water table. The vertical discretization distinguishes the main UZ layers, which are each discretized in greater detail. The model accounts for variations in saturations associated with variations in permeability, capillary pressure, porosity, and fracture spacing for both fractures and matrix in each geologic layer. Transport of radionuclides accounts for dispersion, decay, diffusion, and sorption. Uncertainty in sorption in the UZ is represented in the logic tree approach as retardation (Kozak and Kessler 2005 [DIRS 178580], Figure 2-3) which includes sorption in the SZ. In the EPRI TSPA Analysis, sorption coefficients (K_d) are defined for specific radionuclides for volcanic rocks in the UZ and SZ and for the alluvium in the SZ. Only for neptunium are sorption coefficients given for individual layers and as low, median, and high values represented in the logic-tree analysis. A comparison of the K_d values used in the EPRI TSPA Analysis and in the TSPA-LA Model is given in Table M-6. Median K_d values for uranium, plutonium, and thorium are significantly lower in the EPRI TSPA Analysis compared to the median values in the TSPA-LA Model, whereas the Kd value for neptunium is only slightly greater.

7.7.3.9 Saturated Zone Transport

The SZ submodel in the EPRI TSPA Analysis (SZ code) consists of two segments, representing the fractured tuff (15 km downgradient) and the other subsequent alluvial segment (5 km), which is 2 km beyond the location of the RMEI. For transport simulation in the tuff, the model considers steady-state groundwater flow in the fracture only. Boundary conditions for the transport simulation include prescribed mass fluxes from the UZ model along the footprint of the repository, and infiltration (boundary condition Type III, Cauchy condition) is prescribed along the entire water table. Similar to the UZ model, transport is affected by fracture flow and sorption in the tuff and in the alluvium. Uncertainty in the K_d values in the SZ is included in the logic-tree analysis that is combined with the UZ Kds. A comparison of the sorption coefficients between those used in the EPRI TSPA Analysis and those used in TSPA-LA Model are summarized in Table M-7. In general, median K_d values are similar for both fractured volcanic rocks and alluvium between the EPRI TSPA Analysis and TSPA-LA Model.

7.7.3.10 Biosphere

The conversion of radionuclide concentration to dose is through the BDCFs for the RMEI living approximately 18 km downstream of the repository. For this, a representative volume of 3,000 acre-feet per year for consumption by the RMEI is assumed. The BDCFs used in the EPRI TSPA Analysis and those used in the TSPA-LA Model are compared in Table M-8. Overall, the EPRI BDCFs are higher than those used in TSPA-LA Model, which would result in higher doses in the EPRI TSPA Analysis for the same concentration.

7.7.3.11 Mean Annual Dose Comparison—Nominal Case

The computed mean radionuclide doses for the EPRI nominal scenario is given on Figure 5-10 in Apted and Ross (2005 [DIRS 182229]). In comparison, the results from the TSPA-LA Model for the computed mean annual doses for the combined Nominal Scenario Modeling Case and the Waste Package EF Modeling Case are shown on Figure 7.7.3-3. The results indicate a similar pattern for the nominal scenario characterized by a significant increase in dose after 100,000 years. The early failure dose is represented by the dose increase after about 1,000 years in the TSPA-LA Model (Figure 7.7.3-3), which is somewhat delayed in the EPRI TSPA Analysis (Apted and Ross 2005 [DIRS 182229], Figure 5-10). The mean annual dose in the EPRI TSPA Analysis is about 2.0×10^{-2} mrem/yr compared to about 4.0×10^{-1} mrem/yr in the TSPA-LA Model after one-million years. The main contributor to mean annual dose at late time is ^{129}I in both cases.

The differences between the EPRI TSPA Analysis and the TSPA-LA Model results can be accounted for by differences in:

- Seepage rates through the repository
- Early-failure representation and EBS failure curves
- Inventory, both in terms of waste type and individual radionuclides
- Solubility limits and sorption characteristics in the UZ and SZ.

As shown in Figure 7.7.3-1, seepage rates used in the EPRI TSPA Analysis are significantly lower than the corresponding rates used in the TSPA-LA Model, whereby the seepage rates in the EPRI TSPA Analysis are based on previous analysis and/or model report results. This causes a delay in radionuclide release from the EBS.

The EPRI TSPA Analysis only accounts for CSNF waste and considers failure of DS, WP, and cladding, whereas the TSPA-LA Model accounts for CSNF, DSNF, and HLW WPs, but does not take credit for cladding in CSNF WPs. Consequently, the overall dose release in the EPRI TSPA Analysis is delayed both during early failure case and for the nominal case, where the WP failure curve indicates that only about 5,300 CSNF packages failed after one-million years, whereas the TSPA-LA Model indicates that on average about 50 percent of WPs have failed.

The EPRI TSPA Analysis only considers 12 radionuclides compared to 26 radionuclides in the TSPA-LA Model (Table M-4). During early failure ^{14}C is shown to contribute significantly to total dose in the TSPA-LA Model, which is not considered in the EPRI TSPA Analysis. At late time, the dominant radionuclides contributing to mean annual dose include ^{129}I, ^{99}Tc, ^{135}Cs, ^{79}Se, ^{242}Pu, and ^{237}Np in the TSPA-LA Model. The dominant radionuclides in the EPRI TSPA Analysis include ^{129}I followed by ^{237}Np, ^{233}U, and ^{229}Th. However, the EPRI TSPA Analysis does not consider ^{135}Cs and ^{79}Se.

Solubility limits used in the EPRI TSPA Analysis indicate significantly lower values for neptunium, plutonium, and thorium compared to the range given in the TSPA-LA Model. On the other hand, sorption characteristics used in the EPRI TSPA Analysis for the UZ are significantly lower for uranium and plutonium compared to those in the TSPA-LA Model. However, this does not affect ^{129}I, ^{99}Tc, and ^{135}Cs, which represent the main contributors to mean annual dose in the TSPA-LA Model.

In general, the main features of the dose release curves for the nominal scenario compares reasonably well with the TSPA-LA Model. The differences can be related mostly to differences in seepage and in different implementation of the inventory and EBS failure characteristics. This is partly due to the fact that the EPRI TSPA Analysis uses earlier analysis and/or model report results.

Table 7.7.3-1. Model Components and Processes Represented in the TSPA-LA Model and the EPRI TSPA Analysis

TSPA-LA Model[1]	EPRI TSPA Analysis
Unsaturated Zone Flow	**Climate, Net Infiltration, and Percolation** Parametric representation of: Time-history of infiltration rate Flow focusing factor Seepage fraction
Engineered Barrier System Environment Waste Package and Drip Shield Degradation	**Engineered Barrier System Degradation** Degradation processes represented by mean failure curves for: Drip shield Waste-Packages Cladding
Waste Form Degradation and Mobilization Engineered Barrier System Flow and Transport	**Near-field Model and Coupling** *Compartment model to: compute mass transfer across the different near-field components:* *Waste* *Corrosion Products* *Pallet/Basalt* *Invert* *Nearfield rock matrix/fractures*
Unsaturated Zone Transport	**Lower Unsaturated Zone Model and Coupling** UZ-Code: 1-D unsaturated-zone flow and transport, representing four unsaturated horizons: tsw35, tsw38, ch1Vl, Ch2Ze.
Saturated Zone Transport	**Saturated Zone Model and Coupling** SZ-Code: 2-D saturated flow and transport representing fractured tuff segment and alluvial segment
Biosphere	**Biosphere Model and Coupling** Determination of radionuclide-specific set of Biosphere Dose Conversion Factors for the Reasonably Maximally Exposed Individual based on assessment of relevant radiation exposure media

[1]Relevant processes used in the TSPA-LA Model are described in Section 6.

INTENTIONALLY LEFT BLANK

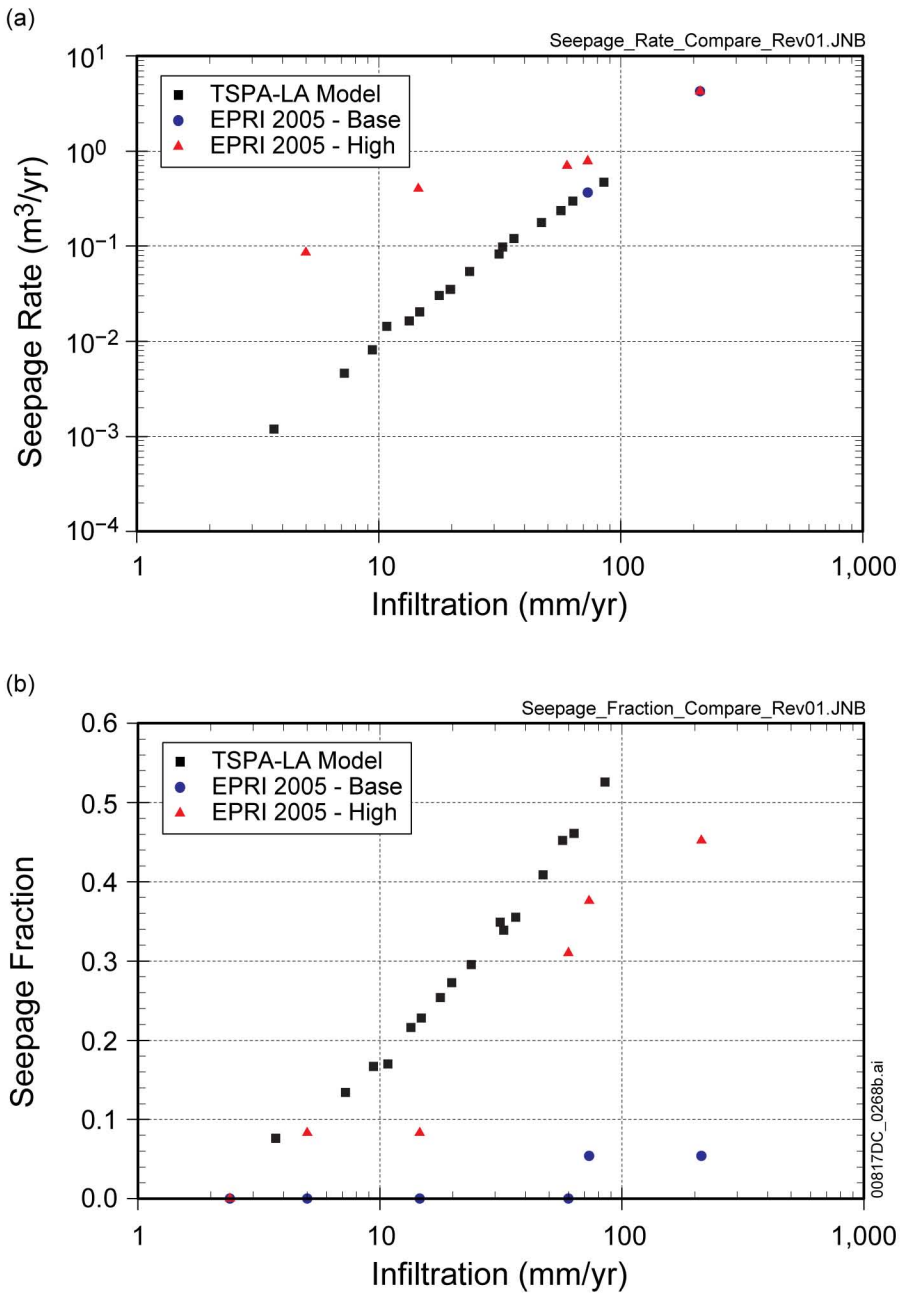

Sources: Kozak and Kessler 2005 [DIRS 178580], Table 3-2; CRWMS M&O 2001 [DIRS 154291], Table 4.3.1-1; and SNL 2007 [DIRS 181244], Tables 6-5[a] and 6-6[a].

Figure 7.7.3-1 Comparisons of (a) Seepage Rate and (b) Seepage Fraction versus Infiltration Rates as Used in the EPRI Analysis and the TSPA-LA Model

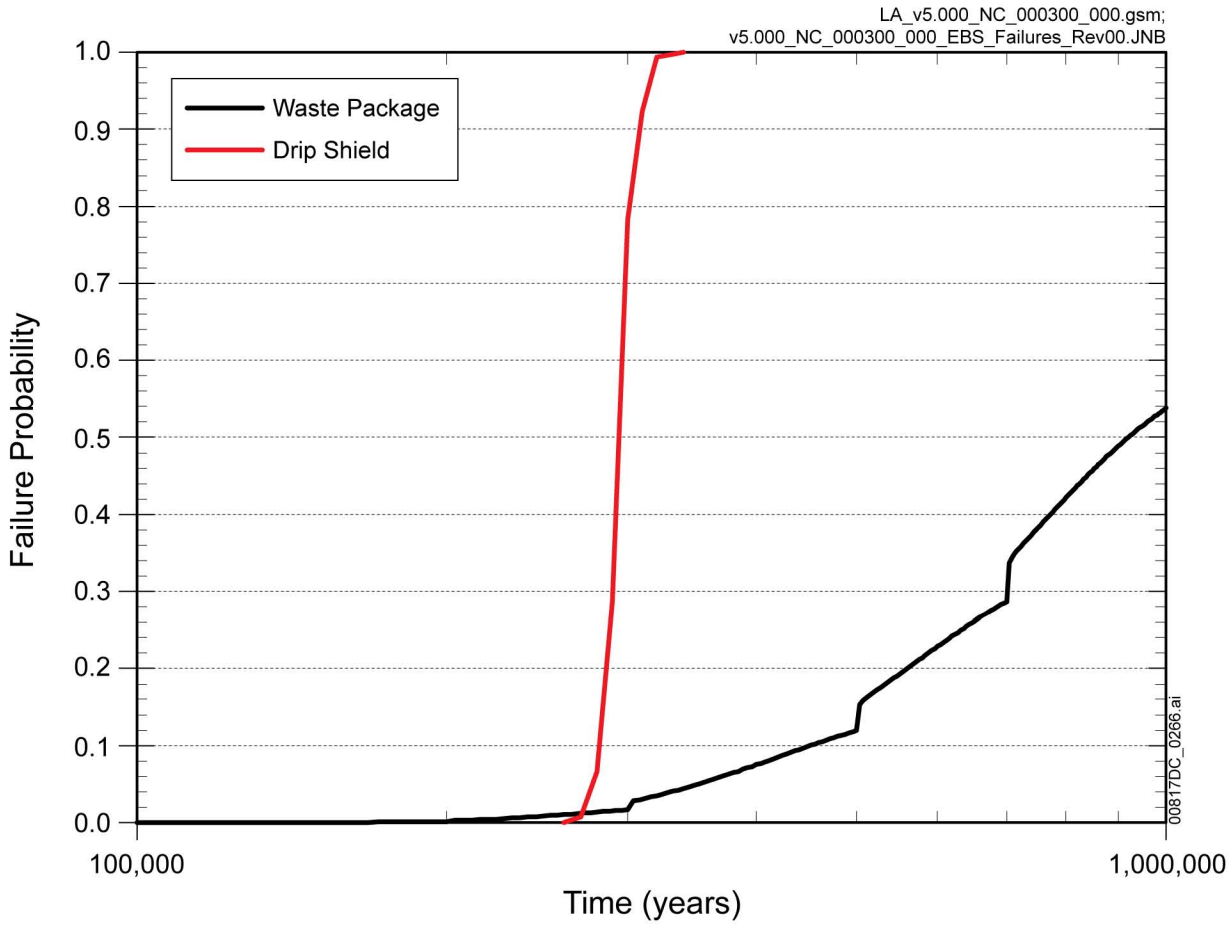

Source: Output DTN: MO0709TSPAREGS.000 [DIRS 182976].

Figure 7.7.3-2. TSPA-LA Nominal Scenario Class Mean Failure Curves for the Drip Shield and Waste Package

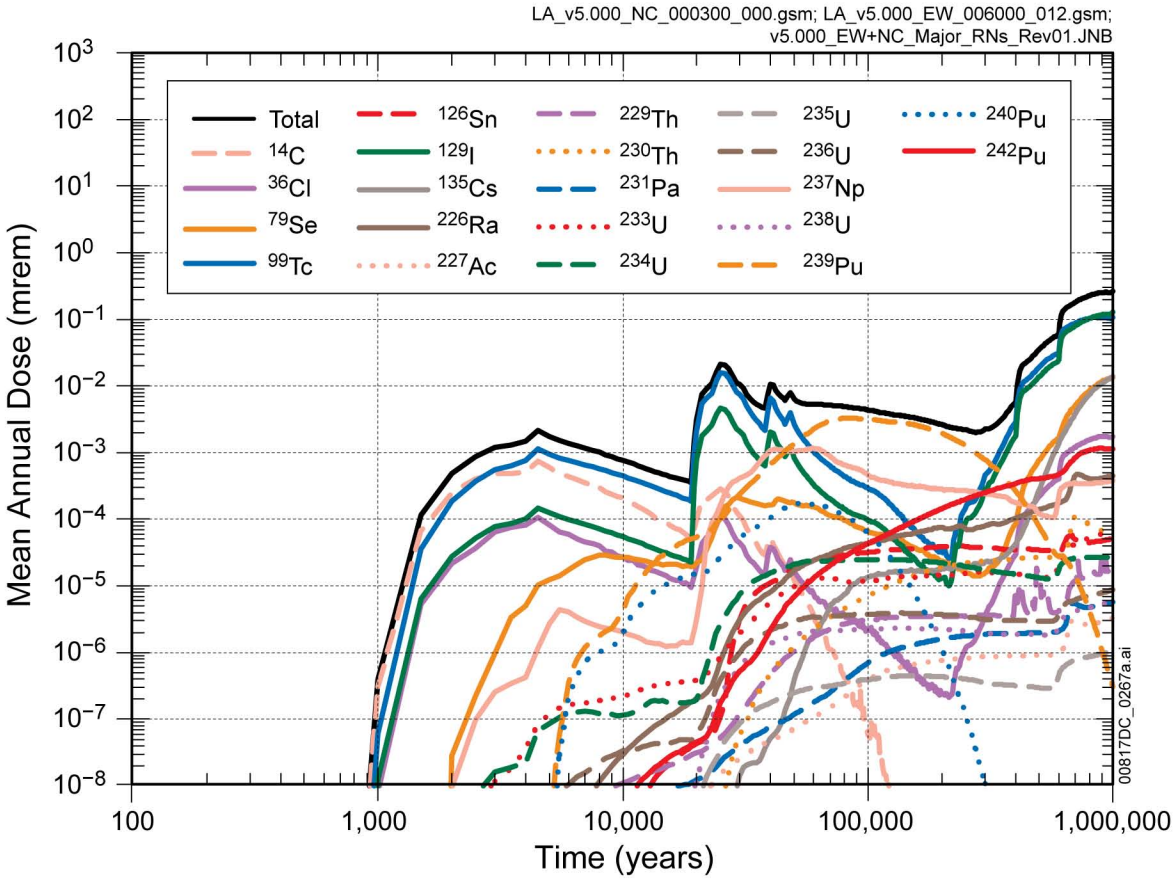

Source: Output DTN: MO0709TSPAREGS.000 [DIRS 182976].

Figure 7.7.3-3. TSPA-LA Mean Dose Histories for Major Radionuclides for the Combined Early Failure and Nominal Scenario Classes

INTENTIONALLY LEFT BLANK

7.7.4 Performance Margin Analysis

The judicious use of reasonable conservative assumptions, play an important role in the development of the TSPA-LA Model, and building confidence in the TSPA-LA results. Conservative assumptions were introduced in the formulation of the TSPA submodels and in selected submodel parameters to compensate for epistemic uncertainties, but more importantly, to ensure that the potential radiological risks would not be underestimated. Individual conservatisms introduced at the submodel level, however, can be attenuated differently to the system level performance measures, i.e., total mean annual dose. Consequently, it was necessary to carefully and quantitatively evaluate the significant explicit and implicit conservatisms of the type discussed in Section 6.3. More specifically, the selected conservatisms were evaluated to:

1. Confirm that, when propagated individually through the TSPA-LA Model, they are conservative with respect to the total system performance measures (e.g., total mean annual dose)

2. Quantify the extent to which the conservatisms, individually and collectively, overestimate the total mean annual dose, relative to the model projections presented in the performance demonstration described in Section 8.0

3. Assess that evaluated conservatisms did not introduce any inappropriate risk dilution in the TSPA-LA results presented in support of the LA (e.g., reduce the peak total mean annual doses).

To perform these evaluations, a separate set of TSPA calculations were conducted and referred to as the Performance Margin Analysis (PMA). The PMA calculations paralleled those of the TSPA-LA Model (Section 8.0), but focused on scrutinizing the impact of select conservatisms embedded in TSPA model components and submodels and utilized by the modeling cases to calculate annual doses. In addition, the PMA was intended to gauge the collective impact of the conservatisms, and thereby give a perspective on the potential performance margin embedded in the TSPA-LA dose-risk projections.

Most of the conservatisms in the TSPA-LA Model were introduced during submodel development and/or derivation of parameter uncertainty characterizations as discussed in Section 6.3. For the most part, these conservatisms are implemented to bound the effects of processes that promote radionuclide release and transport. Other conservatisms were also introduced as a result of not taking credit for processes or conditions, which may potentially enhance containment and isolation. Additional submodels were developed for inclusion in the PMA for the specific purpose of evaluating implicit conservatisms. It is important to state, however, that while these additional submodels and data have been through the required quality assurance (QA) process, in some cases they have a limited technical foundation and/or may use an unqualified software (Section C3), and are only used as a quantitative tool for the PMA.

The PMA was conducted by first modifying selected submodels and parameters of the TSPA-LA Model, including the additional submodels and parameters for the PMA, and then repeating a select set of modeling cases that were run for the TSPA-LA. The total mean annual dose was recalculated replacing the selected set of TSPA-LA modeling cases with PMA results. The

collective impact of the major assumptions was quantified by comparison of the total mean annual dose (for example Figure 7.7.4-2). The PMA results are compared to the mean annual dose results of the TSPA-LA Model. Thus, the PMA is one aspect of the validation work supporting the TSPA-LA Model. The detailed PMA are presented in Volume III, Appendix C.

Changes to the TSPA-LA submodels necessary to conduct the PMA are embedded in the following principal model components defined in Section 6.0 and Figure 6-1:

- Drift-Scale UZ Flow (C6.2)
  - Reduction of seepage flux to WP based on a reduced hydrologic cross-section for the representation of collapsed drift geometry (Drift Seepage Submodel)
- Waste Package and Drip Shield Degradation (C6.3)
  - Modification of corrosion rates based on fluoride ion concentration threshold instead of fixed and pervasive condition of aggressive corrosion
  - Implementation of a lower WP Alloy 22 (UNS N06022) general corrosion rate based on weight loss coupon data instead of conservative crevice corrosion data
  - Implementation of SCC of Alloy 22 using a less conservative representative yield stress threshold
  - Inclusion of a mechanistic approach to the calculated distribution of breached area as a result of localized corrosion on the WP outer barrier
- EBS Flow (C6.4)
  - Inclusion of a detailed in-package water balance to more accurately account for the mass fluxes of water through the WPs
- Waste Form Degradation and Mobilization (C6.5)
  - Modification of In-Package Chemistry Model that accounts for the extent of material degradation and the availability of water inside a WP
  - Inclusion of long-term degradation rate models for CSNF and HLW glass waste forms
  - Inclusion of credit for initial clad failure fractions in place of conservatively assuming all cladding is failed at time of emplacement; applied to first 20,000 years only
  - Reduction of uncertainties for thermodynamic properties of neptunium, uranium, and plutonium
- UZ Flow and Transport Submodel (C6.6)

- Enhanced matrix diffusion effects on radionuclide transport
- Addition of colloid diversity model and retardation of irreversibly sorbed radionuclides
- Addition of detailed model for water table rise

- SZ Transport Submodel (C6.7)
  - Addition of discrete interface for redistribution of the diffusive mass released from the UZ matrix to SZ fractures
  - Addition of colloid diversity model and retardation of reversible and irreversibly sorbed radionuclides
  - Addition of enhanced radionuclide sorption in potential reducing zone
  - Implementation of less conservative distribution for flowing interval porosity
  - Inclusion of correlation between flowing interval porosity and groundwater specific discharge

- Seismic Scenario Class (C6.8)
  - Inclusion of an alternative conceptual model for the crack-area density model in the Seismic Damage Abstraction.

Discussion of each change and how they were addressed in terms of modifications to the above submodels is presented in Volume III, Appendix C.6, PMA Model Description.

7.7.4.1 Projections of the TSPA-LA Performance Margin

In the PMA the postclosure performance was analyzed over a select set of modeling cases to evaluate the changes listed above. The objective of the PMA is to carefully and quantitatively evaluate the significance of the major explicit and implicit conservatisms which would be otherwise very difficult to address given the range of uncertainties and long-term projections inherent in a model of this magnitude.

Scenario Classes and Modeling Cases Considered

The TSPA-LA demonstration of performance for the individual protection standard is based on the total mean annual dose summed over seven scenario modeling cases: (1) Nominal, (2) Waste Package EF, (3) Drip Shield EF, (4) Igneous Intrusion, (5) Volcanic Eruption, (6) Seismic GM, and (7) Seismic FD (Section 8.1). As required by the disposal standards, for the TSPA-LA the postclosure performance is quantified for time periods of 10,000-years and 1,000,000-years after closure. Likewise the PMA was conducted over the 10,000 year and 1,000,000 year postclosure periods for comparison with the TSPA-LA. Drawing from the evaluation presented in Section 8.0, the PMA was exercised using five modeling cases (the Seismic GM Modeling Case

includes the effects of the nominal processes when run for 1,000,000-years postclosure). The Volcanic Eruption Modeling Case was not evaluated in the PMA, because none of the changes included in the PMA have any impact on the Volcanic Eruption Modeling Case.

In addition, a sensitivity analysis was conducted to evaluate the use of weight-loss Alloy 22 general corrosion data (as noted above). This analysis was conducted for two additional simulations: a Seismic GM and a Nominal Modeling Case were run for a period of 1,000,000 years after repository closure. These simulations are documented in Volume III, Appendix C, Section C.7.1.2.

In summary, the performance margin demonstration for the TSPA-LA Model considered projections of radionuclide releases for five modeling cases for the time period of 10,000 years and for the time period after 10,000 years and through the period of geologic stability.

Calculation of Total Mean Annual Dose

The PMA total mean annual dose was calculated replacing the selected set of TSPA-LA modeling cases (identified above) with PMA results. The TSPA-LA results for the Volcanic Eruption Modeling Cases were combined with the PMA results to calculate the PMA total mean annual dose. A detailed discussion of the method used to calculate the total mean annual doses for the TSPA-LA and the PMA, is presented in Appendix J. The total mean annual dose was evaluated to assess the potential performance margin embedded in the TSPA-LA Model results (presented in Section C7).

Performance Margin in the Total Mean Annual Dose for 10,000-years Postclosure

The main result of the simulation process is a set of expected annual dose histories shown on Figure 7.7.4-1, along with curves for the mean, median, 5th- and 95th-percentiles. The total mean annual dose history, which is plotted as the red curve, was computed by taking the 'arithmetic average' of the 300 expected annual dose values, for individual time planes along the curves (Appendix J). A comparison of the total mean annual dose history for the PMA and the TSPA-LA is shown on Figure 7.7.4-2. The peak total mean annual dose to the RMEI is estimated by the PMA to be about 0.02 mrem for the 10,000-year disposal period. Important performance margin insights can be gained by comparison of the total mean annual dose curves between the PMA and the TSPA-LA, which are shown on Figure 7.7.4-2 over the 10,000-years postclosure period. From those dose curves, the following general observations can be drawn about the performance margin demonstration:

- The PMA total mean annual doses are generally lower by nearly an order of magnitude over the first 10,000 years compared with the total mean annual dose from the TSPA-LA Model.

- The peak PMA total mean annual doses calculated over 10,000 years are lower by over an order of magnitude over the largest total mean annual dose from the TSPA-LA Model.

- Total mean annual doses calculated for 10,000 years are dominated by projected releases for the Igneous Intrusion Modeling Case (Appendix C, Figure C7-7).

The radionuclides which contribute the most to the total mean annual dose depend on time frame being evaluated, i.e., 10,000-years or 1,000,000-years after closure, because of the effect of decay on activities. From dose curves shown on Figure 7.7.4-3(b), the principal contributors to the peak total mean annual dose in the PMA for 10,000 years, ranked from highest to lowest, are: ^{99}Tc, ^{129}I, ^{14}C, ^{237}Np, ^{239}Pu, ^{240}Pu, and ^{234}U. Though the relative importance is different, collectively, the dominant radionuclides shown in the PMA results are the same dominant radionuclides that are found in the TSPA-LA Model total mean dose. The similarity between the dominant radionuclides in the PMA and the TSPA-LA Model indicates that the EBS and Natural System components are behaving the same, but the lower total mean annual dose for the PMA would suggest that the reduction in the conservative assumptions embedded in these component models as the primary factor accounting for the lower dose and are responsible for the margin in the TSPA-LA results.

Performance Margin in the Total Mean Annual Dose after 10,000 years through the Period of Geologic Stability

The set of expected annual dose histories for the time period after 10,000 years and through the period of geologic stability are shown on Figure 7.7.4-4. The peak total mean annual dose to the RMEI after 10,000 years, but within the period of geologic stability, is estimated by the PMA to be about 1.1 mrem. Comparison of the total mean annual dose curves between the PMA and the TSPA-LA is shown on Figure 7.7.4-5 for the 1,000,000-year time period. From this comparison plot, the following general observations can be drawn about the performance margin demonstration:

- The PMA total mean annual doses are generally lower by nearly an order of magnitude over the first 200,000 years compared with the total mean annual dose from the TSPA-LA Model.

- The peak PMA total mean annual doses calculated over 1,000,000 years are lower by a factor of two over the largest total mean annual dose from the TSPA-LA Model.

In general, the radionuclides in the nuclear waste that dominate the calculation of annual doses typically have a combination of unique characteristics such as: (1) large initial inventories in the nuclear waste, (2) moderately to highly soluble, (3) very long half-lives (e.g., $\geq 10^5$ yrs), and (4) low sorbing to non-sorbing properties. The important radionuclides vary according to time frame, i.e., 10,000 years or 1,000,000 years after closure, because of the effect of decay on activity. From dose curves shown on Figure 7.7.4-6(b), that the principal contributors to the peak total mean dose in the PMA for 1,000,000 yrs, ranked from highest to lowest, are: ^{226}Ra, ^{242}Pu, ^{237}Np, ^{129}I, ^{233}U, ^{135}Cs, ^{99}Tc, ^{229}Th and ^{230}Th. Through their relative importance changes, these PMA dominant radionuclides are the same dominant radionuclides that are found in the TSPA-LA Model total mean dose. This similarity between dominant radionuclides indicates that the EBS and Natural System components behave in an analogous manner. Moreover, the lower peak total mean annual dose projected for the PMA demonstrates the impact of this reduction in the degree of conservatism.

Scenario Specific Insights to the Performance Margin

Additional important insights to the performance margin can be gained by disaggregating the total mean annual dose into the total mean annual dose curves for the individual modeling cases and conducting a systematic evaluation of the effects of the changes incorporated into the PMA. This detailed analysis is included in Appendix C and the following general observations can be drawn about the PMA results:

- Total mean annual doses calculated for both 10,000 years and 1,000,000 years are dominated by projected releases for the Igneous Intrusion Modeling Case.

- Total mean annual dose projected for Seismic GM Modeling Case is on the order of 10^{-1} mrem or less and is the second largest contributor to the calculated total mean annual dose 1,000,000-years after closure.

- Total mean annual dose projected for Waste Package EF Modeling Case is on the order of 10^{-3} mrem or less and is the second largest contributor to the calculated total mean annual dose calculated until 10,000-years after closure.

- Total mean annual doses for the Drip Shield EF, Seismic FD, and Volcanic Eruption Modeling Cases are relatively small and are estimated to be on the order of 10^{-4} mrem or less for both 10,000-years and 1,000,000-years after closure.

A comparison between the observations listed above for the PMA and the TSPA-LA results yields some notable differences. With regards to the TSPA-LA results, the Seismic GM Modeling Case dominates the total mean annual dose for the 10,000-year time period, whereas for 1,000,000 years the Seismic GM and Igneous Intrusion Modeling Cases contribute equally to the total mean annual dose to the RMEI (Section 8.1.1.2). However, in the PMA results, the Igneous Intrusion Modeling Case dominates the total mean annual dose for the time period of 10,000 years. For the time period after 10,000 years and through the period of geologic stability the Igneous Intrusion Modeling Case dominates the total mean annual dose with a small contribution from the Seismic GM Modeling Case beginning around 225,000 years. This difference is primarily due to a lower incidence of WP failure (Appendix C6.8 and C.7.2) and WP cracking during a seismic event for the PMA (Appendix C6.8 and C.7.2). The remaining cases combined, have a negligible contribution for both the PMA and TSPA-LA total mean annual dose results.

7.7.4.2 Summary of the TSPA-LA Performance Margin

The differences in the relative contributions to the total mean annual dose from each of the scenario modeling cases between the PMA and the TSPA-LA Model indicates that the reduction in the selected conservative assumptions embedded in these TSPA-LA component models exposed a larger performance margin for the Early Failure and Seismic Scenario Classes than that may be contained within the Igneous Scenario Class. With respect to the specified objectives of the PMA:

1. The PMA results confirm that submodel conservatisms propagated through the TSPA-LA Model, are also conservative with respect to the total system performance measures (e.g., total mean annual dose).

2. Relative to the TSPA-LA Model results, the peak PMA total mean annual dose is lower by over an order of magnitude for the 10,000 year time period and lower by a factor of two for the time period after 10,000 years.

3. The evaluated conservatisms did not introduce any inappropriate risk dilution in the TSPA results presented in support of the LA as demonstrated by the absence of higher peak mean annual doses in the PMA results for both the probabilistic projections of the total dose histories and the comparison of the projected total mean dose history for the PMA relative to the TSPA-LA.

The collective impact of the major assumptions was quantified by comparison with the TSPA-LA results. The assessment of the potential performance margin embedded in the TSPA-LA Model results is presented in detail in Volume III, Appendix C.

INTENTIONALLY LEFT BLANK

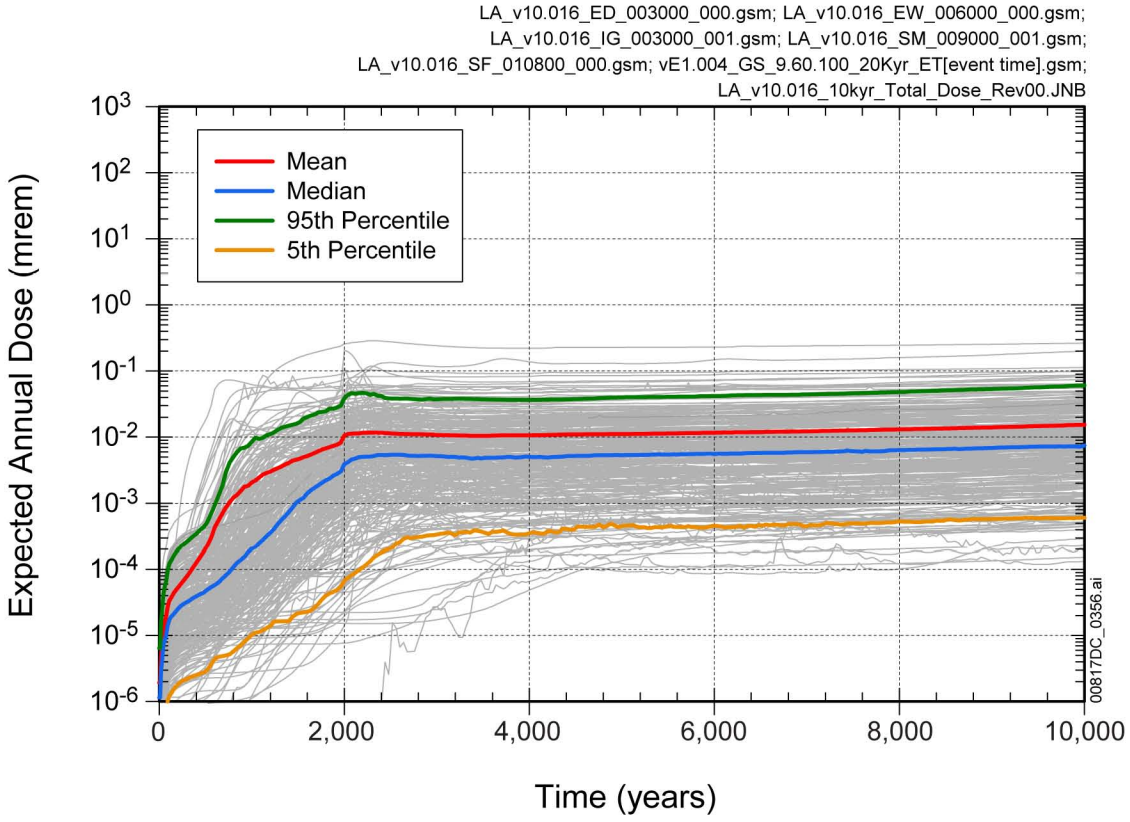

Source: Corroborative DTN: MO0709MARGANAL.000 [DIRS 182978]; and Output DTN: MO0709TSPAREGS.000 [DIRS 182976].

Figure 7.7.4-1. Total Expected Annual Dose for the Performance Margin Analysis for 10,000 Years after Repository Closure

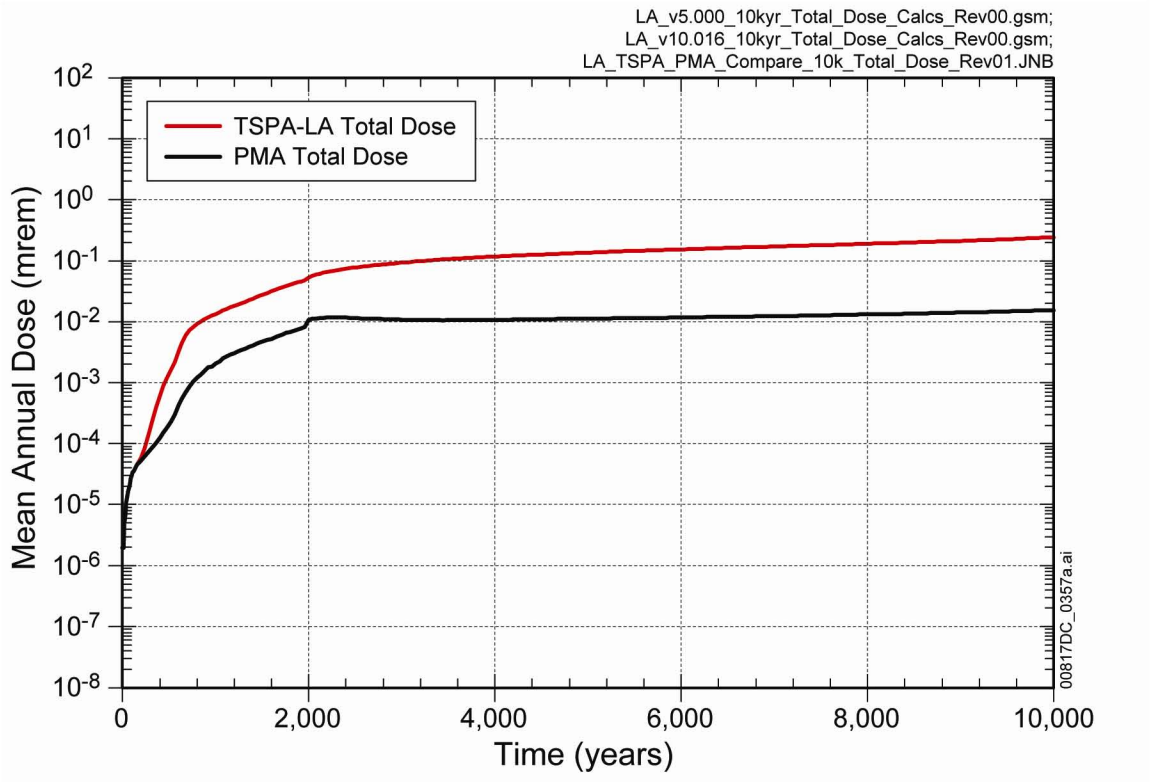

Source: Output DTN: MO0709TSPAPLOT.000 [DIRS 183010]; and Corroborative DTN: MO0709MARGANAL.000 [DIRS 182978].

Figure 7.7.4-2. Comparison of the Total Mean Annual Dose for the TSPA-LA Model to the Performance Margin Analysis 10,000 Years after Repository Closure

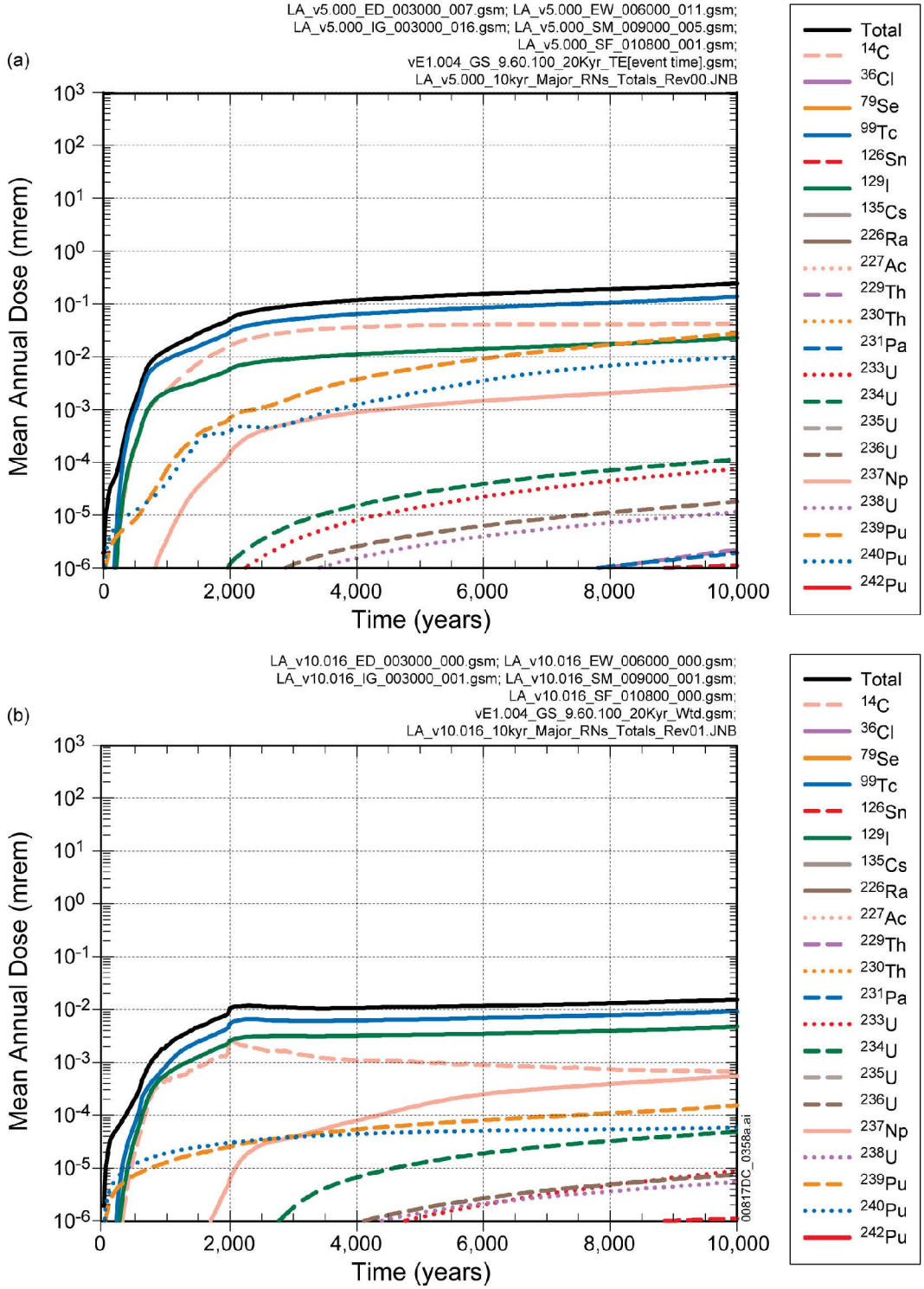

Source: Output DTN: MO0709TSPAREGS.000 [DIRS 182976]; and Corroborative DTN: MO0709MARGANAL.000 [DIRS 182978].

Figure 7.7.4-3. Contributions of Individual Radionuclides to Total Mean Annual Dose for (a) the TSPA-LA Model and (b) the Performance Margin Analysis 10,000 Years after Repository Closure

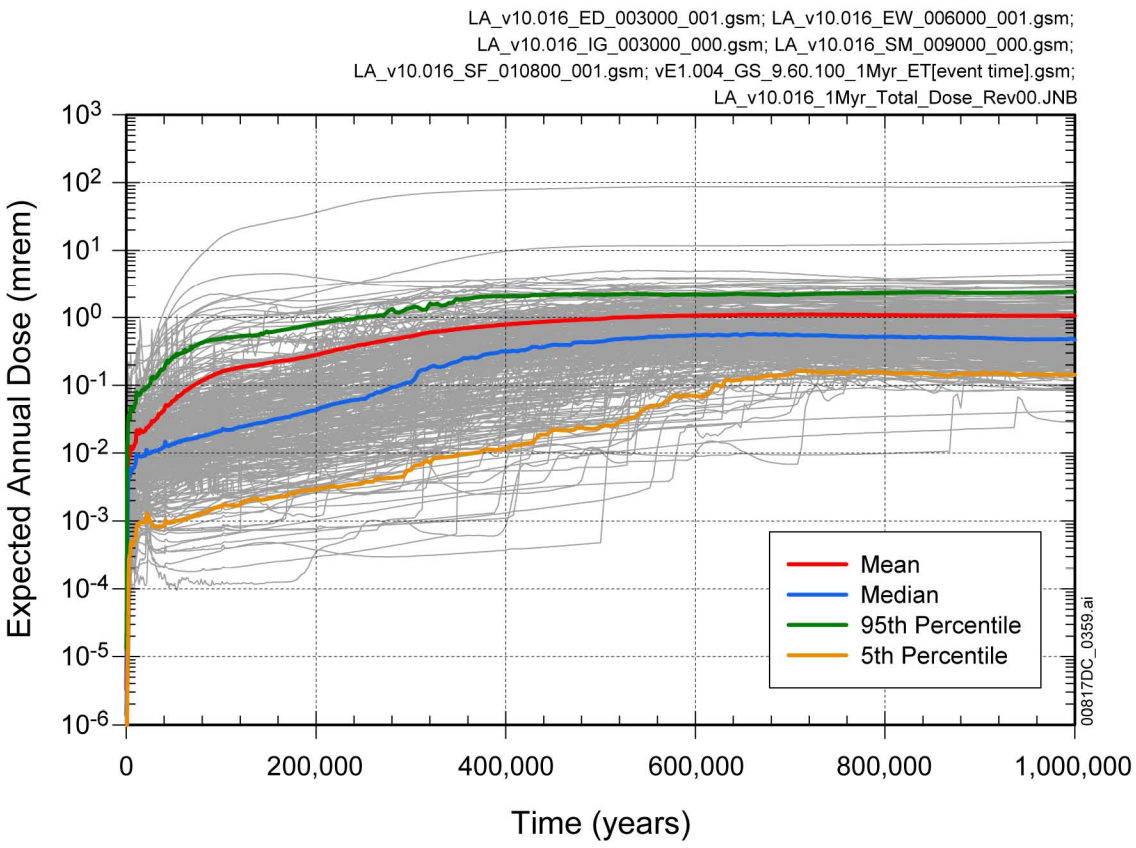

Source: Corroborative DTN: MO0709MARGANAL.000 [DIRS 182978]; and Output DTN: MO0709TSPAREGS.000 [DIRS 182976].

Figure 7.7.4-4. Total Expected Annual Dose for the Performance Margin Analysis for 1,000,000 Years after Repository Closure

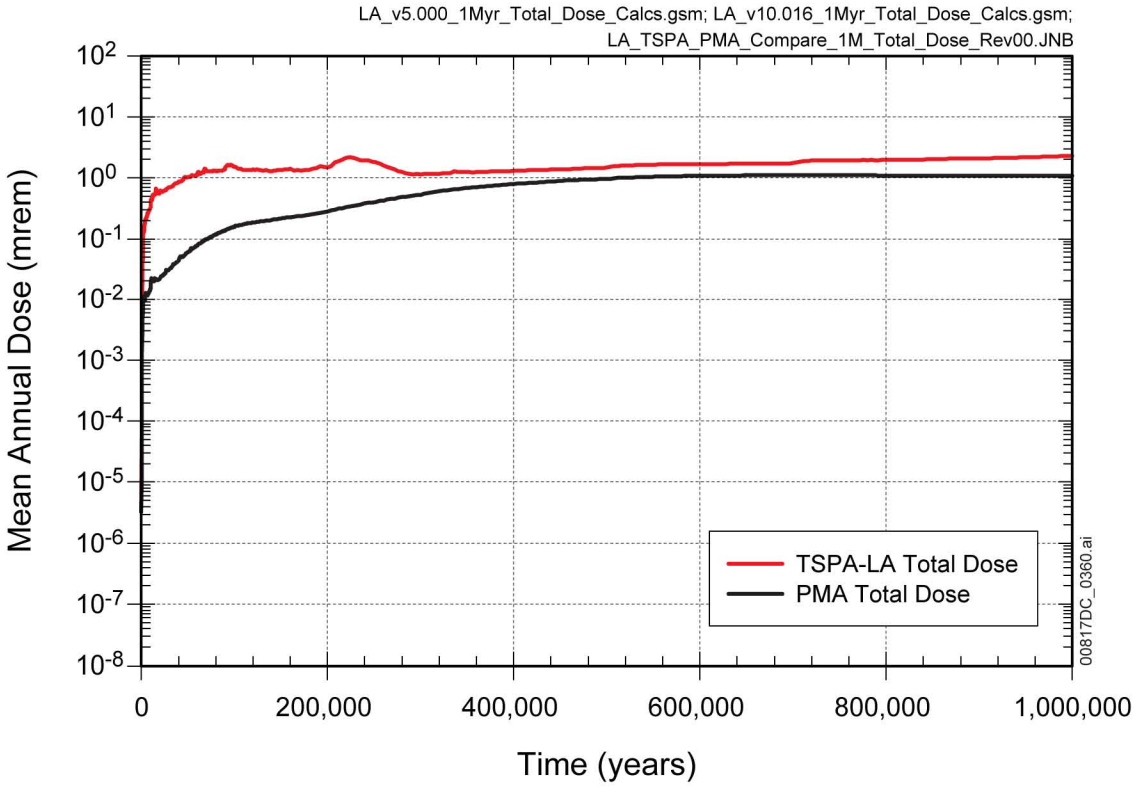

Source: Output DTN: MO0709TSPAPLOT.000 [DIRS 183010]]; and Corroborative DTN: MO0709MARGANAL.000 [DIRS 182978].

Figure 7.7.4-5. Comparison of the Total Mean Annual Dose for the TSPA-LA Model to the Performance Margin Analysis 1,000,000 Years after Repository Closure

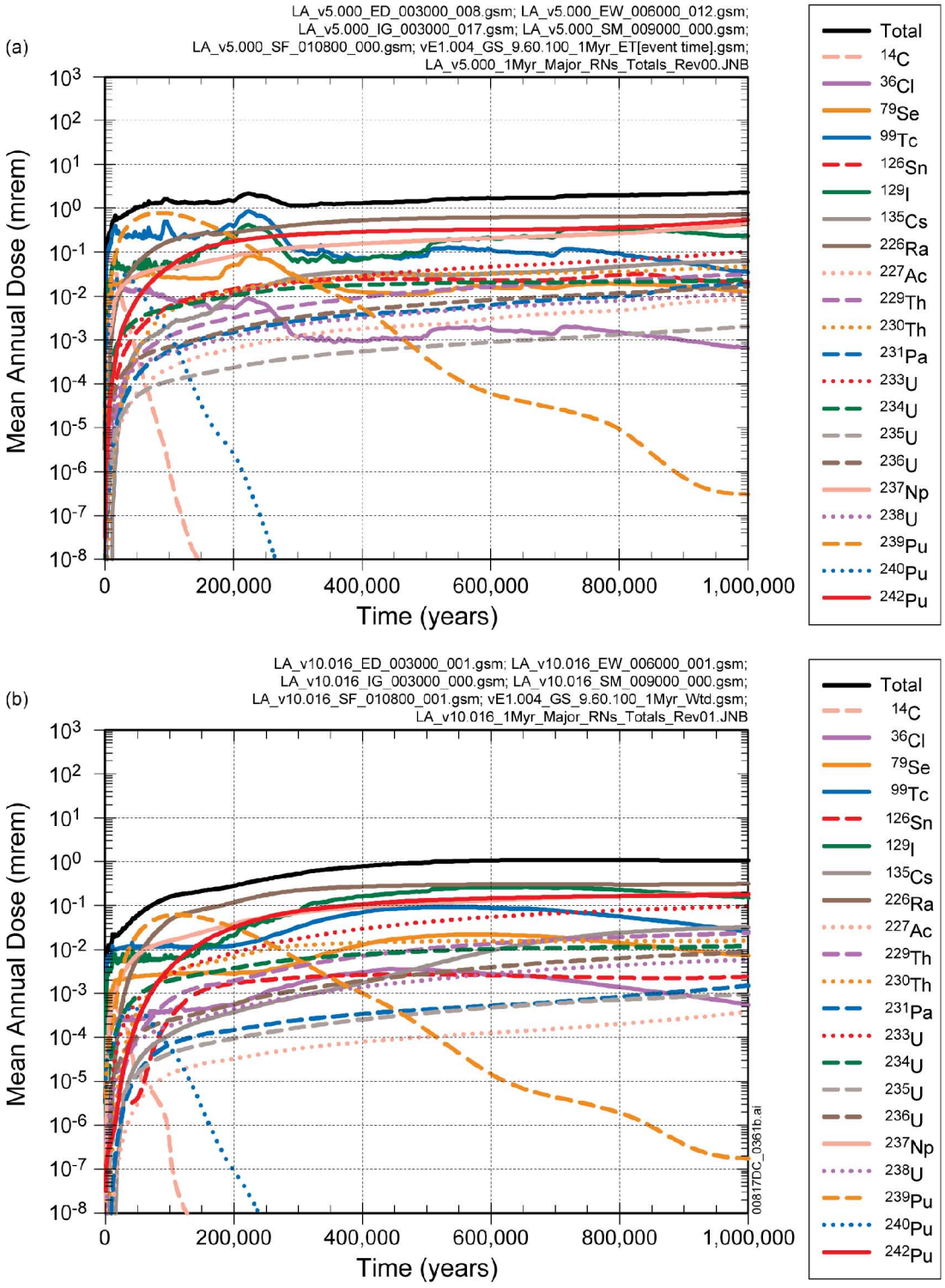

Source: Output DTN: MO0709TSPAREGS.000 [DIRS 182976]; and Corroborative DTN: MO0709MARGANAL.000 [DIRS 182978].

Figure 7.7.4-6. Contributions of Individual Radionuclides to Total Mean Annual Dose for (a) the TSPA-LA Model and (b) the Performance Margin Analysis 1,000,000 Years after Repository Closure

7.8 NATURAL ANALOGUES

The TSPA-LA Model accounts for the uncertainty in making long-term projections of the performance of the repository and simulates the performance of the Yucca Mountain repository for hundreds of thousands of years. Validation of the predicted performance of the repository at these time scales requires less than absolute proof because absolute proof is impossible to attain for disposal due to the uncertainty of projecting long-term performance (NRC Proposed Rule 10 CFR 63.304(1) [DIRS 180319]). Natural analogues to repository conditions and materials, both natural and anthropogenic, provide a means to compare repository conditions and materials to observed conditions and materials for time periods relevant to the lifetime of the repository. In the case of natural analogues, the National Research Council has endorsed the use of natural analogues as "natural test cases, geological settings in which naturally occurring radioactive materials have been subjected to environmental forces for millions of years" (National Research Council 1990 [DIRS 100061], p. 27). Analogues can provide quantitative and/or qualitative evidence to corroborate and assess expected repository performance covering geologic time scales. Analogues, although not the same as controlled laboratory or field experiments, can build confidence in the conceptual and numerical models that are used to represent processes and events that could affect repository performance.

Confidence in and corroboration of the predicted results of the TSPA-LA Model of the Yucca Mountain repository can be gained, in part, through comparison with natural and anthropogenic analogues to the processes, conditions, and materials affecting repository performance. The results of natural analogue analyses relevant to the long-term geologic storage of nuclear waste have served as corroborative input to several of the analysis and model reports that support the model components and submodels of the TSPA-LA Model. Natural analogues that are relevant to the assessment of the long-term performance of the Yucca Mountain repository are discussed in *Natural Analogue Synthesis Report* (BSC 2004 [DIRS 169218]). Some of the analogues to the process models and submodels of the TSPA-LA Model are summarized below. Following these discussions, Sections 7.8.1 and 7.8.2 describe two investigations of natural analogues that describe geologic processes that could possibly affect the performance of the Yucca Mountain repository. These analogues, which provide corroborative evidence for the TSPA-LA Model, are the simulation of the 1995 volcanic eruption at Cerro Negro, Nicaragua (Section 7.8.1), and the investigation of seepage and radionuclide transport at the Nopal I uranium deposit in the Sierra Peña Blanca in Chihuahua, northern Mexico (Section 7.8.2).

Drift Stability—The Nominal Scenario Class Modeling Case simulates the performance of the emplacement drifts as stable throughout the simulation period. The ability of underground openings, such as caves and engineered mines, to remain open and stable under ambient conditions depends on: (1) rock strength; (2) size, shape, and orientation of the opening; (3) orientation, length, and frequency of fractures; and (4) effectiveness of ground support. Cave and/or mine collapses are common occurrences but, depending on geology, natural caves and engineered mines and tunnels may remain stable and open for hundreds to thousands of years. Radiometric analyses of minerals found in cave floors indicate that natural openings, larger than those at Yucca Mountain, have remained stable and open for millions of years. Collapse of openings tends to occur where fracture density is high. Neolithic flint mines (approximately 4,000 to 3,000 B.C.), and Roman mines and aqueducts demonstrate that man-made underground openings can remain open and stable for thousands of years also, as summarized in *Natural*

Analogue Synthesis Report (BSC 2004 [DIRS 169218], Section 15.7.1). Stuckless (2000 [DIRS 151957]) provides examples of archeological analogues including enhanced caves, burial chambers, and underground temples that have been stable for several thousand years. The stability of structures like the Yucca Mountain repository, such as mines and tunnels, is individually dependent on geology, seismicity, quality of ground support, and local hydrogeology. There are no quantitative measures for these structures with respect to the repository.

Waste Form Degradation—The reaction path of the alteration of SNF at Yucca Mountain will be similar to that of geologically young lead-free uraninite, with schoepite and becquerelite forming as intermediate products, followed by uranyl silicates. Natural uraninite and its alteration products, found at the Nopal I uranium deposit at Peña Blanca, have these characteristics, making this deposit an appropriate analogue to the alteration of uranium oxide spent fuel. At Shinkolobwe, Zaire, more than 50 uranium phases were identified; however, because the deposit is 1.8 billion years old, lead-bearing phases have played a role in sequestering the uranium as shown in *Natural Analogue Synthesis Report* (BSC 2004 [DIRS 169218], Section 15.7.2).

The concentrations of fission products can be used as tracers in minerals precipitated in the rock matrix and in dissolved radionuclides in groundwater surrounding naturally occurring uraninite deposits. Geochemical analysis of these minerals and groundwater chemistries provides a means of estimating natural dissolution rates at some natural analogue sites. When this approach was used at the uranium ore deposits at Cigar Lake, Canada, and Koongarra, Australia, where these ore deposits are found under reducing and oxidizing conditions, respectively, the dissolution rate was found to be more rapid under the oxidizing conditions at Koongarra. Other lines of evidence from geochemical investigations concerning dissolution at the natural-analogue uraninite ore deposit at Oklo, Gabon, indicate that dissolution of the ore minerals has been slight over the past two billion years. Under radiolysis conditions occurring at the time of criticality at Oklo, the estimated mobilization of the original uranium for transport was only several percent as given in *Natural Analogue Synthesis Report* (BSC 2004 [DIRS 169218], Section 15.7.2). Uranium, plutonium, neptunium, and americium were retained in the reactor zone for almost two billion years in the reduced environment of the Oklo reactor zones. There has been limited migration of technetium, ruthenium, rhodium, and palladium, and there has been considerable migration of cesium, rubidium, strontium, and barium (the rare earth elements). Although conditions at Oklo's reactor zones are not like those expected at Yucca Mountain, study of the migration patterns for specific radionuclides give useful insights regarding the behaviors of these species in various environments (BSC 2004 [DIRS 169218], Section 15.7.2).

Although natural glasses are different in composition than borosilicate HLW glass, studies of natural glass alteration indicate that HLW glass will be stable in the Yucca Mountain repository environment. Natural geologic glasses tend to be more stable than archaeological glass, especially with regard to changing environments relative to humidity. In both natural and borosilicate glass, higher stability is favored by higher silica and alumina content and by lower alkali and water content. However, analogue studies have not considered radiation effects on glass over long time periods and, thus, cannot be used to confirm experimental results showing that radiation has little effect on HLW glass stability (BSC 2004 [DIRS 169218], Section 15.7.2).

WP Degradation—The analogues to common metals serve mainly to demonstrate that under ambient to slightly elevated temperatures, these metals can be stable for thousands of years, even under oxidizing conditions. The survival of metal archaeological artifacts over prolonged periods of time is related to the corrosion-resistant properties of metals and metal alloys, the development of protective passive film coatings with the onset of corrosion, and the location of artifacts in arid to semiarid environments. Such features were used in the selection of materials and design configuration to enhance the durability of WPs designed for the Yucca Mountain repository (BSC 2004 [DIRS 169218], Section 15.7.3).

Metal alloys similar to the alloys being considered for the WPs to be used at Yucca Mountain have few analogues found in nature. Some meteorites contain metal alloys that are analogues of WP materials (Johnson and Francis 1980 [DIRS 125291], Section 6.4). However, the composition of most meteorites is not analogous to the current suite of alloys being considered for use in the Yucca Mountain repository. Josephinite, a complex rock found in remnants of the earth's mantle in Josephine County, Oregon, contains several nickel-iron alloys. The survival of the naturally occurring ordered nickel-iron alloy in josephinite for millions of years, with only relatively minor amounts of surface oxidation, indicates that this material is highly resistant to oxidation and other forms of corrosion that occur in its geologic environment. Although the composition of the nickel-iron alloy in josephinite differs from Alloy 22 (UNS N06022) in that it does not contain chromium, molybdenum, or tungsten, it does provide evidence that a similar alloy can remain passive over prolonged periods of time under conditions similar to those expected at the Yucca Mountain repository (BSC 2004 [DIRS 169218], Section 15.7.3).

The instability of chromium-bearing materials is illustrated by the observed natural release of chromium from chromite in the Sierra de Guanajuato, in Guanajuato State, central Mexico, ultramafic rocks under ambient conditions. Corrosion was observed to be concentrated along exsolution rims, which are analogues to structural defects on metal surfaces. However, although the chromite has undergone some alteration, it has survived for more than 140 million years (BSC 2004 [DIRS 169218], Section 15.7.3).

EBS Components—Although the invert's crushed devitrified welded tuff does not have high concentrations of zeolite and clay minerals, the high surface area of crushed tuff is expected to provide sorption sites that will retard radionuclide transport. Adsorption of actinides in a gravel bed at Los Alamos, New Mexico, provides qualitative evidence of radionuclide retardation at the contact between an invert-like material and underlying bedrock as seen in *Natural Analogue Synthesis Report* (BSC 2004 [DIRS 169218], Section 15.7.4).

The Pocos de Caldas, Brazil, analogue illustrates that iron-bearing colloids may retard the transport of uranium and other spent-fuel components by forming colloids that are then filtrated from suspension at short distances. Degradation of steel structural elements in the EBS could conceivably contribute to this process (BSC 2004 [DIRS 169218], Section 15.7.4).

Drift Seepage—An important variable related to the preservation, or lack of preservation, of engineered materials in underground openings is relative humidity. If ventilation reduces the relative humidity in the emplacement drifts to less than 100 percent, seepage of liquid water will be reduced or completely suppressed. Most caves have close to, but less than, 100 percent humidity. Thus, the amount of seepage in caves found in ventilated and unsaturated

environments has been observed to be low. This would also be true at Yucca Mountain as long as ventilation is maintained (BSC 2004 [DIRS 169218], Section 15.7.5).

Analogues of the UZ support the hypothesis that most of the infiltrating water in the UZ is diverted around underground openings, and does not enter into these openings. The analogues show that this is true even for areas with much greater precipitation rates than those at Yucca Mountain. Although there are examples where large amounts of seepage can be observed, such as in the Mission Tunnel, California, and at Mitchell Caverns, California, and cave minerals formed by water are common in unsaturated environments, these hydrogeologic settings are very different from those at Yucca Mountain and, thus, are not appropriate analogues. However, for analogues that have some water, at least some of the water that enters underground openings does not drip but, rather, flows down the walls as can be seen at dwellings excavated in tuffs at Goreme, Cappadocia, Turkey, and in efflorescent salts found in the leaking vaulted construction in Building 810 at the Denver Federal Center, Colorado (BSC 2004 [DIRS 169218], Section 8.3). In the few instances where dripping has been noted in settings that are analogous to Yucca Mountain, the drips can be attributed to asperities in the surface of the roof and ceiling of the openings such as seen at Carlsbad Caverns, New Mexico (BSC 2004 [DIRS 169218], Section 8.3). Whether or not water flows on walls or drips depends on conditions affecting the variables that determine drop formation and drop detachment, such as surface tension, roughness angle, and saturation. Thus, although most water would most likely flow around emplacement drifts at Yucca Mountain, the analogue information indicates that the expected small amount of water that could occur would primarily flow down the walls of the drifts. In the few instances where dripping may occur, it would be expected to occur at asperities on emplacement drift walls (BSC 2004 [DIRS 169218], Section 15.7.5).

UZ Flow and Transport—The UZ Flow and the UZ Transport Model Components of the TSPA-LA Model contain submodels with modeling approaches that are corroborated by analogue investigations that build confidence in those approaches. This analogue information provides a body of data for validating the conceptual and numerical models incorporated in the TSPA-LA Model.

The quantitative analogue investigation using related data sets gathered at the Idaho National Laboratory (INL) provides confidence in the dual-permeability approach used for the Yucca Mountain UZ Flow Model. The INL test site is analogous to Yucca Mountain in hydrogeology, precipitation, infiltration, rock types, and perching horizons. Hydrographs of ponded water and ^{75}Se breakthrough curves measured during the pond-infiltration test conducted at INL were analyzed to determine parameters controlling unsaturated flow and transport. Analysis of this data involved building a numerical model using TOUGH2 in a dual-permeability modeling approach used to simulate flow and transport at Yucca Mountain (BSC 2004 [DIRS 169218], Section 9.1).

The UZ Flow Model Component (Table 6-1) at Yucca Mountain considers a range of infiltration rates that are then used to bound the range of percolation flux. The Paintbrush nonwelded unit (PTn) at Yucca Mountain has a damping effect on downward flow to the Topopah Spring welded unit (TSw). Although, the INL transport calculations predicted retardation factors for neptunium and uranium that are orders of magnitude higher than retardation factors for other radionuclides, radionuclide retardation is supported by radionuclide migration experiments under unsaturated

conditions conducted in a 30-cm block of Calico Hills nonwelded tuff from the Busted Butte Test Facility near Yucca Mountain (BSC 2004 [DIRS 169218], Section 10.1). The Calico Hills nonwelded tuff lies below the repository at Yucca Mountain. These studies indicated conservative transport of TcO_4^-, but retardation of Np^{+4} by a factor of three more than the conservative tracer used for field tests.

The Peña Blanca natural analogue site, described in Section 7.8.2, has conditions similar to those at Yucca Mountain. The Nopal I mine at Peña Blanca has groundwater chemistry that is analogous to the groundwater chemistry in the Yucca Mountain hydrogeologic system. Chemical analyses of samples of groundwater from beneath the ore deposit indicate that radionuclides leached from the deposit are mostly sorbed or re-precipitated in the rocks surrounding the ore deposit and that there is little UZ transport. Nopal I also displays discrete alteration zones in fractured rocks intersected by likely groundwater flow paths (BSC 2004 [DIRS 169218], Section 15.7.11). The application of information describing the Peña Blanca natural analogue with respect to validation of the TSPA-LA Model is described in Section 7.8.2.

Coupled Processes—Geothermal systems illustrate a variety of thermal-hydrologic-chemical (THC) processes that are relevant to Yucca Mountain. Yellowstone, Wyoming, and other geothermal systems in welded ash flow tuffs or other low-permeability rocks indicate that the fluid flow is controlled by interconnected fractures. Alteration in low-permeability rocks is typically focused along fracture flow pathways. Only a small portion of the fracture volume needs sealing by precipitated minerals to retard fluid flow effectively. The principal minerals predicted to precipitate in the near field of the Yucca Mountain repository are amorphous silica and calcite, which are also commonly found as sealing minerals in geothermal systems as in *Natural Analogue Synthesis Report* (BSC 2004 [DIRS 169218], Section 15.7.7).

Sealing in geothermal fields can occur over a geologically short time frame in the order of a few days to several years. The unsaturated conditions, lower temperatures, and much lower fluid-flow rates predicted for the Yucca Mountain system, in comparison to the conditions in geothermal systems, should result in less extensive water-rock interaction than is observed in geothermal systems. Fracturing and sealing occur episodically in geothermal systems. Most of the mineralization at Yucca Mountain is predicted to occur 1,000 to 2,000 years after waste emplacement, when temperatures would reach boiling in the vicinity of the emplacement drifts (BSC 2004 [DIRS 169218], Section 15.7.7).

Coupled processes are expected to have a much smaller effect on hydrogeologic properties at Yucca Mountain than are observed at Yellowstone. However, development of a heat pipe above emplacement drifts at Yucca Mountain under a higher temperature operating mode could lead to increased chemical reaction and transport in the near field. Condensate reflux and boiling of silica-bearing fluids within the near field at Yucca Mountain could cause fracture plugging and consequent changing of fluid flow paths. Geochemical modeling of fluid compositions has been used to successfully predict observed alteration mineral assemblages at Yellowstone. The THC simulations conducted to date for the Yucca Mountain repository suggest that only 1 to 3 percent reduction in fracture porosity and less than one order of magnitude reduction in permeability are expected to occur in the near field as a result of the precipitation of amorphous silica and calcite. Changes in permeability, porosity, and sorptive capacity are expected to be relatively minor at the mountain scale, where thermal perturbations will be reduced. This THC result applies to

both the higher and lower temperature sub-boiling operating conditions. These predicted changes in hydrogeologic properties should not negatively affect repository performance (BSC 2004 [DIRS 169218], Section 15.7.7).

Preliminary results from a one-dimensional THC dual-continuum model of the interaction of country rock with heat released from an intrusive complex emplaced above the water table demonstrated the possibility of forming opal-filled veins with the silica derived from the host-rock matrix. However, because of the irregularities caused by the kinetic barrier, effects associated with the geochemical reaction of glass (BSC 2004 [DIRS 169218], Section 15.7.7) provide information that compares and contrasts a number of different sites that provide general conclusions regarding mineral alteration. For example, the Marysvale hydrothermal uranium-molybdenum ore deposit in Utah, tuffaceous rocks in hydrothermal systems at the Long Valley caldera, California, and the Valles caldera, New Mexico, suggest that uranium was concentrated and was liberated from siliceous rocks in response to hydrothermal circulation and then concentrated in ferruginous and carbonaceous zones. The Valles and Long Valley studies indicate localized mobility of uranium and daughter products in tuff and underlying sedimentary rocks at temperatures comparable to those expected in a nuclear waste repository environment (BSC 2004 [DIRS 169218], Section 11.5).

SZ Transport—Some of the Uranium Mill Tailings Remedial Action Program sites may be useful in the evaluation of radionuclide transport in the alluvial portion of the Yucca Mountain flow system. The conclusions derived from an analysis of the Gunnison, Colorado, site are: (1) a fraction of the uranium originating at the site is transported in the alluvial aquifer at a rate similar to the rate at which a conservative constituent is transported and (2) there is little evidence for lateral dispersion of contaminants in the downgradient direction. For the New Rifle, Colorado site, the main conclusions are: (1) dilution occurs in the downgradient direction and (2) uranium is transported at almost the same rate as conservative constituents of natural groundwater. The conclusions regarding uranium transport distances relative to conservative constituents must be tempered by uncertainties regarding the presence of complexing agents (BSC 2004 [DIRS 169218], Section 15.7.8).

Although several natural analogue studies have demonstrated the effects of sorption and precipitation processes on fracture surfaces, none has been able to distinguish clearly between these processes or to provide quantitative information on retardation with respect to the transport of trace elements in natural waters. However, these studies do highlight which mineral phases are most active and provide useful information on the effect of the interaction between solutes and rock surfaces on fractures (BSC 2004 [DIRS 169218], Section 15.7.8).

In most studies of natural systems, a proportion of the total uranium, thorium, and rare earth elements in groundwater have been associated with colloids. Colloids can serve as sorbers of radionuclides and could be agents either of retardation or of fast transport. Unambiguous evidence from natural systems indicating colloidal transport over kilometer-scale distances is limited. Observations from Los Alamos, New Mexico, and the Nevada Test Site lend support to the concept that radionuclide transport in the SZ can be facilitated by colloids, but no natural analogue studies have been able to quantify the importance of this process (BSC 2004 [DIRS 169218], Section 15.7.8).

Biosphere—The Chernobyl, Ukraine, observations regarding hot-particle atmospheric dispersal and dust transport showed that radionuclides get attached to dust particles and are dispersed with these particles. Aspects of models of atmospheric contaminant dispersal, radionuclide fallout, radionuclide resuspension, and particle-size distributions may be relevant to constraining modeling for radionuclide resuspension affecting ash deposits that could result from a volcanic eruption through the Yucca Mountain repository.

The half-lives of radionuclides provide conservative estimates of radionuclide removal from soils in the Yucca Mountain Biosphere Model Component. An increase in the concentrations of radionuclides in soils during irrigation was observed in the southern Ukraine, a locality with environmental conditions more similar to those at Yucca Mountain than they are at Chernobyl. These increases in radionuclide concentrations confirm the concept of the radionuclide buildup factor used in the Yucca Mountain Biosphere Model Component (BSC 2004 [DIRS 169218], Section 15.7.9).

A literature survey regarding the behavior of radionuclides in soils, in the Chernobyl, Ukraine, area suggests that soil type influences the ecological half-life of radionuclides in the biosphere, both in regard to soil bioaccumulation factors, and with respect to advective and diffusive transport properties that limit radionuclide transfer to plant roots. Agricultural methods, including irrigation, tillage, and the types of crops that may play an important role in radionuclide resuspension, could have an effect on rural populations. Radionuclide resuspension is likely to increase the contamination of plant surfaces and would increase the inhalation dose for agricultural workers, especially for plutonium as given in *Natural Analogue Synthesis Report* (BSC 2004 [DIRS 169218], Section 15.7.9).

Estimated transport of groundwater from sources of contamination could result in radionuclide-contaminated water being used as a source for drinking water, irrigation, animal watering, and for domestic applications, thus increasing the likelihood of ingestion uptake of radionuclides by humans. Chernobyl observations showed that the ingestion pathway constitutes a small part of the total radiation dose, as the direct exposure to radiation is predominant within the Chernobyl Exclusion Zone. Chernobyl observations on the atmospheric distribution of contaminants, and their fallout and redistribution in soils and plants, may be considered as an analogue for the release of radionuclides caused by a volcanic eruption at Yucca Mountain. The Chernobyl observations are also useful in understanding the atmospheric dispersal of contaminants into the environment during posteruption ash fallout onto the land surface (BSC 2004 [DIRS 169218], Section 15.7.9).

Volcanism and Seismic Effects on Drifts—Natural analogue investigations are part of the effort to understand volcanism in the Yucca Mountain area. Analogues have been used to assess the probability of dike eruption, plausible eruption styles, eruption parameters, and magma compositions, factors that have been used to increase confidence in the use of the ASHPLUME model (SNL 2007 [DIRS 177431]), to simulate atmospheric dispersal following a theoretical eruption at Yucca Mountain (Section 7.8.1).

For seismic events, examples from observations of underground openings demonstrate that such openings are able to withstand ground shaking for peak ground acceleration as high as 0.4 G. The ability of underground openings to withstand ground shaking is increased by the thickness of

overburden, competence of the rock surrounding the opening(s), decreased earthquake magnitude, and increased distance of the opening(s) from the earthquake epicenter. The bulk of evidence from analogue examples of seismic impacts to underground openings, particularly in settings similar to Yucca Mountain, such as responses to the Little Skull Mountain earthquake, demonstrates that damage to repository drifts due to ground shaking during the postclosure period would be minimal or unlikely (BSC 2004 [DIRS 169218], Section 15.7.10).

Summary—The information from natural analogues has contributed to the understanding of drift stability, waste form and EBS degradation, seepage, UZ flow and transport, coupled processes, SZ transport, the biosphere, and disruptive events, such as igneous intrusions, volcanic eruption and seismic events. This information was used to develop the abstractions that are fed to the TSPA-LA Model through the analysis and model reports. The use of this information during the development of the TSPA-LA submodels ensures that the submodels are grounded in reality and provide confidence in the TSPA-LA Model results. In addition to the confidence provided by the examples of natural analogues on a qualitative basis, a performance comparison with two selected analogues, the Cerro Negro volcanic eruption and the Nopal I uranium mine at Peña Blanca, provides additional confidence in the TSPA-LA Model.

7.8.1 Performance Assessment Comparison with Ash Fall at Cerro Negro

The Cerro Negro volcano is one of a number of active basaltic volcanoes in a volcanic mountain range in Nicaragua. Cerro Negro is located on the Caribbean tectonic plate, and the volcanic activity expressed within this long volcanic mountain range, which extends from southern Mexico to Costa Rica, is directly related to subduction of the Pacific tectonic plate under the Caribbean tectonic plate. Volcanism at Cerro Negro has a 150-year history, with at least 22 documented eruptions. The eruption in 1995 produced a tephra volume of 0.004 km^3 (Hill et al. 1998 [DIRS 151040]), a volume similar to, but less than, the volume from the Lathrop Wells cone, which was approximately 0.07 km^3, as described in *Characterize Eruptive Processes at Yucca Mountain, Nevada* (SNL 2007 [DIRS 174260], Appendix C, Section C.7). The 1995 Cerro Negro eruption may be analogous to the type of eruption that could occur at the Yucca Mountain repository however, Cerro Negro's long history, shape, and magma-production rate suggest that it may represent a young composite volcano rather than a simple, long-lived cinder cone (McKnight and Williams 1997 [DIRS 162827]). Because of the uncertainties associated with the atmospheric and eruption conditions of the Cerro Negro event, comparison of ash-fall thicknesses between the observed distribution and the ASHPLUME result is qualitative. However, this comparison provides confidence that the ASHPLUME software code can give a reasonable representation of ash deposition for the type of eruption that could occur at Yucca Mountain.

The two-dimensional Advection-Dispersion Model of Suzuki (1983 [DIRS 100489]) is implemented by the ASHPLUME code. The following two versions of the code were used to simulate the Cerro Negro ash thickness measurements.

1. Version 1.4LV (STN: 10022-1.4LV-02 [DIRS 161296]) uses the volume and density of the ash to determine ash column height and mass, as described in *Atmospheric Dispersal and Deposition of Tephra from a Potential Volcanic Eruption at Yucca Mountain, Nevada* (SNL 2007 [DIRS 177431], Section 1.2.1).

2. Version 2.0 (STN: 10022-2.0-00 [DIRS 152844]) uses eruption power and event duration to determine column height and mass of ejecta (SNL 2007 [DIRS 177431], Section 1.2.1).

To evaluate the differences in the two ASHPLUME models and demonstrate that they can reasonably predict the ash fall distribution from the eruption of a basaltic cinder cone volcano, these two versions of ASHPLUME were used to simulate a Cerro Negro eruption, and the results were compared to Cerro Negro ash thickness measurements. A slightly different version, ASHPLUME_DLL_LA Version 2.1 (STN: 11117-2.1-00 [DIRS 181035]), was used for the TSPA-LA Model to calculate ash fall for the Volcanic Eruption Modeling Case. ASHPLUME_DLL_LA Versions 2.1 and ASHPLUME Version 2.0 are identical computationally. ASHPLUME_DLL_LA Version 2.1 only differs in its ability to interface with the Fortymile Wash Ash Redistribution code (FAR) for TSPA calculations.

Input parameter values from Hill et al. (1998 [DIRS 151040]), for each ASHPLUME version used in the Cerro Negro ash dispensing calculations, are compared in Table 7.8-1. The ASHPLUME_DLL_LA Version 2.0 [DIRS 152844] simulation was completed first, producing a value for the total mass of ash erupted, based on observed eruption parameters (e.g., total duration and ash column height). Next, the ASHPLUME_DLL_LA Version 1.4LV [DIRS 161296] simulation was performed using the same parameter set and a value for ash volume equal to the total mass of ash produced in the Version 2.0 [DIRS 181034] calculation as in *Atmospheric Dispersal and Deposition of Tephra from a Potential Volcanic Eruption at Yucca Mountain, Nevada* (SNL 2007 [DIRS 177431], Appendix L).

As shown on Figure 7.8-1, the ASHPLUME calculations compare well with the observed thicknesses for distances from the volcanic vent greater than 10 km. For distances less than 10 km, the ASHPLUME results give ash thickness values greater than the observed thicknesses. The lobe on the northern side of the map of measured ash thickness is interpreted to be a result of a variation in wind direction or speed, or both, that occurred during the eruption. This variation accounts for some of the discrepancy, because ASHPLUME assumes a constant wind speed and direction for a given simulation. Figure 7.8-1 compares ASHPLUME V1.4LV and ASHPLUME V2.0 to show the overall consistency between the two versions.

The results generally show that the ASHPLUME model can reasonably predict the ash-fall distribution and ash-fall thickness from the eruption of a basaltic cinder cone volcano similar to Cerro Negro. The Cerro Negro ash-fall calculation method was used to simulate eruptive releases of ash either near the Yucca Mountain repository or through the repository involving WP destruction and aerial distribution of radionuclides. Figure 7.8-2 provides a schematic illustration of the modeling elements that are included in the TSPA-LA Model for the Volcanic Eruption Modeling Case at Yucca Mountain.

ASHPLUME was used in two additional natural analogue studies performed for the Lathrop Wells Cone in Nevada and Cinder Cone in California, as documented in *Atmospheric Dispersal and Deposition of Tephra from a Potential Volcanic Eruption at Yucca Mountain, Nevada* (SNL 2007 [DIRS 177431], Sections 7.3.1.2 and 7.3.1.3). The comparisons of prehistoric ash thickness distribution with simulations using ASHPLUME V2.0 provide confidence that the ASHPLUME code can estimate ash thickness for simulated possible future volcanic eruptions involving the Yucca Mountain repository.

7.8.2 Nopal I Uranium Mine at Peña Blanca, Chihuahua, Mexico

The Peña Blanca natural analogue is a naturally occurring uranium ore deposit, Nopal I, that is analogous to the Yucca Mountain repository. The Nopal I site provides a means to estimate the fate of SNF when it is placed in a geologic repository. Hydrogeologic investigations accompanied by the installation of observation wells have provided opportunities to test the strength of the analogy between Nopal I and the repository, and attempt to provide confidence in the performance of the Yucca Mountain repository with respect to the fate and transport of radionuclides that could be released from the repository.

The Peña Blanca natural analogue Nopal I uranium mine, is located in the Sierra Peña Blanca range, approximately 50 km north of Chihuahua City, Chihuahua, Mexico (Murphy 1995 [DIRS 121310]). The Peña Blanca Nopal I uranium deposit is geologically, climatically, geochemically, and hydrologically analogous to Yucca Mountain, and its approximately 3 million years of exposure to oxidation (Murphy et al. 1991 [DIRS 151772]; and *Natural Analogue Synthesis Report* (BSC 2004 [DIRS 169218], Section 10.4) makes it temporally analogous to the more than one-million-year "period of geologic stability" of the Yucca Mountain repository defined in NRC Proposed Rule 10 CFR 63.302 [DIRS 178394] required for performance assessment in 10 CFR 63.342(c) [DIRS 178394]. Reports by Pickett and Murphy (1997 [DIRS 109989]); Murphy and Pearcy (1992 [DIRS 151773]); Leslie et al. (1993 [DIRS 101714]); Green et al. (1995 [DIRS 149528]); and Murphy (1995 [DIRS 121310]), describe the mineralogy and paragenesis of the uranium-bearing phases, as well as the source term for hydrochemical migration in the near-field area of the Nopal I ore body.

The Nopal I uranium deposit (Murphy and Codell, 1999 [DIRS 149529]) originally consisted of uraninite (uranium oxide) a mineral directly analogous to SNF, which is largely composed of uranium oxide. The essence of the analogue of Nopal I to Yucca Mountain, as described in *Uranium Mineralogy of the Nopal I Natural Site, Chihuahua, Mexico* (Pearcy et al. 1993 [DIRS 151774]); and *Natural Analogue Synthesis Report* (BSC 2004 [DIRS 169218], Section 10.4) is as follows:

- Climate—Nopal I and Yucca Mountain are located in arid to semi-arid regions. Annual rainfall at Nopal I is approximately 240 mm/year (Murphy et al. 1990 [DIRS 151772], p 271) and annual rainfall at Yucca Mountain between 100 and 300 mm/yr (BSC 2004 [DIRS 169734], Figure 7.6).

- Geology—The Peña Blanca district containing the Nopal I mine and Yucca Mountain are fault blocks in the Basin and Range structural geological province. The Nopal I mine and Yucca Mountain contain Tertiary volcanic rocks consisting of welded and non-welded ash-flow tuffs, and both overlie older carbonate rocks.

- Hydrogeology—The Nopal I mine and Yucca Mountain are located in the UZ under oxidizing conditions more than 100 m above the SZ.

- Geochemistry—The uraninite ore at the Nopal I mine has been altered to secondary uranium minerals such as the oxyhydroxide schoepite and uranyl silicates such as boltwoodite and uranophane. The SNF at Yucca Mountain will be primarily uranium

oxide, which is essentially uraninite, and the fuel is also expected to be altered to schoepite and uranyl silicates (Ebert et al. 2005 [DIRS 173071], Executive Summary).

7.8.2.1 Background

The Peña Blanca Nopal I ore deposit lies in high desert terrain in the Basin and Range geologic province shown on Figures 7.8-3 and 7.8-4 (Pearcy et al. 1993 [DIRS 151774]). The Nopal I ore body is located in the Peña Blanca uranium district on the southeast side of the Sierra Peña Blanca, which is named for the white color of oxidized mineral deposits in the range. Field observations indicate that the pre-mining land surface at the Nopal I deposit exposed a small portion of the ore body. The deposit lies in fractured, welded, and altered rhyolitic ash-flow tuffs analogous to the volcanic rocks at Yucca Mountain (George-Aniel et al. 1991 [DIRS 105636]).

When the Nopal I ore deposit was excavated and mined in the late 1970s and early 1980s, two prominent benches were cut across the ore body at the 0-m and +10-m levels (local, vertical mine coordinates). Two adits enter the mined area from land surface at the 0-m and 70-m levels, and the one principal shaft connects the 0-m adit with adits at the 20-m, 40-m, and 70-m levels, as shown on Figure 7.8-5 (Reyes-Cortes 1997 [DIRS 149533], Figure 25, p. 205). The total depth of the main mineshaft is approximately 110 m from the –20-m level.

The Nopal I ore deposit has been estimated to be approximately 32 ± 8 million years old (Fayek 2006 [DIRS 181367], p. 57). Examination of the weathering mineralogy of the ore body indicates that the deposit was stable and under reducing conditions until approximately 3 million years ago, when it was exposed to oxidizing groundwater, infiltration from precipitation, and weathering processes (Murphy and Codell 1999 [DIRS 149529]). Since that time, the oxidation of the uranium oxide ore proceeded through a progression of uranium minerals from schoepite to uranyl silicates dominated by uranophane (Pearcy et al. 1994 [DIRS 151774]; Murphy and Codell 1999 [DIRS 149529]).

The geologic characterization of the Nopal I ore body is described in *Geology of the Peña Blanca Uranium Deposits, Chihuahua, Mexico* (Goodell 1981 [DIRS 149484]), and shown on Figure 7.8-6. The ore deposit occurs in ignimbritic ash-flow tuffs similar to those found at the Yucca Mountain site (DOE 1998 [DIRS 100550]). The top 30 m of the deposit lie in the Nopal Formation, a fractured rhyolitic tuff, and the lower 70 m lies in the Coloradas Formation, a weakly welded, fractured, ignimbritic tuff. The deposit, and probably the lower several meters of the ore body, is underlain by 60 m of the Pozos Formation, a silicified, detrital conglomerate, composed principally of altered limestone clasts, which lies on Cretaceous limestone. A near vertical fault, with greater than 10 m of offset, intersects the hill containing the ore body and lies to the east of the deposit, but does not appear to cut the ore body. Minor faults and fractures are observed in the vertical walls of the open faces of the mine above the 0-m and 10-m levels.

The ore body can be approximately described as a roughly cylindrical, breccia-pipe-like form, approximately 18 m by 30 m in the horizontal plane and 100 m in the vertical dimension. The deposit is presently estimated to contain 333 metric tons of uranium (George-Aniel et al. 1991 [DIRS 105636]). Uranium comprises approximately 0.23 percent of the deposit by volume (George-Aniel et al. 1991 [DIRS 105636]). Using analyses of oxidized uranium minerals,

Pearcy et al. (1993 [DIRS 151774]); and Murphy and Codell (1999 [DIRS 149529]) estimated that the unoxidized ore body contained 408 metric tons of uranium as uranium oxide.

Elements of the site hydrogeology are presented in *Hydraulic Characterization of Hydrothermally Altered Nopal Tuff* (Green et al. 1995 [DIRS 149528]); and *Uranium Mineralogy of the Nopal I Natural Analog Site, Chihuahua, Mexico* (Pearcy et al. 1993 [DIRS 151774]). The Nopal I ore deposit lies in the UZ, and boreholes drilled in 2003 established that the water table is approximately 122 m below the ore deposit (BSC 2004 [DIRS 169218], Section 10.4). Green and Rice (1995 [DIRS 149485]), conducted an artificial recharge study at the Nopal I mine, and the field observations were used to estimate the hydraulic properties of the intact and oxidized portions of the ore body. Their investigations indicated that the porosity of the ore deposit ranged from 0.05 to 0.08 for unaltered rock, to 0.30 for altered rock. The saturated hydraulic conductivity ranged from 6×10^{-12} cm/s for the unaltered rock, to 1×10^{-7} cm/s for the altered rock.

Previous studies of the Nopal I deposit have focused on the geochemical aspects of the oxidation, transport, and reprecipitation of uranium mineral phases in the matrix and bedrock (Pearcy et al. 1993 [DIRS 151774]; Pickett and Murphy 1997 [DIRS 109989]; Pearcy 1994 [DIRS 149523]; Goldstein et al. 2003 [DIRS 168528]). These studies show that uranium, protactinium, and thorium have low groundwater concentrations. The analysis of rock samples collected from fractures exposed on the exposed 0.0 and +10 benches show that actinides released from the ore deposit precipitated in fracture filling minerals within a few tens of meters from the deposit (Goldstein et al. 2003 [DIRS 168528]).

Three boreholes were drilled at the Nopal I site in 2003. Borehole PB1 was drilled immediately adjacent to the ore body continuously cored to total depth approximately 20 m below the top of the SZ. Borehole PB2 was drilled approximately 50 m uphill from PB1 and borehole PB3 was drilled approximately 50 m downhill from PB1. The total well depths of these boreholes ranged from 243 m to 255 m, and they were all completed to approximately 20 m below the observed water table. The cuttings and core samples from the three boreholes were used to characterize the lithologic and hydrogeologic properties of the UZ. In addition, well PB4 located about 1.3 km southeast of the ore deposit was reconditioned to serve to measure the depth to the water table and collect water samples. Water samples have been collected from these four boreholes, and other wells in the area, since 2003. The locations of observation wells PB1 to PB4, and the Pozos Ranch windmill-operated, ranch-supply well, are shown on Figure 7.8-7 (BSC 2004 [DIRS 169218], Figure 10.4-4).

7.8.2.1.1 Climate/Infiltration

Precipitation infiltration has not been estimated at the Nopal I site, but the vegetation and soil of the area indicate that some infiltration is likely (Leslie et al. 1999 [DIRS 109967]). The climate of the Peña Blanca region is arid, with an estimated 250 mm/yr of precipitation (Pearcy et al. 1993 [DIRS 151774]). The presence of perched water in shot holes drilled into the open bench of the +10-m level indicates that precipitation infiltration occurs in the area of the Nopal I mine (Pickett and Murphy 1999 [DIRS 110009]). Because of the climatic similarity of Sierra Peña Blanca and the Yucca Mountain site, and because there have been no long-term infiltration

studies at the Nopal I mine site, the infiltration observations made at Yucca Mountain are considered to apply at the Nopal I site (CRWMS M&O 1998 [DIRS 100356]).

The physiography of the Peña Blanca district is similar to that of the Great Basin where long-term information on climate and precipitation patterns was assembled as part of the TSPA-LA, as summarized in *Yucca Mountain Site Description* (BSC 2004 [DIRS 169734], Sections 2.1.2 and 3.2.1, physiography, Sections 6.3 and 6.4, modern and past climate, respectively). Because of similarities in geography and physiography and the lack of local observations for the state of Chihuahua, the long-term infiltration patterns observed at Yucca Mountain and reported in the Yucca Mountain site description are considered to be adequate for the performance assessment analysis of the Peña Blanca natural analogue.

7.8.2.1.2 Unsaturated Zone

Ghezzehei et al. 2006 [DIRS 179134] conducted a passive seepage study that investigated the ore deposit's near-field UZ to examine patterns of responses to precipitation events. The investigation analyzed seepage in the mine adits using 240 water collectors installed in a gridded pattern. The results of the investigation indicated that there are very heterogeneous seepage volumes and arrival times after a precipitation event. The infiltration into the mine in the area of the ore body displayed slower seepage at a relatively constant rate. Faster flow paths and larger volumes of water were observed away from the ore body. Ghezzehei et al. 2006 ([DIRS 179134], p. 110) modeled the faster seepage locations as having discrete fracture flow and the slower seepage locations as indicative of matrix flow. The longer residence times at the slower seepage locations are consistent with higher uranium concentration and Uranium isotope disequilibrium observed in analyses of water samples collected at these locations.

The vertical UZ section of rock below the ore body is approximately 230-m thick based on the logs of the observation wells drilled in 2003. Figure 7.8-8 shows the stratigraphy of observation and sampling well PB1, as observed in core samples collected during drilling, as well as the results of geophysical logging in PB1 *Natural Analogue Synthesis Report* (BSC 2004 [DIRS 169218], Figure I-1). The UZ is composed both of the lower part of the tuff and volcanic conglomerate of the Pozos Formation and of the upper part of the Cretaceous limestone that underlies this region of northern Mexico. The UZ below the Nopal I deposit has heterogeneous hydrogeologic properties. Green and Rice (1995 [DIRS 149485]) calculated percolation flux based on measured hydrogeologic properties for samples of altered tuff and simulated water flow through partially saturated media in the upper part of the UZ. However, the heterogeneous nature of the UZ is illustrated by observations made during pumping of the three observation wells installed within 100 m of the ore deposit. The water levels in the three wells are not in agreement. Further, the inconsistent responses of the water levels in these wells that were observed during pumping to collect groundwater samples indicate that one of these wells, PB3, is not well connected to PB1 and PB2, despite their proximity to one another (Goldstein et al. 2006 [DIRS 181364], p. 218).

7.8.2.1.3 Saturated Zone

The SZ beneath the volcanic tuffs containing the uranium deposit at the Nopal I site lies near the base of the Pozos Conglomerate, from about 8 m to 20 m above the Cretaceous limestone as

reported in *Natural Analogue Synthesis Report* (BSC 2004 [DIRS 169218], Table 10.4-4, Figures I-1, I-4, and I-5). The water table is in the Cretaceous limestone in PB4. The water-table elevations of wells PB1 to PB4 are within 6 m of one another, with the highest elevation in PB1 and the lowest values in PB2 and PB4 (BSC 2004 [DIRS 169218], Table 10.4-5) Despite the apparent lower elevation in PB2, the data appear to indicate a flow gradient to the southeast.

The Nopal I ore deposit at the Peña Blanca natural analogue, in a manner similar to that at Yucca Mountain, could theoretically transport the water flowing through the ore deposit to the UZ, and any radionuclides released from the ore deposit and transported by water moving through the UZ would be passed to the SZ at the water table in a manner analogous to that expected beneath the Yucca Mountain repository (Sections 6.3.9.1 and 6.3.10.2). The estimated leachate from the Nopal I deposit would primarily contain uranium isotopes and potentially other radionuclides released from the ore deposit. The theoretically contaminated groundwater would flow eastward in the SZ through the Cretaceous limestone according to the hydraulic gradient (Green et al. 1995 [DIRS 149528], Figure 4.8).

7.8.2.1.4 Hydrogeology

The performance assessment analysis of Nopal I assumed the Peña Blanca area to be located in an area where there is lateral to vertically downward groundwater flow (Green et al. 1995 [DIRS 149528], Section 5, paragraph 1). The site of the Nopal I mine is in a recharge condition relative to the regional groundwater flow (Green et al. 1995 [DIRS 149528]). A significant playa, Playa Cuervo, exists east of the Sierra Peña Blanca, and is the likely regional discharge location for groundwater in the Peña Blanca area, and appears to be the local sink for groundwater flow in the Sierra Peña Blanca (Reyes-Cortes 1997 [DIRS 149533], Section I, pp. 24 to 27, Figure 6).

Although there is not sufficient water-level data from the region around the Peña Blanca district to provide an accurate direction of groundwater flow, the regional information indicates that, in general, flow is from west to east. Rodriguez-Piñeda et al. (2005 [DIRS 181366]) collected water-level data from the Encenillas Basin, immediately west of the Peña Blanca district, and these data indicate an overall higher water-table elevation in this basin compared to that in the El Cuervo Basin east of the Peña Blanca district. The regional water-level data (Figure 7.8-9) showed that the groundwater elevation is approximately 1,560 m above sea level (masl) in the Encinillas Basin, 1,240 to 1,243 masl at Nopal I, and 1,230 masl in the El Cuervo Basin. Therefore, if recharge to the Nopal I ore deposit mobilizes radionuclides from the deposit, it is likely that these radionuclides would be transported to the SZ and then eastward to the El Cuervo Basin.

7.8.2.2 Peña Blanca Analysis

The performance assessment analysis of the Nopal I ore deposit as a confidence-building analogue treats the original and present uraninite in the ore body as having been subject to oxidation and dissolution following the change from reducing to oxidizing conditions approximately 3 million years ago. The analogy is predicated on the supposition that alteration of the Nopal I ore deposit was followed by the release of uranium species, and that these

processes will be replicated in a manner similar to the degradation of the SNF waste forms in the WPs that will be placed in the Yucca Mountain repository. Past and recent investigations conducted at the Nopal I site support this conceptualization of the Peña Blanca natural analogue.

Pickett and Murphy (1997 [DIRS 109989]), and Pearcy et al. (1995 [DIRS 110223]) conclude that the Nopal I ore deposit has been exposed to oxidizing conditions over the last 3.2 to 3.4 million years (and indicate that uranium-mineral alteration of the Nopal I ore deposit has resulted in local-scale migration of uraniferous species involving precipitation of secondary uranium minerals and sorption of released uranyl species after tens of meters of lateral travel. Fayek et al. (2006 [DIRS 181367], p. 57) analyzed core samples obtained from the drilling of PB1 in 2003 as reported in *Natural Analogue Synthesis Report* (BSC 2004 [DIRS 169218], Section 10.4). These analyses provide age determinations for alteration minerals such as uranophane. However, the mineralogic analysis reveals a more complex sequence of mineral alteration and reprecipitation of uranium-bearing minerals, suggesting episodic alteration of the Nopal I ore deposit. The mineralogic analysis revealed that secondary uraninite was deposited under reducing conditions in the Pozos Conglomerate about 100 m beneath the main ore body and about 25 m above the present water table approximately 1.6 million years ago. Subsequently, this secondary deposit was subjected to continued oxidation resulting in the precipitation of schoepite and other uranium secondary minerals. Fayek et al. (2006 [DIRS 181367], p. 57-58) suggest that the secondary uraninite may have been precipitated under lower temperature conditions than were present when the main ore body was emplaced under hydrothermal conditions. Thus, this secondary uraninite zone could represent post ore-emplacement deposition of uranium mobilized under oxidative conditions. The work of Fayek et al. (2006 [DIRS 181367] p. 58) thus suggests that the Nopal I ore body has undergone a complex history of emplacement, oxidation, remobilization, and reprecipitation and that transport of much of the uranium in the original ore body has, despite mobilization, not been transported very far from the initial site of deposition.

The Peña Blanca analysis did not consider dose-to-receptor values as did the TSPA-LA Model analyses, because the goal of the investigation was to estimate concentrations in groundwater of uranium and other radionuclides at selected distances from the Nopal I mine. Radionuclides released from the ore body were reported in groundwater samples collected beneath the ore body and at approximately 50 m and approximately 1 km downgradient from the ore body (Goldstein et al. 2006 [DIRS 181364], Table1).

7.8.2.2.1 Source Term Dissolution and Radionuclide Inventory

The source term for the Peña Blanca natural analogue is a uranium mineral, primarily uraninite, ore body that has been the source for the alteration of the primary uraninite and the release of radionuclides since the ore body was exposed at or near land surface approximately three million years ago. Uranium-oxide degradation was the likely operating mechanism for degradation and dissolution of the Nopal I ore body. The sequence of uraninite alteration at Nopal I is similar to that of CSNF and the uranium-oxide fuel analyzed in the laboratory tests, and the corrosion products derived from the uranium-oxide fuel in the laboratory tests are the same mineral phases that are seen at Nopal I (BSC 2004 [DIRS 169987]). Wronkiewicz et al. (1996 [DIRS 102047], p. 92) compared the reaction paragenesis observed in laboratory experiments with the paragenesis of uranium minerals at Nopal I (Pearcy et al. 1994 [DIRS 100486], p 725).

Figure 7.8-10 illustrates these comparable paragenetic sequences. Wronkiewicz et al. (1996 [DIRS 102047], p. 94) conclude that SNF could be readily altered when exposed to moisture in an unsaturated repository and that, "The migration of fission products from a breached spent fuel package may be significantly retarded by the formation of secondary uranyl phases . . . ."

The approach for modeling CSNF waste form dissolution and release of radionuclides for the performance assessment of the Yucca Mountain repository was developed in *CSNF Waste Form Degradation: Summary Abstraction* (BSC 2004 [DIRS 169987]). The method consisted of using experimental measurements from flow-through dissolution rates for a set of specific spent fuels and for unirradiated uranium oxide for a range of controlled water chemistries and temperature. These measurements were used to develop a rate-law expression for the dependence of the corrosion rate on experimental factors. The dependent variables of the dissolution rate were determined to be pH, total carbonate concentration, temperature, and oxygen fugacity. The spent fuel dissolution rate model developed in *CSNF Waste Form Degradation: Summary Abstraction* (BSC 2004 [DIRS 169987]) is:

$$\text{Log (DR)} = a_0 + a_1 \times \text{IT} + a_2 \times \text{pCO}_3 + a_3 \times \text{pO}_2 + a_4 \times \text{pH} \qquad \text{(Eq. 7.8-1)}$$

where

DR is the dissolution rate

a_0, a_1, a_2, a_3, and a_4 are regression parameters and are considered to be uncertain in the Peña Blanca Analogue Model

IT is 1/temperature

pCO_3 is the negative log of total carbonate molar concentration (uncertain parameter)

pO_2 is the negative log of oxygen fugacity

pH is the negative log of hydrogen ion concentration (uncertain parameter).

Dissolution of the Nopal I ore body likely followed processes similar to that described by the CSNF dissolution equation used in the Yucca Mountain Performance Assessment (Equation 7.8-1). Because the Nopal I ore deposit has been at or near land surface for about 3 million years, the mineral alteration and transport of radionuclides has occurred at ambient temperature. An analogous alteration of the ore deposit would have occurred under similar conditions and using similar parameter values as were used for the corresponding fuel-dissolution rate calculation used for SNF in the Yucca Mountain performance assessment.

French et al. 2006 [DIRS 181362], examined transport of radionuclides from an isolated high-grade boulder that had been part of the high-grade ore stockpile placed near the Nopal I mine during operations in the 1980s. When the high-grade ore was removed from the mine site during the 1990s, an isolated boulder rolled off the stockpile and was left behind on unlined, previously undisturbed soil. The boulder provided a point source for radionuclides to be transported to the soil beneath and around the boulder within the last approximately 25 years. Gamma-ray characterization of soil samples revealed the presence of U-series radionuclides and

their intermediate daughters ^{210}Pb, ^{234}U, ^{234}Th, ^{230}Th, ^{226}Ra, ^{214}Pb, ^{214}Bi, and ^{234}Pa. French et al. (2006 [DIRS 181362], p. 68) conclude that the mobilization of radionuclides was due to leaching from precipitation and other weathering processes. Analysis of the concentrations and distribution of the radionuclides in the soil in the immediate vicinity of the boulder indicates that the boulder is the source of those radionuclides. Further, the investigations indicate that there has been multistage mobilization of radionuclides, and that they have not traveled far from the source before being fixed onto clays and organic material in the soil zone.

Another means by which radionuclides have been mobilized from the high-grade ore stockpile is through plant uptake. Leslie et al. 1999 [DIRS 109967] investigated radioactive plants that were growing on the high-grade ore stockpile under ambient conditions. The investigation of the vegetation residues from the plants growing on the high-grade stockpile together with radiochemical analyses of the ore from the Nopal I ore piles provided a radionuclide inventory of uranium species and some daughter products in the ore body. The inventory determined by the vegetation investigation found the uranium series radionuclides, including daughters such as thorium and protactinium, and the results agree with the data presented by French et al. (2006 [DIRS 181362]).

7.8.2.2.2 Water Sample Analyses

Figure 7.8-11 shows the observed concentrations of uranium reported for water samples collected from boreholes PB1, PB2, and PB3, from the mining camp supply well, PB4, and the Pozos Ranch well at the edge of the El Cuervo Basin to the east of the Nopal I mine. These chemical data are reported in Goldstein et al. (2006 [DIRS 181364], p. 217). The high initial concentrations of uranium in PB1, PB2, and PB3 are likely due to drilling contamination. The gradual decay of concentrations seen in these boreholes reflects post-drilling dilution by groundwater flow through the boreholes. Therefore, the late-time samples on Figure 7.8-11, as well as the concentrations at the Pozos Ranch well approximately 3.5 km east of Nopal I (Figure 7.8-7), are more representative of natural background concentrations. The uranium concentrations of less than 300 parts per billion at the distances of the Nopal I boreholes, 50 m from the ore body, show likely sorption or other sequestration of uranium. As shown on Figure 7.8-11, uranium concentrations at the mining-camp well PB4 about 1 km approximately downgradient, as shown on Figure 7.8-7, from the Nopal I ore deposit are negligible, potentially indicating very little downgradient transport of radionuclides from the ore body under active oxidation conditions. Although, PB4 is not directly east of PB1, PB2, and PB3, generally easterly flow from a large point source such as Nopal I, could be reasonably expected to produce a plume of concentration that would intersect PB4.

7.8.2.3 Summary and Discussion

Radionuclide transport by groundwater is the most likely off-site transport mechanism that could possibly affect the performance of the Yucca Mountain repository. Despite some uncertainty in the estimated direction and gradient of groundwater flow, the Peña Blanca natural analogue site offers a unique opportunity to examine the groundwater flow and transport of uranium and its daughter products in a climatic and geologic setting very similar to that of Yucca Mountain. Both sites are set in volcanic tuff in an oxidizing UZ, and they are in similar semi-arid

environments. The Peña Blanca natural analogue at the Nopal I uranium deposit displays the following contrasts and similarities with respect to the Yucca Mountain repository:

- A fully loaded Yucca Mountain repository will likely contain 154 times more uranium than the Nopal I mine (Murphy and Codell 1999 [DIRS 149529]).

- The time scale at Nopal I is on the order of 3 million years. The performance for the Yucca Mountain repository is 10,000 years for compliance with NRC Proposed Rule 10 CFR 63.342(b) [DIRS 178394], and project the performance assessment for the period of geologic stability of 1 million years postclosure per 10 CFR 63.342(c) [DIRS 178394].

- The hydrogeologic configuration of the Nopal I mine is relatively simple. The ore body is exposed at land surface with an approximately 200-m-thick UZ above the SZ. The SZ at Yucca Mountain is at a comparable distance below the repository, mainly in volcanic rocks underlain by Paleozoic carbonate rocks, whereas, at Nopal I, the SZ is primarily in the Cretaceous limestone found in and beneath the Sierra Peña Blanca.

- There are no naturally occurring radioactive ore deposits in the host rocks for the Yucca Mountain repository (BSC 2004 [DIRS 169734], Section 3.6.2), although there are occurrences of radioactive elements in minerals in the host rocks and fracture fillings. Thus, radionuclide transport calculations through the tuffs below the repository horizon are, of necessity, approximations of what could occur in the event that waste was emplaced at the repository. At Nopal I, the natural uranium from the ore body not only dissolves and migrates but also produces and transports its daughter products.

- The regional, surface-water-discharge location for the Nopal I ore deposit is approximately 10 km from the deposit, versus, an approximate 60 km to 80 km travel distance to the nearest surface-water discharge for the Yucca Mountain flow system at the Franklin Lake Playa (DOE 2000 [DIRS 155970], Section 5.3).

Observations at the Nopal I uranium-ore deposit at the Sierra Peña Blanca provide insight with which to estimate the migration and/or sequestration of uranium and other radionuclides from the Yucca Mountain repository. The paragenesis of uraninite at the Nopal I site parallels the paragenetic degradation sequence observed for uranium-oxide spent fuel in laboratory experiments simulating a moist unsaturated repository.

Studies regarding both large ore-bearing boulders and other uraniferous material removed from the Nopal I mine indicate that uranium and other radionuclides are mobile and can be transported in the soil and shallow bedrock or subject to plant uptake. The observations show that uranium leached from the ore deposit is apparently exchanging with uranium minerals that precipitate in fractures around the ore deposit. The analysis of water samples from observation wells at the Nopal I site show that despite the precipitation of radionuclides, there is sufficient uranium available for uranium and some of its daughter products to be transported through the Cretaceous limestone below the Sierra Peña Blanca. However, the observed groundwater concentrations are very low, probably due to reprecipitation and/or sorption of uranium and other radionuclides in the UZ and SZ.

The Nopal I mine was originally composed of uraninite, which is essentially the same material as SNF. Hydrogeologic and geochemical investigations at the Nopal I natural analogue indicate that there has been relatively little transport of the radionuclides from the ore deposit, and that few radionuclides have traveled very far from their sources. There are observed concentrations of uranium in the groundwater beneath the Nopal I ore body but the concentrations are relatively low. In addition, the original ore body composed of uranium oxide has been altered to relatively stable uranyl silicates that do not provide large amounts of radionuclides for transport. Geologic investigations of core samples indicate that oxidative leaching of the uraninite in the ore body was followed by a later lower-temperature precipitation of uraninite in the UZ above the SZ. The analysis of water samples collected from wells completed in the SZ beneath and downgradient from the ore deposit show that although there are radionuclides present in the groundwater, their concentrations are generally in the parts per billion range. In addition, the heterogeneous nature of the UZ provides opportunities for leached radionuclides to be naturally sequestered in mineralized fractures or the bedrock matrix. Analyses of soil and vegetation in the vicinity of stockpiles of high-grade uranium ore indicate that the leached radionuclides and radionuclides taken up in vegetation are sequestered and kept from transport.

The Peña Blanca Natural Analogue provides an example of the dissolution, fate, and transport of radionuclides released from the Nopal I mine through a UZ and SZ that are analogous to the Yucca Mountain repository site. The degradation and leaching of the Nopal I ore deposit is analogous to the expected fate of nuclear material to be emplaced at the Yucca Mountain repository. The Nopal I site indicates that material with a composition very similar to SNF has been subject to dissolution, but the leached material has been largely sequestered by paragenesis, mineral precipitation, or sorption onto clays or other minerals in the near vicinity of the ore body. Considering the analogous nature of the Nopal I site with respect to the Yucca Mountain repository, and that the Nopal I site is at land surface, the apparent immobilization and sequestering of uranium and other radionuclides leached from the ore deposit indicate that radionuclides released from the uranium deposit do not migrate far from their sources. Thus, the performance observed at the Nopal I Peña Blanca provides insight and confidence in the long-term performance of the Yucca Mountain repository.

INTENTIONALLY LEFT BLANK

Table 7.8-1. ASHPLUME Parameters Used for Cerro Negro Comparison

Parameter	Version 1.4LV	Version 2.0
Ash density (g/cm^3)	1.2	1.2
Particle shape factor	0.5	0.5
Air density (g/cm^3)	0.001293	0.001293
Air viscosity, g/cm-s	0.00018	0.00018
Constant C ($cm^2/s^{5/2}$)	400.0	400.0
Constant beta	10.0	10.0
Lower limit on column height (km)	0.001	0.001
Mean ash particle diameter (cm)	0.07	0.07
Particle diameter standard deviation	0.8	0.8
Wind speed (cm/s)	900.0	900.0
Initial eruption velocity (cm/s)	10,000.0	10,000.0
Eruption power (watts)	NA	7.34×10^9
Event duration (s)	NA	3.46×10^5
Eruption volume (km^3)	0.00288	NA

Source: SNL 2007 [DIRS 177431], Appendix L. Parameter values are from Hill et al. 1998 [DIRS 151040].

NOTE: NA = not applicable.

INTENTIONALLY LEFT BLANK

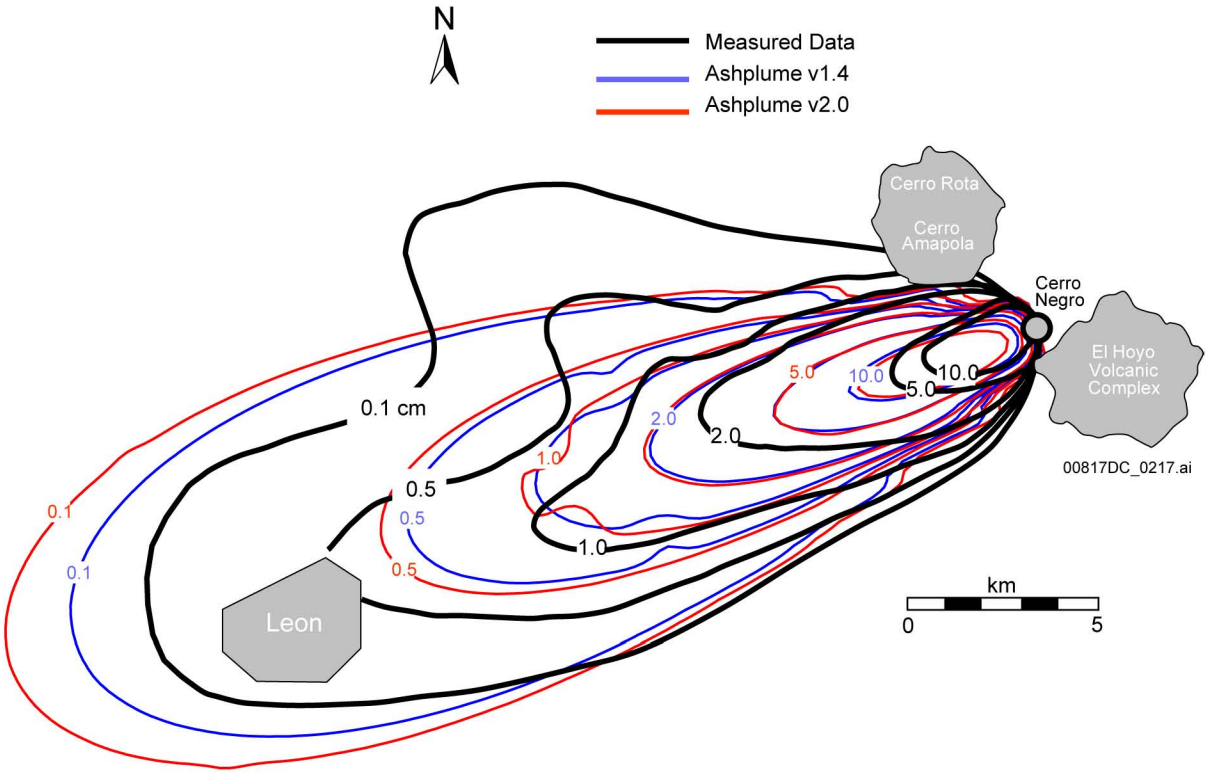

Source: SNL 2007 [DIRS 177431], Appendix L.

Figure 7.8-1. Comparison of Ash Fall at Cerro Negro with ASHPLUME Simulated Results

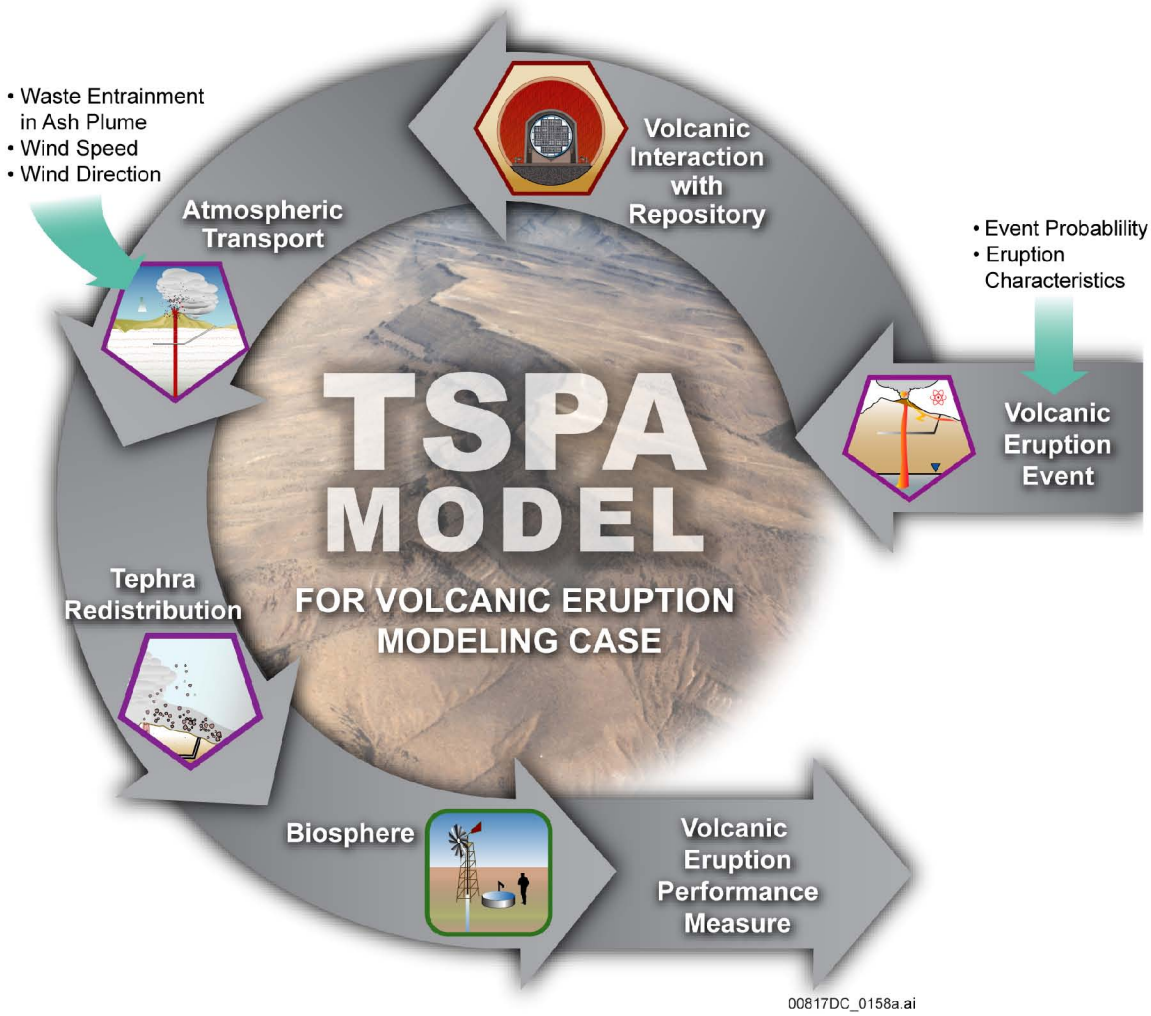

Figure 7.8-2. TSPA-LA Model for the Igneous Scenario Class Volcanic Eruption Modeling Case

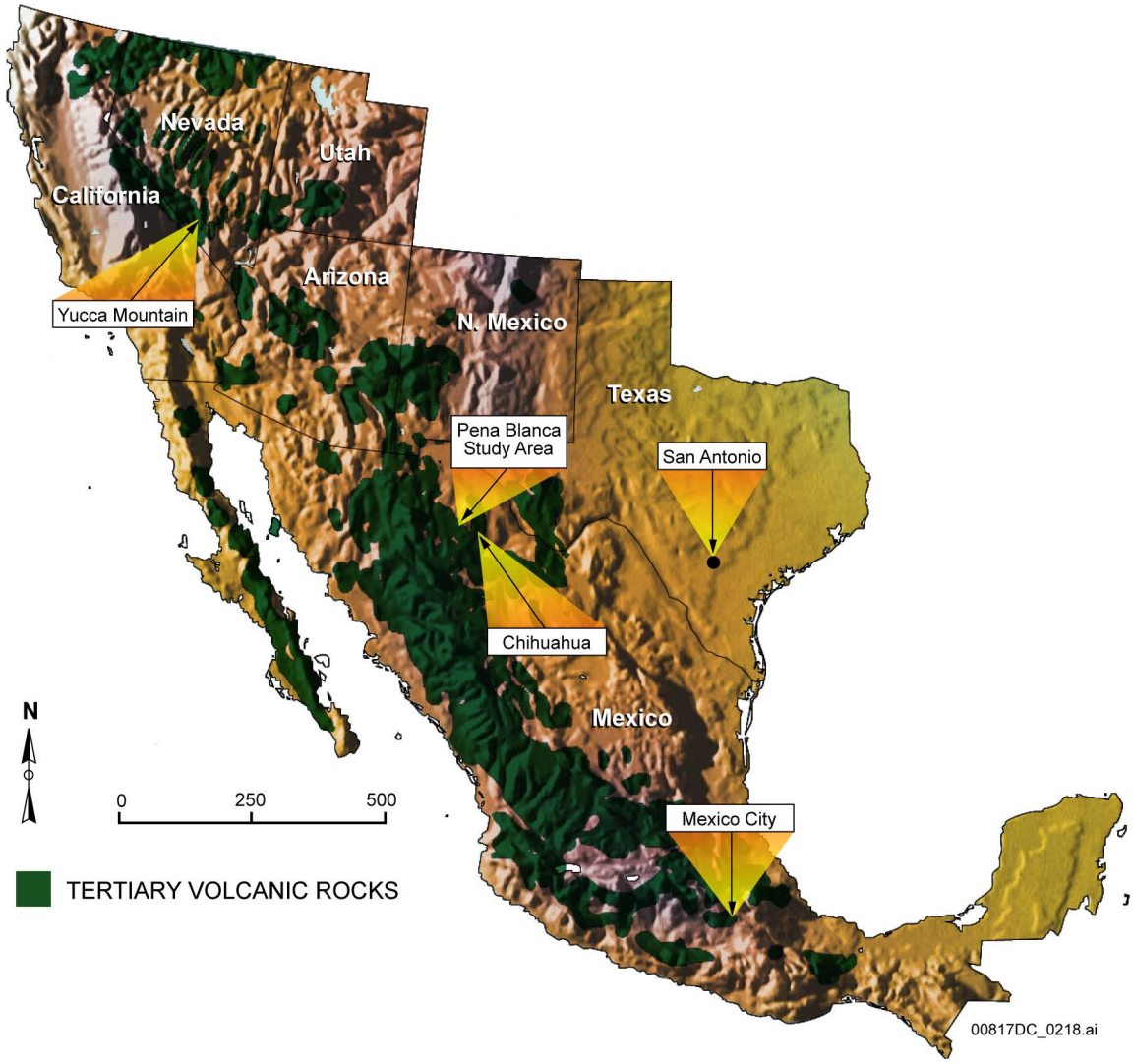

Source: Pearcy 1994 [DIRS 149523], pp. 1 and 2.

Figure 7.8-3. Location of Peña Blanca Study Area

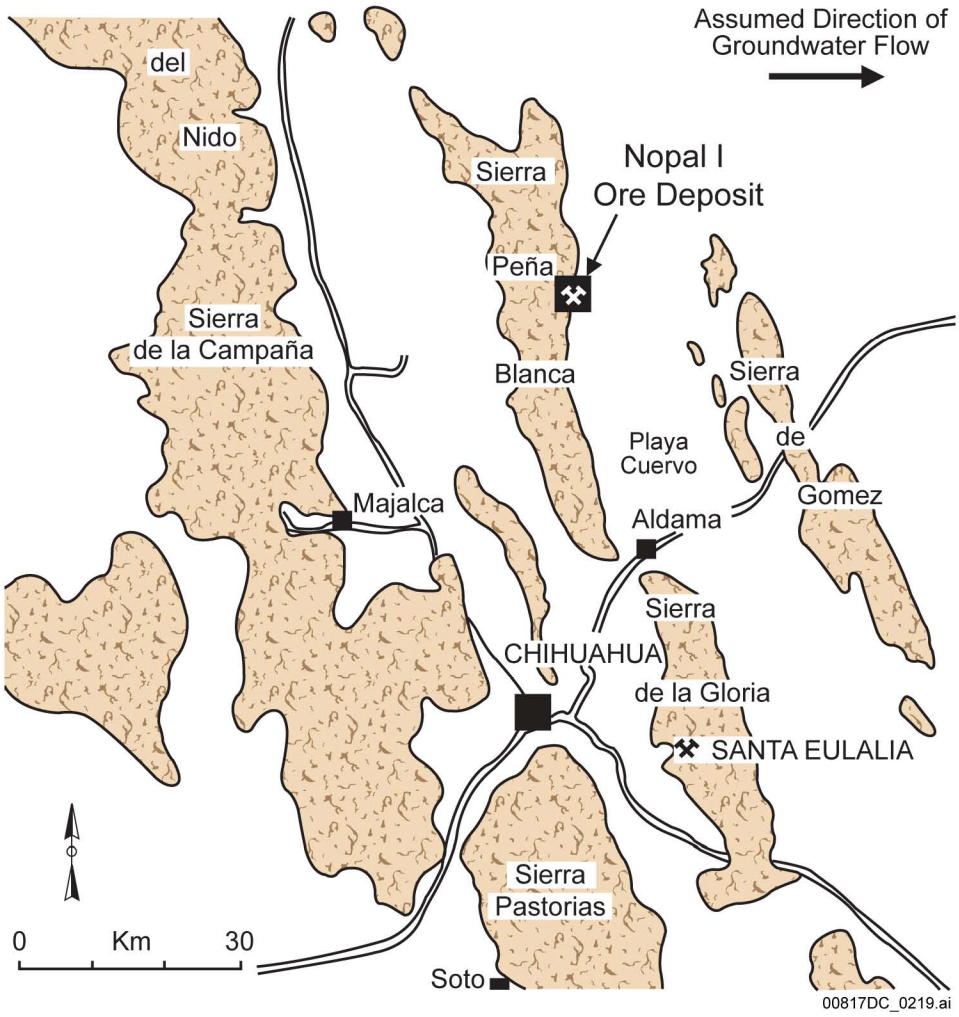

Source: Modified from George-Aniel et al. 1991 [DIRS 105636], Figure 1.

Figure 7.8-4. Location of Peña Blanca Nopal I Ore Deposit

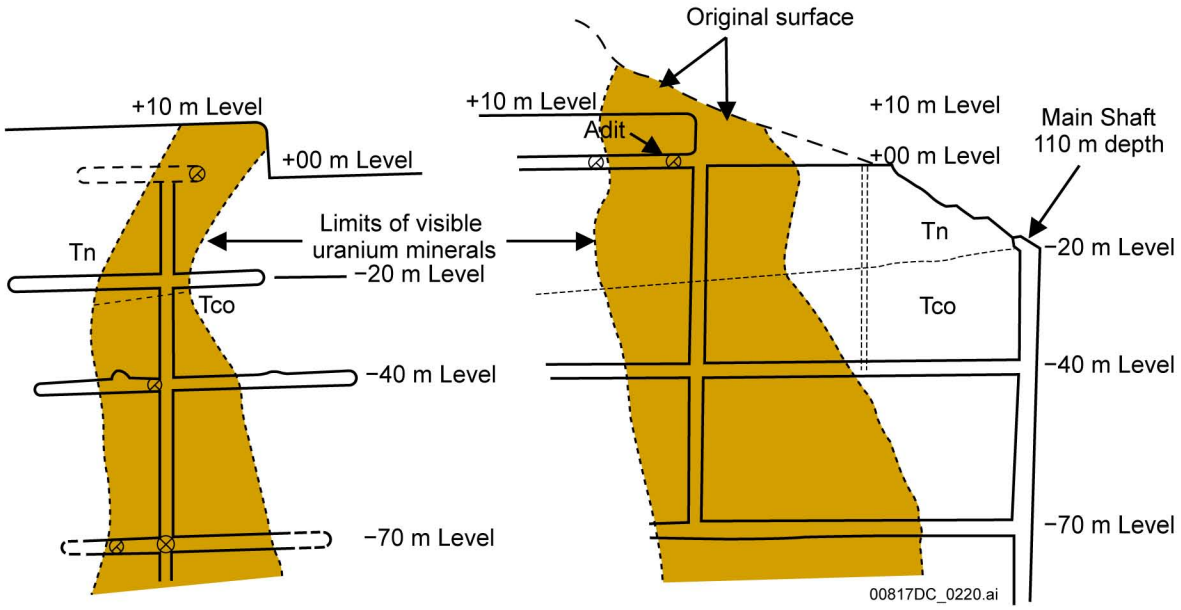

N 5120'E Section showing the accessible main adit at +00 level

N 3840'E Section showing +00 levels and the main shaft at −20 level

Source: Modified from Reyes-Cortes 1997 [DIRS 149533], Figure 25, p. 205.

Figure 7.8-5. Peña Blanca Mine Shaft Schematic

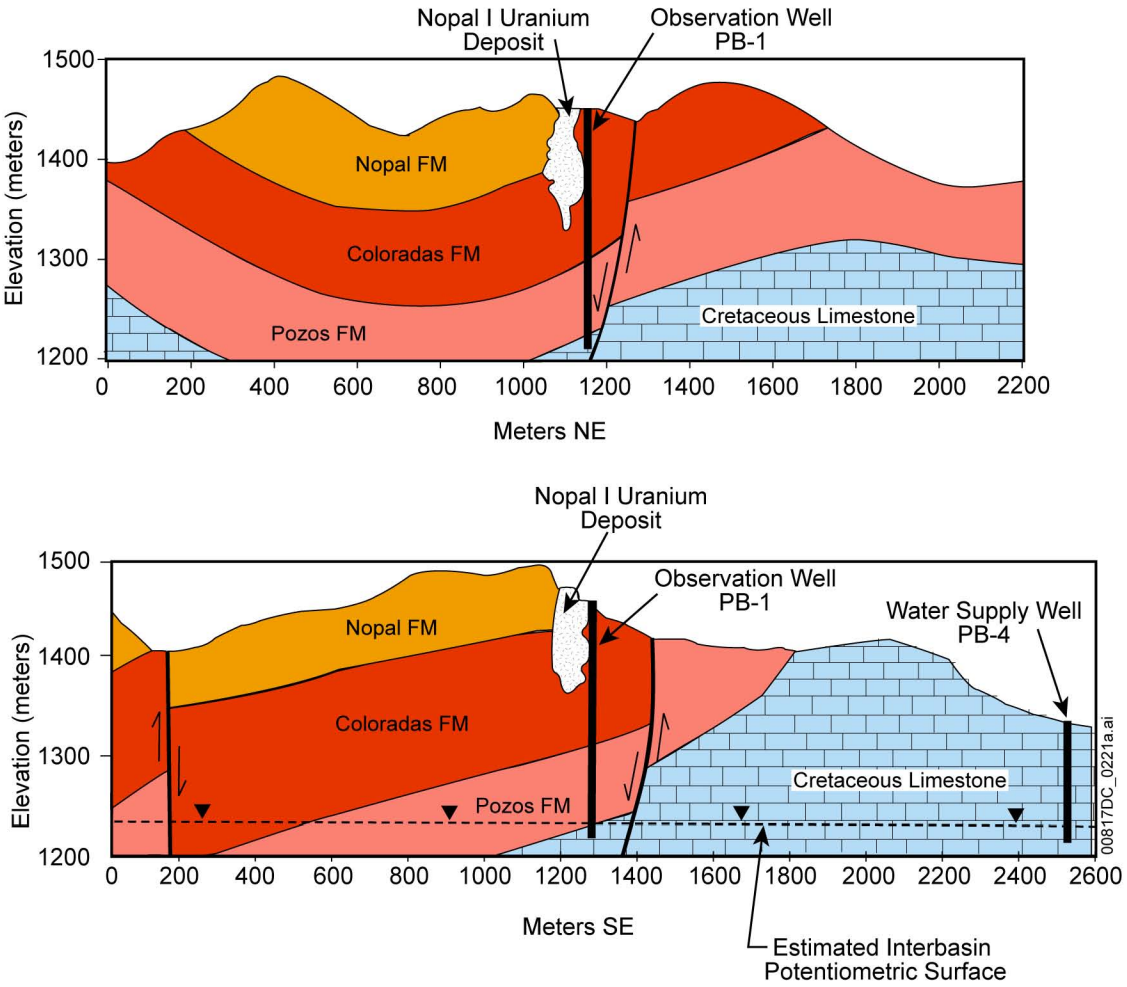

Source: Modified from Pearcy et al. 1993 [DIRS 151774], p. 1-4.

Figure 7.8-6. Geologic Characterization of Nopal I Ore Body

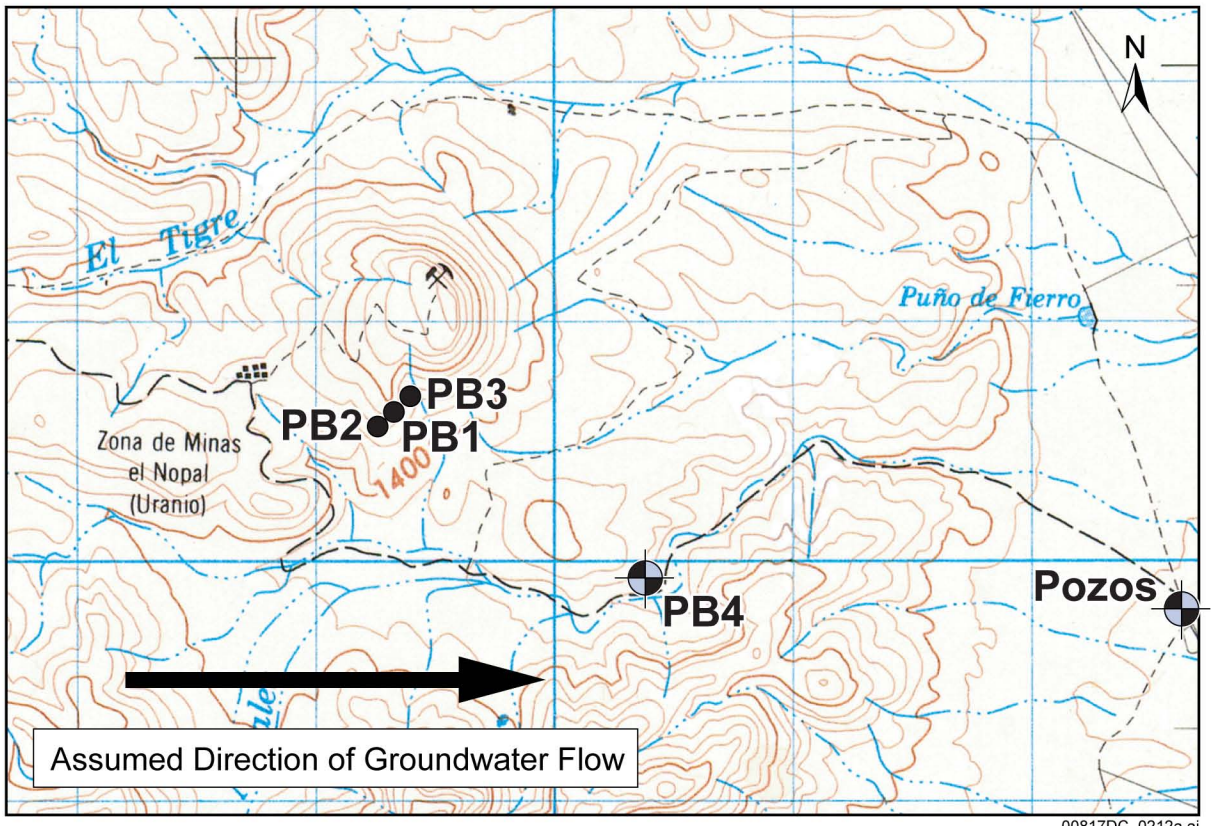

El Sauz 1:50,000 Topographic Map (H13C46)
North American 1927 datum

Legend
- Existing Wells
- New Peña Blanca Boreholes

Source: Modified from BSC 2004 [DIRS 169218], Figure 10.4-4.

NOTE: PB1, PB2, and PB3 were drilled in 2003. PB1 was cored continuously to total depth. PB4 is a former water supply well drilled in the early 1980s.

Figure 7.8-7. Location of Observation Wells at the Nopal I Mine in the Peña Blanca Uranium District

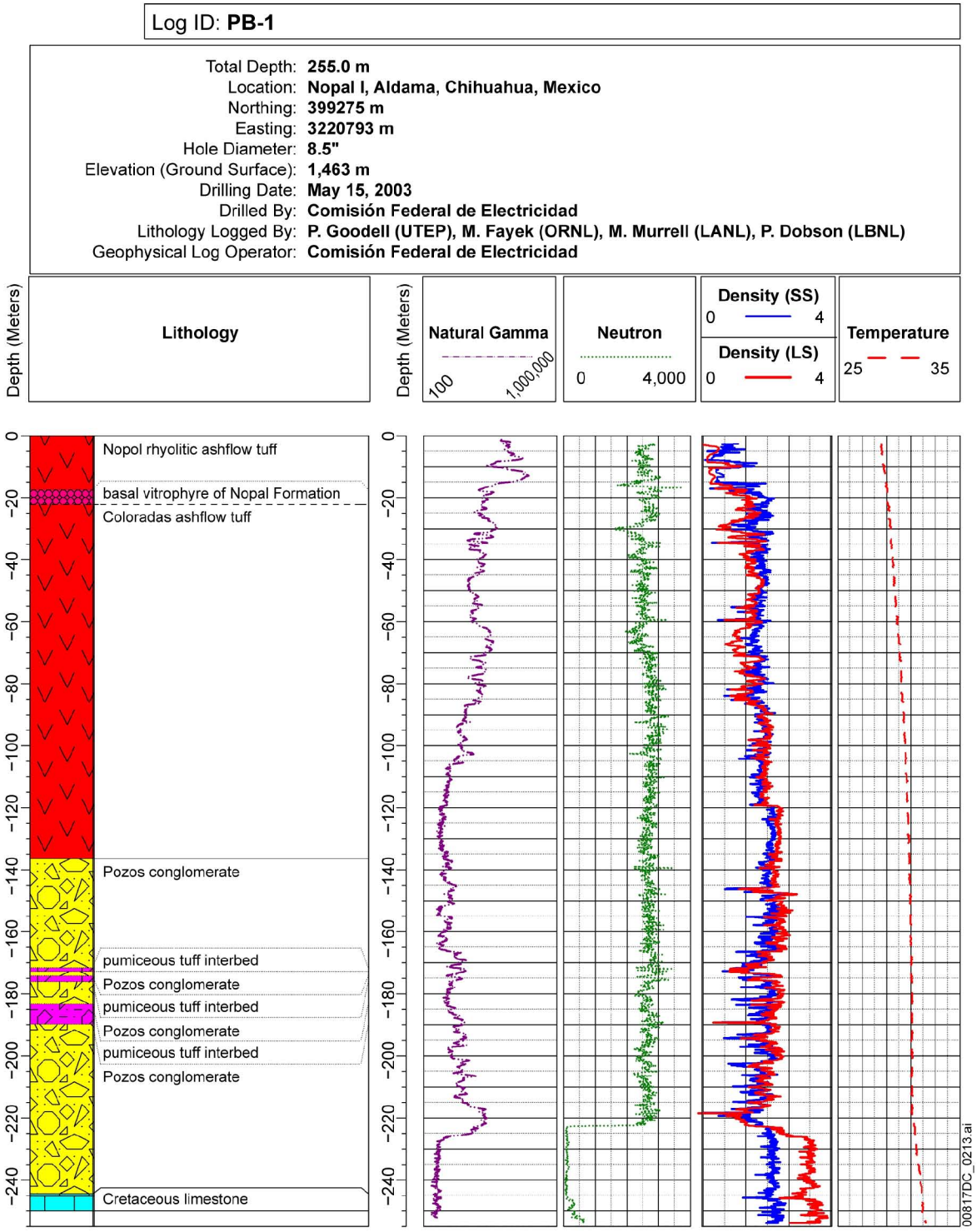

Source: BSC 2004 [DIRS 169218], Figure I-1.

Figure 7.8-8. Geophysical and Geologic Logs of Observation Well PB1

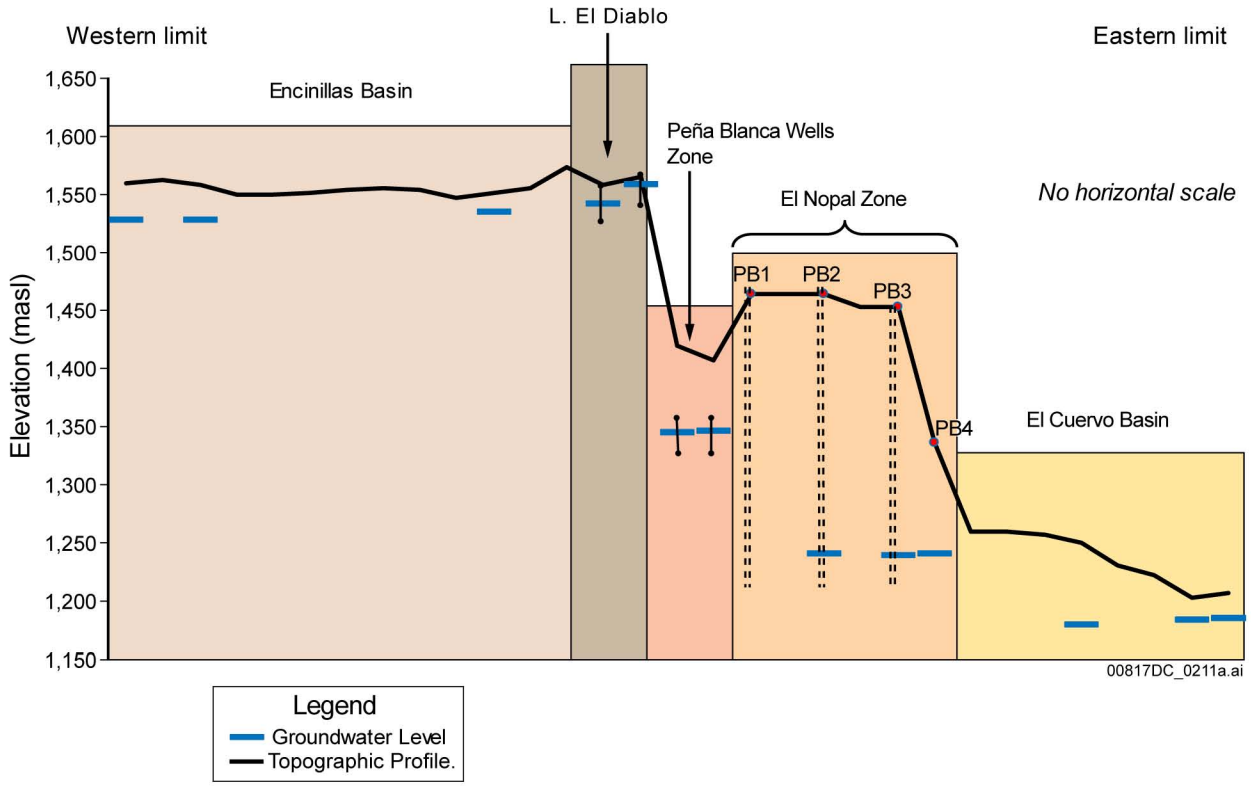

Source: Based on Geological Society of America 2005 [DIRS 181366].

Figure 7.8-9. Schematic Northwest to Southeast Cross Section of the Sierra Peña Blanca Showing the Relative Position of the Water Table in the Encinillas Basin, the Nopal I District, and the El Cuervo Basin

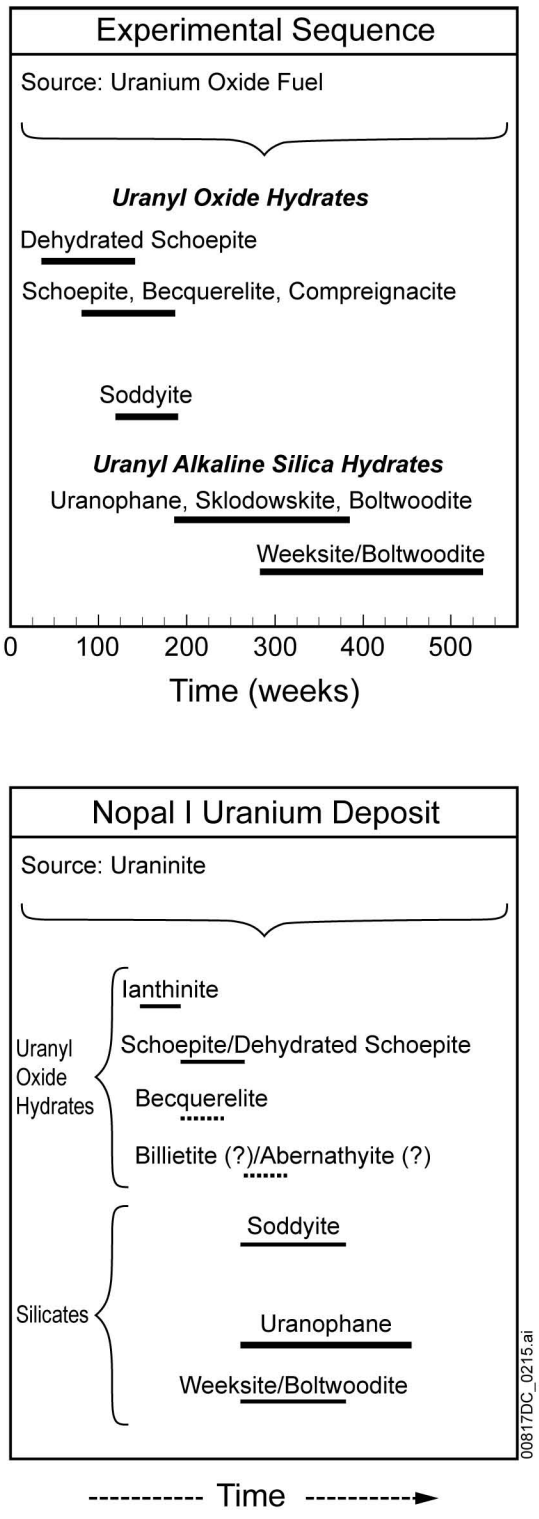

Source: Modified from Wronkiewicz et al. 1996 [DIRS 102047].

Figure 7.8-10. Comparative Reaction Paragenetic Sequences for Uranium Alteration Phases

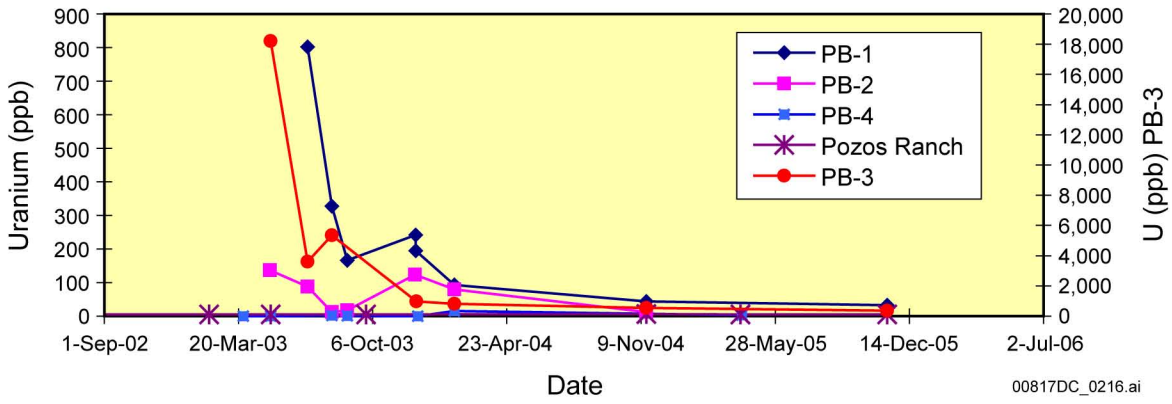

Source: Data from Goldstein et al. 2006 [DIRS 181364], p. 217.

Figure 7.8-11. Uranium Concentration Determined in Groundwater Samples from Wells at and Near the Nopal I Ore Deposit

INTENTIONALLY LEFT BLANK

7.9 TECHNICAL REVIEWS SUMMARY

Section 7.9 summarizes the empanelled technical reviews that were performed by the YMP during the last decade on its TSPA methodology-development approach for producing valid models. These reviews, conducted by teams of experts, were undertaken in order to ensure that the TSPA Model produced by the YMP applying the methodology was credible, defensible to the regulatory authorities, and respected by the technical community. The following sections chronologically describe the reviews, which are the cumulative results that supported the development of the TSPA-LA Model documented in this model report.

Section 7.9.1 addresses the first of these three reviews, namely the peer review of the TSPA-VA, which was completed in 1999. This review was conducted to evaluate whether the TSPA was sufficiently describing the postclosure behavior of the repository. The TSPA-VA review contributed to the development of the TSPA-SR. The TSPA-SR was then subjected to a peer review conducted by an IRT in 2001. The IRT review, described in Section 7.9.2, was undertaken to evaluate the soundness of the Project's decision for site recommendation and, more especially, to seek recommendations from the international perspective for preparation of the next TSPA for LA, which is the TSPA-LA Model documented in this model report. In turn, the earlier drafts of the TSPA-LA Model, along with their supporting analyses and model reports, were subjected to a technical review conducted by an IVRT as mentioned in Section 7.1. The IVRT review was convened in order to gain insight into the state of the validation status of the model as reflected in its early drafts and seek comments and recommendations that were to be applied to the development of the TSPA-LA Model. The IVRT was completed in 2006. The IVRT review is presented in Section 7.9.3.

Before the individual reviews are presented, some discussion on the function of technical reviews in model validation and evolution of the TSPA-LA Model as a result of the Project's previous technical reviews is provided below in order to put the presentation into perspective.

Technical Reviews and Model Validation Requirements

During the last decade the YMP conducted three empanelled technical reviews on the previous versions of the TSPA that led to the current TSPA-LA Model. The reviews were conducted by teams of experts. Although the emphasis and criteria for the reviews varied somewhat from one review to the next as the TSPA Model development process progressively matured from the viability assessment to site recommendation to LA, the underlying single common purpose for all reviews remained the same. That purpose was to continue to improve the model development process as envisioned in the NRC guidance for preparation of model development (Eisenberg et al. 1999 [DIRS 155354]) in order to ultimately develop the TSPA-LA Model, via a successful TSPA-SR, that would comply with the requirements for an LA to the NRC for authorizing construction of the repository at the Yucca Mountain site.

SCI-PRO-006 requires performing two of the activities that are identified therein for the post-model development phase. Technical reviews may be included as one of the activities undertaken in order to produce a valid model. A brief summary of the requirements for developing a valid TSPA Model is included below in order to provide a perspective on the TSPA-LA Model validation strategy (Section 7.1) and the role of technical review in that strategy.

Development of a valid model is an iterative process as described by the NRC (Eisenberg et al. 1999 [DIRS 155354]) and alluded to in Section 7.1. The iterative process involves continuing to validate the model, often with change in compliance strategy, to enhance confidence that the model would meet and exceed the goal for its intended use. In the case of developing a model for a system with a high potential human health and environmental consequence, such as the postclosure performance of a geologic repository for disposal of high-level radioactive waste, the progressive model development process must be controlled by an established quality assurance procedure in order to ensure a high degree of traceability and transparency of the model development process. The development of the TSPA-LA Model evolved through such a controlled iterative process. The TSPA-LA Model development and validation process is guided by *Quality Assurance Requirements and Description* (QARD) (DOE 2007 [DIRS 182051], Supplement SIII-2) and implemented by the QA procedures developed for the purpose. As discussed in Section 7.1, SCI-PRO-006, which controls the development of the TSPA-LA Model, requires that the needed pre- and post-development model verification and validation activities are identified and described in the TSPA-LA technical work plan (SNL 2008 [DIRS 184920]). The technical work plan identified and described the activities required for developing and validating the TSPA-LA Model. The TSPA-LA Model validation approach is presented on Figure 7.1-2.

The governing procedure for the TSPA-LA Model development (SCI-PRO-006 by reference to SCI-PRO-002) identified six criteria to ensure that the model is valid for its intended purpose. At least two of the nine post-development activities identified are required to ensure that the model is valid for its intended purpose.

Two of the nine post-development validation activities identified by SCI-PRO-006 involve a technical review of two kinds. The first is the critical review for which the instructions are described in Attachment 4 of this procedure. The second kind of optional review is peer review, which is governed by SO-PRO-001, *Peer Review*. The earlier versions of the TSPA models received both types of technical reviews. The TSPA-VA and the TSPA-SR models each received a peer review, and the earlier drafts of the TSPA-LA Model received a critical review. SCI-PRO-006 (Section 6.4.10) requires an independent technical reviewer as a part of the model development activities regardless of whether or not a critical review or a peer review is used as one of the post-development model validation criteria. The independent technical review ensured that the TSPA-LA Model was developed as per the requirements stated in the technical work plan (SNL 2008 [DIRS 184920]), and confirms the adequacy of the validation portion of the model documentation.

The TSPA-LA technical work plan (SNL 2008 [DIRS 184920]) incorporated the required criteria for the development of the TSPA-LA Model. As mentioned earlier, the technical work plan did not select a technical review as one of the activities for post-development validation of the

TSPA-LA Model. The rationale for this decision is that another technical review on the TSPA-LA Model was deemed unnecessary given that during the past decade of its iterative development the predecessor TSPA models, as well as their input process models, underwent a number of technical reviews, including the recent IVRT review on the early drafts of the TSPA-LA Model as discussed below. Instead, as a post-development validation criteria, the technical work plan required documenting the Project responses to the comments and implementation of the recommendations from the reviews already conducted on the predecessor TSPAs; in particular, responding to the remaining IVRT issues and continuing to implement the IVRT recommendations.

The technical work plan (SNL 2008 [DIRS 184920]) selected a number of post-development model validation activities from among the nine identified by SCI-PRO-006 (Section 7.1, Figure 7.1-2) to build confidence in the TSPA-LA Model (Section 7.1, Figure 7.1-2). These technical work plan activities include: (1) corroborating the TSPA-LA direct input abstraction results with those of the respective underlying process models (Section 7.6); (2) auxiliary analyses (Section 7.7) that include (a) analyses of single realizations, (b) comparison of the TSPA-LA Model with a separately developed Simplified TSPA-LA Analysis, (c) comparison of the TSPA-LA Model with a TSPA Model for the repository independently developed by EPRI using their own code (IMARC), and (d) the PMA; and (3) evaluation of man-made and natural analogues that are relevant to the different components of the TSPA-LA Model (Section 7.8). In addition, post-development model validation criteria presented in the technical work plan (SNL 2008 [DIRS 184920]) required documenting the Project to the comments and implementation of the recommendations from the prior reviews of the past Project TSPAs to enhance confidence in the final product.

Past Technical Reviews and Evolution of Methodology for the TSPA-LA Model

The TSPA methodology is iterative, as mentioned above. The general TSPA process adopted by the DOE follows the methodology developed by the NRC (Codell et al. 1992 [DIRS 103714] and Westcott et al. 1995 [DIRS 100476]). Over time, the methodology has been enhanced and applied to numerous Projects by various international organizations involved in radioactive waste management. The TSPA-LA Model was developed to analyze the ability of the natural and engineered systems of the Yucca Mountain repository to isolate nuclear waste following repository closure. Performance assessments and related supplemental analyses of the Yucca Mountain repository have been conducted following the publication of the Nuclear Waste Policy Act as Amended in 1987, Public Law No. 100-203 [DIRS 100016]. The TSPAs of the Yucca Mountain repository have been iterative and periodically updated, each building on and extending the scope and results of the previous TSPA. The iterative assessments incorporate both an improved understanding of the processes affecting repository performance and, through additional field observations and laboratory analyses, better identification and quantification of the values of the parameters used in the TSPA.

Early iterations of probabilistic TSPAs for the Yucca Mountain repository include TSPA-91 (Barnard et al. 1992 [DIRS 100309]); TSPA-93 (Wilson et al. 1994 [DIRS 100191]); TSPA-95 (CRWMS M&O 1995 [DIRS 100198]); and *Total System Performance Assessment – Viability Assessment of a Repository at Yucca Mountain* (DOE 1998 [DIRS 100550], Volume 3). The more recent TSPA iterations include *Total System Performance Assessment for the Site*

Recommendation (CRWMS M&O 2000 [DIRS 153246]) and the application of the Total System Performance Assessment-Site Recommendation Model to the Final Environmental Impact Statement for the Yucca Mountain Repository (Williams 2001 [DIRS 157307]).

TSPA iterations are evaluated and independently reviewed by technical staff and various independent organizations. Reviewers generally make recommendations for improvements for consideration in future TSPA iterations. Examples of empanelled technical reviews that contributed to the development of the TSPA-LA Model include the peer review of the TSPA-VA completed in 1999 by a panel of experts and an evaluation of the TSPA-SR by an IRT of peers completed in 2002. More recently, an IVRT performed a critical review of the initial drafts of the TSPA-LA Model. The IVRT review was completed in 2006. The TSPA-VA, IRT, and IVRT reviews are discussed below in Sections 7.9.1, 7.9.2, and 7.9.3, respectively.

In addition to the three empanelled reviews, the Nuclear Waste Technical Review Board (NWTRB) performs routine reviews on key areas of the Project as mandated by Congress. The NWTRB focuses its review effort on three broad technical areas of the Project: Preclosure Operations, Postclosure Repository Performance, and System Integration. The NWTRB reviews on the TSPA effort are captured by its focus on postclosure repository performance. The NWTRB comments on the TSPA, and the Project responses to their comments along with the implementation of the recommendations, are captured in the NWTRB reports and correspondences presented in the NWTRB websites: http://www.nwtrb.gov/reports/reports.html and http://www.nwtrb.gov/corr/corr.html, respectively. These comments and recommendations made significant contributions to the development of the TSPA-LA Model on an on-going basis.

7.9.1 TSPA-VA Review

This section summarizes the TSPA-VA peer review with respect to the scope and methodology of the review, the comments and recommendations made by the review panel, and the Project's response to the comments and implementation of the recommendations. The details are documented in the panel report (Budnitz et al. 1999 [DIRS 102726]) and the Project's response document (CRWMS M&O 1999 [DIRS 153111]).

7.9.1.1 Scope and Methodology for the TSPA-VA Peer Review

The TSPA-VA peer review was conducted to provide a formal, independent evaluation and critique of the TSPA-VA. The peer review was planned and managed by the DOE Management and Operating Contractor at that time. The specific scope was for the review panel to conduct a phased review over a two-year period to observe the development and completion of the TSPA-VA. The comments, concerns, conclusions, and recommendations of the review panel were to be provided in a final report to the Management and Operating Contractor to support the eventual development and conduct of the TSPA-LA. The panel was expected to evaluate the TSPA-VA Model for its analytical approach, including the following within the context of their significance to the long-term performance of the repository:

- Physical events and processes considered in analyses
- Use of appropriate and relevant data
- Assumptions made

- Abstraction of process models into total system models
- Application of accepted analytical methods
- Treatment of uncertainties.

In addition to the review of the TSPA analytical approach, the panel was also to consider traceability and transparency of the TSPA-VA analyses.

The TSPA-VA peer review was conducted in accordance with the Management and Operating Contractor QAP-3-3, *Peer Review,* that was in effect at that time and consistent with the NRC guidance for conducting peer reviews (Altman et al. 1988 [DIRS 103597]). The peer review was conducted during the period 1997 through 1998, with the final panel report submitted in early 1999. As a part of the phased approach of the peer review, the panel submitted three interim reports that were based on observations on the draft documents supporting the TSPA-VA and formal and informal interactions with the Project technical staff, which collectively led to the final TSPA-VA report (DOE 1998 [DIRS 100550], Volume 3) on which the panel's final report was based.

The panel was comprised of six members distinguished in their individual area of expertise. Details of the purpose, methods, panel members, and findings of the peer review on the TSPA-VA model are provided in the panel's final report (Budnitz et al. 1999 [DIRS 102726]). The final report includes the major points from the three interim reports, updated as appropriate, as well as the new findings the panel developed during its review of the TSPA-VA (DOE 1998 [DIRS 100550], Volume 3).

7.9.1.2 TSPA-VA Panel Comments and Recommendations and the Project Responses

The objective of the TSPA-VA review panel in reviewing the completed TSPA-VA (DOE 1998 [DIRS 100550], Volume 3) was to provide comments, concerns, conclusions, and recommendations that could be used in the development of a TSPA Model that would ultimately support development of the LA. The panel drew no conclusion regarding acceptability of the proposed repository or readiness for preparation of the LA and stated that the comments and recommendations it made should be considered with that fact in mind.

The TSPA-VA review panel's key conclusions include:

- Overall, the approach demonstrated in the TSPA-VA for assessing the behavior of the repository during the postclosure period was sound (Budnitz et al. 1999 [DIRS 102726], Section C, p. 3).

- The panel stated that "it is unlikely that the TSPA-VA, taken as a whole, describes the long-term probable behavior of the proposed repository". In the panel's judgment, a number of components of the TSPA-VA analysis were not supported by adequate evidence that they represent systems, components, and processes they were designed to represent. In addition, several of the component models were likely to be conservative and others non-conservative. For these reasons, the panel stated that the decisions based on the TSPA-VA should be made cautiously (Budnitz et al. 1999 [DIRS 102726], Section B, p. 1).

- The TSPA-VA was a necessary and useful step in evolving the understanding of how a repository could be expected to perform at Yucca Mountain. It has produced valuable insights into performance of the various repository components and helped identify issues where additional data and analyses could improve understanding of the repository performance and where additional work is unlikely to make significant contributions (Budnitz et al. 1999 [DIRS 102726], Section B, p. 1). The panel noted the inherent difficulty in developing the TSPA Model that is required to predict the repository behavior such a long time into the future (Budnitz et al. 1999 [DIRS 102726], Section B, p. 1). (Note that 10,000 years after the repository closure was the regulatory compliance period at that time).

- The panel noted the many experiments that were planned to be performed, which would be valuable in confirming, calibrating, or invalidating models that were developed for analyses of conditions at the proposed repository (Budnitz et al. 1999 [DIRS 102726], Section B, p. 2).

The Project reviewed and identified the comments and recommendations that were presented in a discussion format in the panel's final report (Budnitz et al. 1999 [DIRS 102726]) and listed them in the comment-response report (CRWMS M&O 1999 [DIRS 153111]). As mentioned earlier, the panel viewed that the objective of the TSPA-LA Model was to demonstrate that the repository would comply with the applicable regulatory standards with reasonable assurance rather than to describe the probable behavior of the repository system, which was the objective of the TSPA-VA Model. The panel thought the TSPA-LA Model objective would be significantly different from the TSPA-VA Model (DOE 1998 [DIRS 100550], Volume 3) objective and recommended the following approaches for achieving the upcoming TSPA-LA objective (Budnitz et al. 1999 [DIRS 102726], Section D, p. 40):

- Updating the component models
- Expanding the quality and quantity of data for analyses
- Using bounding assumption
- Making design changes
- Incorporating the defense-in-depth concept.

The panel also stated: (1) efforts should be made where improvements are feasible in the component models or underlying data if such efforts would affect the overall assessment, (2) it may not be cost effective to make additional efforts where conservative bounding analyses do not result in unduly pessimistic estimates of total system performance, and (3) for complex issues where development of realistic models supported by data is not feasible, a combination of bounding analyses and design changes should be applied.

The YMP found the panel recommendations were consistent with the Project's strategy for development of the postclosure safety cases for the upcoming site recommendation and subsequent LA and the design selection and work-prioritization efforts that were underway for developing the safety case.

The YMP fully implemented the panel recommendations as demonstrated in the significant updates of the component models based on the highly expanded site-scale test data collection

efforts. This collection of test data came from the ESF; single-heater and drift-scale thermal tests; ECRB tests; various (radionuclide-surrogate) tracer tests in the UZ and SZ of the natural system such as the Busted Butte tests, Alluvium Tracer tests, and Natural Gradient tests; and also several supporting laboratory tests (e.g., the long-term corrosion tests). Some of these tests in the ESF and ECRB are ongoing long-term tests and will continue as a part of the Performance Confirmation program after the LA submittal. The Project also made significant design changes since the panel recommendations. The key changes include the use of a DS and, more recently, incorporating the TAD canister to enhance safety during waste transportation to the repository site, aging at the site, and finally the disposal in the underground repository. Parallel to and complementing these data collection and design-change efforts, the Project significantly improved its ability to treat uncertainty in the TSPA Model and its submodels; enhanced the ability of the TSPA-LA computational software; and improved implementation of quality assurance procedures and issue-identification, tracking, and the correcting process such as the Corrective Action Program. The Project vigorously incorporated the defense-in-depth concept in order to increase the safety margin. For the TSPA, the effort included (a) incorporating the design-changes mentioned above in the TSPA computations, (b) performing additional auxiliary analyses of the total system and its subsystems to better understand the TSPA results and reduce the associated uncertainty, (c) ensuring qualitative and quantitative comparison of the TSPA Model components with several man-made and natural analogues, and (d) performing empanelled technical reviews such as the peer review of the TSPA-SR by an IRT, and more recently, the critical review of the earlier drafts of this TSPA-LA Model by an IVRT. The purpose and outcome of the IRT and IVRT reviews are described below.

Utilizing input from the TSPA-VA review group and, where appropriate, modifying modeling and design elements, the Project has subsequently produced much improved TSPAs, which in turn made achieving significant Project goals possible, for example, the submittal of the TSPA-SR (CRWMS M&O 2000 [DIRS 153246]) and the Environmental Impact Statement (EIS) (DOE 2002 [DIRS 155970]) supporting the Site Recommendation. This resulted in the Presidential and Congressional approval of the repository site and authorizing the DOE to proceed with the LA for the NRC authorization to begin construction of the repository. The TSPA-LA Model is the latest product of the above mentioned testing, modeling, and documentation activities performed during the last decade.

7.9.2 International Review Team Peer Review

This section summarizes the IRT peer review with respect to the scope and methodology of the review, the comments and recommendations made by the IRT, and the Project's response to these comments and implementation of the recommendations. The details are referred to in the IRT final report (OECD and IAEA 2002 [DIRS 158098]); Appendix E (TSPA-LA, Volume III) provides the effort the Project made in implementing the IRT recommendations.

7.9.2.1 Scope and Methodology for the International Review Team Peer Review

The IRT peer review was requested by the Project and conducted by a team of experts organized by a Joint Secretariat formed by the NEA and IAEA. The overall objective of the IRT review was to provide, based on the available international standards and guidance as appropriate, an independent assessment of the methodology developed by the Yucca Mountain Site

Characterization Project, as reported in *Total System Performance Assessment for the Site Recommendation* (CRWMS M&O 2000 [DIRS 153246]). The IRT peer review entailed a review and critical analysis of the performance assessment methodology and rationale being used in support of the site-recommendation decision-process.

The IRT review was conducted while taking into account the international experience in preparing for and conducting system-level postclosure performance assessments. In addition, the IRT was to consider in its review the requirements proposed at that time by the EPA and NRC for disposal of high-level radioactive waste in a geologic repository. The IRT was to identify consistencies and inconsistencies between methods being used by the Project and those being considered or developed in international recommendations, standards, or practices. More importantly, the IRT review was to comment on the adequacy of the overall performance assessment approach for supporting the programmatic decision for site recommendation. In addition, recommendations were expected on specific technical improvements that would help the Project's performance assessment effort better support the next programmatic decision point (i.e., the preparation and submission of an LA, specifically the TSPA-LA Model documented in this report).

The IRT review was primarily based on the TSPA-SR (CRWMS M&O 2000 [DIRS 153246]) Model and some of its key scientific basis documents selected by the IRT panel. Consistent with the IRT review objective and scope in conducting the review, the IRT considered (OECD and IAEA 2002 [DIRS 158098], Appendix 1, Section 3):

- The technical basis for the performance assessment, including identification and justification of the conditions and characteristics modeled at the system level. This would include a review of the abstractions of the adopted design and the scientific basis for determining future environments in the system and its materials and natural systems behavior.

- The development of the key conceptual models, including the assumptions made with respect to the representations of relevant FEPs.

- The adequacy of the treatment of the undisturbed and disturbed system performance.

- The adequacy of the methods used and the cases considered in sensitivity and uncertainty evaluations.

- The overall clarity and completeness of the technical report describing this system-level performance evaluation.

The IRT review was conducted through interactions with the technical and management staff, as necessary, and a site visit and meetings open to the public where technical presentations were made by the Project staff and a few invited public participants. As reported in the IRT final report (OECD and IAEA 2002 [DIRS 158098]), the review was performed during June 2001 through December 2001, culminating in a final review report presented to the DOE in January 2002. Additional detail on the scope and methodology of the IRT review is presented in the IRT final review report (OECD and IAEA 2002 [DIRS 158098]).

International Review Team Comments and Recommendation and the Project Responses

The IRT made several recommendations (OECD and IAEA 2002 [DIRS 158098], Section 5.1) on the rationale the Project was pursuing in developing the SR, specifically the TSPA-SR Model; methodology to be used in developing the ensuing TSPA-LA; and the EPA and NRC proposed regulations for the repository. The IRT made these recommendations from the international perspective of the performance assessment methods being considered or recommendations, standards, or practices being developed. The IRT made the following statement (OECD and IAEA 2002 [DIRS 158098], Section 5.2) regarding the overall performance assessment approach used in the TSPA-SR:

> "While presenting room for improvement, the TSPA-SR methodology is soundly based and has been implemented in a competent manner. Moreover, the modeling incorporates many conservatisms, including the extent to which water is able to contact the WPs, performance of engineered barriers, and retardation provided by the geosphere.
>
> Overall, the international review team considers that the implemented performance assessment approach provides an adequate basis for supporting a statement on likely compliance within the regulatory period of 10,000 years and, accordingly, for the site recommendation decision.
>
> On the basis of a growing international consensus, the international review team stressed that understanding the repository system and its performance and how it provides for safety should be emphasized more in future iterations, both during and beyond the regulatory period. Also, further work would be required to increase confidence in the robustness of the TSPA."

The IRT made a set of 27 specific recommendations in its final report (OECD and IAEA 2002 [DIRS 158098], Section 5.3) for future improvements in the preparation and submission of the LA. The Project implemented these recommendations. Table E-1 in Appendix E (Volume III of the TSPA-LA Model report) tabulates the IRT recommendations and describes the work the Project completed implementing these recommendations and provides references to where the work is documented.

7.9.3 Independent Validation Review Team Review

This section summarizes the IVRT review with respect to the review scope as provided by the prevailing TSPA technical work plan, methodology of the review, comments and recommendations made by the review panel, and the Project's response to these comments and implementation of the recommendations. The details are presented in the draft TSPA-LA Model (Gibson 2007 [DIRS 181099]). The IVRT final report is included as Appendix C of the draft TSPA-LA Model, Rev 01E (Gibson 2007 [DIRS 181099]). In addition, a complete tabulation of the IVRT comments and the Project responses, as well as the Project positions on several difficult-to-resolve issues raised early during the review process, are presented in an interoffice memorandum from T.C. Booth (2006 [DIRS 176638]). Several IVRT issues were not fully addressed according to the IVRT panel when these documentations were completed. The Project

has since planned, performed, and documented the additional work to address these issues as discussed below and summarized in Table 7.9-1.

7.9.3.1 Scope and Methodology for the IVRT Review

The IVRT performed the review during 2004, 2005, and 2006 on the earlier draft of the TSPA-LA Model and its supporting draft documentations. The draft material was prepared for the 10,000-year postclosure compliance period rather than the 10,000 year and 1,000,000 year compliance periods covered by the TSPA-LA Model for the current proposed regulations. Therefore, the TSPA-LA Model is based on a changed compliance strategy from the one the IVRT review drafts were based. In developing the TSPA-LA Model, the Project fully utilized the perspective gained from the IVRT review. The Project considered and responded to all IVRT comments and implemented all of its recommendations as described under IVRT Panel Comments and Recommendation and the Project Responses below.

The IVRT conducted its review in two parts. The 2004 part consisted of reviewing the process models that supported the initial TSPA-LA Model that was being drafted at that time and some of their submodels. This 2004 part of the IVRT review was incorporated as a part of the Repository Integration Team (RIT) review that was ongoing independent of the IVRT at the time the IVRT was convened. The 2004 part of the IVRT review was governed by the review criteria in *Technical Work Plan for: TSPA-LA Model Development, Initial Use, and Documentation* (BSC 2004 [DIRS 168449]). The second part of the review conducted in 2005 and 2006 was governed by the review criteria in the technical work plan revised in March 2005 (BSC 2005 [DIRS 173309]). The entire IVRT review was performed in accordance with the then effective LP-SIII.10Q-BSC, *Models.*

The IVRT adopted the iterative model validation process described in *Regulatory Perspectives on Model Validation in High-Level Radioactive Waste Management Programs: a Joint NRC/SKI White Paper* (Eisenberg et al. 1999 [DIRS 155354]) as the strategy for conducting its review. In addition to the RIT part of the IVRT review conducted in 2004 during its review period, the IVRT reviewed several versions of the draft TSPA-LA Model that resulted from the IVRT comment resolutions starting with the 2004 initial draft. The IVRT comments and recommendations for these drafts were incorporated into the draft TSPA-LA (Gibson 2007 [DIRS 181099]), as mentioned earlier. The IVRT review documented in its draft final report of 2005, which incorporated the results of the 2004 review, was conducted within the context of whether or not the TSPA-LA drafts satisfy the intended purpose specifically included in the following two model validation goals (BSC 2005 [DIRS 173309], Section 2.10.1):

1. Describe the postclosure performance of the repository system for the nominal, igneous, and seismic scenario classes.

2. Produce an estimate of mean dose (and other performance measures, as appropriate) that is consistent with the degree of conservatism representative of the component abstraction models and parameters (and their uncertainty) that are input to the TSPA-LA Model.

In July 2004, the IVRT produced a draft report documenting the findings of its review based on the information it had examined up to that time and as per the scope of the 2004 technical work

plan (BSC 2004 [DIRS 168449]). The IVRT focused its review of 2005 drafts of the TSPA-LA Model on evaluating the compliance status of the 20 review criteria given in the 2005 technical work plan (BSC 2005 [DIRS 173309], Section 2.10.1). Ten of these criteria are in the TSPA draft under review, five are in the submodels area, and the remaining five were of general category. Specifically, the technical work plan (BSC 2005 [DIRS 173309]) identified the following as the objective for the technical review (BSC 2005 [DIRS 173309], Section 2.10.1, pp. 17 and 18):

1. The independent review team should determine and document:
   - Whether or not, in their judgment, the criteria are met
   - Whether or not, in their judgment, the TSPA-LA Model is valid for its intended purpose
   - How the judgment for each criterion was weighted in reaching the valid or not-valid decision for the overall TSPA-LA Model.
2. The independent review team was to categorize their judgments regarding whether or not each criterion has been met as follows:
   - Meeting the criterion is significant for the intended purpose of estimating conservative mean dose and the criterion is met.
   - Meeting the criterion is not significant for the intended purpose of estimating conservative mean dose.
   - Meeting the criterion is significant for the intended purpose of estimating conservative mean dose and the criterion is not met.

In August 2005, the IVRT provided interim information to the project that updated the 2004 review and concluded that an evaluation against the review criteria in the 2005 TWP (BSC 2005 [DIRS 173309]) indicated that the model, as then documented, was not valid for its intended purpose. The IVRT findings are documented in the draft final report. Based on a number of information exchanges between the Management and Operating Contractor technical staff and IVRT panel members on comment resolution and the adverse findings by the IVRT documented in the draft final report, the Management and Operating Contractor requested the IVRT to provide recommendations for future improvements for the TSPA-LA Model validation status. In response to this request, the IVRT revised the 2005 draft final report to reiterate their conclusion that the model had not satisfied all review criteria and to include a total of seven recommendations. This report was submitted to records as the IVRT's final report (Gibson 2007 [DIRS 181099], Appendix C).

The following section provides a summary of the IVRT comments and recommendations and the Project responses to these comments and implementation of the recommendations in developing this TSPA-LA Model.

7.9.3.2 IVRT Panel Comments and Recommendations and the Project Response

The detail of the IVRT comments on the TSPA material and its RIT review of the supporting process models and submodels are in the IVRT final report (Gibson 2007 [DIRS 181099], Appendix C). A summary of the IVRT conclusions and the Project status of addressing the IVRT comments and implementation of its recommendations is presented below.

As mentioned earlier, in July 2004 the IVRT produced a draft report documenting the findings of its review based on the information it had examined up to that time. That draft IVRT report was incorporated in the IVRT final report cited above, which was submitted by the IVRT in February 2006. In the course of its RIT and TSPA-LA initial draft reviews in 2004, the IVRT concluded in its final report that, as of December 2004, "the IVRT found that the technical issues that caused some review criteria to be not met were not significant to the determination of validity and that the TSPA Model as configured at that time was valid for its intended purpose, given that the IVRT believed that the model provided a highly conservative estimate of mean dose and that the intended purpose was to demonstrate compliance with the quantitative requirements at 10 CFR 63.311 [DIRS 178394], and 10 CFR 63.331 [DIRS 180319]. The IVRT therefore determined that, notwithstanding the many concerns it had with the TSPA Model, it nonetheless met the established validation goals due to a number of extreme conservatisms embedded in the model."

The IVRT stated in the final report (Gibson 2007 [DIRS 181099]) that in response to the RIT and the IVRT comments the Project modified the draft TSPA Model to remove some extreme conservatism and made numerous other changes, thereby revising the compliance strategy. The Project also performed a series of impact analyses to provide objective evidence of the effect of apparently significant conservatisms on mean dose as well as to provide responses to the IVRT's comments on the submodel reports, thereby generating additional information. The IVRT further noted that one of the most significant changes to the TSPA Model from 2004 to 2005 was the removal of several of the extreme conservatisms embedded in the model. The IVRT felt that the removal of these extreme conservatisms substantially relaxed the conservative basis that the IVRT had relied on for its 2004 conclusion regarding model validity. The Project incorporated these changes in the revised drafts of the TSPA-LA Model that were produced in 2005, which the IVRT reviewed as mentioned above, and developed its draft final report in late 2005.

In the draft final report, the IVRT concluded that, unlike its conclusion documented in the July 2004 draft report, the draft 2005 TSPA Model could no longer be considered valid for its intended purpose because the information available at the time did not adequately support a conclusion that the drafts of the 2005 TSPA Model they reviewed met the two validation goals mentioned earlier. The IVRT reached this conclusion because the 2005 TSPA Model drafts appeared to contain potentially significant optimisms as well as conservatisms and there were no estimates of the performance measures that the IVRT could use as a basis for comparison and for determining the degree of conservatism of the model. This gap of information led the panel to conclude that it could no longer consider the model valid for its intended purpose.

The Project documented, analyzed, responded to all, and resolved most of the IVRT comments, which numbered in excess of 500, before the panel was dissolved with the submittal of its final report. However, some issues remained not fully addressed according to the panel. As

mentioned earlier, based on the IVRT's adverse conclusion regarding the validation status of the 2005 draft TSPA-LA Model in the draft IVRT final report, the Management and Operating Contractor (Bechtel SAIC Company, LLC) requested the IVRT to provide recommendations for future work that could generate additional information to address the most salient issues that led the IVRT to the new conclusion documented in the 2005 draft IVRT final report. In response, the IVRT revised its draft final report to include seven recommendations for potential future work and submitted the final report in February 2006. The IVRT noted in the final report that the iterative approach that was followed in its review was consistent with the model validation process described in NUREG-1636 (Eisenberg et al. 1999 [DIRS 155354]). The IVRT observed in its final report that "Consistent with the model validation process documented in Addendum C.I, the Project will undertake a number of activities that may result in a revised compliance strategy. It is the IVRT's opinion that this is a prudent approach for achieving the goal of developing and implementing an acceptable TSPA Model for supporting a license application."

The Project agreed with the IVRT that successful completion of additional activities planned for FY06 to FY07 would help achieve the goal of a credible TSPA Model for supporting the LA. The Project has since planned and completed these activities as summarized below and shown in Table 7.9-1. The results of these completed additional activities, along with the continued implementation of the IVRT recommendation for improvements, significantly contributed to the TSPA-LA Model as documented in the three volumes of this report.

Subsequent to the IVRT review, the Project revised the draft version of the TSPA-LA Model the IVRT commented on into the draft TSPA-LA Model report (Gibson 2007 [DIRS 181099]). The draft TSPA-LA Model report contains the IVRT final report (summary in Section 7.7 and full report as Appendix C) and the Project's status of responses to the IVRT comments that were in the IVRT final report. Section 7.8 of the TSPA-LA Model report provides a detailed discussion on the Project responses to the IVRT comments and recommendations especially in the context of the validation status of the draft TSPA-LA Model at that time. Implementation of all seven recommendations was substantially completed by the Project at that time, as indicated and discussed in Section 7.7 and Section 7.8 of TSPA-LA Model report (Gibson 2007 [DIRS 181099]). In March 2006, the Project completed documenting (Booth 2006 [DIRS 176638]) all comments that were generated by the IVRT during its review. Booth (2006 [DIRS 176638]) also documented the Project responses to the IVRT comments, including the ones that were considered by the IVRT not fully addressed at the time when the IVRT submitted its final report in February 2006. In addition, Booth (2006 [DIRS 176638]) shows the Project position statements on the difficult-to-address RIT comments generated in 2004. As mentioned earlier, by the close of the IVRT review with its final report submitted in February 2006, a relatively small number of issues remained not fully addressed according to the IVRT panel members (Booth 2006 [DIRS 176638]). The Project continued to work on the remaining issues and implementation of the IVRT recommendations after the IVRT was dissolved and the current status is discussed below.

As mentioned above and in its final report (Gibson 2007 [DIRS 181099], Appendix C), the IVRT made a total of seven recommendations in response to the Project request to improve the validation status of the TSPA-LA Model. Details of these recommendations are discussed in the final IVRT report. In response to the Project request, the IVRT designed the recommendations

so that when implemented, they would remove the key factors that were responsible for the IVRT-designated overall not-met validation status of the 2005 drafts of the TSPA-LA Model. The IVRT recommendations and their implementation by the Project are summarized below.

Three of the IVRT recommendations (numbers 4, 5, and 6) were related to the potential impact on the model due to changes in GoldSim (V. 8.02.500, STN: 10344-8.02-05 [DIRS 174650]), timely identification and managing model file errors, and performing analysis of impact, if any, due to the errors. The remaining four recommendations (numbers 1, 2, 3, and 7) focused on resolving the technical issues that led the IVRT to conclude that the 2005 drafts of the TSPA Model could not be considered valid for the model's intended use based on the review criteria in the governing technical work plan (BSC 2005 [DIRS 173309]). The discussion on the four recommendations to resolve technical issues is presented first, followed by the discussion on the recommendations on GoldSim software and the related modeling file error management issues.

7.9.3.3 Implementation of the IVRT Recommendations

The IVRT recommendations to resolve technical issues and the status of implementation of these recommendations are as follows.

IVRT Recommendation #1: Conduct a sensitivity analysis for the Nominal and Early Failure Modeling Cases in a manner similar to that used in the analysis for the seismic ground motion and igneous intrusion modeling cases in Appendix M of the 2005 drafts of the TSPA-LA Model report. Include the results of the expanded sensitivity analysis in Appendix M of the next revision of the TSPA Model report. The IVRT suggested this expanded sensitivity analysis in response to concerns regarding not-met Review Criteria 1.5, 3.8, and 3.9 (BSC 2005 [DIRS 173309]).

Status: The Project provided supplemental information to the IVRT along with an expanded version of Appendix M as documented in the draft TSPA-LA Model (Gibson 2007 [DIRS 181099]). The IVRT examined the information and concluded that this activity yielded satisfactory results. The Project continued to perform relevant uncertainty and sensitivity analyses (Appendix K in Volume III of this TSPA-LA Model report) in order to enhance the TSPA-LA Model description and especially the confidence in its results. The TSPA-LA Model contains early failure analysis for DS as well as WP barriers. In addition, the appropriateness and reliability of the TSPA-LA Model was evaluated by a set of auxiliary analyses as discussed in Section 7.7.

IVRT Recommendation #2: Examine the potential for risk dilution for all important uncertain parameters identified in the expanded Appendix M sensitivity analyses described in Recommendation #1. The IVRT suggested this risk dilution analysis in response to the concerns regarding not-met technical work plan Review Criteria 1.1 and 3.3 (BSC 2005 [DIRS 173309]). Risk dilution is a potential nonconservatism that is a concern in a performance assessment model.

Status: In support of the IVRT concerns, the Project reported preliminary findings to the IVRT that indicated (1) the original process of including a normative expert may not have been fully utilized to ensure a consistent treatment of uncertainty, (2) the uncertainty describing some

parameters has a conservative bias, and (3) some parameters may need to be evaluated in TSPA sensitivity analyses as they may have inappropriate ranges with the potential for introducing risk dilution in TSPA calculations. Condition Report 7538 was filed to document these preliminary findings and track the completion of the work. The Project reported that as part of the condition report closure, additional work in this area might be required during the next TSPA Model revision cycle for any parameters found to be contributing to risk dilution. The condition report was closed with the completion of the planned work. The Project has since then initiated more rigorous additional analyses to ensure elimination of the potential for risk dilution concerns. For example, the TSPA-LA Model is supported by a number of auxiliary analyses as discussed in Section 7.7. Section 7.7.4 (with details in Appendix C of the TSPA-LA Model report, Volume III) includes a set of PMA that was specifically conducted to ensure that the TSPA-LA results are reasonable, reliable, and do not result from unmanaged optimistic and conservative modeling approaches. The PMA provides objective evidence for assessing performance margin and the degree of conservatism or non-conservatism in the TSPA-LA compliance model.

The Project established a parameter uncertainty team consisting of a group of the Project's subject matter experts in order to ensure uniform treatment of the uncertainty associated with the TSPA parameters. The parameter uncertainty team performed the uncertainty analyses (Section 6.1.3) and remediated the issues.

IVRT Recommendation #3: Revisit the screening arguments for EBS FEPs that were screened out on the basis of low consequence and provide substantiated arguments, preferably quantitative, that confirm they were of low consequence relative to mean dose. The IVRT suggested this analysis in response to concerns regarding not-met technical work plan Review Criterion 1.1 (BSC 2005 [DIRS 173309]). The objective of this recommendation was to ensure that there are no significant non-conservatisms indirectly included in the total system conceptual model because FEPs that could have potentially significant effects, if included, had been screened out on the basis of low consequence.

Status: The Project completed an initial re-evaluation of certain EBS FEPs that were excluded on the basis of low consequence and initiated condition report 7523 to track the completion of the work. The Project also re-evaluated several other FEPs in addition to those recommended by IVRT in order to further strengthen the Project's FEPs screening results. The condition report was closed as planned. Since the time this effort was completed, the Project has revised its entire FEPs database (SNL 2008 [DIRS 179476]) in order to implement a further enhanced screening process of the FEPs on the repository performance as well as the transparency and traceability of the individual FEPs' screening logic.

IVRT Recommendation #7: Perform an uncertainty and sensitivity analysis using the 2005 draft TSPA Model with model and input modifications proposed by the IVRT. The IVRT believed that the proposed uncertainty and sensitivity analysis addressed those fundamental issues responsible for the IVRT's not-valid decision on the 2005 drafts of the TSPA-LA Model. Achieving these goals requires performing uncertainty analyses for all modeling cases and the related Appendix M sensitivity analyses referred to in Recommendation #1 plus interpretation of all results. The IVRT has provided the TSPA department with a design for this uncertainty and sensitivity analysis, which was included in the IVRT final report (Gibson 2007 [DIRS 181099], Appendix C, Addendum C.III).

Status: The Project evaluated the IVRT recommended design for the uncertainty and sensitivity analysis analyses and responded to the IVRT by presenting a plan for performing the work needed to implement Recommendation 7 during FY06 to FY07. The proposed work plan consisted of two parts as summarized below:

- Revisions to process models and the TSPA Model placed a high priority on evaluating and mitigating potential non-conservatisms in the models. The work scope includes activities to: (1) address potential optimism in the representation of DS degradation, including improper emplacement as well as advective flow through cracks; (2) address potential optimism in the WP degradation representation, including advective flow through cracks; (3) obtain additional laboratory data to strengthen the basis for not including corrosion due to dust deliquescence in the TSPA Model, if possible; (4) include sorption on degraded corrosion products in the revised model, although changes to the EBS due to the incorporation of multipurpose TAD canisters are expected to result in modifications to the models for radionuclide mobilization and transport; (5) strengthen the basis for use of NpO_2 as the controlling phase for neptunium solubility in the in-package solubility model and address the unrealistic approach to solubility caps; and 6) revise the ash redistribution model to provide a more defensible representation for the effect of alluvial fan depositional and erosional processes on ash fall.

- Supplemental analysis to be performed using the TSPA Model. Expert judgment would be used to define alternative models and parameter ranges for input to the TSPA Model to address topics where the IVRT has expressed concerns relevant to recommendation #7 (e.g., incorporate additional realism). Results from this case could be used as a basis for comparison to results from the base case to provide improved understanding of sources of margin and to gain further insights into other impacts of conservatisms in the base case model.

As a result of the proposed implementation of some aspects of the modifications recommended by the IVRT, the model validation process evolved from the not-valid-for-intended purpose conclusion in the 2005 IVRT draft final report toward a new iteration of the validation process. This new iteration in turn would involve revising the compliance strategy, which would then result in revising the TSPA Model. The IVRT noted that although the revised TSPA Model resulting from the proposed work scope by the Project might not include all of the model modifications recommended by the IVRT, the progress made at that time in undertaking the activity suggested in Recommendation #7 was a positive step toward developing a TSPA Model adequate for supporting the LA.

The Project has since revised the technical work plans of the relevant supporting models in order to document the plans for completing the work mentioned in the first bullet and completed the planned work as documented in the respective revised supporting model reports referenced in Table 7.9-1. The Project also completed the initial supplemental analyses mentioned in the second bullet, which have been since superseded by additional auxiliary analyses (Section 7.7). The auxiliary analyses include a set of performance margin analyses (Section 7.7.4 and Appendix C). The performance margin analysis was designed to provide objective evidence for assessing performance margin and degree of conservatism or non-conservatism in the TSPA-LA

Model. As mentioned earlier, the Project also continued to perform other relevant uncertainty and sensitivity analyses (Appendix K in Volume III of the TSPA-LA Model report) in order enhance the TSPA-LA Model description, and especially the confidence in its results.

It was mentioned earlier that a relatively small number of IVRT issues remained not fully addressed according to the responsible IVRT panel members (Booth 2006 [DIRS 176638]). The Project continued to work on these remaining issues since the IVRT was closed with its final report in February 2006 (Gibson 2007 [DIRS 181099], Appendix C). As mentioned in the preceding paragraph, the Project revised the technical work plans (Table 7.9-1) for the relevant process models to include a plan for the work needed to address these remaining issues. The planned work has been completed and documented in the respective supporting model reports. Table 7.9-1 summarizes the nature of these remaining IVRT issues and identifies the technical work plan where the work was planned and the model reports where the completed work is documented. There were a few IVRT issues for which no additional work was deemed necessary by the Project and the reasons for this decision are also provided in Table 7.9-1.

Recommendations on GoldSim Software and the Related Modeling File Error Management Issues

It should be noted that the TSPA-LA Model is based on an updated version of GoldSim (V. 9.60, STN: 10344-9.60-00 [DIRS 181903]) with advanced features, as well as a number of supporting model softwares. However, the Project considered that the IVRT recommendations are also applicable to model execution using the updated versions of these softwares.

IVRT Recommendation #4: Provide objective evidence that the changes in the TSPA Model do not change the current TSPA Model results obtained using earlier GoldSim service packs used in the drafts of the TSPA-LA Model the IVRT reviewed.

Status: The Project provided the IVRT with plots comparing results from GoldSim V. 8.02.400 (STN: 10344-8.02-04 [DIRS 173352]) (using Service Pack 4) with GoldSim V. 8.02.500 (STN: 10344-8.02-05 [DIRS 174650]) (using Service Pack 5). Comparisons of calculated mean dose were provided for the nominal early failure, igneous intrusive, volcanic eruption, and seismic mechanical damage modeling cases. No differences were observed between the results for any of the cases. The IVRT concluded that the current TSPA Model results were not changed by the changes in the TSPA Model.

IVRT Recommendation #5: The IVRT should be kept informed on a timely basis (within one week) if additional GoldSim model file errors are identified.

Status: The Project response to the IVRT stated that during model development, any errors found in the model file are identified internally as the in-process model evolves. It further stated that the TSPA department has provided the IVRT with access to the model file error log during the IVRT review and provided monthly updates on an ongoing basis. The response further stated that as part of the Performance Document Management System process, formalized desktop instructions would document this developmental error-tracking process via Condition Report 7539. In addition, the response stated that after the model is finalized and the document is

approved, any further errors would also be identified in the Corrective Action Program. Condition Report 7539 was subsequently closed as planned.

IVRT Recommendation #6: Any new model file errors identified should be evaluated for impact on modeling cases reported in the TSPA-LA (Gibson 2007 [DIRS 181099], Appendix C]).

Status: The Project explained to the IVRT the procedure that is followed by the TSPA department to identify and log errors and conduct updates to the model and correct the errors as necessary. After the model is finalized and the document is approved, further identification of errors would require documentation in the Corrective Action Program. The response to the IVRT indicated that Performance Document Management System planned to formalize this process into a desktop instruction via Condition Report 7539. The IVRT considered filing a condition report regarding formalizing the developmental error tracking and impact assessment process as a positive step toward ensuring the constructive resolution of this issue. The Project since then formalized the process in the TSPA Configuration Management Desktop Guide, desktop Error Tracking and Evaluation for TSPA Modeling Activities, and Condition Report 7539 was closed.

Summarizing, the IVRT review comments and recommendations, which have been addressed and implemented by the Project, strengthened the TSPA-LA Model as intended. The iterative model development process that the Project pursued during the last decade, of which the IVRT review was an integral part, resulted in the TSPA-LA Model documented in this report. The TSPA-LA Model is based on a sound technical database, fully compliant with the quality assurance requirements, and verified and valid for its intended use by a number of criteria applied during and after the model development. The three empanelled reviews presented in this section played an important role in the development of the TSPA-LA Model.

Table 7.9-1. Summary of Responses to the Remaining IVRT Comments

Remaining IVRT Comment	Additional Work Conducted since the IVRT Review and Documentation where the Work is Located
Remaining IVRT Comments (1) Booth (2006 [DIRS 176638]) provides a full description of all IVRT comments, including those that remained not fully addressed as per the IVRT panel members. These remaining comments are listed here. See Booth (2006 [DIRS 176638]) for full descriptions of the individual remaining comments, which are only abstracted below for brevity. (2) For certain comments, the comment numbers in Booth (2006 [DIRS 176638]) have a zero in front of the number. For example, SZT-02 and UZF-01 in Booth (2006 [DIRS 176638]) are same as SZT-2, UZF-1, respectively, in Section 7.8 of the TSPA-LA (Gibson 2007 [DIRS 181099]).	**Additional Work Conducted since the IVRT Review and Documentation where the Work is Located.** (Note: The project responded to all of the IVRT comments and developed position statements on some of the comments that were difficult to resolve. The IVRT reviewed the Project responses and positions, and found that a relatively small set of comments were not fully addressed to their satisfaction when the IVRT was closed in February 2006. These comment-responses are documented in *Independent Validation Review Team (IVRT) Issues, Bechtel-SAIC Responses, and IVRT Assessment of Responses Related to Review of the TSPA Model and Supporting Analyses and Model Reports* (Booth 2006 [DIRS 176638]). Since the time the IVRT review was closed, the Project completed additional work to address the remaining comments and documented that work as shown below).
Natural Barrier System	
SZT-02: The IVRT was concerned that the 1-D model was not compared to either the 3-D model or the Site-Scale Transport Model under multiple climate changes or with intermittent WP failure and radionuclide release.	The project completed the work planned (BSC 2006 [DIRS 177375]) to address this comment. The comparison work for the base-case model is documented in the *Saturated Zone Flow and Transport Model Abstraction* (SNL 2008 [DIRS 183750], Section 7). The implementation of the 1-D model in dose calculations for the following modeling cases is presented in this TSPA-LA as follows: DS and WP early failure modeling cases in Sections 6.4.1 and 6.4.2, respectively; the disruptive events due to igneous and seismic events in Sections 6.5.1 and 6.5 and Sections 6.6.1 and 6.6.2, respectively; and human intrusion in Sections 6.7.1 and 6.7.2.
UZF-01: The IVRT was concerned that the UZ Flow Model and Submodels analysis and/or model reports do not demonstrate that the three calibrated flow fields developed to address uncertainty in the infiltration rates also capture the uncertainty in the flow fields.	Booth 2006 [DIRS 176638] concluded that the project position was appropriate and that no further work was needed. However, the project subsequently developed a new infiltration model (SNL 2007 [DIRS 182145]) and expanded the treatment of uncertainty in the UZ (SNL 2007 [DIRS 184614]) to use four, rather than three, calibrated flow fields.
UZF-02: The IVRT felt that the comparison between matrix properties measured at Busted Butte with properties calculated for the CHnv did not justify a lack of fracture flow in the CHnv because there was little evidence that hydrologic conditions in the CHnv at Busted Butte are similar to hydrologic conditions in the deeply buried CHnv beneath the repository location, and no correlation was presented between matrix and fracture properties at either location.	The project completed planned (BSC 2006 [DIRS 177465]) work to address this comment. A dual continuum model replaced the single fracture flow model approach that was used in the version of the UZ Flow analysis and/or model report that the IVRT reviewed. The work is documented in *UZ Flow Models and Submodels* (SNL 2007 [DIRS 184614], Sections 6 and 7).

Table 7.9-1. Summary of Responses to the Remaining IVRT Comments (Continued)

Remaining IVRT Comment	Additional Work Conducted since the IVRT Review and Documentation where the Work is Located
Natural Barrier System (Continued)	
CPMS-09(CPM-16): As in UZF-1, this comment deals with uncertainty in UZ flow fields. The remaining questions related to this comment are: (1) whether uncertainty in unsaturated zone flow fields is adequately captured through the use of three calibrated property sets for the low, mean, and high infiltration cases; and (2) the appropriateness of using relaxed constraints for measurements with large uncertainties to develop calibrated property sets for a given infiltration rate.	The project position presented in Booth (2006 [DIRS 176638]) adequately addressed the remaining two parts of this comment. The uncertainties in the flow fields and calibrated properties are not hydraulically significant relative to the uncertainty in the magnitude of the infiltration, which is being addressed in UZ flow with discrete flow fields spanning different climates. Consequently, no additional work is planned on the calibrated properties model.
CPMS-14(CPM-21): This comment deals with uncertainty in UZ flow calibrated parameters. The IVRT was concerned that while the individual parameter uncertainties were used to bound the calibration process, it was not clear that all of the types of parameter uncertainty mentioned in its comment were adequately captured in the CPM.	The project position presented in Booth (2006 [DIRS 176638]) addressed the remaining parts of the comment, especially by the comparison with the bore-hole data approach used. Additional work was considered not likely to make a significant contribution because the uncertainties in the flow fields and calibrated properties are not hydraulically significant relative to the uncertainty in the magnitude of the infiltration, which is being addressed in UZ flow with discrete flow fields spanning different climates.
Disruptive Events—Volcanic Eruption (VE) and Igneous Activity (IGI)	
CMT-062105-112723-09: The IVRT was concerned with the lack of treatment of the possible effects of dike swarms due to future igneous intrusion on the UZ and SZ flow and transport and how the treatment would impact the TSPA results.	The IVRT and TSPA were unable to reach a compromise resolution acceptable to both parties. This impasse was to be recorded in the TSPA-LA Model report as a part of Section 7 with a response from the Project as to its significance in the overall validation of the TSPA-LA Model (Booth 2006 [DIRS 176638]). The project response as to the significance of the comment in the overall validation of the TSPA-LA Model is as follows: The disruptive event FEP disposition argument for 1.2.10.02.0A, Hydrologic Response to Igneous Activity (BSC 2005 [DIRS 173981], Section 6.2.2.10), addressed the comment. The basis argument is that at the scale of the UZ site scale model or the SZ regional model, the effects of dikes on UZ and SZ flow, if they occur at all, are too localized to affect TSPA results. Analyses based on analog results show that mineralogical changes in the host rock adjacent to contacts with dikes typically extend for a few tens of cm to perhaps a couple of meters into the host. Again, at the scales of the SZ and UZ models, the extent of such effects is negligible. Much of the analog work is documented in (SNL 2007 [DIRS 174260], Appendix F).

Table 7.9-1. Summary of Responses to the Remaining IVRT Comments (Continued)

Remaining IVRT Comment	Additional Work Conducted since the IVRT Review and Documentation where the Work is Located
Disruptive Events—Volcanic Eruption (VE) and Igneous Activity (IGI) (Continued)	
IGI-01: The IVRT was concerned that the Project treated dike intrusion effect conservatively; the repository block is a strong monolith, but the path of dike ascent will be structurally controlled to follow primary faults such that few if any dikes will penetrate the Yucca Mountain structural block and can be demonstrated readily by numerical analysis.	The planned work that addresses this IVRT concern is in *Technical Work Plan for: Igneous Activity Assessment for Disruptive Events* (BSC 2006 [DIRS 182219]). The report, *Characterize Eruptive Processes at Yucca Mountain, Nevada* (SNL 2007 [DIRS 174260], Section 6.3.3), includes analog information about the relationship between dike propagation and geologic structures and the tendency of dikes to follow pre-existing structures. Revision 02 of *Dike/Drift Interactions* (SNL 2007 [DIRS 177430]) includes descriptions of analyses of 2 D dike propagation driven by compressible magma, a 2 D model of a rising dike encountering faults and/or stratigraphic discontinuities, and an extension of an analysis of secondary breakout consistent with higher magma pressures described in Revision 01 (BSC 2004 [DIRS 177430], Section 6.5). These discussions show that the repository block does not behave as a strong monolith and will support the abstraction that an ascending dike would propagate through the repository. The analysis in *Dike/Drift Interactions* (SNL 2007 [DIRS 177430], Section 6.3.4) shows that dikes will not be diverted into faults in the rocks of Yucca Mountain except for steeply dipping faults at depths of only a few hundred meters.
IGI-02: As in the case of IGI-01, the IVRT was concerned that an ascending dike will tend to follow pre-existing fractures that it encounters.	The planned work that addresses this IVRT concern, is in *Technical Work Plan for: Igneous Activity Assessment for Disruptive Events* (BSC 2006 [DIRS 182219]), which discusses the differences between the conceptual models and TSPA implementation of dike interactions with rock. *Characterize Eruptive Processes at Yucca Mountain, Nevada* (SNL 2007 [DIRS 174260], Section 6.3.3) includes results of analogue work that shows an ascending dike will tend to follow preexisting fractures. *Dike/Drift Interactions* (SNL 2007 [DIRS 177430], Section 6) provides descriptions of 3D representation of dike propagation driven by compressible magma, a 2 D model of a rising dike encountering faults and/or stratigraphic discontinuities, and topographic effects on dike propagation. The results of these investigations will address the nature of interactions between ascending dikes and intruded rocks. The analysis in *Dike/Drift Interactions* (SNL 2007 [DIRS 177430], Section 6.3.4), shows that dikes will not be diverted into faults in the rocks of Yucca Mountain except for steeply dipping faults at depths of only a few hundred meters.

Table 7.9-1. Summary of Responses to the Remaining IVRT Comments (Continued)

Remaining IVRT Comment	Additional Work Conducted since the IVRT Review and Documentation where the Work is Located
Disruptive Events—Volcanic Eruption (VE) and Igneous Activity (IGI) (Continued)	
IGI-05: The IVRT question asked for the basis for assuming the behavior of the WP to be radically different in the Igneous Intrusion Modeling Case compared with the Nominal Modeling Case. The IVRT believed that additional analyses were necessary to re-evaluate WP performance under magmatic conditions with more representative confining pressures generated by magma filling the drifts and would help address the comment.	The planned work that addresses this IVRT concern is in *Technical Work Plan for: Igneous Activity Assessment for Disruptive Events* (BSC 2006 [DIRS 182219]). Analyses of WP degradation after magma intrusion, described in *Dike/Drift Interactions* (SNL 2007 [DIRS 177430]), provides descriptions of an analysis that shows the TAD canister lid weld fails after exposure to magmatic temperatures and effusive and multiphase flow conditions. That analysis provides the basis for the assumption about WP damage after contact by magma. The 2 D model for magma cooling considers the effects of hot and cold WPs. *Dike/Drift Interactions* (SNL 2007 [DIRS 177430]) also includes an estimate of invert performance. An estimate of WP degradation after combined (igneous + seismic) events (SNL 2007 [DIRS 177432]), includes an assumption about the severity of WP damage following an intrusion. Magmatic pressures following an intrusion are discussed in *Dike/Drift Interactions* (SNL 2007 [DIRS 177430], Section 6.4.8.1). The effect of magmatic temperatures, pressures, and gas composition on the WPs and waste form is discussed in Section 6.4.8.3 of *Dike/Drift Interactions* (SNL 2007 [DIRS 177430]). An analysis of WP failure due to external pressurization is included in Appendix E in *Dike/Drift Interactions* (SNL 2007 [DIRS 177430]).
IGI-WP/WF-04: The IVRT felt that the disconnect on how the WP responds to the magma was still remaining in that magma does not contact the waste, but there is no impedance to the flow of water through the magma-filled drift and the WP. Additionally, in Appendix J of *Atmospheric Dispersal and Deposition of Tephra from a Potential Volcanic Eruption at Yucca Mountain, Nevada* (BSC 2005 [DIRS 174067], a historic document cited for background information), it is stated that the WP is breached and magma enters the WP before the dike turns into a volcanic event; again a disconnect between different parts of the TSPA.	The planned work that addresses this IVRT concern is in *Technical Work Plan for: Igneous Activity Assessment for Disruptive Events* (BSC 2006 [DIRS 182219]). *Dike/Drift Interactions* (SNL 2007 [DIRS 177430]) includes descriptions of the mechanism of TAD canister failures at end cap welds. This failure mechanism is the basis for an assumption that WPs contacted by magma provide no protection for waste, which is documented in *Number of Waste Packages Hit by Igneous Intrusion* (SNL 2007 [DIRS 177432], Section 5.1). In addition, the TSPA-LA Section 6.5 includes descriptions of assumptions about the form of radionuclides suspended in cooled basalt. The radionuclide inventory is available in the first TSPA timestep, but the magnitude of release is controlled by radionuclide solubilities. An analysis of WP failure due to external pressurization is included in Appendix E of *Dike/Drift Interactions* (SNL 2007 [DIRS 177430], Section 6.4.8.3.1).

Table 7.9-1. Summary of Responses to the Remaining IVRT Comments (Continued)

Remaining IVRT Comment	Additional Work Conducted since the IVRT Review and Documentation where the Work is Located
Disruptive Events—Volcanic Eruption (VE) and Igneous Activity (IGI) (Continued)	
IGI-WP/WF-05: The IVRT was concerned that no impact analysis was done to account for the heat sink effect of the WP.	The planned work that addresses this IVRT concern is in *Technical Work Plan for: Igneous Activity Assessment for Disruptive Events* (BSC 2006 [DIRS 182219]). *Dike/Drift Interactions* (SNL 2007 [DIRS 177430]) provides and documents an alternative model that is a tabulation of drift centerline temperatures based on a 2 D model for magma cooling, while considering effects of hot and cold WPs (SNL 2007 [DIRS 177430], Section 6.4.7.2). The analysis results support an assumption about the severity of WP damage following contact with magma (SNL 2007 [DIRS 177432], Section 5.1).
VE-01: This IVRT comment is similar to IGI-01. The geologic block containing the repository was chosen for its strong monolithic qualities, as discussed in the 'siting' criteria; however, in the Igneous Intrusion Modeling Case, the repository geologic block is assumed to be a weak monolith and, therefore, a dike would penetrate the block rather than follow planes of weakness within the surrounding formation. There seems to be an inconsistency in the assumption made for the Igneous Intrusion Modeling Case and the 'siting' criteria.	The relevant work plan is the *Technical Work Plan for: Igneous Activity Assessment for Disruptive Events* (BSC 2006 [DIRS 182219]). The report, *Characterize Eruptive Processes at Yucca Mountain, Nevada* (SNL 2007 [DIRS 174260]), includes analogue information about the relationship between dike propagation and geologic structures and the tendency of dikes to follow pre-existing structures. *Dike/Drift Interactions* (SNL 2007 [DIRS 177430]) includes descriptions of analyses of 2 D dike propagation driven by compressible magma (Section 6.3), a model of a rising dike encountering faults and/or stratigraphic discontinuities (Section 6.3), and an extension of analysis of secondary breakout consistent with higher magma pressures (SNL 2007 [DIRS 177430], Section 6.5). These discussions show that the repository block does not behave as a strong monolith and will support the abstraction that an ascending dike would propagate through the repository.
VE-02: The IVRT was concerned with the extreme mass balance error in the old tephra redistribution model.	The relevant work plan is the *Technical Work Plan for: Igneous Activity Assessment for Disruptive Events* (BSC 2006 [DIRS 182219]). The report, *Redistribution of Tephra and Waste by Geomorphic Processes Following a Potential Volcanic Eruption at Yucca Mountain, Nevada* (SNL 2007 [DIRS 179347], Section 6.5), documents a new ash redistribution model that provides estimates of the amount of waste in remobilized tephra for each cell in the model grid and includes geomorphic processes for landscape features characteristic of the Fortymile Wash watershed. Tephra-soil mixing rates (dilution) are explicitly addressed in the new ash redistribution model. The new model eliminates the mass balance error that was inherent in the previous model by using a mass conservative analytical method to calculate diffusion into the soil on distributary channels and interchannel divides at the RMEI location.

Table 7.9-1. Summary of Responses to the Remaining IVRT Comments (Continued)

Remaining IVRT Comment	Additional Work Conducted since the IVRT Review and Documentation where the Work is Located
Disruptive Events—Volcanic Eruption (VE) and Igneous Activity (IGI) (Continued)	
VE-03: The IVRT commented that the ash distribution model they reviewed for leaching radionuclides from ash deposits and redepositing them in the underlying soil does not seem to account for residence time, rainfall, and depletion of radionuclides in the overlying ash. The current model most likely overestimates the amount and duration of exposure to radionuclides from an ash deposit, perhaps significantly.	Work has been planned in *Technical Work Plan for: Igneous Activity Assessment for Disruptive Events* (BSC 2006 [DIRS 182219]) to address the ash leaching aspect. *Redistribution of Tephra and Waste by Geomorphic Processes Following a Potential Volcanic Eruption at Yucca Mountain, Nevada* (SNL 2007 [DIRS 179347], Section 6.5) documents a new ash redistribution model that addresses the temporal near-surface and at-depth concentrations of fuel (waste) in soil at the location of the RMEI. In the modeling method, a single value of diffusivity is applied to fuel (waste), representing all radionuclides. Support for this approximation comes from measurements that indicate that different radionuclide species are dispersed in the soil column at similar rates (Anspaugh et al. 2002 [DIRS 169793]). Diffusion is assumed to occur within a finite thickness corresponding to the distance from the surface to impermeable soil horizons at depth (with a different thickness for the divide and channel).
VE-04: The IVRT was concerned that active alluvial fans are distributary environments with long-term deposition rather than erosion, as apparently assumed in the TSPA model. It believes that floodwaters rework stream channel gravels and transport them downstream, replacing them with upstream gravel. When the deposited gravel sufficiently raises the channel bed, water will escape and create a new channel. The net effect is to build the fan higher while continually mixing gravel and moving it toward the toe. The process is much more dynamic than what is captured in the TSPA conceptual model.	The work planned in the *Technical Work Plan for: Igneous Activity Assessment for Disruptive Events* (BSC 2006 [DIRS 182219]) to address the comment of alluvial fan deposition was completed. *Redistribution of Tephra and Waste by Geomorphic Processes Following a Potential Volcanic Eruption at Yucca Mountain, Nevada* (SNL 2007 [DIRS 179347], Section 6.5), documents a new ash redistribution model that is based on detailed geomorphic descriptions of the upper part of the Fortymile Wash alluvial fan. The work includes a description of the stability of interchannel divides and erosion/deposition rates for distributary channels.

Table 7.9-1. Summary of Responses to the Remaining IVRT Comments (Continued)

Remaining IVRT Comment	Additional Work Conducted since the IVRT Review and Documentation where the Work is Located
Disruptive Events—Volcanic Eruption (VE) and Igneous Activity (IGI) (Continued)	
VE-05: The IVRT comment deals with the instantaneous incorporation of waste in ash. The IVRT was concerned that the Project treatment of instantaneous incorporation of waste (radionuclides) into erupted ash is not justified and inconsistent with the regulatory expectation that the DOE should use a full range of defensible and reasonable parameters in their performance model rather than relying on extreme physical situations and parameter values. Project treatment of instantaneous incorporation of waste is an example where the use of extreme assumptions leads to results that may be very difficult to defend.	The comment has been addressed by the analyses documented in *Atmospheric Dispersal and Deposition of Tephra from a Potential Volcanic Eruption at Yucca Mountain, Nevada* (SNL 2007 [DIRS 177431]), as described below. Significant progress has been made in defining the processes for the incorporation of exposed waste into the tephra transported in the ASHPLUME model and adding realism in how they are incorporated into the eruptive case model. An analysis of the effects of contact with a WP and the waste form in the intrusion scenario indicates that the integrity of the WP would be compromised (SNL 2007 [DIRS 177430], Section 6.4.8.3). For the Volcanic Eruption Modeling Case, once intrusion of the repository occurs, a volcanic conduit does not form immediately, but rather forms gradually as continued magma flow locally widens the dike. This process may take hours to days to reach the repository depth. If a developing conduit intersects an emplacement drift, the WPs located partially or entirely within the conduit would experience elevated temperatures (1,000°C) for an extended period (100s of hours) as well as other degrading conditions. The WPs located within the boundaries of the developing conduit would also be subjected to magma pressure fluctuations, differential movement by unsteady magma flow, impact by failing wall-rock, and physical degradation by fragmenting melt particles (SNL 2007 [DIRS 174260], Appendix F); (SNL 2007 [DIRS 177430], Section 6.4.8.3.2)). Physical damage to the WP in this energetic conduit environment is assumed to result in failure of the WPs and entrainment of fragmented waste within the rising magma (SNL 2007 [DIRS 177431], Section 5.1.2). A review of international literature on waste form particle size indicates that the likely range resulting from magma/waste interaction in the conduit is 0.0001 cm to 0.2 cm, based on studies of spent fuel pellet size, mechanical shock, crushing and milling, dry and aqueous oxidation/corrosion, and the Chernobyl reactor accident analogue (SNL 2007 [DIRS 177431], Appendix F). Some portion of these waste particles is assumed to be suspended and well-mixed with the magma, carried to the surface through the conduit, and erupted at the vent. The waste particles within the magma are treated as refractory particles (analogous to xenoliths) that form a component of tephra particles upon fragmentation of the magma (SNL 2007 [DIRS 177431], Section 6.5.2.6). The value for the input parameter, waste incorporation ratio, has therefore been revised to reflect a neutral combination of the tephra and waste particle size distributions. The ASHPLUME model abstraction assumes that the various eruption phases are condensed into a single violent Strombolian phase (SNL 2007 [DIRS 177431], Section 5.1.1) with concurrent effusion of lava, sustained eruption column, and construction of a scoria cone. The waste incorporated into the magma is therefore distributed among the various eruptive products—scoria cone, lava flows, and tephra blanket—over the course of the eruption. Accounting is made, by means of a magma partitioning factor, for the proportion of waste-containing magma that is eventually deposited in geologically resistant eruptive products (scoria cone, lava flows) that do not contribute to dose (SNL 2007 [DIRS 177431], Section 6.5.2.22).

Table 7.9-1. Summary of Responses to the Remaining IVRT Comments (Continued)

Remaining IVRT Comment	Additional Work Conducted since the IVRT Review and Documentation where the Work is Located
Disruptive Events—Volcanic Eruption (VE) and Igneous Activity (IGI) (Continued)	
CMT-062105-124045-60; CMT-062005-125053-19; CMT-062105-112025-93; CMT-062105-112302-53; CMT-062105-124255-71; CMT-062105-124619-89: These similar IVRT comments deal with inconsistent treatment of basalt properties in the drift and above and below it. Response to IGI-06 addressed the subsurface aspects of these comments. See Booth (2006 [DIRS 176638]) and the material presented in the column at the right for the specific aspects associated with the unresolved parts of the individual comments and the corresponding work the Project completed to address these parts.	The following analysis and model reports were updated to address the remaining parts of the comments in this group: *Characterize Eruptive Processes at Yucca Mountain, Nevada* (SNL 2007 [DIRS 174260]); *Dike/Drift Interactions* (SNL 2007 [DIRS 177430]); *Magma Dynamics at Yucca Mountain, Nevada* (Dartevelle and Valentine 2007 [DIRS 182090]); *Number of Waste Packages Hit by Igneous Intrusion* (SNL 2007 [DIRS 177432]); *Atmospheric Dispersal and Deposition of Tephra from a Potential Volcanic Eruption at Yucca Mountain, Nevada* (SNL 2007 [DIRS 177431]); and the model report, *Redistribution of Tephra and Waste by Geomorphic Processes Following a Potential Volcanic Eruption at Yucca Mountain, Nevada* (SNL 2007 [DIRS 179347]). The work completed in response to the individual comments in this group is summarized below. **CMT-062105-124045-60:** Comment items related to inconsistent properties of intrusive and eruptive phases, magma characteristics, and eruption energies associated with various eruption phases are described in *Characterize Eruptive Processes at Yucca Mountain, Nevada* (SNL 2007 [DIRS 174260], Section 6.3.2). Partitioning of erupted material into lava, cone forming facies (scoria), and tephra (ash), consistent with the eruption phases described in *Characterize Eruptive Processes at Yucca Mountain, Nevada* (SNL 2007 [DIRS 174260], Section C.9), was used in *Atmospheric Dispersal and Deposition of Tephra from a Potential Volcanic Eruption at Yucca Mountain, Nevada* (SNL 2007 [DIRS 177431]) to divide the mass of entrained waste among the erupted products and provide consistency between the erupted products and eruption phases. **CMT-062005-125053-19:** For the Igneous Intrusion Modeling Case, this comment (i.e., inconsistent properties of intrusive and eruptive phases, magma characteristics, and eruption energies associated with various eruption phases) is addressed (SNL 2007 [DIRS 177430], Section 6) by clarifying that the magma in the drift offers no additional resistance to flow beyond that of the surrounding host rock. In the case of the Hawaiian dike complexes, water table elevations are found to be as much as 1,000 m higher inside the complexes as compared with locations outside the dike complexes (Booth 2006 [DIRS 176638], pp. 349 to 351). Water table elevation changes caused by dike complexes in more arid climates such as Yucca Mountain are expected to be much smaller and should be bound by the existing rise in the water table as modeled for future climates (SNL 2008 [DIRS 184748], Section 6.4.8). Intrusive dikes have been observed to reach the ground surface in Hawaii (Booth 2006 [DIRS 176638], pp. 349 to 351). Nevertheless, surface eruptions by dikes have not led to large surface impoundments of water in Hawaii despite high levels of rainfall that occur on some parts of the islands. Based on these observations, the effects of dikes on surface water flow at Yucca Mountain are not expected to result in significant changes in infiltration behavior or the generation of significant surface water impoundments. Therefore, the effects of dikes on unsaturated zone flow, radionuclide transport, and infiltration are expected to be beneficial to the performance of the natural barriers, but minimal. However, the overall effects on changes in drift seepage are less certain.

Table 7.9-1. Summary of Responses to the Remaining IVRT Comments (Continued)

Remaining IVRT Comment	Additional Work Conducted since the IVRT Review and Documentation where the Work is Located
	The comment is beyond the scope considered in the analyses of the Volcanic Eruption Modeling Case, which examines the direct deposition and redistribution of contaminated waste on the ground surface but does not include percolation through the subsurface components of an igneous event. *Dike/Drift Interactions* (SNL 2007 [DIRS 177430], Section 5.4.1) said, "The permeability of any contact metamorphic aureole surrounding the intruded drifts is assumed to be as great as that of the bulk host rock. The basalt will undoubtedly fracture during cooling, but will fracture to such an extent that the resulting secondary permeability will not provide an additional impediment to seepage." That was an assumption that was used in the seepage water section that has been converted into a literature review. The assumption was, therefore, no longer needed for Revision 02 of *Dike/Drift Interactions* (SNL 2007 [DIRS 177430]) and was not included. **CMT-062105-112025-93:** TSPA-LA Model for the Igneous Scenario Class—FEPs disposition. The surface effects are addressed in the Volcanic Eruption Modeling Case by inclusion of the partitioning of erupted products into lava, cone forming facies, and tephra (ash) in *Atmospheric Dispersal and Deposition of Tephra from a Potential Volcanic Eruption at Yucca Mountain, Nevada* (SNL 2007 [DIRS 177431]), and by redistribution of contaminated ash as described in the new FAR model report, *Redistribution of Tephra and Waste by Geomorphic Processes Following a Potential Volcanic Eruption at Yucca Mountain, Nevada* (SNL 2007 [DIRS 179347]). For the lava, data from field observations indicate that the surfaces of flows are geomorphically stable for long time periods. Hence, the bulk of radionuclides in lava flows would be isolated from redistributed materials moved into distributary channels. In addition, lava flows in the immediate vicinity of Yucca Mountain are of small volume and aerially restricted. If a future volcano penetrated the repository, such flows, if they occurred, would be localized and distant from the location of the RMEI. For the cone-forming facies, a user-defined parameter (radius) in the tephra redistribution model determines the amount of the cone-forming material that is prevented from being redistributed. Cone forming material beyond this user-defined radius is treated the same as tephra dispersed during the eruption. The steepness of the pre-eruption slopes is compared with a critical slope angle and material on slopes equal to or greater than the critical angle that is considered available for redistribution. Partitioning of erupted material into lava, cone forming facies (scoria), and tephra (ash), consistent with the eruption phases described in *Characterize Eruptive Processes at Yucca Mountain, Nevada* (SNL 2007 [DIRS 174260], Section C.9), was used in *Atmospheric Dispersal and Deposition of Tephra from a Potential Volcanic Eruption at Yucca Mountain, Nevada* (SNL 2007 [DIRS 177431]) to divide the mass of entrained waste among the erupted products and provide consistency between the erupted products and eruption phases. The parts of the comment that deal with development of potential fast pathways for groundwater flow in cooled basalt are beyond the scope considered in analyses of the eruption modeling case, which examines the direct deposition and redistribution of contaminated waste on the ground surface but does not include percolation through the subsurface components of an igneous event. Those effects are described for CMT-062005-125053-19. **CMT-062105-112302-53:** This comment addresses long-term (post-cooling) effects of igneous activity on

Table 7.9-1. Summary of Responses to the Remaining IVRT Comments (Continued)

Remaining IVRT Comment	Additional Work Conducted since the IVRT Review and Documentation where the Work is Located
	groundwater flow and transport during the postclosure period. The parts of the comment that are related to the flow of groundwater through cooled basalt and the potential for development of fast pathways are addressed by the response to IGI-06. Analog information included in *Dike/Drift Interactions* (SNL 2007 [DIRS 177430], Section 6.7) addresses changes to groundwater chemistry resulting from percolation through cooled basalt. However, *Dike/Drift Interactions* (SNL 2007 [DIRS 177430]) will no longer include basalt-water chemistry as an abstraction for TSPA, and the text specified above is not needed. The text was included in the TSPA model report (Section 6.5). The TSPA inputs for pH and ionic strength of water that has reacted with cooled basalt is provided by the *In-Package Chemistry Abstraction* (SNL 2007 [DIRS 180506], Section 6[a]). **CMT-062105-124255-71:** This comment is addressed by the response to comment IGI-06. **CMT-062105-124619-89:** This comment was addressed consistent with responses to CMT-062005-125053-19 and IGI-06 in Booth (2006 [DIRS 176638]). The Project noted that the TSPA and DDI reports treat the flux the same. The flux entering the drift is assumed to be the percolation flux from the base of the PTn. The flux remains the same through the magma filled drift (after wall rock and magma cool to below boiling). The confusion lies with the statement in *Dike/Drift Interactions* (SNL 2007 [DIRS 177430]), "the magma in the drift offers no resistance to flow." This statement is misleading and was modified to state (SNL 2007 [DIRS 177430], Section 6) that the magma in the drift offers no additional resistance to flow beyond that of the surrounding host rock. The text in the TSPA-LA (Section 6.5.1) states that the intruded basalt in the drift is assumed to provide no resistance to water flow; because the entire WP and DS are failed, the entire seepage flux enters the WP and is available for advective transport of radionuclides from the EBS (SNL 2007 [DIRS 181244], Section 6.7.1.1).

Table 7.9-1. Summary of Responses to the Remaining IVRT Comments (Continued)

Remaining IVRT Comment	Additional Work Conducted since the IVRT Review and Documentation where the Work is Located
Engineered Barrier System	
CMT-062105-121205-14 and CMT-062105-113319-24: The IVRT was concerned that even though the TSPA Seismic Scenario Class represented a commendable attempt to address a very complex problem and state of the art modeling was used intelligently to provide a reasonable assessment of damage due to severe ground motions, the key assumption that translates the predictions is the assumption of stress corrosion cracking that eliminates advective flow as a result of the damage to vibratory ground motion. The IVRT felt that this assumption needed to be more fully described and justified.	The Project has made a significant enhancement of the FEPs screening process and revised the FEPs database since the IVRT review was closed. The advective flow and transport of radionuclides through the WP as a result of the damage due to vibratory ground motionwas evaluated and screened out. A detailed discussion of the FEPs screening process, including the WP and DS degradation due to stress corrosion cracking, is presented in the FEPs database (DTN: MO0706SPAFEPLA.001 [DIRS 181613]).
EBS-21, CMT-062005-130513-66, CMT-062105-104839-19, CMT-062105-100225-22, and CMT-062105-100349-08: In these similar comments, the IVRT expressed the concern that the Project's treatment of radionuclides transport due to the processes of irreversible and reversible sorption to colloids was inconsistent across the EBS components.	The planned work to address this IVRT concern is in *Technical Work Plan for: Near-Field Environment: Engineered Barrier System: Radionuclide Transport Abstraction Model Report* (BSC 2006 [DIRS 177739]) and *Technical Work Plan for Waste Form Testing and Modeling* (BSC 2006 [DIRS 177389]). The planned work was completed. Colloids assisted radionuclide transport through the EBS components is treated consistently as due to equilibrium and kinetic sorption processes as appropriate (SNL 2007 [DIRS 177407], Section 6.3.4.4).
EBS-29, EBS-49, and CMT-062105-101939-31: The IVRT concern for these comments is similar—water balance within WP. The IVRT was concerned that the basis for the (1) rind product from the reacted spent nuclear fuel becoming fully saturated quickly with water in both seep and non-seep environments reported in the reviewed version of *EBS Radionuclide Transport Abstraction* (SNL 2007 [DIRS 177407]). Section 6.5.3 was not provided and felt that this assumption may result in very conservative-release concentrations for radionuclides not controlled by solubility limits (Tc, I, and C) and discard a more realistic conceptual model (Section 6.6.2 of the reviewed check copy draft of EBS Radionuclide Transport Abstraction), and (2) diffusive release of colloids of larger diameter than the assumed thin water film, was not provided.	The planned work to address this IVRT concern is in *Technical Work Plan for: Near-Field Environment: Engineered Barrier System: Radionuclide Transport Abstraction Model Report* (BSC 2006 [DIRS 177739]) and the *Technical Work Plan for Waste Form Testing and Modeling* (BSC 2006 [DIRS 177389]). The planned work was completed. A detailed discussion on the water saturation of the DSNF and CSNF degradation products (i.e., rind) in seep and non-seep conditions is provided in *EBS Radionuclide Transport Abstraction* (SNL 2007 [DIRS 177407], Section 6.3.4.6)

Table 7.9-1. Summary of Responses to the Remaining IVRT Comments (Continued)

Remaining IVRT Comment	Additional Work Conducted since the IVRT Review and Documentation where the Work is Located
Engineered Barrier System (Continued)	
CMT-062105-100851-03: The IVRT was concerned that there seemed to be a lack of a consistent treatment of water saturation degree in different parts of the EBS system. In CNSF, the saturation degree in corrosion products is calculated using a sorption isotherm of water onto hematite surfaces, while in the DSNF, it is just simply set to 1, though both domains consist of the same material. In addition, in the invert, the van Genuchten moisture retention relationship is used to calculate the intergranular water saturation. This comment is related to those of comments EBS-49 and CLAD-05b discussed above.	See pages 364 and 365 of Booth (2006 [DIRS 176638]) for the Project technical position on the comment where the Project justified the saturation states used in the different parts of EBS. Nonetheless, the Project planned the additional work to further enhance consistency of the degree of water saturation across the EBS. The work has been completed as planned and is reported in the *EBS Radionuclide Transport Abstraction* (SNL 2007 [DIRS 177407], Sections 6.2.4.6 and 6.5.2.2); and *In-Package Chemistry Abstraction* (SNL 2007 [DIRS 180506], Sections 6.6.1[a] and 6.10.9.1 [a]) model reports.
IDC-01: The comment IDC-01 is the same as the last part of comment IDC-02. They both deal with possible compositional differences between the fracture and matrix water. The IVRT was concerned that the compositional differences were not considered.	The comment was addressed in the revised version of *Engineered Barrier System: Physical and Chemical Environment* (SNL 2007 [DIRS 177412], Section 6.6).
IDC-02: In addition to the fracture-matrix water compositional differences comment mentioned above in IDC-01, the IVRT commented that since more data have become available, it would be helpful to show that with more data accumulated the original assumption of equal probability for five waters is still justified. Since no seepage is assumed for temperature greater than100°C, the water compositions calculated from the THC model for temperatures greater than 100°C should be excluded in the P&CE model analysis.	The planned work (SNL 2007 [DIRS 179287]) was completed to address both parts of the comment and is documented in *Engineered Barrier System: Physical and Chemical Environment* (SNL 2007 [DIRS 177412], Section 6.6). The cited section provides a detailed description of how the four end-member starting waters were selected for the Near-Field Chemistry Model based on the latest available pore-water database.

Table 7.9-1. Summary of Responses to the Remaining IVRT Comments (Continued)

Remaining IVRT Comment	Additional Work Conducted since the IVRT Review and Documentation where the Work is Located
Engineered Barrier System (Continued)	
IDC-04: The IVRT stated that the initial draft P&CE model they reviewed takes the water compositions calculated by the THC model as inputs to its evaporation calculations. These water compositions are calculated using a given set of values of reaction rate constants, which generally vary over several orders of magnitude. No sensitivity analysis has been done on how these reaction rate constants affect the calculated water chemistry. They mentioned that in the P&CE Model a small change in the initial water composition could result in quite a different chemical divide pathway.	The work planned in *Technical Work Plan for: Revision of Model Reports for Near-Field and In-Drift Water Chemistry* (SNL 2007 [DIRS 179287]) to address the comment was completed by performing sensitivity studies on THC seepage and is documented in *Drift-Scale THC Seepage Model* (SNL 2007 [DIRS 177404]). The PC&E Model uses the Near-Field Chemistry Model, which was developed independent of the THC model. The results of the THC model were used to corroborate the Near-Field Chemistry Model with agreeable results (SNL 2007 [DIRS 177412], Section 7.1.3 and Figure 7.1-10).
IDC-10: The IVRT stated that the water chemistry calculations in the P&CE Model (REV 02, DRAFT A) are valid only for drift-center temperatures; however, they are also applied at the drift ends. It is not clear how applicable water chemistries at elevated temperatures (i.e., the center of the drift) can be applicable at lower temperatures (i.e., at the end of the drift). This is believed to be conservative because this assumption should result in more corrosive water conditions; however, the adequacy of this assumption has not been demonstrated. Similarly, chemistry is passed as a function of time, yet in reality it is a function of the thermal history (which is spatially variable). The chemistry is for the center of the drift and it is not clear how it applies across the entire drift.	The work planned in *Technical Work Plan for: Revision of Model Reports for Near-Field and In-Drift Water Chemistry* (SNL 2007 [DIRS 179287]), as a part of the work needed to close Condition Report 7037, was completed. The completed work is documented in *Drift-Scale THC Seepage Model* (SNL 2007 [DIRS 177404]). The variations of the modeled water composition at the repository center and edge as the repository heats up and cools off as a function of time are discussed in Section 6.5.5.4 and shown on Figures 6.5-10 through 6.5-24 of the *Drift-Scale THC Seepage Model* (SNL 2007 [DIRS 177404], Section 6.5).

Table 7.9-1. Summary of Responses to the Remaining IVRT Comments (Continued)

Remaining IVRT Comment	Additional Work Conducted since the IVRT Review and Documentation where the Work is Located
Engineered Barrier System (Continued)	
IDC-11: The IVRT was concerned that different types of brines (e.g., NaCl, $CaCl_2$) would be quite different in total volumes, which reflect relative probabilistic distributions. This volume constraint on probabilistic distributions is not captured in the TSPA conceptual model. A similar comment can also be raised for the dust deliquescence model. It is expected that the amount of water potentially condensed on dust will be very small, perhaps not enough to form a continuous water film for metal corrosion.	The total volume of brine that may be residing on the WP due to seepage is not currently determinable. There are several dynamic processes that are occurring simultaneously (e.g., intermittent seepage flow events, seepage flowing off the package, evaporation, mineral precipitation), so the conceptual model falls back to an equilibrium brine composition that covers the entire seeped-on area and results in the most concentrated brine that has the highest potential to trigger localized corrosion. Thus, the brine volumes from different seepage compositions are reasonably assumed to be irrelevant in determining localized corrosion of the WP (SNL 2007 [DIRS 178519], Section 5.5). The IVRT comment no longer applies to dust deliquescence as there are no dust brines chemistry being modeled. Dust brines are all excluded from TSPA because they are of low-consequence, where low brine volume is a part of that justification (SNL 2007 [DIRS 181267], Sections 7.1).
IDC-12: The IVRT was of the opinion that there was a large inconsistency in water chemistries among the P&CE Model (REV 02, DRAFT A), the long-term corrosion testing to support the *WAPDEG Analysis of Waste Package and Drip Shield Degradation Model* (BSC 2003 [DIRS 161317] , a historic document cited for background information), the general corrosion and localized corrosion of WP outer barrier model which they reviewed, the *In-Package Chemistry Abstraction Model* (BSC 2003 [DIRS 161962] , a historic document cited for background information), and the *Dissolved Concentration Limits of Radioactive Elements* (BSC 2003 [DIRS 163152] , a historic document cited for background information). These inconsistencies must be addressed and the analysis and/or model reports for these affected models made consistent, and/or the justification for the inconsistencies being inconsequential.	The Project position (Booth 2006 [DIRS 176638]) is that the alleged inconsistencies no longer exist. Nonetheless, the Project made strides to further consistency between the WP localized corrosion model and seepage chemistry (SNL 2007 [DIRS 177412]) and utilized the same pH scales, which were the largest chemical disconnect.
IDC-19: The IVRT was concerned that the treatment of invert chemistry based on surface evaporation might have resulted in unrealistically high ionic strength, which may overly predict colloidal instability, which is not conservative.	The work needed to address the comment was planned in *Technical Work Plan for: Revision of Model Reports for Near-Field and In-Drift Water Chemistry* (SNL 2007 [DIRS 179287]) and completed. As part of this effort, pH and *p*CO2 covariance was evaluated to constrain, to the extent possible, the uncertainty of conditions that control radionuclide solubility and colloids stability in the invert. This new abstraction was based on fracture and matrix water compositions from the THC seepage model for the drip and no-drip cases, respectively. The work is documented in *Engineered Barrier System: Physical and Chemical Environment* (SNL 2007 [DIRS 177412], Section 6.15.2).

Table 7.9-1. Summary of Responses to the Remaining IVRT Comments (Continued)

Remaining IVRT Comment	Additional Work Conducted since the IVRT Review and Documentation where the Work is Located
Engineered Barrier System (Continued)	
Clad-05b: The IVRT was of the opinion that the Project calculations showed that assuming the rind was always saturated, regardless of temperature, had no effect on the peak mean dose to the RMEI. Therefore, it is not conservative to assume that the rind is saturated. Furthermore, the IVRT believed that it is not physically reasonable to assume that the rind is saturated given that the spent fuel rods are the hottest part of the repository.	No work is needed for this comment because no performance credit due to cladding will be claimed in the TSPA-LA Model (Section 6.3.8). However, additional work was performed by the Project to enhance water-balance treatment as mentioned in this table under the IVRT comments IPC-08, EBS-29, and EBS-49. In addition, Appendix C 5.6 of the TSPA-LA Model includes performance margin analysis on cladding degradation.
IPC-01: The IVRT was of the opinion that no model validation has been provided in the version of the In-Package Chemistry Abstraction model report the IVRT reviewed. The data used for validation in Sections 7-1 to 7-4 of the reviewed TSPA model are not specific, or not relevant, to the system to be validated.	The work planned in *Technical Work Plan for Waste Form Testing and Modeling* (BSC 2006 [DIRS 177389]) to address the comment was completed. The work included enhancing the model validation by incorporating quantitative comparisons of the in-package chemistry modeling results with laboratory data as discussed in Section 7.4[a] of *In-Package Chemistry Abstraction* (SNL 2007 [DIRS 180506]). In addition, the model results by EQ6 were corroborated with the model results from an independently developed code (PHREEQC) as discussed in *In-Package Chemistry Abstraction* (SNL 2007 [DIRS 180506], Section 7.10[a]).
IPC-08: The IVRT concern was the same as in CLAD-05b above and deals with the general water balance comment within the EBS. The related comments are EBS-29 and EBS-49.	Work was planned in *Technical Work Plan for Waste Form Testing and Modeling* (BSC 2006 [DIRS 177389]) to address the comment and was completed as reported above under the comments EBS-29 and EBS-49.
IPC-09: The IVRT was concerned that the version of the In-Package Chemistry Abstraction report that the IVRT reviewed assumed no evaporation inside a WP. This is not consistent with the EBS physical and chemical environment report the IVRT reviewed. No convincing justification has been provided. This comment is also similar to the IVRT comments CLAD-05b, EBS-29, EBS-49, and IPC-08—all related to a more general comment of water balance inside the drift.	Additional work was performed by the Project to enhance water-balance treatment as mentioned in this table under the IVRT comments CLAD-05b, IPC-08, EBS-29, and EBS-49. The objective of the PMA is to obtain a realistic estimate of the quantity of water available inside a breached WP for interaction with waste components and, consequently, radionuclide transport. This analysis involves the fully coupling of thermal evolution, waste degradation, and water transport. The amount of water is modeled as a function of RH in the engineered barrier system, dripping rate, distribution of failed openings on the WP outer layers, and extent of waste degradation.

Table 7.9-1. Summary of Responses to the Remaining IVRT Comments (Continued)

Remaining IVRT Comment	Additional Work Conducted since the IVRT Review and Documentation where the Work is Located
Engineered Barrier System (Continued)	
RNS-02: The IVRT was concerned that although uncertainty in fluoride concentration as a function of pH was explicitly accounted for in the models of Pu, Np, U, Th, and Am dissolved concentration limits, these uncertainties were not correlated. Because every modeled radio element will experience the same fluoride concentration and because the concentration of every modeled radioelement increases with increasing fluoride concentration, these uncertainties should be correlated.	Work has been planned in *Technical Work Plan for Waste Form Testing and Modeling* (BSC 2006 [DIRS 177389]) to address the comment. The planned work was completed and documented in *Dissolved Concentration Limits of Radioactive Elements* (SNL 2007 [DIRS 177418]). The work entailed evaluation of fluoride uncertainty with new values from *In-Package Chemistry Abstraction* (SNL 2007 [DIRS 180506]). The resolution approach was to add a statement to the model report and output DTN that fluoride uncertainties are to be correlated. The impact to TSPA from this change was that, when sampling fluoride, the same fluoride concentration was used for all radionuclides in a WP instead of allowing fluoride to differ for different radionuclides in any one package. The update to achieve consistency with in-package chemistry changed the fluoride uncertainty parameter values (Epsilon 2 parameters). No additional validation is required; this change only affects the implementation of the sampling of uncertainty distributions associated with the effects of fluoride on dissolved concentration limits.
RNS-04: The IVRT was concerned that the *Dissolved Concentration Limits of Radioactive Elements* (REV 03A) suggested using an unconstrained concentration for the chemical condition outside the valid ranges. This treatment will cause serious problems for the Igneous Intrusion Modeling Case, where pH can be around 10, which falls outside the model's valid pH range for some radionuclides. It is not physically credible for radionuclide solubilities under this condition to be unconstrained. Solubilities must have a finite value!	The work was planned in *Technical Work Plan for Waste Form Testing and Modeling* (BSC 2006 [DIRS 177389]) to address the comment. The planned work was completed and reported in Dissolved Concentration Limits of Radioactive Elements (SNL 2007 [DIRS 177418]). The scientific approach used was to set caps, (i.e., setting limits on dissolved concentrations (SNL 2007 [DIRS 177418], Section 6.22)) by exploring the maximum concentration of radionuclides that are possible based on using all the available water to solvate the solute ions. This approach would still give a conservative upper bound for the dissolved concentration while lowering the caps significantly. The resulting change in the numerical values used in TSPA from the metal densities to lower values based on maximum utilization of the available water for salvation of solute ions was implemented.
RNS-07: The IVRT was concerned that the proposed extension of B-dot model calculations to ionic strength up to 3 M was stretchy. The justification provided in Section 6.3.3.4 of the *Dissolved Concentration Limits of Radioactive Elements* (BSC 2004 [DIRS 169425, a historic document cited for background information]) was not fully convincing.	Work was planned in *Technical Work Plan for Waste Form Testing and Modeling* (BSC 2006 [DIRS 177389]) to address the comment. The objective of the planned work was to augment the technical basis for assessing the effects of higher ionic strength (greater than 1 Molal) on confidence in activity coefficients calculated using the B-dot equation. The planned work was completed and documented in *Dissolved Concentration Limits of Radioactive Elements* (SNL 2007 [DIRS 177418], Sections 6.3.3.4 and 6.4.4).

Table 7.9-1. Summary of Responses to the Remaining IVRT Comments (Continued)

Remaining IVRT Comment	Additional Work Conducted since the IVRT Review and Documentation where the Work is Located
Engineered Barrier System (Continued)	
CMT-062705-091834-96: The IVRT was concerned that the general corrosion rate of the order of 0.0001 mm/year was based on the extrapolation of data taken over a period of 1 to 5 years and at temperatures of 60°C and 90°C, to time periods of up to 35,000 years and high temperatures without sufficient justification.	No additional work on this comment is planned. Use of short-term data relative to the regulatory time frame will always be a consideration in performance assessment. The IVRT should reconsider this comment. In addition, this comment is of little consequence to the current TSPA Model because only 1/3 of the thickness of the DS will be corroded in 10,000 years. Because the rates used in TSPA are early time rates and rates decrease with time, the use of lower corrosion rates will only reduce the thickness corroded. The CDF is based on data collected between temperatures of 60°C and 90°C and is constant. However, the general corrosion rate is a function of temperature. The repository temperature drops (Section 6.3.2) to this range (60°C to 90°C) within 1,000 years making it reasonable to use data collected in this temperature range for the whole duration. Moreover, the chemistry becomes less corrosive with time and the corrosion rate should decrease with time.
CMT-062105-123501-09: The IVRT's concern was that it is not known how appropriate it is to apply the evaporation look-up tables directly to the invert since the invert is a porous medium and the capillary effect should play an important role in controlling water saturation degrees.	The comment is not applicable since the Project does not use evaporation look-up tables the IVRT referred to any longer. This is now accomplished by using a relationship between relative humidity and water saturation, as explained in a 9/7-8/2005 meeting between IVRT and TSPA staff as documented in *Independent Validation Review Team (IVRT) Issues, Bechtel-SAIC Responses, and IVRT Assessment of Responses Related to Review of the TSPA Model and Supporting Analyses and Model Reports* (Booth 2006 [DIRS 176638]). Consequently, no additional work was deemed necessary.
General Comment	
CMT-062005-120938-57: The IVRT was concerned that many of the pdfs for characterizing uncertainty in parameter values in analysis and/or model report submodels where very broad pdfs were developed that often (1) were not supported by the existing data or information and (2) does not provide evidence that risk dilution is not likely to occur when implementing the TSPA-LA Model. In addition, the submodel analysis and/or model reports did not seem to have followed and applied the guidelines for developing pdfs presented in *Guidelines for Developing and Documenting Alternative Conceptual Models, Model Abstractions, and Parameter Uncertainty in the Total System Performance Assessment for the License Application* (BSC 2002 [DIRS 158794]), and adequate justification was not provided for why these guidelines were not followed.	The Project conducted an initial scoping evaluation of pdfs for 60 key parameters among the 388 parameters used in the draft TSPA-LA report, which the IVRT reviewed. Sensitivity to dose was analyzed on six of these 60 parameters. The six parameters were selected for their high significance to dose. This initial scoping work was the subject of a Condition Report 7538, which was closed as planned after the initial work was completed. The Project since then undertook a focused effort by a team of SMEs to ensure that the uncertainty-treatment and the pdf development for the TSPA-LA input parameters are uniformly performed. The uncertainty treatment is discussed in Section 6.1.3 and an uncertainty characterization review is presented in Section 7.4 of this TSPA-LA Model report. The review in Section 7.4 was aimed at making an evaluation of the manner in which the uncertainty associated with the TSPA input parameters were treated in developing the TSPA Model, and ensuring that any inconsistencies or inappropriateness in the treatment of uncertainty was detected and corrected so that the TSPA-LA Model results are reliable and reasonable.

Table 7.9-1. Summary of Responses to the Remaining IVRT Comments (Continued)

Remaining IVRT Comment	Additional Work Conducted since the IVRT Review and Documentation where the Work is Located
General Comment (Continued)	
CMT-062005-143936-34: The IVRT commented that the five observed pore waters in the THC-seepage abstraction model were selected only to capture the variability of water samples and no probability was associated with the original selection. Therefore, the equal probability for these five waters is not justified. These five waters were selected from limited early field measurements. Since more data have become available, it would be helpful to show that with more data accumulated, the original assumption of equal probability for five waters is still justified.	This comment is similar to the part of the comment IDC-2 dealing with the probability assignment of the five water samples and the use of the more water data now available to justify the equal probability assignment made. The work planned in *Technical Work Plan for: Revision of Model Reports for Near-Field and In-Drift Water Chemistry* (SNL 2007 [DIRS 179287]) to address the comment was completed and documented in *Engineered Barrier System: Physical and Chemical Environment* (SNL 2007 [DIRS 177412], Section 6.6). The cited section provides a detailed description of how the four end-member starting waters were selected for the Near-Field Chemistry Model (CFM) based on the latest available pore-water database.
CMT-062705-093311-25: The IVRT thought that the basis for using NpO2, summarized in Section 6.6 and Appendix IV in the version of the *Dissolved Concentration Limits of Radioactive Elements* model report that the IVRT reviewed, was not convincing.	Additional work on the subject was planned in *Technical Work Plan for: Revision of Model Reports for Near-Field and In-Drift Water Chemistry* (BSC 2006 [DIRS 179287]) to address the comment. The technical objective of the neptunium testing work was to enhance the technical basis for using NpO2 (as opposed to Np2O5) as the pure neptunium phase limiting the dissolved concentration of neptunium inside the WPs. The technical objective also included determination of the effective activation energy for NpO2 precipitation in systems where active reductants may be scarce or absent. The scope involved examination of the behavior of neptunium in corroded spent fuel samples and assessing the homogenous and heterogeneous precipitation kinetics for precipitation of Np(IV) from Np(V) solutions. The goal was to obtain an improved scientific basis for the redox behavior and precipitation kinetics of neptunium in heterogeneous environments similar to those inside the breached WP and in the low-temperature environments outside the WP, where active reductants may be scarce or absent. The planned work was completed and documented in *Dissolved Concentration Limits of Radioactive Elements* (SNL 2007 [DIRS 177418], Section 6.6).
CMT-062705-093723-54: The IVRT comment was that using solubility equal to the density of the solid metal violated basic physical principles (Darcy's Law and Fick's law) in terms of radionuclide transport as a dilute species. Other related submodels that assume transport of dilute solutions are, therefore, incorrectly linked.	This is an expansion of RNS-04. Work was planned in *Technical Work Plan for: Revision of Model Reports for Near-Field and In-Drift Water Chemistry* (BSC 2006 [DIRS 179287], Section 1.2.1) to address the comment. The planned work was completed and reported in *Dissolved Concentration Limits of Radioactive Elements* (SNL 2007 [DIRS 177418]). The scientific approach used was to set caps that set limits on dissolved concentrations (SNL 2007 [DIRS 177418], Section 6.22) to the maximum concentration of radionuclides that are possible, based on using all the available water to solvate the solute ions. This approach would still give a conservative upper bound for the dissolved concentration while lowering the caps significantly. The resulting change in the numerical values used in TSPA from the metal densities to lower values based on maximum utilization of the available water for solvation of solute ions was implemented.

Table 7.9-1. Summary of Responses to the Remaining IVRT Comments (Continued)

Remaining IVRT Comment	Additional Work Conducted since the IVRT Review and Documentation where the Work is Located
General Comment (Continued)	
CMT-062105-100625-71: The IVRT was concerned that with respect to radionuclides transport in the EBS, the two-cell model used by the Project may not be appropriate because in reality, Cell 1 and Cell 2 in the EBS Transport Model are not completely physically separated in space. Even with a purely advective flow, the water will percolate through multiple fuel rods and corrosion product domains and significant flow mixing is expected.	In order to model this type of transport, two distinct domains are needed: one that acts as a source of dissolved mass and the other that acts as the porous medium. The Project believes the approach (i.e., relying on multiple batch-reactor cells for EBS transport modeling) used is reasonable and consistent with the conceptualization of the in-package environment. The Project's current approach, which is somewhat modified, is discussed in *Technical Work Plan for: Near-Field Environment: Engineered Barrier System: Radionuclide Transport Abstraction Model Report* (BSC 2006 [DIRS 177739]). The planned work was completed and presented in *EBS Radionuclide Transport Abstraction* (SNL 2007 [DIRS 177407], Section 6).

INTENTIONALLY LEFT BLANK

7.10 SUMMARY OF MODEL CONFIDENCE BUILDING

The intended purpose of the TSPA-LA Model, as defined in *Technical Work Plan for: Total System Performance Assessment FY 07-08 Activities* (SNL 2008 [DIRS 184920], Section 2.3.5), is to provide the TSPA-LA Model appropriate for use in the evaluations of compliance with the quantitative postclosure requirements of NRC Proposed Rule 10 CFR Part 63 ([DIRS 178394] and [DIRS 180319]). The TSPA-LA Model was validated by performing activities required by SCI-PRO-006, *Models*. The *Technical Work Plan for: Total System Performance Assessment FY 07-08 Activities* (SNL 2008 [DIRS 184920], Section 2.3.5) implements these procedural requirements and describes and plans the tests and analyses activities that are to be performed to build confidence in the TSPA-LA Model and ensure that the model is valid for its intended purpose. As described in Section 2, results of the activities presented in Sections 7.2 through 7.9 are summarized below, in order to assess the validation status of the TSPA-LA Model for its intended purpose. Once the during-development activities were performed and it was established that the requirements of the technical work were satisfied, the relative significance of the post-development activities in building confidence in the reasonableness of the TSPA-LA Model results were evaluated and determined to meet the required Level II validation status of the model as specified in SCI-PRO-006. While the results of all four groups of the post-development validation activities, summarized below added confidence in making the decision on whether the model achieved the required validation status, the auxiliary analyses and in particular the performance margin analyses (PMA) results, were of special significance in this regard. As required by the technical work plan, the PMA utilized revisions to selected component models in the TSPA-LA compliance model including conceptual or uncertainty alternatives, to assess the performance margin in the compliance model, and to evaluate whether the compliance model dose is underestimated. The cumulative results of the pre- and post-development activities led the responsible performance assessment manager to the conclusion that the TSPA-LA Model indeed satisfied the Level II validation requirements and met its intended purpose.

Section 7.10 summarizes the above validation activities. Section 7.10.1 provides a synopsis of the validation strategy. Sections 7.10.2 through 7.10.9 summarize the validation activities performed. Concluding remarks are presented in Section 7.10.10. Validation of the TSPA-LA Model consisted of a series of activities to provide confidence in the analysis of transport processes for radionuclides that occur between the waste form in the repository and the RMEI. The validation process begins with the verification of model input and verification that the valid supporting models and analyses and their abstractions are incorporated properly into the TSPA-LA Model (Section 7.2). Supporting models, analyses, and abstractions undergo appropriate verification and validation prior to their final implementation in the TSPA-LA Model. The TSPA-LA model is then evaluated for statistical, temporal, and spatial stability (i.e., number of realizations, timesteps, and spatial discretization) and accuracy of the calculated dose (Section 7.3). Treatment of uncertainty in the development of the TSPA-LA Model is documented in Section 6.1.3. Uncertainty characterization reviews on the TSPA-LA Model direct-input parameters were conducted in order to ensure that uncertainty with respect to the input parameters was treated uniformly and consistently throughout the TSPA-LA Model (Section 7.4). Additionally, uncertainty and sensitivity analyses were conducted to gain confidence that uncertainty in parameters, models, and scenarios were propagated correctly into the results provided by the TSPA-LA Model (Section 7.4 and Appendix K). The uncertainty

and sensitivity analyses examined subsystem radionuclide release and transport processes and system results to gain confidence in the TSPA-LA Model results. Surrogate waste form analyses representing the DOE spent fuel Categories 2 through 11 and the NSNF, Category 1, ensured that the TSPA-LA Model appropriately incorporates these waste types (Section 7.5).

Post-development activities are conducted to ensure that the TSPA-LA Model is valid for its intended purpose. The results of these validation activities are documented in Sections 7.6 through 7.9. Section 7.6 documents corroboration of the direct input abstraction parameters with their respective underlying validated process models and demonstrates that the results are consistent with these supporting models. Several auxiliary analyses were conducted to: (1) determine that the submodels are coupled as intended by evaluating selected key single-realization curves that contribute to the calculation of mean annual dose (Section 7.7.1); (2) compare the TSPA-LA Model mean annual dose results with the results from a simplified, independently developed TSPA analysis (Section 7.7.2); (3) compare model results with a TSPA developed independently by the EPRI (Section 7.7.3); and (4) provide objective evidence for assessing a performance margin analysis, and the degree of conservatism or non-conservatism in the TSPA compliance model (Section 7.7.4). In addition, analogues were examined to provide confidence in the results provided by the TSPA-LA Model (Section 7.8).

As an additional confidence-building activity, reviews by three independent teams of external experts were described (Section 7.9) showing that the comments and recommendations from these reviews were addressed in the development of the TSPA-LA Model. This summary includes a description of the implementation of the work planned to address the several remaining comments from the most recent IVRT review of earlier drafts of the TSPA-LA Model.

Validation of the TSPA-LA Model applies directly to the estimates of the performance measures for the Yucca Mountain repository as established by NRC Proposed Rule 10 CFR Part 63 ([DIRS 178394] and [DIRS 180319]). The TSPA-LA Model provides estimates of the groundwater protection performance measures in terms of groundwater concentration and dose. The last step in the annual dose calculation is the conversion of radionuclide concentrations in the groundwater to an annual dose to the RMEI using a BDCF. Thus, a model that is valid for the calculation of annual dose is also valid for calculation of groundwater protection performance measures in terms of concentration and dose (Section 8.1.2).

The activities described in Section 7 are conducted to gain confidence in the TSPA-LA Model through the model validation activities required by SCI-PRO-006. These activities examine the internal supporting models and components of the TSPA-LA Model separately and in combination to determine whether or not they are producing plausible and reasonable inputs to the TSPA-LA Model. The results of the activities demonstrate that the TSPA-LA Model inputs represent the underlying process models as expected; the inputs were accurately implemented in the TSPA-LA Model; the TSPA-LA Model is numerically, temporally, and spatially stable; and the resultant dose calculations are accurate. The subsequent post-development validation activities (Table7.1-1) demonstrate that the TSPA-LA Model produces reliable estimates of repository performance compliance measures such as estimates of the individual and groundwater protection standards.

7.10.1 Validation Strategy

This section summarizes the approach applied to validate the TSPA-LA Model as required by SCI-PRO-006 and as planned in the TSPA-LA technical work plan (SNL 2008 [DIRS 184920]) that implements the procedural requirements. The technical work plan identifies the general activities that need to be performed during and after the model development in order to ensure that the TSPA-LA Model is valid for its intended purpose. This section highlights the tests and analyses that are performed (Table 7.1-1) in support of these activities.

7.10.1.1 Introduction

The general TSPA process adopted by the DOE follows the methodology developed by Cranwell et al. (1990 [DIRS 101234], Sections 2 and 3). Over time, the methodology has been enhanced and applied to numerous projects by various international organizations involved in radioactive waste management. The TSPA-LA Model was developed to analyze the ability of the natural and engineered systems of the Yucca Mountain repository to safely isolate nuclear waste following repository closure. Performance assessments and related supplemental analyses of the Yucca Mountain repository were conducted following the publication of the Nuclear Waste Policy Amendments Act of 1987 (Public Law No. 100-203 [DIRS 100016]). The TSPAs of the Yucca Mountain repository have been iterative and periodically updated, each building on and extending the scope and results of the previous TSPAs. The iterative assessments incorporate both an improved understanding of the processes affecting repository performance and, through additional field observations and laboratory analyses, better identification and quantification of the values of the parameters used in the TSPA models.

The TSPA iterations have been evaluated and independently reviewed by technical staff and various external organizations, and these reviewers have made recommendations for improvements for consideration in future TSPAs. Examples include a TSPA peer review conducted of the TSPA-VA by Budnitz et al. (1999 [DIRS 102726]), an evaluation of the TSPA-SR by an IRT (OECD and IAEA 2002 [DIRS 158098]), and a technical review of the earlier drafts of the TSPA-LA Model by an IVRT (Gibson 2007 [DIRS 181099]). The criteria for these independent technical reviews were designed within the framework of procedural compliance as required by the prevailing model development procedure (precursors of SCI-PRO-006, and per the requirements of the QARD applicable at the time) and the respective technical work plans that were in effect during the review periods. The review criteria especially focused on evaluating two critical aspects of the TSPA under review: (1) the adequacy of the TSPA methodology being developed, and (2) whether the TSPA satisfied its intended purposes. Section 7.9 describes the criteria used for the TSPA-VA, IRT, and IVRT reviews. The TSPA-VA, TSPA-SR, and the early drafts of the TSPA-LA models were developed to assess the repository performance for a 10,000-year postclosure compliance period reflecting the regulations in effect at that time. The TSPA-LA Model assesses repository performance with respect to the NRC Proposed Rule 10 Part CFR 63 ([DIRS 178394] and [DIRS 180319]) for a postclosure compliance period of 10,000 years and the period of geologic stability, defined as 1,000,000 years at NRC Proposed Rule 10 CFR 63.302 [DIRS 178394]. Nonetheless, the comments and recommendations made by these reviews that were implemented in development of the TSPA-LA Model contributed to the development of the TSPA-LA Model as valid for its intended purpose.

Validation of the TSPA-LA Model consists of a sequence of activities that are designed to build confidence in the results of the model. The TSPA-LA Model analyzes the FEPs expected to affect the repository system; that is, the FEPs leading to the development of the Nominal Scenario Class. TSPA-LA Model analyses include the Nominal Scenario Class Modeling Case, the low probability Drip Shield EF and Waste Package EF Modeling Cases, as well as the low probability modeling cases due to postclosure disruptive events that could occur at the Yucca Mountain repository site, such as those represented by the Igneous Intrusion Modeling Case, Volcanic Eruption Modeling Case, Seismic GM Modeling Case, and Seismic FD Modeling Case. The TSPA-LA Model analyses also include evaluation of a Human Intrusion Scenario per NRC Proposed Rule 10 CFR 63.322 [DIRS 180319].

Validation of a computer model for a physical system involves a series of steps designed to generate and enhance confidence in the model's results during and after model development. The modeling process starts with the developer's understanding of the physical system. A model is then conceptualized based on available information using appropriate assumptions, simplifications, and idealizations. The conceptual model is formulated into a mathematical model and then into a numerical model. An appropriate computer code/software suite is selected or developed to implement the numerical model. The input to the computer code is prepared, and the code is executed to obtain the model results.

A well-designed, correctly implemented numerical model should produce results that are explainable and are appropriate for the model's intended use. Validation of the TSPA-LA Model is a process of establishing that the results provided by the model, which requires performance prediction for many thousands of years into the future, are plausible and reasonable. Consequently, in contrast to modeling activities where validation may be achieved by comparing model results with direct measurements, such measurements are impossible to obtain at the temporal and spatial scales of interest for postclosure repository performance assessment. Instead, confidence in the results of the TSPA-LA Model is based on the successful completion of required activities described in the technical work plan (SNL 2008 [DIRS 184920], that are based on SCI-PRO-006. These activities are designed to ensure that the TSPA-LA Model is developed consistent with its intended use for the LA; that it captures the relevant features, events and processes (FEPs) through the implementation of its validated submodel components in which the FEPs are addressed; and that the confidence in the TSPA-LA Model results is demonstrated by independent lines of corroborative information after the model development. There are two main categories of procedural activities to validate the TSPA-LA Model (Figure 7.1-2): (1) those conducted during development of the model, and (2) those conducted after development of the model.

7.10.1.2 During-Development Model Validation Activities

The during-development activities listed in the technical work plan (SNL 2008 [DIRS 184920], Section 2.3.5.1), which are performed to demonstrate the TSPA-LA Model validation in relationship to the model's intended use and required level of confidence, are as follows:

1. Selection of input parameters and/or input data and a discussion of how the selection process builds confidence in the model (SCI-PRO-002, *Planning for Science Activities*, Attachment 3, Level 1, Validation 1).

2. Description of calibration activities, and/or initial boundary condition runs, and/or run convergences, and a discussion of how the activity or activities build confidence in the model. Includes a discussion of impacts of any run non-convergences (SCI-PRO-002, Attachment 3, Level 1,Validation 5).

3. Discussion of the impacts of uncertainties on model results (SCI-PRO-002, Attachment 3, Level 1, Validations 4 and 6).

Two additional factors are incorporated as appropriate during development of the TSPA-LA Model:

1. Formulation of defensible assumptions and simplifications (SCI-PRO-002, Attachment 3, Level 1, Validation 2).

2. Consistency with physical principles, such as conservation of mass, energy, and momentum (SCI-PRO-002, Attachment 3, Level 1, Validation 3).

Selection of input parameters and/or input data provides parameters and initial and boundary conditions for submodels and components that calculate input parameters and boundary conditions for successive submodels and model components. Based on analyses that show that these submodels and components are working as intended (Section 7.10.2), the model is then tested for stability (i.e., appropriate number of realizations, timesteps, and spatial discretization) (Section 7.10.3). The uncertainty characterization review ensures that uncertainty associated with the direct-input TSPA-LA parameters is being characterized adequately and uniformly, and the uncertainty and sensitivity analyses examine impacts of uncertainty on subsystem radionuclide release and transport processes, and the system results to gain confidence in the TSPA-LA Model. (Section 7.4 and Appendix K). These during-development activities test the integration of the submodels and components into the overall system model.

Completion of these during-development activities demonstrates that: (1) the input parameters for the model are correctly implemented into the model from source documents, including those parameters that are internally calculated; (2) the model is stable in terms of the number of realizations, length of timesteps, spatial discretization, that calculated doses are accurate; and the radionuclide transport model using the particle tracking method with FEHM code is stable; and (3) uncertainty in model inputs is treated properly and uniformly and is propagated through the model and correctly accounted for in the model results.

7.10.1.3 Post-Development Model Validation Activities

Post-development model validation activities (SNL 2008 [DIRS 184920], Sections 2.3.5.2 and 2.3.5.3) include activities that may be used to validate the TSPA-LA Model. For the TSPA-LA Model, the required level of confidence and validation falls into the Level II validation category (SCI-PRO-002, Attachment 3) that requires use of at least two of the activities from Section 6.3.2 of SCI-PRO-006. In order to provide confidence beyond the procedural requirements, the TSPA-LA Model utilized several post-development model validation activities:

- Corroboration of the direct-input abstraction results with the validated mathematical model or process model from which the abstraction was derived (Section 7.6)

- Auxiliary analyses for corroborating the results with the TSPA-LA Model or model abstractions and/or submodels used in the TSPA-LA (Section 7.7)

- Comparison of the relevant portions of the TSPA-LA Model with appropriate analogue information (Section 7.8)

- As an additional confidence-building exercise, the comments and recommendations by the past technical reviews, including those by the more recent IVRT on earlier drafts of this TSPA-LA Model were addressed and implemented as appropriate (Section 7.9).

The results of these post-development activities demonstrate that the overall system model is functioning as intended and the results are explainable and reasonable. Addressing the independent technical review comments and recommendations covers both during- and post-development activities and, along with auxiliary analyses, the natural analogues and the during-development activities mentioned earlier that provide confidence that the TSPA-LA Model is valid for its intended use.

In addition to the validation activities mentioned above, potential impact on the TSPA-LA Model results due to issues identified after the model runs were completed was evaluated as stated in *Technical Work Plan for: Total System Performance Assessment FY 07-08 Activities* (SNL 2008 [DIRS 184920], Section 2.3.5.3). Appendix P contains the results of this evaluation. No significant impact on the TSPA-LA results was noted. As a part of the continuing improvement effort by the Project, the impact on the results of this version of the TSPA-LA Model will be included in an addendum.

The goal of the model validation activities is to support the demonstration that the results of the procedurally validated TSPA-LA Model satisfy the applicable individual dose and groundwater protections requirements set by the NRC. The activities are also to address the applicable TSPA-LA Model acceptance criteria identified by the NRC in its Yucca Mountain Review Plan. Table H-1 in Appendix H provides a roadmap of the NRC requirements and the Yucca Mountain Review Plan acceptance criteria applicable to the TSPA-LA Model.

7.10.2 Code and Input Verification

The code and input verification was conducted to provide confidence in the software and the input used in the TSPA-LA Model and to comply with the requirements of SCI-PRO-006, Section 6.3.2. This includes: (1) verification of the integrated system software (GoldSim) that is the software platform for the TSPA-LA Model, (2) verification of DLLs from source documents and DLLs that are generated within the TSPA-LA Model, and (3) verification of model inputs from the TSPA Input Database. Submodels that originate from a source analysis and/or model report were verified by comparing submodel results from the TSPA-LA Model with results provided in the analysis and/or model report. Coupling between submodels was examined by verifying that the information generated by one submodel is input correctly to successive submodels and that this information does not exceed the applicable range of the successive

submodel. In other words, these activities were conducted to verify that the computer codes and model inputs that originated from an outside source (analysis and/or model reports), or are generated internally within the TSPA-LA Model, are implemented correctly. The results of these activities are as follows:

- GoldSim was selected as the TSPA integration code based on its capabilities and use in similar applications. GoldSim V9.60.100 (STN: 10344-9.60-01 [DIRS 181903]) was qualified per IM-PRO-004, *Qualification of Software.*

- Output of DLLs from other sources (analysis and/or model reports and DTNs) was found to be exact.

- Output of DLLs that calculate results within the TSPA-LA Model was found to be within the acceptance criteria (e.g., within five percent).

- Individual submodels were validated and documented in their respective analysis and/or model reports.

- Results from submodels within the TSPA-LA Model were compared to results contained in model reports (stand-alone or simple models) and were found to agree within the acceptance criteria.

- Outputs from one submodel to another were found to be correct and either does not exceed the valid range of the successive submodel or the value used is fixed within the range or at the upper bound of the range of the successive submodel.

- Input in the TSPA Input Database was verified to correspond with source data.

An important aspect of the during-development model validation identified in the technical work plan (SNL 2008 [DIRS 184920], Section 2.3.5.1) is the appropriate selection of input parameters and how the selection process builds confidence in the model. In the case of the TSPA-LA Model, this is a function of the selection process of each of the model abstractions and the appropriateness (i.e., validity) of those abstractions. This process included the formal review by TSPA technical staff of all supporting models and analyses used as input to the TSPA-LA Model. In addition, a formal review of the appropriate subsections of the TSPA-LA Model description, Sections 6.3, 6.4, 6.5, 6.6, and 6.7, was conducted by a SME responsible for these inputs to ensure the information was appropriately implemented in the TSPA-LA Model. This review is summarized and discussed in Section 4.

The activities above demonstrated that the system software for the TSPA-LA Model is appropriate and valid, that input is correct and verified, that the internal transfer of information within the model is correct and within the valid range of successive submodels, and that submodels are valid per their respective source analysis and/or model reports. In other words, incorporation of information and submodels from other sources into the TSPA-LA Model has not altered the validity of the information or the submodels or both.

7.10.3 Model Stability Testing

Demonstration of stability of the TSPA-LA Model is essential to validation and confidence building of the model results. As discussed in Section 7.3, the TSPA-LA Model computes mean annual dose in four steps: (1) selection of values for epistemic parameters and aleatory uncertainties; (2) numerically solving a complex, coupled system of differential equations describing radionuclide decay, flow, transport, and other physical processes; (3) integration over aleatory uncertainty, carried out either by quadrature or Monte Carlo techniques; and (4) integration over epistemic uncertainty, conducted by a Monte Carlo technique. Section 7.3 discusses the details of how the stability of the TSPA-LA Model is verified through implementation of the four steps during the TSPA-LA Model computations. TSPA-LA Model stability verification involved five different analyses: (1) statistical stability of mean annual dose, (2) numerical accuracy of expected annual dose, (3) temporal stability, (4) spatial stability, and (5) stability of the FEHM particle tracking model. A summary of each of these stability tests and their results obtained from them are provided below

Statistical Stability

A replicated sampling procedure was used to determine the statistical stability of the TSPA-LA Model results. With this procedure, the LHS is repeatedly generated with different random seeds. Mean annual dose is computed for each modeling case with each LHS. Confidence intervals for the mean annual dose are then estimated with the *t*-distribution.

Replicate sampling runs were performed in the GoldSim code for each of the TSPA-LA modeling cases: Nominal Modeling Case, Waste Package EF Modeling Case, Drip Shield EF Modeling Case, Igneous Intrusion Modeling Case, Volcanic Eruption Modeling Case, Seismic GM Modeling Case, Seismic FD Modeling Case, and Human Intrusion Modeling Case. The details of the stability analyses for these modeling cases are presented in Section 7.3.1. Results are presented for each modeling case and for total mean annual dose (summed over all modeling cases) in Section 7.3.1. The analysis concludes that the sample size used in the Monte Carlo technique is adequate to estimate mean annual dose in each modeling case as well as to estimate the total mean annual dose. Therefore, the results of the TSPA-LA Model are statistically stable.

Numerical Accuracy of Expected Annual Dose

Detailed discussions on the numerical accuracy analyses for each of the TSPA-LA modeling cases are provided in Section 7.3.2. The results are summarized below.

Because the expected annual dose for the Nominal Modeling Case is computed directly with the GoldSim code, the numerical accuracy of the mean annual dose for the Nominal Modeling Case was evaluated by increasing the size of the LHS size from 300 (used for the base case) to 1,000. The results show that the mean annual dose based on 300 realizations is adequate and numerically stable. The expected annual dose for the Waste Package EF Modeling Case and Drip Shield EF Modeling Case is calculated by summation rather than numeric integration, making the calculated expected annual dose exact, thus requiring no estimate of numerical accuracy.

For the Igneous Intrusion Modeling Case, the accuracy of the calculation of expected annual dose by numeric integration was verified by increasing the number of igneous intrusion times from 10 (base case) to 50. The similarity of the shape of the dose history curves for different times of intrusions within a climate period indicates that the interpolation techniques used within the EXDOC software are justified, and the 10 intrusion times are sufficient to obtain a numerically accurate expected dose. For the Volcanic Eruption Modeling Case, sufficiency of the LHS size for aleatory parameters is demonstrated by increasing the LHS size from 40 to 80. The results show that the LHS sample size of 40 used in the base case is adequate to estimate expected dose. Because the dose from volcanic eruption constitutes most of the total dose during the first 1,000 years, the accuracy of the first 1,000-year dose was verified by increasing the number of eruption events with no significant change in dose. The results imply that the expected dose for 1,000,000 years is also numerically stable.

Accuracy of both the 10,000-year and 1,000,000-year expected annual dose results was verified for the Seismic GM Modeling Case. Detailed discussions on execution of the steps performed for the verification and the results are provided in Section 7.3.2.6. For the 10,000-year Seismic GM Modeling Case, several steps were performed to verify accuracy of the expected annual dose for the 10,000-year modeling case. Summarizing here,

1. Demonstrated that increasing the number of times of seismic events (from 6 to 12) and damage fractions (from 5 to 8) does not change the expected dose calculation for any realization, verifying that the discretization used to calculate expected dose is adequate.

2. Justified the use of the assumption that the dose from a sequence of seismic events is reasonably approximated by the sum of the doses from each event where each event is modeled separately.

3. Justified the simplifications to the *Seismic Consequences Abstraction* (SNL 2007 [DIRS 176828]) by evaluating the effects of corrosion processes; the effects of DS plate or framework failure; magnitude of the volume of rockfall; the consequences of rupture and puncture of WPs; and seismic damage to TAD WPs.

For the 1,000,000-year Seismic GM Modeling Case, numerical stability of the expected annual dose calculated by the Monte Carlo technique was investigated by increasing the aleatory sample size from 30 to 90 for a suitable epistemic realization. Although the expected annual dose for each realization did not converge to a stable value, the results demonstrate that the sample size used in the base case calculation produces a statistically stable mean annual dose for the 1,000,000-year Seismic GM Modeling Case (Section 7.3.2.6.2).

In the case of the Seismic FD Modeling Case, it was shown that increasing the event size would result in an improved dose accuracy. However, given the relatively low significance of this modeling case, the event size used for the base case produces an adequate result. The numerical stability of the expected annual dose for the Human Intrusion Modeling Case was computed by the Monte Carlo technique. The results show no significant difference by increasing the size of the aleatory sample from 30 to 90.

Temporal Stability

Evaluation of temporal stability of the TSPA-LA Model was performed conducting simulations of the Waste Package EF Modeling Case, Igneous Intrusion Modeling Case, Seismic GM Modeling Case, and Human Intrusion Modeling Case. These modeling cases have the most influence on the system performance and are likely to be influenced by the changes in the timestep size used. The simulations were conducted by reducing the TSPA-LA Model timestep size to examine the timestep size sensitivity. The annual dose from the TSPA-LA Model runs with different timestep sizes were compared graphically with the base case results to determine the effect of refining the timesteps. The details of the approach and results are provided in Section 7.3.3. The results for the four modeling cases are summarized below.

In the case of the Waste Package EF Modeling Cases of the CDSP and CSNF WPs, comparison of the annual dose curves resulting from the refined two-timestep scheme runs shows that the temporal discretization used in the Waste Package EF Modeling Case for the TSPA-LA Model is suitable. In the Igneous Intrusion Modeling Case, temporal stability was tested for 1,000,000 years (with the intrusion fixed at 400,000 years) and 20,000 years (with the intrusion fixed at 1,000 years) and then applying separate sets of alternate timestep schemes in both cases. An increase of annual dose was observed for the alternate timesteps immediately after the intrusion events, and the increase was found to be insignificant to either the expected dose or the mean dose. Similarly for the 20,000-year three timestep runs, the overall shape of the dose history is very similar for all three timestep schemes. The results show that the timestep scheme used in the Igneous Intrusion Modeling Case is adequate. In the Seismic GM Modeling Case for 20,000 years, the annual dose is computed by employing three separate timesteps with the seismic event time fixed at 1,000 years and the damage fraction at 10^{-6}. The results demonstrate that the timestep scheme used in the 20,000-year dose calculation is adequate. The test results for the Human Intrusion Modeling Case also confirms that the timestep scheme used for dose calculation in this modeling case is adequate.

Spatial Stability

Section 7.3.4 describes the spatial discretization schemes of the process model abstractions (Mountain-Scale UZ Flow Submodel, the EBS TH Environment Submodel, the UZ Transport Submodel, and the SZ Flow and Transport Submodel) that feed the TSPA-LA Model. No impact on the TSPA-LA Model results due to these inherited (and verified as documented in their respective source documents) spatial discretizations are expected because they were used unchanged in the TSPA-LA Model simulations.

In addition, the TSPA-LA Model implements its own spatial discretization scheme to accommodate the use of the comprehensive EBS TH data set (provided by the MSTHM Process Model) by abstracting a representative TH data set that would capture the variability of the EBS TH environment across the repository footprint, while at the same time minimizing the computational burden associated with each additional subregion. This was accomplished and validated by two activities: (1) spatial discretization of the repository into a minimum but adequate number of subregions with percolation flux as a basis for discretization and binning percolation subregions by quantiles 0.0 to 0.05, 0.05 to 0.3, 0.3 to 0.7, 0.7 to 0.95, and 0.95 to 1.0; and (2) comparing TH-parameter curves (for single CSNF WP and a single CDSP WP for

each of the five percolation subregions) based on the representative TH data set with the corresponding curves based on the comprehensive EBS TH data set. The results demonstrate that the representative TH dataset can be used as a surrogate for the comprehensive EBS TH data set. The difference in EBS release times due to using the comprehensive EBS TH data set and the representative TH data set used in the TSPA-LA Model is insignificant.

Stability of FEHM Particle Tracking Model

Radionuclide transport processes in the TSPA-LA Model were modeled using the FEHM particle-tracking methodology. The model accuracy of this methodology increases with the number of particles released from the source until a plateau is reached, indicating stability. The maximum number of particles used in TSPA-LA Model for any species modeled is computationally limited to 900,000 particles. The UZ Radionuclide Transport Model was rerun in GoldSim with a lower number of released particles (500,000 and 750,000), and the results were compared with the 900,000-particle base case TSPA-LA Model runs to test stability of the FEHM Particle Tracking Model results of the TSPA-LA Model. The runs were made for the Drip Shield EF Modeling Case, Igneous Intrusion Modeling Case, and Seismic GM Modeling Case, and with the radionuclides ^{99}Tc, ^{233}U, ^{234}U, ^{237}Np, and Total ^{239}Pu (combined reversible and slow and fast irreversible colloids). The tests and test results are discussed in Section 7.3.5. A summary of the results is provided below.

The particle-tracking stability test indicates that the use of 900,000 particles in the TSPA-LA Model analyses provides stable results with respect to the number of particles used in all three of the modeling cases (Drip Shield EF Modeling Case, Igneous Intrusion Modeling Case, and Seismic GM Modeling Case). A reduction of the maximum number of particles to 750,000 or 500,000 is shown to have little effect on the annual dose results. Likewise, peak dose results showed that the reductions in the maximum number of particles used to represent the EBS releases had little influence on the TSPA-LA Model results. Therefore, the FEHM particle tracking model is stable. A detailed comparison of annual dose for representative radionuclide species and UZ mass flux releases shows that slight differences in particle tracking results associated with the reductions to the number of particles representing source releases (and in-growth contributions) represent differences in the refinement of source terms to the SZ. This difference in the source terms is dampened by the time mass has been transported 18 km.

7.10.4 Uncertainty Characterization Reviews and Sensitivity Analyses

Uncertainty Characterization Reviews

A substantive effort to systematically review the uncertainty/variability characterizations of the direct-input parameters for consistency, defensibility, and traceability was made for the TSPA-LA Model. These reviews resulted in ensuring that the inputs to the TSPA-LA Model are technically sound and appropriately reflect any significant uncertainty associated with the input parameters. Parameter uncertainty and sensitivity analyses were performed during and after the TSPA-LA Model development to ensure the uncertainty was propagated properly and its sensitivity on the dose calculations were represented accurately. A detailed discussion of the uncertainty characterization reviews, and the sensitivity analyses is presented in Section 7.4. A summary is provided below.

A multi-disciplinary team of scientists and engineers was formed to conduct the parameter uncertainty reviews. The skill composition of the review team was chosen to ensure relevant large breadth of expertise, experience, and knowledge needed to perform the review. While the uncertainty characterization reviews primarily focused on scrutinizing the technical basis, they also included consistency aspects of the NRC Review Method for data uncertainty described in the *Yucca Mountain Review Plan, Final Report* (NRC 2003 [DIRS 163274]) for the 14 abstraction topics. Parameter uncertainty and variability characterizations were judged appropriate based on the criteria consistent with the NRC Acceptance Criterion for data uncertainty. More specifically, the criteria consisted of: (1) must be technically defensible and reasonably account for major sources of uncertainties and variabilities, and (2) will not introduce inappropriate risk dilution when propagated through the TSPA-LA Model. The major scenario classes and their associated modeling cases were ranked according to their potential contribution to the overall dose-risk. Three disruptive scenario modeling cases were chosen as the focus of the formal uncertainty characterization reviews: (1) Seismic GM Modeling Case, (2) Igneous Intrusion Modeling Case, and (3) Volcanic Eruption Modeling Case. The Nominal Scenario Class was added to the list because many of its component models are used in the seismic and igneous modeling cases.

The uncertainty characterization review ensured that the uncertainty associated with the TSPA-LA input parameters was properly and consistently characterized and propagated, and the observed significant issues were addressed. For example, for the seismic hazard curve it was observed that while use of a bounded curve in the TSPA-LA Model may be conservative (with respect to the total dose CDF), this particular treatment of uncertainty is inconsistent with approaches used in other scenario classes. As a result of this finding, additional seismic analyses were performed and a quantitative representation of uncertainty in the mean hazard curve developed. Because this new result provides a better treatment of uncertainty, it was included in the TSPA calculations for the PMA (Appendix C, Volume III). The PMA calculation gives a perspective on the level of conservatism introduced by the bounded hazard curve approach. As a result of the review, the Igneous Intrusion Modeling Case and Drip Shield EF Modeling Case account for both aleatory and epistemic uncertainties, the effects of which are explicitly propagated to the dose CDF. In the case of the Nominal Scenario Class modeling cases, the review findings helped develop improved CDFs for stainless and carbon steel corrosion rates for EBS Transport Model, the groundwater specific discharge (GWSPD) parameter, and the flowing interval spacing (FISVO) parameter for the SZ Flow model.

Sensitivity Analyses

The detail of the final results of sensitivity analyses are documented in Appendix K. The during-development analyses followed the analysis scheme presented in Appendix K. The during-development sensitivity analyses generally confirmed that the uncertainty reviews had covered all key uncertain inputs. In addition, the during-development analyses provided a measure of confirmation that important uncertain inputs are propagated appropriately through the process models, and that the effects of these uncertainties are consistent with physical principles underlying the models. The during-development sensitivity analyses also uncovered a number of implementation errors in developmental versions of the model, which were subsequently corrected before the TSPA-LA Model became final. After model development, a final sensitivity analysis was conducted, and is documented in Appendix K. This analysis identifies the

dominant sources of uncertainty in total expected dose to the RMEI. The final sensitivity analysis confirms that uncertain inputs are propagated through the TSPA-LA Model and that the effects of uncertainty in these inputs are consistent with physical principles. The confirmation is demonstrated through causal explanations of the relationships between input and output variables. The final sensitivity analysis also identified a relatively small number of implementation errors present in version 5.000 of the TSPA-LA Model. The errors were found not to significantly affect the performance measures (i.e., mean dose, dominant modeling cases, etc) from the TSPA-LA Model (Appendix P).

7.10.5 Surrogate Waste Form Validation

The three waste forms included in the TSPA-LA Model are CSNF (stainless steel and Zircaloy clad), DSNF surrogates, and HLW. Of the DSNF fuel categories, the naval spent fuel (Category 1) is represented in the TSPA-LA Model by a CSNF surrogate. The remaining DSNF (Categories 2 through 11) packages are represented by a surrogate with a radionuclide inventory that is the average of the radionuclide inventories of Categories 2 through 11. The dissolution rate of the surrogates is instantaneous based on the rapid dissolution of Category 7 DSNF (i.e., uranium metal).

The analyses presented in Section 7.5 show that the use of surrogates to represent naval spent fuel and Categories 2 through 11 of DSNF is appropriate. The analyses of NSNF show that mean annual dose from NSNF is bounded by that from the Zircaloy-clad CSNF surrogate. In the analyses of Categories 2 through 11, the DSNF show that the surrogate spent fuel used in the TSPA-LA Model is a reasonable representation of the weighted sum of these categories of DSNF.

7.10.6 Corroboration of Abstraction Results with Validated Process Models

Abstraction is a quantitative simplification process utilized for numerical implementation of many of the process models in the TSPA-LA Model. Therefore, it is essential to ensure that the abstraction results corroborate with the underlying process models. That is, the abstractions represent their respective process models before and after their implementation in the TSPA-LA Model and, when applied together as the integral components of the TSPA-LA Model, they function coherently so that the TSPA-LA Model results are stable and properly represent the contributing abstractions. This consistency is achieved by ensuring that the individual abstractions are validated for their intended use in the TSPA-LA Model, performing input-verification activities during their implementation in the TSPA-LA Model and performing TSPA-LA Model stability-testing during its development process. After the integrity of the underlying process models is ensured through the abstraction validation and the TSPA-LA Model implementation processes, and the individual abstractions can be shown to be functioning correctly when they are applied together as TSPA-LA Model components and result in the needed stability of the TSPA-LA Model, certain post-development validation and confidence building activities that are unrelated to the TSPA-LA Model development activities need to be performed in order to determine that the TSPA-LA Model is appropriate for its intended use. Ensuring the integrity of the direct-input process models through abstractions and their successful application in the TSPA-LA Model is the first step towards defining and executing these follow-up post-development validation and confidence-building activities. As a follow up,

the technical work plan (SNL 2008 [DIRS 184920], Section 2.3.5.2) identified corroboration of abstractions with validated process models as a post-development TSPA-LA Model validation criterion in order to demonstrate that the actual abstraction results of the process models do, in fact, corroborate with the respective underlying process models that were abstracted. To accomplish this confirmation, the abstraction results were qualitatively and quantitatively compared with the respective process models. Details of the corroboration method applied and results are presented in Section 7.6 and summarized in Table 7.6-1.

The corroboration effort was performed for the process models and analyses that served as direct inputs (Table 4-1) to the TSPA-LA Model. The results demonstrate that the process model abstractions are validated and corroborated with their underlying process models. The results also show that the relevant analyses that support the TSPA-LA Model are also verified. Details of these validation and verification activities are documented in their respective source documents (Table 7.6-1). In summary, the results of the corroboration study documented in Section 7.6 confirm that the abstractions implemented in the TSPA-LA Model do, in fact, corroborate qualitatively and quantitatively with their underlying validated process models and analyses.

7.10.7 Corroboration of Results with Auxiliary Analyses

The auxiliary analyses are an important aspect of determining whether the TSPA-LA Model is yielding reasonable results (e.g., that the model is producing the results that would be expected). Four different sets of auxiliary analyses were performed: (1) single realization analysis (Section 7.7.1), (2) comparison of the results of the TSPA-LA Model with a Simplified TSPA Analysis (Section 7.7.2), (3) comparison of the results of the TSPA-LA Model with the TSPA independently developed by EPRI (Section 7.7.3), and (4) PMA (Section 7.7.4) of the TSPA-LA modeling cases. The sections cited above describe in detail the analytical approach applied and observations made regarding the reasonableness of the TSPA-LA Model construction and the results it produced. A summary of the auxiliary analyses is provided below.

Single Realization Analysis

A comprehensive explanation detailing how the transport of key radionuclides is affected by coupling various submodel components of the EBS, UZ, and SZ domains in the TSPA Model, following the WP failure under varying physical-chemical-thermal-mechanical conditions, provides confidence that these model components are working as expected and the aggregate TSPA-LA Model results (in terms of dose) are reflective of the model components. Single realization analyses provide insight into the inner workings of the model and allow one to describe the transport of key radionuclide in a transparent manner. Through examination and explanation of key aspects affecting the release of radionuclides, it is demonstrated that the TSPA-LA Model is functioning as intended and that the submodels are coupled correctly to yield the system level results. This demonstration provides confidence that the TSPA-LA Model is functioning as designed and helps validate the model.

Single realization analyses have been performed on four modeling cases that were chosen to cover the range of WP failure mechanisms considered in TSPA-LA and to highlight the various processes affecting and controlling the radionuclide releases under varying

thermal-physical-chemical conditions. The four modeling cases are: (1) Waste Package EF Modeling Case (Section 7.7.1.1), (2) Drip Shield EF Modeling Case (Section 7.7.1.2), (3) Igneous Intrusion Modeling Case (Section 7.7.1.3), and (4) Seismic GM Modeling Case (Section 7.7.1.4). Details of the analyses and ensuing results are discussed in the sections cited above. The Waste Package EF Modeling Case and Drip Shield EF Modeling Case typically highlight the processes and controls on transport at early times when the repository is at an elevated temperature, along with the effects of climate changes while the DS is still intact. In contrast, the Igneous Intrusion Modeling Case and Seismic GM Modeling Case show the effects of various processes occurring late in time and when the DSs are breached but with variable damage on the WP.

A realization for analysis is selected that has behavior similar to the mean expected dose and represents a unique combination of epistemic and aleatory uncertainty. The description of aleatory uncertainty is different for each modeling case. It represents (1) a spatial location in the Waste Package and Drip Shield EF Modeling Cases, (2) timing of the disruptive event in the Igneous Intrusion Modeling Case, and (3) a sequence of randomly generated seismic events of varying magnitudes in the Seismic GM Modeling Case. After selecting a particular realization, the analysis provides a comprehensive explanation on the WP and DS failure mechanism, determination of failure opening area, and how the various waste forms degrade under varying thermal-physical-chemical conditions. The mass release of key radionuclides and their transport characteristics in the EBS, UZ, and SZ as modified by sorption, radioactive decay, decay-chain ingrowth, dispersion, and dilution, are described in detail under conditions that are unique to the modeling cases. The effects of solubility and sorption in controlling the release of certain radionuclides from the EBS are especially highlighted along with transport through various subdomains in the EBS Transport Model. The partitioning of mass going into the UZ fractures versus UZ matrix at the EBS-UZ boundary is described, and then the mass released is tracked in the UZ and SZ to underscore their barrier capability with respect to various radionuclides for selected parameter values. The concentrations at the RMEI location in the SZ are calculated from which the dose to RMEI is determined.

The qualitative and quantitative aspect of mass transport of various selected radionuclides is described in each of the three barriers. Describing the coupling of various submodels, such as in-package chemistry with solubility and sorption calculations under given thermal-physical-chemical conditions, provides the transparency and traceability that the models are coupled together and are working together as expected. The retardation effects in the UZ and SZ, along with the effect of fracture-matrix interaction, are also described. In all modeling cases the early release following the WP breach is dominated by non-sorbing and non-solubility limited radionuclides such as ^{99}Tc and ^{129}I, while the late time release is dominated by longer-lasting solubility-limited radionuclides that undergo sorption such as ^{242}Pu, ^{237}Np, and ^{239}Pu.

Comparison with Simplified TSPA Analysis

Comparison of the TSPA-LA Model results to a stand-alone Simplified TSPA Analysis (Section 7.7.2 and Appendix L) was conducted to further confidence in the TSPA-LA Model. The Simplified TSPA Analysis, based on a stand-alone computer program written in FORTRAN 90 and compiled/linked using Compaq Visual Fortran, was developed to corroborate the TSPA-LA Model. In developing the TSPA-LA Model, a complex numerical model is

required to appropriately solve the couple differential equations while taking into account the spatial variability in properties and processes. The Simplified TSPA Analysis is a higher level abstraction than the TSPA-LA Model. The difference between the two models is described in Section 7.7.2 with additional detail provided in Appendix L. Briefly, the simplification primarily involves removing a considerable amount of detail included in the TSPA-LA Model to capture spatial and temporal variability and treating the repository system with a more average representation. In addition, process level modeling results are further abstracted for inclusion in the Simplified TSPA Analysis. Although its technical bases are identical to those of the TSPA-LA Model, the Simplified TSPA Analysis is different than the TSPA-LA Model both in its structure and computational method.

The Simplified TSPA Analysis simulated four TSPA-LA modeling cases: (1) Nominal Modeling Case, which considered degradation of the WPs and DSs from corrosion processes only. Early WP failure, mechanical damage of the DS and WP, and seismic induced rockfall and its subsequent effects on seepage were not considered. (2) Waste Package EF Modeling Case, which evaluated repository performance considering only those WPs that experience early failure, and no failure of the WPs is considered to occur due to general corrosion, SCC, or seismic mechanical damage. (3) Seismic GM Modeling Case, which considered (a) degradation of the WP and DSs from corrosion processes; (b) effects of seismic ground motion, including mechanical damage to the WPs and DSs, and seismic induced rockfall; (c) random sampling of both aleatory and epistemic uncertainty in each realization; and (d) assuming seismic events of varying magnitude to occur randomly following a Poisson. The subsequent effects on rockfall, DS damage, and WP damage were then calculated. (4) Igneous Intrusion Modeling Case, which (a) considered the degradation of the engineered barriers as a result of an intruding magma dike; (b) did not consider degradation of the WP and DSs due to corrosion processes, seismic mechanical damage, and early WP failure; and (c) randomly sampled both aleatory and epistemic uncertainty in each realization. A single igneous intrusion was assumed to occur randomly over the simulation period resulting in the failure of all DSs and WPs.

The results of the Simplified TSPA Analysis show that for all four modeling cases the total mean annual dose and the individual radionuclide mean annual dose are similar in magnitude to those obtained for the corresponding TSPA-LA modeling cases. In addition, the most significant radionuclides are also similar in the respective modeling cases of both the Simplified TSPA Analysis and TSPA-LA Model. Section 7.7.2 provides detailed discussion on the comparative results for the individual modeling cases for the Simplified TSPA Analysis and the TSPA-LA Model, as well as the minor differences in the prominence of certain radionuclides and mean annual doses calculated by the two approaches. The differences are found to be consistent with the simplifications made in the Simplified TSPA Analysis**.** Three examples of this follow: (1) reflective of the differences in the approaches in the two TSPAs, the Waste Package EF Modeling Case of the Simplified TSPA Analysis yields higher mean annual total and individual radionuclide doses than those of the TSPA-LA Model. (2) The Simplified TSPA Analysis for the Seismic GM Modeling Case indicates that the trend in the mean annual dose for the key radionuclides is similar with the TSPA-LA Model although the magnitude of their mean annual doses may be slightly different. For example, the TSPA-LA results do not show ^{229}Th to be a dominant radionuclide towards the end of the simulation period and that ^{239}Pu is a second-order contributor to the total mean annual dose, always less than ^{129}I and ^{99}Tc. The minor differences in the prominence of certain radionuclides and mean annual doses by the Simplified TSPA

Analysis are consistent with the simplifications made in the models as discussed in detail in Section 7.7.2. (3) For the Igneous Intrusion Modeling Case, the results indicate that the total probability-weighted mean annual dose is similar in magnitude to that obtained for the nominal scenario simulated over a 1,000,000-year period with the TSPA-LA Model. The most significant radionuclides for the Simplified TSPA Analysis show the same trends as for the TSPA-LA Model, but the latter has ^{229}Th being of lesser importance after 200,000 years following repository closure. The increased importance of ^{229}Th is attributed to how its transport in the natural system is being modeled in the Simplified TSPA Analysis.

Comparison with EPRI TSPA Analysis

The EPRI TSPA Analysis was developed independently by EPRI based on its own modeling approach and total systems performance code, Integrated Multiple Assumptions and Release Code (IMARC). The EPRI TSPA Analysis results available in the public domain were compared with those of the TSPA-LA for building further confidence in the TSPA-LA Model results. Like TSPA-LA Model, EPRI identifies scenario class modeling cases. The key features of the EPRI TSPA nominal modeling case were compared with the corresponding TSPA-LA modeling case (Section 7.7.3.2) in order to develop an understanding of the basis for the doses in the EPRI TSPA Analysis and TSPA-LA Model. The EPRI TSPA Analysis is based on the YMP data available in the earlier analysis and/or model reports that were primarily used for preparation of TSPA for the Site Recommendation (TSPA-SR), not the information used in the TSPA-LA. In general, the EPRI Analysis represents a more simplified implementation of the various process models and associated uncertainty compared to the TSPA-LA Model. It does not explicitly consider aleatory uncertainty, whereas the TSPA-LA Model considers both epistemic and aleatory uncertainty. Detail of the similarities and differences between the EPRI TSPA Analysis and the TSPA-LA Model is discussed in Section 7.7.3, with additional detail provided in Appendix M. For dose comparison, no model was rerun using the EPRI TSPA data. Rather, a preliminary comparison was made with the tables and figures in the EPRI report available on the EPRI website with the appropriate parts of the TSPA-LA Model results. The TSPA-LA Model mean annual doses of the Nominal Modeling Class and Waste Package EF Modeling Case were compared with those from the EPRI report.

The results show general similarities of dose curves and radionuclides trend as well as and some differences between the results from the two models. However, the differences in model results can broadly be accounted for by the differences between the two models in seepage rates through the repository; early-failure representation and EBS failure; inventory, both in terms of waste type and individual radionuclides; and solubility limits and sorption characteristics in the UZ and SZ as discussed in Section 7.7.3. For example, the results of the comparison indicate a similar pattern for the nominal scenario characterized by a significant increase in dose after 100,000 years. The early-failure dose is represented by the dose increase after about 1,000 years in the TSPA-LA Model, which is somewhat delayed in the EPRI TSPA Analysis. Overall, the total dose in the EPRI TSPA Analysis is about 0.02 mrem/yr compared to about 0.4 mrem/yr at one million years by the TSPA-LA Model. The main contributor to total dose at late time is ^{129}I in both cases.

Performance Margin Analysis

The PMA was developed to quantitatively evaluate the differences in repository performance due to significant explicit and implicit conservatisms, and simplifications embedded in the TSPA-LA Model subcomponents. The PMA (1) evaluated conservatism with respect to the mean annual dose of the TSPA-LA Model; (2) quantified the extent to which conservatisms and simplifications individually and collectively might overestimate the projected annual dose; and (3) assessed that the evaluated conservatisms and simplifications did not introduce any inappropriate risk dilution in the TSPA-LA results presented in support of the LA. The PMA was conducted by first modifying selected submodels and parameters of the TSPA-LA Model, including the additional submodels and parameters for the PMA and then repeating the sequence of calculation for a select set of modeling cases that were run for the TSPA-LA. PMA was conducted for both 10,000-year and 1,000,000-year time periods and on the same set of modeling cases as the TSPA-LA Model. The details of approach and results of the PMA are presented in Section 7.7.4 with additional supporting material in Appendix C. Summarizing here, the results show that the conservatisms and simplifications evaluated in the PMA are indeed conservative with respect to the total system performance measures (e.g., mean annual dose), as the largest doses calculated in the PMA for the 10,000 year and 1,000,000 year are significantly lower than the doses used in compliance demonstration. The largest calculated PMA mean annual doses are lower by over an order of magnitude and a factor of two over the largest mean annual dose relative to the TSPA-LA Model (Section 8.0) for the time periods of 10,000 years and 1,000,000 years, respectively. Further, the PMA analysis demonstrated that the conservatisms evaluated did not introduce risk dilution in the TSPA-LA results presented (Section 8.1.1 in Volume III) in support of compliance with the regulatory dose requirement, as demonstrated by the absence of higher peak doses in the PMA results for both the probabilistic projections of the expected annual dose and the comparison of the projected total mean annual dose for the PMA relative to the TSPA-LA. The PMA results also have different significant modeling cases than the TSPA-LA Model due primarily to the items selected for modification in PMA.

7.10.8 Corroboration of Results with Natural Analogues

Corroboration of the results of the TSPA-LA Model can be gained, in part, through comparison with characteristics of relevant analogues. Analogue information serves as indirect input to several of the process models and analyses that support the TSPA-LA Model and is used in validation and confidence building of these process models and analyses. The detail of description of the analogues and their application is provided in the source model and analysis reports cited in Table 6-1 and *Natural Analogue Synthesis Report* (BSC 2004 [DIRS 169218]).

Summarizing the results of the corroboration effort with the relevant analogues, the information from natural analogues has contributed to confidence in the submodels for drift stability, waste form and EBS degradation, seepage, UZ flow and transport, coupled processes, SZ transport, the biosphere, and disruptive events due to volcanism and seismicity. The use of this information during the development of these TSPA-LA submodels ensures that the submodels are grounded in reality and provides confidence that the TSPA-LA Model produces reasonable results. In addition to applying the relevant analogues on a qualitative basis for building confidence in the

TSPA-LA supporting process models and analyses, detailed comparisons were conducted with the Cerro Negro volcanic eruption and the Nopal I uranium mine at Peña Blanca (Section 7.8).

The ASHPLUME Model was used to simulate ash-fall thickness from the 1995 eruption of the Cerro Negro volcano. The results show that the ASHPLUME Model can reasonably predict the ash-fall distribution and ash-fall thickness from the eruption of a basaltic cinder cone volcano similar to Cerro Negro. The Cerro Negro ash-fall calculation method is used to simulate eruptive releases of ash either near the Yucca Mountain repository or through the repository involving WP destruction and aerial distribution of radionuclides. The uraninite degradation process at the analogue Peña Blanca Nopal I ore body appears to be similar to that described by the metal-fuel dissolution submodel used in the TSPA-LA Model. The measured values of uranium concentration in the groundwater beneath the Nopal I ore body and in boreholes downgradient on the groundwater flow path from the ore body appear to show, consistent with similar observations in other natural analogues, that uranium and its decay products are sequestered by natural geologic processes and do not migrate significant distances away from the source, even for geologically long times. The Peña Blanca analogue analysis provides confidence in the ability of the TSPA-LA Model to reasonably simulate the processes involved, and the outcome of the transport of radionuclides from the Yucca Mountain repository through a UZ and an SZ to a receptor location.

7.10.9 Technical Reviews Summary

Section 7.9 summarizes the empanelled technical reviews that were performed by the Project during the last decade on its TSPA methodology-development approach for ultimately producing a valid TSPA-LA Model. These reviews, conducted by teams of external experts, were undertaken in order to ensure that the TSPA-LA Model produced by the Project applying the methodology was credible, defensible to the regulatory authorities, and respected by the technical community.

The empanelled TSPA technical reviews that support development of the TSPA-LA Model include the TSPA-VA review completed in 1999, the TSPA-SR review by an IRT completed in 2002, and the critical review performed on initial drafts of the TSPA-LA Model by an IVRT completed in 2006. The TSPA-VA, IRT, and IVRT reviews are discussed in Sections 7.9.1, 7.9.2, and 7.9.3, respectively. In addition to the three empanelled reviews, the NWTRB performs routine reviews on key areas of the Project as mandated by Congress. These NWTRB comments and recommendations make significant contributions to the development of the TSPA-LA Model on an on-going basis. It is to be noted here that the TSPA-VA, TSPA-SR, and the initial drafts of the TSPA-LA were prepared for the 10,000 years after the repository closure period, which was the regulatory compliance period at that time. A summary of the TSPA-VA, IRT, and IVRT reviews are provided below.

TSPA-VA Peer Review

The TSPA-VA peer review was conducted to provide a formal, independent evaluation and critique of the TSPA-VA. The specific scope was for the review panel to conduct a phased review over a two-year period to observe the development and completion of the TSPA-VA. The TSPA-VA review panel's key conclusions include: (1) overall, the approach demonstrated

in the TSPA-VA for assessing the behavior of the repository during the postclosure period was sound; (2) the panel stated that, "it is unlikely that the TSPA-VA, taken as a whole, describes the long-term probable behavior of the proposed repository". In the panel's judgment, a number of components of the TSPA-VA analysis were not supported by adequate evidence that they represent systems, components, and processes they were designed to represent. In addition, several of the component models were likely to be conservative and others non-conservative. For these reasons, the panel stated that the decisions based on the TSPA-VA should be made cautiously (Budnitz et al. 1999 [DIRS 102726], Section B, p. 1); (3) the TSPA-VA was a necessary and useful step in the evolving understanding of how a repository could be expected to perform at Yucca Mountain. It has produced valuable insights into performance of the various repository components and helped identify issues where additional data and analyses could improve understanding of the repository performance and where additional work is unlikely to make significant contributions (Budnitz et al. 1999 [DIRS 102726], Section B, p. 1); (4) the panel noted the inherent difficulty in developing the TSPA model that is required to predict the repository behavior such a long time into the future (Budnitz et al. 1999 [DIRS 102726], Section B, p. 1); and (5) the panel noted the many experiments that were planned to be performed, which would be valuable in confirming, calibrating, or invalidating models that were developed for analyses of conditions at the proposed repository (Budnitz et al. 1999 [DIRS 102726], Section B, p. 2).

The Project responded to the comments (CRWMS M&O 1999 [DIRS 153111]) and found the panel recommendations consistent within the strategy for development of the postclosure safety cases for the upcoming site recommendation and subsequent LA and the design selection, and work-prioritization efforts that were underway for developing the safety cases. The Project fully implemented the panel recommendations as demonstrated in the significant updates of the component models based on the highly expanded site-scale test data collection efforts (Section 7.9.1.2). These bold and positive steps by the Project produced a much improved TSPA, which in turn made achieving significant Project goals possible. The most remarkable achievement is the submittal of the SR (Abraham, S 2002 [DIRS 159915]) and the associated Environmental Impact Statement (EIS) (DOE 2002 [DIRS 155970]). This resulted in the Presidential and Congressional approval of the repository site and authorization to the DOE to proceed with the LA for the NRC authorization of construction of the repository in accordance with the stipulations of NRC Proposed Rule 10 CFR Part 63 [DIRS 178394] and [DIRS 180319].

International Review Team Peer Review

The overall objective of the IRT review was to provide, based on the available international standards and guidance, as appropriate, an independent assessment of the methodology developed by the Yucca Mountain Site Characterization Project, as reported in *Total System Performance Assessment for the Site Recommendation* (CRWMS M&O 2000 [DIRS 153246]). Based on its review, the IRT made several recommendations (OECD and IAEA 2002 [DIRS 158098], Section 5.1) on the rationale the Project was pursuing in developing the SR, specifically the TSPA-SR Model, methodology to be used in developing the ensuing TSPA-LA, and the prevailing EPA and NRC proposed regulations at that time for the repository. The details of these observations are presented in Section 7.9.2. The key ITR included the following: (1) while presenting room for improvement, the TSPA-SR methodology is soundly based and has been implemented in a competent manner; (2) the performance assessment approach

provides an adequate basis for supporting a statement on likely compliance within the regulatory period of 10,000 years and, accordingly, for the site recommendation decision; and, (3) the IRT stressed that understanding the repository system and its performance and how it provides for safety should be emphasized more in future iterations, both during and beyond the regulatory period, and further work would be required to increase confidence in the robustness of the TSPA. The IRT made a set of 27 specific recommendations for future improvements in preparation and submission of the LA. The Project addressed these recommendations (Section 7.9.2.1 and Appendix E).

IVRT Technical Review

The IVRT review scope was defined by the then available TSPA technical work plans for the draft TSPA-LA Model under preparation and was conducted within the context of whether or not the TSPA-LA drafts satisfy the intended purpose specifically included in the following two model validation goals (BSC 2005 [DIRS 173309], Section 2.10.1): (1) describe the postclosure performance of the repository system for the Nominal, Igneous, and Seismic Scenario Classes; and, (2) produce an estimate of mean dose (and other performance measures, as appropriate) that is consistent with the degree of conservatism representative of the component abstraction models and parameters (and their uncertainty) that are input to the TSPA-LA Model. The details of the review are presented in Section 7.9.3. A summary is provided below.

The IVRT developed many comments and submitted seven recommendations (Section 7.9.3.2 and 7.9.3.3). The Project responded to these comments and implemented the recommendations as discussed in Section 7.9.3.2 and 7.9.3.3. The IVRT believed that the model provided highly conservative estimates of mean dose. In 2005, the IVRT issued a draft final report. The Project responded to the IVRT comments and additional changes were made to the process models and the TSPA Model. In their draft final report, the IVRT concluded that unlike its conclusion documented in the July 2004 they determined that the 2005 TSPA Model draft appeared to contain potentially significant optimisms as well as conservatisms and that there was no basis for determining the degree of conservatism of the model. The IVRT included seven recommendations as mentioned above, in its final report of February 2006. The Project recognized that successful completion of additional activities planned for FY06 to FY07 would help achieve the goal of a credible TSPA-LA Model for supporting a LA. The Project has since planned and completed these activities and fully implemented the seven IVRT recommendations (Section 7.9).

7.10.10 Conclusions

The TSPA-LA Model is a product of more than a decade of iterative TSPA development effort by the YMP. The during-development and post-development model validation activities presented in Section 7 of the TSPA-LA Model report are identified in the technical work plan to ensure that the TSPA-LA Model is developed and validated for its intended purpose and as required by procedure. The intended purpose is to provide the TSPA-LA Model for use in evaluations of compliance with the quantitative postclosure requirements of U.S. Nuclear Regulatory Commission (NRC) Proposed Rule 10 CFR Part 63 (DIRS [178394] and DIRS [180319]). The activities are also to address the applicable TSPA-LA Model acceptance criteria identified by the NRC in the Yucca Mountain Review Plan.

The activities presented in Section 7 examine the internal supporting models and components of the TSPA-LA Model separately and in combination to determine whether or not they are producing reasonable and plausible inputs to the TSPA-LA Model. These during-development TSPA-LA Model activities included (a) verification of the GoldSim code and the inputs used in computation of the TSPA-LA Model results using the code; (b) statistical, temporal and spatial stability and numerical accuracy of the computed results, and the radionuclide transport computation applying the particle-tracking method by the FEHM code produces reliable results; (c) performing uncertainty characterization reviews and implementing the review findings to ensure that the uncertainty associated with the TSPA-LA input parameters are properly and uniformly characterized; and, (d) verifying and validating the use of the CSNF and DSNF surrogates to represent the Navy and the DSNF wastes categories respectively, to be disposed of in the repository. The results of these during-development activities demonstrate that the GoldSim code functions as intended, inputs were accurately implemented in the TSPA-LA Model; the TSPA-LA Model is numerically, temporally, and spatially stable; and the resultant dose calculations are accurate for meeting the regulatory standards for disposing the high-level radioactive wastes.

The subsequent post-development validation activities included (a) documenting the demonstration that the abstracted direct inputs to the TSPA-LA Model do represent the respective supporting process models; (b) a number auxiliary analyses to examine that the TSPA-LA Model produces reasonable and plausible results and included several analyses of single realizations, comparison of the TSPA-LA Model results with a Simplified TSPA Analysis using a FORTRAN code and the EPRI TSPA Analysis, and a set of performance margin analyses to ensure that the TSPA-LA Model results are free of inadvertent risk dilution; (c) qualitative and quantitative evaluation of the component-models of TSPA-LA Model with the relevant natural analogues to provide additional confidence in the reasonableness of the TSPA-LA Model; and (d) implementing the recommendations and responding to the review comments by the independent national and international panels of experts on the methodology and validity of the Project's past TSPA models. The results of these post-development corroborative activities demonstrate and provide confidence that the TSPA-LA Model is valid for its intended purpose. A roadmap of the TSPA-LA sections to the applicable NRC requirements and the Yucca Mountain Review Plan acceptance criteria is provided in Table H-1 of Appendix H.

QA: QA

MDL-WIS-PA-000005 REV00

January 2008

Total System Performance Assessment Model/Analysis for the License Application

Volume III

Prepared for:
U.S. Department of Energy
Office of Civilian Radioactive Waste Management
Office of Repository Development
1551 Hillshire Drive
Las Vegas, Nevada 89134-6321

Prepared by:
Sandia National Laboratories
OCRWM Lead Laboratory for Repository Systems
1180 Town Center Drive
Las Vegas, Nevada 89144

Under Contract Number
DE-AC04-94AL85000

DISCLAIMER

This report was prepared as an account of work sponsored by an agency of the United States Government. Neither the United States Government nor any agency thereof, nor any of their employees, nor any of their contractors, subcontractors or their employees, makes any warranty, express or implied, or assumes any legal liability or responsibility for the accuracy, completeness, or any third party's use or the results of such use of any information, apparatus, product, or process disclosed, or represents that its use would not infringe privately owned rights. Reference herein to any specific commercial product, process, or service by trade name, trademark, manufacturer, or otherwise, does not necessarily constitute or imply its endorsement, recommendation, or favoring by the United States Government or any agency thereof or its contractors or subcontractors. The views and opinions of authors expressed herein do not necessarily state or reflect those of the United States Government or any agency thereof.

QA: QA

Total System Performance Assessment Model/Analysis for the License Application

Volume III

MDL-WIS-PA-000005 REV00

January 2008

CONTENTS

Page

8. POSTCLOSURE PERFORMANCE DEMONSTRATION 8-1
8.1 CONFORMANCE WITH RADIATION PROTECTION STANDARDS 8.1-1
8.1.1 Individual Protection Standard 8.1-2
8.1.2 Groundwater Protection 8.1-12
8.1.3 Human Intrusion Protection 8.1-18
8.2 PROJECTIONS FOR INDIVIDUAL MODELING CASES 8.2-1
8.2.1 Nominal Modeling Case 8.2-2
8.2.2 Early Failure Scenario Class Modeling Cases 8.2-3
8.2.3 Igneous Scenario Class Modeling Cases 8.2-6
8.2.4 Seismic Scenario Class Modeling Cases 8.2-8
8.3 DESCRIPTION OF MULTIPLE BARRIER CAPABILITY 8.3-1
8.3.1 Radionuclides Selected to Demonstrate Multiple Barrier Capability 8.3-2
8.3.2 Identification of Barriers for Yucca Mountain Repository System 8.3-4
8.4 VALIDITY AND DEFENSIBILITY OF PERFORMANCE DEMONSTRATION 8.4-1
8.4.1 Validation of TSPA Model and Component Models 8.4-2
8.4.2 Verification and Validation of TSPA Software and Input Data 8.4-3
8.4.3 Uncertainty Characterization Reviews 8.4-5
8.4.4 Corroboration of TSPA-LA Model Results 8.4-6
8.4.5 Reviews of YMP TSPA Methodology 8.4-10

9. INPUTS AND REFERENCES 9-1
9.1 DOCUMENTS CITED 9-1
9.2 CODES, STANDARDS, REGULATIONS, AND PROCEDURES 9-58
9.3 SOFTWARE CODES 9-60
9.4 SOURCE DATA LISTED BY DATA TRACKING NUMBER 9-62

APPENDIX A—ACRONYMS AND ABBREVIATIONS A-1

APPENDIX B—DATA TRACKING NUMBERS FOR THE TSPA-LA MODEL B-1

APPENDIX C—PERFORMANCE MARGIN ANALYSIS C-1

APPENDIX D—PARAMETER LISTING D-1

APPENDIX E—RESPONSE TO REVIEW COMMENTS FROM THE INTERNATIONAL REVIEW TEAM E-1

APPENDIX F—DYNAMICALLY LINKED LIBRARIES DESCRIPTION AND FEEDS F-1

APPENDIX G—WIRING DIAGRAMS FOR MODEL INFORMATION FEEDS G-1

CONTENTS (Continued)

Page

APPENDIX H—YUCCA MOUNTAIN REVIEW PLAN ACCEPTANCE CRITERIA H-1

APPENDIX I—FEATURES, EVENTS, AND PROCESSES MAPPED TO THE TSPA-LA MODEL I-1

APPENDIX J—CONCEPTUAL STRUCTURE OF THE TSPA-LA J-1

APPENDIX K—UNCERTAINTY AND SENSITIVITY ANALYSIS RESULTS K-1

APPENDIX L—SIMPLIFIED TSPA L-1

APPENDIX M—COMPARISON WITH THE ELECTRIC POWER RESEARCH INSTITUTE MODEL M-1

APPENDIX N—DERIVATION OF IMPLEMENTING EQUATIONS FOR WASTE PACKAGE PARSING AND AVERAGE DAMAGE AREA N-1

APPENDIX O—LOCALIZED CORROSION INITIATION UNCERTAINTY ANALYSIS O-1

APPENDIX P— IMPACT ASSESSMENTS P-1

FIGURES

Page

8-1. Illustration of the Multiple Barriers of Yucca Mountain Repository System F8-1

8.1-1. Probabilistic Projections of Total Expected Annual Dose for 10,000 Years after Closure F8.1-1
8.1-2. Probabilistic Projections of Total Expected Annual Dose for 1,000,000 Years after Closure F8.1-2
8.1-3. Relative Contributions of Scenario Modeling Cases to Total Mean Annual Dose for (a) 10,000 Years and (b) 1,000,000 Years after Repository Closure F8.1-3
8.1-4. Histogram of Drip Shield Failure for the Nominal and Seismic Ground Motion Modeling Cases F8.1-4
8.1-5. Fraction of (a) CDSP WPs and (b) CSNF WPs Failed for by Seismic Crack Damage as a Function of Time for Percolation Subregion 3 ..... F8.1-5
8.1-6. Contribution of Individual Radionuclides to Total Mean Annual Dose for 10,000 Years after Repository Closure F8.1-6
8.1-7. Contribution of Individual Radionuclides to Total Mean Annual Dose for 1,000,000 Years after Repository Closure F8.1-7
8.1-8. Radium Mass Breakthrough Curves (upper) and Median Transport Times (lower) at the RMEI Location F8.1-8
8.1-9. Probabilistic Projections of Activity Concentrations Total Radium (^{226}Ra and ^{228}Ra) in Groundwater, Excluding Natural Background, for 10,000 Years after Closure F8.1-9
8.1-10. Probabilistic Projections of Activity Concentration of Gross Alpha and ^{226}Ra (Excluding Radon and Uranium) in Groundwater for 10,000 Years after Closure F8.1-10
8.1-11. Probabilistic Projections of Annual Drinking Water Doses for Combined Beta and Photon Emitting Radionuclides for 10,000 Years after Closure F8.1-11
8.1-12. Probabilistic Projections for Expected Annual Doses for the Human Intrusion Scenario for 1,000,000 Years after Closure with Drilling Event at 200,000 Years F8.1-12
8.1-13. Contribution of Individual Radionuclides to Mean Annual Dose for the Human Intrusion Scenario for 1,000,000 Years after Repository Closure F8.1-13

8.2-1. Probabilistic Projections of Expected Annual Dose for the Nominal Modeling Case for 1,000,000 Years after Repository Closure F8.2-1
8.2-2. Contribution of Individual Radionuclides to Mean Annual Dose for the Nominal Modeling Case for 1,000,000 Years after Repository Closure F8.2-2
8.2-3. Probabilistic Projections of Expected Annual Dose for the Drip Shield Early Failure Modeling Case for (a) 10,000 Years and (b) 1,000,000 Years after Repository Closure F8.2-3
8.2-4. Contribution of Individual Radionuclides to Mean Annual Dose for Drip Shield Early Failure Modeling Case for (a) 10,000 Years and (b) 1,000,000 Years After Repository Closure F8.2-4

FIGURES (Continued)

Page

8.2-5. Probabilistic Projections of Expected Annual Dose for Waste Package Early Failure Modeling Case for (a) 10,000 Years and (b) 1,000,000 Years after Repository Closure....F8.2-5
8.2-6. Contribution of Individual Radionuclides to Mean Annual Dose for Waste Package Early Failure Modeling Case for (a) 10,000 Years and (b) 1,000,000 Years after Repository Closure....F8.2-6
8.2-7. Probabilistic Projections of Expected Annual Dose for the Igneous Intrusion Modeling Case for (a) 10,000 Years and (b) 1,000,000 Years after Repository Closure....F8.2-7
8.2-8. Contribution of Individual Radionuclides to Mean Annual Dose for the Igneous Intrusion Modeling Case for (a) 10,000 Years and (b) 1,000,000 Years After Repository Closure....F8.2-8
8.2-9. Probabilistic Projections of Expected Annual Dose for the Volcanic Eruption Modeling Case for (a) 10,000 Years and (b) 1,000,000 Years after Repository Closure....F8.2-9
8.2-10. Contribution of Individual Radionuclides to Mean Annual Dose for the Volcanic Eruption Modeling Case for (a) 10,000 Years and (b) 1,000,000 Years after Repository Closure....F8.2-10
8.2-11. Probabilistic Projections of Expected Annual Dose for the Seismic Ground Motion Modeling Case for (a) 10,000 Years and (b) 1,000,000 Years after Repository Closure....F8.2-11
8.2-12. Contribution of Individual Radionuclides to Mean Annual Dose for the Seismic Ground Motion Modeling Case for (a) 10,000 Years and (b) 1,000,000 Years after Repository Closure....F8.2-12
8.2-13. Probabilistic Projections of Expected Annual Dose for the Seismic Fault Displacement Modeling Case for (a) 10,000 Years and (b) 1,000,000 Years after Repository Closure....F8.2-13
8.2-14. Contribution of Individual Radionuclides to Mean Annual Dose for the Seismic Fault Displacement Modeling Case for (a) 10,000 Years and (b) 1,000,000 Years After Repository Closure....F8.2-14

8.3-1. Mean Radionuclide Activities in the Nuclear Waste as a Function of Time for (a) 10,000 Years and (b) 1,000,000 Years after Repository Closure....F8.3-1
8.3-2. Mean Radionuclide Contributions to Total Inventory as a Function of Time for (a) 10,000 Years and (b) 1,000,000 Years after Repository Closure....F8.3-2

B-1. Road Map of TSPA-LA Model Data Tracking Numbers.... B-9
B-2. Road Map of Performance Margin Analysis Data Tracking Numbers.... B-10

C6-1. Schematic Illustration of Expected Flow Behavior of Seepage in a Rubble-Filled Collapsed Drift.... FC-1
C6-2. Mean Seepage Rate for (a) Intact Drift, (b) Collapsed Drift with Seepage Collected over 11-Meter Wide Drift, and (c) Collapsed Drift with Seepage Collected over 5.5-Meter Wide Center Section of Drift.... FC-2

FIGURES (Continued)

Page

C6-3. General Corrosion Rate Distribution Resulting from Fitting of Five-year Exposed Weight-Loss Sample Data FC-3
C6-4. Empirical Cumulative Distribution for General Corrosion Rate of Alloy 22 Weight-Loss and Crevice Samples after Five-Year Exposure in Long-Term Corrosion Test Facility FC-4
C6-5. Schematic Diagram of Modeling System for In-Package Water Balance FC-5
C6-6. Fraction of Water Entering Waste Package Estimated from the Sheet-Flow Model FC-6
C6-7. Temperature Difference between the Inside and Outside of a Waste Package FC-7
C6-8. Illustration of the Approach to Steady State pH and Ionic Strength as a Function of Pore Volumes Flushed FC-8
C6-9. Comparison of Performance Margin Analysis Model for High-Level Waste Glass Dissolution FC-9
C6-10. Plot of Log Transformed PuO_2(am) Solubility vs. pH FC-10
C6-11. Plot of Log Transformed Differences (Log Predicted−Log Observed) for PuO_2(am) Solubility FC-11
C6-12. Comparison of Predicted (EQ3/6) and Observed Values for NpO_2 Solubility along with Uncertainty Bounds FC-12
C6-13. Comparison of Predicted (EQ3/6) and Observed Values for Np_2O_5 Solubility along with Uncertainty Bounds FC-13
C6-14. Comparison of Predicted (EQ3/6) and Observed Values for Na-Boltwoodite Solubility along with Uncertainty Bounds FC-14
C6-15. Comparison of Predicted (EQ3/6) and Observed Values for $Na_4UO_2(CO_3)_3$ Solubility along with Uncertainty Bounds FC-15
C6-16. Decrease in Relative Dissolution Rate as a Function of Critical Reaction-Rind Thickness for Each of Three Values for the Final Reaction Affinity FC-16
C6-17. Colloid Filtration Rate Constants and Fractional Recoveries vs. Unretarded Groundwater Travel Times (Determined from Conservative Solute Tracers) from Tracer Experiments in Saturated Fractured Volcanics FC-17
C6-18. Colloid Detachment Rate Constants and Retardation Factors vs. Unretarded Groundwater Travel Times (Determined from Conservative Solute Tracers) from Tracer Experiments in Saturated Fractured Volcanics FC-18
C6-19. Colloid Filtration Rate Constants and Fractional Recoveries vs. Unretarded Groundwater Travel Times (Determined from Conservative Solute Tracers) from Tracer Experiments in Saturated Alluvium FC-19
C6-20. Colloid Detachment Rate Constants and Retardation Factors vs. Unretarded Groundwater Travel Times (Determined from Conservative Solute Tracers) from Tracer Experiments in Saturated Alluvium FC-20
C6-21. Colloid Filtration Rate Constants and Fractional Recoveries Unretarded Groundwater Travel Times for Saturated Fractured Volcanics (Data Replotted from Figure C6-17) FC-21
C6-22. Colloid Filtration Rate Constants and Fractional Recoveries Unretarded Groundwater Travel Times for Saturated Alluvium (Data Replotted from Figure C6-19) FC-22

FIGURES (Continued)

Page

C6-23. Volcanic and Alluvium Log Fractional Recoveries vs. Log Groundwater Travel Time Plotted Together and Fitted by Linear Regression Separately and Together FC-23
C6-24. Log Fractional Recoveries versus Log Ground Travel Time FC-24
C6-25. Colloid Filtration Rate Constant Cumulative Distribution Functions Associated with (1), (2), and (3) from Figure C6-24 Plotted along with the Actual Cumulative Distribution Function of the Filtration Rate Constants (Data Points) FC-25
C6-26. Minimum, Central, and Maximum Cumulative Distribution Functions of Colloid Retardation Factors Associated with a 100-Year Groundwater Travel Times FC-26
C6-27. Results of Sampling a Discretized Version of the Retardation Factor CDF Two Times to Obtain an Effective Retardation Distribution in the Combined Unsaturated Zone and Saturated Zone FC-27
C6-28. Cumulative Distribution Functions of Uncertainty in Water Table Rise for Individual Workshop Participants FC-28
C6-29. Cumulative Distribution Functions of Uncertainty in Water Table Rise by Consensus FC-29
C6-30. Map Showing Locations of Wells with Oxidizing and Reducing Groundwaters FC-30
C6-31. Saturated Zone Matrix Block Used as a Conduit for Unsaturated Matrix Mass Flux to the Saturated Zone FC-31
C6-32. Schematic Diagram Showing Conceptual Dual-Porosity Model for the Unsaturated Zone to Saturated Zone Mass Flux FC-32
C6-33. Configuration of Unsaturated Zone to Saturated Zone Matrix Diffusion FC-33
C6-34. Structure of the GoldSim Saturated Zone1-D Transport Model Setup for the Compliance Model FC-34
C6-35. Structure of the GoldSim Saturated Zone1-D Transport Model with Modifications for the Reducing Zones Model FC-35
C7-1. Probabilistic Projections of the Performance Margin Analysis Total Dose for 10,000 Years after Repository Closure FC-36
C7-2. Probabilistic Projections of Performance Margin Analysis Total Dose for 1,000,000 Years after Repository Closure FC-37
C7-3. Comparison of the Projected Total Mean Annual Dose for the TSPA-LA Model Relative to the Performance Margin Analysis for 10,000 Years after Repository Closure FC-38
C7-4. Comparison of the Projected Total Mean Annual Dose for the TSPA-LA Relative to the Performance Margin Analysis for 1,000,000 Years after Repository Closure FC-39
C7-5. Contributions of Individual Radionuclides to Total Mean Annual Dose for (a) the TSPA-LA and (b) the Performance Margin Analysis 10,000 Years after Repository Closure FC-40

FIGURES (Continued)

Page

C7-6. Contributions of Individual Radionuclides to Total Mean Annual Dose History for (a) the TSPA-LA and (b) the Performance Margin Analysis for 1,000,000 Years after Repository Closure FC-41
C7-7. Comparison of Scenario Modeling Cases to Projected Total Mean Annual Dose 10,000 Years after Repository Closure for (a) Drip Shield Early Failure, (b) Waste Package Early Failure, (c) Seismic Ground Motion, (d) Seismic Fault Displacement, (e) Igneous Intrusion, and (f) Relative Contributions of Scenario Modeling Cases to the Projected Mean Annual Dose for the Performance Margin Analysis. FC-42
C7-8. Comparison of Scenario Modeling Cases to Projected Total Mean Annual Dose 1,000,000 Years after Repository Closure for (a) Drip Shield Early Failure, (b) Waste Package Early Failure, (c) Seismic Ground Motion, (d) Seismic Fault Displacement, (e) Igneous Intrusion, and (f) Relative Contributions of Scenario Modeling Cases to the Projected Mean Annual Dose for the Performance Margin Analysis FC-43
C7-9. PMA Scenario Modeling Cases to Radionuclide Contributions to Projected Total Mean Annual Dose 10,000 Years after Repository Closure for (a) Drip Shield Early Failure, (b) Waste Package Early Failure, (c) Seismic Ground Motion, (d) Seismic Fault Displacement, (e) Igneous Intrusion, and (f) Total Mean Annual Dose for the Performance Margin Analysis FC-44
C7-10. PMA Scenario Modeling Cases to Radionuclide Contributions to Projected Total Mean Annual Dose 1,000,000 Years after Repository Closure for (a) Drip Shield Early Failure, (b) Waste Package Early Failure, (c) Seismic Ground Motion, (d) Seismic Fault Displacement, (e) Igneous Intrusion, and (f) Total Mean Annual Dose for the Performance Margin Analysis FC-45
C7-11. TSPA-LA Scenario Modeling Cases Radionuclide Contributions to Projected Total Mean Annual Dose 10,000 Years after Repository Closure for (a) Drip Shield Early Failure, (b) Waste Package Early Failure, (c) Seismic Ground Motion, (d) Seismic Fault Displacement, and (e) Igneous Intrusion FC-46
C7-12. TSPA-LA Scenario Modeling Cases Radionuclide Contributions to Projected Total Mean Annual Dose 1,000,000 Years after Repository Closure for (a) Drip Shield Early Failure, (b) Waste Package Early Failure, (c) Seismic Ground Motion, (d) Seismic Fault Displacement, and (e) Igneous Intrusion FC-47
C7-13. Comparison of Seismic Ground Motion Modeling Cases to Projected Total Mean Annual Dose 1,000,000 Years after Repository Closure for TSPA-LA, Performance Margin Analysis, and the Performance Margin Analysis, including General Corrosion Weight-Loss Data FC-48
C7-14. Comparison of Nominal Modeling Cases to Projected Total Mean Annual Dose History 1,000,000 Years after Repository Closure for TSPA-LA, Performance Margin Analysis, and the Performance Margin Analysis, including General Corrosion Weight-Loss Data FC-49

G-1. Illustration of the Transfer of Information between Model Components and Submodels of the TSPA-LA Model for the Nominal Scenario Class G-4

FIGURES (Continued)

Page

G-2. Illustration of the Transfer of Information between Model Components and Submodels of the TSPA-LA Model for the Early Failure Scenario Class G-5

G-3. Illustration of the Transfer of Information between Model Components and Submodels of the TSPA-LA Model for the Igneous Intrusion Modeling Case..... G-6

G-4. Illustration of the Transfer of Information between Model Components and Submodels of the TSPA-LA Model for the Seismic Ground Motion and Fault Displacement Modeling Cases..... G-7

G-5. Illustration of the Transfer of Information between Model Components and Submodels of the TSPA-LA Model for the Human Intrusion Scenario Class G-8

G-6. Illustration of the Transfer of Information on Water Fluxes between Model Components and Submodels of the TSPA-LA Model..... G-9

G-7. Illustration of the Transfer of Information on Radionuclide Fluxes between Model Components and Submodels of the TSPA-LA Model G-10

G-8. Illustration of the Transfer of Information between Model Components and Submodels of the TSPA-LA Model for Factors that Affect Flow through the EBS G-11

G-9. Illustration of the Transfer of Information between Model Components and Submodels of the TSPA-LA Model that affect Radionuclide Transport through the EBS..... G-12

G-10. Illustration of the Transfer of Information between Model Components and Submodels of the TSPA-LA Model, Nominal Scenario Class, for Factors that Affect Waste Form Degradation for CSNF WPs..... G-13

G-11. Illustration of the Transfer of Information between Model Components and Submodels of the TSPA-LA Model, Nominal Scenario Class, for Factors that Affect Waste Form Degradation for CDSP WPs..... G-14

I-1. Implementation of Features, Events, and Processes in the TSPA-LA Model I-3

J3.4-1. Example CCDF: plot of probability $prob_A(c > C)$ that a consequence with a value larger then C will occur..... FJ-1

J3.4-2. Approximation of a CCDF with a random sample of size 1,000..... FJ-1

J3.5-1. Different values of CCDF defined by Equation J3.4-5 that derive from different values of e. FJ-2

J3.5-2. Example of an LHS of size $nLHS = 10$ from variables U and V with U normal on [−1, 1] (mean = 0, 0.01 quantile = −1, 0.99 quantile = 1) and V triangular on [0, 4] (mode = 1) (Figure 4, Helton 1999 [DIRS 159042]) FJ-2

J5-1. Estimate obtained with LHS of size $nLHS = 300$ showing epistemic uncertainty in dose $D_N(\tau|\mathbf{a}_N, \mathbf{e}_M)$ to RMEI for $0 \le \tau \le 10^6$ yr that results when only nominal conditions are considered: (a) $D_N(\tau|\mathbf{a}_N, \mathbf{e}_{Mi})$, $i = 1, 2, \ldots, nLHS = 300$, (b) dose $D_N(\tau|\mathbf{a}_N, \mathbf{e}_{Mi})$, $i = 1, 2, \ldots, 50$, (c) exceedance probabilities $p_E[D < D_N(\tau|\mathbf{a}_N, \mathbf{e}_M)]$ and quantiles $Q_q[D_N(\tau|\mathbf{a}_N, \mathbf{e}_M)]$, $q = 0.05, 0.5, 0.95$, for $\tau = 6.0 \times 10^5$ yr, and (d) expected (mean) dose $\bar{\bar{D}}_N(\tau)$ and quantiles $Q_q[D_N(\tau|\mathbf{a}_N, \mathbf{e}_M)]$, $q = 0.05, 0.5, 0.95$..... FJ-3

FIGURES (Continued)

Page

J5-2. Summary of results obtained with LHS of size $nLHS = 300$ showing epistemic uncertainty in dose $D_N(\tau|\mathbf{a}_N, \mathbf{e}_M)$ to RMEI for $0 \le \tau \le 10^6$ yr that results when only nominal conditions are considered. FJ-4

J5-3. Estimate obtained with LHS of size $nLHS = 300$ of epistemic uncertainty in dose $D_{Nr}(\tau|\mathbf{a}_N, \mathbf{e}_M)$ to RMEI for $0 \le \tau \le 10^6$ yr with r corresponding to ^{129}I that results when only nominal conditions are considered: (a) dose $D_{Nr}(\tau|\mathbf{a}_N, \mathbf{e}_{Mi})$, $i = 1, 2, \ldots, nLHS = 300$, (b) dose $D_{Nr}(\tau|\mathbf{a}_N, \mathbf{e}_{Mi})$, $i = 1, 2, \ldots, 50$, (c) exceedance probabilities $p_E[D < D_{Nr}(\tau|\mathbf{a}_N, \mathbf{e}_M)]$ and quantiles $Q_q[D_{Nr}(\tau|\mathbf{a}_N, \mathbf{e}_M)]$, $q = 0.05, 0.5$ and 0.95, for $\tau = 6.0 \times 10^5$ yr, and (d) expected (mean) dose $\bar{\bar{D}}_{Nr}(\tau)$ and quantiles $Q_q[D_{Nr}(\tau|\mathbf{a}_N, \mathbf{e}_M)]$, $q = 0.05, 0.5, 0.95$..... FJ-5

J5-4. Estimates obtained with LHS of size $nLHS = 300$ of expected (mean) dose $\bar{\bar{D}}_{Nr}(\tau|\mathbf{a}_N)$ to RMEI for $0 \le \tau \le 10^6$ yr for individual radioactive species that result when only nominal conditions are considered. FJ-6

J5-5. Assessment with replicated sampling of numerical error associated with use of an LHS of size $nLHS = 300$ to determine epistemic uncertainty in dose $D_N(\tau|\mathbf{a}_N, \mathbf{e}_M)$ to RMEI for $0 \le \tau \le 10^6$ yr that results when only nominal conditions are considered: (a) Replicated estimates of expected (mean) dose $\bar{\bar{D}}_N(\tau|\mathbf{a}_N)$ and quantiles $Q_q[D_N(\tau|\mathbf{a}_N, \mathbf{e}_M)]$, $q = 0.05, 0.5, 0.95$, and (b) confidence intervals for estimates of expected (mean) dose $\bar{\bar{D}}_N(\tau|\mathbf{a}_N)$. FJ-7

J6.2-1. Complementary cumulative distribution functions (CCDFs) for number nEW of WPs with early failure associated with individual elements of LHS of size $nLHS = 300$ in Equation J.4.9-1: (a) CCDFs for all 300 LHS elements, and (b) CCDFs for first 50 LHS elements. FJ-9

J6.2-2. Summary of results obtained with LHS of size $nLHS = 300$ showing epistemic uncertainty in doses $D_{EW}(\tau|[1, r, 3, t], \mathbf{e}_M)$ for $0 \le \tau \le 20{,}000$ yr: (a) CSNF WP in bin 3 under nondripping conditions (i.e., $D_{EW}(\tau|[1, 1, 3, 0], \mathbf{e}_{Mi})$, $i = 1, 2, \ldots, nLHS = 300$), (b) CSNF WP in bin 3 under dripping conditions (i.e., $D_{EW}(\tau|[1, 1, 3, 1], \mathbf{e}_{Mi})$, $i = 1, 2, \ldots, nLHS = 30)0$, (c) CDSP WP in bin 3 under nondripping conditions (i.e., $D_{EW}(\tau|[1, 2, 3, 0], \mathbf{e}_{Mi})$, $i = 1, 2, \ldots, nLHS = 300$), and (d) CDSP WP in bin 3 under dripping conditions (i.e., $D_{EW}(\tau|[1, 2, 3, 1], \mathbf{e}_{Mi})$, $i = 1, 2, \ldots, nLHS = 300$). FJ-10

FIGURES (Continued)

Page

J6.2-3. Box plots (Description: Box extends from 0.25 to 0.75 quantile; left and right bar and whisker extend to 0.1 and 0.9 quantile, respectively; ×'s represent values outside 0.1 to 0.9 quantile range; median and mean are indicated by light and dark vertical lines, respectively) summarizing results obtained with LHS of size $nLHS = 300$ showing epistemic uncertainty in doses $D_{EW}(\tau|[1, r, s, t], \mathbf{e}_{Mi})$ for selected values of τ, $r = 1, 2$, $s = 1, 2, 3, 4, 5$, $t = 0, 1$, and $i = 1, 2, \ldots, nLHS = 300$: (a, c, e) CSNF WPs at $\tau = 10{,}000$, 15,000 and 20,000 yr, and (b, d, f) CDSP WPs at $\tau = 2000$, 5000 and 10,000 yr. FJ-11

J6.2-4. Estimate of $\bar{D}_{EW}(\tau|\mathbf{e}_1)$ for LHS element $\mathbf{e}_1 = [\mathbf{e}_{A1}, \mathbf{e}_{M1}]$ and $0 \le \tau \le 20{,}000$ yr with integration-based procedure indicated in Equation J6.2-2..... FJ-12

J6.2-5. Estimate obtained with LHS of size $nLHS = 300$ showing epistemic uncertainty in expected dose $\bar{D}_{EW}(\tau|\mathbf{e})$ to RMEI for $0 \le \tau \le 20{,}000$ yr that at results when only early WP failure is considered: (a) expected dose $\bar{D}_{EW}(\tau|\mathbf{e}_i)$, $i = 1, 2, \ldots, nLHS = 300$, (b) expected dose $\bar{D}_{EW}(\tau|\mathbf{e}_i)$, $i = 1, 2, \ldots, 50$, (c) exceedance probabilities $p_E[D < \bar{D}_{EW}(\tau|\mathbf{e})]$ and quantiles $Q_q[\bar{D}_{EW}(\tau|\mathbf{e})]$, $q = 0.05$, 0.5 and 0.95, for $\tau = 10^4$ yr, and (d) expected (mean) dose $\bar{\bar{D}}_{EW}(\tau)$ and quantiles $Q_q[\bar{\bar{D}}_{EW}(\tau|\mathbf{e})]$, $q = 0.05$, 0.5, 0.95. ..... FJ-13

J6.2-6. Summary of results obtained with LHS of size $nLHS = 300$ showing epistemic uncertainty in expected dose $\bar{D}_{EW}(\tau|\mathbf{e})$ to RMEI for $0 \le \tau \le 20{,}000$ yr that results when only early WP failure is considered..... FJ-14

J6.2-7. Estimate obtained with LHS of size $nLHS = 300$ showing epistemic uncertainty in expected dose $\bar{D}_{EW,r}(\tau|\mathbf{e})$ to RMEI for $0 \le \tau \le 20{,}000$ yr with r corresponding to ^{99}Tc that results when only early WP failure is considered: (a) expected dose $\bar{D}_{EW,r}(\tau|\mathbf{e}_i)$, $i = 1, 2, \ldots, nLHS = 300$, (b) expected dose $\bar{D}_{EW,r}(\tau|\mathbf{e}_i)$, $i = 1, 2, \ldots, 50$, (c) exceedance probabilities $p_E[D < \bar{D}_{EW}(\tau|\mathbf{e})]$ and quantiles $Q_q[\bar{D}_{EW,r}(\tau|\mathbf{e})]$, $q = 0.05$, 0.5 and 0.95, for $\tau = 10^4$ yr, and (d) expected (mean) dose $\bar{\bar{D}}_{EW,r}(\tau)$ and quantiles $Q_q[\bar{D}_{EW,r}(\tau|\mathbf{e})]$, $q = 0.05$, 0.5, 0.95..... FJ-15

J6.2-8. Estimates obtained with LHS of size $nLHS = 300$ of expected (mean) dose $\bar{\bar{D}}_{EW,r}(\tau)$ to RMEI for $0 \le \tau \le 20{,}000$ yr for individual radioactive species that result when only early WP failure is considered. FJ-16

J6.2-9. Results associated with $D_{EW}(\tau|\mathbf{a}_{EW}, \mathbf{e}_{M1})$ for LHS element $\mathbf{e}_1 = [\mathbf{e}_{A1}, \mathbf{e}_{M1}]$ obtained with sampling-based (Monte Carlo) procedures: (a) CCDF for $D_{EW}(10^4 \text{ yr}|\mathbf{a}_{EW}, \mathbf{e}_{M1})$ with exceedance probabilities $p_A[D < D_{EW}(10^4 \text{ yr}|\mathbf{a}, \mathbf{e}_{M1})|\mathbf{e}_{A1}]$ defined in Equation (J6.2-12), and (b) expected dose $\bar{D}_{EW}(10^4 \text{ yr}|\mathbf{e}_1)$ associated with $D_{EW}(10^4 \text{ yr}|\mathbf{a}_{EW}, \mathbf{e}_{M1})$ as defined in Equation (J6.2-10)..... FJ-17

FIGURES (Continued)

Page

J6.2-10. Results associated with $D_{EW}(10^4 \text{ yr}|\mathbf{a}_{EW}, \mathbf{e}_M)$ obtained with sampling-based (Monte Carlo) procedures for an LHS of size $nLHS = 300$: (a) CCDFs for $D_{EW}(10^4 \text{ yr}|\mathbf{a}_{EW}, \mathbf{e}_{Mi})$ with exceedance probabilities $p_A[D < D_{EW}(10^4 \text{ yr}|\mathbf{a}, \mathbf{e}_{Mi})|\mathbf{e}_{Ai}]$ defined in Equation J6.2-12 for $i = 1, 2, \ldots, nLHS = 300$, (b) CCDFs for $D_{EW}(10^4 \text{ yr}|\mathbf{a}_{EW}, \mathbf{e}_{Mi})$ with exceedance probabilities $p_A[D < D_{EW}(10^4 \text{ yr}|\mathbf{a}, \mathbf{e}_{Mi})|\mathbf{e}_{Ai}]$ defined in Equation J6.2-13 for $i = 1, 2, \ldots, 50$, and (c) expected (mean) CCDF and quantile curves, $q = 0.05, 0.5, 0.95$, for CCDFs in (a). FJ-18

J6.2-11. Assessment with replicated sampling of numerical error associated with use of an LHS of size $nLHS = 300$ to determine epistemic uncertainty in expected dose $\bar{D}_{EW}(\tau|\mathbf{e})$ to RMEI for $0 \le \tau \le 20{,}000$ yr that results when only early WP failure is considered: (a) Replicated estimates of expected (mean) dose $\bar{\bar{D}}_{EW}(\tau)$ and quantiles $Q_q[\bar{D}_{EW}(\tau|\mathbf{e})]$, $q = 0.05, 0.5, 0.95$, and (b) confidence intervals for estimates of expected (mean) dose $\bar{\bar{D}}_{EW}(\tau)$. FJ-19

J6.2-12. Summary of results obtained with LHS of size $nLHS = 300$ showing epistemic uncertainty in doses $D_{EW}(\tau|[1, r, s, t], \mathbf{e}_M)$ for $0 \le \tau \le 10^6$ yr: (a) CSNF WP in bin 3 under nondripping conditions (i.e., $D_{EW}(\tau|[1, 1, 3, 0], \mathbf{e}_{Mi})$, $i = 1, 2, \ldots, nLHS = 300$), (b) CSNF WP in bin 3 under dripping conditions (i.e., $D_{EW}(\tau|[1, 1, 3, 1], \mathbf{e}_{Mi})$, $i = 1, 2, \ldots, nLHS = 300$), (c) CDSP WP in bin 3 under nondripping conditions (i.e., $D_{EW}(\tau|[1, 2, 3, 0], \mathbf{e}_{Mi})$, $i = 1, 2, \ldots, nLHS = 300$), and (d) CDSP WP in bin 3 under dripping conditions (i.e., $D_{EW}(\tau|[1, 2, 3, 1], \mathbf{e}_{Mi})$, $i = 1, 2, \ldots, nLHS = 300$). FJ-20

J6.2-13. Box plots (see Figure J6.2-3 for description) summarizing results obtained with LHS of size $nLHS = 300$ showing epistemic uncertainty in doses $D_{EW}(\tau|[1, r, s, t], \mathbf{e}_{Mi})$ for $\tau = 5 \times 10^4, 2 \times 10^5, 5 \times 10^5$ yr, $r = 1, 2$, $s = 1, 2, 3, 4, 5$, $t = 0, 1$, and $i = 1, 2, \ldots, nLHS = 300$: (a, c, e) CSNF WPs for $\tau = 5 \times 10^4, 2 \times 10^5, 5 \times 10^5$ yr, and (b, d, f) CDSP WPs for $\tau = 5 \times 10^4, 2 \times 10^5, 5 \times 10^5$ yr. FJ-21

J6.2-14. Estimate of $\bar{D}_{EW}(\tau|\mathbf{e}_1)$ for LHS element $\mathbf{e}_1 = [\mathbf{e}_{A1}, \mathbf{e}_{M1}]$ and $0 \le \tau \le 10^6$ yr with integration-based procedure indicated in Equation (J6.2-2). FJ-22

J6.2-15. Estimate obtained with LHS of size $nLHS = 300$ showing epistemic uncertainty in expected dose $\bar{D}_{EW}(\tau|\mathbf{e})$ to RMEI for $0 \le \tau \le 10^6$ yr that at results when only early WP failure is considered: (a) expected dose $\bar{D}_{EW}(\tau|\mathbf{e}_i)$, $i = 1, 2, \ldots, nLHS = 300$, (b) expected dose $\bar{D}_{EW}(\tau|\mathbf{e}_i)$, $i = 1, 2, \ldots, 50$, (c) exceedance probabilities $p_E[D < \bar{D}_{EW}(\tau|\mathbf{e})]$ and quantiles $Q_q[\bar{D}_{EW}(\tau|\mathbf{e})]$, $q = 0.05, 0.5$ and 0.95, for $\tau = 5 \times 10^5$ yr, and (d) expected (mean) dose $\bar{\bar{D}}_{EW}(\tau)$ and quantiles $Q_q[\bar{D}_{EW}(\tau|\mathbf{e})]$, $q = 0.05, 0.5, 0.95$. FJ-23

FIGURES (Continued)

Page

J6.2-16. Summary of results obtained with LHS of size $nLHS = 300$ showing epistemic uncertainty in expected dose $\bar{D}_{EW}(\tau|\mathbf{e})$ to RMEI for $0 \le \tau \le 10^6$ yr that results when only early WP failure is considered. FJ-24

J6.2-17. Estimate obtained with LHS of size $nLHS = 300$ showing epistemic uncertainty in expected dose $\bar{D}_{EW,r}(\tau|\mathbf{e})$ to RMEI for $0 \le \tau \le 10^6$ yr with r corresponding to ^{242}Pu that results when only early DS failure is considered: (a) expected dose $\bar{D}_{EW,r}(\tau|\mathbf{e}_i)$, $i = 1, 2, \ldots, nLHS = 300$, (b) expected dose $\bar{D}_{EW,r}(\tau|\mathbf{e}_i)$, $i = 1, 2, \ldots, 50$, (c) exceedance probabilities $p_E[D < \bar{D}_{EW,r}(\tau|\mathbf{e})]$ and quantiles $Q_q[\bar{D}_{EW,r}(\tau|\mathbf{e})]$, $q = 0.05$, 0.5 and 0.95, for $\tau = 5 \times 10^5$ yr, and (d) expected (mean) dose $\bar{\bar{D}}_{EW,r}(\tau)$ and quantiles $Q_q[\bar{D}_{EW,r}(\tau|\mathbf{e})]$, $q = 0.05$, 0.5, 0.95 ..... FJ-25

J6.2-18. Estimates obtained with LHS of size $nLHS = 300$ of expected (mean) dose $\bar{\bar{D}}_{EW,r}(\tau)$ to RMEI for $0 \le \tau \le 10^6$ yr for individual radioactive species that result when only early WP failure is considered. FJ-26

J6.2-19. Results associated with $D_{EW}(\tau|\mathbf{a}_{EW}, \mathbf{e}_{M1})$ for LHS element $\mathbf{e}_1 = [\mathbf{e}_{A1}, \mathbf{e}_{M1}]$ obtained with sampling-based (Monte Carlo) procedures: (a) CCDF for $D_{EW}(5 \times 10^5 \text{ yr}|\mathbf{a}_{EW}, \mathbf{e}_{M1})$ with exceedance probabilities $p_A[D < D_{EW}(5 \times 10^5 \text{ yr}|\mathbf{a}, \mathbf{e}_{M1})|\mathbf{e}_{A1}]$ defined in Equation (J6.2-12), and (b) expected dose $\bar{D}_{EW}(5 \times 10^5 \text{ yr}|\mathbf{e}_1)$ associated with $D_{EW}(5 \times 10^5 \text{ yr}|\mathbf{a}_{EW}, \mathbf{e}_{M1})$ as defined in Equation (J6.2-10) FJ-27

J6.2-20. Results associated with $D_{EW}(5 \times 10^5 \text{ yr}|\mathbf{a}_{EW}, \mathbf{e}_M)$ obtained with sampling-based (Monte Carlo) procedures for an LHS of size $nLHS = 300$: (a) CCDFs for $D_{EW}(5 \times 10^5 \text{ yr}|\mathbf{a}_{EW}, \mathbf{e}_{Mi})$ with exceedance probabilities $p_A[D < D_{EW}(5 \times 10^5 \text{ yr}|\mathbf{a}, \mathbf{e}_{Mi})|\mathbf{e}_{Ai}]$ defined in Equation J66.2-12 for $i = 1, 2, \ldots, nLHS = 300$, (b) CCDFs for $D_{EW}(10^4 \text{ yr}|\mathbf{a}_{EW}, \mathbf{e}_{Mi})$ with exceedance probabilities $p_A[D < D_{EW}(5 \times 10^5 \text{ yr}|\mathbf{a}, \mathbf{e}_{Mi})|\mathbf{e}_{Ai}]$ defined in Equation J6.2-20 for $i = 1, 2, \ldots, 50$, and (c) expected (mean) CCDF and quantile curves, $q = 0.05$, 0.5, 0.95, for CCDFs in (a). FJ-28

J6.2-21. Assessment with replicated sampling of numerical error associated with use of an LHS of size $nLHS = 300$ to determine epistemic uncertainty in expected dose $\bar{D}_{EW}(\tau|\mathbf{e})$ to RMEI for $0 \le \tau \le 10^6$ yr that results when only early WP failure is considered: (a) Replicated estimates of expected (mean) dose $\bar{\bar{D}}_{EW}(\tau)$ and quantiles $Q_q[\bar{D}_{EW}(\tau|\mathbf{e})]$, $q = 0.05$, 0.5, 0.95, and (b) confidence intervals for estimates of expected (mean) dose $\bar{\bar{D}}_{EW}(\tau)$. FJ-29

FIGURES (Continued)

Page

J6.3-1. Complementary cumulative distribution functions (CCDFs) for number *nED* of DSs with early failure associated with individual elements of LHS of size *nLHS* = 300 in Equation J4.9-1: (a) CCDFs for all 300 LHS elements, and (b) CCDFs for first 50 LHS elements. FJ-30

J6.3-2. Summary of results obtained with LHS of size *nLHS* = 300 showing epistemic uncertainty in doses $D_{ED}(\tau|[1, r, s, 1], \mathbf{e}_M)$ for $0 \le \tau \le 20{,}000$ yr: (a) CSNF WP in bin 3 under dripping conditions (i.e., $D_{ED}(\tau|[1, 1, 3, 1], \mathbf{e}_{Mi})$, $i = 1, 2, \ldots, nLHS = 300$), and (b) CDSP WP in bin 3 under dripping conditions (i.e., $D_{ED}(\tau|[1, 2, 3, 1], \mathbf{e}_{Mi})$, $i = 1, 2, \ldots, nLHS = 300$). FJ-31

J6.3-3. Box plots (see Figure J6.2-3 for description) summarizing results obtained with LHS of size *nLHS* = 300 showing epistemic uncertainty in doses $D_{ED}(\tau|[1, r, s, 1], \mathbf{e}_{Mi})$ for $\tau = 2000$, 5000, 10,000 yr, $r = 1, 2$, $s = 1, 2, 3, 4, 5$, $t = 1$, and $i = 1, 2, \ldots, nLHS = 300$: (a, c, e) CSNF WPs at $\tau = 2000$, 5000 and 10,000 yrs, and (b, d, f) CDSP WPs at $\tau = 2000$, 5000 and 10,000 yrs. FJ-32

J6.3-4. Estimate of $\bar{D}_{ED}(\tau|\mathbf{e}_1)$ for LHS element $\mathbf{e}_1 = [\mathbf{e}_{A1}, \mathbf{e}_{M1}]$ and $0 \le \tau \le 20{,}000$ yr with integration-based procedure indicated in Equation (J6.3-2). FJ-33

J6.3-5. Estimate obtained with LHS of size *nLHS* = 300 showing epistemic uncertainty in expected dose $\bar{D}_{ED}(\tau|\mathbf{e})$ to RMEI for $0 \le \tau \le 20{,}000$ yr that results when only early DS failure is considered: (a) expected dose $\bar{D}_{ED}(\tau|\mathbf{e}_i)$, $i = 1, 2, \ldots, nLHS = 300$, (b) expected dose $\bar{D}_{ED}(\tau|\mathbf{e}_i)$, $i = 1, 2, \ldots, 50$, (c) exceedance probabilities $p_E[D < \bar{D}_{ED}(\tau|\mathbf{e})]$ and quantiles $Q_q[\bar{D}_{ED}(\tau|\mathbf{e})]$, $q = 0.05$, 0.5 and 0.95, for $\tau = 10^4$ yr, and (d) expected (mean) dose $\bar{\bar{D}}_{ED}(\tau)$ and quantiles $Q_q[\bar{D}_{ED}(\tau|\mathbf{e})]$, $q = 0.05$, 0.5, 0.95. ..... FJ-34

J6.3-6. Summary of results obtained with LHS of size *nLHS* = 300 showing epistemic uncertainty in expected dose $\bar{D}_{ED}(\tau|\mathbf{e})$ to RMEI for $0 \le \tau \le 20{,}000$ yr that results when only early DS failure is considered. FJ-35

J6.3-7. Estimate obtained with LHS of size *nLHS* = 300 showing epistemic uncertainty in expected dose $\bar{D}_{ED,r}(\tau|\mathbf{e})$ to RMEI for $0 \le \tau \le 20{,}000$ yr with r corresponding to ^{99}Tc that results when only early DS failure is considered: (a) expected dose $\bar{D}_{ED,r}(\tau|\mathbf{e}_i)$, $i = 1, 2, \ldots, nLHS = 300$, (b) expected dose $\bar{D}_{ED,r}(\tau|\mathbf{e}_i)$, $i = 1, 2, \ldots, 50$, (c) exceedance probabilities $p_E[D < \bar{D}_{ED,r}(\tau|\mathbf{e})]$ and quantiles $Q_q[\bar{D}_{ED,r}(\tau|\mathbf{e})]$, $q = 0.05$, 0.5 and 0.95, for $\tau = 10^4$ yr, and (d) expected (mean) dose $\bar{\bar{D}}_{ED,r}(\tau)$ and quantiles $Q_q[\bar{D}_{ED,r}(\tau|\mathbf{e})]$, $q = 0.05$, 0.5, 0.95. ..... FJ-36

J6.3-8. Estimates obtained with LHS of size *nLHS* = 300 of expected (mean) dose $\bar{\bar{D}}_{ED,r}(\tau)$ to RMEI for $0 \le \tau \le 20{,}000$ yr for individual radioactive species that result when only early DS failure is considered. FJ-37

FIGURES (Continued)

Page

J6.3-9. Results associated with $D_{ED}(\tau|\mathbf{a}_{ED}, \mathbf{e}_{M1})$ for LHS element $\mathbf{e}_1 = [\mathbf{e}_{A1}, \mathbf{e}_{M1}]$ obtained with sampling-based (Monte Carlo) procedures: (a) CCDF for $D_{ED}(10^4 \text{ yr}|\mathbf{a}_{ED}, \mathbf{e}_{M1})$ with exceedance probabilities $p_A[D < D_{ED}(10^4 \text{ yr}|\mathbf{a}, \mathbf{e}_{M1})|\mathbf{e}_{A1}]$ defined similarly to $p_A[D < D_{EW}(\tau|\mathbf{a}, \mathbf{e}_{M1})|\mathbf{e}_{A1}]$ in Equation (J6.2-12), and (b) expected dose $\bar{D}_{ED}(10^4 \text{ yr}|\mathbf{e}_1)$ associated with $D_{ED}(10^4 \text{ yr}|\mathbf{a}_{ED}, \mathbf{e}_{M1})$ defined similarly to $\bar{D}_{EW}(\tau|\mathbf{e}_1)$ in Equation (J6.2-10). FJ-38

J6.3-10. Results associated with $D_{ED}(10^4 \text{ yr}|\mathbf{a}_{ED}, \mathbf{e}_M)$ obtained with sampling-based (Monte Carlo) procedures for an LHS of size $nLHS = 300$: (a) CCDFs for $D_{ED}(10^4 \text{ yr}|\mathbf{a}_{ED}, \mathbf{e}_{Mi})$ with exceedance probabilities $p_A[D < D_{ED}(10^4 \text{ yr}|\mathbf{a}, \mathbf{e}_{Mi})|\mathbf{e}_{Ai}]$ defined similarly to $p_A[D < D_{EW}(\tau|\mathbf{a}, \mathbf{e}_{M1})|\mathbf{e}_{A1}]$ in Equation (J6.2-12) for $i = 1, 2, \ldots, nLHS = 300$, (b) CCDFs for $D_{ED}(10^4 \text{ yr}|\mathbf{a}_{ED}, \mathbf{e}_{Mi})$ with exceedance probabilities $p_A[D < D_{ED}(10^4 \text{ yr}|\mathbf{a}, \mathbf{e}_{Mi})|\mathbf{e}_{Ai}]$ defined similarly to $p_A[D < D_{EW}(\tau|\mathbf{a}, \mathbf{e}_{M1})|\mathbf{e}_{A1}]$ in Equation (J6.2-12) for $i = 1, 2, \ldots, 50$, and (c) expected (mean) CCDF and quantile curves, $q = 0.05, 0.5, 0.95$, for CCDFs in (a). FJ-39

J6.3-11. Assessment with replicated sampling of numerical error associated with use of an LHS of size $nLHS = 300$ to determine epistemic uncertainty in expected dose $\bar{D}_{ED}(\tau|\mathbf{e})$ to RMEI for $0 \le \tau \le 20{,}000$ yr that results when only early DS failure is considered: (a) Replicated estimates of expected (mean) dose $\bar{\bar{D}}_{ED}(\tau)$ and quantiles $Q_q[\bar{D}_{ED}(\tau|\mathbf{e})]$, $q = 0.05, 0.5, 0.95$, and (b) confidence intervals for estimates of expected (mean) dose $\bar{\bar{D}}_{ED}(\tau)$. FJ-40

J6.3-12. Summary of results obtained with LHS of size $nLHS = 300$ showing epistemic uncertainty in doses $D_{ED}(\tau|[1, r, s, 1], \mathbf{e}_M)$ for $0 \le \tau \le 10^6$ yr: (a) CSNF WP in bin 3 under dripping conditions (i.e., $D_{ED}(\tau|[1, 1, 3, 1], \mathbf{e}_{Mi})$, $i = 1, 2, \ldots, nLHS = 300$) and (b) CDSP WP in bin 3 under dripping conditions (i.e., $D_{ED}(\tau|[1, 2, 3, 1], \mathbf{e}_{Mi})$, $i = 1, 2, \ldots, nLHS = 300$). FJ-41

J6.3-13. Box plots (see Figure J6.2-3 for description) summarizing results obtained with LHS of size $nLHS = 300$ showing epistemic uncertainty in doses $D_{ED}(\tau|[1, r, s, 1], \mathbf{e}_{Mi})$ for $\tau = 5 \times 10^4, 2 \times 10^5, 5 \times 10^5$ yr, $r = 1, 2$, $s = 1, 2, 3, 4, 5$, $t = 1$, and $i = 1, 2, \ldots, nLHS = 300$: (a, c, e) CSNF WPs at 5×10^4, 2×10^5, 5×10^5 yr, and (b, d, f) CDSP WPs at 5×10^4, 2×10^5, 5×10^5 yr. FJ-42

J6.3-14. Estimate of $\bar{D}_{ED}(\tau|\mathbf{e}_1)$ for LHS element $\mathbf{e}_1 = [\mathbf{e}_{A1}, \mathbf{e}_{M1}]$ and $0 \le \tau \le 10^6$ yr with integration-based procedure indicated in EquationJ6.2-2 ..... FJ-43

J6.3-15. Estimate obtained with LHS of size $nLHS = 300$ showing epistemic uncertainty in expected dose $\bar{D}_{ED}(\tau|\mathbf{e})$ to RMEI for $0 \le \tau \le 10^6$ yr that results when only early DS failure is considered: (a) expected dose $\bar{D}_{ED}(\tau|\mathbf{e}_i)$, $i = 1, 2, \ldots, nLHS = 300$, (b) expected dose $\bar{D}_{ED}(\tau|\mathbf{e}_i)$, $i = 1, 2, \ldots, 50$, (c)

FIGURES (Continued)

Page

exceedance probabilities $p_E[D < \bar{D}_{ED}(\tau|\mathbf{e})]$ and quantiles $Q_q[\bar{D}_{ED}(\tau|\mathbf{e})]$, q = 0.05, 0.5 and 0.95, for $\tau = 5 \times 10^5$ yr, and (d) expected (mean) dose $\bar{\bar{D}}_{ED}(\tau)$ and quantiles $Q_q[\bar{D}_{ED}(\tau|\mathbf{e})]$, q = 0.05, 0.5, 0.95. ..... FJ-44

J6.3-16. Summary of results obtained with LHS of size $nLHS$ = 300 showing epistemic uncertainty in expected dose $\bar{D}_{ED}(\tau|\mathbf{a})$ to RMEI for $0 \le \tau \le 10^6$ yr that results when only early DS failure is considered. FJ-45

J6.3-17. Estimate obtained with LHS of size $nLHS$ = 300 showing epistemic uncertainty in expected dose $\bar{D}_{ED,r}(\tau|\mathbf{e})$ to RMEI for $0 \le \tau \le 10^6$ yr with r corresponding to ^{242}Pu that results when only early DS failure is considered: (a) expected dose $\bar{D}_{ED,r}(\tau|\mathbf{e}_i)$, i = 1, 2, …, $nLHS$ = 300, (b) expected dose $\bar{D}_{ED,r}(\tau|\mathbf{e}_i)$, i = 1, 2, …, 50, (c) exceedance probabilities $p_E[D < \bar{D}_{ED,r}(\tau|\mathbf{e})]$ and quantiles $Q_q[\bar{D}_{ED,r}(\tau|\mathbf{e})]$, q = 0.05, 0.5 and 0.95, for $\tau = 5 \times 10^5$ yr, and (d) expected (mean) dose $\bar{\bar{D}}_{ED,r}(\tau)$ and quantiles $Q_q[\bar{D}_{ED,r}(\tau|\mathbf{e})]$, q = 0.05, 0.5, 0.95 ..... FJ-46

J6.3-18. Estimates obtained with LHS of size $nLHS$ = 300 of expected (mean) dose $\bar{\bar{D}}_{ED,r}(\tau)$ to RMEI for $0 \le \tau \le 10^6$ yr for individual radioactive species that result when only early DS failure is considered. FJ-47

J6.3-19. Results associated with $D_{ED}(\tau|\mathbf{a}_{ED}, \mathbf{e}_{M1})$ for LHS element $\mathbf{e}_1 = [\mathbf{e}_{A1}, \mathbf{e}_{M1}]$ obtained with sampling-based (Monte Carlo) procedures: (a) CCDF for $D_{ED}(5 \times 10^5$ yr$|\mathbf{a}_{ED}, \mathbf{e}_{M1})$ with exceedance probabilities $p_A[D < D_{ED}(5 \times 10^5$ yr$|\mathbf{a}, \mathbf{e}_{M1})|\mathbf{e}_{A1}]$ defined similarly to $p_A[D < D_{EW}(\tau|\mathbf{a}, \mathbf{e}_{M1})|\mathbf{e}_{A1}]$ in Equation (J6.2-12), and (b) expected dose $\bar{D}_{ED}(5 \times 10^5$ yr$|\mathbf{e}_1)$ associated with $D_{ED}(5 \times 10^5$ yr $|\mathbf{a}_{ED}, \mathbf{e}_1)$ defined similarly to $\bar{D}_{EW}(\tau|\mathbf{e}_1)$ in Equation (J6.2-10). FJ-48

J6.3-20. Results associated with $D_{ED}(5 \times 10^5$ yr$|\mathbf{a}_{ED}, \mathbf{e}_M)$ obtained with sampling-based (Monte Carlo) procedures for an LHS of size $nLHS$ = 300: (a) CCDFs for $D_{ED}(5 \times 10^5$ yr$|\mathbf{a}_{ED}, \mathbf{e}_{Mi})$ with exceedance probabilities $p_A[D < D_{ED}(5 \times 10^5$ yr$|\mathbf{a}_{ED}, e_{Mi})|\mathbf{e}_{Ai}]$ defined similarly to $p_A[D < D_{EW}(\tau|\mathbf{a}, \mathbf{e}_{M1})|\mathbf{e}_{A1}]$ in Equation (J6.2-12) for i = 1, 2, …, $nLHS$ = 300, (b) CCDFs for $D_{ED}(10^4$ yr$|\mathbf{a}_{ED}, \mathbf{e}_{Mi})$ with exceedance probabilities $p_A[D < D_{ED}(5 \times 10^5$ yr$|\mathbf{a}_{ED}, e_{Mi})|\mathbf{e}_{Ai}]$ defined similarly to $p_A[D < D_{EW}(\tau|\mathbf{a}, \mathbf{e}_{M1})|\mathbf{e}_{A1}]$ in Equation (J6.2-12) for i = 1, 2, …, 50, and (c) expected (mean) CCDF and quantile curves, q = 0.05, 0.5, 0.95, for CCDFs in (a) FJ-49

J6.3-21. Assessment with replicated sampling of numerical error associated with use of an LHS of size $nLHS$ = 300 to determine epistemic uncertainty in expected dose $\bar{D}_{ED}(\tau|\mathbf{e})$ to RMEI for $0 \le \tau \le 10^6$ yr that results when only early DS

FIGURES (Continued)

Page

failure is considered: (a) Replicated estimates of expected (mean) dose $\bar{\bar{D}}_{ED}(\tau)$ and quantiles $Q_q[\bar{D}_{ED}(\tau|\mathbf{e})]$, q = 0.05, 0.5, 0.95, and (b) confidence intervals for estimates of expected (mean) dose $\bar{\bar{D}}_{ED}(\tau)$. FJ-50

J6.4-1. Estimate obtained with LHS of size $nLHS$ = 300 showing epistemic uncertainty in expected dose $\bar{D}_E(\tau|\mathbf{e})$ to RMEI for $0 \le \tau \le 20{,}000$ yr that results when only early WP and early DS failures are considered: (a) expected dose $\bar{D}_E(\tau|\mathbf{e}_i)$, i = 1, 2, …, $nLHS$ = 300, (b) expected dose $\bar{D}_E(\tau|\mathbf{e}_i)$, i = 1, 2, …, 50, (c) exceedance probabilities $p_E[D < \bar{D}_E(\tau|\mathbf{e})]$ and quantiles $Q_q[\bar{D}_E(\tau|\mathbf{e})]$, q = 0.05, 0.5 and 0.95, for $\tau = 10^4$ yr, and (d) expected (mean) dose $\bar{\bar{D}}_E(\tau)$ and quantiles $Q_q[\bar{D}_E(\tau|\mathbf{e})]$, q = 0.05, 0.5, 0.95 ..... FJ-51

J6.4-2. Estimate obtained with LHS of size $nLHS$ = 300 showing epistemic uncertainty in expected dose $\bar{D}_E(\tau|\mathbf{e})$ to RMEI for $0 \le \tau \le 1{,}000{,}000$ yr that results when only early WP and early DS failures are considered: (a) expected dose $\bar{D}_E(\tau|\mathbf{e}_i)$, i = 1, 2, …, $nLHS$ = 300, (b) expected dose $\bar{D}_E(\tau|\mathbf{e}_i)$, i = 1, 2, …, 50, (c) exceedance probabilities $p_E[D < \bar{D}_E(\tau|\mathbf{e})]$ and quantiles $Q_q[\bar{D}_E(\tau|\mathbf{e})]$, q = 0.05, 0.5 and 0.95, for τ = 500,000 yr, and (d) expected (mean) dose $\bar{\bar{D}}_E(\tau)$ and quantiles $Q_q[\bar{D}_E(\tau|\mathbf{e})]$, q = 0.05, 0.5, 0.95. ..... FJ-52

J6.4-3. Estimate obtained with LHS of size $nLHS$ = 300 showing epistemic uncertainty in expected dose $\bar{D}_{NE}(\tau|\mathbf{e})$ to RMEI for $0 \le \tau \le 1{,}000{,}000$ yr that results when only nominal process failures and early WP and early DS failures are considered: (a) expected dose $\bar{D}_{NE}(\tau|\mathbf{e}_i)$, i = 1, 2, …, $nLHS$ = 300, (b) expected dose $\bar{D}_{NE}(\tau|\mathbf{e}_i)$, i = 1, 2, …, 50, (c) exceedance probabilities $p_E[D < \bar{D}_{NE}(\tau|\mathbf{e})]$ and quantiles $Q_q[\bar{D}_{NE}(\tau|\mathbf{e})]$, q = 0.05, 0.5 and 0.95, for τ = 500,000 yr, and (d) expected (mean) dose $\bar{\bar{D}}_{NE}(\tau)$ and quantiles $Q_q[\bar{D}_{NE}(\tau|\mathbf{e})]$, q = 0.05, 0.5, 0.95. ..... FJ-53

J6.5-1. Box plots (see Figure J6.2-3 for description) summarizing probabilities $p_A(A_{ED}|\mathbf{e}_{Ai})$, $p_A(A_{EW}|\mathbf{e}_{Ai})$ and $p_A(A_E|\mathbf{e}_{Ai})$ for scenario classes A_{ED}, A_{EW} and A_E obtained with LHS of size $nLHS$ = 300. ..... FJ-54

J7.2-1. Dose to RMEI $D_{II}(\tau|[1, t_k, nWP], \mathbf{e}_{Mi})$ from igneous intrusive events at times t_k = 10, 600, 2000, 4000, 6000 and 10,000 yr for i = 1, 2, …, $nLHS$ = 300: (a) 10 yr, (b) 600 yr, (c) 2000 yr, (d) 4000 yr, (e) 6000 yr, and (f) 10,000 yr. FJ-55

J7.2-2. Illustration of interpolation procedure used to obtain estimated doses $\hat{D}_{II}(\tau|[1, \hat{t}_k, nWP], \mathbf{e}_{M1})$ from calculated doses $D_{II}(\tau|[1, t_k, nWP], \mathbf{e}_{M1})$ indicated in Equation J7.2-18 for LHS element $\mathbf{e}_1 = [\mathbf{e}_{A1}, \mathbf{e}_{M1}]$ and the time interval [0, 2.0×10^4 yr]: (a) $D_{II}(\tau|[1, t_k, nWP], \mathbf{e}_{M1})$, k = 1, 2, …, 10, (b) interpolated values $\hat{D}_{II}(\tau|[1, \hat{t}_k, nWP], \mathbf{e}_{M1})$ for $\hat{t}_k$ between t_7 = 6000 and t_{8+1} = 10,000,

FIGURES (Continued)

Page

and (c) interpolated values $\hat{D}_{II}(\tau|[1, \hat{t}_k, nWP], \mathbf{e}_{M1})$ for $\hat{t}_k$ between 10 yr and 2.0×10^4 yr. FJ-56

J7.2-3. Determination of $\bar{D}_{II}(\tau|\mathbf{e}_1)$ as indicated in conjunction with Equations J7.2-7, J7.2-9 and J7.2-19 from calculated doses $D_{II}(\tau|[1, t_k, nWP], \mathbf{e}_{M1})$ shown in Equation J7.2-18 for LHS element $\mathbf{e}_1 = [\mathbf{e}_{A1}, \mathbf{e}_{M1}]$ and the time interval [0, 2.0×10^4 yr]. FJ-57

J7.2-4. Estimate obtained with LHS of size $nLHS = 300$ showing epistemic uncertainty in expected dose $\bar{D}_{II}(\tau|\mathbf{e})$ to RMEI for $0 \le \tau \le 20{,}000$ yr that results when only igneous intrusion events are considered: (a) expected dose $\bar{D}_{II}(\tau|\mathbf{e}_i)$, $i = 1, 2, \ldots, nLHS = 300$, (b) expected dose $\bar{D}_{II}(\tau|\mathbf{e}_i)$, $i = 1, 2, \ldots, 50$, (c) exceedance probabilities $p_E[D < \bar{D}_{II}(\tau|\mathbf{e})]$ and quantiles $Q_q[\bar{D}_{II}(\tau|\mathbf{e})]$, $q =$ 0.05, 0.5 and 0.95, for $\tau = 10^4$ yr, and (d) expected (mean) dose $\bar{\bar{D}}_{II}(\tau)$ and quantiles $Q_q[\bar{D}_{II}(\tau|\mathbf{e})]$, $q = 0.05, 0.5, 0.95$. FJ-58

J7.2-5. Summary presentation of epistemic uncertainty in expected dose $\bar{D}_{II}(\tau|\mathbf{e})$ to RMEI that results when only igneous intrusion is considered for $0 \le \tau \le$ 2.0×10^4 yr. FJ-59

J7.2-6. Estimate obtained with LHS of size $nLHS = 300$ showing epistemic uncertainty in expected dose $\bar{D}_{II,r}(\tau|\mathbf{e})$ to RMEI for $0 \le \tau \le 20{,}000$ yr with r corresponding to ^{99}Tc that results when only igneous intrusive events are considered: (a) expected dose $\bar{D}_{II,r}(\tau|\mathbf{e}_i)$, $i = 1, 2, \ldots, nLHS = 300$, (b) expected dose $\bar{D}_{II,r}(\tau|\mathbf{e}_i)$, $i = 1, 2, \ldots, 50$, (c) exceedance probabilities $p_E[D <$ $\bar{D}_{II,r}(\tau|\mathbf{e})]$ and quantiles $Q_q[\bar{D}_{II,r}(\tau|\mathbf{e})]$, $q = 0.05$, 0.5 and 0.95, for $\tau = 10^4$ yr, and (d) expected (mean) dose $\bar{\bar{D}}_{II,r}(\tau)$ and quantiles $Q_q[\bar{D}_{II,r}(\tau|\mathbf{e})]$, $q = 0.05$, 0.5, 0.95. ..... FJ-60

J7.2-7. Estimates obtained with LHS of size $nLHS = 300$ of expected (mean) dose $\bar{\bar{D}}_{II,r}(\tau)$ to RMEI for $0 \le \tau \le 20{,}000$ yr for individual radioactive species that result when only igneous intrusive events are considered. FJ-61

J7.2-8. Results associated with $\bar{D}_{II}(\tau|\mathbf{e}_1)$ for LHS element $\mathbf{e}_1 = [\mathbf{e}_{A1}, \mathbf{e}_{M1}]$ obtained with sampling-based (Monte Carlo) procedures: (a) CCDF for $D_{II}(10^4$ yr$|\mathbf{a}_{II}, \mathbf{e}_{M1})$ with exceedance probabilities $p_A[D < D_{II}(10^4$ yr$|\mathbf{a}, \mathbf{e}_{M1})|\mathbf{e}_{A1}]$ defined in Equation J7.2-23, and (b) expected dose $\bar{D}_{II}(10^4$ yr$|\mathbf{e}_1)$ associated with $D_{II}(10^4$ yr$|\mathbf{a}_{II}, \mathbf{e}_{M1})$ as defined in Equation J7.2-21. ..... FJ-62

J7.2-9. Results associated with $D_{II}(10^4$ yr$|\mathbf{a}_{II}, \mathbf{e}_M)$ obtained with sampling-based (Monte Carlo) procedures for an LHS of size $nLHS = 300$: (a) CCDFs for $D_{II}(10^4$ yr$|\mathbf{a}_{II}, \mathbf{e}_{Mi})$ with exceedance probabilities $p_A[D < D_{II}(10^4$ yr$|\mathbf{a},$ $\mathbf{e}_{Mi})|\mathbf{e}_{Ai}]$ defined in Equation J7.2-23 for $i = 1, 2, \ldots, nLHS = 300$, (b)

FIGURES (Continued)

Page

CCDFs for $D_{II}(10^4 \text{ yr}|\mathbf{a}_{II}, \mathbf{e}_{Mi})$ with exceedance probabilities $p_A[D < D_{II}(10^4 \text{ yr}|\mathbf{a}, \mathbf{e}_{Mi})|\mathbf{a}_{Ai}]$ defined in Equation J7.2-23 for $i = 1, 2, \ldots, 50$, and (c) expected (mean) CCDF and quantile curves, $q = 0.05, 0.5, 0.95$, for CCDFs in (a). FJ-63

J7.2-10. Assessment with replicated sampling of numerical error associated with use of an LHS of size $nLHS = 300$ to determine epistemic uncertainty in expected dose $\bar{D}_{II}(\tau|\mathbf{e})$ to RMEI for $0 \le \tau \le 20{,}000$ yr that results when only igneous intrusive events are considered: (a) Replicated estimates of expected (mean) dose $\bar{\bar{D}}_{II}(\tau)$ and quantiles $Q_q[\bar{D}_{II}(\tau|\mathbf{e})]$, $q = 0.05, 0.5, 0.95$, and (b) confidence intervals for estimates of expected (mean) dose $\bar{\bar{D}}_{II}(\tau)$. FJ-64

J7.2-11. Dose to RMEI $D_{II}(\tau|[1, t_k, nWP], \mathbf{e}_{Mi})$ from igneous intrusive events at times $t_k = 10{,}000, 40{,}000, 100{,}000, 200{,}000, 400{,}000$ and $800{,}000$ yr for $i = 1, 2, \ldots, nLHS = 300$: (a) 10,000 yr, (b) 40,000 yr, (c) 100,000 yr, (d) 200,000 yr, (e) 400,000 yr, and (f) 800,000 yr. FJ-65

J7.2-12. Illustration of interpolation procedure used to obtain estimated doses $\hat{D}_{II}(\tau|[1, \hat{t}_k, nWP], \mathbf{e}_{M1})$ from calculated doses $D_{II}(\tau|[1, t_k, nWP], \mathbf{e}_{M1})$ indicated in Equation J7.2-18 for LHS element $\mathbf{e}_1 = [\mathbf{e}_{A1}, \mathbf{e}_{M1}]$ and the time interval $[0, 10^6 \text{ yr}]$: (a) $D_{II}(\tau|[1, t_k, nWP], \mathbf{e}_{M1})$, $k = 1, 2, \ldots, 10$, (b) interpolated values $\hat{D}_{II}(\tau|[1, \hat{t}_k, nWP], \mathbf{e}_{M1})$ for $\hat{t}_k$ between $t_8 = 200{,}000$ yr and $t_9 = 400{,}000$, and (c) interpolated values $\hat{D}_{II}(\tau|[1, \hat{t}_k, nWP], \mathbf{e}_{M1})$ for $\hat{t}_k$ between 250 yr and 10^6 yr. FJ-66

J7.2-13. Determination of $\bar{D}_{II}(\tau|\mathbf{e}_1)$ as indicated in conjunction with Equations J7.2-7, J7.2-9 and J7.2-19 from calculated doses $D_{II}(\tau|[1, t_k, nWP], \mathbf{e}_{M1})$ shown in Equation J7.2-18 for LHS element $\mathbf{e}_1 = [\mathbf{e}_{A1}, \mathbf{e}_{M1}]$ and the time interval $[0, 10^6 \text{ yr}]$. FJ-67

J7.2-14. Estimate obtained with LHS of size $nLHS = 300$ showing epistemic uncertainty in expected dose $\bar{D}_{II}(\tau|\mathbf{e})$ to RMEI for $0 \le \tau \le 10^6$ yr that results when only igneous intrusion is considered: (a) expected dose $\bar{D}_{II}(\tau|\mathbf{e}_i)$, $i = 1, 2, \ldots, nLHS = 300$, (b) expected dose $\bar{D}_{II}(\tau|\mathbf{e}_i)$, $i = 1, 2, \ldots, 50$, (c) exceedance probabilities $p_E[D < \bar{D}_{II}(\tau|\mathbf{e})]$ and quantiles $Q_q[\bar{D}_{II}(\tau|\mathbf{e})]$, $q = 0.05, 0.5$ and 0.95, for $\tau = 5 \times 10^5$ yr, and (d) expected (mean) dose $\bar{\bar{D}}_{II}(\tau)$ and quantiles $Q_q[\bar{D}_{II}(\tau|\mathbf{e})]$, $q = 0.05, 0.5, 0.95$. FJ-68

J7.2-15. Summary presentations of epistemic uncertainty in expected dose $\bar{D}_{II}(\tau|\mathbf{e})$ to RMEI that results when only igneous intrusion is considered for $0 \le \tau \le 10^6$ yr. FJ-69

FIGURES (Continued)

Page

J7.2-16. Estimate obtained with LHS of size $nLHS = 300$ showing epistemic uncertainty in expected dose $\bar{D}_{II,r}(\tau|\mathbf{e})$ to RMEI for $0 \le \tau \le 10^6$ yr with r corresponding to ^{226}Ra that results when only igneous intrusion is considered: (a) expected dose $\bar{D}_{II,r}(\tau|\mathbf{e}_i)$, $i = 1, 2, \ldots, nLHS = 300$, (b) expected dose $\bar{D}_{II,r}(\tau|\mathbf{e}_1)$, $i = 1, 2, \ldots, 50$, (c) exceedance probabilities $p_E[D < \bar{D}_{II,r}(\tau|\mathbf{e})]$ and quantiles $Q_q[\bar{D}_{II,r}(\tau|\mathbf{e})]$, $q = 0.05$, 0.5 and 0.95, for $\tau = 5 \times 10^5$ yr, and (d) expected (mean) dose $\bar{\bar{D}}_{II,r}(\tau)$ and quantiles $Q_q[\bar{D}_{II,r}(\tau|\mathbf{e})]$, $q =$ 0.05, 0.5, 0.95 ..... FJ-70

J7.2-17. Estimates obtained with LHS of size $nLHS = 300$ of expected (mean) dose $\bar{\bar{D}}_{II,r}(\tau)$ to RMEI for $0 \le \tau \le 10^6$ yr for individual radioactive species that result when only igneous intrusive events are considered. FJ-71

J7.2-18. Results associated with $\bar{D}_{II}(\tau|\mathbf{e}_1)$ for LHS elements $\mathbf{e}_1 = [\mathbf{e}_{A1}, \mathbf{e}_{M1}]$ obtained with sampling-based (Monte Carlo) procedures: (a) CCDF for $D_{II}(5 \times 10^5$ yr$|\mathbf{a}_{II}, \mathbf{e}_{M1})$ with exceedance probabilities $p_A[D < D_{II}(5 \times 10^5$ yr$|\mathbf{a}, \mathbf{e}_{M1})|\mathbf{e}_{A1}]$ defined in Equation J7.2-23, and (b) expected dose $\bar{D}_{II}(5 \times 10^5$ yr$|\mathbf{e}_1)$ associated with $D_{II}(5 \times 10^5$ yr$|\mathbf{a}_{II}, \mathbf{e}_{M1})$ as defined in Equation J7.2-21. ..... FJ-72

J7.2-19. Results associated with $D_{II}(5 \times 10^5$ yr$|\mathbf{a}_{II}, \mathbf{e}_M)$ obtained with sampling-based (Monte Carlo) procedures for an LHS of size $nLHS = 300$: (a) CCDFs for $D_{II}(5 \times 10^5$ yr$|\mathbf{a}_{II}, \mathbf{e}_{Mi})$ with exceedance probabilities $p_A[D < D_{II}(5 \times 10^5$ yr$|\mathbf{a}, \mathbf{e}_{Mi})|\mathbf{e}_{Ai}]$ defined in Equation J7.2-23 for $i = 1, 2, \ldots, nLHS = 300$, (b) CCDFs for $D_{II}(5 \times 10^5$ yr$|\mathbf{a}_{II}, \mathbf{e}_{Mi})$ with exceedance probabilities $p_A[D < D_{II}(5 \times 10^5$ yr$|\mathbf{a}, \mathbf{e}_{Mi})|\mathbf{a}_{Ai}]$ defined in Equation J7.2-23 for $i = 1, 2, \ldots, 50$, and (c) expected (mean) CCDF and quantile curves, $q = 0.05$, 0.5, 0.95, for CCDFs in (a). FJ-73

J7.2-20. Assessment with replicated sampling of numerical error associated with use of an LHS of size $nLHS = 300$ to determine epistemic uncertainty in expected dose $\bar{D}_{II}(\tau|\mathbf{e})$ to RMEI for $0 \le \tau \le 10^6$ yr that results when only igneous intrusion is considered: (a) Replicated estimates of expected (mean) dose $\bar{\bar{D}}_{II}(\tau)$ and quantiles $Q_q[\bar{D}_{II}(\tau|\mathbf{e})]$, $q = 0.05$, 0.5, 0.95, and (b) confidence intervals for estimates of expected (mean) dose $\bar{\bar{D}}_{II}(\tau)$. FJ-74

J7.3-1. Dose results $D_{IE}(\tau|[1, t_k, 1, \mathbf{u}_l], \mathbf{e}_{M1})$ obtained for times $t_k = 100$, 1000, 4000, 10,000 yr, igneous eruptive properties $\mathbf{u}_l$, $l = 1, 2, \ldots, nU = 40$, and LHS element $\mathbf{e}_1 = [\mathbf{e}_{A1}, \mathbf{e}_{M1}]$: (a) $t_k = 100$ yr, (b) $t_k = 1000$ yr, (c) $t_k = 4000$ yr, and (d) $t_k = 10{,}000$ yr. FJ-75

FIGURES (Continued)

Page

J7.3-2. Illustration of interpolation procedure used to obtain estimates $\hat{S}(\tau|\hat{t}_k, \mathbf{e}_{M1})$ of conditional expected dose $S(\tau|t, \mathbf{e}_{M1})$ to RMEI (mrem/yr) for LHS element $\mathbf{e}_1 = [\mathbf{e}_{A1}, \mathbf{e}_{M1}]$ and the time interval [0, 20,000 yr]: (a) $S(\tau|t_k, \mathbf{e}_{M1})$, $k = 1, 2, \ldots, 10$, (b) interpolated values $\hat{S}(\tau|\hat{t}_k, \mathbf{e}_{M1})$ for $\hat{t}_k$ between t_7 = 6000 yr and t_8 = 10,000 yr, and (c) interpolated values $\hat{S}(\tau|\hat{t}_k, \mathbf{e}_{M1})$ for $\hat{t}_k$ between 10 yr and 20,000 yr. FJ-76

J7.3-3. Estimate of $\bar{D}_{IE}(\tau|\,\mathbf{e}_1)$ for LHS element $\mathbf{e}_1 = [\mathbf{e}_{A1}, \mathbf{e}_{M1}]$ and $0 \le \tau \le 20{,}000$ yr with integration-based procedure indicated in Equations J7.3-9 and J7.3-16. ..... FJ-77

J7.3-4. Estimate obtained with LHS of size $nLHS = 300$ showing epistemic uncertainty in expected dose $\bar{D}_{IE}(\tau|\mathbf{e})$ to RMEI for $0 \le \tau \le 20{,}000$ yr that results when only igneous eruptive events are considered: (a) expected dose $\bar{D}_{IE}(\tau|\mathbf{e}_i)$, $i = 1, 2, \ldots, nLHS = 300$, (b) expected dose $\bar{D}_{IE}(\tau|\mathbf{e}_i)$, $i = 1, 2, \ldots, 50$, (c) exceedance probabilities $p_E[D < \bar{D}_{IE}(\tau|\mathbf{e})]$ and quantiles $Q_q[\bar{D}_{IE}(\tau|\mathbf{e})]$, $q = 0.05$, 0.5 and 0.95, for $\tau = 10^4$ yr, and (d) expected (mean) dose $\bar{\bar{D}}_{IE}(\tau)$ and quantiles $Q_q[\bar{D}_{IE}(\tau|\mathbf{e})]$, $q = 0.05, 0.5, 0.95$. FJ-78

J7.3-5. Summary of results obtained with LHS of size $nLHS = 300$ showing epistemic uncertainty in expected dose $\bar{D}_{IE}(\tau|\mathbf{e})$ to RMEI for $0 \le \tau \le 20{,}000$ yr that results when only igneous eruptive events are considered. FJ-79

J7.3-6. Estimates obtained with LHS of size $nLHS = 300$ of expected (mean) dose $\bar{\bar{D}}_{IE,r}(\tau)$ to RMEI for $0 \le \tau \le 20{,}000$ yr for individual radioactive species that result when only igneous eruptive events are considered. FJ-80

J7.3-7. Results associated with $D_{IE}(\tau|\mathbf{a}_{IE}, \mathbf{e}_1)$ for LHS element $\mathbf{e}_1 = [\mathbf{e}_{A1}, \mathbf{e}_{M1}]$ obtained with sampling-based (Monte Carlo) procedures: (a) CCDF for $D_{IE}(10^4 \text{ yr}|\mathbf{a}_{IE}, \mathbf{e}_1)$ with exceedance probabilities $p_A[D < D_{IE}(10^4 \text{ yr}|\mathbf{a}, \mathbf{e}_{M1})|\mathbf{e}_{A1}]$ defined in Equation J7.3-20, and (b) expected dose $\bar{D}_{IE}(10^4 \text{ yr}|\mathbf{e}_1)$ associated with $D_{IE}(10^4 \text{ yr}|\mathbf{a}_{IE}, \mathbf{e}_1)$ as defined in Equation J7.3-18. ..... FJ-81

J7.3-8. Results associated with $D_{IE}(10^4 \text{ yr}|\mathbf{a}_{IE}, \mathbf{e}_M)$ obtained with sampling-based (Monte Carlo) procedures for an LHS of size $nLHS = 300$: (a) CCDFs for $D_{IE}(10^4 \text{ yr}|\mathbf{e}_{IE}, \mathbf{e}_{Mi})$ with exceedance probabilities $p_A[D < D_{IE}(10^4 \text{ yr}|\mathbf{a}, \mathbf{e}_{Mi})|\mathbf{e}_{Ai}]$ defined in Equation J7.3-20 for $i = 1, 2, \ldots, nLHS = 300$, (b) CCDFs for $D_{IE}(10^4 \text{ yr}|\mathbf{a}_{IE}, \mathbf{e}_{Mi})$ with exceedance probabilities $p_A[D < D_{IE}(10^4 \text{ yr}|\mathbf{a}, \mathbf{e}_{Mi})|\mathbf{e}_{Ai}]$ defined in Equation J7.3-20 for $i = 1, 2, \ldots, 50$, and (c) expected (mean) CCDF and quantile curves, $q = 0.05, 0.5, 0.95$, for CCDFs in (a). FJ-82

J7.3-9. Assessment with replicated sampling of numerical error associated with use of an LHS of size $nLHS = 300$ to determine epistemic uncertainty in expected

FIGURES (Continued)

Page

dose $\bar{D}_{lE}(\tau)$ to RMEI for $0 \le \tau \le 20{,}000$ yr that results when only igneous eruptive events are considered: (a) Replicated estimates of expected (mean) dose $\bar{D}_{lE}(\tau)$ and quantiles $Q_q[\bar{D}_{lE}(\tau|\mathbf{e})]$, $q = 0.05, 0.5, 0.95$, and (b) confidence intervals for estimates of expected (mean) dose $\bar{\bar{D}}_{lE}(\tau)$. FJ-83

J7.3-10. Dose results $D_{IE}(\tau|[1, t_k, 1, \mathbf{u}_l], \mathbf{e}_{M1})$ obtained for times $t_k = 40{,}000$, 100,000, 200,000, 400,000 yr, igneous eruptive properties $\mathbf{u}_l$, $l = 1, 2, \ldots, nU = 40$, and LHS element $\mathbf{e}_1 = [\mathbf{e}_{A1}, \mathbf{e}_{M1}]$: (a) $t_k = 40{,}000$ yr, (b) $t_k = 100{,}000$ yr, (c) $t_k = 200{,}000$ yr, and (d) $t_k = 400{,}000$ yr. FJ-84

J7.3-11. Illustration of interpolation procedure used to obtain estimates $\hat{S}(\tau|\hat{t}_k, \mathbf{e}_{Mi})$ of conditional expected dose $S(\tau|t, \mathbf{e}_{M1})$ to RMEI (mrem/yr) for LHS element $\mathbf{e}_1 = [\mathbf{e}_{A1}, \mathbf{e}_{M1}]$ and the time interval $[0, 10^6$ yr]: (a) $S(\tau|t_k, \mathbf{e}_{M1})$, $k = 1, 2, \ldots, 10$, (b) interpolated values $\hat{S}(\tau|\hat{t}_k, \mathbf{e}_{M1})$ for $\hat{t}_k$ between $t_8 = 200{,}000$ yr and $t_9 = 400{,}000$ yr, and (c) interpolated values $\hat{S}(\tau|\hat{t}_k, \mathbf{e}_{M1})$ for $\hat{t}_k$ between 250 yr and 10^6 yr. FJ-85

J7.3-12. Estimate of $\bar{D}_{lE}(\tau|\mathbf{e}_1)$ for LHS element $\mathbf{e}_1 = [\mathbf{e}_{A1}, \mathbf{e}_{M1}]$ and $0 \le \tau \le 10^6$ yr with integration-based procedure indicated in Equations J7.3-9 and J7.3-16. ..... FJ-86

J7.3-13. Estimate obtained with LHS of size $nLHS = 300$ showing epistemic uncertainty in expected dose $\bar{D}_{lE}(\tau|\mathbf{e})$ to RMEI for $0 \le \tau \le 10^6$ yr that results when only igneous eruptive events are considered: (a) expected dose $\bar{D}_{lE}(\tau|\mathbf{e}_i)$, $i = 1, 2, \ldots, nLHS = 300$, (b) expected dose $\bar{D}_{lE}(\tau|\mathbf{e}_i)$, $i = 1, 2, \ldots, 50$, (c) exceedance probabilities $p_E[D < \bar{D}_{lE}(\tau|\mathbf{e})]$ and quantiles $Q_q[\bar{D}_{lE}(\tau|\mathbf{e})]$, $q = 0.05, 0.5$ and 0.95, for $\tau = 500{,}000$ yr, and (d) expected (mean) dose $\bar{\bar{D}}_{lE}(\tau)$ and quantiles $Q_q[\bar{D}_{lE}(\tau|\mathbf{e})]$, $q = 0.05, 0.5, 0.95$. FJ-87

J7.3-14. Summary of results obtained with LHS of size $nLHS = 300$ showing epistemic uncertainty in expected dose $\bar{D}_{lE}(\tau|\mathbf{e})$ to RMEI for $0 \le \tau \le 10^6$ yr that results when only igneous eruptive events are considered. FJ-88

J7.3-15. Estimates obtained with LHS of size $nLHS = 300$ of expected (mean) dose $\bar{\bar{D}}_{lE,r}(\tau)$ to RMEI for $0 \le \tau \le 10^6$ yr for individual radioactive species that result when only igneous eruptive events are considered. FJ-89

J7.3-16. Results associated with $D_{IE}(\tau|\mathbf{a}_{IE}, \mathbf{e}_{M1})$ for LHS element $\mathbf{e}_1 = [\mathbf{e}_{A1}, \mathbf{e}_{M1}]$ obtained with sampling-based (Monte Carlo) procedures: (a) CCDF for $D_{IE}(500{,}000$ yr$|\mathbf{a}_{IE}, \mathbf{e}_{M1})$ with exceedance probabilities $p_A[D < D_{IE}(500{,}000$ yr$|\mathbf{a}, \mathbf{e}_{M1})|\mathbf{e}_{A1}]$ defined in Equation J7.3-20, and (b) expected dose $\bar{D}_{lE}(500{,}000$ yr$|\mathbf{e}_1)$ associated with $D_{IE}(500{,}000$ yr$|\mathbf{a}_{IE}, \mathbf{e}_{M1})$ as defined in Equation J7.3-18. ..... FJ-90

J7.3-17. Results associated with $D_{IE}(500{,}000$ yr$|\mathbf{a}_{IE}, \mathbf{e}_M)$ obtained with sampling-based (Monte Carlo) procedures for an LHS of size $nLHS = 300$: (a) CCDFs

FIGURES (Continued)

Page

for $D_{IE}(10^4$ yr$|\mathbf{a}_{IE}, \mathbf{e}_{Mi})$ with exceedance probabilities $p_A[D < D_{IE}(500{,}000$ yr$|\mathbf{a}, \mathbf{e}_{Mi})|\mathbf{e}_{Ai}]$ defined in Equation J7.3-20 for $i = 1, 2, \ldots, nLHS = 300$, (b) CCDFs for $D_{IE}(500{,}000$ yr$|\mathbf{a}_{IE}, \mathbf{e}_{Mi})$ with exceedance probabilities $p_A[D < D_{IE}(500{,}000$ yr$|\mathbf{a}, \mathbf{e}_{Mi})|\mathbf{e}_{Ai}]$ defined in Equation J7.3-20 for $i = 1, 2, \ldots, 50$, and (c) expected (mean) CCDF and quantile curves, $q = 0.05, 0.5, 0.95$, for CCDFs in (a). FJ-91

J7.3-18. Assessment with replicated sampling of numerical error associated with use of an LHS of size $nLHS = 300$ to determine epistemic uncertainty in expected dose $\bar{\bar{D}}_{IE}(\tau)$ to RMEI for $0 \le \tau \le 10^6$ yr that results when only igneous eruptive events are considered: (a) Replicated estimates of expected (mean) dose $\bar{\bar{D}}_{IE}(\tau)$ and quantiles $Q_q[\bar{D}_{IE}(\tau|\mathbf{e})]$, $q = 0.05, 0.5, 0.95$, and (b) confidence intervals for estimates of expected (mean) dose $\bar{\bar{D}}_{IE}(\tau)$. FJ-92

J7.5-1. Box plots summarizing probabilities $p_A[A_{II}(0, \tau)|\mathbf{e}_{Ai}]$, $p_A[\tilde{A}_{II}(0, \tau)|\mathbf{e}_{Ai}]$, $p_A[A_{IE}(0, \tau)|\mathbf{e}_{Ai}]$ and $p_A[\tilde{A}_{IE}(0, \tau)|\mathbf{e}_{Ai}]$ for scenario classes $A_{II}(0, \tau)$, $\tilde{A}_{II}(0, \tau)$, $A_{IE}(0, \tau)$ and $\tilde{A}_{IE}(0, \tau)$ defined for the time intervals [0, 20,000 yr] and [0, 1,000,000 yr] obtained with LHS of size $nLHS = 300$. FJ-93

J8.3-1. Summary of results for damage to CDSP WPs obtained with LHS of size $nLHS = 300$ showing epistemic uncertainty in doses $D_{SG}(\tau|[1, t_r, A_S], \mathbf{e}_{Mi})$ for $0 \le \tau \le 20{,}000$ yr damaged area $A_S = (10^{-6})$ (32.6 m^2) and the following values for event time t_r: (a) 200 yr, (b) 1000 yr, (c) 3000 yr, (d) 6000 yr, (e) 12,000 yr, and (f) 18,000 yr. FJ-95

J8.3-2. Box plots (see Figure J6.2-3 for description) summarizing results for damage to CDSP WPs obtained with LHS of size $nLHS = 300$ showing epistemic uncertainty in dose $D_{SG}(\tau|[1, t_r, A_S], \mathbf{e}_{Mi})$ with $t_r = 200$, 1000, 3000, and 6000 yrs, $A_S = 10^{-8+s}$ (32.6 m^2) for $s = 1, 2, 3, 4, 5$, and $i = 1, 2, \ldots, nLHS = 300$, where 32.6 m^2 is the assumed surface area for a CDSP WP: (a) $t_r = 200$ yrs, (b) $t_r = 1000$ yrs, (c) $t_r = 3000$ yrs, and (d) $t_r = 6000$ yrs. FJ-96

J8.3-3. Illustration of interpolation procedure to obtain estimated integrals $\hat{I}_1(\tau|t, \mathbf{e}_{M1})$ from calculated doses $D_{SG}(\tau|[1, t_r, A_S], \mathbf{e}_{M1})$ indicated in Equation J8.3-9 for LHS element $\mathbf{e}_1 = [\mathbf{e}_{A1}, \mathbf{e}_{M1}]$ and the time interval $[0, 2.0 \times 10^4$ yr]: (a) $D_{SG}(\tau|[1, t_r, A_S], \mathbf{e}_{M1})$, $r = 1, 2, \ldots, 6$ and $s = 1, 2, \ldots, 5$, (b) $\hat{I}_1(\tau|t_r, \mathbf{e}_{M1})$, $r = 1, 2, \ldots, 6$, (c) interpolated values $\hat{I}_1(\tau|\hat{t}_k, \mathbf{e}_{M1})$ for $\hat{t}_k$ between $t_4 =$ 6000 yrs and $t_5 = 12{,}000$ yrs, and (d) interpolated values for $\hat{I}_1(\tau|\hat{t}_k, \mathbf{e}_1)$ for $\hat{t}_k$ between = 100 yrs and 20,000 yrs. FJ-97

J8.3-4. Estimate of $\bar{D}_{SG}(\tau|\mathbf{e}_1)$ for LHS element $\mathbf{e}_1 = [\mathbf{e}_{A1}, \mathbf{e}_{M1}]$ and $0 \le \tau \le 20{,}000$ yr with integration-based procedure indicated in Equation J8.3-13. ..... FJ-98

FIGURES (Continued)

Page

J8.3-5. Estimate obtained with LHS of size $nLHS = 300$ showing epistemic uncertainty in expected dose $\bar{D}_{SG}(\tau|\mathbf{e})$ to RMEI for $0 \le \tau \le 20{,}000$ yr that results when only seismic ground motion events are considered: (a) expected dose $\bar{D}_{SG}(\tau|\mathbf{e}_i)$, $i = 1, 2, \ldots, nLHS = 300$, (b) expected dose $\bar{D}_{SG}(\tau|\mathbf{e}_i)$, $i = 1, 2, \ldots, 50$, (c) exceedance probabilities $p_E[D < \bar{D}_{SG}(\tau|\mathbf{e})]$ and quantiles $Q_q[\bar{D}_{SG}(\tau|\mathbf{e})]$, $q = 0.05$, 0.5 and 0.95, for $\tau = 10^4$ yr, and (d) expected (mean) dose $\bar{\bar{D}}_{SG}(\tau)$ and quantiles $Q_q[\bar{D}_{SG}(\tau|\mathbf{e})]$, $q = 0.05, 0.5, 0.95$. FJ-99

J8.3-6. Summary of results obtained with LHS of size $nLHS = 300$ showing epistemic uncertainty in expected dose $\bar{D}_{SG}(\tau|\mathbf{e})$ to RMEI for $0 \le \tau \le 20{,}000$ yr that results when only seismic ground motion events are considered. FJ-100

J8.3-7. Estimate obtained with LHS of size $nLHS = 300$ showing epistemic uncertainty in expected dose $\bar{D}_{SG,r}(\tau|\mathbf{e})$ to RMEI for $0 \le \tau \le 20{,}000$ yr with r corresponding to ^{99}Tc that results when only seismic ground motion events are considered: (a) expected dose $\bar{D}_{SG,r}(\tau|\mathbf{e}_i)$, $i = 1, 2, \ldots, nLHS = 300$, (b) expected dose $\bar{D}_{SG,r}(\tau|\mathbf{e}_i)$, $i = 1, 2, \ldots, 50$, (c) exceedance probabilities $p_E[D < \bar{D}_{SG,r}(\tau|\mathbf{e})]$ and quantiles $Q_q[\bar{D}_{SG,r}(\tau|\mathbf{e})]$, $q = 0.05$, 0.5 and 0.95, for $\tau = 10^4$ yr, and (d) expected (mean) dose $\bar{\bar{D}}_{SG,r}(\tau)$ and quantiles $Q_q[\bar{D}_{SG,r}(\tau|\mathbf{e})]$, $q = 0.05, 0.5, 0.95$ FJ-101

J8.3-8. Estimates obtained with LHS of size $nLHS = 300$ of expected (mean) dose $\bar{\bar{D}}_{SG,r}(\tau)$ to RMEI for $0 \le \tau \le 20{,}000$ yr for individual radioactive species that result when only seismic ground motion events are considered. FJ-102

J8.3-9. Results associated with $D_{SG}(\tau|\mathbf{a}_{SG}, \mathbf{e}_{M1})$ for LHS element $\mathbf{e}_1 = [\mathbf{e}_{A1}, \mathbf{e}_{M1}]$ obtained with sampling-based (Monte Carlo) procedures: (a) CCDF for $D_{SG}(10^4 \text{ yr}|\mathbf{a}_{SG}, \mathbf{e}_{M1})$ with exceedance probabilities $p_A[D < D_{SG}(10^4 \text{ yr}|\mathbf{a}, \mathbf{e}_{M1})|\mathbf{e}_1]$ defined in Equation J8.3-22, and (b) expected dose $\bar{D}_{SG}(10^4 \text{ yr}|\mathbf{e}_1)$ associated with $D_{SG}(10^4 \text{ yr}|\mathbf{a}_{SG}, \mathbf{e}_{M1})$ defined in Equation J8.3-20 ..... FJ-103

J8.3-10. Results associated with $D_{SG}(10^4 \text{ yr}|\mathbf{a}_{SG}, \mathbf{e}_M)$ obtained with sampling-based (Monte Carlo) procedures for an LHS of size $nLHS = 300$: (a) CCDFs for $D_{SG}(10^4 \text{ yr}|\mathbf{a}_{SG}, \mathbf{e}_{Mi})$ with exceedance probabilities $p_A[D < D_{SG}(10^4 \text{ yr}|\mathbf{a}, \mathbf{e}_{Mi})|\mathbf{e}_{Ai}]$ defined in Equation J4.5-19 for $i = 1, 2, \ldots, nLHS = 300$, (b) CCDFs for $D_{SG}(10^4 \text{ yr}|\mathbf{a}_{SG}, \mathbf{e}_{Mi})$ with exceedance probabilities $p_A[D < D_{SG}(10^4 \text{ yr}|\mathbf{a}, \mathbf{e}_{Mi})|\mathbf{e}_{Ai}]$ defined in Equation J4.5-19 for $i = 1, 2, \ldots, 50$, and (c) expected (mean) CCDF and quantile curves, $q = 0.05, 0.5, 0.95$, for CCDFs in (a). FJ-104

J8.3-11. Assessment with replicated sampling of numerical error associated with use of an LHS of size $nLHS = 300$ to determine epistemic uncertainty in expected dose $\bar{D}_{SG}(\tau|\mathbf{e})$ to RMEI for $0 \le \tau \le 20{,}000$ yr that results when only seismic

FIGURES (Continued)

Page

ground motion events are considered: (a) Replicated estimates of expected (mean) dose $\bar{\bar{D}}_{SG}(\tau)$ and quantiles $Q_q[\bar{D}_{SG}(\tau|\mathbf{e})]$, q = 0.05, 0.5, 0.95, and (b) confidence intervals for estimates of expected (mean) dose $\bar{\bar{D}}_{SG}(\tau)$..... FJ-105

J8.4-1. Doses $D_{SG}(\tau|\mathbf{a}_{SG,ik}, \mathbf{e}_{Mi})$, k = 1, 2, …, nR = 30, and estimated expected doses $\bar{D}_{SG}(\tau|\mathbf{e}_i)$ to the RMEI for $0 \le \tau \le 10^6$ yr for selected LHS elements $\mathbf{e}_i = [\mathbf{e}_{Ai}, \mathbf{e}_{Mi}]$ when only nominal processes and seismic ground motion events are considered: (a) $\mathbf{e}_1$, (b) $\mathbf{e}_2$, (c) $\mathbf{e}_3$, (d) $\mathbf{e}_4$, (e) $\mathbf{e}_5$, and (f) $\mathbf{e}_6$..... FJ-106

J8.4-2. Estimate obtained with LHS of size $nLHS$ = 300 showing epistemic uncertainty in expected dose $\bar{D}_{SG}(\tau|\mathbf{e})$ to RMEI for $0 \le \tau \le 10^6$ yr that results when only nominal processes and seismic ground events are considered: (a) expected dose $\bar{D}_{SG}(\tau|\mathbf{e}_i)$, i = 1, 2, …, $nLHS$ = 300, (b) expected dose $\bar{D}_{SG}(\tau|\mathbf{e}_i)$, i = 1, 2, …, 50, (c) exceedance probabilities $p_E[D < \bar{D}_{SG}(\tau|\mathbf{e})]$ and quantiles $Q_q[\bar{D}_{SG}(\tau|\mathbf{e})]$, q = 0.05, 0.5 and 0.95, for τ = 500,000 yr, and (d) expected (mean) dose $\bar{\bar{D}}_{SG}(\tau)$ and quantiles $Q_q[\bar{D}_{SG}(\tau|\mathbf{e})]$, q = 0.05, 0.5, 0.95..... FJ-107

J8.4-3. Summary of results obtained with LHS of size $nLHS$ = 300 showing epistemic uncertainty in expected dose $\bar{D}_{SG}(\tau|\mathbf{e})$ to RMEI for $0 \le \tau \le 10^6$ yr that results when only nominal processes and seismic ground events are considered..... FJ-108

J8.4-4. Estimate obtained with LHS of size $nLHS$ = 300 showing epistemic uncertainty in expected dose $\bar{D}_{SG,r}(\tau|\mathbf{e}$ to RMEI for $0 \le \tau \le 10^6$ yr with r corresponding to ^{99}Tc that results when only nominal processes and seismic ground events are considered: (a) expected dose $\bar{D}_{SG,r}(\tau|\mathbf{e}_i)$, i = 1, 2, …, $nLHS$ = 300, (b) expected dose $\bar{D}_{SG,r}(\tau|\mathbf{e}_i)$, i = 1, 2, …, 50, (c) exceedance probabilities $p_E[D < \bar{D}_{SG,r}(\tau|\mathbf{e})]$ and quantiles $Q_q[\bar{D}_{SG,r}(\tau|\mathbf{e})]$, q = 0.05, 0.5 and 0.95, for τ = 500,000 yr, and (d) expected (mean) dose $\bar{\bar{D}}_{SG,r}(\tau)$ and quantiles $Q_q[\bar{D}_{SG,r}(\tau|\mathbf{e})]$, q = 0.05, 0.5, 0.95..... FJ-109

J8.4-5. Estimates obtained with LHS of size $nLHS$ = 300 of expected (mean) dose $\bar{\bar{D}}_{SG,r}(\tau)$ to RMEI for $0 \le \tau \le 10^6$ yr for individual radioactive species that result when only nominal proceses and seismic ground events are considered. . FJ-110

J8.4-6. Assessment with replicated sampling of numerical error associated with use of an LHS of size $nLHS$ = 300 to determine epistemic uncertainty in expected dose $\bar{D}_{SG}(\tau|\mathbf{e})$ to RMEI for $0 \le \tau \le 10^6$ yr that results when only nominal processes and seismic ground motion events are considered: (a) Replicated estimates of expected (mean) dose $\bar{\bar{D}}_{SG}(\tau)$ and quantiles $Q_q[\bar{D}_{SG}(\tau|\mathbf{e})]$, q = 0.05, 0.5, 0.95, and (b) confidence intervals for estimates of expected (mean) dose $\bar{\bar{D}}_{SG}(\tau)$..... FJ-111

FIGURES (Continued)

Page

J8.6-1. Summary of results for fault displacement damage of CSNF and CDSP WPs obtained with LHS of size $nLHS = 300$ showing epistemic uncertainty in doses $D_{SF,r}(\tau|[1, t_j, 100, A_r/3, \sim]|\mathbf{e}_{Mi})$ for $0 \le \tau \le 20{,}000$ yr, $r = 1, 2$, with 1 ~ CSNF WPs and $r = 2$ ~ CDSP WPs, $A_1 = 2.78$ m^2 and $A_2 = 3.28$ m^2, and $i = 1, 2, \ldots, nLHS = 300$: (a, c, e) CSNF WPs for $t_j = 200$, 2000 and 8000 yrs and (b, d, f) CDSP WPs for $t_j = 200$, 2000 and 8000 yrs. FJ-112

J8.6-2. Box plots (see Figure J6.2-3 for description) summarizing results for fault displacement damage to CSNF and CDSP WPs obtained with LHS of size $nLHS = 300$ showing epistemic uncertainty in dose $D_{SF,r}(10^4 \text{ yr}|[1, t_j, 100, A_{rk}, \sim]|\mathbf{e}_{Mi})$ for $t_j = 200$, 2000, 4000 and 8000 yrs, $r = 1, 2$, with 1 ~ CSNF WPs and $r = 2$ ~ CDSP WPs, $A_{rk} = A_r/3, 2A_r/3, A_r$, with $A_1 = 2.78$ m^2 and $A_2 = 3.28$ m^2, and $i = 1, 2, \ldots, nLHS = 300$: (a) $t_j = 200$ yr, (b) $t_j = 2000$ yr, (c) $t_j = 4000$ yr, and (d) $t_j = 8000$ yr. FJ-113

J8.6-3. Illustration of interpolation procedure to estimate integrals $\hat{I}_r(\tau|t, \mathbf{e}_{Mi})$ and expected dose $\bar{D}_{SF}(\tau|\mathbf{e}_i)$ from calculated doses $D_{SF,r}(\tau|[1, t_j, 100, A_{rk}, 1, \sim], \mathbf{e}_{Mi})$ in Equation J8.6-18 for LHS element $\mathbf{e}_1 = [\mathbf{e}_{A1}, \mathbf{e}_{M1}]$ and the time interval $[0, 2.0 \times 10^4$ yr]: (a) $D_{SF,1}(\tau|[1, t_j, 100, A_{rk}, 1, \sim], \mathbf{e}_{M1})$ for $j = 1, 2, \ldots, 6$ and $k = 1, 2, 3$ (Notes: Results overlay for A_{1k}, $k = 1, 2, 3$, for each t_j, and results for t_1 and t_2 also overlay), (b) Interpolated values $\hat{I}_1(\tau|\hat{t}_k, \mathbf{e}_{M1})$ for $\hat{t}_k$ between $t_4 =$ 4000 yr and $t_5 = 8000$ yr, (c) Interpolated values for $\hat{I}_1(\tau|\hat{t}_k, \mathbf{e}_{M1})$ for $\hat{t}_k$ between 200 and 20,000 yr, and (d) estimates for $\bar{D}_{SF,1}(\tau|\mathbf{e}_i)$ for CSNF WPs, $\bar{D}_{SF,2}(\tau|\mathbf{e}_i)$ for CDSP WPs and $\bar{D}_{SF}(\tau|\mathbf{e}_i)$ for CSNF and CDSP WPs. FJ-114

J8.6-4. Estimate of $\bar{D}_{SF}(\tau|\mathbf{e}_1)$ for LHS element $\mathbf{e}_1 = [\mathbf{e}_{A1}, \mathbf{e}_{M1}]$ and $0 \le \tau \le 20{,}000$ yr with integration-based procedure indicated in Equations J8.6-17 and J8.6-25 ..... FJ-115

J8.6-5. Estimate obtained with LHS of size $nLHS = 300$ showing epistemic uncertainty in expected dose $\bar{D}_{SF}(\tau|\mathbf{e})$ to RMEI for $0 \le \tau \le 20{,}000$ yr that at results when only fault displacement events are considered: (a) expected dose $\bar{D}_{SF}(\tau|\mathbf{e}_i)$, $i = 1, 2, \ldots, nLHS = 300$, (b) expected dose $\bar{D}_{SF}(\tau|\mathbf{e}_i)$, $i = 1, 2, \ldots, 50$, (c) exceedance probabilities $p_E[D < \bar{D}_{SG}(\tau|\mathbf{e})]$ and quantiles $Q_q[\bar{D}_{SF}(\tau|\mathbf{e})]$, $q = 0.05$, 0.5 and 0.95, for $\tau = 10^4$ yr, and (d) expected (mean) dose $\bar{\bar{D}}_{SF}(\tau)$ and quantiles $Q_q[\bar{D}_{SF}(\tau|\mathbf{e})]$, $q = 0.05$, 0.5, 0.95. ..... FJ-116

J8.6-6. Summary of results obtained with LHS of size $nLHS = 300$ showing epistemic uncertainty in expected dose $\bar{D}_{SF}(\tau|\mathbf{e})$ to RMEI for $0 \le \tau \le 20{,}000$ yr that results when only fault displacement events are considered. FJ-117

J8.6-7. Estimate obtained with LHS of size $nLHS = 300$ showing epistemic uncertainty in expected dose $\bar{D}_{SF,r}(\tau|\mathbf{e})$ to RMEI for $0 \le \tau \le 20{,}000$ yr with r

FIGURES (Continued)

Page

corresponding to ^{99}Tc that results when only fault displacement events are considered: (a) expected dose $\bar{D}_{SF,r}(\tau|\mathbf{e}_i)$, i = 1, 2, …, $nLHS$ = 300, (b) expected dose $\bar{D}_{SF,r}(\tau|\mathbf{e}_i)$, i = 1, 2, …, 50, (c) exceedance probabilities $p_E[D < \bar{D}_{SG,r}(\tau|\mathbf{e})]$ and quantiles $Q_q[\bar{D}_{SF,r}(\tau|\mathbf{e})]$, q = 0.05, 0.5 and 0.95, for $\tau = 10^4$ yr, and (d) expected (mean) dose $\bar{\bar{D}}_{SF,r}(\tau)$ and quantiles $Q_q[\bar{D}_{SF,r}(\tau|\mathbf{e})]$, q = 0.05, 0.5, 0.95 ..... FJ-118

J8.6-8. Estimates obtained with LHS of size $nLHS$ = 300 of expected (mean) dose $\bar{\bar{D}}_{SF,r}(\tau)$ to RMEI for $0 \le \tau \le 20{,}000$ yr for individual radioactive species that result when only seismic ground motion events are considered. FJ-119

J8.6-9. Results associated with $D_{SF}(\tau|\mathbf{a}_{SF}, \mathbf{e}_{M1})$ for LHS element $\mathbf{e}_1 = [\mathbf{e}_{A1}, \mathbf{e}_{M1}]$ obtained with sampling-based (Monte Carlo) procedures: (a) CCDF for $D_{SF}(10^4 \text{ yr}|\mathbf{a}_{SF}, \mathbf{e}_{M1})$ with exceedance probabilities $p_A[D < D_{SF}(10^4 \text{ yr}|\mathbf{a}, \mathbf{e}_{M1})|\mathbf{e}_{A1}]$ defined in Equations J4.5-19 and J8.6-36, and (b) expected dose $\bar{D}_{SF}(10^4 \text{ yr}|\mathbf{e}_1)$ associated with $D_{SF}(10^4|\mathbf{a}_{SF}, \mathbf{e}_{M1})$ as defined in Equation J4.5-20. ..... FJ-120

J8.6-10. Results associated with $D_{SF}(10^4 \text{ yr}|\mathbf{a}_{SF}, \mathbf{e}_M)$ obtained with sampling-based (Monte Carlo) procedures for an LHS of size $nLHS$ = 300: (a) CCDFs for $D_{SF}(10^4 \text{ yr}|\mathbf{a}_{SF}, \mathbf{e}_{Mi})$ with exceedance probabilities $p_A[D < D_{SF}(10^4 \text{ yr}|\mathbf{a}, \mathbf{e}_{Mi})|\mathbf{e}_{Ai}]$ defined in Equation J4.5-19 for i = 1, 2, …, $nLHS$ = 300, (b) CCDFs for $D_{SF}(10^4 \text{ yr}|\mathbf{a}_{SF}, \mathbf{e}_{Mi})$ with exceedance probabilities $p_A[D < D_{SF}(10^4 \text{ yr}|\mathbf{a}, \mathbf{e}_{Mi})|\mathbf{e}_{Ai}]$ defined in Equation J4.5-19 for i = 1, 2, …, 50, and (c) expected (mean) CCDF and quantile curves, q = 0.05, 0.5, 00.95, for CCDFs in (a). FJ-121

J8.6-11. Assessment with replicated sampling of numerical error associated with use of an LHS of size $nLHS$ = 300 to determine epistemic uncertainty in expected dose $\bar{D}_{SF}(\tau|\mathbf{e})$ to RMEI for $0 \le \tau \le 20{,}000$ yr that results when only seismic ground motion events are considered: (a) Replicated estimates of expected (mean) dose $\bar{\bar{D}}_{SF}(\tau)$ and quantiles $Q_q[\bar{D}_{SF}(\tau|\mathbf{e})]$, q = 0.05, 0.5, 0.95, and (b) confidence intervals for estimates of expected (mean) dose $\bar{\bar{D}}_{SF}(\tau)$. FJ-122

J8.6-12. Summary of results for fault displacement damage of CSNF and CDSP WPs obtained with LHS of size $nLHS$ = 300 showing epistemic uncertainty in doses $D_{SF,r}(\tau|[1, t_j, 100, A_r/3, \sim], \mathbf{e}_{Mi})$ for $0 \le \tau \le 20{,}000$ yr, r = 1, 2, with r = 1 ~ CSNF WPs and r = 2 ~ CDSP WPs, A_1 = 2.78 m^2 and A_2 = 3.28 m^2 and i = 1, 2, …, $nLHS$ = 300: (a, c, e) CSNF WPs for t_j = 1000, 80,000 and 200,000 yrs and (b, d, f) CDSP WPs for t_j = 1000, 80,000 and 200,000 yrs. FJ-123

J8.6-13. Box plots (see Figure J6.2-3 for description) summarizing results for fault displacement damage to CSNF and CDSP WPs obtained with LHS of size

FIGURES (Continued)

Page

nLHS = 300 showing epistemic uncertainty in dose $D_{SF,r}(10^4$ yr$|[1, t_j, 100, A_{rk}, \sim], \mathbf{e}_{Mi})$ for t_j =1000, 80,000, 200,000 and 400,000 yrs, r = 1, 2 with r = 1 ~ CSNF WPs and r = 2 ~ CDSP WPs, $A_{rk} = A_r/3, 2A_r/3, A_r$, with A_1 = 2.78 m^2 A_2 = 3.28 m^2, and i = 1, 2, …, *nLHS* = 300: (a) t_j = 1000 yr, (b) t_j = 80,000 yr, (c) t_j = 200,000 yr, and (d) t_j = 400,000 yr..... FJ-124

J8.6-14. Illustration of interpolation procedure to estimate integrals $\hat{I}_r(\tau|t, \mathbf{e}_{M1})$ and expected dose $\bar{D}_{SF}(\tau|\mathbf{e}_i)$ from calculated doses $D_{SF,r}(\tau|[1, t_j, 100, A_{rk}, 1, \sim], \mathbf{e}_{M1})$ in Equation J8.6-18 for LHS element $\mathbf{e}_1 = [\mathbf{e}_{A1}, \mathbf{e}_{M1}]$ and the time interval $[0, 1.0 \times 10^6$ yr]: (a) $D_{SF,1}(\tau|[1, t_j, 100, A_{rk}, 1, \sim], \mathbf{e}_{M1})$ for j = 1, 2, …, 6 and k = 1, 2, 3 (Notes: Results overlay for A_{1k}, k = 1, 2, 3, for each t_j, and results for t_1 and t_2 also overlay), (b) Interpolated values $\hat{I}_1(\tau|\hat{t}_k, \mathbf{e}_{M1})$ for $\hat{t}_k$ between $t_4 = 2.0 \times 10^5$ yr and $t_5 = 4.0 \times 10^5$ yr, (c) Interpolated values for $\hat{I}_1(\tau|\hat{t}_k, \mathbf{e}_{M1})$ for $\hat{t}_k$ between 1000 and 1.0×10^6 yr, and (d) estimates for $\bar{D}_{SF,1}(\tau|\mathbf{e}_i)$ for CSNF WPs, $\bar{D}_{SF,2}(\tau|\mathbf{e}_i)$ for CDSP WPs and $\bar{D}_{SF}(\tau|\mathbf{e}_i)$ for CSNF and CDSP WPs. FJ-125

J8.6-15. Estimate of $\bar{D}_{SF}(\tau|\mathbf{e}_1)$ for LHS element $\mathbf{e}_1 = [\mathbf{e}_{A1}, \mathbf{e}_{M1}]$ and $0 \le \tau \le 10^6$ yr with integration-based procedure indicated in Equations J8.6-17 and J8.6-25..... FJ-126

J8.6-16. Estimate obtained with LHS of size *nLHS* = 300 showing epistemic uncertainty in expected dose $\bar{D}_{SF}(\tau|\mathbf{e})$ to RMEI for $0 \le \tau \le 10^6$ yr that at results when only fault displacement events are considered: (a) expected dose $\bar{D}_{SF}(\tau|\mathbf{e}_i)$, i = 1, 2, …, *nLHS* = 300, (b) expected dose $\bar{D}_{SF}(\tau|\mathbf{e}_i)$, i = 1, 2, …, 50, (c) exceedance probabilities $p_E[D < \bar{D}_{SG}(\tau|\mathbf{e})]$ and quantiles $Q_q[\bar{D}_{SF}(\tau|\mathbf{e})]$, q = 0.05, 0.5 and 0.95, for $\tau = 5 \times 10^5$ yr, and (d) expected (mean) dose $\bar{\bar{D}}_{SF}(\tau)$ and quantiles $Q_q[\bar{D}_{SF}(\tau|\mathbf{e})]$, q = 0.05, 0.5, 0.95. ..... FJ-127

J8.6-17. Summary of results obtained with LHS of size *nLHS* = 300 showing epistemic uncertainty in expected dose $\bar{D}_{SF}(\tau|\mathbf{e})$ to RMEI for $0 \le \tau \le 10^6$ yr that results when only fault displacement events are considered. FJ-128

J8.6-18. Estimate obtained with LHS of size *nLHS* = 300 showing epistemic uncertainty in expected dose $\bar{D}_{SF,r}(\tau|\mathbf{e})$ to RMEI for $0 \le \tau \le 10^6$ yr with r corresponding to ^{242}Pu that results when only fault displacement events are considered: (a) expected dose $\bar{D}_{SF,r}(\tau|\mathbf{e}_i)$, i = 1, 2, …, *nLHS* = 300, (b) expected dose $\bar{D}_{SF,r}(\tau|\mathbf{e}_i)$, i = 1, 2, …, 50, (c) exceedance probabilities $p_E[D < \bar{D}_{SG,r}(\tau|\mathbf{e})]$ and quantiles $Q_q[\bar{D}_{SF,r}(\tau|\mathbf{e})]$, q = 0.05, 0.5 and 0.95, for τ = 500,000 yr, and (d) expected (mean) dose $\bar{\bar{D}}_{SF,r}(\tau)$ and quantiles $Q_q[\bar{D}_{SF,r}(\tau|\mathbf{e})]$, q = 0.05, 0.5, 0.95. ..... FJ-129

FIGURES (Continued)

Page

J8.6-19. Estimates obtained with LHS of size $nLHS = 300$ of expected (mean) dose $\bar{\bar{D}}_{SF,r}(\tau)$ to RMEI for $0 \le \tau \le 10^6$ yr for individual radioactive species that result when only seismic ground motion events are considered. FJ-130

J8.6-20. Results associated with $D_{SF}(\tau|\mathbf{a}_{SF}, \mathbf{e}_{M1})$ for LHS element $\mathbf{e}_1 = [\mathbf{e}_{A1}, \mathbf{e}_{M1}]$ obtained with sampling-based (Monte Carlo) procedures: (a) CCDF for $D_{SF}(5 \times 10^5 \text{ yr}|\mathbf{a}_{SF}, \mathbf{e}_{M1})$ with exceedance probabilities $p_A[D < D_{SF}(5 \times 10^5 \text{ yr}|\mathbf{a}, \mathbf{e}_{M1})|\mathbf{e}_{A1}]$ defined in Equations J4.5-19 and J8.6-36, and (b) expected dose $\bar{D}_{SF}(5 \times 10^5 \text{ yr}|\mathbf{e}_1)$ associated with $D_{SF}(5 \times 10^5 \text{ yr}|\mathbf{a}_{SF}, \mathbf{e}_{M1})$ defined in Equation J4.5-20. ..... FJ-131

J8.6-21. Results associated with $D_{SG}(5 \times 10^5 \text{ yr}|\mathbf{a}_{SF}, \mathbf{e}_M)$ obtained with sampling-based (Monte Carlo) procedures for an LHS of size $nLHS = 300$: (a) CCDFs for $D_{SF}(5 \times 10^5 \text{ yr}|\mathbf{a}_{SF}, \mathbf{e}_{Mi})$ with exceedance probabilities $p_A[D < D_{SF}(5 \times 10^5 \text{ yr}|\mathbf{a}, \mathbf{e}_{Mi})|\mathbf{e}_{Ai}]$ defined in Equation J4.5-19 for $i = 1, 2, \ldots, nLHS = 300$, (b) CCDFs for $D_{SF}(10^4 \text{ yr}|\mathbf{a}_{SF}, \mathbf{e}_{Mi})$ with exceedance probabilities $p_A[D < D_{SF}(5 \times 10^5 \text{ yr}|\mathbf{a}, \mathbf{e}_{Mi})|\mathbf{e}_{Ai}]$ defined in Equation J4.5-19 for $i = 1, 2, \ldots, 50$, and (c) expected (mean) CCDF and quantile curves, $q = 0.05, 0.5, 00.95$, for CCDFs in (a). FJ-132

J8.6-22. Assessment with replicated sampling of numerical error associated with use of an LHS of size $nLHS = 300$ to determine epistemic uncertainty in expected dose $\bar{D}_{SF}(\tau|\mathbf{e})$ to RMEI for $0 \le \tau \le 10^6$ yr that results when only seismic ground motion events are considered: (a) Replicated estimates of expected (mean) dose $\bar{\bar{D}}_{SF}(\tau)$ and quantiles $Q_q[\bar{D}_{SF}(\tau|\mathbf{e})]$, $q = 0.05, 0.5, 0.95$, and (b) confidence intervals for estimates of expected (mean) dose $\bar{\bar{D}}_{SF}(\tau)$. FJ-133

J9.2-1. Estimate obtained with LHS of size $nLHS = 300$ showing epistemic uncertainty in expected dose $\bar{D}(\tau|\mathbf{e})$ to RMEI for $0 \le \tau \le 20{,}000$ yr that results when all futures are considered: (a) expected dose $\bar{D}(\tau|\mathbf{e}_i)$, $i = 1, 2, \ldots, nLHS = 300$, (b) expected dose $\bar{D}(\tau|\mathbf{e}_i)$, $i = 1, 2, \ldots, 50$, (c) exceedance probabilities $p_E[D < \bar{D}(\tau|\mathbf{e})]$ and quantiles $Q_q[\bar{D}(\tau|\mathbf{e})]$, $q = 0.05, 0.5$ and 0.95, for $\tau = 10^4$ yr, and (d) expected (mean) dose $\bar{\bar{D}}(\tau)$ and quantiles $Q_q[\bar{D}(\tau|\mathbf{e})]$, $q = 0.05, 0.5, 0.95$ FJ-135

J9.2-2. Summary of results obtained with LHS of size $nLHS = 300$ showing epistemic uncertainty in expected dose $\bar{D}(\tau|\mathbf{e})$ to RMEI for $0 \le \tau \le 20{,}000$ yr that results when all futures are considered. FJ-136

J9.2-3. Estimates obtained with LHS of size $nLHS = 300$ of expected (mean) dose $\bar{\bar{D}}_r(\tau)$ to RMEI for $0 \le \tau \le 20{,}000$ yr for individual radioactive species that result when all futures are considered. FJ-137

FIGURES (Continued)

Page

J9.2-4. Assessment with replicated sampling of numerical error associated with use of an LHS of size *nLHS* = 300 to determine epistemic uncertainty in expected dose $\bar{D}(\tau|\mathbf{e})$ to RMEI for $0 \le \tau \le 20{,}000$ yr that results when all futures are considered: (a) Replicated estimates of expected (mean) dose $\bar{\bar{D}}(\tau)$ and quantiles $Q_q[\bar{D}(\tau|\mathbf{e})]$, q = 0.05, 0.5, 0.95, and (b) confidence intervals for estimates of expected (mean) dose $\bar{\bar{D}}(\tau)$. FJ-138

J9.3-1. Estimate obtained with LHS of size *nLHS* = 300 showing epistemic uncertainty in expected dose $\bar{D}(\tau|\mathbf{e})$ to RMEI for $0 \le \tau \le 1{,}000{,}000$ yr that results when all futures are considered: (a) expected dose $\bar{D}(\tau|\mathbf{e}_i)$, i = 1, 2, …, *nLHS* = 300, (b) expected dose $\bar{D}(\tau|\mathbf{e}_i)$, i = 1, 2, …, 50, (c) exceedance probabilities $p_E[D < \bar{D}(\tau|\mathbf{e})]$ and quantiles $Q_q[\bar{D}(\tau|\mathbf{e})]$, q = 0.05, 0.5 and 0.95, for $\tau = 10^4$ yr, and (d) expected (mean) dose $\bar{\bar{D}}(\tau)$ and quantiles $Q_q[\bar{D}(\tau|\mathbf{e})]$, q = 0.05, 0.5, 0.95 ..... FJ-139

J9.3-2. Summary of results obtained with LHS of size *nLHS* = 300 showing epistemic uncertainty in expected dose $\bar{D}(\tau|\mathbf{e})$ to RMEI for $0 \le \tau \le 1{,}000{,}000$ yr that results when all futures are considered. FJ-140

J9.3-3. Estimates obtained with LHS of size *nLHS* = 300 of expected (mean) dose $\bar{D}_r(\tau)$ to RMEI for $0 \le \tau \le 1{,}000{,}000$ yr for individual radioactive species that result when all futures are considered. FJ-141

J9.3-4. Assessment with replicated sampling of numerical error associated with use of an LHS of size *nLHS* = 300 to determine epistemic uncertainty in expected dose $\bar{D}(\tau|\mathbf{e})$ to RMEI for $0 \le \tau \le 1{,}000{,}000$ yr that results when all futures are considered: (a) Replicated estimates of expected (mean) dose $\bar{\bar{D}}(\tau)$ and quantiles $Q_q[\bar{D}(\tau|\mathbf{e})]$, q = 0.05, 0.5, 0.95, and (b) confidence intervals for estimates of expected (mean) dose $\bar{D}(\tau|\mathbf{e})$ FJ-142

J11.2-1. Estimate obtained with LHS of size *nLHS* = 300 showing epistemic uncertainty in expected dose $\bar{D}_{HI}(\tau|\mathbf{e})$ to RMEI for $0 \le \tau \le 1{,}000{,}000$ yr that results from a single drilling intrusion at 200,000 years FJ-143

J11.2-2. Assessment with replicated sampling of numerical error associated with use of an LHS of size *nLHS* = 300 to determine epistemic uncertainty in expected dose $\bar{D}_{HI}(\tau|\mathbf{e})$ to RMEI for $0 \le \tau \le 1{,}000{,}000$ yr that results from a single drilling intrusion at 200,000 years: (a) Replicated estimates of expected (mean) dose $\bar{\bar{D}}_{HI}(\tau)$ and quantiles $Q_q[\bar{D}_{HI}(\tau|\mathbf{e})]$, q = 0.05, 0.5, 0.95, and (b) confidence intervals for estimates of expected (mean) dose $\bar{\bar{D}}_{HI}(\tau)$. FJ-144

K2-1. Illustration of uncertainty and sensitivity analysis results for time-dependent number of failed CSNF WPs in percolation bin 3 under nominal conditions: (a) *NCSFL* for all (i.e., 300) sample elements, (b) PRCCs for *NCSFL*, (c) stepwise rank regressions for *NCSFL* at 600,000, 800,000 and 1,000,000 years, and (d, e) scatterplots for (*WDGA22*, *NCSFL*) at 600,000 and 1,000,000 years. FK-1

FIGURES (Continued)

Page

K4.2-1. Uncertainty and sensitivity analysis results for DS failure time (*DSFLTM*, yr) under nominal conditions: (a) CCDF for *DSFLTM*, (b) Stepwise rank regression for *DSFLTM*, and (c,d,e) Selected scatterplots for *DSFLTM*.....FK-2

K4.2-2. Time-dependent numbers of failed CSNF WPs (*NCSFL*) and failed CDSP WPs (*NCDFL*) in percolation bin 3 under nominal conditions: (a, b) *NCSFL* and *NCDFL* for all (i.e., 300) sample elements, (c, d) *NCSFL* and *NCDFL* for first 50 sample elements, and (e, f) PRCCs for *NCSFL* and *NCDFL*.....FK-3

K4.2-3. Stepwise rank regression analyses and selected scatterplots for number of failed CSNF WPs (*NCSFL*) in percolation bin 3 under nominal conditions: (a) Regressions for *NCSFL* at 6×10^5, 8×10^5 and 1×10^6 years, and (b, c, d) Scatterplots for *NCSFL* at 6×10^5, 8×10^5 and 1×10^6 years.....FK-4

K4.2-4. Time-dependent numbers of failed CSNF WPs experiencing dripping conditions (*NCSFLAD*) and nondripping conditions (*NCSFLND*) in percolation bin 3 under nominal conditions: (a, b) *NCSFLAD* and *NCSFLND* for all (i.e., 300) sample elements, (c, d) *NCSFLAD* and *NCSFLND* for first 50 sample elements, and (e, f) PRCCs for *NCSFLAD* and *NCSFLND*. FK-5

K4.2-5. Stepwise rank regression analyses and selected scatterplots for numbers of failed CSNF WPs experiencing dripping conditions (*NCSFLAD*) and nondripping conditions (*NCSFLND*) in percolation bin 3 under nominal conditions: (a, b) Regressions for *NCSFLAD* and *NCSFLND* at 6×10^5, 8×10^5 and 1×10^6 years, and (c, d, e, f) Scatterplots for *NCSFLAD* and *NCSFLND* at 8×10^5 years, and (g, h) Scatterplots comparing *NCSFLAD* and *NCSFLND* at 6×10^5 and 8×10^5 years. FK-6

K4.2-6. Time-dependent average breached area on failed CSNF WPs experiencing dripping conditions (*BACSFLAD*) and nondripping conditions (*BACSFLND*) in percolation bin 3 under nominal conditions: (a) *BACSFLAD* for all (i.e., 300) sample elements, (b) *BACSFLAD* for first 50 sample elements, (c) PRCCs for *BACSFLAD*, and (d) Scatterplot comparing *BACSFLAD* and *BACSFLND* at 1×10^6 years. FK-8

K4.2-7. Stepwise rank regression analyses and selected scatterplots for average breached area on failed CSNF WPs experiencing dripping conditions (*BACSFLAD*) in percolation bin 3 under nominal conditions: (a) Regressions for *BACSFLAD* at 6×10^5, 8×10^5 and 1×10^6 years, and (b, c) Scatterplots for *BACSFLAD* and *NCSFLND* at 8×10^5 years. FK-9

K4.3-1. Time-dependent seepage rates (m^3/yr/WP) into the repository above CSNF WPs (*SPRATECS*) and CDSP WPs (*SPRATECD*) in percolation bin 3 under nominal conditions: (a, b) *SPRATECS* and *SPRATECD* for all (i.e., 300) sample elements, (c, d) *SPRATECS* and *SPRATECD* for first 50 sample elements, and (e, f) PRCCs for *SPRATECS* and *SPRATECD*. FK-10

K4.3-2. Stepwise rank regression analyses and selected scatterplots for seepage rate (m^3/yr/WP) into the repository above CSNF WPs (*SPRATECS*) in percolation bin 3 under nominal conditions: (a) Regressions for *SPRATECS*

FIGURES (Continued)

Page

at 1000, 5000 and 100,000 years, and (b, c, d, e) Scatterplots for *SPRATECS* at 1000 years. FK-11

K4.3-3. Time-dependent seepage rates (m^3/yr/WP) into the repository above CSNF WPs (*SPRATECS*) in percolation bins 1, 2, 4 and 5 under nominal conditions: (a, c, e, g) *SPRATECS* for all (i.e., 300) sample elements, and (b, d, f, h) *SPRATECS* for first 50 sample elements FK-12

K4.3-4. Time-dependent seepage rates (m^3/yr/WP) into the repository above CDSP WPs (*SPRATECD*) in percolation bins 1, 2, 4 and 5 under nominal conditions: (a, c, e, g) *SPRATECD* for all (i.e., 300) sample elements, and (b, d, f, h) *SPRATECD* for first 50 sample elements..... FK-13

K4.3-5. Time-dependent temperatures in percolation bin 3 under nominal conditions for CSNF WPs at the drift wall (*TMPCSWL*), on the WP (*TMPCSWP*) and in the invert beneath the WP (*TMPCSINV*) and similarly for CDSP WPs at the drift wall (*TMPCDWL*), on the WP (*TMPCDWP*) and in the invert beneath the WP (*TMPCDINV*): (a, c, e) *TMPCSWL*, *TMPCSWP* and *TMPCSINV*, and (b, d, f) *TMPCDWL*, *TMPCDWP* and *TMPCDINV* FK-14

K4.3-6. Time-dependent relative humidities in percolation bin 3 under nominal conditions for CSNF WPs on the WP (*RHCSWP*) and in the invert beneath the WP (*RHCSINV*) and similarly for CDSP WPs on the WP (*RHCDWP*) and in the invert beneath the WP (*RHCDINV*): (a, c) *RHCSWP* and *RHCSINV*, and (b, d) *RHCDWP* and *RHCDINV* FK-15

K4.3-7. Time-dependent partial pressures for CO_2 (bars) in the invert for dripping conditions for CSNF WPs (*PCO2CSIA*) and CDSP WPs (*PCO2CDIA*) in percolation bin 3 under nominal conditions: (a, b) *PCO2CSIA* and *PCO2CDIA* for all (i.e., 300) sample elements, (c, d) *PCO2CSIA* and *PCO2CDIA* for first 50 sample elements, and (e, f) PRCCs for *PCO2CSIA* and *PCO2CDIA* FK-16

K4.3-8. Stepwise rank regression analyses and selected scatterplots for CO_2 partial pressure (bars) in the invert under dripping conditions for CSNF WPs (*PCO2CSIA*) in percolation bin 3 under nominal conditions: (a) Regressions for *PCO2CSIA* at 1000, 5000 and 10,000 years, and (b, c) Scatterplots for *PCO2CSIA* at 1000 and 10,000 years. FK-17

K4.3-9. Time-dependent ionic strength (mol/kg) in the invert for CSNF WPs experiencing nondripping conditions (*ISCSINND*) and dripping conditions (*ISCSINAD*) in percolation bin 3 under nominal conditions: (a, b) *ISCSINND* and *ISCSINAD* for all (i.e., 300) sample elements, (c, d) *ISCSINND* and *ISCSINAD* for first 50 sample elements, and (e, f) PRCCs for *ISCSINND* and *ISCSINAD*. FK-18

K4.3-10. Time-dependent ionic strength (mol/kg) in the invert for CDSP WPs experiencing nondripping conditions (*ISCDINND*) and dripping conditions (*ISCDINAD*) in percolation bin 3 under nominal conditions: (a, b) *ISCDINND* and *ISCDINAD* for all (i.e., 300) sample elements, (c, d) *ISCDINND* and *ISCDINAD* for first 50 sample elements, and (e, f) PRCCs for *ISCDINND* and *ISCDINAD*. FK-19

FIGURES (Continued)

Page

K4.3-11. Stepwise rank regression analyses and selected scatterplots for ionic strength (mol/kg) in the invert for CSNF WPs experiencing dripping conditions (*ISCSINAD*) in percolation bin 3 under nominal conditions: (a) Regressions for *ISCSINAD* at 1000, 50,000 and 500,000 years, and (b, c, d) Scatterplots for *ISCSINAD* at 1000, 50,000 and 500,000 years. FK-20

K4.3-12. Time-dependent pH in the invert for CSNF WPs experiencing nondripping conditions (*PHCSINND*) and dripping conditions (*PHCSINAD*) in percolation bin 3 under nominal conditions: (a, b) *PHCSINND* and *PHCSINAD* for all (i.e., 300) sample elements, (c, d) *PHCSINND* and *PHCSINAD* for first 50 sample elements, and (e, f) PRCCs for *PHCSINND* and *PHCSINAD*. FK-21

K4.3-13. Stepwise rank regression analyses and selected scatterplots for pH in the invert for CSNF WPs experiencing nondripping conditions (*PHCSINND*) and dripping conditions (*PHCSINAD*) in percolation bin 3 under nominal conditions: (a, b) Regressions for *PHCSINND* and *PHCSINAD* at 1000, 50,000 and 500,000 years, and (c-j) Scatterplots for *PHCSINND* and *PHCSINAD* at 1000, 50,000 and 500,000 years. FK-22

K4.3-14. Time-dependent pH in the invert for CDSP WPs experiencing nondripping conditions (*PHCDINND*) and dripping conditions (*PHCDINAD*) in percolation bin 3 under nominal conditions: (a, b) *PHCDINND* and *PHCDINAD* for all (i.e., 300) sample elements, (c, d) *PHCDINND* and *PHCDINAD* for first 50 sample elements, and (e, f) PRCCS for *PHCDINND* and *PHCDINAD*..... FK-24

K4.4-1. Time-dependent release rates (*ESNP237*, g/yr) and cumulative (i.e., integrated) releases (*ESNP237C*, g) for movement of dissolved ^{237}Np from the EBS to the UZ under nominal conditions: (a, b) *ESNP237* and *ESNP237C* for all (i.e., 300) sample elements, (c, d) *ESNP237* and *ESNP237C* for first 50 sample elements, and (e, f) PRCCs for *ESNP237* and *ESNP237C*. FK-25

K4.4-2. Stepwise rank regression analyses and selected scatterplots for release rates (*ESNP237*, g/yr) and cumulative (i.e., integrated) releases (*ESNP237C*, g) for movement of dissolved ^{237}Np from the EBS to the UZ under nominal conditions: (a, b) Regressions for *ESNP237* and *ESNP237C* at 400,000, 600,000 and 800,000 years, and (c-h) Scatterplots for *ESNP237* and *ESNP237C* at 800,000 years. FK-26

K4.5-1. Dose to RMEI (*DOSTOT*, mrem/yr) for all radioactive species under nominal conditions: (a) *DOSTOT* for all (i.e., 300) sample elements, (b) *DOSTOT* for first 50 sample elements, and (c) PRCCs for *DOSTOT*. FK-28

K4.5-2. Stepwise rank regression analyses and selected scatterplots for dose to RMEI (*DOSTOT*, mrem/yr) for all radioactive species under nominal conditions: (a) Regressions for *DOSTOT* at 400,000, 600,000 and 800,000 years, and (b,c,d) Scatterplots for *DOSTOT* at 400,000, 600,000 and 800,000 years. FK-29

K4.5-3. Selected scatterplots for dose to RMEI (*DOSTOT*, mrem/yr) for all radioactive species under nominal conditions at 800,000 and 1,000,000 years. .. FK-30

FIGURES (Continued)

Page

K5.2-1 Time-dependent ionic strength (mol/kg) in the invert for CSNF WPs (*ISCSINAD*) and CDSP WPs (*ISCDINAD*) experiencing an early drip shield failure under dripping conditions in percolation bin 3: (a, b) *ISCSINAD* and *ISCDINAD* for all (i.e., 300) sample elements, (c, d) *ISCSINAD* and *ISCDINAD* for first 50 sample elements, and (e, f) PRCCs for *ISCSINAD* and *ISCDINAD* FK-31

K5.2-2 Time-dependent pH in the invert for CSNF WPs (*PHCSINAD*) and CDSP WPs (*PHCDINAD*) experiencing an early DS failure under dripping conditions in percolation bin 3: (a, b) *PHCSINAD* and *PHCDINAD* for all (i.e., 300) sample elements, (c, d) *PHCSINAD* and *PHCDINAD* for first 50 sample elements, and (e, f) PRCCs for *PHCSINAD* and *PHCDINAD*..... FK-32

K5.3.1-1. Time-dependent release rates (*ESIC239*, g/yr) and cumulative (i.e., integrated) releases (*ESIC239C*, g) over 20,000 years for the movement of ^{239}Pu irreversibly attached to glass/waste form colloids from the EBS to the UZ resulting from a single early DS failure above a CDSP WP in percolation bin 3 under dripping conditions: (a, b) *ESIC239* and *ESIC239C* for all (i.e., 300) sample elements, (c, d) *ESIC239* and *ESIC239C* for first 50 sample elements, and (e, f) PRCCs for *ESIC239* and *ESIC239C*. FK-33

K5.3.1-2. Stepwise rank regression analyses and selected scatterplots for time-dependent release rates (*ESIC239*, g/yr) and cumulative (i.e., integrated) releases (*ESIC239C*, g) for the movement of ^{239}Pu irreversibly attached to glass/waste form colloids from the EBS to the UZ resulting from a single early DS failure above a CDSP WP in percolation bin 3 under dripping conditions : (a, b) Regressions for *ESIC239* and *ESIC239C* at 3000, 5000 and 10,000 years, and (c-h) Scatterplots for *ESIC239* and *ESIC239C* at 10,000 years. FK-34

K5.3.1-3. Removed. FK-36

K5.3.1-4. Removed FK-37

K5.3.1-5. Time-dependent release rates (*ESNP237*, g/yr) and cumulative (i.e., integrated) releases (*ESNP2379C*, g) over 20,000 years for the movement of dissolved ^{237}Np from the EBS to the UZ resulting from a single early DS failure above a CDSP WP in percolation bin 3 under dripping conditions: (a, b) *ESNP237* and *ESNP237C* for all (i.e., 300) sample elements, (c, d) *ESNP237* and *ESNP237C* for first 50 sample elements, and (e, f) PRCCs for *ESNP237* and *ESNP237C*. FK-38

K5.3.1-6. Stepwise rank regression analyses and selected scatterplots for time-dependent release rates (*ESNP237*, g/yr) and cumulative (i.e., integrated) releases (*ESNP237C*, g) for the movement of dissolved 237Np from the EBS to the UZ resulting from a single early DS failure above a CDSP WP in percolation bin 3 under dripping conditions: (a, b) Regressions for *ESNP237* and *ESNP237C* at 3000, 5000 and 10,000 years, and (c-h) Scatterplots for *ESNP237* and *ESNP237C* at 10,000 years..... FK-39

K5.3.1-7. Time-dependent release rates (*ESPU239*, g/yr) and cumulative (i.e., integrated) releases (*ESPU239C*, g) over 20,000 years for the movement of

FIGURES (Continued)

Page

dissolved ^{239}Pu from the EBS to the UZ resulting from a single early DS failure above a CDSP WP in percolation bin 3 under dripping conditions: (a, b) *ESPU239* and *ESPU239C* for all (i.e., 300) sample elements, (c, d) *ESPU239* and *ESPU239C* for first 50 sample elements, and (e, f) PRCCs for *ESPU239* and *ESPU239C*.....FK-41

K5.3.1-8. Stepwise rank regression analyses and selected scatterplots for time-dependent release rates (*ESPU239*, g/yr) and cumulative (i.e., integrated) releases (*ESPU239*, g) for the movement of dissolved ^{239}Pu from the EBS to the UZ resulting from a single early DS failure above a CDSP WP in percolation bin 3 under dripping conditions: (a, b) Regressions for *ESPU239* and *ESPU239C* at 3000, 5000 and 10,000 years, and (c-h) Scatterplots for *ESPU239* and *ESPU239C* at 10,000 years.....FK-42

K5.3.1-9. Time-dependent release rates (*ESTC99*, g/yr) and cumulative (i.e., integrated) releases (*ESTC99C*, g) over 20,000 years for the movement of dissolved ^{99}Tc from the EBS to the UZ resulting from a single early DS failure above a CDSP WP in percolation bin 3 under dripping conditions: (a, b) *ESTC99* and *ESTC99C* for all (i.e., 300) sample elements, (c, d) *ESTC99* and *ESTC99C* for first 50 sample elements, and (e, f) PRCCs for *ESTC99* and *ESTC99C*.....FK-44

K5.3.1-10. Stepwise rank regression analyses and selected scatterplots for time-dependent release rates (*ESTC99*, g/yr) and cumulative (i.e., integrated) releases (*ESTC99*, g) for the movement of dissolved ^{99}Tc from the EBS to the UZ resulting from a single early DS failure above a CDSP WP in percolation bin 3 under dripping conditions: (a, b) Regressions for *ESTC99* and *ESTC99C* at 3000, 5000 and 10,000 years, and (c-h) Scatterplots for *ESTC99* and *ESTC99C* at 10,000 years.....FK-45

K5.3.2-1. Time-dependent release rates (*ESIC239*, g/yr) and cumulative (i.e., integrated) releases (*ESIC239C*, g) over 20,000 years for the movement of ^{239}Pu irreversibly attached to glass/waste form colloids from the EBS to the UZ resulting from a single early DS failure above a CSNF WP in percolation bin 3 under dripping conditions: (a, b) *ESIC239* and *ESIC239C* for all (i.e., 300) sample elements, (c, d) *ESIC239* and *ESIC239C* for first 50 sample elements, and (e, f) PRCCs for *ESIC239* and *ESIC239C*.....FK-47

K5.3.2-2. Removed.....FK-48

K5.3.2-3. Time-dependent release rates (*ESNP237*, g/yr) and cumulative (i.e., integrated) releases (*ESNP237C*, g) over 20,000 years for the movement of dissolved ^{237}Np from the EBS to the UZ resulting from a single early DS failure above a CNSF WP in percolation bin 3 under dripping conditions: (a, b) *ESNP237* and *ESNP237C* for all (i.e., 300) sample elements, (c, d) *ESNP237* and *ESNP237C* for first 50 sample elements, and (e, f) PRCCs for *ESNP237* and *ESNP237C*.....FK-49

K5.3.2-4. Time-dependent release rates (*ESPU239*, g/yr) and cumulative (i.e., integrated) releases (*ESPU239C*, g) over 20,000 years for the movement of dissolved ^{239}Pu from the EBS to the UZ resulting from a single early DS

FIGURES (Continued)

Page

failure above a CNSF WP in percolation bin 3 under dripping conditions: (a, b) *ESPU239* and *ESPU239C* for all (i.e., 300) sample elements, (c, d) *ESPU239* and *ESPU239C* for first 50 sample elements, and (e, f) PRCCs for *ESPU239* and *ESPU239C*.....FK-50
K5.3.2-5. Time-dependent release rates (*ESTC99*, g/yr) and cumulative (i.e., integrated) releases (*ESTC99C*, g) over 20,000 years for the movement of dissolved ^{99}Tc from the EBS to the UZ resulting from a single early DS failure above a CNSF WP in percolation bin 3 under dripping conditions: (a, b) *ESTC99* and *ESTC99C* for all (i.e., 300) sample elements, (c, d) *ESTC99* and *ESTC99C* for first 50 sample elements, and (e, f) PRCCs for *ESTC99* and *ESTC99C*.....FK-51
K5.3.3-1. Removed.....FK-52
K5.3.3-2. Removed.....FK-53
K5.3.3-3. Time-dependent release rates (*ESNP237*, g/yr) and cumulative (i.e., integrated) releases (*ESNP237C*, g) over 20,000 years for the movement of dissolved ^{237}Np from the EBS to the UZ resulting from the early failure of a CDSP WP in percolation bin 3 under dripping conditions: (a, b) *ESNP237* and *ESNP237C* for all (i.e., 300) sample elements, (c, d) *ESNP237* and *ESNP237C* for first 50 sample elements, and (e, f) PRCCs for *ESNP237* and *ESNP237C*.....FK-54
K5.3.3-4. Time-dependent release rates (*ESPU239*, g/yr) and cumulative (i.e., integrated) releases (*ESPU239C*, g) over 20,000 years for the movement of dissolved ^{239}Pu from the EBS to the UZ resulting from the early failure of a CDSP WP in percolation bin 3 under dripping conditions: (a, b) *ESPU239* and *ESPU239C* for all (i.e., 300) sample elements, (c, d) *ESPU239* and *ESPU239C* for first 50 sample elements, and (e, f) PRCCs for *ESPU239* and *ESPU239C*.....FK-55
K5.3.3-5. Time-dependent release rates (*ESTC99*, g/yr) and cumulative (i.e., integrated) releases (*ESTC99C*, g) over 20,000 years for the movement of dissolved ^{99}Tc from the EBS to the UZ resulting from the early failure of a CDSP WP in percolation bin 3 under dripping conditions: (a, b) *ESTC99* and *ESTC99C* for all (i.e., 300) sample elements, (c, d) *ESTC99* and *ESTC99C* for first 50 sample elements, and (e, f) PRCCs for *ESTC99* and *ESTC99C*.....FK-56
K5.3.5-1. Removed.....FK-57
K5.3.5-2. Removed.....FK-58
K5.3.5-3. Time-dependent release rates (*ESNP237*, g/yr) and cumulative (i.e., integrated) releases (*ESNP237C*, g) over 20,000 years for the movement of dissolved ^{237}Np from the EBS to the UZ resulting from the early failure of a CSNF WP in percolation bin 3 under dripping conditions: (a, b) *ESNP237* and *ESNP237C* for all (i.e., 300) sample elements, (c, d) *ESNP237* and *ESNP237C* for first 50 sample elements, and (e, f) PRCCs for *ESNP237* and *ESNP237C*.....FK-59
K5.3.5-4. Time-dependent release rates (*ESPU239*, g/yr) and cumulative (i.e., integrated) releases (*ESPU239C*, g) over 20,000 years for the movement of

FIGURES (Continued)

Page

dissolved ^{239}Pu from the EBS to the UZ resulting from the early failure of a CSNF WP in percolation bin 3 under dripping conditions: (a, b) *ESPU239* and *ESPU239C* for all (i.e., 300) sample elements, (c, d) *ESPU239* and *ESPU239C* for first 50 sample elements, and (e, f) PRCCs for *ESPU239* and *ESPU239C*. FK-60

K5.3.5-5. Time-dependent release rates (*ESTC99*, g/yr) and cumulative (i.e., integrated) releases (*ESTC99C*, g) over 20,000 years for the movement of dissolved ^{99}Tc from the EBS to the UZ resulting from the early failure of a CSNF WP in percolation bin 3 under dripping conditions: (a, b) *ESTC99* and *ESTC99C* for all (i.e., 300) sample elements, (c, d) *ESTC99* and *ESTC99C* for first 50 sample elements, and (e, f) PRCCs for *ESTC99* and *ESTC99C*. FK-61

K5.3.7-1. Time-dependent release rates (*ESNP237*, g/yr) and cumulative (i.e., integrated) releases (*ESNP237C*, g) over 1,000,000 years for the movement of dissolved ^{237}Np from the EBS to the UZ resulting from a single early DS failure above a CDSP WP in percolation bin 3 under dripping conditions: (a, b) *ESNP237* and *ESNP237C* for all (i.e., 300) sample elements, (c, d) *ESNP237* and *ESNP237C* for first 50 sample elements, and (e, f) PRCCs for *ESNP237* and *ESNP237C* FK-63

K5.3.7-2. Time-dependent release rates (*ESPU239*, g/yr) and cumulative (i.e., integrated) releases (*ESPU239C*, g) over 200,000 years for the movement of dissolved ^{239}Pu from the EBS to the UZ resulting from a single early DS failure above a CDSP WP in percolation bin 3 under dripping conditions: (a, b) *ESPU239* and *ESPU239C* for all (i.e., 300) sample elements, (c, d) *ESPU239* and *ESPU239C* for first 50 sample elements, and (e, f) PRCCs for *ESPU239* and *ESPU239C*..... FK-64

K5.3.8-1. Time-dependent release rates (*ESNP237*, g/yr) and cumulative (i.e., integrated) releases (*ESNP237C*, g) over 1,000,000 years for the movement of dissolved ^{237}Np from the EBS to the UZ resulting from a single early DS failure above a CSNF WP in percolation bin 3 under dripping conditions: (a, b) *ESNP237* and *ESNP237C* for all (i.e., 300) sample elements, (c, d) *ESNP237* and *ESNP237C* for first 50 sample elements, and (e, f) PRCCs for *ESNP237* and *ESNP237C*. FK-65

K5.3.8-2. Time-dependent release rates (*ESPU239*, g/yr) and cumulative (i.e., integrated) releases (*ESPU239C*, g) over 200,000 years for the movement of dissolved ^{239}Pu from the EBS to the UZ resulting from a single early DS failure above a CSNF WP in percolation bin 3 under dripping conditions: (a, b) *ESPU239* and *ESPU239C* for all (i.e., 300) sample elements, (c, d) *ESPU239* and *ESPU239C* for first 50 sample elements, and (e, f) PRCCs for *ESPU239* and *ESPU239C*..... FK-66

K5.3.9-1. Time-dependent release rates (*ESNP237*, g/yr) and cumulative (i.e., integrated) releases (*ESNP237C*, g) over 1,000,000 years for the movement of dissolved ^{237}Np from the EBS to the UZ resulting from the early failure of a CDSP WP in percolation bin 3 under dripping conditions: (a, b)

FIGURES (Continued)

Page

ESNP237 and *ESNP237C* for all (i.e., 300) sample elements, (c, d) *ESNP237* and *ESNP237C* for first 50 sample elements, and (e, f) PRCCs for *ESNP237* and *ESNP237C*. FK-67

K5.3.9-2. Time-dependent release rates (*ESPU239*, g/yr) and cumulative (i.e., integrated) releases (*ESPU239C*, g) over 200,000 years for the movement of dissolved ^{239}Pu from the EBS to the UZ resulting from the early failure of a CDSP WP in percolation bin 3 under dripping conditions: (a, b) *ESPU239* and *ESPU239C* for all (i.e., 300) sample elements, (c, d) *ESPU239* and *ESPU239C* for first 50 sample elements, and (e, f) PRCCs for *ESPU239* and *ESPU239C*. FK-68

K5.3.10-1. Time-dependent release rates (*ESNP237*, g/yr) and cumulative (i.e., integrated) releases (*ESNP237C*, g) over 1,000,000 years for the movement of dissolved ^{237}Np from the EBS to the UZ resulting from the early failure of a CDSP WP in percolation bin 3 under nondripping conditions: (a, b) *ESNP237* and *ESNP237C* for all (i.e., 300) sample elements, (c, d) *ESNP237* and *ESNP237C* for first 50 sample elements, and (e, f) PRCCs for *ESNP237* and *ESNP237C*. FK-69

K5.3.10-2. Time-dependent release rates (*ESPU239*, g/yr) and cumulative (i.e., integrated) releases (*ESPU239C*, g) over 200,000 years for the movement of dissolved ^{239}Pu from the EBS to the UZ resulting from the early failure of a CDSP WP in percolation bin 3 under nondripping conditions: (a, b) *ESPU239* and *ESPU239C* for all (i.e., 300) sample elements, (c, d) *ESPU239* and *ESPU239C* for first 50 sample elements, and (e, f) PRCCs for *ESPU239* and *ESPU239C*. FK-70

K5.3.11-1. Time-dependent release rates (*ESNP237*, g/yr) and cumulative (i.e., integrated) releases (*ESNP237C*, g) over 1,000,000 years for the movement of dissolved ^{237}Np from the EBS to the UZ resulting from the early failure of a CSNF WP in percolation bin 3 under dripping conditions: (a, b) *ESNP237* and *ESNP237C* for all (i.e., 300) sample elements, (c, d) *ESNP237* and *ESNP237C* for first 50 sample elements, and (e, f) PRCCs for *ESNP237* and *ESNP237C*. FK-71

K5.3.11-2. Time-dependent release rates (*ESPU239*, g/yr) and cumulative (i.e., integrated) releases (*ESPU239C*, g) over 200,000 years for the movement of dissolved ^{239}Pu from the EBS to the UZ resulting from the early failure of a CSNF WP in percolation bin 3 under dripping conditions: (a, b) *ESPU239* and *ESPU239C* for all (i.e., 300) sample elements, (c, d) *ESPU239* and *ESPU239C* for first 50 sample elements, and (e, f) PRCCs for *ESPU239* and *ESPU239C* FK-72

K5.3.12-1. Time-dependent release rates (*ESNP237*, g/yr) and cumulative (i.e., integrated) releases (*ESNP237C*, g) over 1,000,000 years for the movement of dissolved ^{237}Np from the EBS to the UZ resulting from the early failure of a CSNF WP in percolation bin 3 under nondripping conditions: (a, b) *ESNP237* and *ESNP237C* for all (i.e., 300) sample elements, (c, d) *ESNP237*

FIGURES (Continued)

Page

and *ESNP237C* for first 50 sample elements, and (e, f) PRCCs for *ESNP237* and *ESNP237C*.....FK-73
K5.3.12-2. Time-dependent release rates (*ESPU239*, g/yr) and cumulative (i.e., integrated) releases (*ESPU239C*, g) over 200,000 years for the movement of dissolved ^{239}Pu from the EBS to the UZ resulting from the early failure of a CSNF WP in percolation bin 3 under nondripping conditions: (a, b) *ESPU239* and *ESPU239C* for all (i.e., 300) sample elements, (c, d) *ESPU239* and *ESPU239C* for first 50 sample elements, and (e, f) PRCCs for *ESPU239* and *ESPU239C*. FK-74
K5.4.1-1. Time-dependent release rates (*UZIC239*, g/yr) and cumulative (i.e., integrated) releases (*UZIC239C*, g) over 20,000 years for the movement of ^{239}Pu irreversibly attached to slow colloids from the UZ to the SZ resulting from a single early DS failure above a CDSP WP in percolation bin 3 under dripping conditions: (a, b) *UZIC239* and *UZIC239C* for all (i.e., 300) sample elements, (c, d) *UZIC239* and *UZIC239C* for first 50 sample elements, and (e, f) PRCCs for *UZIC239* and *UZIC239C*.....FK-75
K5.4.1-2. Stepwise rank regression analyses and selected scatterplots for time-dependent release rates (*UZIC239*, g/yr) and cumulative (i.e., integrated) releases (*UZIC239C*, g) for the movement of ^{239}Pu irreversibly attached to slow colloids from the UZ to the SZ resulting from a single early DS failure above a CDSP WP in percolation bin 3 under dripping conditions: (a, b) Regressions for *UZIC239* and *UZIC239C* at 3000, 5000 and 10,000 years, and (c-h) Scatterplots for *UZIC239* and *UZIC239C* at 10,000 years. FK-76
K5.4.1-3. Comparison of cumulative releases of ^{239}Pu irreversibly attached to slow colloids into the UZ (*ESSL239C*, g) and out of the UZ (*UZIC239C*, g) at (a) 1000 years, (b) 3000 years, (c) 5000 years and (d) 10,000 years for a single early DS failure above a CDSP WP in percolation bin 3 under dripping conditions.....FK-78
K5.4.1-4. Time-dependent release rates (*UZIF239*, g/yr) and cumulative (i.e., integrated) releases (*UZIF239C*, g) over 20,000 years for the movement of ^{239}Pu irreversibly attached to fast colloids from the UZ to the SZ resulting from a single early DS failure above a CDSP WP in percolation bin 3 under dripping conditions: (a, b) *UZIF239* and *UZIF239C* for all (i.e., 300) sample elements, (c, d) *UZIF239* and *UZIF239C* for first 50 sample elements, and (e, f) PRCCs for *UZIF239* and *UZIF239C*. FK-79
K 5.4.1-5. Stepwise rank regression analyses and selected scatterplots for time-dependent release rates (*UZIF239*, g/yr) and cumulative (i.e., integrated) releases (*UZIF239C*, g) for the movement of ^{239}Pu irreversibly attached to fast colloids from the UZ to the SZ resulting from a single early DS failure above a CDSP WP in percolation bin 3 under dripping conditions : (a, b) Regressions for *UZIF239* and *UZIF239C* at 3000, 5000 and 10,000 years, and (c-h) Scatterplots for *UZIF239* and *UZIF239C* at 10,000 years.....FK-80

FIGURES (Continued)

Page

K5.4.1-6. Comparison of cumulative releases of ^{239}Pu irreversibly attached to fast colloids into the UZ (*ESFA239C*, g) and out of the UZ (*UZIF239C*, g) at (a) 1000 years, (b) 3000 years, (c) 5000 years and (d) 10,000 years for a single early DS failure above a CDSP WP in percolation bin 3 under dripping conditions. FK-82

K5.4.1-7. Time-dependent release rates (*UZNP237*, g/yr) and cumulative (i.e., integrated) releases (*UZNP237C*, g) over 20,000 years for the movement of dissolved ^{237}Np from the UZ to the SZ resulting from a single early DS failure above a CDSP WP in percolation bin 3 under dripping conditions: (a, b) *UZNP237* and *UZNP237C* for all (i.e., 300) sample elements, (c, d) *UZNP237* and *UZNP237C* for first 50 sample elements, and (e, f) PRCCs for *UZNP237* and *UZNP237C*. FK-83

K 5.4.1-8. Stepwise rank regression analyses and selected scatterplots for time-dependent release rates (*UZNP237*, g/yr) and cumulative (i.e., integrated) releases (*UZNP237C*, g) for the movement of dissolved ^{237}Np from the EBS to the UZ resulting from a single early DS failure above a CDSP WP in percolation bin 3 under dripping conditions: (a, b) Regressions for *UZNP237* and *UZNP237C* at 3000, 5000 and 10,000 years, and (c-h) Scatterplots for *UZNP237* and *UZNP237C* at 10,000 years. FK-84

K5.4.1-9. Comparison of cumulative releases of dissolved ^{237}Np into the UZ (*ESNP237C*, g) and out of the UZ (*UZNP237C*, g) at (a) 1000 years, (b) 3000 years, (c) 5000 years and (d) 10,000 years for a single early DS failure above a CDSP WP in percolation bin 3 under dripping conditions. FK-86

K5.4.1-10. Time-dependent release rates (*UZPU239*, g/yr) and cumulative (i.e., integrated) releases (*UZPU239C*, g) over 20,000 years for the movement of dissolved ^{239}Pu from the UZ to the SZ resulting from a single early DS failure above a CDSP WP in percolation bin 3 under dripping conditions: (a, b) *UZPU239* and *UZPU239C* for all (i.e., 300) sample elements, (c, d) *UZPU239* and *UZPU239C* for first 50 sample elements, and (e, f) PRCCs for *UZPU239* and *UZPU239C*. FK-87

K5.4.1-11. Stepwise rank regression analyses and selected scatterplots for time-dependent release rates (*UZPU239*, g/yr) and cumulative (i.e., integrated) releases (*UZPU239*, g) for the movement of dissolved ^{239}Pu from the UZ to the SZ resulting from a single early DS failure above a CDSP WP in percolation bin 3 under dripping conditions: (a, b) Regressions for *UZPU239* and *UZPU239C* at 3000, 5000 and 10,000 years, and (c-h) Scatterplots for *UZPU239* and *UZPU239C* at 10,000 years. FK-88

K5.4.1-12. Comparison of cumulative releases of dissolved ^{239}Pu into the UZ (*ESPU239C*, g) and out of the UZ (*UZPU239C*, g) at (a) 1000 years, (b) 3000 years, (c) 5000 years and (d) 10,000 years for a single early DS failure above a CDSP WP in percolation bin 3 under dripping conditions. FK-90

K5.4.1-13. Time-dependent release rates (*UZTC99*, g/yr) and cumulative (i.e., integrated) releases (*UZTC99C*, g) over 20,000 years for the movement of

FIGURES (Continued)

Page

dissolved ^{99}Tc from the UZ to the SZ resulting from a single early DS failure above a CDSP WP in percolation bin 3 under dripping conditions: (a, b) *UZTC99* and *UZTC99C* for all (i.e., 300) sample elements, (c, d) *UZTC99* and *UZTC99C* for first 50 sample elements, and (e, f) PRCCs for *UZTC99* and *UZTC99C*. FK-91

K5.4.1-14. Stepwise rank regression analyses and selected scatterplots for time-dependent release rates (*UZTC99*, g/yr) and cumulative (i.e., integrated) releases (*UZTC99*, g) for the movement of dissolved ^{99}Tc from the UZ to the SZ resulting from a single early DS failure above a CDSP WP in percolation bin 3 under dripping conditions: (a, b) Regressions for *UZTC99* and *UZTC99C* at 3000, 5000 and 10,000 years, and (c-h) Scatterplots for *UZTC99* and *UZTC99C* at 10,000 years. FK-92

K5.4.1-15. Comparison of cumulative releases of dissolved ^{99}Tc into the UZ (*ESTC99C*, g) and out of the UZ (*UZTC99C*, g) at (a) 1000 years, (b) 3000 years, (c) 5000 years and (d) 10,000 years for a single early DS failure above a CDSP WP in percolation bin 3 under dripping conditions. FK-94

K5.5.1-1. Time-dependent release rates (*SZIC239*, g/yr) and cumulative (i.e., integrated) releases (*SZIC239C*, g) over 20,000 years for the movement of ^{239}Pu irreversibly attached to slow colloids across a subsurface plane at the location of the RMEI resulting from a single early DS failure above a CDSP WP in percolation bin 3 under dripping conditions: (a, b) *SZIC239* and *SZIC239C* for all (i.e., 300) sample elements, (c, d) *SZIC239* and *SZIC239C* for first 50 sample elements, and (e, f) PRCCs for *SZIC239* and *SZIC239C*. FK-95

K5.5.1-2. Time-dependent release rates (*SZIF239*, g/yr) and cumulative (i.e., integrated) releases (*SZIF239C*, g) over 20,000 years for the movement of ^{239}Pu irreversibly attached to fast colloids across a subsurface plane at the location of the RMEI resulting from a single early DS failure above a CDSP WP in percolation bin 3 under dripping conditions: (a, b) *SZIF239* and *SZIF239C* for all (i.e., 300) sample elements, (c, d) *SZIF239* and *SZIF239C* for first 50 sample elements, and (e, f) PRCCs for *SZIF239* and *SZIF239C*. FK-96

K5.5.1-3. Time-dependent release rates (*SZNP237*, g/yr) and cumulative (i.e., integrated) releases (*SZNP237C*, g) over 20,000 years for the movement of dissolved ^{237}Np across a subsurface plane at the location of the RMEI resulting from a single early DS failure above a CDSP WP in percolation bin 3 under dripping conditions: (a, b) *SZNP237* and *SZNP237C* for all (i.e., 300) sample elements, (c, d) *SZNP237* and *SZNP237C* for first 50 sample elements, and (e, f) PRCCs for *SZNP237* and *SZNP237C*. FK-97

K5.5.1-4. Time-dependent release rates (*SZPU239*, g/yr) and cumulative (i.e., integrated) releases (*SZPU239C*, g) over 20,000 years for the movement of dissolved ^{239}Pu across a subsurface plane at the location of the RMEI resulting from a single early DS failure above a CDSP WP in percolation bin 3 under dripping conditions: (a, b) *SZPU239* and *SZPU239C* for all (i.e., 300)

FIGURES (Continued)

Page

sample elements, (c, d) *SZPU239* and *SZPU239C* for first 50 sample elements, and (e, f) PRCCs for *SZPU239* and *SZPU239C*. FK-98

K5.5.1-5. Time-dependent release rates (*SZTC99*, g/yr) and cumulative (i.e., integrated) releases (*SZTC99C*, g) over 20,000 years for the movement of dissolved ^{99}Tc across a subsurface plane at the location of the RMEI resulting from a single early DS failure above a CDSP WP in percolation bin 3 under dripping conditions: (a, b) *SZTC99* and *SZTC99C* for all (i.e., 300) sample elements, (c, d) *SZTC99* and *SZTC99C* for first 50 sample elements, and (e, f) PRCCs for *SZTC99* and *SZTC99C*. FK-99

K5.6.1-1. Time-dependent dose to the RMEI (*DOIC239*, mrem/yr) over 20,000 years for the movement of ^{239}Pu irreversibly attached to slow colloids across a subsurface plane at the location of the RMEI resulting from a single early DS failure above a CDSP WP in percolation bin 3 under dripping conditions: (a) *DOIC239* for all (i.e., 300) sample elements, (b) *DOIC239* for first 50 sample elements, and (c) PRCCs for *DOIC239*. FK-100

K5.6.1-2. Time-dependent dose to the RMEI (*DOIF239*, mrem/yr) over 20,000 years for the movement of ^{239}Pu irreversibly attached to fast colloids across a subsurface plane at the location of the RMEI resulting from a single early DS failure above a CDSP WP in percolation bin 3 under dripping conditions: (a) *DOIF239* for all (i.e., 300) sample elements, (b) *DOIF239* for first 50 sample elements, and (c) PRCCs for *DOIF239*. FK-101

K5.6.1-3. Time-dependent dose to the RMEI (*DONP237*, mrem/yr) over 20,000 years for the movement of dissolved ^{237}Np across a subsurface plane at the location of the RMEI resulting from a single early DS failure above a CDSP WP in percolation bin 3 under dripping conditions: (a) *DONP237*for all (i.e., 300) sample elements, (b) *DONP237*for first 50 sample elements, and (c) PRCCs for *DONP237*. FK-102

K5.6.1-4. Time-dependent dose to the RMEI (*DOPU239*, mrem/yr) over 20,000 years for the movement of dissolved ^{239}Pu across a subsurface plane at the location of the RMEI resulting from a single early DS failure above a CDSP WP in percolation bin 3 under dripping conditions: (a) *DOPU239* for all (i.e., 300) sample elements, (b) *DOPU239* for first 50 sample elements, and (c) PRCCs for *DOPU239*. FK-103

K5.6.1-5. Time-dependent dose to the RMEI (*DOTC99*, mrem/yr) over 20,000 years for the movement of dissolved ^{99}Tc across a subsurface plane at the location of the RMEI resulting from a single early DS failure above a CDSP WP in percolation bin 3 under dripping conditions: (a) *DOTC99* for all (i.e., 300) sample elements, (b) *DOTC99* for first 50 sample elements, and (c) PRCCs for *DOTC99*. FK-104

K5.7.1-1. Expected dose to RMEI (*EXPDOSE*, mrem/yr) over [0, 20,000 yr] for all radioactive species resulting from early DS failure: (a) *EXPDOSE* for all (i.e., 300) sample elements, (b) *EXPDOSE* for first 50 sample elements, and (c) PRCCs for *EXPDOSE*..... FK-105

FIGURES (Continued)

Page

K5.7.1-2. Stepwise rank regression analyses and selected scatterplots for expected dose to RMEI (*EXPDOSE*, mrem/yr) over [0, 20,000 yr] for all radioactive species resulting from early DS failure: (a) Regressions for *EXPDOSE* at 3000, 5000 and 10,000 years, and (b,c,d) Scatterplots for *EXPDOSE* at 10,000 years..... FK-106
K5.7.1-3. Expected dose to RMEI (*EXPDOSE*, mrem/yr) over [0, 1,000,000 yr] for all radioactive species resulting from early DS failure: (a) *EXPDOSE* for all (i.e., 300) sample elements, (b) *EXPDOSE* for first 50 sample elements, and (c) PRCCs for *EXPDOSE*..... FK-107
K5.7.1-4. Stepwise rank regression analyses and selected scatterplots for expected dose to RMEI (*EXPDOSE*, mrem/yr) over [0, 1,000,000 yr] for all radioactive species resulting from early DS failure: (a) Regressions for *EXPDOSE* at 50,000, 200,000 and 500,000 years, and (b,c,d) Scatterplots for *EXPDOSE* at 500,000 years. FK-108
K5.7.2-1. Expected dose to RMEI (*EXPDOSE*, mrem/yr) over [0, 20,000 yr] for all radioactive species resulting from early WP failure: (a) *EXPDOSE* for all (i.e., 300) sample elements, (b) *EXPDOSE* for first 50 sample elements, and (c) PRCCs for *EXPDOSE*. FK-110
K5.7.2-2. Stepwise rank regression analyses and selected scatterplots for expected dose to RMEI (*EXPDOSE*, mrem/yr) over [0, 20,000 yr] for all radioactive species resulting from early WP failure: (a) Regressions for *EXPDOSE* at 3000, 5000 and 10,000 years, and (b,c,d) Scatterplots for *EXPDOSE* at 10,000 years..... FK-111
K5.7.2-3. Expected dose to RMEI (*EXPDOSE*, mrem/yr) over [0, 1,000,000 yr] for all radioactive species resulting from early WP failure: (a) *EXPDOSE* for all (i.e., 300) sample elements, (b) *EXPDOSE* for first 50 sample elements, and (c) PRCCs for *EXPDOSE*. FK-112
K5.7.2-4. Stepwise rank regression analyses and selected scatterplots for expected dose to RMEI (*EXPDOSE*, mrem/yr) over [0, 1,000,000 yr] for all radioactive species resulting from early WP failure: (a) Regressions for *EXPDOSE* at 50,000, 200,000 and 500,000 years, and (b,c,d) Scatterplots for *EXPDOSE* at 500,000 years. FK-113
K5.7.3-1. Expected dose to RMEI (*EXPDOSE*, mrem/yr) over [0, 20,000 yr] for all radioactive species resulting from both early DS failure and early WP failure: (a) *EXPDOSE* for all (i.e., 300) sample elements, (b) *EXPDOSE* for first 50 sample elements, and (c) PRCCs for *EXPDOSE*..... FK-115
K5.7.3-2. Stepwise rank regression analyses and selected scatterplots for expected dose to RMEI (*EXPDOSE*, mrem/yr) over [0, 20,000 yr] for all radioactive species resulting from both early DS failure and early WP failure: (a) Regressions for *EXPDOSE* at 3000, 5000 and 10,000 years, and (b,c,d) Scatterplots for *EXPDOSE* at 10,000 years..... FK-116
K5.7.3-3. Expected dose to RMEI (*EXPDOSE*, mrem/yr) over [0, 1,000,000 yr] for all radioactive species resulting from both early DS failure and early WP failure: (a) *EXPDOSE* for all (i.e., 300) sample elements, (b) *EXPDOSE* for first 50 sample elements, and (c) PRCCs for *EXPDOSE*..... FK-118

FIGURES (Continued)

Page

K5.7.3-4. Stepwise rank regression analyses and selected scatterplots for expected dose to RMEI (*EXPDOSE*, mrem/yr) over [0, 1,000,000 yr] for all radioactive species resulting from both early DS failure and early WP failure: (a) Regressions for *EXPDOSE* at 50,000, 200,000 and 500,000 years, and (b,c,d) Scatterplots for *EXPDOSE* at 500,000 years. FK-119

K5.7.4-1. Expected dose to RMEI (*EXPDOSE*, mrem/yr) over [0, 1,000,000 yr] for all radioactive species resulting from early DS failure, early WP failure and nominal process WP failure: (a) *EXPDOSE* for all (i.e., 300) sample elements, (b) *EXPDOSE* for first 50 sample elements, and (c) PRCCs for *EXPDOSE* FK-121

K5.7.4-2. Stepwise rank regression analyses and selected scatterplots for expected dose to RMEI (*EXPDOSE*, mrem/yr) over [0, 1,000,000 yr] for all radioactive species resulting from early DS failure, early WP failure and nominal process WP failure: (a) Regressions for *EXPDOSE* at 50,000, 200,000 and 500,000 years, and (b,c,d) Scatterplots for *EXPDOSE* at 500,000 years. FK-122

K6.2-1. Time-dependent temperatures in percolation bin 3 for CSNF WPs at the drift wall (*TMPCSWL*), on the WP (*TMPCSWP*) and in the invert beneath the WP (*TMPCSINV*) and similarly for CDSP WPs at the drift wall (*TMPCDWL*), on the WP (*TMPCDWP*) and in the invert beneath the WP (*TMPCDINV*) resulting from an igneous intrusive event at 250 years that destroys all WPs in the repository: (a, c, e) *TMPCSWL*, *TMPCSWP* and *TMPCSINV*, and (b, d, f) *TMPCDWL*, *TMPCDWP* and *TMPCDINV* FK-125

K6.2-2. Time-dependent seepage rates (m^3/yr/WP) into the repository above CSNF WPs (*SPRATECS*) resulting from an igneous intrusive event at 250 years that destroys all WPs in the repository: (a) Bin 1, (b) Bin 2, (c) Bin 3, (d) Bin 4, and (e) Bin 5 ..... FK-126

K6.2-3. Time-dependent ionic strength (mol/kg) under dripping conditions in the invert for CSNF WPs (*ISCSINAD*) and CDSP WPs (*ISCDINAD*) in percolation bin 3 resulting from an igneous intrusive event at 250 years that destroys all WPs in the repository: (a, b) *ISCSINAD* and *ISCDINAD* for all (i.e., 300) sample elements, (c, d) *ISCSINAD* and *ISCDINAD* for first 50 sample elements, and (e, f) PRCCs for *ISCSINAD* and *ISCDINAD* FK-127

K6.2-4. Time-dependent pH under dripping conditions in the invert for CSNF WPs (*PHCSINAD*) and CDSP WPs (*PHCDINAD*) in percolation bin 3 resulting from an igneous intrusive event at 250 years that destroys all WPs in the repository: (a, b) *PHCSINAD* and *PHCDINAD* for all (i.e., 300) sample elements, (c, d) *PHCSINAD* and *PHCDINAD* for first 50 sample elements, and (e, f) PRCCs for *PHCSINAD* and *PHCDINAD* FK-128

K6.3.1-1. Time-dependent release rates (*ESIC239*, g/yr) and cumulative (i.e., integrated) releases (*ESIC239C*, g) over 20,000 years for the movement of ^{239}Pu irreversibly attached to glass/ waste form colloids from the EBS to the UZ resulting from an igneous intrusive event at 10 years that destroys all WPs in the repository: (a, b) *ESIC239* and *ESIC239C* for all (i.e., 300)

FIGURES (Continued)

Page

sample elements, (c, d) *ESIC239* and *ESIC239C* for first 50 sample elements, and (e, f) PRCCs for *ESIC239* and *ESIC239C* FK-129
K6.3.1-2. Stepwise rank regression analyses and selected scatterplots for time-dependent release rates (*ESIC239*, g/yr) and cumulative (i.e., integrated) releases (*ESIC239C*, g) for the movement of ^{239}Pu irreversibly attached to glass/ waste form colloids from the EBS to the UZ resulting from an igneous intrusive event at 10 years that destroys all WPs in the repository: (a, b) Regressions for *ESIC239* and *ESIC239C* at 3000, 5000 and 10,000 years, and (c-h) Scatterplots for *ESIC239* and *ESIC239C* at 10,000 years..... FK-130
K6.3.1-3. Removed FK-132
K6.3.1-4. Removed FK-133
K6.3.1-5. Time-dependent release rates (*ESNP237*, g/yr) and cumulative (i.e., integrated) releases (*ESNP237C*, g) over 20,000 years for the movement of dissolved ^{237}Np from the EBS to the UZ resulting from an igneous intrusive event at 10 years that destroys all WPs in the repository: (a, b) *ESNP237* and *ESNP237C* for all (i.e., 300) sample elements, (c, d) *ESNP237* and *ESNP237C* for first 50 sample elements, and (e, f) PRCCs for *ESNP237* and *ESNP237C* FK-135
K6.3.1-6. Stepwise rank regression analyses and selected scatterplots for time-dependent release rates (*ESNP237*, g/yr) and cumulative (i.e., integrated) releases (*ES NP237C*, g) for the movement of dissolved ^{237}Np from the EBS to the UZ resulting from an igneous intrusive event at 10 years that destroys all WPs in the repository: (a, b) Regressions for *ESNP237* and *ESNP237C* at 3000, 5000 and 10,000 years, and (c-h) Scatterplots for *ESNP237* and *ESNP237C* at 10,000 years FK-136
K6.3.1-7. Time-dependent release rates (*ESPU239*, g/yr) and cumulative (i.e., integrated) releases (*ESPU239C*, g) over 20,000 years for the movement of dissolved ^{239}Pu from the EBS to the UZ resulting from an igneous intrusive event at 10 years that destroys all WPs in the repository: (a, b) *ESPU239* and *ESPU239C* for all (i.e., 300) sample elements, (c, d) *ESPU239* and *ESPU239C* for first 50 sample elements, and (e, f) PRCCs for *ESPU239* and *ESPU239C* FK-138
K6.3.1-8. Stepwise rank regression analyses and selected scatterplots for time-dependent release rates (*ESPU239*, g/yr) and cumulative (i.e., integrated) releases (*ESPU239*, g) for the movement of dissolved ^{239}Pu from the EBS to the UZ resulting from an igneous intrusive event at 10 years that destroys all WPs in the repository: (a, b) Regressions for *ESPU239* and *ESPU239C* at 3000, 5000 and 10,000 years, and (c-h) Scatterplots for *ESPU239* and *ESPU239C* at 10,000 years..... FK-139
K6.3.1-9. Time-dependent release rates (*ESTC99*, g/yr) and cumulative (i.e., integrated) releases (*ESTC99C*, g) over 20,000 years for the movement of dissolved ^{99}Tc from the EBS to the UZ resulting from an igneous intrusive event at 10 years that destroys all WPs in the repository: (a, b) *ESTC99* and *ESTC99C* for all

FIGURES (Continued)

Page

(i.e., 300) sample elements, (c, d) *ESTC99* and *ESTC99C* for first 50 sample elements, and (e, f) PRCCs for *ESTC99* and *ESTC99C*. FK-141

K6.3.1-10. Stepwise rank regression analyses and selected scatterplots for time-dependent release rates (*ESTC99*, g/yr) and cumulative (i.e., integrated) releases (*ESTC99C*, g) for the movement of dissolved ^{99}Tc from the EBS to the UZ resulting from an igneous intrusive event at 10 years that destroys all WPs in the repository: (a, b) Regressions for *ESTC99* and *ESTC99C* at 3000, 5000 and 10,000 years, and (c-h) Scatterplots for *ESTC99* and *ESTC99C* at 10,000 years. FK-142

K6.3.2-1. Time-dependent release rates (*ESIC239*, g/yr) and cumulative (i.e., integrated) releases (*ESIC239C*, g) over 200,000 years for the movement of ^{239}Pu irreversibly attached to glass/ waste form colloids from the EBS to the UZ resulting from an igneous intrusive event at 250 years that destroys all WPs in the repository: (a, b) *ESIC239* and *ESIC239C* for all (i.e., 300) sample elements, (c, d) *ESIC239* and *ESIC239C* for first 50 sample elements, and (e, f) PRCCs for *ESIC239* and *ESIC239C*. FK-144

K6.3.2-2. Removed. FK-145

K6.3.2-3. Time-dependent release rates (*ESNP237*, g/yr) and cumulative (i.e., integrated) releases (*ESNP237C*, g) over 1,000,000 years for the movement of dissolved ^{237}Np from the EBS to the UZ resulting from an igneous intrusive event at 250 years that destroys all WPs in the repository: (a, b) *ESNP237* and *ESNP237C* for all (i.e., 300) sample elements, (c, d) *ESNP237* and *ESNP237C* for first 50 sample elements, and (e, f) PRCCs for *ESNP237* and *ESNP237C*. FK-146

K6.3.2-4. Time-dependent release rates (*ESPU239*, g/yr) and cumulative (i.e., integrated) releases (*ESPU239C*, g) over 200,000 years for the movement of dissolved ^{239}Pu from the EBS to the UZ resulting from an igneous intrusive event at 250 years that destroys all WPs in the repository: (a, b) *ESPU239* and *ESPU239C* for all (i.e., 300) sample elements, (c, d) *ESPU239* and *ESPU239C* for first 50 sample elements, and (e, f) PRCCs for *ESPU239* and *ESPU239C*. FK-147

K6.4.1-1. Time-dependent release rates (*UZIC239*, g/yr) and cumulative (i.e., integrated) releases (*UZIC239C*, g) over 20,000 years for the movement of ^{239}Pu irreversibly attached to slow colloids from the UZ to the SZ resulting from an igneous intrusive event at 10 years that destroys all WPs in the repository: (a, b) *UZIC239* and *UZIC239C* for all (i.e., 300) sample elements, (c, d) *UZIC239* and *UZIC239C* for first 50 sample elements, and (e, f) PRCCs for *UZIC239* and *UZIC239C* FK-149

K6.4.1-2. Stepwise rank regression analyses and selected scatterplots for time-dependent release rates (*UZIC239*, g/yr) and cumulative (i.e., integrated) releases (*UZIC239C*, g) for the movement of ^{239}Pu irreversibly attached to slow colloids from the UZ to the SZ resulting from an igneous intrusive event at 10 years that destroys all WPs in the repository: (a, b) Regressions for

FIGURES (Continued)

Page

UZIC239 and *UZIC239C* at 3000, 5000 and 10,000 years, and (c-h) Scatterplots for *UZIC239* and *UZIC239C* at 10,000 years FK-150
K6.4.1-3. Comparison of cumulative releases of ^{239}Pu irreversibly attached to slow colloids into the UZ (*ESSL239C*, g) and out of the UZ (*UZIC239C*, g) at (a) 1000 years, (b) 3000 years, (c) 5000 years and (d) 10,000 years for an igneous intrusive event at 10 years that destroys all WPs in the repository FK-152
K6.4.1-4. Time-dependent release rates (*UZIF239*, g/yr) and cumulative (i.e., integrated) releases (*UZIF239C*, g) over 20,000 years for the movement of ^{239}Pu irreversibly attached to fast colloids from the UZ to the SZ resulting from an igneous intrusive event at 10 years that destroys all WPs in the repository: (a, b) *UZIF239* and *UZIF239C* for all (i.e., 300) sample elements, (c, d) *UZIF239* and *UZIF239C* for first 50 sample elements, and (e, f) PRCCs for *UZIF239* and *UZIF239C* FK-153
K6.4.1-5. Stepwise rank regression analyses and selected scatterplots for time-dependent release rates (*UZIF239*, g/yr) and cumulative (i.e., integrated) releases (*UZIF239C*, g) for the movement of ^{239}Pu irreversibly attached to fast colloids from the UZ to the SZ resulting from an igneous intrusive event at 10 years that destroys all WPs in the repository: (a, b) Regressions for *UZIF239* and *UZIF239C* at 3000, 5000 and 10,000 years, and (c-h) Scatterplots for *UZIF239* and *UZIF239C* at 10,000 years FK-154
K6.4.1-6. Comparison of cumulative releases of ^{239}Pu irreversibly attached to fast colloids into the UZ (*ESFA239C*, g) and out of the UZ (*UZIF239C*, g) at (a) 1000 years, (b) 3000 years, (c) 5000 years and (d) 10,000 years for an igneous intrusive event at 10 years that destroys all WPs in the repository FK-156
K6.4.1-7. Time-dependent release rates (*UZNP237*, g/yr) and cumulative (i.e., integrated) releases (*UZNP237C*, g) over 20,000 years for the movement of dissolved ^{237}Np from the UZ to the SZ resulting from an igneous intrusive event at 10 years that destroys all WPs in the repository: (a, b) *UZNP237* and *UZNP237C* for all (i.e., 300) sample elements, (c, d) *UZNP237* and *UZNP237C* for first 50 sample elements, and (e, f) PRCCs for *UZNP237* and *UZNP237C* FK-157
K6.4.1-8. Stepwise rank regression analyses and selected scatterplots for time-dependent release rates (*UZNP237*, g/yr) and cumulative (i.e., integrated) releases (*UZNP237C*, g) for the movement of dissolved ^{237}Np from the EBS to the UZ resulting from an igneous intrusive event at 10 years that destroys all WPs in the repository: (a, b) Regressions for *UZNP237* and *UZNP237C* at 3000, 5000 and 10,000 years, and (c-h) Scatterplots for *UZNP237* and *UZNP237C* at 10,000 years FK-158
K6.4.1-9. Comparison of cumulative releases of dissolved ^{237}Np into the UZ (*ESNP237C*, g) and out of the UZ (*UZNP237C*, g) at (a) 1000 years, (b) 3000 years, (c) 5000 years and (d) 10,000 years for an igneous intrusive event at 10 years that destroys all WPs in the repository FK-160
K6.4.1-10. Time-dependent release rates (*UZPU239*, g/yr) and cumulative (i.e., integrated) releases (*UZPU239C*, g) over 20,000 years for the movement of

FIGURES (Continued)

Page

dissolved ^{239}Pu from the UZ to the SZ resulting from an igneous intrusive event at 10 years that destroys all WPs in the repository: (a, b) *UZPU239* and *UZPU239C* for all (i.e., 300) sample elements, (c, d) *UZPU239* and *UZPU239C* for first 50 sample elements, and (e, f) PRCCs for *UZPU239* and *UZPU239C* FK-161

K6.4.1-11. Stepwise rank regression analyses and selected scatterplots for time-dependent release rates (*UZPU239*, g/yr) and cumulative (i.e., integrated) releases (*UZPU239*, g) for the movement of dissolved ^{239}Pu from the UZ to the SZ resulting from an igneous intrusive event at 10 years that destroys all WPs in the repository: (a, b) Regressions for *UZPU239* and *UZPU239C* at 3000, 5000 and 10,000 years, and (c-h) Scatterplots for *UZPU239* and *UZPU239C* at 10,000 years FK-162

K6.4.1-12. Comparison of cumulative releases of dissolved ^{239}Pu into the UZ (*ESPU239C*, g) and out of the UZ (*UZPU239C*, g) at (a) 1000 years, (b) 3000 years, (c) 5000 years and (d) 10,000 years for an igneous intrusive event at 10 years that destroys all WPs in the repository FK-164

K6.4.1-13. Time-dependent release rates (*UZTC99*, g/yr) and cumulative (i.e., integrated) releases (*UZTC99C*, g) over 20,000 years for the movement of dissolved ^{99}Tc from the UZ to the SZ resulting from an igneous intrusive event at 10 years that destroys all WPs in the repository: (a, b) *UZTC99* and *UZTC99C* for all (i.e., 300) sample elements, (c, d) *UZTC99* and *UZTC99C* for first 50 sample elements, and (e, f) PRCCs for *UZTC99* and *UZTC99C* FK-165

K6.4.1-14. Stepwise rank regression analyses and selected scatterplots for time-dependent release rates (*UZTC99*, g/yr) and cumulative (i.e., integrated) releases (*UZTC99*, g) for the movement of dissolved ^{99}Tc from the UZ to the SZ resulting from an igneous intrusive event at 10 years that destroys all WPs in the repository: (a, b) Regressions for *UZTC99* and *UZTC99C* at 3000, 5000 and 10,000 years, and (c-h) Scatterplots for *UZTC99* and *UZTC99C* at 10,000 years FK-166

K6.4.1-15. Comparison of cumulative releases of dissolved ^{99}Tc into the UZ (*ESTC99C*, g) and out of the UZ (*UZTC99C*, g) at (a) 1000 years, (b) 3000 years, (c) 5000 years and (d) 10,000 years for an igneous intrusive event at 10 years that destroys all WPs in the repository FK-168

K6.5.1-1. Time-dependent release rates (*SZIC239*, g/yr) and cumulative (i.e., integrated) releases (*SZIC239C*, g) over 20,000 years for the movement of ^{239}Pu irreversibly attached to slow colloids across a subsurface plane at the location of the RMEI resulting from an igneous intrusive event at 10 years that destroys all WPs in the repository: (a, b) *SZIC239* and *SZIC239C* for all (i.e., 300) sample elements, (c, d) *SZIC239* and *SZIC239C* for first 50 sample elements, and (e, f) PRCCs for *SZIC239* and *SZIC239C* FK-169

K6.5.1-2. Stepwise rank regression analyses and selected scatterplots for time-dependent release rates (*SZIC239*, g/yr) and cumulative (i.e., integrated) releases (*SZIC239C*, g) for the movement of ^{239}Pu irreversibly attached to slow colloids across a subsurface plane at the location of the RMEI resulting

FIGURES (Continued)

Page

from an igneous intrusive event at 10 years that destroys all WPs in the repository: (a, b) Regressions for *SZIC239* and *SZIC239C* at 3000, 5000 and 10,000 years, and (c-h) Scatterplots for *SZIC239* and *SZIC239C* at 10,000 years FK-170

K6.5.1-3. Comparison of cumulative releases of ^{239}Pu irreversibly attached to slow colloids into the SZ (*UZIC239C*, g) and across a subsurface plane at the location of the RMEI (*SZIC239C*, g) at (a) 1000 years, (b) 3000 years, (c) 5000 years and (d) 10,000 years for an igneous intrusive event at 10 years that destroys all WPs in the repository FK-172

K6.5.1-4. Time-dependent release rates (*SZIF239*, g/yr) and cumulative (i.e., integrated) releases (*SZIF239C*, g) over 20,000 years for the movement of ^{239}Pu irreversibly attached to fast colloids across a subsurface plane at the location of the RMEI resulting from an igneous intrusive event at 10 years that destroys all WPs in the repository: (a, b) *SZIF239* and *SZIF239C* for all (i.e., 300) sample elements, (c, d) *SZIF239* and *SZIF239C* for first 50 sample elements, and (e, f) PRCCs for *SZIF239* and *SZIF239C* FK-173

K6.5.1-5. Stepwise rank regression analyses and selected scatterplots for time-dependent release rates (*SZIF239*, g/yr) and cumulative (i.e., integrated) releases (*SZIF239C*, g) for the movement of ^{239}Pu irreversibly attached to fast colloids across a subsurface plane at the location of the RMEI resulting from an igneous intrusive event at 10 years that destroys all WPs in the repository: (a, b) Regressions for *SZIF239* and *SZIF239C* at 3000, 5000 and 10,000 years, and (c-h) Scatterplots for *SZIF239* and *SZIF239C* at 10,000 years FK-174

K6.5.1-6. Comparison of cumulative releases of ^{239}Pu irreversibly attached to fast colloids into the SZ (*UZIF239C*, g) and across a subsurface plane at the location of the RMEI (*SZIF239C*, g) at (a) 1000 years, (b) 3000 years, (c) 5000 years and (d) 10,000 years for an igneous intrusive event at 10 years that destroys all WPs in the repository FK-176

K6.5.1-7. Time-dependent release rates (*SZNP237*, g/yr) and cumulative (i.e., integrated) releases (*SZNP237C*, g) over 20,000 years for the movement of dissolved ^{237}Np across a subsurface plane at the location of the RMEI resulting from an igneous intrusive event at 10 years that destroys all WPs in the repository: (a, b) *SZNP237* and *SZNP237C* for all (i.e., 300) sample elements, (c, d) *SZNP237* and *SZNP237C* for first 50 sample elements, and (e, f) PRCCs for *SZNP237* and *SZNP237C* FK-177

K6.5.1-8. Stepwise rank regression analyses and selected scatterplots for time-dependent release rates (*SZNP237*, g/yr) and cumulative (i.e., integrated) releases (*SZNP237C*, g) for the movement of dissolved ^{237}Np across a subsurface plane at the location of the RMEI resulting from an igneous intrusive event at 10 years that destroys all WPs in the repository: (a, b) Regressions for *SZNP237* and *SZNP237C* at 3000, 5000 and 10,000 years, and (c-h) Scatterplots for *SZNP237* and *SZNP237C* at 10,000 years FK-178

K6.5.1-9. Comparison of cumulative releases of dissolved ^{237}Np into the SZ (*UZNP237C*, g) and across a subsurface plane at the location of the RMEI

FIGURES (Continued)

Page

(*SZNP237C*, g) at (a) 1000 years, (b) 3000 years, (c) 5000 years and (d) 10,000 years for an igneous intrusive event at 10 years that destroys all WPs in the repository FK-180

K6.5.1-10. Time-dependent release rates (*SZPU239*, g/yr) and cumulative (i.e., integrated) releases (*SZPU239C*, g) over 20,000 years for the movement of dissolved ^{239}Pu across a subsurface plane at the location of the RMEI resulting from an igneous intrusive event at 10 years that destroys all WPs in the repository: (a, b) *SZPU239* and *SZPU239C* for all (i.e., 300) sample elements, (c, d) *SZPU239* and *SZPU239C* for first 50 sample elements, and (e, f) PRCCs for *SZPU239* and *SZPU239C* FK-181

K6.5.1-11. Stepwise rank regression analyses and selected scatterplots for time-dependent release rates (*SZPU239*, g/yr) and cumulative (i.e., integrated) releases (*SZPU239C*, g) for the movement of dissolved ^{239}Pu across a subsurface plane at the location of the RMEI resulting from an igneous intrusive event at 10 years that destroys all WPs in the repository: (a, b) Regressions for *SZPU239* and *SZPU239C* at 3000, 5000 and 10,000 years, and (c-h) Scatterplots for *SZPU239* and *SZPU239C* at 10,000 years FK-182

K6.5.1-12. Comparison of cumulative releases of dissolved ^{239}Pu into the SZ (*UZPU239C*, g) and across a subsurface plane at the location of the RMEI (*SZPU239C*, g) at (a) 1000 years, (b) 3000 years, (c) 5000 years and (d) 10,000 years for an igneous intrusive event at 10 years that destroys all WPs in the repository FK-184

K6.5.1-13. Time-dependent release rates (*SZTC99*, g/yr) and cumulative (i.e., integrated) releases (*SZTC99C*, g) over 20,000 years for the movement of dissolved ^{99}Tc across a subsurface plane at the location of the RMEI resulting from an igneous intrusive event at 10 years that destroys all WPs in the repository: (a, b) *SZTC99* and *SZTC99C* for all (i.e., 300) sample elements, (c, d) *SZTC99* and *SZTC99C* for first 50 sample elements, and (e, f) PRCCs for *SZTC99* and *SZTC99C* FK-185

K6.5.1-14. Stepwise rank regression analyses and selected scatterplots for time-dependent release rates (*SZTC99*, g/yr) and cumulative (i.e., integrated) releases (*SZTC99C*, g) for the movement of dissolved ^{99}Tc across a subsurface plane at the location of the RMEI resulting from an igneous intrusive event at 10 years that destroys all WPs in the repository: (a, b) Regressions for *SZTC99* and *SZTC99C* at 3000, 5000 and 10,000 years, and (c-h) Scatterplots for *SZTC99* and *SZTC99C* at 10,000 years FK-186

K6.5.1-15. Comparison of cumulative releases of dissolved ^{99}Tc into the SZ (*UZTC99C*, g) and across a subsurface plane at the location of the RMEI (*SZTC99C*, g) at (a) 1000 years, (b) 3000 years, (c) 5000 years and (d) 10,000 years for an igneous intrusive event at 10 years that destroys all WPs in the repository FK-188

K6.5.2-1. Time-dependent release rates (*SZIC239*, g/yr) and cumulative (i.e., integrated) releases (*SZIC239C*, g) over 200,000 years for the movement of ^{239}Pu irreversibly attached to slow colloids across a subsurface plane at the location of the RMEI resulting from an igneous intrusive event at 250 years

FIGURES (Continued)

Page

that destroys all WPs in the repository: (a, b) *SZIC239* and *SZIC239C* for all (i.e., 300) sample elements, (c, d) *SZIC239* and *SZIC239C* for first 50 sample elements, and (e, f) PRCCs for *SZIC239* and *SZIC239C* FK-189

K6.5.2-2. Time-dependent release rates (*SZIF239*, g/yr) and cumulative (i.e., integrated) releases (*SZIF239C*, g) over 200,000 years for the movement of ^{239}Pu irreversibly attached to fast colloids across a subsurface plane at the location of the RMEI resulting from an igneous intrusive event at 250 years that destroys all WPs in the repository: (a, b) *SZIF239* and *SZIF239C* for all (i.e., 300) sample elements, (c, d) *SZIF239* and *SZIF239C* for first 50 sample elements, and (e, f) PRCCs for *SZIF239* and *SZIF239C* FK-190

K6.5.2-3. Time-dependent release rates (*SZNP237*, g/yr) and cumulative (i.e., integrated) releases (*SZNP237C*, g) over 1,000,000 years for the movement of dissolved ^{237}Np across a subsurface plane at the location of the RMEI resulting from an igneous intrusive event at 250 years that destroys all WPs in the repository: (a, b) *SZNP237* and *SZNP237C* for all (i.e., 300) sample elements, (c, d) *SZNP237* and *SZNP237C* for first 50 sample elements, and (e, f) PRCCs for *SZNP237* and *SZNP237C* FK-191

K6.5.2-4. Time-dependent release rates (*SZPU239*, g/yr) and cumulative (i.e., integrated) releases (*SZPU239C*, g) over 200,000 years for the movement of dissolved ^{239}Pu across a subsurface plane at the location of the RMEI resulting from an igneous intrusive event at 250 years that destroys all WPs in the repository: (a, b) *SZPU239* and *SZPU239C* for all (i.e., 300) sample elements, (c, d) *SZPU239* and *SZPU239C* for first 50 sample elements, and (e, f) PRCCs for *SZPU239* and *SZPU239C* FK-192

K6.6.1-1. Time-dependent dose to the RMEI (*DOIC239*, mrem/yr) over 20,000 years for the movement of ^{239}Pu irreversibly attached to slow colloids across a subsurface plane at the location of the RMEI resulting from an igneous intrusive event at 10 years that destroys all WPs in the repository: (a) *DOIC239* for all (i.e., 300) sample elements, (b) *DOIC239* for first 50 sample elements, and (c) PRCCs for *DOIC239* FK-193

K6.6.1-2. Stepwise rank regression analyses and selected scatterplots for time-dependent dose to the RMEI (*DOIC239*, mrem/yr) for the movement of ^{239}Pu irreversibly attached to slow colloids across a subsurface plane at the location of the RMEI (*SZIC239*, g/yr) resulting from an igneous intrusive event at 10 years that destroys all WPs in the repository: (a) Regressions for *DOIC239* at 3000, 5000 and 10,000 years, (b,c,d) Scatterplots for *DOIC239* at 10,000 years, and (e) Scatterplot comparing *SZIC239* and *DOIC239* at 10,000 years .. FK-194

K6.6.1-3. Time-dependent dose to the RMEI (*DOIF239*, mrem/yr) over 20,000 years for the movement of ^{239}Pu irreversibly attached to fast colloids across a subsurface plane at the location of the RMEI resulting from an igneous intrusive event at 10 years that destroys all WPs in the repository: (a) *DOIF239* for all (i.e., 300) sample elements, (b) *DOIF239* for first 50 sample elements, and (c) PRCCs for *DOIF239* FK-196

FIGURES (Continued)

Page

K6.6.1-4. Stepwise rank regression analyses and selected scatterplots for time-dependent dose to the RMEI (*DOIF239*, mrem/yr) for the movement of ^{239}Pu irreversibly attached to fast colloids across a subsurface plane at the location of the RMEI (*SZIF239*, g/yr) resulting from an igneous intrusive event at 10 years that destroys all WPs in the repository: (a) Regressions for *DOIF239* at 3000, 5000 and 10,000 years, (b,c,d) Scatterplots for *DOIF239* at 10,000 years, and (e) Scatterplot comparing *SZIF239* and *DOIF239* at 10,000 years... FK-197

K6.6.1-5. Time-dependent dose to the RMEI (*DONP237*, mrem/yr) over 20,000 years for the movement of dissolved ^{237}Np across a subsurface plane at the location of the RMEI resulting from an igneous intrusive event at 10 years that destroys all WPs in the repository: (a) *DONP237* for all (i.e., 300) sample elements, (b) *DONP237*for first 50 sample elements, and (c) PRCCs for *DONP237*..... FK-198

K6.6.1-6. Stepwise rank regression analyses and selected scatterplots for time-dependent dose to the RMEI (*DONP237*, mrem/yr) for the movement of dissolved ^{237}Np across a subsurface plane at the location of the RMEI (*SZNP237*, g/yr) resulting from an igneous intrusive event at 10 years that destroys all WPs in the repository: (a) Regressions for *DONP237* at 3000, 5000 and 10,000 years, (b,c,d) Scatterplots for *DONP237* at 10,000 years, and (e) Scatterplot comparing *SZNP237* and *DONP237* at 10,000 years..... FK-199

K6.6.1-7. Time-dependent dose to the RMEI (*DOPU239*, mrem/yr) over 20,000 years for the movement of dissolved ^{239}Pu across a subsurface plane at the location of the RMEI resulting from an igneous intrusive event at 10 years that destroys all WPs in the repository: (a) *DOPU239* for all (i.e., 300) sample elements, (b) *DOPU239* for first 50 sample elements, and (c) PRCCs for *DOPU239* FK-201

K6.6.1-8. Stepwise rank regression analyses and selected scatterplots for time-dependent dose to the RMEI (*DOPU239*, mrem/yr) for the movement of dissolved ^{239}Pu across a subsurface plane at the location of the RMEI (*SZPU239*, g/yr) resulting from an igneous intrusive event at 10 years that destroys all WPs in the repository: (a) Regressions for *DOPU239*at 3000, 5000 and 10,000 years, (b,c,d) Scatterplots for *DOPU239* at 10,000 years, and (e) Scatterplot comparing *SZPU239* and *DOPU239* at 10,000 years FK-202

K6.6.1-9. Time-dependent dose to the RMEI (*DOTC99*, mrem/yr) over 20,000 years for the movement of dissolved ^{99}Tc across a subsurface plane at the location of the RMEI resulting from an igneous intrusive event at 10 years that destroys all WPs in the repository: (a) *DOTC99* for all (i.e., 300) sample elements, (b) *DOTC99* for first 50 sample elements, and (c) PRCCs for *DOTC99* FK-204

K6.6.1-10. Stepwise rank regression analyses and selected scatterplots for time-dependent dose to the RMEI (*DOTC99*, mrem/yr) for the movement of dissolved ^{99}Tc across a subsurface plane at the location of the RMEI (*SZTC99*, g/yr) resulting from an igneous intrusive event at 10 years that destroys all WPs in the repository: (a) Regressions for *DOTC99* at 3000,

FIGURES (Continued)

Page

5000 and 10,000 years, (b,c,d) Scatterplots for *DOTC99* at 10,000 years, and (e) Scatterplot comparing *SZTC99* and *DOTC99* at 10,000 years FK-205
K6.6.2-1. Time-dependent dose to the RMEI (*DOIC239*, mrem/yr) over 200,000 years for the movement of ^{239}Pu irreversibly attached to slow colloids across a subsurface plane at the location of the RMEI resulting from an igneous intrusive event at 250 years that destroys all WPs in the repository: (a) *DOIC239* for all (i.e., 300) sample elements, (b) *DOIC239* for first 50 sample elements, and (c) PRCCs for *DOIC239* FK-207
K6.6.2-2. Time-dependent dose to the RMEI (*DOIF239*, mrem/yr) over 200,000 years for the movement of ^{239}Pu irreversibly attached to fast colloids across a subsurface plane at the location of the RMEI resulting from an igneous intrusive event at 250 years that destroys all WPs in the repository: (a) *DOIF239* for all (i.e., 300) sample elements, (b) *DOIF239* for first 50 sample elements, and (c) PRCCs for *DOIF239* FK-208
K6.6.2-3. Time-dependent dose to the RMEI (*DONP237*, mrem/yr) over 1,000,000 years for the movement of dissolved ^{237}Np across a subsurface plane at the location of the RMEI resulting from an igneous intrusive event at 250 years that destroys all WPs in the repository: (a) *DONP237*for all (i.e., 300) sample elements, (b) *DONP237*for first 50 sample elements, and (c) PRCCs for *DONP237* FK-209
K6.6.2-4. Time-dependent dose to the RMEI (*DOPU239*, mrem/yr) over 200,000 years for the movement of dissolved ^{239}Pu across a subsurface plane at the location of the RMEI resulting from an igneous intrusive event at 250 years that destroys all WPs in the repository: (a) *DOPU239* for all (i.e., 300) sample elements, (b) *DOPU239* for first 50 sample elements, and (c) PRCCs for *DOPU239* FK-210
K6.7.1-1. Expected dose to RMEI (*EXPDOSE*, mrem/yr) over [0, 20,000 yr] for all radioactive species resulting from igneous intrusion: (a) *EXPDOSE* for all (i.e., 300) sample elements, (b) *EXPDOSE* for first 50 sample elements, and (c) PRCCs for *EXPDOSE* FK-211
K6.7.1-2. Stepwise rank regression analyses and selected scatterplots for expected dose to RMEI (*EXPDOSE*, mrem/yr) over [0, 20,000 yr] for all radioactive species resulting from igneous intrusion: (a) Regressions for *EXPDOSE* at 3000, 5000 and 10,000 years, and (b,c,d) Scatterplots for *EXPDOSE* at 10,000 years FK-212
K6.7.2-1. Expected dose to RMEI (*EXPDOSE*, mrem/yr) over [0, 1,000,000 yr] for all radioactive species resulting from igneous intrusion: (a) *EXPDOSE* for all (i.e., 300) sample elements, (b) *EXPDOSE* for first 50 sample elements, and (c) PRCCs for *EXPDOSE* FK-214
K6.7.2-2. Stepwise rank regression analyses and selected scatterplots for expected dose to RMEI (*EXPDOSE*, mrem/yr) over [0, 1,000,000 yr] for all radioactive species resulting from igneous intrusion: (a) Regressions for *EXPDOSE* at 50,000, 200,000 and 500,000 years, and (b,c,d) Scatterplots for *EXPDOSE* at 500,000 years FK-215

FIGURES (Continued)

Page

K6.8.1-1. Expected dose to RMEI (*EXPDOSE*, mrem/yr) over [0, 20,000 yr] for all radioactive species resulting from igneous eruption: (a) *EXPDOSE* for all (i.e., 300) sample elements, (b) *EXPDOSE* for first 50 sample elements, and (c) PRCCs for *EXPDOSE* FK-217
K6.8.1-2. Stepwise rank regression analyses and selected scatterplots for expected dose to RMEI (*EXPDOSE*, mrem/yr) over [0, 20,000 yr] for all radioactive species resulting from igneous eruption: (a) Regressions for *EXPDOSE* at 3000, 5000 and 10,000 years, and (b,c,d) Scatterplots for *EXPDOSE* at 10,000 years..... FK-218
K6.8.2-1. Expected dose to RMEI (*EXPDOSE*, mrem/yr) over [0, 1,000,000 yr] for all radioactive species resulting from igneous eruption: (a) *EXPDOSE* for all (i.e., 300) sample elements, (b) *EXPDOSE* for first 50 sample elements, and (c) PRCCs for *EXPDOSE* FK-219
K6.8.2-2. Stepwise rank regression analyses and selected scatterplots for expected dose to RMEI (*EXPDOSE*, mrem/yr) over [0, 1,000,000 yr] for all radioactive species resulting from igneous eruption: (a) Regressions for *EXPDOSE* and (b,c,d) Scatterplots for *EXPDOSE* at 500,000 years..... FK-220
K7.3-1. Removed FK-221
K7.3-2. Removed FK-222
K7.3-3. Removed FK-223
K7.3-4. Removed FK-224
K7.3-5. Time-dependent release rates (*ESNP237*, g/yr) and cumulative (i.e., integrated) releases (*ESNP237C*, g) over 20,000 years for the movement of dissolved ^{237}Np from the EBS to the UZ resulting from a seismically induced fractional damaged area of 10^{-6}(32.6 m^2) at 200 years to all CDSP WPs in the repository: (a, b) *ESNP237* and *ESNP237C* for all (i.e., 300) sample elements, (c, d) *ESNP237* and *ESNP237C* for first 50 sample elements, and (e, f) PRCCs for *ESNP237* and *ESNP237C* FK-225
K7.3-6. Stepwise rank regression analyses and selected scatterplots for time-dependent release rates (*ESNP237*, g/yr) and cumulative (i.e., integrated) releases (*ES NP237C*, g) for the movement of dissolved ^{237}Np from the EBS to the UZ resulting froma seismically induced fractional damaged area of 10^{-6}(32.6 m^2) at 200 years to all CDSP WPs in the repository: (a, b) Regressions for *ESNP237* and *ESNP237C* at 3000, 5000 and 10,000 years, and (c-h) Scatterplots for *ESNP237* and *ESNP237C* at 10,000 years FK-226
K7.3-7. Time-dependent release rates (*ESPU239*, g/yr) and cumulative (i.e., integrated) releases (*ESPU239C*, g) over 20,000 years for the movement of dissolved ^{239}Pu from the EBS to the UZ resulting from a seismically induced fractional damaged area of 10^{-6}(32.6 m^2) at 200 years to all CDSP WPs in the repository: (a, b) *ESPU239* and *ESPU239C* for all (i.e., 300) sample elements, (c, d) *ESPU239* and *ESPU239C* for first 50 sample elements, and (e, f) PRCCs for *ESPU239* and *ESPU239C* FK-228
K7.3-8. Stepwise rank regression analyses and selected scatterplots for time-dependent release rates (*ESPU239*, g/yr) and cumulative (i.e., integrated) releases (*ESPU239*, g) for the movement of dissolved ^{239}Pu from the EBS to

FIGURES (Continued)

Page

the UZ resulting from a seismically induced fractional damaged area of 10^{-6}(32.6 m^2) at 200 years to all CDSP WPs in the repository: (a, b) Regressions for *ESPU239* and *ESPU239C* at 3000, 5000 and 10,000 years, and (c-h) Scatterplots for *ESPU239* and *ESPU239C* at 10,000 years FK-229

K7.3-9. Time-dependent release rates (*ESTC99*, g/yr) and cumulative (i.e., integrated) releases (*ESTC99C*, g) over 20,000 years for the movement of dissolved ^{99}Tc from the EBS to the UZ resulting from a seismically induced fractional damaged area of 10^{-6}(32.6 m^2) at 200 years to all CDSP WPs in the repository: (a, b) *ESTC99* and *ESTC99C* for all (i.e., 300) sample elements, (c, d) *ESTC99* and *ESTC99C* for first 50 sample elements, and (e, f) PRCCs for *ESTC99* and *ESTC99C* FK-231

K7.3-10. Stepwise rank regression analyses and selected scatterplots for time-dependent release rates (*ESTC99*, g/yr) and cumulative (i.e., integrated) releases (*ESTC99*, g) for the movement of dissolved ^{99}Tc from the EBS to the UZ resulting from a seismically induced fractional damaged area of 10^{-6}(32.6 m^2) at 200 years to all CDSP WPs in the repository: (a, b) Regressions for *ESTC99* and *ESTC99C* at 3000, 5000 and 10,000 years, and (c-h) Scatterplots for *ESTC99* and *ESTC99C* at 10,000 years FK-232

K7.4-1. Time-dependent release rates (*UZIC239*, g/yr) and cumulative (i.e., integrated) releases (*UZIC239C*, g) over 20,000 years for the movement of ^{239}Pu irreversibly attached to glass colloids from the UZ to the SZ resulting from a seismically induced fractional damaged area of 10^{-6}(32.6 m^2) at 200 years to all CDSP WPs in the repository: (a, b) *UZIC239* and *UZIC239C* for all (i.e., 300) sample elements, (c, d) *UZIC239* and *UZIC239C* for first 50 sample elements, and (e, f) PRCCs for *UZIC239* and *UZIC239C* FK-234

K7.4-2. Time-dependent release rates (*UZIF239*, g/yr) and cumulative (i.e., integrated) releases (*UZIF239C*, g) over 20,000 years for the movement of ^{239}Pu irreversibly attached to glass colloids from the UZ to the SZ resulting from a seismically induced fractional damaged area of 10^{-6}(32.6 m^2) at 200 years to all CDSP WPs in the repository: (a, b) *UZIF239* and *UZIF239C* for all (i.e., 300) sample elements, (c, d) *UZIC239* and *UZIC239C* for first 50 sample elements, and (e, f) PRCCs for *UZIF239* and *UZIF239C* FK-235

K7.4-3. Time-dependent release rates (*UZNP237*, g/yr) and cumulative (i.e., integrated) releases (*UZNP2379C*, g) over 20,000 years for the movement of dissolved ^{237}Np from the UZ to the SZ resulting from a seismically induced fractional damaged area of 10^{-6}(32.6 m^2) at 200 years to all CDSP WPs in the repository: (a, b) *UZNP237* and *UZNP237C* for all (i.e., 300) sample elements, (c, d) *UZNP237* and *UZNP237C* for first 50 sample elements, and (e, f) PRCCs for *UZNP237* and *UZNP237C* FK-236

K7.4-4. Time-dependent release rates (*UZPU239*, g/yr) and cumulative (i.e., integrated) releases (*UZPU239C*, g) over 20,000 years for the movement of dissolved ^{239}Pu from the UZ to the SZ resulting from a seismically induced fractional damaged area of 10^{-6}(32.6 m^2) at 200 years to all CDSP WPs in the repository: (a, b) *UZPU239* and *UZPU239C* for all (i.e., 300) sample

FIGURES (Continued)

Page

elements, (c, d) *UZPU239* and *UZPU239C* for first 50 sample elements, and (e, f) PRCCs for *UZPU239* and *UZPU239C* FK-237

K7.4-5. Time-dependent release rates (*UZTC99*, g/yr) and cumulative (i.e., integrated) releases (*UZTC99C*, g) over 20,000 years for the movement of dissolved ^{99}Tc from the UZ to the SZ resulting from a seismically induced fractional damaged area of 10^{-6}(32.6 m^2) at 200 years to all CDSP WPs in the repository: (a, b) *UZTC99* and *UZTC99C* for all (i.e., 300) sample elements, (c, d) *UZTC99* and *UZTC99C* for first 50 sample elements, and (e, f) PRCCs for *UZTC99* and *UZTC99C* FK-238

K7.5-1. Time-dependent release rates (*SZIC239*, g/yr) and cumulative (i.e., integrated) releases (*SZIC239C*, g) over 20,000 years for the movement of ^{239}Pu irreversibly attached to glass colloids across a subsurface plane at the location of the RMEI resulting from a seismically induced fractional damaged area of 10^{-6}(32.6 m^2) at 200 years to all CDSP WPs in the repository: (a, b) *SZIC239* and *SZIC239C* for all (i.e., 300) sample elements, (c, d) *SZIC239* and *SZIC239C* for first 50 sample elements, and (e, f) PRCCs for *SZIC239* and *SZIC239C* FK-239

K7.5-2. Time-dependent release rates (*SZIF239*, g/yr) and cumulative (i.e., integrated) releases (*SZIF239C*, g) over 20,000 years for the movement of ^{239}Pu irreversibly attached to glass colloids across a subsurface plane at the location of the RMEI resulting from a seismically induced fractional damaged area of 10^{-6}(32.6 m^2) at 200 years to all CDSP WPs in the repository: (a, b) *SZIF239* and *SZIF239C* for all (i.e., 300) sample elements, (c, d) *SZIC239* and *SZIC239C* for first 50 sample elements, and (e, f) PRCCs for *SZIF239* and *SZIF239C* FK-240

K7.5-3. Time-dependent release rates (*SZNP237*, g/yr) and cumulative (i.e., integrated) releases (*SZNP2379C*, g) over 20,000 years for the movement of dissolved ^{237}Np across a subsurface plane at the location of the RMEI resulting from a seismically induced fractional damaged area of 10^{-6}(32.6 m^2) at 200 years to all CDSP WPs in the repository: (a, b) *SZNP237* and *SZNP237C* for all (i.e., 300) sample elements, (c, d) *SZNP237* and *SZNP237C* for first 50 sample elements, and (e, f) PRCCs for *SZNP237* and *SZNP237C* FK-241

K7.5-4. Time-dependent release rates (*SZPU239*, g/yr) and cumulative (i.e., integrated) releases (*SZPU239C*, g) over 20,000 years for the movement of dissolved ^{239}Pu across a subsurface plane at the location of the RMEI resulting from a seismically induced fractional damaged area of 10^{-6}(32.6 m^2) at 200 years to all CDSP WPs in the repository: (a, b) *SZPU239* and *SZPU239C* for all (i.e., 300) sample elements, (c, d) *SZPU239* and *SZPU239C* for first 50 sample elements, and (e, f) PRCCs for *SZPU239* and *SZPU239C* FK-242

K7.5-5. Time-dependent release rates (*SZTC99*, g/yr) and cumulative (i.e., integrated) releases (*SZTC99C*, g) over 20,000 years for the movement of dissolved ^{99}Tc from across a subsurface plane at the location of the RMEI resulting from a

FIGURES (Continued)

Page

seismically induced fractional damaged area of 10^{-6}(32.6 m^2) at 200 years to all CDSP WPs in the repository: (a, b) *SZTC99* and *SZTC99C* for all (i.e., 300) sample elements, (c, d) *SZTC99* and *SZTC99C* for first 50 sample elements, and (e, f) PRCCs for *SZTC99* and *SZTC99C* FK-243

K.7.6-1. Time-dependent dose to the RMEI (*DOIC239*, mrem/yr) over 20,000 years for the movement of ^{239}Pu irreversibly attached to slow colloids across a subsurface plane at the location of the RMEI resulting from a seismically induced fractional damaged area of 10^{-6}(32.6 m^2) at 200 years to all CDSP WPs in the repository: (a) *DOIC239* for all (i.e., 300) sample elements, (b) *DOIC239* for first 50 sample elements, and (c) PRCCs for *DOIC239* FK-245

K.7.6-2. Time-dependent dose to the RMEI (*DOIF239*, mrem/yr) over 20,000 years for the movement of ^{239}Pu irreversibly attached to fast colloids across a subsurface plane at the location of the RMEI resulting from a seismically induced fractional damaged area of 10^{-6}(32.6 m^2) at 200 years to all CDSP WPs in the repository: (a) *DOIF239* for all (i.e., 300) sample elements, (b) *DOIF239* for first 50 sample elements, and (c) PRCCs for *DOIF239* FK-246

K.7.6-3. Time-dependent dose to the RMEI (*DONP237*, mrem/yr) over 20,000 years for the movement of dissolved ^{237}Np across a subsurface plane at the location of the RMEI resulting from a seismically induced fractional damaged area of 10^{-6}(32.6 m^2) at 200 years to all CDSP WPs in the repository: (a) *DONP237*for all (i.e., 300) sample elements, (b) *DONP237*for first 50 sample elements, and (c) PRCCs for *DONP237* FK-247

K.7.6-4. Time-dependent dose to the RMEI (*DOPU239*, mrem/yr) over 20,000 years for the movement of dissolved ^{239}Pu across a subsurface plane at the location of the RMEI resulting from a seismically induced fractional damaged area of 10^{-6}(32.6 m^2) at 200 years to all CDSP WPs in the repository: (a) *DOPU239* for all (i.e., 300) sample elements, (b) *DOPU239* for first 50 sample elements, and (c) PRCCs for *DOPU239* FK-248

K.7.6-5. Time-dependent dose to the RMEI (*DOTC99*, mrem/yr) over 20,000 years for the movement of dissolved ^{99}Tc across a subsurface plane at the location of the RMEI resulting from a seismically induced fractional damaged area of 10^{-6}(32.6 m^2) at 200 years to all CDSP WPs in the repository: (a) *DOTC99*for all (i.e., 300) sample elements, (b) *DOTC99* for first 50 sample elements, and (c) PRCCs for *DOTC99* FK-249

K.7.7.1-1. Expected dose to RMEI (*EXPDOSE*, mrem/yr) over [0, 20,000 yr] for all radioactive species resulting from seismic ground motion: (a) *EXPDOSE* for all (i.e., 300) sample elements, (b) *EXPDOSE* for first 50 sample elements, and (c) PRCCs for *EXPDOSE* FK-250

K.7.7.1-2. Stepwise rank regression analyses and selected scatterplots for expected dose to RMEI (*EXPDOSE*, mrem/yr) over [0, 20,000 yr] for all radioactive species resulting from seismic ground motion: (a) Regressions for *EXPDOSE* at 3000, 5000 and 10,000 years, and (b,c,d) Scatterplots for *EXPDOSE* at 10,000 years FK-251

FIGURES (Continued)

Page

K.7.7.2-1. Expected dose to RMEI (*EXPDOSE*, mrem/yr) over [0, 1,000,000 yr] for all radioactive species resulting from seismic ground motion: (a) *EXPDOSE* for all (i.e., 300) sample elements, (b) *EXPDOSE* for first 50 sample elements, and (c) PRCCs for *EXPDOSE* FK-253
K.7.7.2-2. Stepwise rank regression analyses and selected scatterplots for expected dose to RMEI (*EXPDOSE*, mrem/yr) over [0, 1,000,000 yr] for all radioactive species resulting from seismic ground motion: (a) Regressions for *EXPDOSE* at 50,000, 200,000 and 500,000 years, and (b,c,d) Scatterplots for *EXPDOSE* at 500,000 years FK-254
K.7.8.1-1. Expected dose to RMEI (*EXPDOSE*, mrem/yr) over [0, 20,000 yr] for all radioactive species resulting from seismic fault displacement: (a) *EXPDOSE* for all (i.e., 300) sample elements, (b) *EXPDOSE* for first 50 sample elements, and (c) PRCCs for *EXPDOSE* FK-256
K.7.8.1-2. Stepwise rank regression analyses and selected scatterplots for expected dose to RMEI (*EXPDOSE*, mrem/yr) over [0, 20,000 yr] for all radioactive species resulting from seismic fault displacement: (a) Regressions for *EXPDOSE* at 3000, 5000 and 10,000 years, and (b,c,d) Scatterplots for *EXPDOSE* at 10,000 years FK-257
K.7.8.2-1. Expected dose to RMEI (*EXPDOSE*, mrem/yr) over [0, 1,000,000 yr] for all radioactive species resulting from seismic fault displacement: (a) *EXPDOSE* for all (i.e., 300) sample elements, (b) *EXPDOSE* for first 50 sample elements, and (c) PRCCs for *EXPDOSE* FK-259
K.7.8.2-2. Stepwise rank regression analyses and selected scatterplots for expected dose to RMEI (*EXPDOSE*, mrem/yr) over [0, 1,000,000 yr] for all radioactive species resulting from seismic fault displacement: (a) Regressions for *EXPDOSE* at 50,000, 200,000 and 500,000 years, and (b,c,d) Scatterplots for *EXPDOSE* at 500,000 years FK-260
K.8.1-1 Expected dose to RMEI (*EXPDOSE*, mrem/yr) over [0, 20,000 yr] for all scenario classes: (a) *EXPDOSE* for all (i.e., 300) sample elements, (b) *EXPDOSE* for first 50 sample elements, and (c) PRCCs for *EXPDOSE* FK-262
K.8.1.-2 Stepwise rank regression analyses and selected scatterplots for expected dose to RMEI (*EXPDOSE*, mrem/yr) over [0, 20,000 yr] for all scenario classes: (a) Regressions for *EXPDOSE* at 3000, 5000 and 10,000 years, and (b,c,d) Scatterplots for *EXPDOSE* at 10,000 years FK-263
K.8.2-1 Expected dose to RMEI (*EXPDOSE*, mrem/yr) over [0, 1,000,000 yr] for all scenario classes: (a) *EXPDOSE* for all (i.e., 300) sample elements, (b) *EXPDOSE* for first 50 sample elements, and (c) PRCCs for *EXPDOSE* FK-265
K.8.2-2 Stepwise rank regression analyses and selected scatterplots for expected dose to RMEI (*EXPDOSE*, mrem/yr) over [0, 1,000,000 yr] for all scenario classes: (a) Regressions for *EXPDOSE* at 50,000, 200,000 and 500,000 years, and (b,c,d) Scatterplots for *EXPDOSE* at 500,000 years FK-266

FIGURES (Continued)

Page

L-1. Percolation Flux over the Repository Area....L-101
L-2. CSNF and Defense HLW Waste Package Surface Temperatures, 10th Percentile Infiltration Scenario, Medium Thermal Conductivity....L-102
L-3. CSNF and Defense HLW Peak Waste Package Surface Temperature Distribution, 10th Percentile Infiltration Scenario, Medium Thermal Conductivity....L-103
L-4. CSNF and Defense HLW Waste Package Surface Temperature Range, 10th Percentile Infiltration Scenario....L-104
L-5. Average CSNF and Defense HLW Peak Waste Package Surface Temperature, 10th Percentile Infiltration Scenario....L-105
L-6. Maximum CO_2 Partial Pressure: (a) Group 1 Starting Water, (b) Group 2 Starting Water, (c) Group 3 Starting Water, and (d) Group 4 Starting Water....L-106
L-7. Depth Where Stress Corrosion Cracks Can Initiate and Propagate Along the Circumference of the Waste Package Outer Lid Closure Weld Region....L-108
L-8. CSNF Waste Form Degradation for Expected Value Coefficients with Varying pH....L-109
L-9. Defense HLW Waste Form Degradation for Expected Value Coefficients at Different Temperatures....L-110
L-10. Fraction of Seepage that Can Enter a Waste Package with General Corrosion Breaches....L-111
L-11. Dissolved Concentration Limits....L-112
L-12. General Schematic Diagram of a Single EBS Radionuclide Transport Network in Simplified TSPA....L-113
L-13. General Schematic Diagram of a Single EBS Radionuclide Transport Network Used in the Simplified TSPA....L-114

N-1. Venn diagram of overlapping damage modes....N-15

O-1. Fraction of Locations with the Potential for Localized Corrosion Initiation: (a) Bin1, CDSP; (b) Bin1, CSNF; (c) Bin2, CDSP; (d) Bin2, CSNF; (e) Bin3, CDSP; (f) Bin3, CSNF; (g) Bin4, CDSP; (h) Bin4, CSNF; (i) Bin5, CDSP; and (j) Bin5, CSNF....O-7
O-2. Fraction of Locations in Each Percolation Subregion with the Potential for Localized Corrosion Initiation....O-12
O-3. Average Delta E for Percolation Subregion 3, CSNF, for 300 Epistemic Realizations....O-13

P-1. (a) Comparison of the Mean Annual Dose for the Impact Evaluation Case with the Base Case for the Waste Package EF Modeling Case and (b) Major Radionuclide Dose Contributors for the Corrected Case....P-39
P-2. (a) Comparison of the Mean Annual Dose for the Impact Evaluation Case with the Base Case for the Drip Shield EF Modeling Case and (b) Major Radionuclide Dose Contributors for the Corrected Case....P-40

FIGURES (Continued)

Page

P-3. (a) Comparison of the Mean Annual Dose for the Impact Evaluation Case with the Base Case for the Seismic FD Modeling Case and (b) Major Radionuclide Dose Contributors for the Corrected Case P-41

P-4. (a) Comparison of the Mean Annual Dose for the Impact Evaluation Case with the Base Case for the Seismic GM Modeling Case and (b) Major Radionuclide Dose Contributors for the Corrected Case P-42

P-5. (a) Comparison of the Mean Annual Dose for the Impact Evaluation Case with the Base Case for the Igneous Intrusion Modeling Case and (b) Major Radionuclide Dose Contributors for the Corrected Case P-43

P-6. Mean Annual Dose for the Igneous Intrusion Modeling Case: Base Case and Probability of the Igneous Event set to 10^{-7} per year for (a) 20,000 Years and (b) 1,000,000 Years P-44

P-7. Mean Annual Dose for the Volcanic Eruption Modeling Case: Base Case and Probability of the Igneous Event set to 10^{-7} per year for (a) 20,000 Years and (b) 1,000,000 Years P-45

P-8. Mean Annual Dose Comparison for the Base Case and the Impact Evaluation Case with Updated Longitudinal Dispersivity for the Igneous Intrusion Modeling Case P-46

P-9. Comparison of Mean Annual Dose Contribution from ^{226}Ra and ^{230}Th for the Base Case and the Impact Evaluation Case with Updated Longitudinal Dispersivity for the Igneous Intrusion Modeling Case P-47

P-10. Major Radionuclide Dose Contributors for the Impact Evaluation Case with Updated Longitudinal Dispersivity for the Igneous Intrusion Modeling Case P-48

P-11. Mean Seepage Flux Comparison for Percolation Subregion 3 for the Base Case and the Impact Evaluation Case for the Seismic FD Modeling Case P-49

P-12. Mean Annual Dose Comparisons for the Base Case and the Impact Evaluation Case for the Seismic FD Modeling Case P-50

P-13. Mean Annual Dose Comparisons for the Base Case and the Impact Evaluation Case for the Igneous Intrusion Modeling Case P-51

P-14. Mean Annual Dose Comparisons for the Base Case and the Impact Evaluation Case for the Seismic Ground Motion Modeling Case to Evaluate the Impact of the GoldSim Solver Error P-52

P-15. Mean Annual Dose Comparisons for the Base Case and the Impact Evaluation Case for the Igneous Intrusion Modeling Case to Evaluate the Impact of the GoldSim Solver Error P-53

P-16. Mean Annual Dose Comparisons for the Base Case and the Impact Evaluation Case for the Seismic GM Modeling Case to Evaluate the Impact of UZ Transport Delay of some Radionuclides through the Fault Zones P-54

P-17. Mean Annual Dose Comparisons of Major Radionuclides for the Base Case and the Impact Evaluation Case for the Seismic Ground Motion Modeling Case to Evaluate the Impact of Unsaturated Zone Transport Error through the Fault Zones P-55

FIGURES (Continued)

Page

P-18. Mean Annual Dose Comparisons for the Base Case and the Impact Evaluation Case for the Igneous Intrusion Modeling Case to Evaluate the Impact of Unsaturated Zone Transport Error through the Fault Zones P-56
P-19. Mean Annual Dose Comparisons of Major Radionuclides for the Base Case and the Impact Evaluation Case for the Igneous Intrusion Modeling Case to Evaluate the Impact of Unsaturated Zone Transport Error through the Fault Zones..... P-57

TABLES

Page

8.1-1. Performance Demonstration Results for Individual Protection Standard T8.1-1
8.1-2. Performance Demonstration Results for Groundwater Protection Standard T8.1-1
8.1-3. Performance Demonstration Results for Human Intrusion Standard with Drilling Event at 200,000 years After Closure T8.1-1
8.1-4. Uncertainty in Projections of Peak Mean Annual Dose (mrem) for Individual Protection Standard T8.1-1
8.1-5. Uncertainty Importance Ranking as a function of time for Key TSPA-LA Model Parameters T8.1-2

8.3-1. Decay of Total Curie Inventory as a Function of Time and Dominant Contributors to Total Curie Inventory T8.3-1

C3-1. Software Codes Specific to the PMA TC-1
C3-2. TSPA-LA Model Software Codes used in the PMA TC-1
C3-3. Unqualified Software TC-2
C3-4. FEHM Software Documents TC-2
C3-5. TSPA_Input_DBv2.2 Software Documents TC-3
C3-6. iTough V5.0 Software Documents TC-3
C4-1. TSPA-LA Model Parameters Changed or Deleted for the PMA TC-4
C4-2. Input Parameters Added for the PMA TC-13
C4-3. Sources and Parameter Entry Form Numbers for the PMA-Specific Direct Inputs TC-53
C5-1. Assumptions Identified as Potentially Conservative and Significant to Annual Dose Rate TC-58
C6-1. Relative Humidity Threshold for 0.5mM Fluoride Concentration TC-67
C6-2. Stoichiometries of Waste Degradation Reactions TC-69
C6-3. Parameter Values Used in Diffusion-Dominated Simulations TC-69
C6-4. Parameter Values Used in Liquid Influx Simulations TC-70
C6-5. Controlling Factors for CSNF Dissolution TC-70
C6-6. Controlling Parameter Distributions for CSNF Degradation TC-71
C6-7. Distribution of T_{RC} Used in the Glass Degradation Model for PMA TC-71
C6-8. Recommended Uncertainties for Radionuclide Solubilities TC-72
C6-9. Uncertain Parameters for the Impacts of Reducing Zones in the PMA TC-73
C6-10. Cumulative Distribution for FPVO for Use in the PMA (log_{10}-transformed) TC-73
C9-1. Impact Assessment Summary Table TC-74

E-1. Summary of Responses to International Review Team Summary Review Comments E-3

F-1. Summary of the Dynamically Linked Libraries used in the TSPA-LA Model F-19
F-2. *fehmn_v2_24-01.dll* Input Files F-20
F-3. *MFCP_LA.dll* Input Files F-26
F-4. *SEEPAGEDLL_LA.dll* Input Files F-27

TABLES (Continued)

Page

F-5. sz_conv_3.10.dll Input Files F-28
F-6. *wapdeg.dll* Input Files F-30
F-7. *MkTable_LA.dll* Input Files F-30
F-8. *SCCD.dll* Input Files F-31
F-9. PREWAP_LA.exe Output Files F-31
F-10. PassTable1D_LAv2.dll Input Files F-32
F-11. PassTable3D LAv2.dll Input Files F-32
F-12. GetThk.dll Input Files F-32
F-13. FAR_1-2.dll Input Files F-33

H-1. Applicable Regulatory Requirements of 10 CFR Part 63 and NUREG-1804 Acceptance Criteria Addressed in this Document H-7

I-1. Explanation of the Column Headings in Table I-2 ..... I-5
I-2. Model Implementation for Included Features, Events, and Processes I-6

K3-1. High-Level Summary of Epistemically Uncertain Variables (i.e., elements of **e**) Considered in the TSPA-LA (Sensitivity Analysis Name) TK-1
K3-2. High-Level Summary of Epistemically Uncertain Variables (i.e., elements of **e**) Considered in the TSPA-LA (TSPA Parameter Name) TK-27
K3-3. Detailed Summary of Epistemically Uncertain Variables (i.e., elements of **e**) Considered in the TSPA-LA (TSPA Parameter Name) TK-53
K3-4. Alphabetic Listing of the Various TSPA-LA Model Results Considered in Uncertainty and Sensitivity Analyses for Nominal (N), Drip Shield Early Failure (ED), Waste Package Early Failure (EW), Igneous Intrusive (II), Igneous Eruptive (IE), Seismic Ground Motion (SG), and Seismic Fault Displacement (SF) Modeling Cases in Appendix K4, K5, K6, and K7 ..... TK-115
K4.1-1. Summary of TSPA-LA Model Results Considered in Uncertainty and Sensitivity Analyses for the Nominal Scenario Class TK-119

K5.1-1. Summary of TSPA-LA Model Results Considered in Uncertainty and Sensitivity Analyses for the Early Failure Scenario Classes TK-121
K5.1-2 Summary of Uncertainty and Sensitivity Analysis Results for the Early Failure Scenario Class for Release from the Engineered Barrier System TK-124
K5.1-3 Summary of Uncertainty and Sensitivity Analysis Results for Radionuclide Movement from the UZ to the SZ Resulting from Early DS Failure Above a CDSP WP Under Dripping Conditions TK-130
K5.1-4 Summary of Uncertainty and Sensitivity Analysis Results for Radionuclide Movement in the SZ Across a Subsurface Plane at the Location of the RMEI Resulting from Early DS Failure Above a CDSP WP Under Dripping Conditions TK-132
K5.1-5 Summary of Uncertainty and Sensitivity Analysis Results for Dose to the RMEI from Selected Radionuclides Resulting from Early DS Failure Above a CDSP WP Under Dripping Conditions TK-134

TABLES (Continued)

Page

K5.1-6 Summary of Uncertainty and Sensitivity Analysis Results for Expected Dose to the RMEI (*EXPDOSE*, mrem/yr) Resulting from Early Failures TK-135

K6.1-1. Summary of TSPA-LA Model Results Considered in Uncertainty and Sensitivity Analyses for the Igneous Scenario Classes TK-137

K6.1-2 Summary of Uncertainty and Sensitivity Analysis Results for Radionuclide Movement from the EBS to the UZ Resulting from an Igneous Intrusive Event that Destroys All WPs in the Repository TK-139

K6.1-3 Summary of Uncertainty and Sensitivity Analysis Results for Radionuclide Movement from the UZ to the SZ Resulting from an Igneous Intrusive Event that Destroys all WPs in the Repository. TK-141

K6.1-4 Summary of Uncertainty and Sensitivity Analysis Results for Radionuclide Movement in the SZ Across a Subsurface Plane at the Location of the RMEI Resulting from an Igneous Intrusive Event That Destroys all WPs in the Repository. TK-143

K6.1-5 Summary of Uncertainty and Sensitivity Analysis Results for Dose to the RMEI from Selected Radionuclides Resulting from an Igneous Intrusive Event that Destroys All WPs in the Repository TK-145

K6.1-6 Summary of Uncertainty and Sensitivity Analysis Results for Effected Dose to the RMEI (*EXPDOSE*, mrem/yr) Resulting from Igneous Events TK-146

K7.1-1. Summary of TSPA-LA Model Results Considered in Uncertainty and Sensitivity Analyses for the Seismic Scenario Classes TK-147

K7.1-2 Summary of Uncertainty and Sensitivity Analysis Results for Radionuclide Movement from the EBS to the UZ Resulting from a Seismically Induced Damaged Area of 10^{-6} (32.6 m^2) at 10 yrs to All CDSP WPs in the Repository TK-149

K7.1-3 Summary of Uncertainty and Sensitivity Analysis Results for Radionuclide Movement from the UZ to the SZ Resulting from a Seismically Induced Damaged Area of 10^{-6} (32.6 m^2) at 10 yrs to All CDSP WPs in the Repository TK-150

K7.1-4 Summary of Uncertainty and Sensitivity Analysis Results for Radionuclide Movement in the SZ Across a Subsurface Plane at the Location of the RMEI Resulting from a Seismically Induced Damaged Area of 10^{-6} (32.6 m^2) at 10 yrs to All CDSP WPs in the Repository TK-153

K7.1-5 Summary of Uncertainty and Sensitivity Analysis Results for Dose to the RMEI from Selected Radionuclides Resulting from a Seismically Induced Damaged Area of 10^{-6} (32.6 m^2) at 10 yrs to All CDSP WPs in the Repository. TK-155

K7.1-6 Summary of Uncertainty and Sensitivity Analysis Results for Expected Dose to the RMEI (*EXPD05*, mrem/yr) Resulting from Seismic Events TK-156

K9-1. Summary of Selected Sensitivity Analysis Results TK-157

TABLES (Continued)

Page

L-1. Bounded Hazard Curve for Horizontal Peak Ground Velocity at the Emplacement Drifts L-57
L-2. Average Percolation Rate over the Repository Area L-57
L-3. Spatial Variability and Uncertainty Distributions for 1/α for Methods A, B, C, and D L-58
L-4. Spatial Variability and Uncertainty Distributions Fracture Permeability (log (k [m2])) L-58
L-5. Flow Focusing Factor L-59
L-6. Drip Shield General Corrosion Rate Ratio for Titanium Grade 29 Frame Material L-59
L-7. Probability of Failure for the Drip Shield Plates L-60
L-8. Probability of Failure for the Drip Shield Framework L-61
L-9. Weibull Parameters for Alloy 22 Waste Package Outer Barrier General Corrosion L-62
L-10. Time that Relative Humidity Exceeds 75 percent Threshold L-62
L-11. Stress and Stress Intensity Factor Coefficients L-62
L-12. Average Depth Where SCC Cracks Can Initiate and Propagate L-63
L-13. Probability of Nonzero Damage for the Waste Package Surrounded by Rubble L-64
L-14. Conditional Damaged Areas on the Waste Package Surrounded by Rubble L-64
L-15. Probability of TAD-Bearing and CDSP Waste Package Rupture (17-mm-Thick Waste Package Outer Barrier, Degraded Internals) L-65
L-16. Probability of Nonzero Damage for the TAD-bearing Waste Package, Free Movement Underneath the Drip Shield L-66
L-17. Probability of Nonzero Damage for the CDSP Waste Package, Free Movement Underneath the Drip Shield L-67
L-18. Conditional Damage Area on TAD-bearing and CDSP Waste Packages When Damaged Due to Free Motion Underneath the Drip Shield L-68
L-19. Initial Radionuclide Inventory and Treatment L-69
L-20. Uncertainty Multipliers for Grams per Waste Package for Each Waste Type L-71
L-21. Gap and Grain Boundary Fractions for CSNF Waste Forms L-71
L-22. Coefficients in CSNF Degradation Rate Model L-71
L-23. CSNF Waste Form Degradation Covariance Matrix for Alkaline Conditions L-71
L-24. CSNF Waste Form Degradation Covariance Matrix for Acidic Conditions L-72
L-25. DHLW Glass Degradation Parameters L-72
L-26. Dissolved Concentration Limits (without Uncertainty) L-73
L-27. Dissolved Concentration Limit Uncertainty Terms L-73
L-28. Mixing Cell Steel Parameters Used in Calculation of Corrosion Product Mass and Volume of Water L-74
L-29. Metal Mass Fractions and Atomic Weights Used in Calculation of Corrosion Product Mass and Volume of Water L-74
L-30. Properties of Corrosion Product Used in Calculation of Corrosion Product Mass and Volume of Water L-74
L-31. Free Water Diffusion Coefficients L-75

TABLES (Continued)

Page

L-32. Calculation of Average Unsaturated Zone Layer Thickness L-76
L-33. Layer Contact and Thickness from the GFM2000 Contact Information L-77
L-34. Layer Average Residual Saturation L-79
L-35. Unsaturated Zone Layer Average Properties for Determination of Matrix Hydraulic Conductivity L-80
L-36. Unsaturated Zone Layer Average Matrix and Fracture Porosity L-88
L-37. Unsaturated Zone Layer Fracture and Matrix Percolation Flux (mm/yr) L-89
L-38. Unsaturated Zone Fracture and Matrix Groundwater Velocity L-90
L-39. Unsaturated Zone Layer Groundwater Travel Times (yr) L-92
L-40. Unsaturated Zone Layer Average Rock Density L-93
L-41. Unsaturated Zone Layer Distribution Coefficients L-94
L-42. Average Specific Discharge in Flow Path Segments L-95
L-43. Saturated Zone Horizontal Anisotropy L-95
L-44. Saturated Zone Specific Discharge Multiplier L-96
L-45. Saturated Zone Flowing Interval Porosity L-96
L-46. Saturated Zone Distribution Coefficients in mL/g L-97
L-47. Groundwater Biosphere Dose Conversion Factors for the Present-Day Climate L-99

M-1. Net Infiltration Rates (mm/yr) used in the Integrated Multiple Assumptions and Release Code Event Tree Branches for Infiltration M-16
M-2. Infiltration Rates (mm/yr) used in TSPA-LA (Modified from Table L-2) M-17
M-3a. Seepage Fraction and Flow Rate as a Function of Infiltration Rate M-18
M-3b. Summary Statistics for Probabilistic Seepage Evaluation (Intact Drifts) M-19
M-4. Comparison of Solubility Limits used in TSPA-LA and EPRI M-20
M-5. Inventory used in EPRI Model (Based on SNL 2007) and in TSPA-LA Model M-21
M-6. Unsaturated Zone Layer Distribution Coefficients M-22
M-7. Saturated Zone Layer Distribution Coefficients M-22
M-8. BDCFs used in EPRI Model M-23

P-1. Comparison of Mean Seepage Fraction for Various Percolation Subregions for Nominal Conditions P-27
P-2. Comparison of Mean Seepage Fraction for Various Percolation Subregions for Seismic Fault Displacement Modeling Case P-27
P-3. Comparison of Mean Seepage Fraction for Various Percolation Subregions for the Seismic Ground Motion Modeling Case P-27
P-4. Comparison of Mean Seepage Flux (m^3/yr) at 1,000,000 years for Various Percolation Subregions for the Seismic Ground Motion Modeling Case P-28
P-5. Quantitative Evaluation of the Impact of GoldSim Software Error on Various Modeling Cases Based on Dose P-28
P-6. Discussion of Other Minor Implementation Errors P-29
P-7. Impact Assessment Summary Table P-37

TABLES (Continued)

Page

INTENTIONALLY LEFT BLANK

8. POSTCLOSURE PERFORMANCE DEMONSTRATION

As stated in the introduction (Section 1.0), this Total System Performance Assessment for the License Application (TSPA-LA) report provides the technical basis to support the License Application (LA) for a nuclear waste repository at Yucca Mountain. This particular section of the report presents the postclosure performance assessment results and, in doing so, addresses the fundamental risk triplet (Kaplan and Garrick 1982 [DIRS 100557]), namely: (1) what can happen, (2) how likely is it to happen, and (3) what are the consequences if it does happen. The first two elements of the risk triplet are addressed via consideration of scenario classes, which represent a broad spectrum of potential future system states, and by accounting for the major sources of aleatory uncertainty. The third component is addressed by utilizing Total System Performance Assessment (TSPA) submodels of key processes (e.g., water flow, radionuclide mobilization and release, dissolved and colloidal phase transport through the natural barriers, and radiologic dose) and by accounting for the epistemic uncertainty in the current knowledge of those processes. Risk insights are developed based on:

- Projections of annual doses to the reasonably maximally exposed individual (RMEI) for a set of release scenarios, which are grouped into four classes
- Identifying the scenario classes and modeling cases that produce the most significant releases and dominate the projected doses
- Determining the sources of uncertainty that are most influential in producing the spread of the distribution of projected doses
- Identifying the key radionuclides that contribute the most to the projected annual doses.

The four scenario classes include Nominal, Early Failure, Seismic, and Igneous. Detailed descriptions of the technical basis of these scenario classes and their associated modeling cases are presented in Sections 6.3 through 6.6. These scenario classes collectively encompass all the included features, events, and processes (FEPs) that affect postclosure performance. The procedure used to screen the FEPs is discussed in Section 6.1.1; all the identified FEPs and the screening arguments are documented in Appendix I.

The TSPA presented herein focused on quantifying the postclosure performance of the repository system, which is composed of three major barriers, namely: (1) upper natural barrier, (2) engineered barrier system (EBS), and (3) lower natural barrier. The upper natural barrier consists of the topography and surface soils of the mountain, the unsaturated tuff units above the repository, and rock strata in which the repository is constructed. The EBS includes the waste packages (WPs), drip shields (DSs), waste forms, cladding (associated with the commercial spent nuclear fuel [CSNF], DOE spent nuclear fuel [DSNF], and naval spent nuclear fuel [NSNF]), and the drift invert; no credit is taken, however, for cladding performance. The lower natural barrier below the repository includes the unsaturated rock layers beneath the repository as well as the volcanic rock units and the alluvial material in the saturated zone (SZ) that extends from the repository site to the designated accessible environment boundary. A depiction of these three major barriers and the fundamental processes contributing to postclosure performance is presented on Figure 8-1.

The postclosure performance of this system of multiple barriers was analyzed for scenarios representing a broad range of likely and unlikely conditions. At a fundamental level, the postclosure performance of the repository is quantified through a detailed computer analysis of:

- How the system of multiple barriers would function in response to changes in the hydrologic, geologic, and geochemical conditions expected to be induced by the decay heat, as well as by projected future climate changes
- How the multiple barriers could be affected by likely and unlikely disruptive events potentially induced by seismic and igneous activity at or near the site area
- How radionuclides could be released from the EBS, migrate through the multiple barriers, and potentially enter the biosphere pathways at the designated RMEI location.

As required by the disposal standards, the postclosure performance is quantified for time periods of 10,000 years and 1,000,000 years after closure.

Because of the inherent uncertainties in making such long-term projections, this TSPA is largely based on a probabilistic modeling approach that accounts for uncertainties in parameters and in future conditions. Other sources of uncertainty, such as potential early failure of the EBS components arising from undetected defects, are included in the early failure scenario class. In addition, a TSPA projection was developed for a human intrusion scenario. This separate TSPA addresses the regulatory requirement to demonstrate performance for a hypothetical inadvertent drilling event, which is assumed to release radionuclides directly to the groundwater.

It is important to note that this TSPA utilizes the knowledge base, site characterization data, and EBS design compiled over the past two plus decades. Since the inception of the Yucca Mountain Project, scientists and engineers at the U.S. Department of Energy (DOE) national laboratories and other organizations have been refining the technical basis in preparation for this performance demonstration. The technical basis has been critically reviewed by both internal and external peer review groups to ensure that it is scientifically defensible. In addition, it has been documented in a manner that is traceable and auditable. The technical basis that directly supports the TSPA-LA Model is documented in Volumes I and II, as well as in the numerous analysis and modeling reports that are explicitly cited throughout this document.

In this section, the postclosure performance demonstration results for the proposed Yucca Mountain repository are presented and explained. Probabilistic projections of annual doses and activity concentrations (i.e., radionuclide activity per unit volume) in groundwater, at the designated location of the RMEI, were developed for comparison to the applicable radiation protection standards. The demonstration of conformance with the radiation protection standards is presented using the following regulatory and statistical metrics:

1. Projected annual dose and activity concentration histories at the RMEI location (based on the propagation of epistemic and aleatory uncertainties through the TSPA-LA Model)
2. Statistical metrics for the projected distributions, including the mean, median, and 5th and 95th percentiles of the annual dose and activity concentration

3. Largest or peak mean annual doses computed for comparison with the dose limits specified for 10,000 years after closure and the largest median annual doses for post 10,000 years but within the period of geologic stability (i.e., 1,000,000 years)

4. Peak of the mean activity concentrations computed for comparison with the groundwater protection limits specified for 10,000 years after closure.

With regard to the probabilistic projections of the dose metrics, the following mathematical terminology is used in the subsequent sections: (1) annual dose is the projected annual dose to the RMEI conditional on one specific sampled value of aleatory (irreducible or stochastic) and epistemic (reducible or lack of knowledge) uncertainty; (2) expected annual dose is the expected value of annual dose to the RMEI over aleatory uncertainty, conditional on epistemic uncertainty; (3) mean annual dose is the expected value of annual dose computed over both the aleatory and epistemic uncertainty; and (4) median annual dose is the median of the distribution of expected annual dose.

As demonstrated in Section 7.3.1, the probabilistic projections are statistically stable. Stability is determined by comparing TSPA-LA Model results computed using three independent samples of uncertain parameters, termed replicates. Because the comparison showed that the TSPA-LA Model results are statistically stable, any of the three replicates could be chosen for presentation and comparison with the radiation protection standards. Results from the first replicate are presented in this section and are the subject of analyses reported in the appendices.

Comparisons of the TSPA projections with the applicable U.S. Nuclear Regulatory Commission (NRC) radiation protection standards are presented first and in a summary manner (Section 8.1). Explanation of the performance demonstration results is developed based on the probabilistic projections for the individual scenario classes and modeling cases (Section 8.2). Additional insights to the factors affecting the isolation characteristics of the repository system are developed by examining the performance capabilities of the natural and engineered barriers (Section 8.3). The final part of this section highlights the technical basis for confidence, credibility, and defensibility of the performance demonstration (Section 8.4).

INTENTIONALLY LEFT BLANK

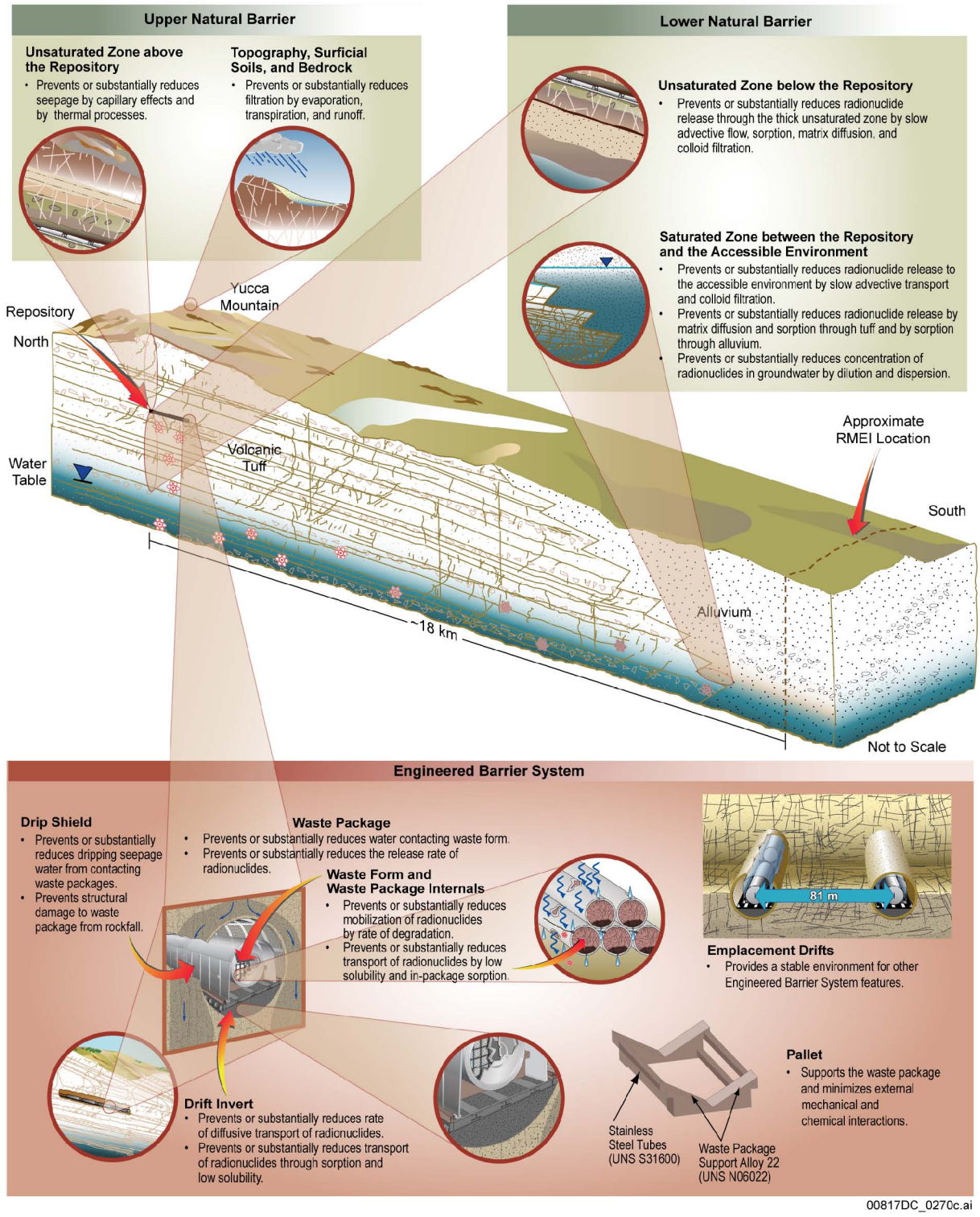

Figure 8-1. Illustration of the Multiple Barriers of Yucca Mountain Repository System

INTENTIONALLY LEFT BLANK

8.1 CONFORMANCE WITH RADIATION PROTECTION STANDARDS

The U.S. Environmental Protection Agency (EPA) and NRC regulations for a high-level radioactive waste (HLW) repository at Yucca Mountain require that DOE demonstrate a reasonable expectation of compliance with the applicable radiation protection standards. The proposed EPA regulation 40 CFR Part 197 (2005 [DIRS 175755]) establishes three separate and distinct radiation protection standards for the Yucca Mountain Repository. As the licensing agency, the NRC adopted these three radiation protection standards as follows:

- Individual Protection Standard After Permanent Closure (10 CFR 63.311 [DIRS 178394]), which considers the required characteristics of the RMEI as described in 10 CFR 63.312 [DIRS 180319].
- Individual Protection Standard for Human Intrusion (10 CFR 63.321 [DIRS 178394]) according to the Human Intrusion Scenario described in 10 CFR 63.322 [DIRS 180319].
- Separate Standards for Protection of Ground Water (10 CFR 63.331 [DIRS 180319]) using the representative volume specified in 10 CFR 63.332 [DIRS 180319].

The EPA and NRC proposed regulations for Individual Protection and Human Intrusion establish two sets standards for annual doses to the RMEI corresponding to: (1) the time period of 10,000 years after closure, and (2) the time period after 10,000 years but within the period of geologic stability, defined as 1,000,000 years in 10 CFR 63.302 [DIRS 178394]. In contrast, the Separate Standards for Protection of Ground Water set limits for annual dose and activity concentrations (i.e., radionuclide activity per unit volume) for only the 10,000-year period following repository closure. For the purpose of making performance projections for these time periods, the characteristics of the RMEI are defined in 10 CFR 63.312 [DIRS 180319] and the RMEI is taken to reside approximately 18 km (11 mi) downgradient of the repository.

Detailed probabilistic projections developed for this postclosure performance demonstration will be presented and explained in the subsequent sections. At this point, however, it is beneficial to preview the high-level results in a tabulation of peak mean and largest median values for annual doses and activity concentrations for direct comparisons with the numerical limits set in three radiation protection standards. Comparisons of the projected performance metrics and regulatory limits are summarized in Tables 8.1-1 through 8.1-3. To highlight the spread in the computed distribution of expected annual doses, additional statistical parameters are presented in Table 8.1-4 to better clarify the comparison with the limits of the Individual Protection Standard.

As shown in the tabular comparisons, the numerical limits prescribed in all three standards are met, with the peak annual doses and activity concentrations falling well below the limits. These numerical comparisons, however, represent only a part of the postclosure performance demonstration and many detailed calculations and graphical outputs are presented in Sections 8.2 to elucidate the comparisons with the regulatory requirements. For the purposes of explaining the basis for a reasonable expectation of compliance, this section and the subsequent sections address the following fundamental questions regarding the TSPA of the repository and the probabilistic projections of the regulatory metrics:

1. What scenario classes and modeling cases were considered and how were they analyzed to make probabilistic performance projections?

2. What processes or site characteristics modeled in the scenario class were most important to postclosure performance?

3. What multiple-barrier attributes and/or characteristics were most influential in reducing the radionuclide release rates, rate of water or radionuclide movement?

4. What radionuclides in the nuclear waste inventory contribute the most to the annual doses and why?

5. What model parameters are most dominant in determining the uncertainty or spread in the projected performance metrics?

In addition, it is important to identify the plausible and potentially important conservatisms incorporated into the TSPA-LA Model, as well as to explain how the performance projections have been cross-checked to ensure that they are technically sound and defensible.

The next sections describe and explain the projections that constitute the postclosure performance demonstration for the three radiation protection standards. The exposure models and conversion factors used to calculate annual dose and activity concentrations in groundwater are summarized in the Biosphere Component Model section (Section 6.3.11) and described in detail in *Biosphere Model Report* (SNL 2007 [DIRS 177399], Sections 6.11 and 6.12). The annual doses to the RMEI are calculated for two separate exposure scenarios, namely, groundwater and volcanic (SNL 2007 [DIRS 177399], Section 6.1.3).

8.1.1 Individual Protection Standard

To provide a postclosure performance demonstration for the Individual Protection Standard (10 CFR 63.311 [DIRS 178394]), a comprehensive TSPA-LA Model (Sections 1 through 6) of the repository system was developed and applied to:

- Analyze potential releases of radionuclides from the EBS
- Evaluate all potential pathways of radionuclide transport through the multiple barriers and to the accessible environment
- Project (i.e., analyze and calculate as a function of time) the annual doses to the RMEI.

The NRC Proposed Rule 10 CFR 63.311(a) [DIRS 178394] states "(a) DOE must demonstrate, using performance assessment, that there is a reasonable expectation that the reasonably maximally exposed individual receives no more than the following annual dose from releases from the undisturbed Yucca Mountain disposal system: (1) 0.15 mSv (15 mrem) for 10,000 years following disposal; and (2) 3.5 mSv (350 mrem) after 10,000 years, but within the period of geologic stability."

NRC Proposed Rule 10 CFR 63.311(b) [DIRS 178394] specifies that the "performance assessment must include all potential environmental pathways of radionuclide transport and exposure." It is important to clarify that, in NRC Proposed Rule 10 CFR 63.311(a) [DIRS 178394], "undisturbed Yucca Mountain disposal system" means that the repository is not affected by human intrusion (10 CFR 63.322 [DIRS 180319]), which is addressed separately in Section 8.1.3. This term is distinct from the regulatory definition of undisturbed performance (10 CFR 63.302 [DIRS 180319]).

To demonstrate compliance with this standard, the peak or largest *mean value* of the projected annual doses to the RMEI is used as the primary performance metric for comparisons with the above numerical limits for 10,000 years and the largest *median value* is used for comparison with the post-10,000-year limit; these metrics are in accordance with 10 CFR 63.303 [DIRS 178394]. The projections of postclosure performance take into account both likely and unlikely FEPs (10 CFR 63.342 [DIRS 178394]) (Appendix I). These FEPs and their affects on waste isolation are quantified in four scenario classes: Nominal, Early Failure, Seismic, and Igneous. Detailed descriptions of the technical basis of these scenario classes and their associated modeling cases are presented in Sections 6.3 through 6.6.

8.1.1.1 Scenario Classes Considered and Calculation of Total Annual Doses

As described in Section 6.1.2, probabilistic projections of the total expected annual dose to the RMEI are computed as a combination of the calculated expected annual doses for each of the four scenario classes; the expectation is taken over all aleatory (i.e., randomly occurring in time) uncertainties. Mathematically, the total expected annual dose to the RMEI, denoted by $\bar{D}_T(\tau \mid \mathbf{e})$ for time τ in years, is defined as the sum of the expected annual doses for each scenario class (Section 6.1.2.2 and Appendix J4.6):

$$\bar{D}_T(\tau \mid \mathbf{e}) = \bar{D}_N(\tau \mid \mathbf{e}) + \bar{D}_E(\tau \mid \mathbf{e}) + \bar{D}_I(\tau \mid \mathbf{e}) + \bar{D}_S(\tau \mid \mathbf{e}) \quad \text{(Eq. 8.1.1-1)}$$

In the above equation, the terms $\bar{D}_N(\tau \mid \mathbf{e})$, $\bar{D}_E(\tau \mid \mathbf{e})$, $\bar{D}_I(\tau \mid \mathbf{e})$, and $\bar{D}_S(\tau \mid \mathbf{e})$ represent the expected annual dose estimates for the four Scenario Classes, namely, Nominal, Early Failure, Igneous, and Seismic, respectively. The term $\mathbf{e}$ represents the set of the epistemically uncertain model parameters, sampled in the probabilistic simulation of postclosure performance.

While the term for the Nominal Scenario Class, $\bar{D}_N(\tau \mid \mathbf{e})$, consists of only one modeling case, the other expected annual dose terms in Equation 8.1.1-1 are the sum of expected values for the various modeling cases. Specifically, the doses for the Early Failure, Igneous, and Seismic Scenario Classes are computed as following:

$$\bar{D}_E(\tau \mid \mathbf{e}) = \bar{D}_{WP}(\tau \mid \mathbf{e}) + \bar{D}_{DS}(\tau \mid \mathbf{e}) \quad \text{(Eq. 8.1.1-2)}$$

$$\bar{D}_I(\tau \mid \mathbf{e}) = \bar{D}_{II}(\tau \mid \mathbf{e}) + \bar{D}_{VE}(\tau \mid \mathbf{e}) \quad \text{(Eq. 8.1.1-3)}$$

$$\bar{D}_S(\tau \mid \mathbf{e}) = \bar{D}_{GM}(\tau \mid \mathbf{e}) + \bar{D}_{FD}(\tau \mid \mathbf{e}) \quad \text{(Eq. 8.1.1-4)}$$

where the terms $\bar{D}_{WP}(\tau|\mathbf{e})$ and $\bar{D}_{DS}(\tau|\mathbf{e})$ are the expected annual dose estimates for the Waste Package and Drip Shield Early Failure (EF) Modeling Cases, respectively; $\bar{D}_{II}(\tau|\mathbf{e})$ and $\bar{D}_{VE}(\tau|\mathbf{e})$ are the expected annual dose estimates for the Igneous Intrusion and Volcanic Eruption Modeling Cases; and $\bar{D}_{GM}(\tau|\mathbf{e})$ and $\bar{D}_{FD}(\tau|\mathbf{e})$ are the expected annual dose estimates for the Seismic Ground Motion (GM) and Seismic Fault Displacement (FD) Modeling Cases, respectively.

A very important point regarding the TSPA-LA Model implementation of Equation 8.1.1-1 is that, although the expected annual dose for the Nominal Modeling Case, $\bar{D}_N(\tau|\mathbf{e})$, is calculated for the post-10,000-year compliance period, $\bar{D}_N(\tau|\mathbf{e})$ is not added into the total dose calculation for $\bar{D}_T(\tau|\mathbf{e})$. Rather, for the post-10,000-year period, the TSPA-LA Model implicitly produces the sum $\bar{D}_N(\tau|\mathbf{e})+\bar{D}_S(\tau|\mathbf{e})$ instead of calculating the individual quantities $\bar{D}_N(\tau|\mathbf{e})$ and $\bar{D}_S(\tau|\mathbf{e})$ separately. This combination of modeling cases was performed to ensure proper coupling between the WP and DS damage abstractions in the Seismic GM Modeling Case and the corrosion processes in the Nominal Modeling Case. The damage abstraction takes into account the increased susceptibility to seismic damage as a result of corrosion induced thinning of the WP outer barrier, DS plate, and frame (Section 6.6.1.2.2).

8.1.1.2 Projections of Annual Doses and Major Observations

Projections of postclosure performance for comparison with the Individual Protection Standard were developed using the Monte Carlo simulation methodology, which is described in Appendix J. This methodology incorporates aleatory and epistemic uncertainties into the projections in two separate computational loops: (1) an outer calculational loop that samples probability distributions for model parameters with epistemic uncertainty using the Latin hypercube sampling technique (Helton and Davis 2002 [DIRS 163475]), and (2) an inner loop that evaluates expected annual dose accounting for distributions representing quantities with aleatory uncertainties. The methodology produced an ensemble of expected annual dose outcomes for each scenario class, which were then combined using Equation 8.1.1-1, using the separate terms $\bar{D}_N(\tau|\mathbf{e})$ and $\bar{D}_S(\tau|\mathbf{e})$ for 10,000-year results and including the combined term $\bar{D}_N(\tau|\mathbf{e})+\bar{D}_S(\tau|\mathbf{e})$ for post-10,000-year results.

The main result of the Monte Carlo simulation process is a set of realizations for the expected annual dose histories for the RMEI, which are generally plotted in the form of a multi-realization plot. The multi-realization plots developed for demonstrating compliance with the Individual Protection Standard are shown on Figure 8.1-1 for 10,000 years after closure and Figure 8.1-2 for the post-10,000-year period (i.e., after 10,000 years but within the period of geologic stability [defined by the proposed NRC rule [DIRS 178394] to end at one million years]). Curves for the mean, median, and 5th and 95th percentiles dose histories are superimposed on each multi-realization plot. The total mean annual dose history, which is plotted as the red curve, was computed by taking the arithmetic average of the 300 expected annual dose values, for individual time planes along the curves. Similarly, the median dose history, plotted as the blue curve, was constructed from points obtained by sorting the 300 expected values from lowest to highest, and

then averaging the two middle values. Curves for the 5th and 95th percentiles are also plotted to illustrate the spread in the expected annual dose histories; 90 percent (or 270 of the 300 epistemic realizations) of the projected dose histories fall between these two percentile curves. For a detailed description of the calculation of total annual dose see Section 6.1.2.2.

For the 10,000-year disposal period, the largest mean and median annual doses to the RMEI are estimated to be about 0.2 mrem and 0.15 mrem, respectively; these projected doses are below the individual protection limit of 15 mrem. Similarly, the largest mean and median annual doses for the post-10,000-year period but within the period of geologic stability are estimated to be about 2 mrem and 1 mrem, respectively; these projected peak values are also below the individual protection limit of 350 mrem. To provide a perspective of the epistemic uncertainty of the performance projections, the annual dose history curves corresponding to the 5th and 95th percentiles are included in the multi-realization plots.

Important risk insights can be gained by disaggregating the total annual doses into the mean annual dose histories for the individual modeling cases; these individual projections are shown on Figure 8.1-3. From those dose curves, the following general observations can be drawn about the projected postclosure performance demonstration:

- Total mean annual doses calculated for both the 10,000-year and post-10,000-year time periods are dominated by releases for the Seismic GM and Igneous Intrusion Modeling Cases.
- Mean annual doses for the Waste Package EF and Seismic FD Modeling Cases are relatively small and are estimated to be on the order of 10^{-2} mrem or less for both the 10,000-year and post-10,000-year time periods.
- Mean annual doses projected for Drip Shield EF and Igneous Volcanic Eruption Modeling Cases are on the order of 10^{-3} mrem or less for both the 10,000-year and post-10,000-year time periods.

With regards to the first observation, the Seismic GM Modeling Case dominates the total mean annual dose for 10,000 years after closure, whereas for the post-10,000-year period, the Igneous Intrusion Modeling Case dominates the total mean annual dose to the RMEI for most of the time period.

An important clarification regarding the projections for the Seismic GM Modeling Case is that the expected annual doses for the 10,000-year time period are only from releases from the damaged co-disposed (CDSP) WPs (Table 6.3.7-1). The contribution to expected annual doses from the commercial spent nuclear fuel (CSNF) WPs were evaluated and found to be insignificant, due to the very low frequency of seismic induced failures of the transportation, aging, and disposal (TAD) packages. The basis for the low frequency is addressed in the following sections and explained in greater detail in Section 7.3.2.6.1.3.7, which examines probability of damage to CSNF WPs by seismic events during the 10,000-year period and the contribution to expected annual dose of these events.

Additional discussion and explanation of the projections for the seven modeling cases is presented in Section 8.2.

8.1.1.3 Disruptive Events Important to Postclosure Performance

From a cause-and-effect view point, clearly the most important disruptive events potentially impacting postclosure performance are the vibratory ground motion and igneous intrusion (i.e., magmatic dike rising through the earth's crust and intersecting the repository). Based on the FEPs screening process, the seismic and igneous disruptions only affect the EBS. In the case of vibratory ground motion, the important aspect is the cumulative damage and failure of the WPs and DSs. It is important to clarify, however, that while WP and DS failures could be caused by a single extreme ground motion event, failure would more typically occur as a result of a sequence of many small to moderate vibratory ground motions over a period of time with stress corrosion cracking (SCC) accumulating from these events. In the case of the igneous intrusion into the repository area, however, the damage and failure of the EBS is a single discrete event that causes complete failure of both WPs and DSs.

For the purposes of risk insights, it is valuable to examine the estimated annual frequencies for these disruptive events and processes. The occurrence of seismic events is described as a Poisson process with the smallest peak ground velocity (PGV) having an annual exceedance frequency of 4.287×10^{-4}/yr and largest PGV with an exceedance frequency of 10^{-8}/yr (Figure 6.6-6; and SNL 2007 [DIRS 176828], Figure 6-7). During the first 10,000 years after closure, only four potentially damaging seismic ground motion events are expected to occur; whereas for the 1,000,000-year period, approximately 430 potentially damaging seismic events are expected to occur. In contrast, the mean annual frequency of a dike intersecting the repository is estimated to be 1.7×10^{-8}/yr (BSC 2004 [DIRS 169989]). This frequency is just slightly greater than the NRC frequency of 10^{-8}/yr for very unlikely events and processes, which are excluded from the performance assessment for the LA by regulation (10 CFR 63.342(b) [DIRS 178394]). While both disruptive events are possible, the potential impacts of seismic ground motion events are much more probable and, therefore, these events are the focus of the subsequent discussion.

Seismically Induced Damage and Failure Mechanisms—Vibratory ground motions can lead to drift degradation and rockfall accumulation on the DS. Subsequent failure of the DS can occur as a result of dynamic loading and deformation and/or by static loading by accumulated rockfall. The ability of the DS to withstand the static and dynamic loading diminishes with time because general corrosion reduces the thickness of the titanium DS plate and framework. Ultimately, the DSs will fail as a result of load-induced buckling or rupture. A histogram of DS failures for the Seismic GM Modeling Case is shown on Figure 8.1-4; the histogram for the Nominal Modeling Case is also shown for the purposes of comparison. As shown, DS failures occur earlier due to the combined effects of nominal and seismic ground motion as compared to nominal process alone. These probabilistic projections of DS and WP failures are described and explained in more detail in Section 8.2.

Seismically induced damage of the WPs is most likely to occur from deformation or denting of the outer wall. These localized areas of deformation or denting develop residual stresses that are susceptible to SCC. Rupture of a WP could potentially occur as a result of kinematic loading caused by package-to-pallet and/or package-to-package impacts. It is important to understand that in the case of the WP, seismic crack damage is more likely to occur than rupture. Projections of CDSP and CSNF WP failures by seismic crack damage as a function of time are

shown on Figure 8.1-5. As can be noted by comparing Figure 8.1-5(a) and Figure 8.1-5(b), the CSNF WP is much less likely to be damaged than is the CDSP WP. A detailed discussion of seismic related damage and failure mechanisms is presented in Section 6.6.1.1.2 and in *Seismic Consequence Abstraction* (SNL 2007 [DIRS 176828]).

All of these potential degradation, damage, and failure mechanisms have been evaluated for this performance demonstration (Section 6.6). The technical basis for the performance analysis of seismic and igneous intrusion consequences are documented in *Seismic Consequence Abstraction* (SNL 2007 [DIRS 176828]) and *Number of Waste Packages Hit by Igneous Intrusion* (SNL 2007 [DIRS 177432]), respectively.

8.1.1.4 Multiple Barrier Processes that Contribute to Postclosure Performance

The multiple barrier processes that are important to postclosure performance have largely been identified in previous TSPAs (Williams 2001[DIRS 157307]) of the Yucca Mountain repository. The modeling studies conducted in support of this TSPA-LA have provided additional insights and understanding, particularly with regard to individual features of natural and engineered barriers. From a high-level perspective, some of the fundamental barrier processes and characteristics that are typically influential in determining how well the system of multiple barriers isolates (i.e., contains and confines) the nuclear waste are:

- Net infiltration into the unsaturated zone (UZ) and seepage into the drifts
- Mechanical strength and corrosion rate properties of the WPs and DSs
- Solubilities for key radioelements such as neptunium, uranium, and plutonium
- Radionuclide sorption onto corrosion products inside the WPs
- Diffusion limited radionuclide releases from failed WPs
- Sorption and matrix diffusion properties of the UZ and SZ underlying the repository.

With regard to infiltration and seepage, these attributes are important because they determine: (1) dripping and non-dripping environments on WP and DS surfaces, and (2) water flow into a failed WP and the ensuant mobilization and release of radionuclides. The strength properties of the WP outer barrier (i.e., Alloy 22 [UNS N06022]) and DS plate (i.e., Titanium Grade 7) and frame (i.e., Titanium Grade 29) determine their capability to withstand dynamic and static loads induced by vibratory ground motion (Section 6.6.1.2). General corrosion and SCC are important processes affecting WP structural integrity because they progressively reduce metal barrier thickness over a period of time. The general corrosion rate of the WP outer barrier is temperature-dependent, which makes the WP surface temperature an important factor. The importance of radioelement solubilities is derived from the fact that they limit the release rates from the waste form. Solubilities of such radioelements as neptunium, uranium, and plutonium are particularly important because they have relatively large initial inventories and produce radionuclide species that have very long half-lives. Corrosion of the WP internals produces metal oxides that provide sorption sites for a variety of fission products and actinide elements (Section 6.3.8). Diffusional release of radionuclides from a failed WP is a function of the breach geometry (e.g., cracks and patches) and effectively limits the rate of release to the natural barrier. The sorption properties of the volcanic tuff and alluvium layers in the UZ and SZ influence the rate of subsurface migration to the RMEI location.

8.1.1.5 Radionuclides Important to Postclosure Performance

In general, the radionuclides in the nuclear waste that dominate the calculation of annual doses typically have a combination of unique characteristics such as: (1) large initial inventories in the nuclear waste, (2) moderately to highly soluble, (3) very long half-lives (e.g., $\geq 10^5$ years), and (4) low to non-sorbing properties. The radionuclides that become important to dose also depend on the time frame considered (i.e., 10,000 years or 1,000,000 years after closure), because of the effect of radionuclide decay on the activity concentrations. In-growth of radionuclides via chain decay, over a very long period of time, can also be an important process that determines the role and importance of actinide elements in the actinium, uranium, neptunium, and thorium series (Figure 6.3.7-4). For the three modeling cases involving groundwater releases, the basic transport processes of advection, dispersion, matrix diffusion, and sorption can play an important role. Moreover, the specific modes (e.g., dissolved and colloidal phases) of transport can also be important; the modes analyzed for each radionuclide are listed in Table 6.3.7-6.

The contributions of the individual radionuclides to the total mean annual dose is shown on Figure 8.1-6 and 8.1-7 for 10,000 years and post-10,000 years, respectively. It is important to acknowledge that some questionable, potentially unrealistic, values of mass dispersivity were found to have been sampled in the probabilistic calculation of the decay chain transport through the SZ; in addition, three radionuclides, namely ^{36}Cl, ^{79}Se, and ^{126}Sn, were inadvertently omitted from the initial TSPA-LA Model runs for the 10,000-year time period. The issues of the dispersivity value and three omitted radionuclides were addressed in a Condition Report (CR 11152). The impact of these issues on the overall analysis is discussed in Appendix P.

Important Radionuclides for the 10,000-Year Performance Projection—From the dose curves shown on Figure 8.1-6, it is clear that the principal contributors to the total mean annual dose, ranked from highest to lowest, are: ^{99}Tc (half-life 2.13×10^5 years), ^{14}C (half-life 5,715 years), ^{239}Pu (half-life 2.41×10^4 years), ^{129}I (half-life 1.57×10^7 years), and ^{240}Pu (half-life 6.56×10^3 years). Collectively, these five radionuclides account for about 98 percent of the peak of the total mean annual dose, which occurs at the end of 10,000 years. The single largest contributor is ^{99}Tc, which accounts for about 56 percent of the peak of the total mean annual dose to the RMEI.

The fission products, ^{99}Tc and ^{129}I, and the activation product, ^{14}C, collectively represent about 83 percent of the total mean annual dose. Their large contribution to total mean annual dose is largely explained by the fact that they are very soluble in water, do not sorb in earth materials, and have long half-lives relative to the 10,000-year time frame. The significance of the technetium, iodine, and carbon radioelements being very soluble is because their release rates are limited only by: (1) the waste form degradation rate, (2) rate and extent of water ingress into the WP, and (3) mass transport mechanism (i.e., diffusion and/or advection) out of the WP. The non-sorbing property is important because these radionuclides are transported from the EBS, through the natural barrier, and to the RMEI at the rate at which the groundwater naturally travels (i.e., no delay by chemical retardation). Their relatively long half-lives, compared to 10,000 years, means that decay would not appreciably reduce their activity level. In contrast to its mobility characteristics, ^{99}Tc has the smallest mean biosphere dose conversion factor (BDCF) (SNL 2007 [DIRS 177399], Figure 6.13-2) of all the major radionuclides; the mean BDCF for ^{14}C is the second lowest. On a mass per package basis, ^{99}Tc has a larger initial inventory than

the ^{129}I and ^{14}C inventory (Table 6.3.7-5), which in part explains the ranking of these three radionuclides.

The two actinides, ^{239}Pu and ^{240}Pu, together contribute about 14 percent to the total mean annual dose with ^{239}Pu by itself contributing about 11 percent. The contribution of these two plutonium species to total mean annual dose is explained by their large initial inventory (Table 6.3.7-5), mode (i.e., dissolved and colloidal) of transport in groundwater, and broad range of transport times in the SZ. With regard to mode of transport, plutonium species are transported through groundwater in dissolved phase and reversible colloids, as well as fast (i.e., not retarded by matrix diffusion or attachment/detachment process) and slow irreversible colloids (Table 6.3.7-6). Detailed probabilistic simulations of plutonium transport through the SZ as reversible colloids, which neglect effects of decay, indicate median transport times ranging from 3,000 years to greater than 1,000,000 years, with a median among all realizations of about 95,000 years (SNL 2007 [DIRS 183750], Table 6-10[a]). In the case of plutonium species in the form of slow irreversible colloids, probabilistic simulations of transport through the SZ that neglect effects of decay indicate transport times ranging from 100 years to about 500,000 years, with a median among all realizations of about 4,500 years (SNL 2007 [DIRS 183750], Table 6-10[a]). In contrast, the simulations for the fast irreversible plutonium colloids range from 10 years to about 1,800 years, with a median among all realizations of about 60 years (SNL 2007 [DIRS 183750], Table 6-10[a]). The TSPA-LA Model projections indicate that the dissolved phase and reversible colloids account for the larger fraction of the contribution to total mean annual dose.

Important Radionuclides for the Post-10,000-Year Performance Projection—Figure 8.1-7 shows the contributors to the total mean annual dose. Ranked from highest to lowest, the four main contributors at 1,000,000 years are: ^{226}Ra (half-life 1,600 years), ^{242}Pu (half-life 3.75×10^5 years), ^{237}Np (half-life 2.14×10^6 years), and ^{129}I (half-life 1.57×10^7 years). These four radionuclides collectively account for nearly 80 percent of the peak mean dose. In marked contrast to ^{242}Pu, ^{237}Np, and ^{129}I, ^{226}Ra has a very small initial inventory in the nuclear waste, relatively short half-life, and sorbs strongly on the geologic media, yet it accounts for about 31 percent of the mean annual dose at 1,000,000 years. This seemingly contrary outcome is explained by: (1) its unique nuclear and chemical properties, and (2) its relatively large BDCF. The nuclear properties of ^{226}Ra explain its persistence in the nuclear waste for potentially millions of years, while its chemical properties explain its rate of migration in the UZ and SZ.

A key nuclear property of ^{226}Ra is that it exhibits in-growth from other radionuclides in the uranium series decay chain (Figure 6.3.7-4). The relevant part of that decay chain consists of the following:

$$^{234}U \text{ (half-life 240,000 yrs)} \rightarrow {}^{230}Th \text{ (half-life 77,000 yrs)} \rightarrow {}^{226}Ra \text{ (half-life 1,600 yrs).}$$

This decay chain is significant because it means that even after ^{226}Ra depletes its initial inventory, it will be continuously replenished so long as there is a source of ^{230}Th and ^{234}U. While both ^{226}Ra and ^{230}Th have relatively small initial inventories in the nuclear waste, the precursor ^{234}U has a significant initial inventory. Also, the large contrast in half-lives between ^{226}Ra and ^{230}Th means that ^{226}Ra will ultimately reach a state of secular equilibrium with ^{230}Th. Similarly, after ^{230}Th depletes its initial inventory, its activity will be in secular equilibrium with

its precursor ^{234}U. The net effect is that ^{226}Ra will persist in the waste form for potentially millions of years.

One of the important chemical properties of ^{226}Ra is that it exhibits high sorption in the unsaturated tuff layers, particularly in the Zeolitic and devitrified tuff (Table 6.3.9-2). This high sorption is also exhibited in the volcanic units and alluvium of the SZ (Table 6.3.10-2). These sorption properties have the effect of greatly slowing the ^{226}Ra rate of migration through the lower natural barrier, to the extent that the activity concentrations of ^{226}Ra would diminish by simple decay before reaching the RMEI location. This transport delay effect is demonstrated in the probabilistic analysis of breakthrough curves (SNL 2007 [DIRS 183750], Figure 6-14[a]) for ^{226}Ra migration through the SZ and to the RMEI location.

The breakthrough curves for ^{226}Ra are reproduced on Figure 8.1-8. It is important to note that the breakthrough curves shown on Figure 8.1-8 do not account for decay during transport; rather, the decay is accounted for when the time-dependent releases of ^{226}Ra from the UZ are computed (SNL 2007 [DIRS 183750], Section 6.5). A statistical analysis of these projections shows that the majority of the ^{226}Ra transport times at the RMEI location are much greater than 10,000 years; more specifically for individual realizations, the median transport times (i.e., the times when relative mass equals 0.5 on Figure 8.1-8a) in the SZ range from 18,000 years to more than 1,000,000 years (SNL 2007 [DIRS 183750], Table 6-10[a]). The 50th percentile of the median ^{226}Ra transport times among all realizations is estimated to be about 731,000 years (SNL 2007 [DIRS 183750], Table 6-10[a]). For these magnitudes of transport times, ^{226}Ra would experience from about 11 to more than 600 half-lives of decay before reaching the RMEI, thus reducing the activity concentration by factors $(1/2)^{11}$ to $(1/2)^{600}$. These decay factors suggest that ^{226}Ra activity concentrations, and dose to the RMEI results from decay during transport of the parents.

To understand how ^{226}Ra actually becomes important to dose, one needs to examine the transport characteristics of its two precursors—^{230}Th and ^{234}U. The radionuclide ^{230}Th is transported in water as a reversible colloidal phase and a solute (Table 6.3.7-6); whereas ^{234}U is transported only as a solute. Because ^{234}U is weakly sorbed in the geologic media, it is transported through the UZ and SZ at rates many times faster than ^{230}Th or ^{226}Ra. A statistical analysis of the probabilistic breakthrough curves (SNL 2007 [DIRS 183750], Table 6-10[a]) for the SZ that neglect effects of decay shows that the median transport times (through the SZ) for ^{230}Th range from about 1,000 years to over 1,000,000 years, with the 50th percentile of the median transport times among all realizations being greater than 1,000,000 years. In contrast, the median transport times for ^{234}U ranges from 200 to more than 900,000 years; the 50th percentile of the median transport times for all realizations is about 8,900 years. Thus, it follows that the doses from ^{226}Ra are primarily the direct result of the mobilization and groundwater transport of ^{234}U (and to a lesser extent ^{230}Th) with subsequent chain decay to ^{226}Ra. This pattern of radionuclide in-growth occurs along the groundwater flow path.

As noted earlier, ^{226}Ra has a relatively large BDCF value. This is in part due to the fact that its BDCF accounts for several decay products (SNL 2007 [DIRS 177399], Table 6.12-1). In fact, the ^{226}Ra and one of its nuclear progeny, ^{210}Pb, have the highest BDCF values (SNL 2007 [DIRS 177399], Figure 6.13-2) of all the radionuclides considered in the groundwater exposure calculation; moreover, as implemented in the TSPA-LA Model, the ^{226}Ra BDCF includes the

contribution of ^{210}Pb, which on average accounts for about 42 percent of the composite BDCF value.

The results discussed herein contain additional issues identified during analysis. The issues and potential impacts are discussed in Appendix P, in particular in Section P15. Incorporation of any changes related to these issues may modify the interpretation of these results.

8.1.1.6 Model Parameters Influencing Uncertainty in Expected Annual Doses

Uncertainty and sensitivity analyses were conducted to identify the TSPA-LA Model parameters that were most influential in determining the spread in the total expected annual dose projections (Appendix K). Based on those analyses, three model parameters were identified as having the largest influence on the overall uncertainty in the total expected annual doses to the RMEI. These three parameters are (1) occurrence rate of igneous events, IGRATE; (2) residual stress threshold for Alloy 22, SCCTHRP; and (3) temperature dependence parameter for Alloy 22 general corrosion rate, WDGCA22. The importance ranking of these three model parameters varies with time, which is illustrated in Table 8.1-5. Appendix K, Figure K8.1-2, provides information for times prior to 20,000 years, and Figure K8.2-2 provides information for times after 20,000 years. These model parameters are described below; Table K3-4 provides additional details.

IGRATE Parameter—This parameter is the estimated annual frequency of an igneous dike intersecting the repository, which is characterized as an epistemic uncertain quantity. The annual frequency of an igneous event intersecting the repository ranges from approximately 7.4×10^{-10}/yr to 5.5×10^{-8}/yr for the 5th and 95th percentiles, respectively, with a mean annual frequency of 1.7×10^{-8}/yr. In a given epistemic realization, the annual frequency of an igneous event is sampled from the cumulative distribution function (CDF) for IGRATE, and is used to determine the probability that an igneous event occurs. As discussed in Section 6.5.1, the Igneous Intrusion Modeling Case assumes that any intrusion penetrating the repository footprint would destroy all DSs and WPs and, therefore, the raw waste form would be exposed to seepage with ensuant radionuclide transport.

SCCTHRP Parameter—This parameter is the residual stress threshold for the Alloy-22 WP outer barrier, which is represented as an epistemically uncertain value. This parameter represents the initiation threshold for the onset of SCC. Thus, when the residual stress in the outer barrier of a WP exceeds this threshold, then SCC is presumed to occur. As explained in Section 6.3.5, the primary causes of residual stresses in the WP outer barrier would be low-frequency, high-peak ground velocity seismic ground motions, which could cause impacts from WP-to-WP, from WP-to-emplacement pallet, and from WP-to-DS; these impacts could potentially cause dynamic loads that dent the outer barrier, which could result in creation of residual stresses. The uncertainty in this model parameter is represented using a uniform distribution.

WDGCA22 Parameter—This parameter relates to the temperature dependence for the general corrosion rate of the Alloy 22 WP outer barrier, which is characterized as an epistemically uncertain quantity. As explained in Section 6.3.5, this parameter determines the magnitude of this temperature dependence and directly influences the short-term and long-term general

corrosion rates of the Alloy 22. Larger values of this parameter correspond to higher general corrosion rates while WP temperatures are above 60 °C, and to lower general corrosion rates when WP temperatures are below 60 °C. This parameter is sampled from a truncated normal distribution

It is important to clarify that the parameter names IGRATE, SCCTHRP, and WDGCA22 are those used in the uncertainty and sensitivity analyses. The corresponding parameter names used in the TSPA-LA Model and the TSPA Input database are Igneous_Event_Prob_a, Stress_Thresh_A22_a, and C1_GenCorr_A22_a, respectively. More detailed discussion of the importance of these and other model parameters is given in Appendix K.

8.1.2 Groundwater Protection

The performance demonstration for the Groundwater Protection Standard was conducted in a manner consistent with the NRC requirements of 10 CFR 63.331 [DIRS 180319]. The radiation protection limits, set in the Groundwater Protection Standard, are restricted to the first 10,000 years after closure; thus, a performance demonstration for this standard beyond this time period was not conducted. The NRC implementation of this standard requires that the DOE TSPA: (1) evaluate potential releases for undisturbed performance, and (2) show a reasonable expectation that the level of radioactivity in a representative volume of groundwater does not exceed the numerical limits in 10 CFR 63.331 ([DIRS 180319], Table 1).

NRC Table 1 establishes limits for selected radionuclides and specific types of radiation emitted. More specifically, Table 1 limits radionuclides in the representative volume in terms of three performance metrics:

1. Combined ^{226}Ra and ^{228}Ra activity concentrations (pCi/L) in groundwater is $\leq$ 5 pCi/L (natural background included)

2. Gross alpha activity (including ^{226}Ra but excluding radon and uranium isotopes) concentration is $\leq$ 15 pCi/L (natural background included)

3. Combined beta- and photon-emitting radionuclides doses to the whole body or any organ (based on drinking 2 liters of water per day from the representative volume) is $\leq$ 4 mrem.

Performance calculations for all three regulatory metrics are for the point of highest concentration in the plume of contamination in the accessible environment. The calculations of whole body and organ doses are based on using the representative volume of groundwater of 3,000 acre-ft/yr, as specified in 10 CFR 63.332 [DIRS 180319].

It is important to clarify that the term undisturbed performance, as defined in the NRC regulations (10 CFR 63.302 [DIRS 180319]), means that "human intrusion or the occurrence of unlikely natural features, events, and processes do not disturb the disposal system." The NRC defines unlikely as "features, events, and processes, or sequences of events and processes, i.e., those that are estimated to have less than one chance in 10 and at least one chance in 10,000 of occurring within 10,000 years" (10 CFR 63.342(b) [DIRS 178394]). Simply stated, the performance demonstration for the groundwater protection standard requires that the TSPA

assess radionuclide releases caused by "likely" FEPs (i.e., having an annual frequency of 10^{-5}/yr or greater).

Scenario Classes and Modeling Cases Considered—The regulatory definitions for undisturbed performance and unlikely FEPs were used to select specific modeling cases for inclusion in the performance demonstration for this standard. The results of that screening are summarized below:

- Nominal Modeling Case included
- Waste Package EF Modeling Case included
- Drip Shield EF Modeling Case included
- Igneous Intrusion Modeling Cases excluded
- Volcanic Eruption Modeling Cases excluded
- Seismic GM Modeling Case included (for PGVs with annual frequency greater than 10^{-5}/yr only)
- Seismic FD Modeling Case excluded.

The Nominal Modeling Case by definition represents all the expected or likely FEPs. However, because of the inherent characteristics of the natural barrier and performance of the EBS, the effects of corrosion on the WPs (and DSs) are expected to be very small and thus the WPs and DSs are not expected to fail within the 10,000 years for this modeling case.

The Waste Package and Drip Shield EF Modeling Cases were selected for inclusion in the performance demonstration because the probability of an early failure of a WP or DS is greater than 10^{-5} (Section 6.4).

Both the Igneous Intrusion and the Volcanic Eruption Modeling Cases have mean annual frequencies of occurrence that are much less than 10^{-5} per year (Section 6.5). In fact, these two modeling cases are characterized by unlikely FEPs with estimated mean annual frequencies of slightly greater than 10^{-8} per year (Section 6.5). On this basis, the two igneous modeling cases were excluded from consideration in the performance demonstration for groundwater protection.

The Seismic GM Modeling Case represents events and processes with mean exceedance frequencies in the range from 10^{-8} to 4.287×10^{-4} per year (SNL 2007 [DIRS 176828], Section 6.4.3). In contrast, the Seismic FD Modeling Case represents events that do not occur with mean exceedance frequencies greater than 10^{-7} per year (Section 6.6.1.2.3). Therefore, the Seismic GM Modeling Case events with mean exceedance frequencies in the range from 10^{-5} to 4.3×10^{-4} per year are considered to be likely and are included in the TSPA for the groundwater protection standard. The Seismic FD Modeling Case is excluded because of its low annual exceedance frequency near 10^{-7} per year (SNL 2007 [DIRS 176828], Table 6-67).

In summary, the performance demonstration for the Groundwater Protection Standard considered radionuclide releases for FEPs that were represented in the Waste Package and Drip Shield EF

Modeling Cases, and the Seismic GM Modeling Case. The early failure and ground motion modeling cases are implemented in a probabilistic manner to determine the number of WPs failed as a function of time in a given realization (Sections 6.4 and 6.6). As indicated previously, the projections for this standard are based on considering releases only from the damaged CDSP WPs; the potential releases from the CSNF WPs were omitted because the contribution to expected annual dose from seismic damage to CSNF WPs has been shown to be insignificant (Section 7.3.2.6.1.3).

Probabilistic projections for the three groundwater protection metrics were developed for the time period of 10,000 years and compared to the specified numerical limits. Those comparisons are presented and explained below.

8.1.2.1 Projections for Combined ^{226}Ra and ^{228}Ra

The performance demonstration for this first metric of the Groundwater Protection Standard is based on the combined activity concentration for ^{226}Ra and ^{228}Ra. The probabilistic projections of the time history of the activity concentrations are presented on Figure 8.1-9. The curves shown are background, mean, and 95th percentile activity concentrations of combined radium species (excluding background). As shown on Figure 8.1-9, the 95th percentile value for the combined radium concentration is less than the mean value. This result was a consequence of a few realizations that projected relatively high, but still small, radium concentrations that skewed the distribution of radium concentrations and caused the mean value to be higher than the 95th percentile value.

The curves on Figure 8.1-9 show that the peak mean groundwater concentration of combined ^{226}Ra and ^{228}Ra at the RMEI location is less than 10^{-5} pCi/L, which is well below the 5 pCi/L limit found in 10 CFR 331 ([DIRS 180319], Table 1). The naturally occurring background activity concentration of combined radium at the site is estimated to be ~0.5 pCi/L (SNL 2008 [DIRS 183750], Section 6.8.5, Table 6-18). At this background level, the projected peak radium activity concentrations of less than 10^{-5} pCi/L for the postulated repository releases would not make any measurable change to the background level in groundwater at the RMEI location. The fundamental reasons for the very low combined radium concentrations at the RMEI location are as follows:

^{228}Ra Activity Concentration—The chemical and nuclear properties of ^{228}Ra, together with its very small inventory, largely explain its small contribution to the total radium activity concentrations. As previously stated, the radioelement radium sorbs very strongly in the geologic media (Tables 6.3.9-2 and 6.3.10-2). This chemical property translates into ^{228}Ra taking very long transport times to migrate through the lower natural barrier. As previously stated, the projected mass breakthrough curves for radium through the SZ alone are predominantly greater than 10,000 years. However, if one postulates a hypothetical fast pathway with a very unlikely transport time, for example, of 500 years, then ^{228}Ra, with a half-life of 5.8 years, would experience about 86 half-lives of decay before reaching the RMEI location. This would reduce its activity by a factor of $(1/2)^{86} \sim 10^{-26}$. The initial total inventory ^{228}Ra in the CDSP WPs can be estimated by multiplying its specific activity (Table 6.3.7-5) times the number of grams of ^{228}Ra per package (Table 6.3.7-5) times the total number of CDSPs (Table 6.3.7-1) or $(2.72 \times 10^{2}$ Ci/g $\times \sim 2 \times 10^{-5}$ g/pkg $\times$ 3416 pkg) = 18.6 Ci or less than 20 Ci. This means that,

after 86 half-lives of decay, the original quantity of ^{228}Ra would be reduced to 2×10^{-13} pCi. Mixing this activity in the representative volume of 3,000 acre-ft would suggest that the ^{228}Ra activity concentration in the groundwater would likely be undetectable.

Considering that ^{228}Ra is a member of the thorium series, it could potentially reach the RMEI location via transport of its precursor ^{232}Th and subsequent in-growth. The relevant part of the decay chain is:

$$^{232}\text{Th (half-life } 1.4 \times 10^{10} \text{ years)} \rightarrow {}^{228}\text{Ra}$$

Because of its extraordinarily long half-life, the ^{232}Th is for all practical purposes a stable element for time periods of 10,000 years. For this reason, it is conservatively assumed that ^{228}Ra and ^{232}Th are in secular equilibrium and the activity of ^{228}Ra is the same as the ^{232}Th.

In the absence of ^{228}Ra inventory regeneration by in-growth and considering characteristically long radium transport times (through the SZ alone), it is reasonable to expect the activity concentrations for ^{228}Ra to show effectively undetectable levels for 10,000 years after disposal.

^{226}Ra Activity Concentration—The explanation for the projected low ^{226}Ra activity concentrations is similar to that for ^{228}Ra. The primary difference is that ^{226}Ra is a member of the uranium series with its two primary precursors being ^{234}U (half-life 240,000 years) and ^{230}Th (half-life 7.54×10^4 years). Over a time period of 10,000 years, the ^{234}U activity would experience a decay change of about 3 percent, which is a relatively small amount of in-growth to ^{230}Th. Similarly, about 9 percent of ^{230}Th activity would decay to ^{226}Ra in 10,000 years. In contrast, ^{226}Ra activity would diminish by almost 99 percent over the 10,000 years.

As noted previously, the median ^{226}Ra transport times through SZ for individual Monte Carlo realizations range from 18,000 years to more than 1,000,000 years, with the median over all realizations exceeding 700,000 years. The median ^{230}Th transport times through SZ for individual realizations range from about 1,000 years to more than 1,000,000 years, with a median for all realizations of greater than 1,000,000 years. Because the ^{226}Ra will be inventory limited, and its projected long transport times in the SZ, it is reasonable to expect that ^{226}Ra activity concentration would be low. Moreover, ^{226}Ra is limited by the small in-growth from ^{230}Th, occurring along the groundwater flow path.

Thus, the probabilistic projections for the combined radium groundwater standard demonstrate a reasonable expectation that the level of radioactivity in a representative volume of groundwater (i.e., 3,000 acre-ft) would not exceed the numerical limit of 5 pCi/L for groundwater protection.

8.1.2.2 Projections for Gross Alpha Activity

The performance demonstration for this metric of the Groundwater Protection Standard is based on a calculation of the gross alpha activity, including ^{226}Ra but excluding ^{222}Rn and Uranium species (10 CFR 63.331). The TSPA Biosphere Component Model, documented in DTN: MO0702PAGWPROS001_R0 [DIRS 179328], identifies 15 primary radionuclides that have one or more alpha emitters in their decay chain to the next tracked radionuclide. The specific alpha emitting radionuclides to consider in estimating the gross alpha are:

- ^{210}Pb (half-life 22.3 years)
- ^{226}Ra (half-life 1,600 years)
- ^{227}Ac (half-life 21.8 years)
- ^{228}Th (half-life 1.913 years)
- ^{229}Th (half-life 7,300 years)
- ^{230}Th (half-life 75,400 years)
- ^{232}Th (half-life 1.4×10^{10} years)
- ^{231}Pa (half-life 32,800 years)
- ^{237}Np (half-life 2.14×10^{6} years)
- ^{238}Pu (half-life 87.7 years)
- ^{239}Pu (half-life 24,100 years)
- ^{240}Pu (half-life 6,560 years)
- ^{242}Pu (half-life 3.75×10^{5} years)
- ^{241}Am (half-life 433 years)
- ^{243}Am (half-life 7,370 years).

The probabilistic projections for gross alpha activity concentrations over the 10,000-year time period are shown on Figure 8.1-10. The activity concentration for gross alpha was calculated based on the annual mass flux of the alpha emitting radionuclides across the boundary of the accessible environment and collected in the representative groundwater volume of 3,000 acre-ft/yr. The plot on this figure shows curves for the mean and 95th percentile for gross alpha activity concentration. The peak mean activity concentration is projected to be less than 1×10^{-4} pCi/L (excluding background). This activity concentration is below the ground-water protection standard of 15 pCi/L (found in 10 CFR 331 [DIRS 180319], Table 1) for gross alpha and well below the natural background level of ~0.5 pCi/L in the site groundwater. As a result, the postulated releases of the alpha emitting radionuclides are effectively limited by the EBS and sufficiently confined to the lower natural barrier.

The radionuclides making the largest contributions to mean gross alpha activity are ^{237}Np, ^{239}Pu, ^{240}Pu, and ^{242}Pu. These four radionuclides have relatively large initial inventories (in the CSNF waste form) and long to very long half-lives. Moreover, the three plutonium species are transported through the groundwater pathway in both dissolved and colloidal phases. The low contributions of the other alpha emitters can be plausibly explained by examining their initial inventories (Table 6.3.7-5), decay chain properties (Figure 6.3.7-4), half-lives (Figure 6.3.7-4), and sorption properties (Tables 6.3.9-2 and 6.3.10-2) (i.e., distribution coefficient or K_d). A qualitative examination leads to the following observations and inferences explained below.

Low Inventory, Short Half-Lives, and Strong Sorption—The alpha emitting radionuclide ^{228}Th is easily eliminated as a potentially significant contributor to gross alpha because its very short half-life of 1.913 years and low initial inventory (provided by the decay of ^{245}Cm) will most likely deplete before loss of containment. Similarly, the radionuclides ^{238}Pu and ^{241}Am have relatively short half-lives; equally important is the fact that they are strongly sorbed in the UZ rock layers and in the volcanic units and alluvium of the SZ. Thus, it is reasonable to expect that these two alpha emitters are not likely to reach the accessible environment in most TSPA-LA realizations. Thus, based on these qualitative arguments, ^{228}Th, ^{238}Pu, and ^{241}Am will likely not make a significant contribution to the gross alpha activity concentrations.

Secular Equilibrium and Sorption—The alpha emitting radionuclides ^{210}Pb, ^{226}Ra, and ^{227}Ac are not likely to be significant contributors to gross alpha because their activity is controlled via secular equilibrium with their precursor radionuclides, namely:

$$^{232}\text{Th (half-life } 1.4 \times 10^{10} \text{ years)} \rightarrow {}^{228}\text{Ra (half-life 5.8 years)} \rightarrow {}^{210}\text{Pb}$$

$$^{230}\text{Th (half-life 77,000 years)} \rightarrow {}^{226}\text{Ra}$$

$$^{231}\text{Pa (half-life 32,800 years)} \rightarrow {}^{227}\text{Ac.}$$

As was explained earlier for the combined radium groundwater standard, these radionuclide species are unlikely to produce significant activity concentrations at the accessible environment boundary because of the sorption properties of both radium and its precursor thorium. In the case of the radioelement protactinium, its initial inventory in the WPs is low and its sorption properties in the unsaturated rock layers is relatively high (e.g., mean K_ds of ~5,000 mL/g), which suggests that the precursors (^{232}Th, ^{230}Th, and ^{231}Pa) or the daughters (^{210}Pb, ^{226}Ra, and ^{227}Ac) are not likely to contribute appreciably to the gross alpha activity levels.

Very High Sorption—The radioelement americium has the property of being very strongly sorbed in the unsaturated rock layers (e.g., mean K_ds of 400 to about 5,000 mL/g), as well as in the volcanic units (e.g., mean K_ds of 400 to about 5,000 mL/g) and alluvium (e.g., mean K_ds of ~5,000 mL/g) of the SZ. On the other hand, this radioelement has a significant initial inventory in the CSNF and can also be transported in colloidal phase (i.e., reversible and irreversible).

Thus, the probabilistic projections for this regulatory performance metric show a reasonable expectation that the level of radioactivity in a representative volume of groundwater would not exceed the numerical limit of 15 pCi/L for groundwater protection.

8.1.2.3 Projections for Combined Beta- and Photon-Emitting Radionuclides

The performance demonstration for this metric of the Groundwater Protection Standard is based on combined beta- and photon-emitting radionuclides; both the primary beta emitters and any daughter products that decay by beta-emission are considered. The annual doses from exposure to beta-photon emitters are quantified in terms of both whole body and organ dose. The TSPA Biosphere Component Model documented in the *Biosphere Model Report* (SNL 2007 [DIRS 177399], Table 6.15-4), identifies a total of 19 primary radionuclides that are used to compute this groundwater protection metric.

Some of the more prominent beta emitters are: ^{14}C, ^{36}Cl, ^{79}Se, ^{90}Sr, ^{99}Tc, ^{129}I, ^{135}Cs, and ^{137}Cs. Of this set, only ^{90}Sr and ^{137}Cs have short half-lives (~ 30 years) relative to the 10,000 year time period. Some of the beta-photon emitters are daughter products of alpha and beta emitters (SNL 2007 [DIRS 177399], Table 6.15-4) such as ^{137m}Ba, ^{228}Ac, ^{212}Pb, and ^{208}Tl. Because this group of radioisotopes has half-lives ranging from minutes to several hours, they are not included in radionuclide transport calculations; however, the associated conversion factors are included in calculating the beta-photon dose. The projections of annual doses for these radionuclides are evaluated as a function of the release rates from the repository, in-growth, and groundwater transport to the accessible environment.

Probabilistic projections for the mean whole body and thyroid annual doses for the 10,000-year time period are shown on Figure 8.1-11; a curve for the 95th percentile is also shown. These annual doses were calculated by summing all the annual doses from the beta- and photon-emitting radionuclides included in the TSPA-LA Model. The peak mean annual drinking water dose to the thyroid is estimated to be about 0.2 mrem. The whole body dose shown on the same figure takes into account the effect on all organs and includes the organ-dose weighting factors. The peak mean annual drinking water dose to the whole body in this case is estimated to be about 4×10^{-2} mrem. The radionuclide that dominates the mean thyroid dose is ^{129}I, whereas ^{99}Tc dominates the mean whole body dose.

Thus, the probabilistic projections for combined beta-photon dose demonstrate a reasonable expectation that the annual doses to the whole body or any organ would not exceed the numerical limit of 4 mrem.

8.1.3 Human Intrusion Protection

As required by the proposed NRC regulation, a performance demonstration was developed for the Human Intrusion Standard (10 CFR 63.321 [DIRS 178394]). The probabilistic projections provide an estimate of the annual dose to the RMEI resulting from a stylized human intrusion drilling scenario and compare the result to the dose limits that the geologic repository at the Yucca Mountain site must meet. The EPA regulation 40 CFR Part 197 (2005 [DIRS 175755]) clarifies that the performance assessment for the Human Intrusion Scenario is to be presented separately and not integrated into the TSPA for the Individual Protection Standard.

The Human Intrusion Standard parallels the Individual Protection Standard in that the same numerical limits for annual dose must be met. More specifically, the Human Intrusion Standard (10 CFR 63.321 (a) and (b) in the proposed NRC regulation [DIRS 178394]) specifies that the DOE must:

1. Determine the earliest time after disposal that a WP would degrade sufficiently that a drilling intrusion could occur without recognition by the drillers

2. Demonstrate a reasonable expectation that the RMEI, as a result of the human intrusion, will not receive an annual dose of:

    a. 0.15 mSv (15 mrem) for 10,000 years following disposal

    b. 3.5 mSv (350 mrem) after 10,000 years, but within the period of geologic stability

3. Include all potential environmental pathways of radionuclide transport and exposure subject to the requirements of 10 CFR 63.322 [DIRS 180319].

The characteristics and assumptions of the stylized Human Intrusion Scenario are specified in the NRC regulation 10 CFR 63.322 [DIRS 180319]. That section of the regulation prescribes the following scenario characteristics for the drilling event:

- There is a single human intrusion as a result of exploratory drilling for ground water, per 10 CFR 63.322(a).
- The intruders drill a borehole directly through a degraded WP into the uppermost aquifer underlying the Yucca Mountain Repository, per 10 CFR 63.322 (b).
- The drillers use the common techniques and practices that are currently employed in exploratory drilling for ground water in the region surrounding Yucca Mountain, per 10 CFR 63.322 (c).
- Careful sealing of the borehole does not occur, instead natural degradation processes gradually modify the borehole, per 10 CFR 63.322 (d).
- No particulate waste material falls into the borehole, per 10 CFR 63.322 (e).
- The exposure scenario includes only those radionuclides transported to the SZ by water (e.g., water enters the WP, releases radionuclides, and transports radionuclides by way of the borehole to the SZ), per 10 CFR 63.322 (f).
- No releases are included which are caused by unlikely natural processes and events, per 10 CFR 63.322 (g).

With regard to the last specification, the NRC regulation defines unlikely natural processes and events as those having a probability of less than one chance in 10 and at least one chance in 10,000 of occurring within 10,000 years of disposal, as defined in 10 CFR 63.342(b) [DIRS 178394]. This probability statement is equivalent to a cut-off annual frequency criterion of $\leq 10^{-5}$/yr for exclusion of unlikely processes and events.

For the purposes of the TSPA, it is assumed that inadvertent drilling into the repository results in a penetration of the DS and WP, as well as creating a direct pathway to the groundwater. The conceptualization of the scenario includes radionuclides transported vertically through the UZ, horizontally along the SZ, and then withdrawn with the groundwater at the location of the RMEI. The exposure characteristics for the RMEI are as defined in 10 CFR 63.312(a) through (e) [DIRS 180319].

8.1.3.1 Determination of Earliest Time for Drilling Intrusion

A detailed technical study was conducted to establish a technical basis to address the first requirement of the Human Intrusion Standard (i.e., 10 CFR 63.321(a) [DIRS 178394]). That study, which is presented in Section 6.7.2, examined three general aspects of the hypothetical drilling intrusion, namely:

1. Capability of intact DSs and WPs to resist penetration by drilling technology typically used in groundwater exploration
2. Drilling operating characteristics (i.e., change-in-conditions) that would or would not indicate drill-bit impingement on a metallic anthropogenic structure

3. Degradation of DSs and WPs by nominal processes and likely disruptive events that could provide a physical pathway for a drill-bit to penetrate the WP without recognition by the drillers.

With regard to the scenario conditions, likely processes and events refers to those events with a frequency of occurrence greater than or equal to 10^{-5}/yr, as specified by the NRC regulation.

The technical basis, which is summarized herein, was used to develop a bounding estimate of 200,000 years for the earliest time of WP penetration (without recognition by drillers). That bounding estimate was used in the probabilistic projections of annual dose to the RMEI, which are presented in Section 8.1.3.2

Capability of Intact DSs and WPs to Resist Drilling Penetration

The 15-mm (0.59 in.) thick Titanium Grade 7 DS plate and 25-mm (0.98 in.) thick Alloy 22 WP outer barrier constitutes a significant double barrier to potential groundwater drilling intrusion. In the case of the CSNF package, which is a canister within a canister, there would be an additional 50.8-mm (2 in.) thick stainless steel barrier to resisting potential drilling intrusion. The capability of the DS and WP barriers to resist a drilling penetration was examined from two perspectives: (1) drill-bits typically used in groundwater exploration in rock formations, and (2) scenario of drill string free-fall through an open drift and potentially penetrating a DS and WP.

Drilling Technology—Drilling technology that would be used in drilling water wells through welded tuff at Yucca Mountain would typically utilize roller bits (IADC 1992 [DIRS 155232]) to drill through the rock formations. Roller bits are very effective in drilling through welded tuff formations and basically cause brittle failure of the rock matrix and break and crush the rock to facilitate removal. This type of drill-bit, however, would be ineffective in attempting to bore through the metal barriers because of the high compressive strength and ductility of titanium and stainless steel. Penetration of these intact metal barriers would require a drill-bit designed to induce metal failure; such types of drill-bits are not typically used in exploratory drilling for water in the Southwestern United States. Moreover, attempts to drill through intact DSs and/or WPs would result in significant changes to the drilling operation characteristics, which would be clear indicators of the drill-string encountering a metallic anthropogenic structure.

Drill-String Free-Fall and Impingement on WP—A drill-string entering an open emplacement drift could experience a free-fall and, in turn, directly impacting the intact DS and WP. The potential for WP penetration was evaluated for the case of a 300 m, 14-metric ton drill-string assembly (i.e., drill pipe, drill collar, and drill-bit) assuming no DS present with drop heights of 1.8 m (i.e., approximate distance to CSNF) and 1.6 m (i.e., approximate distance to CDSP). A bound for the maximum impact velocity of such a drill-string free-fall was estimated to be about 5.9 m/s for both the CSNF and CDSP packages.

The potential for rupture of the WP outer barrier for the above conditions was evaluated by utilizing calculational results from detailed structural analyses for WP-to-pallet impacts (SNL 2007 [DIRS 178851], Section 6.3.2), which provide strain-based rupture conditions as a function of impact velocities. This comparative analysis indicates that the drill-string impact would not penetrate an intact WP. A more likely outcome of a drill-string free-fall would be impingement on and deformation of the DS. In the unlikely event that the DS was actually penetrated by the drill-string, it would absorb the impact energy, which would reduce the impact velocity, and further reduce the potential for penetration of the WP.

Drilling Operating Characteristics

Drilling operations generally involve monitoring of the bit operating conditions as the drill-string penetrates the rock formations. Typical characteristics that are monitored by drillers include circulating fluid properties and rates, drilling stability, bit weight, and rotary speed. Significant changes in any of these types of operating characteristics generally prompt the driller to examine and resolve the change in operating characteristics. In the case of a drill-string entering an open emplacement drift and impinging the DS and/or WP, the following changes in the operating characteristics would likely occur:

- Loss of circulation fluid
- Sudden changes in rotary speed
- Rapid increase in drill-string vibration.

Moreover, driller attempts to correct volumetric problems with the circulating fluid (i.e., by spot cementing and setting cases) would be largely thwarted by the large drift volume and physical presence of the DS and WP. These problems would likely prompt the driller to remove the drill-string from the borehole and examine the drill-bit. Such diagnostic actions by the driller would lead to recognition that a metallic anthropogenic structure had been encountered.

Under conditions of a drift collapse, however, changes in some operational characteristics could be muted and, therefore, less recognizable. For example, the loss of circulating fluid in a collapsed drift (i.e., filled with rubble) would still occur but could be mitigated by the driller. Changes in drill-bit rotation speed would be unaffected until the drill-bit encountered the DS, at which time the drill-string would exhibit vibration. Drift collapse would primarily occur as a result of cumulative effects of seismic events (i.e., vibratory ground motion) in the lithophysal regions of the repository. Such drift collapse events are currently projected to occur in the post-10,000-year time period.

Degradation of Drip Shields and Waste Packages by Nominal and Disruptive Scenario Conditions

The study considered four scenarios for WP and DS degradation: (1) nominal degradation of the DSs and WPs, (2) DS early failures (i.e., having an undetected defect that could cause an early failure), (3) DS and WP failures as a result of igneous intrusion disruptive events, and (4) DS and

WP failures as a result of seismic events (i.e., seismic ground motion and seismic fault displacement). Of these scenario conditions, three were screened-out because their frequency of occurrence was less than the NRC cut-off of 1 chance in 10 in 10,000 years or 10^{-5}/yr, namely:

- Early Failure: The probability that a drilling intrusion encounters a DS early failure occurring at the same location is estimated to be 7×10^{-6}
- Igneous Intrusion: Exceedance frequency of igneous events in the repository footprint estimated to be less than 10^{-5}/yr but greater than 10^{-8}/yr
- Seismic Fault displacement: Exceedance frequency of seismic fault displacement in the repository footprint is estimated to be less than 2.5×10^{-7}/yr.
- Seismic Ground Motion: (1) peak ground velocities, with exceedance frequencies greater than or equal to 10^{-5}/yr, are relatively low and unlikely to induce dynamic loads sufficient to cause DS plate failure, and (2) exceedance frequency of seismic-induced large block movements, which could rupture DSs and damage WPs, are less than 1.17×10^{-6}/yr (DTN MO0712PBANLNWP.000_R0 [DIRS 184664], file *Nonlith LC Calculation Rev03.xmcd*).

Thus, nominal degradation processes are the most probable way that a penetration (i.e., opening) could develop in the DSs and WPs that could potentially a serve as a physical pathway to groundwater drilling—facilitating a penetration without recognition by the drillers.

In the case of the DSs, thinning of the titanium DS plate would occur over geologic time periods. Over a period of 10,000 years, for example, the extent of thinning of the 15-mm-thick DS plate by general corrosion is projected to be approximately 0.66 mm or a thinning of about 4 percent of the total thickness. This projection is based on a high corrosion rate corresponding to a 0.9999 quantile (Section 6.3.5.1.3). Assuming this same corrosion rate, the DS plate failure time is projected to occur at about 230,000 years; this estimate is corroborated by more detailed probabilistic projections for nominal conditions that calculate the first DS plate failure occurring at about 270,000 years (Figure 8.1-4). Those detailed probabilistic projections, also for nominal conditions, indicate that the mean failure time of the first penetration of WP outer barrier by general corrosion patches occurs at about 440,000 years (DTN: MO0709TSPAWPDS.000 [DIRS 183170]).

Based on the above considerations and evaluations, the estimate of the earliest time a driller could penetrate a WP, without recognition by the driller, was taken to be 200,000 years. This time is a conservative bound to DS fail time and neglects the lifetime of the WPs.

8.1.3.2 Projections of Annual Doses for Human Intrusion

To address the second requirement of the Human Intrusion Standard (10 CFR 63.321(b) [DIRS 178394]), a probabilistic TSPA methodology, analogous to that used to demonstrate

performance with the Individual Protection and Groundwater Protection Standards, was used to make projections of the annual dose. The calculations of annual dose to the RMEI were performed for all environmental pathways, as specified in 10 CFR 63.321(c) [DIRS 178394]. Based on the analysis described above, the earliest time after disposal for the drilling intrusion was taken to be 200,000 years.

As described in Section 6.1.2.5, the type of WP (i.e., CSNF or CDSP) assumed to be penetrated is sampled in the analysis so that probabilistic projections of annual dose reflect the radionuclide releases from the various waste forms (Section 6.3.5). Based on the proportion of WP types, the probability of sampling a CSNF WP is ~0.7, whereas the probability of selecting a CDSP WP is ~0.3. The location of the penetration in the repository footprint was also sampled so as to reflect the range of percolation fluxes that would induce waste dissolution and releases.

The probabilistic projections of expected annual dose for the Human Intrusion Scenario are presented on Figure 8.1-12. The plots show the curves for the mean, median, and 5th and 95th percentiles of the distribution of expected annual doses for the period of geologic stability. The peak of the mean annual dose to the RMEI occurs within a few thousand years after inclusion. The peak mean and median annual individual doses are projected to be less than 0.008 mrem and 0.006 mrem, respectively, well below the regulatory limit of 350 mrem. The annual doses at the 5th and 95th percentiles are calculated to be approximately 0.001 mrem and 0.017 mrem, respectively.

The contributions of individual radionuclides to the total mean annual dose for the Human Intrusion Scenario for 1,000,000 years after repository closure, is shown on Figure 8.1-13. ^{99}Tc (half-life 2.13×10^5 yrs), ^{129}I (half-life 1.57×10^7 yrs), ^{36}Cl (half-life 3.01×10^5 yrs), and ^{237}Np (half-life 2.14×10^6 yrs) dominate the mean annual dose from 200,000 years to about 300,000 years; thereafter, dominance then transitions to ^{79}Se (half-life 2.95×10^5 yrs), ^{135}Cs (half-life 2.30×10^6 yrs), ^{242}Pu (half-life 3.75×10^5 yrs), and ^{237}Np (half-life 2.14×10^6 yrs). The ^{242}Pu, which is transported through the SZ in both dissolved and colloidal form, dominates the peak mean annual dose at 1,000,000 years.

Thus, these projections demonstrate that there is a reasonable expectation that the mean annual doses to the RMEI would be well below the limits for the Human Intrusion Standard. Moreover, the projections indicate that the system of multiple barriers would be sufficiently robust and resilient to limit annual doses for the prescribed Human Intrusion Scenario.

INTENTIONALLY LEFT BLANK

Table 8.1-1. Performance Demonstration Results for Individual Protection Standard

Time After Closure (yrs)	Projected Peak Mean Annual Dose (mrem)	Time of Peak Mean Annual Dose (yr)	Projected Peak Median Annual Dose (mrem)	Time of Peak Median Annual Dose (yr)	Limit for Annual Dose (mrem)
10,000	0.24	10,000	0.12	10,000	15 (mean)
1,000,000	2.30	1,000,000	0.99	~760,000	350 (median)

Source: Output DTN: MO0709TSPAREGS.000 [DIRS 182976]; Regulatory Limits from 10 CFR 63.311(a) ([DIRS 178394])

Table 8.1-2. Performance Demonstration Results for Groundwater Protection Standard

Type of Limit	Projected Peak Mean Activity Concentration or Annual Dose	Natural Background Level	Limit for Activity Concentration or Annual Dose
Combined Ra-226 & Ra-228	$<10^{-5}$ pCi/L	0.5 pCi/L	5 pCi/L
Gross Alpha Activity	$<10^{-4}$ pCi/L	0.5 pCi/L	15 pCi/L
Dose from Combined Beta & Photon Emitting Radionuclides	Whole Body ~ 0.04 mrem Thyroid ~ 0.17 mrem	Background level excluded in regulatory requirement	4 mrem

Source: Output DTN: MO0709TSPAREGS.000 [DIRS 182976]; Regulatory Limits from 10 CFR 63.331 ([DIRS 180319])

Table 8.1-3. Performance Demonstration Results for Human Intrusion Standard with Drilling Event at 200,000 years After Closure

Time After Closure (yrs)	Projected Peak Mean Annual Dose (mrem)	Limit for Annual Dose (mrem)
10,000	0	15 (mean)
1,000,000	$< 10^{-2}$	350 (median)

Source: Output DTN: MO0709TSPAREGS.000 [DIRS 182976]; Regulatory Limits from 10 CFR 63.321(b) ([DIRS 178394])

Table 8.1-4. Uncertainty in Projections of Peak Mean Annual Dose (mrem) for Individual Protection Standard

Time After Closure (yrs)	Mean	Median	5th Percentile	95th Percentile
10,000	0.24	0.12	6.43×10^{-3}	0.71
1,000,000	2.30	0.88	0.18	9.55

Source: Output DTN: MO0709TSPAREGS.000 [DIRS 182976]

Table 8.1-5. Uncertainty Importance Ranking as a function of time for Key TSPA-LA Model Parameters

Time After Closure (yrs)	Two Most Important Parameters at the Selected Time	
3,000	SCCTHRP	IGRATE
5,000	SCCTHRP	IGRATE
10,000	SCCTHRP	IGRATE
125,000	IGRATE	SCCTHRP
250,000	WDGCA22	IGRATE
500,000	IGRATE	WDGCA22
1,000,000	IGRATE	WDGCA22

Source: Output DTN: MO0709TSPASENS.000 [DIRS 182982]

NOTE: IGRATE = occurrence rate of igneous events

SCCTHRP = SCC stress threshold

WDGCA22 = temperature dependence parameter for alloy 22 general corrosion rate

Importance related to expected dose to RMEI for all scenario classes.

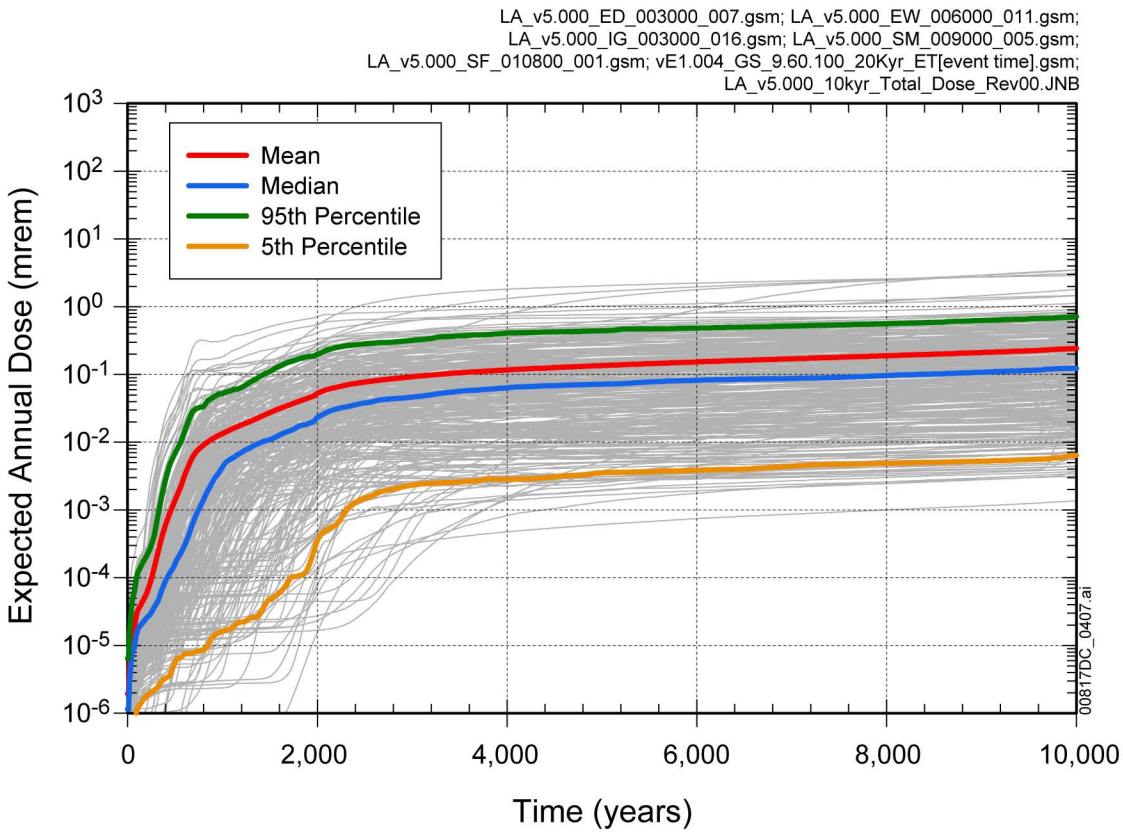

Source: Output DTN: MO0709TSPAREGS.000 [DIRS 182976].

Figure 8.1-1. Probabilistic Projections of Total Expected Annual Dose for 10,000 Years after Closure

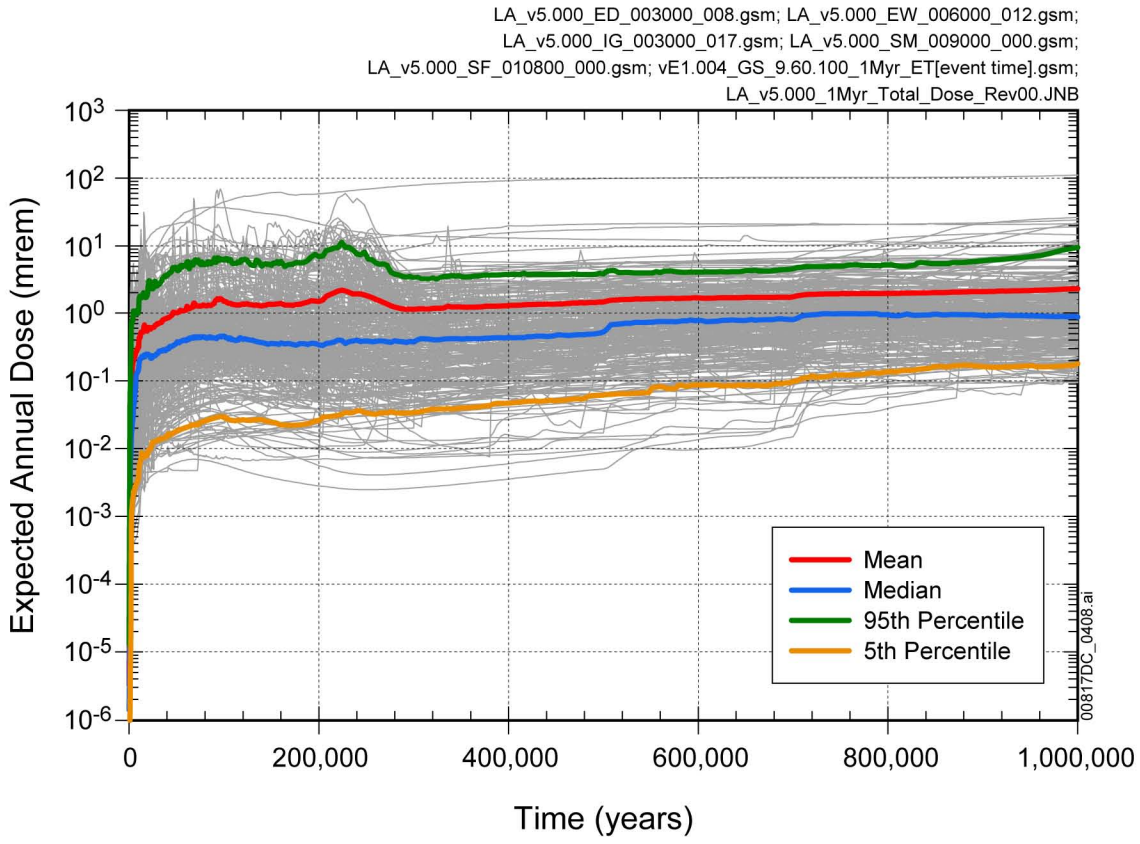

Source: Output DTN: MO0709TSPAREGS.000 [DIRS 182976].

Figure 8.1-2. Probabilistic Projections of Total Expected Annual Dose for 1,000,000 Years after Closure

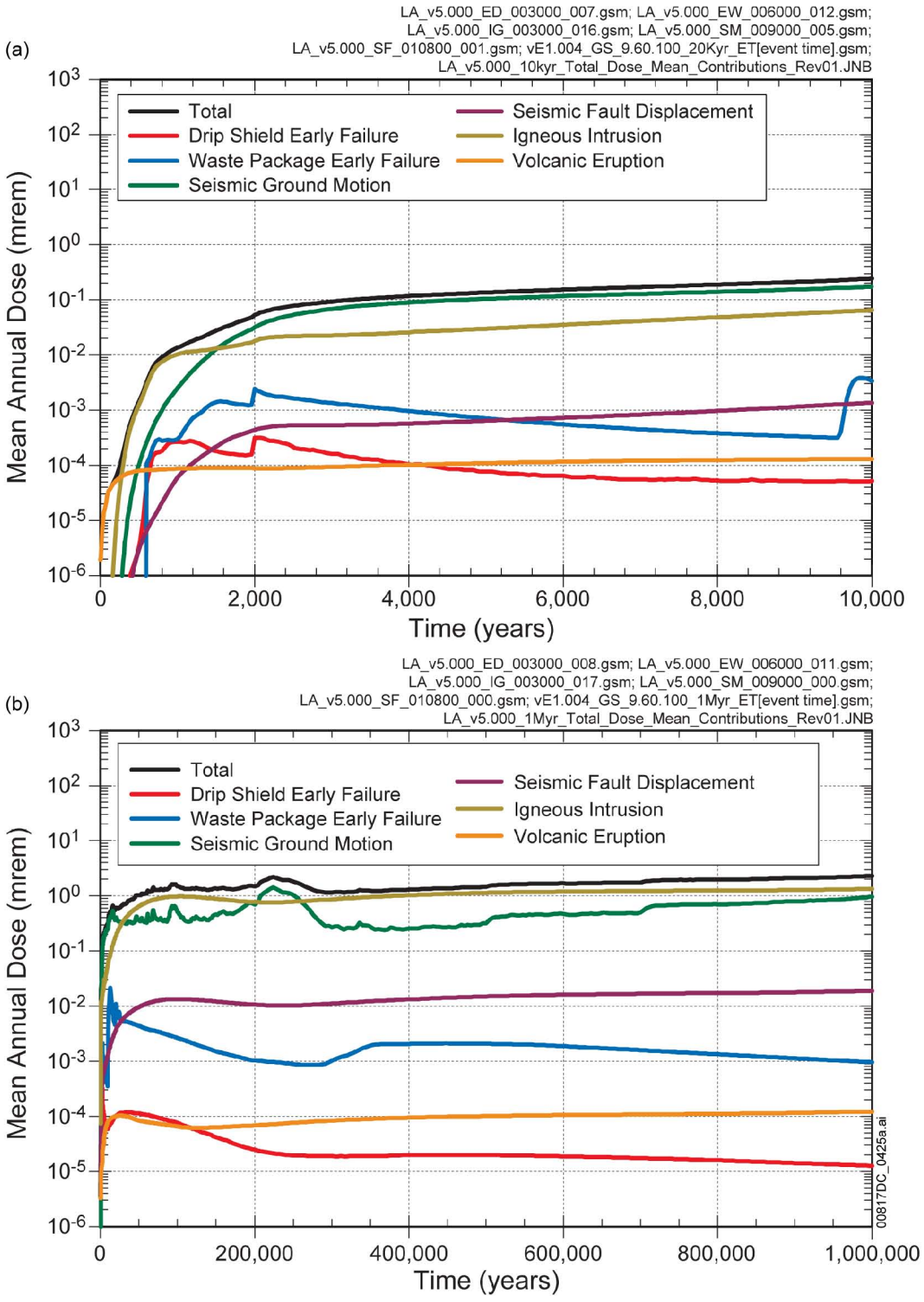

Source: Output DTN: MO0709TSPAREGS.000 [DIRS 182976].

Figure 8.1-3. Relative Contributions of Scenario Modeling Cases to Total Mean Annual Dose for (a) 10,000 Years and (b) 1,000,000 Years after Repository Closure

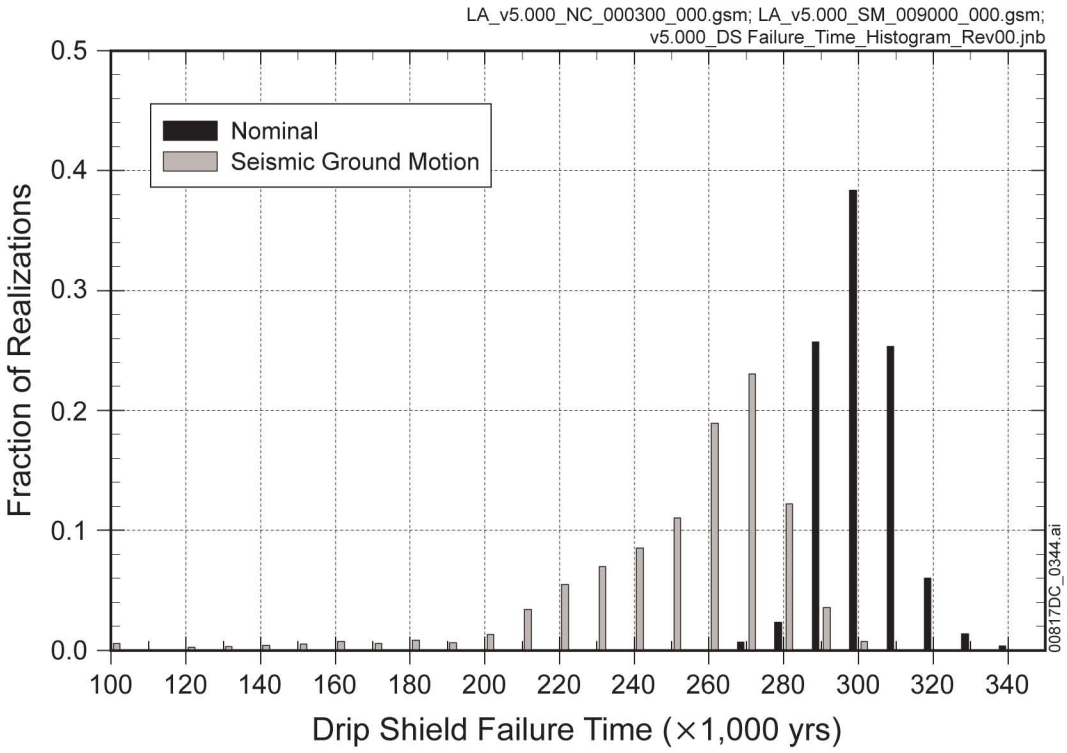

Source: Output DTN: MO0709TSPAREGS.000 [DIRS 182976].

NOTE: Nominal failures are due to general corrosion. Seismic ground motion failures are caused by the combined effects of general corrosion, vibratory ground motion, and rockfall.

Figure 8.1-4. Histogram of Drip Shield Failure for the Nominal and Seismic Ground Motion Modeling Cases

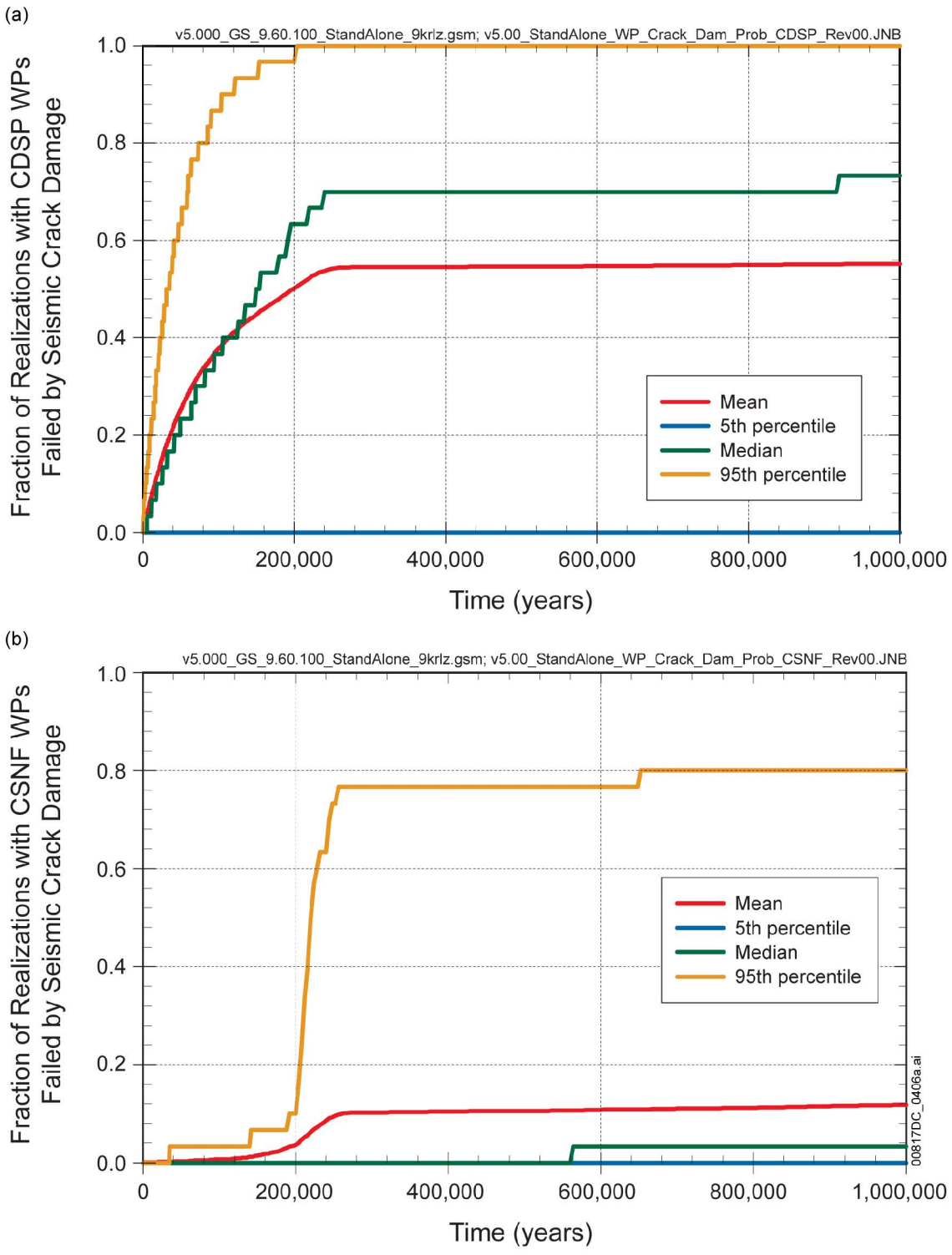

Source: Output DTNs: MO0709TSPAREGS.000 [DIRS 182976]; and MO0709TSPAWPDS.000 [DIRS 183170].

Figure 8.1-5. Fraction of (a) CDSP WPs and (b) CSNF WPs Failed for by Seismic Crack Damage as a Function of Time for Percolation Subregion 3

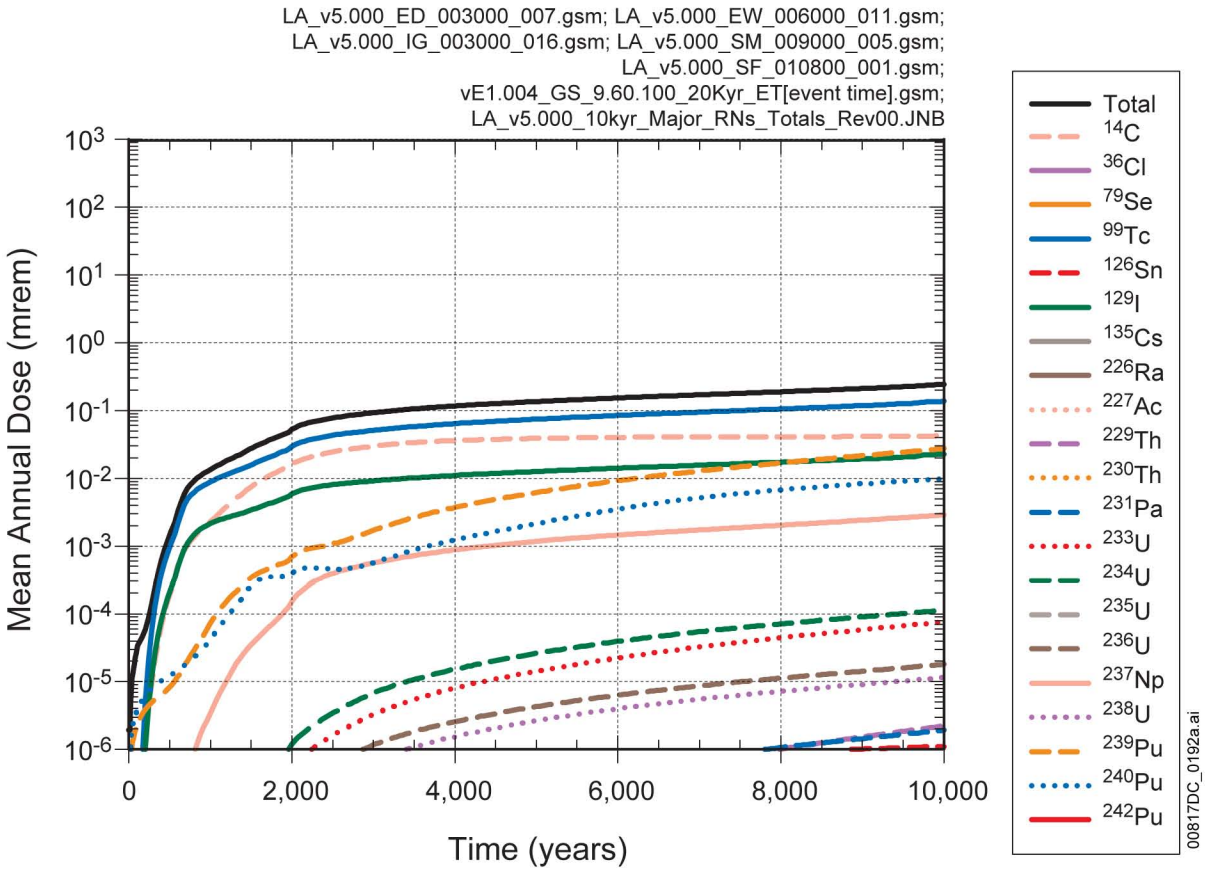

Source: Output DTN: MO0709TSPAREGS.000 [DIRS 182976].

Figure 8.1-6. Contribution of Individual Radionuclides to Total Mean Annual Dose for 10,000 Years after Repository Closure

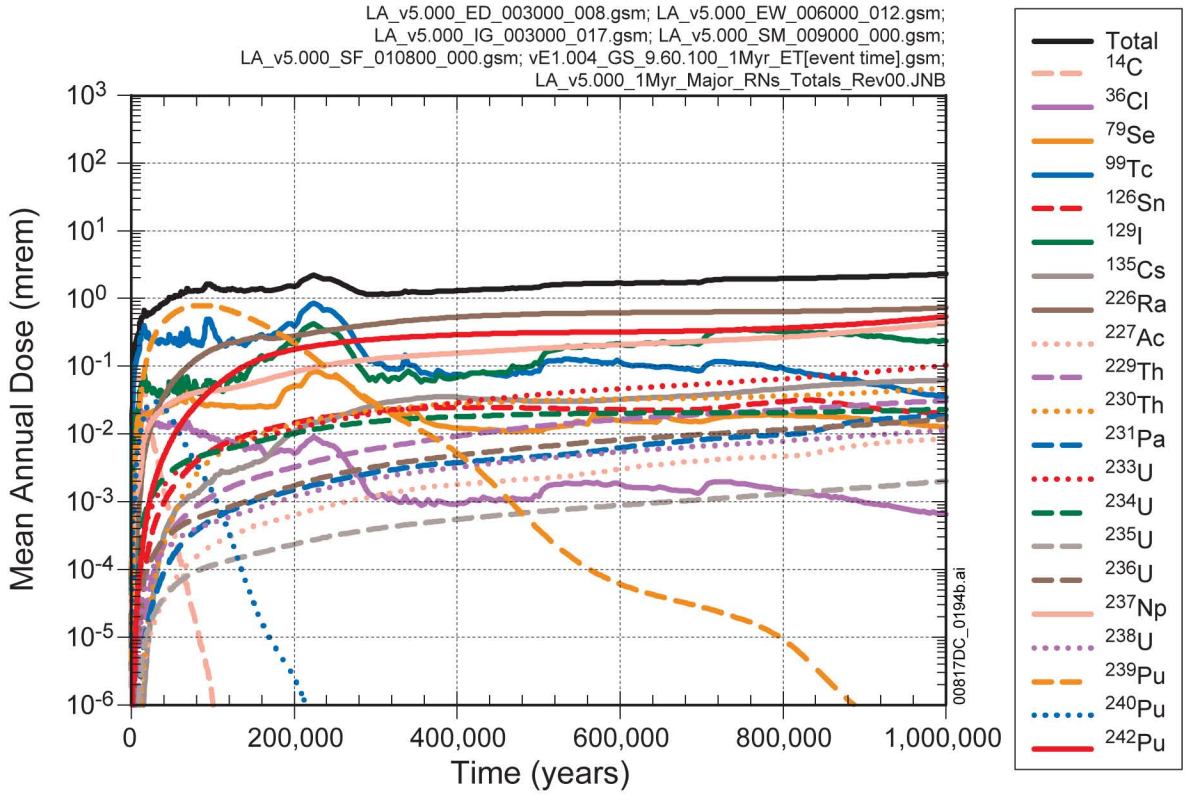

Source: Output DTN: MO0709TSPAREGS.000 [DIRS 182976].

Figure 8.1-7. Contribution of Individual Radionuclides to Total Mean Annual Dose for 1,000,000 Years after Repository Closure

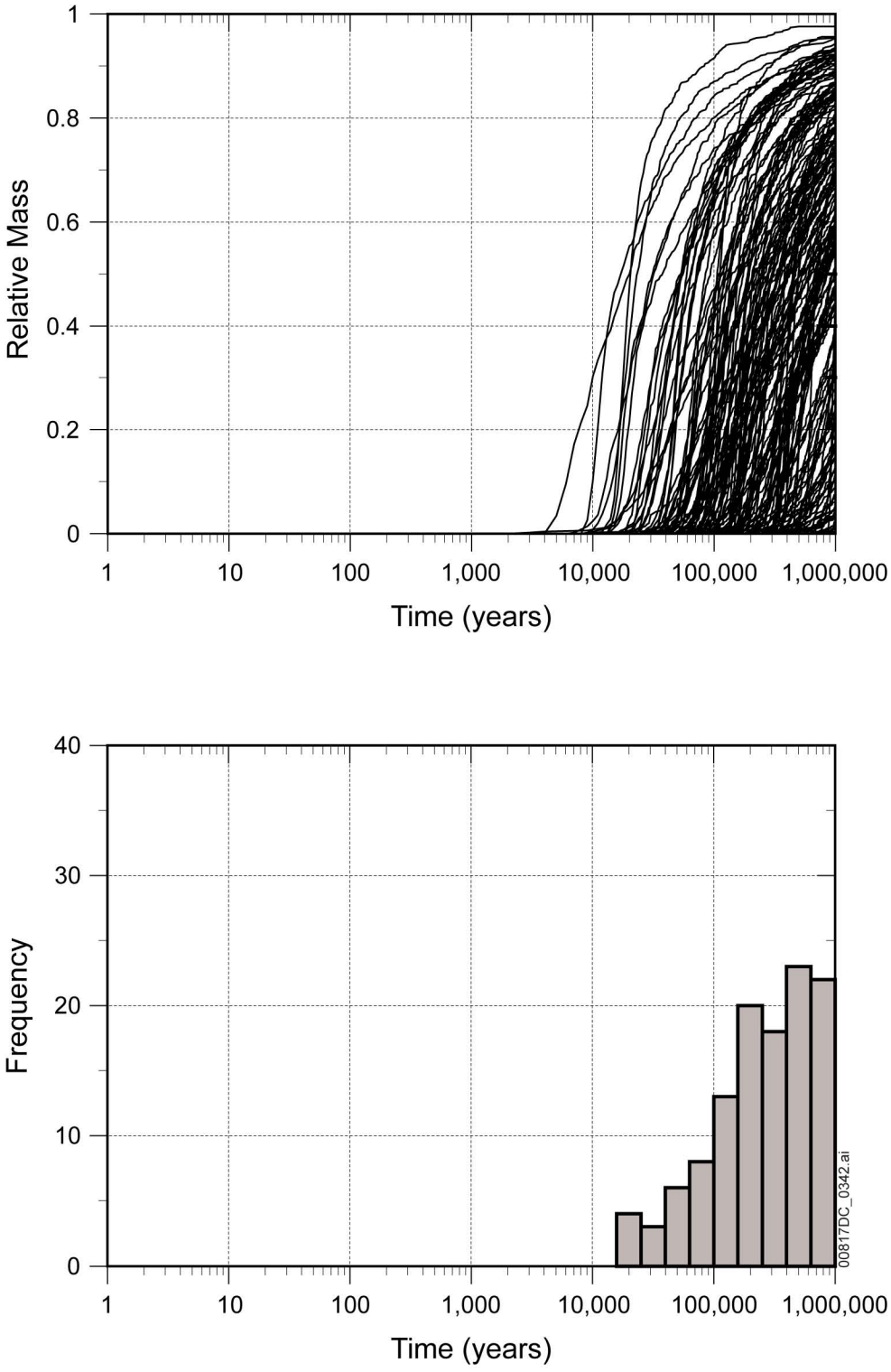

Sources: SNL 2007 [DIRS 183750], Figure 6-14[a].

Figure 8.1-8. Radium Mass Breakthrough Curves (upper) and Median Transport Times (lower) at the RMEI Location

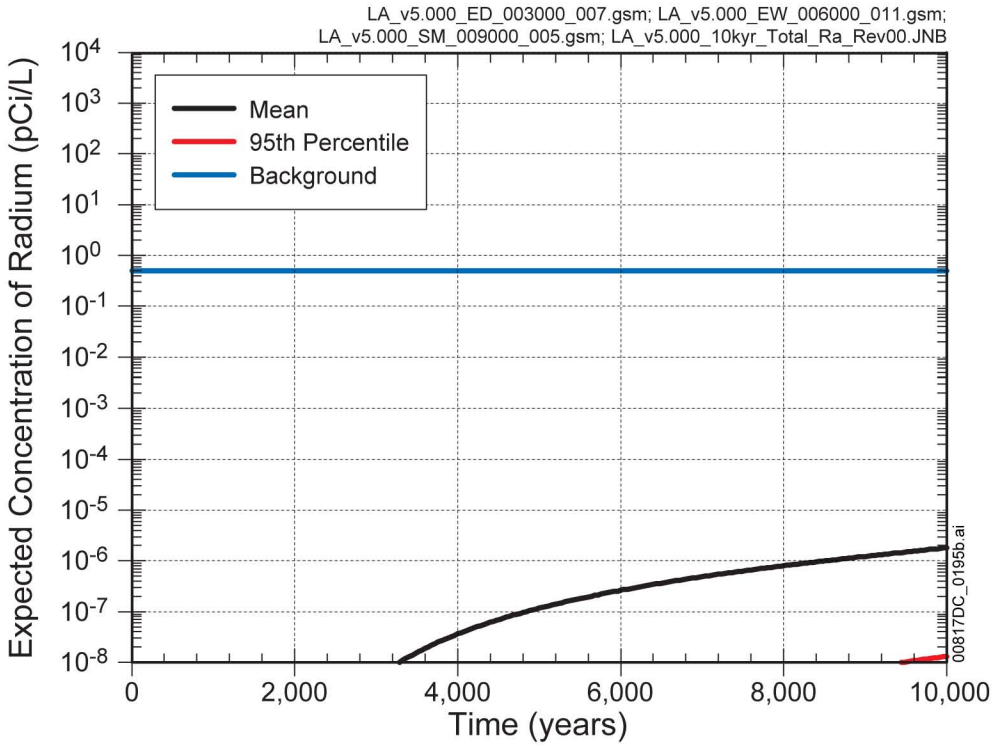

Source: Output DTN: MO0709TSPAREGS.000 [DIRS 182976].

Figure 8.1-9. Probabilistic Projections of Activity Concentrations Total Radium (^{226}Ra and ^{228}Ra) in Groundwater, Excluding Natural Background, for 10,000 Years after Closure

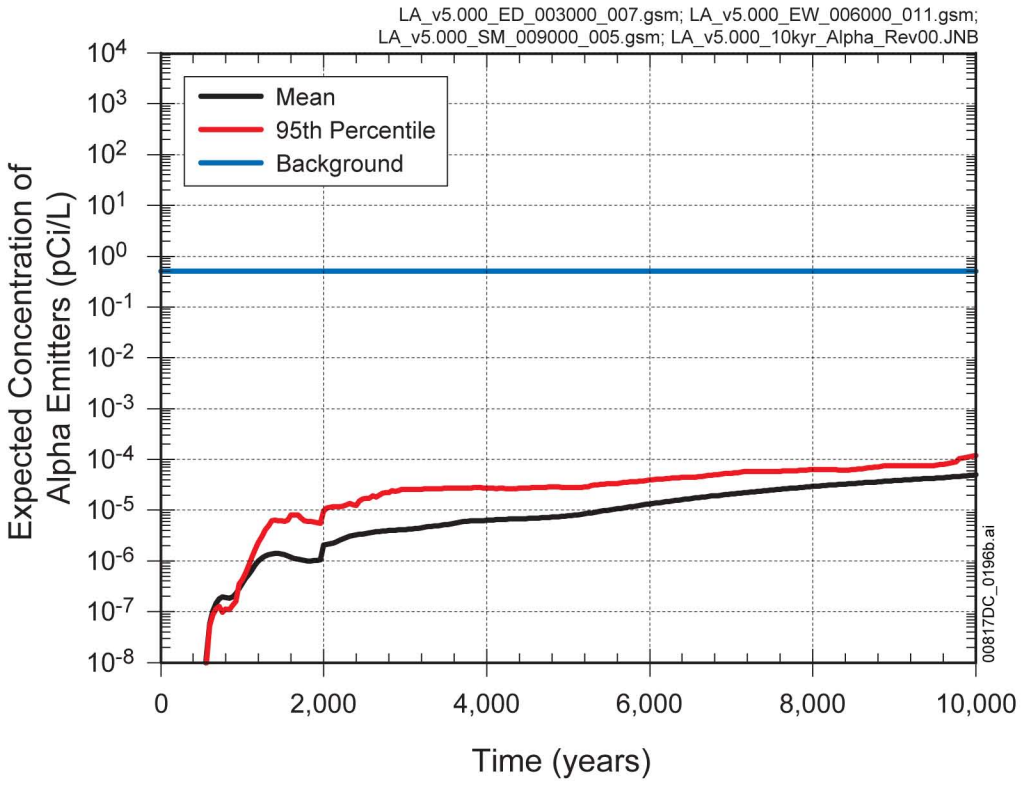

Source: Output DTN: MO0709TSPAREGS.000 [DIRS 182976].

Figure 8.1-10. Probabilistic Projections of Activity Concentration of Gross Alpha and ^{226}Ra (Excluding Radon and Uranium) in Groundwater for 10,000 Years after Closure

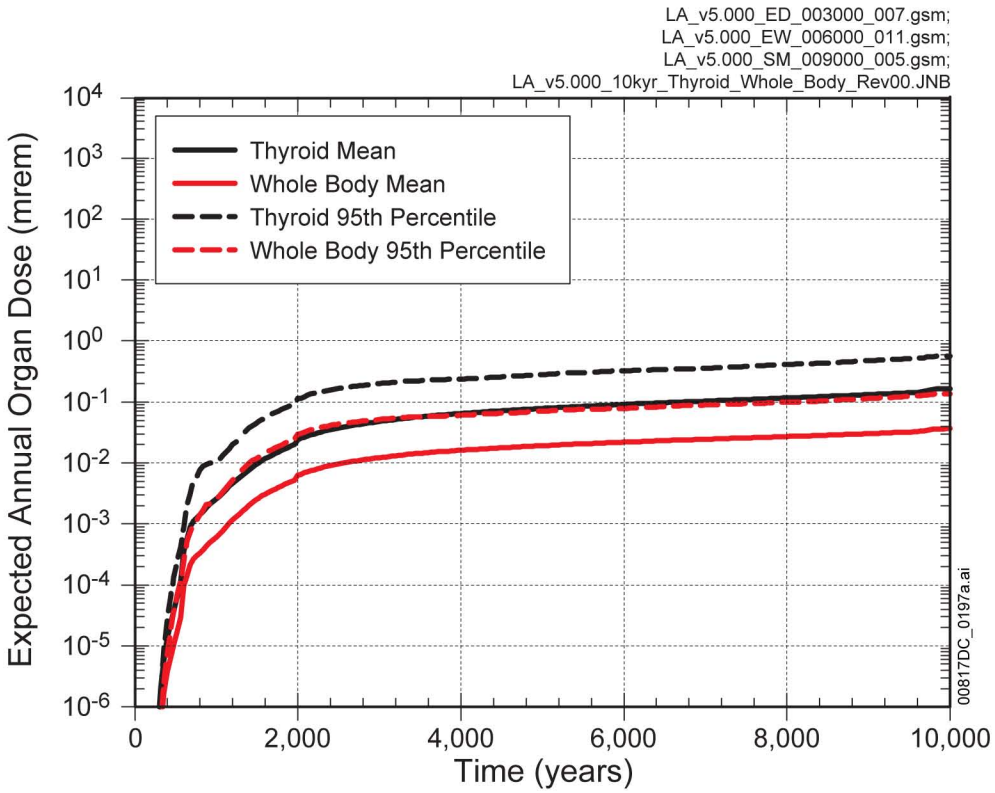

Source: Output DTN: MO0709TSPAREGS.000 [DIRS 182976].

Figure 8.1-11. Probabilistic Projections of Annual Drinking Water Doses for Combined Beta and Photon Emitting Radionuclides for 10,000 Years after Closure

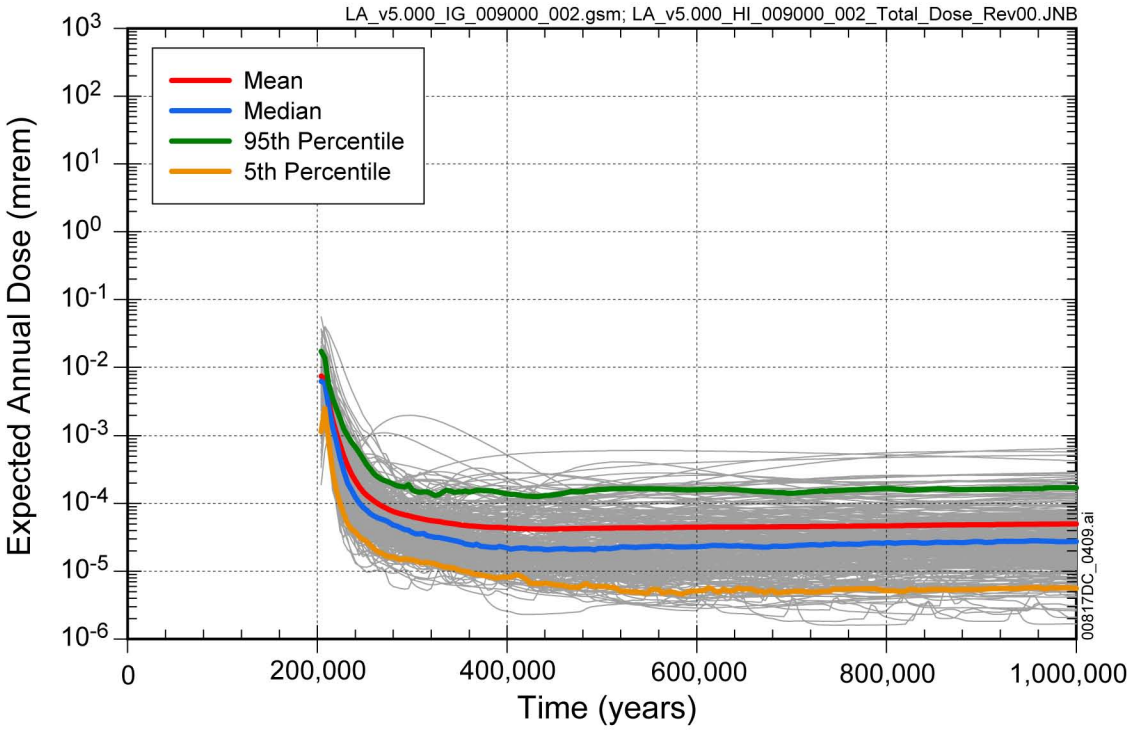

Source: Output DTN: MO0709TSPAREGS.000 [DIRS 182976].

Figure 8.1-12. Probabilistic Projections for Expected Annual Doses for the Human Intrusion Scenario for 1,000,000 Years after Closure with Drilling Event at 200,000 Years

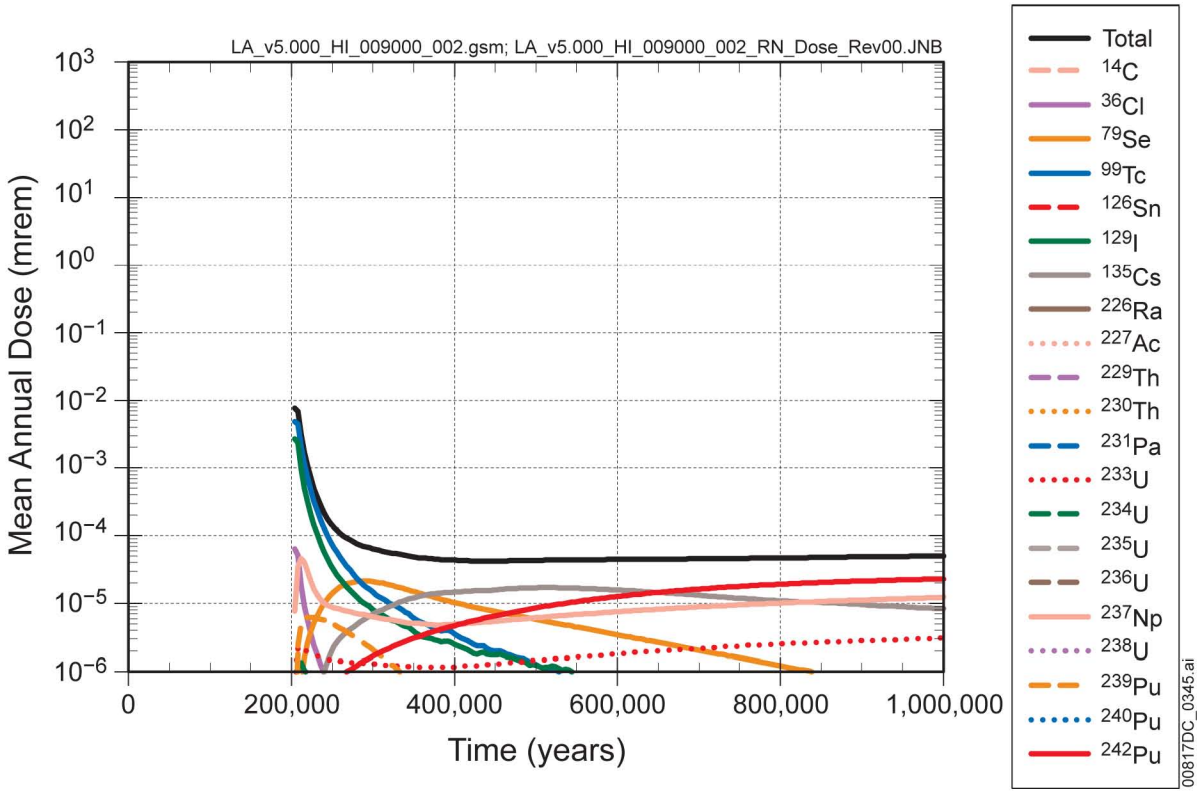

Source: Output DTN: MO0709TSPAREGS.000 [DIRS 182976].

Figure 8.1-13. Contribution of Individual Radionuclides to Mean Annual Dose for the Human Intrusion Scenario for 1,000,000 Years after Repository Closure

INTENTIONALLY LEFT BLANK

8.2 PROJECTIONS FOR INDIVIDUAL MODELING CASES

To clarify and help explain the performance demonstration for the EPA Individual Protection Standard, this section presents the probabilistic projections for the individual modeling cases. As indicated previously, the projections of total expected annual dose to the RMEI are based on a summation (Equation 8.1.1-1) of the expected annual doses over scenario modeling cases. The individual scenario class modeling cases include: (1) Nominal, (2) Waste Package EF, (3) Drip Shield EF, (4) Igneous Intrusion, (5) Volcanic Eruption, (6) Seismic GM, and (7) Seismic FD. As stated earlier, the Nominal Modeling Case is not explicitly included in the sum of total expected annual doses because it is embedded in the Seismic GM Modeling Case.

The performance projections presented herein for these modeling cases are organized in a manner so as to address the five fundamental performance questions identified earlier in Section 8.1. The supporting technical basis for the inferences and observations made regarding characteristics important to postclosure performance are also presented or cited. As will be explained in subsections that follow, the examination of the expected annual doses for the individual modeling cases leads to the following fundamental observations about relative importance of these modeling cases:

- Total mean annual doses to the RMEI for time periods after a few hundred years are largely dominated by Seismic GM and Igneous Intrusion Modeling Cases
- Mean annual doses for Waste Package EF and Seismic FD Modeling Cases are similar and estimated to contribute about 10^{-2} mrem or less to the total mean annual dose
- Mean annual doses for the Drip Shield EF and Volcanic Eruption Modeling Cases are estimated to contribute less than 10^{-3} mrem to the total mean annual dose.

For the 10,000-year period, the Seismic GM Modeling Case contributed about 71 percent and the Igneous Intrusion Modeling Case contributed about 27 percent of the peak total mean annual dose (i.e., 0.2 mrem). In contrast, for the post-10,000-year period, the Seismic GM and Igneous Intrusion Modeling Cases contributed almost equally to the peak total mean annual dose of 1 to 2 mrem.

For the Seismic GM Modeling Case, the important phenomenon is the accumulated WP damage induced by the vibratory ground motion. As indicated on Figure 8.1-5, the CDSP WPs, which contain the defense high-level waste (DHLW) glass and DOE spent nuclear fuel (DSNF), have a higher probability of failure from vibratory ground motion than the more robust CSNF WPs. The probabilistic projections for this modeling case are presented later in Section 8.2.4.

With regard to the Igneous Intrusion Modeling Case, it is important to understand that this particular modeling case represents the consequences of unlikely disruptive events with a mean annual frequency estimated to be 1.7×10^{-8} per year (Section 6.5.1.1). Moreover, the TSPA submodel for these phenomena assumes that all the 3,416 CDSP WPs and 8,213 CSNF WPs (Table 6.3.7-1) are completely failed by the hypothetical magmatic intrusion.

8.2.1 Nominal Modeling Case

The Nominal Scenario Class consists of a single modeling case that is a representation of a set of possible repository futures in which: (1) disruptive events and conditions and (2) DS and WP early failures are excluded. Moreover, the Nominal Modeling Case serves as a 'reference system state' from which all other modeling cases are developed. The system attributes for the Nominal Modeling Case are defined in terms of likely and unlikely FEPs that describe natural evolution of the natural and engineered barriers over geologic time frames, in the absence of disruptive events. That evolution includes changes in climate, infiltration and seepage into the drifts, exposure of the EBS components to water, progressive chemical degradation, and failure of the DSs and WPs, with eventual mobilization, release, and migration of radionuclides; this evolution of the reference state is included in the other modeling cases. The technical description for the representation of this nominal evolution is summarized in Section 6.3.

From a high-level point of view, this modeling case basically describes the evolution of the nuclear waste and repository system in the absence of disruptive events and processes. The system response for the Nominal Modeling Case is a function of a spectrum of processes:

1. Climate changes and attendant changes in net infiltration into the Upper Natural Barrier
2. Seepage of percolating water into the repository drifts
3. Changes to the water chemistry induced by repository heating
4. Progressive degradation of the engineered barriers by corrosion processes (i.e., general corrosion, localized corrosion, and stress corrosion cracking [SCC]) and failure
5. Accumulation of moisture inside the WPs, degradation and dissolution of the waste forms, and mobilization of the radionuclides
6. Migration of dissolved and colloidal-phase radionuclides from the EBS
7. Water flow and radionuclide transport through the Lower Natural Barrier and to the accessible environment
8. Water withdrawal and exposure to the RMEI.

The detailed technical basis (i.e., conceptual models, model abstractions, supporting data, and TSPA model parameter values and their uncertainty characterizations) for the Nominal Modeling Case is documented in numerous analysis and/or modeling reports.

The probabilistic projections of expected annual dose for this modeling case are shown on Figure 8.2-1. As can be seen from this plot, there are no doses to the RMEI in the 10,000-year regulatory time period. This is consistent with calculations for the EBS performance that indicate no realizations of DS failures in the 10,000-year time period (Section 8.1, Figure 8.1-4 and DTN: MO0709TSPAWPDS.000 [DIRS 183170]). With the DSs intact, the WPs would experience very little degradation by general corrosion in a humid-air environment.

The first realization with a failed (i.e., creation of a breach) CDSP or CSNF WP by nominal corrosion processes is projected to occur between 100,000 years to 150,000 years. The WP failure mechanism is typically SCC of the closure-lid welds. The extent of cracking gradually increases with time, leading to the ingress of moisture inside the WP and attendant diffusive radionuclide releases. Realizations with WP failures by corrosion penetrations through the Alloy 22 outer barrier are observed at about 450,000 years. By 1,000,000 years, approximately 60 percent of the WPs are projected to be failed by SCC and about 10 percent by general corrosion breaches. The projections indicate that the DSs are intact until about 270,000 years (Figure 8.1-4), with failure occurring by thinning of the 15-mm thick titanium DS (Section 6.3.5.1). All the DSs are projected to be completely failed by about 340,000 years.

The probabilistic projections for the post-10,000-year period indicate that there is no radiologic exposure until after about 140,000 years after closure. The peak mean and median annual doses for this reference modeling case are 0.5 mrem and 0.3 mrem, respectively. The peak mean annual dose at the RMEI location occurs at about 730,000 years, with two radionuclides dominating the peak annual dose. These radionuclides are the highly soluble, long-lived, and mobile radionuclide species ^{129}I and ^{99}Tc. The second order contributors to this peak dose value are ^{135}Cs and ^{79}Se (Figure 8.2-2). This peak is a modeling artifact driven by the time stepping and WP failure methodology but is similar to the overall peak at 1,000,000 years.

It is very important to differentiate the Nominal Modeling Case results from those for other modeling cases. The Nominal Modeling Case projection of mean annual dose should not be taken as a representation of compliance with radiation protection limits. The mean annual dose for the Nominal Modeling Case is not included in the calculation of the total mean annual doses for the 10,000-year period because there are no projected WP failures by nominal degradation processes in this time period. Rather, the effect of nominal DS and WP corrosion processes for the post-10,000-year period are accounted for in the Seismic GM Modeling Case. The Nominal Modeling Case only provides a reference system state for comparison with the other six modeling cases.

8.2.2 Early Failure Scenario Class Modeling Cases

The projections for early failure modeling cases demonstrate postclosure performance for conditions of DS and WP early failures. As described in Section 6.4, DS and WP early failures are generally attributed to the presence of undetected flaws (e.g., weld flaws and improper weld filler material) and manufacturing defects. Such undetected flaws and defects could possibly be introduced during manufacturing or construction of the barriers, or possibly during handling and emplacement (e.g., damaged welds). In the case of a DS, this type of defect would diminish the DS's ability to withstand the dynamic and static loadings; however, such defects are treated in the TSPA-LA Model as having failed immediately. Similarly, a WP with a defective closure-lid weld, for example, would lead to a shorter period of containment than for nominal performance, but also is treated as an immediate failure at the time of closure.

The DS and WP early failures were simulated in the TSPA-LA Model as a random process described by a Poisson distribution; thus, the number of failed DSs and WPs is a random variable and is sampled from applicable probability distributions (Sections 6.4.1 and 6.4.2). The

following information and calculations (Sections 6.4.1 and 6.4.2, Tables 6.4-1 and 6.4-2) are useful in developing risk insights to DS and WP early failures:

Drip Shield Early Failure

- Probability of 1 or more DS early failures: 0.0166
- Expected number of DS early failures: 0.0181
- Expected number of DS early failures conditional on one or more occurring: 1.09
- Mean probability of DS early failure: 1.56×10^{-6}

Waste Package Early Failure

- Probability of 1 or more WP early failures: 0.442
- Expected number of WP early failures: 1.09
- Expected number of WP early failures conditional on one or more occurring: 2.46
- Mean probability of WP early failure: 9.36×10^{-5}.

The results listed above are documented in output DTN: MO0707WPDRIPSD.000 [DIRS 183005].

For these two early failure modeling cases, the repository system response is developed by applying the process models described for the Nominal Modeling Case to the DSs and WPs that are affected by early failure. Generally speaking, the two early failure modeling cases describe the repository system response as a function of:

1. Changes of climate states, net infiltration, seepage into the drift, and water chemistry as represented in the Nominal Modeling Case (except no degradation of WPs by corrosion)

2. Total number of DS early failures in each realization

3. Total number of CDSP WP and CSNF WP early failures in each realization

4. Ingress of water to the failed WPs, mobilization, and the eventual release of radionuclides from the EBS

5. Water flow and transport of dissolved and colloidal phase radionuclides through the Lower Natural Barrier and to the accessible environment

6. Water withdrawal and radiologic exposure at the RMEI location.

It is important to emphasize that WPs associated with early failed DSs are also assumed to be failed in the TSPA-LA Model. The associated radionuclide releases from these early failed DSs and WPs are assumed to occur at the time of repository closure.

The models and TSPA methodology used to simulate the occurrence of early failures and their impacts on the performance of the affected WPs and DSs are presented in Section 6.4. Section 6.4 also summarizes the supporting technical basis for the abstraction of early failures.

Model parameter values and their uncertainty characterizations are documented in *Analysis of Mechanisms for Early Waste Package/Drip Shield Failure* (SNL 2007 [DIRS 178765]).

8.2.2.1 Drip Shield Early Failure Modeling Case

As indicated by probabilistic analysis of early failures, the total number of DS early failures is estimated to be very small. For example, the probability of three or more DS early failures is about 2×10^{-4} (Table 6.4-1). As implemented in the TSPA-LA Model, the DS early failures are accounted for by simply removing the DS as a barrier to seepage for a given realization. In its implementation, the number of 'n' failed DSs means that the associated 'n' WPs are also assumed to have failed; thus, 'n' failed DSs define the inventory at risk for this modeling case.

The expected annual dose histories for the Drip Shield EF Modeling Case are shown in Figure 8.2-3; this plot shows multi-realization projections for both the (a) 10,000-year period after closure, and (b) post-10,000 years to 1,000,000 years. The mean, median, and 5th and 95th percentile curves are superimposed on the plot to illustrate the central tendency and uncertainty. The uncertainty or spread reflects the epistemic uncertainty in the TSPA-LA Model parameters and representation of the evolution of the future conditions. The projections for the first 10,000 years show an early peak around 1,000 years (not the peak annual dose for the time period, however), which is primarily due to contribution from early failed CDSP WPs (see Section 7.7.1.1). Because the CDSP WPs produce less decay heat than the CSNF WPs, the relative humidity in the CDSP WP emplacement locations goes above 95 percent and diffusive transport of radionuclide starts before 10,000 years. The peak mean and median annual doses of about 3×10^{-4} mrem and 4×10^{-5} mrem, respectively, occur at approximately 2,000 years; the mean and median annual doses decline thereafter and drop to about 4×10^{-5} mrem and 7×10^{-6} mrem, respectively, at 10,000 years. The abrupt increase in the dose histories at 2,000 years is due to the change in the climate (monsoonal to glacial transition). In the post-10,000-year period, the figure shows a second peak occurring at about 40,000 years with a mean of $\sim 10^{-4}$ mrem and median of $\sim 10^{-5}$ mrem.

The primary radionuclides that contribute to the mean annual dose for the Drip Shield EF Modeling Case are shown on Figure 8.2-4. In the first 2,000 years after repository closure, three soluble and mobile radionuclides dominate dose: ^{99}Tc, ^{129}I, and ^{14}C. From 2,000 years to 10,000 years, the ^{14}C drops in importance and is replaced by ^{239}Pu. At the outset of the post-10,000-year period, the mean annual dose is dominated by ^{239}Pu and ^{99}Tc. The radionuclide ^{239}Pu creates the secondary peak mean annual dose at about 40,000 years, but diminishes in importance by about 200,000 years due to radionuclide decay. From that point forward, ^{242}Pu, ^{237}Np, and ^{226}Ra dominate the mean annual doses.

8.2.2.2 Waste Package Early Failure Modeling Case

From the probabilistic analysis of early failures, the number of WP early failures is estimated to be relatively small. For example, the probability of three or more WP early failures is about 0.12 (Table 6.4-1). As implemented in the TSPA-LA Model, the WP early failure is conceptualized as complete failure with respect to radionuclide containment (Section 6.4.2.2), at the time of repository closure. The overlying DS is not affected by the early failure of the WP. The number of early failed WPs defines the radionuclide source term for this modeling case. The

radionuclide releases from these WP early failures occur by diffusive transport from the waste form with sorbing radionuclides delayed by sorption on corrosion products (Section 6.3.8).

The expected annual dose histories for this modeling case are shown in the multi-realization projections in Figure 8.2-5 for both the (a) 10,000-year period after closure, and (b) post-10,000 years. The expected annual doses account for aleatory uncertainties associated with characteristics of the early failed WPs, such as the number of early failed WPs, type of early failed WPs (CDSP or CSNF), and their locations in the repository. The mean, median, and 5th and 95th percentile curves are shown on Figure 8.2-5 to highlight the uncertainty in the expected annual doses.

For the first 10,000 years after repository closure, there is an initial peak between 1,000 and 2,000 years which is primarily due to contribution from early failed CDSP WPs. Because the CDSP WPs produce less decay heat than the CSNF WPs, the relative humidity in the CDSP WP emplacement locations goes above 95 percent and diffusive transport of radionuclides starts. The abrupt jump in the dose histories at 2,000 years is due to the change in the climate state (monsoonal to glacial transition). Between 9,000 and 10,000 years, the dose histories increase with the peak mean and median annual doses estimated to be about 4×10^{-3} mrem and 2×10^{-4} mrem. This peak is due to the early failed CSNF WPs, which have cooled and have relative humidity environments that promote diffusive transport. For post-10,000 years, the peak mean and median annual doses reach levels of approximately 2×10^{-2} mrem and 4×10^{-3} mrem, respectively, at about 12,000 years and then gradually decline. At about 260,000 years the mean annual dose curve again ascends forming one last broad peak at about 450,000 years; the onset of this increase coincides with the onset of DS failures by general corrosion at about 270,000 years (Figure 8.1-4) and, in turn, seepage directly onto the early failed WPs. The mean and median doses at one million years are about 1×10^{-3} mrem and 2×10^{-4} mrem, respectively.

The major radionuclides that contribute to the mean annual dose for the Waste Package EF Modeling Case are shown on Figure 8.2-6. In the first 10,000 years postclosure, soluble and mobile radionuclides, in particular, ^{99}Tc, ^{14}C, and ^{129}I, dominate the estimate of mean annual dose. In the post-10,000-year period, after ^{99}Tc and ^{129}I decline, the peak mean annual dose is dominated by ^{239}Pu up to about 200,000 years; thereafter, ^{242}Pu, ^{226}Ra, and ^{237}Np are the primary contributors to the peak mean annual dose.

8.2.3 Igneous Scenario Class Modeling Cases

The projections for the Igneous Scenario Class demonstrate postclosure performance for unlikely igneous events and processes that could disrupt the repository system. As noted earlier, the estimated annual frequency of igneous activity at the repository site is 1.7×10^{-8} /yr (Section 6.5.1.1). This frequency is just slightly greater than the NRC frequency of 10^{-8} /yr for very unlikely events and processes, which are excluded from the performance demonstration for the LA by regulation (10 CFR 63.342 [DIRS 178394]). As described in Section 6.5, the Igneous Scenario Class consists of two modeling cases: (1) the Igneous Intrusion Modeling Case that represents the interaction of a hypothetical intrusive magma with the repository and attendant release of radionuclides to the groundwater pathway, and (2) the Volcanic Eruption Modeling Case that represents a hypothetical volcanic eruption at the land surface and the release of radionuclides to the atmospheric pathway.

8.2.3.1 Igneous Intrusion Modeling Case

In this modeling case, a simulated magmatic dike intersects the footprint of the repository causing failure of the EBS. Radionuclide releases that are attributed to the intrusion, and are transported away from the repository, are analyzed in a manner analogous to that for the Nominal Modeling Case, but differ in the conceptualization of the EBS failure. There are two main components to the model: (1) the behavior of the WPs and other EBS elements damaged by an igneous intrusion, and (2) groundwater flow and radionuclide transport away from the WPs. For the purposes of ensuring conservatism in the annual doses to the RMEI, the modeling case assumes that all the WPs in the repository are completely destroyed, exposing the waste forms to percolating groundwater with subsequent degradation, radionuclide mobilization, and transport.

Radionuclide transport occurs through the invert and into the UZ, depending on solubility limits and the rate of water flux through the intruded drifts. It is assumed that the drifts do not act as a capillary barrier, and the seepage water flux into a magma-intruded drift is equal to the percolation flux in the overlying host rock. No barrier performance credit is taken for water diversion by the remnants of the DS or WP, and cladding is assumed to be fully degraded. Because the thermal, chemical, hydrological, and mechanical conditions in the drift following igneous intrusion are uncertain, the EBS is assumed to be completely failed.

The expected annual dose histories for the Igneous Intrusion Modeling Case are shown in Figure 8.2-7 for both the (a) 10,000-year period and (b) post-10,000-year period. The mean, median, and 5th and 95th percentile curves are displayed on a multi-realization plot. The expected annual dose to the RMEI takes into account aleatory uncertainty associated with characteristics of the igneous intrusion, such as the number of future events and the time at which they may occur. These figures indicate that the peak mean annual dose to the RMEI for the 10,000-year time period is less than 0.1 mrem and for the post-10,000-year time period is about 1.3 mrem. The median annual dose at 1,000,000 years is about 0.4 mrem.

The radionuclides that contribute most to the mean annual dose are shown on Figure 8.2-8. Figure 8.2-8a shows that radionuclides ^{99}Tc and ^{129}I dominate the estimate of the mean for the first 4,000 years and ^{239}Pu, ^{99}Tc, and ^{240}Pu dominate the estimate of the mean for the remainder of the 10,000-year postclosure period. Figure 8.2-8b shows that ^{239}Pu, which is transported both in dissolved and colloidal form, dominates the peak mean annual dose for the first 200,000 years and radionuclides ^{242}Pu, ^{237}Np, and ^{226}Ra dominate the estimate of the mean for the remainder of the post-10,000-year time period.

8.2.3.2 Volcanic Eruption Modeling Case

In this modeling case, the disruption is conceptualized as a volcanic eruptive conduit intersecting the repository footprint resulting in the dispersal of waste-contaminated tephra in the atmosphere, with attendant deposition of contaminated ash on the land surface. The performance projections evaluate the post-eruption consequences due to waste redistributed from upstream in the Fortymile Wash watershed and deposited at the RMEI location. WPs in the direct path of the conduit are assumed to be destroyed and entrained into the hypothetical eruption. As described in Section 6.3.11, the radiologic exposure scenario is that the RMEI exposure arises from

contaminated volcanic ash deposited on surface soil and the subsequent radionuclide transport from surface soil to other environmental media (e.g., air and plants).

As noted in Section 6.5.2.1.1, the probabilistic calculations of igneous disruptions indicate that there is about a 70 percent probability that no WPs would be hit by a volcanic conduit intersecting the repository. The small conduit diameters relative to drift spacing implies that 70 percent of the conduits potentially intersecting the repository footprint would intersect between drifts and therefore not impact any WPs. In the 30 percent of the realizations in which one or more packages are intersected, the most likely number hit is four and the maximum number hit is seven.

The expected annual dose histories for this modeling case are shown on Figure 8.2-9 for both the (a) 10,000-year period and (b) post-10,000-year period. The expected annual dose takes into account aleatory uncertainty associated with characteristics of the eruption such as number of WPs intersected by the eruption, the fraction of waste-containing magma ejected in the atmosphere, eruption power, wind direction, and wind speed. The mean, median, and 5th and 95th percentile curves on Figure 8.2-9 show uncertainty in the value of the expected annual dose, taking into account epistemic uncertainty associated with incomplete knowledge of the behavior of the physical system during and after the disruptive event. These figures show that the mean annual dose for 10,000 years postclosure is about 1×10^{-4} mrem and is largely uniform for the post-10,000-year time period with the peak mean less than 2×10^{-4} mrem. The median annual dose is less than 6×10^{-5} mrem at 1,000,000 year.

The radionuclides contributions to the mean annual dose are shown on Figure 8.2-10. Because transport of radionuclides to the location of the RMEI is more rapid in the Volcanic Eruption Modeling Case than in the Igneous Intrusion Modeling Case, radionuclides with short half-lives are able to contribute to the estimate of the mean annual dose estimate. Examples of two short-lived radionuclides are ^{137}Cs and ^{238}Pu, which make significant contributions to the dose at early times, but their contributions drop off rapidly because of radioactive decay. At 300 years, ^{241}Am dominates the total, but its contribution rapidly diminishes after about 1,000 years, also due to radioactive decay. These short-lived radionuclides are able to reach the location of the RMEI before they decay because atmospheric transport to this location is relatively rapid. After 1,000 years, ^{239}Pu and ^{240}Pu are the dominant contributors until approximately 100,000 years; thereafter ^{226}Ra, ^{229}Th, and ^{237}Np become the dominant contributors out to 1,000,000 years.

8.2.4 Seismic Scenario Class Modeling Cases

The probabilistic projections for the Seismic Scenario Class demonstrate postclosure performance for likely and unlikely seismic events. As described in Section 6.6, the Seismic Scenario Class consists of two modeling cases: (1) Seismic GM Modeling Case, and (2) Seismic FD Modeling Case. These modeling cases take into account the aleatory uncertainty of the timing of these events, effects of the seismic events on DSs and WPs, and attendant radionuclide releases. This scenario class also takes into account changes in seepage, WP degradation, and flow in the EBS, as well as the conditions associated with the nominal evolution of the repository system. The likelihood and intensity/magnitude of these seismic events are defined by hazard curves, which were developed as part of the probabilistic seismic hazard analysis (CRWMS M&O 1998 [DIRS 103731]).

8.2.4.1 Seismic Ground Motion Modeling Case

The Seismic GM Modeling Case focuses on postclosure performance as a function of disruptions caused by vibratory ground motion. As described in Section 6.6.1, the likelihood and intensity of ground motion is defined by the mean seismic hazard curve (i.e., relation of peak ground velocities to exceedance frequencies (Figure 6.6-6)). Depending on the timing, sequence, and intensity of the ground motion events, the DSs and WPs can accumulate damage and/or fail. In the case of the DSs, seismic ground motion could cause damage or failure by dynamic loading and/or static loading by rockfall resulting in bucking or rupture (Section 6.6.1.1.2). Similarly, the WPs could be damaged or fail by: (1) local strain that exceeds ultimate tensile strength, (2) deformations creating residual stresses that induce SCC, and (3) lithostatic loading from rubble that causes a puncture of the outer barrier by the WP internals (Section 6.6.1.1.2). Both the DSs and WPs are also degraded by the general corrosion (Section 6.6.2.3). The number of failed CDSP and CSNF WPs determine the source term for the radionuclide transport calculations and projections of expected annual dose to the RMEI.

The expected annual dose histories for the Seismic GM Modeling Case are shown on Figure 8.2-11; multi-realization projections are presented for both the (a) 10,000-year period, and (b) post-10,000-year period. The expected annual dose histories take into account aleatory uncertainty associated with characteristics of future events such as number of events, times of events, and the peak ground velocity of the event. The mean, median, and 5th and 95th percentile curves on Figure 8.2-11 show uncertainty in the value of the expected annual dose, taking into account epistemic uncertainty associated with the incomplete knowledge of the behavior of the physical system during and after the disruptive event. These figures show that the mean annual dose for 10,000 years postclosure is less than 0.2 mrem, while for the post-10,000-year period it is less than 2 mrem. The median annual dose at one million years is less than 0.5 mrem.

The radionuclides that contribute most to the estimate of mean annual dose for this modeling case are presented on Figure 8.2-12. The mean dose curves on Figure 8.2-12a illustrate that three radionuclides, ^{99}Tc, ^{14}C, and ^{129}I, contribute the most to the peak mean annual dose for the 10,000-year time period; during this time period CDSP WPs are the primary containers damaged because the CSNF WPs are much more resistant to seismic damage. The predominant mechanism causing damage to the CDSP WPs and CSNF WPs consisted of small cracks that result in releases from the WPs by diffusion. As can be seen on Figure 8.2-12b, the dominant radionuclides contributing to the peak at approximately 230,000 years are ^{99}Tc, ^{129}I, and ^{79}Se. From 200,000 years to about 800,000 years, the dominant radionuclides are ^{99}Tc, ^{129}I, ^{226}Ra, ^{135}Cs, and ^{242}Pu. After 800,000 years, ^{242}Pu, ^{129}I, and ^{237}Np are the three major contributors to the mean annual dose for this modeling case.

8.2.4.2 Seismic Fault Displacement Modeling Case

The Seismic FD Modeling Case demonstrates postclosure performance as a function of disruptions caused by fault displacement. As described in Section 6.6.1, the characterization of the fault is based on data from known faults in the vicinity of the site area. The disruption in this modeling case is conceptualized as a sudden discontinuity in the profile of the repository. The location and magnitude of the fault displacement determines the number of DSs and WPs that

are disrupted. A mean displacement hazard curve provides the basis for calculating the magnitude of the simulated fault displacement. The WPs are presumed to be sheared if the displacement exceeds a threshold value. As noted in Section 6.6.1.2.3, damage of the DSs and WPs by fault displacement is not expected to occur if the mean annual frequency is greater than 2.5×10^{-7}/yr.

The expected annual dose histories for the Seismic FD Modeling Case are shown on Figure 8.2-13; the figure shows expected annual dose to the RMEI for both the (a) 10,000-year period, and (b) post-10,000-year period. The expected annual dose takes into account aleatory uncertainty associated with characteristics associated with the number of DSs and WPs disrupted. The mean, median, and 5th and 95th percentile curves on Figure 8.2-13 show uncertainty in the value of the expected annual dose, taking into account epistemic uncertainty associated with incomplete knowledge of the behavior of the physical system during and after the disruptive event. These figures show that the mean annual dose for 10,000 years postclosure is less than 2×10^{-3} mrem and for 1,000,000 years postclosure less than 2×10^{-2} mrem. The peak median annual dose for the 1,000,000-year time period is approximately 10^{-2} mrem.

The contribution of individual radionuclides to mean annual dose are shown in the results presented on Figure 8.2-14 for both the 10,000-year and post-10,000-year period after closure. The plot for the 10,000-year period (Figure 8.2-14(a)) shows that ^{99}Tc and ^{129}I dominate the dose for the first 4,000 years after closure, and ^{99}Tc, ^{239}Pu, ^{129}I, and ^{240}Pu are the dominant radionuclides contributing to dose at 10,000 years. As can be noted from Figure 8.2-14b, ^{239}Pu dominates the mean annual doses up to about 200,000 years; thereafter, the radionuclides ^{242}Pu, ^{226}Ra, and ^{237}Np remain dominant contributors for the remainder of the 1,000,000 years.

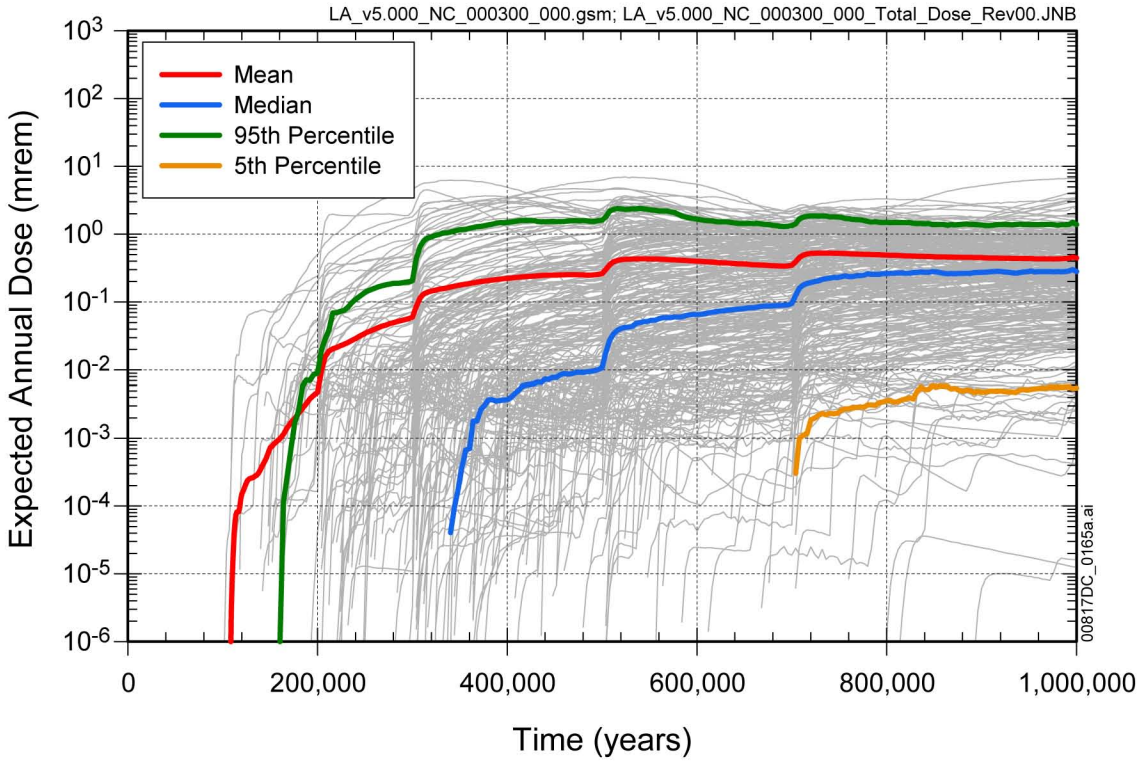

Source: Output DTN: MO0709TSPAREGS.000 [DIRS 182976]

Figure 8.2-1. Probabilistic Projections of Expected Annual Dose for the Nominal Modeling Case for 1,000,000 Years after Repository Closure

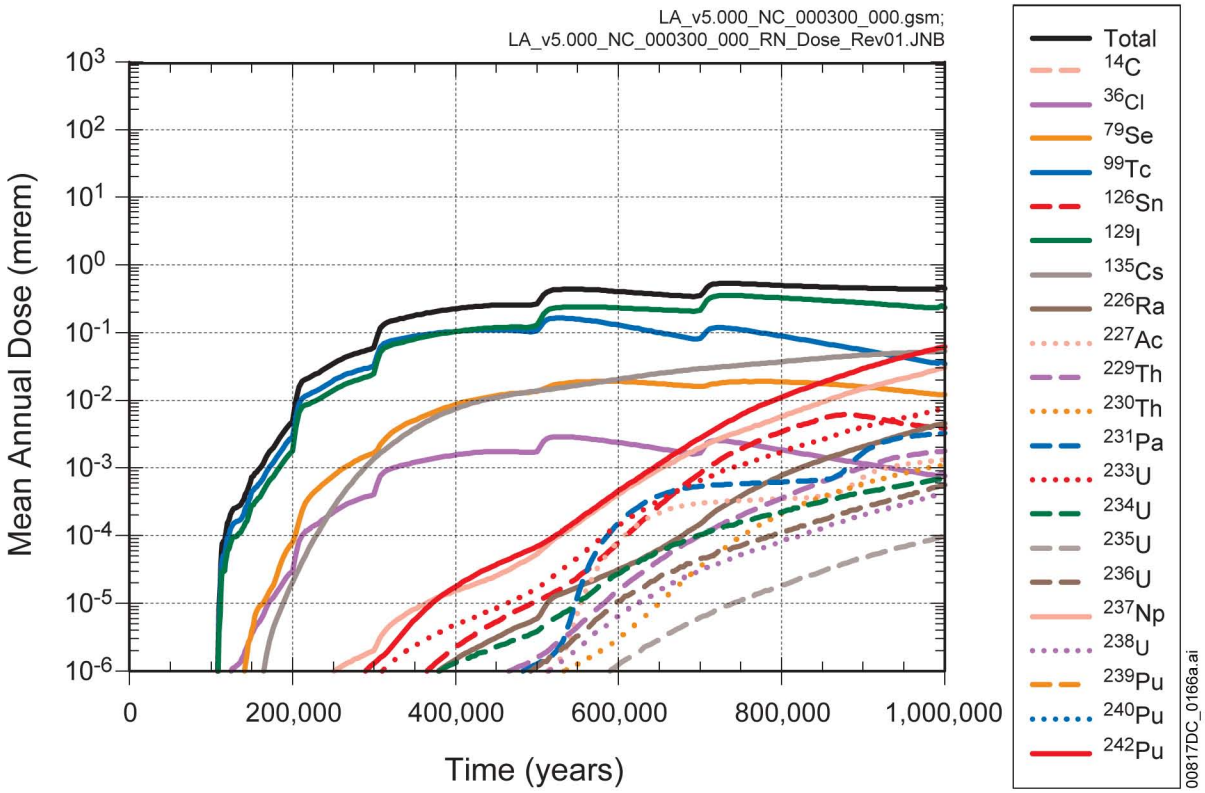

Source: Output DTN: MO0709TSPAREGS.000 [DIRS 182976]

Figure 8.2-2. Contribution of Individual Radionuclides to Mean Annual Dose for the Nominal Modeling Case for 1,000,000 Years after Repository Closure

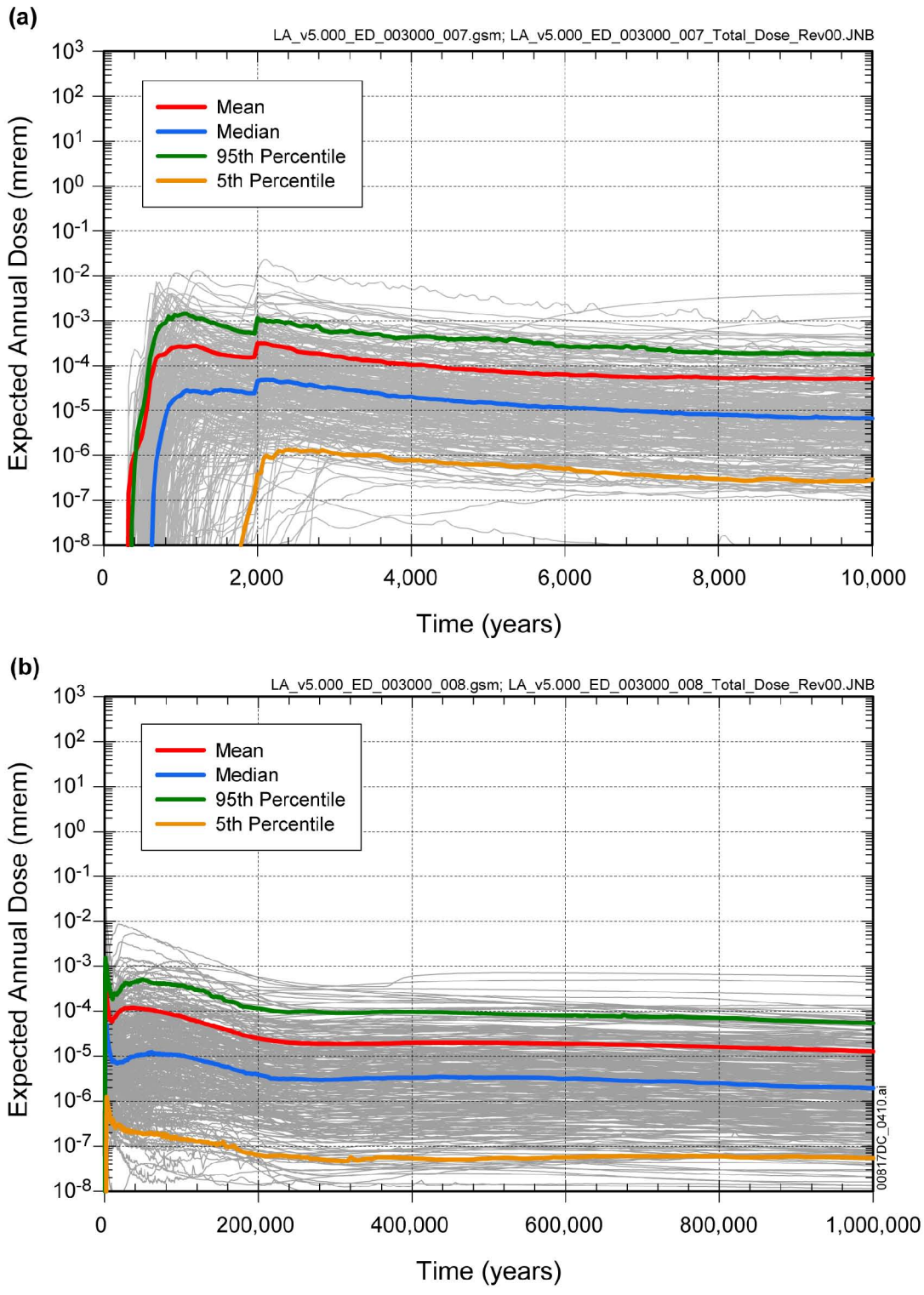

Source: Output DTN: MO0709TSPAREGS.000 [DIRS 182976]

Figure 8.2-3. Probabilistic Projections of Expected Annual Dose for the Drip Shield Early Failure Modeling Case for (a) 10,000 Years and (b) 1,000,000 Years after Repository Closure

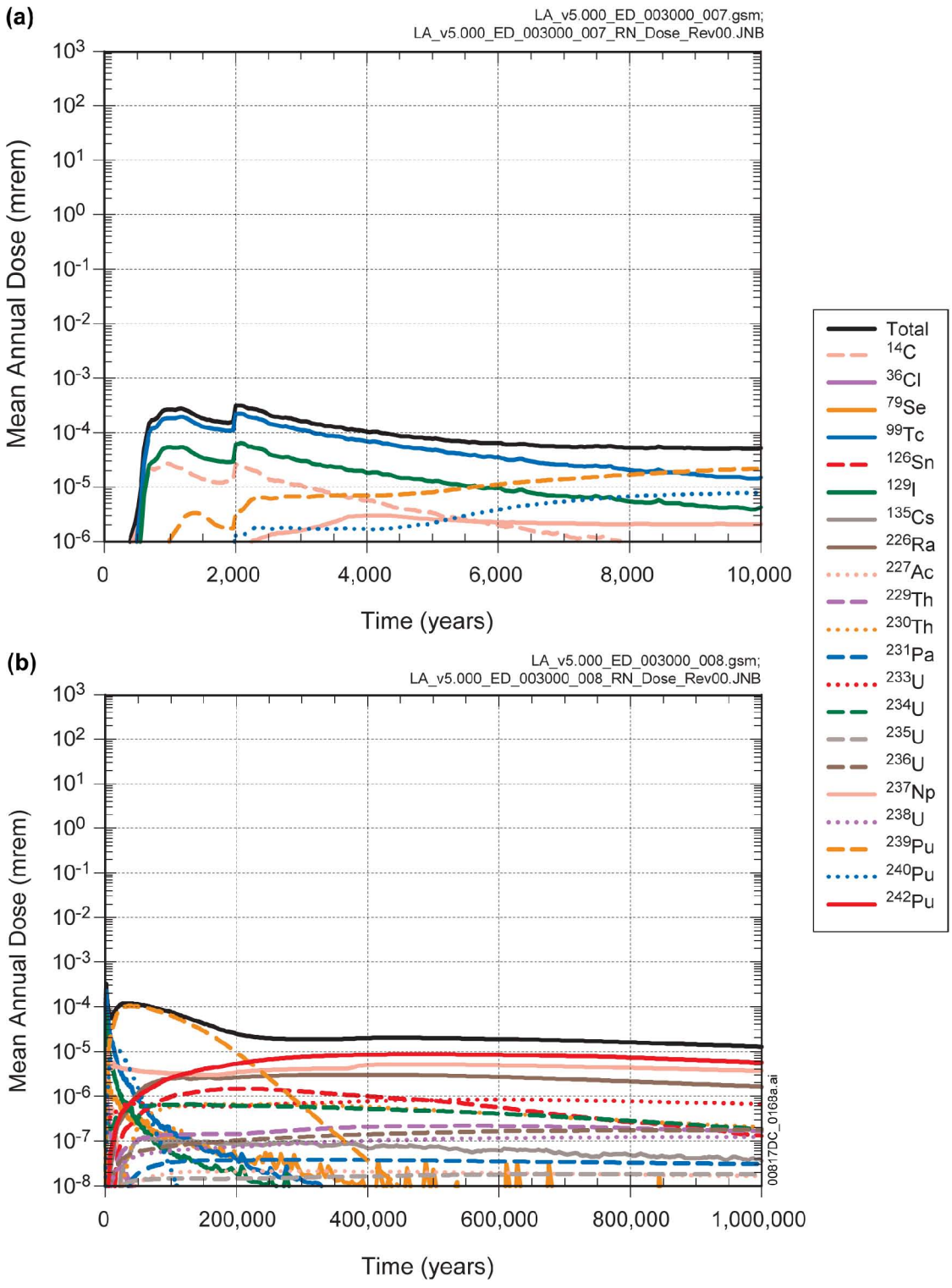

Source: Output DTN: MO0709TSPAREGS.000 [DIRS 182976]

Figure 8.2-4. Contribution of Individual Radionuclides to Mean Annual Dose for Drip Shield Early Failure Modeling Case for (a) 10,000 Years and (b) 1,000,000 Years After Repository Closure

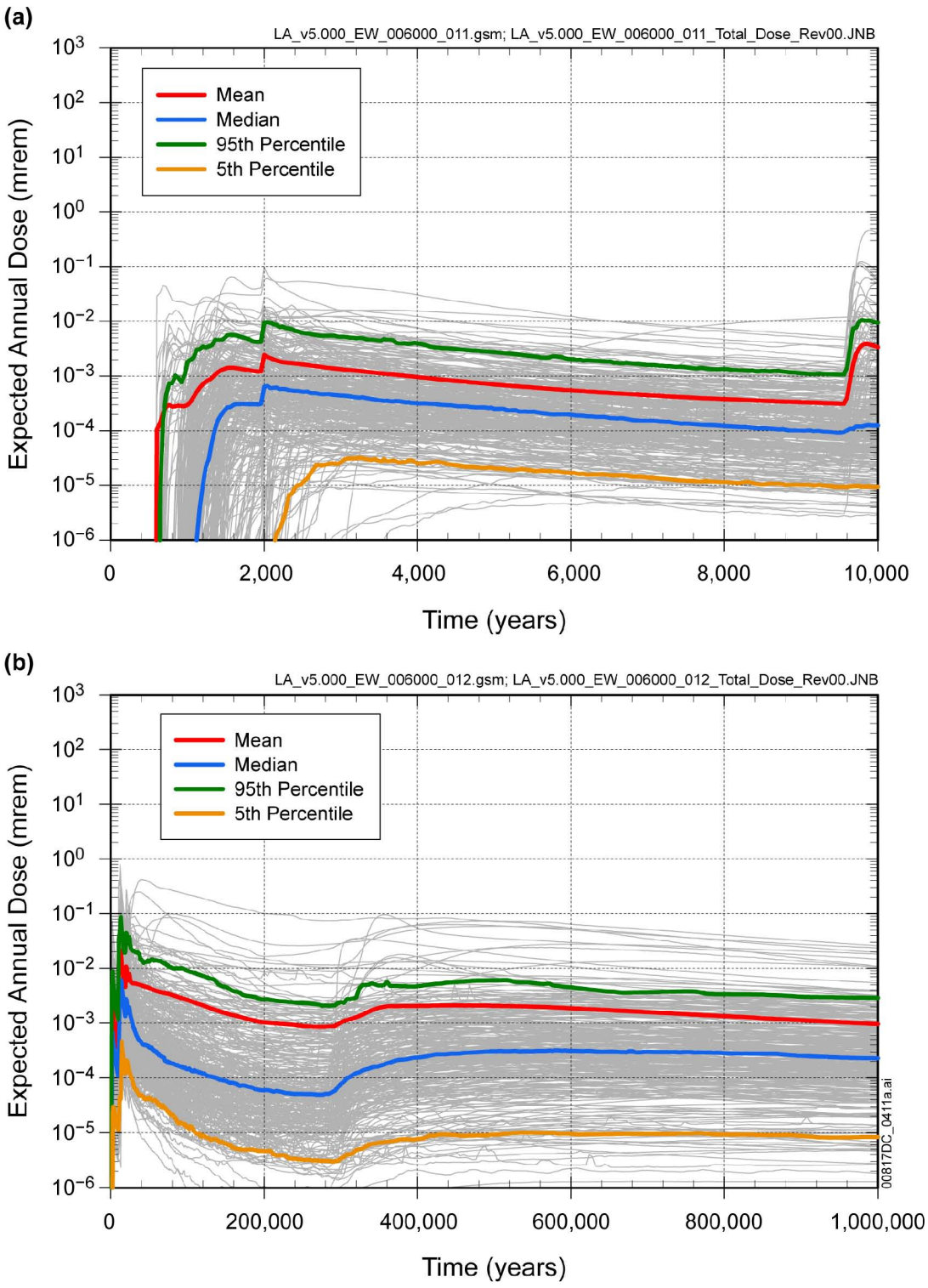

Source: Output DTN: MO0709TSPAREGS.000 [DIRS 182976]

Figure 8.2-5. Probabilistic Projections of Expected Annual Dose for Waste Package Early Failure Modeling Case for (a) 10,000 Years and (b) 1,000,000 Years after Repository Closure

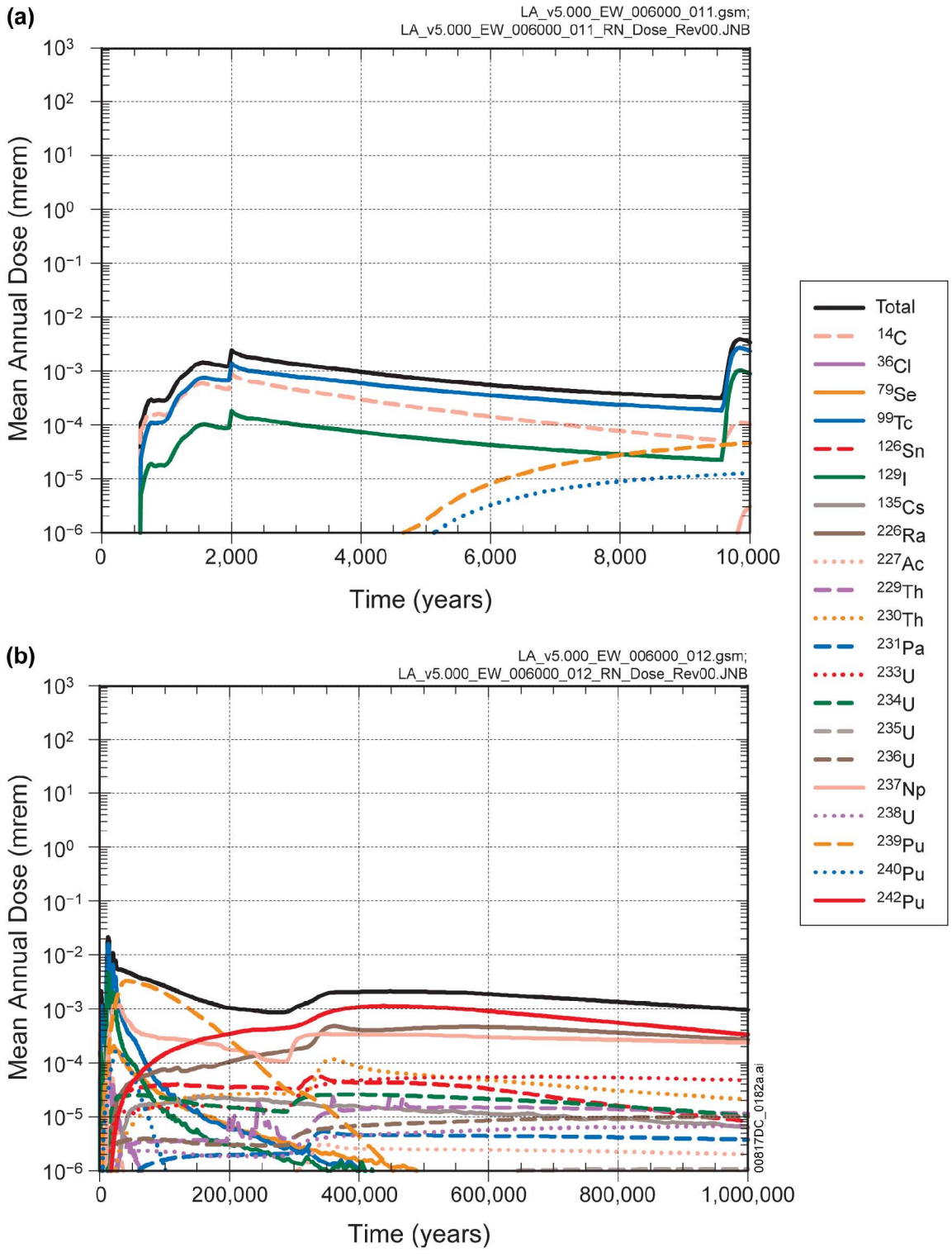

Source: Output DTN: MO0709TSPAREGS.000 [DIRS 182976]

Figure 8.2-6. Contribution of Individual Radionuclides to Mean Annual Dose for Waste Package Early Failure Modeling Case for (a) 10,000 Years and (b) 1,000,000 Years after Repository Closure

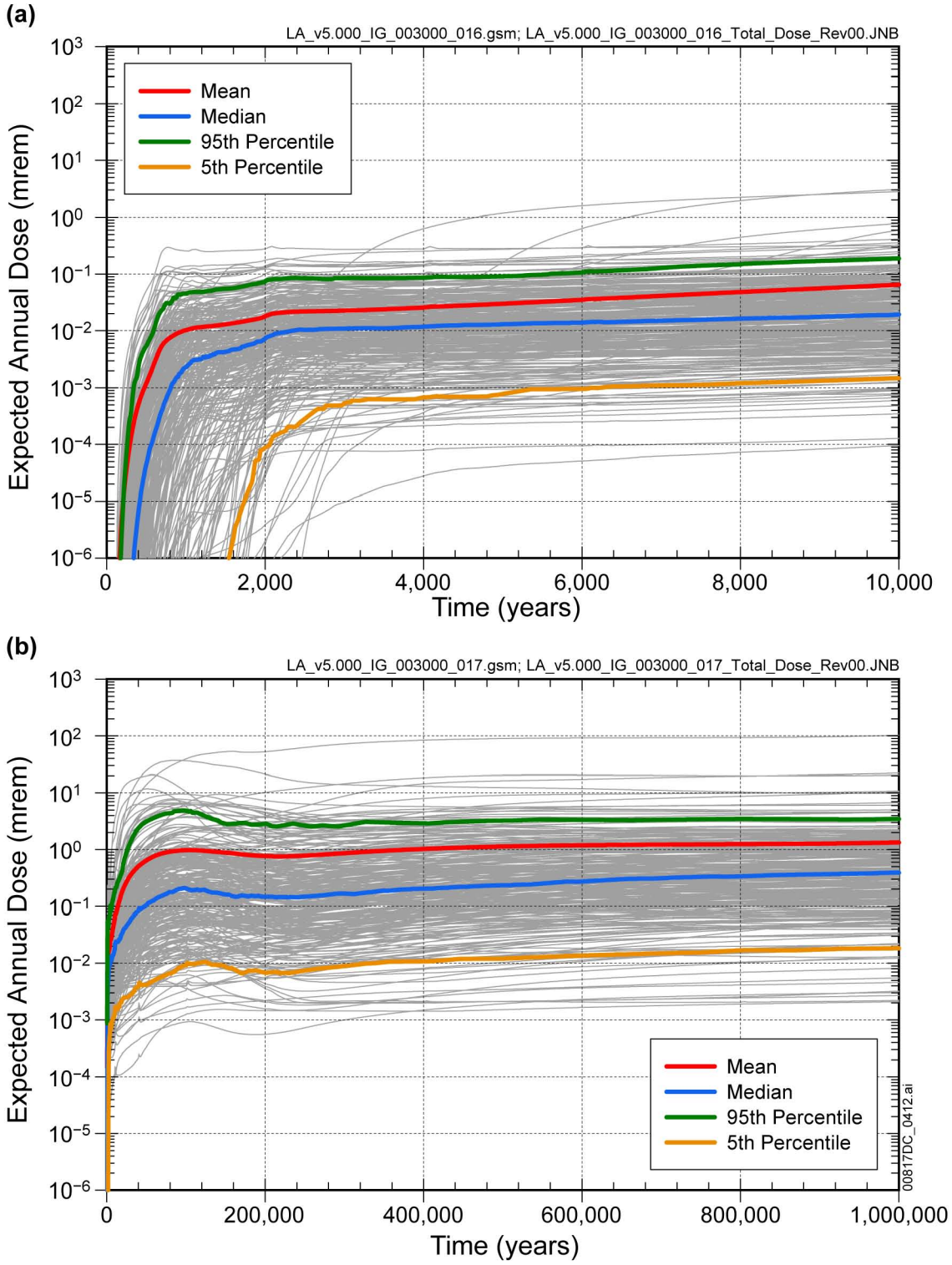

Source: Output DTN: MO0709TSPAREGS.000 [DIRS 182976]

Figure 8.2-7. Probabilistic Projections of Expected Annual Dose for the Igneous Intrusion Modeling Case for (a) 10,000 Years and (b) 1,000,000 Years after Repository Closure

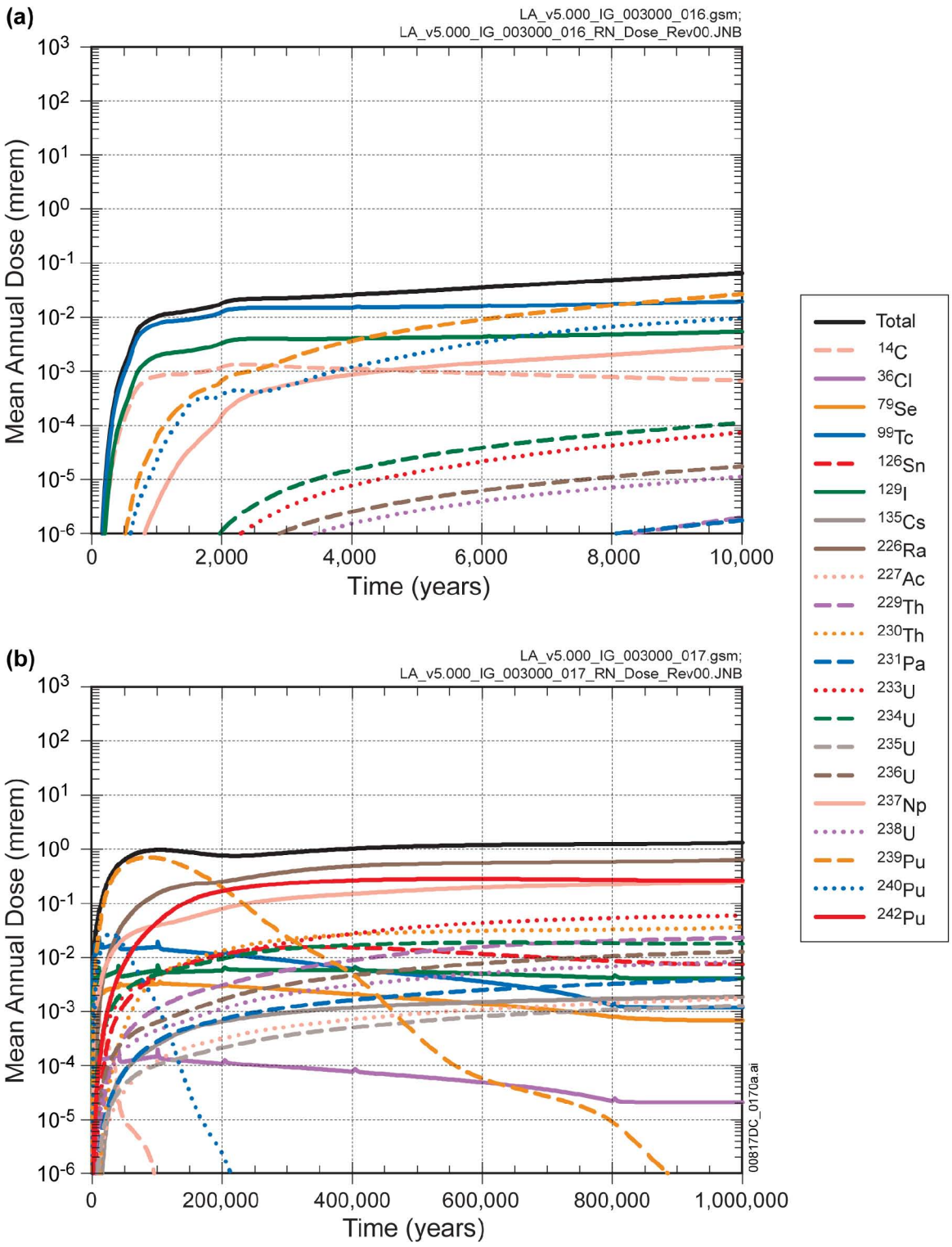

Source: Output DTN: MO0709TSPAREGS.000 [DIRS 182976]

Figure 8.2-8. Contribution of Individual Radionuclides to Mean Annual Dose for the Igneous Intrusion Modeling Case for (a) 10,000 Years and (b) 1,000,000 Years After Repository Closure

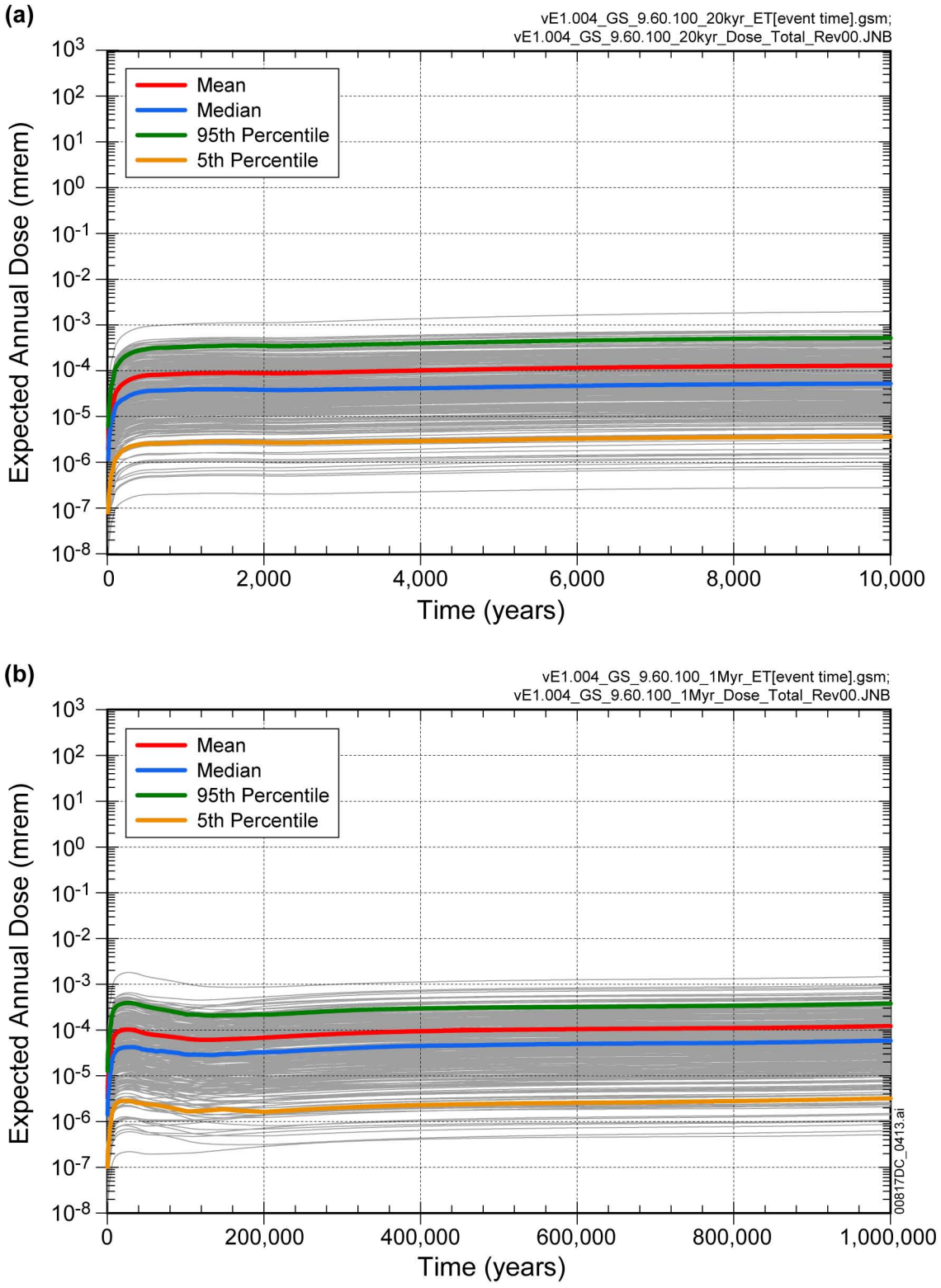

Source: Output DTN: MO0709TSPAREGS.000 [DIRS 182976]

Figure 8.2-9. Probabilistic Projections of Expected Annual Dose for the Volcanic Eruption Modeling Case for (a) 10,000 Years and (b) 1,000,000 Years after Repository Closure

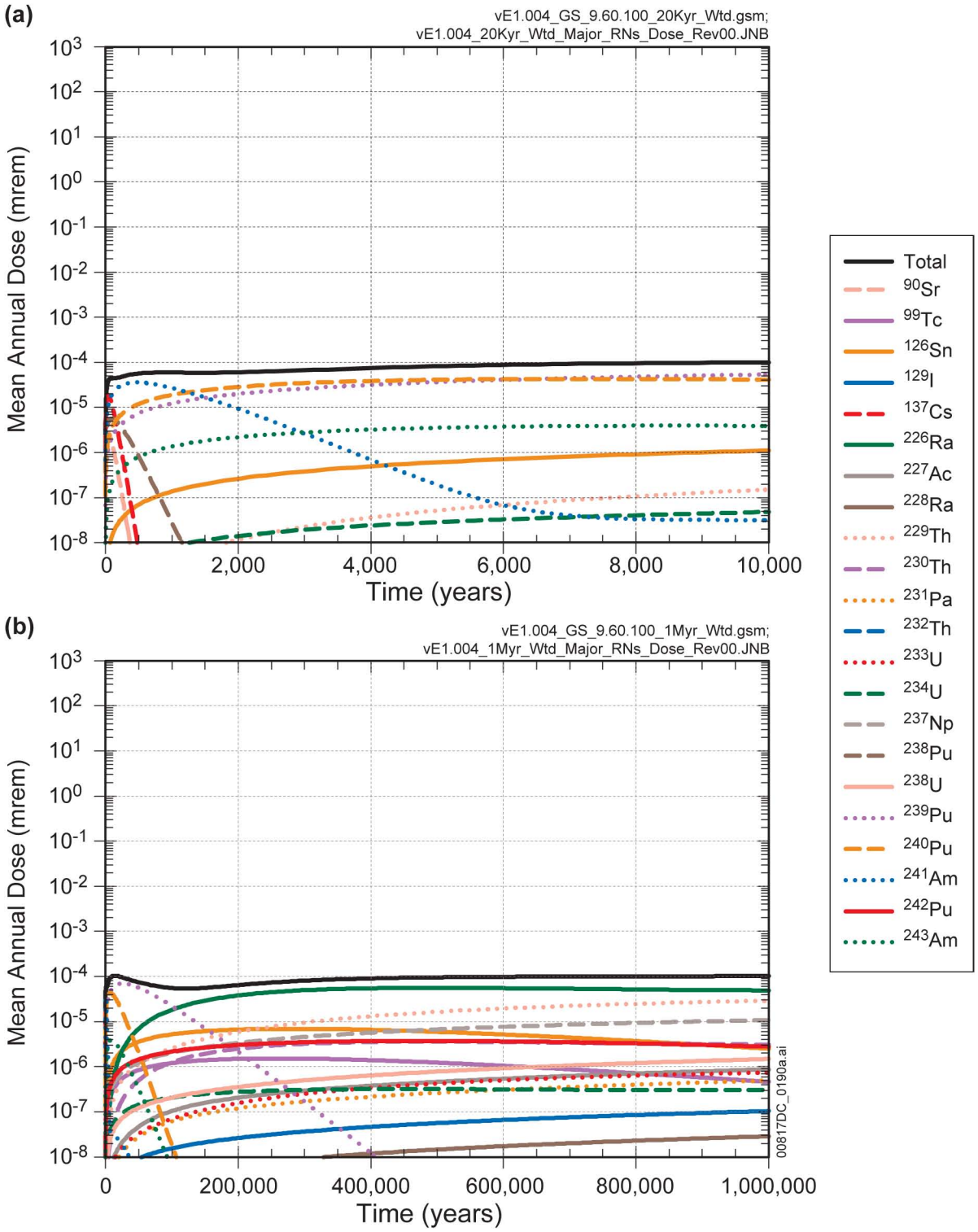

Source: Output DTN: MO0709TSPAREGS.000 [DIRS 182976]

Figure 8.2-10. Contribution of Individual Radionuclides to Mean Annual Dose for the Volcanic Eruption Modeling Case for (a) 10,000 Years and (b) 1,000,000 Years after Repository Closure

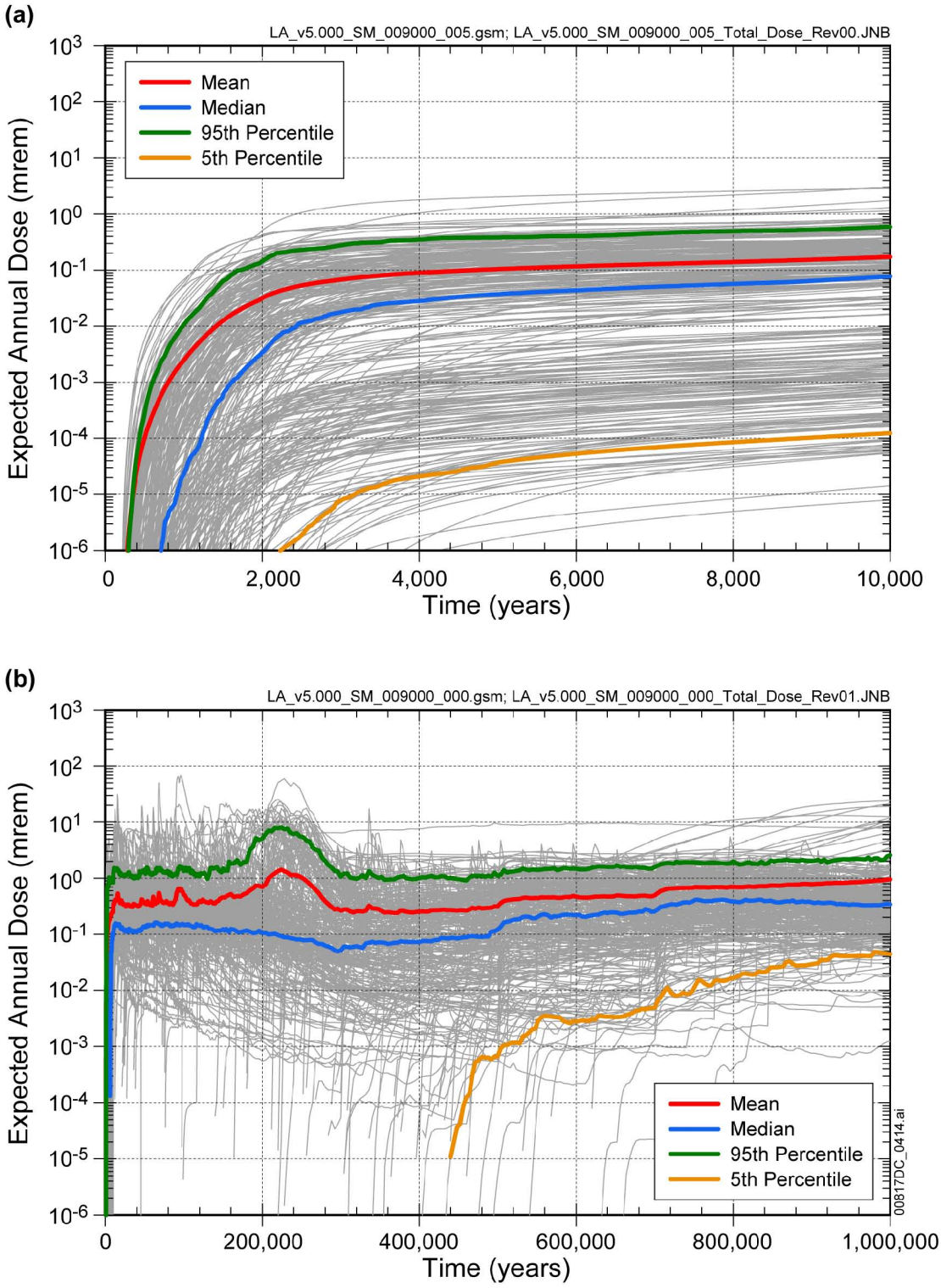

Source: Output DTN: MO0709TSPAREGS.000 [DIRS 182976]

Figure 8.2-11. Probabilistic Projections of Expected Annual Dose for the Seismic Ground Motion Modeling Case for (a) 10,000 Years and (b) 1,000,000 Years after Repository Closure

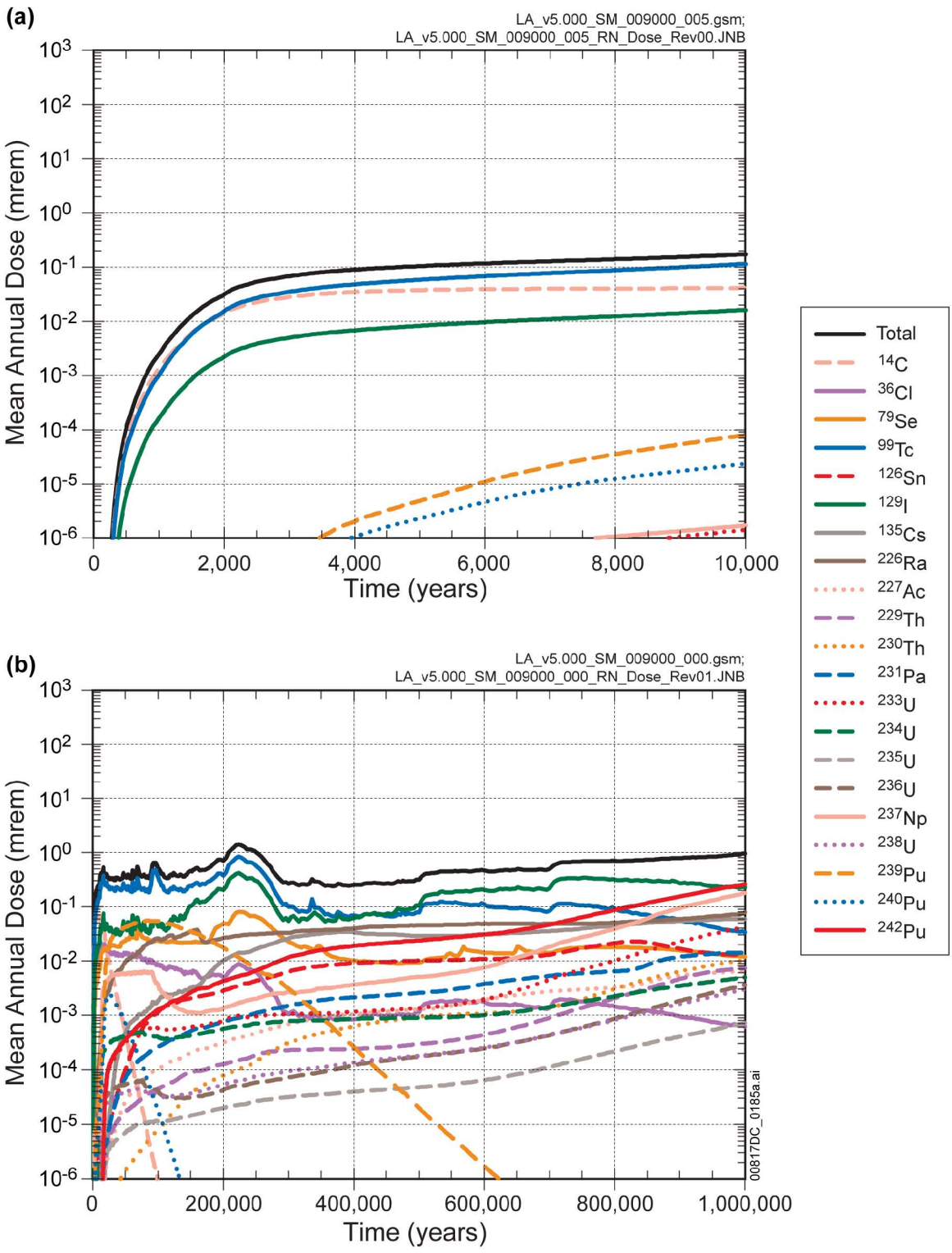

Source: Output DTN: MO0709TSPAREGS.000 [DIRS 182976]

Figure 8.2-12. Contribution of Individual Radionuclides to Mean Annual Dose for the Seismic Ground Motion Modeling Case for (a) 10,000 Years and (b) 1,000,000 Years after Repository Closure

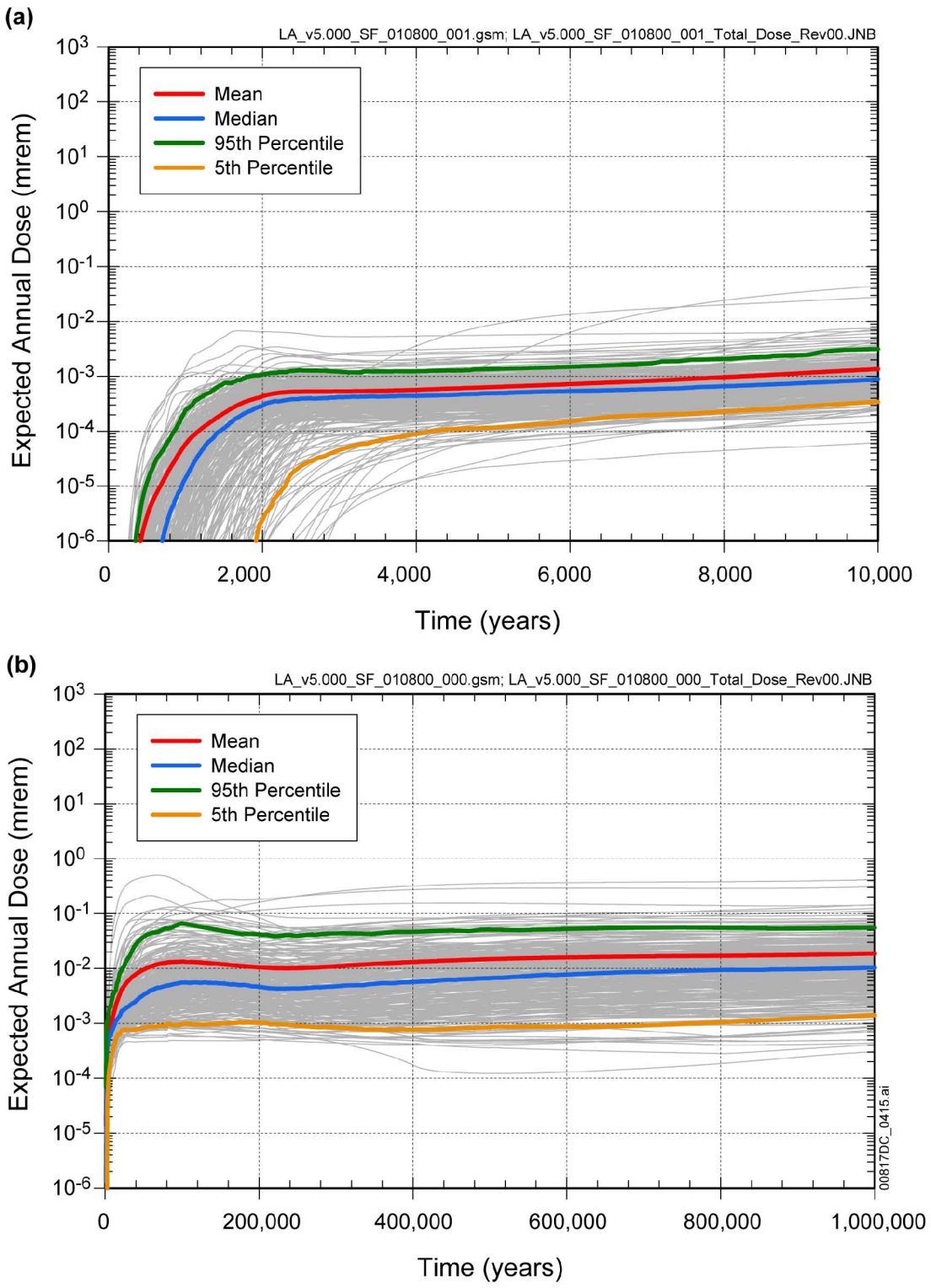

Source: Output DTN: MO0709TSPAREGS.000 [DIRS 182976]

Figure 8.2-13. Probabilistic Projections of Expected Annual Dose for the Seismic Fault Displacement Modeling Case for (a) 10,000 Years and (b) 1,000,000 Years after Repository Closure

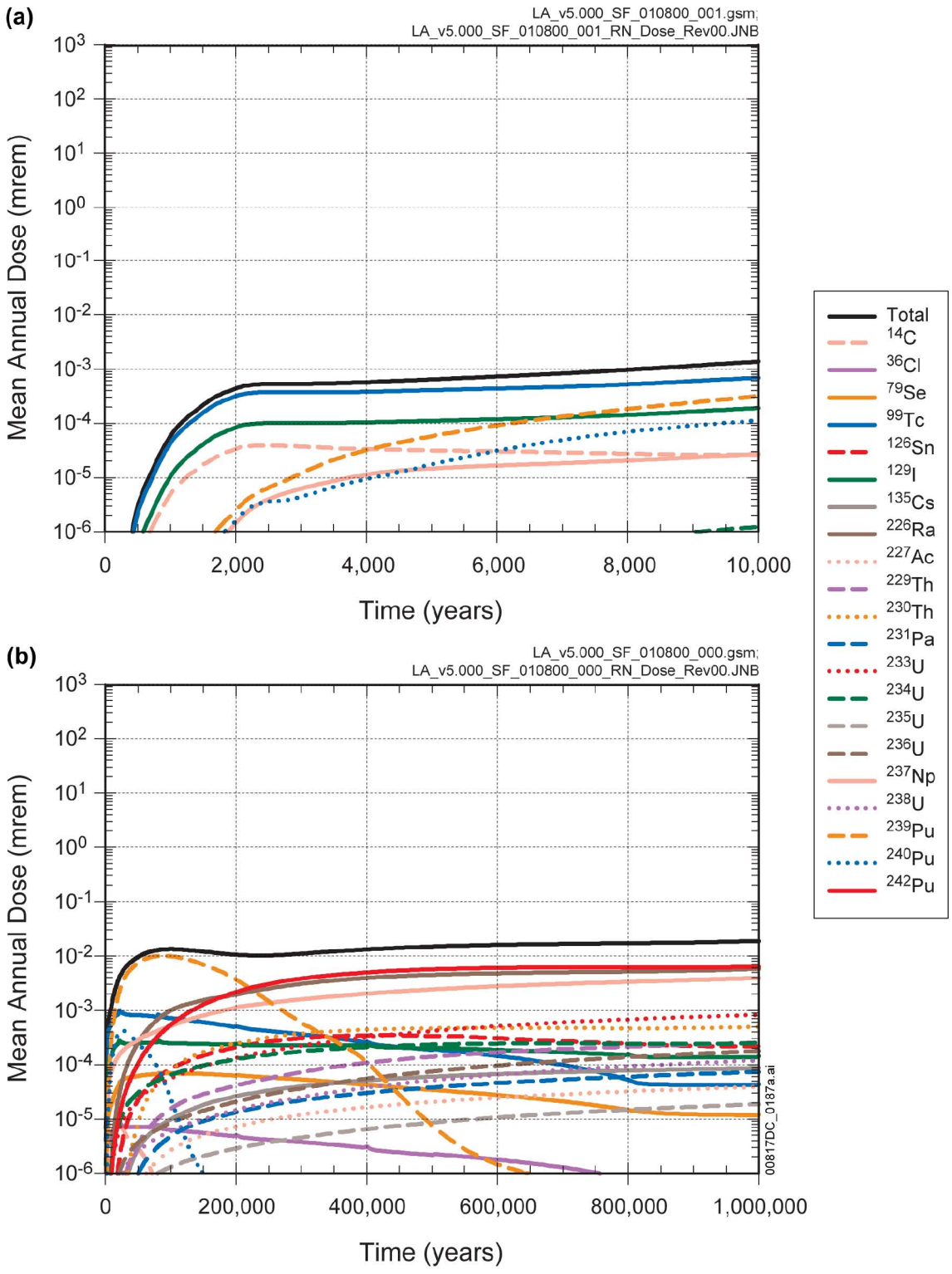

Source: Output DTN: MO0709TSPAREGS.000 [DIRS 182976]

Figure 8.2-14. Contribution of Individual Radionuclides to Mean Annual Dose for the Seismic Fault Displacement Modeling Case for (a) 10,000 Years and (b) 1,000,000 Years After Repository Closure

8.3 DESCRIPTION OF MULTIPLE BARRIER CAPABILITY

In the previous sections of this report, the DOE performance demonstrations for the three NRC radiation protections standards: (1) Individual-Protection (10 CFR 63.311) [DIRS 178394], (2) Human-Intrusion (10 CFR 63.321) [DIRS 178394], and (3) Groundwater Protection (10 CFR 63.331) [DIRS 180319], were presented and explained. The performance projections for these three standards demonstrated the isolation capability of the multiple barriers acting as an integrated system. In this section, both qualitative and quantitative descriptions are presented to explain the performance characteristics and capabilities of the individual barriers. In addition to providing valuable insights to barrier capability, this information also addresses the NRC requirements of 10 CFR 63.115 [DIRS 180319] for multiple barriers, which specifies that the DOE demonstration of compliance must:

- "(a) Identify those design features of the engineered barrier system, and natural features of the geologic setting, that are considered barriers important to waste isolation.
- (b) Describe the capability of barriers, identified as important to waste isolation, to isolate waste, taking into account uncertainties in characterizing and modeling the behavior of the barriers.
- (c) Provide the technical basis for the description of the capability of barriers, identified as important to waste isolation, to isolate waste. The technical basis for each barrier's capability shall be based on and consistent with the technical basis for the performance assessments used to demonstrate compliance with 10 CFR 63.113 (b) and (c)."

Identifying the multiple barriers is a relatively straightforward task, and a brief discussion of the Upper Natural Barrier, EBS, and Lower Natural Barrier, as well as their key features, is given in a subsequent section. With regard to providing the technical bases for barrier capability, that information is extensive and consists of site characterization data and numerous modeling studies that have been conducted over the past two decades. The technical bases for the multiple barriers are documented in numerous Yucca Mountain Project (YMP) reports, many of which are cited in Sections 1 through 6 of this report.

The main purpose of this section is to describe and explain the performance capability of the individual barriers and their barrier features. For this reason, this section is organized into four general parts:

1. Description of the major radionuclides selected to illustrate barriers capability
2. Identification of multiple barriers and their primary barrier features
3. Description of barrier capability in the absence of disruptive events, as defined by a composite modeling case of the Nominal Modeling Case plus Early Failure Modeling Cases
4. Description of barrier capability in the presence of disruptive events, as defined by Seismic GM Modeling Case.

With regard to item 4, the Seismic GM Modeling case was selected to illustrate barrier capability because: (1) frequencies of occurrence of seismic events are much greater than those for other disruptive events and (2) seismic ground motion has been shown to be important to postclosure performance (Section 8.1.1.2).

Selected performance projections of barrier capability will be presented, which highlight each barrier's inherent capability to isolate (i.e., contain and/or confine) the radionuclides that may pose the most risk over the range of plausible future system states. These projections also provide an additional technical basis for the performance demonstration results presented in Sections 8.1 and 8.2. Because of current programmatic and computational constraints, however, the TSPA-LA results for parts (3) and (4) will be documented in a separate addendum to this report.

8.3.1 Radionuclides Selected to Demonstrate Multiple Barrier Capability

One of the basic and important functions of the multiple barriers is to prevent or substantially reduce the rate of radionuclide movement from the repository to the accessible environment. To demonstrate the range of barrier capability but yet limit the number of calculations, a small subset of radionuclides was selected for the barrier performance demonstrations. That subset was selected from two lists: (1) radionuclides identified as dominating the mean annual doses to the RMEI for the 10,000-year and post-10,000-year time periods, and (2) radionuclides identified as dominating the curie inventory for the 10,000-year and post-10,000-year time periods. The first list of important radionuclides was developed directly from the probabilistic projections of mean annual dose (Section 8.1, Figure 8.1-7). The second list was compiled by examining the inventory decay histories, which is discussed herein.

Calculations of inventory decay histories for the major radionuclides are shown on Figure 8.3-1 for the two compliance periods of 10,000 years and post-10,000 years (i.e., after 10,000 years but within 1,000,000 years). The time dependent behavior of individual radionuclides is the result of simple radioactive decay and, in some cases, decay chain in-growth. From the curves on these plots, one can note that in the first 100 years, two fission products, ^{90}Sr (half-life of 28.8 years) and ^{137}Cs (half-life of 30 years), dominate the inventory; thereafter, the actinide radionuclide ^{241}Am (half-life of 432.7 years) dominates to about 1,000 years, ^{240}Pu (half-life of 6,560 years) dominates to about 7,000 years, and then ^{239}Pu (half-life of 2.41×10^4 years) dominates to about 115,000 years. Dominance then shifts to the fission product ^{99}Tc (half-life of 2.13×10^5 years) for the majority of time in the 1,000,000-year time period.

More refined insights to inventory dominance can be gained by examining plots of the fraction of total activity, at time 't', for each radionuclide; two plots are shown on Figure 8.3-2 for 10,000 years and 1,000,000 years. From these plots, it is evident that the dominant radionuclides in the curie inventory, grouped by compliance period, are:

1. For 10,000 years: ^{137}Cs and ^{90}Sr, ^{241}Am, ^{240}Pu and ^{239}Pu
2. For post-10,000 years: ^{239}Pu, ^{99}Tc, ^{237}Np, ^{233}U, and ^{229}Th.

At closure, the three radionuclides, ^{137}Cs, ^{90}Sr, and ^{241}Am, collectively represent about 85 percent of the total curie inventory with ^{137}Cs representing about 46 percent, ^{90}Sr about 29

percent, and ^{241}Am about 10 percent. From Figure 8.3-2(a), it can be clearly seen that ^{241}Am dominates the curie inventory in the interval from 100 to 1,000 years. Dominance shifts to ^{240}Pu and ^{239}Pu from 1,000 years to 10,000 years with these two actinides alone representing more than 90 percent of the inventory at the end of 10,000 years. As shown on Figure 8.3-2 (b), ^{239}Pu dominance peaks at about 50,000 years. From roughly 100,000 years to 1,000,000 years, the inventory dominance shifts to ^{99}Tc (half-life of 2.13×10^5 years) until roughly 850,000 years then transitions to dominance by three actinides: ^{237}Np (half-life of 2.14×10^6 years), ^{233}U (half-life of 1.59×10^5 years), and ^{229}Th (half-life of 7.3×10^3 years); the curves for ^{233}U and ^{229}Th overlay due to secular equilibrium. The latter three actinides are members of a decay chain in the neptunium series (Figure 6.3.7-4). A summary of the decay history of the total curie inventory and the major contributors is presented in Table 8.3-1; the percentages shown in the table were calculated directly from the data files used to create Figure 8.3-1.

Comparing the above radionuclides that dominate the inventory with the radionuclides identified as important to mean annual doses to the RMEI, namely, for the 10,000-year compliance period: ^{99}Tc, ^{14}C, ^{129}I, ^{239}Pu, ^{36}Cl, ^{79}Se, and ^{240}Pu, and for the post-10,000-year compliance period: ^{226}Ra, ^{242}Pu, ^{237}Np, ^{129}I, ^{233}U, ^{135}Cs, ^{230}Th, ^{99}Tc, ^{229}Th, and ^{231}Pa; it can be noted that the radionuclides that dominate the inventory also appear in the list of radionuclides important to dose, with the exception of the short-lived ^{137}Cs, ^{90}Sr, and ^{241}Am.

Based on the above considerations, the following subset of radionuclides was selected for use in describing barrier capabilities with regards to reducing or substantially reducing the rate of radionuclide movement:

These radionuclides represent a broad range of nuclear properties, geochemical behavior, and transport characteristics including:

- Large initial inventory and short half-life: ^{137}Cs, ^{90}Sr, ^{241}Am, ^{240}Pu
- Highly soluble, non-sorbing, long half-life and major contributor to dose: ^{99}Tc
- Solubility limited, strongly sorbed, long half-life, transported in dissolved and colloidal phases, and important contributor to dose: ^{239}Pu and ^{242}Pu
- Moderately soluble, low sorbing, very long half-life, and transported in dissolved phase: ^{237}Np and ^{234}U
- Low initial inventory, strongly sorbed, and important contributor to colloids or decay chain in-growth: ^{243}Am, ^{230}Th, and ^{226}Ra.

The primary barrier performance metrics that will be used are: seepage flux, DS and WP lifetimes and radionuclide release rates. The release rates are computed at the following barrier interfaces: (1) EBS outer boundary, (2) UZ and SZ interface, and (3) SZ and accessible environment interface.

8.3.2 Identification of Barriers for Yucca Mountain Repository System

As noted earlier, the Yucca Mountain Repository system is comprised of three barriers, namely, the Upper Natural Barrier, the EBS, and the Lower Natural Barrier (Figure 8-1). Collectively, these three barriers function to: (1) prevent or substantially reduce the rate of movement of water or radionuclides from the repository to the accessible environment, or (2) prevent or substantially reduce the release rate of radionuclides from the repository. A brief description of these barriers and their features is given below:

1. Upper Natural Barrier—Barrier features include the topography and surface soils of the mountain, the unsaturated tuff units above the repository, and the rock in which the repository is constructed.

2. EBS—Barrier features include the emplacement drifts, DSs, WPs, waste forms, cladding (associated with CSNF, DSNF, and NSNF), WP pallets, and ballast in the emplacement drift inverts.

3. Lower Natural Barrier—Barrier features include the volcanic rock in the UZ beneath the repository and the volcanic rock and alluvial material in the SZ between the repository and the accessible environment.

It is important to clarify that the Upper Natural Barrier is the portion of the geologic strata that extends from land surface to the bottom of the repository emplacement horizon. The Lower Natural Barrier extends from the base of the repository horizon to the water table and includes the SZ below the water table that extends from the repository footprint to the accessible environment boundary at approximately 18 km.

For the Upper Natural Barrier, the capability of the barrier features is described with respect to how they prevent or substantially reduce the rate and amount of water that may seep into the repository drifts and, ultimately, to the accessible environment. In contrast, the capability of the EBS features is described with respect to how they prevent or substantially reduce the release rate of radionuclides from the WPs. In the case of the Lower Natural Barrier, the capability of the barrier features is described in terms of how they prevent or substantially reduce the rate of movement of radionuclides from the repository to the accessible environment.

8.3.2.1 Upper Natural Barrier

The Upper Natural Barrier serves to prevent or substantially reduce the rate of water percolating downward through the UZ. More specifically, this barrier is important to postclosure performance because percolating water and the ensuant drift seepage are the only means by which radionuclides could be mobilized from the nuclear waste and transported by groundwater to the accessible environment. This barrier is the thick UZ formation of Yucca Mountain, which is composed of surficial soils and the unsaturated tuffs; namely, the Tiva Canyon welded (TCw), Paintbrush nonwelded (PTn), and Topopah Springs welded (TSw) units.

The location and elevation of the repository provide further advantage to the favorable and unique barrier characteristics of the geologic and hydrogeologic setting of the Yucca Mountain site. These favorable barrier characteristics include:

- A semiarid climate with limited precipitation and significant evapotranspiration
- A thickness of rock and soil above the repository of at least 200 m and up to more than 400 m
- Geologic, geochemical, and geomechanical characteristics that are compatible with the design and construction of an effective EBS
- Geomechanical and thermal characteristics that provide a stable facility with adequate capacity for waste disposal.

The semiarid climate in the Yucca Mountain is characterized by mean annual precipitation rates of 100 to 300 mm/yr (BSC 2004 [DIRS 169734], Figure 7-6).

Topography and Surficial Soils—The topography and surficial soils play a significant role as barriers to water because they limit the net infiltration into the UZ. The surficial soils function as a barrier by diverting (as runoff) some of the water that arrives as precipitation and run-on, and by storage in the soil, some of which is returned to the atmosphere as evapotranspiration. Thus, the volume of water that is diverted or evaporated would not percolate into the UZ rock layers as net infiltration. Recent studies of infiltration (SNL 2007 [DIRS 182145]) for the Yucca Mountain site indicate that the surficial soils are a very effective natural barrier to surface infiltration. For example, detailed water balance calculations for present-day climate shows that the mean net infiltration rate is less than 10 percent of the mean precipitation rate (SNL 2007 [DIRS 182145], Table 6.5.7.4-1); these water balance calculations also indicate that the processes of evapotranspiration and runoff reduce the net infiltration rate by as much as 88 percent.

Unsaturated Tuff Units—Water flow in the fractured welded tuffs that host the repository (i.e., TSw hydrogeologic unit) occurs primarily in widely distributed fractures (e.g., fracture density, spacing, and apertures). In contrast, the PTn hydrogeologic unit (located above the TSw hydrogeologic unit) is characterized by matrix-dominated flow. The matrix-dominated flow in the PTn unit attenuates, or dampens, the amplitude of pulses of percolation caused by variable infiltration and lateral heterogeneity.

As part of the UZ Flow Model development over the past decade, the steady-state nature of the flow fields and the damping of transient pulses were evaluated in different studies. The work of Wang and Narasimhan (1985 [DIRS 108835]; 1993 [DIRS 106793], Figure 7.4.7), for example, indicates that effects of infiltration pulses at the surface are damped by the underlying tuff units, especially the PTn. The welded tuff of the repository horizon exhibited only small changes in saturations, pressures, and potentials from steady-state values in response to the transient pulses. Pan et al. (1997 [DIRS 164181]) investigated transient flow behavior for downward water flow through sloping layers in the UZ.

Wu et al. (2002 [DIRS 161058], pp. 35-1 to 35-12) analyzed the capillary barrier capacities in unsaturated units and indicated that, on average, it took several thousand years for water to travel through the PTn. Wu et al. (2000 [DIRS 154918]; 2002 [DIRS 161058]) analyzed the implications of capillary barrier development in subunits of the PTn for lateral diversion of flow in the PTn. Along sloping layers, strong capillary barriers, if formed, will promote lateral diversions. A more recent study, conducted by Zhang et al. (2006 [DIRS 180273]) using three-dimensional and one-dimensional model results, shows that the PTn can attenuate episodic infiltration pulses significantly, most percolating water is damped by the subunits at the top of the PTn, and a small percentage of that water flux is diverted into faults.

Within the repository horizon, ambient unsaturated flow and thermo-hydrologic processes are favorable to the natural barrier function of preventing or substantially reducing the movement of water into emplacement drifts. Thermo-hydrologic (TH) analyses (SNL 2007 [DIRS 181383]) of the postclosure thermal period, for example, show that the decay heat will raise host rock temperatures and create dry-out zones around the emplacement drifts (Figure 6.3.3-3). These dry-out zones would vaporize locally percolating water and induce water (liquid and vapor) flow away from the drift. Current analyses of TH processes indicate that dry-out zones or vaporization barriers may effectively extend upwards of about 11 meters (Section 6.3.2.1) into the host rock and would persist for several centuries (SNL 2007 [DIRS 181383], Table 6.3-50[a]). As the host rock cools to temperature below boiling, the locally percolating water would create a zone of increased saturation at the drift crown and around the drift opening, resulting in the formation of a capillary-barrier (SNL 2007 [DIRS 181244], Section 6.1.4). The extent of the capillary-barrier effect would be limited to a relatively thin layer around the opening but would be sufficiently effective to divert flow around the drift (Figure 6.3.3-4); this diversion of ambient water flow, in turn, would reduce the seepage flux to drift.

8.3.2.2 Engineered Barrier System

The primary features of the EBS include the emplacement drifts, DSs, WPs, cladding, waste forms, WP pallets, and the drift invert. While the WPs remain without a major breach (e.g., an opening or tear/puncture created by general corrosion or seismic loading), none of the waste can be exposed to water, and no release of radionuclides can occur. The WP outer barrier will be made of Alloy 22, a corrosion-resistant nickel alloy. Even if some WPs were to be breached, the intact DSs would prevent seepage from contacting the waste. Similarly, the Titanium Grade 7 DS is sufficiently resistant to both general corrosion and localized corrosion and should not be breached by either of these nominal processes for more than 10,000 years. The barrier capability of the EBS features, however, can be diminished by potential disruptive events and processes, such as seismic ground motion, fault displacement, and igneous intrusion.

The favorable barrier characteristics of the EBS include:

- A stable thermal, mechanical hydrologic, and chemical environment affected principally by the thermal effects of radioactive decay
- Corrosion resistant metals that are designed to perform and function in the thermal, mechanical, hydrologic, and chemical environments expected in the emplacement drifts

- DS, WP, and cladding materials with designs and fabrication methods that reduce the potential effects of SCC, and other physical-chemical degradation processes

- Generally low radionuclide solubility and high sorption characteristics of radionuclides (on corrosion products) delaying or preventing their release even in rare early breach of WPs

- Delayed transport of radionuclides through the EBS due to low rates of water advection through the EBS features, and the slow diffusion of radionuclides through any continuous water film that is expected to be highly tortuous.

Evidence from natural and man-made openings in unsaturated underground environments indicates that such openings effectively limit the movement of water and often create stable conditions in which fragile materials may be preserved for tens of thousands of years. Analogue data from Pena Blanca indicate that underground openings provide a significant reduction in seepage compared to the amount of water infiltration that enters the UZ (SNL 2007 [DIRS 181244], Section 7.3[a] and 8.1[a]). Emplacement drifts provide the thermal, mechanical, hydrologic, and chemical environment in which the rest of the EBS features function. These environments are affected by the heat caused by the decay of radioactive materials in the waste, in particular, in the CSNF waste form. Although these environments are expected to change with time, in the absence of unlikely disruptive events such as low probability seismic or igneous events, the rate of change is very slow.

Drip Shields—The corrosion resistant Titanium Grade 7 DSs are installed over the WPs prior to repository closure. The DSs divert any potential seepage from the Upper Natural Barrier and water condensate (that may form from the water vapor in the air) around the WPs to the emplacement drift invert. In addition, the DS protects the WP from the potential effects of rockfall.

Waste Packages—As long as they remain without a major breach, WPs prevent contact between water and the waste form and prevent the release of radionuclides. Should water contact the WPs, any resultant corrosion of the Alloy 22 WP is expected to proceed slowly under the nominal corrosion degradation conditions and result in initial breaches in the form of hairline cracks that still limit the movement of water that could potentially contact the waste form, and thus, reduce the release rate of radionuclides from the WPs. Note that localized corrosion of WPs is not expected to occur under the repository condition (Section 6.3.5.2.3). The 50-mm thick stainless steel WP inner vessel and the 25-mm thick transport, aging, and disposal (TAD) canister are expected to provide some performance benefit for waste containment, and could potentially contribute to the reduction of the rate of radionuclide release after WPs are breached. The performance benefit of these specific WP components, much like CSNF cladding, are not considered in the TSPA-LA Model.

Cladding—Zircaloy cladding is a highly corrosion-resistant component of the CSNF that prevents or substantially reduces the contact of water with the waste form and reduces the release rate of radionuclides. For the purposes of conservatism, no performance credit is taken in the TSPA-LA Model for CSNF cladding effects on release rate.

Waste Forms—The waste forms that will be disposed of, include spent nuclear fuel (SNF) and HLW glass (vitrified). These waste forms are solid materials that generally degrade slowly in the unsaturated environment of the repository, thus reducing the release rate of radionuclides, although the DSNF is assumed to degrade instantaneously in the TSPA-LA Model.

Pallets—The WP pallet provides stability of the WP in the case of a seismic event and keeps the WP elevated above the floor of the emplacement drift as well. Thus, direct contact between the WP and the invert is not possible until the pallet degrades. This behavior is not considered in the TSPA-LA Model.

Inverts—The emplacement drift invert is composed of two parts: a steel invert structure and ballast (or fill). In the unsaturated repository environment, the granular materials in the invert slow the diffusive movement of radionuclides into the Lower Natural Barrier.

The features described above give the EBS the ability to prevent or significantly reduce the seepage water from contacting the waste forms, thereby substantially reducing the potential radionuclide release and rate of release from the waste into the Lower Natural Barrier.

8.3.2.3 Lower Natural Barrier

The features of the Lower Natural Barrier include the UZ tuff layers immediately below the repository and the SZ that extends downgradient from the repository to the accessible environment. The UZ includes a portion of the Topopah Springs welded (TSw) and Calico Hills nonwelded (CHn), and Crater Flat undifferentiated (CFu) units (Ortiz et al. 1985 [DIRS 101280]). These unsaturated rock layers represent a total vertical transport path of 250 to 380 m across the repository footprint with an average of about 300 m to the water table for present-day climate conditions. Under the wetter climates, however, the travel distance through the UZ may be as much as 120 m less due to a higher water table under the glacial transition climate. The SZ is composed of volcanic units and alluvial sediments (Section 6.3.10) with the flow path extending a distance of about 18 km to the accessible environment boundary. The first 12 to 14 km of the SZ flow path is in fractured volcanic rocks, while the remainder of the flow path is through alluvial sediments. The projected direction of the groundwater transport pathway is southeast from the repository site, transitioning to a southerly direction towards the designated accessible environment boundary in the Amargosa Desert.

The role of the Lower Natural Barrier is to prevent or substantially reduce the rate of movement of radionuclides from the repository to the accessible environment. The Lower Natural Barrier performs this role through the intrinsic site characteristics that are directly reflected by such factors as: (1) slow advective water transport, (2) matrix diffusion and sorption of dissolved phase radionuclides, (3) dispersion/dilution of dissolved and colloidal phase radionuclides, (4) reversible filtration of irreversible colloidal phase radionuclides, and (5) radioactive decay and ingrowth. Section 6.3.9.1 discusses the flow and transport processes involved in determining the capability of the UZ, while the relevant SZ processes are discussed in Section 6.3.10.1.

Some of the fundamental and important performance characteristics of the Yucca Mountain Lower Natural Barrier include:

- Low deep percolation rates through the UZ as a result of hydrologic efficiency of the Upper Natural Barrier (i.e., surficial soils with characteristically high evapotranspiration, matrix flow through the PTn, and lateral flow focusing into faults in the northern part of the repository footprint)

- High porosity vitric rock layers (i.e., CHn in southern half of repository) and low permeability zeolitic rock layers (i.e., CHn and CFu), both types of rock layers that have capability to strongly sorb a variety of radionuclides and delay transport

- Long transport path through the SZ volcanic units with capability to delay radionuclides as dissolved radionuclides diffuse into and out of the pores in the rock, increasing the likelihood of sorption onto mineral surfaces, as well as promoting retardation of irreversible colloids (via reversible filtration)

- Lower advective transport through the higher porosity SZ alluvium, with capability to delay radionuclides via sorption of selected radionuclides on mineral particle surfaces and dilution as a result of longitudinal and transverse dispersion.

The performance characteristics of the UZ units below the repository have been analyzed using detailed three-dimensional flow and transport modeling studies. The rates of radionuclide movement through the UZ portion have bee studied using a particle tracking technique which is documented in *Particle Transport Model and Abstraction of Transport Processes* (SNL 2008 [DIRS 184748]). That report presents sensitivity analysis for breakthrough times for various radionuclide species. Analogous studies have been performed for the SZ to develop an understanding radionuclide transport to the accessible environment. Those studies are documented in *Saturated Zone Flow and Transport Model Abstraction* (SNL 2008 [DIRS 183750]).

INTENIONALLY LEFT BLANK

Table 8.3-1. Decay of Total Curie Inventory as a Function of Time and Dominant Contributors to Total Curie Inventory

Time After Closure (yrs)	Percent of Total Initial Curie Inventory	Major Contributors to Total Inventory at Time after Closure
0	100.00	Cs -137 (46%), Sr-90 (29%), Am-241 (10%)
10	81.2	Cs -137 (45%), Sr-90 (28%), Am241 (12%)
100	20.75	Am-241 (41%), Cs -137 (22 %), Sr-90 (13%), Pu-238 (11%))
1,000	4.20	Am-241 (48%), Pu-240 (29%), Pu-239 (19%)
10,000	1.18	Pu-239 (52%), Pu-240 (40%)
100,000	0.10	Pu-239 (46%), Tc-99 (27%)
500,000	0.03	Tc-99 (26%), Th-229 (9%), Th-230 (9%), Ra-226 (9%), U-233 (9%), Np-237 (9%), Pu-242 (8%), U-234 (7%)
1,000,000	0.02	U-233 (15%), Th-229 (15%), Np-237 (14%), Tc-99 (9%), Th-230 (7%), Ra-226 (7%), Cs-135 (7%), U-236 (6%), Pu-242 (6%)

Source: Output DTN: MO0709TSPAREGS.000 [DIRS 182976]

INTENTIONALLY LEFT BLANK

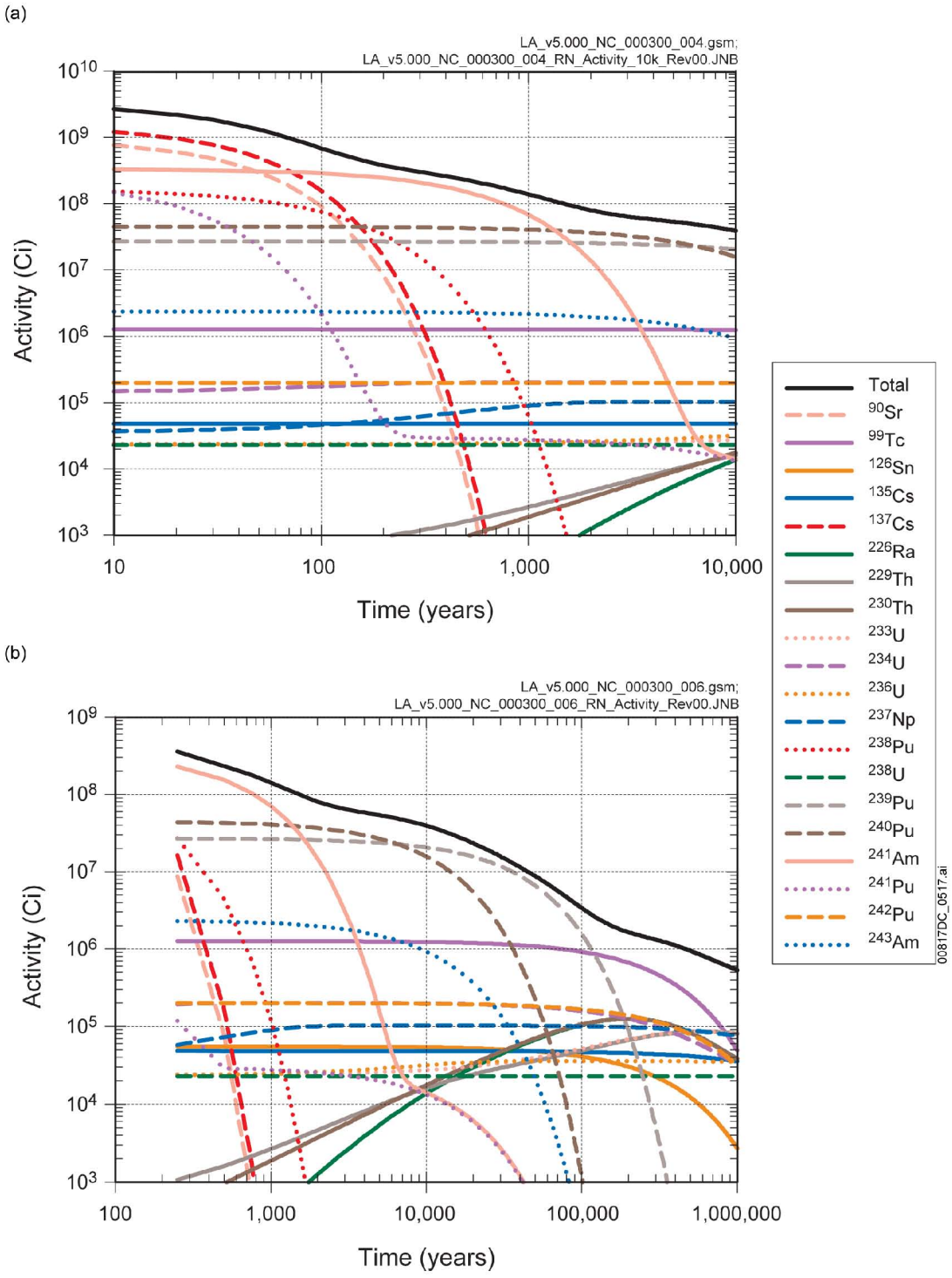

Source: Output DTN: (a) MO0708TSPAVALI.000 [DIRS 182985]; and (b) MO0709TSPALAMO.000 [DIRS 182981].

Figure 8.3-1. Mean Radionuclide Activities in the Nuclear Waste as a Function of Time for (a) 10,000 Years and (b) 1,000,000 Years after Repository Closure

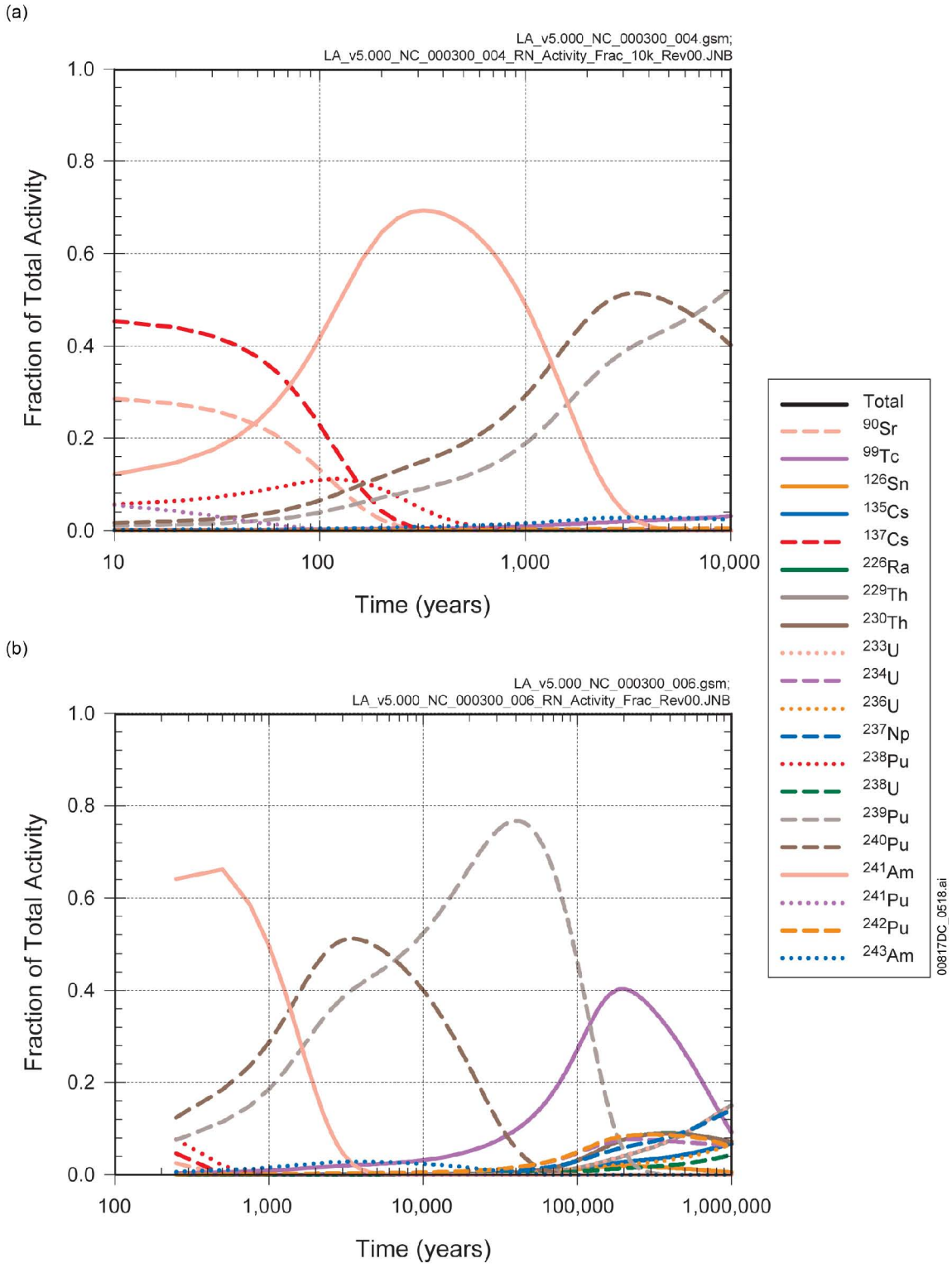

Source: Output DTN: MO0709TSPAREGS.000 [DIRS 182976]

Figure 8.3-2. Mean Radionuclide Contributions to Total Inventory as a Function of Time for (a) 10,000 Years and (b) 1,000,000 Years after Repository Closure

8.4 VALIDITY AND DEFENSIBILITY OF PERFORMANCE DEMONSTRATION

This section outlines the YMP activities that were conducted to ensure that the postclosure performance demonstration for the Yucca Mountain repository would be technically sound and defensible and, therefore, suitable to support the LA. In preparation for the LA, the YMP planned and successfully completed several programmatic activities to ensure that the:

1. TSPA-LA Model and its component models were validated for their intended use, controlled, and documented.

2. Software that implements the TSPA-LA Model was verified and validated through computational testing.

3. Models and input parameters account for the major sources of aleatory and epistemic uncertainties, are supported by appropriate evidence, and are maintained in a controlled database.

4. Performance projections are corroborated, to the extent possible, by other independent means, including auxiliary analyses and comparison with other separate TSPAs.

5. Technical basis for the TSPA-LA methodology was peer reviewed to ensure it is based on well established scientific principles, captures the important phenomena and couplings, and was supported by site characterization data.

The above programmatic activities are presented in Section 7, Volume II, of this report. The description of the TSPA-LA Model is presented in Section 6 of this report; the technical basis for the component models and TSPA input database is documented in several supporting analysis and/or model reports and TSPA Data Input Packages. Moreover, the supporting documentation was prepared in a manner that would ensure the technical basis is auditable and traceable so as to facilitate the licensing review.

Since the issuance of the *Total System Performance Assessment for the Site Recommendation* (CRWMS M&O 2000 [DIRS 143665]), the YMP's TSPA methodology (i.e., models, uncertainty treatment and propagation, code/software, and input parameters) has been significantly improved and refined as a result of:

- Continued scrutiny of the conceptual and mathematical models through internal and external peer reviews

- Further development and testing of TSPA-LA component models and submodels

- Statistical analysis of data and development of improved characterizations of uncertainty.

In addition, plausible and potentially significant model conservatisms have been identified, the rationale for their use explained, and their impact on postclosure performance metrics evaluated.

This section provides a summary of the specific YMP technical and programmatic activities conducted to ensure that the DOE postclosure performance demonstration is suitable to support the LA for the nuclear waste repository at Yucca Mountain.

8.4.1 Validation of TSPA Model and Component Models

At present, the applicable NRC regulation, NRC Proposed Rule 10 CFR Part 63 ([DIRS 178394] and [DIRS 180319]), does not contain requirements for model validation. However, the joint NRC/SKI white paper (Eisenberg et al. 1999 [DIRS 155354], p. 31) notes two essential elements for model validation: (1) procedures for the development of confidence in models, and (2) documentation of results from confidence building activities. These validation elements are incorporated in *Technical Work Plan for: Total System Performance Assessment FY 07-08 Activities* (SNL 2008 [DIRS 184920], Section 2.3.5) and are in accordance with:

- SCI-PRO-002, *Planning for Science Activities*
- SCI-PRO-006, *Models*.

Development and validation of the TSPA-LA Model and its components were planned and controlled in accordance with SCI-PRO-002 and documented in accordance with SCI-PRO-006. It is important to clarify and emphasize that model validation should be viewed as a progressive confidence building process and not an end-state.

The full range of model validation activities conducted for the TSPA-LA is illustrated on Figure 7.1-2. Some of the primary model validation requirements from the two procedures are highlighted here.

During-Development Model Validation—Activities in this first phase of model validation encompassed planning, reviewing, checking, and documenting, which focused on:

- Ensuring the model formulation, assumptions, and simplifications are defensible.
- Ensuring the model theory is consistent with fundamental scientific principles, such as conservation of mass, energy, and momentum.
- Documenting the selection of input parameters and/or input data and explaining how the selection process builds confidence in the model.
- Documenting plans for model calibration activities, and/or initial boundary condition runs, and/or run convergences, and a discussion of how the activity or activities build confidence in the model. Activities also included a discussion of impacts of any run non-convergences.
- Identifying and documenting the potential impacts of uncertainties on model results.

A detailed description of the during-development model validation activities is presented in Section 7.1.2 (Volume II).

Post-Development Model Validation—In this stage of model validation, technical activities involve conducting various computational analyses and evaluations to ensure that the processes modeled are understood and appropriately described. Moreover, the analyses and evaluations demonstrate that the required level of model validation has been fully achieved. The major activities performed for the post-development model validation include:

- Corroborating the abstraction model results to the results of the validated mathematical model or process model from which the abstraction model was derived (Section 7.6)
- Performing auxiliary analyses to corroborate the results with the TSPA-LA Model and/or submodels (Section 7.7)
- Comparing the relevant TSPA-LA component models or submodels with available analogue information (Section 7.8)
- Utilizing internal and external peer reviews to evaluate defensibility of models and identifying potential areas of component model or submodel development improvement (Section 7.9).

More information on the post-development model validation activities is presented in Section 7.1.3.

The TSPA-LA Model and the 11 component models (Section 6) have been validated in accordance with the appropriate procedures. Documentation of the model validation is presented in each of the supporting analysis and/or model reports and includes a description of the validation procedure, validation criteria, and validation results.

8.4.2 Verification and Validation of TSPA Software and Input Data

The TSPA-LA Model and its component models are integrated into the GoldSim software (GoldSim 2007 [DIRS 181903]). The version of the GoldSim software used for the TSPA-LA was verified by the vendor, GoldSim Technology Group, by conducting a broad spectrum of computational tests. The software verification consisted of over 250 tests that covered the program's capabilities, including the user interface, user-defined expressions, internal functions, and distributed processing capabilities. These tests included:

- 93 basic functional tests
- 23 time and Monte Carlo tests
- 130 contaminant transport tests
- 17 reliability module tests.

As part of the verification testing, the software was run through tests that exercise the graphical user interface, internal functions, stochastic processes, contaminant transport code, and result displays for the purpose of demonstrating that the software performed its numerical, logical, and input/output operation correctly. All verification tests were performed in accordance with a verification plan (DOE 2007 [DIRS 181107]).

The YMP staff reran all the verification test cases to provide an independent check; the software testing was performed in accordance with IM-PRO-004, *Qualification of Software*. For added confidence, key functions and capabilities of the simulation software were combined into four TSPA-developed tests, and the results were compared to independently generated results. The independent tests are described in the *Design Document for: GoldSim v9.60* (DOE 2007 [DIRS 181107], Section 7.2.1), and the results are shown in *Software Validation Report for: GoldSim v9.60 on Windows 2000* (DOE 2007 [DIRS 181109], Sections 4.2.34 through 4.2.37). The integrated system software (GoldSim) was qualified in accordance with IM-PRO-004. In addition to verification of the software, testing was performed to verify the computational stability and convergence. This included testing the:

1. Stability of the statistical sampling used in the Monte Carlo simulations (Section 7.3.1)

2. Numerical accuracy of the expected dose calculation (Section 7.3.2)

3. Convergence of the time stepping used in the numerical integration of the model equations (Section 7.3.3)

4. Spatial discretization of the repository system (Section 7.3.4).

5. Stability of transport models using the FEHM particle-tracking methodology (Section 7.3.5).

All of this computational testing was performed for the various modeling cases to ensure that the GoldSim model was ready for use in the performance demonstration for the LA.

The input database for the GoldSim software stores all the TSPA-LA input parameter values and distributions. This input database is used to categorize, store, and retrieve fixed and distributed values of the TSPA-LA Model parameters. The database is programmed with user controls featuring read and write access and audit trails. These controls were designed to ensure the security, integrity, and traceability of the information used in the TSPA-LA Model analyses. A controlled, standalone TSPA Input Database was developed using a commercially available desktop database manager, Microsoft Access 2000. It is a Microsoft Windows based, multi-user relational database solution that allows data entry, viewing, and querying, as well as report preparation. The TSPA Input Database was qualified in accordance with IM-PRO-004.

The parameter values are obtained from controlled sources maintained by the project data and information systems, such as project documents, the Technical Data Management System (TDMS), and the Technical Information Center. The TDMS database is a project-wide database, whereas the TSPA Input Database is used only for the TSPA-LA Model. Each of the parameter sets used in the TSPA Input Database has a data tracking number (DTN) to provide the link to the TDMS database or a reference to the controlled source of the information, such as an analysis and/or model report. The TDMS maintains the qualification status all of its contents. The TSPA Model inputs are controlled and well documented by using the TSPA Input Database. An important configuration management feature of the TSPA Input Database is that it supports the independent verification of every parameter value used in the TSPA-LA Model.

GoldSim software and the TSPA input database have been verified. Additional information on the validation and verification is presented in Section 7.

8.4.3 Uncertainty Characterization Reviews

In preparation for the LA, the Lead Laboratory undertook a substantive effort to systematically review the TSPA uncertainty and variability characterizations for consistency, defensibility, and traceability. A special review team was formed to carefully examine parameter uncertainty and variability representations, correct or modify them as necessary, and ensure that the supporting documentation would facilitate the regulatory review.

The central objective of the uncertainty characterization reviews was to ensure that the treatment of parameter uncertainty and variability was of suitable quality for the LA. To accomplish this objective, the review team focused on:

- Confirming that the stochastic parameter representations appropriately reflect the major sources of uncertainty and/or variability
- Verifying that the probability distributions were supported by appropriate evidence and derived using sound statistical methods and interpretations
- Ensuring that model parameter representations (i.e., probability distributions) were reasonable and defensible, as opposed to depicting extreme variations that could potentially introduce risk dilution (i.e., wider distribution and lower peak mean annual dose).

Uncertainty characterizations were also reviewed with respect to appropriate up-scaling, data modeling, and use of professional judgment in assigning subjective distributions.

A core team of five senior staff members was formed with special expertise in probability and statistics, uncertainty analysis, TSPA modeling, and knowledge of the regulatory guidance regarding consistent treatment of uncertainty and variability. In addition, a small group of SMEs were used to support the core team and to facilitate the reviews of data, parameters, and model abstractions. The review team conducted fifteen formal reviews that were performed to scrutinize the uncertainty characterizations of some forty TSPA input parameters and their associated abstractions.

Because of the relatively large number (~400) of probabilistic parameters used in the TSPA-LA Model, it was necessary to prioritize the parameters for review. The prioritization was developed based on the importance ranking of the scenario modeling cases and parameters within those modeling cases. The ranking of the scenario modeling cases was as follows (from highest to lowest):

1. Seismic Scenario Class, Seismic GM Modeling Case
2. Igneous Scenario Class, Igneous Intrusion Modeling Case
3. Igneous Scenario Class, Volcanic Eruption Modeling Case
4. Early Failure Scenario Class, Waste Package EF Modeling Case

5. Early Failure Scenario Class, Drip Shield EF Modeling Case
6. Seismic Scenario Class, Seismic FD Modeling Case
7. Nominal Scenario Class, Nominal Modeling Case.

A list of 40 plus TSPA-LA parameters (Section 7.4, Tables 7.4-1 through 7.4-3) was compiled. The review focused on parameters whose uncertainty or variability (when propagated through the TSPA-LA Model) would have the greatest influence on the magnitude of the dose results, and the uncertainty in the dose results.

The 15 reviews produced several findings, recommendations, and corrective actions that resulted in improvement in the technical basis and documentation of the parameter uncertainty characterizations. A few of the key improvements to parameter uncertainty characterizations included:

- Unsaturated zone (UZ)—effective soil depth for surface infiltration and weighting factors for UZ flow fields
- Engineered Barrier System (EBS)—general corrosion of the drip shield and waste package internals
- Saturated zone (SZ)—groundwater specific discharge multiplier and flowing interval thickness.

A more detailed discussion of the uncertainty characterization reviews conducted for the TSPA-LA is presented in Section 7.4.

8.4.4 Corroboration of TSPA-LA Model Results

A number of methods (Section 7.0) have been utilized to build confidence in the TSPA-LA Model. One of those approaches is based on corroborating the TSPA-LA performance projections using a simplified and independent computer model (Section 7.7). Performance projections presented in Sections 8.1 and 8.2 were corroborated through: (1) use of a simplified TSPA-LA analysis, and (2) comparison with the Electric Power Research Institute (EPRI) independent assessment of postclosure performance for the proposed repository. The simplified TSPA-LA analysis and the EPRI results have been used to check for consistency of results for the important modeling cases.

The confidence building achieved through these corroborations of the TSPA-LA Model results is emphasized in the following paragraphs.

8.4.4.1 Comparison with Simplified TSPA Analysis Results

A separate and simpler implementation of the performance assessment of postclosure performance (Appendix L) was developed for the specific purpose of corroborating the performance projection results produced with the TSPA-LA Model. That implementation is in a standalone and separate computer code designated as the Simplified TSPA. The Simplified TSPA code uses a Monte Carlo approach to incorporate epistemic and aleatory uncertainties to the probabilistic calculation of mean annual doses. While the formulation of its component

models generally parallels those of the TSPA-LA Model, the Simplified TSPA code employs several simplifications. A detailed enumeration of the differences between the TSPA-LA Model and Simplified TSPA is presented in Section 7.7.2, Table 7.7.2-1. Three important simplifications are: (1) the repository is represented as a single homogeneous region, (2) flow and transport through UZ and SZ are one-dimensional, and (3) approximation for decay chain transport is more conservative.

Thus far, the Simplified TSPA has only been applied to four of the seven TSPA-LA modeling cases (Section 6.1.2) to calculate the mean annual doses to the RMEI. More specifically, the Simplified TSPA has been applied to: Nominal, Waste Package EF, Seismic GM, and Igneous Intrusion. These specific modeling cases were selected because previous TSPAs indicated they would have the greatest influence on the total mean annual doses to the RMEI. This observation is also confirmed in the TSPA-LA results presented in Section 8.1.

Nominal Modeling Case Results—The TSPA-LA Model projections for this case are shown on Figure 8.2-1 and for Simplified TSPA on Figure 7.7.2-5. The TSPA-LA Model projects a dose history where the exposure begins at about 130,000 years and increases, reaching a peak at 1,000,000 years. The Simplified TSPA results show a similar trend, but the WP failures occur later, so exposures are delayed until roughly 300,000 years. TSPA-LA Model results show that a peak mean annual dose for this modeling case is about 0.4 mrem, which compares reasonably well with the Simplified TSPA projection of about 0.2 mrem. A time-slice comparison between the two mean annual dose projections is discussed Section 7.7.2.2 and shown on Figure 7.7.2-6. With regard to radionuclides important to dose, the TSPA-LA Model results show ^{129}I as the main contributor, with small contributions from ^{99}Tc, ^{135}Cs, and ^{242}Pu. The Simplified TSPA results also show the mean annual dose to be dominated by ^{129}I, with lesser contributions from ^{242}Pu. The main difference between the two model results for the Nominal Modeling Case is the timing of WP failures and radionuclide releases. This is explained by the fact that the Simplified TSPA represents the repository as a single block with average properties, and as such does not account for spatial variability.

Waste Package Early Failure Modeling Case Results—For this modeling case, the TSPA-LA Model results are shown on Figure 8.2-5 and the Simplified TSPA results on Figure 7.7.2-2. The TSPA-LA Model results show a relatively flat mean annual dose history over the 1,000,000-year time period, with doses varying from about 10^{-3} to 10^{-1} mrem. The Simplified TSPA shows a similar trend, but the doses vary from about 10^{-2} to 10^{-1} mrem. A time-slice comparison between the two mean annual dose projections is discussed Section 7.7.2.1 and shown on Figure 7.7.2-3. The TSPA-LA Model results indicate that ^{242}Pu, ^{226}Ra (daughter product of ^{230}Th), and ^{237}Np dominate the mean annual dose. In the Simplified TSPA projections, the mean annual dose at 1,000,000 years is dominated by ^{229}Th (daughter product of ^{233}U) and ^{242}Pu and with lesser contributions from ^{237}Np. The differences in radionuclides contributing to the dose are attributed to how the decay chain transport is approximated in the Simplified TSPA code.

Seismic Ground Motion Modeling Case Results—Graphical results for this modeling case are shown on Figure 8.2-11 for the TSPA-LA Model and on Figure 7.7.2-8 for the Simplified TSPA. Both the TSPA-LA Model and Simplified TSPA results show the mean annual doses histories to rise to a peak mean value and then remain relatively flat. However, the TSPA-LA Model shows a peak mean annual dose of about 0.1 mrem, whereas the Simplified TSPA shows a higher value

of about 1 mrem. A time-slice comparison between the two mean annual dose projections is discussed Section 7.7.2.3 and shown on Figure 7.7.2-9. The TSPA-LA Model results show ^{99}Tc and ^{129}I as the main contributors to dose for the majority of the 1,000,000-year time period, whereas the Simplified TSPA dose history is largely dominated by ^{242}Pu, ^{237}Np, and ^{229}Th.

Igneous Intrusion Modeling Case Results—For this modeling case, the TSPA-LA Model results are shown on Figure 8.2-7 and the Simplified TSPA results on Figure 7.7.2-11. The TSPA-LA Model results show a mean annual dose history that rises until reaching a peak of 1 mrem at about 80,000 years and then remaining relatively flat thereafter. The Simplified TSPA results indicate a similar trend but reach a peak mean annual dose of 10 mrem. A time-slice comparison between the two mean annual dose projections is discussed Section 7.7.2.4 and shown on Figure 7.7.2-12. In both the TSPA-LA Model and Simplified TSPA projections, the initial peak dose is attributed to ^{239}Pu. From about 200,000 years to 1,000,000 years, the TSPA-LA Model results show that dose is largely attributed to ^{226}Ra, ^{242}Pu, and ^{237}Np. For this same time interval, the Simplified TSPA results show ^{242}Pu, ^{237}Np, and ^{229}Th as dominating the dose. As noted previously, the daughter products, such as ^{229}Th and ^{226}Ra, are computed differently in the two transport codes, which explain the differences.

Summary of Corroboration—For most of the modeling cases, the performance projections for two separate models compare reasonably well both in terms of the mean annual dose levels and the radionuclides important to the dose. The few differences noted are explainable and attributed to use of different approaches for calculating decay chain transport (i.e., differential transport of precursor and daughter product).

A more detailed discussion of the corroboration of the TSPA-LA Model results using the Simplified TSPA Analysis is presented Section 7.7.2.

8.4.4.2 Comparison with Electric Power Research Institute TSPA Analysis

The EPRI developed its own TSPA Analysis, which is implemented in the Integrated Multiple Assumptions and Release Code (IMARC) (EPRI 2005 [DIRS 178580]). EPRI developed IMARC to provide an independent assessment of key technical and scientific issues associated with the proposed repository at Yucca Mountain. Like the TSPA-LA Model, the EPRI TSPA Analysis uses coupled component models to simulate the response of the repository to changing conditions and disruptive events. With regard to treatment of uncertainty, the EPRI TSPA Analysis accounts for epistemic uncertainties in the model parameters but does not consider aleatory uncertainties associated with occurrence of disruptive events. At present, the EPRI TSPA Analysis only considers four scenarios consisting of nominal, igneous, seismic, and human intrusion. In contrast to the TSPA-LA Model, the EPRI TSPA Analysis for the nominal scenario includes early failure of one WP and one DS. The available EPRI documentation presents a simulation of postclosure performance for the combined nominal and early failure modeling case for a 1,000,000-year time period.

Combined Nominal and Early Failure Modeling Case Results—The TSPA-LA Model projections for this case are shown on Figure 7.7.3-3 and for IMARC on Figure 5-10 of *Program on Technology Innovation: Evaluation of a Spent Fuel Repository at Yucca Mountain, Nevada, 2005 Progress Report* (EPRI 2005 [DIRS 182229]). The mean annual dose history curves for

TSPA-LA Model and IMARC show a similar trend in the dose histories, with a significant increase in dose to the RMEI after about 100,000 years. The TSPA-LA Model projections indicate a peak mean annual dose of 0.4 mrem at 1,000,000 years, whereas the IMARC result shows a peak of about 0.02 mrem. In both the TSPA-LA Model and IMARC model results, the peak mean annual dose is dominated by a single radionuclide, ^{129}I. In addition to peak dose, the other notable difference between the two performance results is the initial breakthrough; the TSPA-LA Model results indicate dose exposure starting at about 400 to 500 years, whereas the IMARC results occur at about 7,000 years.

The main differences in the two independent projections are largely attributed to a distinct technical basis for the EBS and release rate calculation. For example, the EPRI TSPA Analysis only accounts for CSNF waste and considers failure of DS, WP, and cladding, whereas the TSPA-LA Model accounts for CSNF, DSNF, and HLW, but does not take credit for cladding in CSNF WPs. In addition, seepage rates used in the EPRI TSPA Analysis are significantly lower than the corresponding rates used in the TSPA-LA Model, which appear to cause a delay in radionuclide release from the EBS. There are other differences related to the abstraction of features and processes. It is important to keep in mind that the performance projections published by EPRI were intended to status the development of their independent capability and not to present a performance demonstration in accordance with NRC regulation.

Summary of Corroboration—The comparisons of performance projections generally corroborate the TSPA-LA results and therefore provide additional confidence in the validity and defensibility of the performance demonstration. A more detailed discussion of the comparison of the EPRI TSPA Analysis and TSPA-LA Model results is presented in Section 7.7.3

Performance Margin Analysis

A Performance Margin Analysis (PMA) was conducted to quantitatively evaluate the differences in repository performance due to significant explicit and implicit conservatisms embedded in the TSPA-LA Model subcomponents. The conservatisms were evaluated to (1) confirm that they are conservative with respect to the mean annual dose of the TSPA-LA Model; (2) quantify the extent to which they, individually and collectively, overestimate the projected annual dose; and (3) assess that the evaluated conservatisms did not introduce any inappropriate risk dilution in the TSPA-LA results presented in support of the LA. The PMA was conducted by first modifying selected submodels and parameters of the TSPA-LA Model, including the additional submodels and parameters for the PMA and then repeating the sequence of calculation for a select set of modeling cases that were run for the TSPA-LA. PMA was conducted for both 10,000-year and 1,000,000-year time periods and on the same set of modeling cases as the TSPA-LA Model. The details of approach and results of the PMA are presented in Section 7.7.4 with additional supporting material in Appendix C. Summarizing here, the results show that the conservatism evaluated in the PMA are indeed conservative with respect to the total system performance measures (e.g., peak mean annual dose), as the largest doses calculated in the PMA for the 10,000 year and 1,000,000 year are significantly lower than the doses used in compliance demonstration. The largest calculated PMA mean annual doses are lower by over an order of magnitude and a factor of two over the largest mean annual dose relative to the TSPA-LA Model (Section 8.1) for the time periods of 10,000 years and 1,000,000 years, respectively. Further, the PMA analysis demonstrated that the significant conservatisms did not introduce risk dilution in

the TSPA-LA results presented (Section 8.1.1 in Volume III) in support of compliance with the regulatory dose requirement, as demonstrated by the absence of higher peak doses in the PMA results for both the probabilistic projections of the expected annual dose and the comparison of the projected total mean annual dose for the PMA relative to the TSPA-LA. The PMA results also have different significant modeling cases than the TSPA-LA Model due primarily to the items selected for modification in PMA.

8.4.5 Reviews of YMP TSPA Methodology

Independent reviews have played an important role in the development and advancement of the TSPA-LA methodology, as well as in improving its overall conceptual framework. Peer reviews conducted by teams of external experts were commissioned by the YMP in order to ensure that the TSPA methodology would be based on well-established principles, evidence supported, and be technically defensible for the licensing review. Various national and international expert groups have participated in formal reviews of the TSPA methodology and its supporting technical basis. Moreover, various federal oversight and regulatory agencies have regularly reviewed the TSPA methodology. These agencies have included the Nuclear Waste Technical Review Board (NWTRB), NRC's Advisory Committee on Nuclear Waste, and NRC's Division of Nuclear Materials, Safety, and Safeguards staff.

In the subsequent text, three of the comprehensive reviews that were conducted by groups independent of the TSPA-LA Model development are summarized.

8.4.5.1 TSPA-Viability Assessment Peer Review

The first independent and formal evaluation of the TSPA methodology was conducted in support of the DOE Viability Assessment of the Yucca Mountain site (DOE 1998 [DIRS 101779]). The six member peer review group, designated as the TSPA-Viability Assessment (VA) Review Panel, conducted a phased review of the YMP's TSPA methodology over a two-year period. The TSPA-VA peer review was conducted in accordance with the Management and Operating Contractor's QA procedure, QAP-3-3, *Peer Review*, which was in effect at that time of the review.

With regard to the TSPA-VA methodology, the review panel concluded that the "overall performance assessment framework and the approach used to developing the TSPA-VA were sound and followed accepted methods" (Budnitz et al. 1999 [DIRS 102726], p. 2). However, the panel identified deficiencies in some of the component models; these aspects were judged deficient because they, in the view of the panel, lacked an adequate theoretical basis. Some of the review panel's major comments included: (1) TSPA component models and their adequacy to capture relevant phenomena, (2) proper coupling between TSPA component models and submodels, (3) testing and evaluation of the modeled behavior, (4) adequacy and completeness of the supporting database, (5) treatment of model and parameter uncertainties, and (6) potential non-conservative approaches.

Some of the panel's specific recommendations for improving the YMP's TSPA methodology included:

- Make the TSPA submodels more realistic, where supported by data
- Reduce uncertainty (i.e., epistemic) through additional data collection
- Perform additional auxiliary analyses and sensitivity analyses to better understand complex system behavior
- Perform qualitative and quantitative comparisons of the TSPA model components with several man-made and natural analogues
- Conduct follow-on peer reviews of the TSPA methodology.

The YMP implemented the review panel's recommendations for improving the TSPA methodology, as well as those for additional field and laboratory data collection. The review panel's final report is entitled *Peer Review of the Total System Performance Assessment-Viability Assessment Final Report* (Budnitz et al. 1999 [DIRS 102726]). The YMP staff responses to the review panel's comments and recommendations are documented in *Comment Response on the Final Report: Peer Review of the Total System Performance Assessment-Viability Assessment (TSPA-VA)* (CRWMS M&O 1999 [DIRS 153111]).

Additional information on the TSPA-VA review panel comments is presented in Section 7.9.1 of Volume II.

8.4.5.2 Joint Nuclear Energy/International Atomic Energy Agency Peer Review

At the request of DOE, the Organization for Economic Cooperation and Development's (OECD's) Nuclear Energy Agency (NEA) and the International Atomic Energy Agency (IAEA) assembled a team of experts to peer review the TSPA Model for Yucca Mountain. That version of the TSPA Model was to be used for the assessment conducted to support the DOE site recommendation (SR) process. The 10-member international review group, designated as the International Review Team (IRT), reviewed the following aspects of the TSPA-SR model:

- Technical basis for the performance assessment, including identification and justification of the conditions and characteristics modeled at the system level
- Development of the key conceptual models, including the assumptions made with respect to the representations of relevant FEPs
- Adequacy of the treatment of the undisturbed and disturbed system performance
- Adequacy of the methods used, and the cases considered, in sensitivity and uncertainty evaluations
- Overall clarity and completeness of the technical report describing this system-level performance evaluation.

The IRT review was conducted during June 2001 through December 2001. As indicated in their final report, the IRT concluded that "the TSPA-SR methodology is soundly based and has been implemented in a competent manner" (OECD and IAEA 2002 [DIRS 158098], p. 10). In their final report, the IRT made a total of 27 major recommendations for future improvements of the TSPA methodology. Some of the general recommendations for improvements included:

1. A more systematic treatment of uncertainties
2. An investigation of potential risk dilution
3. Improved characterization of the waste forms
4. Use of natural analogues.

The YMP addressed all of the IRT recommendations in developing the TSPA-LA model and in preparing the postclosure demonstration for the LA. The improved systematic treatment of aleatory and epistemic uncertainties is reflected in Section 6.1.2 (Volume I) and Appendix J (Volume III). The investigation of potential risk dilution was largely accomplished through a critical review of the TSPA parameter uncertainty characterizations, which is discussed in Section 8.4.3. Improved characterization of the waste forms is discussed in Section 6.3.7. The use of natural analogs is described in Section 7.8.

A more detailed summary of the IRT review comments and recommendations is presented in Section 7.9.2.

8.4.5.3 Independent Validation Review Team Technical Review

In early preparations for the LA, the YMP commissioned an independent and comprehensive review of the TSPA methodology with the objectives of: (1) examining the defensibility of the TSPA methodology, (2) implementing a model validation strategy, and (3) making a determination of model validity based on a technical review. The critical review of the technical basis was to be based on reviews of the supporting analysis and/or model reports. Implementation of the model validation strategy would follow the applicable process steps outlined in the NRC/SKI white paper on model validation (Eisenberg et al. 1999 [DIRS 155354], pp. 21 to 26). A determination of TSPA Model validity was to be based on conformance with detailed technical criteria. An independent group, designated as the Independent Validation Review Team (IVRT), was formed and chartered to accomplish the review objectives. This team was independent of the TSPA-LA Model development.

The in-depth critical reviews of the TSPA methodology were largely conducted in 2004, while the implementation of a model validation strategy and determination of model validity was performed in 2005. The technical review was conducted in accordance with the then effective QA procedure, LP-SIII.10Q-BSC, *Models*. The IVRT issued their final report in February 2006 (Booth 2006 [DIRS 176638]).

The following is a summary of the IVRT's major recommendations and findings that lead to further improvements of the TSPA-LA methodology.

Review TSPA Methodology and Technical Basis—The IVRT critical reviews of the TSPA technical basis were largely conducted in parallel with the preparation of the supporting analysis and/or model reports and the TSPA component models. The concurrent review and development

efforts had the advantage that the IVRT comments and recommendations could be addressed and incorporated in the final analysis and/or model reports and in the updated version of the TSPA Model. With regard to the TSPA methodology, the IVRT critique and recommendations lead to significant improvements (Booth 2006 [DIRS 176638]) in the defensibility of:

- Conceptual framework and mathematical formulation of the seismic ground motion and igneous intrusion component models
- Formulation and coupling of in-package chemistry and the radionuclide transport abstraction
- Biosphere dose conversion factors and number of key radionuclides considered in the calculation of organ dose
- Uncertainty characterizations for the igneous and seismic events.

The IVRT thoroughly reviewed all the draft analysis and/or model reports and provided nearly 400 technical comments; addressing those comments improved the defensibility of the technical basis as well as the transparency of analysis and/or model reports. One of the more important benefits of this part of the IVRT review was the careful scrutiny of the plausible conservatisms, identification of potential optimisms, and inconsistencies in draft component models. As a result of these comments, the TSPA staff corrected the inconsistencies and conducted impact analyses to evaluate the significance of the conservatisms and potential optimisms in terms of the relative movement of the mean dose curve.

Model Validation Process and Determination of Model Validity—As directed by the YMP, the IVRT critically reviewed the TSPA methodology against 20 technical criteria grouped into three categories (BSC 2005 [DIRS 173309], pp. 18 to 20), namely: (1) general criteria for the TSPA Model framework, (2) specific criteria for the component models and submodels, and (3) specific criteria for the total system model. A total of five general criteria were specified for the model framework that focused on examining the appropriateness and reasonableness of the overall conceptual model, identification of FEPs and inclusion in the models, consistency of the process models and derived abstractions, and confidence-building analyses. The specific criteria for submodels, which consisted of five criteria, focused on the mathematical basis of the models (e.g., assumptions and technical bases, time step and spatial discretization, and consistency of simulation outputs and model abstraction). The 10 specific criteria for the total system model covered such aspects as statistical sampling of uncertain parameters, initial and boundary conditions, parameter distributions, number of realizations, and verification of the TSPA-LA Model software.

The IVRT findings with respect to the general and specific review criteria are presented in the attachment to the memo containing reference to the TSPA-LA (Booth 2006 [DIRS 176638], Attachment draft Rev 01E, Sections C.5.1 through C.5.3, pp. C-39 through C-116). The IVRT determinations regarding the 20 criteria being met, or not met, were used to make a peer group judgment with respect to conformance with two key model validation goals (BSC 2005 [DIRS 173309], Section 2.10.1), namely:

1. To describe the postclosure performance of the repository system for the nominal, igneous, and seismic scenario classes

2. To produce an estimate of mean dose (and other performance measures, as appropriate) that is consistent with the degree of conservatism representative of the component abstraction models and parameters (and their uncertainty) that are input to the TSPA-LA Model.

The IVRT interpreted the first goal as to "require an approach to TSPA Model development that produced estimates of the performance measures of interest with neither pessimistic nor optimistic bias" (Booth 2006 [DIRS 176638], Attachment draft REV 01E, Section C.5.0.2, p. C-37). The second goal was interpreted by the IVRT to "require an approach to model development that did not underestimate the performance measures because the component [model] abstraction and parameter probability density functions were developed with a conservative bias" (Booth 2006 [DIRS 176638], Attachment draft REV 01E, Section C.5.0.2, p. C-37).

The IVRT finding for these two model validation goals was that they had not been met by the 2005 version of the TSPA Model. The rationale for their finding centered on their views that:

- Uncertainty was not characterized as realistically as available information and data allowed

- Inconsistent treatment of uncertainty among the barrier components

- Model appeared to contain potentially significant optimisms and conservatisms.

For the most part, the IVRT views were attributed to deficiencies in the component models for the DS and WP, which were not sufficiently mature at the time of the review. The optimisms referred to by the IVRT were attributed to the: (1) DS component model not accounting for degradation and failure mechanisms, and (2) DS and WP component models not accounting for early failures. With regard to conservatisms, the IVRT noted that the representation of the natural barriers was underestimated to the extent of being extremely conservative (Booth 2006 [DIRS 176638], Attachment draft REV 01E, Section C.5.1.1.2.1, p. C-42).

The IVRT's findings on the two model validation goals prompted additional work to improve the uncertainty treatment, remove the excessive model conservatisms and optimisms. Moreover, the IVRT's finding altered the TSPA compliance strategy from one that relied heavily on conservatism to one that used more realistic models and more rigorous representation of uncertainties.

Additional information on the IVRT review comments and recommendations are presented in Section 7.9.3.

9. INPUTS AND REFERENCES

9.1 DOCUMENTS CITED

159915 Abraham, S. 2002. Recommendation for Approval of the Yucca Mountain Site for the Development of a Nuclear Waste Repository, Along with a Comprehensive Statement of the Basis of Recommendation. Letter from S. Abraham (DOE) to The President, February 14, 2002, with attachment. ACC: HQO.20020325.0001; HQO.20020325.0002.

109715 Ahlers, C.F.; Finsterle, S.; and Bodvarsson, G.S. 1999. "Characterization and Prediction of Subsurface Pneumatic Response at Yucca Mountain, Nevada." *Journal of Contaminant Hydrology, 38,* (1-3), 47-68. New York, New York: Elsevier. TIC: 244160.

180383 Alekseenko, S.V.; Markovich, D.M.; Nakoryakov, V.E.; and Shtork, S.I. 1998. "Rivulet Flow of Liquid on the Outer Surface of an Inclined Cylinder." *Journal of Applied Mechanics and Technical Physics, 38,* (4), 649-653. [New York, New York]: Plenum Publishing. TIC: 259289.

103597 Altman, W.D.; Donnelly, J.P.; and Kennedy, J.E. 1988. *Peer Review for High-Level Nuclear Waste Repositories: Generic Technical Position.* NUREG-1297. Washington, D.C.: U.S. Nuclear Regulatory Commission. TIC: 200651.

169668 Anderson, T.W. 1984. *An Introduction to Multivariate Statistical Analysis.* 2nd Edition. New York, New York: John Wiley & Sons. TIC: 244809.

180487 Anovitz, L.M.; Riciputi, L.R.; Cole, D.R.; Gruszkiewicz, M.S.; and Elam, J.M. 2006. "The Effect of Changes in Relative Humidity on the Hydration Rate of Pachuca Obsidian." *Journal of Non-Crystalline Solids, 352,* 5652-5662. [New York, New York]: Elsevier. TIC: 259330.

169793 Anspaugh, L.R.; Simon, S.L.; Gordeev, K.I.; Likhtarev, I.A.; Maxwell, R.M.; and Shinkarev, S.M. 2002. "Movement of Radionuclides in Terrestrial Ecosystems by Physical Processes." *Health Physics, 82,* (5), 669-679. [Baltimore, Maryland: Lippincott Williams & Wilkins]. TIC: 256136.

107506 Apostolakis, G. 1990. "The Concept of Probability in Safety Assessments of Technological Systems." *Science, 250,* 1359-1364. Washington, D.C.: American Association for the Advancement of Science. TIC: 212560.

107710 Apostolakis, G.E. 1989. "Uncertainty in Probabilistic Safety Assessment." *Nuclear Engineering and Design, 115,* (1), 173-179. Amsterdam, The Netherlands: Elsevier. TIC: 245806.

182227 Apted, M. 2006. *Program on Technology Innovation: Effects of Multiple Seismic Events and Rockfall on Long-Term Performance of the Yucca Mountain Repository.* EPRI TR 1013444. Palo Alto, California: Electric Power Research Institute. TIC: 259559.

182327 Apted, M. and Kessler, J. 2005. *Program on Technology Innovation: Potential Igneous Processes Relevant to the Yucca Mountain Repository: Intrusive-Release Scenario, Analysis and Implications.* EPRI TR 1011165. Palo Alto, California: Electric Power Research Institute. TIC: 259646.

182228 Apted, M. and Kessler, M. 2005. *Program on Technology Innovation: Effects of Seismicity and Rockfall on Long-Term Performance of the Yucca Mountain Repository, 2005 Progress Report.* EPRI TR 1011812. Palo Alto, California: Electric Power Research Institute. TIC: 259560.

182229 Apted, M. and Ross, A. 2005. *Program on Technology Innovation: Evaluation of a Spent Fuel Repository at Yucca Mountain, Nevada, 2005 Progress Report.* EPRI TR 1010074. Palo Alto, California: Electric Power Research Institute. TIC: 259561.

182231 Apted, M.; Ross, A.; and Kessler, J. 2006. *Program on Technology Innovation: EPRI Yucca Mountain Spent Fuel Repository Evaluation, 2006 Progress Report.* EPRI TR 1013445. Palo Alto, California: Electric Power Research Institute. TIC: 259562.

141615 ASM International 1990. *Properties and Selection: Nonferrous Alloys and Special-Purpose Materials.* Volume 2 of *ASM Handbook.* Formerly Tenth Edition, Metals Handbook. 5th Printing 1998. [Materials Park, Ohio]: ASM International. TIC: 241059.

133378 ASM International. 1987. *Corrosion.* Volume 13 of *ASM Handbook.* Formerly 9th Edition, Metals Handbook. [Materials Park, Ohio]: ASM International. TIC: 240704.

145103 ASME (American Society of Mechanical Engineers) 1998. *1998 ASME Boiler and Pressure Vessel Code.* 1998 Edition with 1999 and 2000 Addenda. New York, New York: American Society of Mechanical Engineers. TIC: 247429.

105725 ASTM C 1174-97. 1998. *Standard Practice for Prediction of the Long-Term Behavior of Materials, Including Waste Forms, Used in Engineered Barrier Systems (EBS) for Geological Disposal of High-Level Radioactive Waste.* West Conshohocken, Pennsylvania: American Society for Testing and Materials. TIC: 246015.

103508 Avallone, E.A. and Baumeister, T., III, eds. 1987. *Marks' Standard Handbook for Mechanical Engineers.* 9th Edition. New York, New York: McGraw-Hill. TIC: 206891.

159379 Aziz, P.M. 1956. "Application of the Statistical Theory of Extreme Values to the Analysis of Maximum Pit Depth Data for Aluminum." *Corrosion, 12,* (10), 35-46. Houston, Texas: National Association of Corrosion Engineers. TIC: 241560.

100309 Barnard, R.W.; Wilson, M.L.; Dockery, H.A.; Gauthier, J.H.; Kaplan, P.G.; Eaton, R.R.; Bingham, F.W.; and Robey, T.H. 1992. *TSPA 1991: An Initial Total-System Performance Assessment for Yucca Mountain.* SAND91-2795. Albuquerque, New Mexico: Sandia National Laboratories. ACC: NNA.19920630.0033.

156269 Bear, J. 1972. *Dynamics of Fluids in Porous Media.* Environmental Science Series. Biswas, A.K., ed. New York, New York: Elsevier. TIC: 217356.

166708 Beer, F.P. and Johnston, E.R., Jr. 1981. *Mechanics of Materials.* New York, New York: McGraw-Hill. TIC: 255414.

180397 Belton, J.W. 1935. "The Surface Tensions of Ternary Solutions. Part I. The Surface Tensions of Aqueous Solutions of (a) Sodium and Potassium Chlorides, (b) Sodium Chloride and Hydrochloric Acid.." *Transactions of the Faraday Society, XXXI,* 1413-1419. Edinburgh, Scotland: Gurney and Jackson. TIC: 259689.

105742 Bernstein, P.L. 1996. *Against the Gods: The Remarkable Story of Risk.* New York, New York: John Wiley & Sons. TIC: 245429.

179825 Beven, K.; Freer, J.; Hankin, B.; and Schulz, K. 2000. "The Use of Generalised Likelihood Measures for Uncertainty Estimation in High-Order Models of Environmental Systems." *Nonlinear and Nonstationary Signal Processing.* Fitzgerald, W.J.; Smith, R.L.; Walden, A.T.; and Young, P.C.; eds. Pages 115-151. New York, New York: Cambridge University Press. TIC: 259258.

154522 BIOMASS (Biosphere Modelling and Assessment) 2000. *Example Reference Biosphere 2A: Agricultural Well, Constant Biosphere.* Draft TECDOC. BIOMASS/T1/WD08. Vienna, Austria: International Atomic Energy Agency, Division of Radiation and Waste Safety. TIC: 249456.

168563 BIOMASS (Biosphere Modelling and Assessment) 2003. *"Reference Biospheres" for Solid Radioactive Waste Disposal, Report of BIOMASS Theme 1 of the BIOsphere Modelling and ASSessment (BIOMASS) Programme, Part of the IAEA Co-ordinated Research Project on Biosphere Modelling and Assessment (BIOMASS).* IAEA-BIOMASS-6. Vienna, Austria: International Atomic Energy Agency, Waste Safety Section. TIC: 255411.

180470 Blake, C.A.; Coleman, C.F.; Brown, K.B.; Hill, D.G.; Lowrie, R.S.; and Schmitt, J.M. 1956. "Studies in the Carbonate-Uranium System." *Journal of the American Chemical Society, 78,* 5978-5983. [Washington, D.C.: American Chemical Society]. TIC: 219100.

162477 Bodvarsson, G.S.; Kwicklis, E.; Shan, C.; and Wu, Y.S. 2003. "Estimation of Percolation Flux from Borehole Temperature Data at Yucca Mountain, Nevada." *Journal of Contaminant Hydrology, 62-63,* 3-22. New York, New York: Elsevier. TIC: 254205.

159041 Bonano, E.J. and Apostolakis, G.E. 1991. "Theoretical Foundations and Practical Issues for Using Expert Judgements in Uncertainty Analysis of High-Level Radioactive Waste Disposal." *Radioactive Waste Management and the Nuclear Fuel Cycle, 16,* (2), 137-158. [New York, New York]: Harwood Academic Publishers. TIC: 252826.

176638 Booth, T.C. 2006. "Independent Validation Review Team (IVRT) Issues, Bechtel-SAIC Responses, and IVRT Assessment of Responses Related to Review of the TSPA Model and Supporting Analyses and Model Reports (AMRs)." Interoffice memorandum from T.C. Booth (BSC) to File, March 16, 2006, 0315068011, with enclosures. ACC: MOL.20060320.0115.

155233 Bourgoyne, A.T., Jr.; Millheim, K.K.; Chenevert, M.E.; and Young, F.S., Jr. 1986. "Rotary Drilling Bits." *Applied Drilling Engineering.* [SPE Textbook Series Volume 2]. Pages 190-245. Richardson, Texas: Society of Petroleum Engineers. TIC: 250085.

155318 Boyer, H.E. and Gall, T.L., eds. [1984]. *Metals Handbook.* Desk Edition. 10th Printing 1997. Metals Park, Ohio: American Society for Metals. TIC: 250192.

107727 Breeding, R.J.; Helton, J.C.; Gorham, E.D.; and Harper, F.T. 1992. "Summary Description of the Methods Used in the Probabilistic Risk Assessments for NUREG-1150." *Nuclear Engineering and Design, 135,* 1-27. New York, New York: Elsevier. TIC: 246312.

159576 Brocoum, S. 2001. "Transmittal of Report Addressing Key Technical Issues (KTI) Structural Deformation and Seismicity (SDS)." Letter from S. Brocoum (DOE/YMSCO) to C.W. Reamer (NRC), October 25, 2001, OL&RC:TCG-0140, with enclosure. ACC: MOL.20020304.0297; MOL.20030714.0094.

162420 Brossia, C.S. and Cragnolino, G.A. 2001. "Effects of Environmental and Metallurgical Conditions on the Passive and Localized Dissolution of Ti-0.15%Pd." *Corrosion, 57,* (9), 768-776. Houston, Texas: National Association of Corrosion Engineers. TIC: 254028.

180832 Brossia, C.S. and Cragnolino, G.A. 2004. "Effect of Palladium on the Corrosion Behavior of Titanium." *Corrosion Science, 46,* 1693-1711. [New York, New York]: Elsevier. TIC: 259423.

154657 BSC (Bechtel SAIC Company) 2001. *FY01 Supplemental Science and Performance Analyses, Volume 1: Scientific Bases and Analyses.* TDR-MGR-MD-000007 REV 00. Las Vegas, Nevada: Bechtel SAIC Company. ACC: MOL.20010712.0062.

167572 BSC (Bechtel SAIC Company) 2001. *MKTABLE Software Management Report.* SDN: 10505-SMR-1.00-00. Las Vegas, Nevada: Bechtel SAIC Company. ACC: MOL.20010712.0055.

161068 BSC (Bechtel SAIC Company) 2002. *Design Document (DD) for iTOUGH2 V5.0.* DI: 10003-DD-5.0-00. Las Vegas, Nevada: Bechtel SAIC Company. ACC: MOL.20020923.0144.

167547 BSC (Bechtel SAIC Company) 2002. *Design Document for WAPDEG 4.07.* SDN: 10000-DD-04.07-00. Las Vegas, Nevada: Bechtel SAIC Company. ACC: MOL.20030409.0229; MOL.20040427.0343.

158794 BSC (Bechtel SAIC Company) 2002. *Guidelines for Developing and Documenting Alternative Conceptual Models, Model Abstractions, and Parameter Uncertainty in the Total System Performance Assessment for the License Application.* TDR-WIS-PA-000008 REV 00 ICN 01. Las Vegas, Nevada: Bechtel SAIC Company. ACC: MOL.20020904.0002.

167548 BSC (Bechtel SAIC Company) 2002. *Installation Test Plan for WAPDEG 4.07.* SDN: 10000-ITP-4.07-01. Las Vegas, Nevada: Bechtel SAIC Company. ACC: MOL.20030409.0231; MOL.20040427.0343.

161067 BSC (Bechtel SAIC Company) 2002. *Requirements Document (RD) for iTOUGH2 V5.0-00.* DI: 10003-RD-5.0-0. Las Vegas, Nevada: Bechtel SAIC Company. ACC: MOL.20020923.0143.

167545 BSC (Bechtel SAIC Company) 2002. *Requirements Document for WAPDEG 4.07.* SDN: 10000-RD-4.07-00. Las Vegas, Nevada: Bechtel SAIC Company. ACC: MOL.20030409.0228; MOL.20040427.0343.

161066 BSC (Bechtel SAIC Company) 2002. *User's Manual (UM) for iTOUGH2 V5.0.* DI: 10003-UM-5.0-00. Las Vegas, Nevada: Bechtel SAIC Company. ACC: MOL.20020923.0147.

162606 BSC (Bechtel SAIC Company) 2002. *Users' Manual for WAPDEG 4.07.* SDN: 10000-UM-4.07-00. Las Vegas, Nevada: Bechtel SAIC Company. ACC: MOL.20030409.0233; MOL.20040427.0343.

167542 BSC (Bechtel SAIC Company) 2002. *Validation Test Plan for WAPDEG 4.07.* SDN: 10000-VTP-4.07-00. Las Vegas, Nevada: Bechtel SAIC Company. ACC: MOL.20030409.0232; MOL.20040427.0343.

160437 BSC (Bechtel SAIC Company) 2002. *Validation Test Report (VTR) for iTOUGH2 V5.0.* 10003-VTR-5.0-00. Las Vegas, Nevada: Bechtel SAIC Company. ACC: MOL.20020923.0148.

167554 BSC (Bechtel SAIC Company) 2002. *Validation Test Report for WAPDEG 4.07.* SDN: 10000-VTR-4.07-00. Las Vegas, Nevada: Bechtel SAIC Company. ACC: MOL.20030409.0234; MOL.20040427.0343.

163152 BSC (Bechtel SAIC Company) 2003. *Dissolved Concentration Limits of Radioactive Elements.* ANL-WIS-MD-000010 REV 02. Las Vegas, Nevada: Bechtel SAIC Company. ACC: DOC.20030624.0003.

161962 BSC (Bechtel SAIC Company) 2003. *In-Package Chemistry Abstraction.* ANL-EBS-MD-000037 REV 02. Las Vegas, Nevada: Bechtel SAIC Company. ACC: DOC.20030723.0003.

161727 BSC (Bechtel SAIC Company) 2003. *Repository Design, Repository/PA IED Subsurface Facilities.* 800-IED-EBS0-00402-000-00B. Las Vegas, Nevada: Bechtel SAIC Company. ACC: MOL.20030109.0146.

161317 BSC (Bechtel SAIC Company) 2003. *WAPDEG Analysis of Waste Package and Drip Shield Degradation.* ANL-EBS-PA-000001 REV 01. Las Vegas, Nevada: Bechtel SAIC Company. ACC: DOC.20031208.0004.

170038 BSC (Bechtel SAIC Company) 2004. *Analysis of Hydrologic Properties Data.* ANL-NBS-HS-000042 REV 00. Las Vegas, Nevada: Bechtel SAIC Company. ACC: DOC.20041005.0004; DOC.20050815.0003.

170024 BSC (Bechtel SAIC Company) 2004. *Analysis of Mechanisms for Early Waste Package/Drip Shield Failure.* CAL-EBS-MD-000030 REV 00C. Las Vegas, Nevada: Bechtel SAIC Company. ACC: DOC.20040913.0006; DOC.20050606.0005; DOC.20050830.0002.

169857 BSC (Bechtel SAIC Company) 2004. *Calibrated Properties Model.* MDL-NBS-HS-000003 REV 02. Las Vegas, Nevada: Bechtel SAIC Company. ACC: DOC.20041006.0004.

169989 BSC (Bechtel SAIC Company) 2004. *Characterize Framework for Igneous Activity at Yucca Mountain, Nevada.* ANL-MGR-GS-000001 REV 02. Las Vegas, Nevada: Bechtel SAIC Company. ACC: DOC.20041015.0002; DOC.20050718.0007.

170035 BSC (Bechtel SAIC Company) 2004. *Conceptual Model and Numerical Approaches for Unsaturated Zone Flow and Transport.* MDL-NBS-HS-000005 REV 01. Las Vegas, Nevada: Bechtel SAIC Company. ACC: DOC.20040922.0006; DOC.20050307.0009.

169987 BSC (Bechtel SAIC Company) 2004. *CSNF Waste Form Degradation: Summary Abstraction.* ANL-EBS-MD-000015 REV 02. Las Vegas, Nevada: Bechtel SAIC Company. ACC: DOC.20040908.0001; DOC.20050620.0004.

169988 BSC (Bechtel SAIC Company) 2004. *Defense HLW Glass Degradation Model.* ANL-EBS-MD-000016 REV 02. Las Vegas, Nevada: Bechtel SAIC Company. ACC: DOC.20041020.0015; DOC.20050922.0002.

169855 BSC (Bechtel SAIC Company) 2004. *Development of Numerical Grids for UZ Flow and Transport Modeling.* ANL-NBS-HS-000015 REV 02. Las Vegas, Nevada: Bechtel SAIC Company. ACC: DOC.20040901.0001.

169425 BSC (Bechtel SAIC Company) 2004. *Dissolved Concentration Limits of Radioactive Elements.* ANL-WIS-MD-000010 REV 03. Las Vegas, Nevada: Bechtel SAIC Company. ACC: DOC.20041109.0006.

166107 BSC (Bechtel SAIC Company) 2004. *Drift Degradation Analysis.* ANL-EBS-MD-000027 REV 03. Las Vegas, Nevada: Bechtel SAIC Company. ACC: DOC.20040915.0010; DOC.20050419.0001; DOC.20051130.0002; DOC.20060731.0005.

170040 BSC (Bechtel SAIC Company) 2004. *Drift-Scale Radionuclide Transport.* MDL-NBS-HS-000016 REV 01. Las Vegas, Nevada: Bechtel SAIC Company. ACC: DOC.20040927.0031; DOC.20050927.0003.

172453 BSC (Bechtel SAIC Company) 2004. *DSNF and Other Waste Form Degradation Abstraction.* ANL-WIS-MD-000004 REV 04. Las Vegas, Nevada: Bechtel SAIC Company. ACC: DOC.20041201.0007.

170002 BSC (Bechtel SAIC Company) 2004. *Future Climate Analysis.* ANL-NBS-GS-000008 REV 01. Las Vegas, Nevada: Bechtel SAIC Company. ACC: DOC.20040908.0005.

169218 BSC (Bechtel SAIC Company) 2004. *Natural Analogue Synthesis Report.* TDR-NBS-GS-000027 REV 01. Las Vegas, Nevada: Bechtel SAIC Company. ACC: DOC.20040524.0008.

172452 BSC (Bechtel SAIC Company) 2004. *Performance Confirmation Plan.* TDR-PCS-SE-000001 REV 05. Las Vegas, Nevada: Bechtel SAIC Company. ACC: DOC.20041122.0002.

170006 BSC (Bechtel SAIC Company) 2004. *Saturated Zone Colloid Transport.* ANL-NBS-HS-000031 REV 02. Las Vegas, Nevada: Bechtel SAIC Company. ACC: DOC.20041008.0007; DOC.20051215.0005.

167652 BSC (Bechtel SAIC Company) 2004. *Seepage Model for PA Including Drift Collapse.* MDL-NBS-HS-000002 REV 03. Las Vegas, Nevada: Bechtel SAIC Company. ACC: DOC.20040922.0008; DOC.20051205.0001.

170950 BSC (Bechtel SAIC Company) 2004. *Technical Work Plan for: Near-Field Environment and Transport In-Drift Heat and Mass Transfer Model and Analysis Reports Integration.* TWP-MGR-PA-000018 REV 01. Las Vegas, Nevada: Bechtel SAIC Company. ACC: DOC.20040729.0006.

167969 BSC (Bechtel SAIC Company) 2004. *Technical Work Plan for: Performance Assessment Unsaturated Zone.* TWP-NBS-HS-000003 REV 02 [Errata 001]. Las Vegas, Nevada: Bechtel SAIC Company. ACC: MOL.20030102.0108; DOC.20040121.0001.

168449 BSC (Bechtel SAIC Company) 2004. *Technical Work Plan for: TSPA-LA Model Development, Initial Use, and Documentation.* TWP-MGR-PA-000012 REV 00. Las Vegas, Nevada: Bechtel SAIC Company. ACC: DOC.20040322.0003.

169861 BSC (Bechtel SAIC Company) 2004. *UZ Flow Models and Submodels.* MDL-NBS-HS-000006 REV 02. Las Vegas, Nevada: Bechtel SAIC Company. ACC: DOC.20041101.0004; DOC.20050629.0003.

169996 BSC (Bechtel SAIC Company) 2004. *WAPDEG Analysis of Waste Package and Drip Shield Degradation.* ANL-EBS-PA-000001 REV 02. Las Vegas, Nevada: Bechtel SAIC Company. ACC: DOC.20041004.0005.

169734 BSC (Bechtel SAIC Company) 2004. *Yucca Mountain Site Description.* TDR-CRW-GS-000001 REV 02 ICN 01. Two volumes. Las Vegas, Nevada: Bechtel SAIC Company. ACC: DOC.20040504.0008.

174067 BSC (Bechtel SAIC Company) 2005. *Atmospheric Dispersal and Deposition of Tephra from a Potential Volcanic Eruption at Yucca Mountain, Nevada.* MDL-MGR-GS-000002 REV 02. Las Vegas, Nevada: Bechtel SAIC Company. ACC: DOC.20050825.0001; DOC.20050908.0001; DOC.20060306.0008.

172827 BSC (Bechtel SAIC Company) 2005. *Characteristics of the Receptor for the Biosphere Model.* ANL-MGR-MD-000005 REV 04. Las Vegas, Nevada: Bechtel SAIC Company. ACC: DOC.20050405.0005.

173800 BSC (Bechtel SAIC Company) 2005. *Development of the Total System Performance Assessment-License Application Features, Events, and Processes.* TDR-WIS-MD-000003 REV 02. Las Vegas, Nevada: Bechtel SAIC Company. ACC: DOC.20050829.0004.

172232 BSC (Bechtel SAIC Company) 2005. *Drift-Scale Coupled Processes (DST and TH Seepage) Models.* MDL-NBS-HS-000015 REV 02. Las Vegas, Nevada: Bechtel SAIC Company. ACC: DOC.20050114.0004; DOC.20051115.0002.

173981 BSC (Bechtel SAIC Company) 2005. *Features, Events, and Processes: Disruptive Events.* ANL-WIS-MD-000005 REV 03. Las Vegas, Nevada: Bechtel SAIC Company. ACC: DOC.20050830.0008.

173303 BSC (Bechtel SAIC Company) 2005. *IED Interlocking Drip Shield and Emplacement Pallet [Sheet 1 of 1].* 800-IED-WIS0-00401-000-00E. Las Vegas, Nevada: Bechtel SAIC Company. ACC: ENG.20050301.0007.

174101 BSC (Bechtel SAIC Company) 2005. *Mountain-Scale Coupled Processes (TH/THC/THM) Models.* MDL-NBS-HS-000007 REV 03. Las Vegas, Nevada: Bechtel SAIC Company. ACC: DOC.20050825.0007.

173309 BSC (Bechtel SAIC Company) 2005. *Technical Work Plan for: TSPA-LA FY 05-06 Activities.* TWP-MGR-PA-000031 REV 00. Las Vegas, Nevada: Bechtel SAIC Company. ACC: DOC.20050401.0006.

178275 BSC (Bechtel SAIC Company) 2006. *Analysis of Alcove 8/Niche 3 Flow and Transport Tests.* ANL-NBS-HS-000056 REV 00. Las Vegas, Nevada: Bechtel SAIC Company. ACC: DOC.20060901.0003.

178672 BSC (Bechtel SAIC Company) 2006. *Impacts of Solubility and Other Geochemical Processes on Radionuclide Retardation in the Natural System – Rev 01.* Las Vegas, Nevada: Bechtel SAIC Company. ACC: MOL.20060105.0022.

177101 BSC (Bechtel SAIC Company) 2006. *Inhalation Exposure Input Parameters for the Biosphere Model.* ANL-MGR-MD-000001 REV 04. Las Vegas, Nevada: Bechtel SAIC Company. ACC: DOC.20060605.0011.

177375 BSC (Bechtel SAIC Company) 2006. *Technical Work Plan for Saturated Zone Flow and Transport Modeling.* TWP-NBS-MD-000006 REV 02. Las Vegas, Nevada: Bechtel SAIC Company. ACC: DOC.20060519.0002.

177389 BSC (Bechtel SAIC Company) 2006. *Technical Work Plan for Waste Form Testing and Modeling.* TWP-WIS-MD-000018 REV 01. Las Vegas, Nevada: Bechtel SAIC Company. ACC: DOC.20060817.0001.

178448 BSC (Bechtel SAIC Company) 2006. *Technical Work Plan for: Igneous Activity Assessment for Disruptive Events.* TWP-WIS-MD-000007 REV 09 ICN 01. Las Vegas, Nevada: Bechtel SAIC Company. ACC: DOC.20060814.0018.

177739 BSC (Bechtel SAIC Company) 2006. *Technical Work Plan for: Near-Field Environment: Engineered Barrier System: Radionuclide Transport Abstraction Model Report.* TWP-MGR-PA-000020 REV 03. Las Vegas, Nevada: Bechtel SAIC Company. ACC: DOC.20060915.0005.

177465 BSC (Bechtel SAIC Company) 2006. *Technical Work Plan for: Unsaturated Zone Flow, Drift Seepage and Unsaturated Zone Transport Modeling.* TWP-MGR-HS-000004 REV 04. Las Vegas, Nevada: Bechtel SAIC Company. ACC: DOC.20060824.0001.

178693 BSC (Bechtel SAIC Company) 2007. *Subsurface Geotechnical Parameters Report.* ANL-SSD-GE-000001 REV 00. Las Vegas, Nevada: Bechtel SAIC Company. ACC: ENG.20070115.0006.

102726 Budnitz, B.; Ewing, R.C.; Moeller, D.W.; Payer, J.; Whipple, C.; and Witherspoon, P.A. 1999. *Peer Review of the Total System Performance Assessment-Viability Assessment Final Report.* Las Vegas, Nevada: Total System Performance Assessment Peer Review Panel. ACC: MOL.19990317.0328.

103635 Budnitz, R.J.; Apostolakis, G.; Boore, D.M.; Cluff, L.S.; Coppersmith, K.J.; Cornell, C.A.; and Morris, P.A. 1997. *Recommendations for Probabilistic Seismic Hazard Analysis: Guidance on the Uncertainty and Use of Experts.* NUREG/CR-6372. Two volumes. Washington, D.C.: U.S. Nuclear Regulatory Commission. TIC: 235076; 235074.

159728 Bureau of the Census. 2002. "2000 Summary File 3 (SF 3) Sample Data, Amargosa Valley CCD, Nye County, Nevada." Washington, D.C.: U.S. Department of Commerce, Bureau of the Census. Accessed August 28, 2002. TIC: 253098. URL: http://factfinder.census.gov/servlet/DTTable?_ts=48597952130

163209 Byers, C.D.; Jercinovic, M.J.; Ewing, R.C.; and Keil, K. 1985. "Basalt Glass: An Analogue for the Evaluation of the Long-Term Stability of Nuclear Waste Form Borosilicate Glasses." *Scientific Basis for Nuclear Waste Management VIII, Symposium held November 26-29, 1984, Boston, Massachusetts.* Jantzen, C.M.; Stone, J.A.; and Ewing, R.C., eds. *44,* 583-590. Pittsburgh, Pennsylvania: Materials Research Society. TIC: 203665.

179405 Campbell, G.S. 1974. "A Simple Method for Determining Unsaturated Conductivity from Moisture Retention Data." *Soil Science, 117,* (6), 311-314. Baltimore, Maryland: Williams & Wilkins]. TIC: 259680.

180398 Campbell, G.S. and Shiozawa, Sho 1992. "Prediction of Hydraulic Properties of Soils Using Particle-Size Distribution and Bulk Density Data." *Indirect Methods for Estimating the Hydraulic Properties of Unsaturated Soils, Proceedings of the International Workshop on Indirect Methods for Estimating the Hydraulic Properties of Unsaturated Soils, Riverside, Californaia, October 11-13, 1989.* van Genuchten, M.Th.; Leij, F.J.; and Lund, L.J., eds. Pages 317-328. Riverside, California: U.S. Department of Agriculture, Agricultural Research Service. TIC: 259691.

106346 Chen, F.; Ewing R.C.; and Clark S.B. 1999. "The Gibbs Free Energies and Enthalpies of Formation of U6+ Phases: An Empirical Method of Prediction." *American Mineralogist, 84,* (4), 650-664. Washington, D.C.: American Mineralogist. TIC: 245800.

103714 Codell, R.; Eisenberg, N.; Fehringer, D.; Ford, W.; Margulies, T.; McCartin, T.; Park, J.; and Randall, J. 1992. *Initial Demonstration of the NRC's Capability to Conduct a Performance Assessment for a High-Level Waste Repository.* NUREG-1327. Washington, D.C.: U.S. Nuclear Regulatory Commission. TIC: 204809.

102646 Connor, C.B. and Hill, B.E. 1995. "Three Nonhomogeneous Poisson Models for the Probability of Basaltic Volcanism: Application to the Yucca Mountain Region, Nevada." *Journal of Geophysical Research, 100,* (B6), 10,107-10,125. Washington, D.C.: American Geophysical Union. TIC: 237682.

158968 Cooke, R.M. 1991. *Experts in Uncertainty, Opinion and Subjective Probability in Science.* Oxford, New York: Oxford University Press. TIC: 252710.

101234 Cranwell, R.M.; Guzowski, R.V.; Campbell, J.E.; and Ortiz, N.R. 1990. *Risk Methodology for Geologic Disposal of Radioactive Waste, Scenario Selection Procedure.* NUREG/CR-1667. Washington, D.C.: U.S. Nuclear Regulatory Commission. ACC: NNA.19900611.0073.

100720 Criscenti, L.J.; Laniak, G.F.; and Erikson, R.L. 1996. "Propagation of Uncertainty through Geochemical Code Calculations." *Geochimica et Cosmochimica Acta, 60,* (19), 3551-3568. New York, New York: Pergamon Press. TIC: 239507.

163211 Crovisier, J.L.; Fritz, B.; Grambow, B.; and Eberhart, J.P. 1986. "Dissolution of Basaltic Glass in Seawater: Experiments and Thermodynamic Modelling." *Scientific Basis for Nuclear Waste Management IX, Symposium held September 9-11, 1985, Stockholm, Sweden.* Werme, L.O., ed. *50,* 273-280. Pittsburgh, Pennsylvania: Materials Research Society. TIC: 203664.

180488 Crovisier, J-L.; Advocat, T.; and Dussossoy, J-L. 2003. "Nature and Role of Natural Alteration Gels Formed on the Surface of Ancient Volcanic Glasses (Natural Analogs of Waste Containment Glasses)." *Journal of Nuclear Materials, 321,* 91-109. [New York, New York]: Elsevier. TIC: 259328.

100198 CRWMS M&O 1995. *Total System Performance Assessment - 1995: An Evaluation of the Potential Yucca Mountain Repository.* B00000000-01717-2200-00136 REV 01. Las Vegas, Nevada: CRWMS M&O. ACC: MOL.19960724.0188.

100116 CRWMS M&O 1996. *Probabilistic Volcanic Hazard Analysis for Yucca Mountain, Nevada.* BA0000000-01717-2200-00082 REV 0. Las Vegas, Nevada: CRWMS M&O. ACC: MOL.19971201.0221.

101111 CRWMS M&O 1997. *Saturated Zone Flow and Transport Expert Elicitation Project.* Las Vegas, Nevada: CRWMS M&O. ACC: MOL.19980224.0353.

123196 CRWMS M&O 1998. "Geology and Geochronology of Basaltic Volcanism in the Yucca Mountain Region." Chapter 2 of *Synthesis of Volcanism Studies for the Yucca Mountain Site Characterization Project.* Deliverable 3781MR1. Las Vegas, Nevada: CRWMS M&O. ACC: MOL.19990511.0400.

100356 CRWMS M&O 1998. "Unsaturated Zone Hydrology Model." Chapter 2 of *Total System Performance Assessment-Viability Assessment (TSPA-VA) Analyses Technical Basis Document.* B00000000-01717-4301-00002 REV 01. Las Vegas, Nevada: CRWMS M&O. ACC: MOL.19981008.0002.

103731 CRWMS M&O 1998. *Probabilistic Seismic Hazard Analyses for Fault Displacement and Vibratory Ground Motion at Yucca Mountain, Nevada.* Milestone SP32IM3, September 23, 1998. Three volumes. Las Vegas, Nevada: CRWMS M&O. ACC: MOL.19981207.0393.

100353 CRWMS M&O 1998. *Saturated Zone Flow and Transport Expert Elicitation Project.* Deliverable SL5X4AM3. Las Vegas, Nevada: CRWMS M&O. ACC: MOL.19980825.0008.

105347 CRWMS M&O 1998. *Synthesis of Volcanism Studies for the Yucca Mountain Site Characterization Project.* Deliverable 3781MR1. Las Vegas, Nevada: CRWMS M&O. ACC: MOL.19990511.0400.

100349 CRWMS M&O 1998. *Waste Package Degradation Expert Elicitation Project.* Rev. 1. Las Vegas, Nevada: CRWMS M&O. ACC: MOL.19980727.0002.

153111 CRWMS M&O 1999. *Comment Response on the Final Report: Peer Review of the Total System Performance Assessment-Viability Assessment (TSPA-VA).* B00000000-01717-5700-00037 REV 01. Las Vegas, Nevada: CRWMS M&O. ACC: MOL.19990920.0197.

152499 CRWMS M&O 2000. *SCCD Software Routine Report.* SDN: 10343-SRR-2.01-00. Las Vegas, Nevada: CRWMS M&O. ACC: MOL.20010205.0113.

143665 CRWMS M&O 2000. *Total System Performance Assessment for the Site Recommendation.* TDR-WIS-PA-000001 REV 00. Las Vegas, Nevada: CRWMS M&O. ACC: MOL.20001005.0282.

153246 CRWMS M&O 2000. *Total System Performance Assessment for the Site Recommendation.* TDR-WIS-PA-000001 REV 00 ICN 01. Las Vegas, Nevada: CRWMS M&O. ACC: MOL.20001220.0045.

154291 CRWMS M&O 2001. *Abstraction of Drift Seepage.* ANL-NBS-MD-000005 REV 01. Las Vegas, Nevada: CRWMS M&O. ACC: MOL.20010309.0019.

153263 CRWMS M&O 2001. *EQ6 Calculations for Chemical Degradation of N Reactor (U-metal) Spent Nuclear Fuel Waste Packages.* CAL-EDC-MD-000010 REV 00. Las Vegas, Nevada: CRWMS M&O. ACC: MOL.20010227.0017.

160149 Czarnecki, J.B. 1985. *Simulated Effects of Increased Recharge on the Ground-Water Flow System of Yucca Mountain and Vicinity, Nevada-California.* Water-Resources Investigations Report 84-4344. Denver, Colorado: U.S. Geological Survey. TIC: 203222.

100131 D'Agnese, F.A.; Faunt, C.C.; Turner, A.K.; and Hill, M.C. 1997. *Hydrogeologic Evaluation and Numerical Simulation of the Death Valley Regional Ground-Water Flow System, Nevada and California.* Water-Resources Investigations Report 96-4300. Denver, Colorado: U.S. Geological Survey. ACC: MOL.19980306.0253.

120425 D'Agnese, F.A.; O'Brien, G.M.; Faunt, C.C.; and San Juan, C.A. 1999. *Simulated Effects of Climate Change on the Death Valley Regional Ground-Water Flow System, Nevada and California.* Water-Resources Investigations Report 98-4041. Denver, Colorado: U.S. Geological Survey. TIC: 243555.

182090 Dartevelle, S. and Valentine, G. A. 2007. *Interaction of Multiphase Magmatic Flows with Underground Openings at the Proposed Yucca Mountain Radioactive Waste Repository (Southern Nevada, USA).* LA-UR-07-3579. Los Alamos, New Mexico: Los Alamos National Laboratory. ACC: LLR.20070807.0153.

100027 Day, W.C.; Dickerson, R.P.; Potter, C.J.; Sweetkind, D.S.; San Juan, C.A.; Drake, R.M., II; and Fridrich, C.J. 1998. *Bedrock Geologic Map of the Yucca Mountain Area, Nye County, Nevada.* Geologic Investigations Series I-2627. Denver, Colorado: U.S. Geological Survey. ACC: MOL.19981014.0301.

182065 De Windt, L.; Schneider, H.; Ferry, C.; Catalette, H.; Lagneau, V.; Poinssot, C.; Poulesquen, A.; and Jegou, C. 2006. "Modeling Spent Nuclear Fuel Alteration and Radionuclide Migration in Disposal Conditions." *Radiochimica Acta, 94,* 787-794. München, Germany: Oldenbourg Wissenschaftsverlag. TIC: 259598.

171480 Dillmann, Ph.; Mazaudier, F.; and Hœrlé, S. 2004. "Advances in Understanding Atmospheric Corrosion of Iron. I. Rust Characterisation of Ancient Ferrous Artefacts Exposed to Indoor Atmospheric Corrosion." *Corrosion Science, 46,* 1401 - 1429. [New York, New York]: Elsevier. TIC: 256483.

100550 DOE (U.S. Department of Energy) 1998. *Total System Performance Assessment.* Volume 3 of *Viability Assessment of a Repository at Yucca Mountain.* DOE/RW-0508. Washington, D.C.: U.S. Department of Energy, Office of Civilian Radioactive Waste Management. ACC: MOL.19981007.0030.

101779 DOE (U.S. Department of Energy) 1998. *Viability Assessment of a Repository at Yucca Mountain.* DOE/RW-0508. Overview and five volumes. Washington, D.C.: U.S. Department of Energy, Office of Civilian Radioactive Waste Management. ACC: MOL.19981007.0027; MOL.19981007.0028; MOL.19981007.0029; MOL.19981007.0030; MOL.19981007.0031; MOL.19981007.0032.

118968 DOE (U.S. Department of Energy) 2000. *DOE Spent Nuclear Fuel Grouping in Support of Criticality, DBE, TSPA-LA.* DOE/SNF/REP-046, Rev. 0. Idaho Falls, Idaho: U.S. Department of Energy, Idaho Operations Office. ACC: DOC.20030905.0021.

155970 DOE (U.S. Department of Energy) 2002. *Final Environmental Impact Statement for a Geologic Repository for the Disposal of Spent Nuclear Fuel and High-Level Radioactive Waste at Yucca Mountain, Nye County, Nevada.* DOE/EIS-0250. Washington, D.C.: U.S. Department of Energy, Office of Civilian Radioactive Waste Management. ACC: MOL.20020524.0314; MOL.20020524.0315; MOL.20020524.0316; MOL.20020524.0317; MOL.20020524.0318; MOL.20020524.0319; MOL.20020524.0320.

167603 DOE (U.S. Department of Energy) 2003. *Design Document for: ASHPLUME_DLL_LA Version 2.0, Rev. No. 00.* Document ID: 11117-DD-2.0-00. Las Vegas, Nevada: U.S. Department of Energy, Office of Repository Development. ACC: MOL.20031212.0439.

167588 DOE (U.S. Department of Energy) 2003. *Design Document for: SZ_CONVOLUTE Version 3.0.* 10207-DD-3.0-00. Las Vegas, Nevada: U.S. Department of Energy, Office of Repository Development. ACC: MOL.20030717.0479.

167590 DOE (U.S. Department of Energy) 2003. *Installation Test Process for: SZ_CONVOLUTE Version 3.0.* 10207-ITP-3.0-00. Las Vegas, Nevada: U.S. Department of Energy, Office of Repository Development. ACC: MOL.20030717.0480.

167606 DOE (U.S. Department of Energy) 2003. *Installation Test Process for: ASHPLUME_DLL_LA Version 2.0.* Document ID: 11117-ITP-2.0-00. Las Vegas, Nevada: U.S. Department of Energy, Office of Repository Development. ACC: MOL.20031212.0440.

167587 DOE (U.S. Department of Energy) 2003. *Requirements Document for: SZ_CONVOLUTE Version 3.0.* 10207-RD-3.0-00. Las Vegas, Nevada: U.S. Department of Energy, Office of Repository Development. ACC: MOL.20030717.0478.

167601 DOE (U.S. Department of Energy) 2003. *Requirements Document for: ASHPLUME_DLL_LA, V2.0, Rev. No. 00.* Document ID: 11117-RD-2.0-00. Las Vegas, Nevada: U.S. Department of Energy, Office of Repository Development. ACC: MOL.20031212.0438.

167597 DOE (U.S. Department of Energy) 2003. *Software Management Report, MFCP_LA, V1.0.* DI: 11071-SMR-1.0-00. Las Vegas, Nevada: U.S. Department of Energy, Office of Repository Development. ACC: MOL.20030529.0258.

167564 DOE (U.S. Department of Energy) 2003. *Software Management Report: CWD Version Number 2.0.* Document ID: 10363-SMR-2.0-00. Las Vegas, Nevada: U.S. Department of Energy, Office of Repository Development. ACC: MOL.20030501.0182.

163377 DOE (U.S. Department of Energy) 2003. Source Term Estimates for DOE Spent Nuclear Fuels. DOE/SNF/REP-078, Rev. 0. Idaho Falls, Idaho: U.S. Department of Energy, Idaho Operations Office. TIC: 254275.

167607 DOE (U.S. Department of Energy) 2003. *User's Manual for: ASHPLUME_DLL_LA Version 2.0, UM Rev. No.: 00.* Document ID: 11117-UM-2.0-00. Las Vegas, Nevada: U.S. Department of Energy, Office of Repository Development. ACC: MOL.20031212.0444.

167591 DOE (U.S. Department of Energy) 2003. *Users Manual, SZ_CONVOLUTE Version 3.0.* 10207-UM-3.0-00. Las Vegas, Nevada: U.S. Department of Energy, Office of Repository Development. ACC: MOL.20030717.0483.

167589 DOE (U.S. Department of Energy) 2003. *Validation Test Process for: SZ_CONVOLUTE Version 3.0.* 10207-VTP-3.0-00. Las Vegas, Nevada: U.S. Department of Energy, Office of Repository Development. ACC: MOL.20030717.0481.

167604 DOE (U.S. Department of Energy) 2003. *Validation Test Process for: ASHPLUME_DLL_LA Version 2.0.* Document ID: 11117-VTP-2.0-01. Las Vegas, Nevada: U.S. Department of Energy, Office of Repository Development. ACC: MOL.20031212.0441.

166506 DOE (U.S. Department of Energy) 2003. *Validation Test Report for: ASHPLUME_DLL_LA Version 2.0.* 11117-VTR-2.0-00. Las Vegas, Nevada: U.S. Department of Energy, Office of Repository Development. ACC: MOL.20031212.0443.

167593 DOE (U.S. Department of Energy) 2003. *Validation Test Report for: SZ_CONVOLUTE.* 10207-VTR-3.0-0.0. Las Vegas, Nevada: U.S. Department of Energy, Office of Repository Development. ACC: MOL.20030717.0484.

168977 DOE (U.S. Department of Energy) 2004. *Software Management Report for: SOILEXP_LA, V1.0, SMR REV. NO.: 00.* Document ID: 10933-SMR-1.0-00. Las Vegas, Nevada: U.S. Department of Energy, Office of Repository Development. ACC: MOL.20040227.0046.

168978 DOE (U.S. Department of Energy) 2004. *Software Management Report for: PassTable1D_LA, V1.0.* Document ID: 11142-SMR-1.0-00. Las Vegas, Nevada: U.S. Department of Energy, Office of Repository Development. ACC: MOL.20040310.0105.

168981 DOE (U.S. Department of Energy) 2004. *Software Management Report for: PassTable3D_LA, V1.0, SMR Rev. No.: 00.* Document ID: 11143-SMR-1.0-00. Las Vegas, Nevada: U.S. Department of Energy, Office of Repository Development. ACC: MOL.20040317.0127.

168988 DOE (U.S. Department of Energy) 2004. *Software Management Report, INTERPZDLL_LA, V1.0, STN: 11107-1.0-00, Rev. 00.* Document ID: 11107-SMR-1.0-00. Las Vegas, Nevada: U.S. Department of Energy, Office of Repository Development. ACC: MOL.20040130.0403.

169354 DOE (U.S. Department of Energy) 2004. *Source Term Estimates for DOE Spent Nuclear Fuels.* DOE/SNF/REP-078, Rev. 1. Three volumes. Idaho Falls, Idaho: U.S. Department of Energy, Idaho Operations Office. ACC: MOL.20040524.0451.

173440 DOE (U.S. Department of Energy) 2005. *Design Document for: FEHM V2.23.* Document ID: 10086-DD-2.23-00. Las Vegas, Nevada: U.S. Department of Energy, Office of Repository Development. ACC: MOL.20050301.0043.

174594 DOE (U.S. Department of Energy) 2005. *Design Document for: MVIEW V4.0.* Document ID: 10072-DD-4.0-00. Las Vegas, Nevada: U.S. Department of Energy, Office of Repository Development. ACC: MOL.20050712.0025.

173464 DOE (U.S. Department of Energy) 2005. *Design Document for: SEEPAGEDLL_LA V1.2.* Document ID: 11076-DD-1.2-00. Las Vegas, Nevada: U.S. Department of Energy, Office of Repository Development. ACC: MOL.20050406.0440.

173450 DOE (U.S. Department of Energy) 2005. *Design Document for: TSPA_Input_DB Version 2.0.* Document ID: 10931-DD-2.0-00. Las Vegas, Nevada: U.S. Department of Energy, Office of Repository Development. ACC: MOL.20050131.0430.

173449 DOE (U.S. Department of Energy) 2005. *Requirements Document for: TSPA_Input_DB Version 2.0.* Document ID: 10931-RD-2.0-00. Las Vegas, Nevada: U.S. Department of Energy, Office of Repository Development. ACC: MOL.20050131.0427.

173465 DOE (U.S. Department of Energy) 2005. *Requirements Document for: SEEPAGEDLL_LA V1.2.* Document ID: 11076-RD-1.2-00. Las Vegas, Nevada: U.S. Department of Energy, Office of Repository Development. ACC: MOL.20050406.0437.

174593 DOE (U.S. Department of Energy) 2005. *Requirements Document for: MVIEW V4.0.* Document ID: 10072-RD-4.0-01. Las Vegas, Nevada: U.S. Department of Energy, Office of Repository Development. ACC: MOL.20050712.0023.

174616 DOE (U.S. Department of Energy) 2005. *Requirements Document for: FEHM V2.23.* Document ID: 10086-RD-2.23-00. Las Vegas, Nevada: U.S. Department of Energy, Office of Repository Development. ACC: MOL.20050301.0040.

173442 DOE (U.S. Department of Energy) 2005. *Software Validation Report for: FEHM V2.23.* Document ID: 10086-SVR-2.23-00-Win2000. Las Vegas, Nevada: U.S. Department of Energy, Office of Repository Development. ACC: MOL.20050301.0049.

173462 DOE (U.S. Department of Energy) 2005. *Software Validation Report for: SEEPAGEDLL_LA V1.2.* Document ID: 11076-SVR-1.2-00. Las Vegas, Nevada: U.S. Department of Energy, Office of Repository Development. ACC: MOL.20050406.0429.

173463 DOE (U.S. Department of Energy) 2005. *User Information Document for: SEEPAGEDLL_LA V1.2.* Document ID: 11076-UID-1.2-00. Las Vegas, Nevada: U.S. Department of Energy, Office of Repository Development. ACC: MOL.20050406.0425.

173441 DOE (U.S. Department of Energy) 2005. *User Information for: FEHM V2.23.* Document ID: 10086-UID-2.23-00. Las Vegas, Nevada: U.S. Department of Energy, Office of Repository Development. ACC: MOL.20050301.0046.

174595 DOE (U.S. Department of Energy) 2005. *User Information for: MVIEW 4.0.* Document ID: 10072-UID-4.0-00. Las Vegas, Nevada: U.S. Department of Energy, Office of Repository Development. ACC: MOL.20050712.0027.

181286 DOE (U.S. Department of Energy) 2006. *Design Document for SZ_CONVOLUTE Version 3.10.* Document ID: 10207-DD-3.10-00. Las Vegas, Nevada: U.S. Department of Energy, Office of Repository Development. ACC: MOL.20061106.0219.

181075 DOE (U.S. Department of Energy) 2006. *Design Document for: ASHPLUME_DLL_LA V2.1.* Document ID: 11117-DD-2.1-00. Las Vegas, Nevada: U.S. Department of Energy, Office of Repository Development. ACC: MOL.20061106.0387.

181101 DOE (U.S. Department of Energy) 2006. *Design Document for: GetThk_LA v1.0.* Document ID: 11229-DD-1.0-00. Las Vegas, Nevada: U.S. Department of Energy, Office of Repository Development. ACC: MOL.20060915.0165.

181115 DOE (U.S. Department of Energy) 2006. *Design Document for: MkTable_LA v1.0.* Document ID: 11217-DD-1.0-00. Las Vegas, Nevada: U.S. Department of Energy, Office of Repository Development. ACC: MOL.20060413.0351.

181128 DOE (U.S. Department of Energy) 2006. *Design Document for: PREWAP_LA v1.1.* Document ID: 10939-DD-1.1-00. Las Vegas, Nevada: U.S. Department of Energy, Office of Repository Development. ACC: MOL.20060418.0165.

181132 DOE (U.S. Department of Energy) 2006. *Design Document for: SEEPAGEDLL_LA V1.3.* Document ID: 11076-DD-1.3-00. Las Vegas, Nevada: U.S. Department of Energy, Office of Repository Development. ACC: MOL.20060525.0296.

181284 DOE (U.S. Department of Energy) 2006. *Requirements Document for SZ_CONVOLUTE V. 3.10.* Document ID: 10207-RD-3.10-00. Las Vegas, Nevada: U.S. Department of Energy, Office of Repository Development. ACC: MOL.20061106.0218.

181073 DOE (U.S. Department of Energy) 2006. *Requirements Document for: ASHPLUME_DLL_LA V2.1.* Document ID: 11117-RD-2.1-00. Las Vegas, Nevada: U.S. Department of Energy, Office of Repository Development. ACC: MOL.20061106.0385.

181094 DOE (U.S. Department of Energy) 2006. *Requirements Document for: FEHM V2.24.* Document ID: 10086-RD-2.24-00. Las Vegas, Nevada: U.S. Department of Energy, Office of Repository Development. ACC: MOL.20061127.0272.

181100 DOE (U.S. Department of Energy) 2006. *Requirements Document for: GetThk_LA v1.0.* Document ID: 11229-RD-1.0-00. Las Vegas, Nevada: U.S. Department of Energy, Office of Repository Development. ACC: MOL.20060915.0163.

181114 DOE (U.S. Department of Energy) 2006. *Requirements Document for: MkTable_LA v1.0.* Document ID: 11217-RD-1.0-00. Las Vegas, Nevada: U.S. Department of Energy, Office of Repository Development. ACC: MOL.20060413.0349.

181127 DOE (U.S. Department of Energy) 2006. *Requirements Document for: PREWAP_LA v1.1.* Document ID: 10939-RD-1.1-00. Las Vegas, Nevada: U.S. Department of Energy, Office of Repository Development. ACC: MOL.20060418.0163.

181131 DOE (U.S. Department of Energy) 2006. *Requirements Document for: SEEPAGEDLL_LA V1.3.* Document ID: 11076-RD-1.3-00. Las Vegas, Nevada: U.S. Department of Energy, Office of Repository Development. ACC: MOL.20060525.0294.

181077 DOE (U.S. Department of Energy) 2006. *Software Validation Report for: ASHPLUME_DLL_LA Version 2.1 Operating in GoldSim under the Windows 2000 Environment.* Document ID: 11117-SVR-2.1-00-Win2000. Las Vegas, Nevada: U.S. Department of Energy, Office of Repository Development. ACC: MOL.20070102.0246.

181104 DOE (U.S. Department of Energy) 2006. *Software Validation Report for: GetThk_LA v1.0.* Document ID: 11229-SVR-1.0-00-WIN2000. Las Vegas, Nevada: U.S. Department of Energy, Office of Repository Development. ACC: MOL.20060915.0173.

181105 DOE (U.S. Department of Energy) 2006. *Software Validation Report for: GetThk_LA v1.0.* Document ID: 11229-SVR-1.0-00-WIN2003. Las Vegas, Nevada: U.S. Department of Energy, Office of Repository Development. ACC: MOL.20060915.0171.

181113 DOE (U.S. Department of Energy) 2006. *Software Validation Report for: MFCP_LA v1.0.* Document ID: 11071-SVR-1.0-01-WIN2003. Las Vegas, Nevada: U.S. Department of Energy, Office of Repository Development. ACC: MOL.20061218.0126.

181117 DOE (U.S. Department of Energy) 2006. *Software Validation Report for: MkTable_LA v1.0.* Document ID: 11217-SVR-1.0-00-WIN2000. Las Vegas, Nevada: U.S. Department of Energy, Office of Repository Development. ACC: MOL.20060413.0357.

181120 DOE (U.S. Department of Energy) 2006. *Software Validation Report for: PASSTABLE1D_LA v1.0.* Document ID: 11142-SVR-1.0-01-WIN2003. Las Vegas, Nevada: U.S. Department of Energy, Office of Repository Development. ACC: MOL.20061218.0107.

181130 DOE (U.S. Department of Energy) 2006. *Software Validation Report for: PREWAP_LA v1.1.* Document ID: 10939-SVR-1.1-00-WIN2000. Las Vegas, Nevada: U.S. Department of Energy, Office of Repository Development. ACC: MOL.20060418.0171.

181134 DOE (U.S. Department of Energy) 2006. *Software Validation Report for: SEEPAGEDLL_LA V1.3.* Document ID: 11076-SVR-1.3-00-WIN2000. Las Vegas, Nevada: U.S. Department of Energy, Office of Repository Development. ACC: MOL.20060525.0302.

181139 DOE (U.S. Department of Energy) 2006. *Software Validation Report for: TSPA_Input_DB v2.2.* Document ID: 10931-SVR-2.2-00-WIN2000. Las Vegas, Nevada: U.S. Department of Energy, Office of Repository Development. ACC: MOL.20060222.0422.

181140 DOE (U.S. Department of Energy) 2006. *Software Validation Report for: TSPA_Input_DB v2.2.* Document ID: 10931-SVR-2.2-01-WIN2003. Las Vegas, Nevada: U.S. Department of Energy, Office of Repository Development. ACC: MOL.20061011.0198.

181076 DOE (U.S. Department of Energy) 2006. *User Information Document for: ASHPLUME_DLL_LA Version 2.1.* Document ID: 11117-UID-2.1-00. Las Vegas, Nevada: U.S. Department of Energy, Office of Repository Development. ACC: MOL.20070102.0242.

181102 DOE (U.S. Department of Energy) 2006. *User Information Document for: GetThk_LA v1.0.* Document ID: 11229-UID-1.0-00. Las Vegas, Nevada: U.S. Department of Energy, Office of Repository Development. ACC: MOL.20060915.0169.

181116 DOE (U.S. Department of Energy) 2006. *User Information Document for: MkTable_LA v1.0.* Document ID: 11217-UID-1.0-00. Las Vegas, Nevada: U.S. Department of Energy, Office of Repository Development. ACC: MOL.20060413.0354.

181129 DOE (U.S. Department of Energy) 2006. *User Information Document for: PREWAP_LA v1.1.* Document ID: 10939-UID-1.1-00. Las Vegas, Nevada: U.S. Department of Energy, Office of Repository Development. ACC: MOL.20060418.0169.

181133 DOE (U.S. Department of Energy) 2006. *User Information Document for: SEEPAGEDLL_LA V1.3.* Document ID: 11076-UID-1.3-00. Las Vegas, Nevada: U.S. Department of Energy, Office of Repository Development. ACC: MOL.20060525.0300.

181137 DOE (U.S. Department of Energy) 2006. *User Information Document for: TSPA_Input_DB Version 2.2.* Document ID: 10931-UID-2.2-00. Las Vegas, Nevada: U.S. Department of Energy, Office of Repository Development. ACC: MOL.20060222.0419.

182907 DOE (U.S. Department of Energy) 2007. *Design Document for: EXDOC_LA Version 2.0.* Document ID: 11193-DD-2.0-01. Las Vegas, Nevada: U. S. Department of Energy, Office of Repository Development. ACC: MOL.20070723.0262.

181081 DOE (U.S. Department of Energy) 2007. *Design Document for: FAR Version 1.1.* Document ID: 11190-DD-1.1-00. Las Vegas, Nevada: U.S. Department of Energy, Office of Repository Development. ACC: MOL.20070323.0328.

183118 DOE (U.S. Department of Energy) 2007. *Design Document for: FAR Version 1.2.* Document ID: 11190-DD-1.2-00. Las Vegas, Nevada: U.S. Department of Energy, Office of Repository Development. ACC: MOL.20070919.0327.

181095 DOE (U.S. Department of Energy) 2007. *Design Document for: FEHM V2.24-01.* Document ID: 10086-DD-2.24-01-00. Las Vegas, Nevada: U.S. Department of Energy, Office of Repository Development. ACC: MOL.20070309.0032.

182562 DOE (U.S. Department of Energy) 2007. *Design Document for: FEHM V2.25.* Document ID: 10086-DD-2.25-01. Las Vegas, Nevada: U. S. Department of Energy, Office of Repository Development. ACC: MOL.20070712.0363.

181107 DOE (U.S. Department of Energy) 2007. *Design Document for: GoldSim v9.60.* Document ID: 10344-DD-9.60-01. Las Vegas, Nevada: U.S. Department of Energy, Office of Repository Development. ACC: MOL.20070416.0338.

181122 DOE (U.S. Department of Energy) 2007. *Design Document for: PassTable1D_LA version 2.0.* Document ID: 11142-DD-2.0-01. Las Vegas, Nevada: U.S. Department of Energy, Office of Repository Development. ACC: MOL.20070420.0359.

182917 DOE (U.S. Department of Energy) 2007. *Design Document for: PassTable3D_LA Version 2.0.* Document ID: 11143-DD-2.0-00. Las Vegas, Nevada: U. S. Department of Energy, Office of Repository Development. ACC: MOL.20070816.0247.

182051 DOE (U.S. Department of Energy) 2007. *Quality Assurance Requirements and Description.* DOE/RW-0333P, Rev. 19. Washington, D. C.: U.S. Department of Energy, Office of Civilian Radioactive Waste Management. ACC: DOC.20070717.0006.

181080 DOE (U.S. Department of Energy) 2007. *Requirements Document for: FAR Version 1.1.* Document ID: 11190-RD-1.1-00. Las Vegas, Nevada: U.S. Department of Energy, Office of Repository Development. ACC: MOL.20070323.0326.

181106 DOE (U.S. Department of Energy) 2007. *Requirements Document for: GoldSim v9.60.* Document ID: 10344-RD-9.60-00. Las Vegas, Nevada: U.S. Department of Energy, Office of Repository Development. ACC: MOL.20070416.0330.

181121 DOE (U.S. Department of Energy) 2007. *Requirements Document for: PassTable1D_LA Version 2.0.* Document ID: 11142-RD-2.0-01. Las Vegas, Nevada: U.S. Department of Energy, Office of Repository Development. ACC: MOL.20070420.0357.

182561 DOE (U.S. Department of Energy) 2007. *Requirements Document for: FEHM V2.25.* Document ID: 10086-RD-2.25-01. Las Vegas, Nevada: U. S. Department of Energy, Office of Repository Development. ACC: MOL.20070712.0361.

182906 DOE (U.S. Department of Energy) 2007. *Requirements Document for: EXDOC_LA Version 2.0.* Document ID: 11193-RD-2.0-01. Las Vegas, Nevada: U. S. Department of Energy, Office of Repository Development. ACC: MOL.20070723.0260.

182916 DOE (U.S. Department of Energy) 2007. *Requirements Document for: PassTable3D_LA Version 2.0.* Document ID: 11143-RD-2.0-00. Las Vegas, Nevada: U.S. Department of Energy, Office of Repository Development. ACC: MOL.20070816.0245.

183117 DOE (U.S. Department of Energy) 2007. *Requirements Document for: FAR Version 1.2.* Document ID: 11190-RD-1.2-00. Las Vegas, Nevada: U. S. Department of Energy, Office of Repository Development. ACC: MOL.20070919.0325.

181079 DOE (U.S. Department of Energy) 2007. *Software Validation Report for: CWD v2.0.* Document ID: 10363-SVR-2.0-01-WIN2003. Las Vegas, Nevada: U.S. Department of Energy, Office of Repository Development. ACC: MOL.20070209.0021.

181085 DOE (U.S. Department of Energy) 2007. *Software Validation Report for: FAR Version 1.1.* Document ID: 11190-SVR-1.1-00-Win2000. Las Vegas, Nevada: U.S. Department of Energy, Office of Repository Development. ACC: MOL.20070417.0338.

181087 DOE (U.S. Department of Energy) 2007. *Software Validation Report for: FAR Version 1.1.* Document ID: 11190-SVR-1.1-00-Win2003. Las Vegas, Nevada: U.S. Department of Energy, Office of Repository Development. ACC: MOL.20070417.0340.

181092 DOE (U.S. Department of Energy) 2007. *Software Validation Report for: INTERPZDLL_LA v1.0.* Document ID: 11107-SVR-1.0-01-WIN2003. Las Vegas, Nevada: U.S. Department of Energy, Office of Repository Development. ACC: MOL.20070220.0471.

181097 DOE (U.S. Department of Energy) 2007. *Software Validation Report for: FEHM V2.24-01.* Document ID: 10086-SVR-2.24-01-00-Win2000. Las Vegas, Nevada: U.S. Department of Energy, Office of Repository Development. ACC: MOL.20070309.0047.

181098 DOE (U.S. Department of Energy) 2007. *Software Validation Report for: FEHM V2.24-01.* Document ID: 10086-SVR-2.24-01-00-Win2003. Las Vegas, Nevada: U.S. Department of Energy, Office of Repository Development. ACC: MOL.20070309.0045.

181109 DOE (U.S. Department of Energy) 2007. *Software Validation Report for: GoldSim v9.60 on Windows 2000.* Document ID: 10344-SVR-9.60-00-WIN2000. Las Vegas, Nevada: U.S. Department of Energy, Office of Repository Development. ACC: MOL.20070416.0341.

181110 DOE (U.S. Department of Energy) 2007. *Software Validation Report for: GoldSim v9.60 on Windows Server 2003.* Document ID: 10344-SVR-9.60-00-WIN2003. Las Vegas, Nevada: U.S. Department of Energy, Office of Repository Development. ACC: MOL.20070416.0343.

181111 DOE (U.S. Department of Energy) 2007. *Software Validation Report for: GoldSim v9.60 on Window XP.* Document ID: 10344-SVR-9.60-00-WINXP. Las Vegas, Nevada: U.S. Department of Energy, Office of Repository Development. ACC: MOL.20070416.0345.

181118 DOE (U.S. Department of Energy) 2007. *Software Validation Report for: MkTable_LA v1.0.* Document ID: 11217-SVR-1.0-01-WIN2003. Las Vegas, Nevada: U.S. Department of Energy, Office of Repository Development. ACC: MOL.20070208.0274.

181119 DOE (U.S. Department of Energy) 2007. *Software Validation Report for: MView 4.0.* Document ID: 10072-SVR-4.0-01-WinXP. Las Vegas, Nevada: U.S. Department of Energy, Office of Repository Development. ACC: MOL.20070417.0382.

181124 DOE (U.S. Department of Energy) 2007. *Software Validation Report for: PassTable1D_LA v2.0.* Document ID: 11142-SVR-2.0-00-WIN2000. Las Vegas, Nevada: U.S. Department of Energy, Office of Repository Development. ACC: MOL.20070420.0363.

181125 DOE (U.S. Department of Energy) 2007. *Software Validation Report for: PassTable1D_LA Version 2.0.* Document ID: 11142-SVR-2.0-00-WIN2003. Las Vegas, Nevada: U.S. Department of Energy, Office of Repository Development. ACC: MOL.20070420.0365.

181126 DOE (U.S. Department of Energy) 2007. *Software Validation Report for: PassTable3D_LA v1.0.* Document ID: 11143-SVR-1.0-01-WIN2003. Las Vegas, Nevada: U.S. Department of Energy, Office of Repository Development. ACC: MOL.20070208.0286.

181135 DOE (U.S. Department of Energy) 2007. *Software Validation Report for: SEEPAGEDLL_LA V1.3.* Document ID: 11076-SVR-1.3-01-WIN2003. Las Vegas, Nevada: U.S. Department of Energy, Office of Repository Development. ACC: MOL.20070223.0249.

181141 DOE (U.S. Department of Energy) 2007. *Software Validation Report for: WAPDEG v4.07.* Document ID: 10000-SVR-4.07-01-WIN2003. Las Vegas, Nevada: U.S. Department of Energy, Office of Repository Development. ACC: MOL.20070417.0371.

181275 DOE (U.S. Department of Energy) 2007. *Software Validation Report for: ASHPLUME_DLL_LA Version 2.1 Operating in GoldSim under the Windows Server 2003 Environment.* Document ID: 11117-SVR-2.1-01-Win2003. Las Vegas, Nevada: U.S. Department of Energy, Office of Repository Development. ACC: MOL.20070223.0261.

181277 DOE (U.S. Department of Energy) 2007. *Software Validation Report for: SCCD v2.01.* Document ID: 10343-SVR-2.01-01-WIN2003. Las Vegas, Nevada: U.S. Department of Energy, Office of Repository Development. ACC: MOL.20070209.0013.

182566 DOE (U.S. Department of Energy) 2007. *Software Validation Report for: FEHM V2.25 for Windows 2000.* Document ID: 10086-SVR-2.25-00- Win2000. Las Vegas, Nevada: U.S. Department of Energy, Office of Repository Development. ACC: MOL.20070712.0371.

182567 DOE (U.S. Department of Energy) 2007. *Software Validation Report for: FEHM V2.25 for Windows 2003.* Document ID: 10086-SVR-2.25-00- Win2003. Las Vegas, Nevada: U.S. Department of Energy, Office of Repository Development. ACC: MOL.20070712.0373.

182568 DOE (U.S. Department of Energy) 2007. *Software Validation Report for: FEHM Version 2.25 for Windows XP.* Document ID: 10086-SVR-2.25-00-WinXP. Las Vegas, Nevada: U.S. Department of Energy, Office of Repository Development. ACC: MOL.20070712.0375.

182909 DOE (U.S. Department of Energy) 2007. *Software Validation Report for: EXDOC_LA Version 2.0.* Document ID: 11193-SVR-2.0-00-WIN2000. Las Vegas, Nevada: U. S. Department of Energy, Office of Repository Development. ACC: MOL.20070723.0266.

182910 DOE (U.S. Department of Energy) 2007. *Software Validation Report for: EXDOC_LA Version 2.0.* Document ID: 11193-SVR-2.0-00-WIN2003. Las Vegas, Nevada: U.S. Department of Energy, Office of Repository Development. ACC: MOL.20070723.0268.

182911 DOE (U.S. Department of Energy) 2007. *Software Validation Report for: EXDOC_LA Version 2.0.* Document ID: 11193-SVR-2.0-00-WINXP. Las Vegas, Nevada: U. S. Department of Energy, Office of Repository Development. ACC: MOL.20070723.0270.

182913 DOE (U.S. Department of Energy) 2007. *Software Validation Report for: GoldSim Version 9.60.100 on Windows 2000.* Document ID: 10344-SVR-9.60-01-WIN2000. Las Vegas, Nevada: U.S. Department of Energy, Office of Repository Development. ACC: MOL.20070711.0250.

182914 DOE (U.S. Department of Energy) 2007. *Software Validation Report for: GoldSim Version 9.60.100 Windows Server 2003.* Document ID: 10344-SVR-9.60-01-WIN2003. Las Vegas, Nevada: U.S. Department of Energy, Office of Repository Development. ACC: MOL.20070711.0252.

182915 DOE (U.S. Department of Energy) 2007. *Software Validation Report for: GoldSim Version 9.60.100 on Windows XP.* Document ID: 10344-SVR-9.60-01-WINXP. Las Vegas, Nevada: U. S. Department of Energy, Office of Repository Development. ACC: MOL.20070711.0254.

182919 DOE (U.S. Department of Energy) 2007. *Software Validation Report for: PassTable3D_LA Version 2.0.* Document ID: 11143-SVR-2.0-00-WIN2000. Las Vegas, Nevada: U.S. Department of Energy, Office of Repository Development. ACC: MOL.20070816.0254.

182920 DOE (U.S. Department of Energy) 2007. *Software Validation Report for: PassTable3D_LA Version 2.0.* Document ID: 11143-SVR-2.0-00-WIN2003. Las Vegas, Nevada: U. S. Department of Energy, Office of Repository Development. ACC: MOL.20070816.0256.

183120 DOE (U.S. Department of Energy) 2007. *Software Validation Report for: FAR Version 1.2.* Document ID: 11190-SVR-1.2-00-Win2000. Las Vegas, Nevada: U.S. Department of Energy, Office of Repository Development. ACC: MOL.20070919.0334.

183121 DOE (U.S. Department of Energy) 2007. *Software Validation Report for: FAR Version 1.2.* Document ID: 11190-SVR-1.2-00-Win2003. Las Vegas, Nevada: U.S. Department of Energy, Office of Repository Development. ACC: MOL.20070919.0336.

181289 DOE (U.S. Department of Energy) 2007. *Software Validation Report, SZ_CONVOLUTE Version 3.10.01.* Document ID: 10207-SVR-3.10.01-00-Win2000. Las Vegas, Nevada: U.S. Department of Energy, Office of Repository Development. ACC: MOL.20070501.0392.

181290 DOE (U.S. Department of Energy) 2007. *Software Validation Report, SZ_Convolute Version 3.10.01.* Document ID: 10207-3.10.01-00-Win2003. Las Vegas, Nevada: U.S. Department of Energy, Office of Repository Development. ACC: MOL.20070501.0394.

181084 DOE (U.S. Department of Energy) 2007. *User Information Document for: FAR Version 1.1.* Document ID: 11190-UID-1.1-00. Las Vegas, Nevada: U.S. Department of Energy, Office of Repository Development. ACC: MOL.20070417.0336.

181096 DOE (U.S. Department of Energy) 2007. *User Information Document for: FEHM V2.24-01.* Document ID: 10086-UID-2.24-01-00. Las Vegas, Nevada: U.S. Department of Energy, Office of Repository Development. ACC: MOL.20070309.0037.

181108 DOE (U.S. Department of Energy) 2007. *User Information Document for: GoldSim Version 9.60.* Document ID: 10344-UID-9.60-00. Las Vegas, Nevada: U.S. Department of Energy, Office of Repository Development. ACC: MOL.20070416.0339.

181123 DOE (U.S. Department of Energy) 2007. *User Information Document for: PassTable1D_LA Version 2.0.* Document ID: 11142-UID-2.0-00. Las Vegas, Nevada: U.S. Department of Energy, Office of Repository Development. ACC: MOL.20070420.0361.

181288 DOE (U.S. Department of Energy) 2007. *User Information Document for: SZ_Convolute V. 3.10.* Document ID: 10207-UID-3.10-00. Las Vegas, Nevada: U.S. Department of Energy, Office of Repository Development. ACC: MOL.20070223.0313.

182565 DOE (U.S. Department of Energy) 2007. *User Information Document for: FEHM Version 2.25.* Document ID: 10086-UID-2.25-00. Las Vegas, Nevada: U.S. Department of Energy, Office of Repository Development. ACC: MOL.20070712.0365.

182908 DOE (U.S. Department of Energy) 2007. *User Information Document for: EXDOC_LA Version 2.0.* Document ID: 11193-UID-2.0-00. Las Vegas, Nevada: U. S. Department of Energy, Office of Repository Development. ACC: MOL.20070723.0264.

182918 DOE (U.S. Department of Energy) 2007. *User Information Document for: PassTable3D_LA Version 2.0.* Document ID: 11143-UID-2.0-00. Las Vegas, Nevada: U. S. Department of Energy, Office of Repository Development. ACC: MOL.20070816.0252.

183116 DOE (U.S. Department of Energy) 2007. *User Information Document for: FAR Version 1.2.* Document ID: 11190-UID-1.2-00. Las Vegas, Nevada: U.S. Department of Energy, Office of Repository Development. ACC: MOL.20070919.0332.

116801 Driscoll, F.G. 1986. *Groundwater and Wells.* 2nd Edition. St. Paul, Minnesota: Johnson Filtration Systems. TIC: 217555.

162466 Duan, N. 1982. "Models for Human Exposure to Air Pollution." *Environment International, 8,* 305-309. [New York, New York]: Pergamon Press. TIC: 250558.

179404 Dullien, F.A.L. 1979. *Porous Media: Fluid Transport and Pore Structure.* New York, New York: Academic Press. TIC: 259702.

105483 Dzombak, D.A. and Morel, F.M.M. 1990. *Surface Complexation Modeling, Hydrous Ferric Oxide*. New York, New York: John Wiley & Sons. TIC: 224089.

173071 Ebert, W.L.; Fortner, J.A.; Finch, R.J.; Jerden, J.L., Jr.; and Cunnane, J.C. 2005. *FY 2004 Annual Report for Waste Form Testing Activities.* ANL-05/08. Argonne, Illinois: Argonne National Laboratory. ACC: MOL.20050502.0239.

108015 Efurd, D.W.; Runde, W.; Banar, J.C.; Janecky, D.R.; Kaszuba, J.P.; Palmer, P.D.; Roensch, F.R.; and Tait, C.D. 1998. "Neptunium and Plutonium Solubilities in a Yucca Mountain Groundwater." *Environmental Science & Technology, 32,* (24), 3893-3900. [Easton, Pennsylvania]: American Chemical Society. TIC: 243857.

180746 Ehrenberg, H.; Svoboda, G.; Wltschek, G.; Wiesmann, M.; Trouw, F.; Weitzel, H.; and Fuess, H. 1995. "Crystal and Magnetic Structure of {alpha}-NiMoO{subscript 4}." *Journal of Magetism and Magnetic Materials, 150,* 371-376. [New York, New York]: Elsevier. TIC: 259369.

155354 Eisenberg, N.A.; Lee, M.P.; Federline, M.V.; Wingefors, S.; Andersson, J.; Norrby, S.; Sagar, B.; and Wittmeyer, G.W. 1999. *Regulatory Perspectives on Model Validation in High-Level Radioactive Waste Management Programs: A Joint NRC/SKI White Paper.* NUREG-1636. Washington, D.C.: U.S. Nuclear Regulatory Commission. TIC: 246310.

154149 EPRI (Electric Power Research Institute) 2000. *Evaluation of the Candidate High-Level Radioactive Waste Repository at Yucca Mountain Using Total System Performance Assessment, Phase 5.* 1000802. Palo Alto, California: Electric Power Research Institute. TIC: 249555.

158069 EPRI (Electric Power Research Institute) 2002. *Evaluation of the Proposed High-Level Radioactive Waste Repository at Yucca Mountain Using Total System Performance Assessment, Phase 6.* EPRI TR-1003031. Palo Alto, California: Electric Power Research Institute. TIC: 252239.

171915 EPRI (Electric Power Research Institute) 2004. *Potential Igneous Processes Relevant to the Yucca Mountain Repository: Extrusive-Release Scenario.* EPRI TR-1008169. Palo Alto, California: Electric Power Research Institute. TIC: 256654.

112115 Evans, M.; Hastings, N.; and Peacock, B. 1993. *Statistical Distributions.* 2nd Edition. New York, New York: John Wiley & Sons. TIC: 246114.

146355 Fabryka-Martin, J.T.; Wolfsberg, A.V.; Roach, J.L.; Winters, S.T.; and Wolfsberg, L.E. 1998. "Using Chloride to Trace Water Movement in the Unsaturated Zone at Yucca Mountain." *High-Level Radioactive Waste Management, Proceedings of the Eighth International Conference, Las Vegas, Nevada, May 11-14, 1998.* Pages 264-268. La Grange Park, Illinois: American Nuclear Society. TIC: 237082.

181367 Fayek, M.; Ren, M.; Goodell, P.; Dobson, P.; Saucedo, A.; Kelts, A.; Utsunomiya, S.; Ewing, R.C.; Riciputi, L.R.; and Reyes, I. 2006. "Paragenesis and Geochronology of the Nopal I Uranium Deposit, Mexico." *Proceedings of the 11th International High-Level Radioactive Waste Management Conference (IHLRWM), April 30-May 4, 2006, Las Vegas, Nevada.* Pages 55-62. La Grange Park, Illinois: American Nuclear Society. TIC: 258345.

107822 Feller, W. 1971. *An Introduction to Probability Theory and Its Applications.* 2nd Edition. Volume II. New York, New York: John Wiley & Sons. TIC: 235188.

104385 Fillmore, D.L. 1998. *Parameter Selection for Department of Energy Spent Nuclear Fuel to be Used in the Yucca Mountain Viability Assessment.* INEEL/EXT-98-00666. Idaho Falls, Idaho: Idaho National Engineering and Environmental Laboratory. ACC: MOL.19990511.0296.

127332 Finch, R.J.; Buck, E.C.; Finn, P.A.; and Bates, J.K. 1999. "Oxidative Corrosion of Spent UO2 Fuel in Vapor and Dripping Groundwater at 90°C." *Scientific Basis for Nuclear Waste Management XXII, Symposium held November 30-December 4, 1998, Boston, Massachusetts, U.S.A.* Wronkiewicz, D.J. and Lee, J.H., eds. *556,* 431-438. Warrendale, Pennsylvania: Materials Research Society. TIC: 246426.

109425 Forester, R.M.; Bradbury, J.P.; Carter, C.; Elvidge-Tuma, A.B.; Hemphill, M.L.; Lundstrom, S.C.; Mahan, S.A.; Marshall, B.D.; Neymark, L.A.; Paces, J.B.; Sharpe, S.E.; Whelan, J.F.; and Wigand, P.E. 1999. *The Climatic and Hydrologic History of Southern Nevada During the Late Quaternary.* Open-File Report 98-635. Denver, Colorado: U.S. Geological Survey. TIC: 245717.

168717 Frankel, J.J. 1967. "Forms and Structures of Intrusive Basaltic Rocks." *Basalts, the Poldervaart Treatise on Rocks of Basaltic Composition.* Volume 1. Hess, H.H. and Poldervaart, A., eds. Pages 63-102. New York, New York: Interscience Publishers. TIC: 254505.

101173 Freeze, R.A. and Cherry, J.A. 1979. *Groundwater.* Englewood Cliffs, New Jersey: Prentice-Hall. TIC: 217571.

181362 French, D.; Anthony, E.; and Goodell, P. 2006. "U-Series Disequilibria in Soils, Peña Blanca Natural Analog, Chihuahua, Mexico." *Proceedings of the 11th International High-Level Radioactive Waste Management Conference (IHLRWM), April 30-May 4, 2006, Las Vegas, Nevada.* Pages 63-69. La Grange Park, Illinois: American Nuclear Society. TIC: 258345.

180468 Fujiwara, K.; Yamana, H.; Fujii, T.; and Moriyama, H. 2002. "Solubility Product of Plutonium Hydros Oxide and Its Ionic Strength Dependence." *Radiochim Acta, 90,* (12), 857-861. München, Germany: Oldenbourg Wissenschaftsverlag. TIC: 252601.

105636 George-Aniel, B.; Leroy, J.L.; and Poty, B. 1991. "Volcanogenic Uranium Mineralizations in the Sierra Pena Blanca District, Chihuahua, Mexico: Three Genetic Models." *Economic Geology, 86,* (2), 233-248. El Paso, Texas: Economic Geology Publishing. TIC: 237050.

179134 Ghezzehei, T.A.; Dobson, P.F.; Rodriguez, J.A.; and Cook, P.J. 2006. "Infiltration and Seepage through Fractured Welded Tuff." *Proceedings of the 11th International High-Level Radioactive Waste Management Conference (IHLRWM), April 30 - May 4, 2006, Las Vegas, Nevada.* Pages 105-110. La Grange Park, Illinois: American Nuclear Society. TIC: 258345.

181099 Gibson, P. 2007. "Re: Memo Containing Reference to Draft TSPA-LA REV 01E." E-mail from P. Gibson to B. Mukhopadhyay, May 17, 2007, with attachment. ACC: LLR.20070518.0132; MOL.20060519.0089.

171782 Gisch, R.G. 2004. Postclosure Source Term Information for Naval Spent Fuel with Attachment Entitled "NNPP Postclosure Source Term Discussion for Seismic Disruptive Event Scenario". Letter from R.G. Gisch (DOE) to W.J. Arthur, III (DOE/ORD), September 2, 2004, 09130043151, NA:FA:KAKenney U#04-02635, with attachment. ACC: MOL.20040922.0363.

184807 GoldSim Technology Group 2007. *Radioactive and Hazardous Waste Management Applications Using GoldSim.* White Paper. [Issaquah, Washington]: GoldSim Technology Group. TIC: 260020.

183214 GoldSim Technology Group 2007. *GoldSim Contaminant Transport Module.* Version 4.20. Issaquah, Washington: GoldSim Technology Group. TIC: 259223.

181727 GoldSim Technology Group 2007. *User's Guide, GoldSim Probabilistic Simulation Environment.* Version 9.60. Two volumes. Issaquah, Washington: GoldSim Technology Group. TIC: 259221.

181364 Goldstein, S.J.; Luo, S.; Ku, T.L.; and Murrell, M.T. 2006. "Uranium-Series Constraints on Radionuclide Transport and Groundwater Flow at the Nopal I Uranium Deposit, Sierra Peña Blanca, Mexico." *International High-Level Radioactive Waste Management Conference (IHLRWM), April 30-May 4, 2006, Las Vegas, Nevada.* Pages 215-222. La Grange Park, Illinois: American Nuclear Society. TIC: 258345.

168528 Goldstein, S.J.; Murrell, M.T.; Simmons, A.M.; Oliver, R.D.; Dobson, P.F.; Reyes, I.A.; and de la Garza, R. 2003. "Evidence for Radium Mobility at the Nopal I Uranium Deposit, Peña Blanca, Mexico." *Abstracts with Programs - Geological Society of America, 35,* (6), 436. Boulder, Colorado: Geological Society of America. TIC: 254862.

149484 Goodell, P.C. 1981. "Geology of the Peña Blanca Uranium Deposits, Chihuahua, Mexico." *Uranium in Volcanic and Volcaniclastic Rocks, [Symposium held in El Paso, Texas, February 25-27, 1980].* Goodell, P.C. and Waters, A.C., eds. AAPG Studies in Geology No. 13. Pages 275-291. [Tulsa, Oklahoma]: American Association of Petroleum Geologists. TIC: 247861.

176673 Gordon, S.J. and Brady, P.V. 2002. "In Situ Determination of Long-Term Basaltic Glass Dissolution in the Unsaturated Zone." *Chemical Geology, 190,* ([1-4]), 113-122. [New York, New York]: Elsevier. TIC: 258314.

163257 Grambow, B. 1985. "A General Rate Equation for Nuclear Waste Glass Corrosion." *Scientific Basis for Nuclear Waste Management VIII, Symposium held November 26-29, 1984, Boston, Massachusetts.* Jantzen, C.M.; Stone, J.A.; and Ewing, R.C., eds. *44,* 15-27. Pittsburgh, Pennsylvania: Materials Research Society. TIC: 203665.

181381 Grambow, B. 2006. "Nuclear Waste Glasses - How Durable?" *Elements, 2,* (6), 357-364. Québec, Canada: Mineralogical Society of America. TIC: 259580.

171412 Grambow, B. and Müller, R. 2001. "First-Order Dissolution Rate Law and the Role of Surface Layers in Glass Performance Assessment." *Journal of Nuclear Materials, 298,* 112-124. [New York, New York]: Elsevier. TIC: 256444.

163258 Grambow, B.; Jercinovic, M.J.; Ewing, R.C.; and Byers, C.D. 1986. "Weathered Basalt Glass: A Natural Analogue for the Effects of Reaction Progress on Nuclear Waste Glass Alteration." *Scientific Basis for Nuclear Waste Management IX, Symposium held September 9-11, 1985, Stockholm, Sweden.* Werme, L.O., ed. *50,* 263-272. Pittsburgh, Pennsylvania: Materials Research Society. TIC: 203664.

113255 Grandstaff, D.E. 1976. "A Kinetic Study of the Dissolution of Uraninite." *Economic Geology and the Bulletin of The Society of Economic Geologists, 71,* (8), 1493-1506. El Paso, Texas: Economic Geology Publishing. TIC: 246339.

183165 Grant Prideco 2003. Drill Collars. Pages 97-108. [Houston, Texas]: Grant Prideco. TIC: 259728.

149485 Green, R.T. and Rice, G. 1995. "Numerical Analysis of a Proposed Percolation Experiment at the Pena Blanca Natural Analog Site." *High Level Radioactive Waste Management, Proceedings of the Sixth Annual International Conference, Las Vegas, Nevada, April 30-May 5, 1995.* Pages 226-228. La Grange Park, Illinois: American Nuclear Society. TIC: 215781.

149528 Green, R.T.; Meyer-James, K.A.; and Rice, G. 1995. *Hydraulic Characterization of Hydrothermally Altered Nopal Tuff.* NUREG/CR-6356. San Antonio, Texas: Center for Nuclear Regulatory Analyses. TIC: 247869.

101671 Grenthe, I.; Fuger, J.; Konings, R.J.M.; Lemire, R.J.; Muller, A.B.; Nguyen-Trung, C.; and Wanner, H. 1992. *Chemical Thermodynamics of Uranium.* Volume 1 of *Chemical Thermodynamics.* Wanner, H. and Forest, I., eds. Amsterdam, The Netherlands: North-Holland Publishing Company. TIC: 224074.

168382 Guillaumont, R.; Fanghänel, T.; Fuger, J.; Grenthe, I.; Neck, V.; Palmer, D.A.; and Rand, M.H. 2003. *Update on the Chemical Thermodynamics of Uranium, Neptunium, Plutonium, Americium and Technetium.* Mompean, F.J.; Illemassene, M.; Domenech-Orti, C.; and Ben Said, K., eds. Chemical Thermodynamics 5. Amsterdam, The Netherlands: Elsevier. TIC: 255230.

156830 Guimerà, J. and Carrera, J. 2000. "A Comparison of Hydraulic and Transport Parameters Measured in Low-Permeability Fractured Media." *Journal of Contaminant Hydrology, 41,* ([3-4]), 261-281. [New York, New York]: Elsevier. TIC: 251013.

107512 Hacking, I. 1975. *The Emergence of Probability: A Philosophical Study of Early Ideas About Probability, Induction and Statistical Inference.* New York, New York: Cambridge University Press. TIC: 245428.

146529 Hahn, G.J. and Shapiro, S.S. 1967. *Statistical Models in Engineering.* New York, New York: John Wiley & Sons. TIC: 247729.

158798 Hamby, D.M. 1994. "A Review of Techniques for Parameter Sensitivity Analysis of Environmental Models." *Environmental Monitoring and Assessment, 32,* (2), 135-154. Dordrecht, The Netherlands: Kluwer Academic. TIC: 251324.

182008 Hanson, B.D.; Friese, J.I.; and Soderquist, C.Z. 2004. "Initial Results from Dissolution Testing of Spent Fuel Under Acidic Conditions." *Scientific Basis for Nuclear Waste Mangement XXVIII, Symposium, April 13-16, 2004, San Francisco, California, U.S.A.* Hanchar, J.M.; Stroes-Gascoyne, S.; and Browning, L., eds. *824,* 113-118. Warrendale, Pennsylvania: Materials Research Society. TIC: 256855.

179403 Harris, R.F. 1985. "Effect of Water Potential on Microbial Growth and Activity." Chapter 2 of *Water Potential Relations in Soil Microbiology.* SSSA Special Publication Number 9. Kral, D.M. and M.K. Cousin, eds. Madison, Wisconsin: Soil Science Society of America. TIC: 259690.

117826 Haukwa, C.; Wu, Y.S.; Hinds, J.J.; Zhang, W.; Ritcey, A.C.; Pan, L.H.; Simmons, A.M.; and Bodvarsson, G.S. 1998. *Results of Sensitivity Studies of Thermo-Hydrologic Behavior Conducted on Hydrologic Parameter Sets.* Milestone SP3CK5M4. Berkeley, California: Lawrence Berkeley National Laboratory. ACC: MOL.19980918.0001.

101995 Haynes International 1988. Hastelloy Alloy C-22. Kokomo, Indiana: Haynes International. TIC: 239938.

100452 Helton, J.C. 1993. "Uncertainty and Sensitivity Analysis Techniques for Use in Performance Assessment for Radioactive Waste Disposal." *Reliability Engineering and System Safety, 42,* (2-3), 327-367. Barking, Essex, England: Elsevier. TIC: 237878.

107739 Helton, J.C. 1994. "Treatment of Uncertainty in Performance Assessments for Complex Systems." *Risk Analysis, 14,* (4), 483-511. New York, New York: Plenum Press. TIC: 245848.

107823 Helton, J.C. 1996. "Probability, Conditional Probability and Complementary Cumulative Distribution Functions in Performance Assessment for Radioactive Waste Disposal." *Reliability Engineering and System Safety, 54,* 145-163. Oxford, United Kingdom: Elsevier. TIC: 246183.

107496 Helton, J.C. 1997. "Uncertainty and Sensitivity Analysis in the Presence of Stochastic and Subjective Uncertainty." *Journal of Statistical Computation and Simulation, 57,* (1-4), 3-76. New York, New York: Gordon and Breach Science Publishers. TIC: 245958.

159042 Helton, J.C. 1999. "Uncertainty and Sensitivity Analysis in Performance Assessment for the Waste Isolation Pilot Plant." *Computer Physics Communications, 117,* ([1-2]), 156-180. New York, New York: Elsevier. TIC: 253133.

170558 Helton, J.C. 2003. "Mathematical and Numerical Approaches in Performance Assessment for Radioactive Waste Disposal: Dealing with Uncertainty." Chapter 12 of *Modelling Radioactivity in the Environment.* Scott, E.M., ed. Radioactivity in the Environment. New York, New York: Elsevier. TIC: 256241.

107498 Helton, J.C. and Burmaster, D.E. 1996. "Guest Editorial: Treatment of Aleatory and Epistemic Uncertainty in Performance Assessments for Complex Systems." *Reliability Engineering and System Safety, 54,* 91-94. New York, New York: Elsevier. TIC: 245900.

156572 Helton, J.C. and Davis, F.J. 2000. *Sampling-Based Methods for Uncertainty and Sensitivity Analysis.* SAND99-2240. Albuquerque, New Mexico: Sandia National Laboratories. TIC: 251256.

183872 Helton, J.C. and Davis, F.J. 2002. "Illustration of Sampling-Based Methods for Uncertainty and Sensitivity Analysis." *Risk Analysis, 22,* (3), 591-622. [Malden, Massachusetts: Blackwell Publishing]. TIC: 259830.

163475 Helton, J.C. and Davis, F.J. 2002. *Latin Hypercube Sampling and the Propagation of Uncertainty in Analyses of Complex Systems.* SAND2001-0417. Albuquerque, New Mexico: Sandia National Laboratories. TIC: 254367.

170518 Helton, J.C. and Davis, F.J. 2003. "Latin Hypercube Sampling and the Propagation of Uncertainty in Analyses of Complex Systems." *Reliability Engineering & System Safety, 81,* ([1]), 23-69. [New York, New York]: Elsevier. TIC: 256239.

171759 Helton, J.C. and Marietta, M.G. 2000. "The 1996 Performance Assessment for the Waste Isolation Pilot Plant." *Reliability Engineering and System Safety, 69,* 1-3. [New York, New York]: Elsevier. TIC: 256585.

159560 Helton, J.C.; Johnson, J.D.; McKay, M.D.; Shiver, A.W.; and Sprung, J.L. 1995. "Robustness of an Uncertainty and Sensitivity Analysis of Early Exposure Results with the MACCS Reactor Accident Consequence Model." *Reliability Engineering & System Safety, 48,* ([2]), 129-148. [New York, New York]: Elsevier. TIC: 253092.

183873 Helton, J.C.; Johnson, J.D.; Sallaberry, C.J.; and Storlie, C.B. 2006. "Survey of Sampling-Based Methods for Uncertainty and Sensitivity Analysis." *Reliability Engineering and System Safety, 91,* 1175-1209. [New York, New York]: Elsevier. TIC: 259831.

151040 Hill, B.E.; Connor, C.B.; Jarzemba, M.S.; La Femina, P.C.; Navarro, M.; and Strauch, W. 1998. "1995 Eruptions of Cerro Negro Volcano, Nicaragua, and Risk Assessment for Future Eruptions." *Geological Society of America Bulletin, 110,* (10), 1231-1241. Boulder, Colorado: Geological Society of America. TIC: 245102.

107502 Hoffman, F.O. and Hammonds, J.S. 1994. "Propagation of Uncertainty in Risk Assessments: The Need to Distinguish Between Uncertainty Due to Lack of Knowledge and Uncertainty Due to Variability." *Risk Analysis, 14,* (5), 707-712. New York, New York: Plenum. TIC: 246313.

100902 Hora, S.C. and Iman, R.L. 1989. "Expert Opinion in Risk Analysis: The NUREG-1150 Methodology." *Nuclear Science and Engineering, 102,* 323-331. La Grange Park, Illinois: American Nuclear Society. TIC: 236031.

167022 Hua, F.; Mon, K.; Pasupathi, V.; Gordon, G.; and Shoesmith, D. 2004. "Corrosion of Ti Grade 7 and Other Ti Alloys in Nuclear Waste Repository Environments - A Review." *Corrosion/2004, 59th Annual Conference & Exposition, March 28-April 1, 2004, New Orleans.* Paper No. 04689. Houston, Texas: NACE International. TIC: 255943.

155232 IADC (International Association of Drilling Contractors) 1992. *Drilling Manual.* 11th Edition. [Houston, Texas]: International Association of Drilling Contractors. TIC: 232344.

153705 ICRP (International Commission on Radiological Protection) 1994. *Human Respiratory Tract Model for Radiological Protection.* Volume 24, Nos. 1-3 of *Annals of the ICRP.* Smith, H., ed. ICRP Publication 66. [New York, New York]: Pergamon. TIC: 249223.

178810 Ilton, E.S.; Liu, C.; Yantasee, W.; Wang, Z.; Moore, D.A.; Felmy, A.R.; and Zachara, J.M. 2006. "The Dissolution of Synthetic Na-Boltwoodite in Sodium Carbonate Solutions." *Geochimica et Cosmochimica Acta, 70,* 4836-4849. [New York, New York]: Elsevier. TIC: 259016.

146012 Iman, R.L. 1982. "Statistical Methods for Including Uncertainties Associated with the Geologic Isolation of Radioactive Waste Which Allow for a Comparison with Licensing Criteria." *Proceedings of the Symposium on Uncertainties Associated with the Regulation of the Geologic Disposal of High-Level Radioactive Waste, Gatlinburg, Tennessee, March 9-13, 1981.* Kocher, D.C., ed. NUREG/CP-0022. Pages145-157. Washington, D.C.: U.S. Nuclear Regulatory Commission. TIC: 213069.

158984 Iman, R.L. 1992. "Uncertainty and Sensitivity Analysis for Computer Modeling Applications." *Reliability Technology, 1992, Presented at the Winter Annual Meeting of the American Society of Mechanical Engineers, Anaheim, California, November 8-13, 1992.* Cruse, T.A., ed. AD-Vol. 28. Pages 153-168. New York, New York: American Society of Mechanical Engineers. TIC: 252828.

124158 Iman, R.L. and Conover, W.J. 1982. "A Distribution-Free Approach to Inducing Rank Correlation Among Input Variables." *Communications in Statistics, Simulation and Computation, 11,* (3), 311-334. New York, New York: Marcel Dekker. TIC: 243311.

159050 Iman, R.L. and Davenport, J.M. 1982. "Rank Correlation Plots for Use with Correlated Input Variables." *Communications in Statistics, Simulation and Computation, 11,* (3), 335-360. New York, New York: Marcel Dekker. TIC: 252829.

159052 Iman, R.L. and Helton, J.C. 1988. "An Investigation of Uncertainty and Sensitivity Analysis Techniques for Computer Models." *Risk Analysis, 8,* (1), 71-90. [New York, New York: Plenum Press]. TIC: 252831.

159039 Iman, R.L. and Helton, J.C. 1991. "The Repeatability of Uncertainty and Sensitivity Analyses for Complex Probabilistic Risk Assessments." *Risk Analysis, 11,* (4), 591-606. [New York, New York: Plenum Press]. TIC: 252830.

163337 Incropera, F.P. and DeWitt, D.P. 2002. *Fundamentals of Heat and Mass Transfer.* 5th Edition. [New York, New York]: John Wiley & Sons. TIC: 254280.

100987 Jarzemba, M.S.; LaPlante, P.A.; and Poor, K.J. 1997. *ASHPLUME Version 1.0—A Code for Contaminated Ash Dispersal and Deposition, Technical Description and User's Guide.* CNWRA 97-004, Rev. 1. San Antonio, Texas: Center for Nuclear Waste Regulatory Analyses. ACC: MOL.20010727.0162.

182066 Jégou, C.; Peuget, S.; Broudic, V.; Roudil, D.; Deschanels, X.; and Bart, J.M. 2004. "Identification of the Mechanism Limiting the Alteration of Clad Spent Fuel Segments in Aerated Carbonated Groundwater." *Journal of Nuclear Materials, 326,* 144-155. [New York, New York]: Elsevier. TIC: 259605.

125291 Johnson, A.B., Jr. and Francis, B. 1980. *Durability of Metals from Archaeological Objects, Metal Meteorites, and Native Metals.* PNL-3198. Richland, Washington: Pacific Northwest Laboratory. TIC: 229619.

167761 Kahraman, S.; Balci, C.; Yazici, S.; and Bilgin, N. 2000. "Prediction of the Penetration Rate of Rotary Blast Hole Drills Using a New Drillability Index." *International Journal of Rock Mechanics and Mining Sciences, 37,* ([5]), 729-743. [New York, New York]: Pergamon. TIC: 255709.

107741 Kaplan, S. 1993. "Formalisms for Handling Phenomenological Uncertainties: The Concepts of Probability, Frequency, Variability, and Probability of Frequency." *Nuclear Technology, 102,* (1), 137-142. La Grange Park, Illinois: American Nuclear Society. TIC: 245866.

100557 Kaplan, S. and Garrick, B.J. 1981. "On the Quantitative Definition of Risk." *Risk Analysis, 1,* (1), 11-27. New York, New York: Plenum Press. TIC: 241205.

180396 Katz, D.M.; Watts, F.J.; and Burroughs, E.R. 1995. "Effects of Surface Roughness and Rainfall Impact on Overland Flow." *Journal of Hydraulic Engineering, 121,* (7), 546-553. [Reston, Virginia]: American Society of Civil Engineers. TIC: 259291.

159053 Keeney, R.L. and von Winterfeldt, D. 1991. "Eliciting Probabilities from Experts in Complex Technical Problems." *IEEE Transactions on Engineering Management, 38,* (3), 191-201. [New York, New York: Institute of Electrical and Electronics Engineers]. TIC: 253205.

103282 Kersting, A.B.; Efurd, D.W.; Finnegan, D.L.; Rokop, D.J.; Smith, D.K.; and Thompson, J.L. 1999. "Migration of Plutonium in Ground Water at the Nevada Test Site." *Nature, 397,* ([6714]), 56-59. [London, England: Macmillan Journals]. TIC: 243597.

179402 Kimball, B.A.; Jackson, R.D.; Reginato, R.J.; Nakayama, F.S.; and Idso, S.B. 1976. "Comparison of Field-Measured and Calculated Soil–Heat Fluxes." *Soil Science Society of America Journal, 40,* (1), 18-28. [Madison, Wisconsin]: Soil Science Society of America. TIC: 259679.

159054 Kleijnen, J.P.C. and Helton, J.C. 1999. "Statistical Analyses of Scatterplots to Identify Important Factors in Large-Scale Simulations, 1: Review and Comparison of Techniques." *Reliability Engineering & System Safety, 65,* ([2]), 147-185. [New York, New York]: Elsevier. TIC: 253203.

160094 Klepeis, N.E. 1999. "An Introduction to the Indirect Exposure Assessment Approach: Modeling Human Exposure Using Microenvironmental Measurements and the Recent National Human Activity Pattern Survey." *Environmental Health Perspectives, 107,* (Supplement 2), 365-374. [Research Park Triangle, North Carolina: National Institute of Environmental Health Sciences, National Institutes of Health]. TIC: 250567.

100909 Kotra, J.P.; Lee, M.P.; Eisenberg, N.A.; and DeWispelare, A.R. 1996. *Branch Technical Position on the Use of Expert Elicitation in the High-Level Radioactive Waste Program.* NUREG-1563. Washington, D.C.: U.S. Nuclear Regulatory Commission. TIC: 226832.

178580 Kozak, M. and Kessler, J. 2005. *Program on Technology Innovation: EPRI Yucca Mountain Total System Performance Assessment Code (IMARC) Version 8, Model Description.* 1011813. Palo Alto, California: Electric Power Research Institute. TIC: 259558.

182054 Kuechler, R. and Noack, K. 2007. "Comparison of the Solution Behaviour of a Pyrite-Calcite Mixture in Batch and Unsaturated Sand Column." *Journal of Contaminant Hydrology, 90,* 203-220. [New York, New York]: Elsevier. TIC: 259604.

100051 Langmuir, D. 1997. *Aqueous Environmental Geochemistry.* Upper Saddle River, New Jersey: Prentice Hall. TIC: 237107.

167579 LANL (Los Alamos National Laboratory) 2003. *Software Users Manual (UM) for the FEHM Application Version 2.21.* Document ID: 10086-UM-2.21-00. Los Alamos, [New Mexico]: Los Alamos National Laboratory. ACC: MOL.20031031.0266.

160187 Lasaga, A.C. 1981. "Transition State Theory." Chapter 4 of *Kinetics of Geochemical Processes.* Lasaga, A.C., and Kirkpatrick, R.J., eds. Reviews in Mineralogy Volume 8. Washington, D.C.: Mineralogical Society of America. TIC: 239318.

100913 Lee, J.H.; Chambre, P.L.; and Andrews, R.W. 1996. "Mathematical Models for Diffusive Mass Transfer from Waste Package Container with Multiple Perforations." *Proceedings of the 1996 International Conference on Deep Geological Disposal of Radioactive Waste, September 16-19, 1996, Winnipeg, Manitoba, Canada.* Pages 5-61–5-72. Toronto, Ontario, Canada: Canadian Nuclear Society. TIC: 233923.

100464 Leigh, C.D.; Thompson, B.M.; Campbell, J.E.; Longsine, D.E.; Kennedy, R.A.; and Napier, B.A. 1993. *User's Guide for GENII-S: A Code for Statistical and Deterministic Simulations of Radiation Doses to Humans from Radionuclides in the Environment.* SAND91-0561. Albuquerque, New Mexico: Sandia National Laboratories. ACC: MOL.20010721.0031.

101714 Leslie, B.W.; Pearcy, E.C.; and Prikryl, J.D. 1993. "Oxidative Alteration of Uraninite at the Nopal I Deposit, Mexico: Possible Contaminant Transport and Source Term Constraints for the Proposed Repository at Yucca Mountain." *Scientific Basis for Nuclear Waste Management XVI, Symposium held November 30-December 4, 1992, Boston, Massachusetts.* Interrante, C.G. and Pabalan, R.T., eds. *294,* 505-512. Pittsburgh, Pennsylvania: Materials Research Society. TIC: 208880.

109967 Leslie, B.W.; Pickett, D.A.; and Pearcy, E.C. 1999. "Vegetation-Derived Insights on the Mobilization and Potential Transport of Radionuclides from the Nopal I Natural Analog Site, Mexico." *Scientific Basis for Nuclear Waste Management XXII, Symposium held November 30-December 4, 1998, Boston, Massachusetts, U.S.A.* Wronkiewicz, D.J. and Lee, J.H., eds. *556,* 833-842. Warrendale, Pennsylvania: Materials Research Society. TIC: 246426.

100053 Levy, S.S. 1991. "Mineralogic Alteration History and Paleohydrology at Yucca Mountain, Nevada." *High Level Radioactive Waste Management, Proceedings of the Second Annual International Conference, Las Vegas, Nevada, April 28-May 3, 1991. 1,* 477-485. La Grange Park, Illinois: American Nuclear Society. TIC: 204272.

121006 Lichtner, P.C.; Keating, G.; and Carey, B. 1999. *A Natural Analogue for Thermal-Hydrological-Chemical Coupled Processes at the Proposed Nuclear Waste Repository at Yucca Mountain, Nevada.* LA-13610-MS. Los Alamos, New Mexico: Los Alamos National Laboratory. TIC: 246032.

178081 Lide, D.R., ed. 2006. *CRC Handbook of Chemistry and Physics.* 87th Edition. Boca Raton, Florida: CRC Press. TIC: 258634.

172722 Lieser, K.H. and Bauscher, C. 1987. "Technetium in the Hydrosphere and in the Geosphere. I. Chemistry of Technetium and Iron in Natural Waters and Influence of the Redox Potential on the Sorption of Technetium." *Radiochimica Acta, 42,* (4), 205-213. München, Germany: R. Oldenbourg Verlag. TIC: 256859.

106684 Lieser, K.H. and Muhlenweg, U. 1988. "Neptunium in the Hydrosphere and in the Geosphere, I. Chemistry of Neptunium in the Hydrosphere and Sorption of Neptunium from Groundwaters on Sediments Under Aerobic and Anaerobic Conditions." *Radiochimica Acta, 43,* 27-35. München, Germany: R. Oldenbourg Verlag. TIC: 236783.

180748 Lin, C.; Leslie, B.; Codell, R.; Arlt, H.; and Ahn, T. 2003. "Potential Importance of Fluoride to Performance of the Drip Shield." *Proceedings of the 10th International High-Level Radioactive Waste Management Conference (IHLRWM), March 30-April 2, 2003, Las Vegas, Nevada.* Pages 646-652. La Grange Park, Illinois: American Nuclear Society. TIC: 254559.

109440 Litwin, R.J.; Smoot, J.P.; Durika, N.J.; and Smith, G.I. 1999. "Calibrating Late Quaternary Terrestrial Climate Signals: Radiometrically Dated Pollen Evidence from the Southern Sierra Nevada, USA." *Quaternary Science Reviews, 18,* 1151-1171. New York, New York: Pergamon Press. TIC: 245700.

169948 Liu, H.H.; Bodvarsson, G.S.; and Zhang, G. 2004. "Scale Dependency of the Effective Matrix Diffusion Coefficient." *Vadose Zone Journal, 3,* ([1]), 312-315. Madison, Wisconsin: Soil Science Society of America. TIC: 256150.

105729 Liu, H.H.; Doughty, C.; and Bodvarsson, G.S. 1998. "An Active Fracture Model for Unsaturated Flow and Transport in Fractured Rocks." *Water Resources Research, 34,* (10), 2633-2646. Washington, D.C.: American Geophysical Union. TIC: 243012.

162470 Liu, H-H.; Haukwa, C.B.; Ahlers, C.F.; Bodvarsson, G.S.; Flint, A.L.; and Guertal, W.B. 2003. "Modeling Flow and Transport in Unsaturated Fractured Rock: An Evaluation of the Continuum Approach." *Journal of Contaminant Hydrology, 62-63,* 173-188. New York, New York: Elsevier. TIC: 254205.

162478 Liu, J.; Sonnenthal, E.L.; and Bodvarsson, G.S. 2003. "Calibration of Yucca Mountain Unsaturated Zone Flow and Transport Model Using Porewater Chloride Data." *Journal of Contaminant Hydrology, 62-63,* 213-235. New York, New York: Elsevier. TIC: 254205.

170258 LLNL (Lawrence Livermore National Laboratory) 2000. *Validation Test Plan, The Prediction of Thermohydrologic Behavior—NUFT 3.0.1s.* Document Number: 10130-VTP-3.0.1s-00. North Las Vegas, Nevada: U.S. Department of Energy, Yucca Mountain Site Characterization Office. ACC: MOL.20010905.0180.

170259 LLNL (Lawrence Livermore National Laboratory) 2002. *Validation Test Plan, The Prediction of Thermohydrologic Behavior—NUFT 3.0s, Rev 02.* Software Document Number: 10088-VTP-3.0s-02. North Las Vegas, Nevada: U.S. Department of Energy, Yucca Mountain Site Characterization Office. ACC: MOL.20031024.0397.

168999 Loo, H.H.; MacKay, N.S.; and Wheatley, P.D. 2004. *Additional DOE Spent Nuclear Fuel Information in Support of TSPA-LA Analysis.* DOE/SNF/REP-081, Rev. 0. Idaho Falls, Idaho: U.S. Department of Energy, DOE Idaho Operations Office. ACC: DOC.20040202.0007.

166315 Lu, N.; Conca, J.; Parker, G.R.; Leonard, P.A.; Moore, B.; Strietelmeier, B.; and Triay, I.R. 2000. *Adsorption of Actinides onto Colloids as a Function of Time, Temperature, Ionic Strength, and Colloid Concentration, Waste Form Colloids Report for Yucca Mountain Program (Colloid Data Summary from 1999 to 2000 Research).* LA-UR-00-5121. Los Alamos, New Mexico: Los Alamos National Laboratory. ACC: MOL.20031204.0108.

125923 Lutze, W.; Grambow, B.; Ewing, R.C.; and Jercinovic, M.J. 1987. "The Use of Natural Analogues in the Long-Term Extrapolation of Glass Corrosion Processes." *Natural Analogues in Radioactive Waste Disposal, Symposium held in Brussels on 28-30 April 1987.* Côme, B. and Chapman, N.A., eds. EUR 11037 EN. Pages 142-152. Norwell, Massachusetts: Graham & Trotman. TIC: 247254.

162465 Mage, D.T. 1985. "Concepts of Human Exposure Assessment for Airborne Particulate Matter." *Environment International, 11,* 407-412. [New York, New York]: Pergamon Press. TIC: 250582.

182155 Manepally, C.; Bradbury, K.; Colton, S.; Dinwiddle, C.; Green, R.; McGinnis, R.; Sims, D.; Smart, K.; and Walter, G. 2007. *The Nature of Flow in the Faulted and Fractured Paintbrush Nonwelded Hydrogeologic Unit.* San Antonio, Texas: Center for Nuclear Waste Regulatory Analyses. ACC: LLR.20070725.0014.

159031 Martinez, L.J.; Meertens, C.M.; and Smith, R.B. 1998. "Rapid Deformation Rates Along the Wasatch Fault Zone, Utah, from First GPS Measurements with Implications for Earthquake Hazard." *Geophysical Research Letters, 25,* (4), 567-570. [Washington, D.C.]: American Geophysical Union. TIC: 246585.

111885 Mattsson, H. and Olefjord, I. 1990. "Analysis of Oxide Formed on Ti During Exposure in Bentonite Clay-I. The Oxide Growth." *Werkstoffe und Corrosion, 41,* (7), 383-390. Weinheim, Germany: VCH Verlagsgesellschaft mbH. TIC: 246290.

179401 Matubayasi, N.; Matsuo, H.; Yamamoto, K.; Yamaguchi, S.; and Matuzawa, A. 1999. "Thermodynamic Quantities of Surface Formation of Aqueous Electrolyte Solutions I. Aqueous Solutions of NaCl, MgCl{subscript 2} and LaCl{subscript 3}." *Journal of Colloid and Interface Science, 209,* 398-402. [New York, New York]: Academic Press. TIC: 259292.

127905 McKay, M.D.; Beckman, R.J.; and Conover, W.J. 1979. "A Comparison of Three Methods for Selecting Values of Input Variables in the Analysis of Output from a Computer Code." *Technometrics, 21,* (2), 239-245. Alexandria, Virginia: American Statistical Association. TIC: 221741.

182657 McKenzie, J.M. 2007. Postclosure Radionuclide Release Source Term for Representative Naval SNF Waste Package - Igneous Intrusive and Nominal/Early Failure Scenarios. Letter from J.M. McKenzie to E.F. Sproat, III, August 22, 2007, NR:RA:GFHOLDEN U#07-03303, with enclosure. ACC: LLR.20070823.0027.

162827 McKnight, S.B. and Williams, S.W. 1997. "Old Cinder Cone or Young Composite Volcano?: The Nature of Cerro Negro, Nicaragua." *Geology, 25,* (4), 339–342. [Boulder, Colorado: Geological Society of America]. TIC: 254104.

181382 McLoughlin, S.D.; Hyatt, N.C.; Hand, R.J.; and Lee, W.E. 2006. "Corrosion of Archaeological Model Glasses After 32 Years of Burial at Ballidon." *Scientific Basis for Nuclear Waste Management XXIX, Symposime held September 12-16, 2005, Ghent, Belgium.* Iseghem, P.V.; ed. *932,* 1065-1072. Warrendale, Pennsylvania: Materials Research Society. TIC: 259526.

180862 Meinrath, G. 2001. "Measurement Uncertainty of Thermodynamic Data." *Fresenius Journal of Analytical Chemistry,* (369), 690-697. [New York, New York]: Springer-Verlag. TIC: 259386.

180861 Meinrath, G.; Ekberg, C.; Landgren, A.; and Liljenzin, J.O 2000. "Assessment of Uncertainty in Parameter Evaluation and Prediction." *Talanta, 51,* 231-246. [New York, New York]: Elsevier. TIC: 259387.

110460 Meyer, M.A. and Booker, J.M. 1991. *Eliciting and Analyzing Expert Judgement, A Practical Guide.* Volume 5 of *Knowledge-Based Systems.* Boose, J. and Gaines, B., eds. San Diego, California: Academic Press. TIC: 235911.

105462 Miller, G.A. 1977. *Appraisal of the Water Resources of Death Valley, California-Nevada.* Open-File Report 77-728. Menlo Park, California: U.S. Geological Survey. ACC: HQS.19880517.1934.

161678 Molecke, M.A.; Ruppen, J.A.; and Diegle, R.B. 1982. *Materials for High-Level Waste Caister/Overpacks in Salt Formations.* SAND82-0429. Albuquerque, New Mexico: Sandia National Laboratories. TIC: 231459.

159055 Mosleh, A.; Bier, V.M.; and Apostolakis, G. 1988. "A Critique of Current Practice for the Use of Expert Opinions in Probabilistic Risk Assessment." *Reliability Engineering and System Safety, 20,* 63-85. [New York, New York]: Elsevier. TIC: 253204.

121310 Murphy, W.M. 1995. "Contributions of Thermodynamic and Mass Transport Modeling to Evaluation of Groundwater Flow and Groundwater Travel Time at Yucca Mountain, Nevada." *Scientific Basis for Nuclear Waste Management XVIII, Symposium held October 23-27, 1994, Kyoto, Japan.* Murakami, T. and Ewing, R.C., eds. *353,* 419-426. Pittsburgh, Pennsylvania: Materials Research Society. TIC: 216341.

149529 Murphy, W.M. and Codell, R.B. 1999. "Alternate Source Term Models for Yucca Mountain Performance Assessment Based on Natural Analog Data and Secondary Mineral Solubility." *Scientific Basis for Nuclear Waste Management XXII, Symposium held November 30-December 4, 1998, Boston, Massachusetts.* Wronkiewicz, D.J. and Lee, J.H., eds. *556,* 551-558. Warrendale, Pennsylvania: Materials Research Society. TIC: 246426.

151773 Murphy, W.M. and Pearcy, E.C. 1992. "Source-Term Constraints for the Proposed Repository at Yucca Mountain, Nevada, Derived from the Natural Analog at Pena Blanca, Mexico." *Scientific Basis for Nuclear Waste Management XV, Symposium held November 4-7, 1991, Strasbourg, France.* Sombret, C.G., ed. *257,* 521-527. Pittsburgh, Pennsylvania: Materials Research Society. TIC: 204618.

151772 Murphy, W.M.; Pearcy, E.C.; and Goodell, P.C. 1991. "Possible Analog Research Sites for the Proposed High-Level Nuclear Waste Repository in Hydrologically Unsaturated Tuff at Yucca Mountain, Nevada." *Nuclear Science and Technology, Fourth Natural Analogue Working Group Meeting and Pocos de Caldas Project Final Workshop, Pitlochry, 18 to 22 June 1990, Scotland, Final Report.* Come, B. and Chapman N.A., eds. EUR 13014 EN. Pages 267-276. Brussels, [Belgium]: Commission of European Communities. TIC: 248757.

181017 Myers, T.G. 2002. "Modeling Laminar Sheet Flow Over Rough Surfaces." *Water Resources Research, 38,* (11), 12-1 - 12-12. Washington, D.C.: American Geophysical Union. TIC: 259426.

157927 Napier, B.A.; Peloquin, R.A.; Strenge, D.L.; and Ramsdell, J.V. 1988. *Conceptual Representation.* Volume 1 of *GENII - The Hanford Environmental Radiation Dosimetry Software System.* PNL-6584. Richland, Washington: Pacific Northwest Laboratory. TIC: 252237.

177331 Napier, B.A.; Strenge, D.L.; Ramsdell, J.V., Jr.; Eslinger, P.W.; and Fosmire, C. 2006. *GENII Version 2 Software Design Document.* PNNL-14584, Rev. 1. [Richland, Washington]: Pacific Northwest National Laboratory. ACC: MOL.20060815.0035.

179400 Nassar, I.N. and Horton, R. 1989. "Water Transport in Unsaturated Nonisothermal Salty Soil: II. Theoretical Development." *Soil Science Society of America Journal, 53,* 1330-1337. [Madison, Wisconsin]: Soil Science Society of America. TIC: 259678.

152309 NEA (Nuclear Energy Agency) 1999. *An International Database of Features, Events and Processes.* Paris, France: Organisation for Economic Co-operation and Development. TIC: 248820.

180924 Neymark, L.A.; Paces, J.B.; Marshall, B.D.; Peterman, Z.E.; and Whelan, J.F. 2005. "Geochemical and C, O, Sr, and U-series Isotopic Evidence for the Meteoric Origin of Calcrete at Solitario Wash, Crater Flat, Nevada, USA." *Environmental Geology, 48,* 450-465. [New York, New York]: Springer-Verlag. TIC: 258003.

100809 Nguyen, S.N.; Silva, R.J.; Weed, H.C.; and Andrews, J.E., Jr. 1992. "Standard Gibbs Free Energies of Formation at the Temperature 303.15 K of Four Uranyl Silicates: Soddyite, Uranophane, Sodium Boltwoodite, and Sodium Weeksite." *Journal of Chemical Thermodynamics, 24,* (1-6), 359-376. New York, New York: Academic Press. TIC: 238507.

155218 Nitsche, H.; Gatti, R.C.; Standifer, E.M.; Lee, S.C.; Müller, A.; Prussin, T.; Deinhammer, R.S.; Maurer, H.; Becraft, K.; Leung, S.; and Carpenter, S.A. 1993. *Measured Solubilities and Speciations of Neptunium, Plutonium, and Americium in a Typical Groundwater (J-13) from the Yucca Mountain Region.* LA-12562-MS. Los Alamos, New Mexico: Los Alamos National Laboratory. ACC: NNA.19930507.0136.

144515 Nitsche, H.; Roberts, K.; Prussin, T.; Muller, A.; Becraft, K.; Keeney, D.; Carpenter, S.A.; and Gatti, R.C. 1994. *Measured Solubilities and Speciations from Oversaturation Experiments of Neptunium, Plutonium, and Americium in UE-25P #1 Well Water from the Yucca Mountain Region Milestone Report 3329-WBS1.2.3.4.1.3.1.* LA-12563-MS. Los Alamos, New Mexico: Los Alamos National Laboratory. TIC: 210589.

160556 Ogden, H.R. 1960. "Titanium and Its Alloys." In *Materials,* Volume I, Chapter 30 of *Reactor Handbook.* 2nd Edition. New York, New York: Interscience Publishers. TIC: 245052.

180494 Ojovan, M.I.; Hand, R.J.; Ojovan, N.V.; and Lee, W.E. 2005. "Corrosion of Alkali-Borosilicate Waste Glass K-26 in Non-Saturated Conditions." *Journal of Nuclear Materials, 340,* 12-24. [New York, New York]: Elsevier. TIC: 259324.

101280 Ortiz, T.S.; Williams, R.L.; Nimick, F.B.; Whittet, B.C.; and South, D.L. 1985. *A Three-Dimensional Model of Reference Thermal/Mechanical and Hydrological Stratigraphy at Yucca Mountain, Southern Nevada.* SAND84-1076. Albuquerque, New Mexico: Sandia National Laboratories. ACC: MOL.19980602.0331.

159057 Owen, A.B. 1992. "A Central Limit Theorem for Latin Hypercube Sampling." *Journal of the Royal Statistical Society: Series B, Statistical Methodology, 54,* (2), 541-551. London, England: Royal Statistical Society. TIC: 253131.

174513 Paces, J.B. and Neymark, L.A. 2004. "U-Series Evidence of Water-Rock Interaction at Yucca Mountain, Nevada, USA." *Proceedings of the Eleventh International Symposium on Water-Rock Interaction, WRI-11, 27 June-2 July 2004.* Wanty, R.B. and Seal, R.R., II, eds. *1,* 475-479. New York, New York: A.A. Balkema Publishers. TIC: 257516.

174071 Painter, S.; Cvetkovic, V.; Pickett, D.; and Turner, D.R. 2002. "Significance of Kinetics for Sorption of Inorganic Colloids: Modeling and Experiment Interpretation Issues." *Environmental Science & Technology, 36,* (24), 5369-5375. [Washington, D.C.]: American Chemical Society. TIC: 257438.

164181 Pan, L.; Warrick, A.W.; and Wierenga, P.J. 1997. "Downward Water Flow Through Sloping Layers in the Vadose Zone: Time-Dependence and Effect of Slope Length." *Journal of Hydrology, 199,* ([1-2]), 36-52. [New York, New York]: Elsevier. TIC: 254555.

180455 Pan, P. and Campbell, A.B. 1998. "The Characterization of Np{subscript 2}O{subscript 5}(c) and Its Dissolution in CO{subscript 2}-Free Aqueous Solutions at pH 6 to 13 and 25°C." *Radiochimica Acta, 81,* (2), . München, Germany: R. Oldenbourg Verlag. TIC: 259301.

179398 Papendick, R.I. and Campbell, G.S. 1981. "Theory and Measurement of Water Potential." Chapter 1 of *Water Potential Relations in Soil Microbiology.* SSSA Special Publication Number 9. Pages 1-22. Madison, Wisconsin: Soil Science Society of America. TIC: 218386.

103896 Parrington, J.R.; Knox, H.D.; Breneman, S.L.; Baum, E.M.; and Feiner, F. 1996. *Nuclides and Isotopes, Chart of the Nuclides.* 15th Edition. San Jose, California: General Electric Company and KAPL, Inc. TIC: 233705.

159059 Parry, G.W. and Winter, P.W. 1981. "Characterization and Evaluation of Uncertainty in Probabilistic Risk Analysis." *Nuclear Safety, 22,* (1), 28-41. Washington, D.C.: U.S. Department of Energy, Technical Information Center. TIC: 252834.

170519 Paté-Cornell, M.E. 1986. "Probability and Uncertainty in Nuclear Safety Decisions." *Nuclear Engineering and Design, 93,* ([2-3]), 319-327. Amsterdam, The Netherlands: North-Holland. TIC: 256240.

107499 Paté-Cornell, M.E. 1996. "Uncertainties in Risk Analysis: Six Levels of Treatment." *Reliability Engineering and System Safety, 54,* 95-111. New York, New York: Elsevier. TIC: 245961.

149523 Pearcy, E.C. 1994. *Fracture Transport of Uranium at the Nopal I Natural Analog Site.* CNWRA 94-011. San Antonio, Texas: Center for Nuclear Waste Regulatory Analyses. TIC: 247808.

110223 Pearcy, E.C.; Prikryl, J.D.; and Leslie, B.W. 1995. "Uranium Transport Through Fractured Silicic Tuff and Relative Retention in Areas with Distinct Fracture Characteristics." *Applied Geochemistry, 10,* 685-704. Oxford, United Kingdom: Elsevier. TIC: 246848.

151774 Pearcy, E.C.; Prikryl, J.D.; Murphy, W.M.; and Leslie, B.W. 1993. *Uranium Mineralogy of the Nopal I Natural Analog Site, Chihuahua, Mexico.* CNWRA 93-012. San Antonio, Texas: Center for Nuclear Waste Regulatory Analyses. TIC: 246628.

100486 Pearcy, E.C.; Prikryl, J.D.; Murphy, W.M.; and Leslie, B.W. 1994. "Alteration of Uraninite from the Nopal I Deposit, Pena Blanca District, Chihuahua, Mexico, Compared to Degradation of Spent Nuclear Fuel in the Proposed U.S. High-Level Nuclear Waste Repository at Yucca Mountain, Nevada." *Applied Geochemistry, 9,* 713-732. New York, New York: Elsevier. TIC: 236934.

109989 Pickett, D.A. and Murphy, W.M. 1997. "Isotopic Constraints on Radionuclide Transport at Pena Blanca." *Seventh EC Natural Analogue Working Group Meeting: Proceedings of an International Workshop held in Stein am Rhein, Switzerland from 28 to 30 October 1996.* von Maravic, H. and Smellie, J., eds. EUR 17851 EN. Pages 113-122. Luxembourg, Luxembourg: Office for Official Publications of the European Communities. TIC: 247461.

110009 Pickett, D.A. and Murphy, W.M. 1999. "Unsaturated Zone Waters from the Nopal I Natural Analog, Chihuahua, Mexico - Implications for Radionuclide Mobility at Yucca Mountain." *Scientific Basis for Nuclear Waste Management XXII, Symposium held November 30-December 4, 1998, Boston, Massachusetts.* Wronkiewicz, D.J. and Lee, J.H., eds. *556,* 809-816. Warrendale, Pennsylvania: Materials Research Society. TIC: 246426.

182055 Pierce, E.M.; Icenhower, J.P.; Serne, R.J.; and Catalano, J.G. 2005. "Experimental Determination of UO{subscript 2}(cr) Dissolution Kinetics: Effects of Solution Saturation State and pH." *Journal of Nuclear Materials, 345,* 206-218. [New York, New York]: Elsevier. TIC: 259597.

107812 PLG (Pickard, Lowe, and Garrick) 1982. *Indian Point Probabilistic Safety Study.* Irvine, California: Pickard, Lowe, and Garrick. TIC: 247144.

107813 PLG (Pickard, Lowe, and Garrick) 1983. *Seabrook Station Probabilistic Safety Assessment.* PLG-0300, Rev. 2. Sections 4-13. Irvine, California: Pickard, Lowe and Garrick. TIC: 247143.

148063 PLG (Pickard, Lowe, and Garrick) 1983. *Seabrook Station Probabilistic Safety Assessment, Main Report.* PLG-0300, Rev. 2. Sections 1-3. Irvine, California: Pickard, Lowe and Garrick. TIC: 247420.

103316 Press, W.H.; Teukolsky, S.A.; Vetterling, W.T.; and Flannery, B.P. 1992. *Numerical Recipes in Fortran 77, The Art of Scientific Computing.* Volume 1 of *Fortran Numerical Recipes.* 2nd Edition. Cambridge, United Kingdom: Cambridge University Press. TIC: 243606.

104250 Pruess, K. 1999. "A Mechanistic Model for Water Seepage Through Thick Unsaturated Zones in Fractured Rocks of Low Matrix Permeability." *Water Resources Research, 35,* (4), 1039-1051. Washington, D.C.: American Geophysical Union. TIC: 244913.

167791 Putot, C.J.M.; Guesnon, J.; Perreau, P.J.; and Constantinescu, A. 2000. "Quantifying Drilling Efficiency and Disruption: Field Data vs. Theoretical Model." *SPE Drilling & Completion, 15,* (2), 118-125. [Richardson, Texas]: Society of Petroleum Engineers. TIC: 255897.

122768 Rai, D. 1984. "Solubility Product of Pu(IV) Hydrous Oxide and Equilibrium Constants of Pu (IV)/Pu (V), Pu (IV)/Pu (VI), and Pu (V)/Pu (VI) Couples." *Radiochimica Acta, 35,* 97-106. München, Germany: R. Oldenbourg Verlag. TIC: 219109.

137138 Rai, D. and Ryan, J.L. 1985. "Neptunium (IV) Hydrous Oxide Solubility under Reducing and Carbonate Conditions." *Inorganic Chemistry, 24,* (3), 247-251. Washington, D.C.: American Chemical Society. TIC: 246852.

168392 Rai, D.; Moore, D.A.; Felmy, A.R.; Choppin, G.R.; and Moore, R.C. 2001. "Thermodynamics of the PuO{subscript 2}{superscript +}-Na{superscript +}-OH{superscript -}-Cl{superscript -}-ClO{subscript 4}{superscript -}-H{subscript 2}O System: Use of NpO{subscript 2}{superscript +} Pitzer Parameters for PuO{subscript 2}{superscript +}." *Radiochimica Acta, 89,* ([8]), 491-498. München, Germany: Oldenbourg Wissenschaftsverlag. TIC: 255398.

158380 Reamer, C.W. 2001. "U.S. Nuclear Regulatory Commission/U.S. Department of Energy Technical Exchange and Management Meeting on Total System Performance Assessment and Integration (August 6 through 10, 2001)." Letter from C.W. Reamer (NRC) to S. Brocoum (DOE/YMSCO), August 23, 2001, with enclosure. ACC: MOL.20011029.0281.

145383 Rechard, R.P. 1999. "Historical Relationship Between Performance Assessment for Radioactive Waste Disposal and Other Types of Risk Assessment." *Risk Analysis, 19,* (5), 763-807. New York, New York: Kluwer Academic / Plenum Publishers. TIC: 246972.

147343 Rechard, R.P., ed. 1993. *Initial Performance Assessment of the Disposal of Spent Nuclear Fuel and High Level Waste Stored at Idaho National Engineering Laboratory.* SAND93-2330. Volumes 1 and 2. Albuquerque, New Mexico: Sandia National Laboratories. TIC: 247212.

179246 Reimus, P.W.; Callahan, T.J.; Ware, S.D.; Haga, M.J.; and Counce, D.A. 2007. "Matrix Diffusion Coefficients in Volcanic Rocks at the Nevada Test Site: Influence of Matrix Porosity, Matrix Permeability, and Fracture Coating Minerals." *Journal of Contaminant Hydrology, 93,* 85-95. [New York, New York]: Elsevier. TIC: 259673.

149533 Reyes-Cortes, I.A. 1997. *Geologic Studies in the Sierra de Peña Blanca, Chihuahua, Mexico.* Ph.D. dissertation. El Paso, Texas: University of Texas at El Paso. TIC: 247866.

180698 Robinson, B.A.; Wolfsberg, A.V.; Viswanathan, H.S.; and Reimus, P.W. 2007. "A Colloid-Facilitated Transport Model with Variable Colloid Transport Properties." *Geophysical Research Letters, 34,* 1-5. [Washington, D.C.]: American Geophysical Union. TIC: 259346.

108567 Robinson, R.A. and Stokes, R.H. 1965. *Electrolyte Solutions, The Measurement and Interpretation of Conductance, Chemical Potential and Diffusion in Solutions of Simple Electrolytes.* 2nd Edition (Revised). Washington, D.C.: Butterworth. TIC: 242575.

181366 Rodríguez-Pineda, J.A.; Goodell, P.; Dobson, P.F.; Walton, J.; Oliver, R.D.; De La Garza, R.; and Harder, S. 2005. "Regional Hydrology of the Nopal I Site, Sierra de Peña Blanca, Chihuahua, Mexico." *Abstracts with Programs - Geological Society of America, 37,* (7), 196. Boulder, Colorado: Geological Society of America. TIC: 258167.

172064 Ross, S.M. 1993. *Introduction to Probability Models.* 5th Edition. San Diego, California: Academic Press. TIC: 245879.

182190 Runde, W.; Neu, M.P.; Conradson, S.D.; Clark, D.L.; Palmer, P.D.; Reilly, S.D.; Scott, B.L.; and Tait, C.D. 1997. "Spectroscopic Investigation of Actinide Speciation in Concentrated Chloride Solution." *Scientific Basis for Nuclear Waste Management XX, Symposium held December 2-6 1996, Boston Massachusetts.* Gray, W.J. and Triay, I.R., eds. *465,* 693-703. Pittsburgh, Pennsylvania: Materials Research Society. TIC: 238884.

180747 Ruschak, K.J.; Weinstein, S.J.; and Ng, K. 2001. "Developing Film Flow on an Inclined Plane with a Critical Point." *Journal of Fluids Engineering, 123,* 698-703. [New York, New York]: American Society of Mechanical Engineers. TIC: 259356.

182015 Santos, B.G.; Noël, J.J.; and Shoesmith, D.W. 2006. "The Influence of Calcium Ions on the Development of Acidity in Corrosion Product Deposits on SIMFUEL, UO{subscript 2}." *Journal of Nuclear Materials, 350,* 320-331. [New York, New York]: Elsevier. TIC: 259603.

182052 Santos, B.G.; Noël, J.J.; and Shoesmith, D.W. 2006. "The Influence of Silicate on the Development of Acidity in Corrosion Product Deposits on SIMFUEL (UO{subscript 2})." *Corrosion Science, 48,* 3852-3868. [New York, New York]: Elsevier. TIC: 259602.

100075 Sawyer, D.A.; Fleck, R.J.; Lanphere, M.A.; Warren, R.G.; Broxton, D.E.; and Hudson, M.R. 1994. "Episodic Caldera Volcanism in the Miocene Southwestern Nevada Volcanic Field: Revised Stratigraphic Framework, {superscript 40}Ar/{superscript 39}Ar Geochronology, and Implications for Magmatism and Extension." *Geological Society of America Bulletin, 106,* (10), 1304-1318. Boulder, Colorado: Geological Society of America. TIC: 222523.

162423 Schijven, J.F.; Hoogenboezem, W.; Hassanizadeh, S.M.; and Peters, J.H. 1999. "Modeling Removal of Bacteriophages MS2 and PRD1 by Dune Recharge at Castricum, Netherlands." *Water Resources Research, 35,* (4), 1101-1111. Washington, D.C.: American Geophysical Union. TIC: 252295.

112147 Schutz, R.W. and Thomas, D.E. 1987. "Corrosion of Titanium and Titanium Alloys." In *Corrosion,* Volume 13, Pages 669-706 of *ASM Handbook.* Formerly 9th Edition, Metals Handbook. [Materials Park, Ohio]: ASM International. TIC: 240704.

159070 Shafer, G. 1978. "Non-Additive Probabilities in the Work of Bernoulli and Lambert." *Archive for History of Exact Sciences, 19,* (4), 309-370. New York, New York: Springer-Verlag. TIC: 253047.

161591 Sharpe, S. 2003. *Future Climate Analysis—10,000 Years to 1,000,000 Years After Present.* MOD-01-001 REV 01. [Reno, Nevada: Desert Research Institute]. ACC: MOL.20030407.0055.

159545 Sheppard, M.I.; Sheppard, S.C.; and Amiro, B.D. 1991. "Mobility and Plant Uptake of Inorganic {superscript 14}C and {superscript 14}C-Labelled PCB in Soils of High and Low Retention." *Health Physics, 61,* (4), 481-492. New York, New York: Pergamon Press. TIC: 252687.

119589 Shibata, T. 1996. "Statistical and Stochastic Approaches to Localized Corrosion." *Corrosion, 52,* (11), 813-830. Houston, Texas: National Association of Corrosion Engineers. TIC: 236691.

114445 Shoesmith, D.W. 1999. *Fuel Corrosion Processes Under Waste Disposal Conditions.* AECL-12034. Pinawa, Manitoba, Canada: Whiteshell Laboratories. TIC: 246006.

113368 Shoesmith, D.W. and Sunder, S. 1992. "The Prediction of Nuclear Fuel (UO2) Dissolution Rates Under Waste Disposal Conditions." *Journal of Nuclear Materials, 190,* 20-35. Amsterdam, The Netherlands: Elsevier. TIC: 246431.

164741 Singh, B. 2002. "Nuclear Data Sheets for A = 79." *Nuclear Data Sheets, 96,* (1), 1-240. San Diego, California: Elsevier. TIC: 254728.

109480 Smith, G.I. and Bischoff, J.L., eds. 1997. *An 800,000-Year Paleoclimatic Record from Core OL-92, Owens Lake, Southeast California.* Geological Society of America, Special Paper 317. Boulder, Colorado: Geological Society of America. TIC: 236857.

119483 Smyth, J.R. 1982. "Zeolite Stability Constraints on Radioactive Waste Isolation in Zeolite-Bearing Volcanic Rocks." *Journal of Geology, 90,* (2), 195-201. Chicago, Illinois: University of Chicago Press. TIC: 221104.

177081 SNL (Sandia National Laboratories) 2006. *Data Analysis for Infiltration Modeling: Extracted Weather Station Data Used to Represent Present-Day and Potential Future Climate Conditions in the Vicinity of Yucca Mountain.* ANL-MGR-MD-000015 REV 00. Las Vegas, Nevada: Sandia National Laboratories. ACC: DOC.20070109.0002.

181244 SNL (Sandia National Laboratories) 2007. *Abstraction of Drift Seepage.* MDL-NBS-HS-000019 REV 01 ADD 01. Las Vegas, Nevada: Sandia National Laboratories. ACC: DOC.20070807.0001.

181267 SNL (Sandia National Laboratories) 2007. *Analysis of Dust Deliquescence for FEP Screening.* ANL-EBS-MD-000074 REV 01 AD 01. Las Vegas, Nevada: Sandia National Laboratories. ACC: DOC.20070911.0004; DOC.20070824.0001.

178765 SNL (Sandia National Laboratories) 2007. *Analysis of Mechanisms for Early Waste Package/Drip Shield Failure.* ANL-EBS-MD-000076 REV 00. Las Vegas, Nevada: Sandia National Laboratories. ACC: DOC.20070629.0002; DOC.20071003.0015.

177431 SNL (Sandia National Laboratories) 2007. *Atmospheric Dispersal and Deposition of Tephra from a Potential Volcanic Eruption at Yucca Mountain, Nevada.* MDL-MGR-GS-000002 REV 03. Las Vegas, Nevada: Sandia National Laboratories. ACC: DOC.20071010.0003.

177399 SNL (Sandia National Laboratories) 2007. *Biosphere Model Report.* MDL-MGR-MD-000001 REV 02. Las Vegas, Nevada: Sandia National Laboratories. ACC: DOC.20070830.0007.

179545 SNL (Sandia National Laboratories) 2007. *Calibrated Unsaturated Zone Properties.* ANL-NBS-HS-000058 REV 00. Las Vegas, Nevada: Sandia National Laboratories. ACC: DOC.20070530.0013.

174260 SNL (Sandia National Laboratories) 2007. *Characterize Eruptive Processes at Yucca Mountain, Nevada.* ANL-MGR-GS-000002 REV 03. Las Vegas, Nevada: Sandia National Laboratories. ACC: DOC.20070301.0001.

180616 SNL (Sandia National Laboratories) 2007. *Cladding Degradation Summary for LA.* ANL-WIS-MD-000021 REV 03 ADD 01. Las Vegas, Nevada: Sandia National Laboratories. ACC: DOC.20050815.0002; DOC.20070614.0002.

184077 SNL (Sandia National Laboratories) 2007. *Data Qualification Report for the Qualification of the Preliminary Output from MDL-NBS-HS-000023, REV 01.* TDR-NBS-HS-000020 REV 00. Las Vegas, Nevada: Sandia National Laboratories.

177430 SNL (Sandia National Laboratories) 2007. *Dike/Drift Interactions.* MDL-MGR-GS-000005 REV 02. Las Vegas, Nevada: Sandia National Laboratories. ACC: DOC.20071009.0015.

177418 SNL (Sandia National Laboratories) 2007. *Dissolved Concentration Limits of Elements with Radioactive Isotopes.* ANL-WIS-MD-000010 REV 06. Las Vegas, Nevada: Sandia National Laboratory. ACC: DOC.20070918.0010.

177404 SNL (Sandia National Laboratories) 2007. *Drift-Scale THC Seepage Model.* MDL-NBS-HS-000001 REV 05. Las Vegas, Nevada: Sandia National Laboratories. ACC: DOC.20071010.0004.

177407 SNL (Sandia National Laboratories) 2007. *EBS Radionuclide Transport Abstraction.* ANL-WIS-PA-000001 REV 03. Las Vegas, Nevada: Sandia National Laboratories. ACC: DOC.20071004.0001.

177412 SNL (Sandia National Laboratories) 2007. *Engineered Barrier System: Physical and Chemical Environment.* ANL-EBS-MD-000033 REV 06. Las Vegas, Nevada: Sandia National Laboratories. ACC: DOC.20070907.0003.

179476 SNL (Sandia National Laboratories) 2008. *Features, Events, and Processes for the Total System Performance Assessment: Methods.* ANL-WIS-MD-000026 REV 00. Las Vegas, Nevada: Sandia National Laboratories.

183041 SNL (Sandia National Laboratories) 2008. *Features, Events, and Processes for the Total System Performance Assessment: Analyses.* ANL-WIS-MD-000027 REV 00. Las Vegas, Nevada: Sandia National Laboratories.

178519 SNL (Sandia National Laboratories) 2007. *General Corrosion and Localized Corrosion of Waste Package Outer Barrier.* ANL-EBS-MD-000003 REV 03. Las Vegas, Nevada: Sandia National Laboratories. ACC: DOC.20070730.0003; DOC.20070807.0007.

180778 SNL (Sandia National Laboratories) 2007. *General Corrosion and Localized Corrosion of the Drip Shield.* ANL-EBS-MD-000004 REV 02 ADD 01. Las Vegas, Nevada: Sandia National Laboratories. ACC: DOC.20060427.0002; DOC.20070807.0004; DOC.20071003.0019.

181648 SNL (Sandia National Laboratories) 2007. *In-Drift Natural Convection and Condensation.* MDL-EBS-MD-000001 REV 00 AD 01. Las Vegas, Nevada: Sandia National Laboratories. ACC: DOC.20050330.0001; DOC.20051122.0005; DOC.20070907.0004.

177411 SNL (Sandia National Laboratories) 2007. *In-Drift Precipitates/Salts Model.* ANL-EBS-MD-000045 REV 03. Las Vegas, Nevada: Sandia National Laboratories. ACC: DOC.20070306.0037.

180472 SNL (Sandia National Laboratories) 2007. *Initial Radionuclide Inventories.* ANL-WIS-MD-000020 REV 01 ADD 01. Las Vegas, Nevada: Sandia National Laboratories. ACC: DOC.20050927.0005; DOC.20070801.0001.

180506 SNL (Sandia National Laboratories) 2007. *In-Package Chemistry Abstraction.* ANL-EBS-MD-000037 REV 04 ADD 01. Las Vegas, Nevada: Sandia National Laboratories. ACC: DOC.20070816.0004.

178851 SNL (Sandia National Laboratories) 2007. *Mechanical Assessment of Degraded Waste Packages and Drip Shields Subject to Vibratory Ground Motion.* MDL-WIS-AC-000001 REV 00. Las Vegas, Nevada: Sandia National Laboratories. ACC: DOC.20070917.0006.

177422 SNL (Sandia National Laboratories) 2007. *MOX Spent Nuclear Fuel and LaBS Glass for TSPA-LA.* ANL-WIS-MD-000022 REV 01. Las Vegas, Nevada: Sandia National Laboratories. ACC: DOC.20070220.0007.

181383 SNL (Sandia National Laboratories) 2007. *Multiscale Thermohydrologic Model.* ANL-EBS-MD-000049 REV 03 ADD 01. Las Vegas, Nevada: Sandia National Laboratories. ACC: DOC.20070831.0003.

177432 SNL (Sandia National Laboratories) 2007. *Number of Waste Packages Hit by Igneous Events.* ANL-MGR-GS-000003 REV 03. Las Vegas, Nevada: Sandia National Laboratories. ACC: DOC.20071002.0001.

184748 SNL (Sandia National Laboratories) 2008. *Particle Tracking Model and Abstraction of Transport Processes.* MDL-NBS-HS-000020 REV 02 AD 02. Las Vegas, Nevada: Sandia National Laboratories.

177424 SNL (Sandia National Laboratories) 2007. *Radionuclide Screening.* ANL-WIS-MD-000006 REV 02. Las Vegas, Nevada: Sandia National Laboratories. ACC: DOC.20070326.0003.

177396 SNL (Sandia National Laboratories) 2007. *Radionuclide Transport Models Under Ambient Conditions.* MDL-NBS-HS-000008 REV 02 ADD 01. Las Vegas, Nevada: Sandia National Laboratories. ACC: DOC.20050823.0003; DOC.20070718.0003.

179347 SNL (Sandia National Laboratories) 2007. *Redistribution of Tephra and Waste by Geomorphic Processes Following a Potential Volcanic Eruption at Yucca Mountain, Nevada.* MDL-MGR-GS-000006 REV 00. Las Vegas, Nevada: Sandia National Laboratories. ACC: DOC.20071220.0004.

183750 SNL (Sandia National Laboratories) 2008. *Saturated Zone Flow and Transport Model Abstraction.* MDL-NBS-HS-000021 REV 03 AD 02. Las Vegas, Nevada: Sandia National Laboratories. ACC: DOC.20080107.0006.

177394 SNL (Sandia National Laboratories) 2007. *Saturated Zone In-Situ Testing.* ANL-NBS-HS-000039 REV 02. Las Vegas, Nevada: Sandia National Laboratories. ACC: DOC.20070608.0004.

177391 SNL (Sandia National Laboratories) 2007. *Saturated Zone Site-Scale Flow Model.* MDL-NBS-HS-000011 REV 03. Las Vegas, Nevada: Sandia National Laboratories. ACC: DOC.20070626.0004; DOC.20071001.0013.

176828 SNL (Sandia National Laboratories) 2007. *Seismic Consequence Abstraction.* MDL-WIS-PA-000003 REV 03. Las Vegas, Nevada: Sandia National Laboratories. ACC: DOC.20070928.0011.

182145 SNL (Sandia National Laboratories) 2007. *Simulation of Net Infiltration for Present-Day and Potential Future Climates.* MDL-NBS-HS-000023 REV 01 AD 01. Las Vegas, Nevada: Sandia National Laboratories.

177392 SNL (Sandia National Laboratories) 2007. *Site-Scale Saturated Zone Transport.* MDL-NBS-HS-000010 REV 03. Las Vegas, Nevada: Sandia National Laboratories. ACC: DOC.20070822.0003, DOC.20080117.0002.

181953 SNL (Sandia National Laboratories) 2007. *Stress Corrosion Cracking of Waste Package Outer Barrier and Drip Shield Materials.* ANL-EBS-MD-000005 REV 04. Las Vegas, Nevada: Sandia National Laboratories. ACC: DOC.20070913.0001.

179287 SNL (Sandia National Laboratories) 2007. *Technical Work Plan for: Revision of Model Reports for Near-Field and In-Drift Water Chemistry.* TWP-MGR-PA-000038 REV 02. Las Vegas, Nevada: Sandia National Laboratories. ACC: DOC.20070110.0004.

182219 SNL (Sandia National Laboratories) 2007. *Technical Work Plan for: Igneous Activity Assessment for Disruptive Events.* TWP-WIS-MD-000007 REV 10. Las Vegas, Nevada: Sandia National Laboratories. ACC: DOC.20070830.0002.

184920 SNL (Sandia National Laboratories) 2008. *Technical Work Plan for: Total System Performance Assessment FY 07-08 Activities.* TWP-MGR-PA-000045 REV 01 ICN 02. Las Vegas, Nevada: Sandia National Laboratories. ACC: DOC.20080131.0048.

179354 SNL (Sandia National Laboratories) 2007. *Total System Performance Assessment Data Input Package for Requirements Analysis for Engineered Barrier System In-Drift Configuration.* TDR-TDIP-ES-000010 REV 00. Las Vegas, Nevada: Sandia National Laboratories. ACC: DOC.20070921.0008.

179394 SNL (Sandia National Laboratories) 2007. *Total System Performance Assessment Data Input Package for Requirements Analysis for Transportation Aging and Disposal Canister and Related Waste Package Physical Attributes Basis for Performance Assessment.* TDR-TDIP-ES-000006 REV 00. Las Vegas, Nevada: Sandia National Laboratories. ACC: DOC.20070918.0005.

179412 SNL (Sandia National Laboratories) 2007. *Total System Performance Assessment Data Input Package for Site-Scale Saturated Zone Breakthrough Curves.* TDR-TDIP-NS-000005 REV 00. Las Vegas, Nevada: Sandia National Laboratories. ACC: DOC.20070423.0004.

179466 SNL (Sandia National Laboratories) 2007. *Total System Performance Assessment Data Input Package for Requirements Analysis for Subsurface Facilities.* TDR-TDIP-PA-000001 REV 00. Las Vegas, Nevada: Sandia National Laboratories. ACC: DOC.20070921.0007.

179567 SNL (Sandia National Laboratories) 2007. *Total System Performance Assessment Data Input Package for Requirements Analysis for DOE SNF/HLW and Naval SNF Waste Package Physical Attributes Basis for Performance Assessment.* TDR-TDIP-ES-000009 REV 00. Las Vegas, Nevada: Sandia National Laboratories. ACC: DOC.20070921.0009.

180677 SNL (Sandia National Laboratories) 2007. *Total System Performance Assessment (TSPA) Data Input Package for Saturated Zone 1-D Transport Model.* TDR-TDIP-NS-000006 REV 00. Las Vegas, Nevada: Sandia National Laboratories. ACC: DOC.20070503.0008.

181031 SNL (Sandia National Laboratories) 2007. *Total System Performance Assessment (TSPA) Data Input Package for General Corrosion and Localized Corrosion of Waste Package Outer Barrier.* TDR-TDIP-ES-000001 REV 01. Las Vegas, Nevada: Sandia National Laboratories. ACC: DOC.20070510.0001.

184614 SNL (Sandia National Laboratories) 2007. *UZ Flow Models and Submodels.* MDL-NBS-HS-000006 REV 03 AD 01. Las Vegas, Nevada: Sandia National Laboratories. ACC: DOC.20080108.0003

177423 SNL (Sandia National Laboratories) 2007. *Waste Form and In-Drift Colloids-Associated Radionuclide Concentrations: Abstraction and Summary.* MDL-EBS-PA-000004 REV 03. Las Vegas, Nevada: Sandia National Laboratories. ACC: DOC.20071018.0019.

159400 Snow, J.K. and Wernicke, B.P. 2000. "Cenozoic Tectonism in the Central Basin and Range: Magnitude, Rate, and Distribution of Upper Crustal Strain." *American Journal of Science, 300,* (9), 659-719. New Haven, Connecticut: Yale University, Kline Geology Laboratory. TIC: 253039.

117127 Sonnenthal, E.L. and Bodvarsson, G.S. 1999. "Constraints on the Hydrology of the Unsaturated Zone at Yucca Mountain, NV from Three-Dimensional Models of Chloride and Strontium Geochemistry." *Journal of Contaminant Hydrology, 38,* (1-3), 107-156. New York, New York: Elsevier. TIC: 244160.

159060 Stein, M. 1987. "Large Sample Properties of Simulations Using Latin Hypercube Sampling." *Technometrics, 29,* (2), 143-151. [Alexandria, Virginia]: American Statistical Association. TIC: 253129.

151957 Stuckless, J.S. 2000. *Archaeological Analogues for Assessing the Long-Term Performance of a Mined Geologic Repository for High-Level Radioactive Waste.* Open-File Report 00-181. Denver, Colorado: U.S. Geological Survey. ACC: MOL.20000822.0366.

125332 Stumm, W. and Morgan, J.J. 1996. *Aquatic Chemistry, Chemical Equilibria and Rates in Natural Waters.* 3rd Edition. New York, New York: John Wiley & Sons. TIC: 246296.

100489 Suzuki, T. 1983. "A Theoretical Model for Dispersion of Tephra." *Arc Volcanism: Physics and Tectonics, Proceedings of a 1981 IAVCEI Symposium, August-September, 1981, Tokyo and Hakone.* Shimozuru, D. and Yokoyama, I., eds. Pages 95-113. Tokyo, Japan: Terra Scientific Publishing Company. TIC: 238307.

182056 Sverdrup, H. and Warfvinge, P. 1988. "Weathering of Primary Silicate Minerals in the Natural Soil Environment in Relation to a Chemical Weathering Model." *Water, Air, and Soil Pollution, 38,* 387-408. [Boston, Massachusetts]: Kluwer Academic Publishers. TIC: 259601.

119053 Thatcher, W.; Foulger, G.R.; Julian, B.R.; Svarc, J.; Quilty, E.; and Bawden, G.W. 1999. "Present-Day Deformation Across the Basin and Range Province, Western United States." *Science, 283,* (5408), 1714-1718. Washington, D.C.: American Association for the Advancement of Science. TIC: 246227.

159061 Thorne, M.C. 1993. "The Use of Expert Opinion in Formulating Conceptual Models of Underground Disposal Systems and the Treatment of Associated Bias." *Reliability Engineering and System Safety, 42,* 161-180. [New York, New York]: Elsevier. TIC: 252832.

180513 Tokunaga, T.K.; Olson, K.R.; and Wan, J. 2005. "Infiltration Flux Distributions in Unsaturated Rock Deposits and Their Potential Implications for Fractured Rock Formations." *Geophysical Research Letters, 32,* (L05405), 1-4. [Washington, D.C.]: American Geophysical Union. TIC: 259312.

170136 Truesdell, A.H. and Jones, B.F. 1974. "WATEQ, A Computer Program for Calculating Chemical Equilibria of Natural Waters." *Journal of Research of the U.S. Geological Survey, 3,* (2), 233-248. Menlo Park, California: U.S. Geological Survey. TIC: 224163.

183166 Varel International 2006. Roller Cone Bits, Oil & Gas Products 2006. Carrollton, Texas: Varel International. TIC: 259758.

128494 Vesely, W.E.; Goldberg, F.F.; Roberts, N.H.; and Haasl, D.F. 1981. *Fault Tree Handbook.* NUREG - 0492. Washington, D.C.: U.S. Nuclear Regulatory Commission. TIC: 208328.

164449 Waiting, D.J.; Stamatakos, J.A.; Ferrill, D.A.; Sims, D.W.; Morris, A.P.; Justus, P.S.; and Ibrahim, A.K. 2003. "Methodologies for the Evaluation of Faulting at Yucca Mountain, Nevada." *Proceedings of the 10th International High-Level Radioactive Waste Management Conference (IHLRWM), March 30-April 2, 2003, Las Vegas, Nevada.* Pages 377-387. La Grange Park, Illinois: American Nuclear Society. TIC: 254559.

127454 Walton, J.C. 1994. "Influence of Evaporation on Waste Package Environment and Radionuclide Release from a Tuff Repository." *Water Resources Research, 30,* (12), 3479-3487. Washington, D.C.: American Geophysical Union. TIC: 246921.

108835 Wang, J.S.Y. and Narasimhan, T.N. 1985. "Hydrologic Mechanisms Governing Fluid Flow in a Partially Saturated, Fractured, Porous Medium." *Water Resources Research, 21,* (12), 1861-1874. Washington, D.C.: American Geophysical Union. TIC: 225290.

106793 Wang, J.S.Y. and Narasimhan, T.N. 1993. "Unsaturated Flow in Fractured Porous Media." Chapter 7 of *Flow and Contaminant Transport in Fractured Rock.* Bear, J.; Tsang, C-F.; and de Marsily, G., eds. San Diego, California: Academic Press. TIC: 235461.

155234 Warren, T.M. 1987. "Penetration-Rate Performance of Roller-Cone Bits." *Drilling.* SPE Reprint Series No. 22. Richardson, Texas: Society of Petroleum Engineers. TIC: 250084.

180902 Weber, C.L.; Vanbriesen, J.M.; and Small, M.S. 2006. "A Stochastic Regression Approach to Analyzing Thermodynamic Uncertainty in Chemical Speciation Modeling." *Environmental Science & Technology, 40,* (12), 3872-3878. [Washington, D.C.]: American Chemical Society. TIC: 259389.

100476 Wescott, R.G.; Lee, M.P.; Eisenberg, N.A.; McCartin, T.J.; and Baca, R.G., eds. 1995. *NRC Iterative Performance Assessment Phase 2, Development of Capabilities for Review of a Performance Assessment for a High-Level Waste Repository.* NUREG-1464. Washington, D.C.: U.S. Nuclear Regulatory Commission. ACC: MOL.19960710.0075.

182943 Wheatley, P.D. 2007. "Transmittal of Document EDF-NSNF-035, Radionuclide Inventory Calculation Checkes, SFD Version 5.0.1, Rev. 1." Letter from P.D. Wheatley (INL) to K. Knowles (SNL) and R.M. Kacich (BSC), August, 23, 2007, CCN 210849, with enclosure. ACC: RPM.20070828.0160.

168088 White, A.F. and Brantley, S.L. 2003. "The Effect of Time on the Weathering of Silicate Minerals: Why Do Weathering Rates Differ in the Laboratory and Field?" *Chemical Geology, 202,* ([3-4]), 479-506. [New York, New York]: Elsevier. TIC: 255730.

157307 Williams, N.H. 2001. "Contract No. DE-AC08-01RW12101 – Total System Performance Assessment – Analyses for Disposal of Commercial and DOE Waste Inventories at Yucca Mountain – Input to Final Environmental Impact Statement and Site Suitability Evaluation REV 00 ICN 02." Letter from N.H. Williams (BSC) to J.R. Summerson (DOE/YMSCO), December 11, 2001, RWA:cs-1204010670, with enclosure. ACC: MOL.20011213.0056.

157389 Williams, N.H. 2001. "Contract No. DE-AC08-01RW12101 – Uncertainty Analyses and Strategy Letter Report, REV 00, Activity #SA011481M4." Letter from N.H. Williams (BSC) to S.J. Brocoum (DOE/YMSCO), November 19, 2001, JM:cs-1116010483, with enclosure. ACC: MOL.20020109.0064.

115085 Wilson, C.N. and Gray, W. J. 1990. "Measurement of Soluble Nuclide Dissolution Rates from Spent Fuel." *Scientific Basis for Nuclear Waste Management XIII, Symposium held November 27-30, 1989, Boston, Massachusetts.* Oversby, V.M. and Brown, P.W., eds. *176,* 489-498. Pittsburgh, Pennsylvania: Materials Research Society. TIC: 203658.

100191 Wilson, M.L.; Gauthier, J.H.; Barnard, R.W.; Barr, G.E.; Dockery, H.A.; Dunn, E.; Eaton, R.R.; Guerin, D.C.; Lu, N.; Martinez, M.J.; Nilson, R.; Rautman, C.A.; Robey, T.H.; Ross, B.; Ryder, E.E.; Schenker, A.R.; Shannon, S.A.; Skinner, L.H.; Halsey, W.G.; Gansemer, J.D.; Lewis, L.C.; Lamont, A.D.; Triay, I.R.; Meijer, A.; and Morris, D.E. 1994. *Total-System Performance Assessment for Yucca Mountain – SNL Second Iteration (TSPA-1993).* SAND93-2675. Executive Summary and two volumes. Albuquerque, New Mexico: Sandia National Laboratories. ACC: NNA.19940112.0123.

174895 Wittman, R.S.; Buck, E.C.; and Hanson, B.D. 2005. *Data Analysis of Plutonium Sorption on Colloids in a Minimal Kinetics Model.* PNNL-15285. Richland, Washington: Pacific Northwest National Laboratory. ACC: MOL.20050811.0087.

174800 Wong, L.L.; Lian, T.; Fix, D.V.; Sutton, M.; and Rebak, R.B. 2004. "Surface Analysis of Alloy 22 Coupons Exposed for Five Years to Concentrated Ground Waters." *Corrosion/2004, 59th Annual Conference & Exposition, March 28 - April 1, 2004, New Orleans.* Paper No. 04701. Houston, Texas: NACE International. TIC: 255943.

163662 Woods, A.W.; Sparks, S.; Bokhove, O.; LeJeune, A-M.; Conner, C.B.; and Hill, B.E. 2002. "Modeling Magma-Drift Interaction at the Proposed High-Level Radioactive Waste Repository at Yucca Mountain, Nevada, USA." *Geophysical Research Letters, 29,* (13), 19-1 through 19-4. [Washington, D.C.]: American Geophysical Union. TIC: 254467.

102047 Wronkiewicz, D.J.; Bates, J.K.; Wolf, S.F.; and Buck, E.C. 1996. "Ten-Year Results from Unsaturated Drip Tests with UO{subscript 2} at 90°C: Implications for the Corrosion of Spent Nuclear Fuel." *Journal of Nuclear Materials, 238,* (1), 78-95. Amsterdam, The Netherlands: North-Holland. TIC: 243361.

117161 Wu, Y.S.; Haukwa, C.; and Bodvarsson, G.S. 1999. "A Site-Scale Model for Fluid and Heat Flow in the Unsaturated Zone of Yucca Mountain, Nevada." *Journal of Contaminant Hydrology, 38,* (1-3), 185-215. New York, New York: Elsevier. TIC: 244160.

156399 Wu, Y.S.; Liu, H.H.; Bodvarsson, G.S.; and Zellmer, K.E. 2001. *A Triple-Continuum Approach for Modeling Flow and Transport Processes in Fractured Rock.* LBNL-48875. Berkeley, California: Lawrence Berkeley National Laboratory. TIC: 251297.

117167 Wu, Y.S.; Ritcey, A.C.; and Bodvarsson, G.S. 1999. "A Modeling Study of Perched Water Phenomena in the Unsaturated Zone at Yucca Mountain." *Journal of Contaminant Hydrology, 38,* (1-3), 157-184. New York, New York: Elsevier. TIC: 244160.

160195 Wu, Y-S.; Pan, L.; Zhang, W.; and Bodvarsson, G.S. 2002. "Characterization of Flow and Transport Processes within the Unsaturated Zone of Yucca Mountain, Nevada, Under Current and Future Climates." *Journal of Contaminant Hydrology, 54,* ([3-4]), 215-247. [New York, New York]: Elsevier. TIC: 253316.

154918 Wu, Y-S.; Zhang, W.; Pan, L.; Hinds, J.; and Bodvarsson, G.S. 2000. *Capillary Barriers in Unsaturated Fractured Rocks of Yucca Mountain, Nevada.* LBNL-46876. Berkeley, California: Lawrence Berkeley National Laboratory. TIC: 249912.

161058 Wu, Y-S.; Zhang, W.; Pan, L.; Hinds, J.; and Bodvarsson, G.S. 2002. "Modeling Capillary Barriers in Unsaturated Fractured Rock." *Water Resources Research, 38,* (11), 35-1 through 35-12. [Washington, D.C.]: American Geophysical Union. TIC: 253854.

159465 Yu, C.; Zielen, A.J.; Cheng, J.-J.; LePoire, D.J.; Gnanapragasam, E.; Kamboj, S.; Arnish, J.; Wallo, A., III; Williams, W.A.; and Peterson, H. 2001. *User's Manual for RESRAD Version 6.* ANL/EAD-4. Argonne, Illinois: Argonne National Laboratory. TIC: 252702.

180273 Zhang, K.; Wu, Y-S.; and Pan, L. 2006. "Temporal Damping Effect of the Yucca Mountain Fractured Unsaturated Rock on Transient Infiltration Pulses." *Journal of Hydrology, 327,* 235-248. [New York, New York]: Elsevier. TIC: 259283.

154702 Zheng, C. and Bennett, G.D. 1995. *Applied Contaminant Transport Modeling, Theory and Practice.* New York, New York: Van Nostrand Reinhold. TIC: 249865.

100615 Zyvoloski, G.A.; Robinson, B.A.; Dash, Z.V.; and Trease, L.L. 1997. *User's Manual for the FEHM Application–A Finite-Element Heat- and Mass-Transfer Code*. LA-13306-M. Los Alamos, New Mexico: Los Alamos National Laboratory. TIC: 235999.

9.2 CODES, STANDARDS, REGULATIONS, AND PROCEDURES

180319 10 CFR 63. 2007. Energy: Disposal of High-Level Radioactive Wastes in a Geologic Repository at Yucca Mountain, Nevada. Internet Accessible.

173176 40 CFR 197. 2004. Protection of Environment: Public Health and Environmental Radiation Protection Standards for Yucca Mountain, Nevada: ACC: MOL.20050324.0101.

175755 40 CFR 197. 2005. Protection of Environment: Public Health and Environmental Radiation Protection Standards for Yucca Mountain, Nevada. ACC: MOL.20051121.0084.

155216 66 FR 32074. 40 CFR Part 197, Public Health and Environmental Radiation Protection Standards for Yucca Mountain, NV; Final Rule. ACC: MOL.20050418.0113.

156671 66 FR 55732. Disposal of High-Level Radioactive Wastes in a Proposed Geologic Repository at Yucca Mountain, NV, Final Rule. 10 CFR Parts 2, 19, 20, 21, 30, 40, 51, 60, 61, 63, 70, 72, 73, and 75. ACC: MOL.20050324.0102; MOL.20050418.0124.

177357 70 FR 49014. Public Health and Environmental Radiation Protection Standards for Yucca Mountain, NV. Internet Accessible.

178394 70 FR 53313. Implementation of a Dose Standard After 10,000 Years. Internet Accessible.

122137 DOE (U.S. Department of Energy) 1995. *The Nuclear Waste Policy Act, as Amended, with Appropriations Acts Appended.* DOE/RW-0438, Rev. 1. Washington, D.C.: U.S. Department of Energy, Office of Civilian Radioactive Waste Management. ACC: HQO.19950124.0001.

100975 DOE 1996. *Title 40 CFR Part 191 Compliance Certification Application for the Waste Isolation Pilot Plant.* DOE/CAO-1996-2184. Twenty-one volumes. Carlsbad, New Mexico: U.S. Department of Energy, Carlsbad Area Office. TIC: 240511.

100017 Energy Policy Act of 1992. Public Law No. 102-486, 106 Stat. 2776. TIC: 233191.

116135 EPA (U.S. Environmental Protection Agency) 1997. *Activity Factors.* Volume III of *Exposure Factors Handbook.* EPA/600/P-95/002Fc. Washington, D.C.: U.S. Environmental Protection Agency. TIC: 241062.

175544 EPA (U.S. Environmental Protection Agency) 2002. *Federal Guidance Report 13, CD Supplement, Cancer Risk Coefficients for Environmental Exposure to Radionuclides, EPA.* EPA-402-C-99-001, Rev. 1. [Washington, D.C.]: U.S. Environmental Protection Agency. ACC: MOL.20051013.0016.

100061 National Research Council. 1990. *Rethinking High-Level Radioactive Waste Disposal, A Position Statement of the Board on Radioactive Waste Management.* Washington, D.C.: National Academy Press. TIC: 205153.

100018 National Research Council. 1995. *Technical Bases for Yucca Mountain Standards.* Washington, D.C.: National Academy Press. TIC: 217588.

107799 NRC (U.S. Nuclear Regulatory Commission) 1975. *Reactor Safety Study: An Assessment of Accident Risks in U.S. Commercial Nuclear Power Plants.* WASH-1400. Washington, D.C.: U.S. Nuclear Regulatory Commission. TIC: 236923.

107798 NRC (U.S. Nuclear Regulatory Commission) 1990. *Severe Accident Risks: An Assessment for Five U.S. Nuclear Power Plants.* NUREG-1150. Washington, D.C.: U.S. Nuclear Regulatory Commission. TIC: 214826.

163274 NRC (U.S. Nuclear Regulatory Commission) 2003. *Yucca Mountain Review Plan, Final Report.* NUREG-1804, Rev. 2. Washington, D.C.: U.S. Nuclear Regulatory Commission, Office of Nuclear Material Safety and Safeguards. TIC: 254568.

182132 NRC (U.S. Nuclear Regulatory Commission) 2007. *Igneous Activity at Yucca Mountain: Technical Basis for Decisionmaking.* [Washington, D.C.]: U.S. Nuclear Regulatory Commission, Advisory Committee on Nuclear Waste and Materials. ACC: LLR.20070725.0023.

176542 *Nuclear Energy Institute, Inc., Petitioner v. U.S. Environmental Protection Agency, Respondent,* No. 01-1258 (U.S. Court of Appeals for the District of Columbia Circuit). Argued January 14, 2004 and Decided July 9, 2004. Internet Accessible.

131951 Nuclear Waste Policy Act of 1982. 42 U.S.C. 10101-10133. (1988). Internet Accessible.

100016 Nuclear Waste Policy Amendments Act of 1987. Public Law No. 100-203, 101 Stat. 1330. TIC: 223717.

103445 OECD (Organization for Economic Co-operation and Development) 1997. *Lessons Learnt From Ten Performance Assessment Studies.* Paris, France: Organization for Economic Co-operation and Development. TIC: 243964.

158098 OECD (Organization for Economic Co-operation and Development) and IAEA (International Atomic Energy Agency) 2002. *An International Peer Review of the Yucca Mountain Project TSPA-SR, Total System Performance Assessment for the Site Recommendation (TSPA-SR).* Paris, France: Organization for Economic Co-operation and Development, Nuclear Energy Agency. TIC: 252385.

159027 OECD (Organization for Economic Co-operation and Development, Nuclear Energy Agency) 2001. *Chemical Thermodynamics of Neptunium and Plutonium.* Volume 4 of *Chemical Thermodynamics.* New York, New York: Elsevier. TIC: 209037.

154158 USDA (U.S. Department of Agriculture) 2000. *Food and Nutrient Intakes by Individuals in the United States, 1994-1996.* Nationwide Food Surveys Report No. 96-3. Two volumes. [Washington, D.C.: U.S. Department of Agriculture]. TIC: 249498.

9.3 SOFTWARE CODES

181034 ASHPLUME_DLL_LA V. 2.0. 2003. WINDOWS 2000. STN: 11117-2.0-00.

181035 ASHPLUME_DLL_LA V. 2.1. 2006. WinDOWS 2000/XP. STN: 11117-2.1-00.

180147 ASHPLUME_DLL_LA V. 2.1. 2007. WINDOWS 2003. STN: 11117-2.1-01.

162809 CWD V. 2.0. 2003. WINDOWS 2000. STN: 10363-2.0-00.

181037 CWD V. 2.0. 2007. WINDOWS 2003. STN: 10363-2.0-01.

162228 EQ3/6 V. 8.0. 2003. WINDOWS 2000, WIN NT 4.0, WIN 98, WIN 95. STN: 10813-8.0-00.

176889 EQ3/6 V. 8.1. 2005. WINDOWS 2000. STN: 10813-8.1-00.

159731 EQ6 V. 7.2bLV. 2002. WINDOWS 2000, NT. STN: 10075-7.2bLV-02.

182102 EXDOC_LA V. 2.0. 2007. WINDOWS XP, WINDOWS 2000 & WINDOWS 2003. STN: 11193-2.0-00.

180002 FAR V. 1.1. 2007. WINDOWS 2000 & 2003. STN: 11190-1.1-00.

182225 FAR V. 1.2. 2007. WINDOWS 2000 & WINDOWS 2003. STN: 11190-1.2-00.

173139 FEHM V. 2.23. 2005. WINDOWS 2000. STN: 10086-2.23-00.

179419 FEHM V. 2.24-01. 2007. WIN2003, 2000, & XP, Red Hat Linux 2.4.21, OS 5.9. STN: 10086-2.24-01-00.

182477 FEHM V. 2.25. 2007. Win2000, WinXP, Win2003, SunOS5.9, Linux2.4.21. STN: 10086-2.25-00.

159684 FEPS Database Software Program V. .2. 2002. WINDOWS 2000. STN: 10418-.2-00.

181089 FEPS Viewer V. 1.0. 2007. Windows 2000/XP. STN: 611664-1.0-00.

164315 FLUENT V. 6.0.12. 2003. Redhat Linux V7.3. STN: 10550-6.0.12-01.

181040 GetThk_LA V. 1.0. 2006. WINDOWS 2000 & WINDOWS 2003. STN: 11229-1.0-00.

173352 GOLDSIM V. 8.02.400. 2005. WINDOWS 2000. STN: 10344-8.02-04.

174650 GoldSim V. 8.02.500. 2005. WINDOWS 2000. STN: 10344-8.02-05.

180224 GoldSim V. 9.60. 2007. WINDOWS 2000, WINDOWS XP, WINDOWS 2003. STN: 10344-9.60-00.

181903 Goldsim V. 9.60.100. 2007. WIN 2000, 2003, XP. STN: 10344-9.60-01.

167885 InterpZdll_LA V. 1.0. 2004. WINDOWS 2000. STN: 11107-1.0-00.

181043 InterpZdll_LA V. 1.0. 2007. WINDOWS 2003. STN: 11107-1.0-01.

160106 iTOUGH2 V. 5.0. 2002. SunOS 5.5.1, OSF1 V5.1, RedHat V7.2 and V7.3. STN: 10003-5.0-00.

167884 MFCP_LA V. 1.0. 2003. WINDOWS 2000. STN: 11071-1.0-00.

181045 MFCP_LA V. 1.0. 2006. WINDOWS 2003. STN: 11071-1.0-01.

174528 MkTable V. 1.00. 2003. WINDOWS 2000. STN: 10505-1.00-00.

181047 MkTable_LA V. 1.0. 2006. WINDOWS 2000. STN: 11217-1.0-00.

181048 MkTable_LA V. 1.0. 2007. WINDOWS 2003. STN: 11217-1.0-01.

164274 MSTHAC V. 7.0. 2002. SUN O.S. 5.8. STN: 10419-7.0-00.

181049 MView V. 4.0. 2007. WINDOWS XP. STN: 10072-4.0-01.

169130 PassTable1D_LA V. 1.0. 2004. WINDOWS 2000. STN: 11142-1.0-00.

181050 PassTable1D_LA V. 1.0. 2006. WINDOWS 2003. STN: 11142-1.0-01.

181051 PassTable1D_LA V. 2.0. 2007. WINDOWS 2000 & WINDOWS 2003. STN: 11142-2.0-00.

168980 PassTable3D_LA V. 1.0. 2004. WINDOWS 2000. STN: 11143-1.0-00.

181052 PassTable3D_LA V. 1.0. 2007. WINDOWS 2003. STN: 11143-1.0-01.

182556 PassTable3D_LA V. 2.0. 2007. WINDOWS 2000 & WINDOWS 2003. STN: 11143-2.0-00.

181053 PREWAP_LA V. 1.1. 2006. WINDOWS 2000. STN: 10939-1.1-00.

181157 SCCD V. 2.01. 2003. WINDOWS 2000. STN: 10343-2.01-00.

181054 SCCD V. 2.01. 2007. WINDOWS 2003. STN: 10343-2.01-01.

173435 SEEPAGEDLL_LA V. 1.2. 2005. WINDOWS 2000. STN: 11076-1.2-00.

180318 SEEPAGEDLL_LA V. 1.3. 2006. WINDOWS 2000. STN: 11076-1.3-00.

181058 SEEPAGEDLL_LA V. 1.3. 2007. WINDOWS 2003. STN: 11076-1.3-01.

152844 Software Code: ASHPLUME V. 2.0. 2001. PC. STN: 10022-2.0-00.

161296 Software Code: ASHPLUME V1.4LV. 2002. PC, Windows 2000/NT/98. STN: 10022-1.4LV-02.

153964 Software Code: EQ3/6 V. 7.2b. 1999. UCRL-MA-110662 (LSCR198).

167883 Soilexp_LA V. 1.0. 2004. WINDOWS 2000. STN: 10933-1.0-00.

164180 Software Code: SZ_Convolute V. 3.0. 2003. PC, Windows 2000. 10207-3.0-00.

181060 SZ_CONVOLUTE V. 3.10.01. 2007. WINDOWS 2000 & WINDOWS 2003. STN: 10207-3.10.01-00.

146654 T2R3D V. 1.4. 1999. UNIX, WINDOWS 95/98NT 4.0. STN: 10006-1.4-00.

161491 TOUGH2 V. 1.6. 2003. DOS Emulation (win95/98), SUN OS 5.5.1., OSF1 V4.0. STN: 10007-1.6-01.

181061 TSPA_Input_DB V. 2.2. 2006. WINDOWS 2000. STN: 10931-2.2-00.

181062 TSPA_Input_DB V. 2.2. 2006. WINDOWS 2003. STN: 10931-2.2-01.

161240 WAPDEG V. 4.07. 2002. WINDOWS NT 4.0. STN: 10000-4.07-00.

181774 WAPDEG V. 4.07. 2003. Windows 2000. STN: 10000-4.07-00.

181064 WAPDEG V. 4.07. 2007. WINDOWS SERVER 2003. STN: 10000-4.07-01.

9.4 SOURCE DATA LISTED BY DATA TRACKING NUMBER

151139 GS000308315121.003. Meteorological Stations Selected to Represent Future Climate States at Yucca Mountain, Nevada. Submittal date: 03/14/2000.

165226 GS030408312272.002. Analysis of Water-Quality Samples for the Period from July 2002 to November 2002. Submittal date: 05/07/2003.

165624 LA0303HV831352.003. Fraction of Colloids that Travel Unretarded. Submittal date: 03/31/2003.

164362 LA0306SK831231.001. SZ Site-Scale Transport Model, FEHM Files for Base Case. Submittal date: 06/25/2003.

164713 LA0307BY831811.001. Characterize Igneous Framework Additional Output. Submittal date: 07/29/2003.

171584 LA0408AM831341.001. Unsaturated Zone Distribution Coefficients (Kds) for U, Np, Pu, Am, Pa, Cs, Sr, Ra, and Th. Submittal date: 08/24/2004.

179987 LA0612DK831811.001. Magma and Eruption Properties for Potential Volcano at Yucca Mountain. Submittal date: 03/23/2007.

180497 LA0701PANS02BR.003. UZ Transport Parameters. Submittal date: 04/23/2007.

184763 LA0702AM150304.001. Probability Distribution Functions and Correlations for Sampling of Sorption Coefficient Probability Distributions of Radionuclides in the SZ at the YM. Submittal date: 01/17/2008.

179495 LA0702PADE01EG.001. Igneous Temperatures. Submittal date: 02/01/2007.

179496 LA0702PADE01EG.002. EBS Failure Fractions. Submittal date: 02/02/2007.

179980 LA0702PADE03GK.002. Input Parameter Values for the ASHPLUME V2.1_DLL_LA Model for TSPA. Submittal date: 03/23/2007.

180322 LA0702PANS02BR.001. Repository and Water Table Bins. Submittal date: 04/16/2007.

159525 LB0205REVUZPRP.001. Fracture Properties for UZ Model Layers Developed from Field Data. Submittal date: 05/14/2002.

159526 LB0207REVUZPRP.001. Revised UZ Fault Zone Fracture Properties. Submittal date: 07/03/2002.

159672 LB0207REVUZPRP.002. Matrix Properties for UZ Model Layers Developed from Field and Laboratory Data. Submittal date: 07/15/2002.

163047 LB03033DSSFF9I.001. 3-D Site Scale UZ Flow Fields for 9 Infiltration Scenarios: Simulations Using Alternative Hydraulic Properties. Submittal date: 03/28/2003.

163687 LB0304SMDCREV2.002. Seepage Modeling for Performance Assessment, Including Drift Collapse: Summary Plot Files and Tables. Submittal date: 04/11/2003.

180511 LB0307SEEPDRCL.001. Seepage into Collapsed Drift: Simulations. Submittal date: 07/21/2003.

166116 LB0310AMRU0120.002. Mathcad 11 Spreadsheets for Probabilistic Seepage Evaluation. Submittal date: 10/23/2003.

173280 LB0407AMRU0120.001. Supporting Calculations and Analysis for Seepage Abstraction and Summary of Abstraction Results. Submittal date: 07/29/2004.

180502 LB0610UZDSCP10.001. Drift-Scale Calibrated Property Set for the 10-Percentile Infiltration Map. Submittal date: 11/02/2006.

179180 LB0610UZDSCP30.001. Drift-Scale Calibrated Property Set for the 30-Percentile Infiltration Map. Submittal date: 11/02/2006.

178586 LB0611MTSCHP10.001. Mountain Scale Calibrated Property Set for the 10-Percentile Infiltration Map. Submittal date: 11/28/2006.

180293 LB0611MTSCHP30.001. Mountain Scale Calibrated Property Set for the 30-Percentile Infiltration Map. Submittal date: 11/28/2006.

183948 LB0611UZDSCP50.001. Drift-Scale Calibrated Property Set for the 50-Percentile Infiltration Map. Submittal date: 11/28/2006.

180294 LB0612MTSCHP50.001. Mountain Scale Calibrated Property Set for the 50-Percentile Infiltration Map. Submittal date: 12/19/2006.

180295 LB0612MTSCHP90.001. Mountain Scale Calibrated Property Set for the 90-Percentile Infiltration Map. Submittal date: 12/20/2006.

180296 LB0612MTSCHPFT.001. Calibrated UZ Fault Property Sets. Submittal date: 12/07/2006.

179296 LB0612PDFEHMFF.001. Flow-Field Conversions from TOUGH2 to FEHM Format for Present Day 10-, 30-, 50-, and 90-Percentile Infiltration Maps. Submittal date: 12/19/2006.

183949 LB0612UZDSCP90.001. Drift-Scale Calibrated Property Set for the 90-Percentile Infiltration Map. Submittal date: 12/20/2006.

179160 LB0701GTFEHMFF.001. Flow-Field Conversions from TOUGH2 to FEHM Format for Glacial Transition Climate 10th-, 30th-, 50th-, and 90th-Percentile Infiltration Maps. Submittal date: 01/05/2007.

179297 LB0701MOFEHMFF.001. Flow-Field Conversions from TOUGH2 to FEHM Format for Monsoon Climate 10th-, 30th-, 50th-, and 90th-Percentile Infiltration Maps. Submittal date: 01/05/2007.

179299 LB0701PAKDSESN.001. Unsaturated Zone Sorption Coefficients for Selenium and Tin. Submittal date: 01/31/2007.

179283 LB0701PAWFINFM.001. Weighting Factors for Infiltration Maps. Submittal date: 01/25/2007.

179507 LB0702PAFEM10K.002. Flow Field Conversions to FEHM Format for Post 10,000 Year Peak Dose Fluxes in the Unsaturated Zone for Four Selected Infiltration Rates. Submittal date: 02/15/2007.

179511 LB0702PASEEP01.001. New Extended-Range Seepage Look-Up Tables for Intact and Collapsed Drifts Plus Supporting Files. Submittal date: 02/20/2007.

181635 LB0702PASEEP02.001. Seepage Abstraction for Degraded Drifts. Submittal date: 06/29/2007.

180776 LB0702PAUZMTDF.001. Unsaturated Zone Matrix Diffusion Coefficients. Submittal date: 05/10/2007.

163712 LL030412512251.057. LTCTF Corrosion Rate Calculations for Five-Year Exposed Alloy C22 Specimens Cleaned Under TIP-CM-51. Submittal date: 05/28/2003.

179590 LL0702PA027MST.082. Output for ANL-EBS-MD-000049 Multiscale Thermohydrologic Model for the Mean Host-Rock Thermal Conductivity, 10-Percentile Percolation Flux, Collapsed-Drift, High and Low Rubble Thermal Conductivity Cases. Submittal date: 02/15/2007.

179853 LL0703PA011MST.006. Output for ANL-EBS-MD-000049 REV 04 Multiscale Thermohydrologic Model for the Mean Host-Rock Thermal Conductivity, 10-Percentile Percolation Flux Case. Submittal date: 03/07/2007.

179854 LL0703PA012MST.007. Output for ANL-EBS-MD-000049 REV 04 Multiscale Thermohydrologic Model for the Mean Host-Rock Thermal Conductivity, 30-Percentile Percolation Flux Case. Submittal date: 03/13/2007.

179855 LL0703PA013MST.008. Output for ANL-EBS-MD-000049 REV 04 Multiscale Thermohydrologic Model for the Mean Host-Rock Thermal Conductivity, 50-Percentile Percolation Flux Case. Submittal date: 03/13/2007.

179856 LL0703PA014MST.009. Output for ANL-EBS-MD-000049 REV 04 Multiscale Thermohydrologic Model for the Mean Host-Rock Thermal Conductivity, 90-Percentile Percolation Flux Case. Submittal date: 03/13/2007.

179857 LL0703PA015MST.010. Output for ANL-EBS-MD-000049 REV 04 Multiscale Thermohydrologic Model for the Low Host-Rock Thermal Conductivity, 10-Percentile Percolation Flux Case. Submittal date: 03/13/2007.

179858 LL0703PA016MST.011. Output for ANL-EBS-MD-000049 REV 04 Multiscale Thermohydrologic Model for the High Host-Rock Thermal Conductivity, 90-Percentile Percolation Flux Case. Submittal date: 03/13/2007.

179859 LL0703PA017MST.012. Output for ANL-EBS-MD-000049 REV 04 Multiscale Thermohydrologic Model for the High Host-Rock Thermal Conductivity, 10-Percentile Percolation Flux Case. Submittal date: 03/13/2007.

179981 LL0703PA026MST.013. Weighting Factors for Low (10-Percentile), Mean, and High (90-Percentile) Host-Rock Thermal Conductivity Cases for ANL-EBS-MD-000049 Multiscale Thermohydrologic Model. Submittal date: 03/28/2007.

179982 LL0703PA034MST.016. Output for ANL-EBS-MD-000049 Multiscale Thermohydrologic Model for the Low Host-Rock Thermal Conductivity, 30-Percentile Percolation Flux (P30L) Case. Submittal date: 03/22/2007.

179985 LL0703PA035MST.017. Output for ANL-EBS-MD-000049 Multiscale Thermohydrologic Model for the High Host-Rock Thermal Conductivity, 30-Percentile Percolation Flux (P30H) Case. Submittal date: 03/22/2007.

179986 LL0703PA036MST.018. Output for ANL-EBS-MD-000049 Multiscale Thermohydrologic Model for the Low Host-Rock Thermal Conductivity, 50-Percentile Percolation Flux (P50L) Case. Submittal date: 03/22/2007.

179989 LL0703PA037MST.019. Output for ANL-EBS-MD-000049 Multiscale Thermohydrologic Model for the High Host-Rock Thermal Conductivity, 50-Percentile Percolation Flux (P50H) Case. Submittal date: 03/22/2007.

179992 LL0703PA038MST.020. Output for ANL-EBS-MD-000049 Multiscale Thermohydrologic Model for the Low Host-Rock Thermal Conductivity, 90-Percentile Percolation Flux (P90L) Case. Submittal date: 03/22/2007.

148850 MO0003RIB00071.000. Physical and Chemical Characteristics of Alloy 22. Submittal date: 03/13/2000.

152926 MO0003RIB00073.000. Physical and Chemical Characteristics of Ti Grades 7 and 16. Submittal date: 03/13/2000.

153044 MO0003RIB00076.000. Physical and Chemical Characteristics of Type 316N Grade. Submittal date: 03/14/2000.

148744 MO0003SZFWTEEP.000. Data Resulting from the Saturated Zone Flow and Transport Expert Elicitation Project. Submittal date: 03/06/2000.

165800 MO0310MWDWAPAN.002. WAPDEG Analysis of Waste Package and Drip Shield Degradation. Submittal date: 10/16/2003.

169007 MO0404ANLSF001.001. CSNF Radionuclide Release Model. Submittal date: 04/09/2004.

171483 MO0408MWDDDMIO.002. Drift Degradation Model Inputs and Outputs. Submittal date: 08/31/2004.

171751 MO0408SPADRWSD.002. Desert Rock Wind Speed and Wind Direction Analyses for Years 1978 - 2003. Submittal date: 08/19/2004.

180755 MO0411SPACLDDG.003. Updated TSPA-LA Parameters from Clad Degradation-Summary and Abstraction for LA, ANL-WIS-MD-000021 REV 03. Submittal date: 05/10/2007.

172682 MO0501BPVELEMP.001. Bounded Horizontal Peak Ground Velocity Hazard at the Repository Waste Emplacement Level. Submittal date: 01/11/2005.

172830 MO0502ANLGAMR1.016. HLW Glass Degradation Model. Submittal date: 02/08/2005.

172893 MO0502SPAINPCA.000. In-Package Chemistry Abstraction. Submittal date: 02/25/2005.

173893 MO0505SPAROCKM.000. Rock Mass and Invert Properties for TSPA-LA. Submittal date: 05/23/2005.

174806 MO0506MWDPPMSV.000. PREWAP Processing of MSTHM Files for Spatial Variability Analyses. Submittal date: 06/27/2005.

174809 MO0506MWDTLMV3.000. TSPA-LA Model V3. Submittal date: 06/15/2005.

173958 MO0506SPAROCKU.000. Rock Unit, Radionuclide, and Colloid Parameters for Particle Tracking. Submittal date: 06/03/2005.

175064 MO0508SEPFEPLA.002. LA FEP List and Screening. Submittal date: 08/22/2005.

182281 MO0605SPAFORTY.000. Fortymile Wash Drainage Basin Dem. Submittal date: 08/02/2007.

182035 MO0612WPOUTERB.000. Output from General and Localized Corrosion of Waste Package Outer Barrier Report. Submittal date: 07/18/2007.

180439 MO0701PACSNFCP.000. CSNF Colloid Parameters. Submittal date: 04/17/2007.

180393 MO0701PAGLASWF.000. Glass Waste Form Colloid Parameters. Submittal date: 04/17/2007.

179310 MO0701PAGROUND.000. Groundwater Colloid Concentration Parameters. Submittal date: 01/18/2007.

180440 MO0701PAIRONCO.000. Colloidal Iron Corrosion Products Parameters. Submittal date: 04/17/2007.

180392 MO0701PAKDSUNP.000. Colloidal KDS for U, NP, RA and SN. Submittal date: 04/17/2007.

180508 MO0701PASHIELD.000. Waste Package/Drip Shield Early Failure Probabilities. Submittal date: 04/24/2007.

180391 MO0701PASORPTN.000. Colloidal Sorption Coefficients for PU, AM, TH, CS, and PA. Submittal date: 04/17/2007.

179334 MO0701RLTSCRNA.000. Results of Screening Analysis. Submittal date: 01/30/2007.

179358 MO0702PADISCON.001. Dissolved Concentration Limits of Elements with Radioactive Isotopes. Submittal date: 02/15/2007.

182578 MO0702PAFARDAT.001. FAR Data. Submittal date: 08/21/2007.

181219 MO0702PAFLUORI.000. Fluoride Uncertainty Associated with Dissolved Concentration Limits. Submittal date: 06/01/2007.

181588 MO0702PAFRACSS.000. FRAC_CSNF_PKGS_SS. Submittal date: 06/28/2007.

179327 MO0702PAGBDCFS.001. Groundwater Biosphere Dose Conversion Factors. Submittal date: 02/09/2007.

179328 MO0702PAGWPROS.001. Groundwater Protection Standards Conversion Factors. Submittal date: 02/06/2007.

179329 MO0702PAINHALA.001. Inhalation Dose Factors. Submittal date: 02/15/2007.

180377 MO0702PALOVERT.000. Condensation Abstraction: Well-Ventilated Drip Shield; Low Invert Transport, (0-10,000 Years). Submittal date: 04/16/2007.

180376 MO0702PALV010K.000. Condensation Abstraction: Unventilated Drip Shield; Low Invert Transport, (0-10,000 Years). Submittal date: 04/16/2007.

179925 MO0702PASTREAM.001. Waste Stream Composition and Thermal Decay Histories for LA. Submittal date: 02/15/2007.

180514 MO0702PASTRESS.002. Output DTN of Model Report, "Stress Corrosion Cracking of Waste Package Outer Barrier and Drip Shield Materials," ANL-EBS-MD-000005. Submittal date: 04/24/2007.

179330 MO0702PAVBPDCF.000. Volcanic Biosphere Dose Conversion Factors. Submittal date: 02/21/2007.

181990 MO0703PAEVSIIC.000. Evaluation of Stage II Condensation. Submittal date: 07/16/2007.

182029 MO0703PAGENCOR.001. Output from General Corrosion and Localized Corrosion of Waste Package Outer Barrier 2007 Second Version. Submittal date: 07/18/2007.

182093 MO0703PAHYTHRM.000. Hydrological and Thermal Properties of the Invert. Submittal date: 07/19/2007.

183148 MO0703PASDSTAT.001. Statistical Analyses for Seismic Damage Abstractions. Submittal date: 09/21/2007.

183156 MO0703PASEISDA.002. Seismic Damage Abstractions for TSPA Compliance Case. Submittal date: 09/21/2007.

184647 MO0704PAFEHMBR.001. FEHM Model and Input. Submittal date: 01/10/2008.

180442 MO0704PAPTTFBR.002. Particle Tracking Transfer Functions. Submittal date: 04/12/2007.

182149 MO0704PASCOURD.000. Scour Depth. Submittal date: 07/25/2007.

180389 MO0704PASOLCAP.000. In-Package Solubility "Caps" for Pu, Np, U, Th, Am, and Pa. Submittal date: 04/06/2007.

181281 MO0705GOLDSIMB.000. Goldsim Biosphere Model Files for Calculating Groundwater and Volcanic Biosphere Dose Conversion Factors. Submittal date: 05/08/2007.

181613 MO0706SPAFEPLA.001. FY 2007 LA FEP List and Screening. Submittal date: 06/20/2007.

184664 MO0712PBANLNWP.000. Probabilistic Analysis of Navy Waste Packages. Submittal date: 12/13/2007.

163563 SN0302T0502203.001. Saturated Zone Anisotropy Distribution Near the C-Wells. Submittal date: 02/26/2003.

165640 SN0308T0503100.008. Revised Frequency Distributions for Net Infiltrations and Weighting Factors Applied to Lower, Mean, and Upper Climates. Submittal date: 08/28/2003.

168763 SN0310T0502103.009. Revised Saturated Zone Transport Abstraction Model Uncertain Inputs. Submittal date: 10/09/2003.

168761 SN0310T0505503.004. Initial Radionuclide Inventories for TSPA-LA. Submittal date: 10/27/2003.

178850 SN0612T0502404.014. Thermodynamic Database Input File for EQ3/6 - DATA0.YMP.R5. Submittal date: 12/15/2006.

180523 SN0701PAEBSPCE.001. PCE TDIP Potential Seepage Water Chemistry Lookup Tables. Submittal date: 04/25/2007.

179425 SN0701PAEBSPCE.002. PCE TDIP PCO2 and Total Carbon Lookup Tables. Submittal date: 01/30/2007.

182961 SN0701PAWPHIT1.001. Number of Waste Packages Hit by Igneous Events. Submittal date: 09/13/2007.

180451 SN0702PAIPC1CA.001. In-Package Chemistry Calculations and Abstractions. Submittal date: 04/19/2007.

179504 SN0702PASZFTMA.001. Saturated Zone Flow and Transport Model Abstraction. Submittal date: 02/06/2007.

183471 SN0702PASZFTMA.002. Saturated Zone 1-D Transport Model. Submittal date: 10/15/2007.

181571 SN0703PAEBSPCE.006. Physical and Chemical Environment (PCE) TDIP Water-Rock Interaction Parameter Table and Salt Separation Tables with Supporting Files. Submittal date: 06/27/2007.

184141 SN0703PAEBSPCE.007. Physical and Chemical Environment (PCE) TDIP Uncertainty Evaluations and Supporting Files. Submittal date: 11/30/2007.

183217 SN0703PAEBSRTA.001. Inputs Used in the Engineered Barrier System (EBS) Radionuclide Transport Abstraction. Submittal date: 09/28/2007.

182122 SN0704PADSGCMT.001. Drip Shield General Corrosion Models Based on 2.5-Year Titanium Grade 7 Corrosion Rates. Submittal date: 07/24/2007.

182188 SN0704PADSGCMT.002. Drip Shield General Corrosion Rate Multiplier for Titanium Grade 29. Submittal date: 07/27/2007.

181837 SN0706PAEBSPCE.016. P&CE Invert Relative Humidity (RH) Boundary Table. Submittal date: 06/28/2007.

183485 SN0710PASZFTMA.003. Updated Saturated Zone 1-D Transport Model. Submittal date: 10/10/2007.

APPENDIX A
ACRONYMS AND ABBREVIATIONS

A. ACRONYMS

ACM	alternative conceptual model
BDCF	biosphere dose conversion factor
BWR	boiling water reactor
CCDF	complementary cumulative distribution function
CDF	cumulative distribution function
CDSP	co-disposed
CSNF	commercial spent nuclear fuel
CSNF-SS	commercial spent nuclear fuel-stainless steel
CSNF-Z	commercial spent nuclear fuel-Zircaloy (zirconium-based cladding)
DI	document identifier
DIRS	Document Input Reference System
DLL	dynamically linked library
DOE	U.S. Department of Energy
DS	drip shield
DSNF	DOE spent nuclear fuel
DTN	data tracking number
EBS	engineered barrier system
ECRB	Enhanced Characterization of Repository Block
EF	early failure (only used in modeling cases)
EIS	Environmental Impact Statement
EPA	U.S. Environmental Protection Agency
EPRI	Electric Power Research Institute
ESF	Exploratory Studies Facility
FD	fault displacement (only used in modeling cases)
FEHM	Finite Element, Heat and Mass (Model)
FEIS	Final Environmental Impact Statement
FEP	feature, event, or process
GM	ground motion (only used in modeling cases)
GLUE	generalized likelihood uncertainty estimation
HLW	high-level radioactive waste
IAEA	International Atomic Energy Agency
IDPS	in-drift precipitated salts
IMARC	Integrated Multiple Assumptions and Release Code
INEEL	Idaho National Engineering and Environmental Laboratory
IRT	International Review Team
IVRT	Independent Validation Review Team
LA	License Application

ACRONYMS (Continued)

LaBS	lanthanide borosilicate
LHS	Latin hypercube sample
MIC	microbially influenced corrosion
MINC	Multiple Interacting Continua
MOX	mixed oxide fuel
MSTHM	Multiscale Thermohydrologic Model
NEA	Nuclear Energy Agency
NRC	U.S. Nuclear Regulatory Commission
NSNF	naval spent nuclear fuel
NWTRB	Nuclear Waste Technical Review Board
OCRWM	Office of Civilian Radioactive Waste Management
ODBC	Open Database Connectivity
OCB	outer corrosion barrier
PA	Performance Assessment
P&CE	Physical & Chemical Environment (as in P&CE container)
PDF	Parameter Documentation Form
PEF	Parameter Entry Form
pdf	Probability Density Function
PGA	peak ground acceleration
PGV	peak ground velocity
PMA	Performance Margin Analysis
PIF	Parameter Identification Form
PRCC	Partial Rank Correlation Coefficient
PSHA	Probabilistic Seismic Hazard Analysis
PVEF	Parameter Value Entry Form
PVF	Parameter Verification Form
PVHA	probabilistic volcanic hazard analysis
PWR	pressurized water reactor
QA	quality assurance
QARD	Quality Assurance Requirements and Description
RAM	random access memory
RMEI	reasonably maximally exposed individual
RST	residual stress threshold
SAR	Safety Analysis Report
SCC	stress corrosion cracking
SCM	Software Configuration Management
SD	standard deviation
SME	subject matter expert
SNF	spent nuclear fuel

ACRONYMS (Continued)

SNL	Sandia National Laboratories
SRC	Standardized Regression Coefficient
SRRC	Standardized Rank Regression Coefficient
SZ	saturated zone
TAD	Transportation, aging, and disposal
TDMS	Technical Data Management System
TH	thermal-hydrologic
THC	thermal-hydrologic-chemical
TSPA	Total System Performance Assessment
TSPA-LA	Total System Performance Assessment for the License Application
TSPA-SR	Total System Performance Assessment for the Site Recommendation
TSPA-VA	Total System Performance Assessment for the Viability Assessment
TWP	Technical Work Plan
UTM	Universal Transverse Mercator grid
UZ	unsaturated zone
WAPDEG	waste package degradation model
WP	waste package
YMP	Yucca Mountain Project

INTENTIONALLY LEFT BLANK

A2. ABBREVIATIONS

acre-ft	acre-foot
atm	atmospheres
C	Celsius
Ci	curie
cm	centimeter
F	Fahrenheit
fco_2	fugacity of CO_2
f_{ff}	flow focusing factor
ft	foot
G	constant of gravity
g	gram
gal	gallon
GB	gigabytes
Gbps	gigabytes per second
GHz	gigahertz
GWd	gigawatt-day
hr	hour
Hz	hertz
in.	inch
K	Kelvin
K_d	distribution coefficient (mL/g)
kg	kilogram
kJ	kilojoules
km	kilometer
kVA	kilovolt ampere
kW	kilowatt
L	liter
lb	pound
log( )	logarithm
ln()	natural logarithm
m	meter
Mbps	megabits per second
mg	milligram
MHz	megahertz
mi	mile
mL	milliliter
M_L	local magnitude

ABBREVIATIONS (Continued)

mm	millimeter
M_{max}	maximum magnitude
M_{min}	minimum magnitude
mol/L	molarity
mol/kg	molality
mph	mile per hour
mrem	millirem
mSv	millisievert
mT	metric tons
MTHM	metric tons of heavy metal
MW	megawatt
M_w	moment magnitude
µm	micrometer (micron)
nm	nanometer
Pa	pascal
pCi	picocurie
pCO_2	negative log of the partial pressure of CO_2
Pco_2	partial pressure of CO_2
pH	scale of acidity and alkalinity (hydrogen ion concentration notation)
pO_2	negative log of the partial pressure of O_2
Po_2	partial pressure of O_2
ppb	parts per billion
ppm	parts per million
psi	pounds per square inch
rem	roentgen equivalent man
s or sec	second
TB	terabyte
t, τ	time
W	watt
yr	year

APPENDIX B

DATA TRACKING NUMBERS FOR THE TSPA-LA MODEL

B1. INTRODUCTION

Appendix B describes the interrelationships among the Total System Performance Assessment for the License Application (TSPA-LA) Model output data tracking numbers (DTNs) for the TSPA-LA Model. Figure B-1 shows the information flow among the output DTNs submitted to the Technical Data Management System (TDMS).

The DTNs contain work products (e.g., Microsoft Excel spreadsheets, TSPA Model files, etc.) that are not captured directly in the *Total System Performance Assessment Model/Analysis for the License Application*. The DTNs have been submitted to TDMS.

The following sections contain brief descriptions of the contents of the DTNs. The respective ReadMe.doc file located in each DTN provides more detailed information on the contents of each DTN. Figures B-1 and B-2 provide an overview of the relationships between the DTNs.

B2. DESCRIPTIONS OF THE DATA TRACKING NUMBERS

The following text supports Figures B-1 and B-2. Each block on Figures B-1 and B-2 is described below.

B2.1 MODEL DEVELOPMENT RECORDS PACKAGE

Reference Figure B-1, Block 1, and Figure B-2, Block 105—This records package documents each of the model changes that were generated since v3.007 of the Model, which is documented in DTN: MO0506MWDTLMV3.000_R0 [DIRS 174809]. In order to clearly demark the first step toward building a 10,000-year/peak dose model, the versioning started with v4.000. This records package contains v4.000 through v4.047 of the Groundwater Model and v.E1.000 through vE1.003 of the Eruptive Model. All model versions generally follow the same folder content. For example, the content for a typical folder would contain a Master Folder and the specific case folders that were appropriate at that stage of model development. Examples of case folders are as follows: (1) HI 1Myr, (2) Ign 1Myr, (3) Nominal 1Myr, and (4) Seismic EF 10kyr. Each Master Folder generally contains the following:

- One or more change approval forms
- Change checklist
- Checking checklist
- Conceptual checklist
- Conceptual description
- GoldSim model file
- GoldSim version report
- Additional information directory (optional)

This records package feeds output DTN: MO0709TSPAREGS.000_R0 [DIRS 182976], which contains the final versions of the Groundwater Model (v5.000) and the Eruptive Model (vE1.004). This records package also feeds output DTN: MO0708TSPAPOST.000_R0 [DIRS 182986], which contains the Post Implementation Verification Tests.

B2.2 V4.042 AND VE1.003 RECORDS PACKAGE

Reference Figure B-1, Block 2—Block 2 is on Figure B-1 to clearly indicate which versions of the model were used for this activity. The justifications for the versions used are discussed in Section 7.2.

B2.3 TSPA-LA MODEL POST IMPLEMENTATION VERIFICATION TESTS: OUTPUT DTN: MO0708TSPAPOST.000_R0 [DIRS 182986]

Reference Figure B-1, Block 3—This DTN contains the model cases and supporting checking documentation for the post-implementation verification tests discussed in Section 7.2.

B2.4 PLOTS AND FIGURES FOR THE TSPA-LA DOCUMENT: OUTPUT DTN: MO0709TSPAPLOT.000_R0 [DIRS 183010]

Reference Figure B-1, Block 4 and Figure B-2 Block 109—This DTN contains the official version of the sigma plot files for all the plots used in this document. In addition, any checklists used for checking of the plots will also be included.

B2.5 TSPA-LA PARAMETER SENSITIVITY ANALYSIS: OUTPUT DTN: MO0709TSPASENS.000_R0 [DIRS 182982]

Reference Figure B-1, Block 5—This DTN contains analyses to evaluate the significant uncertain parameters in the TSPA-LA Groundwater and Eruptive Models that are documented in output DTN: MO0709TSPAREGS.000_R0 [DIRS 182976].

B2.6 TSPA-LA MODEL CASES THAT EVALUATE NAVAL SPENT NUCLEAR FUEL: OUTPUT DTN: MO0707NAVYFUEL.000_R0 [DIRS 182991]

Reference Figure B-1, Block 6—This DTN contains the TSPA-LA Model cases, including checking documentation, that were run to evaluate the representation of naval spent nuclear fuel in the TSPA-LA Model as discussed in Section 7.5.3.

B2.7 TSPA-LA GW & E WITH FINAL DOCUMENTATION: OUTPUT DTN: MO0708GWEFINAL.000_R0 [DIRS 182977]

Reference Figure B-1, Block 7—This is the version of the TSPA-LA Groundwater and Eruptive Model (v5.000 and vE1.004) that is used to generate the GoldSim Player Files that supports the TSPA-LA. The differences between the GoldSim files in this DTN versus output DTN: MO0709TSPAREGS.000_R0 [DIRS 182976] are that this DTN contains only the master files for v5.000 and E1.004. These master files have been modified to update the explanatory text. The explanatory text that is in output DTN MO0709TSPAREGS.000_R0 [DIRS 182976] should be ignored, since it is not current. The enclosed master files have not been run; therefore, there are no results in this DTN. The value in providing un-run files is the files can be opened on most current model personal computers. The value in adding the documentation is an interested party can read the embedded text to obtain an overview of how the model is constructed. Also included is a data-only copy of the TSPA Input Database. The value of the data-only version of the TSPA Input Database is an interested party can review the input parameters to quickly

determine the numerical value of a parameter as well as the product that the value is documented within. In most cases, the product is an output DTN from a model and/or analysis report.

B2.8 TSPA GENERATED INPUTS AND POST-PROCESSED INPUTS: OUTPUT DTN: MO0708TSPAGENT.000_R0 [DIRS 183000]

Reference Figure B-1, Block 8—This DTN contains inputs that fall into two categories: (1) TSPA-LA Model-generated inputs and (2) Post-Processed inputs. TSPA-LA Model-generated inputs do not have any external inputs used to create the input values. Post-Processed inputs do have external inputs supplied by supporting Analysis and Model Reports. These external inputs must be Post-Processed for use in the TSPA-LA Model.

B2.9 DECAY OF WASTE FORM INVENTORIES FROM FINAL EMPLACEMENT TO CLOSURE: OUTPUT DTN: MO0707EMPDECAY.000_R0 [DIRS 182995]

Reference Figure B-1, Block 9—This DTN contains the GoldSim files used to decay the TSPA-LA waste form inventories from their time of emplacement to repository closure (i.e., the start of postclosure). The decayed inventory is an input to the TSPA-LA Model. This calculation is discussed in more detail in Section 6.3.7.1.2.1.

B2.10 PREWAP PROCESSING OF MSTHM FILES: OUTPUT DTN: MO0707PREWAPMS.000_R0 [DIRS 183002]

Reference Figure B-1, Block 10—This DTN contains the Multiscale Thermohydrologic Model (MSTHM) input files that are processed by PREWAP software and the resultant output files that are an input to the TSPA-LA Model. The DTN includes a description of how PREWAP was run. This calculation is discussed in more detail in Section 6.3.2.3.

B2.11 TSPA-LA REPRESENTATION OF DOE SPENT NUCLEAR FUEL: OUTPUT DTN: MO0707TSPADSNF.000_R0 [DIRS 182992]

Reference Figure B-1, Block 11—This DTN contains the TSPA-LA Model cases, including checking documentation, that were run to evaluate Categories 2 through 11 of U.S. Department of Energy spent nuclear fuel as discussed in Section 7.5.4.

B2.12 TSPA RESULTS FOR SEIS: DTN: MO0708TSPASEIS.000_R0 [DIRS 183009]

Reference Figure B-1, Block 12—This DTN contains the identical GoldSim files that are included in the Regulatory Compliance output DTN MO0709TSPAREGS.000_R0 [DIRS 182976] plus some additional supporting information such as the sigma plot files, and an evaluation of the important uncertain parameters.

B2.13 TSPA-LA MODEL (GROUNDWATER AND ERUPTIVE) USED FOR REGULATORY COMPLIANCE: OUTPUT DTN: MO0709TSPAREGS.000_R0 [DIRS 182976]

Reference Figure B-1, Block 13—This is the version of Groundwater (v5.000) and Eruptive (vE1.004) Models that is used for Regulatory Compliance that is presented in Section 8. This DTN contains all the modeling cases and supporting checking documentation.

B2.14 UZ KD CORRELATION MATRIX FOR THE TSPA-MODEL: OUTPUT DTN: MO0707UZKDCORR.000_R0 [DIRS 183003]

Reference Figure B-1, Block 14—This DTN contains two MathCad worksheets that are used to produce two unsaturated zone Kd (distribution coefficient (mL/g)) correlation matrices that are used as an input to the TSPA LA Model, as well as a description of the calculation. This calculation is discussed in more detail in Section 6.3.9.3.

B2.15 TSPA-LA PREPROCESSING OF PERCOLATION FLUXES FOR THE DRIFT WALL CONDENSATION SUBMODEL: OUTPUT DTN: MO0707PERCFLUX.000_R0 [DIRS 183001]

Reference Figure B-1, Block 15—This DTN contains the GoldSim files used to extract the percolation fluxes from the MSTHM files and provide one-dimensional percolation flux tables, which are inputs to the Drift Wall Condensation Submodel in the TSPA-LA Model (Section 6.3.3.2.3).

B2.16 TSPA LA WASTE PACKAGE AND DRIP SHIELD DEGRADATION: OUTPUT DTN: MO0707WPDRIPSD.000_R0 [DIRS 183005]

Reference Figure B-1, Block 16—This DTN contains the TSPA-LA Waste Package (WP) and Drip Shield Degradation Inputs.

B2.17 TSPA LOCALIZED CORROSION ANALYSIS: OUTPUT DTN: MO0709TSPALOCO.000_R0 [DIRS 182994]

Reference Figure B-1, Block 17—This DTN contains the GoldSim run that is used to confirm that localized corrosion is addressed by the Compliance Model that is documented in output DTN MO0709TSPAREGS.000_R0 [DIRS 182976].

B2.18 TSPA-LA MODEL GROUNDWATER AND ERUPTIVE STABILITY ANALYSIS: OUTPUT DTN: MO0709TSPASTAB.000_R0 [DIRS 182983]

Reference Figure B-1, Block 18—This DTN contains the GoldSim runs that confirm that the Compliance Model is statistically stable as discussed in Section 7.3.1.

B2.19 TSPA-LA MODEL VALIDATION AND ANALYSES CASES: OUTPUT DTN: MO0708TSPAVALI.000_R0 [DIRS 182985]

Reference Figure B-1, Block 19—This DTN contains GoldSim files that address the following subjects that support model validation:

- Single Realizations (Discussed in Section 7.7.1)
- Accuracy of Expected Dose (Discussed in Section 7.3.2)
- FEHM Particle Stability (Discussed in Section 7.3.5)
- Validation of the number of Timesteps (Discussed in Section 7.3.3)
- Spatial Discretization (Discussed in Section 7.3.4)
- Statistical Stability (output DTN MO0709TSPASTAB.000_R0 [DIRS 182983])

B2.20 TSPA LA MODEL IMPACT ANALYSIS: OUTPUT DTN: MO0709TSPALAMO.000_R0 [DIRS 182981]

Reference Figure B-1, Block 20—This DTN contains GoldSim Files that are evaluating errors and potential future improvements to the Compliance Model contained in output DTN MO0709TSPAREGS.000_R0 [DIRS 182976].

B2.21 CO-DISPOSED SEISMIC DAMAGE CALCULATION: OUTPUT DTN: MO0708CDSPSEIS.000 [DIRS 183007]

Reference Figure B-1, Block 21—This DTN contains the calculations related to the co-disposed WP damage frequency and damage (area) crack fraction distributions for both an intact and degraded state of the WP.

B2.22 SEISMIC FREQUENCY CALCULATION OF WASTE PACKAGE CONTAINERS, OUTPUT DTN: MO0708FREQCALC.000_R0 [DIRS 183006]

Reference Figure B-1, Block 22—In the TSPA-LA, to calculate the expected dose for the Seismic Ground Motion Modeling Case for 10,000 years, a number of simplifications were made in the implementation of the seismic consequences abstraction. Among these simplifications were omitting damage to transportation, aging, and disposal canisters and rupture and puncture of WPs. As documented in the TSPA-LA Section 7.3.2, the use of these simplifications is justified by analysis relying on calculations of the frequency of these various events. This DTN contains the calculations that support the analysis reported in Section 7.3.2.

B2.23 SIMPLIFIED TSPA ANALYSIS: OUTPUT DTN: MO0708SIMPLIFI.000_R0 [DIRS 182980]

Reference Figure B-1, Block 23—This DTN contains the source and executable code for the Simplified TSPA Analysis, the spreadsheets used to develop aspects of that model, input files required to execute the model, and output files for the four modeling cases executed with the model. This DTN is discussed in more detail in Section 7.7.2.

B2.24 TSPA-LA WASTE PACKAGE AND DRIP SHIELD STANDALONE: OUTPUT DTN: MO0709TSPAWPDS.000_R0 [DIRS 183170]

Reference Figure B-1, Block 24—A streamlined version of the v5.000 model file (v5.000_GS_9.60.100.gsm) was made to model the WP and DS degradation. This stand-alone model runs more quickly and is used to perform analyses of WP and DS degradation mechanisms and to generate plots for use in the TSPA-LA. Two versions of the standalone model were created, one for DS only degradation calculations and one for WP degradation calculations. The DS only model did not require the WAPDEG software and the run time was even more reduced.

B2.25 TSPA PERFORMANCE MARGIN ANALYSIS (PMA) GENERATED INPUTS AND POST PROCESSED INPUTS, CORROBORATIVE DTN: MO0708TSPAPROC.000_R0 [DIRS 182979]

Reference Figure B-2, Block 100—This DTN contains inputs that fall into two categories: (1) TSPA LA PMA generated inputs and (2) Post-Processed inputs. TSPA-LA PMA-generated inputs do not have any external inputs used to create the input values. Post-Processed inputs do have external inputs supplied by supporting analysis and/or model reports. These external inputs must be Post-Processed for use in the TSPA-LA Model.

B2.26 FRACTION OF WASTE PACKAGES CONTAINING STAINLESS STEEL CLADDING AND INITIAL ROD FAILURES FOR THE COMPLIANCE CASE: OUTPUT DTN: MO0702PAFRACSS.000_R1 [DIRS 181588]

Reference Figure B-2, Block 101—This DTN contains values for the percentage of WPs containing stainless steel and the fraction of rods assumed failed upon receipt at the repository.

B2.27 COMMERICAL SPENT NUCLEAR FUEL DISSOLUTION RATE PARAMETER DESCRIPTION FOR PMA CORROBORATIVE DTN: SN0707PMACSNFD.001_R0 [DIRS 183045]

Reference Figure B-2, Block 102—This DTN contains Excel spreadsheets describing the parameter distribution effective surface area long-term dissolution scaling factor (F1), and radiolysis scaling factor (F2).

B2.28 IN-PACKAGE CHEMISTRY ABSTRACTION FOR PERMANCE MARGIN ANALYSIS: CORROBORATIVE DTN: SN0704PMAIPCAB.001_R1 [DIRS 182602]

Reference Figure B-2, Block 103—This DTN contains the in-package chemistry abstraction files for the TSPA performance margin analysis. They are used to predict ph and ionic strength in the pore water of degradation products inside commercial spent nuclear fuel and co-disposed WP.

B2.29 SATURATED ZONE FLOW AND TRANSPORT ABSTRACTION FOR THE PERFORMANCE MARGIN ANALYSIS: CORROBORATIVE DTN: SN0704PMASZFTA.001_R1 [DIRS 184395]

Reference Figure B-2, Block 104—This DTN contains input, output, and radionuclide breakthrough curves from the Saturated Zone Flow and Transport Abstraction Model and parameters for the Saturated Zone 1-D Transport Model.

B2.30 V4.044 FROM RECORDS PACKAGE

Reference Figure B-2, Block 106—This records package is the same records package described in Section B2.1.

B2.31 COMPLIANCE MODEL TSPA-GENERATED DTNS

Reference Figure B-2, Block 107—This block represents the DTNs listed from Figure B-1. The contents of each of these DTNs are described in their respective sections.

B2.32 PERFORMANCE MARGIN ANALYSIS: CORROBORATIVE DTN: MO0709MARGANAL.000_R0 [DIRS 182978]

Reference Figure B-2, Block 108—This DTN contains all the runs used for the Performance Margin Analysis.

B2.33 NEW EXTENDED-RANGE SEEPAGE LOOK-UP TABLE FOR SEEPAGE INTO 5.5-M-WIDE CENTER PORTION OF COLLAPSED DRIFT PLUS SUPPORTING FILES: CORROBORATIVE DTN: LB0704PASEEP02.001_R1 [DIRS 181093]

Reference Figure B-2, Block 110—This DTN contains a seepage look-up table that gives seepage results (i.e., seepage percentage and seepage rate) as a function of seepage-relevant parameters capillary strength, permeability, and percolation flux.

B2.34 UZ TRANSPORT MODEL, UNCERTAINTY DISTRIBUTION PARAMETERS AND FEHM FILES FOR PMA ANALYSIS: CORROBORATIVE DTN: MO0704PAUZFEHM.000_R0 [DIRS 182790]

Reference Figure B-2, Block 111—This DTN contains the PMA UZ Transport Model FEHM files.

B2.35 GLASS DEGRADATION MODEL FOR PERFORMANCE MARGIN ANALYSIS (PMA): CORROBORATIVE DTN: SN0704PMAGDEGM.001_R2 [DIRS 183955]

Reference Figure B-2, Block 112—This DTN contains a revised expression for calculating releases of radionuclides from high-level radioactive waste glass as it dissolves when contacted by water. Release rates for radionuclides are calculated as the product of three terms:

- Surface area of glass contacted by water
- Glass dissolution rate
- Mass Fraction of each radionuclide in the glass

B2.36 ALTERNATIVE UNCERTAINTY EVALUATION FOR THE SOLUBILITIES OF PUO2 (HYD, AGED), NPO2, NP2O5, NANPO2CO3, SCHOEPITE, NA-BOLTWOODITE, AND NA4UO2 (CO3)3, CORROBORATIVE DTN: SN0704PMASOLUB.001_R1 [DIRS 182787]

Reference Figure B-2, Block 113—This DTN contains spreadsheets and EQ3/6 input/output files used in the evaluation of alternative uncertainties for the solubility of NP(IV), NP(V), PU(IV), AND U (VI) solubility-controlling solids.

B2.37 SUPPORTING DATA AND CALCULATIONS FOR WATER BALANCE EVALUATION, CORROBORATIVE DTN: SN0704PMAWBCAL.001_R2 [DIRS 182335]

Reference Figure B-2, Block 114—This DTN contains supporting data files and excel spreadsheets for evaluation of water mass balance calculations.

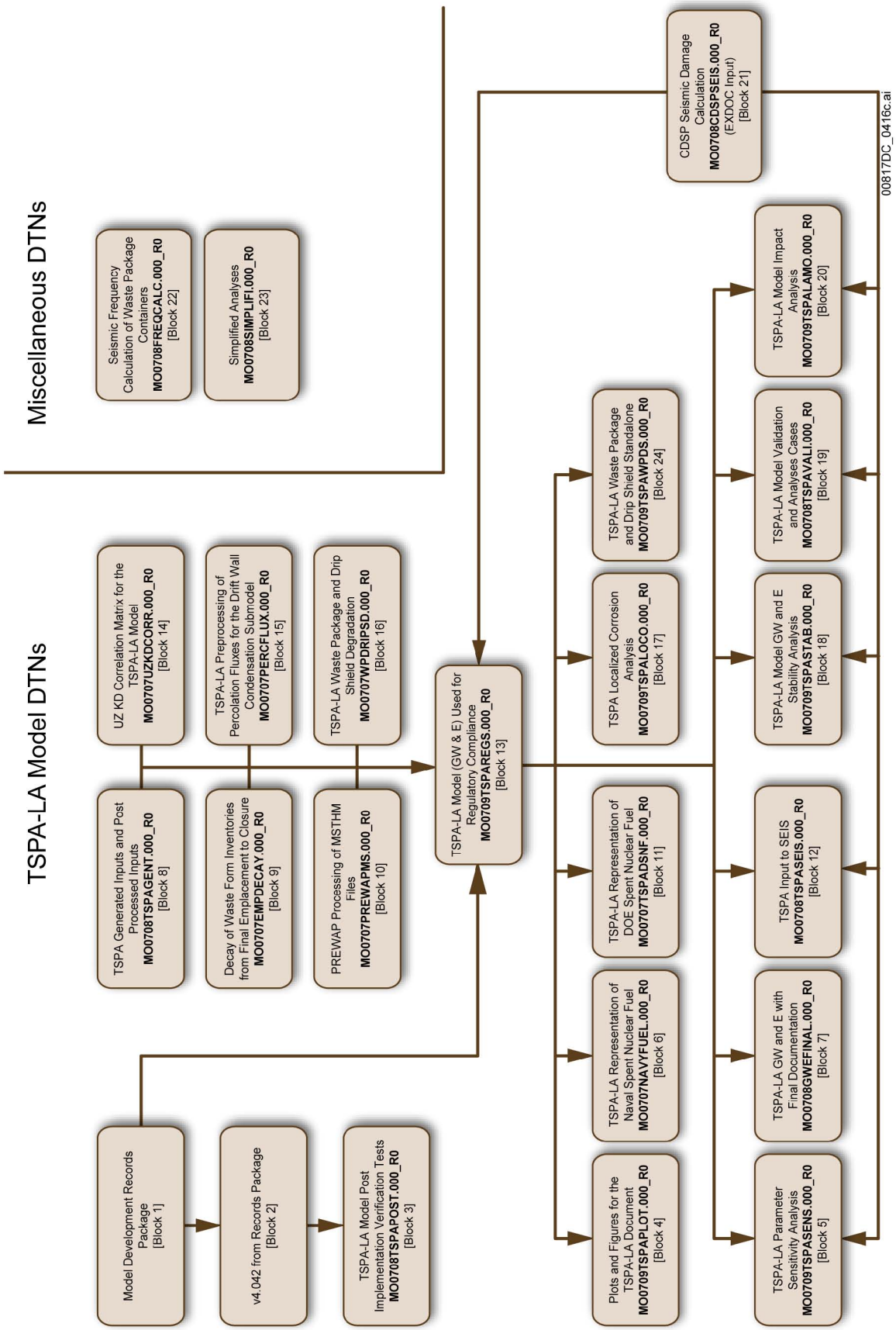

Figure B-1. Road Map of TSPA-LA Model Data Tracking Numbers

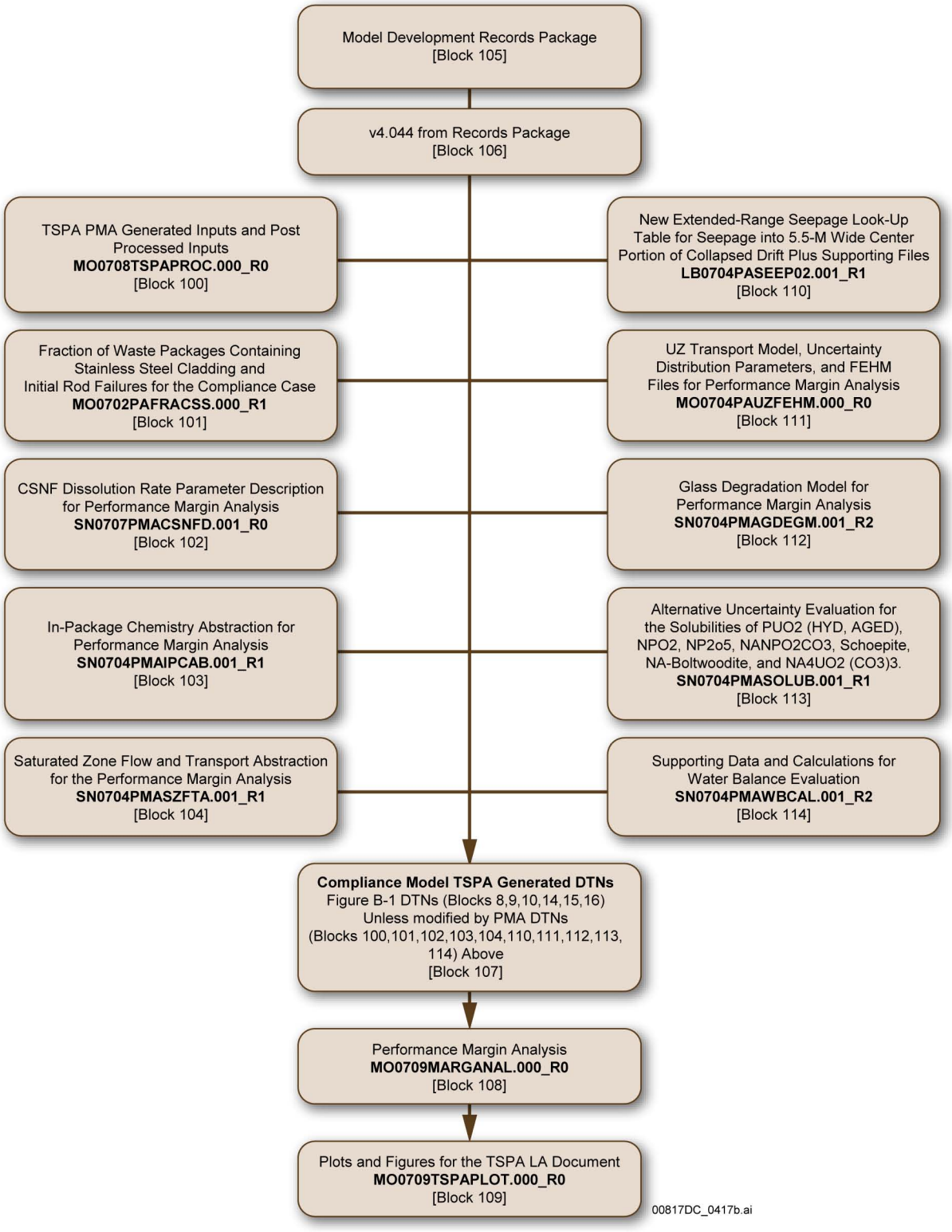

Figure B-2. Road Map of Performance Margin Analysis Data Tracking Numbers

APPENDIX C
PERFORMANCE MARGIN ANALYSIS

C.1 PURPOSE AND OBJECTIVE

The judicious use of conservative assumptions has played an important role in enhancing the confidence and defensibility of the Total System Performance Assessment for the License Application (TSPA-LA) Model. As discussed in Section 6.3, conservative assumptions in the TSPA-LA were generally introduced in the formulation of the TSPA-LA submodels and in the derivation of selected submodel parameter ranges in order to simplify the model formulations or compensate for the epistemic uncertainties that are difficult to quantify. Conservative assumptions must be used judiciously; more importantly, the use must ensure that the potential radiological risks are not underestimated. Individual conservatisms introduced at the submodel level can be attenuated differently to the system-level performance measures (i.e., projected annual dose). Thus, the objective of this Performance Margin Analysis (PMA) is to evaluate the significance of the major explicit and implicit conservatisms of the type identified in Section 5.0 and Section 6.3. Specifically, the PMA was designed to:

1. Confirm that when propagated individually through the TSPA-LA Model, the conservatisms introduced at submodel levels are conservative with respect to the total system performance measures (e.g., mean annual dose).

2. Quantify the extent to which the conservatisms, individually and collectively, overestimate the projected annual dose relative to the model projections presented in the performance demonstration (Section 8.0). The delta in annual dose between the TSPA-LA Model and the PMA is a measure of the performance margin.

3. Assess whether the evaluated conservatisms introduce any inappropriate risk dilution in the TSPA-LA results presented in support of the LA (e.g., reduce the peak total mean annual doses).

The PMA is comprised of an exclusive set of TSPA calculations from those conducted for the TSPA-LA (Section 8.0). The PMA calculations were intended to gauge both individual and collective impacts of major conservatisms embedded in the TSPA-LA model and thereby give a perspective on the potential performance margin included in the TSPA-LA dose projections.

Most of the conservatisms in the TSPA-LA Model were introduced during submodel development and/or derivation of parameter uncertainty characterizations as discussed in Section 6.3. For the most part, these conservatisms are implemented to bound the effects of processes that promote radionuclide release and transport. Other conservatisms were also introduced as a result of not taking credit for processes or conditions, which may potentially enhance containment and isolation. Additional submodels were developed for inclusion in the PMA for the specific purpose of evaluating implicit conservatism. It is important to state, that while these additional submodels and data were developed in accordance with applicable quality assurance (QA) requirements, in some cases they represent new models with limited technical foundation, verification, and validation. Consistent with the requirements of SCI-PRO-006, *Models,* Section 6.2.1.O, PMA submodels may use software (Section C3) that is controlled but not qualified.

The PMA was conducted by first modifying selected submodels and parameters of the TSPA-LA Model, including the addition of submodels and parameters for PMA, and then repeating a select set of modeling cases that were run for the TSPA-LA. The PMA results are compared to the mean annual dose results of the TSPA-LA Model. Thus, the PMA is one aspect of the validation work supporting the TSPA-LA Model (Section 7.0).

C.2 QUALITY ASSURANCE

Technical Work Plan for: Total System Performance Assessment FY 07-08 Activities (SNL 2008 [DIRS 184920]) describes applicable Quality Assurance requirements for the TSPA-LA. Consistent with the requirements of the TWP, this section details measures taken to ensure appropriate controls were in place for the PMA.

C2.1 CONFIGURATION MANAGEMENT

The development of the PMA required the same organization, control, and accountability that was necessary for the development of the TSPA-LA Model (Section 2.0). The PMA used the same configuration management processes that were used for the TSPA-LA Model. Those configuration management processes included software control, change control for making modifications to the TSPA-LA Model, control of inputs to the TSPA-LA Model, and error tracking and evaluation. Refer to Section 2.1 (Configuration Management) for details on these configuration management processes.

The PMA utilized software that was used for the TSPA-LA Model runs as well as additional software specifically for the PMA. All of the software used for the PMA was placed under Software Configuration Management (SCM) control. Refer to Section C.3 (Use of Software) for details on the controlled and baselined software used, qualification status, and any limitations on the use of software for the PMA.

Changes to the TSPA-LA Model for the purpose of the PMA were implemented upon receipt of written approval from the TSPA Department Manager, TSPA Model Calculations Lead, and TSPA Configuration Management Lead.

As in the TSPA-LA Model, the input parameter values used in the PMA are controlled through the TSPA Input Database. The database provides the parameter values and distributions necessary for the PMA. The TSPA Input Database categorizes, stores, and retrieves fixed and distributed values of the model parameters and allows authorized analysts to review and update the values. The TSPA Input Database has strict user controls that feature read and write access and audit trails that ensure the security, integrity, and traceability of the information used in the PMA.

C.3 USE OF SOFTWARE

Software that was necessary for the development and execution of the TSPA-LA Model is documented in Section 3.0. Three additional qualified software items, listed in Table C.3-1, were used specifically to support the development and execution of the PMA for the TSPA-LA. One was used to provide supporting information, and the other was directly implemented in the TSPA-LA Model and coupled to the GoldSim simulation software. These three items are

qualified and have been placed under the control of SCM per IM-PRO-003. The qualified software used to support the PMA, including qualified software used in the TSPA-LA, is listed in Table C.3-2, along with their unique software tracking numbers (STNs). Qualification documentation for each piece of software is available in SCM as well as the Records Processing Center. All qualified software was obtained from SCM, was appropriate for use in this analysis, and each was used within the software's range of validation.

TSPA-LA software was installed on TSPA-LA department computers in accordance with a qualified process. The installation process for each software code listed in Table C.3-2 was followed to ensure that there was a proper, qualified (i.e., in accordance with governing project procedures and controlled by SCM) installation by personnel authorized by SCM (Section 3.0).

The discussion below describes the three qualified software codes listed in Tables C.3-1 and C.3-2 that are in addition to or replaces qualified software used in the TSPA-LA Model (i.e., FEHM, TSPA_dB, and iTough). Each software discussion identifies the following information: (1) name of software; (2) brief description of software; (3) relationship to the PMA (i.e., used for PMA model development only, PMA model development and final component, or final component only); (4) location of software documentation; and (5) statement regarding use of software within the range of validation.

In addition, two unqualified software items were used in the development of the saturated zone (SZ) breakthrough curves that were used for post-processing, which was required to include the redox conditions in the SZ (Section C6.7). The two codes are listed in Table C3-3. Per SCI-PRO-006, *Models*, Section 6.2.1.O unqualified, non-exempt software may be used to corroborate model results. The PMA is a corroborative effort and the use of unqualified software is permissible.

C3.1 FEHM

C3.1.1 Description of Software

The finite element heat and mass transfer code (FEHM) used in the PMA documented in this report has the following general capabilities:

- Is called from another program that conforms to the external interface method and function calls described in the *User's Guide, GoldSim Probabilistic Simulation Environment* (GoldSim Technology Group 2007 [DIRS 183214])
- Provides GoldSim with the ability to perform calculations not included in the standard capabilities of GoldSim
- Calculates the transport of radionuclides through the unsaturated zone (UZ)
- Transfers information to and from the GoldSim software when the PMA is running.

C3.1.2 Relationship to the Performance Margin Analysis

The computer software code, which implements the UZ transport abstraction model for the TSPA-LA Model is based, is FEHM V2.24-01 [DIRS 179419]. The software used for the UZ PMA is FEHM V 2.25-00 (STN: 10086-2.25-00 [DIRS 182477]). The qualification status of this and other software is indicated in the electronic Document Input Reference System (DIRS) database. This version of FEHM has updates (relative to V2.24-01) that incorporate the colloid diversity model and the feature to enable the water table rise to be provided as input, either through the input file or through the interface between FEHM and GoldSim (GoldSim 2007 [DIRS 181903]).

C3.1.3 Software Documentation

The software qualification documents for the version of FEHM mentioned in Section C3.1.2 are listed in Table C3-4.

C3.1.4 Range of Validation

The range of validation for FEHM V 2.25-01 (STN: 10086-2.25-00 [DIRS 182477] listed in Section C3.1.2 is defined by the documented functionality (i.e., requirements) and range(s) of acceptable inputs. The requirements are located in the respective documents listed in Table C3-4. The range(s) of acceptable inputs are discussed in the respective design and user documents listed in Table C3-4.

C3.2 TSPA_INPUT_DBV2.2

C3.2.1 Description of Software

All versions of TSPA_Input_DB used in the TSPA-LA Model documented in this report are a Microsoft Access database that is used as a quality-controlled storage area for the TSPA-LA Model input parameters. The parameter values are maintained as originally entered (i.e., no manipulations or post-processing of the parameter values are performed). The database is capable of interfacing via open database connectivity (ODBC) for automated download to the TSPA-LA Model.

C3.2.2 Relationship to the Performance Margin Analysis

TSPA_Input_DB V2.2 (STN: 10931-2.2-00 [DIRS 181061]) was used for the TSPA-LA Model development and TSPA-LA Model validation and analysis cases. TSPA_Input_DB V2.2 (STN: 10931-2.2-01 [DIRS 181062]) was also used for the TSPA-LA Model validation and analysis cases. For the PMA, a new copy of the TSPA_Input_DB was created to store additional PMA input values and data files, TSPA_PMA_Input_DBv2.2. The PMA downloads input from both the TSPA-LA Model DB and the PMA DB. The TSPA_PMA_Input_DBv2.2 uses the same software (TSPA_Input_DB V2.2, STN: 10931-2.2-01 [DIRS 181062]); however, it is populated with the data that are specific to the PMA (Section 4.0).

C3.2.3 Software Documentation

The software documents for the versions of the TSPA_Input_DB mentioned in Section C3.2.2 are listed in Table C3-5. This documentation is the same for the TSPA_PMA_Input_DBv2.2 since it uses the same software as the TSPA_LA_Input_DBv2.2.

C3.2.4 Range of Validation

The ranges of validation for the versions of TSPA_Input_DB listed in Section C3.2.2 are defined by the documented functionality (i.e., requirements) and range(s) of acceptable inputs. The requirements are located in the respective requirements documents listed in Table C3-54. The range(s) of acceptable inputs is discussed in the respective design and user documents listed in Table C3-5. This range of validation is the same for the TSPA_PMA_Input_DBv2.2 since it uses the same software as the TSPA_LA_Input_DBv2.2.

C3.3 ITOUGH2 V5.0

C3.3.1 Description of Software

iTOUGH2 V5.0 (STN: 10003-5.0-00 [DIRS 160106]) is a computer program that provides inverse modeling capabilities for the TOUGH2 code.

C3.3.2 Relationship to the Performance Margin Analysis

iTOUGH2 V5.0 (STN: 10003-5.0-00 [DIRS 160106]) implemented for the Seepage Model for Performance Assessment (SMPA) simulations conducted to develop the PMA seepage look-up table for collapsed drifts, based on the same methodology and procedure as the TSPA-LA simulations for collapsed drifts described in *Seepage Model for PA Including Drift Collapse* (BSC 2004 [DIRS 167652]). Systematic seepage simulations were then conducted using iTOUGH2 V5.0 to calculate steady-state seepage rates for the 5.5-m wide center section of the 11-m wide collapsed drift for twelve realizations of heterogeneous permeability fields and 2,550 combinations of seepage-relevant parameters.

C3.3.3 Software Documentation

The software documents for the version of iTOUGH2 V5.0 mentioned in Section C3.3.2 are listed in Table C3-6.

C3.3.4 Range of Validation

The range of validation for the versions of iTOUGH2 V5.0 listed in Section C3.3.2 is defined by the documented functionality (i.e., requirements) and range(s) of acceptable inputs. The requirements are located in the respective requirements documents listed in Table C3-6. The range(s) of acceptable inputs is discussed in the respective design and user documents listed in Table C3-6.

C3.4 UNQUALIFIED SOFTWARE

Per SCI-PRO-006, *Models*, 6.2.1.O unqualified, non-exempt software may be used to corroborate model results. The PMA is a corroborative effort and the use of unqualified software is therefore permissible. The two codes used to support this analysis were placed under configuration control, and following the configuration management plan (Appendix C2) are included in the PMA output. These codes were only used in the PMA to generate the input data used for the Saturated Zone Transport Abstraction (Appendix C6.7).

C.3.4.1 SZ_Post_NonQ

SZ_Post_NonQ, Version 3.1 (STN: LL2000) is the code that was used for post-processing radionuclide transport simulation results to produce breakthrough curve files for irreversible colloids.

C.3.4.2 Reduce_Track_NonQ

Reduce_Track_NonQ, Version 00 (STN LL2001) is the code that was used to compute the average track length through the reducing zone of the SZ. The output of the software was used to determine the path length of the reducing zone for use in the one-dimensional SZ transport model.

C.4 INPUTS

This PMA utilizes the TSPA-LA Model with changes to certain inputs and models for the purpose of quantifying the performance margin inherent in the TSPA-LA Model. Therefore, most of the inputs are already given in Section 4, Volume I (Inputs), along with a description of how the inputs are managed. This section presents those inputs that have been changed from those used in the TSPA-LA Model and additional inputs necessary to support the PMA. Table C4-1 lists the input parameters to the TSPA-LA Model that have been changed or deleted for the PMA. Table C4-2 lists input parameters that have been added to the TSPA-LA Model for the PMA. The PMA contains both qualified and unqualified data. The data traceability, as described in Sections C4.1 (Performance Margin Analysis Input Database) and C.4.2 (Parameter Entry Forms), provides a mapping from the PMA parameters to the data source.

C.4.1 PERFORMANCE MARGIN ANALYSIS INPUT DATABASE

Section 4.7, Volume I, provides a summary of the TSPA Input Database. The PMA utilizes both the TSPA Input Database (TSPA_Input_DB, Output DTN: MO0708GWEFINAL.000 [DIRS 182977]) and a PMA-specific input database (TSPA_PMA_Input_DB, Corroborative DTN: MO0709MARGANAL.000 [DIRS 182978]). The TSPA Input Database and the PMA Input Database are used to support the PMA by providing the parameter values and distributions necessary for the PMA. Additional detail on its design and operation can be found in the software documents listed in Section C.3. The database is used to categorize, store, and retrieve fixed and distributed values of the PMA parameters.

C.4.2 PARAMETER ENTRY FORMS

All parameter names, values, and references used in support of the PMA are documented in Parameter Entry Forms (PEFs) and contained in the PMA Input Database. PEFs document both parameters that were downloaded from the PMA Input Database and parameters that were entered directly into the PMA. Table C.4-3 lists the direct inputs that are specific to the PMA and associates each with a reference (source) and a PEF number. The PEFs listed in Section 4.0 (Volume I) and in Table C.4-3 collectively contain all parameters used as input to the PMA. Each PEF references the specific locations of the parameters within a reference document or DTN to aid in the traceability of the direct inputs. The original signed PEFs are in the records package for this document; however, the TSPA Input Database and the PMA Input Database can be used to generate any PEF, as described in Section 4.7 (Volume I).

C.5 ASSUMPTIONS

The assumptions that support the TSPA-LA are documented either in Section 5, Sections 6.3 through 6.6, or in related process model reports. All these assumptions except those listed in Table C5-1 remain the same for the PMA. Those listed in the table were identified to be conservative and potentially significant to the overall performance of the repository. In the PMA, these assumptions were replaced with less conservative ones based on additional data and alternative model analyses or eliminated by development of process models or abstractions. It is important to reiterate, that while these additional submodels and data were developed in accordance with applicable quality assurance (QA) requirements, in some cases they represent models with limited technical foundation, verification, and validation. Consistent with the requirements of SCI-PRO-006, *Models,* Section 6.2.1.O, PMA submodels may use software (Section C3) that is controlled but not qualified. Detailed descriptions of the changes are documented in Section C.6.

C.6 PERFORMANCE MARGIN ANALYSIS DESCRIPTION

C6.1 METHODOLOGY

In the TSPA-LA Model projections presented in the performance demonstration (Section 8.0), postclosure performance is analyzed for time periods of 10,000 years and 1,000,000 years after closure. Because of the inherent uncertainties in making such long-term projections, the TSPA is largely based on a probabilistic modeling approach that accounts for uncertainties in parameters and in future conditions. In the PMA, the postclosure performance is analyzed over a selected set of modeling cases with the removal of a selected set of conservatisms included in the TSPA-LA. The objective of the PMA is to carefully and quantitatively evaluate the significance of these conservatisms that would be otherwise difficult to address given the range of uncertainties and long-term projections inherent in a model of this magnitude. The methodology used to accomplish this task included two primary steps:

- Identify the modeling cases that produce the most significant releases and dominate the projected doses

- Identify the sources of uncertainty and/or conservatisms that are most influential in producing the spread of the distribution of projected doses for these modeling cases.

The TSPA-LA includes four scenario classes: Nominal, Early Failure, Seismic, and Igneous. Detailed descriptions of the technical basis of these scenario classes, and their associated modeling cases, are presented in Sections 6.3 through 6.6 of Volume I. Section 8.0 presents the postclosure performance assessment results to support the LA for a nuclear waste repository at Yucca Mountain. The TSPA-LA demonstration of performance for the individual protection standard is based on the total mean annual dose computed by summing the results for seven modeling cases: (1) Nominal, (2) Waste Package EF, (3) Drip Shield EF, (4) Igneous Intrusion, (5) Volcanic Eruption, (6) Seismic GM, and (7) Seismic FD (Section 8.1). As required by the disposal standards for the TSPA-LA, the postclosure performance is quantified for time periods of 10,000 years and 1,000,000 years after closure. Likewise, the PMA was conducted over the 10,000-year and 1,000,000-year postclosure periods for comparison with the TSPA-LA. Drawing from the evaluation presented in Section 8.0, the PMA was exercised using five modeling cases (the Seismic GM Modeling Case includes the effects of the nominal processes when run for 1,000,000 years postclosure). The Volcanic Eruption Modeling Case was not evaluated in the PMA because none of the changes included in the PMA have any impact on the Volcanic Eruption Modeling Case. To demonstrate the performance margin inherent in the TSPA-LA, the mean of the projected total annual doses to the RMEI (i.e., sum of the expected annual doses projected for each scenario class) is used to evaluate the performance margin for the period within 10,000 years after disposal and over the period after 10,000 years through the period of geologic stability (Section 8.1, Equation 8.1.1-1). The PMA total mean annual dose was calculated replacing the selected set of TSPA-LA modeling cases (identified above) with PMA results. The TSPA-LA results for the Volcanic Eruption Modeling Case were combined with the PMA results to calculate the PMA total mean annual dose. The method used to calculate the total mean annual doses for the TSPA-LA Model and the PMA is presented in Appendix J. The total mean annual dose was evaluated to assess the potential performance margin embedded in the TSPA-LA Model (presented in Section C7).

The next step in the PMA process was to identify potentially conservative assumptions embedded in the TSPA-LA Model that may be significant contributors to the dose. Table C5-1 lists the conservative assumptions embedded in the parameters and submodels of the TSPA Model that were changed or modified for evaluation of their potential to impact the performance margin for the TSPA. The identification of these conservatisms came from the underlying model reports and from professional judgment of subject matter experts. In order to assess the effect of the listed conservatisms in the TSPA-LA Model, changes to submodels and parameter values were formulated. The changes to the TSPA inputs for the PMA primarily focus on the following:

- Include additional coupling between physical and chemical processes
- Reduce discontinuities in scale between submodels
- Represent the expected performance in existing models by reducing the uncertainty distributions in cases where conservative bounding values were assumed

- Include alternative conceptual models (ACMs) that have been screened out in favor of a more conservative model.

In the subsections that follow, each conservatism in the TSPA-LA Model that was assessed for the PMA is discussed along with the changes implemented in the TSPA-LA Model, the basis for the changes, and how those changes were implemented.

The PMA was conducted by first modifying selected submodels and parameters of the TSPA-LA Model. In some cases, the addition of new submodels and parameters was necessary for the PMA changes to the TSPA-LA Model. The second step was to repeat the selected set of modeling cases that were run for the TSPA-LA. The significance of the individual conservatisms was evaluated by examining the results for each modeling case (Section C.7, Results). The collective impact of the major assumptions was quantified by combining the PMA projections for annual dose for all modeling cases and then comparing the total mean dose curves against those of the TSPA-LA Model.

For the most part, the changes were incorporated in the submodels included in the TSPA-LA Nominal Modeling Case (Volume I, Section 1.5.1). More specifically, the changes for the PMA are embedded in the following model components:

- Drift-Scale UZ Flow (C6.2)
  - Reduction of seepage flux to waste package (WP) based on a reduced hydrologic cross-section for the representation of collapsed drift geometry (Drift Seepage Submodel)
- Waste Package and Drip Shield Degradation (C6.3)
  - Modification of corrosion rates based on fluoride ion concentration threshold instead of fixed and pervasive condition of aggressive corrosion
  - Implementation of a lower WP Alloy 22 (UNS N06022) general corrosion rate based on weight loss coupon data instead of crevice corrosion data
  - Implementation of stress corrosion cracking (SCC) of Alloy 22 using a higher representative yield stress threshold
  - Inclusion of a mechanistic approach to the calculated distribution of breached area as a result of localized corrosion on the WP outer barrier
- Engineered Barrier System (EBS) Flow (C6.4)
  - Inclusion of a detailed in-package water balance to account for the mass fluxes of water through the WPs
- Waste Form Degradation and Radionuclide Mobilization (C6.5)

  - Modification of the in-package chemistry model that accounts for the extent of material degradation and the availability of water inside a waste package
  - Inclusion of long-term degradation rate models for commercial spent nuclear fuel (CSNF) and high-level (radioactive) waste (HLW) glass waste forms
  - Inclusion of credit for initial clad failure fractions in place of assuming all cladding is failed at time of emplacement; applied to first 20,000 years only
  - Reduction of uncertainties for thermodynamic properties of neptunium, uranium, and plutonium

- UZ Transport Submodel (C6.6)
  - Enhanced matrix diffusion effects on radionuclide transport
  - Addition of colloid diversity model and retardation of irreversibly sorbed radionuclides
  - Addition of detailed model for water table rise

- SZ Transport Submodel (C6.7)
  - Addition of discrete interface for redistribution of the diffusive mass relaeased from the UZ matrix to SZ fractures
  - Addition of colloid diversity model and retardation of reversible and irreversibly sorbed radionuclides
  - Addition of enhanced radionuclide sorption in potential reducing zone
  - Implementation of an alternative distribution for flowing interval porosity
  - Inclusion of correlation between flowing interval porosity and groundwater specific discharge

- Seismic Scenario Class (C6.8)
  - Inclusion of an Alternative Conceptual Model for the crack-area density model in the Seismic Damage Abstraction.

It should be acknowledged that this list of modifications by no means is exhaustive; some other assumptions in the TSPA-LA Model may also benefit from additional detail or be conservative; for example, the assumption of complete WP failure in an igneous intrusion case and possible reduction of waste package damage due to the depth of the repository in a seismic ground motion case. The exclusion of these examples from the PMA is generally based on the consideration of lack of sufficient technical data for supporting such analyses. A discussion of each conservatism listed above and how it has been addressed with a modification to the above submodels follows.

C6.2 DRIFT-SCALE UNSATURATED ZONE FLOW

C6.2.1 Conceptual Model

In the TSPA-LA model, seepage abstraction accounts for the possible collapse of drifts in lithophysal units using a specific seepage look-up table (SNL 2007 [DIRS 181244], Section 6.4.2.4). This collapsed-drift look-up table was generated from seepage simulations conducted with the seepage model for performance assessment (BSC 2004 [DIRS 167652]), assuming a rubble-filled circular opening with an 11-m diameter as the final state after collapse. In the TSPA-LA seepage component, the total flow of liquid water from the fractured formation into the rubble-filled opening is considered seepage, independent of the actual seepage location, and subsequent TSPA-LA components, such as those for radionuclide mobilization and transport, use this total seepage rate. Use of an 11-m diameter results in a treatment that over-predicts the seepage flux over the 5.5-m drift, since the mostly gravity-driven flow in the rubble-filled opening would effectively prohibit contact of water with the WPs or waste forms for off-center seepage locations. This treatment of seepage was chosen in the TSPA-LA model to account for possible uncertainties in the seepage modeling approach for collapsed drifts.

The lithophysal rocks at Yucca Mountain are relatively deformable with a low compressive strength (SNL 2007 [DIRS 176828], Section 6.7.1). As a result, drifts located in lithophysal units are expected to collapse in case of severe, possibly repeated seismic events (SNL 2007 [DIRS 166107]). During collapse, either sudden or gradual, the rock mass above an underground opening is expected to disintegrate into a number of fragments that fall down and begin to fill the open space. Because there are large voids between the rock fragments, the bulk porosity of the fragmented rubble is expected to be much larger than the intact rock. Examination of the mean volume as presented in Section 6.6 and shown on Figure 6.6-7 shows that rock volume in the lithophysal units will accumulate fairly rapidly. When this occurs, the broken rock provides backpressure, which prevents further collapse of the rock mass (SNL 2007 [DIRS 166107], Section 6.4.2.5). After complete drift collapse, the original opening has increased in size, but is filled, either partially or fully, with fragmented rock blocks with sizes on the order of centimeters or decimeters with large voids between them. The solid wall rock surrounding the rubble-filled opening will remain largely intact, with a potential increase in permeability and a reduction in capillary strength due to the dynamic motion and the stress redistribution. For convenience, the rubble-filled opening is referred to as a 'collapsed drift,' although technically there is no drift after collapse. In collapsed drifts, seepage is defined as the flow of water from the intact fractured formation into the rubble-filled drift. The simulated profiles of collapsed drifts (see Appendix R of SNL 2007 [DIRS 166107]) were approximated, for seepage purposes, as rubble-filled openings of circular shape with a diameter of 11 m, which represents the largest diameter predicted.

For the TSPA-LA Model, seepage simulations were conducted for the selected collapsed-drift conditions, for the full set of seepage parameter combinations (with capillary strength values ranging from 100 Pa to 1,000 Pa, mean permeability values ranging from -14 to -10 (in $\log_{10} m^2$), and percolation flux values ranging from 1 mm/year to 1,000 mm/year, and a seepage look-up table was developed for use in the TSPA (BSC 2004 [DIRS 167652], Section 5). A capillary strength parameter of 100 Pa was assumed for the fragmented rock material within the collapsed drift (BSC 2004 [DIRS 167652], Section 5). Simulations conducted with the Seepage Model for

Performance Assessment indicated that, for the conditions at Yucca Mountain, the seepage into collapsed drifts is smaller than the percolation flux arriving at the drift crown (i.e., despite the changes in drift size and shape, most of the flux is diverted around the rubble-filled opening). However, the seepage rates have significantly increased compared to the intact-drift (SNL 2007 [DIRS 181244], Section 6.4.2.4.2). The larger the drift size, the more seepage can be expected because (1) the total amount of percolation flux arriving at the drift increases with the horizontal size, and (2) flow diversion is less effective for a larger drift.

As mentioned above, the total flow of liquid water from the fractured formation into the rubble-filled opening is considered seepage in the TSPA seepage component, independent of the actual seepage location. The possibility that only a fraction of the seepage water may actually come into contact with the WPs in the center of the drifts is currently not considered in the TSPA. The larger the horizontal extent of a drift, the higher the possibility that seepage water would bypass the center section of the drift in case seepage occurs at off-center ceiling locations.

Figure C6-1 schematically illustrates the potential migration paths of water within the rubble-filled opening depending on its seepage location along the ceiling. Water flow in the rubble is expected to be primarily gravity-driven, because of the coarseness of the rubble material and the large voids between them, corresponding to a weak capillarity. As a result, flow paths should be mostly vertical and highly focused (i.e., dispersion should be limited and the cross-sectional area of the flow should be rather small). This assessment is supported by laboratory experiments examining unsaturated flow behavior in packs of rock blocks with up to a 20 cm size (Tokunaga et al., 2005 [DIRS 180513]). These experiments demonstrated that single point infiltration of water at the top would branch out laterally no more than a few rock blocks, and that merging and splitting of flow paths would stabilize after about five rock layers in the vertical, to be followed by a dynamic stationary state exhibiting dominantly gravity-driven vertical flow. The observed final flux distributions were remarkably reproducible among numerous different rock packings and infiltration rates. Thus, one may assume that lateral dispersion of flow in rubble-filled collapsed drifts is limited and that the contact of seepage water with the WP or waste form should only be possible for seepage locations near the center of the collapsed opening.

It follows that the TSPA-LA Model for seepage—allowing all water entering a collapsed drift to influence drip shield (DS)/WP degradation and radionuclide mobilization/transport—is conservative (Section 6.3.3.1). A less conservative TSPA seepage model would be to assume that only water that enters the drift in the 5.5-m wide center section should be considered seepage (i.e., only then would it be considered in subsequent TSPA components with an impact on DS/WP degradation and radionuclide mobilization/transport). Water that seeps outside of this center section would be neglected because it would bypass drift shields and waste packages in the drift center. To evaluate the importance of the above conservatism, an alternative seepage look-up table for collapsed drifts, developed from revised Seepage Model for Performance Assessment simulations, was included in the PMA. The alternative (or PMA) look-up table gives seepage only when the seepage location is in the 5.5-m wide center section of the rubble-filled opening (Figure C6-1). The conceptual model of water fluxes within the EBS remains the same as the TSPA-LA Model, but with a reduced seepage flux.

The Seepage Model for Performance Assessment simulations conducted to develop the PMA seepage look-up table for collapsed drifts are based on the same methodology and procedure as the TSPA-LA simulations for collapsed drifts described in *Seepage Model for PA Including Drift Collapse* (BSC 2004 [DIRS 167652]). In both simulations, the seepage rate for a certain simulation case is calculated by adding up the seepage fluxes between rock and drift elements. In the PMA Seepage Model for Performance Assessment simulations, seepage is calculated by adding up only those rock-drift fluxes that occur in the 5.5-m wide center section of the 11-m wide collapsed drift. In contrast, the TSPA-LA Seepage Model for Performance Assessment simulations added up as seepage any rock-drift flux that occurred over the entire 11-m wide collapsed drift. The revision involves a change in the post-processing calculation for the seepage simulations, not a change in the simulation methodology and procedure. Thus, the technical basis for the Seepage Model for Performance Assessment simulations, including the model concept, numerical methods, discretization, assumptions, inputs, parameters, validation work, and limitations, has not changed from the description given in *Seepage Model for PA Including Drift Collapse* (BSC 2004 [DIRS 167652], Sections 3, 4, 5, and 6).

The revised Seepage Model for Performance Assessment simulation runs were conducted using various script files and model input files given in the data tracking number (DTN): LB0307SEEPDRCL.001 [DIRS 180511]. This DTN contains supporting files for mesh generation and seepage simulation for the TSPA-LA Seepage Model for Performance Assessment runs. Minor modifications were made to script files and model input files to accommodate the necessary changes. Systematic seepage simulations were then conducted using iTOUGH2 V5.0 to calculate steady-state seepage rates for the 5.5-m wide center section of the 11-m wide collapsed drift for twelve realizations of heterogeneous permeability fields and for 2,550 combinations of seepage-relevant parameters. These parameter combinations are the same as before; they include a variation of capillary-strength values (100 Pa to 1,000 Pa in steps of 100 Pa), mean permeability values (-14 to -10 in steps of 0.25, given in log10 with permeability in the unit m^2), and percolation flux values (1, 5, 10, 20, 50, and 100 through 1,000 mm/year in steps of 100 mm/year).

The seepage results from the PMA simulations, including all necessary supporting files for the iTOUGH2 model, are given in corroborative DTN: LB0704PASEEP01.001_Rev01 [DIRS 181223]. The necessary steps to conduct the simulations and perform some post-processing operations are explained in the Readme file and its Appendix provided in this DTN. Summary results of seepage rates and seepage percentages, for individual realizations as well as averaged over all realizations, are given in file LookupTableSeepageCollapsedDriftCenter.xls. Seepage rates and seepage percentages are provided for a reference drift section of a 5.5-m width (in the center of the collapsed drift) and 5.1-m length, the latter corresponding to the approximate length of a WP plus the 0.1 m spacing between canisters. The seepage rate gives the total amount of water seeping into the reference drift section per unit of time (in kg/yr/WP). The seepage percentage is defined as the ratio of seepage rate divided by percolation rate across a reference area multiplied by 100. Here, the reference area is given by the 5.5-m wide and 5.1-m long drift section over which seepage is calculated. Note that in the TSPA-LA collapsed-drift look-up table, seepage percentage was calculated using a reference area of 11 m wide and 5.1 m long (i.e., the total width of the collapsed drift was used). This is an important point when converting seepage rate into seepage percentage and vice versa. Example results from the

revised Seepage Model for Performance Assessment simulations are compared with the TSPA-LA seepage simulations for intact and collapsed drifts on Figure C6-2.

Figure C6-2 gives contours of the simulated seepage rate as a function of the capillary-strength parameter and the mean fracture permeability (in log10) for a selected percolation flux of 5 mm/year. In all cases, as expected, the seepage rate increases with decreasing capillary strength and decreasing permeability. Compared to the intact drift case, both collapsed drift simulations arrive at higher seepage rates because flow diversion is less effective for a larger opening. When comparing the two collapsed-drift cases, seepage collected over the 11-m total width of the rubble-filled opening is much higher than seepage collected over the 5.5-m wide center section. For example, for the parameter case with a permeability value of -12.5 in log10 m^2 and a capillary strength of 500 Pa, the average seepage rate into an intact drift is less than 5 kg/yr/WP, the average seepage rate into the 11-m wide collapsed drift is above 50 kg/yr/WP, and the average seepage rate collected over the 5.5-m wide center section of an 11-m wide collapsed drift is about 20 kg/yr/WP.

C6.2.2 Model Implementation

Section 6.3.3 details the Drift Scale UZ Flow Submodel for the TSPA-LA. Implementation of the PMA seepage model follows the same process described in Section 6.3.3 with the exception of the data contained in the Seepage Model for Performance Assessment file. The PMA seepage look-up table developed in Section C6.2.1 covers a percolation flux range from 1 mm/yr up to 1,000 mm/yr. As pointed out in *Abstraction of Drift Seepage* (SNL 2007 [DIRS 181244]), this upper limit may be exceeded in the TSPA calculations because revised infiltration estimates have resulted in larger percolation fluxes for certain climate and infiltration conditions. If a sampled parameter value within TSPA would fall outside of the Seepage Model for Performance Assessment range, the outlier value would need to be truncated to the respective upper limit. To avoid (or limit) such truncations, the PMA seepage look-up table developed above is modified to comprise an extended percolation flux range. The data manipulations necessary to develop these extended-range tables are identical to those previously performed for seepage look-up tables in corroborative DTN: LB0702PASEEP01.001_R0 [DIRS 179511], as documented in *Abstraction of Drift Seepage* (SNL 2007 [DIRS 181244]). The modification of the look-up tables is based on the notion that the resulting seepage percentages from the Seepage Model for Performance Assessment are identical for simulation cases that have the same ratio of percolation flux $q_{perc,ff}$ (in mm/yr) over permeability k (in m^2). This is because the steady-state capillary pressure and saturation conditions are determined by the ratio of percolation flux over permeability, not by the individual flux and permeability values.

The new extended-range look-up table for seepage into the 5.5-m wide center section of a collapsed drift is provided in corroborative DTN: LB0705PASEEP02.001 [DIRS 181093]. The new look-up table is given in file:

ResponseSurfaceSMPA_Collapsed_DriftCenter_ExtendedFlux.dat

In the PMA, this file replaces the collapsed-drift look-up table provided in DTN: LB0702PASEEP01.001_R0 [DIRS 179511]. Seepage rates for the PMA are interpolated from the new look-up table.

C6.3 WASTE PACKAGE AND DRIP SHIELD DEGRADATION

C6.3.1 Conceptual Model

Drip Shield General Corrosion Rates

The DS design utilizes Titanium Grade 7 for the plate and Titanium Grade 29 for the frame materials. The general corrosion degradation of the DSs is evaluated for both the underside and topside surface of the DS. General corrosion (or passive corrosion) is the uniform thinning of the material at its open-circuit corrosion potential (E_{corr}), and it can potentially occur when a liquid film exists on the surface of the DS. The titanium general corrosion model is based upon corrosion rates for Titanium Grade 7 determined by weight-loss measurement after 2.5 years of controlled exposure. The rate data supports two environmentally distinct corrosion rates, one for a relatively aggressive aqueous environment, the other corresponding to a rather benign environment. The detailed description of the corrosion model for the TSPA-LA can be found in *General Corrosion and Localized Corrosion of the Drip Shield* (SNL 2007 [DIRS 180778]).

The aqueous environments for DS corrosion are defined on the basis of dissolved fluoride concentrations. The 'steady-state' passive current density measurements of Titanium Grade 7 from a series of long-term (approximately 20 days) potentiostatic polarization tests showed that the passive corrosion rate of the alloy is low and not much affected by chloride ion concentration and pH; however, the passive corrosion rate increases significantly with an increase in the fluoride ion concentrations of water contacting the alloy (Brossia and Cragnolino 2001 [DIRS 162420], Figure 10; Brossia and Cragnolino 2004 [DIRS 180832], Figures 8 to 10). The critical (or minimum) fluoride ion concentration that causes a marked increase in the passive corrosion rate is about 0.5 millimolar (mM), and the passive corrosion rate increase levels off at about 0.01 molar (or 10 mM) fluoride ion concentration (Brossia and Cragnolino 2004 [DIRS 180832], Figure 9). The passive corrosion behaviors of Titanium Grade 2 and Grade 7 were about the same for the environments tested by the above investigators. Thus, for the PMA modeling purpose, an environmental condition that could lead to elevated fluoride ion concentrations in the water contacting DS is defined as an 'aggressive environmental condition' for the DS general corrosion. Any other environmental condition is defined as a 'benign environmental condition.' The critical (or minimum) fluoride ion concentration that causes a marked increase in the passive corrosion rate is set to 0.5 mM or 9.5 mg/L.

The chemical composition of the seepage water that enters the drifts will change in response to evaporation, mineral precipitation, or both. Throughout the thermal period (depending on the relative humidity in the drifts), evaporative concentration of seepage can occur in the EBS. Evaporation increases aqueous species concentrations, mineral precipitation, and the concentration of the most soluble components in brines. In accordance with the geochemical divide theory, the composition of the seepage water changes according to the sequence of minerals that should precipitate from that solution as a function of initial water composition, thermal conditions, relative humidity, and gas composition where the evaporation occurs (SNL 2007 [DIRS 177412], Section 6.3.3.1). An aggressive corrosion environment would only be present when the topside surface of the DS is exposed to dripping water with an evaporative concentration of seepage. However, for simplicity, the TSPA-LA Model applies the aggressive environment DS general corrosion rate to the topside surface of DSs when they are exposed to

seepage dripping, regardless of the changes in water chemistry due to the thermal evolution of the repository. The aggressive environment DS general corrosion rate is also applied to the topside surface of DSs for locations in the repository that are not exposed to dripping seepage. The benign environment DS general corrosion rate is applied to the underside surfaces of the DS at all locations. This treatment results in an earlier failure of DSs. Note that fluoride concentrations in the initial (i.e., with no evaporation) pore waters are all significantly lower than the critical value of 9.5 mg/L for aggressive corrosion (SNL 2007 [DIRS 177412], Table 4.1-3).

The temporal evolution of the physical and chemical environmental conditions within the waste emplacement drifts of the repository, including the DS and WP surfaces, is documented in *Engineered Barrier System: Physical and Chemical Environment* (SNL 2007 [DIRS 177412]). The near-field chemistry model defines four starting waters as representative of the potential range of the Topopah Spring pore-water compositions (SNL 2007 [DIRS 177412]). As water percolates down through from the surface, it interacts with the rock. The water-rock interactions modify the water composition. The normal compositions due to water-rock interactions are further modified by the repository heating as the water passes through the thermal field in the TSw. Ultimately, this thermally altered water is what enters the drift and controls the chemical conditions in the drift. Output seepage water compositions span the natural variability of pore-water compositions in repository units. The data in Table 4.1-3 of *Engineered Barrier System: Physical and Chemical Environment* (SNL 2007 [DIRS 177412]) show that fluoride concentrations in the 34 pore water samples from the Topopah Spring Tuff used to define the four starting waters all range from 0.36 to 4.8 mg/L, with the majority between 1-2 mg/L. Therefore, it is likely that the benign conditions will prevail in the repository after the radiation heat attenuates and the repository returns to near ambient conditions. In the PMA, the chemical environment for DS general corrosion is determined explicitly from the incoming seepage water compositions calculated by the EBS Chemical Environment Submodel (Section 6.3.4). For DSs whose topside surface is exposed to dripping seepage water, the general corrosion environment (e.g. aggressive or benign) is determined as a function of the seepage water chemistry. When the fluoride concentration exceeds 0.5 mM, an aggressive environment is assumed to be present on the topside of the DS. As seepage water compositions return to near ambient conditions, the fluoride concentration drops below 0.5 mM and the environment is switched to benign conditions.

Weight-loss Data for General Corrosion of the Waste Packages

The Alloy 22 general corrosion rates used in the TSPA-LA Model are represented by one of three cumulative distribution functions (CDFs) determined from the five-year crevice geometry samples (Section 6.3.5.1.3 and SNL 2007 [DIRS 178519], Sections 6.4.3). The observed general corrosion rates of the crevice specimens are higher than those of the 'plain' weight-loss specimens (SNL 2007 [DIRS 178519], Figure 6-22). This may have been caused by the difference in surface-polishing treatments between these two groups of test specimens (Wong et al. 2004 [DIRS 174800]). The weight-loss specimens were polished on both sides while the crevice specimens were polished only on one side. Thus, the unpolished surface of the crevice specimens retained the finishing given at the mill (by the primary metal producer) at the time of their immersion into the test electrolytes (i.e., the crevice specimens were tested without removing the mill-annealed oxide coating from their surface) (SNL 2007 [DIRS 178519], Section 6.4.3.2). It is possible that the removal of this mill-annealed oxide film from the

unpolished side of the crevice specimens during post-test specimen cleaning caused a greater amount of weight-loss for these specimens. This, in turn, could have resulted in derivation of higher general corrosion rates for the crevice specimens.

The PMA includes an alternative model using the corrosion rates of weight-loss samples to derive the R_o distribution for use in the general corrosion model of WP outer barrier (Alloy 22). These rates are documented in *General Corrosion and Localized Corrosion of Waste Package Outer Barrier* (SNL 2007 [DIRS 178519], Section 6.4.3.5.2). The weight-loss data is fit to a Weibull distribution using maximum likelihood estimators (i.e., using the same methods applied to the crevice sample data). The results of this fitting procedure found that the scale parameter, *b*, and a shape parameter, *c*, are 3.447 nm/yr and 1.318, respectively (SNL 2007 [DIRS 178519], Section 6.4.3.5.2 and Appendix VI). A plot of the general corrosion rate distribution resulting from fitting the five-year exposed weight-loss sample data and the data themselves is shown on Figure C6-3. A comparison of the weight-loss data with the crevice sample data shows that the weight-loss data show less corrosion relative to the TSPA-LA general corrosion model (Figure C6-4). This evaluation of the effects of the exclusion of the weight-loss data from the TSPA-LA was conducted using two alternative PMA modeling cases that evaluated the affects on the Seismic GM and Nominal Modeling Cases. The PMA results discussed in Section C.7.1 and Section C.7.2 do not include the weight-loss data in the WP general corrosion submodel calculations. Evaluation of this data is contained in Section C7.3, General Corrosion of the Waste Packages.

Localized Corrosion WP Failure Area

Localized corrosion is a phenomenon in which corrosion progresses at discrete sites or in a non-uniform manner (SNL 2007 [DIRS 178519], Sections 6.4.4). The area of the Alloy 22 WP outer barrier that is contacted by seepage is potentially subject to localized corrosion (SNL 2007 [DIRS 178519], Sections 6.3.5 and 6.4.4.8.3). In the TSPA-LA Model, it is assumed the maximum available area for localized corrosion (i.e., the area of the WP wetted by seepage) is the area of the WP damaged by localized corrosion (SNL 2007 [DIRS 178519], Section 6.3.5.2.2). Therefore, the entire surface area of the WP is removed as a barrier to water inflow and transport of radionuclides from a localized corrosion damaged WP.

In the PMA, the results of an ACM are used to establish a minimum WP area subject to crevice corrosion processes from localized corrosion (SNL 2007 [DIRS 178519], Sections 6.4.4.8.3). The ACM considers a minimum WP creviced surface area based on the WP-to-emplacement pallet contact area (SNL 2007 [DIRS 178519], Sections 6.4.4.8.3). The calculated minimum WP-pallet contact area is 1.924×10^4 mm^2 (SNL 2007 [DIRS 178519], Sections 6.4.4.8.3). Therefore, the minimum creviced area is about 0.05 percent of the total WP surface area of 36.074 m^2 for the transportation, aging, and disposal (TAD) canister-bearing WP configuration. The maximum available area for localized corrosion is the area of the WP wetted by seepage. In the absence of specific information regarding local environments on the WP, for the PMA the area of the WP failed by localized corrosion was assumed to have a log-uniform distribution that was sampled between the range of the entire WP surface area that is exposed to seepage (100 percent) and the calculated ACM minimum of 0.05 percent of the WP surface area (SNL 2007 [DIRS 178519], Section 6.4.4.8.3).

Alloy 22 Residual Stress Threshold

The damage abstractions for the seismic scenario will define the total damaged area on the WP barrier. The presence of high residual tensile stress has the potential to result in potential SCC. This combined mechanical-corrosion failure mechanism is expected to be a cause of damage to the WP and DS from impact processes caused by vibratory ground motions and by rockfall induced by vibratory ground motions. The areas that exceed the residual tensile stress threshold are considered damaged areas. The damaged or deformed area that exceeds a residual stress threshold is conceptualized to result in a tightly spaced network of stress corrosion cracks (SNL 2007 [DIRS 176828], Sections 6.1.4). Application of a residual tensile stress threshold for seismic failures is non-mechanistic in the sense that detailed calculations for potential crack initiation and potential crack propagation are not used to determine the actual failure time after a seismic event. Rather, a network of stress corrosion cracks is considered to immediately form once the residual tensile stress threshold is exceeded, providing potential pathways for radionuclide transport and release (SNL 2007 [DIRS 176828], Sections 6.1.4). The residual tensile stress threshold is often referred to as the residual stress threshold, with the understanding that the principal residual stress must always be tensile to initiate the potential for SCC. The structural response calculations for the WP exposed to seismic induced vibratory ground motions were evaluated for three values of the residual stress threshold for Alloy 22: 90 percent, 100 percent, and 105 percent of the yield strength of Alloy 22 (SNL 2007 [DIRS 176828], Sections 6.1.4). The residual stress threshold range for Alloy 22 is provided in *Stress Corrosion Cracking of the Waste Package Outer Barrier and Drip Shield Materials* (SNL 2007 [DIRS 181953], Section 6.2.2 and Table 8-1). The SCC threshold stress initiation criterion for Alloy 22 is defined as 1.05 YS(T) (at-temperature yield strength) (SNL 2007 [DIRS 181953], Section 8.1.1). The Alloy 22 residual stress threshold associated with the initiation of SCC was established by applying a safety factor to the maximum long-term applied stress without failure. Results obtained from the constant-load tests were used because the conditions were shown to be conservative relative to the expected repository environment and failure was not observed in this data (SNL 2007 [DIRS 181953], Section 6.2.2). In addition, to appropriately reflect uncertainty, a range from 0.9 YS(T) to 1.05 YS(T) with a uniform distribution between these values was selected for use in the TSPA-LA Model (SNL 2007 [DIRS 181953], Section 6.2.2). For the PMA, a range from 100 percent to 105 percent of the yield strength of Alloy 22 was used to evaluate damage to the WP outer barrier during a seismic event. The narrower range of uncertainty is justified for use in the PMA since the residual stress threshold for Alloy 22 was defined at 105 percent already including a safety factor of 2.0 (SNL 2007 [DIRS 181953], Section 6.2.2). The seismic damage abstraction calculates the probability of nonzero damage to a WP as a function of the sampled residual stress threshold. A lower residual stress threshold results in a greater probability of damage to the WP (SNL 2007 [DIRS 176828], Table 6-11 and Table 6-26). Application of the reduced range for residual stress threshold in the PMA will decrease the number of WP damaged during a seismic event.

C6.3.2 Model Implementation

Drip Shield General Corrosion Rates

The temporal evolution of the physical and chemical environmental conditions within the waste emplacement drifts of the repository, including the DS and WP surfaces, is documented in

Engineered Barrier System: Physical and Chemical Environment (EBS P&CE) (SNL 2007 [DIRS 177412]). The EBS Chemical Environment Submodel is described in Section 6.3.4. There are 396 in-drift precipitated salts (IDPS) look-up tables for seepage water composition spanning combinations of Pco_2 and temperature for each of four starting water types, 11 water-rock interaction parameter bins, and nine combinations of three Pco_2 values and three temperatures. The IDPS tables for TSPA-LA use are part of DTN: SN0701PAEBSPCE.001_R1 [DIRS 180523], and the guidance for using these inputs is provided in EBS P&CE (SNL 2007 [DIRS 177412], Section 6.15).

The local calculations of the EBS Chemical Environment Submodel determine the Pco_2 pH, $[Cl^-]$, and $[NO_3^-]$ of the crown seepage water. The TSPA-LA Model only requires pH, ionic strength, $[Cl^-]$, and $[NO_3^-]$ of the crown seepage water. The look-up tables included in the EBS Chemical Environment Submodel only include these parameters extracted from the chemical parameters contained in the 396 IDPS look-up tables (DTN: SN0701PAEBSPCE.001_R1 [DIRS 180523]). To correlate the DS general corrosion environment with the fluoride concentrations in the seepage waters, the fluoride concentration needed to be extracted for use in the PMA. Each IDPS look-up table is defined for a specific starting water type, temperature, and Pco_2. The tables are defined for Pco_2 values of 10^{-2}, 10^{-3}, and 10^{-4} bar and temperature values of 30°C, 70°C, and 100°C. There are 99 tables for all possible combinations for each of the four starting waters. For any combination of temperature and Pco_2 values, the fluoride concentration of the seepage water increases with decreasing relative humidity (e.g., evaporative water compositions prevail). Table C6-1 contains the minimum relative humidity below which the fluoride concentration exceeds 0.5 mM for the 99 possible combinations for each of the four starting waters.

To calculate the DS surface general corrosion environment for each repository subregion, the DS surface temperature, drift Pco_2, and DS relative humidity are fed into the look-up table. When the DS relative humidity exceeds the minimum value defined in Table C6-1, the benign environment for DS general corrosion is applied to the topside surface of the DS for all locations. When the relative humidity is below the minimum value, aggressive conditions are applied to the topside of the DS in all locations. For the underside of the DS, the general corrosion rate corresponding to the benign environment is applied for the entire simulation, identical to the TSPA-LA Model.

The EBS Thermal-Hydrologic (TH) Environment Submodel (Section 6.3.2) contains the DS temperatures and relative humidity values used to evaluate the DS corrosion environment for the PMA. The PREWAP_LA V1.1 software (PREWAP_LA V1.1, STN: 10939-1.1-00 [DIRS 181053]) creates environment-history files containing the WP and DS temperature and relative humidity histories as well as the drift wall temperature.

Weight-Loss Data for General Corrosion of the Waste Packages

For each percolation subregion, the WAPDEG V4.07 software simulates corrosion degradation of WPs by patch penetration (due to general corrosion) (Section 6.3.5.1.3). The model implementation is identical to the TSPA-LA Model, with the exception that only one rate distribution is chosen for each realization. This distribution is sampled by the WAPDEG V4.07 software for every patch on each WP. Two additional external files were added to the TSPA

PMA_dB, *WDlnR_ESC_WL_cdf* and *WDlnR_ASC_WL_cdf*, which represent the weight loss general corrosion rate CDFs (corroborative DTN: MO0708TSPAPROC.000 [DIRS 182979]). The first data set represents the scaled rate used in the WP/DS Degradation Submodel WP general corrosion calculations (Section 6.3.5), and the second data set is used to calculate the average WP thickness in the Seismic Damage Abstraction (Section 6.6). The development of the WAPDEG input vector and associated files is documented in corroborative DTN: MO0708TSPAPROC.000 [DIRS 182979]. This evaluation of the effects of the exclusion of the weight-loss data from the TSPA-LA was conducted using two alternative PMA modeling cases that evaluated the affects on the Seismic GM and Nominal Modeling Cases. The PMA results discussed in Section C.7.1 and Section C.7.2 do not include the weight-loss data in the WP general corrosion submodel calculations. Evaluation of this data is contained in Section C7.3, General Corrosion of the Waste Packages.

Localized Corrosion Waste Package Failure Area

The implementation of the localized corrosion WP failure area affects only the Drip Shield EF Modeling Case. However, localized corrosion of the WP outer barrier was simulated for all modeling cases in the Nominal, Early Failure and Seismic Scenario Classes. The Localized Corrosion Initiation and Propagation Submodel (Section 6.3.5.2.3) calculates the likelihood of localized corrosion on the WP outer surfaces which will lead to WP failure as a function of the EBS Chemical Environment, Seepage, and EBS TH Submodels. The primary output from the Localized Corrosion Initiation and Propagation Submodel is the fraction of CSNF WPs and CDSP WPs that fail by localized corrosion due to seepage, as a function of time, in each percolation subregion. These fractions are used to define the number of WPs that fail by localized corrosion during the simulation time and their average breach areas as a function of time. Localized corrosion is not included in the Nominal, Seismic GM and Waste Package EF cases because the DSs remain intact over the time frame in which the seepage water composition was calculated to potentially initiate localized corrosion. For the Igneous Scenario, both the DS and the entire WP is assumed to be destroyed; therefore, localized corrosion is not included.

Modifications to the TSPA-LA Model to include the PMA distribution of localized corrosion WP failure areas for the Drip Shield EF Modeling Case are outlined here. A new stochastic parameter was added to the model in the *Epistemic_Params* container (*f_WP_failed_area_EF_DS_PMA_a*) with a log-uniform distribution [0.0005-1]. The Drip Shield EF Modeling Case parameter *f_WP_Dam_EF_DS* in the EBS submodel container *\Global_Inputs_and_Calcs\ Global_Events \Global_EF\ Model_Input_EF* was modified to select the distribution for the fraction of the WP surface area failed from localized corrosion during a Drip Shield EF Modeling Case. These parameters feed the EBS Flow and EBS Transport Submodel calculations (Section 6.3.6 & Section 6.3.8) with the appropriate advective and diffusive areas used to calculate radionuclide release and transport.

Alloy 22 Residual Stress Threshold

The implementation of the Alloy 22 residual stress threshold involves both the Nominal and Seismic GM Modeling Cases. Modifications to the TSPA-LA Model to include the PMA value for the residual stress threshold of Alloy 22 are outlined here.

In the *Epistemic_Params* container, the Alloy 22 residual stress threshold parameter (*Stress_Thres_SCC_a*) was changed from a uniform distribution between 315.9 MPa to 368.55 MPa (equivalent to 0.90 to 1.05 stress threshold) to 351 MPa to 368.55 MPa (or 1.00 to 1.05 stress threshold values). These parameters feed the Nominal WP and DS Degradation Submodel calculations (Section 6.3.5) and the Seismic Damage Abstraction (Section 6.6).

C6.4 ENGINEERED BARRIER SYSTEM FLOW

C6.4.1 Conceptual Model

Water, whether in liquid or vapor state, can be transported in and out of a breached WP by both diffusive and/or advective percolation through failed areas on the outer layers of WPs. Accurate knowledge of these water mass fluxes is inherently important to constrain the amount of water that would interact with waste components. At an early stage of the repository, when a significant amount of heat generated by radiation still remains, this transport will be affected by the temperature gradient across WP barriers; that is, higher temperatures inside a WP will tend to prevent water vapor condensation onto waste components. The amount of water available inside a WP will ultimately determine the extent of waste degradation and the subsequent release and transport of radionuclides from the WPs. Waste degradation may modify the water potential inside a WP by releasing hydroscopic salts into water, affecting water vapor transport across the WP barriers. The objective of this PMA is to obtain an estimate of the quantity of water available inside a breached WP for waste degradation, and radionuclide transport. This analysis involves coupling the thermal evolution, waste degradation, and water transport. The amount of water is modeled as a function of relative humidity in the EBS, dripping rate, distribution of failed openings on the WP outer layers, and extent of waste degradation. In general, the model is somewhat similar to those developed for water or moisture transport in soils or in other analogous subsurface unsaturated porous media. Walton (1994 [DIRS 127454]) also applies a similar approach in an attempt to describe the potential effect of evaporation on the water chemistry interacting with WP components. The following processes are included in the model:

- In-package water condensation or evaporation as controlled by thermal evolution
- Water diffusion and advection through failed openings on WPs
- Water consumption by chemical reactions
- Capillary and osmotic effects on water saturation in alteration products
- Dripping water run-off onto WP surface.

In the TSPA-LA Model, the failure patches of the WP outer layer are assumed to have no resistance to advective seepage flows (SNL 2007 [DIRS 177407], Section 6.3.3.2.5). The TSPA-LA Model also assumes that the condensation of water vapor inside a WP is controlled by water sorption onto corrosion products (SNL 2007 [DIRS 177407], Section 6.3.4.3.2) and no water will be consumed by corrosion reactions (SNL 2007 [DIRS 177407], Section 5.4).

Different from the TSPA-LA model, the PMA water balance analysis: (1) assumes that a failure patch will be filled with porous corrosion products, which will provide additional resistance to water percolation into a breached WP; (2) accounts for water consumption by reactions; and (3) fully couples hydrologic effects (e.g., the sheet flow on the WP surface and capillarity effect of porous corrosion products) and chemical processes (e.g., water consumption and salt release by reactions; the depression of water activity with increasing dissolved salt concentration). The modeling system for in-package water balance is shown in Figure C6-5.

Water Potentials

It is assumed that water vapor inside a WP will remain in equilibrium with liquid water in pore space of waste degradation products, and the pore space of the alteration products will be the only space for holding liquid water. Additional liquid water beyond the capacity of pore space will percolate through the whole WP. This assumption is justified if the failed openings are distributed equally on both the upper and lower surface of the WP. This assumption maximizes the water flux out of the WP.

By analog to unsaturated soils, it is also assumed that the total water potential (ψ, in bars) inside the pores of waste degradation or metal corrosion products is determined by both the matrix potential of water (ψ_m, in bars) in the porous degradation products and the osmotic potential (ψ_o, bars) due to the presence of dissolved salts in the pore water (Nassar and Horton 1989 [DIRS 179400]):

$$\psi = \psi_m + \psi_o . \qquad \text{(Eq. C6.4-1)}$$

The matric potential is related to water saturation degree (s_w) by a water retention function. For simplicity, Campbell's function (Campbell 1974 [DIRS 179405]) is adopted:

$$\psi_m = \psi_e (s_w)^{-b} \qquad \text{(Eq. C6.4-2)}$$

where ψ_e and b are constants. ψ_e can be further related to the particle size of the porous material (Campbell and Shiozawa 1992 [DIRS 180398]): $\psi_e = 0.0003 d^{-1.5}$ in the unit of m (1 m water head = 0.0978 bar), where d is the mean particle diameter (mm). For a non-isothermal case, Equation C6.4-2 needs to be corrected for the effects of elevated temperature and dissolved salt on water surface tension. Since the capillarity and matric potential in an unsaturated porous medium are proportional to the surface tension of water (Dullien 1979 [DIRS 179404]) and also because the surface tension of water linearly decreases with the temperature and increases with dissolved salt concentration (m, molality) over the parameter ranges of interest (Belton 1935 [DIRS 180397]; Matubayasi et al. 1999 [DIRS 179401]), such effects can be captured by modifying Equation C6.4-2 into:

$$\psi_m = \psi_e (s_w)^{-b} [1 - \alpha (T_{in} - T_0)](1 + \beta m) \qquad \text{(Eq. C6.4-3)}$$

where α and β are constants; T_{in} is the temperature inside the WP (K); and T_0 is the reference temperature (298.15 K).

For a simple electrolyte solution, the osmotic potential of water can be calculated using the van't Hoff relation (Papendick and Campbell 1981 [DIRS 179398], p. 17):

$$\psi_o = \omega \eta m \rho_{water} R T_{in} \quad \text{(Eq. C6.4-4)}$$

where ω is the osmotic coefficient; η is the number of osmotically active species per molecule of solute (e.g., 2 for NaCl); and R is the gas constant (82.06 cm^3.atm/mole/K). The osmotic coefficient weakly depends on salt concentration (Papendick and Campbell 1981 [DIRS 179398], p. 17; Robinson and Stokes 1965 [DIRS 108567]):

$$\omega = 0.006m^2 + 0.0251m + 0.9102 \quad \text{(Eq. C6.4-5)}$$

(corroborative DTN: SN0704PMAWBCAL.001 [DIRS 182335]). Equation C6.4-4 has been widely used in modeling salt and moisture distributions in soils (Papendick and Campbell 1981 [DIRS 179398]). For simplification, NaCl is chosen to represent dissolved salts in WPs.

The total water potentials calculated from Equations C6.4-1 to C6.4-5 can then be related to the relative humidity inside a WP (RH_{in}) by (Harris 1980 [DIRS 179403]):

$$RH_{in} = \frac{\rho_{in}}{\rho_s(T_{in})} = e^{-\frac{\psi v_w^0}{RT_{in}}} \quad \text{(Eq. C6.4-6)}$$

where ρ_{in} is the water vapor density inside the WP (kg/m^3); ρ_s is the saturated water vapor density of pure water (kg/m^3); and v_w^0 is the molar volume of water (m^3/mole), which is assumed to be constant over the temperature range of interest. ρ_s (kg/m^3) can be calculated as a function of temperature T (K) by (corroborative DTN: SN0704PMAWBCAL.001 [DIRS 182335]; Kimball et al. 1976 [DIRS 179402]; and Nassar and Horton 1989 [DIRS 179400]):

$$\rho_s(T) = 10^{-3} e^{19.83 - 5000/T} \quad (\text{kg/m}^3). \quad \text{(Eq. C6.4-7)}$$

The analysis result for a special case indicates that water saturation is sensitive to the temperature difference across the outer layers of the WP and dissolved salt concentration. In this analysis, vapor density is assumed to be in equilibrium between the inside of the WP and drift. One degree difference in temperature may effectively reduce water vapor condensation on waste components (corroborative DTN: SN0704PMAWBCAL.001 [DIRS 182335]).

Water Consumption by Chemical Reactions

The reactions during the degradation of waste forms and WP materials consume water. Based on inventory estimates (SNL 2007 [DIRS 180506], Table 6-9), four major components are included in the calculation of water consumption: CSNF, N-reactor, HLW glass, and Stainless Steel Type 316. The degradation of each component can be represented by an overall stoichiometric reaction:

1 kg waste component i + n_i^w (mole) H_2O → n_i^s (m^3) solids + n_i^{salt} (mole) salt (Eq. C6.4-8)

where stoichiometric coefficients n_i^w, n_i^s, and n_i^{salt} can be evaluated with EQ3/6 (STN: 10813-8.1-00 [DIRS 176889]) calculations (Table C6-2).

Mass Balance Equations

The water balance inside a breached WP can be described by:

$$\frac{dQ}{dt} = \rho_{water}\left(F_{in}^{adv} - F_{out}^{adv}\right) + \frac{D\phi^{5/3}A}{L}(\rho_{out} - \rho_{in}) - M_w \sum_i n_i^w S_i R_i \qquad \text{(Eq. C6.4-9)}$$

with

$$Q = \frac{V_s \phi}{1-\phi}\left[s_w \rho_{water} + (1-s_w)\rho_{in}\right] + V_{void}\rho_{in} \qquad \text{(Eq. C6.4-10)}$$

where Q is the mass of water as either liquid or vapor inside the WP (kg); t is the time (year); V_s is the total volume of degradation products (m^3) inside the WP; ϕ is the porosity of degradation products, assumed to uniformly distribute over [0.35, 0.5]; ρ_{water} is the density of liquid water (kg/m^3); V_{void} is the volume of void space outside the fuel rods and corrosion rinds (m^3); F_{in}^{adv} and F_{out}^{adv} are the advective fluxes of liquid water into and out of the WP (m^3/year); ρ_{out} is the water vapor density outside the WP (kg/m^3) calculated by multiplying the relative humidity on the waste package outer surface to the saturated water vapor density at a given temperature; D is the molecular diffusivity of water vapor in air (m^2/year); A is the cross-sectional area of failure patches on the outer layers of the package for water vapor transport (m^2); L is the thickness of the outer layers (m); M_w is the molecular weight of water (kg/mole); S_i is the surface area of waste component i (m^2); and R_i is the degradation rate of component i (kg/m^2/year). The left-side term of Equation C6.4-9 represents the accumulation rate of water mass inside the WP. The three terms on the right side of the equation represent the water flux by advective flows, water flux by vapor diffusion, and water consumption rate, respectively.

The factor $\phi^{5/3}$ includes the effect of tortuosity (e.g., Nassar and Horton 1989 [DIRS 179400]). The molecular diffusivity of water vapor in air can be calculated by (Kimball et al. 1976 [DIRS 179402]):

$$D = 722 * (T_{in} + T_{out})/2/273.15)^{1.75} \ (m^2/\text{year}) \qquad \text{(Eq. C6.4-11)}$$

where T_{out} is the temperature in the drift (K). It is assumed in Equation C6.4-9 that no significant advective vapor flow will be induced by water evaporation or consumption. This assumption is justified for two reasons: First, for water vapor to advectively flow out, the gas pressure inside the WP must be higher than the ambient pressure. This would be possible only when a large volume of liquid water were introduced into a hot (>100°C) WP. However, this is unlikely because water seepage will not occur until the drift temperature is below the boiling temperature of water. Below the boiling point, it is not possible for evaporation inside the WP to generate air

pressures larger than those outside in the drift since the saturated water vapor pressure is always lower than 1 atm (Lide 2006 [DIRS 178081]). Second, water consumption by chemical reactions could create a pressure gradient between the inside and outside of the WP, which may induce an incoming advective gas flow. This is unlikely because water vapor partial pressure only accounts for a small fraction of total gas pressure (e.g., <10 percent for temperatures < 40°C) (Lide 2006 [DIRS 178081]), and the total pressure gradient created by reactions, if any, will be small in magnitude. This small gradient will be further compensated by the in-package accumulation of non-reactive air components that will be brought in by advective flows. Furthermore, as discussed below, with 10 percent of the WP surface failed, vapor diffusion can only transport up to 756 liters of water into a WP per year. Such a large diffusive flux is expected to overwhelm water-consuming reactions, resulting in an even smaller total pressure gradient.

Similarly, the mass balance for other quantities can be formulated as follows:

$$\frac{dV_s}{dt} = \sum_i n_i^s S_i R_i \qquad \text{(Eq. C6.4-12)}$$

$$\frac{dW_i}{dt} = -S_i R_i \qquad \text{(Eq. C6.4-13)}$$

$$\frac{dV_{void}}{dt} = \sum_i \left(\frac{1}{\rho_i^{waste}} - n_i^s \right) S_i R_i \qquad \text{(Eq. C6.4-14)}$$

$$\frac{dM_{salt}}{dt} = 1000(F_{in}^{adv} m_{seep} - F_{out}^{adv} m) + \sum_i n_i^{salt} S_i R_i \qquad \text{(Eq. C6.4-15)}$$

$$m = \frac{M_{salt}(1-\phi)}{\rho_{water} V_s s_w \phi} \qquad \text{(Eq. C6.4-16)}$$

where W_i is the total mass of material component *i* inside a WP (kg); M_{salt} is the total mass of salt dissolved in the pore water (moles); m_{seep} is the concentration of dissolved salt in the seepage water; and ρ_i^{waste} is the density of waste component *i* (kg/m^3). The initial values of V_s and M_{salt} are set to zero. The initial value of W_i is set to the initial inventory of material component *i*. The initial void space, V_{void}, is estimated to be 6.72 m^3 for a CSNF package and 8.49 m^3 for the co-disposed (CDSP) WP (corroborative DTN: SN0704PMAWBCAL.001 [DIRS 182335]).

Advective Water Influx (F_{in}^{adv}): A Sheet-Flow Model

For a dripping case, it is crucial to evaluate the advective water influx term (F_{in}^{adv}) in Equation C6.4-9. The evaluation assumes that:

- A drip falling on the WP surface will form a rivulet with a thickness of h (m) and a surface area of A_w (m^2), which will move down across the package surface.
- Upon the rivulet flowing over the failure openings of WP, a certain fraction of water will be able to percolate into the package through filling corrosion products, with the rest running off the package surface.
- The corrosion products filling the failure openings can be treated as a porous medium for water percolation. It should be recognized that little is known about the hydraulic permeability of corrosion products. Based on the observations on the rust of ancient ferrous artifacts exposed to atmospheric corrosion, porous corroded material could have the pore size ranging from a few nanometers to tens of microns with the porosity generally less than 15 percent (Dillman et al. 2004 [DIRS 171480], Table 7). For the PMA purpose, the hydraulic permeability of corrosion products is assumed to be 10^{-14} to 10^{-10} m^2, equivalent to that of silty sand (Freeze and Cherry 1979 [DIRS 101173]). The porosity of corrosion products is chosen to be 0.35 to 0.5. Since the values chosen here are likely higher than actual ones, the PMA water balance may overestimate the water flux percolating through WPs.

The velocity of a rivulet movement (v, m/s) can be described by (Ruschak et al. 2001 [DIRS 180747]; Lin et al. 2003 [DIRS 180748]):

$$v = \frac{\rho_{water} g h^2 \sin(\frac{\pi}{2} - \theta)}{3\mu} \qquad \text{(Eq. C6.4-17)}$$

where g is the gravity acceleration (9.81 m/s^2); θ is the angle as shown on Figure C6-5; and μ is the viscosity of water (Pa s = $kg \cdot m^{-1} \cdot s^{-1}$). The evolution of the rivulet can be described by:

$$\frac{d(A_w h)}{dt} = -\phi A_w f K_c^s \sin\theta \qquad \text{(Eq. C6.4-18)}$$

$$\frac{d\theta}{dt} = -\frac{v}{2\pi R_{wp}} \qquad \text{(Eq. C6.4-19)}$$

where f is the fraction of failed openings on the WP total surface area; K_c^s is the hydraulic conductivity of the corrosion products filling the failure openings at water saturated conditions (m/s); and R_{wp} is the radius of the WP. Equation C6.4-18 describes the volume change of water rivulet due to water percolation into the WP through the failure openings under the water head of $\sin\theta$ $(= L\sin\theta / L)$. Equation C6.4-19 converts the linear velocity of water rivulet to the radian velocity. For simplification, it is assumed that the thickness of water film will remain

approximately constant $\left(\frac{dh}{dt}=0\right)$ as the rivulet moves across the surface of the WP. The uncertainty related to this approximation is captured by uniformly sampling h over the range of 0.1 mm to 3 mm. This sampling range is constrained from both laboratory and natural analog observations (Katz et al. 1995 [DIRS 180396]; Alekseenko et al. 1998 [180383]). Then, Equation C6.4-18 reduces to:

$$\frac{d(A_w)}{dt}=\frac{-\phi A_w f K_c^s \sin\theta}{h}. \qquad \text{(Eq. C6.4-20)}$$

By combining Equations C6.4-17, C6.4-19, and C6.4-20, the following relation is obtained:

$$\frac{dA_w}{d\theta}=\frac{6\pi R_{wp}\phi A_w f K_p^s \tan\theta}{h^3}=\lambda A_w \tan\theta \qquad \text{(Eq. C6.4-21)}$$

with

$$\lambda=\frac{6\pi R_{wp}\phi f K_p^s}{h^3} \qquad \text{(Eq. C6.4-22)}$$

where K_p^s ($=\mu K_c^s/\rho_{water}g$) is the permeability of the corrosion products (m^2). By integrating Equation C.6.4-21 for A_w over [θ_0, 0], one obtains:

$$\frac{A_w}{A_w^0}=(\cos\theta_0)^{\lambda} \qquad \text{(Eq. C6.4-23)}$$

where A_w^0 is the initial area of the water film and θ_0 corresponds to the angle θ at the dripping location onto the WP surface. Assuming that the dripping is uniformly distributed over the footprint of the WP, one can calculate the fraction of dripping water that can enter a WP:

$$f_{in}^{adv}=1-\int_{\pi/2}^{0}(-\sin\theta_0)(\cos\theta_0)^{\lambda}d\theta_0=\frac{\lambda}{1+\lambda}. \qquad \text{(Eq. C6.4-24)}$$

For a given dripping rate Q_d (m^3/wp/year), the quantity of water that can enter a breached WP can then be calculated by:

$$F_{in}^{adv}=f_{in}^{adv}Q_d. \qquad \text{(Eq. C6.4-25)}$$

Equation C6.4-17 was originally established for a smooth surface but later extended to a rough surface (e.g., by correcting the water film thickness for surface roughness (Myers 2002 [DIRS 181017]). Given the maximum general corrosion rate of Alloy 22 (23 nm/year) (SNL 2007 [DIRS 178519]), the layer thickness of corrosion products on WP surfaces will remain less than 0.5 mm over at least the first 20,000 years. Thus, the validity of the proposed sheet-flow model is justified. Furthermore, the thickness of water film is generally found to be

on the scale of a few millimeters for various systems (Katz et al. 1995 [DIRS 180396]; Alekseenko et al. 1997 [DIRS 180383]). For the PMA, this thickness is chosen to range from 0.1 mm to 5 mm.

As illustrated on Figure C6-6, the fraction of seepage water that can enter a WP, calculated with Eq. C6.4-24, is relatively small, and the majority of the water will run off over the package surface. Consider an extreme case where the DS is completely neutralized and the maximum seepage rate is 1,000 liters/WP/year. For a typical water film thickness of 1 mm, the water influx F_{in}^{adv} is estimated to be < 1 liter/WP/year, which is small compared to the possible maximum vapor diffusion flux ($D\phi^{5/3}A\rho_d / L$) ~756 liters/WP/year under the same conditions with 10 percent of water package surface failed. Thus, vapor diffusion can potentially become a major source of water supply for waste degradation

Advective Water Out-Flux (F_{out}^{adv})

Assuming that the advective water flux is induced by the gravitational force only, the advective water flux out of the WP (F_{out}^{adv}) in Equation C6.4-9 can be calculated by:

$$F_{out}^{adv} = A_{out} K_c(s_w) \text{ for } s_w < 1 \qquad \text{(Eq. C6.4-26)}$$

where A_{out} is the opening area at the lower part of the WP surface. In reality, water drainage would create a gradient in the degree of water saturation that would prevent further drainage; thus, the water flux calculated from Equation C6.4-26 tends to be greater than would be expected. The hydraulic conductivity K_c is a function of water saturation s_w (Campbell 1974 [DIRS 179405]):

$$K_c = K_c^s (s_w)^{2b+3} \qquad \text{(Eq. C6.4-27)}$$

where b is the Campbell constant in Equation C6.4-2. For s_w = 1 (i.e., the pores of the degradation products are not sufficient for holding all incoming water), the extra water is assumed to percolate through the WP without any accumulation in the void space. From Equations C6.4-9 and C6.4-10, the advective flow F_{out}^{adv} can then be calculated by:

$$\begin{aligned} F_{out}^{adv} = F_{in}^{adv} &+ \frac{1}{\rho_{water}} \left[\frac{D\phi^{5/3} A}{L} (\rho_{out} - \rho_{in}) - M_w \sum_i n_i^w S_i R_i \right] \\ &+ \frac{1}{\rho_{water} \Delta t} \left[Q(t - \Delta t) - \frac{V_s \phi \rho_{water}}{1 - \phi} - V_{void} \rho_{in} \right] \end{aligned} \qquad \text{(Eq. C6.4-28)}$$

where $Q(t - \Delta t)$ is the mass of water accumulated at the previous timestep. The above formulation implies that, even for a non-dripping case (F_{in}^{adv} = 0), an advective out-flux is possible if the water inside a WP contains high enough hygroscopic salts, which may create a significant water vapor density gradient ($\rho_{out} - \rho_{in}$) across the outer layers of a WP barrier and

cause water condensation inside the package. This may happen for HLW packages since the HLW releases could generate a considerable amount of salt during dissolution, as indicated in Table C6-2.

Solid-Water Ratio

The volume ratio of solid to water ($r_{s/w}$) is an important parameter for establishing the chemical conditions inside a WP. This ratio can be calculated by:

$$r_{s/w} = \frac{1-\phi}{s_w \phi}. \qquad \text{(Eq. C6.4-29)}$$

After the thermal event, s_w will remain more or less constant and so will the solid-water ratio, possibly leading to relatively narrow in-package chemical conditions.

Temperature Difference across Waste Package Outer Barrier Layers

As discussed above in this section, the temperature difference between the inside and the outside of a WP may have a significant effect on the water potential inside the WP. For a steady-state heat conduction, this temperature difference (ΔT) can be estimated by:

$$\Delta T = T_{in} - T_{out} = \frac{1000 Q_h L}{2\pi D_c R_{wp}} \qquad \text{(Eq. C6.4-30)}$$

where Q_h is the linear thermal load (kW/m) and D_c is the thermal conductivity of the package materials (W/m/K). Equation C6.4-30 is derived by equating the linear thermal load to the heat flux across the package outer layer. As shown on Figure C6-7, the temperature difference across the outer barrier layers of the WP will be less than 2°K and diminish quickly after ~100 years. Note that the thermal load used in the calculation is the average value over the whole repository. These values are close to the thermal loads for CSNF WPs because they constitute a dominant fraction of the overall inventory. The HLW generally has a lower thermal load than the CSNF, and the temperature difference across the outer layers of HLW WPs is expected to be smaller. Therefore, in the PMA, the temperature difference (ΔT) between the inside and the outside of a WP is set to zero.

C6.4.2 Model Implementation

The water balance model presented in the previous section is solved iteratively using a Newton-Raphson method. The iteration algorithm is implemented in GoldSim with a looping container. The water balance model feeds (1) water saturation to the waste form and EBS water volume calculation, (2) advective water out-fluxes to both the In-Package Chemistry Submodel and Radionuclide Transport Submodel, and (3) the ionic strength to both the radionuclide solubility model and the colloid transport model.

Let us consider a discretization in time for Equation C6.4-9 using a first order backward difference in time. Let the solution be known at time level n and the solution be required at time level $n+1$. A fully implicit discretization of Equation C6.4-9 is

$$\frac{V_s\phi}{1-\phi}\left[s_w^{n+1}\rho_{water}+\left(1-s_w^{n+1}\right)\rho_{in}^{n+1}\right]+V_{void}\rho_{in}^{n+1}-\frac{V_s\phi}{1-\phi}\left[s_w^{n}\rho_{water}+\left(1-s_w^{n}\rho_{in}^{n}\right)\right]-V_{void}\rho_{in}^{n}$$

$$=\Delta t\left\{\rho_{water}\left(F_{in}^{adv}-F_{out}^{adv}\left(s_w^{n+1}\right)\right)+\frac{D\phi^{5/3}A}{L}\left(\rho_{out}-\rho_{in}^{n+1}\right)-M_w\sum_i n_i^w S_i R_i\right\} \quad \text{(Eq. C6.4-31)}$$

Similarly, a discretization of Equation C6.4-15 yields

$$M_{salt}^{n+1}=M_{salt}^{n}+\Delta t\rho_{water}\left(F_{in}^{adv}m_{seep}-F_{out}^{adv}m\right)+\Delta t\sum_i n_i^{salt}S_iR_i\,. \quad \text{(Eq. C6.4-32)}$$

Equation 6.4-16 is used to eliminate the variable m from Equation C6.4-32, yielding moles of salt as a function of water saturation

$$M_{salt}^{n+1}=\frac{M_{salt}^{n}+\Delta t\rho_{water}F_{in}^{adv}m_{seep}+\Delta t\sum_i n_i^{salt}S_iR_i}{1+\dfrac{\Delta t(1-\phi)F_{out}^{adv}\left(s_w\right)}{V_s s_w\phi}}\,. \quad \text{(Eq. C6.4-33)}$$

When the moles of salt are calculated from Equation C6.4-33, then the salt concentration is computed from Equation C6.4-16.

The discretized water balance (Equation C6.4-31) and water vapor density (Equation C6.4-6) are nonlinear algebraic equations in s_w^{n+1} and ρ_{in}^{n+1}. In order to solve these nonlinear system equations, together with auxiliary Equations C6.4-16 and C6.4-33, a Newton-Raphson method is applied. Consequently, the mass balance equation, Equation C6.4-10, is written as

$$F_1(s_w^{n+1},\rho_{in}^{n+1})=\frac{V_s\phi}{1-\phi}\left[s_w^{n+1}\rho_{water}+\left(1-s_w^{n+1}\right)\rho_{in}^{n+1}\right]+V_{void}\rho_{in}^{n+1}$$

$$-\frac{V_s\phi}{1-\phi}\left[s_w^{n}\rho_{water}+\left(1-s_w^{n}\rho_{in}^{n}\right)\right]-V_{void}\rho_{in}^{n}$$

$$-\Delta t\left\{\rho_{water}\left(F_{in}^{adv}-F_{out}^{adv}\left(s_w^{n+1}\right)\right)+\frac{D\phi^{5/3}A}{L}\left(\rho_{out}-\rho_{in}^{n+1}\right)\right.$$

$$\left.-M_w\sum_i n_i^w S_i R_i\right\}=0\,. \quad \text{(Eq. C6.4-34)}$$

The water vapor density equation, Equation C6.4-6, is written in the form

$$F_2\left(s_w^{n+1},\rho_{in}^{n+1}\right)=\rho_{in}^{n+1}$$

$$-\rho_s(T_{in})exp\left\{-\frac{v_w^0}{RT_{in}}\left[\frac{\psi_e}{(s_w^{n+1})^b}(1-\alpha(T_{in}-T_0))(1+\beta m)+\omega\eta m\rho_{water}RT_{in}\right]\right\}=0. \quad \text{(Eq. C6.4-35)}$$

The mole salt accumulated (Equation C6.4-33) and salt concentration (Equation C6.4-16) is updated at each Newton-Raphson iteration.

Let the solution vector be denoted

$$\mathbf{x}=\begin{pmatrix} s_w^{n+1} \\ \rho_{in}^{n+1} \end{pmatrix} \quad \text{(Eq. C6.4-36)}$$

and the vector equation written as

$$\mathbf{F}(\mathbf{x})=\begin{pmatrix} F_1(\mathbf{x}) \\ F_2(\mathbf{x}) \end{pmatrix}=\mathbf{0}. \quad \text{(Eq. C6.4-37)}$$

The Newton-Raphson iteration is

$$\mathbf{x}^{(k+1)}=\mathbf{x}^{(k)}-\mathbf{J}^{-1}(\mathbf{x}^{(k)})\mathbf{F}(\mathbf{x}^{(k)}) \quad \text{(Eq. C6.4-38)}$$

where the initial iteration is taken to be the value at the n-time level

$$\mathbf{x}^{(0)}=\begin{pmatrix} s_w^n \\ \rho_{in}^n \end{pmatrix}. \quad \text{(Eq. C6.4-39)}$$

The Jacobian matrix is

$$\mathbf{J}(\mathbf{x})=\begin{pmatrix} \frac{\partial F_1}{\partial s_w} & \frac{\partial F_1}{\partial \rho_{in}} \\ \frac{\partial F_2}{\partial s_w} & \frac{\partial F_2}{\partial \rho_{in}} \end{pmatrix}. \quad \text{(Eq. C6.4-40)}$$

The elements of the Jacobian matrix are computed as

$$\frac{\partial F_1}{\partial s_w}=\frac{V_s\phi}{1-\phi}(\rho_{water}-\rho_{in})+\Delta t\rho_{water}\frac{\partial F_{out}^{adv}}{\partial s_w}, \quad \text{(Eq. C6.4-41)}$$

$$\frac{\partial F_1}{\partial \rho_{in}}=\frac{V_s\phi}{1-\phi}(1-s_w)+V_{void}+\Delta t\frac{D\phi^{5/3}A}{L}, \quad \text{(Eq. C6.4-42)}$$

$$\frac{\partial F_2}{\partial s_w}=(F_2(s_w,\rho_{in})-\rho_s(T_{in}))\left\{-\frac{v_w^0}{T_{in}R}\left[-\frac{b}{s_w^{b+1}}\psi_e[1-\alpha(T_{in}-T_0)](1+\beta m)\right.\right.$$

$$+\frac{\psi_e}{s_w^b}(1-\alpha(T_{in}-T_0))\beta\frac{\partial m}{\partial s_w}+\omega\eta\rho_{water}RT_{in}\frac{\partial m}{\partial s_w}\Bigg]\Bigg\} \quad \text{(Eq. C6.4-43)}$$

$$\frac{\partial F_2}{\partial \rho_{in}}=1 \quad \text{(Eq. C6.4-44)}$$

where

$$\frac{\partial F_{out}^{adv}}{\partial s_w}=A_{out}K_c^s(2b+3)s_w^{2b+2} \quad \text{(Eq. C6.4-45)}$$

$$\frac{\partial m}{\partial s_w}=-\frac{M_{salt}(1-\phi)}{\rho_{water}V_s\phi s_w^2}+\frac{1-\phi}{\rho_{water}V_s\phi s_w}\frac{\partial M_{salt}}{\partial s_w} \quad \text{(Eq. C6.4-46)}$$

$$\frac{\partial M_{salt}}{\partial s_w}=-\Delta t\rho_{water}\left(F_{out}^{adv}\frac{\partial m}{\partial s_w}+m\frac{\partial F_{out}^{adv}}{\partial s_w}\right). \quad \text{(Eq. C6.4-47)}$$

Combining Equations C6.5-46 and C6.5-47, one obtains:

$$\frac{\partial m}{\partial s_w}=-\frac{\frac{M_{salt}(1-\phi)}{\rho_{water}V_s\phi s_w^2}+\frac{\Delta t(1-\phi)}{V_s\phi s_w}m(s_w)\frac{\partial F_{out}^{adv}}{\partial s_w}}{1+\frac{\Delta t(1-\phi)}{V_s\phi s_w}F_{out}^{adv}(s_w)}. \quad \text{(Eq. C6.4-48)}$$

The iteration is repeated until a convergence criterion is satisfied:

$$\max\left(s_w^{(k+1)}-s_w^{(k)},\rho_{in}^{(k+1)}-\rho_{in}^{(k)}\right)<\varepsilon. \quad \text{(Eq. C6.4-49)}$$

In the model simulation, ε is set to 10^{-8}, which is small enough since s_w varies from 0.05 to 1.0 and ρ_{in} from 0.0 to 1.2 kg/m^3.

C6.5 WASTE FORM DEGRADATION AND RADIONUCLIDE MOBILIZATION

C6.5.1 Conceptual Model

In-Package Chemistry

The TSPA-LA Model for in-package chemistry is documented in *In-Package Chemistry Abstraction* (SNL 2007 [DIRS 180506]). In the TSPA-LA, the pH inside a breached waste package is uniformly sampled over the range constrained from equilibrium with two major buffering mineral phases. The PMA, however, assumes that over the constrained range the in-package pH has a triangular distribution with the most probable value calculated as function of the extent of waste degradation, the pore water volume in waste degradation products, and the rate of water percolation through a waste package. As in the TSPA-LA Model, the predicted pH

is used to calculate concentrations of radionuclides and colloids. Unlike the TSPA-LA Model, the PMA in-package chemistry model no longer calculates the ionic strength inside a WP; this parameter is now provided by the water balance model (Section C6.4).

As in the TSPA-LA Model, the PMA in-package chemistry model is a batch reactor model that calculates the result of mixing the components within the waste-form cells of the WP with water and atmospheric gases to predict equilibrium solution compositions (SNL 2007 [DIRS 180506]). This model is applied to a total of three well-mixed reaction cells in two types of WPs: CSNF WPs and CDSP WPs. The CDSP WPs are represented by the WPs comprised of two multicanister overpacks (MCO) and two defense high-level waste (DHLW) glass logs. The three cells are:

1. CSNF cell 1. This cell contains all materials within and including the baskets inside the CSNF WP, excluding the guides. This includes the fuel basket assembly of neutron moderator material and thermal shunts, fuel basket tubes, and CSNF assemblies.

2. CDSP cell 1A. This cell comprises two containers of defense high-level waste (DHLW) glass and their canisters, as designed for the 2MCO/2DHLW WP.

3. CDSP cell 1B. This cell comprises two MCO containers of N reactor fuel and their canisters, as designed for the 2MCO/2DHLW WP.

The two CDSP cells are modeled separately because the CDSP waste forms are physically separated and their initial distribution within the WP is highly heterogeneous. Justification details are provided in *In-Package Chemistry Abstraction* (SNL 2007 [DIRS 180506], Section 6.3.1.1). Material volumes, properties, degradation rates, and surface areas are obtained from files *Rates CSNF Cell 1.xls, Rates 2DHLW cell.xls*, and *Rates 2MCO Cell 1b.xls* in DTN: SN0702PAIPC1CA.001_R2 [DIRS 180451]. Compositions of Stainless Steel 304B4 and HLW glass are taken from *304B4 Comp and Reaction.xls* and *CDSP_HLWGlass_Sensitivity r2.xls* in DTN: SN0702PAIPC1CA.001_R2 [DIRS 180451]. Other material compositions are obtained from Tables 6-4 and 6-6 of SNL (2007 [DIRS 180506]) and from Table 3 of the referenced document (CRWMS M&O 2001 [DIRS 153263]).

A modification of the *data0.ymp.R5* database, named *data0.R5f*, was used for all EQ3/6 simulations. Most of the modifications were incorporated in the *data0.R5f* database generated in *In-Package Chemistry Abstraction* (SNL 2007 [DIRS 180506], Section 6.3.1.1) and documented in DTN: SN0702PAIPC1CA.001 [DIRS 180451]. This database was further modified (but not renamed) by adding missing molar volumes for $NiMoO_4$ and Nontronite-H, two minerals that can account for a significant fraction of V_s in the PMA in-package chemistry simulations. The molar volume of $NiMoO_4$ is from Ehrenberg et al. (1995 [DIRS 180746]). The molar volume of Nontronite-H is assumed to be equivalent to the molar volume of Nontronite-Na, whose molar volume was already in the database. The modified database, *data0.R5f,* and its associated binary file, *data1.R5f,* are included in corroborative DTN: SN0704PMAIPCPM.001 [DIRS 180745].

The scope of the PMA in-package chemistry calculations is similar to that of the TSPA-LA model. The same three waste-form cells are considered for in-package chemistry (SNL 2007 [DIRS 180506], Section 1.0). The ranges of independent parameters, such as the partial pressure

of CO_2 (g) (10^{-4} to $10^{-1.5}$ bars), temperature (25°C), and flow rate (0 to >100 L/yr), are also similar. The primary difference between the two models is that in the PMA, liquid water is assumed to be restricted to the pores of the degradation products. The minimum ratio of the volume of degradation products, V_s, to the volume of liquid water, V_w, is set at V_s/V_p, where V_p is the volume of pore space. In these simulations V_s/V_p is 1.5, corresponding to a porosity of 0.4. Thus, V_s/V_w is 1.5 when the pores are fully saturated with water. The high range of V_s/V_w ($\geq$ 1.5) in the PMA in-package chemistry model is accomplished by decreasing the amount of water in the simulations.

The PMA calculations for in-package chemistry consist of two parts: The first part is used to construct the functional dependence of pH on waste degradation kinetics for the cases where vapor diffusion is a dominant mechanism for water transport through a breached WP; The second part is to establish the relationship between the water chemistry and the flux of liquid water that percolates the WP. The calculation results are documented in two corroborative DTNs: (1) SN0704PMAIPCPM.001 [DIRS 180745] contains the process model simulations and results, and (2) SN0704PMAIPCAB.001 [DIRS 182602] contains the abstractions.

Diffusion-Dominated Cases—For the diffusion-dominated cases, liquid influx (q) was set to zero in the EQ3/6 simulations. One liter of pure water (to simulate water from water vapor) was reacted at a fixed pCO_2 with cell materials for a period of time to allow degradation products to accumulate. The actual amount of time was immaterial because the equilibrium pH and ionic strength in this model are only a function of the following variables: (1) pCO_2, (2) the relative amount of materials degraded (defined by ratios of k_{wf}, k_{ss}, and k_{al}), and 3) the ratio of the volume of water in the cell, V_w, to the total amount of degradation. The total amount of degradation can be represented by the total volume of degradation products, V_s.

A simulated ten years of reaction and accumulation was used as a starting point from which V_s/V_w was adjusted. To adjust V_s/V_w, H_2O was incrementally removed from the cell. Because the PMA in-package chemistry application considers water only in the pores of the degradation products and the porosity of the degradation products is assumed to be 0.4, the useful range of process model outputs is limited to V_s/V_w greater than or equal to 1.5. At 1.5, the pores are saturated with water. Above 1.5, the pores are unsaturated.

The simulations were performed over large ranges of pCO_2, relative degradation rates, and V_s/V_w so that the effects of these variables could be captured in the vapor influx abstraction. Table C6-3 shows the ranges simulated for each cell. The k_{ss}/k_{wf} ratio was varied from low values to high values in each cell except for the 2MCO cell. Because stainless steel will degrade much more slowly than N reactor fuel, the maximum k_{ss}/k_{wf} ratio simulated was 0.01 in the 2MCO cell. More finely discretized values of k_{ss}/k_{wf} were simulated in the CSNF and 2DHLW cells where pH outputs were highly sensitive to k_{ss}/k_{wf}. H_2O removal in the simulations was terminated at high values of V_s/V_w (e.g., greater than 20) or when the ionic strength reached ~4 molal. Application of the model over this ionic strength range is sufficiently accurate for the purposes of the in-package chemistry model (SNL 2007 [DIRS 180506], Section 6.3.1.1).

Liquid-Advection Dominated Cases—Liquid influx occurs when q is finite. This rate was varied in the liquid influx process model simulations to determine its effect (in combination with variations in degradation rates and pCO_2) on pH. In addition, the composition of the liquid

influx was varied. For condensed water, pure water was used. For seepage, the SD9 pore water of the TSPA-LA model was used as the incoming liquid. The composition of the SD9 water is from pore water sample SD-9/1184.7-1184.8/UC in DTN: GS030408312272.002 [DIRS 165226].

With respect to V_s and V_w, the liquid influx model assumes all water is located in the pores of the degradation products, all pores are filled with water, and the porosity of the degradation products is 0.4. Thus, for the liquid influx simulations, V_s/V_w was maintained at 1.5. Because EQ3/6 requires a constant volume of 1 liter of water for steady-state flow-through calculations, initialization of the cell was more involved than for the vapor influx model. To achieve an initial V_s/V_w of 1.5, degradation was simulated until V_s increased to 1.5 liters. In addition, because degradation reactions consume H_2O, additional H_2O was added to maintain 1 liter of water. From this point, flow-through of condensate or seepage was initiated and kinetically simulated for approximately 9 pore volumes for a given pCO_2, liquid influx rate, and set of degradation rates. By 9 pore volumes, the pH and ionic strength essentially level off and the system is approximately at steady state, as shown in the example on Figure C6-8.

Simulations were performed over large ranges of pCO_2, relative degradation rates, and liquid influx rates so that the effects of these variables could be captured in the liquid influx abstraction. Table C6-3 shows the ranges simulated for each cell. The ranges of k_{ss}/k_{wf} simulated span the variation in pH generated from the reactions, as determined in the diffusion-dominated simulations. The values of q simulated are generally in the range where flushing of the cell with seepage or condensed water controls the steady-state pH and ionic strength.

The degree to which the reactions or liquid influx rate affects the steady-state pH and ionic strength is controlled by the ratio of kinetic reaction rates to the liquid influx rate. This ratio is generally known as the Damkohler number. High values of this ratio (e.g., >100 when dimensionless) imply that the concentrations of the pertinent aqueous components are controlled by the kinetic reactions (i.e., dissolution reactions of structural materials and waste forms), while low values (e.g., <0.01 when dimensionless) imply that concentrations are controlled by the composition of the liquid influx. There are additional processes that affect pH and ionic strength, namely the heterogeneous equilibrium reactions involving precipitation and dissolution of degradation products. These processes are assumed to be instantaneous; thus, regardless of the Damkohler number, the steady-state pH and ionic strength will be affected by these equilibrium reactions.

Time-invariant pH and ionic strength is calculated using the EQ3/6 flow-through mode when the Damkohler number is extremely low or extremely high. When it is extremely low, as in the liquid influx simulations performed using the parameter values in Table C6-4, the composition of the liquid influx and the equilibrium reactions control the pH. When the Damkohler number is extremely high, the time-invariant pH is approximated by the vapor influx model where the liquid influx rate is zero (Table C6-3). In the middle range between extreme Damkohler numbers, the flushing rate is low but relevant. In this range, a long period of time is required to achieve 9 pore volume flushes, the point at which steady state values are approximated. This large amount of time causes V_s to substantially increase. At the same time, V_w stays constant due to a limitation of the EQ3/6 flow-through mode. Because V_s substantially increases and V_w stays

constant in the simulations, the V_s/V_w ratio also substantially increases, which conflicts with the developed liquid influx model that sets the V_s/V_w ratio at 1.5. Consequently, estimates of pH and ionic strength between the two Damkohler number extremes are obtained by interpolation.

The PMA in-package chemistry outputs of the vapor influx and liquid influx models are not a function of time. The absolute amounts of materials degraded and volumes of degradation products and water in the cell (V_s and V_w) are immaterial to the pH and ionic strength calculations. The vapor influx model is essentially an equilibrium model. For a given combination of pCO_2 and relative degradation ratio of stainless steel to waste form, a unique pH and ionic strength are determined for each V_s/V_w analyzed. The liquid influx model is a steady-state model. As long as steady state is achieved, a unique steady-state pH and ionic strength can be determined for a given combination of pCO_2, liquid influx rate, and set of relative degradation rates.

Commercial Spent Nuclear Fuel Cladding

Cladding prevents the environment from interacting with the fuel pellets by limiting the water or moist air from contacting and interacting with the fuel pellets and reduces radionuclide transport by reducing the diffusion area. All CSNF currently in use in the United States (both pressurized water reactor and boiling water reactor fuel) consists of assemblies of Zircaloy tubing filled with UO_2 fuel pellets (SNL 2007 [DIRS 180616], Section 6.1[a]). The cladding is completely sealed and only fuel with failed cladding can interact with water or moist air. Some cladding could be damaged before it is received at the repository. The distribution of failed cladding as-received has an expected value of 0.1 percent (SNL 2007 [DIRS 180616], Section 4.0[a]). After repository closure, additional cladding failure will occur due to mechanical causes. Mechanical failure occurs from events associated with seismic activities such as rockfall or rock overburden. The seismic events and associated rockfall can occur at any time and are addressed in a specific seismic scenario (Section 6.6). However, in the TSPA-LA model, no credit is taken for CSNF cladding as a barrier in all scenario classes (Section 5.0, Assumption 5.1.3). The as-received condition of the CSNF cladding is used in the PMA to evaluate the impact of this assumption.

The PMA repository performance is evaluated using the set of scenario classes defined in Section 6.1.2. Unfailed (not perforated) cladding is assumed to remain intact for the 10,000-year regulatory period in the absence of mechanical damage mechanisms from seismic ground motion and/or rockfall since the intact cladding only starts to split when the cladding fails and only after waste package failure (SNL 2007 [DIRS 180616], Section 6.2.4]). Any further cladding failure is the result of physical processes, including mechanical damage to the intact cladding caused during seismic events (SNL 2007 [DIRS 180616], Section 6.2.3[a]). Therefore, applying the assumption that all CSNF cladding failed for the 10,000-year Nominal and Early Failure Scenario Classes in the TSPA-LA Model is bounding. In the PMA analysis, the as-received cladding condition is assumed to be the only cladding failed for CSNF for the Nominal and Early Failure Scenario Classes during the first 10,000 years postclosure. WP failures do not occur in the Nominal Scenario Class during the first 10,000 years postclosure; therefore, the assumption in the TSPA-LA Model that all cladding is failed has no impact on dose. In the Seismic GM Modeling Case, DSs do not fail during the first 10,000 years postclosure. The probability of CSNF WP failure under an intact DS with intact internals is nonzero only for large events (Section 6.6.1.2.2.2 and Figure 6.6-10(a)). The probability of occurrence of a large enough event

in the first 10,000 years postclosure is small since these types of seismic events occur, on average, every 23,000 years. In the Seismic FD Modeling Case, the WP failures are caused by the shearing of WPs (Section 6.6.1.1.2) and cladding is likely to be failed as well. The as-received failed fuel rods undergo instantaneous clad splitting when the WP fails. The exposed fuel is available for waste form degradation. No cladding credit is taken for stainless steel clad fuel. The as-received cladding condition and stainless steel cladding distribution is provided by *Cladding Degradation Summary for LA* (SNL 2007 [DIRS 180616], Section 6.2[a] and Section 7.0[a]).

Degradation Rate of Commercial Spent Nuclear Fuel

CSNF constitutes a major portion of the total waste inventory. The degradation rate of this waste form is therefore expected to have a significant impact on the overall performance of the Yucca Mountain repository. In the TSPA-LA model, this rate is calculated as a function of temperature, oxygen fugacity, total carbonate concentration, and pH (BSC 2004 [DIRS 169987]). In the PMA, the functional dependence on water chemistry remains the same as in the TSPA-LA model. However, the distribution range of the effective surface area of CSNF is modified, and two additional scaling factors are included to capture the effect of long-term dissolution and the decrease in radiolysis, based on the synthesis of literature data.

Dissolution Kinetics—Oxidative dissolution of CSNF undergoes numerous chemical and physical transformations. The factors that have major impacts on waste dissolution are listed in Table C6-5. The PMA specifically considers the following factors: the effective surface areas, the effect of long-term dissolution, and the changes in radiolysis. In the PMA, the matrix dissolution rate of CSNF is calculated as:

$$\log(F) = Log(A) - Log(f_1) - Log(f_2) + a_0 + a_1 IT + a_2.pCO_3 + a_3.pO_2 + a_4.pH \qquad \text{(Eq. C6.5-1)}$$

where F is the fractional dissolution rate of the fuel (d^{-1}); A is the effective surface area of the fuel (m^2/mg); f_1 is the scaling factor for the effect of long-term dissolution; f_2 is the scaling factor for the attenuation of gamma and beta radiations; IT is the inverse temperature (K^{-1}); pCO_3 is the negative base 10 logarithm of total carbonate (molar); and pO_2 is the negative base 10 logarithm of oxygen partial pressure (atm). The PMA uses the same functional form as the TSPA-LA model for the rate dependence on temperature, pCO_3, pO_2, and pH, and thus the last five terms in Equation C6.5-1 (a_0 through a_4) remain the same as in the TSPA-LA model. These five terms were determined from short-term and far-from-equilibrium flow-through tests with rates normalized to surface areas obtained either by geometric or Brunauer-Emmett-Teller (BET) methods (BSC 2004 [DIRS 169987]). The first three terms on the right side of Equation C6.5-1 are described below in this section.

Effective Surface Area (A)—The effective surface area refers to the portion of total surface area that is directly contacted by water and participates in fuel dissolution. The effective surface area is always less than the total surface area for several reasons. First of all, the spent fuel contains various impurities such as plutonium, zirconium, and molybdenum; these metal cations tend to accumulate on the surface of the spent fuel during dissolution and block reactive surface sites (Grandstaff 1992 [DIRS 113255]). Some elements in groundwater (e.g., calcium and silicon) can also exert a similar effect on a surface site (Santos et al. 2006 [DIRS 182015]; Santos et al.

2006 [DIRS 182052]). These impurities usually have high affinities for sorption to the dissolution surface and form a protective surface layer, which could result in a large decrease in dissolution rate (Wilson and Gray 1990 [DIRS 115085]). Furthermore, not all surfaces of fuel grains are accessible by reactants. In many cases, the rate of a dissolution reaction is limited by the diffusion of chemical species either toward or away from the reaction front, and the reaction front does not necessarily coincide with grain boundaries (Finch et al. 1999 [DIRS 127332]). In addition, fuel dissolution takes place at a solid-water interface; as the water saturation decreases, the contact area between fuel and water also decreases (Kuechler and Noack 2007 [DIRS 182054]; Sverdrup and Warfvinge 1988 [DIRS 182056]). For all these reasons, accurately determining the effective surface area for a chemical reaction, particularly in environments with variable degrees of saturation, is generally subject to large uncertainties.

In the TSPA-LA Model, the effective surface area is determined from a combination of geometrical calculation, particle size distribution, BET measurements, and fractional release measurements (BSC 2004 [DIRS 169987]). The TSPA-LA Model chooses the geometric-specific surface of the cracked fragments in irradiated pellets as a most probable value for the effective surface area. The lower and upper limits are constrained from the fractional release measurements and particle size distributions, respectively. The distribution of log (A m^2/mg) for the TSPA-LA model is assumed to be triangular with a low of -7.3, apex of -6.7, and maximum of -5.4. This distribution is conservative, especially for the upper limit, because it assumes that all the surfaces of individual fuel fragments are accessible by reactants. Such scenarios are unlikely, since fuel dissolution takes place at a reaction front rather than pervasively on the surface of each individual particle, as discussed above.

To remove these conservatisms in the TSPA-LA model, the PMA derives the effective surface area from the fractional release rate measurements in fuel rod segment tests and further assumes this to be the most probable value. This assumption is reasonable because the fractional release rate is a parameter that is directly measured in leaching experiments. The reliability of these measurements has been confirmed by their consistency with the fuel fragment tests (BSC 2004 [DIRS 169987], Tables 6-10 and 6-11). The effective surface area therefore should be chosen to reflect these measurements. Second, dissolution rates depend on the physical configuration of the fuel, and the rod segment tests may more accurately mimic the likely state of spent fuels in a breached WP.

Based on the above discussion, the PMA used the following equation to calculate the effective surface area for spent fuel dissolution:

$$A = A_s . s_w \qquad \text{(Eq. C6.5-2)}$$

where A_s is the effective surface area under water-saturated conditions, and s_w is the water saturation in spent corrosion products calculated in the Water Balance Model (Section C6.4.1). The distribution of log (A_s) is assumed to be right triangular with values at the low and apex end of -7.3 and at the upper bound of -6.7. A right triangular distribution is assumed here as to weigh more on the low value as it was determined from leaching experiments. The upper limit is chosen to be the geometric-specific surface of the cracked fragments in irradiated pellets. A relationship similar to Equation C6.5-2 has been proposed for modeling mineral dissolution in

soils (Kuechler and Noack 2007 [DIRS 182054]; Sverdrup and Warfvinge 1988 [DIRS 182056]).

Scaling Factor for Long-Term Dissolution (f1)—The dissolution rate of spent fuel in a leaching test generally decreases with time (Hanson et al. 2004 [DIRS 182008]; Jégou et al. 2004 [DIRS 182066]). This decrease could be caused by the accumulation of impurities or the formation of coating layers on the dissolving surface of the fuel. For example, precipitation of a schoepite layer may slow down spent fuel dissolution (De Windt et al. 2006 [DIRS 182065]). Hanson et al. (2004 [DIRS 182008]) conducted flow-through dissolution tests using solutions with pH in the range 2 to 7 on a moderate burnup Light Water Reactor spent fuel. They found that the release rates of cesium, strontium, technetium, and plutonium all systematically decreased with time. Over a testing period of 140 days, the release rates for Cs were reduced by a factor of 3 to 10 (Hanson et al. 2004 [DIRS 182008], Figure 1). Therefore, for the PMA, it is recommended that the scaling factor for long-term dissolution be chosen to be 3 to 10 with a uniform distribution over this range. Note that this distribution range is considered conservative because the dissolution rate is expected to decrease further for longer time periods.

Scaling Factor for the Change In Radiolysis (f2)—It has been observed that the rate of UO_2 dissolution is enhanced by both gamma and beta radiolysis even in oxygenated solutions (Shoesmith and Sunder 1992 [DIRS 113368]; Shoesmith 2000 [DIRS 114445]). Note that the dose rate from these radiations in CSNF will diminish after a few hundred years. This implies that laboratory measurements on relatively fresh fuels have inevitably included the enhancing effect of gamma and beta radiolysis and have likely over-estimated the CSNF dissolution rates that are used for long-term performance assessments. To remove this conservatism, the PMA uses a scaling factor (f_2) to account for the diminishing effect of gamma and beta radiations on the CSNF dissolution rate.

In an oxygenated solution, the dissolution rate of UO_2 is found to linearly decrease with the dose rate of external gamma radiation on a log-log scale (Shoesmith and Sunder 1992 [DIRS 113368]; Shoesmith 2000 [DIRS 114445]). The gamma dose rate at the surface of fresh fuel is estimated to be ~10^3 Gy/h, which diminishes to approximately 10 Gy/h after about 800 years (Shoesmith 2000 [DIRS 114445], Figure 6). This decrease in gamma-dose rate is sufficient to reduce the dissolution rate of spent fuel by a factor of ~10 (Shoesmith 2000 [DIRS 114445], Figure 32; Shoesmith and Sunder 1992 [DIRS 113368], Figure 6). It is therefore recommended for the PMA that the scaling factor for the change in radiolysis be set to 5 to 10 with a uniform distribution over this range.

Degradation Rate of High-Level Waste Glass

The glass-degradation model developed in this section provides an expression for calculating releases of radionuclides from a single canister of HLW glass as it dissolves when contacted by water. Key parameters used by the TSPA-LA Model for glass degradation are based on short-term experimental dissolution rate data for a variety of HLW glasses. Because laboratory dissolution rates tend to be many times faster than long-term field rates reported for natural glasses, the TSPA-LA model for glass degradation may be conservative, especially at long times (e.g., greater than several hundred years) following breach of a WP.

Dissolution Mechanism of High-Level Glass—The TSPA-LA model for the dissolution of HLW glass (BSC 2004 [DIRS 169988], Section 6.3) is based on the transition-state theory, which was applied to the dissolution of borosilicate waste glass by Grambow (1985 [DIRS 163257]). Transition-state theory is founded on the concept of an activated complex that is transitional between two or more stable complexes but that has a configuration through which one species (species-1 of a certain configuration) must pass in order to achieve the configuration of a second species (species-2). Although species-2 has a lower free energy than species-1, the energy of the activated complex (or transition-state energy) is higher than both, and the energy difference between species-1 and the activated complex represents the activation energy (E_a) for the reaction, *species-1* ⇨ *species-2* (Lasaga 1981 [DIRS 160187]).

In the case of glass dissolution, Grambow (1985 [DIRS 163257]) proposed that the rate-limiting step, the transition state with the greatest activation energy, is the transition from a partly hydrolyzed complex that is part of the glass (surface) to a fully hydrolyzed complex dissolved in the water. Because silica comprises the essential structural framework of borosilicate glasses, the rate-limiting reaction proposed by Grambow (1985 [DIRS 163257]) is: ≡Si-O-Si(OH)$_3$ + H_2O → ≡Si-OH + Si(OH)$_{4(aq)}$, where [≡Si-O] represents a surface complex that is part of the structural framework. Thus, the rate-limiting step for glass dissolution is the detachment of orthosilicic acid from the glass surface, and the activation energy for that detachment is E_a.

At infinite dilution (and ignoring transport-limiting effects such as diffusion), the detachment of orthosilicic acid will proceed at a forward rate. The forward rate (k_f) depends on the activation energy of the rate-limiting step (E_a), temperature, pH, and glass composition. The forward rate constant, k_f, is defined by the following equation (BSC 2004 [DIRS 169988], Equation 11, p. 6-14):

$$k_f = \vec{k}_0 \times 10^{n \cdot pH} \times \exp\left(\frac{-E_a}{RT}\right). \qquad \text{(Eq. C6.5-3)}$$

The intrinsic rate constant, k_0, depends only on the glass composition (E_a and η are assumed to be independent of glass composition and temperature).

Experimental evidence indicates that, as the concentration of dissolved silica in the solution contacting the glass increases, the (apparent) rate of glass dissolution decreases (the dissolution rate is commonly determined from the rate of release into a solution of silica or boron). Grambow (1985 [DIRS 163257]) then proposed that as the silica concentration in solution approaches saturation with respect to amorphous silica, the rate at which orthosilicic acid detaches from the glass surface will be approximately equal to the rate at which it condenses back onto the surface.

Employing the concept of a mineral saturation index, Q/K, in which K is a solubility constant and Q is the ion activity product in solution, the (apparent) dissolution rate will slow as Q/K approaches unity (i.e., saturation). Grambow (1985 [DIRS 163257]) suggested that because the dissolution of the glass matrix is controlled by the detachment of orthosilicic acid, the value for Q is taken as the activity of orthosilicic acid in solution, and the corresponding value of K is the activity of orthosilicic acid in that same solution saturated with respect to amorphous silica [$SiO_{2(am)}$]. Thus, the precipitation of silica on the glass surface represents the re-attachment

(condensation) of orthosilicic acid and accounts for the common observation of silica-rich layers on surfaces of experimentally altered glasses.

Because glass does not have an equilibrium solubility, the value for K is essentially arbitrary and, recognizing this, Grambow (1985 [DIRS 163257]) proposed including a long-term rate (k_{long}) to account for the fact that the glass matrix will continue to dissolve at some constant (but slow) rate even when the solution is fully saturated with respect to amorphous silica. Thus, taking into account the silica saturation and long-term rate, the following general rate equation can be applied to glass dissolution:

$$rate_G = k_f\left(1-\frac{Q}{K}\right)+k_{long} \qquad \text{(Eq. C6.5-4)}$$

where k_f is defined in Equation C6.5-3.

The term (1-Q/K) has been called the reaction affinity (Grambow 1985 [DIRS 163257]) and is related to the Gibbs free energy of the reaction (ΔG_r) through the saturation index:

$$\Delta G_r = RT\ln\left(\frac{Q}{K}\right) \qquad \text{(Eq. C6.5-5)}$$

where R is the gas constant and T is temperature in Kelvin (note that the equilibrium constant, K, is also a function of temperature). As Q/K approaches unity, the Gibbs free energy of reaction—and the reaction affinity—approaches zero.

The long-term rate constant, k_{long}, introduced by Grambow (1985 [DIRS 163257]) must have a functionality similar to that of the forward rate constant, k_f; however, determining the dependence of k_{long} on pH, temperature, and glass composition requires appropriate long-term dissolution-rate data. Although long term is not uniquely defined, it is assumed for the purposes of repository-relevant time scales to be on the order of a few thousand to several tens of thousands of years (or even longer). Such long-term dissolution rates are unavailable from laboratory experiments but can be inferred from observations of natural glasses (e.g., basaltic glasses) that have been altered in nature (Gordon and Brady 2003 [DIRS 176673]). Unfortunately, it is impossible to determine from such observations a reliable rate dependence on pH and temperature because sufficient knowledge about such environmental variables is rarely obtainable for ancient natural systems. In fact, these environmental variables are subject to change over time, both long term and short term (e.g., T can fluctuate diurnally and annually as well as over considerably longer time frames).

In order to implement the Grambow model in the TSPA-LA model (BSC 2004 [DIRS 169988], Equation 13, p. 6-14) combines k_0 and (1-Q/K) into an effective rate constant, k_E:

$$rate_{glass} = k_E \times 10^{n\cdot pH} \times \exp\left(\frac{-E_a}{RT}\right) \qquad \text{(Eq. C6.5-6)}$$

where values for k_E, η, and Ea are determined by fitting experimental data; specifically, data for dissolution rates measured in the laboratory. All three parameters are assumed constant for all temperatures between 25°C and 90°C (the temperature range over which experimental data used to develop the model are obtained). Dependence of k_E on glass and solution compositions is accounted for by evaluating k_E from a variety of experiments conducted on various glasses under a range of experimental conditions. Furthermore, k_E used in the current rate model is assigned different values depending on which pH range, either acid or alkaline, is being considered. This is based on the inherent assumption that the reaction affinity, (1-Q/K), takes on different values above and below pH 6.8.

It is readily apparent that the long-term rate constant proposed by Grambow (1985 [DIRS 163257]), k_{long}, is not included in the dissolution-rate equation in the TSPA-LA Model. Although it is well documented that the rate of glass dissolution slows as Q approaches K, this dependency is also unavailable in Equation C6.5-6 (BSC 2004 [DIRS 169988], Equation 13, p. 6-14). Therefore, it is not possible to model a reduction in the dissolution rate through the affinity term. By using Equation C6.5-6 to model glass dissolution, there is no change in the glass dissolution rate over time (despite a preponderance of evidence to the contrary). Instead, the reaction affinity is incorporated into k_E by fitting rate data from glass-corrosion experiments conducted under a variety of experimental conditions where Q/K assumes various values and k_E is treated as an epistemic uncertainty represented by two triangular distributions, one for each pH condition (i.e., pH less than 6.8 and greater than 6.8 at 25°C). The experimentally determined range of k_E values is intended to reflect the potential range of silica saturation expected under repository-relevant conditions: from Q/K near zero, where $k_E \approx k_f$, to Q/K near one (approaching saturation), for which $k_E << k_f$. However, because the range of k_E values is treated as a random variable with a distribution (given by the range of k_E values), there is no rule by which lower values of k_E are preferentially used as an HLW glass log reacts with water that contains increasing silica concentrations as a function of contact time. In addition, the current glass dissolution model does not account for the concentration of dissolved silica in natural groundwater and pore waters expected to enter the repository.

Natural Glasses—Dissolution rates of HLW glasses intended for permanent disposal in a geologic repository are currently modeled as dissolving at rates derived solely from laboratory experiments. In an effort to estimate rates at which HLW glasses are likely to dissolve in a geologic repository over the timescales of interest for geologic disposal (several thousands to tens of thousands of years), a comparison of dissolution rates determined for naturally occurring glasses can provide a range of likely long-term HLW glass dissolution rates more consistent with those observed in the natural environment over repository relevant timescales.

Considerable evidence exists from the study of naturally occurring minerals and glasses in their native environments that the rates at which solids dissolve (or corrode or alter) in nature appears to be substantially slower than rates determined in laboratory experiments (e.g., White and Brantley 2003 [DIRS 168088]; Gordon and Brady 2003 [DIRS 176673]). It is common for initial dissolution rates of minerals and glasses to slow over laboratory timescales; however, even the slowest laboratory rates may be one or more orders of magnitude faster than dissolution rates of analogous materials after thousands of years of weathering in nature. A full explanation for such differences remains a topic of debate; however, Grambow (2006 [DIRS 181381]) notes that, "The main reasons are the progressive *depletion of reactive surface sites*, the *accumulation*

of leached layers, the *formation of secondary precipitates*, the *low permeability and high mineral/fluid ratios*, and *increased solute concentration over time*." (emphasis added). These are primarily time-dependent processes. Grambow (2006 [DIRS 181381]) further notes that "it has been estimated that it would take about 1,000 years for the laboratory-measured rates to decrease to rates observed in the field." He goes on to say that, "Linear, long-term glass dissolution rates are used as a worst-case, upper limit of future behavior."

A primary goal of the PMA is to introduce a reasonable time dependence into the overall model for the rate of glass dissolution, such that the long-term dissolution rate approaches that observed for many natural glasses (primarily of basaltic composition, as these are considered to be reasonable chemical analogues of HLW glasses, largely due to their similar silica and alkali contents) (Byers et al. 1985 [DIRS 163209]; Crovisier et al. 1985 [DIRS 163211]; Lutze et al. 1987 [DIRS 125923]; Grambow et al. 1985 [DIRS 163258]; Gordon and Brady 2003 [DIRS 176673]; and Crovisier et al. 2003 [DIRS 180488]).

Dissolution Rate—In the PMA, the rate expression for HLW dissolution at timestep (t_i) is given by:

$$rate_G(t_i) = k_f \left(1 - \frac{Q}{K}\right)_{t_i} \qquad \text{(Eq. C6.5-7)}$$

where the forward rate is calculated with Equation C6.5-3. The intrinsic rate constant ($\vec{k}_0$) in Equation C6.5-3 is assigned a value of 1×10^7 g/m^{-2}·d^{-1}.

Separate sets of parameter values are used to calculate forward reaction rates in acidic and basic solutions, and the pH value at which the acid and basic rates are equal (pH_{eq}) depends on temperature, as given by the following relationship:

$$pH_{eq} = 7.3\text{-}0.02 \times T\,(°C) \qquad \text{(Eq. C6.5-8)}$$

which, for 25°C, gives a value for pH_{eq} equal to 6.8 (pH_{eq} equals 5.5 at 90°C).

Constant values of $\eta = -0.49$ and $E_a = 31$ kJ/mol are used for acidic solutions ($pH < pH_{eq}$), and constant values of $\eta = 0.49$ and $E_a = 69$ kJ/mol are used for basic solutions ($pH > pH_{eq}$) (values are from BSC 2004 [DIRS 169988], Table 8-1). Substituting these constant values into Equation C6.5-6 yields the forward rate as a function of pH and temperature:

$$k_{f_acidic} = 1 \times 10^7 \times 10^{-0.49 \cdot pH} \times \exp(-31/RT) \qquad \text{(Eq. C6.5-9a)}$$

$$k_{f_alkaline} = 1 \times 10^7 \times 10^{0.49 \cdot pH} \times \exp(-69/RT). \qquad \text{(Eq. C6.5-9b)}$$

The forward rates calculated with Equations C6.5-9a or C6.5-9b (depending on pH range) are substituted for k_f in Equation C6.5-7 in order to calculate the degradation rate for the applicable range of pH. The pH and temperature are variables in the glass dissolution model and their values are obtained from another model; R is the gas constant.

Reaction Affinity—The reaction affinity at timestep (t_i) in Equation C6.5-7 is split into two parts representing both short and long-term water chemistry respectively:

$$\left(1-\frac{Q}{K}\right)_{t_i} = \left(1-\frac{Q}{K}\right)_{Final} + \left(1-\frac{Q}{K}\right)_{Initial} \times e^{-\left(\frac{T_R}{T_{RC}}\right)} \qquad \text{(Eq. C6.5-10)}$$

where T_R is the thickness of the reaction rind before the current timestep (in millimeters) and T_{RC} is the rind thickness at which solute transport begins to dominate the concentration of silica (and, therefore, Q) at the surface of the dissolving glass. The value of $(1 - Q/K)_{t_i}$ is constant for a given timestep and is incremented for each successive timestep (beginning after water first contacts the glass following the breach of a WP), with subsequent values decreasing exponentially over the course of a realization and approaching a value that represents near-saturation conditions within the alteration rind. Alternatively, as noted above, the time dependence of the reaction affinity is a measure of how the Gibbs free energy of reaction is expected to decrease over time, and the rate at which the reaction affinity term approaches zero corresponds to the rate at which the reaction approaches equilibrium. Because glass can never reach equilibrium with water, the final value of the reaction affinity, $(1-Q/K)_{Final}$, is chosen to ensure that the glass dissolution rate never equals zero but merely slows to a long-term rate.

The initial value of (1-Q/K) in J-13 groundwater is 0.5 ([Si] = 0.001 M), whereas (1-Q/K) is unity (Q = 0) for water condensed from humid air. Because the release of glass constituents occurs for pristine glass exposed to silica-saturated waters, the initial value of the reaction affinity for exposure to groundwater is taken as being greater than that of J-13. $(1-Q/K)_{Final}$ corresponds to the long-term reaction affinity for which Q is assumed to be approximately equal to the concentration of dissolved silica in the corrosion rind. Therefore, the value of the reaction affinity, $(1-Q/K)_{Final}$, is assumed to be near (but not at) saturation with respect to amorphous silica (log[Si] ≈ -2.7 (Stumm and Morgan 1996 [DIRS 125332], pp. 667 and 668). Long-term reaction rates reported for natural basalt glasses after approximately 1,000 to 3,000 years of sub-aerial weathering are on the order of 10^{-5} to 10^{-8} $g \cdot m^{-2} \cdot d^{-1}$ for reaction temperatures commonly reported to be between approximately 0°C and 10°C (Gordon and Brady 2003 [DIRS 176673]). These rates are used to constrain the long-term affinities for HLW degradation. Therefore, the values of reaction affinity can be chosen as:

Humid Air: $(1-Q/K)_{HA_Initial} = 1.0$
Groundwater: $(1-Q/K)_{GW_Initial} = 0.8$
Long-term reaction affinity: $(1-Q/K)_{Final} = 5 \times 10^{-4}$ (most probable value).

The exponential factor, T_R/T_{RC}, establishes the rate at which the affinity term approaches the long-term value, $(1-Q/K)_{Final}$. The parameter T_R is the total thickness of the reaction rind formed since the beginning of the realization (prior to the current timestep, (t_i)) and T_{RC} is the rind thickness at which solute transport (e.g., diffusion) begins to dominate silica concentration at the surface of the dissolving glass and, thereby, begins to dominate the reaction affinity term. The rate dependence establishes that the reaction affinity will (nearly) reach its minimum value, $(1-Q/K)_{Final}$, after the reaction rind has achieved a thickness approximately five times T_{RC} after which the glass dissolves at a constant long-term (minimum) rate.

The reaction affinity derived from Equation C6.5-10 is substituted into Equation C6.5-7 for $(1 - Q/K)_{t_i}$ in order to calculate the dissolution rate for each timestep, (t_i), and is incremented after each timestep. The long-term rate is simply

$$R_{long} = k_f(1-Q/K)_{Final.} \quad \text{(Eq. C6.5-11)}$$

For example, a value of $(1-Q/K)_{Final}$ equal to 0.005 (which corresponds to a final Gibbs energy of reaction equal to -0.00134 kJ/mol) results in a long-term dissolution rate (R_{long}) that is 0.5 percent of the forward rate. The glass dissolution rate model given by Equations C6.5-7 through C6.5-11 is valid over the pH range 1 to 14, over the temperature range 10°C to 150°C, and over the relative humidity range 44 percent to 100 percent.

Reactive Surface Area—As noted above, the reaction rate must be multiplied by a surface-area term in order to scale the normalized rate to dissolution of a specific glass sample (HLW glass log). As in the TSPA-LA model, the PMA calculates the reactive surface area, $S(t_i)$ (in square meters), of the mass of glass that reacts during a given timestep, (t_i), as follows:

$$S(t_i) = f_{exposure} \times S_{SP} \times M(t_{i-1}) \quad \text{(Eq. C6.5-12)}$$

where

S_{SP} = the specific surface area of the glass (2.70×10^{-3} m^2/kg). S_{SP} is a constant value calculated from the internal geometry of an average glass canister and is calculated from the nominal dimensions and initial mass of glass, based on a weighted average of anticipated waste glasses in short and long canisters.

$f_{exposure}$ = a dimensionless multiplier that accounts for the reactive surface area being greater than S_{SP} due to cracking caused by thermal effects and handling. The value of $f_{exposure}(t_i)$ is sampled over a triangular distribution with both the low and the most probable values of 4 and the high value of 17.

$M(t_{i-1})$ The mass of (undissolved) glass at timestep t_{i-1}.

***M_d*: Mass of Glass Dissolved**—The mass of glass that will have degraded at the end of the current timestep is calculated with:

$$\Delta M_D(t_i) = rate_G(t_i) \times \Delta t_i \times S(t_i) \quad \text{(Eq. C6.5-13)}$$

where $rate_G(t_i)$ is the rate of glass dissolution applied during timestep (t_i), $S(t_i)$ is the surface area available at the beginning of timestep (t_i), and Δt_i is the duration of timestep (t_i).

The mass of undissolved glass that remains at the end of the current timestep, $M(t_i)$, is calculated by:

$$M(t_i) = M(t_{i-1}) - \Delta M_D(t_i) \quad \text{(Eq. C6.5-14)}$$

where $M(t_{i-1})$ is the total mass of undissolved glass prior to the current timestep.

Glass Alteration Layer: Reaction Rind—A description of the reaction rind is given in *Defense HLW Glass Degradation Model* (BSC 2004 [DIRS 169988], Appendix D), including equations to calculate the volume, thickness, and water content of the alteration layer, in terms of the mass of HLW glass that dissolves in a single canister. The volume of the alteration layer is given by:

$$V_R \text{ (in m}^3\text{)} = 3.7 \times 10^{-4} \times M_D(t) \text{ kg.} \qquad \text{(Eq. C6.5-15)}$$

The volume of pore water within the alteration layer is:

$$V_w \text{ (in m}^3\text{)} = 6.3 \times 10^{-5} \times M_D(t) \text{ kg.} \qquad \text{(Eq. C6.5-16)}$$

The thickness of the alteration layer, T_R, is determined from Equation C6.5-17 (BSC 2004 [DIRS 169988], *cf.* Equation D-17, Appendix D, p. D-8):

$$TR \text{ (in meters)} = 0.30 - [0.090 - (3.0 \times 10{-}5) \times MD(t)]/2. \qquad \text{(Eq. C6.5-17)}$$

Relative Humidity—As in the TSPA-LA model, glass degradation is not applied (i.e., $rate_G(t_i) = 0$) if the relative humidity is below 44 percent. For relative humidity greater than or equal to 44 percent, the same rate expression (Equation C6.5-7) is used to calculate the degradation rate whether the glass is exposed to humid air, dripping water, or is immersed. At temperatures between 100°C (100 percent relative humidity for water at 0.1 MPa total pressure) and 125°C (44 percent relative humidity), Equation C6.5-7 is used with the pH fixed at 10 (consistent with the TSPA-LA model).

As a cautionary note, Anovitz et al. (2006 [DIRS 180487]), who studied hydration of obsidian over a wide range of relative humidities, state in their *Conclusions* that,

> "... if nuclear waste storage glasses behave in a manner similar to obsidian, large reductions of relative humidity (below about 20 percent relative humidity) will be needed before significant reductions in the rate of glass corrosion due to water diffusion, including the rate of perlite formation, are observed. This should be true even in a vapor-dominated atmosphere, where water-mediated corrosion due to leaching is expected to be minimal."

However, Anovitz et al. (2006 [DIRS 180487]) also acknowledge that the extent to which their data, obtained on an alkali aluminosilicate glass, might apply to glasses of vastly different compositions is not clear.

The PMA developed here can be considered a reasonable approximation of expected glass dissolution over time, and yet may be moderately conservative in several aspects, based on discussions below in this section; therefore, no adjustment is recommended to change the lower limit of relative humidity for initiating glass degradation from that already used in the TSPA-LA glass degradation model.

Model Values for k_0, $(1\text{-}Q/K)_{Final}$, and T_{RC}—The glass degradation model in the PMA introduces a time dependence to the reaction affinity (through a growing reaction rind); whereas,

with the exception of k_0, all other model parameters and assumptions are identical to those in the TSPA-LA model. A value for the intrinsic rate constant, k_0, is required for this model because, in order to reintroduce the reaction affinity term, (1-Q/K), the parameter k_E in the TSPA-LA model has been separated into its constituent factors [$k_E = k_0(1\text{-}Q/K)$]. The value for k_0 recommended is essentially equal to the value of k_E used for the acid leg rate equation in the TSPA-LA model (i.e., $k_{E_acid} = 1.15 \times 10^7$ g m^{-2} d^{-1}; BSC 2004 [DIRS 169988], Table 8-1). The value for k_0 recommended is 1×10^7 g m^{-2} d^{-1}. Because k_0 is considered an intrinsic property independent of pH and temperature (Grambow 1985 [DIRS 163257]), k_0 is the same for both pH legs in the model. One result of this constancy in k_0 is to eliminate a discontinuity in the calculated dissolution rate across pH legs that arise from different values of k_E being used for acid versus basic pH legs. Such a discontinuity has never been observed in experiments on glass dissolution.

The most probable value for the final reaction affinity, $(1\text{-}Q/K)_{Final}$ ($= 5 \times 10^{-4}$), is chosen such that the long-term rate (defined by Equation C6.5-11) is approximately equal to long-term reaction rates reported for basaltic glass in nature (Gordon and Brady 2003 [DIRS 176673], Table 4, field rates). Considerable variability in reported rates for natural glasses, combined with uncertainty about the effectiveness of the reaction rind to limit access of water to the glass surface under the variety of potential conditions over repository relevant timescales, the reaction affinity term is assumed to have a log-normal distribution centered on the most probable value, with a minimum value of 10^{-5} and a maximum value of 10^{-2}. Such a distribution results in long-term dissolution rates that bracket those reported in Table 4 of Gordon and Brady (2003 [DIRS 176673]) for natural basaltic glasses.

The value for T_{RC}, the critical reaction-rind thickness, is the thickness of the reaction rind for which mass transport through the reaction rind begins to dominate the exchange of glass constituents between the bulk glass and solution and, therefore, begins dominating control on the reaction affinity, (1-Q/K). The role of the reaction rind in this model is to establish the long-term dissolution rate, which occurs when $T_R \approx 5T_{RC}$. For the purposes of the model, the reaction rind is considered to include any precipitated phases (amorphous silica and clays) on the glass surface, as well as depleted and leached zones below the surface of reacted glass. The value of T_{RC} used in the model is based on observations of reaction rinds from a variety of glass dissolution experiments. McLoughlin et al. (2006 [DIRS 181382]) measured the reaction rind thicknesses of three archeological glasses after 32 years of burial in a soil. These measurements represent the longest-term reaction rinds formed under well constrained conditions of pH (9.5 to 9.7) and temperature (0.7°C to 18.9°C). The three glasses examined by McLoughlin et al. (2006 [DIRS 181382], Figures 4, 5, 6, and 7) displayed different reaction rind (and depleted zone) thicknesses, from less than 10 to greater than 30 micrometers, with differences attributed to differences in glass composition. Based on diffusion constants from Grambow and Müller (2001 [DIRS 171412], fig. 7), a 30 micrometer thick reaction layer is sufficiently thick that diffusion will dominate glass alteration. However, McLoughlin et al. (2006 [DIRS 181382]) notes that, whereas two of the three glasses with thinner reaction rinds appeared to have reached steady state, the one glass with the thickest layer had apparently not, despite the observation that this 30 μm layer was substantially depleted in alkalis and alkaline earths and strongly enriched in silica. The composition of this latter glass is more like that of a HLW glass than is the composition of the least reacted glass studied by McLoughlin et al. (2006 [DIRS 181382]). The minimum value for the critical reaction rind thickness, T_{RC}, for the model is therefore chosen to

be the thickness of the thickest reaction layer reported by McLoughlin et al. (2006 [DIRS 181382]): 30 micrometers [0.03 mm]. This is an estimate of a rind thickness for which diffusion just begins to dominate the reaction affinity term. The model applies to the entire glass surface available for dissolution. In reality, the reaction rind is likely to vary in both thickness and extent, so another factor of approximately three is applied to T_{RC} to arrive at the most probable value of 0.1 mm. The maximum value for T_{RC} is 0.3 mm, considered to be well beyond the rind thickness necessary to establish diffusion as the predominant mechanism controlling the reaction affinity term.

Comparing Model Predictions Against Long-Term Glass Corrosion—Ojovan et al. (2005 [DIRS 180494]) reported dissolution rates for a low-level (radioactive) waste (LLW) glass that has been buried in water-saturated soil for 16 years. The dissolution rates gradually diminished from 9.4 x 10^{-7} g/cm^2/day over the first year to 2.2 x 10^{-7} g/cm^2/day over 16 years of tests. Radionuclide Cs losses obey a square root time dependence indicating a diffusion-controlled release mechanism. The main parameters, which control the corrosion of waste glass in the near-surface repository, are the effective diffusion coefficient of radiocaesium and the rate of glass hydrolysis. Diffusion is predicted to be dominant for about 16 years after which diffusion and hydrolytic dissolution are expected to be similarly important. This mixed stage is predicted to continue for about 260years after which hydrolytic dissolution will be the dominant mechanism. Figure C6-9 illustrates the PMA for HLW glass dissolution developed here for temperature and pH conditions equivalent to those reported by Ojovan et al. (2005 [DIRS 180494]) (6.5°C and pH 7.6). In order to best fit the LLW glass data, the T_{RC} value of 0.3 mm and the $f_{exposure}$ of 17 were used. Dissolution-rate data reported by Ojovan et al. (2005 [DIRS 180494]) are shown as filled triangles (1 year and 16 years), and steady-state rates that they expect to occur after approximately 262 years of burial are shown as well (hollow triangle). Also shown on Figure C6-9 are dissolution rates for natural basalt glasses (filled squares) reported in Table 4 of Gordon and Brady (2003 [DIRS 176673]) that correspond to temperatures of approximately 10°C. The long-term dissolution rate predicted by the PMA developed here is also shown on Figure C6-9 (dashed line); however, that model rate is not achieved until after about two million years at this temperature. The long-term rate shown on Figure C6-9 is also within a factor of five of the long-term reaction rate for basaltic glasses in seawater (0.1 μm yr^{-1}) estimated by Grambow et al. (1985 [DIRS 163258], Figure 3). The fit of the PMA to the data of Ojovan et al. (2005 [DIRS 180494] is excellent; however, model rates remain well above dissolution rates estimated for natural basaltic glasses, and the time for the model rates to reach a rate comparable to the estimated long-term rates of natural basalts is about 1,000 times longer than achieved in nature. Such a result suggests that, while a reasonable approximation of long-term LLW glass dissolution, the PMA developed here remains conservative with respect to observed natural basaltic glass degradation rates and, by inference, with respect to anticipated HLW glass degradation rates.

Uncertainty Associated with Uranium(VI), Plutonium(IV), Neptunium(IV), and Neptunium(V) Solubility Limits

The objective of this submodel update in the PMA is to reconsider the uncertainties assigned to the solubilities of some actinide-bearing solids considered in *Dissolved Concentration Limits of Radioactive Elements* (SNL 2007 [DIRS 177418]). The uncertainties for the solubilities of solids controlling the concentrations of the radionuclides uranium(VI) (solids: schoepite,

Na-boltwoodite, $Na_4UO_2(CO_3)_3$); Pu(IV) (solid: PuO_2(am) or PuO_2(hyd,aged)); neptunium(IV) (solid: NpO_2); and neptunium (V) (solids: Np_2O_5 and $NaNpO_2CO_3$) have been assessed by comparisons between the EQ3/6 code predictions using the thermodynamic database *data0.ymp.R5* (DTN: SN0612T0502404.014 [DIRS 178850]) and solubility data available in the peer-review scientific literature. In cases where solubility data are limited or not available, uncertainties in log K values advanced by the source (in this case, the thermodynamic data compilation by the Organization for Economic Cooperation and Development/Nuclear Energy Agency compilation of thermodynamic data) are used as the basis for the uncertainty evaluations of the affected phases. These Organization for Economic Cooperation and Development/Nuclear Energy Agency uncertainties are mainly based on their evaluation of thermodynamic data of the relevant solid and aqueous species.

In general, solubility data for actinide solids are scant. In many cases data are given at specific redox conditions and solution compositions, thus restricting their use to specific chemical conditions. Still, some of the available solubility data can be used to evaluate and reasonably bound the predicted actinide solubilities using the computer code EQ3/6 and thermodynamic database *data0.ymp.R5* (DTN: SN0612T0502404.014 [DIRS 178850]). The analysis report, *Dissolved Concentration Limits of Radioactive Elements* (SNL 2007 [DIRS 177418]) assessed uncertainties on the solubility of the above-mentioned solids. The assessment was mainly based on potential sources of uncertainty effecting solubility and/or solubility calculations. These include uncertainties due to: (1) thermodynamic data in the solubility calculations, (2) variations in solution chemistry, (3) temperature effects, and (4) calculations of activity coefficients at different ionic strengths. The assessment of uncertainty due to thermodynamic data is captured by the parameter ε_1. This parameter is estimated from the uncertainty rolled in the log K computed from the uncertainties in thermodynamic data of the individual chemical species composing the solubility reaction. The uncertainty in water chemistry is represented by ε_2, which explicitly accounts for the effect of F^- concentration in solution. Finally, the uncertainty in the activity coefficients is defined by the difference between those predicted by the EQ3/6 code using the b-dot activity coefficient model and mean salt activity coefficients calculated by the method of Truesdell and Jones (1974 [DIRS 170136]). The uncertainty due to temperature effects is assessed in the analysis report *Dissolved Concentration Limits of Radioactive Elements* (SNL 2007 [DIRS 177418]) but is implemented in a qualitative discussion of its magnitude relative to the bounding nature of the model results. In general, the appropriate treatment of all these uncertainties as to unequivocally discern their effects on solubility calculations is a difficult problem. Equally important is how these uncertainties could have downstream effects on EQ3/6 or other geochemical code calculations given the wide range of water compositions estimated for the near-field environment. Examination of these downstream effects of uncertainties in geochemical code calculations is often difficult, given the complexities of how these propagate when, for example, solubilities are determined as a function of pH. For instance, substantial changes in the aqueous speciation due to the presence of carbonate in solution with increasing pH can have a significant effect on solubility. Moreover, the selection of different sets of aqueous species representing a given chemical system (sometimes the case between different thermodynamic databases) could also influence uncertainty propagation in solubility calculations. In addition, the effects of ionic strength on activity coefficients can also affect uncertainty, particularly when the relative proportion of highly charged aqueous species in solution could be large. A rigorous assessment of parameter uncertainty, whether it involves the

retrieval of thermodynamic data or a model output, could encompass an extensive statistical analysis using techniques involving sampling approaches (e.g., jackknife, bootstrap, Markov Chain Monte Carlo) and evaluations of residuals by regression methods among others (Meinrath et al. 2000 [DIRS 180861]; Meinrath 2001 [DIRS 180862]; Weber et al. 2006 [DIRS 180902]). An additional complexity is the nature of uncertainty propagation in the determination of thermodynamic parameters from analytical measurements (e.g., log K data) and, consequently, how these propagate within an aqueous speciation model intrinsic to the chemical system of interest (Criscenti et al. 1996 [DIRS 100720]).

An uncertainty evaluation comprising some form of rigorous statistical approach as mentioned above could translate into a large effort given the rather diverse applications of geochemical models in the Yucca Mountain Project. For example, geochemical calculations are utilized in the evaluation of water chemistries during waste degradation, water/rock interactions in the near-field, and in the assessment of solubilities of actinide solids. One potential limitation in using any of the aforementioned statistical approaches to evaluate uncertainty is that the solubility data needed in the assessments of uncertainties may be limited or non-existent, therefore precluding the useful applicability of these methods. As a result, addressing explicitly the effect of all these uncertainties not only goes beyond the scope of the current effort but could end up being impractical given the large number of parameters in geochemical modeling and their dependencies on solution concentration. However, for a relatively simple system, estimation of uncertainties in geochemical calculations based simply on data (e.g., solubilities) should reasonably correspond to that derived from propagated uncertainties evaluated using other rigorous statistical approaches. This is because the actual uncertainty in the result depends more on the weighted uncertainties of the chemical species that contribute significantly to the result (Criscenti et al. 1996 [DIRS 100720], p. 3552, 3rd Para.). *Dissolved Concentration Limits of Elements with Radioactive Isotopes* (SNL 2007 [DIRS 177418]) captures the extent of various uncertainties by combining them additively (in log-space) to generate an uncertainty envelope encompassing some of the above-mentioned effects. However, because these uncertainties would not simply be additive, this method probably overestimates the actual uncertainty in any single result. It is the purpose of this PMA work to use a more simplistic method to reasonably bound uncertainties based on comparisons with solubility data or use those advanced by a sanctioning body such as the Organization for Economic Cooperation and Development/Nuclear Energy Agency in their thermodynamic data compilations when solubility data are lacking.

The uncertainty advanced in this work, to a large extent, is similar to the ε_1 uncertainty parameter in *Dissolved Concentration Limits of Elements with Radioactive Isoptopes* (SNL 2007 [DIRS 177418]). The approach taken here is mainly based on direct comparisons with available solubility data. In cases where solubility data for a given solid can be evaluated in a sufficiently large number of observations as a function of pH, then a statistically based approach is used to estimate the standard error of the EQ3/6 code prediction. This is the case for the phase PuO_2(hyd,aged). In cases where solubility data are either limited or simply not available for a particular phase, the uncertainty advanced by the Organization for Economic Cooperation and Development/Nuclear Energy Agency data compilation on the relevant solid is used in the evaluation. In such cases, comparisons with available solubility data for a similar phase (i.e., a hydrated form of the evaluated phase) are used to constrain the uncertainty bounds. Although the latter cannot be considered an explicitly valid comparison because of obvious differences in the exact composition of the solid, it is by itself a reasonable approach to evaluating the

uncertainty limits based on the solubility of a similar phase. It is also assumed that the resulting uncertainty envelope appropriately represents the bounds as a function of pH. There was no attempt to propagate explicit uncertainties in the values of pH and ionic strength because (1) solubility and related uncertainty data for the solids of interest are not abundant, and (2) it would require a more involved analysis in the characterization of uncertainty propagation as a result of changes in aqueous speciation. Overall, it was noted that moderate changes in ionic strength (e.g., 0.5 to 1 molal) did not result in significant changes in the predicted solubilities as to invalidate the recommended uncertainty envelope.

Explicit representation of uncertainty to relatively large values of ionic strength (i.e., values much larger than 1 molal) is not currently possible except for a few actinide solids for which solubility data exist but require the use of a different activity coefficient model (i.e., Pitzer model). At this point, it is assumed that ionic strength effects are relatively insignificant and captured within the recommended uncertainty. This is based on analyses regarding the behavior of the model at various ionic strengths. An example of this is the prediction of $NaUO_2(CO_3)_3$ solubility (Figure C6-15) up to an ionic strength of 4 molal using the b-dot approach. The predicted solubility is well represented by the EQ3/6 results in comparison with the solubility data. However, one must be cautious in extending this result to other cases given that the main electrolyte is NaCl, which is symmetrical, and the b-dot activity coefficient prediction does not suffer much from the expected breakdown with increasing ionic strength. Mixed (unsymmetrical) electrolytes with large proportions of aqueous species having valences larger than unity could result in the breakdown of the b-dot activity coefficient model.

Solution chemistry could be considered a major contributor in the uncertainty estimates. The variations in solution chemistry for the different sets of solubility data, specifically in the case of PuO_2(hyd,aged), appear to be captured by the recommended uncertainty limits. In the PMA, the effect of solution chemistry is assumed to be captured within the recommended uncertainty limits. No additional uncertainties are assigned beyond what is determined on the basis of comparisons with reported solubilities, or uncertainties evaluated based on information in the Organization for Economic Cooperation and Development/Nuclear Energy Agency data compilations. It should be noted that direct propagation of the pH uncertainty is not treated here within the uncertainties evaluated for the solubility prediction. Such uncertainties due to the independent parameters of the solubility-limited dissolved concentration models are evaluated explicitly within the TSPA calculation based on the abstractions that constrain those parameter values.

Uncertainty Estimate of PuO_2(am) Solubility—The solubility of PuO_2(am) at 25°C at pH ~3 to ~8.5 has been addressed by various experimental studies. Notice that PuO_2(hyd,aged) is sometimes used instead of PuO_2(am) in the spreadsheet given its designation in the *data0.ymp.R5* (DTN: SN0612T0502404.014 [DIRS 178850]) thermodynamic database. The uncertainty evaluation of PuO_2(am) solubility was assessed based on comparisons with the solubility data by Rai et al. (2001 [DIRS 168392]), Rai et al. (1984 [DIRS 122768]), Efurd et al. (1998 [DIRS 108015]), Nitsche et al. (1993 [DIRS 155218]), and Nitsche et al. (1994 [DIRS 144515]) and obtained at a temperature of 25°C. The selected value for log fO_2(g) of -7 is used in this evaluation. The basis for using this log fO_2(g) is to obtain an Eh-pH range in the generation of the solubility curve using the EQ3/6 reaction path calculations that closely corresponds to that in the study of Rai (1984 [DIRS 122768]). The corresponding values

calculated in Eh units (Volts) from those reported by Rai (1984 [DIRS 122768]) in pe units range from 0.957 at pH 2.3 to 0.864 at pH 3.8 (Corroborative DTN: SN0704PMASOLUB.001 [DIRS 182787] 'Recommended_Uncertainties_Pu_Np_U_Rev01.xls, worksheet: T.Bernot_PuO2 Solub_data_ Comp). This range in particular is closely reflected by the resultant Eh-pH trajectory that is represented by the curves on Figure C6-10. It must be noted that a few observations from Rai (1984 [DIRS 122768]) for corresponding Eh values at pH higher than 3.8 are slightly lower than those expected from a linear Eh-pH relation. Although these data deviated from the Eh-pH trend of the EQ3/6 reaction path calculation, they were still considered in the uncertainty evaluation. The chosen log $fCO_2(g)$ in this evaluation equals -3.5 assuming equilibrium with air. The similarity in solubility trends as a function of pH between data obtained from different sources adds further confidence in the use of the data. Finally, a comparison with a recent set of solubility data from Fujiwara et al. (2002 [DIRS 180468]), although obtained under different experimental conditions, indicates good agreement with other data sets strengthening the confidence in the selected data.

The EQ3/6 runs were conducted with a solution composition having ~0.4 molal NaCl in agreement with Rai et al. (1984 [DIRS 122768]) solubility experiments. Runs with relatively more dilute NaCl concentrations yield similar solubility curves except in the high pH range (e.g., pH > 8). Given the nature of the solubility with respect to its variation as a function of pH, the solubility values for both EQ3/6 predictions and experimental observation were transformed to a logarithmic (base 10) scale. A log normal distribution is assumed and is evaluated by plotting the difference of the log-transformed values (log predicted–log observed) for total plutonium concentrations as a function of pH (Figure C6-11). This plot shows that most of the data lie below the solubility curve with a slight skewing of the data at low pH. Still, the apparent skewing does not preclude the use of a log normal distribution to capture the range of observed solubilities for this phase at this low pH range. The sum of log transformed differences squared divided by the number of experimental observations given by Equation C6.5-18 was calculated with respect to the actual predicted solubility value computed by EQ3/6 at a given pH value:

$$\text{Sum of Squared Differences} = \frac{\sum\left(log[Pu]_{obs} - log[Pu]_{pred}\right)^2}{40}. \qquad \text{(Eq. C6.5-18)}$$

where $log[Pu]_{obs}$ and $log[Pu]_{pred}$ correspond to the observed and predicted log of total plutonium concentration, respectively. The value of 40 represents the total number of observed measurements used in the analysis. This formulation is slightly different from that used to calculate a variance that uses an average of the data. The standard error of the EQ3/6 prediction (not to be confused with standard deviation in this case) of the whole solubility data population is calculated by taking the square root of Equation C6.5-18 (see spreadsheet Recommended_Uncertainties_Pu_Np_U_Rev01.xls, worksheet PuO2(hyd,aged)_summary, corroborative DTN: SN0704PMASOLUB.001 [DIRS 182787]):

$$\text{Standard Error} = \sqrt{\frac{\sum\left(log[Pu]_{obs} - log[Pu]_{pred}\right)^2}{40}} \qquad \text{(Eq. C6.5-19)}$$

The value obtained from Equation C6.5-19 is ±0.79 and is applied to the whole pH range for which the solubility curve is computed. To evaluate the confidence interval of the solubility

curve, the estimated standard error (±0.79) is applied to the mean of the log solubility in molal units and compared to the reported solubilities as seen on Figure C6-11. Overall, an uncertainty of ±0.79 appears to capture most of the data, generally within the lower confidence bound. Notice on Figure C6-10 that no data lie outside the upper confidence bound for the pH range comprised by the reported solubilities. It should be noted that many of the experimental solubilities used in this analysis correspond to chemical conditions that are different with respect to each other. For example, the solubility data sets include solubilities measured in NaCl and $NaClO_4$ electrolyte matrices (Rai et al. 2001 [DIRS 168392]) and in J-13 water composition (Nitsche et al. (1993 [DIRS 155218]). Moreover, the Eh-pH relations in these studies are relatively variable and in many cases deviate from the assumed trend in the reaction path model with a fixed log $fO_2(g)$ value. In addition, the lower uncertainty bound appears to capture a large fraction of the solubility data by Fujiwara et al. (2002 [DIRS 180468]) that was obtained under more reduced conditions and in solutions with higher ionic strength. Therefore, even with these variations in solutions chemistry and redox potentials, the selected confidence interval is sufficiently adequate as to reasonably capture most of the observed solubility data for this phase. It should be noted that the data by Fujiwara et al. (2002 [DIRS 180468]) are used for comparison purposes only and did not take part in the uncertainty analysis. The EQ3/6 runs were conducted without suppressing any aqueous species. It was noted that some code run results at ionic strength values close to or slightly larger than unity results in the shift of the solubility curve at pH>8. The recommended uncertainty distribution for the solubility of this phase is given in Table C6-8. For a log normal distribution with the mean set at zero, the value for σ based on the computed standard error is ±0.79 and truncated at $\pm 1\sigma$.

Uncertainty Estimate of NpO_2 Solubility—The log K value for NpO_2 in the thermodynamic database *data0.ymp.R5* (DTN: SN0612T0502404.014 [DIRS 178850]) is based on thermochemical measurements on the solid and not from solubility data. On the other hand, solubility data only exist for amorphous and/or hydrated forms of NpO_2. The study of Rai and Ryan (1985 [DIRS 137138]) reports the solubility of NpO_2*H_2O with and without carbonate in solution. The log K value for the reaction $NpO_2 + 4H^+ = Np^{++++} + 2H_2O$ is determined from the Gibbs energies of formation for each component in the reaction. The log K value evaluated by the Organization for Economic Cooperation and Development/Nuclear Energy Agency (Guillaumont et al. 2003 [DIRS 168382], Section 10.2.2.2.1, p. 297, 1st paragraph) for the reaction $NpO_2 + 2H_2O = Np^{++++} + 4OH^-$ is -65.75 ±1.07. Converting this reaction in the form consistent with the EQ3/6 thermodynamic database requires combining the above expression with the one for H_2O dissociation having the stoichiometric coefficients multiplied by 4. Assuming the uncertainties for the log K value of the water dissociation reaction are negligible relative to those of the NpO_2 reaction, the adopted uncertainty from the Organization for Economic Cooperation and Development/Nuclear Energy Agency source is ±1.07 log solubility in molality units. The comprehensive evaluation by the Organization for Economic Cooperation and Development/Nuclear Energy Agency thermodynamic data compilation (Guillaumont et al. 2003 [DIRS 168382], Section 10.2.2.2) renders this source as sufficiently adequate as to justify the use of this uncertainty value in this work. For comparison with a similar phase, the solubility data of Rai and Ryan (1985 [DIRS 137138]) are shown with the predicted solubility curve calculated by EQ3/6 (Figure C6-12). The log $fO_2(g)$ value used in the EQ3/6 calculations is -0.7, which results in more oxidized conditions relative to those of the Rai and Ryan (1985 [DIRS 137138]) experiments. Therefore, the predicted solubility of this anhydrous phase is upper

bound at this redox condition. The differences are relatively small for most of the data, and the uncertainty bounds capture all the data in the pH range of 6.9 through 7.7 (Figure C6-12). The EQ3/6 runs were conducted without suppressing any aqueous species. It should be noted that these solubility data were not used in the uncertainty analysis since it pertains to a different phase, but it is used for qualitative purposes remarking how the uncertainty bounds capture the solubility of the hydrated Np(IV) oxide solid. The recommended uncertainty distribution for the solubility of this phase is given in Table C6-8. For a triangular distribution in the range a through c, a equals -1.07, b is set to zero, and c is 1.07. A triangular distribution is recommended to emphasize the average, and the limits (a and c) provide for truncation of the distribution at values different from those in the implementation of a normal distribution. In addition, this type of distribution seems to be appropriate given the limited amount of data used in the comparison.

Uncertainty Estimate of Np_2O_5 Solubility—The log K value for Np_2O_5 in the thermodynamic database *data0.ymp.R5* (DTN: SN0612T0502404.014 [DIRS 178850]) is also based on thermochemical measurements on the solid and not from solubility data. Like in the case of NpO_2, there are some solubility studies on hydrated forms of Np_2O_5 by Efurd et al. (1998 [DIRS 108015]). Pan and Campbell (1998 [DIRS 180455]) reported solubilities for Np_2O_5 in CO_2-free solutions that are about a log unit more soluble than that calculated using the Organization for Economic Cooperation and Development/Nuclear Energy Agency thermodynamic data and those given by Efurd et al. (1998 [DIRS 108015]). A discussion in the Organization for Economic Cooperation and Development/Nuclear Energy Agency source (Guillaumont et al. 2003 [DIRS 168382], p.585) mentions the solubility data from Pan and Campbell (1998 [DIRS 180455]), but they select the constant based on thermochemical measurements and estimations. Guillaumont et al. (2003 [DIRS 168382], Section 10.2.2.1, p. 297) make remarks on the agreement of their selected log K value based on thermochemical data with the log K value given by Efurd et al. (1998 [DIRS 108015]) based on solubility data, even if it is for a hydrous phase. The recommended uncertainty for the Organization for Economic Cooperation and Development/Nuclear Energy Agency log K value is ±2 for the solubility reaction adopted in the *data0.ymp.R5* (DTN: SN0612T0502404.014 [DIRS 178850]) thermodynamic database $Np_2O_5 + 2H^+ = 2NpO_2^+ + H_2O$. This uncertainty interval is rather large and it appears to be mainly based on the uncertainty of the thermochemical data for the solid. The Organization for Economic Cooperation and Development/Nuclear Energy Agency compilation of Guillaumont et al. (2003 [DIRS 168382], Section 10.2.2.1, p. 297) selected their log K value on the grounds that it is in good agreement with that obtained in the study of Efurd et al. (1998 [DIRS 108015]). The same rationale is adopted in this evaluation but recommends an uncertainty of ±1 for the calculated solubility of this phase in molality units (Figure C6-13). The reason for recommending an uncertainty value half of that advanced by Guillaumont et al. (2003 [DIRS 168382], Section 10.2.2.1, p. 297) is because it is considered sufficient to encompass the data by Efurd et al. (1998 [DIRS 108015]). However, the upper bound underestimates Pan and Campbell (1998 [DIRS 180455]) solubility data by ~1 log unit. Guillaumont et al. (2003 [DIRS 168382], Section 10.2.2.1, p. 297) does not provide any arguments on why the solubility data of Pan and Campbell (1998 [DIRS 180455]) were not used in their analysis to constrain solubilities even when the authors report Np_2O_5(cr) as the equilibrium phase in their experiments. The solubility data given by Pan and Campbell (1998 [DIRS 180455]) at pH values larger than 9, do not follow the expected trend of increasing solubility with pH. A possible explanation for this is that these solubility experiments were conducted under CO_2-free

conditions and Np-carbonate complexation would not be expected in the alkaline pH range. Although Pan and Campbell (1998 [DIRS 180455]) noticed this behavior in the solubility data, they did not offer an explanation for the cause of such trend except to say that it opposes the observed increase in solubility in the alkaline pH range. The data by Nitsche et al. (1993 [DIRS 155218]) tabulated in Efurd et al. (1998 [DIRS 108015]) is shown in the graph since it was also considered by Efurd et al. (1998 [DIRS 108015]) for comparison with their results. The study by Nitsche et al. (1993 [DIRS 155218]) reports X-ray diffraction analysis of the solids for the solubility experiments at 25°C and concludes that better agreement of the X-ray diffraction patterns is obtained for hydrated Na-Np(IV)-carbonate phases. Therefore, the relevance of these data to the solubility of Np_2O_5 is small but it is shown for comparison purposes only. No suppressions were used in the EQ3/6 runs. The recommended uncertainty distribution for the solubility of this phase is given in Table C6-4. For a triangular distribution in the range a through c, a equals -1, b is set to zero, and c is 1. A triangular distribution is recommended to emphasize the average, and the limits (a and c) provide for truncation of the distribution at values different from those in the implementation of a normal distribution. In addition, this type of distribution seems to be appropriate given the limited amount of data used in the comparison.

Uncertainty Estimate of $NaNpO_2CO_3$ Solubility—The log K value for $NaNpO_2CO_3$ selected by the Organization for Economic Cooperation and Development/Nuclear Energy Agency compilation (Guillaumont et al. 2003 [DIRS 168382], Section 10.6.2.1.1, p. 305) is based on the solubility study at various CO_3^{--} concentrations in NaCl solutions. The adopted uncertainty of ±0.5 is that evaluated by the Organization for Economic Cooperation and Development/Nuclear Energy Agency Guillaumont et al. (2003 [DIRS 168382], Section 10.6.2.1.1) for the log K, which is applied to the log of the solubility in molality units to be obtained from the EQ3/6 predictions. The available solubility data for this phase has already been evaluated by OECD (2001 [DIRS 159027]) and Guillaumont et al. (2003 [DIRS 168382], Section 10.6.2.1.1) for the retrieval of thermodynamic data for this phase. The recommended uncertainty distribution for the solubility of this phase is given in Table C6-8. Note that this uncertainty of ±0.5 given by the Organization for Economic Cooperation and Development/Nuclear Energy Agency Guillaumont et al. (2003 [DIRS 168382], Section 10.6.2.1.1) is at the 95 percent confidence level. The recommended distribution is log normal truncated at 2σ.

Uncertainty Estimate of Schoepite ($UO_3 \cdot 2H_2O$) Solubility—Evaluation of log K values for schoepite has been largely determined from solubility studies. However, the log K value adopted in the thermodynamic database *data0.ymp.R5* (DTN: SN0612T0502404.014 [DIRS 178850]) from the Organization for Economic Cooperation and Development/Nuclear Energy Agency compilation (Guillaumont et al. 2003 [DIRS 168382], Section 9.3.2.1.5.1, p. 179) is derived from thermochemical measurements as evaluated by Grenthe et al. (1992 [DIRS 101671]). Guillaumont et al. (2003 [DIRS 168382], Section 9.3.2.1.5.1) considered the log K value calculated using the thermodynamic data advanced by Grenthe et al. (1992 [DIRS 101671]) adequate based on comparisons with various log K values determined from solubility data. At this point, the evaluation of schoepite solubility has been reasonably extensive in the Organization for Economic Cooperation and Development/Nuclear Energy Agency thermodynamic data reviews by Grenthe et al. (1992 [DIRS 101671]) and Guillaumont et al. (2003 [DIRS 168382], Section 9.3.2.1.5.1). The uncertainties advanced by Guillaumont et al. (2003 [DIRS 168382], Section 9.3.2.1.5.1) for their tabulated reaction log K of ±0.4 is applied to the solubility of this phase in molality units is adopted in this evaluation. This uncertainty is less

than that advanced by *Dissolved Concentration Limits of Radioactive Elements* (SNL 2007 [DIRS 177418]) for the log K value of this solid. The uncertainty analysis in this report for the U(VI)-bearing phases (schoepite, Na-boltwoodite, and $Na_4UO_2(CO_3)_3$) is somewhat different in the sense that it combines the uncertainty of two solids when their solubility overlaps as a function of pH and fCO_2. However, this 'crossover' uncertainty (as referred in the aforementioned report) is not treated explicitly in their report (SNL 2007 [DIRS 177418]) and a total uncertainty of ±0.99 units is then applied to all log total uranium concentrations. In the analysis described here, all uncertainties are explicitly assigned to each U(VI)-bearing phase. For the PMA implementation, the sampling of uncertainties among schoepite, Na-boltwoodite, and $Na_4UO_2(CO_3)_3$ will be perfectly correlated to ensure the continuity of uranium solubility in mineral phase transitions. The recommended uncertainty distribution for the solubility of this phase is given in Table C6-8. For a triangular distribution in the range a through c, a equals -0.4, b is set to zero, and c is 0.4. A triangular distribution is recommended to emphasize the average, and the limits (a and c) provide for truncation of the distribution at values different from those in the implementation of a normal distribution. Also, this type of distribution seems to be appropriate given the limited amount of data used in the comparison.

Uncertainty Estimate of Na-Boltwoodite ($NaUO_2SiO_3OH \cdot 1.5H_2O$) Solubility—Thermodynamic data for Na-boltwoodite have been largely based on the solubility data. However, the log K value in the thermodynamic database *data0.ymp.R5* (DTN: SN0612T0502404.014 [DIRS 178850]) is based on the Gibbs energy of formation for this phase given in the Organization for Economic Cooperation and Development/Nuclear Energy Agency compilation (Guillaumont et al. 2003 [DIRS 168382], p. 443). It should be noted that this value estimated in the work by Chen et al. (1999 [DIRS 106346]) and Guillaumont et al. (2003 [DIRS 168382], p. 442 to 443) does not select this datum in their tabulations even when it is discussed in this volume. The main reason for not selecting this value in Guillaumont et al. (2003 [DIRS 168382], p. 441 to 443) is the need of more work or further re-evaluation of the thermodynamic data for this solid. The more recent study of the solubility of this phase by Ilton et al. (2006 [DIRS 178810]) calculates a log K value at 25°C (log K = 5.86 ±0.24) that is in good agreement with that adopted in the thermodynamic database *data0.ymp.R5* (log K = 6.08 (DTN: SN0612T0502404.014 [DIRS 178850])). Moreover, this value is in good agreement with that advanced by the solubility study of Nguyen et al. (1992 [DIRS 100809], Table 6, p. 374) of log K ≥5.82(±0.16). It should be noted that the uncertainty range given by Ilton et al. (2006 [DIRS 178810]) is not represented on Figure C6-14, and the size of the symbol is arbitrary.

As seen on Figure C6-14, the EQ3/6 solubility predictions, as a function of pH tend to over-predict the solubility at pH 6.7 to 7.5 where transitions from predominantly uranyl-hydroxy-carbonate to uranyl-carbonate-aqueous species occur. At pH above 7.5, the difference between predicted and observed solubilities is relatively small, and the predicted solubility trend conforms well to that of the experimental data. The recommended uncertainty distribution for the solubility of this phase is given in Table C6-8. For a triangular distribution in the range a through c, a equals -0.5, b is set to zero, and c is 0.3. Note that a slightly larger uncertainty of-0.5 is assigned to the unsaturated side of the solubility curve where a larger difference between predicted and observed data exists at pH ~6.6 to 7. This was determined by examination of an uncertainty range that captures the bulk of the data at undersaturated conditions relative to the EQ3/6 code prediction. Similarly, the uncertainty value 0.3 was

obtained in the same manner. To avoid confusion, there is little or no relationship of the recommended uncertainty in this evaluation with the one given by Ilton et al. (2006 [DIRS 178810]). Since these larger differences apply to two points lying outside the lower solubility bound, the predicted solubility curve in this narrow pH range could be considered conservative. Additional solubility data could provide better reconciliation of these differences as well as data scatter as a function of pH. Differences in predicted solubility values are anticipated considering that the log K value retrieved by Ilton et al. (2006 [DIRS 178810]) of K = 5.86 is somewhat smaller than that adopted in the thermodynamic database *data0.ymp.R5* (DTN: SN0612T0502404.014 [DIRS 178850]) with a log K value equal to 6.0800 at 25°C. Even with these differences in log K data of 0.22 log units, the predicted solubilities along with assigned uncertainties are in good agreement with their solubility data. Although these differences in log K values can cause the discrepancy between predictions and observations, other factors such as analytical uncertainties and solution chemistry can also have non-negligible effects on this deviation. Once more, the limited amount of experimental data along with its uncertainty makes it difficult to explain these discrepancies. Even with the limited amount of data and their associated uncertainties, solubility predictions do not show trends of either gross under- or over-prediction beyond the uncertainty range advanced by Ilton et al. (2006 [DIRS 178810]). It should be noted that Ilton et al. (2006 [DIRS 178810]) used variable concentrations of bicarbonate in their solubility experiments. Even with this variation in solution chemistry, the solubility predictions and associated uncertainties appear to reasonably capture this effect as a function of pH. A triangular distribution is recommended as to weigh more on the average and their limits (a and c) provide for truncation of the distribution at values different from those in the implementation of a normal distribution. In addition, this type of distribution seems to be appropriate given the limited amount of data used in the comparison.

There is an overlap in solubilities between schoepite and Na-boltwoodite in the TSPA implementation of the solubility model. For the PMA implementation, the larger uncertainty between schoepite and Na-boltwoodite will be applied when the solubilities of these two phases overlap.

Uncertainty Estimate of $Na_4UO_2(CO_3)_3$ Solubility—The log K value for $Na_4UO_2(CO_3)_3$ selected by the Organization for Economic Cooperation and Development/Nuclear Energy Agency compilation (Guillaumont et al. 2003 [DIRS 168382], Table 3-2, p. 75) traces back to another Organization for Economic Cooperation and Development/Nuclear Energy Agency compilation by Grenthe et al. (1992 [DIRS 101671]) for uranium. The log K value in the thermodynamic database *data0.ymp.R5* (DTN: SN0612T0502404.014 [DIRS 178850]) is based on the thermodynamic data given by Grenthe et al. (1992 [DIRS 101671]) who retrieved the thermodynamic parameters for this phase using data from the solubility study by Blake et al. (1956 [DIRS 180470]). Therefore, it is not surprising to obtain a good agreement between prediction and observed solubility (Figure C6-15). Consequently, this comparison is more of a confirmation of the predictive capability of the EQ3/6 code calculation along with the adopted thermodynamic data of aqueous species for this phase. Figure C6-15 shows that there is some level of discrepancy between the EQ3/6 prediction and experimental data. Further discussion on this is given below.

The Organization for Economic Cooperation and Development/Nuclear Energy Agency compilation (Guillaumont et al. 2003 [DIRS 168382]) selects a log K value for this phase. Given

the sanctioning status of such compilation of thermodynamic data, its use in this work is justified for its intended use. The EQ3/6 results tend to under predict the solubility at low NaCl concentration, but the difference between prediction and reported solubility tend to decrease with increasing NaCl concentration. Although the b-dot activity coefficient model should not be used at ionic strengths exceeding 1 molal, the electrolyte considered in the model and experiment (i.e., NaCl) is symmetric and the accuracy of the extrapolation should not suffer significantly as opposed to unsymmetrical electrolytes. Additional solubility data in a $NaClO_4$ solution (Blake et al. 1956 [DIRS 180470], Table II) shows that the differences in solubility between two different electrolytes are overall minimal, and the range is captured by the recommended uncertainty range. The recommended uncertainties for the log value of solubility in molality units are given in Table C6-8. For a triangular distribution in the range a through c, a equals-0.3, b is set to zero, and c is 0.3. The limits (a and c) provide for truncation of the distribution at values different from those in the implementation of a normal distribution.

The uncertainty values were assessed by examining a range that can capture the bulk of the solubility data relative to the EQ3/6 model prediction as depicted on Figure C6-15. The source (Grenthe et al. 1992 [DIRS 101671], p. 327) advances a lower uncertainty of ±0.16 for the log K value of the reaction $Na_4UO_2(CO_3)_3 = 4\ Na^+ + UO_2(CO_3)_3^{---}$ from the analysis of Blake et al. (1956 [DIRS 180470]) data. Figure C6-15 indicates that there is some level of discrepancy between the EQ3/6 prediction and experimental data. Examination of the sources of thermodynamic data for uranium(VI) hydroxide and carbonate aqueous species in the thermodynamic database *data0.ymp.R5* (DTN: SN0612T0502404.014 [DIRS 178850]) indicates that all are consistent with the source Grenthe et al. (1992 [DIRS 101671]). This is also the case for the solid $Na_4UO_2(CO_3)_3$ as already discussed above. Thermodynamic data U(VI) hydroxide aqueous species were not updated in Guillaumont et al. (2003 [DIRS 168382]). However, thermodynamic data for uranium (VI) carbonate complexes were updated, but the differences in the Gibbs energies of formation and resulting log K values for the corresponding reactions are relatively minor. In fact, the differences are within the uncertainties given by both authors. Knowing that thermodynamic data for the solid and aqueous species used in the solubility calculation are consistent with one source (i.e., Grenthe et al. (1992 [DIRS 101671])), then it is unlikely that the discrepancy is due to inconsistency in the thermodynamic data. A possible factor influencing this deviation is the different activity coefficient models used in the retrieval of thermodynamic parameters in the source data and that used in the EQ3/6 solubility calculation. The retrieval of thermodynamic data in the studies by Grenthe et al. (1992 [DIRS 101671]) and Guillaumont et al. (2003 [DIRS 168382]) use the specific ion interaction theory and the EQ3/6 code uses the b-dot equation. Differences in activity coefficient estimations between the two approaches as a function of NaCl concentration were not assessed here, but it is assumed that these would be relatively minor. Another difference is that the tabulated solubility data by Blake et al. (1956 [DIRS 180470]) is given in molarity units. However, the difference in solution density would be rather small, even up to 4 molal NaCl, and the resulting correction to molality units would be too small except in fairly concentrated electrolytes. It should be noted that the retrieval of the log K value for $Na_4UO_2(CO_3)_3$ by Grenthe et al. (1992 [DIRS 101671]) was based on the solubility runs in the $NaClO_4$ electrolyte solutions and a better agreement should be expected with these data. In summary, it is not evident why there is systematic deviation from the predicted solubility and the solubility data except to say that it is relatively small. The regression by Grenthe et al. (1992 [DIRS 101671]) to obtain the infinite dilution log K value for this phase using the specific ion interaction theory

indicates that there are indeed minor deviations from the solubility data as specified in their computed uncertainties. Therefore, some sort of discrepancy would also be expected from the EQ3/6 solubility predictions. Interestingly, the Gibbs energy of formation and log K for the reaction $Na_4UO_2(CO_3)_3 = 4Na^+ + UO_2(CO_3)_3^{----}$, plus their corresponding uncertainties, are identical between the sources Grenthe et al. (1992 [DIRS 101671]) and Guillaumont et al. (2003 [DIRS 168382]) even when the values for Gibbs energy of formation for $UO_2(CO_3)_3^{----}$ in each source are slightly different.

Since the current EQ3/6 prediction tends to underestimate part of the experimental data of Blake et al. (1956 [DIRS 180470]), it seems reasonable to adopt an uncertainty of ±0.3 to capture the bulk of the solubility data relative to the predicted solubility curve. This uncertainty is approximately twice that advanced by Grenthe et al. (1992 [DIRS 101671]) of ±0.16. The lower uncertainty in the latter is expected since it is based on the analysis of solubility data and is not relative to a model prediction as evaluated in this work. The use of a triangular distribution is recommended as to weigh more on the average, and the limits (a and c) provide for truncation of the distribution at values different from those in the implementation of a normal distribution. For the PMA implementation, the sampling of uncertainties among schoepite, Na-boltwoodite, and $Na_4UO_2(CO_3)_3$ will be perfectly correlated.

C6.5.2 Model Implementation

In-Package Chemistry

The calculations of in-package pH are abstracted into lookup tables for the PMA. The set of independent variables for the PMA in-package chemistry abstractions is different from those in the TSPA-LA model. The variables q and pCO_2 are retained and additional parameters for degradation rates, degradation amounts, and volumes of water and degradation products are used. In addition, the PMA in-package chemistry abstractions do not utilize the time since breach parameter.

The type of output in the PMA in-package chemistry abstractions is also modified in one respect. Instead of calculating the maximum and minimum pH, the most likely pH value is calculated. The TSPA-LA Model relies on major buffer reactions to establish the maximum and minimum pH but refrains from predicting the most likely pH.

The PMA in-package chemistry abstractions are split into three flow regimes: vapor diffusion-dominated cases, liquid advection cases, and the cases in between. The diffusion dominated regime is represented by the vapor influx abstraction described in Section C6.5.1. The outputs for this regime are primarily controlled by degradation and heterogeneous equilibrium reactions. The high-flow liquid influx regime is represented by the high-flow liquid influx abstraction (Section 6.5.1). Its outputs are primarily controlled by heterogeneous equilibrium reactions and liquid influx composition. The abstraction for the cases in between is an interpolation between the vapor influx and high-flow liquid influx abstractions. Its outputs are controlled to varying degrees by degradation reactions, heterogeneous equilibrium reactions, and liquid influx composition.

Diffusion-Dominated Cases—The vapor influx abstraction consists of a look-up table for each combination of pCO_2 and k_{ss}/k_{wf} in each cell in Table C6-3. The look-up tables provide pH, ionic strength, and concentrations of uranium, plutonium, neptunium, and fluorine as a function of V_s/V_w. Only pH is used in the PMA. The k_{ss}/k_{wf} ratio is represented in the look-up tables as R_{sw}, which is the ratio of the cumulative moles of stainless steel degraded in the cell, n_{ss}, to the cumulative moles of waste form degraded, n_{wf}. For the process model, these ratios are equivalent because they are held constant for the entire simulation. In the PMA simulation, these ratios will not always be the same because the rate ratio is an instantaneous ratio while the mole ratio is cumulative. In the PMA, instantaneous rates change with time and will go to zero when the associated material is completely degraded. It is appropriate to use the ratio of the moles of degraded materials to determine pH and ionic strength in this case because dissolved materials are not flushed out of the pore space under vapor influx conditions. Instead, the water composition in the pore space should reflect the cumulative degradation of materials in the cell.

V_s/V_w increases for each successive row in the look-up tables because each row represents an equilibrium condition after an additional aliquot of water is removed. Many of the rows at the tops of these tables are not applicable to the PMA because V_s/V_w is less than 1.5 until a sufficient amount of water is removed. V_s is calculated by EQ3/6 and included in the output. V_w is estimated from the mass of solvent in the EQ3/6 output assuming a density of 1 kg/L and negligible volume effects from dissolved constituents.

Liquid-Advection Dominated Cases—The high-flow liquid influx abstraction provides look-up tables to determine steady-state pH when the degradation rates are low compared to the flush rate (i.e., when the Damkohler number is low enough that degradation rates do not considerably affect the steady-state pH). To determine quantitatively the range of the high-flow liquid influx abstraction, process model steady-state results were plotted (in **Da.xls* spreadsheets in corroborative DTN: SN0704PMAIPCPM.001 [DIRS 180745]) as a function of an empirical Damkohler ratio, Da:

$$Da = \frac{(k_{ss} + k_{wf})}{q/V_p} \qquad \text{(Eq. C6.5-20)}$$

where the numerator is the sum of the degradation rates of the stainless steel and waste form in the cell and the denominator is the flush rate or turnover rate (q/V_p). Da has units of moles. The flush rate is used in the denominator instead of q because it is a much better indicator of how fast aqueous components are removed from the cell as the pore volume changes with time.

The EQ3/6 simulations indicate that below a Da value of 0.1, degradation rates negligibly affect the steady-state pH and ionic strength for each cell and at each pCO_2. Thus, when TSPA determines that Da is less than or equal to 0.1, then the pH and ionic strength values in the look-up tables of the high-flow liquid influx abstraction are defined to be the most likely pH and ionic strength values in the cell at the given time. These most likely values are used in combination with the uncertainties defined in the section below to determine the sampled pH values in TSPA calculations.

Intermediate Cases—For the cases with intermediate liquid flow rates, the pH is calculated through a linear interpolation between the output values in the vapor diffusion abstraction and

those in the liquid advection abstraction. This abstraction applies when Da is between 0.1 and 100. The detail of the interpolation process is explained in the Low-Flow Abstraction worksheet of *IPC PMA Flow Abstraction r1.xls*. The advective flux of liquid water is provided by the water balance model in Section 6.4. For simplicity, at the high advective flow end, only the lookup tables calculated with condensed water (deionized water) are used, since the difference in the predicted pH between the condensed water and the seepage water is insignificant.

Uncertainties—The output uncertainty is determined based on uncertainties in the inputs, uncertainties in the model, and ranges observed in sensitivity simulations. These uncertainties are adopted from the TSPA-LA model. The in-package chemistry model for TSPA-LA was designed to determine the maximum and minimum pH values in the vicinity of the waste form. The TSPA-LA model does this by identifying and quantifying the major pH-buffering reactions that cannot be overcome by possible sources of acid or base. The secondary minerals that accumulate in each In-Package Chemistry cell are primarily responsible for the buffer capacities, which are quantified by titrating accumulated minerals with hypothetical additions of acid and base. The hypothetical additions are extreme and exceed anticipated sources so that maximum and minimum pH limits are determined with a high degree of confidence.

Sensitivity analyses confirm that the established maximum and minimum pH limits are reasonable (SNL 2007 [DIRS 180506], Section 6.6). Sensitivity simulations for each of the three In-Package Chemistry cells involved varying liquid flux rates from 0.1 to 1,000 L/yr, varying degradation rates of the In-Package Chemistry cell materials and waste forms from minimum to maximum values, and varying the composition of the liquid influx among a range of compositions. Sensitivity analyses for liquid flux rate and degradation rates included variations in liquid flux composition.

For the PMA In-Package Chemistry abstraction, the maximum and minimum pH values determined in the TSPA-LA model are used to bound the pH uncertainty. The pH distribution is defined as triangular with the most probable value equal to the pH value determined in the PMA In-Package Chemistry abstraction (corroborative DTN: SN0704PMAIPCAB.001 [DIRS 182602]) and the maximum and minimum values equal to the values established in the TSPA-LA model (SNL 2007 [DIRS 180506], Section 6.10.1).

Commercial Spent Nuclear Fuel Cladding

In the PMA, the Cladding Degradation Submodel is invoked in both the Waste Package EF and Drip Shield EF Modeling Cases. Since no WP failures are predicted to occur during the first 10,000 years postclosure, the Cladding Submodel was not used in the Nominal Scenario Class. Input parameters include the fraction of predisposal failures (as-received failure fraction) and the fraction of CSNF WPs containing stainless-steel-clad fuel. The groups of WPs represented in the TSPA have an initial percentage of failed rods defined by the log uniform distribution with a range 0.01 percent to 1 percent (SNL 2007 [DIRS 180616], Table 7-1[a]). In addition, 1.0 to 2.0 percent (uniformly distributed) of the WPs are predicted to contain stainless-steel-clad fuel rods and the total amount of stainless-steel-clad fuel is fixed at 1.0 percent of the total CSNF (SNL 2007 [DIRS 180616], Table 7-1[a]).

The early failed WPs are partitioned into three fuel groups. The CDSP WPs containing HLW glass and DSNF canisters are assigned to the one fuel group. The CSNF WPs containing only Zircaloy-clad fuel are assigned to a second fuel group. The CSNF WPs containing both Zircaloy and stainless-steel-clad fuel are assigned to a third fuel group. In the PMA, each WP is assigned an initial fraction of failed cladding, sampled from a log-uniform distribution (f_2). This parameter represents epistemic uncertainty and is sampled once per realization. It applies to all Zircaloy-clad CSNF fuel. The third group contains both Zircaloy-clad and stainless-steel-clad fuel. The stainless-steel-clad fuel is modeled with cladding that is completely degraded. The fraction of WPs containing stainless-steel-clad fuel is sampled from a uniform distribution, representing epistemic uncertainty. This parameter is sampled once per realization. The fraction of total CSNF inventory that is stainless-steel clad is not uncertain. The ratio of these two parameters gives the fraction of stainless-steel-clad fuel in each of the WPs in the third fuel group. This fraction is added to the predisposal failure fraction assigned to the Zircaloy-clad fuel to give the total initial fraction of failed rods in each of the WPs in the third fuel group, f_3.

The structure of the TSPA-LA Model file does not permit the modeling of two SNF fuel groups. Therefore, the two groups are combined and the resulting cladding failure fraction, F_{fail}, is taken to be a weighted sum of the individual failure fractions for the two WP groups:

$$F_{fail} = \frac{N_2 \cdot f_2 + N_3 \cdot f_3}{N_2 + N_3} \qquad \text{(Eq. C6.5-21)}$$

where N_2 and N_3 are the number of WPs assigned to the second and third fuel groups, respectively, and f_2 and f_3 are the clad failure fractions for the second and third fuel groups, respectively.

Degradation Rate of Commercial Spent Nuclear Fuel

As discussed in Section C6.5.1, the functional dependence of the dissolution rate on water chemistry in the PMA remains the same as in the TSPA-LA model. The distribution range of the effective surface area of CSNF is modified, and two additional scaling factors are included to account for the effect of long-term dissolution and the temporal evolution of gamma and beta radiation fields. The distributions of the three parameters are recommended as listed in Table C6-6.

Degradation Rate of High-Level Waste Glass

The conceptual model for HLW glass dissolution described in Section C6.5.1 is based on chemical and physical feedback caused by formation of an increasing reaction rind on the surface of the glass. The rate at which the reaction rind forms is a function of solution chemistry (primarily pH and temperature), with the most aggressive conditions leading to the most rapid formation of the rind. Conceptually, such conditions should lead to the most rapid reductions in dissolution rate; however, the modeled rate at which the rind thickness provides feedback is a function of the timestep (Δt_i), so that the longer the timestep, the longer a fixed dissolution rate is applied to the mass of glass remaining. Under aggressive chemical conditions and relatively

long timesteps, this can lead to a physically unrealistic mass of glass being dissolved in a single timestep. This potential effect can be mitigated by separating the glass into two components, each of which dissolves at a different rate. The 'fast fraction' is that portion of the mass of a glass log that is assumed to dissolve at the forward rate (for which the reaction affinity term is unity), and the 'slow fraction' is the remaining portion of glass, assumed to dissolve at the long-term rate.

Depending on the value of the final reaction affinity, $(1\text{-}Q/K)_{final}$, the long-term reaction rate, $R_{long} = k_f(1\text{-}Q/K)_{final}$, is achieved once the reaction rind has attained between 5 and 15 times the critical reaction-rind thickness, T_{RC}, with the larger thickness required when the lowest value of $(1\text{-}Q/K)_{final}$ is used (Figure C6-16). Therefore, we can calculate the maximum mass of one glass log necessary to achieve a reaction-rind thickness sufficient to impose the long-term rate on the remaining mass of glass:

$$\text{Rate}_{glass} \leq 1.1R_{long} \text{ when } T_R = 15T_{RC}. \quad \text{(Eq. C6.5-22)}$$

The mass of glass dissolved is given by the volume of glass dissolved times the glass density:

$$M_D = V_{MD} \times \rho. \quad \text{(Eq. C6.5-23)}$$

The volume of dissolved glass is equal to the surface area of the glass log (assumed equal to $2\pi r_o L_o$, from the current document) times the rind thickness:

$$V_{MD} = 2\pi r_o L_o \times T_R. \quad \text{(Eq. C6.5-24)}$$

So that

$$M_D = = 2\pi r_o L_o \times T_R \times \rho \quad \text{(Eq. C6.5-25)}$$

Letting $r_o = 0.3$ m, $L_o = 3.9$ m, $\rho = 2{,}700$ kg/m^3, and $T_R = 15T_{RC}$ gives

$$M_D = 2\pi(0.3)(3.9) \text{ m}^2 \times 15T_{RC} \text{ m} \times 2{,}700 \text{ kg/m}^3 \quad \text{(Eq. C6.5-26)}$$

$$M_D \text{ (kg)} = 110T_{RC} \text{ m}^3 \times 2{,}700 \text{ kg/m}^3 = 297{,}000 \times T_{RC}. \quad \text{(Eq. C6.5-27)}$$

The proportion of a glass log that must be dissolved in order to approach the long-term rate is

$$M_D/M_0 = (297{,}000/2710) \times T_{RC} = 110 \text{ m}^{-1} \times T_{RC} \text{ m} \quad \text{(Eq. C6.5-28)}$$

where M_0 is the initial mass of an average glass log (2710 kg) and T_{RC} is the critical rind thickness in meters.

For the distribution of T_{RC} used in the PMA glass degradation model (Table C6-7), this gives a distribution for the proportion of glass to be assigned as the fast fraction; that is, the fraction of glass that dissolves at the forward rate (k_f). The fraction of glass where the long-term rate ($R_{long} = k_f(1\text{-}Q/K)_{final}$) is applied is simply one minus the fast fraction; this is the slow fraction. The intrinsic reaction rate constant k_0 in Equation C6.5-3 is set to $1\text{x}10^7$ g/m^2/d as discussed in the Conceptual Description. Multiplying the forward and long-term rates (g/m^2/d) by the specific

surface area (and the appropriate exposure factor) gives the fractional degradation rate (d^{-1}) used in the PMA. Thus,

Forward fractional rate: $rate_{forward} = S_{SP} \times f_{exposure} \times k_f$ (Eq. C6.5-29)

Long-term fraction rate: $rate_{long\text{-}term} = S_{SP} \times f_{exposure} \times k_f \times (1\text{-}Q/K)_{final}$. (Eq. C6.5-30)

These are the fractional degradation rates applied to the fast and slow fractions, respectively.

Uncertainty Associated with Uranium(VI), Plutonium(IV), Neptunium(IV), and Neptunium(V) Solubility Limits

As discussed in the Conceptual Description, the PMA provides uncertainties on selected actinide solid solubilities that are based on available experimental solubility and thermodynamic data reported in the scientific literature or in specialized data compilations. The recommended uncertainties and associated distributions for the relevant actinide solids in log solubility (given in molality units) were in essence based on comparisons of EQ3/6 code predictions with measured solubilities. EQ3/6 run outputs are given in corroborative DTN: SN0704PMASOLUB.001 [DIRS 182787]. In cases where solubility data were either not available or too limited for a valid statistical comparison, the uncertainties were then based on the evaluations of thermodynamic data described in the Organization for Economic Cooperation and Development/Nuclear Energy Agency compilations for the actinide solid of interest. The assigned uncertainty bounds were implemented in a continuous form as a function of pH and fCO_2. No additional uncertainty was assigned to explicitly capture the effects of any particular component given the lack of solubility data for many of these actinide solids as a function of solution chemistry. The recommended PMA solubility uncertainties are given in Table C6-8.

C6.6 UNSATURATED ZONE TRANSPORT

C6.6.1 Conceptual Model

The UZ Transport Model component of the PMA modifies certain elements of the TSPA-LA model thought to be conservative by using an alternate conceptual model. The resulting representation of the UZ transport consists of a different set of computer input files, a different version of the FEHM code, and accompanying documentation that allows a complete TSPA analysis model run to be performed with the changes defined herein in place. Many of the modeling assumptions and implementation details for the PMA are identical to those of the TSPA-LA model. Those components that have been changed to implement the PMA include: the colloid diversity model for colloid-facilitated radionuclide transport, the use of an alternate conceptual model and a matrix diffusion enhancement factor that represents the effects of small-scale fractures, and a new approach and parameter distribution for water table rise under future climate conditions.

Colloid Diversity Model (CDM) for Colloid-Facilitated Transport

In the TSPA-LA model (SNL 2008 [DIRS 184748], Section 6.4.5), radionuclides assumed to be affected by colloid-facilitated transport are handled using a composite of three individual components: 1) the reversibly sorbed species, 2) a fraction that is governed by irreversible

attachment to colloids that undergo retardation due to colloid attachment/detachment processes, and 3) a 'fast fraction' of colloids that were assumed to transport conservatively (without any filtration or retardation). The fast fraction was calculated by assuming that the CDF of observed filtration rate constants (from the same lab and field experiments and using the same weighting approach) reflects a typical population of colloids with filtration rate constants that are distributed according to the CDF of observed rate constants. The rate constant CDF was then extrapolated to estimate the cumulative probability associated with a rate constant less than or equal to the reciprocal of a specified groundwater travel time, and the resulting probability was taken to be the value of the fast fraction associated with that travel time. The fast fraction was calculated for a combined UZ/SZ groundwater travel time of 100 years and was assumed to apply to all TSPA realizations. The remaining colloids containing radionuclides (one minus the fast fraction) were all assumed to transport with a single retardation factor that is randomly sampled from the retardation factor CDFs developed from the experimental data, but truncated at the low end to avoid retardation factors of one (which were accounted for in the fast fraction). Details of the approach are provided in *Particle Tracking Model and Abstraction of Transport Processes* (SNL 2008 [DIRS 184748]).

This approach is modified in the PMA to address technical issues that could underestimate performance of the natural barriers for colloid-facilitated radionuclides. Principally, the model is considered to be conservative because it does not account, except in a coarse way, for the inherent variability of transport properties of individual colloids in a colloid population. In the PMA, the treatment of colloid-facilitated contaminant transport represents the variability of mobility of individual colloids as a process that is inherent to the colloid population, rather than as observations that lead to uncertainty in the transport properties within a conventional, single-valued parameter. The process of retardation via attachment and detachment of colloids on immobile surfaces is often modeled with time and space invariant parameters; here it is modeled assuming a diverse population of transport properties that account for the inherent variability of colloid size, surface charge and chemical properties, mineralogy, and the concomitant impact on colloid mobility. The critical concept is the assumption that the transport properties of colloids in nature are heterogeneous. Therefore, a single set of colloid transport parameters is insufficient to capture the composite transport behavior of a contaminant that is sorbing or is intrinsically bound to colloidal material. The colloid diversity treatment is formulated to account for these heterogeneities.

Robinson et al. (2007 [DIRS 180698]) introduced an approach called the 'colloid diversity' model, in which colloids are assigned a wide range of retardation factors (rather than single retardation factors for volcanics and alluvium) reflecting the diversity in retardation factors inherent in the experimental data. Instead of this variability being transformed into parameter uncertainty, the variability itself is built into the model. With regard to the implementation in the PMA, transport of species taken to be affected by colloid-facilitated transport is still handled by subdividing the species into up to three components: the reversibly sorbed component; the irreversibly sorbed component, which undergoes colloid retardation; and the fast fraction, a portion of the inventory assumed to irreversibly sorb radionuclides, with no colloid retardation. For isotopes of plutonium and americium, all three components are simulated; whereas for isotopes of cesium, protactinium, thorium, and tin, only the reversibly sorbed species are included. For all three components, the colloid diversity model changes the way the simulation

is performed. The implementation of each of these components in the colloid diversity model is outlined below.

Fast Fraction—As in the TSPA-LA model, the fast-fraction ('If') species travel through the system unaffected by sorption, filtration, or diffusion processes. The computational approach describing the fast fraction is identical to that developed in *Particle Tracking Model and Abstraction of Transport Processes* (SNL 2008 [DIRS 184748]), except that the size exclusion option is not active. Instead, it is assumed that all processes related to the transport of colloids through the system are governed by the colloid diversity model, which assigns specific characteristics to each individual colloid that determines its subsequent transport behavior. For the specific case of the fast-fraction species, this subpopulation is defined as the fraction of all individual colloids that transport with an effective retardation factor of 2 (the minimum value possible in this model analysis) for a given realization. Thus, in contrast with the TSPA-LA model, individual colloid transport processes in the TSPA-LA model are assumed to be subsumed in the colloid diversity model. Also, in contrast to the TSPA-LA model, the proportion of the mass that is assigned to the fast fraction varies from one realization to the next, and depends on the colloid diversity model parameters of that realization.

Irreversibly Sorbed Fraction—This fraction, represented by the 'Ic' species, applies only to isotopes of plutonium and americium and is subject to the colloid diversity model. This approach, implemented in FEHM V 2.25 (STN: 10086-2.25-00 [DIRS 182477]), assigns each particle in an Ic species a unique value of the retardation factor R_{coll} by sampling from the statistical distribution function defining R_{coll} for that particular species. Transport of the colloidal particles through the system is subject to spreading due to the variability of R_{coll} among the total population of colloids for each specific radioisotope. In the SZ part of the colloid diversity model, an option exists to be able to employ a stratified sampling strategy in which particles throughout the entire range of R_{coll} values are assigned, with weights established in order to reproduce the desired distribution. This approach can dramatically improve the numerical accuracy of the solution when the range of R_{coll} values spans several orders of magnitude. For the UZ, this option is not available in FEHM V 2.25 because difficulties associated with the simulation of decay chains make this implementation considerably more complex. Instead, in the UZ, uniform weighting and sampling from the distribution is used. This current limitation should not significantly impact the UZ PMA because TSPA simulations use a large number of particles (10^5 or more).

Observations and data used in the development of the R_{coll} distribution in the TSPA-LA Model were revisited. Those data are interpreted with respect to the forward and reverse rate constants, k_f and k_r, respectively. These parameters are related to R_{coll} using the following expression:

$$R_{coll} = 1 + \frac{k_f}{k_r}. \qquad \text{(Eq. C6.6-1)}$$

As in the TSPA-LA Model, the colloids associated with the Ic species are assumed not to undergo diffusion. In addition, the size exclusion and filtration at matrix interfaces is also not applied. Instead, the size exclusion and filtration processes are implicitly included in the colloid diversity model through the use of new parameters defining the CDF for the colloid retardation

factor. Therefore, it is assumed that transport processes such as these are all subsumed within the colloid diversity approach to modeling transport. Alternatively, the analysis could have been developed such that the size exclusion process or the filtration at matrix interfaces had been left as individual processes explicitly simulated. However, this approach would not have been consistent with the approach embodied in the colloid diversity model, which foregoes a process-by-process depiction of colloid transport in favor of a phenomenological approach involving retardation factors that can be parameterized so that it is consistent with lab and field observations.

Reversibly Sorbed Species—These species transport through the system subject to reversible sorption on the colloids and on the rock matrix. When the mass is in the aqueous phase, diffusion can also occur. As in the TSPA-LA model, these species are governed by a transport equation that was developed in *Particle Tracking Model and Abstraction of Transport Processes* (SNL 2008 [DIRS 184748], Section 6.4.5, Equation 6-15a):

$$\left(\frac{R_f + K_c R_{coll}}{1 + K_c}\right)\frac{\partial C}{\partial t} = D_{eff}\frac{\partial^2 C}{\partial z^2} - v\frac{\partial C}{\partial z} - \frac{q}{b(1+K_c)} \qquad \text{(Eq. C6.6-2)}$$

where R_f is the retardation factor of the dissolved contaminant (assumed to be 1 for the fractured medium and governed by the retardation factor for sorption in the matrix), K_c is the sorption partition coefficient onto colloids, C is concentration, v is velocity, D_{eff} is the effective dispersion coefficient, q is the flux term to or from the matrix due to diffusion, and b is the fracture half aperture. The factor multiplying the time derivative is the effective retardation factor for a reversibly sorbed species. This mathematical expression is identical to that used in the TSPA-LA model, and the parameters K_c, R_f, and b are determined in an identical fashion as the TSPA-LA model. The one significant difference in the PMA for reversibly sorbed species is that the colloid diversity approach is used to determine an effective colloid retardation factor that is used in Equation C6.6-2. This parameter, which we call $\overline{R}_{coll}$ to distinguish it from the retardation factor of individual colloids, is now discussed. The first assumption is that the colloid diversity model governs the range of transport properties of colloids involved in the transport of reversibly sorbed species. The assumption of reversible equilibrium sorption means that radionuclide sorbs and desorbs rapidly on and off the colloids, resulting in an effective colloid retardation factor $\overline{R}_{coll}$ governing the behavior. We further assume that, in the absence of detailed data to the contrary, the equilibrium sorption coefficient for sorption of a radionuclide onto colloids is independent of that of the colloid's retardation factor (R_{coll}). These simplifications lead to the following expression for the effective colloid retardation factor for reversibly sorbed species:

$$\overline{R}_{coll} = \int_{R_l}^{R_u} \eta(R_{coll}) dR_{coll} \qquad \text{(Eq. C6.6-3)}$$

where R_l and R_u are the minimum and maximum values of R_{coll} in the distribution and $\eta(R_{coll})$ is the density function for R_{coll}; that is, $\eta(R_{coll})dR_{coll}$ is the fraction of the colloid population possessing a value of R_{coll} between R_{coll} and $R_{coll} + dR_{coll}$. Thus, when the assumptions outlined above are made, the effective value of colloid retardation factor reduces to the mean value in the population. This relationship is implemented in FEHM V 2.25 so that the value varies from realization to realization, subject to the distribution of R_{coll} discussed below.

Development of Parameter Uncertainty Distributions

In the PMA, the development of the retardation factor distributions has been modified to better address the considerable uncertainty in the colloid experimental data, and particularly in the extrapolation of these data to TSPA time and distance scales. The retardation factor distributions, and also the fast fractions, are now realization-dependent because they are travel time dependent. In the TSPA-LA model, colloid retardation factor distributions for colloids with irreversibly-sorbed radionuclides were developed by constructing CDFs of retardation factors observed in lab and field experiments, with field data being given twice the weight as lab data because of their more relevant distance and time scales. These CDFs were assumed to be uncertainty distributions for the retardation of colloids due to attachment-detachment processes occurring for colloids carrying radionuclides. In the development below, the same data used previously are re-examined using the colloid diversity model approach to develop the parameter uncertainty distributions for the PMA. Note that as in the TSPA-LA model, data collected under saturated conditions are assumed to be appropriate for both the UZ and SZ systems.

Figure C6-17 shows plots of colloid filtration rate constants (k_f, hr^{-1}) and fractional recoveries as a function of groundwater travel time in laboratory and field tracer tests conducted in saturated fractured volcanics. These plots reflect the same data that were used to develop filtration rate constant and retardation factor distributions for saturated volcanics (BSC 2004 [DIRS 170006]). Figure C6-18 shows plots of retardation factors (R_{coll}) and detachment rate constants (k_r, hr^{-1}) as a function of travel time for the same experiments as Figure C6-17. These two parameters are inherently more uncertain than k_f values because the detachment rate constants are poorly constrained in most of the experiments, and the retardation factors are calculated using the detachment rate constants. Figures C6-19 and C6-20 are analogous plots to Figures C6-17 and C6-18 for saturated alluvium experiments. Again, the data are the same used to develop filtration rate constant and retardation factor distributions for alluvium in *Saturated Zone Colloid Transport* (BSC 2004 [DIRS 170006]), except new data points (output DTN: LA0705PR150304.001 [DIRS 181744]) are added for field experiments in the saturated alluvium south of Yucca Mountain (labeled YMP 22S Field in the plots).

The important points from all these plots are:

- Although the experiments involved a wide range of colloid compositions and sizes and significantly different distance scales, there is a clear tendency for both filtration rate constants and fractional recoveries to decrease as travel times increase.

- There is no clear correlation of retardation factors with time scale, although there appear to be trends within some data sets, including the Schijven data sets.

- Detachment rate constants appear to have a weak negative correlation with time/distance scales, and with the exception of three of the C-wells field data points, the detachment rate constants never exceed 1/travel time. Note that the nonconforming C-wells data points are all associated with attempts to fit a double-peaked breakthrough curve that was unique to all the data sets and required splitting the colloid mass into separate 'pathways' that had different detachment rate constants (SNL 2007 [DIRS 177394], Appendix D). These complications may be the reason that these data points do not conform to the general trend. This result is considered to be a factor in assessing the uncertainty of the parameters in the colloid diversity model but does not invalidate the approach.

Figure C6-21 shows the k_f values and fractional recoveries for the fractured volcanics, where data points associated with the same colloids in the same flow system (but with different travel times) are connected by lines. The field data in these plots are colored and the lab data are black. These plots show that there is an even better case for k_f values and recoveries decreasing with increasing time scales when different types of colloids and different flow systems are not viewed as a single data set. Figure C6-22 shows analogous plots for saturated alluvium. Only a few experiments contradict the general trends. In some cases, the colloids used in the experiments were so nonreactive that they were essentially fully recovered at the two different travel times studied (e.g., the natural colloids and 190-nm CML microspheres in the alluvium lab experiments), suggesting that the travel times were not long enough to discern a trend (although such a trend could only be downward with increasing time).

Because the colloid 'fast fraction' is essentially equivalent to the fractional recovery of colloids that are not retarded, it was decided that the best approach to obtaining a distribution of filtration rate constants for a colloid diversity model was *not* to simply construct a CDF of all experimental filtration rate constants (as was previously done) but rather to deduce a distribution that yielded a recovery versus travel time dependence consistent with the plots of Figures C6-21 and C6-22. It was also desirable from an implementation standpoint to have a single rate constant and retardation factor distribution rather than separate ones for the volcanics and alluvium. Figure C6-23 shows the log recovery data as a function of log time for both the volcanics and the alluvium on a single plot along with linear regression fits to each individual data set as well as a single linear regression fit to the combined data set. The upper and lower 95 percent confidence intervals, associated with the latter fit, are shown as the light dashed lines, and the 95 percent confidence intervals associated with the slope of the linear fit are shown as the dark dashed lines. The combined fit was forced to pass through the origin (forcing a fractional recovery of 1.0 at a time of 1 hour). The individual alluvium fit has a much steeper negative slope than the individual volcanic fit, mainly because of several laboratory alluvium tests involving natural smectite colloids and 190-nm fluorescent carboxylate modified polystyrene latex (CML) microspheres that had essentially complete fractional recoveries and several low recovery data points corresponding to virus transport over different distance/time scales in a sandy aquifer in the Netherlands (Schijven et al., 1999 [DIRS 162423]). The latter data are the only data that are not specific to the Nevada Test Site. These data were included

because they were previously used in the absence of any site-specific alluvium field data (a data gap that has since been addressed by data from a crosshole tracer test at Nye County Site 22, labeled YMP 22S Field on Figures C6-19 and C6-20), and they also serve to illustrate trends of decreasing recovery and filtration rate constant with time and distance under natural-gradient conditions.

The CDF of all filtration rate constants (assuming twice the weight for field data versus lab data) was previously shown to follow a linear trend on a log-log plot of probability versus rate constant (top figures of Figures C6-17 and C6-19), so a CDF P, with intercept b and slope m, of the following form was assumed to represent the diversity of rate constants in a colloid population:

$$\log_{10} P = b + m \cdot \log_{10}(k_f). \qquad \text{(Eq. C6.6-4)}$$

Equation C6.6-4 has a long tail at the low probability end of the distribution, consistent with a small fraction of colloids having small filtration rate constants and, hence, equilibrium retardation factors approaching unity.

Figure C6-24 shows the fractional recovery versus travel time superimposed over all the data from Figure C6-23 for three CDFs that approximately match (1) the best linear fit (passing through the origin) to the combined data set, (2) the CDF of all rate constants (with twice the weight given to field data), and (3) the best fit to the 2 highest recovery data points associated with the field tracer test in the fractured volcanics at the ER-20-6 site, which had the highest recoveries of any of the field tests. Fits (1) and (3) were chosen to represent the lower and upper bound CDFs, respectively, for the colloid diversity model.

Although it would seem justified to use CDFs that result in lower recoveries than (1), which is effectively only the 'mean' CDF that is consistent with the data, the use of CDFs with lower recoveries than (1) resulted in negligible recoveries/fast fractions for travel times exceeding a few years. Because most of the data (including all the field data) are associated with synthetic organic colloids (microspheres and viruses) rather than inorganic colloids, this approach was considered prudent. The approach also inherently de-emphasizes the virus data from a shallow sandy aquifer in favor of colloids in more relevant settings. Furthermore, the approach implicitly weights the field data sets more heavily than the lab data sets because the field data exert more influence on the slope of the best-fitting line through the data (owing to their greater distance from the origin) and also because the upper bound CDF is based on a fit to the field data set with the highest recoveries. Finally, the observations of the colloid-facilitated transport of plutonium over ~1 km in ~30 years from a nuclear test cavity at the Nevada Test Site (Kersting et al., 1999 [DIRS 103282]) provides a good argument for weighting the data such that the filtration rate constant CDFs emphasize the higher recovery data. The CDFs associated with (1), (2), and (3) above are plotted along with the actual CDF of the filtration rate constants (with twice the weight given to field data) on Figure C6-25.

To generate CDFs of colloid retardation factors based on the filtration rate constant CDFs, it is necessary to assume (1) some uncertainty in the latter CDFs (captured as slope and/or intercept uncertainty), and (2) a distribution of colloid detachment rate constants. To address (1), it is

assumed that the slope of the filtration rate constant CDF versus k_f on a log-log scale is subject to an uncertainty distribution given by a triangular distribution with values [0.17, 0.51, 0.85], which correspond to the negative of the slopes of the three lines on Figure C6-24. Because the intercept has a lesser effect on the filtration rate constant CDF than the slope, it was assumed to be fixed at a value of 0.2. To address (2), uncertainty in the detachment rate constants are assumed to be governed by a triangular distribution with a minimum value of 0.01/travel time (hr^{-1}), mode of 0.1/travel time (hr^{-1}), and maximum of 1/travel time (hr^{-1}) for any specified travel time. The latter serves as a reasonable upper bound for detachment rate constants, which were shown on Figures C6-18 and C6-20 to never exceed 1/travel time except for the C-wells tracer test involving two tracer peaks. The mode of 0.1/travel time is greater than many of the data points on Figures C6-18 and C6-20, but this value, extending down to the minimum of 0.01/travel time, is justified because of the poorly constrained nature of the detachment rate constants.

Figure C6-26 shows the resulting minimum, central, and maximum CDFs of colloid retardation factors associated with a 100-year travel time. The minimum CDF corresponds to a slope of 0.85 for the k_f CDF and a value of 0.01/travel time (hr^{-1}) for k_r, and the maximum CDF corresponds to a value of 0.17 for the k_f CDF slope and a value of 1/travel time (hr^{-1}) for k_r. The central CDF corresponds to the modes of the distributions of slope and k_r. Clearly, there is a great deal of uncertainty associated with the retardation factor CDFs. This uncertainty reflects the considerable scatter in the available data sets as well as the uncertainty associated with the extrapolation of the data to much longer time and distance scales. The large retardation factors associated with each of the CDF realizations will result in some filtration of colloids that are essentially permanent, which is a desirable effect that is considered to improve the colloid diversity model.

Because there are no colloid transport data associated with the UZ, it is assumed that the same retardation factor CDFs apply to both the UZ and SZ, and the CDFs ideally should be based on the combined UZ and SZ travel time in a given TSPA realization. This assumption may be conservative because of filtration and retardation processes that could be present in the UZ that do not occur in the SZ, such as colloid attachment to air-water interfaces, thin-film straining, and imbibition into the matrix during wetting-drying cycles.

Another implementation issue for the PMA concerns the independent/decoupled nature of the UZ and SZ systems. This implementation, rather than a single, unified UZ/SZ system, poses problems for simulating transport of colloids using the colloid diversity model. If the same retardation factor CDF is sampled once for the UZ and again for the SZ, there will be a strong tendency to eliminate the portion of the distribution with small retardation factors. That is, the probability of sampling small retardation factors in both the UZ and SZ and thus obtaining a small combined retardation factor is exceedingly small. The consistent approach is one in which fast-moving colloids in the UZ remain fast moving in the SZ.

To ensure that the fast portion of the colloid distribution is not under-sampled, leading to non-conservative results, the fast fraction species is retained, even though, in principle, this fraction could fall out naturally from the colloid diversity approach. Instead, for the PMA, the fast fraction is defined as the cumulative probability associated with a retardation factor of 2, the

minimum value in the distribution. Then, for the Ic species, a method is required that yields the appropriate overall CDF for the combined UZ/SZ system. Two approaches are taken to confront this issue. In both cases, the travel time used to establish the CDF for retardation factor is taken to be that of the SZ. In the first approach, the colloid diversity model for the Ic species is applied only to the SZ system, whereas for the UZ, the Ic species is conservatively taken to be governed by all R_{coll} values equal to 2. This assumption is valid if the travel time is dominated by the SZ portion of the flow path. However, if the travel times are equal to one another, then the process of individually sampling the CDFs in the UZ and SZ can be overcome by altering the CDF such that the composite behavior is the one that is desired. It can be shown that this altered CDF can be obtained by using a CDF that is sampled independently for both the UZ and SZ that has the retardation factors from the original CDF (combined UZ and SZ) but assigns the square root of the cumulative probabilities as the cumulative probability associated with each retardation factor. Figure C6-27 presents an example calculation that demonstrates that this approach reproduces the original combined UZ and SZ CDF when the distribution is randomly sampled twice.

Water Table Rise for Future Climate

In the TSPA-LA model, future climate conditions are simulated assuming that the system instantaneously changes from one steady state flow field to another at the time the climate changes. Future climates, termed the monsoonal and glacial-transition climate states, are represented by adopting a flow field in which infiltration rates are elevated compared to the present-day conditions for that realization. In the UZ flow model area, the present-day water table varies from less than 730 m to greater than 980 m above mean sea level (BSC 2004 [DIRS 169855] Figure 6.2). Within the repository fingerprint, the present-day water table varies from around 730 m to 850 m above mean sea level (BSC 2004 [DIRS 169855] Figure 6.2). Note that the bottom boundary for the flow models of all climate states is the present day water table. For use in conjunction with FEHM's multi-species particle tracking model the flow-field files for the monsoon, glacial-transition, and post-10,000-year climate flow fields from the UZ Flow Model Abstraction are post-processed to approximate the affects of a rising water table. The rising water table is approximated by constraining the water table to a minimum elevation of 850 m above mean sea level (SNL 2008 [DIRS 184748] Section 6.4.8). That is for future climates, any locations where the present-day water table is below 850 m it is set to 850 m and any locations where the present-day water table is above 850 m, the water table is not adjusted from the present day level (see BSC 2004 [DIRS 169855]). In the TSPA-LA model, the rise of up to 120 m above a nominal level of 730 m was adopted without uncertainty. This approach was considered to be conservative with respect to the UZ transport times, because 850 m was considered to be an upper bound, and the higher water table shortens the travel distance and travel times through the UZ. In the PMA, the water table elevation is taken as an uncertain parameter with a distribution that results in most realizations being conducted with a minimum water table elevation that is less than 850 m. This change should lead to an analysis that is less conservative with respect to UZ transport times than the TSPA-LA Model and one which incorporates the uncertainty in water table elevation.

A workshop was conducted on August 23, 2006, to quantify uncertainty in past water table rise at Yucca Mountain for use in the TSPA Model for future climatic conditions. This was accomplished by convening a group of Project participants who are technical experts in the areas of hydrology, geochemistry, mineralogy, and statistics/uncertainty to represent and consider the

multiple lines of evidence regarding this process. The workshop consisted of a series of presentations on previous studies and new geochemical information relevant to past water table rise at Yucca Mountain, followed by a quantitative assessment of uncertainty in water table rise by the entire group:

- James Paces (USGS)
- Leonid Neymark (USGS)
- Kenneth Rehfeldt (LANL)
- Robert Roback (LANL)
- Schön Levy (LANL)
- Srikanta Mishra (INTERA)
- Bill Arnold (SNL)
- Drew Coleman (DOE).

It was noted in the technical presentations that:

- The water table rise parameter for this discussion is defined as being the average water table rise in the area beneath the repository and is to be applied as a uniform increase in the water table elevation in the site-scale UZ transport model.

- A 'warm-up' exercise, in estimating the 90 percent confidence intervals for answers to a set of random questions by the participants, was conducted and confirmed a common outcome in which participants routinely underestimate their uncertainty in the answers.

- Differences in scale at which measurements are made and the scale of model parameters complicate the assessment of uncertainty for some parameters.

- Discussion among the participants concluded that uncertainty in water table rise is primarily epistemic (related to lack of knowledge) uncertainty.

- Previous studies relevant to water table rise include evidence from calcite morphology, Sr isotopes, zeolite mineralogy, paleospring deposits, packrat middens, and numerical models. More recent data indicate reevaluation the conclusions from the original analysis may be necessary.

- Large-scale areas of recharge occur generally to the north and east of Yucca Mountain and areas of natural discharge occur to the south.

- Schematic analyses indicate that with wetter climatic conditions and greater groundwater flow rates, the rise in the water table would be expected to be greater at locations upstream from springs, than at the springs.

- The original estimates of maximum standing water level rise published in 1991 (about 60 m to 100 m) were based on visual examination of cuttings from well H-6 (Levy 1991 [DIRS 100053]).

- Modeling studies by Czarnecki (1985 [DIRS 160149]) resulted in simulated water table rise of about 130 m.

- The three-dimensional regional-scale groundwater flow model of D'Agnese et al. (1999 [DIRS 120425]) simulated steady-state flow for full-glacial conditions (21,000 years ago), used increased precipitation estimates from an atmospheric general circulation model, and head-dependent sinks at inferred potential discharge locations. These studies indicated water table rise of 60 m to 150 m beneath the repository.

- CRWMS M&O (1997 [DIRS 101111]) gave a general endorsement of estimated water table rise in the range of 80 to 120 m, based on geochemical and existing paleodischarge evidence.

During and following these presentations, there were discussions among the participants about the uncertainties and persuasiveness of various lines of evidence regarding past water table rise beneath the repository. It was generally acknowledged by the group that no single line of evidence was definitive, but individual participants expressed greater or lesser confidence in different types of information. In particular, James Paces expressed doubt in the reliability of results from the numerical modeling of groundwater flow. Bill Arnold stated that it was unpersuasive to extrapolate the maximum rise in the water table at paleospring deposits to the area beneath the repository. Because the interpretation of water table rise based on patterns of zeolitic alteration by Schön Levy depends on the difference in water levels across the Solitario Canyon Fault, Dr. Levy acknowledged some uncertainty in the quantitative estimates in her presentation.

Next, each workshop participant completed a subjective probability assessment worksheet provided by Srikanta Mishra. This worksheet contains a table with seven quantiles to be filled in by each participant individually. The results of these subjective assessments of water table rise are shown as the light-colored curves on Figure C6-28.

Following completion of the worksheets, the results were entered into a spreadsheet, displayed graphically on a projector, and discussed by the entire group. In particular, each participant discussed the rationale used for the upper bound, lower bound, and median value. It was recognized that the lower bounds chosen by James Paces and Schön Levy differed significantly from the values chosen by other participants. Similarly, the upper bound chosen by James Paces was significantly different than the values from other participants.

Srikanta Mishra explained that there were two options available for defining the aggregate uncertainty in water table rise among the participants. The first option involved allowing each participant to reconsider his or her individual uncertainty distribution and then mathematically 'averaging' the results. The second option was to agree upon a consensus uncertainty distribution. The group decided to use the second option and a consensus uncertainty distribution was constructed through a process of graphical display, discussion, and trial-and-error variations in the quantile values. The resulting consensus uncertainty distribution in water table rise for use in the PMA is shown as a dark solid line on Figure C6-28.

However, for the PMA, this distribution is slightly modified for the following reason. It is desirable to use the FEHM input files for the TSPA-LA model that assigned the water table node bins so that these files do not have to be reworked. However, those files (DTN: MO0704PAFEHMBR.001_R3 [DIRS 184647]) assumed that the water table would be elevated no higher than 120 m higher than the minimum value in the present-day water table (730 m). Therefore, any water table elevations in the new analysis that extend beyond 730+120=850 m would be problematic because a grid node higher than this value would not be flagged as a repository node, leading to mass leaving the UZ system but not recorded in the output. To prevent this from happening while still enabling the use of the water table bins developed previously, it is required that the water table elevation be restricted to no more than 120 m. However, the 'consensus distribution developed earlier, extends to 150 m water table rise. To accommodate this limitation, the distribution is adjusted to linearly extend the high end of the CDF to unity at 120 m. The revised distribution is plotted as a dashed curve alongside the original 'consensus' curve on Figure C6-29. This is the CDF that is used in the PMA to capture uncertainty in water table rise. This necessary change to the distribution to accommodate limitations in the water table bins developed previously opens the possibility of roughly 5 percent of the realizations that would have been given a water table elevation between 850 m and 880 m being forced to be no greater than 850 m. For the purposes of examining the sensitivity of the UZ breakthrough curves to water table elevation, this change is an acceptable compromise. This is especially true if the dependence of transport results to the water table elevation is modest.

The distribution required for use in the PMA is the water table elevation, rather than the water table rise. These data are labeled 'Water Table Elevation' in the Excel spreadsheet in corroborative DTN: MO0704PAUZFEHM.000 [DIRS 182790] and is paired with the 'Consensus Quantile' column to define the CDF to be used in the PMA. It is computed by adding the water table elevation to the nominal value of the present-day repository beneath the repository, 730 m (SNL 2008 [DIRS 184748], Section 6.4.8). Figure C6-29 is the CDF to be used for water table elevation.

Matrix Diffusion Submodel

This section describes the changes to the diffusion model to be used in the PMA, compared to the TSPA-LA model. Changes include the addition of a diffusion-enhancement factor and the use of the Discrete Fracture Model as an alternate conceptual model for fracture/matrix interaction.

Effective Matrix Diffusion Coefficient

In the TSPA-LA Model (SNL 2008 [DIRS 184748]), the diffusion coefficient is based on a segregation of the rock units below the repository into three groups of similar properties, and a diffusion coefficient for each radioelement is computed as the product of the diffusive tortuosity τ_D and the free-water diffusion coefficient D_{free}:

$$D_{eff} = \tau_D D_{free} . \qquad \text{(Eq. C6.6-5)}$$

In the model, the diffusive tortuosity differs for each of the three rock units but is independent of radioelement; whereas the free-water diffusion coefficient is a property of the radioelement. Values for these parameters are developed in DTN: LB0702PAUZMTDF.001_R1 [DIRS 180776]. Studies have shown that laboratory based matrix-diffusion coefficients may underestimate field-scale matrix diffusion coefficients used to simulate field tests (SNL 2008 [DIRS 184614] Section 6.8 [a] and BSC 2006 [DIRS 178275] Section 6.4.1). Wu et al. (2001 [DIRS 156399]) and Liu et al. (2003[DIRS 162470]) indicated that the existence of many small-scale fractures may be the major reason for relatively large diffusion coefficient calculated from field data. For the PMA, the effect of a presumed increase in the effective diffusion coefficient D_{eff} due to the effects of small-scale fractures is modeled by applying a multiplication factor to this expression:

$$D_{eff} = f_d \tau_D D_{free} \quad \text{(Eq. C6.6-6)}$$

where f_d is the enhancement factor for matrix diffusion. In the PMA implementation of this enhancement factor, the GoldSim model is used to generate values of f_d and τ_D subject to the parameter uncertainty distribution described herein for f_d and in DTN: LB0702PAUZMTDF.001 [DIRS 180776] for τ_D, and the product of these two terms is passed to FEHM in the parameter input table.

To assign a parameter uncertainty distribution for f_d, the modeling efforts to reconcile the results of UZ transport field tests have been examined. In Section 7.8 of *UZ Flow Models and Submodels* (SNL 2007 [DIRS 184614]), a flow and transport field test and model are presented for a percolation and tracer test conducted along a fault in Alcove 8/Niche 3. A Multiple Interacting Continua model was developed for simulating flow and transport during the test. The fault was explicitly included, along with finely discretized grid spacings in the matrix adjacent to the fault. An analysis is presented of the influence of matrix diffusion and the parameter ranges required to match the breakthrough curves of two conservative, diffusing tracers with different diffusion coefficients in free water. *UZ Flow Models and Submodels* (SNL 2007 [DIRS 184614], Figure 7.8-9) shows that in order to obtain a good match to the tracer tests, the interface area had to be increased by a factor of 45 above that of the original data. Likewise, in *Radionuclide Transport Models Under Ambient Conditions* (SNL 2007 [DIRS 177396], Section 7.3), the same analysis is provided, and in both reports, a discussion on the need for adjusting the interface area is provided. In Liu et al. (2004 [DIRS 169948]), this need to enhance the diffusion coefficient or interface area is described in the form of an increase in the matrix diffusion coefficient, but the description in the paper postulates that the increase could be due to the increase in available surface area for diffusion as a solute encounters a greater number of fractures during its transit through a fractured medium.

Analysis of Alcove 8/Niche 3 Flow and Transport Tests (BSC 2006 [DIRS 178275]) describes a second round of testing at this field site, away from the location of the fault zone tested previously. The test, called the large-infiltration-plot test, consisted of flow and transport studies similar to those in the fault zone, to examine the behavior of rock in a relatively unfaulted zone, although the rock mass contained numerous fractures. A numerical model using the Multiple Interacting Continua conceptualization was developed to simulate the flow and transport

behavior. Like the discrete fracture representation above, the Multiple Interacting Continua approach employs a grid that includes fine discretization near the fractures, which in this case are represented as an equivalent continuum. From the standpoint of matrix diffusion, the Multiple Interacting Continua model is similar to that of the discrete fracture model in that it captures fine gradients in solute concentration away from the fractures. Although this test yielded seepage flow information, unfortunately no tracer breakthrough was observed during the test. Therefore, a transport model of this test could only be used to bound the diffusion coefficient. It was noted in transport simulations that if the laboratory based matrix diffusion coefficient was used, tracer breakthrough was predicted by the model. Transport models with diffusion coefficients increased by a factor of 45 (the same as that found in the fault zone test) resulted in predicted concentrations that were low enough that they would probably go undetected in the experiment (i.e., the concentrations would be within the background levels). From this result, the study concluded that this modeling exercise corroborated the reasonableness of the factor of 45 for the test.

The use of an enhancement factor of the diffusion coefficient (or, equivalently for an individual fracture zone, the interface area) is an attempt to parameterize a commonly used transport model formulation to explain the observed field results. In the PMA, to include this effect, it should be recognized that other parameters besides the diffusion coefficient influence the matrix diffusion coefficient, including the fracture aperture, spacing, and Active Fracture Model parameter γ. Therefore, it could be argued that uncertainties in these transport parameters already capture the uncertainty in the phenomena that lead to the need to increase the diffusion coefficient. In other words, it is possible that the difference between field-scale effective diffusion coefficients and lab-scale values is actually a geometric effect related to fracture area that is already included in the TSPA-LA Model analysis in the form of uncertainty in aperture. Alternatively, the enhancement factor may represent features such as the effects of small-scale fractures not simulated by the model, in which case the enhancement parameter needs to be explicitly included. An additional piece of information is available from an analysis of the Alcove 1 tracer test (Liu et al. 2003 [DIRS 162470]), which suggested that a multiplier of the diffusion term in the range of 2 to 4 provided a reasonable match to the data. The range of values determined from these tests, combined with the uncertainty in the tracer test interpretations themselves, suggest that a lower bound of the enhancement factor should be set to 1 (no enhancement considered), whereas the upper bound should be set to 45 to match the value obtained in the analysis of the fault test and corroborated as reasonable for the large-infiltration-plot test. Given the lack of systematic measurements to provide further constraints on this distribution, it is reasonable to assume a uniform distribution of the enhancement factor from 1 to 45.

Since the analyses leading to the value of 45 were obtained using models with fine discretization near the flowing fracture(s), this parameter uncertainty distribution is only compatible with the Discrete Fracture Model conceptual model incorporated in the UZ component of the PMA. The TSPA-LA model uses a dual-k conceptualization, for which higher values of the scale factor would likely be needed to match the field data. No attempt has been made to estimate the enhancement factor with a dual continuum transport model, so the uncertainty distribution developed herein is only compatible with the Discrete Fracture Model conceptual model for fracture/matrix interaction.

Discrete Fracture Model Fracture/Matrix Interaction Model Conceptualization

The matrix diffusion in the PMA is implemented with the Discrete Fracture Model. The TSPA-LA Model was developed using the dual-permeability (*k*) conceptualization because the only Mountain-scale, process model simulations available for comparison were performed with the dual continuum model option in T2R3D [DIRS 146654]. *Particle Tracking Model and Abstraction of Transport Processes* (SNL 2008 [DIRS 184748]) also developed a set of breakthrough curves using a discrete fracture representation of transport in the matrix. The choice of conceptual model used for the simulation is simply made by invoking the Discrete Fracture Model transfer function curves. For the PMA, the Discrete Fracture Model transfer function is selected because it is desirable to eliminate the conservatism that the dual-k model represents (greater breakthrough at short travel times), and because the Discrete Fracture Model transfer function is compatible with the enhancement factor uncertainty distribution developed in the previous section.

The Discrete Fracture Model transfer function has been used in a variety of tests to ensure that it performs as expected. A series of comparisons of the FEHM particle tracking model (with the Discrete Fracture Model transfer function) show favorable comparisons to a discrete fracture model with a completely different numerical formulation (SNL 2008 [DIRS 184748], Section 7.2.1). In a two-dimensional cross section model, the Discrete Fracture Model results showed reasonable comparison, especially at late travel times, to a Multiple Interacting Continua transport model and to a particle tracking model that employed a completely different numerical algorithm (SNL 2008 [DIRS 184748], Section 7.2.2). Finally, in the three-dimensional model validation runs presented in *Particle Tracking Model and Abstraction of Transport Processes* (SNL 2008 [DIRS 184748], Section 7.2.3), the Discrete Fracture Model runs, when compared to the validated dual-k transport model runs, exhibited behavior that is understandable given the nature of these two conceptual models: later first arrivals in the breakthrough curves, with convergence of the two breakthrough curves at long travel times. This series of model runs provides confidence that the particle-tracking model with the Discrete Fracture Model transfer function is behaving as expected and is suitable for use in the PMA.

The underlying mathematical development and the theoretical considerations related to the use of transfer functions to represent fracture/matrix interactions in the TSPA abstraction model for UZ transport are described in *Particle Tracking Model and Abstraction of Transport Processes* (SNL 2008 [DIRS 184748], Section 6.4.3). The inputs associated with this data are direct inputs to the UZ component of the PMA. They are invoked from within an FEHM data input file specified in the fehm_PMATSPA.mptr input file for the UZ transport abstraction.

The method for generating the transfer functions is described in detail in *Particle Tracking Model and Abstraction of Transport Processes* (SNL 2008 [DIRS 184748], Appendix C). The differences in the transfer-function parameter matrix from the analysis and/or model reports to the TSPA-LA model were discussed in *Particle Tracking Model and Abstraction of Transport Process* (SNL 2008 [DIRS 184748]. The treatment of this parameter in the PMA is identical to that used in the TSPA-LA model.

C6.6.2 Model Implementation

Colloid Diversity Model for Colloid-Facilitated Transport

The implementation of the colloid diversity model in the PMA is accomplished with the following steps. For the PMA, Steps 1 to 6 are evaluated within the SZ, as discussed in Section C6.7.2. Steps 7 and 8 apply only to the UZ PMA implementation.

1. For a given realization, determine the median SZ travel time, τ (hr), from the calculation of the If species in each Monte Carlo realization and store each travel time in a table.

2. Use τ (hr) as the total travel time through the UZ and SZ, equivalent to assuming that, for the purposes of assigning the colloid diversity distribution parameters, the SZ travel times are much longer than UZ travel times.

3. Randomly sample a triangular distribution with parameters (0.17, 0.51, 0.85) and use the resulting value as the slope m in Equation C6.6-4 to define a CDF for the colloid filtration rate constants (hr^{-1}). Use a value of b = 0.2 for all realizations.

4. Randomly sample from a triangular distribution [$log_{10}(0.01/\tau$ (hr^{-1})), $log_{10}(0.1/\tau$ (hr^{-1})), and $log_{10}(1/\tau$ (hr^{-1}))], and use the resulting value as the log_{10}(colloid detachment rate constant).

5. Transform the filtration rate constant CDF to a retardation factor CDF using Equation C6.6-1, which yields, after applying Equation C6.6:

$$\log_{10} P = b + m \cdot \log_{10}\left[k_r (R_{coll} - 1)\right]. \qquad \text{(C6.6-7)}$$

6. Compute the fast fraction as the cumulative probability associated with a retardation factor of 2.

7. Define a new retardation factor CDF that can be independently sampled for the UZ and SZ by using the CDF from Step 5 with cumulative probabilities equal to the square root of the probabilities of the CDF from Step 5. This approach is executed by choosing this option in FEHM V 2.25. Alternatively, apply the colloid diversity model to the Ic species of the SZ system, and apply a uniform value of 2 for the Ic species in the UZ. The latter approach is used in the PMA.

8. Compute the value of $\overline{R}_{coll}$ for the reversibly sorbing species using Equation C6.6-3. This is done by supplying the retardation factor distribution parameters to FEHM V 2.25 and selecting the appropriate option in the input for the reversible species.

Water Table Rise for Future Climate

To implement this change for the PMA, the water table elevation under future climate conditions is now passed from GoldSim to FEHM during the simulation. FEHM V 2.25 now has the provision, which is invoked in the PMA, to change the flow field representation during the

simulation to accommodate the water table elevation at runtime. This requires that the template for information passing between GoldSim and FEHM be changed from that described in Table 6-2 of SNL 2008 [DIRS 184748] to accommodate the passing of an additional variable, called wt_elevation (corroborative DTN: MO0704PAUZFEHM.000 [DIRS 182790]).

Matrix Diffusion Submodel

The enhancement factor for the effective matrix diffusion coefficient for the PMA is implemented by the addition of a GoldSim stochastic element to the TSPA-LA Model. The stochastic element is used to sample a uniform distribution between 1 and 45 to choose a scaling factor, f_d, which is applied to the effective matrix diffusion coefficient as noted in Equation C6.6-6. The new effective matrix diffusion coefficient values will become part of a FEHM external file that is generated during a preprocessing PMA run (Sections 6.3.9.3 and F.2.1.1.13).

The switch to the Discrete Fracture Model fracture/matrix interaction alternative conceptual model is readily implemented in the TSPA-LA Model by replacing the FEHM external input file uz_tfcurves_nn_dualk_4680.in (DTN: MO0704PAPTTFBR.002_R0 [DIRS 180442]: Particle Tracking Transfer Functions) used in the TSPA-LA model with the alternate file uz_tfcurves_nn_dualk_4680.in (DTN: MO0704PAPTTFBR.002_R0 [DIRS 180442]: Particle Tracking Transfer Functions). This procedure is readily implemented using the MFCP-LA DLL that copies the desired Transfer Function curves file into a generically named file found in the FEHM external multi-species particle tracking files (Section F.2.1.11).

C6.7 SATURATED ZONE FLOW AND TRANSPORT

C6.7.1 Conceptual Model

Radionuclide Mass Flux from the UZ to the SZ

In the SZ TSPA TSPA-LA Model (Section 6.3.10), the radionuclide mass reaching the water table in both the matrix and fractures of the UZ released from the UZ Transport Model is transferred to flow through the fractures in the SZ radionuclide transport model. This is equivalent to assuming that the radionuclide mass instantly diffuses out of the UZ matrix and into the SZ fractures at the interface between the UZ and SZ. This approximation reduces the transport time expected if mass diffused from UZ matrix into SZ matrix. The analysis described in this section documents modification of the TSPA-LA Model by introducing matrix transport at the interface between the UZ and SZ. The modified model channels the radionuclide mass release from the UZ to the SZ three-dimensional and one-dimensional transport models and accounts for transport in the matrix.

In the SZ TSPA-LA Model (Section 6.3.10), the source of radionuclides in the SZ is modeled as the radionuclide mass released from the UZ at the water table (i.e., the interface between UZ and SZ). The UZ radionuclide transport model calculates the rate and spatial distribution of radionuclide releases to the SZ. The area beneath the repository is subdivided into four source regions, and the released mass from the UZ is directed to one of these four regions to be transported to the SZ. For the SZ three-dimensional transport model, the UZ released

time-varying radionuclide mass is combined with the SZ unit-source radionuclide breakthrough curves in a convolution integral to model radionuclide transport to the accessible environment. For the SZ one-dimensional transport model, the UZ radionuclide mass release is directly used as the source to the one-dimensional transport model within the TSPA Model. Radionuclide ingrowth is calculated in the one-dimensional transport model.

The UZ Transport Model primarily uses the dual-continuum approach that models transport in both the fractures and rock matrix. The dual-continuum approach is implemented using a numerical grid that consists of fracture and matrix cells, with each fracture cell connected to a corresponding matrix cell. Thus, in the dual-continuum numerical grid, the radionuclide mass released at the water table is through both fracture and matrix cells. The TSPA-LA Model combines the releases from the UZ fracture and matrix cells and directly feeds the output to both the SZ three-dimensional and one-dimensional transport models. For the PMA analysis, the radionuclide mass releases from the UZ matrix cells will be separated from the releases through fracture cells. The release from the matrix cells at the water table will then be routed through a sub-model that will simulate diffusion from the UZ matrix into the SZ fractures. This is done by introducing new GoldSim cell pathways in the TSPA Model. A GoldSim cell pathway is an element in the Contaminant Transport Module of GoldSim that is used to transport contaminant species. A network of cells, are mathematically equivalent to a finite difference network of nodes. The submodel contains a discretized scheme with five cells in series (to reduce numerical dispersion) at the UZ/SZ boundary that is used to transport mass from the UZ matrix to the SZ fractures (Figure C6-32). The new cells simulate transport by diffusion in a dual porosity environment. The output of the new cells is directed to both the SZ three-dimensional and one-dimensional transport models. The mass is applied to the four SZ regions. No change is made to the mass flux from the fractures of the UZ as the UZ-SZ interface accurately handles the mass flux transfer from the UZ fractures to the SZ.

Colloid Transport of Irreversibly Sorbed Radionuclides

In the SZ Flow and Transport Model Abstraction, radionuclides are transported in the SZ as solutes in groundwater or sorbed onto colloids (SNL 2008 [DIRS 183750], Section 6.3). For transport through colloids, the radionuclides are either reversibly or irreversibly sorbed onto colloids. The latter mode of colloid transport is the subject of this section. The TSPA SZ transport model simulation of colloid transport with irreversibly sorbed radionuclides has been applied to the radionuclides plutonium and americium (SNL 2008 [DIRS 183750], Section 6.5.2.11). A large fraction of the colloids are retarded by sorption while a small fraction, known as fast-fraction, are transported unretarded. In the TSPA-LA Model (SNL 2008 [DIRS 183750], Section 6.5.2.11), transport of irreversible colloids for the retarded fraction in both the volcanic units and alluvium is calculated using single retardation factors per realization (one for the volcanic units and another for the alluvium). Current data analysis shows that use of single retardation factors for all non-fast-fraction colloids in the volcanic rocks and alluvium does not fit experimental observations (corroborative DTN: LA0705PR150304.001 [DIRS 181744). Moreover, the TSPA-LA colloid model does not account for scale dependence of filtration rate or retardation factors. The data have been gathered from lab and field experiments (i.e., relatively small distances) and consideration of length (distance) scales may be more appropriate than directly applying them to large scale modeling grids.

In the PMA, colloid filtration (retardation) in the SZ is modeled with a colloid diversity model. The details of the colloid diversity model for both UZ and SZ is summarized in Section C6.6. In this model, colloids are assigned a wide range of retardation factors within a given TSPA realization in recognition of their diverse sizes, shapes, compositions, and surface properties (Robinson et al. 2007 [DIRS 180698]). In addition, the development of the colloid retardation factor distributions will be modified to better address the considerable uncertainty in the colloid transport experimental data and, particularly, in the extrapolation of these data to the TSPA time and distance scales. The retardation factor distributions, and also the fast fractions, will now be travel time dependent. This colloid diversity approach is implemented in the SZ three-dimensional and one-dimensional models.

The PMA implementation of a distribution of colloid retardation factors in the three-dimensional SZ transport model is accomplished with a modification of the FEHM software code (V. 2.25). For the SZ one-dimensional transport, the colloid diversity model is implemented by duplicating the GoldSim SZ 1-D pipe setup into 10 sets of pipes each with a different retardation factor, derived from the distribution of retardation factors, applied to each set of pipes. A GoldSim pipe pathway is an element in the Contaminant Transport Module that is used to simulate advectively dominated one-dimensional conduit. Implementation details with steps to be followed are given in Section C6.7.2. The SZ one-dimensional model implementation consists of a set of GoldSim pipe pathways with three pipe segments representing each of the four source regions. The three pipe segments represent the distance from the UZ-SZ boundary to the accessible environment. The lengths of each pipe segment are given in *Saturated Zone Flow and Transport Model Abstraction* (SNL 2008 [DIRS 183750], Table 6-6[a]).

Redox Conditions and Impacts on Radionuclide Transport

Potential variations in redox conditions in the SZ could have an impact on the migration of redox-sensitive radionuclide species released from the repository at Yucca Mountain (BSC 2006 [DIRS 178672]). For example, under reducing geochemical conditions, the solubility limit can be much lower and the sorption coefficient can be much higher for radioelements such as technetium and neptunium. Potential precipitation from lower solubility limits and retardation from enhanced sorption would lead to longer transport times in the SZ if groundwater flow paths from beneath the repository encountered reducing conditions before reaching the boundary of the accessible environment.

The base-case conceptual model of SZ transport developed for the TSPA-LA Model is implicitly taken to be oxidizing conditions in the SZ, based on the uncertainty distributions for sorption coefficients of technetium and neptunium (SNL 2008 [DIRS 183750]). In the TSPA-LA Model, technetium is modeled with no sorption (i.e., no retardation) in both the volcanic units and the alluvium. The objective is to modify the SZ Flow and Transport Abstraction Model and the SZ one-dimensional transport model for the PMA to simulate the transport of technetium and neptunium with enhanced sorption in zones of reducing geochemical conditions. Uncertainty in the transport of these redox-sensitive species is evaluated with regard to the location and size of a potential reducing zone in the SZ and uncertainty in the sorption coefficients within the reducing zone.

Redox conditions in the SZ, as measured by the reduction/oxidation potential of groundwater samples, are variable in the area near and downgradient from Yucca Mountain. Although apparent non-equilibrium redox conditions are observed in many wells, an approach based on a preponderance of evidence can be used to identify oxidizing and reducing locations in the SZ (BSC 2006 [DIRS 178672], Section 2.1). Measurements of dissolved oxygen, Eh from inert platinum electrode, and total iron concentration, along with manganese and nitrite/nitrate redox couples, are used to infer redox conditions in wells.

Results of the analysis of redox conditions in the SZ indicate that oxidizing conditions prevail in most characterized locations in the SZ but that there are several wells to the east and south of Yucca Mountain with reducing conditions. The assessment of redox conditions in wells near Yucca Mountain is summarized on the map shown on Figure C6-30 (BSC 2006 [DIRS 178672], Figure 2.1-2). The area of inferred reducing conditions, including Wells b#1, H-4, WT-17, and WT-12, is located along potential groundwater flow pathways in the SZ from beneath the proposed repository and it is this area in the tuff that is of greatest potential significance to the transport of redox-sensitive radionuclides. A working hypothesis is that the zone of observed reducing conditions is related to the presence of minor primary pyrite in the Tram Tuff and its reaction with dissolved oxygen in groundwater (BSC 2006 [DIRS 178672], Section 2.1). The solubility of both technetium and neptunium have much lower under reducing conditions, relative to oxidizing conditions (BSC 2006 [DIRS 178672], Section 2.2). Precipitation of these radioelements in the SZ could occur if their concentrations in upstream oxidizing groundwater exceeded the solubility limit as flow enters the reducing zone. Although the conceptual model of transport of redox-sensitive species acknowledges the possibility of precipitation of these radionuclides under reducing conditions in the SZ, a simplified approach that does not implement the precipitation process is used in the numerical modeling. This is because radionuclide concentrations are not explicitly simulated in the SZ Flow and Transport Abstraction Model and because enhanced sorption is probably the dominant process with regard to radionuclide retardation in reducing zones.

Experimental results and surface complexation modeling indicate that values of sorption coefficients for technetium and neptunium are significantly higher under reducing conditions (BSC 2006 [DIRS 178672], Section 2.3). The conceptual model used in the PMA is that the resulting enhanced sorption for these redox-sensitive radioelements would occur in the tuff matrix of the fractured volcanic units in reducing zones within the SZ. As with all radionuclides, diffusion from the fractures into the rock matrix must occur for the enhanced sorption of technetium and neptunium onto the tuff in the SZ (SNL 2008 [DIRS 183750], Section 6.3). For the purposes of the PMA and associated enhanced sorption of technetium and neptunium, reducing conditions are defined as geochemical conditions in which the Eh is less than approximately 100 mV (BSC 2006 [DIRS 178672], Section 2.3).

Flowing Interval Porosity (Fracture Porosity in Volcanic Units)

The flowing interval porosity is defined as the volume of the pore space through which significant groundwater flow occurs, relative to the total volume. It characterizes the flowing intervals rather than all fractures. Estimates of this parameter were based on theoretical models, pumping tests, and tracer data. For the TSPA-LA model, a cumulative distribution in the range 10^{-5} to $10^{-1}$was used (SNL 2008 [DIRS 183750], Table 6-8). To define the lower bound value,

estimates of fracture porosity of intact cores of volcanic rock were used. More details can be found in *Saturated Zone Flow and Transport Model Abstraction* (SNL 2008 [DIRS 183750], Section 6.5.2.5).

It has been pointed out that the lower bound might be low for bulk average parameter value (i.e., average value over the volcanic zone) that is being applied at the km scale (i.e., the model domain) (SNL 2008 [DIRS 183750], Section 6.5.2.5). A study of the cumulative distribution function plot for parameter flowing interval porosity in the *Saturated Zone Flow and Transport Model Abstraction* (SNL 2008 [DIRS 183750], Figure 6-13) shows that less weight is given to the bottom of the distribution (i.e., low flowing interval porosity) than the rest of the distribution. The 0.5 probability value of 10^{-3} is considered to be representative of the smallest values of fracture porosity estimated from the exploratory studies facility data and field tests (SNL 2008 [DIRS 183750], Section 6.5.2.5). Guimera and Carrera (2000 [DIRS 156830]) analyzed 90 tracer experiments performed in low-permeability fractured rocks The experimental data indicate that most of the porosity data were in the range of 10^{-4} to 10^{-2}, and few points were below porosity of 10^{-4}. The tracer tests represent distances in the range of 2 m to 346 m with an average distance of 41 m. Applying the measured porosity data to km scale would probably result in an even higher lower bound bulk porosity. As a result, using a lower bound porosity value of 10^{-4} would be appropriate for the purpose of this study. Therefore, for the PMA, the lower bound is raised from 10^{-5} to 10^{-4}.

In the TSPA-LA Model, the ground water specific discharge (which is the function of permeability) and flowing interval porosity are uncorrelated variables (SNL 2008 [DIRS 183750], Section 6.5.2). In a fractured flow aquifer, there are theoretical and geometric arguments that suggest the two parameters are at least partially correlated. As fracture density and apertures increase, one would expect both flowing interval porosity and permeability to also increase. An uncorrelated model could generate parameter combinations (large specific discharge and small flowing interval porosity) that are not physically consistent. A correlation factor applicable for Yucca Mountain conditions is considered in PMA for simulation of flow and transport in the SZ.

The relationship between permeability and porosity has been the subject of numerous studies. One of the most widely accepted relationships is the Kozeny-Carman equation that relates permeability to porosity and other characteristics of the porous medium (Bear 1972 [DIRS 156269], p. 166). The Kozeny-Carman equation is a porous medium modification of the cubic law relationship. Experimental data are not currently available for the development of a permeability-porosity correlation for the SZ volcanic and alluvial units; therefore, a literature review was conducted to find experimental data that are applicable to the Yucca Mountain setting. For this study the work of Guimera and Carrera (2000 [DIRS 156830]) that used experimental data performed in low-permeability fractured rocks has been adapted. The Guimera and Carrera study (2000 [DIRS 156830]) used data from 90 tracer experiments to explore correlations among parameters controlling flow and transport. The authors reported that the data from the first arrival time was more applicable to a permeability-porosity relationship. Most of the porosity data were in the range of 10^{-4} to 10^{-2}, and few points were below a porosity of 10^{-4} (Guimera and Carrera 2000 [DIRS 156830], Figure 1). For the PMA study, the literature data compiled by Guimera and Carrera (2000 [DIRS 156830]) was used. The data set was copied into an Excel spreadsheet and Rank Correlation performed. Rank correlation was used

because that is the method used in the TSPA-LA Model. The resulting correlation value was 0.64.

C6.7.2 Model Implementation

Radionuclide Mass Flux from the UZ to the SZ

To simulate matrix diffusion at the UZ and SZ boundary, an SZ submodel has been set up in GoldSim within the TSPA-LA Model. The PMA submodel allows routing of the radionuclide mass release from UZ matrix cells at the water table through an intermediate stage before reaching the SZ Transport Model. This approach does not change the transfer of radionuclide mass release at the water table from UZ fracture cells to the SZ. The PMA submodel simulates radionuclide transport by diffusion in a dual porosity environment. The submodel is represented by an SZ matrix block with total dimensions of 250 m × 250 m × 10 m (thickness) (Figure C6-31). The grid dimensions are the horizontal grid dimensions and the thickness of the first layer below the water table, used in the SZ three-dimensional flow and transport models (SNL 2007 [DIRS 177392], Section 6.3) and are appropriate for use for the purpose of the PMA.

The diffusive length and diffusive area for the model are evaluated as shown in Equations C6.7-5 and C6.7-6. The evaluation is done in the same way as with the SZ matrix diffusion model in the TSPA-LA model (Section 6.3.10).

$$\text{Diffusive length} = \text{FISVO}/2 \qquad \text{(Eq. C6.7-1)}$$

$$\text{Diffusive area} = \text{block length} \times \text{block thickness} \times (\text{block length}/\text{FISVO}) \times 2 \qquad \text{(Eq. C6.7-2)}$$

where FISVO is the flowing interval spacing (SNL 2008 [DIRS 183750], Section 6.5.2.4), and the block dimensions are as shown on Figure C6-31 and Table C4-2. The diffusive length is the distance to the middle of the flowing interval spacing. The diffusive area represents the cross-sectional area for diffusion, which includes two faces. Using a single block to model radionuclide transport by diffusion could introduce numerical dispersion. The alternative is to discretize the block into a number of cells that would diminish numerical dispersion. For this work, a five-cell discretization scheme has been considered. Figure C6-32 shows a conceptual model of the dual-porosity system with the discretization scheme. In the figure it is assumed that FISVO equals the total block length, which is 250 m. The figure shows half of the block length on either side of the fracture. The horizontal arrows show the direction of SZ matrix diffusion. Figure C6-33 shows the discretized system representation with five matrix cells as implemented in TSPA. In this model, the mass flux from the UZ is divided by five and applied to each SZ matrix cell. The total mass flux passes through the last cell to the SZ. The water volume and the matrix volume of each cell have also been divided by five. Since the five cells are in series, the diffusive length is divided by 5, while the diffusive area is the same for all the discretized cells. The output of the new scheme is simultaneously directed to the SZ convolution integral (three-dimensional) and the SZ one-dimensional transport system. The model has been applied to the four SZ regions.

Additional changes have also been made in other parts of the SZ transport section and the UZ transport section of the TSPA Model to allow flow of information between the new model and other sections of the TSPA Model.

Colloid Transport of Irreversibly Sorbed Radionuclides

The implementation of the colloid diversity model for the SZ is summarized below. The first four steps were followed for both the SZ three-dimensional and one-dimensional transport models.

1. For a given realization, determine the median SZ travel time, τ, using the mass breakthrough curves for the fast fraction of irreversible colloids. τ is an average of the median travel times of the four SZ regions and is given in hours.

2. Use τ as the total travel time through the SZ.

3. Randomly sample a triangular distribution defined by [0.17, 0.51, and 0.85] and use the resulting value as the slope m in Equation C6.7-1 to define a CDF for the colloid filtration rate constants. Use a value of b = 0.2 for all realizations.

4. Randomly sample a triangular distribution defined by [$\log_{10}(0.01/\tau)$, $\log_{10}(0.1/\tau)$, and $\log_{10}(1/\tau)$], and use 10 raised to the resulting value as the colloid detachment rate constant.

5. In the next step, the one-dimensional transport model is discussed. For the one-dimensional model, first calculate the probability P using the following procedure:

    a. Get the minimum probability value that corresponds to the minimum retardation factor, which is selected for this study to be equal to 2:

$$P_{\min} = 10^{b}\left[(R_l - 1)k_{\det}\right]^{m} = 10^{b}k_{\det}^{m} \qquad \text{(Eq. C6.7-3)}$$

where

P_{min} = minimum probability value

R_l = lower bound retardation factor = 2

    b. Divide the probability space into ten equal parts:

$$P_{diff} = (1.0 - P_{\min})/10 \qquad \text{(Eq. C6.7-4)}$$

where

P_{diff} = is the interval between two probability points, to get 10 equal parts

    c. Get 10 uncertainty uniform distributions with bin size as shown below. First the probability space is divided into ten bins (intervals). The range of each bin is as given below. Once the bins are defined the next step is to make a uniform distribution for each bin with

        i. $P_{\min}$ to $P_{\min} + P_{diff}$

ii. $P_{\min} + P_{diff}$ to $P_{\min} + 2P_{diff}$

iii. $P_{\min} + 2P_{diff}$ to $P_{\min} + 3P_{diff}$

iv. $P_{\min} + 3P_{diff}$ to $P_{\min} + 4P_{diff}$

v. $P_{\min} + 4P_{diff}$ to $P_{\min} + 5P_{diff}$

vi. $P_{\min} + 5P_{diff}$ to $P_{\min} + 6P_{diff}$

vii. $P_{\min} + 6P_{diff}$ to $P_{\min} + 7P_{diff}$

viii. $P_{\min} + 7P_{diff}$ to $P_{\min} + 8P_{diff}$

ix. $P_{\min} + 8P_{diff}$ to $P_{\min} + 9P_{diff}$

x. $P_{\min} + 9P_{diff}$ to $P_{\min} + 10P_{diff}$.

6. Retardation factors R_{f1} to R_{f10}: For each bin, randomly sample across the probability range assuming a uniform distribution between the lower and upper probability limits of the bin. Once the detachment rate constant (Step 4 above) and the sampled probabilities for each bin are evaluated, the retardation factor for each bin is calculated using Equation C6.7-4.

7. For the one-dimensional SZ transport model, use 10 one-dimensional pipe sets with retardation factors calculated using Step 6. Note that a pipe set for the 1-D SZ Model is as defined in the Conceptual Description. The mass flux is divided equally to the 10 pipe sets. The calculated 10 retardation factors, which are realization dependent, replace the TSPA-LA parameters CORVO and CORAL (SNL 2008 [DIRS 183750], Section 6.5.2.11). The parameters CORVO and CORAL are the single colloid retardation factors in the volcanic units and alluvium defined in *Saturated Zone Flow and Transport Model Abstraction* (SNL 2008 [DIRS 183750], Section 6.5.2.11). For the PMA, no distinction is made between the volcanic units and alluvium values of colloid retardation for irreversibly sorbed radionuclides.

8. For the three-dimensional SZ Flow and Transport Model, use the detachment rate constant, slope m, y-intercept b, and minimum and maximum retardation factor values to implement the CDM. As with the one-dimensional model, the minimum retardation factor is 2.0. The maximum retardation factor is derived using Equations C6.7-1 and C6.7-3 in conjunction with the maximum probability value of 1.0. For the three-dimensional model, the CDM is implemented in the particle tracking 'sptr' module of the code FEHM V. 2.25 (STN: 10086-2.25-00 [DIRS 182477]). Each simulation is conducted using a user-defined number of particles (500 in this case). FEHM generates 500 retardations (one for each particle) using the minimum and maximum retardations as two of the retardation coefficient values. The remaining 498 retardation values are derived by dividing the range of the retardation into 499 equal intervals ($LogR_{Interval}$) in log space, where

$$\log R_{Interval} = \log 10(R_{\max} / R_{\min}) / 499. \qquad \text{(Eq. C6.7-5)}$$

The retardation values are then found by taking the antilogs of these values. Except for the particles assigned the minimum and maximum retardation, the value of each particle is

then weighted based upon the difference between probabilities ($P_{i-1/2}$ and $P_{i+1/2}$) of retardation (from Equations C6.7-1 and C6.7-3) representing the midpoints (in log space) between a selected retardation (R_i) and the retardation an the interval below it (R_{i-1}) and the retardation an interval above (R_{i+1}) where i = 2 - 499. The weighting factor Wi can be defined as:

$$W_i = (P_{i+1/2} - P_{i-1/2}) . \quad \text{(Eq. C6.7-6)}$$

The weighting factors for the minimum retardation and the maximum retardation are in turn defined as follows:

$$W_1 = (P_{1+1/2} - P_1) \quad \text{(Eq. C6.7-7)}$$

and

$$W_{500} = (P_{500} - P_{500-1/2}) . \quad \text{(Eq. C6.7-8)}$$

The normalized weighting factors, w_i, used in the model are then defined as

$$w_i = \frac{500 W_i}{\sum_{j=1,500} W_j} . \quad \text{(Eq. C6.7-9)}$$

Redox Conditions and Impacts on Radionuclide Transport

The PMA for the effects of potential reducing conditions on the transport of redox-sensitive species is implemented in the PMA by modifying the SZ Flow and Transport Abstraction Model and the SZ one-dimensional transport model to incorporate these effects. A zone of uncertain dimensions is defined in the three-dimensional SZ flow and transport abstraction model to represent the location of reducing conditions. A separate value for the sorption coefficients in the volcanic matrix is assigned within this zone, relative to the values assigned to the volcanic units and alluvium under oxidizing conditions. The SZ one-dimensional transport model is modified by subdividing the GoldSim pipe elements such that separate pipe segments exist for oxidizing and reducing conditions. The length of the pipe segment with reducing conditions is assigned to approximate the flow path length through the reducing zone in the three-dimensional SZ Flow and Transport Abstraction Model for each realization.

Uncertainty in radionuclide transport related to potential reducing conditions in the SZ is incorporated into the PMA by defining uncertainty distributions for key parameters and sampling from these uncertainty distributions in the Monte Carlo realizations. These uncertainty distributions are summarized in Table C6-9.

The potential reducing zone in the SZ is approximated by a rectangular area that includes several wells in which reducing conditions have been inferred from groundwater samples. This zone is elongated in the north-south direction and encompasses Wells b#1, H-4, WT-17, and WT-12, as shown on Figure C6-30. The potential zone extends over the elevation from 200 m to ~730 m (where the water table is located) in that area. The eastern boundary of the reducing zone varies

from a maximum of 550,000 m to a minimum of 548,200 m (in Universal Transverse Mercator [UTM] coordinates), corresponding to a maximum width of 2,800 m and a minimum width of 0 m. The southern boundary of the reducing zone varies from a minimum of 4,069,200 m to a maximum of 4,073,300 m UTM, and the northern boundary varies from 4,077,300 m to 4,080,000 m. These ranges of geographical uncertainty in the boundaries of the reducing zone include the potential for misinterpretation of redox conditions in one to all of the wells used to infer the location of the reducing zone. The implementation of the SZ reducing zone in the PMA utilizes the synthesis and conclusions of *Impacts of Solubility and Other Geochemical Processes on Radionuclide Retardation in the Natural System – Rev 01* (BSC 2006 [DIRS 178672]) as direct input but also incorporates a potentially large degree of uncertainty in those conclusions. The unitless uncertain parameters for the boundaries of the reducing zone given in Table C6-9 are used as multiplying factors to the ranges given above in meters in defining the boundaries of the reducing zone for each realization.

The elements technetium and neptunium can exist in several oxidation states in groundwaters depending on the redox potential (Eh) of the groundwater, and their mobility highly depends on their oxidation states. Under oxidizing conditions, technetium exists primarily in the +7 oxidation state while neptunium exists primarily in the +6 oxidation state. Under sufficiently reducing conditions (Eh = < 100 mv) in near-neutral groundwaters (pH = 7.0 +/-2), both technetium and neptunium exist primarily in the +4 oxidation state. Although sorption experiments under reducing conditions have not been carried out for these two elements using samples from Yucca Mountain, sorption coefficients for these elements under reducing conditions have been reported in the literature. Lieser and Bauscher (1988 [DIRS 172722]) have reported on sorption coefficients for technetium under reducing conditions, and Lieser and Muhlenweg (1988 [DIRS 106684]) reported on sorption coefficients for neptunium under reducing conditions. These estimates of the sorption coefficients were obtained using sediment samples from the Gorleben site in Germany. The sediments were composed mainly of quartz with lesser amounts of other minerals including orthoclase, plagioclase, kaolinite, muscovite, calcite, chlorite, and dolomite. This mineralogy is not unlike the mineralogy of many of the tuffs at Yucca Mountain (BSC 2006 [DIRS 178672], Section 2.3.2). The surface areas of the Gorleben samples ranged from 0.011 to 0.025 m^2/g. Although several different groundwater compositions were used in the experiments including two with chemistry similar to groundwaters at Yucca Mountain, the sorption coefficients obtained for technetium and neptunium under reducing conditions did not show much sensitivity to groundwater composition. The sorption coefficients obtained by Lieser and Bauscher (1988 [DIRS 172722]) for technetium under reducing conditions averaged about 1,000 +/- 200 mL/g. For neptunium, Lieser and Muhlenweg (1988 [DIRS 106684]) obtained sorption coefficients ranging from 1,060 to 1,600 mL/g.

The uncertainty distributions for the sorption coefficients of technetium and neptunium under reducing conditions (Table C6-9) are based primarily on the experimental results of Lieser and Bauscher (1987 [DIRS 172722]) and Lieser and Muhlenweg (1988 [DIRS 106684]), respectively. These results show that the average value of the sorption coefficient under reducing conditions is about 1,000 mL/g for both technetium and neptunium. The uncertainty distributions are inclusive of the Lieser and Bauscher (1987 [DIRS 172722]) and Lieser and Muhlenweg (1988 [DIRS 106684]) values of sorption coefficients measured under reducing conditions. The values of sorption coefficients from these uncertainty distributions are likely underestimates because the tuffs and sediments at Yucca Mountain have surface areas 100-1,000

times larger than the surface areas of the Gorleben sediments (SNL 2007 [DIRS 177392], Appendix A). In addition, surface complexation modeling for neptunium sorption on quartz, as a function of Eh, quantitatively confirmed the high values of the sorption coefficient from the experimental sources (BSC 2006 [DIRS 178672], Section 2.3.2).

The SZ Flow and Transport Abstraction Model for the TSPA-LA model (DTN: SN0702PASZFTMA.001_R0 [DIRS 179504]) formed the basis for the model developed for the SZ PMA. Parameter values for the SZ Flow and Transport Abstraction Model were resampled, including the additional parameters related to the impacts of the reducing zone listed in Table C6-9. The resampled parameters for the reducing zones model, are included in the file SZ_Sampled_Vectors_PMA.txt in corroborative DTN: SN0704PMASZFTA.001_R1 [DIRS 184395]. The main input files to the FEHM software code used in the SZ Flow and Transport Abstraction Model were modified to include a zonal definition for the reducing zone to describe the coordinates. The input files controlling radionuclide transport in the FEHM code for technetium and neptunium were modified to assign the value of the sorption coefficients under reducing conditions to all volcanic hydrogeologic units within the reducing zone. A complete set of simulated radionuclide breakthrough curves was generated by the SZ Flow and Transport Abstraction Model for technetium and neptunium, as in the case for the TSPA-LA model runs (SNL 2008 [DIRS 183750], Section 6.6).

The structure of the SZ one-dimensional transport model was modified to insert additional pipe segments to represent the reducing zone within the volcanic units. Figure C6-34 shows the unmodified GoldSim structure used for the TSPA-LA model. The SZ three-dimensional model uses an external software (SZ_Convolute [DIRS 181060]) to calculate flow and transport through the SZ. The element *SZ_External* is a call to SZ_Convolute [DIRS 181060], which simulates the breakthrough of radionuclides 18 km away from the repository. The mass flux returned from SZ_Convolute [DIRS 181060] for each source region is then fed to cell *SZOUT*. A small volume and large flow rates (inflow and outflow) are assigned to *SZOUT*, which ensures that all mass entering *SZOUT* is flushed into cell *Sink* at every timestep. The one-dimensional transport model represents a network of four pathways, one for each source region. Each pathway consists of three GoldSim pipe segments. The first two pipes in each of the four pathways represent two distinct volcanic sections of the SZ and the third pipe simulates flow and transport through the saturated zone. The mass fluxes exiting the last pipe of each of the four one-dimensional model pathways are collected in element *Sink*. The *Sink* cell represents an unlimited volume into which all radionuclide mass exiting the two flow and transport models can flow without constraints. The total mass flux exiting the SZ from the one-dimensional model is calculated as a sum of the four mass fluxes exiting the last pipes.

Since the reducing zone path length could extend from Pipe_ax to parts of Pipe_bx on Figure C6-34, where x represents the source regions, the PMA divides both Pipe_ax and Pipe_bx into two parts, as shown on Figure C6-35, to accommodate variable path length of reducing zones. The resampled parameter values used in the SZ Flow and Transport Abstraction Model are also applied to the modified SZ one-dimensional transport model for consistency. The resulting modified version of the SZ one-dimensional transport model is inserted into the GoldSim model for PMA. The tabulated data representing the reducing zone path length for the one-dimensional transport model is given in the EXCEL spreadsheet

RZ_1-D_Average_Length.xls in corroborative DTN: SN0704PMASZFTA.001_R1 [DIRS 184395].

Flowing Interval Porosity (Fracture Porosity in Volcanic Units)

Based on the discussion above, the cumulative distribution (log_{10}-transformed) of the flowing interval porosity was revised and given in Table C6-10. This new distribution was used in the generation of the SZ breakthrough curves that feed TSPA and was also used for the SZ one-dimensional transport model. The correlation factor of 0.64 between the parameters flowing interval porosity and groundwater specific discharge multiplier was used during parameter sampling (corroborative DTN: SN0704PMASZFTA.001_R1 [DIRS 184395]).

C6.8 SEISMIC SCENARIO CLASS

The Seismic Scenario Class describes future performance of the repository system in the event of seismic activity that could disrupt the repository system (Section 6.6). The Seismic Scenario Class represents the direct effect of vibratory ground motion and fault displacement associated with seismic activity. The Seismic Scenario Class considers the effects of the seismic hazards on DSs and WPs because damage to or failure of these components has the potential to initiate or increase releases of radionuclides by forming new diffusive or advective transport pathways. The Seismic Scenario Class estimates the mean annual dose due to seismic activity by accounting for the probability of occurrence of activity expressed in terms of its mean annual exceedance frequency. The estimate of mean annual dose takes into account the relevant processes that affect system performance.

C6.8.1 Conceptual Model

Seismic Crack Area Density for Alloy 22

The seismic crack density model of the WP estimates the crack opening area on a WP damaged by a seismic event. The cracks within the damaged area are assumed to be caused as a result of stresses induced by a seismic event. The areas of the WP outer barrier that exceed the residual tensile stress threshold are considered damaged area (Section 6.6). The damaged or deformed area that exceeds a residual stress threshold is conceptualized to result in a tightly spaced network of stress corrosion cracks (SNL 2007 [DIRS 176828], Sections 6.1.4). In order to assess the potential for radionuclide release through these cracks, it is necessary to assess the possible number of cracks in the damaged area and the opening areas of these cracks.

The TSPA-LA Model samples a uniform distribution from 3.27×10^{-3} to 1.31×10^{-2} for the crack area density for WP seismic damage area. This distribution includes an upper bound allowing for uncertainties, such as the potential for crack overlap and deviations from a regular array of identically shaped cracks, to be appropriately accounted for (SNL 2007 [DIRS 181953], Section 6.7.3.3). This crack density model, used in the seismic damage analyses, includes the use of lower yield strength values for Alloy 22 (Haynes International 1988 [DIRS 101995], p. 15) leading to greater calculated damaged area. The yield strength is considered conservative because the process of crack initiation and through-wall crack propagation will result in significant reduction in the residual stress (SNL 2007 [DIRS 181953], Section 6.7.3.3). The yield strength of the material should be used as a reasonable estimate for the stress component in

the crack area density calculation (SNL 2007 [DIRS 181953], Section 6.7.3.3). The crack length used in the calculation of the lower bound allows for cracks, if they lie in the same plane, to just touch without overlapping (SNL 2007 [DIRS 181953], Section 6.7.3.1). The upper bound considers a crack length that allows for significant overlap (SNL 2007 [DIRS 181953], Section 6.7.3.2). For both the upper and lower bounds, the room temperature range of crack area density was used in the TSPA-LA as this choice yields higher crack area densities (SNL 2007 [DIRS 181953], Section 6.7.3.3). Additionally, because the hexagonal array used in the crack area density model for TSPA-LA represents a high effective density (close spacing) of individual cracks, this hexagonal geometry, with crack center spacings set at the plate thickness is considered a conservative representation (SNL 2007 [DIRS 181953], Section 6.7.2).

An alternative model for the crack area density considers a damaged area with a circular geometry circumscribed by a single through-wall crack and yields crack area density at a room temperature of 7.22×10^{-3} (SNL 2007 [DIRS 181953], Section 6.7.4). This is considered a limiting realistic case (SNL 2007 [DIRS 181953], Section 6.7.2). For the PMA, the crack area density was changed to a constant value equal to the lower bound used in the TSPA-LA Model, 3.27×10^{-3}. This lower bound more closely resembles the ACM results.

C6.8.2 Model Implementation

Seismic Crack Area Density for Alloy 22

The implementation of the crack area density affects only the Seismic GM Modeling Cases. The seismic crack area density model of the WP estimates the crack opening area on a WP damaged by a seismic event. In the *Epistemic_Params* container, the selector element, *WP_Crack_Area_Density*, was added to select between the TSPA-LA Model value (a uniform distribution from 3.27×10^{-3} to 1.31×10^{-2}) represented by the stochastic parameter, *WP_Crack_Area_Density_a*, and a constant value of 3.27×10^{-3}, used for the PMA included in the data element *WP_Crack_Area_Density_PMA*. The crack area density parameter only affects diffusive releases from WPs damaged during a Seismic GM Modeling Case. These parameters feed the Seismic Damage Abstraction calculations (Section 6.6).

C.7 RESULTS

Detailed probabilistic projections developed for the PMA are presented and explained in the subsequent sections. The *mean value* of the projected PMA annual doses to the RMEI is used as the primary metric for comparison with the TSPA-LA Model. The mean annual dose is quantified using four scenario classes: Nominal, Early Failure, Seismic, and Igneous. Detailed descriptions of the technical basis of these scenario classes and their associated modeling cases are presented in Sections 6.3 through 6.6 of Volume I of this report. In addition, a detailed discussion of the TSPA-LA Model dose is documented in Section 8.0 of this report.

The projection of total mean annual dose for the Individual Protection Standard is based on summing the expected annual doses over seven modeling cases: (1) Nominal, (2) Drip Shield EF, (3) Waste Package EF, (4) Seismic GM, (5) Seismic FD, (6) Igneous Intrusion, and (7) Volcanic Eruption. As required by the disposal standards, the postclosure performance is quantified for time periods of 10,000 years and 1,000,000 years after closure. Drawing from the evaluation

presented in Section 8.2, the PMA is exercised over modeling cases that are anticipated to have significant contributions to annual dose over the specified regulatory time periods. As discussed in Section C6.1, the performance margin of the TSPA-LA model can be largely quantified with results from the Seismic GM and Igneous Intrusion modeling cases since these two cases dominate the projected mean annual doses to the RMEI for time periods after a few hundred years (Sections 8.1 and 8.2). The results of this scenario class and modeling case screening for the performance margin analysis are summarized below:

- Nominal Modeling Case *included* (included in the Seismic GM Modeling Case)
- Drip Shield EF Modeling Case *included*
- Waste Package EF Modeling Case *included*
- Seismic GM Modeling Case *included*
- Seismic FD Modeling Case *included*
- Igneous Intrusion Modeling Case *included*
- Volcanic Eruption Modeling Case *excluded.*

The Seismic GM Modeling Case includes the effects of the nominal processes when run for 1,000,000 years after closure.

C7.1 PERFORMANCE MARGIN IN TOTAL ANNUAL DOSE PREDICTIONS

As described in Section 6.1.2 (Volume I), probabilistic projections of the expected (in the statistical sense) total annual dose to the RMEI are computed as a combination of the calculated expected annual doses for each of the four scenario classes; the expectation is taken over all aleatory (i.e., randomly occurring in time) uncertainties.

The main result of the simulation process is a plot of a set of expected annual dose histories. On each plot, dose curves for the mean, median, 5th and 95th percentiles are superimposed. The mean annual dose history was computed by taking the *arithmetic average* of the 300 expected annual dose values for individual time planes along the curves. Similarly, the *median* dose history was constructed from points obtained by sorting the 300 expected values from lowest to highest, and then averaging the two middle values. Curves for the 5th and 95th percentiles are also plotted to illustrate the spread in the expected annual dose histories; 90 percent (or 270 of the 300 epistemic realizations) of the projected dose histories fall between these two percentile curves. The plots obtained from the PMA are shown on Figure C7-1 for 10,000 years and on Figure C7-2 for 1,000,000 years.

The largest *mean* annual dose to the RMEI is estimated by the PMA to be about 0.02 mrem for the 10,000-year disposal period. Similarly, the largest *mean* annual doses to the RMEI after 10,000 years but within the period of geologic stability is estimated by the PMA to be about 1.0 mrem. To provide importance of the epistemic uncertainty of the performance projections, the annual dose histories corresponding to the 5th- and 95th- percentiles are also shown in the plots.

Important performance margin insights can be gained by comparison of the mean annual dose curves between the PMA and the TSPA-LA, which are shown on Figure C7-3 for 10,000 years

and on Figure C7-4 for 1,000,000 years. From those dose curves, the following general observations can be drawn about the PMA:

- The PMA mean annual doses are generally nearly an order of magnitude lower than the mean annual dose from the TSPA-LA Model over the first 250,000 years.
- The largest PMA mean annual doses calculated over 10,000 years are an order of magnitude lower than the largest mean annual dose from the TSPA-LA Model.
- The largest PMA mean annual doses calculated over 1,000,000 years are lower by a factor of two than the largest mean annual dose from the TSPA-LA Model.

As shown on Figures C.7-5(b) and C.7-6(b), the major contributors to the mean annual dose in the PMA ranked from highest to lowest, are: ^{99}Tc, ^{129}I, ^{14}C, ^{237}Np, ^{239}Pu, ^{240}Pu, and ^{234}U for the first 10,000 years and ^{226}Ra, ^{242}Pu, ^{237}Np, ^{129}I, ^{233}U, ^{135}Cs, ^{99}Tc, ^{229}Th, and ^{230}Th for the time period of 1,000,000 years. These radionuclides typically have a combination of unique characteristics such as: (1) large initial inventories in the nuclear waste, (2) moderate to high solubililities, (3) relatively long half-lives (e.g., $\geq 10^5$ years), and (4) low to non-sorbing properties. The dominant radionuclides identified in the PMA are similar to those found in the TSPA-LA Model (Figures C.7-5(a) and C.7-6(a)), indicating that the modifications made for the PMA do not alter the fundamental behavior of the repository system and thus add additional confidence in the TSPA-LA Model results. The lower annual doses estimated by the PMA, however, confirm that the conservatisms identified in Table C5-1 have potentially significant impacts on the repository performance. The PMA also confirms that, when propagated through the TSPA-LA Model, the conservatisms addressed in this analysis are conservative with respect to the total system performance measures (e.g., peak mean annual dose).

Additional insights into the performance margin can be gained by disaggregating the total annual doses into the mean annual dose curves for individual modeling cases, which are shown on Figure C7-7 for 10,000 years after closure and on Figure C7-8 for 1,000,000 years after closure. From those dose curves, the following general observations can be made about the projected postclosure performance for the PMA:

- The Igneous Intrusion Modeling Case is the dominant contributor to the calculated mean annual dose for both 10,000 years and 1,000,000 years.
- Mean annual doses for the Drip Shield EF, Seismic FD, and Volcanic Eruption Modeling Cases are relatively small and are estimated to be on the order of 10^{-4} mrem or less for both 10,000 years and 1,000,000 years after closure.
- Mean annual dose projected for the Waste Package EF Modeling Case is on the order of 10^{-3} mrem or less and is the second largest contributor to the calculated total mean annual dose until 10,000 years after closure.
- Mean annual dose projected for the Seismic GM Modeling Case is on the order of 10^{-1} mrem or less and is the second largest contributor to the calculated total mean annual dose for 1,000,000 years after closure.

In the TSPA-LA Model, the Seismic GM Modeling Case dominates the mean annual dose for the 10,000-year time period; whereas for 1,000,000 years, the Seismic GM and Igneous Intrusion Modeling Cases contribute equally to the total mean annual dose to the RMEI (Section 8.1.1.2). The PMA, however, shows that the Igneous Intrusion Modeling Case dominates the mean annual dose for the 10,000-year time period; whereas for 1,000,000 years, the Seismic GM and Igneous Intrusion Modeling Cases start to dominate after 200,000 years. The remaining cases combined have a negligible contribution.

Although the Igneous Intrusion Modeling Case dominates the calculated annual dose in the PMA, it is important to note, for the purpose of risk insights, that the mean annual frequency for a dike to intersect the repository is estimated to be 1.7×10^{-8} per year (Section 8.1.1.3). This frequency is only slightly greater than the NRC frequency threshold (10^{-8}) for unlikely FEPS that can be omitted by regulation.

C7.2 PERFORMANCE MARGIN ANALYSIS—MODELING CASE RESULTS

It is necessary to disaggregate the PMA results by modeling case to quantify the extent to which the conservatisms, individually and collectively, affect the projected annual dose, relative to the TSPA-LA Model projections presented in Section 8.1. In this section, the PMA results are examined for each individual modeling case in comparison with the TSPA-LA results.

Drip Shield EF Modeling Case—In this modeling case, the defective drip shields are assumed to fail at the time of repository closure (Section 6.4.1, Volume I). WPs under an early-failed DS are assumed to experience localized corrosion as soon as seepage contacts the WP, since the area of the Alloy 22 WP outer barrier that is contacted by seepage is potentially subject to localized corrosion (Section 6.4, Volume I). The mean annual dose histories calculated in the PMA are presented on Figures C7-7(a) and C7-8(a), together with those obtained in the TSPA-LA calculations. It can be clearly seen in the figures that the TSPA-LA Model predicts a higher mean annual dose than the PMA by more than one order of magnitude over both 10,000-year and 1,000,000-year time frames. The radionuclides that contribute most to the PMA Drip Shield EF Modeling Case mean annual dose are shown on Figures C7-9(a) and C7-10(a). In the first 10,000 years after repository closure, soluble radionuclides ^{99}Tc, ^{14}C, and ^{129}I are the primary contributors to the Drip Shield EF Modeling Case mean annual dose; while over the 1,000,000-year time period, the mean annual dose is dominated by ^{242}Pu, ^{129}I, ^{126}Sn, ^{237}Np, ^{135}Cs, and ^{233}U. Compared to the TSPA-LA Model, Figures C7-11(a) and C7-12(a), the total dose contributions from soluble radionuclides, are reduced in the PMA results for the Drip Shield EF Modeling Case by more than one order of magnitude for the first 10,000 years, while the contributions from solubility-controlled radionuclides, such as plutonium, neptunium, and uranium, are reduced by about two orders of magnitude. In the TSPA-LA Drip Shield EF Modeling Case, the entire area of the Alloy 22 WP outer barrier that is contacted by seepage is assumed to be failed since it is potentially subject to localized corrosion (Section 6.4, Volume I). In the PMA, the localized corrosion failure area is uncertain and generally much smaller than the entire WP surface area (Section C6.3). In addition, unfailed (not perforated) CSNF cladding is assumed to remain intact for the 10,000-year regulatory period in the absence of mechanical damage mechanisms from seismic ground motion and/or rockfall (Section C.6.5). The lower dose results in the PMA are primarily controlled by these changes.

Waste Package EF Modeling Case—In the Waste Package EF Modeling Case, an early-failed WP is considered breached at the beginning of the simulation, and its entire surface area is considered degraded (Section 6.4.2, Volume I). General corrosion of the DSs due to nominal corrosion processes (Section 6.3.5.1.2) is included in the Waste Package EF Modeling Case. The mean annual dose histories calculated in the PMA are presented on Figures C7-7(b) and C7-8(b), together with those obtained in the TSPA-LA calculations. The figures indicate that the TSPA-LA Model slightly exceeds the mean dose as compared to the PMA over the first 9,000 years, after which the TSPA-LA model exceeds the PMA predicted dose by one order of magnitude. The radionuclides that contribute most to the PMA Waste Package EF Modeling Case mean annual dose are shown on Figures C7-9(b) and C7-10(b). In the first 10,000 years after repository closure, soluble radionuclides ^{99}Tc, ^{14}C, and ^{129}I are the primary contributors to the Waste Package EF Modeling Case mean annual dose; while over the 1,000,000-year time period, the mean annual dose is dominated by ^{242}Pu, ^{129}I, ^{99}Tc, ^{237}Np, ^{135}Cs, and ^{239}Pu. Compared to the TSPA-LA Model Figures C7-11(b) and C7-12(b), the total dose contributions from soluble radionuclides are slightly reduced in the PMA results for the Waste Package EF Modeling Case over the first 9,000 years; while the contributions from solubility-controlled radionuclides, such as plutonium, neptunium, and uranium, are reduced by one to two orders of magnitude over most of the 1,000,000-year time period. In the Waste Package EF Modeling Case, releases from the waste packages by diffusion control the dose results as diffusive transport of dissolved radionuclides through the WP using the entire surface area is sufficiently high that there are minimal differences between the PMA and TSPA-LA mean annual dose results over the first 9,000 years. In the PMA unfailed (not perforated) CSNF, cladding is assumed to remain intact for the 10,000-year regulatory period (Section C.6.5), which explains the sudden increase in the dose in the TSPA-LA when the CSNF WP begins to release radionuclides; whereas there is no corresponding increase in the PMA results at approximately 9,000 years. The lower dose results in the PMA over the 1,000,000-year time period are primarily controlled by a cumulative effect from reductions in the saturation used to calculate the diffusive releases and a reduction in the WF degradation rates (Section C7.3).

Seismic GM Modeling Case—This modeling case represents DSs and WPs that fail from mechanical damage associated with seismic vibratory ground motion (Section 6.6, Volume I). Depending on the timing, sequence, and intensity of the ground motion events, the DSs and WPs can accumulate damage and/or cause a failure. In the case of the DSs, seismic ground motions could cause damage or failure by: (1) buckling and rupture, (2) exceeding residual stress threshold, and (3) deformation or rupture by large block rockfall. Similarly, the WPs could be damaged or fail by: (1) local strain that exceeds ultimate tensile strength, (2) deformations creating residual stresses that induce SCC, and (3) lithostatic loading from rubble that causes a rupture of the outer barrier by WP internals. Both the DSs and WPs are also degraded by the nominal corrosion processes (e.g., general corrosion and localized corrosion). The total mean annual dose history for the Seismic GM Modeling Case calculated in the PMA is presented on Figures C7-7(c) and C7-8(c), together with those obtained in the TSPA-LA calculations. Comparison of the total mean annual dose curves shown in the figure indicate that the TSPA-LA Model results exceed the PMA mean annual dose by three orders of magnitude over the first 10,000 years. The difference between the PMA and the TSPA-LA model dose results decreases over the time period from 10,000 years to 700,000 years after repository closure. The radionuclides that contribute most to the PMA Seismic GM Modeling Case mean annual dose are shown on Figures C7-9(c) and C7-10(c). In the first 10,000 years after repository closure,

soluble radionuclides ^{14}C, ^{99}Tc, and ^{129}I are the primary contributors to the PMA Seismic GM Modeling Case mean annual dose; while over the 1,000,000-year time period, the mean annual dose is dominated by ^{129}I, ^{99}Tc, ^{79}Se, ^{135}Cs, ^{36}Cl, ^{242}Pu, and ^{237}Np. Compared to the TSPA-LA Model Figures C7-11(c) and C7-12(c), the total mean annual dose contributions from soluble radionuclides are reduced in the PMA results by three orders of magnitude over the first 10,000 years, while the contributions from solubility-controlled radionuclides, such as plutonium, neptunium, and uranium, are reduced by a factor of one to two orders of magnitude over most of the 1,000,000-year time period. The CDSP WPs are the primary container damaged during the 10,000-year period in both the PMA and the TSPA-LA modeling cases. The CSNF WPs are much more resistant to seismic damage than the CDSP WPs (Section 6.6, Volume I). The predominate mechanism causing damage to the CDSP and CSNF WPs in the TSPA-LA Seismic GM Modeling Case consisted of small cracks (SCC) when the residual stress threshold on the WP outer barrier was exceeded (Section 8.2.4.1). In the PMA, the residual stress threshold necessary for SCC is higher than the TSPA-LA (Section C6.8), as well as a reduction in the SCC density on damaged WPs (Section C6.8). The lower dose results in the PMA are primarily controlled by these changes.

Seismic FD Modeling Case—This modeling case includes disruption of the WPs and DSs by the displacement of faults. As described in Section 6.6.1 (Volume I), the characterization of the fault is based on data from known faults in the vicinity of the site area. The disruption in this modeling case is conceptualized as a sudden discontinuity in the profile of the repository. The location and magnitude of the fault displacement determines the number of DSs and WPs that are disrupted. The total mean annual dose history for the Seismic FD Modeling Case calculated in the PMA is presented on Figures C7-7(d) and C7-8(d), together with those obtained in the TSPA-LA calculations. Comparison of the total mean annual dose curves shown on the figures indicate that the TSPA-LA Model results exceed the PMA mean annual dose by one to two orders of magnitude over both the first 10,000 years and the first 1,000,000 years after repository closure. The radionuclides that contribute most to the PMA Seismic FD Modeling Case total mean annual dose are shown on Figures C7-9(d) and C7-10(d). In the first 10,000 years after repository closure, soluble radionuclides ^{14}C, ^{99}Tc, and ^{129}I are the primary contributors to the PMA Seismic FD Modeling Case mean annual dose; while over the 1,000,000-year time period, the mean annual dose is dominated by ^{129}I, ^{99}Tc, ^{242}Pu, ^{79}Se, ^{239}Pu, ^{237}Np, and ^{135}Cs. Compared to the TSPA-LA Model Figures C7-11(d) and C7-12(d), the total mean annual dose contributions from soluble radionuclides are reduced in the PMA by about a factor of 10 for the first 10,000 years, while the contributions from solubility-controlled radionuclides, such as plutonium, neptunium, and uranium, are reduced by a factor of one to two orders of magnitude over the most part of the 1,000,000-year time period. The Seismic FD Modeling Case includes the destruction of both the WP and DS (Section 6.6, Volume I). The radionuclide releases in both the TSPA-LA and PMA are controlled by the advective releases from the EBS. The PMA is primarily driven by a reduced seepage flux to WP based on a smaller hydrologic cross section used for the representation of collapsed drift geometry (Section C.6.2) and the result of the PMA predicting much lower advective water flux percolating through breached WPs (Section C.6.4). A discussion of these affects in Section C.7.3 follows.

Igneous Intrusion Modeling Case—As described in Section 6.5.1 (Volume I) in this modeling case, a simulated magmatic dike intersects the footprint of the repository causing failure of the EBS. Radionuclide releases attributed to the intrusion and transport away from the repository

are analyzed in a manner analogous to that for the Nominal Modeling Case but differ in the conceptualization of the EBS failure. The modeling case assumes that all the WPs in the repository are completely destroyed, exposing the waste forms to percolating groundwater with subsequent degradation, radionuclide mobilization, and transport. The total mean annual dose history for the Igneous Intrusion Modeling Case calculated in the PMA is presented in Figures C7-7(e) and C7-8(e), together with those obtained in the TSPA-LA calculations. Comparison of the total mean annual dose curves shown on the figures indicates that the TSPA-LA Model results systematically exceed the PMA mean annual dose by a factor of two to a factor of ten for both the first 10,000 years and the first 1,000,000 years after repository closure. The radionuclides that contribute most to the PMA Igneous Intrusion Modeling Case total mean annual dose results are shown on Figures C7-9(e) and C7-10(e). In the first 10,000 years after repository closure, soluble radionuclides ^{99}Tc, ^{129}I, and ^{14}C are the primary contributors to the PMA Igneous Intrusion Modeling Case mean annual dose; while over the 1,000,000-year time period, the mean annual dose is dominated by ^{226}Ra, ^{242}Pu, ^{237}Np, ^{233}U, and ^{239}Pu. The domination of ^{226}Ra is due to the fact that in the Igneous Intrusion Modeling Case all WPs will be damaged and subjected to large percolating water fluxes, resulting in quick depletion of soluble radionuclides ^{99}Tc, ^{129}I, and ^{14}C and accumulation of a large quantity of ^{238}U and ^{234}U in both the UZ and SZ, which will give rise to a high dose contribution of ^{226} Ra (a daughter product of ^{238}U and ^{234}U). Compared to the TSPA-LA Model Figures C7-11(d) and C7-12(d), the total mean annual contributions from soluble radionuclides remain practically the same in the PMA, while the contributions from solubility-controlled radionuclides, such as plutonium, neptunium, and uranium, are slightly decreased in the PMA results. It is worth noting that the contribution from ^{239}Pu is reduced by a factor of approximately 10, partly due to reduction in waste-form colloid transport as a result of the implementation of the colloid diversity model in the SZ (C6.7).

C7.3 KEY FACTORS AFFECTING THE PERFORMANCE MARGIN

Mechanical Damage of Waste Packages—For the PMA, the Seismic GM Modeling Case contributes a much lower dose over the first 250,000 years compared with the TSPA-LA results, as can be seen on Figure C7-8 (c). For the TSPA-LA Model results, the predominate mechanism causing damage to the CDSP and CSNF WPs consisted of small cracks (SCC) that result in releases from the WPs by diffusion (Section 8.2.4.1). Diffusive transport of dissolved radionuclides through the cracks is sufficiently high that they contribute significantly to the mean annual dose. In the Seismic GM Modeling Case for the PMA, fewer WP are damaged by SCC. The PMA uses an increase for the lower bound of the range for the residual stress threshold, which is used to evaluate the SCC along the closure welds. In addition, the damaged area on WPs used in the PMA is generally smaller, resulting in fewer openings in a failed WP (Section C6.8). Seismic induced SCC failure of both of CDSP and transportation-, aging-, and disposal-bearing WPs are dependent upon the stress threshold for Alloy 22. At approximately 200,000 years after closure, the PMA Seismic GM Modeling Case begins to contribute to the PMA Total Dose. The timing is significant in that not until enough WPs begin to fail due to general corrosion effects, after approximately 100,000 years, will the GM damage begin to occur to the transportation, aging, and disposal WPs. The PMA Seismic GM Modeling Case dose continues to rise from 200,000 to approximately 600,000 years after closure, as a result of seismic ground motion damage to the WPs. The use of slower DS corrosion rates in the PMA (Section C6.3) increases the lifetime of a DS, which in turn will increase the damage area for

failed WPs under intact DSs. This damage mechanism, referred to as kinematic damage, is invoked when WPs are free to move beneath and intact DSs (SNL 2007 [DIRS 178851], Section 6.5.1 through Section 6.5.4 and Section 6.6.1 through 6.6.4). The Seismic Damage Submodel in the TSPA calculates the damage area WPs with degraded internals and intact DSs (Section 6.6.1.2.2.2). The increase in damage area that is calculated as a result of the longer DSs life time mitigates some of the margin gained by the longer WP life spans, as can be seen by the rise in the dose from approximately 200,000 years to its peak at approximately 600,000 years after closure. However, the dominant effect of increasing WP durability through the modified SCC threshold is significant for accounting for the margin in both the 10,000-year and 1,000,000-year time periods for PMA. The Seismic GM Modeling Case is reduced by two orders of magnitude below the Igneous Intrusion Modeling Case dose results over the 10,000-year time period (Figure C7-7(f)).

General Corrosion of Waste Packages—The PMA considers an ACM included in *General Corrosion and Localized Corrosion of Waste Package Outer Barrier* (SNL 2007 [DIRS 178519], Section 6.4.3.5.2), which uses the corrosion rates of weight-loss samples to derive the R_o distribution for use in the General Corrosion Model of the WP outer barrier (Section C6.3). This ACM does not involve the use of a conceptual model that differs from that used in the WP General Corrosion Model but does make use of a different distribution for Alloy 22 general corrosion rates. This evaluation of the effects of the exclusion of the weight-loss data from the TSPA-LA was conducted using two alternative PMA modeling cases that evaluated the affects on the Seismic GM and Nominal Modeling Cases. The baseline PMA results discussed above (Section C.7.1 and Section C.7.2) do not include the weight-loss data in the WP general corrosion submodel calculations. The Seismic GM Modeling Case was chosen since it is one of the dominant dose contributors to the total mean annual dose for both 10,000 years and 1,000,000 years postclosure. In addition, the Nominal Modeling Case was selected so that the general corrosion effects could be evaluated without any interference from other WP failure mechanisms.

Figure C7-13 shows a comparison of the total mean annual dose for the Seismic GM Modeling Cases for the TSPA-LA and the PMA with and without using weight-loss corrosion data. In the TSPA-LA Model results, the most likely failure mechanism from a seismic event was accelerated SCC in the damaged areas that exceed the residual stress threshold for Alloy 22 (the waste package outer barrier). The PMA increased the lower bound for the residual stress threshold (RST) for Alloy 22 and reduced the crack density for the damaged areas that exceed the RST (Section C6.3). The effect of these changes are seen between 0 and approximately 100,000 years postclosure as the PMA is two orders of magnitude below the TSPA-LA mean dose for the Seismic GM Modeling Case (Figure C7-13). In all three modeling cases shows on Figure C7-13, the ground motion enhanced SCC accounts for all the WP failures before 100,000 years and thus, the PMA with the weight-loss data shows a nearly identically dose history as the PMA Seismic GM Modeling Case with the TSPA-LA WP general corrosion model. After, approximately 120,000 years, the PMA Seismic GM Modeling Case shows the effects of the addition of the WPs failed from general corrosion as can be seen by a change in the slope of the mean annual dose curve shown on Figure C7-13. In contrast, the mean annual dose curve for the PMA Seismic GM Modeling Case using the alternative weight-loss general corrosion data does not change slope at approximately 140,000 years; rather, there is a more subtle change in the slope at approximately 220,000 years postclosure. The weight-loss general corrosion data yields a result that includes the first WP failure

at approximately 200,000 years postclosure while the TSPA-LA WP General Corrosion Submodel calculates the first WP failures to occur at approximately 100,000 years postclosure. This is demonstrated on Figure C7-14, which shows a comparison of the total mean annual dose for the Nominal Modeling Cases for the TSPA-LA and the PMA for a period of 1,000,000 years postclosure.

Advective Water Flux and Waste Form Degradation Rates—As discussed in Section C6.4, by incorporating additional hydrologic/chemical processes as well as water balance model parameters, the PMA predicts much lower advective water flux percolating through breached WPs than the TSPA-LA Model. In addition, the PMA reduces waste form degradation rates for both the CSNF and the HLW glass. The PMA calculations show that the combination of reduced water flux and waste form degradation rates has a notable effect on the predicted total annual dose over the first 10,000 years for the Drip Shield EF, Seismic GM, and Seismic FD Modeling Cases. This can be best seen for soluble radionuclides such as ^{99}Tc, ^{129}I, and ^{14}C, the release rates of which highly depend on the waste form degradation rate. As shown on Figure C7-9, the annual dose contributions from these three radionuclides for the first 10,000 years are systematically lower as compared to the TSPA-LA model results (Figure C7-11 and Figure C7-12) for the Drip Shield EF, Seismic GM, and Seismic FD Modeling Cases. As can be seen by comparison of the solubility controlled species (^{237}Np and ^{239}Pu), the lower water flux results in a lower dose in these cases, including during the late stage of WP failure, all of which involve advective water flows. Based on the discussion in Section C7.2, the performance margin gain from a the updated water balance model and waste degradation rates is estimated to be more than one order of magnitude for soluble radionuclides.

Note that the water balance model described in Section C6.4 was not applied to the Igneous Intrusion Modeling Case. In addition, it is likely that the reduced waste form degradation rates were not invoked in both the TSPA-LA and the PMA simulations for the Igneous Intrusion Modeling Case because the thermal pulse due to magmatic intrusion causes waste forms to degrade at a pre-specified maximum rate. Therefore, the dependence of dose contributions from soluble radionuclides on the newly implemented water balance model and the reduced waste form degradation rates is not observed for this modeling case.

Radionuclide Solubility—Solubility-controlled radionuclides such as ^{242}Pu, ^{239}Pu, ^{237}Np, and ^{233}U are expected to quickly reach their solubility limits after WP breaching, given the repository condition of high solid/water ratio as well as the relatively large inventories of these radionuclides. The release of these radionuclides, therefore, is mainly controlled by their solubility limits and the rate of water percolating through WPs. The release of these radionuclides is insensitive to the rates of waste form degradation. As discussed in Section C7.2, compared to the TSPA-LA Model, the total dose contributions from plutonium, neptunium, and uranium are reduced by one to two orders of magnitude for the time period of 1,000,000 years. By excluding the potential effect of reduced water flux as discussed above, the performance margin gain from using a narrower range of solubility uncertainties is estimated to be about one order of magnitude for radionuclides ^{242}Pu, ^{239}Pu, ^{237}Np, and ^{233}U.

It is important to note that the PMA only narrowed the uncertainty ranges of radionuclide solubility but did not change the solubilities themselves. The PMA results thus indicate that the dose contributions from ^{242}Pu, ^{239}Pu, ^{237}Np, and ^{233}U are sensitive to the upper limits of their

solubilities. This is reasonable based on the consideration that the solubility uncertainties are sampled on a logarithmic scale while the mean dose is calculated from radionuclide concentrations in a linear space. As a result, the mean dose calculated as such is expected to be influenced significantly by a few realizations with extremely high resultant radionuclide solubilities.

Irreversible Waste Form Colloids—It is important to mention that for the Igneous Intrusion Modeling Case only an early dose reduction is observed, which is primarily a function of a reduction in the amount of plutonium that reaches the accessible environment in the PMA. This effect can be seen by comparing Figure C7-9(e) and Figure C7-10(e) with Figure C7-11(e) and Figure C7-12(e). This early dose reduction is due to the colloid diversity model used for transport through the natural system (Section C6.6) as well as the reduction in the dissolved concentration limit uncertainty applied to plutonium isotopes (Section C6.5). The PMA calculations show that the dose contribution from ^{239}Pu-embedded waste form colloids is significantly reduced as compared to the TSPA-LA results. Both ^{239}Pu and ^{242}Pu are present mainly in waste form colloids for the first 10,000 years and then in dissolved forms over the rest of the 1,000,000-year time period.

Redox Conditions in SZ—As described in Section C6.7, the PMA includes the potential effect of reducing environments that may exist in the flow pathway in the SZ. These reducing environments can potentially affect the mobility of redox-sensitive radionuclides such as ^{99}Tc and ^{237}Np. In the PMA, this effect is captured by using appropriate sorption coefficients for ^{99}Tc and ^{237}Np in the SZ Radionuclide Transport Model. It is important to bear in mind that a sorption process generally delays the breakthrough time of sorbed radionuclides. Since no significant delay for ^{99}Tc and ^{237}Np in the SZ was observed in the PMA (Figure C7-3(b) and Figure C7-6(b)) as compared to the TSPA-LA Model (Figure C7-3(a) and Figure C7-6(a)), it appears that reducing environments in the SZ flow pathway have little effect on radionuclide doses.

C.8 SUMMARY

The objective of this PMA is to carefully and quantitatively evaluate the significance of the major explicit and implicit conservatisms embedded in the TSPA-LA model. This analysis was performed in two steps: (1) identifying the scenario classes and modeling cases that produce the most significant releases and dominate the projected doses, and (2) determining the sources of uncertainty and/or conservatisms that are most influential in producing the spread of the distribution of projected doses for these modeling cases. The PMA performed a separate set of TSPA calculations in parallel to those of the TSPA-LA for the modeling cases of Drip Shield EF, Waste Package EF, Seismic GM, Seismic FD, and Igneous Intrusion Modeling Cases. The performance margin of the TSPA-LA model was evaluated by comparing the mean values of the projected annual doses to the RMEI obtained from the PMA to those from TSPA-LA.

The PMA calculations have show that (1) the PMA mean annual doses are nearly an order of magnitude lower than the mean annual dose from the TSPA-LA Model for the first 250,000 years, (2) the largest PMA mean annual doses calculated over 10,000 years are lower by an order of magnitude than the largest mean annual dose from the TSPA-LA Model, and (3) the largest PMA mean annual doses calculated over 1,000,000 years are lower by a factor of two

than the largest mean annual dose from the TSPA-LA Model. Thus, the PMA calculations confirm that, when propagated individually through the TSPA-LA Model, the conservatisms introduced at submodel levels are conservative with respect to the total system performance measures (e.g., peak mean annual dose). In the PMA, the Igneous Intrusion Modeling Case contributes the most to the calculated mean annual doses for both 10,000 years and 1,000,000 years. The mean annual dose projected for the Seismic GM Modeling Case is on the order of 10^{-1} mrem or less and is the second largest contributor to the calculated total mean annual dose for 1,000,000 years after closure. The total dose contribution from other modeling cases is negligible over that time period. The major contributors to the peak mean dose in the PMA, ranked from highest to lowest, are: ^{99}Tc, ^{129}I, ^{14}C, ^{239}Pu, ^{240}Pu, ^{237}Np, and ^{234}U for the first 10,000 years and ^{226}Ra, ^{242}Pu, ^{237}Np, ^{129}I, ^{233}U, ^{135}Cs, ^{99}Tc, ^{229}Th, and ^{230}Th for the time period of 1,000,000 years, in the same order as the TSPA-LA Model predicts.

It is important to evaluate the performance margin of the TSPA-LA Model for each individual modeling case. Although the Igneous Intrusion Modeling Case dominates the calculated annual dose in the PMA and results in a relatively small performance margin, it is important to bear in mind that the mean annual frequency for a dike to intersect the repository is estimated to be 1.7×10^{-8} per year. This frequency is only slightly greater than the NRC frequency threshold for unlikely FEPs, which can be omitted by regulation. It is important to notice that the performance margins of the TSPA-LA Model for other modeling cases, especially the Drip Shield EF, Waste Package EF, and Seismic FD, are apparently much larger than that for the Igneous Intrusion Modeling Case. The factors that can significantly affect the performance margin include: mechanical damage of WPs by seismic ground motion, general corrosion rates of the WP outer barrier layer, in-package water balance, waste form degradation rates, radionuclide solubility uncertainties, and Colloidal Diversity Model for the SZ. Reducing environments in the SZ has little effect on radionuclide transport due to the already rapid transport in the SZ.

C.9 IMPACT ANALYSIS

After the PMA was completed and its feeds were frozen, several issues were identified in the TSPA-LA Model during post-model development checking activities that are related to errors in implementation and changes in parameter values. These issues are addressed in Appendix P as per the review criteria outlined in Sections 2.1.4 and 2.3.5.2.1 of the *Technical Work Plan for: Total System Performance Assessment FY 07-08 Activities* (SNL 2008 [DIRS 184920]). Since the PMA modifications were performed using a copy of the TSPA-LA Model, the issue descriptions and impact analyses in Appendix P apply equally to the PMA. In addition, PMA post-model development checking activities identified errors in implementation and changes in parameter values specific to the PMA. Table C9-1 summarizes the known PMA model errors and provides a qualitative assessment of the expected impact on the PMA. None of the issues evaluated on Table C9-1 or in Appendix P present a significant impact on the assessment of the performance margin or to the conclusions presented in Section C8. Thus, the confidence in the PMA results as an estimator of the performance margin in the mean dose to the reasonably RMEI can be maintained.

Table C3-1. Software Codes Specific to the PMA

Code	Version	Software Tracking Number	Operating System	DIRS Number
FEHM	2.25-00	STN: 10086-2.25-00	Windows 2000 Windows 2003 Windows XP	DIRS 182477
iTough	5.0	STN: 10003-5.0-00	SUN OS 5.5.1, OSF1 V5.1, RedHat V7.2 and V7.3	DIRS 160106

Table C3-2. TSPA-LA Model Software Codes used in the PMA

Code	Version	Software Tracking Number	Operating System	DIRS Number
CWD[a]	2.0	STN: 10363-2.0-00	Windows 2000	DIRS 162809
CWD[a]	2.0	STN: 10363-2.0-01	Windows 2003	DIRS 181037
EXDOC_LA[b]	2.0	STN: 11193-2.0-00	Windows 2000 Windows 2003 Windows XP	DIRS 182102
FEHM[a,c]	2.24-01	STN: 10086-2.24-00	Windows 2000 Windows 2003 Windows XP	DIRS 179419
GetThk_LA[a]	1.0	STN: 11229-1.0-00	Windows 2000 Windows 2003	DIRS 181040
GoldSim[a]	9.60.100	STN: 10344-9.60-01	Windows 2000 Windows 2003 Windows XP	DIRS 181903
InterpZdll_LA[a]	1.0	STN: 11107-1.0-00	Windows 2000	DIRS 167885
InterpZdll_LA[a]	1.0	STN: 11107-1.0-01	Windows 2003	DIRS 181043
MFCP_LA[a]	1.0	STN: 11071-1.0-00	Windows 2000	DIRS 167884
MFCP_LA[a]	1.0	STN: 11071-1.0-01	Windows 2003	DIRS 181045
MkTable_LA[a]	1.0	STN: 11217-1.0-00	Windows 2000	DIRS 181047
MkTable_LA[a]	1.0	STN: 11217-1.0-01	Windows 2003	DIRS 181048
MView[b]	4.0	STN: 10072-4.0-01	Windows XP	DIRS 181049
PassTable1D_LA[a]	2.0	STN: 11142-2.0-00	Windows 2000 Windows 2003	DIRS 181051
PassTable3D_LA[a]	2.0	STN: 11143-2.0-00	Windows 2000 Windows 2003	DIRS 182556
PREWAP_LA[b]	1.1	STN: 10939-1.1-00	Windows 2000	DIRS 181053
SCCD[a]	2.01	STN: 10343-2.01-00	Windows 2000	DIRS 181157
SCCD[a]	2.01	STN: 10343-2.01-01	Windows 2003	DIRS 181054
SEEPAGEDLL_LA[a]	1.3	STN: 11076-1.3-00	Windows 2000	DIRS 180318

Table C3-2. TSPA-LA Model Software Codes use in the PMA (Continued)

Code	Version	Software Tracking Number	Operating System	DIRS Number
SEEPAGEDLL_LA[a]	1.3	STN: 11076-1.3-01	Windows 2003	DIRS 181058
SZ_Convolute[a]	3.10.01	STN: 10207-3.10.01-00	Windows 2000/ Windows 2003	DIRS 181060
TSPA_Input_DB[a]	2.2	STN: 10931-2.2-00	Windows 2000	DIRS 181061
TSPA_Input_DB[a]	2.2	STN: 10931-2.2-01	Windows 2003	DIRS 181062
WAPDEG[a]	4.07	STN: 10000-4.07-00	Windows 2000	DIRS 181774
WAPDEG[a]	4.07	STN: 10000-4.07-01	Windows 2003	DIRS 181064

[a] Codes used in the TSPA-LA Model that are used for TSPA-LA Model development and to develop results and conclusions in Section 8.

[b] Code is a pre- or post-processor that does not require GoldSim to run codes that are used for TSPA-LA Model development and to develop results and conclusions in Section 8.

[c] Codes used in the PMA Model that are not used in the TSPA-LA Model development and to develop results and conclusions in Section 8.

Table C3-3. Unqualified Software

Description	Status	Software Tracking Number
SZ_Post_NonQ	Unqualified	STN: LL2000
Reduce_Track_NonQ	Unqualified	STN LL2001

Unqualifed software used for corroborative PMA analyses per SCI-PRO-006, *Models*.

Table C3-4. FEHM Software Documents

Version 2.25 Windows 2000, XP, and 2003 (STN: 10086-2.25-00)			
Description	**Document ID**	**DIRS Number**	**Tracking Number**
Requirements Document (RD)	10086-RD-2.25-01	DIRS 182561	MOL.20070712.0361
Design Document (DD)	10086-DD-2.25-01	DIRS 182562	MOL.20070712.0363
User Information Document (UID)	10086-UID-2.25-00	DIRS 182565	MOL.20070712.0365
Software Validation Report (SVR)	10086-SVR-2.25-00 WIN2000	DIRS 182566	MOL.20070712.0371
Software Validation Report (SVR)	10086-SVR-2.25-00-WIN2003	DIRS 182567	MOL.20070712.0373
Software Validation Report (SVR)	10086-SVR-2.25-00-WINXP	DIRS 182568	MOL.20070712.0375

Table C3-5. TSPA_Input_DBv2.2 Software Documents

Version 2.2 Windows 2000 (STN:10931-2.2-00)*			
Description	**Document ID**	**DIRS Number**	**Tracking Number**
Requirements Document (RD)	10931-RD-2.0-00	DIRS 173449	MOL.20050131.0427
Design Document (DD)	10931-DD-2.0-00	DIRS 173450	MOL.20050131.0430
User Information Document (UID)	10931-UID-2.2-00	DIRS 181137	MOL.20060222.0419
Software Validation Report (SVR)	10931-SVR-2.2-00-WIN2000	DIRS 181139	MOL.20060222.0422
Version 2.2 Windows 2003 (STN:10931-2.2-01)*			
Requirements Document (RD)	Same as above	NA	NA
Design Document (DD)	Same as above	NA	NA
User Information Document (UID)	Same as above	NA	NA
Software Validation Report (SVR)	10931-SVR-2.2-01-WIN2003	DIRS 181140	MOL.20061011.0198

* The PMA uses the same software for the model input database as the TSPA-LA Model database (TSPA_Input_DBv2.2).

Table C3-6. iTough V5.0 Software Documents

Version 5.0 SUN OS 5.5.1, OSF1 V5.1, and RedHat V7.2 and V7.3 (STN:10003-5.0-00)			
Description	**Document ID**	**DIRS Number**	**Tracking Number**
Requirements Document (RD)	10003-RD-5.0-00	DIRS 161067	MOL.20020923.0143
Design Document (DD)	10003-DD-5.0-00	DIRS 161068	MOL.20020923.0144
Users Manual (UM)	10003-UM-5.0-00	DIRS 161066	MOL.20020923.0147
Validation Test Report (VTR)	10003-VTR-5.0-00	DIRS 160437	MOL.20020923.0148

Table C4-1. TSPA-LA Model Parameters Changed or Deleted for the PMA

Parameter Name in TSPA-LA Compliance Model	Description	Parameter Value for Compliance Model (including DTN)	Parameter Value for PMA Model (including DTN)	Rationale for Changes
Drift Scale UZ Flow				
SMPA_C.dat	An alternative extended range seepage lookup table that considers seepage into only a 5.5-m wide center section of a collapsed drift.	Lookup Table (DTN: LB0702PASEEP01.001_R0 [DIRS 179511])	Lookup Table (Corroborative DTN: LB0704PASEEP02.001_R1 [DIRS 181093])	This PMA option assumes that when the drift is in a collapsed state, water moves vertically downward and the waste package is affected only by seepage from directly above it.
Waste Form Degradation and Radionuclide Mobilization				
Np2O5_Eps_1_high_a	RN Solubility, Np, epsilon 1, high ionic strength (1-3 mol/kg).	Normal [0, 0.85], truncated at +/- 2σ, MO0702PADISCON.001_R0 [DIRS 179358]	Replaced by new PMA parameters	The PMA uses more realistic uncertainty ranges for radionuclide solubility limits.
Np2O5_Eps_1_low_a	RN Solubility, Np, epsilon 1, low ionic strength (<1 mol/kg).	Normal [0, 0.8], truncated at +/- 2σ, MO0702PADISCON.001_R0 [DIRS 179358]	Replaced by new PMA parameters	The PMA uses more realistic uncertainty ranges for radionuclide solubility limits.
Np2O5_Eps_2_CDSP_ High_a	RN Solubility, Np2O5, epsilon 2, CDSP, I >= 0.004m, Cell 1b.	Triangular [0, 0, 853], MO0702PAFLUORI.000_R1 [DIRS 181219]	Replaced by new PMA parameters	The PMA uses more realistic uncertainty ranges for radionuclide solubility limits.
Np2O5_Eps_2_CSNF_ High_a	RN Solubility, Np2O5, epsilon 2, CSNF, I >= 0.2m.	Triangular [0, 0, 197], MO0702PAFLUORI.000_R1 [DIRS 181219]	Replaced by new PMA parameters	The PMA uses more realistic uncertainty ranges for radionuclide solubility limits.
Np2O5_Eps_2_Glass_L ow_a	RN Solubility, Np2O5, epsilon 2, CDSP cell 1a, CDSP I < 0.004m Cell 1b, CSNF I < 0.2m.	Triangular [0, 0, 11], MO0702PAFLUORI.000_R1 [DIRS 181219]	Replaced by new PMA parameters	The PMA uses more realistic uncertainty ranges for radionuclide solubility limits.
NpO2_Eps_1_high_a	RN Solubility, Np, epsilon 1, high ionic strength (1-3 mol/kg).	Normal [0, 0.67], truncated at +/- 2σ, MO0702PADISCON.001_R0 [DIRS 179358]	Replaced by new PMA parameters	The PMA uses more realistic uncertainty ranges for radionuclide solubility limits.
NpO2_Eps_1_low_a	RN Solubility, Np, epsilon 1, low ionic strength (<1 mol/kg).	Normal [0, 0.6], truncated at +/- 2σ, MO0702PADISCON.001_R0 [DIRS 179358]	Replaced by new PMA parameters	The PMA uses more realistic uncertainty ranges for radionuclide solubility limits.

Table C4-1. TSPA-LA Model Parameters Changed or Deleted for the PMA (Continued)

Parameter Name	Description	Parameter Value for Compliance Model (including DTN)	Parameter Value for PMA Model (including DTN)	Rationale for Changes
Waste Form Degradation and Radionuclide Mobilization (Continued)				
NpO2_Eps_2_CDSP_High_a	RN Solubility, Np2O5, epsilon 2, CDSP, I >= 0.004m, Cell 1b, Invert.	Triangular [0, 0, 1,093.5], MO0702PAFLUORI.000_R1 [DIRS 181219]	Replaced by new PMA parameters	The PMA uses more realistic uncertainty ranges for radionuclide solubility limits.
NpO2_Eps_2_CSNF_High_a	RN Solubility, Np2O5, epsilon 2, CSNF, I >= 0.2m, Invert.	Triangular [0, 0, 255.8], MO0702PAFLUORI.000_R1 [DIRS 181219]	Replaced by new PMA parameters	The PMA uses more realistic uncertainty ranges for radionuclide solubility limits.
NpO2_Eps_2_Glass_Low_a	RN Solubility, Np2O5, epsilon 2, CDSP cell 1a, CDSP I < 0.004m Cell 1b, CSNF I < 0.2m.	Triangular [0, 0, 14.1], MO0702PAFLUORI.000_R1 [DIRS 181219]	Replaced by new PMA parameters	The PMA uses more realistic uncertainty ranges for radionuclide solubility limits.
Pu_Eps_1_high_a	RN Solubility, Pu, epsilon 1, high ionic strength (1-3 mol/kg).	Normal [0, 0.76], truncated at +/- 2σ, MO0702PADISCON.001_R0 [DIRS 179358]	Replaced by new PMA parameters	The PMA uses more realistic uncertainty ranges for radionuclide solubility limits.
Pu_Eps_1_low_a	RN Solubility, Pu, epsilon 1, low ionic strength (<1 mol/kg).	Normal [0, 0.7], truncated at +/- 2σ, MO0702PADISCON.001_R0 [DIRS 179358]	Replaced by new PMA parameters	The PMA uses more realistic uncertainty ranges for radionuclide solubility limits.
Pu_Eps_2_CSNF_High_a	RN Solubility, Pu, epsilon 2, CSNF, I > = 0.2m, Invert.	Triangular [0, 0, 1,374], MO0702PAFLUORI.000_R1 [DIRS 181219]	Replaced by new PMA parameters	The PMA uses more realistic uncertainty ranges for radionuclide solubility limits.
Pu_Eps_2_CDSP_High_a	RN Solubility, Pu, epsilon 2, CDSP, I > = 0.004m, Cell 1b, Invert.	Triangular [0, 0, 5,460], MO0702PAFLUORI.000_R1 [DIRS 181219]	Replaced by new PMA parameters	The PMA uses more realistic uncertainty ranges for radionuclide solubility limits.
Pu_Eps_2_Glass_Low_a	RN Solubility, Pu, epsilon 2, CDSP cell 1a, CDSP I < 0.004m Cell 1b, CSNF I < 0.2m.	Triangular [0, 0, 79], MO0702PAFLUORI.000_R1 [DIRS 181219]	Replaced by new PMA parameters	The PMA uses more realistic uncertainty ranges for radionuclide solubility limits.

Table C4-1. TSPA-LA Model Parameters Changed or Deleted for the PMA (Continued)

Parameter Name	Description	Parameter Value for Compliance Model (including DTN)	Parameter Value for PMA Model (including DTN)	Rationale for Changes
Waste Form Degradation and Radionuclide Mobilization (Continued)				
U_Eps_1_high_Other_a	RN Solubility, U, epsilon 1, high ionic strength (1-3 mol/kg).	Normal [0, 0.6], truncated at +/- 2σ, MO0702PADISCON.001_R0 [DIRS 179358]	Replaced by new PMA parameters	The PMA uses more realistic uncertainty ranges for radionuclide solubility limits.
U_Eps_1_low_Other_a	RN Solubility, U, epsilon 1, low ionic strength (<1 mol/kg).	Normal [0, 0.5], truncated at +/- 2σ, MO0702PADISCON.001_R0 [DIRS 179358]	Replaced by new PMA parameters	The PMA uses more realistic uncertainty ranges for radionuclide solubility limits.
U_Eps_2_Schoepite_CSNF_High_a	RN Solubility, U-Schoepite, epsilon 2, CSNF, I >= 0.2m, Invert.	Triangular [0, 0, 1,361], MO0702PAFLUORI.000_R1 [DIRS 181219]	Replaced by new PMA parameters	The PMA uses more realistic uncertainty ranges for radionuclide solubility limits.
U_Eps_2_Schoepite_CDSP_High_a	RN Solubility, U-Schoepite, epsilon 2, CDSP, I >= 0.004m, Cell 1b, Invert.	Triangular [0, 0, 5,385], MO0702PAFLUORI.000_R1 [DIRS 181219]	Replaced by new PMA parameters	The PMA uses more realistic uncertainty ranges for radionuclide solubility limits.
U_Eps_2_Boltwoodite_CSNF_Hig_a	RN Solubility, U-Na-Boltwoodite, epsilon 2, CSNF, I >= 0.2m, Invert.	Triangular [0, 0, 57.01], MO0702PAFLUORI.000_R1 [DIRS 181219]	Replaced by new PMA parameters	The PMA uses more realistic uncertainty ranges for radionuclide solubility limits.
U_Eps_2_Boltwoodite_CDSP_Hig_a	RN Solubility U-Na-Boltwoodite, epsilon 2, CDSP, I >= 0.004m, Cell 1b, Invert.	Triangular [0, 0, 272.3], MO0702PAFLUORI.000_R1 [DIRS 181219]	Replaced by new PMA parameters	The PMA uses more realistic uncertainty ranges for radionuclide solubility limits.
U_Eps_2_Schoepite_Glass_Low_a	RN Solubility, U-Schoepite, epsilon 2, CDSP cell 1a, CDSP I < 0.004m Cell 1b, CSNF I < 0.2m.	Triangular [0, 0, 78], MO0702PAFLUORI.000_R1 [DIRS 181219]	Replaced by new PMA parameters	The PMA uses more realistic uncertainty ranges for radionuclide solubility limits.
U_Eps_2_Boltwoodite_Glass_Lo_a	RN Solubility, U-Na-Boltwoodite, epsilon 2, CDSP cell 1a, CDSP I < 0.004m Cell 1b, CSNF I < 0.2m.	Triangular [0, 0, 6.13], MO0702PAFLUORI.000_R1 [DIRS 181219]	Replaced by new PMA parameters	The PMA uses more realistic uncertainty ranges for radionuclide solubility limits.

Table C4-1. TSPA-LA Model Parameters Changed or Deleted for the PMA (Continued)

Parameter Name	Description	Parameter Value for Compliance Model (including DTN)	Parameter Value for PMA Model (including DTN)	Rationale for Changes
Waste Form Degradation and Radionuclide Mobilization (Continued)				
U_Eps_1_high_Nominal_a	RN Solubility, U, epsilon 1, high ionic strength (1-3 mol/kg).	Normal [0, 0.6], truncated at +/- 2σ, MO0702PADISCON.001_R0 [DIRS 179358]	Replaced by new PMA parameters	The PMA uses more realistic uncertainty ranges for radionuclide solubility limits.
U_Eps_1_low_Nominal_a	RN Solubility, U, epsilon 1, low ionic strength (<1 mol/kg).	Normal [0, 0.5], truncated at +/- 2σ, MO0702PADISCON.001_R0 [DIRS 179358]	Replaced by new PMA parameters	The PMA uses more realistic uncertainty ranges for radionuclide solubility limits.
U_Eps_2_CSNF_Low_Nominal_a	RN Solubility, U, epsilon 2, CSNF, I < 0.2m, Invert, nominal seismic.	Triangular [0, 0, 78], MO0702PAFLUORI.000_R1 [DIRS 181219]	Replaced by new PMA parameters	The PMA uses more realistic uncertainty ranges for radionuclide solubility limits.
U_Eps_2_CSNF_High_Nominal_a	RN Solubility, U, epsilon 2, CSNF, I >= 0.2m, Invert, nominal seismic.	Triangular [0, 0, 1,361], MO0702PAFLUORI.000_R1 [DIRS 181219]	Replaced by new PMA parameters	The PMA uses more realistic uncertainty ranges for radionuclide solubility limits.
SZ Flow and Transport Parameters				
FPVO	Flowing interval porosity.	CDF (Log_{10} – transformed) with Probability (0, .05, .5, .8,1) and Value (-5, -4, -3, -2, -1) (SN0702PASZFTMA.002_R1 [DIRS 183471]).	CDF (Log_{10} – transformed) with Probability (0, .5, .8, 1) and Value (-4, -3, -2, -1) (Corroborative DTN: SN0704PMASZFTA.00_R1 [DIRS 184395])	The lower bound of the compliance model might be very low for bulk average parameter value (i.e., average value over the volcanic zone) that is being applied at the km scale (i.e., the model domain). Thus, the lower bound flowing interval porosity was set at 1e-4.
FPVO	Correlation coefficient between the flowing interval porosity and the groundwater specific discharge multiplier, GWSPD.	N/A (a value of 0 is used by default in the TSPA-LA model)	0.64 (Corroborative DTN: SN0704PMASZFTA.001_R1 [DIRS 184395])	In a fractured flow aquifer, there are theoretical and geometric arguments that suggest the two parameters are at least partially correlated. As fracture density and apertures increase, one would expect both flowing interval porosity and permeability to also increase. Thus, a correlation factor was obtained from literature survey.

Table C4-1. TSPA-LA Model Parameters Changed or Deleted for the PMA (Continued)

Parameter Name	Description	Parameter Value for Compliance Model (including DTN)	Parameter Value for PMA Model (including DTN)	Rationale for Changes
SZ Flow and Transport Parameters (Continued)				
SZ_01_01	SZ, Breakthrough Curves, C, I, Cl, SR1.	Table (SN0702PASZFTMA.001_R0 [DIRS 179504])	Table (Corroborative DTN: SN0704PMASZFTA.001_R1 [DIRS 184395])	New breakthrough curves that incorporated PMA changes.
SZ_01_02	SZ, Breakthrough Curves, C, I, Cl, SR2.	Table (SN0702PASZFTMA.001_R0 [DIRS 179504])	Table (Corroborative DTN: SN0704PMASZFTA.001_R1 [DIRS 184395])	New breakthrough curves that incorporated PMA changes.
SZ_01_03	SZ, Breakthrough Curves, C, I, Cl, SR3.	Table (SN0702PASZFTMA.001_R0 [DIRS 179504])	Table (Corroborative DTN: SN0704PMASZFTA.001_R1 [DIRS 184395])	New breakthrough curves that incorporated PMA changes.
SZ_01_04	SZ, Breakthrough Curves, C, I, Cl, SR4.	Table (SN0702PASZFTMA.001_R0 [DIRS 179504])	Table (Corroborative DTN: SN0704PMASZFTA.001_R1 [DIRS 184395])	New breakthrough curves that incorporated PMA changes.
SZ_02_01	SZ, Breakthrough Curves, Am, Th, Pa, SR1.	Table (SN0702PASZFTMA.001_R0 [DIRS 179504])	Table (Corroborative DTN: SN0704PMASZFTA.001_R1 [DIRS 184395])	New breakthrough curves that incorporated PMA changes.
SZ_02_02	SZ, Breakthrough Curves, Am, Th, Pa, SR2.	Table (SN0702PASZFTMA.001_R0 [DIRS 179504])	Table (Corroborative DTN: SN0704PMASZFTA.001_R1 [DIRS 184395])	New breakthrough curves that incorporated PMA changes.
SZ_02_03	SZ, Breakthrough Curves, Am, Th, Pa, SR3.	Table (SN0702PASZFTMA.001_R0 [DIRS 179504])	Table (Corroborative DTN: SN0704PMASZFTA.001_R1 [DIRS 184395])	New breakthrough curves that incorporated PMA changes.
SZ_02_04	SZ, Breakthrough Curves, Am, Th, Pa, SR4.	Table (SN0702PASZFTMA.001_R0 [DIRS 179504])	Table (Corroborative DTN: SN0704PMASZFTA.001_R1 [DIRS 184395])	New breakthrough curves that incorporated PMA changes.
SZ_03_01	SZ, Breakthrough Curves, Cs, SR1.	Table (SN0702PASZFTMA.001_R0 [DIRS 179504])	Table (Corroborative DTN: SN0704PMASZFTA.001_R1 [DIRS 184395])	New breakthrough curves that incorporated PMA changes.
SZ_03_02	SZ, Breakthrough Curves, Cs, SR2.	Table (SN0702PASZFTMA.001_R0 [DIRS 179504])	Table (Corroborative DTN: SN0704PMASZFTA.001_R1 [DIRS 184395])	New breakthrough curves that incorporated PMA changes.

Table C4-1. TSPA-LA Model Parameters Changed or Deleted for the PMA (Continued)

Parameter Name	Description	Parameter Value for Compliance Model (including DTN)	Parameter Value for PMA Model (including DTN)	Rationale for Changes
SZ_03_03	SZ, Breakthrough Curves, Cs, SR3.	Table (SN0702PASZFTMA.001_R0 [DIRS 179504])	Table (Corroborative DTN: SN0704PMASZFTA.001_R1 [DIRS 184395])	New breakthrough curves that incorporated PMA changes.
SZ Flow and Transport Parameters (Continued)				
SZ_03_04	SZ, Breakthrough Curves, Cs, SR4.	Table (SN0702PASZFTMA.001_R0 [DIRS 179504])	Table (Corroborative DTN: SN0704PMASZFTA.001_R1 [DIRS 184395])	New breakthrough curves that incorporated PMA changes.
SZ_04_01	SZ, Breakthrough Curves, Pu, SR1.	Table (SN0702PASZFTMA.001_R0 [DIRS 179504])	Table (Corroborative DTN: SN0704PMASZFTA.001_R1 [DIRS 184395])	New breakthrough curves that incorporated PMA changes.
SZ_04_02	SZ, Breakthrough Curves, Pu, SR2.	Table (SN0702PASZFTMA.001_R0 [DIRS 179504])	Table (Corroborative DTN: SN0704PMASZFTA.001_R1 [DIRS 184395])	New breakthrough curves that incorporated PMA changes.
SZ_04_03	SZ, Breakthrough Curves, Pu, SR3.	Table (SN0702PASZFTMA.001_R0 [DIRS 179504])	Table (Corroborative DTN: SN0704PMASZFTA.001_R1 [DIRS 184395])	New breakthrough curves that incorporated PMA changes.
SZ_04_04	SZ, Breakthrough Curves, Pu, SR4.	Table (SN0702PASZFTMA.001_R0 [DIRS 179504])	Table (Corroborative DTN: SN0704PMASZFTA.001_R1 [DIRS 184395])	New breakthrough curves that incorporated PMA changes.
SZ_05_01	SZ, Breakthrough Curves, Np, SR1.	Table (SN0702PASZFTMA.001_R0 [DIRS 179504])	Table (Corroborative DTN: SN0704PMASZFTA.001_R1 [DIRS 184395])	New breakthrough curves that incorporated PMA changes.
SZ_05_02	SZ, Breakthrough Curves, Np, SR2.	Table (SN0702PASZFTMA.001_R0 [DIRS 179504])	Table (Corroborative DTN: SN0704PMASZFTA.001_R1 [DIRS 184395])	New breakthrough curves that incorporated PMA changes.
SZ_05_03	SZ, Breakthrough Curves, Np, SR3.	Table (SN0702PASZFTMA.001_R0 [DIRS 179504])	Table (Corroborative DTN: SN0704PMASZFTA.001_R1 [DIRS 184395])	New breakthrough curves that incorporated PMA changes.
SZ_05_04	SZ, Breakthrough Curves, Np, SR4.	Table (SN0702PASZFTMA.001_R0 [DIRS 179504])	Table (Corroborative DTN: SN0704PMASZFTA.001_R1 [DIRS 184395])	New breakthrough curves that incorporated PMA changes.

Table C4-1. TSPA-LA Model Parameters Changed or Deleted for the PMA (Continued)

Parameter Name	Description	Parameter Value for Compliance Model (including DTN)	Parameter Value for PMA Model (including DTN)	Rationale for Changes
SZ_06_01	SZ, Breakthrough Curves, IcPu, IcAm, IcTh, SR1.	Table (SN0702PASZFTMA.001_R0 [DIRS 179504])	Table (Corroborative DTN: SN0704PMASZFTA.001_R1 [DIRS 184395])	New breakthrough curves that incorporated PMA changes.
SZ_06_02	SZ, Breakthrough Curves, IcPu, IcAm, IcTh, SR2.	Table (SN0702PASZFTMA.001_R0 [DIRS 179504])	Table (Corroborative DTN: SN0704PMASZFTA.001_R1 [DIRS 184395])	New breakthrough curves that incorporated PMA changes.
SZ Flow and Transport Parameters (Continued)				
SZ_06_03	SZ, Breakthrough Curves, IcPu, IcAm, IcTh, SR3.	Table (SN0702PASZFTMA.001_R0 [DIRS 179504])	Table (Corroborative DTN: SN0704PMASZFTA.001_R1 [DIRS 184395])	New breakthrough curves that incorporated PMA changes.
SZ_06_04	SZ, Breakthrough Curves, IcPu, IcAm, IcTh, SR4.	Table (SN0702PASZFTMA.001_R0 [DIRS 179504])	Table (Corroborative DTN: SN0704PMASZFTA.001_R1 [DIRS 184395])	New breakthrough curves that incorporated PMA changes.
SZ_07_01	SZ, Breakthrough Curves, Ra, SR1.	Table (SN0702PASZFTMA.001_R0 [DIRS 179504])	Table (Corroborative DTN: SN0704PMASZFTA.001_R1 [DIRS 184395])	New breakthrough curves that incorporated PMA changes.
SZ_07_02	SZ, Breakthrough Curves, Ra, SR2.	Table (SN0702PASZFTMA.001_R0 [DIRS 179504])	Table (Corroborative DTN: SN0704PMASZFTA.001_R1 [DIRS 184395])	New breakthrough curves that incorporated PMA changes.
SZ_07_03	SZ, Breakthrough Curves, Ra, SR3.	Table (SN0702PASZFTMA.001_R0 [DIRS 179504])	Table (Corroborative DTN: SN0704PMASZFTA.001_R1 [DIRS 184395])	New breakthrough curves that incorporated PMA changes.
SZ_07_04	SZ, Breakthrough Curves, Ra, SR4.	Table (SN0702PASZFTMA.001_R0 [DIRS 179504])	Table (Corroborative DTN: SN0704PMASZFTA.001_R1 [DIRS 184395])	New breakthrough curves that incorporated PMA changes.
SZ_08_01	SZ, Breakthrough Curves, Sr, SR1.	Table (SN0702PASZFTMA.001_R0 [DIRS 179504])	Table (Corroborative DTN: SN0704PMASZFTA.001_R1 [DIRS 184395])	New breakthrough curves that incorporated PMA changes.
SZ_08_02	SZ, Breakthrough Curves, Sr, SR2.	Table (SN0702PASZFTMA.001_R0 [DIRS 179504])	Table (Corroborative DTN: SN0704PMASZFTA.001_R1 [DIRS 184395])	New breakthrough curves that incorporated PMA changes.

Table C4-1. TSPA-LA Model Parameters Changed or Deleted for the PMA (Continued)

Parameter Name	Description	Parameter Value for Compliance Model (including DTN)	Parameter Value for PMA Model (including DTN)	Rationale for Changes
SZ_08_03	SZ, Breakthrough Curves, Sr, SR3.	Table (SN0702PASZFTMA.001_R0 [DIRS 179504])	Table (Corroborative DTN: SN0704PMASZFTA.001_R1 [DIRS 184395])	New breakthrough curves that incorporated PMA changes.
SZ_08_04	SZ, Breakthrough Curves, Sr, SR4.	Table (SN0702PASZFTMA.001_R0 [DIRS 179504])	Table (Corroborative DTN: SN0704PMASZFTA.001_R1 [DIRS 184395])	New breakthrough curves that incorporated PMA changes.
SZ_09_01	SZ, Breakthrough Curves, U, SR1.	Table (SN0702PASZFTMA.001_R0 [DIRS 179504])	Table (Corroborative DTN: SN0704PMASZFTA.001_R1 [DIRS 184395])	New breakthrough curves that incorporated PMA changes.
SZ Flow and Transport Parameters (Continued)				
SZ_09_02	SZ, Breakthrough Curves, U, SR2.	Table (SN0702PASZFTMA.001_R0 [DIRS 179504])	Table (Corroborative DTN: SN0704PMASZFTA.001_R1 [DIRS 184395])	New breakthrough curves that incorporated PMA changes.
SZ_09_03	SZ, Breakthrough Curves, U, SR3.	Table (SN0702PASZFTMA.001_R0 [DIRS 179504])	Table (Corroborative DTN: SN0704PMASZFTA.001_R1 [DIRS 184395])	New breakthrough curves that incorporated PMA changes.
SZ_09_04	SZ, Breakthrough Curves, U, SR4.	Table (SN0702PASZFTMA.001_R0 [DIRS 179504])	Table (Corroborative DTN: SN0704PMASZFTA.001_R1 [DIRS 184395])	New breakthrough curves that incorporated PMA changes.
SZ_10_01	SZ, Breakthrough Curves, IfPu, IfAm, IfTh, SR1.	Table (SN0702PASZFTMA.001_R0 [DIRS 179504])	Table (Corroborative DTN: SN0704PMASZFTA.001_R1 [DIRS 184395])	New breakthrough curves that incorporated PMA changes.
SZ_10_02	SZ, Breakthrough Curves, IfPu, IfAm, IfTh, SR2.	Table (SN0702PASZFTMA.001_R0 [DIRS 179504])	Table (Corroborative DTN: SN0704PMASZFTA.001_R1 [DIRS 184395])	New breakthrough curves that incorporated PMA changes.
SZ_10_03	SZ, Breakthrough Curves, IfPu, IfAm, IfTh, SR3.	Table (SN0702PASZFTMA.001_R0 [DIRS 179504])	Table (Corroborative DTN: SN0704PMASZFTA.001_R1 [DIRS 184395])	New breakthrough curves that incorporated PMA changes.
SZ_10_04	SZ, Breakthrough Curves, IfPu, IfAm, IfTh, SR4.	Table (SN0702PASZFTMA.001_R0 [DIRS 179504])	Table (Corroborative DTN: SN0704PMASZFTA.001_R1 [DIRS 184395])	New breakthrough curves that incorporated PMA changes.

Table C4-1. TSPA-LA Model Parameters Changed or Deleted for the PMA (Continued)

Parameter Name	Description	Parameter Value for Compliance Model (including DTN)	Parameter Value for PMA Model (including DTN)	Rationale for Changes
SZ_11_01	SZ, Breakthrough Curves, Se, SR1.	Table (SN0702PASZFTMA.001_R0 [DIRS 179504])	Table (Corroborative DTN: SN0704PMASZFTA.001_R1 [DIRS 184395])	New breakthrough curves that incorporated PMA changes.
SZ_11_02	SZ, Breakthrough Curves, Se, SR2.	Table (SN0702PASZFTMA.001_R0 [DIRS 179504])	Table (Corroborative DTN: SN0704PMASZFTA.001_R1 [DIRS 184395])	New breakthrough curves that incorporated PMA changes.
SZ_11_03	SZ, Breakthrough Curves, Se, SR3.	Table (SN0702PASZFTMA.001_R0 [DIRS 179504])	Table (Corroborative DTN: SN0704PMASZFTA.001_R1 [DIRS 184395])	New breakthrough curves that incorporated PMA changes.
SZ_11_04	SZ, Breakthrough Curves, Se, SR4.	Table (SN0702PASZFTMA.001_R0 [DIRS 179504])	Table (Corroborative DTN: SN0704PMASZFTA.001_R1 [DIRS 184395])	New breakthrough curves that incorporated PMA changes.
SZ Flow and Transport Parameters (Continued)				
SZ_12_01	SZ, Breakthrough Curves, Sn, SR1.	Table (SN0702PASZFTMA.001_R0 [DIRS 179504])	Table (Corroborative DTN: SN0704PMASZFTA.001_R1 [DIRS 184395])	New breakthrough curves that incorporated PMA changes.
SZ_12_02	SZ, Breakthrough Curves, Sn, SR2.	Table (SN0702PASZFTMA.001_R0 [DIRS 179504])	Table (Corroborative DTN: SN0704PMASZFTA.001_R1 [DIRS 184395])	New breakthrough curves that incorporated PMA changes.
SZ_12_03	SZ, Breakthrough Curves, Sn, SR3.	Table (SN0702PASZFTMA.001_R0 [DIRS 179504])	Table (Corroborative DTN: SN0704PMASZFTA.001_R1 [DIRS 184395])	New breakthrough curves that incorporated PMA changes.
SZ_12_04	SZ, Breakthrough Curves, Sn, SR4.	Table (SN0702PASZFTMA.001_R0 [DIRS 179504])	Table (Corroborative DTN: SN0704PMASZFTA.001_R1 [DIRS 184395])	New breakthrough curves that incorporated PMA changes.

NOTE: SZ = saturated zone; Ic = irreversible colloids; If = fast fraction of irreversible colloids; SR = source region; C = carbon; I = iodine; Cl = chlorine; Am = americium; Th = thorium; Pa = protactinium; Cs = cesium; Pu = plutonium; Np = neptunium; Ra = radium; Sr = strontium; U = uranium; Se = selenium; Sn = tin; FPVO = fracture porosity in volcanic units; and GWSPD = ground water specific discharge multiplier.

Table C4-2. Input Parameters Added for the PMA

Parameter Name	Description	Parameter Distribution	Rationale for Inclusion	Data Source
EBS Thermal-Hydrology Parameters				
B1_CSNF_REP_P10_PMA.ou	PREWAP output file for representative TH (DS T and RH)	File	Files re-generated to include the DS RH values used in the DS corrosion rate model for PMA.	LL0703PA011MST.006_R0 [DIRS 179853]
B1_CSNF_REP_P10H_PMA.ou	PREWAP output file for representative TH (DS T and RH)	File	Same as above.	LL0703PA017MST.012_R0 [DIRS 179859]
B1_CSNF_REP_P10L_PMA.ou	PREWAP output file for representative TH (DS T and RH)	File	Same as above.	LL0703PA015MST.010_R0 [DIRS 179857]
B1_CSNF_REP_P30_PMA.ou	PREWAP output file for representative TH (DS T and RH)	File	Same as above.	LL0703PA012MST.007_R0 [DIRS 179854]
B1_CSNF_REP_P30H_PMA.ou	PREWAP output file for representative TH (DS T and RH)	File	Same as above.	LL0703PA035MST.017_R0 [DIRS 179985]
B1_CSNF_REP_P30L_PMA.ou	PREWAP output file for representative TH (DS T and RH)	File	Same as above.	LL0703PA034MST.016_R0 [DIRS 179982]
B1_CSNF_REP_P50_PMA.ou	PREWAP output file for representative TH (DS T and RH)	File	Same as above.	LL0703PA013MST.008_R0 [DIRS 179855]
B1_CSNF_REP_P50H_PMA.ou	PREWAP output file for representative TH (DS T and RH)	File	Same as above.	LL0703PA037MST.019_R0 [DIRS 179989]
B1_CSNF_REP_P50L_PMA.ou	PREWAP output file for representative TH (DS T and RH)	File	Same as above.	LL0703PA036MST.018_R0 [DIRS 179986]
B1_CSNF_REP_P90_PMA.ou	PREWAP output file for representative TH (DS T and RH)	File	Same as above.	LL0703PA014MST.009_R0 [DIRS 179856]
B1_CSNF_REP_P90H_PMA.ou	PREWAP output file for representative TH (DS T and RH)	File	Same as above.	LL0703PA016MST.011_R0 [DIRS 179858]
B1_CSNF_REP_P90L_PMA.ou	PREWAP output file for representative TH (DS T and RH)	File	Same as above.	LL0703PA038MST.020_R0 [DIRS 179992]
B1_DHLW_REP_P10_PMA.ou	PREWAP output file for representative TH (DS T and RH)	File	Same as above.	LL0703PA011MST.006_R0 [DIRS 179853]
B1_DHLW_REP_P10H_PMA.ou	PREWAP output file for representative TH (DS T and RH)	File	Same as above.	LL0703PA017MST.012_R0 [DIRS 179859]
B1_DHLW_REP_P10L_PMA.ou	PREWAP output file for representative TH (DS T and RH)	File	Same as above.	LL0703PA015MST.010_R0 [DIRS 179857]

Table C4-2. Input Parameters Added for the PMA (Continued)

Parameter Name	Description	Parameter Distribution	Rationale for Inclusion	Data Source
EBS Thermal-Hydrology Parameters (Continued)				
B1_DHLW_REP_P30_PMA.ou	PREWAP output file for representative TH (DS T and RH)	File	Same as above.	LL0703PA012MST.007_R0 [DIRS 179854]
B1_DHLW_REP_P30H_PMA.ou	PREWAP output file for representative TH (DS T and RH)	File	Same as above.	LL0703PA035MST.017_R0 [DIRS 179985]
B1_DHLW_REP_P30L_PMA.ou	PREWAP output file for representative TH (DS T and RH)	File	Same as above.	LL0703PA034MST.016_R0 [DIRS 179982]
B1_DHLW_REP_P50_PMA.ou	PREWAP output file for representative TH (DS T and RH)	File	Same as above.	LL0703PA013MST.008_R0 [DIRS 179855]
B1_DHLW_REP_P50H_PMA.ou	PREWAP output file for representative TH (DS T and RH)	File	Same as above.	LL0703PA037MST.019_R0 [DIRS 179989]
B1_DHLW_REP_P50L_PMA.ou	PREWAP output file for representative TH (DS T and RH)	File	Same as above.	LL0703PA036MST.018_R0 [DIRS 179986]
B1_DHLW_REP_P90_PMA.ou	PREWAP output file for representative TH (DS T and RH)	File	Same as above.	LL0703PA014MST.009_R0 [DIRS 179856]
B1_DHLW_REP_P90H_PMA.ou	PREWAP output file for representative TH (DS T and RH)	File	Same as above.	LL0703PA016MST.011_R0 [DIRS 179858]
B1_DHLW_REP_P90L_PMA.ou	PREWAP output file for representative TH (DS T and RH)	File	Same as above.	LL0703PA038MST.020_R0 [DIRS 179992]
B2_CSNF_REP_P10_PMA.ou	PREWAP output file for representative TH (DS T and RH)	File	Same as above.	LL0703PA011MST.006_R0 [DIRS 179853]
B2_CSNF_REP_P10H_PMA.ou	PREWAP output file for representative TH (DS T and RH)	File	Same as above.	LL0703PA017MST.012_R0 [DIRS 179859]
B2_CSNF_REP_P10L_PMA.ou	PREWAP output file for representative TH (DS T and RH)	File	Same as above.	LL0703PA015MST.010_R0 [DIRS 179857]
B2_CSNF_REP_P30_PMA.ou;	PREWAP output file for representative TH (DS T and RH)	File	Same as above.	LL0703PA012MST.007_R0 [DIRS 179854]
B2_CSNF_REP_P30H_PMA.ou	PREWAP output file for representative TH (DS T and RH)	File	Same as above.	LL0703PA035MST.017_R0 [DIRS 179985]
B2_CSNF_REP_P30L_PMA.ou	PREWAP output file for representative TH (DS T and RH)	File	Same as above.	LL0703PA034MST.016_R0 [DIRS 179982]
B2_CSNF_REP_P50_PMA.ou;	PREWAP output file for representative TH (DS T and RH)	File	Same as above.	LL0703PA013MST.008_R0 [DIRS 179855]

Table C4-2. Input Parameters Added for the PMA (Continued)

Parameter Name	Description	Parameter Distribution	Rationale for Inclusion	Data Source
EBS Thermal-Hydrology Parameters (Continued)				
B2_CSNF_REP_P50H_PMA.ou	PREWAP output file for representative TH (DS T and RH)	File	Same as above.	LL0703PA037MST.019_R0 [DIRS 179989]
B2_CSNF_REP_P50L_PMA.ou	PREWAP output file for representative TH (DS T and RH)	File	Same as above.	LL0703PA036MST.018_R0 [DIRS 179986]
B2_CSNF_REP_P90_PMA.ou	PREWAP output file for representative TH (DS T and RH)	File	Same as above.	LL0703PA014MST.009_R0 [DIRS 179856]
B2_CSNF_REP_P90H_PMA.ou	PREWAP output file for representative TH (DS T and RH)	File	Same as above.	LL0703PA016MST.011_R0 [DIRS 179858]
B2_CSNF_REP_P90L_PMA.ou	PREWAP output file for representative TH (DS T and RH)	File	Same as above.	LL0703PA038MST.020_R0 [DIRS 179992]
B2_DHLW_REP_P10_PMA.ou	PREWAP output file for representative TH (DS T and RH)	File	Same as above.	LL0703PA011MST.006_R0 [DIRS 179853]
B2_DHLW_REP_P10H_PMA.ou	PREWAP output file for representative TH (DS T and RH)	File	Same as above.	LL0703PA017MST.012_R0 [DIRS 179859]
B2_DHLW_REP_P10L_PMA.ou	PREWAP output file for representative TH (DS T and RH)	File	Same as above.	LL0703PA015MST.010_R0 [DIRS 179857]
B2_DHLW_REP_P30_PMA.ou	PREWAP output file for representative TH (DS T and RH)	File	Same as above.	LL0703PA012MST.007_R0 [DIRS 179854]
B2_DHLW_REP_P30H_PMA.ou	PREWAP output file for representative TH (DS T and RH)	File	Same as above.	LL0703PA035MST.017_R0 [DIRS 179985]
B2_DHLW_REP_P30L_PMA.ou	PREWAP output file for representative TH (DS T and RH)	File	Same as above.	LL0703PA034MST.016_R0 [DIRS 179982]
B2_DHLW_REP_P50_PMA.ou	PREWAP output file for representative TH (DS T and RH)	File	Same as above.	LL0703PA013MST.008_R0 [DIRS 179855]
B2_DHLW_REP_P50H_PMA.ou	PREWAP output file for representative TH (DS T and RH)	File	Same as above.	LL0703PA037MST.019_R0 [DIRS 179989]
B2_DHLW_REP_P50L_PMA.ou	PREWAP output file for representative TH (DS T and RH)	File	Same as above.	LL0703PA036MST.018_R0 [DIRS 179986]
B2_DHLW_REP_P90_PMA.ou	PREWAP output file for representative TH (DS T and RH)	File	Same as above.	LL0703PA014MST.009_R0 [DIRS 179856]
B2_DHLW_REP_P90H_PMA.ou	PREWAP output file for representative TH (DS T and RH)	File	Same as above.	LL0703PA016MST.011_R0 [DIRS 179858]

Table C4-2. Input Parameters Added for the PMA (Continued)

Parameter Name	Description	Parameter Distribution	Rationale for Inclusion	Data Source
EBS Thermal-Hydrology Parameters (Continued)				
B2_DHLW_REP_P90L_PMA.ou	PREWAP output file for representative TH (DS T and RH)	File	Same as above.	LL0703PA038MST.020_R0 [DIRS 179992]
B3_CSNF_REP_P10_PMA.ou	PREWAP output file for representative TH (DS T and RH)	File	Same as above.	LL0703PA011MST.006_R0 [DIRS 179853]
B3_CSNF_REP_P10H_PMA.ou	PREWAP output file for representative TH (DS T and RH)	File	Same as above.	LL0703PA017MST.012_R0 [DIRS 179859]
B3_CSNF_REP_P10L_PMA.ou	PREWAP output file for representative TH (DS T and RH)	File	Same as above.	LL0703PA015MST.010_R0 [DIRS 179857]
B3_CSNF_REP_P30_PMA.ou	PREWAP output file for representative TH (DS T and RH)	File	Same as above.	LL0703PA012MST.007_R0 [DIRS 179854]
B3_CSNF_REP_P30H_PMA.ou	PREWAP output file for representative TH (DS T and RH)	File	Same as above.	LL0703PA035MST.017_R0 [DIRS 179985]
B3_CSNF_REP_P30L_PMA.ou	PREWAP output file for representative TH (DS T and RH)	File	Same as above.	LL0703PA034MST.016_R0 [DIRS 179982]
B3_CSNF_REP_P50_PMA.ou	PREWAP output file for representative TH (DS T and RH)	File	Same as above.	LL0703PA013MST.008_R0 [DIRS 179855]
B3_CSNF_REP_P50H_PMA.ou	PREWAP output file for representative TH (DS T and RH)	File	Same as above.	LL0703PA037MST.019_R0 [DIRS 179989]
B3_CSNF_REP_P50L_PMA.ou	PREWAP output file for representative TH (DS T and RH)	File	Same as above.	LL0703PA036MST.018_R0 [DIRS 179986]
B3_CSNF_REP_P90_PMA.ou	PREWAP output file for representative TH (DS T and RH)	File	Same as above.	LL0703PA014MST.009_R0 [DIRS 179856]
B3_CSNF_REP_P90H_PMA.ou	PREWAP output file for representative TH (DS T and RH)	File	Same as above.	LL0703PA016MST.011_R0 [DIRS 179858]
B3_CSNF_REP_P90L_PMA.ou	PREWAP output file for representative TH (DS T and RH)	File	Same as above.	LL0703PA038MST.020_R0 [DIRS 179992]
B3_DHLW_REP_P10_PMA.ou	PREWAP output file for representative TH (DS T and RH)	File	Same as above.	LL0703PA011MST.006_R0 [DIRS 179853]
B3_DHLW_REP_P10H_PMA.ou	PREWAP output file for representative TH (DS T and RH)	File	Same as above.	LL0703PA017MST.012_R0 [DIRS 179859]
B3_DHLW_REP_P10L_PMA.ou	PREWAP output file for representative TH (DS T and RH)	File	Same as above.	LL0703PA015MST.010_R0 [DIRS 179857]

Table C4-2. Input Parameters Added for the PMA (Continued)

Parameter Name	Description	Parameter Distribution	Rationale for Inclusion	Data Source
EBS Thermal-Hydrology Parameters (Continued)				
B3_DHLW_REP_P30_PMA .ou;	PREWAP output file for representative TH (DS T and RH)	File	Same as above.	LL0703PA012MST.007_R0 [DIRS 179854]
B3_DHLW_REP_P30H_P MA.ou	PREWAP output file for representative TH (DS T and RH)	File	Same as above.	LL0703PA035MST.017_R0 [DIRS 179985]
B3_DHLW_REP_P30L_PM A.ou	PREWAP output file for representative TH (DS T and RH)	File	Same as above.	LL0703PA034MST.016_R0 [DIRS 179982]
B3_DHLW_REP_P50_PMA .ou	PREWAP output file for representative TH (DS T and RH)	File	Same as above.	LL0703PA013MST.008_R0 [DIRS 179855]
B3_DHLW_REP_P50H_P MA.ou	PREWAP output file for representative TH (DS T and RH)	File	Same as above.	LL0703PA037MST.019_R0 [DIRS 179989]
B3_DHLW_REP_P50L_PM A.ou	PREWAP output file for representative TH (DS T and RH)	File	Same as above.	LL0703PA036MST.018_R0 [DIRS 179986]
B3_DHLW_REP_P90_PMA .ou	PREWAP output file for representative TH (DS T and RH)	File	Same as above.	LL0703PA014MST.009_R0 [DIRS 179856]
B3_DHLW_REP_P90H_P MA.ou	PREWAP output file for representative TH (DS T and RH)	File	Same as above.	LL0703PA016MST.011_R0 [DIRS 179858]
B3_DHLW_REP_P90L_PM A.ou	PREWAP output file for representative TH (DS T and RH)	File	Same as above.	LL0703PA038MST.020_R0 [DIRS 179992]
B4_CSNF_REP_P10_PMA .ou	PREWAP output file for representative TH (DS T and RH)	File	Same as above.	LL0703PA011MST.006_R0 [DIRS 179853]
B4_CSNF_REP_P10H_PM A.ou	PREWAP output file for representative TH (DS T and RH)	File	Same as above.	LL0703PA017MST.012_R0 [DIRS 179859]
B4_CSNF_REP_P10L_PM A.ou	PREWAP output file for representative TH (DS T and RH)	File	Same as above.	LL0703PA015MST.010_R0 [DIRS 179857]
B4_CSNF_REP_P30_PMA .ou	PREWAP output file for representative TH (DS T and RH)	File	Same as above.	LL0703PA012MST.007_R0 [DIRS 179854]
B4_CSNF_REP_P30H_PM A.ou	PREWAP output file for representative TH (DS T and RH)	File	Same as above.	LL0703PA035MST.017_R0 [DIRS 179985]
B4_CSNF_REP_P30L_PM A.ou	PREWAP output file for representative TH (DS T and RH)	File	Same as above.	LL0703PA034MST.016_R0 [DIRS 179982]
B4_CSNF_REP_P50_PMA .ou	PREWAP output file for representative TH (DS T and RH)	File	Same as above.	LL0703PA013MST.008_R0 [DIRS 179855]

Table C4-2. Input Parameters Added for the PMA (Continued)

Parameter Name	Description	Parameter Distribution	Rationale for Inclusion	Data Source
EBS Thermal-Hydrology Parameters (Continued)				
B4_CSNF_REP_P50H_PMA.ou	PREWAP output file for representative TH (DS T and RH)	File	Same as above.	LL0703PA037MST.019_R0 [DIRS 179989]
B4_CSNF_REP_P50L_PMA.ou	PREWAP output file for representative TH (DS T and RH)	File	Same as above.	LL0703PA036MST.018_R0 [DIRS 179986]
B4_CSNF_REP_P90_PMA.ou	PREWAP output file for representative TH (DS T and RH)	File	Same as above.	LL0703PA014MST.009_R0 [DIRS 179856]
B4_CSNF_REP_P90H_PMA.ou	PREWAP output file for representative TH (DS T and RH)	File	Same as above.	LL0703PA016MST.011_R0 [DIRS 179858]
B4_CSNF_REP_P90L_PMA.ou	PREWAP output file for representative TH (DS T and RH)	File	Same as above.	LL0703PA038MST.020_R0 [DIRS 179992]
B4_DHLW_REP_P10_PMA.ou	PREWAP output file for representative TH (DS T and RH)	File	Same as above.	LL0703PA011MST.006_R0 [DIRS 179853]
B4_DHLW_REP_P10H_PMA.ou	PREWAP output file for representative TH (DS T and RH)	File	Same as above.	LL0703PA017MST.012_R0 [DIRS 179859]
B4_DHLW_REP_P10L_PMA.ou	PREWAP output file for representative TH (DS T and RH)	File	Same as above.	LL0703PA015MST.010_R0 [DIRS 179857]
B4_DHLW_REP_P30_PMA.ou	PREWAP output file for representative TH (DS T and RH)	File	Same as above.	LL0703PA012MST.007_R0 [DIRS 179854]
B4_DHLW_REP_P30H_PMA.ou	PREWAP output file for representative TH (DS T and RH)	File	Same as above.	LL0703PA035MST.017_R0 [DIRS 179985]
B4_DHLW_REP_P30L_PMA.ou	PREWAP output file for representative TH (DS T and RH)	File	Same as above.	LL0703PA034MST.016_R0 [DIRS 179982]
B4_DHLW_REP_P50_PMA.ou	PREWAP output file for representative TH (DS T and RH)	File	Same as above.	LL0703PA013MST.008_R0 [DIRS 179855]
B4_DHLW_REP_P50H_PMA.ou	PREWAP output file for representative TH (DS T and RH)	File	Same as above.	LL0703PA037MST.019_R0 [DIRS 179989]
B4_DHLW_REP_P50L_PMA.ou	PREWAP output file for representative TH (DS T and RH)	File	Same as above.	LL0703PA036MST.018_R0 [DIRS 179986]
B4_DHLW_REP_P90_PMA.ou	PREWAP output file for representative TH (DS T and RH)	File	Same as above.	LL0703PA014MST.009_R0 [DIRS 179856]
B4_DHLW_REP_P90H_PMA.ou	PREWAP output file for representative TH (DS T and RH)	File	Same as above.	LL0703PA016MST.011_R0 [DIRS 179858]

Table C4-2. Input Parameters Added for the PMA (Continued)

Parameter Name	Description	Parameter Distribution	Rationale for Inclusion	Data Source
EBS Thermal-Hydrology Parameters (Continued)				
B4_DHLW_REP_P90L_PMA.ou	PREWAP output file for representative TH (DS T and RH)	File	Same as above.	LL0703PA038MST.020_R0 [DIRS 179992]
B5_CSNF_REP_P10_PMA.ou	PREWAP output file for representative TH (DS T and RH)	File	Same as above.	LL0703PA011MST.006_R0 [DIRS 179853]
B5_CSNF_REP_P10H_PMA.ou	PREWAP output file for representative TH (DS T and RH)	File	Same as above.	LL0703PA017MST.012_R0 [DIRS 179859]
B5_CSNF_REP_P10L_PMA.ou	PREWAP output file for representative TH (DS T and RH)	File	Same as above.	LL0703PA015MST.010_R0 [DIRS 179857]
B5_CSNF_REP_P30_PMA.ou	PREWAP output file for representative TH (DS T and RH)	File	Same as above.	LL0703PA012MST.007_R0 [DIRS 179854]
B5_CSNF_REP_P30H_PMA.ou	PREWAP output file for representative TH (DS T and RH)	File	Same as above.	LL0703PA035MST.017_R0 [DIRS 179985]
B5_CSNF_REP_P30L_PMA.ou	PREWAP output file for representative TH (DS T and RH)	File	Same as above.	LL0703PA034MST.016_R0 [DIRS 179982]
B5_CSNF_REP_P50_PMA.ou;	PREWAP output file for representative TH (DS T and RH)	File	Same as above.	LL0703PA013MST.008_R0 [DIRS 179855]
B5_CSNF_REP_P50H_PMA.ou	PREWAP output file for representative TH (DS T and RH)	File	Same as above.	LL0703PA037MST.019_R0 [DIRS 179989]
B5_CSNF_REP_P50L_PMA.ou	PREWAP output file for representative TH (DS T and RH)	File	Same as above.	LL0703PA036MST.018_R0 [DIRS 179986]
B5_CSNF_REP_P90_PMA.ou	PREWAP output file for representative TH (DS T and RH)	File	Same as above.	LL0703PA014MST.009_R0 [DIRS 179856]
B5_CSNF_REP_P90H_PMA.ou	PREWAP output file for representative TH (DS T and RH)	File	Same as above.	LL0703PA016MST.011_R0 [DIRS 179858]
B5_CSNF_REP_P90L_PMA.ou	PREWAP output file for representative TH (DS T and RH)	File	Same as above.	LL0703PA038MST.020_R0 [DIRS 179992]
B5_DHLW_REP_P10_PMA.ou	PREWAP output file for representative TH (DS T and RH)	File	Same as above.	LL0703PA011MST.006_R0 [DIRS 179853]
B5_DHLW_REP_P10H_PMA.ou	PREWAP output file for representative TH (DS T and RH)	File	Same as above.	LL0703PA017MST.012_R0 [DIRS 179859]
B5_DHLW_REP_P10L_PMA.ou	PREWAP output file for representative TH (DS T and RH)	File	Same as above.	LL0703PA015MST.010_R0 [DIRS 179857]

Table C4-2. Input Parameters Added for the PMA (Continued)

Parameter Name	Description	Parameter Distribution	Rationale for Inclusion	Data Source
EBS Thermal-Hydrology Parameters (Continued)				
B5_DHLW_REP_P30_PMA.ou	PREWAP output file for representative TH (DS T and RH)	File	Same as above.	LL0703PA012MST.007_R0 [DIRS 179854]
B5_DHLW_REP_P30H_PMA.ou	PREWAP output file for representative TH (DS T and RH)	File	Same as above.	LL0703PA035MST.017_R0 [DIRS 179985]
B5_DHLW_REP_P30L_PMA.ou	PREWAP output file for representative TH (DS T and RH)	File	Same as above.	LL0703PA034MST.016_R0 [DIRS 179982]
B5_DHLW_REP_P50_PMA.ou	PREWAP output file for representative TH (DS T and RH)	File	Same as above.	LL0703PA013MST.008_R0 [DIRS 179855]
B5_DHLW_REP_P50H_PMA.ou	PREWAP output file for representative TH (DS T and RH)	File	Same as above.	LL0703PA037MST.019_R0 [DIRS 179989]
B5_DHLW_REP_P50L_PMA.ou	PREWAP output file for representative TH (DS T and RH)	File	Same as above.	LL0703PA036MST.018_R0 [DIRS 179986]
B5_DHLW_REP_P90_PMA.ou	PREWAP output file for representative TH (DS T and RH)	File	Same as above.	LL0703PA014MST.009_R0 [DIRS 179856]
B5_DHLW_REP_P90H_PMA.ou	PREWAP output file for representative TH (DS T and RH)	File	Same as above.	LL0703PA016MST.011_R0 [DIRS 179858]
B5_DHLW_REP_P90H_PMA.ou	PREWAP output file for representative TH (DS T and RH)	File	Same as above.	LL0703PA038MST.020_R0 [DIRS 179992]
MFCP_LA_Input.txt	Simulation Settings: Master File Control Program support file.	File	Same as above.	Corroborative DTN: MO0708TSPAPROC.000_R0 [DIRS 182979]
pass_table_master_PMA.in	List of TH files for DS temperature and RH.	File	Same as above.	Corroborative DTN: MO0708TSPAPROC.000_R0 [DIRS 182979]
Drift Scale UZ Flow Parameters				
SMPA_C_PMA.dat	Seepage model input for performance assessment used for PMA collapsed-drift look-up table.	File	Necessary to implement the PMA seepage model.	Corroborative DTN: LB0704PASEEP02.001_R1 [DIRS 181093]

Table C4-2. Input Parameters Added for the PMA (Continued)

Parameter Name	Description	Parameter Distribution	Rationale for Inclusion	Data Source
EBS Flow and Transport Parameters				
WB_Campbell_b_a	Campbell parameter.	Uniform [3.5, 5]	Necessary for developing a more realistic water balance model.	Corroborative DTN: SN0704PMAWBCAL.001_R 2 [DIRS 182335]
WB_Ionic_strength_seep_a	Ionic strength of seepage water.	Uniform [0.001 mol/kg, 0.02 mol/kg]	Necessary for developing a more realistic water balance model.	Corroborative DTN: SN0704PMAWBCAL.001_R 2 [DIRS 182335]
WB_Mean_Particle_Diam_a	Mean particle diameter for water balance model.	Log-uniform [0.001 mm, 1 mm]	Necessary for developing a more realistic water balance model.	Corroborative DTN: SN0704PMAWBCAL.001_R 2 [DIRS 182335]
WB_Permeability_CP_a	Corrosion product permeability.	Log-uniform [1E-014 m^2, 1E-010 m^2]	Necessary for developing a more realistic water balance model.	Corroborative DTN: SN0704PMAWBCAL.001_R 2 [DIRS 182335]
WB_Porosity_Deg_Prod_a	Porosity of the degradation product.	Uniform [0.35, 0.5]	Necessary for developing a more realistic water balance model.	Corroborative DTN: SN0704PMAWBCAL.001_R 2 [DIRS 182335]
WB_Salt_CDSP_a	Moles of salt released from 1 kg HLW degraded.	Uniform [0.062 mol/kg, 1.078 mol/kg]	Necessary for developing a more realistic water balance model.	Corroborative DTN: SN0704PMAWBCAL.001_R 2 [DIRS 182335]
WB_Salt_SS_a	Moles of salt released from 1 kg SS degraded.	Uniform [0.062 mol/kg, 0.133 mol/kg]	Necessary for developing a more realistic water balance model.	Corroborative DTN: SN0704PMAWBCAL.001_R 2 [DIRS 182335]
WB_Water_Film_Thickness_a	Water film thickness.	Uniform [0.1 mm, 3 mm]	Necessary for developing a more realistic water balance model.	Corroborative DTN: SN0704PMAWBCAL.001_R 2 [DIRS 182335]
WB_Alpha_Potential	Alpha potential.	0.002332021	Necessary for developing a more realistic water balance model.	Corroborative DTN: SN0704PMAWBCAL.001_R 2 [DIRS 182335]
WB_Beta_Potential	Beta potential.	0.023762087	Necessary for developing a more realistic water balance model.	Corroborative DTN: SN0704PMAWBCAL.001_R 2 [DIRS 182335]
WB_Bulk_Volume_DSNF	Initial bulk volume of the DSNF waste form.	0.749727 m^3	Necessary for developing a more realistic water balance model.	Corroborative DTN: SN0704PMAWBCAL.001_R 2 [DIRS.182335]

Table C4-2. Input Parameters Added for the PMA (Continued)

Parameter Name	Description	Parameter Distribution	Rationale for Inclusion	Data Source
EBS Flow and Transport Parameters (Continued)				
WB_Density_CDSP	Density of CDSP.	3.34 g/cm^3	Necessary for developing a more realistic water balance model.	Corroborative DTN: SN0704PMAWBCAL.001_R 2 [DIRS.182335]
WB_Density_CSNF	Density of CSNF.	10.08 g/cm^3	Necessary for developing a more realistic water balance model.	Corroborative DTN: SN0704PMAWBCAL.001_R 2 [DIRS.182335]
WB_Density_Steel	Density of steel.	7.98 g/cm^3	Necessary for developing a more realistic water balance model.	Corroborative DTN: SN0704PMAWBCAL.001_R 2 [DIRS.182335]
WB_Density_water	Density of liquid water.	0.99707 g/cm^3	Necessary for developing a more realistic water balance model.	Corroborative DTN: SN0704PMAWBCAL.001_R 2 [DIRS.182335]
WB_Initial_Void_Vol_CDSP_WP	Initial void volume in CDSP waste package.	8.49117 m^3	Necessary for developing a more realistic water balance model.	Corroborative DTN: SN0704PMAWBCAL.001_R 2 [DIRS.182335]
WB_Initial_Void_Vol_CSNF_WP	Initial void volume in CSNF waste package.	6.723077 m^3	Necessary for developing a more realistic water balance model.	Corroborative DTN: SN0704PMAWBCAL.001_R 2 [DIRS.182335]
WB_Mol_Wt_Water	Molecular weight of water.	18.01534 g/mol	Necessary for developing a more realistic water balance model.	Corroborative DTN: SN0704PMAWBCAL.001_R 2 [DIRS.182335]
WB_Molar_Vol_Water	Molar volume of water.	1.80683e-005 m^3/mol	Necessary for developing a more realistic water balance model.	Corroborative DTN: SN0704PMAWBCAL.001_R 2 [DIRS.182335]
WB_Num_Active_Species	Number of osmotically active species.	2	Necessary for developing a more realistic water balance model.	Corroborative DTN: SN0704PMAWBCAL.001_R 2 [DIRS.182335]
WB_Radius_WP_CDSP	CDSP waste package radius.	1.06 m	Necessary for developing a more realistic water balance model.	Corroborative DTN: SN0704PMAWBCAL.001_R 2 [DIRS.182335]
WB_Radius_WP_CSNF	CSNF waste package radius.	0.9408 m	Necessary for developing a more realistic water balance model.	Corroborative DTN: SN0704PMAWBCAL.001_R 2 [DIRS 182335]

Table C4-2. Input Parameters Added for the PMA (Continued)

Parameter Name	Description	Parameter Distribution	Rationale for Inclusion	Data Source
EBS Flow and Transport Parameters (Continued)				
WB_Ref_Temp	Waste package reference temperature.	25 C	Necessary for developing a more realistic water balance model.	Corroborative DTN: SN0704PMAWBCAL.001_R 2 [DIRS 182335]
WB_Residual_water_conte nt	Residual water content in degradation products.	0.05	Necessary for developing a more realistic water balance model.	Corroborative DTN: SN0704PMAWBCAL.001_R 2 [DIRS 182335]
WB_Salt_CSNF	Moles of salt released from 1 kg CSNF.	0.034 mol/kg	Necessary for developing a more realistic water balance model.	Corroborative DTN: SN0704PMAWBCAL.001_R 2 [DIRS 182335]
WB_Vol_CP_Per_Kg_SS	Volume of corrosion products from 1 kg stainless steel.	0.00033 m^3/kg	Necessary for developing a more realistic water balance model.	Corroborative DTN: SN0704PMAWBCAL.001_R 2 [DIRS 182335]
WB_Vol_Degrad_prod_Per _Kg_CDSP	Solid volume produced from 1 kg of CDSP degraded.	0.00059 m^3/kg	Necessary for developing a more realistic water balance model.	Corroborative DTN: SN0704PMAWBCAL.001_R 2 [DIRS 182335]
WB_Vol_Degrad_prod_Per _Kg_CSNF	Solid volume produced from 1 kg of CSNF degraded.	0.000239 m^3/kg	Necessary for developing a more realistic water balance model.	Corroborative DTN: SN0704PMAWBCAL.001_R 2 [DIRS 182335]
WB_Water_Consum_Per_ Kg_CDSP	Moles of water consumed per kg CDSP degraded.	10.52 mol/kg	Necessary for developing a more realistic water balance model	Corroborative DTN: SN0704PMAWBCAL.001_R 2 [DIRS 182335]
WB_Water_Consum_Per_ Kg_CSNF	Moles of water consumed per kg CSNF degraded.	7.23 mol/kg	Necessary for developing a more realistic water balance model.	Corroborative DTN: SN0704PMAWBCAL.001_R 2 [DIRS182335]
WB_Water_Consum_Per_ Kg_SS	Moles of water consumed per kg stainless steel degraded.	14.15 mol/kg	Necessary for developing a more realistic water balance model.	Corroborative DTN: SN0704PMAWBCAL.001_R 2 [DIRS 182335]

Table C4-2. Input Parameters Added for the PMA (Continued)

Parameter Name	Description	Parameter Distribution	Rationale for Inclusion	Data Source
Waste Package and Drip Shield Degradation Parameters				
Gp1_RH_Threshold_table	RH threshold for fluoride activity.	Lookup Table (1D)	DS corrosion is a function of F ion concentration which was correlated to RH for use in selecting the DS corrosion rates.	Corroborative DTN: MO0708TSPAPROC.000_R 0 [DIRS 182979]
Gp2_RH_Threshold_table	RH threshold for fluoride activity.	Lookup Table (1D)	Same as above.	Corroborative DTN: MO0708TSPAPROC.000_R 0 [DIRS 182979]
Gp3_RH_Threshold_table	RH threshold for fluoride activity.	Lookup Table (1D)	Same as above.	Corroborative DTN: MO0708TSPAPROC.000_R 0 [DIRS 182979]
Gp4_RH_Threshold_table	RH threshold for fluoride activity. f_WP_failed_area_EF_DS_PMA_a	Lookup Table (1D)	Same as above.	Corroborative DTN: MO0708TSPAPROC.000_R 0 [DIRS 182979]
f_WP_failed_area_EF_DS_ PMA_a	Fraction of waste package area failed by localized corrosion in the early failed drip shield modeling case.	Log-Uniform [0.0005, 1]	Used ACM for localized corrosion failure area provided in *General Corrosion and Localized Corrosion of Waste Package Outer Barrier*, ANL-EBS-MD-000003 REV 03 [DIRS 178519].	ANL-EBS-MD-000003 REV 03 [DIRS 178519]
WAP_file	List of filenames for GoldSim-WAPDEG file transfer.	File	Necessary to for Weight Loss data based corrosion model.	Corroborative DTN: MO0708TSPAPROC.000_R 0 [DIRS 182979]
WDInR_ASC_WL_cdf	CDF for the natural logarithm of the GC rate for Alloy 22 (average patch) using the weight-loss data.	File	Same as above.	Corroborative DTN: MO0708TSPAPROC.000_R 0 [DIRS 182979]
WDInR_ESC_WL_cdf	CDF for the natural logarithm of the GC rate for Alloy 22 (extreme patch) using the weight-loss data.	File	Same as above.	Corroborative DTN: MO0708TSPAPROC.000_R 0 [DIRS 182979]
Stress_Thresh_SCC_PMA _a	Distribution for residual stress threshold.	Uniform [351, 368.55]	Necessary to implement less conservative threshold for stress corrosion cracking.	ANL-EBS-MD-000005 Rev 04 [DIRS 181953]

Table C4-2. Input Parameters Added for the PMA (Continued)

Parameter Name	Description	Parameter Distribution	Rationale for Inclusion	Data Source
Waste Package and Drip Shield Degradation Parameters (Continued)				
Initial_Rod_Failures_PMA_a	Fraction of CSNF Zircaloy-clad fuel rods that are failed upon receipt to the repository (PMA model).	Log-Uniform [0.0001, 0.01]	Necessary to implement cladding credit.	MO0411SPACLDDG.003_R1 [DIRS 180755]
Inven_SS	Fraction of CSNF fuel rods that are SS-Clad.	Constant Value [0.01]	Necessary to implement cladding credit.	MO0411SPACLDDG.003_R1 [DIRS 180755]
Frac_CSNF_Pkgs_SS_a	Fraction of CSNF Waste Packages that contain SS-Clad fuel.	Log-Uniform [0.01, 0.02]	Necessary to implement cladding credit.	MO0702PAFRACSS.000_R1 [DIRS 181588]
HLW_Fast_Fraction_a	Fraction of glass waste form that dissolves at the forward reaction rate.	Triangular [0.0033, 0.011, 0.033]	Necessary for developing a more realistic water balance model	Corroborative DTN: SN0704PMAGDEGM.001_R2 [DIRS 183955]
HLW_RA_final_a	Final reaction affinity.	Log-triangular [1E-005, 0.0005, 0.01]	Necessary for developing a more realistic water balance model	Corroborative DTN: SN0704PMAGDEGM.001_R2 [DIRS 183955]
HLW_k0	Intrinsic glass dissolution rate.	10,000,000 $g/m^2/d$	Necessary for developing a more realistic water balance model	Corroborative DTN: SN0704PMAGDEGM.001_R2 [DIRS 183955]
Log_Specific_SA_CSNF_PMA_a	Log of the specific surface area for CSNF.	Triangular [-7.3, -7.3, -6.7]	Necessary for developing a more realistic water balance model	Corroborative DTN: SN0707PMACSNFD.001_R0 [DIRS 183045]
Scaling_Fact_Long_Term_Diss_a	Scaling factor for long-term dissolution.	Uniform [3, 10]	Necessary for developing a more realistic water balance model	Corroborative DTN: SN0707PMACSNFD.001_R0 [DIRS 183045]
Scaling_Fact_Radiolysis_a	Scaling factor for changes in Radiolysis.	Uniform [5, 10]	Necessary for developing a more realistic water balance model	Corroborative DTN: SN0707PMACSNFD.001_R0 [DIRS 183045]
Np2O5_PMA_Eps	Uncertainty of Np_2O_5 solubility for PMA.	Triangular [-1, 0, 1]	New uncertainty ranges derived by comparison of model prediction with experimental data	Corroborative DTN: SN0704PMASOLUB.001_R1[DIRS 182787]
Np_Carbonate_PMA_Eps	Uncertainty of $NaNpO_2CO_3$ for PMA.	Normal [0, 0.25] truncated at +/- 2σ	New uncertainty ranges derived by comparison of model prediction with experimental data	Corroborative DTN: SN0704PMASOLUB.001_R1[DIRS 182787]

Table C4-2. Input Parameters Added for the PMA (Continued)

Parameter Name	Description	Parameter Distribution	Rationale for Inclusion	Data Source
Waste Package and Drip Shield Degradation Parameters (Continued)				
NpO2_PMA_Eps	Uncertainty of NpO_2 solubility for PMA.	Triangular [-1.07, 0, 1.07]	New uncertainty ranges derived by comparison of model prediction with experimental data.	Corroborative DTN: SN0704PMASOLUB.001_R1[DIRS 182787]
Pu_PMA_Eps_a	Uncertainty of Pu solubility model for PMA.	Normal [0, 0.79] truncated at +/- 1σ	New uncertainty ranges derived by comparison of model prediction with experimental data.	Corroborative DTN: SN0704PMASOLUB.001_R1[DIRS 182787]
U_schoepite_PMA_Eps	Uncertainty of schoepite solubility for PMA.	Triangular [-0.4, 0, 0.4]	New uncertainty ranges derived by comparison of model prediction with experimental data.	Corroborative DTN: SN0704PMASOLUB.001_R1[DIRS 182787]
U_Boltwoodite_PMA_Eps	Uncertainty of Na-boltwoodite solubility for PMA.	Triangular [-0.5, 0, 0.3]	New uncertainty ranges derived by comparison of model prediction with experimental data.	Corroborative DTN: SN0704PMASOLUB.001_R[DIRS 182787]
U_Carbonate_PMA_Eps	Uncertainty of $Na_4UO_2(CO_3)_3$ solubility for PMA.	Triangular [-0.3, 0, 0.3]	New uncertainty ranges derived by comparison of model prediction with experimental data.	Corroborative DTN: SN0704PMASOLUB.001_R1[DIRS 182787]
IPC_PMA_pH_2DHLW_HS_Choice	Record which random number to use for the dual triangular distribution of CDSP Cell 1a pH high-dripping.	Discrete [0.5, 1, 0.5,2]	Necessary for calculating more realistic in-package pH values.	Corroborative DTN: SN0704PMAIPCAB.001_R1 [DIRS 182602]
IPC_PMA_pH_2DHLW_HS_Rand_1_a	Sampling for the dual triangular distribution, 2DHLW, High-seepage.	Uniform [0,1]	Necessary for calculating more realistic in-package pH values.	Corroborative DTN: SN0704PMAIPCAB.001_R1 [DIRS 182602]
IPC_PMA_pH_2DHLW_HS_Rand_2_a	Sampling for the dual triangular distribution, 2DHLW, High-seepage.	Uniform [0,1]	Necessary for calculating more realistic in-package pH values.	Corroborative DTN: SN0704PMAIPCAB.001_R1 [DIRS 182602]

Table C4-2. Input Parameters Added for the PMA (Continued)

Parameter Name	Description	Parameter Distribution	Rationale for Inclusion	Data Source
Waste Form Degradation and Radionuclide Mobilization Parameter (Continued)				
IPC_PMA_pH_2DHLW_NS_Choice	Record which random number to use for the dual triangular distribution of CDSP Cell 1a pH no-dripping	Discrete [0.5, 1, 0.5,2]	Necessary for calculating more realistic in-package pH values	Corroborative DTN: SN0704PMAIPCAB.001_R1 [DIRS 182602]
IPC_PMA_pH_2DHLW_NS_Rand_1_a	Sampling for the dual triangular distribution, 2DHLW, Non-seepage	Uniform [0,1]	Necessary for calculating more realistic in-package pH values	Corroborative DTN: SN0704PMAIPCAB.001_R1 [DIRS 182602]
IPC_PMA_pH_2DHLW_NS_Rand_2_a	Sampling for the dual triangular distribution, 2DHLW, Non-seepage	Uniform [0,1]	Necessary for calculating more realistic in-package pH values	Corroborative DTN: SN0704PMAIPCAB.001_R1 [DIRS 182602]
IPC_PMA_pH_2MCO_HS_Choice	Record which random number to use for the dual triangular distribution of CDSP Cell 1b pH high-dripping	Discrete [0.5, 1, 0.5,2]	Necessary for calculating more realistic in-package pH values	Corroborative DTN: SN0704PMAIPCAB.001_R1 [DIRS 182602]
IPC_PMA_pH_2MCO_HS_Rand_1_a	Sampling for the dual triangular distribution, 2MCO, High-seepage	Uniform [0,1]	Necessary for calculating more realistic in-package pH values	Corroborative DTN: SN0704PMAIPCAB.001_R1 [DIRS 182602]
IPC_PMA_pH_2MCO_HS_Rand_2_a	Sampling for the dual triangular distribution, 2MCO, High-seepage	Uniform [0,1]	Necessary for calculating more realistic in-package pH values	Corroborative DTN: SN0704PMAIPCAB.001_R1 [DIRS 182602]
IPC_PMA_pH_2MCO_NS_Choice	Record which random number to use for the dual triangular distribution of CDSP Cell 1b pH no-dripping	Discrete [0.5, 1, 0.5,2]	Necessary for calculating more realistic in-package pH values	Corroborative DTN: SN0704PMAIPCAB.001_R1 [DIRS 182602]
IPC_PMA_pH_2MCO_NS_Rand_1_a	Sampling for the dual triangular distribution, 2MCO, Non-seepage	Uniform [0,1]	Necessary for calculating more realistic in-package pH values	Corroborative DTN: SN0704PMAIPCAB.001_R1 [DIRS 182602]
IPC_PMA_pH_2MCO_NS_Rand_2_a	Sampling for the dual triangular distribution, 2MCO, Non-seepage	Uniform [0,1]	Necessary for calculating more realistic in-package pH values	Corroborative DTN: SN0704PMAIPCAB.001_R1 [DIRS 182602]
IPC_PMA_pH_CSNF_HS_Choice	Record which random number to use for the dual triangular distribution of CSNF Cell 1 pH high-dripping	Discrete [0.5, 1, 0.5,2]	Necessary for calculating more realistic in-package pH values	Corroborative DTN: SN0704PMAIPCAB.001_R1 [DIRS 182602]
IPC_PMA_pH_CSNF_HS_Rand_1_a	Sampling for the dual triangular distribution, CSNF High-seepage	Uniform [0,1]	Necessary for calculating more realistic in-package pH values	Corroborative DTN: SN0704PMAIPCAB.001_R1 [DIRS 182602]

Table C4-2. Input Parameters Added for the PMA (Continued)

Parameter Name	Description	Parameter Distribution	Rationale for Inclusion	Data Source
Waste Form Degradation and Mobilization (Continued)				
IPC_PMA_pH_CSNF_HS_Rand_2_a	Sampling for the dual triangular distribution, CSNF, High-seepage	Uniform [0,1]	Necessary for calculating more realistic in-package pH values	Corroborative DTN: SN0704PMAIPCAB.001_R1 [DIRS 182602]
IPC_PMA_pH_CSNF_NS_Choice	Record which random number to use for the dual triangular distribution of CSNF Cell 1 pH no-dripping	Discrete [0.5, 1, 0.5,2]	Necessary for calculating more realistic in-package pH values	Corroborative DTN: SN0704PMAIPCAB.001_R1 [DIRS 182602]
IPC_PMA_pH_CSNF_NS_Rand_1_a	Sampling for the dual triangular distribution, CSNF, Non-seepage	Uniform [0,1]	Necessary for calculating more realistic in-package pH values	Corroborative DTN: SN0704PMAIPCAB.001_R1 [DIRS 182602]
IPC_PMA_pH_CSNF_NS_Rand_2_a	Sampling for the dual triangular distribution, CSNF, Non-seepage	Uniform [0,1]	Necessary for calculating more realistic in-package pH values	Corroborative DTN: SN0704PMAIPCAB.001_R1 [DIRS 182602]
Density_2DHLW_SS304L	Density of Stainless Steel 304L in CDSP Cell 1a	Single Value, 7.94 g/cm^3	Necessary for calculating more realistic pH values inside a waste package	SN0702PAIPC1CA.001_R2 [DIRS 180451]
Density_2MCO_SS304L	Density of Stainless Steel 304L in CDSP Cell 1b	Single Value, 7.94 g/cm^3	Necessary for calculating more realistic pH values inside a waste package	SN0702PAIPC1CA.001_R2 [DIRS 180451]
Density_CSNF_SS304B	Density of 304B SS, CSNF	Single Value, 7.81 g/cm^3	Necessary for calculating more realistic pH values inside a waste package	SN0702PAIPC1CA.001_R2 [DIRS 180451]
Density_CSNF	Density of CSNF	Single Value, 10080 kg/m^3	Necessary for calculating more realistic pH values inside a waste package	SN0702PAIPC1CA.001_R2 [DIRS 180451]
Density_HLW	Density of HLW*	Single Value, 3340 kg/m^3	Necessary for calculating more realistic pH values inside a waste package	SN0702PAIPC1CA.001_R2 [DIRS 180451]
Density_DSNF	Density of DSNF*	Single Value, 2300 kg/m^3	Necessary for calculating more realistic pH values inside a waste package	SN0702PAIPC1CA.001_R2 [DIRS 180451]
Initial_Mass_2DHLW_SS304	Initial mass of 304L SS, 2DHLW	Single Value, 1490 kg	Necessary for calculating more realistic pH values inside a waste package	SN0702PAIPC1CA.001_R2 [DIRS 180451]

Table C4-2. Input Parameters Added for the PMA (Continued)

Parameter Name	Description	Parameter Distribution	Rationale for Inclusion	Data Source
Waste Form Degradation and Mobilization (Continued)				
Initial_Mass_2MCO_SS304	Initial mass of 304L SS, 2MCO	Single Value, 4720 kg	Necessary for calculating more realistic pH values inside a waste package	SN0702PAIPC1CA.001_R2 [DIRS 180451]
Initial_Mass_CSNF_SS304	Initial mass of 304B4 SS, CSNF	Single Value, 38200 mol	Necessary for calculating more realistic pH values inside a waste package	SN0702PAIPC1CA.001_R2 [DIRS 180451]
Initial_Mass_CSNF_SS316	Initial mass of 316 SS, CSNF	Single Value, 61800 mol	Necessary for calculating more realistic pH values inside a waste package	SN0702PAIPC1CA.001_R2 [DIRS 180451]
Initial_Mass_CSNF	Initial mass of CSNF	Single Value, 110000 mol	Necessary for calculating more realistic pH values inside a waste package	SN0702PAIPC1CA.001_R2 [DIRS 180451]
Initial_Mass_DHLW	Initial mass of HLW	Single Value, 6910 kg	Necessary for calculating more realistic pH values inside a waste package	SN0702PAIPC1CA.001_R2 [DIRS 180451]
Initial_Mass_DSNF	Initial mass of DSNF	Single Value, 13700 kg	Necessary for calculating more realistic pH values inside a waste package	SN0702PAIPC1CA.001_R2 [DIRS 180451]
MW_304B_SS_CSNF	Molecular weight of 304B SS, CSNF	Single Value, 100 g/mol	Necessary for calculating more realistic pH values inside a waste package	ANL-EBS-MD-000037 Rev 04 AD 01, [DIRS 180506],Table 6.5[a]
MW_304L_SS_2DHLW	Molecular weight of 304L SS, 2DHLW	Single Value, 100 g/mol	Necessary for calculating more realistic pH values inside a waste package	ANL-EBS-MD-000037 Rev 04 AD 01, [DIRS 180506],Table 6.5[a]
MW_304L_SS_2MCO	Molecular weight of 304L SS, 2MCO	Single Value, 100 g/mol	Necessary for calculating more realistic pH values inside a waste package	ANL-EBS-MD-000037 Rev 04 AD 01, [DIRS 180506],Table 6.5[a]
MW_316_SS_CSNF	Molecular weight of 316 SS, CSNF	Single Value, 100 g/mol	Necessary for calculating more realistic pH values inside a waste package	ANL-EBS-MD-000037 Rev 04 AD 01, [DIRS 180506],Table 6.5[a]
MW_CSNF_WF	Molecular weight of CSNF	Single Value, 100 g/mol	Necessary for calculating more realistic pH values inside a waste package	ANL-EBS-MD-000037 Rev 04 AD 01, [DIRS 180506],Table 6.5[a]

Table C4-2. Input Parameters Added for the PMA (Continued)

Parameter Name	Description	Parameter Distribution	Rationale for Inclusion	Data Source
Waste Form Degradation and Mobilization (Continued)				
MW_DSNF_WF	Molecular weight of DSNF	Single Value, 100 g/mol	Necessary for calculating more realistic pH values inside a waste package	ANL-EBS-MD-000037 Rev 04 AD 01 , [DIRS 180506], Table 6.5[a]
MW_HLW_WF	Molecular weight HLW	Single Value, 100 g/mol	Necessary for calculating more realistic pH values inside a waste package	ANL-EBS-MD-000037 Rev 04 AD 01 , [DIRS 180506],Table 6.5[a]
Surface_Area_2DHLW	Surface area of DHLW	Single Value, 680000 cm^2	Necessary for calculating more realistic pH values inside a waste package	SN0702PAIPC1CA.001_R2 [DIRS 180451]
Surface_Area_2DHLW_SS304	Surface area of 304 SS, 2DHLW	Single Value, 357000 cm^2	Necessary for calculating more realistic pH values inside a waste package	SN0702PAIPC1CA.001_R2 [DIRS 180451]
Surface_Area_2MCO_SS304	Surface area of 304 SS, 2MCO	Single Value, 271000 cm^2	Necessary for calculating more realistic pH values inside a waste package	SN0702PAIPC1CA.001_R2 [DIRS 180451]
Surface_Area_CSNF	Surface area of CSNF	Single Value, 5030000 cm^2	Necessary for calculating more realistic pH values inside a waste package	SN0702PAIPC1CA.001_R2 [DIRS 180451]
Surface_Area_CSNF_SS304	Surface area of 304 SS, CSNF	Single Value, 881000 cm^2	Necessary for calculating more realistic pH values inside a waste package	SN0702PAIPC1CA.001_R2 [DIRS 180451]
Surface_Area_CSNF_SS316	Surface area of 316 SS, CSNF	Single Value, 1950000 cm^2	Necessary for calculating more realistic pH values inside a waste package	SN0702PAIPC1CA.001_R2 [DIRS 180451]
Surface_Area_2MCO	Surface area of DSNF	Single Value, 9580000 cm^2	Necessary for calculating more realistic pH values inside a waste package	SN0702PAIPC1CA.001_R2 [DIRS 180451]
Da_HF_log	Log Damkohler ratio of high-dripping conditions	Single value, -1 log mole	Necessary for calculating more realistic pH values inside a waste package	Corroborative DTN: SN0702PAIPCAB.001_R1 [DIRS 182602]
Da_NS_log	Log Damkohler ratio of no-dripping	Single value, 2 log mole	Necessary for calculating more realistic pH values inside a waste package	Corroborative DTN: SN0704PMAIPCAB.001_R1 [DIRS 182602]

Table C4-2. Input Parameters Added for the PMA (Continued)

Parameter Name	Description	Parameter Distribution	Rationale for Inclusion	Data Source
Waste Form Degradation and Mobilization (Continued)				
IPC_2DHLW_HiFlo_pH_Cond	pH look-up table under high flow conditions, condensated water, for CDSP Cell 1a	Lookup Table (2D)	Necessary for calculating more realistic pH values inside a waste package	Corroborative DTN: SN0704PMAIPCAB.001_R1 [DIRS 182602]
IPC_2DHLW_pCO2_Thresh_15	pCO_2 (=-log P_{CO2}) threshold value provides input to the DHLW pH routine.	Single Value, 1.5	Necessary for calculating more realistic pH values inside a waste package	Corroborative DTN: SN0704PMAIPCAB.001_R1 [DIRS 182602]
IPC_2DHLW_pCO2_Thresh_2	pCO_2 threshold value provides input to the DHLW pH routine.	Single Value, 2.0	Necessary for calculating more realistic pH values inside a waste package	Corroborative DTN: SN0704PMAIPCAB.001_R1 [DIRS 182602]
IPC_2DHLW_pCO2_Thresh_3	pCO_2 threshold value provides input to the DHLW pH routine.	Single Value, 3.0	Necessary for calculating more realistic pH values inside a waste package	Corroborative DTN: SN0704PMAIPCAB.001_R1 [DIRS 182602]
IPC_2DHLW_pCO2_Thresh_4	pCO_2 threshold value provides input to the DHLW pH routine.	Single Value, 4.0	Necessary for calculating more realistic pH values inside a waste package	Corroborative DTN: SN0704PMAIPCAB.001_R1 [DIRS 182602]
IPC_2MCO_HiFlo_pH_Cond	pH look-up table under high flow conditions, condensated water, for CDSP Cell 1b	Lookup Table (2D)	Necessary for calculating more realistic pH values inside a waste package	Corroborative DTN: SN0704PMAIPCAB.001_R1 [DIRS 182602]
IPC_2MCO_pCO2_Thresh_15	pCO_2 threshold value provides input to the MCO pH routine.	Single Value, 1.5	Necessary for calculating more realistic pH values inside a waste package	Corroborative DTN: SN0704PMAIPCAB.001_R1 [DIRS 182602]
IPC_2MCO_pCO2_Thresh_2	pCO_2 threshold value provides input to the MCO pH routine.	Single Value, 2.0	Necessary for calculating more realistic pH values inside a waste package	Corroborative DTN: SN0704PMAIPCAB.001_R1 [DIRS 182602]
IPC_2MCO_pCO2_Thresh_3	pCO_2 threshold value provides input to the MCO pH routine.	Single Value, 3.0	Necessary for calculating more realistic pH values inside a waste package	Corroborative DTN: SN0704PMAIPCAB.001_R1 [DIRS 182602]
IPC_2MCO_pCO2_Thresh_4	pCO_2 threshold value provides input to the MCO pH routine.	Single Value, 4.0	Necessary for calculating more realistic pH values inside a waste package	Corroborative DTN: SN0704PMAIPCAB.001_R1 [DIRS 182602]
IPC_CSNF_HiFlo_pH_Cond	pH look-up table under high flow conditions, condensated water, for CSNF Cell 1	Lookup Table (2D)	Necessary for calculating more realistic pH values inside a waste package	Corroborative DTN: SN0704PMAIPCAB.001_R1 [DIRS 182602]

Table C4-2. Input Parameters Added for the PMA (Continued)

Parameter Name	Description	Parameter Distribution	Rationale for Inclusion	Data Source
Waste Form Degradation and Mobilization (Continued)				
IPC_CSNF_pCO2_Thresh_15	pCO_2 threshold value provides input to the CSNF pH routine.	Single Value, 1.5	Necessary for calculating more realistic pH values inside a waste package	Corroborative DTN: SN0704PMAIPCAB.001_R1 [DIRS 182602]
IPC_CSNF_pCO2_Thresh_2	pCO_2 threshold value provides input to the CSNF pH routine.	Single Value, 2.0	Necessary for calculating more realistic pH values inside a waste package	Corroborative DTN: SN0704PMAIPCAB.001_R1 [DIRS 182602]
IPC_CSNF_pCO2_Thresh_3	pCO_2 threshold value provides input to the CSNF pH routine.	Single Value, 3.0	Necessary for calculating more realistic pH values inside a waste package	Corroborative DTN: SN0704PMAIPCAB.001_R1 [DIRS 182602]
IPC_CSNF_pCO2_Thresh_4	pCO_2 threshold value provides input to the CSNF pH routine.	Single Value, 4.0	Necessary for calculating more realistic pH values inside a waste package	Corroborative DTN: SN0704PMAIPCAB.001_R1 [DIRS 182602]
IPC_CSNF_Rsw_Thresh_A	Log Rsw (solid/water ratio) threshold value provides input to the CSNF pH routine.	Single Value, -2.0	Necessary for calculating more realistic pH values inside a waste package	Corroborative DTN: SN0704PMAIPCAB.001_R1 [DIRS 182602]
IPC_CSNF_Rsw_Thresh_B	Log Rsw threshold value provides input to the CSNF pH routine.	Single Value, -1.0	Necessary for calculating more realistic pH values inside a waste package	Corroborative DTN: SN0704PMAIPCAB.001_R1 [DIRS 182602]
IPC_CSNF_Rsw_Thresh_C	Log Rsw threshold value provides input to the CSNF pH routine.	Single Value, -0.522878745	Necessary for calculating more realistic pH values inside a waste package	Corroborative DTN: SN0704PMAIPCAB.001_R1 [DIRS 182602]
IPC_CSNF_Rsw_Thresh_D	Log Rsw threshold value provides input to the CSNF pH routine.	Single Value, 0	Necessary for calculating more realistic pH values inside a waste package	Corroborative DTN: SN0704PMAIPCAB.001_R1 [DIRS 182602]
IPC_CSNF_Rsw_Thresh_E	Log Rsw threshold value provides input to the CSNF pH routine.	Single Value, 0.1760912591	Necessary for calculating more realistic pH values inside a waste package	Corroborative DTN: SN0704PMAIPCAB.001_R1 [DIRS 182602]
IPC_CSNF_Rsw_Thresh_F	Log Rsw threshold value provides input to the CSNF pH routine.	Single Value, 0.3010299957	Necessary for calculating more realistic pH values inside a waste package	Corroborative DTN: SN0704PMAIPCAB.001_R1 [DIRS 182602]
IPC_CSNF_Rsw_Thresh_G	Log Rsw threshold value provides input to the CSNF pH routine.	Single Value, 0.4771212547	Necessary for calculating more realistic pH values inside a waste package	Corroborative DTN: SN0704PMAIPCAB.001_R1 [DIRS 182602]

Table C4-2. Input Parameters Added for the PMA (Continued)

Parameter Name	Description	Parameter Distribution	Rationale for Inclusion	Data Source
Waste Form Degradation and Mobilization (Continued)				
IPC_CSNF_Rsw_Thresh_H	Log Rsw hreshold value provides input to the CSNF pH routine.	Single Value, 1	Necessary for calculating more realistic pH values inside a waste package	Corroborative DTN: SN0704PMAIPCAB.001_R1 [DIRS 182602]
IPC_CSNF_Rsw_Thresh_I	Log Rsw hreshold value provides input to the CSNF pH routine.	Single Value, 2	Necessary for calculating more realistic pH values inside a waste package	Corroborative DTN: SN0704PMAIPCAB.001_R1 [DIRS 182602]
IPC_CSNF_pH_Rsw_15_A_LUT	LUT for CSNF pH.	Lookup Table (2D)	Necessary for calculating more realistic pH values inside a waste package	Corroborative DTN: SN0704PMAIPCAB.001_R1 [DIRS 182602]
IPC_CSNF_pH_Rsw_15_B_LUT	Same as above	Lookup Table (2D)	Necessary for calculating more realistic pH values inside a waste package	Corroborative DTN: SN0704PMAIPCAB.001_R1 [DIRS 182602]
IPC_CSNF_pH_Rsw_15_C_LUT	Same as above	Lookup Table (2D)	Necessary for calculating more realistic pH values inside a waste package	Corroborative DTN: SN0704PMAIPCAB.001_R1 [DIRS 182602]
IPC_CSNF_pH_Rsw_15_D_LUT	Same as above	Lookup Table (2D)	Necessary for calculating more realistic pH values inside a waste package	Corroborative DTN: SN0704PMAIPCAB.001_R1 [DIRS 182602]
IPC_CSNF_pH_Rsw_15_E_LUT	Same as above	Lookup Table (2D)	Necessary for calculating more realistic pH values inside a waste package	Corroborative DTN: SN0704PMAIPCAB.001_R1 [DIRS 182602]
IPC_CSNF_pH_Rsw_15_F_LUT	Same as above	Lookup Table (2D)	Necessary for calculating more realistic pH values inside a waste package	Corroborative DTN: SN0704PMAIPCAB.001_R1 [DIRS 182602]
IPC_CSNF_pH_Rsw_15_G_LUT	Same as above	Lookup Table (2D)	Necessary for calculating more realistic pH values inside a waste package	Corroborative DTN: SN0704PMAIPCAB.001_R1 [DIRS 182602]
IPC_CSNF_pH_Rsw_15_H_LUT	Same as above	Lookup Table (2D)	Necessary for calculating more realistic pH values inside a waste package	Corroborative DTN: SN0704PMAIPCAB.001_R1 [DIRS 182602]
IPC_CSNF_pH_Rsw_15_I_LUT	Same as above	Lookup Table (2D)	Necessary for calculating more realistic pH values inside a waste package	Corroborative DTN: SN0704PMAIPCAB.001_R1 [DIRS 182602]

Table C4-2. Input Parameters Added for the PMA (Continued)

Parameter Name	Description	Parameter Distribution	Rationale for Inclusion	Data Source
Waste Form Degradation and Mobilization (Continued)				
IPC_CSNF_pH_Rsw_2_A_LUT	Same as above	Lookup Table (2D)	Necessary for calculating more realistic pH values inside a waste package	Corroborative DTN: SN0704PMAIPCAB.001_R1 [DIRS 182602]
IPC_CSNF_pH_Rsw_2_B_LUT	Same as above	Lookup Table (2D)	Necessary for calculating more realistic pH values inside a waste package	Corroborative DTN: SN0704PMAIPCAB.001_R1 [DIRS 182602]
IPC_CSNF_pH_Rsw_2_C_LUT	Same as above	Lookup Table (2D)	Necessary for calculating more realistic pH values inside a waste package	Corroborative DTN: SN0704PMAIPCAB.001_R1 [DIRS 182602]
IPC_CSNF_pH_Rsw_2_D_LUT	Same as above	Lookup Table (2D)	Necessary for calculating more realistic pH values inside a waste package	Corroborative DTN: SN0704PMAIPCAB.001_R1 [DIRS 182602]
IPC_CSNF_pH_Rsw_2_E_LUT	Same as above	Lookup Table (2D)	Necessary for calculating more realistic pH values inside a waste package	Corroborative DTN: SN0704PMAIPCAB.001_R1 [DIRS 182602]
IPC_CSNF_pH_Rsw_2_F_LUT	Same as above	Lookup Table (2D)	Necessary for calculating more realistic pH values inside a waste package	Corroborative DTN: SN0704PMAIPCAB.001_R1 [DIRS 182602]
IPC_CSNF_pH_Rsw_2_G_LUT	Same as above	Lookup Table (2D)	Necessary for calculating more realistic pH values inside a waste package	Corroborative DTN: SN0704PMAIPCAB.001_R1 [DIRS 182602]
IPC_CSNF_pH_Rsw_2_H_LUT	Same as above	Lookup Table (2D)	Necessary for calculating more realistic pH values inside a waste package	Corroborative DTN: SN0704PMAIPCAB.001_R1 [DIRS 182602]
IPC_CSNF_pH_Rsw_2_I_LUT	Same as above	Lookup Table (2D)	Necessary for calculating more realistic pH values inside a waste package	Corroborative DTN: SN0704PMAIPCAB.001_R1 [DIRS 182602]
IPC_CSNF_pH_Rsw_3_A_LUT	Same as above	Lookup Table (2D)	Necessary for calculating more realistic pH values inside a waste package	Corroborative DTN: SN0704PMAIPCAB.001_R1 [DIRS 182602]
IPC_CSNF_pH_Rsw_3_B_LUT	Same as above	Lookup Table (2D)	Necessary for calculating more realistic pH values inside a waste package	Corroborative DTN: SN0704PMAIPCAB.001_R1 [DIRS 182602]

Table C4-2. Input Parameters Added for the PMA (Continued)

Parameter Name	Description	Parameter Distribution	Rationale for Inclusion	Data Source
Waste Form Degradation and Mobilization (Continued)				
IPC_CSNF_pH_Rsw_3_C_LUT	Same as above	Lookup Table (2D)	Necessary for calculating more realistic pH values inside a waste package	Corroborative DTN: SN0704PMAIPCAB.001_R1 [DIRS 182602]
IPC_CSNF_pH_Rsw_3_D_LUT	Same as above	Lookup Table (2D)	Necessary for calculating more realistic pH values inside a waste package	Corroborative DTN: SN0704PMAIPCAB.001_R1 [DIRS 182602]
IPC_CSNF_pH_Rsw_3_E_LUT	Same as above	Lookup Table (2D)	Necessary for calculating more realistic pH values inside a waste package	Corroborative DTN: SN0704PMAIPCAB.001_R1 [DIRS 182602]
IPC_CSNF_pH_Rsw_3_F_LUT	Same as above	Lookup Table (2D)	Necessary for calculating more realistic pH values inside a waste package	Corroborative DTN: SN0704PMAIPCAB.001_R1 [DIRS 182602]
IPC_CSNF_pH_Rsw_3_G_LUT	Same as above	Lookup Table (2D)	Necessary for calculating more realistic pH values inside a waste package	Corroborative DTN: SN0704PMAIPCAB.001_R1 [DIRS 182602]
IPC_CSNF_pH_Rsw_3_H_LUT	Same as above	Lookup Table (2D)	Necessary for calculating more realistic pH values inside a waste package	Corroborative DTN: SN0704PMAIPCAB.001_R1 [DIRS 182602]
IPC_CSNF_pH_Rsw_3_I_LUT	Same as above	Lookup Table (2D)	Necessary for calculating more realistic pH values inside a waste package	Corroborative DTN: SN0704PMAIPCAB.001_R1 [DIRS 182602]
IPC_CSNF_pH_Rsw_4_A_LUT	Same as above	Lookup Table (2D)	Necessary for calculating more realistic pH values inside a waste package	Corroborative DTN: SN0704PMAIPCAB.001_R1 [DIRS 182602]
IPC_CSNF_pH_Rsw_4_B_LUT	Same as above	Lookup Table (2D)	Necessary for calculating more realistic pH values inside a waste package	Corroborative DTN: SN0704PMAIPCAB.001_R1 [DIRS 182602]
IPC_CSNF_pH_Rsw_4_C_LUT	Same as above	Lookup Table (2D)	Necessary for calculating more realistic pH values inside a waste package	Corroborative DTN: SN0704PMAIPCAB.001_R1 [DIRS 182602]
IPC_CSNF_pH_Rsw_4_D_LUT	Same as above	Lookup Table (2D)	Necessary for calculating more realistic pH values inside a waste package	Corroborative DTN: SN0704PMAIPCAB.001_R1 [DIRS 182602]

Table C4-2. Input Parameters Added for the PMA (Continued)

Parameter Name	Description	Parameter Distribution	Rationale for Inclusion	Data Source
Waste Form Degradation and Mobilization (Continued)				
IPC_CSNF_pH_Rsw_4_E_LUT	Same as above	Lookup Table (2D)	Necessary for calculating more realistic pH values inside a waste package	Corroborative DTN: SN0704PMAIPCAB.001_R1 [DIRS 182602]
IPC_CSNF_pH_Rsw_4_F_LUT	Same as above	Lookup Table (2D)	Necessary for calculating more realistic pH values inside a waste package	Corroborative DTN: SN0704PMAIPCAB.001_R1 [DIRS 182602]
IPC_CSNF_pH_Rsw_4_G_LUT	Same as above	Lookup Table (2D)	Necessary for calculating more realistic pH values inside a waste package	Corroborative DTN: SN0704PMAIPCAB.001_R1 [DIRS 182602]
IPC_CSNF_pH_Rsw_4_H_LUT	Same as above	Lookup Table (2D)	Necessary for calculating more realistic pH values inside a waste package	Corroborative DTN: SN0704PMAIPCAB.001_R1 [DIRS 182602]
IPC_CSNF_pH_Rsw_4_I_LUT	Same as above	Lookup Table (2D)	Necessary for calculating more realistic pH values inside a waste package	Corroborative DTN: SN0704PMAIPCAB.001_R1 [DIRS 182602]
IPC_DHLW_Rsw_Thresh_A	Log Rsw threshold value provides input to the DHLW pH routine.	Single Value, -2.0	Necessary for calculating more realistic pH values inside a waste package	Corroborative DTN: SN0704PMAIPCAB.001_R1 [DIRS 182602]
IPC_DHLW_Rsw_Thresh_B	Log Rsw threshold value provides input to the DHLW pH routine.	Single Value, -1.0	Necessary for calculating more realistic pH values inside a waste package	Corroborative DTN: SN0704PMAIPCAB.001_R1 [DIRS 182602]
IPC_DHLW_Rsw_Thresh_C	Log Rsw threshold value provides input to the DHLW pH routine.	Single Value, 0	Necessary for calculating more realistic pH values inside a waste package	Corroborative DTN: SN0704PMAIPCAB.001_R1 [DIRS 182602]
IPC_DHLW_Rsw_Thresh_D	Log Rsw threshold value provides input to the DHLW pH routine.	Single Value, 1	Necessary for calculating more realistic pH values inside a waste package	Corroborative DTN: SN0704PMAIPCAB.001_R1 [DIRS 182602]
IPC_DHLW_Rsw_Thresh_E	Log Rsw threshold value provides input to the DHLW pH routine.	Single Value, 1.39794000867204	Necessary for calculating more realistic pH values inside a waste package	Corroborative DTN: SN0704PMAIPCAB.001_R1 [DIRS 182602]
IPC_DHLW_Rsw_Thresh_F	Log Rsw threshold value provides input to the DHLW pH routine.	Single Value, 1.6989700043	Necessary for calculating more realistic pH values inside a waste package	Corroborative DTN: SN0704PMAIPCAB.001_R1 [DIRS 182602]

Table C4-2. Input Parameters Added for the PMA (Continued)

Parameter Name	Description	Parameter Distribution	Rationale for Inclusion	Data Source
Waste Form Degradation and Mobilization (Continued)				
IPC_DHLW _Rsw_Thresh_G	Log Rsw threshold value provides input to the DHLW pH routine.	Single Value, 1.8750612634	Necessary for calculating more realistic pH values inside a waste package	Corroborative DTN: SN0704PMAIPCAB.001_R1 [DIRS 182602]
IPC_DHLW _Rsw_Thresh_H	Log Rsw threshold value provides input to the DHLW pH routine.	Single Value, 2	Necessary for calculating more realistic pH values inside a waste package	Corroborative DTN: SN0704PMAIPCAB.001_R1 [DIRS 182602]
IPC_DHLW _Rsw_Thresh_I	Log Rsw threshold value provides input to the DHLW pH routine.	Single Value, 3	Necessary for calculating more realistic pH values inside a waste package	Corroborative DTN: SN0704PMAIPCAB.001_R1 [DIRS 182602]
IPC_DHLW_pH_Rsw_15_A _LUT	LUT for 2DHLW pH	Lookup Table (2D)	Necessary for calculating more realistic pH values inside a waste package	Corroborative DTN: SN0704PMAIPCAB.001_R1 [DIRS 182602]
IPC_DHLW_pH_Rsw_15_B _LUT	Same as above	Lookup Table (2D)	Necessary for calculating more realistic pH values inside a waste package	Corroborative DTN: SN0704PMAIPCAB.001_R1 [DIRS 182602]
IPC_DHLW_pH_Rsw_15_ C_LUT	Same as above	Lookup Table (2D)	Necessary for calculating more realistic pH values inside a waste package	Corroborative DTN: SN0704PMAIPCAB.001_R1 [DIRS 182602]
IPC_DHLW_pH_Rsw_15_ D_LUT	Same as above	Lookup Table (2D)	Necessary for calculating more realistic pH values inside a waste package	Corroborative DTN: SN0704PMAIPCAB.001_R1 [DIRS 182602]
IPC_DHLW_pH_Rsw_15_E _LUT	Same as above	Lookup Table (2D)	Necessary for calculating more realistic pH values inside a waste package	Corroborative DTN: SN0704PMAIPCAB.001_R1 [DIRS 182602]
IPC_DHLW_pH_Rsw_15_F _LUT	Same as above	Lookup Table (2D)	Necessary for calculating more realistic pH values inside a waste package	Corroborative DTN: SN0704PMAIPCAB.001_R1 [DIRS 182602]
IPC_DHLW_pH_Rsw_15_ G_LUT	Same as above	Lookup Table (2D)	Necessary for calculating more realistic pH values inside a waste package	Corroborative DTN: SN0704PMAIPCAB.001_R1 [DIRS 182602]
IPC_DHLW_pH_Rsw_15_ H_LUT	Same as above	Lookup Table (2D)	Necessary for calculating more realistic pH values inside a waste package	Corroborative DTN: SN0704PMAIPCAB.001_R1 [DIRS 182602]

Table C4-2. Input Parameters Added for the PMA (Continued)

Parameter Name	Description	Parameter Distribution	Rationale for Inclusion	Data Source
Waste Form Degradation and Mobilization (Continued)				
IPC_DHLW_pH_Rsw_15_I_LUT	Same as above	Lookup Table (2D)	Necessary for calculating more realistic pH values inside a waste package	Corroborative DTN: SN0704PMAIPCAB.001_R1 [DIRS 182602]
IPC_DHLW_pH_Rsw_2_A_LUT	Same as above	Lookup Table (2D)	Necessary for calculating more realistic pH values inside a waste package	Corroborative DTN: SN0704PMAIPCAB.001_R1 [DIRS 182602]
IPC_DHLW_pH_Rsw_2_B_LUT	Same as above	Lookup Table (2D)	Necessary for calculating more realistic pH values inside a waste package	Corroborative DTN: SN0704PMAIPCAB.001_R1 [DIRS 182602]
IPC_DHLW_pH_Rsw_2_C_LUT	Same as above	Lookup Table (2D)	Necessary for calculating more realistic pH values inside a waste package	Corroborative DTN: SN0704PMAIPCAB.001_R1 [DIRS 182602]
IPC_DHLW_pH_Rsw_2_D_LUT	Same as above	Lookup Table (2D)	Necessary for calculating more realistic pH values inside a waste package	Corroborative DTN: SN0704PMAIPCAB.001_R1 [DIRS 182602]
IPC_DHLW_pH_Rsw_2_E_LUT	Same as above	Lookup Table (2D)	Necessary for calculating more realistic pH values inside a waste package	Corroborative DTN: SN0704PMAIPCAB.001_R1 [DIRS 182602]
IPC_DHLW_pH_Rsw_2_F_LUT	Same as above	Lookup Table (2D)	Necessary for calculating more realistic pH values inside a waste package	Corroborative DTN: SN0704PMAIPCAB.001_R1 [DIRS 182602]
IPC_DHLW_pH_Rsw_2_G_LUT	Same as above	Lookup Table (2D)	Necessary for calculating more realistic pH values inside a waste package	Corroborative DTN: SN0704PMAIPCAB.001_R1 [DIRS 182602]
IPC_DHLW_pH_Rsw_2_H_LUT	Same as above	Lookup Table (2D)	Necessary for calculating more realistic pH values inside a waste package	Corroborative DTN: SN0704PMAIPCAB.001_R1 [DIRS 182602]
IPC_DHLW_pH_Rsw_2_I_LUT	Same as above	Lookup Table (2D)	Necessary for calculating more realistic pH values inside a waste package	Corroborative DTN: SN0704PMAIPCAB.001_R1 [DIRS 182602]
IPC_DHLW_pH_Rsw_3_A_LUT	Same as above	Lookup Table (2D)	Necessary for calculating more realistic pH values inside a waste package	Corroborative DTN: SN0704PMAIPCAB.001_R1 [DIRS 182602]

Table C4-2. Input Parameters Added for the PMA (Continued)

Parameter Name	Description	Parameter Distribution	Rationale for Inclusion	Data Source
Waste Form Degradation and Mobilization (Continued)				
IPC_DHLW_pH_Rsw_3_B_LUT	Same as above	Lookup Table (2D)	Necessary for calculating more realistic pH values inside a waste package	Corroborative DTN: SN0704PMAIPCAB.001_R1 [DIRS 182602]
IPC_DHLW_pH_Rsw_3_C_LUT	Same as above	Lookup Table (2D)	Necessary for calculating more realistic pH values inside a waste package	Corroborative DTN: SN0704PMAIPCAB.001_R1 [DIRS 182602]
IPC_DHLW_pH_Rsw_3_D_LUT	Same as above	Lookup Table (2D)	Necessary for calculating more realistic pH values inside a waste package	Corroborative DTN: SN0704PMAIPCAB.001_R1 [DIRS 182602]
IPC_DHLW_pH_Rsw_3_E_LUT	Same as above	Lookup Table (2D)	Necessary for calculating more realistic pH values inside a waste package	Corroborative DTN: SN0704PMAIPCAB.001_R1 [DIRS 182602]
IPC_DHLW_pH_Rsw_3_F_LUT	Same as above	Lookup Table (2D)	Necessary for calculating more realistic pH values inside a waste package	Corroborative DTN: SN0704PMAIPCAB.001_R1 [DIRS 182602]
IPC_DHLW_pH_Rsw_3_G_LUT	Same as above	Lookup Table (2D)	Necessary for calculating more realistic pH values inside a waste package	Corroborative DTN: SN0704PMAIPCAB.001_R1 [DIRS 182602]
IPC_DHLW_pH_Rsw_3_H_LUT	Same as above	Lookup Table (2D)	Necessary for calculating more realistic pH values inside a waste package	Corroborative DTN: SN0704PMAIPCAB.001_R1 [DIRS 182602]
IPC_DHLW_pH_Rsw_3_I_LUT	Same as above	Lookup Table (2D)	Necessary for calculating more realistic pH values inside a waste package	Corroborative DTN: SN0704PMAIPCAB.001_R1 [DIRS 182602]
IPC_DHLW_pH_Rsw_4_A_LUT	Same as above	Lookup Table (2D)	Necessary for calculating more realistic pH values inside a waste package	Corroborative DTN: SN0704PMAIPCAB.001_R1 [DIRS 182602]
IPC_DHLW_pH_Rsw_4_B_LUT	Same as above	Lookup Table (2D)	Necessary for calculating more realistic pH values inside a waste package	Corroborative DTN: SN0704PMAIPCAB.001_R1 [DIRS 182602]
IPC_DHLW_pH_Rsw_4_C_LUT	Same as above	Lookup Table (2D)	Necessary for calculating more realistic pH values inside a waste package	Corroborative DTN: SN0704PMAIPCAB.001_R1 [DIRS 182602]

Table C4-2. Input Parameters Added for the PMA (Continued)

Parameter Name	Description	Parameter Distribution	Rationale for Inclusion	Data Source
Waste Form Degradation and Mobilization (Continued)				
IPC_DHLW_pH_Rsw_4_D_LUT	Same as above	Lookup Table (2D)	Necessary for calculating more realistic pH values inside a waste package	Corroborative DTN: SN0704PMAIPCAB.001_R1 [DIRS 182602]
IPC_DHLW_pH_Rsw_4_E_LUT	Same as above	Lookup Table (2D)	Necessary for calculating more realistic pH values inside a waste package	Corroborative DTN: SN0704PMAIPCAB.001_R1 [DIRS 182602]
IPC_DHLW_pH_Rsw_4_F_LUT	Same as above	Lookup Table (2D)	Necessary for calculating more realistic pH values inside a waste package	Corroborative DTN: SN0704PMAIPCAB.001_R1 [DIRS 182602]
IPC_DHLW_pH_Rsw_4_G_LUT	Same as above	Lookup Table (2D)	Necessary for calculating more realistic pH values inside a waste package	Corroborative DTN: SN0704PMAIPCAB.001_R1 [DIRS 182602]
IPC_DHLW_pH_Rsw_4_H_LUT	Same as above	Lookup Table (2D)	Necessary for calculating more realistic pH values inside a waste package	Corroborative DTN: SN0704PMAIPCAB.001_R1 [DIRS 182602]
IPC_DHLW_pH_Rsw_4_I_LUT	Same as above	Lookup Table (2D)	Necessary for calculating more realistic pH values inside a waste package	Corroborative DTN: SN0704PMAIPCAB.001_R1 [DIRS 182602]
IPC_MCO_Rsw_Thresh_A	Log Rsw threshold value provides input to the MCO pH routine.	Single Value, -7.0	Necessary for calculating more realistic pH values inside a waste package	Corroborative DTN: SN0704PMAIPCAB.001_R1 [DIRS 182602]
IPC_MCO _Rsw_Thresh_B	Log Rsw threshold value provides input to the MCO pH routine.	Single Value, -6.0	Necessary for calculating more realistic pH values inside a waste package	Corroborative DTN: SN0704PMAIPCAB.001_R1 [DIRS 182602]
IPC_MCO _Rsw_Thresh_C	Log Rsw threshold value provides input to the MCO pH routine.	Single Value, -4.0	Necessary for calculating more realistic pH values inside a waste package	Corroborative DTN: SN0704PMAIPCAB.001_R1 [DIRS 182602]
IPC_MCO _Rsw_Thresh_D	Log Rsw threshold value provides input to the MCO pH routine.	Single Value, -2.0	Necessary for calculating more realistic pH values inside a waste package	Corroborative DTN: SN0704PMAIPCAB.001_R1 [DIRS 182602]
IPC_MCO_pH_Rsw_15_A_LUT	LUT for 2MCO pH	Lookup Table (2D)	Necessary for calculating more realistic pH values inside a waste package	Corroborative DTN: SN0704PMAIPCAB.001_R1 [DIRS 182602]

Table C4-2. Input Parameters Added for the PMA (Continued)

Parameter Name	Description	Parameter Distribution	Rationale for Inclusion	Data Source
Waste Form Degradation and Mobilization (Continued)				
IPC_MCO_pH_Rsw_15_B_LUT	Same as above	Lookup Table (2D)	Necessary for calculating more realistic pH values inside a waste package	Corroborative DTN: SN0704PMAIPCAB.001_R1 [DIRS 182602]
IPC_MCO_pH_Rsw_15_C_LUT	Same as above	Lookup Table (2D)	Necessary for calculating more realistic pH values inside a waste package	Corroborative DTN: SN0704PMAIPCAB.001_R1 [DIRS 182602]
IPC_MCO_pH_Rsw_15_D_LUT	Same as above	Lookup Table (2D)	Necessary for calculating more realistic pH values inside a waste package	Corroborative DTN: SN0704PMAIPCAB.001_R1 [DIRS 182602]
IPC_MCO_pH_Rsw_2_A_LUT	Same as above	Lookup Table (2D)	Necessary for calculating more realistic pH values inside a waste package	Corroborative DTN: SN0704PMAIPCAB.001_R1 [DIRS 182602]
IPC_MCO_pH_Rsw_2_B_LUT	Same as above	Lookup Table (2D)	Necessary for calculating more realistic pH values inside a waste package	Corroborative DTN: SN0704PMAIPCAB.001_R1 [DIRS 182602]
IPC_MCO_pH_Rsw_2_C_LUT	Same as above	Lookup Table (2D)	Necessary for calculating more realistic pH values inside a waste package	Corroborative DTN: SN0704PMAIPCAB.001_R1 [DIRS 182602]
IPC_MCO_pH_Rsw_2_D_LUT	Same as above	Lookup Table (2D)	Necessary for calculating more realistic pH values inside a waste package	Corroborative DTN: SN0704PMAIPCAB.001_R1 [DIRS 182602]
IPC_MCO_pH_Rsw_3_A_LUT	Same as above	Lookup Table (2D)	Necessary for calculating more realistic pH values inside a waste package	Corroborative DTN: SN0704PMAIPCAB.001_R1 [DIRS 182602]
IPC_MCO_pH_Rsw_3_B_LUT	Same as above	Lookup Table (2D)	Necessary for calculating more realistic pH values inside a waste package	Corroborative DTN: SN0704PMAIPCAB.001_R1 [DIRS 182602]
IPC_MCO_pH_Rsw_3_C_LUT	Same as above	Lookup Table (2D)	Necessary for calculating more realistic pH values inside a waste package	Corroborative DTN: SN0704PMAIPCAB.001_R1 [DIRS 182602]
IPC_MCO_pH_Rsw_3_D_LUT	Same as above	Lookup Table (2D)	Necessary for calculating more realistic pH values inside a waste package	Corroborative DTN: SN0704PMAIPCAB.001_R1 [DIRS 182602]

Table C4-2. Input Parameters Added for the PMA (Continued)

Parameter Name	Description	Parameter Distribution	Rationale for Inclusion	Data Source
Waste Form Degradation and Mobilization (Continued)				
IPC_MCO_pH_Rsw_4_A_LUT	Same as above	Lookup Table (2D)	Necessary for calculating more realistic pH values inside a waste package	Corroborative DTN: SN0704PMAIPCAB.001_R1 [DIRS 182602]
IPC_MCO_pH_Rsw_4_B_LUT	Same as above	Lookup Table (2D)	Necessary for calculating more realistic pH values inside a waste package	Corroborative DTN: SN0704PMAIPCAB.001_R1 [DIRS 182602]
IPC_MCO_pH_Rsw_4_C_LUT	Same as above	Lookup Table (2D)	Necessary for calculating more realistic pH values inside a waste package	Corroborative DTN: SN0704PMAIPCAB.001_R1 [DIRS 182602]
IPC_MCO_pH_Rsw_4_D_LUT	Same as above	Lookup Table (2D)	Necessary for calculating more realistic pH values inside a waste package	Corroborative DTN: SN0704PMAIPCAB.001_R1 [DIRS 182602]
IPC_Read_pH_Column_2DHLW	Input value to direct GoldSim to read the pH column of the IPC pH lookup tables	Single Value, 2.0	Necessary for calculating more realistic pH values inside a waste package	Corroborative DTN: SN0704PMAIPCAB.001_R1 [DIRS 182602]
IPC_Read_pH_Column_2MCO	Input value to direct GoldSim to read the pH column of the IPC pH lookup tables	Single Value, 2.0	Necessary for calculating more realistic pH values inside a waste package	Corroborative DTN: SN0704PMAIPCAB.001_R1 [DIRS 182602]
IPC_Read_pH_Column_CSNF	Input value to direct GoldSim to read the pH column of the IPC pH lookup tables	Single Value, 2.0	Necessary for calculating more realistic pH values inside a waste package	Corroborative DTN: SN0704PMAIPCAB.001_R1 [DIRS 182602]
Unsaturated Zone Transport				
kdet	Detachment rate constant used for Colloid Diversity Model. The median travel time τ is obtained from the Pu fast breakthrough curves. (Used in both the UZ and SZ transport models)	Log10 transformed triangular distribution defined by: log10(0.01/τ), log10(0.1/τ), log10(1/τ)]. τ is in hours.	The colloid retardation factor is a function of the detachment rate constant. The distribution is based on experimental data reported in DTN: LA0705PR150304.001 [DIRS 181744].	Corroborative DTN: SN0704PMASZFTA.001_R1 [DIRS 184395]
R_Min	Lower limit of the distribution used for the retardation coefficient	Constant - 2.0	Provides a more realistic distribution for colloid retardation factors in fractures	Corroborative DTN: MO0704PAUZFEHM.000_R0 [DIRS 182790]

Table C4-2. Input Parameters Added for the PMA (Continued)

Parameter Name	Description	Parameter Distribution	Rationale for Inclusion	Data Source
Unsaturated Zone Transport (Continued)				
Slope_m	Slope of the equation approximating the CDF of the filtration rate constant (Used in both the UZ and SZ transport models)	Lookup Table (1D): based on SZ PMA sampling of a triangular distribution with values [0.17, 0.31 51, and 0.85]	Provides a more realistic distribution for colloid retardation factors in fractures	Corroborative DTN: SN0704PMASZFTA.001_R1 [DIRS 184395]
Intercept_b	y-intercept of the equation approximating the CDF of the filtration rate constant	Constant – 0.2	Provides a more realistic distribution for colloid retardation factors in fractures	Corroborative DTN: MO0704PAUZFEHM.000_R 0 [DIRS 182790]
Water_Table_a	Water table elevation after change the Present Day climate ends	Cumulative Distribution: 0 750 0.05 755 0.1 760 0.25 770 0.5 780 0.7 790 0.9 830 0.95 840 1 850	Provides uncertainty to the degree of water table rise associated with climate changes	Section 6.6.1.2 Corroborative DTN: MO0704PAUZFEHM.000_R 0 [DIRS 182790]
ff2100.ini	FEHM external file containing the flow field data for the monsoonal climate 10th percentile infiltration case without water-table adjustment.	External File	Necessary for FEHM code to accurately track the RN species.	DTN: LB0701MOFEHMFF.001_R 0. [DIRS 179297]
ff2200.ini	FEHM external file containing the flow field data for the monsoonal climate 30th percentile infiltration case without water-table adjustment.	External File	Necessary for FEHM code to accurately track the RN species.	DTN: LB0701MOFEHMFF.001_R 0 [DIRS 179297]
ff2300.ini	FEHM external file containing the flow field data for the monsoonal climate 50th percentile infiltration case without water-table adjustment.	External File	Necessary for FEHM code to accurately track the RN species.	DTN: LB0701MOFEHMFF.001_R 0 [DIRS 179297]
ff2400.ini	FEHM external file containing the flow field data for the monsoonal climate 90th percentile infiltration case without	External File	Necessary for FEHM code to accurately track the RN species.	DTN: LB0701MOFEHMFF.001_R 0 [DIRS 179297]

Table C4-2. Input Parameters Added for the PMA (Continued)

Parameter Name	Description	Parameter Distribution	Rationale for Inclusion	Data Source
	water-table adjustment.			
Unsaturated Zone Transport (Continued)				
ff3100.ini	FEHM external file containing the flow field data for the glacial climate 10th percentile infiltration case without water-table adjustment.	External File	Necessary for FEHM code to accurately track the RN species.	DTN: LB0701GTFEHMFF.001_R0 [DIRS 179160]
ff3200.ini	FEHM external file containing the flow field data for the glacial climate 30th percentile infiltration case without water-table adjustment.	External File	Necessary for FEHM code to accurately track the RN species.	DTN: LB0701GTFEHMFF.001_R0 [DIRS 179160]
ff3300.ini	FEHM external file containing the flow field data for the glacial climate 50th percentile infiltration case without water-table adjustment.	External File	Necessary for FEHM code to accurately track the RN species.	DTN: LB0701GTFEHMFF.001_R0 [DIRS 179160]
ff3400.ini	FEHM external file containing the flow field data for the glacial climate 90th percentile infiltration case without water-table adjustment.	External File	Necessary for FEHM code to accurately track the RN species.	DTN: LB0701GTFEHMFF.001_R0 [DIRS 179160]
ff4100.ini	FEHM external file containing the flow field data for the 4th climate 10th percentile infiltration case without water-table adjustment.	External File	Necessary for FEHM code to accurately track the RN species.	DTN: LB0701PAFEM10K.002_R0 [DIRS 179507]
ff4200.ini	FEHM external file containing the flow field data for the 4th climate 30th percentile infiltration case without water-table adjustment.	External File	Necessary for FEHM code to accurately track the RN species.	DTN: LB0701PAFEM10K.002_R0 [DIRS 179507]
ff4300.ini	FEHM external file containing the flow field data for the 4th climate 50th percentile infiltration case without water-table adjustment.	External File	Necessary for FEHM code to accurately track the RN species.	DTN: LB0701PAFEM10K.002_R0 [DIRS 179507]
ff4400.ini	FEHM external file containing the flow field data for the 4th climate 90th percentile infiltration case without water-table adjustment.	External File	Necessary for FEHM code to accurately track the RN species.	DTN: LB0701PAFEM10K.002_R0 [DIRS 179507]
fehmn.gold	GoldSim/FEHM external interface control file containing length of input array used to pass data from GoldSim	External File	Necessary for FEHM code to accurately track the RN species.	Corroborative DTN: MO0708TSPAPROC.000_R0 [DIRS 182979]

Table C4-2. Input Parameters Added for the PMA (Continued)

Parameter Name	Description	Parameter Distribution	Rationale for Inclusion	Data Source
	to FEHM.			
Unsaturated Zone Transport (Continued)				
UZ_Params_Multi_PMA_21_300rlz	FEHM stochastic external file for PMA. 300 rlzs, random seed 1, Colloid Diversity model 2, Interface Area 1.	External File	Necessary for FEHM code to accurately track the RN species.	Corroborative DTN: MO0708TSPAPROC.000_R0 [DIRS 182979]
fehm_PMA_10kyr.mptr	FEHM external file containing the control data, physical params., and chemical params. for multiple-species ingrowth particle tracking in 10,000 yr. non-igneous simulations. The file contains pointer indices for sampled params.	External File	Necessary for FEHM code to accurately track the RN species.	Corroborative DTN: MO0708TSPAPROC.000_R0 [DIRS 182979]
fehm_PMA_10kyr_ef_cdsp.mptr	FEHM external file containing the control data, physical params., and chemical params. for multiple-species ingrowth particle tracking in 10 kyr. non-igneous simulations. The file contains pointer indices for sampled params.	External File	Necessary for FEHM code to accurately track the RN species.	Corroborative DTN: MO0708TSPAPROC.000_R0 [DIRS 182979]
fehm_PMA_10kyr_ef_csnf.mptr	FEHM external file containing the control data, physical params., and chemical params. for multiple-species ingrowth particle tracking in 10 kyr. non-igneous simulations. The file contains pointer indices for sampled params.	External File	Necessary for FEHM code to accurately track the RN species.	Corroborative DTN: MO0708TSPAPROC.000_R0 [DIRS 182979]
fehm_PMA_10kyr_lgn.mptr	FEHM external file containing the control data, physical params., and chemical params. for multiple-species ingrowth particle tracking in 10,000 yr. igneous simulations. The file contains pointer indices for sampled params.	External File	Necessary for FEHM code to accurately track the RN species.	Corroborative DTN: MO0708TSPAPROC.000_R0 [DIRS 182979]
fehm_PMA_10kyr_lgn_ni.mptr	FEHM ext. file containing the control data, physical params., and chemical params. for multiple-species ingrowth particle tracking in 10,000 yr. igneous simulations. The file contains ptr indices for sampled params (no irreversibles).	External File	Necessary for FEHM code to accurately track the RN species.	Corroborative DTN: MO0708TSPAPROC.000_R0 [DIRS 182979]

Table C4-2. Input Parameters Added for the PMA (Continued)

Parameter Name	Description	Parameter Distribution	Rationale for Inclusion	Data Source
Unsaturated Zone Transport (Continued)				
fehm_PMA_10kyr_ni.mptr	FEHM ext. file containing the control data, physical params., and chemical params. for multiple-species ingrowth particle tracking in 10,000 yr. simulations. The file contains ptr indices for sampled params (no irreversibles).	External File	Necessary for FEHM code to accurately track the RN species.	Corroborative DTN: MO0708TSPAPROC.000_R 0 [DIRS 182979]
fehm_PMA_1Myr.mptr	FEHM external file containing the control data, physical params., and chemical params. for multiple-species ingrowth particle tracking in one million yr. non-igneous simulations. The file contains pointer indices for sampled params.	External File	Necessary for FEHM code to accurately track the RN species.	Corroborative DTN: MO0708TSPAPROC.000_R 0 [DIRS 182979]
fehm_PMA_1Myr_ef_cdsp. mptr	FEHM external file containing the control data, physical params., and chemical params. for multiple-species ingrowth particle tracking in one million yr. non-igneous simulations. The file contains pointer indices for sampled params.	External File	Necessary for FEHM code to accurately track the RN species.	Corroborative DTN: MO0708TSPAPROC.000_R 0 [DIRS 182979]
fehm_PMA_1Myr_ef_csnf. mptr	FEHM external file containing the control data, physical params., and chemical params. for multiple-species ingrowth particle tracking in one million yr. non-igneous simulations. The file contains pointer indices for sampled params.	External File	Necessary for FEHM code to accurately track the RN species.	Corroborative DTN: MO0708TSPAPROC.000_R 0 [DIRS 182979]
fehm_PMA_1Myr_lgn.mptr	FEHM external file containing the control data, physical params., and chemical params. for multiple-species ingrowth particle tracking in one million yr. igneous simulations. The file contains pointer indices for sampled params.	External File	Necessary for FEHM code to accurately track the RN species.	Corroborative DTN: MO0708TSPAPROC.000_R 0 [DIRS 182979]

Table C4-2. Input Parameters Added for the PMA (Continued)

Parameter Name	Description	Parameter Distribution	Rationale for Inclusion	Data Source
Unsaturated Zone Transport (Continued)				
fehm_PMA_1Myr_lgn_ni.mptr	FEHM ext. file containing the control data, physical params., and chemical params. for multiple-species ingrowth particle tracking in 1M yr. igneous simulations. The file contains ptr indices for sampled params (no irreversibles).	External File	Necessary for FEHM code to accurately track the RN species.	Corroborative DTN: MO0708TSPAPROC.000_R0 [DIRS 182979]
fehm_PMA_1Myr_ni.mptr	FEHM ext. file containing the control data, physical params., and chemical params. for multiple-species ingrowth particle tracking in 1M yr. simulations. The file contains ptr indices for sampled params (no irreversibles).	External File	Necessary for FEHM code to accurately track the RN species.	Corroborative DTN: MO0708TSPAPROC.000_R0 [DIRS 182979]
fehm_PMA_gs_1Myr.dat	UZ Transport: FEHM external file containing the general control data needed for the one million yr. simulations.	External File	Necessary for FEHM code to accurately track the RN species.	Corroborative DTN: MO0708TSPAPROC.000_R0 [DIRS 182979]
fehm_PMA_gs_20kyr.dat	FEHM external file containing the general control data needed for the 10,000/20,000 yr. simulations.	External File	Necessary for FEHM code to accurately track the RN species.	Corroborative DTN: MO0708TSPAPROC.000_R0 [DIRS 182979]
fehmn.files	FEHM external file containing names of major input and output files used in a simulation.	External File	Necessary for FEHM code to accurately track the RN species.	Corroborative DTN: MO0708TSPAPROC.000_R0 [DIRS 182979]
fehm_TSPA_10kyr.mptr	FEHM external file containing the control data, physical params., and chemical params. for multiple-species ingrowth particle tracking in 10,000 yr. non-igneous simulations. The file contains pointer indices for sampled params.	External File	Slight adjustment from the TSPA-LA compliance file to include reference the expanded file list used for PMA	Corroborative DTN: MO0708TSPAPROC.000_R0 [DIRS 182979]
fehm_TSPA_1Myr.mptr	Same as above for 1,000,000 year simulations.	External File	Same as above	Corroborative DTN: MO0708TSPAPROC.000_R0 [DIRS 182979]
fehm_TSPA_10kyr_ign.mptr	Same as fehm_TSPA_10kyr.mptr adjusted for the igneous simulations	External File	Same as above	Corroborative DTN: MO0708TSPAPROC.000_R0 [DIRS 182979]

Table C4-2. Input Parameters Added for the PMA (Continued)

Parameter Name	Description	Parameter Distribution	Rationale for Inclusion	Data Source
Unsaturated Zone Transport (Continued)				
fehm_TSPA_1Myr_ign.mptr	Same as fehm_TSPA_1Myr.mptr adjusted for the igneous simulations	External File	Same as above	Corroborative DTN: MO0708TSPAPROC.000_R0 [DIRS 182979]
fehm_TSPA_10kyr_ef_cdsp.mptr	FEHM external file containing the control data, physical params., and chemical params. for multiple-species ingrowth particle tracking in 10 kyr.early failure simulations. The file contains pointer indices for sampled params.	External File	Same as above	Corroborative DTN: MO0708TSPAPROC.000_R0 [DIRS 182979]
fehm_TSPA_10kyr_ef_csnf.mptr	Same as above for CSNF WPs.	External File	Same as above	Corroborative DTN: MO0708TSPAPROC.000_R0 [DIRS 182979]
fehm_TSPA_1Myr_ef_cdsp.mptr	Same as above for 1 million year simulations and CDSP WPs.	External File	Same as above	Corroborative DTN: MO0708TSPAPROC.000_R0 [DIRS 182979]
fehm_TSPA_1Myr_ef_csnf.mptr	Same as above for CSNF WPs.	External File	Same as above	Corroborative DTN: MO0708TSPAPROC.000_R0 [DIRS 182979]
SZ Flow and Transport Parameters				
SZ_Block_Length	Block length for matrix diffusion from UZ to SZ	250 m (constant)	The parameter value is the horizontal grid dimension of the saturated zone flow and transport model.	Corroborative DTN: SN0704PMASZFTA.001_R1 [DIRS 184395]
SZ_Block_Thickness	Block thickness for matrix diffusion from UZ to SZ	10 m (constant)	The parameter value reflects the thickness of the top most layer in the SZ below the water table.	Corroborative DTN: SN0704PMASZFTA.001_R1 [DIRS 184395]
kdet	Detachment rate constant used for Colloid Diversity Model. The median travel time τ is obtained from the Pu fast breakthrough curves. (Used in both the UZ and SZ transport models)	Log10 transformed triangular distribution defined by: log10(0.01/τ), log10(0.1/τ), log10(1/τ)]. τ is in hours.	The colloid retardation factor is a function of the detachment rate constant. The distribution is based on experimental data reported in DTN: LA0705PR150304.001 [DIRS 181744].	Corroborative DTN: SN0704PMASZFTA.001_R1 [DIRS 184395]

Table C4-2. Input Parameters Added for the PMA (Continued)

Parameter Name	Description	Parameter Distribution	Rationale for Inclusion	Data Source
SZ Flow and Transport Parameters (Continued)				
Slope_m	Slope of filtration rate constant vs. travel time plot used for the Colloid Diversity Model. (Used in both the UZ and SZ transport models)	Lookup Table (1D)	The colloid retardation factor is a function of the slope of filtration rate constant vs. travel time plot. The distribution is based on experimental data reported in DTN: LA0705PR150304.001 [DIRS 181744].	Corroborative DTN: SN0704PMASZFTA.001_R1 [DIRS 184395]
Intercept_b	Y-intercept of filtration rate constant vs. travel time plot used for the Colloid Diversity Model.	0.2 (constant)	The colloid retardation factor is a function of the intercept of filtration rate constant vs. travel time plot. The distribution is based on experimental data reported in DTN: LA0705PR150304.001 [DIRS 181744].	Corroborative DTN: SN0704PMASZFTA.001_R1 [DIRS 184395]
Rf1 to Rf10	Colloid retardation factors for the Colloid Diversity Model	Table	The parameter values are computed based on the Colloid Diversity Model.	Corroborative DTN: SN0704PMASZFTA.001_R1 [DIRS 184395]
Rl	Lower bound retardation factor used to calculate the minimum probability value for the Colloid Diversity Model.	2.0 (constant)	The lower bound retardation factor was set based on observations of experimental data.	Corroborative DTN: SN0704PMASZFTA.001 [DIRS 184395]
Kd_Tc_RZ	Sorption coefficient for technetium in the reducing zone	Lookup Table (1D)	Technetium sorption coefficient representing areas with reducing conditions. Sorption distribution based on Lieser and Bauscher (1988 [DIRS 172722]).	Corroborative DTN: SN0704PMASZFTA.001_R1 [DIRS 184395]

Table C4-2. Input Parameters Added for the PMA (Continued)

Parameter Name	Description	Parameter Distribution	Rationale for Inclusion	Data Source
SZ Flow and Transport Parameters (Continued)				
KD_Np_RZ	Sorption coefficient for neptunium in the reducing zone	Lookup Table (1D)	Technetium sorption coefficient representing areas with reducing conditions. Sorption distribution based on Lieser and Muhlenweg (1988 [DIRS 106684]).	Corroborative DTN: SN0704PMASZFTA.001_R1 [DIRS 184395]
FPLRZN	Factor for Northern reducing zone boundary	Lookup Table (1D)	Parameter used as a multiplying factor to the ranges given in meters in defining the northern boundaries of the reducing zone for each realization. Dimensions based on BSC (2006 [DIRS 178672]).	Corroborative DTN: SN0704PMASZFTA.001_R1 [DIRS 184395]
FPLRZS	Factor for Southern reducing zone boundary	Lookup Table (1D)	Parameter used as a multiplying factor to the ranges given in meters in defining the southern boundaries of the reducing zone for each realization (BSC 2006 [DIRS 178672]).	Corroborative DTN: SN0704PMASZFTA.001_R1 [DIRS 184395]
FPLRZE	Factor for Eastern reducing zone boundary	Lookup Table (1D)	Parameter used as a multiplying factor to the ranges given in meters in defining the eastern boundaries of the reducing zone for each realization (BSC 2006 [DIRS 178672]).	Corroborative DTN: SN0704PMASZFTA.001_R1 [DIRS 184395]
FPVO_PMA	Flowing interval porosity A	Table	Parameter used for the flowing interval porosity in the Saturated Zone transport model	Corroborative DTN: SN0704PMASZFTA.001_R1 [DIRS 184395]

Table C4-2. Input Parameters Added for the PMA (Continued)

Parameter Name	Description	Parameter Distribution	Rationale for Inclusion	Data Source
SZ Flow and Transport Parameters (Continued)				
RZ_Pipe_Length_Data	Pipe length data for the SZ 1-D transport	Table	Estimation of the reducing zone length for the 1-D SZ transport model based on particle tracking data analysis and the rectangular dimensions of the reducing zone.	Corroborative DTN: SN0704PMASZFTA.001_R 1 [DIRS 184395]
SZ_13_01 to SZ_13_04	SZ, Breakthrough Curves, C,Tc, I, SR1, SR2, SR3, and SR4	File	Breakthrough curves for the SZ PMA model	Corroborative DTN: SN0704PMASZFTA.001_R 1 [DIRS 184395]
SZ_14_01 to SZ_14_04	SZ, Breakthrough Curves, Am, Th, Pa SR1, SR2, SR3, and SR4	File	Breakthrough curves for the SZ PMA model	Corroborative DTN: SN0704PMASZFTA.001_R 1 [DIRS 184395]
SZ_15_01 to SZ_15_04	SZ, Breakthrough Curves, Cs, SR1, SR2, SR3, and SR4	File	Breakthrough curves for the SZ PMA model	Corroborative DTN: SN0704PMASZFTA.001_R 1 [DIRS 184395]
SZ_16_01 to SZ_16_04	SZ, Breakthrough Curves, Pu, SR1, SR2, SR3, and SR4	File	Breakthrough curves for the SZ PMA model	Corroborative DTN: SN0704PMASZFTA.001_R 1 [DIRS 184395]
SZ_17_01 to SZ_17_04	SZ, Breakthrough Curves, Np, SR1, SR2, SR3, and SR4	File	Breakthrough curves for the SZ PMA model	Corroborative DTN: SN0704PMASZFTA.001_R 1 [DIRS 184395]
SZ_18_01 to SZ_18_04	SZ, Breakthrough Curves, IcPu, IcAm SR1, SR2, SR3, and SR4	File	Breakthrough curves for the SZ PMA model	Corroborative DTN: SN0704PMASZFTA.001_R 1 [DIRS 184395]
SZ_19_01 to SZ_19_04	SZ, Breakthrough Curves, Ra, SR1, SR2, SR3, and SR4	File	Breakthrough curves for the SZ PMA model	Corroborative DTN: SN0704PMASZFTA.001_R 1 [DIRS 184395]
SZ_20_01 to SZ_20_04	SZ, Breakthrough Curves, Sr, SR1, SR2, SR3, and SR4	File	Breakthrough curves for the SZ PMA model	Corroborative DTN: SN0704PMASZFTA.001_R 1 [DIRS 184395]
SZ_21_01 to SZ_21_04	SZ, Breakthrough Curves, U, SR1, SR2, SR3, and SR4	File	Breakthrough curves for the SZ PMA model	Corroborative DTN: SN0704PMASZFTA.001_R 1 [DIRS 184395]

Table C4-2. Input Parameters Added for the PMA (Continued)

Parameter Name	Description	Parameter Distribution	Rationale for Inclusion	Data Source
SZ Flow and Transport Parameters (Continued)				
SZ_22_01 to SZ_22_04	SZ, Breakthrough Curves, IfPu, IfAm, SR1, SR2, SR3, and SR4	File	Breakthrough curves for the SZ PMA model	Corroborative DTN: SN0704PMASZFTA.001_R1 [DIRS 184395]
SZ_23_01 to SZ_23_04	SZ, Breakthrough Curves, Se, SR1, SR2, SR3, and SR4	File	Breakthrough curves for the SZ PMA model	Corroborative DTN: SN0704PMASZFTA.001_R1 [DIRS 184395]
SZ_24_01 to SZ_24_04	SZ, Breakthrough Curves, Sn, SR1, SR2, SR3, and SR4	File	Breakthrough curves for the SZ PMA model	Corroborative DTN: SN0704PMASZFTA.001_R1 [DIRS 184395]
SZ_25_01 to SZ_25_04	SZ, Breakthrough Curves, Tc, SR1, SR2, SR3, and SR4	File	Breakthrough curves for the SZ PMA model	Corroborative DTN: SN0704PMASZFTA.001_R1 [DIRS 184395]
sz_convolute2_1Myr_pma.dat	SZ, Control file, 1,000,000 yr duration for PMA model	File	Input file for the SZ PMA model	Corroborative DTN: SN0704PMASZFTA.001_R1 [DIRS 184395]
sz_convolute2_20kyr_pma.dat	SZ, Control file, 20,000 yr duration for PMA model	File	Input file for the SZ PMA model	Corroborative DTN: SN0704PMASZFTA.001_R1 [DIRS 184395]
Seismic Scenario Parameters				
Stress_Thresh_A22_PMA_a	Distribution for residual stress threshold factor.	Uniform [100, 105]	Necessary to implement less conservative threshold for stress corrosion cracking	ANL-EBS-MD-000005 Rev 04 [DIRS 181953]
WP_Crack_Area_Density_PMA	Modified WP SCC crack density.	Constant Value [0.00327]	Value needed to implement alternative crack density model	ANL-EBS-MD-000005 Rev 04 [DIRS 181953]

* It is acknowledged that different density values may have been used for both HLW and DSNF. These values were derived from different assumptions or choices of representative waste components. The use of different values is expected to have little effect on the PMA results.

Table C4-3. Sources and Parameter Entry Form Numbers for the PMA-Specific Direct Inputs

Line #	Document_ID	Reference_Document	Document DIRS	DTN	DTN DIRS	PEF
1	ANL-EBS-MD-000003 REV 03	General Corrosion and Localized Corrosion of Waste Package Outer Barrier	178519	NA	NA	520
2	ANL-EBS-MD-000033 REV06	Engineered Barrier System: Physical and Chemical Environment	177412	SN0701PAEBSPCE.001_R1	180523	513
3	ANL-EBS-MD-000037 REV04 AD01	In-Package Chemistry Abstraction	180506	SN0702PAIPC1CA.001_R2	180451	506
4	ANL-EBS-MD-000049 REV03 AD01	Multiscale Thermohydrologic Model	181383	LL0703PA011MST.006_R0	179853	508
5	ANL-EBS-MD-000049 REV03 AD01	Multiscale Thermohydrologic Model	181383	LL0703PA012MST.007_R0	179854	527
6	ANL-EBS-MD-000049 REV03 AD01	Multiscale Thermohydrologic Model	181383	LL0703PA013MST.008_R0	179855	528
7	ANL-EBS-MD-000049 REV03 AD01	Multiscale Thermohydrologic Model	181383	LL0703PA014MST.009_R0	179856	529
8	ANL-EBS-MD-000049 REV03 AD01	Multiscale Thermohydrologic Model	181383	LL0703PA015MST.010_R0	179857	530
9	ANL-EBS-MD-000005 Rev 04	Stress Corrosion Cracking of Waste Package Outer Barrier and Drip Shield Materials	181953	NA	NA	539
10	ANL-EBS-MD-000049 REV03 AD01	Multiscale Thermohydrologic Model	181383	LL0703PA016MST.011_R0	179858	531
11	ANL-EBS-MD-000049 REV03 AD01	Multiscale Thermohydrologic Model	181383	LL0703PA017MST.012_R0	179859	532
12	ANL-EBS-MD-000049 REV03 AD01	Multiscale Thermohydrologic Model	181383	LL0703PA034MST.016_R0	179982	533

Table C4-3. Sources and Parameter Entry Form Numbers for the PMA-Specific Direct Inputs (Continued)

Line #	Document_ID	Reference_Document	Document DIRS	DTN	DTN DIRS	PEF
13	ANL-EBS-MD-000049 REV03 AD01	Multiscale Thermohydrologic Model	181383	LL0703PA035MST.017_R0	179985	534
14	ANL-EBS-MD-000049 REV03 AD01	Multiscale Thermohydrologic Model	181383	LL0703PA036MST.018_R0	179986	535
15	ANL-EBS-MD-000049 REV03 AD01	Multiscale Thermohydrologic Model	181383	LL0703PA037MST.019_R0	179989	536
16	ANL-EBS-MD-000049 REV03 AD01	Multiscale Thermohydrologic Model	181383	LL0703PA038MST.020_R0	179992	537
17	ANL-WIS-MD-000021 REV03 AD01	Cladding Degradation Summary for LA	180616	MO0411SPACLDDG.003_R1	180755	515
18	ANL-WIS-MD-000021 REV03 AD01	Cladding Degradation Summary for LA	180616	MO0702PAFRACSS.000_R1	181588	522
19	MDL-MGR-GS-000007	Supplemental Earthquake Ground Motion Input for a Geologic Repository at Yucca Mountain	NA	MO0801HCUHSREB.001_R0	184803	538
20	MDL-WIS-PA-000005	Total System Performance Assessment Model/Analysis for the License Application	NA	SN0704PMAIPCAB.001_R1	182602	523
21	MDL-NBS-HS-000006 REV03	UZ Flow Models and Submodels	184614	LB0701GTFEHMFF.001_R0	179160	525
22	MDL-NBS-HS-000006 REV03	UZ Flow Models and Submodels	184614	LB0701MOFEHMFF.001_R0	179297	510
23	MDL-NBS-HS-000006 REV03	UZ Flow Models and Submodels	184614	LB0702PAFEM10K.002_R0	179507	526
24	MDL-NBS-HS-000019 REV01 AD01	Abstraction of Drift Seepage	181244	LB0702PASEEP01.001_R0	179511	514
25	MDL-NBS-HS-000020 REV 02 AD02	Particle Tracking Model and Abstraction of Transport Processes	184748	MO0704PAFEHMBR.001_R3	184647	512
26	MDL-NBS-HS-000021 REV03 AD02	Saturated Zone Flow and Transport Model Abstraction	183750	Corroborative DTN: SN0704PMASZFTA.001_R1	184395	519

Table C4-3. Sources and Parameter Entry Form Numbers for the PMA-Specific Direct Inputs (Continued)

Line #	Document_ID	Reference_Document	Document DIRS	DTN	DTN DIRS	PEF
27	MDL-WIS-PA-000005	Total System Performance Assessment Model/Analysis for the License Application	NA	Corroborative DTN: LB0704PASEEP02.001_R1	181093	516
28	MDL-WIS-PA-000005	Total System Performance Assessment Model/Analysis for the License Application	NA	Corroborative DTN: MO0704PAUZFEHM.000_R0	182790	507, 509, 524
29	MDL-WIS-PA-000005	Total System Performance Assessment Model/Analysis for the License Application	NA	Corroborative DTN: MO0708TSPAPROC.000_R0	182979	507, 508, 509, 512, 513, 517, 518, 519, 521, 527, 528, 529, 530, 531, 532, 533, 534, 535, 536, 537, 538, 541, 542, 543
30	MDL-WIS-PA-000005	Total System Performance Assessment Model/Analysis for the License Application	NA	Corroborative DTN: SN0704PMAGDEGM.001_R2	183955	503

Table C4-3. Sources and Parameter Entry Form Numbers for the PMA-Specific Direct Inputs (Continued)

Line #	Document_ID	Reference_Document	Document DIRS	DTN	DTN DIRS	PEF
31	MDL-WIS-PA-000005	Total System Performance Assessment Model/Analysis for the License Application	NA	Corroborative DTN: SN0704PMAIPCAB.001_R1	182602	500
32	MDL-WIS-PA-000005	Total System Performance Assessment Model/Analysis for the License Application	NA	Corroborative DTN: SN0704PMASOLUB.001_R1	182787	505
33	MDL-WIS-PA-000005	Total System Performance Assessment Model/Analysis for the License Application	NA	Corroborative DTN: SN0704PMASZFTA.001_R1_R0	184395	501
34	MDL-WIS-PA-000005	Total System Performance Assessment Model/Analysis for the License Application	NA	Corroborative DTN: SN0704PMAWBCAL.001_R2	182335	502
35	MDL-WIS-PA-000005	Total System Performance Assessment Model/Analysis for the License Application	NA	Corroborative DTN: SN0707PMACSNFD.001_R0	183045	504
36	MDL-WIS-PA-000005	Total System Performance Assessment Model/Analysis for License Application	NA	NA	NA	511
37	MDL-WIS-PA-000005	In-Package Chemistry Abstraction, ANL-EBS-MD-000037 Rev 04 AD 01	180506	NA	NA	540
38	MDL-NBS-HS-000008, REV 02 ADD 01	Radionuclide Transport Models Under Ambient Conditions	177396	LA0408AM831341.001_R0	171584	509
39	MDL-NBS-HS-000008, REV 02 ADD 01	Radionuclide Transport Models Under Ambient Conditions	177396	LB0701PAKDSESN.001_R0	179299	509
40	MDL-NBS-HS-000020 REV 02 AD02	Particle Tracking Model and Abstraction of Transport Processes	184748	LA0701PANS02BR.003_R2	180497	509

Table C4-3. Sources and Parameter Entry Form Numbers for the PMA-Specific Direct Inputs (Continued)

Line #	Document_ID	Reference_Document	Document DIRS	DTN	DTN DIRS	PEF
41	MDL-NBS-HS-000008, REV 02 ADD 01	Radionuclide Transport Models Under Ambient Conditions	177396	LB0702PAUZMTDF.001_R1	180776	509
42	MDL-WIS-PA-000005	Total System Performance Assessment Model/Analysis for License Application	NA	MO0707UZKDCORR.000_R0	183003	509

Table C5-1. Assumptions Identified as Potentially Conservative and Significant to Annual Dose Rate

Submodel	TSPA-LA Assumption	PMA Treatment	Basis for Change
Drift Seepage	Seepage abstraction collapsed-drift look-up table was generated from seepage simulations conducted with the seepage model for performance assessment (SMPA) (BSC 2004 [DIRS 181244], Section 6.1[a]), assuming a rubble-filled circular opening with 11 m diameter as the final state after collapse.	The PMA model includes this analysis for collapsed drifts using an alternative seepage look-up table developed from revised SMPA simulations. The alternative look-up table gives seepage only when the seepage location at the ceiling is within the 5.5-m wide center section of the rubble-filled opening.	In the TSPA seepage component, the total flow of liquid water from the fractured formation into the rubble-filled opening is considered seepage, independent of the actual seepage location, and subsequent TSPA components, such as those for radionuclide mobilization and transport, use this total seepage rate. This is a conservative treatment of seepage, since the mostly gravity-driven flow in the rubble-filled opening would effectively prohibit contact of water with the waste packages or waste forms for off-center seepage locations. Such conservative treatment was chosen in the TSPA compliance model to account for possible uncertainties in the seepage modeling approach for collapsed drifts.
WF Degradation and Radionuclide Mobilization	All of the CSNF (Zircaloy and Stainless Steel) cladding is assumed to be failed at time of WP failure (Section 5.1.3).	For 10,000 year EF WP and EF DS cases, spent-fuel, zirconium-based (Zircaloy) cladding is assumed to split instantly along the length of a fuel rod only if the cladding is perforated at the time of WP failure based upon the initial failed fraction. No credit is taken for stainless-steel cladding because it is assumed to be failed upon receipt.	It is expected that unfailed (not breached or perforated) Zircaloy cladding will remain intact for at least 10,000 years, in absence of rock fall induced damage (SNL 2007 [DIRS 180616], Section 1.0). The groups of waste packages represented in the TSPA-LA model have an initial percentage of failed rods defined by the log uniform distribution with a range 0.01% to 1%. This fuel rod failure rate is based on historical data on reactor operation and includes uncertainty. It also includes failure from wet and dry storage at the reactor site, and handling (SNL 2007 [DIRS 180616], Section 7.1.1).

Table C5-1. Assumptions Identified as Potentially Conservative and Significant to Annual Dose Rate (Continued)

Submodel	TSPA-LA Assumption	PMA Treatment	Basis for Change
WF Degradation and Radionuclide Mobilization (Continued)	CSNF WF Degradation The commercial SNF waste-form degradation rate is calculated as a function of temperature, oxygen fugacity, total carbonate concentration, and pH (BSC 2004 [DIRS 169987]), based on a set of conservative assumptions that may overestimate the rate and extent of waste degradation.	The functional dependence on water chemistry remains the same as in the compliance model. However, the distribution range of the effective surface area of commercial SNF is modified based on fractional release rate measurements in fuel rod segment tests (BSC 2004 [DIRS 169987]), and two additional scaling factors are included to capture the effect of long-term dissolution and the decrease in radiolysis.	CSNF WF Degradation • The fractional release rate is a parameter that is directly measured in leaching experiments. The effective surface area should be chosen to reflect these measurements. In addition, the rod segment tests may most accurately mimic the likely state of spent fuels in a breached waste package. • The linear dependence of dissolution rate on water saturation has been used in modeling mineral dissolution in soils. • Experimental data show that the degradation rates decrease with time and with a decrease in radiation field.
	HLW WF Degradation Key parameters used by the compliance model for glass degradation are based on short-term experimental dissolution rate data for a variety of HLW glasses.	The PMA model accounts for the long-term effect by including a chemical affinity term and the effect of rind thickness.	Because laboratory dissolution rates tend to be many times faster than long-term field rates reported for natural glasses, the TSPA-LA model for glass degradation may be overly conservative, especially at long times (e.g., greater than several hundred years) following breach of a waste package.
	Np, Pu, U DCL Uncertainty (Section 5.1.3) The uncertainty assessments are mainly based on many potential sources of uncertainty effecting solubility and/or solubility calculations. These include uncertainties due to: (1) thermodynamic data in the solubility calculations, (2) variations in solution chemistry, (3) temperature effects, and (4) calculations of activity coefficients at different ionic strengths.	The uncertainties for the solubilities of solids controlling the concentrations of the radionuclides U(VI), Pu(IV), Np(IV), and Np(V) have been assessed by comparisons between the EQ3/6 code predictions using the thermodynamic database *data0.ymp.R5* and solubility data available in the peer-review scientific literature. The uncertainties estimated as such are considered as total uncertainties.	The TSPA dissolved concentration limits submodel captures the extent of various uncertainties in thermodynamic data by combining them additively (in log-space) to generate an uncertainty envelope. However, because these uncertainties may not simply be additive, this method may overestimate the uncertainty in any single result.

Table C5-1. Assumptions Identified as Potentially Conservative and Significant to Annual Dose Rate (Continued)

Submodel	TSPA-LA Assumption	PMA Treatment	Basis for Change
WF Degradation and Radionuclide Mobilization (Continued)	The IPC model is a batch reactor model that assumes the bulk in-package chemistry and calculates the result of mixing the components within the waste-form cells of the waste package with water and atmospheric gases to predict equilibrium solution compositions. The effect of water/rock ratio is not included.	The PMA calculations for in-package chemistry consist of two parts: The first part is used to construct the functional dependence of pH on waste degradation kinetics for the cases where vapor diffusion is a dominant mechanism for water transport through a breached waste package. The second part is to establish the relationship between the water chemistry and the flux of liquid water that percolates the waste package.	The modified in-package chemistry abstraction was necessary to support the in-package water balance abstraction, the liquid water is assumed to be restricted to the pores of the available degradation products. Rather than using the bulk chemistry based in-package chemistry abstraction to predict pH in the pore water of waste-form degradation products exposed to liquid or vapor influx.
WP and DS Degradation	The TSPA-LA Model uses a Stress Threshold value for SCC based upon a temperature of 125°C and a stress safety factor of 2.0 (SNL 2007 [DIRS 181953] Section 6.2.2[a]). The SCC stress threshold is conservatively applied with an uncertainty, a range from 0.9 to 1.05 yield strength with a uniform distribution between these values is selected for use in TSPA (SNL 2007 [DIRS 181953], Table 6-3[a], Section 6.2.2[a]).	The PMA model uses a SCC damage threshold range for Alloy 22 of 100-105% of the yield strength.	The narrower range of uncertainty is justified for use in the performance margin analysis since the stress corrosion cracking threshold stress initiation criterion for Alloy 22 was already conservatively defined at 105% by including a safety factor of 2.0 (SNL 2007 [DIRS 181953], Section 6.2.2[a])
	Stress Corrosion Cracking of Waste Package outer Barrier and Drip Shield Materials (SNL 2007 [DIRS 181953], Section 6.7.3.3) provide estimates of the crack area through analysis of networks of cracks arranged in hexagonal and circular geometries, respectively, circumscribed by a single through-wall crack. The TSPA-LA Model crack density ranges from 3.27×10^{-3} to 1.31×10^{-2}.	In the PMA model the crack area density was changed to a constant value equal to the lower bound used in the TSPA-LA model, 3.27×10^{-3}.	Because the hexagonal array represents a high effective density (close spacing) of individual cracks, this hexagonal case, with crack center spacing is considered a conservative representation (SNL 2007 [DIRS 181953], Sections 8.4.2). An alternative model for the crack area density yields a value at room temperature of 7.22×10^{-3} (SNL 2007 [DIRS 181953], Section 6.7.4). This is considered a limiting case (SNL 2007 [DIRS 181953], Section 6.7.2). This lower bound (3.27×10^{-3}) used in the PMA represents a less conservative value and more closely resembles the results of the alternative model.

Table C5-1. Assumptions Identified as Potentially Conservative and Significant to Annual Dose Rate (Continued)

Submodel	TSPA-LA Assumption	PMA Treatment	Basis for Change
WP and DS Degradation (Continued)	It is assumed that using only the crevice specimen data is sufficient for the GC model for TSPA-LA. Differences in surface-polishing treatments between weight-loss and crevice samples are not evaluated and the conservative crevice data (i.e., higher) corrosion rates are used (SNL 2007 [DIRS 178519], Section 6.4.3.2).	The PMA includes an alternative model using the corrosion rates of weight-loss samples to derive the Ro distribution for use in the general corrosion model of WP outer barrier (Alloy 22). These rates are documented in *General Corrosion and Localized Corrosion of Waste Package Outer Barrier* (SNL 2007 [DIRS 178519], Section 6.4.3.5.2).	The observed general corrosion rates of the crevice specimens are higher than those of the plain weight-loss specimens (SNL 2007 [DIRS 178519], Section 6.4.3.2). The use of only higher general corrosion rates of the crevice specimens in the TSPA-LA is conservative and an evaluation of the weight-loss data is justified.
	The TSPA-LA Model applies the "aggressive-environment" drip shield general corrosion rate to the topside surface of the drip shields when they are exposed to seepage dripping, regardless of the changes in water chemistry due to the thermal evolution of the repository (SNL 2007 [DIRS 180778], Section 6.1.2[a]).	PMA model explicitly evaluates the chemical environment for on the drip shield surface and only applies the aggressive DS corrosion rates to the topside of the DS when the seepage chemistry exceeds the critical (or minimum) fluoride ion concentration of 0.5 millimolar (mM) (SNL 2007 [DIRS 180778], Section 6.1.2[a]).	Application of aggressive conditions to all topside surfaces, with benign conditions only applied to the underside surfaces applies the higher corrosion rate from aggressive conditions to more of the drip shield surfaces is conservative, i.e., it results in an earlier failure of a portion of the drip shields (SNL 2007 [DIRS 180778], Section 6.1.2[a]). The fluoride ion concentrations of the ambient water at the repository horizon have a range of 0.02 to 0.17 mM (SNL 2007 [DIRS 177412], Table 4.1-3). The repository is expected to return to near ambient conditions are after 10,000 years post-closure. Applying the aggressive DS GC rates to for 1e6 year modeling cases is conservative.

Table C5-1. Assumptions Identified as Potentially Conservative and Significant to Annual Dose Rate (Continued)

Submodel	TSPA-LA Assumption	PMA Treatment	Basis for Change
EBS Flow and Transport	The TSPA-LA Model assumes that (Section 5.1.4): 1) Evaporation of water from the surface or interior of a WP does not occur; 2) Water consumption by chemical reactions is negligible; 3) Water vapor is in equilibrium between the inside and the outside of a waste package; 4) Rind saturation is controlled by surface adsorption; and 5)There is no resistance to water percolation over WP failures.	The PMA water balance: (1) accounts for water consumption by reactions; and (2) fully couples hydrologic effects (e.g., the sheet flow on the waste package surface and capillarity effect of porous corrosion products) and chemical processes (e.g., water consumption and salt release by reactions; the depression of water activity with increasing dissolved salt concentration).	Water availability and water flux are two important parameters for predicting the extents of chemical reactions and the transport of radionuclides inside a breached waste package. The objective of this performance margin analysis submodel is to obtain a more detailed estimate of the quantity of water available inside a breached waste package for waste degradation and radionuclide transport in order to evaluate the potential conservatism in the TSPA-LA Model water balance assumptions.

Table C5-1. Assumptions Identified as Potentially Conservative and Significant to Annual Dose Rate (Continued)

Submodel	TSPA-LA Assumption	PMA Treatment	Basis for Change
UZ Transport	In the TSPA-LA model, the diffusive tortuosity differs for each of the three UZ rock units, but is independent of radioelement, whereas the free-water diffusion coefficient is a property of the radioelement (SNL 2008 [DIRS 184748], Section 6.5.5). In the TSPA-LA model, laboratory based values of matrix diffusion coefficients, which are derived as the product of tortuosity and free-water diffusion coefficient, are utilized. Added effects of small scale fractures are not considered.	For the PMA model, the effect of a presumed increase in the effective diffusion coefficient due to small-scale fractures (BSC 2006 [DIRS 178275], Section 6.4.1) is modeled by applying an alternate conceptual model and enhancement factor for matrix diffusion.	In Section 7.6 of *UZ Flow Models and Submodels* (SNL 2007 [DIRS 184614]), a flow and transport field test and model is presented for a percolation and tracer test conducted along a fault in Alcove 8/Niche 3. A Multiple Interacting Continua (MINC) discrete fracture model was developed for simulating flow and transport during the test. The fault was explicitly included, along with finely discretized grid spacings in the matrix adjacent to the fault. An analysis is presented regarding the influence of matrix diffusion and the parameter ranges required to match the breakthrough curves of two conservative, diffusing tracers with different diffusion coefficients in free water. Figure 7.8-9 of SNL (2007 [DIRS 184614]) shows that in order to obtain a good match to the tracer tests, the interface area had to be increased by a factor of 45 above that of the original data. Likewise, in Section 7.3 of SNL (2007 [DIRS 177396]), the same analysis is provided; in both reports, a discussion of the reasons for the need to adjust the interface area is provided. In Liu et al. (2004 [DIRS 169948]), this scale effect is described in the form of an increase in the matrix diffusion coefficient, but the description in the paper postulates that the increase could be due to the increase in available surface area for diffusion as a solute encounters a greater number of fractures during its transit through a fractured medium.

Table C5-1. Assumptions Identified as Potentially Conservative and Significant to Annual Dose Rate (Continued)

Submodel	TSPA-LA Assumption	PMA Treatment	Basis for Change
UZ Transport (Continued)	In the compliance model (SNL 2008 [DIRS 184748], Section 6.4.5), radionuclides assumed to be affected by colloid-facilitated transport are handled using a composite of three individual components: 1) the reversibly sorbed species, 2) a fraction that is governed by irreversible attachment to colloids that undergo retardation due to colloid attachment/detachment processes, and 3) a 'fast fraction' of colloids that were assumed to transport conservatively (without any filtration or retardation).	Colloid-facilitated contaminant transport in the PMA treats the variability of mobility of individual colloids as a process that is inherent to the colloid population, rather than as observations that lead to uncertainty in the transport properties within a conventional, single-valued parameter. The process of retardation via attachment and detachment of colloids on immobile surfaces is modeled assuming a diverse population of transport properties that account for the inherent variability of colloid size, surface charge and chemical properties, mineralogy, and their concomitant impact on colloid mobility.	This approach is modified in the PMA to address technical issues that could lead to overly conservative performance of the natural barriers for colloid-facilitated radionuclides. Principally, the TSPA-LA model is considered to be conservative because it does not account, except in a coarse way, for the inherent variability of transport properties of individual colloids in a colloid population.
	The water table in the UZ Transport Model under the future climate states is assumed to rise to a level of 850 m for all realizations, a nominal rise of 120 m from the present-day value. In the compliance model, the rise of 120 m was adopted without uncertainty (SNL 2008 [DIRS 184748], Section 6.6.2.1).	In the PMA model, the water table elevation is taken as an uncertain parameter with a distribution that results in most realizations being conducted with a water table elevation that is less than 850 m.	This approach for the TSPA-LA Model was considered to be conservative with respect to the UZ transport times, because 850 m was considered to be an upper bound, and the higher water table shortens the travel distance and travel times through the UZ. This change for PMA creates a model analysis that is more realistic with respect to UZ transport times than the compliance model, and one in which the uncertainty in water table elevation is more faithfully represented.
SZ Flow and Transport	The change in groundwater flow in the SZ from one climatic state to another occurs rapidly and is approximated by a shift from one steady-state flow condition to another steady-state flow condition over one timestep (Section 5.1.5).	In the PMA model, the water table elevation is taken as an uncertain parameter with a distribution that results in most realizations being conducted with a water table elevation that is less than 850 m.	This approach for the TSPA-LA Model was considered to be conservative with respect to the SZ transport times, because the entire RN mass between the lower and the higher water table elevations was put in the SZ in one timestep which shortens the travel distance and travel times (SNL 2008 [DIRS 183750], Section 6.5, p. 6-18).

Table C5-1. Assumptions Identified as Potentially Conservative and Significant to Annual Dose Rate (Continued)

Submodel	TSPA-LA Assumption	PMA Treatment	Basis for Change
SZ Flow and Transport (Continued)	The radionuclide mass reaching the water table in both the matrix and fractures of the UZ released from the UZ Transport Model is transferred to flow through the fractures in the SZ Radionuclide Transport Model (SNL 2008 [DIRS 183750], Sections 6.3.3 and 6.5.2.13).	The PMA model channels the radionuclide mass release from the UZ to the SZ three-dimensional and one-dimensional transport models and accounts for transport in the matrix.	The model assumption in the TSPA-LA Model is equivalent to assuming that the radionuclide mass instantly diffuses out of the UZ matrix and into the SZ fractures at the interface between the UZ and SZ. This approximation is conservative as it reduces the transport time (SNL 2008 [DIRS 183750], Sections 6.3.3 and 6.5.2.13).
	A large fraction of the colloids are retarded by sorption while a small fraction, known as fast-fraction, are transported unretarded. In the TSPA-LA Model (SNL 2008 [DIRS 183750], Section 6.5.2.11), transport of irreversible colloids for the retarded fraction in both the volcanic units and alluvium is calculated using single retardation factors per realization	Using a Colloid Diversity Model, colloids are assigned a wide range of retardation factors within a given TSPA realization in recognition of their diverse sizes, shapes, compositions, and surface properties.	There is significant variability (diversity) in the attachment/detachment rate constants resulting from differences in water chemistry, colloid size, colloid mineralogy, colloid surface charge, and characteristics of sorption sites on the aquifer media (Robinson et al. 2007 [DIRS 180698]). Implementation of a single retardation factor for all nonfast-fraction colloids in the volcanic rocks and alluvium is conservative.
	The base-case conceptual model of SZ transport developed for the TSPA-LA model is implicitly taken to be oxidizing conditions in the SZ, based on the uncertainty distributions for sorption coefficients of technetium and neptunium (SNL 2008 [DIRS 183750]).	The PMA model adapts the SZ Flow and Transport Abstraction Model to simulate the transport of technetium and neptunium with enhanced sorption in zones of potentially reducing geochemical conditions. Uncertainty in the transport of these redox-sensitive species is evaluated with regard to the location and size of a potential reducing zone in the SZ and uncertainty in the sorption coefficients within the reducing zone.	Potential variations in redox conditions in the SZ could have significant impacts on the migration of redox-sensitive radionuclide species released from the repository at Yucca Mountain (BSC 2006 [DIRS 178672]). Under reducing geochemical conditions, the solubility limit can be much lower and the sorption coefficient can be much higher for radioelements such as technetium and neptunium. Ignoring the effects of encountering potential reducing zones in the SZ such as precipitation from lower solubility limits and retardation from enhanced sorption would lead to conservative transport times in the SZ before reaching the boundary of the accessible environment.

Table C5-1. Assumptions Identified as Potentially Conservative and Significant to Annual Dose Rate (Continued)

Submodel	TSPA-LA Assumption	PMA Treatment	Basis for Change
SZ Flow and Transport (Continued)	The flowing interval porosity (FPVO) is defined as the volume of the pore space through which significant groundwater flow occurs. To define the lower bound value, estimates of fracture porosity of intact cores of volcanic rock were used. More details can be found in *Saturated Zone Flow and Transport Model Abstraction* (SNL 2008 [DIRS 183750], Section 6.5.2.5).	For the PMA, the lower bound will be raised from 10^{-5} to 10^{-4}, which increases the lower bound by an order of magnitude.	A study of the cumulative distribution function plot for parameter FPVO (SNL 2008 [DIRS 183750], Figure 6-13) shows that less weight is given to the bottom of the distribution (i.e. very low FPVO) than the rest of the distribution. This is based on data from the Experimental Studies Facility (ESF) as well as data from other sources (i.e. theoretical models, pumping tests and tracer tests). The 0.5 probability value of 10^{-3} is considered to be representative of the smallest values of fracture porosity estimated from the ESF data and field tests (SNL 2008 [DIRS 183750], Section 6.5.2.5).
	In the TSPA-LA Model, the ground water specific discharge (which is the function of permeability) and flowing interval porosity are uncorrelated variables (SNL 2008 [DIRS 183750], Sections 6.5.2.1 and 6.5.2.5).	For the PMA value of 0.64 was used as the correlation factor for the parameters FPVO and GWSPD during parameter sampling This affects the SZ breakthrough curves as well as sampled data used in the SZ one-dimensional pipe model.	In a fractured flow aquifer, as fracture density and apertures increase, both flowing interval porosity and permeability to also increase. An uncorrelated model could generate parameter combinations (large specific discharge and small flowing interval porosity) that are not physically consistent. An uncorrelated model could generate parameter combinations (large specific discharge and small flowing interval porosity) that are not physically consistent.

Table C6-1. Relative Humidity Threshold for 0.5mM Fluoride Concentration

Look-up tables* for water 1		RH Threshold	Look-up tables for water 2		RH Threshold	Look-up tables for water 3		RH Threshold	Look-up tables for water 4		RH Threshold
1	1bp2t1.xls	0.99155	1	2bp2t1.xls	0.459231	1	3bp2t1.xls	0.38266	1	4bp2t1.xls	0.559223
2	1bp2t30.xls	0.990971	2	2bp2t30.xls	0.459281	2	3bp2t30.xls	0.44001	2	4bp2t30.xls	0.556413
3	1bp2t70.xls	0.991264	3	2bp2t70.xls	0.427894	3	3bp2t70.xls	0.417156	3	4bp2t70.xls	0.517622
4	1bp3t1.xls	0.991775	4	2bp3t1.xls	0.459335	4	3bp3t1.xls	0.382874	4	4bp3t1.xls	0.559247
5	1bp3t30.xls	0.991533	5	2bp3t30.xls	0.457475	5	3bp3t30.xls	0.440007	5	4bp3t30.xls	0.556864
6	1bp3t70.xls	0.991761	6	2bp3t70.xls	0.425404	6	3bp3t70.xls	0.401144	6	4bp3t70.xls	0.517596
7	1bp4t1.xls	0.991368	7	2bp4t1.xls	0.45937	7	3bp4t1.xls	0.382895	7	4bp4t1.xls	0.559253
8	1bp4t30.xls	0.991944	8	2bp4t30.xls	0.426394	8	3bp4t30.xls	0.388749	8	4bp4t30.xls	0.55688
9	1bp4t70.xls	0.991744	9	2bp4t70.xls	0.425895	9	3bp4t70.xls	0.401212	9	4bp4t70.xls	0.517528
10	1cp2t1.xls	0.991357	10	2cp2t1.xls	0.476173	10	3cp2t1.xls	0.380135	10	4cp2t1.xls	0.558955
11	1cp2t30.xls	0.990736	11	2cp2t30.xls	0.462071	11	3cp2t30.xls	0.440003	11	4cp2t30.xls	0.556412
12	1cp2t70.xls	0.991053	12	2cp2t70.xls	0.428376	12	3cp2t70.xls	0.420008	12	4cp2t70.xls	0.517607
13	1cp3t1.xls	0.991593	13	2cp3t1.xls	0.475998	13	3cp3t1.xls	0.380356	13	4cp3t1.xls	0.558975
14	1cp3t30.xls	0.991333	14	2cp3t30.xls	0.450614	14	3cp3t30.xls	0.440009	14	4cp3t30.xls	0.556865
15	1cp3t70.xls	0.991575	15	2cp3t70.xls	0.426551	15	3cp3t70.xls	0.407961	15	4cp3t70.xls	0.517692
16	1cp4t1.xls	0.991164	16	2cp4t1.xls	0.47617	16	3cp4t1.xls	0.380376	16	4cp4t1.xls	0.558998
17	1cp4t30.xls	0.991761	17	2cp4t30.xls	0.418463	17	3cp4t30.xls	0.425837	17	4cp4t30.xls	0.55688
18	1cp4t70.xls	0.991557	18	2cp4t70.xls	0.426235	18	3cp4t70.xls	0.408021	18	4cp4t70.xls	0.517699
19	1dp2t1.xls	0.990947	19	2dp2t1.xls	0.517331	19	3dp2t1.xls	0.33659	19	4dp2t1.xls	0.558053
20	1dp2t30.xls	0.990234	20	2dp2t30.xls	0.5568	20	3dp2t30.xls	0.477803	20	4dp2t30.xls	0.556413
21	1dp2t70.xls	0.990604	21	2dp2t70.xls	0.442767	21	3dp2t70.xls	0.416811	21	4dp2t70.xls	0.517951
22	1dp3t1.xls	0.991206	22	2dp3t1.xls	0.517304	22	3dp3t1.xls	0.336916	22	4dp3t1.xls	0.55809
23	1dp3t30.xls	0.990909	23	2dp3t30.xls	0.556865	23	3dp3t30.xls	0.449625	23	4dp3t30.xls	0.556865
24	1dp3t70.xls	0.991178	24	2dp3t70.xls	0.442582	24	3dp3t70.xls	0.422049	24	4dp3t70.xls	0.518003
25	1dp4t1.xls	0.99073	25	2dp4t1.xls	0.517284	25	3dp4t1.xls	0.460022	25	4dp4t1.xls	0.558092
26	1dp4t30.xls	0.991369	26	2dp4t30.xls	0.55688	26	3dp4t30.xls	0.481359	26	4dp4t30.xls	0.55688
27	1dp4t70.xls	0.991159	27	2dp4t70.xls	0.442424	27	3dp4t70.xls	0.422094	27	4dp4t70.xls	0.518015
28	1ep2t1.xls	0.990592	28	2ep2t1.xls	0.529443	28	3ep2t1.xls	0.336589	28	4ep2t1.xls	0.561883
29	1ep2t30.xls	0.99527	29	2ep2t30.xls	0.5568	29	3ep2t30.xls	0.505668	29	4ep2t30.xls	0.556412
30	1ep2t70.xls	0.990215	30	2ep2t70.xls	0.524391	30	3ep2t70.xls	0.414621	30	4ep2t70.xls	0.518674
31	1ep3t1.xls	0.99087	31	2ep3t1.xls	0.528825	31	3ep3t1.xls	0.33688	31	4ep3t1.xls	0.561791
32	1ep3t30.xls	0.990539	32	2ep3t30.xls	0.556865	32	3ep3t30.xls	0.453249	32	4ep3t30.xls	0.556864
33	1ep3t70.xls	0.990833	33	2ep3t70.xls	0.524333	33	3ep3t70.xls	0.415086	33	4ep3t70.xls	0.518671
34	1ep4t1.xls	0.990354	34	2ep4t1.xls	0.528903	34	3ep4t1.xls	0.336896	34	4ep4t1.xls	0.561779
35	1ep4t30.xls	0.991028	35	2ep4t30.xls	0.556877	35	3ep4t30.xls	0.428995	35	4ep4t30.xls	0.55688
36	1ep4t70.xls	0.990812	36	2ep4t70.xls	0.52425	36	3ep4t70.xls	0.415105	36	4ep4t70.xls	0.518693
37	1fp2t1.xls	0.990079	37	2fp2t1.xls	0.565735	37	3fp2t1.xls	0.384397	37	4fp2t1.xls	0.567246
38	1fp2t30.xls	0.991139	38	2fp2t30.xls	0.556799	38	3fp2t30.xls	0.505668	38	4fp2t30.xls	0.550692
39	1fp2t70.xls	0.989651	39	2fp2t70.xls	0.530004	39	3fp2t70.xls	0.500638	39	4fp2t70.xls	0.52025
40	1fp3t1.xls	0.990384	40	2fp3t1.xls	0.565712	40	3fp3t1.xls	0.383386	40	4fp3t1.xls	0.567252
41	1fp3t30.xls	0.990384	41	2fp3t30.xls	0.565712	41	3fp3t30.xls	0.383386	41	4fp3t30.xls	0.567252
42	1fp3t70.xls	0.990384	42	2fp3t70.xls	0.565712	42	3fp3t70.xls	0.383386	42	4fp3t70.xls	0.567252

Table C6-1. Relative Humidity Threshold for 0.5mM Fluoride Concentration (Continued)

Look-up tables for water 1		RH Threshold	Look-up tables for water 2		RH Threshold	Look-up tables for water 3		RH Threshold	Look-up tables for water 4		RH Threshold
43	1fp4t1.xls	0.990384	43	2fp4t1.xls	0.565712	43	3fp4t1.xls	0.383386	43	4fp4t1.xls	0.567252
44	1fp4t30.xls	0.990384	44	2fp4t30.xls	0.565712	44	3fp4t30.xls	0.383386	44	4fp4t30.xls	0.567252
45	1fp4t70.xls	0.990384	45	2fp4t70.xls	0.565712	45	3fp4t70.xls	0.383386	45	4fp4t70.xls	0.567252
46	1gp2t1.xls	0.990384	46	2gp2t1.xls	0.565712	46	3gp2t1.xls	0.383386	46	4gp2t1.xls	0.567252
47	1gp2t30.xls	0.990384	47	2gp2t30.xls	0.565712	47	3gp2t30.xls	0.383386	47	4gp2t30.xls	0.567252
48	1gp2t70.xls	0.990384	48	2gp2t70.xls	0.565712	48	3gp2t70.xls	0.383386	48	4gp2t70.xls	0.567252
49	1gp3t1.xls	0.990384	49	2gp3t1.xls	0.565712	49	3gp3t1.xls	0.383386	49	4gp3t1.xls	0.567252
50	1gp3t30.xls	0.990384	50	2gp3t30.xls	0.565712	50	3gp3t30.xls	0.383386	50	4gp3t30.xls	0.567252
51	1gp3t70.xls	0.989604	51	2gp3t70.xls	0.522893	51	3gp3t70.xls	0.497909	51	4gp3t70.xls	0.51394
52	1gp4t1.xls	0.989046	52	2gp4t1.xls	0.565013	52	3gp4t1.xls	0.53999	52	4gp4t1.xls	0.556558
53	1gp4t30.xls	0.989804	53	2gp4t30.xls	0.638204	53	3gp4t30.xls	0.648868	53	4gp4t30.xls	0.541255
54	1gp4t70.xls	0.989578	54	2gp4t70.xls	0.522839	54	3gp4t70.xls	0.49796	54	4gp4t70.xls	0.5131
55	1hp2t1.xls	0.988313	55	2hp2t1.xls	0.555012	55	3hp2t1.xls	0.539994	55	4hp2t1.xls	0.608822
56	1hp2t30.xls	0.986973	56	2hp2t30.xls	0.603528	56	3hp2t30.xls	0.652043	56	4hp2t30.xls	0.603527
57	1hp2t70.xls	0.9877	57	2hp2t70.xls	0.541019	57	3hp2t70.xls	0.555884	57	4hp2t70.xls	0.582732
58	1hp3t1.xls	0.988703	58	2hp3t1.xls	0.555023	58	3hp3t1.xls	0.540003	58	4hp3t1.xls	0.608848
59	1hp3t30.xls	0.988136	59	2hp3t30.xls	0.603691	59	3hp3t30.xls	0.652386	59	4hp3t30.xls	0.603689
60	1hp3t70.xls	0.98858	60	2hp3t70.xls	0.54102	60	3hp3t70.xls	0.555924	60	4hp3t70.xls	0.582756
61	1hp4t1.xls	0.987944	61	2hp4t1.xls	0.555025	61	3hp4t1.xls	0.540005	61	4hp4t1.xls	0.608838
62	1hp4t30.xls	0.988787	62	2hp4t30.xls	0.603733	62	3hp4t30.xls	0.652438	62	4hp4t30.xls	0.60372
63	1hp4t70.xls	0.98855	63	2hp4t70.xls	0.541013	63	3hp4t70.xls	0.600666	63	4hp4t70.xls	0.582745
64	1ip2t1.xls	0.986787	64	2ip2t1.xls	0.720004	64	3ip2t1.xls	0.586237	64	4ip2t1.xls	0.608062
65	1ip2t30.xls	0.990796	65	2ip2t30.xls	0.607439	65	3ip2t30.xls	0.604172	65	4ip2t30.xls	0.579992
66	1ip2t70.xls	0.986018	66	2ip2t70.xls	0.620008	66	3ip2t70.xls	0.570486	66	4ip2t70.xls	0.586302
67	1ip3t1.xls	0.987243	67	2ip3t1.xls	0.720006	67	3ip3t1.xls	0.586285	67	4ip3t1.xls	0.608067
68	1ip3t30.xls	0.98651	68	2ip3t30.xls	0.899994	68	3ip3t30.xls	0.603691	68	4ip3t30.xls	0.579993
69	1ip3t70.xls	0.987056	69	2ip3t70.xls	0.617002	69	3ip3t70.xls	0.570494	69	4ip3t70.xls	0.586242
70	1ip4t1.xls	0.986337	70	2ip4t1.xls	0.71999	70	3ip4t1.xls	0.586279	70	4ip4t1.xls	0.60807
71	1ip4t30.xls	0.987257	71	2ip4t30.xls	0.939993	71	3ip4t30.xls	0.603738	71	4ip4t30.xls	0.58
72	1ip4t70.xls	0.987019	72	2ip4t70.xls	0.617094	72	3ip4t70.xls	0.570497	72	4ip4t70.xls	0.586259
73	1jp2t1.xls	0.984584	73	2jp2t1.xls	0.984522	73	3jp2t1.xls	0.613285	73	4jp2t1.xls	0.980003
74	1jp2t30.xls	0.982339	74	2jp2t30.xls	0.98398	74	3jp2t30.xls	0.610202	74	4jp2t30.xls	0.960001
75	1jp2t70.xls	0.983577	75	2jp2t70.xls	0.984197	75	3jp2t70.xls	0.610609	75	4jp2t70.xls	0.980001
76	1jp3t1.xls	0.985126	76	2jp3t1.xls	0.984658	76	3jp3t1.xls	0.613262	76	4jp3t1.xls	0.980003
77	1jp3t30.xls	0.989258	77	2jp3t30.xls	0.9843	77	3jp3t30.xls	0.610389	77	4jp3t30.xls	0.980003
78	1jp3t70.xls	0.984822	78	2jp3t70.xls	0.984495	78	3jp3t70.xls	0.61066	78	4jp3t70.xls	0.980002
79	1jp4t1.xls	0.984024	79	2jp4t1.xls	0.984438	79	3jp4t1.xls	0.613248	79	4jp4t1.xls	0.980003
80	1jp4t30.xls	0.985008	80	2jp4t30.xls	0.984575	80	3jp4t30.xls	0.610447	80	4jp4t30.xls	0.980002
81	1jp4t70.xls	0.984778	81	2jp4t70.xls	0.984778	81	3jp4t70.xls	0.610732	81	4jp4t70.xls	0.980002
82	1Lp2t1.xls	0.980009	82	2Lp2t1.xls	0.96	82	3Lp2t1.xls	0.940004	82	4Lp2t1.xls	0.960004
83	1Lp2t30.xls	0.98	83	2Lp2t30.xls	0.960094	83	3Lp2t30.xls	0.939998	83	4Lp2t30.xls	0.960006
84	1Lp2t70.xls	0.979998	84	2Lp2t70.xls	0.960006	84	3Lp2t70.xls	0.940001	84	4Lp2t70.xls	0.960003

Table C6-1. Relative Humidity Threshold for 0.5mM Fluoride Concentration (Continued)

Look-up tables for water 1		RH Threshold	Look-up tables for water 2		RH Threshold	Look-up tables for water 3		RH Threshold	Look-up tables for water 4		RH Threshold
85	1Lp3t1.xls	0.98001	85	2Lp3t1.xls	0.973538	85	3Lp3t1.xls	0.940001	85	4Lp3t1.xls	0.959994
86	1Lp3t30.xls	0.98	86	2Lp3t30.xls	0.963402	86	3Lp3t30.xls	0.939999	86	4Lp3t30.xls	0.960005
87	1Lp3t70.xls	0.980008	87	2Lp3t70.xls	0.960001	87	3Lp3t70.xls	0.940002	87	4Lp3t70.xls	0.960003
88	1Lp4t1.xls	0.979995	88	2Lp4t1.xls	0.960003	88	3Lp4t1.xls	0.94	88	4Lp4t1.xls	0.960002
89	1Lp4t30.xls	0.980006	89	2Lp4t30.xls	0.964723	89	3Lp4t30.xls	0.94611	89	4Lp4t30.xls	0.959999
90	1Lp4t70.xls	0.980425	90	2Lp4t70.xls	0.960001	90	3Lp4t70.xls	0.940003	90	4Lp4t70.xls	0.959997
91	10p2t1.xls	0.980425	91	20p2t1.xls	0.960001	91	30p2t1.xls	0.940003	91	40p2t1.xls	0.959997
92	10p2t30.xls	0.980425	92	20p2t30.xls	0.960001	92	30p2t30.xls	0.940003	92	40p2t30.xls	0.959997
93	10p2t70.xls	0.980425	93	20p2t70.xls	0.960001	93	30p2t70.xls	0.940003	93	40p2t70.xls	0.959997
94	10p3t1.xls	0.980425	94	20p3t1.xls	0.960001	94	30p3t1.xls	0.940003	94	40p3t1.xls	0.959997
95	10p3t30.xls	0.980425	95	20p3t30.xls	0.960001	95	30p3t30.xls	0.940003	95	40p3t30.xls	0.959997
96	10p3t70.xls	0.980425	96	20p3t70.xls	0.960001	96	30p3t70.xls	0.940003	96	40p3t70.xls	0.959997
97	10p4t1.xls	0.980425	97	20p4t1.xls	0.960001	97	30p4t1.xls	0.940003	97	40p4t1.xls	0.959997
98	10p4t30.xls	0.980425	98	20p4t30.xls	0.960001	98	30p4t30.xls	0.940003	98	40p4t30.xls	0.959997
99	10p4t70.xls	0.980425	99	20p4t70.xls	0.960001	99	30p4t70.xls	0.940003	99	40p4t70.xls	0.959997

Source: DTN: SN0701PAEBSPCE.001_R1 [DIRS 180523]

Table C6-2. Stoichiometries of Waste Degradation Reactions

Waste/WP Component	Water Consumed (mole)	Volume of Corrosion Products Produced (m^3)	Hygroscopic Salt Released (Mole NaCl Equivalent)
1 kg CSNF reacted	7.23	2.39×10^{-4}	0.034
1 kg N-reactor reacted	8.40	2.78×10^{-4}	0
1 kg HLW reacted	10.52	5.9×10^{-4}	0.062-1.078
1 kg SS316 reacted	14.15	3.3×10^{-4}	0.062-0.133

Source: Corroborative DTN: SN0704PMAWBCAL.001_R2 [DIRS 182335]

Table C6-3. Parameter Values Used in Diffusion-Dominated Simulations

Variable	Units	CSNF	2DHLW	2MCO
pCO_2	Negative log bar	1.5, 2, 3, and 4	1.5, 2, 3, and 4	1.5, 2, 3, and 4
q	L/yr	0	0	0
k_{ss}/k_{wf}	Nondimensional	0.01, 0.1, 0.3, 1, 1.5, 2, 3, 10, and 100	0.01, 0.1, 1, 10, 25, 50, 75, 100, and 1,000	1×10^{-2}, 1×10^{-4}, 1×10^{-6}, and 1×10^{-7}
V_s/V_w	Nondimensional	≥ 1.5 (continuous)	≥ 1.5 (continuous)	≥ 1.5 (continuous)

Source: Corroborative DTN: SN0704PMAIPCPM.001 [DIRS 180745]

Table C6-4. Parameter Values Used in Liquid Influx Simulations

Parameter	Units	CSNF	2DHLW	2MCO
pCO2	Log bar	1.5, 3, and 4	1.5, 3, and 4	1.5, 3, and 4
q	L/yr	0.1, 1, 10, 100, and 1,000	0.01, 0.1, 1, 10, and 100	1, 10, 100, and 1,000
kss/kwf	nondimensional	0.1, 1.5, and 10	10 and 100	$1x10^{-2}$, $1x10^{-4}$, and $1x10^{-7}$
Vs/Vw	nondimensional	1.5	1.5	1.5

Source: Corroborative DTN: SN0704PMAIPCPM.001 [DIRS 180745]

Table C6-5. Controlling Factors for CSNF Dissolution

Process/Parameter	Impact on Dissolution	Treatment in Compliance Model	Treatment in PMA
Water chemistry (e.g., oxygen fugacity, total carbonate molar concentration, and pH)	The rate of CSNF dissolution depends on temperature, oxygen fugacity, total carbonate molar concentration, and pH (BSC 2004 [DIRS 169987]).	Explicitly included in a0 through a4.	Use the same functional dependence as in the compliance model.
Water chemistry (e.g., dissolved Ca, Si)	Dissolved Ca and Si tend to inhibit CSNF dissolution (Wilson and Gray 1990 [DIRS 115085]).	At least partly included in a0 through a4 since simulated groundwater is used in leaching tests.	The same as the compliance model.
Fuel chemistry—Non-uranium cation effect	Non-uranium cations such as Pu, Zr, and Mo are known to inhibit CSNF dissolution (Grandstaff 1976 [DIRS 113255]).	At least partly included in a0 through a4 since actual fuels are used in leaching tests.	The same as the compliance model.
Chemical affinity	The overall dissolution rate decreases as the dissolved uranium concentration approaches saturation with respect to secondary reaction products (Pierce et al. 2005 [DIRS 182055]).	Not included	Not included
Effective surface areas	The dissolution rate is directly proportional to the effective surface area of the fuel (BSC 2004 [DIRS 169987]).	The distribution of effective surface area is conservatively derived from fractional release measurements, geometrical calculations, and particle size distributions.	Constrained from fractional release measurements from rod segment tests. Included in As.
Water saturation	Dissolution takes place at the water-solid interface. As water saturation decreases, the effective surface area also decreases (Kuechler and Noack 2007 [DIRS 182054]; Sverdrup and Warfvinge 1988 [DIRS 182056]).	Not included	Included in Eq. C6.5-2. The effective surface area is set to be proportional to water saturation.

Table C6-5. Controlling Factors for CSNF Dissolution (Continued)

Process/Parameter	Impact on Dissolution	Treatment in Compliance Model	Treatment in PMA
Long-term effect	The rate of CSNF dissolution decreases with time (Hanson et al. 2004 [DIRS 182008]).	Not include	Included in a scaling factor (f1).
Changes in radiolysis	Both gamma and beta radiations enhance fuel dissolution (Shoesmith and Sunder 1992 [DIRS 113368]; Shoesmith 2000 [DIRS 114445]). As a result, the actual rates of CSNF dissolution will be lower than those measured in the lab.	Not included	Included in a scaling factor (f2)
Diffusion limit	Diffusion through the layer of degradation products could potentially limit dissolution reactions as the corrosion layer builds up.	Not included	Partly included as a long-term effect (f1).

Table C6-6. Controlling Parameter Distributions for CSNF Degradation

Parameter	Distribution
Log (A_s m^2/mg)	Triangular Low: -7.3 Apex: -7.3 High: -6.7
f_1	Uniform Low: 3 High: 10
f_2	Uniform Low: 5 High: 10

Source: Corroborative DTN: SN0704PMAGDEGM.001_R2 [DIRS 183955]

Table C6-7. Distribution of T_{RC} Used in the Glass Degradation Model for PMA

T_{RC} (mm)	T_{RC} (m)	M_D/M_0 (Fast Fraction)	Distribution (triangular)	Corresponding Slow Fraction
0.03	0.00003	0.0033 (0.33 %)	Minimum	99.67 %
0.1	0.0001	0.011 (1.10 %)	Most probable	98.90 %
0.3	0.0003	0.033 (3.3 %)	Maximum	96.70 %

Source: Corroborative DTN: SN0704PMAGDEGM.001_R2 [DIRS 183955]

Table C6-8. Recommended Uncertainties for Radionuclide Solubilities

Solid	Distribution
PuO_2(aged,hyd)	Log normal, truncated at ±1σ Mean (μ): 0 Standard deviation (σ): 0.79
NpO_2	Triangular a: -1.07 b: 0 c: 1.07
Np_2O_5	Triangular a: -1 b: 0 c: 1
$NaNpO_2CO_3$	Log normal, truncated at ±1σ Mean (μ): 0 Standard deviation (σ): 0.25
Schoepite	Triangular a: -0.4 b: 0 c: 0.4
Na-Boltwoodite	Triangular a: -0.5 b: 0 c: 0.3
$NaNpO_2CO_3$	Triangular a: -0.3 b: 0 c: 0.3

Source: Corroborative DTN: SN0704PMASOLUB.001 [DIRS 182787]

Table C6-9. Uncertain Parameters for the Impacts of Reducing Zones in the PMA

Parameter Name	Input Description	Values	Units
FPLRZN	Northern boundary of the reducing zone used for the 3-D model	Uniform: Minimum: 0.0 Maximum: 1.0	NA
FPLRZS	Southern boundary of the reducing zone used for the 3-D model	Uniform: Minimum: 0.0 Maximum: 1.0	NA
FPLRZE	Eastern boundary of the reducing zone used for the 3-D model	Uniform: Minimum: 0.0 Maximum: 1.0	NA
KD_TC_RZ	Sorption coefficient for technetium in the reducing zone	Normal: Mean: 1,000 Standard Deviation: 150	mL/g
KD_NP_RZ	Sorption coefficient for neptunium in the reducing zone	Normal: Mean: 1.000 Standard Deviation: 150	mL/g

Source: Corroborative DTN: SN0704PMASZFTA.001_R1 [DIRS 184395]

Table C6-10. Cumulative Distribution for FPVO for Use in the PMA (log_{10}-transformed)

Probability	Value
0.0	-4.0
0.50	-3.0
0.80	-2.0
1.0	-1.0

Source: Corroborative DTN: SN0704PMASZFTA.001_R1 [DIRS 184395]

Table C9-1. Impact Assessment Summary Table

	ISSUE DESCRIPTION	IMPACT ASSESSMENT
1	Fifteen of the sixteen UZ_Params_Multi_PMA tables, input files to FEHM DLL (version 2.25), need to be populated at run time according to the model simulation specific settings.	This issue does not impact the TSPA-LA PMA dose calculation which uses the appropriate updated UZ_Params file for 300 epistemic realizations. The UZ_Params_Multi files, tables of sampled values of epistemically uncertain parameters, are only used when the PMA model is run with the compliance implementation of the UZ.
2	The 4 external FEHM .mptr input files for the EF 10k and 1Myr cases need to be updated to point to the correct UZ_Params_Multi_PMA file to use.	This modification only impacts EF EXDOC PMA simulations that turn the PMA UZ implementation off (i.e compliance UZ implementation is used). This feature was not used for the PMA dose calculations, but was intended for future sensitivity analyses. This change needs to occur in conjunction with populating the UZ_Params_Mult files identified in issue #1. This issue does not have any impact on dose results.
3	The selector containing the logic for the determination of the CDSP WP Seismic first damage time is incorrectly set.	The first switch in the selector element, Seismic_1st_Dam_Time_CDSP is incorrectly set to suppress any seismic events. The correct setting should select the EXDOC table, Seismic_Time_A1_Spec, which specifies the sampling configuration for the Seismic GM 10,000-year simulation. This issue, which only applies to the 10,000-year Seismic GM simulation, was corrected prior to running the model, and therefore has no impact on dose.
4	UZ tortuosity parameters, UZ_Tortuosity_RG2_a and UZ_Tortuosity_RG3_a were incorrectly set (v10.002) (err#-case# 001-10.002 needs to change to 002-10.002)	The UZ tortuosity parameters should Correct settings: min(1.0,(10^(UZDC_Mean_RG2+UZDC_STN_RG2*UZDC_SD_RG2))) The expression for UZ_Tortuosity_RG3_a should be min(1.0,(10^(UZDC_Mean_RG3+UZDC_STN_RG3*UZDC_SD_RG3))) This error should have negligible or no impact in all modeling cases.
5	The IWPD submodel selector elements for the timing of the first Igneous or Seismic event are incorrectly set to supress events until 400,000 years. To correct this, the first two switches in the selector elements, Event_Time_Feed_IWPD_CDSP and Event_Time_Feed_IWPD_CSNF need to be deleted. (err#-case# 002-10.016)	This issue is scenario specific to the Igneous, Seismic-FD, and Seismic-GM 10,000-year simulations, as well as the Seismic-FD 1, 000,000 year simulations. The model file for each of the affected cases was corrected prior to running the file, and therefore does not impact the dose calculations.

Table C9-1. Impact Assessment Summary Table (Continued)

	ISSUE DESCRIPTION	IMPACT ASSESSMENT
6	ExDoc type runs for both 1Myr EF cases are run with the PMA cladding failure submodel calculations turned on. (err#-case# 003-10.016)	This is not an error and is not applicable to the impact evaluation.
7	The RH threshold for the fluoride ion calculation is incorrect in nineteen of the tables.	Most of these incorrect values were not used in the actual simulations because these values, both the incorrect and the corrected ones, are low (<0.65). At such low RH, the temperatures in the drift will be still high (> 96 $^{\circ}$ C) and there will be no seepage water dripping. For the other incorrect values, the differences between the incorrect and the correct ones are small (<0.012). Therefore, the impact on dose is expected to be negligible.
8	The PMA early failure scenarios distribute the EBS mass released to the UZ nodes unevenly within a given percolation subregion.	Although the EBS mass released to the UZ nodes is distributed unevenly within a given percolation subregion in each realization, the even distribution is captured by calculating the annual mean dose from 300 realizations sampling uncertainty uniformly. Therefore no dose impact is expected.
9	Certain parameters within the model were not connected to the PMA database.	The PMA simulations use the correct values for the parameters listed below, and therefore this issue does not affect the dose calculations. The parameters that need to be linked to the PMA database include, FPLRZN, FPLRZS, FPLRZE, FPVO_PMA, Rf1-Rf10, Kd_Np_RZ, Kd_Np_RZ, SZ_Block_Length, SZ_Block_Thickness, Viscosity_water_T, Sat_Vap_Density_Outside_WP, Water_Vap_Diff_Coeff, Water_Vap_Diff_Cond, Air_Entry_Potential, Sat_Vap_Density_Inside_WP, Osmotic_Coeff, pH_eq
10	Certain parameters within the model were not locked on to the PMA database. GoldSim allows you to “lock onto” the file that is being referenced by a file element. When you lock onto a file (by checking the Lock onto this file option in the File element dialog), the following additional information regarding the referenced file is saved with the element: File and path name; Date the file was created; Date the file was last modified; File size; and CRC signature. Once you have locked onto a file, this information is displayed in a tool-tip when you hold your cursor over the filename in the dialog.	The PMA simulations used the correct files because they were downloaded from the controlled PMA database when the model was run, and therefore this issue does not affect the dose calculations.

Table C9-1. Impact Assessment Summary Table (Continued)

	ISSUE DESCRIPTION	IMPACT ASSESSMENT
11	The pH regression equation contains incorrect coefficients.	The coefficients in the regression for pH_eq need to be corrected. The value of 7.2625 should be rounded to 7.3. The value of 0.00185 has an extra zero and should also be rounded to 0.02. pH_eq is the pH where the acid and the alkaline dissolution rates cross over, and this pH weakly depends on temperature. For the most part of repository time period, the resulting difference in pH_eq due to the error is less than one unit, which is within the uncertainty range of predicted in-package pH values. Therefore, the impact on annual dose is expected to be negligible.
12	There are incorrect values in some of the tables used in the in-package chemistry calculations.	Some of the inputs in the PMA database for the lookup tables named: IPC_XXX_pH_Rsw_YY_Z_LUT (where XXX = CSNF, DHLW, or MCO; YY = 15, 2, 3, or 4; and Z = A-I) has some rows with erroneous data. The DTN that supplied the tables had some independent variables that were duplicated in multiple rows. GoldSim could not read tables with these duplicate independent variables. The DTN supplier indicated that it was acceptable to average these rows together. The error occurred because the analyst who averaged these rows failed to expand out each cell to display the maximum number of significant figures. Therefore some rows were rounded together that did not need to be. No impacts to the dose results are expected. More information is provided in PEF 500. The PEF has a Roadmap to the TSPA-produced DTN that holds the modified lookup tables. This DTN now has two file sets: Uncorrected and Corrected. To correct this error, replace the PMA database entries with the tables in the Corrected folder.
13	The parameter specifying the value of Np Carbonate Eps is incorrect.	The input in the PMA database for parameter “Np_Carbonate_PMA_Eps” is not correct. It should be a triangular distribution with a=-0.5 and b=0 and c=0.5 rather than a truncated normal distribution. The truncated normal distribution is equally well justified. No impacts to the dose results are expected.
14	In determining whether the drift chemical environment is benign or aggressive for drip shield general corrosion, 5 mM dissolved fluoride concentration is used instead of 0.5 mM as suggested in C6.3.1.	The value of 5 mM is justifiable because this value is close to the middle point of the fluoride concentration interval within which the corrosion rate starts to increase at the lower bound (0.5 mM) and then levels off at the upper bound (5 mM). Furthermore, this error only affects one out four initial seepage waters used in the model and this effect will diminish as the seepage water composition returns to the ambient conditions after the thermal event. Therefore, the impact of this error is negligible.

INTENTIONALLY LEFT BLANK

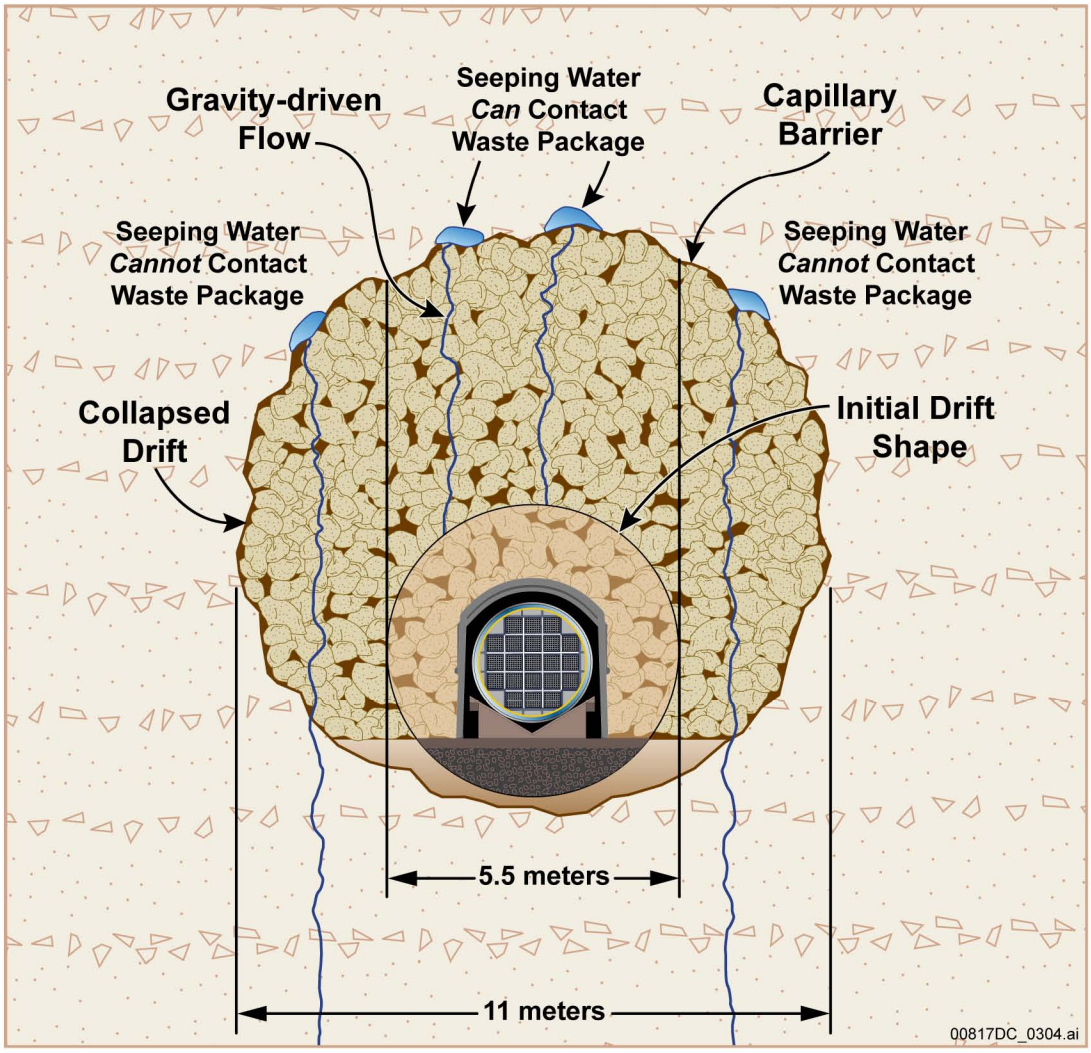

Figure C6-1. Schematic Illustration of Expected Flow Behavior of Seepage in a Rubble-Filled Collapsed Drift

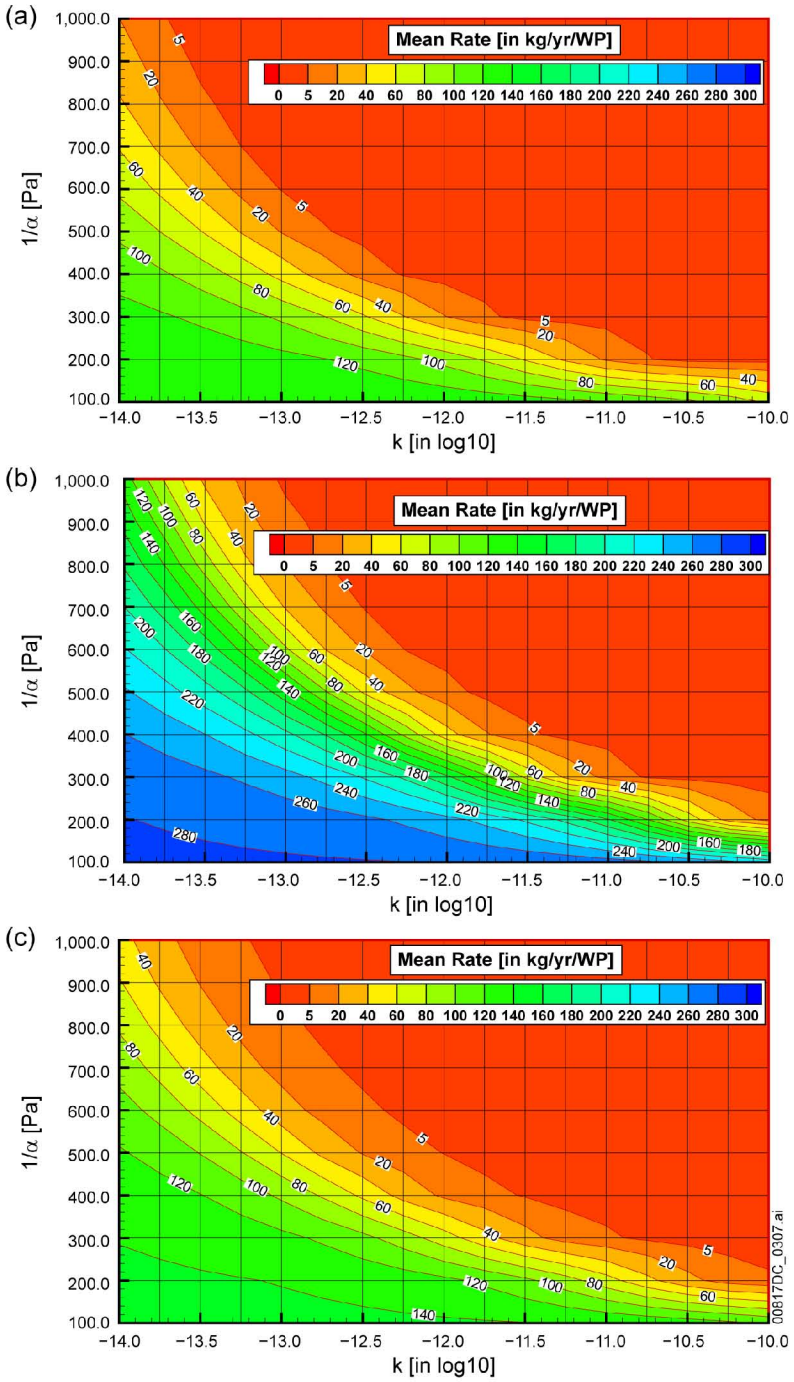

Source: (a) DTN: LB0304SMDCREV2.002 [DIRS 163687], file: Fig6-3to6-8.dat, (b) DTN: LB0307SEEPDRCL.002 [DIRS 180511], file: ResponsSurfaceSMPACollapsedDrift.dat, (c) Corroborative DTN: LB0704PASEEP01.001 [DIRS 181223], file: LookupTableSeepageCollapsedDriftCenter.xls.

NOTES: Seepage Rate Shown as a Function of Capillary-Strength Parameter and Mean Permeability for a Percolation Flux of 5 mm/year. Plots conducted with Tecplot V9.0 graphical software. Horizontal and vertical lines indicate simulated SMPA parameter combinations. Permeability values in log10 of unit m^2.

Figure C6-2. Mean Seepage Rate for (a) Intact Drift, (b) Collapsed Drift with Seepage Collected over 11-Meter Wide Drift, and (c) Collapsed Drift with Seepage Collected over 5.5-Meter Wide Center Section of Drift

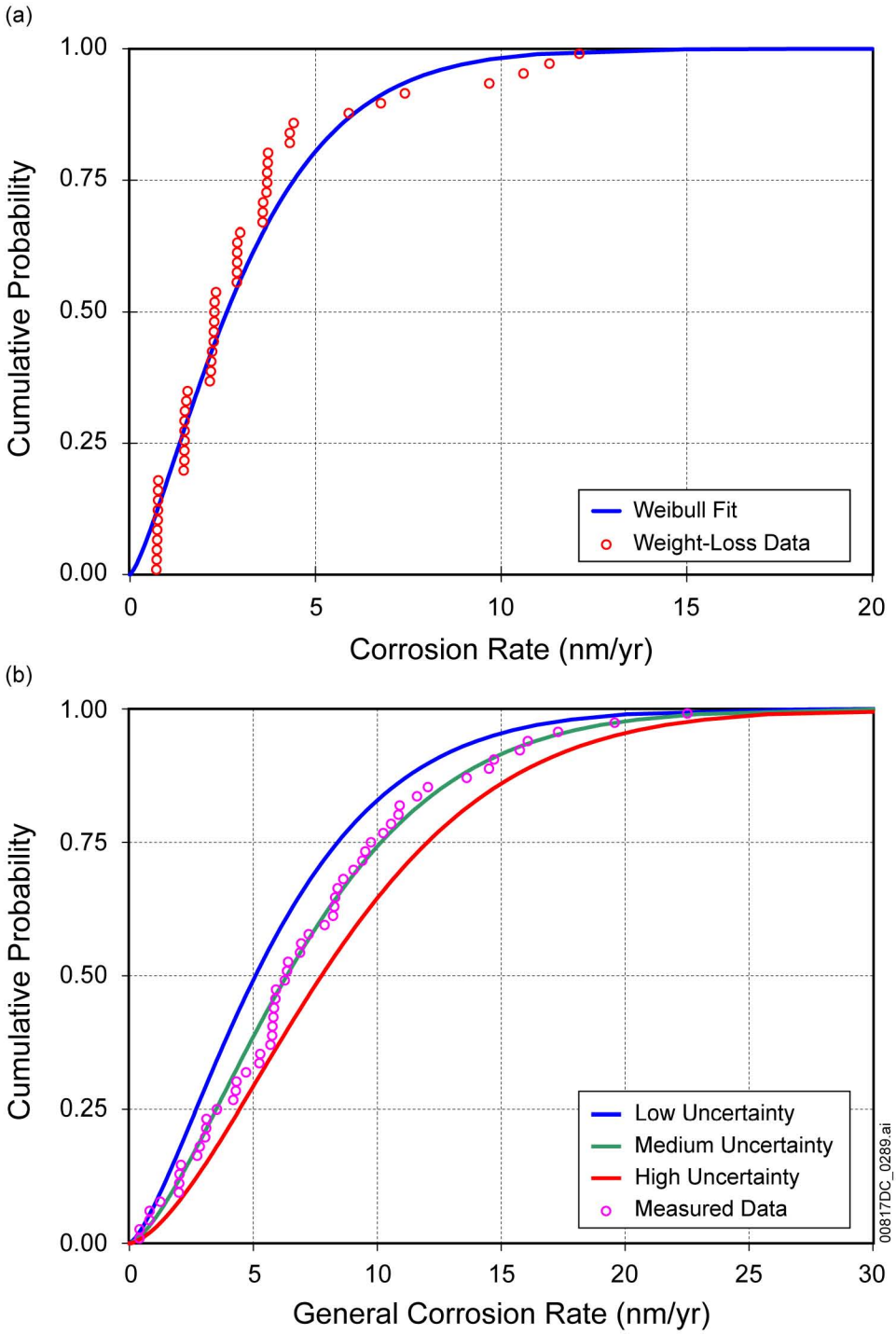

Sources: DTN: LL03041251251.057 [DIRS 163712], *C22 5 Year Coupon Corrosion Rates 4-14-03.xls*;
DTN: MO0612WPOUTERB.000, [DIRS 182035], *ACM GC Rate CDF.xls*.

Figure C6-3. General Corrosion Rate Distribution Resulting from Fitting of Five-year Exposed Weight-Loss Sample Data

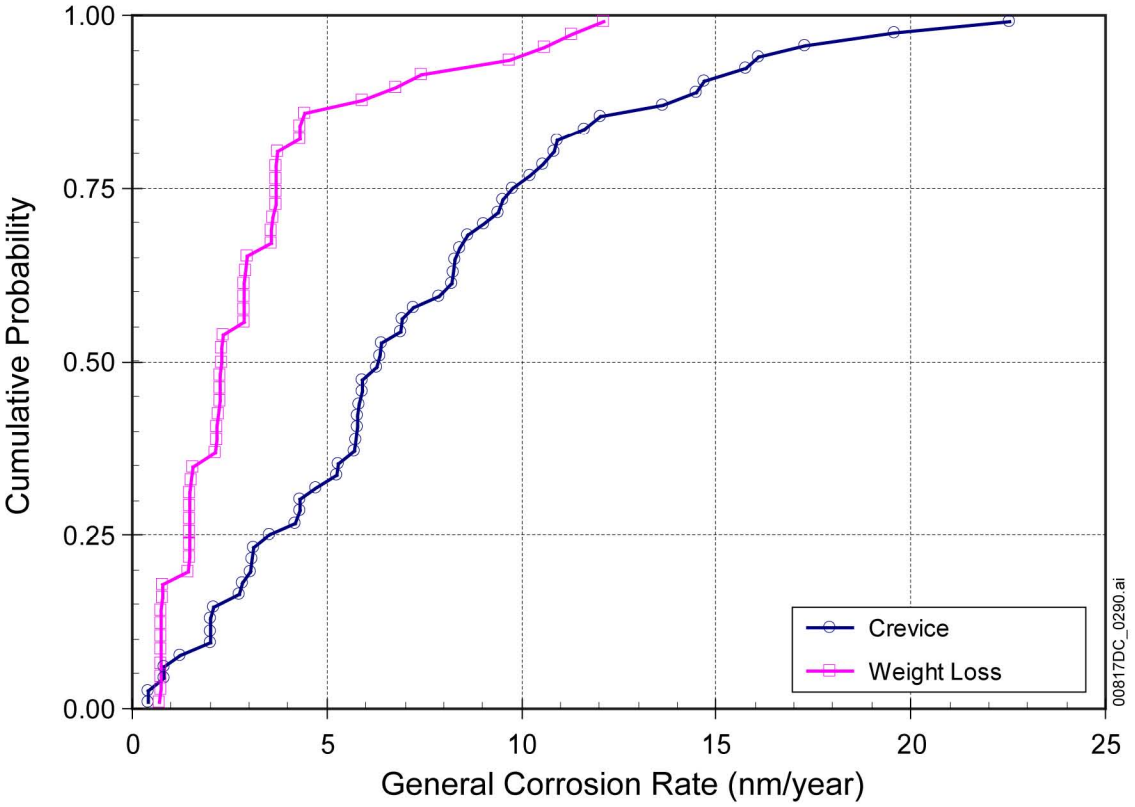

Sources: DTN: MO0612WPOUTERB.000 [DIRS 182035], *Alloy22_5yr_CreviceAnalysis.xls*.

Figure C6-4. Empirical Cumulative Distribution for General Corrosion Rate of Alloy 22 Weight-Loss and Crevice Samples after Five-Year Exposure in Long-Term Corrosion Test Facility

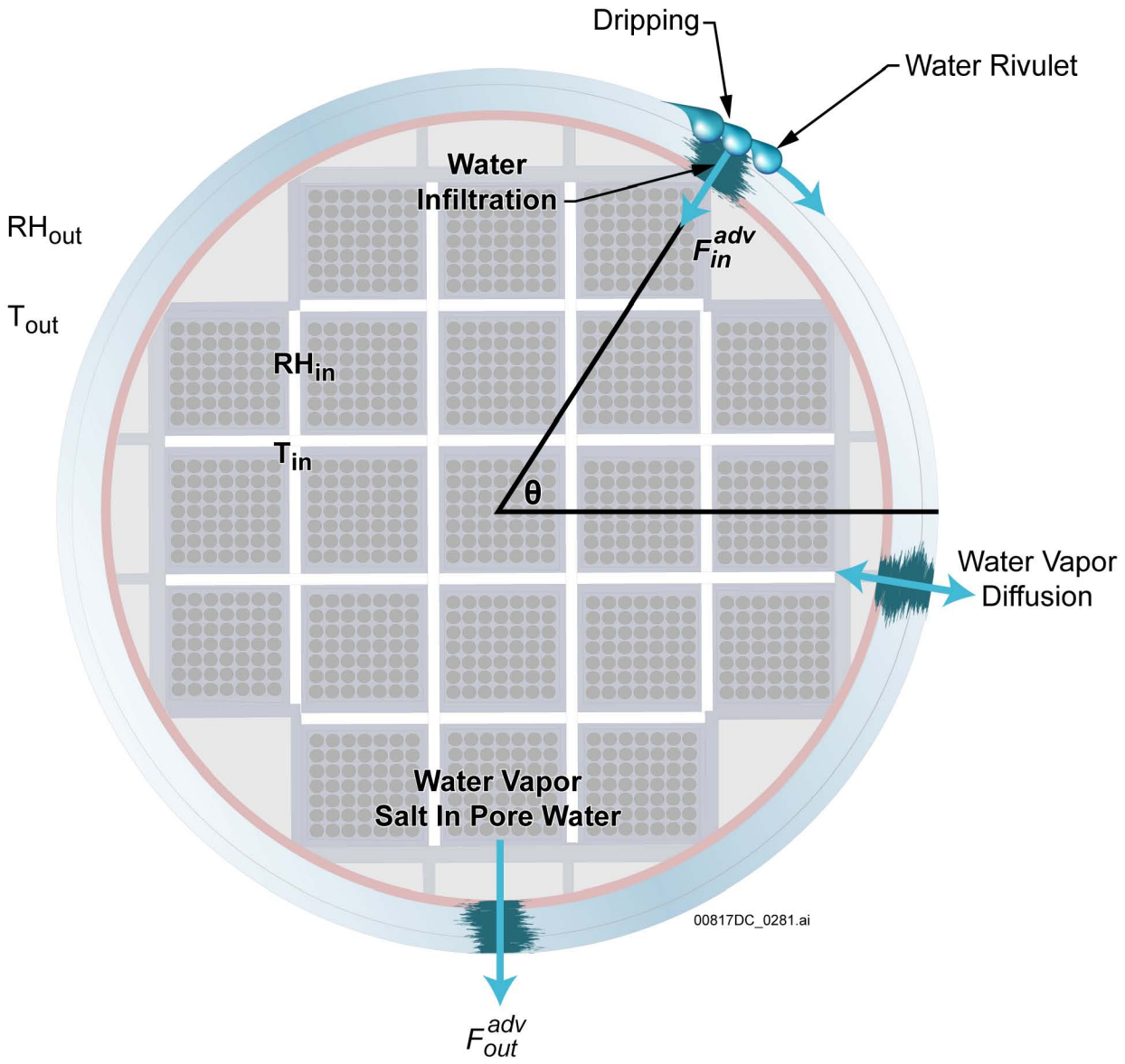

Figure C6-5. Schematic Diagram of Modeling System for In-Package Water Balance

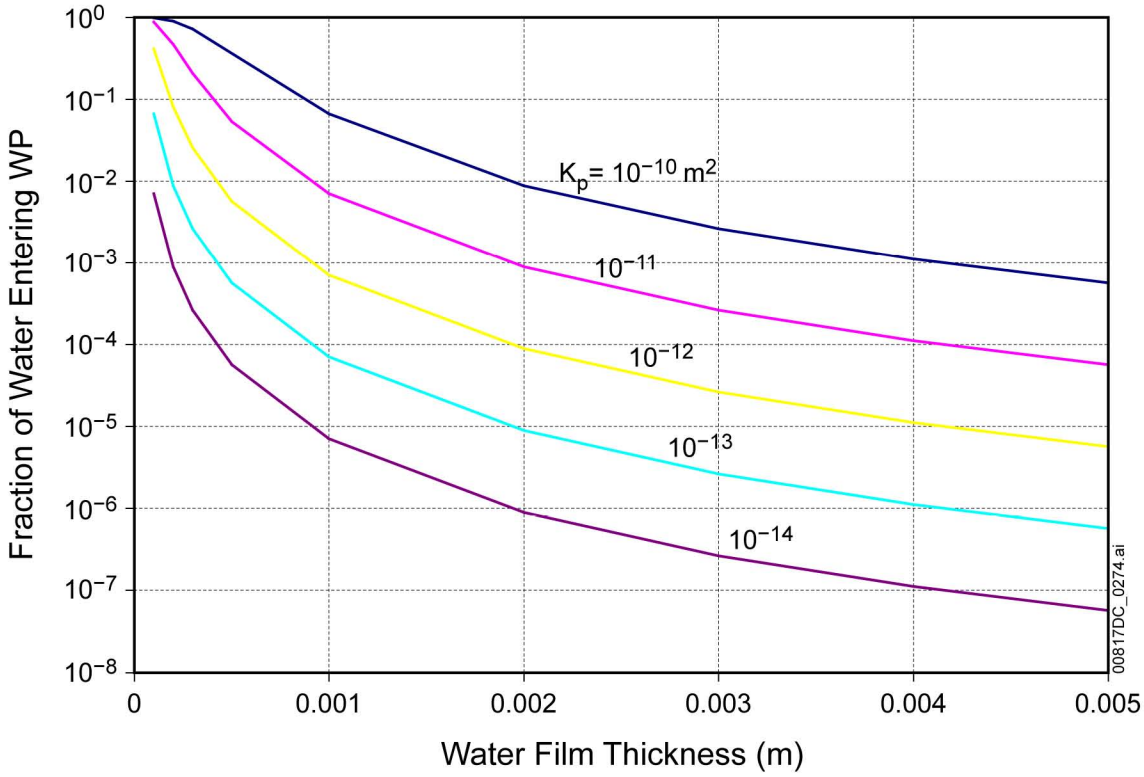

Source: Corroborative DTN: SN0704PMAWBCAL.001_R1 [DIRS 182335], file: *inputs_to_water_balance model.xls, worksheet "water-flux"*.

NOTES: f = 0.1 and ϕ = 0.4

Figure C6-6. Fraction of Water Entering Waste Package Estimated from the Sheet-Flow Model

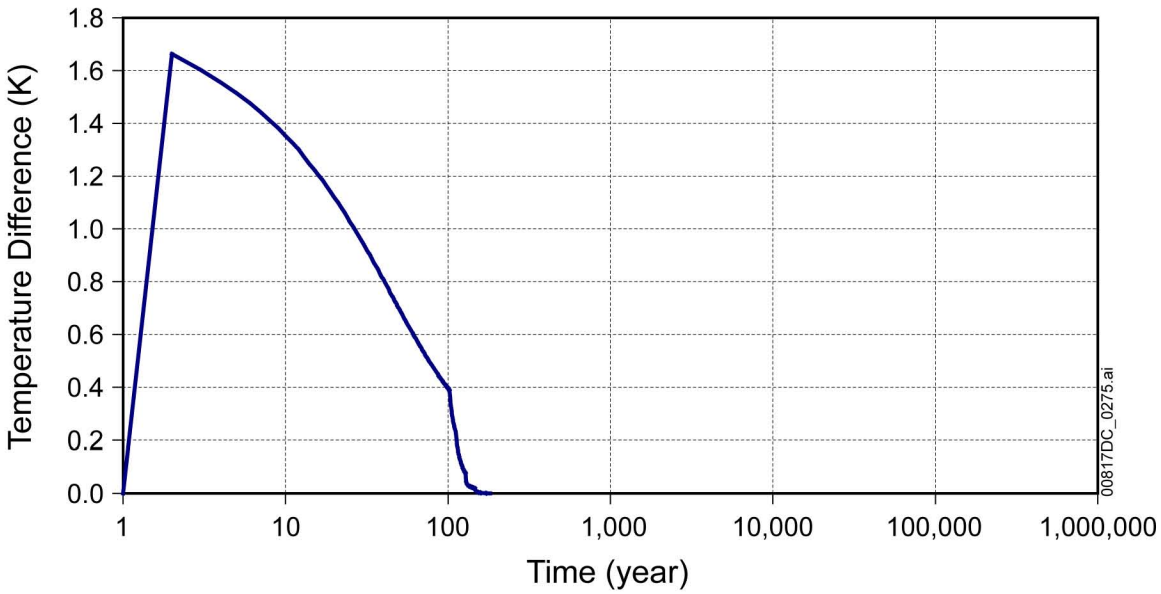

Source: Corroborative DTN: SN0704PMAWBCAL.001 [DIRS 182335], file: *inputs_to_water_balance model.xls, worksheet "Thermal Evolution"*.

Figure C6-7. Temperature Difference between the Inside and Outside of a Waste Package

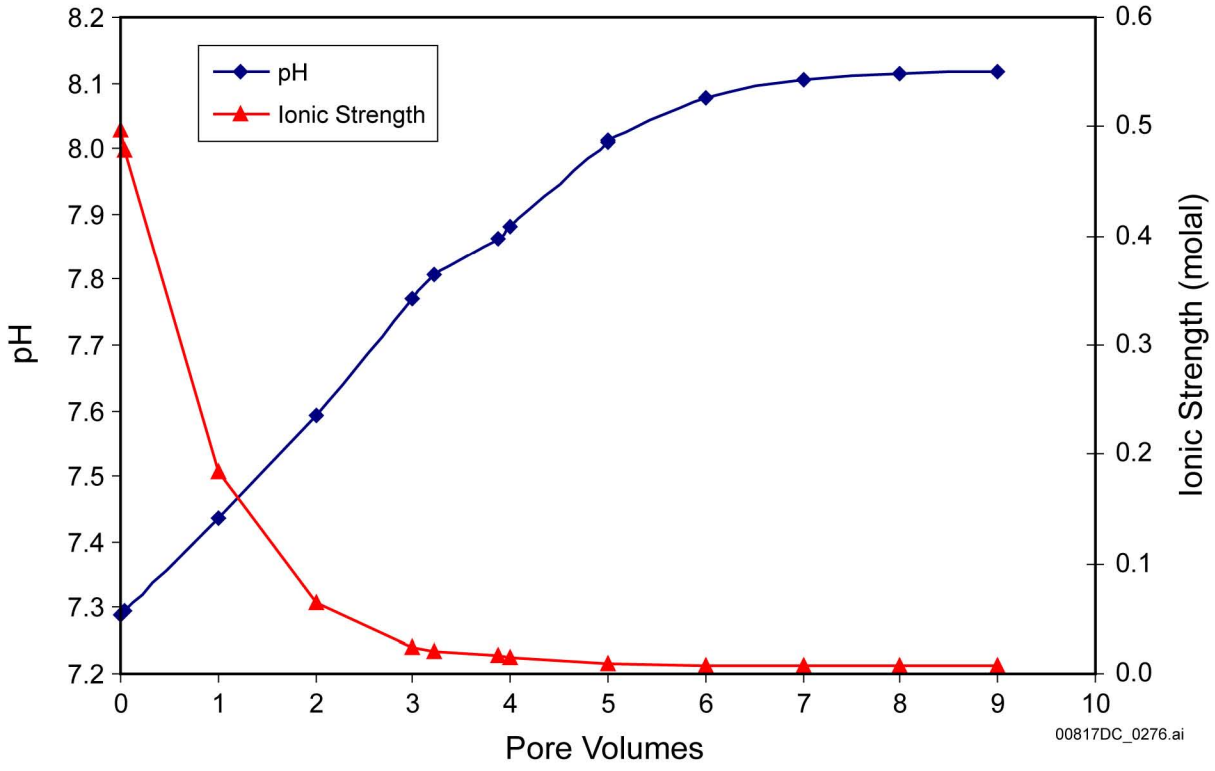

Source: Corroborative DTNs: SN0704PMAIPCPM.001_R0 [DIRS 180745], file: *p0c3fp0s.elem_aqu.xls*; MO0709MARGANAL.000_R0 [DIRS 182978].

Figure C6-8. Illustration of the Approach to Steady State pH and Ionic Strength as a Function of Pore Volumes Flushed

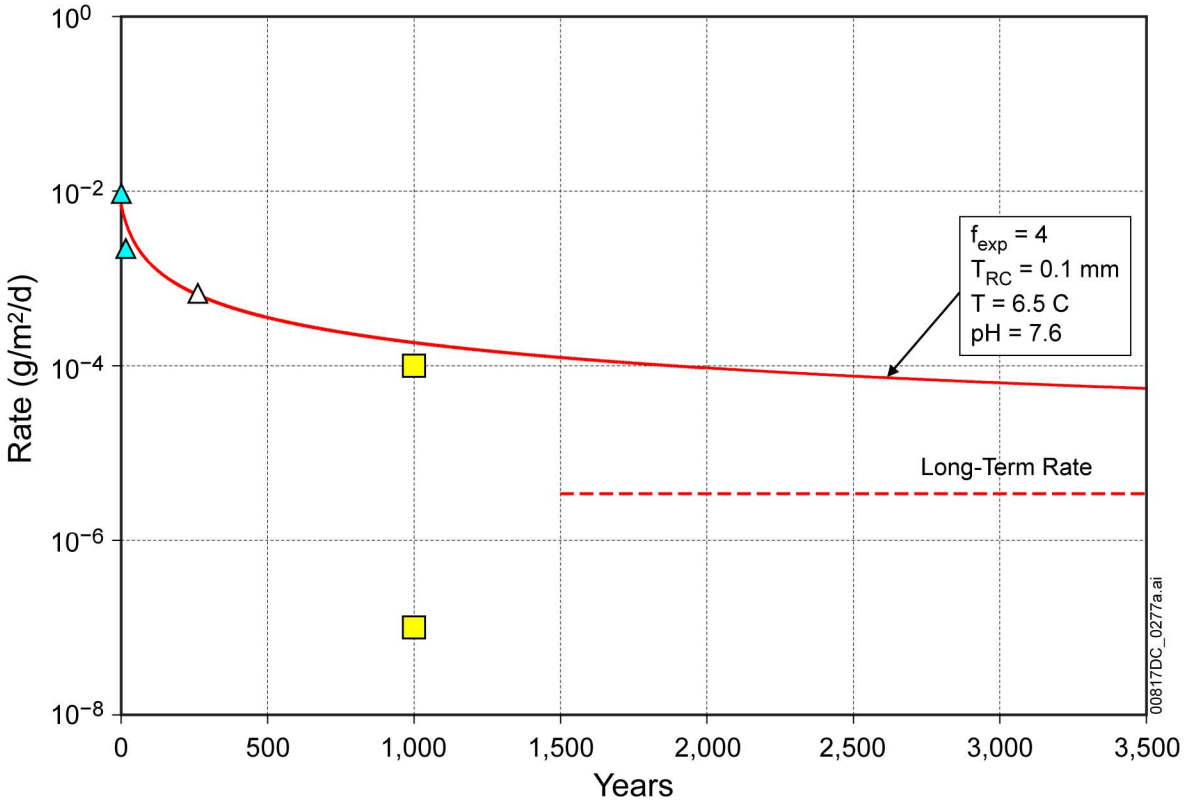

Sources: Triangles from Ojovan et al. (2005 [DIRS 180494]); squares from Gordon and Brady (2003 [DIRS 176673], Table 4); Corroborative DTN: SN0704PMAGDEGM.001_R2 [DIRS 183955], file: *PMA model_revised.xls, worksheet "rate(PMA)"*.

Figure C6-9. Comparison of Performance Margin Analysis Model for High-Level Waste Glass Dissolution

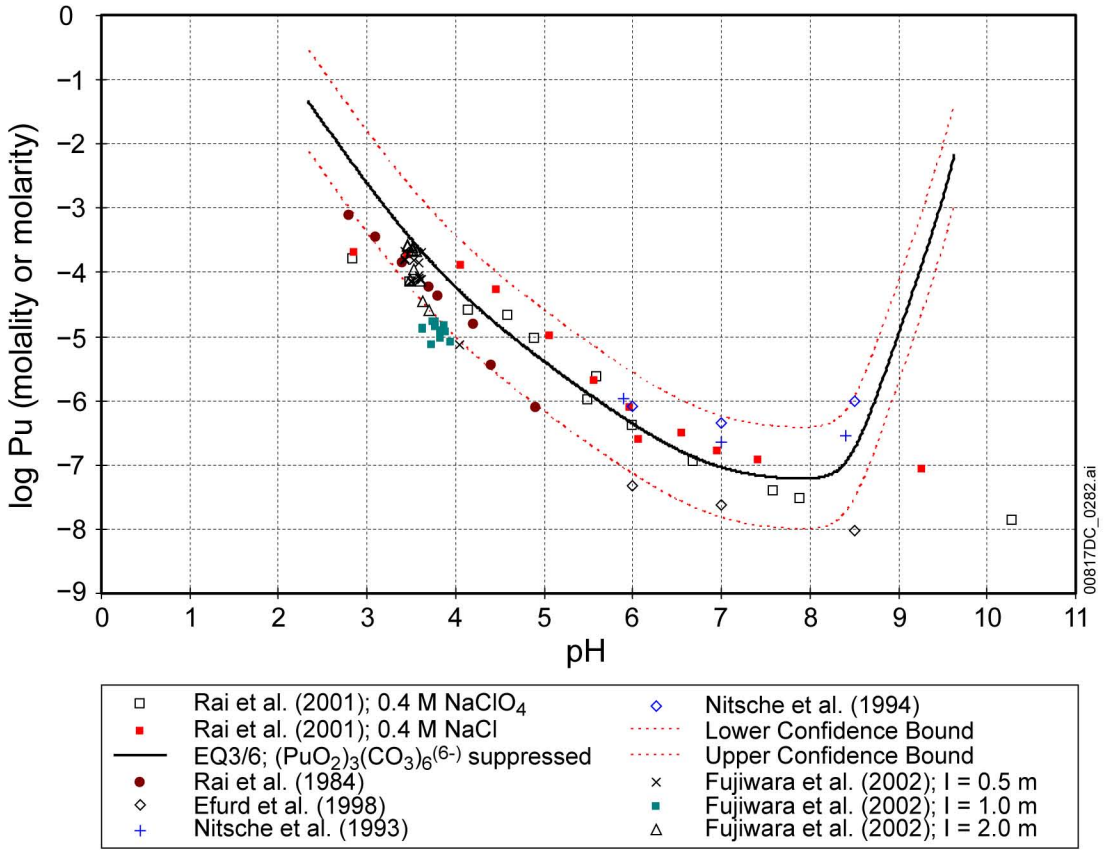

Source: Corroborative DTN: SN0704PMASOLUB.001_R1 [DIRS 182787], file: *Recommended_Uncertainties_Pu_Np_U_Rev01.xls, worksheet "PuO2(hyd,aged)_Summary".*

NOTE: Computed solubility curve is in molality units ($logfO_2(aq)$=-7; $logPCO_2$=-3.5 bars).

Figure C6-10. Plot of Log Transformed PuO_2(am) Solubility vs. pH

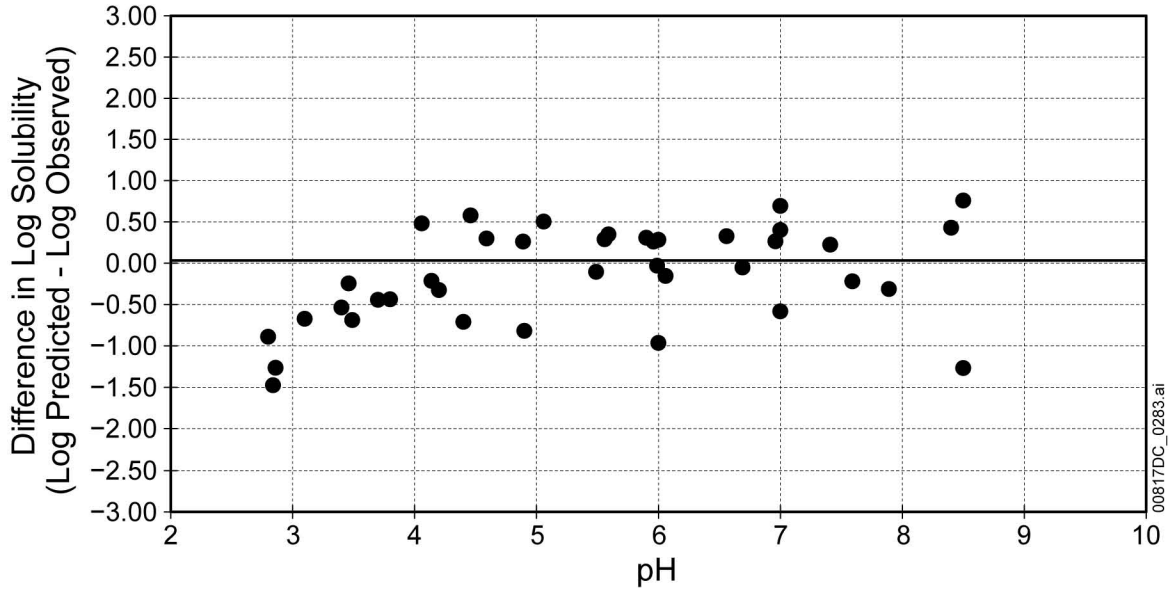

Source: Corroborative DTN: SN0704PMASOLUB.001_R1 [DIRS 182787], file: *Recommended_Uncertainties_Pu_Np_U_Rev01.xls, worksheet "PuO2(hyd,aged)_Summary".*

NOTE: Log predicted stands for solubility values obtained by EQ3/6 simulations. Log observed is the reported solubilities by various sources.

Figure C6-11. Plot of Log Transformed Differences (Log Predicted−Log Observed) for PuO_2(am) Solubility

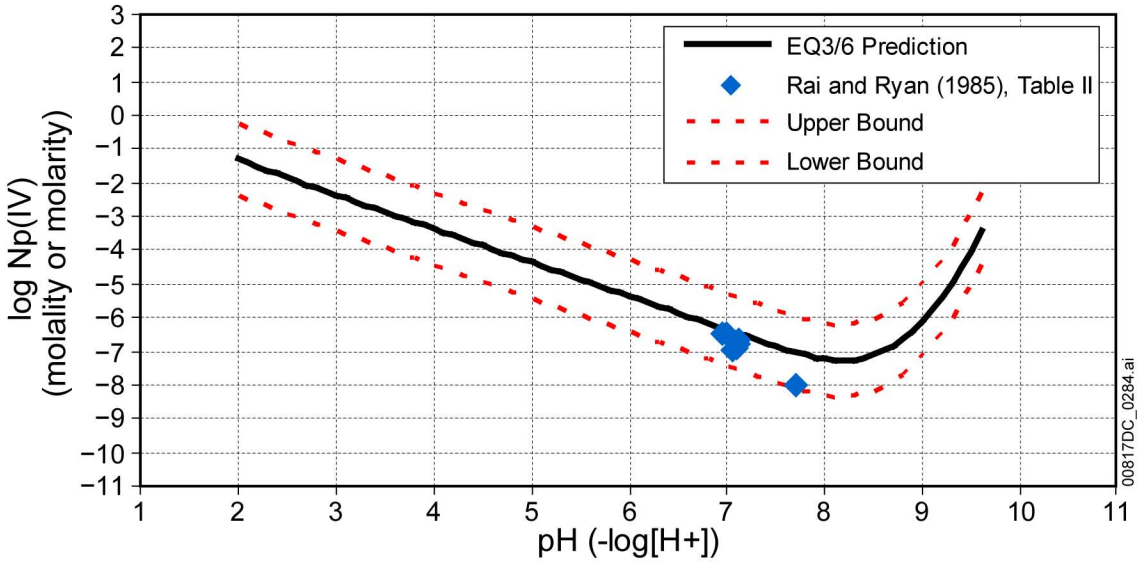

Source: DTN: SN0612T0502404.014 [DIRS 178850]; Corroborative DTN: SN0704PMASOLUB.001_R1 [DIRS 182787], file: *Recommended_Uncertainties_Pu_Np_U_Rev01.xls, worksheet "Np_summary"*.

NOTE: The predicted solubility by EQ3/6 is calculated using the thermodynamic database *data0.ymp.R5* (DTN: SN0612T0502404.014 [DIRS 178850]). The summary of calculations is given in Corroborative DTN: SN0704PMASOLUB.001_R1 [DIRS 182787].

Figure C6-12. Comparison of Predicted (EQ3/6) and Observed Values for NpO_2 Solubility along with Uncertainty Bounds

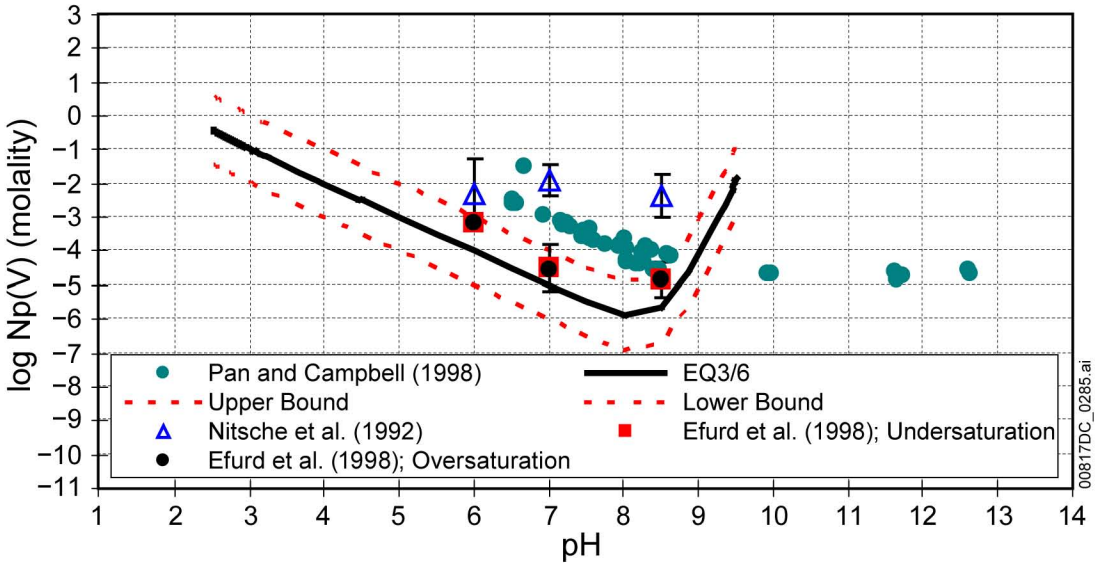

Source: DTN: SN0612T0502404.014 [DIRS 178850]; Corroborative DTN: SN0704PMASOLUB.001_R1 [DIRS 182787], file: *Recommended_Uncertainties_Pu_Np_U_Rev01.xls, worksheet "Np_summary"*.

NOTE: The predicted solubility by EQ3/6 is calculated using the thermodynamic database *data0.ymp.R5* (DTN: SN0612T0502404.014 [DIRS 178850]). Vertical error bars represent one standard deviation. The summary of calculations is given in Corroborative DTN: SN0704PMASOLUB.001_R1 [DIRS 182787].

Figure C6-13. Comparison of Predicted (EQ3/6) and Observed Values for Np_2O_5 Solubility along with Uncertainty Bounds

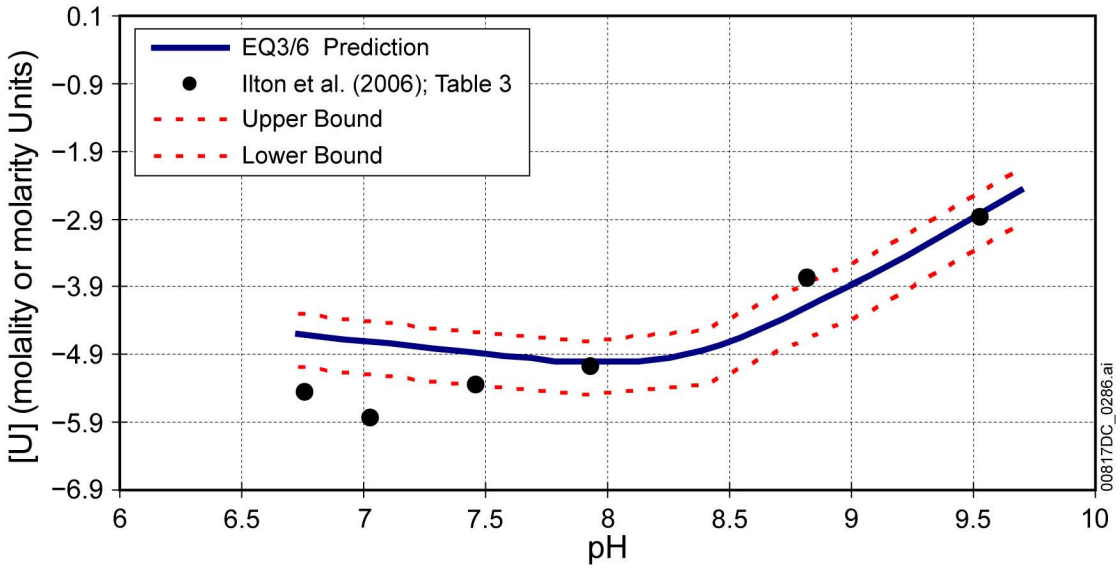

Source: DTN: SN0612T0502404.014 [DIRS 178850]; Corroborative DTN: SN0704PMASOLUB.001_R1 [DIRS 182787], file: *Recommended_Uncertainties_Pu_Np_U_Rev01.xls, worksheet* "U(VI)_*summary*".

NOTE: The predicted solubility by EQ3/6 is calculated using the thermodynamic database *data0.ymp.R5* (DTN: SN0612T0502404.014 [DIRS 178850]). The summary of calculations is given in Corroborative DTN: SN0704PMASOLUB.001_R1 [DIRS 182787].

Figure C6-14. Comparison of Predicted (EQ3/6) and Observed Values for Na-Boltwoodite Solubility along with Uncertainty Bounds

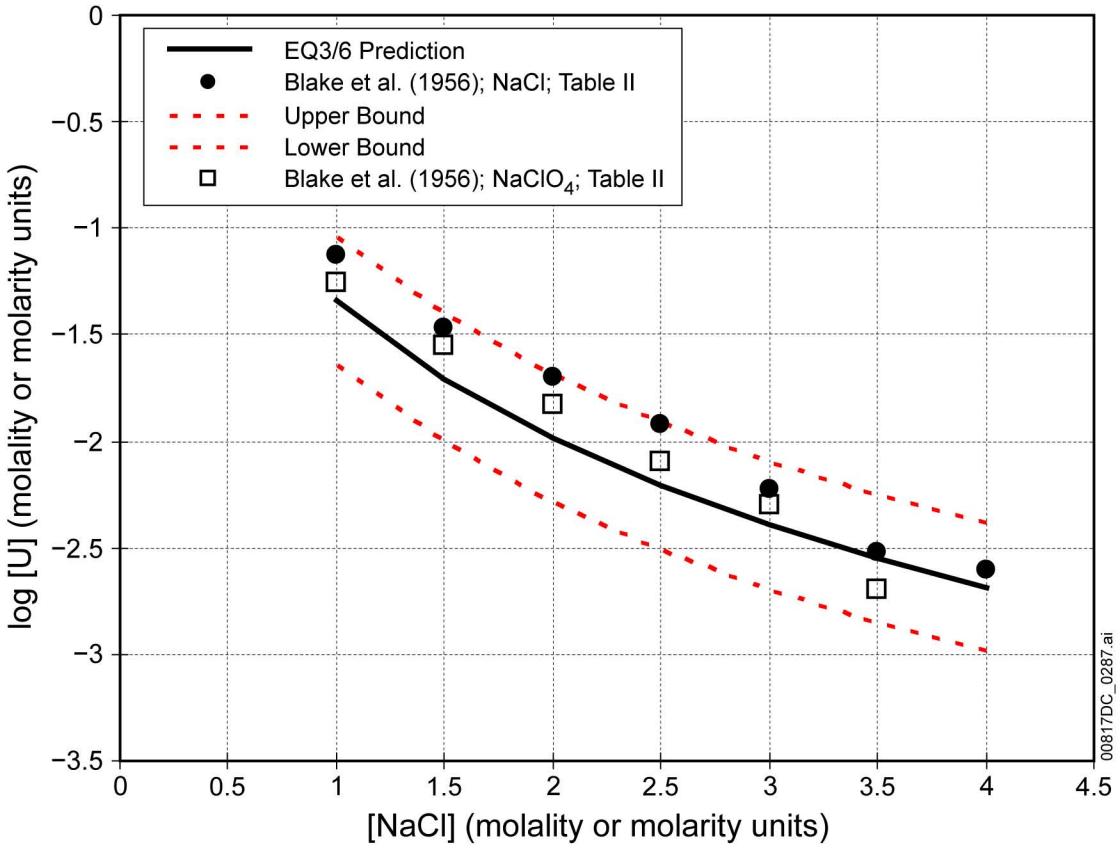

Source: DTN: SN0612T0502404.014 [DIRS 178850]; Corroborative DTN: SN0704PMASOLUB.001_R1 [DIRS 182787], file: *Recommended_Uncertainties_Pu_Np_U_Rev01.xls, worksheet* "U(VI)_*summary*".

NOTE: The predicted solubility by EQ3/6 is calculated using the thermodynamic database *data0.ymp.R5* (DTN: SN0612T0502404.014 [DIRS 178850]). The summary of calculations is given in Corroborative DTN: SN0704PMASOLUB.001_R1 [DIRS 182787].

Figure C6-15. Comparison of Predicted (EQ3/6) and Observed Values for $Na_4UO_2(CO_3)_3$ Solubility along with Uncertainty Bounds

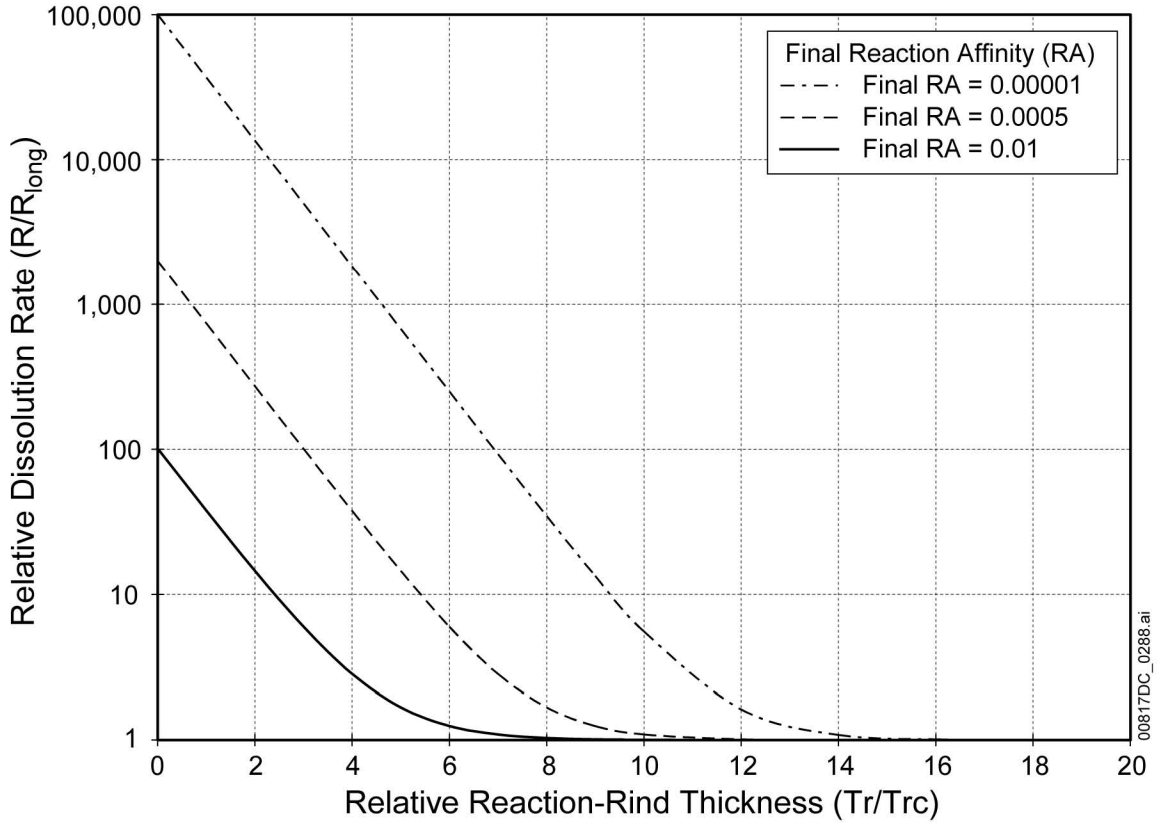

Source: Corroborative DTNs: SN0704PMAGDEGM.001_R2 [DIRS 183955], file: *PMA Model_revised.xls, worksheet "L-T rate"*; MO0709MARGANAL.000 [DIRS 182978].

Figure C6-16. Decrease in Relative Dissolution Rate as a Function of Critical Reaction-Rind Thickness for Each of Three Values for the Final Reaction Affinity

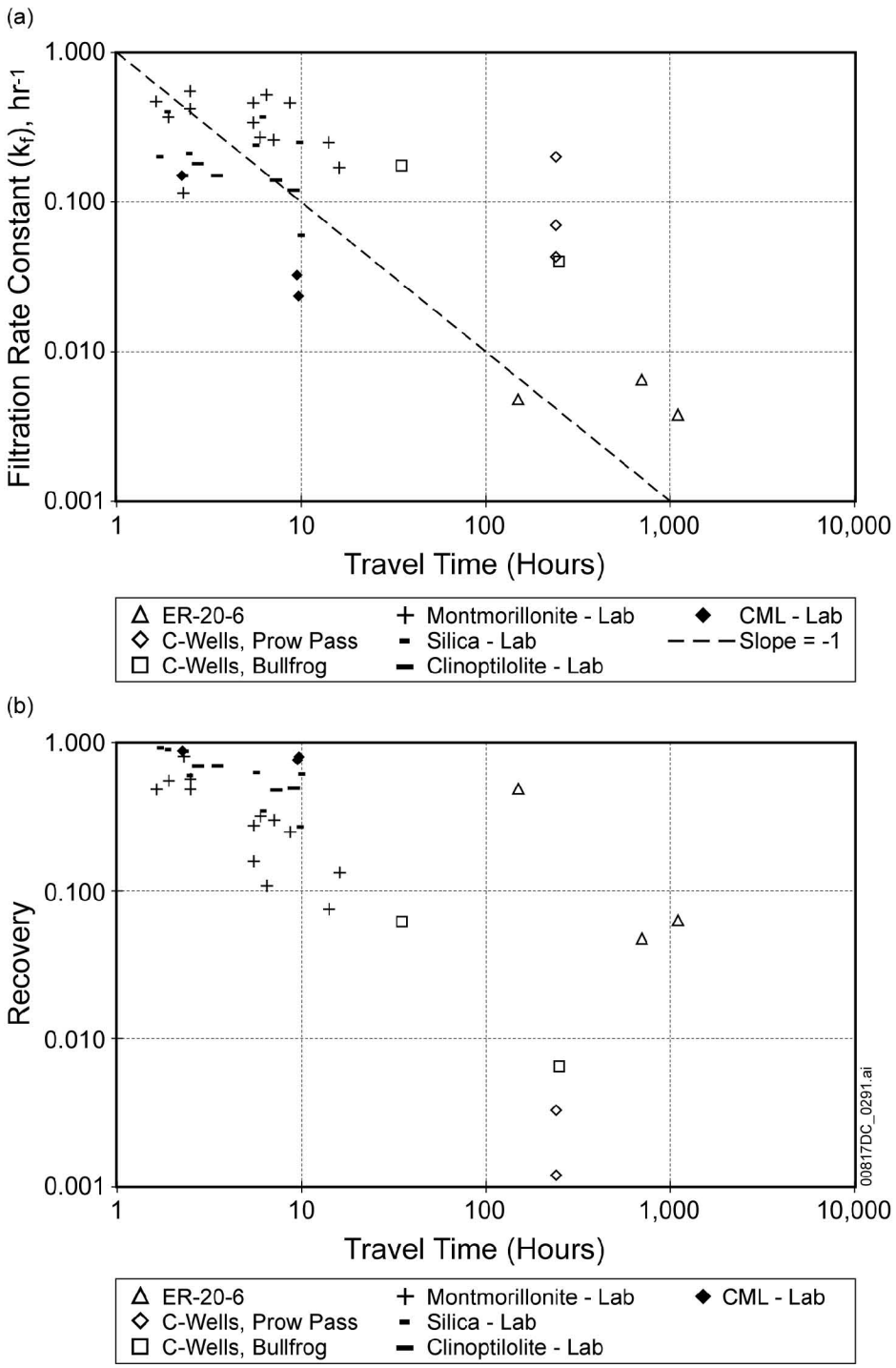

Source: Output DTN: LA0705PR150304.001 [DIRS 181744], file: *Colloid_Diversity_Parameters.xls, worksheet "Volcanics Data*; and Corroborative DTN: MO0709MARGANAL.000 [DIRS 182978].

NOTE: Travel times in field tests are peak conservative tracer travel times.

Figure C6-17. Colloid Filtration Rate Constants and Fractional Recoveries vs. Unretarded Groundwater Travel Times (Determined from Conservative Solute Tracers) from Tracer Experiments in Saturated Fractured Volcanics

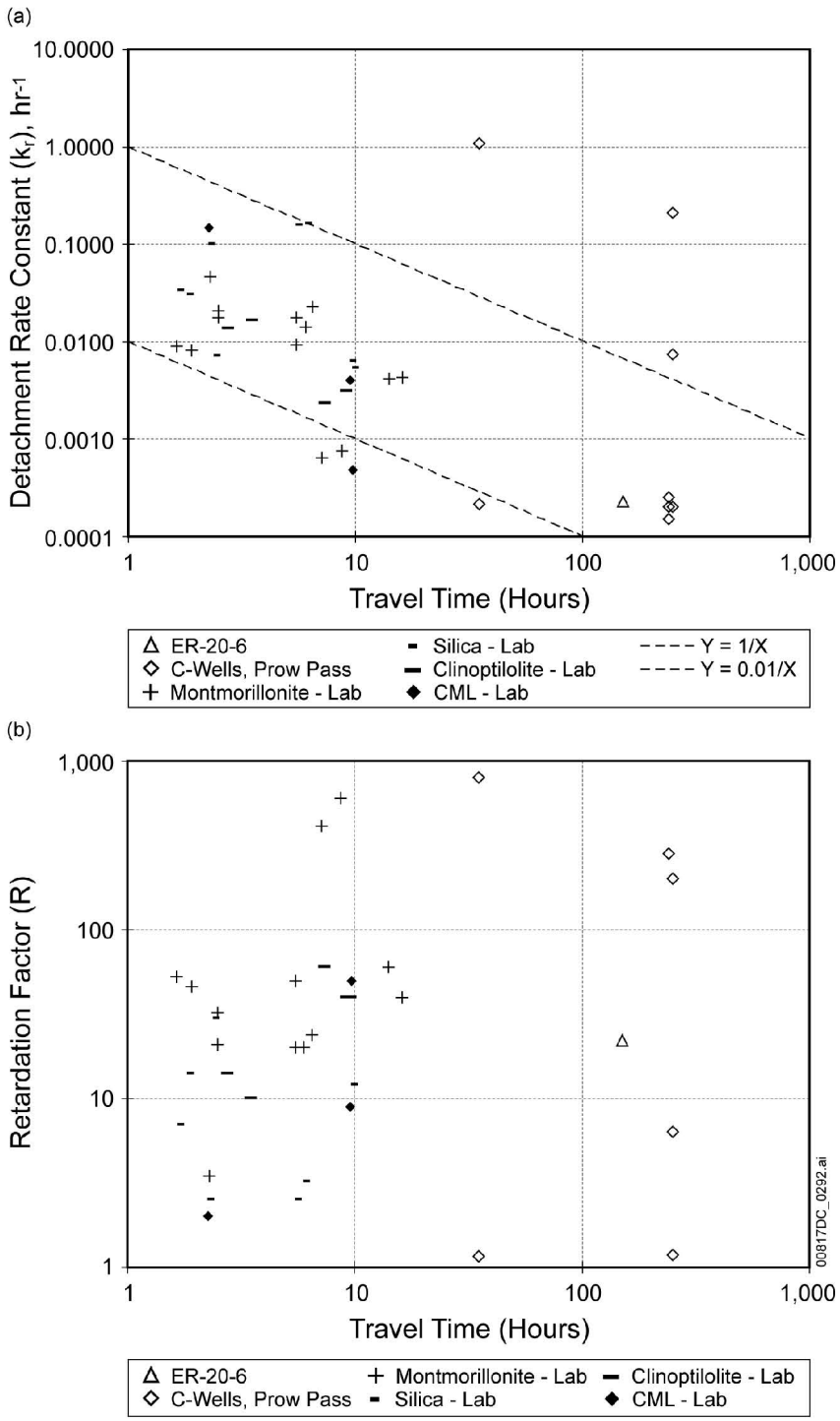

Source: Output DTN: LA0705PR150304.001 [DIRS 181744], file: *Colloid_Diversity_Parameters.xls, worksheet "Volcanics Data"*; and Corroborative DTN: MO0709MARGANAL.000 [DIRS 182978].

NOTE: Travel times in field tests are peak conservative tracer travel times.

Figure C6-18. Colloid Detachment Rate Constants and Retardation Factors vs. Unretarded Groundwater Travel Times (Determined from Conservative Solute Tracers) from Tracer Experiments in Saturated Fractured Volcanics

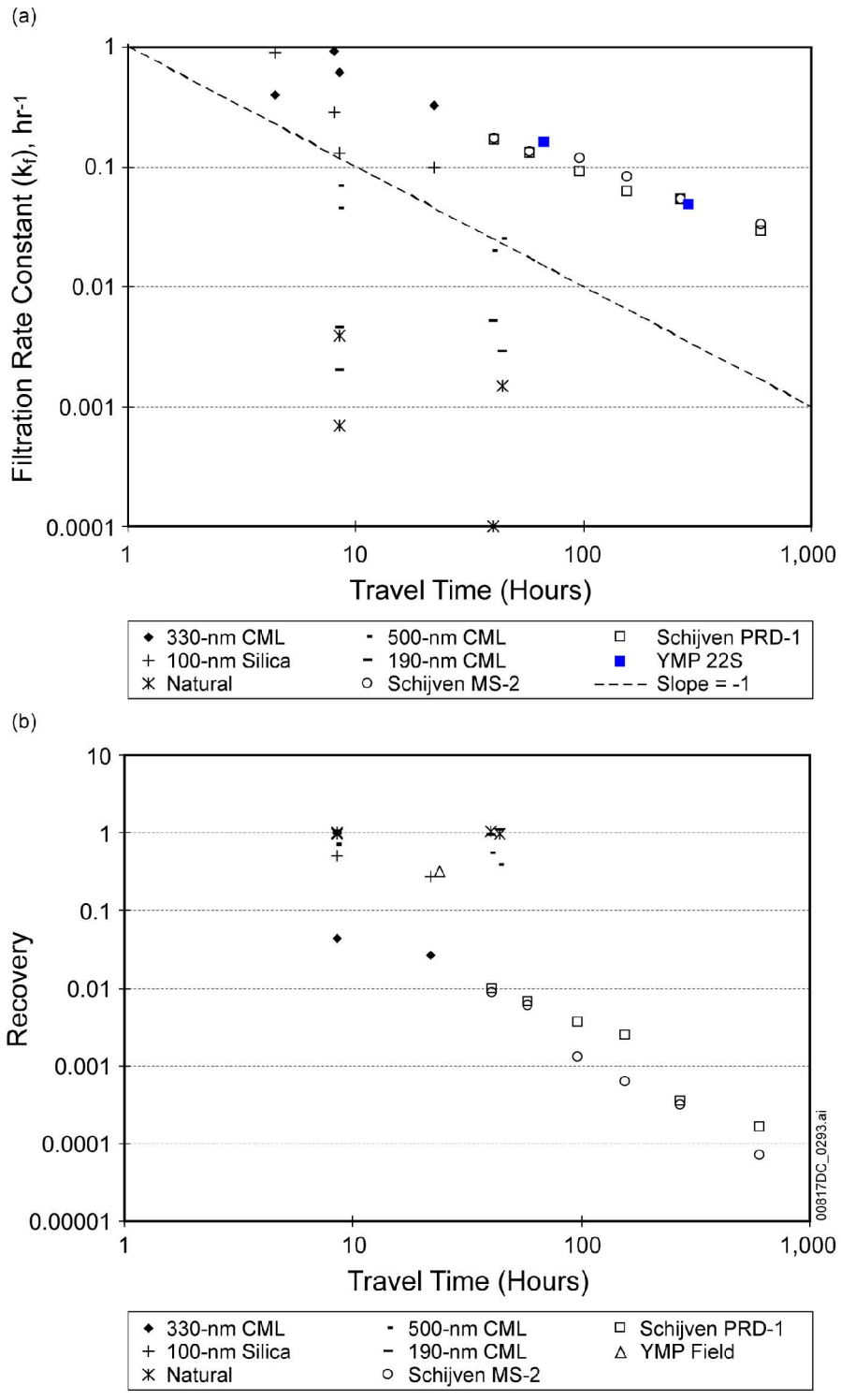

Source: Output DTN: LA0705PR150304.001 [DIRS 181744], file: *Colloid_Diversity_Parameters.xls, worksheet "Alluvium Data"*; and Corroborative DTN: MO0709MARGANAL.000 [DIRS 182978].

Figure C6-19. Colloid Filtration Rate Constants and Fractional Recoveries vs. Unretarded Groundwater Travel Times (Determined from Conservative Solute Tracers) from Tracer Experiments in Saturated Alluvium

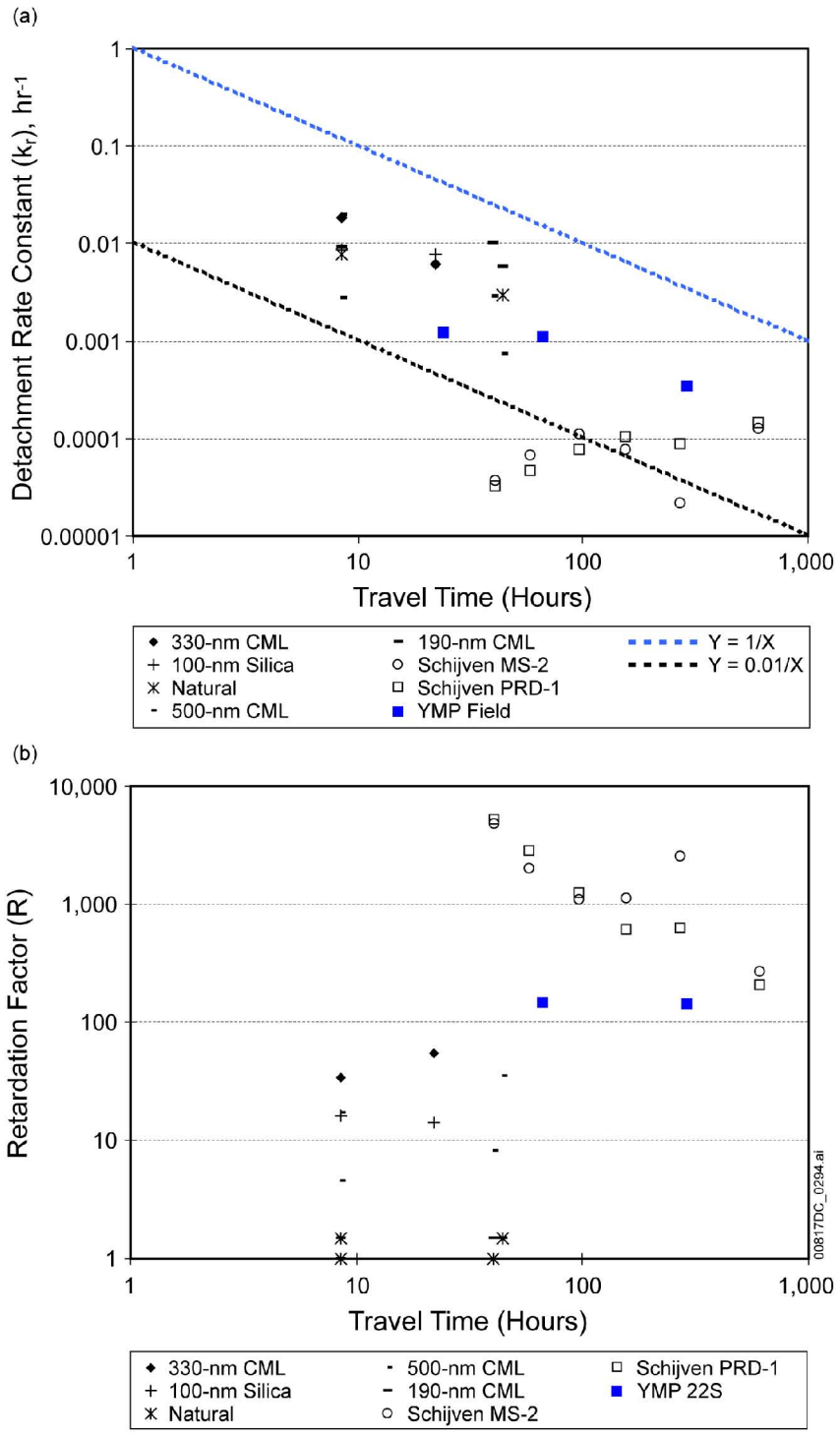

Source: DTN: LA0705PR150304.001 [DIRS 181744], file: *Colloid_Diversity_Parameters.xls, worksheet "Alluvium Data"*; and Corroborative DTN: MO0709MARGANAL.000 [DIRS 182978].

NOTE: Travel times in field tests are peak conservative tracer travel times.

Figure C6-20. Colloid Detachment Rate Constants and Retardation Factors vs. Unretarded Groundwater Travel Times (Determined from Conservative Solute Tracers) from Tracer Experiments in Saturated Alluvium

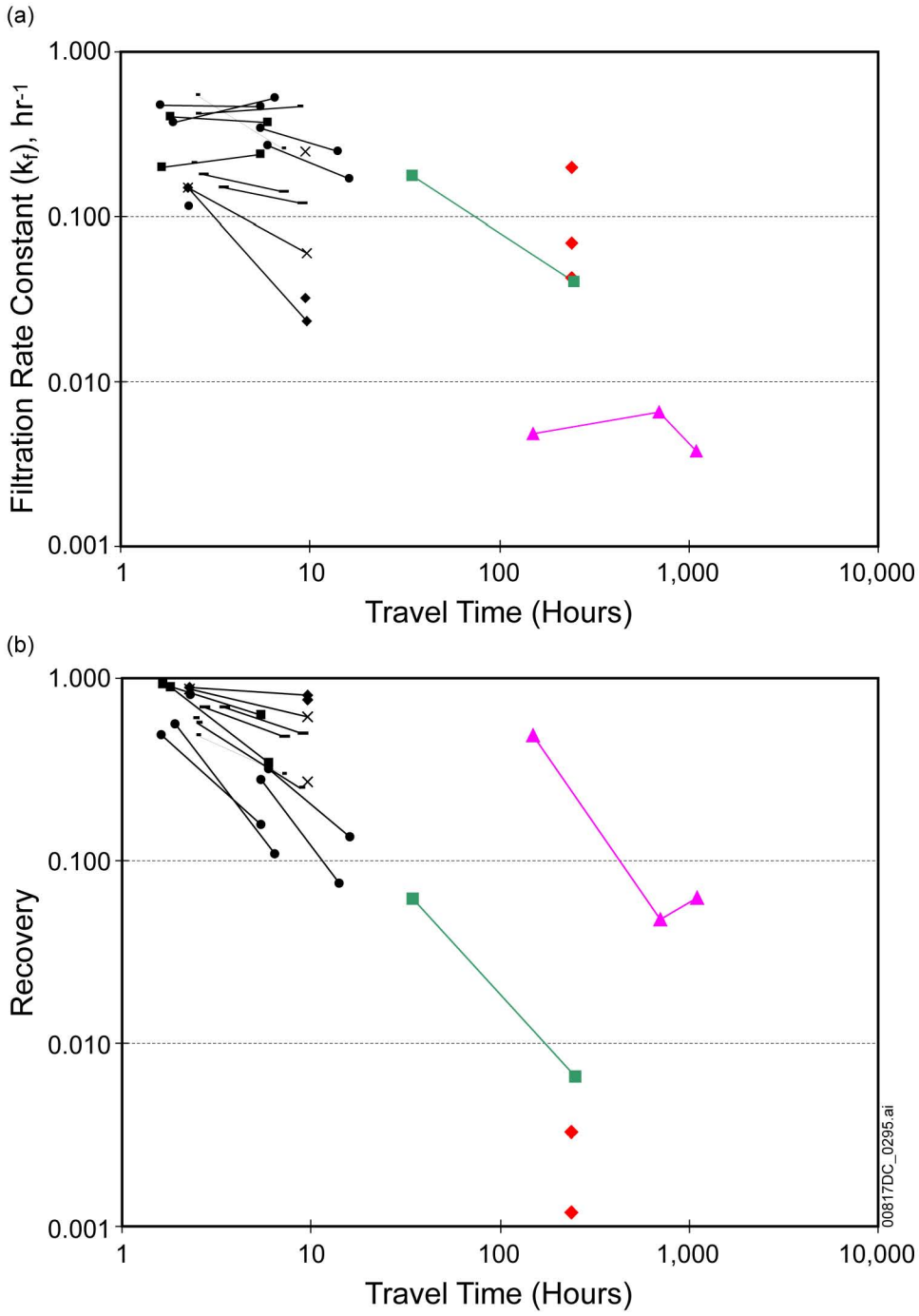

Source: Output DTN: LA0705PR150304.001 [DIRS 181744], file: *Colloid_Diversity_Parameters.xls, worksheet "Volcanics Data"*; and Corroborative DTN: MO0709MARGANAL.000 [DIRS 182978].

NOTE: Lines have been drawn to connect experiments conducted with the same colloids in the same flow system. Colored data are for field tests.

Figure C6-21. Colloid Filtration Rate Constants and Fractional Recoveries Unretarded Groundwater Travel Times for Saturated Fractured Volcanics (Data Replotted from Figure C6-17)

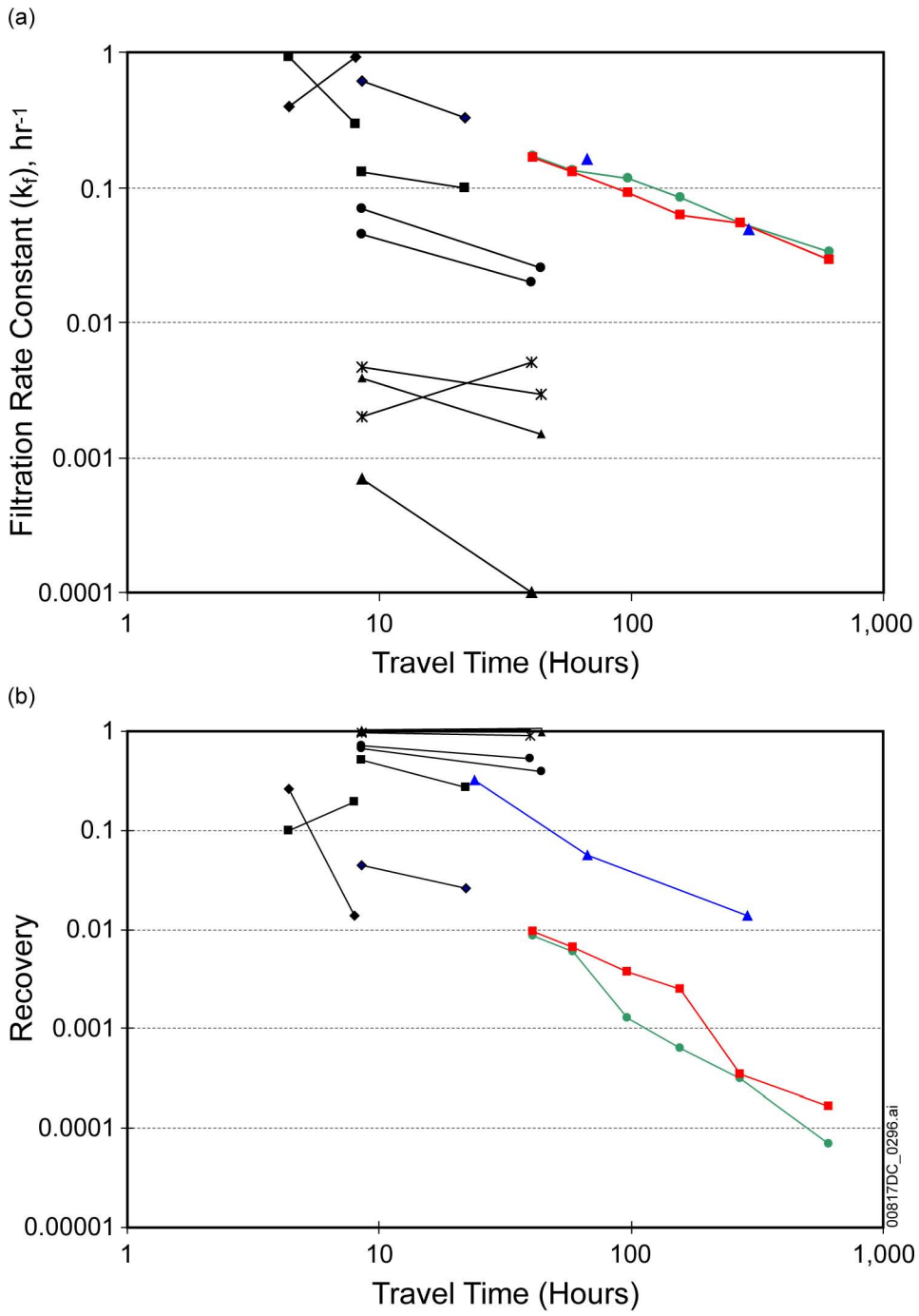

Source: Output DTN: LA0705PR150304.001 [DIRS 181744], file: *Colloid_Diversity_Parameters.xls, worksheet "Alluvium Data"*; and Corroborative DTN: MO0709MARGANAL.000 [DIRS 182978].

NOTE: Lines have been drawn to connect experiments conducted with the same colloids in the same flow system. Colored data are for field tests.

Figure C6-22. Colloid Filtration Rate Constants and Fractional Recoveries Unretarded Groundwater Travel Times for Saturated Alluvium (Data Replotted from Figure C6-19)

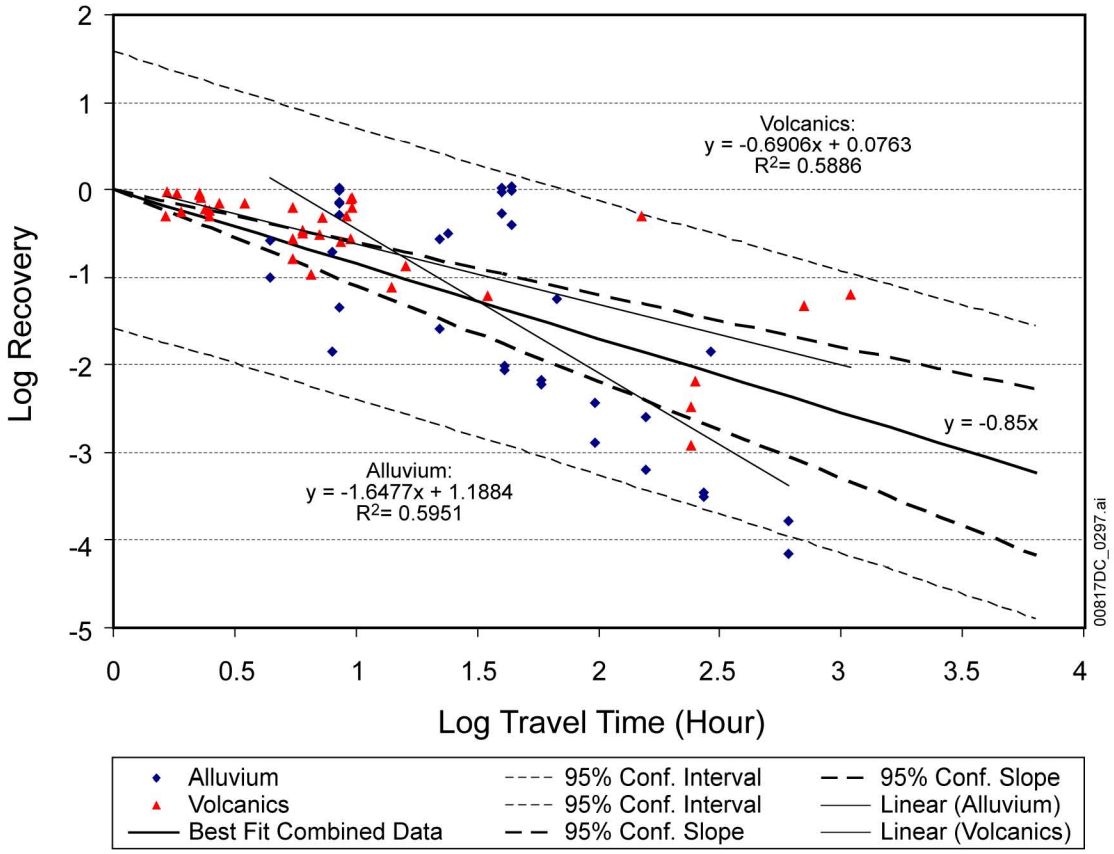

Source: Output DTN: LA0705PR150304.001 [DIRS 181744], file: *Colloid_Diversity_Parameters.xls, worksheet "Alluvium&Volcanics"*; and Corroborative DTN: MO0709MARGANAL.000 [DIRS 182978].

NOTE: The combined fit is forced to go through the origin. The light dashed lines are the 95 percent confidence intervals for the combined fit, and the dark dashed lines are plotted using the 95 percent confidence intervals for the slope of the combined fit.

Figure C6-23. Volcanic and Alluvium Log Fractional Recoveries vs. Log Groundwater Travel Time Plotted Together and Fitted by Linear Regression Separately and Together

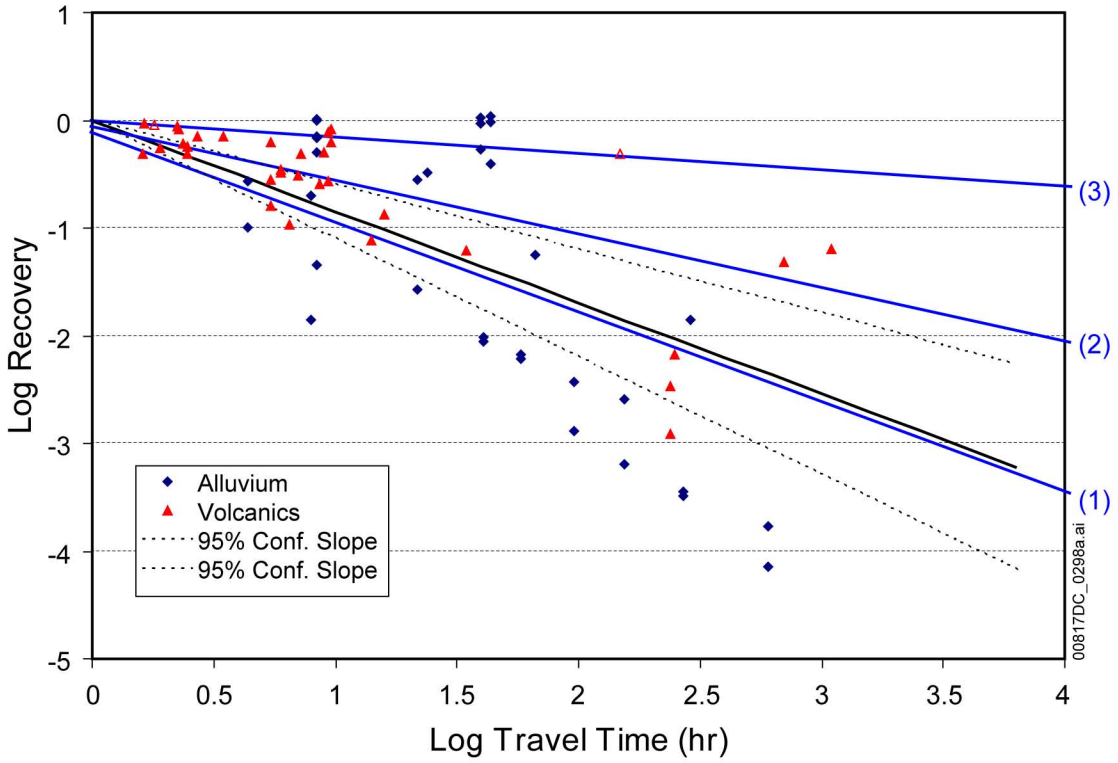

Source: Output DTN: LA0705PR150304.001 [DIRS 181744], file: *Colloid_Diversity_Parameters.xls, worksheet "Alluvium&Volcanics"*; and Corroborative DTN: MO0709MARGANAL.000 [DIRS 182978].

NOTES: Log Fractional Recoveries vs. Log Ground Travel Time for Filtration Rate Constant CDFs Associated with (1) Best Linear Fit (passing through the origin) to the combined alluvium and volcanic data (slope of approximately 0.85), (2) CDF of all rate constants (with twice the weight given to field data; slope of approximately 0.51), and (3) Best fit to the two highest recovery data points associated with the filed tracer test in the fractured volcanics at the ER-20-6 site (open triangles), which had the highest recoveries of any of the field tests (Slope of Approximately 0.17).

Figure C6-24. Log Fractional Recoveries versus Log Ground Travel Time

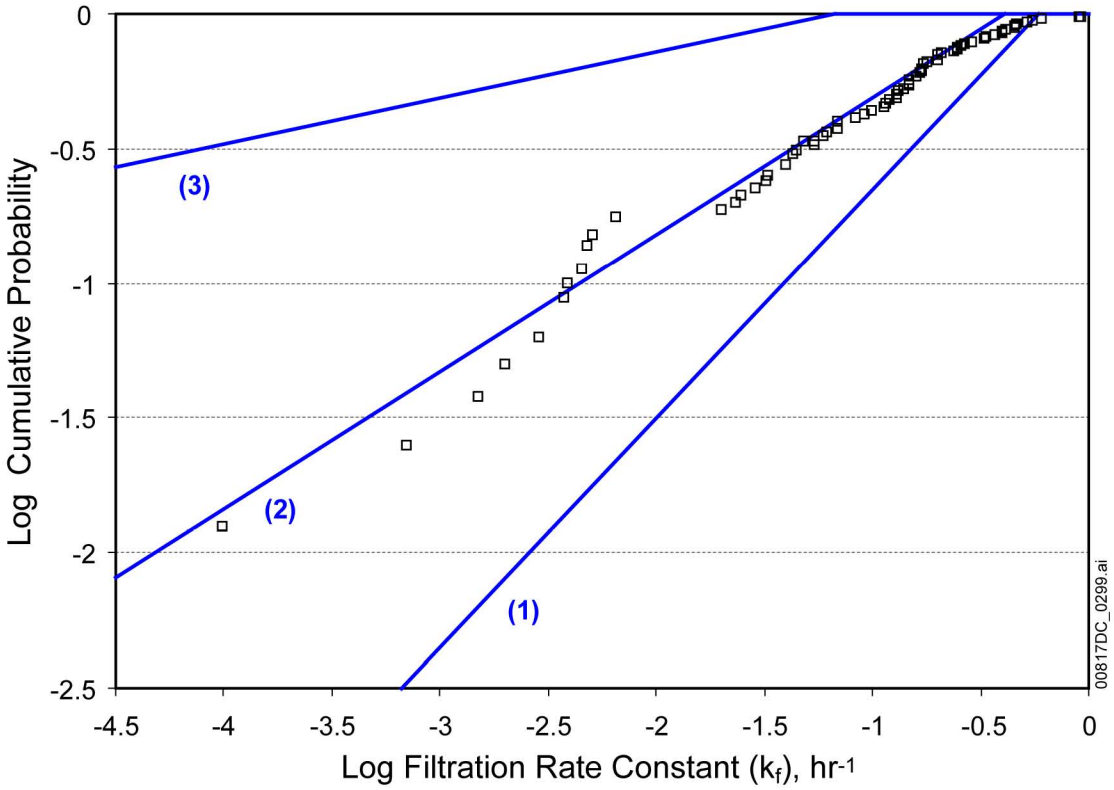

Source: Output DTN: LA0705PR150304.001 [DIRS 181744], file: *Colloid_Diversity_Parameters.xls, worksheet "kfCDF"*; and Corroborative DTN: MO0709MARGANAL.000 [DIRS 182978].

NOTE: The data CDF was generated by assigning twice the probabilistic weight to field data relative to laboratory data. The slopes of the lines are the negative of the slopes of the corresponding lines in the previous figure (0.85, 0.51, and 0.17).

Figure C6-25. Colloid Filtration Rate Constant Cumulative Distribution Functions Associated with (1), (2), and (3) from Figure C6-24 Plotted along with the Actual Cumulative Distribution Function of the Filtration Rate Constants (Data Points)

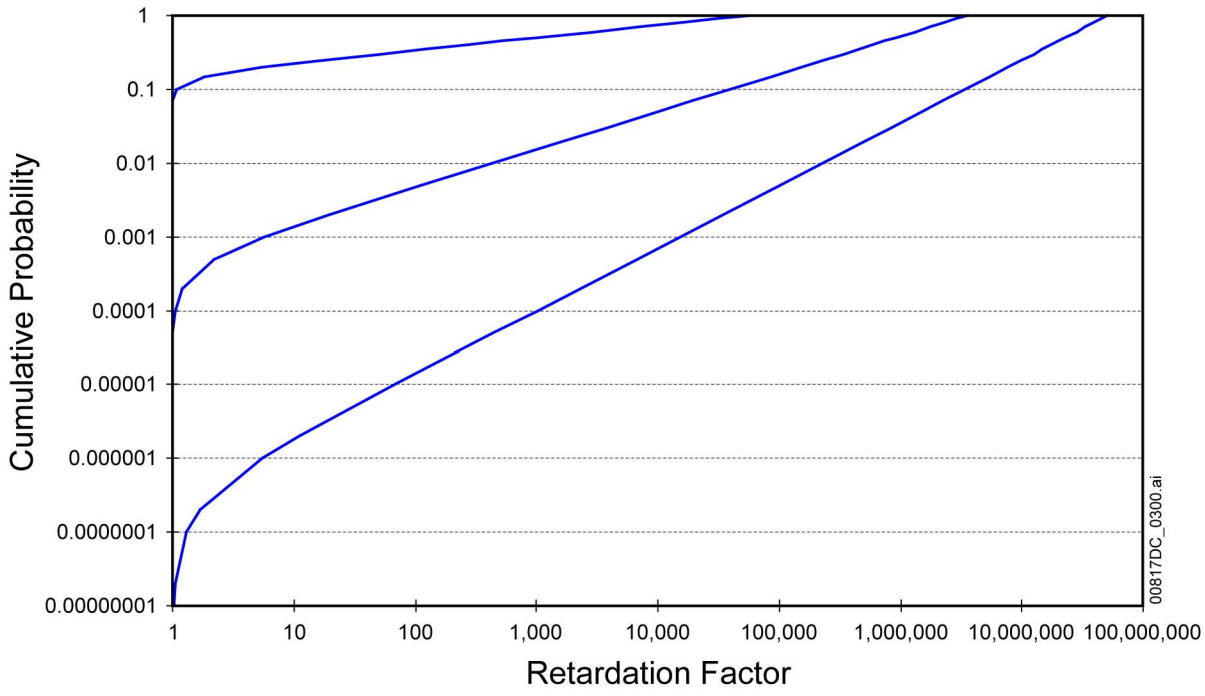

Source: Output DTN: LA0705PR150304.001 [DIRS 181744], file: *Colloid_Diversity_Parameters.xls, worksheet "Alluvium&Volcanics"*; and Corroborative DTN: MO0709MARGANAL.000 [DIRS 182978].

Figure C6-26. Minimum, Central, and Maximum Cumulative Distribution Functions of Colloid Retardation Factors Associated with a 100-Year Groundwater Travel Times

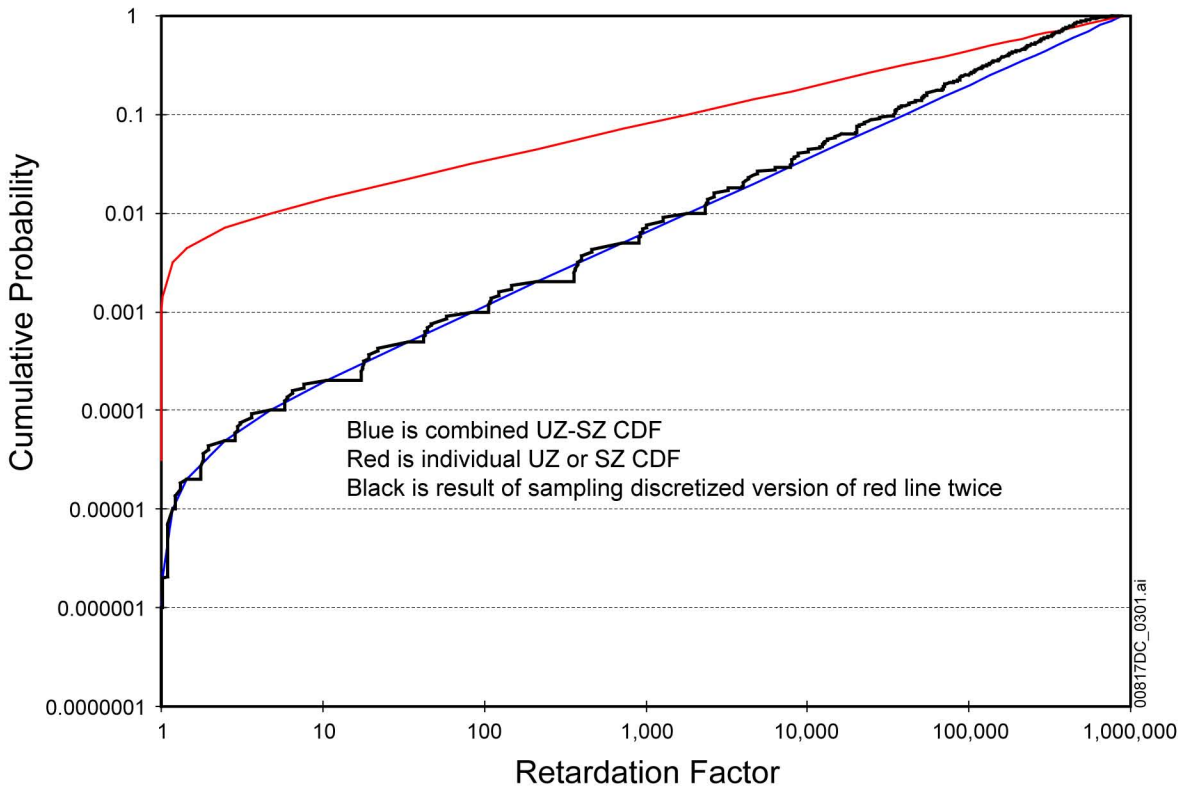

Source: Output DTN: LA0705PR150304.001 [DIRS 181744], file: *Colloid_Diversity_Parameters.xls, worksheet "Alluvium&Volcanics"*; and Corroborative DTN: MO0709MARGANAL.000 [DIRS 182978].

NOTE: The black line is the discretized combined CDF obtained numerically, and the blue line is the original combined unsaturated zone-saturated zone CDF from the approach developed herein.

Figure C6-27. Results of Sampling a Discretized Version of the Retardation Factor CDF Two Times to Obtain an Effective Retardation Distribution in the Combined Unsaturated Zone and Saturated Zone

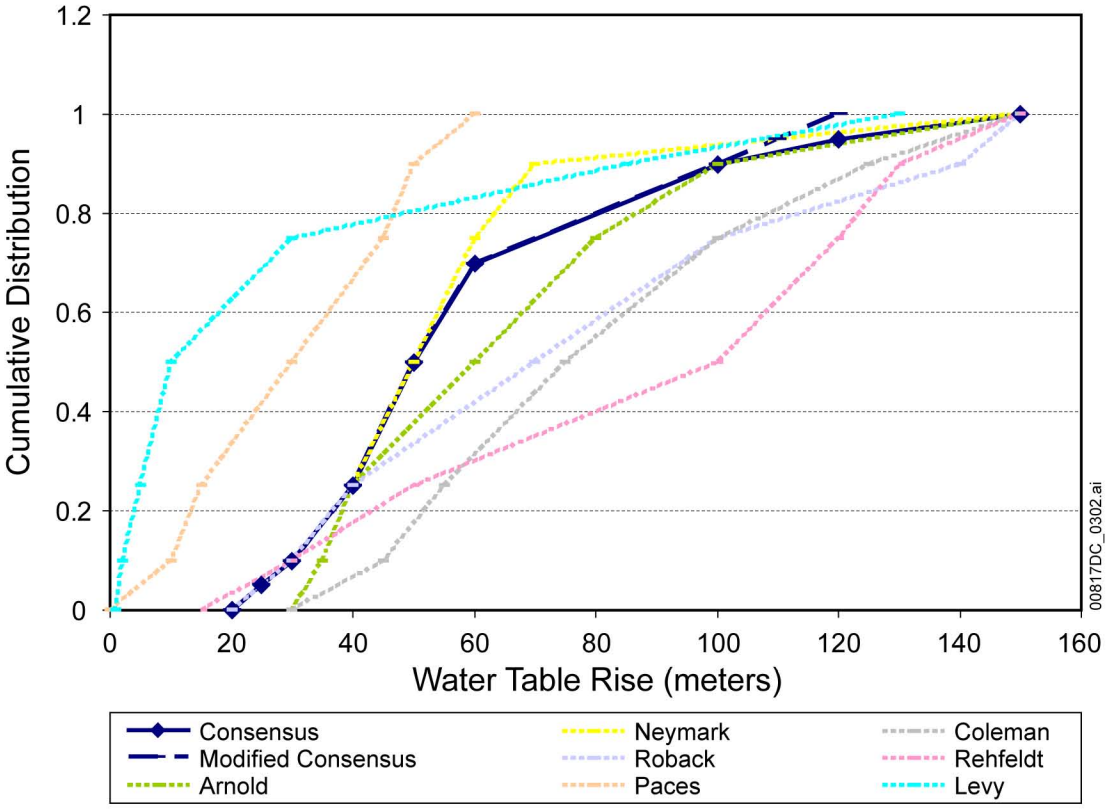

Source: Corroborative DTN: MO0704PAUZFEHM.000 [DIRS 182790], file: *water_table_rise_uncert_summaryDTN.xls, worksheet "sheet1"*.

Figure C6-28. Cumulative Distribution Functions of Uncertainty in Water Table Rise for Individual Workshop Participants

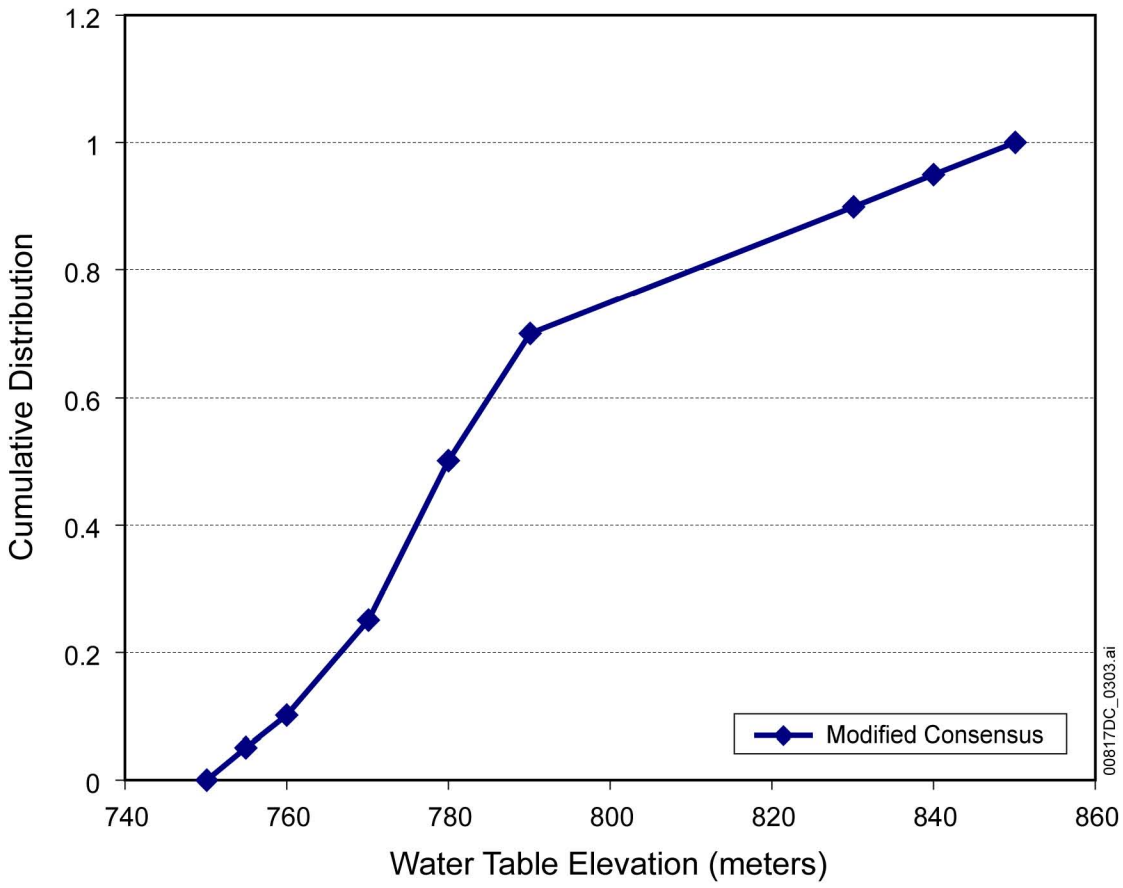

Source: Corroborative DTN: MO0704PAUZFEHM.000 [DIRS 182790], file: *water_table_rise_uncert_summaryDTN.xls, worksheet "sheet1".*

Figure C6-29. Cumulative Distribution Functions of Uncertainty in Water Table Rise by Consensus

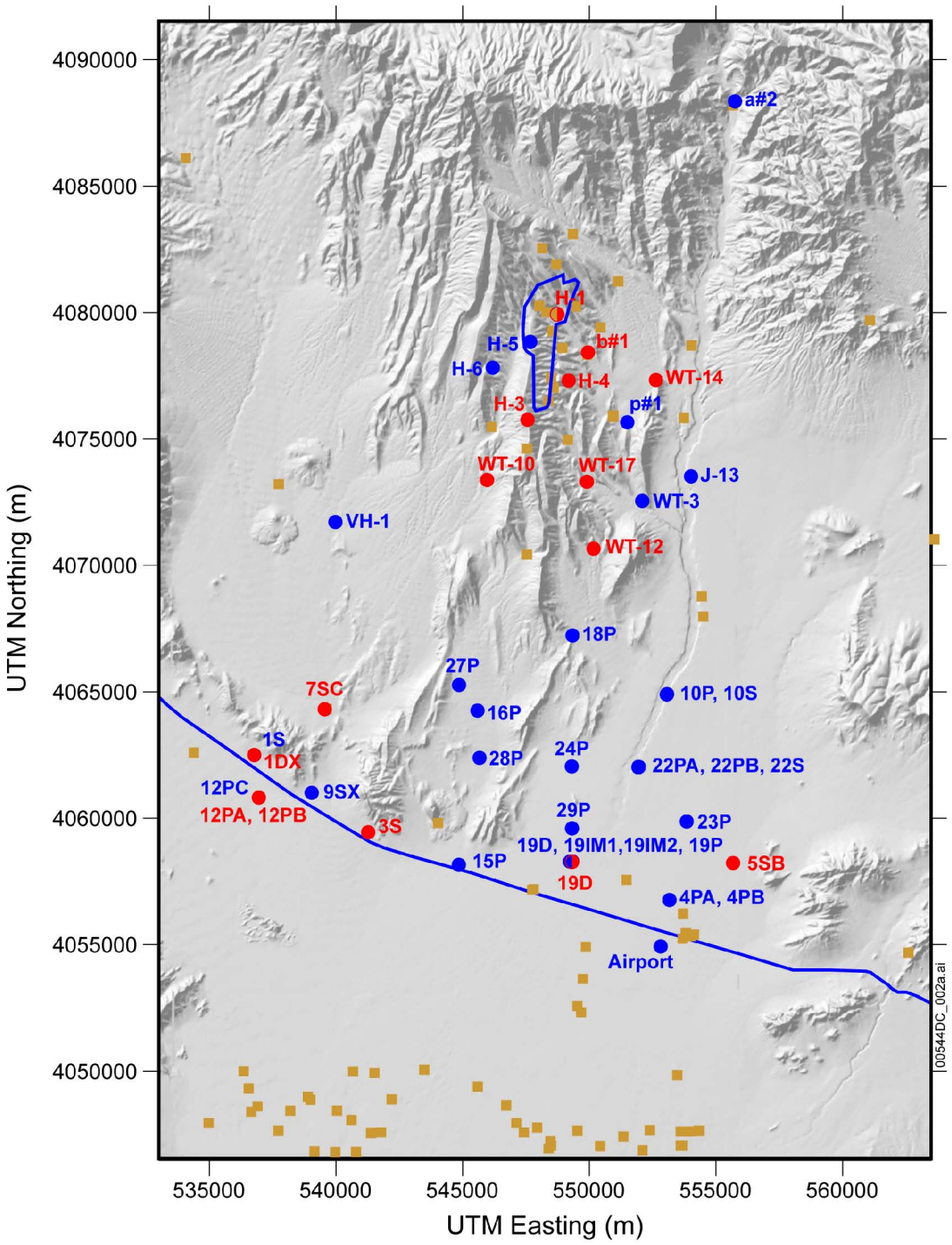

Source: BSC 2006 [DIRS 178672], Figure 2.1-2, p. F-2.

NOTES: Wells with oxidizing groundwater are shown with blue filled circles, wells with reducing groundwater are shown with red filled circles, and wells in which redox conditions have not been measured are shown with brown filled squares. Wells with both oxidizing and reducing conditions (H-1 and 19-D) are shown with half-filled circles. The repository is outlined in blue in the north-central part of the map, and Highway 95 is shown as the blue line in the southern part of the map.

Figure C6-30. Map Showing Locations of Wells with Oxidizing and Reducing Groundwaters

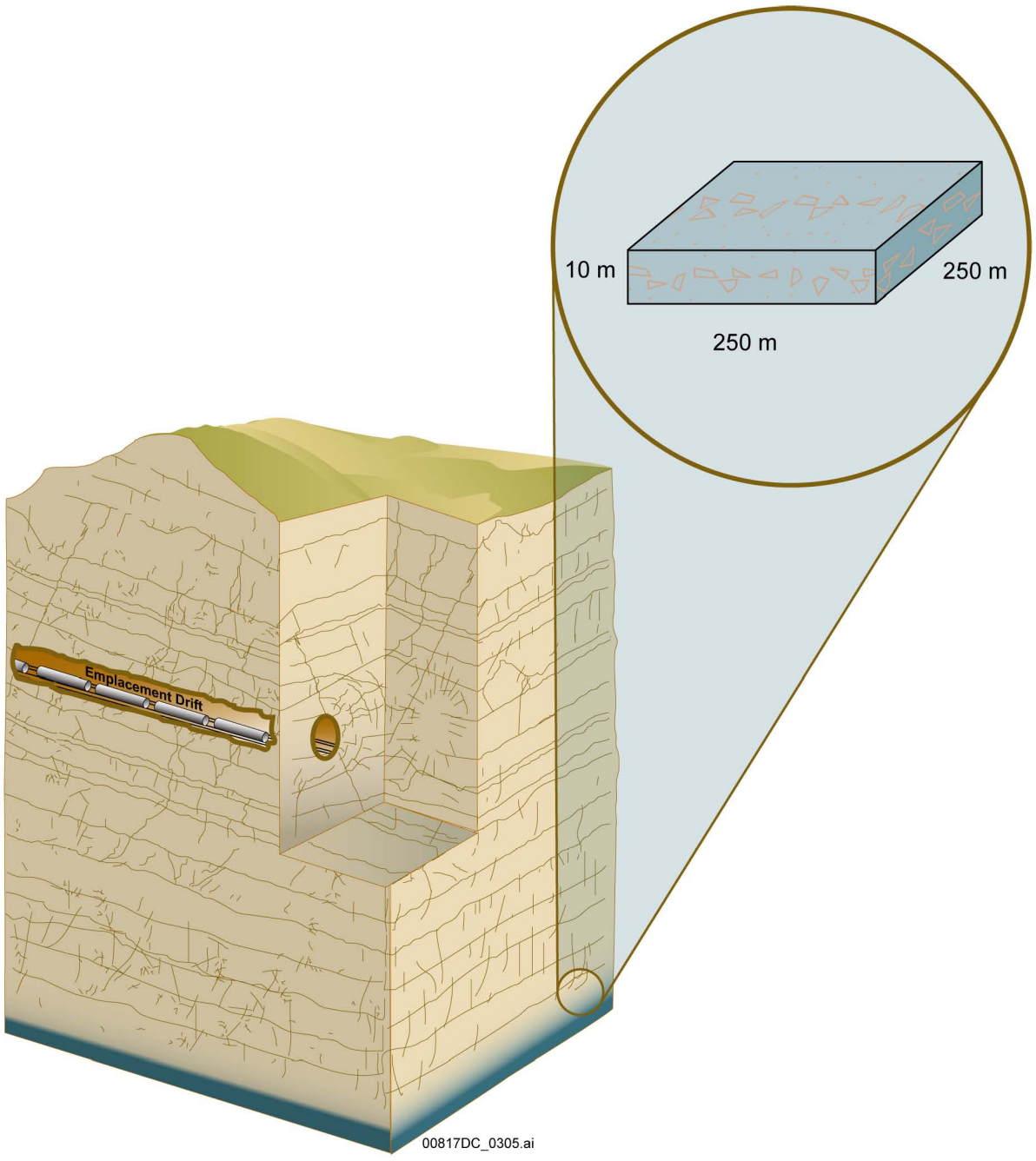

Figure C6-31. Saturated Zone Matrix Block Used as a Conduit for Unsaturated Matrix Mass Flux to the Saturated Zone

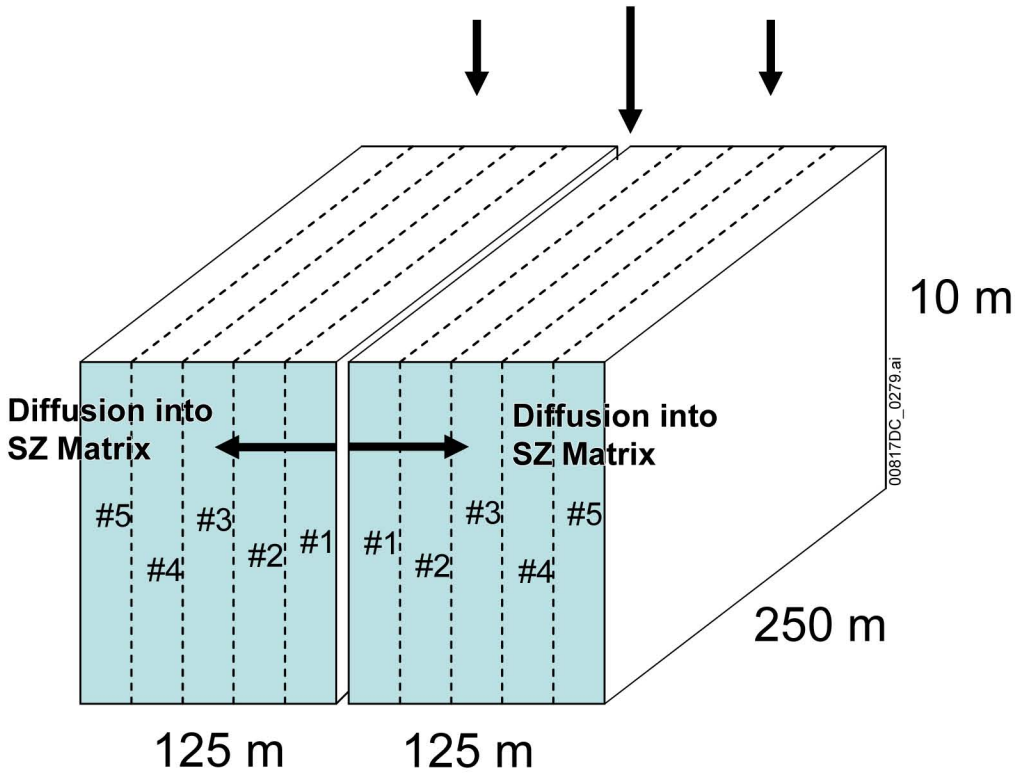

NOTE: The 125 m length represents half of the total block length. In this example, FISVO, which is the total length between fractures, is 250 m.

Figure C6-32. Schematic Diagram Showing Conceptual Dual-Porosity Model for the Unsaturated Zone to Saturated Zone Mass Flux

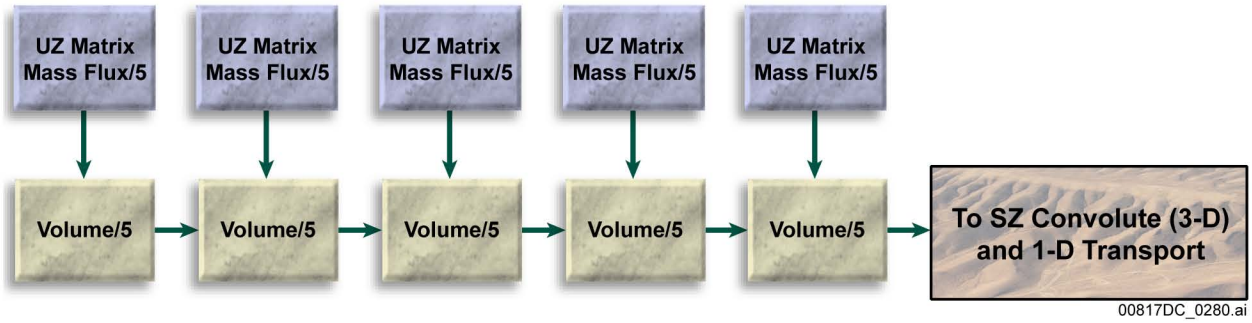

Figure C6-33. Configuration of Unsaturated Zone to Saturated Zone Matrix Diffusion

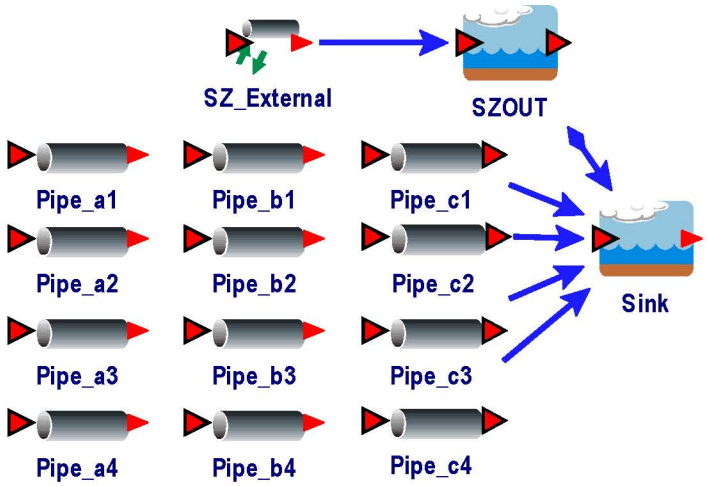

Figure C6-34. Structure of the GoldSim Saturated Zone1-D Transport Model Setup for the Compliance Model

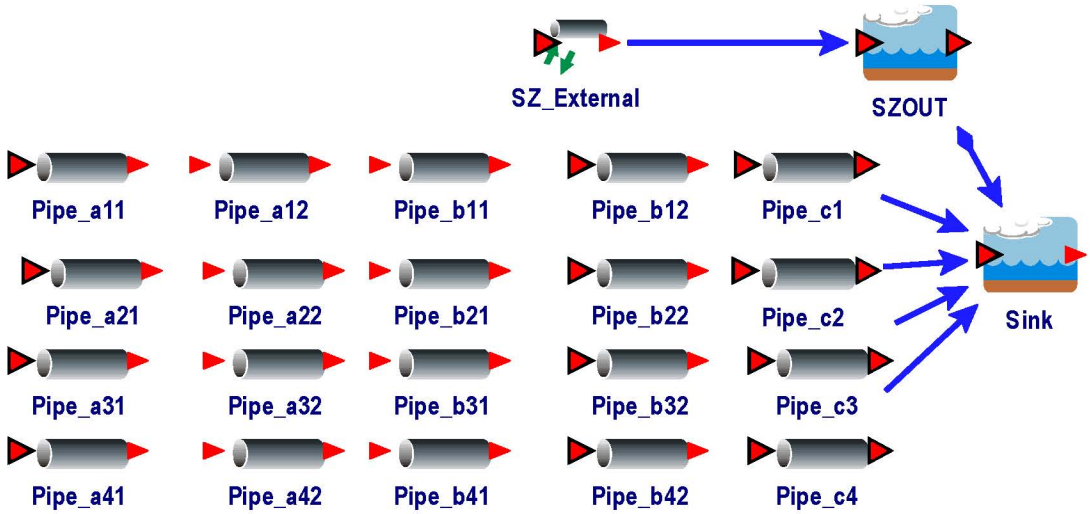

Figure C6-35. Structure of the GoldSim Saturated Zone1-D Transport Model with Modifications for the Reducing Zones Model

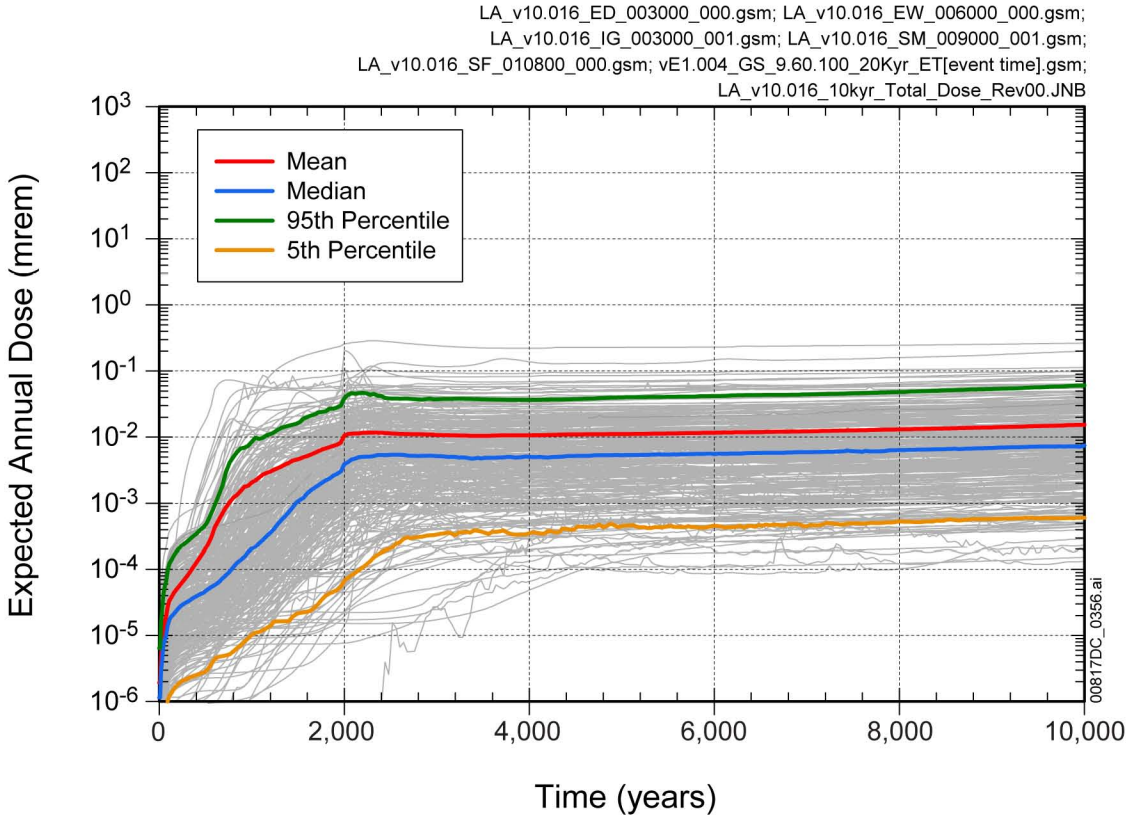

Source: Corroborative DTN: MO0709MARGANAL.000 [DIRS 182978]; and Output DTN: MO0709TSPAREGS.000 [DIRS 182976].

Figure C7-1. Probabilistic Projections of the Performance Margin Analysis Total Dose for 10,000 Years after Repository Closure

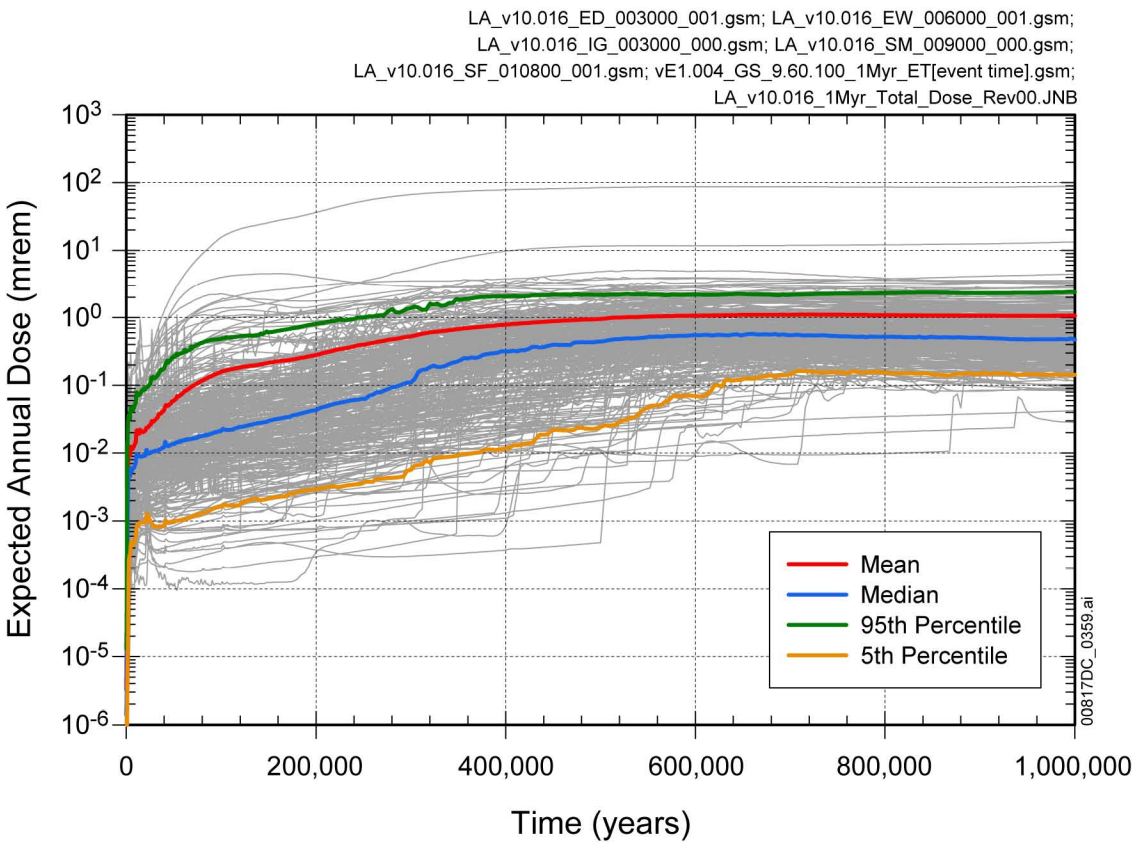

Source: Corroborative DTN: MO0709MARGANAL.000 [DIRS 182978]; and Output DTN: MO0709TSPAREGS.000 [DIRS 182976].

Figure C7-2. Probabilistic Projections of Performance Margin Analysis Total Dose for 1,000,000 Years after Repository Closure

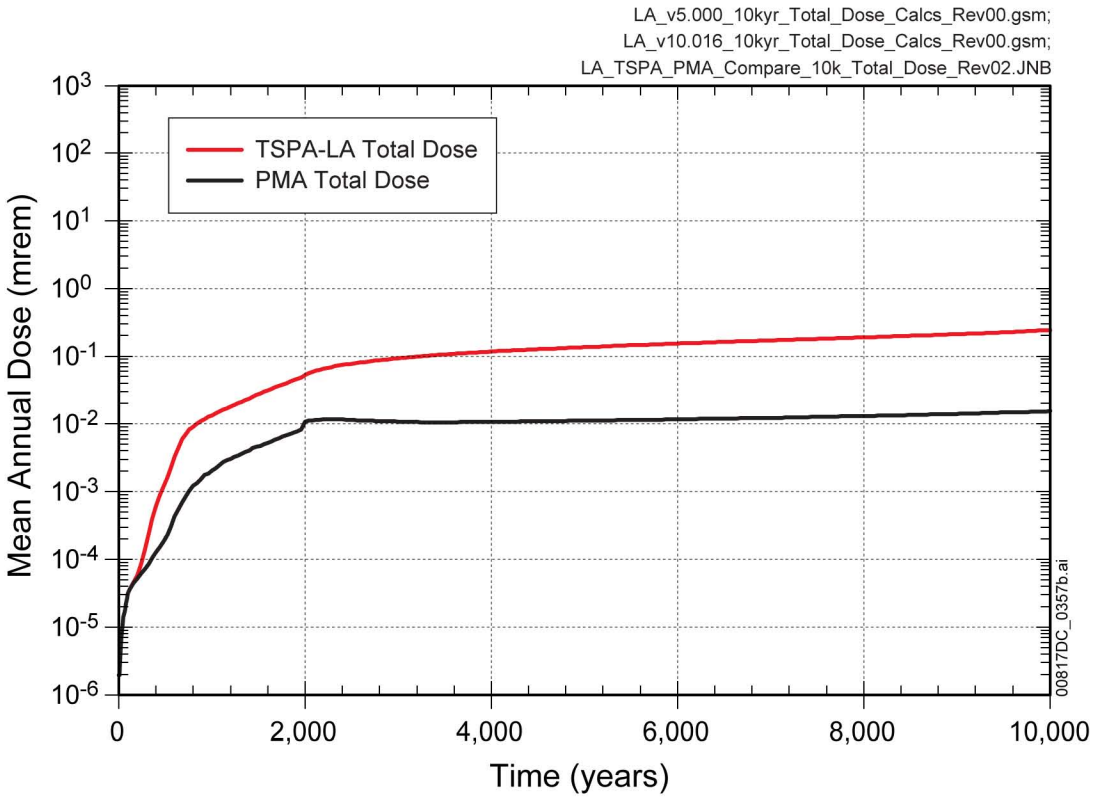

Source: Output DTN: MO0709TSPAPLOT.000 [DIRS 183010].

Figure C7-3. Comparison of the Projected Total Mean Annual Dose for the TSPA-LA Model Relative to the Performance Margin Analysis for 10,000 Years after Repository Closure

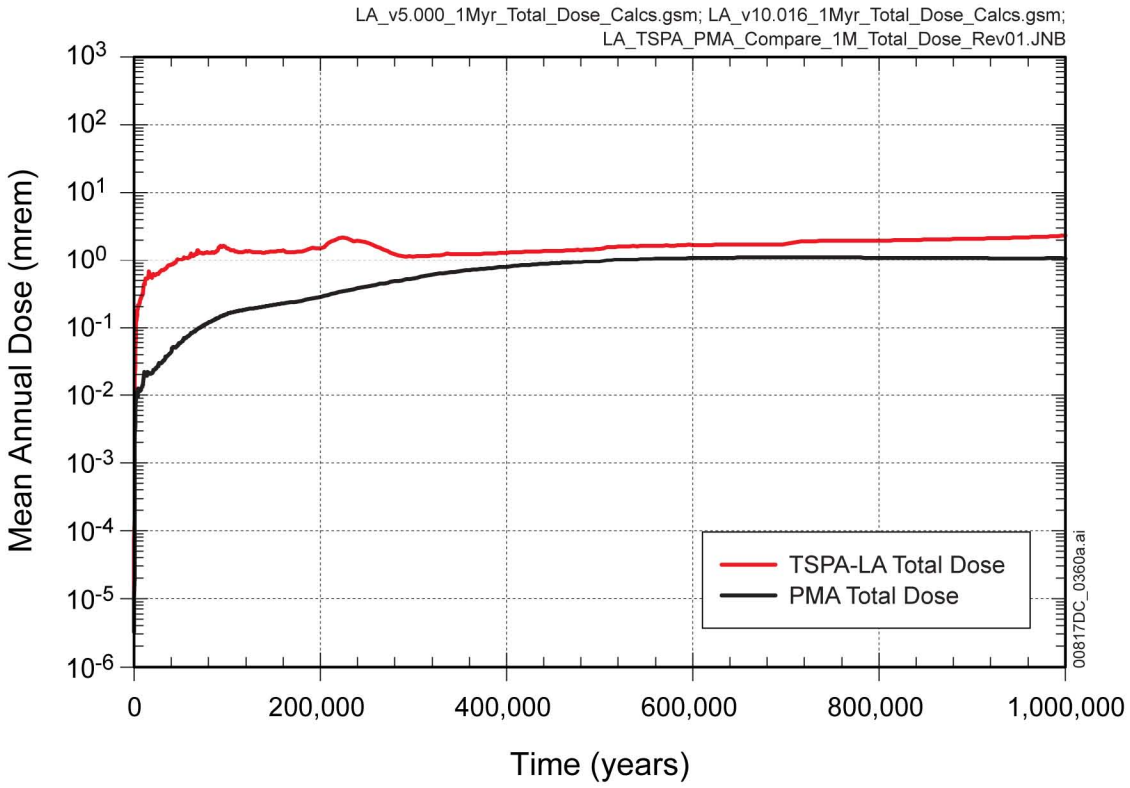

Source: Output DTN: MO0709TSPAPLOT.000 [DIRS 183010].

Figure C7-4. Comparison of the Projected Total Mean Annual Dose for the TSPA-LA Relative to the Performance Margin Analysis for 1,000,000 Years after Repository Closure

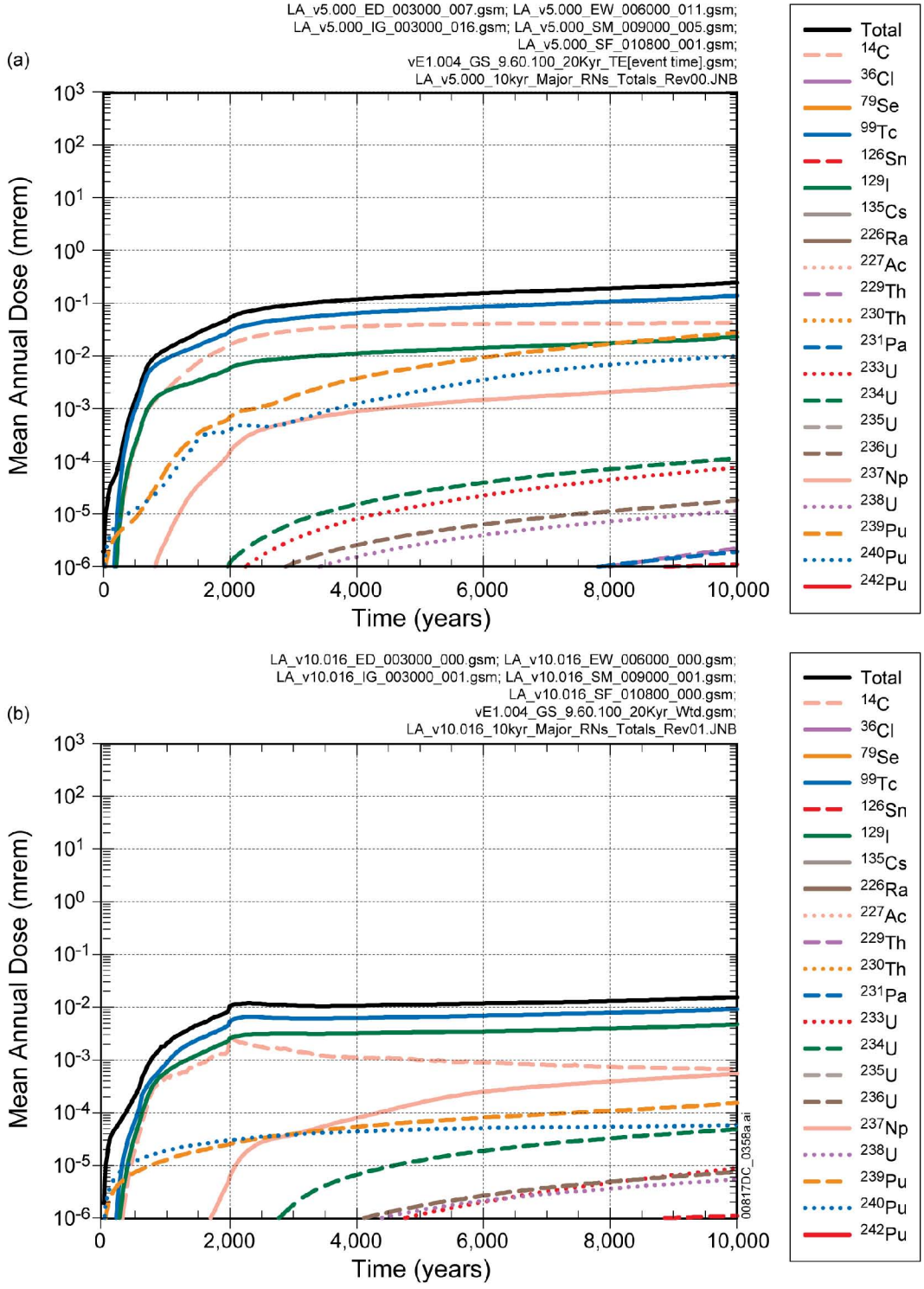

Source: Corroborative DTN: MO0709MARGANAL.000 [DIRS 182978]; and Output DTN: MO0709TSPAREGS.000 [DIRS 182976].

Figure C7-5. Contributions of Individual Radionuclides to Total Mean Annual Dose for (a) the TSPA-LA and (b) the Performance Margin Analysis 10,000 Years after Repository Closure

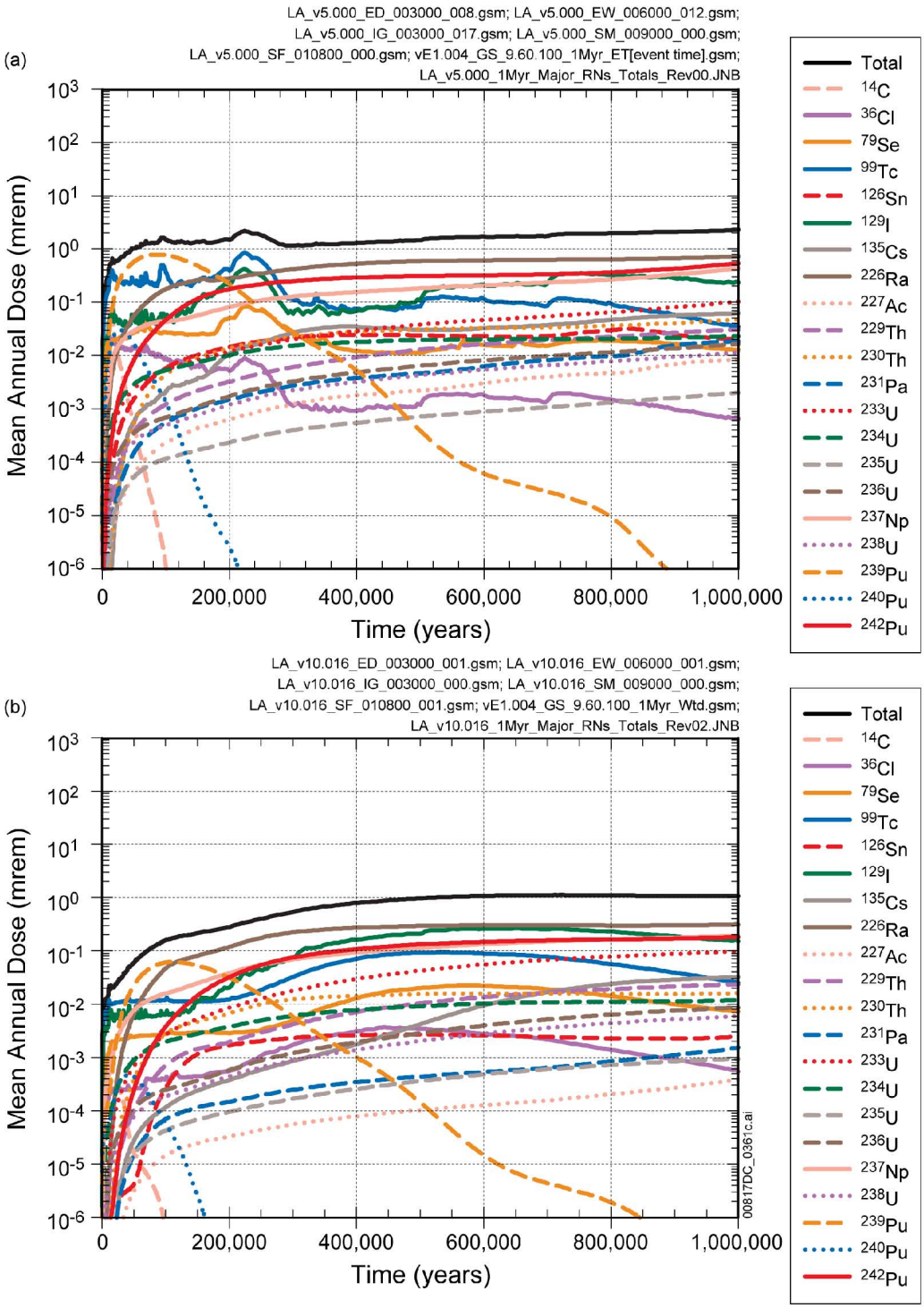

Source: Corroborative DTN: MO0709MARGANAL.000 [DIRS 182978]; and Output DTN: MO0709TSPAREGS.000 [DIRS 182976].

Figure C7-6. Contributions of Individual Radionuclides to Total Mean Annual Dose History for (a) the TSPA-LA and (b) the Performance Margin Analysis for 1,000,000 Years after Repository Closure

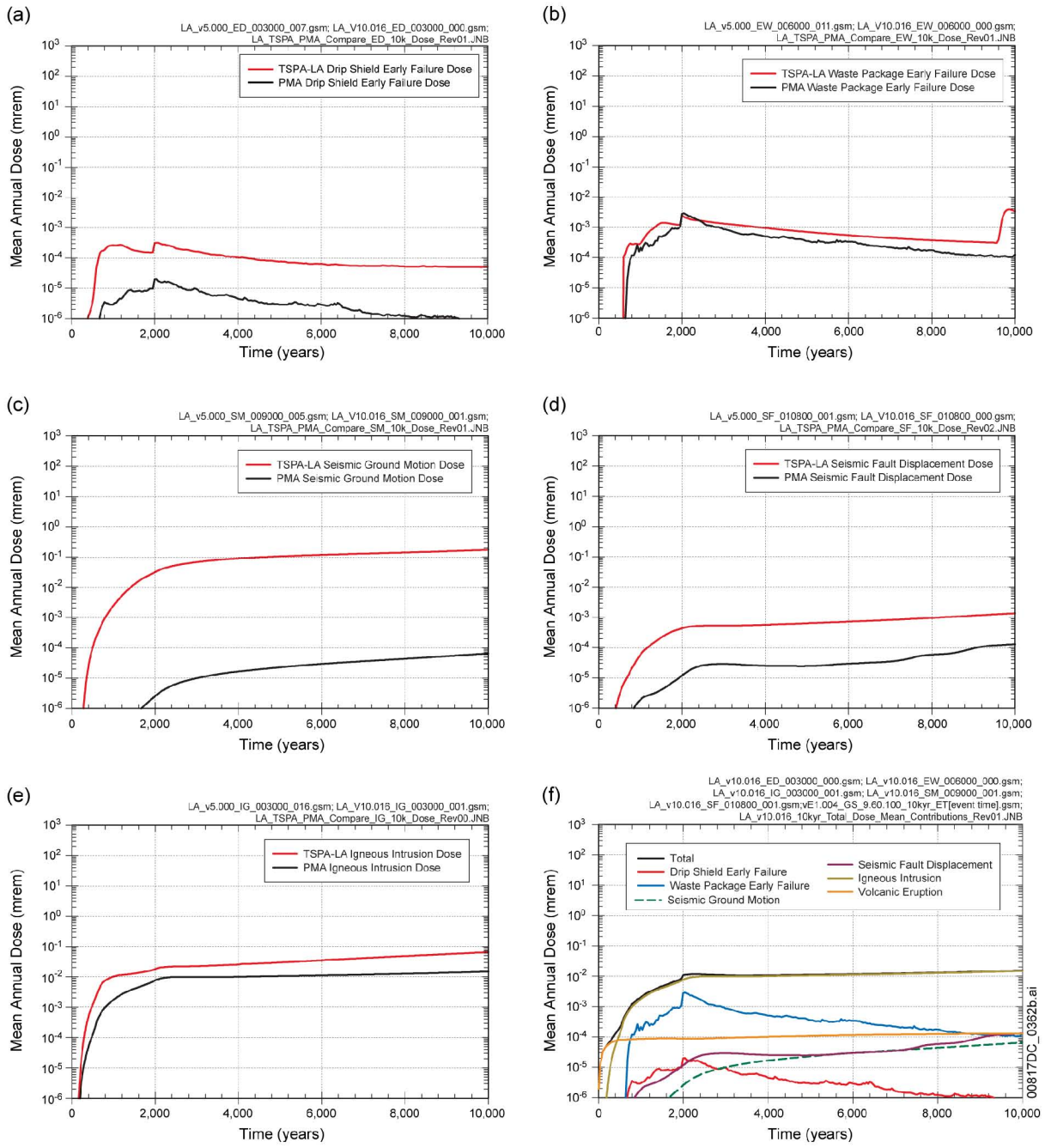

Source: Output DTN: MO0709TSPAREGS.000 [DIRS 182976]; and Corroborative DTN: MO0709MARGANAL.000 [DIRS 182978].

Figure C7-7. Comparison of Scenario Modeling Cases to Projected Total Mean Annual Dose 10,000 Years after Repository Closure for (a) Drip Shield Early Failure, (b) Waste Package Early Failure, (c) Seismic Ground Motion, (d) Seismic Fault Displacement, (e) Igneous Intrusion, and (f) Relative Contributions of Scenario Modeling Cases to the Projected Mean Annual Dose for the Performance Margin Analysis.

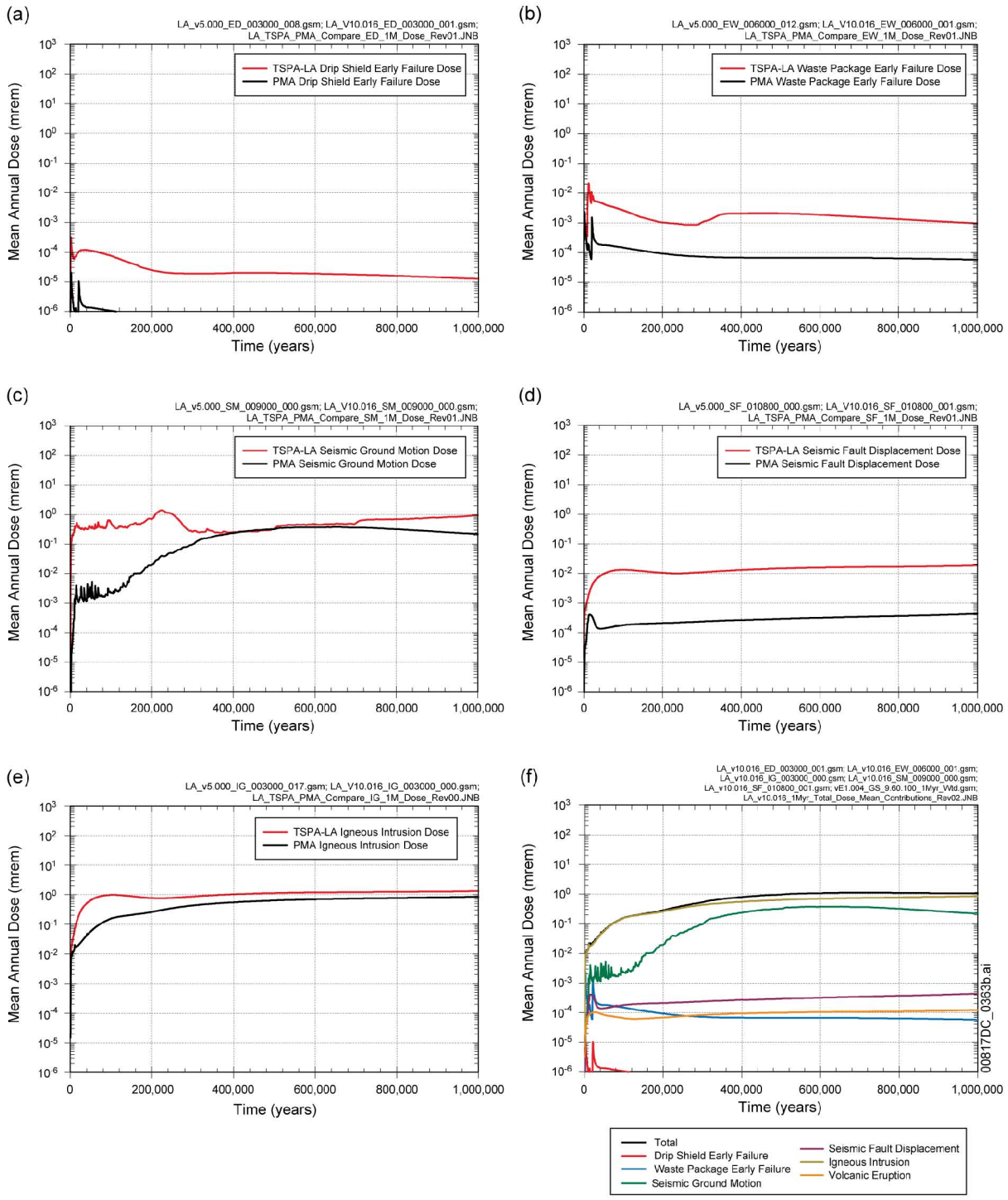

Source: Output DTN: MO0709TSPAREGS.000 [DIRS 182976] and Corroborative DTN: MO0709MARGANAL.000 [DIRS 182978].

Figure C7-8. Comparison of Scenario Modeling Cases to Projected Total Mean Annual Dose 1,000,000 Years after Repository Closure for (a) Drip Shield Early Failure, (b) Waste Package Early Failure, (c) Seismic Ground Motion, (d) Seismic Fault Displacement, (e) Igneous Intrusion, and (f) Relative Contributions of Scenario Modeling Cases to the Projected Mean Annual Dose for the Performance Margin Analysis

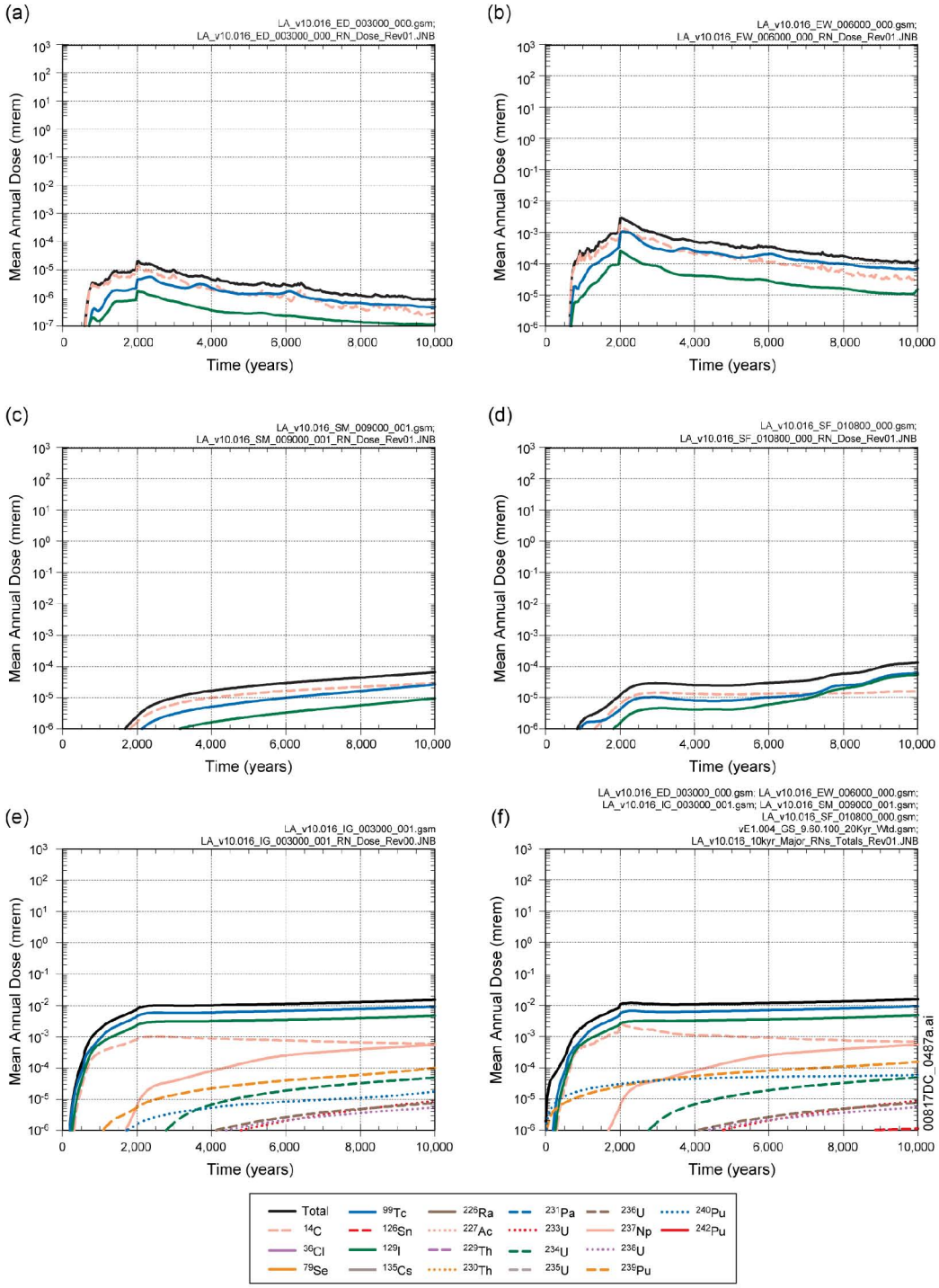

Source: Corroborative DTN: MO0709MARGANAL.000 [DIRS 182978]; and Output DTN: MO0709TSPAREGS.000 [DIRS 182976].

Figure C7-9. PMA Scenario Modeling Cases to Radionuclide Contributions to Projected Total Mean Annual Dose 10,000 Years after Repository Closure for (a) Drip Shield Early Failure, (b) Waste Package Early Failure, (c) Seismic Ground Motion, (d) Seismic Fault Displacement, (e) Igneous Intrusion, and (f) Total Mean Annual Dose for the Performance Margin Analysis

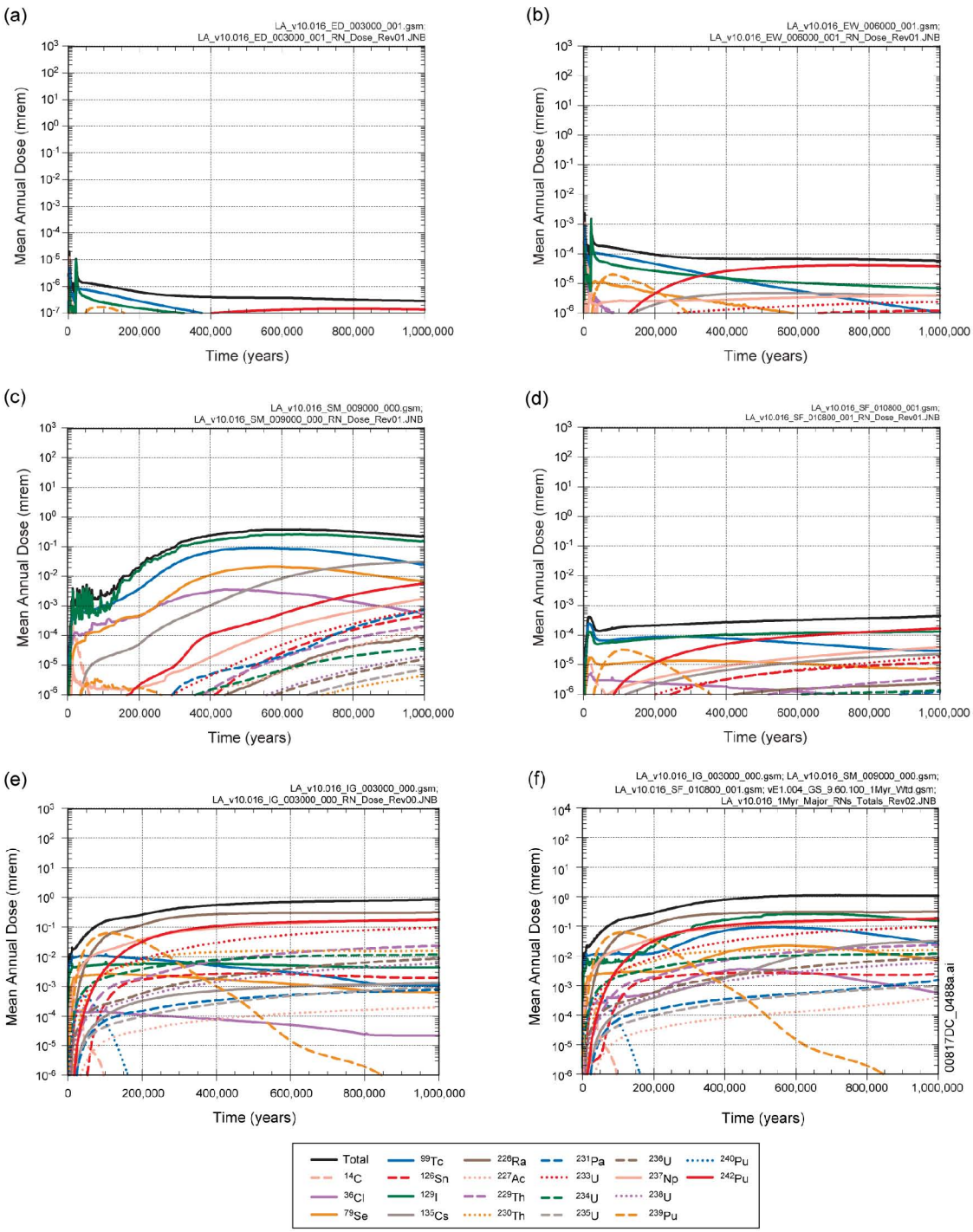

Source: Corroborative DTN: MO0709MARGANAL.000 [DIRS 182978]; and Output DTN: MO0709TSPAREGS.000 [DIRS 182976].

Figure C7-10. PMA Scenario Modeling Cases to Radionuclide Contributions to Projected Total Mean Annual Dose 1,000,000 Years after Repository Closure for (a) Drip Shield Early Failure, (b) Waste Package Early Failure, (c) Seismic Ground Motion, (d) Seismic Fault Displacement, (e) Igneous Intrusion, and (f) Total Mean Annual Dose for the Performance Margin Analysis

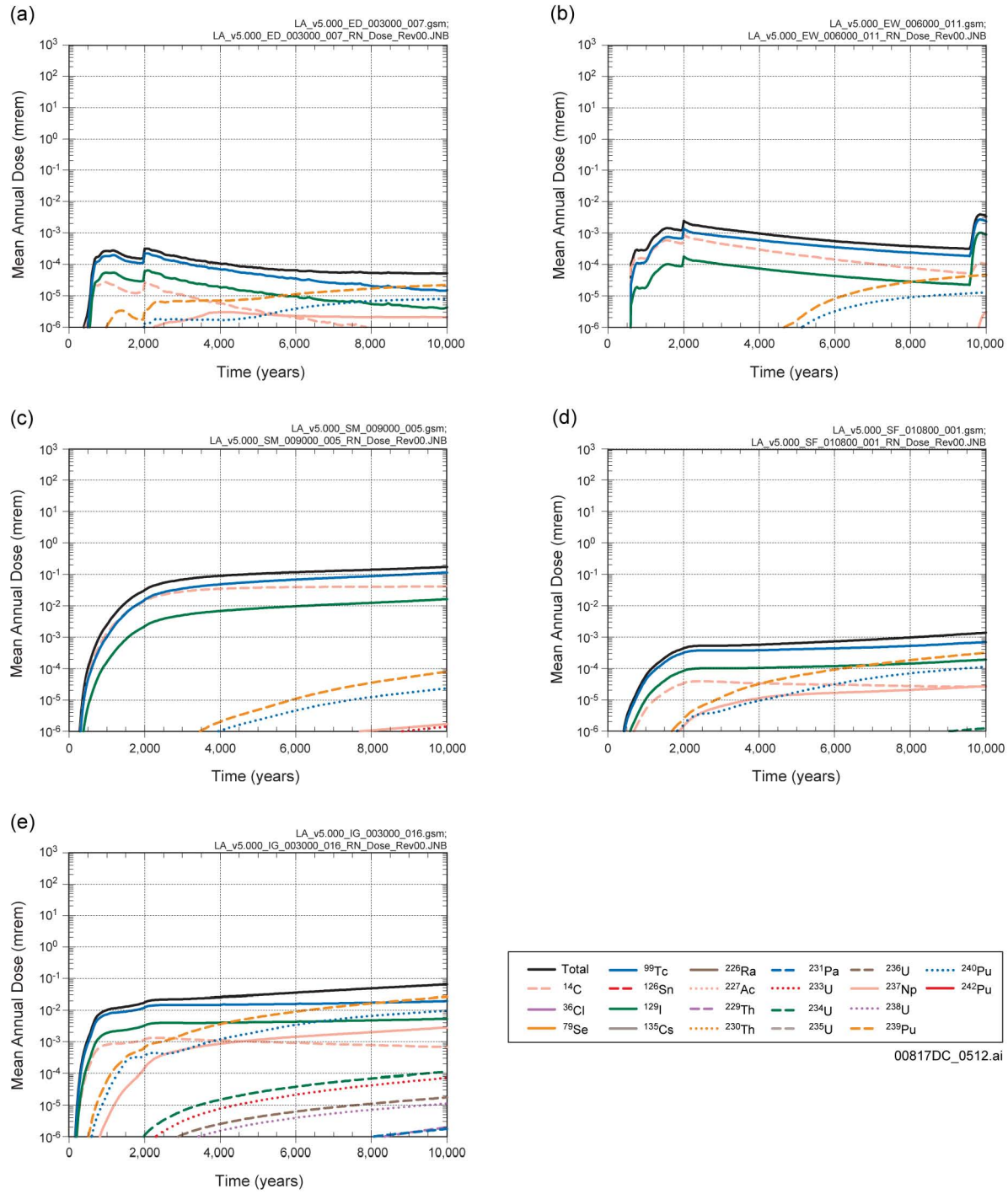

Source: Output DTN: MO0709TSPAREGS.000 [DIRS 182976].

Figure C7-11. TSPA-LA Scenario Modeling Cases Radionuclide Contributions to Projected Total Mean Annual Dose 10,000 Years after Repository Closure for (a) Drip Shield Early Failure, (b) Waste Package Early Failure, (c) Seismic Ground Motion, (d) Seismic Fault Displacement, and (e) Igneous Intrusion

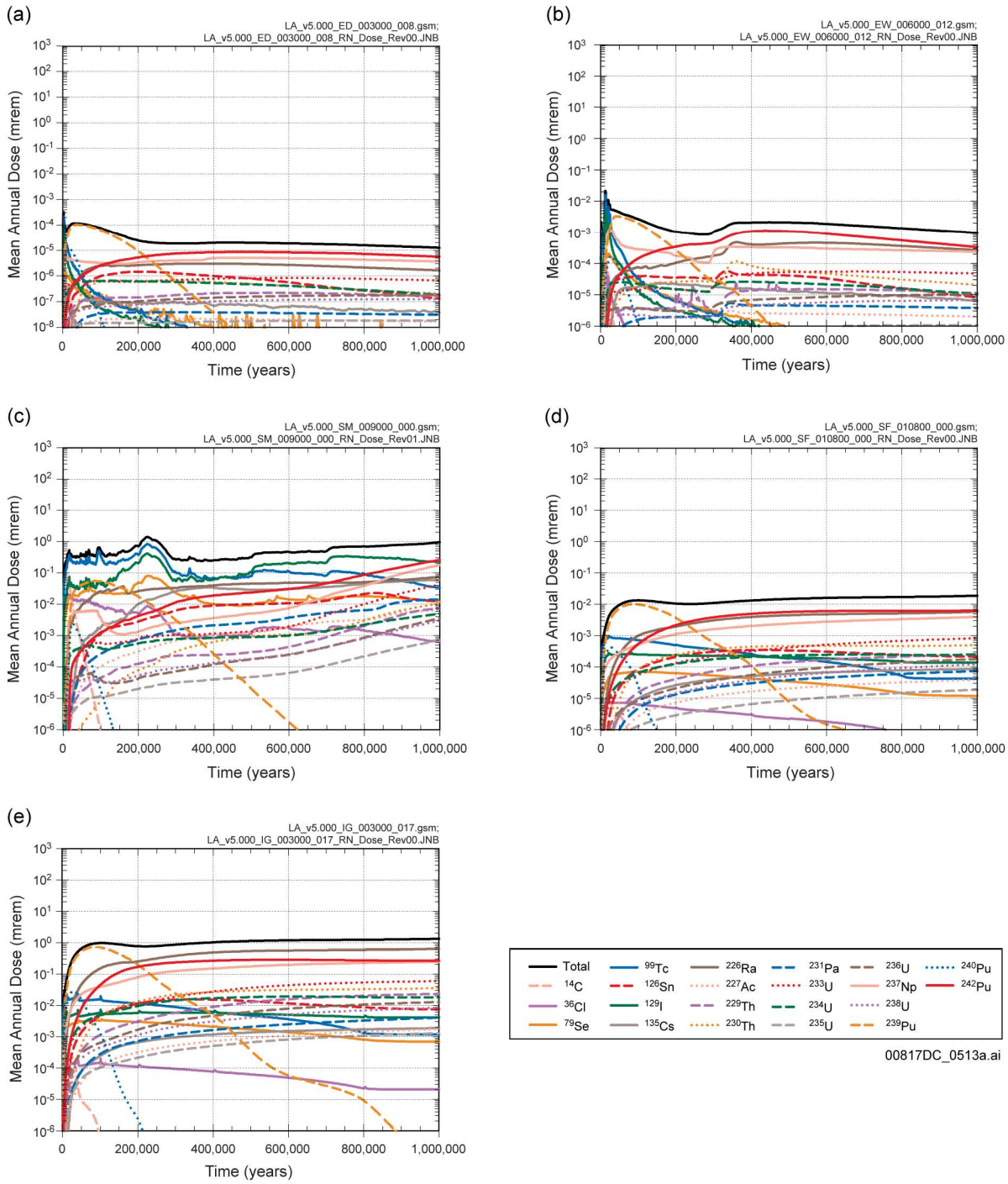

Source: Output DTN: MO0709TSPAREGS.000 [DIRS 182976].

Figure C7-12. TSPA-LA Scenario Modeling Cases Radionuclide Contributions to Projected Total Mean Annual Dose 1,000,000 Years after Repository Closure for (a) Drip Shield Early Failure, (b) Waste Package Early Failure, (c) Seismic Ground Motion, (d) Seismic Fault Displacement, and (e) Igneous Intrusion

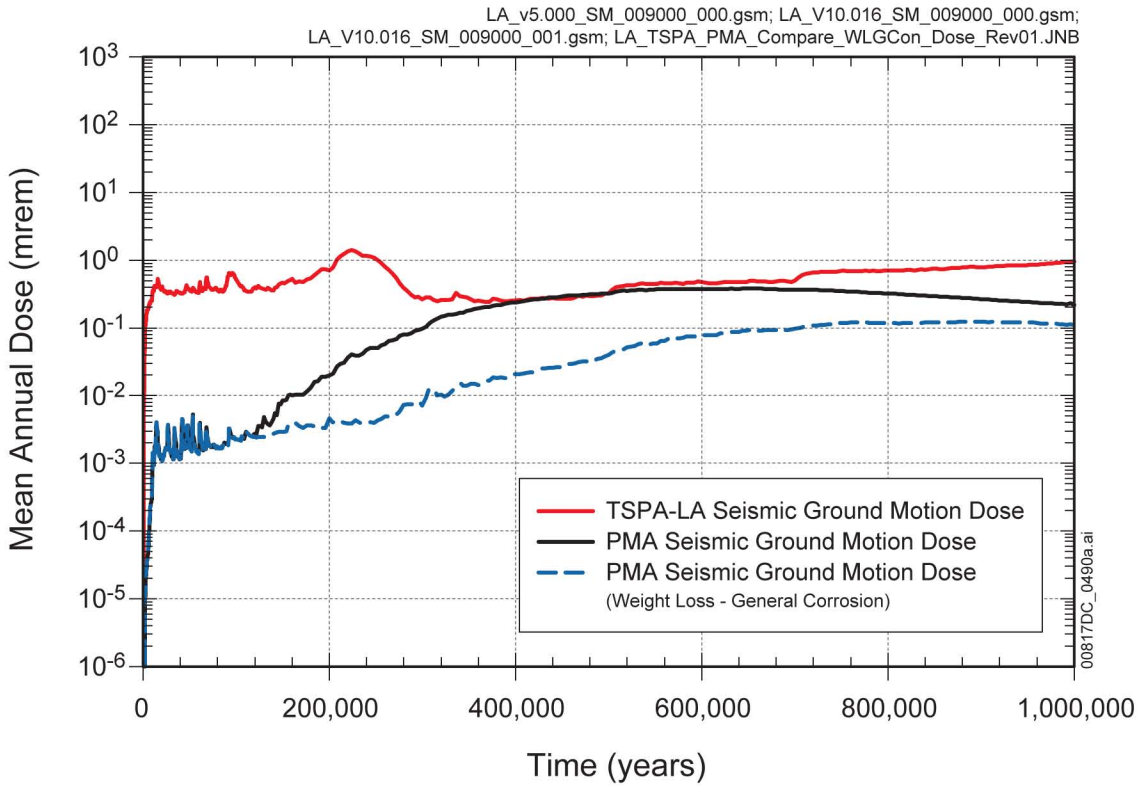

Source: Output DTN: MO0709TSPAREGS.000 [DIRS 182976] and Corroborative DTN: MO0709MARGANAL.000 [DIRS 182978].

Figure C7-13. Comparison of Seismic Ground Motion Modeling Cases to Projected Total Mean Annual Dose 1,000,000 Years after Repository Closure for TSPA-LA, Performance Margin Analysis, and the Performance Margin Analysis, including General Corrosion Weight-Loss Data

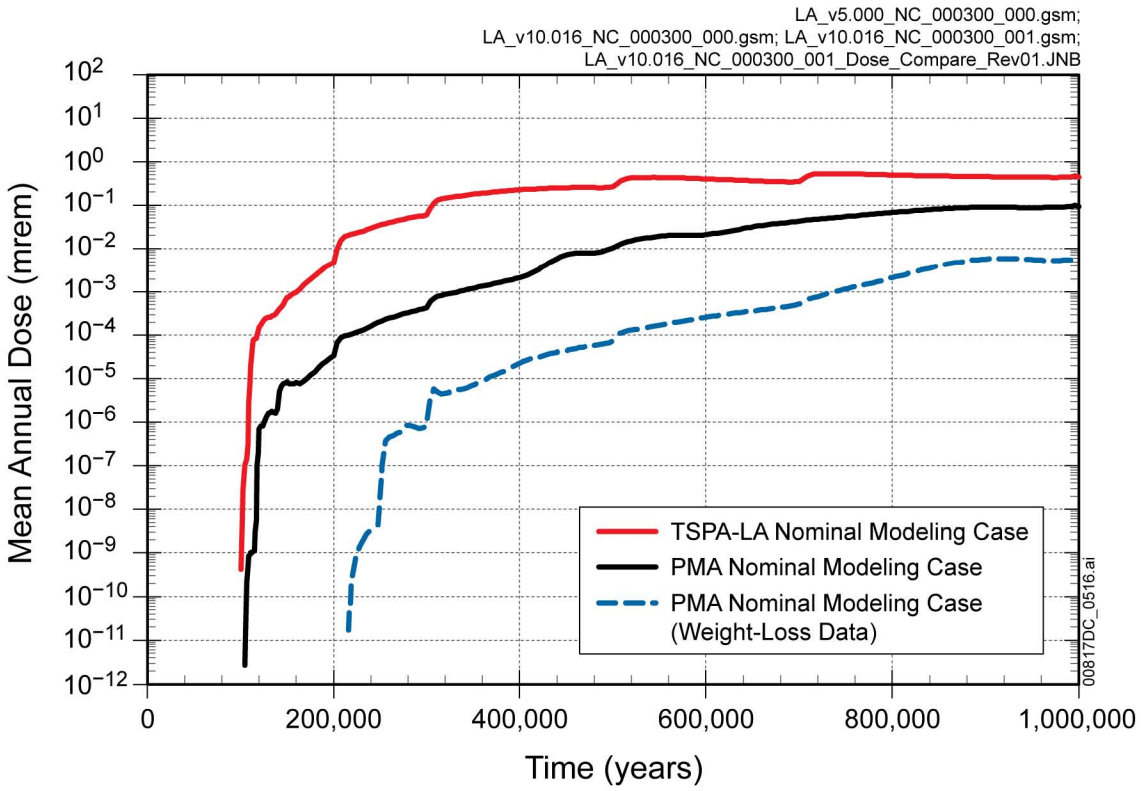

Source: Output DTN: MO0709TSPAREGS.000 [DIRS 182976] and Corroborative DTN: MO0709MARGANAL.000 [DIRS 182978].

Figure C7-14. Comparison of Nominal Modeling Cases to Projected Total Mean Annual Dose History 1,000,000 Years after Repository Closure for TSPA-LA, Performance Margin Analysis, and the Performance Margin Analysis, including General Corrosion Weight-Loss Data

INTENTIONALLY LEFT BLANK

APPENDIX D
PARAMETER LISTING

D1. INTRODUCTION

The Total System Performance Assessment (TSPA) Input Database contains the list of parameters used in the TSPA-LA Model. The details of this database are described in Section 4. Additionally, Appendix K contains two tables that describe the significant uncertain parameters (Tables K.3-1 and K.3-2.).

INTENTIONALLY LEFT BLANK

APPENDIX E
RESPONSE TO REVIEW COMMENTS FROM THE INTERNATIONAL REVIEW TEAM

E1. INTRODUCTION

The Total System Performance Assessment for the License Application (TSPA-LA) Model has evolved from the numerous TSPA models that were completed during the past decade (Sections ES2 and 1.1). In the summer of 2001, an International Review Team (IRT) jointly organized by the Nuclear Energy Agency of the Organization for Economic Cooperation and Development, and the International Atomic Energy Agency of the United Nations, met in Paris, France, and conducted an evaluation of the most recent performance assessment of the Yucca Mountain Repository, the Total System Performance Assessment for the Site Recommendation (TSPA-SR), and the accompanying TSPA-SR performance-assessment model. The IRT's evaluation is documented in: *An International Peer Review of the Yucca Mountain Project TSPA-SR* (OECD/IAEA 2002 [DIRS 158098]). The conclusions of the summary document support the TSPA methodology used for the Yucca Mountain Repository, and also provide a number of recommendations for future TSPA analyses and models related to the repository (OECD/IAEA 2002 [DIRS 158098], pp. 63 to 66). This appendix provides a summary of the recommendations provided by the IRT, and also identifies actions undertaken in response to those recommendations.

The Yucca Mountain Project conducted numerous analyses, evaluations, and impact analyses in response to many of the IRT recommendations. The recommendations from IRT were used, along with improvements in the understanding of the processes and engineered systems related to Yucca Mountain, to develop the TSPA-LA Model and its supporting submodels and analyses.

Table E-1 summarizes the status of the additional work conducted in response to the recommendations provided by the IRT.

INTENTIONALLY LEFT BLANK

Table E-1. Summary of Responses to International Review Team Summary Review Comments

IRT Recommendation Number	IRT Comment	Additional DOE Work Conducted since Review	Documentation
General	In particular, the IRT recommends that the inclusion of a diffusion pathway, in the absence of any advective flow onto or into the WP or the presence of any liquid water, should be independently reviewed to determine if it is credible and whether the complexity serves a valid purpose. If this over conservatism is removed, the calculated repository performance beyond 10,000 years could improve substantially.	The TSPA-LA Model is a modification of the TSPA-SR Model but is still conservative. The inclusion of a diffusion pathway in the absence of advective flow has not yet been independently reviewed. The current diffusion model is a key component of the *EBS Radionuclide Transport Abstraction* and is described in Section 7.2.1 and Appendix L of that report. Some aspects of the diffusion model that the IRT found to be very conservative were retained, including: (1) diffusion through thin water films that cover all EBS surfaces (SNL 2007 [DIRS 177407], Sections 6.3.1.2 and 6.3.4); (2) the presence of an emplacement pallet that was ignored in the EBS Radionuclide Transport assessment (SNL 2007 [DIRS 177407], Sections 6.1.1 and 6.3.1.2); (3) placing the WPs on the surface of invert (SNL 2007 [DIRS 177407], Sections 6.3.2.2 and 6.3.1.2); and (4) not allowing evaporation from DSs or WPs (SNL 2007 [DIRS 177407], Sections 6.3.2.4 and 6.3.3.2). Although conservative, the approach is appropriate for bounding analyses of repository performance for 10,000 years after repository closure and until the period of geologic stability per NRC Proposed Rule at 10 CFR 63.302 [DIRS 178394].	*EBS Radionuclide Transport Abstraction* (SNL 2007 [DIRS 177407], Sections 6.1, 6.3, 7.2.1, and Appendix L)
General	One aspect that has not been given sufficient attention is the possibility for any liquid water to exist on and within WPs over long periods of time. The probability of extraordinarily high seepage should be investigated in more depth. Design fixes, such as capillary barrier backfill, could be considered for the areas where seepage could be too high.	The *Multiscale Thermohydrologic Model* (SNL 2007 [DIRS 181383], Sections 6.1.3 and 6.3.16[a]) summarizes the relationship between percolation flux and seepage that contributes to Section 6.3.1. High percolation flux scenarios were not found to cause or encourage extraordinarily high seepage into repository drifts (Section 6.3.1.1). In addition, Section 6.3.1.2 shows that heat does not enhance seepage. Further, high percolation causes boiling duration to be shorter at the drift walls. Conversely, a low flux may encourage boiling for a longer period of time. In addition, thermal conductivity greatly affects how heat is dissipated in rock. Design fixes, such as capillary barrier backfill, were not included. Although a range of design alternatives may be evaluated by DOE, the basis for the License Application design of the repository is limited by the approved conceptual design found in *Total System Performance Assessment Data Input Package for Requirements Analysis for EBS In-Drift Configuration* (SNL 2007 [DIRS 179354], which serves as a source for the relevant model abstractions.	Engineered Barrier System: Physical and Chemical Environment Model: *Engineered Barrier System: Physical and Chemical Environment* (SNL 2007 [DIRS 177412], Sections 6.6, 6.9, and 6.15.1) Engineered Barrier System: *Multiscale Thermohydrologic Model* (SNL 2007 [DIRS 181383], Sections 6.1.3 and 6.3.16[a])

Table E-1. Summary of Responses to International Review Team Summary Review Comments (Continued)

IRT Recommendation Number	IRT Comment	Additional DOE Work Conducted since Review	Documentation
1	Include more disaggregation of TSPA-LA Model results and a more realistic assessment of the likely performance of the repository.	The evaluation of postclosure performance provided in this document includes a detailed presentation of subsystem results and other disaggregation of system-level results. Sections 7.1 to 7.4 and 7.7 and Appendix K provide information regarding assessments of the subsystems of the TSPA-LA Model. Because of the nature of the information provided to the TSPA and the overall approach required for an LA, the analysis includes some conservatisms. These conservatisms are noted as appropriate in subsections of Section 6.3, and their effect is qualitatively discussed.	Sections 6.3, 7.1 to 7.4 and 7.7 and Appendix K
2	Take steps to enhance the use of prior project information.	The project approach is to use available, quality information to conduct the performance assessment for the LA.	NA
3	Develop a safety case similar to the Nuclear Energy Agency approach.	This is a strategic project issue. No TSPA action is necessary.	NA

Table E-1. Summary of Responses to International Review Team Summary Review Comments (Continued)

IRT Recommendation Number	IRT Comment	Additional DOE Work Conducted since Review	Documentation
4	Develop and implement a comprehensive and systematic method for identification and treatment of uncertainty.	The approach developed in part, in response to the IRT recommendation, resulted in *Guidelines for Developing and Documenting Alternative Conceptual Models, Model Abstractions, and Parameter Uncertainty in the Total System Performance Assessment for the License Application*, and further specified for the TSPA in the *Technical Work Plan for: Total System Performance Assessment FY 07 to 08 Activities*. Uncertainty was incorporated in the development and implementation of the supporting models and abstractions and in the TSPA-LA Model. As part of this implementation, TSPA analysts reviewed relevant model abstractions and evaluated each input. When introducing uncertain parameters, the guidelines provided in the aforementioned documentation were followed. Section 6.1.2 discusses how uncertainty is incorporated in the calculation of mean annual dose using the TSPA-LA Model, and subsections to Section 6.3 contain discussions of the implementation of uncertainty with respect to the process models and submodels. Section 7.3 considers variability in terms of uncertainty and statistical stability (Section 7.3.1), variable numbers of Latin Hypercube samples with respect to the numerical accuracy of the calculation of mean annual dose (7.3.2), and temporal and spatial variability (Sections 7.3.3 and 7.3.4, respectively). Section 7.4 describes how uncertainty is incorporated into the modeling cases that are used to analyze the TSPA-LA Model scenario classes.	Sections 6.1.2, 7.3.1, 7.3.2, 7.3.3, 7.3.4, and 7.4 *Guidelines for Developing and Documenting Alternative Conceptual Models, Model Abstractions, and Parameter Uncertainty in the Total System Performance Assessment for the License Application* (BSC 2002 [DIRS 158794], Section 4) *Technical Work Plan for: Total System Performance Assessment FY 07 to 08 Activities* (SNL 2008 [DIRS 184920])

Table E-1. Summary of Responses to International Review Team Summary Review Comments (Continued)

IRT Recommendation Number	IRT Comment	Additional DOE Work Conducted since Review	Documentation
5	Quantitatively evaluate the importance of risk dilution.	The potential for risk dilution was minimized in the TSPA-LA process by evaluating and propagating realistic uncertainty in the distributions and ranges of the parameter values used in the TSPA-LA Model. One of the objectives of the Appendix C Performance Margin Analysis (PMA) as described in Section 7.7.4 was to ensure that the removal of the evaluated conservatisms did not introduce any inappropriate risk dilution in the TSPA-LA Model results as demonstrated by the absence of higher peak mean annual doses in the PMA results for both the probabilistic projections of the total dose histories and the comparison of the projected total mean dose history for the PMA relative to the TSPA-LA. The inclusion of uncertainty was significantly enhanced from previous TSPA models and follows the guidelines in *Guidelines for Developing and Documenting Alternative Conceptual Models, Model Abstractions, and Parameter Uncertainty in the Total System Performance Assessment for the License Application.* Section 6.1.2 describes the calculation of total mean annual dose and total median annual dose for the defined scenario classes for the TSPA-LA Model. In Section 7.7.4, the PMA also examines the sensitivity of the TSPA-LA Model with respect to conservatisms, parameter values, and model integration. These analyses provide comparisons between the base-case TSPA-LA Model and models that quantify the impact of various modeling issues. Furthermore, uncertainty within the TSPA-LA Model is quantitatively analyzed in Appendix K. Appendix K provides sensitivity analyses and discussions of parameters that were assessed to be important to the uncertainty of the model results. The TSPA-LA Model results include analyses of the impact of these parameters on the dose calculations.	Sections 6.1.2 and 7.7.4 and Appendix K *Guidelines for Developing and Documenting Alternative Conceptual Models, Model Abstractions, and Parameter Uncertainty in the Total System Performance Assessment for the License Application* (BSC 2002 [DIRS 158794])
6	Establish a program-wide focus on the reduction of uncertainty where it has the greatest effect.	Uncertainty in the TSPA-LA Model is addressed and described in Sections 6.1.2, 7.3.1, 7.3.2, 7.3.3, 7.3.4, and 7.4. Performance Confirmation testing and monitoring will assess the adequacy of the information used in the LA. Performance Confirmation test plans identify importance and/or relevance to the safety case and quantify parameters and condition limits for each test activity. If information obtained during Performance Confirmation challenges the information used in the licensing basis, the impact on repository performance will be evaluated and the regulator will be notified.	Sections 6.1.2, 7.3.1, 7.3.2, 7.3.3, 7.3.4, and 7.4 *Performance Confirmation Plan*, BSC 2004 [DIRS 172452]

Table E-1. Summary of Responses to International Review Team Summary Review Comments (Continued)

IRT Recommendation Number	IRT Comment	Additional DOE Work Conducted since Review	Documentation
7	Review and improve the EBS Transport Submodel.	Transport modeling through the EBS has been enhanced, including an Invert Diffusion Submodel, a section on retardation in the EBS, an In-Package Diffusion Submodel for Commercial Spent Nuclear Fuel Waste Packages, and sections discussing colloidal transport, transport through stress corrosion cracks, and transport through the waste-form rind. Supporting analyses and discussions are presented in *EBS Radionuclide Transport Abstraction* (SNL 2007 [DIRS 177407].	*EBS Radionuclide Transport Abstraction* (SNL 2007 [DIRS 177407], Section 6.3.4)
8	Improve the SZ regional model and the site-scale flow model. Run the model for in-spatial variability analysis, not just with a large uncertainty factor.	Although the SZ Regional and Site-Scale Models were developed outside the scope of the TSPA, the reference document supports the SZ Flow and Transport Model, the SZ Transport Model Component, and the SZ Flow and Transport Model Component. The SZ Regional and Site-Scale Models were updated with a number of modifications to: (1) reflect the current understanding of the SZ flow; (2) enhance model validation and uncertainty analyses; and (3) incorporate new data collected since the TSPA-SR. Changes introduced since the TSPA-SR Model report include the following: • Use of field and laboratory tests (hydraulic and tracer data collected since the TSPA-SR Model report) to establish and confirm the conceptual model for flow, constrain model parameter calibration, and provide data for model validation. • For validation purposes, use of recently collected hydraulic and geologic data that were obtained from the Nye County Early Warning Drilling Program. Despite these improvements, there remains uncertainty concerning the SZ flow component of the SZ flow model. This uncertainty represents a current lack of knowledge regarding the geophysical and hydrologic properties of the SZ. This uncertainty is represented in the assumptions in the reference document and in this TSPA-LA Model document, along with the bases and rationales for these assumptions.	*Saturated Zone Site-Scale Flow Model* (SNL 2007 [DIRS 177391], Sections 5, 6.4.3, 6.5, 6.7, and 7.2.2)

Table E-1. Summary of Responses to International Review Team Summary Review Comments (Continued)

IRT Recommendation Number	IRT Comment	Additional DOE Work Conducted since Review	Documentation
9	Develop a realistic understanding of radionuclide transport in a closed basin utilizing natural analogues.	Work is continuing on the evaluation of natural analogues and on the overall hydrogeologic system. In particular, the Peña Blanca Natural Analogue ongoing investigations include water sampling, rock and water analyses, and plans for PA modeling to assess groundwater flow and transport as part of studies under the DOE Office of Science and Technology (Goldstein et al. 2006 [DIRS 181364], p. 217). Section 7.8 contains a discussion of relevant natural analogues.	Section 7.8 Goldstein et al. 2006 ([DIRS 181364], p. 217) *Natural Analogue Synthesis Report* (BSC 2004 [DIRS 169218], Section 10)
10	Develop various levels of documentation, including a summary document.	The TSPA-LA Model documentation is supported by individual submodels and subordinate analysis and/or model reports. Section 6 of this report describes the essence of the main features of the TSPA-LA Model Section 1 and the Executive Summary provide summary descriptions of the TSPA-LA Model and its components as well as descriptions of the TSPA methodology.	Executive Summary and Section 6
11	Discuss design improvements and their role in the safety strategy in future documents.	The design of the repository is beyond the scope of this document. Quality Assurance processes are in place to ensure proper updating of controlled design inputs to the TSPA Model based on modifications to repository design. The scope of the documentation regarding design improvements is developed by the TSPA department and coordinated with DOE through mechanisms such as the Technical Management Review Board.	CC-PRO-1001, Rev. 2, *Technical Management Review Board Operations*
12	Long-term corrosion tests should be carried out on WP and DS materials, and the scientific understanding of corrosion mechanisms should be improved.	Long-term corrosion testing was conducted for both general corrosion and localized corrosion and more testing is scheduled in the Performance Confirmation Plan. There are about 5 years of corrosion data for WP and DS materials and about 10 years of data relating to stress corrosion cracking. The results of the corrosion testing are incorporated in the WP and DS models used in the TSPA-LA Model.	*Analysis of Dust Deliquescence for FEP Screening* (SNL 2007 [DIRS 181267]) *General Corrosion and Localized Corrosion of the Drip Shield* (SNL 2007 [DIRS 180778]) *General Corrosion and Localized Corrosion of Waste Package Outer Barrier* (SNL 2007 [DIRS 178519]) *Performance Confirmation Plan* (BSC 2004 [DIRS 172452])

Table E-1. Summary of Responses to International Review Team Summary Review Comments (Continued)

IRT Recommendation Number	IRT Comment	Additional DOE Work Conducted since Review	Documentation
13	The inventory screening procedure should be reviewed and amended, as appropriate, so that all potentially important radionuclides are included in the analysis.	The radionuclide screening procedure was reviewed, resulting in revised starting inventories for screening and a revised list of screened-in radionuclides. The revised list includes 32 nuclides (DTN: SN0310T0505503.004_R0 [DIRS 168761]. Thus, radionuclide screening analysis included (screen in) or removed radionuclides from further consideration (screen out) as contributors to radiation dose to the public from a nuclear waste repository at Yucca Mountain. The radionuclide screening analysis separately considered two different postclosure time periods: the 10,000-year period and the period from 10,000 years up to 1 million years after emplacement. Four release scenarios were considered: (1) the nominal scenario, (2) the human-intrusion scenario, (3) an intrusive igneous event, and (4) an eruptive igneous event. A radionuclide is screened out for a particular screening set, a grouping of radionuclides for a given waste form according to transport characteristics of each radionuclide, and waste form at a particular time. For comparison of results, the screening for the groundwater scenarios was used as the reference case to compare results. Of the 20 radionuclides collectively identified by the 10 studies, 13 were screened in for groundwater scenarios during the 10,000-year regulatory compliance period: ^{227}Ac, ^{243}Am, ^{14}C, ^{135}Cs, ^{129}I, ^{237}Np, ^{231}Pa, ^{239}Pu, ^{240}Pu, ^{226}Ra, ^{99}Tc, ^{229}Th, and ^{233}U. Four more were screened in for times up to 1,000,000 years: ^{36}Cl, ^{242}Pu, ^{79}Se, and ^{236}U. A fine-screen test, using a 99% cutoff level (contributes less than 1% of the dose), indicated that ^{36}Cl is potentially of marginal importance in the groundwater scenarios during the 10,000-year regulatory compliance period. OECD (Organization for Economic Co-operation and Development) 1997 ([DIRS 103445], Section 2.11) identified the radionuclides that contributed most to dose rate in “reference” studies of 10 repository performance assessments. Only one of the 10 studies found ^{94}Nb to be a major contributor to dose. *Radionuclide Screening* (SNL 2007 [DIRS 177424] developed the following results.	*Initial Radionuclide Inventories* (SNL 2007 [DIRS 180472], Table 6-2[a]) *Radionuclide Screening* (SNL 2007 [DIRS 177424], Sections 6.2.1, 6.7.2, and 7)

Table E-1. Summary of Responses to International Review Team Summary Review Comments (Continued)

IRT Recommendation Number	IRT Comment	Additional DOE Work Conducted since Review	Documentation
13 (Continued)		• ^{94}Nb is screened out for all scenarios and times. However, ^{94}Nb is found to be potentially of marginal importance for the groundwater scenarios after the 10,000-year regulatory compliance period. • ^{107}Pd is screened out for all scenarios and all times, and is not identified as marginally important by the fine-screen test. • ^{223}Ra has a half-life less than 10 years, and it is accounted for in the groundwater scenario only as a decay daughter from parents, such as ^{227}Ac. • For the waste forms considered and the physical processes employed in making the screening decision, ^{223}Ra is excluded as a primary radionuclide. • ^{245}Cm, ^{246}Cm, or ^{59}Ni are not important contributors to dose. • In addition to the radionuclides identified by the screening analysis, ^{241}Pu, ^{245}Cm, ^{228}Ra, and ^{235}U, were included in the radionuclide inventory to account for screened-in daughter products or due to augmentation from a screened-in precursor radionuclide. Also, ^{228}Ra was included because it is included in the groundwater protection standard.	
14	Further work should be carried out to strengthen confidence in the role of the cladding as a long-term containment barrier.	The cladding degradation analysis for the TSPA-LA Model starts with a discussion of cladding as a barrier and discusses the various parts of the cladding degradation abstraction analysis. The analysis document includes discussions of alternative scientific approaches, a summary of included FEPs, and a discussion of uncertainty. The document relies on 25 cladding-related documents for the sources of information used to develop and corroborate the analysis of cladding performance for the TSPA-LA Model. However, Cladding Degradation Summary for LA [DIRS 180616] conservatively concludes that, "For the no-cladding-credit compliance case, all fuel is taken to be failed upon receipt at the repository and the cladding is split when the waste package fails." Thus, the TSPA-LA Model does not take credit for spent fuel cladding.	*Cladding Degradation Summary for LA* (SNL 2007 [DIRS 180616])

Table E-1. Summary of Responses to International Review Team Summary Review Comments (Continued)

IRT Recommendation Number	IRT Comment	Additional DOE Work Conducted since Review	Documentation
15	More experimental data should be obtained to validate thermodynamic modeling, especially with regard to the complex interactions between the waste form and components of the WP.	Work to improve validation of thermodynamic modeling has continued, including thermal testing in the Exploratory Studies Facility (ESF). However, the need to increase knowledge of in-package interactions between the waste form and the components of the WP persists. To satisfy this need, the Performance Confirmation program includes plans for continued laboratory waste-form testing, including WP coupled effects (see Performance Confirmation Plan Activity ID #226).	*Multiscale Thermohydrologic Model* (SNL 2007 [DIRS 181383], Section 6.2.3.1, 6.3.3, 7.1, and 8.4.2[a]) *In-Package Chemistry Abstraction* (SNL 2007 [DIRS 180506], Sections 6.3.2.1.1, 6.3.1.1[a], and 7.2[a]) *Performance Confirmation Plan* (BSC 2004 [DIRS 172452])
16 and 17	Additional experiments should be performed to enhance confidence in the model of flow and transport in the UZ. Head measurements in the rock matrix and water extraction by the ventilation system should be used to test the 3-D UZ Flow and Transport Model.	The validation activities for the UZ Flow Model Component include corroboration with experimental data and modeling studies using the following: 1. Observational data from the transverse cross drift above the repository horizon, the Enhanced Characterization Repository Block (ECRB) drift, conducted within the validation activities for the UZ Flow Model Component, which includes corroboration within the ESF; 2. Perched-water data from borehole WT-24; 3. Gas-flow data from boreholes SD-12 and UZ-7a; 4. Measured ^{14}C borehole data. In addition, validation efforts were also performed for the calcite model, and strontium model. The following demonstrations met the validation criteria: 1. Simulated water potential values are within the range of measurements along the ECRB drift (*Technical Work Plan for: Performance Assessment Unsaturated Zone*, Attachment I-1-2-1).	Unsaturated Zone Transport: *UZ Flow Models and Submodels* (SNL2007 [DIRS 184614], Section 7) *Radionuclide Transport Models Under Ambient Conditions* (SNL 2007 [DIRS 177396], Section 7) *Technical Work Plan for: Performance Assessment Unsaturated Zone* (BSC 2004 [DIRS 167969])

Table E-1. Summary of Responses to International Review Team Summary Review Comments (Continued)

IRT Recommendation Number	IRT Comment	Additional DOE Work Conducted since Review	Documentation
16 and 17 (Continued)		2. Simulated perched water elevation matches the observed value within 10 m (*Technical Work Plan for: Performance Assessment Unsaturated Zone*, Attachment I-1-2-1). 3. Simulated gas pressures and their patterns of variations consistently compare closely with observed values. Simulations consistently reproduce increases and decreases resulting from changes in barometric pressure at the ground surface (*Technical Work Plan for: Performance Assessment Unsaturated Zone*, Attachment I-1-2-1). 4. The comparison between simulated matrix pore-water age and observed ^{14}C ages indicates that with active fracture parameter, ã = 0.4 (for UZ Model layers TSw32 to TSw38), the simulated tracer transport time can reasonably represent the measured ^{14}C ages of boreholes UZ-1 and SD-12. In addition, the simulated matrix pore-water age is sensitive to ã. Water potential data were collected from heat dissipation probes installed in the tunnel wall along the ECRB drift inside the ESF. Water potential data were collected from heat dissipation sensors that were calibrated for matrix potential. The validation activities of the conservative UZ Transport Model component demonstrated adequate reproduction of field transport test results relative to the Busted Butte test series, and Alcove 8-Niche 3 tests as described in *Radionuclide Transport Models Under Ambient Conditions*. As part of the 3-D flow and transport modeling validation process, modeled results of water potentials were compared to field observation data collected from the tunnel wall to check the accuracy of the modeling predictions. Even though the data available for comparison at the ECRB drift are limited, results indicated that the UZ Flow and Transport Model Component predicted the observed range of the water potential data collected in field studies.	

Table E-1. Summary of Responses to International Review Team Summary Review Comments (Continued)

IRT Recommendation Number	IRT Comment	Additional DOE Work Conducted since Review	Documentation
18	The probability of bimodal basaltic-rhyolitic volcanism should be estimated and, if relevant, analyzed.	The Yucca Mountain Project does not agree with this peer review recommendation because, "It is inferred that a volcano that might form at Yucca Mountain … will exhibit similar eruptive processes to those recorded in the deposits at Lathrop Wells volcano" (SNL 2007 [DIRS 174260] Section 6.3), which is a distinctly basaltic volcano. Therefore, DOE did not estimate or analyze the probability of bimodal basaltic-rhyolitic volcanism. More discussion on the magmatic sequence at Yucca Mountain is included in NRC 2007 [DIRS 182132], Section 3.2.1.	Disruptive Events-Igneous: *Characterize Framework for Igneous Activity at Yucca Mountain, Nevada* (BSC 2004 [DIRS 169989], Section 6.1.1) Disruptive Events-Igneous: *Characterize Eruptive Processes at Yucca Mountain, Nevada* (SNL 2007 [DIRS 174260], Appendix F.2.6) *Igneous Activity at Yucca Mountain: Technical Basis for Decision Making* (NRC 2007 [DIRS 182132], Section 3.2.1)
19	Direct flow of surface water into a human-intrusion borehole should be considered in future assessments.	The conditions for analyzing the Human Intrusion Scenario are specified in NRC Proposed Rule 10 CFR 63.322 [DIRS 180319]. The specifications do not include surface water down the borehole. Therefore, this circumstance was not included in the TSPA-LA Model analysis of the Human Intrusion Scenario. Further, this condition would not occur under "the common techniques and practices that are currently employed in exploratory drilling for groundwater in the region surrounding Yucca Mountain" (10 CFR 63.322(c) [DIRS 180319]) because current practice would call for a surface seal, which would prevent water from falling into the borehole.	Section 6.7 FEPs DTN: MO0706SPAFEPLA.001; FEP Numbers 1.4.04.01.0A and 1.1.11.00.0A [DIRS 181613] NRC Proposed Rule 10 CFR 63.322 [DIRS 180319]
20	Conduct additional work at Peña Blanca.	Section 7.8.2 provides a summary of completed work at Peña Blanca, which provides confidence in the PA of the Yucca Mountain Repository using the TSPA-LA Model. Additional field data are being collected at the Peña Blanca natural analogue site as described in Goldstein et al. 2006 ([DIRS 181364], p. 217). The additional investigations will continue to support the Yucca Mountain project.	Section 7.8.2 *Natural Analogue Synthesis Report* (BSC 2004 [DIRS 169218], Section 10) Goldstein et al., 2006 ([DIRS 181364], p. 217)

Table E-1. Summary of Responses to International Review Team Summary Review Comments (Continued)

IRT Recommendation Number	IRT Comment	Additional DOE Work Conducted since Review	Documentation
21	Continue the investigation of naturally occurring uranium and its progeny in Yucca Mountain tuffs.	In addition to the work already conducted and presented in Paces and Neymark 2004 [DIRS 174513], and Neymark et al. 2005 [DIRS 180924], USGS researchers are collecting and analyzing additional field data.	Paces, J.B. and Neymark, L.A. 2004. "U-Series Evidence of Water-Rock Interaction at Yucca Mountain, Nevada, USA" [DIRS 174513] Neymark, L.A.; Paces, J.B.; Marshall, B.D.; Peterman, Z.E.; and Whelan, J.F. 2005. "Geochemical and C, O, Sr, and U-series Isotopic Evidence for the Meteoric Origin of Calcrete at Solitario Wash, Crater Flat, Nevada, USA." [DIRS180924]
22	Screen FEPs in two stages: (1) all FEPs required for understanding, and (2) regulatory considerations.	The Yucca Mountain Project FEP database was reviewed in accordance with the recommended two-stage process as part of the development of the TSPA-LA. FEP screening decisions were reviewed and documented. The results are incorporated in DTN: MO0706SPAFEPLA.001 [DIRS 181613].	FEPS descriptions, screening arguments, and dispositions are consolidated in DTN: MO0706SPAFEPLA.001 [DIRS 181613]
23	Present a best estimate or most probable dose range, plus the upper limit value at an appropriate percentile, as a measure of maximum reasonably expected value.	NRC Proposed Rule 10 CFR Part 63 ([DIRS 178394] and [DIRS 180319]) require that the results of the PA analyses present annual dose to the RMEI in terms of the mean annual dose for the first 10,000 years postclosure, and as the median annual dose for the period from 10,000 years to the period of geologic stability (10 CFR 63.303 [DIRS 178394]). In addition, the TSPA-LA Model calculates at the 5th and 95th percentiles of dose to the RMEI.	NRC Proposed Rule 10 CFR Part 63 [DIRS 178394] and [DIRS 180319]

Table E-1. Summary of Responses to International Review Team Summary Review Comments (Continued)

IRT Recommendation Number	IRT Comment	Additional DOE Work Conducted since Review	Documentation
24	Base the probabilistic analysis on realistic rather than conservative representation.	The realistic analysis is not required by current regulations (10 CFR 63.114(b) [DIRS 178394]). However, the general approach for the TSPA-LA Model is to improve realism by reducing the number of conservative assumptions. Regardless of this general approach, it should be noted that "simplifications and assumptions are involved out of necessity..." (40 CFR Part 197 [DIRS 173176]). This results in the TSPA-LA Model being a hybrid "conservative/probabilistic" Model in which reasonable incorporation of conservatism is used when necessary. Further, Appendix C presents the results of a Performance Margin Analysis, summarized in Section 7.7.4, which uses less conservative, i.e., more "realistic," values of some TSPA-LA Model parameters to estimate the range of performance with respect to choices of parameter values, thus indicating the potential performance margin embedded in the TSPA-LA Model's dose calculations.	10 CFR Part 63 [DIRS 178394] and [DIRS 180319] 40 CFR Part 197 [DIRS 173176]
25	Use a more formal approach to determine convergence of probabilistic results. Consider using alternative sampling schemes and larger numbers of realizations.	The approach to be utilized is described, and the results of the statistical stability analysis are presented in Section 7.3.1. Larger numbers of realizations and alternative sampling schemes were utilized. Section 7.3.2 considers variable numbers of Latin hypercube sample, and TSPA-LA Model realizations with respect to the numerical accuracy of the calculation of mean annual dose. In addition, temporal and spatial variability are addressed in Sections 7.3 and 7.4, respectively. After establishing the stability of the calculation methodology, the TSPA-LA Model utilizes enough realizations to provide statistically stable results.	Sections 7.3.1, 7.3.2, 7.3.3, and 7.3.4

Table E-1. Summary of Responses to International Review Team Summary Review Comments (Continued)

IRT Recommendation Number	IRT Comment	Additional DOE Work Conducted since Review	Documentation
26	Present probability density function of calculated doses.	The complete array of annual doses used in calculating the mean annual dose for each modeling case is provided in Section 8.2 and Appendix K. These plots present the same relevant data that could alternatively be displayed as probability density function curves, although these data are not presented in that form in Section 8 or Appendix K. In addition, the distribution of calculated annual doses at 10,000 and 1,000,000 years after repository closure is provided for each modeling case in Sections 8.2 and Appendix K.	Section 8.2 and Appendix K
27	Use sensitivity analysis to assist in building an integrated and comprehensive understanding of the relative importance and role of different barriers and processes.	Such analyses were conducted and are described in Section 8.3 and Appendix K.	Section 8.3 and Appendix K

APPENDIX F

DYNAMICALLY LINKED LIBRARIES DESCRIPTION AND FEEDS

F1. INTRODUCTION

Appendix F provides a summary of the dynamically linked libraries (DLLs) used in the Total System Performance Assessment for the License Application (TSPA-LA) Model and their associated input files. Each DLL is identified by software name and version, software tracking number (STN), and Document Input Reference System (DIRS) number. Some DLL names differ slightly from their corresponding software names. Appendix F also includes tables that list the input file(s) used by each DLL. Since only input files are described, the DLLs that do not use input files are briefly identified for completeness.

Table F-1 provides a brief description of each DLL and identifies the subsequent table that contains the input files for the DLL. Tables F-2 through F-13 contain a list of the input files used by each DLL, a description of the files, the Data Tracking Number (DTN) containing the files, and a list of the control information and data within the input files. For TSPA-LA Model V5.000, the DLLs are identified as DLL Set 35 and their input files are identified as Input File Set 62. Some TSPA-LA Model V5.000 groundwater transport simulations used DLL Set 34 and Input File Set 61. These DLLs and associated input files are the same for the groundwater transport analyses as in DLL Set 35 and Input File Set 62. The only differences between these sets are with respect to the Volcanic Eruption Modeling case.

The TSPA-LA Model V5.000 simulations were processed using GoldSim V9.60.100 (STN: 10344-9.60-01 [DIRS 181903]) as described in Section 3.1.2. During a TSPA-LA Model multi-realization simulation, the DLLs and their associated input files are automatically downloaded from a controlled computer network area into the primary run directory on the master processor. The file-transfer process utilizes the GoldSim model file elements to ensure that the external supporting files to GoldSim, including both the DLL executable files and their associated input files used in a simulation, are directly accessed from a controlled environment. These files are in turn passed from the master processor to slaves when the GoldSim *Distributed Process Module* is utilized. This automated file transfer process allows GoldSim to provide an 'audit trail' of the DLL executable files and associated input files used in any simulation. In addition, the TSPA-LA Model utilizes the file-locking option of the GoldSim file elements, which permits the simulation to proceed only if the file being used for the simulation is exactly the same as the file that the element was initially locked onto. The names of the DLL executable files and their associated input files are parameters in the TSPA-LA Model Input Database (Section 4.7), which are directly accessed by the GoldSim file elements.

F2. INPUT FILES BY DYNAMICALLY LINKED LIBRARY

F2.1 FEHMN_V2_24-01.DLL

The DLL fehmn_v2_24-01.dll (FEHM V 2.24-01, STN: 10086-2.24-01-00 [DIRS 179419]) is designed to perform radionuclide transport calculations. Transport through the unsaturated zone (UZ) is simulated in the TSPA-LA Model using a residence-time, transfer-function particle-tracking technique as described in *Particle Tracking Model and Abstraction of Transport Processes* (SNL 2008 [DIRS 184748]). A complete description of fehmn_v2_24-01.dll and the input files is documented in *Software Users Manual (UM) for the*

FEHM Application Version 2.21 (LANL 2003 [DIRS 167579]) and *User Information for: FEHM V2.24-01* (DOE 2007 [DIRS 181096]).

In TSPA-LA Model simulations, GoldSim and fehmn_v2_24-01.dll (also generally abbreviated as FEHM for Finite Element, Heat and Mass Model) are coupled through a predefined interface. Data passed from GoldSim directly through the interface for each timestep includes: (1) the simulation time; (2) a flow-field index (instructing FEHM which flow-field file to read for the present timestep and infiltration scenario; (3) two random seeds, one used to initiate sampling for particle-tracking logic and one used to initialize logic for determining the source release location; (4) the number of source bins; (5) the number of waste packages (WPs) contributing mass to the engineered barrier system (EBS) release to the UZ for each percolation subregion; (6) the fraction of mass in each source bin for each species entering the UZ that is applied to the fractures; and (7) the EBS mass release rates. Additional control data for the number of WP early failures are also passed, but the option is not used in the TSPA-LA Model as indicated by the passed control index. For efficiency, FEHM does not simulate the flow fields. Instead, FEHM reads pre-existing flow fields at the start of each realization and at times of climate changes. These flow fields were generated in advance using TOUGH2 V1.6 (LBNL 2003 [DIRS 161491]). At the end of each simulation timestep, FEHM passes the radionuclide mass fluxes generated at the water table back to GoldSim through the interface.

The fehmn_v2_24-01.dll input stream is controlled by two main files. The input file fehmn.files contains a list of the main input and output files used by FEHM. The input file fehm_TSPA_template.dat is a generic file that contains both FEHM input parameters and input file names, where additional parameters are found. For the TSPA-LA Model, either fehm_TSPA_gs_20kyr.dat for 10,000/20,000-year simulations or fehm_TSPA_gs_1Myr.dat for one-million-year simulations is automatically copied into fehm_TSPA_template.dat.

The following subsections describe the input files used by fehmn_v24_2.-01.dll. The file names used refer to actual UZ Transport Submodel files. A complete list of these files and their contents is presented in Table F-2.

F2.1.1 Control Data File for Primary Inputs and Outputs

As described in Table F-2, the input file fehmn.files is the default fehmn_v2_24-01.dll control file read at the start of a run. It contains names of the main input data file, grid file, initial zone file, output file, flow-field (or restart) file, updated restart file, simulation history file, stiffness matrix file, Solute history output file, and check file; contour files (if used); a screen output indicator and information on supplementary subroutines. See the user's manual (LANL 2003 [DIRS 167579], Section 6.2.1) for a description of the file.

F2.1.2 Control Data Files for Input Parameters

As described in Table F-2, the two input files fehm_TSPA_gs_20kyr.dat and fehm_TSPA_gs_1Myr.dat contain control information and data for 10,000/20,000-year and one-million year simulations. The two files are based on the template file fehm_TSPA_template.dat obtained from DTN: MO0704PAFEHMBR.001_R3 [DIRS 184647], which is an output DTN from *Particle Tracking Model and Abstraction of Transport Processes*

(SNL 2008 [DIRS 184748]). Minor modifications were made to the template file to create the two input files that allow the TSPA-LA Model to control the time stepping. At the start of each TSPA-LA Model simulation, the appropriate file for the chosen simulation time length is copied into a generic file named in the control file fehmn.files (described in Section F2.1.1). Both of the input files contain simulation control information and names of parameter files containing data for rock properties, a dual permeability option, a colloid interface-filtration model, a spatial zonation of properties, and a generic multiple-species particle tracking transport model. See the user's manual (LANL 2003 [DIRS 167579], Section 6.0) for a description of the file.

To enhance the input process, FEHM contains a macro control structure for data input. The macro command structure is based on a set of control statements that is recognized by the program. When a macro control statement (or keyword) is encountered in an input file, the input control module reads in a specific set of data in a prescribed order. This allows the user to set up an input file or set of files using structured blocks of data assembled in any order. Except for macro control statements, data within each block are read in by free format. This adds to the flexibility of the model, but dictates that values be added for all input variables. In addition, because the model allows the user to assign data by node, groups of nodes, or for the entire system, data lists are generally followed by blank lines indicating to the model that no more data of that specific type follows. Within blocks of data, the user can include the keyword 'file', followed by a file name, indicating that the next data expected by the input module are contained in the file noted.

Basic macros controlled by parameters listed in the above data control files include: (1) *perm*, which assigns default permeabilities to all zones; (2) *rlp*, the relative permeability and capillary pressure model; (3) *time*, the which sets up the timesteps for and ending time of the simulation; (4) *itfc*, which controls colloid filtration at matrix interfaces; (5) *ctrl*, which lists the general run parameters needed for equation solver and matrix solver routines; (6) *sol*, which defines the solution type and element integration method; (7) *rflo*, which signifies that the flow field will be read in; (8) *airwater,* which signifies that the problem is two-phased; and (9) *node*, which can be used to assign specific nodes for output. Note that many of the parameters associated with the above macros are not used in the coupled GoldSim/FEHM simulations.

F2.1.3 Nodal-Coordinate Data File

As described in Table F-2, the input file fehmn.grid contains a list of the grid node numbers and their associated location coordinates and elevations. The nodal-coordinates are based on the Nevada State Plane eastings (m), northings (m), and elevations (meters above mean sea level). Note that only the node numbers for the fracture media are listed. The node number for the spatially equivalent matrix node is found by adding 120,711 to the fracture medium node number. Although the element connectivities are defined in this file, they are not used in the particle-tracking model. See the user's manual (LANL 2003 [DIRS 167579], Section 6.2.12) for a complete description.

F2.1.4 Zone Data File – Initial

As described in Table F-2, the input file fehmn.zone is the initial material zone file. See the user's manual (LANL 2003 [DIRS 167579], Section 6.2.74) for a description of the input parameters.

The zones defined below are used for all zone-based property assignments until superseded by another zone file listed in the main input file. All zone-based property assignments following a new zone-file assignment will be based upon the new file until a new zone file occurs in the input stream. The data are in the form of a list of nodes for each zone. As listed below, there are 96 material zones in the model. The first 46 represent rock matrix, the second 46 represent the corresponding fractures overlaying the same space, and zones 93 through 96 represent fault zones.

1. tcwM1-Tiva Canyon Layer 1 welded tuff rock matrix
2. tcwM2-Tiva Canyon Layer 2 welded tuff rock matrix
3. tcwM3-Tiva Canyon Layer 3 welded tuff rock matrix
4. ptnM1-Paintbrush Layer 1 nonwelded tuff rock matrix
5. ptnM2-Paintbrush Layer 2 nonwelded tuff rock matrix
6. ptnM3-Paintbrush Layer 3 nonwelded tuff rock matrix
7. ptnM4-Paintbrush Layer 4 nonwelded tuff rock matrix
8. ptnM5-Paintbrush Layer 5 nonwelded tuff rock matrix
9. ptnM6-Paintbrush Layer 6 nonwelded tuff rock matrix
10. tswM1-Topopah Springs Layer 1 welded tuff rock matrix
11. tswM2-Topopah Springs Layer 2 welded tuff rock matrix
12. tswM3-Topopah Springs Layer 3 welded tuff rock matrix
13. tswM4-Topopah Springs Layer 4 welded tuff rock matrix
14. tswM5-Topopah Springs Layer 5 welded tuff rock matrix
15. tswM6-Topopah Springs Layer 6 welded tuff rock matrix
16. tswM7-Topopah Springs Layer 7 welded tuff rock matrix
17. tswM8-Topopah Springs Layer 8 welded tuff rock matrix
18. tswMz-Topopah Springs Layer 9 zeolitized tuff rock matrix
19. tswMz-Topopah Springs Layer 9 vitric tuff rock matrix
20. ch1Mz-Calico Hills Layer 1 zeolitized tuff rock matrix
21. ch1Mv-Calico Hills Layer 1 vitric tuff rock matrix
22. ch2Mv-Calico Hills Layer 2 vitric tuff rock matrix
23. ch3Mv-Calico Hills Layer 3 vitric tuff rock matrix
24. ch4Mv-Calico Hills Layer 4 vitric tuff rock matrix
25. ch5Mv-Calico Hills Layer 5 vitric tuff rock matrix
26. ch2Mz-Calico Hills Layer 2 zeolitized tuff rock matrix
27. ch3Mz-Calico Hills Layer 3 zeolitized tuff rock matrix

28. ch4Mz-Calico Hills Layer 4 zeolitized tuff rock matrix
29. ch5Mz-Calico Hills Layer 5 zeolitized tuff rock matrix
30. ch6Mz-Calico Hills Layer 6 zeolitized tuff rock matrix
31. ch6Mv-Calico Hills Layer 6 vitric tuff rock matrix
32. pp4Mz-Prow Pass Layer 4 zeolitized tuff rock matrix
33. pp3Md-Prow Pass Layer 3 differentiated tuff rock matrix
34. pp2Md-Prow Pass Layer 2 differentiated tuff rock matrix
35. pp1Mz-Prow Pass Layer 1 zeolitized tuff rock matrix
36. bf3Md-Bull Frog Layer 3 differentiated tuff rock matrix
37. bf2Mz-Bull Frog Layer 2 zeolitized tuff rock matrix
38. tr3Md-Tram Layer 3 differentiated tuff rock matrix
39. tr2Mz-Tram Layer 2 zeolitic tuff rock matrix
40. pcM38-Perched water layer corresponding to Topopah Springs Layer 8 rock matrix
41. pcM39-Perched water layer corresponding to Topopah Springs Layer 9 rock matrix
42. pcM1z-Perched water layer corresponding to Calico Hills zeolitic Layer 1 matrix
43. pcM2z-Perched water layer corresponding to Calico Hills zeolitic Layer 2 matrix
44. pcM5z-Perched water layer corresponding to Calico Hills zeolitic Layer 5 matrix
45. pcM6z-Perched water layer corresponding to Calico Hills zeolitic Layer 6 matrix
46. pcM4p-Perched water layer corresponding to Prow Pass zeolitic Layer 4 matrix
47. tcwF1-Tiva Canyon Layer 1 welded tuff fractures
48. tcwF2-Tiva Canyon Layer 2 welded tuff fractures
49. tcwF3-Tiva Canyon Layer 3 welded tuff fractures
50. ptnF1-Paintbrush Layer 1 nonwelded tuff fractures
51. ptnF2-Paintbrush Layer 2 nonwelded tuff fractures
52. ptnF3-Paintbrush Layer 3 nonwelded tuff fractures
53. ptnF4-Paintbrush Layer 4 nonwelded tuff fractures
54. ptnF5-Paintbrush Layer 5 nonwelded tuff fractures
55. ptnF6-Paintbrush Layer 6 nonwelded tuff fractures
56. tswF1-Topopah Springs Layer 1 welded tuff fractures
57. tswF2-Topopah Springs Layer 2 welded tuff fractures
58. tswF3-Topopah Springs Layer 3 welded tuff fractures
59. tswF4-Topopah Springs Layer 4 welded tuff fractures
60. tswF5-Topopah Springs Layer 5 welded tuff fractures
61. tswF6-Topopah Springs Layer 6 welded tuff fractures
62. tswF7-Topopah Springs Layer 7 welded tuff fractures
63. tswF8-Topopah Springs Layer 8 welded tuff fractures
64. tswFz-Topopah Springs Layer 9 zeolitized tuff fractures
65. tswFv-Topopah Springs Layer 9 vitric tuff fractures

66. ch1Fz-Calico Hills Layer 1 zeolitized tuff fractures
67. ch1Fv-Calico Hills Layer 1 vitric tuff fractures
68. ch2Fv-Calico Hills Layer 2 vitric tuff fractures
69. ch3Fv-Calico Hills Layer 3 vitric tuff fractures
70. ch4Fv-Calico Hills Layer 4 vitric tuff fractures
71. ch5Fv-Calico Hills Layer 5 vitric tuff fractures
72. ch2Fz-Calico Hills Layer 2 zeolitized tuff fractures
73. ch3Fz-Calico Hills Layer 3 zeolitized tuff fractures
74. ch4Fz-Calico Hills Layer 4 zeolitized tuff fractures
75. ch5Fz-Calico Hills Layer 5 zeolitized tuff fractures
76. ch6Fz-Calico Hills Layer 6 zeolitized tuff fractures
77. ch6Fv-Calico Hills Layer 6 vitric tuff fractures
78. pp4Fz-Prow Pass Layer 4 zeolitized tuff fractures
79. pp3Fd-Prow Pass Layer 3 differentiated tuff fractures
80. pp2Fd-Prow Pass Layer 2 differentiated tuff fractures
81. pp1Fz-Prow Pass Layer 1 zeolitized tuff fractures
82. bf3Fd-Bull Frog Layer 3 differentiated tuff fractures
83. bf2Fz-Bull Frog Layer 2 zeolitized tuff fractures
84. tr3Fd-Tram Layer 3 differentiated tuff fractures
85. tr2Fz-Tram Layer 2 zeolitized tuff fractures
86. pcF38-Perched water layer corresponding to Topopah Springs Layer 8 fractures
87. pcF39-Perched water layer corresponding to Topopah Springs Layer 9 fractures
88. pcF1z-Perched water layer corresponding to Calico Hills Layer 1 zeolitic fractures
89. pcF2z-Perched water layer corresponding to Calico Hills zeolitic Layer 2 fractures
90. pcF5z-Perched water layer corresponding to Calico Hills zeolitic Layer 5 fractures
91. pcF6z-Perched water layer corresponding to Calico Hills zeolitic Layer 6 fractures
92. pcF4p-Perched water layer corresponding to Prow Pass zeolitic Layer 4 fractures
93. tcwFf–Faults in Tiva Canyon welded hydrologic units
94. ptnFf-Faults in Paintbrush nonwelded hydrologic units
95. tswFf-Faults in Topopah Spring welded hydrologic units
96. chnFf-Faults in Calico Hills nonwelded hydrologic units.

F2.1.5 Initialization Files

As described in Table F-2, the 16 input files ffij00.ini are restart/initialization files that contain nodal pressure and saturation data for each node and flux data for each pair of adjacent nodes. These data are used to describe the flow field for different climates and infiltration scenarios. The data initializes at the beginning of each model realization and at each timestep when the climate changes. For this analysis, the initialization files contain the flow fields generated by TOUGH2 in FEHM format that are read by FEHM at run time. Although pressure data is

required, it is not used in the particle-tracking analysis. The structure of the flow-field files is consistent with the structure of restart records written by FEHM. Particle tracking records written to the restart files are not part of the flow-field files used in the coupled GoldSim/FEHM runs. See the user's manual (LANL 2003 [DIRS 167579], Section 7.2) for a description of the file.

The naming convention, ffij00.ini, is used for the coupled GoldSim/FEHM analyses. The saturation and flux data are used to describe the flow field as follows:

i = 1 (present-day climate)
i = 2 (monsoon climate)
i = 3 (glacial-transition climate)
i = 4 (post-10,000 years)
j = 1 (10th percentile infiltration scenario)
j = 2 (30th percentile infiltration scenario)
j = 3 (50th percentile infiltration scenario)
j = 4 (90th percentile infiltration scenario).

Note that the classification of 10th, 30th, 50th, and 90th percentile infiltration scenarios is based on the infiltration maps used to develop the flow fields for the first three climates. For the post-10,000-year climate, the four equivalent flow fields are generated using the scaled 90th percentile present-day, 50th percentile Glacial Transition, 90th percentile glacial transition, and the 90th percentile monsoon infiltration maps, respectively (see Section 6.3.1). The flow-field index, ij00, is passed from GoldSim to FEHM at each timestep. When the index changes from its original value to ij00, FEHM will reinitialize the flow field with the contents of ffij00.ini. The flow field input files are renamed from the original file names and are found in the output DTN: MO0708TSPAGENT.000 [DIRS 183000]. The files are grouped as follows:

Present-day files ff1100.ini, ff1200.ini, ff1300.ini, and ff1400.ini are equivalent to the original files pd10.ini, pd30.ini, pd50.ini, and pd90.ini (DTN: LB0612PDFEHMFF.001_R0 [DIRS 179296]), respectively.

Monsoon-climate files ff2100.ini, f2200.ini, ff2300.ini, and ff2400.ini are equivalent to the original files mo10wtrise.ini, mo30wtrise.ini, mo50wtrise.ini, and mo90wtrise.ini (DTN: LB0701MOFEHMFF.001_R0 [DIRS 179297]), respectively.

Glacial-transition climate flow field files, ff3100.ini, ff3200.ini, ff3300.ini, and ff3400.ini are equivalent to the original files gt10wtrise.ini, gt30wtrise.ini, gt50wtrise.ini, and gt90wtrise.ini (gt10wtrise.ini, gt30wtrise.ini, gt50wtrise.ini, gt90wtrise.ini (DTN: LB0701GTFEHMFF.001_R0 [DIRS 179160]), respectively.

Post-10,000 year flow fields, ff4100.ini, ff4200.ini, ff4300.ini, and ff4400.ini are equivalent to the original files post10kWTRISEpkdq1.ini, post10kWTRISEpkdq2.ini, post10kWTRISEpkdq3.ini, and post10kWTRISEpkdq4.ini (DTN: LB0702PAFEM10K.002_R0 [DIRS 179507]), respectively.

F2.1.6 Stiffness Matrix Data File

As described in Table F-2, the input file fehmn.stor contains the pre-calculated stiffness matrix data associated with the grid file used in the UZ transport calculation. This input file contains finite element coefficients designed to speed-up the execution of the software. Note that dummy area coefficients are also included in this file. See the user's manual (LANL 2003 [DIRS 167579], Section 7.7) for a description of the file.

The stiffness matrix file contains two required text lines describing information about the file and the following data:

1. Number of storage locations needed to store geometric input types (974,283).
2. Number of fracture (or matrix) nodes (120,711).
3. Number of positions for which information needs to be stored (1,094,995).
4. Volume associated with each node.
5. Nodal connectivity information including array positions followed by the node numbers grouped by connectivity.
6. Finite element geometric coefficients along with their starting positions for each node and the position of the primary nodes in the connectivity array. Note that the geometric coefficients are all set to -1.0 for the multiple-species particle tracking model.

F2.1.7 Double Porosity/Double Permeability Data File

As described in Table F-2, the input file fehm_TSPA.dpdp contains dual porosity/dual permeability geometric data for each fracture zone identified in Section F2.1.4 (zones 47 through 96). The first set of data defines the volume fraction (unitless) of the effective nodal volume taken up by the fracture. The volume fraction is used to define the accumulation (storage) terms. The second set of data defines the length scale of matrix nodes. See the user's manual (LANL 2003 [DIRS 167579], Section 6.2.14) for a description of the file.

F2.1.8 Rock Data File

As described in Table F-2, the input file fehm_TSPA.rock contains rock bulk density, specific heat, and porosity data for each zone defined in fehmn.zone (described in Section F.2.1.4). See the user's manual (LANL 2003 [DIRS 167579], Section 6.2.58) for a description of the file.

F2.1.9 Pore Size Data Files

As described in Table F-2, the 16 input files contain pore-size (filtration) cumulative probability data for the various rock matrix zones used to determine which size of colloidal particles will be filtered out during the rock layer contact filtration analysis. The pore-size distribution data are used to simulate the effect of colloid filtration at matrix interfaces on radionuclide transport. See the user's manual (LANL 2003 [DIRS 167579], Section 6.2.40) for a description of the file.

F2.1.10 Zone Data File – Updated

As described in Table F-2, the input file fehm.zone2 is an updated zone file that contains the same zone data as fehmn.zone described in Section F2.1.4*)*, plus two supplemental sets of zones at the end of the file. See the user's manual (LANL 2003 [DIRS 167579], Section 6.2.74) for a description of the file.

The first supplemental set of zones defines fracture zones (Zones 501 through 505) and matrix radionuclide release zones (Zones 601 through 605) for mass entering the UZ from the EBS. Note that for the TSPA-LA Model analysis, only the fracture zones 501 through 505 are used. The nodal numbering convention indicates the number of the matrix node that is spatially equivalent to a specified fracture node, which can be derived as $node\#_{matrix} = node\#_{fracture} + 120{,}711$, where 120,711 is the number of fault or matrix nodes.

The second supplemental set of zones (Zones 701 through 704) contains the nodes from which the radionuclide mass flux is summed for each zone to provide four source terms for the Saturated Zone (SZ) Flow and Transport Submodel. The nodes in these bins are found at or below the water table. The areal distribution of the four bins is as follows:

Bin #701–NSP Easting(m) < 171190 and NSP Northing(m) > 233460
Bin #702–NSP Easting(m) > 171190 and NSP Northing(m) > 233460
Bin #703–NSP Easting(m) < 171190 and NSP Northing(m) < 233460
Bin #704–NSP Easting(m) > 171190 and NSP Northing(m) < 233460.

F2.1.11 Multiple-Species Particle Tracking Data Files

As described in Table F-2, the 8 input files contain parameter values and names of parameter files containing data used for multiple-species particle tracking transport simulations. The input files are based on TSPA-LA Model modifications to the template file fehm_TSPA.mptr obtained from DTN: MO0704PAFEHMBR.001_R3 [DIRS 184647]. During a TSPA-LA Model simulation, the appropriate file based on simulation length and scenario type is automatically copied into a generic file by MFCP_LA.dll (MFCP_LA V1.0, STN: 11071-1.0-00 [DIRS 167884]), as described in Section F2.2. See the User Information Document (DOE 2007 [DIRS 181096], Section 2.5.1) for a description of the file.

The file fehm_TSPA_10kyr.mptr is identical to fehm_TSPA.mptr, except it has been updated from UNIX to PC format. The files with *ign* (for igneous simulations) and *ef* (for early failure simulations) in the filename contain updates associated with the assignment of particles by mass, as opposed to by timestep, for the radionuclides ^{99}Tc and ^{129}I. The difference between the igneous and early failure files, and the other files, is the manner with which particles are assigned for ^{129}I and ^{99}Tc. Because the igneous model generates short-duration spike-type source terms for ^{129}I and ^{99}Tc, the number of particles released for each timestep is based upon the mass released. As described in the User Information Document (DOE 2007 [181096] Section 2.5.1), the value for the input variable CONFACTOR is chosen to assign a specific number of particles per mole based on the maximum number of moles that could possibly be released from the repository.

In some of the early failure simulations, only a single WP is failed so that for ^{129}I and ^{99}Tc the maximum possible mass release for one package is used as the basis for determining the number of moles of radionuclides that each particle represents. The calculations used to determine CONFACTOR values for these early failure simulations are based on the maximum number of moles per WP that could be released. For all other species in the igneous and early failure simulations and all species in other simulations, the particles are assigned based upon a function of the size of the timestep, the number of years remaining in the simulation, and the number of particles left.

Other changes to the original files are associated with the need to increase the array allocation lengths for specific arrays that are dimensioned based on a function of the number of timesteps. These array sizes are increased for the 1,000,000-year simulations.

The multiple-species particle tracking files contain species-independent control and transport parameters and species-dependent control and transport parameters (or indices pointing to the transport parameters) for particle tracking simulations.

The species-independent control parameters include the number of species simulated, the maximum number of property zones, the maximum number of particles that can be released per species, an index indicating whether FEHM is being used in conjunction with GoldSim, the maximum allowable length for timestep dependent one-dimensional arrays, activation control of the active fracture model, output control parameters, and the names of input files for specific multiple-species particle tracking options. The output control parameters include basic file format instructions and as well as more specific controls indicating what zones are considered output (mass release zones). In the coupled FEHM/GoldSim simulations, species-specific mass releases for each defined zone are returned from FEHM to GoldSim at the end of each timestep.

Particle tracking files defined in the multiple-species particle tracking input file include the transfer function file and the sampled parameters used in the UZ particle tracking analysis as described in Section F2.1.13. The sampled parameters are in turn referenced by the multiple-species particle tracking files using column indices (as indicated by a negative sign) in lieu of deterministic values. The random seed for the particle tracking analysis is also found in the multiple-species particle tracking files, but this value is not used in a coupled GoldSim/FEHM simulation where sampled random-seed values are passed from GoldSim to fehmn_v2_24-01.dll. Additionally, data property zone assignments for repository and water-table collection zones are listed in the multiple-species particle tracking files.

Species-independent transport data found in the multiple-species particle tracking files include x-direction, y-direction, and z-direction dispersivities; values for fracture apertures; porosities within fractures; residual saturations; and active fracture model gammas. These transport parameters are assigned by rock property zones.

Inputs grouped by species alone include the fluid phase type, radionuclide half life, index of daughter product, ratio of particles per mole (for use with particle assignment by mass option), the radionuclide atomic weight, a factor for saving a percentage of species-based storage allocation for ingrowth products and the storage length for timestep dependent arrays. Additional species dependent input data include colloid size distributions.

Control and transport data grouped by both species and rock property zones include the transport conceptual model, matrix sorption coefficients, fracture retardation coefficients, matrix diffusion coefficients, colloid distribution parameters, colloid retardation coefficients, and colloid fracture-matrix filtration parameters.

F2.1.12 Transfer Function Curve Data Files

As described in Table F-2, the input files uz_tfcurves_nn_dualk_4680.in and uz_tfcurves_nn_4680.in are used for the dual k (dual permeability) and discrete fracture models, respectively. These files contain transfer function curve data to be read by fehmn_v2_24-01.dll at run time for matrix diffusion simulations. Although both files have the same file format, uz_tfcurves_nn_4680.in is not presently used in the TSPA-LA Model, but included here for completeness. The transfer function curves are comprised of time/concentration pairs for each set of three dimensionless parameter values used to generate the curves as described in Appendix C of *Particle Tracking Model and Abstraction of Transport Processes* (SNL 2008 [DIRS 184748]). See the user's manual (LANL 2003 [DIRS 167579], Section 6.2.3) for a description of the file.

F2.1.13 Sampled Parameter File

As described in Table F-2, the input files UZ_Pa_LA_300rlz_rs1_042307.txt and UZ_Pa_LA_1000rlz_rs1_042307.txt are sampled parameters for 300 and 1,000 realizations, respectively, to be used by the TSPA-LA Model. The sampled parameter file is an alternate transport parameter file containing sampled parameters for multiple realizations. *UZ_Params_Multi_LA_Compliance* is the generic file name that the TSPA-LA Model uses to copy a number of realizations-specific alternate transport parameter files to be read by FEHM and used as instructed in the multiple-species particle tracking file. A file of material properties is generated by GoldSim using uncertainty distributions. These properties consist of fracture apertures, active fracture-model gamma parameters, sorption coefficients, matrix diffusion coefficients, colloid distribution parameter, and colloid retardation factors. Sampling procedures and uncertainty distributions used in the sampling of parameters are described in Section 6.3.9. See the user's manual (LANL 2003 [DIRS 167579], Sections 6.2.44 and 6.2.54) for a description of the file.

F2.1.14 Interface Control File

As described in Table F-2, the input file fehmn.gold is a GoldSim/FEHM interface control file. The only active input in this file is the first line, which indicates the number of parameters that will be passed to fehmn_v2_24-01.dll in front of the mass releases from the EBS. The second input indicates whether added concentration average mass flux and peak concentration data are to be returned to GoldSim. See the user's manual (LANL 2003 [DIRS 167579], Section 6.1.1.4) for a complete description.

F2.2 MFCP_LA.DLL

The DLL MFCP_LA.dll (MFCP_LA Vl.0, STN: 11071-1.0-00 [DIRS 167884] and MFCP_LA Vl.0, STN: 11071-1.0-01 [DIRS 181045]) is designed to select the correct version of parameter-dependent input files for all TSPA-LA Model run types. This DLL uses GoldSim

modeling control parameters to select the correct (scenario and/or realization dependent) file from a suite of files and then copies its contents to a generic file name. A complete description of MFCP_LA.dll and the input file is documented in *Software Management Report, MFCP_LA, V1.0* (DOE 2003 [DIRS 167597]). As described in Table F-3, MFCP_LA.dll uses only one input file called MFCP_LA_input.txt.

F2.3 SEEPAGEDLL_LA.DLL

The DLL SEEPAGEDLL_LA.dll (SEEPAGEDLL_LA V1.3, STN: 11076-1.3-00 [DIRS 180318] for Windows 2000 and SEEPAGEDLL_LA V1.3, STN: 11076-1.3-01 [DIRS 181058] for Windows 2003) is designed to calculate the average seepage flux per WP for each fuel type in each percolation subregion, the fraction of WPs that have seepage for each fuel type in each percolation subregion, and the fraction of WPs emplaced in lithophysal units. A complete description of SEEPAGEDLL_LA.dll and the input files is documented in *User Information Document for: SEEPAGEDLL_LA V1.3* (DOE 2006 [DIRS 181133]).

As described in Table F-4, SEEPAGEDLL_LA.dll uses five input files. The first three files listed are control files that also contain a list of the PREWAP (PREWAP_LA V1.1, STN: 10939-1.1-00 [DIRS 181053]) output files (Appendix F2.8) to be read by the DLL. The realization dependent choice of the three files is then copied by *MFCP_LA.dll* into a generic file named *SEEPAGE_MASTER_INPUT.IN*. The last two files are the seepage look-up tables for nominal and collapsed drift conditions. SEEPAGEDLL_LA.dll interpolates seepage rates from the look-up tables based on percolation rates from the PREWAP output files and values of capillary strengths and log permeabilities passed from GoldSim.

F2.4 SZ_CONV_3.10.DLL

The DLL sz_conv_3.10.dll (SZ_CONVOLUTE V3.10.01, STN: 10207-3.10.01-00 [DIRS 181060]) is designed to calculate radionuclide mass flux rates in the SZ between the Yucca Mountain repository and specified locations downgradient from the repository. A complete description of sz_conv_3.10.dll and the input files is documented in *User Information Document for: SZ_Convolute V. 3.10* (DOE 2007 [DIRS 181288]).

As described in Table F-5, sz_conv_3.10.dll uses 50 input files in conjunction with the TSPA-LA Model. Of these files, two are control files for 10,000-year simulations (sz_convolute2_20kyr.dat) and one-million-year simulations (sz_convolute2_1Myr.dat). The simulation-length dependent choice of the files is then copied by MFCP_LA.dll into a generic file named SZ_CONVOLUTE2.DAT. The 10,000-year simulations are actually run for 20,000 years so that any changes in results immediately after the 10,000-year compliance timeframe can be assessed.

The remaining forty-eight files contain predefined static breakthrough curve data (e.g., SZ_03_04). Each of these files contains 200 sets each of three cumulative mass flux breakthrough curves generated using the streamlined particle tracking option in FEHM V2.24-01 [DIRS 179419]. The three curves are representative of mass fluxes in the SZ integrated over time at three distinct distances downgradient from the repository. The 200 sets of curves reflect 200 realizations of data sampling performed using GoldSim V.9.60.100 [DIRS 181903].

The 18 km compliance distance used in the TSPA-LA Model is represented by the second of the three sets of curves. The cumulative mass flux breakthrough curves are also used in conjunction with mass releases from the UZ Transport Submodel. This is done to derive time histories of radionuclide mass fluxes at the 18 km compliance distance using a convolution integral approach described in *Saturated Zone Flow and Transport Model Abstraction* (SNL 2008 [DIRS 183750], Sections 6 and 8).

F2.5 WAPDEG.DLL

The DLL wapdeg.dll (WAPDEG V4.07, STN: 10000-4.07-00 [DIRS 181774] and WAPDEG V4.07, STN: 10000-4.07-01 [DIRS 181064]) is designed to perform WP and drip shield (DS) degradation calculations. This DLL reads several input control files, cumulative distribution functions, and look-up table files. A complete description of *wapdeg.dll* and the input files is documented in *Users' Manual for WAPDEG 4.07* (BSC 2002 [DIRS 162606]).

As described in Table F-6, *wapdeg.dll* uses three input files. The initially empty file, WD4DLL.dbg, is used to record an echo of the run. Although this file is initially empty, it is populated by a DLL run and subsequently used to debug any problems with the run. The WD4DLL.wap file lists names of files that contain thermal-hydrologic (TH) exposure history data, cumulative distribution functions, probability density functions, or look-up tables. The initially empty file, WD4DLL.thk, is used to record WP thickness data at run time. Although this file is initially empty, it is populated by a DLL run.

F2.6 MKTABLE_LA.DLL

The DLL MkTable_LA.dll (MkTable_LA V. 1.0, STN: 11217-1.0-00 [DIRS 181047] and MkTable_LA V. 1.0, STN: 11217-1.0-01 [DIRS 181048]) is designed to randomly select a subset of files from an existing set of TH history files. A complete description of mktable_LA.dll and the input files is documented in *User Information Document for: MkTable_LA v1.0* (DOE 2006 [DIRS 181116]).

As described in Table F-7, MkTable_LA.dll uses 13 input files. The 12 TH history file names are obtained from rows 11 through 23 of the WD4DLL.wap file described in Section F2.5. These 12 files correspond to combinations of the 10th, 30th, 50th, and 90th percentile infiltration scenarios and the low, medium, and high thermal conductivities. The choice of which of these files to be used by MkTable_LA.dll is controlled by MFCP_LA.dll (Section F2.2). For example, WDhist.inp.P10 contains the list of PREWAP (described in Section F2.8) output files for the 10th percentile infiltration scenario and the mean thermal conductivity case.

The file THFiles.in is a text file containing a list of 16 file names. These 16 files contain the incremental temperatures and relative humidities that are added to the temperatures and relative humidities in the TH history files, after the drift fills with lithophysal rubble. The order of the file names in THFiles.in matches the order of the TH history data tables.

F2.7 SCCD.DLL

The DLL *SCCD.dll* (SCCD V2.01, STN: 10343-2.01-00 [DIRS 181157] and SCCD V2.01, STN: 10343-2.01-01 [DIRS 181054]) is designed to implement the stress and stress intensity

factor analysis for the Alloy 22 closure-lid welds on the WP outer surface. A complete description of SCCD.dll and the input files is documented in *SCCD Software Routine Report* (CRWMS M&O 2000 [DIRS 152499]). As described in Table F-8, *SCCD.dll* uses only one input file, WDKIinO.fil.

F2.8 PREWAP_LA.EXE

The executable file PREWAP_LA.exe (PREWAP_LA V1.1, STN: 10939-1.1-00 [DIRS 181053]) is designed to process and format the output files produced by the Multiscale Thermohydrologic Abstraction Code (MSTHAC V7.0, STN: 10419-7.0-00 [DIRS 164274]) to be read by other TSPA-LA Model DLLs. The resulting files are inputs to MkTable_LA.dll, SEEPAGEDLL_LA.dll, and PassTable1D_LAv2.dll (PassTable1D_LA V2.0, STN: 11142-2.0-00 [DIRS 181051]). These files contain TH histories for the repository and percolation rates. Although PREWAP_LA.exe is not a DLL used directly by the TSPA-LA Model, it is described here because of its relationship to several TSPA-LA Model DLLs. A complete description of PREWAP_LA.exe and the input and output files is documented in *User Information Document for:* PREWAP_LA v1.1 (DOE 2006 [DIRS 181129]).

As described in Table F-9, PREWAP_LA.exe generates 240 output files. These files are composed of the following: 12 percolation flux/host rock thermal conductivity scenarios (10th, 30th, 50th, and 90th percentile percolation flux with low, mean, and high thermal conductivity); two WP types (co-disposed [CDSP] and commercial spent nuclear fuel [CSNF]); five percolation subregions (1 through 5); and two types of TH data (representative TH and WP degradation TH). Two examples of these files are B1_DHLW_REP_P30L.ou (30th percentile percolation flux, low thermal conductivity, representative CDSP WP type, and percolation Subregion 1) and B3_CSNF_WAPDEG_P10H.ou (10th percentile percolation flux, high thermal conductivity, CSNF WP type used in WP degradation calculations, and percolation subregion 3).

The inputs to PREWAP_LA.exe are the output DTNs generated by the Multiscale Thermohydrologic Model (Sandia 2007 [DIRS 181383]) listed below and identified in the DTN shown on Table F-9.

LL0703PA011MST.006_R0 [DIRS 179853]
LL0703PA012MST.007_R0 [DIRS 179854]
LL0703PA013MST.008_R0 [DIRS 179855]
LL0703PA014MST.009_R0 [DIRS 179856]
LL0703PA015MST.010_R0 [DIRS 179857]
LL0703PA016MST.011_R0 [DIRS 179858]
LL0703PA017MST.012_R0 [DIRS 179859]
LL0703PA034MST.016_R0 [DIRS 179982]
LL0703PA035MST.017_R0 [DIRS 179985]
LL0703PA036MST.018_R0 [DIRS 179986]
LL0703PA037MST.019_R0 [DIRS 179989]
LL0703PA038MST.020_R0 [DIRS 179992]

F2.9 PASSTABLE1D_LAV2.DLL

The DLL PassTable1D_LAv2.dll (PassTable1D_LA V 2.0, STN: 11142-2.0-00 [DIRS 181051]) is designed to reformat one-dimensional tabular information from an input file and pass that information into GoldSim. The reformatted data is in the form of a one-dimensional look-up table element that conforms to the external interface method and function calls described in the *User's Guide, GoldSim Probabilistic Simulation Environment* (GoldSim Technology Group 2007 [DIRS 181727], Chapter 10 and Appendix C).

PassTable1D_LAv2.dll supports the evaluation of localized corrosion initiation on the WPs, the WP thickness calculations for the seismic calculations, the thermo hydrology parameters for the EBS environment calculations, and the volcanic eruption calculations. A complete description of PassTable1D_LAv2.dll and the input files is documented in *User Information Document for:* PassTable1D_LA Version 2.0 (DOE 2007 [DIRS 181123]).

As described in Table F-10, PassTable1D_LAv2.dll uses five input files. The pass_table_master.in input file contains a list of 240 PREWAP output file names that contain data for input to the TH model. These files are comprised of two data sets, one for all appropriate locations and the other for only representative locations. Each set contains 120 file names for cases defined by five percolation bins, two fuel types, three thermal conductivity scenarios, and four infiltration scenarios ($5 \times 2 \times 3 \times 4 = 120$). The pass_table_master1.in input file contains a list of 30 localized corrosion failure fraction files that are used to find the maximum WP failure fraction occurring at the simulation duration time. These files are defined by the five percolation bins, the two fuel types, and three modeling cases (Nominal, Seismic Ground Motion, and Seismic Fault Displacement). The pass_table_master2.in input file contains a list of 10 file names for files containing the WP thickness versus time for 5 percolation subregions and 2 fuel types.

For the Volcanic Eruption Modeling Case, the input file pass_table_master_eruptive.in contains data for a 20,000-year simulation and pass_table_master1_eruptive.in contains data for a one-million-year simulation. These files each identify the names of two files containing time-series data of concentration calculated for an eruptive event occurring at time zero. These data are used to calculate concentrations for later event times.

F2.10 PASSTABLE3DV2.DLL

The DLL PassTable3Dv2.dll (PassTable3D_LA V. 2.0, STN: 11143-2.0-00 [DIRS 182556]) is designed to reformat three-dimensional tabular information from an input file and pass that information into GoldSim. The reformatted information is in the form of a three-dimensional look-up table element that conforms to the external interface method and function calls described in the *User's Guide, GoldSim Probabilistic Simulation Environment* (GoldSim Technology Group 2007 [DIRS 181727], Chapter 10 and Appendix C).

PassTable3Dv2.dll is used only in the stand-alone Localized Corrosion Initiation Submodel file. This DLL supports the evaluation of localized corrosion on the WPs by reading the nominal and collapsed drift-seepage data files described in Section F2.3 and returning four three-dimensional look-up tables containing mean seepages and standard deviations for both the nominal and

collapsed drifts. A complete description of PassTable3Dv2.dll and the input file is documented in *User Information Document for: PassTable3D_LA Version 2.0* (DOE 2007 [DIRS 182918]).

As described in Table F-11, PassTable3Dv2.dll uses only one input file, pass_table_3d_master.in, that provides the file names of the external data files to be processed.

F2.11 GETTHK_LA.DLL

The DLL GetThk_LA.dll (GetThk_LA V. 1.0, STN: 11229-1.0-00 [DIRS 181040]) is designed to process the file WD4DLL.thk generated by the wapdeg.dll described in Section F2.5. This file contains sets of WP barrier thicknesses as a function of time. The output from GetThk_LA.dll includes barrier thickness data and thickness statistics as a function of time. Output also includes a single value for the number of timesteps per data set that is used for controlling the sequence of calling DLLs within GoldSim. A complete description of GetThk_LA.dll and the input file is documented in *User Information Document for: GetThk_LA v1.0* (DOE 2006 [DIRS 181102]). As described in Table F-12, GetThk_LA.dll uses only one input file.

F2.12 FAR_1-2.DLL

The DLL FAR_1-2.dll (FAR V1.2, STN: 11190-1.2-00 [DIRS 182225]) is designed to evaluate the redistribution of volcanic ash and associated radionuclides within the Fortymile Wash drainage area and the subsequent radionuclide migration in the soil at the location of the reasonably maximally exposed individual on the Fortymile Wash fan. A complete description of FAR_1-2.dll and the input file is documented in *User Information Document for: FAR Version 1.2* (DOE 2007 [DIRS 183116]).

As described in Table F-13, FAR_1-2.dll uses only one input file, farinputdem.txt, that contains a Digital Elevation Model (DEM) at a 30-meter-resolution. The DEM covers the Fortymile Wash drainage basin extending to the latitude of the Fortymile Wash fan apex. The DEM file contains topographical elevations at coordinates within the Fortymile Wash watershed and null values of -9999.0 at coordinates located outside of the watershed.

F2.13 ASHPLUME21_DLL_LA.DLL

The DLL Ashplume21_dll_la.dll (ASHPLUME_DLL_LA V2.1, STN: 11117-2.1-00 [DIRS 181035] and ASHPLUME_DLL_LA V2.1, STN: 11117-2.1-01 [DIRS 180147]) is designed to calculate the waste and ash areal depositional densities on the ground surface from a hypothetical volcanic eruption through the repository. The DLL is called from another program that conforms to the external interface method and function calls described in the *User's Guide, GoldSim Probabilistic Simulation Environment* (GoldSim Technology Group 2007 [DIRS 181727], Chapter 10 and Appendix C).

A complete description of Ashplume21_dll_la.dll and the inputs is documented in *User Information Document for: ASHPLUME_DLL_LA Version 2.1* (DOE 2006 [DIRS 181076]). As described in Table F-1, Ashplume21_dll_la.dll uses specific parameters as input instead of an input file.

F2.14 CWD.DLL

The DLL CWD.dll (CWD V2.0, STN: 10363-2.0-00 [DIRS 162809] and CWD V2.0, STN: 10363-2.0-01 [DIRS 181037]) is designed to implement the abstraction results of the probability of occurrence and size of manufacturing defects in the closure lid welds of the Alloy 22 WP outer surface. The DLL is called from GoldSim and conforms to the external interface method and function calls described in the *User's Guide, GoldSim Probabilistic Simulation Environment* (GoldSim Technology Group 2007 [DIRS 181727], Chapter 10 and Appendix C).

A complete description of CWD.dll and the inputs is documented in *Software Management Report: CWD Version Number 2.0* (DOE 2003 [DIRS 167564]). As described in Table F-1, CWD.dll uses specific parameters as input instead of an input file.

F2.15 INTERPZDLL_LA.DLL

The DLL InterpZdll_LA.dll (InterpZdll_LA V1.0, STN: 11107-1.0-00 [DIRS 167885] and InterpZdll_LA V1.0, STN: 11107-1.0-01 [DIRS 181043] is designed to provide interpolation capabilities for the EBS Chemical Environment Submodel of the TSPA-LA Model. The DLL is called from GoldSim and conforms to the external interface method and function calls described in the *User's Guide, GoldSim Probabilistic Simulation Environment* (GoldSim Technology Group 2007 [DIRS 181727], Chapter 10 and Appendix C).

A complete description of InterpZdll_LA.dll and the inputs is documented in *Software Management Report, INTERPZDLL_LA V1.0* (DOE 2004 [DIRS 168988]). As described in Table F-1, InterpZdll_LA.dll uses specific parameters as input instead of an input file.

INTENTIONALLY LEFT BLANK

Table F-1. Summary of the Dynamically Linked Libraries used in the TSPA-LA Model

DLL File Name	Description	Location
Ashplume21_dll_la.dll	Calculates fuel and ash deposition and areal concentrations from a volcanic eruption.	None [a]
CWD.dll	Performs closure weld defect probability calculations.	None [a]
FAR_1-2.dll	Evaluates redistribution of volcanic ash and associate radionuclides within the Fortymile Wash drainage area; models redistribution of radionuclides in soil at the location of a reasonably maximally exposed individual on the Fortymile Wash fan.	Table F-13
fehmn_v2_24-01.dll	Performs radionuclide transport calculations through the UZ using FEHM's multi-species, particle-tracking option.	Table F-2
GetThk_LA.dll	Processes the file WD4DLL.thk by extracting barrier thickness data, generating thickness statistics based on these data, and outputting tables containing these statistics. In addition, a single value for the number of timesteps per data set is generated to be used for controlling the sequence of calling DLLs within GoldSim.	Table F-12
InterpZdll_LA.dll	Performs a four point linear interpolation that can accommodate any single missing point in the data.	None [a]
MFCP_LA.dll	Conducts the selection and implementation of input files for DLLs that are part of the TSPA-LA Model.	Table F-3
MkTable_LA.dll	Performs sampling of the TH time history files used as input to WAPDEG for performing WP degradation calculations.	Table F-7
PassTable1D _LAv2.dll	Extracts columns from tabular input files and converts the data into the format required by a GoldSim for a one-dimensional look-up table element.	Table F-10
PassTable3Dv2.dll	Reformats a file containing tabular information into the format required by GoldSim for a three-dimensional look-up table element.	Table F-11
PREWAP_LA.exe [b]	Reformats TH data into files for input to MkTable_LA.dll, SEEPAGEDLL_LA.dll, and PassTable1D_LAv2.dll.	Table F-9
SCCD.dll	Applies the analysis of the Alloy 22 WP outer surface stress intensity factors to the TSPA-LA Model.	Table F-8
SEEPAGEDLL_LA.dll	Performs drift-seepage calculations.	Table F-4
sz_conv_3.10.dll	Performs radionuclide mass flux rate calculations in the SZ between the Yucca Mountain repository and specified locations downgradient from the repository.	Table F-5
wapdeg.dll	Performs WP degradation calculations.	Table F-6

NOTES: [a] Input is not in the form of files.

[b] Executable file used as a preprocessor for other DLLs and listed for completeness.

Table F-2. *fehmn_v2_24-01.dll* Input Files

File(s)	Description	Data Source	Inputs
fehmn.files	Control file specifying FEHM main input and output file names.	DTN: MO0704PAFEHMBR.001_R3 [DIRS 184647]	Controls: List of input and output files
fehm_TSPA_gs_20kyr.dat fehm_TSPA_gs_1Myr.dat	General control information and data for 10,000/20,000-year and one-million-year simulations.	Output DTN: MO0708TSPAGENT.000_R0 [DIRS 183000]	Data: Permeability data Residual liquid saturation Residual vapor saturation Maximum liquid saturation Maximum vapor saturation Capillary pressure at zero saturation Saturation that defines zero capillary pressure Equation solver control data Control data for FEHM linear equation solver Reference temperature and pressure Controls: Input file names Initial timestep Final simulation time Maximum number of timesteps allowed Printout interval for dependent variables Simulation start year Simulation start month Initial time of startup Species subject to filtration Files containing filtration or size exclusion data

Table F-2. *fehmn_v2_24-01.dll* Input Files (Continued)

File(s)	Description	Data Source	Inputs
fehmn.grid	Nodal coordinate and finite element connectivity data.	DTN: MO0704PAFEHMBR.001_R3 [DIRS 184647]	Data: Nodal-coordinate data: (NSP Easting, NSP Northing [m] and elevation) Finite element connectivity data
fehmn.zone	Defines material zones and nodes contained in each declared zone.	DTN: MO0704PAFEHMBR.001_R3 [DIRS 184647]	Controls: List of nodes for each material zone
ff1100.ini ff1200.ini ff1300.ini ff1400.ini ff2100.ini ff2200.ini ff2300.ini ff2400.ini ff3100.ini ff3200.ini ff3300.ini ff3400.ini ff4100.ini ff4200.ini ff4300.ini ff4400.ini	A restart/initialization file containing nodal pressure, saturation, and adjacent node flux data used to describe the flow field for the different climates and infiltration scenarios as derived from the TOUGH2 generated flow fields.	Output DTN: MO0708TSPAGENT.000 _R0 [DIRS 183000]	Data: Saturation values in the fracture nodes Saturation values in the rock-matrix nodes Total pressures in the fracture nodes Total pressures in the rock-matrix nodes Water flux data

Table F-2. *fehmn_v2_24-01.dll* Input Files (Continued)

File(s)	Description	Data Source	Inputs
fehmn.stor	Precalculated stiffness matrix associated with the grid file used during the UZ transport calculation.	DTN: MO0704PAFEHMBR.001_R3 [DIRS 184647]	Data: Volume data for each node Finite element geometric coefficients Finite element geometric coefficients for stress module Controls: Nodal connectivity data Starting position for each connection Position of element in connectivity array for each node
fehmn_TSPA.dpdp	Fracture geometry data for each defined fracture zone in the dual permeability model.	DTN: MO0704PAFEHMBR.001_R3 [DIRS 184647]	Data: Volume fraction of effective nodal volume taken up by the fractures Length scale of matrix nodes
fehm_TSPA.rock	Rock bulk density, specific heat, and porosity data for both matrix and fracture material zones defined in the file *fehmn.zone*.	DTN: MO0704PAFEHMBR.001_R3 [DIRS 184647]	Data: Rock bulk density Rock specific heat Porosity

Table F-2. *fehmn_v2_24-01.dll* Input Files (Continued)

File(s)	Description	Data Source	Inputs
ltfc_tsw4.txt ltfc_tsw5.txt ltfc_tsw6.txt ltfc_tsw7.txt ltfc_tsw8.txt ltfc_tsw9.txt ltfc_chv.txt ltfc_chz.txt ltfc_ch1.txt ltfc_ch6.txt ltfc_pp1.txt ltfc_pp2.txt ltfc_pp3.txt ltfc_pp4.txt ltfc_bf2.txt ltfc_bf3.txt	Pore-size cumulative probability data for the following rock units: Topopah Springs (tsw) layers 4 through 9 Calico Hills (ch*) layers vitric, zeolitic, 1, and 6 Prow Pass (pp) layers 1 through 4 Bull Frog (bf) layers 2 and 3.	DTN: MO0704PAFEHMBR.001_R3 [DIRS 184647]	Data: Pore-size Cumulative probability data
fehm.zone2	fehmn.zone data plus radionuclide source releases zones and water table collecting zones defined at the UZ-SZ interface.	DTN: LA0702PANS02BR.001_R1 [DIRS 180322]	Controls: List of node numbers for each material zone Fracture and matrix radionuclide EBS release zone data Node numbers within UZ collecting (mass exit) zones when found beneath the water table
fehm_TSPA_10kyr.mptr fehm_TSPA_10kyr_ign.mptr fehm_TSPA_1Myr.mptr fehm_TSPA_1Myr_ign.mptr fehm_TSPA_10kyr_ef_cdsp.mptr	Parameter values and files used for multiple species particle-tracking transport simulations for lower-bound infiltration rate simulations. Automatically assigns particles based upon timestep length, total time of analysis, ingrowth, and maximum number of particles. The '_ign_' and '_ef_' files assign particles for ^{99}Tc and ^{129}I by mass and timestep for the other. All other files assign particles by timestep.	Output DTN: MO0708TSPAGENT.000 [DIRS 183000]	Data: A 6-digit random seed Start/end times for particle tracking Start/end times for disabling the flow solution X-direction dispersivity

Table F-2. *fehmn_v2_24-01.dll* Input Files (Continued)

File(s)	Description	Data Source	Inputs
fehm_TSPA_1Myr_ef_cdsp.mptr fehm_TSPA_10kyr_ef_csnf.mptr fehm_TSPA_1Myr_ef_csnf.mptr			Y-direction dispersivity Z-direction dispersivity Mean fracture aperture Matrix porosity Residual saturation Exponent in active fracture model Zone to rock property link data Rock property to repository water table collecting zone assignments Species index Fluid-phase type Radionuclide half-life data Index of daughter products Conversion factors Atomic weights Decay-ingrowth particle release factors Species names Cumulative probability of colloid sizes Zone numbers Transport analysis flag Matrix sorption coefficients Fracture retardation factor Matrix diffusion coefficient Ratio of radionuclide colloid mass to aqueous mass Colloidal retardation factor Colloidal filtration factor Number of particles or moles

Table F-2. *fehmn_v2_24-01.dll* Input Files (Continued)

File(s)	Description	Data Source	Inputs
			to be input at each location Injection start and end times Controls: Input file names Number of species Maximum number of property zones Maximum number of particles that can be used Parameter to define transfer function curve Number of zones for breakthrough curve data List of zone numbers Array size declarations
uz_tfcurves_nn_dualk_4680.in uz_tfcurves_nn_4680.in	Dual permeability transfer function curve data used in matrix diffusion simulations. Note that the file for the discrete fracture model (*uz_tfcurves_nn_4680.in*) is currently not used.	DTN: MO0704PAPTTFBR.002_R0 [DIRS 180442]	Data: Transfer function time and data pairs Controls: Curve scaling factor Normalization control parameters Interpolation scheme
UZ_Pa_LA_300rlz_rs1_042307.txt UZ_Pa_LA_1000rlz_rs1_042307.txt Corresponding parameter names: UZ_Params_Multi_LA_300rlz UZ_Params_Multi_LA_1000rlz	Sampled parameters for 300 and 1,000 realizations using a random seed of 1.	Output DTN: MO0708TSPAGENT.000_R0 [DIRS 183000]	Data: Fracture apertures Matrix diffusion coefficients Active fracture gamma sorption coefficients K_d values Colloid distribution parameter (Ratio of radionuclide colloid mass to aqueous mass) Colloid retardation coefficient

Table F-2. *fehmn_v2_24-01.dll* Input Files (Continued)

File(s)	Description	Data Source	Inputs
fehmn.gold	Input and output control data for variables passed from GoldSim to FEHM and from FEHM to GoldSim.	Output DTN: MO0708TSPAGENT.000_R0 [DIRS 183000]	Controls: Index parameter indicating number of parameters passed to FEHM Output control parameter indicating only time vs. mass flux results

Table F-3. *MFCP_LA.dll* Input Files

File(s)	Description	Data Source	Inputs
MFCP_LA_input.txt	List of control parameter-dependent input files.	Output DTN: MO0708TSPAGENT.000_R0 [DIRS 183000]	Controls: Input file names Number of file sets Number of names per set

Table F-4. *SEEPAGEDLL_LA.dll* Input Files

File(s)	Description	Data Source	Inputs
Seepage_Master_Input_File_LKT.in Seepage_Master_Input_File_MKT.in Seepage_Master_Input_File_HKT.in	List of input files for low, medium, and high thermal k.	Output DTN: MO0708TSPAGENT.000_R0 [DIRS 183000]	Controls: Input file names Number of fuel types Number of bins per fuel type Number of climates Times when climates change Number of infiltration types
SMPA_N.dat SMPA_C.dat	Seepage model for performance assessment response surfaces for non-collapsed and collapsed drift conditions.	DTN: LB0702PASEEP01.001_R0 [DIRS 179511]	Data: Log permeability Capillary strength Percolation Mean seepage Standard deviation seepage

Table F-5. sz_conv_3.10.dll Input Files

File(s)	Description	Data Source	Inputs
sz_convolute2_20kyr.dat sz_convolute2_1Myr.dat	Climate, time, and radionuclide species data for 10,000-year and one-million-year simulations.	DTN: SN0702PASZFTMA.001_R0 [DIRS 179504]	Controls: Output file name Maximum number of climate states Maximum number of timesteps Maximum number of SZ points Smallest timestep Number of species Number of breakthrough curves Number of climate states Data: Climate multiplier values Climate concentration multiplier Total simulation time Initial timestep size Half-life data for each species

Table F-5. sz_conv_3.10.dll Input Files (Continued)

SZ_**xx_yy** Total of 48 files for 12 solute types in each of 4 regions	Breakthrough curve data for: Solute xx (below) and Region yy = 01 to 04 01 = solute C 02 = Kc_Am 03 = Kc_Cs 04 = Kc_Pu 05 = Np 06 = solute Pu 07 = solute Ra 08 = solute Sr 09 = solute U 10 = solute Pu_fast 11 = solute Se 12 = solute Sn.	DTN: SN0702PASZFTMA.001_R0 [DIRS 179504]	Controls: Region identifier and number Number of realizations in the file Data: Percent of solute transported at a given timestep

Table F-6. *wapdeg.dll* Input Files

File(s)	Description	Data Source	Inputs
WD4DLL.dbg	Initially empty debug file used to record an echo of a run.	Output DTN: MO0707WPDRIPSD.000_R0 [DIRS 183005]	None
WD4DLL.wap	List of all input and intermediate file names previously produced by *CWD.dll*, *SCCD.dll*, and *mktable_LA.dll*.	Output DTN: MO0707WPDRIPSD.000_R0 [DIRS 183005]	Controls: Input file names
WD4DLL.thk	Initially empty capture file used to record WP thicknesses generated by a run.	Output DTN: MO0707WPDRIPSD.000_R0 [DIRS 183005]	None

Table F-7. *MkTable_LA.dll* Input Files

File(s)	Description	Data Source	Inputs
THFiles.in	List of 16 file names that contain the incremental temperatures and relative humidities to be added to the temperatures and relative humidities in the TH history files after the drift fills with lithophysal rubble.	Output DTN: MO0707WPDRIPSD.000_R0 [DIRS 183005]	Controls: Input file names
WDhist.inp.P10L WDhist.inp.P10 WDhist.inp.P10H WDhist.inp.P30L WDhist.inp.P30 WDhist.inp.P30H WDhist.inp.P50L WDhist.inp.P50 WDhist.inp.P50H WDhist.inp.P90L WDhist.inp.P90 WDhist.inp.P90H	List of PREWAP output file names for TH history data sets associated with each of the 12 percolation flux/host rock thermal conductivity combinations (10th, 30th, 50^{t}h, and 90th percentile percolation flux with low, mean, and high thermal conductivity).	Output DTN: MO0707WPDRIPSD.000_R0 [DIRS 183005]	Controls: Maximum number of tables Bin parameters PREWAP file names

Table F-8. *SCCD.dll* Input Files

File(s)	Description	Data Source	Inputs
WDKlinO.fil	One-dimensional table containing stress intensity factors (KI) vs. depths for the WP outer lid. The corresponding parameter name is WDKlinO.	DTN: MO0702PASTRESS.002_R2 [DIRS 180514]	Data: Stress intensity factors Depths

Table F-9. PREWAP_LA.exe Output Files

File(s)	Description	Data Source	Inputs
B**x**_CSNF_WAPDEG_P**y**L.ou B**x**_CSNF_WAPDEG_P**y**.ou B**x**_CSNF_WAPDEG_P**y**H.ou B**x**_DHLW_WAPDEG_P**y**L.ou B**x**_DHLW_WAPDEG_P**y**.ou B**x**_DHLW_WAPDEG_P**y**H.ou	TH properties in percolation subregion **x** for each CSNF and CDSP WP modeled at each MSTHM location: where **x** = 1 to 5 and **y** = 10, 30, 50, or 90 for a total of 5 × 4 x 6 = 120 files.	Output DTN: MO0707PREWAPMS.000_R0 [DIRS 183002]	Controls: Time WP temperature WP relative humidity DS temperature DS relative humidity Drift-wall temperature Percolation rates
B**x**_CSNF_REP_P**y**L.ou B**x**_CSNF_REP_P**y**.ou B**x**_CSNF_REP_P**y**H.ou B**x**_DHLW_REP_P**y**L.ou B**x**_DHLW_REP_P**y**.ou B**x**_DHLW_REP_P**y**H.ou	TH properties in percolation subregion **x** for each CSNF and CDSP WP modeled at representative MSTHM location: where **x** = 1 to 5 and **y** = 10, 30, 50, or 90 for a total of 5 × 4 x 6 = 120 files.		

Table F-10. PassTable1D_LAv2.dll Input Files

File(s)	Description	Data Source	Inputs
pass_table_master.in *pass_table_master1.in* *pass_table_master2.in*	List of PREWAP output files containing TH data. Localized corrosion (LC) failure fraction histories. WP thickness versus time.	Output DTN: MO0708TSPAGENT.000_R0 [DIRS 183000]	Controls: PREWAP file names, LC failure fraction file names, WP thickness file names.
pass_table_master_eruptive.in *pass_table_master1_eruptive.in*	Time-series data of concentration for an eruptive event that occurs at time = 0 for 20,000-year and one-million-year simulations.	Output DTN: MO0708TSPAGENT.000_R0 [DIRS 183000]	Controls: Concentration file names

Table F-11. PassTable3Dv2.dll Input Files

File(s)	Description	Data Source	Inputs
pass_table_3d_master.in	Seepage data input file names for nominal and collapsed drifts.	Output DTN: MO0708TSPAGENT.000_R0 [DIRS 183000]	Controls: Input file names

Table F-12. GetThk_LA.dll Input Files

File(s)	Description	Data Source	Inputs
WD4DLL.thk	Generic file generated by *wapdeg.dll* during TSPA-LA Model simulations that contains multiple time-series of WP barrier thicknesses.	Output DTN: MO0707WPDRIPSD.000_R0 [DIRS 183005]	Data: Number of WP thickness data sets Time series of WP barrier thicknesses

Table F-13. FAR_1-2.dll Input Files

File(s)	Description	Data Source	Inputs
farinputdem.txt	DEM file covering the Fortymile Wash drainage basin at a 30-meter resolution.	DTN: MO0605SPAFORTY.000_R1 [DIRS 182281]	Data: Elevation data

INTENTIONALLY LEFT BLANK

APPENDIX G
WIRING DIAGRAMS FOR MODEL INFORMATION FEEDS

G1. INTRODUCTION

Appendix G provides a set of diagrams that illustrate in detail the information flow between model components and submodels within the Total System Performance Assessment for the License Application (TSPA-LA) Model.

Figure G-1 is an overall TSPA-LA Model information flow diagram and provides a schematic description of the model structure for the Nominal Scenario Class, with boxes representing model components and submodels, and arrows representing the flow of data. The Nominal Scenario Class represents the expected initial starting conditions for the repository system, and is, therefore, the primary focus of Appendix G. Information flow diagrams are also provided for the Early Failure Scenario Class (Figure G-2), Igneous Intrusion Modeling Case (Figure G-3), Seismic Scenario Class (Figure G-4), and the Human Intrusion Scenario (Figure G-5). Additionally, information flow diagrams showing only the flow of water (Figure G-6) and radionuclides (Figure G-7) are also presented.

Within the schematic diagrams, white boxes indicate models external to the TSPA-LA Model and grey boxes represent TSPA-LA Model components and submodels. The general philosophy used throughout the *Total System Performance Assessment Model/Analysis for the License Application* is that this TSPA-LA Model is comprised of eight principal model component areas that are combined to evaluate repository system performance for the Nominal, Early Failure, Igneous, and Seismic Scenario Classes, and the Human Intrusion Scenario. The colored areas shown on these figures are used to group the model components and submodels into these eight areas. The eight areas, as depicted in the legend, are as follows: unsaturated zone (UZ) flow, engineered barrier system (EBS), waste package (WP) and drip shield (DS) degradation, waste form degradation and mobilization, EBS flow and transport, UZ transport, saturated zone (SZ) flow and transport, and biosphere.

The colors of the arrows on the flow diagrams indicate the type of information passed between the model components and submodels. Water flux (blue) and radionuclide flux (red) are the main data types presented. EBS-related components include data flows representing thermal-hydrologic (TH) data, water chemistry, DS and/or WP failure, and other model information (e.g., number of failed WPs).

TSPA-LA Model components and submodels shown with a dashed line on the overall flow diagram for the Nominal Scenario Class are presented in further detail as separate information flow diagrams. The overall factors affecting flow through the EBS are shown on Figure G-8. The overall factors affecting the radionuclide transport through the EBS are shown on Figure G-9. The Waste Form Degradation and Mobilization Model Component has two associated submodel flow diagrams representing CSNF waste forms (Figure G-10) and CDSP waste forms (Figure G-11).

INTENTIONALLY LEFT BLANK

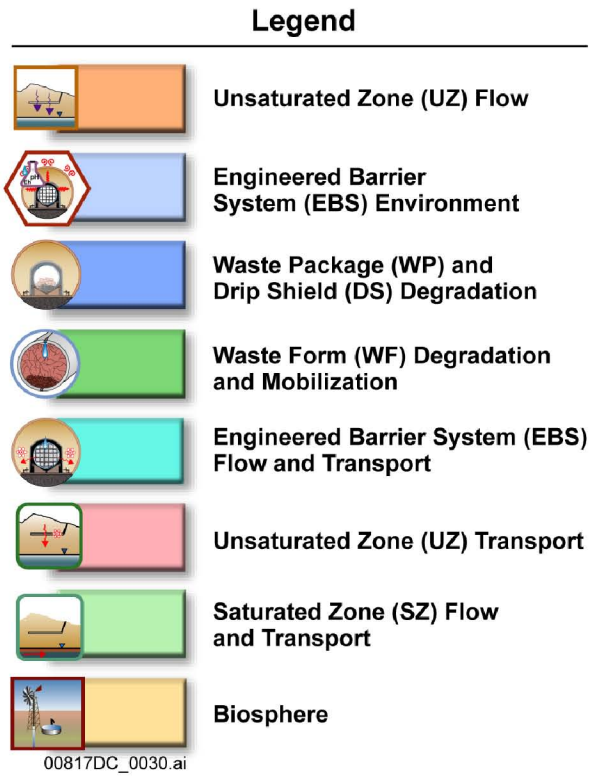

NOTE: This legend explains the colors and icons appearing in the following figures. The icons and colors are used throughout the document and are intended to provide consistency and to assist the reader with understanding how all the various components interact with each other.

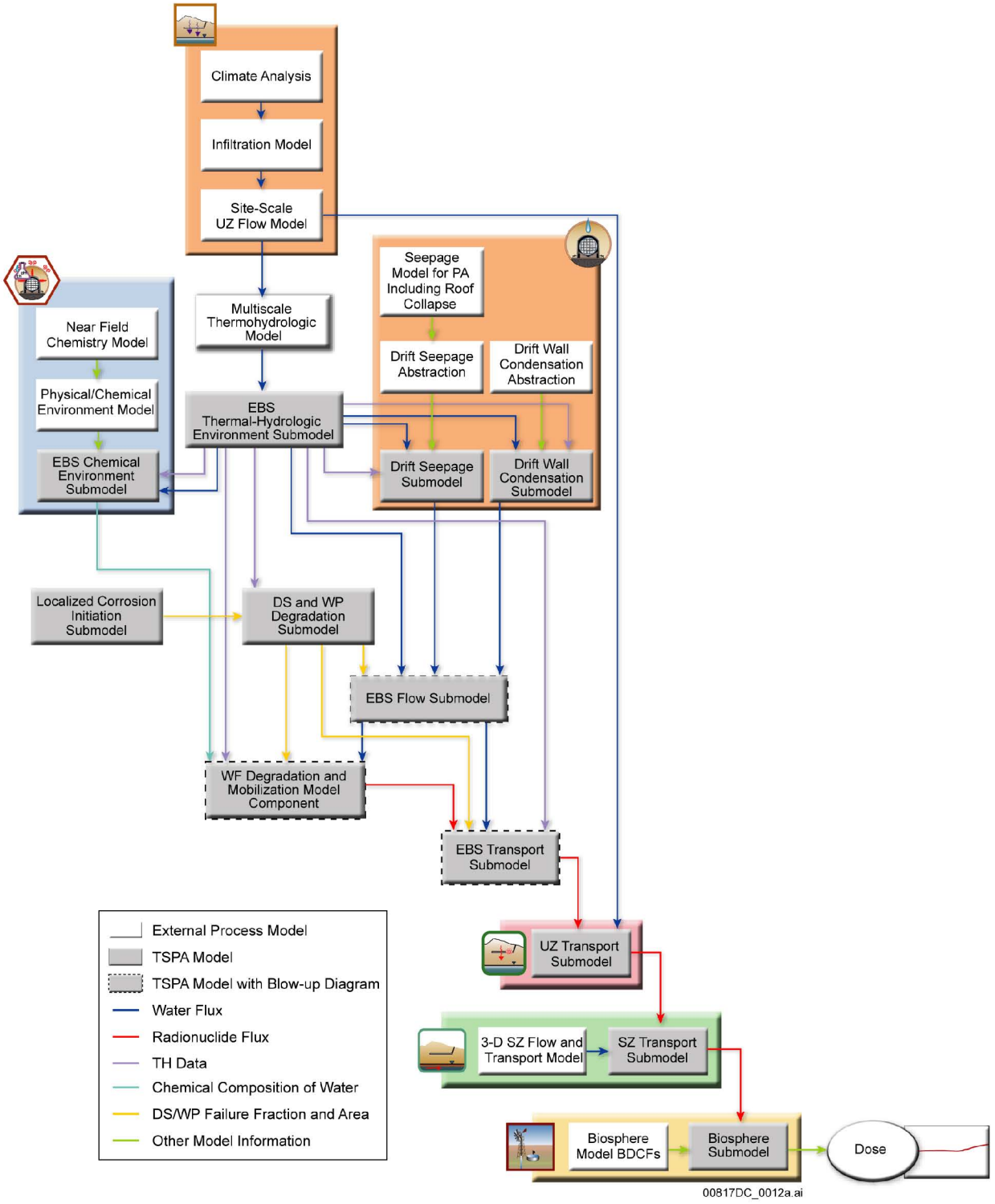

Figure G-1. Illustration of the Transfer of Information between Model Components and Submodels of the TSPA-LA Model for the Nominal Scenario Class

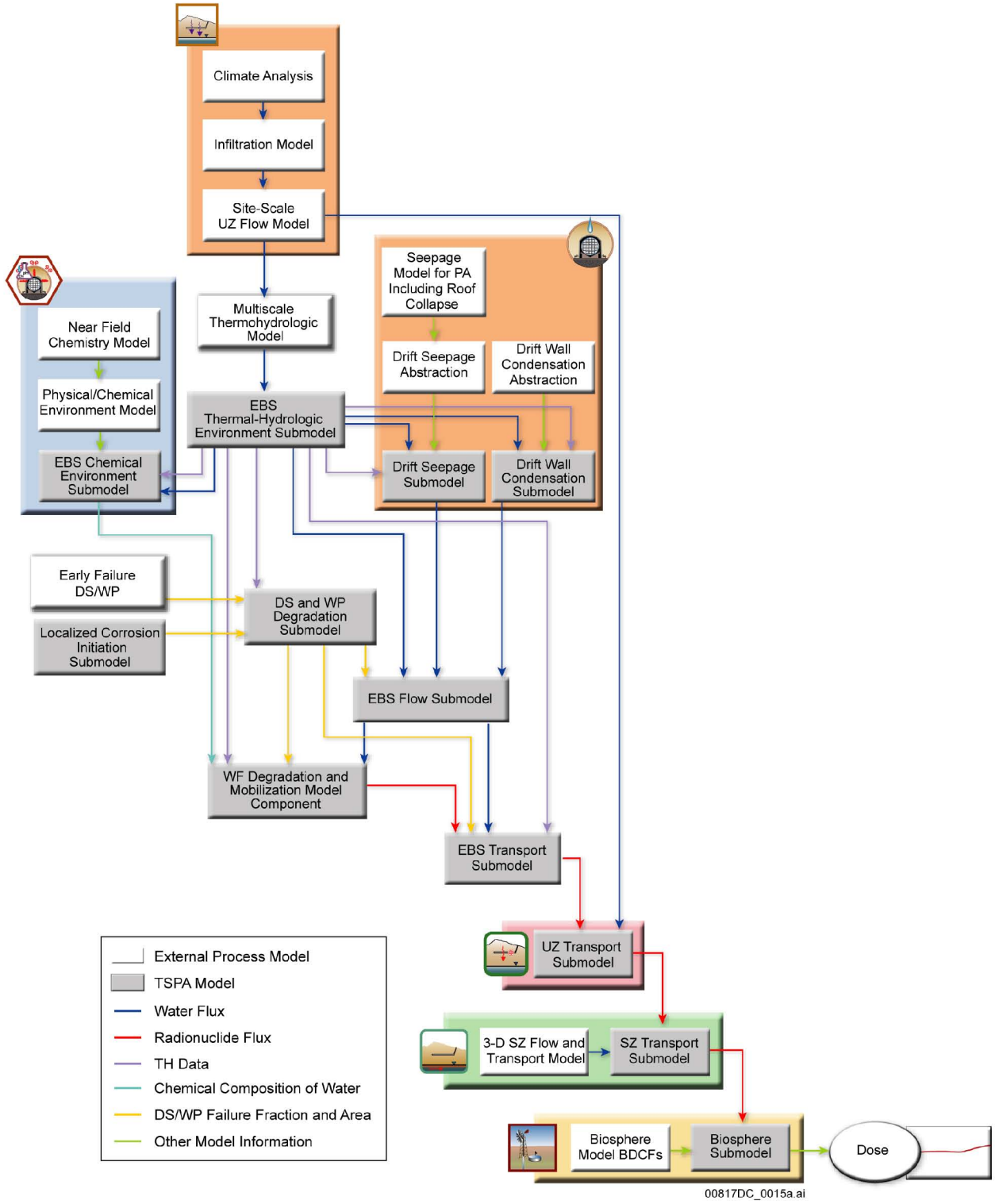

Figure G-2. Illustration of the Transfer of Information between Model Components and Submodels of the TSPA-LA Model for the Early Failure Scenario Class

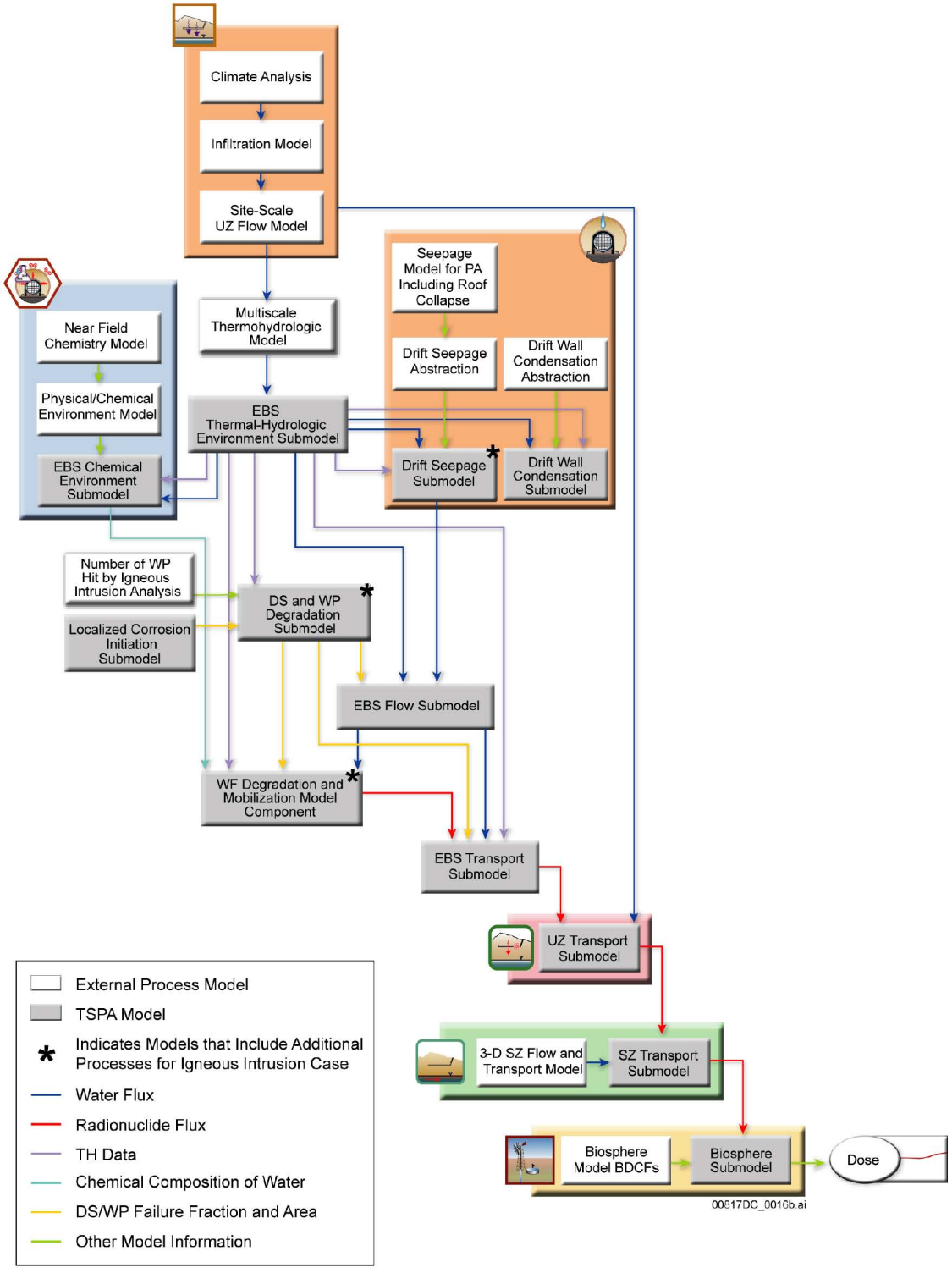

Figure G-3. Illustration of the Transfer of Information between Model Components and Submodels of the TSPA-LA Model for the Igneous Intrusion Modeling Case

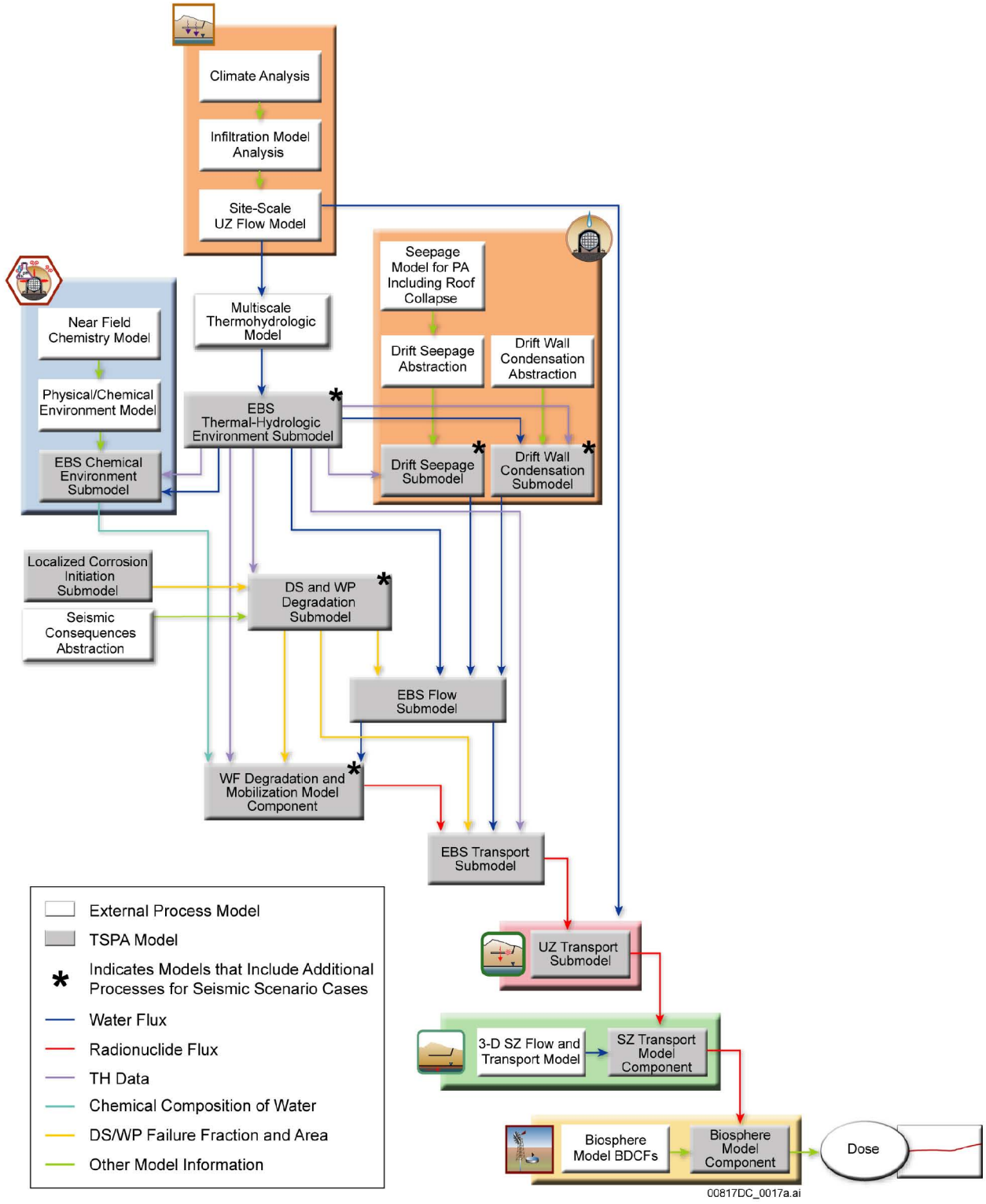

Figure G-4. Illustration of the Transfer of Information between Model Components and Submodels of the TSPA-LA Model for the Seismic Ground Motion and Fault Displacement Modeling Cases

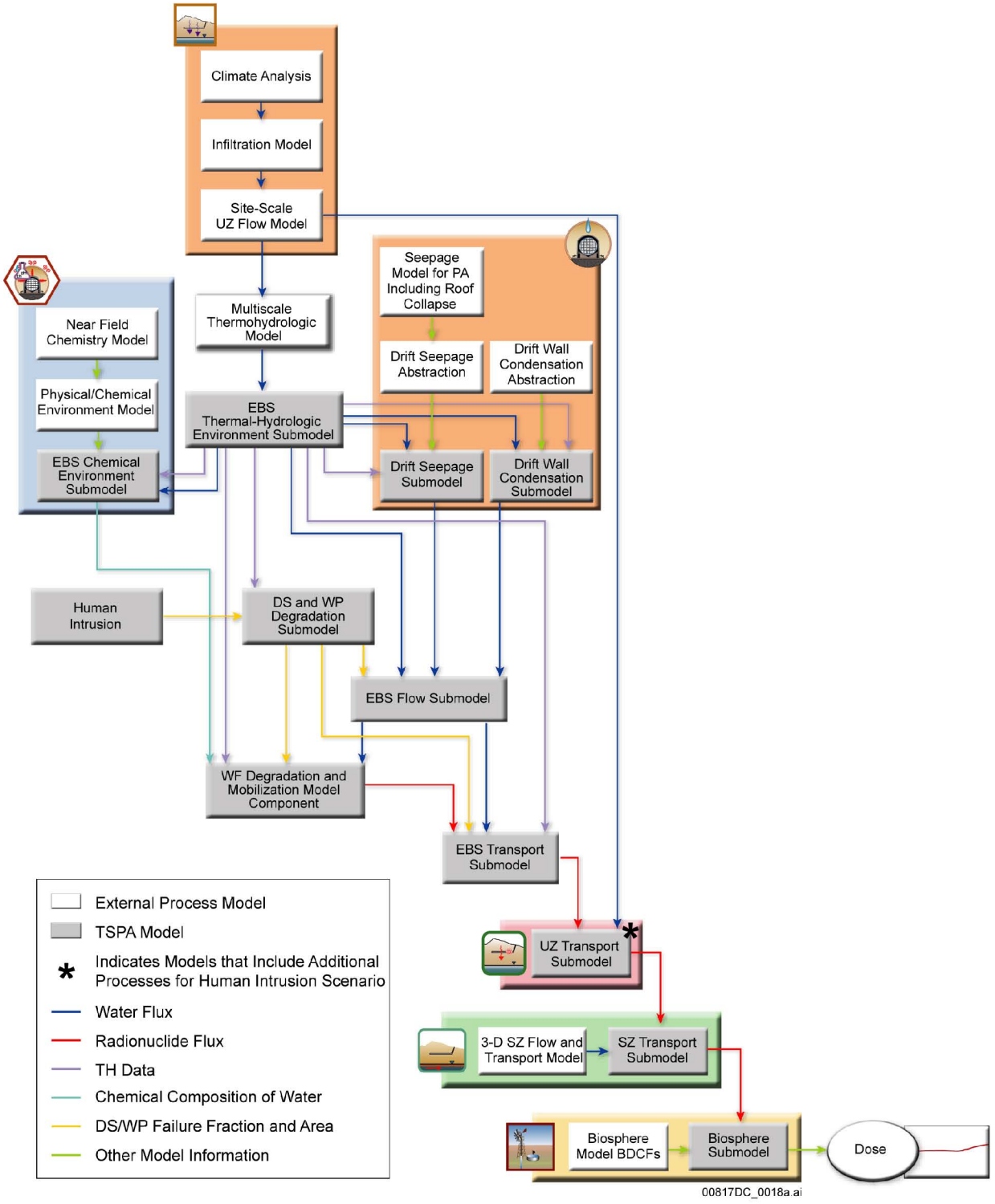

Figure G-5. Illustration of the Transfer of Information between Model Components and Submodels of the TSPA-LA Model for the Human Intrusion Scenario Class

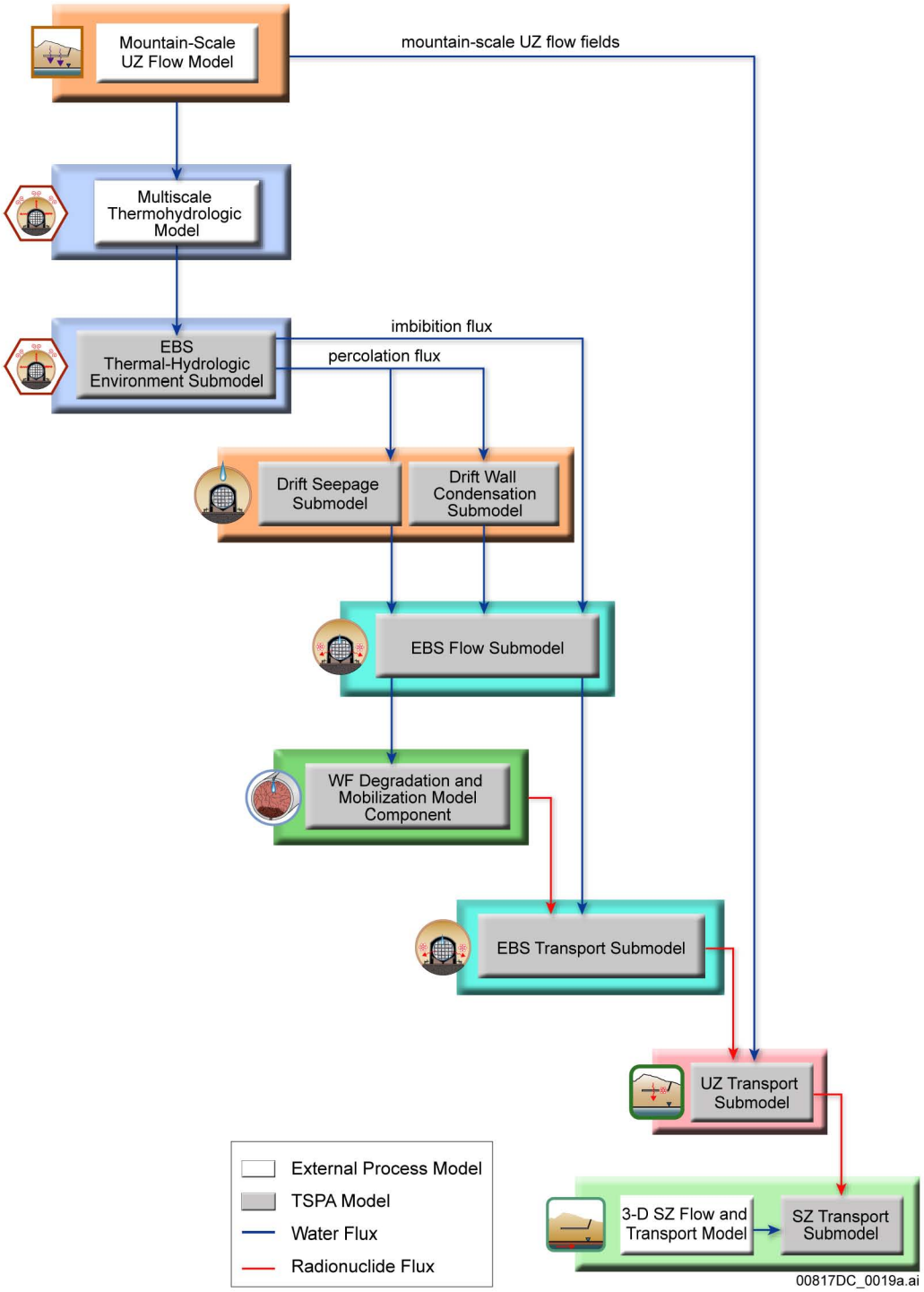

Figure G-6. Illustration of the Transfer of Information on Water Fluxes between Model Components and Submodels of the TSPA-LA Model

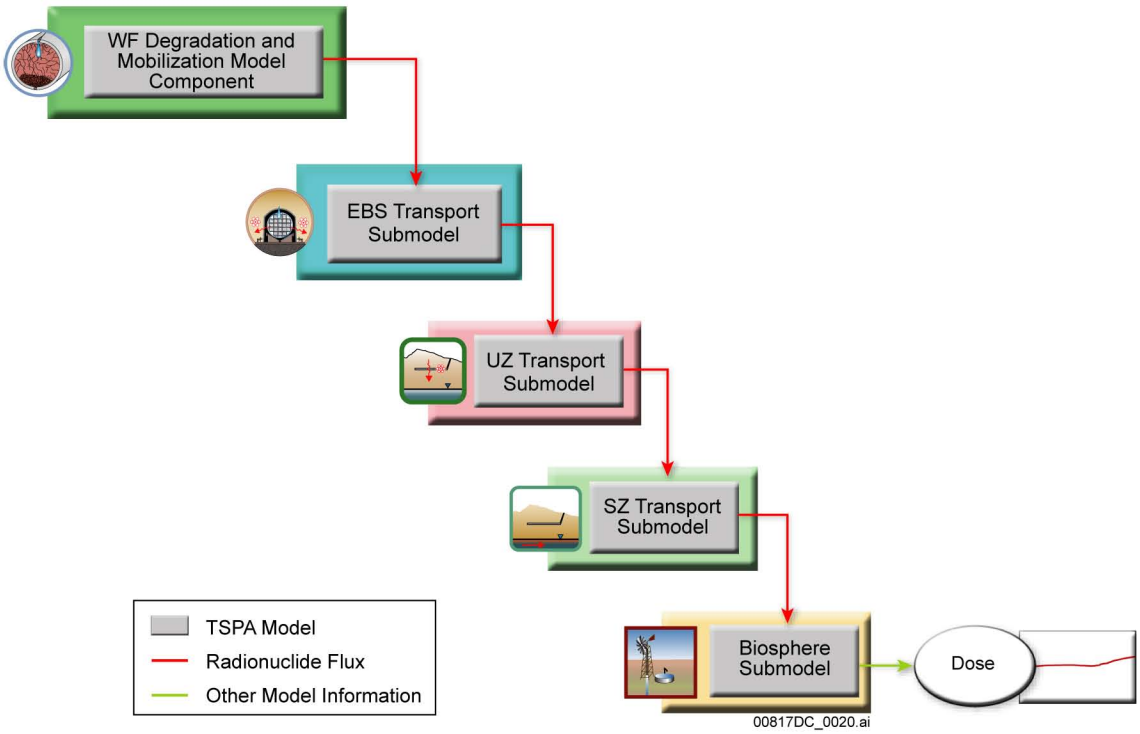

Figure G-7. Illustration of the Transfer of Information on Radionuclide Fluxes between Model Components and Submodels of the TSPA-LA Model

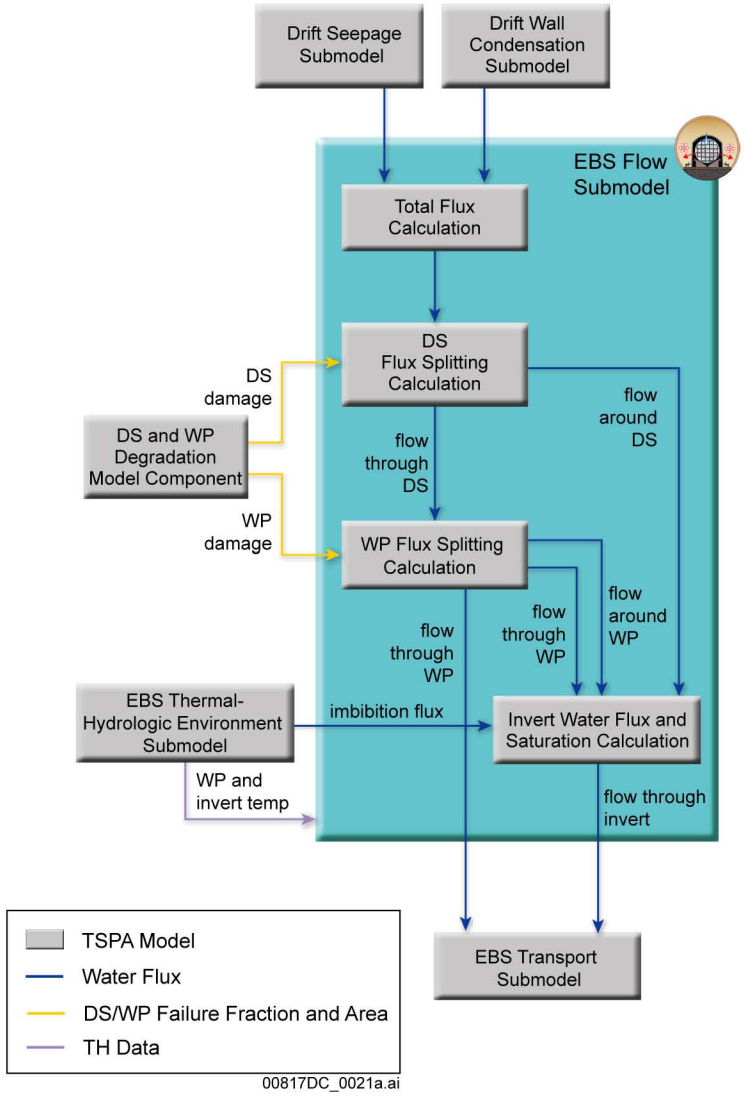

Figure G-8. Illustration of the Transfer of Information between Model Components and Submodels of the TSPA-LA Model for Factors that Affect Flow through the EBS

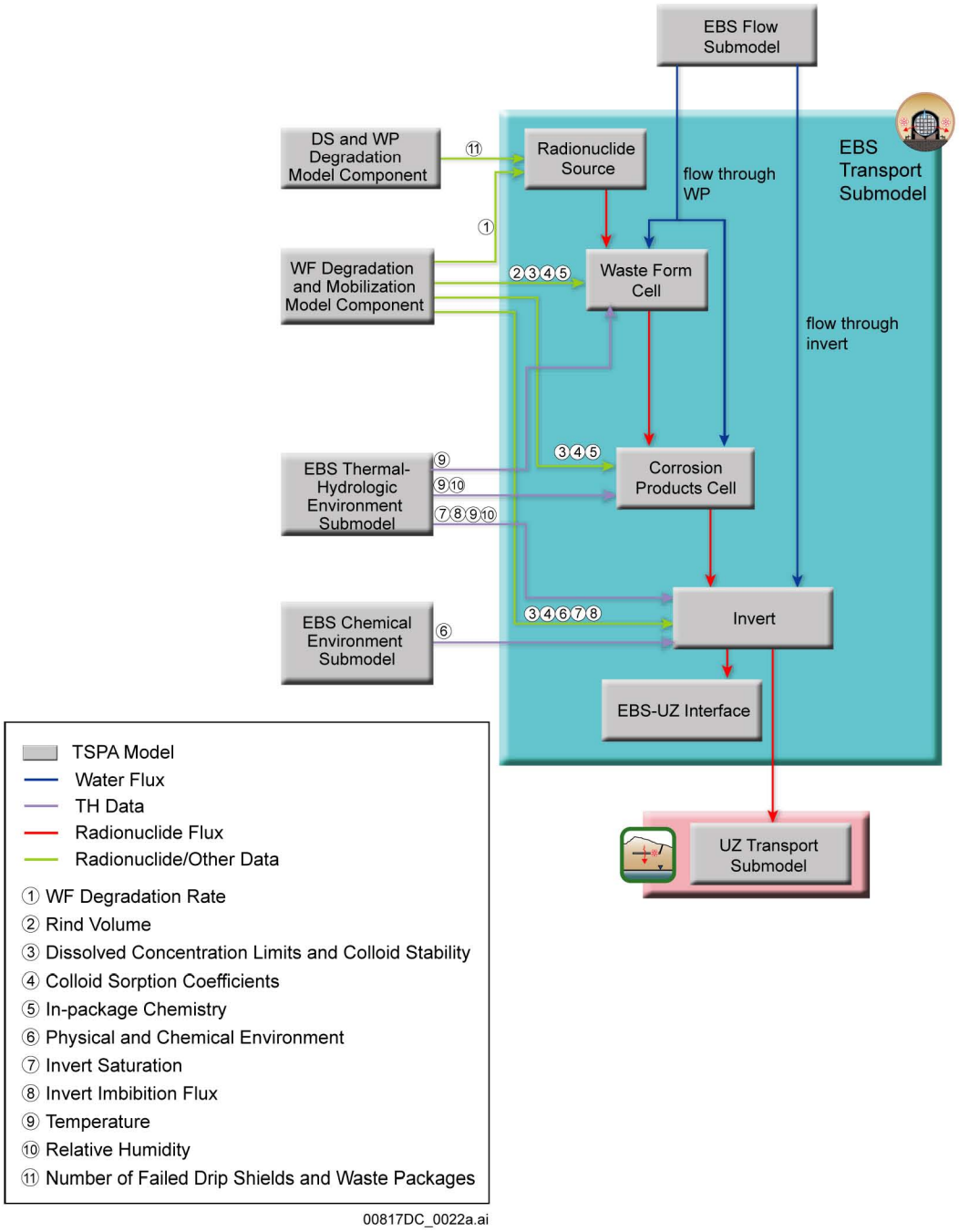

Figure G-9. Illustration of the Transfer of Information between Model Components and Submodels of the TSPA-LA Model that affect Radionuclide Transport through the EBS

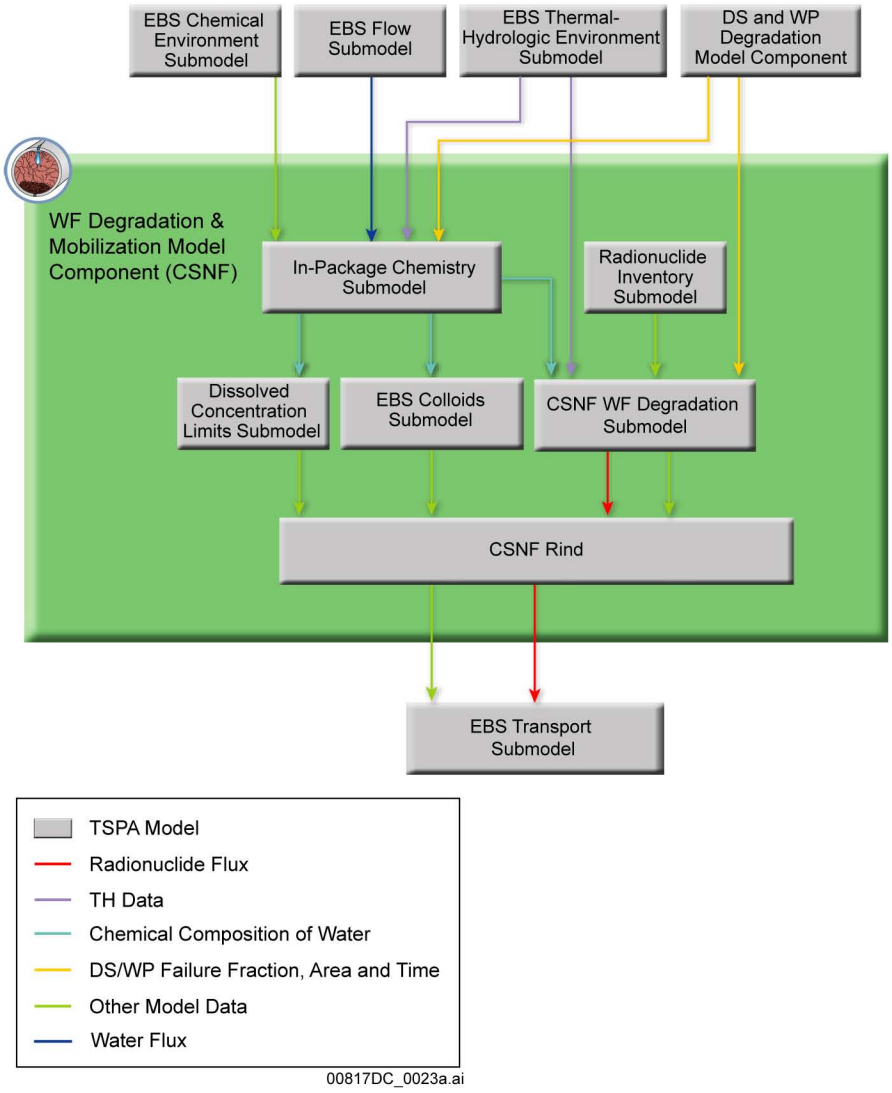

Figure G-10. Illustration of the Transfer of Information between Model Components and Submodels of the TSPA-LA Model, Nominal Scenario Class, for Factors that Affect Waste Form Degradation for CSNF WPs

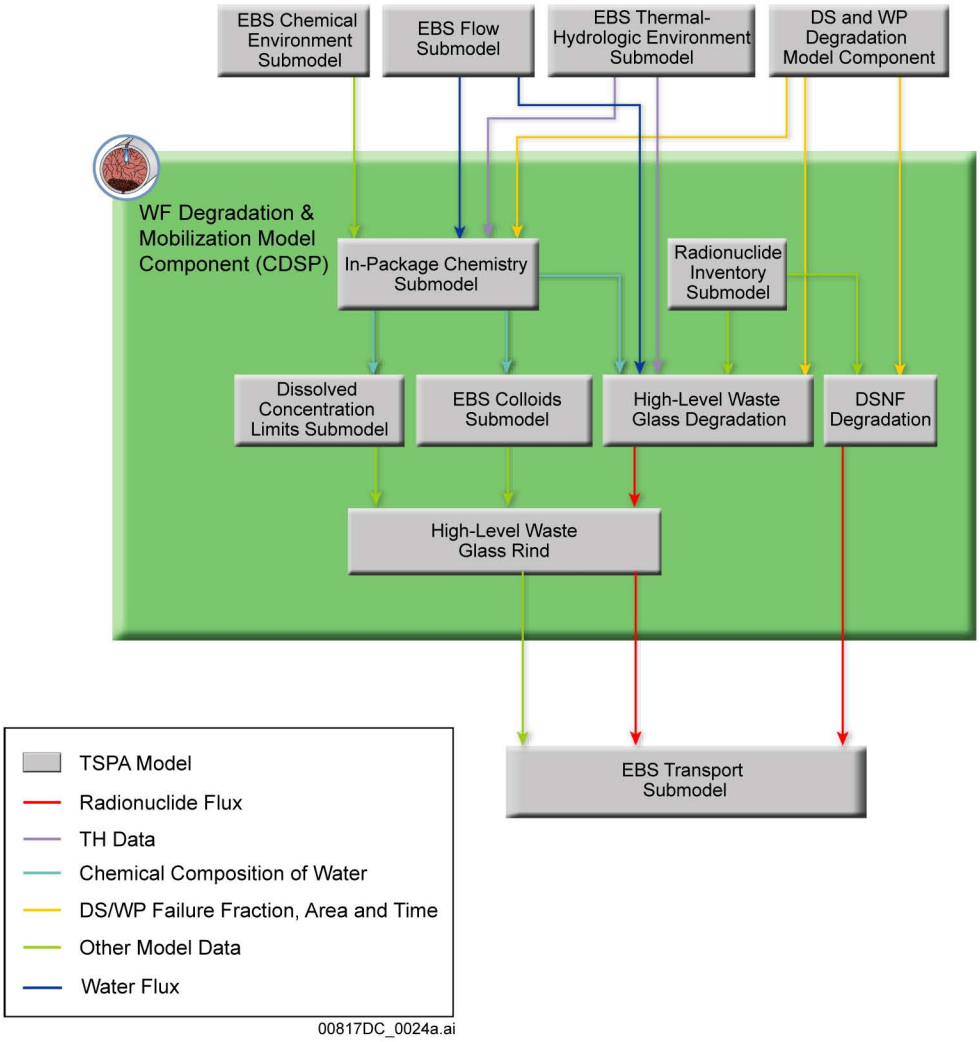

Figure G-11. Illustration of the Transfer of Information between Model Components and Submodels of the TSPA-LA Model, Nominal Scenario Class, for Factors that Affect Waste Form Degradation for CDSP WPs

APPENDIX H

YUCCA MOUNTAIN REVIEW PLAN ACCEPTANCE CRITERIA

H1. EVALUATION OF THE TOTAL SYSTEM PERFORMANCE ASSESSMENT FOR THE LICENSE APPLICATION MODEL DOCUMENT AGAINST REGULATORY REQUIREMENTS

Pursuant to the Technical Work Plan (SNL 2008 [DIRS 184920], Section 3.3 and Table 3.3-1), for the TSPA-LA Model, the *Total System Performance Assessment Model/Analysis for the License Application* is to be evaluated against sections of Subpart E—Technical Criteria of the U.S. Nuclear Regulatory Commission (NRC) Proposed Rule 10 CFR Part 63 ([DIRS 178394] and [DIRS 180319]). In particular, 10 CFR 63.113(a), (b), (c), and (d); and 10 CFR 63.115(a), and (b) [DIRS 180319] and to the acceptance criteria specified in the *Yucca Mountain Review Plan, Final Report* (NUREG-1804) (NRC 2003 [DIRS 163274]) that apply to these requirements. NUREG-1804 (NRC 2003 [DIRS 163274]) acceptance criteria addressed in the *Total System Performance Assessment Model/Analysis for the License Application* and their correlation with the sections of Subpart E of 10 CFR Part 63 ([DIRS 178394] and [DIRS 180319]) are summarized in Table H-1. The following sections provide pointers to the sections of the *Total System Performance Assessment Model/Analysis for the License Application* that address the specified sections of the NRC Rule and the associated acceptance criteria.

Section H1.1 points to the sections of the *Total System Performance Assessment Model/Analysis for the License Application* related to NRC Rule 10 CFR 63.113(a); and 10 CFR 63.115(a) and (b) [DIRS 180319]. The identified sections of this model report provide information that can be used in evaluating the multiple barriers against the NUREG-1804 (NRC 2003 [DIRS 163274]) acceptance criteria.

Section H1.2 points to the sections of the *Total System Performance Assessment Model/Analysis for the License Application* related to 10 CFR 63.113(b) [DIRS 180319]. The identified sections of this model report provide information that can be used in evaluating NUREG-1804 (NRC 2003 [DIRS 163274]) acceptance criteria regarding the postclosure performance objective associated with protection of the reasonably maximally exposed individual (RMEI).

Section H1.3 points to the sections of the *Total System Performance Assessment Model/Analysis for the License Application* related to 10 CFR 63.113(c) [DIRS 180319]. The identified sections of the *Total System Performance Assessment Model/Analysis for the License Application* provide information that can be used in evaluating NUREG-1804 (NRC 2003 [DIRS 163274]) acceptance criteria regarding the postclosure performance objective associated with protection of the groundwater.

Section H1.4 points to the sections of this model report related to 10 CFR 63.113(d) [DIRS 180319]. The identified sections of this model report provide information that can be used in evaluating NUREG-1804 (NRC 2003 [DIRS 163274]) acceptance criteria regarding the postclosure performance objective associated with protection of the RMEI if there is a human intrusion into the repository.

H1.1. EVALUATION AGAINST 10 CFR 63.113(A); 10 CFR 63.115(A); AND 10 CFR 63.115(B)

The requirements given in 10 CFR 63.113(a); and 10 CFR 63.115(a) and (b) [DIRS 180319] address the multiple barriers. The NRC's review of the information provided will focus on these requirements according to NUREG-1804 (NRC 2003 [DIRS 163274], Section 2.2.1.1) (see Table H-1). The following sections of this model report provide information relevant to the acceptance criteria specified in this section of NUREG-1804.

Acceptance Criterion 1–Identification of Barriers is Adequate—Section 8.3 identifies barriers important to waste isolation. These barriers are the Upper Natural Barrier, the Engineered Barrier System (EBS), and the Lower Natural Barrier. The discussion in Section 8.3 therefore, provides information for evaluating Acceptance Criterion 1.

Acceptance Criterion 2–Description of Barrier Capability to Isolate Waste is Acceptable—Section 8.3 discusses the capability of the barriers identified as important to waste isolation. This section summarizes the capabilities of the barriers that are important to waste isolation to prevent or substantially reduce the rate of radionuclide movement from the Yucca Mountain Repository to the accessible environment, or to prevent the release or substantially reduce the release rate of radionuclides from the waste. The discussion in Section 8.3 therefore, provides information useful for evaluating Acceptance Criterion 2.

Acceptance Criterion 3–Technical Basis for Barrier Capability is Adequately Presented—Section 6.3 summarizes the model components of the TSPA-LA Model, which include the submodels used to evaluate barrier capability. The technical basis for these models is provided in the analysis and model reports referenced in Section 6.3.

H1.2. EVALUATION AGAINST 10 CFR 63.113(B)

The requirements given in NRC Rule 10 CFR 63.113(b) [DIRS 180319], address the postclosure performance objectives associated with protection of the RMEI. The review by the NRC, of the information provided, will focus on the individual protection requirements according to NUREG-1804 (NRC 2003 [DIRS 163274], Section 2.2.1.4.1) (Table H-1). The following sections of this model report provide information relevant to the acceptance criteria specified in this section of NUREG-1804.

Acceptance Criterion 1–Scenarios Used in the Calculation of the Annual Dose as a Function of Time are Adequate—Section 8.1.1 describes the mean annual dose history calculated for the repository system. This mean annual dose history is a sum of the mean annual dose histories for all modeling cases that represent the scenario classes determined to be sufficiently probable or to have a sufficient effect on overall performance, and therefore, were included in the analyses. Section 6.1.2 discusses the summing of results for these modeling cases and shows that the contribution to mean annual dose properly accounts for the random time of occurrence of the disruptive events. Section 6.1.2 also summarizes the probabilities of all scenario classes and shows that the approach in the TSPA-LA Model provides an appropriate sum of these probabilities.

Acceptance Criterion 2–An Adequate Demonstration is Provided that the Annual Dose to the Reasonably Maximally Exposed Individual in Any Year During the Compliance Period Does Not Exceed the Exposure Standard—The analyses in Sections 7.3 and 8.1.1 show that mean annual dose is calculated with a sufficient number of realizations for each scenario class modeling case to ensure that the results of the calculations are statistically stable. The analyses in Section 8.1.1 also address the uncertainty in the estimate of mean annual dose and Sections 8.2.1 through 8.2.4 show the range of annual doses used to estimate mean annual dose in each of the TSPA-LA Model modeling cases. This range represents the full range of uncertainty in each estimate of mean annual dose. Subsystem analyses in Sections 8.3.1 through 8.3.4 show that the performances of individual components and subsystems are consistent and reasonable. The results in Section 8.1.1, Sections 8.2.1 through 8.2.4, and Sections 8.3.1 through 8.3.4, therefore provide information useful in evaluating this acceptance criterion.

Acceptance Criterion 3–The Total System Performance Assessment (TSPA) Code Provides a Credible Representation of Repository Performance—Section 5 discusses the general assumptions used in the TSPA-LA Model development and justification for these assumptions. Sections 6.3, 6.4, 6.5, 6.6, and 6.7, document the use of these assumptions and the parameter values that differ among components and submodels of the TSPA-LA Model. Section 6.1 provides an overview of the conceptual TSPA-LA Model. The subsections of Section 6.1 describe the transfer of information among the TSPA-LA Model components. Section 6.3 provides details of the components of the TSPA-LA Model for the Nominal Scenario Class. Section 6.4 presents the detail for the Early Failure Scenario Class, with Section 6.4.1 discussing the Drip Shield Early Failure Modeling Case, and Section 6.4.2 discussing the Waste Package Early Failure Modeling Case. Section 6.5 provides details for the Igneous Scenario Class and Section 6.6 presents the Seismic Scenario Class information. Section 6.7 discusses the details for the Human Intrusion Scenario, including the conceptual model in Section 6.7.1, and the TSPA-LA Model implementation in Section 6.7.2. Section 7.2 confirms that the TSPA-LA Model is properly verified and that information transfer between and among components and submodels, is conducted properly. Section 7.4 provides results of the uncertainty analyses, and corrective actions implemented when appropriate. Section 7.4 also shows that the estimate of the uncertainty in the performance assessment results is consistent with the model and the uncertainty in parameter values. Section 6.1.3 shows that a Latin hypercube sampling approach addresses all quantified uncertainties, and that this approach ensures that parameter values are sampled across their ranges of uncertainty. Section 7.10 summarizes the validation of the TSPA-LA Model and provides confidence that the TSPA-LA Model adequately represents the physical processes of the repository system. The overview of the TSPA-LA Model in Section 6 and the model validation and confidence building information in Section 7 therefore, provide information useful in evaluating this acceptance criterion.

H1.3. EVALUATION AGAINST 10 CFR 63.113(C)

The requirements at NRC Rule 10 CFR 63.113(c) [DIRS 180319] address the postclosure performance objective associated with protection of groundwater. 10 CFR 63.113(c) [DIRS 180319] points to the requirements of the NRC Rule 10 CFR 63.331 [DIRS 180319], which address the standards for groundwater protection, and the requirements at 10 CFR 63.332 [DIRS 180319], which define the representative volume. The review by the NRC of the

information that will be provided in the TSPA-LA Model and the *Total System Performance Assessment Model/Analysis for the License Application* will focus on these groundwater protection requirements according to NUREG-1804 (NRC 2003 [DIRS 163274], Section 2.2.1.4.3) (Table H-1). The following sections of the *Total System Performance Assessment Model/Analysis for the License Application* provide information relevant to the acceptance criteria specified in this section of NUREG-1804.

Acceptance Criterion 1–An Adequate Demonstration is Provided that the Expected Concentration of Combined ^{226}Ra and ^{228}Ra, Expected Concentration of Specified Alpha–Emitting Radionuclides, and Expected Whole Body or Organ–Specific Doses from any Photon– or Beta–Emitting Radionuclides at Any Year During the Compliance Period Do Not Exceed the Separate Groundwater Protection Standards—Section 8.1.2 presents the results of analyses addressing the groundwater protection standards. In particular, Section 8.1.2 shows the estimate of groundwater radioactivity for the representative volume of groundwater that includes combined ^{226}Ra and ^{228}Ra, gross alpha activity (including due to ^{226}Ra, but excluding that due to radon and uranium), and combined beta- and photon-emitting radionuclides. Sections 6.3 and 8.1.2 discuss the methods, assumptions, models, and data used in calculating these estimates. Sections 6.3 and 8.1.2 show that these estimates are consistent with the repository performance assessment calculations for likely processes and events that may occur after disposal, and that the calculations are supported by an adequate technical basis. Therefore, the material in Sections 6.3 and 8.1.2 provides information useful in evaluating Acceptance Criterion 1.

Acceptance Criterion 2–The Methods and Assumptions Used to Determine the Position of the Representative Volume of Groundwater are Credible and Consistent, and the Representative Volume of Groundwater Includes the Highest Concentration Level in the Plume of Contamination in the Accessible Environment—Section 6.3.10 discusses the methods and assumptions for determination of groundwater concentrations in the representative volume that is located along the radionuclide migration path from the repository at Yucca Mountain to the accessible environment. Section 8.1.2 provides results and a detailed evaluation of the concentrations in the context of the groundwater concentration standards. In the TSPA-LA Model, a conservative approach is used in which radionuclide concentrations are estimated by assuming the entire annual release from the repository system is discharged into the representative volume, located 18 km from the repository. Therefore, the estimated radionuclide concentrations provide an upper bound to the groundwater concentrations needed to assess the groundwater protection requirements. This approach eliminates the need to specify the dimensions of the representative volume or the water usage by the RMEI (Section 1.1.1). The information provided in Sections 6.3.10 and 8.1.2 therefore, supports evaluation of Acceptance Criterion 2 by the NRC.

Acceptance Criterion 3–The Methods and Assumptions Used to Calculate the Physical Dimensions of the Representative Volume of Groundwater are Credible and Consistent—The dose results presented in Section 8.1.2 are estimated by assuming that the entire annual release from the repository system is discharged into the representative volume. Therefore, the associated concentrations provide an upper bound to the groundwater concentrations needed to assess the groundwater protection requirements. This approach eliminates the need to specify the physical dimensions of the representative volume or the water

usage by the RMEI (Section 1.1.1). The information in Section 8.1.2 therefore, supports evaluation of this Acceptance Criterion 3.

H1.4. EVALUATION AGAINST 10 CFR 63.113(D)

The requirements given in NRC Rule 10 CFR 63.113(d) [DIRS 180319] address the postclosure performance objective associated with protection of the RMEI due to a human intrusion into the repository. Section 63.113(d) [DIRS 180319] points to the requirements: (1) in 10 CFR 63.321 [DIRS 178394], which address the selection of the time of occurrence of the human intrusion, (2) for conducting the TSPA for the human intrusion separately from the overall TSPA, and meets the requirements for performance assessments (PA) specified in NRC Proposed Rule 10 CFR 63.114 [DIRS 178394], which are the same as for the overall TSPA, and (3) in 10 CFR 63.322 [DIRS 180319], which specifies the Human Intrusion Scenario for the DOE to use in addressing the postclosure individual protection standard. The review by the NRC of the information that will be provided in the TSPA-LA Model and the *Total System Performance Assessment Model/Analysis for the License Application*, will focus on these requirements according to NUREG-1804 (NRC 2003 [DIRS 163274], Section 2.2.1.4.2) (Table H-1). The following sections of the TSPA-LA Model report provide information relevant to the acceptance criteria specified in Section 2.2.1.4.2 of NUREG-1804.

Acceptance Criterion 1–Evaluation of the Time of an Intrusion Event—Section 6.7.2 provides the technical basis and associated analyses in support of the selection of time of occurrence of the human intrusion, as specified in 10 CFR 63.321 [DIRS 178394]. Specifically, Section 6.7.2.1 describes the TSPA-LA analysis for drip shield (DS) and waste package (WP) degradation. Section 6.7.2.2 discusses the unlikely events-related damage mechanisms. Section 6.7.2.3 describes the potential for WP penetration during drilling. Section 6.7.2.4 provides the earliest time of WP penetration by a human intrusion. The information provided in Section 6.7.2 therefore supports evaluation of Acceptance Criterion 1.

Acceptance Criterion 2–Evaluation of an Intrusion Event Demonstrates That the Annual Dose to the Reasonably Maximally Exposed Individual in Any Year During the Compliance Period Is Acceptable—Sections 6.7 and 8.1.3 discuss how the TSPA-LA Model addresses the Human Intrusion Scenario, the implementation, and how the resultant RMEI dose complies with the requirement of this acceptance criterion. Section 6.7.3 specifically discusses implementation of the TSPA-LA Model for human intrusion separately from the overall TSPA, and is consistent with the requirements for PAs, as specified in 10 CFR 63.114 [DIRS 178394]. Sections 6.7.3 and 6.7.4 show that the TSPA for human intrusion is identical as applicable to the TSPA for individual protection, except that it assumes the occurrence of a postulated human intrusion event with characteristics as defined in 10 CFR 63.322 [DIRS 180319], and excludes the consideration of 10 CFR 63.342 [DIRS 178394] for unlikely natural features, events, or processes (6.7.2.2). Sections 7.3 and 8.1.1 provide information regarding the fact that a sufficient number of realizations have been run using the TSPA-LA Model, to ensure that the results of the calculations are statistically stable. Section 8.1.3 discusses the overall system performance analyses and presents the resulting annual dose curves for the Human Intrusion Scenario. The information provided in Sections 6.7 and 8.1 supports confirmation that the repository system meets performance objectives specified in 10 CFR 63.321 [DIRS 178394] for a human intrusion into the repository.

Acceptance Criterion 3—The Total System Performance Assessment Code Provides a Credible Representation of the Intrusion Event—Sections 5, 6.7.1 through 6.7.5, 7.2, 7.4, and 7.7, provide the information needed to evaluate this acceptance criterion as shown in Table H-1. Section 6.7.3 describes the implementation of the TSPA-LA Model for simulating the Human Intrusion Scenario. The parameter sampling for the TSPA-LA Model is discussed in Section 6.1.3. Section 6.7.4 provides information on the assessment of the impact due to the assumptions used, and model and parameter uncertainty on the dose calculated by the TSPA-LA Model, which are reflected in modeling the Human Intrusion Scenario. Section 6.7.4 discusses the consistency among model components and submodels, and identifies the conservative assumptions in abstractions, process models, and parameter sets supporting the modeling case for the Human Intrusion Scenario. Section 7.2 documents the TSPA-LA Model verification activities in order to ensure that the TSPA-LA Model inputs are properly verified providing confidence that the code was modeling the physical processes in the repository system in a manner that is consistent with the characteristics of the postulated human intrusion event. The information in Section 7.3 ensures that the individual dose curves do indeed represent the model and are not due to errors and lack of transfer of data (coupling) between the modules of the code. Section 6.1.3 discusses the treatment of uncertainty in the TSPA-LA Model input parameters. Section 7.4 presents an uncertainty characterization review and remedial actions implemented. Section 6.7.4 discusses the application of the uncertainty treatment, and characterization reviews to the Human Intrusion Scenario. The measures described above together provide the information needed to support evaluation of this Acceptance Criterion 3.

Table H-1. Applicable Regulatory Requirements of 10 CFR Part 63 and NUREG-1804 Acceptance Criteria Addressed in this Document

Applicable Sections of 10 CFR Part 63	Associated Section of NUREG-1804 Acceptance Criterion	NUREG-1804 Acceptance Criterion		Section of Report Addressing NUREG-1804 Acceptance Subcriterion
		Criterion	Subcriterion	
10 CFR 63.113(a), 10 CFR 63.115(a), and 10 CFR 63.115(b) [DIRS 180319]	2.2.1.1.3 System Description and Demonstration of Multiple Barriers	1. Identification of Barriers	1. Identification of barriers	8.3
		2. Description of Barrier Capability	1. Time period of applicable function	8.3
			2. Uncertainty in barrier capability	8.3
			3. Description consistent with the TSPA-LA Model	8.3
			4. Description consistent with barrier definition	8.3
		3. Technical Basis for Barrier Capability	1. Technical basis for barrier capability	6.3
10 CFR 63.113(b) [DIRS 180319]	2.2.1.4.1.3 Demonstration of Compliance with Postclosure Individual Protection Standard	1. Scenario Classes	1. Scenario class screening	6.1.2
			2. Combining mean annual dose from scenario classes	6.1.2 and 8.1.1.1
		2. Mean Annual Doses	1. Number of realizations	8.1.1.2, 7.3
			2. Uncertainty in mean annual dose	6.1.3 and 8.1.1.2
			3. Performance of components and subsystems	8.2 – 8.4
			4. Comparison with individual protection standard	8.1.1.2
		3. Credible TSPA-LA Model	1. Consistency of assumptions	5, 6.3 to 6.6
			2. Model verification	7.2
			3. Uncertainty analysis	6.1.3 and 7.4
			4. Parameter sampling	6.1.3
10 CFR 63.113(c) [DIRS 180319]	2.2.1.4.3.3 Demonstration of Compliance with Groundwater Protection Standards	1. Groundwater Protection Standards	1. Compliance with concentration and dose standards	8.1.2.1 to 8.1.2.2, and 8.1.2.3
			2. Methods and assumptions	8.1.2
			3. Comparison with groundwater protection standards	8.1.2
		2. Position of Representative Volume	1. Along radionuclide migration path	6.3.10
			2. Method of locating position	6.3.10
			3. Highest concentration	6.3.10
		3. Dimensions of Representative Volume	1. Specifications on representative volume	8.1.2
			2. Method to determine dimensions	6.3.10 and 8.1.2
			3. Consistency with water usage	8.1.2 and 6.3.11

Table H-1. Applicable Regulatory Requirements of 10 CFR Part 63 and NUREG-1804 Acceptance Criteria Addressed in this Document (Continued)

Applicable Sections of 10 CFR Part 63	Associated Section of NUREG-1804 Acceptance Criterion	NUREG-1804 Acceptance Criterion		Section of Report Addressing NUREG-1804 Acceptance Subcriterion
		Criterion	Subcriterion	
10 CFR 63.113(d) [DIRS 180319]	2.2.1.4.2 Demonstration of Compliance with the Human Intrusion Standard	1. Evaluation of the Time of a Human Intrusion Event	1. The technical basis and associated analyses adequately support the selection of the time of occurrence of a human intrusion, as specified in 10 CFR 63.321 [DIRS 178394].	6.7.2
		2. Evaluation of an Intrusion Event Demonstrates That the Annual Dose to the RMEI in Any Year During the Compliance Period Is Acceptable	1. The TSPA for the Human Intrusion Scenario is performed separately from the overall TSPA, and meets the requirements for performance assessments, specified in 10 CFR 63.114 [DIRS 178394].	6.7.3 and 6.7.4
			2. The TSPA for Human Intrusion Scenario is identical to the TSPA for individual protection, except that it assumes the occurrence of a postulated human intrusion event with characteristics, as defined in 10 CFR 63.322 [DIRS 180319] and excludes the consideration of unlikely natural features, events, or processes in 10 CFR 63.342 [DIRS 178394].	6.7.2.2, 6.7.3, and 6.7.4
			3. A sufficient number of realizations have been run using the TSPA code, to ensure that the results of the calculations are statistically stable.	8.1.1.2 and 7.3
			4. The estimated repository performance is reasonable and consistent with the analysis of overall repository performance, and with the characteristics of the postulated Human Intrusion Scenario.	8.1.3.2
			5. The annual dose curve for limited human intrusion confirms that the repository system meets performance objectives, specified in 10 CFR 63.321 [DIRS 178394], for limited human intrusion events.	8.1.3.2

Table H-1. Applicable Regulatory Requirements of 10 CFR Part 63 and NUREG-1804 Acceptance Criteria Addressed in this Document (Continued)

Applicable Sections of 10 CFR Part 63	Associated Section of NUREG-1804 Acceptance Criterion	NUREG-1804 Acceptance Criterion		Section of Report Addressing NUREG-1804 Acceptance Subcriterion
		Criterion	Subcriterion	
		3. The TSPA Code Provides a Credible Representation of a Human Intrusion Event.	1. Assumptions made on the method of transport from a breached WP within the TSPA for evaluating the postulated intrusion event are consistent among different modules of the code. The use of assumptions and parameter values that differ among modules of the code is adequately documented.	5, 6.7.1 to 6.7.5, and 7.7
			2. The TSPA code for evaluating human intrusion is properly verified, such that there is confidence that the code is modeling the physical processes in the repository system in a manner that is consistent with the characteristics of the postulated intrusion event. The transfer of data between modules of the code is conducted properly.	7.2
			3. The estimate of uncertainty in the performance assessment results is consistent with the uncertainties considered in the characteristics of the postulated intrusion event, and with model and parameter uncertainty.	8.1.3, 6.7.3 ,6.1.3, and 7.4
			4. The sampling method used in the TSPA ensures that sampled parameters of the postulated intrusion event have been sampled across their ranges of uncertainty.	6.1.3, 6.7, and 7.4

Sources: 10 CFR Part 63 [DIRS 178394 and DIRS 180319]; NUREG-1804 (NRC 2003 [DIRS 163274])

INTENTIONALLY LEFT BLANK

APPENDIX I

FEATURES, EVENTS, AND PROCESSES MAPPED TO TSPA-LA MODEL

I1. FEATURES, EVENTS, AND PROCESSES MAPPED TO TSPA-LA MODEL

I1.1. INTRODUCTION

This appendix provides summary information about how features, events, and processes (FEPs) are implemented in the Total System Performance Assessment for the License Application (TSPA-LA) Model. Section 6.1.1 discusses the process of FEP screening and development. Section 6.1.1 also lists the criteria used to determine whether or not individual FEPs are included in or excluded from the TSPA-LA Model. The FEPs that are included as a result of the FEPs screening process are implemented in the TSPA-LA Model in various ways (Figure I-1). A FEP may be included by direct incorporation into the GoldSim simulation software (STN: 10344-9.60-01[DIRS 181903]) model file, such as in a parameter in a functional relation. (Throughout Appendix I, all references to GoldSim and the GoldSim model file refer to V9.60.100 (STN: 10344-9.60-01[DIRS 181903]) unless otherwise noted.) A FEP may also be included in the TSPA-LA Model by incorporation into a dynamically linked library (DLL) that is called by the GoldSim model file. A FEP may also be included in the TSPA-LA Model by incorporation into an abstraction of a process model. The development process for the TSPA-LA Model utilizes the development of several process models, as discussed in Section 6.1.5 (TSPA-LA Model File Architecture), which are abstracted for inclusion into the GoldSim model file. For example, FEP 1.1.02.02.0A, Preclosure Ventilation, is included in the Multiscale Thermohydrologic Model (MSTHM) Process Model and analysis that is used to develop the thermal hydrologic (TH) abstraction for the TSPA. Preclosure ventilation is included in the MSTHM analysis by accounting for the removal of heat in the energy source term.

Complete documentation for the FEPs abstracted in this appendix can be found in *Features, Events, and Processes for the Total System Performance Assessment: Methods* (SNL 2008 [DIRS 179476]), and *Features, Events, and Processes for the Total System Performance Assessment: Analyses* (SNL 2008 [DIRS 183041]). These documents contain information on the FEP screening process, applicable criteria, pertinent regulations, and detailed discussions of all 374 FEPs, including screening decisions, screening justifications, and full text TSPA dispositions. The TSPA disposition contains information on how each included FEP is implemented in a particular submodel or submodels. This information is also consolidated in the FEP data set (DTN: MO0706SPAFEPLA.001 [DIRS 181613]), which can be viewed using the FEPS database software program (STN: 611664-1.0-00 [DIRS 181089]).

The FEPs included in the TSPA-LA Model, require inclusion in one or more performance assessments conducted to demonstrate compliance with the proposed individual protection standard (10 CFR 63.311 [DIRS 178394]), groundwater protection standard (10 CFR 63.331 [DIRS 180319]), and/or the proposed individual protection standard for human intrusion (10 CFR 63.321 [DIRS 178394]). The results of this evaluation are incorporated in this appendix. Section 6.1.1 further explains this process and the regulatory requirements.

Figure I-1 pictorially describes the incorporation of an included FEP in the TSPA-LA Model. Table I-2 contains a brief description of how each included FEP is implemented in the TSPA-LA Model. More detailed TSPA dispositions are provided in the FEP data set (DTN: MO0706SPAFEPLA.001 [DIRS 181613]), which is too lengthy to include in its entirety

in this appendix. Information in this appendix provides a path to a location within the GoldSim model file where a FEP is implemented. The details of implementation for specific submodels are best understood by direct review of the TSPA-LA Model implementation within GoldSim, also known as a GoldSim model file. The text within the GoldSim model files described in this report was updated after the models were run. The updated GoldSim models with the descriptive text are part of output DTN: MO0708GWEFINAL.000 [DIRS 182977].

Sections 6.3.1 through 6.3.11, and 6.4 through 6.7 of this report describe the submodels included in the TSPA-LA Model. Each subsection also discusses the implementation of the submodels in the TSPA-LA Model and provides a pathway to the appropriate location in the GoldSim model file, allowing a detailed review of the implementation. In addition, the GoldSim model file includes descriptions of the inputs and calculations being performed within each submodel. Table 6.1.5-1 provides the GoldSim model file locations containing submodel documentation.

Table I-1 explains the information contained in the table headings used in Table I-2, and Table I-2 gives the TSPA implementation information for each FEP included in the TSPA-LA Model. The GoldSim model path listed is provided to guide the reader to the submodel within the TSPA-LA Model file. Different types of information will be found at these path locations depending on how the individual FEP is implemented or how broad the FEP is in nature. Implementation of each FEP, whether directly in the GoldSim model file, indirectly by a process model abstraction, or through a DLL, results in variations in the GoldSim model file paths identified in Table I-2. The GoldSim model paths shown for each FEP provides a location of the submodel where the feature, event or process is included. FEPs are not listed specifically in the GoldSim model file.

FEPs can be implemented by more than one submodel, and therefore can appear more than once in Table I-2. Effort was made to indicate only those FEPs that are directly implemented in a particular submodel and not include all downstream implementation of the same FEP. Additionally, FEPs identified in the nominal scenario class are, in general, included in the disruptive scenario classes. See sections 6.4- 6.7 for more information.

The GoldSim model file has evolved during the development of the TSPA-LA Model and this evolution has resulted in some inconsistencies in the use of terminology. For instance, Section 6 describes percolation subregions and discusses how they are defined and used in the TSPA-LA Model. In the GoldSim model file, these are referred to as bins. There is also legacy coding in the GoldSim model file that is no longer being used but was retained to allow for future sensitivity analyses or other investigations. Text has been added to the GoldSim model file to identify these special situations.

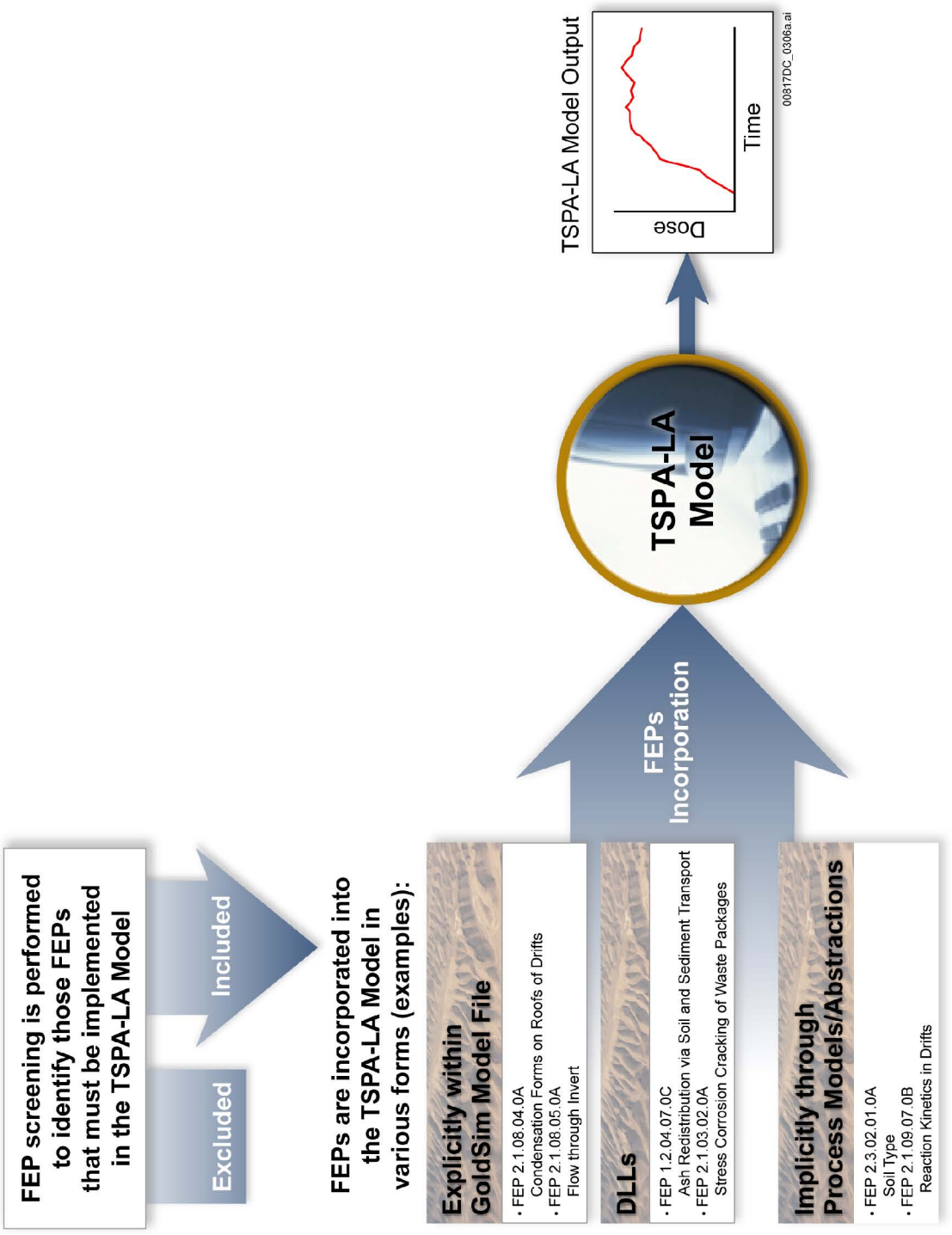

Figure I-1. Implementation of Features, Events, and Processes in the TSPA-LA Model

INTENTIONALLY LEFT BLANK

Table I-1. Explanation of the Column Headings in Table I-2

Column Heading	Explanation
Submodel implemented in the TSPA-LA Model and Section Number	This is the name of the submodel where the FEP is implemented. The number below the submodel name represents the section in this document where submodel information can be found.
Path in GoldSim Model File	The GoldSim path showing where the FEP is implemented in the GoldSim model. This is meant to provide a sampling of important paths. Other implementation paths may exist that are not shown in this column. Some FEP implementations are in multiple parallel locations in the GoldSim model because they contain multiple waste forms and multiple discrete repository regions.
FEPs included in the Submodel	The numbers and titles of the features, events and processes that are implemented in the TSPA-LA Model through the appropriate submodel.
TSPA Inclusion Explanation	A short description of how the FEP is implemented in the TSPA-LA Model.
Performance Assessment Standard	This column identifies the relevant regulatory standard the FEP is addressing: Groundwater Protection Standard (10 CFR 63.331 [DIRS 180319]), proposed Individual Protection Standard (10 CFR 63.311 [DIRS 178394]), or proposed Individual Protection Standard for Human Intrusion (10 CFR 63.321 [DIRS 178394]).
TSPA-LA Model Implementation	This column indicates how the FEP is implemented in the TSPA-LA Model; GSM = directly into the GoldSim model; MA = Process Model Abstraction; DLL= Dynamically Linked Library.

Table I-2. Model Implementation for Included Features, Events, and Processes

Submodel implemented in the TSPA-LA Model and Section Number	Path in GoldSim Model File	FEPs Included in the Submodel	TSPA Inclusion Explanation	Performance Assessment Standard[a]	TSPA-LA Model Implementation
UZ Flow Fields Abstraction 6.3.1	Epistemic: \Input_Params_Epistemic\Epistemic_Params_UZ_Flow EBS: \Time_Zero\EBS_PS_Loop\Static_Calcs_PS_Loop\Static_Calcs_UZ_Flow \Global_Inputs_and_Calcs\Global_UZ_Flow	1.3.01.00.0A Climate change	Climate change is addressed in the TSPA based on the record of climate changes in the past, which are used to predict the expected changes in climate for the future. Climate modeling is incorporated into TSPA through the site-scale unsaturated zone (UZ) flow fields which use different infiltration maps (water-flux boundary condition maps) corresponding to four different climates: present-day, monsoon, and glacial-transition, and the post-10,000-year climate.	10 CFR 63.311 10 CFR 63.331 10 CFR 63.321	GSM
UZ Flow Fields Abstraction for Human Intrusion assessment 6.7		1.3.07.02.0B Water table rise affects UZ	The water table will be higher in future climate states that have greater infiltration rates. To include this predicted water table rise in the TSPA calculations, the water table elevation is instantaneously increased up to 120m when the climate changes from present-day to monsoon climate, and the glacial-transition climate state. Water table changes are implemented in the TSPA by allowing the water table to change elevation instantaneously upon change in climate affecting the unsaturated flow and pathways in the UZ.	10 CFR 63.311 10 CFR 63.331 10 CFR 63.321	GSM
		1.4.01.01.0A Climate modification increases recharge	The Infiltration Model includes the effects of climate change. These effects are captured in the net infiltration map outputs that are used as upper boundary condition water-flux inputs for the Site-Scale UZ Flow Model. The Site-Scale UZ Flow Model is used to develop UZ flow fields corresponding to the four uncertainty cases for water flux at the upper boundary of the UZ Flow Model and four distinct climate states: present-day, monsoon, and glacial-transition, as well as the post-10,000-year period. These flow fields are used directly by the TSPA-LA Model.	10 CFR 63.311 10 CFR 63.331 10 CFR 63.321	GSM

Table I-2. Model Implementation for Included Features, Events, and Processes (Continued)

Submodel implemented in the TSPA-LA Model and Section Number	Path in GoldSim Model File	FEPs Included in the Submodel	TSPA Inclusion Explanation	Performance Assessment Standard[a]	TSPA-LA Model Implementation
UZ Flow Fields Abstraction 6.3.1 (Continued)	Epistemic: \Input_Params_Epistemic\Epistemic_Params_UZ_Flow EBS: \Time_Zero\EBS_PS_Loop\Static_Calcs_PS_Loop\Static_Calcs_UZ_Flow \Global_Inputs_and_Calcs\Global_UZ_Flow	1.2.02.01.0A Fractures	Fractures are included in the Site-Scale UZ Flow Model by using models based on the dual-permeability concept, with fractures represented by a distinct continuum. The fracture continuum models spatially averaged flow through discrete fractures. The fracture continuum interacts with the matrix continuum, which represents matrix blocks separated by the network of fractures. Fracture porosity, fracture spacing, and fracture volume fraction, measured in the field and within different stratigraphic units, determine geometrical parameters of fractures that are incorporated. The flow fields generated by the Site-Scale UZ Flow Model are used directly by the TSPA.	10 CFR 63.311 10 CFR 63.331 10 CFR 63.321	MA
		1.2.02.02.0A Faults	Stratigraphic displacement, dip-slip, strike-slip, and detachments due to faulting within the model domain are explicitly discretized in the Site-Scale UZ Flow Model. Specific hydrogeologic properties are assigned to the fault zones, supported by measurements within fault zones or across faults. The flow fields generated by the Site-Scale UZ Flow Model are used directly by the TSPA.	10 CFR 63.311 10 CFR 63.331 10 CFR 63.321	MA
		2.1.08.01.0A Water influx at the repository	Spatial and temporal changes in UZ flow are represented by the Site-Scale UZ Flow Model. The flow fields generated by the Site-Scale UZ Flow Model are used directly by the TSPA-LA Model. The local percolation flux at the repository for different climate states and different locations within the repository is provided by these flow fields. In the TSPA-LA Model these percolation fluxes are used by the Drift Seepage Submodel to calculate the influx of water into the repository.	10 CFR 63.311 10 CFR 63.331 10 CFR 63.321	MA

Table I-2. Model Implementation for Included Features, Events, and Processes (Continued)

Submodel implemented in the TSPA-LA Model and Section Number	Path in GoldSim Model File	FEPs Included in the Submodel	TSPA Inclusion Explanation	Performance Assessment Standard[a]	TSPA-LA Model Implementation
UZ Flow Fields Abstraction 6.3.1 (Continued)	Epistemic: \Input_Params_Epistemic\Epistemic_Params_UZ_Flow EBS: \Time_Zero\EBS_PS_Loop\Static_Calcs_PS_Loop\Static_Calcs_UZ_Flow \Global_Inputs_and_Calcs\Global_UZ_Flow	2.2.03.01.0A Stratigraphy	Stratigraphic units and layers provide the structural basis for the Site-Scale UZ Flow Model grid. Hydrologic properties corresponding to each unit and layer are also assigned to the flow model grid. The flow fields generated by the Site-Scale UZ Flow Model are used directly by the TSPA.	10 CFR 63.311 10 CFR 63.331 10 CFR 63.321	MA
		2.2.03.02.0A Rock properties of host rock and other units	Rock properties are defined for each of the stratigraphic units and layers and associated with the model grid for the Site-Scale UZ Flow Model. Heterogeneity is modeled in terms of the sequence of hydrogeologic units and discrete faults. The flow fields generated by the Site-Scale UZ Flow Model are used directly by the TSPA.	10 CFR 63.311 10 CFR 63.331 10 CFR 63.321	MA
		2.2.07.02.0A Unsaturated groundwater flow in the geosphere	The three-dimensional the Site-Scale UZ Flow Model represents flow in a heterogeneous dual-permeability system that includes fractures and discrete fault zones that allow for a realistic description of flow pathways in the UZ. The flow fields generated by the Site-Scale UZ Flow Model are used directly by the TSPA.	10 CFR 63.311 10 CFR 63.331 10 CFR 63.321	GSM

Table I-2. Model Implementation for Included Features, Events, and Processes (Continued)

Submodel implemented in the TSPA-LA Model and Section Number	Path in GoldSim Model File	FEPs Included in the Submodel	TSPA Inclusion Explanation	Performance Assessment Standard[a]	TSPA-LA Model Implementation
UZ Flow Fields Abstraction 6.3.1 (Continued)	Epistemic: \Input_Params_Epistemic\Epistemic_Params_UZ_Flow EBS: \Time_Zero\EBS_PS_Loop\Static_Calcs_PS_Loop\Static_Calcs_UZ_Flow \Global_Inputs_and_Calcs\Global_UZ_Flow	2.2.07.03.0A Capillary rise in the UZ	Capillary forces are included in the Site-Scale UZ Flow Model. These forces affect the distribution of water in the UZ through capillary effects on water flow, also known as capillary wicking. Parameters used for capillarity modeling are incorporated within the matrix properties and fracture properties. These parameters are used as direct input to the Site-Scale UZ Flow Model. The flow fields generated by the Site-Scale UZ Flow Model are used directly by the TSPA.	10 CFR 63.311 10 CFR 63.331 10 CFR 63.321	MA
		2.2.07.04.0A Focusing of unsaturated flow (fingers, weeps)	Large-scale flow focusing caused by flow in faults and fractures are represented in the Site-Scale UZ Flow Model. Faults are included in the Site-Scale UZ Flow Model as discrete features. Fractures are included by using the dual-permeability concept, with fractures represented by a distinct continuum. Flow focused model results indicate that, as flow moves downward through the UZ, the flow tends to focus into fractures and fault zones. Intermediate-scale focusing of flow from the site scale to the drift scale is accounted for in the seepage abstraction (Section 6.3.3 by using appropriate flow-focusing factors). The flow fields generated by the Site-Scale UZ Flow Model are used directly by the TSPA. Large scale focusing is included in human intrusion because percolation flux in the UZ above the repository at the base of the PTn is used to determine the flux downward through the borehole. Intermediate-scale focusing is not included in human intrusion because the seepage model is not implemented for this assessment.	10 CFR 63.311 10 CFR 63.331 10 CFR 63.321	MA

Table I-2. Model Implementation for Included Features, Events, and Processes (Continued)

Submodel implemented in the TSPA-LA Model and Section Number	Path in GoldSim Model File	FEPs Included in the Submodel	TSPA Inclusion Explanation	Performance Assessment Standard[a]	TSPA-LA Model Implementation
UZ Flow Fields Abstraction 6.3.1 (Continued)	Epistemic: \Input_Params_Epistemic\Epistemic_Params_UZ_Flow EBS: \Time_Zero\EBS_PS_Loop\Static_Calcs_PS_Loop\Static_Calcs_UZ_Flow \Global_Inputs_and_Calcs\Global_UZ_Flow	2.2.07.07.0A Perched water develops	Perched water bodies above the repository were not observed and are not included in the flow fields predicted by the Site-Scale UZ Flow Model. The effects of existing perched-water zones below the repository are included, as are potential changes in these perched-water zones caused by climate. Lateral diversion of flow is associated with low permeability zeolites immediately above and within the CHn unit. Because of low permeability, perched water may form at the contacts with CHn zeolitic (CHnz) tuffs, and a large portion of the percolating flux may be diverted laterally to the east. The low permeability zeolitic layers are represented by the Site-Scale UZ Flow Model grid. The flow fields generated by the Site-Scale UZ Flow Model are used directly by the TSPA. The effects of underlying low permeability layers are not included in human intrusion because flow and transport is down the borehole from the repository to the SZ.	10 CFR 63.311 10 CFR 63.331	MA
		2.2.07.08.0A Fracture flow in the UZ	Fracture flow in the UZ is included in the Site-Scale UZ Flow Model by using models based on the dual-permeability concept, with fractures represented by a distinct continuum. The fracture continuum, models spatially averaged flow through discrete fractures. The fracture continuum interacts with the matrix continuum, which represents matrix blocks separated by the network of fractures. Fracture porosity, fracture spacing, and fracture volume fraction measured in the field and within different stratigraphic units determine geometrical parameters of fractures that are incorporated in the model. The flow fields generated by the Site-Scale UZ Flow submodel are used directly by the TSPA-LA Model	10 CFR 63.311 10 CFR 63.331 10 CFR 63.321	GSM

Table I-2. Model Implementation for Included Features, Events, and Processes (Continued)

Submodel implemented in the TSPA-LA Model and Section Number	Path in GoldSim Model File	FEPs Included in the Submodel	TSPA Inclusion Explanation	Performance Assessment Standard[a]	TSPA-LA Model Implementation
UZ Flow Fields Abstraction 6.3.1 (Continued)	Epistemic: \Input_Params_Epistemic\Epistemic_Params_UZ_Flow EBS: \Time_Zero\EBS_PS_Loop\Static_Calcs_PS_Loop\Static_Calcs_UZ_Flow \Global_Inputs_and_Calcs\Global_UZ_Flow	2.2.07.09.0A Matrix imbibition in the UZ	Matrix imbibition is included in the Site-Scale UZ Flow Model. Matrix imbibition refers to the movement of water into the matrix as a result of capillary forces. Capillary forces are represented by characteristic curves for the fracture and matrix continua that are a function of saturation. This process affects the distribution of flow between fractures and matrix in a dual-permeability flow model for fractured rock. The flow fields generated by the Site-Scale UZ Flow Model are used directly by the TSPA.	10 CFR 63.311 10 CFR 63.331 10 CFR 63.321	MA
		2.2.07.19.0A Lateral flow from Solitario Canyon Fault enters drift	The Site-Scale UZ Flow Model contains potential hydrogeologic connections between the Solitario Canyon Fault and the waste emplacement horizon. The potential connection is captured using a property set of the PTn unit with calibrated fracture-matrix properties that favor lateral flow. Therefore, flow from this fault to waste emplacement locations is addressed. This water may seep into waste emplacement drifts if the flux is sufficient to overcome the capillary barrier represented in the drift seepage model. The lateral flow effect is incorporated in the output flow fields generated by the Site-Scale UZ Flow Model and used directly by the TSPA.	10 CFR 63.311 10 CFR 63.331 10 CFR 63.321	MA

Table I-2. Model Implementation for Included Features, Events, and Processes (Continued)

Submodel implemented in the TSPA-LA Model and Section Number	Path in GoldSim Model File	FEPs Included in the Submodel	TSPA Inclusion Explanation	Performance Assessment Standard[a]	TSPA-LA Model Implementation
UZ Flow Fields Abstraction 6.3.1 (Continued)	Epistemic: \Input_Params_Epistemic\Epistemic_Params_UZ_Flow EBS: \Time_Zero\EBS_PS_Loop\Static_Calcs_PS_Loop\Static_Calcs_UZ_Flow \Global_Inputs_and_Calcs\Global_UZ_Flow	2.2.10.03.0B Natural geothermal effects on flow in the UZ	Natural geothermal effects, observed as the natural temperature profile in the UZ, are included in the Site-Scale UZ Model calibration. The temperature profile is primarily determined by the ground surface temperature, the water table temperature, water flux through the UZ, and the thermal conductivity from layer to layer. The influence of water flux on temperature is utilized to calibrate the probabilities for different surface water flux boundary conditions for the UZ Flow Model. The calibration is based on the generalized likelihood uncertainty estimation (GLUE) methodology, utilizing temperature observations and model predictions as well as chloride observations and model predictions. The probabilities for surface water flux are applied as flow weighting factors for UZ flow fields in the TSPA, which are used for present-day, monsoon, and glacial-transition, and post-10,000-year climates.	10 CFR 63.311 10 CFR 63.331 10 CFR 63.321	MA
		2.3.01.00.0A Topography and morphology	Topographical features, precipitation, and surficial permeability distribution are incorporated into the Infiltration Model. Topographical features are captured in the net Infiltration Model using digital elevation data. The impacts of topography and morphology on preferential flow and percolation in the UZ are incorporated into the TSPA through the UZ flow fields that use the net Infiltration Model results as upper boundary conditions.	10 CFR 63.311 10 CFR 63.331 10 CFR 63.321	MA
		2.3.11.01.0A Precipitation	Precipitation affects the net infiltration. Precipitation is captured in the net infiltration map outputs used as boundary condition water-flux inputs for the Site-Scale UZ Flow Model. The flow fields generated by the Site-Scale UZ Flow Model include the affects of precipitation and are used directly by the TSPA.	10 CFR 63.311 10 CFR 63.331 10 CFR 63.321	MA

Table I-2. Model Implementation for Included Features, Events, and Processes (Continued)

Submodel implemented in the TSPA-LA Model and Section Number	Path in GoldSim Model File	FEPs Included in the Submodel	TSPA Inclusion Explanation	Performance Assessment Standard[a]	TSPA-LA Model Implementation
UZ Flow Fields Abstraction 6.3.1 (Continued)	Epistemic: \Input_Params_Epistemic\Epistemic_Params_UZ_Flow EBS: \Time_Zero\EBS_PS_Loop\Static_Calcs_PS_Loop\Static_Calcs_UZ_Flow \Global_Inputs_and_Calcs\Global_UZ_Flow	2.3.11.02.0A Surface runoff and evapotranspiration	Surface runoff and flooding affect the net infiltration. These effects are captured in the net infiltration map outputs used as inputs for the Site-Scale UZ Flow Model. The flow fields generated by the Site-Scale UZ Flow Model are used directly by the TSPA.	10 CFR 63.311 10 CFR 63.331 10 CFR 63.321	MA
		2.3.11.03.0A Infiltration and recharge	The hydrologic effects of infiltration and recharge are included in the Infiltration Model. The Infiltration Model includes the effects of seasonal and climate variations, climate change, surface-water runoff, and site topology, such as hill slopes and washes. The time dependence of infiltration results are linked to the timing of climate change. These effects are captured in the net infiltration map outputs used as upper boundary condition inputs for the Site-Scale UZ Flow Model. The flow fields generated by the Site-Scale UZ Flow Model are used directly by the TSPA.	10 CFR 63.311 10 CFR 63.331 10 CFR 63.321	MA

Table I-2. Model Implementation for Included Features, Events, and Processes (Continued)

Submodel implemented in the TSPA-LA Model and Section Number	Path in GoldSim Model File	FEPs Included in the Submodel	TSPA Inclusion Explanation	Performance Assessment Standard[a]	TSPA-LA Model Implementation
Infiltration Submodel 6.3.1	Epistemic: \Input_Params_Epistemic\Epistemic_Params_UZ_Flow\Uncertain_Params_Infiltration EBS: \Time_Zero\EBS_PS_Loop\Static_Calcs_PS_Loop\Static_Calcs_UZ_Flow\Infiltration \Global_Inputs_and_Calcs\Global_UZ_Flow\Infiltration	1.4.01.01.0A Climate modification increases recharge	The effects of climate changes on UZ flux through the repository are incorporated through the explicit simulations of UZ flow fields corresponding to the 10th, 30th, 50th, and 90th percentile infiltrations of four distinct climates: present-day, monsoon, and glacial-transition, in addition to the post-10,000-year climate. **Note**: Infiltration processes are included in the TSPA-LA Model through the UZ flow fields abstraction and that the Infiltration Submodel in the TSPA-LA Model implements epistemic uncertainty in the net infiltration rates by sampling the different UZ flow fields once per realization based on the probability weighting factors as described in Section 6.3.1.3	10 CFR 63.311 10 CFR 63.331 10 CFR 63.321	GSM
Climate Submodel 6.3.1	EBS: \Global_Inputs_and_Calcs\Global_UZ_Flow\Climate Other: \TSPA_Model\UZ_Flow\Climate	1.3.01.00.0A Climate change	Global climate change is addressed in the TSPA-LA Model using a climate analysis based on the record of climate changes in the past, which is used to forecast the expected changes in climate for the future. The climate analysis is incorporated into the TSPA-LA Model through UZ flow fields having different surface-water infiltration as a result of different climates that correspond to four distinct future climate states: present-day (from 0 to 600 years after present), monsoon (from 600 to 2,000 years after present), and glacial-transition (from 2,000 to 10,000 years after present and the post-10,000-year climate.	10 CFR 63.311 10 CFR 63.331 10 CFR 63.321	GSM

Table I-2. Model Implementation for Included Features, Events, and Processes (Continued)

Submodel implemented in the TSPA-LA Model and Section Number	Path in GoldSim Model File	FEPs Included in the Submodel	TSPA Inclusion Explanation	Performance Assessment Standard[a]	TSPA-LA Model Implementation
Drift Seepage Submodel 6.3.3.1 Note: This model is not implemented for human intrusion	Epistemic: \Input_Params_Epistemic\Epistemic_Params_UZ_Flow\Input_Params_Seepage_Uncert \Input_Params_Epistemic\Epistemic_Params_UZ_Flow\Uncertain_Params_Seepage EBS: \Time_Zero\EBS_PS_Loop\Static_Calcs_PS_Loop\Static_Calcs_UZ_Flow\Drift_Seepage \Global_Inputs_and_Calcs\Global_UZ_Flow\Drift_Seepage	1.1.02.02.0A Preclosure ventilation	Preclosure ventilation in drifts will remove a considerable amount of the heat output from the waste packages (WPs). The ventilation period following emplacement is 50 years, during which a large fraction of the heat energy supplied to the rock by the waste is removed from the drifts by ventilation. This heat removal effect of preclosure ventilation is explicitly simulated with the Thermal Seepage Model. Thus, the thermal seepage modeling results inherently include these effects. The abstraction of thermal seepage utilizes these modeling results to develop a simplified thermal-seepage abstraction for the TSPA. The thermal seepage abstraction is implemented in the TSPA by setting drift seepage to zero when drift-wall temperature is greater than 100°C. Initial rock drying in the drift vicinity as a result of evaporation effects due to ventilation is not explicitly addressed, which conservatively overestimates the quantity of water available for drift seepage early in the postclosure period.	10 CFR 63.311 10 CFR 63.331	MA

Table I-2. Model Implementation for Included Features, Events, and Processes (Continued)

Submodel implemented in the TSPA-LA Model and Section Number	Path in GoldSim Model File	FEPs Included in the Submodel	TSPA Inclusion Explanation	Performance Assessment Standard[a]	TSPA-LA Model Implementation
Drift Seepage Submodel 6.3.3.1 (Continued)	Epistemic: \Input_Params_Epistemic\Epistemic_Params_UZ_Flow\Input_Params_Seepage_Uncert \Input_Params_Epistemic\Epistemic_Params_UZ_Flow\Uncertain_Params_Seepage EBS: \Time_Zero\EBS_PS_Loop\Static_Calcs_PS_Loop\Static_Calcs_UZ_Flow\Drift_Seepage \Global_Inputs_and_Calcs\Global_UZ_Flow\Drift_Seepage	1.2.02.01.0A Fractures	The seepage calibration model and seepage model for performance assessment are stochastic fracture continuum models that include fracture properties. These models provide the basis for the Seepage Abstraction Model. Fracture properties and their effects on drift seepage are included in the Drift Seepage Abstraction Model implemented in the TSPA-LA Model.	10 CFR 63.311 10 CFR 63.331	MA
		1.3.01.00.0A Climate change	The effects of climate change on seepage are included explicitly in the TSPA through the UZ flow fields that are used to evaluate the local percolation fluxes. The local percolation flux is explicitly evaluated for different climate states and different locations within the repository. The local percolation flux is used to evaluate seepage into waste emplacement drifts as provided in lookup tables from the seepage abstraction model for performance assessment.	10 CFR 63.311 10 CFR 63.331 10 CFR 63.321	GSM

Table I-2. Model Implementation for Included Features, Events, and Processes (Continued)

Submodel implemented in the TSPA-LA Model and Section Number	Path in GoldSim Model File	FEPs Included in the Submodel	TSPA Inclusion Explanation	Performance Assessment Standard[a]	TSPA-LA Model Implementation
Drift Seepage Submodel 6.3.3.1 (Continued)	Epistemic: \Input_Params_Epistemic\Epistemic_Params_UZ_Flow\Input_Params_Seepage_Uncert \Input_Params_Epistemic\Epistemic_Params_UZ_Flow\Uncertain_Params_Seepage EBS: \Time_Zero\EBS_PS_Loop\Static_Calcs_PS_Loop\Static_Calcs_UZ_Flow\Drift_Seepage \Global_Inputs_and_Calcs\Global_UZ_Flow\Drift_Seepage	1.4.01.01.0A Climate modification increases recharge	The effects of climate changes on seepage are included explicitly in the TSPA through the UZ flow fields that are used to evaluate the local percolation fluxes. The local percolation flux is explicitly evaluated for different climate states and different locations within the repository. The local percolation flux is used to evaluate seepage into waste emplacement drifts as provided in lookup tables from the seepage abstraction model for performance assessment.	10 CFR 63.311 10 CFR 63.331 10 CFR 63.321	GSM
		2.1.08.01.0A Water influx at the repository	The local percolation flux is one of the key factors affecting drift seepage and a key input to the Drift Seepage Abstraction Model. Spatial and temporal changes in the local percolation flux are thus included in the TSPA-LA Model. The local percolation flux is explicitly evaluated for different climate states and different locations within the repository. Moreover, the local percolation flux is modified to account for random, intermediate-scale flow-focusing effects and the impact of small-scale heterogeneity. The local percolation flux is used to evaluate seepage into waste emplacement drifts as provided in lookup tables from the seepage abstraction model for performance assessment.	10 CFR 63.311 10 CFR 63.331	DLL
		2.1.08.02.0A Enhanced influx at the repository	The impact of an underground opening on the unsaturated flow field (including capillary barrier effect and the related flow diversion around the drifts) and its relevance for seepage is explicitly captured in the seepage calibration model and seepage model for performance assessment, which provide the basis for the drift seepage abstraction implementation in the TSPA-LA Model.	10 CFR 63.311 10 CFR 63.331	DLL

Table I-2. Model Implementation for Included Features, Events, and Processes (Continued)

Submodel implemented in the TSPA-LA Model and Section Number	Path in GoldSim Model File	FEPs Included in the Submodel	TSPA Inclusion Explanation	Performance Assessment Standard[a]	TSPA-LA Model Implementation
Drift Seepage Submodel 6.3.3.1 (Continued)	Epistemic: \Input_Params_Epistemic\Epistemic_Params_UZ_Flow\Input_Params_Seepage_Uncert \Input_Params_Epistemic\Epistemic_Params_UZ_Flow\Uncertain_Params_Seepage EBS: \Time_Zero\EBS_PS_Loop\Static_Calcs_PS_Loop\Static_Calcs_UZ_Flow\Drift_Seepage \Global_Inputs_and_Calcs\Global_UZ_Flow\Drift_Seepage	2.1.08.03.0A Repository dryout due to waste heat	The process of dryout due to waste heat is explicitly simulated with the thermal seepage model. Using this model, the impact of such coupled processes on seepage is assessed for various simulation cases. These simulations provide the basis for the simplified thermal seepage abstraction implemented in the TSPA-LA Model (i.e., no seepage when the drift-wall temperature is greater than 100°C, and ambient seepage when the drift wall temperature is less than 100°C. Thus, the thermal seepage modeling results inherently include these effects.	10 CFR 63.311 10 CFR 63.331	GSM
		2.1.08.11.0A Repository resaturation due to waste cooling	The Thermal Seepage Model includes dryout of the repository followed by resaturation as the WPs cool. The Thermal Seepage Model provides the technical basis for the thermal seepage abstraction implemented in the TSPA-LA Model. The thermal seepage abstraction is implemented by setting drift seepage to zero when drift-wall temperature is greater than 100°C and to ambient seepage when the drift wall temperature is less than 100°C.	10 CFR 63.311 10 CFR 63.331	MA

Table I-2. Model Implementation for Included Features, Events, and Processes (Continued)

Submodel implemented in the TSPA-LA Model and Section Number	Path in GoldSim Model File	FEPs Included in the Submodel	TSPA Inclusion Explanation	Performance Assessment Standard[a]	TSPA-LA Model Implementation
Drift Seepage Submodel 6.3.3.1 (Continued)	Epistemic: \Input_Params_Epistemic\Epistemic_Params_UZ_Flow\Input_Params_Seepage_Uncert \Input_Params_Epistemic\Epistemic_Params_UZ_Flow\Uncertain_Params_Seepage EBS: \Time_Zero\EBS_PS_Loop\Static_Calcs_PS_Loop\Static_Calcs_UZ_Flow\Drift_Seepage \Global_Inputs_and_Calcs\Global_UZ_Flow\Drift_Seepage	2.1.11.01.0A Heat generation in EBS	Heat generation is explicitly simulated in the Thermal Seepage Model that provides the technical basis for the thermal seepage abstraction implemented in the TSPA-LA Model. The thermal seepage abstraction is implemented by setting drift seepage to zero when drift wall temperature is greater than 100°C and to ambient seepage when the drift-wall temperature is less than 100°C.	10 CFR 63.311 10 CFR 63.331 10 CFR 63.321	MA
		2.2.01.01.0A Mechanical effects of excavation and construction in the near field	Excavation effects and their impacts on seepage are included in the thermal and ambient drift seepage process models for through the use of seepage-relevant parameters calibrated for the excavation-disturbed zone around niches and drifts. These models and properties are used to develop the Drift Seepage Abstraction for implementation in the TSPA-LA Model.	10 CFR 63.311 10 CFR 63.331	MA
		2.2.07.02.0A Unsaturated groundwater flow in the geosphere	The impact of unsaturated flow at the repository level on seepage is included in the TSPA-LA Model through the use of local percolation fluxes, which are derived from site-scale unsaturated flow fields, intermediate-scale flow-focusing factors, and small-scale flow simulations with a heterogeneous fracture permeability field.	10 CFR 63.311 10 CFR 63.331	DLL
		2.2.07.03.0A Capillary rise in the UZ	Capillary forces and their impact on seepage are explicitly included in the thermal and ambient Drift Seepage process models. These models are used to generate simulations of capillary- and gravity-driven water flow toward, around, and into waste emplacement drifts. These simulations are used as the basis for the Drift Seepage Abstraction for implementation in the TSPA-LA Model.	10 CFR 63.311 10 CFR 63.331	MA

Table I-2. Model Implementation for Included Features, Events, and Processes (Continued)

Submodel implemented in the TSPA-LA Model and Section Number	Path in GoldSim Model File	FEPs Included in the Submodel	TSPA Inclusion Explanation	Performance Assessment Standard[a]	TSPA-LA Model Implementation
Drift Seepage Submodel 6.3.3.1 (Continued)	Epistemic: \Input_Params_Epistemic\Epistemic_Params_UZ_Flow\Input_Params_Seepage_Uncert \Input_Params_Epistemic\Epistemic_Params_UZ_Flow\Uncertain_Params_Seepage EBS: \Time_Zero\EBS_PS_Loop\Static_Calcs_PS_Loop\Static_Calcs_UZ_Flow\Drift_Seepage \Global_Inputs_and_Calcs\Global_UZ_Flow\Drift_Seepage	2.2.07.04.0A Focusing of unsaturated flow (fingers, weeps)	The site-scale UZ flow fields represent the large-scale redistribution of infiltrating water as it percolates through hydrogeologic layers, with matrix, fractures, and faults explicitly taken into account. Intermediate-scale focusing of flow from the site scale to the drift scale is accounted for in the drift seepage abstraction by using a distribution of flow-focusing factors, which were determined from high-resolution simulations of flow in a heterogeneous fracture continuum. Preferential flow induced by small-scale heterogeneity is explicitly accounted for in the suite of seepage process models that feed the drift seepage abstraction and TSPA by using multiple, stochastic, heterogeneous fracture permeability fields. Thus, preferential flow is addressed in the seepage lookup tables and in the thermal component of the drift seepage abstraction.	10 CFR 63.311 10 CFR 63.331	DLL
		2.2.07.08.0A Fracture flow in the UZ	Fractures as potential conduits for fluid flow are explicitly accounted for in the Site-Scale UZ Flow Model providing the large-scale percolation flux distribution and the drift seepage process models used to evaluate seepage under ambient and thermal conditions. The fact that water may only flow through a portion of the fracture network is accounted for through the use of (1) the active fracture model (on the site-scale), (2) flow-focusing factors (on the intermediate scale), and (3) explicit simulation of preferential flow (on the drift scale). Thus, fracture flow and its spatial distribution are embedded in the lookup tables for seepage and propagated to TSPA.	10 CFR 63.311 10 CFR 63.331 10 CFR 63.321	DLL

Table I-2. Model Implementation for Included Features, Events, and Processes (Continued)

Submodel implemented in the TSPA-LA Model and Section Number	Path in GoldSim Model File	FEPs Included in the Submodel	TSPA Inclusion Explanation	Performance Assessment Standard[a]	TSPA-LA Model Implementation
Drift Seepage Submodel 6.3.3.1 (Continued)	Epistemic: \Input_Params_Epistemic\Epistemic_Params_UZ_Flow\Input_Params_Seepage_Uncert \Input_Params_Epistemic\Epistemic_Params_UZ_Flow\Uncertain_Params_Seepage EBS: \Time_Zero\EBS_PS_Loop\Static_Calcs_PS_Loop\Static_Calcs_UZ_Flow\Drift_Seepage \Global_Inputs_and_Calcs\Global_UZ_Flow\Drift_Seepage	2.2.07.09.0A Matrix imbibition in the UZ	Imbibition of water into the matrix is included in the UZ Flow Model which provides the percolation flux for the drift seepage process models, however, the ambient seepage models are stochastic fracture continuum models. The impact of the matrix on seepage during both the liquid-release tests used for model calibration and the calculation of steady-state ambient seepage into waste emplacement drifts is considered small enough that it can be lumped into seepage-relevant parameters applied to the fracture continuum. The Thermal Seepage Model, on the other hand, includes the rock matrix because the matrix impacts heat transfer and provides a source for water that evaporates during above-boiling temperature conditions. Thus, matrix imbibition is embedded in the lookup tables for the seepage abstraction implemented in the TSPA-LA Model.	10 CFR 63.311 10 CFR 63.331	MA
		2.2.07.10.0A Condensation zone forms around drifts	The coupled thermal-hydrologic processes of vapor condensation during the thermal period, which potentially leads to water accumulation above the drifts and shedding between drifts, is explicitly simulated with the Thermal Seepage Model that provides the basis for a simplified thermal drift seepage abstraction in the TSPA-LA Model. The Thermal seepage abstraction is implemented in the TSPA-LA Model by setting drift seepage to zero when drift wall temperature is greater than 100°C.	10 CFR 63.311 10 CFR 63.331	DLL

Table I-2. Model Implementation for Included Features, Events, and Processes (Continued)

Submodel implemented in the TSPA-LA Model and Section Number	Path in GoldSim Model File	FEPs Included in the Submodel	TSPA Inclusion Explanation	Performance Assessment Standard[a]	TSPA-LA Model Implementation
Drift Seepage Submodel 6.3.3.1 (Continued)	Epistemic: \Input_Params_Epistemic\Epistemic_Params_UZ_Flow\Input_Params_Seepage_Uncert \Input_Params_Epistemic\Epistemic_Params_UZ_Flow\Uncertain_Params_Seepage EBS: \Time_Zero\EBS_PS_Loop\Static_Calcs_PS_Loop\Static_Calcs_UZ_Flow\Drift_Seepage \Global_Inputs_and_Calcs\Global_UZ_Flow\Drift_Seepage	2.2.07.11.0A Resaturation of geosphere dry-out zone	Resaturation of the dryout zone around drifts and the potential of return flow from the condensation zone back to the drifts are explicitly simulated in the Thermal Seepage Model that feeds into the seepage abstraction implemented in the TSPA-LA Model. Thus, the thermal seepage modeling results inherently include these effects. The abstraction of thermal seepage utilizes these modeling results to develop an appropriate thermal seepage abstraction methodology. The thermal seepage abstraction is implemented in the TSPA-LA Model by setting drift seepage to zero when drift-wall temperature is greater than 100°C.	10 CFR 63.311 10 CFR 63.331	DLL
		2.2.07.18.0A Film flow into the repository	The impact of film flow through the fracture network leading to potential drop detachment at the drift wall is implicitly accounted for in the seepage-relevant parameters estimated by the seepage calibration model, which is calibrated against seepage-rate data from liquid-release tests. These seepage-rate data include film flow water appearing at and detaching from the drift wall. The seepage-relevant parameters thus include the effect of film flow; these parameters are propagated to the Drift Seepage Abstraction Model that is implemented in the TSPA-LA Model.	10 CFR 63.311 10 CFR 63.331	MA

Table I-2. Model Implementation for Included Features, Events, and Processes (Continued)

Submodel implemented in the TSPA-LA Model and Section Number	Path in GoldSim Model File	FEPs Included in the Submodel	TSPA Inclusion Explanation	Performance Assessment Standard[a]	TSPA-LA Model Implementation
Drift Seepage Submodel 6.3.3.1 (Continued)	Epistemic: \Input_Params_Epistemic\Epistemic_Params_UZ_Flow\Input_Params_Seepage_Uncert \Input_Params_Epistemic\Epistemic_Params_UZ_Flow\Uncertain_Params_Seepage EBS: \Time_Zero\EBS_PS_Loop\Static_Calcs_PS_Loop\Static_Calcs_UZ_Flow\Drift_Seepage \Global_Inputs_and_Calcs\Global_UZ_Flow\Drift_Seepage	2.2.07.20.0A Flow diversion around repository drifts	The impact of flow diversion around underground openings and its relevance for seepage are explicitly captured by the suite of seepage process models that provide the technical basis for the drift seepage abstraction implemented in the TSPA-LA Model. The seepage calibration model and seepage model for performance assessment simulate water flow driven by capillary forces and gravity, which are the main processes leading to flow diversion around and seepage into waste emplacement drifts. Site-specific, seepage-relevant parameters characterizing the capillary-barrier and flow-diversion effects are estimated from seepage-rate data and are used to develop the Drift Seepage Abstraction Model that is implemented in the TSPA-LA Model.	10 CFR 63.311 10 CFR 63.331	DLL
		2.2.10.03.0B Natural geothermal effects on flow in the UZ	The natural geothermal gradient in the UZ is explicitly included in boundary conditions for the Thermal Seepage Model in Drift-Scale Coupled Processes (DST and TH Seepage) Models (BSC 2005 [DIRS 172232], Section 6.5.2). Using this model, the impact of thermal and coupled processes on seepage is assessed for various simulation cases. These simulations provide the basis for the simplified thermal seepage abstraction implemented in the TSPA-LA Model (i.e., no seepage when the drift wall temperature is greater than 100°C, and ambient seepage when the drift wall temperature is less than 100°C). Thus, the seepage abstraction model implemented in the TSPA-LA Model inherently includes the effects of the natural thermal gradient in the UZ.	10 CFR 63.311 10 CFR 63.331	GSM

Table I-2. Model Implementation for Included Features, Events, and Processes (Continued)

Submodel implemented in the TSPA-LA Model and Section Number	Path in GoldSim Model File	FEPs Included in the Submodel	TSPA Inclusion Explanation	Performance Assessment Standard[a]	TSPA-LA Model Implementation
Drift Seepage Submodel 6.3.3.1 (Continued)	Epistemic: \Input_Params_Epistemic\Epistemic_Params_UZ_Flow\Input_Params_Seepage_Uncert \Input_Params_Epistemic\Epistemic_Params_UZ_Flow\Uncertain_Params_Seepage EBS: \Time_Zero\EBS_PS_Loop\Static_Calcs_PS_Loop\Static_Calcs_UZ_Flow\Drift_Seepage \Global_Inputs_and_Calcs\Global_UZ_Flow\Drift_Seepage	2.2.10.10.0A Two-phase buoyant flow/heat pipes	The coupled processes causing heat-pipe behavior are explicitly simulated with the thermal seepage model that provides the basis for the simplified thermal seepage abstraction implemented in the TSPA-LA Model (i.e., no seepage when the drift wall temperature is greater than 100°C and ambient seepage when the drift-wall temperature is less than 100°C).	10 CFR 63.311 10 CFR 63.331	GSM
		2.2.10.12.0A Geosphere dryout due to waste heat	The coupled processes of vaporization, dryout, and resaturation are explicitly simulated with the Thermal Seepage Model. Using this model, the impact of such coupled processes on seepage is assessed for various simulation cases. These simulations provide the basis for the simplified thermal seepage abstraction implemented in the TSPA-LA Model (i.e., no seepage when the drift-wall temperature is greater than 100°C and ambient seepage when the drift wall temperature is less than 100°C.).	10 CFR 63.311 10 CFR 63.331	GSM

Table I-2. Model Implementation for Included Features, Events, and Processes (Continued)

Submodel implemented in the TSPA-LA Model and Section Number	Path in GoldSim Model File	FEPs Included in the Submodel	TSPA Inclusion Explanation	Performance Assessment Standard[a]	TSPA-LA Model Implementation
Drift Seepage Submodel 6.3.3.1 (Continued)	Epistemic: \Input_Params_Epistemic\Epistemic_Params_UZ_Flow\Input_Params_Seepage_Uncert \Input_Params_Epistemic\Epistemic_Params_UZ_Flow\Uncertain_Params_Seepage EBS: \Time_Zero\EBS_PS_Loop\Static_Calcs_PS_Loop\Static_Calcs_UZ_Flow\Drift_Seepage \Global_Inputs_and_Calcs\Global_UZ_Flow\Drift_Seepage	2.2.03.01.0A Stratigraphy	Stratigraphic information is used in the TSPA-LA Model to evaluate seepage into waste emplacement drifts located in specific hydrogeologic units. Seepage-relevant parameters (permeability and capillary strength) are evaluated separately for lithophysal and nonlithophysal rock units, and the percolation flux used to determine seepage is taken from the UZ flow fields, which incorporate stratigraphic information. Seepage is evaluated for specific repository locations, capturing their respective host rock unit.	10 CFR 63.311 10 CFR 63.331	MA
		2.2.03.02.0A Rock properties of host rock and other units	Properties affecting seepage are defined for each of the repository rock units. The impact of intermediate-scale heterogeneity on flow and seepage is included through the use of flow-focusing factors; the impact of small-scale heterogeneity is explicitly modeled in the seepage calibration model and the seepage abstraction model for performance assessment, which provide the basis for the seepage evaluation in the TSPA-LA Model. The impact of potential changes in the physical properties as a result of coupled thermal, mechanical, and chemical processes has been evaluated and considered insignificant.	10 CFR 63.311 10 CFR 63.331	MA

Table I-2. Model Implementation for Included Features, Events, and Processes (Continued)

Submodel implemented in the TSPA-LA Model and Section Number	Path in GoldSim Model File	FEPs Included in the Submodel	TSPA Inclusion Explanation	Performance Assessment Standard[a]	TSPA-LA Model Implementation
Drift Seepage Submodel 6.3.3.1 (Continued)		2.3.11.03.0A Infiltration and recharge	The infiltration process is simulated by the net infiltration model MASSIF, which includes the effects of climate variations. The infiltration model output is in the form of infiltration maps that are used to provide input to the UZ flow model, which simulates the spatial distribution of percolation fluxes within the unsaturated zone. Percolation fluxes are used to calculate seepage fluxes into the repository by TSPA.	10 CFR 63.311 10 CFR 63.331	MA
Drift Wall Condensation Submodel 6.3.3.2 This model is not implemented in human intrusion	Epistemic: \Input_Params_Epistemic\Epistemic_Params_UZ_Flow\Uncertain_Params_DWC EBS: \Global_Inputs_and_Calcs\Global_UZ_Flow\Drift_Wall_Condensation	1.1.02.02.0A Preclosure ventilation	A 50-year preclosure period with ventilation, as abstracted in the Ventilation Model and Analysis Report is included at the beginning of the MSTHM analyses and is accounted for in the input to the TSPA model. The ventilation model and the MSTHM therefore address the effect of ventilation on the removal of waste package heat during the preclosure period. The TSPA model uses the abstraction results starting at the time of closure (at the end of the ventilation period).	10 CFR 63.311 10 CFR 63.331	GSM
		1.3.01.00.0A Climate Change	The effects of climate change on drift wall condensation are included in the TSPA through the UZ flow fields, which are used to evaluate the local percolation fluxes. The local percolation flux is explicitly evaluated for different climate states and different locations within the repository.	10 CFR 63.311 10 CFR 63.331	GSM
		1.4.01.01.0A Climate modification increases recharge	The effects of climate changes are included explicitly in the TSPA through the UZ flow fields developed by the Site-Scale UZ Flow Model. These flow fields are used to evaluate the t local percolation flux. The local percolation flux is an input to the drift-wall condensation model implemented in the TSPA-LA Model and is evaluated for different climate states and different locations within the repository.	10 CFR 63.311 10 CFR 63.331	GSM

Table I-2. Model Implementation for Included Features, Events, and Processes (Continued)

Submodel implemented in the TSPA-LA Model and Section Number	Path in GoldSim Model File	FEPs Included in the Submodel	TSPA Inclusion Explanation	Performance Assessment Standard[a]	TSPA-LA Model Implementation
Drift Wall Condensation Submodel 6.3.3.2 (Continued)	Epistemic: \Input_Params_Epistemic\Epistemic_Params_UZ_Flow\Uncertain_Params_DWC EBS: \Global_Inputs_and_Calcs\Global_UZ_Flow\Drift_Wall_Condensation	2.1.06.06.0A Effects of drip shield on flow	The role of the drip shield on flow processes in the in-drift environment is implemented in the TSPA-LA Model through the in-drift natural convection and condensation model, which develops a computational fluid dynamics model of natural convection during the postclosure period. The drift wall condensation rate is combined with the drift seepage rate in the EBS flow submodel to yield a total dripping rate onto the drip shield in the TSPA. The fraction of the total dripping rate that is diverted by the drip shield when breaches in the drip shield exist is also calculated in the TSPA using the EBS flow model.	10 CFR 63.311 10 CFR 63.331	MA
		2.1.08.01.0A Water influx at the repository	Water influx at the repository is included explicitly in the TSPA through the UZ flow fields developed by the Site-Scale UZ Flow Model. These flow fields are used to evaluate the local percolation flux. The local percolation flux is an input to the drift-wall condensation model implemented in the TSPA-LA Model and is evaluated for different climate states and different locations within the repository.	10 CFR 63.311 10 CFR 63.331	GSM
		2.1.08.04.0A Condensation forms on roofs of drifts (drift-scale cold traps)	The coupled processes of vapor condensation forming condensation and cold traps on the drift walls are simulated with the in-drift condensation process model. Using this model, the impact of condensation and its contributions to seepage are assessed for various simulation cases. These simulations are used to develop the drift-wall condensation abstraction model implemented in the TSPA-LA Model.	10 CFR 63.311 10 CFR 63.331	GSM

Table I-2. Model Implementation for Included Features, Events, and Processes (Continued)

Submodel implemented in the TSPA-LA Model and Section Number	Path in GoldSim Model File	FEPs Included in the Submodel	TSPA Inclusion Explanation	Performance Assessment Standard[a]	TSPA-LA Model Implementation
Drift Wall Condensation Submodel 6.3.3.2 (Continued)	Epistemic: \Input_Params_Epistemic\Epistemic_Params_UZ_Flow\Uncertain_Params_DWC EBS: \Global_Inputs_and_Calcs\Global_UZ_Flow\Drift_Wall_Condensation	2.1.08.04.0B Condensation forms at repository edges (repository-scale cold traps)	Condensation at the repository edges is included in the TSPA through application of the in-drift condensation model, which provides correlation functions representing the probability of condensation on the drift wall, and the magnitude of condensation where it occurs. This abstraction is used in conjunction with the abstracted output from the MSTHM, which describes the temperature evolution at WP locations. Condensation can occur only where the drift-wall temperature has cooled through the local boiling temperature (96°C), which happens first near the repository edges. The condensation rate is generally greater on cooler WPs, and the effect of repository edge cooling on drift-wall temperature is represented in the in-drift condensation model. The implementation in the TSPA uses repository-wide condensation frequency and magnitude distributions, which are not specific to WP location, applied to representative WPs based on correlation with percolation flux. The effect of repository-scale edge cooling on condensation is thus included in the TSPA-LA Model, in order to represent the potential effects on radionuclide transport in the invert and transport coupling to the UZ.	10 CFR 63.311 10 CFR 63.331	GSM
		2.1.11.01.0A Heat generation in EBS	The in-drift natural convection and condensation model uses an averaged line-load to calculate the wall temperatures through a heated drift and the individual heat generation rates for different packages to calculate the temperatures of the individual packages.	10 CFR 63.311 10 CFR 63.331	GSM

Table I-2. Model Implementation for Included Features, Events, and Processes (Continued)

Submodel implemented in the TSPA-LA Model and Section Number	Path in GoldSim Model File	FEPs Included in the Submodel	TSPA Inclusion Explanation	Performance Assessment Standard[a]	TSPA-LA Model Implementation
Drift Wall Condensation Submodel 6.3.3.2 (Continued)	Epistemic: \Input_Params_Epistemic\Epistemic_Params_UZ_Flow\Uncertain_Params_DWC EBS: \Global_Inputs_and_Calcs\Global_UZ_Flow\Drift_Wall_Condensation	2.1.11.02.0A Non-uniform heat distribution in EBS	Non-uniform heat distribution in EBS is included in the TSPA through application of the in-drift condensation model, which calculates a probability of condensate on the drift walls at any location and, if condensation occurs, the rate of condensation. The probability of occurrence of condensation and the condensation rate are abstracted as functions of the percolation flux.	10 CFR 63.311 10 CFR 63.331	GSM
		2.1.03.11.0A Physical form of waste package and drip shield	The effects of heat dissipation from the waste package and its impact on drift wall condensation are addressed in the in-drift natural convection and condensation process model implemented in the TSPA-LA Model.	10 CFR 63.311 10 CFR 63.331	MA
		2.1.11.09.0A Thermal effects on flow in the EBS	Thermal gradients in the repository could lead to localized accumulation of moisture within the cooler regions of the emplacement drifts. Such effects are represented in the TSPA by the condensation model. The abstraction of the condensation model defines the condensation rate and the likelihood of condensation on the drift wall, under the drip shield (DS), and on the WPs, and the rate of condensation should it occur. The condensation abstraction includes algorithms used in the TSPA for interpolating the condensation rates and probabilities, and specifies how parameters are used and where they are obtained.	10 CFR 63.311 10 CFR 63.331	GSM

Table I-2. Model Implementation for Included Features, Events, and Processes (Continued)

Submodel implemented in the TSPA-LA Model and Section Number	Path in GoldSim Model File	FEPs Included in the Submodel	TSPA Inclusion Explanation	Performance Assessment Standard[a]	TSPA-LA Model Implementation
Drift Wall Condensation Submodel 6.3.3.2 (Continued)	Epistemic: \Input_Params_Epistemic\Epistemic_Params_UZ_Flow\Uncertain_Params_DWC EBS: \Global_Inputs_and_Calcs\Global_UZ_Flow\Drift_Wall_Condensation	2.1.11.09.0C Thermally driven flow (convection) in drifts	The in-drift natural convection and condensation submodel includes explicit representation of two-dimensional and three-dimensional natural convection driven by temperature differences. Results from this model are used to develop an effective thermal conductivity for air that captures the heat transfer effects from natural convection, and is subsequently used in submodels of MSTHM. Temperature and relative humidity conditions derived from the MSTHM are used in the TSPA-LA Model calculations.	10 CFR 63.311 10 CFR 63.331	GSM
		2.3.11.03.0A Infiltration and recharge	Percolation fluxes are used to calculate seepage fluxes into the repository and condensation onto the drift walls. These processes are all affected by changes in infiltration, which are modeled in TSPA in the form of infiltration maps. The infiltration maps provide input to the UZ flow model, which calculates the spatial distribution of percolation fluxes within the unsaturated zone. The probability of occurrence and the rate of condensation on drift walls are abstracted in the TSPA-LA Model as functions of the percolation flux.	10 CFR 63.311 10 CFR 63.331	MA

Table I-2. Model Implementation for Included Features, Events, and Processes (Continued)

Submodel implemented in the TSPA-LA Model and Section Number	Path in GoldSim Model File	FEPs Included in the Submodel	TSPA Inclusion Explanation	Performance Assessment Standard[a]	TSPA-LA Model Implementation
EBS TH Environment Submodel 6.3.2	Epistemic: \Input_Params_Epistemic\Epistemic_Params_EBS_Environ\Uncertain_Params_TH EBS: \Global_Inputs_and_Calcs\Global_EBS_Environ\EBS_Environment\ThermoHydrology	1.1.02.02.0A Preclosure ventilation	Preclosure ventilation in drifts will remove a considerable amount of the heat output from the WPs. The ventilation period following emplacement is 50 years, during which a large fraction of the heat energy supplied to the rock by the waste is removed from the drifts by ventilation. This heat removal effect of preclosure ventilation is explicitly simulated with the MSTHM Process Model. Thus, the thermal-hydrologic modeling results inherently include these effects. The abstraction of thermal-hydrologic processes utilizes these modeling results to develop a simplified thermal-hydrologic abstraction that is implemented in the TSPA-LA Model.	10 CFR 63.311 10 CFR 63.331 10 CFR 63.321	MA
		1.2.02.01.0A Fractures	Fractures are included in MSTHM Process Model for predicting conditions in the EBS. The MSTHM Process Model is based on a dual-permeability concept, with fractures represented by a continuum. The fracture continuum represents the spatially averaged flow and heat transfer through discrete fractures. The fracture continuum interacts with the matrix continuum, which represents matrix blocks separated by fracture. Output results from the Multiscale Thermohydrologic process model are used to develop the TH abstraction implemented in the TSPA-LA Model.	10 CFR 63.311 10 CFR 63.331 10 CFR 63.321	MA
		1.3.01.00.0A Climate change	The effects of climate changes on TH conditions are included in the TSPA through the UZ flow fields, which are used to evaluate the local percolation fluxes. The local percolation flux is explicitly evaluated for different climate states and different locations within the repository. The local percolation flux is used to provide a flux boundary condition for the MSTHM process model. Output results from the MSTHM process model are used to develop the MSTHM abstraction that is implemented in the TSPA-LA Model.	10 CFR 63.311 10 CFR 63.331 10 CFR 63.321	GSM

Table I-2. Model Implementation for Included Features, Events, and Processes (Continued)

Submodel implemented in the TSPA-LA Model and Section Number	Path in GoldSim Model File	FEPs Included in the Submodel	TSPA Inclusion Explanation	Performance Assessment Standard[a]	TSPA-LA Model Implementation
EBS TH Environment Submodel 6.3.2 (Continued)	Epistemic: \Input_Params_Epistemic\Epistemic_Params_EBS_Environ\Uncertain_Params_TH EBS: \Global_Inputs_and_Calcs\Global_EBS_Environ\EBS_Environment\ThermoHydrology	1.4.01.01.0A Climate modification increases recharge	The effects of climate changes on UZ flux through the repository are incorporated through the explicit simulations of UZ flow fields using the Site-Scale UZ Flow Model corresponding to the 10th, 30th, 50th, and 90th percentile infiltration cases of four different climates: present-day, monsoon, and glacial-transition, and the post-10,000 year climate. MSTHM process model simulations are implemented for each of these infiltration cases using the UZ flow fields to prescribe boundary condition water fluxes at the top of the MSTHM process model domain. These simulations are used to develop the TH abstraction implemented in the TSPA-LA Model.	10 CFR 63.311 10 CFR 63.331 10 CFR 63.321	GSM
		2.1.03.11.0A Physical form of waste package and drip shield	Physical form of waste package and drip shield and its relevance for TH conditions in the EBS are explicitly captured in the MSTHM process model simulations. The MSTH process model captures repository thermal conditions during post-closure. These processes are reflected in model output variables of temperature in the near field host rock. Multiscale TH process simulations are used to develop the TH abstraction implemented in the TSPA-LA Model.	10 CFR 63.311 10 CFR 63.331 10 CFR 63.321	MA
		2.1.08.01.0A Water influx at the repository	Water influx at the repository is included explicitly in the TSPA through the UZ flow fields developed by the Site-Scale UZ Flow Model. These flow fields are used to evaluate the t local percolation flux. The local percolation flux is used to provide the upper water flux boundary condition for the MSTHM process model simulations. These simulations are used to develop the TH abstraction model implemented in the TSPA-LA Model.	10 CFR 63.311 10 CFR 63.331 10 CFR 63.321	GSM

Table I-2. Model Implementation for Included Features, Events, and Processes (Continued)

Submodel implemented in the TSPA-LA Model and Section Number	Path in GoldSim Model File	FEPs Included in the Submodel	TSPA Inclusion Explanation	Performance Assessment Standard[a]	TSPA-LA Model Implementation
EBS TH Environment Submodel 6.3.2 (Continued)	Epistemic: \Input_Params_Epistemic\Epistemic_Params_EBS_Environ\Uncertain_Params_TH EBS: \Global_Inputs_and_Calcs\Global_EBS_Environ\EBS_Environment\ThermoHydrology	2.1.08.03.0A Repository dryout due to waste heat	The impact of repository dryout due to waste heat and its relevance for TH conditions in the EBS are explicitly captured in the MSTHM process model simulations. The MSTH process model captures repository dryout during the heating phase and rewetting during the cooling phase. These processes are reflected in model output variables of temperature and liquid-phase flux in the near field host rock. Multiscale TH process simulations are used to develop the TH abstraction implemented in the TSPA-LA Model.	10 CFR 63.311 10 CFR 63.331 10 CFR 63.321	GSM
		2.1.08.05.0A Flow through Invert	Flow through the invert is included in the TSPA through the use of two models: the radionuclide transport abstraction and the MSTHM. The radionuclide transport abstraction is implemented directly within the TSPA to simulate the flow pathways through the EBS. Flow through the invert consists of flux diverted by the DS and by the WP and the flux through the WP, and is reduced by any evaporation from the invert. Water saturation and water flux through the invert, for the case of no drift seepage or condensation, is provided to TSPA by the MSTHM abstraction model, which includes capillary wicking from the host rock. In the human intrusion assessment flow and transport from the WP through the EBS is within the borehole, so the human intrusion assessment does not apply.	10 CFR 63.311 10 CFR 63.331	GSM

Table I-2. Model Implementation for Included Features, Events, and Processes (Continued)

Submodel implemented in the TSPA-LA Model and Section Number	Path in GoldSim Model File	FEPs Included in the Submodel	TSPA Inclusion Explanation	Performance Assessment Standard[a]	TSPA-LA Model Implementation
EBS TH Environment Submodel 6.3.2 (Continued)	Epistemic: \Input_Params_Epistemic\Epistemic_Params_EBS_Environ\Uncertain_Params_TH EBS: \Global_Inputs_and_Calcs\Global_EBS_Environ\EBS_Environment\ThermoHydrology	2.1.08.06.0A Capillary effects (wicking) in EBS	The MSTHM process model includes the processes that cause wicking from the host rock to the invert. The MSTHM process model results provide the basis for the MSTHM abstraction implemented in the TSPA. This abstraction also provides input to the radionuclide transport abstraction, which is implemented directly in the TSPA-LA Model to evaluate the fluxes through the invert. Capillary effects are included in all three assessments. However, capillary effects associated with the invert and water flux through the invert are not included in the human intrusion assessment. In the human intrusion assessment flow and transport from the WP through the EBS is within the borehole.	10 CFR 63.311 10 CFR 63.331	MA
		2.1.08.11.0A Repository resaturation due to waste cooling	The MSTHM process model includes processes controlling dryout of the repository followed by resaturation as the WPs cool. Dryout and resaturation effects are captured by running simulations for all climate states and infiltration cases. Results of these simulations are used to develop the MSTHM abstraction that is implemented in the TSPA-LA Model to predict relative humidity, temperature, and liquid saturations and fluxes, inside the emplacement drift.	10 CFR 63.311 10 CFR 63.331 10 CFR 63.321	GSM
		2.1.11.01.0A Heat generation in EBS	Heat generation and its thermal effects on TH environment in the EBS are calculated by the MSTHM process model. The thermal effects on TH are assessed by multiple MSTHM process model simulations. These simulations are used to develop the TH Abstraction implemented in the TSPA-LA Model.	10 CFR 63.311 10 CFR 63.331 10 CFR 63.321	GSM

Table I-2. Model Implementation for Included Features, Events, and Processes (Continued)

Submodel implemented in the TSPA-LA Model and Section Number	Path in GoldSim Model File	FEPs Included in the Submodel	TSPA Inclusion Explanation	Performance Assessment Standard[a]	TSPA-LA Model Implementation
EBS TH Environment Submodel 6.3.2 (Continued)	Epistemic: \Input_Params_Epistemic\Epistemic_Params_EBS_Environ\Uncertain_Params_TH EBS: \Global_Inputs_and_Calcs\Global_EBS_Environ\EBS_Environment\ThermoHydrology	2.1.11.02.0A Non-uniform heat distribution in EBS	The MSTHM process model predicts the repository thermal-hydrologic environment, including thermal gradients from the repository center to the edges and corners of the repository. Thus, the impact of uneven heating and cooling during both the thermal peak and the cool-down period is captured in the MSTHM process model outputs (e.g., temperature and relative humidity). These outputs are used to develop the MSTHM abstraction used by the TSPA.	10 CFR 63.311 10 CFR 63.331 10 CFR 63.321	GSM
		2.1.11.09.0A Thermal effects on flow in the EBS	Thermal effects on flow in the EBS are calculated by the MSTHM process model. Water flow within the drift is influenced by temperature and evaporation. Water fluxes in the invert are influenced by temperature and capillary pressure (wicking) processes. The thermal effects on flow are assessed by multiple MSTHM process model simulations. These simulations are used to develop the MSTHM Abstraction implemented in the TSPA-LA Model.	10 CFR 63.311 10 CFR 63.331 10 CFR 63.321	GSM
		2.1.11.09.0C Thermally driven flow (convection) in drifts	The MSTHM process model uses an average equivalent thermal conductivity correlation that is based on convection analyses. The effects of convection (in two-dimensional drift cross section) are assessed by multiple MSTHM process model simulations. These simulations are used to develop the MSTHM Abstraction implemented in the TSPA-LA Model.	10 CFR 63.311 10 CFR 63.331 10 CFR 63.321	GSM

Table I-2. Model Implementation for Included Features, Events, and Processes (Continued)

Submodel implemented in the TSPA-LA Model and Section Number	Path in GoldSim Model File	FEPs Included in the Submodel	TSPA Inclusion Explanation	Performance Assessment Standard[a]	TSPA-LA Model Implementation
EBS TH Environment Submodel 6.3.2 (Continued)	Epistemic: \Input_Params_Epistemic\Epistemic_Params_EBS_Environ\Uncertain_Params_TH EBS: \Global_Inputs_and_Calcs\Global_EBS_Environ\EBS_Environment\ThermoHydrology	2.2.03.01.0A Stratigraphy	This FEP is included in the UZ flow model by use of the grids developed with the information contained in the geologic framework model. The stratigraphic unit and layers are developed into the UZ flow model grid. Since the assignment of hydrologic properties is associated with the grid used for the UZ flow model, the stratigraphy information is embedded in the TSPA through the output flow fields. The Multiscale Thermohydrologic models Process Model uses the flow fields to define the upper flux boundary condition, as well as the grid layers from the UZ flow model. Output results from the MSTHM process model are used to develop the MSTHM abstraction that is implemented in the TSPA-LA Model.	10 CFR 63.311 10 CFR 63.331 10 CFR 63.321	MA
		2.2.03.02.0A Rock properties of host rock and other units	Rock properties used are defined for each of the stratigraphic units/layers classified in the geologic framework model, which is further developed into a model grid for the Site-Scale UZ Flow Model and the MSTHM process model. Heterogeneity is modeled in terms of the sequence of hydrogeologic units and discrete faults. Therefore, rock properties are embedded in the TSPA through the output flow fields, which are used to prescribe the upper boundary condition water fluxes for the MSTHM, with site-scale layering and faults explicitly taken into account and through the multiscale TH simulations. MSTHM process model simulations are used to develop the TH abstraction implemented in the TSPA-LA Model.	10 CFR 63.311 10 CFR 63.331 10 CFR 63.321	MA

Table I-2. Model Implementation for Included Features, Events, and Processes (Continued)

Submodel implemented in the TSPA-LA Model and Section Number	Path in GoldSim Model File	FEPs Included in the Submodel	TSPA Inclusion Explanation	Performance Assessment Standard[a]	TSPA-LA Model Implementation
EBS TH Environment Submodel 6.3.2 (Continued)	Epistemic: \Input_Params_Epistemic\Epistemic_Params_EBS_Environ\Uncertain_Params_TH EBS: \Global_Inputs_and_Calcs\Global_EBS_Environ\EBS_Environment\ThermoHydrology	2.2.07.02.0A Unsaturated groundwater flow in the geosphere	The Site-Scale UZ Flow Model uses a three-dimensional, steady flow in a heterogeneous dual-permeability system that includes discrete fault zones and allows for a realistic description of flow pathways in the UZ. The flow fields generated by the Site-Scale UZ Flow Model are used to prescribe the upper boundary condition water fluxes for the MSTHM process model. This process model also calculates processes of UZ flow and their effects on TH conditions in the EBS. MSTHM process model simulations are used to develop the MSTHM abstraction implemented in the TSPA-LA Model.	10 CFR 63.311 10 CFR 63.331 10 CFR 63.321	GSM
		2.2.07.08.0A Fracture flow in the UZ	The MSTHM process model is based on the dual-permeability concept, with the fractures represented by a continuum. The fracture continuum represents the spatially averaged flow through discrete fractures. The fracture continuum interacts with the matrix continuum, which represents matrix blocks separated by fractures. MSTHM process model simulations are used to develop the MSTHM abstraction implemented in the TSPA-LA Model.	10 CFR 63.311 10 CFR 63.331 10 CFR 63.321	GSM
		2.2.07.09.0A Matrix imbibition in the UZ	The impact of matrix imbibition in the UZ and in the invert due to capillary pressure differences and its relevance for thermal hydrologic conditions in the EBS are explicitly captured in the MSTHM process model simulations. These simulations are used to develop the MSTHM abstraction implemented in the TSPA-LA Model. Matrix imbibition is also captured explicitly in the Site-Scale UZ Flow Model and the UZ flow fields that are used to prescribe the upper boundary condition water fluxes to the MSTHM process model simulations.	10 CFR 63.311 10 CFR 63.331 10 CFR 63.321	MA

Table I-2. Model Implementation for Included Features, Events, and Processes (Continued)

Submodel implemented in the TSPA-LA Model and Section Number	Path in GoldSim Model File	FEPs Included in the Submodel	TSPA Inclusion Explanation	Performance Assessment Standard[a]	TSPA-LA Model Implementation
EBS TH Environment Submodel 6.3.2 (Continued)	Epistemic: \Input_Params_Epistemic\Epistemic_Params_EBS_Environ\Uncertain_Params_TH EBS: \Global_Inputs_and_Calcs\Global_EBS_Environ\EBS_Environment\ThermoHydrology	2.2.07.10.0A Condensation zone forms around drifts	The coupled processes of vapor condensation forming a condensation cap in the fractured rock above the drifts are explicitly simulated with the MSTHM process model. Using this model, the impact of condensation and shedding on TH conditions is assessed for various simulation cases. These modeling results are used to develop the MSTHM abstraction implemented in the TSPA-LA Model.	10 CFR 63.311 10 CFR 63.331 10 CFR 63.321	MA
		2.2.07.11.0A Resaturation of geosphere dry-out zone	Resaturation of the dryout zone around drifts and the potential for return flow from the condensation zone back to the drifts are explicitly represented in the MSTHM process model. This model is used to generate simulations of TH processes, including dryout. These simulations are used as the basis for the MSTHM Abstraction implemented in the TSPA-LA Model.	10 CFR 63.311 10 CFR 63.331 10 CFR 63.321	DLL
		2.2.07.20.0A Flow diversion around repository drifts	The impact of flow diversion around the drifts due to capillary pressure differences and its relevance for thermal-hydrologic conditions in the EBS are explicitly captured in the MSTHM process model simulations. These simulations are used to develop the MSTHM abstraction implemented in the TSPA-LA Model.	10 CFR 63.311 10 CFR 63.331 10 CFR 63.321	DLL
		2.2.10.03.0B Natural geothermal effects on flow in the UZ	Natural geothermal effects are included in the MSTHM process model used to describe the effects of waste heat in the repository. The MSTHM contains the natural geothermal gradient in its initialization. This gradient is primarily determined by the ground surface temperature, the water table temperature, water flux through the UZ, and the thermal conductivity from layer to layer. MSTHM process model simulations are used as the basis for the MSTHM abstraction implemented in the TSPA-LA Model.	10 CFR 63.311 10 CFR 63.331 10 CFR 63.321	MA

Table I-2. Model Implementation for Included Features, Events, and Processes (Continued)

Submodel implemented in the TSPA-LA Model and Section Number	Path in GoldSim Model File	FEPs Included in the Submodel	TSPA Inclusion Explanation	Performance Assessment Standard[a]	TSPA-LA Model Implementation
EBS TH Environment Submodel 6.3.2 (Continued)	Epistemic: \Input_Params_Epistemic\Epistemic_Params_EBS_Environ\Uncertain_Params_TH EBS: \Global_Inputs_and_Calcs\Global_EBS_Environ\EBS_Environment\ThermoHydrology	2.2.10.10.0A Two-phase buoyant flow/heat pipes	The coupled processes causing heat-pipe behavior are explicitly simulated with the MSTHM process model. This model is used to assess the impact of heat-pipe behavior on TH conditions in the drift for various simulation cases. These simulations are used to develop the MSTHM abstraction implemented in the TSPA-LA Model.	10 CFR 63.311 10 CFR 63.331 10 CFR 63.321	MA
		2.2.10.12.0A Geosphere dryout due to waste heat	The impact of geosphere dryout due to waste heat and the coupled processes of vaporization, dryout, and resaturation and their relevance for thermal hydrologic conditions in the EBS are explicitly captured in the MSTHM process model simulations. These processes are reflected in output variables of temperature and liquid-phase flux in the near field host rock. MSTHM process simulations are used to develop the MSTHM abstraction implemented in the TSPA-LA Model.	10 CFR 63.311 10 CFR 63.331 10 CFR 63.321	MA

Table I-2. Model Implementation for Included Features, Events, and Processes (Continued)

Submodel implemented in the TSPA-LA Model and Section Number	Path in GoldSim Model File	FEPs Included in the Submodel	TSPA Inclusion Explanation	Performance Assessment Standard[a]	TSPA-LA Model Implementation
EBS Chemical Environment Submodel 6.3.4	Epistemic: \Input_Params_Epistemic\Epistemic_Params_EBS_Environ\Uncertain_Params_EBS_CE Aleatory: \Input_Params_Aleatory\Input_Params_EBS_Environ\Input_Params_EBS_CE EBS: \Global_Inputs_and_Calcs\Global_EBS_Environ\EBS_Environment\EBS_Chemical_Environment	1.1.02.02.0A Preclosure ventilation	Preclosure ventilation in drifts will remove a considerable amount of the heat output from the WPs. Heat removal by ventilation during the ventilation period is modeled in the near field chemistry model by extracting vertical temperature profiles at various timesteps which are implemented directly into TSPA by the Physical and Chemical Environment submodel.	10 CFR 63.311 10 CFR 63.321 10 CFR 63.331	GSM
		1.3.01.00.0A Climate change	The near field chemistry submodel examines the water-rock interactions at 20 different sets of percolation fluxes each representing four climate states. This is computed at many different waste package locations throughout the repository and the abstractions are included in the Physical and Chemical Environment submodel in the TSPA-LA Model.	10 CFR 63.311 10 CFR 63.331 10 CFR 63.321	MA

Table I-2. Model Implementation for Included Features, Events, and Processes (Continued)

Submodel implemented in the TSPA-LA Model and Section Number	Path in GoldSim Model File	FEPs Included in the Submodel	TSPA Inclusion Explanation	Performance Assessment Standard[a]	TSPA-LA Model Implementation
EBS Chemical Environment Submodel 6.3.4	Epistemic: \Input_Params_Epistemic\Epistemic_Params_EBS_Environ\Uncertain_Params_EBS_CE Aleatory: \Input_Params_Aleatory\Input_Params_EBS_Environ\Input_Params_EBS_CE EBS: \Global_Inputs_and_Calcs\Global_EBS_Environ\EBS_Environment\EBS_Chemical_Environment	1.4.01.01.0A Climate modification increases recharge	The near field chemistry submodel examines the water-rock interactions at 20 different sets of percolation fluxes each representing four climate states. This is computed at many different waste package locations throughout the repository and the abstractions are included in the physical and chemical environment submodel in the TSPA-LA Model.	10 CFR 63.311 10 CFR 63.331 10 CFR 63.321	MA
		2.1.03.11.0A Physical form of waste package and drip shield	The physical form of waste packages and drip shields and their relevance to the chemical environment in the EBS are explicitly captured in the EBS Chemical environment model during post-closure. The radionuclide sorption characteristics of the corrosion products of waste package internal components are dependent on the CO_2 partial pressure provided by the EBS chemical environment submodel.	10 CFR 63.311 10 CFR 63.331 10 CFR 63.321	MA
		2.1.08.06.0A Capillary effects (wicking) in EBS	The invert chemistry abstraction includes evaluation of pore-water chemistry in the invert, which is affected by capillary condensation/wicking in the invert. This abstraction has two lookup tables: one for water entering the drift by crown seepage and the other for water entering the invert by capillary condensation and/or wicking. Flow and transport through the invert is not included in the human intrusion assessment.	10 CFR 63.311 10 CFR 63.331	GSM

Table I-2. Model Implementation for Included Features, Events, and Processes (Continued)

Submodel implemented in the TSPA-LA Model and Section Number	Path in GoldSim Model File	FEPs Included in the Submodel	TSPA Inclusion Explanation	Performance Assessment Standard[a]	TSPA-LA Model Implementation
EBS Chemical Environment Submodel 6.3.4 (Continued)	Epistemic: \Input_Params_Epistemic\Epistemic_Params_EBS_Environ\Uncertain_Params_EBS_CE Aleatory: \Input_Params_Aleatory\Input_Params_EBS_Environ\Input_Params_EBS_CE EBS: \Global_Inputs_and_Calcs\Global_EBS_Environ\EBS_Environment\EBS_Chemical_Environment	2.1.08.11.0A Repository resaturation due to waste cooling	The impact of repository resaturation due to waste cooling and the coupled processes of vaporization, dryout, and their relevance for thermal hydrologic conditions in the EBS are explicitly captured in the MSTHM process model simulations. These processes are reflected in output variables of temperature and liquid-phase flux in the near field host rock. MSTHM process simulations are used to develop the MSTHM abstraction implemented in the TSPA-LA Model.	10 CFR 63.311 10 CFR 63.331 10 CFR 63.321	GSM
		2.1.09.01.0A Chemical characteristics of water in drifts	The composition of water entering the drift by crown seepage, and subsequent evaporation, is determined in the TSPA through implementation of the seepage dilution/evaporation abstraction look-up tables provided by the Physical and Chemical Environment submodel. The composition of water entering within the invert is determined in the TSPA-LA Model through implementation of the invert chemistry abstraction look-up tables. Potential carrier plume effects are considered in the evaluation of seepage water interaction with stainless steel and carbon steel structural materials. Cementitious materials are not considered because they are not part of the repository design.	10 CFR 63.311 10 CFR 63.331 10 CFR 63.321	GSM

Table I-2. Model Implementation for Included Features, Events, and Processes (Continued)

Submodel implemented in the TSPA-LA Model and Section Number	Path in GoldSim Model File	FEPs Included in the Submodel	TSPA Inclusion Explanation	Performance Assessment Standard[a]	TSPA-LA Model Implementation
EBS Chemical Environment Submodel 6.3.4 (Continued)	Epistemic: \Input_Params_Epistemic\Epistemic_Params_EBS_Environ\Uncertain_Params_EBS_CE Aleatory: \Input_Params_Aleatory\Input_Params_EBS_Environ\Input_Params_EBS_CE EBS: \Global_Inputs_and_Calcs\Global_EBS_Environ\EBS_Environment\EBS_Chemical_Environment	2.1.09.06.0B Reduction-oxidation potential in drifts	The reduction-oxidation potential in the drifts is included in the Physical and Chemical Environment submodel abstractions, which are implemented directly in the TSPA. In particular, the gas abstraction accounts for redox potential in its oxygen mass balance. Oxidizing conditions are predicted to occur indefinitely in the in-drift environment, based on corrosion of carbon steel (which is rate-limited by oxygen supply) as the principal representative cause of oxygen consumption.	10 CFR 63.311 10 CFR 63.331 10 CFR 63.321	MA
		2.1.09.07.0B Reaction kinetics in drifts	The effects of reaction kinetics are implicitly included in each geochemical submodel developed in Engineered Barrier System: Physical and Chemical Environment submodel. In reaction path geochemical modeling calculations using an EQ3/6 equilibrium model of the water compositions resulting from seepage evaporation, reaction kinetics are implicitly included through suppression of individual mineral phases. Individual mineral phases were suppressed if those phases are kinetically inhibited from forming under repository conditions. The choice of mineral suppressions directly affects the modeled evolution of the in-drift waters, and hence the water compositions that are passed to the TSPA in the form of look-up tables. In addition, the kinetics of corrosion of committed materials was examined with respect to its effect on in-drift water and atmosphere compositions. Seepage water interactions with Stainless Steel Type 316L ground barrier components and low alloy invert steels were found to be of low consequence.	10 CFR 63.311 10 CFR 63.331 10 CFR 63.321	MA
		2.1.11.01.0A Heat generation in EBS	The Physical and Chemical Environment submodel uses vertical thermal profiles generated by the Near Field chemistry submodel. At each waste package location, the thermal profile is evaluated by summing the contribution of the heat generated by each of the 108 drifts within the repository lay-out, using an averaged line load of each drift.	10 CFR 63.311 10 CFR 63.331 10 CFR 63.321	MA

Table I-2. Model Implementation for Included Features, Events, and Processes (Continued)

Submodel implemented in the TSPA-LA Model and Section Number	Path in GoldSim Model File	FEPs Included in the Submodel	TSPA Inclusion Explanation	Performance Assessment Standard[a]	TSPA-LA Model Implementation
EBS Chemical Environment Submodel 6.3.4 (Continued)	Epistemic: \Input_Params_Epistemic\Epistemic_Params_EBS_Environ\Uncertain_Params_EBS_CE Aleatory: \Input_Params_Aleatory\Input_Params_EBS_Environ\Input_Params_EBS_CE EBS: \Global_Inputs_and_Calcs\Global_EBS_Environ\EBS_Environment\EBS_Chemical_Environment	2.1.11.08.0A Thermal effects on chemistry and microbial activity in the EBS	The Physical and Chemical Environment submodel abstractions capture the impact of temperature on the evolution of potential seepage chemistries within the EBS. The effects of temperature on mineral stabilities and chemical reaction rates are also included in the geochemical modeling used to create the seepage dilution/evaporation and invert chemistry abstractions. Temperature is one of the parameters required as input to implement these abstractions in the TSPA-LA Model.	10 CFR 63.311 10 CFR 63.331 10 CFR 63.321	GSM
		2.1.11.09.0C Thermally driven flow (convection) in drifts	Temperature and relative humidity conditions derived from the MSTHM are used to extract parameters of the in-drift chemical environment from the lookup-tables generated by the in-drift seepage dilution/evaporation model, developed in the Physical and Chemical Environment submodel and implemented by TSPA.	10 CFR 63.311 10 CFR 63.331 10 CFR 63.321	GSM

Table I-2. Model Implementation for Included Features, Events, and Processes (Continued)

Submodel implemented in the TSPA-LA Model and Section Number	Path in GoldSim Model File	FEPs Included in the Submodel	TSPA Inclusion Explanation	Performance Assessment Standard[a]	TSPA-LA Model Implementation
EBS Chemical Environment Submodel 6.3.4 (Continued)	Epistemic: \Input_Params_Epistemic\Epistemic_Params_EBS_Environ\Uncertain_Params_EBS_CE Aleatory: \Input_Params_Aleatory\Input_Params_EBS_Environ\Input_Params_EBS_CE EBS: \Global_Inputs_and_Calcs\Global_EBS_Environ\EBS_Environment\EBS_Chemical_Environment	2.2.07.02.0A Unsaturated groundwater flow in the geosphere	The effects of unsaturated groundwater flow are included in the submodel for seepage water chemistry. The approach used is a plug flow model that has a transport velocity equal to the percolation flux divided by the product of the average porosity and the average water saturation. The effects of flow on the water chemistry are evaluated in terms of the amount of feldspar dissolution that occurs during flow through the TSw. The amount of feldspar dissolution is passed to TSPA in a lookup table, as the water-rock interaction parameter, or WRIP.	10 CFR 63.311 10 CFR 63.331 10 CFR 63.321	GSM
		2.2.07.08.0A Fracture flow in the unsaturated zone	Flow processes in fractures or other channels and their effects on the water chemistry are evaluated by the thermal-hydrologic-chemical seepage process model. Thermal-hydrologic-chemical effects on fracture flow processes are evaluated in terms of the amount of feldspar dissolution that occurs during flow through the TSw. The starting point for evaluating potential water compositions in the near field is the composition of ambient pore waters in the TSw. The amount of feldspar dissolution is passed to TSPA in a lookup table, as the water-rock interaction parameter (WRIP).	10 CFR 63.311 10 CFR 63.331 10 CFR 63.321	GSM

Table I-2. Model Implementation for Included Features, Events, and Processes (Continued)

Submodel implemented in the TSPA-LA Model and Section Number	Path in GoldSim Model File	FEPs Included in the Submodel	TSPA Inclusion Explanation	Performance Assessment Standard[a]	TSPA-LA Model Implementation
EBS Chemical Environment Submodel 6.3.4 (Continued)	Epistemic: \Input_Params_Epistemic\Epistemic_Params_EBS_Environ\Uncertain_Params_EBS_CE Aleatory: \Input_Params_Aleatory\Input_Params_EBS_Environ\Input_Params_EBS_CE EBS: \Global_Inputs_and_Calcs\Global_EBS_Environ\EBS_Environment\EBS_Chemical_Environment	2.2.07.11.0A Resaturation of geosphere dry-out zone	The MSTHM model provides in-drift temperature and relative humidity inputs used by TSPA to extract water composition data from lookup tables generated by the seepage dilution/evaporation model. This submodel, in turn, evaluates in-drift processes and provides lookup tables for in-drift aqueous chemistry to TSPA.	10 CFR 63.311 10 CFR 63.331 10 CFR 63.321	GSM
		2.2.08.01.0B Chemical characteristics of groundwater in the UZ	The seepage dilution/evaporation abstraction model provided by the Physical and Chemical Environment submodel was developed using four different input water compositions spanning the range of compositions in the repository units. The variability of pore-water compositions reflects the spatial variations in rock mineralogy, temperature, and infiltration rates. The four input water compositions capture that variability as well as uncertainty, which are propagated to the TSPA through the seepage dilution/evaporation abstraction look-up tables created using results from the Physical and Chemical Environment submodel.	10 CFR 63.311 10 CFR 63.331 10 CFR 63.321	GSM

Table I-2. Model Implementation for Included Features, Events, and Processes (Continued)

Submodel implemented in the TSPA-LA Model and Section Number	Path in GoldSim Model File	FEPs Included in the Submodel	TSPA Inclusion Explanation	Performance Assessment Standard[a]	TSPA-LA Model Implementation
EBS Chemical Environment Submodel 6.3.4 (Continued)	Epistemic: \Input_Params_Epistemic\Epistemic_Params_EBS_Environ\Uncertain_Params_EBS_CE Aleatory: \Input_Params_Aleatory\Input_Params_EBS_Environ\Input_Params_EBS_CE EBS: \Global_Inputs_and_Calcs\Global_EBS_Environ\EBS_Environment\EBS_Chemical_Environment	2.2.08.12.0A Chemistry of water flowing into the drift	The near field chemistry submodel in the Physical and Chemical Environment model component evaluates the effects of the thermal-hydrologic-chemical processes in the rock on the chemistry of potential seepage water entering the drift. The seepage dilution/evaporation abstraction uses these waters to generate lookup tables of in-drift water chemistry couple TH processes and chemical processes for the TSPA-LA Model.	10 CFR 63.311 10 CFR 63.331 10 CFR 63.321	DLL
		2.2.10.12.0A Geosphere dryout due to waste heat	In the near-field chemistry submodel, the effect of dryout is implemented by adjusting the length of the flow pathway considered for water-rock interactions; however, the seepage compositions that are predicted during the boiling period are not used, because the abstraction of drift seepage does not predict seepage when the drift-wall temperature exceeds the boiling point.	10 CFR 63.311 10 CFR 63.331 10 CFR 63.321	DLL

Table I-2. Model Implementation for Included Features, Events, and Processes (Continued)

Submodel implemented in the TSPA-LA Model and Section Number	Path in GoldSim Model File	FEPs Included in the Submodel	TSPA Inclusion Explanation	Performance Assessment Standard[a]	TSPA-LA Model Implementation
EBS Chemical Environment Submodel 6.3.4 (Continued)	Epistemic: \Input_Params_Epistemic\Epistemic_Params_EBS_Environ\Uncertain_Params_EBS_CE Aleatory: \Input_Params_Aleatory\Input_Params_EBS_Environ\Input_Params_EBS_CE EBS: \Global_Inputs_and_Calcs\Global_EBS_Environ\EBS_Environment\EBS_Chemical_Environment	2.3.11.03.0A Infiltration and recharge	Changes in infiltration rate in the UZ could affect the composition of groundwater passing through the repository. The seepage dilution/evaporation abstraction model provided by the Physical and Chemical Environment submodel was developed using four different input water compositions spanning the range of compositions in the repository units. The variability of pore-water compositions reflects the spatial variations in rock mineralogy, temperature, and infiltration rates. The four input water compositions capture that variability as well as uncertainty, which are propagated to the TSPA through the seepage dilution/evaporation abstraction look-up tables created using results from the Physical and Chemical Environment submodel.	10 CFR 63.311 10 CFR 63.331 10 CFR 63.321	DLL

Table I-2. Model Implementation for Included Features, Events, and Processes (Continued)

Submodel implemented in the TSPA-LA Model and Section Number	Path in GoldSim Model File	FEPs Included in the Submodel	TSPA Inclusion Explanation	Performance Assessment Standard[a]	TSPA-LA Model Implementation
WP and DS Degradation Submodel 6.3.5	Epistemic: \Input_Params_Epistemic\Epistemic_Params_WP_DS_Deg\ Aleatory: \Model_Calcs_Aleatory\Aleatory_Calcs_WP_DS_Deg EBS: \Time_Zero\EBS_PS_Loop\Static_Calcs_PS_Loop\Static_Calcs_WP_DS_Deg \Global_Inputs_and_Calcs\Global_WP_DS_Deg\Global_IWPD	2.1.03.01.0A General corrosion of waste packages	General corrosion of WPs is modeled as uniform thinning of the WP outer barrier. The general corrosion model is constructed around crevice-corrosion geometry weight-loss corrosion data with a temperature-dependent term. The general corrosion rate is represented as constant versus time under a given temperature. General corrosion is modeled by dividing the WP surface into subareas (patches) that are used to simulate variability across the barrier surfaces.	10 CFR 63.311 10 CFR 63.331	DLL
		2.1.03.01.0B General corrosion of drip shields	General corrosion of the DS is modeled as uniform thinning of the DS. The general corrosion rate is modeled as constant with time and temperature and constructed around weight-loss data determined from long term corrosion tests. The general corrosion of the DS is modeled separately for the inner surface and the outer surfaces to reflect the less corrosive environment that will be present on the underside of the DS. Each DS is modeled as a single entity with no spatial variability. General corrosion of the DS is included implicitly in the assessment of the earliest time at which a WP could be penetrated without being detected by the driller.	10 CFR 63.311 10 CFR 63.331 10 CFR 63.321	DLL

Table I-2. Model Implementation for Included Features, Events, and Processes (Continued)

Submodel implemented in the TSPA-LA Model and Section Number	Path in GoldSim Model File	FEPs Included in the Submodel	TSPA Inclusion Explanation	Performance Assessment Standard[a]	TSPA-LA Model Implementation
WP and DS Degradation Submodel 6.3.5 (Continued)	Epistemic: \Input_Params_Epistemic\Epistemic_Params_WP_DS_Deg\ Aleatory: \Model_Calcs_Aleatory\Aleatory_Calcs_WP_DS_Deg EBS: \Time_Zero\EBS_PS_Loop\Static_Calcs_PS_Loop\Static_Calcs_WP_DS_Deg \Global_Inputs_and_Calcs\Global_WP_DS_Deg\Global_IWPD	2.1.03.02.0A Stress corrosion cracking of the waste packages	Stress corrosion cracking (SCC) of WPs is modeled as the initiation and propagation of cracks due to a sustainable tensile stress. The threshold stress, threshold stress intensity factor, and parameters associated with the slip dissolution/film rupture crack growth model are inputs to the TSPA SCC abstraction in WAPDEG, which is implemented by TSPA. SCC of the WP outer barrier closure weld region is modeled to initiate at incipient flaws or weld flaws in the closure weld region. Each WP closure lid is represented as a collection of approximately 40 patches. It is conservatively modeled that, when the first crack on a given patch penetrates through-wall, all possible through-wall cracks on that patch are considered to penetrate through-wall. SCC is excluded from the human intrusion assessment because SCC does not significantly alter the yield strength of the WP, and therefore, a driller would recognize penetration by the drill bit.	10 CFR 63.311 10 CFR 63.331	DLL
		2.1.03.05.0A Microbially induced corrosion of waste packages	Microbially influenced corrosion is modeled in the TSPA-LA Model as an enhancement factor uniformly distributed between 1 and 2 due to uncertainty. The factor is applied to the entire WP outer barrier general corrosion rate when the relative humidity at the WP outer corrosion barrier surface is equal to a threshold value represented by, and sampled from, a uniform distribution ranging from 75 percent to 90 percent. Microbially induced corrosion of the WP is not implemented directly in the assessment of human intrusion, however, it is included implicitly as part of general corrosion in the assessment of the earliest time at which a WP could be penetrated.	10 CFR 63.311 10 CFR 63.331	DLL

Table I-2. Model Implementation for Included Features, Events, and Processes (Continued)

Submodel implemented in the TSPA-LA Model and Section Number	Path in GoldSim Model File	FEPs Included in the Submodel	TSPA Inclusion Explanation	Performance Assessment Standard[a]	TSPA-LA Model Implementation
WP and DS Degradation Submodel 6.3.5(Continued)	Epistemic: \Input_Params_Epistemic\Epistemic_Params_WP_DS_Deg\ Aleatory: \Model_Calcs_Aleatory\Aleatory_Calcs_WP_DS_Deg EBS: \Time_Zero\EBS_PS_Loop\Static_Calcs_PS_Loop\Static_Calcs_WP_DS_Deg \Global_Inputs_and_Calcs\Global_WP_DS_Deg\Global_IWPD	2.1.03.11.0A Physical form of waste package and drip shield	General corrosion of WPs and DS are modeled as uniform thinning of the WP outer barrier, and uniform thinning of the DS. The WP general corrosion model is constructed around crevice-corrosion geometry weight-loss corrosion data with a temperature-dependent term. The general corrosion rate is represented as constant versus time under a given temperature. General corrosion of the WP is modeled by dividing the WP surface into subareas (patches) that are used to simulate variability across the barrier surfaces. The general corrosion rate of the DS is modeled as constant with time and temperature and constructed around weight-loss data determined from long term corrosion tests. The general corrosion of the DS is modeled separately for the inner surface and the outer surfaces to reflect the less corrosive environment that will be present on the underside of the DS. Each DS is modeled as a single entity with no spatial variability.	10 CFR 63.311 10 CFR 63.331 10 CFR 63.321	GSM

Table I-2. Model Implementation for Included Features, Events, and Processes (Continued)

Submodel implemented in the TSPA-LA Model and Section Number	Path in GoldSim Model File	FEPs Included in the Submodel	TSPA Inclusion Explanation	Performance Assessment Standard[a]	TSPA-LA Model Implementation
LC Initiation Submodel 6.3.5.2	Epistemic: \Input_Params_Epistemic\Epistemic_Params_WP_DS_Deg\ EBS: \Time_Zero\EBS_PS_Loop\Static_Calcs_PS_Loop\Static_Calcs_WP_DS_Deg \Global_Inputs_and_Calcs\Global_WP_DS_Deg\Global_LC	2.1.03.03.0A Localized corrosion of waste packages	Localized corrosion of WPs is implemented in the TSPA-LA Model using an initiation model and a propagation model. Localized corrosion can only be initiated when seepage contacts a WP during the thermal period, thus requiring a failed DS prior to 10,000 years. DSs potentially fail within 10,000 years in the Seismic Scenario Class and Early Failure Scenario Class only. The initiation model is a regression model that involves the following dependent variables: nitrate concentration, chloride concentration, temperature, pH, and nitrate to chloride ratio. Values for these time-dependent quantities are provided by the seepage dilution/evaporation abstraction model. Upon initiation of localized corrosion, the propagation depth is modeled using a constant rate and a distribution function to address uncertainty ranges found in the literature. The area affected by localized corrosion resulting from seepage brines is modeled as the entire WP surface area. In the case of an early-failed DS it is assumed that the underlying WP fails immediately due to localized corrosion.	10 CFR 63.311 10 CFR 63.331	GSM
Radionuclide Inventory Submodel 6.3.7.1	Epistemic: \Input_Params_Epistemic\Epistemic_Params_WF_Deg_Mob\Uncertain_Params_RN_Inventory EBS: \Global_Inputs_and_Calcs\Global_WF_Deg_Mob\RN_Inventory	2.1.01.01.0A Waste inventory	The TSPA models three representative waste form inventories: CSNF, DSNF, and HLW. Naval SNF is conservatively treated as CSNF. More than 100 radionuclides (e.g., fission products, actinides, and activation products) are screened for importance to expected dose. The abstraction is treated with uncertainty ranges for each waste form.	10 CFR 63.311 10 CFR 63.331 10 CFR 63.321	GSM

Table I-2. Model Implementation for Included Features, Events, and Processes (Continued)

Submodel implemented in the TSPA-LA Model and Section Number	Path in GoldSim Model File	FEPs Included in the Submodel	TSPA Inclusion Explanation	Performance Assessment Standard[a]	TSPA-LA Model Implementation
Radionuclide Inventory Submodel 6.3.7.1 (Continued)	Epistemic: \Input_Params_Epistemic\Epistemic_Params_WF_Deg_Mob\Uncertain_Params_RN_Inventory	2.1.01.03.0A Heterogeneity of waste inventory	TSPA considers the gross heterogeneity between the waste form types: CSNF, DSNF, and HLW. Radionuclide inventory and degradation rates are provided for each waste form type. Heterogeneity is acknowledged in uncertainty parameters in each of these models.	10 CFR 63.311 10 CFR 63.331 10 CFR 63.321	GSM
	EBS: \Global_Inputs_and_Calcs\Global_WF_Deg_Mob\RN_Inventory	2.1.03.11.0A Physical form of waste package and drip shield	The effect of the physical form of the waste package is considered in the TSPA in representing all waste packages by two types—TADs for CSNF and 5-DHLW/DOE SNF – Long for codisposal. By using the most common CSNF waste package and the largest (as well as most common) codisposal waste package, the full radionuclide inventory is reasonably represented in the TSPA.	10 CFR 63.311 10 CFR 63.331 10 CFR 63.321	GSM
		3.1.01.01.0A Radioactive decay and ingrowth	Radioactive decay and ingrowth were considered in screening which radionuclides to include in the TSPA. The TSPA accounts for decay and ingrowth in the EBS using built-in functions of GoldSim. During execution, the GoldSim model automatically calculates decay and ingrowth of the included isotopes.	10 CFR 63.311 10 CFR 63.331 10 CFR 63.321	GSM

Table I-2. Model Implementation for Included Features, Events, and Processes (Continued)

Submodel implemented in the TSPA-LA Model and Section Number	Path in GoldSim Model File	FEPs Included in the Submodel	TSPA Inclusion Explanation	Performance Assessment Standard[a]	TSPA-LA Model Implementation
In Package Chemistry Submodel 6.3.7.2	Epistemic: \Input_Params_Epistemic\Epistemic_Params_WF_Deg_Mob\Uncertain_Params_InPkg_Chem Aleatory: NA EBS: \Global_Inputs_and_Calcs\Global_WF_Deg_Mob\In_Package_Chemistry	2.1.01.02.0B Interactions between co-disposed waste	The In-Package Chemistry Process Model provides the interactions between co-disposed wastes. These interactions and their relevance to in-package chemistry are assessed in multiple simulations. These simulations are used to develop the in-package chemistry abstraction implemented in the TSPA-LA Model. The DSNF degradation is modeled as insensitive to in-package chemistry and is modeled as instantaneous. The degradation rate of HLW depends on pH, which in turn is dependent on all materials within the package. Degradation of HLW tends to raise the in-package pH while degradation of disposal canisters and other in-package metals tends to lower the pH. Degradation of DSNF and surface complexation on corrosion products tends to bring the pH back toward neutral.	10 CFR 63.311 10 CFR 63.331 10 CFR 63.321	GSM
		2.1.03.11.0A Physical form of waste	The effect of waste package and drip shield materials on the chemical behavior of the disposal area is included in the in-package chemistry abstraction implemented in the TSPA-LA Model.	10 CFR 63.311 10 CFR 63.331 10 CFR 63.321	MA
		2.1.09.06.0A Reduction-oxidation potential in waste package	As long as there are reduced fuels and metals within the breached WP, there will be strong redox gradients between them and the atmosphere, providing the driving force for the reactions calculated in the In-Package Chemistry Process Model simulations. The In-Package Chemistry Process Model uses the bounding approximation that the bulk water within the package is in equilibrium with the atmosphere. In-Package Chemistry Process Model simulations are used to develop the In-Package Chemistry Abstraction implemented in TSPA.	10 CFR 63.311 10 CFR 63.331 10 CFR 63.321	MA

Table I-2. Model Implementation for Included Features, Events, and Processes (Continued)

Submodel implemented in the TSPA-LA Model and Section Number	Path in GoldSim Model File	FEPs Included in the Submodel	TSPA Inclusion Explanation	Performance Assessment Standard[a]	TSPA-LA Model Implementation
In Package Chemistry Submodel 6.3.7.2 (Continued)	Epistemic: \Input_Params_Epistemic\Epistemic_Params_WF_Deg_Mob\Uncertain_Params_InPkg_Chem Aleatory: NA EBS: \Global_Inputs_and_Calcs\Global_WF_Deg_Mob\In_Package_Chemistry	2.1.02.09.0A Chemical effects of void space in waste packages	Upon WP breach, the inert gas escapes and is replaced with humid air. The reaction of this air with WP internals and the resulting changes in water chemistry are modeled with the In-Package Chemistry Process Model. In-Package Chemistry Process Model simulations are used to develop the In-Package Chemistry Abstraction implemented in the TSPA-LA Model.	10 CFR 63.311 10 CFR 63.331 10 CFR 63.321	MA
		2.1.09.01.0B Chemical characteristics of water in waste package	The In-Package Chemistry Process Model accounts for the reaction of incoming water and air with the waste forms and metals within the WP. In-Package Chemistry Process Model simulations are used to develop the In-Package Chemistry Abstraction implemented in the TSPA-LA Model.	10 CFR 63.311 10 CFR 63.331 10 CFR 63.321	GSM
		2.1.09.07.0A Reaction kinetics in waste package	The In-Package Chemistry Process Model accounts for the impact of reaction kinetics on the resulting pH and ionic strength from the reaction of metals and waste forms with air and water within the package. . In-Package Chemistry Process Model simulations are used to develop the In-Package Chemistry Abstraction implemented in the TSPA-LA Model.	10 CFR 63.311 10 CFR 63.331 10 CFR 63.321	MA
		2.1.09.02.0A Chemical interaction with corrosion products	The chemical influence of corrosion products inside the package is modeled in the In-Package Chemistry Process Model. . In-Package Chemistry Process Model simulations are used to develop the In-Package Chemistry Abstraction implemented in the TSPA-LA Model.	10 CFR 63.311 10 CFR 63.331 10 CFR 63.321	GSM

Table I-2. Model Implementation for Included Features, Events, and Processes (Continued)

Submodel implemented in the TSPA-LA Model and Section Number	Path in GoldSim Model File	FEPs Included in the Submodel	TSPA Inclusion Explanation	Performance Assessment Standard[a]	TSPA-LA Model Implementation
In Package Chemistry Submodel 6.3.7.2 (Continued)	Epistemic: \Input_Params_Epistemic\Epistemic_Params_WF_Deg_Mob\Uncertain_Params_InPkg_Chem Aleatory: NA EBS: \Global_Inputs_and_Calcs\Global_WF_Deg_Mob\In_Package_Chemistry	2.2.08.12.0B Chemistry of water flowing into the waste package	Different representative initial water compositions were used to represent the chemistry of the water flowing into the WP. In-package chemistry simulations were used to asses the impact of these water compositions on chemistry of the evolving water in the WP. Results of these simulations verified that in-package chemistry was not significantly affected by starting water composition. Thus the In-Package Chemistry Abstraction implemented in the TSPA-LA Model does not require initial water composition as an input.	10 CFR 63.311 10 CFR 63.331 10 CFR 63.321	GSM
Waste Form Degradation Submodel 6.3.7.4	Epistemic: \Input_Params_Epistemic\Epistemic_Params_WF_Deg_Mob\Uncertain_Params_HLW_WF EBS: \Global_Inputs_and_Calcs\Global_WF_Deg_Mob\WF_Degradation\Input_Params_HLW_WF	2.1.01.02.0B Interactions between co-disposed waste	The In-Package Chemistry Process Model assesses the interaction between co-disposed wastes and its impact on in-package chemistry. The In-Package Chemistry Abstraction is used to represent these interactions in the TSPA-LA Model and provide inputs to the waste form degradation models. The DSNF degradation is modeled as insensitive to in-package chemistry and is modeled as instantaneous. The degradation rate of HLW depends on pH, which in turn is dependent on all materials within the package. Degradation of HLW tends to raise the in-package pH while degradation of disposal canisters and other in-package metals tends to lower the pH. Degradation of DSNF and surface complexation on corrosion products tends to bring the pH back toward neutral.	10 CFR 63.311 10 CFR 63.331 10 CFR 63.321	GSM

Table I-2. Model Implementation for Included Features, Events, and Processes (Continued)

Submodel implemented in the TSPA-LA Model and Section Number	Path in GoldSim Model File	FEPs Included in the Submodel	TSPA Inclusion Explanation	Performance Assessment Standard[a]	TSPA-LA Model Implementation
Waste Form Degradation Submodel 6.3.7.4 (Continued)	Epistemic: \Input_Params_Epistemic\Epistemic_Params_WF_Deg_Mob\Uncertain_Params_CSNF_WF	2.1.01.03.0A Heterogeneity of waste inventory	TSPA considers the gross heterogeneity between the waste form types: CSNF, DSNF, and HLW. Radionuclide inventory and degradation rates are provided for each waste form type. In-package chemistries and radionuclide solubilities are defined for each WP type: CSNF and CDSP.	10 CFR 63.311 10 CFR 63.331 10 CFR 63.321	GSM
	EBS: \Global_Inputs_and_Calcs\Global_WF_Deg_Mob\WF_Degradation\CSNF_WF_Dissolution	2.1.02.01.0A DSNF degradation (alteration, dissolution, and radionuclide release)	Naval SNF is conservatively treated as CSNF in the TSPA-LA Model calculations. The degradation rate of all DSNF except naval is bounded in the TSPA-LA Model as instantaneous. With the exception of naval SNF, no credit is given for DSNF cladding in the TSPA-LA Model. In addition, no credit is taken for any disposal canisters, including high-integrity canisters.	10 CFR 63.311 10 CFR 63.331 10 CFR 63.321	GSM
	EBS: \Global_Inputs_and_Calcs\Global_WF_Deg_Mob\WF_Degradation\Input_Params_DSNF_WF	2.1.02.02.0A CSNF degradation (alteration, dissolution, and radionuclide release)	TSPA uses an empirical CSNF degradation rate model that is a function of surface area, temperature, oxygen, carbonate concentration, and pH. Data for the empirical model are taken from several test programs.	10 CFR 63.311 10 CFR 63.331 10 CFR 63.321	GSM
	Epistemic: \Input_Params_Epistemic\Epistemic_Params_WF_Deg_Mob\Uncertain_Params_HLW_WF	2.1.02.03.0A HLW glass degradation (alteration, dissolution, and radionuclide release)	TSPA uses an empirical glass degradation rate model that is a function of surface area, temperature, and pH. Data used to develop the degradation model was collected under conditions similar to those expected for the repository.	10 CFR 63.311 10 CFR 63.331 10 CFR 63.321	GSM
	EBS: \Global_Inputs_and_Calcs\Global_WF_Deg_Mob\WF_Degradation\Input_Params_HLW_WF	2.1.02.05.0A HLW glass cracking	The increase in surface area due to cracking is included in the exposure factor, fexposure. A range of values is applied to account for experimental evidence.	10 CFR 63.311 10 CFR 63.331 10 CFR 63.321	GSM

Table I-2. Model Implementation for Included Features, Events, and Processes (Continued)

Submodel implemented in the TSPA-LA Model and Section Number	Path in GoldSim Model File	FEPs Included in the Submodel	TSPA Inclusion Explanation	Performance Assessment Standard[a]	TSPA-LA Model Implementation
Waste Form Degradation Submodel 6.3.7.4 (Continued)	Epistemic: \Input_Params_Epistemic\Epistemic_Params_WF_Deg_Mob\Uncertain_Params_CSNF_WF	2.1.02.07.0A Radionuclide release from gap and grain boundaries	The fraction of cesium, iodine, technetium, and strontium that resides in the gap and grain boundaries is represented in the TSPA-LA Model by the instantaneous release fractions. The fraction of CSNF that comprises this instantaneous release inventory is specified by four triangular distributions. The computed uncertain fraction is released instantly upon breach of the WP.	10 CFR 63.311 10 CFR 63.331 10 CFR 63.321	GSM
	EBS: \Global_Inputs_and_Calcs\Global_WF_Deg_Mob\WF_Degradation\CSNF_WF_Dissolution	2.1.02.12.0A Degradation of cladding prior to disposal	These cladding FEPs are included in the TSPA in a bounding way by assuming they provide no capability to prevent of reduce the flow of water or release of radionuclides. The cladding of all CSNF and DSNF is assumed to be failed upon arrival at the repository.	10 CFR 63.311 10 CFR 63.331 10 CFR 63.321	No barrier capability credit taken for cladding
	EBS: \Global_Inputs_and_Calcs\Global_WF_Deg_Mob\WF_Degradation\Input_Params_DSNF_WF	2.1.02.23.0A Cladding unzipping	These cladding FEPs are included in the TSPA in a bounding way by assuming they provide no capability to prevent of reduce the flow of water or release of radionuclides. The cladding of all CSNF and DSNF is assumed to be failed upon arrival at the repository.	10 CFR 63.311 10 CFR 63.331 10 CFR 63.321	No barrier capability credit taken for cladding

Table I-2. Model Implementation for Included Features, Events, and Processes (Continued)

Submodel implemented in the TSPA-LA Model and Section Number	Path in GoldSim Model File	FEPs Included in the Submodel	TSPA Inclusion Explanation	Performance Assessment Standard[a]	TSPA-LA Model Implementation
Waste Form Degradation Submodel 6.3.7.4 (Continued)	Epistemic: \Input_Params_Epistemic\Epistemic_Params_WF_Deg_Mob\Uncertain_Params_HLW_WF EBS: \Global_Inputs_and_Calcs\Global_WF_Deg_Mob\WF_Degradation\Input_Params_HLW_WF	2.1.02.25.0B Naval cladding	This FEP is included in the TSPA in a bounding way by assuming cladding provides no capability to prevent of reduce the flow of water or release of radionuclides. The cladding of all CSNF and DSNF is assumed to be failed upon arrival at the repository.	10 CFR 63.311 10 CFR 63.331 10 CFR 63.321	No barrier capability credit taken for cladding
	Epistemic: \Input_Params_Epistemic\Epistemic_Params_WF_Deg_Mob\Uncertain_Params_CSNF_WF	2.1.02.28.0A Grouping of DSNF waste types into categories	DSNF is composed of a variety of fuel types and the quantities of each fuel type are considered when compiling the nominal radionuclide inventory in grams per package and uncertainty distributions for radionuclides important to dose calculations for the TSPA. For degradation rate determination, the various DSNF types have been classified into eleven groups for TSPA analyses	10 CFR 63.311 10 CFR 63.331 10 CFR 63.321	MA
		2.1.03.11.0A Physical form of waste package and drip shield	The physical form of waste package internal waste containers and their degradation is modeled in the TSPA by two representative waste package types (TADs and the 5-DHLW/DOE SNF – Long), which are the most common waste packages. The two types of waste packages also account for the predominant waste forms (CSNF, DSNF, and DHLW).	10 CFR 63.311 10 CFR 63.331 10 CFR 63.321	MA
		2.1.09.02.0A Chemical interaction with corrosion products	Chemical interaction with corrosion products is implemented in the waste form degradation submodel by using the results of tests from the defense HLW glass degradation abstraction when determining model parameter values for pH dependence in acidic and alkaline solutions.	10 CFR 63.311 10 CFR 63.331 10 CFR 63.321	MA

Table I-2. Model Implementation for Included Features, Events, and Processes (Continued)

Submodel implemented in the TSPA-LA Model and Section Number	Path in GoldSim Model File	FEPs Included in the Submodel	TSPA Inclusion Explanation	Performance Assessment Standard[a]	TSPA-LA Model Implementation
Waste Form Degradation Submodel 6.3.7.4 (Continued)	EBS: \Global_Inputs_and_Calcs\Global_WF_Deg_Mob\WF_Degradation\CSNF_WF_Dissolution EBS: \Global_Inputs_and_Calcs\Global_WF_Deg_Mob\WF_Degradation\Input_Params_DSNF_WF	2.1.11.08.0A Thermal effects on chemistry and microbial activity in the EBS	Test data show that the reaction rates for CSNF and HLW glass degradation are temperature dependent. Temperature dependence was included in degradation abstraction models implemented in the TSPA-LA Model for both waste forms. Total carbonate concentration, which is an input for CSNF degradation, is also temperature dependent.	10 CFR 63.311 10 CFR 63.331 10 CFR 63.321	GSM
Dissolved Concentration Limits Submodel 6.3.7.5	Epistemic: \Input_Params_Epistemic\Epistemic_Params_WF_Deg_Mob\Uncertain_Params_Solubility EBS: \Global_Inputs_and_Calcs\Global_WF_Deg_Mob\Global_Solubility	2.1.09.04.0A Radionuclide solubility, solubility limits, and speciation in the waste form and EBS	In the TSPA-LA Model, inventory concentrations of radioactive elements released from the waste forms (CSNF, DSNF, and HLW glass) are calculated according to the dissolution or degradation rates of waste forms and the volume of water within the (breached) WP and radionuclide inventory. Then the radioelement concentrations are compared against their solubility limits. If the concentration is greater than its solubility limit, then the amount of that radioactive element in excess of the solubility limit will precipitate, potentially available for transport at a later time. In the TSPA-LA Model, solubility limits are enforced in the WP and in the invert. This FEP is included in the human intrusion assessment for the WP. However, radionuclide solubility and flow and transport through the invert (EBS) are not included in the human intrusion assessment.	10 CFR 63.311 10 CFR 63.331 10 CFR 63.321	GSM

Table I-2. Model Implementation for Included Features, Events, and Processes (Continued)

Submodel implemented in the TSPA-LA Model and Section Number	Path in GoldSim Model File	FEPs Included in the Submodel	TSPA Inclusion Explanation	Performance Assessment Standard[a]	TSPA-LA Model Implementation
Dissolved Concentration Limits Submodel 6.3.7.5	Epistemic: \Input_Params_Epistemic\Epistemic_Params_WF_Deg_Mob\Uncertain_Params_Solubility EBS: \Global_Inputs_and_Calcs\Global_WF_Deg_Mob\Global_Solubility	2.1.09.06.0A Reduction-Oxidation potential in waste packages	Reduction-oxidation potential in WPs FEP is implemented in the Dissolved Concentration Limits Submodel by examining redox potential as it pertains to repository conditions, and develops an adjusted Eh model based on experimental data and natural analog information. This adjusted Eh model is used for the solubility calculations in the TSPA-LA Model.	10 CFR 63.311 10 CFR 63.331 10 CFR 63.321	GSM
		2.1.09.07.0A Reaction kinetics in waste package	Dissolution kinetics is included in the TSPA in-package chemistry submodel abstraction. The in-package chemistry submodel uses kinetic expressions – linear or transition state theory rate laws - to describe SNF degradation, DHLW glass degradation, and steel degradation. Kinetics is taken into account in the dissolved concentrations model when secondary phases that are kinetically inhibited from forming under repository conditions are suppressed in the calculations. The adjusted Eh model takes account of kinetic controls over Pu speciation.	10 CFR 63.311 10 CFR 63.331 10 CFR 63.321	GSM
		2.2.08.12.0B Chemistry of water flowing into the waste package	Four different initial water compositions were used to represent the chemistry of the water flowing into the waste package in the in-package chemistry abstraction The variability of the incoming water composition is included in the in-package chemistry abstraction passed to the TSPA, which then feeds these results to the solubility, colloid, CSNF, and HLW glass submodels.	10 CFR 63.311 10 CFR 63.331 10 CFR 63.321	GSM

Table I-2. Model Implementation for Included Features, Events, and Processes (Continued)

Submodel implemented in the TSPA-LA Model and Section Number	Path in GoldSim Model File	FEPs Included in the Submodel	TSPA Inclusion Explanation	Performance Assessment Standard[a]	TSPA-LA Model Implementation
Engineered Barrier System Colloids Submodel 6.3.7.6	Epistemic: \Input_Params_Epistemic\Epistemic_Params_EBS_F_and_T\Uncertain_Params_Colloids EBS: \Global_Inputs_and_Calcs\Global_EBS_F_and_T\Model_Input_EBS_Transport\Input_Params_Colloids	2.1.09.02.0A Chemical interaction with corrosion products	Corrosion products provide sorption sites along the transport pathway for radionuclide release from the waste form to the invert. In the TSPA-LA Model, sorption of radionuclides onto corrosion products retards radionuclide migration, while sorption onto mobile corrosion product colloids facilitates migration.	10 CFR 63.311 10 CFR 63.331 10 CFR 63.321	GSM
		2.1.09.16.0A Formation of pseudo-colloids (natural) in EBS	In the TSPA-LA Model, seepage water colloids included in the Colloid Model are modeled with reversible radionuclide attachment using linear sorption coefficients Kd.	10 CFR 63.311 10 CFR 63.331 10 CFR 63.321	GSM
		2.1.09.17.0A Formation of pseudo-colloids (corrosion product) in EBS	In the TSPA-LA Model, corrosion product colloids included in the Colloid Model are modeled with both reversible and irreversible radionuclide attachments.	10 CFR 63.311 10 CFR 63.331 10 CFR 63.321	GSM
		2.1.09.23.0A Stability of colloids in EBS	In the TSPA-LA Model, the stability of smectite colloids, which is applicable for the repository groundwater colloids and waste form colloids, is determined primarily by ionic strength but also to an extent by pH. The stability of iron-(hydr)oxide colloids, which is applicable to corrosion-product colloids, is determined by both ionic strength and pH.	10 CFR 63.311 10 CFR 63.331 10 CFR 63.321	GSM
		2.1.09.25.0A Formation of colloids (waste form) by co-precipitation in EBS	Colloids formed from the corrosion of HLW glass and the degradation of CSNF were found to contain embedded radionuclide-carrying phases. In the TSPA-LA Model, these radionuclides are modeled as irreversibly attached to the colloids.	10 CFR 63.311 10 CFR 63.331 10 CFR 63.321	GSM

Table I-2. Model Implementation for Included Features, Events, and Processes (Continued)

Submodel implemented in the TSPA-LA Model and Section Number	Path in GoldSim Model File	FEPs Included in the Submodel	TSPA Inclusion Explanation	Performance Assessment Standard[a]	TSPA-LA Model Implementation
EBS Flow Submodel 6.3.6	Epistemic: \Input_Params_Epistemic\Epistemic_Params_EBS_F_and_T\Uncertain_Params_Flux_Split EBS: \Time_Zero\EBS_PS_Loop\Static_Calcs_PS_Loop\Static_Calcs_EBS_F_and_T\EBS_Flow \Global_Inputs_and_Calcs\Global_EBS_F_and_T\Model_Feeds_EBS_Flow	2.1.06.06.0A Effects of drip shield on flow	The EBS Flow Abstraction Model implemented in the TSPA-LA Model accounts for the flow of water through and around the DS. An algorithm referred to as the DS flux-splitting submodel is developed for calculating the fraction of flow diverted by the DS when breaches in the DS exist, and is directly included in the TSPA-LA Model.	10 CFR 63.311 10 CFR 63.331	GSM
		2.1.08.04.0A Condensation forms on roofs of drifts (drift-scale cold traps)	Condensation represents one source of input into the dripping flux presented by the EBS radionuclide transport abstraction. The EBS RTA is used to quantify the release of radionuclides from the EBS to the UZ. Dripping flux comprises a major source of liquid flow into the EBS. The EBS flow model is implemented directly in TSPA.	10 CFR 63.311 10 CFR 63.331	GSM
		2.1.08.04.0B Condensation forms at repository edges (repository-scale cold traps)	Condensation represents one source of input into the dripping flux presented by the EBS radionuclide transport abstraction. The EBS RTA is used to quantify the release of radionuclides from the EBS to the UZ. Dripping flux comprises a major source of liquid flow into the EBS. The EBS flow model is implemented directly in TSPA.	10 CFR 63.311 10 CFR 63.331	GSM

Table I-2. Model Implementation for Included Features, Events, and Processes (Continued)

Submodel implemented in the TSPA-LA Model and Section Number	Path in GoldSim Model File	FEPs Included in the Submodel	TSPA Inclusion Explanation	Performance Assessment Standard[a]	TSPA-LA Model Implementation
EBS Flow Submodel 6.3.6	Epistemic: \Input_Params_Epistemic\Epistemic_Params_EBS_F_and_T\Uncertain_Params_Flux_Split EBS: \Time_Zero\EBS_PS_Loop\Static_Calcs_PS_Loop\Static_Calcs_EBS_F_and_T\EBS_Flow \Global_Inputs_and_Calcs\Global_EBS_F_and_T\Model_Feeds_EBS_Flow	2.1.08.05.0A Flow through invert	The EBS Flow Model explicitly models flow through the invert and the advective transport of radionuclides. Flow through the invert consists of the fluxes diverted by the DS and WP, the flux through the WP, and the imbibition flux from the UZ. Each of these terms is accounted for in the EBS Flow Abstraction Model, which is implemented in the TSPA-LA Model.	10 CFR 63.311 10 CFR 63.331	GSM
		2.1.08.06.0A Capillary effects (wicking) in EBS	The MSTHM process model includes wicking from the host rock to the invert. The MSTHM results are used to develop the TH abstraction implemented in the TSPA-LA Model. Wicking of water from the host rock to the invert is accounted for in the EBS Flow Model through the prediction of the matrix saturation of the invert provided by the TH abstraction. Matrix saturation is directly applied in the calculation of diffusion coefficient in both the WP and the invert.	10 CFR 63.311 10 CFR 63.331	GSM

Table I-2. Model Implementation for Included Features, Events, and Processes (Continued)

Submodel implemented in the TSPA-LA Model and Section Number	Path in GoldSim Model File	FEPs Included in the Submodel	TSPA Inclusion Explanation	Performance Assessment Standard[a]	TSPA-LA Model Implementation
EBS Flow Submodel (continued) 6.3.6	Epistemic: \Input_Params_Epistemic\Epistemic_Params_EBS_F_and_T\Uncertain_Params_Flux_Split EBS: \Time_Zero\EBS_PS_Loop\Static_Calcs_PS_Loop\Static_Calcs_EBS_F_and_T\EBS_Flow \Global_Inputs_and_Calcs\Global_EBS_F_and_T\Model_Feeds_EBS_Flow	2.1.08.07.0A Unsaturated flow in the EBS	Unsaturated flow is included in the TSPA through the flow component of the EBS radionuclide flow and transport abstraction. In the flow model, no explicit distinction between saturated and unsaturated flow is made. However, water saturations along the flow pathway, in the WP and in the invert, are typically less than one (fully saturated conditions). Invert and EBS/UZ interface aspects of this FEP are not implemented in the human intrusion assessment.	10 CFR 63.311 10 CFR 63.331	GSM
		2.1.11.09.0A Thermal effects on flow in the EBS	In the TSPA-LA Model, the temperature history in the EBS is calculated by the TH abstraction model. When drift wall temperatures exceed 100°C, seepage is not allowed to enter the drift, and flow in the EBS is assumed not to occur.	10 CFR 63.311 10 CFR 63.331	GSM
EBS Transport Submodel 6.3.8	Epistemic: \Input_Params_Epistemic\Epistemic_Params_EBS_F_and_T EBS: \Global_Inputs_and_Calcs\Global_EBS_F_and_T\Model_Input_EBS_Transport	2.1.03.11.0A Physical form of waste package and drip shield	The effect of the physical form of waste package is accounted for in the EBS transport submodel, in which different diffusive path lengths are used for each of the two representative waste packages (TADs for CSNF and 5-DHLW/DOE SNF – Long for codisposal). Radionuclide transport is impacted by the materials used in the waste package by means of material-specific degradation rates, diffusive properties, and radionuclide sorption characteristics implemented in the TSPA.	10 CFR 63.311 10 CFR 63.331 10 CFR 63.321	GSM

Table I-2. Model Implementation for Included Features, Events, and Processes (Continued)

Submodel implemented in the TSPA-LA Model and Section Number	Path in GoldSim Model File	FEPs Included in the Submodel	TSPA Inclusion Explanation	Performance Assessment Standard[a]	TSPA-LA Model Implementation
EBS Transport Submodel 6.3.8 (Continued)	Epistemic: \Input_Params_Epistemic\Epistemic_Params_EBS_F_and_T EBS: \Global_Inputs_and_Calcs\Global_EBS_F_and_T\Model_Input_EBS_Transport	2.1.08.07.0A Unsaturated flow in the EB	Unsaturated flow is included in the TSPA through the flow component of the EBS radionuclide flow and transport abstraction. In the flow model, no explicit distinction between saturated and unsaturated flow is made. However, water saturations along the flow pathway, in the WP and in the invert, are typically less than one (fully saturated conditions). This water flow is used by the EBS Transport abstraction model to advect radionuclides along the transport pathway from the waste form to the EBS/UZ interface. Invert and EBS-UZ interface aspects of this FEP are not implemented in the human intrusion assessment.	10 CFR 63.311 10 CFR 63.331 10 CFR 63.321	GSM
		2.1.09.01.0B Chemical characteristics of water in waste package	Chemical characteristics of water in waste package are implemented in the TSPA model through the in-package chemistry abstraction, which estimates pH in the waste form. In the EBS radionuclide transport abstraction, a range of waste form effluents is numerically equilibrated with waste package corrosion products to parameterize pH as a function of ambient carbon dioxide levels and corrosion product surface properties to estimate the distribution of radionuclides among colloids, stationary corrosion products, and the solution	10 CFR 63.311 10 CFR 63.331 10 CFR 63.321	MA
		2.1.09.02.0A Chemical interaction with corrosion products	The effect of corrosion products on the transport of radionuclides internal to the waste package is included in the TSPA-LA Model through the EBS radionuclide transport abstraction. No radionuclide sorption is modeled to occur on corrosion products in the invert. The EBS radionuclide transport abstraction models retardation of radionuclides in the waste package corrosion products using site-limited, competitive sorption coefficients for radionuclides on corrosion products.	10 CFR 63.311 10 CFR 63.331 10 CFR 63.321	MA

Table I-2. Model Implementation for Included Features, Events, and Processes (Continued)

Submodel implemented in the TSPA-LA Model and Section Number	Path in GoldSim Model File	FEPs Included in the Submodel	TSPA Inclusion Explanation	Performance Assessment Standard[a]	TSPA-LA Model Implementation
EBS Transport Submodel 6.3.8 (Continued)	Epistemic: \Input_Params_Epistemic\Epistemic_Params_EBS_F_and_T EBS: \Global_Inputs_and_Calcs\Global_EBS_F_and_T\Model_Input_EBS_Transport	2.1.09.08.0A Diffusion of dissolved radionuclides in EBS	Diffusive transport of dissolved radionuclides in the EBS is a major component of the EBS Transport model. Uncertainty in diffusive transport is incorporated via parameters for invert diffusion coefficient uncertainty, stainless steel and carbon steel corrosion rates, diffusive path length through corrosion products inside a WP, and the specific surface area of steel corrosion products. These parameters are sampled in TSPA-LA Model, and the model for diffusive transport of radionuclides is implemented directly in TSPA-LA Model Invert and EBS/UZ interface aspects of this FEP are not implemented in the human intrusion assessment.	10 CFR 63.311 10 CFR 63.331 10 CFR 63.321	GSM
		2.1.09.19.0B Advection of colloids in EBS	Advective transport of radionuclide-bearing colloids in the EBS is determined in the EBS Transport Model. The advective transport moves colloids (and the associated radionuclides) at about the same velocity as the liquid flux through the EBS. The concentration of colloids in EBS components, together with the water flow rates through each component, determines the rate of advective releases of colloids from the EBS. In the assessment of human intrusion, advection of colloids is included in the transport of colloids down the borehole from the WP to the UZ	10 CFR 63.311 10 CFR 63.331 10 CFR 63.321	GSM
		2.1.09.08.0B Advection of dissolved radionuclides in EBS	Advective transport, which depends on the fluxes through breaches in the DS and WP, is directly included in TSPA. The flux splitting submodel determines the fraction of the seepage flux that flows through the WP. Flux splitting submodel is not included in the human intrusion assessment	10 CFR 63.311 10 CFR 63.331 10 CFR 63.321	GSM

Table I-2. Model Implementation for Included Features, Events, and Processes (Continued)

Submodel implemented in the TSPA-LA Model and Section Number	Path in GoldSim Model File	FEPs Included in the Submodel	TSPA Inclusion Explanation	Performance Assessment Standard[a]	TSPA-LA Model Implementation
EBS Transport Submodel 6.3.8 (Continued)	Epistemic: \Input_Params_Epistemic\Epistemic_Params_EBS_F_and_T EBS: \Global_Inputs_and_Calcs\Global_EBS_F_and_T\Model_Input_EBS_Transport	2.1.09.05.0A Sorption of dissolved radionuclides in EBS	Sorption of dissolved radionuclides in the EBS is captured by two sorption models. In the WP, a complexation-based sorption submodel relates the mass concentration of a radionuclide component in a solid phase to the dissolved concentration of the same component in a contacting phase as a function of aqueous phase chemistry. This submodel accounts for sorption of radionuclides onto corrosion products in the WP. A linear sorption model accounts for sorption on crushed tuff in the invert. The proportionality constant in this submodel is the distribution coefficient (Kd). The Kds are uncertain parameters sampled in the TSPA-LA Model and used as input to the radionuclide transport calculation in TSPA. Sorption retards the transport of radionuclides through the EBS and thus has a direct impact on estimated releases of radionuclides from the EBS. Sorption to invert not included in the human intrusion assessment; however, sorption to corrosoion products inside the waste package in included for the human intrusion assessment	10 CFR 63.311 10 CFR 63.331 10 CFR 63.321	GSM

Table I-2. Model Implementation for Included Features, Events, and Processes (Continued)

Submodel implemented in the TSPA-LA Model and Section Number	Path in GoldSim Model File	FEPs Included in the Submodel	TSPA Inclusion Explanation	Performance Assessment Standard[a]	TSPA-LA Model Implementation
EBS Transport Submodel 6.3.8 (Continued)	Epistemic: \Input_Params_Epistemic\Epistemic_Params_EBS_F_and_T EBS: \Global_Inputs_and_Calcs\Global_EBS_F_and_T\Model_Input_EBS_Transport	2.1.09.24.0A Diffusion of Colloids in EBS	Diffusion of colloids in the EBS is determined by the EBS Transport model and implemented directly in TSPA. Three types of colloids are anticipated to exist in the EBS: (a) waste form colloids from degradation of HLW glass and CSNF, (b) iron oxyhydroxide colloids due to products from the corrosion of steel WPs, and (c) groundwater or seepage water colloids. On all three types of colloids, radionuclides may undergo reversible, or equilibrium, sorption. The waste form colloids may also contain embedded radionuclides that are not removable. General colloid-facilitated diffusive transport model is implemented in TSPA. In the assessment of human intrusion, diffusion of colloids is included in the transport of colloids down the borehole from the WP to the UZ	10 CFR 63.311 10 CFR 63.331 10 CFR 63.321	GSM
		2.2.07.06.0B Long-term release of radionuclides from the repository	The EBS radionuclide transport abstraction (RTA) is used to quantify the time-dependent radionuclide releases from a failed waste package and their subsequent transport through the EBS to the emplacement drift wall/UZ interface. The RTA model, which is implemented directly into the TSPA GoldSim model, allows quantification of radionuclide releases from a failed waste package over the entire compliance period.	10 CFR 63.311 10 CFR 63.331 10 CFR 63.321	GSM

Table I-2. Model Implementation for Included Features, Events, and Processes (Continued)

Submodel implemented in the TSPA-LA Model and Section Number	Path in GoldSim Model File	FEPs Included in the Submodel	TSPA Inclusion Explanation	Performance Assessment Standard[a]	TSPA-LA Model Implementation
EBS-UZ Interface Submodel 6.3.8 This submodel is not implemented in human intrusion assessment	Epistemic: \Input_Params_Epistemic\Epistemic_Params_EBS_F_and_T\Uncertain_Params_EBS_UZ_Trans EBS: \Global_Inputs_and_Calcs\Global_EBS_F_and_T\EBS_UZ_Transport_Inputs	1.2.02.01.0A Fractures	In TSPA, the EBS-UZ interface domain is included beneath the invert domain to establish a boundary condition for calculating the diffusive flux from the invert to the UZ and to compute the radionuclide mass flux fraction going into each of the UZ fracture and matrix continua.	10 CFR 63.311 10 CFR 63.331	GSM
		2.1.09.08.0A Diffusion of dissolved radionuclides in EBS	Diffusive transport of dissolved radionuclides from EBS to the UZ is determined by the EBS-UZ Interface Submodel. Uncertainty in diffusive transport is incorporated via parameters for invert diffusion coefficient uncertainty and UZ invert diffusion coefficient uncertainty. These parameters are sampled in TSPA, and the model for diffusive transport of radionuclides to the UZ is implemented directly in the TSPA-LA Model	10 CFR 63.311 10 CFR 63.331	GSM
		2.1.09.08.0B Advection of dissolved radionuclides in EBS	The EBS radionuclide transport abstraction is used to quantify the time-dependent radionuclide releases from a failed waste package and their subsequent transport through the EBS to the emplacement drift wall/UZ interface. The basic inputs to the RTA model consist of the drift seepage and drift-wall condensation flux, the environmental conditions in the drift (temperature, relative humidity, and water chemistry), and the degradation state of the EBS components. Outputs from the RTA are used in the TSPA to calculate the rates of radionuclide releases to the UZ. The RTA model is implemented directly into the TSPA GoldSim model to compute the radionuclide release rates from the EBS.	10 CFR 63.311 10 CFR 63.331	GSM

Table I-2. Model Implementation for Included Features, Events, and Processes (Continued)

Submodel implemented in the TSPA-LA Model and Section Number	Path in GoldSim Model File	FEPs Included in the Submodel	TSPA Inclusion Explanation	Performance Assessment Standard[a]	TSPA-LA Model Implementation
EBS-UZ Interface Submodel 6.3.8 (Continued) Model not implemented in human intrusion assessment	Epistemic: \Input_Params_Epistemic\Epistemic_Params_EBS_F_and_T\Uncertain_Params_EBS_UZ_Trans EBS: \Global_Inputs_and_Calcs\Global_EBS_F_and_T\EBS_UZ_Transport_Inputs	2.1.09.19.0B Advection of colloids in EBS	Advective transport of radionuclide-bearing colloids from the EBS to the UZ is determined EBS-UZ Interface Submodel. The advective transport moves colloids (and the associated radionuclides) from the EBS to the UZ at about the same velocity as the liquid flux through the invert.	10 CFR 63.311 10 CFR 63.331	GSM
		2.1.09.24.0A Diffusion of Colloids in EBS	Diffusive transport of dissolved colloids from EBS to the UZ is determined by the EBS-UZ Interface Submodel. The diffusion coefficient for colloidal particles is estimated to be a factor of 100 less than the diffusion coefficient for dissolved radionuclides. Uncertainty in diffusive transport is incorporated via parameters for invert diffusion coefficient uncertainty and UZ invert diffusion coefficient uncertainty. These parameters are sampled in TSPA, and the model for diffusive transport of radionuclides to the UZ is implemented directly in the TSPA-LA Model	10 CFR 63.311 10 CFR 63.331	GSM
UZ Transport Submodel (groundwater protection and individual protection assessment) 6.3.9	Epistemic: \Input_Params_Epistemic\Epistemic_Params_UZ_Transport Other: \TSPA_Model\UZ_Transport	1.2.02.01.0A Fractures	The influence of fractures on radionuclide transport is included in the UZ Transport Particle Tracking Transport Abstraction Model through the dual- permeability model for UZ flow and transport. Fracture aperture, porosity, and frequency are treated directly in the UZ radionuclide particle tracking transport abstraction model.	10 CFR 63.311 10 CFR 63.331	DLL

Table I-2. Model Implementation for Included Features, Events, and Processes (Continued)

Submodel implemented in the TSPA-LA Model and Section Number	Path in GoldSim Model File	FEPs Included in the Submodel	TSPA Inclusion Explanation	Performance Assessment Standard[a]	TSPA-LA Model Implementation
UZ Transport submodel for Human Intrusion Assessment 6.3.9 In the human intrusion assessment UZ transport is implemented using a 1D pipe model in GoldSim	Epistemic: \Input_Params_Epistemic\Epistemic_Params_UZ_Transport Other: \TSPA_Model\UZ_Transport	1.2.02.01.0A Fractures	The influence of fractures in the UZ on transport down the borehole is included in the 1D pipe model for human intrusion.	10 CFR 63.321	GSM

Table I-2. Model Implementation for Included Features, Events, and Processes (Continued)

Submodel implemented in the TSPA-LA Model and Section Number	Path in GoldSim Model File	FEPs Included in the Submodel	TSPA Inclusion Explanation	Performance Assessment Standard[a]	TSPA-LA Model Implementation
UZ Transport Submodel 6.3.9 (continued)	Epistemic: \Input_Params_Epistemic\Epistemic_Params_UZ_Transport Other: \TSPA_Model\UZ_Transport	1.2.02.02.0A Faults	The influence of faults on radionuclide transport is included in the UZ Transport Particle Tracking Transport Abstraction Model through the use of the dual-permeability flow model that directly represents the effects of faults on UZ flow. Fracture aperture, porosity, and frequency within faults are treated directly in the UZ radionuclide particle tracking transport abstraction model.	10 CFR 63.311 10 CFR 63.331	DLL
		1.3.01.00.0A Climate change	The effect of climate change on radionuclide transport in the UZ is included in the UZ Transport Particle Tracking Transport Abstraction Model by using pre-generated flow fields for different climates. Shorter term climate changes are incorporated in the range of uncertainty for all climate states.	10 CFR 63.311 10 CFR 63.331	DLL
		1.3.01.00.0A Climate change	In the human intrusion assessment the effect of climate change is included in the calculation of water flux through the borehole. Water flux through the borehole is determined from the percolation flux at the base of the PTn. See the UZ Flow Field Abstraction Submodel.	10 CFR 63.321	GSM
		1.3.07.02.0B Water table rise affects unsaturated zone	The effect of water table rise on transport in the UZ is included by shortening the length of the transport pathway between the EBS and UZ by the amount of water table rise. Also, all radionuclides that are contained in the UZ region captured by the water table rise are assumed to be released instantaneously into the SZ. Water table changes are implemented in the TSPA by allowing the water table to change elevation instantaneously upon change in climate, concurrent with changes in infiltration.	10 CFR 63.311 10 CFR 63.331	DLL

Table I-2. Model Implementation for Included Features, Events, and Processes (Continued)

Submodel implemented in the TSPA-LA Model and Section Number	Path in GoldSim Model File	FEPs Included in the Submodel	TSPA Inclusion Explanation	Performance Assessment Standard[a]	TSPA-LA Model Implementation
UZ Transport Submodel 6.3.9 (Continued)	Epistemic: \Input_Params_Epistemic\Epistemic_Params_UZ_Transport Other: \TSPA_Model\UZ_Transport		Water table rise affects the UZ as it impacts the water level in the borehole and is included in the human intrusion assessment. See the UZ Flow Field Abstraction Submodel.	10 CFR 63.321	
		1.4.01.01.0A Climate modification increases recharge	The effect of climate changes is included in the UZ Transport Particle Tracking Transport Abstraction Model in the form of increased recharge and is included in the UZ radionuclide transport abstraction model for TSPA through the use of pre-generated flow fields.	10 CFR 63.311 10 CFR 63.331	DLL
			The effect of climate modification and its impact on water flux down the borehole is included in the human intrusion assessment. See the UZ Flow Field Abstraction Submodel.	10 CFR 63.321	
		2.1.08.01.0A Water influx at the repository	The influence of water influx at the repository on radionuclide transport is included in the UZ Transport Particle Tracking Transport Abstraction Model through the use of pregenerated flow fields under different climates in the UZ Radionuclide Transport Abstraction Model.	10 CFR 63.311 10 CFR 63.331	DLL
			The effect of percolation flux above the repository and its impact on water flux down the borehole is included in the human intrusion assessment. See the UZ Flow Field Abstraction Submodel.	10 CFR 63.321	
		2.2.03.01.0A Stratigraphy	Stratigraphy is included in the UZ radionuclide transport abstraction model through the use of pre-generated flow fields.	10 CFR 63.311 10 CFR 63.331	MA

Table I-2. Model Implementation for Included Features, Events, and Processes (Continued)

Submodel implemented in the TSPA-LA Model and Section Number	Path in GoldSim Model File	FEPs Included in the Submodel	TSPA Inclusion Explanation	Performance Assessment Standard[a]	TSPA-LA Model Implementation
UZ Transport Submodel 6.3.9 (Continued)	Epistemic: \Input_Params_Epistemic\Epistemic_Params_UZ_Transport Other: \TSPA_Model\UZ_Transport	2.2.03.02.0A Rock properties of host rock and other units	Rock properties of host rock and other units are included and used in the TSPA simulations of radionuclide transport through the UZ. Matrix porosity, rock density, fracture porosity, fracture spacing, and aperture data are incorporated into the transport simulations.	10 CFR 63.311 10 CFR 63.331	MA
			In the human intrusion assessment the borehole is conceptualized to be filled with the rubble of collapsed matrix blocks that have preferential pathways such as fractures similar to the fractures in the undisturbed host rock near the drift. Fracture properties such as fracture aperture, porosity, and frequency are assumed to be the same as that for the rock type near the drift (such as the TSw unit).	10 CFR 63.321	
		2.2.07.02.0A Unsaturated groundwater flow in the geosphere	Water flow is the driving force for radionuclide transport through the UZ. This process is included through the use of pregenerated flow fields for transport. The effect of percolation flux above the repository and its impact on water flux down the borehole is included in the human intrusion assessment. See the UZ Flow Field Abstraction Submodel.	10 CFR 63.311 10 CFR 63.331 10 CFR 63.321	DLL
		2.2.07.04.0A Focusing of unsaturated flow (fingers, weeps)	The effect of focusing unsaturated flow is included through the use of pregenerated flow fields in the TSPA UZ transport simulations. Large scale focusing is included in human intrusion because percolation flux in the UZ above the repository at the base of the PTn is used to determine the flux downward through the borehole. Intermediate-scale focusing is not included in human intrusion because the seepage model is not implemented for this assessment	10 CFR 63.311 10 CFR 63.331 10 CFR 63.321	DLL

Table I-2. Model Implementation for Included Features, Events, and Processes (Continued)

Submodel implemented in the TSPA-LA Model and Section Number	Path in GoldSim Model File	FEPs Included in the Submodel	TSPA Inclusion Explanation	Performance Assessment Standard[a]	TSPA-LA Model Implementation
UZ Transport Submodel 6.3.9 (Continued)	Epistemic: \Input_Params_Epistemic\Epistemic_Params_UZ_Transport Other: \TSPA_Model\UZ_Transport	2.2.07.06.0B Long-term release of radionuclides from the repository	The effects of WP breaches over a long period of time are included in the source term model for TSPA, which affects the source term of radionuclide mass for the UZ radionuclide transport abstraction model implemented in TSPA.	10 CFR 63.311 10 CFR 63.331	DLL
		2.2.07.07.0A Perched water develops	Perched water is included through the use of pre-generated flow fields in the TSPA UZ transport simulations.	10 CFR 63.311 10 CFR 63.331	DLL
		2.2.07.08.0A Fracture flow in the unsaturated zone	The effects of fracture flow on radionuclide transport (advection) is included in the UZ radionuclide transport abstraction model implemented in the TSPA-LA Modelthrough the use of pre-generated unsaturated flow fields that include the occurrence of perched water.	10 CFR 63.311 10 CFR 63.331 10 CFR 63.321	DLL
		2.2.07.09.0A Matrix imbibition in the unsaturated zone	Matrix imbibition in the UZ is included through the use of pre-generated flow fields in the TSPA UZ transport simulations.	10 CFR 63.311 10 CFR 63.331	DLL
		2.2.07.15.0B Advection and dispersion in the unsaturated zone	Dispersion is incorporated in the UZ radionuclide transport abstraction model implemented in the TSPA-LA Model through the use of a transfer function based on an analytical solution to the advection-dispersion equation.	10 CFR 63.311 10 CFR 63.331 10 CFR 63.321	DLL
		2.2.08.01.0B Chemical characteristics of groundwater in the unsaturated zone	The effects of groundwater composition are incorporated into the probability distributions for radionuclide sorption in the UZ sampled in TSPA.	10 CFR 63.311 10 CFR 63.331 10 CFR 63.321	GSM
		2.2.08.06.0B Complexation in the unsaturated zone	The effects of complexation are included in the experimental data used to derive radionuclide sorption coefficients sampled in the TSPA-LA Model for sorption in the UZ.	10 CFR 63.311 10 CFR 63.331 10 CFR 63.321	DLL

Table I-2. Model Implementation for Included Features, Events, and Processes (Continued)

Submodel implemented in the TSPA-LA Model and Section Number	Path in GoldSim Model File	FEPs Included in the Submodel	TSPA Inclusion Explanation	Performance Assessment Standard[a]	TSPA-LA Model Implementation
UZ Transport Submodel 6.3.9 (Continued)	Epistemic: \Input_Params_Epistemic\Epistemic_Params_UZ_Transport Other: \TSPA_Model\UZ_Transport	2.2.08.08.0B Matrix diffusion in the UZ	Transfer functions that are used in the UZ radionuclide transport abstraction model for TSPA include the mechanism of matrix diffusion.	10 CFR 63.311 10 CFR 63.331 10 CFR 63.321	DLL
		2.2.08.09.0B Sorption in the unsaturated zone	Linear, equilibrium sorption is accounted for in the rock matrix continuum, with no sorption conservatively used in the fractures. Sorption coefficients are implemented in the TSPA-LA Model in terms of probability distributions for the sorption coefficient of each element of interest among the three major rock types (devitrified, zeolitic, and vitric) found in the UZ. The probability distributions account for uncertainties in water chemistry, mineralogy, and sorption mechanisms. In the human intrusion assessment, sorption of radionuclides in the UZ is modeled using the devitrified UZ Kd values as representative for the entire pathway. Sorption occurs on the matrix only.	10 CFR 63.311 10 CFR 63.331 10 CFR 63.321	DLL
		2.2.08.10.0B Colloid transport in the UZ	Colloid-facilitated radionuclide transport included in the TSPA-LA Model treats both radionuclides permanently attached to colloids and radionuclides that partition between colloids, the aqueous phase, and the rock matrix. Diffusion of colloids into the rock matrix is not included, which leads to greater facilitation of radionuclide transport by colloids. Colloid transport down the borehole through the UZ is included in the human intrusion assessment.	10 CFR 63.311 10 CFR 63.331 10 CFR 63.321	DLL

Table I-2. Model Implementation for Included Features, Events, and Processes (Continued)

Submodel implemented in the TSPA-LA Model and Section Number	Path in GoldSim Model File	FEPs Included in the Submodel	TSPA Inclusion Explanation	Performance Assessment Standard[a]	TSPA-LA Model Implementation
UZ Transport Submodel 6.3.9 (Continued)	Epistemic: \Input_Params_Epistemic\Epistemic_Params_UZ_Transport Other: \TSPA_Model\UZ_Transport	2.3.11.03.0A Infiltration and recharge	The hydrologic effects of infiltration and recharge are included in the Infiltration Model which includes the effects of seasonal and climate variations, climate change, surface-water runoff, and site topology, such as hill slopes and washes. The effects of climate change included in the TSPA through the UZ flow fields that are used to evaluate the local percolation fluxes. Percolation fluxes are used to calculate radionuclide transport from the repository to the SZ.	10 CFR 63.311 10 CFR 63.331 10 CFR 63.321	DLL
		3.1.01.01.0A Radioactive decay and ingrowth	Both simple decay and radionuclide chain-decay are directly included in the UZ Transport Model implemented in TSPA. Although the UZ Transport Submodel Is not implemented in the human intrusion assessment, radioactive decay and ingrowth down the borehole through the UZ is included in the human intrusion assessment.	10 CFR 63.311 10 CFR 63.331 10 CFR 63.321	DLL
SZ Flow and Transport Submodel 6.3.10	Epistemic: \Input_Params_Epistemic\Epistemic_Params_SZ_Transport Other: \TSPA_Model\SZ_Transport	1.2.02.01.0A Fractures	Groundwater flow through fractures in the volcanic units is included in the SZ flow and transport model which is implemented directly into the TSPA-LA model through an effective continuum flow model. Observations at Yucca Mountain indicate that flow is primarily through the fracture network instead of the matrix. The characteristics of the fracture properties, such as fracture orientation, aperture size, degree of infilling, and tortuosity are modeled through probabilistically modeled parameters.	10 CFR 63.311 10 CFR 63.331 10 CFR 63.321	GSM

Table I-2. Model Implementation for Included Features, Events, and Processes (Continued)

Submodel implemented in the TSPA-LA Model and Section Number	Path in GoldSim Model File	FEPs Included in the Submodel	TSPA Inclusion Explanation	Performance Assessment Standard[a]	TSPA-LA Model Implementation
SZ Flow and Transport Submodel (continued) 6.3.10	Epistemic: \Input_Params_Epistemic\Epistemic_Params_SZ_Transport Other: \TSPA_Model\SZ_Transport	1.2.02.02.0A Faults	In general, large-scale hydraulic features (e.g., major faults, fault zones, zones of chemical alteration) have been incorporated into the Site-Scale Saturated Zone (SZ) Flow Model as zones of enhanced or reduced permeability. The faults were generally modeled as anisotropic features with high conductivity along the fault (strike) and low conductivity in the direction across the fault. These features are reflected in the flow fields used in the SZ flow model abstraction implemented in TSPA.	10 CFR 63.311 10 CFR 63.331 10 CFR 63.321	GSM
		1.3.01.00.0A Climate Change	The effects of climate change are incorporated into the SZ flow and transport abstraction model and the SZ one-dimensional transport model as implemented in the TSPA by assuming instantaneous change from one steady-state flow condition to another steady-state condition in the SZ. Changes in climate state are assumed to affect the magnitude of groundwater flux through the SZ system but have a negligible impact on flow paths. The effect of changes in groundwater flux is incorporated into the SZ flow and transport abstraction model by scaling the timing of radionuclide mass breakthrough curves proportionally to the change in SZ-specific discharge	10 CFR 63.311 10 CFR 63.331 10 CFR 63.321	GSM
		1.3.07.02.0A Water table rise affects SZ	Water table rise and the effect of increased flow (due to wetter future climate conditions) on the SZ breakthrough curves are modeled using scaling factors representing the future climate states. The scaling factors used in this approach are the ratio of average SZ groundwater flow under the future climatic conditions to the flow under present conditions. The scaling factors are a direct input to TSPA.	10 CFR 63.311 10 CFR 63.331 10 CFR 63.321	GSM

Table I-2. Model Implementation for Included Features, Events, and Processes (Continued)

Submodel implemented in the TSPA-LA Model and Section Number	Path in GoldSim Model File	FEPs Included in the Submodel	TSPA Inclusion Explanation	Performance Assessment Standard[a]	TSPA-LA Model Implementation
SZ Flow and Transport Submodel (continued) 6.3.10	Epistemic: \Input_Params_Epistemic\Epistemic_Params_SZ_Transport Other: \TSPA_Model\SZ_Transport	1.4.01.01.0A Climate modification increases recharge	Climate modification is expected to lead to an increase in precipitation and net infiltration Increased net infiltration will become increased recharge to the saturated zone, and as more recharge enters the saturated zone, the water table may rise increasing the volumetric flow of groundwater. The larger flow in the saturated zone is simulated by a groundwater specific discharge scaling factor that increases the flow of water in the saturated zone corresponding to future climate conditions without changing the position of the water table. These scaling factors are a direct input to the TSPA.	10 CFR 63.311 10 CFR 63.331 10 CFR 63.321	GSM
		1.4.07.02.0A Wells	Dilution of radionuclide concentrations in groundwater used by the reasonable maximally exposed individual (RMEI) occurs both during transport in the SZ because of dispersion and in the process of extracting groundwater from wells. The Site-Scale SZ Flow Model domain was made sufficiently large to include wells in the Amargosa Valley at the southern end of the modeled area. At the accessible environment, located about 18 km south of Yucca Mountain, the RMEI is postulated to use well water that is extracted from the aquifer. In the TSPA, all radionuclide mass reaching the downgradient accessible environment is captured by the wells of the receptor group.	10 CFR 63.311 10 CFR 63.331 10 CFR 63.321	GSM
		2.2.03.01.0A Stratigraphy	The site-scale HFM is a representation of the hydrogeologic units and major structural features within the SZ flow system, encompassed by the domain of the Site-Scale SZ Flow Model. To represent the geologic heterogeneity introduced by stratigraphy in a groundwater model, geologic units were simplified into hydrogeologic units on the basis of similar hydrogeologic properties. The stratigraphy is reflected in the flow fields used in the SZ Flow Model abstraction implemented in TSPA.	10 CFR 63.311 10 CFR 63.331 10 CFR 63.321	MA

Table I-2. Model Implementation for Included Features, Events, and Processes (Continued)

Submodel implemented in the TSPA-LA Model and Section Number	Path in GoldSim Model File	FEPs Included in the Submodel	TSPA Inclusion Explanation	Performance Assessment Standard[a]	TSPA-LA Model Implementation
SZ Flow and Transport Submodel 6.3.10 (Continued)	Epistemic: \Input_Params_Epistemic\Epistemic_Params_SZ_Transport Other: \TSPA_Model\SZ_Transport	2.2.03.02.0A Rock properties of host rock and other units	Geologic features and heterogeneous hydrostratigraphic units are included in the SZ flow and transport abstraction model as cells with specific hydrologic parameter values in a configuration based on the hydrogeologic framework. Available geologic information of rock properties that affect saturated zone flow and transport in the Yucca Mountain region is used to determine the 23 hydrostratigraphic units modeled in the site-scale saturated zone flow domain. Rock properties are reflected in the flow fields used in the SZ Flow Model abstraction implemented in TSPA.	10 CFR 63.311 10 CFR 63.331 10 CFR 63.321	MA
		2.2.07.12.0A Saturated groundwater flow in the geosphere	Steady-state, saturated, three-dimensional groundwater flow within the Yucca Mountain vicinity is modeled through the Site-Scale SZ Flow Model. Flow through fractures is modeled through an effective continuum flow model. The continuum approach allows the use of widely accepted mathematical equations describing groundwater flow through porous medium as the mathematical basis for the Site-Scale SZ Flow Model.	10 CFR 63.311 10 CFR 63.331 10 CFR 63.321	GSM
		2.2.07.13.0A Water-conducting features in the SZ	To represent discrete features and regions having distinct hydrologic properties within the Site-Scale SZ Flow Model domain, a set of 17 hydrogeologic features complementary to the HFM were identified and incorporated into the Site-Scale SZ Flow Model. These features are reflected in the flow abstraction model implemented in TSPA. The SZ Flow and Transport Abstraction Model is implemented by the 1-D SZ Flow and Transport Model Component that is implemented in GoldSim and the 3-D SZ Flow and Transport Model component implemented by the SZ convolute DLL.	10 CFR 63.311 10 CFR 63.331 10 CFR 63.321	GSM/DLL

Table I-2. Model Implementation for Included Features, Events, and Processes (Continued)

Submodel implemented in the TSPA-LA Model and Section Number	Path in GoldSim Model File	FEPs Included in the Submodel	TSPA Inclusion Explanation	Performance Assessment Standard[a]	TSPA-LA Model Implementation
SZ Flow and Transport Submodel 6.3.10 (Continued	Epistemic: \Input_Params_Epistemic\Epistemic_Params_SZ_Transport Other: \TSPA_Model\SZ_Transport	2.2.07.15.0A Advection and dispersion in the SZ	The processes of advection and dispersion are modeled in the SZ transport models using the advective-dispersive transport equations and reflected in the SZ breakthrough curves implemented in the TSPA-LA Model. The processes are implemented using the FEHM code. Parameters used in the models related to dispersion are longitudinal dispersivity, horizontal transverse dispersivity, and vertical transverse dispersivity.	10 CFR 63.311 10 CFR 63.331 10 CFR 63.321	DLL
		2.2.07.16.0A Dilution of radionuclides in groundwater	In TSPA, dilution of radionuclide concentrations in groundwater used by the RMEI occurs both during transport in the SZ because of dispersion and in the process of extracting groundwater from wells.	10 CFR 63.311 10 CFR 63.331 10 CFR 63.321	GSM
		2.2.07.17.0A Diffusion in the SZ	The molecular diffusion coefficient is included as a component of the dispersion coefficient in SZ radionuclide transport simulations used to develop the 3D breakthrough curves implemented in the TSPA-LA Model via the convolution integral method and in the 1D SZ pipe model abstraction implemented by GoldSim. In both cases, the dispersion coefficient is dominated by the hydrodynamic dispersion component for most groundwater flow rates.	10 CFR 63.311 10 CFR 63.331 10 CFR 63.321	GSM
		2.2.08.01.0A Chemical characteristics of groundwater in the SZ	Hydrochemical data and chemical data on rock types in the flow system are used to corroborate groundwater flow patterns and flow rates, and to provide input to determine the sorption coefficient distributions. The effect of chemical characteristics of groundwater in the SZ on sorption coefficients is reflected in the uncertainty distributions used in the SZ transport abstraction model implemented in TSPA.	10 CFR 63.311 10 CFR 63.331 10 CFR 63.321	GSM

Table I-2. Model Implementation for Included Features, Events, and Processes (Continued)

Submodel implemented in the TSPA-LA Model and Section Number	Path in GoldSim Model File	FEPs Included in the Submodel	TSPA Inclusion Explanation	Performance Assessment Standard[a]	TSPA-LA Model Implementation
SZ Flow and Transport Submodel 6.3.10 (Continued	Epistemic: \Input_Params_Epistemic\Epistemic_Params_SZ_Transport Other: \TSPA_Model\SZ_Transport	2.2.08.06.0A Complexation in the SZ	Variations in groundwater chemistry may influence complexation of radionuclides with other aqueous species. Complexation can impact the sorption of radionuclides onto the aquifer material. In particular, the sorption behavior of uranium, neptunium, and plutonium is sensitive to bicarbonate and carbonate concentrations in groundwater. The influence of these variations is incorporated into the uncertainty distributions developed for SZ sorption coefficients implemented in TSPA.	10 CFR 63.311 10 CFR 63.331 10 CFR 63.321	GSM
		2.2.08.08.0A Matrix diffusion in the SZ	Diffusion in the SZ is implemented through a dual porosity effective continuum approach. The SZ Transport Model includes matrix diffusion in the volcanic rock matrix and is parameterized by the effective diffusion coefficient to distinguish it from the free water diffusion coefficient. Matrix diffusion is captured by the breakthrough curves generated by the SZ Transport Model and implemented in TSPA. Parameters used in the transport models related to matrix diffusion are flowing interval spacing, effective diffusion coefficient, and matrix porosity.	10 CFR 63.311 10 CFR 63.331 10 CFR 63.321	DLL
		2.2.08.09.0A Sorption in the SZ	Sorption is modeled in the SZ transport models using the linear sorption isotherm with sorption coefficient parameters that appear in the equations being treated as effective variables appropriate for the model scale. In TSPA, sorption is modeled to occur in the matrix of fractured volcanic rocks and in the porous medium of the alluvium. Sorption coefficients are primarily based on laboratory measurements using samples from the Yucca Mountain site. These data are combined with information on the variability and uncertainty in hydrochemical and mineralogical composition to assess the uncertainty in sorption coefficients.	10 CFR 63.311 10 CFR 63.331 10 CFR 63.321	GSM

Table I-2. Model Implementation for Included Features, Events, and Processes (Continued)

Submodel implemented in the TSPA-LA Model and Section Number	Path in GoldSim Model File	FEPs Included in the Submodel	TSPA Inclusion Explanation	Performance Assessment Standard[a]	TSPA-LA Model Implementation
SZ Flow and Transport Submodel 6.3.10 (Continued	Epistemic: \Input_Params_Epistemic\Epistemic_Params_SZ_Transport Other: \TSPA_Model\SZ_Transport	2.2.08.10.0A Colloid transport in the SZ	The impact of colloid filtration in the SZ is incorporated in transport simulations of radionuclides irreversibly attached to colloids with the colloid retardation factor parameter. Radionuclides that are reversibly sorbed onto colloids are modeled as temporarily attached to the surface of colloids. Colloid-facilitated transport of radionuclides reversibly attached to colloids is a function of two parameters: the concentration of colloids in the groundwater and the sorption coefficient for that radionuclide onto colloids. The SZ transport models use a semi-analytical method to include retardation due to diffusion and sorption and colloid-facilitated transport in a random-walk model.	10 CFR 63.311 10 CFR 63.331 10 CFR 63.321	GSM
		2.2.10.03.0A Natural geothermal effects on flow in the SZ	Representative hydrologic properties were assigned to each node in the SZ computational grid. For flow modeling, these properties include permeability, porosity, and viscosity. Because the viscosity of groundwater depends on temperature, the nodal values for viscosity were assigned based on the expected temperature distribution in the subsurface.	10 CFR 63.311 10 CFR 63.331 10 CFR 63.321	MA
		2.2.12.00.0B Undetected features in the SZ	The HFM contains an inherent level of uncertainty that is a function of data distribution and geologic complexity. Uncertainty in the HFM is addressed in the Site-Scale Flow Model. Through the definition and assemblage of the hydrogeologic units integral to its construction, the HFM provides an internally consistent, volume-filling representation of the spatial distribution of block-averaged hydrologic properties within the Site-Scale SZ Flow Model domain. In general, large-scale hydraulic features (e.g., major faults, fault zones, zones of chemical alteration) have been incorporated into the Site-Scale Model as zones of enhanced or reduced permeability.	10 CFR 63.311 10 CFR 63.331 10 CFR 63.321	MA

Table I-2. Model Implementation for Included Features, Events, and Processes (Continued)

Submodel implemented in the TSPA-LA Model and Section Number	Path in GoldSim Model File	FEPs Included in the Submodel	TSPA Inclusion Explanation	Performance Assessment Standard[a]	TSPA-LA Model Implementation
SZ Flow and Transport Submodel 6.3.10 (Continued	Epistemic: \Input_Params_Epistemic\Epistemic_Params_SZ_Transport Other: \TSPA_Model\SZ_Transport	2.3.11.03.0A Infiltration and recharge	The effect of increased flow in the SZ due to increased recharge (caused by climate change) from the UZ is modeled using scaling factors to increase specific discharge in the SZ. The scaling factors used in this approach are the ratio of average SZ groundwater flow under the future climatic conditions to the flow under present conditions. The scaling factors are a direct input from the SZ Flow and Transport Abstraction Model to TSPA.	10 CFR 63.311 10 CFR 63.331 10 CFR 63.321	MA
		3.1.01.01.0A Radioactive decay and ingrowth	The 1-D SZ Transport Model is used to calculate the mass of daughter products from the radioactive decay of several radionuclides. The one-dimensional model, which is implemented directly in the TSPA simulations, simulates the radioactive decay and in-growth of radionuclides in four decay chains. Radioactive decay is also applied to radionuclide mass flux calculated with the convolution integral method in the SZ Flow and Transport Abstraction Model.	10 CFR 63.311 10 CFR 63.331 10 CFR 63.321	GSM
Biosphere Submodel 6.3.11	Epistemic: \Input_Params_Epistemic\Epistemic_Params_Biosphere Other: \TSPA_Model\Biosphere	1.2.04.07.0A Ashfall	This FEP is dispositioned in the biosphere component of the TSPA-LA Model through the use of Biosphere Dose Conversion factors (BDCFs) that are direct inputs to the TSPA. Volcanic ash is the initial source of contamination for the eruption case of the volcanic scenario. Ash characteristics and depth were considered in development of the input parameters for the surface soil and air submodels.	10 CFR 63.311	GSM

Table I-2. Model Implementation for Included Features, Events, and Processes (Continued)

Submodel implemented in the TSPA-LA Model and Section Number	Path in GoldSim Model File	FEPs Included in the Submodel	TSPA Inclusion Explanation	Performance Assessment Standard[a]	TSPA-LA Model Implementation
Biosphere Submodel 6.3.11 (Continued)	Epistemic: \Input_Params_Epistemic\Epistemic_Params_Biosphere Other: \TSPA_Model\Biosphere	1.3.07.02.0A Water table rise affects SZ	The water table will likely be higher in future climate states that have greater infiltration rates. To include water table rise in the TSPA calculations, the water table elevation is instantaneously increased up to 120m when the climate changes from present-day to monsoon climate. This rise reduces the transport length in the UZ. This treatment is consistent with the instantaneous change of UZ flow fields. Water table rise also captures the radionuclides present in the UZ below the new water table elevation. The captured radionuclides are input as a source term to the SZ transport simulation.	10 CFR 63.311 10 CFR 63.331 10 CFR 63.321	GSM
		1.4.07.01.0A Water management activities	Water management activities conducted in the Yucca Mountain region (e.g., irrigation and fish farming) were incorporated throughout the conceptual and mathematical model and considered in the development of parameter values for the plant uptake and fish uptake submodels. All FEPs considered in the biosphere model and its input parameters are collectively included in BDCFs	10 CFR 63.311 10 CFR 63.321	GSM
		1.4.07.02.0A Wells	A well is the source of groundwater for domestic and agricultural uses in the groundwater exposure scenario. All FEPs considered in the Biosphere Model and its input parameters are collectively included in BDCFs	10 CFR 63.311 10 CFR 63.331 10 CFR 63.321	GSM
		2.2.08.01.0A Chemical characteristics of the groundwater in the SZ	The source of radionuclides in the biosphere groundwater scenario is the groundwater pumped from wells. The model addresses radionuclide accumulation and transport within and between biosphere compartments culminating in an annual dose to a defined receptor. All FEPs considered in the Biosphere Model and its input parameters are collectively included in BDCFs that are implemented in TSPA.	10 CFR 63.311 10 CFR 63.331 10 CFR 63.321	MA

Table I-2. Model Implementation for Included Features, Events, and Processes (Continued)

Submodel implemented in the TSPA-LA Model and Section Number	Path in GoldSim Model File	FEPs Included in the Submodel	TSPA Inclusion Explanation	Performance Assessment Standard[a]	TSPA-LA Model Implementation
Biosphere Submodel 6.3.11 (Continued)	Epistemic: \Input_Params_Epistemic\Epistemic_Params_Biosphere Other: \TSPA_Model\Biosphere	2.3.02.03.0A Soil and sediment transport in the biosphere	Soil and sediment transport via erosion were included in the surface soil and air submodels. All FEPs considered in the Biosphere Model and its input parameters are collectively included in BDCFs that are implemented in TSPA.	10 CFR 63.311 10 CFR 63.321	MA
		2.3.02.01.0A Soil type	This feature was included through the consideration of the soil characteristics in the reference biosphere in the development of parameter values for the surface soil, plant uptake, and ^{14}C submodels. All FEPs considered in the Biosphere Model and its input parameters are collectively included in BDCFs that are implemented in TSPA.	10 CFR 63.311 10 CFR 63.321	MA
		2.3.02.02.0A Radionuclide accumulation in soils	Accumulation of radionuclides in soil from deposition of irrigation water and volcanic ash was modeled in the surface soil submodel. All FEPs considered in the Biosphere Model and its input parameters are collectively included in BDCFs that are implemented in TSPA.	10 CFR 63.311 10 CFR 63.321	MA
		2.3.04.01.0A Surface water transport and mixing	The groundwater scenario implicitly included water transport because the model applied to the use of any water containing radionuclides, regardless of the origin, if the reference biosphere, water-use practices, and characteristics of the RMEI remain unchanged. The model did not consider mixing of contaminated and uncontaminated water. All FEPs considered in the Biosphere Model and its input parameters are collectively included in BDCFs	10 CFR 63.311 10 CFR 63.321	MA

Table I-2. Model Implementation for Included Features, Events, and Processes (Continued)

Submodel implemented in the TSPA-LA Model and Section Number	Path in GoldSim Model File	FEPs Included in the Submodel	TSPA Inclusion Explanation	Performance Assessment Standard[a]	TSPA-LA Model Implementation
Biosphere Submodel 6.3.11 (Continued)	Epistemic: \Input_Params_Epistemic\Epistemic_Params_Biosphere Other: \TSPA_Model\Biosphere	2.3.11.01.0A Precipitation	Levels of precipitation consistent with current knowledge of the reference biosphere were considered in the development of input parameter distributions for the surface soil, plant uptake, and ^{14}C submodels. All FEPs considered in the Biosphere Model and its input parameters are collectively included in BDCFs that are implemented in TSPA.	10 CFR 63.311 10 CFR 63.321	MA
		2.3.13.01.0A Biosphere characteristics	The principal components, conditions, and characteristics of the reference biosphere that influence radionuclide transport were represented in the conceptual and mathematical models. Current knowledge of the conditions in the reference biosphere was considered in the development of parameter distributions for all submodels. All FEPs considered in the Biosphere Model and its input parameters are collectively included in BDCFs that are implemented in TSPA.	10 CFR 63.311 10 CFR 63.321	MA
		2.3.13.02.0A Radionuclide alteration during biosphere transport	Changes in the physical and chemical form of radionuclides during transfer among biosphere components were incorporated throughout the conceptual and mathematical models. This FEP was also implicitly incorporated through the use of radionuclide-specific transfer factors in the plant uptake and animal uptake submodels. All FEPs considered in the Biosphere Model and its input parameters are collectively included in BDCFs that are implemented in TSPA.	10 CFR 63.311 10 CFR 63.321	MA
		2.4.01.00.0A Human characteristics (physiology, metabolism)	Metabolic and physiologic considerations consistent with present knowledge of adults, as per 10 CFR 63.312(e) [DIRS 180319], were used in the development of parameter distributions for the external exposure, inhalation, and ingestion submodels. The characteristics in these parameters are propagated to the BDCFs which are direct inputs to the TSPA for the scenario classes involving radionuclide release to the groundwater.	10 CFR 63.311 10 CFR 63.331 10 CFR 63.321	MA

Table I-2. Model Implementation for Included Features, Events, and Processes (Continued)

Submodel implemented in the TSPA-LA Model and Section Number	Path in GoldSim Model File	FEPs Included in the Submodel	TSPA Inclusion Explanation	Performance Assessment Standard[a]	TSPA-LA Model Implementation
Biosphere Submodel 6.3.11 (Continued)	Epistemic: \Input_Params_Epistemic\Epistemic_Params_Biosphere Other: \TSPA_Model\Biosphere	2.4.04.01.0A Human lifestyle	Activities representative of the living style of the residents of the Town of Amargosa Valley were incorporated throughout the conceptual and mathematical model. The living style of Amargosa Valley residents was considered in the development of parameter distributions for the air, external exposure, inhalation, and ingestion submodels. The characteristics in these parameters are propagated to the BDCFs which are direct inputs to the TSPA for the scenario classes involving radionuclide release to the groundwater.	10 CFR 63.311 10 CFR 63.321	MA
		2.4.07.00.0A Dwellings	Characteristics of dwellings representative of the living style of the residents of the Town of Amargosa Valley were considered in the development of input parameters for the air, external exposure, and inhalation submodels. The characteristics in these parameters are propagated to the BDCFs which are direct inputs to the TSPA for the scenario classes involving radionuclide release to the groundwater.	10 CFR 63.311 10 CFR 63.321	MA
		2.4.08.00.0A Wild and natural land and water use	Wild and natural land and water use (e.g., use of natural lands, ingestion of game animals) by the residents of the Town of Amargosa Valley was incorporated into the air, external exposure, and ingestion submodels. These lifestyle characteristics were considered in the development of parameters for those submodels. The characteristics in these parameters are propagated to the BDCFs which are direct inputs to the TSPA for the scenario classes involving radionuclide release to the groundwater.	10 CFR 63.311 10 CFR 63.321	MA

Table I-2. Model Implementation for Included Features, Events, and Processes (Continued)

Submodel implemented in the TSPA-LA Model and Section Number	Path in GoldSim Model File	FEPs Included in the Submodel	TSPA Inclusion Explanation	Performance Assessment Standard[a]	TSPA-LA Model Implementation
Biosphere Submodel 6.3.11 (Continued)	Epistemic: \Input_Params_Epistemic\Epistemic_Params_Biosphere Other: \TSPA_Model\Biosphere	2.4.09.01.0B Agricultural land use and irrigation	Agricultural land use and irrigation practices of the residents of the Town of Amargosa Valley were incorporated into the soil, air, plant uptake, animal uptake, ^{14}C, and fish uptake submodels. These practices were considered in the development of parameters for those submodels. All FEPs considered in the Biosphere Model and its input parameters are collectively included in BDCFs that are implemented in TSPA.	10 CFR 63.311 10 CFR 63.321	MA
		2.4.09.02.0A Animal farms and fisheries	Animal farm and fishery practices of the residents of the Town of Amargosa Valley were incorporated into the animal uptake and fish uptake submodels. These practices were considered in the development of parameters for those submodels. All FEPs considered in the Biosphere Model and its input parameters are collectively included in BDCFs	10 CFR 63.311 10 CFR 63.321	MA
		2.4.10.00.0A Urban and industrial land and water use	Land and water use in urban and industrial settings of the residents of the Town of Amargosa Valley were incorporated into the soil, air, ^{14}C, external exposure, inhalation, and ingestion submodels. These lifestyle characteristics were considered in the development of parameters for those submodels. All FEPs considered in the Biosphere Model and its input parameters are collectively included in BDCFs that are implemented in TSPA.	10 CFR 63.311 10 CFR 63.321	MA

Table I-2. Model Implementation for Included Features, Events, and Processes (Continued)

Submodel implemented in the TSPA-LA Model and Section Number	Path in GoldSim Model File	FEPs Included in the Submodel	TSPA Inclusion Explanation	Performance Assessment Standard[a]	TSPA-LA Model Implementation
Biosphere Submodel 6.3.11 (Continued)	Epistemic: \Input_Params_Epistemic\Epistemic_Params_Biosphere Other: \TSPA_Model\Biosphere	3.1.01.01.0A Radioactive decay and ingrowth	This FEP is dispositioned in the biosphere component of the TSPA-LA Model through the use of groundwater exposure scenario BDCFs that are direct inputs to the TSPA for the scenario classes involving radionuclide release to the groundwater. Annual doses are calculated as the product of radionuclide concentration in groundwater and BDCFs. The present-day climate BDCFs are used for the assessment of doses to the RMEI for the entire period of geologic stability. Radioactive decay and ingrowth is also included in the TSPA through the use of the conversion factors for evaluating compliance with the groundwater protection standards.	10 CFR 63.311 10 CFR 63.331 10 CFR 63.321	GSM
		3.2.10.00.0A Atmospheric transport of contaminants	The processes of atmospheric transport of radionuclides from resuspension of soil and ash particles, gaseous emission of radionuclides from soil, and generation of aerosols from evaporative coolers were included in the air and ^{14}C submodels. All FEPs considered in the Biosphere Model and its input parameters are collectively included in BDCFs that are implemented in TSPA.	10 CFR 63.311 10 CFR 63.321	GSM
		3.3.01.00.0A Contaminated drinking water, foodstuffs, and drugs	Consumption of contaminated water and soil and consumption of locally produced crops, animal products, and fish were included in the ingestion submodel. Consumption rates were based on the diet of the residents of the Town of Amargosa Valley and the requirements of 10 CFR 63.312 [DIRS 180319]. All FEPs considered in the Biosphere Model and its input parameters are collectively included in BDCFs that are implemented in TSPA.	10 CFR 63.311 10 CFR 63.331 10 CFR 63.321	MA
		3.3.02.01.0A Plant uptake	The process of plant uptake of radionuclides was included in the plant uptake and ^{14}C submodels. All FEPs considered in the Biosphere Model and its input parameters are collectively included in BDCFs that are implemented in TSPA.	10 CFR 63.311 10 CFR 63.321	MA

Table I-2. Model Implementation for Included Features, Events, and Processes (Continued)

Submodel implemented in the TSPA-LA Model and Section Number	Path in GoldSim Model File	FEPs Included in the Submodel	TSPA Inclusion Explanation	Performance Assessment Standard[a]	TSPA-LA Model Implementation
Biosphere Submodel 6.3.11 (Continued)	Epistemic: \Input_Params_Epistemic\Epistemic_Params_Biosphere Other: \TSPA_Model\Biosphere	3.3.02.02.0A Animal uptake	The animal uptake submodel included the process of radionuclide uptake by farm animals. All FEPs considered in the Biosphere Model and its input parameters are collectively included in BDCFs	10 CFR 63.311 10 CFR 63.321	MA
		3.3.02.03.0A Fish uptake	The fish uptake submodel included the bioaccumulation of radionuclides in fish. All FEPs considered in the Biosphere Model and its input parameters are collectively included in BDCFs that are implemented in TSPA.	10 CFR 63.311 10 CFR 63.321	MA
		3.3.03.01.0A Contaminated non-food products and exposure	The external exposure submodel bounded exposure to the few nonfood products produced in Amargosa Valley that may contain radionuclides by assuming that the RMEI would be exposed to contaminated soil at all times while in the biosphere. All FEPs considered in the Biosphere Model and its input parameters are collectively included in BDCFs	10 CFR 63.311 10 CFR 63.321	MA
		3.3.04.01.0A Ingestion	The ingestion submodel included ingestion of contaminated food, drinking water, and soil. All FEPs considered in the Biosphere Model and its input parameters are collectively included in BDCFs that are implemented in TSPA.	10 CFR 63.311 10 CFR 63.331 10 CFR 63.321	MA
		3.3.04.02.0A Inhalation	The inhalation submodel includes inhalation of gaseous ^{14}C and radon decay products from radon exhalation from the ground, contaminated resuspended particles, and contaminated aerosols from evaporative coolers. All FEPs considered in the Biosphere Model and its input parameters are collectively included in BDCFs that are implemented in TSPA.	10 CFR 63.311 10 CFR 63.321	MA

Table I-2. Model Implementation for Included Features, Events, and Processes (Continued)

Submodel implemented in the TSPA-LA Model and Section Number	Path in GoldSim Model File	FEPs Included in the Submodel	TSPA Inclusion Explanation	Performance Assessment Standard[a]	TSPA-LA Model Implementation
Biosphere Submodel 6.3.11 (continued)	Epistemic: \Input_Params_Epistemic\Epistemic_Params_Biosphere Other: \TSPA_Model\Biosphere	3.3.04.03.0A External exposure	The external exposure submodel included external exposure to contaminated materials. The characteristics in these parameters are propagated to the BDCFs which are direct inputs to the TSPA for the scenario classes involving radionuclide release to the groundwater.	10 CFR 63.311 10 CFR 63.321	MA
		3.3.05.01.0A Radiation doses	Calculation of the predicted annual dose for a unit activity concentration of a radionuclide (i.e., BDCF) was conducted in the external exposure, inhalation, and ingestion submodels. All FEPs considered in the Biosphere Model and its input parameters are collectively included in BDCFs that are implemented in TSPA.	10 CFR 63.311 10 CFR 63.331 10 CFR 63.321	GSM
		3.3.08.00.0A Radon and radon decay product exposure	Exposure to radon (^{222}Rn) and radon decay products is included in the air and inhalation submodels of the groundwater and volcanic ash exposure scenarios. Concentrations of radon and radon decay products are calculated in the air submodels for the groundwater and volcanic ash exposure scenarios. This FEP is included in the biosphere component of the TSPA model through the use of groundwater exposure scenario BDCFs that are direct inputs to the TSPA for the scenario classes involving radionuclide release to the groundwater	10 CFR 63.311 10 CFR 63.331 10 CFR 63.321	GSM

Table I-2. Model Implementation for Included Features, Events, and Processes (Continued)

Submodel implemented in the TSPA-LA Model and Section Number	Path in GoldSim Model File	FEPs Included in the Submodel	TSPA Inclusion Explanation	Performance Assessment Standard[a]	TSPA-LA Model Implementation
WP Early Failure Submodel 6.4.2 Note: FEPS included here for the Early failure scenario class are in addition to the FEPS described above in sections 6.3.x	Epistemic: \Input_Params_Epistemic\Epistemic_Params_Events\Epistemic_Parameters_EF Aleatory: \Input_Params_Aleatory\Aleatory_Params_Events\Aleatory_Params_EF EBS: \Time_Zero\EBS_PS_Loop\Static_Calcs_PS_Loop\Static_Calcs_Events\Static_Calcs_EF \Global_Inputs_and_Calcs\Global_Events\Global_EF	2.1.03.08.0A Early failure of the waste package	Early failure of WPs due to manufacturing or handling-induced defects is modeled based on possible defects identified from literature and human error probability data. The resultant probability of early failure is evaluated by a log normal distribution with a median of 4.14×10^{-5} and an error factor of 8.17. These inputs are adjusted to conform to implementation requirements of GoldSim for log-normal distributions, which require geometric mean and geometric standard deviation as parameters. For WP early failure, the WPs are divided into two fuel-type groups denoted by CSNF early-failed WPs and CDSP early-failed WPs.	10 CFR 63.311 10 CFR 63.331	GSM
		2.1.03.11.0A Physical form of waste package and drip shield	The physical form of waste packages is represented in the TSPA by two nominal waste package configurations. For waste package early failure, the waste packages are divided into two fuel-type groups denoted by CSNF early-failed waste packages and CDSP early-failed waste packages.	10 CFR 63.311 10 CFR 63.331	GSM

Table I-2. Model Implementation for Included Features, Events, and Processes (Continued)

Submodel implemented in the TSPA-LA Model and Section Number	Path in GoldSim Model File	FEPs Included in the Submodel	TSPA Inclusion Explanation	Performance Assessment Standard[a]	TSPA-LA Model Implementation
DS Early Failure Submodel 6.4.1 Note: FEPS included here for the Early failure scenario class are in addition to the FEPS described above in sections 6.3.x	Epistemic: \Input_Params_Epistemic\Epistemic_Params_Events\Epistemic_Parameters_EF Aleatory: \Input_Params_Aleatory\Aleatory_Params_Events\Aleatory_Params_EF EBS: \Time_Zero\EBS_PS_Loop\Static_Calcs_PS_Loop\Static_Calcs_Events\Static_Calcs_EF \Global_Inputs_and_Calcs\Global_Events\Global_EF	2.1.03.08.0B Early failure of drip shields	Early failure of DSs due to manufacturing or handling-induced defects or errors in emplacement is modeled based on possible defects identified from literature and human error probability data. The resultant probability of early failure is evaluated by a log normal distribution with a median of 4.3×10^{-7} and an error factor of 14. These inputs are adjusted to conform to implementation requirements of GoldSim for log-normal distributions, which require geometric mean and geometric standard deviation as parameters. The rate of DS early failure is sampled in the TSPA-LA Model from this log-normal distribution. Early failed DSs are randomly placed in the repository. Early failure is assumed to occur at time zero and allows the full volume of seepage to contact the underlying WP. The underlying WP is also assumed to fail at time zero.	10 CFR 63.311 10 CFR 63.331	GSM
		2.1.03.11.0A Physical form of waste package and drip shield	Early failure of drip shields due to manufacturing or handling-induced defects or errors in emplacement, as identified from literature and human error probability data, is dependent on the specific form of the drip shield.	10 CFR 63.311 10 CFR 63.331	GSM

Table I-2. Model Implementation for Included Features, Events, and Processes (Continued)

Submodel implemented in the TSPA-LA Model and Section Number	Path in GoldSim Model File	FEPs Included in the Submodel	TSPA Inclusion Explanation	Performance Assessment Standard[a]	TSPA-LA Model Implementation
Igneous Intrusion Submodel 6.5.1 FEPS included here for the Igneous scenario class are in addition to the FEPS described above in sections 6.3.x	Epistemic: \Input_Params_Epistemic\Epistemic_Params_Events\Epistemic_Params_Igneous_Intr Aleatory: \Input_Params_Aleatory\Aleatory_Params_Events\Aleatory_Params_Igneous_Intr EBS: \Time_Zero\EBS_PS_Loop\Static_Calcs_PS_Loop\Static_Calcs_Events\Igneous_Intrusion\Global_Inputs_and_Calcs\Global_Events\Igneous_Scenario	1.2.04.03.0A Igneous intrusion into repository	The Igneous intrusion submodel includes the in-drift conditions that would accompany the intersection of one or more emplacement drifts by an ascending basaltic dike and subsequent cooling and solidification of the basaltic intrusion. This section also addresses estimating the number of WPs damaged in the intersected drifts.	10 CFR 63.311	GSM
Igneous Event Time and Probability Submodel 6.5.1 FEPS included here for the Igneous scenario class are in addition to the FEPS described above in sections 6.3.x		1.2.04.04.0A Igneous intrusion interacts with EBS components	In-drift conditions that would accompany intersection of one or more emplacement drifts by an ascending basaltic dike are described. The expected behavior of WPs exposed to magma is described. This supports the TSPA assumption that WPs, DSs, and cladding in intersected drifts provide no protection for the waste.	10 CFR 63.311	GSM
		1.2.04.06.0A Eruptive conduit to surface intersects repository	The modeling of eruption, dispersal, and transport of radionuclides is described, as well as the estimation of the number of WPs intersected by eruptive conduits. The descriptions provide the primary inputs for ASHPLUME to model the eruption case in TSPA.	10 CFR 63.311	GSM

Table I-2. Model Implementation for Included Features, Events, and Processes (Continued)

Submodel implemented in the TSPA-LA Model and Section Number	Path in GoldSim Model File	FEPs Included in the Submodel	TSPA Inclusion Explanation	Performance Assessment Standard[a]	TSPA-LA Model Implementation
Igneous Intrusion EBS Damage Submodel 6.5.1 Note: FEPS included here for the Igneous scenario class are in addition to the FEPS described above in sections 6.3.x	Epistemic: \Input_Params_Epistemic\Epistemic_Params_Events\Epistemic_Params_Igneous_Intr The five Volcanic eruption submodels from the Igneous Scenario Class are contained in a separate GoldSim model file:Aleatory: \Input_Params_Aleatory\Aleatory_Params_Events\Aleatory_Params_Igneous_Intr EBS: \Time_Zero\EBS_PS_Loop\Static_Calcs_PS_Loop\Static_Calcs_Events\Igneous_Intrusion\Global_Inputs_and_Calcs\Global_Events\Igneous_Scenario	1.2.04.03.0A Igneous intrusion into repository	The in-drift temperature conditions that would accompany the intersection of one or more emplacement drifts are represented in the TSPA-LA Model by the igneous intrusion thermal condition abstraction model.	10 CFR 63.311	GSM
		1.2.04.04.0A Igneous intrusion interacts with EBS components	TSPA implements the assumption that WPs and DSs in intersected drifts provide no protection for the waste immediately upon intrusion.	10 CFR 63.311	GSM
		2.1.03.11.0A Physical form of waste package and drip shield	In the igneous intrusion modeling case, magma from dikes is assumed to engulf all drip shields and waste packages in the repository, rendering them incapable of protecting their contents. Conceptually, the codisposal waste packages and CSNF waste packages no longer act to prevent or slow the rate of advective transport, leaving radionuclides available for transport by groundwater downward through the unsaturated zone to the water table. Both the geometry of the waste form (which is important for diffusive transport) and the formation of corrosion products from degradation of the waste package internal components (which impacts both diffusive transport and retardation due to sorption of radionuclides) are assumed to be the same as in the nominal scenario class.	10 CFR 63.311	GSM

Table I-2. Model Implementation for Included Features, Events, and Processes (Continued)

Submodel implemented in the TSPA-LA Model and Section Number	Path in GoldSim Model File	FEPs Included in the Submodel	TSPA Inclusion Explanation	Performance Assessment Standard[a]	TSPA-LA Model Implementation
EBS Chemical Environment Submodel Modifications for Igneous Intrusion 6.5.1 Note: FEPS included here for the Igneous scenario class are in addition to the FEPS described above in sections 6.3.x	Epistemic: \Input_Params_Epistemic\Epistemic_Params_Events\Epistemic_Params_Igneous_Intr The five Volcanic eruption submodels from the Igneous Scenario Class are contained in a separate GoldSim model file:Aleatory: \Input_Params_Aleatory\Aleatory_Params_Events\Aleatory_Params_Igneous_Intr EBS: \Time_Zero\EBS_PS_Loop\Static_Calcs_PS_Loop\Static_Calcs_Events\Igneous_Intrusion\Global_Inputs_and_Calcs\Global_Events\Igneous_Scenario	1.2.04.04.0B Chemical effects of magma and magmatic volatiles	Chemistry of water percolating into drifts that have cooled after an igneous intrusion could be affected by basalt-water interactions. Analogue data on basalt-water chemistry is included to support the abstraction of basalt-water chemistry used in the TSPA.	10 CFR 63.311	GSM

Table I-2. Model Implementation for Included Features, Events, and Processes (Continued)

Submodel implemented in the TSPA-LA Model and Section Number	Path in GoldSim Model File	FEPs Included in the Submodel	TSPA Inclusion Explanation	Performance Assessment Standard[a]	TSPA-LA Model Implementation
Volcanic Interaction with the Repository Submodel 6.5.2.1.1 FEPS included here for the Volcanic scenario class are in addition to the FEPS described above in sections 6.3.x	The Volcanic Eruption model is a separate GoldSim file: vE1.004_GS_9.60.100.gsm Epistemic: \Model_Uncertainties\EU\Inventory_Uncertainty and \Model_Uncertainties\EU\Eruptive_Case_Uncertainty Aleatory: \Model_Uncertainties\AU Other: \Eruptive_Model\Igneous_Erupt_Input and \Eruptive_Model\Igneous_Erupt_Calcs	1.2.04.04.0A Igneous intrusion interacts with EBS components	In the TSPA-LA Model the number of WPs intersected by magmatic conduits is a function of conduit area, the number of conduits, and the conduit location within the repository. Only WPs located partially or entirely within a magmatic conduit are assumed to be destroyed, making all of the waste in these WPs available for entrainment in the erupting pyroclastic material.	10 CFR 63.311	DLL
		1.2.04.06.0A Eruptive conduit to surface intersects repository	The consequences of an igneous intrusion through the repository and an associated eruptive event are explicitly included in the TSPA-LA Model through modeling of aerial dispersion followed by deposition and redistribution of potentially contaminated pyroclastic materials; the consequences are appropriately weighted by the probability of occurrence of the event.	10 CFR 63.311	DLL
Atmospheric Transport Submodel 6.5.2.1.2		1.2.04.07.0A Ashfall	The eruption model case that includes entrainment of waste in an ascending tephra plume and deposition of contaminated tephra on the land surface is described. The result is the areal concentration of contaminated tephra on the ground surface at the RMEI location.	10 CFR 63.311	DLL
Tephra Redistribution Submodel 6.5.2.1.3		1.2.04.07.0A Ashfall	Atmospheric transport of the tephra-waste mixture is modeled directly in the TSPA-LA Model using ASHPLUME, the atmospheric tephra dispersal model as it evaluates downwind transport of contaminated tephra and radioactive waste and their deposition on the ground surface.	10 CFR 63.311	DLL
		1.2.04.07.0C Ash redistribution via soil and sediment transport	The ash redistribution model is described, as are the results of surficial processes acting on primary tephra deposited on the two primary landforms near the RMEI location: distributary channels and interchannel divides. The model evaluates the effects of surficial processes on concentrations of waste as contaminated tephra is transported to the RMEI location.	10 CFR 63.311	DLL

Table I-2. Model Implementation for Included Features, Events, and Processes (Continued)

Submodel implemented in the TSPA-LA Model and Section Number	Path in GoldSim Model File	FEPs Included in the Submodel	TSPA Inclusion Explanation	Performance Assessment Standard[a]	TSPA-LA Model Implementation
Volcanic Ash Exposure Submodel 6.5.2.1.4	The Volcanic Eruption model is a separate GoldSim file: vE1.004_GS_9.60.100.gsm Epistemic: \Model_Uncertainties\EU\Biosphere_Uncertainty Aleatory: \Model_Uncertainties\AU Biosphere: \Eruptive_Model\Igneous_Erupt_Input\ST_Components and \Dose	1.2.04.07.0A Ashfall	Volcanic ash is the initial source of contamination for the eruption case of the volcanic scenario. Ash characteristics and depth were considered in development of the input parameters for the surface soil and air submodels.	10 CFR 63.311	DLL
		2.3.02.01.0A Soil Type	This FEP is dispositioned in the TSPA volcanic eruption modeling case through BDCFs for the volcanic ash exposure scenarios. Annual doses are calculated in the TSPA as the product of radionuclide concentration in soil contaminated by radionuclides volcanic tephra and the BDCF components. For the volcanic ash exposure scenario, three BDCF components are provided to the TSPA-LA Model that account for various RMEI exposure pathways.	10 CFR 63.311	DLL
		2.3.02.02.0A Radionuclide accumulation in soils	This FEP is dispositioned in the TSPA volcanic eruption modeling case through BDCFs for the volcanic ash exposure scenarios. Annual doses are calculated in the TSPA as the product of radionuclide concentration in soil contaminated by radionuclides volcanic tephra and the BDCF components. For the volcanic ash exposure scenario, three BDCF components are provided to the TSPA-LA Model that account for various RMEI exposure pathways.	10 CFR 63.311	DLL
		2.3.02.03.0A Soil and sediment transport in the biosphere	This FEP is dispositioned in the TSPA volcanic eruption modeling case through BDCFs for the volcanic ash exposure scenarios. Annual doses are calculated in the TSPA as the product of radionuclide concentration in soil contaminated by radionuclides volcanic tephra and the BDCF components. For the volcanic ash exposure scenario, three BDCF components are provided to the TSPA-LA Model that account for various RMEI exposure pathways.	10 CFR 63.311	DLL

Table I-2. Model Implementation for Included Features, Events, and Processes (Continued)

Submodel implemented in the TSPA-LA Model and Section Number	Path in GoldSim Model File	FEPs Included in the Submodel	TSPA Inclusion Explanation	Performance Assessment Standard[a]	TSPA-LA Model Implementation
Volcanic Ash Exposure Submodel 6.5.2.1.4 (Continued)	The Volcanic Eruption model is a separate GoldSim file: vE1.004_GS_9.60.100.gsm Epistemic: \Model_Uncertainties\EU\Biosphere_Uncertainty Aleatory: \Model_Uncertainties\AU Biosphere: \Eruptive_Model\Igneous_Erupt_Input\ST_Components and \Dose	2.3.11.01.0A Precipitation	This FEP is dispositioned in the TSPA Volcanic Eruption Modeling Case through BDCFs for the volcanic ash exposure scenario (because the mass loading levels and some agricultural parameters may depend on precipitation) and the radioactive waste concentration in the soil calculated by the Tephra Redistribution Model. Annual doses are calculated in the TSPA as the product of radionuclide concentration in the soil contaminated by radionuclides in volcanic tephra, the BDCF components, and the mass loading time decrease function. For the volcanic ash exposure scenario, three BDCF components are provided to the TSPA-LA Model that account for various RMEI exposure pathways.	10 CFR 63.311	DLL

Table I-2. Model Implementation for Included Features, Events, and Processes (Continued)

Submodel implemented in the TSPA-LA Model and Section Number	Path in GoldSim Model File	FEPs Included in the Submodel	TSPA Inclusion Explanation	Performance Assessment Standard[a]	TSPA-LA Model Implementation
Volcanic Ash Exposure Submodel 6.5.2.1.4 (Continued)	The Volcanic Eruption model is a separate GoldSim file: vE1.004_GS_9.60.100.gsm Epistemic: \Model_Uncertainties\EU\Biosphere_Uncertainty Aleatory: \Model_Uncertainties\AU Biosphere: \Eruptive_Model\Igneous_Erupt_Input\ST_Components and \Dose	2.3.13.01.0A Biosphere characteristics	The TSPA-LA Model calculates radiation dose as a product of the time-dependent source terms, the source-independent BDCFs, and the mass loading time decay function. For the volcanic ash exposure scenario, three BDCF components are provided to the TSPA-LA Model. The first is for exposure to sources external to the body, and the second and third BDCF components (the short-term and the long-term inhalation components) account for inhaling airborne particulates.	10 CFR 63.311	DLL
		2.3.13.02.0A Radionuclide alteration during biosphere transport	This FEP is dispositioned in the TSPA Volcanic Eruption Modeling Case through BDCFs for the volcanic ash exposure scenario. Annual doses are calculated in the TSPA as the product of radionuclide concentration in soil contaminated by radionuclides in volcanic tephra, the BDCF components, and the mass loading time decrease function. For the volcanic ash exposure scenario, three BDCF components are provided to the TSPA-LA Model that account for various RMEI exposure pathways.	10 CFR 63.311	DLL

Table I-2. Model Implementation for Included Features, Events, and Processes (Continued)

Submodel implemented in the TSPA-LA Model and Section Number	Path in GoldSim Model File	FEPs Included in the Submodel	TSPA Inclusion Explanation	Performance Assessment Standard[a]	TSPA-LA Model Implementation
Volcanic Ash Exposure Submodel 6.5.2.1.4 (Continued)	The Volcanic Eruption model is a separate GoldSim file: vE1.004_GS_9.60.100.gsm Epistemic: \Model_Uncertainties\EU\Biosphere_Uncertainty Aleatory: \Model_Uncertainties\AU Biosphere: \Eruptive_Model\Igneous_Erupt_Input\ST_Components and \Dose	2.4.01.00.0A Human characteristics (physiology, metabolism)	This FEP is dispositioned in the TSPA Volcanic Eruption Modeling Case through BDCFs for the volcanic ash exposure scenario. Annual doses are calculated in the TSPA as the product of radionuclide concentration in soil contaminated by radionuclides in volcanic tephra, the BDCF components, and the mass loading time decrease function. For the volcanic ash exposure scenario, three BDCF components are provided to the TSPA-LA Model that account for various RMEI exposure pathways: exposure to sources external to the body, (ingestion, and inhalation of radon decay products); and the short-term and long-term inhalation components.	10 CFR 63.311	DLL
		2.4.04.01.0A Human Lifestyle	This FEP is dispositioned in the TSPA Volcanic Eruption Modeling Case through BDCFs for the volcanic ash exposure scenario. Annual doses are calculated in the TSPA as the product of radionuclide concentration in soil contaminated by radionuclides in volcanic tephra, the BDCF components, and the mass loading time decrease function. For the volcanic ash exposure scenario, three BDCF components are provided to the TSPA-LA Model that account for various RMEI exposure pathways.	10 CFR 63.311	DLL

Table I-2. Model Implementation for Included Features, Events, and Processes (Continued)

Submodel implemented in the TSPA-LA Model and Section Number	Path in GoldSim Model File	FEPs Included in the Submodel	TSPA Inclusion Explanation	Performance Assessment Standard[a]	TSPA-LA Model Implementation
Volcanic Ash Exposure Submodel 6.5.2.1.4 (Continued)	The Volcanic Eruption model is a separate GoldSim file: vE1.004_GS_9.60.100.gsm Epistemic: \Model_Uncertainties\EU\Biosphere_Uncertainty Aleatory: \Model_Uncertainties\AU Biosphere: \Eruptive_Model\Igneous_Erupt_Input\ST_Components and \Dose	2.4.07.00.0A Dwellings	This FEP is dispositioned in the TSPA Volcanic Eruption Modeling Case through BDCFs for the volcanic ash exposure scenarios. Annual doses are calculated in the TSPA as the product of radionuclide concentration in soil contaminated by radionuclides volcanic tephra and the BDCF components. For the volcanic ash exposure scenario, three BDCF components are provided to the TSPA-LA Model that account for various RMEI exposure pathways	10 CFR 63.311	DLL
		2.4.08.00.0A Wild and natural land and water use	This FEP is dispositioned in the TSPA Volcanic Eruption Modeling Case through BDCFs for the volcanic ash exposure scenarios. Annual doses are calculated in the TSPA as the product of radionuclide concentration in soil contaminated by radionuclides volcanic tephra and the BDCF components. For the volcanic ash exposure scenario, three BDCF components are provided to the TSPA-LA Model that account for various RMEI exposure pathways	10 CFR 63.311	DLL
		2.4.09.01.0B Agricultural land use and irrigation	This FEP is dispositioned in the TSPA Volcanic Eruption Modeling Case through BDCFs for the volcanic ash exposure scenarios. Annual doses are calculated in the TSPA as the product of radionuclide concentration in soil contaminated by radionuclides volcanic tephra and the BDCF components. For the volcanic ash exposure scenario, three BDCF components are provided to the TSPA-LA Model that account for various RMEI exposure pathways	10 CFR 63.311	DLL

Table I-2. Model Implementation for Included Features, Events, and Processes (Continued)

Submodel implemented in the TSPA-LA Model and Section Number	Path in GoldSim Model File	FEPs Included in the Submodel	TSPA Inclusion Explanation	Performance Assessment Standard[a]	TSPA-LA Model Implementation
Volcanic Ash Exposure Submodel 6.5.2.1.4 (Continued)	The Volcanic Eruption model is a separate GoldSim file: vE1.004_GS_9.60.100.gsm Epistemic: \Model_Uncertainties\EU\Biosphere_Uncertainty Aleatory: \Model_Uncertainties\AU Biosphere: \Eruptive_Model\Igneous_Erupt_Input\ST_Components and \Dose	2.4.09.02.0A Animal farms and fisheries	This FEP is dispositioned in the TSPA Volcanic Eruption Modeling Case through BDCFs for the volcanic ash exposure scenarios. For the volcanic ash scenario, a fish consumption pathway is not included. Annual doses are calculated in the TSPA as the product of radionuclide concentration in soil contaminated by radionuclides in volcanic tephra, the BDCF components, and the mass loading time decrease function. For the volcanic ash exposure scenario, three BDCF components are provided to the TSPA-LA Model that account for various RMEI exposure pathways.	10 CFR 63.311	DLL
		2.4.10.00.0A Urban and industrial land and water use	This FEP is dispositioned in the TSPA Volcanic Eruption Modeling Case through BDCFs for the volcanic ash exposure scenarios. Annual doses are calculated in the TSPA as the product of radionuclide concentration in soil contaminated by radionuclides volcanic tephra and the BDCF components. For the volcanic ash exposure scenario, three BDCF components are provided to the TSPA-LA Model that account for various RMEI exposure pathways	10 CFR 63.311	DLL

Table I-2. Model Implementation for Included Features, Events, and Processes (Continued)

Submodel implemented in the TSPA-LA Model and Section Number	Path in GoldSim Model File	FEPs Included in the Submodel	TSPA Inclusion Explanation	Performance Assessment Standard[a]	TSPA-LA Model Implementation
Volcanic Ash Exposure Submodel 6.5.2.1.4 (Continued)	The Volcanic Eruption model is a separate GoldSim file: vE1.004_GS_9.60.100.gsm Epistemic: \Model_Uncertainties\EU\Biosphere_Uncertainty Aleatory: \Model_Uncertainties\AU Biosphere: \Eruptive_Model\Igneous_Erupt_Input\ST_Components and \Dose	3.2.10.00.0A Atmospheric transport of contaminants	This FEP is dispositioned in the TSPA Volcanic Eruption Modeling Case through BDCFs for the volcanic ash exposure scenario. Annual doses are calculated in the TSPA as the product of radionuclide concentration in soil contaminated by radionuclides in volcanic tephra, the BDCF components, and the mass loading time decrease function. For the volcanic ash exposure scenario, three BDCF components are provided to the TSPA-LA Model that account for various RMEI exposure pathways: exposure to sources external to the body, (ingestion, and inhalation of radon decay products); and the short-term and long-term inhalation components	10 CFR 63.311	DLL
		3.3.01.00.0A Contaminated drinking water, foodstuffs and drugs	This FEP is dispositioned in the TSPA Volcanic Eruption Modeling Case through BDCFs for the volcanic ash exposure scenario. Annual doses are calculated in the TSPA as the product of radionuclide concentration in soil contaminated by radionuclides in volcanic tephra, the BDCF components, and the mass loading time decrease function. For the volcanic ash exposure scenario, three BDCF components are provided to the TSPA-LA Model that account for various RMEI exposure pathways.	10 CFR 63.311	DLL

Table I-2. Model Implementation for Included Features, Events, and Processes (Continued)

Submodel implemented in the TSPA-LA Model and Section Number	Path in GoldSim Model File	FEPs Included in the Submodel	TSPA Inclusion Explanation	Performance Assessment Standard[a]	TSPA-LA Model Implementation
Volcanic Ash Exposure Submodel 6.5.2.1.4 (Continued)	The Volcanic Eruption model is a separate GoldSim file: vE1.004_GS_9.60.100.gsm Epistemic: \Model_Uncertainties\EU\Biosphere_Uncertainty Aleatory: \Model_Uncertainties\AU Biosphere: \Eruptive_Model\Igneous_Erupt_Input\ST_Components and \Dose	3.3.02.01.0A Plant uptake	This FEP is dispositioned in the TSPA Volcanic Eruption Modeling Case through BDCFs for the volcanic ash exposure scenario. Annual doses are calculated in the TSPA as the product of radionuclide concentration in soil contaminated by radionuclides in volcanic tephra, the BDCF components, and the mass loading time decrease function. For the volcanic ash exposure scenario, three BDCF components are provided to the TSPA-LA Model that account for various RMEI exposure pathways.	10 CFR 63.311	DLL
		3.3.02.02.0A Animal uptake	This FEP is dispositioned in the TSPA Volcanic Eruption Modeling Case through BDCFs for the volcanic ash exposure scenarios. Annual doses are calculated in the TSPA as the product of radionuclide concentration in soil contaminated by radionuclides in volcanic tephra, the BDCF components, and the mass loading time decrease function. For the volcanic ash exposure scenario, three BDCF components are provided to the TSPA-LA Model that account for various RMEI exposure pathways: short term and long term inhalation, and exposure to sources external to the body.	10 CFR 63.311	DLL

Table I-2. Model Implementation for Included Features, Events, and Processes (Continued)

Submodel implemented in the TSPA-LA Model and Section Number	Path in GoldSim Model File	FEPs Included in the Submodel	TSPA Inclusion Explanation	Performance Assessment Standard[a]	TSPA-LA Model Implementation
Volcanic Ash Exposure Submodel 6.5.2.1.4 (Continued)	The Volcanic Eruption model is a separate GoldSim file: vE1.004_GS_9.60.100.gsm Epistemic: \Model_Uncertainties\EU\Biosphere_Uncertainty Aleatory: \Model_Uncertainties\AU Biosphere: \Eruptive_Model\Igneous_Erupt_Input\ST_Components and \Dose	3.3.03.01.0A Contaminated non-food products and exposure	This FEP is dispositioned in the TSPA Volcanic Eruption Modeling Case through BDCFs for the volcanic ash exposure scenarios. Annual doses are calculated in the TSPA as the product of radionuclide concentration in soil contaminated by radionuclides in volcanic tephra, the BDCF components, and the mass loading time decrease function. For the volcanic ash exposure scenario, three BDCF components are provided to the TSPA-LA Model that account for various RMEI exposure pathways	10 CFR 63.311	DLL
		3.3.04.01.0A Ingestion	This FEP is also dispositioned in the TSPA Volcanic Eruption Modeling Case through BDCFs for the volcanic ash exposure scenario. Annual doses are calculated in the TSPA as the product of radionuclide concentration in soil contaminated by radionuclides in volcanic tephra, the BDCF components, and the mass loading time decrease function. For the volcanic ash exposure scenario, three BDCF components are provided to the TSPA-LA Model that account for various RMEI exposure pathways: exposure to sources external to the body, and short-term and long-term inhalation.	10 CFR 63.311	DLL

Table I-2. Model Implementation for Included Features, Events, and Processes (Continued)

Submodel implemented in the TSPA-LA Model and Section Number	Path in GoldSim Model File	FEPs Included in the Submodel	TSPA Inclusion Explanation	Performance Assessment Standard[a]	TSPA-LA Model Implementation
Volcanic Ash Exposure Submodel 6.5.2.1.4 (Continued)	The Volcanic Eruption model is a separate GoldSim file: vE1.004_GS_9.60.100.gsm Epistemic: \Model_Uncertainties\EU\Biosphere_Uncertainty Aleatory: \Model_Uncertainties\AU Biosphere: \Eruptive_Model\Igneous_Erupt_Input\ST_Components and \Dose	3.3.04.02.0A Inhalation	This FEP is dispositioned in the TSPA Volcanic Eruption Modeling Case through BDCFs for the volcanic ash exposure scenario. Annual doses are calculated in the TSPA as the product of radionuclide concentration in soil contaminated by radionuclides in volcanic tephra, the BDCF components, and the mass loading time decrease function. For the volcanic ash exposure scenario, three BDCF components are provided to the TSPA-LA Model that account for various RMEI exposure pathways: exposure to sources external to the body, ingestion, and inhalation of radon decay products; and the short-term and long-term inhalation components account for the remaining two.	10 CFR 63.311	DLL
		3.3.04.03.0A External exposure	This FEP is dispositioned in the TSPA Volcanic Eruption Modeling Case through BDCFs for the volcanic ash exposure scenarios. Annual doses are calculated in the TSPA as the product of radionuclide concentration in soil contaminated by radionuclides in volcanic tephra, the BDCF components, and the mass loading time decrease function. For the volcanic ash exposure scenario, three BDCF components are provided to the TSPA-LA Model that account for various RMEI exposure pathways, including external exposure.	10 CFR 63.311	DLL

Table I-2. Model Implementation for Included Features, Events, and Processes (Continued)

Submodel implemented in the TSPA-LA Model and Section Number	Path in GoldSim Model File	FEPs Included in the Submodel	TSPA Inclusion Explanation	Performance Assessment Standard[a]	TSPA-LA Model Implementation
Volcanic Ash Exposure Submodel 6.5.2.1.4 (Continued)	The Volcanic Eruption model is a separate GoldSim file: vE1.004_GS_9.60.100.gsm Epistemic: \Model_Uncertainties\EU\Biosphere_Uncertainty Aleatory: \Model_Uncertainties\AU Biosphere: \Eruptive_Model\Igneous_Erupt_Input\ST_Components and \Dose	3.3.05.01.0A Radiation doses	This FEP is dispositioned in the TSPA Volcanic Eruption Modeling Case through BDCFs for the volcanic ash exposure scenario. Because variation in radionuclide concentrations in deposited and redistributed volcanic tephra is not part of the biosphere model, BDCFs are calculated based on a unit radionuclide concentration in the soil, depending on the exposure pathway. The TSPA-LA Model calculates annual radiation dose as a product of the time-dependent source terms, the source-independent BDCFs, and the mass loading time decay function. For the volcanic ash exposure scenario, three BDCF components are provided to the TSPA-LA Model: exposure to sources external to the body, (ingestion, and inhalation of radon decay products) and the short-term and long-term inhalation of airborne particulates.	10 CFR 63.311	DLL
		3.3.08.00.0A Radon and radon decay product exposure	Radon (^{222}Rn) is a decay product of one of the primary radionuclides considered in the TSPA. Human exposure to radon and radon decay products occurs through inhalation. Concentrations of radon and radon decay products are calculated in the air submodels for the volcanic ash exposure scenario. For the volcanic ash exposure scenario, three BDCF components are provided to the TSPA model that account for various RMEI exposure pathways, including inhalation of radon and its decay products	10 CFR 63.311	DLL

Table I-2. Model Implementation for Included Features, Events, and Processes (Continued)

Submodel implemented in the TSPA-LA Model and Section Number	Path in GoldSim Model File	FEPs Included in the Submodel	TSPA Inclusion Explanation	Performance Assessment Standard[a]	TSPA-LA Model Implementation
Ground Motion Damage Submodel 6.6.1.1.1	Epistemic: \Input_Params_Epistemic\Epistemic_Params_Events\Epistemic_Params_Seismic Aleatory: \Input_Params_Aleatory\Aleatory_Params_Events\Input_Params_Seismic_Uncert \Input_Params_Aleatory\Aleatory_Params_Events\Input_Params_Seismic_FD_Uncert EBS: \Time_Zero\EBS_PS_Loop\Static_Calcs_PS_Loop\Static_Calcs_Events\Seismic_Fault_Displacement \Global_Inputs_and_Calcs\Global_Events\Seismic_Scenario	1.2.03.02.0A Seismic ground motion damages EBS components	Structural calculations were used to simulate the response of the DS and WP to vibratory ground motion. These calculations utilize a three-dimensional, dynamic structural analysis model that incorporates the details of the EBS design. Ground motion time histories input into the calculations represent postclosure hazard levels at the emplacement depth. The potential for structural damage and for separation of the DSs is examined. The potential damage to the WP due to ground motion-induced interactions of the WPs, the pallet, and the DS are examined. Surface area damage is determined for input to the abstraction of seismic consequence. Acceleration and potential structural failure of fuel cladding induced by the ground motions is also determined. Results of these studies are used in creating abstractions for TSPA	10 CFR 63.311 10 CFR 63.331	GSM

Table I-2. Model Implementation for Included Features, Events, and Processes (Continued)

Submodel implemented in the TSPA-LA Model and Section Number	Path in GoldSim Model File	FEPs Included in the Submodel	TSPA Inclusion Explanation	Performance Assessment Standard[a]	TSPA-LA Model Implementation
Ground Motion Damage Submodel 6.6.1.1.1 (Continued)	Epistemic: \Input_Params_Epistemic\Epistemic_Params_Events\Epistemic_Params_Seismic Aleatory: \Input_Params_Aleatory\Aleatory_Params_Events\Input_Params_Seismic_Uncert \Input_Params_Aleatory\Aleatory_Params_Events\Input_Params_Seismic_FD_Uncert EBS: \Time_Zero\EBS_PS_Loop\Static_Calcs_PS_Loop\Static_Calcs_Events\Seismic_Fault_Displacement \Global_Inputs_and_Calcs\Global_Events\Seismic_Scenario	1.2.03.02.0C Seismic-induced drift collapse damages EBS components	Drift collapse as a function of seismic shaking is the only mechanism in the TSPA-LA Model for rockfall and DS loading. Abstraction damage models for rock loading of DSs and WPs are provided by the Seismic Consequence Abstraction Model. The loading of the DS and its response to time-dependent drift degradation is represented in the TSPA-LA Model by a DS damage abstraction submodel. If the DS has corroded or collapsed rockfall may also load the WP. The loading of the DS and its response to time-dependent drift degradation is represented in the TSPA-LA Model by a WP damage abstraction submodel.	10 CFR 63.311 10 CFR 63.331	GSM

Table I-2. Model Implementation for Included Features, Events, and Processes (Continued)

Submodel implemented in the TSPA-LA Model and Section Number	Path in GoldSim Model File	FEPs Included in the Submodel	TSPA Inclusion Explanation	Performance Assessment Standard[a]	TSPA-LA Model Implementation
Ground Motion Damage Submodel 6.6.1.1.1 (Continued)	Epistemic: \Input_Params_Epistemic\Epistemic_Params_Events\Epistemic_Params_Seismic Aleatory: \Input_Params_Aleatory\Aleatory_Params_Events\Input_Params_Seismic_Uncert \Input_Params_Aleatory\Aleatory_Params_Events\Input_Params_Seismic_FD_Uncert EBS: \Time_Zero\EBS_PS_Loop\Static_Calcs_PS_Loop\Static_Calcs_Events\Seismic_Fault_Displacement \Global_Inputs_and_Calcs\Global_Events\Seismic_Scenario	1.2.03.03.0A Seismicity associated with igneous activity	Seismicity associated with igneous activity was considered as part of the probabilistic seismic hazard analysis for Yucca Mountain. The seismic source characterization expert teams either included specific seismic sources for seismicity associated with igneous activity or determined that such seismicity was included in their areal source zones representing background seismicity not associated with specific faults. Thus, seismicity associated with igneous activity is included in the ground motion hazard results that form the basis for developing seismic inputs for postclosure analyses.	10 CFR 63.311 10 CFR 63.331	MA
		2.1.06.05.0C Chemical degradation of emplacement pallet	A thickness reduction equal to the WP outer barrier thickness reduction is also applied to the Alloy 22 plates of the emplacement pallet for each analysis in the Seismic Consequence Abstraction. While no parameter was directly sent to TSPA, the seismic damage abstraction has an implicit treatment of chemical degradation of the pallet, that in effect reduces the pallet thickness and hence stiffness at a rate equal to the WP thinning. The thinning of the WP emplacement pallet due to chemical degradation is included in seismic analyses, however, the affect of the emplacement pallet on radionuclide release is not considered.	10 CFR 63.311 10 CFR 63.331	MA
		2.1.03.11.0A Physical form of waste package and drip shield	The seismic consequence abstraction takes into account that when a ground motion event occurs, the drip shield above the affected waste packages is assumed to be ruptured. The releases of radionuclides are mainly due to the failure of the drip shield and the open breach area in the waste package.	10 CFR 63.311 10 CFR 63.331	GSM
Fault Displacement Damage Submodel 6.6.1.1.3		1.2.02.03.0A Fault displacement damages EBS components	An analysis is performed that examines how fault displacement may contribute to mechanical disruption of the EBS. In this analysis, estimates of very low probability fault displacement are compared with the dimensions of the EBS features. Potential damage to the EBS is estimated, and the results are used to create an abstraction for TSPA.	10 CFR 63.311 10 CFR 63.331	GSM

Table I-2. Model Implementation for Included Features, Events, and Processes (Continued)

Submodel implemented in the TSPA-LA Model and Section Number	Path in GoldSim Model File	FEPs Included in the Submodel	TSPA Inclusion Explanation	Performance Assessment Standard[a]	TSPA-LA Model Implementation
Fault Displacement Damage Submodel 6.6.1.1.3		2.1.03.11.0A Physical form of waste package and drip shield	The seismic consequence abstraction takes into account how fault displacement may contribute to mechanical disruption of the WP and DS. In this analysis, estimates of very low probability fault displacement are compared with the dimensions of the EBS features. Potential damage to the EBS is estimated, and the results are used to create an abstraction for TSPA.	10 CFR 63.311 10 CFR 63.331	DLL
Drift Seepage Submodel Modifications for Seismic Disruption 6.6.2.1	Epistemic: \Input_Params_Epistemic\Epistemic_Params_Events\Epistemic_Params_Seismic Aleatory: \Input_Params_Aleatory\Aleatory_Params_Events\Input_Params_Seismic_Uncert \Input_Params_Aleatory\Aleatory_Params_Events\Input_Params_Seismic_FD_Uncert EBS: \Time_Zero\EBS_PS_Loop\Static_Calcs_PS_Loop\Static_Calcs_Events\Seismic_Fault_Displacement \Global_Inputs_and_Calcs\Global_Ev	1.2.03.02.0D Seismic-induced drift collapse alters in-drift thermohydrology	Postclosure ground motion in lithophysal rock could result in substantial or complete drift collapse affecting the hydrologic and thermal environment in the EBS. The potential for drift collapse and its thermal-hydrologic consequences are addressed in by the Multiscale Thermohydrologic Model implemented in TSPA. Changes in seepage behavior caused by seismically induced drift collapse are included in calculations for the lithophysal host rock only. A seepage abstraction is used to represent the range from intact (uncollapsed) to fully collapsed openings. The approach interpolates linearly between the uncollapsed and collapsed abstractions using rockfall volume as modeled in seismic consequence abstraction to define the extent of collapse. Both MSTHM and seismic consequence abstraction are implemented in the TSPA-LA model.	10 CFR 63.311 10 CFR 63.331	DLL
		2.1.08.02.0A Enhanced influx at the repository	The impact of an underground opening on the unsaturated flow field (including capillary barrier effect and the related flow diversion around the drifts) and its relevance for seepage is explicitly captured in the seepage calibration model and seepage model for performance assessment, which provide the basis for the drift seepage abstraction implementation in the TSPA-LA Model The drift seepage abstraction provides a seepage abstraction look-up table for enhanced seepage due to drift collapse as a result of seismic ground motions.	10 CFR 63.311 10 CFR 63.331	DLL

Table I-2. Model Implementation for Included Features, Events, and Processes (Continued)

Submodel implemented in the TSPA-LA Model and Section Number	Path in GoldSim Model File	FEPs Included in the Submodel	TSPA Inclusion Explanation	Performance Assessment Standard[a]	TSPA-LA Model Implementation
EBS TH Environment Submodel Modifications for Seismic Disruption 6.6.2.2	ents\Seismic_Scenario	1.2.03.02.0D Seismic-induced drift collapse alters in-drift thermohydrology	Drift collapse can occur due to seismic-induced large peak ground velocity. Drift collapse can act like backfill and alter the in-drift thermal-hydrologic conditions. This effect is captured explicitly by MSTHM process model simulations. These simulations are used to develop TH abstractions implemented in the TSPA for the Seismic Scenario Class.	10 CFR 63.311 10 CFR 63.331	GSM
Human Intrusion Submodel 6.7	Aleatory: \Input_Params_Aleatory\Aleatory_Params_Events\Aleatory_Params_HI EBS: \Time_Zero\EBS_PS_Loop\Static_Calcs_PS_Loop\Static_Calcs_Events\Human_Intrusion_Events \Global_Inputs_and_Calcs\Global_Events\Human_Intrusion Other: \TSPA_Model\UZ_Transport\UZ_Transport_Calculations\HI_Borehole_Transport	1.4.04.00.0A Drilling activities (human intrusion)	These FEPs are included in a stylized TSPA assessment that is consistent with the requirements described for the human intrusion stylized scenario defined in 10 CFR 63.322 [DIRS 180319] and proposed rule 10 CFR 63.321 [DIRS 178394]. This assessment addresses drilling activities, inadvertent human intrusion and effects of drilling.	10 CFR 63.321	GSM
		1.4.04.01.0A Effects of drilling intrusion		10 CFR 63.321	GSM/MA/ DLL
		1.4.02.02.0A Inadvertent human intrusion		10 CFR 63.321	GSM/MA/ DLL

Table I-2. Model Implementation for Included Features, Events, and Processes (Continued)

Submodel implemented in the TSPA-LA Model and Section Number	Path in GoldSim Model File	FEPs Included in the Submodel	TSPA Inclusion Explanation	Performance Assessment Standard[a]	TSPA-LA Model Implementation
Human Intrusion Submodel 6.7	Aleatory: \Input_Params_Aleatory\Aleatory_Params_Events\Aleatory_Params_HI EBS: \Time_Zero\EBS_PS_Loop\Static_Calcs_PS_Loop\Static_Calcs_Events\Human_Intrusion_Events \Global_Inputs_and_Calcs\Global_Events\Human_Intrusion Other: \TSPA_Model\UZ_Transport\UZ_Transport_Calculations\HI_Borehole_Transport	2.1.03.01.0B General corrosion of drip shields	In the case of human intrusion, the rate of general corrosion is used to determine the earliest time at which intrusion would not be recognized by the drillers. The TSPA-LA Model for general corrosion is the only DS corrosion mechanism modeled. This process is modeled as being independent of temperature and relative humidity and is initiated at the time of repository closure. Because of the low corrosion rate of titanium alloy used for the DSs, the initial breaches of the DSs are not expected to occur until well after 10,000 years.	10 CFR 63.321	GSM/MA/ DLL
		2.1.03.11.0A Physical form of waste package and drip shield	The rate of general corrosion is used to determine the earliest time at which human intrusion would not be recognized by the drillers. The TSPA-LA model for general corrosion is the only drip shield corrosion mechanism modeled. This process is modeled independent of temperature and relative humidity, but is dependent on the specific forms of the drip shields, waste packages, and internal waste containers that are proposed for the Yucca Mountain repository.	10 CFR 63.321	GSM/MA/ DLL
TSPA FEPs	\Model	0.1.02.00.0A Timescales of concern	The simulation durations are set to 20,000 years and 1,000,000 years to cover the regulatory time periods of 10,000 years and 1,000,000 years and to evaluate uncertainties in results after 10,000 years and before 20,000 years.	10 CFR 63.311 10 CFR 63.331 10 CFR 63.321	GSM/MA/ DLL
		0.1.03.00.0A Spatial domain of concern	The spatial domain encompassed and evaluated explicitly in the TSPA and GoldSim model file extends from the land surface through the UZ, through the repository, into the SZ, and laterally away from the repository to the location of the RMEI and to a representative volume of water in the accessible environment	10 CFR 63.311 10 CFR 63.331 10 CFR 63.321	GSM/MA/ DLL

Table I-2. Model Implementation for Included Features, Events, and Processes (Continued)

Submodel implemented in the TSPA-LA Model and Section Number	Path in GoldSim Model File	FEPs Included in the Submodel	TSPA Inclusion Explanation	Performance Assessment Standard[a]	TSPA-LA Model Implementation
TSPA FEPs (continued)	\Model	0.1.09.00.0A Regulatory requirements and exclusions	This is intrinsically included throughout the TSPA-LA Model because these regulations provided requirements for model development. One example of how this FEP was implemented is comparing the mean biosphere dose with the established regulatory limit.	10 CFR 63.311 10 CFR 63.331 10 CFR 63.321	GSM/MA/ DLL
		0.1.10.00.0A Model and data issues	Model and data requirements are addressed specifically at 10 CFR 63.114 [DIRS 178394] and are included in the GoldSim model file. This FEP is very broad in nature and also includes information covered in Sections 5, 6, 7, and 8 of this document.	10 CFR 63.311 10 CFR 63.331 10 CFR 63.321	GSM/MA/ DLL
		1.1.07.00.0A Repository design	This FEP is implemented in many locations in the TSPA-LA Model. Model components reflect the physical dimensions, material characteristics, and evolution of the in-drift environment, all of which stem directly from design considerations. The data element Drift_Diameter is one example of repository design implementation. The dimensions of the invert are another example of the design implementation.	10 CFR 63.311 10 CFR 63.331 10 CFR 63.321	GSM/MA/ DLL
		1.1.13.00.0A Retrievability	Retrievability is implicitly addressed in the TSPA-LA Model through the implementation of the repository design (FEP 1.1.07.00.0A). Particularly applicable to this FEP are the model components for the EBS, WP and DS degradation, waste form degradation and mobilization, and EBS flow and transport. Retrievability is thereby implicitly included in the TSPA.	10 CFR 63.311 10 CFR 63.331 10 CFR 63.321	GSM/MA/ DLL
		1.1.09.00.0A Schedule and planning	Schedule and planning is one of several initial conditions set for the TSPA-LA Model. For example, the waste emplacement schedule and closure of the repository are tied to the TSPA via the assumed post-emplacement ventilation duration and the radiation decay and thermal decay that takes place during preclosure and is accounted for in radionuclide inventories and thermal-hydrological inputs that are provided to TSPA.	10 CFR 63.311 10 CFR 63.331 10 CFR 63.321	GSM/MA/ DLL

Table I-2. Model Implementation for Included Features, Events, and Processes (Continued)

Submodel implemented in the TSPA-LA Model and Section Number	Path in GoldSim Model File	FEPs Included in the Submodel	TSPA Inclusion Explanation	Performance Assessment Standard[a]	TSPA-LA Model Implementation
TSPA FEPs (continued)	\Model	2.1.01.04.0A Repository-scale spatial heterogeneity of emplaced waste	Waste form heterogeneity is addressed through several approaches: (1) the waste form physical, chemical, and radiological properties are addressed through the degradation models for the CSNF waste form, the DSNF waste form, and the HLW form; (2) WP radionuclide inventory heterogeneity is addressed through uncertainty parameters; and (3) effects of WP heterogeneity as a result of differing waste form contents is addressed in the In-Package Chemistry submodel.	10 CFR 63.311 10 CFR 63.331 10 CFR 63.321	GSM

[a] 10 CFR 63.311 Individual Protection (70 FR 53313 [DIRS 178394])

10 CFR 63.331 Groundwater Protection (10 CFR 63 [DIRS 180319])

10 CFR 63.321 Human Intrusion (70 FR 53313 [DIRS 178394])

APPENDIX J
CONCEPTUAL STRUCTURE OF TSPA-LA

J1 INTRODUCTION

Performance assessment (PA) for a complex system requires detailed calculations that bring together a probabilistic description of the events that could affect the system, models for physical processes associated with the system, and an assessment of the level confidence that can be ascribed to individual assumptions that underlie the PA. Owing to its inherent complexity, a PA needs a clear conceptual structure that provides both an overview of what the PA is intended to calculate and guidance on the computational structure required to implement the PA. Without an overarching structure, it is difficult to communicate exactly what a PA is intended to calculate and also to design and carry out a conceptually consistent set of calculations. The purpose of this appendix is to describe the conceptual structure on which the TSPA-LA is based.

J2 REQUIREMENTS UNDERLYING CONCEPTUAL STRUCTURE OF TSPA-LA

The conceptual structure of any PA should derive from the intended use of that PA and the information that the PA is intended to summarize. The TSPA-LA is intended to summarize information about the Yucca Mountain facility for use in a regulatory decision. Thus, the conceptual structure of the TSPA-LA derives from the regulatory requirements that are placed on the Yucca Mountain facility. As initially promulgated, these regulatory requirements have three primary sources: (i) 40 CFR Part 197, *Public Health and Environmental Radiation Protection Standards for Yucca Mountain, NV; Final Rule*, which has been promulgated by the U.S. Environmental Protection Agency (EPA) (66 FR 32074 [DIRS 155216]), (ii) 10 CFR Parts 2, 19, 20, 21, etc., *Disposal of High-Level Radioactive Wastes in a Proposed Geologic Repository at Yucca Mountain, Nevada; Final Rule*, which has been promulgated by the U.S. Nuclear Regulatory Commission (NRC) (66 FR 55732 [DIRS 156671]), and (iii) *Yucca Mountain Review Plan; Final Report*, which has been published by the NRC (NRC 2003 [DIRS 163274], Section 2.2) to guide assessing compliance with 10 CFR Parts 2, 19, 20, 21, etc.

The initial promulgations indicated above specified conditions that the Yucca Mountain facility was required to satisfy for the first 10,000 yr after its closure. In a subsequent suit [DIRS 176542], it was ruled that the EPA did not follow guidance in a National Academy of Science (NAS) study (National Research Council 1995 [DIRS 100018]) as mandated by Congress in the Energy Policy Act of 1992 [DIRS 100017]. In particular, it was ruled that the EPA had failed to follow the guidance in the NAS study that the regulatory period for the Yucca Mountain facility should extend over the period of geologic stability at the facility site, which was suggested to be 10^6 yr. As a result, the initial regulation for the Yucca Mountain facility was remanded to the EPA for revision.

In response to this remand, the EPA promulgated 40 CFR Part 197, *Public Health and Environmental Radiation Protection Standards for Yucca Mountain, Nevada; Proposed Rule* (70 FR 49014 [DIRS 177357]), which contained revised standards for the Yucca Mountain facility. In turn and in consistency with the EPA's revised standard, the NRC promulgated 10 CFR Part 63, *Implementation of a Dose Standard After 10,000 Years* (70 FR 53313 [DIRS 178394]). The EPA's and NRC's regulations proposed in response to the remand left the requirements for the first 10,000 yr after repository closure unchanged. However, new conditions were specified for the time interval [10^4, 10^6 yr].

Because the regulations for the first 10,000 yr after repository closure are unchanged, the regulations and supporting rational for this time period are initially discussed for the EPA (Section J2.1) and the NRC (Section J2.2). This discussion includes quotes from the original regulations and supporting material that provides insights on the type of analysis desired and the implementation of such an analysis. Then, the regulations for the time interval [10^4, 10^6 yr] proposed by the EPA (Section J2.3) and the NRC (Section J2.4) are discussed. Finally, the Yucca Mountain review plan as originally published is discussed (Section J2.5). At present, there has been no change to the review plan in response to the proposed regulations.

J2.1 EPA Requirements: 40 CFR Part 197 Before Remand

As mandated in the Energy Policy Act of 1992 [DIRS 100017], the EPA promulgated public health and safety standards for radioactive material stored or deposed of in the potential repository at Yucca Mountain, NV in 40 CFR Part 197 (66 FR 32074 [DIRS 155216]). In turn, the NRC is required to incorporate these standards into its licensing standards, and the U.S. Department of Energy (DOE) must demonstrate compliance with these standards. Selected requirements and explanatory material from 40 CFR Part 197 (66 FR 32074 [DIRS 155216]) that influence the conceptual structure of the TSPA-LA for postclosure conditions follow. Specifically, the primary focus is on Subpart B of 40 CFR Part 197 (66 FR 32074 [DIRS 155216]), which relates to postclosure requirements.

The core requirement in 40 CFR 197 (66 FR 32074 [DIRS 155216]) that ultimately gives rise to the conceptual structure of the TSPA-LA is an individual-protection standard. Specifically, the following standard was mandated (66 FR 32074 [DIRS 155216], p. 32134):

> **§ 197.20 What standard must DOE meet?**
>
> The DOE must demonstrate, using performance assessment, that there is a reasonable expectation that, for 10,000 years following disposal, the reasonably maximally exposed individual receives no more than an annual committed effective dose equivalent of 150 microsieverts (15 millirems) from releases from the undisturbed Yucca Mountain disposal system. The DOE's analysis must include all potential pathways of radionuclide transport and exposure. (EPA1)

A reading of the preceding requirement immediately gives rise to three questions: (i) "What is a PA?", (ii) "What is reasonable expectation?", and (iii) "What is the reasonably maximally exposed individual (RMEI)?".

In answer to the first question, the EPA defined a PA in 40 CFR Part 197 (66 FR 32074 [DIRS 155216], p. 32133):

> *Performance assessment* means an analysis that:
>
> (1) Identifies the features, events, processes, (except human intrusion), and sequences of events and processes (except human intrusion) that might affect the Yucca Mountain disposal system and their probabilities of occurring during 10,000 years after disposal;

(2) Examines the effects of those features, events, processes, and sequences of events and processes upon the performance of the Yucca Mountain disposal system; and

(3) Estimates the annual committed effective dose equivalent incurred by the reasonably maximally exposed individual, including the associated uncertainties, as a result of releases caused by all significant features, events, processes, and sequences of events and processes, weighted by their probability of occurrence. (EPA2)

In answer to the second question, the EPA defined reasonable expectation in 40 CFR Part 197 (66 FR 32074 [DIRS 155216], p. 32133):

§ 197.14 What is a reasonable expectation?

Reasonable expectation means that NRC is satisfied that compliance will be achieved based upon the full record before it. Characteristics of reasonable expectation include that it:

(a) Requires less than absolute proof because absolute proof is impossible to attain for disposal due to the uncertainty of projecting long-term performance;

(b) Accounts for the inherently greater uncertainties in making long-term projections of the performance of the Yucca Mountain disposal system;

(c) Does not exclude important parameters from assessments and analyses simply because they are difficult to precisely quantify to a high degree of confidence; and

(d) Focuses performance assessments and analyses upon the full range of defensible and reasonable parameter distributions rather than only upon extreme physical situations and parameter values. (EPA3)

Finally, in answer to the third question, the EPA defined the reasonably maximally exposed individual (RMEI) in 40 CFR Part 197 (66 FR 32074 [DIRS 155216], p. 32134):

§ 197.21 Who is the reasonably maximally exposed individual?

The reasonably maximally exposed individual is a hypothetical person who meets the following criteria:

(a) Lives in the accessible environment above the highest concentration of radionuclides in the plume of contamination;

(b) Has a diet and living style representative of the people who now reside in the Town of Amargosa Valley, Nevada. The DOE must use projections based upon surveys of the people residing in the Town of Amargosa Valley,

Nevada, to determine their current diets and living styles and use the mean values of these factors in the assessments conducted for §§ 197.20 and 197.25; and

(c) Drinks 2 liters of water per day from wells drilled into the ground water at the location specified in paragraph (a) of this section. (EPA4)

With respect to the preceding statements, the definitions of PA and reasonable expectation are particularly important with respect to the conceptual structure of the TSPA-LA because they relate to requirements that affect the overall organization of the analysis. In contrast, the definition of the RMEI is less important to the conceptual structure of the analysis because it simply relates to a particular result that must be calculated.

A PA is often described as an analysis intended to answer three questions about a system and one additional question about the analysis itself (Kaplan and Garrick 1981 [DIRS 100557]). The first three questions are:

(i) What could happen? (Q1)

(ii) How likely is it to happen? (Q2)

and

(iii) What are the consequences if it does happen? (Q3)

The fourth question is:

(iv) What is the uncertainty (or equivalently, how much confidence do you have) in the answers to the first three questions? (Q4)

The posing of the first three questions in the definition of a PA in (EPA2) is clearly evident. Specifically, "Identifies features, events and processes" corresponds to answering Q1 and "Identifies… their probabilities of occurring" corresponds to answering Q2. Similarly, "Examines the effects of those features, events and processes" and "Estimates the annual committed effective dose equivalent" correspond to answering Q3. The presence of Q4 is not as immediately obvious but is imbedded in the definition of PA in (EPA2) in the statement "including the associated uncertainties" and in the definition of reasonable expectation in (EPA3) in the statements "Accounts for the inherently greater uncertainties in making long-term projections" and "Focuses performance assessments upon the full range of defensible and reasonable parameter values". The four questions in (Q1) – (Q4) are introduced here because they will later be used as an intuitive lead into the conceptual structure of the TSPA-LA.

The EPA provided the following guidance on the implementation of the postclosure requirements in 40 CFR 197.13 (66 FR 32074 [DIRS 155216], p. 32133):

§ 197.13 How is subpart B implemented?

> The NRC implements this subpart B. The DOE must demonstrate to NRC that there is a reasonable expectation of compliance with this subpart before NRC may issue a license. In the case of the specific numerical requirements in § 197.20 of this subpart, and if performance assessment is used to demonstrate compliance with the specific numerical requirements in §§ 197.25 and 197.30 of this subpart, NRC will determine compliance based upon the mean of the distribution of projected doses of DOE's performance assessments which project the performance of the Yucca Mountain disposal system for 10,000 years after disposal. (EPA5)

Of particular importance is the statement that "In the case of the specific numerical requirements in § 197.20…, NRC will determine compliance based upon the mean of projected doses." This is a very important requirement with respect to the conceptual and computational structure of the TSPA-LA, and a requirement that is not easy to interpret. In particular, a mean is a quantity that is defined by an integral, and it is not immediately obvious exactly what this integral is supposed to be over.

Identifying what is intended by the "mean" indicated in (EPA5) is complicated by the required consideration of two types of uncertainty in the EPA mandated PA for the Yucca Mountain facility. First, there is the uncertainty that arises from the different types of disruptions that could occur at the Yucca Mountain facility in the future. This uncertainty appears in the EPA's definition of PA in (EPA2) in the statements "Identifies features, events and processes … and their probabilities of occurring during 10,000 years after disposal" and "Estimates the annual effective dose equivalent … as a result of releases caused by all significant features, events and processes, and sequences of events and processes, weighted by their probability of occurrence." The latter statement appears to imply a mean, i.e., an integral, over what could happen in the future. This is the uncertainty associated with questions (Q1) and (Q2). Second, there is the uncertainty that arises from a lack of knowledge about properties of the Yucca Mountain site. This uncertainty appears in the EPA's definition of PA in (EPA2) in the statement "including the associated uncertainties" and in the definition of reasonable expectation in (EPA3) in the statements "due to the uncertainty of projecting long-term performance" and "the full range of defensible and reasonable parameter distributions." Given that these uncertainties are to be characterized probabilistically as implied by the last quote, then there would also be a mean over these uncertainties. These are the uncertainties associated with question (Q4).

Possibilities include a mean over what could happen in the future, a mean over uncertainty with respect to parameter values and other modeling assumptions, and a mean over both types of uncertainty. When read in full, the following final part of the definition of PA in (EPA2) suggests, but does not explicitly state, the last of the three indicated possibilities: "Estimates the annual committed effective dose equivalent incurred by the reasonably maximally exposed individual, *including the associated uncertainties*, as a result of releases caused by all significant features, events, processes and sequences of events and processes, *weighted by their probability of occurrence*," with the italics added for emphasis. As a further consideration, doses to the RMEI vary as a function of time, and this variation must be incorporated in some manner in the determination of mean doses.

The EPA does not provide a definitive statement in 40 CFR Part 197 (66 FR 32074 [DIRS 155216]) of what is intended by a mean dose. However, a number of additional

statements are included in 40 CFR Part 197 (66 FR 32074 [DIRS 155216]) that indicate the EPA's emphasis on consideration of a mean dose in assessing compliance:

> In line with our use of the term ''reasonable expectation,'' the fundamental compliance measure consistent with a literal mathematical interpretation of this term would be the mean value of the distribution of calculated doses (66 FR 32074 [DIRS 155216], p. 32125). (EPA6)

> By specifying the mean as the performance measure and probability limits for the processes and events to be considered (§ 197.36), and in concert with the intent of our ''reasonable expectation'' approach in general, we have implied that probabilistic approaches for the disposal system performance assessments are expected (66 FR 32074 [DIRS 155216], p. 32125). (EPA7)

> The mean or median are reasonably conservative measures because they are influenced by high exposure estimates found when analyzing the full range of site conditions and relevant processes, without being geared to exclusively reflect high-end results, as would be the case if we selected as the measure a high-end percentile of the calculated dose distribution (such as the 95th or 99th percentile). Our final rule for Yucca Mountain specifies only that the mean be used, as we believe that it is appropriately conservative in this situation (66 FR 32074 [DIRS 155216], p. 32126). (EPA8)

Thus, although some ambiguity exists with respect to exactly how a mean dose is to be defined and calculated, there is no ambiguity in the EPA's intent that compliance with its dose standard for the RMEI is to be determined with a mean dose. As an aside, it is perhaps worth noting that the statement with respect to the median in (EPA8) is not correct; in particular, the median unlike the mean is not particularly influenced by the high values associated with a skewed distribution.

The discussion of the requirements promulgated by the EPA in 40 CFR Part 197 (66 FR 32074 [DIRS 155216]) ends with several additional quotes that provide insights into the nature of the desired properties of a PA used to assess compliance with the EPA's Yucca Mountain standard:

> It is NRC's responsibility to determine how DOE must demonstrate compliance with our standards; however, we envision the use of a probabilistic assessment for the compliance demonstration. (66 FR 32074 [DIRS 155216], p. 32086) (EPA9)

> DOE and NRC may not assume that future geologic, hydrologic, and climatic conditions will be the same as they are at present. We require that these conditions be varied within reasonably ascertainable bounds over the required compliance period (66 FR 32074 [DIRS 155216], p. 32096). (EPA10)

> If choices are made that make the simulations very unrealistic, the confidence that can be placed on modeling results is very limited. Inappropriate simplifications can mask the effects of processes that will in reality determine disposal system performance, if the uncertainties involved with these simplifications are not recognized. Overly conservative assumptions made in developing performance scenarios can bias the analyses in the direction of unrealistically extreme

> situations, which in reality may be highly improbable, and can deflect attention from questions critical to developing an adequate understanding of the expected features, events, and processes (66 FR 32074 [DIRS 155216], p. 32102), (EPA 11)
>
> The reasonable expectation approach is aimed simply at focusing attention on understanding the uncertainties in projecting disposal system performance so that regulatory decision making will be done with a full understanding of the uncertainties involved (66 FR 32074 [DIRS 155216], p. 32102). (EPA12)

The statement in (EPA9) clearly indicates that the EPA expects a probabilistic analysis. The statement in (EPA10) indicates the need to consider events that can happen in the future (e.g., volcanic eruptions, earthquakes, climatic changes). The statement in (EPA11) is important because it clearly indicates that the EPA does not desire a conservative analysis. The statement in (EPA12) indicates the EPA's desire for an appropriate representation of the uncertainties associated with a PA for the Yucca Mountain site. However, the EPA's desire "that regulatory decision making will be done with a full understanding of the uncertainties involved" as stated in (EPA12) is inconsistent with the intent to regulate on mean results as the calculation of means suppresses the implications of uncertainty.

J2.2 NRC Requirements: 10 CFR Parts 2, 19, 20, 21, etc. Before Remand

As mandated in the Energy Policy Act of 1992 [DIRS 100017], the NRC has promulgated licensing standards for the disposal of radioactive waste at the Yucca Mountain facility that are consistent with the EPA public health and safety standards in 40 CFR Part 197 (66 FR 32074 [DIRS 155216]) (see Section J2.1). Selected requirements and explanatory material from 10 CFR Parts 2, 19, 20, 21, etc. (66 FR 55732 [DIRS 156671]) that influence the conceptual structure of the TSPA-LA for postclosure conditions follow. Specifically, the primary focus is on Subpart L of 10 CFR Part 63 (66 FR 55732 [DIRS 156671]), which relates to postclosure requirements.

The core requirement in 10 CFR Part 63 (66 FR 55732 [DIRS 156671]) that ultimately gives rise to the conceptual structure of the TSPA-LA is an individual protection standard. Specifically, the following standard was mandated (66 FR 55732 [DIRS 156671], p. 55814):

> **§ 63.311 Individual protection standard after permanent closure.**
>
> DOE must demonstrate, using performance assessment, that there is a reasonable expectation that, for 10,000 years following disposal, the reasonably maximally exposed individual receives no more than an annual dose of 0.15 mSv (15 mrem) from releases from the undisturbed Yucca Mountain disposal system. DOE's analysis must include all potential pathways of radionuclide transport and exposure. (NRC1)

The preceding mandate is identical to the corresponding mandate from the EPA in (EPA1) provided the terminology in the two mandates has the same meaning. In particular, the phrases performance assessment, reasonable expectation and reasonably maximally exposed individual (RMEI) appear in both mandates.

Specifically, the NRC defined PA in 10 CFR Part 63.2 (66 FR 55732 [DIRS 156671], p. 55794):

> *Performance assessment* means an analysis that:
>
> (1) Identifies the features, events, processes (except human intrusion), and sequences of events and processes (except human intrusion) that might affect the Yucca Mountain disposal system and their probabilities of occurring during 10,000 years after disposal;
>
> (2) Examines the effects of those features, events, processes, and sequences of events and processes upon the performance of the Yucca Mountain disposal system; and
>
> (3) Estimates the dose incurred by the reasonably maximally exposed individual, including the associated uncertainties, as a result of releases caused by all significant features, events, processes, and sequences of events and processes, weighted by their probability of occurrence. (NRC2)

The preceding definition of PA is identical to the definition given by the EPA in (EPA2) except for the use of "dose" rather than "annual committed effective dose"; presumably, the NRC intends the same dose measure as specified by the EPA. Further, the NRC defined reasonable expectation in 10 CFR Part 63.304 (66 FR 55732 [DIRS 156671], p. 55813):

> **§ 63.304 Reasonable expectation.**
>
> *Reasonable expectation* means that the Commission is satisfied that compliance will be achieved based upon the full record before it. Characteristics of reasonable expectation include that it:
>
> (1) Requires less than absolute proof because absolute proof is impossible to attain for disposal due to the uncertainty of projecting long-term performance;
>
> (2) Accounts for the inherently greater uncertainties in making long-term projections of the performance of the Yucca Mountain disposal system;
>
> (3) Does not exclude important parameters from assessments and analyses simply because they are difficult to precisely quantify to a high degree of confidence; and
>
> (4) Focuses performance assessments and analyses on the full range of defensible and reasonable parameter distributions rather than only upon extreme physical situations and parameter values. (NRC3)

The preceding is identical to the EPA's definition of reasonable expectation in (EPA3) except for the replacement of "NRC" by "the Commission." Finally, the RMEI was defined by the NRC in 10 CFR Part 63.312 (66 FR 55732 [DIRS 156671], p. 55814):

§ 63.312 Required characteristics of the reasonably maximally exposed individual.

The reasonably maximally exposed individual is a hypothetical person who meets the following criteria:

(a) Lives in the accessible environment above the highest concentration of radionuclides in the plume of contamination;

(b) Has a diet and living style representative of the people who now reside in the Town of Amargosa Valley, Nevada. DOE must use projections based upon surveys of the people residing in the Town of Amargosa Valley, Nevada, to determine their current diets and living styles and use the mean values of these factors in the assessments conducted for §§ 63.311 and 63.321;

(c) Uses well water with average concentrations of radionuclides based on an annual water demand of 3000 acre-feet;

(d) Drinks 2 liters of water per day from wells drilled into the ground water at the location specified in paragraph (a) of this section; and

(e) Is an adult with metabolic and physiological considerations consistent with present knowledge of adults. (NRC4)

Except for some additional guidance on the determination of exposure, the definition of the RMEI given by the NRC is the same as the definition given by the EPA in (EPA4).

As a result of the effective identical content of the requirements/definitions given by the NRC in (NRC1) – (NRC4) and the EPA in (EPA1) – (EPA4), both organizations are specifying the same analysis. Hence, the four core questions underlying a PA indicated in (Q1) – (Q4) are present in the requirements of both the NRC and the EPA.

Because the NRC has regulatory authority for the Yucca Mountain facility, it is important to examine any additional requirements and/or specifications that it has made with respect to PA in support of a license application for this facility. The following guidance given in 10 CFR 63.303 (66 FR 55732 [DIRS 156671], p. 55813) on the implementation of postclosure requirements provides a high-level summary of what the NRC expects in a PA for the Yucca Mountain facility:

§ 63.303 Implementation of Subpart L.

DOE must demonstrate that there is a reasonable expectation of compliance with this subpart before a license may be issued. In the case of the specific numerical requirements in § 63.311 of this subpart, and if performance assessment is used to demonstrate compliance with the specific numerical requirements in §§ 63.321 and 63.331 of this subpart, compliance is based upon the mean of the distribution of projected doses of DOE's performance assessments which project the

> performance of the Yucca Mountain disposal system for 10,000 years after disposal. (NRC5)

Except for minor changes in wording, the preceding implementation guidance is identical with the guidance given by the EPA in (EPA5). Of particular importance is the statement that "compliance is based upon the mean of the distribution of projected doses." As discussed in conjunction with (EPA5), this requirement has a major effect on the conceptual and computational structure of the TSPA-LA.

Like the EPA in 40 CFR Part 197 (66 FR 32074 [DIRS 155216]), the NRC does not provide a definitive statement of what is intended by a mean dose. However, it seems reasonable to assume that the NRC was guided by the same perspectives with respect to the concept of a mean as expressed by the EPA in (EPA6) – (EPA8). The following statement by the NRC from 10 CFR Parts 2, 19, 20, 21, etc. (66 FR 55732 [DIRS 156671], p. 55752) actually provides a more specific indication of what is intended by a mean than any of the statements from the EPA:

> The Commission expects that performance assessments conducted by the applicant in support of any potential license application will use probabilistic methods to simulate a wide range of possible future behaviors of the repository system. Each possible future behavior of the repository system is represented by a curve describing the annual dose to the RMEI as a function of time. Generally, but not necessarily, each of the possible curves is assumed to be equally likely. Because none of these possible futures can be demonstrated to describe the actual future behavior of the repository system, the Commission requires that the applicant calculate the mean of these dose versus time curves, properly weighted by their individual probabilities. (NRC6)

This statement specifically describes the weighting of doses by their likelihood of occurrence (i.e., a calculation involving answers to questions (Q1), (Q2) and (Q3)). However, no mention is made of uncertainty in the sense of question (Q4).

The description of a PA by the NRC in (NRC2) is at a very high level. Owing to the central role played by PA in the licensing of the Yucca Mountain facility, it is important to examine any additional statements made by the NRC with respect to the desired characteristics of a PA carried out for this purpose. Such statements help provide guidance with respect to the conceptual and computational structure of the TSPA-LA. Specifically, the following statement given in 10 CFR 63.102 (66 FR 55732 [DIRS 156671], p. 55805) helps provide insights with respect to what the NRC considers to be an appropriately designed and conducted PA:

> (j) *Performance assessment.* Demonstrating compliance with the postclosure performance objective specified at § 63.113(b) requires a performance assessment to quantitatively estimate radiological exposures to the reasonably maximally exposed individual at any time during the compliance period. The performance assessment is a systematic analysis that identifies the features, events, and processes (i.e., specific conditions or attributes of the geologic setting, degradation, deterioration, or alteration processes of engineered barriers, and interactions between the natural and engineered

> barriers) that might affect performance of the geologic repository; examines their effects on performance; and estimates the radiological exposures to the reasonably maximally exposed individual. The features, events, and processes considered in the performance assessment should represent a wide range of both beneficial and potentially adverse effects on performance (e.g., beneficial effects of radionuclide sorption; potentially adverse effects of fracture flow or a criticality event). Those features, events, and processes expected to materially affect compliance with § 63.113(b) or be potentially adverse to performance are included, while events (event classes or scenario classes) that are very unlikely (less than one chance in 10,000 over 10,000 years) can be excluded from the analysis. An event class consists of all possible specific initiating events that are caused by a common natural process (e.g., the event class for seismicity includes the range of credible earthquakes for the Yucca Mountain site). Radiological exposures to the reasonably maximally exposed individual are estimated using the selected features, events, and processes, and incorporating the probability that the estimated exposures will occur. (NRC7)

The first three questions, (Q1) – (Q3), related to PA are clearly imbedded in the preceding description. For example, references to "events" and "event classes" involve the question (Q1): "What can happen?"; the statement "incorporating the probability that the estimated exposures will occur" involves the question (Q2): "How likely is it to happen?"; and statements such as "quantitatively estimate radiological exposures" and "examines their effects on performance" involve answering question (Q3): "What are the consequences if it does happen?".

The NRC's description of PA in (NRC7) does not include any statement that can be identified with question (Q4): "What is the uncertainty in the answers to the first three questions?" However, the answering of this question is clearly intended to be part of the NRC's concept of what a PA should be as indicted in 10 CFR 63.114 (66 FR 55732 [DIRS 156671], p. 55807):

> **§ 63.114 Requirements for performance assessment.**
>
> Any performance assessment used to demonstrate compliance with § 63.113 must:
>
> (a) Include data related to the geology, hydrology, and geochemistry (including disruptive processes and events) of the Yucca Mountain site, and the surrounding region to the extent necessary, and information on the design of the engineered barrier system used to define parameters and conceptual models used in the assessment.
>
> (b) Account for uncertainties and variabilities in parameter values and provide for the technical basis for parameter ranges, probability distributions, or bounding values used in the performance assessment.
>
> (c) Consider alternative conceptual models of features and processes that are consistent with available data and current scientific understanding and

evaluate the effects that alternative conceptual models have on the performance of the geologic repository.

(d) Consider only events that have at least one chance in 10,000 of occurring over 10,000 years.

(e) Provide the technical basis for either inclusion or exclusion of specific features, events, and processes in the performance assessment. Specific features, events, and processes must be evaluated in detail if the magnitude and time of the resulting radiological exposures to the reasonably maximally exposed individual, or radionuclide releases to the accessible environment, would be significantly changed by their omission.

(f) Provide the technical basis for either inclusion or exclusion of degradation, deterioration, or alteration processes of engineered barriers in the performance assessment, including those processes that would adversely affect the performance of natural barriers. Degradation, deterioration, or alteration processes of engineered barriers must be evaluated in detail if the magnitude and time of the resulting radiological exposures to the reasonably maximally exposed individual, or radionuclide releases to the accessible environment, would be significantly changed by their omission.

(g) Provide the technical basis for models used in the performance assessment such as comparisons made with outputs of detailed process-level models and/or empirical observations (e.g., laboratory testing, field investigations, and natural analogs). (NRC8)

Statement (b) clearly involves asking and answering question (Q4). Further, much of the above statement involves the formulation of models used to answer question (Q3), and statement (d) involves obtaining answers to questions (Q1) and (Q2).

The following two statements from 10 CFR 63.101 (66 FR 55732 [DIRS 156671]) also indicate the importance that the NRC attaches to an adequate treatment of uncertainty:

For such long-term performance, what is required is reasonable expectation, making allowance for the time period, hazards, and uncertainties involved, that the outcome will conform with the objectives for postclosure performance for the geologic repository. Demonstrating compliance will involve the use of complex predictive models that are supported by limited data from field and laboratory tests, site-specific monitoring, and natural analog studies that may be supplemented with prevalent expert judgment. Compliance demonstrations should not exclude important parameters from assessments and analyses simply because they are difficult to precisely quantify to a high degree of confidence. The performance assessments and analyses should focus upon the full range of defensible and reasonable parameter distributions rather than only upon extreme physical situations and parameter values (66 FR 55732 [DIRS 156671], p. 55804).(NRC9)

> Once again, although the criteria may be written in unqualified terms, the demonstration of compliance must take uncertainties and gaps in knowledge into account so that the Commission can make the specified finding with respect to paragraph (a)(2) of § 63.31 (66 FR 55732 [DIRS 156671], p. 55804). (NRC10)

Both the preceding statements clearly indicate that a realistic treatment of uncertainty should be a fundamental part of a PA used to support a licensing application for the Yucca Mountain facility.

In addition, a number of statements provided by the NRC as supplementary information with respect to 10 CFR Parts 2, 19, 20, 21, etc. (66 FR 55732 [DIRS 156671]) emphasize the importance that the NRC places on the assessment and representation of uncertainty:

> Part 63 requires consideration of uncertainties in DOE's representation of the repository (uncertainty and variability in parameter values must be taken into account—§63.114(b)) and the events that can happen during the compliance period (consideration of potentially disruptive events with a probability of occurrence as low as one chance in 10,000 of occurring over 10,000 years—§ 63.114(d)) to be directly included in the quantitative estimate of performance (66 FR 55732 [DIRS 156671], p. 55747). (NRC11)

> DOE is expected to conduct uncertainty analyses (i.e., evaluation of how uncertainty in parameter values affects uncertainty in the estimate of dose), including the consideration of disruptive events and associated probability of occurrence (66 FR 55732 [DIRS 156671], p. 55747). (NRC12)

> The approach defined in part 63, which requires DOE to fully address uncertainties in its performance assessment rather than requiring DOE to meet a specific level of uncertainty, is appropriate. The treatment of uncertainty in DOE's performance assessment will be an important part of NRC's review (66 FR 55732 [DIRS 156671], p. 55748). (NRC13)

The statement in (NRC11) is particularly interesting because it involves three distinct concepts related to uncertainty: (i) uncertainty in the epistemic or subjective sense related to knowledge about the appropriateness of assumptions used in an analysis, (ii) spatial variability, and (iii) uncertainty in the aleatory sense related to events that may, or may not, occur in the future. The statement in (NRC12) is informative because it goes beyond asking for an analysis that simply calculates a mean outcome; in particular, it asks for an uncertainty analysis which evaluates "how uncertainty in parameter values affects uncertainty in the estimate of dose," which involves a more complex analysis than simply calculating a mean dose. Finally, the statement in (NRC13) expresses the importance that the NRC places on an adequate treatment of uncertainty.

This section ends by recording several statements by the NRC that relate to the nature of occurrences (i.e., the events of the phrase "features, events and processes") that should, and should not, be included in a PA for the Yucca Mountain facility:

> *Event sequence* means a series of actions and/or occurrences within the natural and engineered components of a geologic repository operations area that could

> potentially lead to exposure of individuals to radiation. An event sequence includes one or more initiating events and associated combinations of repository system component failures, including those produced by the action or inaction of operating personnel (66 FR 55732 [DIRS 156671], p. 55793). (NRC14)
>
> *Initiating event* means a natural or human induced event that causes an event sequence (66 FR 55732 [DIRS 156671], p. 55794). (NRC15)
>
> **§ 63.305 Required characteristics of the reference biosphere.**
>
> (a) Features, events, and processes that describe the reference biosphere must be consistent with present knowledge of the conditions in the region surrounding the Yucca Mountain site.
>
> (b) DOE should not project changes in society, the biosphere (other than climate), human biology, or increases or decreases of human knowledge or technology. In all analyses done to demonstrate compliance with this part, DOE must assume that all of those factors remain constant as they are at the time of submission of the license application.
>
> (c) DOE must vary factors related to the geology, hydrology, and climate based upon cautious, but reasonable assumptions consistent with present knowledge of factors that could affect the Yucca Mountain disposal system over the next 10,000 years.
>
> (d) Biosphere pathways must be consistent with arid or semi-arid conditions (66 FR 55732 [DIRS 156671], p. 55813). (NRC16)
>
> DOE's performance assessments should not include consideration of very unlikely features, events, or processes, i.e., those that are estimated to have less than one chance in 10,000 of occurring within 10,000 years of disposal. (10 CFR 63.342 (66 FR 55732 [DIRS 156671], p. 55815); see also revision dated Oct. 8, 2002) (NRC17)

These statements are included because they relate to what is to be included in the conceptual and computational structure of the TSPA-LA.

Finally, it is important to realize that the NRC does not view a PA in support of a licensing application for the Yucca Mountain facility as a risk assessment in the traditional sense of the phrase. In particular, the dose to the RMEI is used as a means to convert potential radionuclide releases into intuitively interpretable quantities (i.e., doses). However, owing to the prescribed and stylized manner in which doses to the RMEI are defined and calculated, they do not realistically represent actual doses to individuals in the future and thus should not be viewed as the consequence component of a risk calculation. This point is emphasized by the NRC in the following statement:

> However, it should be kept in mind that the performance assessment evaluates "potential" doses, not "actual" doses. For example, part 63 requires the

> performance assessment to assume for the next 10,000 years that the reasonably maximally exposed individual (RMEI) is a member of a community that: (1) Exists where it will intercept potential releases from the repository and (2) uses ground water but never tests the quality of this water nor treats the ground water to remove any contaminants. This specification is considered appropriately conservative for evaluating performance but most likely is not an "accurate" prediction of what will happen during the next 10,000 years (see discussion under RMEI Characteristics and Reference Biosphere for more information on the RMEI). Although the Commission does not require an ''accurate'' prediction of the future, uncertainty in performance estimates cannot be so large that the Commission cannot find a reasonable expectation that the postclosure performance objectives will be met (see discussion under Reasonable Expectation) (66 FR 55732 [DIRS 156671], p. 55748). (NRC18)

Thus, although a PA in support of a licensing application will have the same conceptual and computational structure as a risk assessment, the actual dose results cannot be given a risk-based interpretation.

J2.3 EPA Requirements: 40 CFR Part 197 after Remand

The revised standards for the Yucca Mountain facility proposed by the EPA after the remand leave the dose requirements for the first 10^4 year after repository closure unchanged (i.e., the requirement that the maximum dose to the RMEI is to be less than 15 mrem/yr). However, subsequent to the initial 10^4 year period, a new bounding dose requirement is imposed. This requirement specifies a bound of 350 mrem/yr on the dose to the RMEI after the initial 10^4 year period, with this bound required to hold over the period of geologic stability. Specifically, the requirement in (EPA1) is replaced by the following requirement (70 FR 49014 [DIRS 177357], p. 49063):

> **§ 197.20 What standard must DOE meet?**
>
> (a) The DOE must demonstrate, using performance assessment, that there is a reasonable expectation that the reasonably maximally exposed individual receives no more than the following annual committed effective dose equivalent from releases from the undisturbed Yucca Mountain disposal system:
>
> (1) 150 microsieverts (15 millirems) for 10,000 years following disposal; and
>
> (2) 3.5 millisieverts (350 millirems) after 10,000 years, but within the period of geologic stability.
>
> (b) The DOE's performance assessment must include all potential pathways of radionuclide transport and exposure. (EPA13)

Except for the addition of the 350 mrem/yr dose requirement after 10^4 yr, the above requirement is the same as specified in (EPA1). As noted in conjunction with (EPA1), a careful reading of the

preceding requirement gives rise to three questions: (i) "What is a PA?", (ii) "What is reasonable expectation?", and (iii) "What is the RMEI?". The answers to these questions provided in the proposed revision to 40 CFR Part 197 (70 FR 49014 [DIRS 177357]) are effectively the same as given in the statements (EPA2), (EPA3) and (EPA4) taken from the original promulgation of 40 CFR Part 197 (66 FR 32074 [DIRS 155216]).

In turn, the EPA's original guidance on the implementation of the 10^4 yr dose standards stated in (EPA5) is revised in the proposed standard to include the time period after 10^4 yr. Specifically, the requirement in (EPA5) is replaced by the following requirement (70 FR 49014 [DIRS 177357], p. 49063):

§ 197.13 How is subpart B implemented?

(a) The NRC will determine compliance based upon the arithmetic mean of the projected doses from DOE's performance assessments for the period within 10,000 years after disposal:

(1) For § 197.20 of this subpart; and

(2) For §§ 197.25 and 197.30 of this subpart, if performance assessment is used to demonstrate compliance with either or both of these sections.

(b) NRC will determine compliance based upon the median of the projected doses from DOE's performance assessments for the period after 10,000 years of disposal and through the period of geologic stability:

(1) For § 197.20 of this subpart; and

(2) For § 197.25, if a performance assessment is used to demonstrate compliance. (EPA14)

The part of the preceding statement relating to dose in the initial 10^4 yr time period is effectively the same as the statement in (EPA5) from the original promulgation of 40 CFR Part 197 (66 FR 32074 [DIRS 155216]). However, the second part relating to dose after 10^4 yr is different. Specifically, a bound of 350 mrem/yr on the median dose to the RMEI is imposed.

The interpretation of what is intended by the specification of a mean dose is extensively discussed in Sections J2.1 and J2.2. The actual calculation of mean dose in the TSPA-LA is discussed in detail in Section J4, where the descriptor expected dose rather than mean dose is used for consistency with standard terminology used in probability and statistical theory. As discussed in Section J4, there are actually two expectations that underlie the "mean" dose specified by the EPA: an expectation over random events that could occur in the future (i.e., over aleatory uncertainty) and an expectation over the appropriate values to use for quantities that are assumed to have fixed but poorly known values in the computational implementation of the TSPA-LA (i.e., over epistemic uncertainty). Expected dose over aleatory uncertainty at a specific point in time corresponds to the concept of individual risk that the NAS committee (National Research Council 1995 [DIRS 100018]) recommended as the basis of regulations for the Yucca Mountain facility; specifically, only a scalar multiplier is needed to convert from expected dose

over aleatory uncertainty to individual risk. In turn, the distribution of expected dose over aleatory uncertainty at a specific point in time that results from epistemic uncertainty provides the representation of uncertainty in TSPA-LA results repeatedly requested by the NAS committee, the EPA and the NRC. To have a unique regulatory quantity, the distribution of expected dose over aleatory uncertainty at a specific point in time can itself be reduced to an expected value (i.e., an expected value over both aleatory and epistemic uncertainty). Then, the specified bound of 15 mrem/yr can be applied to the expected doses over aleatory and epistemic uncertainty for the time interval [0, 10^4 yr]. The calculations indicated in this paragraph are extensively discussed and illustrated later in this appendix.

For the post 10^4 yr time period, the EPA specifies that the median dose to the RMEI is to be bounded by 350 mrem/yr. This specification immediately raises the question of how to define median dose to the RMEI. The view taken in the development of the TSPA-LA is that median dose should be defined in a manner consistent with both the NAS committee's recommendations and the calculation of mean dose for the initial 10^4 yr period. Consistent with this view, the median dose at a specific point in time is defined in the TSPA-LA as the median of the expected doses over aleatory uncertainty at that time. Thus, median doses are based on the same conceptual epistemic uncertainty distributions for expected dose over aleatory uncertainty that are used to determine mean doses for the time interval [0, 10^4 yr]. The only difference is that for the [0, 10^4 yr] time interval, the distributions of expected dose over aleatory uncertainty are summarized with their means and for the post 10^4 yr time period, the distributions of expected dose over aleatory uncertainty are summarized with their medians. With this approach, the definition of median dose is consistent with the NAS committee's recommendation that the Yucca Mountain facility should be regulated on the basis of risk to an individual and is also consistent with the determination of mean dose as the determination of mean and median doses use conceptually identical distributions. The calculations indicated in this paragraph are extensively discussed and illustrated later in this appendix.

The preceding definitions indicated for mean and median dose involve summarizing distributions for expected dose over aleatory uncertainty at specific points in time. The following statement appears in the introductory discussion associated with the proposed revisions to 40 CFR Part 197 and could be interpreted as implying different definitions for mean and median dose than those just indicated (70 FR 49014 [DIRS 177357], p. 49042): "A distribution of projected peak doses will result from these analyses, each representing a possible "future" and a dose associated with the specific parameter values chosen for each calculation." This statement appears to imply that a peak dose should be determined for each possible future. Then, means and medians could be extracted from the resulting distributions of peak dose (i.e., one peak dose distribution for the [0, 10^4 yr] time interval and one peak dose distribution for the post 10^4 yr time interval). With this approach, the indicated peak doses could possibly occur at a different time for each future. The TSPA-LA does not use distributions of peak dose defined in this manner for two reasons. First, use of this approach loses the concept of individual risk that is prominent in the recommendations of the NAS committee. Specifically, the combining of likelihood and consequence that is essential to the concept of individual health risk is lost. Second, the effects of half of all possible futures are eliminated from consideration. As a notional example, if 51 percent of all possible futures result in no dose and 49 percent all possible futures result in a peak dose greater than 1000 mrem/yr, then the median dose would be 0 mrem/yr. As long as

51 percent of the possible futures result in no dose, the peak doses associated with the remaining 49 percent of the futures will have no effect on the median peak dose. Because of the preceding considerations, the TSPA-LA bases its determinations of mean and median doses on distributions of expected doses over aleatory uncertainty at individual points in time rather than on distributions of peak dose over time.

In effect, what the EPA refers to as projected doses in (EPA5) and (EPA14) are assumed to be expected doses over aleatory uncertainty in the TSPA-LA for comparisons with the indicated regulatory requirements. Then, means or medians as appropriate for the time interval under consideration are determined. Because of this, the projected doses under consideration are not actual doses but rather are probabilistically weighted doses. However, because it is important not to lose the actual dose results that are being probabilistically weighted, presentations later in this appendix will show both original unweighted doses and the resultant probabilistically weighted doses.

J2.4 NRC Requirements: 10 CFR Parts 2, 19, 20, 21, etc. after Remand

The NRC has revised its standards for the Yucca Mountain facility for consistency with the revised standards proposed by the EPA. As in the EPA's proposed standards, the dose requirements for the first 10^4 yr after repository closure unchanged (i.e., the requirement that the maximum dose to the RMEI is to be less than 15 mrem/yr). However, subsequent to the initial 10^4 yr period, a new bounding dose requirement is imposed. This requirement specifies a bound of 350 mrem/yr on the dose to the RMEI after the initial 10^4 yr period, with this bound required to hold over the period of geologic stability. Specifically, the requirement in (NRC1) is replaced by the following requirement (70 FR 53313 [DIRS 178394], p. 53319):

> **§ 63.311 Individual protection standard after permanent closure.**
>
> (a) DOE must demonstrate, using performance assessment, that there is a reasonable expectation that the reasonably maximally exposed individual receives no more than the following annual dose from releases from the undisturbed Yucca Mountain disposal system:
>
> (1) 0.15 mSv (15 mrem) for 10,000 years following disposal; and
>
> (2) 3.5 mSv (350 mrem) after 10,000 years, but within the period of geologic stability.
>
> (b) DOE's performance assessment must include all potential environmental pathways of radionuclide transport and exposure. (NRC19)

Except for minor differences in wording, the preceding standard is the same as the proposed standard specified by the EPA in (EPA13). Thus, the NRC has simply repeated back the EPA's individual protection standard.

In turn, the NRC's gives the following guidance on implementing the preceding individual protection standard (70 FR 53313 [DIRS 178394], p. 53319):

§ 63.303 Implementation of Subpart L.

(a) Compliance is based upon the arithmetic mean of the projected doses from DOE's performance assessments for the period within 10,000 years after disposal for:

(1) § 63.311(a)(1); and

(2) §§ 63.321(b)(1) and 63.331, if performance assessment is used to demonstrate compliance with either or both of these sections.

(b) Compliance is based upon the median of the projected doses from DOE's performance assessments for the period after 10,000 years of disposal and through the period of geologic stability for:

(1) § 63.311(a)(2); and

(2) § 63.321(b)(2), if performance assessment is used to demonstrate compliance. (NRC20)

Except for minor changes in wording, the preceding implementation guidance is identical with the guidance given by the EPA in (EPA14).

The requirements for the time interval [0, 10^4 yr] are unchanged. Thus, the discussion in Section J2.2 with respect to this time interval remains unchanged. The NRC is rather sparse in its preliminary discussion of it proposed rule change (70 FR 53313 [DIRS 178394]). Thus, it seems reasonable to assume that the core ideas given in the original promulgation of 10 CFR Parts 2, 19, 20, 21, etc. [DIRS 156671] and summarized in Section J2.2 continue to remain valid. The major change to the present NRC's proposed rule is the addition of the bound of 350 mrem/yr on the median dose to the RMEI after the initial 10^4 yr period. In addressing this bound, the TSPA-LA follows the conceptual and computational approach indicated at the end of Section J2.3. A more detailed description the determination of mean and median doses in the TSPA-LA is given in Section J4.

J2.5 Yucca Mountain Review Plan

In addition to the NRC rule 10 CFR Parts 2, 19, 20, 21, etc. (66 FR 55732 [DIRS156671], 70 FR 53313 [DIRS 178394]), the NRC has published an extensive review plan for the Yucca Mountain facility, the *Yucca Mountain Review Plan, Final Report* (YMRP), to guide its assessment of the DOE's license application (NRC 2003 [DIRS 163274]). Selected portions of the YMRP (NRC 2003 [DIRS 163274]) that specifically relate to the conceptual and computational structure of the TSPA-LA are presented in this section. The YMRP (NRC 2003 [DIRS 163274]) is a large and detailed document. No attempt is made to summarize everything in it that relates to the TSPA-LA. Rather, only selected material that specifically relates to the overall structure of the TSPA-LA is presented.

Early in the YMRP, the NRC specifically acknowledges that the DOE's license application is to be based on a detailed PA (NRC 2003 [DIRS 163274], p. 2.2-1):

> **Risk-Informed Review Process for Performance Assessment**—The performance assessment quantifies repository performance, as a means of demonstrating compliance with the postclosure performance objectives at 10 CFR 63.113 [DIRS 180319]. The U.S. Department of Energy performance assessment is a systematic analysis that answers the triplet risk questions: what can happen; how likely is it to happen; and what are the consequences. (YMRP1)

The "triplet" referred to above is the classic Kaplan-Garrick ordered triple definition of risk (Kaplan and Garrick 1981 [DIRS 100557]) that evolved out of the Reactor Safety Study conducted by the NRC in the mid 1970s (NRC 1975 [DIRS 107799]) and other reactor probabilistic risk assessments carried out in the late 1970s and early 1980s (PLG 1983 [DIRS 148063]; PLG 1983 [DIRS 107813]; PLG 1982 [DIRS 107812]). This risk representation also provided the conceptual and organizational basis for the NRC's reassessment of the risk from commercial nuclear power reactors carried out in the late 1980s (i.e., NUREG-1150: NRC 1990 [DIRS 107798]; Breeding et al. 1992 [DIRS 107727]) and the DOE's PA in support of a successful certification application to the EPA for the Waste Isolation Pilot Plant (WIPP) in the mid 1990s (DOE 1996 [DIRS 100975]; Helton and Marietta 2000 [DIRS 171759]). The three indicted questions have already been referred to as questions (Q1), (Q2), and (Q3) in Section J2.1. As a reminder, there is also a fourth question (i.e., Q4): "What is the uncertainty in the answers to the first three questions?", or equivalently, "How much confidence do you have in the answers to the first three questions?".

The NRC provides three acceptance criteria, with multiple subparts, to be used in judging the DOE's success in meeting regulatory standards related to the use of PA to assess compliance with the postclosure individual protection requirement (i.e., NRC1). These criteria follow (NRC 2003 [DIRS 163274], pp. 2.2-133 and 2.2-134):

> **Acceptance Criterion 1:** Scenarios Used in the Calculation of the Annual Dose as a Function of Time Are Adequate.
>
> (1) The annual dose as a function of time includes all scenario classes that have been determined to be sufficiently probable, or to have a sufficient effect on overall performance that they could not be screened from the total system performance assessment analyses; and (YMRP2)
>
> (2) The calculation of the annual dose curve appropriately sums the contribution of each of the disruptive event scenario classes. The contribution to the annual dose from each scenario class calculation properly accounts for the effects that the time of occurrence of the disruptive events comprising the scenario class has on the consequences. The annual probability of occurrence of the events used to calculate the contribution to the annual dose is consistent with the results of the scenario analysis. The probabilities of occurrence of all scenario classes, included in calculating the annual dose curve, sum to one. (YMRP3)

Acceptance Criterion 2: An Adequate Demonstration Is Provided That the Annual Dose to the Reasonably Maximally Exposed Individual in Any Year During the Compliance Period Does Not Exceed the Exposure Standard.

(1) A sufficient number of realizations has been obtained, for each scenario class, using the total system performance assessment code, to ensure that the results of the calculations are statistically stable; (YMRP4)

(2) The annual dose curve includes confidence intervals (e.g., 95th and 5th percentile) to represent the uncertainty in the dose calculations; (YMRP5)

(3) Repository performance and the performance of individual components or subsystems are consistent and reasonable; and (YMRP6)

(4) The total system performance assessment results confirm that the repository performance results in annual dose, to the reasonably maximally exposed individual, in any year, during the compliance period, that does not exceed the postclosure individual protection standard. (YMRP7)

Acceptance Criterion 3: The Total System Performance Assessment Code Provides a Credible Representation of Repository Performance.

(1) Assumptions made within the total system performance assessment code are consistent among different modules of the code. The use of assumptions and parameter values that differ among modules of the code is adequately documented; (YMRP8)

(2) The total system performance assessment code is properly verified, such that there is confidence that the code is modeling the physical processes in the repository system in the manner that was intended. The transfer of data between modules of the code is conducted properly; (YMRP9)

(3) The estimate of the uncertainty in the performance assessment results is consistent with the model and parameter uncertainty; and (YMRP10)

(4) The total system performance assessment sampling method ensures that sampled parameters have been sampled across their ranges of uncertainty.(YMRP11)

The preceding acceptance criteria are basically describing what should be expected of any modern PA. Examples of such PAs include the NRC's reassessment of the risk from commercial nuclear power plants ([DIRS 107798], [DIRS 107727]) and the DOE's successful Compliance Certification Application for the Waste Isolation Pilot Plant ([DIRS 100975], [DIRS 171759]).

J3 TUTORIAL ON PROBABILITY, UNCERTAINTY AND THE STRUCTURE OF PERFORMANCE ASSESSMENTS

As clearly indicated by the material presented in Section J2, probability and the treatment of uncertainty are fundamental components of a PA in support of a licensing application for the

Yucca Mountain facility. In particular, determination of expected (i.e., mean) and median dose to the RMEI is an inherently probabilistic calculation. For convenience and to standardize the use of certain terminology, a brief tutorial on probability and uncertainty follows.

J3.1 Probability and the Representation of Uncertainty

Three basic components are involved in a formal definition of probability: a set $\mathcal{S}$ that contains everything that could occur in the particular universe under consideration; a suitably restricted collection Σ of subsets of $\mathcal{S}$ for which probability is defined; and a function p that defines probability for the elements of Σ (Feller 1971 [DIRS 107822], Section IV.3). At an intuitive level, Σ can be thought of as containing all possible subsets of $\mathcal{S}$. However, to obtain a mathematically rigorous development of probability, Σ and p must have the following properties: (i) if $\mathcal{E} \in \Sigma$, then $\mathcal{E}^c \in \Sigma$, where the superscript c is used to denote the complement of $\mathcal{E}$, (ii) if $\{\mathcal{E}_i\}$ is a countable collection of elements of Σ, then $\cup_i \mathcal{E}_i$ and $\cap \mathcal{E}_i$ are also elements of Σ, (iii) $p(\mathcal{S}) = 1$, (iv) if $\mathcal{E} \in \Sigma$, then $0 \le p(\mathcal{E}) \le 1$, and (v) if $\{\mathcal{E}_i\}$ is a countable collection of disjoint elements of Σ (i.e., $\mathcal{E}_i \cap \mathcal{E}_j = \varnothing$ for $i \neq j$), then $p(\cup_i \mathcal{E}_i) = \sum_i p(\mathcal{E}_i)$. The triple $(\mathcal{S}, \Sigma, p)$ is called a probability space and is the fundamental mathematical structure that underlies a careful development of probability. In the usual terminology of probability theory, $\mathcal{S}$ is called the sample space; elements of $\mathcal{S}$ are called elementary events; elements of Σ are called events; and p is called a probability measure. The idea of a probability space is introduced in this presentation primarily as a notational convenience to facilitate in distinguishing between different uses of probability and in describing the calculation of expected values and distributions.

Although the concept of a probability space is important conceptually and convenient notationally, calculations involving a probability space $(\mathcal{S}, \Sigma, p)$ are often described with a density function d, where

$$p(\mathcal{E}) = \int_{\mathcal{E}} d(\mathbf{x})\, dE \qquad \text{(Eq. J3.1-1)}$$

for $\mathcal{E} \in \Sigma$, $\mathbf{x} \in \mathcal{E}$, and dE corresponding to an increment of volume from $\mathcal{E}$. Then, the expected value, variance, cumulative distribution function (CDF), and complementary cumulative distribution function (CCDF) associated with a real-valued function $y = f(\mathbf{x})$ defined on $\mathcal{S}$ are given by

$$E(y) = E\left[f(\mathbf{x})\right] = \int_{\mathcal{S}} f(\mathbf{x})\, d(\mathbf{x})\, dS, \qquad \text{(Eq. J3.1-2)}$$

$$V(y) = V\left[f(\mathbf{x})\right] = \int_{\mathcal{S}} \left[f(\mathbf{x}) - E(y)\right]^2 d(\mathbf{x})\, dS, \qquad \text{(Eq. J3.1-3)}$$

$$prob(\tilde{y} \le y) = prob\left[f(\mathbf{x}) \le y\right] = \int_{\mathcal{S}} \underline{\delta}_y\left[f(\mathbf{x})\right] d(\mathbf{x})\, dS \qquad \text{(Eq. J3.1-4)}$$

and

$$prob(\tilde{y} > y) = prob[f(\mathbf{x}) > y] = \int_S \bar{\delta}_y[f(\mathbf{x})] d(\mathbf{x})\, dS, \qquad \text{(Eq. J3.1-5)}$$

respectively, where

$$\underline{\delta}_y[f(\mathbf{x})] = \begin{cases} 1 & \text{if } f(\mathbf{x}) \le y \\ 0 & \text{otherwise} \end{cases} \text{ and } \bar{\delta}_y[f(\mathbf{x})] = 1 - \underline{\delta}_y[f(\mathbf{x})] = \begin{cases} 1 & \text{if } f(\mathbf{x}) > y \\ 0 & \text{otherwise} \end{cases} \qquad \text{(Eq. J3.1-6)}$$

and dS represents an increment of volume from S. Specifically, $prob(\tilde{y} \le y)$ denotes the probability that $f(\mathbf{x})$ has a value less than or equal to y; $prob(\tilde{y} > y)$ denotes the probability that $f(\mathbf{x})$ has a value greater than y; the points $[y, prob(\tilde{y} \le y)]$ define the CDF for y; and the points $[y, prob(\tilde{y} > y)]$ define the CCDF for y.

In turn, the q quantile value (e.g., $q = 0.05, 0.5, 0.95$) for $y = f(\mathbf{x})$ is the value y such that

$$q = prob(\tilde{y} \le y) = \int_S \underline{\delta}_y[f(\mathbf{x})] d(\mathbf{x})\, dS. \qquad \text{(Eq. J3.1-7)}$$

Specifically, the value y for which

$$0.5 = prob(\tilde{y} \le y) = \int_S \underline{\delta}_y[f(\mathbf{x})] d(\mathbf{x})\, dS \qquad \text{(Eq. J3.1-8)}$$

is the median value for $y = f(\mathbf{x})$. Notationally, the q quantile value for $y = f(\mathbf{x})$ can be represented by $Q_q(y) = Q_q[f(\mathbf{x})]$. The results in Equations J3.1-7 and J3.1-8 determine $Q_q[f(\mathbf{x})]$ on the basis of the CDF for $y = f(\mathbf{x})$. Equivalently, the value y such that

$$1 - q = prob(\tilde{y} > y) = \int_S \bar{\delta}_y[f(\mathbf{x})] d(\mathbf{x})\, dS \qquad \text{(Eq. J3.1-9)}$$

defines $Q_q[f(\mathbf{x})]$ on the basis of the CCDF for $y = f(\mathbf{x})$.

Results of risk analyses are typically represented with CCDFs rather than CDFs. In particular, a CCDF answers the question "How likely is it to be this bad or worse?", which is usually the question asked with respect to individual consequences in a risk assessment. In contrast, CDFs are usually used as the basis for defining quantiles. However, conversion between CCDFs and CDFs is straightforward as the probabilities defining a CDF are simply one minus the corresponding probabilities defining a CCDF (i.e., $prob(\tilde{y} \le y) = 1 - prob(\tilde{y} > y)$) and vice versa (i.e., $prob(\tilde{y} > y) = 1 - prob(\tilde{y} \le y)$).

As discussed in Section J4, expected values of the form defined in Equation J3.1-2 and medians of the form defined in Equation J3.1-8 are of central importance in the EPA's and the NRC's regulations for the Yucca Mountain facility.

Before continuing, two technical observations are made. First, the preceding development of expected value and related quantities is done at an intuitive level using density functions and the Riemann integral. A more formal development using measure theory and the Lebesgue integral

is also possible but would not be helpful at an intuitive level. Second, the function $\bar{\delta}_y[f(\mathbf{x})]$ defined in Equation J3.1-6 is effectively the same as the Heaviside function and should not be confused with the Dirac delta function.

The representation and incorporation of uncertainty figures prominently in the EPA's and NRC's standards for the Yucca Mountain facility. For example, see references to uncertainty in statements (EPA2), (EPA3), and (EPA5) – (EPA12) by the EPA and in statements (NRC2), (NRC3), and (NRC5) – (NRC13) by the NRC. In addition, statements such as (YMRP1) – (YMRP5), (YMRP10), and (YMRP11) in the NRC's YMRP also relate to the importance attached to the representation of uncertainty.

Examination of the indicated statements shows that three different concepts of uncertainty are involved in PA for the Yucca Mountain facility: (i) uncertainty about what will happen in the future, (ii) uncertainty about parameters, models, and other analysis assumptions, and (iii) variability.

Uncertainty about what will happen in the future can be seen in statements such as (i) "weighted by their probability of occurrence" in (EPA2) and (NRC2), (ii) "Because none of these possible futures can be demonstrated to describe the actual future behavior of the repository system, the Commission requires that the applicant calculate the mean of these dose curves, properly weighted by their individual probabilities" in (NRC6), and (iii) "The probabilities of occurrence of all scenario classes, included in calculating the annual dose curve sum to one" in (YMRP3). Uncertainty of the type indicated in the preceding statements about events whose future occurrence is assumed to be random, at least insofar as our ability to forecast such occurrences is concerned, is called aleatory uncertainty (Helton and Burmaster 1996 [DIRS 107498]; Paté-Cornell 1996 [DIRS 107499]; Helton 1997 [DIRS 107496]). Other descriptors sometimes used in the designation of aleatory uncertainty include stochastic, type A and irreducible. The preceding statements indicate that the EPA and the NRC intend for probability to be used in the mathematical characterization of aleatory uncertainty. Thus, underlying the TSPA-LA, there must be a probability space $(\mathcal{A}, \mathrm{A}, p_A)$ for aleatory uncertainty. The general nature of the probability space $(\mathcal{A}, \mathrm{A}, p_A)$ will be discussed in more detail in Section J3.3.

Uncertainty about parameters, models and other analysis assumptions can be seen in statements such as (i) "focuses performance assessments and analyses upon the full range of defensible and reasonable parameter distributions" in (EPA3) and (NRC3), (ii) "Account for uncertainties and variabilities in parameter values and provide for the technical basis for parameter ranges, probability distributions, or bounding values used in the performance assessment" in (NRC8), (iii) "performance assessments and analyses should focus on the full range of defensible and reasonable parameter distributions" in (NRC9), and (iv) "The estimate of the uncertainty in the performance assessment results is consistent with the model and parameter uncertainty" in (YMRP10). Uncertainty of the type indicated in the preceding statements derives from a lack of knowledge about a quantity, a model or an assumption assumed to have a fixed value in the context of a specific analysis and is usually referred to as epistemic uncertainty (Helton and Burmaster 1996 [DIRS 107498]; Paté-Cornell 1996 [DIRS 107499]; Helton 1997 [DIRS 107496]). Other descriptors sometimes used in the designation of epistemic uncertainty include subjective, state of knowledge, type B and reducible. The preceding statements indicate

that the EPA and the NRC intend for probability to be used in the mathematical characterization of the epistemic uncertainty. Thus, underlying the TSPA-LA, there must be a probability space ($\mathcal{E}$, E, p_E) for epistemic uncertainty. The general nature of the probability space ($\mathcal{E}$, E, p_E) will be discussed in more detail in Section J3.5.

Recognition of the potential importance of variability in assessing the compliance of the Yucca Mountain facility with applicable standards is demonstrated by references to "variability" in (NRC8) and (NRC11). In the two indicated quotes, variability appears in conjunction with uncertainty in the statements "Account for uncertainties and variabilities in parameter values" in (NRC8) and "uncertainty and variability in parameter values must be taken into account" in (NRC11). However, uncertainty in the sense of epistemic uncertainty and variability in the sense of a quantity having different values as a function of space and/or time are very different concepts. In particular, (epistemic) uncertainty involves a lack of knowledge about the appropriate value to use for a quantity that is assumed to have a fixed value in the context of a particular analysis. In the TSPA-LA, probability is used to characterize such uncertainty. In contrast, variability in a quantity is characterized in the TSPA-LA as a function of space and/or time (e.g., $f(x, y), f(x, y, z), f(x, y, z, t), f(t)$, …, where x, y and z correspond to spatial coordinates and t corresponds to time). For some quantities, functions of the form just indicated are used as input to the TSPA-LA (e.g., infiltration is both spatially and temporally variable); for other quantities, spatial and/or temporal variability is reduced to an expected value over space and/or time, and then this expected value is used as input to the TSPA-LA (e.g., quantities involved in ground water flow and transport such as porosities, fracture spacings and distribution coefficients are spatially-averaged quatities).

An important point to recognize is that there is almost always epistemic uncertainty in the characterization of variability. For example, if a function $f(x, y)$ characterizes the two-dimensional variability of some quantity, there are most likely many possible values for this function of varying levels of credibility. Thus, the function $f(x, y)$ characterizes spatial variability, but a lack of knowledge with respect to how to exactly define $f(x, y)$ is epistemic uncertainty. Similarly, there can be, and almost always is, epistemic uncertainty with respect to the values of quantities used in the characterization of aleatory uncertainty. For example, the occurrence of a certain process (e.g., volcanism) might be assumed to follow a Poisson process with a rate constant λ (units: yr^{-1}). The rate constant λ characterizes aleatory uncertainty and gives rise to probabilities of volcanic events occurring over time intervals of different lengths. However, the inability to confidently assign an exact value for λ is epistemic uncertainty.

It is worthwhile to briefly consider the phrases "features, events, and processes, and sequences of events and processes" and "features, events and processes" that appear often in the EPA and NRC standards for the Yucca Mountain facility (e.g., EPA2, NRC2, NRC7, NRC8, and NRC16). As suggested by its name, a feature is a large-scale property of the system under consideration (e.g., a fault, a geologic formation, an aquifer, …). A feature either exists or it does not exist. There can be epistemic uncertainty about whether or not a feature exists (i.e., maybe it is there or maybe it is not there) and also epistemic uncertainty about the properties of a feature (e.g., permeability, porosity, fracture spacing, thermal conductivity, …). Often, there is spatial variability in the properties of a feature. There can also be epistemic uncertainty in how to define such variability. However, as previously discussed, variability and epistemic uncertainty

are distinct concepts. An event is something that occurs over a very short period of time (e.g., igneous or seismic occurrences); in essence, an event is a discontinuity in the behavior of the system that occurs at a specific point in time. The occurrence, or nonoccurrence, of events is considered to be aleatory uncertainty and is distinct from epistemic uncertainty. However, there can be epistemic uncertainty in quantities used to characterize aleatory uncertainty (e.g., means, standard deviations, occurrence rates, …). The reference to "sequence of events" derives from the fact that the occurrence of one or more aleatory events is always considered over some period of time (e.g., 0 to 10,000 yr in parts of the regulations for the Yucca Mountain facility); such sequences of events correspond to elementary events associated with the probability space for aleatory uncertainty. A process is something that takes place continuously over a long period of time (e.g., groundwater flow, heat flow, corrosion, …). Although a process may be, but is not necessarily, initiated by a specific aleatory event, it is usually represented by a model (e.g., a system of ordinary or partial differential equations) that predicts the time-dependent, and often spatially dependent, behavior of the process. Often, there is substantial epistemic uncertainty associated with the model inputs used in modeling complex processes (e.g., dual porosity fluid flow and solute transport in a fractured geologic medium) and there can also be epistemic uncertainty with respect to the choice of a model itself (i.e., model uncertainty as it is sometimes called).

The dual use of probability to represent both aleatory uncertainty and epistemic uncertainty, as is done in the TSPA-LA, can be traced back to the beginnings of the formal development of probability theory in the late sixteen hundreds (Hacking 1975 [DIRS 107512], Section 2; Shafer 1978 [DIRS 159070]; Bernstein 1996 [DIRS 105742], pp. 47 to 56; Rechard 1999 [DIRS 145383]). The use of probability in PAs for complex systems is a topic of wide interest and many references are available that provide additional information and perspectives on this use (Paté-Cornell 1996 [DIRS 107499]; Helton 1997 [DIRS 107496], Section 4; Parry and Winter 1981 [DIRS 159059]; Paté-Cornell 1986 [DIRS 170519]; Apostolakis 1989 [DIRS 107710]; Apostolakis 1990 [DIRS 107506]; Helton 1994 [DIRS 107739]; Hoffman and Hammonds 1994 [DIRS 107502]; Kaplan 1993 [DIRS 107741]).

J3.2 Conceptual Structure of a Performance Assessment

A PA for a radioactive waste disposal facility or some other large engineered facility is a very complex undertaking requiring large amounts of information and a variety of mathematical models. Full documentation of a PA can require 1000s of pages of text. Yet, at a conceptual level, the computational implementation of a PA can be viewed as involving three basic entities: (i) EN1, a probabilistic characterization of what could occur at the facility under consideration; (ii) EN2, mathematical models for estimating the consequences of what could occur; and (iii) EN3, a probabilistic characterization of the uncertainty in the parameters used in the definitions of EN1 and EN2. The term parameter in the definition of EN3 is used broadly enough to include designators for alternative models or model structures. Despite the complexity of a PA, much of the overarching conceptual and computational structure of a PA can be described in terms of the preceding three entities. In particular, EN1 corresponds to the probabilistic characterization of aleatory uncertainty used in the analysis; EN2 corresponds to the mathematical models for physical processes used in the analysis; and EN3 corresponds to the probabilistic characterization of epistemic uncertainty used in the analysis. The nature of EN1,

EN2 and EN3 is discussed further in Sections J3.3 – J3.5. This discussion is adapted in part from Helton (2003 [DIRS 170558]).

J3.3 EN1: Probabilistic Characterization of Aleatory Uncertainty

The first entity, EN1, is the probability space ($\mathcal{A}$, A, p_A) associated with aleatory uncertainty. This probability space is intended to provide a mathematical description of those occurrences that could take place at some time in the future with sufficient likelihood and consequence to merit inclusion in the PA. Typically, these occurrences are constrained to take place over some time interval of interest (e.g., 10,000 yr in parts of the regulations that apply to the Yucca Mountain facility). There are two aspects to the specification of such occurrences: (i) definition of occurrence properties (e.g., time, location, magnitude, …) within the time interval of interest, and (ii) assignment of probabilities to possible occurrences within the time interval of interest.

The development of probabilities requires a careful specification of exactly what probabilities are to be assigned to. As an example, suppose only two occurrences, designated o_1 and o_2, with the following properties were selected for inclusion in a PA: (i) the occurrences of o_1 and o_2 are independent, (ii) the occurrences of o_1 and o_2 follow Poisson processes with rate constants λ_1 (yr^{-1}) and λ_2 (yr^{-1}), respectively, and (iii) a time interval [0, T = 1000 yr] is under consideration. There are many possible patterns of occurrence of o_1 and o_2 over the interval [0, T]. Each possible pattern can be represented by a vector

$$\mathbf{a} = [m, n, t_{11}, t_{12}, \ldots, t_{1m}, t_{21}, t_{22}, \ldots, t_{2n}], \qquad \text{(Eq. J3.3-1)}$$

where (i)

$$0 \le t_{11} \le t_{12} \le \ldots \le t_{1m} \le T = 1000 \text{ yr}$$

and

$$0 \le t_{21} \le t_{22} \le \ldots \le t_{2n} \le T = 1000 \text{ yr}$$

are the times at which o_1 and o_2, respectively, occur, (ii) m = 0 or n =0 indicates that the corresponding occurrence did not take place in the time interval [0, T], and (iii) the symbol **a** for the vector in Equation J3.3-1 is used to be suggestive of aleatory.

Each vector **a** of the form appearing in Equation J3.3-1 represents a possible pattern of occurrences over the time interval [0, T]. The pattern of occurrences characterized by **a** is sometimes referred to as a future in radioactive waste disposal because each **a** is describing one possible future at the facility under consideration. The set

$$\mathcal{A} = \{\mathbf{a} : \mathbf{a} = [m, n, t_{11}, t_{12}, \ldots, t_{1m}, t_{21}, t_{22}, \ldots, t_{2n}]\} \qquad \text{(Eq. J3.3-2)}$$

corresponds to the universe of all possible futures that could occur over the time interval [0, T = 1000 yr] given the assumption that o_1 and o_2 are the only two occurrences to be considered.

The introduction of **a** provides an exact mathematical description (i.e., definition) of occurrence properties within the time interval of interest. The vector **a** in Equation J3.3-1 is quite simple; in general, more properties than initiation times are required to define individual occurrences in a PA. A more general formulation of the example would be

$$\mathbf{a} = [m, n, \mathbf{o}_{11}, \mathbf{o}_{12}, \ldots, \mathbf{o}_{1m}, \mathbf{o}_{21}, \mathbf{o}_{22}, \ldots, \mathbf{o}_{2n}], \qquad \text{(Eq. J3.3-3)}$$

where $\mathbf{o}_{1i}$, i = 1, 2, …, m, and $\mathbf{o}_{2j}$, j = 1, 2, …, n, are vectors of properties associated with the occurrence of o_1 and o_2, respectively. Further, PAs can involve more than two occurrences of interest. However, **a** as defined in Equation J3.3-1 is sufficient as an example.

Introduction of the vector **a** and the set $\mathcal{A}$ is simply a means of providing a mathematical structure to ideas previously introduced by the NRC in the specification of licensing requirements for the Yucca Mountain facility. Such a mathematical structure must be introduced to provide an unambiguous description of the conceptual and computational structure of the TSPA-LA. With respect to the introduction of ideas by the NRC, the vector **a** is a means of giving a formal and mathematically unambiguous description to the concept of "possible future behavior" introduced in (NRC6) and the equivalent concept of an "event sequence" introduced in (NRC14). The elements of individual **a**'s derive from the occurrence of "initiating events" introduced in (NRC15). Although the NRC refers to the **a**'s as future behaviors or event sequences, the standard terminology in probability theory is to refer to the **a**'s as elementary events and to refer to the set $\mathcal{A}$ of all possible **a**'s as the sample space. The NRC refers to "events (event classes or scenario classes)" in (NRC7), "events" in (NRC8), and "scenario classes" in (YMRP2); in each case, what is being referred to is a subset of the sample space $\mathcal{A}$. The standard terminology from probability theory is to refer to such sets as events (technically, events are elements of the set A but, at an intuitive level, an event can be thought of as any subset of $\mathcal{A}$). What is often referred to as a scenario class is an event in the sense that it is a subset of $\mathcal{A}$. Thus, in NRC terminology, the set A of subsets of $\mathcal{A}$ appearing in the formal development of probability simply contains all possible event classes (or, equivalently, scenario classes) for which probability can be defined.

Statements relating to completeness such as "Those features, events and processes expected to materially affect compliance with § 63.113(b) (66 FR 55732 [DIRS 156671]) or be potentially adverse to performance are included, while events (event classes or scenario classes) that are very unlikely (less than one chance in 10,000 over 10,000 years) can be excluded from the analysis" in (NRC7) involve the question of whether or not the **a**'s, and hence $\mathcal{A}$, have been appropriately defined. At a technical level, there are two ways in which unlikely occurrences (e.g., meteor impact) can be formally excluded from an analysis. The first approach is to simply not include such occurrences in the definition of **a**. With this approach, such occurrences are not in the formal structure of the analysis. The second approach is to include such occurrences in the definition of **a** but then to eliminate subsets of $\mathcal{A}$ that involve these occurrences from consideration on the basis of low probability. With this approach, unlikely occurrences are formally included in the structure of the analysis and then eliminated from computational consideration on the basis of low probability. In effect, both approaches are used at different stages of the TSPA-LA analysis, with the second approach constituting part of the screening of

features, events and processes (FEPs) and the first approach underlying the computational implementation of the TSPA-LA.

In this presentation, subsets of $\mathcal{A}$ will be referred to as scenario classes. Thus, with this usage, a scenario class corresponds to what the NRC refers to at various places as events, event classes, or scenario classes (NRC7, NRC8, and YMRP2). The choice of scenario class to designate a subset of $\mathcal{A}$ is based on a desire to emphasize that, in general, a scenario class contains many possible futures (i.e., elementary events). Thus, in documentation for the TSPA-LA, a scenario class corresponds to what is usually referred to as an event in the standard terminology of probability theory.

The assignment of probabilities is now considered. Typically, individual futures of the form illustrated by $\mathbf{a}$ in Equation J3.3-1 have a probability of zero. An important exception to this is the "degenerate vector" corresponding to undisturbed conditions (i.e., the future in which none of the occurrences under consideration take place and thus for which $m = n = 0$), which has a probability close to one in many PAs. Thus, probabilities are used in reference to sets of futures or, equivalently, to subsets $\mathcal{U}$ of the sample space $\mathcal{A}$ defined in Equation J3.3-2. For example, $\mathcal{U}$ might be defined by

$$\mathcal{U} = \left\{ \mathbf{a} = [1, 2, t_{11}, t_{21}, t_{22}] : 0 \le t_{11} \le 500 \text{ yr}, \ 0 \le t_{21} \le t_{22} \le 1000 \text{ yr} \right\}. \quad \text{(Eq. J3.3-4)}$$

Then, under the previously stated assumptions that (i) o_1 and o_2 are independent and follow Poisson processes with rate constants λ_1 and λ_2 and (ii) a time interval of length 1000 yrs is under consideration, the probability $p_A(\mathcal{U})$ of $\mathcal{U}$ is given by

$$\begin{aligned} p_A(\mathcal{U}) &= \left\{ \left[(500\lambda_1)^1 / 1! \right] \left[\exp(-500\lambda_1) \right] \right\}_1 \left\{ \left[(500\lambda_1)^0 / 0! \right] \left[\exp(-500\lambda_1) \right] \right\}_2 \\ &\quad \left\{ \left[(1000\lambda_2)^2 / 2! \right] \left[\exp(-1000\lambda_2) \right] \right\}_3 \\ &= \left\{ \left[(500\lambda_1)^1 / 1! \right] \left[\exp(-1000\lambda_1) \right] \right\} \left\{ \left[(1000\lambda_2)^2 / 2! \right] \left[\exp(-1000\lambda_2) \right] \right\}. \end{aligned} \quad \text{(Eq. J3.3-5)}$$

where $\{\sim\}_1$ is the probability that occurrence o_1 takes place exactly once in the time interval [0, 500 yr], $\{\sim\}_2$ is the probability that occurrence o_1 does not take place in the time interval [500, 1000 yr], and$\{\sim\}_3$ is the probability that occurrence o_2 takes place exactly twice in the time interval [0, 1000 yr].Thus, in this example and more generally in most situations, probability distributions are introduced for the individual elements of $\mathbf{a}$ and then used to define probabilities for sets of $\mathbf{a}$'s. The closed form calculation of such probabilities can be difficult or impossible; often, Monte Carlo techniques or other numerical procedures must be used to calculate approximate probabilities.

References to probabilities of events, event classes and scenario classes repeatedly appear in the EPA and NRC standards for the Yucca Mountain facility. For example "weighted by their probability of occurrence" appears in (EPA2) and (NRC2); related statements appear in (NRC6), (NRC7), (NRC8), (NRC11), (NRC12), (NRC17), and (YMRP1) – (YMRP3). As another

specific example, the statement "Consider only events that have at least one chance in 10,000 of occurring over 10,000 years" in (NRC8) clearly mandates the determination of probabilities of the form indicated in Equation J3.3-5.

To the extent practicable, descriptions of the various parts of a PA should use widely recognized mathematical constructions. Then, the computational implementation of the PA can be viewed as the calculation of approximations to these constructions. For the use of probability to represent aleatory uncertainty, the fundamental mathematical construction is a probability space $(\mathcal{A}, \mathrm{A}, p_A)$, which involves three components as previously indicated in Section J3.1: (i) the set $\mathcal{A}$ that contains everything that could occur in the particular universe under consideration, (ii) the set A of subsets of $\mathcal{A}$ for which probability is defined, and (iii) the function p_A that defines the probability of the individual elements of A. The preceding three components appear in the previous example and, as already indicated, in the EPA and NRC regulatory requirements for the Yucca Mountain facility. In the terminology of probability theory, $\mathcal{A}$ is the sample space; elements $\mathbf{a}$ of $\mathcal{A}$ are elementary events; elements $\mathcal{U}$ of A are events; and p_A is a probability measure. In terminology often used in PA for radioactive waste disposal, elements $\mathbf{a}$ of $\mathcal{A}$ are futures; elements $\mathcal{U}$ of A are scenario classes; the probabilities $p_A(\mathcal{U})$ are scenario probabilities; and questions of "completeness" deal with whether or not $\mathcal{A}$ has been defined in a way that incorporates all significant occurrences at the site under consideration. As previously indicated, the descriptor scenario class instead of scenario is used in the documentation for the TSPA-LA to emphasize that sets containing, in general, many futures are under consideration.

In practice, most probability calculations are based on the distributions assigned to the individual elements of $\mathbf{a}$ and do not rely on the formal properties of the probability space $(\mathcal{A}, \mathrm{A}, p_A)$. For example, the probability space associated with the illustration of aleatory uncertainty for the vector $\mathbf{a}$ in Equation J3.3-1 is defined by distributions D_1 and D_2 of occurrence times for occurrences o_1 and o_2 that derive from the Poisson rate constants λ_1 and λ_2. In actual calculation, it is the mathematical characterization of these distributions that are used rather than the formal properties of the corresponding probability space. However, the introduction of the concept of a probability space provides a way to formally describe what is being done in a PA and also a way to distinguish between different uses of probability within a PA.

The TSPA-LA incorporates three types of disruptions that are treated as aleatory occurrences: early failures of WPs and DSs, igneous events, and seismic events. Descriptions of the formal probabilistic representations used in the TSPA-LA for the occurrence of early failures of WPs and DSs, igneous events, and seismic events are given in later sections.

J3.4 EN2: Mathematical Models for Estimating Consequences of Individual Futures

The entity EN2 corresponds to the mathematical models required to estimate various consequences in a PA for a radioactive waste disposal site or some other facility. Conceptually, EN2 can be viewed as a function $\mathbf{f}$ of the form

$$\mathbf{y} = \mathbf{f}(\mathbf{a}), \qquad \text{(Eq. J3.4-1)}$$

where **a** is a particular future, **f** corresponds to the models used to estimate various outcomes associated with **a**, and **y** is the estimated outcomes. A vector notation is used for **f** and **y** because typically a large number of outcomes are estimated for each future **a**. Often, the elements of **y** include functions of space and/or time. For a radioactive waste disposal site, the models denoted by **f** are often systems of ordinary or partial differential equations used to represent processes such as material deformation, corrosion, fluid flow, radionuclide transport in flowing groundwater, and radionuclide movement and associated human radiation exposure in the surface environment. This is certainly the case in the TSPA-LA for the Yucca Mountain facility.

The models used in a particular PA will depend on many things, including the site under consideration, the resolution of the data available for characterization of the site, the desired resolution in model predictions, and the time and resources available for the analysis. However, most models actually consist of three parts: (i) a formal mathematical representation (e.g., a system of nonlinear partial differential equations), (ii) a numerical procedure that produces approximations to the formal mathematical representation (e.g., a finite difference procedure), and (iii) a computer program that implements the numerical procedure. A common situation is to use physically detailed and computationally demanding models for initial assessment of system behavior and then to incorporate the results obtained from these models into less detailed and less computationally demanding models for use in a final, integrated PA. This type of incorporation process is used extensively in the TSPA-LA and is often referred to as model abstraction.

Given the almost universal use of numerical approximations and computer programs to implement these approximations, a PA typically involves two extensions of the representation in Equation J3.4-1:

$$\mathbf{y} = \hat{\mathbf{f}}(\mathbf{a}) \qquad \text{(Eq. J3.4-2)}$$

and

$$\mathbf{y} = \mathbf{F}(\mathbf{a}), \qquad \text{(Eq. J3.4-3)}$$

where $\hat{\mathbf{f}}$ is used to represent the numerical approximation that replaces **f**, and **F** is used to represent the computer program that implements this approximation and actually produces **y**. For example, if **f** is based on a system of ordinary differential equations, $\hat{\mathbf{f}}$ might correspond to an Adams-Moulten method, a variable order, variable stepsize Runge-Kutta method or a Gear's backward differentiation method, and **F** would correspond to the program that actually implemented the method.

The model **f** indicated in Equation J3.4-1 is almost always the result of the assembly of many individual models. For example, **f** might be of the form

$$\begin{aligned}\mathbf{f}(\mathbf{a}) = {} & \mathbf{f}_1(\mathbf{a}) + \mathbf{f}_2\left[\mathbf{a}, \mathbf{f}_3(\mathbf{a})\right] + \mathbf{f}_4\left\{\mathbf{a}, \mathbf{f}_2\left[\mathbf{a}, \mathbf{f}_3(\mathbf{a})\right], \mathbf{f}_3(\mathbf{a})\right\} + \mathbf{f}_5\left[\mathbf{a}, \mathbf{f}_3(\mathbf{a})\right] \\ & + \mathbf{f}_6\left[\mathbf{a}, \mathbf{f}_3(\mathbf{a})\right] + \mathbf{f}_7\left[\mathbf{a}, \mathbf{f}_3(\mathbf{a})\right] + \mathbf{f}_8\left\{\mathbf{a}_N, \mathbf{f}_9(\mathbf{a}_N), \mathbf{f}_{10}\left[\mathbf{a}, \mathbf{f}_3(\mathbf{a})\right]\right\}, \qquad \text{(Eq. J3.4-4)}\end{aligned}$$

where $\mathbf{a}$ ~ particular future under consideration, $\mathbf{a}_N$ ~ future involving no disruptions, and $\mathbf{f}_1$, $\mathbf{f}_2$, …, $\mathbf{f}_{10}$ ~ individual models from which $\mathbf{f}$ is constructed. The description of the exact form of $\mathbf{f}$ and its many component models in the TSPA-LA is outside the scope of this introductory presentation. However, in concept, the TSPA-LA employs a model structure of the form indicated, and in reality, has a computational structure more complex than that just indicated.

References and allusions to results that must be obtained by the use of models occur throughout the EPA and NRC regulations for the Yucca Mountain facility. The following statement by the NRC in (NRC9) explicitly acknowledges the necessity of using complex numerical procedures: "Demonstrating compliance will involve the use of complex predictive models …". Thus, EN2 unavoidably exists as part of the TSPA-LA for the Yucca Mountain facility.

In a PA, EN1 (i.e., the probability space ($\mathcal{A}$, A, p_A)) provides a probabilistic characterization of what could happen at the facility under consideration, and EN2 (i.e., the function $\mathbf{f}$ indicated in Equation J3.4-1) provides estimates of the consequences associated with individual futures $\mathbf{a}$. In many PAs, a representation of results is desired that provides a display of both consequence and likelihood. The usual mathematical construction used to display this information is a complementary cumulative distribution function (CCDF), which provides a display of the probability that individual consequence values will be exceeded (Figure J3.4-1).

A CCDF can be formally defined by an integral involving EN1 and EN2. Specifically,

$$prob_A(c > C) = \int_{\mathcal{A}} \bar{\delta}_C\left[f(\mathbf{a})\right] d_A(\mathbf{a})\,\mathrm{d}A, \qquad \text{(Eq. J3.4-5)}$$

where $prob_A(c > C)$ is the probability that a future $\mathbf{a}$ yielding a consequence value larger than C will occur, $d_A(\mathbf{a})$ is the density function associated with ($\mathcal{A}$, A, p_A), dA is an incremental (i.e., differential) volume from $\mathcal{A}$,

$$\bar{\delta}_C\left[f(\mathbf{a})\right] = \begin{cases} 1 & \text{if } f(\mathbf{a}) > C \\ 0 & \text{if } f(\mathbf{a}) \le C, \end{cases}$$

a nonbold representation for f is used because a single consequence (i.e., analysis outcome) is considered in the construction of a CCDF (i.e., f is real valued rather than vector valued in this context), and the subscript A indicates that $prob_A(c > C)$ derives from aleatory uncertainty. The effect of the indicator function $\bar{\delta}_C$ is to pick out the subset of $\mathcal{A}$ for which $f(\mathbf{a}) > C$, with the result that the integral yields the desired probability. The preceding is a specific example of the generic CCDF defined in conjunction with Equation J3.1-5.

In practice, the integral in Equation J3.4-5 is too complex to permit a closed-form evaluation. Part of this complexity comes from the properties of ($\mathcal{A}$, A, p_A) and part of it comes from the complexity of f. This complexity typically precludes the use of standard numerical procedures for evaluating integrals. In practice, either Monte Carlo techniques or importance sampling are often used in the evaluation of the integral in Equation J3.4-5.

With the Monte Carlo approach, the integral in Equation J3.4-5 is approximated by

$$prob_A(c > C) \cong \sum_{i=1}^{nR} \bar{\delta}_C\left[f\left(\mathbf{a}_i\right)\right] / nR, \qquad \text{(Eq. J3.4-6)}$$

where $\mathbf{a}_i$, i = 1, 2, …, nR, is a random sample from $\mathcal{A}$ generated in consistency with the definition of ($\mathcal{A}$, A, p_A) (Figure J3.4-2). In practice, generating a random sample from $\mathcal{A}$ in consistency with the definition of ($\mathcal{A}$, A, p_A) means generating a sample using the distributions assigned to the individual elements of $\mathbf{a}$.

In most PAs, evaluation of $f(\mathbf{a})$ is too expensive to permit an evaluation for each sample element $\mathbf{a}_i$ in Equation J3.4-6. Rather, $f(\mathbf{a})$ is evaluated for a relatively small number of elements of $\mathcal{A}$ and then these evaluations are used in the construction (i.e., approximation) of $f(\mathbf{a}_i)$ for use in the summation in Equation J3.4-6. Thus, there are actually three numerical approximations involved: (i) the Monte Carlo procedure to approximate the integral in Equation J3.4-5, (ii) an initial approximation of $f(\mathbf{a})$ for selected elements of $\mathcal{A}$, and (iii) a subsequent approximation of $f(\mathbf{a}_i)$ from these initial approximations for use in the summation in Equation J3.4-6. As indicated earlier, the use of a limited number of complex calculations to cover a number of different situations is used extensively in the TSPA-LA and is referred to as model abstraction.

With importance sampling, $\mathcal{A}$ is divided into disjoint strata $\mathcal{A}_i$, i = 1, 2, …, nS, with $\mathcal{A} = \cup_i \mathcal{A}_i$ and a value $\mathbf{a}_i$, i = 1, 2, …, nS, is selected from each strata. Then, the integral in Equation J3.4-5 is approximated by

$$prob_A\left(c > C\right) = \sum_{i=1}^{nS} \bar{\delta}_C\left[f\left(\mathbf{a}_i\right)\right] p_A\left(\mathcal{A}_i\right), \qquad \text{(Eq. J3.4-7)}$$

where $p_A(\mathcal{A}_i)$ is the probability of $\mathcal{A}_i$. The strata $\mathcal{A}_i$ are simply a collection of scenario classes (i.e., subsets of $\mathcal{A}$) with the properties $\mathcal{A}_i \cap \mathcal{A}_j = \varnothing$ for $i \neq j$ and $\mathcal{A} = \cup_i \mathcal{A}_i$. When the $\mathbf{a}_i$ are randomly selected within the corresponding strata, importance sampling is a variance reduction technique for simple random (i.e., Monte Carlo) sampling. Importance sampling involves the same approximation considerations as the Monte Carlo approach described in conjunction with Equation J3.4-6. The fault tree and event tree techniques (Breeding et. al. 1992 [DIRS 107727]; Vesely et al. 1981 [DIRS 128494]) used extensively in conjunction with PAs for nuclear reactors and other complex engineered systems can be viewed as algorithms for defining an importance sampling procedure over the sample space associated with all possible accidents at these facilities.

Another approach to importance sampling is to reformulate the integral in Equation J3.4-5 as

$$\int_{\mathcal{A}} \bar{\delta}_C\left[f\left(\mathbf{a}\right)\right] d_A\left(\mathbf{a}\right) \mathrm{d}A = \int_{\mathcal{A}} \left[\frac{\bar{\delta}_C\left[f\left(\mathbf{a}\right)\right] d_A\left(\mathbf{a}\right)}{d_I\left(\mathbf{a}\right)}\right] d_I\left(\mathbf{a}\right) \mathrm{d}A, \qquad \text{(Eq. J3.4-8)}$$

where $d_I(\mathbf{a})$ is the density function for a distribution defined on $\mathcal{A}$ selected to accentuate subregions of $\mathcal{A}$ that are believed to be important in the determination of $prob_A(c > C)$. Then, $prob_A(c > C)$ is approximated by

$$prob_A(c > C) \cong \sum_{i=1}^{nR} \left[\frac{\bar{\delta}_C[f(\mathbf{a}_i)]\, d_A(\mathbf{a}_i)}{d_I(\mathbf{a}_i)} \right] \Big/ nR, \qquad \text{(Eq. J3.4-9)}$$

where $\mathbf{a}_i$, $i = 1, 2, \ldots, nR$, is a random sample from $\mathcal{A}$ generated in consistency with the density function $d_I(\mathbf{a})$.

The TSPA-LA uses both random sampling and importance sampling in various integrations involving aleatory uncertainty.

Another possible display of the combined effects of EN1 and EN2 is given by the expected value and variance of a consequence of interest. The expected value $E_A(f) = E_A[f(\mathbf{a})]$ and variance $V_A(f) = V_A[f(\mathbf{a})]$ of a particular consequence that derive from aleatory uncertainty are formally defined by

$$E_A(f) = E_A[f(\mathbf{a})] = \int_{\mathcal{A}} f(\mathbf{a})\, d_A(\mathbf{a})\, \mathrm{d}A \qquad \text{(Eq. J3.4-10)}$$

and

$$V_A(f) = V_A[f(\mathbf{a})] = \int_{\mathcal{A}} [f(\mathbf{a}) - E_A(f)]^2\, d_A(\mathbf{a})\, \mathrm{d}A \qquad \text{(Eq. J3.4-11)}$$

and are easily estimated with the results used in the CCDF approximations in Equations J3.4-6, J3.4-8 and J3.4-9. However, as a large amount of information is lost in the calculation of $E_A(f)$ and $V_A(f)$, the combined effects of EN1 and EN2 are better displayed as CCDFs. The mean and variance defined in Equations J3.4-10 and J3.4-11 are specific examples of the generic results defined in Equations J3.1-2 and J3.1-3.

The NRC's regulations for the Yucca Mountain facility specifically call for the calculation of expected dose to the RMEI (e.g., EPA2, EPA5 – EPA8, NRC2, and NRC5 – NRC7). In particular, the projected doses referred to in (EPA14), (NRC20) and elsewhere are assumed to correspond to expected doses over aleatory uncertainty. Therefore, the TSPA-LA pays special attention to the calculation of expected dose to the RMEI. This is a calculation of the form indicated in Equation J3.4-10. Dose is actually a function of time. Thus, the expected value calculation for dose to the RMEI is perhaps better expressed as

$$\bar{D}(\tau) = E_A[D(\tau|\mathbf{a})] = \int_{\mathcal{A}} D(\tau|\mathbf{a})\, d_A(\mathbf{a})\, \mathrm{d}A, \qquad \text{(Eq. J3.4-12)}$$

where

$D(\tau|\mathbf{a})$ = dose (mrem/yr) at time τ to the RMEI conditional on the occurrence of future **a** (i.e., $\mathbf{a} \in \mathcal{A}$).

In general, dose to the RMEI at time τ changes from future to future, and the indicated expected value $E_A[D(\tau|\mathbf{a})]$ is the expected dose to the RMEI at time τ with the expectation taken over all possible futures (i.e., elements **a** of $\mathcal{A}$).

Application of the approximation procedures indicated in conjunction with Equations J3.4-6, J3.4-7 and J3.4-9 to the integral defining $E_A[D(\tau|\mathbf{a})]$ in Equation J3.4-12 results in the approximations

$$E_A\left[D\left(\tau|\mathbf{a}\right)\right] \cong \sum_{i=1}^{nR} D\left(\tau|\mathbf{a}_i\right)/nR, \qquad \text{(Eq. J3.4-13)}$$

$$E_A\left[D\left(\tau|\mathbf{a}\right)\right] \cong \sum_{i=1}^{nS} D\left(\tau|\mathbf{a}_i\right) p_A\left(\mathcal{A}_i\right) \qquad \text{(Eq. J3.4-14)}$$

and

$$E_A\left[D\left(\tau|\mathbf{a}\right)\right] \cong \sum_{i=1}^{nR}\left[D\left(\tau|\mathbf{a}_i\right) d_A\left(\mathbf{a}_i\right)/d_I\left(\mathbf{a}_i\right)\right]/nR. \qquad \text{(Eq. J3.4-15)}$$

The approximation to $E_A[D(\tau)]$ in Equation J3.4-14 can be viewed as the mathematical implementation of the following NRC statement in (YMRP3): "The calculation of the annual dose curve appropriately sums the contribution of each of the disruptive event scenario classes. … . The probabilities of occurrence of all scenario classes, included in calculating the annual dose curve, sum to one." In particular, $E_A[D(\tau|\mathbf{a}]$ is the (expected) annual dose curve; $D(\tau|\mathbf{a}_i)$ is a dose curve conditional on the event (i.e., scenario class in NRC terminology) $\mathcal{A}_i$; $p_A(\mathcal{A}_i)$ is the probability of $\mathcal{A}_i$; and $\sum_i p_A(\mathcal{A}_i) = 1$ because $\mathcal{A}_i \cap \mathcal{A}_j = \varnothing$ for $i \neq j$ and $\mathcal{A} = \cup_i \mathcal{A}_i$. In general, $\mathbf{a}_i$ is only one of many futures contained in $\mathcal{A}_i$; however, as long as $\mathbf{a}_i$ is selected randomly from $\mathcal{A}_i$, an unbiased estimate for $E_A[D(\tau|\mathbf{a})]$ will be obtained. If one or more futures are randomly selected for each $\mathcal{A}_i$, then the approximation to $E_A[D(\tau|\mathbf{a})]$ in Equation J3.4-14 has the form

$$E_A\left[D\left(\tau|\mathbf{a}\right)\right] \cong \sum_{i=1}^{nS}\left[\sum_{j=1}^{nS(i)} D\left(\tau|\mathbf{a}_{ij}\right)/nS(i)\right] p_A\left(\mathcal{A}_i\right) \qquad \text{(Eq. J3.4-16)}$$

where $\mathbf{a}_{ij}$, $j = 1, 2, \ldots, nS(i)$, are randomly selected from $\mathcal{A}_i$ for $i = 1, 2, \ldots, nS$.

The expressions in Equations J3.4-13 and J3.4-15 provide equally valid approximation procedures for $E_A[D(\tau|\mathbf{a})]$ but do not match the NRC terminology in (YMRP3) as neither scenario classes nor scenario class probabilities are explicitly involved. In particular, $1/nR$ is not a probability but rather a weight used in the estimation of an expected value (e.g., $E_A[D(\tau|\mathbf{a})]$) in a Monte Carlo calculation. The approximation in Equation J3.4-13 is actually closer in spirit to the NRC statement "Each possible future behavior of the repository is represented by a curve describing the annual dose to the RMEI. Generally, but not necessarily, each of the curves is assumed to be equally likely." in (NRC6). In the approximation in Equation J3.4-13, each of the dose curves is assigned an equal weight (i.e., $1/nR$) but not an equal probability. With the exception of the dose curve corresponding to the nominal scenario class, each individual dose curve will typically have a probability of zero.

J3.5 EN3: Probabilistic Characterization of Epistemic Uncertainty

The entity EN3 is the formal outcome of the data development component of a PA and provides a probabilistic characterization of the uncertainty in the many parameters required in the definitions of EN1 (e.g., occurrence rates, parameters in distributions, …) and EN2 (e.g., distribution coefficients, solubilities, …). The term parameter in the description of EN3 is used in a sense that is sufficiently broad to include designators for alternative models or model structures. Formally, EN3 is defined by a probability space ($\mathcal{E}$, E, p_E).

The sample space $\mathcal{E}$ associated with EN3 has the form

$$\mathcal{E} = \{\mathbf{e}: \mathbf{e} \text{ is possibly the correct vector of inputs to use with EN1 and EN2 in the calculation of analysis outcomes}\}. \quad \text{(Eq. J3.5-1)}$$

Further, $\mathbf{e}$ has the form

$$\mathbf{e} = [e_1, e_2, \ldots, e_{nE}], \quad \text{(Eq. J3.5-2)}$$

where each element e_i, $i = 1, 2, \ldots, nE$, of $\mathbf{e}$ is a quantity required in the formulation of EN1 or EN2 that is assumed to have a fixed value in the context of the particular PA under consideration but with this value being imprecisely known. The basic idea is that the PA and the associated definitions of EN1 and EN2 have been developed to the point that appropriate analysis outcomes would be obtained if the appropriate value of $\mathbf{e}$ was used as input to the analysis.

As an example, the representation for the CCDF in Equation J3.4-5 would now become

$$prob_A(c > C \mid \mathbf{e}) = \int_{\mathcal{A}} \bar{\delta}_C[f(\mathbf{a}, \mathbf{e})] d_A(\mathbf{a} \mid \mathbf{e}) \mathrm{d}A, \quad \text{(Eq. J3.5-3)}$$

with the addition of $\mathbf{e}$ to the notation for various quantities in Equation J3.4-5 indicating that the values and/or predictions associated with these quantities are dependent on the value assigned to $\mathbf{e}$. Thus, different values for $\mathbf{e}$ lead to different values for the CCDF in Equation J3.4-1 and other analysis outcomes of interest (Figure J3.5-1). The sample space $\mathcal{E}$ contains all values for $\mathbf{e}$

consistent with available information about the facility under consideration and thus leads to all possible values for the CCDF defined in Equation J3.4-5 and other analysis outcomes of interest.

The vector **e** typically contains elements that affect the value of the analysis outcome under consideration as indicated notationally by $f(\mathbf{a}, \mathbf{e})$ in Equation J3.5-3 and other elements that affect the distribution of **a** as indicated notationally by $d_A(\mathbf{a}|\mathbf{e})$ in Equation J3.5-3. The elements of **e** relevant to the evaluation of $f(\mathbf{a}, \mathbf{e})$ and the elements of **e** relevant to the evaluation of $d_A(\mathbf{a}|\mathbf{e})$ are usually different. To emphasize this distinction, it is often convenient to represent **e** by

$$\mathbf{e} = [\mathbf{e}_A, \mathbf{e}_M], \qquad \text{(Eq. J3.5-4)}$$

where

$$\mathbf{e}_A = \left[e_{A1}, e_{A2}, \ldots, e_{A,nA}\right]$$

and

$$\mathbf{e}_M = \left[e_{M1}, e_{M2}, \ldots, e_{M,nM}\right]$$

are vectors of epistemically uncertain quantities affecting the evaluation of $d_A(\mathbf{a})$ and $f(\mathbf{a})$, respectively. That is, $d_A(\mathbf{a})$ and $f(\mathbf{a})$ notationally have the forms $d_A(\mathbf{a}|\mathbf{e}_A)$ and $f(\mathbf{a}, \mathbf{e}_M)$ to emphasize this dependence. The representation for $prob(c > C|\mathbf{e})$ in Equation J3.5-3 becomes

$$prob_A\left(c > C|\mathbf{e}\right) = \int_{\mathcal{A}} \bar{\delta}_C\left[f\left(\mathbf{a}, \mathbf{e}_M\right)\right] d_A\left(\mathbf{a}|\mathbf{e}_A\right) \mathrm{d}A \qquad \text{(Eq. J3.5-5)}$$

with the addition of this more explicit notation.

The probability space ($\mathcal{E}$, E, p_E) that formally defines EN3 provides a characterization of the uncertainty in the elements of **e**. In practice, ($\mathcal{E}$, E, p_E) is defined by specifying a distribution

$$D_j, j = 1, 2, \ldots, nE, \qquad \text{(Eq. J3.5-6)}$$

for each element e_j of **e**. Correlations and various other restrictions involving the possible values of e_j can also be specified. The purpose of the D_j is to provide, on the basis of all available information, a quantitative (i.e., probabilistic) description of where the possible values for the e_j are located. In contrast, $\mathcal{E}$ only provides a complete compilation of the possible values for the **e** and thus for the e_j. In some instances, it may be possible to use formal statistical procedures to estimate the D_j. However, typically some type of expert review process is needed to develop the D_j (Bonano and Apostolakis 1991 [DIRS 159041]; Cooke 1991 [DIRS 158968]; Hora and Iman 1989 [DIRS 100902]; Keeney and von Winterfeldt 1991 [DIRS 159053]; Meyer and Booker 1991 [DIRS 110460], pp. 4 to 5; Mosleh et al. 1988 [DIRS 159055]; Thorne 1993 [DIRS 159061]).

The EPA and NRC intend for the distributions in Equation J3.5-6 to provide "reasonable" characterizations of uncertainty in the TSPA-LA rather than overtly conservative representations of uncertainty. Here, conservative is used in the designation of assumptions that are contrary to what is believed to be an appropriate representation of system properties and which produce analysis results that are more pessimistic in a regulatory context than should be the case. The EPA and NRC desire for a reasonable characterization of uncertainty is indicated in a number of statements: (i) "Focuses performance assessments and analyses upon the full range of defensible and reasonable parameter distributions rather than only upon extreme physical situations and parameters values." in (EPA3) and (NRC3), (ii) "If choices are made that make simulations very unrealistic the confidence that can be placed on modeling results is limited." and "Overly conservative assumptions made in developing performance scenarios can bias the analyses … and can deflect attention from questions critical to developing an adequate understanding of the expected features, events, and processes." in (EPA11), and (iii) "so that regulatory decision making will be done with a full understanding of the uncertainties involved" in (EPA12). As a result, the goal in defining the distributions in Equation J3.5-6 for the TSPA-LA is to mathematically capture an honest assessment of the epistemic uncertainty associated with the individual elements of **e** without being either deliberately conservative or deliberately nonconservative in this assessment.

For a specific future **a** and a single analysis outcome $f(\mathbf{a}, \mathbf{e}_M)$, the resultant distribution of possible values for $f(\mathbf{a}, \mathbf{e}_M)$ is given by

$$prob_E(c > C \mid \mathbf{a}) = \int_{\mathcal{E}} \bar{\delta}_C\left[f(\mathbf{a}, \mathbf{e}_M)\right] d_E(\mathbf{e})\, dE, \qquad \text{(Eq. J3.5-7)}$$

where $prob_E(c > C|\mathbf{a})$ is the probability that $f(\mathbf{a}, \mathbf{e}_M)$ will have a value larger than C due to the uncertainty in $\mathbf{e}_M$ as characterized by ($\mathcal{E}$, E, p_E), the subscript E indicates that $prob_E(c > C|\mathbf{a})$ derives from epistemic uncertainty, and the remaining terms are defined similarly to those in Equations J3.4-5 and J3.5-2 except that ($\mathcal{E}$, E, p_E) rather than ($\mathcal{A}$, A, p_A) is now under consideration. In concept, this distribution has the same appearance as in Figure J3.4-1 except that $C = f(\mathbf{a}, \mathbf{e}_M)$ appears on the abscissa and $prob_E(c > C|\mathbf{a})$ appears on the ordinate. As a technical point, an element of **e** has no effect on the value of the integral in Equation J3.5-7 if it has no effect on the value of $f(\mathbf{a}, \mathbf{e}_M)$.

In practice, closed form evaluation of $prob_E(c > C|\mathbf{a})$ is not practicable. For example, evaluation of $f(\mathbf{a}, \mathbf{e}_M)$ could require the solution of a complex system of nonlinear partial differential equations. Typically, a sampling-based approach is used to approximate $prob_E(c > C|\mathbf{a})$. For example, a random sample $\mathbf{e}_i = [\mathbf{e}_{Ai}, \mathbf{e}_{Mi}]$, $i = 1, 2, \ldots, nR$, generated in consistency with the definition of ($\mathcal{E}$, E, p_E) (i.e., in consistency with the distributions in Equation J3.5-6 and any associated restrictions) leads to the approximation

$$prob_E(c > C \mid \mathbf{a}) \cong \sum_{i=1}^{nR} \bar{\delta}_C\left[f(\mathbf{a}, \mathbf{e}_{Mi})\right] / nR. \qquad \text{(Eq. J3.5-8)}$$

The resultant approximation is similar in appearance to that shown in Figure J3.4-2 except that $C = f(\mathbf{a}, \mathbf{e}_{Mi})$ appears on the abscissa and $prob_E(c > C|\mathbf{a})$ appears on the ordinate.

The probability space ($\mathcal{E}$, E, p_E) leads to distributions of CCDFs resulting from aleatory uncertainty as indicated in Figure J3.5-1. When viewed formally, such distributions are defined by double integrals involving ($\mathcal{A}$, A, p_A), f, and ($\mathcal{E}$, E, p_E). The formal notation for such integrals is messy (Helton 1996 [DIRS 107823]) and will not be presented here but will be presented in Section J4.

As previously indicated, integrals involving ($\mathcal{A}$, A, p_A) and f are often evaluated with numerical procedures based on random sampling or importance sampling. Integrals involving ($\mathcal{E}$, E, p_E) are often evaluated with procedures based on Latin hypercube sampling (Helton and Davis 2003 [DIRS 163475]; Iman 1992 [DIRS 158984]; McKay et al. 1979 [DIRS 127905]) because of its efficient stratification properties. In particular, Latin hypercube sampling shows less sampling variability than simple random sampling (McKay et al. 1979 [DIRS 127905]; Owen 1992 [DIRS 159057]; Stein 1987 [DIRS 159060]) and has been observed to produce stable results in several large analyses (Iman and Helton 1988 [DIRS 159052]; Iman and Helton 1991 [DIRS 159039]; Helton et al. 1995 [DIRS 159560]).

Latin hypercube sampling operates in the following manner to generate a sample of size *nLHS* from *nE* variables. The range of each variable (i.e., the e_j in Equation J3.5-2) is divided into *nLHS* intervals of equal probability and one value is selected at random from each interval. The *nLHS* values thus obtained for e_1 are paired at random and without replacement with the *nLHS* values obtained for e_2. These *nLHS* pairs are paired at random and without replacement with the *nLHS* values of e_3 to form *nLHS* triples. This process is continued until a set of *nLHS* *nE*-tuples is formed. These *nE*-tuples are of the form

$$\mathbf{e}_i = \left[e_{i1},\ e_{i2},\ \ldots,\ e_{i,nE} \right],\ i = 1,\ \ldots,\ nLHS, \qquad \text{(Eq. J3.5-9)}$$

and constitute the Latin hypercube sample (LHS). The individual e_j must be independent for the preceding construction procedure to work; however, a method for generating LHSs from correlated variables has been developed by Iman and Conover (1982 [DIRS 124158]; Iman and Davenport 1982 [DIRS 159050]). As illustrated in Figure J3.5-2 for an LHS from two variables, Latin hypercube sampling results in a dense stratification across the range of each variable (i.e., there is one value from each equal probability interval).

Once the LHS is generated, PA results are calculated for each sample element. For EN2 and an individual future **a**, this creates a mapping

$$\left[\mathbf{e}_{Mi},\ \mathbf{f}(\mathbf{a},\ \mathbf{e}_{Mi}) \right],\ i = 1,\ 2,\ \ldots,\ nLHS, \qquad \text{(Eq. J3.5-10)}$$

from uncertain inputs to results conditional on the occurrence of **a**. Typically, a relatively small number of futures is selected for detailed analysis of this type (e.g., 5 – 10). As a reminder, **f** is usually quite complex and in practice is composed of many models (e.g., see Equation J3.4-4). Further, all models represented by **f** may not be used in the analysis of all futures selected for

consideration. In particular, different models or suites of models might be used to analyze different futures at the facility under consideration or to calculate different outcomes of interest for a given future.

For CCDFs, a mapping of the form

$$\left[\mathbf{e}_i,\ prob_E\left(c > C \mid \mathbf{e}_i\right)\right],\ i = 1,\ 2,\ \ldots,\ nLHS, \qquad \text{(Eq. J3.5-11)}$$

is created, where $prob_E(c > C|\ \mathbf{e}_i)]$ defines the CCDF for some consequence of interest as indicated in Equations J3.4-5 and J3.5-3 (i.e., a CCDF results when C is allowed to run across all possible values of the consequence). In most PAs, CCDFs are generated for a large number of consequences.

The mappings in Equations J3.5-10 and J3.5-11 provide the basis for both uncertainty analysis and sensitivity analysis. Uncertainty analysis designates the determination of the uncertainty in analysis outcomes that results from uncertainty in analysis inputs. Specifically, uncertainty analysis involves the determination of the effects of the uncertainty characterized by EN3 and thus is providing an answer to question Q4 introduced in Section J2.1 relating to how much confidence should be placed in the results of the analysis. Once the calculations that lead to the mappings in Equations J3.5-10 and J3.5-11 are completed, the presentation of uncertainty analysis results simply involves the plotting of the predicted results with an equal weight (i.e., the reciprocal of the sample size) given to the individual results when either random or Latin hypercube sampling is used in the generation of the sample in Equation J3.5-9. Sensitivity analysis designates the determination of the effects of individual variables contained in **e** on the observed uncertainty in predictions of interest. For sampling-based propagations of uncertainty, sensitivity analysis involves an exploration of mappings of the form appearing in Equations J3.5-10 and J3.5-11 with techniques based on examination of scatterplots, correlation analysis, regression analysis, and the identification of nonrandom patterns (Helton et al. 2006 [DIRS 183873]; Helton and Davis 2002 [DIRS 183872]; Hamby 1994 [DIRS 158798]; Helton 1993 [DIRS 100452]; Kleijnen and Helton 1999 [DIRS 159054]). Extensive analyses of this type are presented in Appendix K.

The importance of uncertainty and sensitivity analyses of the type just indicated is emphasized in many statements made by the EPA and the NRC in their regulations for the Yucca Mountain facility. Examples of such statements include: (i) "Focuses performance assessments and analyses upon the full range of defensible and reasonable parameter distributions" in (EPA3) and (NRC3), (ii) "Account for uncertainties and variabilities in parameter values" in (NRC8), (iii) "the demonstration of compliance must take uncertainties and gaps in knowledge into account" in (NRC10), (iv) "DOE is expected to conduct uncertainty analyses (i.e., evaluation of how uncertainty in parameter values affects the uncertainty in the estimate of dose)" in (NRC12), (v) "The treatment of uncertainty in DOE's performance assessment will be an important part of NRC's review" in (NRC13), and (vi) "The total system performance assessment sampling method ensures that sampled parameters have been sampled across their ranges of uncertainty." in (YMRP11).

The expected dose $\bar{D}(\tau)$ indicated in Equation J3.4-12 depends on the particular vector **e** of epistemically uncertain inputs used in its determination. Thus, $\bar{D}(\tau)$ is actually of the form $\bar{D}(\tau|\mathbf{e})$. Specifically,

$$\bar{D}(\tau|\mathbf{e}) = E_A\left[D(\tau|\mathbf{a}, \mathbf{e}_M)\right] = \int_{\mathcal{A}} D(\tau|\mathbf{a}, \mathbf{e}_M)\, d_A(\mathbf{a}|\mathbf{e}_A)\, \mathrm{d}A \qquad \text{(Eq. J3.5-12)}$$

when the dependence on elements of $\mathbf{e} = [\mathbf{e}_A, \mathbf{e}_M]$ is added to the representation for $\bar{D}(\tau)$ in Equation J3.4-12. In turn, $\bar{D}(\tau|\mathbf{e})$ has a distribution that derives from the probability space ($\mathcal{E}$, E, p_E) (i.e., from the distributions indicated in Equations J3.5-6 assigned to the elements of **e** and collectively represented by the density function $d_E(\mathbf{e})$) with an expected value $\bar{\bar{D}}(\tau)$ defined by

$$\bar{\bar{D}}(\tau) = \int_{\mathcal{E}} \bar{D}(\tau|\mathbf{e})\, d_E(\mathbf{e})\, \mathrm{d}E \qquad \text{(Eq. J3.5-13)}$$

and a q quantile value $Q_q[\bar{D}(\tau|\mathbf{e})]$ defined by the value D such that

$$q = \int_{\mathcal{E}} \delta_D\left[\bar{D}(\tau|\mathbf{e})\right] d_E(\mathbf{e})\, \mathrm{d}E. \qquad \text{(Eq. J3.5-14)}$$

The expected value $\bar{\bar{D}}(\tau)$ and the quantile $Q_q[\bar{D}(\tau|\mathbf{e})]$ are examples of the generic values defined in Equations J3.1-2 and J3.1-7. As discussed in Section J4, $\bar{\bar{D}}(\tau)$ and $Q_{0.5}[\bar{D}(\tau|\mathbf{e})]$ are assumed in the TSPA-LA to correspond to the mean dose and median dose, respectively, specified in (EPA14) and (NRC20).

J3.6 Properties of Poisson Processes

At least two types of disruptions must be considered in PAs for the proposed Yucca Mountain repository: igneous events and seismic events. Both of these disruptions are assumed to have a pattern of occurrence that can be represented as a Poisson process (Ross 1993 [DIRS 172064], Chapter 5). Because the properties of Poisson processes will play an important role in determining expected dose to the RMEI in PAs for the Yucca Mountain repository, it is useful to briefly review these properties at the beginning of this presentation. Then, these properties can be referred to as needed in the subsequent derivation and calculation of expected dose to the RMEI.

The descriptor Poisson process is used to designate a set of potentially realizable sequences of occurrences (e.g., sequences of seismic events occurring at different times in the future) with certain special probabilistic characteristics. For the purposes of this presentation, a Poisson process can be described in terms of a function $N(r, s)$ defined for $0 \le r < s < \infty$, where

$$N(r, s) = \text{ number of occurrences in the time interval } [r, s]. \qquad \text{(Eq. J3.6-1)}$$

Specifically, the potential sequences of occurrences that give rise to different possible values for $N(r, s)$ are said to follow a (stationary or homogeneous) Poisson process provided

$$prob\left[N(r, r+\Delta t)=1\right]=\lambda\Delta t+o(\Delta t), \quad \text{(Eq. J3.6-2)}$$

$$prob\left[N(r, r+\Delta t)\geq 2\right]=o(\Delta t) \quad \text{(Eq. J3.6-3)}$$

and

$$prob\left[N(r,s)=k \text{ and } N(u,v)=l \middle| [r,s]\cap[u,v]=\varnothing\right]=prob\left[N(r,s)=k\right]prob\left[N(u,v)=l\right], \quad \text{(Eq. J3.6-4)}$$

where (i) *prob* denotes probability and the associated vertical line indicates conditionality, (ii) λ is independent of r, and (iii) the $o(\Delta t)$ notation is an abbreviation for

$$\lim_{\Delta t\to 0^+} prob\left[N(r,r+\Delta t)=1\right]/\Delta t=\lambda \quad \text{(Eq. J3.6-5)}$$

and

$$\lim_{\Delta t\to 0^+} prob\left[N(r,r+\Delta t)\geq 2\right]/\Delta t=0 \quad \text{(Eq. J3.6-6)}$$

in Equations J3.6-2 an J3.6-3, respectively.

The conditions in Equations J3.6-2 and J3.6-3 require that, in a small interval of length Δt, the probability of one event occurring is approximately $\lambda\Delta t$ and the probability of two or more events occurring is approximately zero. The condition in Equation J3.6-4 requires independence for the numbers of events occurring in two disjoint intervals. The quantity λ is the defining rate for the process and has units of inverse time (e.g., yr^{-1}).

The following important properties hold for the Poisson process defined by the conditions in Equations J3.6-2 – J3.6-4:

$$prob\left[N(r,s)=0\right]=\exp\left[-\lambda(s-r)\right], \quad \text{(Eq. J3.6-7)}$$

$$prob\left[N(r,s)=1\right]=\lambda(s-r)\exp\left[-\lambda(s-r)\right], \quad \text{(Eq. J3.6-8)}$$

$$prob\left[N(r,s)\geq 1\right]=1-prob\left[N(r,s)=0\right]=1-\exp\left[-\lambda(s-r)\right] \quad \text{(Eq. J3.6-9)}$$

and, in general,

$$prob\left[N(r,s)=k\right]=\left\{\left[\lambda(s-r)\right]^k/k!\right\}\exp\left[-\lambda(s-r)\right] \quad \text{(Eq. J3.6-10)}$$

for $k = 0, 1, 2, \ldots$. Further,

$$E\left[N(r,s)\right] = \lambda(s-r), \qquad \text{(Eq. J3.6-11)}$$

where E denotes expected value. When $\lambda(s - r)$ is small (i.e., much less than one), then $\lambda(s - r)$ approximates $prob[N(r, s) = 1]$; however, $\lambda(s - r)$ ceases to be a valid approximation to $prob[N(r, s) = 1]$ as it increases in size.

An important property of stationary Poisson processes is that, if the process occurs exactly one time in the interval $[r, s]$ (i.e., if $N(r, s) = 1$), then the occurrence time has a uniform distribution on $[r, s]$. Specifically,

$$d\left[t \middle| N(r,s) = 1\right] = 1/(s-r) \qquad \text{(Eq. J3.6-12)}$$

is the density function defined on $[r, s]$ for time of occurrence.

A new Poisson process with rate

$$\lambda = \lambda_1 + \lambda_2 + \ldots + \lambda_n \qquad \text{(Eq. J3.6-13)}$$

can be created by combining n Poisson processes with rates $\lambda_1, \lambda_2, \ldots, \lambda_n$ provided the occurrences across the rates are independent (i.e., the occurrence of an event associated with process i has no effect on the potential occurrence of an event associated with process j and vice versa). Then, λ is the occurrence rate for the process that results when no distinction is made between occurrences associated with the processes characterized by $\lambda_1, \lambda_2, \ldots, \lambda_n$.

The Poisson process defined by the conditions in Equations J3.6-2 – J3.6-4 is referred to as a stationary or homogeneous Poisson to emphasize that the value for λ is constant. A generalization is to replace the condition in Equation J3.6-2 with

$$prob\left[N(r, r+\Delta t) = 1\right] = \lambda(r)\Delta t + o(\Delta t). \qquad \text{(Eq. J3.6-14)}$$

With this formulation, $\lambda(r)$ is now a function of time, and the resultant Poisson process is referred to as a nonstationary or nonhomogeneous Poisson process to emphasize that λ is no longer constant with time. For example, it has been proposed that the occurrence of igneous events in the vicinity of the Yucca Mountain repository can be characterized by a nonstationary Poisson process (Connor and Hill 1995 [DIRS 102646]).

When nonstationary Poisson processes are under consideration, the relationships in Equations J3.6-7 – J3.6-13 have similar but slightly more complicated forms. Specifically,

$$prob\left[N(r,s) = 0\right] = \exp\left[-\int_r^s \lambda(t)\,dt\right], \qquad \text{(Eq. J3.6-15)}$$

$$prob\left[N(r,s)=1\right]=\left[\int_r^s \lambda(t)\,dt\right]\exp\left[-\int_r^s \lambda(t)\,dt\right], \quad \text{(Eq. J3.6-16)}$$

$$prob\left[N(r,s)\geq 1\right]=1-\exp\left[-\int_r^s \lambda(t)\,dt\right], \quad \text{(Eq. J3.6-17)}$$

$$prob\left[N(r,s)=k\right]=\left\{\left[\int_r^s \lambda(t)\,dt\right]^k \Big/ k!\right\}\exp\left[-\int_r^s \lambda(t)\,dt\right], \quad \text{(Eq. J3.6-18)}$$

$$E\left[N(r,s)\right]=\int_r^s \lambda(t)\,dt \quad \text{(Eq. J3.6-19)}$$

and

$$\lambda(t)=\lambda_1(t)+\lambda_2(t)+\ldots+\lambda_n(t). \quad \text{(Eq. J3.6-20)}$$

Further, if a nonstationary Poisson process with rate $\lambda(t)$ occurs exactly one time in the interval $[r, s]$, then

$$d\left[t\,|\,N(r,s)=1\right]=\lambda(t)\Big/\int_r^s \lambda(\tau)\,d\tau \quad \text{(Eq. J3.6-21)}$$

is the density function defined on $[r, s]$ for time of occurrence. The results in Equations J3.6-14 – J3.6-21 reduce to those in Equations J3.6-7 – J3.6-13 when the time-dependent λ's are replaced by constant values.

A Poisson process involves events occurring over intervals of time. A related process involves occurrences (e.g., failures) associated with individual members of a finite population. If the population has n members and each member of the population has the same probability p of experiencing the occurrence under consideration, then probability $prob(m)$ that exactly m members of the population will experience the occurrence is

$$prob(m)=\binom{n}{m}p^m(1-p)^{n-m}. \quad \text{(Eq. J3.6-22)}$$

The preceding defines the density function for the binomial distribution (Ross 1993 [DIRS 172064], p. 27). In turn,

$$prob(i\leq m)=\sum_{i=0}^{m}\binom{n}{i}p^i(1-p)^{n-1} \quad \text{(Eq. J3.6-23)}$$

is the probability of m or fewer occurrences, and

$$prob(m<i)=\sum_{i=m+1}^{n}\binom{n}{i}p^{i}(1-p)^{n-i}$$
$$=1-\sum_{i=0}^{m}\binom{n}{i}p^{i}(1-p)^{n-i} \quad \text{(Eq. J3.6-24)}$$

is the probability of more than m occurrences. An important special case of Equation J3.6-24 is

$$prob(0<i)=1-\binom{n}{0}p^{0}(1-p)^{n-0}$$
$$=1-(1-p)^{n}, \quad \text{(Eq. J3.6-25)}$$

which is the probability of one or more failures. In the TSPA-LA, early WP failures and early DS failures are assumed to follow binomial distributions with occurrence probabilities of the form defined in Equations J3.6-22 – J3.6-25.

For $p \leq 0.1$, the Poisson probability model provides a good approximation to the binomial probability model. Specifically,

$$prob(m)\cong\left[(np)^{m}/m!\right]\exp(-np), \quad \text{(Eq. J3.6-26)}$$

$$prob(i\leq m)\cong\sum_{i=1}^{m}\left[(np)^{i}/i!\right]\exp(-np), \quad \text{(Eq. J3.6-27)}$$

$$prob(m\leq i)\cong\sum_{i=m+1}^{n}\left[(np)^{i}/i!\right]\exp(-np)$$
$$=1-\sum_{i=m+1}^{m}\left[(np)^{i}/i!\right]\exp(-np) \quad \text{(Eq. J3.6-28)}$$

and

$$prob(0<i)\cong 1-\exp(-np). \quad \text{(Eq. J3.6-29)}$$

The preceding approximations are valid independent of the size of n and also hold for $p \geq 0.9$ (Hahn and Shapiro 1967 [DIRS 146529]).

J4 CONCEPTUAL STRUCTURE OF TSPA-LA

J4.1 Three Basic Entities

The following is written to provide a high-level overview of the calculations that will be performed in the TSPA-LA to determine expected dose and other quantities of interest. As discussed in Section J3, the determination of expected dose is based on operations involving three basic mathematical entities: (i) a probabilistic characterization of aleatory uncertainty, (ii) a model that predicts dose to the RMEI conditional on a specific realization of aleatory uncertainty, and (iii) a probabilistic characterization of the epistemic uncertainty present in quantities used in the characterization of aleatory uncertainty and the determination of dose.

In the preceding, aleatory uncertainty is used in the designation of, in so far as our ability to predict the future is concerned, randomness in the possible future conditions that could affect the Yucca Mountain repository. In concept, each possible future at the Yucca Mountain repository can be represented by a vector

$$\mathbf{a} = [a_1, a_2, \ldots, a_{nA}], \qquad \text{(Eq. J4.1-1)}$$

where each a_i is a specific property of the future **a** (e.g., time of a seismic event, size of a seismic event, …). In turn, a subset $\mathcal{S}$ of the set $\mathcal{A}$ of all possible values for **a** constitutes what is referred to as a scenario class in the TSPA-LA. As part of the TSPA-LA development, a probabilistic structure is imposed on the set $\mathcal{A}$. Formally, this corresponds to defining a probability space ($\mathcal{A}$, A, p_A) for aleatory uncertainty. Then, A is the set of all possible scenario classes, and p_A is the function that defines scenario class probability (i.e., scenario class $\mathcal{S}$ is an element of A and $p_A(\mathcal{S})$ is the probability of scenario class $\mathcal{S}$). Formally, the probability space ($\mathcal{A}$, A, p_A) provides a characterization of aleatory uncertainty and constitutes the first of the three basic mathematical entities that underlie the determination of expected dose.

Although useful conceptually and notationally, the probability space ($\mathcal{A}$, A, p_A) is never explicitly defined in the TSPA-LA. Rather, the characterization of aleatory uncertainty enters the analysis through the definition of probability distributions for the individual elements of **a**. Conceptually, the distributions for the elements of **a** lead to a distribution for **a** and an associated density function $d_A(\mathbf{a})$.

The second of the three basic mathematical entities that underlie the determination of expected dose is a model that predicts dose to the RMEI. Formally, this model can be represented by the function

$D(\tau|\mathbf{a})$ = dose to RMEI (mrem/yr) at time τ (yr) conditional on the occurrence of the future represented by **a**. (Eq. J4.1-2)

Technically, $D(\tau|\mathbf{a})$ is the committed 50 yr dose to the RMEI that results from radiation exposure incurred in a single year. In the computational implementation of the TSPA-LA, $D(\tau|\mathbf{a})$ corresponds to the calculation performed with the GoldSim program for the particular analysis

configuration defined for the future **a**. In practice, many results are calculated for **a** in addition to dose to the RMEI. Thus, $D(\tau|\mathbf{a})$ is actually a vector $\mathbf{D}(\tau|\mathbf{a})$ containing at least several thousand elements. For notational convenience, $D(\tau|\mathbf{a})$ is treated as a scalar and referred to as dose to the RMEI; however, other TSPA-LA results can be handled in exactly the same manner as described for dose.

The third of the three basic mathematical entities that underlie the determination of expected dose is a probabilistic characterization of epistemic uncertainty. Here, epistemic uncertainty refers to a lack of knowledge with respect to the appropriate value to use for a quantity that is assumed to have constant or fixed value in the context of a specific analysis — the TSPA-LA in this discussion. Specifically, epistemic uncertainty relates to a vector of the form

$$\begin{aligned}\mathbf{e} &= [\mathbf{e}_A, \mathbf{e}_M] \\ &= [e_{A1}, e_{A2}, \ldots, \cdots e_{A,nAE}, e_{M1}, e_{M2}, \ldots, e_{M,nME}] \\ &= [e_1, e_2, \ldots, e_{nE}],\ nE = nAE + nME,\end{aligned} \qquad \text{(Eq. J4.1-3)}$$

where

$$\mathbf{e}_A = [e_{A1}, e_{A2}, \ldots, e_{A,nAE}]$$

is a vector of epistemically uncertain quantities used in the characterization of aleatory uncertainty (e.g., a rate term that defines a Poisson process) and

$$\mathbf{e}_M = [e_{M1}, e_{M2}, \ldots, e_{M,nME}]$$

is a vector of epistemically uncertain quantities used in the determination of dose (e.g., a distribution coefficient).

Epistemic uncertainty results in a set $\mathcal{E}$ of possible values for **e**. In turn, probability is used to characterize the level of likelihood or credence that can be assigned to various subsets of $\mathcal{E}$. In concept, this leads to a probability space ($\mathcal{E}$, E, p_E) for epistemic uncertainty. Like the probability space ($\mathcal{A}$, A, p_A) for aleatory uncertainty, the probability space ($\mathcal{E}$, E, p_E) for epistemic uncertainty is useful conceptually and notationally but is never explicitly defined in the TSPA-LA. Rather, the characterization of epistemic uncertainty enters the analysis through the definition of probability distributions for the individual elements of **e**. These distributions serve as mathematical summaries of all available information with respect to where the appropriate values for individual elements of **e** are located for use in the TSPA-LA. Conceptually, the distributions for the elements of **e** lead to a distribution for **e** and an associated density function $d_E(\mathbf{e})$.

J4.2 Expected Dose and Related Definitions of Projected Dose, Mean Dose and Median Dose

Now that the characterization of epistemic uncertainty has been introduced, the notations used to represent aleatory uncertainty and dose need to be expanded. Because the representation of aleatory uncertainty depends on elements of the vector $\mathbf{e}_A$, each possible value for $\mathbf{e}_A$ could lead to a different probability space ($\mathcal{A}$, A, p_A) for aleatory uncertainty. For notational convenience, this dependence will be indicated by representing the density function associated with aleatory uncertainty by $d_A(\mathbf{a}|\mathbf{e}_A)$. Similarly, the determination of dose depends on elements of the vector $\mathbf{e}_M$, with each possible value for $\mathbf{e}_M$ potentially leading to different dose results. For notational convenience, this dependence will be indicated by representing the dose function by $D(\tau|\mathbf{a}, \mathbf{e}_M)$.

The probability space ($\mathcal{A}$, A, p_A) for aleatory uncertainty characterized by the density function $d_A(\mathbf{a}|\mathbf{e}_A)$, the dose function $D(\tau|\mathbf{a}, \mathbf{e}_M)$, and the probability space ($\mathcal{E}$, E, p_E) for epistemic uncertainty characterized by the density function $d_E(\mathbf{e})$ constitute the three basic parts of the TSPA-LA that come together in the determination of expected dose to the RMEI and the uncertainty in expected dose to the RMEI. Specifically, the complementary cumulative distribution function (CCDF) for dose at time τ and the expected value for dose at time τ conditional on a specific element $\mathbf{e} = [\mathbf{e}_A, \mathbf{e}_M]$ of $\mathcal{E}$ are given by

$$p_A\left[D < D\left(\tau|\mathbf{a}, \mathbf{e}_M\right)\middle|\mathbf{e}_A\right] = \int_{\mathcal{A}} \bar{\delta}_D\left[D\left(\tau|\mathbf{a}, \mathbf{e}_M\right)\right] d_A\left(\mathbf{a}|\mathbf{e}_A\right) \mathrm{d}A \qquad \text{(Eq. J4.2-1)}$$

and

$$\bar{D}\left(\tau|\mathbf{e}\right) = E_A\left[D\left(\tau|\mathbf{a}, \mathbf{e}_M\right)\middle|\mathbf{e}_A\right] = \int_{\mathcal{A}} D\left(\tau|\mathbf{a}, \mathbf{e}_M\right) d_A\left(\mathbf{a}|\mathbf{e}_A\right) \mathrm{d}A, \qquad \text{(Eq. J4.2-2)}$$

respectively, where

$$\bar{\delta}_D\left[D\left(\tau|\mathbf{a}, \mathbf{e}_M\right)\right] = \begin{cases} 1 & \text{if } D < D\left(\tau|\mathbf{a}, \mathbf{e}_M\right) \\ 0 & \text{otherwise} \end{cases} \qquad \text{(Eq. J4.2-3)}$$

and $E_A[D(\tau|\mathbf{a}, \mathbf{e}_M)|\mathbf{e}_A]$ denotes expectation over aleatory uncertainty.

In turn, the uncertainty associated with the estimation of $\bar{D}(\tau|\mathbf{e})$ can be determined from the properties of the probability space ($\mathcal{E}$, E, p_E) for epistemic uncertainty. In particular, the CCDF for $\bar{D}(\tau|\mathbf{e})$ and the expected value for $\bar{D}(\tau|\mathbf{e})$ that derive from epistemic uncertainty are given by

$$p_E\left[D < \bar{D}\left(\tau|\mathbf{e}\right)\right] = \int_{\mathcal{E}} \bar{\delta}_D\left[\bar{D}\left(\tau|\mathbf{e}\right)\right] d_E\left(\mathbf{e}\right) \mathrm{d}E \qquad \text{(Eq. J4.2-4)}$$

and

$$\bar{\bar{D}}(\tau) = E_E\left[\bar{D}(\tau|\mathbf{e})\right] = \int_{\mathcal{E}} \bar{D}(\tau|\mathbf{e})\, d_E(\mathbf{e})\, \mathrm{d}E, \qquad \text{(Eq. J4.2-5)}$$

respectively, where $\bar{\delta}_D[\bar{D}(\tau|\mathbf{e})]$ is defined as indicated in Equation J4.2-3 and $E_E[\bar{D}(\tau|\mathbf{e})]$ denotes expectation over epistemic uncertainty.

Complementary cumulative distribution functions of the form defined in Equations J4.2-1 and J4.2-4 constitute the standard format used to present the results of a performance assessment because they provide the answer to the following basic question that underlies all performance assessments: "How likely is it to be this bad or worse?"

In addition to CCDFs, cumulative distribution functions (CDFs) are also used in the presentation of results obtained in a performance assessment. Specifically, the CDF for dose at time τ conditional on a specific element $\mathbf{e} = [\mathbf{e}_A, \mathbf{e}_M]$ of $\mathcal{E}$ is given by

$$p_A\left[D(\tau|\mathbf{a}, \mathbf{e}_M) \le D|\mathbf{e}_A\right] = \int_{\mathcal{A}} \underline{\delta}_D\left[D(\tau|\mathbf{a}, \mathbf{e}_M)\right] d_A(\mathbf{a}|\mathbf{e}_A)\, \mathrm{d}A, \qquad \text{(Eq. J4.2-6)}$$

where

$$\underline{\delta}_D\left[D(\tau|\mathbf{a}, \mathbf{e}_M)\right] = \begin{cases} 1 & \text{if } D(\tau|\mathbf{a}, \mathbf{e}_M) \le D \\ 0 & \text{otherwise} \end{cases}$$
$$= 1 - \bar{\delta}_D\left[D(\tau|\mathbf{a}, \mathbf{e}_M)\right]. \qquad \text{(Eq. J4.2-7)}$$

The value of D for which

$$q = p_A\left[D(\tau|\mathbf{a}, \mathbf{e}_M) \le D|\mathbf{e}_A\right] = \int_{\mathcal{A}} \underline{\delta}_D\left[D(\tau|\mathbf{a}, \mathbf{e}_M)\right] d_A(\mathbf{a}|\mathbf{e}_A)\, \mathrm{d}A \qquad \text{(Eq. J4.2-8)}$$

defines the q quantile (e.g., $q = 0.05$, 0.5 or 0.95) for the distribution of dose at time τ conditional on the vector $\mathbf{e} = [\mathbf{e}_A, \mathbf{e}_M]$ of epistemically uncertain analysis inputs. For notational purposes, the value of D corresponding to the q quantile of $D(\tau|\mathbf{a}, \mathbf{e}_M)$ defined in Equation J4.2-8 will be represented by $Q_{Aq}[D(\tau|\mathbf{a}, \mathbf{e}_M)|\mathbf{e}_A]$ with the subscript A indicating that the quantile derives from aleatory uncertainty (i.e., from the possible values of $\mathbf{a}$ conditional on the vector $\mathbf{e} = [\mathbf{e}_A, \mathbf{e}_M]$ of epistemically uncertain analysis inputs).

Similarly, the CDF for expected dose at time τ is given by

$$p_E\left[\bar{D}(\tau|\mathbf{e}) \le D\right] = \int_{\mathcal{E}} \underline{\delta}_D\left[\bar{D}(\tau|\mathbf{e})\right] d_E(\mathbf{e})\, \mathrm{d}E$$
$$= \int_{\mathcal{E}} \underline{\delta}_D\left[\int_{\mathcal{A}} D(\tau|\mathbf{a}, \mathbf{e}_M)\, d_A(\mathbf{a}|\mathbf{e}_A)\, \mathrm{d}A\right] d_E(\mathbf{e})\, \mathrm{d}E \qquad \text{(Eq. J4.2-9)}$$

with $\underline{\delta}_D$ defined in the manner indicated in Equation J4.2-7, and the value of D for which

$$q = p_E\left[\bar{D}(\tau|\mathbf{e}) \le D\right] = \int_{\mathcal{E}} \underline{\delta}_D\left[\bar{D}(\tau|\mathbf{e})\right] d_E(\mathbf{e})\,dE \qquad \text{(Eq. J4.2-10)}$$

defines the q quantile for the distribution of expected dose over epistemically uncertain analysis inputs. For notational purposes, the value of D corresponding to the q quantile of $\bar{D}(\tau|\mathbf{e})$ defined in Equation J4.2-9 will be represented by $Q_q[\bar{D}(\tau|\mathbf{e})]$.

For assessing compliance with the standards in (EPA14) and (NRC20), projected dose is assumed to correspond to the expected doses $\bar{D}(\tau|\mathbf{e})$ defined in Equation J4.2-2, mean dose is assumed to correspond to the expected dose $\bar{\bar{D}}(\tau)$ defined in Equation J4.2-5, and median dose is assumed to correspond to the $q = 0.5$ quantile $D = Q_{0.5}[\bar{D}(\tau|\mathbf{e})]$ defined in Equation J4.2-10. To facilitate distinguishing between the two expected doses, $\bar{D}(\tau|\mathbf{e})$ will be referred to as expected dose, and $\bar{\bar{D}}(\tau)$ will be referred to as expected (mean) dose.

In contrast, if the actual dose $D(\tau|\mathbf{a}, \mathbf{e}_M)$ for each future $\mathbf{a}$ was assumed to correspond to projected dose, then $\bar{D}(\tau|\mathbf{e})$ would correspond to the mean dose specified in (EPA14) and (NRC20) and the CDF defined by Equation J4.2-9 would characterize the uncertainty in mean dose (i.e., in $\bar{D}(\tau|\mathbf{e})$). With $D(\tau|\mathbf{a}, \mathbf{e}_M)$ interpreted as projected dose, the median dose specified in (EPA14) and (EPA20) would then be $Q_{A,0.5}[D(\tau|\mathbf{a}, \mathbf{e}_M)|\mathbf{e}_A]$ as defined in Equation J4.2-6 for $q = 0.5$. In turn, the uncertainty in median dose would be characterized by the CDF defined by

$$p_E\left\{Q_{A,0.5}\left[D(\tau|\mathbf{a}, \mathbf{e}_M)\middle|\mathbf{e}_A\right] \le Q\right\} = \int_{\mathcal{E}} \underline{\delta}_Q\left\{Q_{A,0.5}\left[D(\tau|\mathbf{a}, \mathbf{e}_M)\middle|\mathbf{e}_A\right]\right\} d_E(\mathbf{e})\,dE \qquad \text{(Eq. J4.2-11)}$$

with $\underline{\delta}_Q\{\sim\}$ defined similarly to $\underline{\delta}_D\{\sim\}$ in Equation J4.2-7. Both interpretations of projected dose use the same information; the only difference is how this information is summarized.

J4.3 Probabilities

As a reminder, probabilities are defined for subsets of a sample space. In Equations J4.2-1 and J4.2-6, the sample space is the set $\mathcal{A}$ of possible futures, and the indicated probabilities $p_A[D < D(\tau|\mathbf{a}, \mathbf{e}_M)|\mathbf{e}_A]$ and $p_A[D(\tau|\mathbf{a}, \mathbf{e}_M) \le D|\mathbf{e}_A]$ are probabilities for the sets

$$\bar{\mathcal{A}}_D(\tau, \mathbf{e}_M) = \left\{\mathbf{a} : \mathbf{a} \in \mathcal{A} \text{ and } D < D(\tau|\mathbf{a}, \mathbf{e}_M)\right\} \qquad \text{(Eq. J4.3-1)}$$

and

$$\underline{\mathcal{A}}_D(\tau, \mathbf{e}_M) = \left\{\mathbf{a} : \mathbf{a} \in \mathcal{A} \text{ and } D(\tau|\mathbf{a}, \mathbf{e}_M) \le D\right\}, \qquad \text{(Eq. J4.3-2)}$$

respectively. The sets $\bar{\mathcal{A}}_D(\tau|\mathbf{e}_M)$ and $\underline{\mathcal{A}}_D(\tau|\mathbf{e}_M)$, and hence the probabilities

$$p_A\left[D < D(\tau|\mathbf{a}, \mathbf{e}_M)\middle|\mathbf{e}_A\right] = p_A\left[\bar{\mathcal{A}}_D(\tau, \mathbf{e}_M)\middle|\mathbf{e}_A\right] \qquad \text{(Eq. J4.3-3)}$$

and

$$p_A\left[D\left(\tau\middle|\mathbf{a},\mathbf{e}_M\right)\le D\middle|\mathbf{e}_A\right]=p_A\left[\underline{\mathcal{A}}_D\left(\tau,\mathbf{e}_M\right)\middle|\mathbf{e}_A\right], \qquad \text{(Eq. J4.3-4)}$$

depend on both the time τ at which dose is calculated and the elements of $\mathbf{e}_M$ used in the calculation of dose. As indicated by the conditionality on $\mathbf{e}_A$, the preceding probabilities also depend on epistemically uncertain quantities that are elements of $\mathbf{e}_A$. Similarly, the defining relationships for quantiles in Equation J4.2-8 involves probabilities for sets of the form $\underline{\mathcal{A}}_D(\tau|\mathbf{e}_M)$.

In Equations J4.2-4 and J4.2-9, the sample space is the set $\mathcal{E}$ of epistemically uncertain analysis inputs, and the indicated probabilities $p_E[D < \bar{D}(\tau|\mathbf{e})]$ and $p_E[\bar{D}(\tau|\mathbf{e}) \le D]$ are probabilities for the sets

$$\bar{\mathcal{E}}_D\left(\tau\right)=\left\{\mathbf{e}:\mathbf{e}\in\mathcal{E}\text{ and }D<\bar{D}\left(\tau\middle|\mathbf{e}\right)\right\} \qquad \text{(Eq. J4.3-5)}$$

and

$$\underline{\mathcal{E}}_D\left(\tau\right)=\left\{\mathbf{e}:\mathbf{e}\in\mathcal{E}\text{ and }\bar{D}\left(\tau\middle|\mathbf{e}\right)\le D\right\}, \qquad \text{(Eq. J4.3-6)}$$

respectively. As indicated, the sets $\bar{\mathcal{E}}_D(\tau)$ and $\underline{\mathcal{E}}_D(\tau)$, and hence the probabilities

$$p_E\left[D<\bar{D}\left(\tau\middle|\mathbf{e}\right)\right]=p_E\left[\bar{\mathcal{E}}_D\left(\tau\right)\right] \qquad \text{(Eq. J4.3-7)}$$

and

$$p_E\left[\bar{D}\left(\tau\middle|\mathbf{e}\right)\le D\right]=p_E\left[\underline{\mathcal{E}}_D\left(\tau\right)\right], \qquad \text{(Eq. J4.3-8)}$$

depend on the time τ at which expected dose is calculated. Similarly, the defining relationship for quantiles in Equation J4.2-10 involves probabilities for sets of the form $\underline{\mathcal{E}}_D(\tau)$.

The discussion associated with Equations J4.3-1 – J4.3-8 may seem pedantic. However, probabilities are defined for sets. In turn, there are two important implications to the dependence of probabilities on sets. First, a probability cannot be meaningfully defined unless the set for which it is being defined is clearly described. Second, even if a probability is appropriately defined for a given set, this probability cannot be meaningfully understood unless the underlying set is also known. All of the results discussed in this presentation are based on the assignment of probabilities to scenario classes, which in turn are subsets of the sample space $\mathcal{A}$ for aleatory uncertainty. As a result, the connection between sets and probabilities is fundamental to the conceptual structure and computational implementation of the TSPA-LA.

In practice, the quantities $p_A[D < D(\tau|\mathbf{a}, \mathbf{e}_M)|\mathbf{e}_A]$, $\bar{D}(\tau|\mathbf{e})$ and $p_A[D(\tau|\mathbf{a}, \mathbf{e}_M) \le D|\mathbf{e}_A]$ defined in Equations J4.2-1, J4.2-2 and J4.2-6 are often estimated with sampling-based procedures. Specifically, a random sample

$$\mathbf{a}_j, j = 1, 2, \ldots, nR, \qquad \text{(Eq. J4.3-9)}$$

is generated from $\mathcal{A}$ in consistency with the density function $d_A(\mathbf{a}|\mathbf{e}_A)$ (i.e., in consistency with the definition of the probability space ($\mathcal{A}$, A, p_A) for aleatory uncertainty corresponding to $\mathbf{e}_A$). Then, approximations to $p_A[D < D(\tau|\mathbf{a}, \mathbf{e}_M)|\mathbf{e}_A]$, $\bar{D}(\tau|\mathbf{e})$ and $p_A[D(\tau|\mathbf{a}, \mathbf{e}_M) \le D|\mathbf{e}_A]$ are given by

$$p_A\left[D < D\left(\tau|\mathbf{a}, \mathbf{e}_A\right)\middle|\mathbf{e}_M\right] \cong \sum_{j=1}^{nR} \bar{\delta}_D\left[D\left(\tau|\mathbf{a}_j, \mathbf{e}_M\right)\right] \Big/ nR, \qquad \text{(Eq. J4.3-10)}$$

$$\bar{D}\left(\tau|\mathbf{e}\right) \cong \sum_{j=1}^{nR} D\left(\tau|\mathbf{a}_j, \mathbf{e}_M\right) \Big/ nR \qquad \text{(Eq. J4.3-11)}$$

and

$$p_A\left[D\left(\tau|\mathbf{a}, \mathbf{e}_M\right) \le D\middle|\mathbf{e}_A\right] \cong \sum_{j=1}^{nR} \underline{\delta}_D\left[D\left(\tau|\mathbf{a}_j, \mathbf{e}_M\right)\right] \Big/ nR, \qquad \text{(Eq. J4.3-12)}$$

respectively. In some cases, the use of importance sampling rather than simple random sampling can reduce the sample size required to produce adequate approximations. Further, as indicated in Equation J4.2-8, the approximation in Equation J4.3-12 can be used in the determination of quantile values for $D(\tau|\mathbf{a}, \mathbf{e}_M)$ that derive from the probability distribution over $\mathcal{A}$ defined by $d_A(\mathbf{a}|\mathbf{e}_A)$.

Similarly, the quantitites $p_E[D < \bar{D}(\tau|\mathbf{e})]$, $\bar{\bar{D}}(\tau)$ and $p_E[\bar{D}(\tau|\mathbf{e}) \le D]$ defined in Equations J4.2-4, J4.2-5 and J4.2-9 are usually estimated with sampling-based procedure. As discussed in Section J4.9, the TSPA-LA uses Latin hypercube sampling in the estimation of $p_E[D < \bar{D}(\tau|\mathbf{e})]$, $\bar{\bar{D}}(\tau)$ and $p_E[\bar{D}(\tau|\mathbf{e}) \le D]$.

J4.4 Scenario Classes and the Characterization of Aleatory Uncertainty

The following conditions/occurrences related to aleatory uncertainty are considered in the TSPA-LA: nominal (i.e., undisturbed) conditions, early waste package (WP) failure, early drip shield (DS) failure, igneous intrusive events, igneous eruptive events, seismic ground motion events, and seismic fault displacement events. Consistent with this, each aleatory future $\mathbf{a}$ over a time interval $[a, b]$ (e.g., $[0, 2 \times 10^4$ yr] or $[0, 10^6$ yr]) can be represented by

$$\mathbf{a} = \left[nEW, nED, nII, nIE, nSG, nSF, \mathbf{a}_{EW}, \mathbf{a}_{ED}, \mathbf{a}_{II}, \mathbf{a}_{IE}, \mathbf{a}_{SG}, \mathbf{a}_{SF}\right] \qquad \text{(Eq. J4.4-1)}$$

where, for the time interval $[a, b]$,

nEW = number of early WP failures,

nED = number of early DS failures,

nII = number of igneous intrusive events.

nIE = number of igneous eruptive events,

nSG = number of seismic ground motion events,

nSF = number of seismic fault displacement events,

$\mathbf{a}_{EW}$ = vector defining the nEW early WP failures,

$\mathbf{a}_{ED}$ = vector defining the nED early DS failures,

$\mathbf{a}_{II}$ = vector defining the nII igneous intrusive events,

$\mathbf{a}_{IE}$ = vector defining the nIE igneous eruptive events,

$\mathbf{a}_{SG}$ = vector defining the nSG seismic ground motion events,

$\mathbf{a}_{SF}$ = vector defining the nSF fault displacement events.

Then,

$$\mathcal{A} = \left\{ \mathbf{a} : \mathbf{a} = \left[nEW, nED, nII, nIE, nSG, nSF, \mathbf{a}_{EW}, \mathbf{a}_{ED}, \mathbf{a}_{II}, \mathbf{a}_{IE}, \mathbf{a}_{SG}, \mathbf{a}_{SF} \right] \right\} \quad \text{(Eq. J4.4-2)}$$

is the set of all futures to be considered in the TSPA-LA (i.e., the sample space for aleatory uncertainty). If needed, the expanded notation $\mathcal{A}(a, b)$ can be used to indicate the time interval over which the individual futures are defined (e.g., $\mathcal{A}(0, 20000)$ and $\mathcal{A}(0, 10^6)$ for $[a, b]$ = [0, 20,000 yr] and $[a, b]$ = [0, 10^6 yr], respectively); however, this will not be done when the time interval is clear given the context under consideration.

In turn, the vectors $\mathbf{a}_{EW}$, $\mathbf{a}_{ED}$, $\mathbf{a}_{II}$, $\mathbf{a}_{IE}$, $\mathbf{a}_{SG}$ and $\mathbf{a}_{SF}$ are of the form

$$\mathbf{a}_{EW} = \left[\mathbf{a}_{EW,1}, \mathbf{a}_{EW,2}, \ldots, \mathbf{a}_{EW,nEW} \right], \quad \text{(Eq. J4.4-3)}$$

$$\mathbf{a}_{ED} = \left[\mathbf{a}_{ED,1}, \mathbf{a}_{ED,2}, \ldots, \mathbf{a}_{ED,nED} \right], \quad \text{(Eq. J4.4-4)}$$

$$\mathbf{a}_{II} = \left[\mathbf{a}_{II,1}, \mathbf{a}_{II,2}, \ldots, \mathbf{a}_{II,nII} \right], \quad \text{(Eq. J4.4-5)}$$

$$\mathbf{a}_{IE} = \left[\mathbf{a}_{IE,1}, \mathbf{a}_{IE,2}, \ldots, \mathbf{a}_{IE,nIE}\right], \quad \text{(Eq. J4.4-6)}$$

$$\mathbf{a}_{SG} = \left[\mathbf{a}_{SG,1}, \mathbf{a}_{SG,2}, \ldots, \mathbf{a}_{SG,nSG}\right] \quad \text{(Eq. J4.4-7)}$$

and

$$\mathbf{a}_{SF} = \left[\mathbf{a}_{SF,1}, \mathbf{a}_{SF,2}, \ldots, \mathbf{a}_{SF,nSF}\right], \quad \text{(Eq. J4.4-8)}$$

where

$\mathbf{a}_{EW,j}$ = vector defining early WP failure j for $j = 1, 2, \ldots, nEW$,

$\mathbf{a}_{ED,j}$ = vector defining early DS failure j for $j = 1, 2, \ldots, nED$,

$\mathbf{a}_{II,j}$ = vector defining igneous intrusive event j for $j = 1, 2, \ldots, nII$,

$\mathbf{a}_{IE,j}$ = vector defining igneous eruptive event j for $j = 1, 2, \ldots, nIE$,

$\mathbf{a}_{SG,j}$ = vector defining seismic ground motion event j for $j = 1, 2, \ldots, nSG$,

$\mathbf{a}_{SF,j}$ = vector defining seismic fault displacement event j for $j = 1, 2, \ldots, nSF$.

The vectors $\mathbf{a}_{EW,j}$, $\mathbf{a}_{ED,j}$, $\mathbf{a}_{II,j}$, $\mathbf{a}_{IE,j}$, $\mathbf{a}_{SG,j}$ and $\mathbf{a}_{SF,j}$ will be defined in later sections.

Given an adequate probabilistic characterization of the elements of $\mathbf{a}_{EW,j}$, $\mathbf{a}_{ED,j}$, $\mathbf{a}_{II,j}$, $\mathbf{a}_{IE,j}$, $\mathbf{a}_{SG,j}$ and $\mathbf{a}_{SF,j}$, it is, at least in concept, possible to calculate the probability $p_A(\mathcal{U})$ of any subset $\mathcal{U}$ of $\mathcal{A}$ (modulo certain theoretical restrictions on the nature of $\mathcal{U}$). More generally, the probability of a subset $\mathcal{U}$ of $\mathcal{A}$ is dependent on values for epistemically uncertain analysis inputs and thus has the conditional representation $p_A(\mathcal{U}|\mathbf{e}_A)$ or possibly $p_A(\mathcal{U}|\mathbf{e})$, where $\mathbf{e} = [\mathbf{e}_A, \mathbf{e}_M]$ is the vector of epistemically uncertain analysis inputs defined in Equation J4.1-3.

A scenario class is a subset of the set $\mathcal{A}$ (i.e., an event in the standard terminology of probability theory). The following basic scenario classes are used in the organization of the TSPA-LA: nominal, early failure, igneous, and seismic. In turn, these scenario classes correspond to the following subsets of $\mathcal{A}$:

$$\mathcal{A}_N = \{\mathbf{a} : \mathbf{a} \in \mathcal{A} \text{ and } nEW = nED = nII = nIE = nSG = nSF = 0\} \quad \text{(Eq. J4.4-9)}$$

for the nominal scenario class (i.e., the set containing the single future $\mathbf{a}_N$ that involves no disruption of any kind);

$$\mathcal{A}_E = \{\mathbf{a} : \mathbf{a} \in \mathcal{A} \text{ and } nEW \geq 1 \text{ or } nED \geq 1\} \quad \text{(Eq. J4.4-10)}$$

for the early failure scenario class (i.e., the set containing all elements of $\mathcal{A}$ that involve at least one early WP failure or a least one early DS failure);

$$\mathcal{A}_I = \{\mathbf{a} : \mathbf{a} \in \mathcal{A} \text{ and } nII \geq 1\} \quad \text{(Eq. J4.4-11)}$$

for the igneous scenario class (i.e., the set containing all elements of $\mathcal{A}$ that involve at least one igneous intrusive event, which includes all elements of $\mathcal{A}$ with $nIE \geq 1$ as igneous eruptions only, but not necessarily, occur in conjunction with igneous intrusions); and

$$\mathcal{A}_S = \{\mathbf{a} : \mathbf{a} \in \mathcal{A} \text{ and } nSG \geq 1 \text{ or } nSF \geq 1\} \quad \text{(Eq. J4.4-12)}$$

for the seismic scenario class (i.e., the set containing all elements of $\mathcal{A}$ that involve at least one seismic ground motion event or at least one seismic fault displacement event).

In turn, the early failure scenario class $\mathcal{A}_E$ is underlain by an early WP failure scenario class $\mathcal{A}_{EW}$ and an early DS failure scenario class $\mathcal{A}_{ED}$; the igneous scenario class $\mathcal{A}_I$ is underlain by an igneous intrusive scenario class $\mathcal{A}_{II}$ and an igneous eruptive scenario class $\mathcal{A}_{IE}$; and the seismic scenario class $\mathcal{A}_S$ is underlain by a seismic ground motion scenario class $\mathcal{A}_{SG}$ and a seismic fault displacement scenario class $\mathcal{A}_{SF}$. Specifically, these scenario classes correspond to the following subsets of $\mathcal{A}$:

$$\mathcal{A}_{EW} = \{\mathbf{a} : \mathbf{a} \in \mathcal{A} \text{ and } nEW \geq 1\} \quad \text{(Eq. J4.4-13)}$$

for the early WP failure scenario class;

$$\mathcal{A}_{ED} = \{\mathbf{a} : \mathbf{a} \in \mathcal{A} \text{ and } nED \geq 1\} \quad \text{(Eq. J4.4-14)}$$

for the early DS failure scenario class;

$$\mathcal{A}_{II} = \mathcal{A}_I = \{\mathbf{a} : \mathbf{a} \in \mathcal{A} \text{ and } nII \geq 1\} \quad \text{(Eq. J4.4-15)}$$

for the igneous intrusive scenario class;

$$\mathcal{A}_{IE} = \{\mathbf{a} : \mathbf{a} \in \mathcal{A} \text{ and } nIE \geq 1\} \quad \text{(Eq. J4.4-16)}$$

for the igneous eruptive scenario class;

$$\mathcal{A}_{SG} = \{\mathbf{a} : \mathbf{a} \in \mathcal{A} \text{ and } nSG \geq 1\} \quad \text{(Eq. J4.4-17)}$$

for the seismic ground motion scenario class; and

$$\mathcal{A}_{SF} = \{\mathbf{a} : \mathbf{a} \in \mathcal{A} \text{ and } nSF \geq 1\} \quad \text{(Eq. J4.4-18)}$$

for the fault displacement scenario class. The scenario classes $\mathcal{A}_{EW}$, $\mathcal{A}_{ED}$, $\mathcal{A}_{II}$, $\mathcal{A}_{IE}$, $\mathcal{A}_{SG}$ and $\mathcal{A}_{SF}$ defined in Equations J4.4-13 – J4.4-18 and their associated analyses are often referred to as modeling cases in the TSPA-LA.

For the time interval $[a, b]$ underlying the definition of $\mathcal{A}$,

$$p_A(\mathcal{A}_N) = \text{probability of no disruptions of any kind,} \quad \text{(Eq. J4.4-19)}$$

$$p_A(\mathcal{A}_E) = \text{probability of one or more early failures,} \quad \text{(Eq. J4.4-20)}$$

$$p_A(\mathcal{A}_{EW}) = \text{probability of one or more early WP failures,} \quad \text{(Eq. J4.4-21)}$$

$$p_A(\mathcal{A}_{ED}) = \text{probability of one or more early DS failures,} \quad \text{(Eq. J4.4-22)}$$

$$p_A(\mathcal{A}_{II}) = p_A(\mathcal{A}_I) = \text{probability of one or more igneous intrusive events,} \quad \text{(Eq. J4.4-23)}$$

$$p_A(\mathcal{A}_{IE}) = \text{probability of one or more igneous eruptive events,} \quad \text{(Eq. J4.4-24)}$$

$$p_A(\mathcal{A}_S) = \text{probability of one or more seismic events,} \quad \text{(Eq. J4.4-25)}$$

$$p_A(\mathcal{A}_{SG}) = \text{probability of one or more seismic ground motions events,} \quad \text{(Eq. J4.4-26)}$$

and

$$p_A(\mathcal{A}_{SF}) = \text{probability of one or more fault displacement events,} \quad \text{(Eq. J4.4-27)}$$

More generally, the indicated scenario probabilities are conditional on values of epistemically uncertain analysis inputs and thus have conditional representations $p_A(\mathcal{A}_C|\mathbf{e}_A)$ or possibly $p_A(\mathcal{A}_C|\mathbf{e})$ for $C = N, E, EW, ED, I, II, S, SG$ and SF, where $\mathbf{e} = [\mathbf{e}_A, \mathbf{e}_M]$ is the vector of epistemically uncertain analysis inputs defined in Equation J4.1-3. When scenario class probabilities are requested, it is usually some subset of the preceding probabilities that is desired. The determination of these probabilities is discussed in later sections.

J4.5 Scenario Classes and the Determination of Expected Dose

The scenario classes $\mathcal{A}_N$, $\mathcal{A}_{EW}$, $\mathcal{A}_{ED}$, $\mathcal{A}_{II}$, $\mathcal{A}_{IE}$, $\mathcal{A}_{SG}$ and $\mathcal{A}_{SF}$ play a fundamental role in the computational determination of expected dose to the RMEI in the TSPA-LA. Specifically, with the assumption that there are no synergisms between disruptions that have significant effects on the expected dose $\bar{D}(\tau|\mathbf{e})$ defined in Equation J4.2-2, $\bar{D}(\tau|\mathbf{e})$ can be approximated by

$$\bar{D}(\tau|\mathbf{e}) \cong D_N(\tau|\mathbf{a}_N, \mathbf{e}_M) + \bar{D}_{EW}(\tau|\mathbf{e}) + \bar{D}_{ED}(\tau|\mathbf{e}) + \bar{D}_{II}(\tau|\mathbf{e}) + \bar{D}_{IE}(\tau|\mathbf{e}) + \bar{D}_{SG}(\tau|\mathbf{e}) + \bar{D}_{SF}(\tau|\mathbf{e}), \quad \text{(Eq. J4.5-1)}$$

where, conditional on the element $\mathbf{e} = [\mathbf{e}_A, \mathbf{e}_M]$ of $\mathcal{E}$,

$D_N(\tau|\mathbf{a}, \mathbf{e}_M)$ = dose to RMEI (mrem/yr) at time τ resulting from nominal conditions for future $\mathbf{a} \in \mathcal{A}$

$$= D_N(\tau|\mathbf{a}_N, \mathbf{e}_M), \quad \text{(Eq. J4.5-2)}$$

$D_{EW}(\tau|\mathbf{a}, \mathbf{e}_M)$ = dose to RMEI (mrem/yr) at time τ resulting from early WP failure for future $\mathbf{a} \in \mathcal{A}$

$$= D_{EW}(\tau|\mathbf{a}_{EW}, \mathbf{e}_M), \quad \text{(Eq. J4.5-3)}$$

$D_{ED}(\tau|\mathbf{a}, \mathbf{e}_M)$ = dose to RMEI (mrem/yr) at time τ resulting from early DS failure for future $\mathbf{a} \in \mathcal{A}$

$$= D_{ED}(\tau|\mathbf{a}_{ED}, \mathbf{e}_M), \quad \text{(Eq. J4.5-4)}$$

$D_{II}(\tau|\mathbf{a}, \mathbf{e}_M)$ = dose to RMEI (mrem/yr) at time τ resulting from igneous intrusive events for future $\mathbf{a} \in \mathcal{A}$

$$= D_{II}(\tau|\mathbf{a}_{II}, \mathbf{e}_M), \quad \text{(Eq. J4.5-5)}$$

$D_{IE}(\tau|\mathbf{a}, \mathbf{e}_M)$ = dose to RMEI (mrem/yr) at time τ resulting from igneous eruptive events for future $\mathbf{a} \in \mathcal{A}$

$$= D_{IE}(\tau|\mathbf{a}_{IE}, \mathbf{e}_M), \quad \text{(Eq. J4.5-6)}$$

$D_{SG}(\tau|\mathbf{a}, \mathbf{e}_M)$ = dose to RMEI (mrem/yr) at time τ resulting from seismic ground motion events for future $\mathbf{a} \in \mathcal{A}$

$$= D_{SG}(\tau|\mathbf{a}_{SG}, \mathbf{e}_M), \quad \text{(Eq. J4.5-7)}$$

$D_{SF}(\tau|\mathbf{a}, \mathbf{e}_M)$ = dose to RMEI (mrem/yr) at time τ resulting from seismic fault displacement events for future $\mathbf{a} \in \mathcal{A}$

$$= D_{SF}(\tau|\mathbf{a}_{SF}, \mathbf{e}_M), \quad \text{(Eq. J4.5-8)}$$

and in turn

$\bar{D}_{EW}(\tau|\mathbf{e})$ = expected dose to RMEI (mrem/yr) at time τ resulting from early WP failure

$= E_A\left[D_{EW}(\tau|\mathbf{a},\mathbf{e}_M)\middle|\mathbf{e}_A\right]$

$= \int_{\mathcal{A}} D_{EW}(\tau|\mathbf{a},\mathbf{e}_M)\, d_A(\mathbf{a}|\mathbf{e}_A)\,\mathrm{d}A$

$= \int_{\mathcal{A}_{EW}} D_{EW}(\tau|\mathbf{a}_{EW},\mathbf{e}_M)\, d_A(\mathbf{a}|\mathbf{e}_A)\,\mathrm{d}A$, reminder $\mathbf{a}=[\ldots\,\mathbf{a}_{EW}\ldots]$,(Eq. J4.5-9)

$\bar{D}_{ED}(\tau|\mathbf{e})$ = expected dose to RMEI (mrem/yr) at time τ resulting from early DS failure

$= E_A\left[D_{ED}(\tau|\mathbf{a},\mathbf{e}_M)\middle|\mathbf{e}_A\right]$

$= \int_{\mathcal{A}} D_{ED}(\tau|\mathbf{a},\mathbf{e}_M)\, d_A(\mathbf{a}|\mathbf{e}_A)\,\mathrm{d}A$

$= \int_{\mathcal{A}_{ED}} D_{ED}(\tau|\mathbf{a}_{ED},\mathbf{e}_M)\, d_A(\mathbf{a}|\mathbf{e}_A)\,\mathrm{d}A$, reminder $\mathbf{a}=[\ldots\,\mathbf{a}_{ED}\ldots]$, (Eq. J4.5-10)

$\bar{D}_{II}(\tau|\mathbf{e})$ = expected dose to RMEI (mrem/yr) at time τ resulting from igneous intrusive events

$= E_A\left[D_{II}(\tau|\mathbf{a},\mathbf{e}_M)\middle|\mathbf{e}_A\right]$

$= \int_{\mathcal{A}} D_{II}(\tau|\mathbf{a},\mathbf{e}_M)\, d_A(\mathbf{a}|\mathbf{e}_A)\,\mathrm{d}A$

$= \int_{\mathcal{A}_{II}} D_{II}(\tau|\mathbf{a}_{II},\mathbf{e}_M)\, d_A(\mathbf{a}|\mathbf{e}_A)\,\mathrm{d}A$, reminder $\mathbf{a}=[\ldots\,\mathbf{a}_{II}\ldots]$, (Eq. J4.5-11)

$\bar{D}_{IE}(\tau|\mathbf{e})$ = expected dose to RMEI (mrem/yr) at time τ resulting from igneous eruptive events

$= E_A\left[D_{IE}(\tau|\mathbf{a},\mathbf{e}_M)\middle|\mathbf{e}_A\right]$

$= \int_{\mathcal{A}} D_{IE}(\tau|\mathbf{a},\mathbf{e}_M)\, d_A(\mathbf{a}|\mathbf{e}_A)\,\mathrm{d}A$

$= \int_{\mathcal{A}_{IE}} D_{IE}(\tau|\mathbf{a}_{IE},\mathbf{e}_M)\, d_A(\mathbf{a}|\mathbf{e}_A)\,\mathrm{d}A$, reminder $\mathbf{a}=[\ldots\,\mathbf{a}_{IE}\ldots]$, (Eq. J4.5-12)

$\bar{D}_{SG}(\tau|\mathbf{e})$ = expected dose to RMEI (mrem/yr) at time τ resulting from seismic ground motion events

$= E_A\left[D_{SG}(\tau|\mathbf{a},\mathbf{e}_M)\middle|\mathbf{e}_A\right]$

$= \int_{\mathcal{A}} D_{SG}(\tau|\mathbf{a},\mathbf{e}_M)\, d_A(\mathbf{a}|\mathbf{e}_A)\,\mathrm{d}A$

$$= \int_{\mathcal{A}_{SG}} D_{SG}\left(\tau|\mathbf{a}_{SG}, \mathbf{e}_M\right) d_A\left(\mathbf{a}|\mathbf{e}_A\right) \mathrm{d}A, \text{ reminder: } \mathbf{a} = [\ldots \mathbf{a}_{SG} \ldots], \text{ (Eq. J4.5-13)}$$

$\bar{D}_{SF}\left(\tau|\mathbf{e}\right)$ = expected dose to RMEI (mrem/yr) at time τ resulting from seismic fault displacement events

$$= E_A\left[D_{SF}\left(\tau|\mathbf{a}, \mathbf{e}_M\right)\middle|\mathbf{e}_A\right]$$

$$= \int_{\mathcal{A}} D_{SF}\left(\tau|\mathbf{a}, \mathbf{e}_M\right) d_A\left(\mathbf{a}|\mathbf{e}_A\right) \mathrm{d}A$$

$$= \int_{\mathcal{A}_{SF}} D_{SF}\left(\tau|\mathbf{a}_{SF}, \mathbf{e}_M\right) d_A\left(\mathbf{a}|\mathbf{e}_A\right) \mathrm{d}A, \text{ reminder } \mathbf{a} = [\ldots \mathbf{a}_{SF} \ldots]. \quad \text{(Eq. J4.5-14)}$$

In the preceding, $D_{EW}(\tau|\mathbf{a}, \mathbf{e}_M)$ is equivalent to $D_{EW}(\tau|\mathbf{a}_{EW}, \mathbf{e}_M)$ because only dose from early WP failure is under consideration; for the same reason, the integrals over $\mathcal{A}$ and $\mathcal{A}_{EW}$ in Equation J4.4-20 are equivalent. Specifically, possible synergisms between occurrences associated with different scenario classes are not being considered. Analogous equivalencies hold $D_{ED}(\tau|\mathbf{a}, \mathbf{e}_M)$, $D_{II}(\tau|\mathbf{a}, \mathbf{e}_M)$, $D_{IE}(\tau|\mathbf{a}, \mathbf{e}_M)$, $D_{SG}(\tau|\mathbf{a}, \mathbf{e}_M)$, $D_{SF}(\tau|\mathbf{a}, \mathbf{e}_M)$ and associated integrals.

A more compact representation for Equation J4.5-1 is

$$\bar{D}\left(\tau|\mathbf{e}\right) \cong D_N\left(\tau|\mathbf{a}_N, \mathbf{e}_M\right) + \sum_{C \in \mathcal{MC}} \bar{D}_C\left(\tau|\mathbf{e}\right), \quad \text{(Eq. J4.5-15)}$$

where

$$\mathcal{MC} = \{EW, ED, II, IE, SG, SF\}$$

and the symbol $\mathcal{MC}$ is selected in consistency with the designated modeling case.

The justification of the decomposition of expected dose in Equations J4.5-1 and J4.5-15 ultimately depends on both the properties of the individual dose functions $D_N(\tau|\mathbf{a}_N, \mathbf{e}_M)$ and $D_C(\tau|\mathbf{a}, \mathbf{e}_M)$, $C \in \mathcal{MC}$, and the properties of the corresponding scenario classes $\mathcal{A}_N$ and $\mathcal{A}_C$. This justification is discussed in Section J10 after results for $p_A(\mathcal{A}_N)$, $p_A(\mathcal{A}_C)$, $D_N(\tau|\mathbf{a}_N, \mathbf{e}_M)$, $D_C(\tau|\mathbf{a}, \mathbf{e}_M)$, and $\bar{D}_C(\tau|\mathbf{e})$ are available.

The quantities $p_A[D < D_C(\tau|\mathbf{a}, \mathbf{e}_M)|\mathbf{e}_A]$, $\bar{D}_C(\tau|\mathbf{e})$ and $p_A[D_C(\tau|\mathbf{a}, \mathbf{e}_M) \leq D|\mathbf{e}_A]$ for $D_C(\tau|\mathbf{a}, \mathbf{e}_M)$, $C \in \mathcal{MC}$, can be approximated with sampling-based procedures in the same manner as indicated in Equations J4.3-10 – J4.3-12 for $D(\tau|\mathbf{e})$. Specifically,

$$p_A\left[D < D_C\left(\tau|\mathbf{a}, \mathbf{e}_M\right)\middle|\mathbf{e}_A\right] = \int_{\mathcal{A}} \bar{\delta}_D\left[D_C\left(\tau|\mathbf{a}, \mathbf{e}_M\right)\right] d_A\left(\mathbf{a}|\mathbf{e}_A\right) \mathrm{d}A$$
$$\cong \sum_{j=1}^{nR} \bar{\delta}_D\left[D_C\left(\tau|\mathbf{a}_j, \mathbf{e}_M\right)\right] \Big/ nR, \qquad \text{(Eq. J4.5-16)}$$

$$\bar{D}_C\left(\tau|\mathbf{e}\right) = \int_{\mathcal{A}} D_C\left(\tau|\mathbf{a}, \mathbf{e}_M\right) d_A\left(\mathbf{a}|\mathbf{e}_A\right) \mathrm{d}A$$
$$\cong \sum_{j=1}^{nR} D_C\left(\tau|\mathbf{a}_j, \mathbf{e}_M\right) \Big/ nR \qquad \text{(Eq. J4.5-17)}$$

and

$$p_A\left[D_C\left(\tau|\mathbf{a}, \mathbf{e}_M\right) \le D\right] = \int_{\mathcal{A}} \underline{\delta}_D\left[D_C\left(\tau|\mathbf{a}, \mathbf{e}_M\right)\right] d_A\left(\mathbf{a}|\mathbf{e}_A\right) \mathrm{d}A$$
$$\cong \sum_{j=1}^{nR} \underline{\delta}_D\left[D_C\left(\tau|\mathbf{a}_j, \mathbf{e}_M\right)\right] \Big/ nR \qquad \text{(Eq. J4.5-18)}$$

for a random sample $\mathbf{a}_j$, j = 1, 2, …, nR, from $\mathcal{A}$ of the form indicated in Equation J4.3-9. Further, as indicated in Equation J4.2-8, the approximation in Equation J4.5-18 can be used in the determination of quantile values for $D_C(\tau|\mathbf{a}, \mathbf{e}_M)$ that derive from the probability distribution over $\mathcal{A}$ defined by $d_A(\mathbf{a}|\mathbf{e}_A)$.

When a specific scenario class is under consideration, and no synergisms are assumed to exist between the effects associated with individual scenario classes, it is only necessary to sample the components of $\mathbf{a}$ that are involved in the evaluation of dose $D_C(\tau|\mathbf{a}, \mathbf{e}_M)$ for this scenario class (i.e., scenario class C) as the remaining components of $\mathbf{a}$ have no effect on $D_C(\tau|\mathbf{a}, \mathbf{e}_M)$. In this case, the representations for the approximations in Equations J4.5-16 – J4.5-18 become

$$p_A\left[D < D_C\left(\tau|\mathbf{a}, \mathbf{e}_M\right)\middle|\mathbf{e}_A\right] \cong p_A\left(\mathcal{A}_C|\mathbf{e}_A\right) \sum_{j=1}^{nR} \bar{\delta}_D\left[D_S\left(\tau|\mathbf{a}_{Cj}, \mathbf{e}_M\right)\right] \Big/ nR, \qquad \text{(Eq. J4.5-19)}$$

$$\bar{D}_C\left(\tau|\mathbf{e}\right) \cong p_A\left(\mathcal{A}_C|\mathbf{e}_A\right) \sum_{j=1}^{nR} D_S\left(\tau|\mathbf{a}_{Cj}, \mathbf{e}_M\right) \Big/ nR \qquad \text{(Eq. J4.5-20)}$$

and

$$p_A\left[D_C\left(\tau|\mathbf{a}, \mathbf{e}_M\right) \le D\right] \cong p_A\left(\mathcal{A}_C|\mathbf{e}_A\right) \sum_{j=1}^{nR} \underline{\delta}_D\left[D_C\left(\tau|\mathbf{a}_{Cj}, \mathbf{e}_M\right)\right] \Big/ nR, \qquad \text{(Eq. J4.5-21)}$$

where $\mathbf{a}_{Cj}$, $j = 1, 2, \ldots, nR$, is a random sample from $\mathcal{A}_C$ generated in consistency with the part of $d_A(\mathbf{a}|\mathbf{e}_A)$ that applies to the components of $\mathbf{a}$ that enter into the definition of $\mathcal{A}_C$.

Inclusion of the factor $p_A(\mathcal{A}_C|\mathbf{e}_A)$ in Equations J4.5-19 – J4.5-21 is predicated on the assumption that sampling is being carried out conditional on the occurrence of scenario class $\mathcal{A}_C$. In contrast, the factor $p_A(\mathcal{A}_C|\mathbf{e}_A)$ is not included in Equations J4.5-16 – J4.5-18 because sampling is being carried out over the entire sample space $\mathcal{A}$. When $p_A(\mathcal{A}_C|\mathbf{e}_A)$ is small, restriction of sampling to the set $\mathcal{A}_C$ is numerically efficient because it avoids the generation of large numbers of futures $\mathbf{a}$ for which $D_C(\tau|\mathbf{a}, \mathbf{e}_M) = 0$.

Although sampling-based procedures provide one method for estimating $p_A[D < D_C(\tau|\mathbf{a}, \mathbf{e}_M)|\mathbf{e}_A]$, $\bar{D}_C(\tau|\mathbf{e})$ and $p_A[D_C(\tau|\mathbf{a}, \mathbf{e}_M) \le D|\mathbf{e}_A]$, other methods also exist. This is especially true with respect to the estimation of $\bar{D}_C(\tau|\mathbf{e})$. Typically, these methods are designed to achieve computational efficiencies on the basis of specific properties of $D_C(\tau|\mathbf{a}, \mathbf{e}_M)$ and $d_A(\mathbf{a}|\mathbf{e}_A)$. For the TSPA-LA, alternatives to the use of naïve sampling-based procedures are employed to determine $\bar{D}_{EW}(\tau|\mathbf{e})$, $\bar{D}_{ED}(\tau|\mathbf{e})$, $\bar{D}_{II}(\tau|\mathbf{e})$, $\bar{D}_{IE}(\tau|\mathbf{e})$ and $\bar{D}_{SF}(\tau|\mathbf{e})$ for the [0, 2×10^4 yr] and [0, 10^6 yr] time intervals and to determine $\bar{D}_{SG}(\tau|\mathbf{e})$ for the [0, 2×10^4 yr] time interval. However, owing to the complexity of the calculation, $\bar{D}_{SG}(\tau|\mathbf{e})$ could only be determined with a sampling-based calculation for [0, 10^6 yr] time interval.

J4.6 Analysis Decomposition

As previously stated, the approximation in Equations J4.5-1 and J4.5-15 is based on the assumption that there are no synergisms between disruptions that have significant effects on the expected dose $\bar{D}(\tau|\mathbf{e})$ defined in Equation J4.2-2. One way to arrive at this approximation is to start with the assumption that there are no significant synergisms between disruptions that affect the dose $D(\tau|\mathbf{a}, \mathbf{e}_M)$ for individual futures, which is equivalent to the assumption that

$$D(\tau|\mathbf{a}, \mathbf{e}_M) \cong D_N(\tau|\mathbf{a}_N, \mathbf{e}_M) + \sum_{C \in \mathcal{MC}} D_C(\tau|\mathbf{a}, \mathbf{e}_M), \qquad \text{(Eq. J4.6-1)}$$

where $\mathcal{MC}$ is defined in conjunction with Equation J4.5-15. In turn,

$$\bar{D}(\tau|\mathbf{e}) \cong \int_{\mathcal{A}} \left\{ D_N(\tau|\mathbf{a}_N, \mathbf{e}_M) + \sum_{C \in \mathcal{MC}} D_C(\tau|\mathbf{a}, \mathbf{e}_M) \right\} d_A(\mathbf{a}|\mathbf{e}_A)\, \mathrm{d}A$$

$$= D_N(\tau|\mathbf{a}_N, \mathbf{e}_M) + \sum_{C \in \mathcal{MC}} \int_{\mathcal{A}} D_C(\tau|\mathbf{a}, \mathbf{e}_M)\, d_A(\mathbf{a}|\mathbf{e}_A)\, \mathrm{d}A$$

$$= D_N(\tau|\mathbf{a}_N, \mathbf{e}_M) + \sum_{C \in \mathcal{MC}} \int_{\mathcal{A}_C} D_C(\tau|\mathbf{a}, \mathbf{e}_M)\, d_A(\mathbf{a}|\mathbf{e}_A)\, \mathrm{d}A$$

$$= D_N(\tau|\mathbf{a}_N, \mathbf{e}_M) + \sum_{C \in \mathcal{MC}} \bar{D}_C(\tau|\mathbf{e}), \qquad \text{(Eq. J4.6-2)}$$

which is the result in Equations J4.5-1 and J4.5-15. As previously noted, the appropriateness of this approximation to $\bar{D}(\tau|\mathbf{e})$ depends on both the level of synergisms between disruptions and the probabilities associated with the scenario classes $\mathcal{A}_{EW}$, $\mathcal{A}_{ED}$, $\mathcal{A}_{II}$, $\mathcal{A}_{IE}$, $\mathcal{A}_{SG}$ and $\mathcal{A}_{SF}$.

In turn, the expected dose $\bar{\bar{D}}(\tau)$ over both epistemic and aleatory uncertainty defined in Equation J4.2-5 can be approximated by

$$\bar{\bar{D}}(\tau) \cong \int_{\mathcal{E}} \left\{ D_N(\tau|\mathbf{a}_N, \mathbf{e}_M) + \sum_{C \in \mathcal{MC}} \bar{D}_C(\tau|\mathbf{e}) \right\} d_E(\mathbf{e})\, \mathrm{d}E$$

$$= \int_{\mathcal{E}} D_N(\tau|\mathbf{a}_N, \mathbf{e}_M)\, d_E(\mathbf{e})\, \mathrm{d}E + \sum_{C \in \mathcal{MC}} \int_{\mathcal{E}} \bar{D}_C(\tau|\mathbf{e})\, d_E(\mathbf{e})\, \mathrm{d}E$$

$$= \bar{\bar{D}}_N(\tau) + \sum_{C \in \mathcal{MC}} \bar{\bar{D}}_C(\tau), \qquad \text{(Eq. J4.6-3)}$$

where

$$\bar{\bar{D}}_N(\tau) = E_E\left[D_N(\tau|\mathbf{a}_N, \mathbf{e}_M) \right] = \int_{\mathcal{E}} D_N(\tau|\mathbf{a}_N, \mathbf{e}_M)\, d_E(\mathbf{e})\, \mathrm{d}E \qquad \text{(Eq. J4.6-4)}$$

and

$$\bar{\bar{D}}_C(\tau) = E_E\left[\bar{D}_C(\tau|\mathbf{e}) \right] = \int_{\mathcal{E}} \bar{D}_C(\tau|\mathbf{e})\, d_E(\mathbf{e})\, \mathrm{d}E \qquad \text{(Eq. J4.6-5)}$$

for $C \in \mathcal{MC}$.

If desired, the equality

$$\bar{D}(\tau|\mathbf{e}) = D_N(\tau|\mathbf{a}_N, \mathbf{e}_M) + \sum_{C \in \mathcal{MC}} \int_{\mathcal{A}_C} D_C(\tau|\mathbf{a}, \mathbf{e}_M)\, d_A(\mathbf{a}|\mathbf{e}_A)\, \mathrm{d}A \qquad \text{(Eq. J4.6-6)}$$

appearing in Equation J4.6-2 can be reformulated as

$$\begin{aligned}\bar{D}(\tau|\mathbf{e}) &= D_N(\tau|\mathbf{a}_N, \mathbf{e}_M) + \sum_{C \in \mathcal{MC}} p_A(\mathcal{A}_C|\mathbf{e}_A) \int_{\mathcal{A}_C} D_C(\tau|\mathbf{a}, \mathbf{e}_M) \left[d_A(\mathbf{a}|\mathbf{e}_A) / p_A(\mathcal{A}_C|\mathbf{e}_A) \right] \mathrm{d}A \\ &= D_N(\tau|\mathbf{a}_N, \mathbf{e}_M) + \sum_{C \in \mathcal{MC}} p_A(\mathcal{A}_C|\mathbf{e}_A) E_A\left[D_C(\tau|\mathbf{a}, \mathbf{e}_M) \middle| \mathcal{A}_C, \mathbf{e}_A \right], \qquad \text{(Eq. J4.6-7)}\end{aligned}$$

where

$$E_A\left[D_C(\tau|\mathbf{a}, \mathbf{e}_M) \middle| \mathcal{A}_C, \mathbf{e}_A \right] = \int_{\mathcal{A}_C} D_C(\tau|\mathbf{a}, \mathbf{e}_M) \left[d_A(\mathbf{a}|\mathbf{e}_A) / p_A(\mathcal{A}_C|\mathbf{e}_A) \right] \mathrm{d}A$$

is the expected value for $D_C(\tau|\mathbf{a}, \mathbf{e}_M)$ given the occurrence of scenario class $\mathcal{A}_C$ and conditional on $\mathbf{e} = [\mathbf{e}_A, \mathbf{e}_M]$. This is the formulation that underlies the approximation to $\bar{D}_C(\tau|\mathbf{e})$ in Equation J4.5-20.

J4.7 Disjoint and Nondisjoint Scenario Classes

Neither the scenario classes $\mathcal{A}_E$, $\mathcal{A}_I$ and $\mathcal{A}_S$ nor the scenario classes $\mathcal{A}_{EW}$, $\mathcal{A}_{ED}$, $\mathcal{A}_{II}$, $\mathcal{A}_{IE}$, $\mathcal{A}_{SG}$ and $\mathcal{A}_{SF}$ are disjoint. However, it is straightforward to define disjoint scenario classes on the basis of the same disruptive occurrences that define the preceding scenario classes.

Disjoint scenario classes related to $\mathcal{A}_E$, $\mathcal{A}_I$ and $\mathcal{A}_S$ can be defined by sets of the form

$$\begin{aligned}\mathcal{A}(r, s, t) = \{&\mathbf{a}: \mathbf{a} \in \mathcal{A} \text{ with } nEW + nED = 0 \text{ if } r = 0,\ nEW + nED \geq 1 \text{ if } r = 1, \\ &nII = 0 \text{ if } s = 0,\ nII \geq 1 \text{ if } s = 1,\ nSG + nSF = 0 \text{ if } t = 0,\ nSG + \\ &nSF \geq 1 \text{ if } t = 1\} \qquad \text{(Eq. J4.7-1)}\end{aligned}$$

for $r = 0, 1$, $s = 0, 1$, $t = 0, 1$. The preceding defines $2^3 = 8$ disjoint scenario classes on the basis of early failures, igneous events and seismic events. Further, the probabilities $p_A[\mathcal{A}(r, s, t)]$ of these scenario classes sum to one.

In like manner, disjoint scenario classes related to $\mathcal{A}_{EW}$, $\mathcal{A}_{ED}$, $\mathcal{A}_{II}$, $\mathcal{A}_{IE}$, $\mathcal{A}_{SG}$ and $\mathcal{A}_{SF}$ can be defined by sets of the form

$$\begin{aligned}\mathcal{A}(r, s, t, u, v, w) = \{&\mathbf{a}: \mathbf{a} \in \mathcal{A} \text{ with } nEW = 0 \text{ if } r = 0,\ nEW \geq 1 \text{ if } r = 1, \ldots, \\ &nSF = 0 \text{ if } w = 0,\ nSF \geq 1 \text{ if } w = 1\} \qquad \text{(Eq. J4.7-2)}\end{aligned}$$

for $r = 0, 1$, $w = 0, 1$, and similarly for s, t, u and v. The preceding defines $2^6 = 64$ disjoint scenario classes, although all sets of the form $\mathcal{A}(r, s, 0, 1, v, w)$ correspond to the null set because the occurrence of an igneous intrusive event (i.e., $t = 1$) is a necessary, but not sufficient,

condition for the occurrence of an igneous eruptive event (i.e., $u = 1$). As a result, there are only 48 nondegenerate scenario classes of the form $\mathcal{A}(r, s, t, u, v, w)$. Further, the probabilities $p_A[\mathcal{A}(r, s, t, u, v, w)]$ of the 64 scenario classes sum to one.

For perspective, the calculation of expected dose $\bar{D}(\tau|\mathbf{e})$ is illustrated with the disjoint scenario classes $\mathcal{A}(r, s, t)$ defined in Equation J4.7-1. Specifically,

$$\begin{aligned}
\bar{D}(\tau|\mathbf{e}) &= \int_{\mathcal{A}} D(\tau|\mathbf{a},\mathbf{e}_M)\, d_A(\mathbf{a}|\mathbf{e}_A)\,\mathrm{d}A \\
&= \sum_{\mathbf{r}\in\mathcal{R}} \int_{\mathcal{A}(\mathbf{r})} D_{\mathbf{r}}(\tau|\mathbf{a},\mathbf{e}_M)\, d_A(\mathbf{a}|\mathbf{e}_A)\,\mathrm{d}A \\
&= \sum_{\mathbf{r}\in\mathcal{R}} \int_{\mathcal{A}(\mathbf{r})} \left[D_N(\tau|\mathbf{a},\mathbf{e}_M) + \tilde{D}_{\mathbf{r}}(\tau|\mathbf{a},\mathbf{e}_M)\right] d_A(\mathbf{a}|\mathbf{e}_A)\,\mathrm{d}A \\
&= D_N(\tau|\mathbf{a}_N,\mathbf{e}_M) + \sum_{\mathbf{r}\in\tilde{\mathcal{R}}} \int_{\mathcal{A}(\mathbf{r})} \tilde{D}_{\mathbf{r}}(\tau|\mathbf{a},\mathbf{e}_M)\, d_A(\mathbf{a}|\mathbf{e}_A)\,\mathrm{d}A \\
&= D_N(\tau|\mathbf{a}_N,\mathbf{e}_M) + \sum_{C\in\mathcal{MC}} \int_{\mathcal{A}_C} D_C(\tau|\mathbf{a},\mathbf{e}_M)\, d_A(\mathbf{a}|\mathbf{e}_A)\,\mathrm{d}A, \qquad \text{(Eq. J4.7-3)}
\end{aligned}$$

where

$$\begin{aligned}
\mathcal{R} &= \{0,1\}\times\{0,1\}\times\{0,1\} \\
&= \{[0,0,0],[0,0,1],[0,1,0],[0,1,1],[1,0,0],[1,0,1],[1,1,0],[1,1,1]\}, \\
\tilde{\mathcal{R}} &= \{[0,0,1],[0,1,0],[0,1,1],[1,0,0],[1,0,1],[1,1,0],[1,1,1]\},
\end{aligned}$$

$$\begin{aligned}
\tilde{D}_{\mathbf{r}}(\tau|\mathbf{a},\mathbf{e}_M) &= 0 && \text{if } \mathbf{r} = [0,0,0] \\
&= D_{SG}(\tau|\mathbf{a},\mathbf{e}_M) + D_{SF}(\tau|\mathbf{a},\mathbf{e}_M) && \text{if } \mathbf{r} = [0,0,1] \\
&= D_{II}(\tau|\mathbf{a},\mathbf{e}_M) + D_{IE}(\tau|\mathbf{a},\mathbf{e}_M) && \text{if } \mathbf{r} = [0,1,0] \\
&= D_{II}(\tau|\mathbf{a},\mathbf{e}_M) + D_{IE}(\tau|\mathbf{a},\mathbf{e}_M) + D_{SG}(\tau|\mathbf{a},\mathbf{e}_M) + D_{SF}(\tau|\mathbf{a},\mathbf{e}_M) && \text{if } \mathbf{r} = [0,1,1] \\
&= D_{EW}(\tau|\mathbf{a},\mathbf{e}_M) + D_{ED}(\tau|\mathbf{a},\mathbf{e}_M) && \text{if } \mathbf{r} = [1,0,0] \\
&= D_{EW}(\tau|\mathbf{a},\mathbf{e}_M) + D_{ED}(\tau|\mathbf{a},\mathbf{e}_M) + D_{SG}(\tau|\mathbf{a},\mathbf{e}_M) + D_{SF}(\tau|\mathbf{a},\mathbf{e}_M) && \text{if } \mathbf{r} = [1,0,1] \\
&= D_{EW}(\tau|\mathbf{a},\mathbf{e}_M) + D_{ED}(\tau|\mathbf{a},\mathbf{e}_M) + D_{II}(\tau|\mathbf{a},\mathbf{e}_M) + D_{IE}(\tau|\mathbf{a},\mathbf{e}_M) && \text{if } \mathbf{r} = [1,1,0] \\
&= D_{EW}(\tau|\mathbf{a},\mathbf{e}_M) + D_{ED}(\tau|\mathbf{a},\mathbf{e}_M) + D_{II}(\tau|\mathbf{a},\mathbf{e}_M) \\
&\quad + D_{IE}(\tau|\mathbf{a},\mathbf{e}_M) + D_{SG}(\tau|\mathbf{a},\mathbf{e}_M) + D_{SF}(\tau|\mathbf{a},\mathbf{e}_M) && \text{if } \mathbf{r} = [1,1,1]
\end{aligned}$$

and

$$D_{\mathbf{r}}(\tau|\mathbf{a}, \mathbf{e}_M) = D_N(\tau|\mathbf{a}_N, \mathbf{e}_M) + \tilde{D}_{\mathbf{r}}(\tau|\mathbf{a}, \mathbf{e}_M)$$

for $\mathbf{r} \in \mathcal{R}$.

With respect to the preceding representation of $\bar{D}(\tau|\mathbf{e})$, (i) the first equality corresponds to the definition of $\bar{D}(\tau|\mathbf{e})$ in Equation J4.2-2, (ii) the second equality decomposes the defining integral for $\bar{D}(\tau|\mathbf{e})$ into integrals over the eight disjoint scenario classes $\mathcal{A}(r, s, t) = \mathcal{A}(\mathbf{r})$ indexed by elements of the set $\mathcal{R}$, (iii) the third equality involves a division of the dose function $D_{\mathbf{r}}(\tau|\mathbf{a}, \mathbf{e}_M)$ for scenario class $\mathcal{A}(\mathbf{r})$ into a constituent part $D_N(\tau|\mathbf{a}_N, \mathbf{e}_M)$ arising from WP failures resulting from nominal processes and a constituent part $\tilde{D}_{\mathbf{r}}(\tau|\mathbf{a}, \mathbf{e}_M)$ arising from WP failures resulting from the disruptions associated with scenario class $\mathcal{A}(\mathbf{r})$, (iv) the fourth equality divides the preceding integrals into an integral of $D_N(\tau|\mathbf{a}_N, \mathbf{e}_M)$ over $\mathcal{A} = \cup\, \mathcal{A}(\mathbf{r})$, which is equal to $D_N(\tau|\mathbf{a}_N, \mathbf{e}_M)$, and integrals of $\tilde{D}_{\mathbf{r}}(\tau|\mathbf{a}, \mathbf{e}_M)$ over $\mathcal{A}(\mathbf{r})$ for $\mathbf{r} \in \tilde{R}$, and (v) the fifth and final equality involves a regrouping of the constituent dose functions in the definitions of $\tilde{D}_{\mathbf{r}}(\tau|\mathbf{a}, \mathbf{e}_M)$ into integrals over nondisjoint scenario classes indexed by elements of the set $\mathcal{MC}$ defined in conjunction with Equation J4.5-15 on which these constituent dose functions are potentially nonzero. The overall computational structure used in the TSPA-LA to determine expected dose to the RMEI is based on the final representation for $\bar{D}(\tau|\mathbf{e})$ in Equation J4.7-3.

If desired, the generation of disjoint scenario classes illustrated in Equation J4.7-1 and J4.7-2 can be carried farther by changing the definition of $\mathcal{A}(r, s, t, u, v, w)$ in Equation J4.7-2 to

$$\mathcal{A}(r, s, t, u, v, w) = \{\mathbf{a}: \mathbf{a} \in \mathcal{A} \text{ with } nEW = r, nED = s, nII = t, nIE = u, nSG = v, nSF = w\} \quad \text{(Eq. J4.7-4)}$$

for $r = 0, 1, 2, \ldots$, $s = 0, 1, 2, \ldots$, and similarly for t, u, v and w. Further, this is only a small start on the possibilities for defining disjoint scenario classes as many additional event properties (e.g., time of occurrence, size, …) could also be used in the definition of disjoint scenario classes. Actually, this is what is being done in concept when expected doses $\bar{D}(\tau|\mathbf{e})$ and $\bar{D}_C(\tau|\mathbf{e})$, $C \in \mathcal{MC}$, are defined by integrals as indicated in Equations J4.2-2 and J4.5-9 – J4.5-14.

For example, the integral defining $\bar{D}(\tau|\mathbf{e})$ in Equation J4.2-2 is the limit of approximating sums of the form

$$\bar{D}(\tau|\mathbf{e}) \cong \sum_{j=1}^{nS} D(\tau|\mathbf{a}_j, \mathbf{e}_M)\, p_A(\mathcal{A}_j|\mathbf{e}_A) \quad \text{(Eq. J4.7-5)}$$

where (i) $\mathcal{A}_j$, $j = 1, 2, \ldots, nS$, is a sequence of disjoint subsets of $\mathcal{A}$ with $\cup_j \mathcal{A}_j = \mathcal{A}$, (ii) $\mathbf{a}_j$ is a representative element of $\mathcal{A}_j$, and (iii)

$$p_A\left(\mathcal{A}_j \middle| \mathbf{e}_A\right) = \int_{\mathcal{A}_j} d_A\left(\mathbf{a} \middle| \mathbf{e}_A\right) \mathrm{d}A.$$

In this approximation to $\bar{D}(\tau|\mathbf{e})$, the $\mathcal{A}_j$ are disjoint scenario classes, $p_A(\mathcal{A}_j|\mathbf{e}_A)$ is the probability for scenario class $\mathcal{A}_j$, and $\Sigma_j\, p_A(\mathcal{A}_j|\mathbf{e}_A) = 1$. In turn, $\bar{D}(\tau|\mathbf{e})$ results in the limit as increasingly refined scenario classes are used in the summation in Equation J4.7-5 (i.e., as $p_A(\mathcal{A}_j|\mathbf{e}_A) \rightarrow 0$). In practice, the scenario classes $\mathcal{A}_j$ in Equation J4.7-5 may or may not be computationally present in a specific implementation of a numerical approximation to the integral defining $\bar{D}(\tau|\mathbf{e})$ (e.g., if a Monte Carlo procedure is being used). However, they are conceptually present in the definition of $\bar{D}(\tau|\mathbf{e})$. The same conceptual ideas underlie the definition of $\bar{D}_C(\tau|\mathbf{e})$ for $C \in \mathcal{MC}$. The use of integrals in the definition and computational evaluation of $\bar{D}(\tau|\mathbf{e})$ and $\bar{D}_C(\tau|\mathbf{e})$ avoids the messy notational and computational problems that arise when $\bar{D}(\tau|\mathbf{e})$ and $\bar{D}_C(\tau|\mathbf{e})$ are defined and evaluated on the basis of a large number of disjoint scenario classes.

J4.8 Scenario Classes and the Yucca Mountain Review Plan

The NRC's Yucca Mountain Review Plan (YMRP) requests that TSPA-LA results be developed and presented in the context of the Kaplan and Garrick ordered triple representation for risk. With this representation, risk is characterized by a sequence

$$\left(S_j, pS_j, cS_j\right),\ j = 1, 2, \ldots, nS, \qquad \text{(Eq. J4.8-1)}$$

of triples, where (i) S_j is a set of similar occurrences (i.e., futures), (ii) the sets S_j are disjoint and $\cup_j S_j$ contains all possible occurrences for the system under study, (iii) pS_j is the probability of S_j, and (iv) cS_j is the consequence (or, more generally, a vector $\mathbf{cS}_j$ of consequences) of interest. In the terminology of the TSPA-LA, S_j corresponds to a scenario class; $\mathcal{S} = \cup_j S_j$ is the sample space for aleatory uncertainty; pS_j is the probability for scenario class S_j; and cS_j is the consequence associated with scenario class S_j. In turn, the expected consequence $\overline{cS}$ is approximated by

$$\overline{cS} \cong \sum_{j=1}^{nS} pS_j\, cS_j. \qquad \text{(Eq. J4.8-2)}$$

In concept, the preceding approximation improves as $nS \rightarrow \infty$ and the $pS_j \rightarrow 0$ and in the limit becomes

$$\overline{cS} = \int_{\mathcal{S}} cS\left(\mathbf{a}\right) d_S\left(\mathbf{a}\right) \mathrm{d}S, \qquad \text{(Eq. J4.8-3)}$$

where $cS(\mathbf{a})$ denotes the consequence of interest as a function of individual elements (i.e., occurrences or futures) $\mathbf{a}$ contained in $\mathcal{S}$ and $d_S(\mathbf{a})$ denotes the density function associated with the indicated probabilities pS_j.

The ordered triple representation for risk in Equation J4.8-1 is precisely the risk representation that underlies the approximation to $\bar{D}(\tau|\mathbf{e})$ in Equation J4.7-5. Specifically, the corresponding ordered triple representation is

$$\left[\mathcal{A}_j,\ p_A\left(\mathcal{A}_j\middle|\mathbf{e}_A\right),\ D\left(\tau|\mathbf{a}_j,\mathbf{e}_M\right)\right],\ j=1,2,\ldots,nS, \qquad \text{(Eq. J4.8-4)}$$

where $\mathcal{A}_j \sim S_j$, $p_A(\mathcal{A}_j|\mathbf{e}_A) \sim pS_j$ and $D(\tau|\mathbf{a}_j, \mathbf{e}_M) \sim cS_j$. In turn, the approximation to $\bar{D}(\tau|\mathbf{e})$ in Equation J4.7-5 corresponds to the approximation to $\overline{cS}$ in Equation J4.8-2. Similarly, the integral in Equation J4.2-2 that formally defines $\bar{D}(\tau|\mathbf{e})$ corresponds to the integral in Equation J4.8-3 that formally defines $\overline{cS}$.

J4.9 Characterization of Epistemic Uncertainty

As indicated in Equations J4.2-4, J4.2-5 and J4.2-9, $p_E[D < \bar{D}(\tau|\mathbf{e})]$, $\bar{\bar{D}}(\tau)$ and $p_E[\bar{D}(\tau|\mathbf{e}) \le D]$ can be formally defined by integrals over $\mathcal{E}$. In practice, closed form evaluation of these integrals is not feasible; instead, these integrals must be approximated with a sampling-based procedure. In the TSPA-LA, this sampling-based integration is performed with Latin hypercube sampling. Specifically, an LHS

$$\mathbf{e}_i = \left[\mathbf{e}_{Ai}, \mathbf{e}_{Mi}\right],\ i=1,2,\ldots,nLHS, \qquad \text{(Eq. J4.9-1)}$$

is generated in consistency with the definition of the probability space ($\mathcal{E}$, E, p_E) (i.e., in consistency with the distributions defined for the individual elements of $\mathbf{e}$). Then, $p_E[D < \bar{D}(\tau|\mathbf{e})]$, $\bar{\bar{D}}(\tau)$ and $p_E[\bar{D}(\tau|\mathbf{e}) \le D]$ are approximated by

$$p_E\left[D < \bar{D}\left(\tau|\mathbf{e}\right)\right] \cong \sum_{i=1}^{nLHS} \bar{\delta}_D\left[\bar{D}\left(\tau|\mathbf{e}_i\right)\right] / nLHS, \qquad \text{(Eq. J4.9-2)}$$

$$\bar{\bar{D}}(\tau) \cong \sum_{i=1}^{nLHS} \bar{D}\left(\tau|\mathbf{e}_i\right) / nLHS \qquad \text{(Eq. J4.9-3)}$$

and

$$p_E\left[\bar{D}\left(\tau|\mathbf{e}\right) \le D\right] \cong \sum_{i=1}^{nLHS} \underline{\delta}_D\left[\bar{D}\left(\tau|\mathbf{e}_i\right)\right] / nLHS, \qquad \text{(Eq. J4.9-4)}$$

respectively. Further, this sample can be used in a numerical determination of the quantiles $Q_q[\bar{D}(\tau|\mathbf{e})]$ for $\bar{D}(\tau|\mathbf{e})$ defined in Equation J4.2-10.

Similarly, corresponding approximations for $D_N(\tau|\mathbf{a}_N, \mathbf{e}_M)$ are given by

$$p_E\left[D < D_N\left(\tau|\mathbf{a}_N, \mathbf{e}_M\right)\right] = \int_{\mathcal{E}} \bar{\delta}_D\left[D_N\left(\tau|\mathbf{a}_N, \mathbf{e}_M\right)\right] d_E(\mathbf{e})\,\mathrm{d}E$$
$$\cong \sum_{i=1}^{nLHS} \bar{\delta}_D\left[D_N\left(\tau|\mathbf{a}_N, \mathbf{e}_{Mi}\right)\right] / nLHS, \qquad \text{(Eq. J4.9-5)}$$

$$\bar{\bar{D}}_N(\tau) = \int_{\mathcal{E}} D_N\left(\tau|\mathbf{a}_N, \mathbf{e}_M\right) d_E(\mathbf{e})\,\mathrm{d}E$$
$$\cong \sum_{i=1}^{nLHS} D_N\left(\tau|\mathbf{a}_N, \mathbf{e}_{Mi}\right) / nLHS \qquad \text{(Eq. J4.9-6)}$$

and

$$p_E\left[D_N\left(\tau|\mathbf{a}_N, \mathbf{e}_M\right) \le D\right] = \int_{\mathcal{E}} \underline{\delta}_D\left[D_N\left(\tau|\mathbf{a}_N, \mathbf{e}_M\right)\right] d_E(\mathbf{e})\,\mathrm{d}E$$
$$\cong \sum_{i=1}^{nLHS} \underline{\delta}_D\left[D_N\left(\tau|\mathbf{a}_N, \mathbf{e}_{Mi}\right)\right] / nLHS, \qquad \text{(Eq. J4.9-7)}$$

and corresponding approximations for $\bar{D}_C(\tau|\mathbf{e})$ are given by

$$p_E\left[D < \bar{D}_C\left(\tau|\mathbf{e}\right)\right] = \int_{\mathcal{E}} \bar{\delta}_D\left[\bar{D}_C\left(\tau|\mathbf{e}\right)\right] d_E(\mathbf{e})\,\mathrm{d}E$$
$$\cong \sum_{i=1}^{nLHS} \bar{\delta}_D\left[\bar{D}_C\left(\tau|\mathbf{e}_i\right)\right] / nLHS, \qquad \text{(Eq. J4.9-8)}$$

$$\bar{\bar{D}}_C(\tau) = \int_{\mathcal{E}} \bar{D}_C\left(\tau|\mathbf{e}\right) d_E(\mathbf{e})\,\mathrm{d}E$$
$$\cong \sum_{i=1}^{nLHS} \bar{D}_C\left(\tau|\mathbf{e}_i\right) / nLHS \qquad \text{(Eq. J4.9-9)}$$

and

$$p_E\left[\bar{D}_C\left(\tau|\mathbf{e}\right) \le D\right] = \int_{\mathcal{E}} \underline{\delta}_D\left[\bar{D}_C\left(\tau|\mathbf{e}\right)\right] d_E(\mathbf{e})\,\mathrm{d}E$$
$$\cong \sum_{i=1}^{nLHS} \underline{\delta}_D\left[\bar{D}_C\left(\tau_i|\mathbf{e}_i\right)\right] / nLHS \qquad \text{(Eq. J4.9-10)}$$

for $C = EW, ED, II, IE, SG, SF$. Further, the sample can be used in a numerical determination of quantiles for $D_N(\tau|\mathbf{a}_N, \mathbf{e}_M)$ and $\bar{D}_C(\tau|\mathbf{e})$ in the same manner as indicated in Equation J4.2-10 for $\bar{D}(\tau)$.

J4.10 Adequacy of Latin Hypercube Sample Size

The adequacy of an LHS of size *nLHS* can be assessed with a replicated sampling procedure proposed by R.L. Iman (Iman 1982 [DIRS 146012]). Specifically, the goal of the procedure is to determine how much variability exists in estimated analysis outcomes when different LHSs of size *nLHS* are used. The procedure is based on independently generating LHSs of size *nLHS* with different random seeds *nRL* times. At an intuitive level, the adequacy of the sample size can be assessed by simply comparing the results obtained with the individual samples.

At a more formal level, the *t*-distribution can be used to place confidence intervals around summary results (e.g., expected values over epistemic uncertainty) obtained from individual samples. Specifically, assume that the LHS has been replicated *nRL* times to produce $r = 1, 2, \ldots, nRL$ independently generated LHSs

$$\mathbf{e}_{ri} = \left[\mathbf{e}_{Ari}, \mathbf{e}_{Mri}\right], i = 1, 2, \ldots, nLHS, \qquad \text{(Eq. J4.10-1)}$$

of size *nLHS* and that C_r is an analysis result of interest obtained for replicated sample *r*. For example, C might be the expected dose $\bar{\bar{D}}(\tau)$ at time τ that is estimated with use of Latin hypercube sampling and $C_r = \bar{\bar{D}}_r(\tau)$ would be the estimate for $\bar{\bar{D}}(\tau)$ obtained with replicated sample *r*. Then,

$$\bar{C} = \sum_{r=1}^{nRL} C_r / nRL \qquad \text{(Eq. J4.10-2)}$$

and

$$SE\left(\bar{C}\right) = \left\{ \sum_{r=1}^{nRL} \left[C_r - \bar{C}\right]^2 \Big/ nRL\left(nRL - 1\right) \right\}^{1/2} \qquad \text{(Eq. J4.10-3)}$$

provide an additional estimate of C and an estimate of the standard error associated with this additional estimate.

The *t*-distribution with $nRL - 1$ degrees of freedom can now be used to place confidence intervals around the estimate for C in Equation J4.10-2. Specifically, the $1 - \alpha$ confidence interval for C is given by

$$\bar{C} \pm t_{1-\alpha/2} SE\left(\bar{C}\right), \qquad \text{(Eq. J4.10-4)}$$

where $t_{1-\alpha/2}$ is the $1 - \alpha/2$ quantile of the *t*-distribution with $nRL - 1$ degrees of freedom. For example, $t_{1-\alpha/2} = 4.303$ for $\alpha = 0.05$ and $nRL = 3$.

J5 NOMINAL SCENARIO CLASS: $\mathcal{A}_N$

For the nominal scenario class $\mathcal{A}_N$, no disruptions of any kind (i.e., early WP failures, early DS failures, igneous intrusive events, igneous eruptive events, seismic ground motion events, seismic fault displacement events) are assumed to take place. Thus, as discussed in Section J4.4, the vector

$$\mathbf{a}_N = [0, 0, 0, 0, 0, 0] \qquad \text{(Eq. J5-1)}$$

can be used to represent the realization of aleatory uncertainty associated with nominal conditions, where the 0's indicate the complete absence of any disruptions of the repository (see Equation J4.4-1) with $nEW = nED = nII = nIE = nSG = nSF = 0$). As a result, the set $\mathcal{A}_N$ corresponding to the nominal scenario class contains the single element $\mathbf{a}_N$ (see Equation J4.4-9). In turn, $D_N(\tau|\mathbf{a}_N, \mathbf{e}_M)$ is used to represent dose to the RMEI at time τ for the nominal scenario class conditional on the element $\mathbf{e} = [\mathbf{e}_A, \mathbf{e}_M]$ of $\mathcal{E}$ as indicated in Equation J4.5-2. No component of $\mathbf{e}_A$ is involved in the analysis of results for nominal conditions.

Only epistemic uncertainty is involved in the estimation of $D_N(\tau|\mathbf{a}_N, \mathbf{e}_M)$. As a result and given an LHS

$$\mathbf{e}_i = [\mathbf{e}_{Ai}, \mathbf{e}_{Mi}], i = 1, 2, \ldots, nLHS, \qquad \text{(Eq. J5-2)}$$

from $\mathcal{E}$ of the form indicated in Equation J4.9-1, the expected value, CDF and CCDF for $D_N(\tau|\mathbf{a}_N, \mathbf{e}_M)$ that derive from epistemic uncertainty conditional on the occurrence of the nominal scenario class can be estimated as indicated in Equations J4.9-5 – J4.9-7 by

$$\begin{aligned} \bar{\bar{D}}_N(\tau|\mathbf{a}_N) &= E_E\left[D_N(\tau|\mathbf{a}_N, \mathbf{e}_M)\right] \\ &= \int_{\mathcal{E}} D_N(\tau|\mathbf{a}_N, \mathbf{e}_M)\, d_E(\mathbf{e})\, dE \\ &\cong \sum_{i=1}^{nLHS} D_N(\tau|\mathbf{a}_N, \mathbf{e}_{Mi}) / nLHS, \end{aligned} \qquad \text{(Eq. J5-3)}$$

$$\begin{aligned} p_E\left[D_N(\tau|\mathbf{a}_N, \mathbf{e}_M) \le D\right] &= \int_{\mathcal{E}} \underline{\delta}_D\left[D_N(\tau|\mathbf{a}_N, \mathbf{e}_M)\right] d_E(\mathbf{e})\, dE \\ &\cong \sum_{i=1}^{nLHS} \underline{\delta}_D\left[D_N(\tau|\mathbf{a}_N, \mathbf{e}_{Mi})\right] / nLHS \end{aligned} \qquad \text{(Eq. J5-4)}$$

and

$$p_E\left[D < D_N\left(\tau|\mathbf{a}_N, \mathbf{e}_M\right)\right] = \int_{\mathcal{E}} \underline{\delta}_D\left[D_N\left(\tau|\mathbf{a}_N, \mathbf{e}_M\right)\right] d_E(\mathbf{e})\,dE$$
$$\cong \sum_{i=1}^{nLHS} \underline{\delta}_D\left[D_N\left(\tau|\mathbf{a}_N, \mathbf{e}_{Mi}\right)\right] / nLHS, \qquad \text{(Eq. J5-5)}$$

respectively, with $\underline{\delta}_D[\sim]$ and $\overline{\delta}_D[\sim]$ defined as indicated in Equations J4.2-7 and J4.2-3. Quantiles (e.g., q = 0.05, 0.5, 0.95) characterizing epistemic uncertainty in the dose $D_N(\tau|\mathbf{a}_N, \mathbf{e}_M)$ associated with the nominal scenario class can be obtained from the probabilities defined and then approximated in Equation J5-4. Specifically, the q quantile value $Q_q[D_N(\tau|\mathbf{a}_N, \mathbf{e}_M)]$ for the distribution of $D_N(\tau|\mathbf{a}_N, \mathbf{e}_M)$ at time τ over the possible values for $\mathbf{e} = [\mathbf{e}_A, \mathbf{e}_M]$ is formally defined to be the value of D such that

$$q = \int_{\mathcal{E}} \underline{\delta}_D\left[D_N\left(\tau|\mathbf{a}_N, \mathbf{e}_M\right)\right] d_E(\mathbf{e})\,dE \qquad \text{(Eq. J5-6)}$$

and in computational practice is the value of D in the summation in Equation J5-4 for which $p_E[D_N(\tau|\mathbf{a}_N, \mathbf{e}_M) \le D]$ most closely equals q. Equivalently, $Q_q[D_N(\tau|\mathbf{a}_N, \mathbf{e}_M)]$ is the value of D such that

$$1 - q = \int_{\mathcal{E}} \overline{\delta}_D\left[D_N\left(\tau|\mathbf{a}_N, \mathbf{e}_M\right)\right] d_E(\mathbf{e})\,dE \qquad \text{(Eq. J5-7)}$$

and correspondingly is the value of D in the summation in Equation J5-5 for which $p_E[D \le D_N(\tau|\mathbf{a}_N, \mathbf{e}_M)]$ most closely equals $1 - q$.

To support the calculations indicated in conjunction with Equations J5-2 – J5-7, the GoldSim component of the TSPA-LA model calculates and saves

$$D_N\left(\tau|\mathbf{a}_N, \mathbf{e}_{Mi}\right) \qquad \text{(Eq. J5-8)}$$

for $0 \le \tau \le 10^6$ yr and all values of $\mathbf{e}_{Mi}$. In addition, a large number of intermediate results are also saved.

A summary of the resultant dose calculations is given in Figure J5-1. Specifically, Figure J5-1a shows all 300 dose curves (i.e., $D_N(\tau|\mathbf{a}_N, \mathbf{e}_{Mi})$ for $0 \le \tau \le 10^6$ yr and i = 1, 2, …, $nLHS$ = 300); Figure J5-1b shows the first 50 dose curves (i.e., $D_N(\tau|\mathbf{a}_N, \mathbf{e}_{Mi})$ for $0 \le \tau \le 10^6$ yr and i = 1, 2, …, 50; Figure J5-1c shows the expected (mean) value for dose at 6.0×10^5 yr, the CCDF for dose at 6.0×10^5 yr, and selected quantiles for dose at 6.0×10^5 yr (i.e., $\overline{\overline{D}}_N(\tau|\mathbf{a}_N)$, $p_E[D < D_N(6.0 \times 10^5 \text{ yr}|\mathbf{a}_N, \mathbf{e}_M)]$ and $Q_q[D_N(6.0 \times 10^5 \text{ yr}|\mathbf{a}_N, \mathbf{e}_M)]$, q = 0.05, 0.5, 0.95, estimated from $D_N(6.0 \times 10^5 \text{ yr}|\mathbf{a}_N, \mathbf{e}_{Mi})$, i = 1, 2, …, $nLHS$ = 300); and Figure J5-1d shows expected (mean) dose and quantile curves as a function of time (i.e., $\overline{\overline{D}}_N(\tau)$ and $Q_q[D_N(\tau|\mathbf{a}_N, \mathbf{e}_M)]$, q = 0.05, 0.5, 0.95, estimated from $D_N(\tau|\mathbf{a}_N, \mathbf{e}_{Mi})$, i = 1, 2, …, $nLHS$ = 300, for $0 \le \tau \le 10^6$ yr).

The results in Figure J5-1 are conditional on the occurrence of the nominal scenario class $\mathcal{A}_N$ and thus do not incorporate the probability $p_A(\mathcal{A}_N|\mathbf{e}_A)$ of $\mathcal{A}_N$. Because the probability of the seismic ground motion scenario class $\mathcal{A}_{SG}$ is effectively one for the time interval [0, 10^6 yr], the corresponding probability for $\mathcal{A}_N$ is effectively zero (see Section J8.8). However, because nominal processes affect the evolution of the repository and its performance in the seismic scenario class, nominal processes and associated doses are included in the calculation of dose from seismic ground motion events for the time interval [0, 10^6 yr] (see Section J8.4).

Figure J5-1 is in a standard format that is used to summarize the dose results for each scenario class. This format permits (i) display of results for all LHS elements for completeness and results for 50 LHS elements for enhanced resolution of individual dose curves, (ii) selection of a scale on the ordinate that enhances the resolution of individual dose curves, (iii) illustration of the determination of quantiles from a CCDF, and (iv) display of expected (mean) and quantile curves.

In turn, a standardized and more compact display is used to summarize dose results for presentation outside this appendix (Figure J5-2). This display shows all dose curves, the expected (mean) dose curve, and quantile curves in the same plot frame. Further, the same range of values is used on the ordinate for all summary figures of this type. This standardization facilitates the comparison of results across scenario classes but reduces the resolution in the results for individual scenario classes. In contrast, the format used in Figure J5-1 provides better resolution for individual scenario classes but is less convenient for the comparison of results across scenario classes.

Dose $D_N(\tau|\mathbf{a}_N, \mathbf{e}_M)$ to the RMEI is just one of a large number of results that are produced and presented in the TSPA-LA. For example, $D_N(\tau|\mathbf{a}_N, \mathbf{e}_M)$ is defined by the sum

$$D_N\left(\tau|\mathbf{a}_N, \mathbf{e}_M\right) = \sum_{r=1}^{nRS} D_{Nr}\left(\tau|\mathbf{a}_N, \mathbf{e}_M\right), \tag{J5-9}$$

where

nRS = number of radioactive species potentially causing dose to the RMEI,

$D_{Nr}\left(\tau|\mathbf{a}_N, \mathbf{e}_M\right)$ = dose to RMEI (mrem/yr) at time τ for radioactive species r resulting from nominal conditions.

In turn, quantities such as $\bar{\bar{D}}_{Nr}(\tau|\mathbf{a}_N)$, $p_E[D_{Nr}(\tau|\mathbf{a}_N, \mathbf{e}_M) \le D]$, $p_E[D < D_{Nr}(\tau|\mathbf{a}_N, \mathbf{e}_M)]$ and $Q_q[D_{Nr}(\tau|\mathbf{a}_N, \mathbf{e}_M)]$ can be determined for each radioactive species in exactly the same manner as $\bar{\bar{D}}_N(\tau|\mathbf{a}_N)$, $p_E[D_N(\tau|\mathbf{a}_N, \mathbf{e}_M) \le D]$, $p_E[D < D_N(\tau|\mathbf{a}_N, \mathbf{e}_M)]$ and $Q_q[D_N(\tau|\mathbf{a}_N, \mathbf{e}_M)]$ are determined in Equations J5-3 – J5-7.

As an example, a summary of the resultant dose calculations for ^{129}I is given in Figure J5-3, which has exactly the same organization as Figure J5-1. Overall, ^{129}I is the largest contributor to the expected (mean) dose $\bar{\bar{D}}_N(\tau|\mathbf{a}_N)$.

Results of the form shown in Figure J5-3 can be obtained for each radioactive species under consideration. This results in too many figures for a complete presentation. A compact summary of this large amount of information is provided by presenting the expected (mean) doses $\bar{\bar{D}}_{Nr}(\tau|\mathbf{a}_N)$ for all radioactive species in a single plot (Figure J5-4). The curve labeled "Total" in Figure J5-4 corresponds to the expected (mean) dose $\bar{\bar{D}}_N(\tau|\mathbf{a}_N)$ previously presented in Figures J5-1 and J5-2. The remaining curves correspond to expected (mean) doses $\bar{\bar{D}}_{Nr}(\tau|\mathbf{a}_N)$ for individual radioactive species.

As discussed in Section J4.10, the numerical stability of results obtained with Latin hypercube sampling can be assessed with replicated sampling. Specifically, the analysis for nominal conditions was performed with the $nRL = 3$ replicated LHSs indicated in Equation J4.10-1. In turn, this analysis shows that the numerical error in using Latin hypercube sampling to estimate $\bar{\bar{D}}_N(\tau|\mathbf{a}_N)$ is small relative to the epistemic uncertainty associated with the possible values for $D_N(\tau|\mathbf{a}_N, \mathbf{e}_M)$ (Figure J5-5).

Further descriptions of the nominal scenario class $\mathcal{A}_N$ and sources of additional information are available in Section 6.3.

J6 EARLY FAILURE SCENARIO CLASSES: $\mathcal{A}_E$, $\mathcal{A}_{EW}$ AND $\mathcal{A}_{ED}$

J6.1 Relationships Involving $\mathcal{A}_E$, $\mathcal{A}_{EW}$ and $\mathcal{A}_{ED}$

The early WP failure scenario class and the early DS failure scenario class are defined by the sets

$$\mathcal{A}_{EW} = \{\mathbf{a} : \mathbf{a} \in \mathcal{A} \text{ and } nEW \geq 1\} \quad \text{(Eq. J6.1-1)}$$

and

$$\mathcal{A}_{ED} = \{\mathbf{a} : \mathbf{a} \in \mathcal{A} \text{ and } nED \geq 1\} \quad \text{(Eq. J6.1-2)}$$

as indicated in Equations J4.4-13 and J4.4-14. Further, the combined early failure scenario class $\mathcal{A}_E$ is defined by

$$\mathcal{A}_E = \mathcal{A}_{EW} \cup \mathcal{A}_{ED} = \{\mathbf{a} : \mathbf{a} \in \mathcal{A} \text{ and } nEW + nED \geq 1\}. \quad \text{(Eq. J6.1-3)}$$

Then, $p_A(\mathcal{A}_{EW})$ is the probability of one or more early WP failures; $p_A(\mathcal{A}_{ED})$ is the probability of one or more early DS failures; and $p_A(\mathcal{A}_E)$ is the probability of one or more early failures.

The subsets $\mathcal{A}_{EW}$ and $\mathcal{A}_{ED}$ of $\mathcal{A}$ are not disjoint. For the early WP failure scenario class and the early DS failure scenario class to be disjoint from both each other and also from the scenario classes $\mathcal{A}_{II}$, $\mathcal{A}_{IE}$, $\mathcal{A}_{SG}$ and $\mathcal{A}_{SF}$ defined in Equations J4.4-15 – J4.4-18 requires their definitions to be based on the sets

$$\tilde{\mathcal{A}}_{EW} = \{\mathbf{a} : \mathbf{a} \in \mathcal{A},\ nEW \geq 1 \text{ and } nED = nII = nIE = nSG = nSF = 0\} \quad \text{(Eq. J6.1-4)}$$

and

$$\tilde{\mathcal{A}}_{ED} = \{\mathbf{a} : \mathbf{a} \in \mathcal{A},\ nED \geq 1 \text{ and } nEW = nII = nIE = nSG = nSF = 0\}, \quad \text{(Eq. J6.1-5)}$$

respectively. In turn,

$$p_A\left(\tilde{\mathcal{A}}_{EW}\right) = p_A\left(\mathcal{A}_{EW}\right) p_A\left(\{\mathbf{a} : \mathbf{a} \in \mathcal{A} \text{ and } nED = nII = nIE = nSG = nSF = 0\}\right) \quad \text{(Eq. J6.1-6)}$$

and

$$p_A\left(\tilde{\mathcal{A}}_{ED}\right) = p_A\left(\mathcal{A}_{ED}\right) p_A\left(\{\mathbf{a} : \mathbf{a} \in \mathcal{A} \text{ and } nEW = nII = nIE = nSG = nSF = 0\}\right) \quad \text{(Eq. J6.1-7)}$$

under the assumption that the occurrences of early WP failure and early DS failure are independent of both each other and also the other types of disruption under consideration. Specifically, $p_A(\tilde{\mathcal{A}}_{EW})$ is the probability that one or more early WP failures occur and also that no other disruptive events take place, and $p_A(\tilde{\mathcal{A}}_{ED})$ is the probability that one or more early DS failures occur and also that no other disruptive events take place.

When the second term in the products in Equations J6.1-6 and J6.1-7 is small, then $p_A(\tilde{\mathcal{A}}_{EW})$ and $p_A(\tilde{\mathcal{A}}_{ED})$ will be much smaller than $p_A(\mathcal{A}_{EW})$ and $p_A(\mathcal{A}_{ED})$. For this reason, it is the probabilities $p_A(\mathcal{A}_{EW})$ and $p_A(\mathcal{A}_{ED})$ for the scenario classes $\mathcal{A}_{EW}$ and $\mathcal{A}_{ED}$ that are usually of interest rather than the probabilities $p_A(\tilde{\mathcal{A}}_{EW})$ and $p_A(\tilde{\mathcal{A}}_{ED})$ for the more restricted (and disjoint) scenario classes $\tilde{\mathcal{A}}_{EW}$ and $\tilde{\mathcal{A}}_{ED}$. If the question is asked "What is the probability of early WP failure?", then most likely $p_A(\mathcal{A}_{EW})$ is the desired answer. Similarly, if the question is asked "What is the probability of early DS failure?", then most likely the desired answer is $p_A(\mathcal{A}_{ED})$. It is very unlikely that the desired answers are $p_A(\tilde{\mathcal{A}}_{EW})$ and $p_A(\tilde{\mathcal{A}}_{ED})$ as these probabilities provide little useful information about the likelihood of early WP and early DS failures.

No synergisms are assumed to exist between the doses that result from early WP failures and early DS failures. Further, as indicated in conjunction with Equation J4.5-1, no synergisms are assumed to exist between doses that result from early failures and doses that result from other disruptions. As a result,

$$D_E\left(\tau | \mathbf{a}, \mathbf{e}_M\right) = D_{EW}\left(\tau | \mathbf{a}, \mathbf{e}_M\right) + D_{ED}\left(\tau | \mathbf{a}, \mathbf{e}_M\right), \quad \text{(Eq. J6.1-8)}$$

where

$D_E(\tau|\mathbf{a}, \mathbf{e}_M)$ = dose to RMEI (mrem/yr) at time τ resulting from early failures associated with element $\mathbf{a}$ of $\mathcal{A}_E$,

$D_{EW}(\tau|\mathbf{a}, \mathbf{e}_M)$ = dose to RMEI (mrem/yr) at time τ resulting from early WP failures associated with element $\mathbf{a}$ of $\mathcal{A}_E$,

$D_{ED}(\tau|\mathbf{a}, \mathbf{e}_M)$ = dose to RMEI (mrem/yr) at time τ resulting from early DS failures associated with element $\mathbf{a}$ of $\mathcal{A}_E$,

and all results are conditional on the element $\mathbf{e} = [\mathbf{e}_A, \mathbf{e}_M]$ of $\mathcal{E}$. If $\mathbf{a}$ involves no early WP failures (i.e., if $nEW = 0$ or, equivalently, if $\mathbf{a} \notin \mathcal{A}_{EW}$), then $D_{EW}(\tau|\mathbf{a}, \mathbf{e}_M) = 0$; similarly, if $\mathbf{a}$ involves no early DS failures (i.e., if $nED = 0$ or, equivalently, if $\mathbf{a} \notin \mathcal{A}_{ED}$), then $D_{ED}(\tau|\mathbf{a}, \mathbf{e}_M) = 0$.

In turn, the expected dose $\bar{D}_E(\tau|\mathbf{e})$ to the RMEI (mrem/yr) at time τ from early failures is given by

$$\begin{aligned}\bar{D}_E(\tau|\mathbf{e}) &= \int_{\mathcal{A}_E} D_E(\tau|\mathbf{a}, \mathbf{e}_M)\, d_A(\mathbf{a}|\mathbf{e}_A)\, \mathrm{d}A \\ &= \int_{\mathcal{A}_E} \left[D_{EW}(\tau|\mathbf{a}, \mathbf{e}_M) + D_{ED}(\tau|\mathbf{a}, \mathbf{e}_M)\right] d_A(\mathbf{a}|\mathbf{e}_A)\, \mathrm{d}A \\ &= \int_{\mathcal{A}_E} D_{EW}(\tau|\mathbf{a}, \mathbf{e}_M)\, d_A(\mathbf{a}|\mathbf{e}_A)\, \mathrm{d}A + \int_{\mathcal{A}_E} D_{ED}(\tau|\mathbf{a}, \mathbf{e}_M)\, d_A(\mathbf{a}|\mathbf{e}_A)\, \mathrm{d}A \\ &= \bar{D}_{EW}(\tau|\mathbf{e}) + \bar{D}_{ED}(\tau|\mathbf{e}),\end{aligned} \qquad \text{(Eq. J6.1-9)}$$

where (i)

$$\begin{aligned}\bar{D}_{EW}(\tau|\mathbf{e}) &= \int_{\mathcal{A}_E} D_{EW}(\tau|\mathbf{a}, \mathbf{e}_M)\, d_A(\mathbf{a}|\mathbf{e}_A)\, \mathrm{d}A \\ &= \int_{\mathcal{A}_{EW}} D_{EW}(\tau|\mathbf{a}, \mathbf{e}_M)\, d_A(\mathbf{a}|\mathbf{e}_A)\, \mathrm{d}A\end{aligned} \qquad \text{(Eq. J6.1-10)}$$

is the expected dose to the RMEI (mrem/yr) at time τ resulting from early WP failures as previously indicated in Equation J4.5-9, (ii)

$$\begin{aligned}\bar{D}_{ED}(\tau|\mathbf{e}) &= \int_{\mathcal{A}_E} D_{ED}(\tau|\mathbf{a}, \mathbf{e}_M)\, d_A(\mathbf{a}|\mathbf{e}_A)\, \mathrm{d}A \\ &= \int_{\mathcal{A}_{ED}} D_{ED}(\tau|\mathbf{a}, \mathbf{e}_M)\, d_A(\mathbf{a}|\mathbf{e}_A)\, \mathrm{d}A\end{aligned} \qquad \text{(Eq. J6.1-11)}$$

is the expected dose to the RMEI (mrem/yr) at time τ resulting from early DS failures as previously indicated in Equation J4.5-10, and (iii) all results are conditional on the element $\mathbf{e} = [\mathbf{e}_A, \mathbf{e}_M]$ of $\mathcal{E}$. The conversion from an integral over $\mathcal{A}_E$ to an integral over $\mathcal{A}_{EW}$ in Equation

J6.1-10 is possible because $D_{EW}(\tau|\mathbf{a}, \mathbf{e}_M) = 0$ if $\mathbf{a} \notin \mathcal{A}_{EW}$; similarly, the conversion from an integral over $\mathcal{A}_E$ to an integral over $\mathcal{A}_{ED}$ in Equation J6.1-11 is possible because $D_{ED}(\tau|\mathbf{a}, \mathbf{e}_M) = 0$ if $\mathbf{a} \notin \mathcal{A}_{ED}$.

The general form of the elements $\mathbf{a}$ of $\mathcal{A}$ is shown in Equations J4.4-1 – J4.4-8. However, because no synergisms between disruptions are assumed in the determination of $\bar{D}_{EW}(\tau|\mathbf{e})$ and $\bar{D}_{ED}(\tau|\mathbf{e})$, the representations for the elements of $\mathcal{A}_{EW}$ and $\mathcal{A}_{ED}$ can be simplified to

$$\mathbf{a}_{EW} = \left[nEW, \mathbf{a}_{EW,1}, \mathbf{a}_{EW,2}, \ldots, \mathbf{a}_{EW,nEW} \right] \qquad \text{(Eq. J6.1-12)}$$

and

$$\mathbf{a}_{ED} = \left[nED, \mathbf{a}_{ED,1}, \mathbf{a}_{ED,2}, \ldots, \mathbf{a}_{ED,nED} \right], \qquad \text{(Eq. J6.1-13)}$$

respectively. With this notation, the elements $\mathbf{a}_{EW}$ of $\mathcal{A}_{EW}$ only contain representations for early WP failures, and the elements $\mathbf{a}_{ED}$ of $\mathcal{A}_{ED}$ only contain representations for early DS failures.

The preceding representations for $\mathbf{a}_{EW}$ and $\mathbf{a}_{ED}$ lead to computationally useful representations for the doses $D_{EW}(\tau|\mathbf{a}, \mathbf{e}_M)$ and $D_{ED}(\tau|\mathbf{a}, \mathbf{e}_M)$. Specifically,

$$\begin{aligned} D_{EW}\left(\tau|\mathbf{a}, \mathbf{e}_M\right) &= D_{EW}\left(\tau|\mathbf{a}_{EW}, \mathbf{e}_M\right) \\ &= \sum_{j=1}^{nEW} D_{EW}\left(\tau|\left[1, \mathbf{a}_{EW,j}\right], \mathbf{e}_M\right) \end{aligned} \qquad \text{(Eq. J6.1-14)}$$

provided (i) $\mathbf{a}_{EW}$ as defined in Equation J6.1-12 characterizes the early WP failures associated with $\mathbf{a}$, (ii) there are no synergisms between the doses associated with individual early WP failures, and (iii) $D_{EW}(\tau|[1, \mathbf{a}_{EW,j}], \mathbf{e}_M)$ equals the dose to the RMEI (mrem/yr) at time τ from an early failed WP with properties defined by $\mathbf{a}_{EW,j}$. Similarly,

$$\begin{aligned} D_{ED}\left(\tau|\mathbf{a}, \mathbf{e}_M\right) &= D_{ED}\left(\tau|\mathbf{a}_{ED}, \mathbf{e}_M\right) \\ &= \sum_{j=1}^{nED} D_{ED}\left(\tau|\left[1, \mathbf{a}_{ED,j}\right], \mathbf{e}_M\right) \end{aligned} \qquad \text{(Eq. J6.1-15)}$$

provided (i) $\mathbf{a}_{ED}$ as defined in Equation J6.1-13 characterizes the early DS failures associated with $\mathbf{a}$, (ii) there are no synergisms between doses associated with individual early DS failures, and (iii) $D_{ED}(\tau|[1, \mathbf{a}_{ED,j}], \mathbf{e}_M)$ equals the dose to the RMEI (mrem/yr) at time τ from an early failed DS with properties defined by $\mathbf{a}_{ED,j}$. The preceding representations for $D_{EW}(\tau|\mathbf{a}, \mathbf{e}_M)$ and $D_{ED}(\tau|\mathbf{a}, \mathbf{e}_M)$ play a fundamental role in the numerical calculation of $\bar{D}_{EW}(\tau|\mathbf{e})$ and $\bar{D}_{ED}(\tau|\mathbf{e})$.

The expected (mean) dose $\bar{\bar{D}}_E(\tau)$ for the early failure scenario class $\mathcal{A}_E$ over both aleatory and epistemic uncertainty is given by

$$\begin{aligned}\bar{\bar{D}}_E(\tau) &= \int_{\mathcal{E}} \bar{D}_E(\tau|\mathbf{e})\, d_E(\mathbf{e})\, \mathrm{d}E \\ &= \int_{\mathcal{E}} \left[\bar{D}_{EW}(\tau|\mathbf{e}) + \bar{D}_{ED}(\tau|\mathbf{e})\right] d_E(\mathbf{e})\, \mathrm{d}E \\ &= \int_{\mathcal{E}} \bar{D}_{EW}(\tau|\mathbf{e})\, d_E(\mathbf{e})\, \mathrm{d}E + \int_{\mathcal{E}} \bar{D}_{ED}(\tau|\mathbf{e})\, d_E(\mathbf{e})\, \mathrm{d}E \\ &= \bar{\bar{D}}_{EW}(\tau) + \bar{\bar{D}}_{ED}(\tau), \end{aligned} \quad \text{(Eq. J6.1-16)}$$

where

$$\bar{\bar{D}}_{EW}(\tau) = \int_{\mathcal{E}} \bar{D}_{EW}(\tau|\mathbf{e})\, d_E(\mathbf{e})\, \mathrm{d}E \quad \text{(Eq. J6.1-17)}$$

is the expected (mean) dose for the early WP failure scenario class $\mathcal{A}_{EW}$ over both aleatory and epistemic uncertainty as defined in Equation J4.6-5 for $C = EW$ and

$$\bar{\bar{D}}_{ED}(\tau) = \int_{\mathcal{E}} \bar{D}_{ED}(\tau|\mathbf{e})\, d_E(\mathbf{e})\, \mathrm{d}E \quad \text{(Eq. J6.1-18)}$$

is the expected (mean) dose for the early DS failure scenario class $\mathcal{A}_{ED}$ over both aleatory and epistemic uncertainty as defined in Equation J4.5-6 for $C = ED$.

The CCDF and CDF for $\bar{D}_E(\tau|\mathbf{e})$ over epistemic uncertainty are defined by

$$\begin{aligned} p_E\left[D < \bar{D}_E(\tau|\mathbf{e})\right] &= \int_{\mathcal{E}} \bar{\delta}_D\left[\bar{D}_E(\tau|\mathbf{e})\right] d_E(\mathbf{e})\, \mathrm{d}E \\ &= \int_{\mathcal{E}} \bar{\delta}_D\left[\bar{D}_{EW}(\tau|\mathbf{e}) + \bar{D}_{ED}(\tau|\mathbf{e})\right] d_E(\mathbf{e})\, \mathrm{d}E \end{aligned} \quad \text{(Eq. J6.1-19)}$$

and

$$\begin{aligned} p_E\left[\bar{D}_E(\tau|\mathbf{e}) \le D\right] &= 1 - p_E\left[D < \bar{D}_E(\tau|\mathbf{e})\right] \\ &= \int_{\mathcal{E}} \underline{\delta}_D\left[\bar{D}_E(\tau|\mathbf{e})\right] d_E(\mathbf{e})\, \mathrm{d}E \\ &= \int_{\mathcal{E}} \underline{\delta}_D\left[\bar{D}_{EW}(\tau|\mathbf{e}) + \bar{D}_{ED}(\tau|\mathbf{e})\right] d_E(\mathbf{e})\, \mathrm{d}E, \end{aligned} \quad \text{(Eq. J6.1-20)}$$

respectively. However, unlike the result for $\bar{\bar{D}}_E(\tau)$ in Equation J6.1-16, the CCDF and CDF for $\bar{D}_E(\tau|\mathbf{e})$ cannot be decomposed into a sum of separate results for the early WP failure scenario class $\mathcal{A}_{EW}$ and the early DS failure scenario class $\mathcal{A}_{ED}$.

Direct evaluation of the integrals that define $\bar{\bar{D}}_E(\tau)$, $p_E[D < \bar{D}_E(\tau|\mathbf{e})]$ and $p_E[\bar{D}_E(\tau|\mathbf{e}) \le D]$ is not practical. However, the approximations

$$\bar{\bar{D}}_E(\tau) \cong \sum_{i=1}^{nLHS} \bar{D}_E(\tau|\mathbf{e}_i)/nLHS, \qquad \text{(Eq. J6.1-21)}$$

$$p_E\left[D < \bar{D}_E(\tau|\mathbf{e})\right] \cong \sum_{i=1}^{nLHS} \bar{\delta}_D\left[\bar{D}_E(\tau|\mathbf{e}_i)\right]/nLHS \qquad \text{(Eq. J6.1-22)}$$

and

$$p_E\left[\bar{D}_E(\tau|\mathbf{e}) \le D\right] \cong \sum_{i=1}^{nLHS} \underline{\delta}_D\left[\bar{D}_E(\tau|\mathbf{e}_i)\right]/nLHS \qquad \text{(Eq. J6.1-23)}$$

result with use of the LHS in Equation J4.9-1 as previously indicated in conjunction with Equations J4.9-8 – J4.9-10.

Further descriptions of the early failure scenario classes $\mathcal{A}_E$, $\mathcal{A}_{EW}$ and $\mathcal{A}_{ED}$ and sources of additional information are available in Section 6.4.

J6.2 Early WP Failure Scenario Class: $\mathcal{A}_{EW}$

In the TSPA-LA, the individual vectors $\mathbf{a}_{EW,j}$, j = 1, 2, …, nEW, appearing in the definition of $\mathbf{a}_{EW}$ in Equation J6.1-12 are defined by

$$\mathbf{a}_{EW,j} = \left[t_j, b_j, d_j\right] \qquad \text{(Eq. J6.2-1)}$$

and characterize the properties of failed WP j, where t_j designates WP type (i.e., t_j = 1 ~ CSNF WP, t_j = 2 ~ CDSP WP), b_j designates percolation bin in which the failed WP is located (i.e., b_j = k ~ location of failed WP in percolation bin k for k = 1, 2, 3, 4, 5), and d_j designates whether the failed WP experiences nondripping or dripping conditions (i.e., d_j = 0 ~ nondripping conditions and d_j = 1 ~ dripping conditions).

The following quantities are available in the TSPA-LA for the characterization of the probability of early WP failure results of the form defined by $\mathbf{a}_{EW,j}$ in Equation J6.2-1 and hence for use in the determination of $\bar{D}_{EW}(\tau|\mathbf{a}, \mathbf{e})$:

nWP = number of WPs in repository,

nWT = number of WP types (i.e., CSNFs, CDSPs, …),

fWT_r = fraction of WPs of type r, r = 1, 2, …, nWT,

pWT_r = probability that a randomly selected WP of type r, r = 1, 2, …, nWT, will experience an early failure (element of $\mathbf{e}_A$),

nBN = number of percolation bins used for early failure calculations,

fBN_{rs} = fraction of WPs of type r, r = 1, 2, …, nWT, in bin s, s = 1, 2, …, nBN,

$fDRP_{rs}$ = fraction of WPs of type r, r = 1, 2, …, nWT, in bin s, s = 1, 2, …, nBN, experiencing dripping conditions (function of $\mathbf{e}_M$).

The probability pWT_r that a randomly selected WP will experience an early failure constitutes the defining parameter for a binomial probability distribution (see Equations J3.6-22 to J3.6-25) and is treated as being epistemically uncertain in the TSPA, with this uncertainty characterized by a lognormal distribution. In the TSPA-LA, the probability pWT_r is assumed to be the same for CSNF and CDSP WPs (i.e., $pW = pWT_1 = pWT_2$). A different value for this probability (i.e., pW_i) is selected in each LHS element $\mathbf{e}_i = [\mathbf{e}_{Ai}, \mathbf{e}_{Mi}]$ indicated in Equation J4.9-1. In turn, this results in $nLHS$ = 300 CCDFs for the possible number of early WP failures (Figure J6.2-1). No upper bound was specified for pW; as a result, large values are possible if the upper tail of the specified lognormal distribution is sampled. An occurrence of this type can be seen in the outlier CCDF in Figure 6.2-1a.

For a given LHS element $\mathbf{e}_i = [\mathbf{e}_{Ai}, \mathbf{e}_{Mi}]$ of the form indicated in Equation J4.9-1, the expected dose $\bar{D}_{EW}(\tau|\mathbf{e}_i)$ is now given by

$$\begin{aligned}\bar{D}_{EW}\left(\tau|\mathbf{e}_i\right) &= \int_{\mathcal{A}_{EW}} D_{EW}\left(\tau|\mathbf{a}, \mathbf{e}_{Mi}\right) d_A\left(\mathbf{a}|\mathbf{e}_{Ai}\right) \mathrm{d}A \\ &= \sum_{r=1}^{nWT} \sum_{s=1}^{nBN} \sum_{t=0}^{1} pWT_{ri}\ fWT_r\ fBN_{rs}\ pDRP_{rsti}\ nWP\ D_{EW}\left(\tau|[1, r, s, t], \mathbf{e}_{Mi}\right) \\ &= \sum_{r=1}^{2} \sum_{s=1}^{5} \sum_{t=0}^{1} pWT_{ri}\ fWT_r\ fBN_{rs}\ pDRP_{rsti}\ nWP\ D_{EW}\left(\tau|[1, r, s, t], \mathbf{e}_{Mi}\right),\end{aligned}$$

(Eq. J6.2-2)

where (i)

$$pDRP_{rsti} = \begin{cases} 1 - fDRP_{rsi} & \text{if } t = 0 \\ fDRP_{rsi} & \text{if } t = 1 \end{cases}$$

and (ii) the final equality results when nWT = 2 WP types (i.e., CSNFs and CDSPs) and nBN = 5 percolation bins are under consideration, which corresponds to the values for nWT and nBN used in the TSPA-LA. As previously indicated, the probability of early failure is assumed to be the same for the two WP types; thus, $pW_i = pWT_{1i} = pWT_{2i}$.

In turn, the estimates for $\bar{D}_{EW}(\tau|\mathbf{e}_i)$ can be used to estimate $\bar{\bar{D}}_{EW}(\tau)$, $p_E[\bar{D}_{EW}(\tau|\mathbf{e}) \le D]$ and $p_E[D < \bar{\bar{D}}_{EW}(\tau|\mathbf{e})]$. Specifically,

$$\bar{\bar{D}}_{EW}(\tau) \cong \sum_{i=1}^{nLHS} \bar{D}_{EW}(\tau|\mathbf{e}_i)/nLHS, \qquad \text{(Eq. J6.2-3)}$$

$$p_E\left[\bar{D}_{EW}(\tau|\mathbf{e}) \le D\right] \cong \sum_{i=1}^{nLHS} \underline{\delta}_D\left[\bar{D}_{EW}(\tau|\mathbf{e}_i)\right]/nLHS \qquad \text{(Eq. J6.2-4)}$$

and

$$p_E\left[D < \bar{D}_{EW}(\tau|\mathbf{e})\right] \cong \sum_{i=1}^{nLHS} \bar{\delta}_D\left[\bar{D}_{EW}(\tau|\mathbf{e}_i)\right]/nLHS, \qquad \text{(Eq. J6.2-5)}$$

as indicated in Equations J4.9-8 – J4.9-10, where $\bar{\delta}_D(\sim)$ and $\underline{\delta}_D(\sim)$ are defined in Equations J4.2-3 and J4.2-7, respectively. Further, quantiles $Q_q[\bar{D}_{EW}(\tau|\mathbf{e})]$ for $\bar{D}_{EW}(\tau|\mathbf{e})$ can obtained by solving either

$$q = \int_{\mathcal{A}_{EW}} \underline{\delta}_D\left[\bar{D}_{EW}(\tau|\mathbf{e})\right] d_E(\mathbf{e})\,\mathrm{d}E \qquad \text{(Eq. J6.2-6)}$$

or

$$1-q = \int_{\mathcal{A}_{EW}} \bar{\delta}_D\left[\bar{D}_{EW}(\tau|\mathbf{e})\right] d_E(\mathbf{e})\,\mathrm{d}E \qquad \text{(Eq. J6.2-7)}$$

for D. In practice, the solution of Equation J6.2-6 or Equation J6.2-7 to determine D, and hence $Q_q[\bar{D}_{EW}(\tau|\mathbf{e})]$, is based on the approximating sums in Equations J6.2-4 and J6.2-5.

The determination of $\bar{D}_{EW}(\tau|\mathbf{e}_i)$ as indicated in Equation J6.2-2 requires the evaluation of

$$D_{EW}(\tau|[1, r, s, t], \mathbf{e}_{Mi}) \qquad \text{(Eq. J6.2-8)}$$

in GoldSim for selected values of τ, r = 1, 2, …, nWT, s = 1, 2, …, nBN, t = 0, 1, and $\mathbf{e}_{Mi}$, i = 1, 2, …, $nLHS$. The fractions $fDRP_{rst}$ are also determined in GoldSim and are functions of $\mathbf{e}_{Mi}$. Further, a large number of intermediate results are also generated and saved.

The results indicated in conjunction with Equation J6.2-8 were calculated twice, once for the time interval [0, 2.0×10^4 yr] and once for the time interval [0, 10^6 yr]. Owing to its shorter length, results for the 20,000 yr time interval were saved with use of shorter timesteps (i.e., more closely spaced values for τ) than used to compute results for the 10^6 yr time interval. Specifically, timesteps of 10, 40 and 80 yr were used for the 20,000 yr time interval, and timesteps of 250, 500, 1000, 2000 and 4000 yr were used for the 10^6 yr time interval.

Results obtained for the 20,000 yr time interval are presented first; corresponding results for the 10^6 yr time interval are presented at the end of this section. As a result of the consideration of

nWT = 2 waste types, nBN = 5 percolation bins, and $nDRP$ = 2 dripping conditions, (2)(5)(2) = 20 dose calculations are performed by GoldSim for each LHS element. As an example, the values for $D_{EW}(\tau|[1, r, 3, t], \mathbf{e}_{Mi})$ obtained for r = 1, 2, t = 0, 1, and i = 1, 2, …, $nLHS$ = 300 are presented in Figure J6.2-2. Specifically, Figure J6.2-2 shows the epistemic uncertainty in dose to the RMEI that results from the early failure of one WP under four conditions: (i) one early failed CSNF WP in bin 3 under nondripping conditions (Figure J6.2-2a), (ii) one early failed CSNF WP in bin 3 under dripping conditions (Figure J6.2-2b), (iii) one early failed CDSP WP in bin 3 under nondripping conditions (Figure J6.2-2c), and (iv) one early failed CDSP WP in bin 3 under dripping conditions (Figure J6.2-2d).

Only 4 of the 20 dose results calculated by GoldSim for each LHS element are presented in Figure J6.2-2. An alternate presentation format is to use box plots to summarize all 20 dose results in a single figure (Figure J6.2-3). Specifically, Figure J6.2-3 shows the 10 dose results calculated for CSNF WPs at three times (i.e., 10,000, 15,000, 20,000 yr) and the 10 dose results calculated for CDSP WPs at three times (i.e., 2000, 5000, 10,000 yr). Different presentation times are used for CSNF and CDSP WPs because the dose results for CSNF WPs are effectively zero prior to 10,000 yr (Figures J6.2-2a,b and J6.2-3a). Figure J6.2-3 does not present individual dose results at the same level of temporal resolution as Figure J6.2-2. However, Figure J6.2-3 has two important properties. First, it summarizes all 20 dose results in a single figure. Second, the horizontal presentation of the box plots facilitates comparison of dose results obtained under different conditions.

Once the dose results indicated in Equation J6.2-8 and illustrated in Figures J6.2-2 and J6.2-3 are available, $\bar{D}_{EW}(\tau|\mathbf{e}_i)$ can be estimated for each LHS element $\mathbf{e}_i$ as shown in Equation J6.2-2. As an example, the resultant estimate $\bar{D}_{EW}(\tau|\mathbf{e}_1)$ for LHS element $\mathbf{e}_1$ is shown in Figure J6.2-4.

A summary of the calculations involving $\bar{D}_{EW}(\tau|\mathbf{e})$ for all LHS elements is given in Figure J6.2-5. Specifically, Figure J6.2-5a shows all 300 expected dose curves (i.e., $\bar{D}_{EW}(\tau|\mathbf{e}_i)$ for $0 \le \tau \le 20{,}000$ yr and i = 1, 2, …, $nLHS$ = 300); Figure J6.2-5b shows the first 50 expected dose curves (i.e., $\bar{D}_{EW}(\tau|\mathbf{e}_i)$ for $0 \le \tau \le 20{,}000$ yr and i = 1, 2, …, 50); Figure J6.2-5c shows the expected (mean) value, the CCDF and selected quantiles for expected dose at 10,000 yr (i.e., $\bar{\bar{D}}_{EW}(10^4 \text{ yr})$, $p_E[D < \bar{D}_{EW}(10^4 \text{ yr}|\mathbf{e})]$ and $Q_q[\bar{D}_{EW}(10^4 \text{ yr}|\mathbf{e})]$, q = 0.05, 0.5, 0.95, estimated from $\bar{D}_{EW}(10^4 \text{ yr}|\mathbf{e}_i)$, i = 1, 2, …, $nLHS$ = 300); and Figure J6.2-5d shows expected (mean) dose and quantile curves as functions of time (i.e., $\bar{\bar{D}}_{EW}(\tau)$ and $Q_q[\bar{D}_{EW}(\tau|\mathbf{e})]$, q = 0.05, 0.5, 0.95, estimated from $\bar{D}_{EW}(\tau|\mathbf{e}_i)$, i = 1, 2, …, $nLHS$ = 300, for $0 \le \tau \le 20{,}000$ yr).

In turn, the results in Figure J6.2-5 can be summarized in the standard format appearing in Figure J6.2-6. As discussed in conjunction with Figures J5-1 and J5-2, the format in Figure J6.2-5 facilitates the presentation of results for individual scenario classes, and the format in Figure J6.2-6 facilitates the comparison of results across scenario classes.

As previously discussed in conjunction with Equation J5-9 and illustrated in Figures J5-3 and J5-4 for nominal conditions, dose and expected dose to the RMEI is just one of a large number of

results that can be produced and presented in the TSPA-LA. Similarly to $D_N(\tau|\mathbf{a}_N, \mathbf{e}_M)$ in Equation J5-9, the dose $D_C(\tau|\mathbf{a}_C, \mathbf{e}_M)$ to the RMEI for an arbitrary scenario class C (e.g., $C \in \{EW, ED, II, IE, SG, SF\}$) is defined by the sum

$$D_C\left(\tau|\mathbf{a}_C, \mathbf{e}_M\right) = \sum_{r=1}^{nRS} D_{Cr}\left(\tau|\mathbf{a}_C, \mathbf{e}_M\right), \qquad \text{(Eq. J6.2-9)}$$

where

nRS = number of radioactive species potentially causing dose to the RMEI,

$D_{Cr}\left(\tau|\mathbf{a}_C, \mathbf{e}_M\right)$ = dose to RMEI (mrem/yr) at time τ for radioactive species r resulting from conditions associated with scenario class C.

In turn, quantities such as $\bar{D}_{Cr}(\tau|\mathbf{e})$, $p_E[\bar{D}_{Cr}(\tau|\mathbf{e}) \le D]$, $p_E[D < \bar{D}_{Cr}(\tau|\mathbf{e})]$, $Q_q[\bar{D}_{Cr}(\tau|\mathbf{e})]$ and $\bar{\bar{D}}_{Cr}(\tau)$ can be determined for each radioactive species in exactly the same manner as $\bar{D}_C(\tau|\mathbf{e})$, $p_E[\bar{D}_C(\tau|\mathbf{e}) \le D]$, $p_E[D < \bar{D}_C(\tau|\mathbf{e})]$, $Q_q[\bar{D}_C(\tau|\mathbf{e})]$ and $\bar{\bar{D}}_C(\tau)$). For this section, $C = EW$, and the determinations for $\bar{D}_{EW,r}(\tau|\mathbf{e})$, $p_E[\bar{D}_{EW,r}(\tau|\mathbf{e}) \le D]$, $p_E[D < \bar{D}_{EW,r}(\tau|\mathbf{e})]$, $Q_q[\bar{D}_{EW,r}(\tau|\mathbf{e})]$ and $\bar{\bar{D}}_{EW,r}(\tau)$ are made in the same manner as the presented determinations for $\bar{D}_{EW}(\tau|\mathbf{e})$, $p_E[\bar{D}_{EW}(\tau|\mathbf{e}) \le D]$, $p_E[D < \bar{D}_{EW}(\tau|\mathbf{e})]$, $Q_q[\bar{D}_{EW}(\tau|\mathbf{e})]$ and $\bar{\bar{D}}_{EW}(\tau)$.

As an example, a summary of the resultant dose calculations for ^{99}Tc is given in Figure J6.2-7, which has the same organization as Figure J6.2-5. Overall, ^{99}Tc is the largest contributor to the expected (mean) dose $\bar{\bar{D}}_{EW}(\tau)$ for the 20,000 yr time period.

Results of the form shown in Figure J6.2-7 can be obtained for each radioactive species under consideration. This results in too many figures for a complete presentation. As previously done in Figure J5-4 for nominal conditions, a compact summary of this large amount of information is provided by presenting the expected (mean) doses $\bar{\bar{D}}_{EW,r}(\tau)$ for all radioactive species in a single plot (Figure J6.2-8). The curve labeled "Total" in Figure J6-8 corresponds to the expected (mean) dose $\bar{\bar{D}}_{EW}(\tau)$ previously presented in Figures J6.2-5 and J6.2-6. The remaining curves correspond to expected (mean) doses $\bar{\bar{D}}_{EW,r}(\tau)$ for individual radioactive species.

Once the results in Equation J6.2-8 are available, Monte Carlo procedures can also be used to estimate $\bar{D}_{EW}(\tau|\mathbf{e}_i)$, the CDF for $D_{EW}(\tau|\mathbf{a}, \mathbf{e}_{Mi})$, and the CCDF for $D_{EW}(\tau|\mathbf{a}, \mathbf{e}_{Mi})$. Specifically,

$$\bar{D}_{EW}\left(\tau|\mathbf{e}_i\right) \cong p_A\left(\mathcal{A}_{EW}|\mathbf{e}_{Ai}\right)\sum_{k=1}^{nR} D_{EW}\left(\tau|\mathbf{a}_{EW,k},\mathbf{e}_{Mi}\right)\Big/nR$$

$$= p_A\left(\mathcal{A}_{EW}|\mathbf{e}_{Ai}\right)\sum_{k=1}^{nR}\left\{\sum_{j=1}^{nEW_k} D_{EW}\left(\tau|\left[1,t_{jk},b_{jk},d_{jk}\right],\mathbf{e}_{Mi}\right)\right\}\Big/nR, \qquad \text{(Eq. J6.2-10)}$$

$$p_A\left[D_{EW}\left(\tau|\mathbf{a},\mathbf{e}_{Mi}\right)\le D\middle|\mathbf{e}_{Ai}\right] \cong p_A\left(\mathcal{A}_{EW}|\mathbf{e}_{Ai}\right)\sum_{k=1}^{nR}\underline{\delta}_D\left[D_{EW}\left(\tau|\mathbf{a}_{EW,k},\mathbf{e}_{Mi}\right)\right]\Big/nR$$

$$= p_A\left(\mathcal{A}_{EW}|\mathbf{e}_{Ai}\right)\sum_{k=1}^{nR}\underline{\delta}_D\left\{\sum_{j=1}^{nEW_k} D_{EW}\left(\tau|\left[1,t_{jk},b_{jk},d_{jk}\right],\mathbf{e}_{Mi}\right)\right\}\Big/nR \qquad \text{(Eq. J6.2-11)}$$

and

$$p_A\left[D < D_{EW}\left(\tau|\mathbf{a},\mathbf{e}_{Mi}\right)\middle|\mathbf{e}_{Ai}\right] \cong p_A\left(\mathcal{A}_{EW}|\mathbf{e}_{Ai}\right)\sum_{k=1}^{nR}\bar{\delta}_D\left[D_{EW}\left(\tau|\mathbf{a}_{EW,k},\mathbf{e}_{Mi}\right)\right]\Big/nR$$

$$= p_A\left(\mathcal{A}_{EW}|\mathbf{e}_{Ai}\right)\sum_{k=1}^{nR}\bar{\delta}_D\left\{\sum_{j=1}^{nEW_k} D_{EW}\left(\tau|\left[1,t_{jk},b_{jk},d_{jk}\right],\mathbf{e}_{Mi}\right)\right\}\Big/nR, \qquad \text{(Eq. J6.2-12)}$$

as indicated in Equations J4.5-19 – J4.5-21 with $C = EW$, where (i)

$$\mathbf{a}_{EW,k} = \left[nEW_k, \mathbf{a}_{EW,1k}, \mathbf{a}_{EW,2k}, \ldots, \mathbf{a}_{EW,nEW_k,k}\right], k = 1, 2, \ldots, nR,$$

is a random sample from vectors $\mathbf{a}_{EW}$ of the form defined in Equation J6.1-12 generated in consistency with fWT_r, pWT_r, fBN_{rs} and $fDRP_{rs}$ and the assumption that nEW is greater than zero, (ii)

$$\mathbf{a}_{EW,jk} = \left[t_{jk}, b_{jk}, d_{jk}\right]$$

for j = 1, 2, …, nEW_k, and (iii) the indicator functions $\bar{\delta}_D(\sim)$ and $\underline{\delta}_D(\sim)$ are defined in Equations J4.2-3 and (J4.2-7), respectively.

As an example, Figure J6.2-9a shows the CCDF for the dose $D_{EW}(10^4 \text{ yr}|\mathbf{a}_{EW}, \mathbf{e}_{M1})$ to the RMEI at $\tau = 10^4$ yr obtained with LHS element $\mathbf{e}_1$. Specifically, the CCDF in Figure J6.2-9a is a plot of the exceedance probabilities $p_A[D < D_{EW}(10^4 \text{ yr}|\mathbf{a}, \mathbf{e}_{M1})|\mathbf{e}_{A1}]$ defined in Equation J6.2-12 and obtained with a random sample of size $nR = 10^4$ from $\mathcal{A}_{EW}$. In turn, the sampled results used in the construction of the CCDF in Figure J6.2-9a can be reduced to an estimate for the expected

dose $\bar{D}_{EW}(10^4 \text{ yr}|\mathbf{e}_1)$ as indicated in Equation J6.2-10 and illustrated in Figure J6.2-9b. Specifically, Figure J6.2-9b shows the expected dose curve $\bar{D}_{EW}(\tau|\mathbf{e}_1)$, $0 \le \tau \le 20{,}000$ yr, previously presented in Figure J6.2-4 and the value $\bar{D}_{EW}(10^4 \text{ yr}|\mathbf{e}_1)$ calculated with the indicated Monte Carlo procedure. As can be seen, the value for $\bar{D}_{EW}(\tau|\mathbf{e}_1)$ produced by the Monte Carlo procedure is effectively the same as the value for $\bar{D}_{EW}(\tau|\mathbf{e}_1)$ produced by integration procedures. As a result, repeating the Monte Carlo estimation procedure for a sequence of values for τ would result in an estimate for $\bar{D}_{EW}(\tau|\mathbf{e}_1)$ for $0 \le \tau \le 20{,}000$ yr that is effectively the same as the estimate that appears in Figures J6.2-4 and J6.2-9b. The integration-based approach to estimate $\bar{D}_{EW}(\tau|\mathbf{e})$ has the advantage of numerical efficiency but does not provide estimates of CCDFs of the form shown in Figure J6.2-9a. In contrast, the sampling-based approach $\bar{D}_{EW}(\tau|\mathbf{e})$ is less efficient numerically but provides CCDFs that summarize the effects of aleatory uncertainty.

The CCDF in Figure J6.2-9a is for a single LHS element. As shown in Figure J6.2-10a,b, a different CCDF results for $D_{EW}(10^4 \text{ yr}|\mathbf{a}_{EW}, \mathbf{e}_{Mi})$ for each LHS element $\mathbf{e}_i = [\mathbf{e}_{Ai}, \mathbf{e}_{Mi}]$. Collectively, these CCDFs are displaying the epistemic uncertainty associated with the distribution of dose $D_{EW}(10^4 \text{ yr}|\mathbf{a}_{EW}, \mathbf{e}_{Mi})$ to the RMEI at $\tau = 10^4$ yr that results from the different possible values for $\mathbf{a}_{EW}$. In turn, the epistemic uncertainty associated with these CCDFs can be summarized by an expected (mean) CCDF and quantile curves constructed in a manner analogous to the construction of expected (mean) and quantile curves for expected dose $\bar{D}_{EW}(\tau|\mathbf{e})$ (Figure J6.2-10c). The expected (mean) dose $\bar{\bar{D}}_{EW}(10^4 \text{ yr})$ appearing in Figures J6.2-5, J6.2-6 and J6.2-8 is the result of reducing all the information in Figure J6.2-10a to single number (i.e., $\bar{\bar{D}}_{EW}(10^4 \text{ yr})$).

As discussed in Section J4.10, the numerical stability of results obtained with Latin hypercube sampling can be assessed with replicated sampling. Specifically, the analysis for early WP failure was performed with the $nRL = 3$ replicated LHSs indicated in Equation J4.10-1. In turn, this analysis shows that the numerical error in using Latin hypercube sampling to estimate $\bar{\bar{D}}_{EW}(\tau)$ is small relative to the epistemic uncertainty associated with the possible values for $\bar{\bar{D}}_{EW}(\tau|\mathbf{e})$ (Figure J6.2-11).

The results presented in Figures J6.2-2 to J6.2-11 are for the time period $[0, 2.0 \times 10^4 \text{ yr}]$. Corresponding results for the time period $[0, 10^6 \text{ yr}]$ are presented without discussion in Figures J6.2-12 to J6.2-21.

J6.3 Early DS Failure Scenario Class: $\mathcal{A}_{ED}$

The analyses for the early DS failure scenario class $\mathcal{A}_{ED}$ are structurally identical to the analyses for the early WP failure scenario class $\mathcal{A}_{EW}$. The individual elements $\mathbf{a}_{ED,j}$, $j = 1, 2, \ldots, nED$, appearing in the definition of $\mathbf{a}_{ED}$ in Equation J6.1-13 are defined by

$$\mathbf{a}_{ED,j} = \left[t_j, b_j, d_j \right] \qquad \text{(Eq. J6.3-1)}$$

and characterize the properties of failed DS j, where t_j designates WP type (i.e., $t_j = 1 \sim$ CSNF WP, $t_j = 2 \sim$ CDSP WP) underneath the failed DS, b_j designates the percolation bin in which the failed DS is located (e.g., $b_j = k \sim$ location of failed DS in bin k for $k = 1, 2, 3, 4, 5$), and d_j designates whether the failed DS experiences nondripping or dripping conditions (i.e., $d_j = 0 \sim$ nondripping conditions and $d_j = 1 \sim$ dripping conditions).

The quantities nWP, nWT, fWT_r, nBN, fBN_{rs} and $fDRP_{rst}$ are the same as in Section J6.2 and the additional quantity

pD = probability that a randomly selected DS will experience an early failure (element of $\mathbf{e}_A$)

characterizes the occurrence of early DS failure and is analogous to pWT_r. Specifically, early DS failure is assumed to be characterized by a binomial probability model defined by pD (see Equations J3.6-22 to J3.6-25). A different value for pD is selected in each LHS element $\mathbf{e}_i = [\mathbf{e}_{Ai}, \mathbf{e}_{Mi}]$ indicated in Equation J4.9-1. In turn, this results in $nLHS = 300$ CCDFs for the possible number of early DS failures (Figure J6.3-1).

For a given LHS element $\mathbf{e}_i = [\mathbf{e}_{Ai}, \mathbf{e}_{Mi}]$ of the form defined in Equation J4.9-1, the expected dose $\bar{D}_{ED}(\tau|\mathbf{e}_i)$ from early DS failure is given by

$$\begin{aligned}
\bar{D}_{ED}\left(\tau|\mathbf{e}_i\right) &= \int_{\mathcal{A}_{ED}} D_{ED}\left(\tau|\mathbf{a}, \mathbf{e}_{Mi}\right) d_A\left(\mathbf{a}|\mathbf{e}_{Ai}\right) \mathrm{d}A \\
&= \sum_{r=1}^{nWT} \sum_{s=1}^{nBN} \sum_{t=0}^{1} pD_i \; fWT_r \; fBN_{rs} \; pDRP_{rsti} \; nWP \; D_{ED}\left(\tau|[1, r, s, t], \mathbf{e}_{Mi}\right) \\
&= \sum_{r=1}^{2} \sum_{s=1}^{5} \sum_{t=1}^{1} pD_i \; fWT_r \; fBN_{rs} \; pDRP_{rsti} \; nWP \; D_{ED}\left(\tau|[1, r, s, t], \mathbf{e}_{Mi}\right) \\
&= \sum_{r=1}^{2} \sum_{s=1}^{5} pD_i \; fWT_r \; fBN_{rs} \; pDRP_{rs1i} \; nWP \; D_{ED}\left(\tau|[1, r, s, 1], \mathbf{e}_{Mi}\right) \qquad \text{(Eq. J6.3-2)}
\end{aligned}$$

where (i) $pDRP_{rsti}$ is defined in conjunction with Equation J6.2-2, (ii) the third equality results when $nWT = 2$ WP types (i.e., CSNFs and CDSPs) and $nBN = 5$ percolation bins are under consideration, which corresponds to the values for nWT and nBN in the TSPA-LA, and (iii) the fourth and final equality results because releases are only assumed to take place if the DS fails in the presence of dripping conditions, in which case the associated WP is assumed to fail due to localized corrosion.

The determination of $\bar{D}_{ED}(\tau|\mathbf{e}_i)$ as indicated in Equation J6.3-2 requires the evaluation of

$$D_{ED}\left(\tau|[1, r, s, t], \mathbf{e}_{Mi}\right) \qquad \text{(Eq. J6.3-3)}$$

in GoldSim for selected values of τ, $r = 1, 2, \ldots, nWT$, $s = 1, 2, \ldots, nBN$, $t = 1$, and $\mathbf{e}_{Mi}$, $i = 1, 2, \ldots, nLHS$. The fractions $fDRP_{rsti}$ are also determined in GoldSim and are functions of $\mathbf{e}_{Mi}$.

Similarly to the analysis for early WP failure, the results indicated in conjunction with Equation J6.3-3 were calculated twice, once for the time interval [0, 2.0×10^4 yr] and once for the time interval [0, 10^6 yr]. Owing to its shorter length, results for the 20,000 yr time interval were computed with use of shorter timesteps (i.e., more closely spaced values for τ) than used to compute results for the 10^6 yr time interval. Specifically, timesteps of 10, 40 and 80 yr were used for the 20,000 yr time interval, and timesteps of 250, 500, 1000, 2000 and 4000 yr were used for the 10^6 time interval.

Once the results in Equation J6.3-3 are available, $\bar{D}_{ED}(\tau|\mathbf{e}_i)$ can be determined as indicated in Equation J6.3-2. Further, additional results involving early DS failure can be determined in the same manner as corresponding results for early WP failure were determined in Section J6.2. For example $\bar{\bar{D}}_{ED}(\tau)$, $p_E[\bar{D}_{ED}(\tau|\mathbf{e}_i) \le D]$, $p_E[D < \bar{D}_{ED}(\tau|\mathbf{e})]$ and $Q_q[\bar{D}_{ED}(\tau|\mathbf{e})]$ can be determined in the same manner as $\bar{\bar{D}}_{EW}(\tau)$, $p_E[\bar{D}_{EW}(\tau|\mathbf{e}) \le D]$, $p_E[D < \bar{D}_{EW}(\tau|\mathbf{e})]$ and $Q_q[\bar{D}_{EW}(\tau|\mathbf{e})]$ in Equations J6.2-3 – J6.2-7.

For consistency, similar results are presented for early DS failure and early WP failure. Specifically, early DS failure results for $0 \le \tau \le 20{,}000$ yr are presented in Figures J6.3-2 to J6.3-11 and contain results analogous to the results presented in Figures J6.2-2 to J6.2-11 for early WP failure. Similarly, early DS failure results for $0 \le \tau \le 10^6$ yr are presented in Figures J6.3-12 to J6.3-21 and contain results analogous to the results presented in Figures J6.2-12 to J6.2-21 for early WP failure.

J6.4 Early Failure Scenario Class: $\mathcal{A}_E$

As indicated in Equation J6.1-9, the expected dose $\bar{D}_E(\tau|\mathbf{e})$ to the RMEI at time τ from early failures is given by the sum of the expected doses $\bar{D}_{EW}(\tau|\mathbf{e})$ and $\bar{D}_{ED}(\tau|\mathbf{e})$ from early WP failures and early DS failures. The result of this calculation is presented in Figures J6.4-1 and J6.4-2 for the 20,000 and 10^6 yr time intervals, respectively. The organization of Figures J6.4-1 and J6.4-2 is the same as the organization of Figure J6.2-5.

The expected dose resulting from nominal process failures and early failures of WPs and DSs is given by

$$\bar{D}_{NE}(\tau|\mathbf{e}) = D_N(\tau|\mathbf{a}_N, \mathbf{e}_M) + \bar{D}_{EW}(\tau|\mathbf{e}_M) + \bar{D}_{ED}(\tau|\mathbf{e}_M). \qquad \text{(Eq. J6.4-1)}$$

The result of this calculation is presented in Figure J6.4-3, which also has the same organization as Figure J6.2-5.

J6.5 Probabilities Associated with Early Failure Scenario Classes

The probabilities $p_A(\mathcal{A}_{EW}|\mathbf{e}_A)$, $p_A(\mathcal{A}_{ED}|\mathbf{e}_A)$ and $p_A(\mathcal{A}_E|\mathbf{e}_A)$ for the scenario classes $\mathcal{A}_{EW}$, $\mathcal{A}_{ED}$ and $\mathcal{A}_E$ conditional on the element $\mathbf{e} = [\mathbf{e}_A, \mathbf{e}_M]$ of $\mathcal{E}$ are given by

$$p_A\left(\mathcal{A}_{EW}\middle|\mathbf{e}_A\right) \cong 1-\exp\left[-(nWP)(pW)\right], \tag{Eq. J6.5-1}$$

$$p_A\left(\mathcal{A}_{ED}\middle|\mathbf{e}_A\right) \cong 1-\exp\left[-(nDS)(pD)\right] \tag{Eq. J6.5-2}$$

and

$$\begin{aligned} p_A\left(\mathcal{A}_E\middle|\mathbf{e}_A\right) &\cong 1-\exp\left[-(nWP)(pW)-(nDS)(pD)\right] \\ &= 1-\exp\left[-nWP(pW+pD)\right], \end{aligned} \tag{Eq. J6.5-3}$$

where nWP = 11,629 is the number of WPs in the repository, $nDS = nWP$ is the number of DSs (i.e., one DS for each WP), pW is the element of $\mathbf{e}_A$ that corresponds to the probability that an individual WP will experience an early failure, pD is the element of $\mathbf{e}_A$ that corresponds to the probability that an individual DS will experience an early failure, and the approximations in Equations J6.5-1, J6.5-2, and J6.5-3 follow from Equation J3.6-29. The values for $p_A(\mathcal{A}_{EW}|\mathbf{e}_{Ai})$, $p_A(\mathcal{A}_{ED}|\mathbf{e}_{Ai})$ and $p_A(\mathcal{A}_E|\mathbf{e}_{Ai})$ obtained for the LHS in Equation J4.9-1 are summarized in Figure J6.5-1.

J7 IGNEOUS SCENARIO CLASSES: $\mathcal{A}_I$, $\mathcal{A}_{II}$ AND $\mathcal{A}_{IE}$

J7.1 Relationships Involving $\mathcal{A}_I$, $\mathcal{A}_{II}$ and $\mathcal{A}_{IE}$

The igneous intrusive scenario class and the igneous eruptive scenario class are defined by the sets

$$\mathcal{A}_{II} = \{\mathbf{a} : \mathbf{a} \in \mathcal{A} \text{ and } nII \geq 1\} \tag{Eq. J7.1-1}$$

and

$$\mathcal{A}_{IE} = \{\mathbf{a} : \mathbf{a} \in \mathcal{A} \text{ and } nIE \geq 1\} \tag{Eq. J7.1-2}$$

as indicated in Equations J4.4-15 and J4.4-16. Further, the igneous scenario class $\mathcal{A}_I$ is defined by

$$\mathcal{A}_I = \mathcal{A}_{II} \cup \mathcal{A}_{IE} = \{\mathbf{a} : \mathbf{a} \in \mathcal{A} \text{ and } nII \geq 1\} = \mathcal{A}_{II} \tag{Eq. J7.1-3}$$

as indicated in Equation J4.4-11. The equality $\mathcal{A}_I = \mathcal{A}_{II}$ results because the occurrence of an igneous intrusive event is a necessary, but not sufficient, condition for the occurrence of an

igneous eruptive event in the TSPA-LA. In turn, $p_A(\mathcal{A}_I) = p_A(\mathcal{A}_{II})$ is the probability of one or more igneous intrusive events and $p_A(\mathcal{A}_{IE})$ is the probability of one or more igneous eruptive events.

The scenario classes $\mathcal{A}_{II}$ and $\mathcal{A}_{IE}$ are not disjoint. However, if the question is asked "What is the probability of an igneous event?" or "What is the probability of an igneous intrusive event?", then most likely $p_A(\mathcal{A}_{II}) = p_A(\mathcal{A}_I)$ is the desired answer. Similarly, if the question is asked "What is the probability of an igneous eruptive event?", then most likely $p_A(\mathcal{A}_{IE})$ is the desired answer. If desired, disjoint scenario classes involving igneous intrusive and igneous eruptive scenario classes and their associated probabilities can be defined in the same manner as indicated in Equations J6.1-4 – J6.1-7 for early WP failure and early DS failure. Although possible, such definitions are not very useful computationally.

No synergisms are assumed to exist between the doses that result from the intrusive damage to WPs and the doses that result from the eruptive releases to the atmosphere. Further, as indicated in conjunction with Equation J4.5-1, no synergisms are assumed to exist between doses that result from igneous events and doses that result from other disruptions. As a result,

$$D_I\left(\tau|\mathbf{a}, \mathbf{e}_M\right) = D_{II}\left(\tau|\mathbf{a}, \mathbf{e}_M\right) + D_{IE}\left(\tau|\mathbf{a}, \mathbf{e}_M\right), \qquad \text{(Eq. J7.1-4)}$$

where

$D_I(\tau|\mathbf{a}, \mathbf{e}_M)$ = dose to RMEI (mrem/yr) at time τ resulting from igneous events associated with element $\mathbf{a}$ of $\mathcal{A}$,

$D_{II}(\tau|\mathbf{a}, \mathbf{e}_M)$ = dose to RMEI (mrem/yr) at time τ resulting from intrusive damage to WPs for igneous events associated with element $\mathbf{a}$ of $\mathcal{A}$,

$D_{IE}(\tau|\mathbf{a}, \mathbf{e}_M)$ = dose to RMEI (mrem/yr) at time τ resulting from the eruptive releases to the atmosphere for igneous events associated with element $\mathbf{a}$ of $\mathcal{A}$,

and all results are conditional on the element $\mathbf{e} = [\mathbf{e}_A, \mathbf{e}_M]$ of $\mathcal{E}$. If $\mathbf{a}$ involves no igneous intrusive damage to WPs, then $D_{II}(\tau|\mathbf{a}, \mathbf{e}_M) = 0$; similarly, if $\mathbf{a}$ involves no eruptive releases to the atmosphere, then $D_{IE}(\tau|\mathbf{a}, \mathbf{e}_M) = 0$.

In turn, the expected dose $\bar{D}_I(\tau|\mathbf{e})$ to the RMEI (mrem/yr) at time τ is given by

$$\begin{aligned}
\bar{D}_I\left(\tau|\mathbf{e}\right) &= \int_{\mathcal{A}_I} D_I\left(\tau|\mathbf{a}, \mathbf{e}_M\right) d_A\left(\mathbf{a}|\mathbf{e}_A\right) \mathrm{d}A \\
&= \int_{\mathcal{A}_I} \left[D_{II}\left(\tau|\mathbf{a}, \mathbf{e}_M\right) + D_{IE}\left(\tau|\mathbf{a}, \mathbf{e}_M\right)\right] d_A\left(\mathbf{a}|\mathbf{e}_A\right) \mathrm{d}A \\
&= \int_{\mathcal{A}_I} D_{II}\left(\tau|\mathbf{a}, \mathbf{e}_M\right) d_A\left(\mathbf{a}|\mathbf{e}_A\right) \mathrm{d}A + \int_{\mathcal{A}_I} D_{IE}\left(\tau|\mathbf{a}, \mathbf{e}_M\right) d_A\left(\mathbf{a}|\mathbf{e}_A\right) \mathrm{d}A \\
&= \bar{D}_{II}\left(\tau|\mathbf{e}\right) + \bar{D}_{IE}\left(\tau|\mathbf{e}\right), \qquad \text{(Eq. J7.1-5)}
\end{aligned}$$

where (i)

$$\bar{D}_{II}(\tau|\mathbf{e}) = \int_{\mathcal{A}_I} D_{II}(\tau|\mathbf{a}, \mathbf{e}_M)\, d_A(\mathbf{a}|\mathbf{e}_A)\, \mathrm{d}A = \int_{\mathcal{A}_{II}} D_{II}(\tau|\mathbf{a}, \mathbf{e}_M)\, d_A(\mathbf{a}|\mathbf{e}_A)\, \mathrm{d}A \quad \text{(Eq. J7.1-6)}$$

is the expected dose to the RMEI (mrem/yr) at time τ resulting from igneous intrusive events, (ii)

$$\bar{D}_{IE}(\tau|\mathbf{e}) = \int_{\mathcal{A}_I} D_{IE}(\tau|\mathbf{a}, \mathbf{e}_M)\, d_A(\mathbf{a}|\mathbf{e}_A)\, \mathrm{d}A = \int_{\mathcal{A}_{IE}} D_{IE}(\tau|\mathbf{a}, \mathbf{e}_M)\, d_A(\mathbf{a}|\mathbf{e}_A)\, \mathrm{d}A \quad \text{(Eq. J7.1-7)}$$

is the expected dose to the RMEI (mrem/yr) at time τ resulting from igneous eruptive events, and (iii) all results are conditional on the element $\mathbf{e} = [\mathbf{e}_A, \mathbf{e}_M]$ of $\mathcal{E}$. The conversion from an integral over $\mathcal{A}_I$ to an integral over $\mathcal{A}_{II}$ in Equation J7.1-6 is only notational as $\mathcal{A}_I = \mathcal{A}_{II}$; the conversion from an integral over $\mathcal{A}_I$ to an integral over $\mathcal{A}_{IE}$ in Equation J7.1-7 is possible because $D_{IE}(\tau|\mathbf{a}, \mathbf{e}_M) = 0$ if $\mathbf{a} \notin \mathcal{A}_{IE}$.

The general form of the elements $\mathbf{a}$ of $\mathcal{A}$ is shown in Equations J4.4-1 – J4.4-8. However, because no synergisms between disruptions are assumed in the determination of $\bar{D}_{II}(\tau|\mathbf{e})$ and $\bar{D}_{IE}(\tau|\mathbf{e})$, the representations for the elements of $\mathcal{A}_{II}$ and $\mathcal{A}_{IE}$ can be simplified to

$$\mathbf{a}_{II} = \left[nII, \mathbf{a}_{II,1}, \mathbf{a}_{II,2}, \ldots, \mathbf{a}_{II,nII}\right] \quad \text{(Eq. J7.1-8)}$$

and

$$\mathbf{a}_{IE} = \left[nIE, \mathbf{a}_{IE,1}, \mathbf{a}_{IE,2}, \ldots, \mathbf{a}_{IE,nIE}\right], \quad \text{(Eq. J7.1-9)}$$

respectively. With this notation, the elements $\mathbf{a}_{II}$ of $\mathcal{A}_{II}$ only contain representations for igneous intrusive events, and the elements $\mathbf{a}_{IE}$ of $\mathcal{A}_{IE}$ only contain representations for igneous eruptive events.

The expected (mean) dose $\bar{\bar{D}}_I(\tau)$ for the igneous scenario class $\mathcal{A}_I$ over both aleatory and epistemic uncertainty is given by

$$\begin{aligned}\bar{\bar{D}}_I(\tau) &= \int_{\mathcal{E}} \bar{D}_I(\tau|\mathbf{e})\, d_E(\mathbf{e})\, \mathrm{d}E \\ &= \int_{\mathcal{E}} \left[\bar{D}_{II}(\tau|\mathbf{e}) + \bar{D}_{IE}(\tau|\mathbf{e})\right] d_E(\mathbf{e})\, \mathrm{d}E \\ &= \int_{\mathcal{E}} \bar{D}_{II}(\tau|\mathbf{e})\, d_E(\mathbf{e})\, \mathrm{d}E + \int_{\mathcal{E}} \bar{D}_{IE}(\tau|\mathbf{e})\, d_E(\mathbf{e})\, \mathrm{d}E \\ &= \bar{\bar{D}}_{II}(\tau) + \bar{\bar{D}}_{IE}(\tau), \end{aligned} \quad \text{(Eq. J7.1-10)}$$

where

$$\bar{\bar{D}}_{II}(\tau) = \int_{\mathcal{E}} \bar{D}_{II}(\tau|\mathbf{e})\, d_E(\mathbf{e})\, \mathrm{d}E \qquad \text{(Eq. J7.1-11)}$$

is the expected (mean) dose for the igneous intrusive scenario class $\mathcal{A}_{II}$ over both aleatory and epistemic uncertainty and

$$\bar{\bar{D}}_{IE}(\tau) = \int_{\mathcal{E}} \bar{D}_{IE}(\tau|\mathbf{e})\, d_E(\mathbf{e})\, \mathrm{d}E \qquad \text{(Eq. J7.1-12)}$$

is the expected (mean) dose for the igneous eruptive scenario class $\mathcal{A}_{IE}$ over both aleatory and epistemic uncertainty.

The CCDF and CDF for $\bar{D}_I(\tau|\mathbf{e})$ over epistemic uncertainty are defined by

$$\begin{aligned} p_E\left[D < \bar{D}_I(\tau|\mathbf{e})\right] &= \int_{\mathcal{E}} \bar{\delta}_D\left[\bar{D}_I(\tau|\mathbf{e})\right] d_E(\mathbf{e})\, \mathrm{d}E \\ &= \int_{\mathcal{E}} \bar{\delta}_D\left[\bar{D}_{II}(\tau|\mathbf{e}) + \bar{D}_{IE}(\tau|\mathbf{e})\right] d_E(\mathbf{e})\, \mathrm{d}E \end{aligned} \qquad \text{(Eq. J7.1-13)}$$

and

$$\begin{aligned} p_E\left[\bar{D}_I(\tau|\mathbf{e}) < D\right] &= 1 - p_E\left[\bar{D}_I(\tau|\mathbf{e})\right] \\ &= \int_{\mathcal{E}} \underline{\delta}_D\left[\bar{D}_I(\tau|\mathbf{e})\right] d_E(\mathbf{e})\, \mathrm{d}E \\ &= \int_{\mathcal{E}} \underline{\delta}_D\left[\bar{D}_{II}(\tau|\mathbf{e}) + \bar{D}_{IE}(\tau|\mathbf{e})\right] d_E(\mathbf{e})\, \mathrm{d}E, \end{aligned} \qquad \text{(Eq. J7.1-14)}$$

respectively. However, unlike the result for $\bar{\bar{D}}_I(\tau)$ in Equation J7.1-10, the CCDF and CDF for $\bar{D}_I(\tau|\mathbf{e})$ cannot be decomposed into a sum of separate results for the igneous intrusive scenario class $\mathcal{A}_{II}$ and the igneous eruptive scenario class $\mathcal{A}_{IE}$.

Direct evaluation of the integrals that define $\bar{\bar{D}}_I(\tau)$, $p_E[D < \bar{D}_I(\tau|\mathbf{e})]$ and $p_E[\bar{D}_I(\tau|\mathbf{e}) \le D]$ is not practicable. However, the approximations

$$\bar{\bar{D}}_I(\tau) \cong \sum_{i=1}^{nLHS} \bar{D}_I(\tau|\mathbf{e}_i)/nLHS, \qquad \text{(Eq. J7.1-15)}$$

$$p_E\left[D < \bar{D}_I(\tau|\mathbf{e})\right] \cong \sum_{i=1}^{nLHS} \bar{\delta}_D\left[\bar{D}_I(\tau|\mathbf{e}_i)\right]/nLHS \qquad \text{(Eq. J7.1-16)}$$

and

$$p_E\left[\bar{D}_I\left(\tau|\mathbf{e}\right)\le D\right]\cong\sum_{i=1}^{nLHS}\underline{\delta}_D\left[\bar{D}_I\left(\tau|\mathbf{e}_i\right)\right]/nLHS \qquad \text{(Eq. J7.1-17)}$$

result with use of the LHS in Equation J4.9-1 as previously indicated in conjunction with Equations J4.9-8 – J4.9-10.

Further descriptions of the igneous scenario classes $\mathcal{A}_I$, $\mathcal{A}_{II}$ and $\mathcal{A}_{IE}$ and sources of additional information are available in Section 6.5.

J7.2 Igneous Intrusive Scenario Class: $\mathcal{A}_{II}$

The aleatory futures **a** associated with the igneous intrusive scenario class $\mathcal{A}_{II}$ are defined by number of igneous intrusive events, the times of these events, and the number of WPs damaged by each of these events. Specifically, the individual vectors $\mathbf{a}_{II,j}$, j = 1, 2, …, nII, appearing in the definition of $\mathbf{a}_{II}$ in Equation J7.1-8 are defined by

$$\mathbf{a}_{II,j}=\left[t_j, nWD_j\right] \qquad \text{(Eq. J7.2-1)}$$

and characterize the properties of igneous intrusive event j, where t_j (yr) is the time of the event and nWD_j is the number of WPs damaged by the event.

Two quantities define the probabilities associated with $\mathcal{A}_{II}$:

λ_I = rate of occurrence (yr^{-1}) of igneous events that intersect the repository (element of $\mathbf{e}_A$),

$d_{II}(N)$ = density function for number N of WPs damaged by an igneous intrusive event (i.e., $N \sim nWD_j$ in Equation J7.2-1).

Specifically, the occurrence of igneous events that intersect the repository is assumed to follow a Poisson process defined by the rate λ_I. The TSPA-LA assumes that an igneous event that intersects the repository damages all nWP WPs in the repository. For this special situation, $d_{II}(N)$ is defined by

$$d_{II}\left(N\right)=\delta\left(N-nWP\right), \qquad \text{(Eq. J7.2-2)}$$

where $\delta(\sim)$ is the Dirac delta function. However, the general representation $d_{II}(N)$ for the density function for the number of damaged WPs will be used in the initial description of expected dose for the igneous intrusive scenario class $\mathcal{A}_{II}$ for notational generality.

Given λ_I, $d_{II}(N)$ and an LHS element $\mathbf{e}_i = [\mathbf{e}_{Ai}, \mathbf{e}_{Mi}]$ of the form defined in Equation J4.9-1, the expected dose $\bar{D}_{II}(\tau|\mathbf{e}_i)$ is given by

$$\bar{D}_{II}\left(\tau|\mathbf{e}_i\right) = \int_{\mathcal{A}_{II}} D_{II}\left(\tau|\mathbf{a}, \mathbf{e}_{Mi}\right) d_A\left(\mathbf{a}|\mathbf{e}_{Ai}\right) \mathrm{d}A$$
$$= \int_0^{\tau}\left[\int_{\mathcal{N}_{II}} D_{II}\left(\tau|[1, t, N], \mathbf{e}_{Mi}\right) d_{II}\left(N\right) \mathrm{d}N\right] \lambda_I \, \mathrm{d}t, \qquad \text{(Eq. J7.2-3)}$$

where

$\mathcal{N}_{II}$ = set of possible values for number N of damaged WPs consistent with the definition of $d_{II}(N)$,

$D_{II}\left(\tau|[1, t, N], \mathbf{e}_{Mi}\right)$ = dose to RMEI (mrem/yr) at time τ from a single igneous intrusive event that occurs at time t and damages N WPs.

The second integral in Equation J7.2-3 is predicated on the assumption that there are no synergisms between multiple igneous events associated with a given element **a** of $\mathcal{A}_{II}$, which is equivalent to the assumption that each event affects a different group of WPs. In practice, this is satisfied because the probability of the subset of $\mathcal{A}_{II}$ containing values of **a** with two or more igneous events (i.e., $nI \geq 2$) is small. However, because the TSPA-LA assumes that the first igneous event affects all WPs in the repository, Equation J7.2-3 produces a slight overestimate of $\bar{D}_{II}(\tau|\mathbf{e}_i)$.

The second integral in Equation J7.2-3 is based on the approximation

$$\bar{D}_{II}\left(\tau|\mathbf{e}_i\right) \cong \sum_{k=1}^{n}\left[\int_{\mathcal{N}_{II}} D_{II}\left(\tau|[1, t_k, N], \mathbf{e}_{Mi}\right) d_{II}\left(N\right) \mathrm{d}N\right] \lambda_I \Delta t_k, \qquad \text{(Eq. J7.2-4)}$$

where $0 = t_0 < t_1 < t_2 < \ldots < t_n = \tau$. The representation for $\bar{D}_{II}(\tau|\mathbf{e}_i)$ in the second integral in Equation J7.2-3 then results in the limit as $\Delta t_k \rightarrow 0$. Intuitively, $\lambda_I \Delta t_k$ can be thought of as the probability that an igneous event occurs in the time interval $[t_{k-1}, t_k]$. However, $\lambda_I \Delta t_k$ is actually the expected number of igneous events in the time interval $[t_{k-1}, t_k]$. As a result, the second integral representation for $\bar{D}_{II}(\tau|\mathbf{e}_i)$ includes the effects of multiple igneous events. However, as previously indicated, there is an underlying assumption that there are no synergisms between multiple events in a given element **a** of $\mathcal{A}_{II}$.

If it is desired to incorporate the effects of only the first igneous event in the time interval $[0, \tau]$ into $\bar{D}_{II}(\tau|\mathbf{e}_i)$, then the final representation in Equation J7.2-3 becomes

$$\bar{D}_{II}\left(\tau|\mathbf{e}_i\right) = \int_0^{\tau}\left[\int_{\mathcal{N}_{II}} D_{II}\left(\tau|[1, t, N], \mathbf{e}_{Mi}\right) d_{II}\left(N\right) \mathrm{d}N\right] \lambda_I \exp\left[-\lambda_I t\right] \mathrm{d}t. \qquad \text{(Eq. J7.2-5)}$$

The preceding representation for $\bar{D}_{II}(\tau|\mathbf{e}_i)$ derives from the approximation

$$\bar{D}_{II}\left(\tau|\mathbf{e}_i\right) \cong \sum_{k=1}^{n}\left\{\int_{\mathcal{N}_{II}} D_{II}\left(\tau|[1, t_k, N], \mathbf{e}_{Mi}\right) d_{II}\left(N\right) \mathrm{d}N\right\} \times\left\{\left[\exp\left(-\lambda_I t_{k-1}\right)\right]_1\left[\lambda_I \Delta t_k \exp\left(-\lambda_I \Delta t_k\right)\right]_2\right\}, \quad \text{(Eq. J7.2-6)}$$

where

$[\sim]_1$ = probability that no igneous event occurs before time t_{k-1},

$[\sim]_2$ = probability that exactly one igneous event occurs in the time interval Δt_k,

$[\sim]_1[\sim]_2$ = probability that first igneous event occurs in the time interval Δt_k,

and the t_k are defined the same as in Equation J7.2-4. The representation for $\bar{D}_{II}(\tau|\mathbf{e}_i)$ in Equation J7.2-5 then results in the limit as $\Delta t_k \rightarrow 0$.

When $d_{II}(N)$ has the simple form indicated in Equation J7.2-2 and used in the TSPA-LA, the representations for $\bar{D}_{II}(\tau|\mathbf{e}_i)$ in Equations J7.2-3 and J7.2-5 become

$$\bar{D}_{II}\left(\tau|\mathbf{e}_i\right) = \int_0^{\tau} D_{II}\left(\tau|[1, t, nWP], \mathbf{e}_{Mi}\right) \lambda_I \, \mathrm{d}t \quad \text{(Eq. J7.2-7)}$$

and

$$\bar{D}_{II}\left(\tau|\mathbf{e}_i\right) = \int_0^{\tau} D_{II}\left(\tau|[1, t, nWP], \mathbf{e}_{Mi}\right) \lambda_I \exp\left(-\lambda_I t\right) \mathrm{d}t, \quad \text{(Eq. J7.2-8)}$$

respectively. The representation for $\bar{D}_{II}(\tau|\mathbf{e}_i)$ in Equation J7.2-7 actually overestimates the expected value over aleatory uncertainty for $D_{II}(\tau|[1, t, nWP], \mathbf{e}_{Mi})$ because it incorporates the effects of multiple events that destroy all WPs in the repository. This overcounting of damaged WPs is corrected for in the representation for $\bar{D}_{II}(\tau|\mathbf{e}_i)$ in Equation J7.2-8. However, if the product $\lambda_I \tau$ is small, there is little difference in the values for the integrals in Equations J7.2-7 and J7.2-8. In turn, the corresponding quadrature approximations for $\bar{D}_{II}(\tau|\mathbf{e}_i)$ as defined in Equations J7.2-7 and J7.2-8 are

$$\bar{D}_{II}\left(\tau|\mathbf{e}_i\right) \cong \sum_{k=1}^{n} D_{II}\left(\tau|\left[1, \hat{t}_k, nWP\right], \mathbf{e}_{Mi}\right) \lambda_I \Delta \hat{t}_k \quad \text{(Eq. J7.2-9)}$$

and

$$\bar{D}_{II}\left(\tau|\mathbf{e}_i\right) \cong \sum_{k=1}^{n} D_{II}\left(\tau|\left[1, \hat{t}_k, nWP\right], \mathbf{e}_{Mi}\right) \lambda_I \exp\left(-\lambda_I \hat{t}_{k-1}\right) \Delta \hat{t}_k, \quad \text{(Eq. J7.2-10)}$$

respectively, where $0 = \hat{t}_0 < \hat{t}_1 < \ldots < \hat{t}_n = \tau$.

In situations where the dose $D_{II}(\tau|[1, t, N], \mathbf{e}_{Mi})$ varies linearly with N, a significant simplification to the representations for $\bar{D}_{II}(\tau|\mathbf{e}_i)$ in Equations J7.2-3 and J7.2-5 is possible. Specifically, the representation for $\bar{D}_{II}(\tau|\mathbf{e}_i)$ in Equation J7.2-3 becomes

$$\begin{aligned}\bar{D}_{II}\left(\tau|\mathbf{e}_i\right) &= \int_0^{\tau}\left[\int_{\mathcal{N}_{II}} D_{II}\left(\tau|[1,t,N],\mathbf{e}_{Mi}\right) d_{II}\left(N\right)\mathrm{d}N\right]\lambda_I\ \mathrm{d}t \\ &= \int_0^{\tau}\left[\int_{\mathcal{N}_{II}} \left(N/N_0\right) D_{II}\left(\tau|[1,t,N_0],\mathbf{e}_{Mi}\right) d_{II}\left(N\right)\mathrm{d}N\right]\lambda_I\ \mathrm{d}t \\ &= \left(\lambda_I \bar{N}/N_0\right)\int_0^{\tau} D_{II}\left(\tau|[1,t,N_0],\mathbf{e}_{Mi}\right)\mathrm{d}t, \end{aligned} \qquad \text{(Eq. J7.2-11)}$$

where N_0 is an arbitrary value for N and

$$\bar{N}_{II} = \int_{\mathcal{N}_{II}} N\, d_{II}\left(N\right)\mathrm{d}N$$

is the expected value for N. Similarly, the representation for $\bar{D}_{II}(\tau|\mathbf{e}_i)$ in Equation J7.2-5 becomes

$$\bar{D}_{II}\left(\tau|\mathbf{e}_i\right) = \left(\lambda_I \bar{N}_{II}/N_0\right)\int_0^{\tau} D_{II}\left(\tau|[1,t,N_0],\mathbf{e}_{Mi}\right)\exp\left(-\lambda_I t\right)\mathrm{d}t. \qquad \text{(Eq. J7.2-12)}$$

When the assumption of linearity in N can be justified, the representations for $\bar{D}_{II}(\tau|\mathbf{e}_i)$ in Equations J7.2-9 and J7.2-10 provide the basis for computational procedures for the approximation of $\bar{D}_{II}(\tau|\mathbf{e}_i)$ that are more efficient than computational procedures based on the representations in Equations J7.2-3 and J7.2-5.

In turn, the estimates for $\bar{D}_{II}(\tau|\mathbf{e}_i)$ can be used to estimate $\bar{\bar{D}}_{II}(\tau)$, $p_E[\bar{D}_{II}(\tau|\mathbf{e}) \le D]$ and $p_E[D < \bar{D}_{II}(\tau|\mathbf{e})]$. Specifically,

$$\bar{\bar{D}}_{II}\left(\tau\right) \cong \sum_{i=1}^{nLHS} \bar{D}_{II}\left(\tau|\mathbf{e}_i\right)/nLHS, \qquad \text{(Eq. J7.2-13)}$$

$$p_E\left[\bar{D}_{II}\left(\tau|\mathbf{e}\right) \le D\right] \cong \sum_{i=1}^{nLHS} \delta_D\left[\bar{D}_{II}\left(\tau|\mathbf{e}_i\right)\right]/nLHS \qquad \text{(Eq. J7.2-14)}$$

and

$$p_E\left[D < \bar{D}_{II}\left(\tau|\mathbf{e}\right)\right] \cong \sum_{i=1}^{nLHS} \bar{\delta}_D\left[\bar{D}_{II}\left(\tau|\mathbf{e}_i\right)\right]/nLHS, \qquad \text{(Eq. J7.2-15))}$$

as indicated in Equations J4.9-8 – J4.9-10, where $\bar{\delta}_D(\sim)$ and $\underline{\delta}_D(\sim)$ are defined in Equations J4.2-3 and J4.2-7, respectively. Further, quantiles $Q_q[\bar{D}_{II}(\tau|\mathbf{e})]$ for $\bar{D}_{II}(\tau|\mathbf{e})$ can be obtained by solving either

$$q = \int_{\mathcal{A}_{II}} \underline{\delta}_D\left[\bar{D}_{II}\left(\tau|\mathbf{e}\right)\right] d_E\left(\mathbf{e}\right) \mathrm{d}E \qquad \text{(Eq. J7.2-16)}$$

or

$$1-q = \int_{\mathcal{A}_{II}} \bar{\delta}_D\left[\bar{D}_{II}\left(\tau|\mathbf{e}\right)\right] d_E\left(\mathbf{e}\right) \mathrm{d}E \qquad \text{(Eq. J7.2-17)}$$

for D. In practice, the solution of Equation J7.2-16 or J7.2-17 to determine D, and hence $Q_q[\bar{D}_{II}(\tau|\mathbf{e})]$, is based on the approximating sums in Equations J7.2-14 and J7.2-15.

The TSPA-LA calculates $\bar{D}_{II}(\tau|\mathbf{e}_i)$ on the basis of the representation in Equation J7.2-7. To support this calculation, $D_{II}(\tau|[1, t, nWP], \mathbf{e}_{Mi})$ is evaluated with GoldSim for a selected sequence of times. Two cases are considered in TSPA-LA: events occurring over the time interval [0, 2.0×10^4 yr] and events occurring over the time interval [0, 1.0×10^6 yr]. For the time interval [0, 2.0×10^4 yr], the results

$$D_{II}\left(\tau\left|\left[1, t_k, nWP\right], \mathbf{e}_{Mi}\right.\right), k = 1, 2, \ldots, 10, i = 1, 2, \ldots, nLHS = 300, \qquad \text{(Eq. J7.2-18)}$$

are calculated for (i) $0 \le \tau \le 2.0 \times 10^4$ yr and (ii) t_k = 10, 100, 600, 1000, 2000, 4000, 6000, 10,000, 14,000 and 18,000 yr. For the time interval [0, 10^6 yr], the results indicated in Equation J7.2-18 are calculated for (i) $0 \le \tau \le 1.0 \times 10^6$ yr and (ii) t_k = 250, 600, 1000, 4000, 10,000, 40,000, 100,000, 200,000, 400,000 and 800,000 yr. The preceding results are then used in numerical integration procedures to evaluate the integral in Equation J2.7-7 over the time intervals [0, 2.0×10^4 yr] and [0, 1.0×10^6 yr] (see Equation J7.2-9).

Results for the 20,000 yr time interval are presented first; corresponding results for the 10^6 yr time interval are presented at the end of this section. As indicated in conjunction with Equation J2.2-18, the results for 20,000 yr are based on evaluations of $D_{II}(\tau|[1, t_k, nWP], \mathbf{e}_{Mi})$ for ten values of t_k. For illustration, the values obtained for $D_{II}(\tau|[1, t_k, nWP], \mathbf{e}_{Mi})$ are shown in Figure J7.2-1 for t_k = 10, 600, 2000, 4000, 6000 and 10,000 yr and i = 1, 2, …, $nLHS$ = 300.

The quadrature approximations for $\bar{D}_{II}(\tau|\mathbf{e}_i)$ indicated in Equations J7.2-9 and J7.2-10 are actually of the form

$$\bar{D}_{II}\left(\tau|\mathbf{e}_i\right) \cong \sum_{k=1}^{n} \hat{D}_{II}\left(\tau|\left[1, \hat{t}_k, nWP\right], \mathbf{e}_{Mi}\right) \lambda_I \Delta\hat{t}_k \qquad \text{(Eq. J7.2-19)}$$

and

$$\bar{D}_{II}\left(\tau|\mathbf{e}_i\right) \cong \sum_{k=1}^{n} \hat{D}_{II}\left(\tau|\left[1, \hat{t}_k, nWP\right], \mathbf{e}_{Mi}\right) \lambda_I \exp\left(-\lambda_I \hat{t}_{k-1}\right) \Delta\hat{t}_k \qquad \text{(Eq. J7.2-20)}$$

in the computational implementation of the TSPA-LA, where $\hat{D}(\tau|[1, \hat{t}_k, nWP], \mathbf{e}_{Mi})$ is an approximation to $D(\tau|[1, \hat{t}_k, nWP], \mathbf{e}_{Mi})$ obtained from interpolations employing the values for $D(\tau|[1, t_k, nWP], \mathbf{e}_{Mi})$ obtained with GoldSim for the 10 values for t_k indicated in conjunction with Equation J7.2-18 (Figure J7.2-2).

Once the dose results indicated in Equation J7.2-18 are available, $\bar{D}_{II}(\tau|\mathbf{e}_i)$ can be approximated with the quadrature procedures indicated in Equations J7.2-19 and J7.2-20, with $\hat{D}_{II}(\tau|[1, \hat{t}_k, nWP], \mathbf{e}_{Mi})$ determined through interpolation as illustrated in Figure J7.2-2. As an example, the resultant estimate $\bar{D}_{II}(\tau|\mathbf{e}_1)$ for LHS element $\mathbf{e}_1$ is shown in Figure J7.2-3.

A summary of the calculations involving $\bar{D}_{II}(\tau|\mathbf{e})$ for all LHS elements is given in Figure J7.2-4. Specifically, Figure J7.2-4a shows all 300 expected dose curves (i.e., $\bar{D}_{II}(\tau|\mathbf{e}_i)$ for $0 \le \tau \le$ 20,000 yr and i = 1, 2, …, $nLHS$ = 300); Figure J7.2-4b shows the first 50 expected dose curves (i.e., $\bar{D}_{II}(\tau|\mathbf{e}_i)$ for $0 \le \tau \le$ 20,000 yr and i = 1, 2, …, 50); Figure J7.2-4c shows the CCDF and selected quantiles for expected dose at 10,000 yr (i.e., $p_E[D < \bar{D}_{II}(10^4 \text{ yr}|\mathbf{e})]$ and $Q_q[\bar{D}_{II}(10^4 \text{ yr}|\mathbf{e})]$, q = 0.05, 0.5, 0.95, estimated from $\bar{D}_{II}(10^4 \text{ yr}|\mathbf{e}_i)$, i = 1, 2, …, $nLHS$ = 300); and Figure J7.2-4d shows expected (mean) dose and quantile curves as a function of time (i.e., $\bar{D}_{II}(\tau)$ and $Q_q[\bar{D}_{II}(\tau|\mathbf{e})]$, q = 0.05, 0.5, 0.95, estimated from $\bar{D}_{II}(\tau|\mathbf{e}_i)$, i = 1, 2, …, $nLHS$ = 300, for $0 \le \tau \le$ 20,000 yr).

In turn, the results in Figure J7.2-4 can be summarized in the standard format appearing in Figure J7.2-5. As discussed in conjunction with Figures J5-1 and J6-2, the format in Figure J7.2-4 facilitates the presentation of results for individual scenario classes, and the format in Figure J7.2-5 facilitates the comparison of results across scenario classes.

As previously discussed in conjunction with Equations J5-9 and J6.2-9, dose and expected dose to the RMEI are just two of a large number of results that can be produced and presented in the TSPA-LA. As an example, a summary of the resultant dose calculations for ^{99}Tc is given in Figure J7.2-6, which has exactly the same organization as Figure J7.2-4. Overall, ^{99}Tc is one of the largest contributors to the expected (mean) dose $\bar{\bar{D}}_{II}(\tau)$ for the 20,000 yr time period.

Results of the form shown in Figure J7.2-6 can be obtained for each radioactive species under consideration. This results in too many results for a complete presentation. As previously done in Figure J5-4 and other similar figures, a compact summary of this large amount of information is provided by presenting the expected (mean) dose $\bar{\bar{E}}_{II,r}(\tau)$ for each radioactive species in a single plot (Figure J7.2-7). The curve labeled "Total" in Figure J7.2-7 corresponds to the expected (mean) dose $\bar{\bar{E}}_{II}(\tau)$ previously presented in Figures J7.2-4 and J7.2-5. The remaining curves correspond to expected (mean) dose $\bar{\bar{E}}_{II,r}(\tau)$ for individual radioactive species.

Once the results in Equation J7.2-18 are available, Monte Carlo procedures can also be used to estimate $\bar{D}_{II}(\tau|\mathbf{e}_i)$, the CDF for $D_{II}(\tau|\mathbf{a}, \mathbf{e}_{Mi})$ and the CCDF for $D_{II}(\tau|\mathbf{a}, \mathbf{e}_{Mi})$. For illustration, an arbitrary distribution is assumed for N as is done in Equations J7.2-11 and J7.2-12. Then,

$$\begin{aligned}\bar{D}_{II}\left(\tau|\mathbf{e}_i\right) &\cong p_A\left(\mathcal{A}_{II}|\mathbf{e}_{Ai}\right)\sum_{k=1}^{nR} D_{II}\left(\tau|\mathbf{a}_{II}, \mathbf{e}_{Mi}\right)\Big/nR \\ &\cong p_A\left(\mathcal{A}_{II}|\mathbf{e}_{Ai}\right)\sum_{k=1}^{nR}\left\{\sum_{j=1}^{nII_k}\left(N_{jk}/nWP\right)\hat{D}_{II}\left(\tau|\left[1, t_{jk}, nWP\right], \mathbf{e}_{Mi}\right)\right\}\Big/nR,\end{aligned}$$

(Eq. J7.2-21)

$$\begin{aligned}p_A\left[D_{II}\left(\tau|\mathbf{a}, \mathbf{e}_{Mi}\right) \le D\middle|\mathbf{e}_{Ai}\right] &= 1 - p_A\left[D < D_{II}\left(\tau|\mathbf{a}, \mathbf{e}_{Mi}\right)\middle|\mathbf{e}_{Ai}\right] \\ &\cong p_A\left(\mathcal{A}_{II}|\mathbf{e}_{Ai}\right)\sum_{k=1}^{nR}\underline{\delta}_D\left[D_{II}\left(\tau|\mathbf{a}_{II,k}, \mathbf{e}_{Mi}\right)\right]\Big/nR \\ &\cong p_A\left(\mathcal{A}_{II}|\mathbf{e}_{Ai}\right)\sum_{k=1}^{nR}\underline{\delta}_D\left\{\sum_{j=1}^{nII_k}\left(N_{jk}/nWP\right)\hat{D}_{II}\left(\tau|\left[1, t_{jk}, nWP\right], \mathbf{e}_{Mi}\right)\right\}\Big/nR\end{aligned}$$

(Eq. J7.2-22)

and

$$\begin{aligned}p_A\left[D < D_{II}\left(\tau|\mathbf{a}, \mathbf{e}_{Mi}\right)\middle|\mathbf{e}_{Ai}\right] &\cong p_A\left(\mathcal{A}_{II}|\mathbf{e}_{Ai}\right)\sum_{k=1}^{nR}\bar{\delta}_D\left[D_{II}\left(\tau|\mathbf{a}_{II,k}, \mathbf{e}_{Mi}\right)\right]\Big/nR \\ &\cong p_A\left(\mathcal{A}_{II}|\mathbf{e}_{Ai}\right)\sum_{k=1}^{nR}\bar{\delta}_D\left\{\sum_{j=1}^{nII_k}\left(N_{jk}/nWP\right)\hat{D}_{II}\left(\tau|\left[1, t_{jk}, nWP\right], \mathbf{e}_{Mi}\right)\right\}\Big/nR\end{aligned}$$

(Eq. J7.2-23)

as indicated in Equations J4.5-19 – J4.5-21 with $C = II$, where (i)

$$\mathbf{a}_{II,k} = \left[nII_k, \mathbf{a}_{II,1k}, \mathbf{a}_{II,2k}, \ldots, \mathbf{a}_{II,nII_k,k}\right], k = 1, 2, \ldots, nR,$$

is a random sample from vectors $\mathbf{a}_{II}$ of the form defined in Equation J7.1-8 generated in consistency with λ_I and $d_{II}(N)$ and with elements

$$\mathbf{a}_{II,jk} = \left[t_{jk}, N_{jk} \right]$$

for $j = 1, 2, \ldots, nII_k$, (ii) $\hat{D}_{II}(\tau|[1, t_{jk}, nWP], \mathbf{e}_{Mi})$ is obtained by interpolation from the results in Equation J7.2-18 with procedures of the form illustrated in Figure J7.2-2, and (iii) the indicator functions $\bar{\delta}_D(\sim)$ and $\underline{\delta}_D(\sim)$ are defined in Equations J4.2-3 and J4.2-7, respectively. If considered appropriate, the requirement $nII_k = 1$ could be imposed.

As an example, Figure J7.2-8a shows the CCDF for the dose $D_{II}(10^4 \text{ yr}|\mathbf{a}_{II}, \mathbf{e}_{M1})$ to the RMEI at $\tau = 10^4$ yr obtained with LHS element $\mathbf{e}_1$. Specifically, the CCDF in Figure J7.2-8a is a plot of the exceedance probabilities $p_A[D < D_{II}(10^4 \text{ yr}|\mathbf{a}, \mathbf{e}_{M1})|\mathbf{e}_{A1}]$ defined in Equation J7.2-23 and obtained with a random sample of size $nR = 10^4$ from $\mathcal{A}_{II}$. In turn, the sampled results used in the construction of the CCDF in Figure J7.2-8a can be reduced to an estimate for the expected dose $\bar{D}_{II}(10^4 \text{ yr}|\mathbf{e}_1)$ as indicated in Equation J7.2-21 and illustrated in Figure J7.2-8b. Specifically, Figure J7.2-8a shows the expected dose curve $\bar{D}_{II}(\tau|\mathbf{e}_1)$, $0 \le \tau \le 20{,}000$ yr, previously presented in Figure J7.2-3 and the expected dose $\bar{D}_{II}(10^4 \text{ yr}|\mathbf{e}_1)$ calculated with the indicated Monte Carlo procedure. As can be seen, the value for $\bar{D}_{II}(10^4 \text{ yr}|\mathbf{e}_1)$ produced by the Monte Carlo procedure is effectively the same as the value for $\bar{D}_{II}(10^4 \text{ yr}|\mathbf{e}_1)$ produced by integration procedures. As a result, repeating the Monte Carlo estimation procedure for a sequence of values for τ would result in an estimate for $\bar{D}_{II}(\tau|\mathbf{e}_1)$ for $0 \le \tau \le 20{,}000$ yr that is effectively the same as the estimate that appears in Figures J7.2-3 and J7.2-8b. The integration-based approach to estimating $\bar{D}_{II}(\tau|\mathbf{e})$ has the advantage of numerical efficiency but does not provide estimates of CCDFs of the form shown in Figure J7.2-8a. In contrast, the sampling-based approach to estimating $\bar{D}_{II}(\tau|\mathbf{e})$ is less efficient numerically but provides CCDFs that summarize the effects of aleatory uncertainty.

The CCDF in Figure J7.2-8a is for a single LHS element. As shown in Figure J7.2-9a,b, a different CCDF results for $D_{II}(10^4 \text{ yr}|\mathbf{a}_{II}, \mathbf{e}_{Mi})$ for each LHS element $\mathbf{e}_i = [\mathbf{e}_{Ai}, \mathbf{e}_{Mi}]$. Collectively, these CCDFs are displaying the epistemic uncertainty associated with the distribution of dose $D_{II}(10^4 \text{ yr}|\mathbf{a}_{II}, \mathbf{e}_{Mi})$ to the RMEI at $\tau = 10^4$ yr that results from the different possible values for $\mathbf{a}_{II}$. In turn, the epistemic uncertainty associated with these CCDFs can be summarized by an expected (mean) CCDF and quantile curves constructed in a manner analogous to the construction of expected (mean) and quantile curves for expected dose $\bar{D}_{II}(\tau|\mathbf{e})$ (Figure J7.2-9c). The expected (mean) dose $\bar{\bar{D}}_{II}(10^4 \text{ yr})$ appearing in Figures J7.2-4, J7.2-5 and J7.2-7 is the result of reducing all the information in Figure J7.2-9a to single number (i.e., $\bar{\bar{D}}_{II}(10^4 \text{ yr})$).

As discussed in Section J4.10, the numerical stability of results obtained with Latin hypercube sampling can be assessed with replicated sampling. Specifically, the analysis for igneous intrusive events was performed with the $nRL = 3$ replicated LHSs indicated in Equation J4.10-1. In turn, this analysis shows that the numerical error in using Latin hypercube sampling to estimate $\bar{\bar{D}}_{II}(\tau)$ is small relative to the epistemic uncertainty associated with the possible values for $\bar{\bar{D}}_{II}(\tau|\mathbf{e})$ (Figure J7.2-10).

The results presented in Figures J7.2-1 to J7.2-10 are for the time period [0, 20,000 yr]. Corresponding results for the time period [0, 10^6 yr] are presented without discussion in Figures J7.2-11 to J7.2-20.

J7.3 Igneous Eruptive Scenario Class: $\mathcal{A}_{IE}$

The aleatory futures associated with the igneous eruptive scenario class $\mathcal{A}_{IE}$ are defined by number of eruptive events (nIE) and, for each eruptive event, by event time, number of WPs intersected by vents leading to the surface, fraction of intersected WP content that is ejected into the atmosphere, eruptive power, eruptive velocity, eruption duration, wind speed and wind direction. Specifically, the individual vectors $\mathbf{a}_{IE,j}$, $j = 1, 2, \ldots, nIE$, appearing in the definition of $\mathbf{a}_{IE}$ in Equation J7.1-9 are defined by

$$\mathbf{a}_{IE,j} = \left[t_j, nWE_j, fP_j, EP_j, EV_j, ED_j, WS_j, WD_j \right], \qquad \text{(Eq. J7.3-1)}$$

where

t_j = event time (yr),

nWE_j = number of WPs intersected by vents leading to the surface,

fP_j = fraction of intersected WP content ejected into the atmosphere,

EP_j = eruptive power (watts),

EV_j = eruptive velocity (cm/s),

ED_j = eruption duration (s),

WS_j = wind speed at maximum plume height (cm/s),

WD_j = wind direction at maximum plume height.

In turn, the following quantities define the probabilities associated with $\mathcal{A}_{IE}$:

$pE\,\lambda_I$ = rate of occurrence (yr^{-1}) of igneous eruptive events that intersect one or more WPs in the repository, where λ_I is the rate of occurrence (yr^{-1}) of igneous

events that intersect the repository and pE is the conditional probability that an igneous intrusive event will also have an eruptive component that ejects waste into the atmosphere (i.e., pE is the probability that waste will be ejected into the atmosphere given that an igneous intrusive event has occurred).

$d_{IE}(N)$ = density function for number N of WPs intersected by vents leading to the surface (i.e., $N \sim nWE_j$ in Equation J7.3-1),

$d_F(F)$ = density function for fraction F of intersected WP content that is ejected into the atmosphere (i.e., $F \sim fP_j$ in Equation J7.3-1),

$d_P(P)$ = density function (watts^{-1}) for eruptive power P (i.e., $P \sim EP_j$ in Equation J7.3-1),

$d_V(V)$ = density function (s/cm) for eruptive velocity V (i.e., $V \sim EV_j$ in Equation J7.3-1),

$d_D(D|P)$ = density function (s^{-1}) for eruption duration (i.e., $D \sim ED_j$ in Equation J7.3-1),

$d_{WS}(WS|H)$ = density function (s/cm) for wind speed at maximum plume height H (km) (i.e., $WS \sim WS_j$ in Equation J7.3-1),

$d_{WD}(WD|H)$ = density function for wind direction WS at maximum plume height H (km) (i.e., $WD \sim WD_j$ in Equation J7.3-1).

As indicated, the density function $d_D(D|P)$ is conditional on eruptive power P, and the density functions $d_{WS}(WS|H)$ and $d_{WD}(WD|H)$ for wind speed and wind direction are conditional on maximum plume height H. In turn, H is a function $H(P)$ of eruptive power P.

Given pE, λ_I, $d_{IE}(N)$, $d_F(F)$, $d_P(P)$, $d_V(V)$, $d_D(D|P)$, $d_{WS}(WS|H)$, $d_{WD}(WD|H)$ and an LHS element $\mathbf{e}_i = [\mathbf{e}_{Ai}, \mathbf{e}_{Mi}]$ of the form indicated in Equation J4.9-1, then $\bar{D}_{IE}(\tau|\mathbf{e}_i)$ formally has the form

$$\bar{D}_{IE}\left(\tau|\mathbf{e}_i\right) = \int_{\mathcal{A}_{IE}} D_{IE}\left(\tau|\mathbf{a}, \mathbf{e}_{Mi}\right) d_A\left(\mathbf{a}|\mathbf{e}_{Ai}\right) \mathrm{d}A, \qquad \text{(Eq. J7.3-2)}$$

where, in concept, the density $d_A(\mathbf{a}|\mathbf{e}_{Ai})$ derives from pE, λ_{Ii}, $d_{IE}(N)$, $d_F(F)$, $d_P(P)$, $d_V(V)$, $d_D(D|P)$, $d_{WS}(WS|H)$, and $d_{WD}(WD)$. The dependence of $d_A(\mathbf{a}|\mathbf{e}_{Ai})$ on $\mathbf{e}_{Ai}$ results in the TSPA-LA because λ_I is an element of $\mathbf{e}_A$.

In turn, the formal representation for $\bar{D}_{IE}(\tau|\mathbf{e}_i)$ in Equation J7.3-2 can be restated as

$$\bar{D}_{IE}(\tau|\mathbf{e}_i) = \int_0^{\tau}\left\{\int_{\mathcal{N}_{IE}}\int_{\mathcal{F}_{IE}}\left[\int_{\mathcal{U}_{IE}} D_{IE}(\tau|[1,t,FN,\mathbf{u},]\,\mathbf{e}_{Mi})\,d_U(\mathbf{u})\,dU\right]_1 d_F(F)\,d_{IE}(N)\,dF\,dN\right\}_2 pE\,\lambda_{Ii}\,dt \quad \text{(Eq. J7.3-3)}$$

where (i) $\mathcal{N}_{IE}$, $\mathcal{F}_{IE}$, $\mathcal{P}_{IE}$, $\mathcal{V}_{IE}$, $\mathcal{D}_{IE}$, $\mathcal{WS}_{IE}$ and $\mathcal{WD}_{IE}$ are the sets of possible values for N, F, P, V, D, WS and WD associated with the density functions $d_{IE}(N)$, $d_F(F)$, $d_P(P)$, $d_V(V)$, $d_D(D|P)$, $d_{WS}(WS|H)$ and $d_{WD}(WD|H)$, (ii) the set $\mathcal{U}_{IE}$ is defined by

$$\begin{aligned}\mathcal{U}_{IE} &= \mathcal{P}_{IE}\times\mathcal{V}_{IE}\times\mathcal{D}_{IE}\times\mathcal{WS}_{IE}\times\mathcal{WD}_{IE}\\ &= \{\mathbf{u}:\mathbf{u}=[P,V,D,WS,WD] \text{ with } p\in\mathcal{P}_{IE}, V\in\mathcal{V}_{IE}, D\in\mathcal{D}_{IE}, WS\in\mathcal{WS}_{IE}, WD\in\mathcal{WD}_{IE}\},\end{aligned}$$

(iii) $d_U(\mathbf{u})$ is the density function on $\mathcal{U}_{IE}$ that derives from $d_P(P)$, $d_V(V)$, $d_D(D|P)$, $d_{WS}(WS|H)$ and $d_{WD}(WD|H)$, and (iv) $D_{IE}(\tau|[1, t, FN, \mathbf{u}], \mathbf{e}_{Mi})$ is the dose to the RMEI (mrem/yr) at time τ that results from a single igneous eruptive event at time t that has the properties defined by the components of the vector $\mathbf{u} = [P, V, D, WS, WD]$, intercepts N WPs in the repository, and ejects a fraction F of these WPs into the atmosphere. In the actual calculations performed for the igneous eruptive scenario class, each intercepted WP is assumed to be a "blended" WP that contains a radionuclide content equal to the fraction $1/nWP$ of the entire radionuclide content in the repository.

In Equation J7.3-3, the integral contained in $[\sim]_1$ is the expected dose to the RMEI at time τ from an event that occurs at time t, intercepts N WPs, and ejects a fraction F of the content of these WPs into the atmosphere. Or, put another way, this integral is the expected dose to the RMEI that derives from the distribution of $\mathbf{u} = [P, V, D, WS, WD]$ over the set $\mathcal{U}$ as defined by $d_U(\mathbf{u})$ *conditional* on t, N and F. In turn, the triple integral contained in $\{\sim\}_2$ is the expected dose to the RMEI at time τ conditional on the occurrence of an igneous eruptive event at time t. Further, the "product" $pE\ \lambda_{Ii}\ dt$ of the occurrence rate $pE\ \lambda_{Ii}$ and the differential on time dt in Equation J7.3-3 results in the conditional expected dose defined by the triple integral in $\{\sim\}_2$ being multiplied by the expected number of igneous eruptive events in a time interval with a length conceptually represented by the differential dt (i.e., in an interval of length Δt_k when a subdivision $0 = t_0 < t_1 < \ldots < t_n = \tau$ of $[0, \tau]$ is used in an approximation of the integral over t in Equation J7.3-3). As a result, the representation for $\bar{D}_{IE}(\tau|\mathbf{e}_i)$ in Equation J7.3-3 derives from the approximation

$$\bar{D}_{IE}(\tau|\mathbf{e}_i) \cong \sum_{k=1}^{n}\left\{\int_{\mathcal{N}_{IE}}\int_{\mathcal{F}_{IE}}\left[\int_{\mathcal{U}_{IE}} D_{IE}(\tau|[1,t_k,FN,\mathbf{u}],\mathbf{e}_{Mi})\,d_U(\mathbf{u})\,dU\right]_1 d_F(F)\,d_{IE}(N)\,dF\,dN\right\}_2 \times pE\,\lambda_{Ii}\Delta t_k \quad \text{(Eq. J7.3-4)}$$

as $\Delta t_k \rightarrow 0$, where $pE\ \lambda_{Ii}\ \Delta t_k$ is the expected number of igneous eruptive events in the time interval $[t_{k-1}, t_k]$ and the triple integral contained in $\{\sim\}_2$ is the conditional expected dose to the RMEI given the occurrence of an igneous eruptive event at time t_k.

The dose $D_{IE}(\tau|[1, t, F\,N, \mathbf{u}], \mathbf{e}_{Mi})$ appearing in Equation J7.3-3 is linear with respect to the term $F\,N$. As a result, the simplification

$$\int_{\mathcal{N}_{IE}} \int_{\mathcal{F}_{IE}} \left[\int_{\mathcal{U}_{IE}} D_{IE}\left(\tau|[1, t_k, F\,N, \mathbf{u}], \mathbf{e}_{Mi}\right) d_U(\mathbf{u})\, \mathrm{d}U \right] d_F(F)\, d_{IE}(N)\, \mathrm{d}F\, \mathrm{d}N$$
$$= \bar{N}_{IE} \bar{F} \int_{\mathcal{U}_{IE}} D_{IE}\left(\tau|[1, t, 1, \mathbf{u}], \mathbf{e}_{Mi}\right) d_U(\mathbf{u})\, \mathrm{d}U \qquad \text{(Eq. J7.3-5)}$$

results for the triple integral contained in $\{\sim\}_2$ in Equation J7.3-3, where

$$\bar{N}_{IE} = \int_{\mathcal{N}_{IE}} N\, d_{IE}(N)\, \mathrm{d}N$$

and

$$\bar{F} = \int_{\mathcal{F}_{IE}} F\, d_F(F)\, \mathrm{dF}$$

are the expected values for N and F, respectively. In turn, the simpler representation

$$\bar{D}_{IE}\left(\tau|\mathbf{e}_i\right) = pE\ \lambda_{Ii}\ \bar{N}_{IE}\ \bar{F} \int_0^{\tau} \left[\int_{\mathcal{U}_{IE}} D_{IE}\left(\tau|[1, t, 1, \mathbf{u}], \mathbf{e}_{Mi}\right) d_U(\mathbf{u})\, \mathrm{d}U \right] \mathrm{d}t$$
$$= pE\ \lambda_{Ii}\ \bar{N}_{IE} \bar{F} \int_{\mathcal{U}_{IE}} \left[\int_0^{\tau} D_{IE}\left(\tau|[1, t, 1, \mathbf{u}], \mathbf{e}_{Mi}\right) \mathrm{d}t \right] d_U(\mathbf{u})\, \mathrm{d}U \qquad \text{(Eq. J7.3-6)}$$

results when the representation in Equation J7.3-5 for the triple integral contained in $\{\sim\}_2$ is substituted into the representation for $D_{IE}(\tau|\mathbf{e}_i)$ in Equation J7.3-3.

The integrals involving $\mathcal{U}_{IE}$ in Equation J7.3-6 can be approximated with a Monte Carlo procedure. Specifically, an LHS

$$\mathbf{u}_l = [P_l, V_l, D_l, WS_l, WD_l], l = 1, 2, \ldots, nU, \qquad \text{(Eq. J7.3-7)}$$

of size nU can be generated from $\mathcal{U}_{IE}$ in consistency with the distributions defined by the density functions $d_P(P)$, $d_V(V)$, $d_D(D|P)$, $d_{WS}(WS|H)$ and $d_{WD}(WD|H)$. In practice, this sample is generated by first constructing an LHS

$$\tilde{\mathbf{u}}_l = [P_l, V_l, p_{1l}, p_{2l}, p_{3l}], l = 1, 2, \ldots, nU, \qquad \text{(Eq. J7.3-8)}$$

from $\tilde{\mathcal{U}}_{IE} = \mathcal{P}_{IE} \times \mathcal{V}_{IE} \times [0, 1] \times [0, 1] \times [0, 1]$ in consistency with the density functions $d_P(P)$ and $d_V(V)$ for P and V and uniform density functions for the pointer variables p_1, p_2 and p_3. Then, D_l is determined with the pointer variable p_{1l} from the distribution for D defined by $d_D(D|P_l)$, and once plume height H_1 is determined as a function of eruptive power P_l, values for WS_l and WD_l are determined with the pointer variables p_{2l} and p_{3l} from the distributions for WS and WD defined by $d_{WS}(WS|H_l)$ and $d_{WD}(WD|H_l)$.

Once the sample in Equation J7.3-7 is generated, $\bar{D}_{IE}(\tau|\mathbf{e}_i)$ can be approximated by

$$\begin{aligned}\bar{D}_{IE}\left(\tau|\mathbf{e}_i\right) &\cong pE\ \lambda_{Ii}\ \bar{N}_{IE}\ \bar{F} \int_0^{\tau} \left[\sum_{l=1}^{nU} D_{IE}\left(\tau|[1, t, 1, \mathbf{u}_l], \mathbf{e}_{Mi}\right)/nU \right] \mathrm{d}t \\ &\cong pE\ \lambda_{Ii}\ \bar{N}_{IE}\ \bar{F} \sum_{k=1}^{n} \left[\sum_{l=1}^{nU} D_{IE}\left(\tau|[1, t_k, 1, \mathbf{u}_l], \mathbf{e}_{Mi}\right)/nU \right] \Delta t_k \end{aligned} \qquad \text{(Eq. J7.3-9)}$$

and also by

$$\begin{aligned}\bar{D}_{IE}\left(\tau|\mathbf{e}_i\right) &\cong pE\ \lambda_{Ii}\ \bar{N}_{IE}\ \bar{F} \sum_{l=1}^{nU} \left[\int_0^{\tau} D_{IE}\left(\tau|[1, t, 1, \mathbf{u}_l], \mathbf{e}_{Mi}\right) \mathrm{d}t \right] \Big/ nU \\ &\cong pE\ \lambda_{Ii}\ \bar{N}_{IE}\ \bar{F} \sum_{l=1}^{nU} \left[\sum_{k=1}^{n} D_{IE}\left(\tau|[1, t_k, 1, \mathbf{u}_l], \mathbf{e}_{Mi}\right) \Delta t_k \right] \Big/ nU \\ &= pE\ \lambda_{Ii}\ \bar{N}_{IE}\ \bar{F} \sum_{k=1}^{n} \left[\sum_{l=1}^{nU} D_{IE}\left(\tau|[1, t_k, 1, \mathbf{u}_l], \mathbf{e}_{Mi}\right)/nU \right] \Delta t_k, \end{aligned} \qquad \text{(Eq. J7.3-10)}$$

where (i) the approximations in Equation J7.3-9 start with the first representation for $\bar{D}_{IE}(\tau|\mathbf{e}_i)$ in Equation J7.3-6, (ii) the approximations in Equation J7.3-10 start with the second representation for $\bar{D}_{IE}(\tau|\mathbf{e}_i)$ in Equation J7.3-6, and (iii) the sequences of approximations in Equations J7.3-9 and J7.3-10 ultimately lead to the same final approximation. The particular approximation for $\bar{D}_{IE}(\tau|\mathbf{e}_i)$ that is used depends on the form in which results from GoldSim are saved.

The TSPA-LA calculates $\bar{D}_{IE}(\tau|\mathbf{e}_i)$ on the basis of the representation in Equation J7.3-9. To support this calculation, $D_{IE}[\tau|[1, t, 1, \mathbf{u}], \mathbf{e}_{Mi})$ is evaluated for a sequence of times and a set of sampled selected values of $\mathbf{u}$ for each time. Two cases are considered in the TSPA-LA: events occurring over the time interval [0, 2.0×10^4 yr] and events occurring over the time interval [0, 1.0×10^6 yr]. For the time interval [0, 2.0×10^4 yr], the results

$$D_{IE}\left(\tau|[1, t_k, 1, \mathbf{u}_l], \mathbf{e}_{Mi}\right), k = 1, 2, \ldots, 10, l = 1, 2, \ldots, nU = 40, i = 1, 2, \ldots, 300, \qquad \text{(Eq. J7.3-11)}$$

are calculated for (i) $0 \le \tau \le 2.0 \times 10^4$ yr, (ii) t_k = 10, 100, 600, 1000, 2000, 4000, 6000, 10,000, 14,000 and 18,000 yr, and (iii) the $\mathbf{u}_l$ an LHS of size $nU = 40$ from $\mathcal{U}_{IE}$. For the time interval [0, 1.0×10^6 yr], the results in Equation J7.3-11 are calculated for (i) $0 \le \tau \le 1.0 \times 10^6$ yr, (ii) t_k = 250, 600, 1000, 4000, 10,000, 40,000, 100,000, 200,000, 400,000 and 800,000 yr, and (iii) the $\mathbf{u}_l$ an LHS of size $nU = 40$ from $\mathcal{U}_{IE}$.

Because of the interpolations involved, it is more efficient to sum over $\mathbf{u}_l$ and then integrate over time as indicated in Equation J7.3-9 than to integrate on time and then sum on $\mathbf{u}_l$ as indicated in Equation J7.3-10. As a result, the approximations to $\bar{D}_{IE}(\tau|\mathbf{e}_i)$ in the TSPA-LA are of the form

$$\bar{D}_{IE}\left(\tau\middle|\mathbf{e}_i\right) \cong pE\ \lambda_{Ii}\ \bar{N}_{IE}\ \bar{F} \sum_{k=1}^{n} \left[\sum_{l=1}^{nU} \hat{D}_{IE}\left(\tau\middle|\left[1, \hat{t}_k, 1, \mathbf{u}_l\right], \mathbf{e}_{Mi}\right) \Big/ nU \right] \Delta\hat{t}_k, \qquad \text{(Eq. J7.3-12)}$$

where (i) $0 = \hat{t}_0 < \hat{t}_1 < \ldots < \hat{t}_n = \tau$ and (ii) and $\hat{D}_{IE}(\tau|[1, \hat{t}_k, 1, \mathbf{u}_l], \mathbf{e}_{Mi})$ is an approximation to $D_{IE}(\tau|[1, \hat{t}_k, 1, \mathbf{u}_l], \mathbf{e}_{Mi})$ obtained by interpolation from the calculated values $D_{IE}(\tau|[1, t_k, 1, \mathbf{u}_l], \mathbf{e}_{Mi})$ indicated in Equation J7.3-11.

For computational efficiency, the quantity

$$\sum_{l=1}^{nU} \hat{D}_{IE}\left(\tau\middle|\left[1, \hat{t}_k, 1, \mathbf{u}_l\right], \mathbf{e}_{Mi}\right) \Big/ nU \qquad \text{(Eq. J7.3-13)}$$

in Equation J7.3-12 is actually obtained by interpolating on the sums

$$S\left(\tau\middle|t_k, \mathbf{e}_{Mi}\right) = \sum_{l=1}^{nU} D_{IE}\left(\tau\middle|\left[1, t_k, 1, \mathbf{u}_l\right], \mathbf{e}_{Mi}\right) \Big/ nU \qquad \text{(Eq. J7.3-14)}$$

rather than on the individual doses $D_{IE}(\tau|[1, t_k, 1, \mathbf{u}_l], \mathbf{e}_{Mi})$, which reduces the number of required interpolations by a factor of nU. Specifically, the interpolated approximation $\hat{S}(\tau|\hat{t}_k, \mathbf{e}_{Mi})$ to $S(\tau|\hat{t}_k, \mathbf{e}_{Mi})$ is given by

$$\begin{aligned}
\hat{S}\left(\tau\middle|\hat{t}_k, \mathbf{e}_{Mi}\right) &= S\left[t_{k-1} + \left(\tau - \hat{t}_k\right)\middle|t_{k-1}, \mathbf{e}_{Mi}\right] \\
&\quad + \left\{\left(\hat{t}_k - t_{k-1}\right)\Big/\left(t_k - t_{k-1}\right)\right\}\left\{S\left[t_k + \left(\tau - \hat{t}_k\right)\middle|t_k, \mathbf{e}_{Mi}\right] - S\left[t_{k-1} + \left(\tau - \hat{t}_k\right)\middle|t_{k-1}, \mathbf{e}_{Mi}\right]\right\} \\
&\cong \sum_{l=1}^{nU} D_{IE}\left(\tau\middle|\left[1, \hat{t}_k, 1, \mathbf{u}_l\right], \mathbf{e}_{Mi}\right) \Big/ nU \\
&\cong \int_{\mathcal{U}_{IE}} D_{IE}\left(\tau\middle|\left[1, \hat{t}_k, 1, \mathbf{u}\right], \mathbf{e}_{Mi}\right) d_U\left(\mathbf{u}\right) \mathrm{d}U
\end{aligned} \qquad \text{(Eq. J7.3-15)}$$

for $\hat{t}_k \le \tau$ and $t_{k-1} < \hat{t}_k < t_k$. In turn,

$$\bar{D}_{IE}\left(\tau|\mathbf{e}_i\right) \cong pE\,\lambda_{Ii}\,\bar{N}_{IE}\,\bar{F}\sum_{k=1}^{n}\hat{S}\left(\tau|\hat{t}_k,\mathbf{e}_{Mi}\right)\Delta\hat{t}_k \qquad \text{(Eq. J7.3-16)}$$

is the resultant approximation to $\bar{D}_{IE}(\tau|\mathbf{e}_i)$.

Results are initially illustrated for the 20,000 yr time period. As indicated in conjunction with Equation J7.3-11, the expected dose results are based on the results $D_{IE}(\tau|[1, t_k, 1, \mathbf{u}_l], \mathbf{e}_{Mi})$. As an example, the values obtained for $D_{IE}(\tau|[1, t_k, 1, \mathbf{u}_l], \mathbf{e}_{Mi})$ for t_k = 100, 1000, 4000 and 10,000 yr and LHS element $\mathbf{e}_1$ are presented in Figure J7.3-1.

As indicated in Equation J7.3-15 and illustrated in Figure J7.3-2 for LHS element $\mathbf{e}_1$, the results $D_{IE}(\tau|[1, t_k, 1, \mathbf{u}_l], \mathbf{e}_{Mi})$ are used in an interpolation procedure to obtain the quantities $\hat{S}(\tau|\hat{t}_k, \mathbf{e}_{Mi})$ used in the approximation to $\bar{D}_{IE}(\tau|\mathbf{e}_i)$ in Equation J7.3-16. Specifically, the following results are shown in Figure J7.3-2 for LHS element $\mathbf{e}_1$: (i) the quantities $S(\tau|t_k, \mathbf{e}_{Mi})$ defined in Equation J7.3-14 for k = 1, 2, …, 10 (Figure J7.3-2a), (ii) the approximations $\hat{S}(\tau|\hat{t}_k, \mathbf{e}_{Mi})$ to $S(\tau|t_k, \mathbf{e}_{Mi})$ defined in Equation J7.3-15 for $\hat{t}_k$ between t_7 = 6000 yr and t_8 = 10,000 yr (Figure J7.3-2b), and (iii) the approximations $\hat{S}(\tau|\hat{t}_k, \mathbf{e}_{Mi})$ defined between 0 and 20,000 yr and used in the approximation to $\bar{D}_{IE}(\tau|\mathbf{e}_i)$ in Equation J7.3-16 (Figure J7.3-2c).

In turn, the results indicated in Equation J7.3-11 can be used to estimate $\bar{D}_{IE}(\tau|\mathbf{e}_i)$ as illustrated in Figure J7.3-3 for LHS element $\mathbf{e}_1$. Further, the results obtained with all $nLHS$ = 300 LHS elements are summarized in Figure J7.3-4 and presented in a standard format in Figure J7.3-5.

As discussed in conjunction with Equations J5-8 and J6.2-9, dose and expected dose to the RMEI are just two of a large number of results that can be produced and presented in the TSPA-LA. As previously done in Figure J5-4 and other similar figures, a compact summary of the expected (mean) dose results $\bar{\bar{D}}_{IE,r}(\tau)$ for the individual radioactive species is provided in Figure J7.3-6, where $\bar{\bar{D}}_{IE,r}(\tau)$ is the expected (mean) dose to the RMEI at time τ resulting from the atmospheric release of radioactive species r due to igneous eruptive events (see Equation J6.2-9 and associated discussion). In concept, the expected (mean) dose results $\bar{\bar{D}}_{IE,r}(\tau)$ for the individual radioactive species are computed using Equation J7.3-10. However, as indicated by Eaution 6.5.2-1, the implementation of this calculation does not produce the intermediate quantities $\bar{D}_{IE,r}(\tau|\mathbf{e}_i)$.

Once the results in Equation J7.3-11 are available, Monte Carlo procedures can also be used to estimate $\bar{D}_{IE}(\tau|\mathbf{e}_i)$, the CDF for $D_{IE}(\tau|\mathbf{a}, \mathbf{e}_{Mi})$, and the CCDF for $D_{IE}(\tau|\mathbf{a}, \mathbf{e}_{Mi})$. Specifically, a sequence

$$\mathbf{a}_{IE,k} = \left[nIE_k, t_{1k}, \mathbf{a}_{IE,1k}, t_{2k}, \mathbf{a}_{IE,2k}, \ldots, t_{nIE_k,k}, \mathbf{a}_{IE,nIE_k,k} \right], k = 1, 2, \ldots, nR, \qquad \text{(Eq. J7.3-17)}$$

of random futures can be generated, where

$$\mathbf{a}_{IE,jk} = \left[N_{jk}, F_{jk}, \mathbf{u}_{jk} \right]$$

for j = 1, 2, …, nIE_k. In generating the indicated sample, the number of igneous eruptive events (nIE_k) would be sampled conditional on the occurrence of one or more events; the number of WPs intersected by vents leading to the surface (N_{jk}) and fraction of intersected WP content ejected into the atmosphere (F_{jk}) would be sampled from their assigned distributions; and the property vectors $\mathbf{u}_{jk}$ would be randomly selected from the vectors $\mathbf{u}_l$ used in the generation of the results in Equation J7.3-11. In practice, the probability that nIE_k will be greater than one is very small. Then,

$$\begin{aligned} \bar{D}_{IE}\left(\tau|\mathbf{e}_i\right) &\cong p_A\left(\mathcal{A}_{IE}|\mathbf{e}_{Ai}\right)\sum_{k=1}^{nR} D_{IE}\left(\tau|\mathbf{a}_{IE,k}, \mathbf{e}_{Mi}\right)/nR \\ &\cong p_A\left(\mathcal{A}_{IE}|\mathbf{e}_{Ai}\right)\sum_{k=1}^{nR}\left\{\sum_{j=1}^{nIE_k}\left(F_{jk}\ N_{jk}\right)\hat{D}_{IE}\left(\tau|\left[1, t_{jk}, 1, \mathbf{u}_{jk}\right], \mathbf{e}_{Mi}\right)\right\}\Big/nR, \end{aligned} \qquad \text{(Eq. J7.3-18)}$$

$$\begin{aligned} p_A\left[D_{IE}\left(\tau|\mathbf{a}, \mathbf{e}_{Mi}\right) \le D\middle|\mathbf{e}_{Ai}\right] &= 1 - p_A\left[D < D_{IE}\left(\tau|\mathbf{a}, \mathbf{e}_{Mi}\right)\middle|\mathbf{e}_{Ai}\right] \\ &\cong p_A\left(\mathcal{A}_{IE}|\mathbf{e}_{Ai}\right)\sum_{k=1}^{nR}\underline{\delta}_D\left[D_{IE}\left(\tau|\mathbf{a}_{IE,k}, \mathbf{e}_{Mi}\right)\right]/nR \\ &\cong p_A\left(\mathcal{A}_{IE}|\mathbf{e}_{Ai}\right)\sum_{k=1}^{nR}\underline{\delta}_D\left\{\sum_{j=1}^{nIE_k}\left(F_{jk}\ N_{jk}\right)\hat{D}_{IE}\left(\tau|\left[1, t_{jk}, 1, \mathbf{u}_{jk}\right], \mathbf{e}_{Mi}\right)\right\}\Big/nR \end{aligned} \qquad \text{(Eq. J7.3-19)}$$

and

$$\begin{aligned} p_A\left[D < D_{IE}\left(\tau|\mathbf{a}, \mathbf{e}_{Mi}\right)\middle|\mathbf{e}_{Ai}\right] &\cong p_A\left(\mathcal{A}_{IE}|\mathbf{e}_{Ai}\right)\sum_{k=1}^{nR}\bar{\delta}_D\left[D_{IE}\left(\tau|\mathbf{a}_{IE,k}, \mathbf{e}_{Mi}\right)\right]/nR \\ &\cong p_A\left(\mathcal{A}_{IE}|\mathbf{e}_{Ai}\right)\sum_{k=1}^{nR}\bar{\delta}_D\left\{\sum_{j=1}^{nIE_k}\left(F_{jk}\ N_{jk}\right)\hat{D}_{IE}\left(\tau|\left[1, t_{jk}, 1, \mathbf{u}_{jk}\right], \mathbf{e}_{Mi}\right)\right\}\Big/nR \end{aligned} \qquad \text{(Eq. J7.3-20)}$$

as indicated in Equations J4.5-19 – J4.5-21 with $\hat{D}_{IE}[\tau|[1, t_{jk}, 1, \mathbf{u}_{jk}], \mathbf{e}_{Mi})$ with interpolation procedures from the results in Equation J7.3-11.

Further, the LHS in Equation J4.9-1 can be used to estimate $\bar{\bar{D}}_{IE}(\tau)$, $p_E[\bar{D}_{IE}(\tau|\mathbf{e}) \le D]$ and $p_E[D < \bar{D}_{IE}(\tau|\mathbf{e})]$. Specifically,

$$\bar{\bar{D}}_{IE}(\tau) \cong \sum_{i=1}^{nLHS} \bar{D}_{IE}(\tau|\mathbf{e}_i)/nLHS, \qquad \text{(Eq. J7.3-21)}$$

$$p_E\left[\bar{D}_{IE}(\tau|\mathbf{e}) \le D\right] \cong \sum_{i=1}^{nLHS} \underline{\delta}_D\left[\bar{D}_{IE}(\tau|\mathbf{e}_i)\right]/nLHS \qquad \text{(Eq. J7.3-22)}$$

and

$$p_E\left[D < \bar{D}_{IE}(\tau|\mathbf{e})\right] \cong \sum_{i=1}^{nLHS} \bar{\delta}_D\left[\bar{D}_{IE}(\tau|\mathbf{e}_i)\right]/nLHS \qquad \text{(Eq. J7.3-23)}$$

as indicated in Equations J4.9-8 – J4.9-10.

As an example, Figure J7.3-7a shows the CCDF for the dose $D_{IE}(10^4 \text{ yr}|\mathbf{a}_{IE}, \mathbf{e}_{M1})$ to the RMEI at $\tau = 10^4$ yr obtained with LHS element $\mathbf{e}_1$. Specifically, the CCDF in Figure J7.3-7 is a plot of the exceedance probabilities $p_A[D < D_{II}(10^4 \text{ yr}|\mathbf{a}, \mathbf{e}_{M1})|\mathbf{e}_{A1}]$ defined in Equation J7.3-20 and obtained with a random sample of size $nR = 10^4$ from $\mathcal{A}_{IE}$. In turn, the sampled results used in the construction of the CCDF in Figure J7.3-7a can be reduced to an estimate for the expected dose $\bar{D}_{IE}(10^4 \text{ yr}|\mathbf{e}_1)$ as indicated in Equation J7.3-18 and illustrated in Figure J7.3-7b. Specifically, Figure J7.3-7a shows the expected dose curve $\bar{D}_{IE}(\tau|\mathbf{e}_1)$, $0 \le \tau \le 20{,}000$ yr, previously presented in Figure J7.3-3 and the expected dose $\bar{D}_{IE}(10^4 \text{ yr}|\mathbf{e}_1)$ calculated with the indicated Monte Carlo procedure. As can be seen, the value for $\bar{D}_{IE}(10^4 \text{ yr}|\mathbf{e}_1)$ produced by the Monte Carlo procedure is effectively the same as the value for $\bar{D}_{IE}(10^4 \text{ yr}|\mathbf{e}_1)$ produced by integration procedures. As a result, repeating the Monte Carlo estimation procedure for a sequence of values for τ would result in an estimate for $\bar{D}_{IE}(\tau|\mathbf{e}_1)$ for $0 \le \tau \le 20{,}000$ yr that is effectively the same as the estimate that appears in Figures J7.3-3 and J7.3-7b. The integration-based approach to estimating $\bar{D}_{IE}(\tau|\mathbf{e})$ has the advantage of numerical efficiency but does not provide estimates of CCDFs of the form shown in Figure J7.3-7a. In contrast, the sampling-based approach to estimating $\bar{D}_{IE}(\tau|\mathbf{e})$ is less efficient numerically but provides CCDFs that summarize the effects of aleatory uncertainty.

The CCDF in Figure J7.3-7a is for a single LHS element. As shown in Figure J7.3-8a,b, a different CCDF results for $D_{IE}(10^4 \text{ yr}|\mathbf{a}_{IE}, \mathbf{e}_{M1})$ for each LHS element $\mathbf{e}_i = [\mathbf{e}_{Ai}, \mathbf{e}_{Mi}]$. Collectively, these CCDFs are displaying the epistemic uncertainty associated with the distribution of dose $D_{IE}(10^4 \text{ yr}|\mathbf{a}_{IE}, \mathbf{e}_{M1})$ to the RMEI at $\tau = 10^4$ yr that results from the different possible values for $\mathbf{a}_{IE}$. In turn, the epistemic uncertainty associated with these CCDFs can be

summarized by an expected (mean) CCDF and quantile curves constructed in a manner analogous to the construction of expected (mean) and quantile curves for expected dose $\bar{D}_{IE}(\tau|\mathbf{e})$ (Figure J7.3-8c). The expected (mean) dose $\bar{\bar{D}}_{IE}(10^4 \text{ yr})$ appearing in Figures J7.3-4, J7.3-5, and J7.3-6 is the result of reducing all the information in Figure J7.3-8a to single number (i.e., $\bar{\bar{D}}_{IE}(10^4 \text{ yr})$).

As discussed in Section J4.10, the numerical stability of results obtained with Latin hypercube sampling can be assessed with replicated sampling. Specifically, the analysis for igneous eruptive events was performed with the $nRL = 3$ replicated LHSs indicated in Equation J4.10-1. In turn, this analysis shows that the numerical error in using Latin hypercube sampling to estimate $\bar{\bar{D}}_{IE}(\tau)$ is small relative to the epistemic uncertainty associated with the possible values for $\bar{\bar{D}}_{IE}(\tau)$ (Figure J7.3-9).

The results presented in Figures J7.3-1 to J7.3-9 are for the time period [0, 2.0×10^4 yr]. Corresponding results for the time period [0, 10^6 yr] are presented without discussion in Figures J7.3-10 and J7.3-18.

J7.4 Igneous Scenario Class: $\mathcal{A}_I$

The results $\bar{D}_{II}(\tau|\mathbf{e}_i)$ and $\bar{\bar{D}}_{II}(\tau)$ obtained for the igneous intrusive scenario class $\mathcal{A}_{II}$ are much larger than the corresponding results $\bar{D}_{IE}(\tau|\mathbf{e}_i)$ and $\bar{\bar{D}}_{IE}(\tau)$ obtained for the igneous eruptive scenario class $\mathcal{A}_{IE}$. As a result, $\bar{D}_I(\tau|\mathbf{e}_i)$ and $\bar{\bar{D}}_I(\tau)$ for the igneous scenario class $\mathcal{A}_I$ are effectively the same as $\bar{D}_{II}(\tau|\mathbf{e}_i)$ and $\bar{\bar{D}}_{II}(\tau)$ and are not presented as separate figures for this reason.

J7.5 Probabilities Associated with Igneous Scenario Classes

The probabilities $p_A(\mathcal{A}_{II}|\mathbf{e}_A)$, $p_A(\mathcal{A}_{IE}|\mathbf{e}_A)$ and $p_A(\mathcal{A}_I|\mathbf{e}_A)$ for the scenario classes $\mathcal{A}_{II}$, $\mathcal{A}_{IE}$ and $\mathcal{A}_I$ conditional on the element $\mathbf{e} = [\mathbf{e}_A, \mathbf{e}_M]$ of $\mathcal{E}$ depend on the time interval under consideration. In the TSPA-LA, the time intervals of primary interest are [0, 20,000 yr] and [0, 1,000,000 yr]. However, for generality, a time interval $[0, \tau]$ is assumed to be under consideration and $\mathcal{A}_{II}(0, \tau)$, $\mathcal{A}_{IE}(0, \tau)$ and $\mathcal{A}_I(0, \tau)$ will represent $\mathcal{A}_{II}$, $\mathcal{A}_{IE}$ and $\mathcal{A}_I$ defined with futures (i.e., igneous event occurrences) restricted to $[0, \tau]$. Formally, this corresponds to restricting the sample spaces (i.e., sets of possible futures) under consideration to futures defined on the time interval $[0, \tau]$.

With the indicated restriction,

$$p_A\left[A_{II}(0,\tau)\middle|\mathbf{e}_A\right] = p_A\left[A_I(0,\tau)\middle|\mathbf{e}_A\right] = 1-\exp(-\lambda_I\tau) \qquad \text{(Eq. J7.5-1)}$$

and

$$p_A\left[A_{IE}(0,\tau)\middle|\mathbf{e}_A\right]=1-\exp(-p_E\lambda_I\tau), \qquad \text{(Eq. J7.5-2)}$$

where λ_I is the element of $\mathbf{e}_A$ that corresponds to the annual frequency of an igneous intrusive event, p_E is the conditional probability that an igneous intrusive event will also have an eruptive component that ejects waste into the atmosphere, and the indicated probabilities are special cases of Equation J3.6-9. In turn, pE is defined by

$$pE = pEC\ pIW = (0.28)\ (0.2968) = 0.083, \qquad \text{(Eq. J7.5-3)}$$

where pEC = 0.28 is the conditional probability that an igneous intrusive event will have an eruptive component and pIW = 0.2968 is the conditional probability that the eruptive component of an igneous intrusive event will intersect waste.

The probabilities $p_A[\mathcal{A}_{II}(0,\ \tau)|\mathbf{e}_A]$ and $p_A[\mathcal{A}_{IE}(0,\ \tau)|\mathbf{e}_A]$ defined in Equations J7.5-1 and J7.5-2 are for one or more events. The corresponding probabilities for exactly one event in the time interval $[0,\ \tau]$ are

$$p_A\left[\tilde{A}_{II}(0,\tau)\middle|\mathbf{e}_A\right]=(\lambda_I\tau)\exp(-\lambda_I\tau) \qquad \text{(Eq. J7.5-4)}$$

and

$$p_A\left[\tilde{A}_{IE}(0,\tau)\middle|\mathbf{e}_A\right]=(p_E\lambda_I\tau)\exp(-p_E\lambda_I\tau), \qquad \text{(Eq. J7.5-5)}$$

where

$$\tilde{\mathcal{A}}_{II}(0,\tau)=\left\{\mathbf{a}_{II}:\mathbf{a}_{II}\in\mathcal{A}_{II}(0,\tau)\ \text{and}\ nII=1\right\},$$

$$\tilde{\mathcal{A}}_{IE}(0,\tau)=\left\{\mathbf{a}_{IE}:\mathbf{a}_{IE}\in\mathcal{A}_{IE}(0,\tau)\ \text{and}\ nIE=1\right\}$$

and the indicated probabilities are special cases of Equation J3.6-8.

The values for $p_A[\mathcal{A}_{II}(0,\ \tau)|\mathbf{e}_{Ai}]$, $p_A[\tilde{\mathcal{A}}_{II}(0,\ \tau)|\mathbf{e}_{Ai}]$, $p_A[\mathcal{A}_{IE}(0,\ \tau)|\mathbf{e}_{Ai}]$ and $p_A[\tilde{\mathcal{A}}_{IE}(0,\ \tau)|\mathbf{e}_{Ai}]$ for the time intervals [0, 20,000 yr] and [0, 1,000,000 yr] obtained for the LHS in Equation J4.9-1 are summarized in Figure J7.5-1.

J8 SEISMIC SCENARIO CLASSES: $\mathcal{A}_S$, $\mathcal{A}_{SG}$ AND $\mathcal{A}_{SF}$

J8.1 Relationships Involving $\mathcal{A}_S$, $\mathcal{A}_{SG}$ and $\mathcal{A}_{SF}$

The seismic ground motion scenario class and the seismic fault displacement scenario class are defined by the sets

$$\mathcal{A}_{SG}=\left\{\mathbf{a}:\mathbf{a}\in\mathcal{A}\ \text{and}\ nSG\geq 1\right\} \qquad \text{(Eq. J8.1-1)}$$

and

$$\mathcal{A}_{SF} = \{\mathbf{a} : \mathbf{a} \in \mathcal{A} \text{ and } nSF \geq 1\} \quad \text{(Eq. J8.1-2)}$$

as indicated in Equations J4.4-17 and J4.4-18. Further, the seismic scenario class $\mathcal{A}_S$ is defined by

$$\mathcal{A}_S = \mathcal{A}_{SG} \cup \mathcal{A}_{SF} = \{\mathbf{a} : \mathbf{a} \in \mathcal{A} \text{ and } nSG \geq 1 \text{ or } nSF \geq 1\} \quad \text{(Eq. J8.1-3)}$$

as indicated in Equation J4.4-12. In turn, $p_A(\mathcal{A}_{SG})$ is the probability of one or more seismic ground motion events; $p_A(\mathcal{A}_{SF})$ is the probability of one or more seismic fault displacement events; and $p_A(\mathcal{A}_S)$ is the probability of one or more seismic events.

The scenario classes $\mathcal{A}_S$, $\mathcal{A}_{SG}$ and $\mathcal{A}_{SF}$ are not disjoint. However, if the question is asked "What is the probability of a seismic event?," then most likely $p_A(\mathcal{A}_S)$ is the desired answer. If the question is asked "What is the probability of a seismic ground motion event?", then most likely $p_A(\mathcal{A}_{SG})$ is the desired answer. Similarly, if the question is asked "What is the probability of a seismic fault displacement event?", then most likely $p_A(\mathcal{A}_{SF})$ is the desired answer. If desired, disjoint scenario classes involving seismic ground motion and their associated probabilities can be defined in the same manner as indicated in Equations J6.1-4 – J6.1-7 for early WP failure and early DS failure.

No synergisms are assumed to exist between the doses that result from the seismic ground motion damage to WPs and the doses that result from seismic fault displacement damage to WPs. Further, as indicated in conjunction with Equation J4.5-1, no synergisms are assumed to exist between doses that result from seismic events and doses that result from other disruptions. As a result,

$$D_S(\tau|\mathbf{a}, \mathbf{e}_M) = D_{SG}(\tau|\mathbf{a}, \mathbf{e}_M) + D_{SF}(\tau|\mathbf{a}, \mathbf{e}_M), \quad \text{(Eq. J8.1-4)}$$

where

$D_S(\tau|\mathbf{a}, \mathbf{e}_M)$ = dose to RMEI (mrem/yr) at time τ resulting from seismic events associated with element $\mathbf{a}$ of $\mathcal{A}$,

$D_{SG}(\tau|\mathbf{a}, \mathbf{e}_M)$ = dose to RMEI (mrem/yr) at time τ resulting from ground motion damage to WPs for seismic events associated with element $\mathbf{a}$ of $\mathcal{A}$,

$D_{SF}(\tau|\mathbf{a}, \mathbf{e}_M)$ = dose to RMEI (mrem/yr) at time τ resulting from fault displacement damage to WPs for seismic events associated with element $\mathbf{a}$ of $\mathcal{A}$,

and all results are conditional on the element $\mathbf{e} = [\mathbf{e}_A, \mathbf{e}_M]$ of $\mathcal{E}$. If $\mathbf{a}$ involves no seismic ground motion damage to WPs, then $D_{SG}(\tau|\mathbf{a}, \mathbf{e}_M) = 0$; similarly, if $\mathbf{a}$ involves no seismic fault displacement damage to WPs, then $D_{SF}(\tau|\mathbf{a}, \mathbf{e}_M) = 0$.

In turn, the expected dose $\bar{D}_S(\tau|\mathbf{e})$ to the RMEI (mrem/yr) at time τ is given by

$$\begin{aligned}\bar{D}_S(\tau|\mathbf{e}) &= \int_{\mathcal{A}_S} D_S(\tau|\mathbf{a}, \mathbf{e}_M)\, d_A(\mathbf{a}|\mathbf{e}_A)\, \mathrm{d}A \\ &= \int_{\mathcal{A}_S} \left[D_{SG}(\tau|\mathbf{a}, \mathbf{e}_M) + D_{SF}(\tau|\mathbf{a}, \mathbf{e}_M)\right] d_A(\mathbf{a}|\mathbf{e}_A)\, \mathrm{d}A \\ &= \int_{\mathcal{A}_S} D_{SG}(\tau|\mathbf{a}, \mathbf{e}_M)\, d_A(\mathbf{a}|\mathbf{e}_A)\, \mathrm{d}A + \int_{\mathcal{A}_S} D_{SF}(\tau|\mathbf{a}, \mathbf{e}_M)\, d_A(\mathbf{a}|\mathbf{e}_A)\, \mathrm{d}A \\ &= \bar{D}_{SG}(\tau|\mathbf{e}) + \bar{D}_{SF}(\tau|\mathbf{e}),\end{aligned} \qquad \text{(Eq. J8.1-5)}$$

where (i)

$$\begin{aligned}\bar{D}_{SG}(\tau|\mathbf{e}) &= \int_{\mathcal{A}_S} D_{SG}(\tau|\mathbf{a}, \mathbf{e}_M)\, d_A(\mathbf{a}|\mathbf{e}_A)\, \mathrm{d}A \\ &= \int_{\mathcal{A}_{SG}} D_{SG}(\tau|\mathbf{a}, \mathbf{e}_M)\, d_A(\mathbf{a}|\mathbf{e}_A)\, \mathrm{d}A\end{aligned} \qquad \text{(Eq. J8.1-6)}$$

is the expected dose to the RMEI (mrem/yr) at time τ resulting from seismic ground motion events, (ii)

$$\begin{aligned}\bar{D}_{SF}(\tau|\mathbf{e}) &= \int_{\mathcal{A}_S} D_{SF}(\tau|\mathbf{a}, \mathbf{e}_M)\, d_A(\mathbf{a}|\mathbf{e}_A)\, \mathrm{d}A \\ &= \int_{\mathcal{A}_{SF}} D_{SF}(\tau|\mathbf{a}, \mathbf{e}_M)\, d_A(\mathbf{a}|\mathbf{e}_A)\, \mathrm{d}A\end{aligned} \qquad \text{(Eq. J8.1-7)}$$

is the expected dose to the RMEI (mrem/yr) at time τ resulting from seismic fault displacement events, and (iii) all results are conditional on the element $\mathbf{e} = [\mathbf{e}_A, \mathbf{e}_M]$ of $\mathcal{E}$. The conversion from an integral over $\mathcal{A}_S$ to an integral over $\mathcal{A}_{SG}$ in Equation J8.1-6 is possible because $D_{SG}(\tau|\mathbf{a}, \mathbf{e}_M) = 0$ if $\mathbf{a} \notin \mathcal{A}_{SG}$; similarly, the conversion from an integral over $\mathcal{A}_S$ to an integral over $\mathcal{A}_{SF}$ in Equation J8.1-7 is possible because $D_{SF}(\tau|\mathbf{a}, \mathbf{e}_M) = 0$ if $\mathbf{a} \notin \mathcal{A}_{SF}$.

The general form of the elements $\mathbf{a}$ of $\mathcal{A}$ is shown in Equations J4.4-1 – J4.4-8. However, because no synergisms between disruptions are assumed in the determination of $\bar{D}_{SG}(\tau|\mathbf{e})$ and $\bar{D}_{SF}(\tau|\mathbf{e})$, the representations for the elements of $\mathcal{A}_{SG}$ and $\mathcal{A}_{SF}$ can be simplified to

$$\mathbf{a}_{SG} = \left[nSG, \mathbf{a}_{SG,1}, \mathbf{a}_{SG,2}, \ldots, \mathbf{a}_{SG,nSG}\right] \qquad \text{(Eq. J8.1-8)}$$

and

$$\mathbf{a}_{SF} = \left[nSF, \mathbf{a}_{SF,1}, \mathbf{a}_{SF,2}, \ldots, \mathbf{a}_{SF,nSF}\right], \qquad \text{(Eq. J8.1-9)}$$

respectively. With this notation, the elements $\mathbf{a}_{SG}$ of $\mathcal{A}_{SG}$ only contain representations for seismic ground motion events, and the elements $\mathbf{a}_{SF}$ of $\mathcal{A}_{SF}$ only contain representations for seismic fault displacement events.

The expected (mean) dose $\bar{\bar{D}}_S(\tau)$ for the seismic scenario class $\mathcal{A}_S$ over both aleatory and epistemic uncertainty is given by

$$\begin{aligned}\bar{\bar{D}}_S(\tau) &= \int_{\mathcal{E}} \bar{D}_S(\tau|\mathbf{e})\, d_E(\mathbf{e})\, \mathrm{d}E \\ &= \int_{\mathcal{E}} \left[\bar{D}_{SG}(\tau|\mathbf{e}) + \bar{D}_{SF}(\tau|\mathbf{e})\right] d_E(\mathbf{e})\, \mathrm{d}E \\ &= \int_{\mathcal{E}} \bar{D}_{SG}(\tau|\mathbf{e})\, d_E(\mathbf{e})\, \mathrm{d}E + \int_{\mathcal{E}} \bar{D}_{SF}(\tau|\mathbf{e})\, d_E(\mathbf{e})\, \mathrm{d}E \\ &= \bar{\bar{D}}_{SG}(\tau) + \bar{\bar{D}}_{SF}(\tau), \end{aligned} \qquad \text{(Eq. J8.1-10)}$$

where

$$\bar{\bar{D}}_{SG}(\tau) = \int_{\mathcal{E}} \bar{D}_{SG}(\tau|\mathbf{e})\, d_E(\mathbf{e})\, \mathrm{d}E \qquad \text{(Eq. J8.1-11)}$$

is the expected (mean) dose for the seismic ground motion scenario class $\mathcal{A}_{SG}$ over both aleatory and epistemic uncertainty and

$$\bar{\bar{D}}_{SF}(\tau) = \int_{\mathcal{E}} \bar{D}_{SF}(\tau|\mathbf{e})\, d_E(\mathbf{e})\, \mathrm{d}E \qquad \text{(Eq. J8.1-12)}$$

is the expected (mean) dose for the seismic fault displacement scenario class $\mathcal{A}_{SF}$ over both aleatory and epistemic uncertainty.

The CCDF and CDF for $\bar{D}_S(\tau|\mathbf{e})$ over epistemic uncertainty are defined by

$$\begin{aligned} p_E\left[D < \bar{D}_S(\tau|\mathbf{e})\right] &= \int_{\mathcal{E}} \bar{\delta}_D\left[\bar{D}_S(\tau|\mathbf{e})\right] d_E(\mathbf{e})\, \mathrm{d}E \\ &= \int_{\mathcal{E}} \bar{\delta}_D\left[\bar{D}_{SG}(\tau|\mathbf{e}) + \bar{D}_{SF}(\tau|\mathbf{e})\right] d_E(\mathbf{e})\, \mathrm{d}E \end{aligned} \qquad \text{(Eq. J8.1-13)}$$

and

$$\begin{aligned} p_E\left[\bar{D}_S(\tau|\mathbf{e}) \le D\right] &= 1 - p_E\left[D < \bar{D}_S(\tau|\mathbf{e})\right] \\ &= \int_{\mathcal{E}} \underline{\delta}_D\left[\bar{D}_S(\tau|\mathbf{e})\right] d_E(\mathbf{e})\, \mathrm{d}E \\ &= \int_{\mathcal{E}} \underline{\delta}_D\left[\bar{D}_{SG}(\tau|\mathbf{e}) + \bar{D}_{SF}(\tau|\mathbf{e})\right] d_E(\mathbf{e})\, \mathrm{d}E, \end{aligned} \qquad \text{(Eq. J8.1-14)}$$

respectively. However, unlike the result for $\bar{\bar{D}}_S(\tau)$ in Equation J8.1-10, the CCDF and CDF for $\bar{D}_S(\tau|\mathbf{e})$ cannot be decomposed into a sum of separate results for the seismic ground motion scenario class $\mathcal{A}_{SG}$ and the seismic fault displacement scenario class $\mathcal{A}_{SF}$.

Direct evaluation of the integrals that define $\bar{\bar{D}}_S(\tau)$, $p_E[D < \bar{D}_S(\tau|\mathbf{e})]$ and $p_E[\bar{D}_S(\tau|\mathbf{e}) \le D]$ is not practicable. However, the approximations

$$\bar{\bar{D}}_S(\tau) \cong \sum_{i=1}^{nLHS} \bar{D}_S(\tau|\mathbf{e}_i)/nLHS, \quad \text{(Eq. J8.1-15)}$$

$$p_E\left[D < \bar{D}_S(\tau|\mathbf{e})\right] \cong \sum_{i=1}^{nLHS} \bar{\delta}_D\left[\bar{D}_S(\tau|\mathbf{e}_i)\right]/nLHS \quad \text{(Eq. J8.1-16)}$$

and

$$p_E\left[\bar{D}_S(\tau|\mathbf{e}) \le D\right] \cong \sum_{i=1}^{nLHS} \underline{\delta}_D\left[\bar{D}_S(\tau|\mathbf{e}_i)\right]/nLHS \quad \text{(Eq. J8.1-17)}$$

result with use of the LHS in Equation J4.9-1 as previously indicated in conjunction with Equations J4.9-8 – J4.9-10.

Further descriptions of the seismic scenario classes $\mathcal{A}_S$, $\mathcal{A}_{SG}$ and $\mathcal{A}_{SF}$ and sources of additional information are available in Section 6.6.

J8.2 Seismic Ground Motion Scenario Class: $\mathcal{A}_{SG}$

As discussed in conjunction with Equation J8.1-1, the seismic ground motion scenario class is defined by the subset $\mathcal{A}_{SG}$ of $\mathcal{A}$. Formally, $\mathcal{A}_{SG}$ contains all elements $\mathbf{a}$ of $\mathcal{A}$ with $nSG > 0$. To fully define $\mathcal{A}_{SG}$, it is necessary to first define the vector $\mathbf{a}_{SG}$ indicated in Equation (J8.1-8) and its associated components $\mathbf{a}_{SG,j}$, $j = 1, 2, \ldots, nS$.

Each component $\mathbf{a}_{SG,j}$ of $\mathbf{a}_{SG}$ is defined by

$$\mathbf{a}_{SG,j} = \left[t_j, v_j, VR_j, AW_{1j}, AW_{2j}, AD_j, RW_{1j}, RW_{2j}, FDP_j, FDF_j\right], \quad \text{(Eq. J8.2-1)}$$

where, for seismic event j occurring at time t_j (yr),

v_j = peak ground velocity (PGV, m/s),

VR_j = volume (m^3/m) of rockfall,

AW_{rj} = damaged area (m^2) on WP type r with $r = 1$ ~ CSNF WP and $r = 2$ ~ CDSP WP,

AD_j = damaged area (m^2) on DSs,

RW_{rj} = indicator variable for rupture of WP type r

$$= \begin{cases} 2 & \text{if rupture occurred} \\ 1 & \text{if incipient rupture occurred} \\ 0 & \text{otherwise,} \end{cases}$$

FDP_j = indicator variable for failure of DS plates

$$= \begin{cases} 1 & \text{if DS plates fail} \\ 0 & \text{otherwise,} \end{cases}$$

FDF_j = indicator variable for failure of DS frame

$$= \begin{cases} 1 & \text{if DS frames fail} \\ 0 & \text{otherwise.} \end{cases}$$

In turn, the distributions for the individual elements of $\mathbf{a}_{SG,j}$ are defined by the following quantities:

$\lambda_G(v)$ = exceedance frequency (yr^{-1}) for PGV v (i.e., $\lambda_G(v)$ is the seismic ground motion hazard curve), (Eq. J8.2-2)

$pRF(v)$ = probability of rockfall conditional on the occurrence of a seismic ground motion event with PGV v, (Eq. J8.2-3)

$d_V(V|v)$ = density function (m/m^3) for volume V of rock (m^3/m) that caves into a drift conditional on the occurrence of a seismic ground motion event with PGV v ($d_V(V|v)$ corresponds to a gamma distribution with a mean $\mu(v)$ and a standard deviation $\sigma(v)$ that are functions of v), (Eq. J8.2-4)

$pWD_r(v|\delta_{Ir}, \delta_{Rr}, WT_r, R)$ = probability of nonzero damaged area on a WP of type r ($r = 1$ ~ CSNF WP and $r = 2$ ~ CDSP WP) conditional on the occurrence of a seismic ground motion event with PGV v given the existence of conditions defined by the following variables: (i) δ_{Ir}, where $\delta_{Ir} = 1$ ~ WPs with degraded internals and $\delta_{Ir} = 0$ ~ WPs with intact internals, (ii) δ_{Rr}, where $\delta_{Rr} = 1$ ~ WPs surrounded by rubble and $\delta_{Rr} = 0$ ~ WPs not surrounded by rubble, (iii) WT_r = outer corrosion barrier thickness (mm) on WP, and (iv) R = residual stress failure threshold, (Eq. J8.2-5)

$d_{Ar}(A|v, \delta_{Ir}, \delta_{Rr}, WT_r, R)$ = density function (m^{-2}) for damaged area A (m^2) on a WP of type r conditional on the occurrence of a seismic ground motion event with PGV v that results in a nonzero damaged area (see $pWD_r(v|\delta_{Ir}, \delta_{Rr}, WT_r, R)$) given the existence of conditions defined by $\delta_{Ir}, \delta_{Rr}, WT_r, R$, (Eq. J8.2-6)

$d_L(L|v, F)$ = density function (Pa^{-1}) for total dynamic load L (Pa) on a DS conditional on the occurrence of a seismic ground motion event with PGV v given that a fraction F of the drift is filled with rubble ($d_L(L|v, F)$ corresponds to a lognormal distribution with parameters that are functions of v and F), (Eq. J8.2-7)

$d_A(A|L, DT)$ = density function (m^{-2}) for damaged area (m^2) on DS conditional on total dynamic load L on DS and DS thickness DT (mm), (Eq. J8.2-8)

$pIRW_r(v|\delta_{Ir}, \delta_{Rr}, WT_r)$ = probability of incipient rupture of a WP of type r conditional on the occurrence of a seismic ground motion event with PGV v given the existence of conditions defined by $\delta_{Ir}, \delta_{Rr}, WT_r$, (Eq. J8.2-9)

$pRW_r(v|\delta_{Ir}, \delta_{Rr}, WT_r)$ = probability of rupture of a WP of type r conditional on the occurrence of a seismic ground motion event with PGV v given the existence of conditions defined by $\delta_{Ir}, \delta_{Rr}, WT_r$, (Eq. J8.2-10)

$pDP(v|F, DT)$ = probability of DS plate failure conditional on the occurrence of a seismic ground motion event with PGV v given the existence of conditions defined by F and DT, (Eq. J8.2-11)

$pDF(v|F, DT)$ = probability of DS frame failure conditional on the occurrence of a seismic ground motion event with PGV v given the existence of conditions defined by F and DT. (Eq. J8.2-12)

As indicated by the definitions of the components of $\mathbf{a}_{SG,j}$ in Equation J8.2-1 and the following definitions in Equations J8.2-2 – J8.2-12 of the quantities that define the distributions for the components of $\mathbf{a}_{SG,j}$, the probabilistic structure for the set $\mathcal{A}_{SG}$ is very complex. This structure is made even more complex by the fact that the distributions for individual components of $\mathbf{a}_{SG,j}$ can depend on both the values for components in $\mathbf{a}_{SG,k}$, $k = 1, 2, \ldots, j-1$, and the repository conditions that derive from these values. For example, WP thickness at time t_j affects values for components of $\mathbf{a}_{SG,j}$ and derives from both values of components in $\mathbf{a}_{SG,k}$, $k = 1, 2, \ldots, j-1$, and the modeling of WP thickness as a function of these values. In concept, there exists a density

function $d_A(\mathbf{a})$ defined on $\mathcal{A}$ that includes the aleatory uncertainty associated with the occurrence of seismic events. Actually, $d_A(\mathbf{a})$ is more appropriately represented by $d_A(\mathbf{a}|\mathbf{e})$ given that the distributions for components of $\mathbf{a}_{SG,j}$ can depend on calculated quantities that in turn depend on components of $\mathbf{e} = [\mathbf{e}_A, \mathbf{e}_M]$. However, in practice, $d_A(\mathbf{a})$, or more generally $d_A(\mathbf{a}|\mathbf{e})$, is too complex to represent in a closed form.

Formally, the expected dose $\bar{D}_{SG}(\tau|\mathbf{e})$ to the RMEI (mrem/yr) at time τ from the seismic ground motion scenario class $\mathcal{A}_{SG}$ is given by

$$\bar{D}_{SG}(\tau|\mathbf{e}) = \int_{\mathcal{A}_{SG}} D_{SG}(\tau|\mathbf{a}, \mathbf{e}_M)\, d_A(\tau|\mathbf{e})\, \mathrm{d}A \qquad \text{(Eq. J8.2-13)}$$

as indicated in Equation J4.4-13, where

$D_{SG}(\tau|\mathbf{a}, \mathbf{e}_M)$ = dose to RMEI (mrem/yr) at time τ resulting from seismic ground motion events associated with element $\mathbf{a}$ of $\mathcal{A}_{SG}$

and all results are conditional on the element $\mathbf{e} = [\mathbf{e}_A, \mathbf{e}_M]$ of $\mathcal{E}$. In the determination of $D_{SG}(\tau|\mathbf{a}, \mathbf{e}_M)$, no synergisms are assumed to exist with other disruptive events that could be associated with elements of $\mathcal{A}_{SG}$. Further, as indicated in Equations J4.5-16 and J4.5-18 with $C = SG$, the CCDF and CDF for $D_{SG}(\tau|\mathbf{a}, \mathbf{e}_M)$ are defined by the probabilities $p_A[D_{SG}(\tau|\mathbf{a}, \mathbf{e}_M) \le D|\mathbf{e}_A]$ and $p_A[D < D_{SG}(\tau|\mathbf{a}, \mathbf{e}_M)|\mathbf{e}_A]$.

In addition, given that $\bar{D}_{SG}(\tau|\mathbf{e})$ can be determined, additional results of the form indicated in Equations J4.9-8 – J4.9-10 with $C = SG$ can also be determined for the seismic ground motion scenario class $\mathcal{A}_{SG}$. For example, the expected (mean) dose $\bar{\bar{D}}_{SG}(\tau)$ to the RMEI (mrem/yr) at time τ for the seismic ground motion scenario class $\mathcal{A}_{SG}$ over both aleatory and epistemic uncertainty is given by

$$\begin{aligned}
\bar{\bar{D}}_{SG}(\tau) &= \int_{\mathcal{E}} \bar{D}_{SG}(\tau|\mathbf{e})\, d_E(\mathbf{e})\, \mathrm{d}E \\
&= \int_{\mathcal{E}} \left[\int_{\mathcal{A}_{SG}} D_{SG}(\tau|\mathbf{a}, \mathbf{e}_M)\, d_A(\mathbf{a}|\mathbf{e})\, \mathrm{d}A \right] d_E(\mathbf{e})\, \mathrm{d}E \\
&\cong \sum_{i=1}^{nLHS} \left[\int_{\mathcal{A}_{SG}} D_{SG}(\tau|\mathbf{a}, \mathbf{e}_{Mi})\, d_A(\mathbf{a}|\mathbf{e}_i)\, \mathrm{d}A \right] \Big/ nLHS, \qquad \text{(Eq. J8.2-14)}
\end{aligned}$$

where $\mathbf{e}_i = [\mathbf{e}_{Ai}, \mathbf{e}_{Mi}]$, $i = 1, 2, \ldots, nLHS$, corresponds to the LHS indicated in Equation J4.9-1.

J8.3 Seismic Ground Motion Scenario Class: 0 to 20,000 yr

Evaluation of the integral in Equation J8.2-13 that defines $\bar{D}_{SG}(\tau|\mathbf{e})$ for $0 \le \tau \le 10^6$ yr with quadrature-based procedures is not possible as a result of the complexity of the futures contained in $\mathcal{A}_{SG}$ and their associated probabilistic structure. However, when τ is restricted to the time interval [0, 20,000 yr], the evaluation of $D_{SG}(\tau|\mathbf{e})$ is significantly simplified. This simplification results because (i) significant reduction in the thicknesses of the WPs and DSs does not take place, (ii) significant accumulation of rock fall does not take place, (iii) the probabilities of WP damage and WP rupture for CSNF WPs are sufficiently low that these potential occurrences do not need to be included in the determination of $\bar{D}_{SG}(\tau|\mathbf{e})$, (iv) the probability of rupture for CDSP WPs is sufficiently low that this potential occurrence does not need to be included in the determination of $\bar{D}_{SG}(\tau|\mathbf{e})$, and (v) the probabilities for DS plate damage, DS plate failure and DS frame failure are sufficiently low that these potential occurrences do not need to be included in the determination of $\bar{D}_{SG}(\tau|\mathbf{e})$. As a result, only damage to CDSP WPs under intact DSs needs to be considered in the determination of $\bar{D}_{SG}(\tau|\mathbf{e})$ for $0 \le \tau \le 20{,}000$ yr.

Given that only damage to CDSP WPs under intact DSs needs to be considered in the determination of $\bar{D}_{SG}(\tau|\mathbf{e})$ for $0 \le \tau \le 20{,}000$ yr, the representation for $\mathbf{a}_{SG,j}$ in Equation J8.2-1 simplifies to

$$\mathbf{a}_{SG,j} = \left[t_j, A_j \right], \qquad \text{(Eq. J8.3-1)}$$

where t_j is the time (yr) of seismic event j and A_j is the resultant damaged area (m^2) on a CDSP WP. As a result, a seismic ground motion future $\mathbf{a}_{SG}$ for the time interval [0, 20,000 yr] is effectively of the form

$$\mathbf{a}_{SG} = \left[nSG, t_1, A_1, t_2, A_2, \ldots, t_{nSG}, A_{nSG} \right]. \qquad \text{(Eq. J8.3-2)}$$

Distributions for t_j and A_j can be derived from quantities characterizing the aleatory uncertainty associated with seismic ground motion events that are given following Equation J8.2-1. The PGV v_j associated with seismic ground motion event j is not included in the definition $\mathbf{a}_{SG,j}$ in Equation J8.3-1. However, the hazard curve defining exceedance probabilities for PGV defines the distribution of event times t_j and also enters into the determination of the distribution of the damaged area A_j given the occurrence of a seismic ground motion event at time t_j.

A distinction is made between WPs with intact internals and WPs with degraded internals. Further, the assumption is made that the internals in a WP degrade as soon as the outer barrier of the WP is damaged. The distinction between WPs with intact internals and degraded internals is potentially important because WPs with degraded internals are assumed to be less resistant to damage than WPs with intact internals. In the context of the representation for $\mathbf{a}_{SG}$ in Equation J8.3-2, the first event at time t_1 involves damage to WPs with intact internals, and the events at times $t_2, t_3, \ldots, t_{nS}$ involve damage to WPs with degraded internals.

Given that seismic ground motion futures $\mathbf{a}_{SG}$ of the form indicated in Equation J8.3-2 are under consideration, the expected dose $\bar{D}_{SG}(\tau|\mathbf{a}, \mathbf{e})$ to the RMEI can be determined with use of the following quantities to characterize the aleatory uncertainty associated with the components of $\mathbf{a}$ that are defined by $\mathbf{a}_{SG}$:

$\lambda_1(\mathbf{e})$ = occurrence rate (yr^{-1}) for seismic ground motion events that cause damage to CDSP WPs with intact internals, (Eq. J8.3-3)

$d_{A1}(A|\mathbf{e})$ = density function (m^{-2}) defined on set $\mathcal{A}1$ for damaged (i.e., diffusive) area on a CDSP WP with intact internals conditional on the occurrence of a damaging seismic ground motion event, (Eq. J8.3-4)

$\lambda_2(\mathbf{e})$ = occurrence rate (yr^{-1}) for seismic ground motion events that cause damage to CDSP WPs with degraded internals, (Eq. J8.3-5)

$d_{A2}(A|\mathbf{e})$ = density function (m^{-2}) defined on set $\mathcal{A}2$ for damaged (i.e., diffusive) area on a CDSP WP with degraded internals conditional on the occurrence of a damaging seismic ground motion event. (Eq. J8.3-6)

As indicated, $\lambda_1(\mathbf{e})$, $d_{A1}(A|\mathbf{e})$, $\lambda_2(\mathbf{e})$ and $d_{A2}(A|\mathbf{e})$ are dependent on elements of $\mathbf{e}$. Derivations of these quantities that incorporate this dependence will be discussed later.

Given the preceding quantities, the expected dose $\bar{D}_{SG}(\tau|\mathbf{e})$ to the RMEI at time τ for $0 \le \tau \le$ 20,000 yr arising from the aleatory uncertainty associated with seismic ground motion events can be approximated by

$$\begin{aligned}\bar{D}_{SG}(\tau|\mathbf{e}) \cong \sum_{k=1}^{n} \Bigg(& \left\{ \exp\left[-\lambda_1(\mathbf{e})\, t_{k-1}\right] \right\}_3 \left\{ \lambda_1(\mathbf{e})(\Delta t_k) \exp\left[-\lambda_1(\mathbf{e})\, \Delta t_k\right] \right\}_4 \Bigg)_1 \\ & \times \Bigg(\left\{ \int_{\mathcal{A}1} D_{SG}(\tau|[1, t_k, A], \mathbf{e}_M)\, d_{A1}(A|\mathbf{e})\, dA \right\}_5 \\ & + \left\{ \int_{t_k}^{\tau} \left[\int_{\mathcal{A}2} D_{SG}(\tau|[1, \tilde{t}, A], \mathbf{e}_M)\, d_{A2}(A|\mathbf{e})\, dA \right] \lambda_2(\mathbf{e})\, d\tilde{t} \right\}_6 \Bigg)_2 \end{aligned} \quad \text{(Eq. J8.3-7)}$$

where $0 = t_0 < t_1 < \ldots < t_n = \tau$, $\Delta t_k = t_{k-1} - t_k$, and $D_{SG}(\tau|[1, t_k, A], \mathbf{e}_M)$ is the dose to the RMEI (mrem/yr) at time τ that results from a damaged (i.e., diffusive) area of size A (m^2) on individual WPs associated with a single seismic ground motion event occurring at time t_k.

In the preceding, $\{\sim\}_3$ is the probability that WPs with intact internals are not damaged in the time interval $[0, t_{k-1}]$, and $\{\sim\}_4$ is the probability that WPs with intact internals are damaged in the time interval $[t_{k-1}, t_k]$. As a result, the product $(\{\sim\}_3\ \{\sim\}_4)_1$ is the probability that the first

seismic ground motion event causing damage to WPs with intact internals occurs in the time internal $[t_{k-1}, t_k]$. The integral contained in $\{\sim\}_5$ is the expected dose to the RMEI at time τ from a seismic ground motion event at time t_k that damages WPs with intact internals, and the double integral contained in $\{\sim\}_6$ is the expected dose to the RMEI at time τ from seismic ground motion events that occur in the time interval $[t_k, \tau]$ and damage WPs with degraded internals. As a result, the sum $(\{\sim\}_5 + \{\sim\}_6)_2$ is the expected dose to the RMEI at time τ conditional on the occurrence of a seismic ground motion event at time t_k that damages WPs with intact internals; specifically, the conditional expected dose $(\{\sim\}_5 + \{\sim\}_6)_2$ includes both the dose from the event at time k and the dose from additional events that can potentially occur in the time interval $[t_k, \tau]$. Given that the "events" corresponding to occurrence in time interval $[t_{k-1}, t_k]$ of first damage to WPs with intact internals are disjoint, it follows that the sum of the products of the probabilities defined by $(\{\sim\}_3\ \{\sim\}_4)_1$ and the conditional expected doses defined by $(\{\sim\}_5 + \{\sim\}_6)_2$ approximates $\bar{D}_{SG}(\tau|\mathbf{e})$. Underlying this approximation is the assumption that the effects of multiple seismic events are additive.

In turn, the integral representation

$$\bar{D}_{SG}(\tau|\mathbf{e}) = \int_0^{\tau} \left(\lambda_1(\mathbf{e}) \exp\left[-\lambda_1(\mathbf{e})t\right]\right) \left(\int_{\mathcal{A}1} D_{SG}(\tau|[1, t, A], \mathbf{e}_M)\, d_{A1}(A|\mathbf{e})\, \mathrm{d}A \right.$$
$$\left. + \int_t^{\tau} \left[\int_{\mathcal{A}2} D_{SG}(\tau|[1, \tilde{t}, A], \mathbf{e}_M)\, d_{A2}(A|\mathbf{e})\, \mathrm{d}A \right] \lambda_2(\mathbf{e})\, \mathrm{d}\tilde{t} \right) \mathrm{d}t \qquad \text{(Eq. J8.3-8)}$$

follows from the approximation in Equation J8.3-7 as $\Delta t_k \to 0$.

The integral defining $\bar{D}_{SG}(\tau|\mathbf{e})$ in Equation J8.3-8 can be efficiently approximated with quadrature-based methods by evaluating $D_{SG}(\tau|[1, t, A], \mathbf{e}_M)$ for selected values of t and A and then using interpolation to obtain $D_{SG}(\tau|[1, t, A], \mathbf{e}_M)$ for additional values of t and A. Specifically, the evaluations

$$D_{SG}(\tau|[1, t_r, A_s], \mathbf{e}_{Mi}), r = 1, 2, \ldots, nT, s = 1, 2, \ldots, nDA, \qquad \text{(Eq. J8.3-9)}$$

are carried out for $0 \le \tau \le 20{,}000$ yr, each element $\mathbf{e}_i = [\mathbf{e}_{Ai}, \mathbf{e}_{Mi}]$ of the LHS in Equation J4.9-1 and damage to CDSP WPs. In the TSPA-LA,

$$t_r = 100, 1000, 3000, 6000, 12000, 18000 \text{ yrs} \qquad \text{(Eq. J8.3-10)}$$

for $r = 1, 2, \ldots, nT = 6$ and

$$A_s = 10^{-8+s}\ (32.6\ \text{m}^2) \qquad \text{(Eq. J8.3-11)}$$

for $s = 1, 2, \ldots, nDA = 5$. Selected results are shown in Figures J8.3-1 and J8.3-2.

In turn, $\bar{D}_{SG}(\tau|\mathbf{e}_i)$ can be approximated by

$$\bar{D}_{SG}\left(\tau|\mathbf{e}_i\right) \cong \sum_{j=1}^{n}\left(\lambda_1\left(\mathbf{e}_i\right)\exp\left[-\lambda_1\left(\mathbf{e}_i\right)\hat{t}_{j-1}\right]\right)\left(\left\{\sum_{l=1}^{n1}\hat{D}_{SG}\left(\tau|\left[1,\hat{t}_j,A_{1l}\right],\mathbf{e}_{Mi}\right)d_{A1}\left(A_{1l}|\mathbf{e}_i\right)\Delta A_{1l}\right\}\right.$$
$$\left.+\left\{\sum_{k=j+1}^{n}\left[\sum_{l=1}^{n2}\hat{D}_{SG}\left(\tau|\left[1,\hat{t}_{k-1},A_{2l}\right],\mathbf{e}_{Mi}\right)d_{A2}\left(A_{2l}|\mathbf{e}_i\right)\Delta A_{2l}\right]\lambda_2\left(\mathbf{e}_i\right)\Delta\hat{t}_k\right\}\right)\Delta\hat{t}_j, \quad \text{(Eq. J8.3-12)}$$

where (i) $0 = \hat{t}_0 < \hat{t}_1 < \ldots < \hat{t}_n = \tau$ is a subdivision of $[0, \tau]$, (ii) $a_1 = A_{10} < A_{11} < \ldots < A_{1,n1} = b_1$ is a subdivision of $\mathcal{A}1 = [a_1, b_1]$, (iii) $a_2 = A_{20} < A_{21} < \ldots < A_{2,n2} = b_2$ is a subdivision of $\mathcal{A}2 = [a_2, b_2]$, and (iv) the doses $\hat{D}_{SG}(\tau|[1, \hat{t}_j, A_{1l}], \mathbf{e}_{Mi})$ and $\hat{D}_{SG}(\tau|[1, \hat{t}_{k-1}, A_{2l}], \mathbf{e}_{Mi})$ are approximations to $D_{SG}(\tau|[1, \hat{t}_j, A_{1l}] \mathbf{e}_{Mi})$ and $D_{SG}(\tau|[1, \hat{t}_{k-1}, A_{2l}], \mathbf{e}_{Mi})$ obtained with interpolation procedures from the results indicated in Equation J8.3-9.

An alternative computational strategy that involves fewer interpolations is to approximate $\bar{D}_{SG}(\tau|\mathbf{e}_i)$ by

$$\bar{D}_{SG}\left(\tau|\mathbf{e}_i\right) \cong \sum_{j=1}^{n}\left(\lambda_1\left(\mathbf{e}_i\right)\exp\left[-\lambda_1\left(\mathbf{e}_i\right)\hat{t}_{j-1}\right]\right)\left(\hat{I}_1\left(\tau|\hat{t}_j,\mathbf{e}_i\right)+\sum_{k=j+1}^{n}\left[\hat{I}_2\left(\tau|\hat{t}_{k-1},\mathbf{e}_i\right)\right]\lambda_2\left(\mathbf{e}_i\right)\Delta\hat{t}_k\right)\Delta\hat{t}_j, \quad \text{(Eq. J8.3-13)}$$

where, for a given event time t, $\hat{I}_1(\tau|t, \mathbf{e}_i)$ and $\hat{I}_2(\tau|t, \mathbf{e}_i)$ are approximations to the integrals

$$I_1\left(\tau|t,\mathbf{e}_i\right) = \int_{\mathcal{A}1} D_{SG}\left(\tau|[1,t,A],\mathbf{e}_{Mi}\right)d_{A1}\left(A|\mathbf{e}_i\right)\mathrm{d}A \quad \text{(Eq. J8.3-14)}$$

and

$$I_2\left(\tau|t,\mathbf{e}_i\right) = \int_{\mathcal{A}2} D_{SG}\left(\tau|[1,t,A],\mathbf{e}_{Mi}\right)d_{A2}\left(A|\mathbf{e}_i\right)\mathrm{d}A, \quad \text{(Eq. J8.3-15)}$$

respectively. For numerical implementation, the approximations

$$\hat{I}_1\left(\tau|t_r,\mathbf{e}_i\right) = \sum_{l=1}^{n1}\hat{D}_{SG}\left(\tau|[1,t_r,A_{1l}],\mathbf{e}_{Mi}\right)d_{A1}\left(A_{1l}|\mathbf{e}_i\right)\Delta A_{1l} \quad \text{(Eq. J8.3-16)}$$

and

$$\hat{I}_2\left(\tau|t_r,\mathbf{e}_i\right) = \sum_{l=1}^{n2}\hat{D}_{SG}\left(\tau|[1,t_r,A_{2l}],\mathbf{e}_{Mi}\right)d_{A2}\left(A_{2l}|\mathbf{e}_i\right)\Delta A_{2l} \quad \text{(Eq. J8.3-17)}$$

can be determined for the times t_r, $r = 1, 2, \ldots, nT = 6$, in Equation J8.3-10 with the areas A_{1l} and A_{2l} defined the same as in Equation J8.3-12. Once values for $\hat{I}_1(\tau|t_r, \mathbf{e}_i)$ and $\hat{I}_2(\tau|t_r, \mathbf{e}_i)$, $r = 1, 2, \ldots, nT = 6$, are determined, the required values for $\hat{I}_1(\tau|\hat{t}_j, \mathbf{e}_i)$ and $\hat{I}_2(\tau|\hat{t}_{k-1}, \mathbf{e}_i)$ in Equation J8.3-13 can be determined by interpolation as illustrated in Figure J8.3-3. Use of the approximation to $\bar{D}_{SG}(\tau|\mathbf{e}_i)$ in Equation J8.3-13 rather than the approximation in Equation J8.3-12 reduces the number of required interpolations by a factor of approximately $nDA = 5$ (see Equation J8.3-11).

As an example, the estimate for $\bar{D}_{SG}(\tau|\mathbf{e}_1)$ obtained for LHS element $\mathbf{e}_1$ with the procedure indicated in Equation J8.3-13 is shown in Figure J8.3-4. Further, the results obtained with all $nLHS = 300$ LHS elements are summarized in Figure J8.3-5 and presented in a standard format in Figure J8.3-6.

As previously discussed in conjunction with Equations J5-8 and J6.2-9, dose and expected dose to the RMEI are just two of a large number of results that can be produced and presented in the TSPA-LA. As an example, a summary of the dose calculations for ^{99}Tc is given in Figure J8.3-7, which has the same organization as Figure J8.3-5. Overall, ^{99}Tc is one of the largest contributors to the expected (mean) dose $\bar{\bar{D}}_{SG}(\tau)$ for the 20,000 yr time period. As previously done in Figure J5-4 and other similar figures, a compact summary of the expected (mean) dose results $\bar{\bar{D}}_{SG,r}(\tau)$ for the individual radioactive species is provided in Figure J8.3-8, where $\bar{\bar{D}}_{SG,r}(\tau)$ is the expected (mean) dose to the RMEI at time τ resulting from the release of radioactive species r due to seismic ground motion events (see Equation J6.2-9 and associated discussion).

An alternative numerical procedure is to use Monte Carlo techniques to estimate the distribution of the dose function $D_{SG}(\tau|\mathbf{a}, \mathbf{e}_M)$ defined in conjunction with Equation J8.3-8 for futures of the form defined in Equation J8.3-2. Specifically, a random sample of futures

$$\mathbf{a}_{SG,k} = \left[nSG_k, t_{1k}, A_{1k}, t_{2k}, A_{2k}, \ldots, t_{nSG_k,k}, A_{nSG_k,k} \right], k = 1, 2, \ldots, nR, \quad \text{(Eq. J8.3-18)}$$

of size nR can be drawn in consistency with the distributions defined by $\lambda_1(\mathbf{e}_i)$, $d_{A1}(A|\mathbf{e}_i)$, $\lambda_2(\mathbf{e}_i)$ and $d_{A2}(A|\mathbf{e}_i)$ for each LHS element $\mathbf{e}_i = [\mathbf{e}_{Ai}, \mathbf{e}_{Mi}]$. Then, $D_{SG}(\tau|\mathbf{a}_{SG,j}, \mathbf{e}_{Mi})$ can be estimated by

$$D_{SG}\left(\tau|\mathbf{a}_{SG,k}, \mathbf{e}_{Mi}\right) \cong \sum_{j=1}^{nSG_k} \hat{D}_{SG}\left(\tau|\left[1, t_{jk}, A_{jk}\right], \mathbf{e}_{Mi}\right) \quad \text{(Eq. J8.3-19)}$$

where the individual doses $\hat{D}_{SG}(\tau|[1, t_{jk}, A_{jk}], \mathbf{e}_{Mi})$ are obtained with interpolation procedures from the results indicated in Equation J8.3-9.

Once the results in Equation J8.3-19 are available, $\bar{D}_{SG}(\tau|\mathbf{e}_i)$, the CDF for $D_{SG}(\tau|\mathbf{a}_{SG}, \mathbf{e}_{Mi})$ and the CCDF for $D_{SG}(\tau|\mathbf{a}_{SG}, \mathbf{e}_{Mi})$ can be determined in the same manner as indicated in Equations J4.5-19 – J4.5-21 with $C = SG$. Specifically,

$$\bar{D}_{SG}\left(\tau|\mathbf{e}_i\right) \cong p_A\left(\mathcal{A}_{SG}|\mathbf{e}_i\right)\sum_{k=1}^{nR} D_{SG}\left(\tau|\mathbf{a}_{SG,k}, \mathbf{e}_{Mi}\right)\Big/nR$$

$$\cong p_A\left(\mathcal{A}_{SG}|\mathbf{e}_i\right)\sum_{k=1}^{nR}\left\{\sum_{j=1}^{nSG_k}\hat{D}_{SG}\left(\tau|\left[1, t_{jk}, \mathcal{A}_{jk}\right], \mathbf{e}_{Mi}\right)\right\}\Big/nR, \quad \text{(Eq. J8.3-20)}$$

$$p_A\left[D_{SG}\left(\tau|\mathbf{a}, \mathbf{e}_{Mi}\right) \le D|\mathbf{e}_i\right] = 1 - p_A\left[D < D_{SG}\left(\tau|\mathbf{a}, \mathbf{e}_{Mi}\right)\Big|\mathbf{e}_i\right]$$

$$\cong p_A\left(\mathcal{A}_{SG}|\mathbf{e}_i\right)\sum_{k=1}^{nR}\underline{\delta}_D\left[D_{SG}\left(\tau|\mathbf{a}_{SG,k}, \mathbf{e}_{Mi}\right)\right]\Big/nR$$

$$\cong p_A\left(\mathcal{A}_{SG}|\mathbf{e}_i\right)\sum_{k=1}^{nR}\underline{\delta}_D\left\{\sum_{j=1}^{nSG_k}\left[\hat{D}_{SG}\left(\tau|\left[1, t_{jk}, A_{jk}\right], \mathbf{e}_{Mi}\right)\right]\right\}\Big/nR \quad \text{(Eq. J8.3-21)}$$

and

$$p_A\left[D < D_{SG}\left(\tau|\mathbf{a}, \mathbf{e}_{Mi}\right)\Big|\mathbf{e}_i\right] \cong p_A\left(\mathcal{A}_{SG}|\mathbf{e}_i\right)\sum_{k=1}^{nR}\bar{\delta}_D\left[D_{SG}\left(\tau|\mathbf{a}_{SG,k}, \mathbf{e}_{Mi}\right)\right]\Big/nR$$

$$\cong p_A\left(\mathcal{A}_{SG}|\mathbf{e}_i\right)\sum_{k=1}^{nR}\bar{\delta}_D\left\{\sum_{j=1}^{nSG_k}\hat{D}_{SG}\left(\tau|\left[1, t_{jk}, A_{jk}\right], \mathbf{e}_{Mi}\right)\right\}\Big/nR, \quad \text{(Eq. J8.3-22)}$$

as indicated in Equations J4.5-19 – J4.5-21 with $C = SG$, where (i)

$$\mathbf{a}_{SG,k} = \left[nSG_k, \mathbf{a}_{SG,1k}, \mathbf{a}_{SG,2k}, \ldots, \mathbf{a}_{SG,nSG_k,k}\right], k = 1, 2, \ldots, nR,$$

is a random sample from vectors $\mathbf{a}_{SG}$ of the form defined in Equation J8.3-18 generated in consistency with $\lambda_1(\mathbf{e}_i)$, $d_{A1}(A|\mathbf{e}_i)$, $\lambda_2(\mathbf{e}_i)$ and $d_{A2}(A|\mathbf{e}_i)$ and with

$$\mathbf{a}_{SG,jk} = \left[t_{jk}, A_{jk}\right]$$

for j = 1, 2, …, nSG_k and (ii) the indicator functions $\bar{\delta}_D(\sim)$ and $\underline{\delta}_D(\sim)$ are defined in Equations J4.2-3 and J4.2-7, respectively. This process is illustrated in Figures J8.3-9 and J8.3-10.

In the preceding, $p_A(\mathcal{A}_{SG}|\mathbf{e}_i)$, $p_A[D_{SG}(\tau|\mathbf{a}, \mathbf{e}_{Mi}) \le D|\mathbf{e}_i]$ and $p_A[D < D_{SG}(\tau|\mathbf{a}, \mathbf{e}_{Mi})|\mathbf{e}_i]$ are indicated as being conditional on $\mathbf{e}_i$ because the values for $\lambda_1(\mathbf{e}_i)$, $d_{A1}(A|\mathbf{e}_i)$, $\lambda_2(\mathbf{e}_i)$ and $d_{A2}(A|\mathbf{e}_i)$ are conditional on the value for $\mathbf{e}_i$. Further, as used in Equations J8.3-20 – J8.3-22, the set (i.e., scenario class) $\mathcal{A}_{SG}$ is assumed to only contain those futures in which one or more CDSP WPs failures occur in the time interval [0, 20,000 yr]. Because of this restriction,

$$p_A\left(\mathcal{A}_{SG}\middle|\mathbf{e}_i\right) = 1 - \exp\left[-20{,}000\,\lambda_1\left(\mathbf{e}_i\right)\right] \qquad \text{(Eq. J8.3-23)}$$

in Equations J8.3-20 – J8.3-22 (see Equation J3.6-9).

As discussed in Section J4.10, the numerical stability of results obtained with Latin hypercube sampling can be assessed with replicated sampling. Specifically, the analysis for seismic ground motion events was performed with the nRL = 3 replicated LHSs indicated in Equation J4.10-1. In turn, this analysis shows that the numerical error in using Latin hypercube sampling to estimate $\bar{\bar{D}}_{SG}(\tau)$ is small relative to the epistemic uncertainty associated with the possible values for $\bar{D}_{SG}(\tau)$ (Figure J8.3-11).

J8.4 Seismic Ground Motion Scenario Class: 0 to 10^6 yr

The expected dose $\bar{D}_{SG}(\tau|\mathbf{e})$ is formally defined by the integral in Equation J8.2-13. For the time interval [0, 10^6 yr], the structure of the elements $\mathbf{a}$ of $\mathcal{A}_{SG}$ is too complex (see definition of $\mathbf{a}_{SG,j}$ in Equation J8.2-1) to allow a quadrature-based approximation for the defining integral for $\bar{D}_{SG}(\tau|\mathbf{e})$. However, a sampling-based (i.e., Monte Carlo) approximation is possible.

As a result, $\bar{D}_{SG}(\tau|\mathbf{e}_i)$ will be approximated in the TSPA-LA for each element $\mathbf{e}_i = [\mathbf{e}_{Ai}, \mathbf{e}_{Mi}]$ of the LHS in Equation J4.9-1 by

$$\bar{D}_{SG}\left(\tau\middle|\mathbf{e}_i\right) \cong \sum_{k=1}^{nR} D_{SG}\left(\tau\middle|\mathbf{a}_{SG,ik}, \mathbf{e}_{Mi}\right)\Big/nR, \qquad \text{(Eq. J8.4-1)}$$

where $\mathbf{a}_{SG,ik}$, k = 1, 2, …, nR, is a random sample from $\mathcal{A}_{SG}$ generated in consistency with the conceptual, but undefined, density function $d_{SG}(\mathbf{a}|\mathbf{e}_i)$. Owing to the complexity of the distributions that define the properties of individual seismic ground motion events, the properties of each seismic ground motion event must be sampled internal to the evaluation of $D_{SG}(\tau|\mathbf{a}_{SG,ik}, \mathbf{e}_{Mi})$ as the properties of the disposal system and the resultant distributions for some of elements of $\mathbf{a}_{SG,ik}$ change through time.

In concept, the following results can be sampled for each future $\mathbf{a}_{SG,ik}$ before the calculation of $D_{SG}(\tau|\mathbf{a}_{SG,ik}, \mathbf{e}_{Mi})$ is initiated: (i) number nSG_{ik} of seismic ground motion events associated with $\mathbf{a}_{SG,ik}$, (ii) times

$$0 \le t_{i1k} \le t_{i2k} \le \cdots \le t_{i,nSG_{ik},k} \le 10^6 \text{ yr} \quad \text{(Eq. J8.4-2)}$$

of seismic ground motion events associated with $\mathbf{a}_{SG,ik}$, (iii) PGVs

$$v_{i1k}, v_{i2k}, \ldots, v_{i,nSG_{ik},k} \quad \text{(Eq. J8.4-3)}$$

for seismic ground motion events associated with $\mathbf{a}_{SG,ik}$, and (iv) rock fall volumes

$$VR_{i1k}, VR_{i2k}, \ldots, VR_{i,nSG_{ik},k} \quad \text{(Eq. J8.4-4)}$$

for seismic ground motion events associated with $\mathbf{a}_{SG,ik}$. The remaining properties associated with individual seismic ground motion events (i.e., AW_{1ijk}, AW_{2ijk}, AD_{ijk}, RW_{1ijk}, $RW2_{ijk}$, FDP_{ijk}, FDF_{ijk} for j = 1, 2, …, nSG_{ik}; see Equation J8.2-1) have distributions that are conditional on repository properties and can only be sampled once these conditions are calculated within the computational structure that underlies the determination of $D_{SG}(\tau|\mathbf{a}_{SG,ik}, \mathbf{e}_{Mi})$.

When the same hazard curve (i.e., the function $\lambda_G(v)$) is used for all LHS elements, an initial set of high-level futures defined by

$$\tilde{\mathbf{a}}_{SG,k} = \left[nSG_{1k}, t_{1k}, v_{1k}, VR_{1k}, t_{2k}, v_{2k}, VR_{2k}, \ldots, t_{nSG_k,k}, v_{nSG_k,k}, VR_{nSG_k,k} \right] \quad \text{(Eq. J8.4-5)}$$

can be sampled for k = 1, 2, …, nR. Then, for each LHS element $\mathbf{e}_i$, the corresponding future $\mathbf{a}_{SG,k}$ can be generated by using the seismic ground motion properties defined by $\tilde{\mathbf{a}}_{SG,k}$ and sampling the additional properties indicated in Equation J8.2-1 on the basis of distributions that are conditional on calculated repository properties at the times t_{jk}, j = 1, 2, …, nSG_k. The result is a sequence of futures

$$\mathbf{a}_{SG,ik},\ i = 1, 2, \ldots, nLHS,\ k = 1, 2, \ldots, nR, \quad \text{(Eq. J8.4-6)}$$

where the seismic ground motion properties associated with $\tilde{\mathbf{a}}_{SG,k}$ are used in the definition of $\mathbf{a}_{SG,ik}$ for each LHS element $\mathbf{e}_i$. This approach has the positive feature that it permits uncertainty and sensitivity analysis results to be obtained conditional on the occurrence of each high level future $\tilde{\mathbf{a}}_{SG,k}$. However, if the hazard curve $\lambda_G(v)$ is treated as being uncertain (i.e., as an element of $\mathbf{e}_A$), the sampled futures $\mathbf{a}_{SG,ik}$ used in the approximation to $\bar{D}_{SG}(\tau|\mathbf{e}_i)$ in Equation J8.4-1 cannot be generated in this manner and the sequences of properties in Equations J8.4-2 – J8.4-3 will change for each LHS element $\mathbf{e}_i$. Similarly, this change would also occur if any of the other distributions that characterize aleatory uncertainty associated with seismic events were treated as being uncertain in an epistemic sense.

However, a negative feature of the preceding approach is that it results in less stable estimates for the expected (mean) dose $\bar{\bar{D}}_{SG}(\tau)$ than is the case when the futures $\mathbf{a}_{SG,ik}$ in Equation J8.4-6 are sampled independently for each LHS element. For this reason, the futures $\mathbf{a}_{SG,ik}$ used in the approximations to $\bar{D}_{SG}(\tau|\mathbf{e}_i)$ in Equation J8.4-1, and hence in the approximation $\bar{\bar{D}}_{SG}(\tau)$, in the TSPA-LA are sampled independently for each LHS element. Specifically, the TSPA-LA uses an independently generated sample

$$\mathbf{a}_{SG,ik},\ k = 1, 2, \ldots, nR = 30, \qquad \text{(Eq. J8.4-7)}$$

of seismic futures of the form defined in Equations J4.4-7 and J8.2-1 for each LHS element $\mathbf{e}_i = [\mathbf{e}_{Ai}, \mathbf{e}_{Mi}]$ in the approximation $\bar{D}_{SG}(\tau|\mathbf{e}_i)$.

The dose function $D_{SG}(\tau|\mathbf{a}_{SG,ik}, \mathbf{e}_{Mi})$ is evaluated for each seismic future indicated in Equation J8.4-7. As illustrated in Figure J8.4-1, this results in $nR = 30$ dose curves for each LHS element. In turn, vertical averaging of the $nR = 30$ dose curves associated with LHS element $\mathbf{e}_i$ results in the estimate of $\bar{D}_{SG}(\tau|\mathbf{e}_i)$ defined in Equation J8.4-1 (Figure J8.4-1). Further, the results obtained with all $nLHS = 300$ LHS elements are summarized in Figure J8.4-2 and presented in a standard format in Figure J8.4-3.

As previously discussed in conjunction with Equations J5-8 and J6.2-9, dose and expected dose to the RMEI are just two of a large number of results that can be produced and presented in the TSPA-LA. As an example, a summary of the dose calculations for ^{99}Tc is given in Figure J8.4-4, which has the same organization as Figure J8.4-2. Overall, ^{99}Tc is one of the largest contributors to the expected (mean) dose $\bar{\bar{D}}_{SG}(\tau)$ for the 10^6 yr time period. As previously done in Figure J5-4 and other similar figures, a compact summary of the expected (mean) dose results $\bar{\bar{D}}_{SG,r}(\tau)$ for the individual radioactive species is provided in Figure J8.4-5, where $\bar{\bar{D}}_{SG,r}(\tau)$ is the expected (mean) dose to the RMEI at time τ resulting from the release of radioactive species r due to seismic ground motion events over 10^6 yr (see Equation J6.2-9 and associated discussion).

As discussed in Section J4.10, the numerical stability of results obtained with Latin hypercube sampling can be assessed with replicated sampling. Specifically, the analysis for seismic ground motion was performed with the $nRL = 3$ replicated LHSs indicated in Equation J4.10-1. In turn, this analysis shows that the numerical error in using Latin hypercube sampling to estimate $\bar{\bar{D}}_{SG}(\tau)$ is small relative to the epistemic uncertainty associated with the possible values for $\bar{D}_{SG}(\tau|\mathbf{e})$ (Figure J8.4-6). However, a large amount of numerical noise is present in the sampling-based integration over aleatory uncertainty for each LHS element. Thus, the estimates for $\bar{D}_{SG}(\tau|\mathbf{e}_i)$ are not fully converged; specifically, $\bar{D}_{SG}(\tau|\mathbf{e}_i)$ will be a smooth curve when the estimation process is fully converged. In concept, convergence can be achieved by using a sample size larger than $nR = 30$ for each LHS element. Other numerical strategies to make more efficient use of the evaluations of $D_{SG}(\tau|\mathbf{a}_{SG}, \mathbf{e}_{Mi})$ are also possible. For example, an obvious

possibility is to use an appropriate smoothing technique (e.g., a running average with a Gaussian kernel) in the estimation of $\bar{D}_{SG}(\tau|\mathbf{e}_i)$ from the results $D_{SG}(\tau|\mathbf{a}_{SG,ik}, \mathbf{e}_{Mi})$, $k = 1, 2, \ldots, nR$, for each LHS element. There is less numerical noise in the estimation of $\bar{\bar{D}}_{SG}(\tau)$ than in the estimation of the individual expected dose curves $\bar{D}_{SG}(\tau|\mathbf{e}_i)$ because the averaging process used to obtain $\bar{\bar{D}}_{SG}(\tau)$ results in a cancellation of some of the random noise associated with the individual expected dose curves $\bar{D}_{SG}(\tau|\mathbf{e}_i)$; in essence, a much larger random sample of futures is used in the estimation of $\bar{\bar{D}}_{SG}(\tau)$ than is used in the estimation of the individual expected dose curves $\bar{D}_{SG}(\tau|\mathbf{e}_i)$.

J8.5 Representation of Aleatory Uncertainty Associated with Seismic Ground Motion Scenario Class $\mathcal{A}_{SG}$

As indicated in conjunction with Equation J8.2-1, a large number of probability distributions are used to characterize the aleatory uncertainty associated with the occurrence of seismic ground motion events. As described in this section, representational and computational simplifications can be achieved by coalescing multiple distributions into a single distribution. These representations are used explicitly in the quadrature method for the time interval $[0, 2 \times 10^4$ yr] but not in the sampling-based method for the time interval $[0, 1 \times 10^6$ yr].

J8.5.1 Occurrence Rates for WP Damage

The occurrence rates (yr^{-1}) for seismic ground motion events that damage WPs derive from the quantities $\lambda_G(v)$ and $pWD_r(v|\delta_{Ir}, \delta_{Rr}, WT_r, R)$ defined in Equations J8.2-2 and J8.2-5, respectively. Specifically,

$\lambda_G(v)$ = exceedance frequency (yr^{-1}) for PGV v (i.e., $\lambda_G(v)$ is the seismic ground motion hazard curve) (Eq. J8.5.1-1)

and

$pWD_r(v|\delta_{Ir}, \delta_{Rr}, WT_r, R)$ = probability of nonzero damaged area on a WP of type r ($r = 1$ ~ CSNF WP and $r = 2$ ~ CDSP WP) conditional on the occurrence of a seismic ground motion event with PGV v given the existence of conditions defined by the following variables: (i) δ_{Ir}, where $\delta_{Ir} = 1$ ~ WPs with degraded internals and $\delta_{Ir} = 0$ ~ WPs with intact internals, (ii) δ_{Rr}, where $\delta_{Rr} = 1$ ~ WPs surrounded by rubble and $\delta_{Rr} = 0$ ~ WPs not surrounded by rubble, (iii) WT_r = outer corrosion barrier thickness (mm) on WP, and (iv) R = residual stress failure threshold. (Eq. J8.5.1-2)

For notational convenience in the following derivation of occurrence rate for WP damage, the dependence of $pWD_r(v|\delta_{Ir}, \delta_{Rr}, WT_r, R)$ on r, δ_{Ir}, δ_{Rr}, WT_r, and R will be suppressed and $pWD_r(v|\delta_{Ir}, \delta_{Rr}, WT_r, R)$ will simply be represented by $pWD(v)$.

Given $\lambda_G(v)$ and $pWD(v)$, the occurrence rate λ_D (yr^{-1}) of seismic ground motion events that damage WPs is approximated by

$$\begin{aligned}\lambda_D &\cong \sum_{j=1}^{n} pWD\left(v_{j-1}\right)\left[\lambda_G\left(v_{j-1}\right)-\lambda_G\left(v_j\right)\right] \\ &= \sum_{j=1}^{n} (-1)\, pWD\left(v_{j-1}\right)\left[\lambda_G\left(v_j\right)-\lambda_G\left(v_{j-1}\right)\right], \end{aligned} \qquad \text{(Eq. J8.5.1-3)}$$

where $[v_{mn}, v_{mx}]$ is the range of values for PGV over which $\lambda_G(v)$ is defined and $v_{mn} = v_0 < v_1 < \ldots < v_n = v_{mx}$. In turn, the representations

$$\begin{aligned}\lambda_D &= \int_{v_{mn}}^{v_{mx}} (-1)\, pWD(v)\, \mathrm{d}\lambda_G(v) \\ &= \int_{v_{mn}}^{v_{mx}} (-1)\, pWD(v)\left[\mathrm{d}\lambda_G(v)/\mathrm{d}v\right] \mathrm{d}v \\ &= \int_{\lambda_G(v_{mn})}^{\lambda_G(v_{mx})} (-1)\, pWD\left[\lambda_G^{-1}(\lambda)\right] \mathrm{d}\lambda \\ &= \int_{\lambda_{mx}}^{\lambda_{mn}} (-1)\, pWD\left[\lambda_G^{-1}(\lambda)\right] \mathrm{d}\lambda \\ &= \int_{\lambda_{mn}}^{\lambda_{mx}} pWD\left[\lambda_G^{-1}(\lambda)\right] \mathrm{d}\lambda \end{aligned} \qquad \text{(Eq. J8.5.1-4)}$$

result as $\Delta v_j \to 0$, where (i) the first integral is a Stieltjes integral, (ii) the second integral is the corresponding Riemann integral, (iii) the third integral is the result of a change of variables from an integral on v to an integral on λ, (iv) the fourth integral is a notational change in the limits of integration based on the equalities $\lambda_{mx} = \lambda_G(v_{mn})$ and $\lambda_{mn} = \lambda_G(v_{mx})$, and (v) the fifth and final integral results from an interchange of the upper and lower limits of integration.

The residual stress failure threshold R appearing in $pWD_r(v|\delta_{Ir}, \delta_{Rr}, WT_r, R)$ affects the definition of probability distributions that characterize aleatory uncertainty and, in particular, affects the definition of λ_D in Equation J8.5.1-4. However, R is fundamentally a physical property of the WPs. Therefore, given that R is treated as being epistemically uncertain in the TSPA-LA, it seems most natural to identify R as an element of $\mathbf{e}_M$ although a case could be made R should be identified as an element of $\mathbf{e}_A$. Computationally, this has no effect on the outcome of the TSPA-LA because, with either identification, R is an element of the vector $\mathbf{e} = [\mathbf{e}_A, \mathbf{e}_M]$ of epistemically uncertain quantities sampled in the LHS indicated in Equation J4.9-1. However, in general although not implemented in the TSPA-LA, the hazard

curve $\lambda_G(v)$ is epistemically uncertain (i.e., $\lambda_G(v)$ is an important analysis input that can never be known with certainty) and thus is appropriately viewed as an element of $\mathbf{e}_A$. As a result, the rate λ_D defined in Equation J8.5.1-4 is actually a function $\lambda_D(\mathbf{e})$ of epistemically uncertain analysis inputs.

The occurrence rates $\lambda_1(\mathbf{e})$ and $\lambda_2(\mathbf{e})$ defined in Equations J8.3-3 and J8.3-5 and appearing in Equations J8.3-7 and J8.3-8 are rates of the form defined in Equation J8.5.1-4. Specifically,

$$\lambda_1(\mathbf{e}) = \int_{\lambda_{mn}}^{\lambda_{mx}} pWD_2\left[\lambda_G^{-1}(\lambda)\middle|\delta_{I2}=0, \delta_{R2}=0, WT_2 = 23 \text{ mm}, R\right] d\lambda \qquad \text{(Eq. J8.5.1-5)}$$

with (i) $r = 2$ indicating CDSP WPs, (ii) $\delta_{I2} = 0$ indicating intact internals, (iii) $\delta_{R2} = 0$ indicating WPs that are free to move beneath the DS, (iv) $WT_2 = 23$ mm corresponding to an essentially undiminished outer corrosion barrier, and (v) R and possibly $\lambda_G(v)$ elements of $\mathbf{e}$. Similarly,

$$\lambda_2(\mathbf{e}) = \int_{\lambda_{mn}}^{\lambda_{mx}} pWD_2\left[\lambda_G^{-1}(\lambda)\middle|\delta_{I2}=1, \delta_{R2}=0, WT_2 = 23 \text{ mm}, R\right] d\lambda, \qquad \text{(Eq. J8.5.1-6)}$$

with (i) r, δ_{R2}, WT_2, R and $\lambda_G(v)$ defined the same as in Equation J8.5.1-5 and (ii) $\delta_{I2} = 1$ indicating degraded internals.

The preceding representations for $\lambda_1(\mathbf{e})$ and $\lambda_2(\mathbf{e})$ use the final integral representation for λ_D in Equation J8.5.1-4; however, the other integral representations for λ_D in Equation J8.5.1-4 provide equally valid representations for $\lambda_1(\mathbf{e})$ and $\lambda_2(\mathbf{e})$. For example, use of the second integral representation in Equation J8.5.1-4 results in

$$\lambda_1(\mathbf{e}) = \int_{v_{mn}}^{v_{mx}} (-1)\, pWD_2\left(v\middle|\delta_{I2}=0, \delta_{R2}=0, WT_2 = 23 \text{ mm}, R\right)\left[d\lambda_G(v)/dv\right] dv \qquad \text{(Eq. J8.5.1-7)}$$

and

$$\lambda_2(e) = \int_{\lambda_{mn}}^{\lambda_{mx}} pWD_2\left(v\middle|\delta_{I2}=1, \delta_{R2}=0, WT_2 = 23 \text{ mm}, R\right)\left[d\lambda_G(v)/dv\right] dv, \qquad \text{(Eq. J8.5.1-8)}$$

which avoids the use of the inverse function $\lambda_G^{-1}(\lambda)$ but requires the determination of the derivative $d\lambda_G(v)/dv$. In many ways, the initial Stieltjes integral in Equation J8.5.1-4 provides the simplest representation for $\lambda_1(\mathbf{e})$ and $\lambda_2(\mathbf{e})$.

J8.5.2 Distributions for PGV

The hazard curve $\lambda_G(v)$ is defined for $v_{mn} \le v \le v_{mx}$, where v_{mn} is the smallest PGV included in the analysis (i.e., the smallest PGV with the potential to affect repository behavior) and v_{mx} is the largest PGV that merits inclusion in the analysis on the basis of probabilistic considerations. In

turn, $\lambda_{mx} = \lambda_G(v_{mn})$ and $\lambda_{mn} = \lambda_G(v_{mx})$ are the exceedance frequencies associated with v_{mn} and v_{mx} as previously used in Section J8.5.1. With $\lambda_G(v)$, it is possible to determine the distribution for PGV conditional on the occurrence of a potentially damaging seismic ground motion event (i.e., an event with a PGV ≥ v_{mn}). Further, with both $\lambda_G(v)$ and the conditional probability of nonzero damage $pWD_r(v|\delta_{Ir}, \delta_{Rr}, WT_r, R)$ defined in Equation J8.5.1-2, it is possible to determine the distributions for PGV conditional on the occurrence of a damaging seismic ground motion event.

The CDF for PGV given a potentially damaging seismic event is defined by probabilities of the form

$$prob\left(\tilde{v} \le v \middle| v_{mn} \le v \le v_{mx}\right) \cong \sum_{j=1}^{n} \left[\lambda_G\left(v_{j-1}\right) - \lambda_G\left(v_j\right)\right] \Big/ \left(\lambda_{mx} - \lambda_{mn}\right)$$

$$= \sum_{j=1}^{n} (-1) \left[\lambda_G\left(v_j\right) - \lambda_G\left(v_{j-1}\right)\right] \Big/ \left(\lambda_{mx} - \lambda_{mn}\right), \quad \text{(Eq. J8.5.2-1)}$$

where $v_{mn} = v_0 < v_1 < \ldots < v_n = v$ and $prob(\tilde{v} \le v|v_{mn} \le v \le v_{mx})$ represents the probability of a PGV that is less than or equal to v given the occurrence of a seismic event with a PGV between v_{mn} and v_{mx}. In turn,

$$prob\left(\tilde{v} \le v \middle| v_{mn} \le v \le v_{mx}\right) = \frac{1}{\lambda_{mx} - \lambda_{mn}} \int_{v_{mn}}^{v} (-1)\, \mathrm{d}\lambda_G\left(\tilde{v}\right)$$

$$= \frac{1}{\lambda_{mx} - \lambda_{mn}} \int_{v_{mn}}^{v} (-1) \left[\mathrm{d}\lambda_G\left(\tilde{v}\right) / \mathrm{d}\tilde{v}\right] \mathrm{d}\tilde{v}$$

$$= \frac{1}{\lambda_{mx} - \lambda_{mn}} \int_{\lambda_G(v_{mn})}^{\lambda_G(v)} (-1)\, \mathrm{d}\lambda$$

$$= \frac{1}{\lambda_{mx} - \lambda_{mn}} \int_{\lambda_G(v)}^{\lambda_{mx}} \mathrm{d}\lambda$$

$$= \left[\lambda_{mx} - \lambda_G\left(v\right)\right] \Big/ \left[\lambda_{mx} - \lambda_{mn}\right] \quad \text{(Eq. J8.5.2-2)}$$

as $\Delta v_i \to 0$.

The density function $d_v(v|P)$ for PGV given a potentially damaging seismic ground motion event (i.e., indicated by the conditionality notation "$|P$") can now be obtained by differentiating the cumulative probability $prob(\tilde{v} \le v|v_{mn} \le v \le v_{mx})$ defined in Equation J8.5-2-2. Specifically,

$$d_v(v|P) = \frac{\mathrm{d}}{\mathrm{d}v}\left[prob\left(\tilde{v} \le v | v_{mn} \le v \le v_{mx}\right)\right]$$
$$= \frac{\mathrm{d}}{\mathrm{d}v}\left(\left[\lambda_{mx} - \lambda_G(v)\right]/\left[\lambda_{mx} - \lambda_{mn}\right]\right)$$
$$= -\left[\mathrm{d}\lambda_G(v)/\mathrm{d}v\right]/\left[\lambda_{mx} - \lambda_{mn}\right] \quad \text{(Eq. J8.5.2-3)}$$

is the density function for PGV given a potentially damaging seismic ground motion event.

The distributions for PGV given a damaging seismic ground motion event are now considered. This development requires use of both $\lambda_G(v)$ and the conditional probability of nonzero damage $pWD_r(v|\delta_{Ir}, \delta_{Rr}, WT_r, R)$ defined in Equation J8.5.1-2. As in Section J8.5.1, the dependence of $pWD_r(v|\delta_{Ir}, \delta_{Rr}, WT_r, R)$ on r, δ_{Ir}, δ_{Rr}, WT_r and R will be suppressed for notational convenience and $pWD_r(v|\delta_{Ir}, \delta_{Rr}, WT_r, R)$ will simply be represented by $pWD(v)$.

The CDF for PGV given a damaging seismic ground motion event is defined by probabilities of the form

$$prob\left(\tilde{v} \le v | D\right) = \int_{v_{mn}}^{v} pWD(\tilde{v}) d_v(\tilde{v}|P)\,\mathrm{d}\tilde{v} \Big/ \int_{v_{mn}}^{v_{mx}} pWD(\tilde{v}) d_v(\tilde{v}|P)\,\mathrm{d}\tilde{v}$$
$$= \int_{v_{mn}}^{v} pWD(\tilde{v})\left[\mathrm{d}\lambda_G(\tilde{v})/\mathrm{d}\tilde{v}\right]\mathrm{d}\tilde{v} \Big/ \int_{v_{mn}}^{v_{mx}} pWD(\tilde{v})\left[\mathrm{d}\lambda_G(\tilde{v})/\mathrm{d}\tilde{v}\right]\mathrm{d}\tilde{v}$$
$$= \left(1/\lambda_D\right)\int_{v_{mn}}^{v} (-1)\, pWD(\tilde{v})\left[\mathrm{d}\lambda_G(\tilde{v})/\mathrm{d}\tilde{v}\right]\mathrm{d}\tilde{v}, \quad \text{(Eq. J8.5.2-4)}$$

where $prob(\tilde{v} \le v|D)$ represents the probability of a PGV less than or equal to v given the occurrence of a seismic ground motion event with a PGV between v_{mn} and v_{mx} that causes WP damage (i.e., indicated by the conditionality notation "$|D$") and λ_D is the frequency of damaging events defined in Equation J8.5.1-4. In turn,

$$d_v(v|D) = \frac{\mathrm{d}}{\mathrm{d}v}\left[prob\left(\tilde{v} \le v | D\right)\right]$$
$$= \frac{\mathrm{d}}{\mathrm{d}v}\left\{\left(1/\lambda_D\right)\int_{v_{mn}}^{v} (-1)\, pWD(\tilde{v})\left[\mathrm{d}\lambda_G(\tilde{v})/\mathrm{d}\tilde{v}\right]\mathrm{d}\tilde{v}\right\}$$
$$= \left(-1/\lambda_D\right) pWD(v)\left[\mathrm{d}\lambda_G(v)/\mathrm{d}v\right] \quad \text{(Eq. J8.5.2-5)}$$

is the density function for PGV conditional on the occurrence of a seismic ground motion event with a PGV between v_{mn} and v_{mx} that causes WP damage.

As a reminder, $d_v(v|D)$ is actually of the form $d_{vr}(v|\delta_{Ir}, \delta_{Rr}, WT_r, R, D)$ because of the dependence on $pWD_r(v|\delta_{Ir}, \delta_{Rr}, WT_r, R)$. Further, $d_v(v|P)$ and $d_v(v|D)$ are generally of the form $d_v(v|P, \mathbf{e})$ and $d_v(v|D, \mathbf{e})$ because of dependencies on epistemically uncertain quantities contained in $\mathbf{e}$.

J8.5.3 Distributions for Damaged Area on WPs

The distributions for damaged area on WPs conditional on the occurrence of a damaging seismic ground motion event derive from the hazard curve $\lambda_G(v)$ (see Equation J8.5.1-1) and the conditional density functions $d_{Ar}(A|v, \delta_{Ir}, \delta_{Rr}, WT_r, R)$, where

$d_{Ar}\left(A\middle|v, \delta_{Ir}, \delta_{Rr}, WT_r, R\right)$ = density function (m^{-2}) for damaged area A (m^2) on a WP of type r conditional on the occurrence of a seismic ground motion event with PGV v that results in a nonzero damaged area (see $pWD_r(v|\delta_{Ir}, \delta_{Rr}, WT_r, R)$) given the existence of conditions defined by δ_{Ir}, δ_{Rr}, WT_r and R. (Eq. J8.5.3-1)

For notational convenience, the dependence of $d_{Ar}(A|v, \delta_{Ir}, \delta_{Rr}, WT_r, R)$ on r, δ_{Ir}, δ_{Rr}, WT_r and R will be suppressed and $d_{Ar}(A|v, \delta_{Ir}, \delta_{Rr}, WT_r, R)$ will simply be represented by $d_A(A|v, D)$, with the conditionality indicated by the notation "$|v, D$".

The CDF for damaged area on a WP given a damaging seismic ground motion event is defined by probabilities of the form

$$prob\left(\tilde{A} \le A\middle|D\right) \cong \sum_{j=1}^{n} prob\left(\tilde{A} \le A\middle|v_j, D\right) d_v\left(v_j\middle|D\right) \Delta v_j$$

$$= \sum_{j=1}^{n} \left[\int_0^A d_A\left(\tilde{A}\middle|v_j, D\right) \mathrm{d}\tilde{A}\right] d_v\left(v_j\middle|D\right) \Delta v_j, \qquad \text{(Eq. J8.5.3-2)}$$

where $v_{mn} = v_0 < v_1 < \ldots < v_n = v_{mx}$, $prob(\tilde{A} \le A|D)$ represents the probability of a damaged area less than or equal to A given the occurrence of a damaging seismic ground motion event, and $prob(\tilde{A} \le A|v_j, D)$ represents the probability of a damaged area less than or equal to A given the occurrence a damaging seismic ground motion event with PGV v_j. In turn,

$$prob\left(\tilde{A} \le A\middle|D\right) \cong \int_{v_{mn}}^{v_{mx}} \left[\int_0^A d_A\left(\tilde{A}\middle|v, D\right) \mathrm{d}\tilde{A}\right] d_v\left(v|D\right) \mathrm{d}v$$

$$= \int_0^A \left[\int_{v_{mn}}^{v_{mx}} d_A\left(\tilde{A}\middle|v, D\right) d_v\left(v|D\right) \mathrm{d}v\right] \mathrm{d}\tilde{A} \qquad \text{(Eq. J8.5.3-3)}$$

as $\Delta v_j \to 0$.

The density function $d_A(A|D)$ for damaged area given a damaging seismic ground motion event can now be obtained by differentiating the cumulative probability $prob(\tilde{A} \le A|D)$ defined in Equation J8.5.3-3. Specifically,

$$d_A\left(A\middle|D\right)=\frac{\mathrm{d}}{\mathrm{d}A}\left\{\int_0^A\left[\int_{v_{mn}}^{v_{mx}} d_A\left(\tilde{A}\middle|v,D\right)d_v\left(v\middle|D\right)\mathrm{d}v\right]\mathrm{d}\tilde{A}\right\}$$
$$=\int_{v_{mn}}^{v_{mx}} d_A\left(A\middle|v,D\right)d_v\left(v\middle|D\right)\mathrm{d}v \qquad \text{(Eq. J8.5.3-4)}$$

is the density function for damaged area on a WP given a damaging seismic ground motion event.

As a reminder, $pWD_r(v|\delta_{Ir}, \delta_{Rr}, WT_r, R)$ and $d_{Ar}(A|v, \delta_{Ir}, \delta_{Rr}, WT_r, R)$ underlie the derivation of $d_A(A|D)$. Further, quantities such as R and $\lambda_G(v)$ that are either actually or potentially elements of **e** are also involved. Thus, when a representation of the underlying conditionalities is included, the complete notation for $d_A(A|D)$ in Equation J8.5.3-4 becomes $d_{Ar}(A|\delta_{Ir}, \delta_{Rr}, WT_r, R, \mathbf{e}, D)$.

The density functions $d_{A1}(A|\mathbf{e})$ and $d_{A2}(A|\mathbf{e})$ defined in Equations J8.3-4 and J8.3-6 and appearing in Equations J8.3-7 and J8.3-8 are density functions of the form defined in Equation J8.5.3-4. Specifically,

$$d_{A1}\left(A\middle|\mathbf{e}\right)=\int_{v_{mn}}^{v_{mx}} d_{A2}\left(A\middle|v,\delta_{I2}=0,\delta_{R2}=0,WT_2=23\text{ mm},R\right)$$
$$\times d_{D2}\left(v\middle|\delta_{I2}=0,\delta_{R2}=0,WT_2=23\text{ mm},R\right)\mathrm{d}v \qquad \text{(Eq. J8.5.3-5)}$$

and

$$d_{A2}\left(A\middle|\mathbf{e}\right)=\int_{v_{mn}}^{v_{mx}} d_{A2}\left(A\middle|v,\delta_{I2}=1,\delta_{R2}=0,WT_2=23\text{ mm},R\right)$$
$$\times d_{D2}\left(v\middle|\delta_{I2}=1,\delta_{R2}=0,WT_2=23\text{ mm},R\right)\mathrm{d}v. \qquad \text{(Eq. J8.5.3-6)}$$

where (i) $d_{A2}(A|v, \delta_{I2}, \delta_{R2}, WT_2, R)$ is defined in Equation J8.2-6 and corresponds to $d_A(A|v, D)$ in Equation J8.5.3-4 and (ii) $d_{D2}(v|\delta_{I2}, \delta_{R2}, WT_2, R)$ is defined by

$$d_{D2}\left(v\middle|\delta_{I2},\delta_{R2},WT_2,R\right)=\frac{pWD_2\left(v\middle|\delta_{I2},\delta_{R2},WT_2,R\right)\left[\mathrm{d}\lambda_G\left(v\right)/\mathrm{d}v\right]}{\int_{v_{mn}}^{v_{mx}} pWD_2\left(\tilde{v}\middle|\delta_{I2},\delta_{R2},WT_2,R\right)\left[\mathrm{d}\lambda_G\left(\tilde{v}\right)/\mathrm{d}\tilde{v}\right]\mathrm{d}\tilde{v}} \qquad \text{(Eq. J8.5.3-7)}$$

as indicated in Equations J8.5.2-5 and J8.5.1-4 with $\lambda_G(v)$ and $pWD_2(v|\delta_{I2}, \delta_{R2}, WT_2, R)$ defined in Equations J8.5.1-1 and J8.5.1-2 and corresponds to $d_v(v|D)$ in Equation J8.5.3-4. In the preceding, R and potentially $\lambda_G(v)$ are elements of **e**.

The density functions $d_{Ar}(A|v, \delta_{Ir}, \delta_{Rr}, WT_r, R)$ for damaged area are not defined directly as input to the TSPA-LA. Rather, density functions $\tilde{d}_{Ar}(A|v, \delta_{Ir}, \delta_{Rr}, WT_r, R)$ for stressed area are defined as input. Then, within the computational implementation of the TSPA-LA, an

epistemically uncertain multiplicative scale factor SF (i.e., SF is an element of **e**) is used to convert from stressed area A_S to damaged area A_D (i.e., $A_D = SF \times A_S$). As a result,

$$d_{Ar}\left(A \middle| v, \delta_{Ir}, \delta_{Rr}, WT_r, R\right) = \left(1/SF\right) \tilde{d}_{Ar}\left(A/SF \middle| v, \delta_{Ir}, \delta_{Rr}, WT_r, R\right). \quad \text{(Eq. J8.5.3-8)}$$

The preceding equality follows from the relationship

$$d_w(w) = f_x\left[h^{-1}(w)\right]\left|\mathrm{d}h^{-1}(w)/\mathrm{d}w\right|, \quad \text{(Eq. J8.5.3-9)}$$

where (i) x has a probability distribution defined over an interval (i.e., the values of x are continuous) with density function $f_x(x)$, (ii) $h(x)$ is a strictly monotonic function such that $w = h(x)$, and (iii) $d_w(w)$ is the density function for the resultant probability space for w (Hahn and Shapiro 1967 [DIRS 146529], Equation 5-7, p. 177). In the context of Equation J8.5.3-8,

$$h\left(A_S\right) = SF \times A_S = A_D, h^{-1}\left(A_D\right) = A_D/SF, \mathrm{d}h^{-1}\left(A_D\right)/\mathrm{d}A_D = 1/SF. \quad \text{(Eq. J8.5.3-10)}$$

In terms of computational implementation, the density functions $d_{A1}(A|\mathbf{e})$ and $d_{A2}(A|\mathbf{e})$ in Equations J8.5.3-5 and J8.5.3-6 can either be (i) defined with $d_{Ar}(A|v, \delta_{Ir}, \delta_{Rr}, WT_r, R)$ as specified in Equation J8.5.3-8, with the result that damaged areas for use in Equations J8.3-7 and J8.3-8 are produced directly or (ii) defined with $\tilde{d}_{Ar}(A|v, \delta_{Ir}, \delta_{Rr}, WT_r, R)$, with the result that stressed areas are produced and the area A indicated in Equations J8.3-7 and J8.3-8 must be replaced by $SF \times A$.

J8.5.4 Distribution of Cumulative Rockfall Volume

The distribution of cumulative rockfall volume (m^3/m) as a function of time derives from the exceedance frequency $\lambda_G(v)$ for PGV v (see Equation J8.2-2), the probability of rockfall $pRF(v)$ conditional on the occurrence of a seismic ground motion event with PGV v (see Equation J8.2-3), and the density function $d_V(V|v)$ for volume V of rock that caves into a drift conditional on PGV v and the occurrence of rockfall (see Equation J8.2-4). Further, $d_V(V|v)$ is assumed to correspond to a gamma distribution with a mean $\mu(v)$ and standard deviation $\sigma(v)$ that are functions of PGV v.

In concept, it is desirable to determine $d_V(V_c|t)$, where $d_V(V_c|t)$ is the density function for cumulative rockfall V_c at time t. However, owing to the complexity of the interplay of $\lambda_G(v)$, $pRV(v)$ and $d_V(V|v)$, a closed form determination for $d_V(V_c|t)$ is difficult. However, the expected value $E_A(V_c|t)$ and variance $V_A(V_c|t)$ of cumulative rockfall volume V_c at time t are relatively easy to determine and so will be determined. Then, by recourse to the Central Limit Theorem, $E_A(V_c|t)$ and $V_A(V_c|t)$ can be used to estimate the distribution for rockfall volume $V_c(t)$ at time t. In the preceding, the subscript "A" on $E_A(V_c|t)$ and $V_A(V_c|t)$ indicates that the mean and variance for V_c derive from aleatory uncertainty.

Rockfall is assumed to follow what is known as a compound Poisson process. In such a process, events occur at a rate λ_R (yr^{-1}) with each event having the same distribution of possible values for an outcome V. Then, if $V_c(t)$ is the cumulative outcome of these events at time t (e.g., cumulative rockfall), the expected value $E_A(V_c|t)$ and variance $V_A(V_c|t)$ at time t for events occurring over the time interval [0, t] is

$$E_A\left(V_c|t\right) = \lambda_R t\, E\left(V\right) \qquad \text{(Eq. J8.5.4-1)}$$

and

$$V_A\left(V_c|t\right) = \lambda_R t\, E\left(V^2\right), \qquad \text{(Eq. J8.5.4-2)}$$

where $E(V)$ and $E(V^2)$ denote the expectation of V and V^2 (Ross1993 [DIRS 172064], pp. 239-241). In this section, the outcomes of interest are rockfall volume V and the associated expected value $E_A(V_c|t)$ and variance $V_A(V_c|t)$ for cumulative rockfall V_c at time t. The subscript A is used to indicate $E_A(V_c|t)$ and $V_A(V_c|t)$ derive from aleatory uncertainty associated with the occurrence of seismic events.

The expectation $E(V)$ is given by

$$E\left(V\right) = \int_{v_{R,mn}}^{v_{R,mx}} \mu\left(v\right) d_v\left(v|R\right) \mathrm{d}v, \qquad \text{(Eq. J8.5.4-3)}$$

where (i) $[v_{R,mn}, v_{R,mx}]$ is the range of PGVs that have the potential to cause rockfall, (ii)

$$\lambda_R = \int_{v_{R,mn}}^{v_{R,mx}} (-1)\, pRF\left(v\right) \mathrm{d}\lambda_G\left(v\right) \qquad \text{(Eq. J8.5.4-4)}$$

is the occurrence rate (yr^{-1}) of rockfall events, and (iii)

$$d_v\left(v|R\right) = \left(-1/\lambda_R\right) pRF\left(v\right)\left[\mathrm{d}\lambda_G\left(v\right)/\mathrm{d}v\right] \qquad \text{(Eq. J8.5.4-5)}$$

is the density function for PGV conditional on the occurrence of rockfall. The derivations for λ_R and $d_v(v|R)$ are analogous to the derivations for λ_D and $d_v(v|D)$ in Equations J8.5.1-4 and J8.5.2-5. In turn, the representation

$$E_A\left(V_c|t\right) = t\left[\int_{v_{R,mn}}^{v_{R,mx}} (-1)\, \mu\left(v\right) pRF\left(v\right)\left[\mathrm{d}\lambda_G\left(v\right)/\mathrm{d}v\right]\mathrm{d}v\right] \qquad \text{(Eq. J8.5.4-6)}$$

results when the values for $E(V)$, λ_R and $d_v(v|R)$ in Equations J8.5.4-3 – J8.5.4-5 are substituted into Equation J8.5.4-1.

The determination of $E(V^2)$ requires the density function $d_V(V|R)$ for rockfall volume V given the occurrence of rockfall. Specifically, $d_V(V|R)$ is given by

$$d_V\left(V\middle|R\right) = \int_{v_{R,mn}}^{v_{R,mx}} d_V\left(V\middle|v\right) d_v\left(v\middle|R\right) \mathrm{d}v, \qquad \text{(Eq. J8.5.4-7)}$$

where $d_V(V|v)$ is the density function for rockfall volume V given the occurrence of a rockfall at a PGV of v (i.e., a gamma distribution with mean $\mu(v)$ and standard deviation $\sigma(v)$ as previously indicated) and $d_v(v|R)$ is the density function for PGV v defined in Equation J8.5.4-5 given the occurrence of rockfall. In turn, $E(V^2)$ is given by

$$\begin{aligned}
E\left(V^2\right) &= \int_{V_{R,mn}}^{V_{R,mx}} V^2 d_V\left(V\middle|R\right) \mathrm{d}V \\
&= \int_{V_{R,mn}}^{V_{R,mx}} V^2 \left\{ \int_{v_{R,mn}}^{v_{R,mx}} d_V\left(V\middle|v\right) d_v\left(v\middle|R\right) \mathrm{d}v \right\} \mathrm{d}V \\
&= \int_{V_{R,mn}}^{V_{R,mx}} V^2 \left\{ \int_{v_{R,mn}}^{v_{R,mx}} d_V\left(V\middle|v\right) \left(-1/\lambda_R\right) pRF\left(v\right) \left[\mathrm{d}\lambda_G\left(v\right)/\mathrm{d}v \right] \mathrm{d}v \right\} \mathrm{d}V \\
&= \left(-1/\lambda_R\right) \int_{V_{R,mn}}^{V_{R,mx}} \int_{v_{R,mn}}^{v_{R,mx}} V^2 d_V\left(V\middle|v\right) pRF\left(v\right) \left[\mathrm{d}\lambda_G\left(v\right)/\mathrm{d}v \right] \mathrm{d}v \mathrm{d}V, \qquad \text{(Eq. J8.5.4-8)}
\end{aligned}$$

where (i) the first integral corresponds to the definition of $E(V^2)$ with $[V_{R,mn}, V_{R,mx}]$ the range of possible values for V, (ii) the second integral results from the replacement of $d_V(V|v)$ by its representation in Equation J8.5.4-7, (iii) the third integral results from the replacement of $d_v(v|R)$ by its representation in Equation J8.5.4-5, and (iv) the final integral is an algebraic rearrangement of the third integral. Once $E(V^2)$ is determined, $V_A(V_c|t)$ can be determined as indicated in Equation J8.5.4-2.

J8.5.5 Probability of CDSP WP Rupture in 10^4 yr

The probability of the rupture of a CDSP WP in the time interval [0, 10^4 yr] is now considered. The probability of a rupture of a CDSP WP with a 23 mm thick outer corrosion barrier (OCB) and intact internals is zero. Thus, as there will be little reduction of OCB thickness in the [0, 10^4 yr] time interval, the probability that an initial seismic ground motion event in this time interval will result in a rupture is zero.

The first seismic ground motion event that damages the OCB is assumed to instantly result in degraded internals (an obviously conservative assumption). Thus, only second and subsequent seismic ground motions events have the potential to cause WP rupture. Such events have the potential to cause two types of damage relevant to the occurrence of rupture: (i) incipient rupture, and (ii) rupture. Incipient rupture corresponds to a condition in which the WP is weakened and thus more susceptible to rupture should additional events occur.

For a CDSP WP with degraded internals, a 23 mm thick OCB and freedom to move beneath the DS that experiences a seismic ground motion event with PGV v, the probabilities of incipient rupture and rupture are

$$pIRW(v) = \begin{cases} (0.0158)(v-1.05)^{1.8586} & \text{if } v \geq 1.05 \text{ m/s} \\ 0 & \text{otherwise} \end{cases} \quad \text{(Eq. J8.5.5-1)}$$

and

$$pRW(v) = \begin{cases} (0.0474)(v-2.44)^{1.8586} & \text{if } v \geq 2.44 \text{ m/s} \\ 0 & \text{otherwise,} \end{cases} \quad \text{(Eq. J8.5.5-2)}$$

respectively. The probabilities $pIRW(v)$ and $pRW(v)$ correspond to $pIRW_2(v|\delta_{I2} = 1, \delta_{R2} = 0, WT_2 = 23 \text{ mm})$ and $pRW_2(v|\delta_{I2} = 1, \delta_{R2} = 0, WT_2 = 23 \text{ mm})$ in Equations J8.2-9 and J8.2-10. In turn, the corresponding frequencies (yr^{-1}) of incipient rupture and rupture are

$$\lambda_{IR} = \int_{1.05}^{4.07} pIRW(v)(-1)\,d\lambda_G(v) \quad \text{(Eq. J8.5.5-3)}$$

and

$$\lambda_R = \int_{2.44}^{4.07} pRW(v)(-1)\,d\lambda_G(v), \quad \text{(Eq. J8.5.5-4)}$$

respectively.

Given λ_R, the probability $pR2(\tau)$ of the rupture of a CDSP WP due to two seismic events in the time interval $[0, \tau]$ with the first event causing WP damage and the second event causing WP rupture is

$$pR2(\tau) = \int_0^{\tau} \left(\exp\left[-\lambda_1(R)t\right]\right) \lambda_1(R)\left\{1-\exp\left[-\lambda_R(\tau-t)\right]\right\} dt, \quad \text{(Eq. J8.5.5-5)}$$

where $\lambda_1(R)$ corresponds to the rate term $\lambda_1(\mathbf{e})$ in Equation J8.3-3 with $\mathbf{e}$ replaced by the residual stress threshold R, which is the only variable in $\mathbf{e}$ that affects the definition of $\lambda_1(\mathbf{e})$ in the TSPA-LA. The rate $\lambda_1(R) = \lambda_1(\mathbf{e})$ is defined in Equation J8.5.1-5.

The preceding representation for $pR2(\tau)$ follows from the approximation

$$pR2 \cong \sum_{i=1}^{n} \left\{ \left(\exp\left[-\lambda_1(R) t_{i-1} \right] \right)_1 \left(1 - \exp\left[-\lambda_1(R) \Delta t_i \right] \right)_2 \right\}_1 \left\{ 1 - \exp\left[-\lambda_R(\tau - t_i) \right] \right\}_2$$

$$\cong \sum_{i=1}^{n} \left\{ \left(\exp\left[-\lambda_1(R) t_{i-1} \right] \right)_1 \left(\lambda_1(R) \Delta t_i \right)_3 \right\}_3 \left\{ 1 - \exp\left[-\lambda_R(\tau - t_i) \right] \right\}_2, \qquad \text{(Eq. J8.5.5-6)}$$

where (i) $0 = t_0 < t_1 < \ldots < t_n = \tau$, (ii) $(\sim)_1$ is the probability that no WP damage occurs in the time interval $[0, t_{i-1}]$, (ii) $(\sim)_2$ is the probability that WP damage occurs in the time interval $[t_{i-1}, t_i]$, (iii) $\{(\sim)_1, (\sim)_2\}_1$ is the probability that the first WP damage occurs in the time interval $[t_{i-1}, t_i]$, (iv) $\{\sim\}_2$ is the probability that an event capable of causing rupture of an already damaged WP occurs in the time interval $[t_i, \tau]$, (v) $\{(\sim)_1, (\sim)_2\}_1 \{\sim\}_2$ is the probability that the first damaging event occurs in the time interval $[t_{i-1}, t_i]$ and is followed by an event that causes rupture in the time interval $[t_i, \tau]$, and (vi) $(\sim)_3$ is an approximation to $(\sim)_2$. The representation for $pR2(\tau)$ in Equation J8.5.5-6 then follows in the limit as $\Delta t_i \to 0$.

Similarly, the probability $pR3(\tau)$ of the rupture of a CDSP WP due to three seismic events in the time interval $[0, \tau]$ with the first event causing WP damage and the next two events causing incipient ruptures (which corresponds to the third event causing rupture) is

$$pR3(\tau) = \int_0^{\tau} \left(\exp\left[-\lambda_1(R) t \right] \right) \lambda_1(R) \left(\int_t^{\tau} \exp\left[-\lambda_{IR}(\tilde{t} - t) \right] \lambda_{IR} \left\{ 1 - \exp\left[-(\tau - \tilde{t}) \lambda_{IR} \right] \right\} d\tilde{t} \right) dt. \qquad \text{(J8.5.5-7)}$$

The derivation of $pR3(\tau)$ is similar to the derivation of $pR2(\tau)$.

As an example, the values of $pR2(\tau)$ for $R = 90$ (i.e., 90 percent of the stress threshold) and $\tau = 10{,}000$ and 20,000 yrs are estimated to be

$$pR2(10{,}000) = 8.3 \times 10^{-5} \qquad \text{(J8.5.5-8)}$$

and

$$pR2(20{,}000) = 1.7 \times 10^{-4} \qquad \text{(J8.5.5-9)}$$

respectively.

J8.6 Seismic Fault Displacement Scenario Class: $\mathcal{A}_{SF}$

As discussed in conjunction with Equation J8.1-2, the seismic fault displacement scenario class is defined by the subset $\mathcal{A}_{SF}$ of $\mathcal{A}$. Formally, $\mathcal{A}_{SF}$ contains all elements $\mathbf{a}$ of $\mathcal{A}$ with $nSF > 0$. To fully define $\mathcal{A}_{SF}$, it is necessary to first define the vector $\mathbf{a}_{SF}$ indicated in Equation J8.1-9 and its associated components $\mathbf{a}_{SF,j}$, $j = 1, 2, \ldots, nSF$.

Each component $\mathbf{a}_{SF,j}$ of $\mathbf{a}_{SF}$ is defined by

$$\mathbf{a}_{SF,j} = \left[t_j, N_{1j}, N_{2j}, A_{1j}, A_{2j}, b_j, d_j \right] \quad \text{(Eq. J8.6-1)}$$

where, for fault displacement event j,

t_j = event time (yr),

N_{rj} = number of WPs of type r damaged (i.e., $r = 1$ ~ CSNF WPs, $r = 2$ ~ CDSP WPs),

A_{rj} = damaged area on a WP of type r,

b_j = indicator variable for percolation bin containing damaged WPs (e.g., $b_j = k$ ~ location of failed WPs in percolation bin k for $k = 1, 2, 3, 4, 5$),

d_j = indicator variable for dripping/nondripping conditions experienced by damaged WPs

$$= \begin{cases} 1 & \text{if dripping conditions} \\ 0 & \text{if nondripping conditions.} \end{cases}$$

The following quantities are used to characterize the aleatory uncertainty associated with the elements of $\mathbf{a}_{SF,j}$:

$\lambda_{SF,r}$ = occurrence rate (yr^{-1}) for fault displacement events that damage WPs of type r, (Eq. J8.6-2)

$d_{Nr}(N_r)$ = density function defined on set $\mathcal{N}_r$ for number of damaged WPs of type r given the occurrence of a fault displacement event, (Eq. J8.6-3)

$d_{Ar}(A_r)$ = density function (m^{-2}) defined on set $\mathcal{A}_r$ for damaged area on a WP of type r damaged by a fault displacement event, (Eq. J8.6-4)

pBN_k = probability that damaged WPs are located in percolation bin k, $k = 1, 2, \ldots, nBN$, given the occurrence of a fault displacement event, (Eq. J8.6-5)

$pDRP_{kl}$ = probability that damaged WPs in percolation bin k experience dripping condition l, $l = 0, 1$, with $l = 0$ ~ nondripping conditions and $l = 1$ ~ dripping conditions. (Eq. J8.6-6)

An alternate formulation is to specify $\lambda_{SF,r}$ and $d_{Nr}(N_r)$ through a hazard curve $\lambda_{SF,r}(N_r)$ defined for $0 < N_{mn,r} \le N_r \le N_{mx,r}$, where $\lambda_{SF,r}(N_r)$ is the frequency (yr^{-1}) of fault displacement events that damage N_r or more WPs of type r and $[N_{mn,r}, N_{mx,r}]$ is the range of possible values for N_r. Then,

$$\lambda_{SF,r} = \lambda_{SF,r}\left(N_{mn,r}\right), \qquad \text{(Eq. J8.6-7)}$$

$$d_{Nr}\left(N_r\right) = \left[-\mathrm{d}\lambda_{SF,r}\left(N_r\right)/\mathrm{d}N_r\right] \Big/ \left[\lambda_{SF,r}\left(N_{mn,r}\right) - \lambda_{SF,r}\left(N_{mx,r}\right)\right] \qquad \text{(Eq. J8.6-8)}$$

provided $\lambda_{SF,r}(N_r)$ is differentiable, and

$$\mathcal{N}_r = \left\{N_r : N_{mn,r} \le N_r \le N_{mx,r}\right\}. \qquad \text{(Eq. J8.6-9)}$$

If the hazard curve $\lambda_{SF,r}(N_r)$ is not continuous over the set $\mathcal{N}_r$, then a modification to the definition of $d_{Nr}(N_r)$ is necessary (e.g., if $\lambda_{SF,r}(N_r)$ is piecewise constant or, equivalently, if $\mathcal{N}_r$ contains a finite number of elements).

Because multiple fault displacement events would damage different WPs at different locations and times, the dose $D_{SF}(\tau|\mathbf{a}_{SF}, \mathbf{e}_M)$ to the RMEI (mrem/yr) at time τ associated with the fault displacement future defined by

$$\mathbf{a}_{SF} = \left[nSF, \mathbf{a}_{SF,1}, \mathbf{a}_{SF,2}, \ldots, \mathbf{a}_{SF,nSF}\right] \qquad \text{(Eq. J8.6-10)}$$

and the vector $\mathbf{e}_M$ of epistemically uncertain quantities can be represented by

$$D_{SF}\left(\tau|\mathbf{a}_{SF}, \mathbf{e}_M\right) = \sum_{j=1}^{nSF} D_{SF}\left(\tau|\left[1, \mathbf{a}_{SF,j}\right], \mathbf{e}_M\right), \qquad \text{(Eq. J8.6-11)}$$

where

$$D_{SF}\left(\tau|\left[1, \mathbf{a}_{SF,j}\right], \mathbf{e}_M\right) = D_{SF}\left(\tau|\left[1, t_j, N_{1j}, N_{2j}, A_{1j}, A_{2j}, b_j, d_j\right], \mathbf{e}_M\right)$$

is the dose to the RMEI (mrem/yr) that derives from the fault displacement event characterized by $\mathbf{a}_{SF,j}$.

Further, given the occurrence of the event characterized by $\mathbf{a}_{SF,j}$, there are no synergisms between the doses that derive from the individual N_{1j} damaged CSNF WPs and the individual N_{2j} damaged CDSP WPs. As a result, the further simplification

$$D_{SF}\left(\tau\middle|\left[1, t_j, N_{1j}, N_{2j}, A_{1j}, A_{2j}, b_j, d_j\right], \mathbf{e}_M\right)$$

$$= \sum_{r=1}^{2} D_{SF,r}\left(\tau\middle|\left[1, t_j, N_{rj}, A_{rj}, b_j, d_j\right], \mathbf{e}_M\right)$$

$$= \sum_{r=1}^{2} \left(N_{rj}/\tilde{N}_r\right) D_{SF,r}\left(\tau\middle|\left[1, t_j, \tilde{N}_r, A_{rj}, b_j, d_j\right], \mathbf{e}_M\right) \qquad \text{(Eq. J8.6-12)}$$

is possible, where

$$D_{SF,1}\left(\tau\middle|\left[1, t_j, N, A_{1j}, b_j, d_j\right], \mathbf{e}_M\right) = D_{SF}\left(\tau\middle|\left[1, t_j, N, 0, A_{1j}, 0, b_j, d_j\right], \mathbf{e}_M\right),$$

$$D_{SF,2}\left(\tau\middle|\left[1, t_j, N, A_{2j}, b_j, d_j\right], \mathbf{e}_M\right) = D_{SF}\left(\tau\middle|\left[1, t_j, 0, N, 0, A_{2j}, b_j, d_j\right], \mathbf{e}_M\right),$$

and $\tilde{N}_r$, r = 1, 2, is some computationally convenient number of damaged WPs (e.g., 1 or 100). The factoring of N_{rj} in Equation J8.6-12 is possible because dose is linear with respect to the number of damaged WPs.

In concept, the expected dose $\bar{D}_{SF}(\tau|\mathbf{e})$ to the RMEI is defined by the integral

$$\bar{D}_{SF}\left(\tau\middle|\mathbf{e}\right) = \int_{\mathcal{A}_{SF}} D_{SF}\left(\tau\middle|\mathbf{a}_{SF}, \mathbf{e}_M\right) d_A\left(\mathbf{a}_{SF}\middle|\mathbf{e}_A\right) \mathrm{d}A. \qquad \text{(Eq. J8.6-13)}$$

In turn, the representations for $D_{SF}(\tau|\mathbf{a}_{SF}, \mathbf{e}_M)$ and $D_{SF}(\tau|[1, t_j, N_{1j}, N_{2j}, A_{1j}, A_{2j}, b_j, d_j], \mathbf{e}_M)$ in Equations J8.6-11 and J8.6-12 permit a more explicit and computationally tractable representation for the defining integral for $\bar{D}_{SF}(\tau|\mathbf{e})$. Specifically, $\bar{D}_{SF}(\tau|\mathbf{e})$ can be represented by

$$\bar{D}_{SF}\left(\tau\middle|\mathbf{e}\right) = \sum_{r=1}^{2} \sum_{k=1}^{nBN} \sum_{l=0}^{1} \left(pBN_k \; pDRP_{kl}\right)$$

$$\times \left(\int_0^{\tau} \left\{ \int_{\mathcal{A}_r} \left[\int_{\mathcal{N}_r} D_{SF,r}\left(\tau\middle|\left[1, t, N_r, A_r, b_k, d_l\right], \mathbf{e}_M\right) d_{Nr}\left(N_r\right) \mathrm{d}N_r \right]_1 d_{Ar}\left(A_r\right) \mathrm{d}A_r \right\}_2 \lambda_{SF,r} \mathrm{d}t \right)_3,$$

(Eq. J8.6-14)

where (i) the integral in $[\sim]_1$ is expected dose at time τ from WP package type r conditional on A_r, b_k, d_l, $\mathbf{e}_M$ and t, (iii) the double integral in $\{\sim\}_2$ is the expected dose at time τ from WP type r conditional on b_k, d_l, $\mathbf{e}_M$ and t, (iii) the triple integral in $(\sim)_3$ is the expected dose at time τ from WP type r conditional on b_k, d_l and $\mathbf{e}_M$. Then, the summations on k and l and the associated

multiplication of $(\sim)_3$ by $pBN_k\ pDRP_{kl}$ removes the conditionality on b_k and d_l for WP type r. Finally, the summation on r combines the expected doses for the individual WP types and leaves only the conditionality on $\mathbf{e}_M$.

In turn, the simpler representation

$$\bar{D}_{SF}\left(\tau|\mathbf{e}\right)=\sum_{r=1}^{2}\left[\bar{N}_r\lambda_{SF,r}/\tilde{N}_r\right]\left[\sum_{k=1}^{nBN}\sum_{l=0}^{1}\left(pBN_k\ pDRP_{kl}\right)\right]$$

$$\times\left(\int_0^{\tau}\left\{\int_{\mathcal{A}_r}D_{SF,r}\left(\tau|\left[1,t,\tilde{N}_r,A_r,b_k,d_l\right],\mathbf{e}_M\right)d_{Ar}\left(A_r\right)\mathrm{d}A_r\right\}\mathrm{d}t\right) \quad \text{(Eq. J8.6-15)}$$

results from the linear relationship between dose and number of damaged WPs indicated in Equation J8.6-12, where

$$\bar{N}_r=\int_{\mathcal{N}_r}N_r d_{Nr}\left(N_r\right)\mathrm{d}N_r \quad \text{(Eq. J8.6-16)}$$

is the expected number of damaged WPs of type r.

For implementation in the TSPA-LA, the division of the repository into multiple percolation bins is not considered for fault displacement events. Rather, the entire repository is treated as a single percolation bin with 100 failed WPs of a given type spread over this "bin." In this implementation, the number nB_k of WPs assigned to each of the k = 1, 2, 3, 4, 5 original percolation bins is $nB_k = pBN_k$ (100). Further, the numbers nB_{kl}, l = 0, 1, of WPs assigned to nondripping ($\sim l$ = 0) and dripping ($\sim l$ = 1) conditions in percolation bin k are $nB_{kl} = pDRP_{kl}\ nB_k$ for l = 0, 1. With this simplification, the representation for $\bar{D}_{SF}(\tau|\mathbf{e})$ in Equation J8.6-15 reduces to

$$\bar{D}_{SF}\left(\tau|\mathbf{e}\right)=\sum_{r=1}^{2}\left(\bar{N}_r\lambda_{SF,r}/100\right)\left(\int_0^{\tau}\left\{\int_{\mathcal{A}_r}D_{SF,r}\left(\tau|[1,t,100,A_r,1,\sim],\mathbf{e}_M\right)d_{Ar}\left(A_r\right)\mathrm{d}A_r\right\}\mathrm{d}t\right)$$

$$=\sum_{r=1}^{2}\bar{D}_{SF,r}\left(\tau|\mathbf{e}\right), \quad \text{(Eq. J8.6-17)}$$

where the "d_l" has been replaced by "~" to indicate that the presence of nondripping and dripping conditions is now incorporated into the locations assigned to the individual WPs and

$$\bar{D}_{SF,r}\left(\tau|\mathbf{e}\right)=\left(\bar{N}_r\lambda_{SF,r}/100\right)\left(\int_0^{\tau}\left\{\int_{\mathcal{A}_r}D_{SF,r}\left(\tau|[1,t,100,A_r,1,\sim],\mathbf{e}_M\right)d_{Ar}\left(A_r\right)\mathrm{d}A_r\right\}\mathrm{d}t\right).$$

In turn, evaluation of the preceding representation for $\bar{D}_{SF}(\tau|\mathbf{e})$ requires the evaluation of two double integrals; specifically, one double integral for CSNF WPs (i.e., for $r = 1$) and one double integral for CDSP WPs (i.e., for $r = 2$).

The preceding integrations must be carried out for each element of the LHS indicated in Equation J4.9-1. To support these integrations,

$$D_{SF,r}\left(\tau\left|\left[1, t_j, 100, A_{rk}, 1, \sim\right], \mathbf{e}_{Mi}\right.\right) \qquad \text{(Eq. J8.6-18)}$$

must be evaluated for (i) $r = 1, 2$, (ii) $0 \le \tau \le 20{,}000$ yr or $0 \le \tau \le 10^6$ yr, (iii) a sequence of event times $0 < t_1 < t_2 < \ldots < t_m$ from the intervals [0, 20,000 yr] and [0, 10^6 yr], (iv) a sequence of damaged areas $0 < A_{r1} < A_{r2} < \ldots < A_{rn}$, where A_{rn} is an upper bound for the set $\mathcal{A}_r$, and (v) $\mathbf{e}_{Mi}$, $i = 1, 2, \ldots, nLHS$.

In the TSPA-LA for the [0, 20,000 yr] time interval, the $m = 6$ event times $t_1, t_2, \ldots, t_m$ are

$$200, 800, 2000, 4000, 8000, 18{,}000 \text{ yrs}; \qquad \text{(Eq. J8.6-19)}$$

the $n = 3$ areas A_{11}, A_{12}, A_{13} are

$$A_1/3, 2A_1/3, A_1, \qquad \text{(Eq. J8.6-20)}$$

where $A_1 = 2.78$ m^2 is the cross-sectional area (m^2) of a CSNF WP; and the $n = 3$ areas A_{21}, A_{22}, A_{23} are

$$A_2/3, 2A_2/3, A_2, \qquad \text{(Eq. J8.6-21)}$$

where $A_2 = 3.28$ m^2 is the cross-sectional area of a CDSP WP. For the [0, 10^6 yr] time interval, the $m = 6$ times $t_1, t_2, \ldots, t_m$ are

$$1000, 20{,}000, 80{,}000, 200{,}000, 400{,}000, 800{,}000 \text{ yrs}; \qquad \text{(Eq. J8.6-22)}$$

and the cross-sectional areas for CSNF and CDSP WPs are the same as in Equations J8.6-20 and J8.6-21, respectively. Selected results for the [0, 20,000 yr] time interval are shown in Figures J8.6-1 and J8.6-2.

Once the preceding results are available, quadrature procedures can be used to evaluate $\bar{D}_{SF}(\tau|\mathbf{e}_{Mi})$ for $i = 1, 2, \ldots, nLHS$. Specifically, the double integral in Equation J8.6-17 is approximated by

$$\int_0^{\tau}\left\{\int_{\mathcal{A}_r} D_{SF,r}\left(\tau\middle|[1, t, 100, A_r, 1, \sim], \mathbf{e}_{Mi}\right) d_{Ar}\left(A_r\right) \mathrm{d}A_r\right\} \mathrm{d}t$$

$$\cong \sum_{k=1}^{n}\left\{\sum_{l=1}^{m} \hat{D}_{SF,r}\left(\tau\middle|\left[1, \hat{t}_k, 100, \hat{A}_{rl}, 1, \sim\right], \mathbf{e}_{Mi}\right)\Delta\hat{A}_{rl}\right\}\Delta\hat{t}_k, \qquad \text{(Eq. J8.6-23)}$$

where $0 = \hat{t}_0 < \hat{t}_1 < \ldots < \hat{t}_n = \tau$ is a subdivision of $[0, \tau]$, (ii) $A_{mn,r} = \hat{A}_{r0} < \hat{A}_{r1} < \ldots < \hat{A}_{rm} = A_{mx,r}$ is a subdivision of $\mathcal{A}_r = [A_{mn,r}, A_{mx,r}]$, and (iii) $\hat{D}(\tau\,|[1, \hat{t}_k, 100, \hat{A}_{rl}, 1, \sim]\,, \mathbf{e}_{Mi})$ is an approximation to $D(\tau\,|[1, \hat{t}_k, 100, \hat{A}_{rl}, 1, \sim]\,, \mathbf{e}_{Mi})$ obtained with interpolation procedures from the results in Equation J8.6-18. Then,

$$\bar{D}_{SF}\left(\tau\middle|\mathbf{e}_i\right) \cong \sum_{r=1}^{2}\left(\bar{N}_r, \lambda_{SF,r}/100\right)\left(\sum_{k=1}^{n}\left\{\sum_{l=1}^{m} \hat{D}_{SF,r}\left(\tau\middle|\left[1, \hat{t}_k, 100, \hat{A}_{rl}, 1, \sim\right], \mathbf{e}_{Mi}\right)\Delta\hat{A}_{rl}\right\}\Delta\hat{t}_k\right) \qquad \text{(Eq. J8.6-24)}$$

is the desired approximation to $\bar{D}_{SF}(\tau|\mathbf{e}_i)$.

An alternative computational strategy that involves fewer interpolations is to approximate $\bar{D}_{SF}(\tau|\mathbf{e}_i)$ by

$$\bar{D}_{SF}\left(\tau\middle|\mathbf{e}_i\right) \cong \sum_{r=1}^{2}\left[\bar{N}_r\, \lambda_{SF,r}/100\right]\left[\sum_{k=1}^{n} \hat{I}_r\left(\tau\middle|\hat{t}_k, \mathbf{e}_{Mi}\right)\Delta\hat{t}_k\right], \qquad \text{(Eq. J8.6-25)}$$

where, for a given time t, $\hat{I}_r(\tau|t, \mathbf{e}_{Mi})$ is an approximation to the integral

$$I_r\left(\tau\middle|t, \mathbf{e}_{Mi}\right) = \int_{\mathcal{A}_r} D_{SF,r}\left(\tau\middle|[1, t, A_r, 1, \sim], \mathbf{e}_{Mi}\right) d_{Ar}\left(A_r\right) \mathrm{d}A_r \qquad \text{(Eq. J8.6-26)}$$

for $r = 1, 2$. For numerical implementation, the approximations

$$\hat{I}_r\left(\tau\middle|t_j, \mathbf{e}_{Mi}\right) = \sum_{l=1}^{m} \hat{D}_{SF,r}\left(\tau\middle|\left[1, t_j, 100, \hat{A}_{rl}, 1, \sim\right], \mathbf{e}_{Mi}\right)\Delta\hat{A}_{rl} \qquad \text{(Eq. J8.6-27)}$$

can be determined for the times t_j, $j = 1, 2, \ldots, 6$, in Equation J8.6-19 with the areas $\hat{A}_{rl}$ determined the same as in Equation J8.6-23. Once the values for $\hat{I}_r(\tau|t_j, \mathbf{e}_{Mi})$ are determined for $r = 1, 2$ and $j = 1, 2, \ldots, 6$, the required values for $\hat{I}_r(\tau|\hat{t}_k, \mathbf{e}_{Mi})$ in Equation J8.6-25 can be determined by interpolation as illustrated in Figure J8.6-3. In addition, the expected doses from the individual WP types are approximated by

$$\bar{D}_{SF,r}\left(\tau|\mathbf{e}_i\right) \cong \left[\bar{N}_r \lambda_{SF,r}/100\right]\left[\sum_{k=1}^{n} \hat{I}_r\left(\tau|\hat{t}_k, \mathbf{e}_{Mi}\right)\right] \qquad \text{(Eq. J8.6-28)}$$

for r = 1, 2. Use of the approximation to $\bar{D}_{SF}(\tau|\mathbf{e}_i)$ in Equation J8.6-25 rather than the approximation in Equation J8.6-24 reduces the number of required interpolations by a factor of approximately 3 (see Equation J8.6-20).

Some additional elaboration on Figure J8.6-3 follows. As noted in the caption for Figure J8.6-3, the results for the three damaged areas under consideration (see Equations J8.6-20 and J8.6-21) are the same for each event time. As a result, the three dose curves for the three damaged areas for each event time exactly overlay in Figure J8.6-3a; if this was not the case, Figure J8.6-3a would look like Figure J8.3-3a but with three rather than five dose curves for each event time. As a result, the integral $I_1(\tau|t_j, \mathbf{e}_{M1})$ in Equation J8.6-26 and its approximation $\hat{I}_1(\tau|t_j, \mathbf{e}_{Mi})$ in Equation J8.6-27 are effectively the same as the dose curves in Figure J8.6-3a. Further, again as noted in the caption to Figure J8.6-3, the results for t_1 and t_2 overlay; thus, Figure J8.6-3a appears to contain five curves when, in actuality, it contains eighteen curves. The results in Figure J8.6-3b,c illustrate interpolated values $\hat{I}_1(\tau|\hat{t}_k, \mathbf{e}_{Mi})$ obtained from $\hat{I}_1(\tau|t_j, \mathbf{e}_{Mi})$. Finally, the expected doses $\bar{D}_{SF,1}(\tau|\mathbf{e}_1)$ and $\bar{D}_{SF,2}(\tau|\mathbf{e}_1)$ for CSNF and CDSP WPs, respectively, defined in Equation J8.6-28 and the expected dose $\bar{D}_{SF}(\tau|\mathbf{e}_1)$ for CSNF and CDSP WPs defined in Equation (J8.6-25) are shown in Figure J8.6-3d.

As an example, the estimate for $\bar{D}_{SF}(\tau|\mathbf{e}_1)$ obtained for LHS element $\mathbf{e}_1$ with the procedure indicated in Equation J8.6-25 is shown in Figure J8.6-4. Further, the results obtained with all *nLHS* = 300 LHS elements are summarized in Figure J8.6-5 and presented in a standard format in Figure J8.6-6.

As previously discussed in conjunction with Equations J5-8 and J6.2-9, dose and expected dose to the RMEI are just two of a large number of results that can be produced and presented in the TSPA-LA. As an example, a summary of the dose calculations for ^{99}Tc is given in Figure J8.6-7, which has the same organization as Figure J8.6-5. Overall, ^{99}Tc is one of the largest contributors to the expected (mean) dose $\bar{\bar{D}}_{SF}(\tau)$ for the 20,000 yr time period. As previously done in Figure J5-4 and other similar figures, a compact summary of the expected (mean) dose results $\bar{\bar{D}}_{SF,r}(\tau)$ for the individual radioactive species is provided in Figure J8.6-8, where $\bar{\bar{D}}_{SF,r}(\tau)$ is the expected (mean) dose to the RMEI at time τ resulting from the release of radioactive species r due to fault displacement events (see Equation J6.2-9 and associated discussion).

The results in Equation J8.6-18 can also be used in a Monte Carlo procedure to provide both (i) an alternate calculation of $\bar{D}_{SF}(\tau|\mathbf{e}_i)$ and (ii) distributions for $D_{SF}(\tau|\mathbf{a}, \mathbf{e}_{Mi})$ at a sequence of values for τ. It is not necessary to consider correlations between the numbers of damaged CSNF

and CDSP WPs in the determination of $\bar{D}_{SF}(\tau|\mathbf{e})$. However, such correlations are potentially important in the determination of distributions for $D_{SF}(\tau|\mathbf{a}, \mathbf{e}_{Mi})$ for individual values of τ.

In the TSPA-LA, the occurrence of fault displacement events is characterized by hazard curves of the form discussed in conjunction with Equations J8.6-7 – J8.6-9. Further, it is specified that there is a perfect correlation between the numbers of damaged WPs obtained from the hazard curves for individual WP types (i.e., CSNF and CDSP WPs in the TSPA-LA). What perfect correlation means with respect to the indicated hazard curves is that the specific numbers of damaged WPs for a given fault displacement event is obtained by selecting a random number on the ordinate of a plot containing the hazard curves and then moving horizontally across the plot to determine the number of damaged WPs of each type.

When the hazard curves are piecewise constant, the sampling procedure indicated in the preceding paragraph results in a finite number of pairs of values $(N_{1j}, N_{2j}), j = 1, 2, \ldots, m$, for the numbers of damaged WPs given the occurrence of a damaging fault displacement event, where N_{1j} is the number of damaged CSNF WPs and N_{2j} is the number of damaged CDSP WPs. Further, each pair (N_{1j}, N_{2j}) has a conditional probability pN_j given the occurrence of a damaging fault displacement event.

In the TSPA-LA, the hazard curves for WP damage from fault displacement are piecewise constant. As a result, the possible combinations of damaged WPs given by a fault displacement event can be described by a sequence of the form

$$\left[pN_j, \left(N_{1j}, N_{2j} \right) \right], j = 1, 2, \ldots, m. \qquad \text{(Eq. J8.6-29)}$$

More specifically, the occurrence rate for damaging fault displacement events is

$$\lambda_{SF} = \max\left\{ \lambda_{SF,1}, \lambda_{SF,2} \right\} = 2.5 \times 10^{-7} \text{ yr}^{-1}. \qquad \text{(Eq. J8.6-30)}$$

Further, the specified hazard curves for CSNF and CDSP WPs result in the following $m = 8$ results in the sequence in Equation J8.6-29: [0.12, (0, 6.5)], [0.24, (19.5, 6.5)], [0.08, (19.5, 9.3)], [0.216, (27.7, 9.3)], [0.032, (27.7, 10.3)], [0.196, (30.7, 10.3)], [0.004, (30.7, 53.2)], [0.112, (158.8, 53.2)].

Given the results in Equation J8.6-29 and the frequency λ_{SF} in Equation J8.6-30, the generation of a sampling based distribution for $D_{SF}(\tau|\mathbf{a}, \mathbf{e}_{Mi})$ and an associated estimate for $\bar{D}_{SF}(\tau|\mathbf{e}_i)$ is straightforward. The probability of a fault displacement event in the time interval $[0, \tau]$ is small. Thus, the appropriate computational strategy is to directly calculate

$$prob_A\left[\mathcal{A}_{SF}(0, \tau) \middle| \mathbf{e}_{Ai} \right] = 1 - \exp(-\lambda_{SF}\, \tau), \qquad \text{(Eq. J8.6-31)}$$

which is the probability that one or more WPs will be damaged by one or more fault displacement events in the time interval $[0, \tau]$ (i.e., the notation $\mathcal{A}_{SF}(0, \tau)$ indicates a restriction

to fault displacement events occurring in the time interval [0, τ]). In turn, the probability of exceeding a dose of size D given a damaging fault displacement event is given by

$$prob_A\left[D < D_{SF}\left(\tau\middle|\mathbf{a}_{SF}\right)\middle|\mathcal{A}_{SF}(0,\tau),\mathbf{e}_i\right] \cong \sum_{k=1}^{nR}\bar{\delta}_D\left[D_{SF}\left(\tau\middle|\mathbf{a}_{SF,k},\mathbf{e}_{Mi}\right)\right]\Big/nR, \qquad \text{(Eq. J8.6-32)}$$

where each sampled future $\mathbf{a}_{SF,k}$ is a future of the form $\mathbf{a}_{SF}$ defined in Equation J4.4-8 with components $\mathbf{a}_{SF,jk}$ of the form indicated in Equation J8.6-1 generated under the assumption that one or more damaging fault displacement events have occurred in the time interval. Specifically, the component vectors

$$\mathbf{a}_{SF,jk} = \left[t_j, N_{1j}, N_{2j}, A_{1j}, A_{2j}, 1, d_j\right], j = 1, 2, \ldots, nSF_k, \qquad \text{(Eq. J8.6-33)}$$

for a sampled future

$$\mathbf{a}_{SF,k} = \left[nSF_k, \mathbf{a}_{SF,1k}, \mathbf{a}_{SF,2k}, \ldots, \mathbf{a}_{SF,nSF_k,k}\right] \qquad \text{(Eq. J8.6-34)}$$

are generated by (i) sampling the event times $0 < t_1 < t_2 < \ldots < t_{nSF_k} < \tau$ in consistency with λ_{SF} and the assumption that one or more damaging fault displacement events have occurred in the time internal [0, τ], (ii) sampling the pairs (N_{1j}, N_{2j}), j = 1, 2, …, nSF_k, in consistency with the probabilities pN_j indicated in Equation J8.6-29, and (iii) sampling the quantities A_{1j}, A_{2j} and d_j in consistency with their assigned distributions for j = 1, 2, …, nSF_k. When $\lambda_{SF}\tau$ is substantially less than one, $\mathbf{a}_{SF,k}$ will have the form $\mathbf{a}_{SF,k}$ = [t, N_1, N_2, A_1, A_2, 1, d] for almost all sampled futures with (i) t having a uniform distribution on [0, τ], (ii) the pair (N_1, N_2) sampled in consistency with the probabilities pN_j indicated in Equation J8.6-29, and (iii) and areas A_1 and A_2 and the dripping indicator sampled in consistency with their assigned distributions. In the current TSPA-LA analysis, the indicator d is not sampled because the effects of dripping/nondripping conditions are incorporated directly into the determination of $D_{SF,r}(\tau|[1, t, 100, A_r, 1, \sim], \mathbf{e}_M)$ as indicated in conjunction with Equation J8.6-17.

The required evaluation of $D_{SF}(\tau|\mathbf{a}_{SF,k}, \mathbf{e}_{Mi})$ in Equation J8.6-32 follows from the relationships

$$D_{SF}\left(\tau\middle|\mathbf{a}_{SF,k},\mathbf{e}_{Mi}\right) = \sum_{j=1}^{nSF_k} D_{SF}\left(\tau\middle|\left[1,\mathbf{a}_{SF,jk}\right],\mathbf{e}_{Mi}\right)$$

$$= \sum_{j=1}^{nSF_k}\sum_{r=1}^{2}\left(N_{rj}/100\right) D_{SF,r}\left(\tau\middle|\left[1,t_j,100,A_{rj},1,\sim\right],\mathbf{e}_{Mi}\right), \qquad \text{(Eq. J8.6-35)}$$

where $D_{SF,r}(\tau|[1, t_j, 100, A_{rj}, 1, \sim], \mathbf{e}_{Mi})$ is defined in conjunction with (J8.6-17) for r = 1 and 2. The specific values for $D_{SF,r}(\tau|[1, t_j, 100, A_{rj}, 1, \sim], \mathbf{e}_{Mi})$ required in the evaluation of

$D_{SF}(\tau|\mathbf{a}_{SF,k}, \mathbf{e}_{Mi})$ in Equation J8.6-35 and hence in Equation J8.6-28 can be obtained with interpolation procedures from the precalculated results indicated in Equations J8.6-18 – J8.6-22 and are denoted by $\hat{D}_{SF,r}(\tau|[1, t_j, 100, A_{rj}, 1, \sim], \mathbf{e}_{Mi})$.

Together, the results in Equations J8.6-31 and J8.6-32 define the CCDF for dose to the RMEI (mrem/yr) at time τ from fault displacement events. Specifically, the probability of exceeding dose D at time τ is given by

$$prob_A\left[D < D_{SF}\left(\tau|\mathbf{a}_{SF}\right)\middle|\mathbf{e}_i\right]$$

$$= prob_A\left[A_{SF}\left(0,\tau\right)\middle|\mathbf{e}_{Ai}\right] prob_A\left[D < D_{SF}\left(\tau|\mathbf{a}_{SF}\right)\middle|A_{SF}\left(0,\tau\right), \mathbf{e}_i\right] \quad \text{(Eq. J8.6-36)}$$

with $prob_A[\mathcal{A}_{SF}(0, \tau)|\mathbf{e}_{Ai}]$ and $prob_A[D < D_{SF}(\tau|\mathbf{a}_{SF})|\mathcal{A}_{SF}(0, \tau), \mathbf{e}_i]$ defined in Equations J8.6-31 and J8.6-32, respectively. The preceding corresponds to the calculation described in conjunction with Equation J4.5-19 with $C = SF$. A similar calculation leads to the CDF for dose to the RMEI for fault displacements as described in conjunction with Equation J4.5-21 for $C = SF$. This process is illustrated in Figures J8.6-9 and J8.6-10.

As discussed in Section J4.10, the numerical stability of results obtained with Latin hypercube sampling can be assessed with replicated sampling. Specifically, the analysis for fault displacement events was performed with the $nRL = 3$ replicated LHSs indicated in Equation J4.10-1. In turn, this analysis shows that the numerical error in using Latin hypercube sampling to estimate $\bar{\bar{D}}_{SF}(\tau)$ is small relative to the epistemic uncertainty associated with the possible values for $\bar{D}_{SF}(\tau|\mathbf{e})$ (Figure J8.6-11).

The results presented in Figures J8.6-1 to J8.6-11 are for the time period [0, 20,000 yr]. Corresponding results for the time period [0, 10^6 yr] are presented without discussion in Figures J8.6-12 to J8.6-22.

J8.7 Seismic Scenario Class: $\mathcal{A}_S$

The results $\bar{D}_{SG}(\tau|\mathbf{e}_i)$ and $\bar{\bar{D}}_{SG}(\tau)$ obtained for the seismic ground motion scenario class $\mathcal{A}_{SG}$ are generally much larger than the corresponding results $\bar{D}_{SF}(\tau|\mathbf{e}_i)$ and $\bar{\bar{D}}_{SF}(\tau)$ obtained for the seismic fault displacement scenario class $\mathcal{A}_{SF}$. The only exceptions to this occur for LHS elements that result in very small values for $\bar{D}_{SG}(\tau|\mathbf{e}_i)$, in which case $\bar{D}_{SG}(\tau|\mathbf{e}_i)$ and $\bar{D}_{SF}(\tau|\mathbf{e}_i)$ have similar values. As a result, $\bar{D}_S(\tau|\mathbf{e}_i)$ and $\bar{\bar{D}}_S(\tau)$ for the seismic scenario class $\mathcal{A}_S$ are effectively the same as $\bar{D}_{SG}(\tau|\mathbf{e}_i)$ and $\bar{\bar{D}}_{SG}(\tau)$ and are not presented as separate figures for this reason.

J8.8 Probabilities Associated with Seismic Scenario Classes

The probabilities $p_A(\mathcal{A}_{SG})$, $p_A(\mathcal{A}_{SF})$ and $p_A(\mathcal{A}_S)$ for the scenario classes $\mathcal{A}_{SG}$, $\mathcal{A}_{SF}$ and $\mathcal{A}_S$ depend on the time interval under consideration. In the TSPA-LA, the time intervals of primary interest are [0, 20,000 yr] and [0, 1,000,000 yr]. However, for generality, a time interval [0, τ] is assumed to be under consideration and $\mathcal{A}_{SG}(0, \tau)$, $\mathcal{A}_{SF}(0, \tau)$ and $\mathcal{A}_S(0, \tau)$ will represent $\mathcal{A}_{SG}$, $\mathcal{A}_{SF}$ and $\mathcal{A}_S$ defined with futures (i.e., seismic event occurrences) restricted to [0, τ]. Formally, this corresponds to restricting the sample spaces (i.e., sets of possible futures) under consideration to futures defined on the time interval [0, τ]. The notation for $p_A(\mathcal{A}_{SG})$, $p_A(\mathcal{A}_{SF})$ and $p_A(\mathcal{A}_S)$ does not include a dependence on the vector **e** of epistemically uncertain analysis inputs because the TSPA-LA does not include any uncertain analysis inputs (i.e., elements of **e**) that affect the values of these probabilities.

The seismic ground motion scenario class $\mathcal{A}_{SG}(0, \tau)$ is assumed to be defined by the properties of seismic ground motion events that have a PGV greater than or equal to 0.219 m/s and an associated exceedance frequency of 4.287×10^{-4} yr^{-1} (i.e., v_{mn} = 0.219 m/s and $\lambda_{mx} = 4.287 \times 10^{-4}$ yr^{-1} in previously used notation). In turn,

$$p_A\left[\mathcal{A}_{SG}(0,\tau)\right] = 1-\exp(-\lambda_{mx}\tau) = \begin{cases} 0.99 & \text{for } \tau = 10^4 \text{ yr} \\ 1.00 & \text{for } \tau = 2\times10^4 \text{ yr} \\ 1.00 & \text{for } \tau = 10^6 \text{ yr} \end{cases} \quad \text{(Eq. J8.8-1)}$$

as indicated in Equation J3.6-9.

The seismic fault displacement scenario class $\mathcal{A}_{SF}(0, \tau)$ is assumed to be defined by the properties of fault displacement events that have an occurrence frequency of $\lambda_{SF} = 2.5 \times 10^{-7}$ yr^{-1}. In turn,

$$p_A\left[\mathcal{A}_{SF}(0,\tau)\right] = 1-\exp(-\lambda_{SF}\tau) = \begin{cases} 2.50\times10^{-3} & \text{for } \tau = 10^4 \text{ yr} \\ 4.99\times10^{-3} & \text{for } \tau = 2\times10^4 \text{ yr} \\ 0.22\times10^{0} & \text{for } \tau = 10^6 \text{ yr} \end{cases} \quad \text{(Eq. J8.8-2)}$$

as indicated in Equation J3.6-9.

If the occurrence of fault displacement events is included in the determination of λ_{mx} for seismic ground motion events, then $p_A[\mathcal{A}_S(0, \tau)] = p_A[\mathcal{A}_{SG}(0, \tau)]$. If the occurrence of fault displacement events is not included in the determination of λ_{mx}, then the occurrence rate λ_S for seismic events

is given by $\lambda_S = \lambda_{mx} + \lambda_{SF}$ as indicated in Equation J3.6-13. However, given that $\lambda_{mx} = 4.287 \times 10^{-4}$ yr^{-1} and $\lambda_{SF} = 2.5 \times 10^{-7}$ yr^{-1}, λ_S in this case is effectively the same as λ_{mx}. As a result, there is no meaningful difference between $p_A[\mathcal{A}_S(0, \tau)]$ and $p_A[\mathcal{A}_{SG}(0, \tau)]$.

J9 EXPECTED DOSE FROM ALL SCENARIO CLASSES

J9.1 Expected Dose from All Scenario Classes: Preliminaries

As indicated in Equation J4.5-1, the TSPA-LA assumes that expected dose to the RMEI at time τ from aleatory uncertainty can be approximated by

$$\bar{D}(\tau|\mathbf{e}) \cong D_N(\tau|\mathbf{a}_N, \mathbf{e}_M) + \bar{D}_{EW}(\tau|\mathbf{e}) + \bar{D}_{ED}(\tau|\mathbf{e}) + \bar{D}_{II}(\tau|\mathbf{e}) + \bar{D}_{IE}(\tau|\mathbf{e}) + \bar{D}_{SG}(\tau|\mathbf{e}) + \bar{D}_{SF}(\tau|\mathbf{e}) \quad \text{(Eq. J9.1-1)}$$

conditional on the element $\mathbf{e} = [\mathbf{e}_A, \mathbf{e}_M]$ of $\mathcal{E}$. In turn, the expected (mean) dose to the RMEI at time τ from aleatory and epistemic uncertainty is approximated by

$$\bar{\bar{D}}(\tau) \cong \bar{\bar{D}}_N(\tau) + \bar{\bar{D}}_{EW}(\tau) + \bar{\bar{D}}_{ED}(\tau) + \bar{\bar{D}}_{II}(\tau) + \bar{\bar{D}}_{IE}(\tau) + \bar{\bar{D}}_{SG}(\tau) + \bar{\bar{D}}_{SF}(\tau) \quad \text{(Eq. J9.1-2)}$$

as indicated in Equation J4.6-3.

In the TSPA-LA, $\bar{D}_N(\tau|\mathbf{e}) = 0$ for $0 \le \tau \le 20{,}000$ yr. Further, for $0 \le \tau \le 1{,}000{,}000$ yr, the effects of nominal processes are incorporated into the determination of $\bar{D}_{SG}(\tau|\mathbf{e})$. As a result, $\bar{D}(\tau|\mathbf{e})$ and $\bar{\bar{D}}(\tau)$ effectively have the forms

$$\bar{D}(\tau|\mathbf{e}) \cong \bar{D}_{EW}(\tau|\mathbf{e}) + \bar{D}_{ED}(\tau|\mathbf{e}) + \bar{D}_{II}(\tau|\mathbf{e}) + \bar{D}_{IE}(\tau|\mathbf{e}) + \bar{D}_{SG}(\tau|\mathbf{e}) + \bar{D}_{SF}(\tau|\mathbf{e}) \quad \text{(Eq. J9.1-3)}$$

and

$$\bar{\bar{D}}(\tau) \cong \bar{\bar{D}}_{EW}(\tau) + \bar{\bar{D}}_{ED}(\tau) + \bar{\bar{D}}_{II}(\tau) + \bar{\bar{D}}_{IE}(\tau) + \bar{\bar{D}}_{SG}(\tau) + \bar{\bar{D}}_{SF}(\tau) \quad \text{(Eq. J9.1-4)}$$

for both the 20,000 yr and 1,000,000 yr calculations.

The same LHS $\mathbf{e}_i = [\mathbf{e}_{Ai}, \mathbf{e}_{Mi}]$, $i = 1, 2, \ldots, nLHS = 300$, is used for all scenario classes. As a result,

$$\bar{D}(\tau|\mathbf{e}_i) \cong \bar{D}_{EW}(\tau|\mathbf{e}_i) + \bar{D}_{ED}(\tau|\mathbf{e}_i) + \bar{D}_{II}(\tau|\mathbf{e}_i) + \bar{D}_{IE}(\tau|\mathbf{e}_i) + \bar{D}_{SG}(\tau|\mathbf{e}_i) + \bar{D}_{SF}(\tau|\mathbf{e}_i) \quad \text{(Eq. J9.1-5)}$$

for $i = 1, 2, \ldots, nLHS = 300$ and

$$\bar{\bar{D}}(\tau) \cong \sum_{i=1}^{300} \bar{D}\left(\tau|\mathbf{e}_i\right)/300. \qquad \text{(Eq. J9.1-6)}$$

Further, quantiles $Q_q[\bar{D}(\tau|\mathbf{e})]$ for $\bar{D}(\tau|\mathbf{e})$ are defined as indicated in Equation J4.2-10 and are approximated by the value D such that

$$q \cong \sum_{i=1}^{300} \underline{\delta}_D\left[\bar{D}\left(\tau|\mathbf{e}_i\right)\right]/300, \qquad \text{(Eq. J9.1-7)}$$

where

$$\underline{\delta}_D\left[\bar{D}\left(\tau|\mathbf{e}_i\right)\right] = \begin{cases} 1 & \text{if } \bar{D}\left(\tau|\mathbf{e}_i\right) \le D \\ 0 & \text{otherwise.} \end{cases} \qquad \text{(Eq. J9.1-8)}$$

Specifically, $Q_q[\bar{D}(\tau|\mathbf{e})]$ is the q quantile value (e.g., 0.05, 0.5, 0.95) for $\bar{D}(\tau|\mathbf{e})$ and is equal to the value of D that most closely satisfies Equation J9.1-7.

The results $\bar{D}_r(\tau|\mathbf{e}_i)$ and $\bar{\bar{D}}_r(\tau)$ for individual radioactive species designated by r can be determined in the same manner as $\bar{D}(\tau|\mathbf{e}_i)$ and $\bar{\bar{D}}(\tau)$ in Equations J9.1-5 and J9.1-6. Specifically,

$$\bar{D}_r\left(\tau|\mathbf{e}_i\right) \cong \bar{D}_{EW,r}\left(\tau|\mathbf{e}_i\right) + \bar{D}_{ED,r}\left(\tau|\mathbf{e}_i\right) + \bar{D}_{II,r}\left(\tau|\mathbf{e}_i\right) + \bar{D}_{IE,r}\left(\tau|\mathbf{e}_i\right) + \bar{D}_{SG,r}\left(\tau|\mathbf{e}_i\right) + \bar{D}_{SF,r}\left(\tau|\mathbf{e}_i\right) \qquad \text{(Eq. J9.1-9)}$$

and

$$\bar{\bar{D}}_r\left(\tau\right) \cong \sum_{i=1}^{300} \bar{D}_r\left(\tau|\mathbf{e}_i\right)/300, \qquad \text{(Eq. J9.1-10)}$$

where $\bar{D}_{EW,r}(\tau|\mathbf{e}_i)$ is the expected dose to the RMEI (mrem/yr) at time τ for radioactive species r resulting from early WP failure conditional on $\mathbf{e}_i$ and the other expected doses in Equation J9.1-9 are defined similarly.

J9.2 Expected Dose from All Scenario Classes: 0 to 20,000 yr

The outcomes of the calculation to determine $\bar{D}(\tau|\mathbf{e}_i)$, $Q_q[\bar{D}(\tau|\mathbf{e})]$ for q = 0.05, 0.5 and 0.95, and $\bar{\bar{D}}(\tau)$ for $0 \le \tau \le 20{,}000$ yr are summarized in Figure J9.2-1. Further, the standard presentation format used for these results is shown in Figure J9.2-2. In addition, the expected (mean) results for the individual radioactive species are presented in Figure J9.2-3.

As described in Section J4.10, the analyses leading to the results in Figures J9.2-1 to J9.2-3 were replicated with three independently generated LHSs to test for stability (Figure J9.2-4). This replication shows than an LHS of size 300 is adequate for the estimation of $Q_q[\bar{D}(\tau|\mathbf{e})]$ and $\bar{\bar{D}}(\tau)$ in this analysis for the 0 to 20,000 yr time interval.

J9.3 Expected Dose from All Scenario Classes: 0 to 1,000,000 yr

The same analyses that lead to Figures J9.2-1 to J9.2-4 for the 20,000 yr time interval were also carried out for the 1,000,000 yr time interval (Figures J9.3-1 to J9.3-4).

J10 JUSTIFICATION FOR ANALYSIS DECOMPOSITION

As discussed in Sections J4.5 and J4.6 and explicitly represented in Equations J4.5-1 and (J4.6-1), the computational structure of the TSPA-LA is based on the assumption that there are no significant synergisms between results conditional on the occurrence of individual scenario classes that materially affect the expected dose $\bar{D}(\tau|\mathbf{e})$ over all scenario classes (i.e., over all possible futures $\mathbf{a}$). Specifically, the assumption is made that

$$\bar{D}(\tau|\mathbf{e}) = D_N(\tau|\mathbf{a}_N, \mathbf{e}_M) + \bar{D}_{EW}(\tau|\mathbf{e}) + \bar{D}_{ED}(\tau|\mathbf{e}) + \bar{\bar{D}}_{II}(\tau|\mathbf{e}) + \bar{D}_{IE}(\tau|\mathbf{e}) + \bar{D}_{SG}(\tau|\mathbf{e}) + \bar{D}_{SG}(\tau|\mathbf{e}), \quad \text{(Eq. J10-1)}$$

where, conditional on the element $\mathbf{e} = [\mathbf{e}_A, \mathbf{e}_M]$ of $\mathcal{E}$,

$D_N(\tau|\mathbf{a}, \mathbf{e}_M)$ = dose to RMEI (mrem/yr) at time τ resulting from nominal conditions for future $\mathbf{a} \in \mathcal{A}$

$$= D_N(\tau|\mathbf{a}_N, \mathbf{e}_M), \quad \text{(Eq. J10-2)}$$

$D_{EW}(\tau|\mathbf{a}, \mathbf{e}_M)$ = dose to RMEI (mrem/yr) at time τ resulting from early WP failure for future $\mathbf{a} \in \mathcal{A}$

$$= D_{EW}(\tau|\mathbf{a}_{EW}, \mathbf{e}_M), \quad \text{(Eq. J10-3)}$$

$D_{ED}(\tau|\mathbf{a}, \mathbf{e}_M)$ = dose to RMEI (mrem/yr) at time τ resulting from early DS failure for future $\mathbf{a} \in \mathcal{A}$

$$= D_{ED}(\tau|\mathbf{a}_{ED}, \mathbf{e}_M), \quad \text{(Eq. J10-4)}$$

$D_{II}(\tau|\mathbf{a}, \mathbf{e}_M)$ = dose to RMEI (mrem/yr) at time τ resulting from igneous intrusive events for future $\mathbf{a} \in \mathcal{A}$

$$= D_{II}(\tau|\mathbf{a}_{II}, \mathbf{e}_M), \quad \text{(Eq. J10-5)}$$

$D_{IE}\left(\tau|\mathbf{a},\mathbf{e}_M\right)$ = dose to RMEI (mrem/yr) at time τ resulting from igneous eruptive events for future $\mathbf{a} \in \mathcal{A}$

$= D_{IE}\left(\tau|\mathbf{a}_{IE},\mathbf{e}_M\right)$, (Eq. J10-6)

$D_{SG}\left(\tau|\mathbf{a},\mathbf{e}_M\right)$ = dose to RMEI (mrem/yr) at time τ resulting from seismic ground motion events for future $\mathbf{a} \in \mathcal{A}$

$= D_{SG}\left(\tau|\mathbf{a}_{SG},\mathbf{e}_M\right)$, (Eq. J10-7)

$D_{SF}\left(\tau|\mathbf{a},\mathbf{e}_M\right)$ = dose to RMEI (mrem/yr) at time τ resulting from seismic fault displacement events for future $\mathbf{a} \in \mathcal{A}$

$= D_{SF}\left(\tau|\mathbf{a}_{SF},\mathbf{e}_M\right)$, (Eq. J10-8)

and in turn

$\bar{D}_{EW}\left(\tau|\mathbf{e}\right)$ = expected dose to RMEI (mrem/yr) at time τ resulting from early WP failure

$= E_A\left[D_{EW}\left(\tau|\mathbf{a},\mathbf{e}_M\right)\middle|\mathbf{e}_A\right]$

$= \int_{\mathcal{A}} D_{EW}\left(\tau|\mathbf{a},\mathbf{e}_M\right) d_A\left(\mathbf{a}|\mathbf{e}_A\right) \mathrm{d}A$

$= \int_{\mathcal{A}_{EW}} D_{EW}\left(\tau|\mathbf{a}_{EW},\mathbf{e}_M\right) d_A\left(\mathbf{a}|\mathbf{e}_A\right) \mathrm{d}A$, reminder $\mathbf{a} = [\ldots \mathbf{a}_{EW} \ldots]$, (Eq. J10-9)

$\bar{D}_{ED}\left(\tau|\mathbf{e}\right)$ = expected dose to RMEI (mrem/yr) at time τ resulting from early DS failure

$= E_A\left[D_{ED}\left(\tau|\mathbf{a},\mathbf{e}_M\right)\middle|\mathbf{e}_A\right]$

$= \int_{\mathcal{A}} D_{ED}\left(\tau|\mathbf{a},\mathbf{e}_M\right) d_A\left(\mathbf{a}|\mathbf{e}_A\right) \mathrm{d}A$

$= \int_{\mathcal{A}_{ED}} D_{ED}\left(\tau|\mathbf{a}_{ED},\mathbf{e}_M\right) d_A\left(\mathbf{a}|\mathbf{e}_A\right) \mathrm{d}A$, reminder $\mathbf{a} = [\ldots \mathbf{a}_{ED} \ldots]$, (Eq. J10-10)

$\bar{D}_{II}\left(\tau|\mathbf{e}\right)$ = expected dose to RMEI (mrem/yr) at time τ resulting from igneous intrusive events

$= E_A\left[D_{II}\left(\tau|\mathbf{a},\mathbf{e}_M\right)\middle|\mathbf{e}_A\right]$

$= \int_{\mathcal{A}} D_{II}\left(\tau|\mathbf{a},\mathbf{e}_M\right) d_A\left(\mathbf{a}|\mathbf{e}_A\right) \mathrm{d}A$

$= \int_{\mathcal{A}_{II}} D_{II}\left(\tau|\mathbf{a}_{II},\mathbf{e}_M\right) d_A\left(\mathbf{a}|\mathbf{e}_A\right) \mathrm{d}A$, reminder $\mathbf{a} = [\ldots \mathbf{a}_{II} \ldots]$, (Eq. J10-11)

$\bar{D}_{IE}(\tau|\mathbf{e})$ = expected dose to RMEI (mrem/yr) at time τ resulting from igneous eruptive events

$$= E_A\left[D_{IE}(\tau|\mathbf{a}, \mathbf{e}_M)\middle|\mathbf{e}_A\right]$$

$$= \int_{\mathcal{A}} D_{IE}(\tau|\mathbf{a}, \mathbf{e}_M)\, d_A(\mathbf{a}|\mathbf{e}_A)\,\mathrm{d}A$$

$$= \int_{\mathcal{A}_{IE}} D_{IE}(\tau|\mathbf{a}_{IE}, \mathbf{e}_M)\, d_A(\mathbf{a}|\mathbf{e}_A)\,\mathrm{d}A, \text{ reminder } \mathbf{a} = [\ldots \mathbf{a}_{IE} \ldots], \quad \text{(Eq. J10-12)}$$

$\bar{D}_{SG}(\tau|\mathbf{e})$ = expected dose to RMEI (mrem/yr) at time τ resulting from seismic ground motion events

$$= E_A\left[D_{SG}(\tau|\mathbf{a}, \mathbf{e}_M)\middle|\mathbf{e}_A\right]$$

$$= \int_{\mathcal{A}} D_{SG}(\tau|\mathbf{a}, \mathbf{e}_M)\, d_A(\mathbf{a}|\mathbf{e}_A)\,\mathrm{d}A$$

$$= \int_{\mathcal{A}_{SG}} D_{SG}(\tau|\mathbf{a}_{SG}, \mathbf{e}_M)\, d_A(\mathbf{a}|\mathbf{e}_A)\,\mathrm{d}A, \text{ reminder: } \mathbf{a} = [\ldots \mathbf{a}_{SG} \ldots], \text{ (Eq. J10-13)}$$

$\bar{D}_{SF}(\tau|\mathbf{e})$ = expected dose to RMEI (mrem/yr) at time τ resulting from seismic fault displacement events

$$= E_A\left[D_{SF}(\tau|\mathbf{a}, \mathbf{e}_M)\middle|\mathbf{e}_A\right]$$

$$= \int_{\mathcal{A}} D_{SF}(\tau|\mathbf{a}, \mathbf{e}_M)\, d_A(\mathbf{a}|\mathbf{e}_A)\,\mathrm{d}A$$

$$= \int_{\mathcal{A}_{SF}} D_{SF}(\tau|\mathbf{a}_{SF}, \mathbf{e}_M)\, d_A(\mathbf{a}|\mathbf{e}_A)\,\mathrm{d}A, \text{ reminder } \mathbf{a} = [\ldots \mathbf{a}_{SF} \ldots]. \quad \text{(Eq. J10-14)}$$

In the preceding, $D_{EW}(\tau|\mathbf{a}, \mathbf{e}_M)$ is equivalent to $D_{EW}(\tau|\mathbf{a}_{EW}, \mathbf{e}_M)$ because only dose from early WP failure is under consideration; for the same reason, the integrals over $\mathcal{A}$ and $\mathcal{A}_{EW}$ in Equation J.4.4-20 are equivalent. Specifically, possible synergisms between occurrences associated with different scenario classes are not being considered. Analogous equivalencies hold $D_{ED}(\tau|\mathbf{a}, \mathbf{e}_M)$, $D_{II}(\tau|\mathbf{a}, \mathbf{e}_M)$, $D_{IE}(\tau|\mathbf{a}, \mathbf{e}_M)$, $D_{SG}(\tau|\mathbf{a}, \mathbf{e}_M)$, $D_{SF}(\tau|\mathbf{a}, \mathbf{e}_M)$ and associated integrals.

The appropriateness of the approximation in Equation J10-1 is now considered. In general, this appropriateness depends on both scenario class probability and the expected doses to the RMEI that result from the futures associated with individual scenario classes.

Nominal processes result in $\bar{D}_N(\tau|\mathbf{a}_N, \mathbf{e}_M) = 0$ mrem/yr prior to 20,000 yr (Figures J5-1 and J5-2). Thus, the separation of $\bar{D}_N(\tau|\mathbf{a}_N, \mathbf{e}_M)$ from the other expected doses in Equation J10-1 has no consequence for the [0, 20,000 yr] time interval. For the determination of $\bar{D}(\tau|\mathbf{e})$ for the

time interval [0, 10^6 yr], releases associated with WP failures that derive from nominal processes are included with releases that derive from seismic ground motion events. As a result, the expected dose $\bar{D}_{SG}(\tau|\mathbf{e})$ for the seismic ground motion scenario class $\mathcal{A}_{SG}$ contains the dose $D_N(\tau|\mathbf{a}_N, \mathbf{e}_M)$ associated with the nominal scenario class. In the determination of the doses $D_{SG}(\tau|\mathbf{a}, \mathbf{e}_M)$ that give rise to $\bar{D}_{SG}(\tau|\mathbf{e})$ for the [0, 10^6 yr] time interval, the synergisms (e.g., effects of WP thinning, inventory depletion, ...) between the effects of nominal processes and seismic events are incorporated into the analysis. Thus, $\bar{D}_{SG}(\tau|\mathbf{e})$ appropriately contains the effects of both nominal processes and seismic ground motion events.

The early failure scenario classes $\mathcal{A}_{EW}$ and $\mathcal{A}_{ED}$ involve failures of small numbers of WPs (Figure J6.2-1) and DSs (Figure J6.3-1) randomly spread through the repository. Because of the small numbers of WPs and DSs involved, there should be no synergisms between early WP failures and early DS failures. As a result, the separation of $\bar{D}_{EW}(\tau|\mathbf{e})$ and $\bar{D}_{ED}(\tau|\mathbf{e})$ is reasonable. Similarly, the fault displacement scenario class $\mathcal{A}_{SF}$ involves the failure of a small number of WPs (see Equation J8.6-29 and associated discussion) as does the igneous eruptive scenario class $\mathcal{A}_{IE}$. As a result, the separation of $\bar{D}_{SF}(\tau|\mathbf{e})$, $\bar{D}_{IE}(\tau|\mathbf{e})$, $\bar{D}_{EW}(\tau|\mathbf{e})$ and $\bar{D}_{ED}(\tau|\mathbf{e})$ is also reasonable. Specifically, the likelihood that a given WP would be affected in a given future **a** by events associated with more than one of these scenario classes is small. Further, as the analysis is designed, the ignoring of this potential interaction results in a small, and insignificant, upward shift in the values for $\bar{D}_{SF}(\tau|\mathbf{e})$, $\bar{D}_{IE}(\tau|\mathbf{e})$, $\bar{D}_{EW}(\tau|\mathbf{e})$ and $\bar{D}_{ED}(\tau|\mathbf{e})$ as a result of slightly overcounting the releases associated with the WPs affected by more than one event.

The seismic ground motion scenario class $\mathcal{A}_{SG}$ involves damage to large numbers of WPs. Specifically, a seismic ground motion event that damages one WP of a given type (i.e., CSNF or CDSP) will generally damage all WPs of that type. As a result, the fraction of WPs damaged by a seismic ground motion event that have been previously affected by an early WP failure, an early DS failure, an igneous eruptive event or a seismic fault displacement event is small. Because of this, correcting for the inventory reduction associated with such precursor events would have little effect on $\bar{D}_{SG}(\tau|\mathbf{e})$. Specifically, ignoring the effects of this inventory correction produces a small, but not significant, upward shift in $\bar{D}_{SG}(\tau|\mathbf{e})$. For the [0, 10^6 yr] time interval, WP failure by nominal processes is included in the determination of $\bar{D}_{SG}(\tau|\mathbf{e})$. With increasing time, many more WPs fail by nominal processes (Figures K4.2-2 and K4.2-4) than fail by early WP failure, early DS failure, seismic fault displacement or igneous eruption. Thus, again, including a correction for the indicated potential precursor events would have little effect on $\bar{D}_{SG}(\tau|\mathbf{e})$ for the [0, 10^6 yr] time interval. As a result, the value for $\bar{D}_{SG}(\tau|\mathbf{e})$ is not significantly affected by precursor events associated with the scenario classes $\mathcal{A}_{EW}$, $\mathcal{A}_{ED}$, $\mathcal{A}_{IE}$ and $\mathcal{A}_{SF}$.

The potential effects of seismic ground motion events on $\bar{D}_{EW}(\tau|\mathbf{e})$ and $\bar{D}_{ED}(\tau|\mathbf{e})$ are limited because the affected WPs are destroyed at the start of the calculation for the early WP failure

scenario class $\mathcal{A}_{EW}$ and both the DS and the WP are destroyed at the start of the calculation for the early DS failure scenario class $\mathcal{A}_{ED}$. Thus, including the potential effects of seismic ground motion events would have little incremental effect on $\bar{D}_{EW}(\tau|\mathbf{e})$ and $\bar{D}_{ED}(\tau|\mathbf{e})$. The most likely effect would be to increase $\bar{D}_{EW}(\tau|\mathbf{e})$ as a result of seismically-induced DS failure. However, this would induce so many more DS failures over additional previously unfailed WPs that the incremental effect on $\bar{D}(\tau|\mathbf{e})$ would be small.

At later times, it is possible that seismic events could reduce the WP inventories that give rise to $\bar{D}_{IE}(\tau|\mathbf{e})$ and $\bar{D}_{SF}(\tau|\mathbf{e})$. However, the values for $\bar{D}_{IE}(\tau|\mathbf{e})$ (Figures J7.3-4 and J7.3-12) and $\bar{D}_{SF}(\tau|\mathbf{e})$ (Figures J8.6-5 and J8.6-16) are already small. As a result, any reductions in $\bar{D}_{IE}(\tau|\mathbf{e})$ and $\bar{D}_{SF}(\tau|\mathbf{e})$ that might occur as a result of correcting for the effects of prior seismic ground motion events would have little effect on $\bar{D}(\tau|\mathbf{e})$.

The potential interactions between seismic ground motion events and igneous intrusive events are now considered. An igneous intrusive event is assumed to destroy all WPs in the repository. When $\bar{D}_{SG}(\tau|\mathbf{e})$ and $\bar{D}_{II}(\tau|\mathbf{e})$ are calculated under the assumptions that $\bar{D}_{SG}(\tau|\mathbf{e})$ is not affected by potential igneous intrusive events and $\bar{D}_{II}(\tau|\mathbf{e})$ is not affected by potential ground motion events, the result is that $\bar{D}_{SG}(\tau|\mathbf{e})$ is slightly overestimated as a result of assuming that seismically-induced releases continue after an igneous intrusion has destroyed all WPs in the repository and $\bar{D}_{II}(\tau|\mathbf{e})$ is slightly overestimated as a result of not correcting for inventory reduction in the WPs that result from the seismically-induced releases.

Because the probability of the seismic ground motion scenario class $\mathcal{A}_{SG}$ is effectively one (Equation J8.8-1) and the probability of the igneous intrusive scenario class is much smaller (Figure J7.5-1), omitting a correction for the effects of igneous intrusive events has a relatively small effect on $\bar{D}_{SG}(\tau|\mathbf{e})$.

In contrast, igneous intrusive events will almost always be preceded by one or more seismic ground motion events. The extent to which these events affect dose from igneous intrusive events depends on the amount of WP inventory released before the igneous intrusive event. At early times (e.g., prior to 10^5 yr), the amount of material released from WPs as a result of seismic ground motion events is likely to be small, with the result that $\bar{D}_{II}(\tau|\mathbf{e})$ will be little affected by prior seismic ground motion events. As time increases, the effect will be larger because of increasing seismic damage, increasing DS and WP failures from nominal processes, and increasing time for radionuclide transport from the WPs and the EBS. To a great extent, this effect will be linear with respect to the amount of radioactive material removed from the WPs and the EBS. As a result, unless prior seismic events result in the release of substantial amounts of radioactive material (e.g., >50 percent of the inventory in the repository), the effect on $\bar{D}_{II}(\tau|\mathbf{e})$ will not be large relative to the epistemic uncertainty in $\bar{D}_{II}(\tau|\mathbf{e})$ that results from the uncertainty associated with $\mathbf{e}$ (Figures J7.2-4 and J7.2-14). As comparison of the igneous dose results in Figures J7.2-1 and J7.2-11 with the seismic dose results in Figures J8.3-1, J8.3-2 and J8.4-1 shows, the doses from igneous intrusive events tend to be much larger than the doses from

seismic events. This observation includes the combined effects of nominal processes and multiple seismic events shown in Figure J8.4-1 for the [0, 10^6 yr] time interval. Because dose is proportional to released inventory, this comparison indicates that correcting WP inventory for the effects of nominal processes and prior seismic events would have little effect on $\bar{D}_{II}(\tau|\mathbf{e})$. In any event, the effect of not correcting for the effects of prior seismic ground motion events results in an overestimate for $\bar{D}_{II}(\tau|\mathbf{e})$.

As previously discussed, the scenario classes $\mathcal{A}_{EW}$, $\mathcal{A}_{ED}$ and $\mathcal{A}_{IE}$ involve damage to small numbers of WPs. In contrast, the igneous intrusive scenario class $\mathcal{A}_{II}$ is assumed to involve damage to all WPs in the repository. As a result, a correction to $\bar{D}_{II}(\tau|\mathbf{e})$ to account for the potential effects of events associated with the scenario classes $\mathcal{A}_{EW}$, $\mathcal{A}_{ED}$ and $\mathcal{A}_{IE}$ would have no discernable effect.

In summary, the only potentially significant synergisms between events associated with individual scenario classes involve the nominal scenario class $\mathcal{A}_N$ and the seismic ground motion scenario class $\mathcal{A}_{SG}$ for the [0, 10^6 yr] time interval. For these two scenario classes, the potential effects of such synergisms are directly incorporated into the determination of $\bar{D}_{SG}(\tau|\mathbf{e})$ for the [0, 10^6 yr] time interval. For the remaining scenario classes, no significant synergisms exist that materially affect the estimation of $\bar{D}(\tau|\mathbf{e})$ by first determining the expected doses $\bar{D}_{EW}(\tau|\mathbf{e})$, $\bar{D}_{ED}(\tau|\mathbf{e})$, $\bar{D}_{II}(\tau|\mathbf{e})$, $\bar{D}_{IE}(\tau|\mathbf{e})$, $\bar{D}_{SG}(\tau|\mathbf{e})$ and $\bar{D}_{SF}(\tau|\mathbf{e})$ and then summing these expected doses as indicated in Equation J10-1. As a reminder, $\bar{D}_N(\tau|\mathbf{a}_N, \mathbf{e}_M) = 0$ mrem/yr for the [0, 20,000 yr] time interval, and the effects of nominal processes are directly incorporated into the determination of $\bar{D}_{SG}(\tau|\mathbf{e})$ for the [0, 10^6 yr] time interval. The result of ignoring inventory corrections for the effects of events associated with individual scenario classes is a slight upward shift in the values for $\bar{D}_{EW}(\tau|\mathbf{e})$, $\bar{D}_{ED}(\tau|\mathbf{e})$, $\bar{D}_{II}(\tau|\mathbf{e})$, $\bar{D}_{IE}(\tau|\mathbf{e})$, $\bar{D}_{SG}(\tau|\mathbf{e})$ and $\bar{D}_{SF}(\tau|\mathbf{e})$ and hence in the value for $\bar{D}(\tau|\mathbf{e})$. However, this effect is small relative to the epistemic uncertainty in $\bar{D}(\tau|\mathbf{e})$ that results from the uncertainty in $\mathbf{e}$ (Figures J9.2-1 and J9.3-1). As a result, the decomposition in Equation J10-1 provides a reasonable and numerically practicable approximation to $\bar{D}(\tau|\mathbf{e})$.

J11 HUMAN INTRUSION SCENARIO

J11.1 Human Intrusion Scenario: Preliminaries

The Human Intrusion Scenario is proscribed by the U.S. Nuclear Regulatory Commission (NRC) proposed rule in 10 CFR 63.322 [DIRS 180319], as follows:

> **§ 63.322 Human intrusion scenario**. For the purposes of the analysis of human intrusion, DOE must make the following assumptions:
>
> (a) There is a single human intrusion as a result of exploratory drilling for groundwater.

(b) The intruders drill a borehole directly through a degraded waste package (WP) into the uppermost aquifer underlying the Yucca Mountain repository.

(c) The drillers use the common techniques and practices that are currently employed in exploratory drilling for groundwater in the region surrounding Yucca Mountain.

(d) Careful sealing of the borehole does not occur; instead natural degradation processes gradually modify the borehole.

(e) No particulate waste material falls into the borehole.

(f) The exposure scenario includes only those radionuclides transported to the saturated Zone (SZ) by water (e.g., water enters the WP, releases radionuclides, and transports radionuclides by way of the borehole to the SZ).

(g) No releases are included that are caused by unlikely natural processes and events.

The results of this scenario are compared with the individual protection standard for a human intrusion of the repository defined in 10 CFR 63.321 [DIRS 178394]:

§ 63.321 Individual protection standard for human intrusion. DOE must determine the earliest time after disposal that the waste package would degrade sufficiently that a human intrusion could occur without recognition by the drillers. DOE must:

(a) Provide the analyses and its technical bases used to determine the time of occurrence of human intrusion (§ 63.322) without recognition by the drillers.

(b) If complete waste package penetration is projected to occur at or before 10,000 years after disposal:

(1) Demonstrate that there is a reasonable expectation that the reasonably maximally exposed individual receives no more than an annual dose of 0.15 mSv (15 mrem) as a result of a human intrusion, at or before 10,000 years after disposal. The analysis must include all potential environmental pathways of radionuclide transport and exposure subject to the requirements at § 63.322; and

(2) If exposures to the reasonably maximally exposed individual occur more than 10,000 years after disposal, include the results of the analysis and its bases in the environmental impact statement for Yucca Mountain as an indicator of long-term disposal system performance.

(c) Include the results of the analysis and its bases in the environmental impact statement for Yucca Mountain as an indicator of long-term disposal system performance, if the intrusion is not projected to occur before 10,000 years after disposal.

The NRC specifies that the U.S. Department of Energy (DOE) must determine the earliest time after disposal that the WP would degrade sufficiently that a human intrusion could occur without recognition by the drillers. In addition, by way of explanation and corroboration per 10 CFR 63.321(a) [DIRS 178394], the DOE must provide the analyses and its technical basis used to determine the time of occurrence of human intrusion, as described in NRC proposed rule in 10 CFR 63.322 [DIRS 180319], without recognition by the drillers. Analysis presented in Section 6.7.2 selects 200,000 yrs after closure as the earliest time of intrusion.

J11.2 Human Intrusion Scenario: Analysis

Conceptually, the Human Intrusion Scenario is structured using the same principles as the other scenario classes in the PA for the Yucca Mountain facility. The Human Intrusion Scenario differs only in the uncertainties considered in the scenario, and in the regulation that the scenario answers. As described in Section J3, the same three basic entities underlie the conceptual structure of this scenario: (i) EN1, a probabilistic characterization of what could occur at the facility under consideration; (ii) EN2, mathematical models for estimating the consequences of what could occur; and (iii) EN3, a probabilistic characterization of the uncertainty in the parameters used in the definitions of EN1 and EN2. In the case of the Human Intrusion Scenario, EN1 is comprised of the probability space describing the uncertainty in the location of the intrusion (because the time of intrusion and number of intrusions are not uncertain, location of the intrusion is the only uncertainty described by EN1); EN2 defines the models used to estimate radionuclide transport after the intrusion occurs; and EN3 provides the possible values of parameters that are used in EN1 and EN2.

In the Human Intrusion Scenario, each aleatory future, $\mathbf{a}_j$, j = 1, 2, …, *nHI*, is a sample element from a sample space $\mathcal{A}_{HI}$, an element of which can be represented by

$$\mathbf{a}_j = \left[r_j, q_j\left(\mathbf{e}_{Mi}\right), SR_j \right] \qquad \text{(Eq. J11.2-1)}$$

where *nHI* is the number of aleatory realizations generated to evaluate the consequences of the Human Intrusion Scenario, r_j designates the type of WP (CDSP WP or transportation, aging, and disposal canister CSNF WP) intersected in the jth aleatory realization, $q_i(\mathbf{e}_{Mi})$ is the percolation rate (mm/yr) in the percolation bin selected in the jth aleatory realization (Section 6.3.2) which depends on the LHS element $\mathbf{e}_i = [\mathbf{e}_{Ai}, \mathbf{e}_{Mi}]$, and SR_j is the SZ source region selected in the jth aleatory realization (Section 6.3.9). The borehole is conceptually represented as a conduit for fluid flow through a WP, through to UZ and into the SZ. The type of WP intersected is determined randomly with the probability of selecting waste package type r_j given by the fraction of WPs of type r_j.

The location of the borehole is described in terms of the percolation bin and the entry point into the SZ. The probability of selecting a percolation bin corresponds to the percentage of WPs located in each bin. Specifically, percolation bins 1 and 5 each contain 5 percent of WPs and are assigned probabilities of 0.05, percolation bins 2 and 4 each contain 25 percent of WPs and are assigned probabilities of 0.25, and percolation bin 3 contains 40 percent of WPs and is assigned probability of 0.40. After selection of a percolation bin into which the intrusion occurs, a UZ node to which mass from the EBS flows is randomly selected, and the percolation rate $q_i(\mathbf{e}_{Ai})$ (mm/yr) at the selected location is determined. Figure 6.3.9-6 illustrates the relationship between percolation bins and their constituent nodes. The percolation rate at a node depends on a number of epistemic uncertainties defined by $\mathbf{e}_{Mi}$.

As described in Section 6.3.9, flow from the UZ into the SZ is numerically represented by use of four SZ source regions, shown in Figure 6.3.10-6. An SZ source region is randomly selected in conjunction with the selection of the percolation bin. The probability of selecting each region is determined by the fraction of the UZ nodes comprising the selected percolation bin that fall within the SZ source region. Figure 6.3.9-6 combined with Figure 6.3.10-6 illustrates the mapping from UZ nodes to SZ source regions.

For a given LHS element $\mathbf{e}_i = [\mathbf{e}_{Ai}, \mathbf{e}_{Mi}]$ of the form indicated in Equation J4.9-1, the expected dose $\bar{D}_{HI}(\tau|\mathbf{e}_i)$ (mrem/yr) is now given by

$$\bar{D}_{HI}\left(\tau|\mathbf{e}_i\right) = \sum_{j=1}^{nHI} D_{HI}\left(\tau\left|\left[1, r_j, q_j\left(\mathbf{e}_{Mi}\right) SR_j\right], \mathbf{e}_i\right.\right) \Big/ nHI \qquad \text{(Eq. J11.2-2)}$$

where $D_{HI}(\tau|[1, r_j, q_j(\mathbf{e}_{Mi}), SB_j], \mathbf{e}_i)$ denotes the dose (mrem/yr) resulting at time τ from a human intrusion that intersects 1 WP of type r_j that experiences percolation rate $q_j(\mathbf{e}_{Mi})$ (mm/yr) and intersects the SZ in source region SR_j. In turn, the estimates for $\bar{D}_{HI}(\tau|\mathbf{e}_i)$ can be used to estimate $\bar{\bar{D}}_{HI}(\tau)$, $p_E[\bar{D}_{HI}(\tau|\mathbf{e}_i) \le D]$ and $p_E[D < \bar{D}_{HI}(\tau|\mathbf{e}_i)]$. Specifically,

$$\bar{\bar{D}}_{HI}\left(\tau\right) \cong \sum_{i=1}^{nLHS} \bar{D}_{HI}\left(\tau|\mathbf{e}_i\right) \Big/ nLHS, \qquad \text{(Eq. J11.2-3)}$$

$$p_E\left[\bar{D}_{HI}\left(\tau|\mathbf{e}\right) \le D\right] \cong \sum_{i=1}^{nLHS} \underline{\delta}_D\left[\bar{D}_{HI}\left(\tau|\mathbf{e}_i\right)\right] \Big/ nLHS \qquad \text{(Eq. J11.2-4)}$$

and

$$p_E\left[D < \bar{D}_{HI}\left(\tau|\mathbf{e}\right)\right] \cong \sum_{i=1}^{nLHS} \bar{\delta}_D\left[\bar{D}_{HI}\left(\tau|\mathbf{e}_i\right)\right] \Big/ nLHS \qquad \text{(Eq. J11.2-5)}$$

as indicated in Equations J4.9-8 – J4.9-10, where $\bar{\delta}_D(\sim)$ and $\underline{\delta}_N(\sim)$ are defined in Equations J4.2-3 and J4.2-7, respectively. Further, quantiles $Q_q[\bar{D}_{HI}(\tau|\mathbf{e})]$ for $\bar{D}_{HI}(\tau|\mathbf{e})$can obtained by solving either

$$q = \int_{\mathcal{A}_{HI}} \underline{\delta}_D\left[\bar{D}_{HI}\left(\tau|\mathbf{e}\right)\right] d_E\left(\mathbf{e}\right) \mathrm{d}E \qquad \text{(Eq. J11.2-6)}$$

or

$$1-q = \int_{\mathcal{A}_{HI}} \bar{\delta}_D\left[\bar{D}_{HI}\left(\tau|\mathbf{e}\right)\right] d_E\left(\mathbf{e}\right) \mathrm{d}E \qquad \text{(Eq. J11.2-7)}$$

for D. In practice, the solution of Equation J11.2-6 or Equation J11.2-7 to determine D, and hence $Q_q[\bar{D}_{HI}(\tau|\mathbf{e})]$, is based on the approximating sums in Equations J11.2-4 and J11.2-5.

The determination of $\bar{D}_{HI}(\tau|\mathbf{e}_i)$as indicated in Equation J11.2-2 requires the evaluation of

$$D_{HI}\left(\tau\left|\left[1, r_j, q_j\left(\mathbf{e}_{Mi}\right), SR_j\right], \mathbf{e}_i\right.\right) \qquad \text{(Eq. J11.2-8)}$$

in GoldSim for selected values of τ, $\mathbf{a}_j = [r_j, q_j(\mathbf{e}_{Mi}), SR_j]$, $j = 1, 2, \ldots, nHI$, and $\mathbf{e}_i = [\mathbf{e}_{Ai}, \mathbf{e}_{Mi}]$, $i = 1, 2, \ldots, nLHS$. Further, a large number of intermediate results are also generated and saved.

The results indicated in conjunction with Equation J11.2-8 were calculated for the time interval [0, 10^6 yr] using timesteps of 4,000 yr after the intrusion event. Section 7.3.3 describes the numerical stability of the GoldSim results with respect to the timesteps. For each sample $\mathbf{e}_i$ $i = 1, 2, \ldots, nLHS = 300$, an aleatory sample $\mathbf{a}_j = [r_j, q_j(\mathbf{e}_{Mi}), SR_j]$, $j = 1, 2, \ldots, nHI = 30$, was independently generated, and the quantities $D_{HI}(\tau|[1, r_j, q_j, (\mathbf{e}_{Mi}), SR_j], \mathbf{e}_i)$ were computed by GoldSim, for a total of 9000 individual dose calculations. Expected dose and expected (mean) dose were computed as defined by Equations J11.2-2 and J11.2-3, respectively (Figure J11.2-1).

As discussed in Section J4.10, the numerical stability of results obtained with Latin hypercube sampling can be assessed with replicated sampling. Specifically, the analysis for human intrusion failure was performed with the $nRL = 3$ replicated LHSs indicated in Equation J4.10-1. In turn, this analysis shows that the numerical error in using Latin hypercube sampling to estimate $\bar{\bar{D}}_{HI}(\tau)$ is small relative to the epistemic uncertainty associated with the possible values for $\bar{D}_{HI}(\tau|\mathbf{e})$ (Figure J11.2-2).

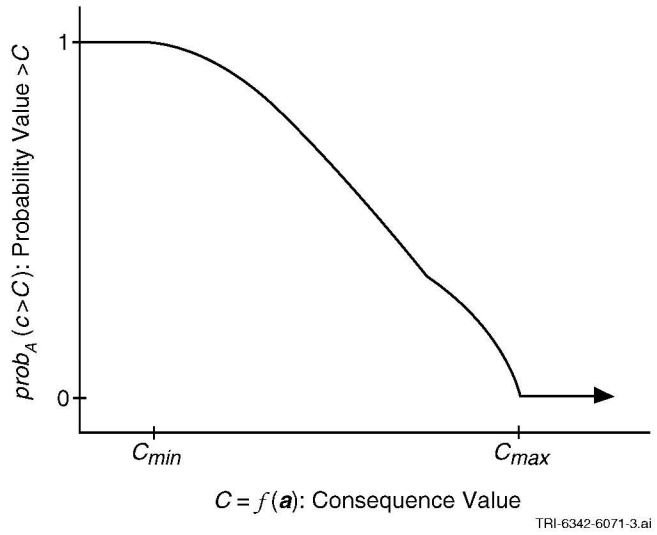

Figure J3.4-1. Example CCDF: plot of probability $prob_A(c > C)$ that a consequence with a value larger then C will occur.

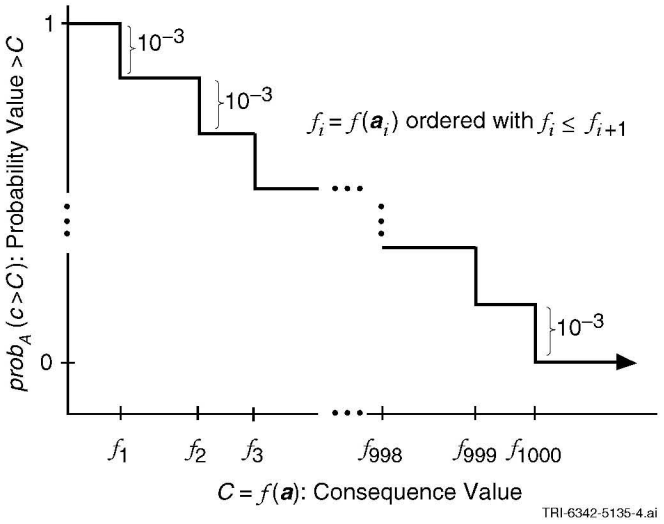

Figure J3.4-2. Approximation of a CCDF with a random sample of size 1,000

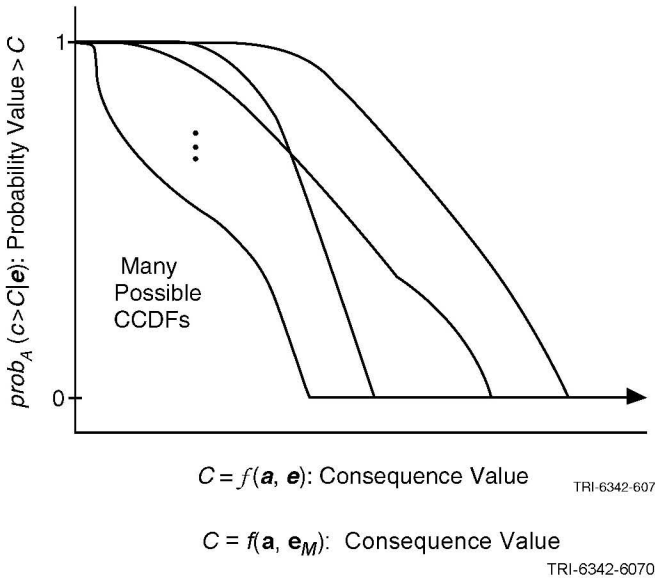

Figure J3.5-1. Different values of CCDF defined by Equation J3.4-5 that derive from different values of e.

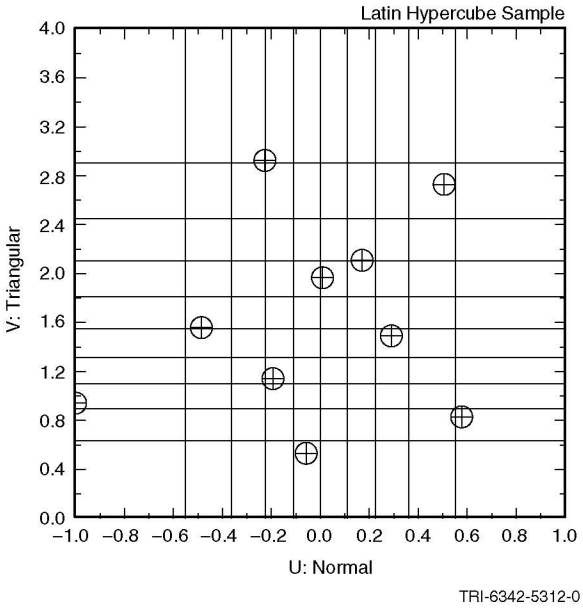

Figure J3.5-2. Example of an LHS of size *nLHS* = 10 from variables *U* and *V* with *U* normal on [–1, 1] (mean = 0, 0.01 quantile = –1, 0.99 quantile = 1) and *V* triangular on [0, 4] (mode = 1) (Figure 4, Helton 1999 [DIRS 159042])

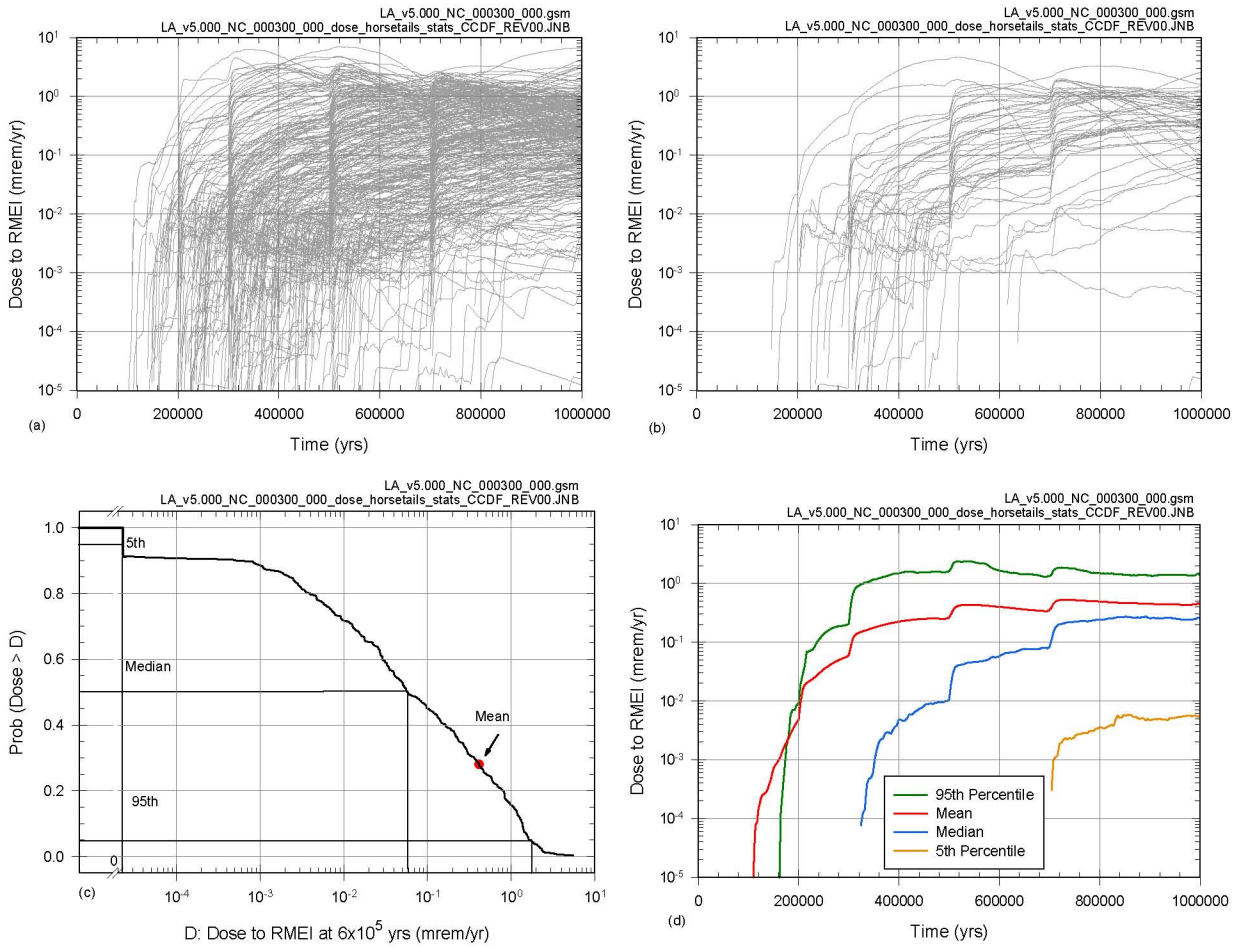

Source: Ouput DTNs: MO0709TSPAPLOT.000 [DIRS 183010]; and MO0709TSPAREGS.000 [DIRS 182976].

Figure J5-1. Estimate obtained with LHS of size *nLHS* = 300 showing epistemic uncertainty in dose $D_N(\tau|\mathbf{a}_N, \mathbf{e}_M)$ to RMEI for $0 \le \tau \le 10^6$ yr that results when only nominal conditions are considered: (a) $D_N(\tau|\mathbf{a}_N, \mathbf{e}_{Mi})$, $i = 1, 2, \ldots, nLHS = 300$, (b) dose $D_N(\tau|\mathbf{a}_N, \mathbf{e}_{Mi})$, $i = 1, 2, \ldots, 50$, (c) exceedance probabilities $p_E[D < D_N(\tau|\mathbf{a}_N, \mathbf{e}_M)]$ and quantiles $Q_q[D_N(\tau|\mathbf{a}_N, \mathbf{e}_M)]$, $q = 0.05, 0.5, 0.95$, for $\tau = 6.0 \times 10^5$ yr, and (d) expected (mean) dose $\bar{D}_N(\tau)$ and quantiles $Q_q[D_N(\tau|\mathbf{a}_N, \mathbf{e}_M)]$, $q = 0.05, 0.5, 0.95$.

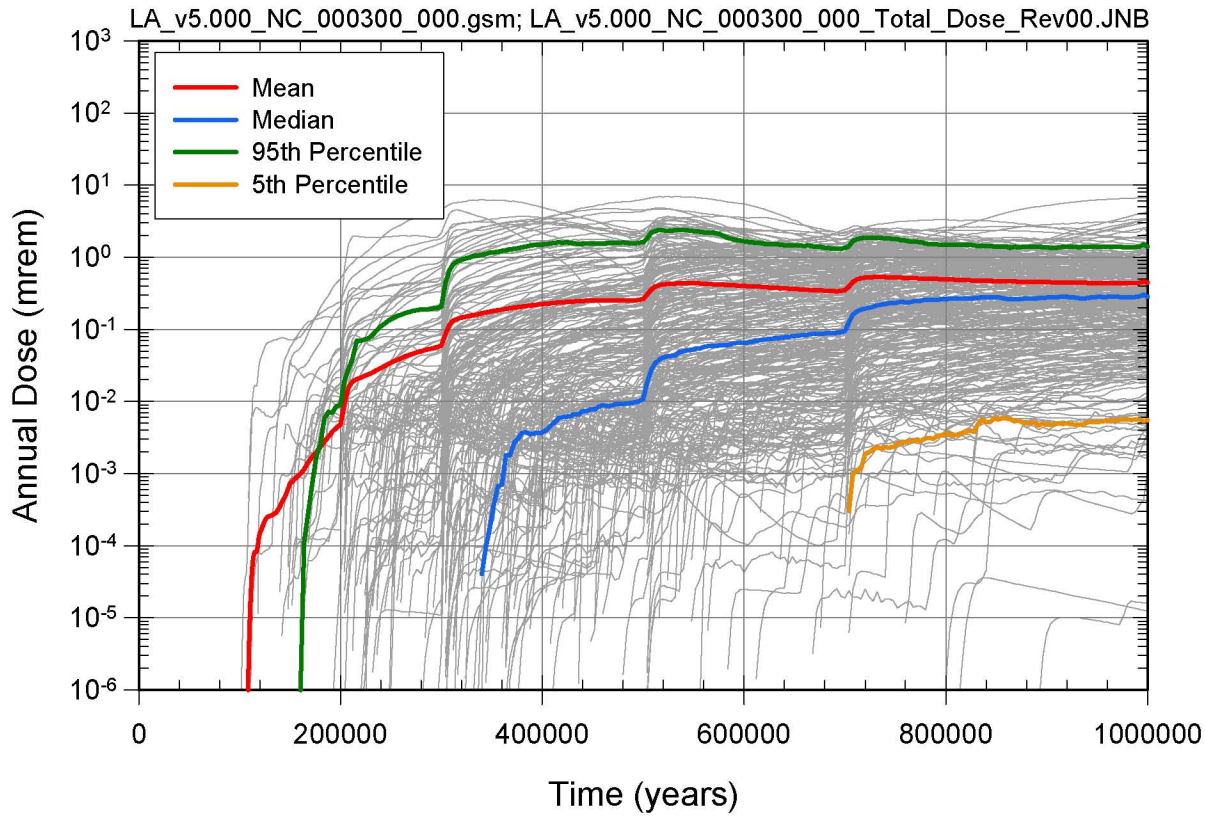

Source: Ouput DTNS: MO0709TSPAPLOT.000 [DIRS 183010]; and MO0709TSPAREGS.000 [DIRS 182976].

Figure J5-2. Summary of results obtained with LHS of size *nLHS* = 300 showing epistemic uncertainty in dose $D_N(\tau|\mathbf{a}_N, \mathbf{e}_M)$ to RMEI for $0 \leq \tau \leq 10^6$ yr that results when only nominal conditions are considered.

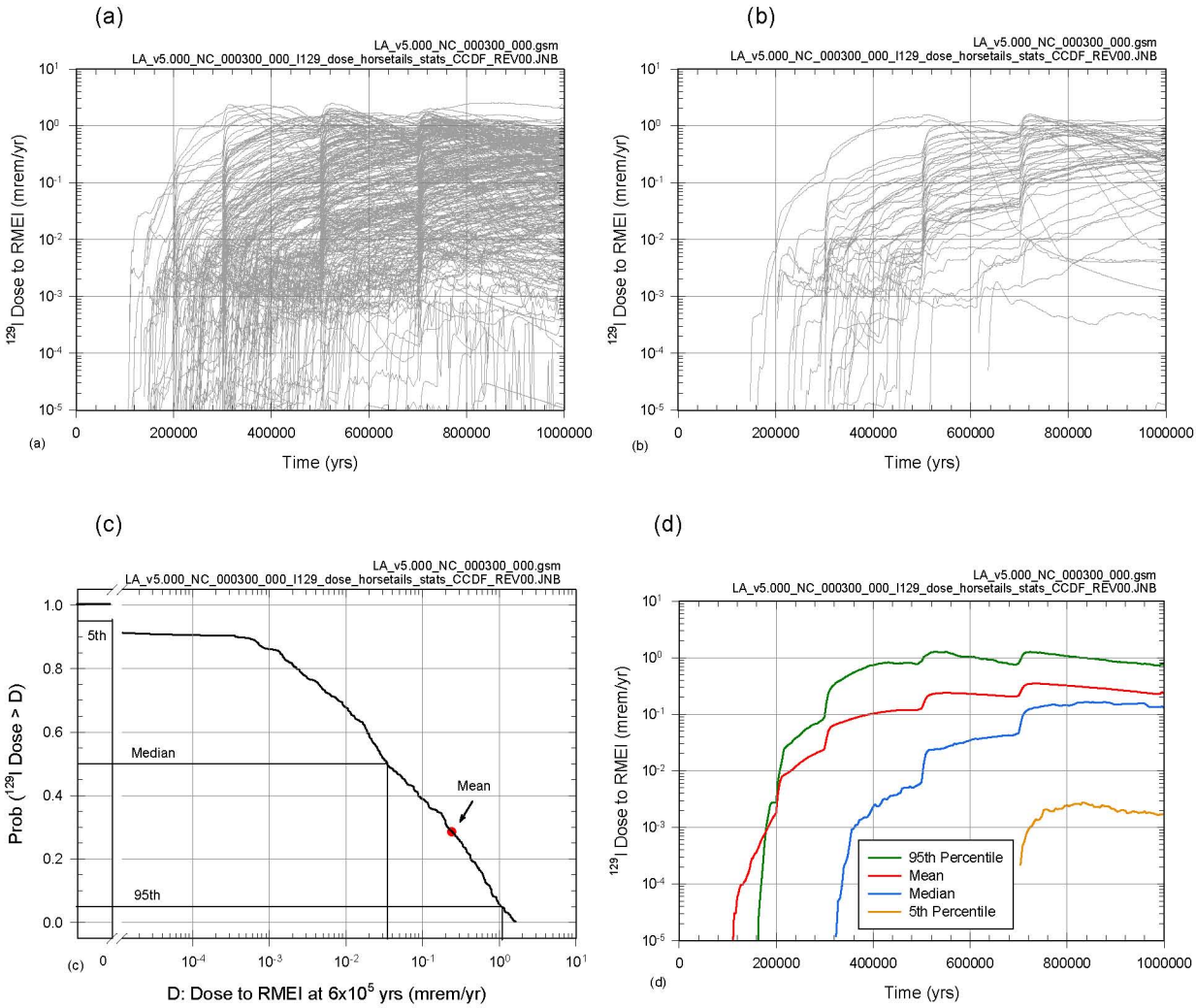

Source: Ouput DTNs: MO0709TSPAPLOT.000 [DIRS 183010]; and MO0709TSPAREGS.000 [DIRS 182976].

Figure J5-3. Estimate obtained with LHS of size *nLHS* = 300 of epistemic uncertainty in dose $D_{Nr}(\tau|\mathbf{a}_N, \mathbf{e}_M)$ to RMEI for $0 \le \tau \le 10^6$ yr with r corresponding to ^{129}I that results when only nominal conditions are considered: (a) dose $D_{Nr}(\tau|\mathbf{a}_N, \mathbf{e}_{Mi})$, i = 1, 2, ..., *nLHS* = 300, (b) dose $D_{Nr}(\tau|\mathbf{a}_N, \mathbf{e}_{Mi})$, i = 1, 2, ..., 50, (c) exceedance probabilities $p_E[D < D_{Nr}(\tau|\mathbf{a}_N, \mathbf{e}_M)]$ and quantiles $Q_q[D_{Nr}(\tau|\mathbf{a}_N, \mathbf{e}_M)]$, q = 0.05, 0.5 and 0.95, for $\tau = 6.0 \times 10^5$ yr, and (d) expected (mean) dose $\overline{D}_{Nr}(\tau)$ and quantiles $Q_q[D_{Nr}(\tau|\mathbf{a}_N, \mathbf{e}_M)]$, q = 0.05, 0.5, 0.95.

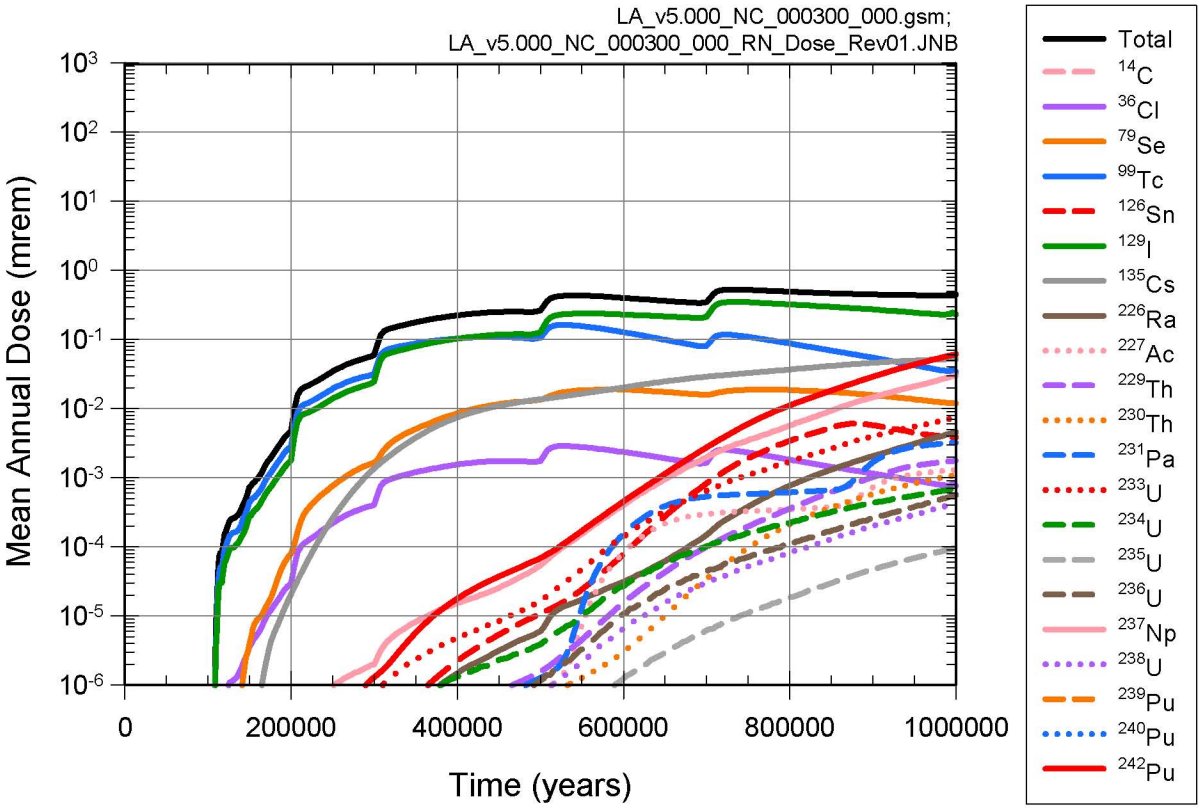

Source: Ouput DTNs: MO0709TSPAPLOT.000 [DIRS 183010]; and MO0709TSPAREGS.000 [DIRS 182976].

Figure J5-4. Estimates obtained with LHS of size *nLHS* = 300 of expected (mean) dose $\bar{\bar{D}}_{Nr}(\tau|\mathbf{a}_N)$ to RMEI for $0 \leq \tau \leq 10^6$ yr for individual radioactive species that result when only nominal conditions are considered.

(a)

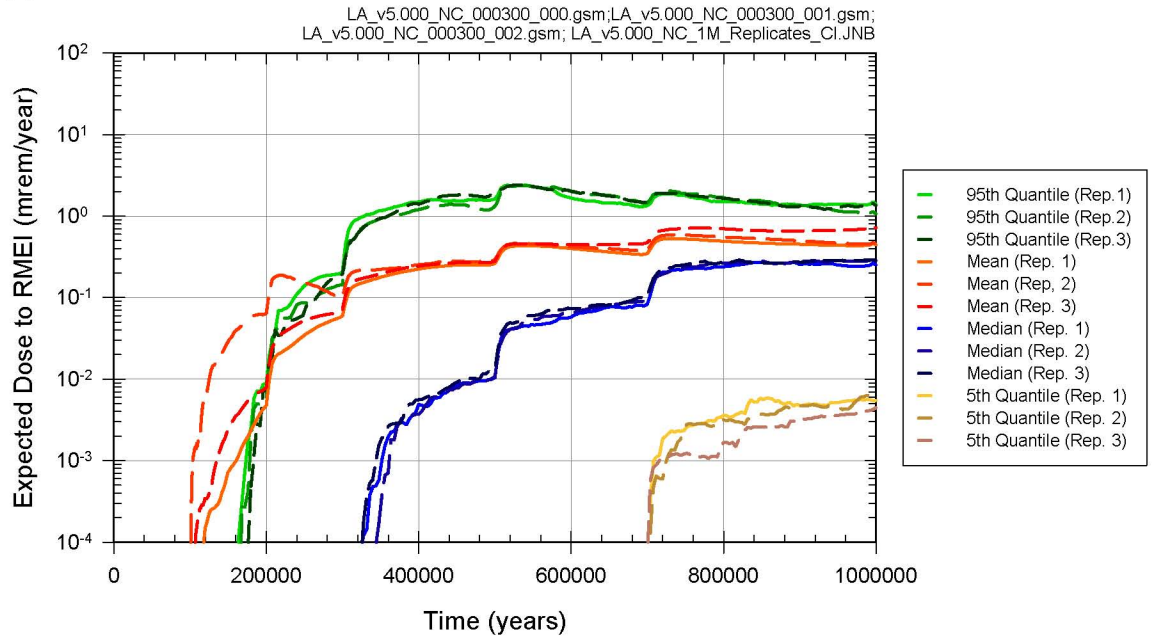

(b)

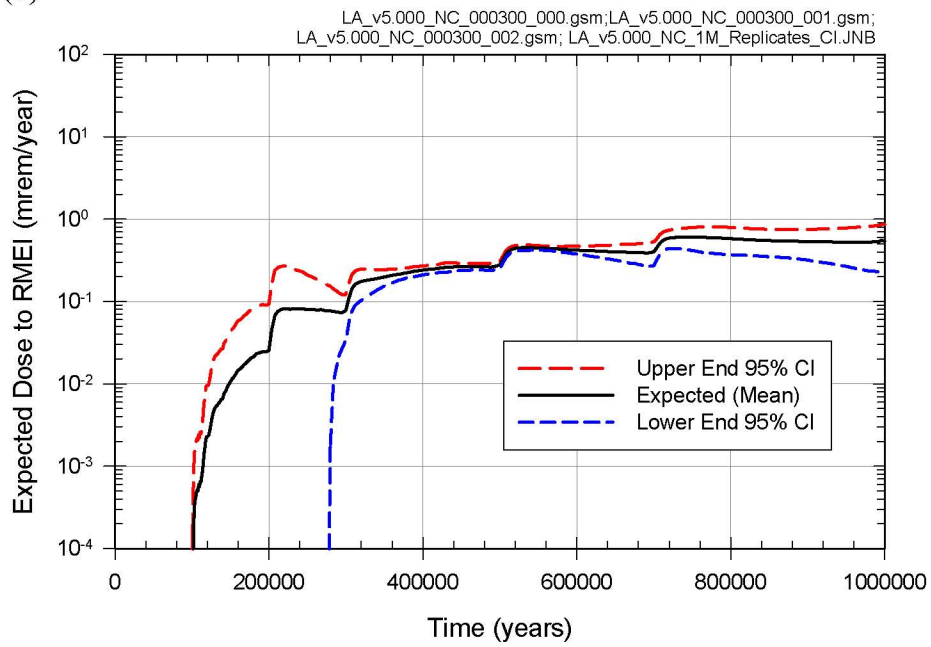

Source: Ouput DTNs: MO0709TSPAPLOT.000 [DIRS 183010]; MO0709TSPAREGS.000 [DIRS 182976]; and MO0709TSPASTAB.000 [DIRS 182983].

Figure J5-5. Assessment with replicated sampling of numerical error associated with use of an LHS of size *nLHS* = 300 to determine epistemic uncertainty in dose $D_N(\tau|\mathbf{a}_N, \mathbf{e}_M)$ to RMEI for $0 \leq \tau \leq 10^6$ yr that results when only nominal conditions are considered: (a) Replicated estimates of expected (mean) dose $\bar{\bar{D}}_N(\tau|\mathbf{a}_N)$ and quantiles $Q_q[D_N(\tau|\mathbf{a}_N, \mathbf{e}_M)]$, q = 0.05, 0.5, 0.95, and (b) confidence intervals for estimates of expected (mean) dose $\bar{\bar{D}}_N(\tau|\mathbf{a}_N)$.

INTENTIONALLY LEFT BLANK

(a)

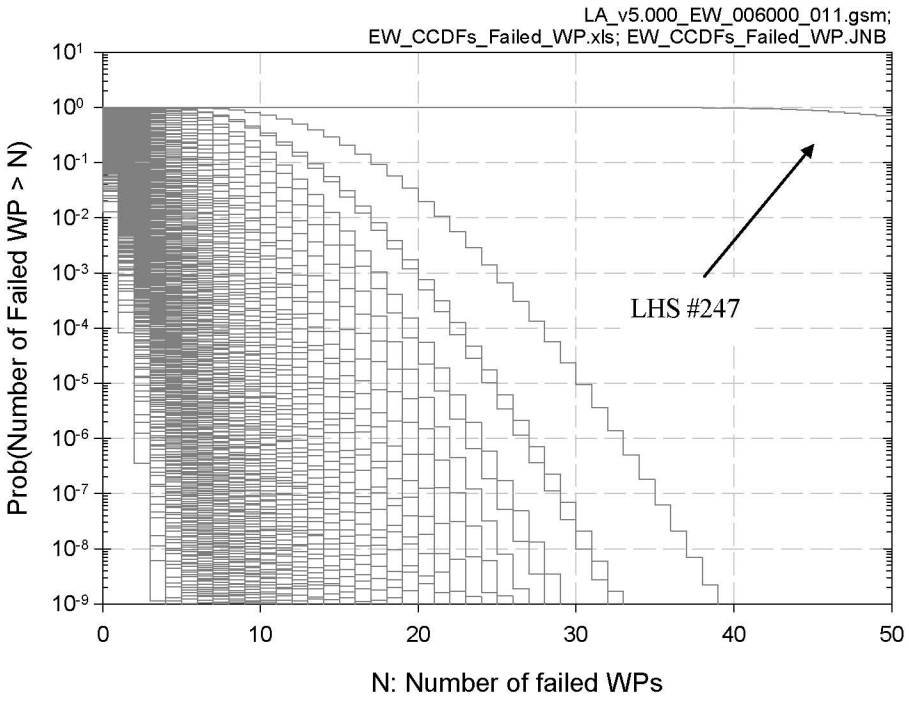

(b)

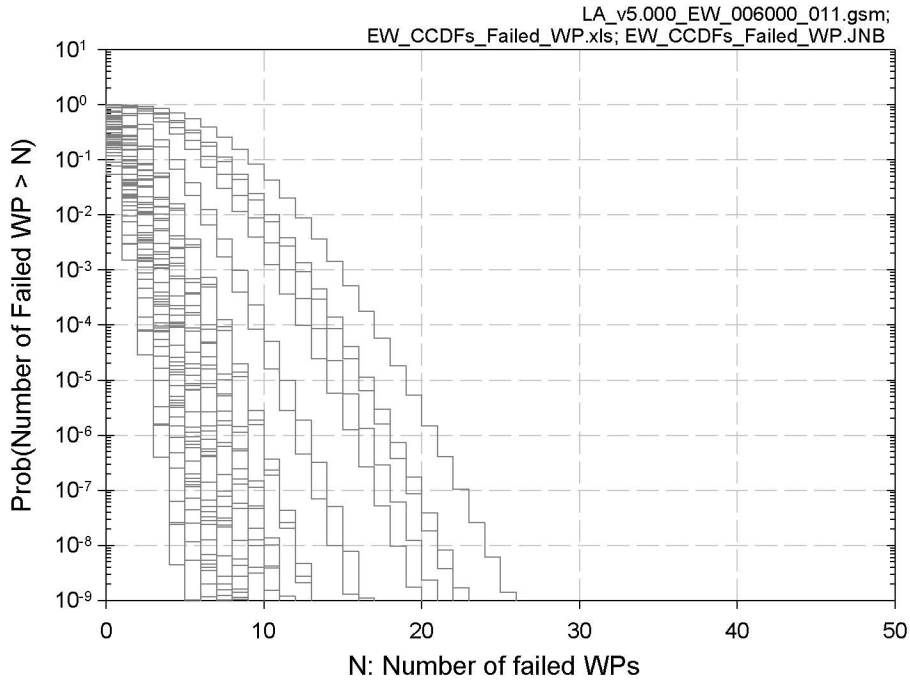

Source: Ouput DTNs: MO0709TSPAPLOT.000 [DIRS 183010]; and MO0709TSPAREGS.000 [DIRS 182976].

Figure J6.2-1. Complementary cumulative distribution functions (CCDFs) for number *nEW* of WPs with early failure associated with individual elements of LHS of size *nLHS* = 300 in Equation J.4.9-1: (a) CCDFs for all 300 LHS elements, and (b) CCDFs for first 50 LHS elements.

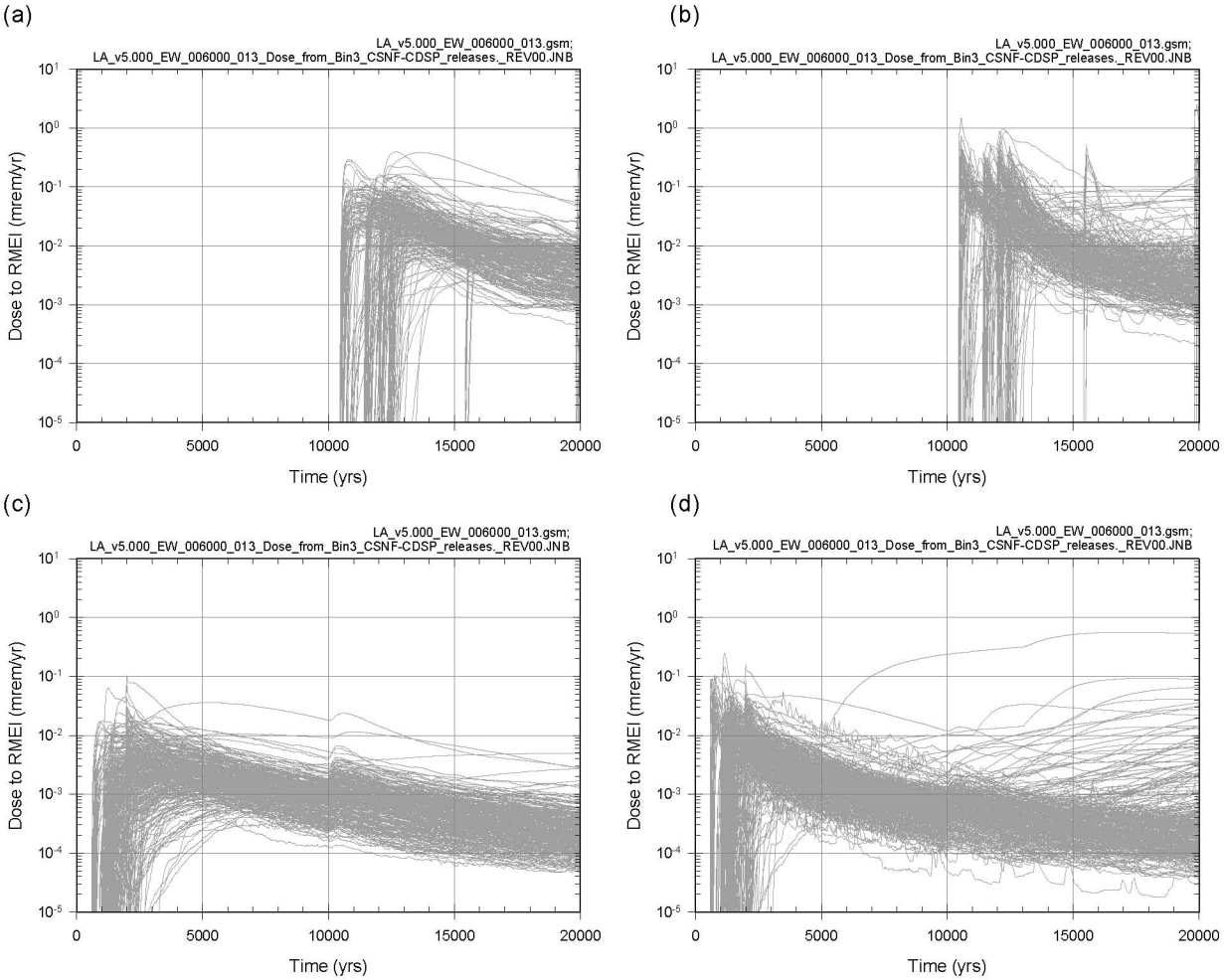

Source: Ouput DTNs: MO0709TSPAPLOT.000 [DIRS 183010]; MO0709TSPASENS.000 [DIRS 182982].

Figure J6.2-2. Summary of results obtained with LHS of size *nLHS* = 300 showing epistemic uncertainty in doses $D_{EW}(\tau|[1, r, 3, t], \mathbf{e}_M)$ for $0 \le \tau \le 20{,}000$ yr: (a) CSNF WP in bin 3 under non-dripping conditions (i.e., $D_{EW}(\tau|[1, 1, 3, 0], \mathbf{e}_{Mi})$, $i = 1, 2, \ldots, nLHS = 300$), (b) CSNF WP in bin 3 under dripping conditions (i.e., $D_{EW}(\tau|[1, 1, 3, 1], \mathbf{e}_{Mi})$, $i = 1, 2, \ldots, nLHS = 30)0$, (c) CDSP WP in bin 3 under nondripping conditions (i.e., $D_{EW}(\tau|[1, 2, 3, 0], \mathbf{e}_{Mi})$, $i = 1, 2, \ldots, nLHS = 300$), and (d) CDSP WP in bin 3 under dripping conditions (i.e., $D_{EW}(\tau|[1, 2, 3, 1], \mathbf{e}_{Mi})$, $i = 1, 2, \ldots, nLHS = 300$).

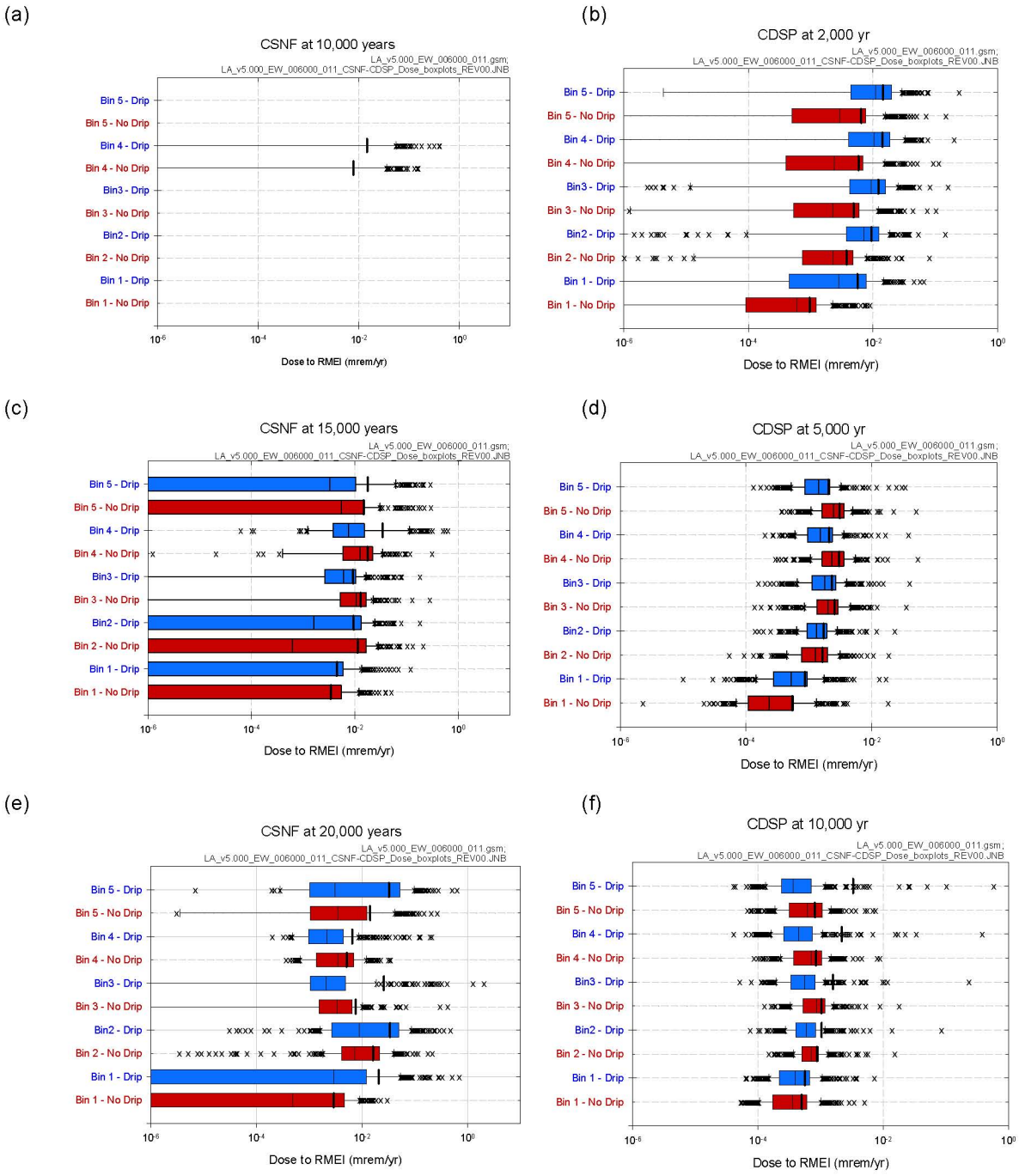

Source: Ouput DTNs: MO0709TSPAPLOT.000 [DIRS 183010]; and MO0709TSPAREGS.000 [DIRS 182976].

Figure J6.2-3. Box plots (Description: Box extends from 0.25 to 0.75 quantile; left and right bar and whisker extend to 0.1 and 0.9 quantile, respectively; ×'s represent values outside 0.1 to 0.9 quantile range; median and mean are indicated by light and dark vertical lines, respectively) summarizing results obtained with LHS of size $nLHS$ = 300 showing epistemic uncertainty in doses $D_{EW}(\tau|[1, r, s, t], \mathbf{e}_{Mi})$ for selected values of τ, r = 1, 2, s = 1, 2, 3, 4, 5, t = 0, 1, and i = 1, 2, …, $nLHS$ = 300: (a, c, e) CSNF WPs at τ = 10,000, 15,000 and 20,000 yr, and (b, d, f) CDSP WPs at τ = 2000, 5000 and 10,000 yr.

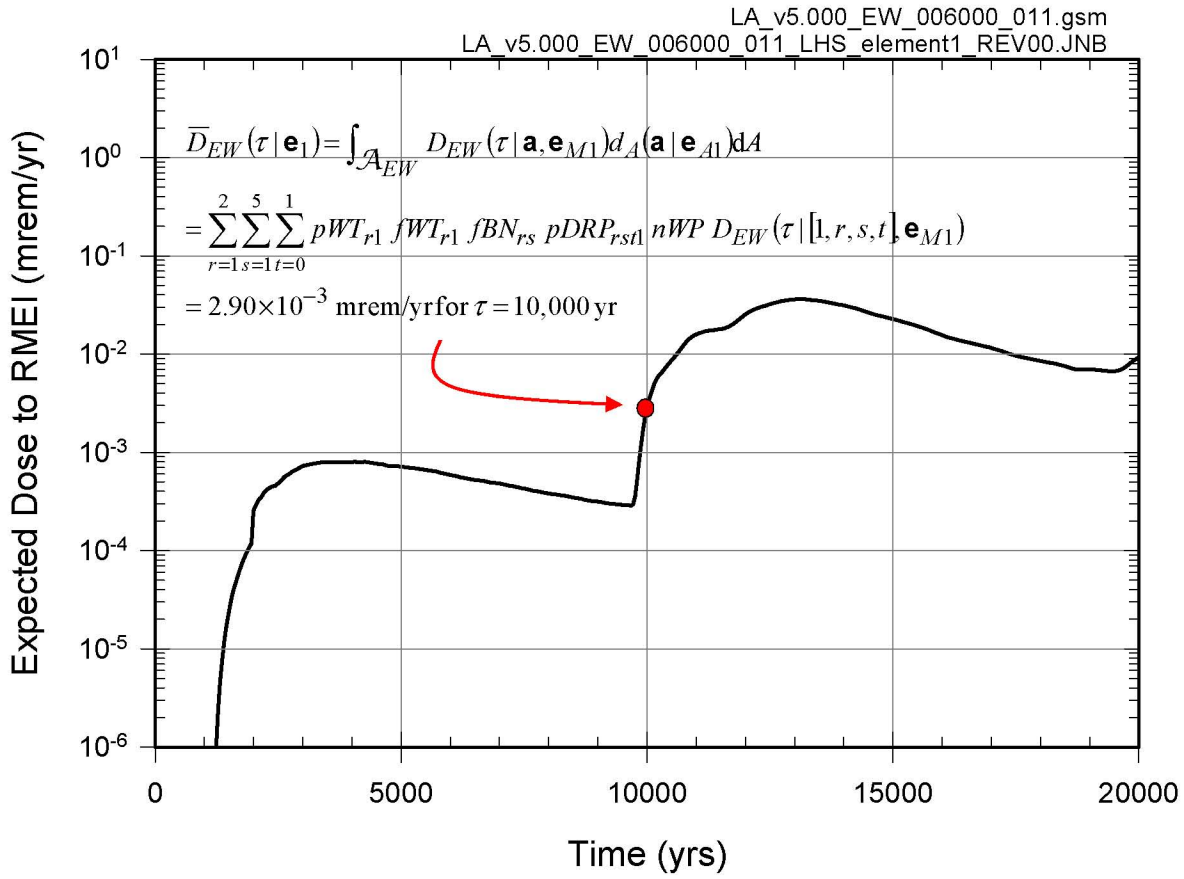

Source: Ouput DTNs: MO0709TSPAPLOT.000 [DIRS 183010]; and MO0709TSPAREGS.000 [DIRS 182976].

Figure J6.2-4. Estimate of $\bar{D}_{EW}(\tau|\mathbf{e}_1)$ for LHS element $\mathbf{e}_1 = [\mathbf{e}_{A1}, \mathbf{e}_{M1}]$ and $0 \le \tau \le 20{,}000$ yr with integration-based procedure indicated in Equation J6.2-2.

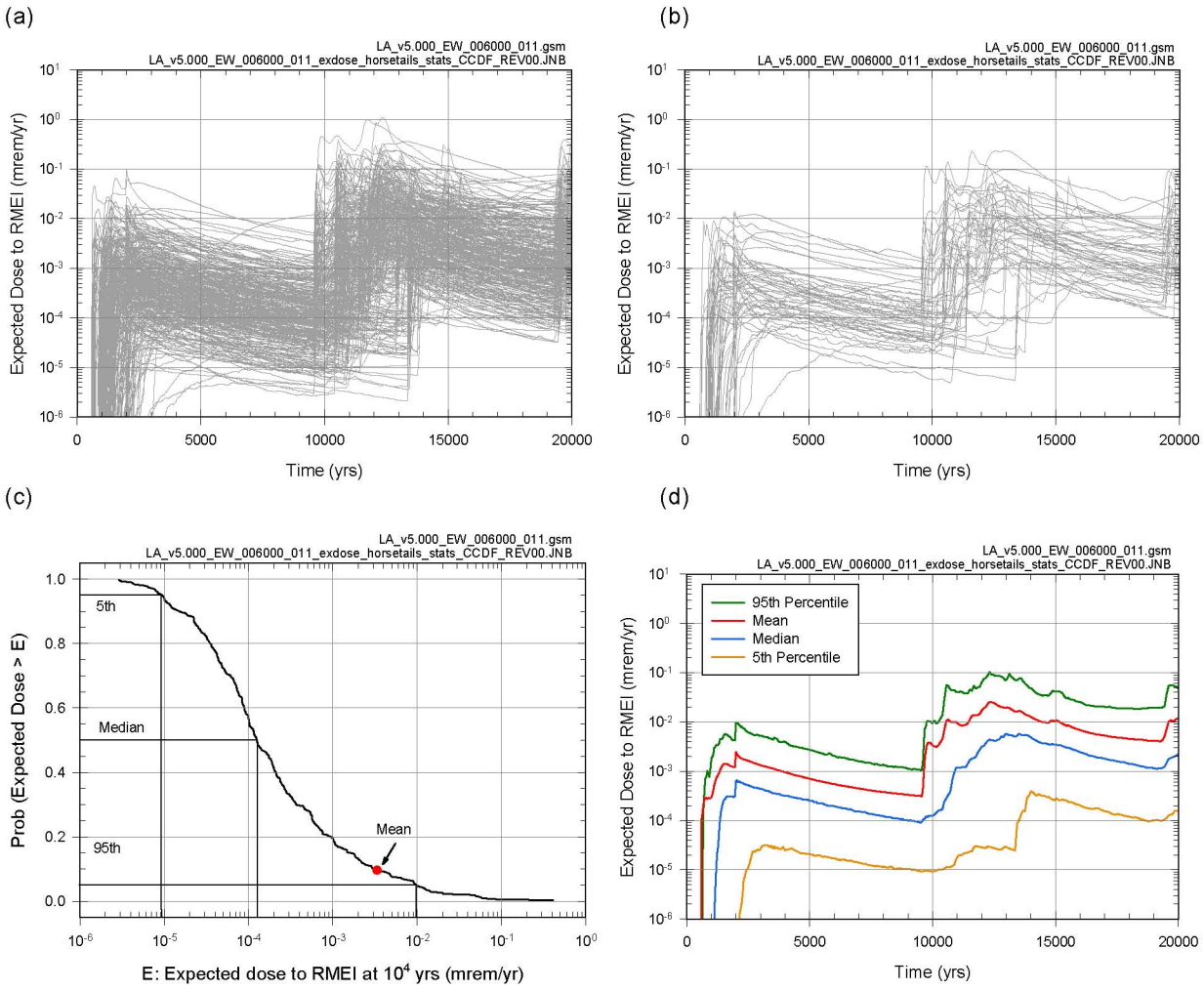

Source: Ouput DTNs: MO0709TSPAPLOT.000 [DIRS 183010]; and MO0709TSPAREGS.000 [DIRS 182976].

Figure J6.2-5. Estimate obtained with LHS of size *nLHS* = 300 showing epistemic uncertainty in expected dose $\bar{D}_{EW}(\tau|\mathbf{e})$ to RMEI for $0 \le \tau \le 20{,}000$ yr that at results when only early WP failure is considered: (a) expected dose $\bar{D}_{EW}(\tau|\mathbf{e}_i)$, i = 1, 2, …, *nLHS* = 300, (b) expected dose $\bar{D}_{EW}(\tau|\mathbf{e}_i)$, i = 1, 2, …, 50, (c) exceedance probabilities $p_E[D < \bar{D}_{EW}(\tau|\mathbf{e})]$ and quantiles $Q_q[\bar{D}_{EW}(\tau|\mathbf{e})]$, q = 0.05, 0.5 and 0.95, for $\tau = 10^4$ yr, and (d) expected (mean) dose $\bar{\bar{D}}_{EW}(\tau)$ and quantiles $Q_q[\bar{\bar{D}}_{EW}(\tau|\mathbf{e})]$, q = 0.05, 0.5, 0.95.

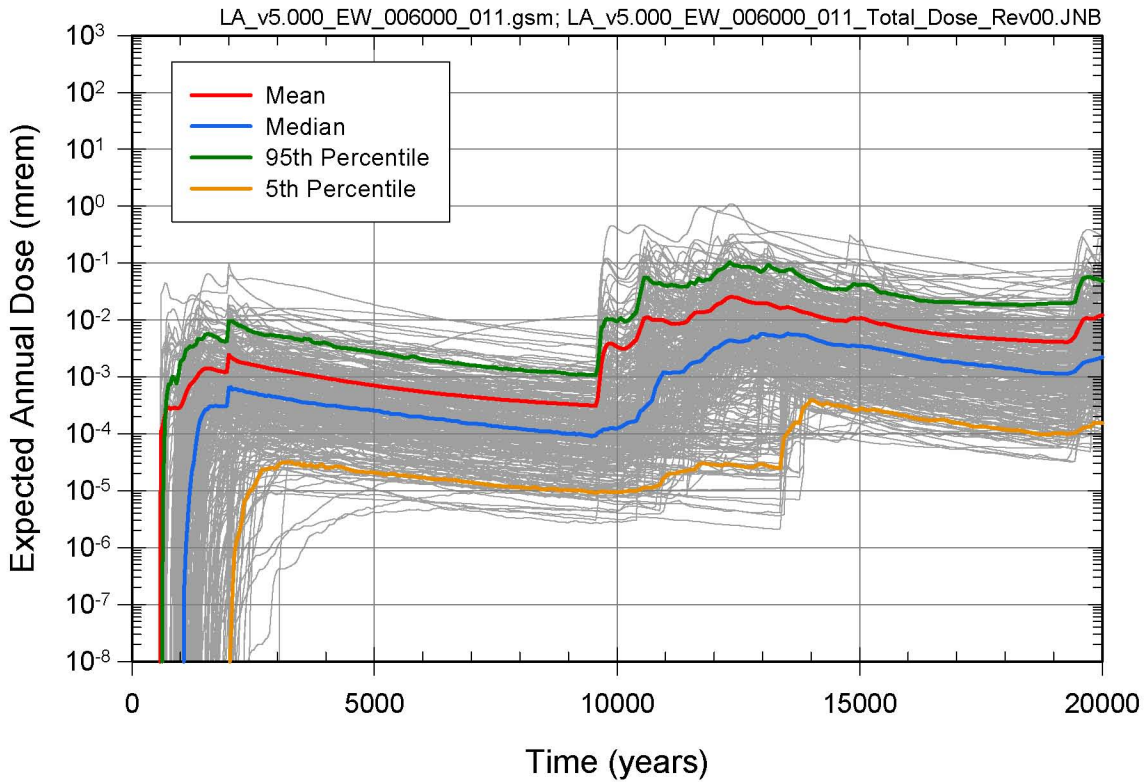

Source: Ouput DTNs: MO0709TSPAPLOT.000 [DIRS 183010]; and MO0709TSPAREGS.000 [DIRS 182976].

Figure J6.2-6. Summary of results obtained with LHS of size *nLHS* = 300 showing epistemic uncertainty in expected dose $\bar{D}_{EW}(\tau|\mathbf{e})$ to RMEI for $0 \leq \tau \leq 20{,}000$ yr that results when only early WP failure is considered.

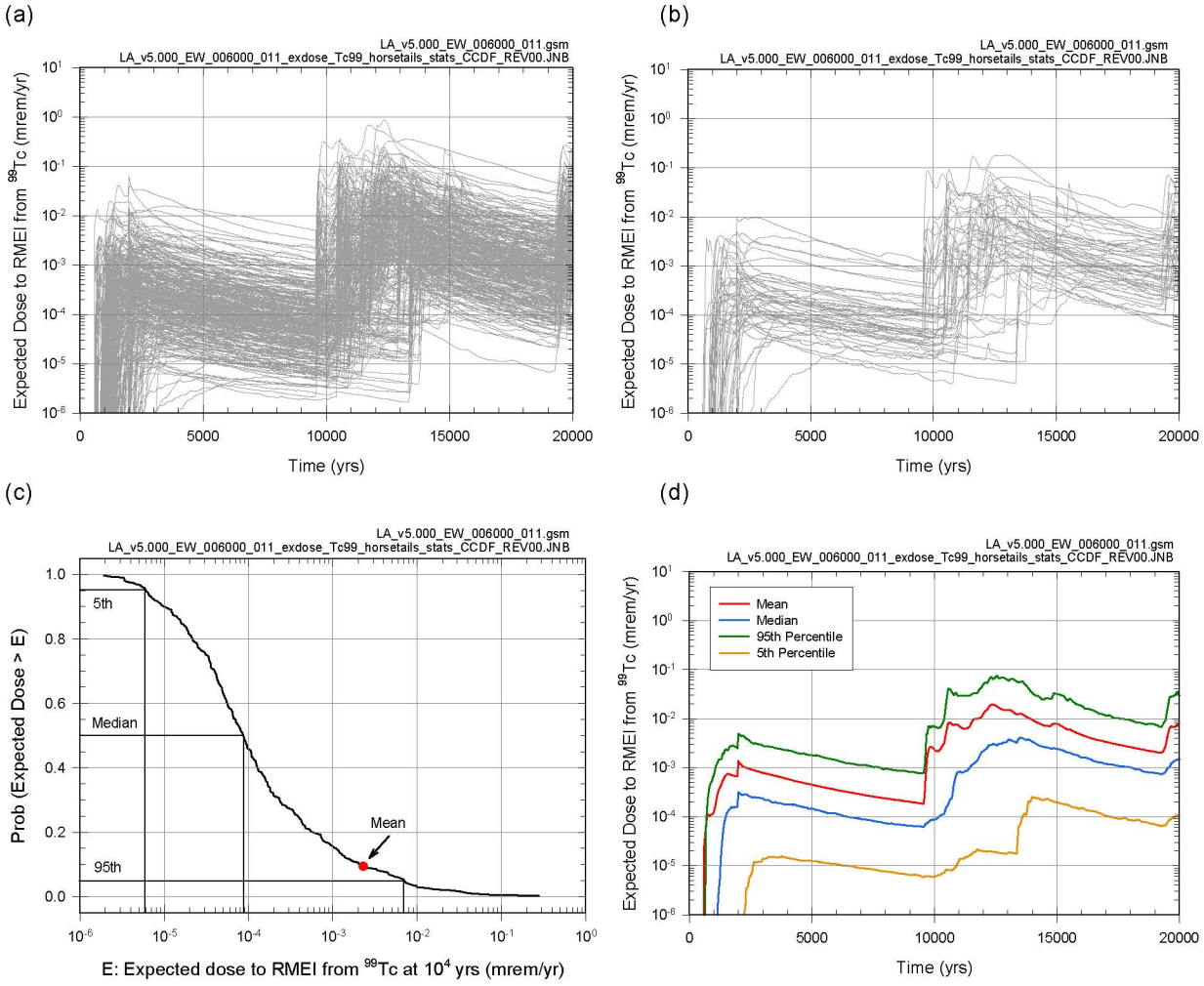

Source: Ouput DTNs: MO0709TSPAPLOT.000 [DIRS 183010]; and MO0709TSPAREGS.000 [DIRS 182976].

Figure J6.2-7. Estimate obtained with LHS of size *nLHS* = 300 showing epistemic uncertainty in expected dose $\bar{D}_{EW,r}(\tau|\mathbf{e})$ to RMEI for $0 \le \tau \le 20{,}000$ yr with r corresponding to ^{99}Tc that results when only early WP failure is considered: (a) expected dose $\bar{D}_{EW,r}(\tau|\mathbf{e}_i)$, i = 1, 2, ..., *nLHS* = 300, (b) expected dose $\bar{D}_{EW,r}(\tau|\mathbf{e}_i)$, i = 1, 2, ..., 50, (c) exceedance probabilities $p_E[D < \bar{D}_{EW}(\tau|\mathbf{e})]$ and quantiles $Q_q[\bar{D}_{EW,r}(\tau|\mathbf{e})]$, q = 0.05, 0.5 and 0.95, for $\tau = 10^4$ yr, and (d) expected (mean) dose $\bar{\bar{D}}_{EW,r}(\tau)$ and quantiles $Q_q[\bar{D}_{EW,r}(\tau|\mathbf{e})]$, q = 0.05, 0.5, 0.95.

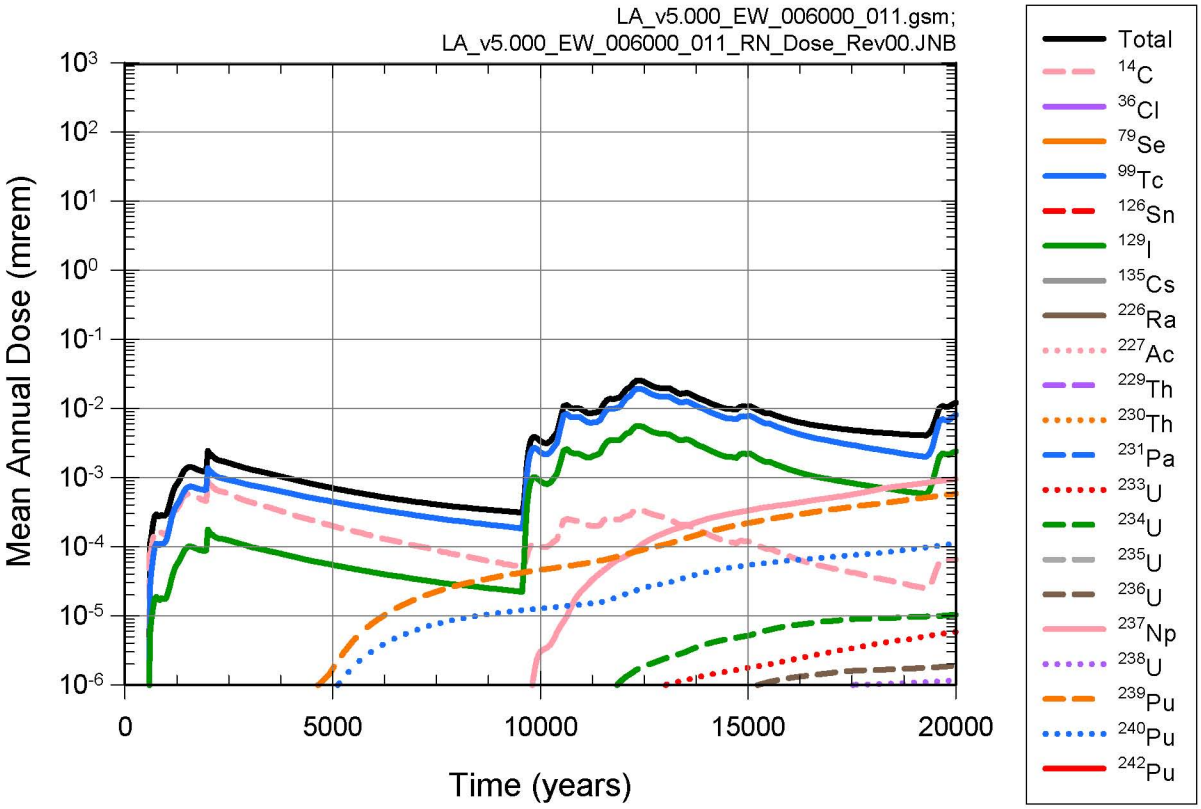

Source: Ouput DTNs: MO0709TSPAPLOT.000 [DIRS 183010]; and MO0709TSPAREGS.000 [DIRS 182976].

Figure J6.2-8. Estimates obtained with LHS of size *nLHS* = 300 of expected (mean) dose $\bar{\bar{D}}_{EW,r}(\tau)$ to RMEI for $0 \leq \tau \leq 20{,}000$ yr for individual radioactive species that result when only early WP failure is considered.

(a)

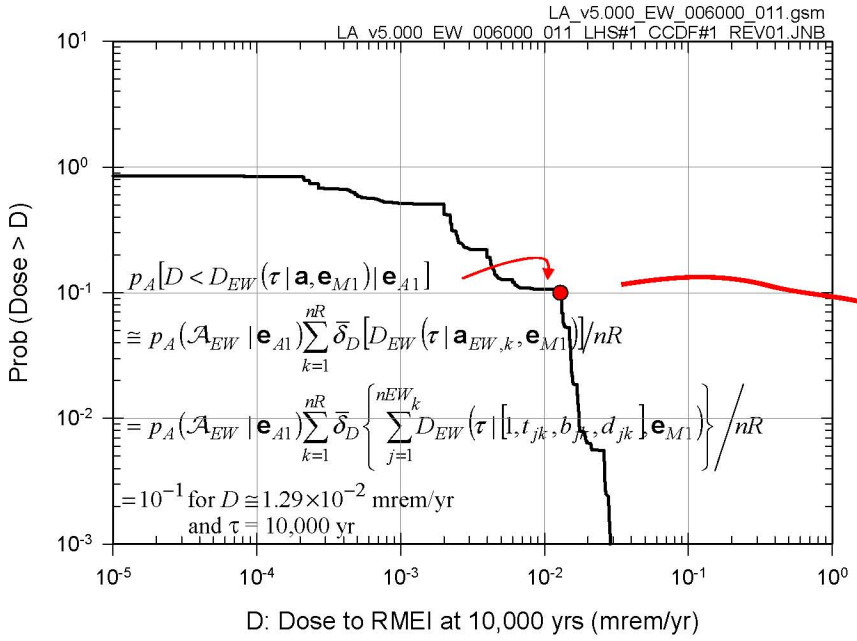

(b)

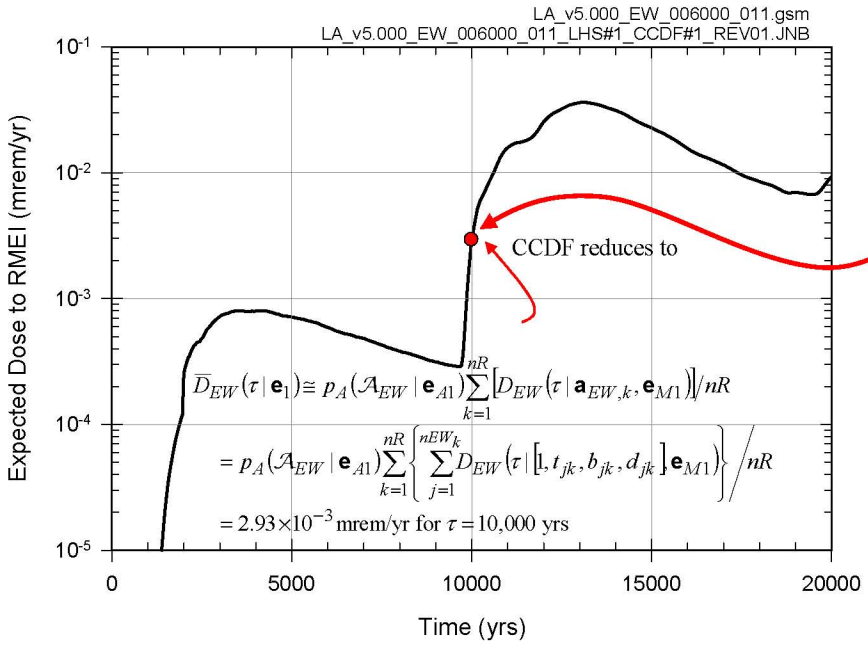

Source: Ouput DTNs: MO0709TSPAPLOT.000 [DIRS 183010]; and MO0709TSPAREGS.000 [DIRS 182976].

Figure J6.2-9. Results associated with $D_{EW}(\tau|\mathbf{a}_{EW}, \mathbf{e}_{M1})$ for LHS element $\mathbf{e}_1 = [\mathbf{e}_{A1}, \mathbf{e}_{M1}]$ obtained with sampling-based (Monte Carlo) procedures: (a) CCDF for $D_{EW}(10^4 \text{ yr}|\mathbf{a}_{EW}, \mathbf{e}_{M1})$ with exceedance probabilities $p_A[D < D_{EW}(10^4 \text{ yr}|\mathbf{a}, \mathbf{e}_{M1})|\mathbf{e}_{A1}]$ defined in Equation (J6.2-12), and (b) expected dose $\bar{D}_{EW}(10^4 \text{ yr}|\mathbf{e}_1)$ associated with $D_{EW}(10^4 \text{ yr}|\mathbf{a}_{EW}, \mathbf{e}_{M1})$ as defined in Equation (J6.2-10).

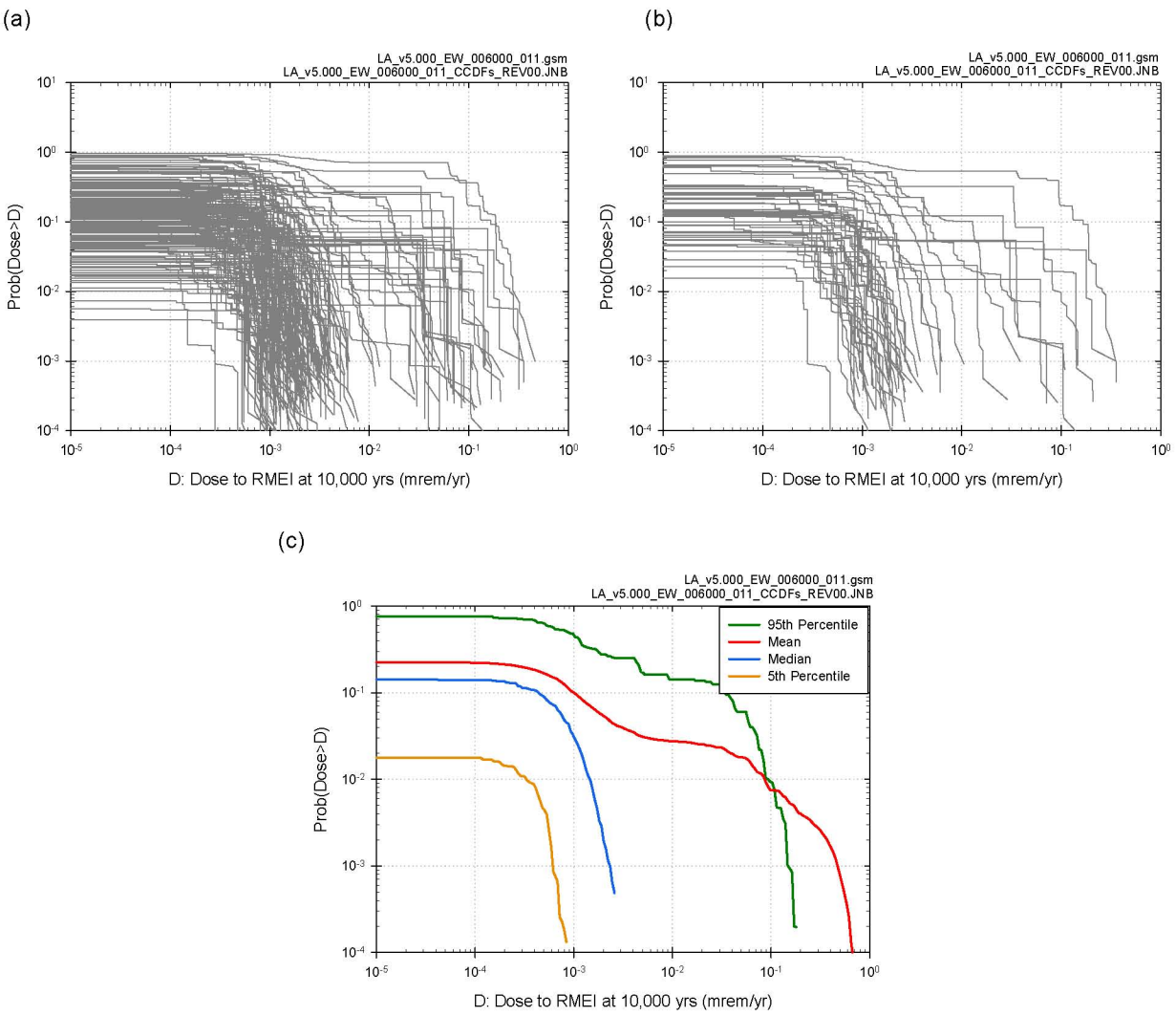

Source: Ouput DTNs: MO0709TSPAPLOT.000 [DIRS 183010]; and MO0709TSPAREGS.000 [DIRS 182976].

Figure J6.2-10. Results associated with $D_{EW}(10^4 \text{ yr}|\mathbf{a}_{EW}, \mathbf{e}_M)$ obtained with sampling-based (Monte Carlo) procedures for an LHS of size $nLHS = 300$: (a) CCDFs for $D_{EW}(10^4 \text{ yr}|\mathbf{a}_{EW}, \mathbf{e}_{Mi})$ with exceedance probabilities $p_A[D < D_{EW}(10^4 \text{ yr}|\mathbf{a}, \mathbf{e}_{Mi})|\mathbf{e}_{Ai}]$ defined in Equation J6.2-12 for $i = 1, 2, \ldots, nLHS = 300$, (b) CCDFs for $D_{EW}(10^4 \text{ yr}|\mathbf{a}_{EW}, \mathbf{e}_{Mi})$ with exceedance probabilities $p_A[D < D_{EW}(10^4 \text{ yr}|\mathbf{a}, \mathbf{e}_{Mi})|\mathbf{e}_{Ai}]$ defined in Equation J6.2-13 for $i = 1, 2, \ldots, 50$, and (c) expected (mean) CCDF and quantile curves, $q = 0.05, 0.5, 0.95$, for CCDFs in (a).

(a)

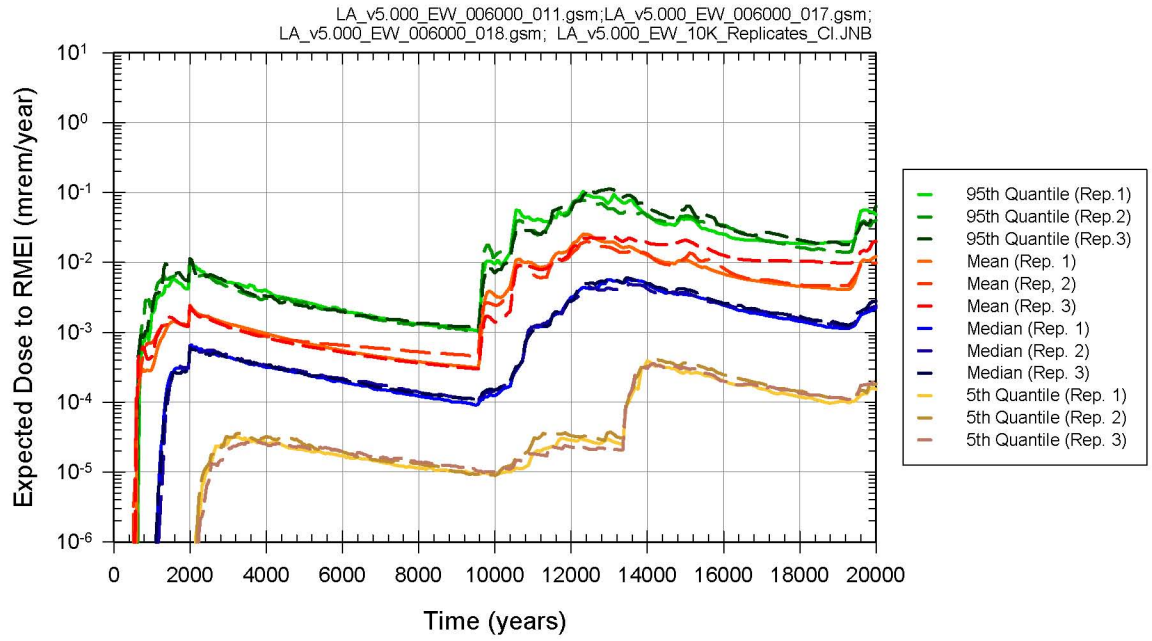

(b)

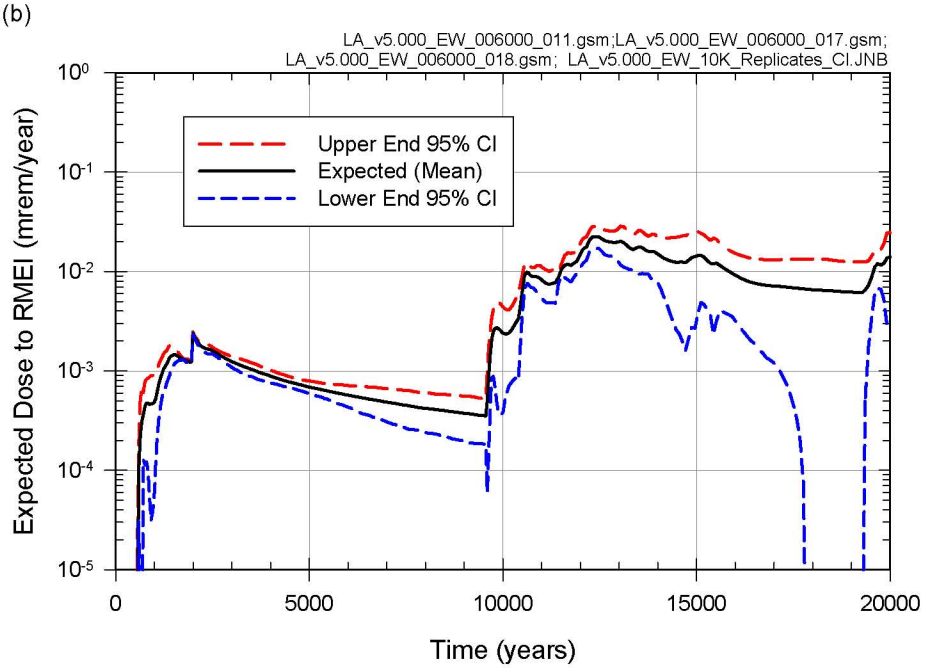

Source: Ouput DTNs: MO0709TSPAPLOT.000 [DIRS 183010]; MO0709TSPAREGS.000 [DIRS 182976]; and MO0709TSPASTAB.000 [DIRS 182983].

Figure J6.2-11. Assessment with replicated sampling of numerical error associated with use of an LHS of size *nLHS* = 300 to determine epistemic uncertainty in expected dose $\bar{D}_{EW}(\tau|\mathbf{e})$ to RMEI for $0 \leq \tau \leq 20{,}000$ yr that results when only early WP failure is considered: (a) Replicated estimates of expected (mean) dose $\bar{\bar{D}}_{EW}(\tau)$ and quantiles $Q_q[\bar{D}_{EW}(\tau|\mathbf{e})]$, q = 0.05, 0.5, 0.95, and (b) confidence intervals for estimates of expected (mean) dose $\bar{\bar{D}}_{EW}(\tau)$.

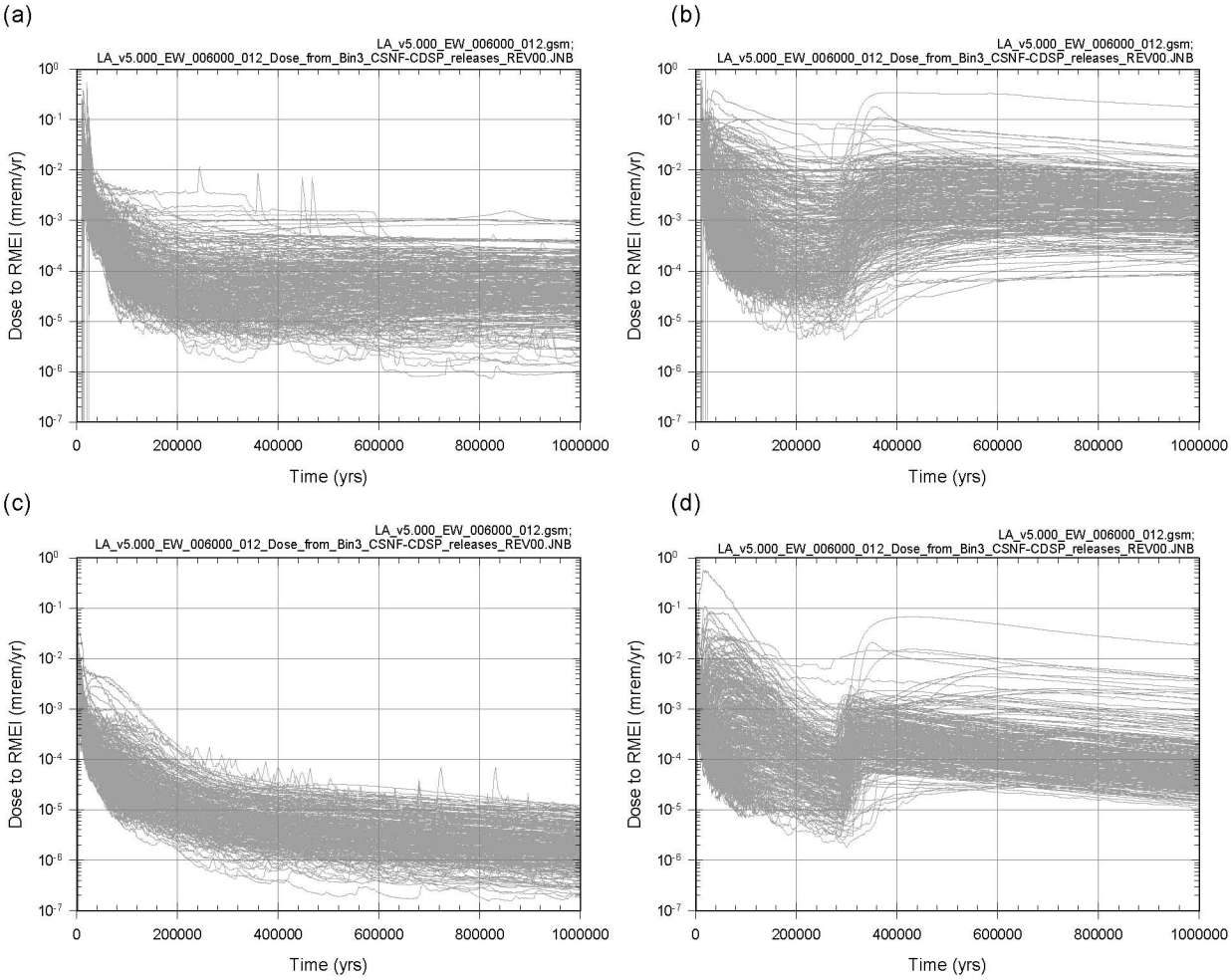

Source: Ouput DTNs: MO0709TSPAPLOT.000 [DIRS 183010]; and MO0709TSPAREGS.000 [DIRS 182976].

Figure J6.2-12. Summary of results obtained with LHS of size *nLHS* = 300 showing epistemic uncertainty in doses $D_{EW}(\tau|[1, r, s, t], \mathbf{e}_M)$ for $0 \le \tau \le 10^6$ yr: (a) CSNF WP in bin 3 under nondripping conditions (i.e., $D_{EW}(\tau|[1, 1, 3, 0], \mathbf{e}_{Mi})$, $i = 1, 2, \ldots, nLHS = 300$), (b) CSNF WP in bin 3 under dripping conditions (i.e., $D_{EW}(\tau|[1, 1, 3, 1], \mathbf{e}_{Mi})$, $i = 1, 2, \ldots, nLHS = 300$), (c) CDSP WP in bin 3 under nondripping conditions (i.e., $D_{EW}(\tau|[1, 2, 3, 0], \mathbf{e}_{Mi})$, $i = 1, 2, \ldots, nLHS = 300$), and (d) CDSP WP in bin 3 under dripping conditions (i.e., $D_{EW}(\tau|[1, 2, 3, 1], \mathbf{e}_{Mi})$, $i = 1, 2, \ldots, nLHS = 300$).

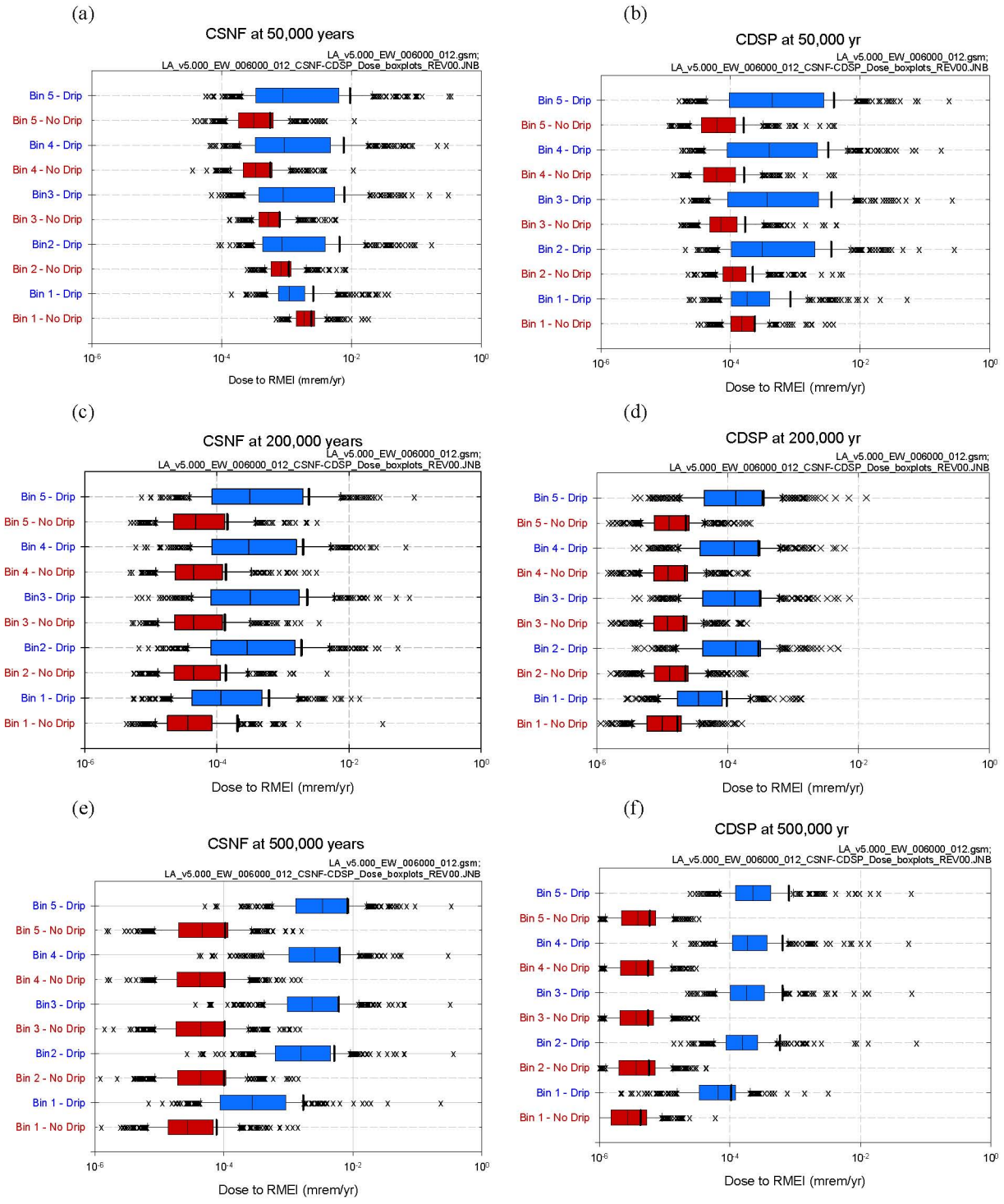

Source: Ouput DTNs: MO0709TSPAPLOT.000 [DIRS 183010]; and MO0709TSPAREGS.000 [DIRS 182976].

Figure J6.2-13. Box plots (see Figure J6.2-3 for description) summarizing results obtained with LHS of size *nLHS* = 300 showing epistemic uncertainty in doses $D_{EW}(\tau|[1, r, s, t], \mathbf{e}_{Mi})$ for $\tau = 5 \times 10^4$, 2×10^5, 5×10^5 yr, $r = 1, 2$, $s = 1, 2, 3, 4, 5$, $t = 0, 1$, and $i = 1, 2, \ldots, nLHS = 300$: (a, c, e) CSNF WPs for $\tau = 5 \times 10^4$, 2×10^5, 5×10^5 yr, and (b, d, f) CDSP WPs for $\tau = 5 \times 10^4$, 2×10^5, 5×10^5 yr.

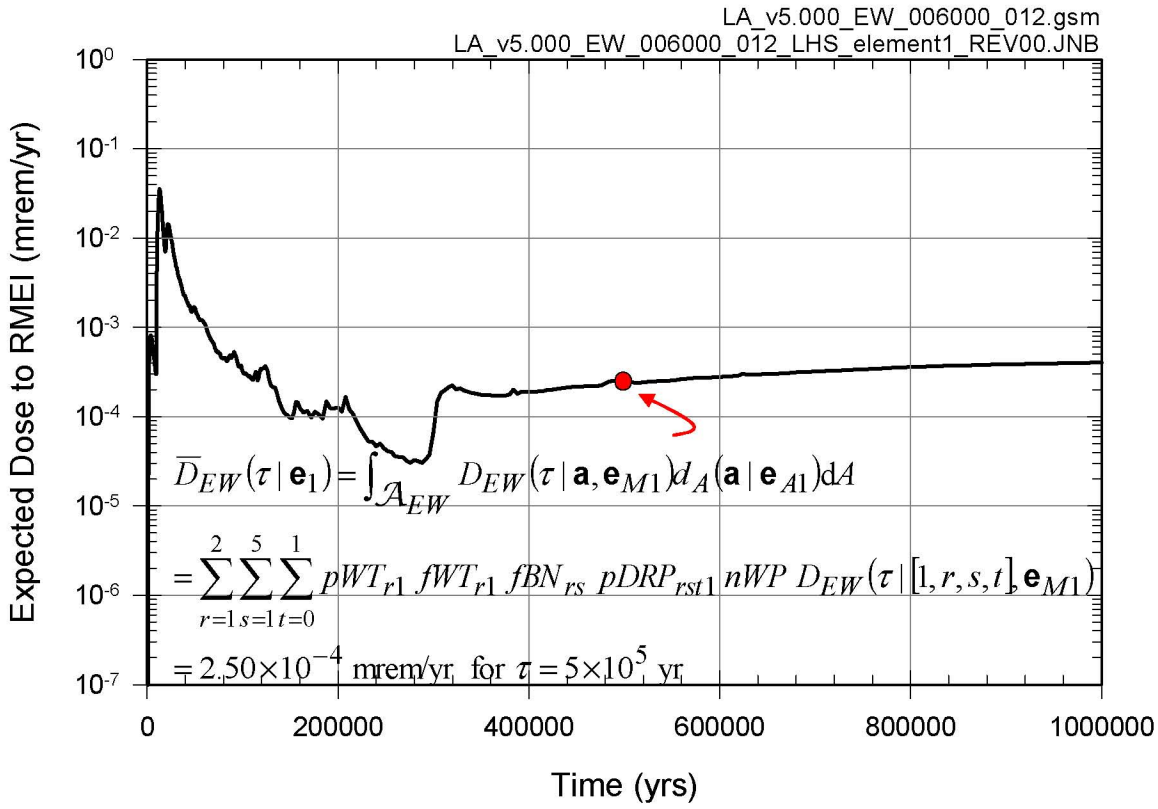

Source: Ouput DTNs: MO0709TSPAPLOT.000 [DIRS 183010]; and MO0709TSPAREGS.000 [DIRS 182976].

Figure J6.2-14. Estimate of $\bar{D}_{EW}(\tau|\mathbf{e}_1)$ for LHS element $\mathbf{e}_1 = [\mathbf{e}_{A1}, \mathbf{e}_{M1}]$ and $0 \le \tau \le 10^6$ yr with integration-based procedure indicated in Equation (J6.2-2).

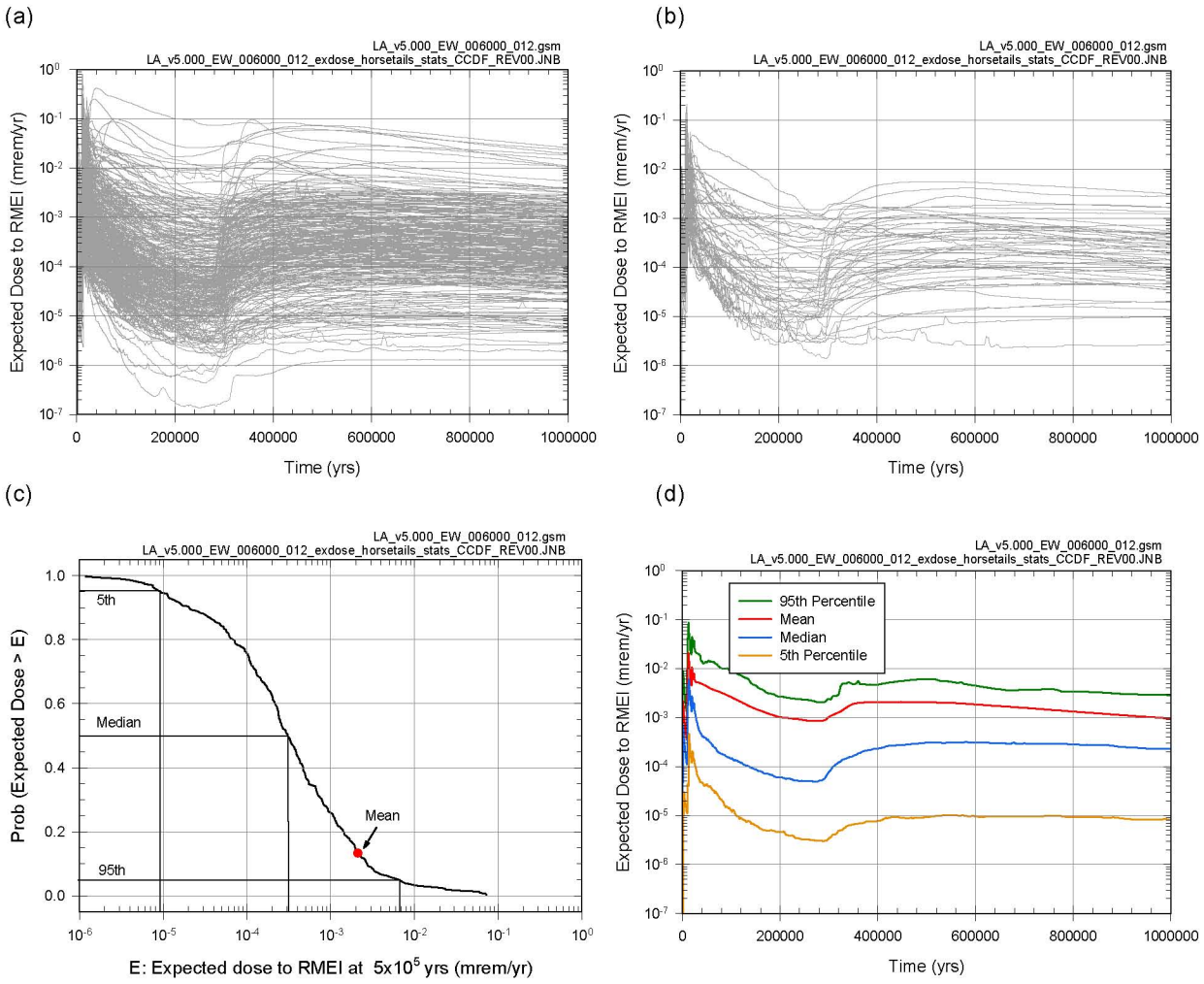

Source: Ouput DTNs: MO0709TSPAPLOT.000 [DIRS 183010]; and MO0709TSPAREGS.000 [DIRS 182976].

Figure J6.2-15. Estimate obtained with LHS of size *nLHS* = 300 showing epistemic uncertainty in expected dose $\bar{D}_{EW}(\tau|\mathbf{e})$ to RMEI for $0 \le \tau \le 10^6$ yr that at results when only early WP failure is considered: (a) expected dose $\bar{D}_{EW}(\tau|\mathbf{e}_i)$, i = 1, 2, …, *nLHS* = 300, (b) expected dose $\bar{D}_{EW}(\tau|\mathbf{e}_i)$, i = 1, 2, …, 50, (c) exceedance probabilities $p_E[D < \bar{D}_{EW}(\tau|\mathbf{e})]$ and quantiles $Q_q[\bar{D}_{EW}(\tau|\mathbf{e})]$, q = 0.05, 0.5 and 0.95, for $\tau = 5 \times 10^5$ yr, and (d) expected (mean) dose $\bar{\bar{D}}_{EW}(\tau)$ and quantiles $Q_q[\bar{D}_{EW}(\tau|\mathbf{e})]$, q = 0.05, 0.5, 0.95.

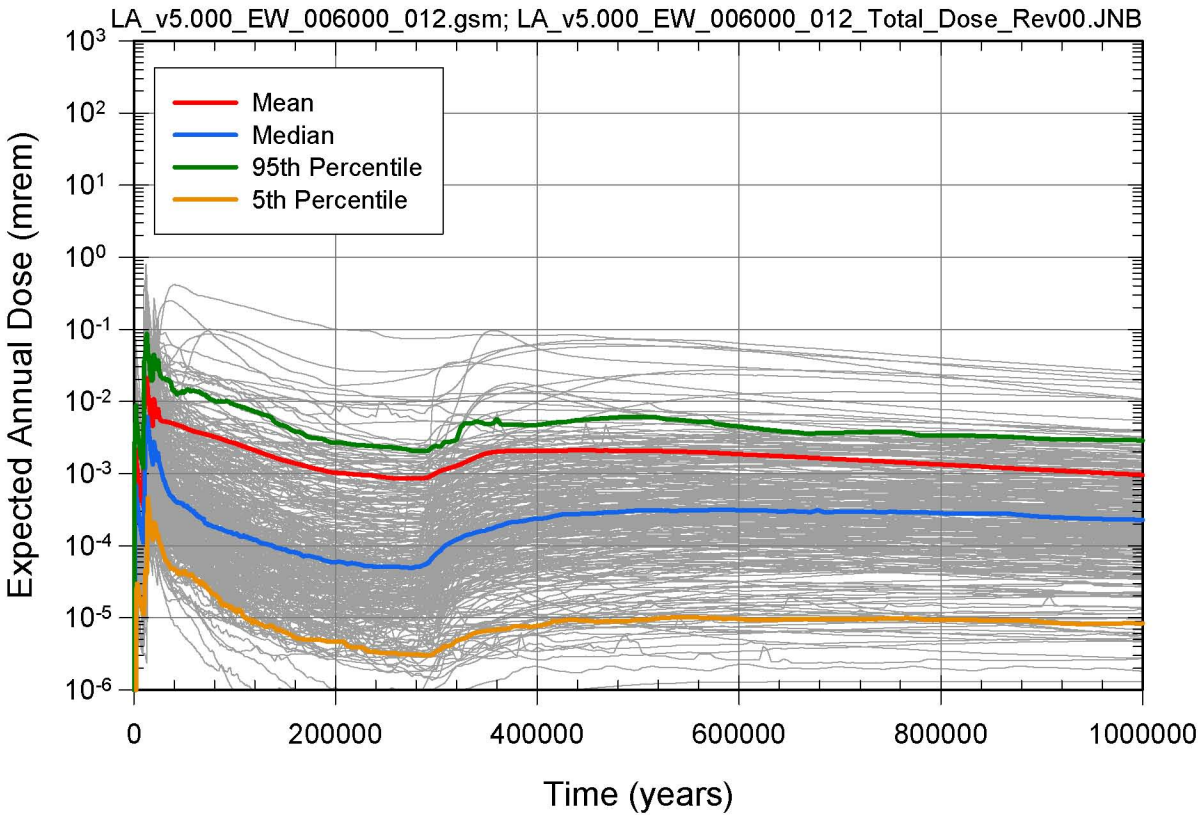

Source: Ouput DTNs: MO0709TSPAPLOT.000 [DIRS 183010]; and MO0709TSPAREGS.000 [DIRS 182976].

Figure J6.2-16. Summary of results obtained with LHS of size *nLHS* = 300 showing epistemic uncertainty in expected dose $\bar{D}_{EW}(\tau|\mathbf{e})$ to RMEI for $0 \leq \tau \leq 10^6$ yr that results when only early WP failure is considered.

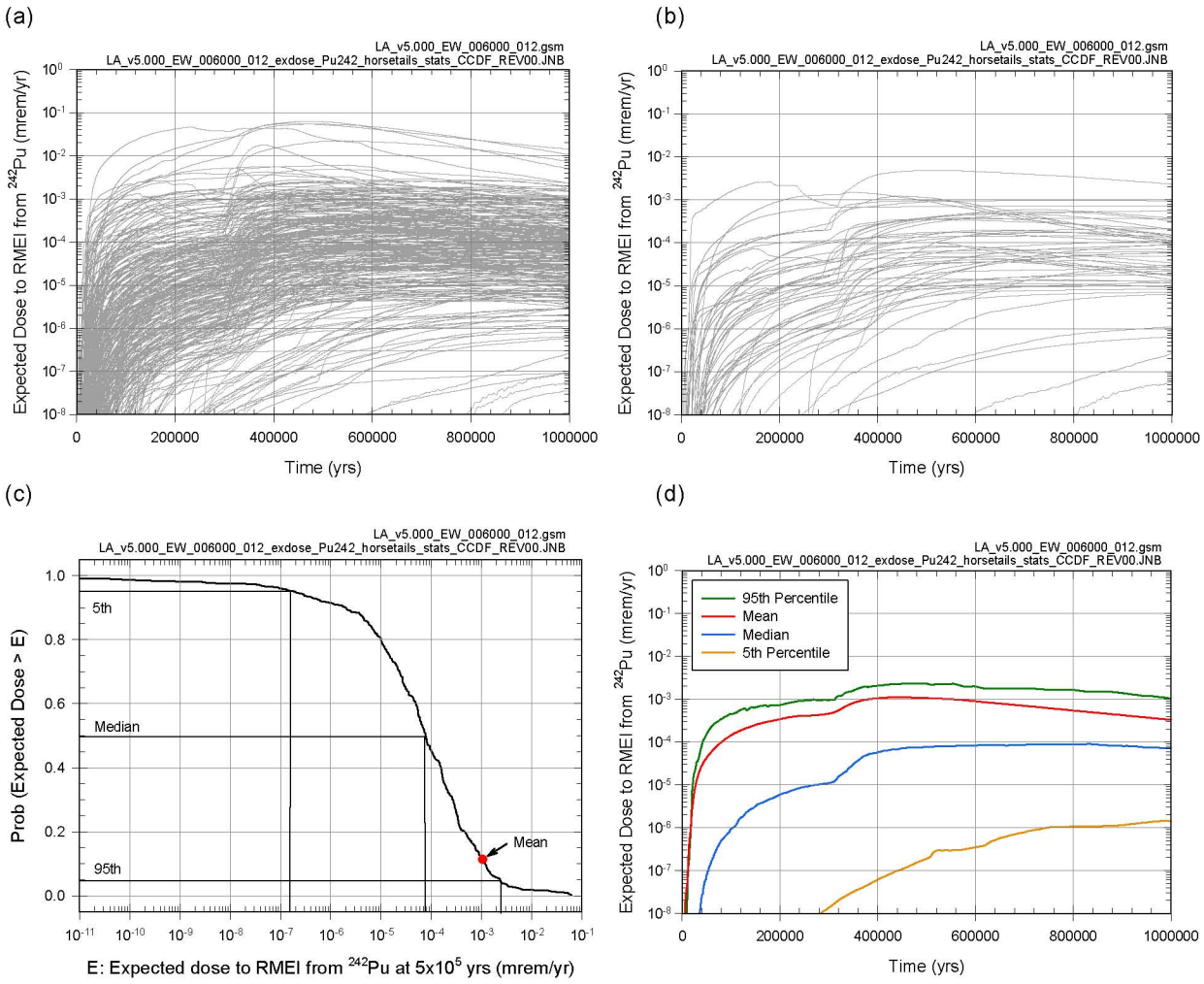

Source: Ouput DTNs: MO0709TSPAPLOT.000 [DIRS 183010]; and MO0709TSPAREGS.000 [DIRS 182976].

Figure J6.2-17. Estimate obtained with LHS of size *nLHS* = 300 showing epistemic uncertainty in expected dose $\bar{D}_{EW,r}(\tau|\mathbf{e})$ to RMEI for $0 \le \tau \le 10^6$ yr with r corresponding to ^{242}Pu that results when only early DS failure is considered: (a) expected dose $\bar{D}_{EW,r}(\tau|\mathbf{e}_i)$, i = 1, 2, ..., *nLHS* = 300, (b) expected dose $\bar{D}_{EW,r}(\tau|\mathbf{e}_i)$, i = 1, 2, ..., 50, (c) exceedance probabilities $p_E[D < \bar{D}_{EW,r}(\tau|\mathbf{e})]$ and quantiles $Q_q[\bar{D}_{EW,r}(\tau|\mathbf{e})]$, q = 0.05, 0.5 and 0.95, for $\tau = 5 \times 10^5$ yr, and (d) expected (mean) dose $\bar{\bar{D}}_{EW,r}(\tau)$ and quantiles $Q_q[\bar{D}_{EW,r}(\tau|\mathbf{e})]$, q = 0.05, 0.5, 0.95.

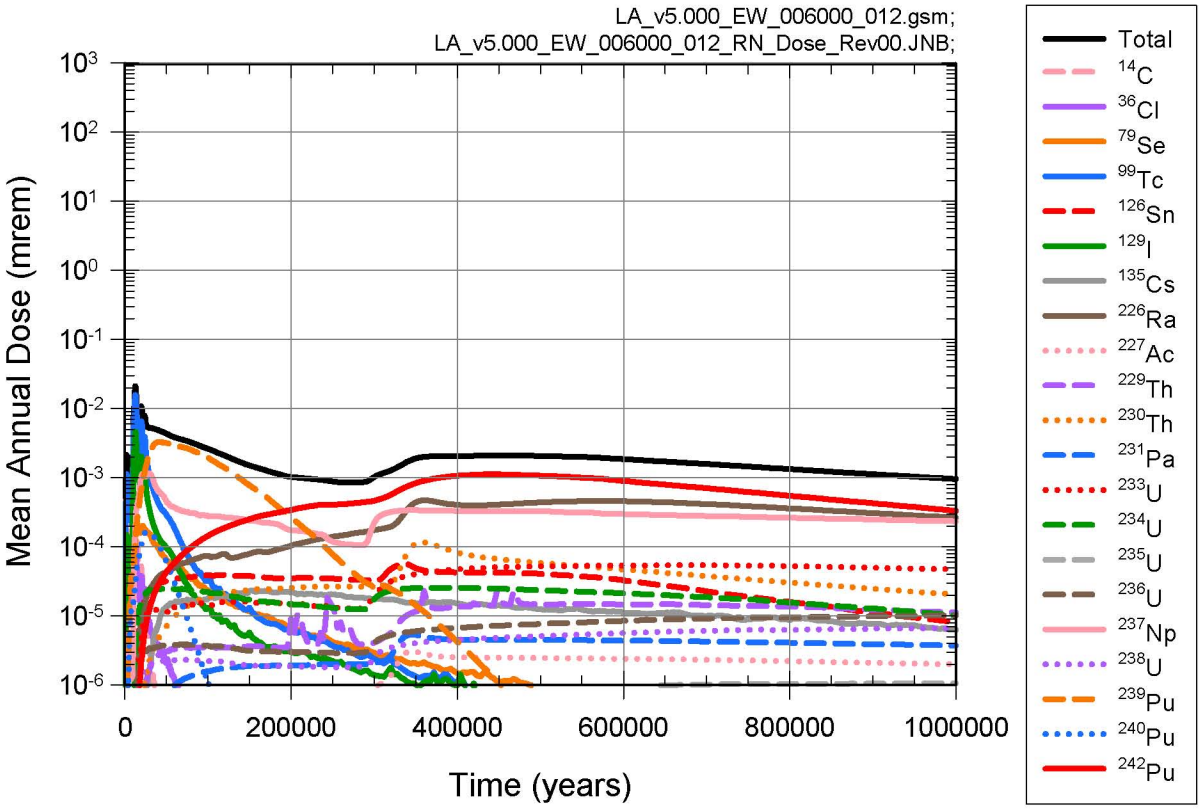

Source: Ouput DTNs: MO0709TSPAPLOT.000 [DIRS 183010]; and MO0709TSPAREGS.000 [DIRS 182976].

Figure J6.2-18. Estimates obtained with LHS of size *nLHS* = 300 of expected (mean) dose $\bar{\bar{D}}_{EW,r}(\tau)$ to RMEI for $0 \leq \tau \leq 10^6$ yr for individual radioactive species that result when only early WP failure is considered.

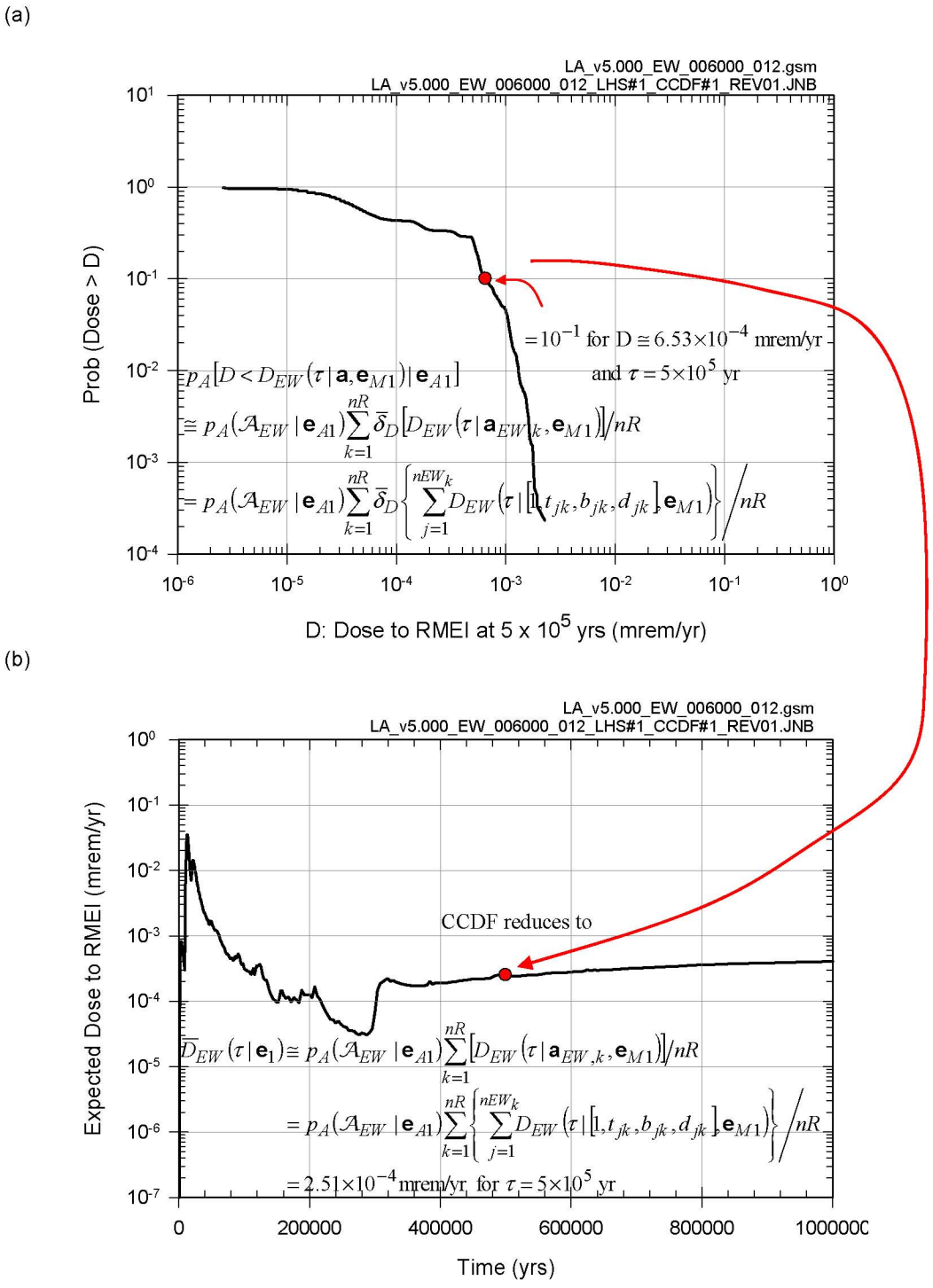

Source: Ouput DTNs: MO0709TSPAPLOT.000 [DIRS 183010]; and MO0709TSPAREGS.000 [DIRS 182976].

Figure J6.2-19. Results associated with $D_{EW}(\tau|\mathbf{a}_{EW}, \mathbf{e}_{M1})$ for LHS element $\mathbf{e}_1 = [\mathbf{e}_{A1}, \mathbf{e}_{M1}]$ obtained with sampling-based (Monte Carlo) procedures: (a) CCDF for $D_{EW}(5 \times 10^5 \text{ yr}|\mathbf{a}_{EW}, \mathbf{e}_{M1})$ with exceedance probabilities $p_A[D < D_{EW}(5 \times 10^5 \text{ yr}|\mathbf{a}, \mathbf{e}_{M1})|\mathbf{e}_{A1}]$ defined in Equation (J6.2-12), and (b) expected dose $\bar{D}_{EW}(5 \times 10^5 \text{ yr}|\mathbf{e}_1)$ associated with $D_{EW}(5 \times 10^5 \text{ yr}|\mathbf{a}_{EW}, \mathbf{e}_{M1})$ as defined in Equation (J6.2-10).

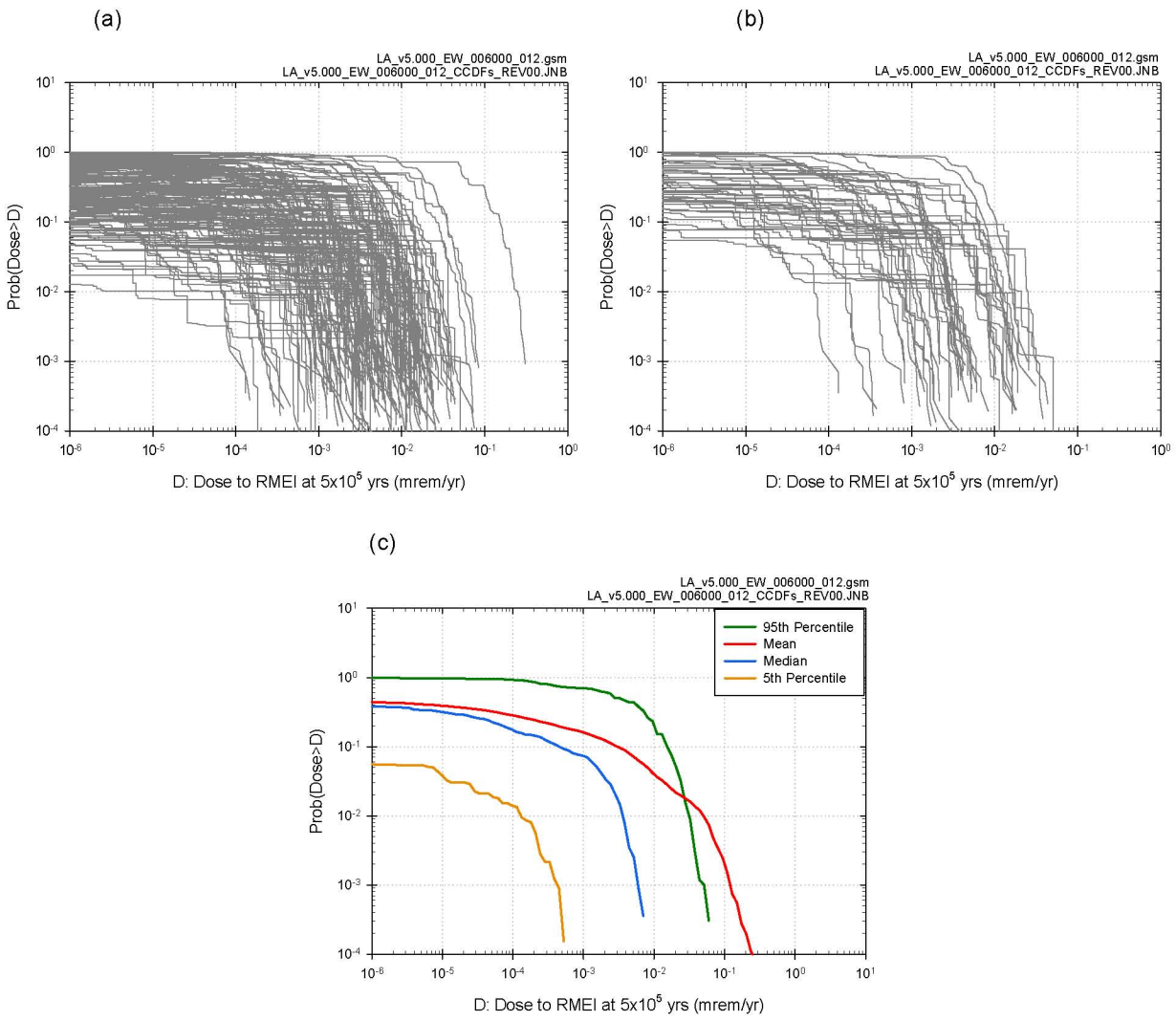

Source: Ouput DTNs: MO0709TSPAPLOT.000 [DIRS 183010]; and MO0709TSPAREGS.000 [DIRS 182976].

Figure J6.2-20. Results associated with $D_{EW}(5 \times 10^5 \text{ yr}|\mathbf{a}_{EW}, \mathbf{e}_M)$ obtained with sampling-based (Monte Carlo) procedures for an LHS of size $nLHS = 300$: (a) CCDFs for $D_{EW}(5 \times 10^5 \text{ yr}|\mathbf{a}_{EW}, \mathbf{e}_{Mi})$ with exceedance probabilities $p_A[D < D_{EW}(5 \times 10^5 \text{ yr}|\mathbf{a}, \mathbf{e}_{Mi})|\mathbf{e}_{Ai}]$ defined in Equation J66.2-12 for $i = 1, 2, \ldots, nLHS = 300$, (b) CCDFs for $D_{EW}(10^4 \text{ yr}|\mathbf{a}_{EW}, \mathbf{e}_{Mi})$ with exceedance probabilities $p_A[D < D_{EW}(5 \times 10^5 \text{ yr}|\mathbf{a}, \mathbf{e}_{Mi})|\mathbf{e}_{Ai}]$ defined in Equation J6.2-20 for $i = 1, 2, \ldots, 50$, and (c) expected (mean) CCDF and quantile curves, $q = 0.05, 0.5, 0.95$, for CCDFs in (a).

(a)

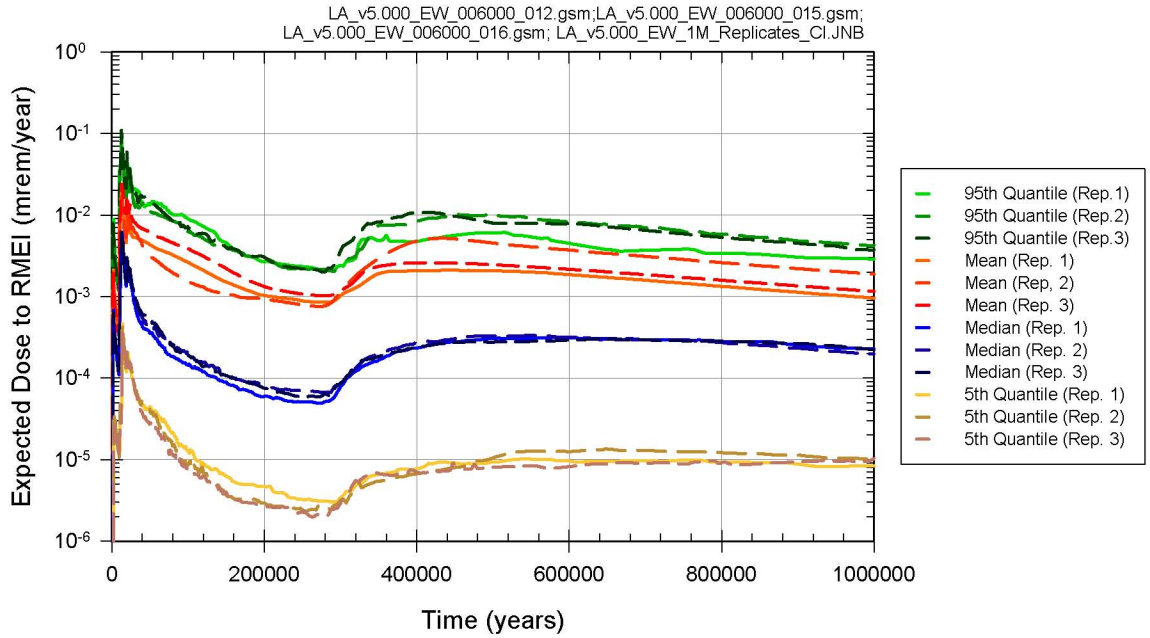

(b)

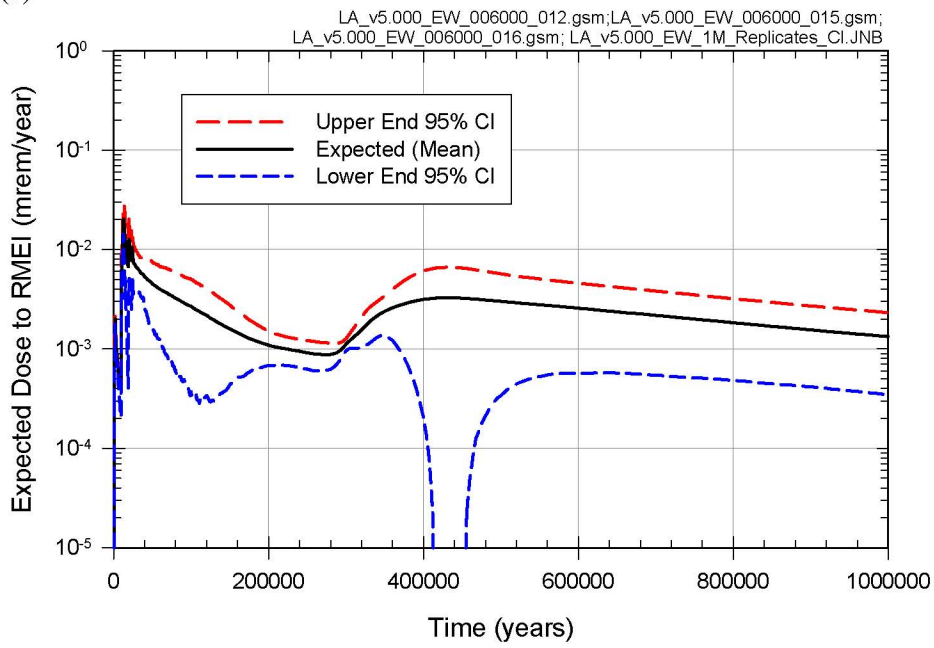

Source: Ouput DTNs: MO0709TSPAPLOT.000 [DIRS 183010]; MO0709TSPASTAB.000 [DIRS 182983]; and MO0709TSPAREGS.000 [DIRS 182976].

Figure J6.2-21. Assessment with replicated sampling of numerical error associated with use of an LHS of size *nLHS* = 300 to determine epistemic uncertainty in expected dose $\bar{D}_{EW}(\tau|\mathbf{e})$ to RMEI for $0 \le \tau \le 10^6$ yr that results when only early WP failure is considered: (a) Replicated estimates of expected (mean) dose $\bar{D}_{EW}(\tau)$ and quantiles $Q_q[\bar{D}_{EW}(\tau|\mathbf{e})]$, q = 0.05, 0.5, 0.95, and (b) confidence intervals for estimates of expected (mean) dose $\bar{\bar{D}}_{EW}(\tau)$.

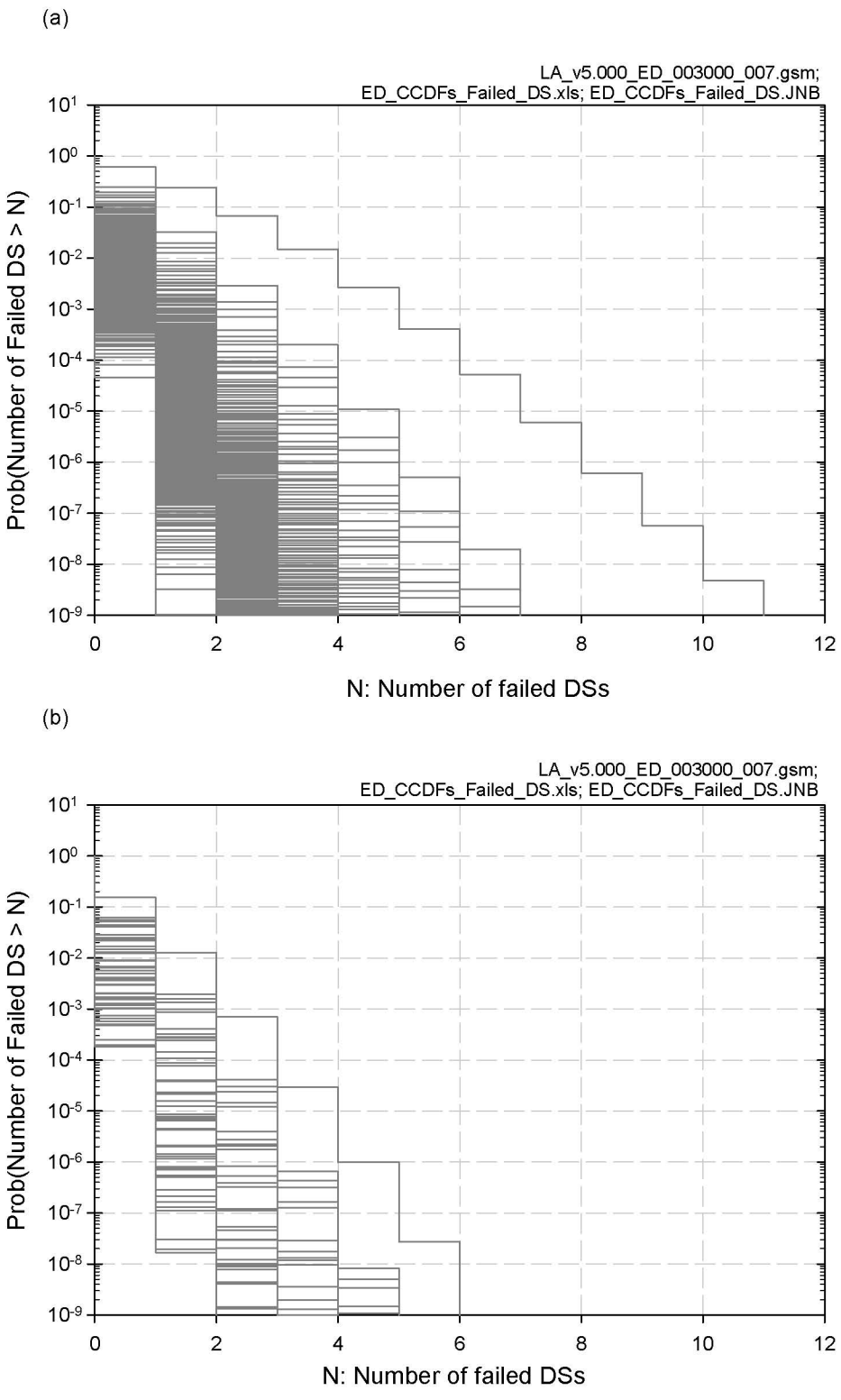

Source: Ouput DTNs: MO0709TSPAPLOT.000 [DIRS 183010]; and MO0709TSPAREGS.000 [DIRS 182976].

Figure J6.3-1. Complementary cumulative distribution functions (CCDFs) for number *nED* of DSs with early failure associated with individual elements of LHS of size *nLHS* = 300 in Equation J4.9-1: (a) CCDFs for all 300 LHS elements, and (b) CCDFs for first 50 LHS elements.

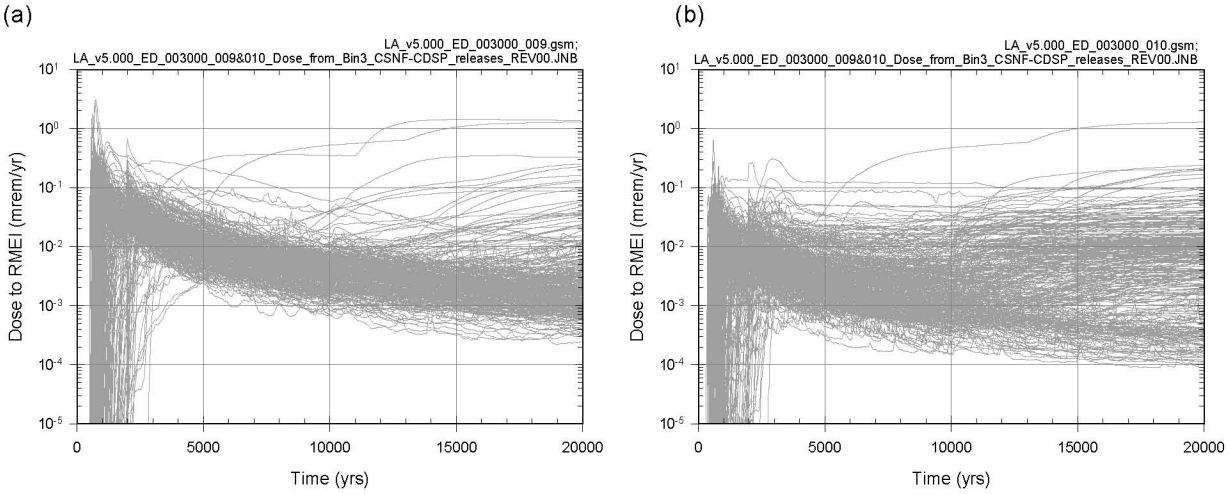

Source: Ouput DTNs: MO0709TSPAPLOT.000 [DIRS 183010]; and MO0709TSPASENS.000 [DIRS 182982].

Figure J6.3-2. Summary of results obtained with LHS of size *nLHS* = 300 showing epistemic uncertainty in doses $D_{ED}(\tau|[1, r, s, 1], \mathbf{e}_M)$ for $0 \leq \tau \leq 20{,}000$ yr: (a) CSNF WP in bin 3 under dripping conditions (i.e., $D_{ED}(\tau|[1, 1, 3, 1], \mathbf{e}_{Mi})$, $i = 1, 2, \ldots, nLHS = 300$), and (b) CDSP WP in bin 3 under dripping conditions (i.e., $D_{ED}(\tau|[1, 2, 3, 1], \mathbf{e}_{Mi})$, $i = 1, 2, \ldots, nLHS = 300$).

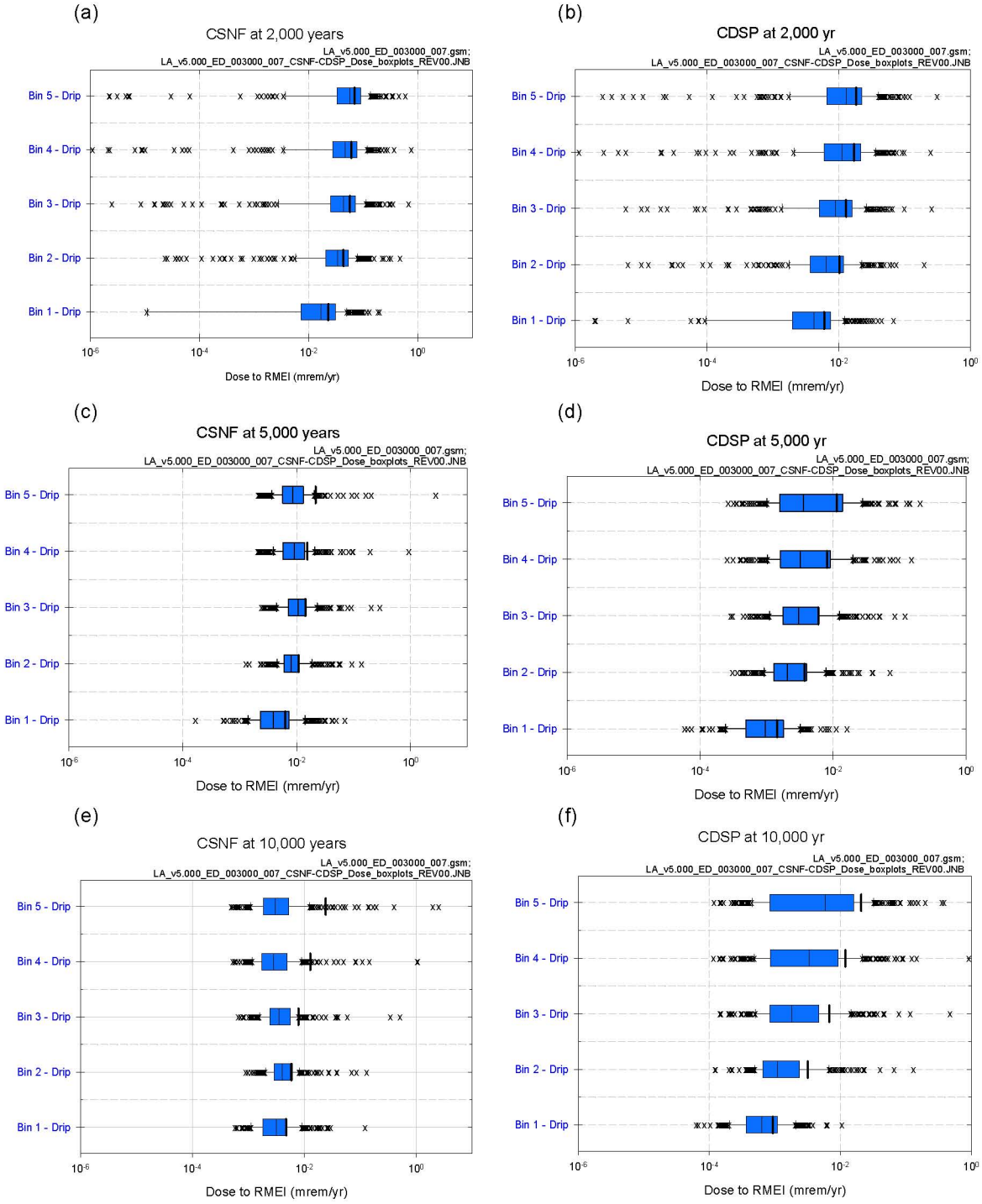

Source: Ouput DTNs: MO0709TSPAPLOT.000 [DIRS 183010]; and MO0709TSPAREGS.000 [DIRS 182976].

Figure J6.3-3. Box plots (see Figure J6.2-3 for description) summarizing results obtained with LHS of size *nLHS* = 300 showing epistemic uncertainty in doses $D_{ED}(\tau|[1, r, s, 1], \mathbf{e}_{Mi})$ for τ = 2000, 5000, 10,000 yr, r = 1, 2, s = 1, 2, 3, 4, 5, t = 1, and i = 1, 2, …, *nLHS* = 300: (a, c, e) CSNF WPs at τ = 2000, 5000 and 10,000 yrs, and (b, d, f) CDSP WPs at τ = 2000, 5000 and 10,000 yrs.

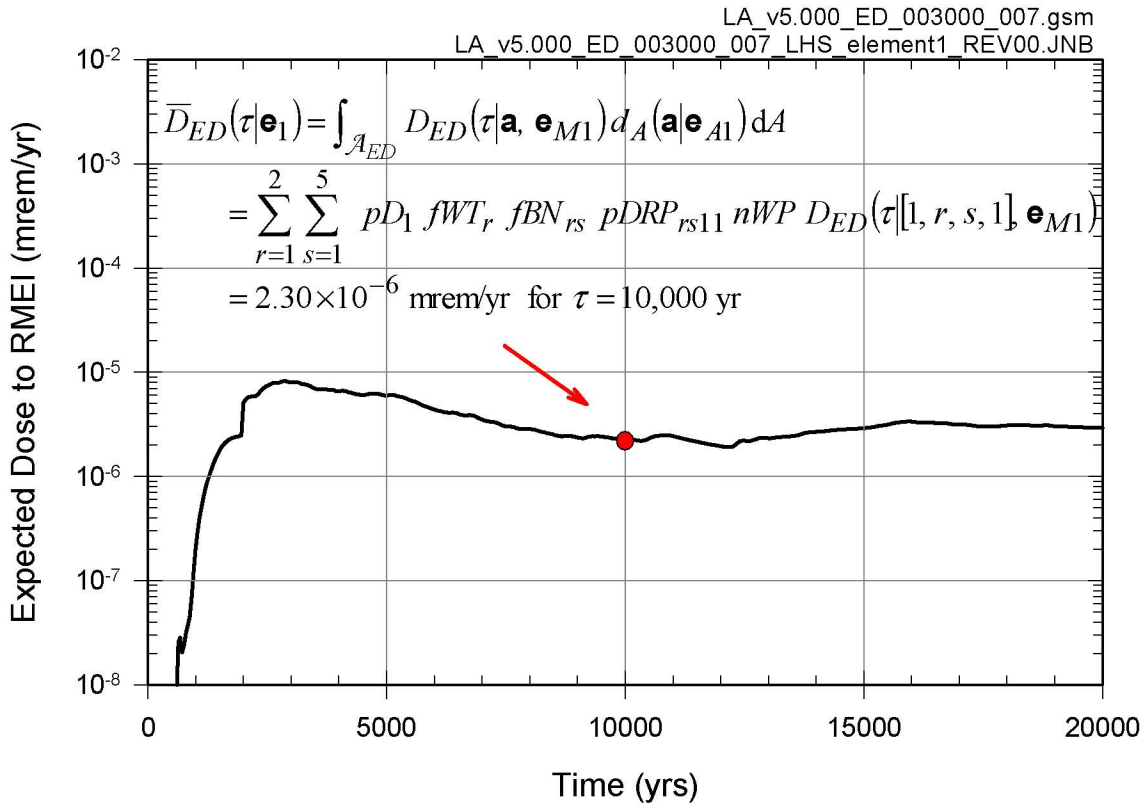

Source: Ouput DTNs: MO0709TSPAPLOT.000 [DIRS 183010]; and MO0709TSPAREGS.000 [DIRS 182976].

Figure J6.3-4. Estimate of $\bar{D}_{ED}(\tau|\mathbf{e}_1)$ for LHS element $\mathbf{e}_1 = [\mathbf{e}_{A1}, \mathbf{e}_{M1}]$ and $0 \le \tau \le 20{,}000$ yr with integration-based procedure indicated in Equation (J6.3-2).

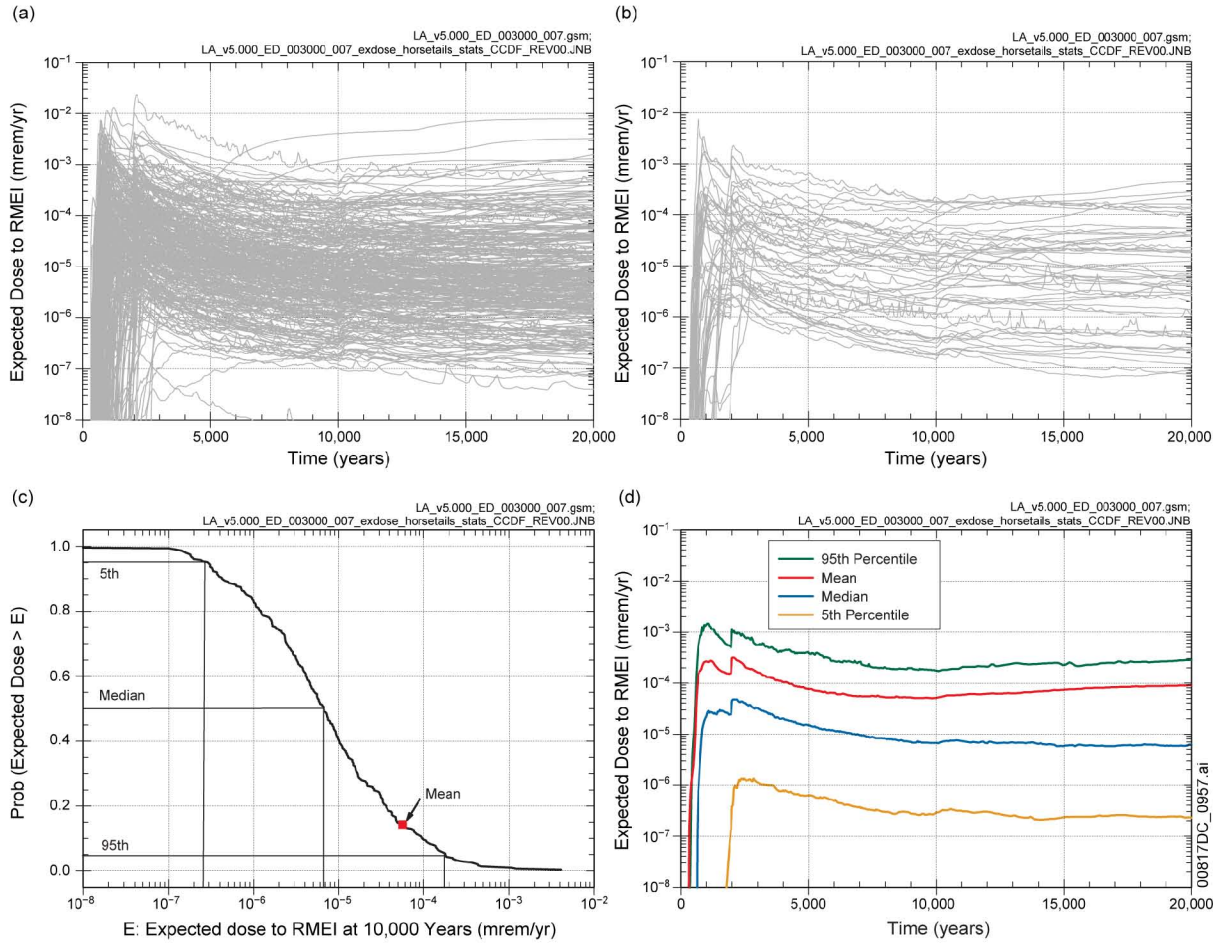

Source: Ouput DTNs: MO0709TSPAPLOT.000 [DIRS 183010]; and MO0709TSPAREGS.000 [DIRS 182976].

Figure J6.3-5. Estimate obtained with LHS of size *nLHS* = 300 showing epistemic uncertainty in expected dose $\bar{D}_{ED}(\tau|\mathbf{e})$ to RMEI for $0 \le \tau \le 20{,}000$ yr that results when only early DS failure is considered: (a) expected dose $\bar{D}_{ED}(\tau|\mathbf{e}_i)$, i = 1, 2, …, *nLHS* = 300, (b) expected dose $\bar{D}_{ED}(\tau|\mathbf{e}_i)$, i = 1, 2, …, 50, (c) exceedance probabilities $p_E[D < \bar{D}_{ED}(\tau|\mathbf{e})]$ and quantiles $Q_q[\bar{D}_{ED}(\tau|\mathbf{e})]$, q = 0.05, 0.5 and 0.95, for $\tau = 10^4$ yr, and (d) expected (mean) dose $\bar{\bar{D}}_{ED}(\tau)$ and quantiles $Q_q[\bar{D}_{ED}(\tau|\mathbf{e})]$, q = 0.05, 0.5, 0.95.

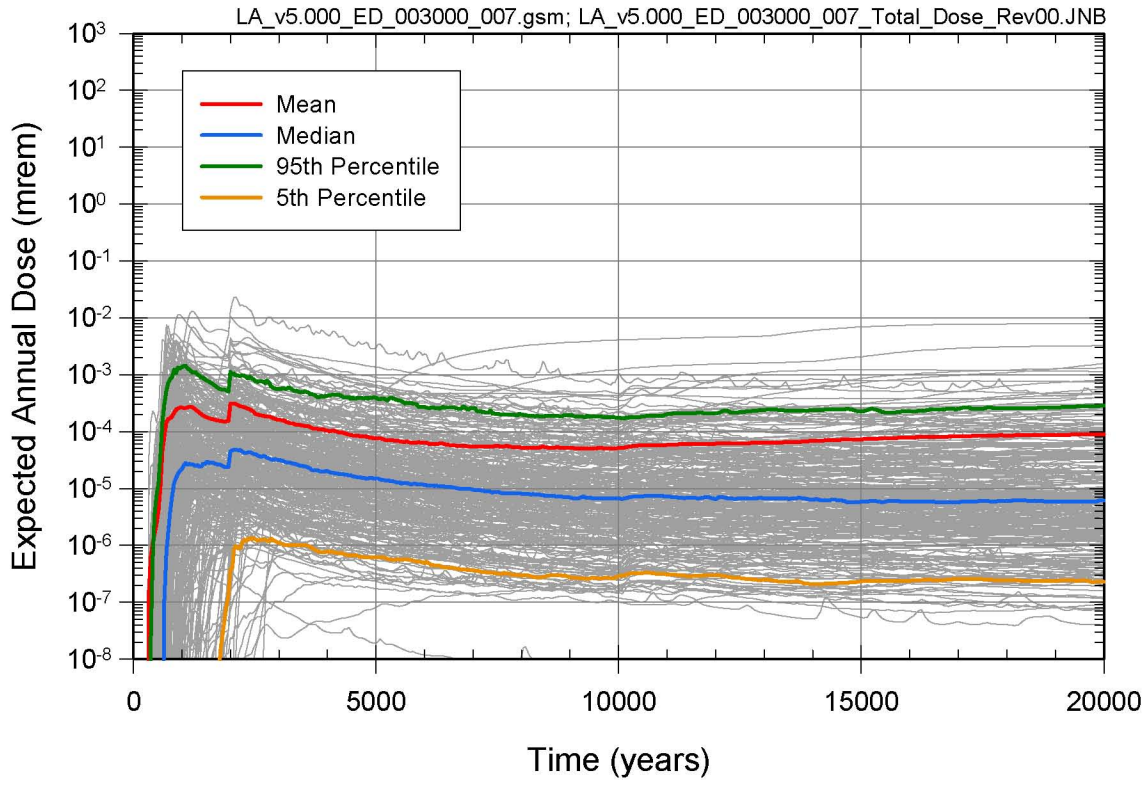

Source: Ouput DTNs: MO0709TSPAPLOT.000 [DIRS 183010]; and MO0709TSPAREGS.000 [DIRS 182976].

Figure J6.3-6. Summary of results obtained with LHS of size *nLHS* = 300 showing epistemic uncertainty in expected dose $\bar{D}_{ED}(\tau|\mathbf{e})$ to RMEI for $0 \leq \tau \leq 20{,}000$ yr that results when only early DS failure is considered.

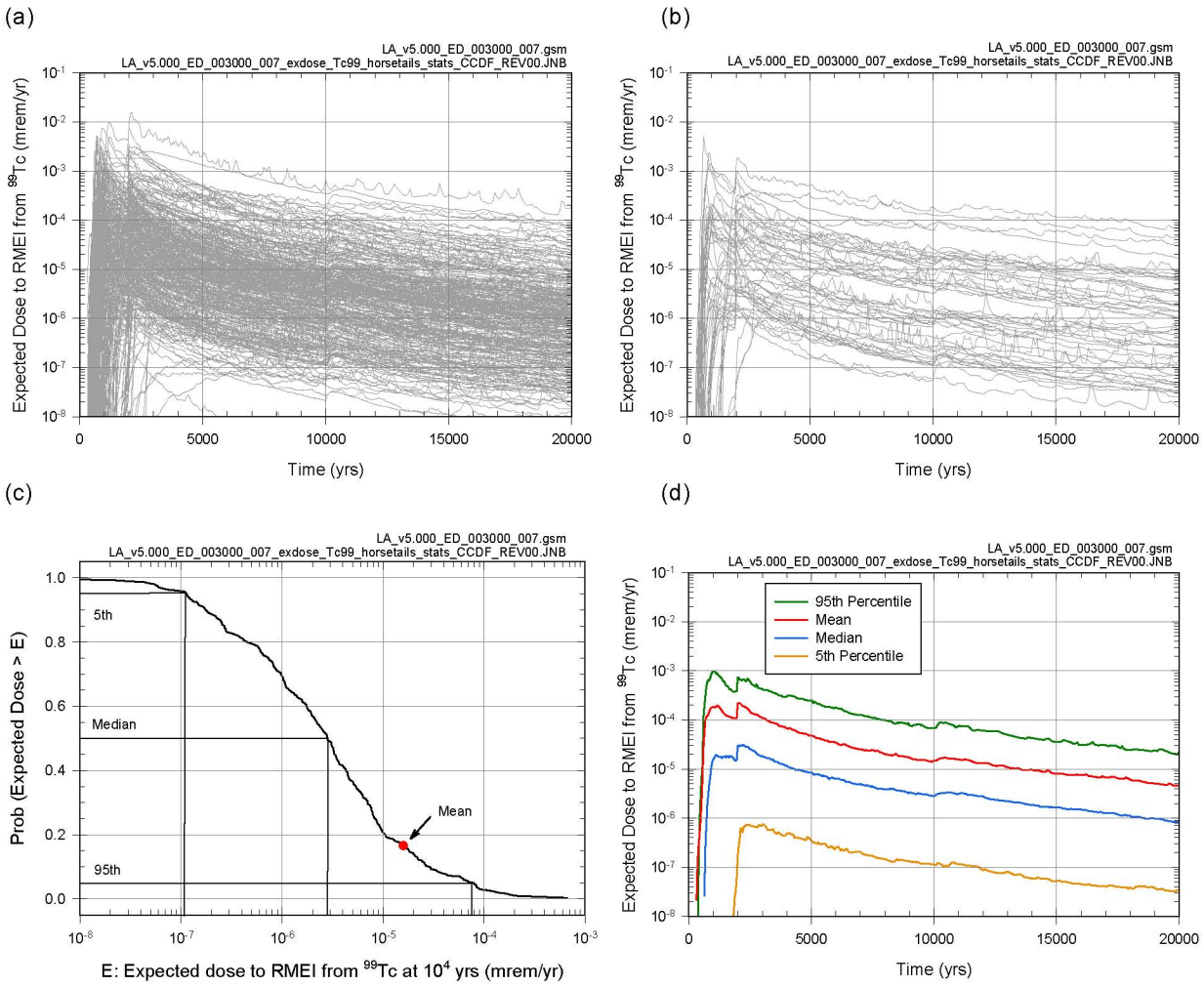

Source: Ouput DTNs: MO0709TSPAPLOT.000 [DIRS 183010]; and MO0709TSPAREGS.000 [DIRS 182976].

Figure J6.3-7. Estimate obtained with LHS of size *nLHS* = 300 showing epistemic uncertainty in expected dose $\bar{D}_{ED,r}(\tau|\mathbf{e})$ to RMEI for $0 \le \tau \le 20{,}000$ yr with r corresponding to ^{99}Tc that results when only early DS failure is considered: (a) expected dose $\bar{D}_{ED,r}(\tau|\mathbf{e}_i)$, i = 1, 2, …, *nLHS* = 300, (b) expected dose $\bar{D}_{ED,r}(\tau|\mathbf{e}_i)$, i = 1, 2, …, 50, (c) exceedance probabilities $p_E[D < \bar{D}_{ED,r}(\tau|\mathbf{e})]$ and quantiles $Q_q[\bar{D}_{ED,r}(\tau|\mathbf{e})]$, q = 0.05, 0.5 and 0.95, for $\tau = 10^4$ yr, and (d) expected (mean) dose $\bar{\bar{D}}_{ED,r}(\tau)$ and quantiles $Q_q[\bar{D}_{ED,r}(\tau|\mathbf{e})]$, q = 0.05, 0.5, 0.95.

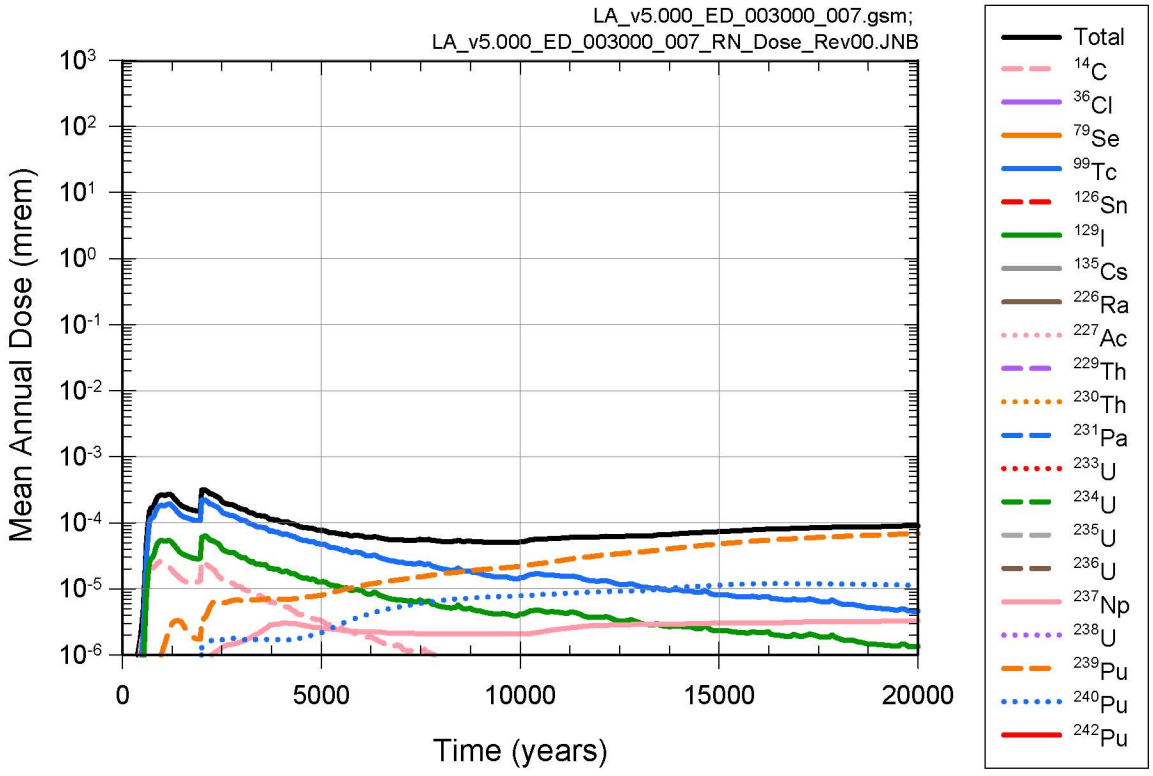

Source: Ouput DTNs: MO0709TSPAPLOT.000 [DIRS 183010]; and MO0709TSPAREGS.000 [DIRS 182976].

Figure J6.3-8. Estimates obtained with LHS of size *nLHS* = 300 of expected (mean) dose $\bar{\bar{D}}_{ED,r}(\tau)$ to RMEI for $0 \leq \tau \leq 20{,}000$ yr for individual radioactive species that result when only early DS failure is considered.

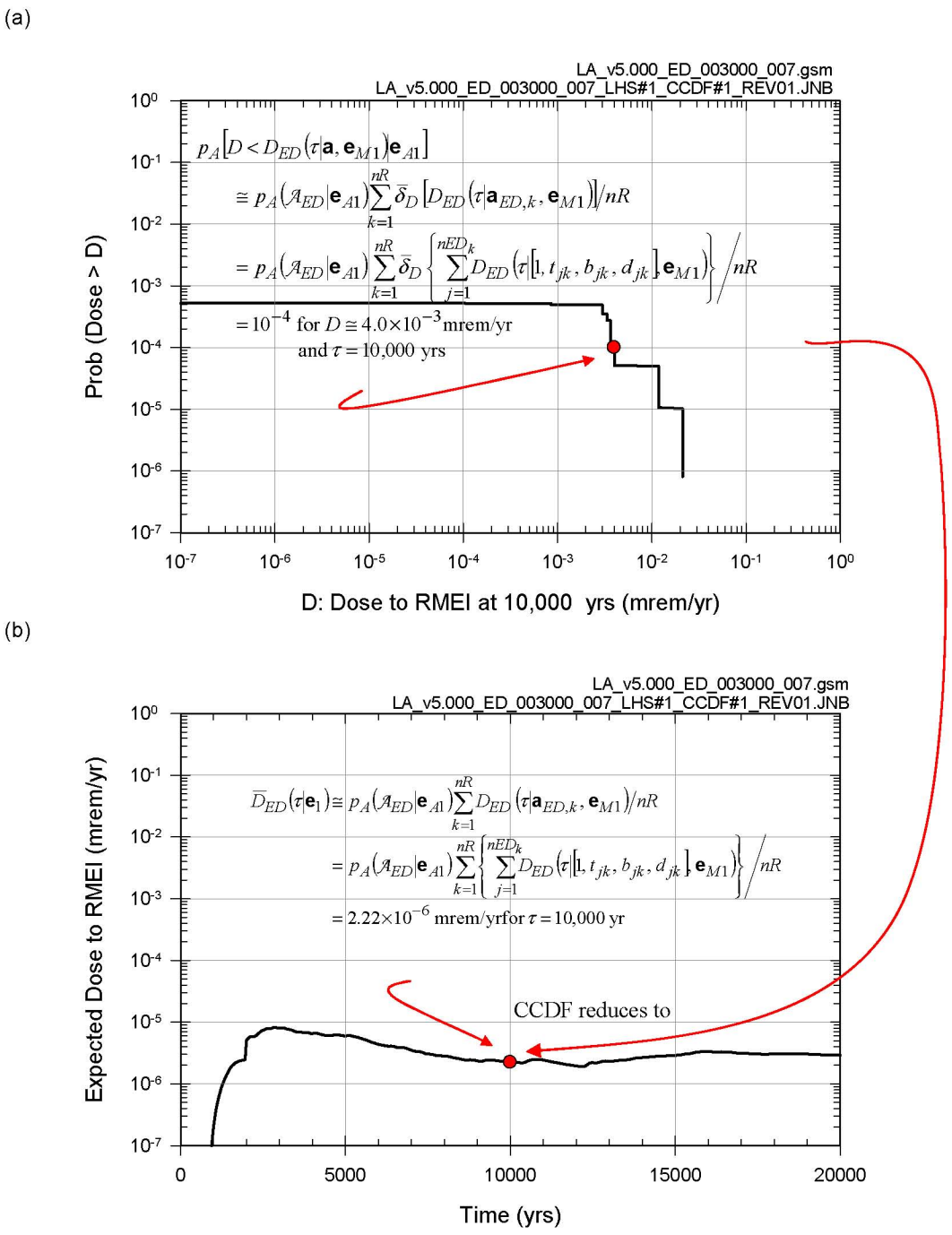

Source: Ouput DTNs: MO0709TSPAPLOT.000 [DIRS 183010]; and MO0709TSPAREGS.000 [DIRS 182976].

Figure J6.3-9. Results associated with $D_{ED}(\tau|\mathbf{a}_{ED}, \mathbf{e}_{M1})$ for LHS element $\mathbf{e}_1 = [\mathbf{e}_{A1}, \mathbf{e}_{M1}]$ obtained with sampling-based (Monte Carlo) procedures: (a) CCDF for $D_{ED}(10^4 \text{ yr}|\mathbf{a}_{ED}, \mathbf{e}_{M1})$ with exceedance probabilities $p_A[D < D_{ED}(10^4 \text{ yr}|\mathbf{a}, \mathbf{e}_{M1})|\mathbf{e}_{A1}]$ defined similarly to $p_A[D < D_{EW}(\tau|\mathbf{a}, \mathbf{e}_{M1})|\mathbf{e}_{A1}]$ in Equation (J6.2-12), and (b) expected dose $\bar{D}_{ED}(10^4 \text{ yr}|\mathbf{e}_1)$ associated with $D_{ED}(10^4 \text{ yr}|\mathbf{a}_{ED}, \mathbf{e}_{M1})$ defined similarly to $\bar{D}_{EW}(\tau|\mathbf{e}_1)$ in Equation (J6.2-10).

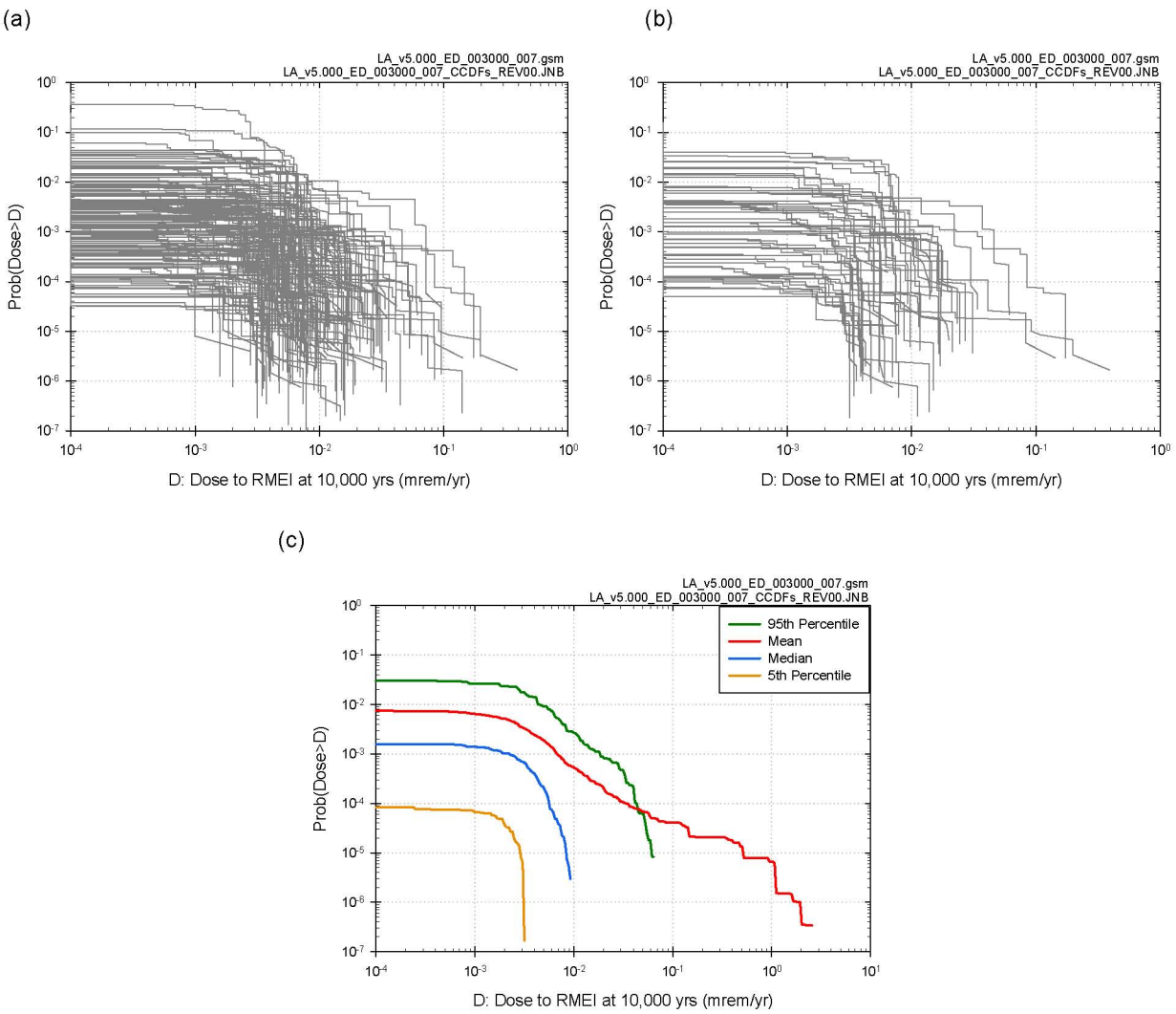

Source: Ouput DTNs: MO0709TSPAPLOT.000 [DIRS 183010]; and MO0709TSPAREGS.000 [DIRS 182976].

Figure J6.3-10. Results associated with $D_{ED}(10^4 \text{ yr}|\mathbf{a}_{ED}, \mathbf{e}_M)$ obtained with sampling-based (Monte Carlo) procedures for an LHS of size $nLHS = 300$: (a) CCDFs for $D_{ED}(10^4 \text{ yr}|\mathbf{a}_{ED}, \mathbf{e}_{Mi})$ with exceedance probabilities $p_A[D < D_{ED}(10^4 \text{ yr}|\mathbf{a}, \mathbf{e}_{Mi})|\mathbf{e}_{Ai}]$ defined similarly to $p_A[D < D_{EW}(\tau|\mathbf{a}, \mathbf{e}_{M1})|\mathbf{e}_{A1}]$ in Equation (J6.2-12) for $i = 1, 2, \ldots, nLHS = 300$, (b) CCDFs for $D_{ED}(10^4 \text{ yr}|\mathbf{a}_{ED}, \mathbf{e}_{Mi})$ with exceedance probabilities $p_A[D < D_{ED}(10^4 \text{ yr}|\mathbf{a}, \mathbf{e}_{Mi})|\mathbf{e}_{Ai}]$ defined similarly to $p_A[D < D_{EW}(\tau|\mathbf{a}, \mathbf{e}_{M1})|\mathbf{e}_{A1}]$ in Equation (J6.2-12) for $i = 1, 2, \ldots, 50$, and (c) expected (mean) CCDF and quantile curves, $q = 0.05, 0.5, 0.95$, for CCDFs in (a).

(a)

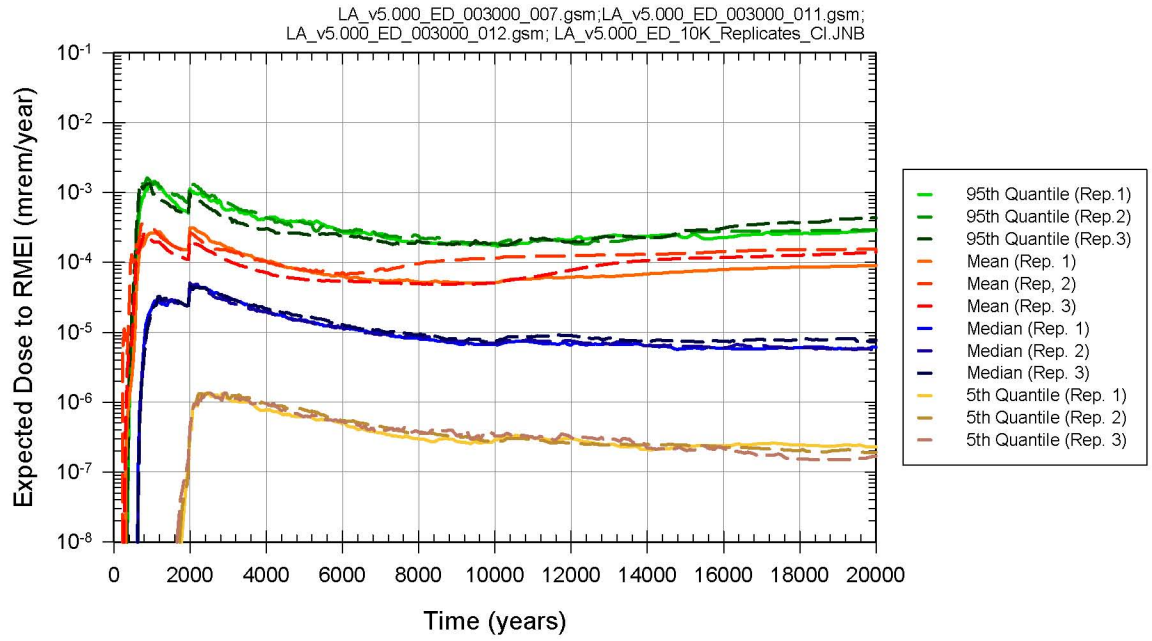

(b)

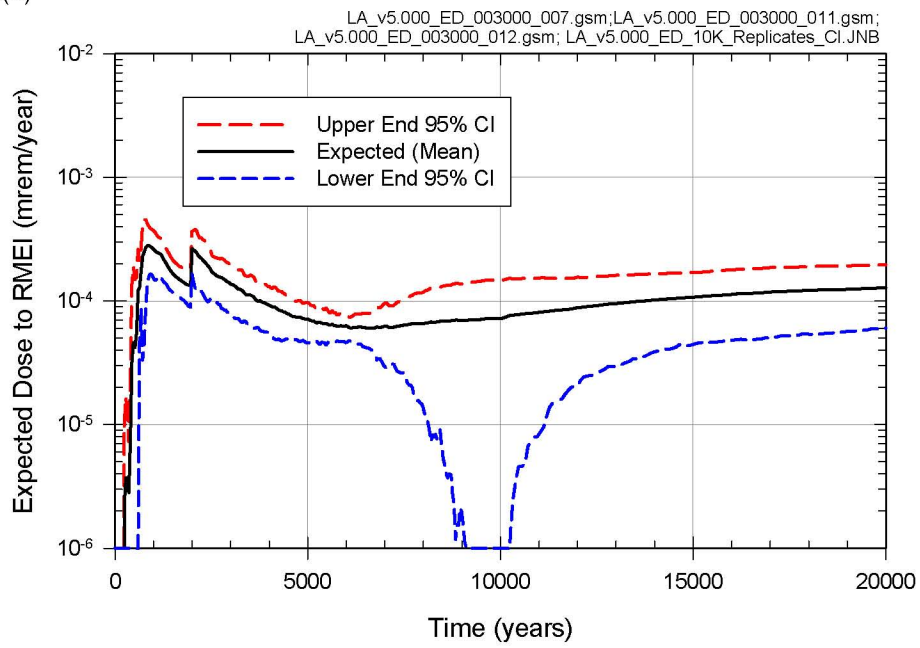

Source: Ouput DTNs: MO0709TSPAPLOT.000 [DIRS 183010]; MO0709TSPAREGS.000 [DIRS 182976]; and MO0709TSPASTAB.000 [DIRS 182983].

Figure J6.3-11. Assessment with replicated sampling of numerical error associated with use of an LHS of size *nLHS* = 300 to determine epistemic uncertainty in expected dose $\bar{D}_{ED}(\tau|\mathbf{e})$ to RMEI for $0 \leq \tau \leq 20{,}000$ yr that results when only early DS failure is considered: (a) Replicated estimates of expected (mean) dose $\bar{\bar{D}}_{ED}(\tau)$ and quantiles $Q_q[\bar{D}_{ED}(\tau|\mathbf{e})]$, q = 0.05, 0.5, 0.95, and (b) confidence intervals for estimates of expected (mean) dose $\bar{\bar{D}}_{ED}(\tau)$.

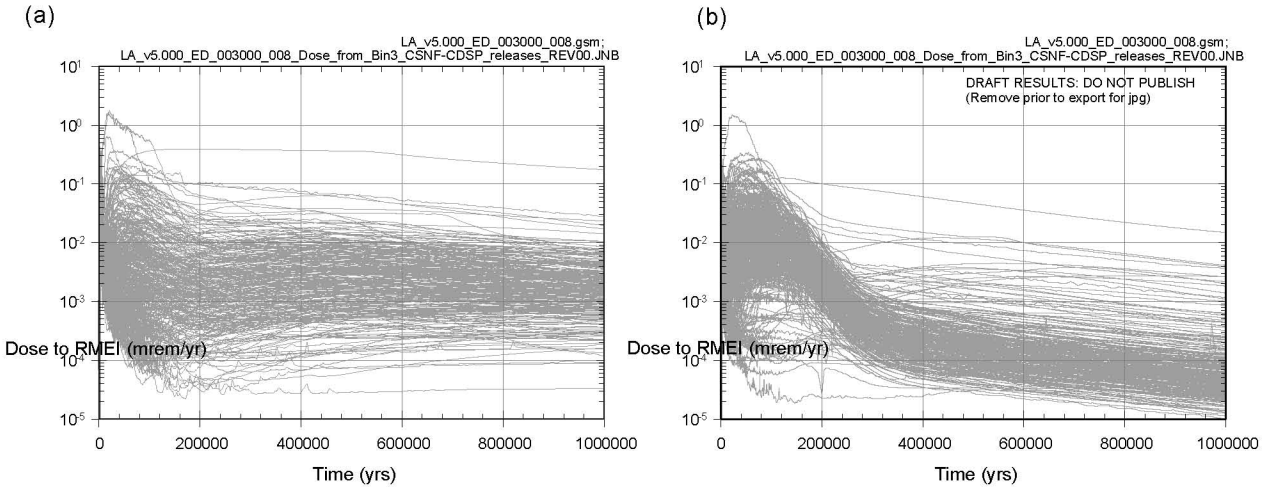

Source: Ouput DTNs: MO0709TSPAPLOT.000 [DIRS 183010]; and MO0709TSPAREGS.000 [DIRS 182976].

Figure J6.3-12. Summary of results obtained with LHS of size *nLHS* = 300 showing epistemic uncertainty in doses $D_{ED}(\tau|[1, r, s, 1], \mathbf{e}_M)$ for $0 \leq \tau \leq 10^6$ yr: (a) CSNF WP in bin 3 under dripping conditions (i.e., $D_{ED}(\tau|[1, 1, 3, 1], \mathbf{e}_{Mi})$, $i = 1, 2, \ldots, nLHS = 300$) and (b) CDSP WP in bin 3 under dripping conditions (i.e., $D_{ED}(\tau|[1, 2, 3, 1], \mathbf{e}_{Mi})$, $i = 1, 2, \ldots, nLHS = 300$).

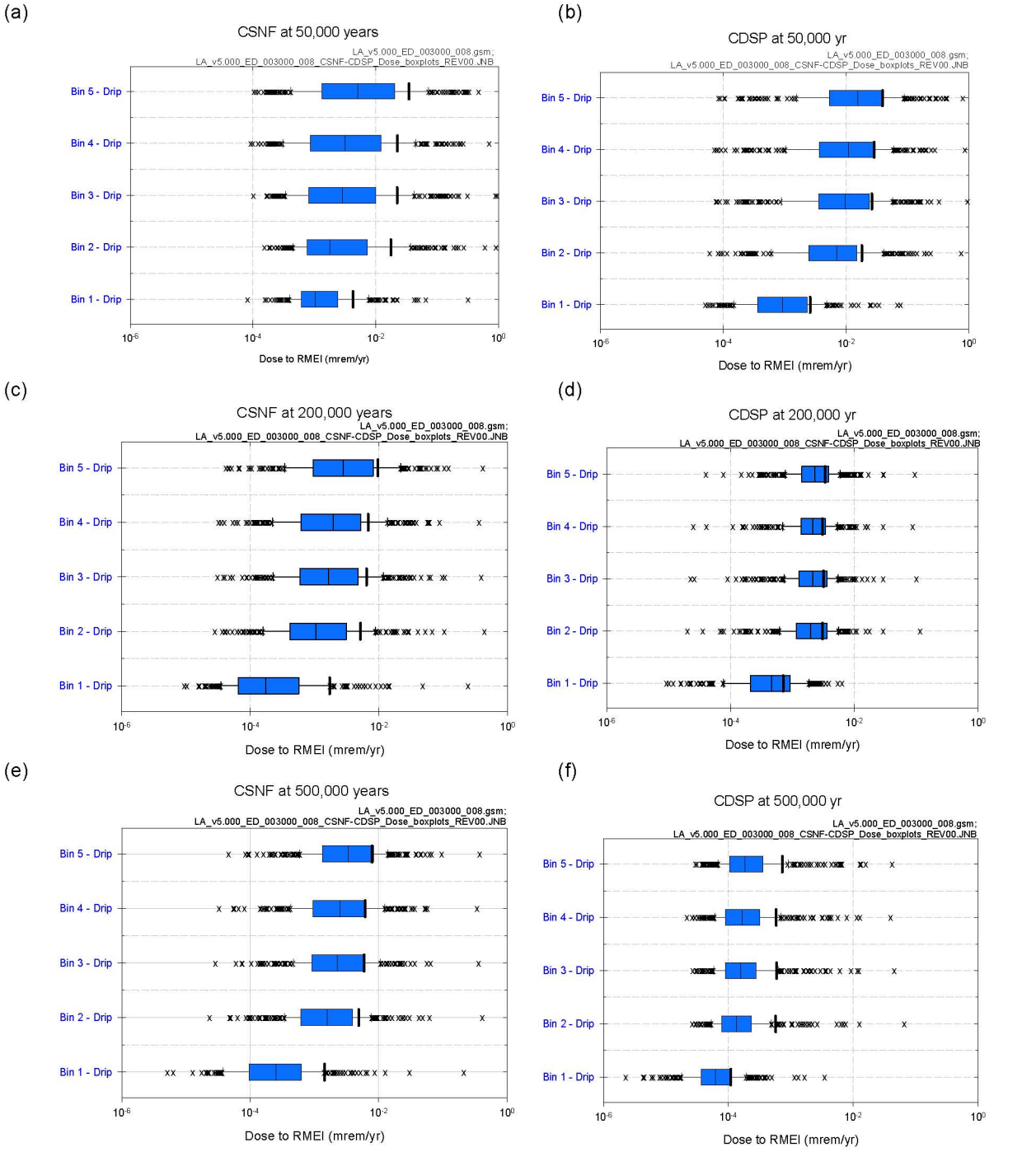

Source: Ouput DTNs: MO0709TSPAPLOT.000 [DIRS 183010]; and MO0709TSPAREGS.000 [DIRS 182976].

Figure J6.3-13. Box plots (see Figure J6.2-3 for description) summarizing results obtained with LHS of size *nLHS* = 300 showing epistemic uncertainty in doses $D_{ED}(\tau|[1, r, s, 1], \mathbf{e}_{Mi})$ for $\tau = 5 \times 10^4$, 2×10^5, 5×10^5 yr, $r = 1, 2$, $s = 1, 2, 3, 4, 5$, $t = 1$, and $i = 1, 2, \ldots, nLHS = 300$: (a, c, e) CSNF WPs at 5×10^4, 2×10^5, 5×10^5 yr, and (b, d, f) CDSP WPs at 5×10^4, 2×10^5, 5×10^5 yr.

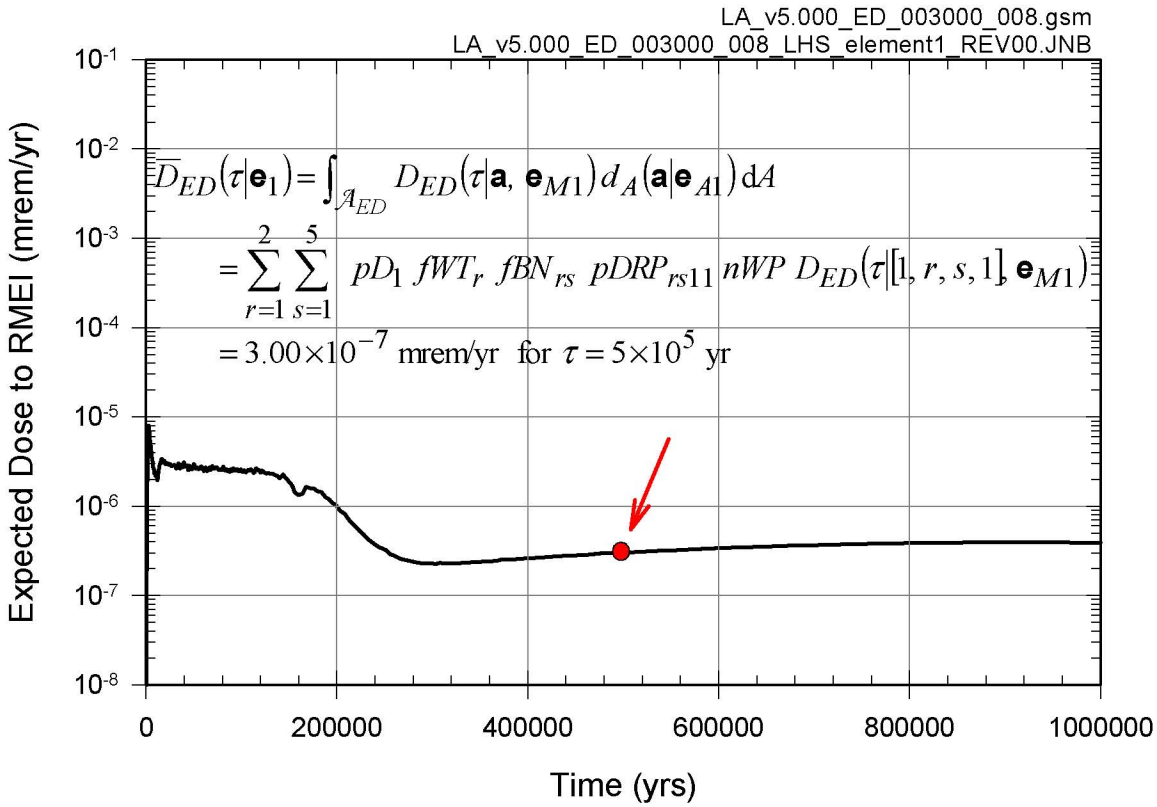

Source: Ouput DTNs: MO0709TSPAPLOT.000 [DIRS 183010]; and MO0709TSPAREGS.000 [DIRS 182976].

Figure J6.3-14. Estimate of $\bar{D}_{ED}(\tau|\mathbf{e}_1)$ for LHS element $\mathbf{e}_1 = [\mathbf{e}_{A1}, \mathbf{e}_{M1}]$ and $0 \leq \tau \leq 10^6$ yr with integration-based procedure indicated in EquationJ6.2-2.

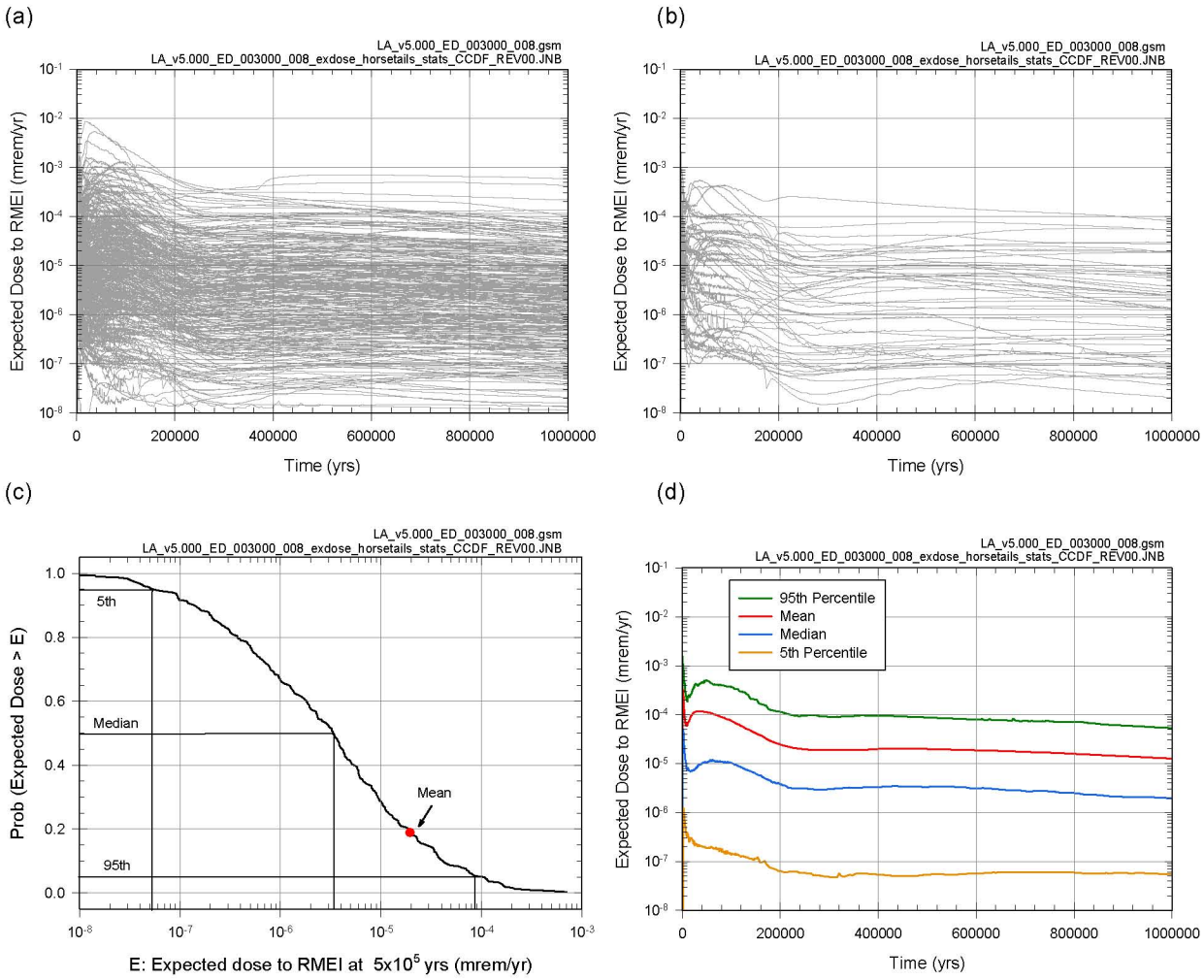

Source: Ouput DTNs: MO0709TSPAPLOT.000 [DIRS 183010]; and MO0709TSPAREGS.000 [DIRS 182976].

Figure J6.3-15. Estimate obtained with LHS of size *nLHS* = 300 showing epistemic uncertainty in expected dose $\bar{D}_{ED}(\tau|\mathbf{e})$ to RMEI for $0 \le \tau \le 10^6$ yr that results when only early DS failure is considered: (a) expected dose $\bar{D}_{ED}(\tau|\mathbf{e}_i)$, i = 1, 2, ..., *nLHS* = 300, (b) expected dose $\bar{D}_{ED}(\tau|\mathbf{e}_i)$, i = 1, 2, ..., 50, (c) exceedance probabilities $p_E[D < \bar{D}_{ED}(\tau|\mathbf{e})]$ and quantiles $Q_q[\bar{D}_{ED}(\tau|\mathbf{e})]$, q = 0.05, 0.5 and 0.95, for $\tau = 5 \times 10^5$ yr, and (d) expected (mean) dose $\bar{\bar{D}}_{ED}(\tau)$ and quantiles $Q_q[\bar{D}_{ED}(\tau|\mathbf{e})]$, q = 0.05, 0.5, 0.95.

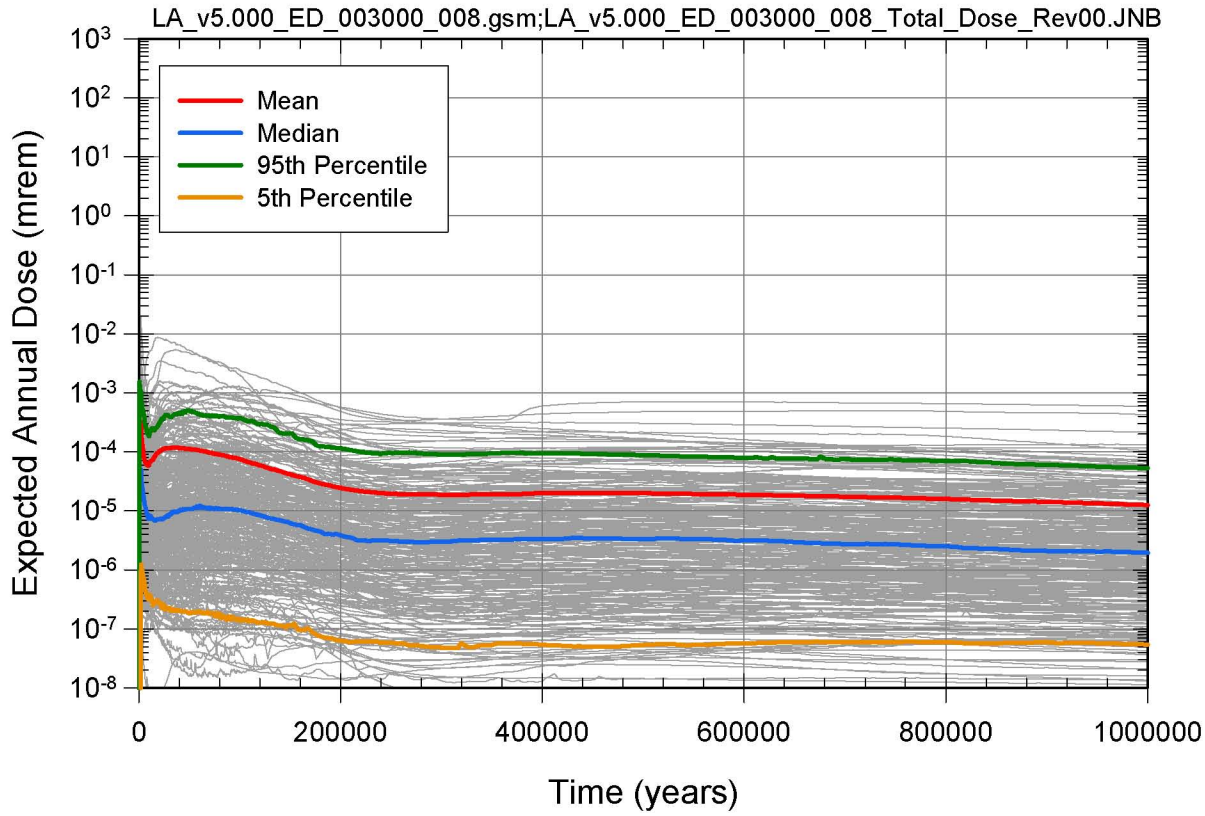

Source: Ouput DTNs: MO0709TSPAPLOT.000 [DIRS 183010]; and MO0709TSPAREGS.000 [DIRS 182976].

Figure J6.3-16. Summary of results obtained with LHS of size *nLHS* = 300 showing epistemic uncertainty in expected dose $\bar{D}_{ED}(\tau|\mathbf{a})$ to RMEI for $0 \leq \tau \leq 10^6$ yr that results when only early DS failure is considered.

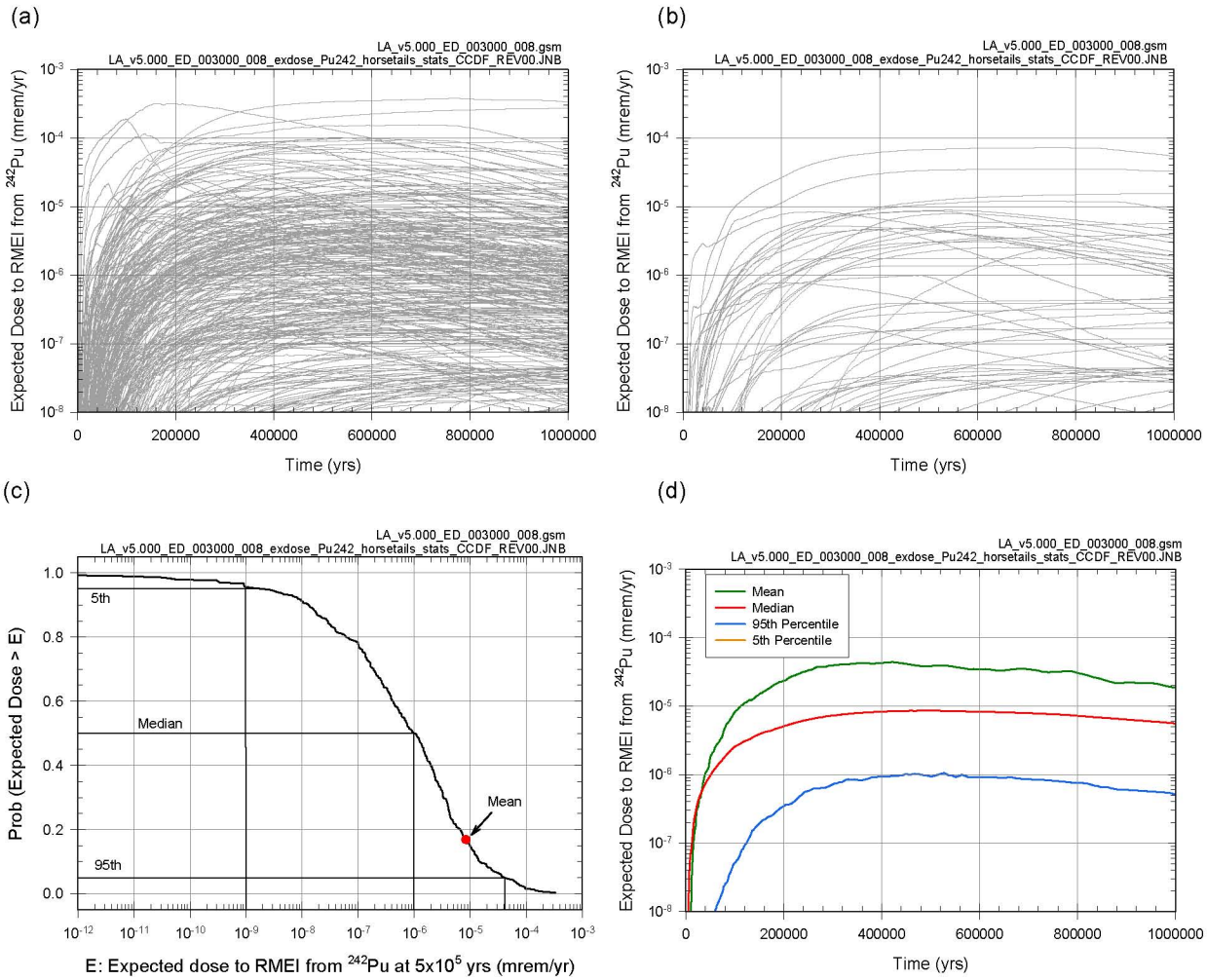

Source: Ouput DTNs: MO0709TSPAPLOT.000 [DIRS 183010]; and MO0709TSPAREGS.000 [DIRS 182976].

Figure J6.3-17. Estimate obtained with LHS of size *nLHS* = 300 showing epistemic uncertainty in expected dose $\bar{D}_{ED,r}(\tau|\mathbf{e})$ to RMEI for $0 \le \tau \le 10^6$ yr with r corresponding to ^{242}Pu that results when only early DS failure is considered: (a) expected dose $\bar{D}_{ED,r}(\tau|\mathbf{e}_i)$, i = 1, 2, …, *nLHS* = 300, (b) expected dose $\bar{D}_{ED,r}(\tau|\mathbf{e}_i)$, i = 1, 2, …, 50, (c) exceedance probabilities $p_E[D < \bar{D}_{ED,r}(\tau|\mathbf{e})]$ and quantiles $Q_q[\bar{D}_{ED,r}(\tau|\mathbf{e})]$, q = 0.05, 0.5 and 0.95, for $\tau = 5 \times 10^5$ yr, and (d) expected (mean) dose $\bar{\bar{D}}_{ED,r}(\tau)$ and quantiles $Q_q[\bar{D}_{ED,r}(\tau|\mathbf{e})]$, q = 0.05, 0.5, 0.95.

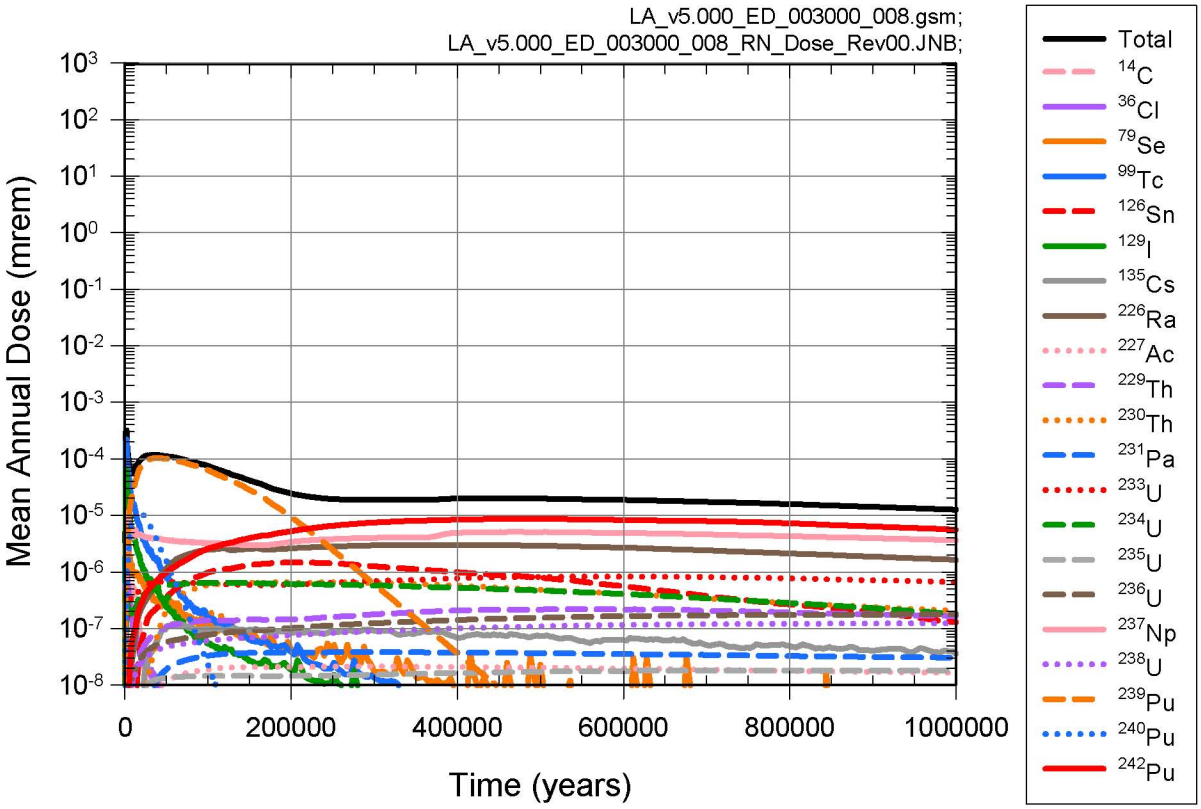

Source: Ouput DTNs: MO0709TSPAPLOT.000 [DIRS 183010]; and MO0709TSPAREGS.000 [DIRS 182976].

Figure J6.3-18. Estimates obtained with LHS of size *nLHS* = 300 of expected (mean) dose $\bar{\bar{D}}_{ED,r}(\tau)$ to RMEI for $0 \leq \tau \leq 10^6$ yr for individual radioactive species that result when only early DS failure is considered.

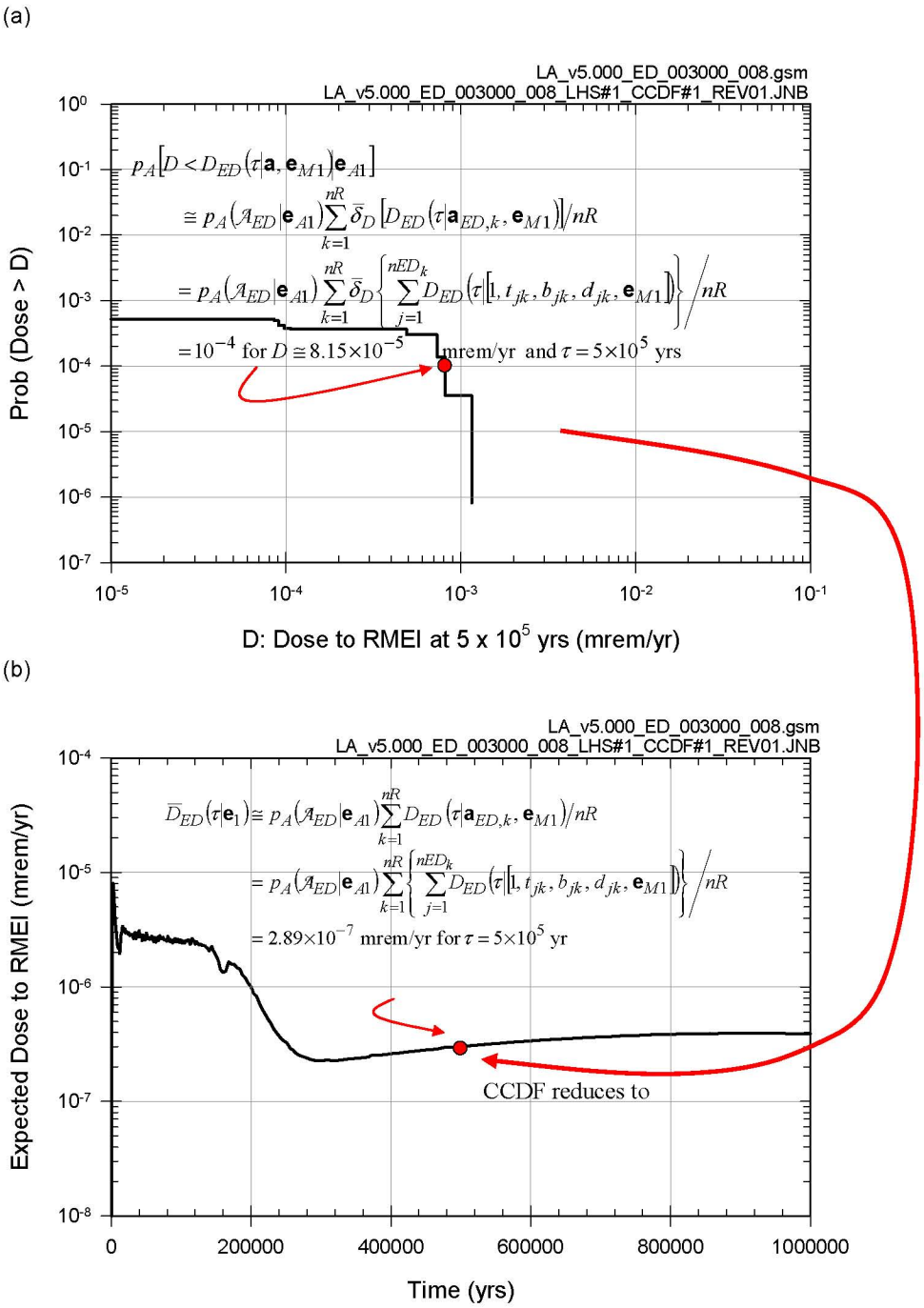

Source: Ouput DTNs: MO0709TSPAPLOT.000 [DIRS 183010]; and MO0709TSPAREGS.000 [DIRS 182976].

Figure J6.3-19. Results associated with $D_{ED}(\tau|\mathbf{a}_{ED}, \mathbf{e}_{M1})$ for LHS element $\mathbf{e}_1 = [\mathbf{e}_{A1}, \mathbf{e}_{M1}]$ obtained with sampling-based (Monte Carlo) procedures: (a) CCDF for $D_{ED}(5 \times 10^5 \text{ yr}|\mathbf{a}_{ED}, \mathbf{e}_{M1})$ with exceedance probabilities $p_A[D < D_{ED}(5 \times 10^5 \text{ yr}|\mathbf{a}, \mathbf{e}_{M1})|\mathbf{e}_{A1}]$ defined similarly to $p_A[D < D_{EW}(\tau|\mathbf{a}, \mathbf{e}_{M1})|\mathbf{e}_{A1}]$ in Equation (J6.2-12), and (b) expected dose $\bar{D}_{ED}(5 \times 10^5 \text{ yr}|\mathbf{e}_1)$ associated with $D_{ED}(5 \times 10^5 \text{ yr}|\mathbf{a}_{ED}, \mathbf{e}_1)$ defined similarly to $\bar{D}_{EW}(\tau|\mathbf{e}_1)$ in Equation (J6.2-10).

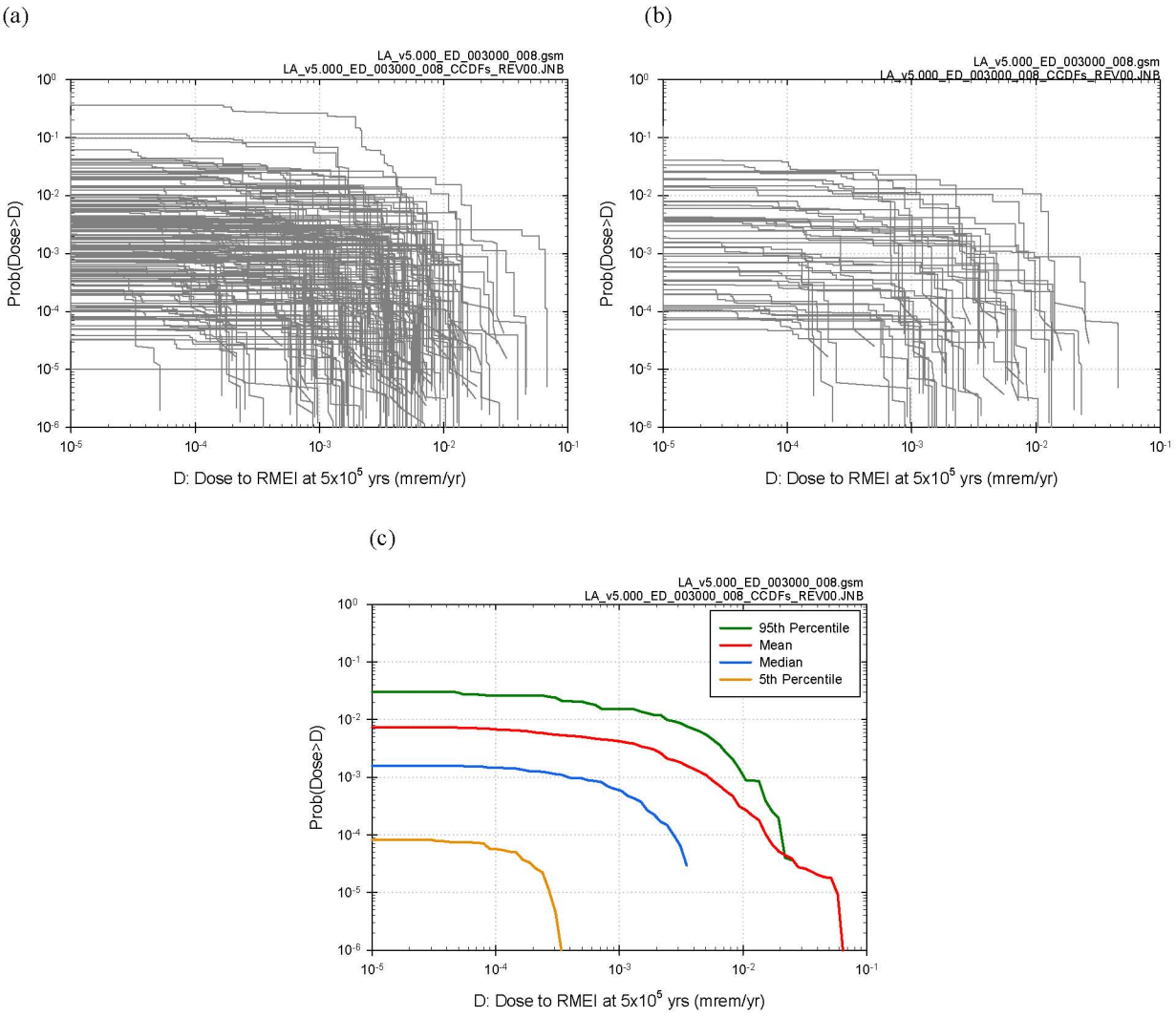

Source: Ouput DTNs: MO0709TSPAPLOT.000 [DIRS 183010]; and MO0709TSPAREGS.000 [DIRS 182976].

Figure J6.3-20. Results associated with $D_{ED}(5 \times 10^5 \text{ yr}|\mathbf{a}_{ED}, \mathbf{e}_M)$ obtained with sampling-based (Monte Carlo) procedures for an LHS of size $nLHS$ = 300: (a) CCDFs for $D_{ED}(5 \times 10^5 \text{ yr}|\mathbf{a}_{ED}, \mathbf{e}_{Mi})$ with exceedance probabilities $p_A[D < D_{ED}(5 \times 10^5 \text{ yr}|\mathbf{a}_{ED}, e_{Mi})|\mathbf{e}_{Ai}]$ defined similarly to $p_A[D < D_{EW}(\tau|\mathbf{a}, \mathbf{e}_{M1})|\mathbf{e}_{A1}]$ in Equation (J6.2-12) for i = 1, 2, …, $nLHS$ = 300, (b) CCDFs for $D_{ED}(10^4 \text{ yr}|\mathbf{a}_{ED}, \mathbf{e}_{Mi})$ with exceedance probabilities $p_A[D < D_{ED}(5 \times 10^5 \text{ yr}|\mathbf{a}_{ED}, e_{Mi})|\mathbf{e}_{Ai}]$ defined similarly to $p_A[D < D_{EW}(\tau|\mathbf{a}, \mathbf{e}_{M1})|\mathbf{e}_{A1}]$ in Equation (J6.2-12) for i = 1, 2, …, 50, and (c) expected (mean) CCDF and quantile curves, q = 0.05, 0.5, 0.95, for CCDFs in (a).

(a)

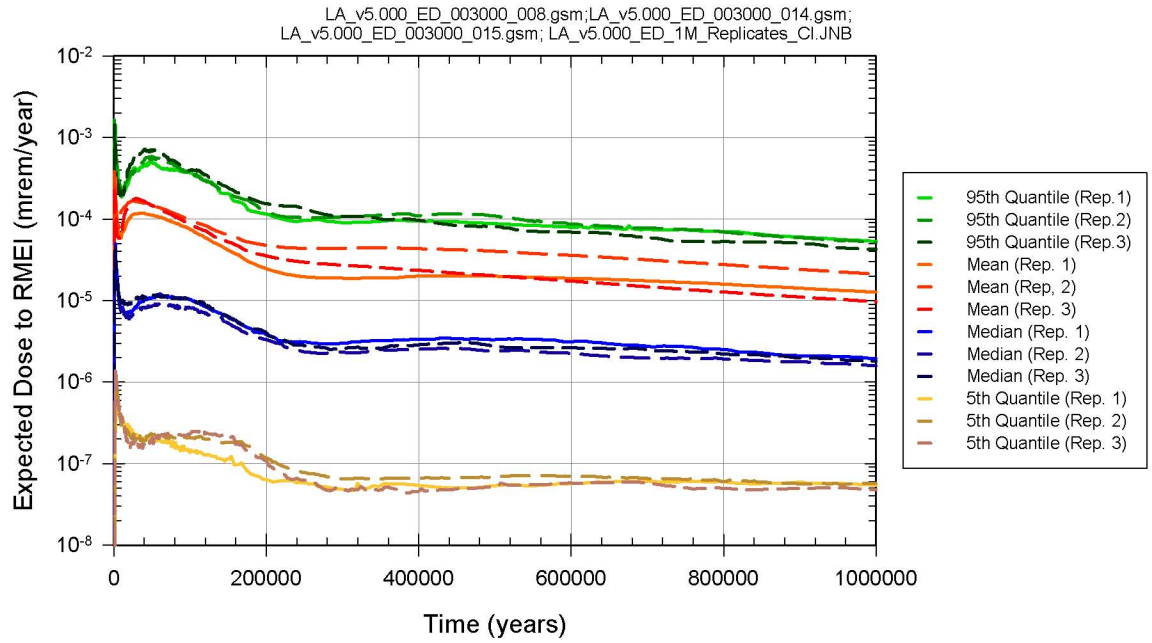

(b)

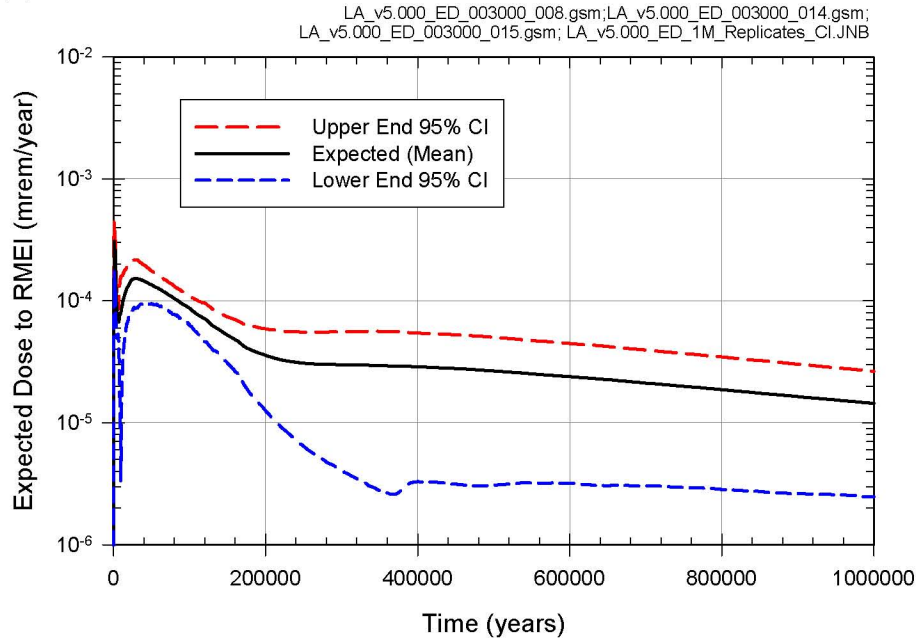

Source: Ouput DTNs: MO0709TSPAPLOT.000 [DIRS 183010]; MO0709TSPAREGS.000 [DIRS 182976]; and MO0709TSPASTAB.000 [DIRS 182983].

Figure J6.3-21. Assessment with replicated sampling of numerical error associated with use of an LHS of size *nLHS* = 300 to determine epistemic uncertainty in expected dose $\bar{D}_{ED}(\tau|\mathbf{e})$ to RMEI for $0 \leq \tau \leq 10^6$ yr that results when only early DS failure is considered: (a) Replicated estimates of expected (mean) dose $\bar{\bar{D}}_{ED}(\tau)$ and quantiles $Q_q[\bar{D}_{ED}(\tau|\mathbf{e})]$, q = 0.05, 0.5, 0.95, and (b) confidence intervals for estimates of expected (mean) dose $\bar{\bar{D}}_{ED}(\tau)$.

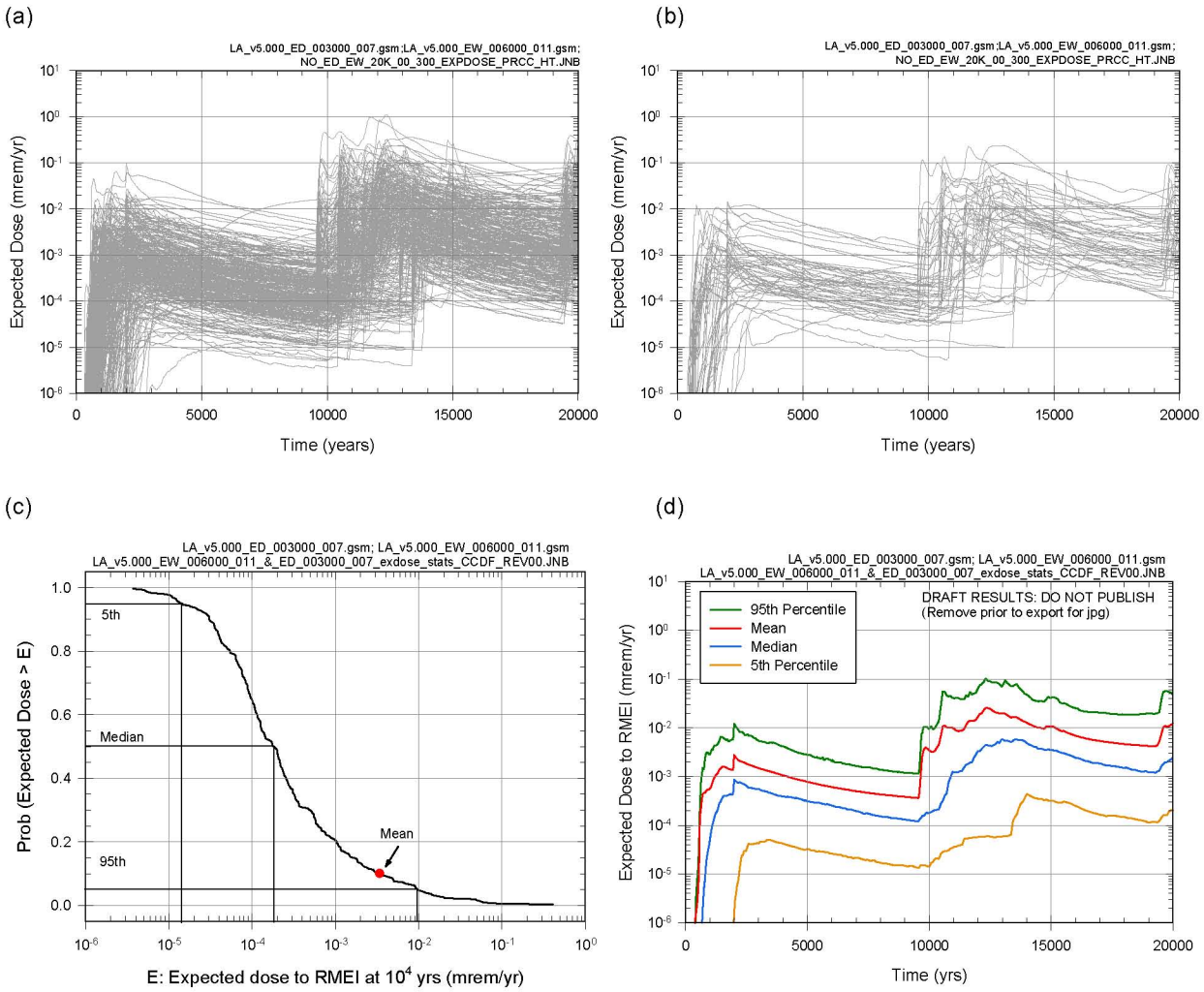

Source: Ouput DTNs: MO0709TSPAPLOT.000 [DIRS 183010]; and MO0709TSPAREGS.000 [DIRS 182976].

Figure J6.4-1. Estimate obtained with LHS of size *nLHS* = 300 showing epistemic uncertainty in expected dose $\bar{D}_E(\tau|\mathbf{e})$ to RMEI for $0 \le \tau \le 20{,}000$ yr that results when only early WP and early DS failures are considered: (a) expected dose $\bar{D}_E(\tau|\mathbf{e}_i)$, $i = 1, 2, \ldots, nLHS = 300$, (b) expected dose $\bar{D}_E(\tau|\mathbf{e}_i)$, $i = 1, 2, \ldots, 50$, (c) exceedance probabilities $p_E[D < \bar{D}_E(\tau|\mathbf{e})]$ and quantiles $Q_q[\bar{D}_E(\tau|\mathbf{e})]$, $q = 0.05, 0.5$ and 0.95, for $\tau = 10^4$ yr, and (d) expected (mean) dose $\bar{\bar{D}}_E(\tau)$ and quantiles $Q_q[\bar{D}_E(\tau|\mathbf{e})]$, $q = 0.05, 0.5, 0.95$.

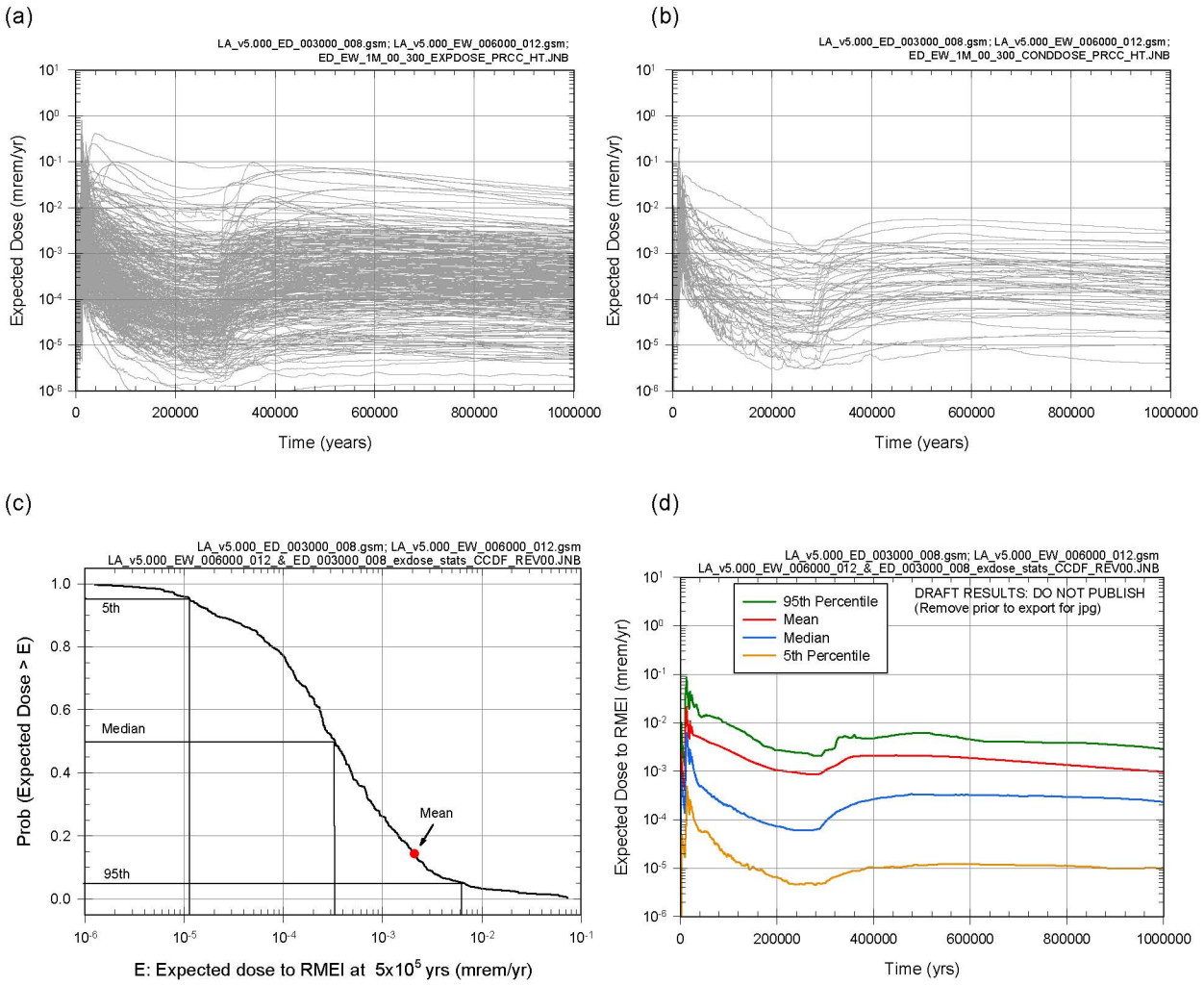

Source: Ouput DTNs: MO0709TSPAPLOT.000 [DIRS 183010]; and MO0709TSPAREGS.000 [DIRS 182976].

Figure J6.4-2. Estimate obtained with LHS of size *nLHS* = 300 showing epistemic uncertainty in expected dose $\bar{D}_E(\tau|\mathbf{e})$ to RMEI for $0 \le \tau \le 1{,}000{,}000$ yr that results when only early WP and early DS failures are considered: (a) expected dose $\bar{D}_E(\tau|\mathbf{e}_i)$, $i = 1, 2, \ldots, nLHS = 300$, (b) expected dose $\bar{D}_E(\tau|\mathbf{e}_i)$, $i = 1, 2, \ldots, 50$, (c) exceedance probabilities $p_E[D < \bar{D}_E(\tau|\mathbf{e})]$ and quantiles $Q_q[\bar{D}_E(\tau|\mathbf{e})]$, $q = 0.05, 0.5$ and 0.95, for $\tau = 500{,}000$ yr, and (d) expected (mean) dose $\bar{\bar{D}}_E(\tau)$ and quantiles $Q_q[\bar{D}_E(\tau|\mathbf{e})]$, $q = 0.05, 0.5, 0.95$.

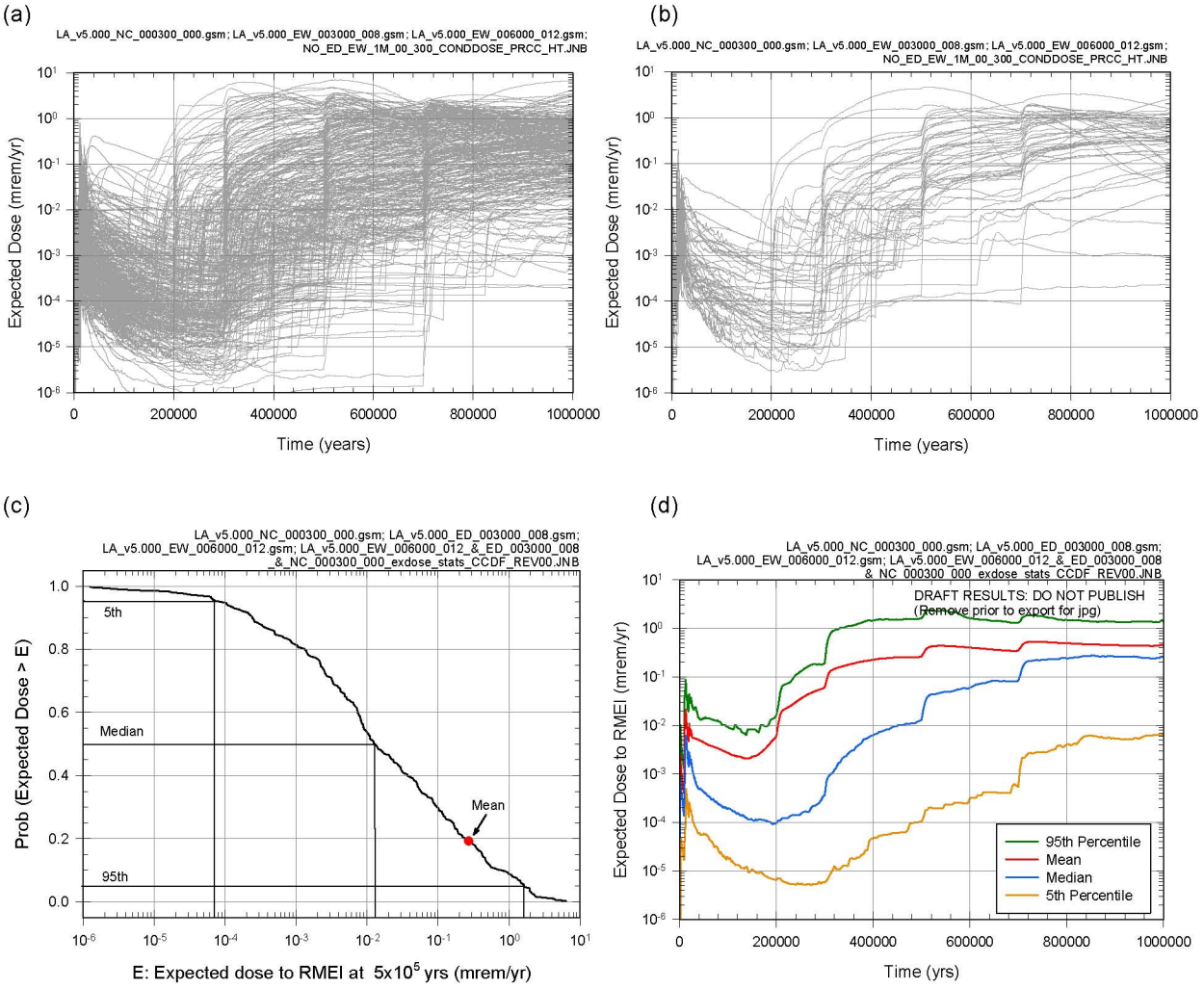

Source: Ouput DTNs: MO0709TSPAPLOT.000 [DIRS 183010]; and MO0709TSPAREGS.000 [DIRS 182976].

Figure J6.4-3. Estimate obtained with LHS of size $nLHS$ = 300 showing epistemic uncertainty in expected dose $\bar{D}_{NE}(\tau|\mathbf{e})$ to RMEI for $0 \le \tau \le 1{,}000{,}000$ yr that results when only nominal process failures and early WP and early DS failures are considered: (a) expected dose $\bar{D}_{NE}(\tau|\mathbf{e}_i)$, i = 1, 2, …, $nLHS$ = 300, (b) expected dose $\bar{D}_{NE}(\tau|\mathbf{e}_i)$, i = 1, 2, …, 50, (c) exceedance probabilities $p_E[D < \bar{D}_{NE}(\tau|\mathbf{e})]$ and quantiles $Q_q[\bar{D}_{NE}(\tau|\mathbf{e})]$, q = 0.05, 0.5 and 0.95, for τ = 500,000 yr, and (d) expected (mean) dose $\bar{\bar{D}}_{NE}(\tau)$ and quantiles $Q_q[\bar{D}_{NE}(\tau|\mathbf{e})]$, q = 0.05, 0.5, 0.95.

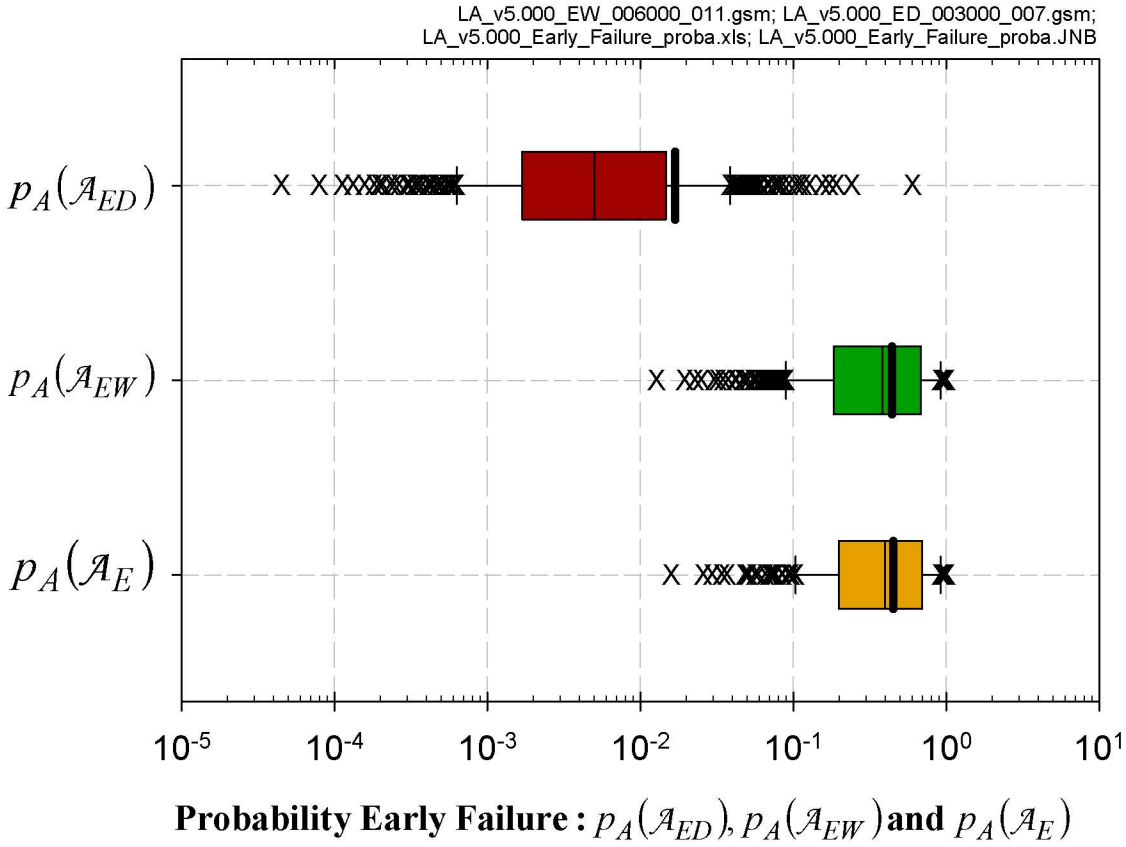

Source: Ouput DTNs: MO0709TSPAPLOT.000 [DIRS 183010]; and MO0709TSPAREGS.000 [DIRS 182976].

Figure J6.5-1. Box plots (see Figure J6.2-3 for description) summarizing probabilities $p_A(\mathcal{A}_{ED}|\mathbf{e}_{Ai})$, $p_A(\mathcal{A}_{EW}|\mathbf{e}_{Ai})$ and $p_A(\mathcal{A}_E|\mathbf{e}_{Ai})$ for scenario classes $\mathcal{A}_{ED}$, $\mathcal{A}_{EW}$ and $\mathcal{A}_E$ obtained with LHS of size *nLHS* = 300.

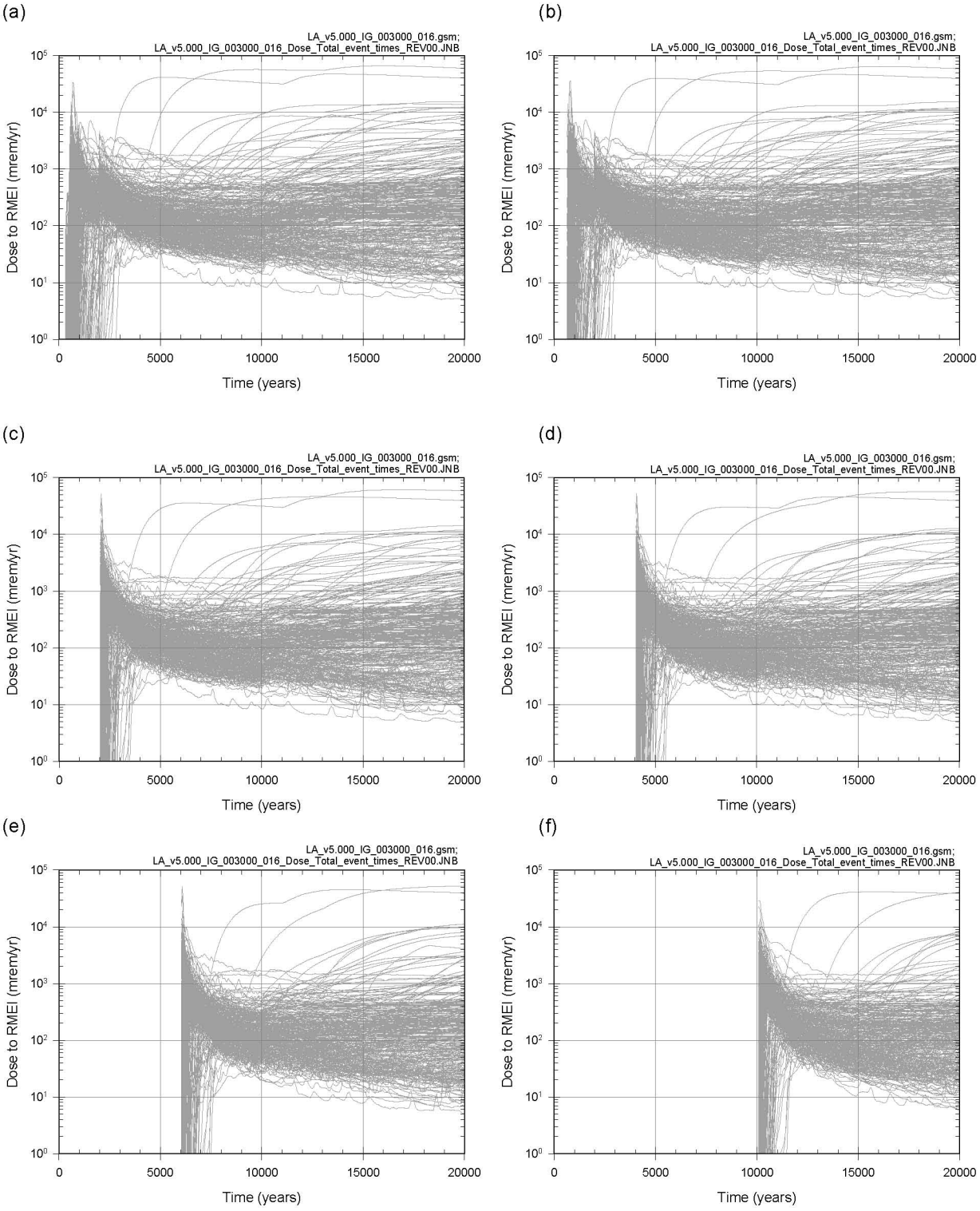

Source: Ouput DTNs: MO0709TSPAPLOT.000 [DIRS 183010]; and MO0709TSPAREGS.000 [DIRS 182976].

Figure J7.2-1. Dose to RMEI $D_{II}(\tau|[1, t_k, nWP], \mathbf{e}_{Mi})$ from igneous intrusive events at times t_k = 10, 600, 2000, 4000, 6000 and 10,000 yr for i = 1, 2, …, $nLHS$ = 300: (a) 10 yr, (b) 600 yr, (c) 2000 yr, (d) 4000 yr, (e) 6000 yr, and (f) 10,000 yr.

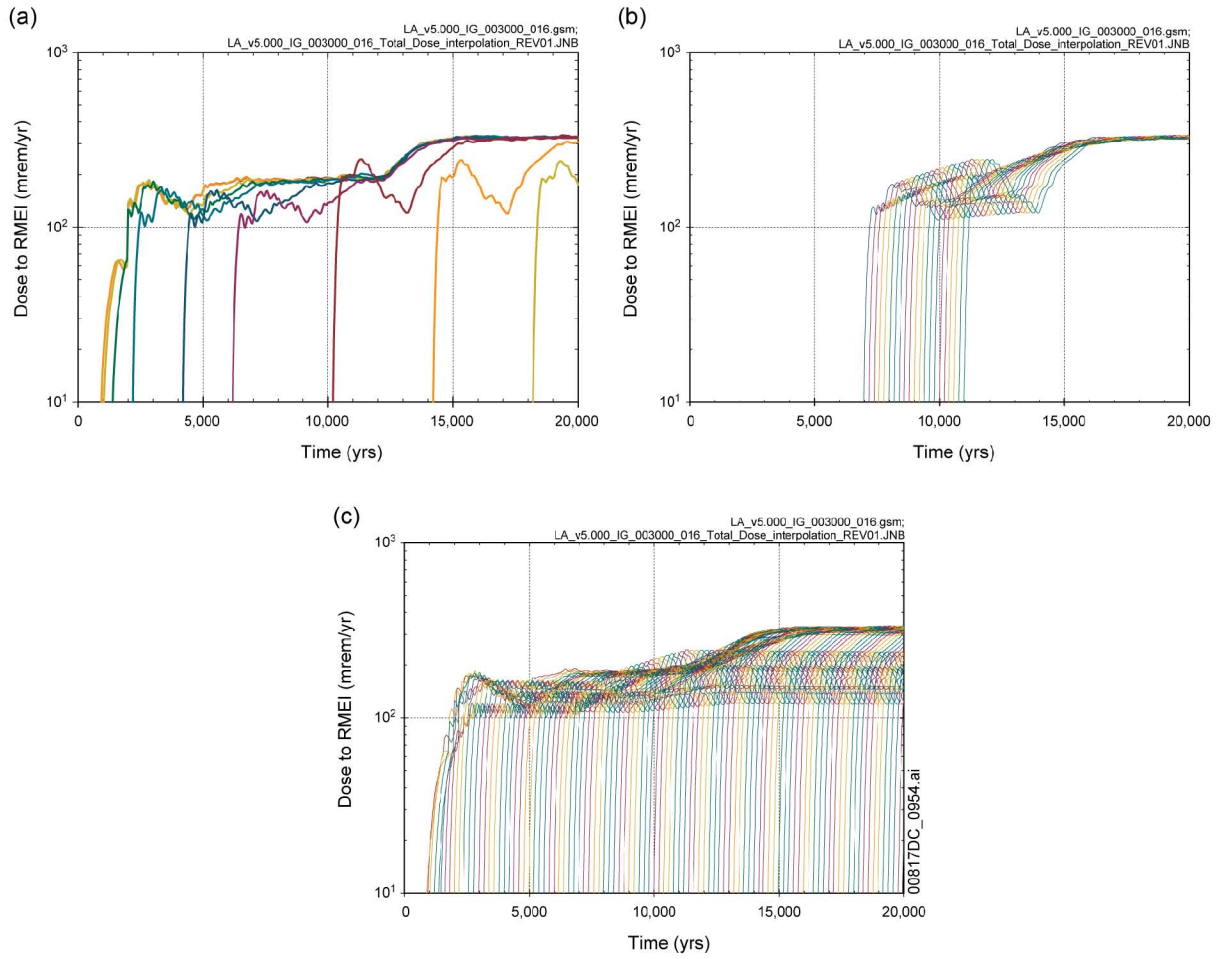

Source: Ouput DTNs: MO0709TSPAPLOT.000 [DIRS 183010]; and MO0709TSPAREGS.000 [DIRS 182976].

Figure J7.2-2. Illustration of interpolation procedure used to obtain estimated doses $\hat{D}_{ll}(\tau|[1, \hat{t}_k, nWP], \mathbf{e}_{M1})$ from calculated doses $D_{ll}(\tau|[1, t_k, nWP], \mathbf{e}_{M1})$ indicated in Equation J7.2-18 for LHS element $\mathbf{e}_1 = [\mathbf{e}_{A1}, \mathbf{e}_{M1}]$ and the time interval [0, 2.0×10^4 yr]: (a) $D_{ll}(\tau|[1, t_k, nWP], \mathbf{e}_{M1})$, $k = 1, 2, \ldots, 10$, (b) interpolated values $\hat{D}_{ll}(\tau|[1, \hat{t}_k, nWP], \mathbf{e}_{M1})$ for $\hat{t}_k$ between $t_7 = 6000$ and $t_{8+1} = 10{,}000$, and (c) interpolated values $\hat{D}_{ll}(\tau|[1, \hat{t}_k, nWP], \mathbf{e}_{M1})$ for $\hat{t}_k$ between 10 yr and 2.0×10^4 yr.

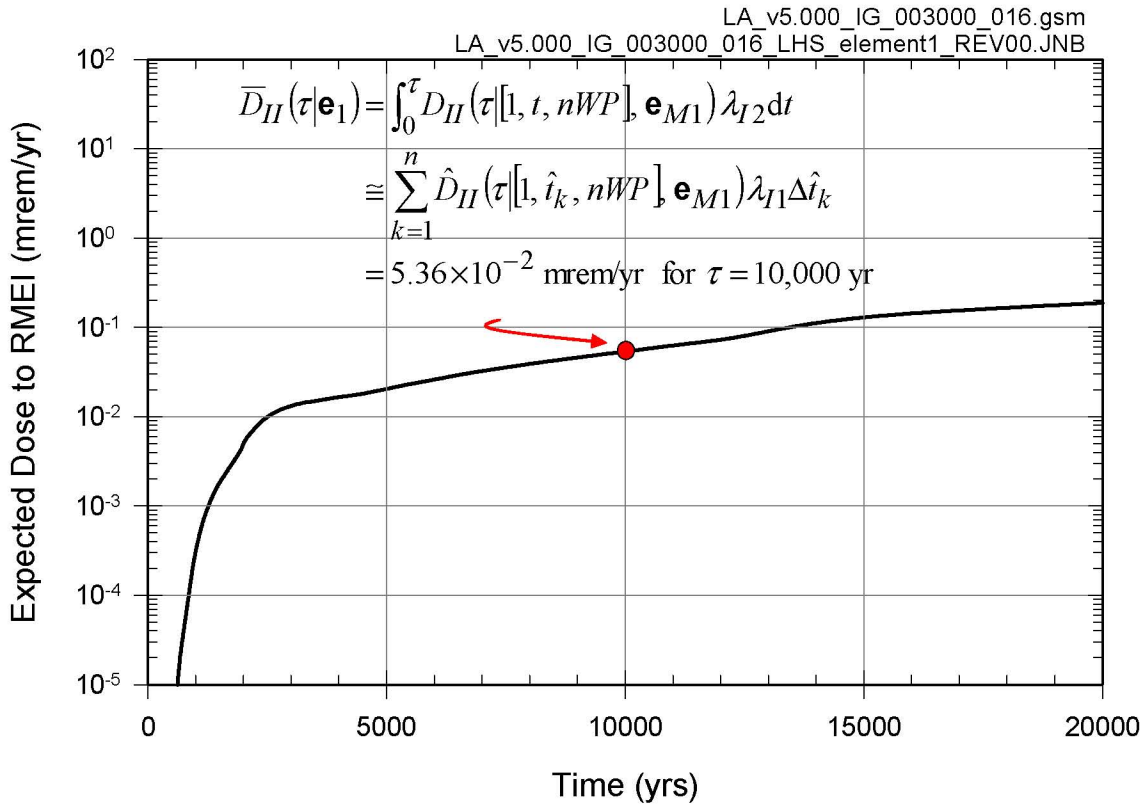

Source: Ouput DTNs: MO0709TSPAPLOT.000 [DIRS 183010]; and MO0709TSPAREGS.000 [DIRS 182976].

Figure J7.2-3. Determination of $\overline{D}_{II}(\tau|\mathbf{e}_1)$ as indicated in conjunction with Equations J7.2-7, J7.2-9 and J7.2-19 from calculated doses $D_{II}(\tau|[1, t_k, nWP], \mathbf{e}_{M1})$ shown in Equation J7.2-18 for LHS element $\mathbf{e}_1 = [\mathbf{e}_{A1}, \mathbf{e}_{M1}]$ and the time interval $[0, 2.0 \times 10^4$ yr].

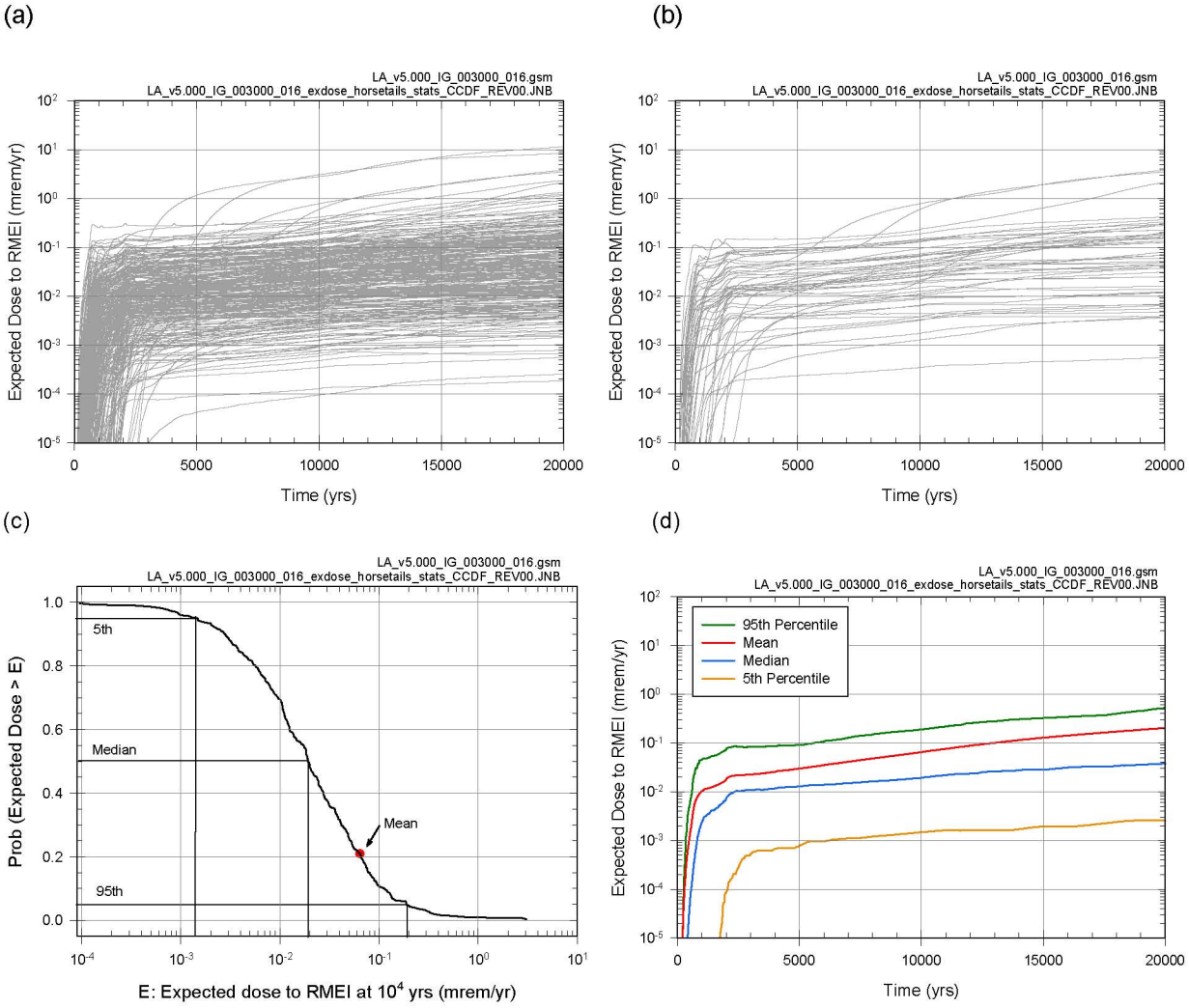

Source: Ouput DTNs: MO0709TSPAPLOT.000 [DIRS 183010]; and MO0709TSPAREGS.000 [DIRS 182976].

Figure J7.2-4. Estimate obtained with LHS of size *nLHS* = 300 showing epistemic uncertainty in expected dose $\bar{D}_{II}(\tau|\mathbf{e})$ to RMEI for $0 \le \tau \le 20{,}000$ yr that results when only igneous intrusion events are considered: (a) expected dose $\bar{D}_{II}(\tau|\mathbf{e}_i)$, $i = 1, 2, \ldots, nLHS = 300$, (b) expected dose $\bar{D}_{II}(\tau|\mathbf{e}_i)$, $i = 1, 2, \ldots, 50$, (c) exceedance probabilities $p_E[D < \bar{D}_{II}(\tau|\mathbf{e})]$ and quantiles $Q_q[\bar{D}_{II}(\tau|\mathbf{e})]$, $q = 0.05$, 0.5 and 0.95, for $\tau = 10^4$ yr, and (d) expected (mean) dose $\bar{D}_{II}(\tau)$ and quantiles $Q_q[\bar{D}_{II}(\tau|\mathbf{e})]$, $q = 0.05, 0.5, 0.95$.

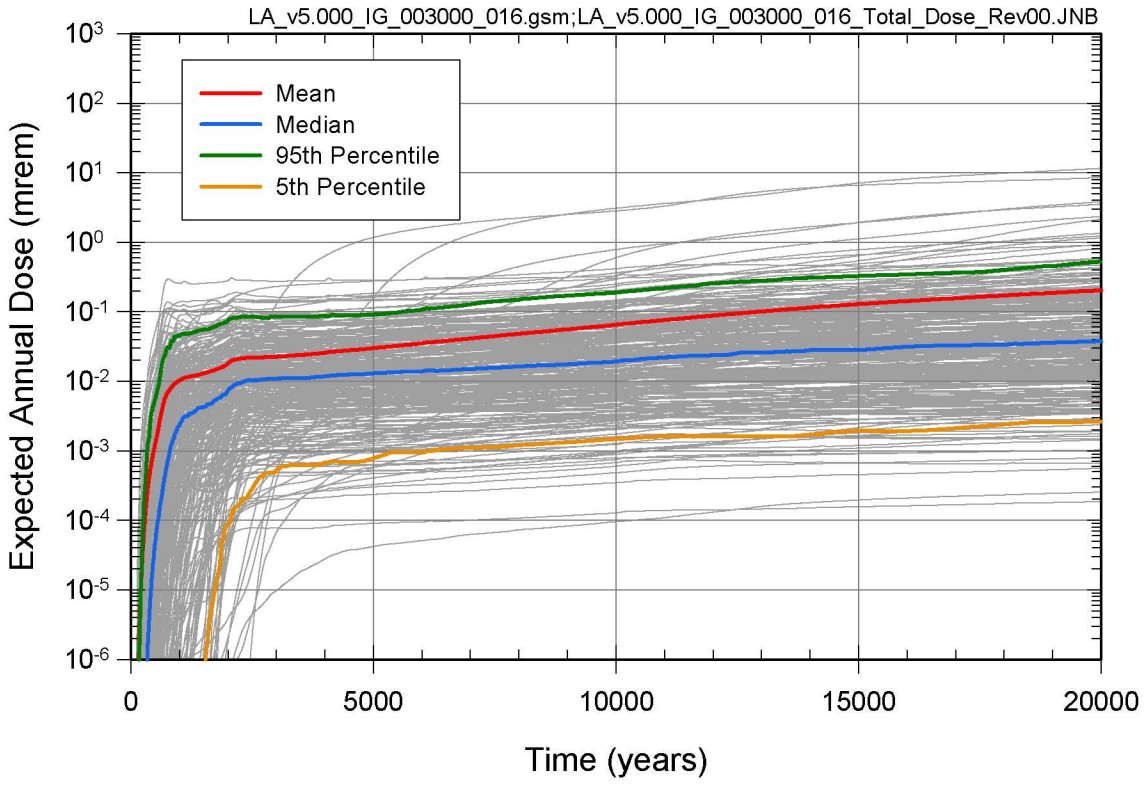

Source: Ouput DTNs: MO0709TSPAPLOT.000 [DIRS 183010]; and MO0709TSPAREGS.000 [DIRS 182976].

Figure J7.2-5. Summary presentation of epistemic uncertainty in expected dose $\bar{D}_{II}(\tau|\mathbf{e})$ to RMEI that results when only igneous intrusion is considered for $0 \leq \tau \leq 2.0 \times 10^4$ yr.

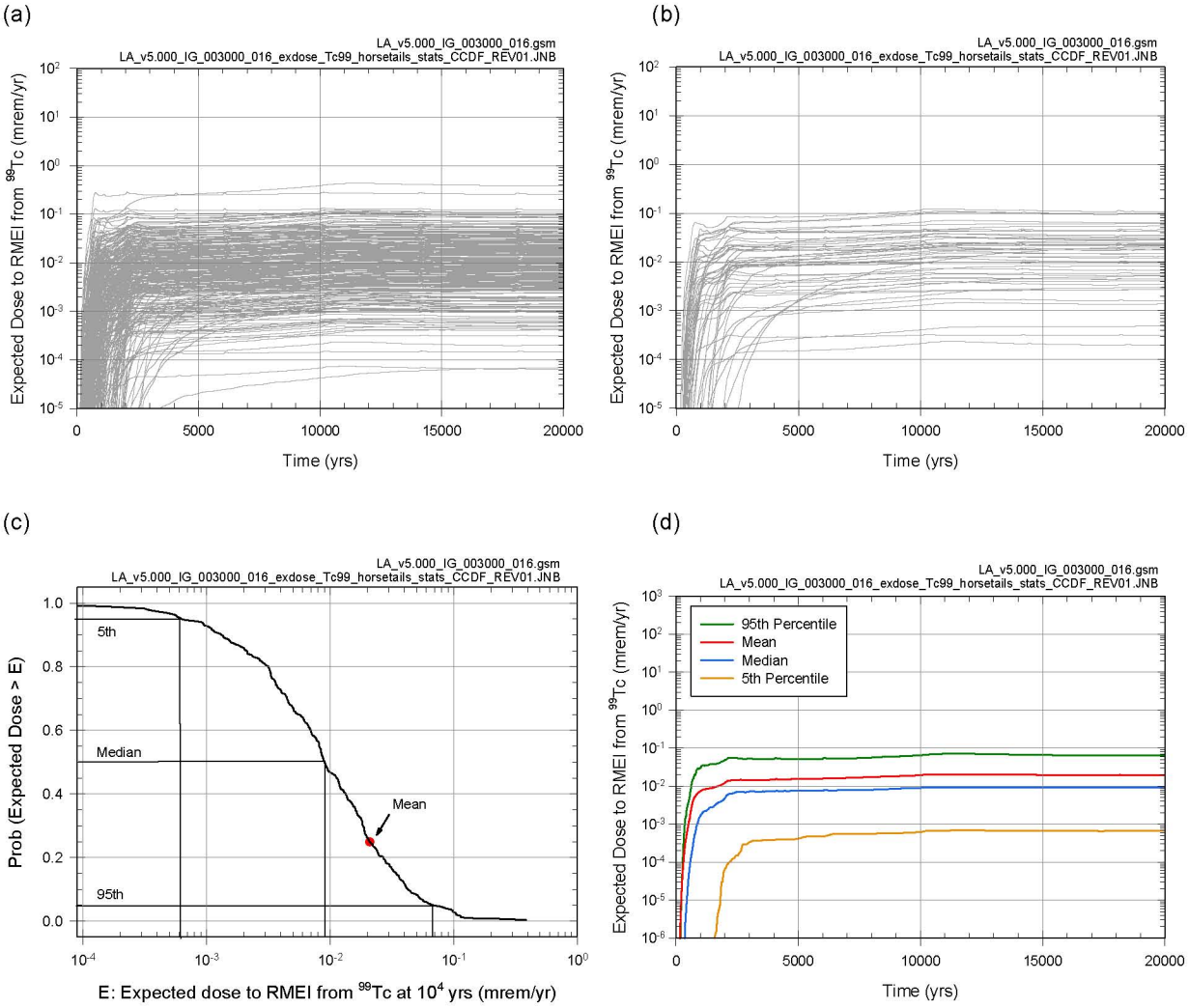

Source: Ouput DTNs: MO0709TSPAPLOT.000 [DIRS 183010]; and MO0709TSPAREGS.000 [DIRS 182976].

Figure J7.2-6. Estimate obtained with LHS of size $nLHS$ = 300 showing epistemic uncertainty in expected dose $\bar{D}_{II,r}(\tau|\mathbf{e})$ to RMEI for $0 \le \tau \le 20{,}000$ yr with r corresponding to ^{99}Tc that results when only igneous intrusive events are considered: (a) expected dose $\bar{D}_{II,r}(\tau|\mathbf{e}_i)$, i = 1, 2, …, $nLHS$ = 300, (b) expected dose $\bar{D}_{II,r}(\tau|\mathbf{e}_i)$, i = 1, 2, …, 50, (c) exceedance probabilities $p_E[D < \bar{D}_{II,r}(\tau|\mathbf{e})]$ and quantiles $Q_q[\bar{D}_{II,r}(\tau|\mathbf{e})]$, q = 0.05, 0.5 and 0.95, for $\tau = 10^4$ yr, and (d) expected (mean) dose $\bar{\bar{D}}_{II,r}(\tau)$ and quantiles $Q_q[\bar{D}_{II,r}(\tau|\mathbf{e})]$, q = 0.05, 0.5, 0.95.

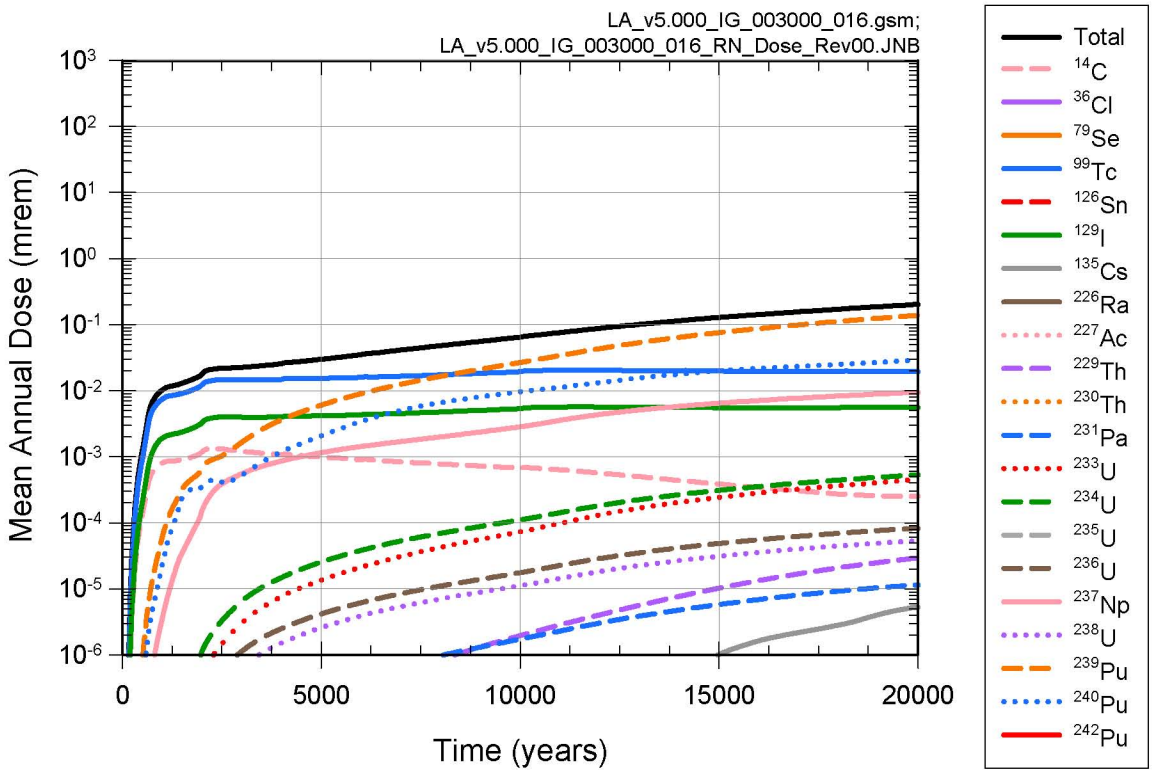

Source: Ouput DTNs: MO0709TSPAPLOT.000 [DIRS 183010]; and MO0709TSPAREGS.000 [DIRS 182976].

Figure J7.2-7. Estimates obtained with LHS of size *nLHS* = 300 of expected (mean) dose $\bar{\bar{D}}_{II,r}(\tau)$ to RMEI for $0 \leq \tau \leq 20{,}000$ yr for individual radioactive species that result when only igneous intrusive events are considered.

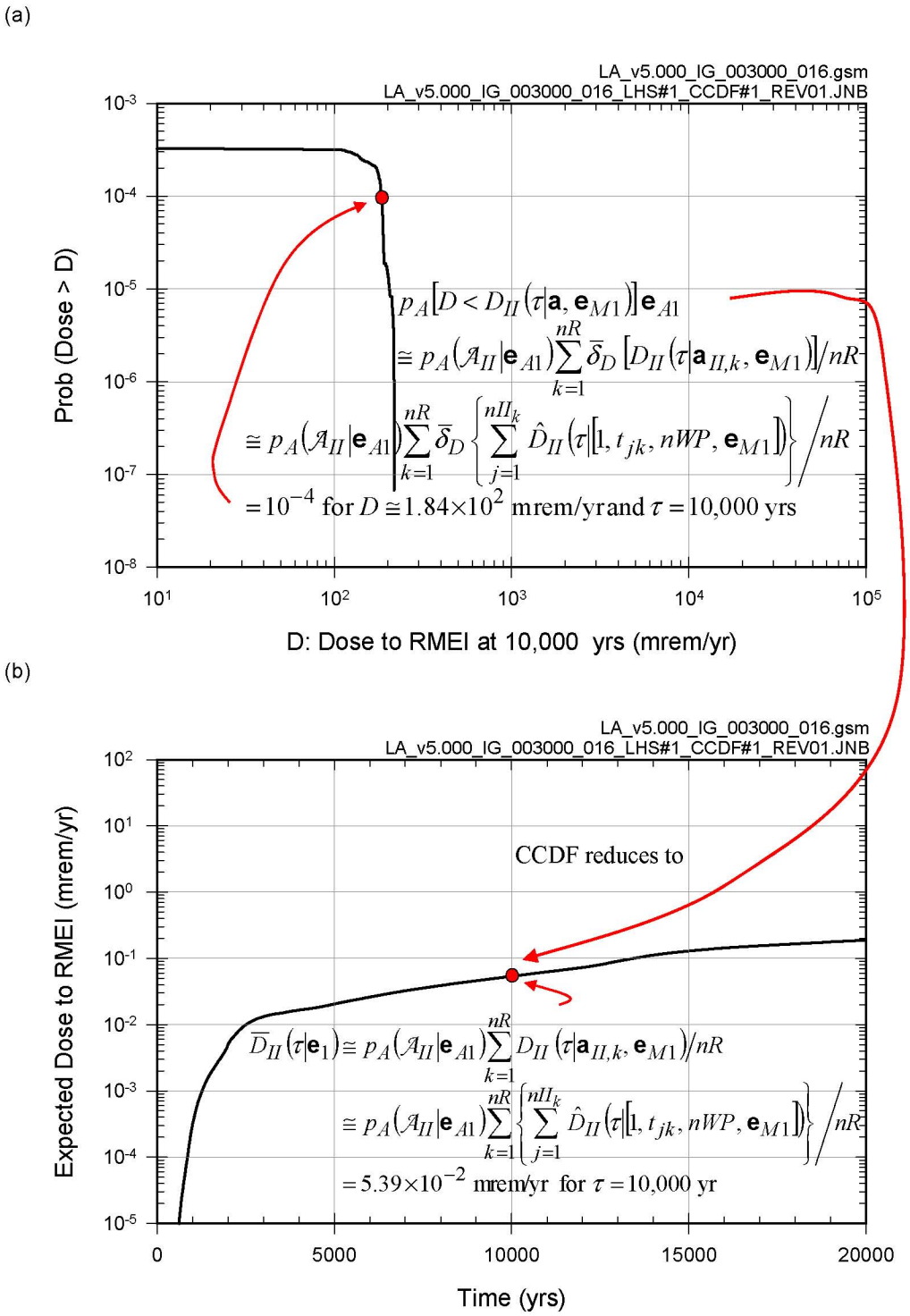

Source: Ouput DTNs: MO0709TSPAPLOT.000 [DIRS 183010]; and MO0709TSPAREGS.000 [DIRS 182976].

Figure J7.2-8. Results associated with $\bar{D}_{II}(\tau|\mathbf{e}_1)$ for LHS element $\mathbf{e}_1 = [\mathbf{e}_{A1}, \mathbf{e}_{M1}]$ obtained with sampling-based (Monte Carlo) procedures: (a) CCDF for $D_{II}(10^4 \text{ yr}|\mathbf{a}_{II}, \mathbf{e}_{M1})$ with exceedance probabilities $p_A[D < D_{II}(10^4 \text{ yr}|\mathbf{a}, \mathbf{e}_{M1})|\mathbf{e}_{A1}]$ defined in Equation J7.2-23, and (b) expected dose $\bar{D}_{II}(10^4 \text{ yr}|\mathbf{e}_1)$ associated with $D_{II}(10^4 \text{ yr}|\mathbf{a}_{II}, \mathbf{e}_{M1})$ as defined in Equation J7.2-21.

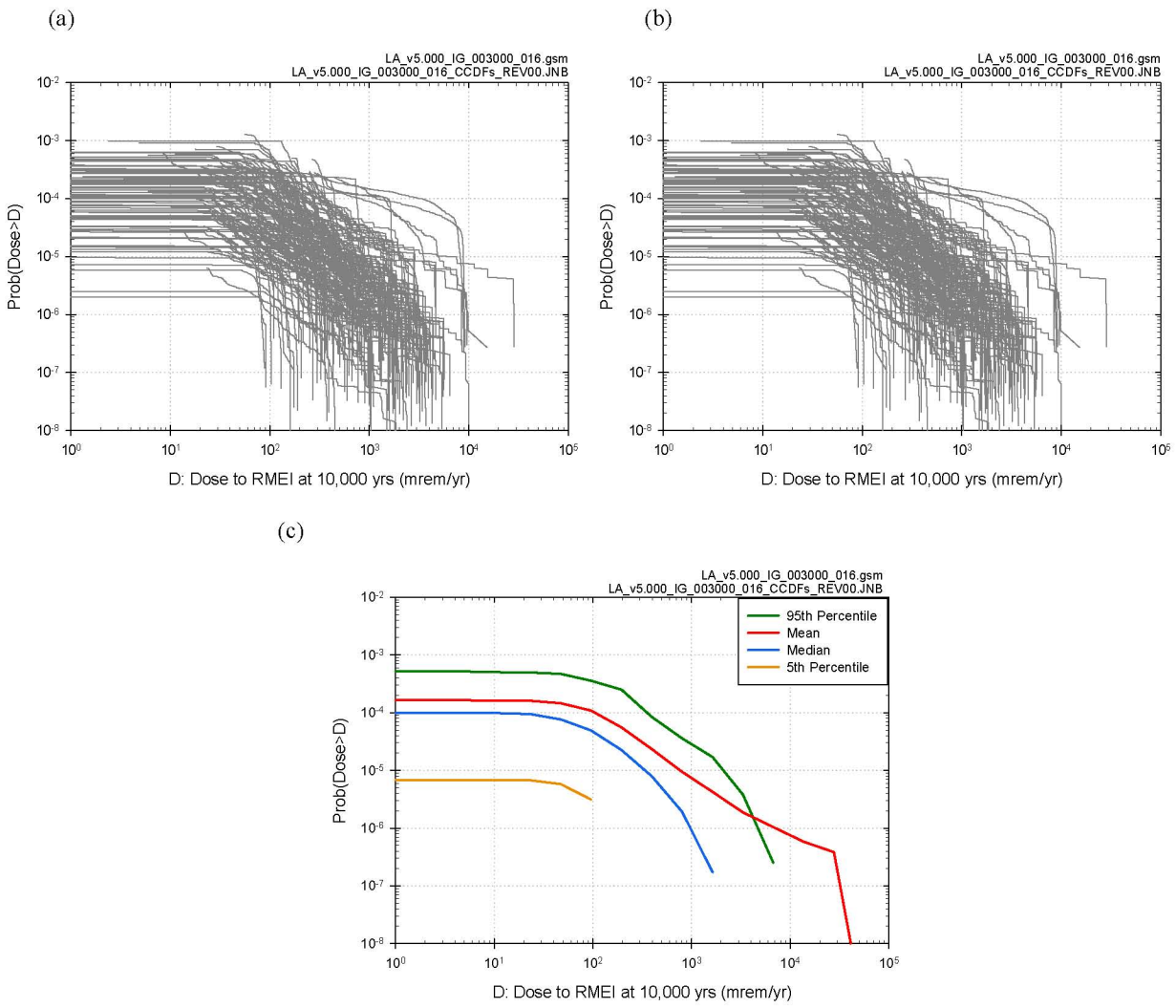

Source: Ouput DTNs: MO0709TSPAPLOT.000 [DIRS 183010]; and MO0709TSPAREGS.000 [DIRS 182976].

Figure J7.2-9. Results associated with $D_{II}(10^4 \text{ yr}|\mathbf{a}_{II}, \mathbf{e}_M)$ obtained with sampling-based (Monte Carlo) procedures for an LHS of size $nLHS = 300$: (a) CCDFs for $D_{II}(10^4 \text{ yr}|\mathbf{a}_{II}, \mathbf{e}_{Mi})$ with exceedance probabilities $p_A[D < D_{II}(10^4 \text{ yr}|\mathbf{a}, \mathbf{e}_{Mi})|\mathbf{e}_{Ai}]$ defined in Equation J7.2-23 for $i = 1, 2, \ldots, nLHS = 300$, (b) CCDFs for $D_{II}(10^4 \text{ yr}|\mathbf{a}_{II}, \mathbf{e}_{Mi})$ with exceedance probabilities $p_A[D < D_{II}(10^4 \text{ yr}|\mathbf{a}, \mathbf{e}_{Mi})|\mathbf{a}_{Ai}]$ defined in Equation J7.2-23 for $i = 1, 2, \ldots, 50$, and (c) expected (mean) CCDF and quantile curves, $q = 0.05, 0.5, 0.95$, for CCDFs in (a).

(a)

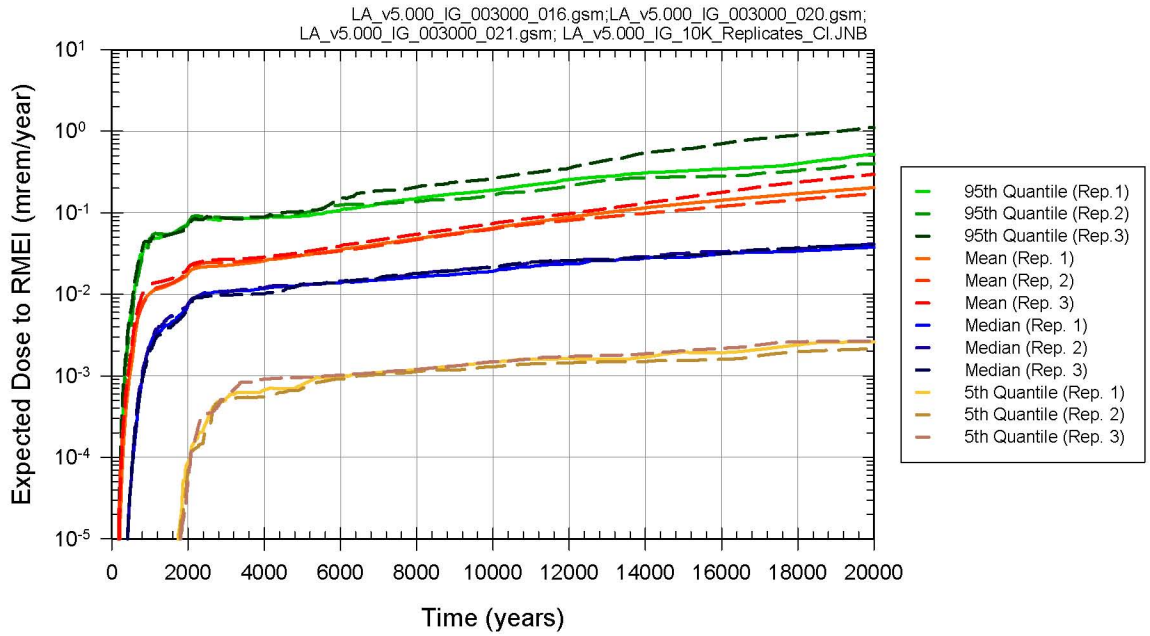

(b)

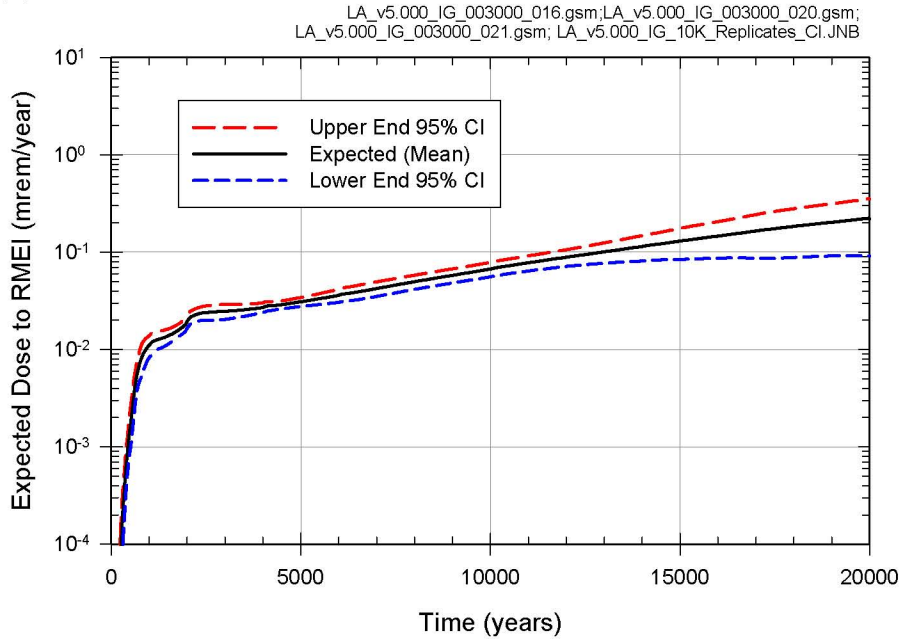

Source: Ouput DTNs: MO0709TSPAPLOT.000 [DIRS 183010]; MO0709TSPAREGS.000 [DIRS 182976]; and MO0709TSPASTAB.000 [DIRS 182983].

Figure J7.2-10. Assessment with replicated sampling of numerical error associated with use of an LHS of size *nLHS* = 300 to determine epistemic uncertainty in expected dose $\bar{D}_{II}(\tau|\mathbf{e})$ to RMEI for $0 \le \tau \le 20{,}000$ yr that results when only igneous intrusive events are considered: (a) Replicated estimates of expected (mean) dose $\bar{\bar{D}}_{II}(\tau)$ and quantiles $Q_q[\bar{D}_{II}(\tau|\mathbf{e})]$, q = 0.05, 0.5, 0.95, and (b) confidence intervals for estimates of expected (mean) dose $\bar{\bar{D}}_{II}(\tau)$.

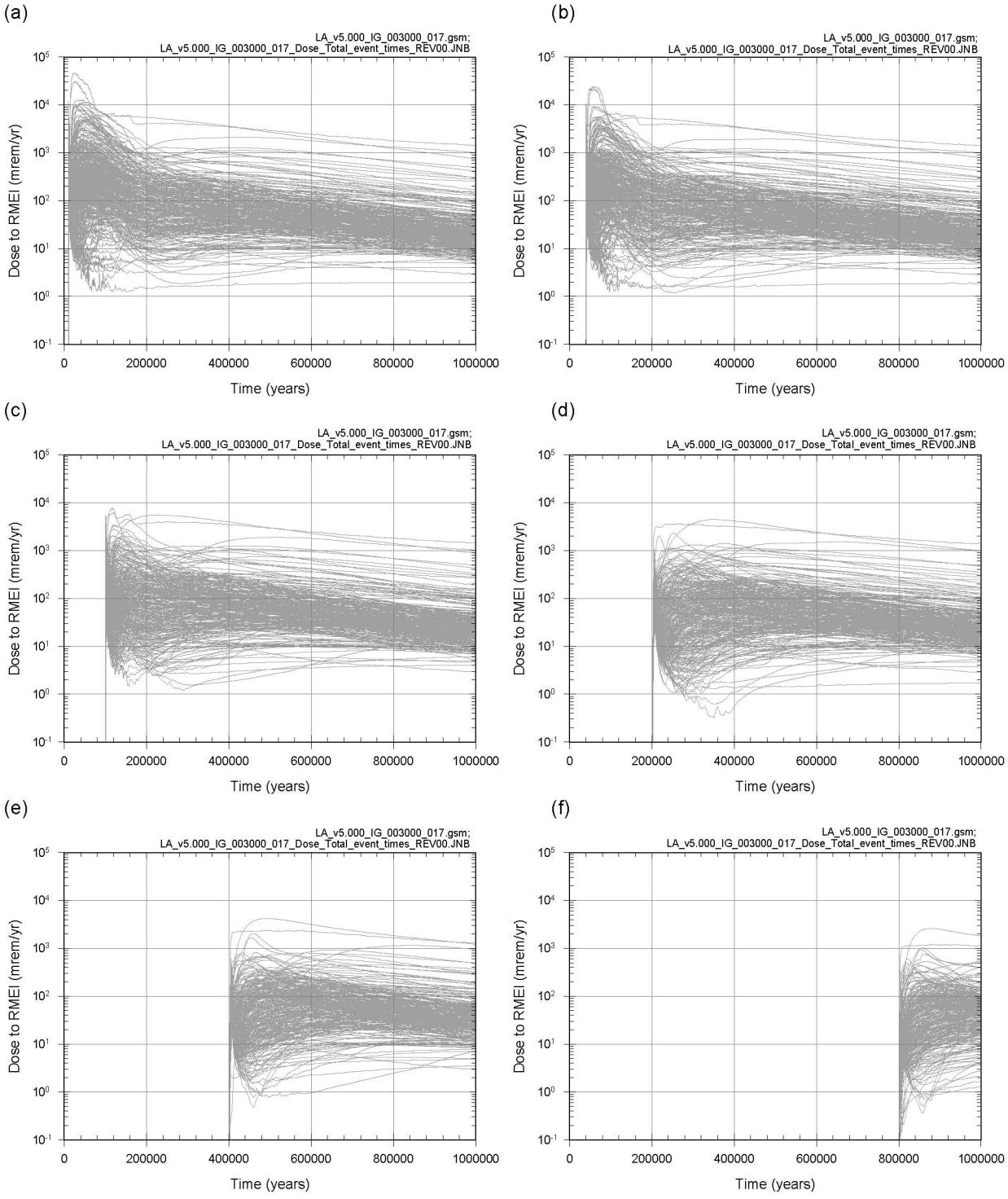

Source: Ouput DTNs: MO0709TSPAPLOT.000 [DIRS 183010]; and MO0709TSPAREGS.000 [DIRS 182976].

Figure J7.2-11. Dose to RMEI $D_{II}(\tau|[1, t_k, nWP], \mathbf{e}_{Mi})$ from igneous intrusive events at times t_k = 10,000, 40,000, 100,000, 200,000, 400,000 and 800,000 yr for i = 1, 2, …, $nLHS$ = 300: (a) 10,000 yr, (b) 40,000 yr, (c) 100,000 yr, (d) 200,000 yr, (e) 400,000 yr, and (f) 800,000 yr.

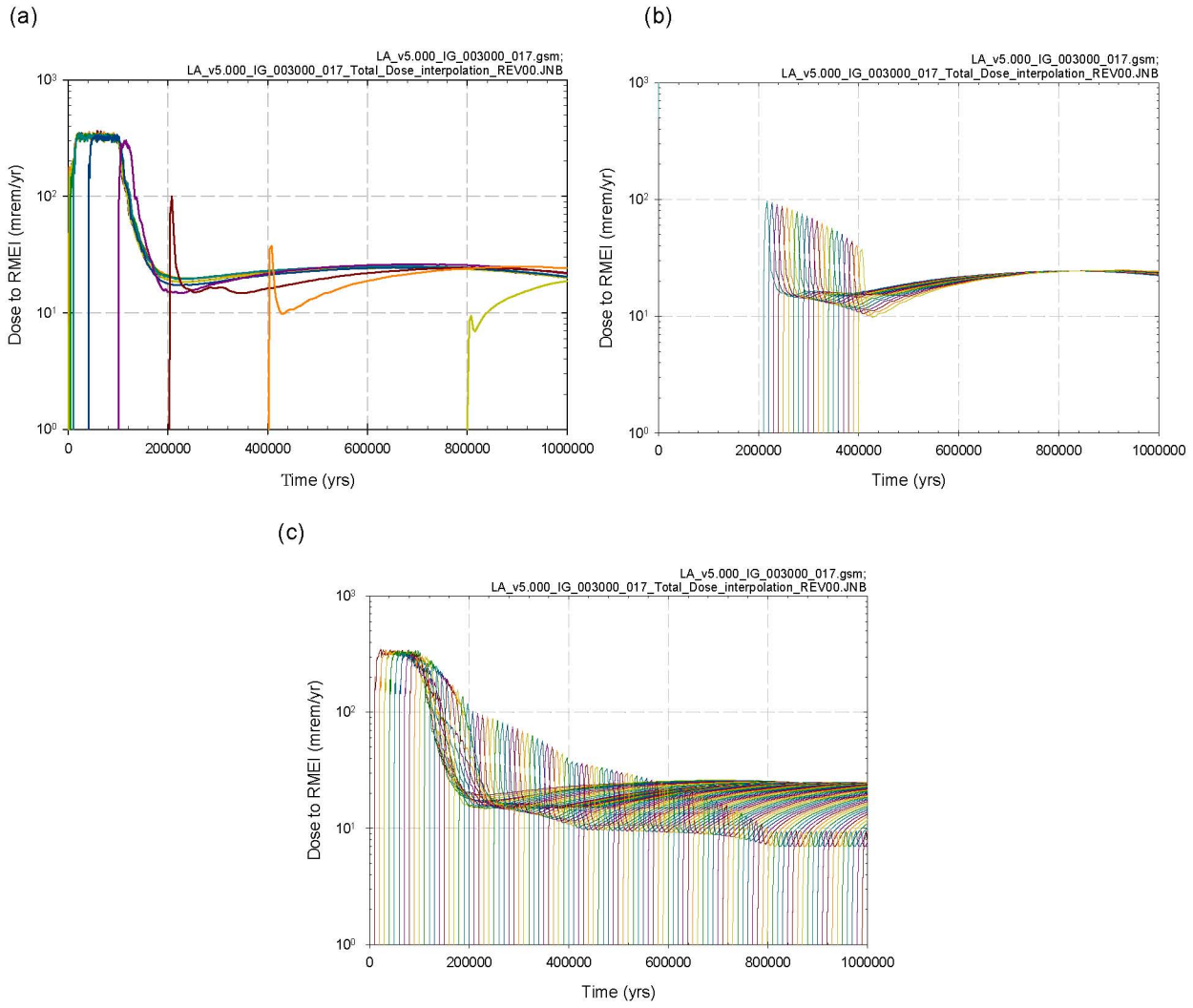

Source: Ouput DTNs: MO0709TSPAPLOT.000 [DIRS 183010]; and MO0709TSPAREGS.000 [DIRS 182976].

Figure J7.2-12. Illustration of interpolation procedure used to obtain estimated doses $\hat{D}_{II}(\tau|[1, \hat{t}_k, nWP], \mathbf{e}_{M1})$ from calculated doses $D_{II}(\tau|[1, t_k, nWP], \mathbf{e}_{M1})$ indicated in Equation J7.2-18 for LHS element $\mathbf{e}_1 = [\mathbf{e}_{A1}, \mathbf{e}_{M1}]$ and the time interval [0, 10^6 yr]: (a) $D_{II}(\tau|[1, t_k, nWP], \mathbf{e}_{M1})$, k = 1, 2, …, 10, (b) interpolated values $\hat{D}_{II}(\tau|[1, \hat{t}_k, nWP], \mathbf{e}_{M1})$ for $\hat{t}_k$ between t_8 = 200,000 yr and t_9= 400,000, and (c) interpolated values $\hat{D}_{II}(\tau|[1, \hat{t}_k, nWP], \mathbf{e}_{M1})$ for $\hat{t}_k$ between 250 yr and 10^6 yr.

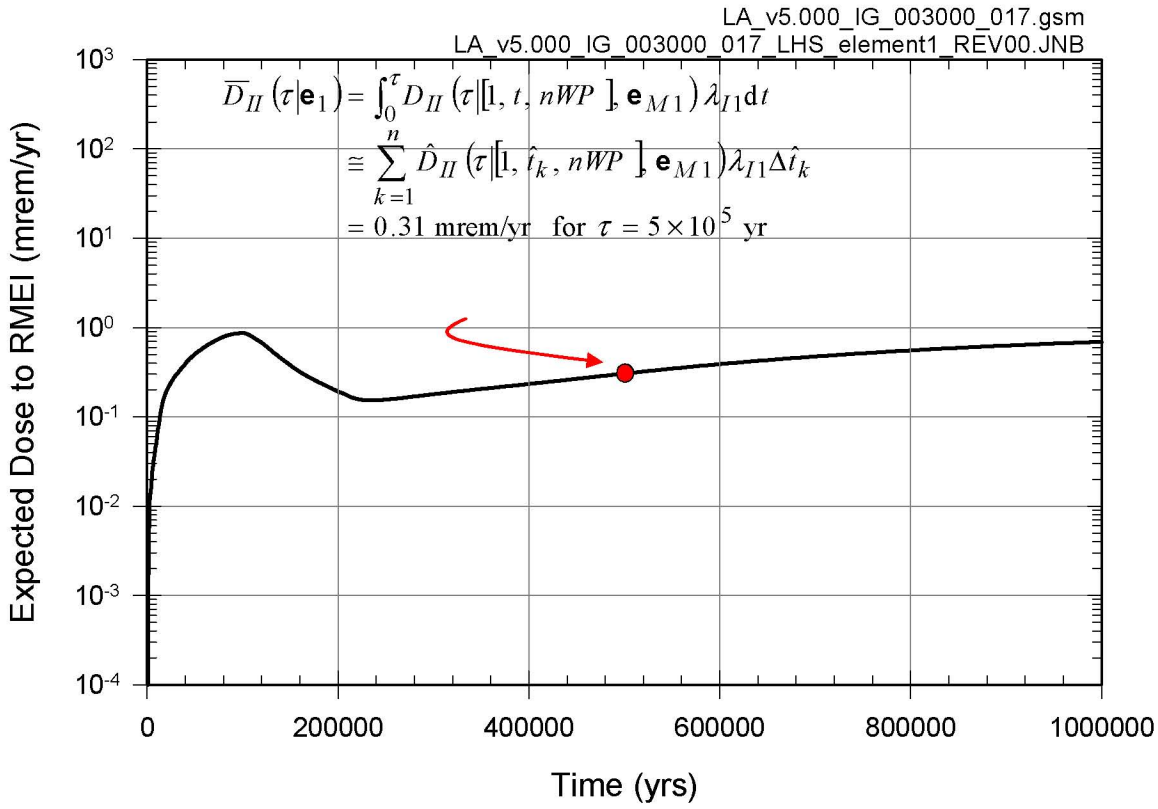

Source: Ouput DTNs: MO0709TSPAPLOT.000 [DIRS 183010]; and MO0709TSPAREGS.000 [DIRS 182976].

Figure J7.2-13. Determination of $\overline{D}_{II}(\tau|\mathbf{e}_1)$ as indicated in conjunction with Equations J7.2-7, J7.2-9 and J7.2-19 from calculated doses $D_{II}(\tau|[1, t_k, nWP], \mathbf{e}_{M1})$ shown in Equation J7.2-18 for LHS element $\mathbf{e}_1 = [\mathbf{e}_{A1}, \mathbf{e}_{M1}]$ and the time interval [0, 10^6 yr].

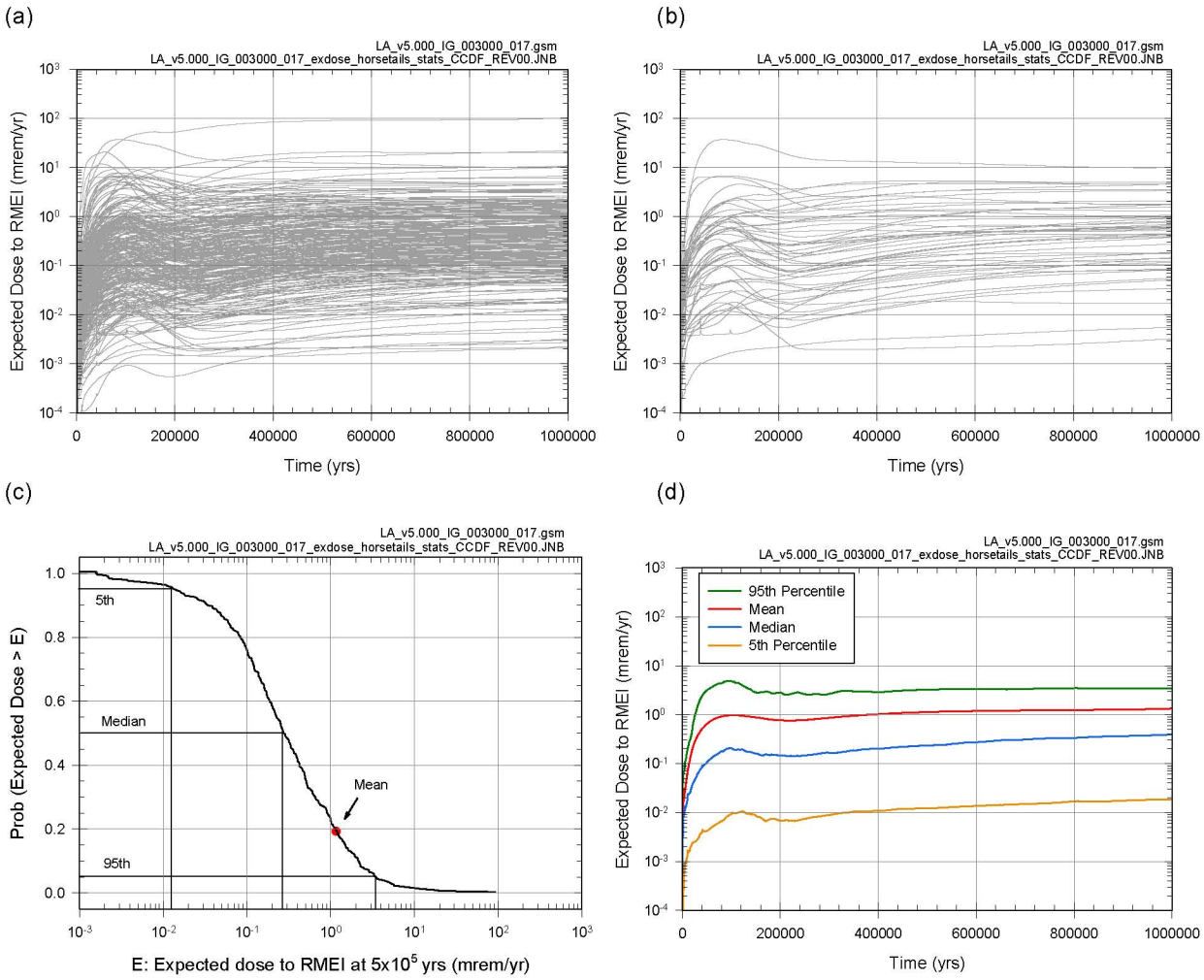

Source: Ouput DTNs: MO0709TSPAPLOT.000 [DIRS 183010]; and MO0709TSPAREGS.000 [DIRS 182976].

Figure J7.2-14. Estimate obtained with LHS of size *nLHS* = 300 showing epistemic uncertainty in expected dose $\bar{D}_{II}(\tau|\mathbf{e})$ to RMEI for $0 \le \tau \le 10^6$ yr that results when only igneous intrusion is considered: (a) expected dose $\bar{D}_{II}(\tau|\mathbf{e}_i)$, i = 1, 2, …, *nLHS* = 300, (b) expected dose $\bar{D}_{II}(\tau|\mathbf{e}_i)$, i = 1, 2, …, 50, (c) exceedance probabilities $p_E[D < \bar{D}_{II}(\tau|\mathbf{e})]$ and quantiles $Q_q[\bar{D}_{II}(\tau|\mathbf{e})]$, q = 0.05, 0.5 and 0.95, for $\tau = 5 \times 10^5$ yr, and (d) expected (mean) dose $\bar{\bar{D}}_{II}(\tau)$ and quantiles $Q_q[\bar{D}_{II}(\tau|\mathbf{e})]$, q = 0.05, 0.5, 0.95.

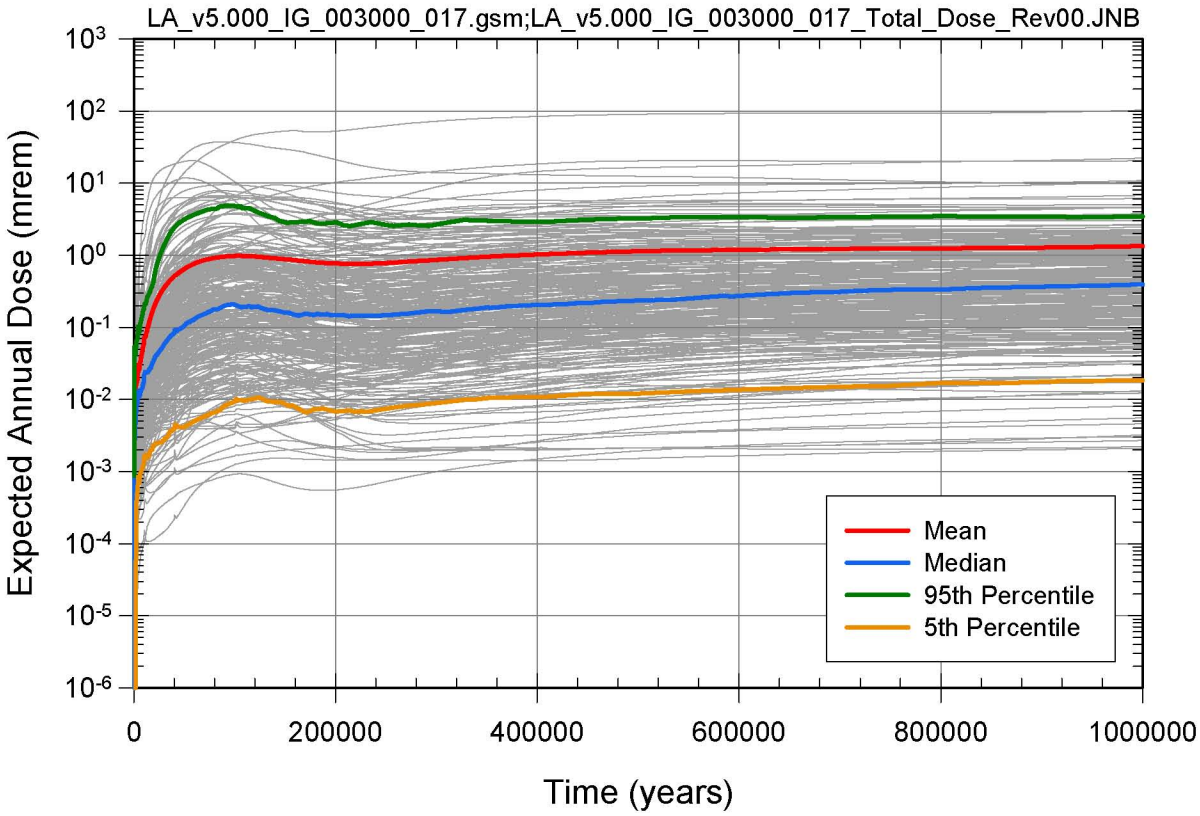

Source: Ouput DTNs: MO0709TSPAPLOT.000 [DIRS 183010]; and MO0709TSPAREGS.000 [DIRS 182976].

Figure J7.2-15. Summary presentations of epistemic uncertainty in expected dose $\bar{D}_{II}(\tau|\mathbf{e})$ to RMEI that results when only igneous intrusion is considered for $0 \leq \tau \leq 10^6$ yr.

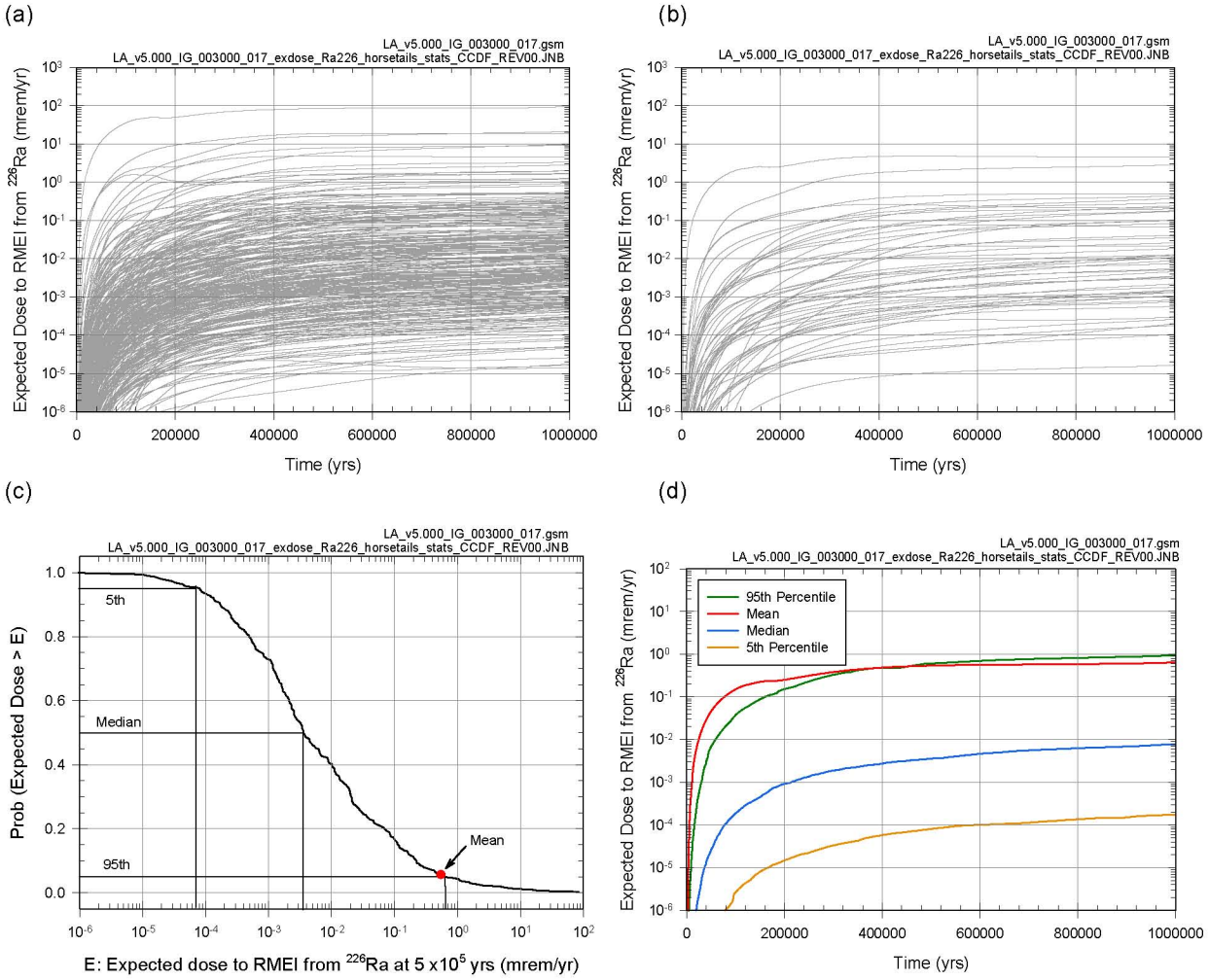

Source: Ouput DTNs: MO0709TSPAPLOT.000 [DIRS 183010]; and MO0709TSPAREGS.000 [DIRS 182976].

Figure J7.2-16. Estimate obtained with LHS of size *nLHS* = 300 showing epistemic uncertainty in expected dose $\bar{D}_{II,r}(\tau|\mathbf{e})$ to RMEI for $0 \le \tau \le 10^6$ yr with r corresponding to ^{226}Ra that results when only igneous intrusion is considered: (a) expected dose $\bar{D}_{II,r}(\tau|\mathbf{e}_i)$, i = 1, 2, …, *nLHS* = 300, (b) expected dose $\bar{D}_{II,r}(\tau|\mathbf{e}_i)$, i = 1, 2, …, 50, (c) exceedance probabilities $p_E[D < \bar{D}_{II,r}(\tau|\mathbf{e})]$ and quantiles $Q_q[\bar{D}_{II,r}(\tau|\mathbf{e})]$, q = 0.05, 0.5 and 0.95, for $\tau = 5 \times 10^5$ yr, and (d) expected (mean) dose $\bar{\bar{D}}_{II,r}(\tau)$ and quantiles $Q_q[\bar{D}_{II,r}(\tau|\mathbf{e})]$, q = 0.05, 0.5, 0.95.

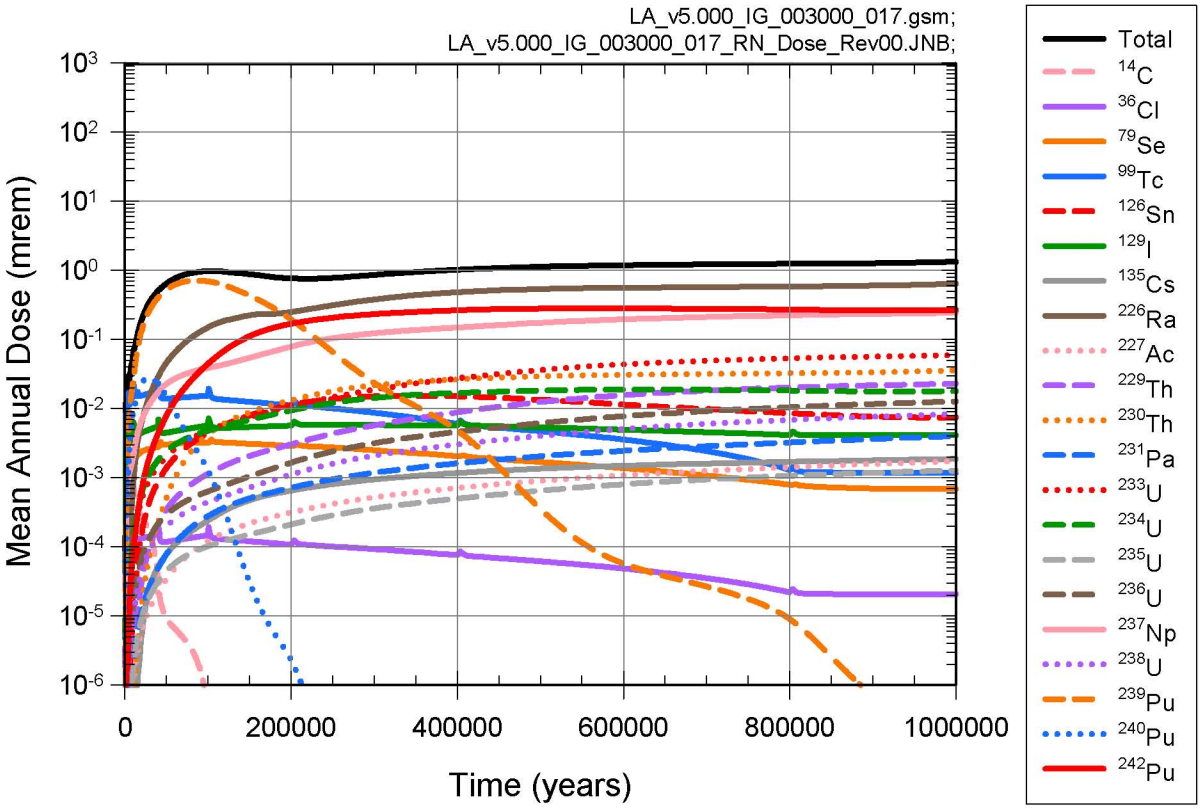

Source: Ouput DTNs: MO0709TSPAPLOT.000 [DIRS 183010]; and MO0709TSPAREGS.000 [DIRS 182976].

Figure J7.2-17. Estimates obtained with LHS of size *nLHS* = 300 of expected (mean) dose $\bar{\bar{D}}_{II,r}(\tau)$ to RMEI for $0 \leq \tau \leq 10^6$ yr for individual radioactive species that result when only igneous intrusive events are considered.

(a)

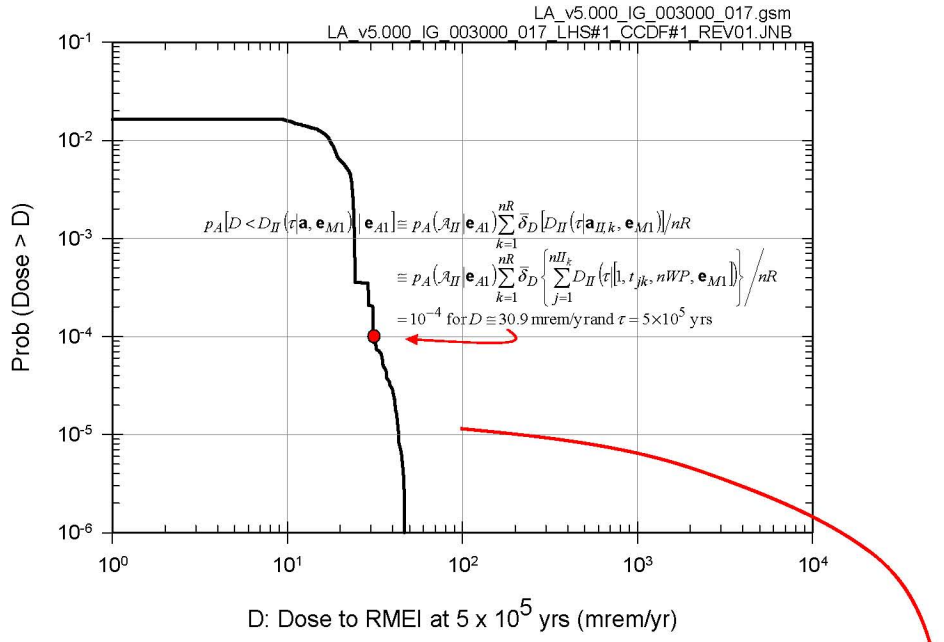

(b)

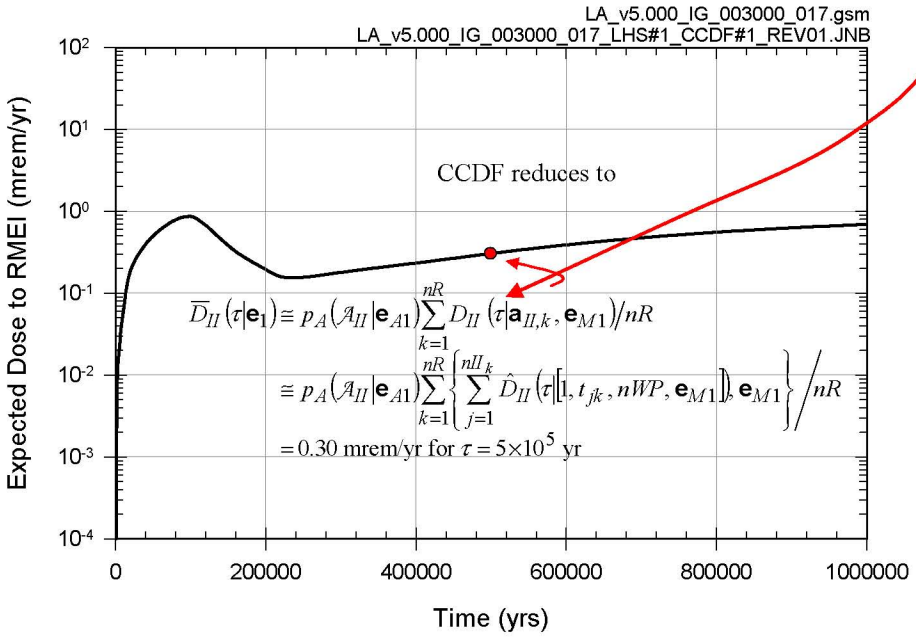

Source: Ouput DTNs: MO0709TSPAPLOT.000 [DIRS 183010]; and MO0709TSPAREGS.000 [DIRS 182976].

Figure J7.2-18. Results associated with $\bar{D}_{II}(\tau|\mathbf{e}_1)$ for LHS elements $\mathbf{e}_1 = [\mathbf{e}_{A1}, \mathbf{e}_{M1}]$ obtained with sampling-based (Monte Carlo) procedures: (a) CCDF for $D_{II}(5 \times 10^5 \text{ yr}|\mathbf{a}_{II}, \mathbf{e}_{M1})$ with exceedance probabilities $p_A[D < D_{II}(5 \times 10^5 \text{ yr}|\mathbf{a}, \mathbf{e}_{M1})|\mathbf{e}_{A1}]$ defined in Equation J7.2-23, and (b) expected dose $\bar{D}_{II}(5 \times 10^5 \text{ yr}|\mathbf{e}_1)$ associated with $D_{II}(5 \times 10^5 \text{ yr}|\mathbf{a}_{II}, \mathbf{e}_{M1})$ as defined in Equation J7.2-21.

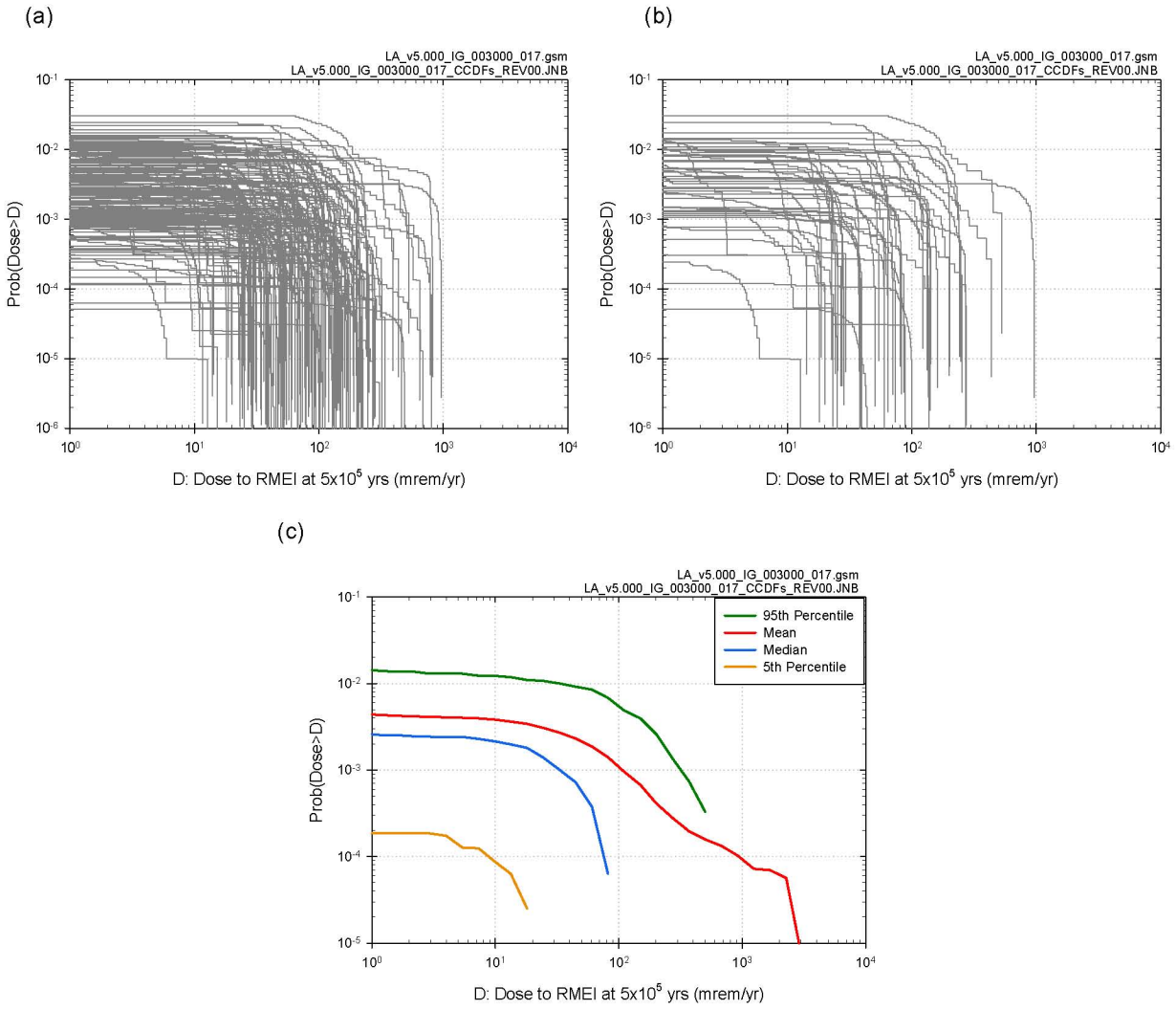

Source: Ouput DTNs: MO0709TSPAPLOT.000 [DIRS 183010]; and MO0709TSPAREGS.000 [DIRS 182976].

Figure J7.2-19. Results associated with $D_{II}(5 \times 10^5 \text{ yr}|\mathbf{a}_{II}, \mathbf{e}_M)$ obtained with sampling-based (Monte Carlo) procedures for an LHS of size $nLHS = 300$: (a) CCDFs for $D_{II}(5 \times 10^5 \text{ yr}|\mathbf{a}_{II}, \mathbf{e}_{Mi})$ with exceedance probabilities $p_A[D < D_{II}(5 \times 10^5 \text{ yr}|\mathbf{a}, \mathbf{e}_{Mi})|\mathbf{e}_{Ai}]$ defined in Equation J7.2-23 for $i = 1, 2, \ldots, nLHS = 300$, (b) CCDFs for $D_{II}(5 \times 10^5 \text{ yr}|\mathbf{a}_{II}, \mathbf{e}_{Mi})$ with exceedance probabilities $p_A[D < D_{II}(5 \times 10^5 \text{ yr}|\mathbf{a}, \mathbf{e}_{Mi})|\mathbf{a}_{Ai}]$ defined in Equation J7.2-23 for $i = 1, 2, \ldots, 50$, and (c) expected (mean) CCDF and quantile curves, $q = 0.05, 0.5, 0.95$, for CCDFs in (a).

(a)

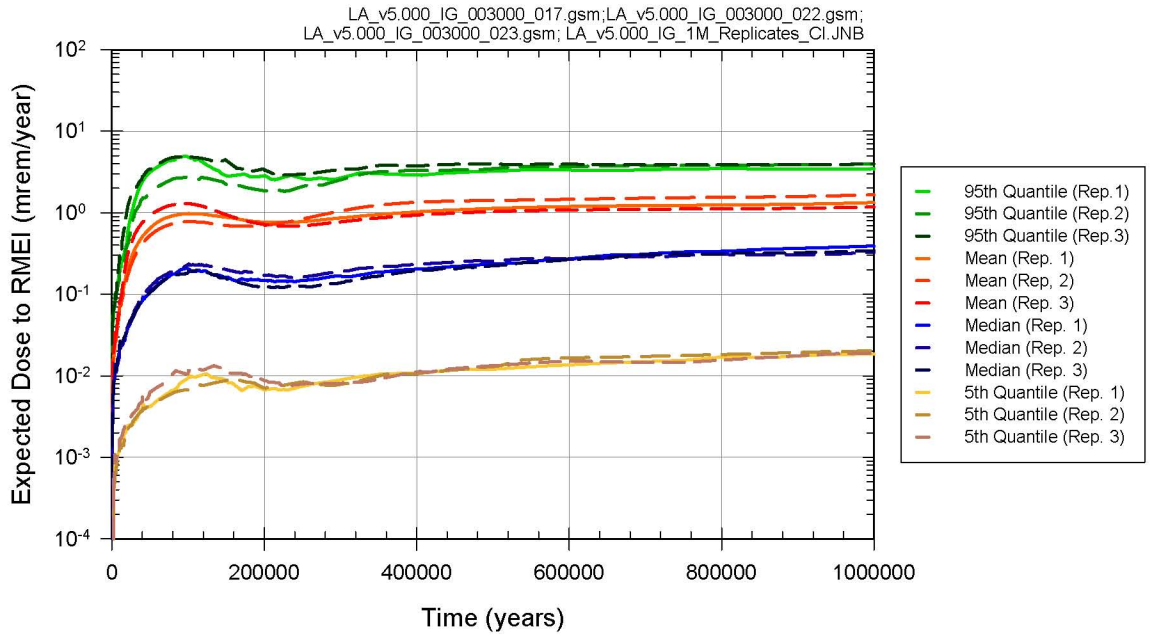

(b)

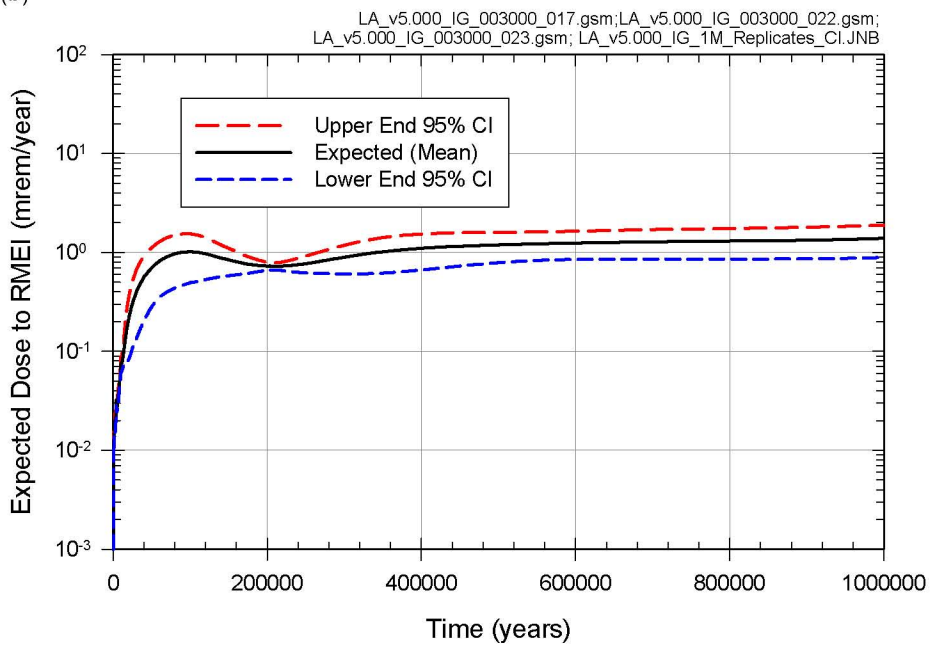

Source: Ouput DTNs: MO0709TSPAPLOT.000 [DIRS 183010]; MO0709TSPAREGS.000 [DIRS 182976]; and MO0709TSPASTAB.000 [DIRS 182983].

Figure J7.2-20. Assessment with replicated sampling of numerical error associated with use of an LHS of size *nLHS* = 300 to determine epistemic uncertainty in expected dose $\bar{D}_{II}(\tau|\mathbf{e})$ to RMEI for $0 \leq \tau \leq 10^6$ yr that results when only igneous intrusion is considered: (a) Replicated estimates of expected (mean) dose $\bar{\bar{D}}_{II}(\tau)$ and quantiles $Q_q[\bar{D}_{II}(\tau|\mathbf{e})]$, q = 0.05, 0.5, 0.95, and (b) confidence intervals for estimates of expected (mean) dose $\bar{\bar{D}}_{II}(\tau)$.

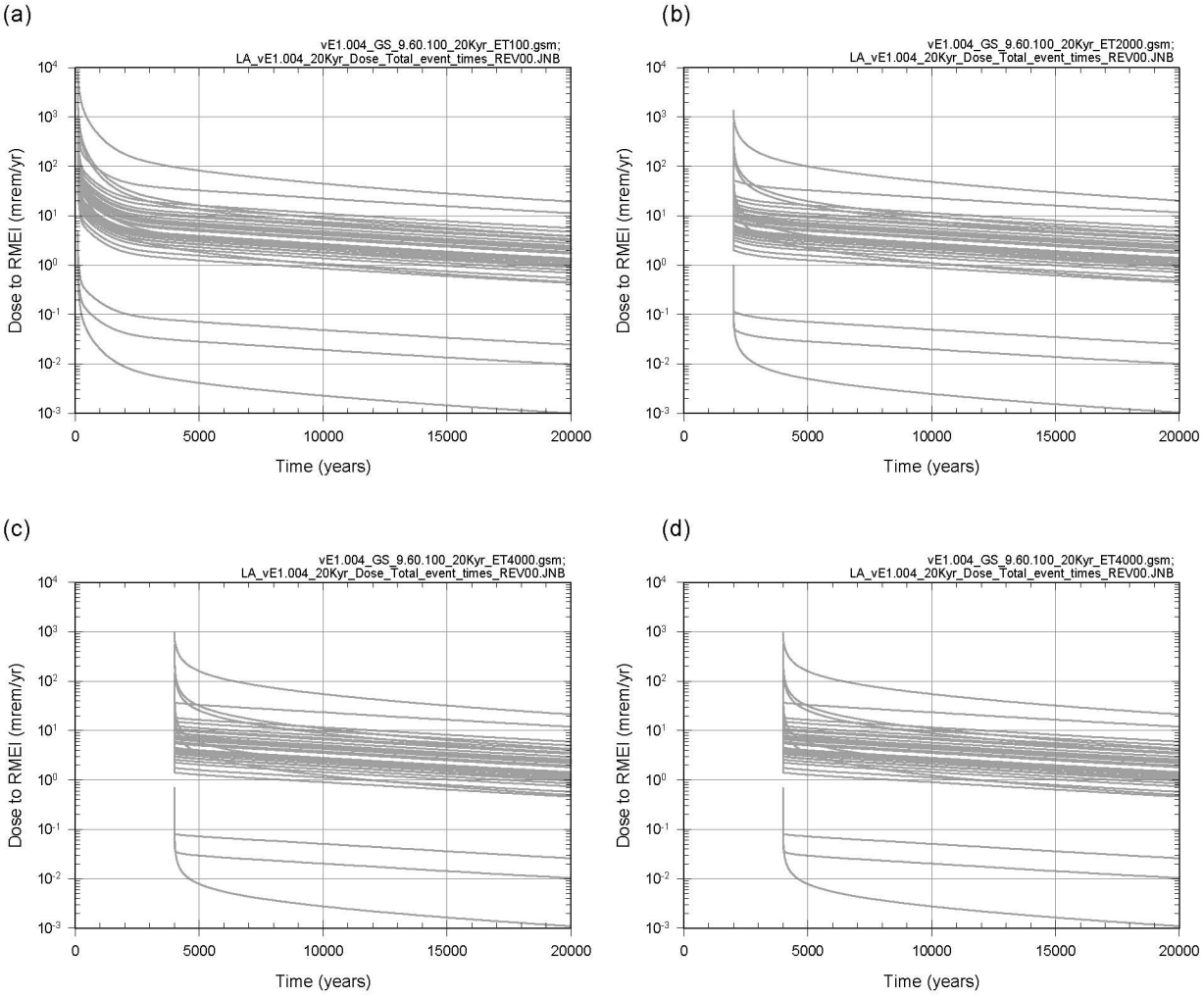

Source: Ouput DTNs: MO0709TSPAPLOT.000 [DIRS 183010]; and MO0709TSPAREGS.000 [DIRS 182976].

Figure J7.3-1. Dose results $D_{lE}(\tau|[1, t_k, 1, \mathbf{u}_l], \mathbf{e}_{M1})$ obtained for times t_k = 100, 1000, 4000, 10,000 yr, igneous eruptive properties $\mathbf{u}_l$, l = 1, 2, …, nU = 40, and LHS element $\mathbf{e}_1 = [\mathbf{e}_{A1}, \mathbf{e}_{M1}]$: (a) t_k = 100 yr, (b) t_k = 1000 yr, (c) t_k = 4000 yr, and (d) t_k = 10,000 yr.

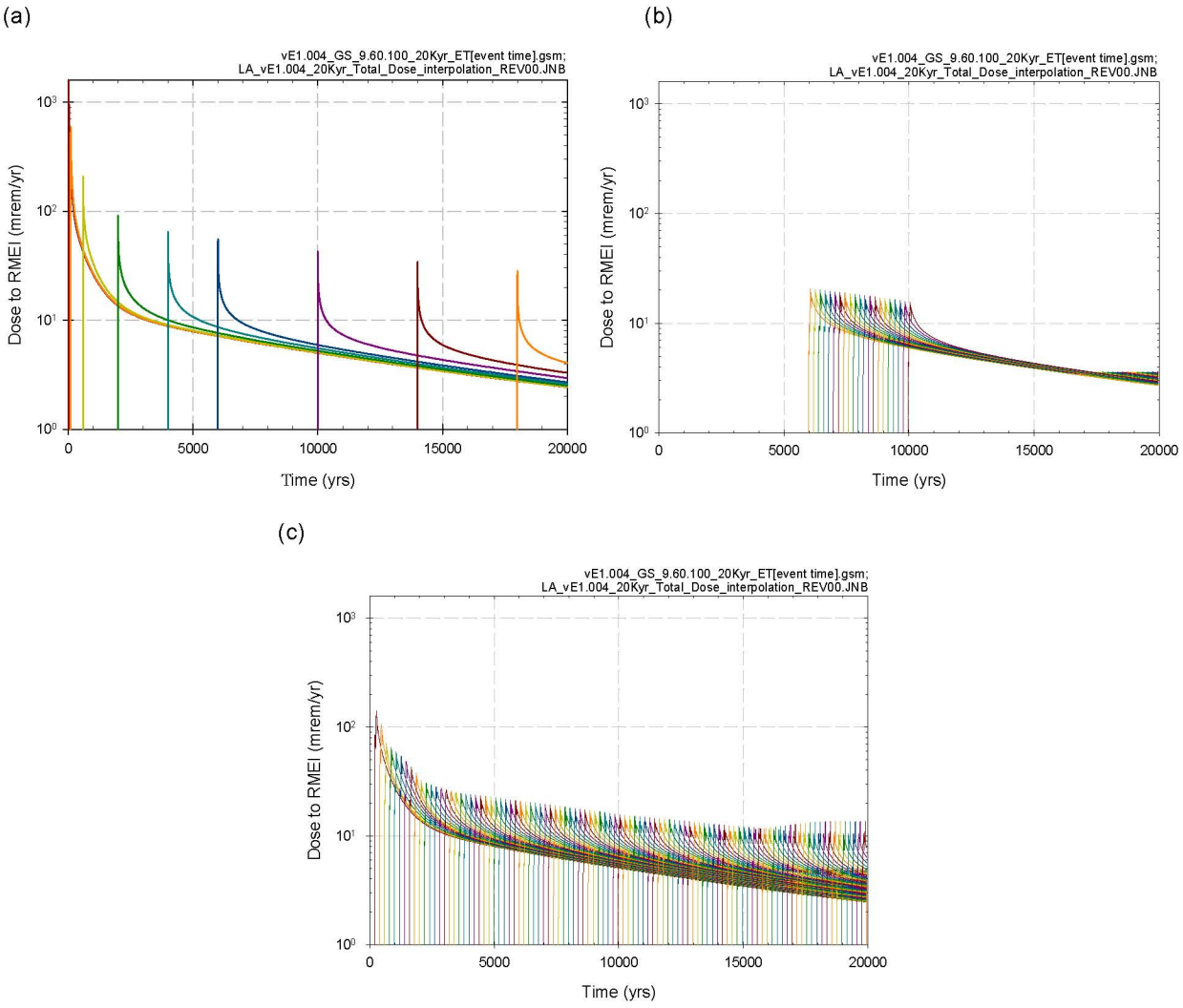

Source: Ouput DTNs: MO0709TSPAPLOT.000 [DIRS 183010]; and MO0709TSPAREGS.000 [DIRS 182976].

Figure J7.3-2. Illustration of interpolation procedure used to obtain estimates $\hat{S}(\tau|\hat{t}_k, \mathbf{e}_{M1})$ of conditional expected dose $S(\tau|t, \mathbf{e}_{M1})$ to RMEI (mrem/yr) for LHS element $\mathbf{e}_1 = [\mathbf{e}_{A1}, \mathbf{e}_{M1}]$ and the time interval [0, 20,000 yr]: (a) $S(\tau|t_k, \mathbf{e}_{M1})$, k = 1, 2, …, 10, (b) interpolated values $\hat{S}(\tau|\hat{t}_k, \mathbf{e}_{M1})$ for $\hat{t}_k$ between t_7 = 6000 yr and t_8 = 10,000 yr, and (c) interpolated values $\hat{S}(\tau|\hat{t}_k, \mathbf{e}_{M1})$ for $\hat{t}_k$ between 10 yr and 20,000 yr.

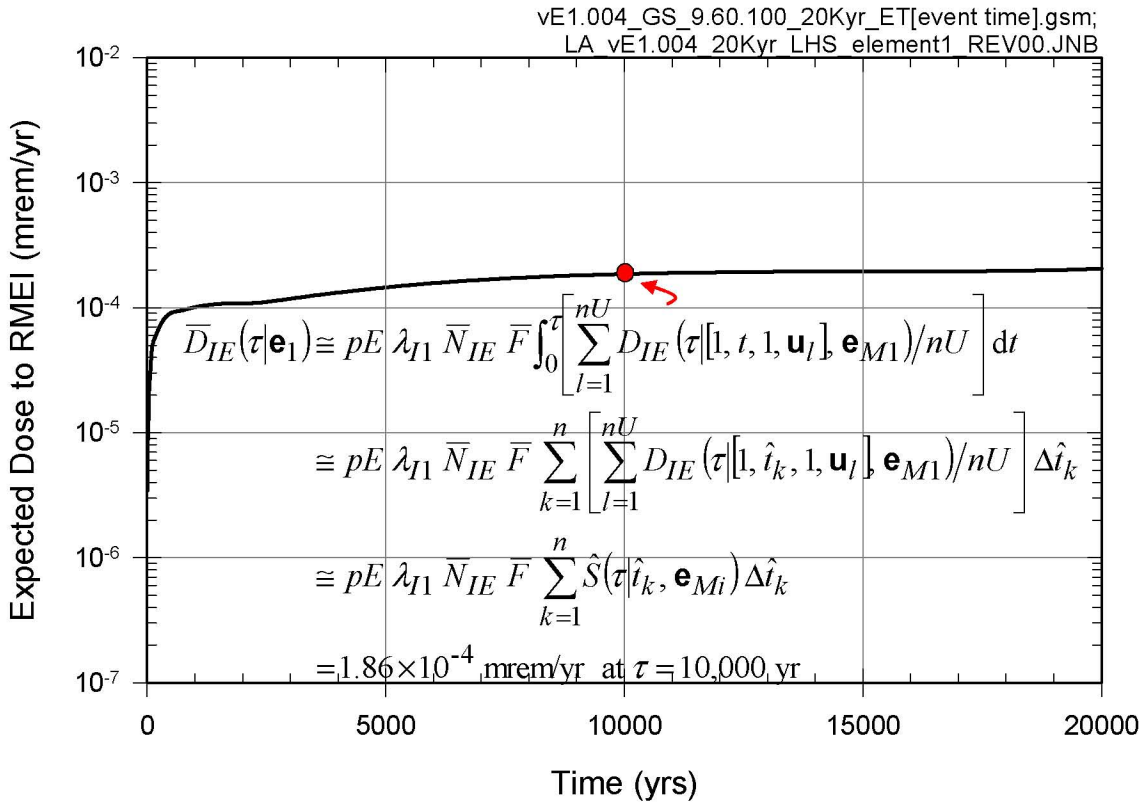

Source: Ouput DTNs: MO0709TSPAPLOT.000 [DIRS 183010]; and MO0709TSPAREGS.000 [DIRS 182976].

Figure J7.3-3. Estimate of $\bar{D}_{IE}(\tau|\,\mathbf{e}_1)$ for LHS element $\mathbf{e}_1 = [\mathbf{e}_{A1}, \mathbf{e}_{M1}]$ and $0 \le \tau \le 20{,}000$ yr with integration-based procedure indicated in Equations J7.3-9 and J7.3-16.

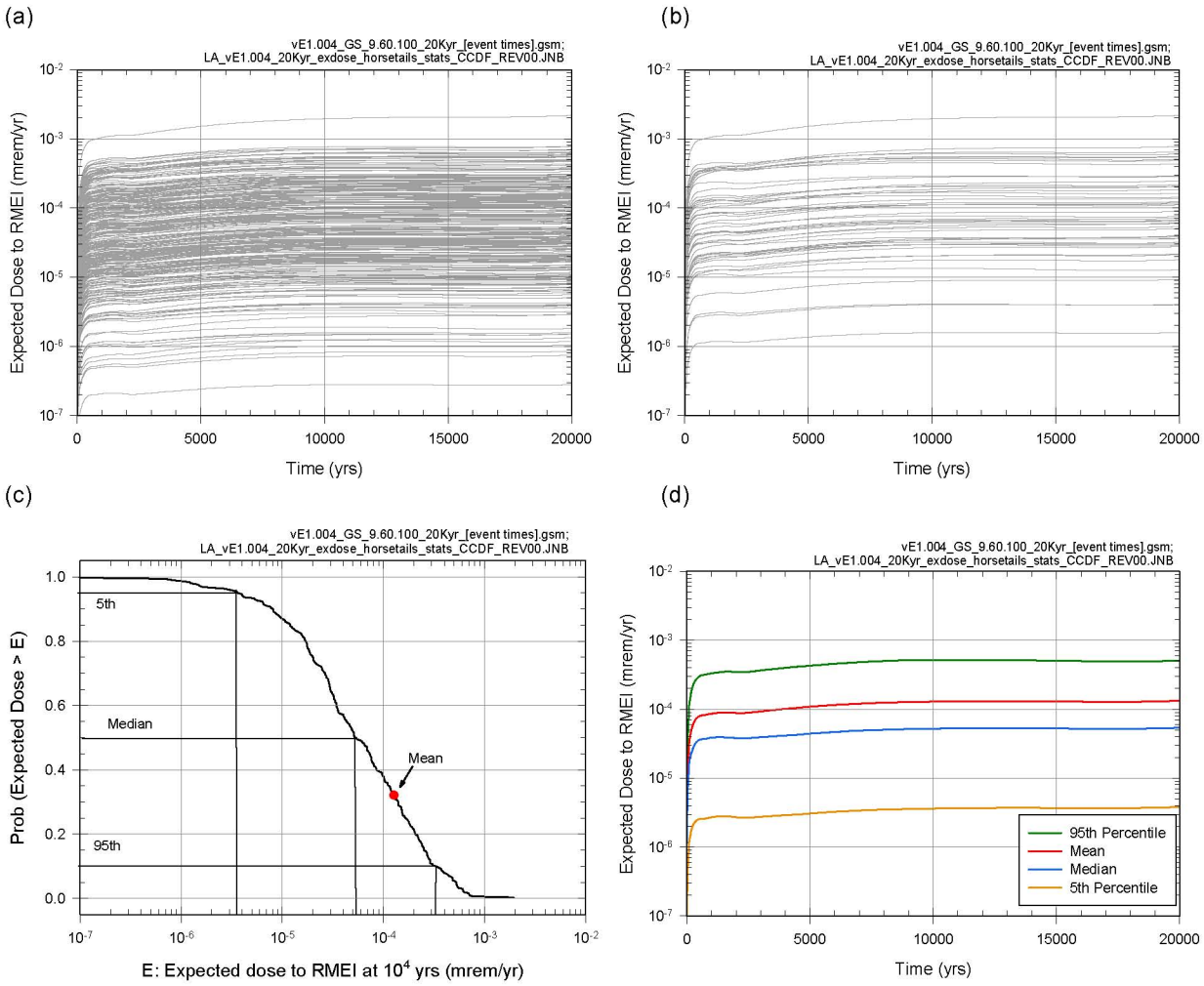

Source: Ouput DTNs: MO0709TSPAPLOT.000 [DIRS 183010]; and MO0709TSPAREGS.000 [DIRS 182976].

Figure J7.3-4. Estimate obtained with LHS of size $nLHS$ = 300 showing epistemic uncertainty in expected dose $\bar{D}_{lE}(\tau|\mathbf{e})$ to RMEI for $0 \le \tau \le 20{,}000$ yr that results when only igneous eruptive events are considered: (a) expected dose $\bar{D}_{lE}(\tau|\mathbf{e}_i)$, i = 1, 2, …, $nLHS$ = 300, (b) expected dose $\bar{D}_{lE}(\tau|\mathbf{e}_i)$, i = 1, 2, …, 50, (c) exceedance probabilities $p_E[D < \bar{D}_{lE}(\tau|\mathbf{e})]$ and quantiles $Q_q[\bar{D}_{lE}(\tau|\mathbf{e})]$, q = 0.05, 0.5 and 0.95, for $\tau = 10^4$ yr, and (d) expected (mean) dose $\bar{\bar{D}}_{lE}(\tau)$ and quantiles $Q_q[\bar{D}_{lE}(\tau|\mathbf{e})]$, q = 0.05, 0.5, 0.95.

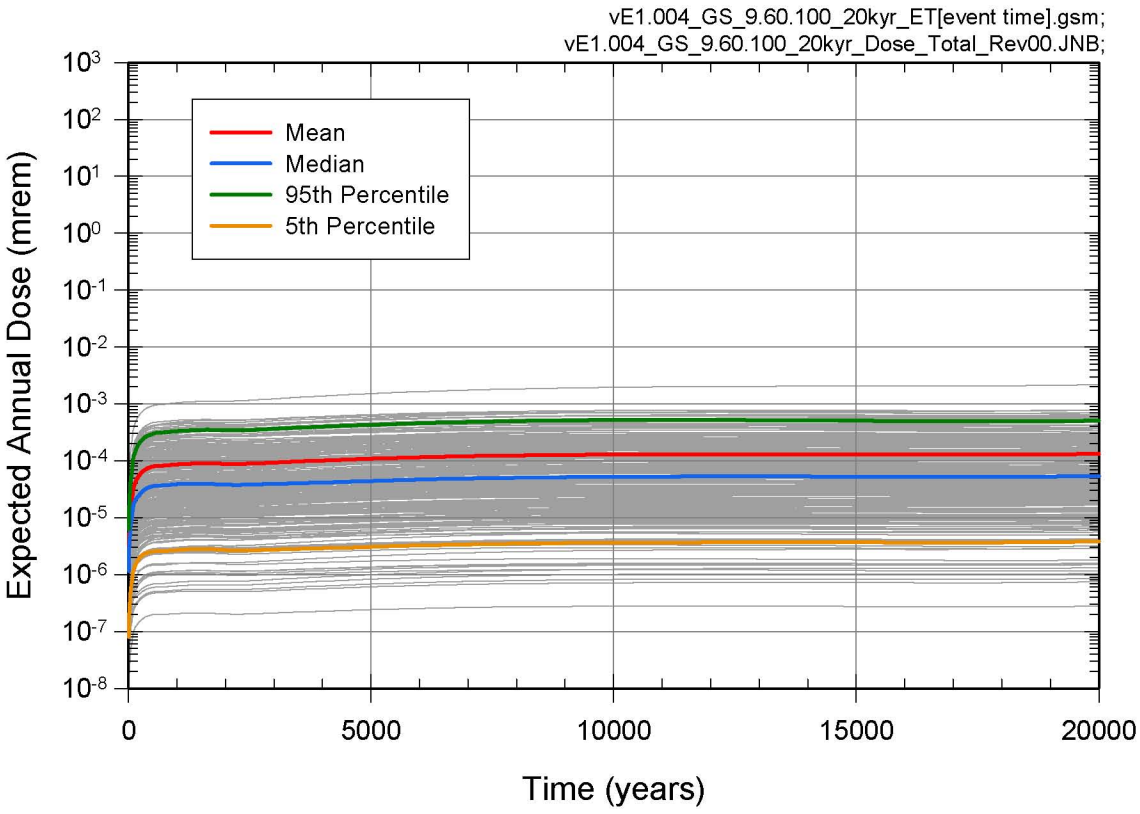

Source: Ouput DTNs: MO0709TSPAPLOT.000 [DIRS 183010]; and MO0709TSPAREGS.000 [DIRS 182976].

Figure J7.3-5. Summary of results obtained with LHS of size *nLHS* = 300 showing epistemic uncertainty in expected dose $\bar{D}_{IE}(\tau|\mathbf{e})$ to RMEI for $0 \leq \tau \leq 20{,}000$ yr that results when only igneous eruptive events are considered.

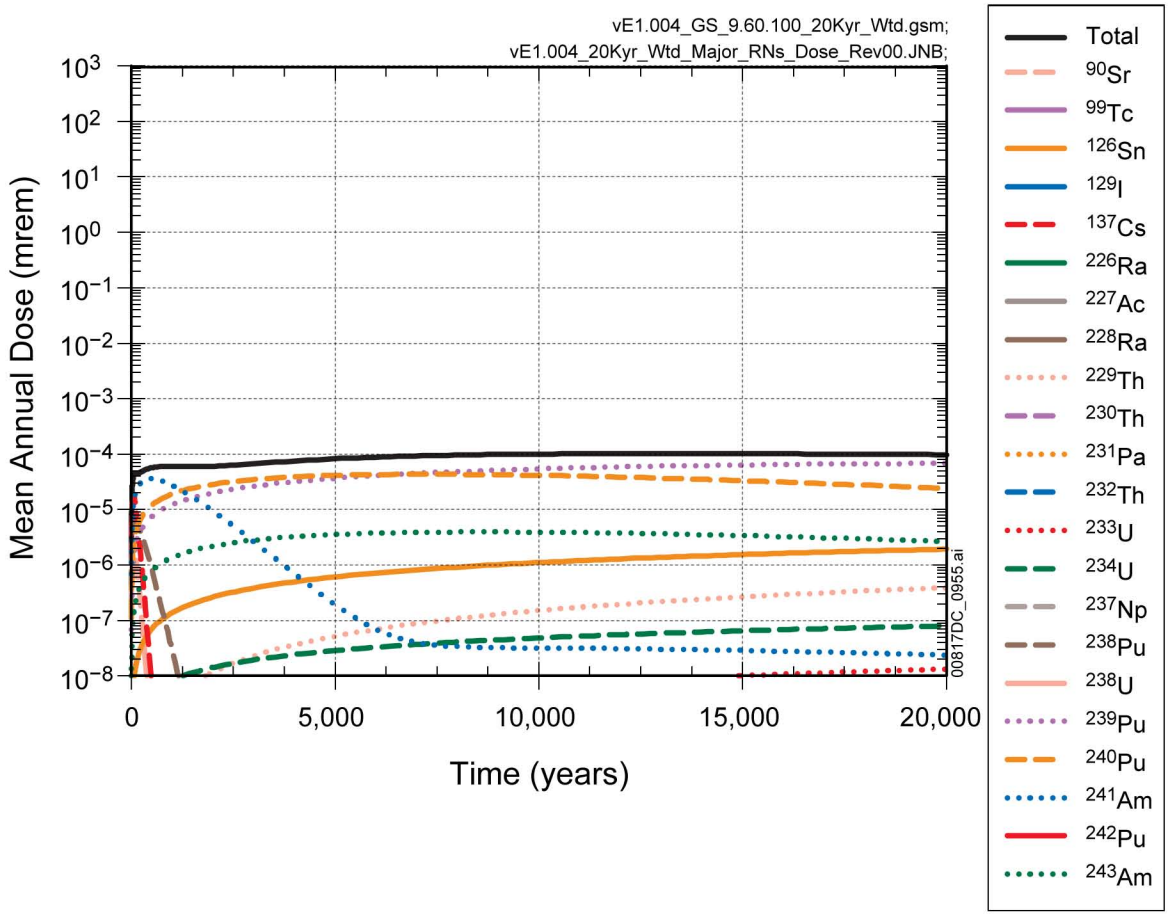

Source: Ouput DTNs: MO0709TSPAPLOT.000 [DIRS 183010]; and MO0709TSPAREGS.000 [DIRS 182976].

Figure J7.3-6. Estimates obtained with LHS of size *nLHS* = 300 of expected (mean) dose $\bar{\bar{D}}_{lE,r}(\tau)$ to RMEI for $0 \leq \tau \leq 20{,}000$ yr for individual radioactive species that result when only igneous eruptive events are considered.

(a)

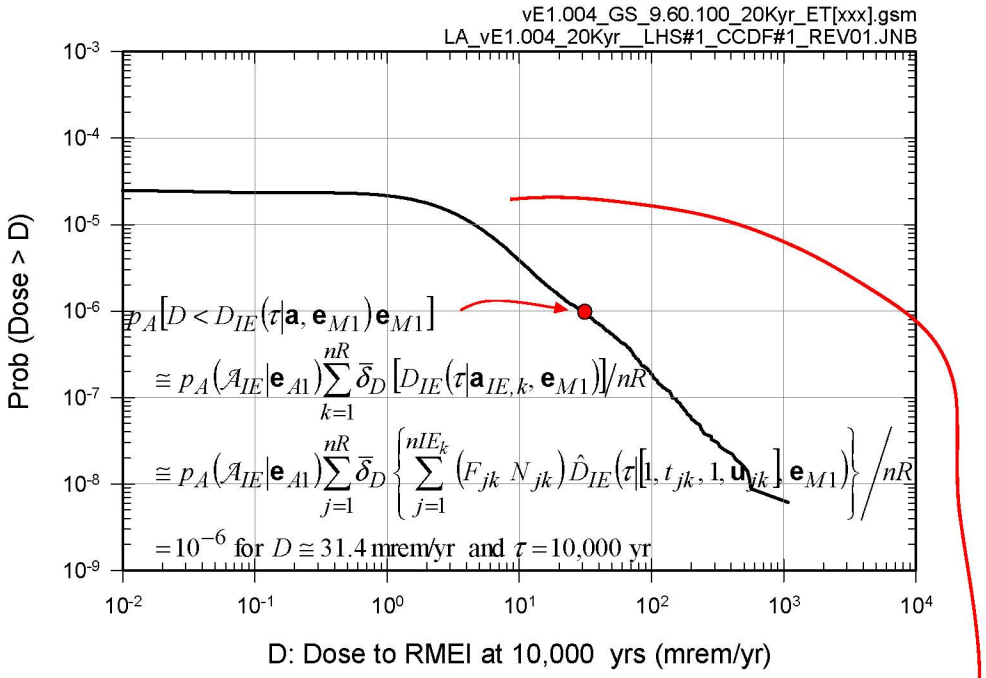

(b)

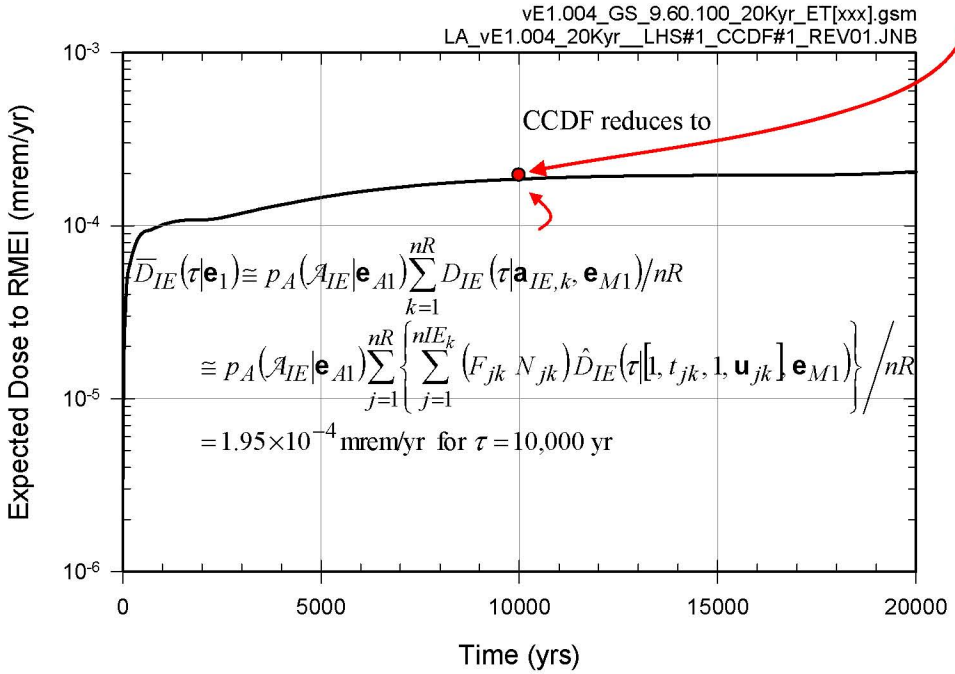

Source: Ouput DTNs: MO0709TSPAPLOT.000 [DIRS 183010]; and MO0709TSPAREGS.000 [DIRS 182976].

Figure J7.3-7. Results associated with $D_{IE}(\tau|\mathbf{a}_{IE}, \mathbf{e}_1)$ for LHS element $\mathbf{e}_1 = [\mathbf{e}_{A1}, \mathbf{e}_{M1}]$ obtained with sampling-based (Monte Carlo) procedures: (a) CCDF for $D_{IE}(10^4 \text{ yr}|\mathbf{a}_{IE}, \mathbf{e}_1)$ with exceedance probabilities $p_A[D < D_{IE}(10^4 \text{ yr}|\mathbf{a}, \mathbf{e}_{M1})|\mathbf{e}_{A1}]$ defined in Equation J7.3-20, and (b) expected dose $\bar{D}_{IE}(10^4 \text{ yr}|\mathbf{e}_1)$ associated with $D_{IE}(10^4 \text{ yr}|\mathbf{a}_{IE}, \mathbf{e}_1)$ as defined in Equation J7.3-18.

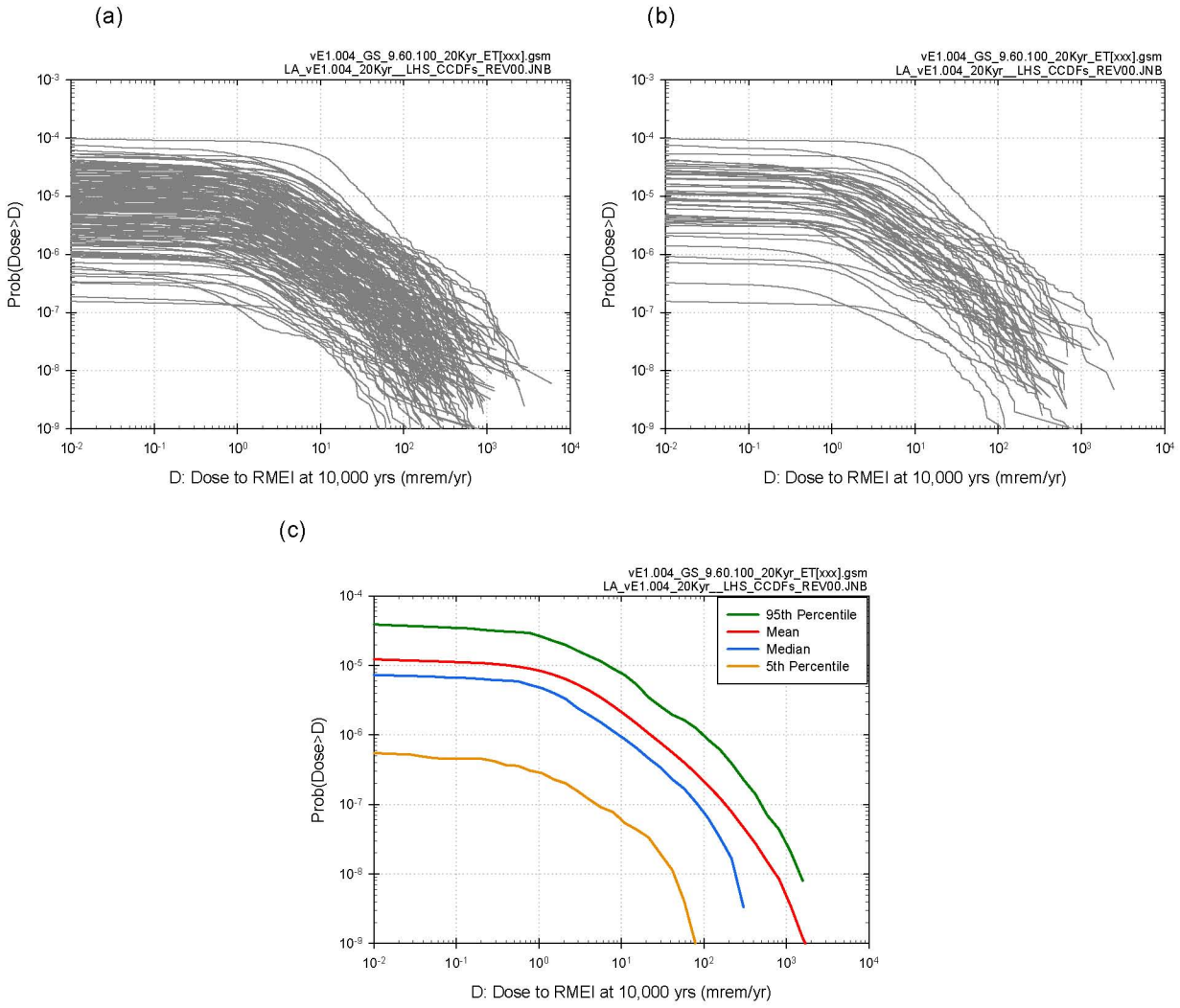

Source: Ouput DTNs: MO0709TSPAPLOT.000 [DIRS 183010]; and MO0709TSPAREGS.000 [DIRS 182976].

Figure J7.3-8. Results associated with $D_{IE}(10^4\ \text{yr}|\mathbf{a}_{IE}, e_M)$ obtained with sampling-based (Monte Carlo) procedures for an LHS of size $nLHS = 300$: (a) CCDFs for $D_{IE}(10^4\ \text{yr}|\mathbf{e}_{IE}, e_{Mi})$ with exceedance probabilities $p_A[D < D_{IE}(10^4\ \text{yr}|\mathbf{a}, \mathbf{e}_{Mi})|\mathbf{e}_{Ai}]$ defined in Equation J7.3-20 for $i = 1, 2, \ldots, nLHS = 300$, (b) CCDFs for $D_{IE}(10^4\ \text{yr}|\mathbf{a}_{IE}, e_{Mi})$ with exceedance probabilities $p_A[D < D_{IE}(10^4\ \text{yr}|\mathbf{a}, \mathbf{e}_{Mi})|\mathbf{e}_{Ai}]$ defined in Equation J7.3-20 for $i = 1, 2, \ldots, 50$, and (c) expected (mean) CCDF and quantile curves, $q = 0.05, 0.5, 0.95$, for CCDFs in (a).

(a)

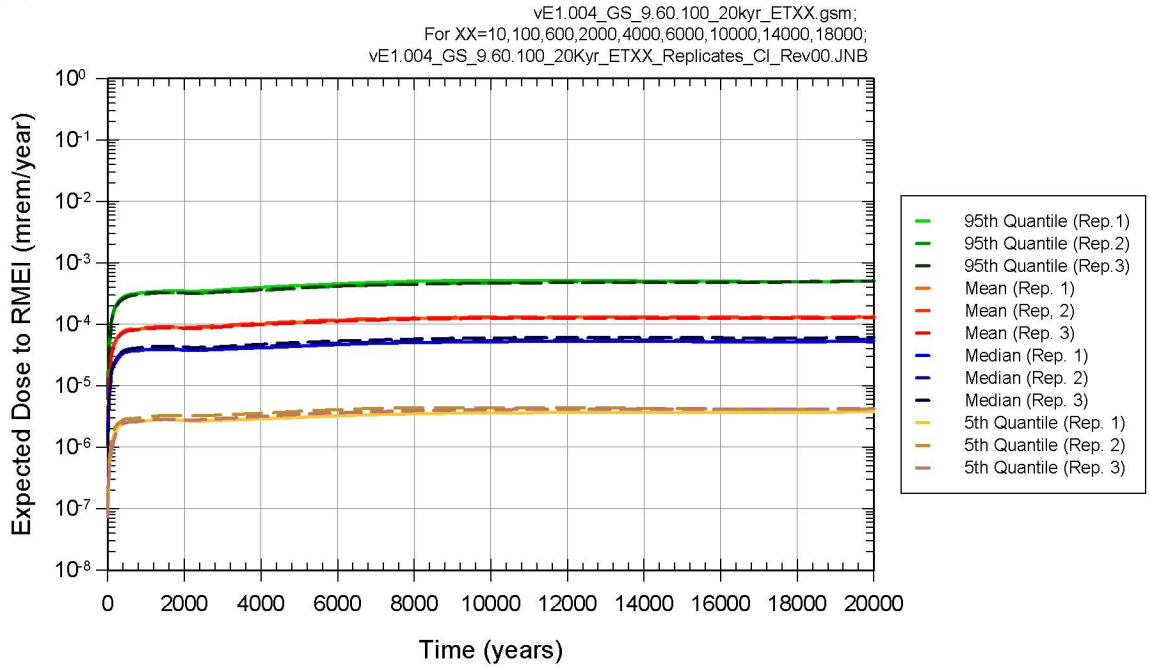

(b)

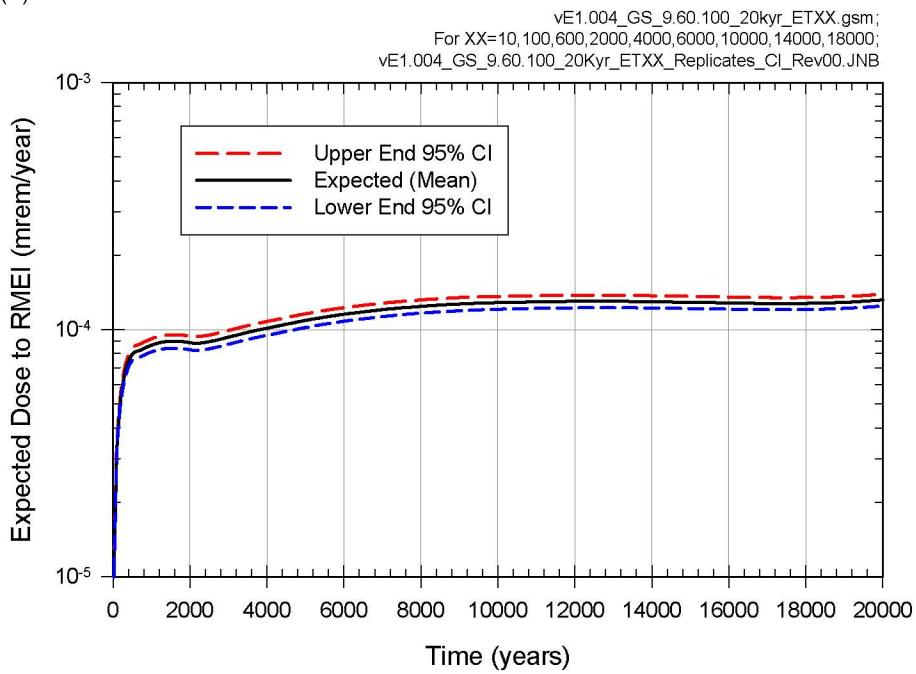

Source: Ouput DTNs: MO0709TSPAPLOT.000 [DIRS 183010]; and MO0709TSPAREGS.000 [DIRS 182976].

Figure J7.3-9. Assessment with replicated sampling of numerical error associated with use of an LHS of size *nLHS* = 300 to determine epistemic uncertainty in expected dose $\bar{D}_{IE}(\tau)$ to RMEI for $0 \leq \tau \leq 20{,}000$ yr that results when only igneous eruptive events are considered: (a) Replicated estimates of expected (mean) dose $\bar{D}_{IE}(\tau)$ and quantiles $Q_q[\bar{D}_{IE}(\tau|\mathbf{e})]$, q = 0.05, 0.5, 0.95, and (b) confidence intervals for estimates of expected (mean) dose $\bar{\bar{D}}_{IE}(\tau)$.

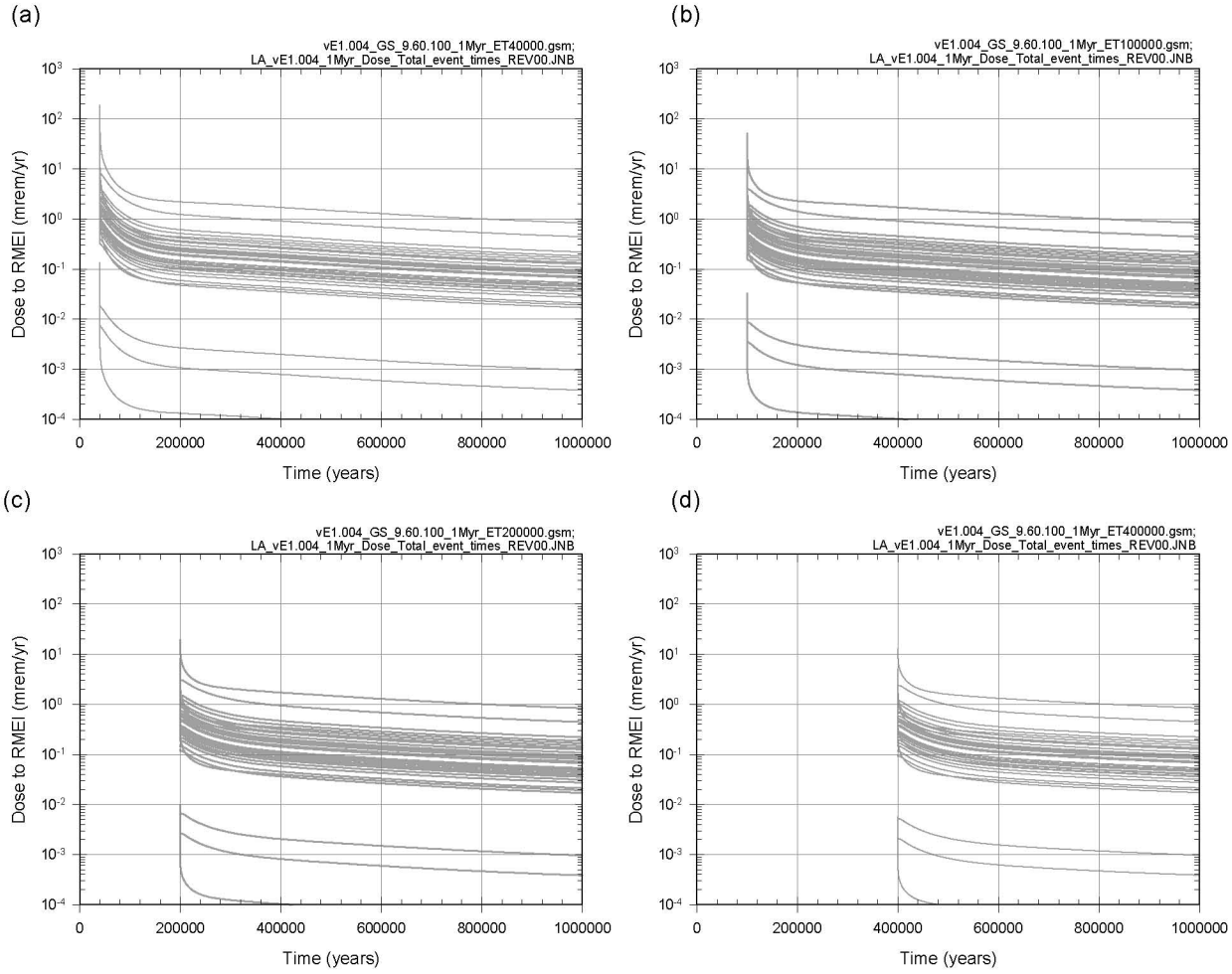

Source: Ouput DTNs: MO0709TSPAPLOT.000 [DIRS 183010]; and MO0709TSPAREGS.000 [DIRS 182976].

Figure J7.3-10. Dose results $D_{lE}(\tau|[1, t_k, 1, \mathbf{u}_l], \mathbf{e}_{M1})$ obtained for times t_k = 40,000, 100,000, 200,000, 400,000 yr, igneous eruptive properties $\mathbf{u}_l$, l = 1, 2, …, nU = 40, and LHS element $\mathbf{e}_1$ = [$\mathbf{e}_{A1}$, $\mathbf{e}_{M1}$]: (a) t_k = 40,000 yr, (b) t_k = 100,000 yr, (c) t_k = 200,000 yr, and (d) t_k = 400,000 yr.

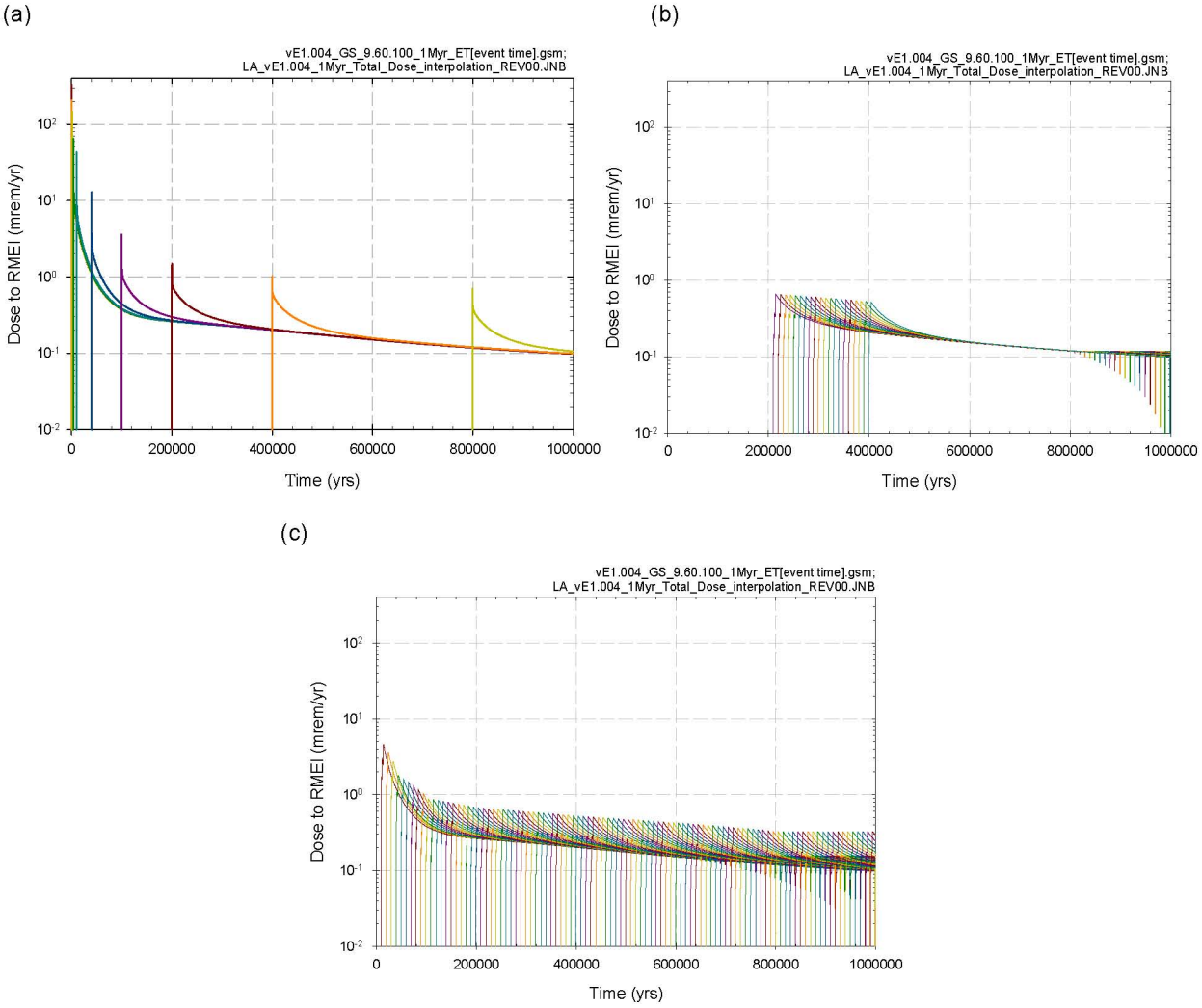

Source: Ouput DTNs: MO0709TSPAPLOT.000 [DIRS 183010]; and MO0709TSPAREGS.000 [DIRS 182976].

Figure J7.3-11. Illustration of interpolation procedure used to obtain estimates $\hat{S}(\tau|\hat{t}_k, \mathbf{e}_{Mi})$ of conditional expected dose $S(\tau|t, \mathbf{e}_{M1})$ to RMEI (mrem/yr) for LHS element $\mathbf{e}_1 = [\mathbf{e}_{A1}, \mathbf{e}_{M1}]$ and the time interval [0, 10^6 yr]: (a) $S(\tau|t_k, \mathbf{e}_{M1})$, k = 1, 2, …, 10, (b) interpolated values $\hat{S}(\tau|\hat{t}_k, \mathbf{e}_{M1})$ for $\hat{t}_k$ between t_8 = 200,000 yr and t_9 = 400,000 yr, and (c) interpolated values $\hat{S}(\tau|\hat{t}_k, \mathbf{e}_{M1})$ for $\hat{t}_k$ between 250 yr and 10^6 yr.

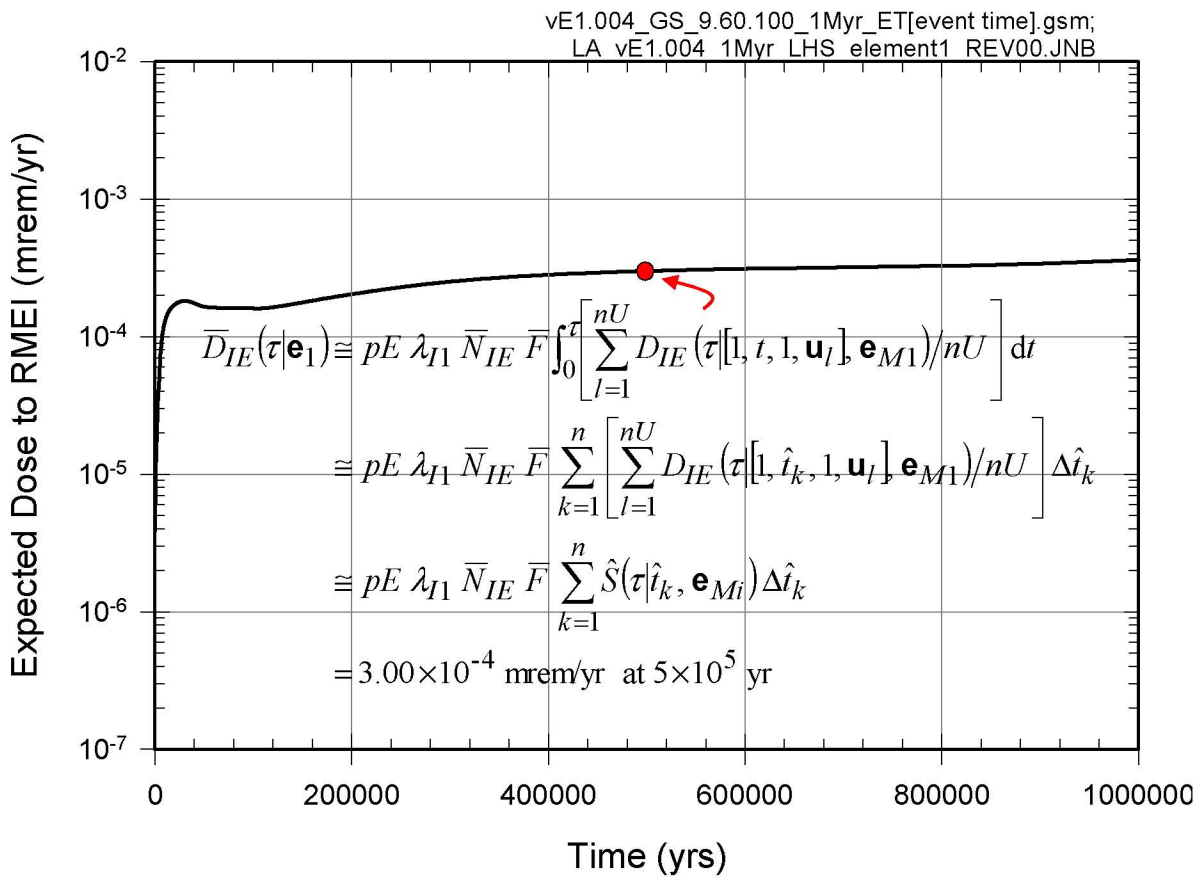

Source: Ouput DTNs: MO0709TSPAPLOT.000 [DIRS 183010]; and MO0709TSPAREGS.000 [DIRS 182976].

Figure J7.3-12. Estimate of $\overline{D}_{IE}(\tau|\mathbf{e}_1)$ for LHS element $\mathbf{e}_1 = [\mathbf{e}_{A1}, \mathbf{e}_{M1}]$ and $0 \le \tau \le 10^6$ yr with integration-based procedure indicated in Equations J7.3-9 and J7.3-16.

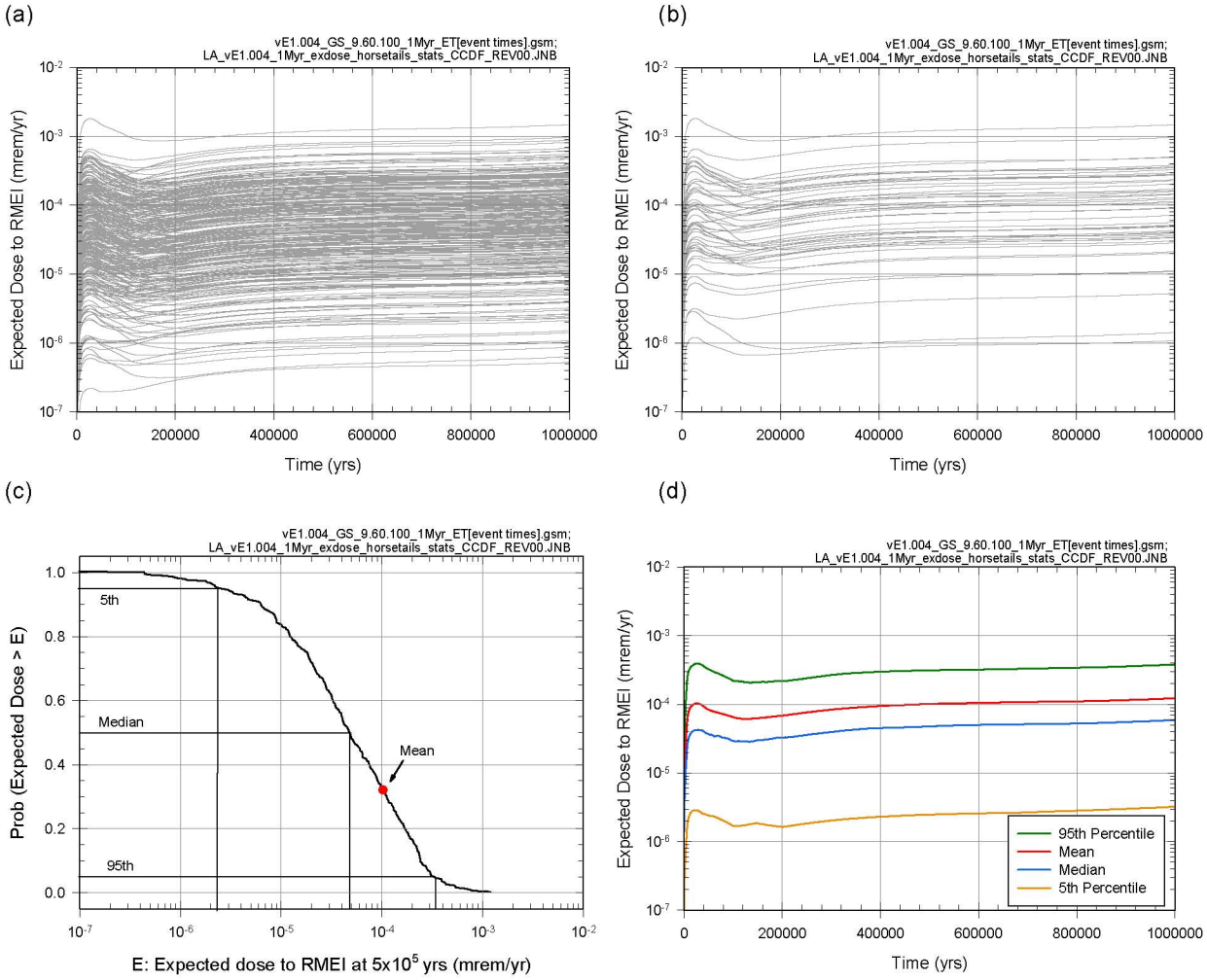

Source: Ouput DTNs: MO0709TSPAPLOT.000 [DIRS 183010]; and MO0709TSPAREGS.000 [DIRS 182976].

Figure J7.3-13. Estimate obtained with LHS of size *nLHS* = 300 showing epistemic uncertainty in expected dose $\bar{D}_{lE}(\tau|\mathbf{e})$ to RMEI for $0 \le \tau \le 10^6$ yr that results when only igneous eruptive events are considered: (a) expected dose $\bar{D}_{lE}(\tau|\mathbf{e}_i)$, i = 1, 2, …, *nLHS* = 300, (b) expected dose $\bar{D}_{lE}(\tau|\mathbf{e}_i)$, i = 1, 2, …, 50, (c) exceedance probabilities $p_E[D < \bar{D}_{lE}(\tau|\mathbf{e})]$ and quantiles $Q_q[\bar{D}_{lE}(\tau|\mathbf{e})]$, q = 0.05, 0.5 and 0.95, for τ = 500,000 yr, and (d) expected (mean) dose $\bar{\bar{D}}_{lE}(\tau)$ and quantiles $Q_q[\bar{D}_{lE}(\tau|\mathbf{e})]$, q = 0.05, 0.5, 0.95.

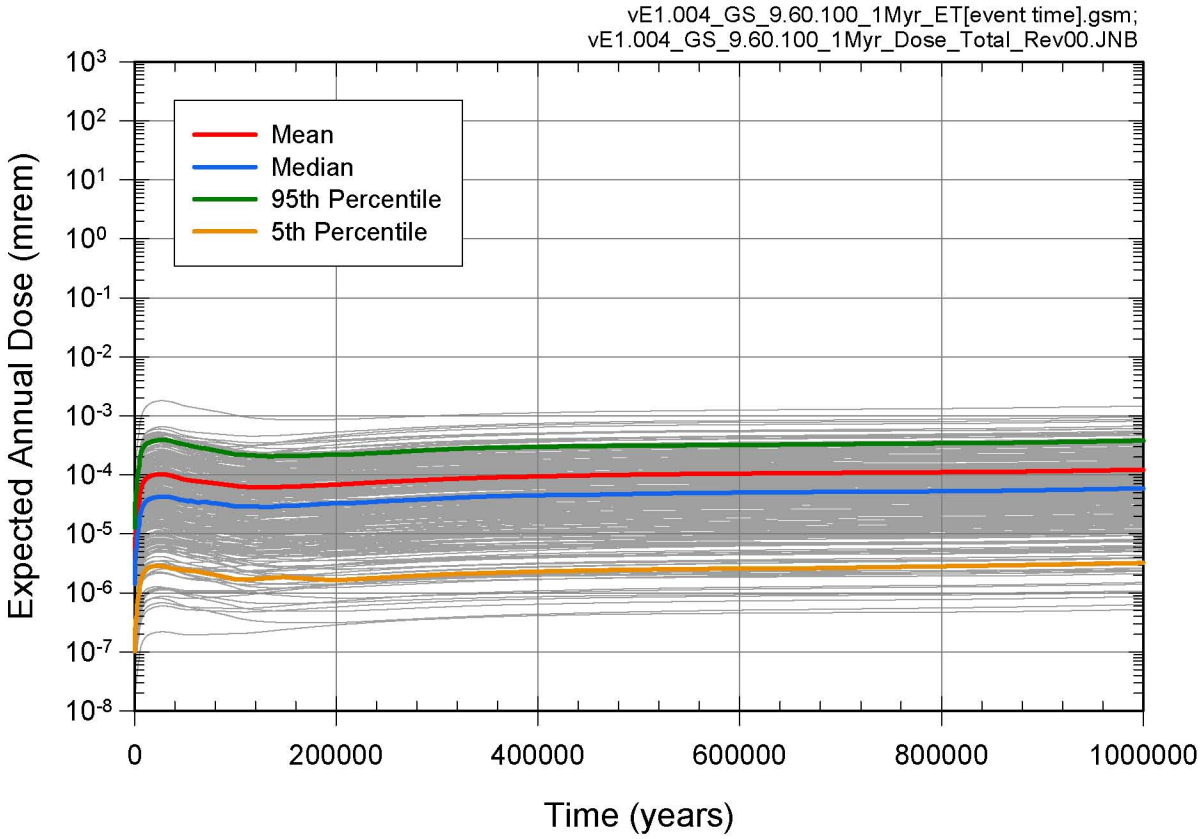

Source: Ouput DTNs: MO0709TSPAPLOT.000 [DIRS 183010]; and MO0709TSPAREGS.000 [DIRS 182976].

Figure J7.3-14. Summary of results obtained with LHS of size *nLHS* = 300 showing epistemic uncertainty in expected dose $\bar{D}_{IE}(\tau|\mathbf{e})$ to RMEI for $0 \leq \tau \leq 10^6$ yr that results when only igneous eruptive events are considered.

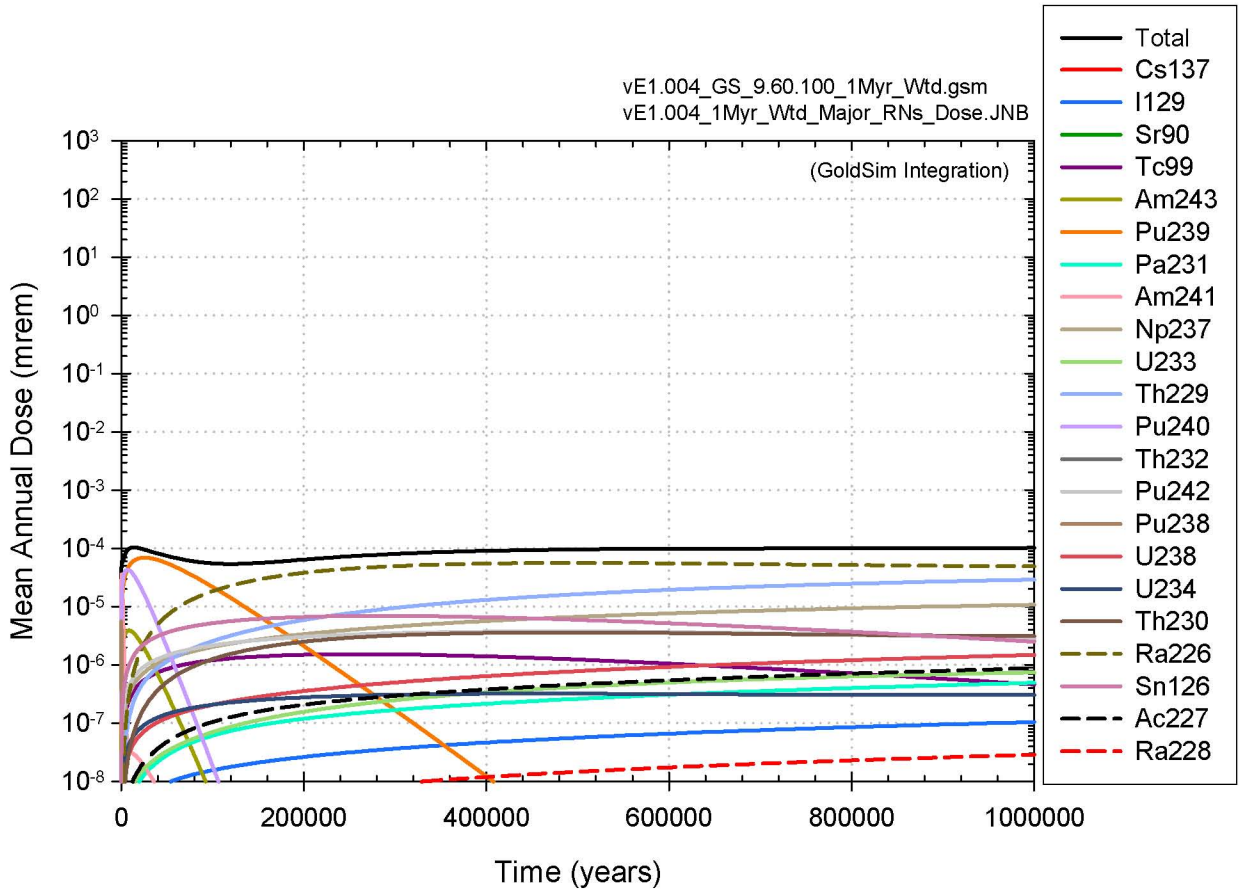

Source: Ouput DTNs: MO0709TSPAPLOT.000 [DIRS 183010]; and MO0709TSPAREGS.000 [DIRS 182976].

Figure J7.3-15. Estimates obtained with LHS of size *nLHS* = 300 of expected (mean) dose $\bar{\bar{D}}_{IE,r}(\tau)$ to RMEI for $0 \leq \tau \leq 10^6$ yr for individual radioactive species that result when only igneous eruptive events are considered.

(a)

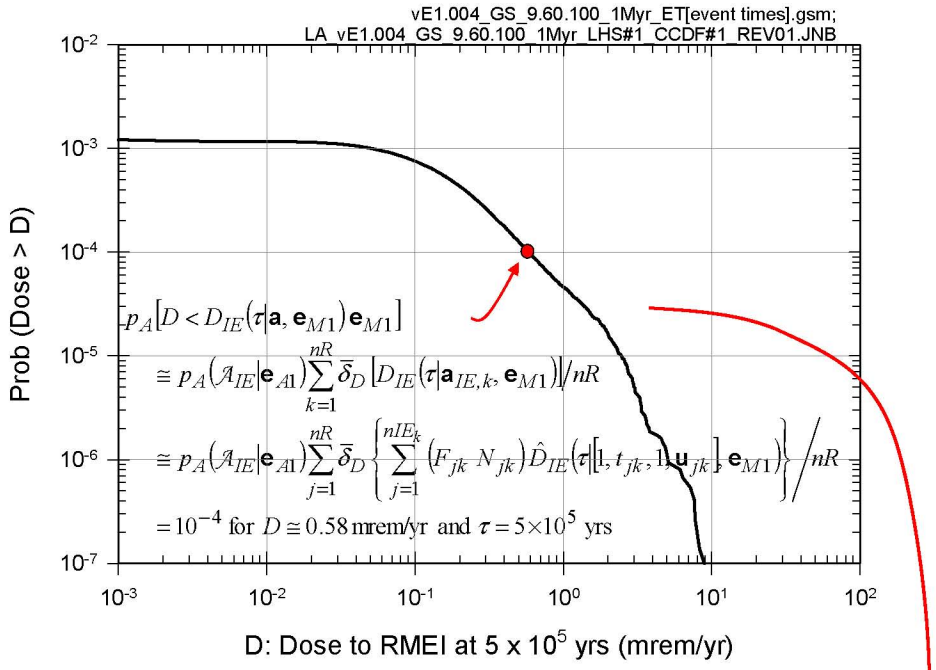

(b)

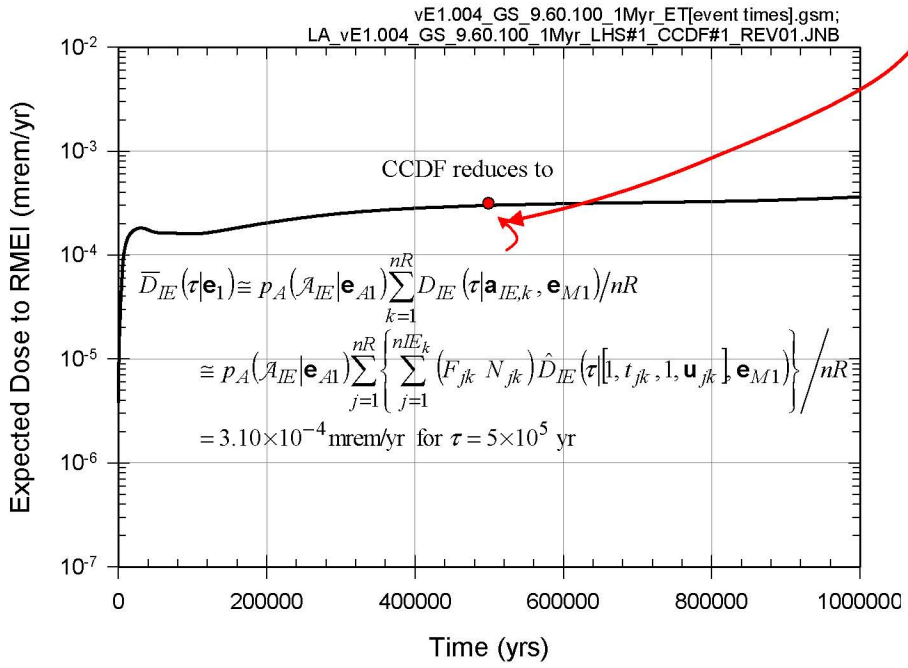

Source: Ouput DTNs: MO0709TSPAPLOT.000 [DIRS 183010]; and MO0709TSPAREGS.000 [DIRS 182976].

Figure J7.3-16. Results associated with $D_{IE}(\tau|\mathbf{a}_{IE}, \mathbf{e}_{M1})$ for LHS element $\mathbf{e}_1 = [\mathbf{e}_{A1}, \mathbf{e}_{M1}]$ obtained with sampling-based (Monte Carlo) procedures: (a) CCDF for $D_{IE}(500{,}000\ \text{yr}|\mathbf{a}_{IE}, \mathbf{e}_{M1})$ with exceedance probabilities $p_A[D < D_{IE}(500{,}000\ \text{yr}|\mathbf{a}, \mathbf{e}_{M1})|\mathbf{e}_{A1}]$ defined in Equation J7.3-20, and (b) expected dose $\bar{D}_{IE}(500{,}000\ \text{yr}|\mathbf{e}_1)$ associated with $D_{IE}(500{,}000\ \text{yr}|\mathbf{a}_{IE}, \mathbf{e}_{M1})$ as defined in Equation J7.3-18.

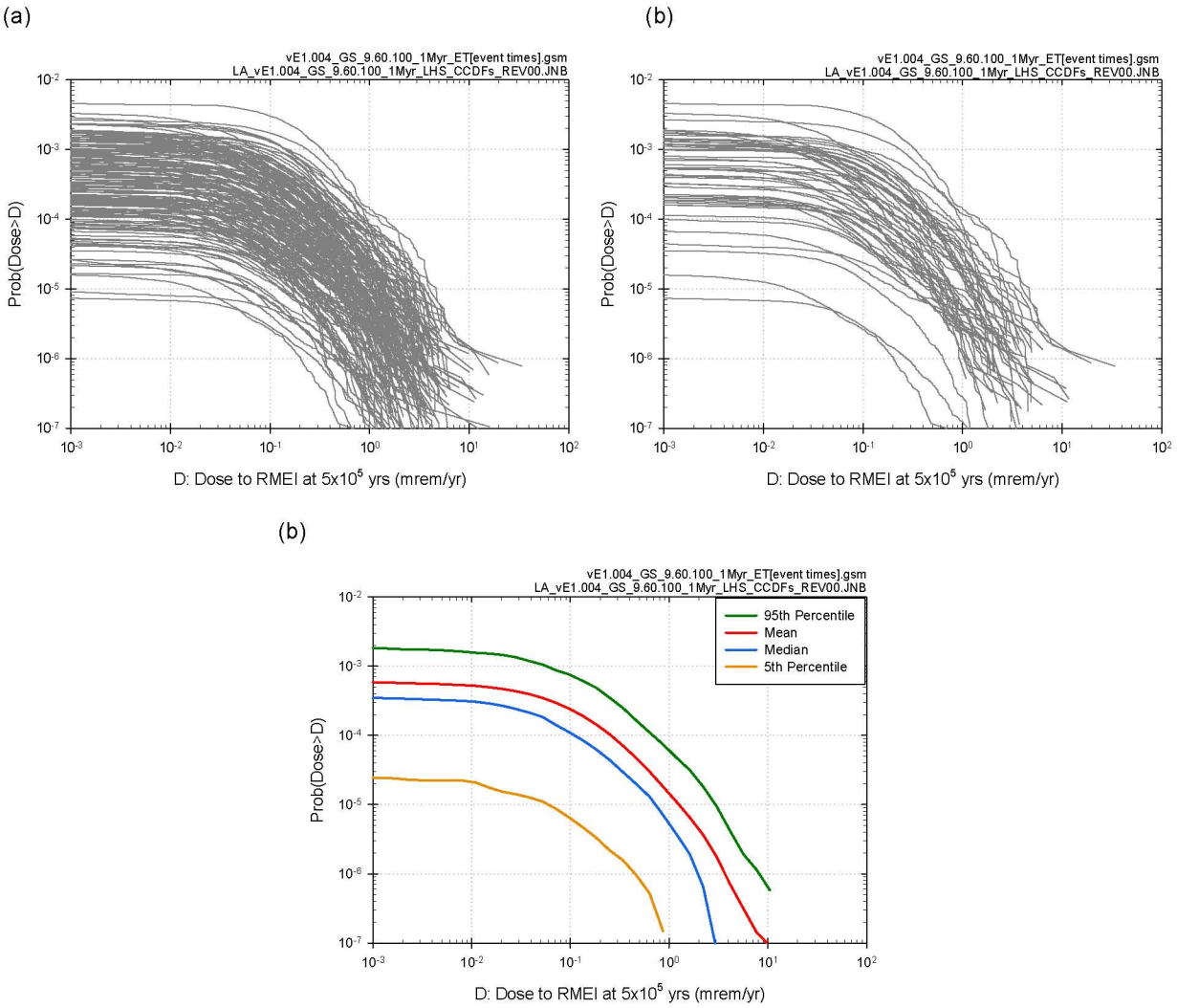

Source: Ouput DTNs: MO0709TSPAPLOT.000 [DIRS 183010]; and MO0709TSPAREGS.000 [DIRS 182976].

Figure J7.3-17. Results associated with $D_{IE}(500{,}000\ \text{yr}|\mathbf{a}_{IE}, \mathbf{e}_M)$ obtained with sampling-based (Monte Carlo) procedures for an LHS of size $nLHS = 300$: (a) CCDFs for $D_{IE}(10^4\ \text{yr}|\mathbf{a}_{IE}, \mathbf{e}_{Mi})$ with exceedance probabilities $p_A[D < D_{IE}(500{,}000\ \text{yr}|\mathbf{a}, \mathbf{e}_{Mi})|\mathbf{e}_{Ai}]$ defined in Equation J7.3-20 for $i = 1, 2, \ldots, nLHS = 300$, (b) CCDFs for $D_{IE}(500{,}000\ \text{yr}|\mathbf{a}_{IE}, \mathbf{e}_{Mi})$ with exceedance probabilities $p_A[D < D_{IE}(500{,}000\ \text{yr}|\mathbf{a}, \mathbf{e}_{Mi})|\mathbf{e}_{Ai}]$ defined in Equation J7.3-20 for $i = 1, 2, \ldots, 50$, and (c) expected (mean) CCDF and quantile curves, $q = 0.05, 0.5, 0.95$, for CCDFs in (a).

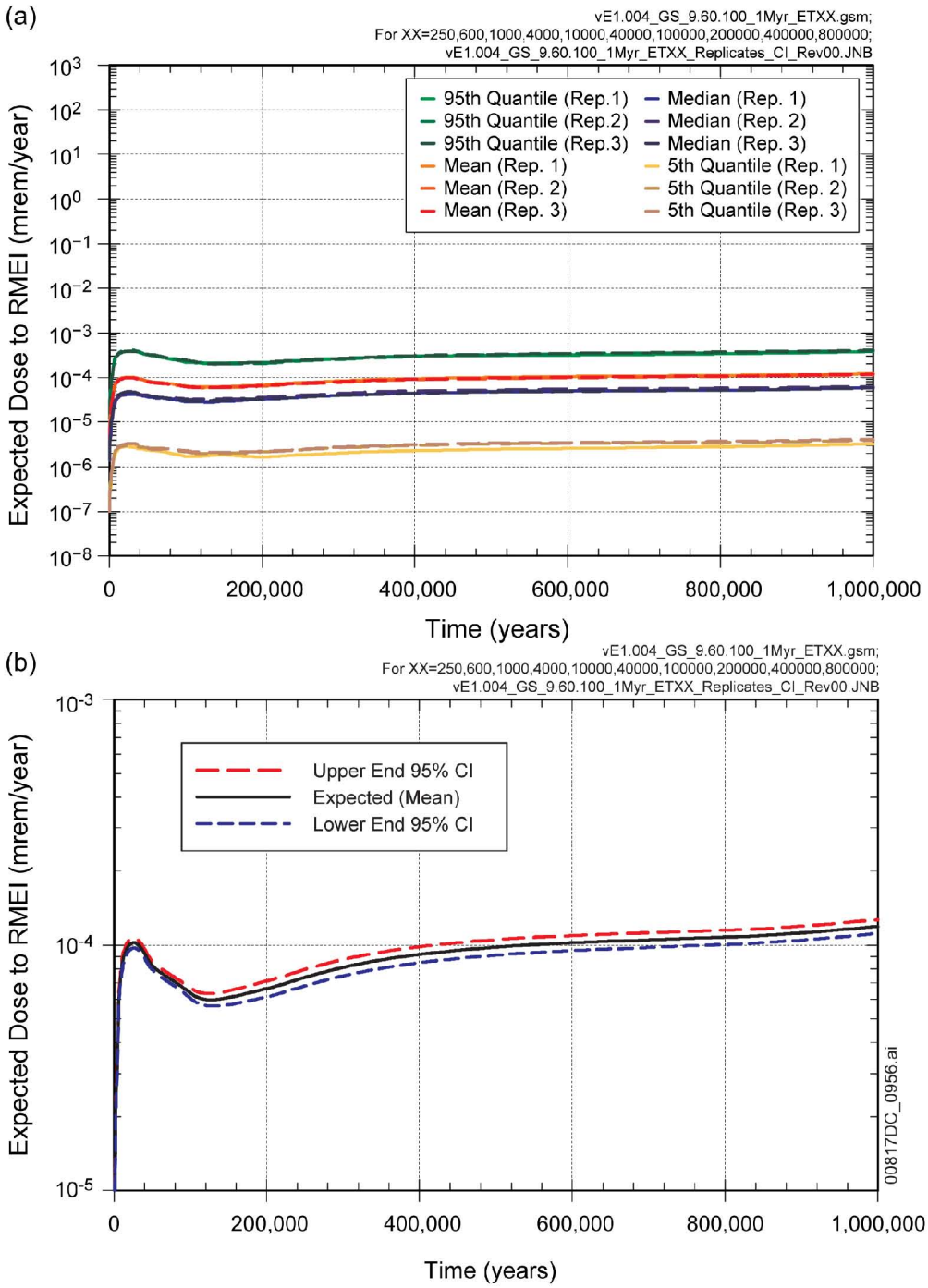

Source: Ouput DTNs: MO0709TSPAPLOT.000 [DIRS 183010]; and MO0709TSPAREGS.000 [DIRS 182976].

Figure J7.3-18. Assessment with replicated sampling of numerical error associated with use of an LHS of size *nLHS* = 300 to determine epistemic uncertainty in expected dose $\bar{\bar{D}}_{IE}(\tau)$ to RMEI for $0 \leq \tau \leq 10^6$ yr that results when only igneous eruptive events are considered: (a) Replicated estimates of expected (mean) dose $\bar{\bar{D}}_{IE}(\tau)$ and quantiles $Q_q[\bar{D}_{IE}(\tau|\mathbf{e})]$, q = 0.05, 0.5, 0.95, and (b) confidence intervals for estimates of expected (mean) dose $\bar{\bar{D}}_{IE}(\tau)$.

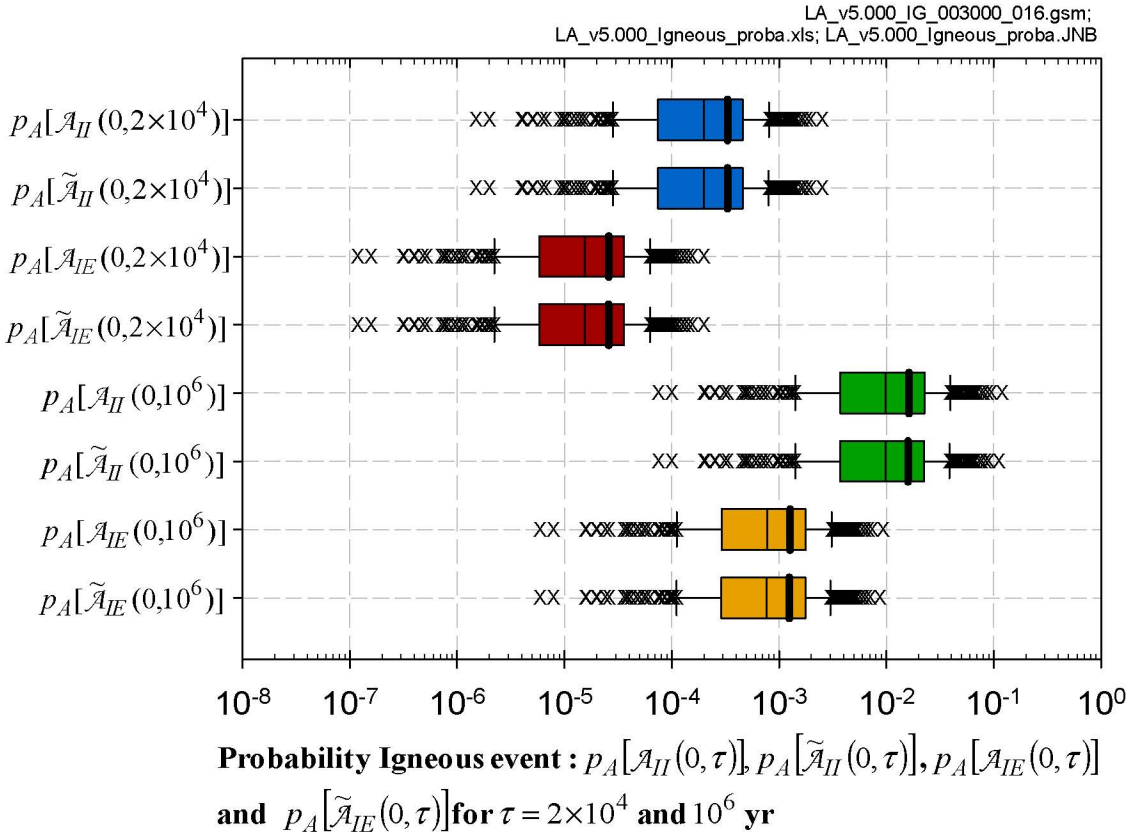

Source: Ouput DTNs: MO0709TSPAPLOT.000 [DIRS 183010]; and MO0709TSPAREGS.000 [DIRS 182976].

Figure J7.5-1. Box plots summarizing probabilities $p_A[\mathcal{A}_{II}(0, \tau)|\mathbf{e}_{Ai}]$, $p_A[\tilde{\mathcal{A}}_{II}(0, \tau)|\mathbf{e}_{Ai}]$, $p_A[\mathcal{A}_{IE}(0, \tau)|\mathbf{e}_{Ai}]$ and $p_A[\tilde{\mathcal{A}}_{IE}(0, \tau)|\mathbf{e}_{Ai}]$ for scenario classes $\mathcal{A}_{II}(0, \tau)$, $\tilde{\mathcal{A}}_{II}(0, \tau)$, $\mathcal{A}_{IE}(0, \tau)$ and $\tilde{\mathcal{A}}_{IE}(0, \tau)$ defined for the time intervals [0, 20,000 yr] and [0, 1,000,000 yr] obtained with LHS of size *nLHS* = 300.

INTENTIONALLY LEFT BLANK

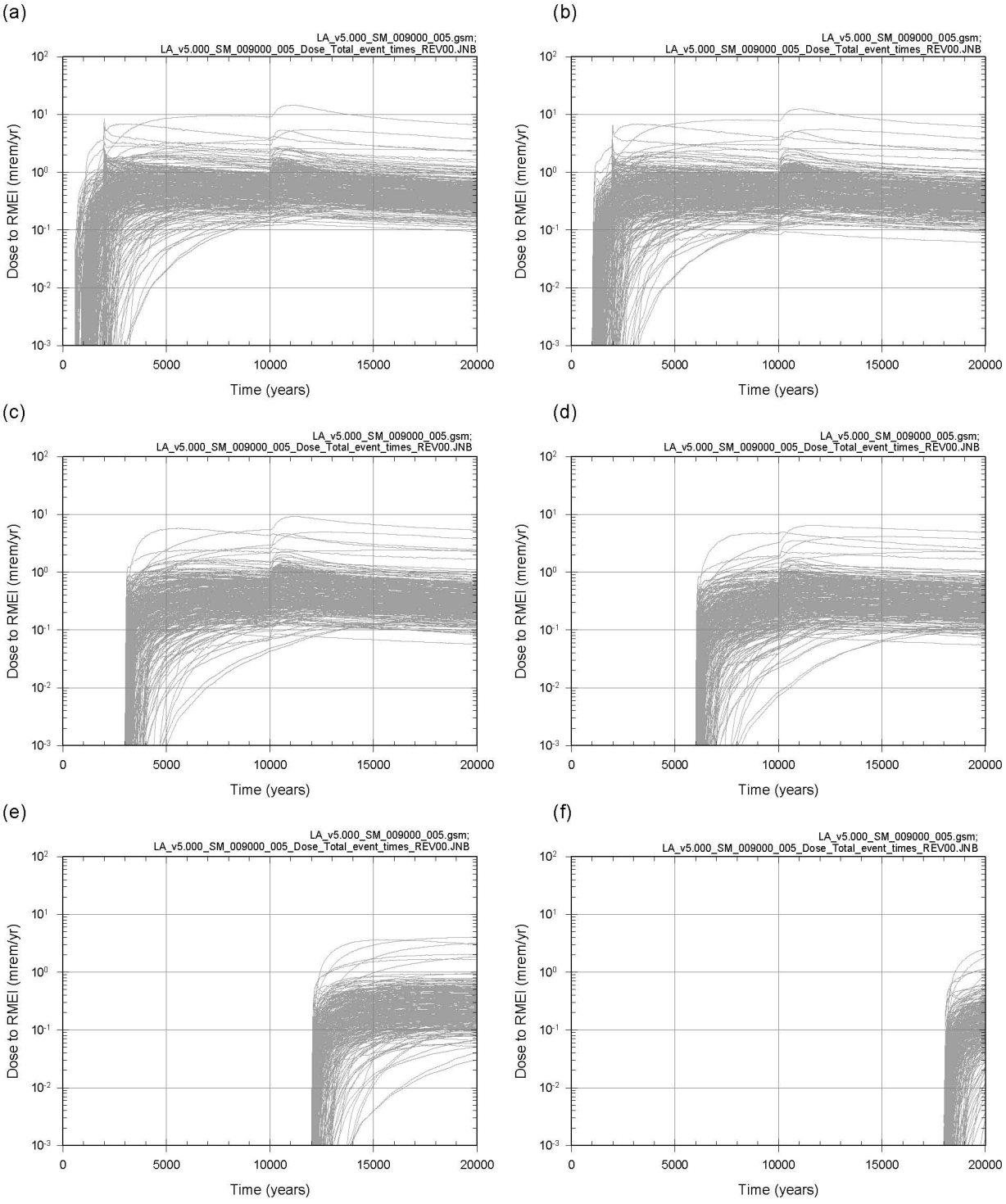

Source: Ouput DTNs: MO0709TSPAPLOT.000 [DIRS 183010]; and MO0709TSPAREGS.000 [DIRS 182976].

Figure J8.3-1. Summary of results for damage to CDSP WPs obtained with LHS of size *nLHS* = 300 showing epistemic uncertainty in doses $D_{SG}(\tau|[1, t_r, A_s], \mathbf{e}_{Mi})$ for $0 \leq \tau \leq 20{,}000$ yr damaged area $A_s = (10^{-6})$ (32.6 m^2) and the following values for event time t_r: (a) 200 yr, (b) 1000 yr, (c) 3000 yr, (d) 6000 yr, (e) 12,000 yr, and (f) 18,000 yr.

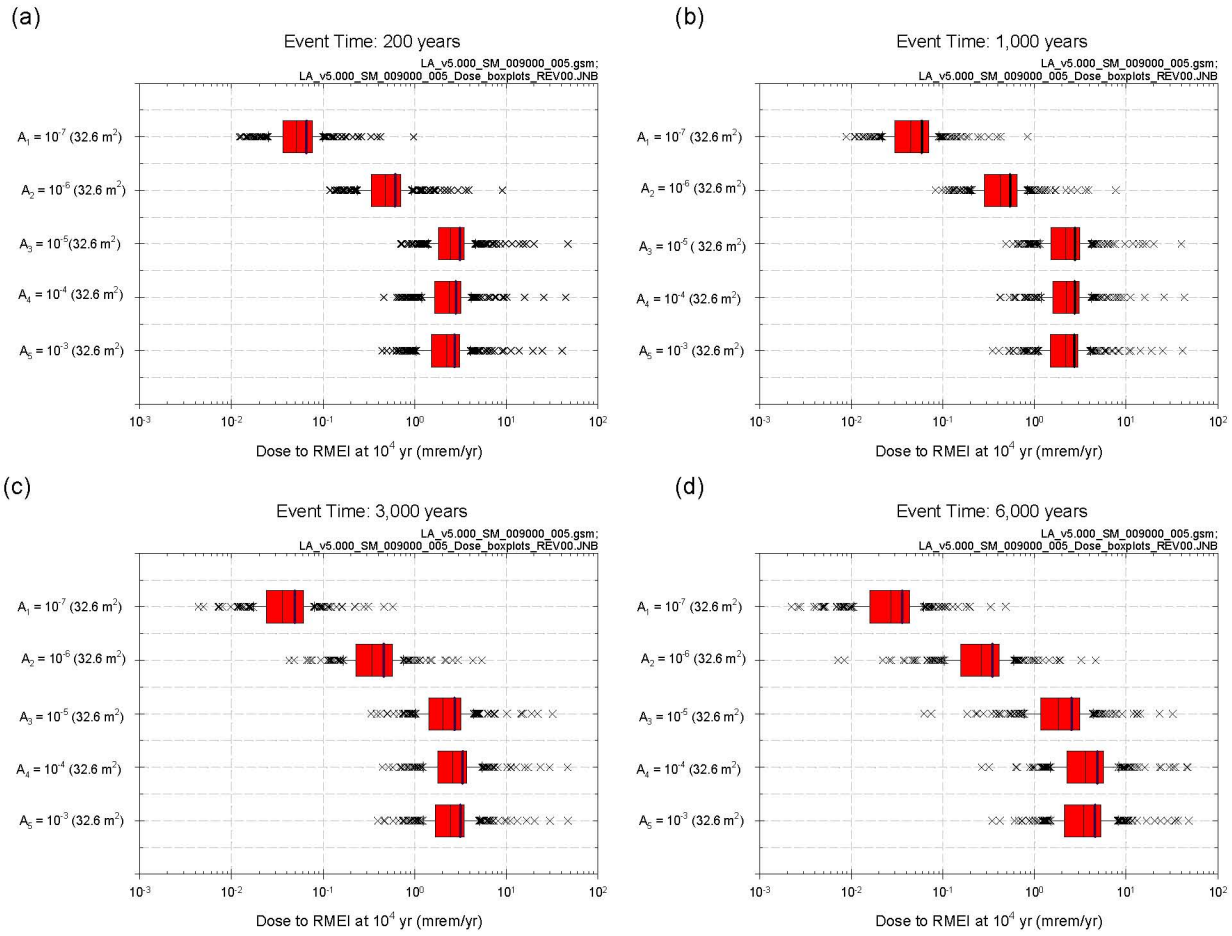

Source: Ouput DTNs: MO0709TSPAPLOT.000 [DIRS 183010]; and MO0709TSPAREGS.000 [DIRS 182976].

Figure J8.3-2. Box plots (see Figure J6.2-3 for description) summarizing results for damage to CDSP WPs obtained with LHS of size *nLHS* = 300 showing epistemic uncertainty in dose $D_{SG}(\tau|[1, t_r, A_s], \mathbf{e}_{Mi})$ with t_r = 200, 1000, 3000, and 6000 yrs, $A_s = 10^{-8+s}$ (32.6 m^2) for s = 1, 2, 3, 4, 5, and i = 1, 2, …, *nLHS* = 300, where 32.6 m^2 is the assumed surface area for a CDSP WP: (a) t_r = 200 yrs, (b) t_r = 1000 yrs, (c) t_r = 3000 yrs, and (d) t_r = 6000 yrs.

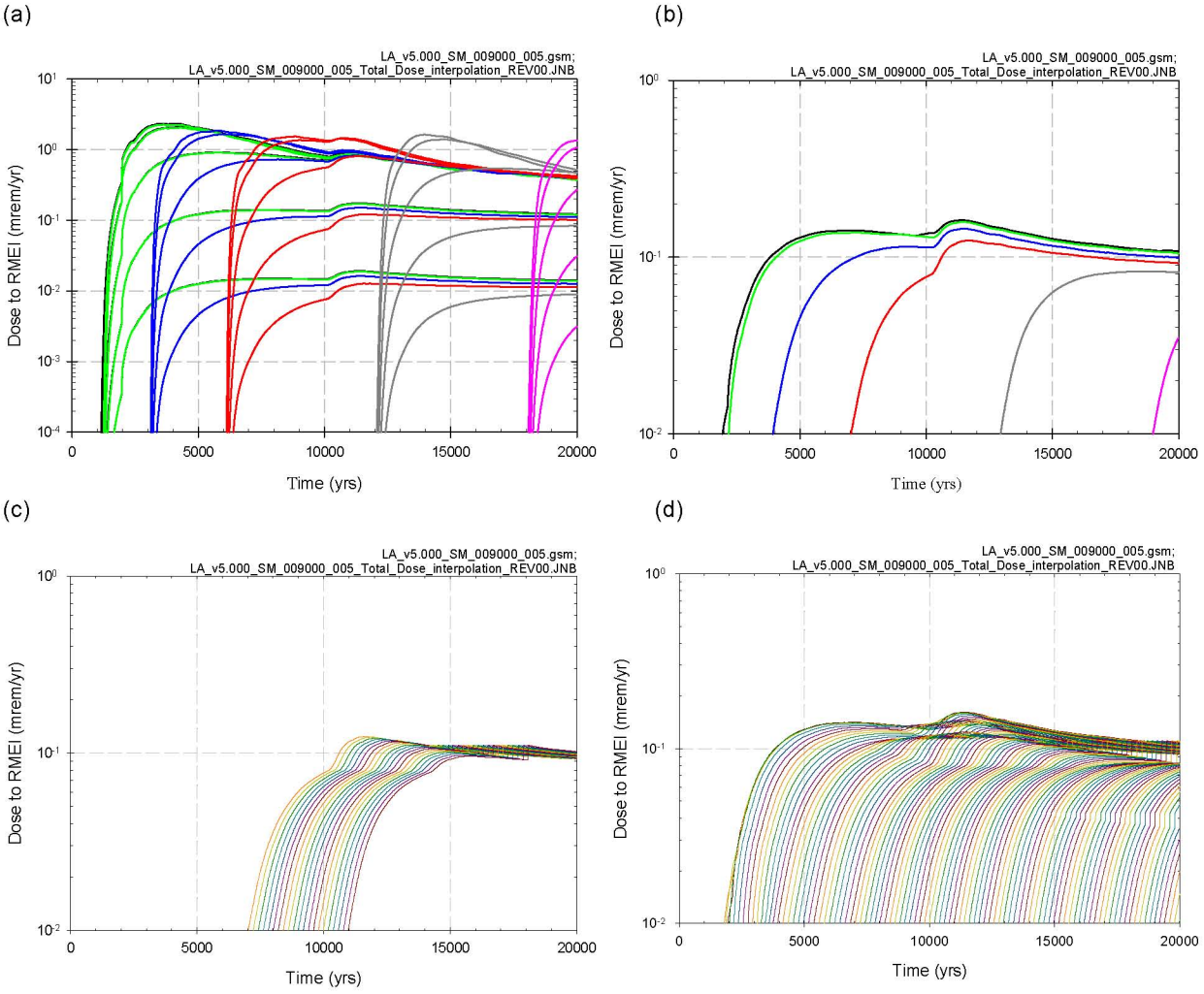

Source: Ouput DTNs: MO0709TSPAPLOT.000 [DIRS 183010]; and MO0709TSPAREGS.000 [DIRS 182976].

Figure J8.3-3. Illustration of interpolation procedure to obtain estimated integrals $\hat{I}_1(\tau|t, \mathbf{e}_{M1})$ from calculated doses $D_{SG}(\tau|[1, t_r, A_s], \mathbf{e}_{M1})$ indicated in Equation J8.3-9 for LHS element $\mathbf{e}_1 = [\mathbf{e}_{A1}, \mathbf{e}_{M1}]$ and the time interval $[0, 2.0 \times 10^4$ yr]: (a) $D_{SG}(\tau|[1, t_r, A_s], \mathbf{e}_{M1})$, $r = 1, 2, \ldots, 6$ and $s = 1, 2, \ldots, 5$, (b) $\hat{I}_1(\tau|t_r, \mathbf{e}_{M1})$, $r = 1, 2, \ldots, 6$, (c) interpolated values $\hat{I}_1(\tau|\hat{t}_k, \mathbf{e}_{M1})$ for $\hat{t}_k$ between $t_4 = 6000$ yrs and $t_5 = 12{,}000$ yrs, and (d) interpolated values for $\hat{I}_1(\tau|\hat{t}_k, \mathbf{e}_1)$ for $\hat{t}_k$ between = 100 yrs and 20,000 yrs.

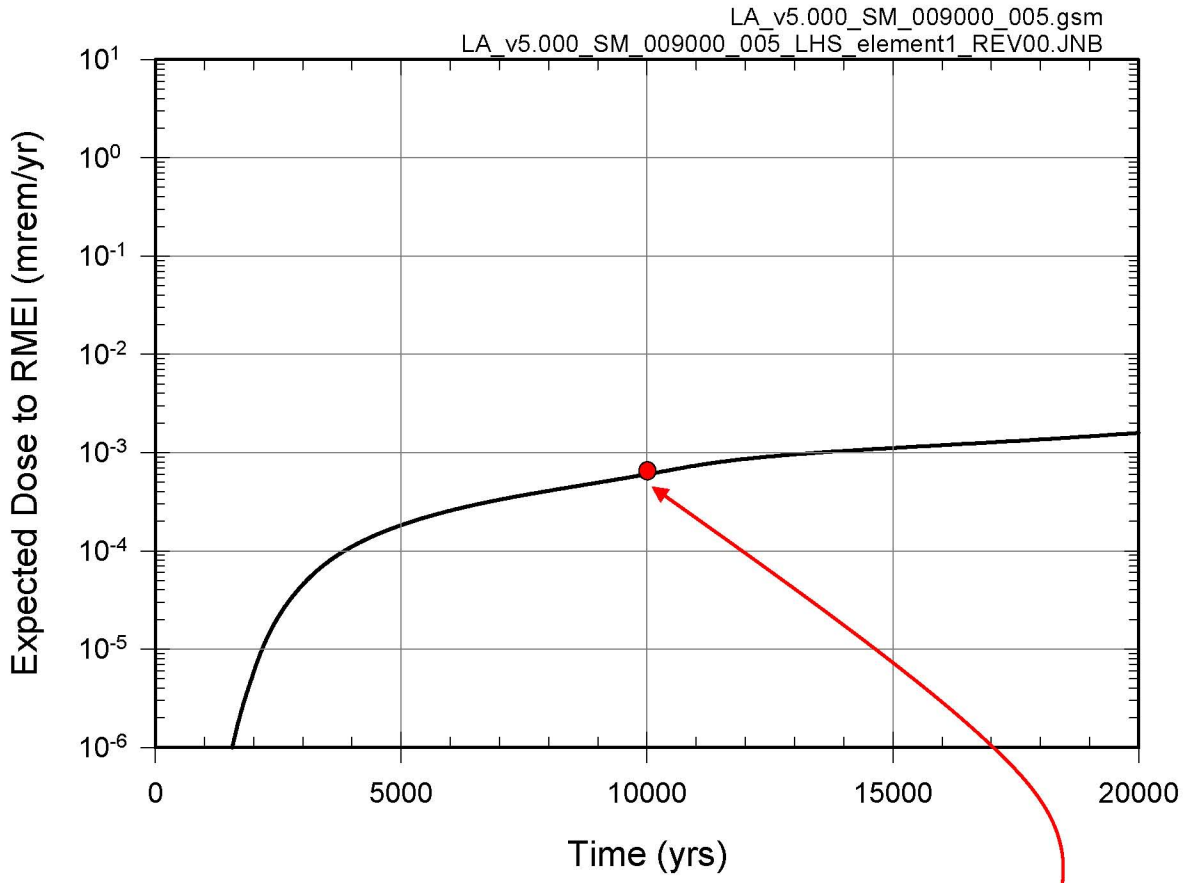

$$\bar{D}_{SG}(\tau|\mathbf{e}_1) = \int_0^{\tau} \left(\lambda_1(\mathbf{e}_1)\exp\left[-\lambda(\mathbf{e}_1)t\right]\right)\left(\int_{\mathcal{A}1} D_{SG}(\tau|[1, t, A], \mathbf{e}_{M1})\, d_{A1}(A|\mathbf{e}_1)\,\mathrm{d}A + \int_0^{\tau}\left[\int_{\mathcal{A}2} D_{SG}(\tau|[1, \tilde{\tau}, A], \mathbf{e}_{M1})\, d_{A2}(A|\mathbf{e}_1)\,\mathrm{d}A\right]\lambda_2(\mathbf{e}_1)\,\mathrm{d}\tilde{\tau}\right)\mathrm{d}t$$

$$\cong \sum_{j=1}^{n}\left(\lambda_1(\mathbf{e}_1)\exp\left[-\lambda_1(\mathbf{e}_1)\hat{t}_{j-1}\right]\right)\left(\hat{I}_1(\tau|\hat{t}_j, \mathbf{e}_1) + \sum_{k=j+1}^{n}\left[\hat{I}_2(\tau|\hat{t}_{k-1}, \mathbf{e}_1)\right]\lambda_2(\mathbf{e}_1)\Delta\hat{t}_k\right)\Delta\hat{t}_j$$

$$= 6.00\times10^{-4}\ \text{mrem/yr} \quad \text{for } \tau = 10{,}000\ \text{yr}$$

Source: Ouput DTNs: MO0709TSPAPLOT.000 [DIRS 183010]; and MO0709TSPAREGS.000 [DIRS 182976].

Figure J8.3-4. Estimate of $\bar{D}_{SG}(\tau|\mathbf{e}_1)$ for LHS element $\mathbf{e}_1$ = [$\mathbf{e}_{A1}$, $\mathbf{e}_{M1}$] and $0 \le \tau \le 20{,}000$ yr with integration-based procedure indicated in Equation J8.3-13.

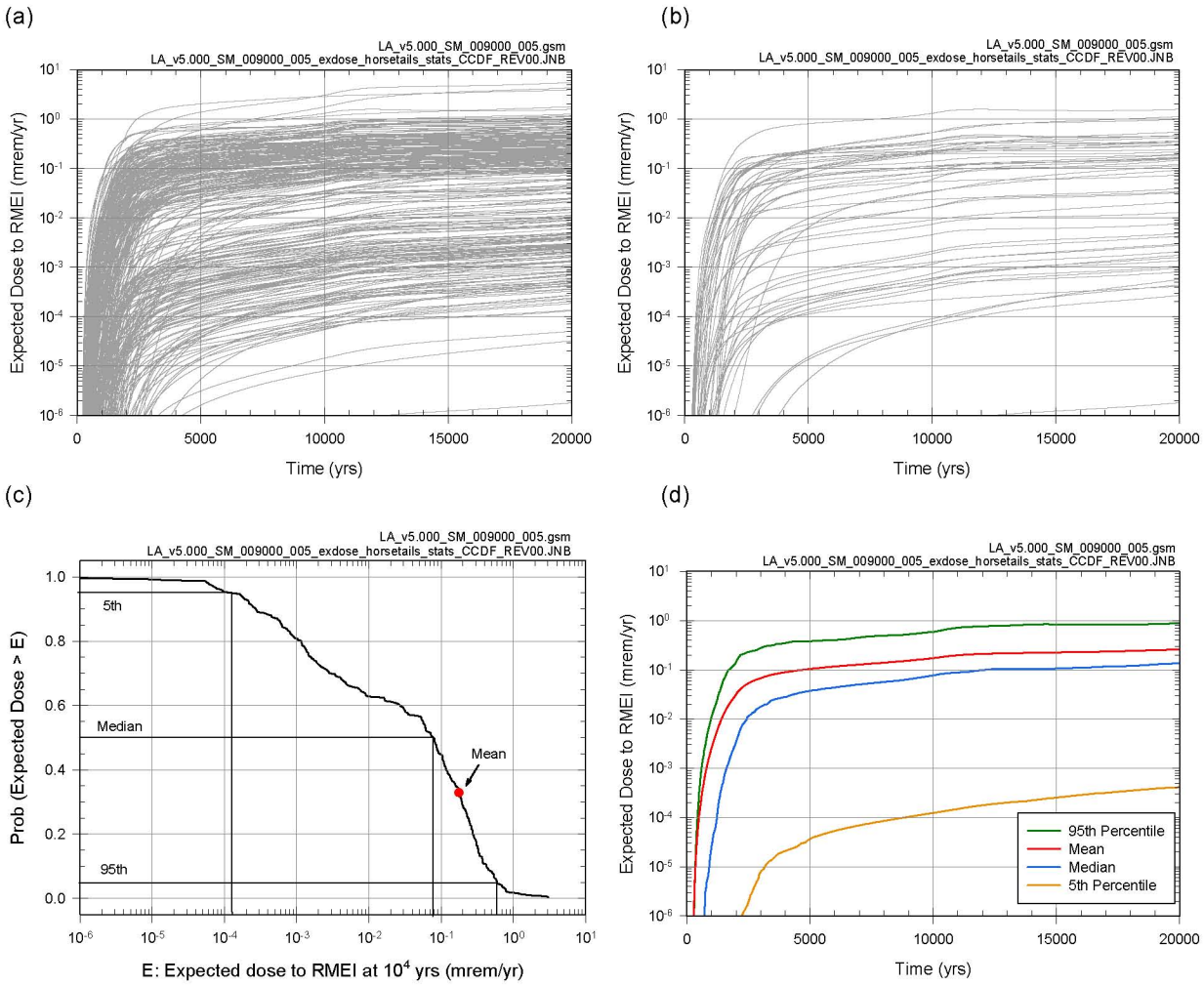

Source: Ouput DTNs: MO0709TSPAPLOT.000 [DIRS 183010]; and MO0709TSPAREGS.000 [DIRS 182976].

Figure J8.3-5. Estimate obtained with LHS of size *nLHS* = 300 showing epistemic uncertainty in expected dose $\bar{D}_{SG}(\tau|\mathbf{e})$ to RMEI for $0 \le \tau \le 20{,}000$ yr that results when only seismic ground motion events are considered: (a) expected dose $\bar{D}_{SG}(\tau|\mathbf{e}_i)$, $i = 1, 2, \ldots, nLHS = 300$, (b) expected dose $\bar{D}_{SG}(\tau|\mathbf{e}_i)$, $i = 1, 2, \ldots, 50$, (c) exceedance probabilities $p_E[D < \bar{D}_{SG}(\tau|\mathbf{e})]$ and quantiles $Q_q[\bar{D}_{SG}(\tau|\mathbf{e})]$, $q = 0.05$, 0.5 and 0.95, for $\tau = 10^4$ yr, and (d) expected (mean) dose $\bar{\bar{D}}_{SG}(\tau)$ and quantiles $Q_q[\bar{D}_{SG}(\tau|\mathbf{e})]$, $q = 0.05, 0.5, 0.95$.

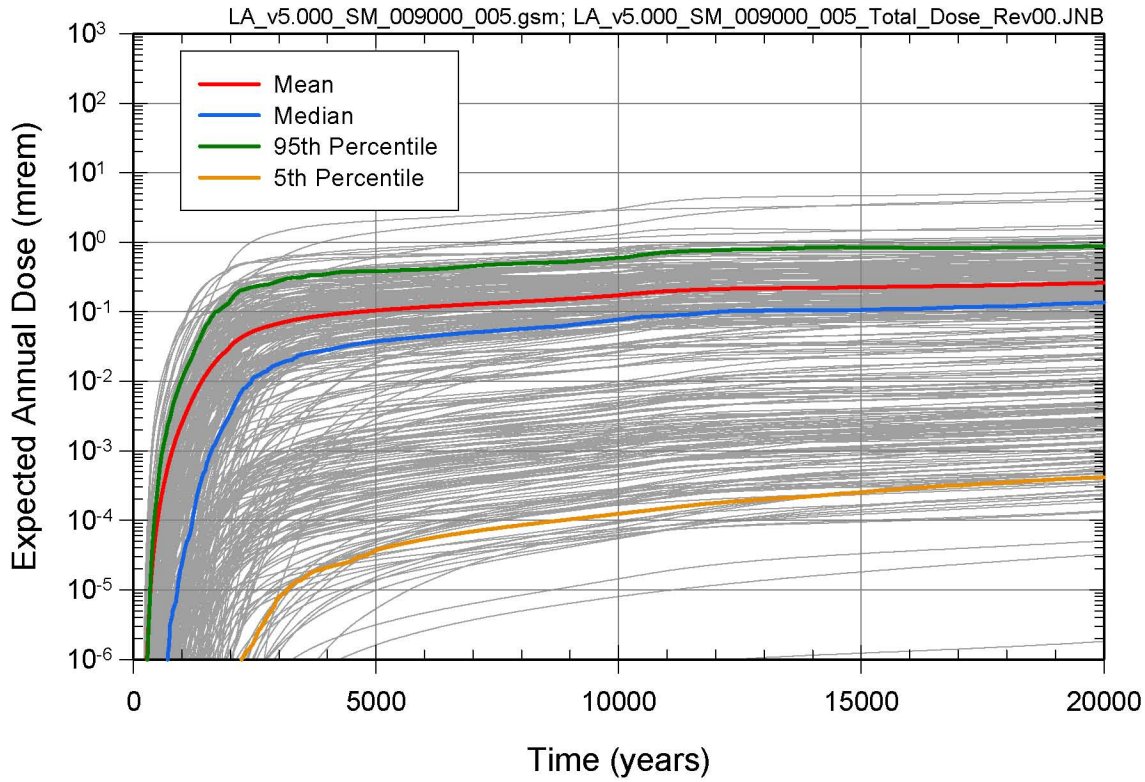

Source: Ouput DTNs: MO0709TSPAPLOT.000 [DIRS 183010]; and MO0709TSPAREGS.000 [DIRS 182976].

Figure J8.3-6. Summary of results obtained with LHS of size *nLHS* = 300 showing epistemic uncertainty in expected dose $\bar{D}_{SG}(\tau|\mathbf{e})$ to RMEI for $0 \leq \tau \leq 20{,}000$ yr that results when only seismic ground motion events are considered.

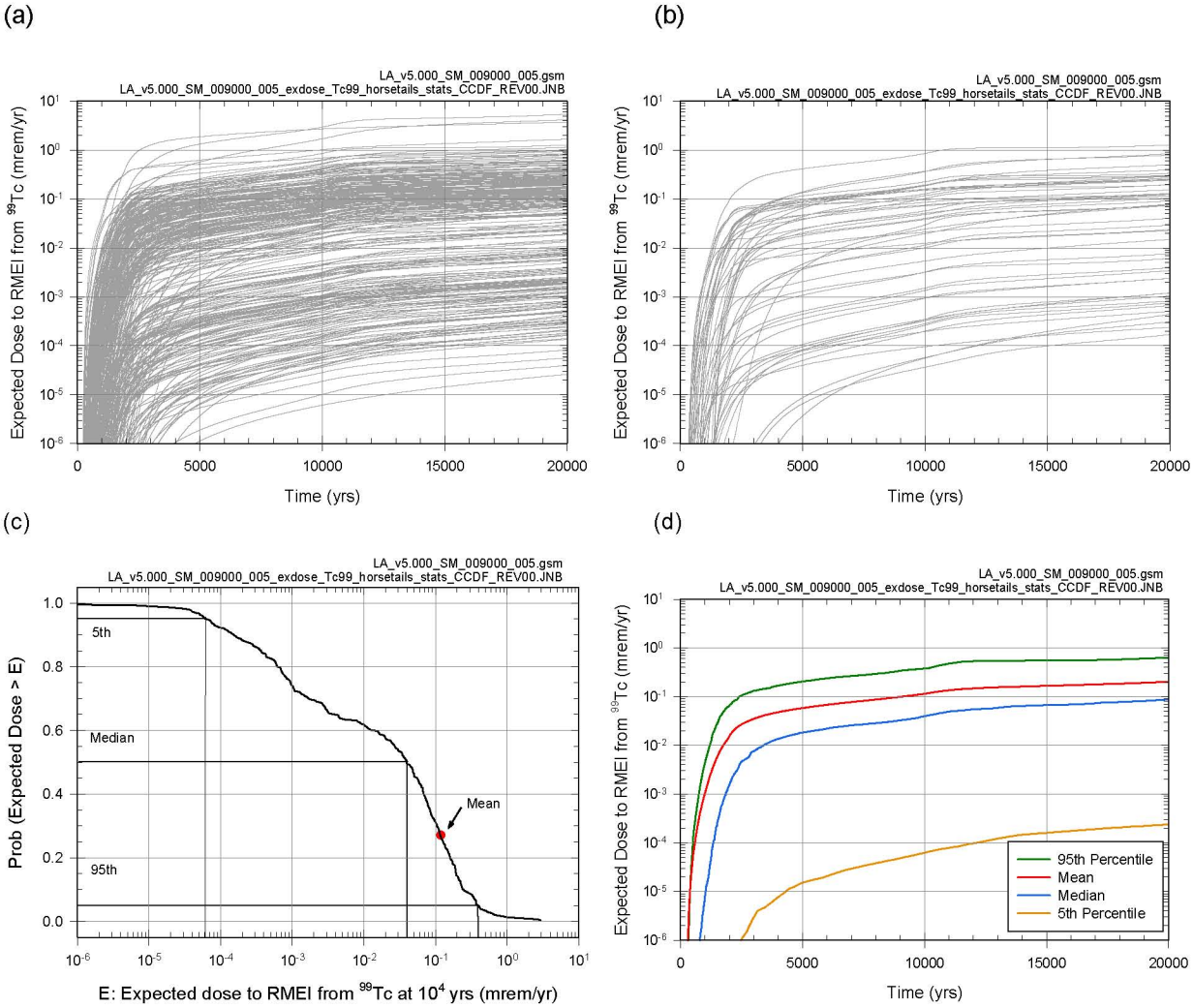

Source: Ouput DTNs: MO0709TSPAPLOT.000 [DIRS 183010]; and MO0709TSPAREGS.000 [DIRS 182976].

Figure J8.3-7. Estimate obtained with LHS of size *nLHS* = 300 showing epistemic uncertainty in expected dose $\bar{D}_{SG,r}(\tau|\mathbf{e})$ to RMEI for $0 \le \tau \le 20{,}000$ yr with r corresponding to ^{99}Tc that results when only seismic ground motion events are considered: (a) expected dose $\bar{D}_{SG,r}(\tau|\mathbf{e}_i)$, i = 1, 2, …, *nLHS* = 300, (b) expected dose $\bar{D}_{SG,r}(\tau|\mathbf{e}_i)$, i = 1, 2, …, 50, (c) exceedance probabilities $p_E[D < \bar{D}_{SG,r}(\tau|\mathbf{e})]$ and quantiles $Q_q[\bar{D}_{SG,r}(\tau|\mathbf{e})]$, q = 0.05, 0.5 and 0.95, for $\tau = 10^4$ yr, and (d) expected (mean) dose $\bar{\bar{D}}_{SG,r}(\tau)$ and quantiles $Q_q[\bar{D}_{SG,r}(\tau|\mathbf{e})]$, q = 0.05, 0.5, 0.95.

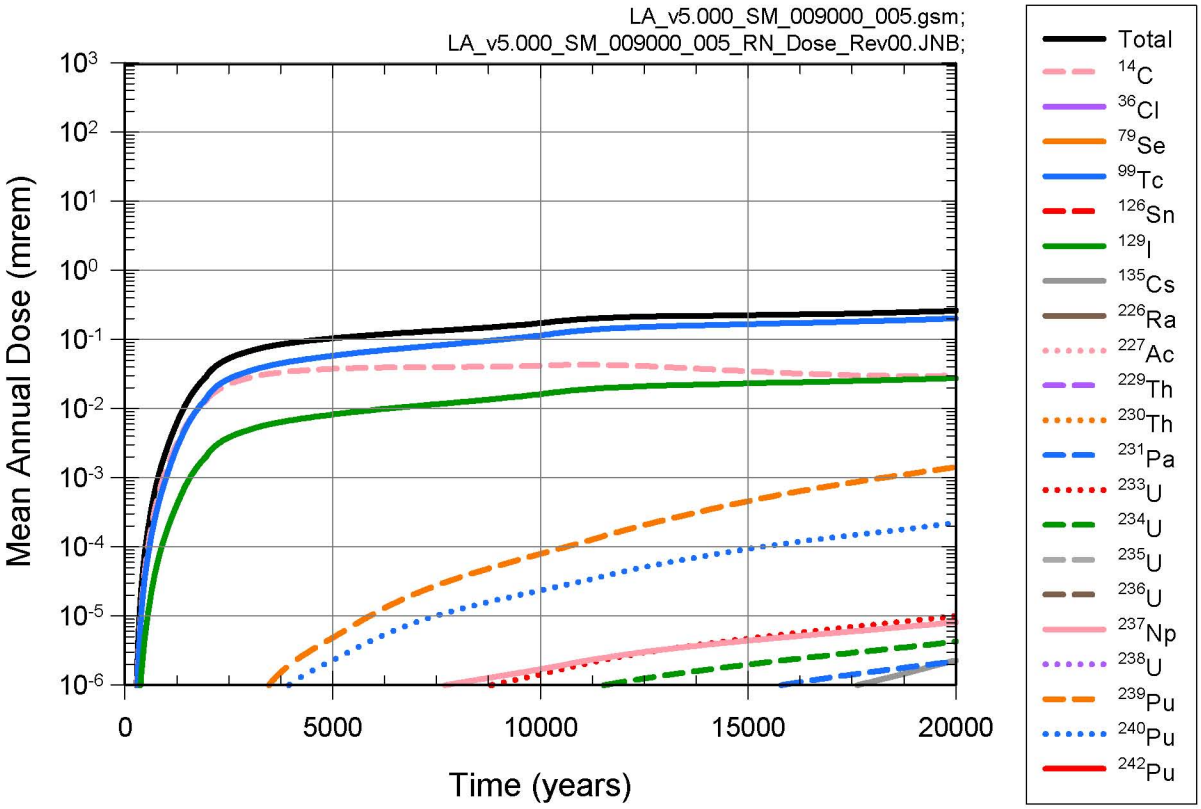

Source: Ouput DTNs: MO0709TSPAPLOT.000 [DIRS 183010]; and MO0709TSPAREGS.000 [DIRS 182976].

Figure J8.3-8. Estimates obtained with LHS of size *nLHS* = 300 of expected (mean) dose $\bar{\bar{D}}_{SG,r}(\tau)$ to RMEI for $0 \leq \tau \leq 20{,}000$ yr for individual radioactive species that result when only seismic ground motion events are considered.

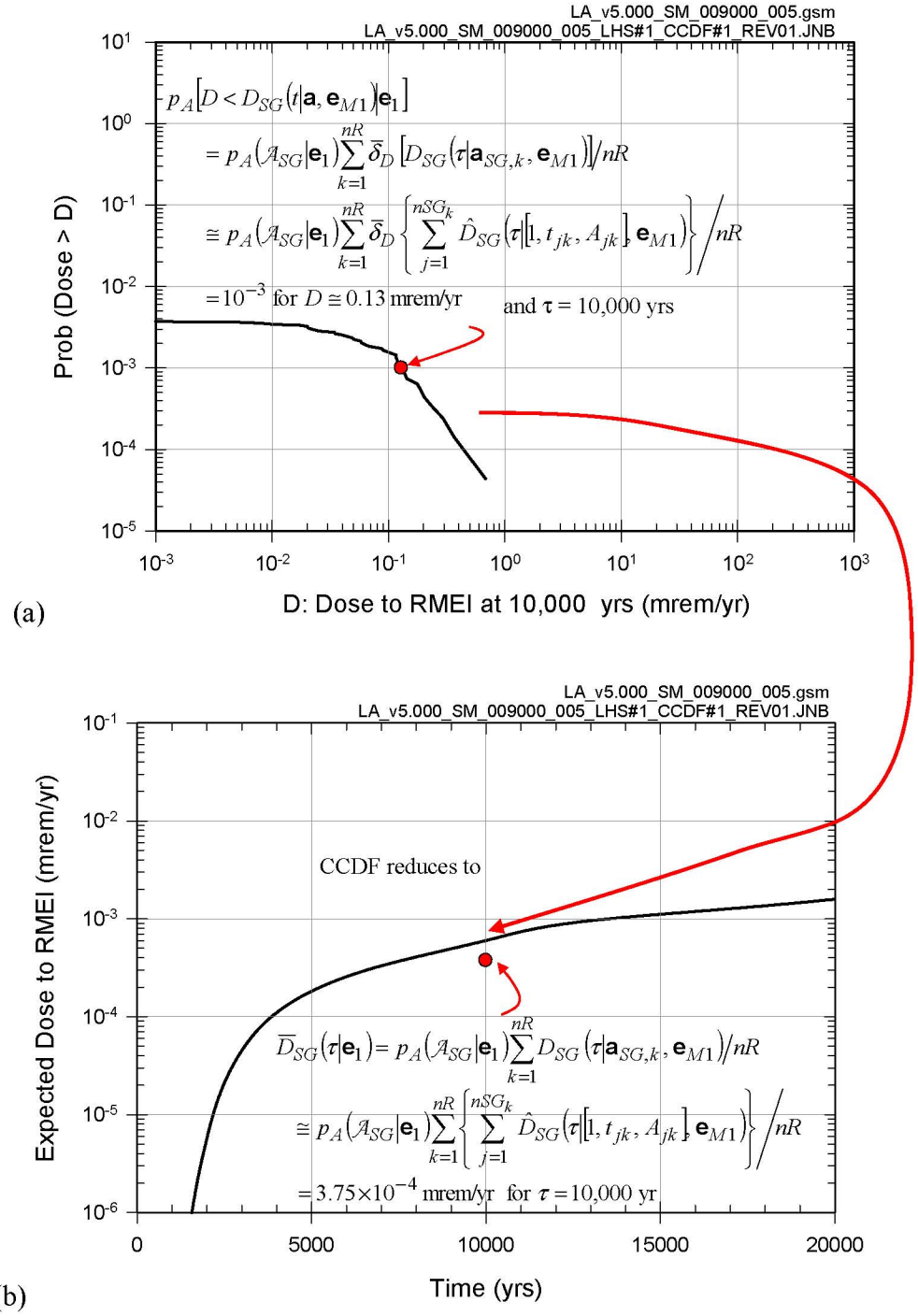

Source: Ouput DTNs: MO0709TSPAPLOT.000 [DIRS 183010]; and MO0709TSPAREGS.000 [DIRS 182976].

Figure J8.3-9. Results associated with $D_{SG}(\tau|\mathbf{a}_{SG}, \mathbf{e}_{M1})$ for LHS element $\mathbf{e}_1 = [\mathbf{e}_{A1}, \mathbf{e}_{M1}]$ obtained with sampling-based (Monte Carlo) procedures: (a) CCDF for $D_{SG}(10^4 \text{ yr}|\mathbf{a}_{SG}, \mathbf{e}_{M1})$ with exceedance probabilities $p_A[D < D_{SG}(10^4 \text{ yr}|\mathbf{a}, \mathbf{e}_{M1})|\mathbf{e}_1]$ defined in Equation J8.3-22, and (b) expected dose $\bar{D}_{SG}(10^4 \text{ yr}|\mathbf{e}_1)$ associated with $D_{SG}(10^4 \text{ yr}|\mathbf{a}_{SG}, \mathbf{e}_{M1})$ defined in Equation J8.3-20.

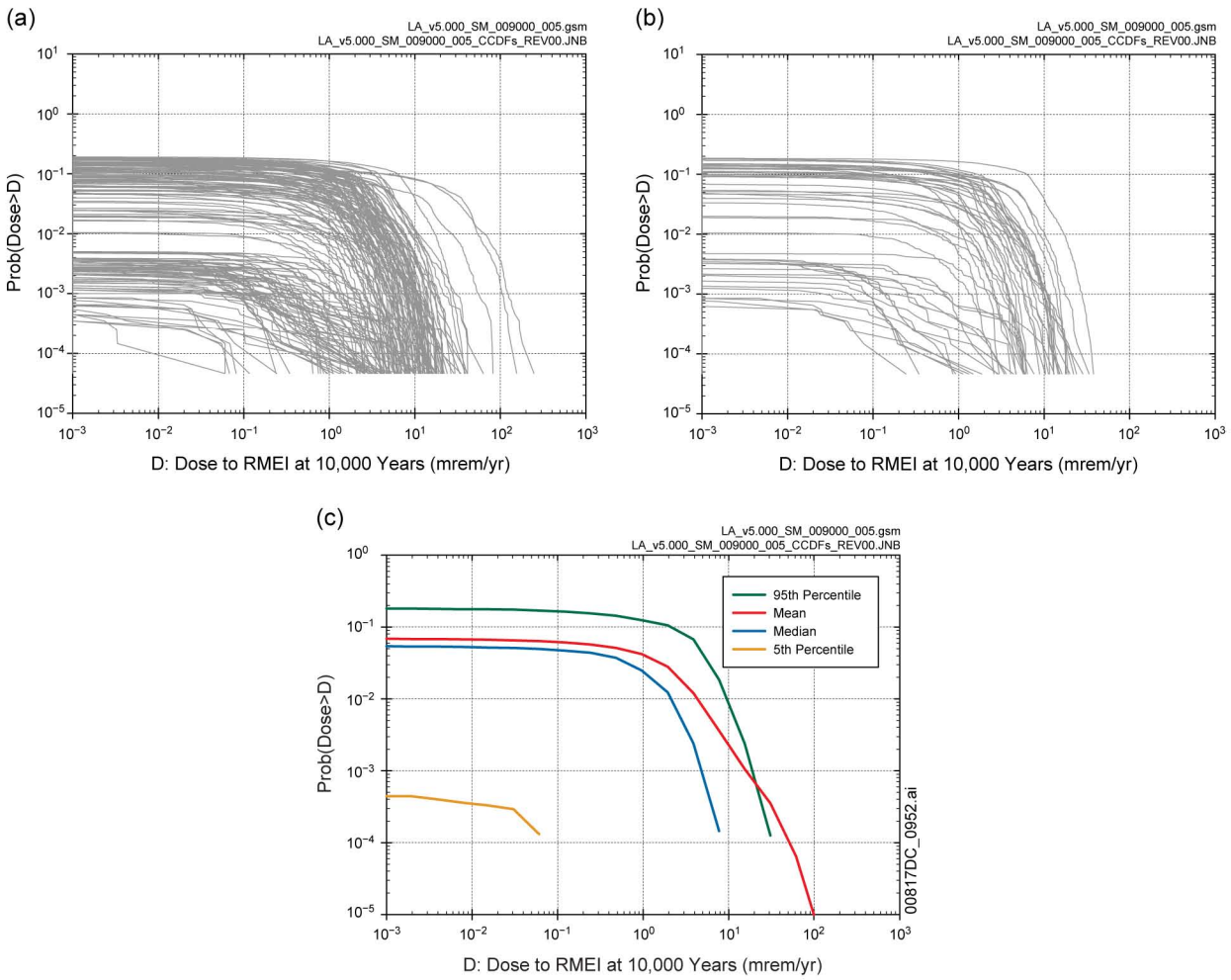

Source: Ouput DTNs: MO0709TSPAPLOT.000 [DIRS 183010]; and and MO0709TSPAREGS.000 [DIRS 182976].

Figure J8.3-10. Results associated with $D_{SG}(10^4 \text{ yr}|\mathbf{a}_{SG}, \mathbf{e}_M)$ obtained with sampling-based (Monte Carlo) procedures for an LHS of size $nLHS = 300$: (a) CCDFs for $D_{SG}(10^4 \text{ yr}|\mathbf{a}_{SG}, \mathbf{e}_{Mi})$ with exceedance probabilities $p_A[D < D_{SG}(10^4 \text{ yr}|\mathbf{a}, \mathbf{e}_{Mi})|\mathbf{e}_{Ai}]$ defined in Equation J4.5-19 for $i = 1, 2, \ldots, nLHS = 300$, (b) CCDFs for $D_{SG}(10^4 \text{ yr}|\mathbf{a}_{SG}, \mathbf{e}_{Mi})$ with exceedance probabilities $p_A[D < D_{SG}(10^4 \text{ yr}|\mathbf{a}, \mathbf{e}_{Mi})|\mathbf{e}_{Ai}]$ defined in Equation J4.5-19 for $i = 1, 2, \ldots, 50$, and (c) expected (mean) CCDF and quantile curves, $q = 0.05, 0.5, 0.95$, for CCDFs in (a).

(a)

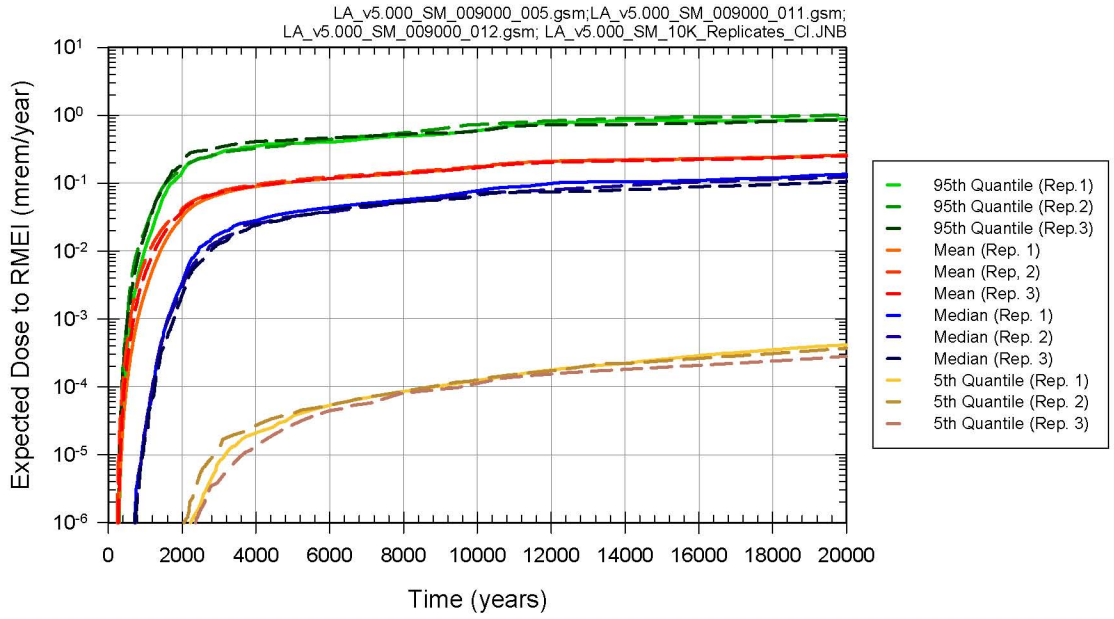

(b)

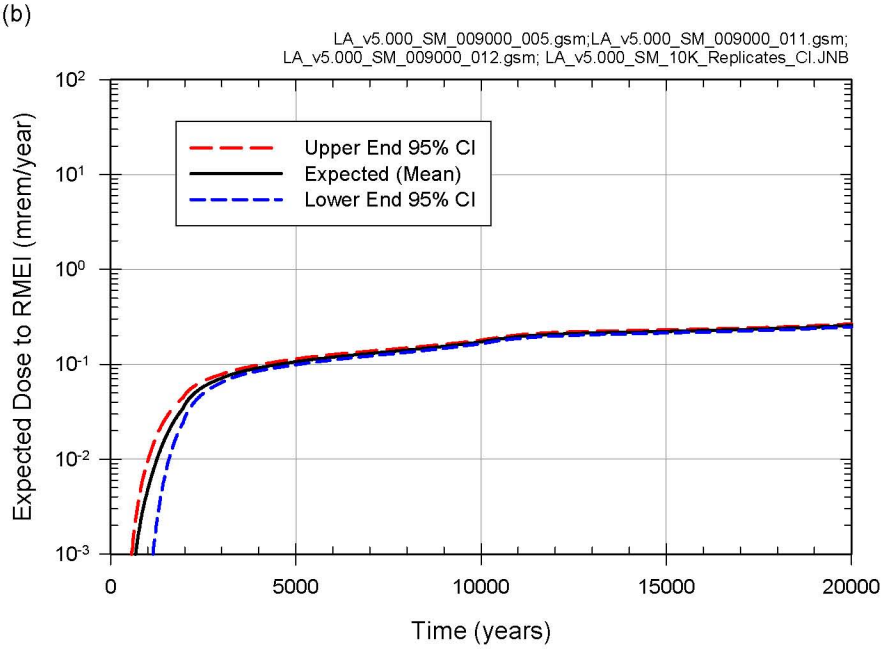

Source: Ouput DTNs: MO0709TSPAPLOT.000 [DIRS 183010]; MO0709TSPAREGS.000 [DIRS 182976]; and MO0709TSPASTAB.000 [DIRS 182983].

Figure J8.3-11. Assessment with replicated sampling of numerical error associated with use of an LHS of size *nLHS* = 300 to determine epistemic uncertainty in expected dose $\bar{D}_{SG}(\tau|\mathbf{e})$ to RMEI for $0 \leq \tau \leq 20{,}000$ yr that results when only seismic ground motion events are considered: (a) Replicated estimates of expected (mean) dose $\bar{\bar{D}}_{SG}(\tau)$ and quantiles $Q_q[\bar{D}_{SG}(\tau|\mathbf{e})]$, q = 0.05, 0.5, 0.95, and (b) confidence intervals for estimates of expected (mean) dose $\bar{\bar{D}}_{SG}(\tau)$.

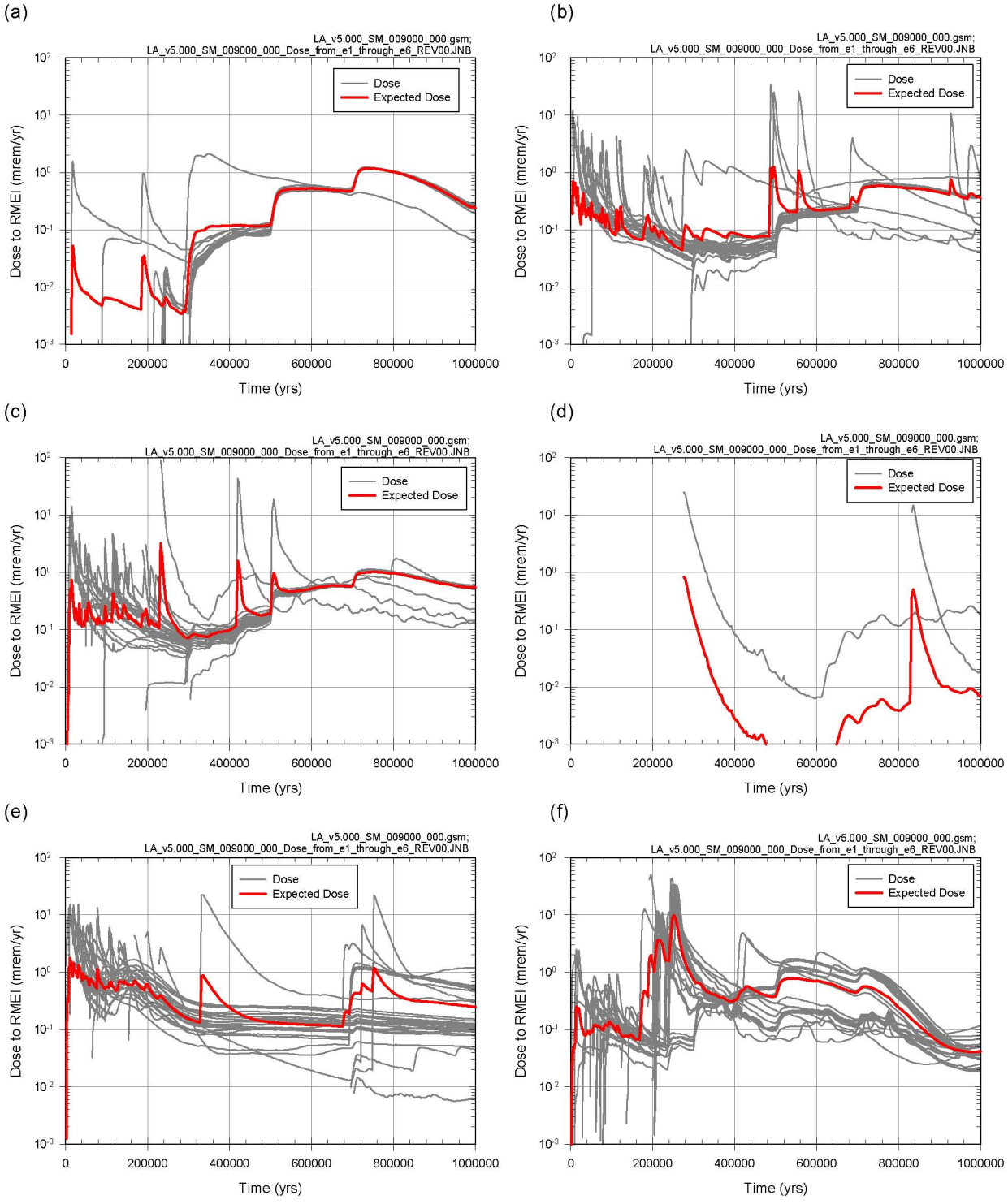

Source: Ouput DTNs: MO0709TSPAPLOT.000 [DIRS 183010]; and MO0709TSPAREGS.000 [DIRS 182976].

Figure J8.4-1. Doses $D_{SG}(\tau|\mathbf{a}_{SG,ik}, \mathbf{e}_{Mi})$, k = 1, 2, …, nR = 30, and estimated expected doses $\bar{D}_{SG}(\tau|\mathbf{e}_i)$ to the RMEI for $0 \le \tau \le 10^6$ yr for selected LHS elements $\mathbf{e}_i = [\mathbf{e}_{Ai}, \mathbf{e}_{Mi}]$ when only nominal processes and seismic ground motion events are considered: (a) $\mathbf{e}_1$, (b) $\mathbf{e}_2$, (c) $\mathbf{e}_3$, (d) $\mathbf{e}_4$, (e) $\mathbf{e}_5$, and (f) $\mathbf{e}_6$.

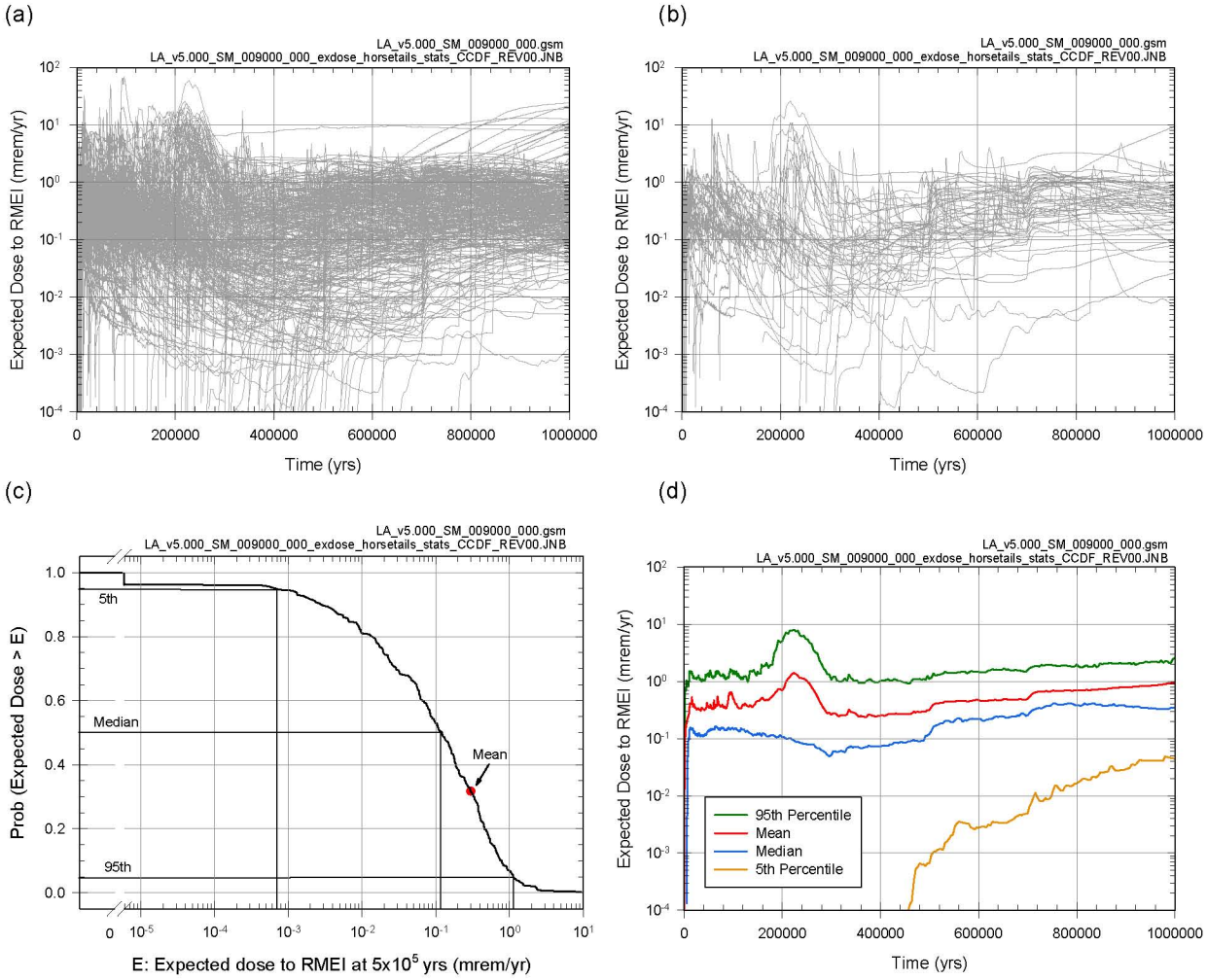

Source: Ouput DTNs: MO0709TSPAPLOT.000 [DIRS 183010]; and MO0709TSPAREGS.000 [DIRS 182976].

Figure J8.4-2. Estimate obtained with LHS of size *nLHS* = 300 showing epistemic uncertainty in expected dose $\bar{D}_{SG}(\tau|\mathbf{e})$ to RMEI for $0 \le \tau \le 10^6$ yr that results when only nominal processes and seismic ground events are considered: (a) expected dose $\bar{D}_{SG}(\tau|\mathbf{e}_i)$, i = 1, 2, …, *nLHS* = 300, (b) expected dose $\bar{D}_{SG}(\tau|\mathbf{e}_i)$, i = 1, 2, …, 50, (c) exceedance probabilities $p_E[D < \bar{D}_{SG}(\tau|\mathbf{e})]$ and quantiles $Q_q[\bar{D}_{SG}(\tau|\mathbf{e})]$, q = 0.05, 0.5 and 0.95, for τ = 500,000 yr, and (d) expected (mean) dose $\bar{\bar{D}}_{SG}(\tau)$ and quantiles $Q_q[\bar{D}_{SG}(\tau|\mathbf{e})]$, q = 0.05, 0.5, 0.95.

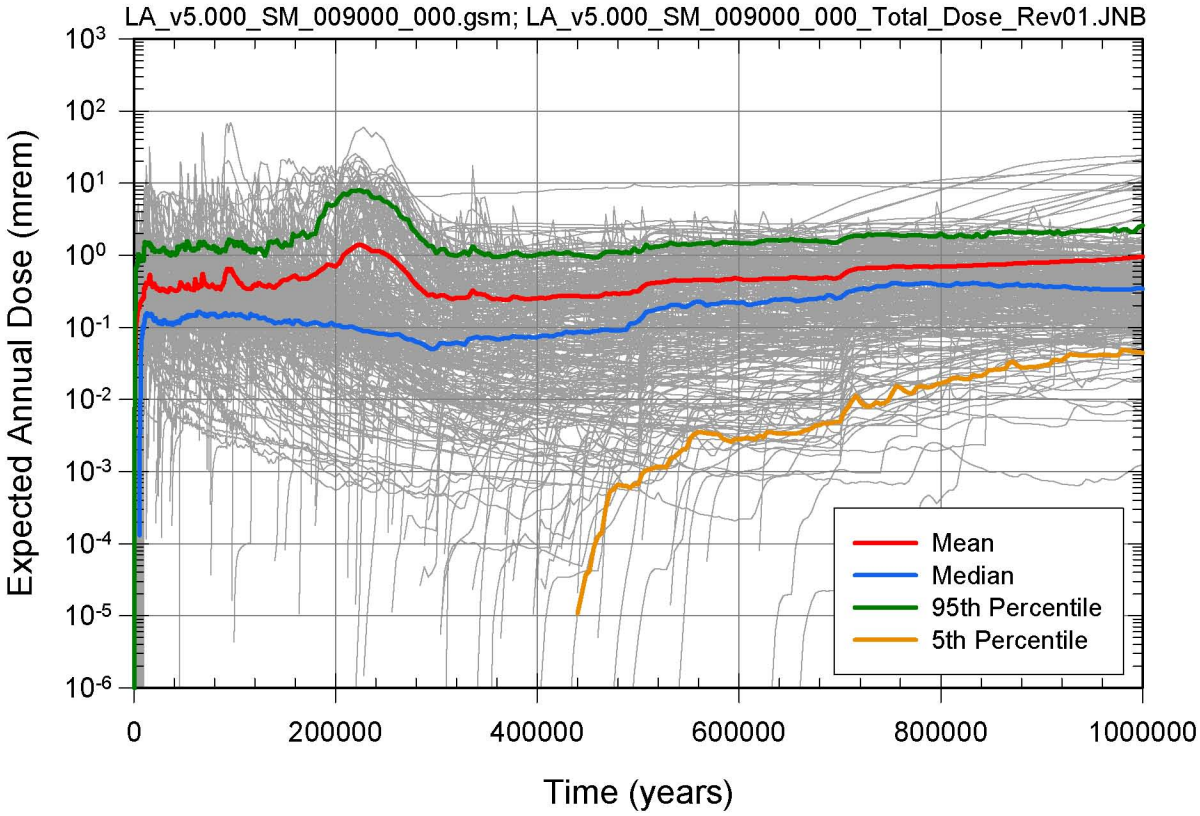

Source: Ouput DTNs: MO0709TSPAPLOT.000 [DIRS 183010]; and MO0709TSPAREGS.000 [DIRS 182976].

Figure J8.4-3. Summary of results obtained with LHS of size *nLHS* = 300 showing epistemic uncertainty in expected dose $\bar{D}_{SG}(\tau|\mathbf{e})$ to RMEI for $0 \leq \tau \leq 10^6$ yr that results when only nominal processes and seismic ground events are considered.

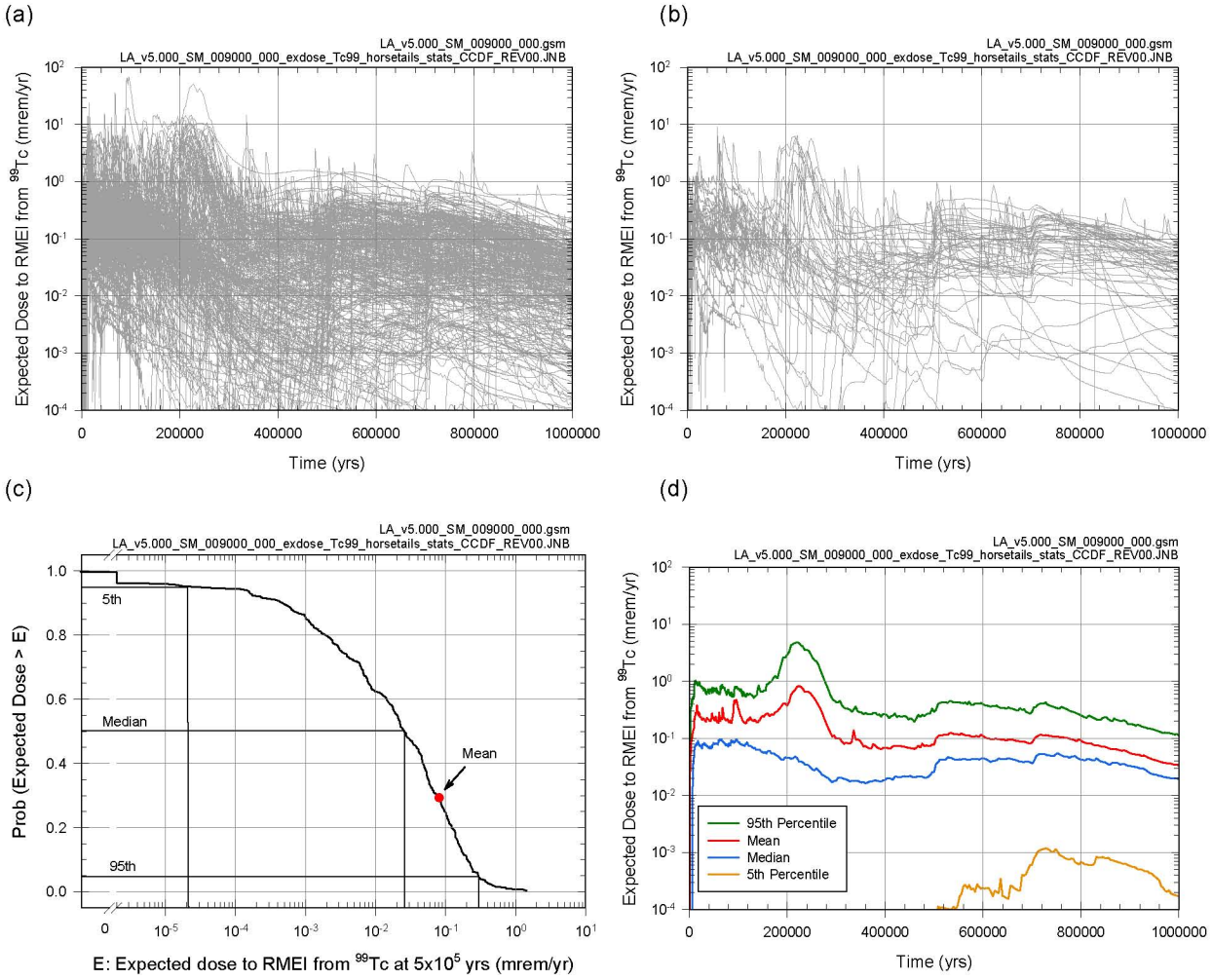

Source: Ouput DTNs: MO0709TSPAPLOT.000 [DIRS 183010]; and MO0709TSPAREGS.000 [DIRS 182976].

Figure J8.4-4. Estimate obtained with LHS of size *nLHS* = 300 showing epistemic uncertainty in expected dose $\bar{D}_{SG,r}(\tau|\mathbf{e}$ to RMEI for $0 \le \tau \le 10^6$ yr with r corresponding to ^{99}Tc that results when only nominal processes and seismic ground events are considered: (a) expected dose $\bar{D}_{SG,r}(\tau|\mathbf{e}_i)$, i = 1, 2, …, *nLHS* = 300, (b) expected dose $\bar{D}_{SG,r}(\tau|\mathbf{e}_i)$, i = 1, 2, …, 50, (c) exceedance probabilities $p_E[D < \bar{D}_{SG,r}(\tau|\mathbf{e})]$ and quantiles $Q_q[\bar{D}_{SG,r}(\tau|\mathbf{e})]$, q = 0.05, 0.5 and 0.95, for τ = 500,000 yr, and (d) expected (mean) dose $\bar{\bar{D}}_{SG,r}(\tau)$ and quantiles $Q_q[\bar{D}_{SG,r}(\tau|\mathbf{e})]$, q = 0.05, 0.5, 0.95.

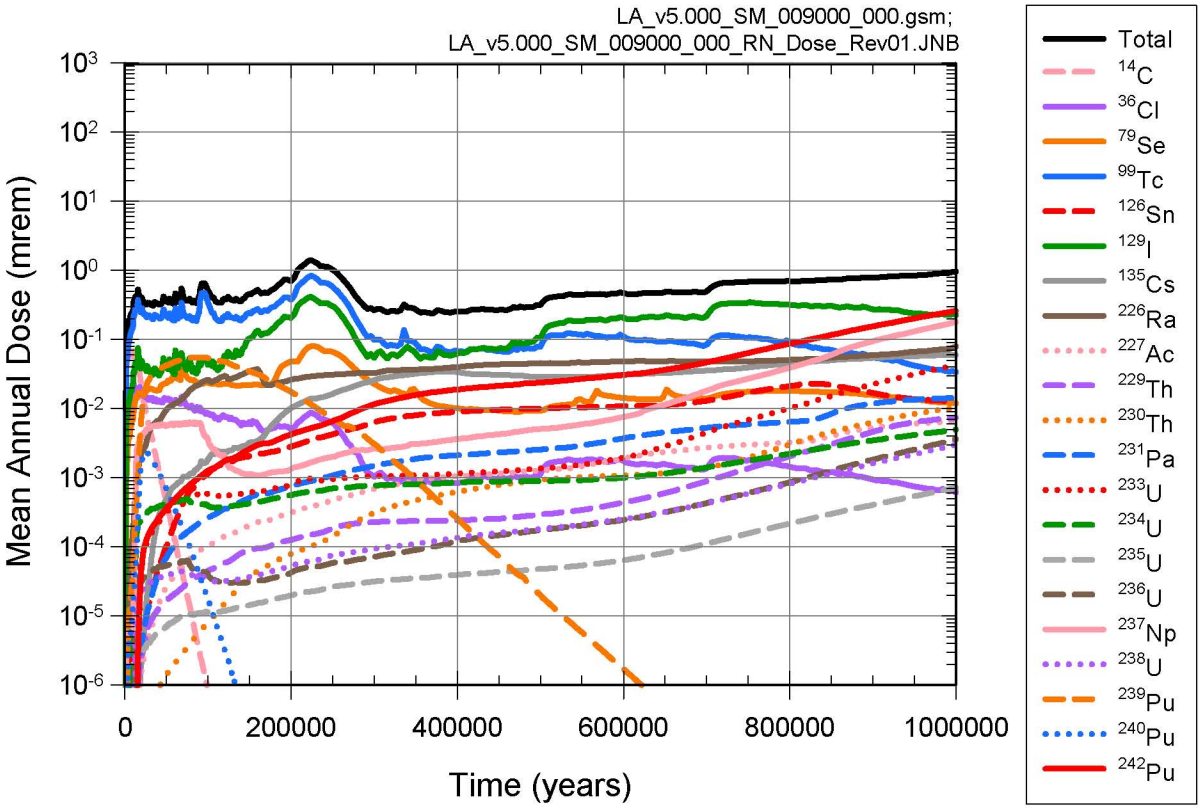

Source: Ouput DTNs: MO0709TSPAPLOT.000 [DIRS 183010]; and MO0709TSPAREGS.000 [DIRS 182976].

Figure J8.4-5. Estimates obtained with LHS of size *nLHS* = 300 of expected (mean) dose $\bar{\bar{D}}_{SG,r}(\tau)$ to RMEI for $0 \leq \tau \leq 10^6$ yr for individual radioactive species that result when only nominal proceses and seismic ground events are considered.

(a)

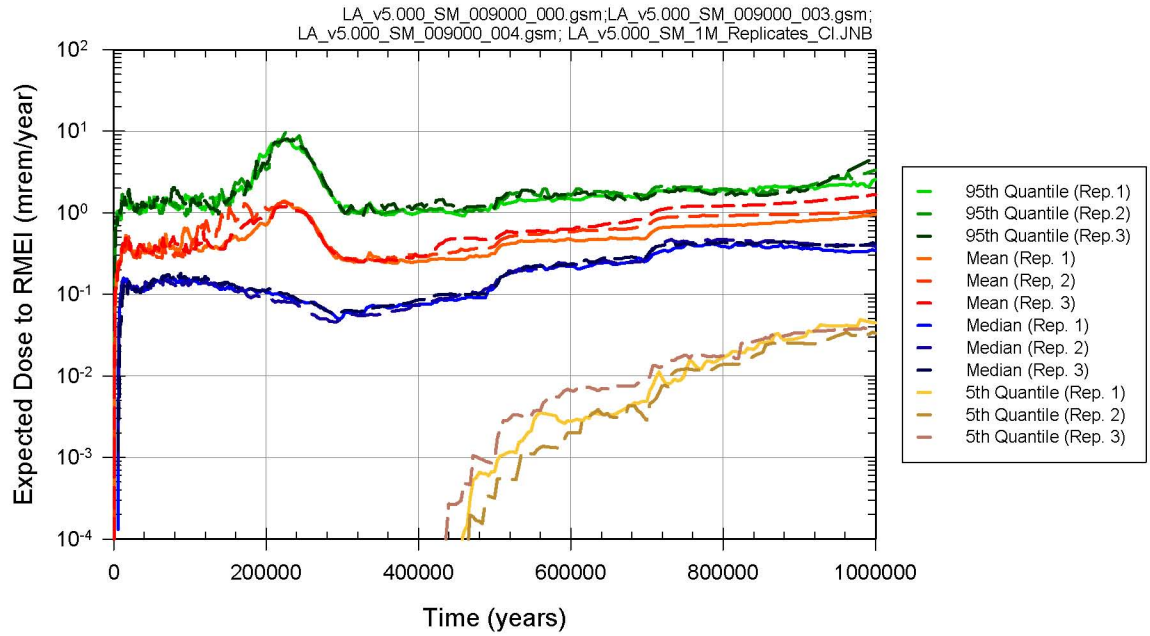

(b)

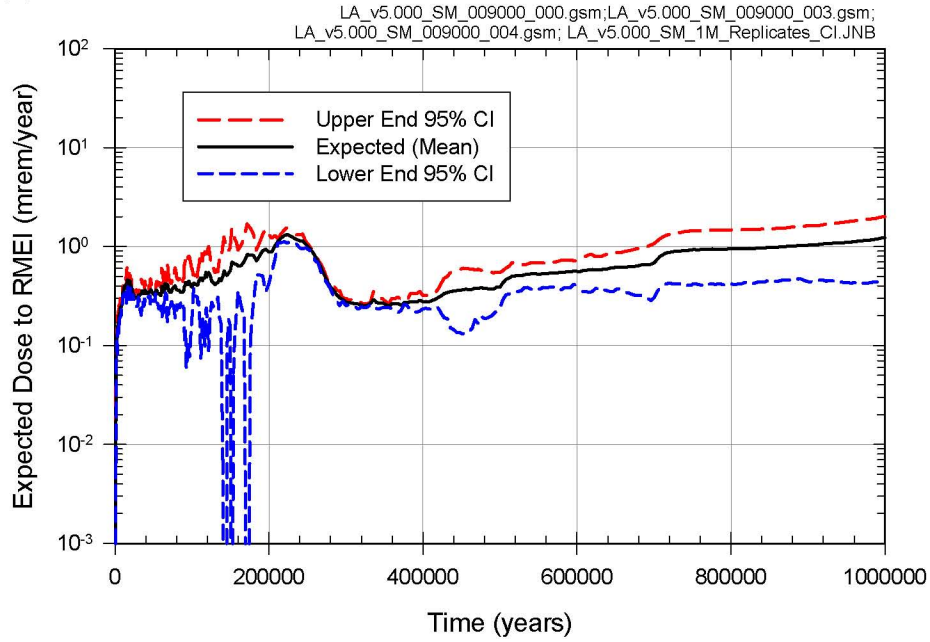

Source: Ouput DTNs: MO0709TSPAPLOT.000 [DIRS 183010]; MO0709TSPAREGS.000 [DIRS 182976]; and MO0709TSPASTAB.000 [DIRS 182983].

Figure J8.4-6. Assessment with replicated sampling of numerical error associated with use of an LHS of size *nLHS* = 300 to determine epistemic uncertainty in expected dose $\bar{D}_{SG}(\tau|\mathbf{e})$ to RMEI for $0 \leq \tau \leq 10^6$ yr that results when only nominal processes and seismic ground motion events are considered: (a) Replicated estimates of expected (mean) dose $\bar{\bar{D}}_{SG}(\tau)$ and quantiles $Q_q[\bar{D}_{SG}(\tau|\mathbf{e})]$, q = 0.05, 0.5, 0.95, and (b) confidence intervals for estimates of expected (mean) dose $\bar{\bar{D}}_{SG}(\tau)$.

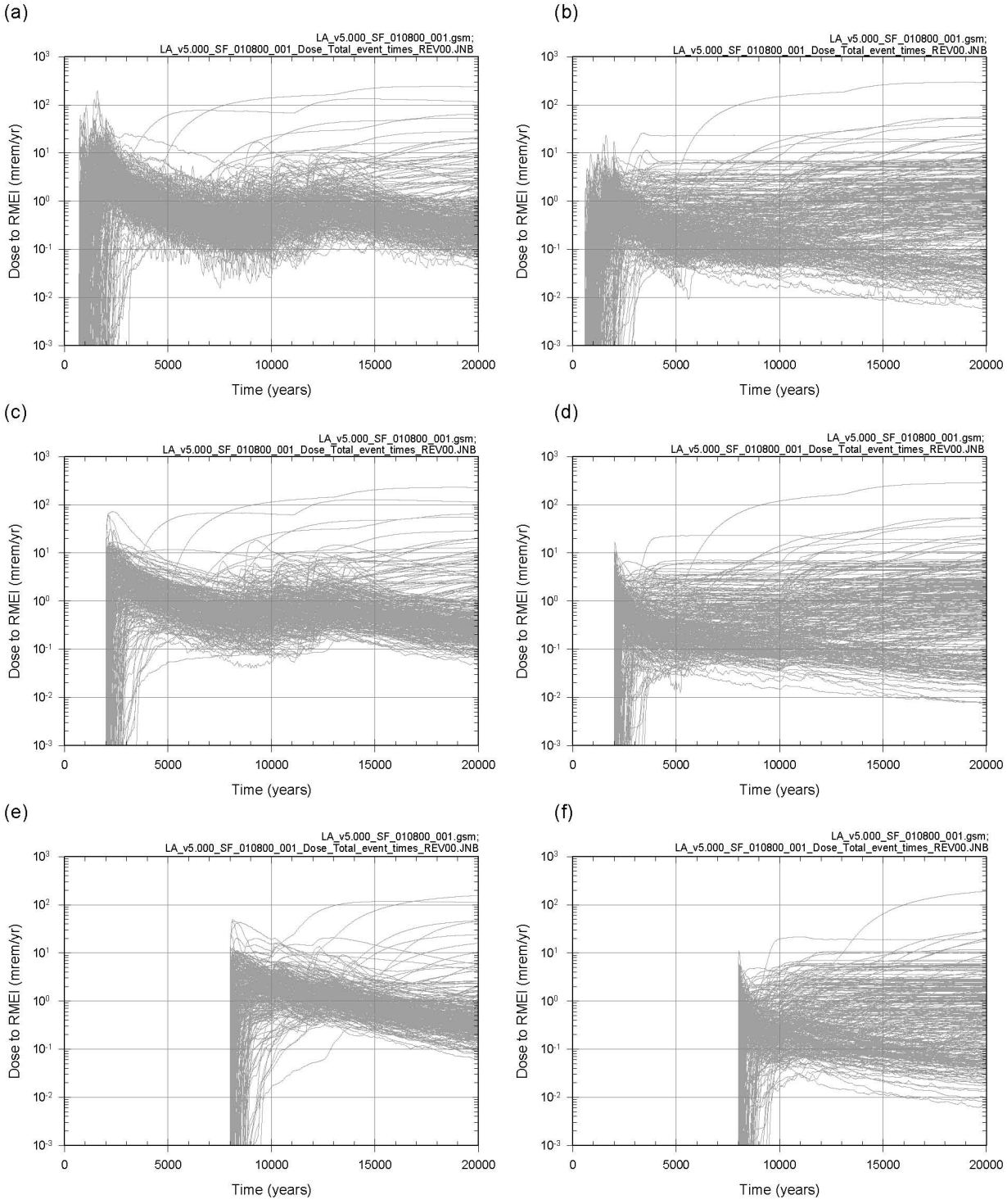

Source: Ouput DTNs: MO0709TSPAPLOT.000 [DIRS 183010]; and MO0709TSPAREGS.000 [DIRS 182976].

Figure J8.6-1. Summary of results for fault displacement damage of CSNF and CDSP WPs obtained with LHS of size *nLHS* = 300 showing epistemic uncertainty in doses $D_{SF,r}(\tau|[1, t_j, 100, A_r/3, \sim]|\mathbf{e}_{Mi})$ for $0 \le \tau \le 20{,}000$ yr, $r = 1, 2$, with 1 ~ CSNF WPs and $r = 2$ ~ CDSP WPs, $A_1 = 2.78$ m^2 and $A_2 = 3.28$ m^2, and $i = 1, 2, \ldots, nLHS = 300$: (a, c, e) CSNF WPs for t_j = 200, 2000 and 8000 yrs and (b, d, f) CDSP WPs for t_j = 200, 2000 and 8000 yrs.

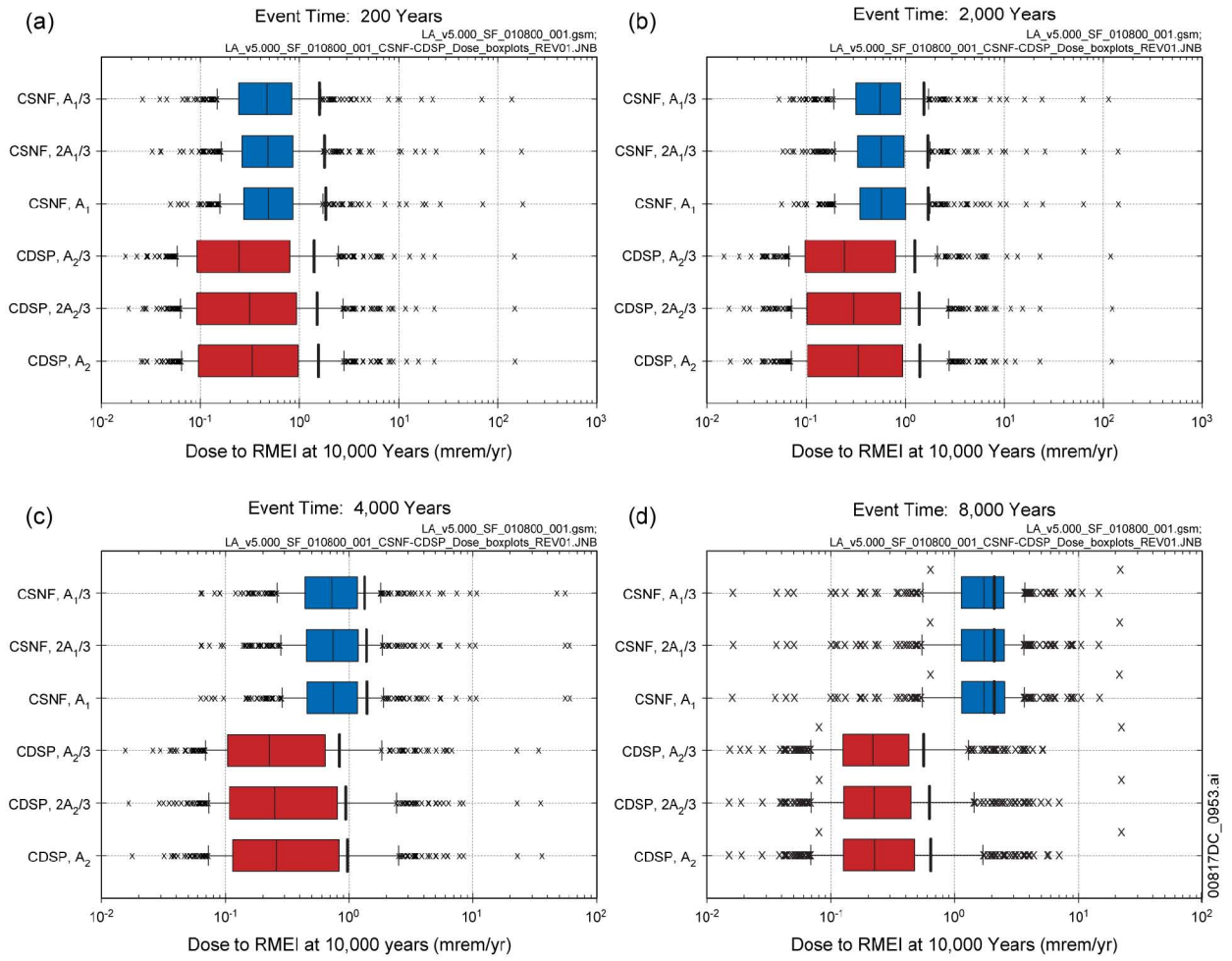

Source: Ouput DTNs: MO0709TSPAPLOT.000 [DIRS 183010]; and MO0709TSPAREGS.000 [DIRS 182976].

Figure J8.6-2. Box plots (see Figure J6.2-3 for description) summarizing results for fault displacement damage to CSNF and CDSP WPs obtained with LHS of size *nLHS* = 300 showing epistemic uncertainty in dose $D_{SF,r}(10^4 \text{ yr}|[1, t_j, 100, A_{rk}, \sim]|\mathbf{e}_{Mi})$ for t_j = 200, 2000, 4000 and 8000 yrs, r = 1, 2, with 1 ~ CSNF WPs and r = 2 ~ CDSP WPs, $A_{rk} = A_r/3, 2A_r/3, A_r$, with A_1 = 2.78 m^2 and A_2 = 3.28 m^2, and i = 1, 2, …, *nLHS* = 300: (a) t_j = 200 yr, (b) t_j = 2000 yr, (c) t_j = 4000 yr, and (d) t_j = 8000 yr.

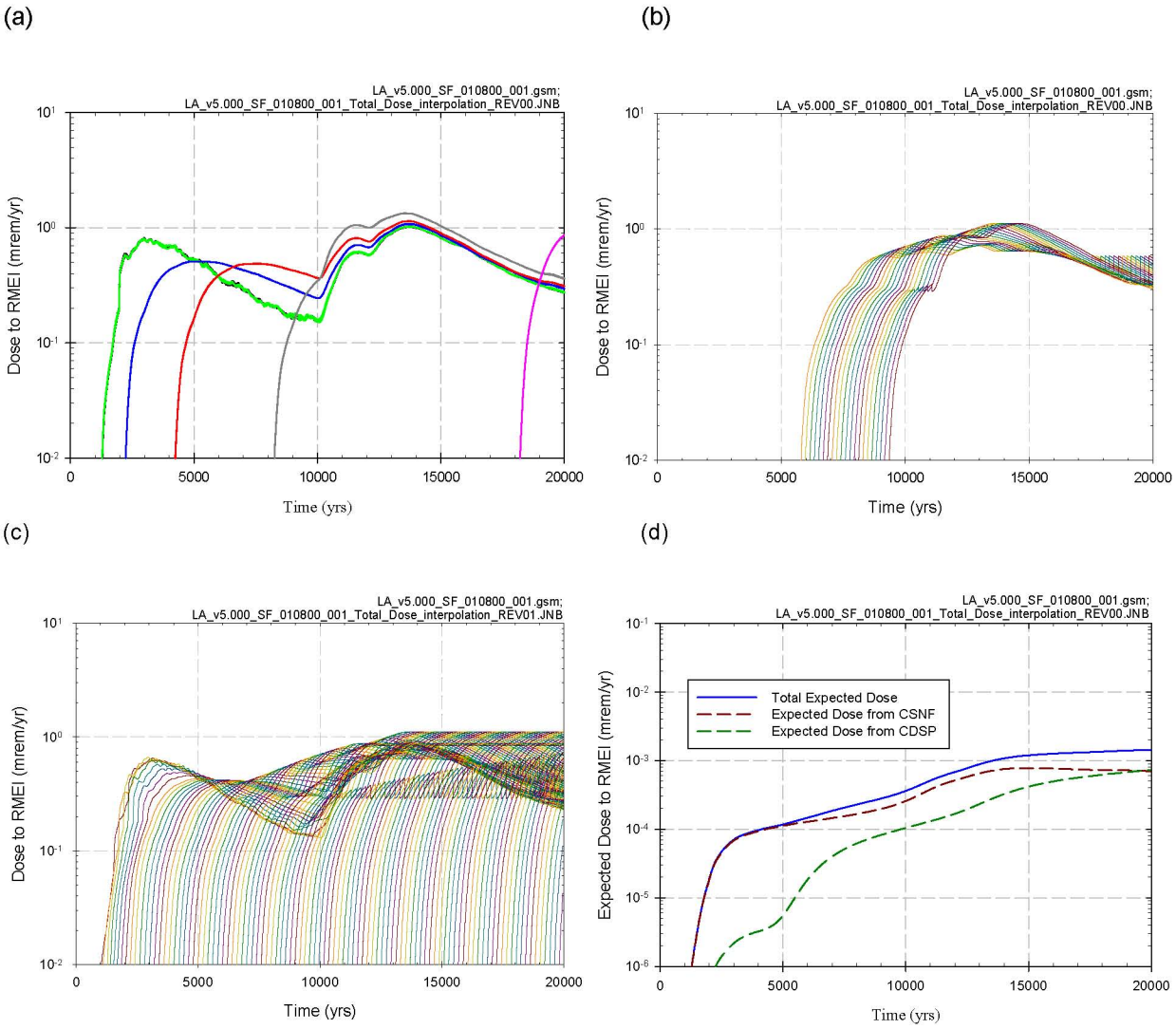

Source: Ouput DTNs: MO0709TSPAPLOT.000 [DIRS 183010]; and MO0709TSPAREGS.000 [DIRS 182976].

Figure J8.6-3. Illustration of interpolation procedure to estimate integrals $\hat{I}_r(\tau|t, \mathbf{e}_{Mi})$ and expected dose $\bar{D}_{SF}(\tau|\mathbf{e}_i)$ from calculated doses $D_{SF,r}(\tau|[1, t_j, 100, A_{rk}, 1, \sim], \mathbf{e}_{Mi})$ in Equation J8.6-18 for LHS element $\mathbf{e}_1 = [\mathbf{e}_{A1}, \mathbf{e}_{M1}]$ and the time interval [0, 2.0×10^4 yr]: (a) $D_{SF,1}(\tau|[1, t_j, 100, A_{rk}, 1, \sim], \mathbf{e}_{M1})$ for $j = 1, 2, \ldots, 6$ and $k = 1, 2, 3$ (Notes: Results overlay for A_{1k}, $k = 1, 2, 3$, for each t_j, and results for t_1 and t_2 also overlay), (b) Interpolated values $\hat{I}_1(\tau|\hat{t}_k, \mathbf{e}_{M1})$ for $\hat{t}_k$ between $t_4 = 4000$ yr and $t_5 = 8000$ yr, (c) Interpolated values for $\hat{I}_1(\tau|\hat{t}_k, \mathbf{e}_{M1})$ for $\hat{t}_k$ between 200 and 20,000 yr, and (d) estimates for $\bar{D}_{SF,1}(\tau|\mathbf{e}_i)$ for CSNF WPs, $\bar{D}_{SF,2}(\tau|\mathbf{e}_i)$ for CDSP WPs and $\bar{D}_{SF}(\tau|\mathbf{e}_i)$ for CSNF and CDSP WPs.

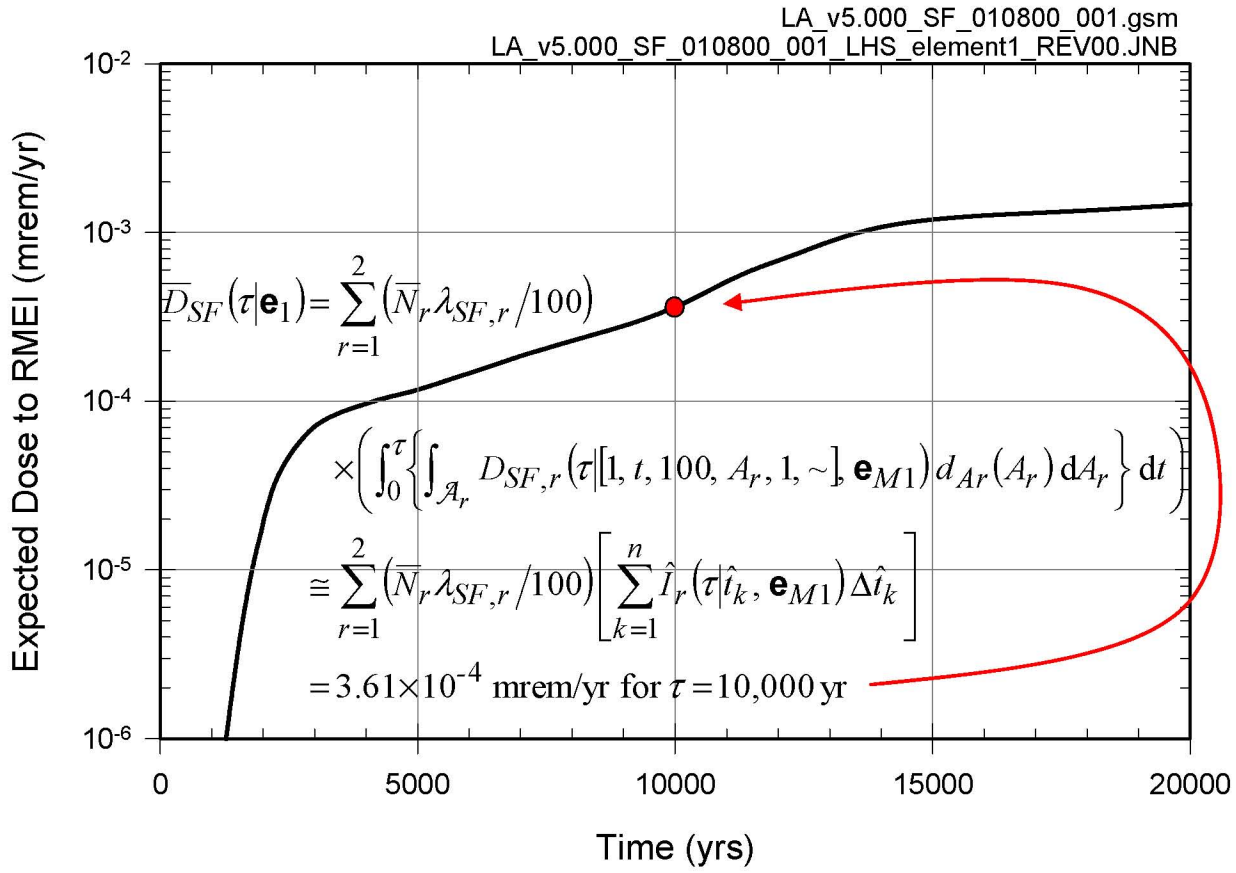

Source: Ouput DTNs: MO0709TSPAPLOT.000 [DIRS 183010]; and MO0709TSPAREGS.000 [DIRS 182976].

Figure J8.6-4. Estimate of $\bar{D}_{SF}(\tau|\mathbf{e}_1)$ for LHS element $\mathbf{e}_1 = [\mathbf{e}_{A1}, \mathbf{e}_{M1}]$ and $0 \le \tau \le 20{,}000$ yr with integration-based procedure indicated in Equations J8.6-17 and J8.6-25.

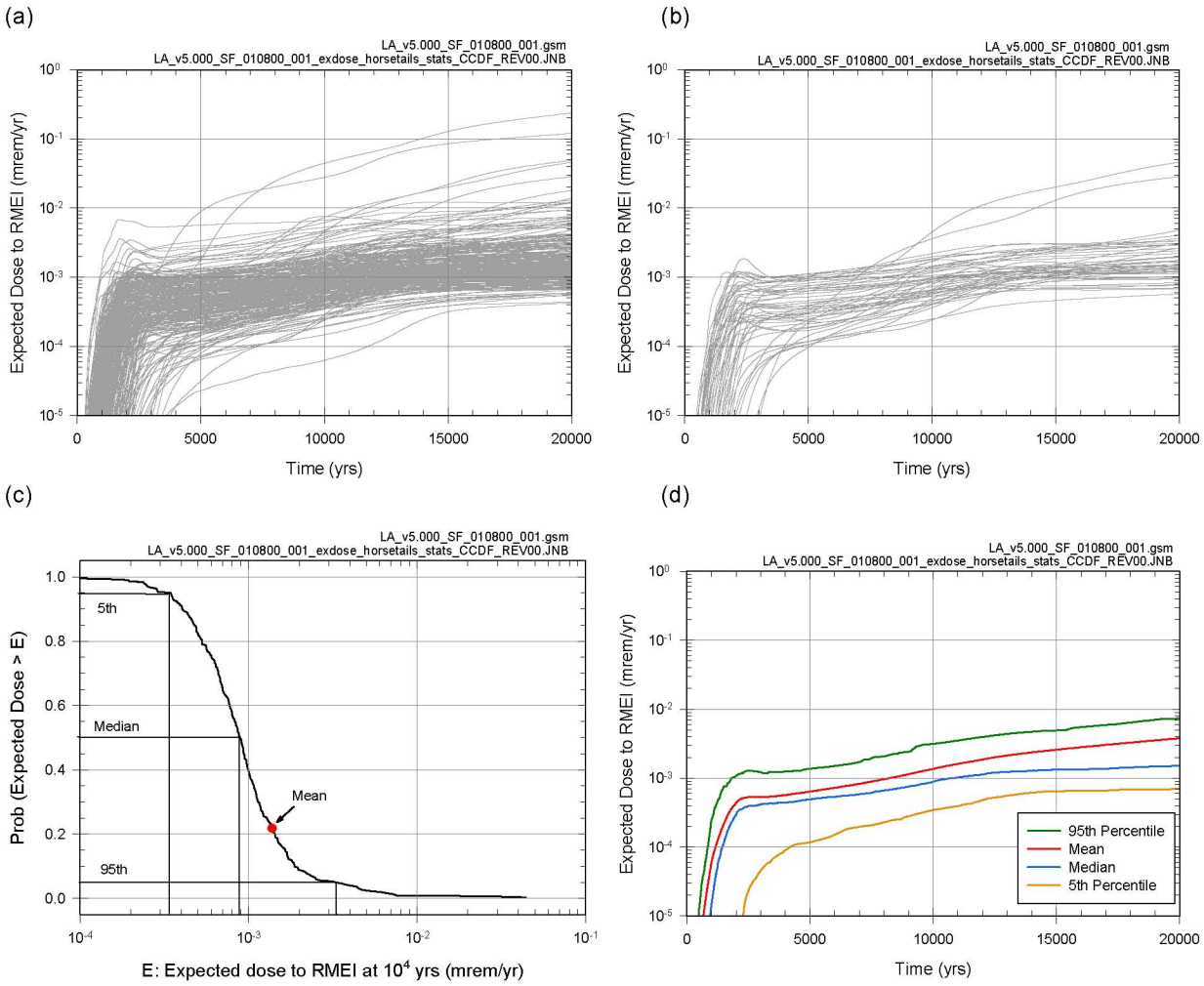

Source: Ouput DTNs: MO0709TSPAPLOT.000 [DIRS 183010]; and MO0709TSPAREGS.000 [DIRS 182976].

Figure J8.6-5. Estimate obtained with LHS of size *nLHS* = 300 showing epistemic uncertainty in expected dose $\bar{D}_{SF}(\tau|\mathbf{e})$ to RMEI for $0 \le \tau \le 20{,}000$ yr that at results when only fault displacement events are considered: (a) expected dose $\bar{D}_{SF}(\tau|\mathbf{e}_i)$, i = 1, 2, …, *nLHS* = 300, (b) expected dose $\bar{D}_{SF}(\tau|\mathbf{e}_i)$, i = 1, 2, …, 50, (c) exceedance probabilities $p_E[D < \bar{D}_{SG}(\tau|\mathbf{e})]$ and quantiles $Q_q[\bar{D}_{SF}(\tau|\mathbf{e})]$, q = 0.05, 0.5 and 0.95, for $\tau = 10^4$ yr, and (d) expected (mean) dose $\bar{\bar{D}}_{SF}(\tau)$ and quantiles $Q_q[\bar{D}_{SF}(\tau|\mathbf{e})]$, q = 0.05, 0.5, 0.95.

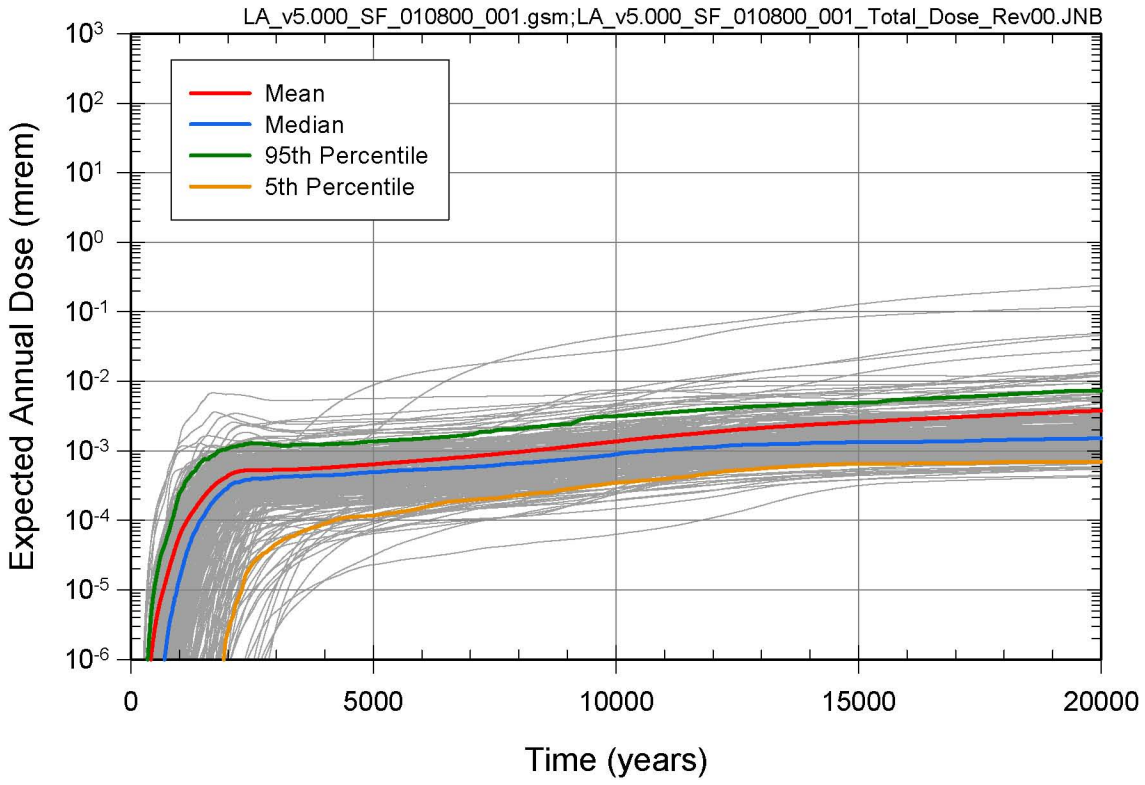

Source: Ouput DTNs: MO0709TSPAPLOT.000 [DIRS 183010]; and MO0709TSPAREGS.000 [DIRS 182976].

Figure J8.6-6. Summary of results obtained with LHS of size *nLHS* = 300 showing epistemic uncertainty in expected dose $\bar{D}_{SF}(\tau|\mathbf{e})$ to RMEI for $0 \leq \tau \leq 20{,}000$ yr that results when only fault displacement events are considered.

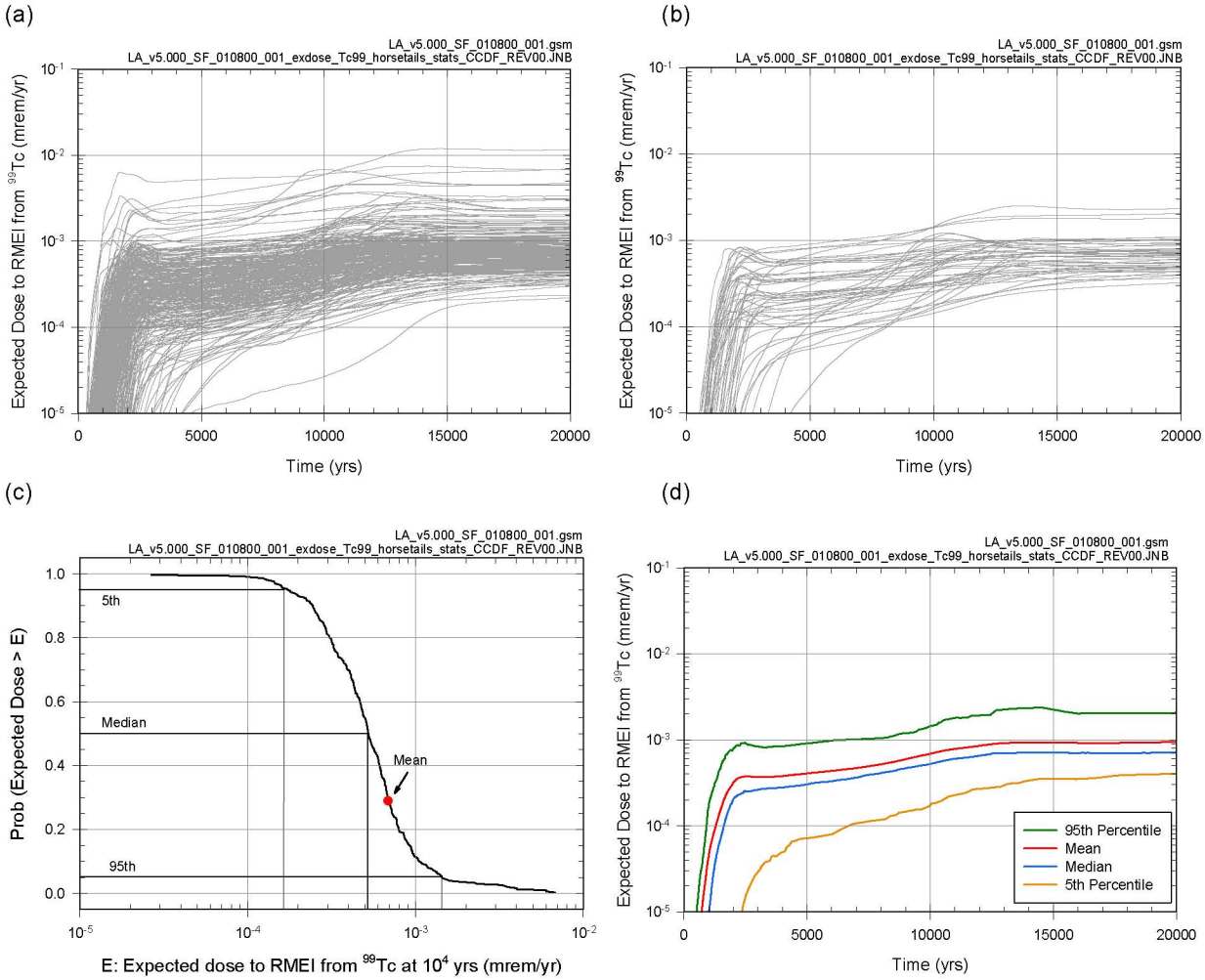

Source: Ouput DTNs: MO0709TSPAPLOT.000 [DIRS 183010]; and MO0709TSPAREGS.000 [DIRS 182976].

Figure J8.6-7. Estimate obtained with LHS of size *nLHS* = 300 showing epistemic uncertainty in expected dose $\bar{D}_{SF,r}(\tau|\mathbf{e})$ to RMEI for $0 \le \tau \le 20{,}000$ yr with r corresponding to ^{99}Tc that results when only fault displacement events are considered: (a) expected dose $\bar{D}_{SF,r}(\tau|\mathbf{e}_i)$, i = 1, 2, …, *nLHS* = 300, (b) expected dose $\bar{D}_{SF,r}(\tau|\mathbf{e}_i)$, i = 1, 2, …, 50, (c) exceedance probabilities $p_E[D < \bar{D}_{SG,r}(\tau|\mathbf{e})]$ and quantiles $Q_q[\bar{D}_{SF,r}(\tau|\mathbf{e})]$, q = 0.05, 0.5 and 0.95, for $\tau = 10^4$ yr, and (d) expected (mean) dose $\bar{\bar{D}}_{SF,r}(\tau)$ and quantiles $Q_q[\bar{D}_{SF,r}(\tau|\mathbf{e})]$, q = 0.05, 0.5, 0.95.

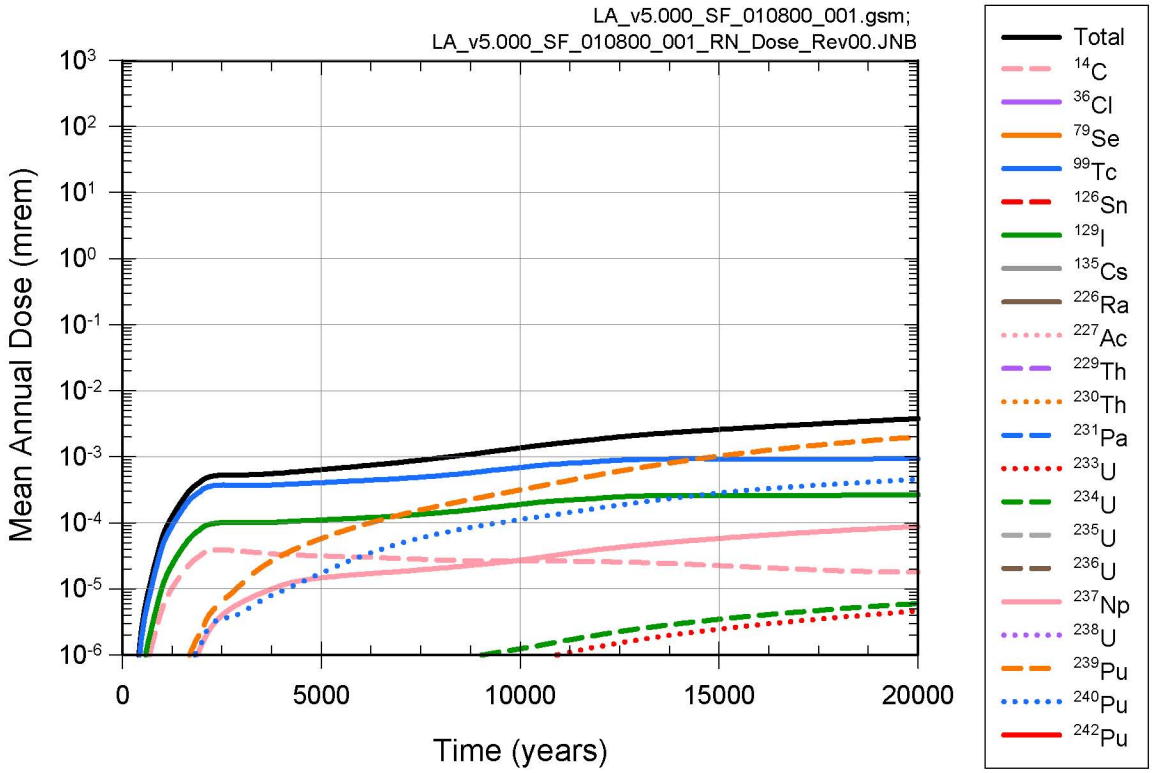

Source: Ouput DTNs: MO0709TSPAPLOT.000 [DIRS 183010]; and MO0709TSPAREGS.000 [DIRS 182976].

Figure J8.6-8. Estimates obtained with LHS of size *nLHS* = 300 of expected (mean) dose $\bar{\bar{D}}_{SF,r}(\tau)$ to RMEI for $0 \leq \tau \leq 20{,}000$ yr for individual radioactive species that result when only seismic ground motion events are considered.

(a)

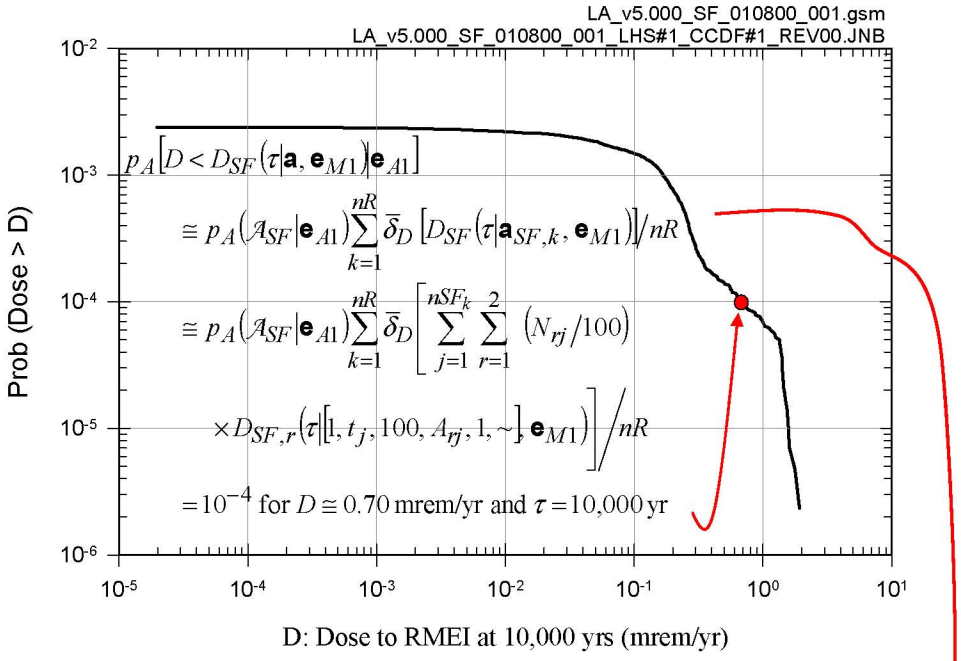

(b)

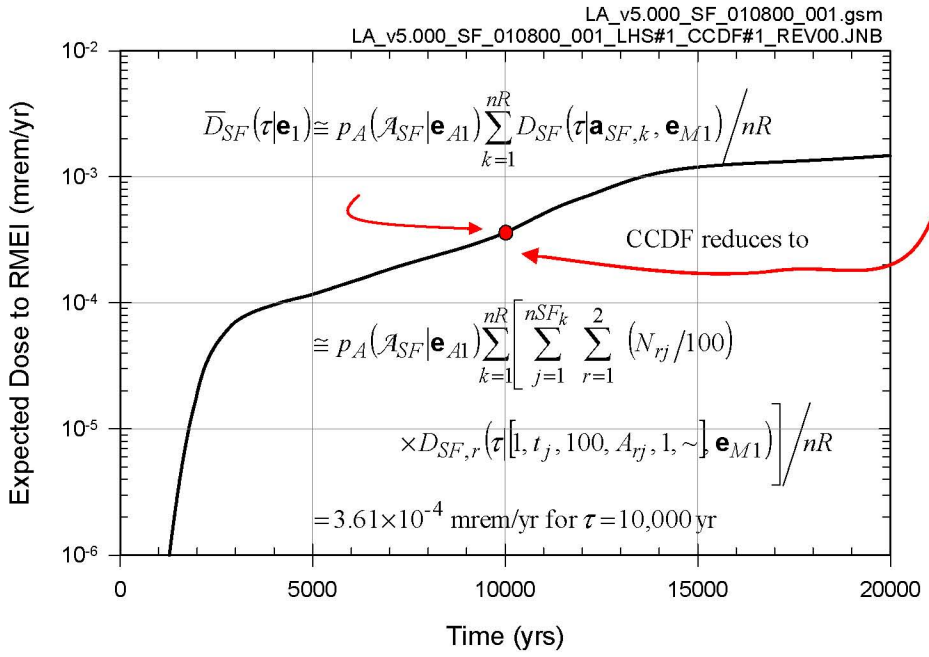

Source: Ouput DTNs: MO0709TSPAPLOT.000 [DIRS 183010]; and MO0709TSPAREGS.000 [DIRS 182976].

Figure J8.6-9. Results associated with $D_{SF}(\tau|\mathbf{a}_{SF}, \mathbf{e}_{M1})$ for LHS element $\mathbf{e}_1 = [\mathbf{e}_{A1}, \mathbf{e}_{M1}]$ obtained with sampling-based (Monte Carlo) procedures: (a) CCDF for $D_{SF}(10^4 \text{ yr}|\mathbf{a}_{SF}, \mathbf{e}_{M1})$ with exceedance probabilities $p_A[D < D_{SF}(10^4 \text{ yr}|\mathbf{a}, \mathbf{e}_{M1})|\mathbf{e}_{A1}]$ defined in Equations J4.5-19 and J8.6-36, and (b) expected dose $\bar{D}_{SF}(10^4 \text{ yr}|\mathbf{e}_1)$ associated with $D_{SF}(10^4|\mathbf{a}_{SF}, \mathbf{e}_{M1})$ as defined in Equation J4.5-20.

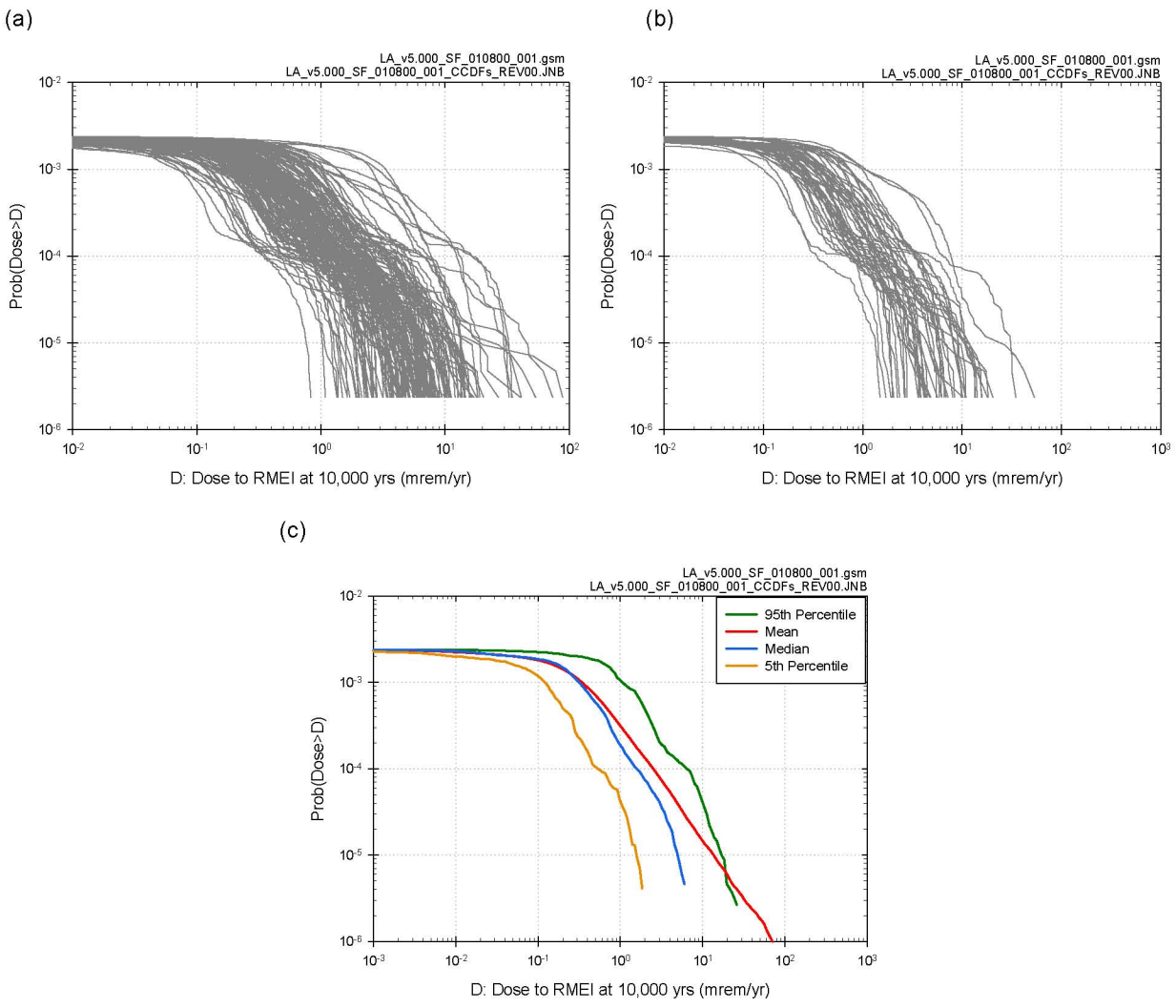

Source: Ouput DTNs: MO0709TSPAPLOT.000 [DIRS 183010]; and MO0709TSPAREGS.000 [DIRS 182976].

Figure J8.6-10. Results associated with $D_{SF}(10^4 \text{ yr}|\mathbf{a}_{SF}, \mathbf{e}_M)$ obtained with sampling-based (Monte Carlo) procedures for an LHS of size $nLHS = 300$: (a) CCDFs for $D_{SF}(10^4 \text{ yr}|\mathbf{a}_{SF}, \mathbf{e}_{Mi})$ with exceedance probabilities $p_A[D < D_{SF}(10^4 \text{ yr}|\mathbf{a}, \mathbf{e}_{Mi})|\mathbf{e}_{Ai}]$ defined in Equation J4.5-19 for $i = 1, 2, \ldots, nLHS = 300$, (b) CCDFs for $D_{SF}(10^4 \text{ yr}|\mathbf{a}_{SF}, \mathbf{e}_{Mi})$ with exceedance probabilities $p_A[D < D_{SF}(10^4 \text{ yr}|\mathbf{a}, \mathbf{e}_{Mi})|\mathbf{e}_{Ai}]$ defined in Equation J4.5-19 for $i = 1, 2, \ldots, 50$, and (c) expected (mean) CCDF and quantile curves, $q = 0.05, 0.5, 00.95$, for CCDFs in (a).

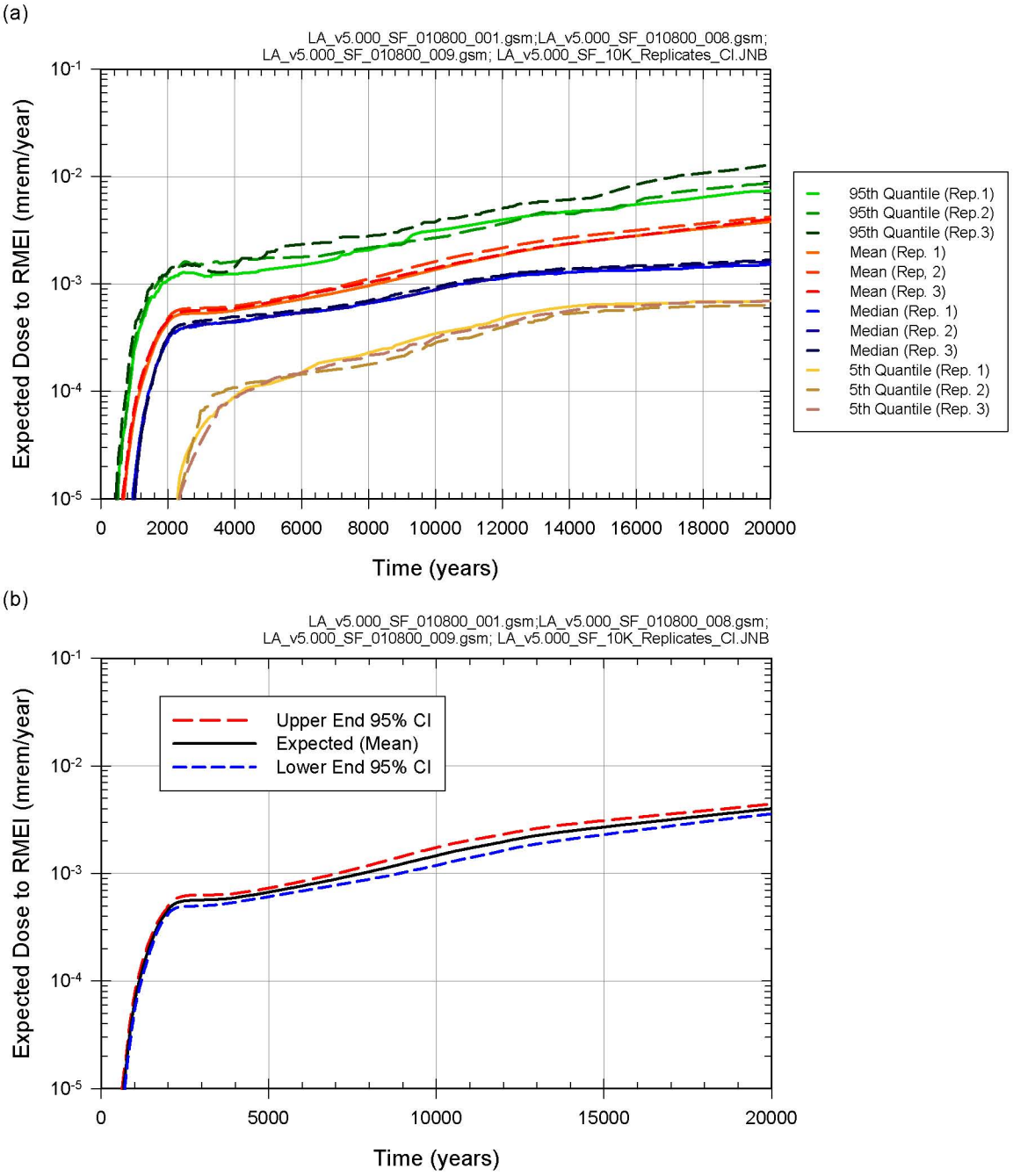

Source: Ouput DTNs: MO0709TSPAPLOT.000 [DIRS 183010]; MO0709TSPAREGS.000 [DIRS 182976]; and MO0709TSPASTAB.000 [DIRS 182983].

Figure J8.6-11. Assessment with replicated sampling of numerical error associated with use of an LHS of size *nLHS* = 300 to determine epistemic uncertainty in expected dose $\bar{D}_{SF}(\tau|\mathbf{e})$ to RMEI for $0 \leq \tau \leq 20{,}000$ yr that results when only seismic ground motion events are considered: (a) Replicated estimates of expected (mean) dose $\bar{\bar{D}}_{SF}(\tau)$ and quantiles $Q_q[\bar{D}_{SF}(\tau|\mathbf{e})]$, q = 0.05, 0.5, 0.95, and (b) confidence intervals for estimates of expected (mean) dose $\bar{\bar{D}}_{SF}(\tau)$.

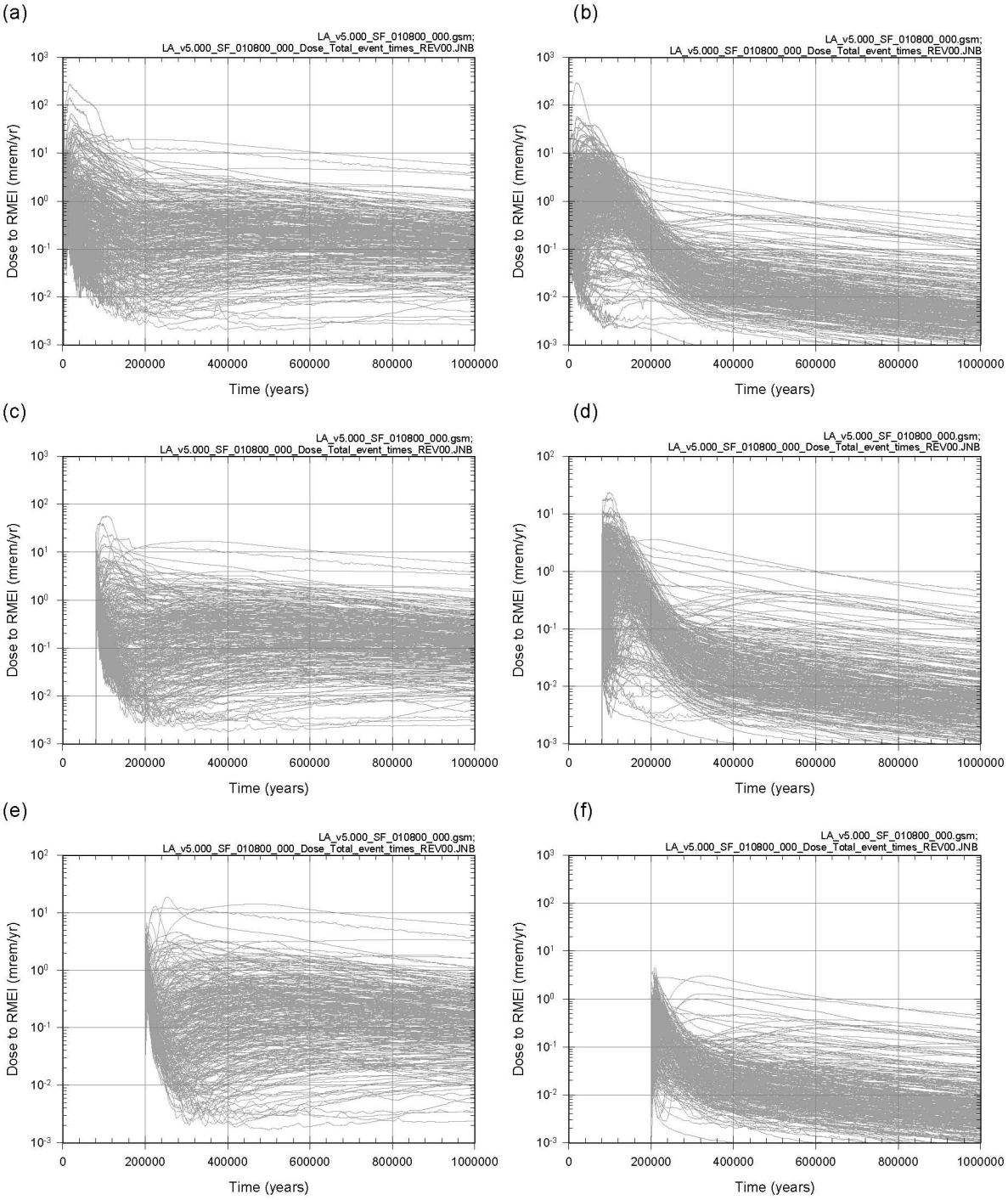

Source: Ouput DTNs: MO0709TSPAPLOT.000 [DIRS 183010]; and MO0709TSPAREGS.000 [DIRS 182976].

Figure J8.6-12. Summary of results for fault displacement damage of CSNF and CDSP WPs obtained with LHS of size *nLHS* = 300 showing epistemic uncertainty in doses $D_{SF,r}(\tau|[1, t_j, 100, A_r/3, \sim], \mathbf{e}_{Mi})$ for $0 \leq \tau \leq 20{,}000$ yr, $r = 1, 2$, with $r = 1 \sim$ CSNF WPs and $r = 2 \sim$ CDSP WPs, $A_1 = 2.78$ m^2 and $A_2 = 3.28$ m^2 and $i = 1, 2, \ldots, nLHS = 300$: (a, c, e) CSNF WPs for $t_j = 1000$, 80,000 and 200,000 yrs and (b, d, f) CDSP WPs for $t_j = 1000$, 80,000 and 200,000 yrs.

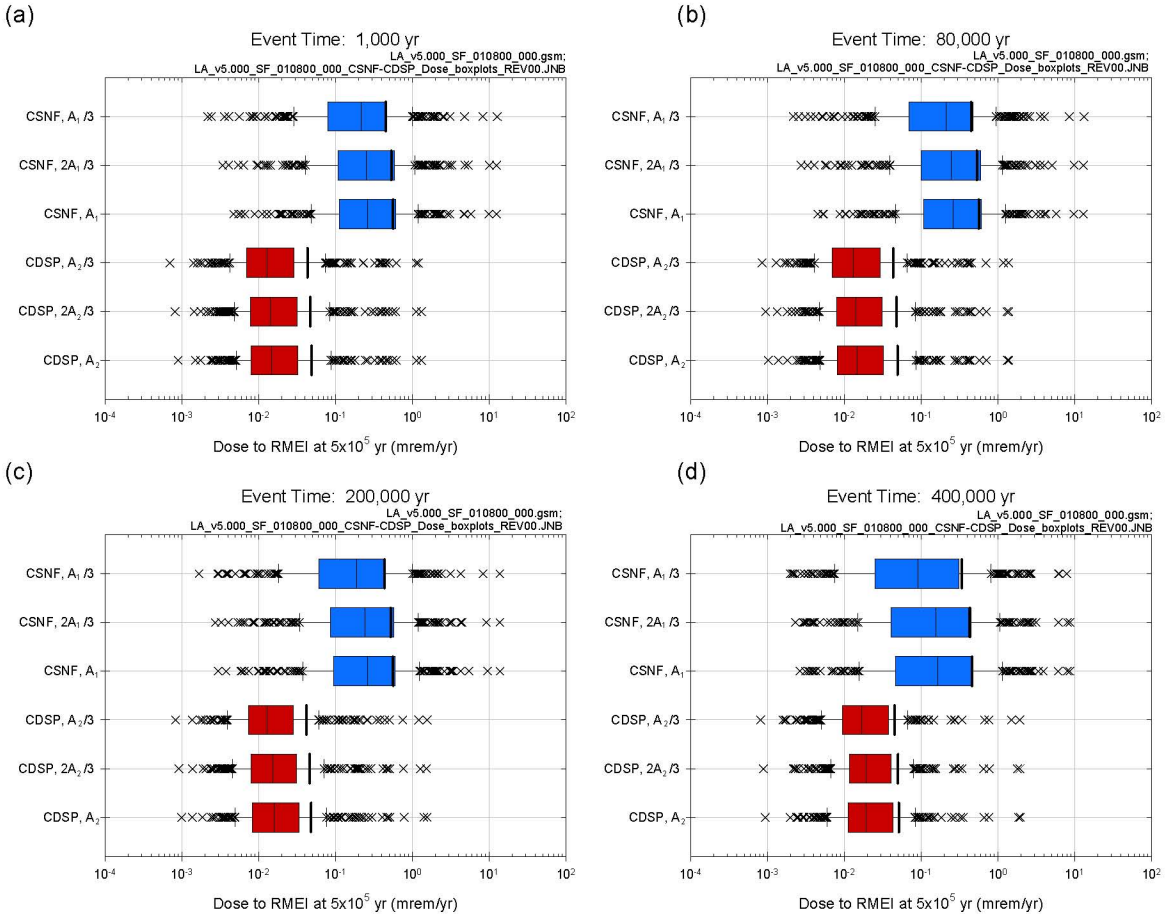

Source: Ouput DTNs: MO0709TSPAPLOT.000 [DIRS 183010]; and MO0709TSPAREGS.000 [DIRS 182976].

Figure J8.6-13. Box plots (see Figure J6.2-3 for description) summarizing results for fault displacement damage to CSNF and CDSP WPs obtained with LHS of size *nLHS* = 300 showing epistemic uncertainty in dose $D_{SF,r}(10^4 \text{ yr}|[1, t_j, 100, A_{rk}, \sim], \mathbf{e}_{Mi})$ for t_j =1000, 80,000, 200,000 and 400,000 yrs, r = 1, 2 with r = 1 ~ CSNF WPs and r = 2 ~ CDSP WPs, A_{rk} = $A_r/3$, $2A_r/3$, A_r, with A_1 = 2.78 m^2 A_2 = 3.28 m^2, and i = 1, 2, …, *nLHS* = 300: (a) t_j = 1000 yr, (b) t_j = 80,000 yr, (c) t_j = 200,000 yr, and (d) t_j = 400,000 yr.

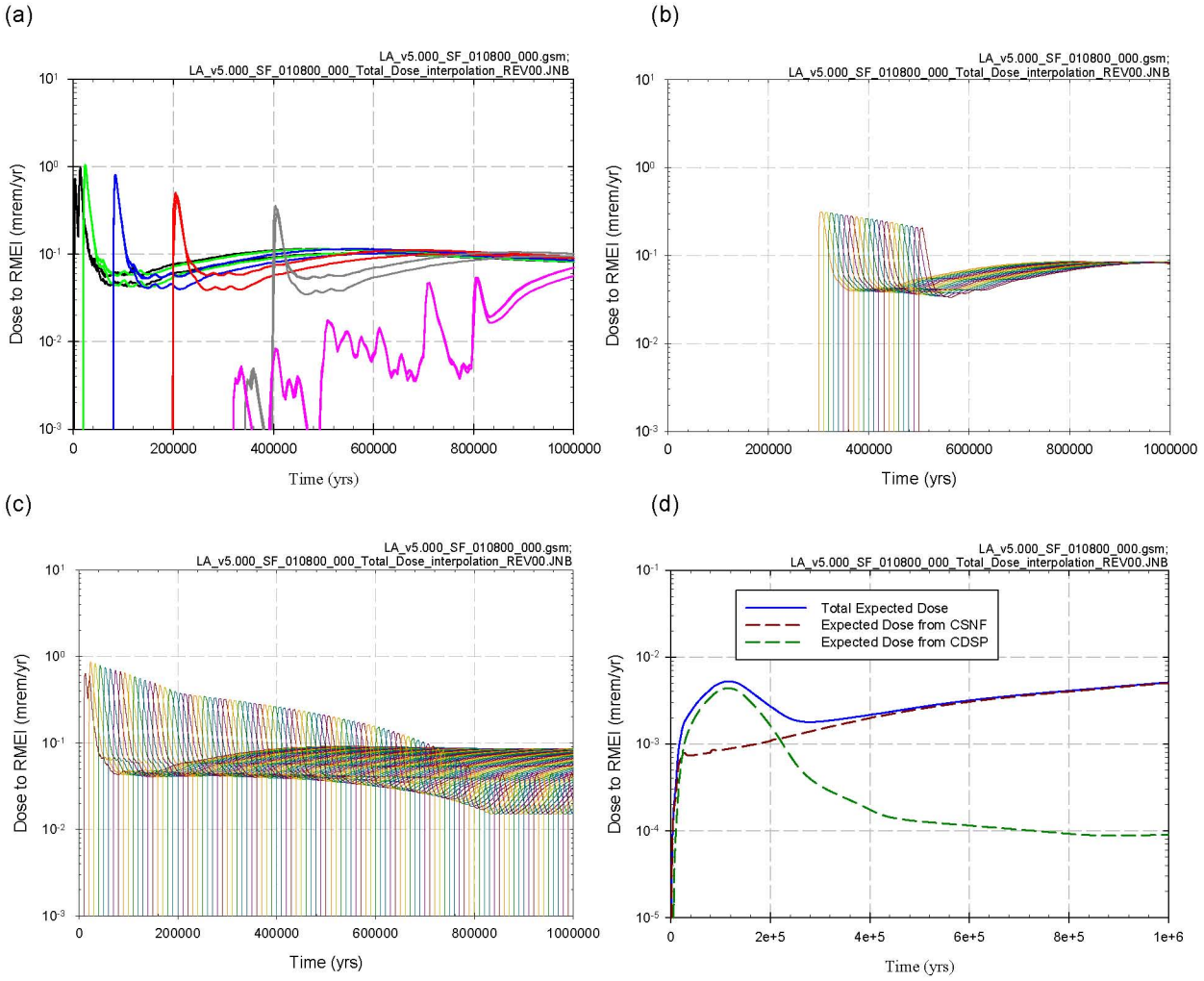

Source: Ouput DTNs: MO0709TSPAPLOT.000 [DIRS 183010]; and MO0709TSPAREGS.000 [DIRS 182976].

Figure J8.6-14. Illustration of interpolation procedure to estimate integrals $\hat{I}_r(\tau|t, \mathbf{e}_{M1})$ and expected dose $\bar{D}_{SF}(\tau|\mathbf{e}_i)$ from calculated doses $D_{SF,r}(\tau|[1, t_j, 100, A_{rk}, 1, \sim], \mathbf{e}_{M1})$ in Equation J8.6-18 for LHS element $\mathbf{e}_1 = [\mathbf{e}_{A1}, \mathbf{e}_{M1}]$ and the time interval [0, 1.0×10^6 yr]: (a) $D_{SF,1}(\tau|[1, t_j, 100, A_{rk}, 1, \sim], \mathbf{e}_{M1})$ for $j = 1, 2, \ldots, 6$ and $k = 1, 2, 3$ (Notes: Results overlay for A_{1k}, $k = 1, 2, 3$, for each t_j, and results for t_1 and t_2 also overlay), (b) Interpolated values $\hat{I}_1(\tau|\hat{t}_k, \mathbf{e}_{M1})$ for $\hat{t}_k$ between $t_4 = 2.0 \times 10^5$ yr and $t_5 = 4.0 \times 10^5$ yr, (c) Interpolated values for $\hat{I}_1(\tau|\hat{t}_k, \mathbf{e}_{M1})$ for $\hat{t}_k$ between 1000 and 1.0×10^6 yr, and (d) estimates for $\bar{D}_{SF,1}(\tau|\mathbf{e}_i)$ for CSNF WPs, $\bar{D}_{SF,2}(\tau|\mathbf{e}_i)$ for CDSP WPs and $\bar{D}_{SF}(\tau|\mathbf{e}_i)$ for CSNF and CDSP WPs.

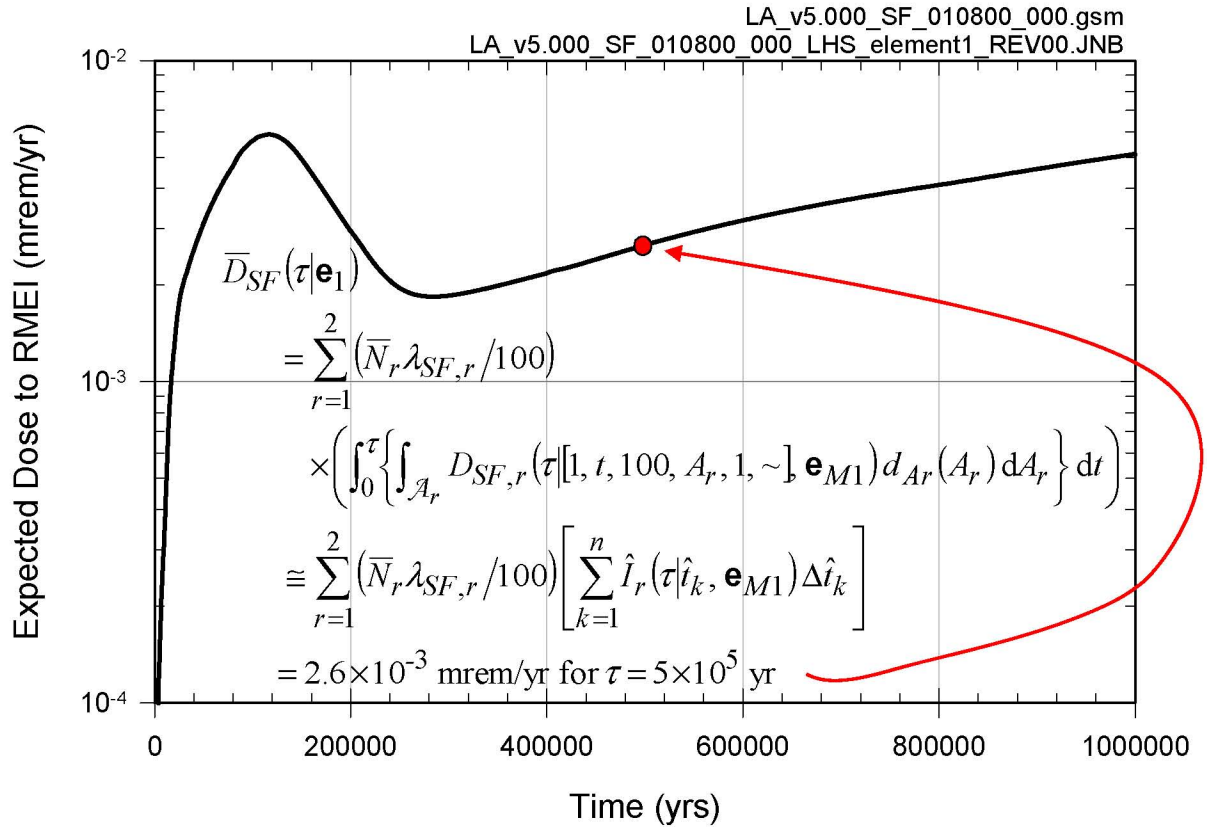

Source: Ouput DTNs: MO0709TSPAPLOT.000 [DIRS 183010]; and MO0709TSPAREGS.000 [DIRS 182976].

Figure J8.6-15. Estimate of $\overline{D}_{SF}(\tau|\mathbf{e}_1)$ for LHS element $\mathbf{e}_1 = [\mathbf{e}_{A1}, \mathbf{e}_{M1}]$ and $0 \le \tau \le 10^6$ yr with integration-based procedure indicated in Equations J8.6-17 and J8.6-25.

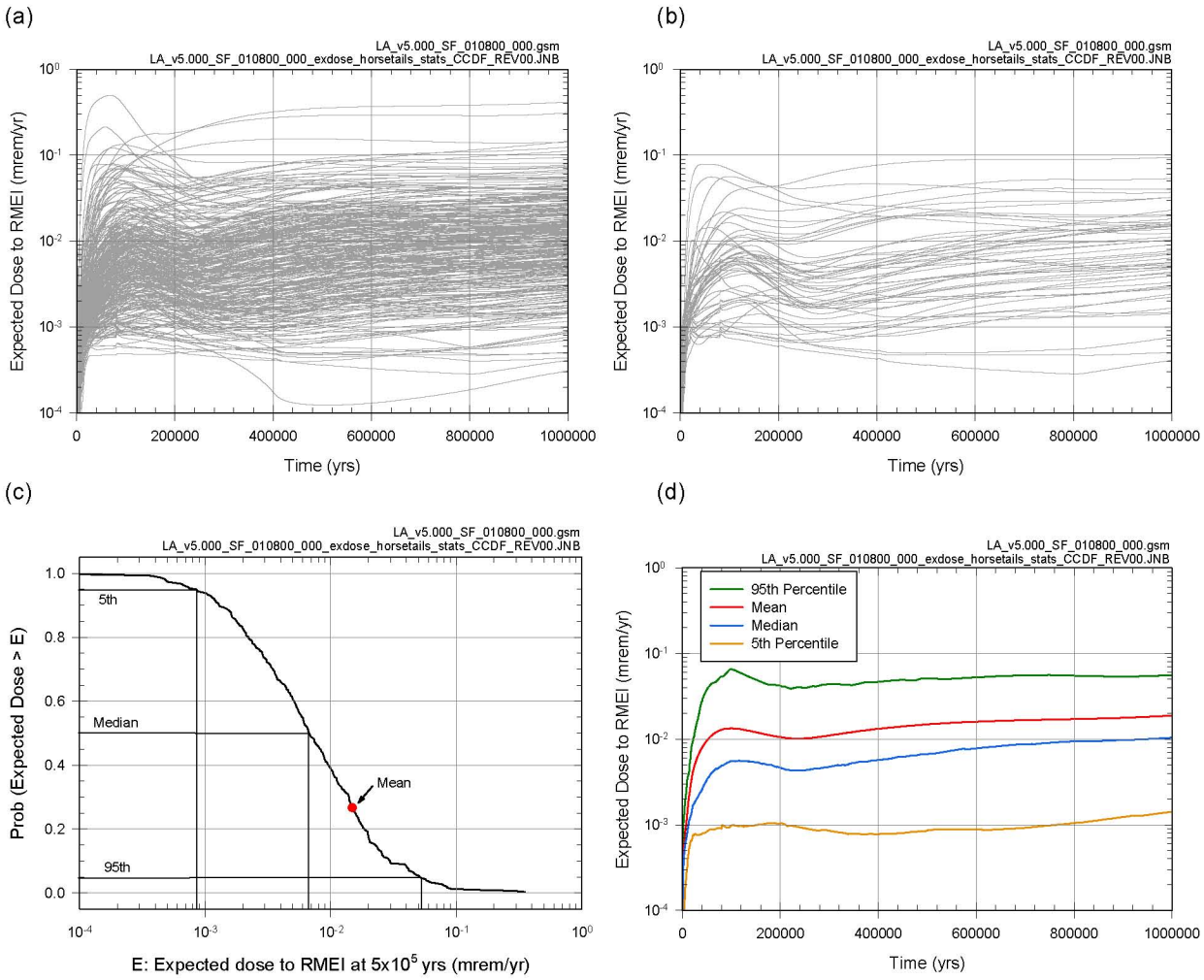

Source: Ouput DTNs: MO0709TSPAPLOT.000 [DIRS 183010]; and MO0709TSPAREGS.000 [DIRS 182976].

Figure J8.6-16. Estimate obtained with LHS of size *nLHS* = 300 showing epistemic uncertainty in expected dose $\bar{D}_{SF}(\tau|\mathbf{e})$ to RMEI for $0 \le \tau \le 10^6$ yr that at results when only fault displacement events are considered: (a) expected dose $\bar{D}_{SF}(\tau|\mathbf{e}_i)$, i = 1, 2, ..., *nLHS* = 300, (b) expected dose $\bar{D}_{SF}(\tau|\mathbf{e}_i)$, i = 1, 2, ..., 50, (c) exceedance probabilities $p_E[D < \bar{D}_{SG}(\tau|\mathbf{e})]$ and quantiles $Q_q[\bar{D}_{SF}(\tau|\mathbf{e})]$, q = 0.05, 0.5 and 0.95, for $\tau = 5 \times 10^5$ yr, and (d) expected (mean) dose $\bar{\bar{D}}_{SF}(\tau)$ and quantiles $Q_q[\bar{D}_{SF}(\tau|\mathbf{e})]$, q = 0.05, 0.5, 0.95.

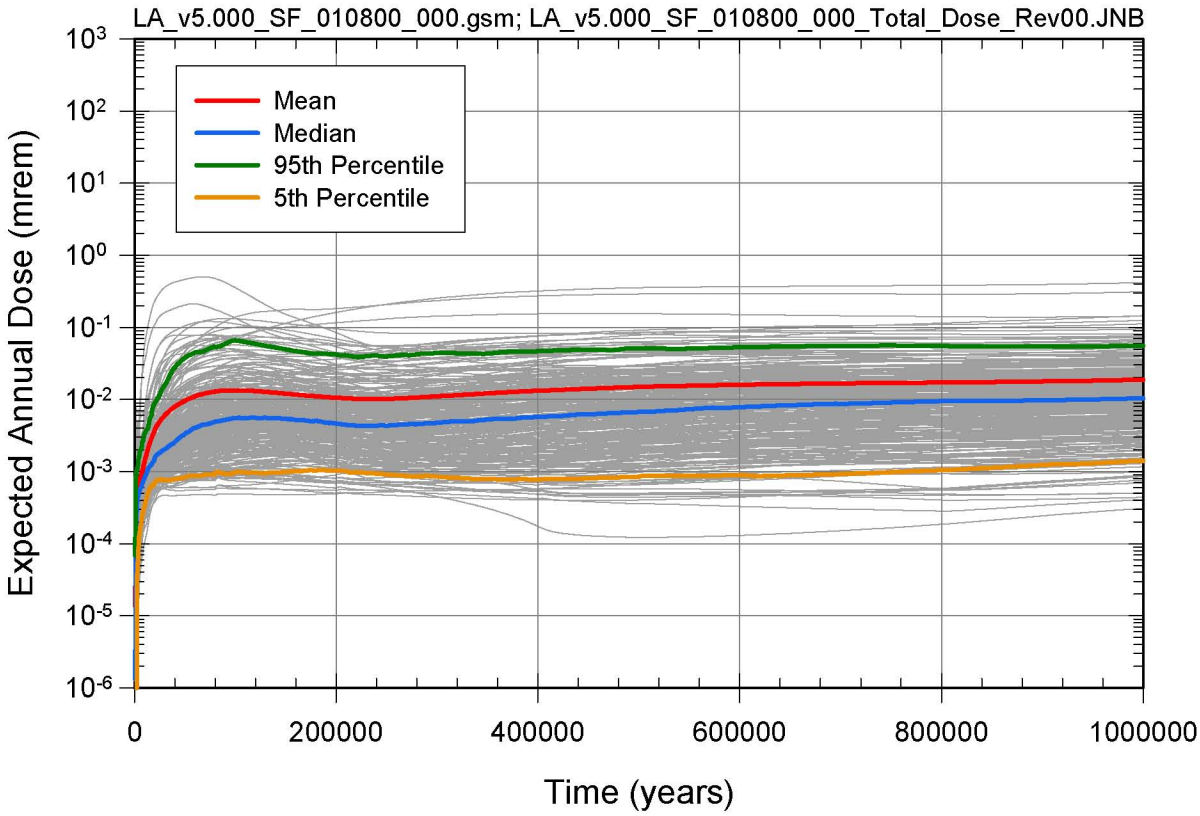

Source: Ouput DTNs: MO0709TSPAPLOT.000 [DIRS 183010]; and MO0709TSPAREGS.000 [DIRS 182976].

Figure J8.6-17. Summary of results obtained with LHS of size *nLHS* = 300 showing epistemic uncertainty in expected dose $\bar{D}_{SF}(\tau|\mathbf{e})$ to RMEI for $0 \leq \tau \leq 10^6$ yr that results when only fault displacement events are considered.

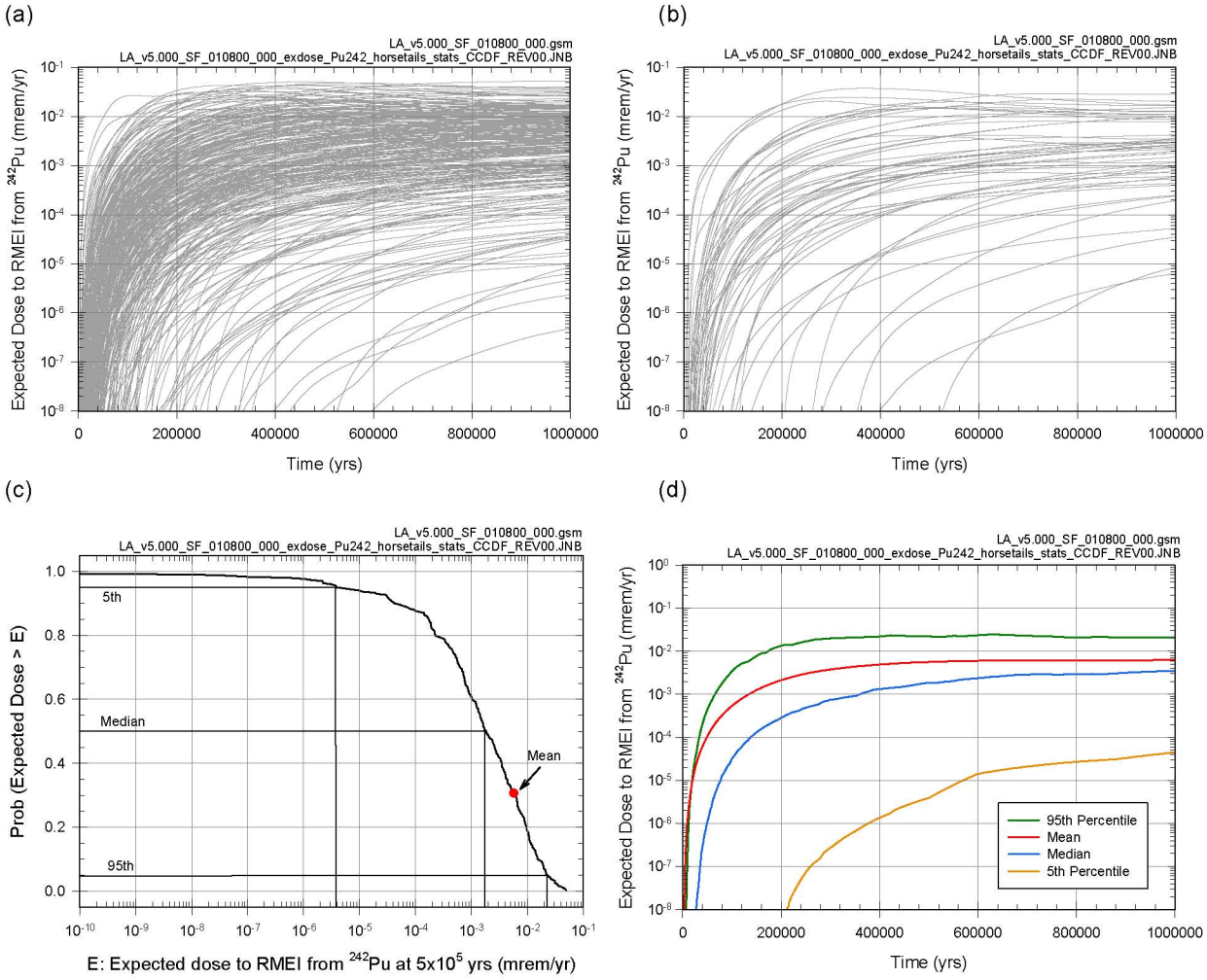

Source: Ouput DTNs: MO0709TSPAPLOT.000 [DIRS 183010]; and MO0709TSPAREGS.000 [DIRS 182976].

Figure J8.6-18. Estimate obtained with LHS of size *nLHS* = 300 showing epistemic uncertainty in expected dose $\bar{D}_{SF,r}(\tau|\mathbf{e})$ to RMEI for $0 \le \tau \le 10^6$ yr with r corresponding to ^{242}Pu that results when only fault displacement events are considered: (a) expected dose $\bar{D}_{SF,r}(\tau|\mathbf{e}_i)$, i = 1, 2, …, *nLHS* = 300, (b) expected dose $\bar{D}_{SF,r}(\tau|\mathbf{e}_i)$, i = 1, 2, …, 50, (c) exceedance probabilities $p_E[D < \bar{D}_{SG,r}(\tau|\mathbf{e})]$ and quantiles $Q_q[\bar{D}_{SF,r}(\tau|\mathbf{e})]$, q = 0.05, 0.5 and 0.95, for τ = 500,000 yr, and (d) expected (mean) dose $\bar{\bar{D}}_{SF,r}(\tau)$ and quantiles $Q_q[\bar{D}_{SF,r}(\tau|\mathbf{e})]$, q = 0.05, 0.5, 0.95.

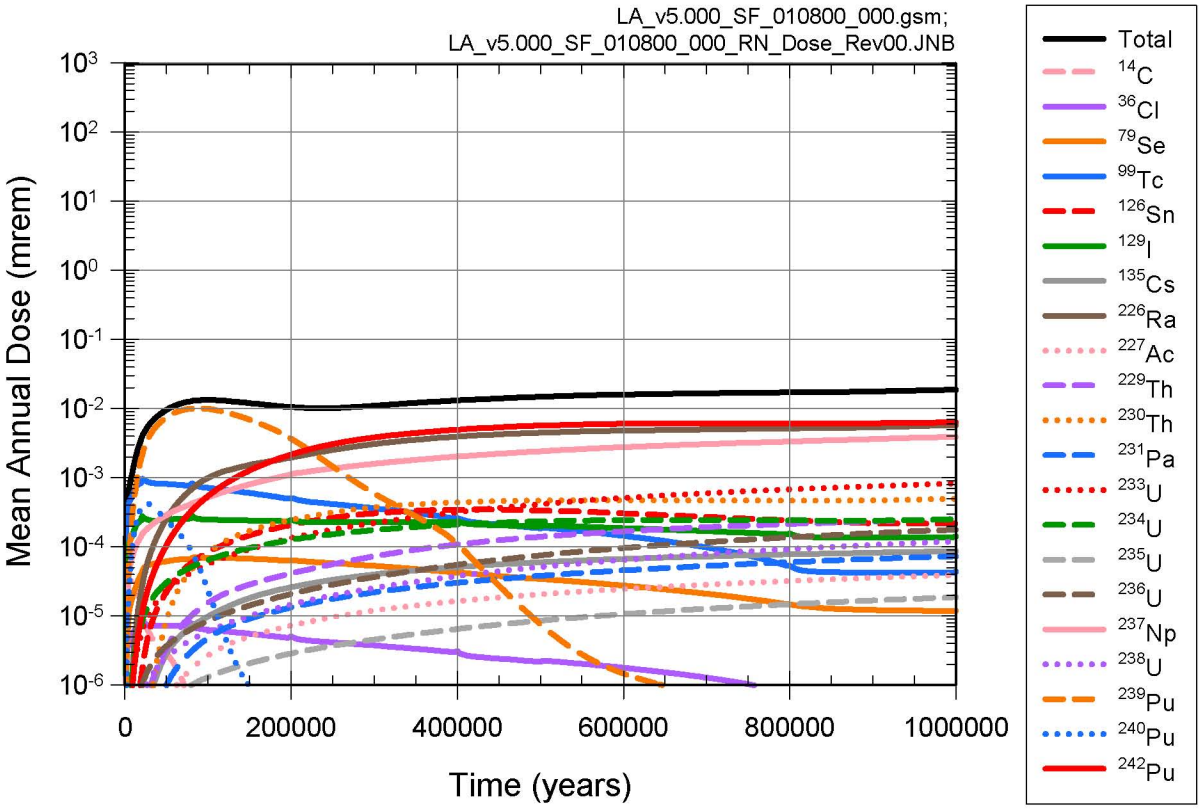

Source: Ouput DTNs: MO0709TSPAPLOT.000 [DIRS 183010]; and MO0709TSPAREGS.000 [DIRS 182976].

Figure J8.6-19. Estimates obtained with LHS of size *nLHS* = 300 of expected (mean) dose $\bar{\bar{D}}_{SF,r}(\tau)$ to RMEI for $0 \leq \tau \leq 10^6$ yr for individual radioactive species that result when only seismic ground motion events are considered.

(a)

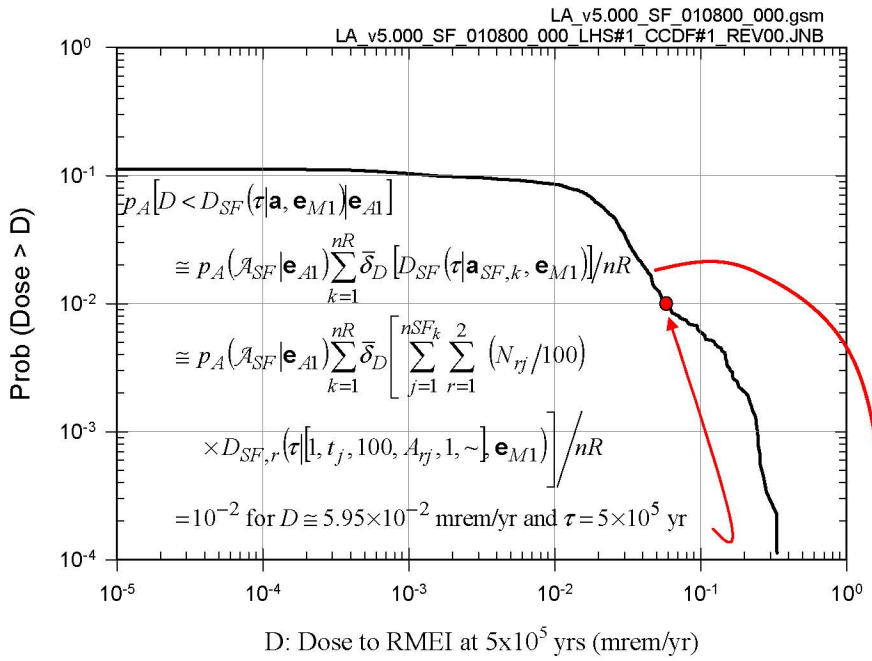

(b)

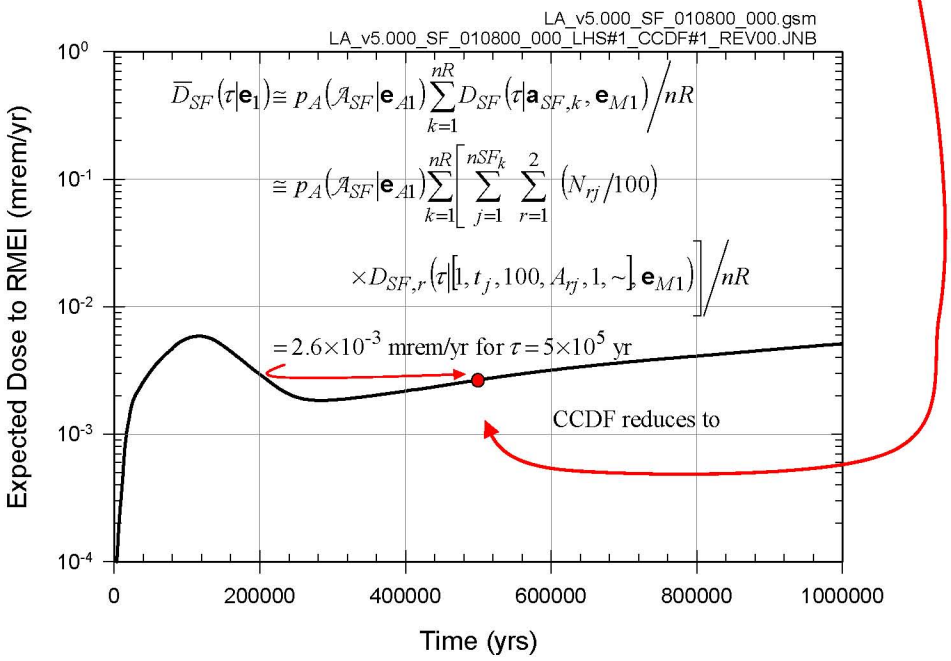

Source: Ouput DTNs: MO0709TSPAPLOT.000 [DIRS 183010]; and MO0709TSPAREGS.000 [DIRS 182976].

Figure J8.6-20. Results associated with $D_{SF}(\tau|\mathbf{a}_{SF}, \mathbf{e}_{M1})$ for LHS element $\mathbf{e}_1 = [\mathbf{e}_{A1}, \mathbf{e}_{M1}]$ obtained with sampling-based (Monte Carlo) procedures: (a) CCDF for $D_{SF}(5 \times 10^5 \text{ yr}|\mathbf{a}_{SF}, \mathbf{e}_{M1})$ with exceedance probabilities $p_A[D < D_{SF}(5 \times 10^5 \text{ yr}|\mathbf{a}, \mathbf{e}_{M1})|\mathbf{e}_{A1}]$ defined in Equations J4.5-19 and J8.6-36, and (b) expected dose $\bar{D}_{SF}(5 \times 10^5 \text{ yr}|\mathbf{e}_1)$ associated with $D_{SF}(5 \times 10^5 \text{ yr}|\mathbf{a}_{SF}, \mathbf{e}_{M1})$ defined in Equation J4.5-20.

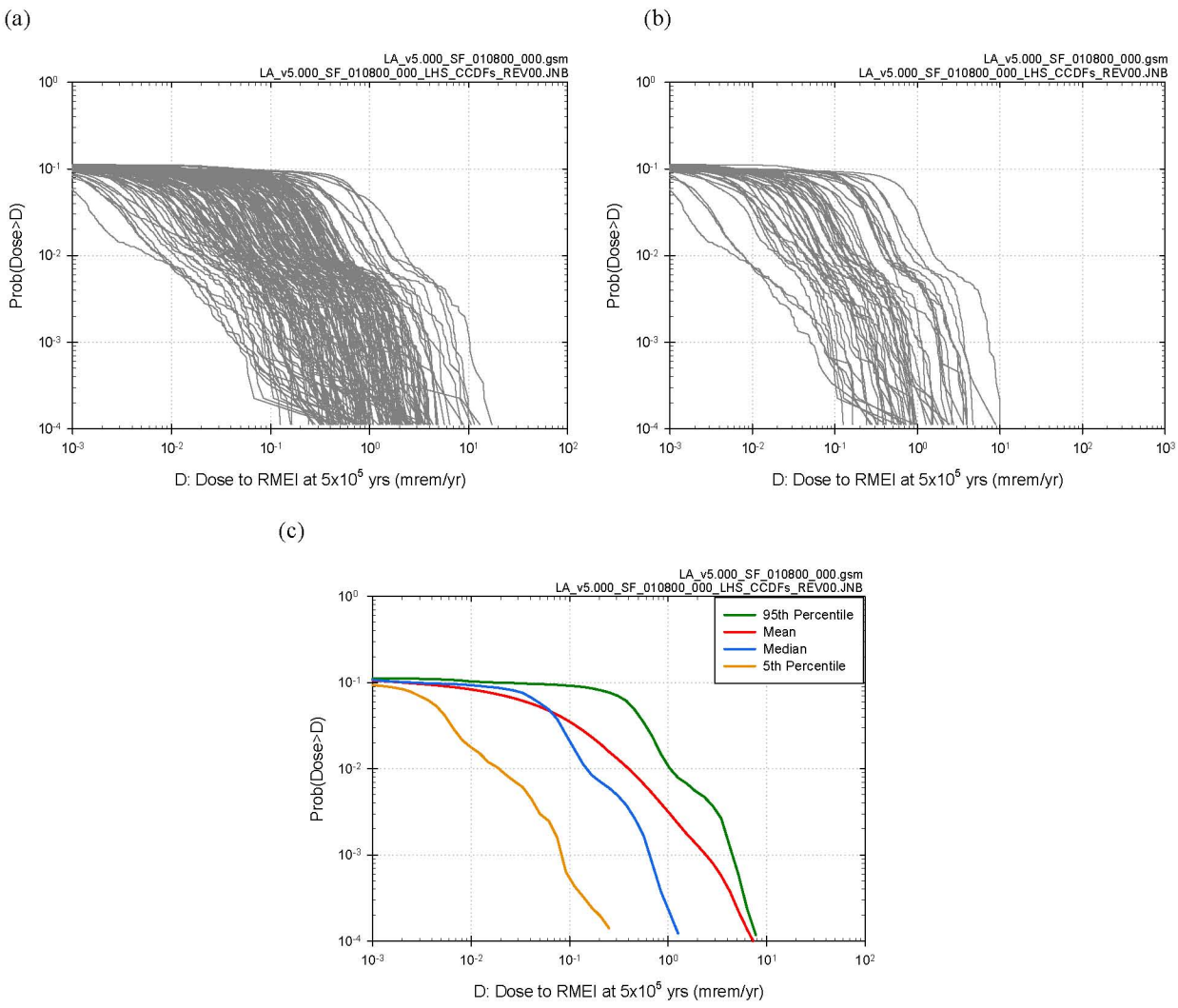

Source: Ouput DTNs: MO0709TSPAPLOT.000 [DIRS 183010]; and MO0709TSPAREGS.000 [DIRS 182976].

Figure J8.6-21. Results associated with $D_{SG}(5 \times 10^5 \text{ yr}|\mathbf{a}_{SF}, \mathbf{e}_M)$ obtained with sampling-based (Monte Carlo) procedures for an LHS of size $nLHS = 300$: (a) CCDFs for $D_{SF}(5 \times 10^5 \text{ yr}|\mathbf{a}_{SF}, \mathbf{e}_{Mi})$ with exceedance probabilities $p_A[D < D_{SF}(5 \times 10^5 \text{ yr}|\mathbf{a}, \mathbf{e}_{Mi})|\mathbf{e}_{Ai}]$ defined in Equation J4.5-19 for $i = 1, 2, \ldots, nLHS = 300$, (b) CCDFs for $D_{SF}(10^4 \text{ yr}|\mathbf{a}_{SF}, \mathbf{e}_{Mi})$ with exceedance probabilities $p_A[D < D_{SF}(5 \times 10^5 \text{ yr}|\mathbf{a}, \mathbf{e}_{Mi})|\mathbf{e}_{Ai}]$ defined in Equation J4.5-19 for $i = 1, 2, \ldots, 50$, and (c) expected (mean) CCDF and quantile curves, $q = 0.05, 0.5, 00.95$, for CCDFs in (a).

(a)

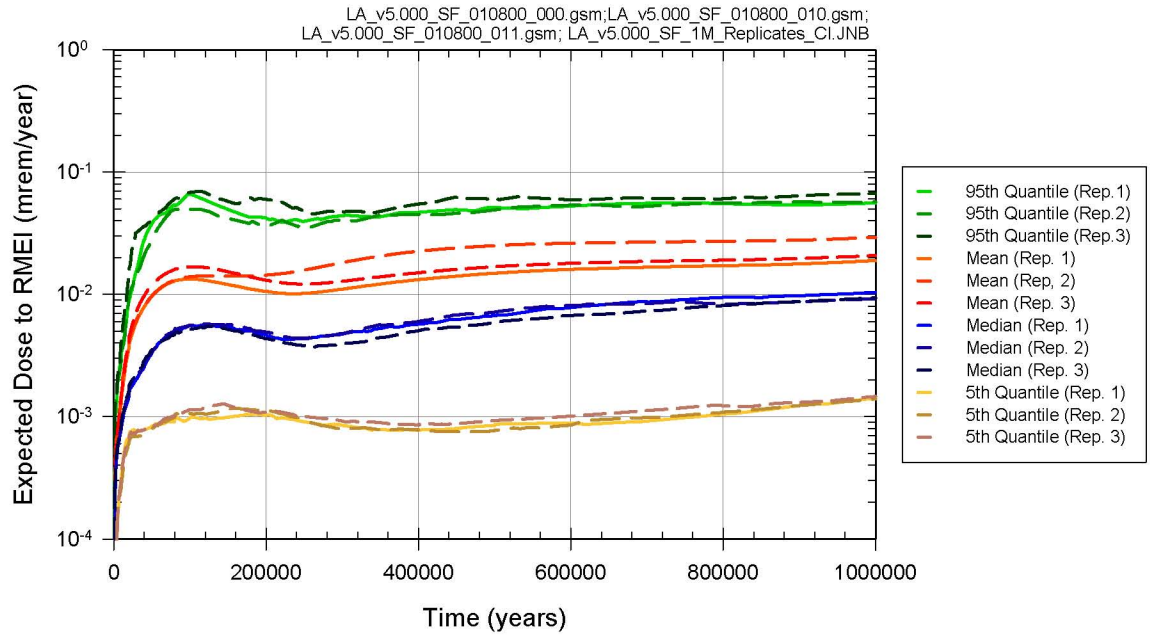

(b)

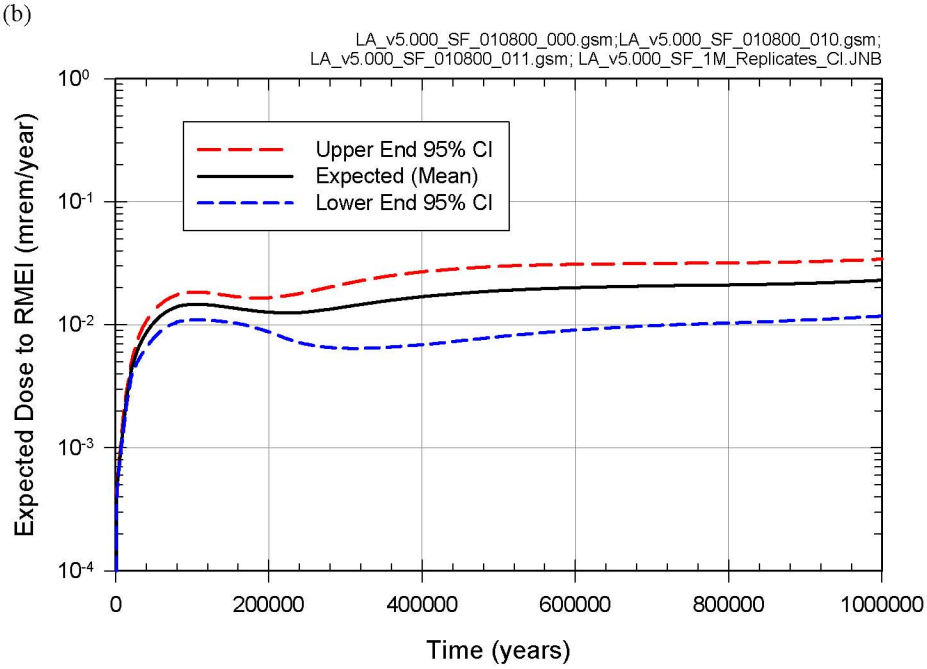

Source: Ouput DTNs: MO0709TSPAPLOT.000 [DIRS 183010]; MO0709TSPAREGS.000 [DIRS 182976]; and MO0709TSPASTAB.000 [DIRS 182983].

Figure J8.6-22. Assessment with replicated sampling of numerical error associated with use of an LHS of size *nLHS* = 300 to determine epistemic uncertainty in expected dose $\bar{D}_{SF}(\tau|\mathbf{e})$ to RMEI for $0 \leq \tau \leq 10^6$ yr that results when only seismic ground motion events are considered: (a) Replicated estimates of expected (mean) dose $\bar{\bar{D}}_{SF}(\tau)$ and quantiles $Q_q[\bar{D}_{SF}(\tau|\mathbf{e})]$, q = 0.05, 0.5, 0.95, and (b) confidence intervals for estimates of expected (mean) dose $\bar{\bar{D}}_{SF}(\tau)$.

INTENTIONALLY LEFT BLANK

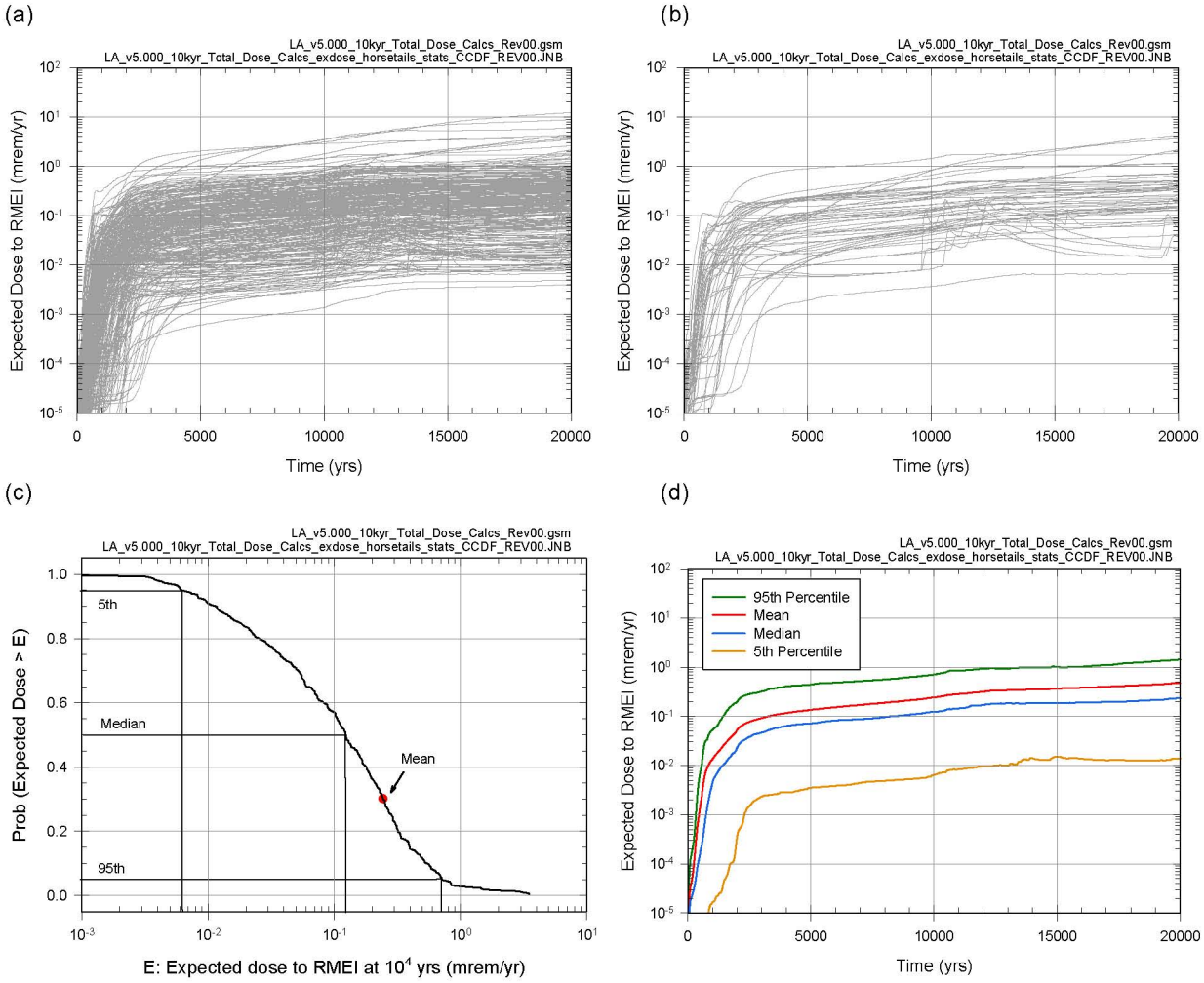

Source: Ouput DTN: MO0709TSPAPLOT.000 [DIRS 183010].

Figure J9.2-1. Estimate obtained with LHS of size *nLHS* = 300 showing epistemic uncertainty in expected dose $\bar{D}(\tau|\mathbf{e})$ to RMEI for $0 \le \tau \le 20{,}000$ yr that results when all futures are considered: (a) expected dose $\bar{D}(\tau|\mathbf{e}_i)$, i = 1, 2, …, *nLHS* = 300, (b) expected dose $\bar{D}(\tau|\mathbf{e}_i)$, i = 1, 2, …, 50, (c) exceedance probabilities $p_E[D < \bar{D}(\tau|\mathbf{e})]$ and quantiles $Q_q[\bar{D}(\tau|\mathbf{e})]$, q = 0.05, 0.5 and 0.95, for $\tau = 10^4$ yr, and (d) expected (mean) dose $\bar{\bar{D}}(\tau)$ and quantiles $Q_q[\bar{D}(\tau|\mathbf{e})]$, q = 0.05, 0.5, 0.95.

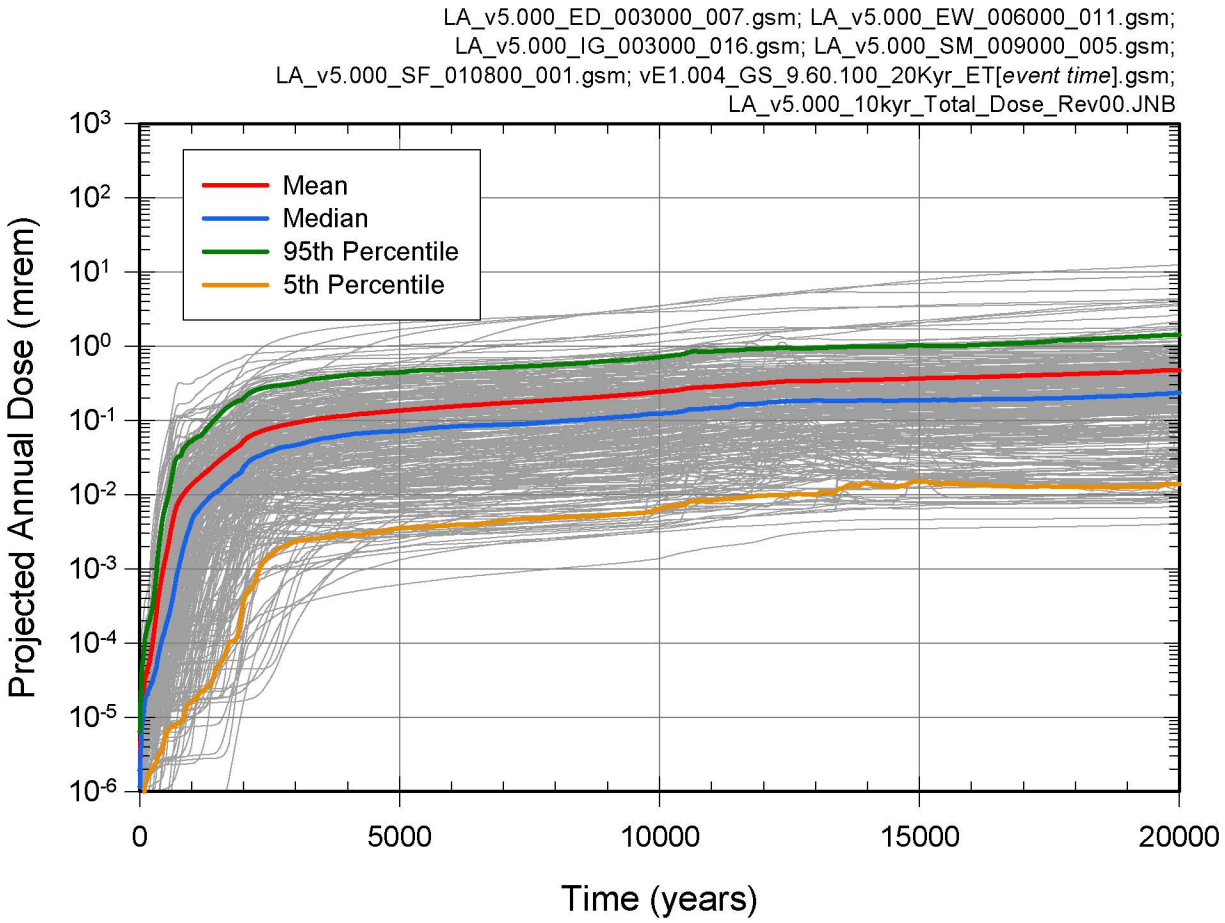

Source: Ouput DTNs: MO0709TSPAPLOT.000 [DIRS 183010]; and MO0709TSPAREGS.000 [DIRS 182976].

Figure J9.2-2. Summary of results obtained with LHS of size *nLHS* = 300 showing epistemic uncertainty in expected dose $\bar{D}(\tau|\mathbf{e})$ to RMEI for $0 \leq \tau \leq 20{,}000$ yr that results when all futures are considered.

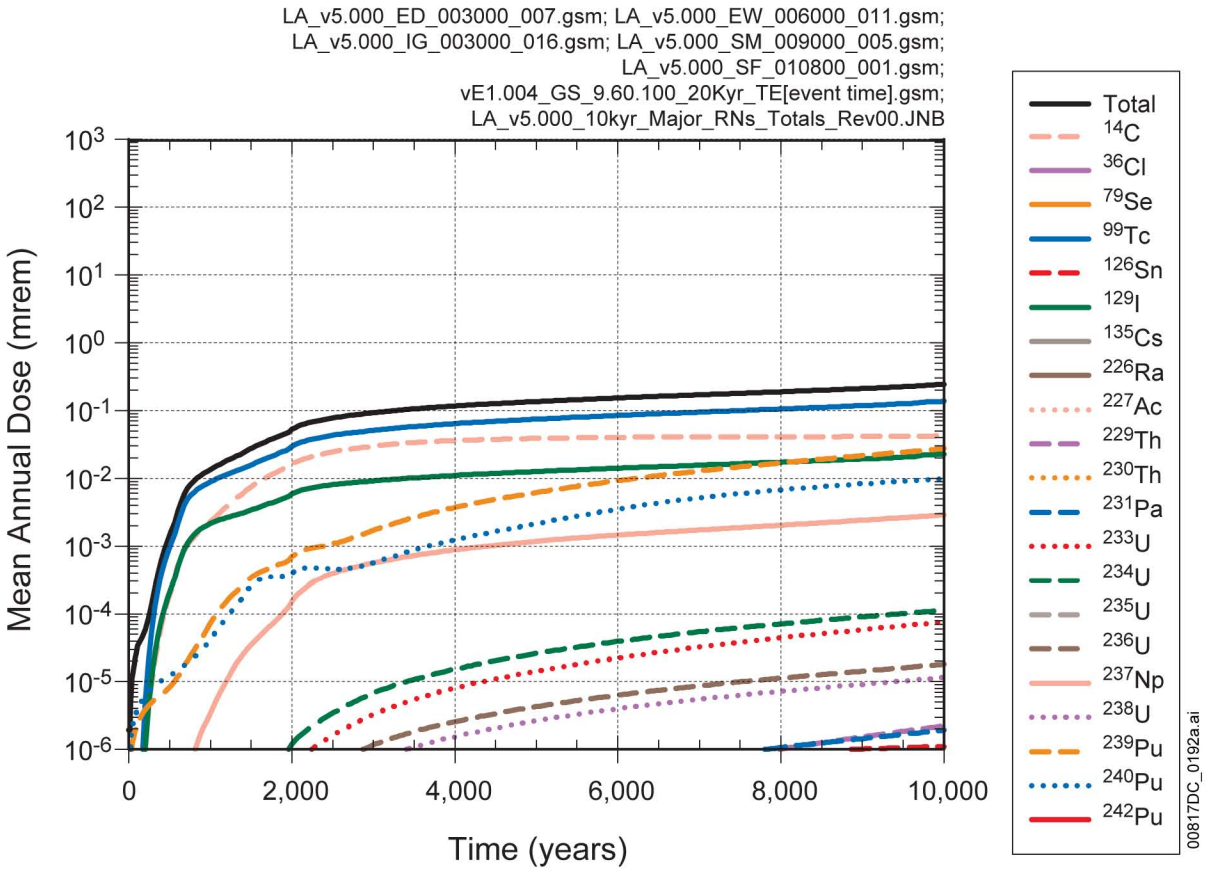

Source: Ouput DTNs: MO0709TSPAPLOT.000 [DIRS 183010]; and MO0709TSPAREGS.000 [DIRS 182976].

Figure J9.2-3. Estimates obtained with LHS of size *nLHS* = 300 of expected (mean) dose $\overline{\overline{D}}_r(\tau)$ to RMEI for $0 \leq \tau \leq 20{,}000$ yr for individual radioactive species that result when all futures are considered.

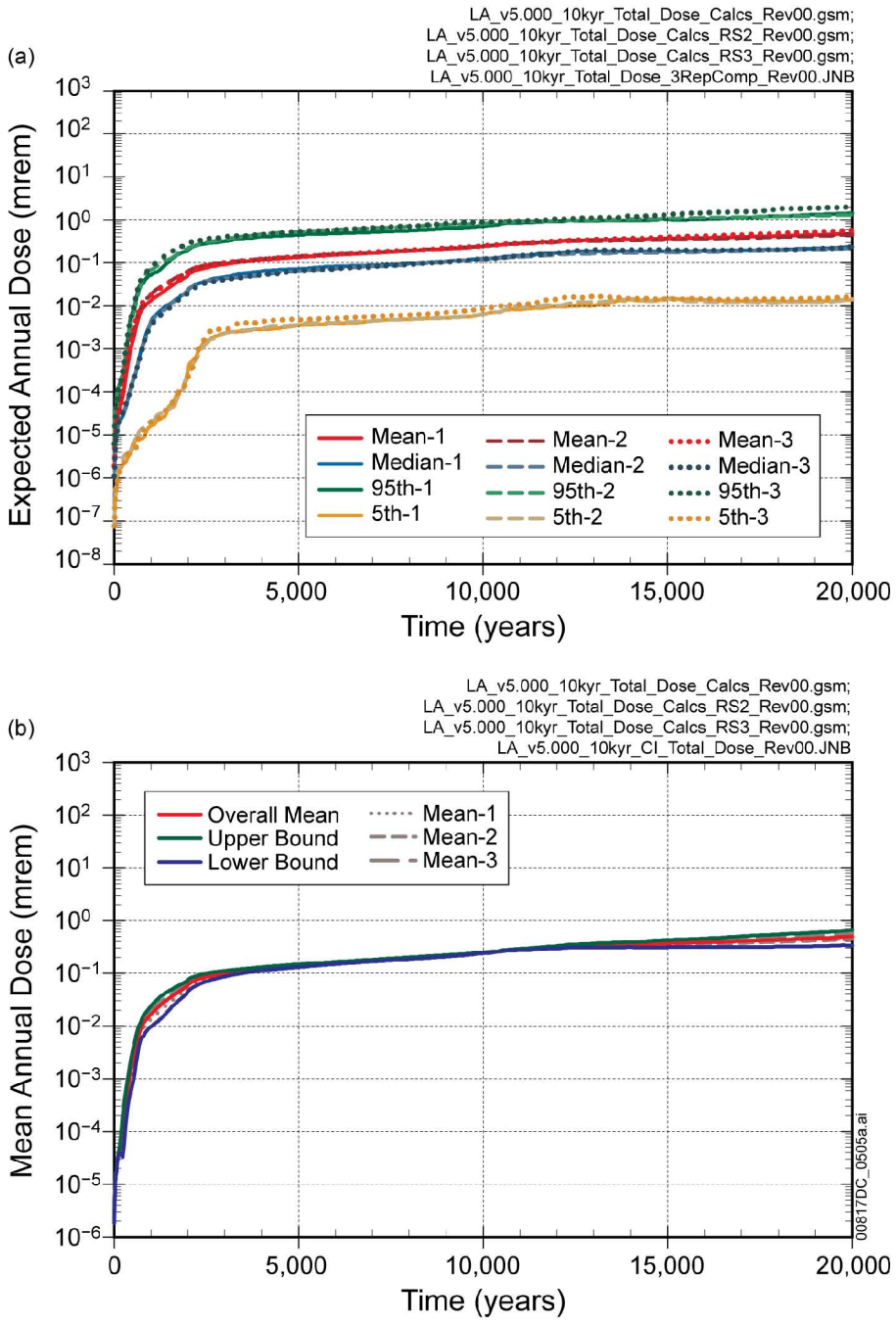

Source: Ouput DTN: MO0709TSPAPLOT.000 [DIRS 183010].

Figure J9.2-4. Assessment with replicated sampling of numerical error associated with use of an LHS of size *nLHS* = 300 to determine epistemic uncertainty in expected dose $\bar{D}(\tau|\mathbf{e})$ to RMEI for $0 \leq \tau \leq 20{,}000$ yr that results when all futures are considered: (a) Replicated estimates of expected (mean) dose $\bar{\bar{D}}(\tau)$ and quantiles $Q_q[\bar{D}(\tau|\mathbf{e})]$, q = 0.05, 0.5, 0.95, and (b) confidence intervals for estimates of expected (mean) dose $\bar{\bar{D}}(\tau)$.

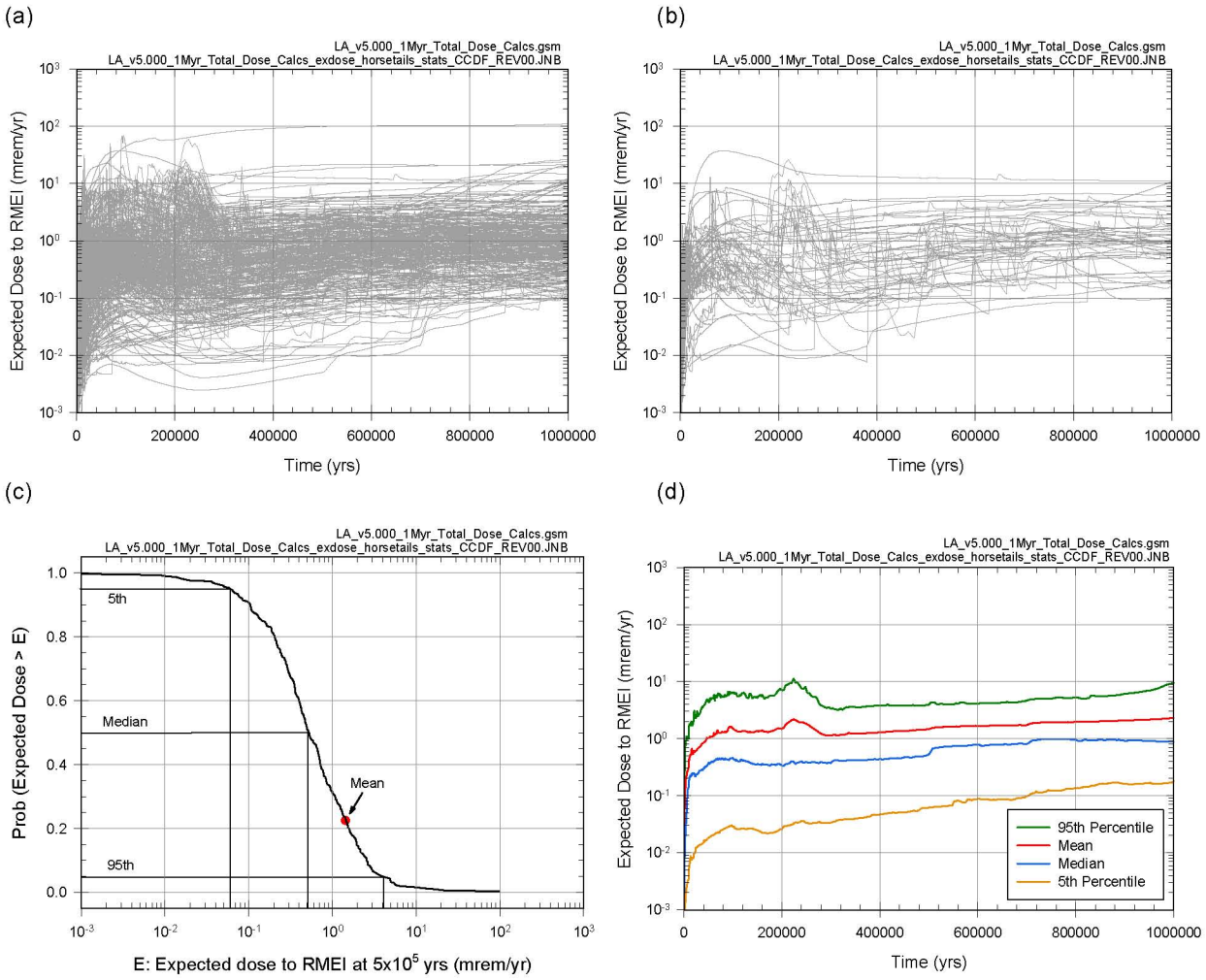

Source: Ouput DTN: MO0709TSPAPLOT.000 [DIRS 183010].

Figure J9.3-1. Estimate obtained with LHS of size *nLHS* = 300 showing epistemic uncertainty in expected dose $\bar{D}(\tau|\mathbf{e})$ to RMEI for $0 \le \tau \le 1{,}000{,}000$ yr that results when all futures are considered: (a) expected dose $\bar{D}(\tau|\mathbf{e}_i)$, i = 1, 2, …, *nLHS* = 300, (b) expected dose $\bar{D}(\tau|\mathbf{e}_i)$, i = 1, 2, …, 50, (c) exceedance probabilities $p_E[D < \bar{D}(\tau|\mathbf{e})]$ and quantiles $Q_q[\bar{D}(\tau|\mathbf{e})]$, q = 0.05, 0.5 and 0.95, for $\tau = 10^4$ yr, and (d) expected (mean) dose $\bar{\bar{D}}(\tau)$ and quantiles $Q_q[\bar{D}(\tau|\mathbf{e})]$, q = 0.05, 0.5, 0.95.

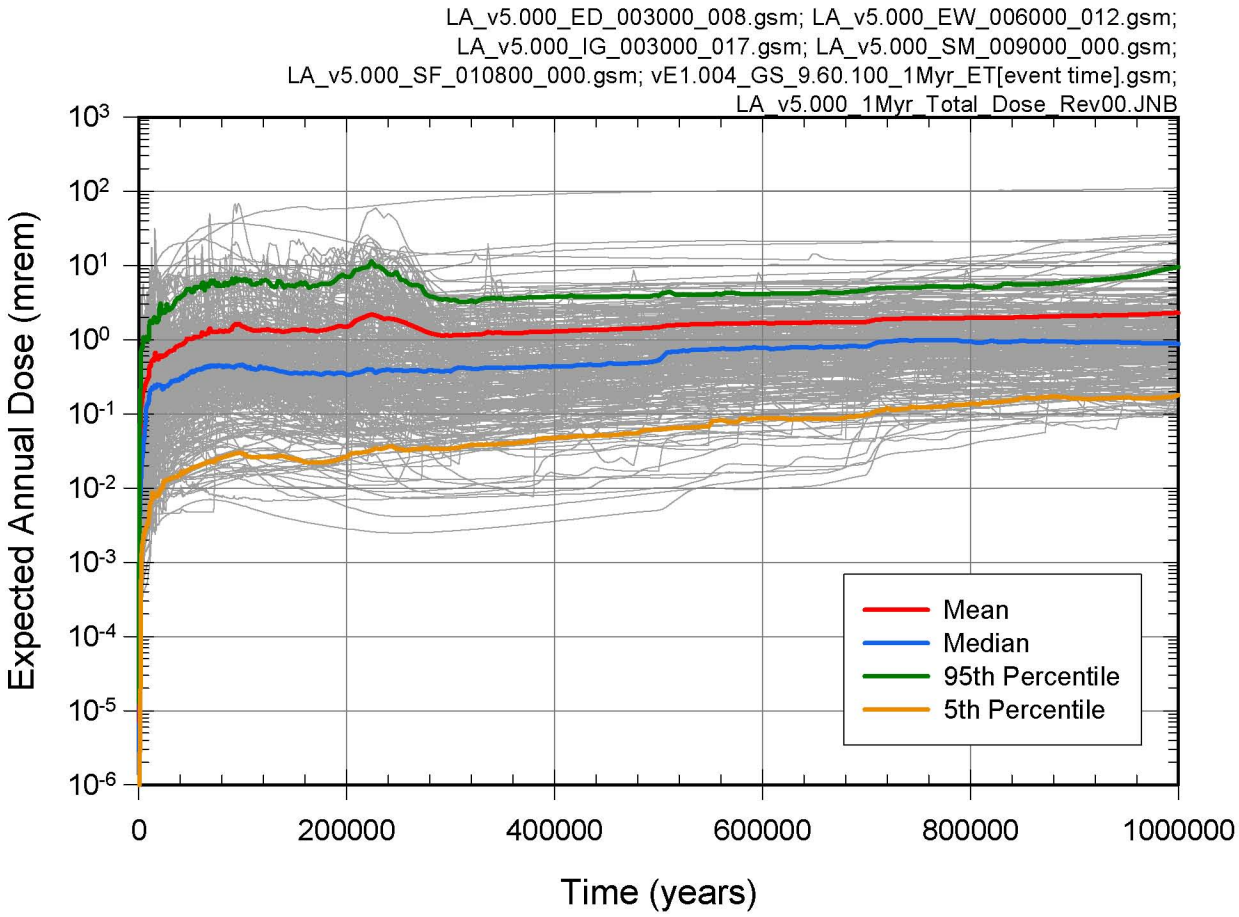

Source: Ouput DTNs: MO0709TSPAPLOT.000 [DIRS 183010]; and MO0709TSPAREGS.000 [DIRS 182976].

Figure J9.3-2. Summary of results obtained with LHS of size *nLHS* = 300 showing epistemic uncertainty in expected dose $\bar{D}(\tau|\mathbf{e})$ to RMEI for $0 \leq \tau \leq 1{,}000{,}000$ yr that results when all futures are considered.

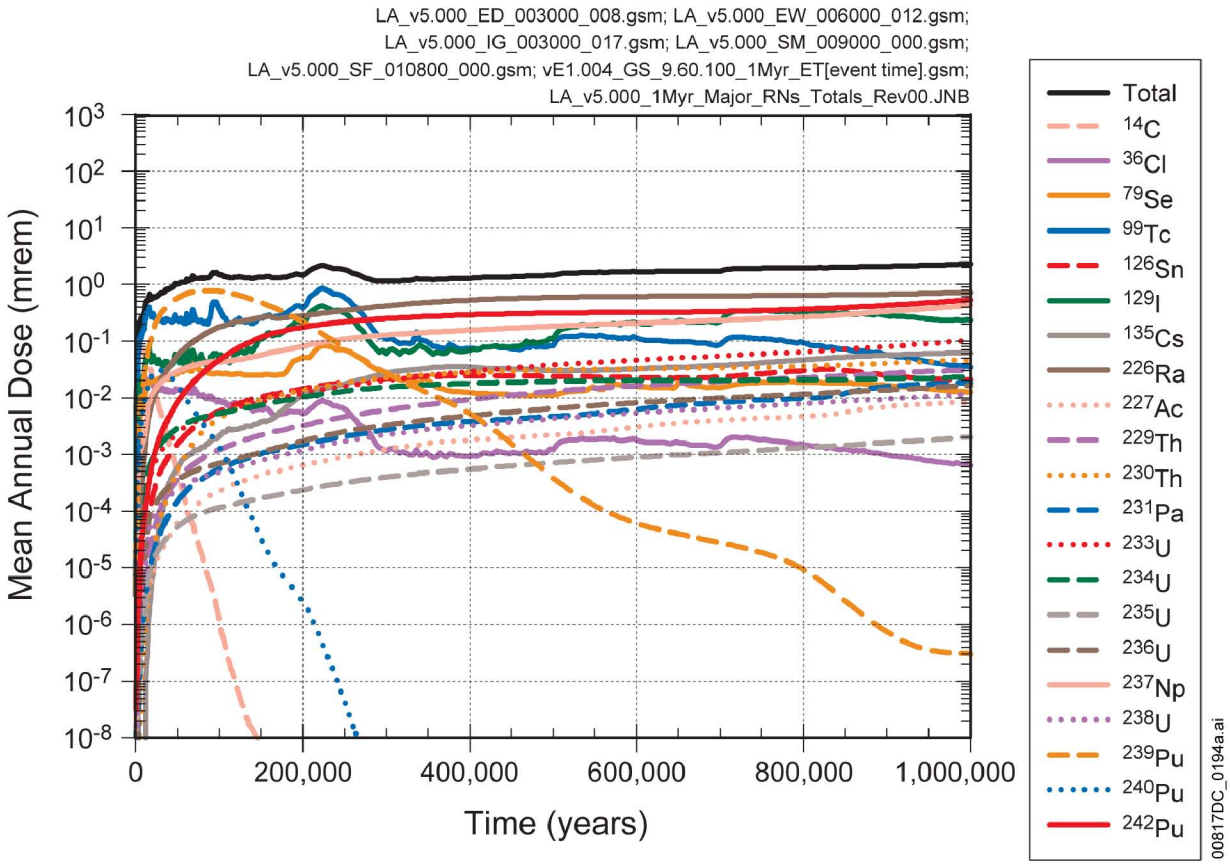

Source: Ouput DTNs: MO0709TSPAPLOT.000 [DIRS 183010]; and MO0709TSPAREGS.000 [DIRS 182976].

Figure J9.3-3. Estimates obtained with LHS of size *nLHS* = 300 of expected (mean) dose $\bar{D}_r(\tau)$ to RMEI for $0 \leq \tau \leq 1{,}000{,}000$ yr for individual radioactive species that result when all futures are considered.

(a)

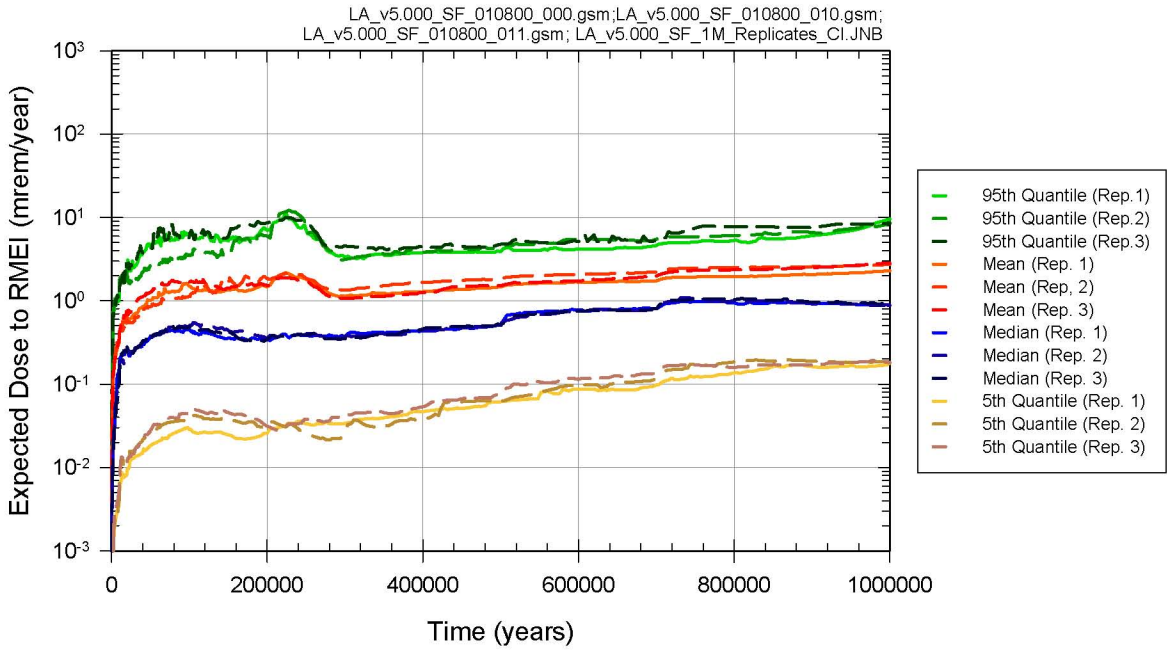

(b)

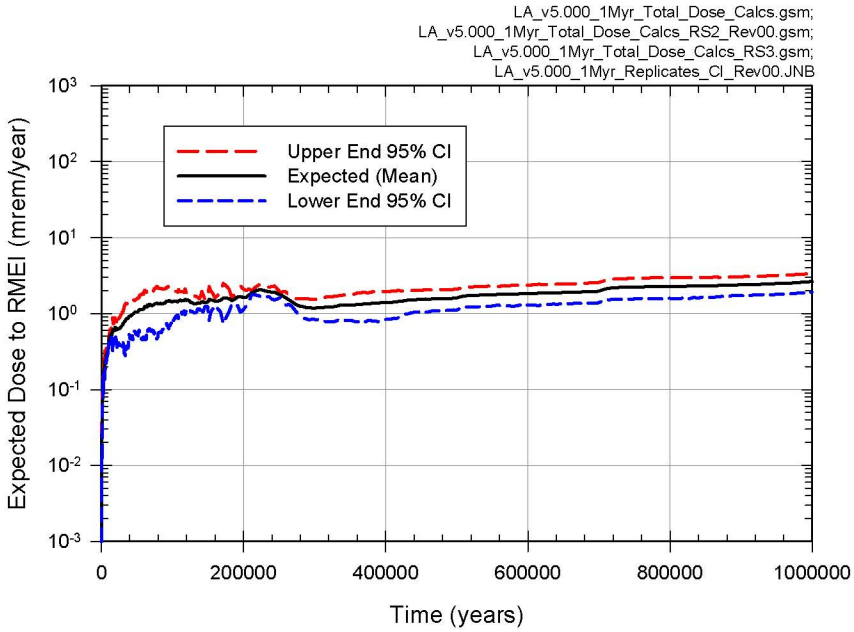

Source: Ouput DTNs: MO0709TSPAPLOT.000 [DIRS 183010]; MO0709TSPAREGS.000 [DIRS 182976]; and MO0709TSPASTAB.000 [DIRS 182983].

Figure J9.3-4. Assessment with replicated sampling of numerical error associated with use of an LHS of size *nLHS* = 300 to determine epistemic uncertainty in expected dose $\bar{D}(\tau|\mathbf{e})$ to RMEI for $0 \leq \tau \leq 1{,}000{,}000$ yr that results when all futures are considered: (a) Replicated estimates of expected (mean) dose $\bar{\bar{D}}(\tau)$ and quantiles $Q_q[\bar{D}(\tau|\mathbf{e})]$, q = 0.05, 0.5, 0.95, and (b) confidence intervals for estimates of expected (mean) dose $\bar{D}(\tau|\mathbf{e})$.

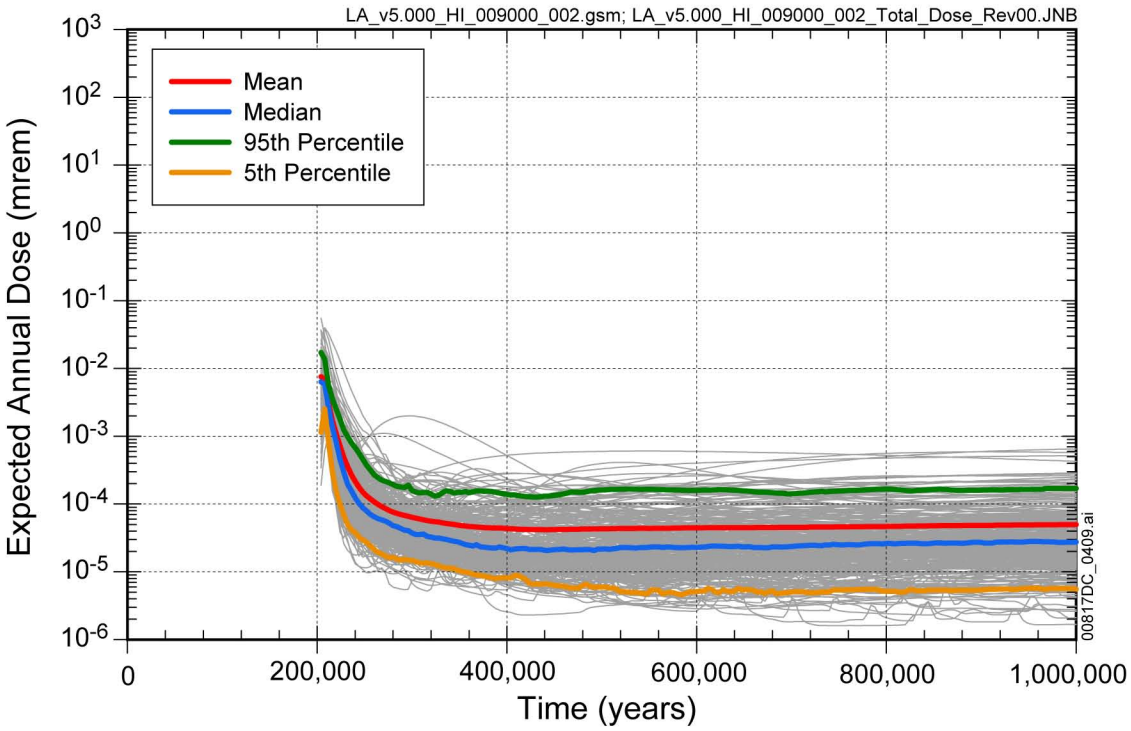

Source: Ouput DTNs: MO0709TSPAPLOT.000 [DIRS 183010]; and MO0709TSPAREGS.000 [DIRS 182976].

Figure J11.2-1. Estimate obtained with LHS of size *nLHS* = 300 showing epistemic uncertainty in expected dose $\bar{D}_{HI}(\tau|\mathbf{e})$ to RMEI for $0 \leq \tau \leq 1{,}000{,}000$ yr that results from a single drilling intrusion at 200,000 years.

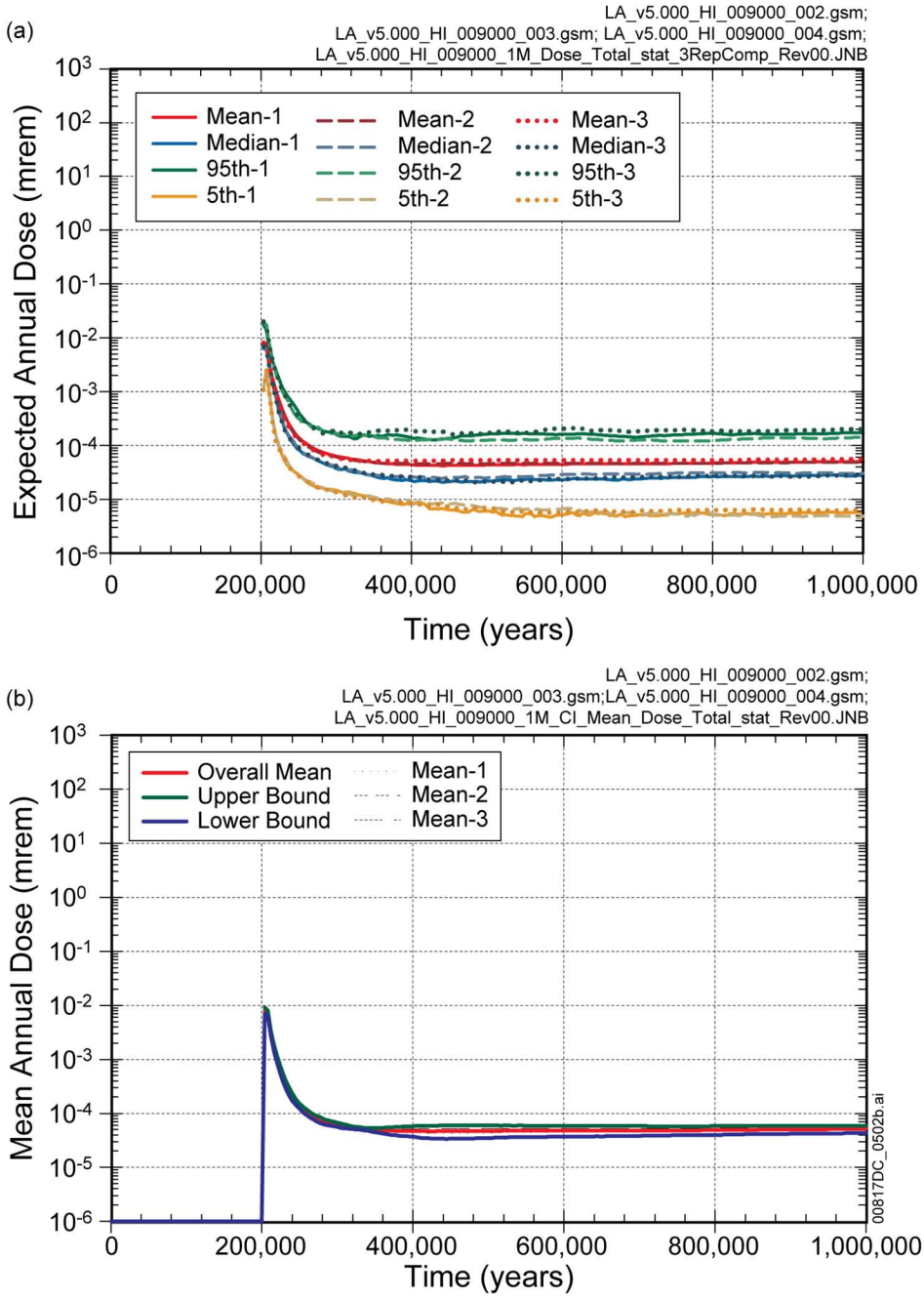

Source: Output DTNs: MO0709TSPASTAB.000 [DIRS 182983]; MO0709TSPAREGS.000 [DIRS 182976]; and MO0709TSPASTAB.000 [DIRS 182983].

Figure J11.2-2. Assessment with replicated sampling of numerical error associated with use of an LHS of size *nLHS* = 300 to determine epistemic uncertainty in expected dose $\bar{D}_{HI}(\tau|\mathbf{e})$ to RMEI for $0 \le \tau \le 1{,}000{,}000$ yr that results from a single drilling intrusion at 200,000 years: (a) Replicated estimates of expected (mean) dose $\bar{\bar{D}}_{HI}(\tau)$ and quantiles $Q_q[\bar{D}_{HI}(\tau|\mathbf{e})]$, q = 0.05, 0.5, 0.95, and (b) confidence intervals for estimates of expected (mean) dose $\bar{\bar{D}}_{HI}(\tau)$.

APPENDIX K:
UNCERTAINTY AND SENSITIVITY ANALYSIS RESULTS

K1 INTRODUCTION

This appendix (Appendix K) presents uncertainty and sensitivity analysis results obtained in support of the Total System Performance Assessment for the License Application (TSPA-LA) based on the analysis structure described in Appendix J and the technical basis described in Section 6. Uncertainty analyses determine the uncertainty in analysis results that derives from uncertainty in analysis inputs. Sensitivity analyses determine the contribution to the uncertainty in analysis results that derives from individual analysis inputs.

The appendix begins with two background sections that briefly describe the uncertainty and sensitivity procedures in use (Section K2) and the independent and dependent variables under consideration (Section K3). These sections also provide references to additional sources of information about sensitivity analysis methods. Then, uncertainty and sensitivity analysis results are presented for the following scenario classes: nominal scenario class (Section K4), early failure scenario classes (Section K5), igneous scenario classes (Section K6), and seismic scenario classes (Section K7). In addition, results are presented for expected dose to the reasonably maximally exposed individual (RMEI) from all sources (Section K8). The appendix concludes with a summary of the analysis results (Section K9).

K2 UNCERTAINTY AND SENSITIVITY ANALYSIS PROCEDURES

Conceptually, the TSPA-LA analysis can be represented by

$$\mathbf{y} = \mathbf{f}(\mathbf{e}), \tag{Eq. K2-1}$$

where

$$\mathbf{e} = [\mathbf{e}_A, \mathbf{e}_M] = [e_1, e_2, \ldots, e_{nE}] \tag{Eq. K2-2}$$

is a vector of epistemically uncertain inputs to the TSPA-LA (see Section J4.9),

$$\mathbf{y} = [y_1, y_2, \ldots, y_{nY}] \tag{Eq. K2-3}$$

is a vector of epistemically uncertain TSPA-LA results, and the function $\mathbf{f}$ denotes the integrated suite of models that constitute the TSPA-LA modeling system. Major categories of epistemic uncertainties represented in $\mathbf{e}$ are summarized in Table 6.1.3-2. The elements of $\mathbf{e}$ are listed in Table K3-1 by the abbreviated name given the element in the sensitivity analyses, and in Table K3-2 by the name given the element in the TSPA-LA Model. Each element is presented in more detail in Table K3-3. Selected elements of $\mathbf{y}$ are summarized in Table K3-, and $\mathbf{f}$ is the function resulting from the integration of the models described in Section 6 of this AMR and in more detail in the cited background references to this section.

The TSPA-LA employs uncertainty and sensitivity analysis procedures based on a mapping between analysis inputs and analysis results generated with use of Latin hypercube sampling. As discussed in Section J4.9, a Latin hypercube sample (LHS)

$$\mathbf{e}_i = [\mathbf{e}_{Ai}, \mathbf{e}_{Mi}], i = 1, 2, \ldots, nLHS, \quad \text{(Eq. K2-4)}$$

is generated from the epistemically uncertain analysis inputs in consistency with the probability space ($\mathcal{E}$, E, p_E) used to characterize epistemic uncertainty (see Equation (J4.1-3) and associated discussion). In the computational implementation of the TSPA-LA, the probability space ($\mathcal{E}$, E, p_E) is, in effect, defined by assigning a probability distribution D_j to each element e_j of **e**. A high-level summary of the elements of **e** and their associated distributions is given in Table K3-1, and a more detailed summary is given in Table K3-3. Additional information on Latin hypercube sampling is available in Helton and Davis (2003) [DIRS 170518].

The TSPA-LA analysis uses an LHS sample of size $nLHS$ = 300 from the elements **e** of $\mathcal{E}$. Further, as discussed in Section J4.10, this sample is replicated nRL = 3 times to test for the stability of analysis results.

Evaluation of TSPA-LA results for each element $\mathbf{e}_i$ = [$\mathbf{e}_{Ai}$, $\mathbf{e}_{Mi}$] of the LHS in Equation K2-4 generates a mapping

$$\mathbf{y}_i = \mathbf{f}(\mathbf{e}_i), \; i = 1, 2, \ldots, nLHS, \quad \text{(Eq. K2-5)}$$

from epistemically uncertain TSPA-LA inputs contained in $\mathbf{e}_i$ to epistemically uncertain TSPA-LA results contained in $\mathbf{y}_i$. Once generated, this mapping forms the basis for both uncertainty analysis and sensitivity analysis. Specifically, the weights associated with the individual LHS elements (i.e., 1/$nLHS$) permit the construction of distributions for elements of **y** that characterize epistemic uncertainty, and the mapping itself can be explored with a variety of sensitivity analysis procedures to determine the effects of individual elements of **e** on elements of **y**. The structure and implementation of analyses of this type are extensively discussed in the review by Helton et al. (2006) [DIRS 183873].

The primary sensitivity analysis procedures in use involve the determination and presentation of partial rank correlation coefficients (PRCCs), stepwise rank regression analyses, and scatterplots.

PRCCs provide a measure of the strength of the monotonic relationships between an independent variable e (i.e., an element of **e**) and a dependent variable y (i.e., an element of **y**) after a correction has been made to remove the monotonic effects of the other independent variables in the analysis (i.e., the elements of **e** other than e). Most of the elements of **y** under consideration are functions of time. For such variables, the presentation of PRCCs as functions of time provides an informative display of sensitivity analysis results (Figure K2-1).

As indicated by the name, PRCCs involve the analysis of rank-transformed data. With this approach, the values for variables are replaced with their ranks and then the PRCCs are calculated with these ranks rather than with the original values for the variables. Specifically, the smallest value of a variable is given a rank of 1; the next largest value is given a rank of 2; equal observations are assigned the average of what their ranks would have been if they had not been equal; and so on up to the largest value, which is given a rank equal to the number of sample elements in use (i.e., $nLHS$ = 300 in Appendix K). The effect of the rank transformation

is to transform monotonic relationships into linear relationships. Further, the rank transform tends to reduce the skewing effects of outliers, which permits the regression analyses to represent the general relationships between the inputs and the output of interest. Although no variable transformation is universally successful in improving the resolution of a sensitivity analysis in the presence of nonlinear relationships, the rank transformation has been found to be a broadly effective and useful means of enhancing the insights in sensitivity analyses based on partial correlation and also in sensitivity analyses based on stepwise regression.

In the example in Figure K2-1, the time-dependent results for the variable under consideration (i.e., *NCSFL*, number of failed commercial spent nuclear fuel (CSNF) waste packages (WPs) in percolation bin 3 under nominal conditions) are presented in the top left frame (i.e., Figure K2-1a) and the corresponding PRCCs are presented in the top right frame (i.e., Figure K2-1b). Figure K2-1a contains 300 time-dependent values for *NCSFL*. Thus, at each time there are 300 values for *NCSFL* for which a PRCC is calculated for each element e of $\mathbf{e}$ (Note: In the calculation of PRCCs for a particular dependent variable y that is not influenced by all elements of $\mathbf{e}$, such as release of a particular radionuclide from the engineered barrier system (EBS), the elements of $\mathbf{e}$ that are known to be unrelated to the determination of the dependent variable y are excluded from this calculation. The exclusion of these elements reduces the occurrence of spurious correlations in the PRCC calculation results). Then, the PRCCs are plotted above the time at which they were calculated and connected for each independent variable e to show the effect of e on the dependent variable (i.e., *NCSFL* in this example) as a function of time. To limit the number of time-dependent PRCC curves in a given plot frame, the PRCC plots in Appendix K only show PRCC curves for the six variables with the largest PRCCs in absolute value over the time interval under consideration. Further, plots are only shown for variables whose PRCCs exceed 0.3 in absolute value at some point in time. Variables with PRCCs less than 0.3 in absolute value have only a limited monotonic effect on the output variable under consideration. In the legend of a figure showing PRCCs, the variables are listed in decreasing order of PRCC, i.e., the variable having the largest PRCC in absolute value over the time interval under consideration is listed first.

Values of PRCCs fall in the interval [−1, 1], with (i) positive PRCCs indicating that two variables tend to increase and decrease together (i.e., the independent variable has a positive effect on the dependent variable), (ii) negative PRCCs indicating that two variables tend to move in opposite directions (i.e., the independent variable has a negative effect on the dependent variable), and (iii) the absolute value of a PRCC indicating the strength of the relationship between two variables (i.e., a PRCC close to 1 in absolute value indicates a strong monotonic relationship between two variables after the removal of the monotonic effects associated with the other independent variables under consideration; a PRCC close to 0 in absolute value indicates no monotonic relationship after the removal of the monotonic effects associated with the other variables under consideration; and the strength of the effect increases as the absolute value of a PRCC increases from 0 to 1). Thus, in the example in Figure K2-1b, *WDGCA22* has a negative effect on *NCSFL* with this effect increasing with time; *WDZOLID* has a positive effect on *NCSFL* with this effect increasing with time; and *INFIL*, *WDNSCC*, *THERMCON* and *SCCTHR* have small negative effects on *NCSFL* with these effects also increasing with time.

An alternative to the use of PRCCs is to carry out stepwise rank regressions to determine the effects of uncertain inputs on analysis results of interest. In analyses of this type, the regressions

are carried out with rank transformed variable values as previously discussed rather than with the original variables.

In a stepwise rank regression, the single independent variable that makes the largest contribution to the uncertainty in the dependent variable is selected in the first step. Then, at the second step, the single independent variable that, in conjunction with the first variable, makes the largest contribution to the uncertainty in the dependent variable is selected. This process then continues until no additional variables are found that make identifiable (i.e., significant) contributions to the uncertainty in the dependent variable; at this point, the stepwise selection process terminates. In Appendix K, a significance level of $\alpha = 0.01$ is used as the criterion for both dropping a previously selected variable from a stepwise regression and for terminating a stepwise regression analysis. Selection of this significance level was based on preliminary sensitivity analyses, in which it was observed that a greater value tended to introduce obviously spurious variables into the regression models. The significance levels were intended to be set at 0.01 for entering variables and 0.02 for departing variables. However, through an oversight, a value of 0.01 was used for both entering and departing variables. Under very unlikely conditions, this inconsistency could cause unintended looping in the stepwise variable selection process if the same variable was repeatedly added and then dropped from the regression model. An examination of the regression analyses showed that such looping did not occur. Thus, the specification of 0.01 rather than 0.02 for the dropping of a previously selected variable has no effect on the presented regression results. In the context of stepwise regression analysis, variable importance is indicated by (i) order of selection in the stepwise selection process, (ii) incremental changes in R^2 values with the successive entry of individual variables into the regression model, and (iii) the sign and size of the standardized regression coefficients, (i.e., standardized rank regression coefficients (SRRCs), when rank regression is being used) in the final regression model.

As an example, stepwise rank regressions for NCSFL at 600,000, 800,000 and 1,000,000 yr are shown in Figure K2-1c. For the analysis at each time, the first column lists the independent variables in the order of selection in the stepwise process; the second column lists the cumulative R^2 value with the entry of each variable into the regression model; and the third column lists the SRRCs for the variables in the final regression model.

The R^2 value corresponds to the fraction of the uncertainty in the dependent variable that is accounted for by a regression model. Thus, R^2 values monotonically increase as additional variables are added to the regression model and, for a very successful regression analysis, approach 1 as additional variables are added to the model. The SRRCs provide a measure of the fractional contribution of individual independent variables to the uncertainty in the dependent variable under consideration. Further, like PRCCs, a positive SRRC indicates that the independent variable and dependent variable tend to increase and decrease together, and a negative SRRC indicates that the independent variable and dependent variable tend to move in opposite directions.

In the analysis that follows, PRCCs are presented as plots of PRCC values over time for the six parameters with the highest absolute PRCC values over the time interval under consideration. The PRCCs are computed at each time at which TSPA-LA Model output is provided. In contrast, SRRCs are computed at 3 fixed times (usually at 2,000, 5,000 and 10,000 years for a

model result calculated out to 20,000 years, and at 50,000 years, 200,000 years and 500,000 years for a model result calculated out to 1,000,000 years). These typical times for SRRC computation were chosen to illustrate the changes in importance of uncertain parameters over time. The same analysis times are generally used for analysis of all TSPA-LA Model output variables to facilitate comparisons between the sensitivity analysis results across output variables. For a few output variables that do not have meaningful values at these typical times, SRRC computations are done at times at which the output variable is meaningful.

Related, but not identical, information is provided by PRCCs and SRRCs. Specifically, PRCCs measure the strength of the monotonic relationship between an independent variable and a dependent variable after correcting for the effects of other independent variables, and SRRCs provide a measure of the fractional contribution of an individual independent variable to the uncertainty in the dependent variable under consideration. Except in rare situations involving SRRCs from a regression model involving multiple correlated variables, PRCCs and SRRCs have the same sign, which indicates either a positive or negative correlation between an input variable and an output variable. Because PRCCs are selected for display based on the maximum absolute value over time, and SRRCs are computed at specific times, the selection and order of important variables indicated by PRCCs and SRRCs may be different between the two analyses. However, when there are no correlations between the independent variables (i.e., the variables in the LHS), then, at a fixed time, an ordering of variable importance based on the absolute value of PRCCs is the same as an ordering of variable importance based on the absolute value of SRRCs.

In addition to PRCCs and stepwise rank regression analyses, Appendix K makes use of scatterplots to present and explain the relationships between independent and dependent variables. A scatterplot is simply a plot of the points (e_i, y_i), $i = 1, 2, \ldots, nLHS$, where e_i are the sampled values for an independent variable and the y_i are the corresponding values for a dependent variable. If e has a significant effect on y, then this will be apparent in the scatterplot; if e does not have a significant effect on y, then the points in the scatterplot will have a random distribution conditional on the marginal distributions for e and y. As an example, scatterplots involving the pair

$$(e_i, y_i) = (WDGA22_i, NCSFL_i), \; i = 1, 2, \ldots, nLHS = 300, \qquad \text{(Eq. K2-6)}$$

for results obtained at 600,000 and 800,000 yr are presented in Figure K2-1d, e. As can be seen, a strong and complex relationship exists between *WDGA22* and *NCSFL*. In some instances, scatterplots can reveal relationships that may be too complex to be adequately captured by the numeric effect summaries provided by PRCCs and stepwise rank regression analyses. An example of such a relationship may be found in Figure K4.5-3, with an explanation provided in the accompanying text.

More detailed information on the sensitivity analysis techniques in use is available in several reviews (Helton et al. 2006 [DIRS 183873]; Helton and Davis 2000 [DIRS 156572]). Further, these reviews describe a number of additional sensitivity analysis techniques that can be used in the exploration of the mapping between analysis inputs and analysis results indicated in Equation (K2-5).

The examples contained in Figure K2-1 are taken from Figures K4.2-2 and K4.2-3. The discussions associated with Figures K4.2-2 and K4.2-3 describe the physical processes underlying the presented results and the roles that the variables identified in the sensitivity analyses have in these processes.

K3 INDEPENDENT AND DEPENDENT VARIABLES

As indicated in conjunction with Equation (J4.1-3), the TSPA-LA involves a large number of epistemically uncertain variables. These variables and their associated distributions collectively define the probability space ($\mathcal{E}$, E, p_E) for epistemic uncertainty. Notationally, the elements of $\mathcal{E}$ can be represented by a vector

$$\begin{aligned}\mathbf{e} &= [\mathbf{e}_A, \mathbf{e}_M] \\ &= \left[e_{A1}, e_{A2}, \ldots, \cdots e_{A,nAE}, e_{M1}, e_{M2}, \ldots, e_{M,nME}\right] \\ &= [e_1, e_2, \ldots, e_{nE}], nE = nAE + nME,\end{aligned} \qquad \text{(Eq. K3-1)}$$

where

$$\mathbf{e}_A = \left[e_{A1}, e_{A2}, \ldots, e_{A,nAE}\right]$$

is a vector of epistemically uncertain quantities used in the characterization of aleatory uncertainty (e.g., a rate term that defines a Poisson process) and

$$\mathbf{e}_M = \left[e_{M1}, e_{M2}, \ldots, e_{M,nME}\right]$$

is a vector of epistemically uncertain quantities used in the determination of dose (e.g., a distribution coefficient).

The vector **e** contains a total of $nE = 387$ elements. Thus, $\mathcal{E}$ is a subset of $R^{nE} = R^{387}$. However, not every element of **e** is used in uncertainty and sensitivity analysis for every scenario class. For example, **e** contains 44 elements corresponding to the dose conversion factors for inhalation pathways used to calculate the dose following an igneous eruptive event. These elements are only used in the igneous eruptive scenario class. In addition, certain of elements of **e** are correlated to other elements of **e**. Each subset of correlated variables is represented in the sensitivity analyses by one member of the set of correlated variables. By excluding variables that are not used in a scenario class and by choosing representatives for correlated sets of variables, the total number of uncertain input variables considered for the sensitivity analysis of a scenario class is less than 387, with the exact number depending on the scenario class.

Table K3-1 provides a high-level summary of the elements of **e**. Of the variables listed in Table K3-1, only *IGRATE*, *PROBDSEF* and *PROBWPEF* are elements of $\mathbf{e}_A$. Thus, $nAE = 3$ and

$$\mathbf{e}_A = [IGRATE, PROBDSEF, PROBWPEF]. \quad \text{(Eq. K3-2)}$$

The remaining variables contained in Table K3-1 constitute the elements of $\mathbf{e}_M$. Thus $nME = nE - 3 = 384$ and

$$\mathbf{e}_M = [ALPHAL, ALPHANL, \ldots, WPFLUX] \quad \text{(Eq. K3-3)}$$

contains all variables in Table K3-1 except for the three elements of $\mathbf{e}_A$. Not all variables listed in Table K3-1 are included in the sensitivity analysis because of correlations between elements of **e**. Table K3-1 and Table K3-2 show an asterisk (*) at the end of a variable name to indicate that the variable is excluded from the sensitivity analysis because of correlations. Table K3-3 provides references to descriptions of the correlations between input variables.

The problems that can result from correlated variables are discussed and illustrated in Section 8.7 of Helton and Davis 2000 [DIRS 156572]. Where correlations exist, only one of the correlated variables is retained as an input variable in the sensitivity analyses. The sensitivity analyses were conducted iteratively to ensure that correlations between input variables were identified and that no significantly correlated pairs of input variables were used in the analyses. Examination of the final regression model produced from a stepwise regression analysis allows the identification of the presence of correlations that affect the assessment of variable importance. In particular, unless there are correlations between the selected variables, the SRRCs for the variables selected in a stepwise regression analysis will monotonically decrease in order of selection in the stepwise process. A significant deviation from a monotonic decrease in the absolute values of the SRRCs indicates that there are correlations between variables that are affecting the structure of the constructed regression models.

Table K3-1 is intended primarily as a quick reference to variable definitions for use in conjunction with the sensitivity analyses presented in the remainder of this appendix. However, Table K3-1 does not provide enough information to actually track an individual variable back through the TSPA-LA analysis and ultimately to its original sources of documentation. To assist with this traceability, Table K3-2 lists the variables by the name given in the TSPA-LA Model, and Table K3-3 provides more information on the individual variables contained in **e**, including references to supporting documentation.

Appendix J concentrated on TSPA-LA results for two analysis outcomes: dose to the RMEI as a function of time and expected dose to the RMEI as a function of time. However, these are only two of a very large number of TSPA-LA results. As indicated in Equation (K2-3), the TSPA-LA actually produces a vector **y** of results, with most of these results functions of time. A subset of the potential elements of **y** is considered in the sensitivity analyses presented in this appendix. The elements of **y** specifically considered in this appendix are listed in Table K3-4. Thus, in the context of this appendix,

$$\mathbf{y} = [BACSFLAD, BACSFLND, \ldots, UZTC99C], \quad \text{(Eq. K3-4)}$$

where *BACSFLAD*, *BACSFLND*, …, *UZTC99C* are defined in Table K3-4. However, even this representation for **y** is a simplification for **y** in two ways. First, most of the elements of **y** are functions of individual scenario classes or specific modeling assumptions and also possibly functions of location within the repository system (e.g., percolation bin). Second, **y** contains only a subset of the TSPA-LA results that could be considered for uncertainty and sensitivity analysis.

The TSPA-LA Model calculations are performed for the two time periods: from 0 years to 20,000 years, and from 0 years to 1,000,000 years after repository closure. Separate calculations are performed for these time periods because of a necessarily coarser temporal discretization in the GoldSim component of the TSPA-LA Model for 1,000,000 years calculations (Section 7.3.3). The calculations for the 20,000-year simulations are extended to 20,000 years to assess whether or not the trends present at the end of 10,000 years continue.

The dependent variables included in the analysis, summarized in Table K3-4, were selected to provide insight into the behavior of the repository system, rather than solely on the basis of the importance of individual variables to repository performance. For scenario class, expected dose to the RMEI is analyzed, and for most scenario classes, results for a select set of radionuclides are also analyzed. The selection of radionuclides considered for analysis was made in part to cover a wide range of radionuclide behavior. As a result, (i) the colloidal forms of ^{239}Pu were selected to allow the examination of the behavior of glass and ferrous colloids in the EBS and the behavior of fast and slow colloids downstream of the EBS, (ii) dissolved ^{239}Pu was selected to allow the consideration of a highly retarded radionuclide with an intermediate half life that is important to dose, (iii) dissolved ^{237}Np was selected to allow the consideration of a retarded radionuclide with a long half life that is important to dose, and (iv) dissolved ^{99}Tc was selected to allow the consideration of an unretarded radionuclide with a long half life that is important to dose. In addition to analyses of expected dose and of individual radionuclides, the discussion of some scenario classes includes analyses of variables related to the state of EBS components (e.g. number of failed WPs) and conditions within the EBS (e.g. temperature, relative humidity).

For scenario classes defined by an event (i.e. igneous intrusive, igneous eruptive, seismic ground motion, and seismic fault displacement scenario classes), analyses of dependent variables other than expected dose are conducted on model results calculated conditional on the occurrence of a specific event. Fixing the aleatory parameters that describe the event allows the sensitivity analyses to determine the effects on model results of the uncertainty in epistemic parameters. In general, events are chosen at the earliest time available in the Goldsim calculations. Because the Goldsim timesteps are necessarily different in 20,000 yr and 1,000,000 yr calculations, and because event times must align with a Goldsim timestep, sensitivity analyses are generally conducted for different event times for the two different calculations.

K4 NOMINAL SCENARIO CLASS

K4.1 Nominal Scenario Class: Summary

The nominal scenario class consists of the future in which no disruptions of any kind (i.e., early drip shield (DS) failures, early WP failures, igneous events, and seismic events) occur

(Section J5). This section (Section K4) presents uncertainty and sensitivity analysis results for selected analysis outcomes associated with the nominal scenario class (Table K4.1-1).

The results of most direct interest to repository performance are DS failure time (*DSFLTM*, yr), numbers of failed CSNF (*NCSFL*) and co-disposed (CDSP) (*NCDFL*) WPs, and dose to the RMEI (*DOSTOT*, mrem/yr). In addition to these analysis results, other results related to environmental conditions in the EBS are presented.

The value for *DSFLTM* is the same for all DSs and falls between 2.65×10^5 and 3.32×10^5 yr (Figure K4.2-1). The uncertainty in *DSFLTM* is completely dominated by *WDDSAGGC* (rate of aggressive general corrosion on top of the DS, nm/yr) and *WDDSBEGC* (rate of benign general corrosion on bottom of the DS, nm/yr).

The values for *NCSFL* and *NCDFL* range from very limited WP failure to failure of all WPs (Figures K4.2-2 to K4.2-5). The uncertainty in *NCSFL* and *NCDFL* is dominated by *WDGCA22* (temperature dependence coefficient associated with general corrosion rate for alloy 22, K). Specifically, the general corrosion rate for alloy 22, and hence the values for *NCSFL* and *NCDFL*, decreases as *WDGCA22* increases.

The values for *DOSTOT* range up to 7 mrem/yr but are much smaller for most sample elements (Figure K4.5-1). The uncertainty in *DOSTOT* is dominated by *WDGCA22* because of its effects on the number of failed WPs.

K4.2 Nominal Scenario Class: Drip Shield and Waste Package Failure

This section presents analysis results for DS failure time, number of failed WPs and the average breached area on failed WPs.

Drip Shield Failure Time: *DSFLTM.* The uncertainty and sensitivity analyses for DS failure time (*DSFLTM*, yr) are summarized in Figure K4.2-1. The possible values for *DSFLTM* fall between 265,000 and 332,000 yr (Figure K4.2-1a). The value for *DSFLTM* is determined by *WDDSAGGC* (rate of aggressive general corrosion on the top of the DS, nm/yr) and *WDDSBEGC* (rate of benign general corrosion on the bottom of the DS, nm/yr) (Figure K4.2-1b,c,d). The uncertainty in the value for *DSFLTM* is dominated by *WDDSAGGC*, which accounts for approximately 64 percent of the uncertainty in *DSFLTM* (i.e., the R^2 value associated with *WDDSAGGC* in the regression in Figure K4.2-1b is 0.64). The addition of *WDDSBEGC* results in a regression model with an R^2 value of 0.93. The regression model does not achieve an R^2 value of 1.00 because of the use of discrete timesteps in GoldSim. The effects of *WDDSAGGC* and *WDDSBEGC* on *DSFLTM* are independent and additive (Figure K4.2-1e).

Number of Failed Waste Packages: *NCSFL*, *NCSFLAD*, *NCSFLND*, *NCDFL*, *NCDFLAD*, *NCDFLND*. The uncertainty and sensitivity analyses for numbers of failed CSNF WPs (*NCSFL*) and failed CDSP WPs (*NCDFL*) in percolation bin 3 are summarized in Figures K4.2-2 and K4.2-3. Percolation bin 3 contains 3285 CSNF WPs and 1366 CDSP WPs (approximately 40 percent of the WPs in the repository), more than any one of the other four percolation bins, and is selected for analysis for this reason. Comparisons of dose results between percolation bins

for early failed WP and DS cases (Figure J6.2-13 and Figure J6.3-13, respectively) indicate little variation in dose among percolation bins for either diffusive dominated (early failed WP) or advective dominated (early failed DS) conditions. The earliest WP failures occur for some, but not all, sample elements approximately 200,000 yr after repository closure (Figure K4.2-2a,b,c,d). However, there is significant uncertainty with respect to when initial WP failure will occur, with initial WP failure occurring after 500,000 yr for many sample elements. Many sample elements result in the failure of all WPs before 1,000,000 yr (Figure K4.2-2a,b,c,d). The jumps in failures evident at 300,000 years, 500,000 years and 700,000 years are due to the timesteps used by the WAPDEG code.

The PRCCs in Figure K4.2-2e,f indicate that the uncertainty in *NCSFL* and *NCDFL* is dominated by *WDGCA22* (temperature dependence coefficient associated with the general corrosion rate for alloy 22, K). Specifically, *WDGCA22* corresponds to a coefficient used to alter the general corrosion rate for alloy 22 as function of temperature, with the alloy 22 general corrosion rate decreasing as *WDGCA22* increases when temperature is below 60 °C. The strong negative effect of *WDGCA22* on *NCSFL* and *NCDFL* is indicated by the associated PRCCs having values very close to −1.0 (Figure K4.2-2e,f). In addition, a lesser positive effect is indicated for *WDZOLID* (scale factor used to incorporate uncertainty into the stress intensity factor for closure-lid weld), with this positive effect resulting because increasing *WDZOLID* increases the stress at the closure lid. Small negative effects are also indicated for *INFIL* (infiltration level), *THERMCON* (host rock thermal conductivity level), *WDNSCC* (stress corrosion cracking growth rate exponent), and *SCCTHR* (stress corrosion cracking threshold, MPa). These negative effects result because (i) increasing *INFIL* and *THERMCON* tends to lower WP temperatures and thus reduce the rate of corrosion, (ii) increasing *WDNSCC* increases the threshold stress intensity factor, which determines the threshold stress at which stress corrosion cracks propagate, and thus reduces failures at the closure-lid weld, and (iii) increasing *SCCTHR* increases the stress level at which stress corrosion cracking initiates and thus reduces failures at the closure-lid weld.

More detailed sensitivity analysis results for *NCSFL* based on stepwise rank regression are presented in Figure K4.2-3a. The results are the same for *NCDFL* and thus are not presented; further, the pattern of results is the same for all five percolation bins as the processes leading to nominal WP failures are not very affected by environmental conditions. As the regressions show, the uncertainty in *NCSFL* is dominated by *WDGCA22*, with *WDGCA22* having R^2 values of 0.86, 0.90 and 0.91 in the three presented regressions. The dominant effect of *WDGCA22* on the uncertainty in *NCSFL* can also been seen in the three presented scatterplots (Figure K4.2-3b,c,d); the horizontal lines of points in the scatterplots result from sample elements in which all CSNF WPs in percolation bin 3 have failed by the time under consideration. The remaining variables selected in the regressions are generally the same as those identified in the analyses with PRCCs in Figure K4.2-2e,f. The changes in the R^2 values associated with entry of these variables into the regression analyses are small (e.g., 0.01 – 0.02) and provide an indication of the extent to which the uncertainty in these variables impacts the uncertainty in *NCSFL*.

The pointer variable *WDGCUA22* used to select the distribution of base corrosion rates of alloy 22 at 60 °C over the patches on the WPs is also identified in all three regressions in

Figure K4.2-3a as having a small positive effect on the uncertainty in *NCSFL*. Specifically, *WDGCUA22* is a pointer variable used to select from three uncertain distributions that derive from both the uncertainty in a base corrosion rate for alloy 22 at 60 °C and the uncertainty that exists in the prediction of small scale variability in chemical and physical conditions across patches used in the modeling of WP degradation. In turn, *WDGCA22* is used in the correction of the corrosion rates defined by the distributions indexed by *WDGCUA22* for temperature effects. It should be noted that the impact of the uncertainty associated with *WDGCA22* is much greater than the impact of the uncertainty associated with *WDGCUA22*.

Uncertainty and sensitivity analyses for numbers of failed CSNF WPs under dripping conditions (*NCSFLAD*) and nondripping conditions (*NCSFLND*) in percolation bin 3 are summarized in Figures K4.2-4 and K4.2-5. The terminal designators *AD* and *ND* in *NCSFLAD* and *NCSFLND* derive from the alternative use of "always dripping" and "never dripping" as designators for dripping and nondripping conditions. Time-dependent values for *NCSFLAD* and *NCSFLND* appear in Figure K4.2-4a,b,c,d. As already indicated, the processes leading to nominal WP failures are not affected by seepage conditions. Because of this, WPs experiencing nondripping conditions have the same likelihood of failure as WPs experiencing dripping conditions. As a result, the division of *NCSFL* into *NCSFLAD* and *NCSFLND* (reminder: *NCSFL* = *NCSFLAD* + *NCSFLND*) is determined by the fractions of WPs that experience dripping and nondripping conditions.

As indicated by the PRCCs in Figure K4.2-4e,f, the uncertainty in *NCSFLAD* and *NCSFLND* is dominated by *WDGCA22*, with the number of failed WPs decreasing as *WDGCA22* increases. In consistency with the analyses for *NCSFL* and *NCDFL*, a small positive effect is indicated for *WDZOLID* and a small negative effect is indicated for *WDNSCC* for both *NCSFLAD* and *NCSFLND*. A small negative effect is also indicated for *THERMCON* for *NCSFLAD*, with this small effect probably resulting from the slower corrosion rate for alloy 22 at reduced temperatures. The effects of *WDGCA22*, *WDZOLID*, *WDNSCC* and *THERMCON* on *NCSFLAD* and *NCSFLND* result from their influence on WP failure.

In contrast, other variables appear in the sensitivity analysis as a result of their effects on the numbers of WPs experiencing dripping or nondripping conditions. For example, *INFIL* has a negative effect on *NCSFLND* because increasing its value decreases the number of WPs experiencing nondripping conditions (Figure K4.2-4f). Two variables identified in the analysis that affect both *NCSFLAD* and *NCSFLND* are *SEEPUNC* (pointer variable used to determine local seepage rates) and *SEEPPRM* (mean fracture permeability in lithophysal rock units, m^2; as sampled, *SEEPPRM* is actually the logarithm of the indicated permeability) (Figure K4.2-4e,f). Increasing *SEEPUNC* tends to increase seepage into the EBS through an upscaling of base seepage rates while increasing *SEEPPRM* tends to decrease seepage into the repository by increasing the diversion of water around the drifts. As a result, increasing *SEEPUNC* has a positive effect on *NCSFLAD* and a negative effect on *NCSFLND*, and in a reverse pattern, increasing *SEEPPRM* has a negative effect on *NCSFLAD* and a positive effect on *NCSFLND*.

More detailed sensitivity analysis results for *NCSFLAD* and *NCSFLND* based on stepwise rank regression are presented in Figure K4.2-5a,b. Although more detailed, these results are consistent with the PRCC results in Figure K4.2-4e,f. In particular, the uncertainty in *NCSFLAD* and *NCSFLND* is dominated by *WDGCA22,* with small incremental contributions to this

uncertainty from a number of additional variables. The dominant effect of *WDGCA22* can be seen in the scatterplots in Figure K4.2-5c,e.

The numbers of WPs experiencing dripping and nondripping conditions varies widely from sample element to sample element (Figure K4.2-5g,h). In particular, the straight lines of points in Figure K4.2-5g,h correspond to sample elements in which all WPs in percolation bin 3 have failed. As examination of the points associated with these lines shows, the possibilities range from almost all failed WPs experiencing dripping conditions to almost all failed WPs experiencing nondripping conditions.

The results presented in Figures K4.2-4 and K4.2-5 are for CSNF WPs in percolation bin 3. Essentially identical results hold for numbers of failed CDSP WPs under dripping conditions (*NCDFLAD*) and nondripping conditions (*NCDFLND*) in percolation bin 3 and are not presented. Similar results also hold for the other percolation bins.

Averaged Breached Area on Failed Waste Packages: *BACSFLAD*, *BACSFLND*, *BACDFLAD*, *BACSFLND*. The uncertainty and sensitivity analyses for average breached area (m^2) on failed CSNF WPs under dripping conditions (*BACSFLAD*) and nondripping conditions (*BACSFLND*) in percolation bin 3 are summarized in Figures K4.2-6 and K4.2-7. As indicated in Figure K4.2-6d, there is no meaningful difference in *BACSFLAD* and *BACSFLND*. For this reason, analyses are presented only for *BACSFLAD*. Further, the uncertainty and sensitivity analyses for average breached area on failed CDSP WPs under dripping conditions (*BACDFLAD*) and nondripping conditions (*BACDFLND*) in percolation bin 3 are the same as those shown in Figures K4.2-6 and K4.2-7 for CSNF WPs and are also not shown.

As shown in Figure K4.2-6a,b, *BACSFLAD* increases monotonically with time and ranges at 1×10^6 yr from less than 10^{-4} m^2 to almost 10 m^2. The uncertainty in *BACSFLAD* is dominated by *WDGCA22* (temperature dependence coefficient associated with the general corrosion rate for alloy 22, K), with *BACSFLAD* tending to increase as *WDGCA22* as decreases (Figures K4.2-6c and K4.2-7a). Specifically, the dominant effect of *WDGCA22* on the uncertainty in *BACSFLAD* is indicated by PRCCs close to -1 in Figure K4.2-6c and R^2 values ranging from 0.81 to 0.91 in Figure K4.2-7a. The dominant effect of *WDGCA22* can also be seen in the scatterplot in Figure K4.2-7b. Smaller effects are also indicated for the following variables: *WDZOLID* (stress intensity factor for closure-lid weld), *INFIL* (infiltration level), *THERMCON* (host rock thermal conductivity level), *WDNSCC* (stress corrosion cracking growth rate exponent), *SCCTHR* (stress corrosion cracking threshold, MPa), and *WDGCUA22* (pointer variable used to select the distribution of base corrosion rates of alloy 22 at 60 °C over the patches on the WPs). The effects of these variables are the same as previously discussed for number of failed WPs (see discussion for *NCSFL* and *NCDFL*).

The results for the other percolation bins are the same as those shown in Figures K4.2-6 and K4.2-7 for percolation bin 3 and, for this reason, are not presented.

K4.3 Nominal Scenario Class: Engineered Barrier System Conditions

This section presents analysis results describing seepage rates, temperature and relative humidity in the drifts, as well as partial pressure of CO_2, ionic strength and pH in the invert.

Seepage Rate into Drifts: *SPRATECS, SPRATECD.* The uncertainty and sensitivity analyses for seepage rate (m^3/yr/WP) into the repository above CSNF WPs (*SPRATECS*) and CDSP WPs (*SPRATECD*) in percolation bin 3 are summarized in Figures K4.3-1 and K4.3-2. The jumps evident at 2,000 years and at 10,000 years are due to modeling the changes in climate as instantaneous changes in UZ flow fields. As examination of Figure K4.3-1 shows, there is effectively no difference in the values for *SPRATECS* and *SPRATECD*. The uncertainty in *SPRATECS* and *SPRATECD* is dominated by *INFIL* (infiltration level). Specifically, the PRCCs for *SPRATECS* and *SPRATECD* are close to 1.0, which indicates that *SPRATECS* and *SPRATECD* tend to increase as *INFIL* increases (Figure K4.3-1e,f). The regression analyses for *SPRATECS* in Figure K4.3-2a also indicate the dominate effect of *INFIL*, with the individual regression analyses having R^2 values of 0.67, 0.73 and 0.68 when only *INFIL* is included in the regression model. Similar regression results exist for *SPRATECD* and are not presented.

In addition to *INFIL*, the following variables have lesser effects on the uncertainty in *SPRATECS* and *SPRATECD*: *THERMCON* (host rock thermal conductivity level), *ALPHAL* (capillary strength parameter in lithophysal rock units), *SEEPPRMN* (mean fracture permeability in nonlithophysal rock units, m^2; as sampled, *SEEPPRMN* is actually the logarithm of the indicated permeability), *SEEPPRM* (mean fracture permeability in lithophysal rock units, m^2; as sampled, *SEEPPRM* is actually the logarithm of the indicated permeability), and *SEEPUNC* (pointer variable used to determine local seepage rates). The variable *THERMCON* has a positive effect at early times (i.e., before 1,000 yr as indicated in Figure K4.3-1e,f), with this effect resulting because increasing *THERMCON* increases the rate at which the repository cools to a temperature level (i.e., less than 100 °C) at which seepage can occur. The negative effect for *ALPHAL* (Figure K4.3-2a) results from increasing the capillary "hold" on water in the drift walls. The negative effects for *SEEPPRMN* and *SEEPPRM* (Figures K4.3-1e,f and K4.3-2a) result from their role in increasing water flow around the drifts. Finally, increasing *SEEPUNC* tends to increase seepage into the EBS through an upscaling of base seepage rates (Figures K4.3-1e,f and K4.3-2a); however, *SEEPUNC* has no effect after 10,000 yr as shown by its PRCC dropping to 0 after this time (Figure K4.3-1e,f). Several spurious variables with no significant effect on the final R^2 values are also selected at the end of the regressions in Figure K4.3-2a.

The dominant effect of *INFIL* can also be seen in the 1,000 yr scatterplots in Figure K4.3-2b,c,d,e; similar patterns of behavior also exist at later times as indicated by the variables selected in the regression analyses for 50,000 and 100,000 yr (Figure K4.3-2a).

Results for the other percolation bins are similar to those shown in Figures K4.3-1 and K4.3-2 for percolation bin 3. However, given the interest in and potential importance of seepage into the repository, seepage rates (i.e., *SPRATECS* and *SPRATECD*) for the other percolation bins are presented without discussion in Figures K4.3-3 and K4.3-4.

Temperature in Drifts: *TMPCSWL, TMPCSWP, TMPCSINV, TMPCDWL, TMPCDWP, TMPCDINV.* The uncertainty and sensitivity analyses for drift temperatures (°C) in percolation bin 3 are summarized in Figure K4.3-5. Specifically, the following results are presented: temperatures for CSNF WPs at the drift wall (*TMPCSWL*), on the WP (*TMPCSWP*) and in the invert beneath the WP (*TMPCSINV*) and similarly temperatures for CDSP WPs at the drift wall (*TMPCDWL*), on the WP (*TMPCDWP*) and in the invert beneath the WP (*TMPCDINV*).

Because of the use of a representative WP to determine the drift-wall temperature in each percolation bin (see Section 6.3.2.2.2), the uncertainty in drift temperature is determined entirely by the variables *INFIL* (infiltration level) and *THERMCON* (host rock thermal conductivity level). The variables *INFIL* and *THERMCON* have 4 and 3 levels, respectively. Specifically, *INFIL* takes on values of 1, 2, 3 and 4, with these values serving as pointers to different time-dependent flow fields, and *THERMCON* takes on values of 1, 2 and 3, with these values serving as pointers to different levels of thermal conductivity in the region surrounding the drifts. In turn, seven heat flow fields were calculated and mapped to the 12 (i.e., 4×3) combinations of *INFIL* and *THERMCON*; the mapping is summarized in Section 6.3.2.2, and is described in detail in *Multiscale Thermohydrologic Model* (SNL 2007 [DIRS 181383], Section 6.3.15[a]). For the sensitivity analysis, these seven heat flow fields are indexed by the variable *TH_INFIL*, which has the possible values of 1, 2, …, 7, corresponding to the seven uncertainty cases computed by the Multiscale Thermohydrology Model. Each possible value for *TH_INFIL* indicates the heat flow field to be used for a specific sample element. In turn, *TH_INFIL* is a function of *INFIL* and *THERMCON* defined by

TH_INFIL = 1 if [*INFIL*, *THERMCON*] = [2, 3], [3, 3] or [4, 2] (uncertainty case P90)

TH_INFIL = 2 if [*INFIL*, *THERMCON*] = [4,3] (uncertainty case P90H)

TH_INFIL = 3 if [*INFIL*, *THERMCON*] = [3,2] (uncertainty case P50)

TH_INFIL = 4 if [*INFIL*, *THERMCON*] = [2,2], [4,1] (uncertainty case P30)

TH_INFIL = 5 if [*INFIL*, *THERMCON*] = [1,1], [2,1] (uncertainty case P10L)

TH_INFIL = 6 if [*INFIL*, *THERMCON*] = [1,3] (uncertainty case P10H)

TH_INFIL = 7 if [*INFIL*, *THERMCON*] = [1,2], [3,1] (uncertainty case P10),

where the uncertainty case descriptions are provided in *Multiscale Thermohydrologic Model* (SNL 2007 [DIRS 181383], Section 6.3.15[a]). As inspection of Figure K4.3-5 shows, the values for *TMPCSWL*, *TMPCSWP*, *TMPCSINV*, *TMPCDWL*, *TMPCDWP* and *TMPCDINV* are completely determined by *TH_INFIL*, with the same temperature values used for both dripping and nondripping conditions. The results for all 300 sample elements are shown in Figure K4.3-5, but only 7 curves appear in each plot frame as a result of the mapping associated with *TH_INFIL*. Overall, higher values for *INFIL* and *THERMCON* tend to be associated with lower temperatures. The temperatures associated with CSNF WPs are slightly higher than those associated with CDSP WPs, but the difference is not large. Similar temperature behavior occurs in all 5 percolation bins; also, dripping and nondripping conditions have the same temperature values for a given value for *TH_INFIL*.

Relative Humidity in Drifts: *RHCSWP*, *RHCSINV*, *RHCDWP*, *RHCDINV*. The uncertainty and sensitivity analyses for relative humidity in percolation bin 3 are summarized in Figure K4.3-6. Specifically, the following relative humidity results are presented: on the WP (*RHCSWP*) and in the invert beneath the WP (*RHCSINV*) for CSNF WPs and, similarly, on the

WP (*RHCDWP*) and in the invert beneath the WP (*RHCDINV*) for CDSP WPs. As for the temperature results in Figure K4.3-5, the uncertainty in *RHCSWP*, *RHCSINV*, *RHCDWP* and *RHCDINV* is completely determined by the heat flow fields indexed by *TH_INFIL*. The results for all 300 sample elements are shown in Figure K4.3-6, but only 7 curves appear in each plot frame as a result of the mapping associated with *TH_INFIL*. Because of assumed thermal effects, relative humidities associated with CDSP WPs tend to be higher at early times than those associated with CSNF WPs. Similar temperature behavior occurs in all 5 percolation bins; also, dripping and nondripping conditions have the same relative humidity values for a given value for *TH_INFIL*.

Partial Pressure of CO_2 in Invert: *PCO2CSIA*, *PCO2CSIN*, *PCO2CDIA*, *PCO2CDIN*. The uncertainty and sensitivity analyses for the partial pressure of CO_2 (bars) in the invert in percolation bin 3 are summarized in Figures K4.3-7 and K4.3-8. Specifically, time-dependent partial pressure results for CSNF WPs under dripping conditions (*PCO2CSIA*) are presented in Figure K4.3-7a,c and corresponding results for CDSP WPs (*PCO2CDIA*) are presented in Figure K4.3-7b,d. As examination of preceding results shows, there is little difference in the partial pressure results for CSNF and CDSP WPs. Similar results were also obtained for nondripping conditions (i.e., for *PCO2CSIN* and *PCO2CDIN* for CSNF and CDSP WPs, respectively, under nondripping conditions); the results are also similar for all 5 percolation bins. The partial pressures initially divide into two groups, which then monotonically converge through time to a partial pressure of 0.001 bar. The grouping of partial pressures results from the use of two bounding models that determine the minimum and maximum values for the partial pressure of CO_2 (bars) in the invert (SNL 2007 [DIRS 177412], Section 6.3.2.8). At each time, partial pressure in the invert is calculated by linearly interpolating between the ambient value of 10^{-3} bar and one of the bounding models, which is selected by the sign of the sampled value of the variable *DELPPCO2* (scale factor used to incorporate uncertainty into the value for the partial pressure of CO_2); the linear interpolation is based on the absolute value of *DELPPCO2*.

The PRCCs in Figure K4.3-7e,f indicate that the uncertainty in *PCO2CSIA* and *PCO2CDIA* is dominated by *DELPPCO2*, with *PCO2CSIA* and *PCO2CDIA* increasing as *DELPPCO2* increases. The dominance of *DELPPCO2* with respect to the uncertainty in *PCO2CSIA* and *PCO2CDIA* is also apparent in the regressions for *PCO2CSIA* in Figure K4.3-8a (i.e., models containing only *DELPPCO2* have R^2 values of 0.99, 0.94 and 0.92) and in the associated scatterplots in Figure K4.3-8b,c. The scatterplots in Figure K4.3-8b,c demonstrate the effect of the linear interpolation between ambient and minimum or maximum partial pressure of CO_2 (bars) using the sampled values of *DELPPCO2*. The banding evident in Figure K4.3-8c for positive values of *DELPPCO2* arises because of differences in temperature among CSNF WPs, which in turn is due to the value for *TH_INFIL* for each sample element. For *TH_INFIL*=1 and *TH_INFIL*=2 (see Figure K4.3-5e), the lower temperatures at 10,000 yr result in the lower band of values for *PCO2CSIA* for positive values of *DELPPCO2*. The scatterplots in Figure K4.3-8b,c also indicate the effects of variables that collectively determine the equilibrium of the gas and aqueous phases of CO_2 at the evaporation front, which include starting water (*SEEPWAT*) and variables which determine temperature, i.e., infiltration level (*INFIL*) and thermal conductivity (*THERMCON*) (SNL 2007 [DIRS 177412], Section 6.15.1).

Ionic Strength in Invert: *ISCSINAD*, *ISCSINND*, *ISCDINAD*, *ISCDINND*. The uncertainty and sensitivity analyses for ionic strength in percolation bin 3 are summarized in Figures K4.3-9, K4.3-10 and K4.3-11. Specifically, the following ionic strength results are presented: in the invert beneath the WP for CSNF WPs under dripping (*ISCSINAD*) and nondripping (*ISCSINND*) conditions (Figure K4.3-9a,b,c,d) and, similarly, in the invert beneath the WP for CDSP WPs under dripping (*ISCDINAD*) and nondripping (*ISCDINND*) conditions (Figure K4.3-10 a,b,c,d). Further, sensitivity analysis results are presented in Figures K4.3-9 e,f (PRCCs for *ISCSINAD* and *ISCSINND*), K4.3-10 (PRCCs for *ISCDINAD* and *ISCDINND*), and K4.3-11 (stepwise rank regression analyses and scatterplots for *ISCSINAD*).

The analyses for *ISCSINAD*, *ISCSINND*, *ISCDINAD* and *ISCDINND* are similar up to the time of DS failure between approximately 260,000 and 300,000 yr (Figures K4.3-9 a,b,c,d and K4.3-10 a,b,c,d; see Figure 4.2-1a for DS failure times). Over the time period prior to approximately 3,000 yr, the values for *ISCSINAD*, *ISCSINND*, *ISCDINAD* and *ISCDINND* are determined primarily by temperatures in the repository, which are indexed by the variable *TH_INFIL* (Figures K4.3-9 a,b,c,d and K4.3-10 a,b,c,d). In turn, *TH_INFIL* is a function of the variables *INFIL* (infiltration level) and *THERMCON* (host rock thermal conductivity level), which is why *INFIL* and *THERMCON* appear in the PRCC analyses prior to approximately 3,000 yr. After 3,000 yr and until the time of DS failure, the values for *ISCSINAD*, *ISCSINND*, *ISCDINAD* and *ISCDINND* for the individual sample elements are almost constant and vary within approximately an order of magnitude (i.e., 5×10^{-3} to 5×10^{-2} mol/kg) across sample elements (Figures K4.3-9 a,b,c,d and K4.3-10 a,b,c,d). During this time, *SEEPWAT* (indicator variable for seepage water type) and *RHI85* (scale factor for ionic strength at humidities above 85 percent; as sampled, *RHI85* is the logarithm of the indicated scale factor) are indicated as having positive effects on *ISCSINND* and *ISCDINND* (Figures K4.3-9e and K4.3-10e). The variables *INFIL* and *THERMCON* also continue to have negative effects on *ISCSINAD* and *ISCSINND* (Figure K4.3-9e,f) and similar but lesser effects on *ISCDINAD* and *ISCDINND* (Figure K4.3-10e,f).

The behavior of *ISCSINAD* and *ISCDINAD* undergoes substantial change at the time of DS failure (Figures K4.3-9 b,d and K4.3-10 b,d), typically around 300,000 years. Specifically, *ISCSINAD* and *ISCDINAD* show sudden increases in value after DS failure. This jump is due to changing the model for determining chemistry in the invert from the EBS Chemical Environment Submodel (Section 6.3.4.2.2) to the In-Package Chemistry Submodel (Section 6.3.7.2.2). This change should have been made only for realizations in which general corrosion patches in the WP outer barrier allow advection through the waste, but due to an error in the GoldSim component of the TSPA-LA Model, all realizations experience the change in models (see Appendix P, Section P5, for a discussion of the error and its effects on the TSPA-LA Model results). An additional step change is evident at later times, after about 500,000 years. This step change is due to switching from vapor influx conditions in the In-Package Chemistry Submodel to liquid influx conditions, which has the effect of lowering the calculated ionic strength.

Although it is hard to read in Figures K4.3-9f and K4.3-10f, *WDDSAGGC* (rate of aggressive general corrosion on the top of the DS, nm/yr) and *WDDSBEGC* (rate of benign general corrosion on the bottom of the DS, nm/yr) (Figure K4.2-1b,c,d) show a brief period of positive effect over the period of DS failure as a result of the jump in the values for *ISCSINAD* and *ISCDINAD* at the time of DS failure. After DS failure, the uncertainty in *ISCSINAD* is

dominated by *ISCSNS* (pointer variable used to determine ionic strength in CSNF WP Cell 1 under vapor influx conditions), and the uncertainty in *ISCDINAD* is dominated by *IS2MCONS* (pointer variable used to determine ionic strength in CDSP WP Cell 2MCO, i.e., Cell 1b, under vapor influx conditions). The vapor influx model is significant even after DS failure because early corrosion failures of WPs generally occur as stress corrosion cracking rather than as a result of general corrosion. As WPs fail by general corrosion, patches open on the WP outer barrier that allow seepage water to flow into the WPs. This effect is evident by the increasing importance of *WDGCA22* (temperature dependence coefficient associated with the general corrosion rate for alloy 22, K) after 500,000 yr. As patches open, the ionic strength is determined by liquid influx conditions with the result that *ISCSNS* becomes less significant.

More detailed sensitivity analyses for *ISCSINAD* based on stepwise rank regression and the examination of scatterplots are presented in Figure K4.3-11.

pH in Invert: *PHCSINAD*, *PHCSINND*, *PHCDINAD*, *PHCDINND*. The uncertainty and sensitivity analyses for pH in the invert for CSNF WPs experiencing nondripping conditions (*PHCSINND*) and dripping conditions (*PHCSINAD*) in percolation bin 3 under nominal conditions are summarized in Figures K4.3-12 and K4.3-13. Further, Figure K4.3-14 provides a summary analogous to the summary in Figure K4.3-12 for pH in the invert for CDSP WPs experiencing nondripping conditions (*PHCDINND*) and dripping conditions (*PHCDINAD*) in percolation bin 3 under nominal conditions.

The time dependent behavior of pH in the invert is similar for both CSNF and CDSP WPs (Figures K4.3-12a,b,c,d and K4.3-14a,b,c,d), with pH showing a bifurcated behavior into a high and a low range of values until the occurrence of DS failures between 260,000 and 300,000 yr. This bifurcation is most obvious prior to 1,000 yr but continues to be visually apparent out to the time of DS failure (Figures K4.3-12a,b,c,d and K4.3-14a,b,c,d).

Neither the PRCCs in Figures K4.3-12e,f and K4.3-14e,f nor the regression analyses in Figure K4.3-13a,b provide a clear indication of the reason for this bifurcated behavior. However, these analyses do indicate that *SEEPWAT* (indicator variable for seepage water type), *RHPH0* (uncertainty factor for pH of in-drift waters at relative humidities less than 65 percent), and *RHPH75* (uncertainty factor for pH of in-drift waters at relative humidities greater than 75 percent) are affecting *PHCSINND*, *PHCSINAD*, *PHCDINND* and *PHCDINAD* prior to DS failure. Fortunately, the needed insights as to what is causing the bifurcated behavior can be obtained by examining the scatterplots involving *SEEPWAT* and *RHPH75* in Figure K4.3-13c,d,e,f,g,h. These scatterplots show that pH divides into high and low values on the basis of seepage water type as specified by *SEEPWAT*. Specifically, high pH values are associated with seepage water type 1, and low pH values are associated with seepage water types 2, 3 and 4 (Figure K4.3-13c,e,g). For a given seepage water type, the uncertainty factors *RHPH0* and *RHPH75* define linear scalings of a base pH value (Figure K4.3-13d,f,h). This scaling is particularly obvious in Figure K4.3-13d,h but is less obvious in Figure K4.3-13f as a result of the presence of different relative humidity conditions at 1,000 yr for different LHS elements. The grouping of pH values associated with each seepage water type into a few distinct, parallel lines, as evident in the scatterplot in Figure K4.3-13d, results from the interpolation technique implemented in the TSPA-LA Model. In particular, pH is determined by interpolation using

tables of values provided in *Engineered Barrier System: Physical and Chemical Environment* (SNL 2007 [DIRS 177412]), with the independent variables being relative humidity, temperature, partial pressure of CO_2, and water-rock interaction parameter. The interpolation is not simultaneous in all four variables. Rather, the relative humidity is determined first, and is then used as a constant in the interpolation involving the other three variables. Because pH is quite sensitive to small changes in relative humidity when relative humidity is very close to unity, this calculation scheme results in the data grouping observed in Figure K4.3-13d.

The PRCC and stepwise analyses correctly identify that *PHCSINND*, *PHCSINAD*, *PHCDINND* and *PHCDINAD* prior to DS failure as being affected by *SEEPWAT*, *RHPH0* and *RHPH75*. However, the effects are indicated as being smaller than they really are as shown by the scatterplots in Figure K4.3-13c,d,e,f,g,h. The reason for this performance is the introduction of complex patterns through the effects of discrete variables that the effectively linear analyses with PRCCs and stepwise rank regressions cannot capture. However, the underlying patterns are revealed by the associated scatterplots. Fortunately, this is often the case when stepwise regression fails to produce a model with a high R^2 value.

There is no change in the behavior of *PHCSINND* and *PHCDINND* after DS failure (Figures K4.3-12a,c and K4.3-14a,c). However, the behavior of *PHCSINAD* and *PHCDINAD* changes significantly after DS failure (Figures K4.3-12b,d and K4.3-14b,d). After DS failure in a dripping location, the chemistry of water in the invert should be determined by the in-package chemistry model if advection occurs through the waste. Otherwise, the invert chemistry model is applied. However, the version of the TSPA-LA model that produced the results displayed in this appendix contains an error discovered after calculations were completed in that, after DS failure in a dripping location, the chemistry of water in the invert is always determined by the in-package chemistry model (see Appendix P Section P5 for a discussion of the error and its effects on the TSPA-LA Model results). The in-package chemistry model computes pH using one of two submodels for estimating water inside the package: a vapor influx model and a liquid influx model. Once the in-package chemistry model is in use (after DS failure), pH is computed using the vapor influx model until general corrosion results in a patch opening in the WP outer barrier, after which time the liquid influx model is used. Hence, the uncertainty in *PHCSINAD* and *PHCDINAD* after DS failure is determined primarily *WDGCA22* (temperature dependence coefficient associated with the general corrosion rate for alloy 22, K) and *PH2RGER* (error term in regression equation used to determine pH of corrosion products domain), with the effects of *WDGCA22* acting as a switch to divide *PHCSINAD* and *PHCDINAD* into two sets of results (vapor influx model for in-package pH and liquid influx model for in-package pH) and *PH2RGER* defining a linear scaling of pH within each set (Figure K4.3-13i,j).

K4.4 Nominal Scenario Class: Release Results for Engineered Barrier System, Unsaturated Zone and Saturated Zone

Release results are available for individual radioactive species for the EBS, the UZ and the SZ. For the nominal scenario class, these results are completely dominated by the time and extent of WP failure, which in turn is determined by *WDGCA22* (temperature dependence coefficient associated with the general corrosion rate for alloy 22, K). As a result, the effects of the physical processes associated with radionuclide transport through the EBS, the UZ and the SZ tend to be obscured by the dominant effects of *WDGCA22*. Because of this, the nominal scenario class

results for the EBS, the UZ and the SZ provide less informative uncertainty and sensitivity analysis results than can be obtained from release results calculated for other scenario classes. For this reason, extensive presentation and discussion of uncertainty and sensitivity analysis results for radionuclide transport in the EBS, the UZ and the SZ will be deferred to later sections.

For perspective on the dominant role played by *WDGCA22* for the nominal scenario class, uncertainty and sensitivity analysis results for the release rate (*ESNP237*, g/yr) and cumulative (i.e., integrated) release (*ESNP237C*, g) of ^{237}Np from the EBS are presented and briefly discussed (Figures K4.4-1 and K4.4-2).

Prior to 400,000 yr, *ESNP237* and *ESNP237C* are very small (Figure K4.4-1a,b,c,d). For example, almost all values for *ESNP237* are less than 10^{-3} g/yr at 400,000 yr (Figure K4.4-1a). The limited release of ^{237}Np from the EBS prior to 400,000 yr results from the absence of DS failures prior to approximately 260,000 yr and the limited number of WP failures prior to 200,000 yr (see Figures K4.2-1a and K4.2-2a). By 300,000 yr, all DSs have failed and the number of failed WPs steadily increases (see Figures K4.2-1a and K4.2-2a). As a result, *ESNP237* tends to show a monotonic increase with time, although there is some nonmonotonicity, especially prior to approximately 500,000 yr, when the release of highly mobile species from the failure of individual WPs still has the potential to dominate the value for *ESNP237*. With increasing time and hence increasing numbers of failed WPs, the value for *ESNP237* tends to be dominated by the slower releases from a large number of previously failed WPs rather than by the quicker releases of highly mobile species from recently failed WPs. As a result, *ESNP237* tends to become increasing monotonic with increasing time.

The sensitivity analysis results for *ESNP237* and *ESNP237C* are very similar. For example, the analysis based on PRCCs in Figure K4.4-1e,f identifies *WDGCA22* as the most important variable with respect to both *ESNP237* and *ESNP237C*, with *ESNP237* and *ESNP237C* decreasing as *WDGCA22* increases. This effect results because increasing *WDGCA22* decreases both the number of failed WPs and the total failed area on failed WPs (see Figures K4.2-2 to K4.2-7). The next most important variable indicated in the analyses with PRCCs is *EP1NPO2* (scale factor used to incorporate uncertainty into NpO_2 solubility below 1 molal ionic strength; as sampled, *EP1NPO2* is actually the logarithm of the indicated scale factor), with *ESNP237* and *ESNP237C* increasing as *EP1NPO2* increases. This effect results because increasing *EP1NPO2* increases the concentration of dissolved ^{237}Np in the EBS, which in turn results in larger values for *ESNP237* and *ESNP237C*.

In addition, the analyses with PRCCs also identify smaller effects for the following four variables: *PHCSNS* (pointer variable used to determine pH in CSNF cell 1 under nondripping conditions), *GOESITED* (density of sorption sites on goethite, sites/nm^2), *WDZOLID* (scale factor used to incorporate uncertainty into the stress intensity factor for closure-lid weld), and *CORRATSS* (stainless steel corrosion rate, μm/yr). The negative effects associated with *PHCSS*, *GOESITED* and *CORRATSS* result because (i) increasing *PHCSNS* reduces the solubility of neptunium in CSNF WPs and thus reduces the dissolved concentration ^{237}Np, (ii) increasing *GOESITED* increases the sorption of neptunium onto goethite and thus reduces the dissolved concentration ^{237}Np, and (iii) increasing *CORRATSS* increases the generation of corrosion products, which turn results in more sorption sites in the WP. The positive effect associated with

WDZOLID results because increasing *WDZOLID* increases the stress at the closure lid, which in turn increases the number of WP failures.

More detailed sensitivity analysis results for *ESNP237* and *ESNP237C* are provided by the regression results in Figure K4.4-2a,b. Specifically, *WDGCA22* is the dominant variable in all six regression analyses in Figure K4.4-2a,b with R^2 values between 0.71 and 0.74. Overall, the results in the regression analyses are very similar to the results obtained with PRCCs. With some minor variations, the regressions initially pick the same six variables as the analyses with PRCCs. After the selection of six variables, the individual regression analyses have R^2 values between 0.80 and 0.86. The incremental R^2 values with the addition of each variable to a regression model provide an indication of variable importance. As examination of the individual regressions shows, the effects of the individual variables selected after *WDGCA22* on the uncertainty in *ESNP237* and *ESNP237C* is relatively small (i.e., incremental R^2 values between 0.05 and 0.01). However, a number of variables with small effects are identified, with the result that the final regression models contain from 10 to 16 variables and have R^2 values from 0.83 to 0.92. The regressions at 400,000 yr have the smaller R^2 values because of the presence of many zero values for *ESNP237* and *ESNP237C* that result from the absence of WP failures for many sample elements, which in turn creates patterns that are difficult for the regression techniques in use to capture.

The dominant effect of *WDGCA22* on *ESNP237* and *ESNP237C* and the lesser effects of *EP1NPO2* and *PHCSNS* on *ESNP237* and *ESNP237C* can be seen in the scatterplots in Figure K4.4-2c,d,e,f,g,h.

K4.5 Nominal Scenario Class: Dose to Reasonably Maximally Exposed Individual

The uncertainty and sensitivity analyses for total dose to the RMEI (*DOSTOT*, mrem/yr) are summarized in Figures K4.5-1 and K4.5-2. Nonzero values for *DOSTOT* begin at about 200,000 yr as a result of WP failure and then show a general tendency to increase (Figure K4.5-1a,b). However, some dose curves and especially some of the curves with the largest values for *DOSTOT*, change from increasing to decreasing at some point in time. This change results from inventory depletion, and hence decreasing or terminating releases, for highly mobile species such as ^{99}Tc and ^{129}I. All curves remain below 10 mrem/yr.

The PRCCs in Figure K4.5-1c indicate that the uncertainty in *DOSTOT* is dominated by *WDGCA22* (temperature dependence coefficient associated with the general corrosion rate for alloy 22, K), with *DOSTOT* tending to decrease as *WDGCA22* increases. This effect results because the general corrosion rate for alloy 22 decreases as *WDGCA22* increases. Smaller effects are indicated for *SCCTHR* (stress corrosion cracking threshold, MPa), *WDZOLID* (scale factor used to incorporate uncertainty into the stress intensity factor for closure-lid weld), *THERMCON* (host rock thermal conductivity level), *WDNSCC* (stress corrosion cracking growth rate exponent), and *INRFRCTC* (initial release fraction for ^{99}Tc in a CSNF WP). The variables *SCCTHR*, *WDZOLID*, *THERMCON* and *WDNSCC* affect *DOSTOT* through their effects on WP failure. Specifically, increasing *SCCTHR* increases the stress level at which stress corrosion cracking initiates and thus reduces failures at the closure-lid weld; increasing *WDZOLID* increases the stress at the closure lid and thus increases failures at the closure-lid weld;

increasing *THERMCON* tends to lower WP temperatures and thus reduce the rate of corrosion; and increasing *WDNSCC* tends to increase the threshold stress intensity factor, which determines the threshold stress at which stress corrosion cracks propagate, and thus to reduce failures at the closure-lid weld. The variable *INRFRCTC* has small effects that are initially positive and then negative on *DOSTOT*. This pattern results because increasing *INRFRCTC* increases the releases of ^{99}Tc at the time of initial WP failure, which causes *INRFRCTC* to have a positive effect on *DOSTOT* at early times. However, early releases of ^{99}Tc reduce the amount of ^{99}Tc that can be released at later points in time, with the result that increasing *INRFRCTC* has a negative effect on *DOSTOT* at later times.

More detailed sensitivity analysis results for *DOSTOT* are provided by the regression results in Figure K4.5-2a. Specifically, *WDGCA22* is the dominant variable with R^2 values of 0.77, 0.84 and 0.60. Actually, the indicated R^2 values tend to under represent the effect of *WDGCA22* because of the nonlinear relationship between *WDGCA22* and *DOSTOT* that can be seen in Figure K4.5-2b and is more apparent in Figure K4.5-3. Specifically, large values of *WDGCA22* result in small values for *DOSTOT* at late times because of limited WP failure and hence limited radionuclide releases, and small values of *WDGCA22* result in small values for *DOSTOT* at late times because of extensive, early WP failure and the resultant reduction in radionuclide inventory by late times.

In addition to *WDGCA22*, the regressions in Figure K4.5-2a indicate small effects for the following variables that affect WP failure: *WDZOLID*, *THERMCON*, *INFIL* (infiltration level), *SCCTHR*, *WDNSCC*, and *WDGCUA22* (pointer variable used to select the distribution of base corrosion rates of alloy 22 at 60 °C over the patches on the WPs). The effects of *WDZOLID*, *THERMCON*, *SCCTHR* and *WDNSCC* have already been discussed in conjunction with Figure K4.5-1c. Like *THERMCON*, the negative effect associated with *INFIL* probably results because increased values for *INFIL* result in lower WP temperatures and thus lower rates of corrosion. The variable *WDGCUA22* has a small positive effect on the uncertainty in *DOSTOT*. Specifically, *WDGCUA22* is a pointer variable used to select from three uncertain distributions that derive from both the uncertainty in a base corrosion rate for alloy 22 at 60 °C and the uncertainty that exists in the prediction of small scale variability in chemical and physical conditions across patches used in the modeling of WP degradation. Increasing *WDGCUA22* results in higher overall corrosion rates and thus higher values for *DOSTOT*. The dominance of *WDGCA22* with respect to the uncertainty associated with *DOSTOT* can be seen in the scatterplots in Figure K4.5-2b,c,d.

The regressions in Figure K4.5-2a also indicate very small effects of several variables related physical processes. However, the effects of these variables are minor given the much larger effects of variables related to WP failure and, in particular, the dominant effect of *WDGCA22* on WP failure.

K5 EARLY FAILURE SCENARIO CLASSES

K5.1 Early Failure Scenario Classes: Summary

The early failure scenario classes are defined on the basis of futures that involve one or more early failure events (Section J6). This section (Section K5) presents uncertainty and sensitivity

analysis results for selected analysis outcomes associated with the early failure scenario classes (Table K5.1-1).

The primary results considered for the early failure scenario classes are radionuclide movement from the EBS to the UZ (Table K5.1-2), radionuclide movement from the UZ to the SZ (Table K5.1-3), radionuclide movement in the SZ at the location of the RMEI (Table K5.1-4), dose to the RMEI from selected radionuclides (Table K5.1-5), and expected dose to the RMEI from all radionuclides (Table K5.1-6). High-level summaries of the uncertainty and sensitivity analysis results presented in this section are provided in Tables K5.1-2 to K5.1-6. Particular emphasis is given to releases from the EBS to the UZ (Table K5.1-2). Additional uncertainty analysis results are also available in Section J6.

From a regulatory perspective, expected dose to the RMEI (*EXPDOS*, mrem/yr) is the analysis outcome of greatest interest associated with the early failure classes (Table K5.1-6).

For the early DS failure scenario class, *EXPDOS* tends to show a sharp early peak prior to 1,000 yr and then monotonically decrease over the time (Figures K5.7.1-1, K5.7.1-3). The observed range of possible values for *EXPDOS* over the time interval [0, 10^6 yr] is approximately [10^{-8}, 0.02 mrem/yr] (Figure K5.7.1-1, K5.7.1-3). For the [0, 20,000 yr] time interval, the dominant variable contributing to the uncertainty in *EXPDOS* for the early DS failure scenario class is *PROBDSEF* (probability that a randomly selected DS will experience an early failure) (Figures K5.7.1-1, K5.7.1-2). For the [0, 10^6 yr] time interval, *INFIL* (infiltration level) is also an important contributor to the uncertainty in *EXPDOS* (Figures K5.7.1-3, K5.7.1-4). A number of additional variables also have small effects on *EXPDOS*.

For the early WP failure scenario class, *EXPDOS* shows two distinct patterns of behavior (Figure K5.7.2-1). Prior to 10^4 yr, *EXPDOS* is dominated by the failure of CDSP WPs and generally falls in the range [10^{-5}, 0.1 mrem/yr]; after 10^4 yr, *EXPDOS* is dominated by the failure of CSNF WPs and generally falls in the range [10^{-4}, 1 mrem/yr] as the failures of the CSNF WPs result in dose to the RMEI. This effect can be seen in the sharp jump in the values for *EXPDOS* that takes place shortly after 10^4 yr (Figure K5.7.2-1). This effect results from the delayed releases from the hotter CSNF WPs. However, the uncertainty in *EXPDOS* over the time interval [0, 20,000 yr] is dominated by *PROBWPEF* (probability that a randomly selected WP will experience an early failure) (Figures K5.7.2-1, K5.7.2-2). After initial peaks, *EXPDOS* tends to decrease with time, although there is a jump in values at beginning at about 2.6×10^5 yr as the DSs start to fail. At 5×10^5 yr, values for *EXPDOS* fall in the range [10^{-6}, 0.1 mrem/yr] (Figure K5.7.2-3). At later times, *PROBWPEF* remains the most important variable with respect to the uncertainty in *EXPDOS*; however, a number of additional variables also have effects (Figures K5.7.2-3, K5.7.2-4).

Expected dose to the RMEI from both early DS failure and early WP failure is also determined (Figures K5.7.3-1, K5.7.3-2, K5.7.3-3, K5.7.3-4). However, as a result of the expected doses from early WP failures being substantially larger than the expected doses from early DS failures, the combined results for expected dose from early WP and early DS failures are similar to the results for early WP failure alone (Figures K5.7.2-1, K5.7.2-2, K5.7.2-3, K5.7.2-4).

An additional analysis considers expected dose to the RMEI from early DS failure, early WP failure and nominal process WP failure (Figures K5.7.4-1, K5.7.4-2). In this case, the results prior to about 2×10^5 yr are essentially the same as the early WP failure analyses and the results after 2×10^5 yr are essentially the same as the analyses for nominal conditions.

K5.2 Early Failure Scenario Classes: Engineered Barrier System Conditions

The environmental conditions in the EBS after early WP failures are the same as discussed and illustrated in Section K4 for nominal conditions.

For early DS failures under dripping conditions, the seepage rates, EBS temperatures, relative humidities and partial pressures for CO_2 are the same as for nominal conditions. However, the ionic strength and pH in the invert associated with a failed DS under dripping conditions are different from the values present in the absence of a failed DS under dripping conditions (i.e., compare results in Figures K5.2-1 and K5.2-2 with the corresponding 0 to 20,000 yr results in Figures K4.3-9, K4.3-10 and K4.3-12).

The uncertainty results for time-dependent ionic strength (mol/kg) in the invert for CSNF WPs (*ISCSINAD*) and CDSP WPs (*ISCDINAD*) experiencing an early DS failure under dripping conditions in percolation bin 3 are similar (Figure K5.2-1a,b). The transient behavior before about 600 yr results from the thermal evolution of the WPs. While the WPs are above 100 °C ionic strength is not computed because no liquid water is present in the waste. During this time period the ionic strength variable is assigned an artificial value of 1.0 to indicate in Goldsim that ionic strength is not computed. The uncertainty in the ionic strength results is dominated by *ISCSS* (pointer variable used to determine ionic strength in CSNF WP Cell 1 under dripping conditions) for CSNF WPs (Figure K5.2-1e) and by *IS2MCOS* (pointer variable used to determine ionic strength in CDSP WP Cell 2MCO, i.e., Cell 1b, under dripping conditions) for CDSP WPs (Figure K5.2-1f), with ionic strength increasing as each of these variables increases.

The uncertainty results for time-dependent pH in the invert for CSNF WPs (*PHCSINAD*) and CDSP WPs (*PHCDINAD*) experiencing an early DS failure under dripping conditions in percolation bin 3 are similar (Figure K5.2-2a,b). The uncertainty in both *PHCSINAD* and *PHCDINAD* is dominated by *PH2RGER* (error term in regression equation for pH of corrosion product domain) and *DELPPCO2* (scale factor used to incorporate uncertainty into the value for the partial pressure of CO_2), with increasing *PH2RGER* having a strong positive effect on *PHCSINAD* and *PHCDINAD* and increasing *DELPPCO2* having a strong negative effect on *PHCSINAD* and *PHCDINAD*.

K5.3 Early Failure Scenario Classes: Release from Engineered Barrier System

This section contains analysis results for EBS releases over the time interval [0, 20,000 yr] resulting from:

- Early DS failure over a CDSP WP in percolation bin 3 under dripping conditions (Section 5.3.1);

- Early DS failure over a CSNF WP in percolation bin 3 under dripping conditions (Section 5.3.2);
- Early failure of a CDSP WP in percolation bin 3 under dripping conditions (Section 5.3.3);
- Early failure of a CSNF WP in percolation bin 3 under dripping conditions (Section 5.3.5).
- For the time interval [0, 1,000,000 yr] results are presented for:
- Early DS failure over a CDSP WP in percolation bin 3 under dripping conditions (Section 5.3.7);
- Early DS failure over a CSNF WP in percolation bin 3 under dripping conditions (Section 5.3.8);
- Early failure of a CDSP WP in percolation bin 3 under dripping conditions (Section 5.3.9);
- Early failure of a CDSP WP in percolation bin 3 under non-dripping conditions (Section 5.3.10);
- Early failure of a CSNF WP in percolation bin 3 under dripping conditions (Section 5.3.11);
- Early failure of a CSNF WP in percolation bin 3 under non-dripping conditions (Section 5.3.12).

K5.3.1 Early Failure Scenario Classes: Release from Engineered Barrier System over the Time Interval [0, 20,000 yr] for Early Drip Shield Failure above a CDSP WP

Movement of ^{239}Pu Irreversibly Attached to Glass (i.e., Ic) Colloids: *ESIC239* and *ESIC239C*. The uncertainty and sensitivity analyses for the time-dependent release rates (*ESIC239*, g/yr) and cumulative releases (*ESIC239C*, g) over the time interval [0, 20,000 yr] for the movement of ^{239}Pu irreversibly attached to glass (i.e., Ic) colloids from the EBS to the UZ resulting from the early failure of one DS above a CDSP WP in percolation bin 3 under dripping conditions are summarized in Figures K5.3.1-1 and K5.3.1-2.

The values for *ESIC239* are small (i.e., $< 10^{-3}$ g/yr) and tend to be constant for each period of constant infiltration (Figure K5.3.1-1a,c). As a result, the values for *ESIC239C* are also small and less than 10 g over 20,000 yr for most sample elements (Figure K5.3.1-1b,d). For some sample elements, drift-wall condensation occurring before 1,000 yr increases water flow through the affected WPs for a short period, which causes the higher releases of ^{239}Pu irreversibly attached to glass colloids during this period. More discussion is provided below in the analysis for the movement of dissolved ^{237}Np.

As indicated by the PRCCs in Figure K5.3.1-1e,f, the uncertainty in *ESIC239* and *ESIC239C* is dominated by *INFIL* (infiltration level) and *CPUCOLWF* (maximum concentration of plutonium irreversibly attached to glass colloids, mol/L), with *ESIC239* and *ESIC239C* increasing as each of these variables increases. These effects result because increasing *INFIL* increases water flow in the EBS and the UZ and increasing *CPUCOLWF* increases the amount of ^{239}Pu that can potentially be irreversibly attached to glass colloids. In addition to *INFIL* and *CPUCOLWF*, negative effects are indicated for *SEEPPRM* (mean fracture permeability in lithophysal rock units, m^2; as sampled, *SEEPPRM* is actually the logarithm of the indicated permeability) and *SEEPPRMN* (mean fracture permeability in nonlithophysal rock units, m^2; as sampled, *SEEPPRMN* is actually the logarithm of the indicated permeability). The negative effects associated with *SEEPPRM* and *SEEPPRMN* result from increasing water flow around the EBS and thus decreasing water flow through the EBS.

The variables *THERMCON* (host rock thermal conductivity level) and *DIAMCOL* (colloid particle diameter, nm) have indicated effects prior to 1,000 yr that may or may not be real. After 1,000 yr, no identifiable effects are indicated for these variables. Prior to 1,000 yr, *ESIC239* and *ESIC239C* have values of zero for many of the sample elements. Performing rank correlations where many output variables have the value zero can cause input variables to appear to have effects when they actually do not. It is also possible that the early positive effect associated with *THERMCON* results from an enhanced cooling of the repository and a resultant earlier initiation of water flow into and out of the EBS, or from a relationship between *THERMCON* and the occurrence of condensation.

More detailed sensitivity analysis results for *ESIC239* and *ESIC239C* are provided by the regression analyses in Figure K5.3.1-2a,b. Specifically, all six regressions contained in Figure K5.3.1-2a,b initially select the following five variables in the same order: *INFIL*, *CPUCOLWF*, *SEEPPRM*, *SEEPPRMN* and *ALPHAL* (capillary strength parameter in lithophysal rock units, Pa). The effects of *INFIL*, *CPUCOLWF*, *SEEPPRM* and *SEEPPRMN* on *ESIC239* and *ESIC239C* have already been discussed in conjunction with Figure K5.3.1-1e,f. Similarly to *SEEPPRM* and *SEEPPRMN*, the negative effect associated with *ALPHAL* results from increasing water diversion around the EBS. The individual regressions containing only *INFIL* and *CPUCOLWF* have R^2 values between 0.83 and 0.86; thus, these two variables account for most of the uncertainty associated with *ESIC239* and *ESIC239C*. The variables *SEEPPRM*, *SEEPPRMN* and *ALPHAL* have smaller effects, and their inclusion in the regression models produces cumulative R^2 values between 0.87 and 0.90. After the first five variables, five of the six regression analyses in Figure K5.3.1-2a,b select additional variables that have very small effects on *ESIC239* and *ESIC239C*. The selection of the pointer variable used to determine pH in cell 1 of CSNF WPs under dripping conditions (*PHCSS*) as the final variable selected in all three regressions for *ESIC239* is probably spurious.

The dominant effects of *INFIL* and *CPUCOLWF* on *ESIC239* and *ESIC239C* and the lesser effect of *SEEPPRM* can be seen in the scatterplots in Figure K5.3.1-2c,d,e,f,g,h.

Movement of ^{239}Pu Irreversibly Attached to Ferrous (i.e., If) Colloids: *ESIF239* and *ESIF239C*. Uncertainty and sensitivity analyses for the movement of ^{239}Pu irreversibly attached to ferrous colloids are not presented due to an error in the GoldSim component of the

TSPA-LA Model that affects the calculation of the stability of ferrous colloids. Consequently, Figure K5.3.1-3 and Figure K5.3.1-4 have been removed from this document. See Appendix P, Section P18, for a discussion of the error and the effect of the error on TSPA-LA Model results.

Movement of Dissolved ^{237}Np: *ESNP237* and *ESNP237C*. The uncertainty and sensitivity analyses for the time-dependent release rates (*ESNP237*, g/yr) and cumulative releases (*ESNP237C*, g) over the time interval [0, 20,000 yr] for the movement of dissolved ^{237}Np from the EBS to the UZ resulting from the early failure of one DS above a CDSP WP in percolation bin 3 under dripping conditions are summarized in Figures K5.3.1-5 and K5.3.1-6.

The values for *ESNP237* exhibit an initial pulse release prior to 1,000 yr, a subsequent increase in rates at 2,000 yr, and then a monotonic decrease with time until 10,000 yr (Figure K5.3.1-5a,c). The initial pulse occurs because of condensation on the drift wall, which adds to the seepage flux falling onto the failed WP. The Drift Wall Condensation Abstraction divides time into three stages: Stage 1 is the initial stage when all WPs in the drift are above 96°C; Stage 2 is the middle stage after the first WP in the drift cools to below 96 °C, but before the last WP in the drift cools to below 96 °C; and Stage 3 is the final stage after all WPs in the drift are below 96 °C (see Section 6.3.3.2.2 for details). Condensation can begin as soon the drift wall temperature falls below 96 °C for at least one WP in a drift, and continues until 2,000 yr. However, the condensation rate varies, with Stage 2 rates applied until the drift wall temperatures for all WPs fall below 96 °C, and Stage 3 ratesapplied from that time until 2,000 yr. Condensation during Stage 2 is generally much larger than during Stage 3, and can be much larger than seepage during the Stage 2 period. The effect of the Stage 2 condensation is to increase water flow into a failed WP, which in turn increases the rate of mass release from the WP during Stage 2. After Stage 3, condensation greatly decreases, resulting in the drop in release rates observed at about 1,000 yr. At 10,000 yr, the climate changes from monsoon to glacial transition, and percolation rates generally increase, which in turn increases seepage and the release rate of ^{237}Np. The initial release of ^{237}Np is primarily from DSNF waste forms, which are conservatively assumed to immediately degrade when the WP is breached. The later releases of ^{237}Np are primarily from high-level radioactive waste (HLW), which degrades slowly over time, and thus allows for other processes to affect the release of ^{237}Np from the WP.

The release rates of ^{237}Np after about 1,000 years generally evolve toward a steady state value, as environmental conditions inside the WP evolve toward steady state. These environmental variables determine the solubility of ^{237}Np as a function of time. This evolution is apparent in the changing values of the PRCCs for *DELPPCO2* (scale factor used to incorporate uncertainty into the value for the partial pressure of CO_2) and *PH2MCOS* (pointer variable used to incorporate uncertainty into pH in cell 1b of CDSP WPs under dripping conditions). The steady state release rate is determined by the balance between waste form degradation and reversible sorption onto ferrous corrosion products as indicated by the PRCCs for *GOESITED* (density of sorption sites on goethite, sites/nm^2) and *HFOSA* (hydrous ferrous oxide surface area, m^2/g).

Movement of Dissolved ^{239}Pu: *ESPU239* and *ESPU239C*. The uncertainty and sensitivity analyses for the time-dependent release rates (*ESPU239*, g/yr) and cumulative releases (*ESPU239C*, g) over the time interval [0, 20,000 yr] for the movement of dissolved ^{239}Pu from

the EBS to the UZ resulting from the early failure of one DS above a CDSP WP in percolation bin 3 under dripping conditions are summarized in Figures K5.3.1-7 and K5.3.1-8.

The values for *ESPU239* display an initial pulse release prior to 1,000 yr and then a monotonic increase with time thereafter toward a steady state value (Figure K5.3.1-7a,c). The pulse occurs because of condensation on the drift wall, and the steady state release rate is due to reversible sorption on corrosion products, as explained in the discussion of ^{237}Np. The initial release of ^{239}Pu is primarily from DSNF waste forms, which are conservatively assumed to immediately degrade when the WP is breached. The later releases of ^{239}Pu are primarily from HLW, which degrades slowly over time. Much of the mobilized plutonium sorbs onto ferrous corrosion products and its subsequent release depends on the rates of desorption. However, because other radionuclides (i.e. uranium) also sorb onto the ferrous corrosion products, there is a complex interplay between the rates of waste degradation, concentrations of radionuclides in solution, and rates of sorption and desorption, which result in the slow but steady increase in the release rates of ^{239}Pu from the WP. At 20,000 yr, *ESPU239* and *ESPU239C* fall below 0.1 g/yr and 1,000 g, respectively, for all sample elements (Figure K5.3.1-7a,b,c,d).

The most important variable with respect to the uncertainty in *ESPU239* and *ESPU239C* is *EP1LOWPU* (scale factor used to incorporate uncertainty into plutonium solubility under low ionic strength conditions; as sampled, *EP1LOWPU* is actually the logarithm of the indicated scale factor), with *ESPU239* and *ESPU239C* tending to increase as *EP1LOWPU* increases (Figures K5.3.1-7e,f and K5.3.1-8a,b) This effect results because increasing *EP1LOWPU* increases the solubility limit for plutonium and hence increases the amount of dissolved ^{239}Pu that is available for movement from the EBS to the UZ. In various orders, all six regressions in Figure K5.3.1-8a,b select *EP1LOWPU*, *DELPPCO2* (scale factor used to incorporate uncertainty into the value for the partial pressure of CO_2), and *INFIL* (infiltration level) as the first three variables in the stepwise process. Both *DELPPCO2* and *INFIL* have positive effects on *ESPU239* and *ESPU239C*. Specifically, increasing *DELPPCO2* increases the solubility limit for plutonium, and increasing *INFIL* increases water flow in the EBS and UZ. The regression models containing *EP1LOWPU*, *DELPPCO2* and *INFIL* have cumulative R^2 values between 0.67 and 0.78.

After *EP1LOWPU*, *DELPPCO2* and *INFIL*, the regression analyses select a number of additional variables that have small effects on *ESPU239* and *ESPU239C* (Figure K5.3.1-8a,b). For example, the analysis for *ESPU239* at 10,000 yr selects the following 10 additional variables: *SEEPPRM* (mean fracture permeability in lithophysal rock units, m^2; as sampled, *SEEPPRM* is actually the logarithm of the indicated permeability), *SEEPPRMN* (mean fracture permeability in nonlithophysal rock units, m^2; as sampled, *SEEPPRMN* is actually the logarithm of the indicated permeability), *GOESITED* (density of sorption sites on goethite, sites/nm^2), *ALPHAL* (capillary strength parameter in lithophysal rock units, Pa), *PH2MCOS* (pointer variable used to incorporate uncertainty into pH in cell 1b of CDSP WPs under dripping conditions), *EBSDIFCF* (scale factor used to incorporate uncertainty into invert diffusion coefficient; as sampled, *EBSDIFCF* is actually the logarithm of the indicated scale factor), *PH2MCOS* (pointer variable used to incorporate uncertainty into pH in cell 1b of CDSP WPs under dripping conditions), *GP2NO3* (ratio of Cl to NO_3 in Group 2 pore waters, dimensionless), *RHPH75* (scale factor used to incorporate uncertainty into pH of in-drift waters at relative

humidities above 75 percent), *GOESA* (specific surface area for goethite, m^2/g), and *DIFPATHL* (diffusive path length from WP outer corrosion barrier to midpoint of invert, m) (Figure K5.3.1-8a). The variables *SEEPPRM*, *SEEPPRMN* and *ALPHAL* have negative effects on *ESPU239* as a result of increasing water flow around the EBS and thus reducing water flow through the EBS. The variables *GOESITED* and *GOESA* have negative effects on *ESPU239* as a result of increasing the sorption of ^{239}Pu on goethite. The variables *EBSDIFCF* and *DIFPATHL* have opposite effects on diffusion in the invert. Specifically, *EBSDIFCF* has a positive effect on *ESPU239* because diffusion in the invert increases as *EBSDIFCF* increases, and *DIFPATHL* has a negative effect on *ESPU239* because diffusion in the invert decreases as *DIFPATHL* increases. The variables *PH2MCOS* and *RHPH75* are involved in the definition of pH in the WP and the invert, respectively. The negative effects associated with *PH2MCOS* and *RHPH75* result because increasing either variable increases pH, which in most realizations decreases Pu solubility, thus decreasing *ESPU239*. Finally, the negative effect associated with *GP2NO3* is spurious as there is no functional relationship in the TSPA-LA Model between transport of ^{239}Pu and the ratio of Cl to NO_3 concentrations. The final regression model for *ESPU239* at 10,000 yr contains 13 variables and has an R^2 value of 0.85; thus most of the uncertainty in *ESPU239* is being accounted for.

The remaining five regressions in Figure K5.3.1-8a,b are similar to the just discussed regression for *ESPU239* at 10,000 yr and will not be discussed. The effects of the three dominant variables *EP1LOWPU*, *DELPPCO2* and *INFIL* on the uncertainty in *ESIC239* and *ESIC239C* at 10,000 yr can be seen in the scatterplots in Figure K5.3.1-8c,d,e,f,g,h.

Movement of Dissolved ^{99}Tc: *ESTC99* and *ESTC99C*. The uncertainty and sensitivity analyses for the time-dependent release rates (*ESTC99*, g/yr) and cumulative releases (*ESTC99C*, g) over the time interval [0, 20,000 yr] for the movement of dissolved ^{99}Tc from the EBS to the UZ resulting from the early failure of one DS above a CDSP WP in percolation bin 3 under dripping conditions are summarized in Figures K5.3.1-9 and K5.3.1-10.

Because technetium is assumed to have no solubility limit and to undergo no retardation in the invert (or anywhere else in the disposal system), released technetium moves very rapidly from the EBS to the UZ. This behavior can be seen in the rapidly decreasing values for *ESTC99* in Figure K5.3.1-9a,c and the rapid approach of *ESTC99C* to an asymptote in Figure K5.3.1-9b,d.

Because of the rapid decrease in *ESTC99*, the sensitivity analysis results for *ESTC99* and *ESTC99C* are very different (e.g., compare the PRCCs for *ESTC99* and *ESTC99C* in Figure K5.3.1-9e,f). For example, *HLWDRALK* (dissolution rate of HLW glass under alkaline conditions, $g/m^2/d$) has a negative effect on *ESTC99* and a positive effect on *ESTC99C*. These contrasting effects result because increasing *HLWDRALK* increases dissolution rate of HLW glass and hence increases the rate of release of ^{99}Tc. This results in a negative effect on *ESTC99* because increasing the amount of ^{99}Tc released at early times reduces the amount of ^{99}Tc that can be released at later times and, as a result, reduces *ESTC99* as time increases. In contrast, increasing *HLWDRALK* increases the total amount of ^{99}Tc released from HLW glass by a given time and thus increases *ESTC99C*.

As an example, the analysis for *ESTC99* at 10,000 yr is discussed in more detail (Figure K5.3.1-10a). The two dominant variables are *HLWDRALK* and *WFDEGEXF* (surface area exposure factor for amount of HLW glass contacted by water). As already discussed, *HLWDRALK* has a negative effect on *ESTC99* at 10,000 yr as a result of increasing the release of ^{99}Tc at earlier times. Similarly, *WFDEGEXF* has a negative effect on *ESTC99* at 10,000 yr as a result of increasing HLW glass degradation and thus increasing the release of ^{99}Tc at earlier times. Together, *HLWDRALK* and *WFDEGEXF* result in a regression model with an R^2 value of 0.47. After *HLWDRALK* and *WFDEGEXF*, the regression analysis indicates small positive effects for *THERMCON* (host rock thermal conductivity level), *PH2DHLS* (pointer variable used to determine pH in Cell 1a, i.e. Cell 2DHLW, of CDSP WPs under dripping conditions), and *SEEPPRMN* (mean fracture permeability in nonlithophysal rock units, m^2; as sampled, *SEEPPRMN* is actually the logarithm of the indicated permeability), and small negative effects for *HLWDRACD* (dissolution rate of HLW glass under acidic conditions, $g/m^2/d$) and *GP4NO3* (ratio of Cl to NO_3 in Group 4 pore waters, dimensionless). The positive effects result because (i) increasing *THERMCON* reduces EBS temperatures, which in turn reduces the degradation rate of HLW glass and thus reduces early releases of ^{99}Tc, (ii) increasing *PH2DHLS* increases pH in the vicinity of HLW glass and thus reduces its rate of degradation and associated early releases of ^{99}Tc, and (iii) increasing *SEEPPRMN* reduces water flow through the EBS and thus reduces early releases of ^{99}Tc. The negative effects result because (i) increasing *HLWDRACD* increases the dissolution of HLW glass and at early times and thus reduces the release of ^{99}Tc at later times. The correlation of *ESTC99* to *GP4NO3* is spurious, as there is no functional relationship in the TSPA-LA Model between transport of ^{99}Tc and the ratio of Cl to NO_3 concentration. The final regression model has a rather low R^2 value of 0.56. This low R^2 value probably results from a lack of resolution in calculating the very small values that exist for *ESTC99* at 10,000 yr as a result of inventory depletion (Figure K5.3.1-9a,c).

The analysis for *ESTC99C* at 10,000 yr is now considered. Overall, the dominant variables are *HLWMASS* (scale factor used to characterize uncertainty in amount of HLW in CDSP WPs), *HLWDRACD*, *DSNFMASS* (scale factor used to characterize uncertainty in amount of DSNF in CDSP WPs), *HLWDRALK*, *WFDEGEXF* and *PH2DHLS*. The variables *HLWMASS* and *DSNFMASS* have positive effects on *ESTC99C* because increasing their values increases the amount of ^{99}Tc in CDSP WPs. The variables *HLWDRACD*, *HLWDRALK*, and *WFDEGEXF* have positive effects on *ESTC99C* because increasing their values increases the amount of ^{99}Tc released from the degradation of HLW glass, which is the opposite of the effect that these variables have on *ESTC99* at 10,000 yr. In contrast, *PH2DHLS* has a negative effect on *ESTC99C* because increasing its value reduces the rate of HLW glass degradation. Collectively, *HLWMASS*, *HLWDRACD*, *DSNFMASS*, *HLWDRALK*, *WFDEGEXF* and *PH2DHLS* result in a model with an R^2 value of 0.79. After these variables, the analysis selects several additional variables with small effects and produces model with an R^2 value of 0.81; thus, most of the uncertainty associated with *ESTC99C* at 10,000 yr is being accounted for.

The remaining four regressions in Figure K5.3.1-10a,b are similar to the just discussed regressions for *ESTC99* and *ESTC99C* at 10,000 yr and will not be discussed. The effects of the first three variables selected in the regression analyses for *ESTC99* and *ESTC99C* at 10,000 yr can be seen in the scatterplots in Figure K5.3.1-10c,d,e,f,g,h.

K5.3.2 Early Failure Scenario Classes: Release from Engineered Barrier System over the Time Interval [0, 20,000 yr] for Early Drip Shield Failure above a CSNF WP

For completeness, this section presents summaries of the uncertainty and sensitivity analyses for release from the EBS over the time interval [0, 20,000 yr] for early DS failure above a CSNF WP without discussion.

Movement of ^{239}Pu Irreversibly Attached to Glass (i.e., Ic) Colloids: *ESIC239* and *ESIC239C*. The uncertainty and sensitivity analyses for the time-dependent release rates (*ESIC239*, g/yr) and cumulative releases (*ESIC239C*, g) over the time interval [0, 20,000 yr] for the movement of ^{239}Pu irreversibly attached to glass (i.e., Ic) colloids from the EBS to the UZ resulting from the early failure of one DS above a CSNF WP in percolation bin 3 under dripping conditions are summarized in Figure K5.3.2-1.

Movement of ^{239}Pu Irreversibly Attached to Ferrous (i.e., If) Colloids: *ESIF239* and *ESIF239C*. Uncertainty and sensitivity analyses for the movement of ^{239}Pu irreversibly attached to ferrous colloids are not presented due to an error in the GoldSim component of the TSPA-LA Model that affects the calculation of stability of ferrous colloids. Consequently, Figure K5.3.2-2 has been removed from this document. See Appendix P, Section P18, for a discussion of the error and the effect of the error on TSPA-LA Model results.

Movement of Dissolved ^{237}Np: *ESNP237* and *ESNP237C*. The uncertainty and sensitivity analyses for the time-dependent release rates (*ESNP237*, g/yr) and cumulative releases (*ESNP237C*, g) over the time interval [0, 20,000 yr] for the movement of dissolved ^{237}Np from the EBS to the UZ resulting from the early failure of one DS above a CSNF WP in percolation bin 3 under dripping conditions are summarized in Figure K5.3.2-3.

Movement of Dissolved ^{239}Pu: *ESPU239* and *ESPU239C*. The uncertainty and sensitivity analyses for the time-dependent release rates (*ESPU239*, g/yr) and cumulative releases (*ESPU239C*, g) over the time interval [0, 20,000 yr] for the movement of dissolved ^{239}Pu from the EBS to the UZ resulting from the early failure of one DS above a CSNF WP in percolation bin 3 under dripping conditions are summarized in Figures K5.3.2-4.

Movement of Dissolved ^{99}Tc: *ESTC99* and *ESTC99C*. The uncertainty and sensitivity analyses for the time-dependent release rates (ESTC99, g/yr) and cumulative releases (ESTC99C, g) over the time interval [0, 20,000 yr] for the movement of dissolved ^{99}Tc from the EBS to the UZ resulting from the early failure of one DS above a CSNF WP in percolation bin 3 under dripping conditions are summarized in Figure K5.3.2-5.

K5.3.3 Early Failure Scenario Classes: Release from Engineered Barrier System over the Time Interval [0, 20,000 yr] for Early Failure of a CDSP Waste Package under Dripping Conditions

For completeness, this section presents summaries of the uncertainty and sensitivity analyses for release from the EBS over the time interval [0, 20,000 yr] for early failure of a CDSP WP under dripping conditions without discussion.

Movement of ^{239}Pu Irreversibly Attached to Glass (i.e., Ic) Colloids: *ESIC239* and *ESIC239C*. Uncertainty and sensitivity analyses for the movement of ^{239}Pu irreversibly attached to glass colloids are not presented when transport is predominantly by diffusion (i.e., for early failed WP and seismic ground motion scenario classes), due to an error in the GoldSim component of the TSPA-LA Model that affects the calculation of concentration of glass colloids when glass colloids are unstable. Consequently, Figure K5.3.3-1 has been removed from this document. See Appendix P, Table P-6, for a discussion of the error and the effect of the error on TSPA-LA Model results.

Movement of ^{239}Pu Irreversibly Attached to Ferrous (i.e., If) Colloids: *ESIF239* and *ESIF239C*. Uncertainty and sensitivity analysis for the movement of ^{239}Pu irreversibly attached to ferrous colloids are not presented due to an error in the GoldSim component of the TSPA-LA Model that affects the calculation of stability of ferrous colloids. Consequently, Figure K5.3.3-2 has been removed from this document. See Appendix P, Section P18, for a discussion of the error and the effect of the error on TSPA-LA Model results.

Movement of Dissolved ^{237}Np: *ESNP237* and *ESNP237C*. The uncertainty and sensitivity analyses for the time-dependent release rates (*ESNP237*, g/yr) and cumulative releases (*ESNP237C*, g) over the time interval [0, 20,000 yr] for the movement of dissolved ^{237}Np from the EBS to the UZ resulting from the early failure of a CDSP WP in percolation bin 3 under dripping conditions are summarized in Figure K5.3.3-3.

Movement of Dissolved ^{239}Pu: *ESPU239* and *ESPU239C*. The uncertainty and sensitivity analyses for the time-dependent release rates (*ESPU239*, g/yr) and cumulative releases (*ESPU239C*, g) over the time interval [0, 20,000 yr] for the movement of dissolved ^{239}Pu from the EBS to the UZ resulting from the early failure of a CDSP WP in percolation bin 3 under dripping conditions are summarized in Figure K5.3.3-4.

Movement of Dissolved ^{99}Tc: *ESTC99* and *ESTC99C*. The uncertainty and sensitivity analyses for the time-dependent release rates (*ESTC99*, g/yr) and cumulative releases (*ESTC99C*, g) over the time interval [0, 20,000 yr] for the movement of dissolved ^{99}Tc from the EBS to the UZ resulting from the early failure of a CDSP WP in percolation bin 3 under dripping conditions are summarized in Figure K5.3.3-5.

K5.3.4 Early Failure Scenario Classes: Release from Engineered Barrier System over the Time Interval [0, 20,000 yr] for Early Failure of a CDSP Waste Package under Nondripping Conditions

Releases from the EBS over the time interval [0, 20,000 yr] for early failure of a CDSP WP under nondripping conditions are small. Therefore, no uncertainty and sensitivity analyses are presented for this case.

K5.3.5 Early Failure Scenario Classes: Release from Engineered Barrier System over the Time Interval [0, 20,000 yr] for Early Failure of a CSNF Waste Package under Dripping Conditions

For completeness, this section presents summaries of the uncertainty and sensitivity analyses for release from the EBS over the time interval [0, 20,000 yr] for early failure of a CSNF WP under dripping conditions without discussion.

Movement of ^{239}Pu Irreversibly Attached to Glass (i.e., Ic) Colloids: *ESIC239* and *ESIC239C*. Uncertainty and sensitivity analysis of movement of ^{239}Pu irreversibly attached to glass colloids are not presented when transport is predominantly by diffusion (i.e. for early failed WP and seismic ground motion scenario classes), due to an error in the GoldSim component of the TSPA-LA Model that affects the calculation of concentration of glass colloids when glass colloids are unstable. Consequently, Figure K5.3.5-1 has been removed from this document. See Appendix P, Table P-6, for a discussion of the error and the effect of the error on TSPA-LA Model results.

Movement of ^{239}Pu Irreversibly Attached to Ferrous (i.e., If) Colloids: *ESIF239* and *ESIF239C*. Uncertainty and sensitivity analyses for the movement of ^{239}Pu irreversibly attached to ferrous colloids are not presented due to an error in the GoldSim component of the TSPA-LA Model that affects the calculation of stability of ferrous colloids. Consequently, Figure K5.3.5-2 has been removed from this document. See Appendix P, Section P18, for a discussion of the error and the effect of the error on TSPA-LA Model results.

Movement of Dissolved ^{237}Np: *ESNP237* and *ESNP237C*. The uncertainty and sensitivity analyses for the time-dependent release rates (*ESNP237*, g/yr) and cumulative releases (*ESNP237C*, g) over the time interval [0, 20,000 yr] for the movement of dissolved ^{237}Np from the EBS to the UZ resulting from the early failure of a CSNF WP in percolation bin 3 under dripping conditions are summarized in Figure K5.3.5-3.

Movement of Dissolved ^{239}Pu: *ESPU239* and *ESPU239C*. The uncertainty and sensitivity analyses for the time-dependent release rates (*ESPU239*, g/yr) and cumulative releases (*ESPU239C*, g) over the time interval [0, 20,000 yr] for the movement of dissolved ^{239}Pu from the EBS to the UZ resulting from the early failure of a CSNF WP in percolation bin 3 under dripping conditions are summarized in Figure K5.3.5-4.

Movement of Dissolved ^{99}Tc: *ESTC99* and *ESTC99C*. The uncertainty and sensitivity analyses for the time-dependent release rates (*ESTC99*, g/yr) and cumulative releases (*ESTC99C*, g) over the time interval [0, 20,000 yr] for the movement of dissolved ^{99}Tc from the EBS to the UZ resulting from the early failure of a CSNF WP in percolation bin 3 under dripping conditions are summarized in Figure K5.3.5-5.

K5.3.6 Early Failure Scenario Classes: Release from Engineered Barrier System over the Time Interval [0, 20,000 yr] for Early Failure of a CSNF Waste Package under Nondripping Conditions

Releases from the EBS over the time interval [0, 20,000 yr] for early failure of a CSNF WP under nondripping conditions are small. Therefore, no uncertainty and sensitivity analyses are presented for this case.

K5.3.7 Early Failure Scenario Classes: Release from Engineered Barrier System over the Time Interval [0, 1,000,000 yr] for Early Drip Shield Failure above a CDSP WP

This section presents summaries of the uncertainty and sensitivity analyses for the releases of dissolved ^{237}Np and dissolved ^{239}Pu from the EBS over the time interval [0, 1,000,000 yr] for early DS failure above a CSNF WP without discussion. Dissolved ^{237}Np is used as an example because of its long half life (2.14×10^6 yr). Dissolved ^{239}Pu is used as an example because of its significant but shorter half life (2.41×10^5 yr). The plutonium colloids are omitted because they involve smaller releases from the EBS than dissolved ^{239}Pu and also, like dissolved ^{239}Pu, their long term releases are dominated by the effects of radioactive decay. Owing to its rapid release from the EBS, there is no reason to show results for ^{99}Tc for the 1,000,000 yr case (see Figures K5.3.1-9a and K5.3.2-5a for results for the time interval [0, 20,000 yr]).

Movement of Dissolved ^{237}Np: *ESNP237* and *ESNP237C*. The uncertainty and sensitivity analyses for the time-dependent release rates (*ESNP237*, g/yr) and cumulative releases (*ESNP237C*, g) over the time interval [0, 1,000,000 yr] for the movement of dissolved 237Np from the EBS to the UZ resulting from the early failure of one DS above a CDSP WP in percolation bin 3 under dripping conditions are summarized in Figure K5.3.7-1.

Movement of Dissolved ^{239}Pu: *ESPU239* and *ESPU239C*. The uncertainty and sensitivity analyses for the time-dependent release rates (*ESPU239*, g/yr) and cumulative releases (*ESPU239C*, g) over the time interval [0, 200,000 yr] for the movement of dissolved 239Pu from the EBS to the UZ resulting from the early failure of one DS above a CDSP WP in percolation bin 3 under dripping conditions are summarized in Figures K5.3.7-2.

K5.3.8 Early Failure Scenario Classes: Release from Engineered Barrier System over the Time Interval [0, 1,000,000 yr] for Early Drip Shield Failure above a CSNF WP

See discussion at start of Section K5.3.7.

Movement of Dissolved ^{237}Np: *ESNP237* and *ESNP237C*. The uncertainty and sensitivity analyses for the time-dependent release rates (*ESNP237*, g/yr) and cumulative releases (*ESNP237C*, g) over the time interval [0, 1,000,000 yr] for the movement of dissolved ^{237}Np from the EBS to the UZ resulting from the early failure of one DS above a CSNF WP in percolation bin 3 under dripping conditions are summarized in Figure K5.3.8-1.

Movement of Dissolved ^{239}Pu: *ESPU239* and *ESPU239C*. The uncertainty and sensitivity analyses for the time-dependent release rates (*ESPU239*, g/yr) and cumulative releases (*ESPU239C*, g) over the time interval [0, 1,000,000 yr] for the movement of dissolved ^{239}Pu from the EBS to the UZ resulting from the early failure of one DS above a CSNF WP in percolation bin 3 under dripping conditions are summarized in Figures K5.3.8-2.

K5.3.9 Early Failure Scenario Classes: Release from Engineered Barrier System over the Time Interval [0, 1,000,000 yr] for Early Failure of a CDSP Waste Package under Dripping Conditions

See discussion at start of Section K5.3.7.

Movement of Dissolved ^{237}Np: *ESNP237* and *ESNP237C*. The uncertainty and sensitivity analyses for the time-dependent release rates (*ESNP237*, g/yr) and cumulative releases (*ESNP237C*, g) over the time interval [0, 1,000,000 yr] for the movement of dissolved ^{237}Np from the EBS to the UZ resulting from the early failure of a CDSP WP in percolation bin 3 under dripping conditions are summarized in Figure K5.3.9-1. The significant increase in release rates around 300,000 yr is due to failure of the DS from general corrosion. Prior to DS failure, dissolved ^{237}Np moves from the EBS primarily by diffusion; after DS failure, advection becomes the dominant mechanism for dissolved ^{237}Np movement. The change in release mechanisms is reflected in the change in PRCCs for *EBSDIFCF* (exponential term representing uncertainty in the invert diffusion coefficient (dimensionless)) and *INFIL* (infiltration level).

Movement of Dissolved ^{239}Pu: *ESPU239* and *ESPU239C*. The uncertainty and sensitivity analyses for the time-dependent release rates (*ESPU239*, g/yr) and cumulative releases (*ESPU239C*, g) over the time interval [0, 200,000 yr] for the movement of dissolved ^{239}Pu from the EBS to the UZ resulting from the early failure of a CDSP WP in percolation bin 3 under dripping conditions are summarized in Figures K5.3.9-2. Results are plotted only to 200,000 yr because most of the ^{239}Pu decays within this time interval.

K5.3.10 Early Failure Scenario Classes: Release from Engineered Barrier System over the Time Interval [0, 1,000,000 yr] for Early Failure of a CDSP Waste Package under Nondripping Conditions

See discussion at start of Section K5.3.7.

Movement of Dissolved ^{237}Np: *ESNP237* and *ESNP237C*. The uncertainty and sensitivity analyses for the time-dependent release rates (*ESNP237*, g/yr) and cumulative releases (*ESNP237C*, g) over the time interval [0, 1,000,000 yr] for the movement of dissolved ^{237}Np

from the EBS to the UZ resulting from the early failure of a CDSP WP in percolation bin 3 under nondripping conditions are summarized in Figure K5.3.10-1. Because these results involve a WP in nondripping conditions, DS failure does not affect the movement of dissolved ^{237}Np.

Movement of Dissolved ^{239}Pu: *ESPU239* and *ESPU239C*. The uncertainty and sensitivity analyses for the time-dependent release rates (*ESPU239*, g/yr) and cumulative releases (*ESPU239C*, g) over the time interval [0, 200,000 yr] for the movement of dissolved ^{239}Pu from the EBS to the UZ resulting from the early failure of a CDSP WP in percolation bin 3 under nondripping conditions are summarized in Figures K5.3.10-2.

K5.3.11 Early Failure Scenario Classes: Release from Engineered Barrier System over the Time Interval [0, 1,000,000 yr] for Early Failure of a CSNF Waste Package under Dripping Conditions

See discussion at start of Section K5.3.7.

Movement of Dissolved ^{237}Np: *ESNP237* and *ESNP237C*. The uncertainty and sensitivity analyses for the time-dependent release rates (*ESNP237*, g/yr) and cumulative releases (*ESNP237C*, g) over the time interval [0, 1,000,000 yr] for the movement of dissolved ^{237}Np from the EBS to the UZ resulting from the early failure of a CSNF WP in percolation bin 3 under dripping conditions are summarized in Figure K5.3.11-1.

Movement of Dissolved ^{239}Pu: *ESPU239* and *ESPU239C*. The uncertainty and sensitivity analyses for the time-dependent release rates (*ESPU239*, g/yr) and cumulative releases (*ESPU239C*, g) over the time interval [0, 200,000 yr] for the movement of dissolved ^{239}Pu from the EBS to the UZ resulting from the early failure of a CSNF WP in percolation bin 3 under dripping conditions are summarized in Figures K5.3.11-2.

K5.3.12 Early Failure Scenario Classes: Release from Engineered Barrier System over the Time Interval [0, 1,000,000 yr] for Early Failure of a CSNF Waste Package under Nondripping Conditions

See discussion at start of Section K5.3.7.

Movement of Dissolved ^{237}Np: *ESNP237* and *ESNP237C*. The uncertainty and sensitivity analyses for the time-dependent release rates (*ESNP237*, g/yr) and cumulative releases (*ESNP237C*, g) over the time interval [0, 1,000,000 yr] for the movement of dissolved ^{237}Np from the EBS to the UZ resulting from the early failure of a CSNF WP in percolation bin 3 under nondripping conditions are summarized in Figure K5.3.12-1.

Movement of Dissolved ^{239}Pu: *ESPU239* and *ESPU239C*. The uncertainty and sensitivity analyses for the time-dependent release rates (*ESPU239*, g/yr) and cumulative releases (*ESPU239C*, g) over the time interval [0, 200,000 yr] for the movement of dissolved ^{239}Pu from the EBS to the UZ resulting from the early failure of a CSNF WP in percolation bin 3 under nondripping conditions are summarized in Figures K5.3.12-2.

K5.4 Early Failure Scenario Classes: Release from Unsaturated Zone

This section contains analysis results for releases from the UZ over the time interval [0, 20,000 yr] resulting from early failure of one DS over a CDSP WP in percolation bin 3 under dripping conditions (Section 5.4.1). Analysis results for other early failures are discussed in Section K5.4.2.

K5.4.1 Early Failure Scenario Classes: Release from Unsaturated Zone over the Time Interval [0, 20,000 yr] for Early Drip Shield Failure above a CDSP WP

Movement of ^{239}Pu Irreversibly Attached to Slow (i.e., Ic) Colloids: *UZIC239* and *UZIC239C*. To understand the presented analyses for colloids in the UZ and SZ, it is important to bear in mind that the ^{239}Pu irreversibly attached to glass (i.e., Ic) and ferrous (i.e., If) colloids in the EBS is reapportioned upon entry into the UZ. Specifically, (i) Ic now designates slow moving colloids, (ii) If now designates fast moving colloids, and (iii) the total amount of ^{239}Pu attached to Ic and If colloids in the EBS is reapportioned so that 99.832 percent of the total ^{239}Pu is attached to slow colloids (i.e., the new Ic colloids) upon entry into the UZ and the remaining 0.168 percent is attached to fast colloids (i.e., the new If colloids) upon entry into the UZ. Because the mass of ^{239}Pu attached to glass colloids in the EBS is much greater than the mass of ^{239}Pu attached to ferrous colloids in the EBS, the mass of ^{239}Pu attached to slow colloids entering the UZ is effectively the same as the mass of ^{239}Pu attached to glass colloids leaving the EBS. However, because the mass of ^{239}Pu attached to glass colloids in the EBS is much greater than the mass of ^{239}Pu attached to ferrous colloids in the EBS, the indicated reapportioning results in the release of ^{239}Pu attached to fast colloids into the UZ having very different properties from the release of ^{239}Pu attached to ferrous colloids out of the EBS.

The uncertainty and sensitivity analyses for the time-dependent release rates (*UZIC239*, g/yr) and cumulative releases (*UZIC239C*, g) over the time interval [0, 20,000 yr] for the movement of ^{239}Pu irreversibly attached to slow (i.e., Ic) colloids from the UZ to the SZ resulting from the early failure of one DS above a CDSP WP in percolation bin 3 under dripping conditions are summarized in Figures K5.4.1-1 and K5.4.1-2.

Retardation of slow colloids in the UZ is illustrated by Figure K5.4.1-3. By 10,000 yr after the breach in the WP, most of the ^{239}Pu that entered the UZ attached to slow colloids has exited the UZ. Consequently, retardation in the UZ is not sufficient to permit significant reduction in ^{239}Pu due to radioactive decay. As a result, the behavior of *UZIC239* and *UZIC239C* shown in Figures K5.4.1-1 and K5.4.1-2 is essentially the same as the behavior of *ESIC239* and *ESIC239C* shown in Figures K5.3.1-1 and K5.3.1-2. Because of this similarity, the discussions for Figures K5.3.1-1 and K5.3.1-2 are also applicable to Figures K5.4.1-1 and K5.4.1-2.

The results for *UZIC239* in Figure K5.4.1-1a,c,e are choppier than the corresponding results for *ESIC239* in Figure K5.3.1-1a,c,e. This choppiness results from the use of a particle tracking algorithm to numerically solve the radionuclide transport equations for the UZ. Despite the choppiness of the results, in Section 7.3.5 the UZ transport model is shown to be stable in the sense that increasing the number of particles does not change the model results. The use of a different numerical solution algorithm may result in less choppy results for *UZIC239*. One

potential way to reduce the choppiness in *UZIC239* and other similar results is to incorporate a smoothing procedure into the particle tracking algorithm that produces a locally weighted average (e.g., with a Gaussian kernel function) of time-dependent releases into the SZ. The results for *UZIC239C* in Figure K5.4.1-1b,d,f are much smoother than the results for *UZIC239* because of the smoothing effect of the integration that defines *UZIC239C*.

Movement of ^{239}Pu Irreversibly Attached to Fast (i.e., If) Colloids: *UZIF239* and *UZIF239C*. The uncertainty and sensitivity analyses for the time-dependent release rates (*UZIF239*, g/yr) and cumulative releases (*UZIF239C*, g) over the time interval [0, 20,000 yr] for the movement of ^{239}Pu irreversibly attached to fast (i.e., If) colloids from the UZ to the SZ resulting from the early failure of one DS above a CDSP WP in percolation bin 3 under dripping conditions are summarized in Figures K5.4.1-4 and K5.4.1-5.

Very little retardation of fast colloids takes place in the UZ (Figure K5.4.1-6). As a result, the behavior of *UZIF239* and *UZIF239C* shown in Figures K5.4.1-4 and K5.4.1-5 has essentially the same structure as the behavior of *ESIC239* and *ESIC239C* shown in Figures K5.3.1-1 and K5.3.1-2 for ^{239}Pu irreversibly attached to glass (i.e., Ic) colloids in the EBS. The behavior of *ESIC239* and *ESIC239C* rather than the behavior of *ESIF239* and *ESIF239C* is relevant to the behavior of *UZIF239* and *UZIF239C* because the previously described reapportioning of ^{239}Pu onto slow and fast colloids upon entry into the UZ results in ^{239}Pu irreversibly attached to glass colloids in the EBS being the primary source of ^{239}Pu irreversibly attached to fast colloids in the EBS. Because of this similarity, the discussions for Figures K5.3.1-1 and K5.3.1-2 are also applicable to Figures K5.4.1-1 and K5.4.1-2.

As previously discussed for *UZIC239* in conjunction with Figure K5.4.1-1a,c,f, the choppiness of the values for *UZIF239* in Figure K5.4.1-4a,c,e results from the use of a particle tracking algorithm to solve the radionuclide transport equations for the UZ.

Movement of Dissolved ^{237}Np: *UZNP237* and *UZNP237C*. The uncertainty and sensitivity analyses for the time-dependent release rates (*UZNP237*, g/yr) and cumulative releases (*UZNP237C*, g) over the time interval [0, 20,000 yr] for the movement of dissolved ^{237}Np from the UZ to the SZ resulting from the early failure of one DS above a CDSP WP in percolation bin 3 under dripping conditions are summarized in Figures K5.4.1-7 and K5.4.1-8.

Dissolved ^{237}Np is somewhat retarded in the UZ (Figure K5.4.1-9). As demonstrated by these scatterplots, by 10,000 years, roughly half or more of the dissolved ^{237}Np that has entered the UZ from the EBS has also moved from the UZ to the SZ. As a result, the mass of dissolved ^{237}Np that leaves the UZ is primarily determined by the mass of dissolved ^{237}Np entering the UZ. Consequently the behavior of *UZNP237* and *UZNP237C* shown in Figures K5.4.1-7 is essentially the same as the behavior of *ESNP237* and *ESNP237C* shown in Figures K5.3.1-5, and the dominant variables in the regression models for *UZNP237* and *UZNP237C* (Figure K5.4.1-8) are generally the same as those in the regression model for *ESNP237* and *ESNP237C* (Figure K5.3.1-6). Because of this similarity, the discussions for Figures K5.3.1-5 and K5.3.1-6 are also applicable to Figures K5.4.1-7 and K5.4.1-8.

As previously discussed for *UZIC239* in conjunction with Figure K5.4.1-1a,c,f, the choppiness of the values for *UZNP237* in Figure K5.4.1-7a,c,e results from the use of a particle tracking algorithm to solve the radionuclide transport equations for the UZ.

Movement of Dissolved ^{239}Pu: *UZPU239* and *UZPU239C*. The uncertainty and sensitivity analyses for the time-dependent release rates (*UZPU239*, g/yr) and cumulative releases (*UZPU239C*, g) over the time interval [0, 20,000 yr] for the movement of dissolved ^{239}Pu from the UZ to the SZ resulting from the early failure of one DS above a CDSP WP in Bin 3 under dripping conditions are summarized in Figures K5.4.1-10 and K5.4.1-11.

Some retardation of dissolved ^{239}Pu takes place in the UZ (Figure K5.4.1-12). For example, *UZKDPUDT* (sorption coefficient for plutonium in devitrified tuff units of UZ, mL/g) appears in the analyses for *UZPU239* and *UZPU239C* with a negative PRCC (Figure K5.4.1-10e,f), and *UZTORRG3* (tortuosity in rock group 3 of the UZ, dimensionless ; as sampled, *UZTORRG3* is actually the logarithm of the indicated tortuosity) also appears in the analysis for *UZPU239C* with a negative PRCC (Figure K5.4.1-10f). These effects result because increasing *UZKDPUDT* results in more retardation of ^{239}Pu in the UZ and increasing *UZTORRG3* results in slower water flow in the UZ. However, the effects associated with *UZKDPUDT* and *UZTORRG3* are small. For example, the inclusion of *UZKDPUDT* in the regression model for *UZPU239* at 10,000 years raises the R^2 value from 0.78 to 0.83 (Figure K5.4.1-11a), and the inclusion of *UZKDPUDT* in the regression model for *UZPU239C* at 10,000 yr raises the R^2 value from 0.73 to 0.80 (Figure K5.4.1-11b). Further, *UZTORRG3* is not selected in any of the regression analyses in Figure K5.4.1-11a,b.

Overall, the behavior of *UZPU239* and *UZPU239C* shown in Figures K5.4.1-10 and K5.4.1-11 is very similar to the behavior of *ESPU239* and *ESPU239C* shown in Figures K5.3.1-7 and K5.3.1-8. Because of this similarity, the discussions for Figures K5.3.1-7 and K5.3.1-8 are also applicable to Figures K5.4.1-10 and K5.4.1-11.

Movement of Dissolved ^{99}Tc: *UZTC99* and *UZTC99C*. The uncertainty and sensitivity analyses for the time-dependent release rates (*UZTC99*, g/yr) and cumulative releases (*UZTC99C*, g) over the time interval [0, 20,000 yr] for the movement of dissolved ^{99}Tc from the UZ to the SZ resulting from the early failure of one DS above a CDSP WP in percolation bin 3 under dripping conditions are summarized in Figures K5.4.1-13 and K5.4.1-14.

The release of ^{99}Tc from the EBS takes place very rapidly (Figure K5.3.1-9a,c). The movement of ^{99}Tc through the UZ takes place at a slower rate. For example, the very small values for *ESTC99* that result at later times for some sample elements (Figure K5.3.1-9a,c) are not present in the values for *UZTC99* (Figure K5.4.1-13a,c) because of the slowing and spreading effect of transport in the UZ. However, almost all ^{99}Tc released to the UZ ultimately is released to the SZ (Figure K5.4.1-15).

The dominant variable with respect to the uncertainty associated with *UZTC99* is *INFIL* (infiltration level). As shown by the PRCCs in Figure K5.4.1-13e, increasing *INFIL* initially has a positive effect on *UZTC99* and then at later times increasing *INFIL* has a negative effect on *UZTC99*. This pattern of effects results because large values for *INFIL* increase water flow in the

EBS and UZ, which speeds ^{99}Tc transport through the EBS and UZ and results in the positive effect for *INFIL* at early times. However, the effect of speeding ^{99}Tc transport through the EBS and UZ at early times is to reduce the amount of ^{99}Tc available to be released to the SZ at later times, which is why *INFIL* has a negative effect on *UZTC99* at later times. The regressions in Figure K5.4.1-14a were performed during the later time period (i.e., after 2000 years) in which *INFIL* has a negative effect on *UZTC99*. In particular, the regression models for *UZTC99* containing only *INFIL* have R^2 values of 0.59, 0.58 and 0.46, respectively, at 3,000, 5,000 and 10,000 yr. After *INFIL*, the regressions select a number of additional variables, with most of these variables having been previously discussed in conjunction with the analyses for *ESTC99* in Figures K5.3.1-9 and K5.3.1-9. The final regression models for *ESTC99* have R^2 values of 0.81, 0.68 and 0.62, respectively, at 3,000, 5,000 and 10,000 yr. The decreasing R^2 values with time probably results for a lack of resolution in the calculation of the small values for *ESTC99* that are present at later times.

With the exception of the positive effect of *INFIL* on *UZTC99C*, the sensitivity analyses for *UZTC99C* in Figures K5.4.1-13 and K5.4.1-14 are generally the same as the sensitivity analyses for *ESTC99C* in Figures K5.3.1-9 and K5.3.1-10. This similarity results because most ^{99}Tc releases to the UZ are transported rapidly and with little reduction to the SZ (Figure K5.4.1-15). The increased importance for *INFIL* with respect to *UZTC99C* over its importance with respect to *ESTC99C* results from the greater transport distances associated with the UZ relative to the transport distances associated with the SZ.

As previously discussed for *UZIC239* in conjunction with Figure K5.4.1-1a,c,f, the choppiness of the values for *ESTC99* in Figure K5.4.1-13a,c,f results from the use of a particle tracking algorithm to solve the radionuclide transport equations for the UZ.

K5.4.2 Early Failure Scenario Classes: Release from Unsaturated Zone (UZ) for Early Failures Considered in Sections K5.3.2- K5.3.12

Results specific to movement through the UZ for the early failures considered in Sections K5.3.2 – K5.3.12 are similar to the results presented in Section K5.3.1 for the early failure of one DS above a CDSP WP in percolation bin 3 under dripping conditions and also to the results presented in Section K6.4.1 for an igneous intrusive event at 10 yr. For this reason, uncertainty and sensitivity analysis results for radionuclide movement in the UZ are not presented for the early failures considered in Sections K5.3.2 – K5.3.12.

K5.5 Early Failure Scenario Classes: Release from Saturated Zone (SZ)

This section contains analysis results for releases from the SZ over the time interval [0, 20,000 yr] resulting from early failure of one DS over a CDSP WP in percolation bin 3 under dripping conditions (Section 5.5.1). Analysis results for other early failures are discussed in Section K5.5.2.

K5.5.1 Early Failure Scenario Classes: Release from Saturated Zone (SZ) over the Time Interval [0, 20,000 yr] for Early Drip Shield Failure above a CDSP WP

This section presents summaries of the uncertainty and sensitivity analyses for radionuclide movement in the SZ without discussion. The same processes operate in the SZ for all scenario classes. Thus, the sensitivity analysis results for the SZ are similar for all scenario classes. However, somewhat sharper results are obtained for the scenario classes that involve large releases from the EBS. In particular, the numerical noise associated with the solution of the transport equations in the UZ for very low radionuclide concentrations is reduced when larger releases from the EBS are under consideration. For this reason, the presentation and discussion of detailed sensitivity results for radionuclide transport in the SZ is delayed to Section K6.5.1, where results associated with the igneous intrusive scenario class are presented and discussed.

Movement of ^{239}Pu Irreversibly Attached to Slow (i.e., Ic) Colloids: *SZIC239* and *SZIC239C*. The uncertainty and sensitivity analyses for the time-dependent release rates (*SZIC239*, g/yr) and cumulative releases (*SZIC239C*, g) over the time interval [0, 20,000 yr] for the movement of ^{239}Pu irreversibly attached to slow (i.e., Ic) colloids across a subsurface plane at the location of the RMEI resulting from the early failure of one DS above a CDSP WP in percolation bin 3 under dripping conditions are summarized in Figure K5.5.1-1. Discussion is provided in conjunction with Figures K6.5.1-1, K6.5.1-2 and K6.5.1-3.

Movement of ^{239}Pu Irreversibly Attached to Fast (i.e., If) Colloids: *SZIF239* and *SZIF239C*. The uncertainty and sensitivity analyses for the time-dependent release rates (*SZIF239*, g/yr) and cumulative releases (*SZIF239C*, g) over the time interval [0, 20,000 years] for the movement of ^{239}Pu irreversibly attached to fast (i.e., If) colloids across a subsurface plane at the location of the RMEI resulting from the early failure of one DS above a CDSP WP in percolation bin 3 under dripping conditions are summarized in Figure K5.5.1-2. Discussion is provided in conjunction with Figures K6.5.1-4, K6.5.1-5 and K6.5.1-6.

Movement of Dissolved ^{237}Np: *SZNP237* and *SZNP237C*. The uncertainty and sensitivity analyses for the time-dependent release rates (*SZNP237*, g/yr) and cumulative releases (*SZNP237C*, g) over the time interval [0, 20,000 yr] for the movement of dissolved ^{237}Np across a subsurface plane at the location of the RMEI resulting from the early failure of one DS above a CDSP WP in percolation bin 3 under dripping conditions are summarized in Figure K5.5.1-3. Discussion is provided in conjunction with Figures K6.5.1-7, K6.5.1-8 and K6.5.1-9.

Movement of Dissolved ^{239}Pu: *SZPU239* and *SZPU239C*. The uncertainty and sensitivity analyses for the time-dependent release rates (*SZPU239*, g/yr) and cumulative releases (*SZPU239C*, g) over the time interval [0, 20,000 yr] for the movement of dissolved ^{239}Pu across a subsurface plane at the location of the RMEI resulting from the early failure of one DS above a CDSP WP in percolation bin 3 under dripping conditions are summarized in Figure K5.5.1-4. Discussion is provided in conjunction with Figures K6.5.1-10, K6.5.1-11 and K6.5.1-12.

Movement of Dissolved ^{99}Tc: *SZTC99* and *SZTC99C*. The uncertainty and sensitivity analyses for the time-dependent release rates (*SZTC99*, g/yr) and cumulative releases (*SZTC99C*, g) over

the time interval [0, 20,000 yr] for the movement of dissolved ^{99}Tc across a subsurface plane at the location of the RMEI resulting from the early failure of one DS above a CDSP WP in percolation bin 3 under dripping conditions are summarized in Figure K5.5.1-5. Discussion is provided in conjunction with Figures K6.5.1-13, K6.5.1-14 and K6.5.1-5.

K5.5.2 Early Failure Scenario Classes: Release from Saturated Zone (SZ) for Early Failures Considered in Sections K5.3.2- K5.3.12

Results specific to movement through the SZ for the early failures considered in Sections K5.3.2 – K5.3.12 are similar to the results presented in Section K5.5.1 for the early failure of one DS above a CDSP WP in percolation bin 3 under dripping conditions, and also to the results presented in Section K6.5.1 for an igneous intrusive event at 10 yr. For this reason, uncertainty and sensitivity analysis results for radionuclide movement in the SZ are not presented here for the early failures considered in Sections K5.3.2 – K5.3.12.

K5.6 Early Failure Scenario Classes: Dose to Reasonably Maximally Exposed Individual

This section contains analysis results for the dose to a RMEI (RMEI) over the time interval [0, 20,000 yr] resulting from an early DS failure over a CDSP WP in percolation bin 3 under dripping conditions (Section K5.6.1). Analysis results for other early failures are discussed in Section K5.6.2.

K5.6.1 Early Failure Scenario Classes: Dose to Reasonably Maximally Exposed Individual over the Time Interval [0, 20,000 yr] for Early Drip Shield Failure above a CDSP WP

This section presents summaries of the uncertainty and sensitivity analyses for dose to the RMEI without discussion. The same processes affect the conversion of radionuclide concentration in groundwater to dose to the RMEI for all scenario classes. Thus, the sensitivity analysis results for dose to the RMEI are similar for all scenario classes. However, somewhat sharper results are obtained for the scenario classes that involve large releases from the EBS. In particular, the numerical noise associated with the solution of the transport equations in the UZ and SZ for very low radionuclide concentrations is reduced when larger releases from the EBS are under consideration. For this reason, the presentation and discussion of detailed sensitivity results for dose to the RMEI is delayed to Section K6.6.1, where results associated with the igneous intrusive scenario class are presented and discussed.

Dose to RMEI from ^{239}Pu Irreversibly Attached to Slow (i.e., Ic) Colloids: *DOIC239*. The uncertainty and sensitivity analyses for dose to the RMEI (*DOIC239*, mrem/yr) over the time interval [0, 20,000 yr] for the movement of ^{239}Pu irreversibly attached to slow (i.e., Ic) colloids across a subsurface plane at the location of the RMEI resulting from the early failure of one DS above a CDSP WP in percolation bin 3 under dripping conditions are summarized in Figure K5.6.1-1. Discussion is provided in conjunction with Figures K6.6.1-1 and K6.6.1-2.

Dose to RMEI from ^{239}Pu Irreversibly Attached to Fast (i.e., Ic) Colloids: *DOIF239*. The uncertainty and sensitivity analyses for dose to the RMEI (*DOIF239*, mrem/yr) over the time

interval [0, 20,000 yr] for the movement of ^{239}Pu irreversibly attached to fast (i.e., Ic) colloids across a subsurface plane at the location of the RMEI resulting from the early failure of one DS above a CDSP WP in percolation bin 3 under dripping conditions are summarized in Figure K5.6.1-2. Discussion is provided in conjunction with Figures K6.6.1-3 and K6.6.1-4.

Dose to RMEI from Dissolved ^{237}Np: *DONP237*. The uncertainty and sensitivity analyses for dose to the RMEI (*DONP237*, mrem/yr) over the time interval [0, 20,000 yr] for the movement of dissolved ^{237}Np across a subsurface plane at the location of the RMEI resulting from the early failure of one DS above a CDSP WP in percolation bin 3 under dripping conditions are summarized in Figure K5.6.1-3. Discussion is provided in conjunction with Figures K6.6.1-5 and K6.6.1-6.

Dose to RMEI from Dissolved ^{239}Pu: *DOPU239*. The uncertainty and sensitivity analyses for dose to the RMEI (*DOPU239*, mrem/yr) over the time interval [0, 20,000 yr] for the movement of dissolved ^{239}Pu across a subsurface plane at the location of the RMEI resulting from the early failure of one DS above a CDSP WP in percolation bin 3 under dripping conditions are summarized in Figure K5.6.1-4. Discussion is provided in conjunction with Figures K6.6.1-7 and K6.6.1-8.

Dose to RMEI from Dissolved ^{99}Tc: *DOTC99*. The uncertainty and sensitivity analyses for dose to the RMEI (*DOTC99*, mrem/yr) over the time interval [0, 20,000 yr] for the movement of dissolved ^{99}Tc across a subsurface plane at the location of the RMEI resulting from the early failure of one DS above a CDSP WP in percolation bin 3 under dripping conditions are summarized in Figure K5.6.1-5. Discussion is provided in conjunction with Figures K6.6.1-9 and K6.6.1-10.

K5.6.2 Early Failure Scenario Classes: Dose to Reasonably Maximally Exposed Individual for Early Failures Considered in Sections K5.3.2- K5.3.12

Results specific to dose to the RMEI for the early failures considered in Sections K5.3.2 - K5.3.12 are similar to the results presented in Section K5.6.1 for the early failure of one DS above a CDSP WP in percolation bin 3 under dripping conditions, and also to results presented in Section K6.6.1 for an igneous intrusive event at 10 yr. For this reason, uncertainty and sensitivity analysis results for radionuclide movement in the UZ are not presented for the early failures considered in Sections K5.3.2 – K5.3.12.

K5.7 Early Failure Scenario Classes: Expected Dose to Reasonably Maximally Exposed Individual

This section contains analysis results for expected dose to a RMEI (RMEI) resulting from early failures. Expected dose is computed as discussed in Section J6.3. The following cases are presented:

- Expected dose to the RMEI for the time intervals [0, 20,000 yr] and [0, 1,000,000 yr] resulting from early DS failure (Section 5.7.1);

- Expected dose to the RMEI for the time intervals [0, 20,000 yr] and [0, 1,000,000yr] resulting from early WP failure (Section 5.7.2);

- Expected dose to the RMEI for the time intervals [0, 20,000 yr] and [0, 1,000,000 yr] resulting from early failures (considering both DSs and WPs) (Section 5.7.3);

- Expected dose to the RMEI for the time intervals [0, 20,000 yr] and [0, 1,000,000 yr] resulting from early failures (considering both DSs and WPs) and nominal processes (Section 5.7.4).

K5.7.1 Early Failure Scenario Classes: Expected Dose to Reasonably Maximally Exposed Individual from Early Drip Shield Failure

Expected Dose to RMEI over [0, 20,000 yr]: *EXPDOSE*. The uncertainty and sensitivity analyses for expected dose to the RMEI (*EXPDOSE*, mrem/yr) over the time interval [0, 20,000 years] resulting from early DS failure are summarized in Figures K5.7.1-1 and K5.7.1-2. There is sharp peak in *EXPDOSE* prior to 1000 yr resulting from the release of ^{99}Tc. At the time of this peak, maximum values for *EXPDOSE* are in the vicinity of 0.01 mrem/yr, although the values for most sample elements are considerably smaller (Figure K5.7.1-1a,b). After the early peak, *EXPDOSE* has values in a range from 10^{-7} to 10^{-3} mrem/yr.

The PRCCs in Figure K5.7.1-1c indicate that the uncertainty in *EXPDOSE* is dominated by *PROBDSEF* (probability that a randomly selected DS will experience an early failure), with the value for *EXPDOSE* increasing as *PROBDSEF* increases. This effect results because increasing *PROBDSEF* increases the expected number of DSs that experience early failure and hence increases *EXPDOSE*.

In addition to *PROBDSEF*, smaller effects are indicated for *SZFIPOVO* (flowing interval porosity in the volcanic unit of the SZ), *SZGWSPDM* (groundwater specific discharge multiplier; as sampled, *SZGWSPDM* is actually the logarithm of the indicated multiplier), *SEEPUNC* (pointer variable used to determine local seepage rates), *THERMCON* (host rock thermal conductivity level), and *INFIL* (infiltration level) (Figure K5.7.1-1c). A negative effect is indicated for *SZFIPOVO* at early times (i.e., prior to 3,000 yr), with this effect then going to zero. This effect results because increasing *SZFIPOVO* increases the time required for the initial releases of mobile species such as ^{99}Tc to reach the location of the RMEI. The positive effect associated with *SZGWSPDM* results from increasing the flow velocity in the SZ, which in turn moves radioactive species more rapidly to the location of the RMEI. This effect is especially pronounced at early times (i.e., prior to 2000 yr) because increasing *SZGWSPDM* decreases the time of first arrival of radioactive species at the location of the RMEI. Both *THERMCON* and *INFIL* have small positive effects on *EXPDOSE* at early times (i.e., prior to 3,000 yr). These effects are possibly related to the influence of these variables on repository temperature and hence the time at which release from the EBS can begin. Specifically, increasing *THERMCON* and *INFIL* tends to reduce EBS temperatures and thus reduce the time at which releases from the EBS can begin. After 3,000 yr, *THERMCON* has no effect on *EXPDOSE*; however, *INFIL* continues to have a small effect, with effect probably resulting from increased water flow through the EBS and UZ that results as *INFIL* increases in value.

More detailed sensitivity analyses for *EXPDOSE* are provided by the regression analyses in Figure K5.7.1-2a. The dominant effect of *PROBDSEF* on the uncertainty in *EXPDOSE* is indicated by R^2 values of 0.74, 0.76 and 0.69 for the regressions containing only *PROBDSEF* at 3,000, 5,000 and 10,000 yr. After *PROBDSEF*, the most important variable is *SEEPUNC*. However the incremental effect associated with *SEEPUNC* is small as the R^2 values for the regression models containing both *PROBDSEF* and *SEEPUNC* are 0.79, 0.82 and 0.75.

After *PROBDSEF* and *SEEPUNC*, smaller effects are indicated for a number of variables (Figure K5.7.1-2a). For example, the following additional variables are indicated as affecting *EXPDOSE* at 10,000 yr: *INFIL*, *SEEPPRM* (mean fracture permeability in lithophysal rock units, m^2; as sampled, *SEEPPRM* is actually the logarithm of the indicated permeability), *ALPHAL* (capillary strength parameter in lithophysal rock units), *MICTC99* (dose conversion factor for ^{99}Tc for modern interglacial climate, (rem/yr)/(pCi/L)), *MICPU239* (dose conversion factor for ^{239}Pu for modern interglacial climate, (rem/yr)/(pCi/L)), *PHCSS* (pointer variable used to determine pH in Cell 1 of CSNF WP under liquid influx conditions), *CPUCOLWF* (concentration of irreversibly attached plutonium on stable glass colloids, mol/L), *SZCOLRAL* (colloid retardation factor in alluvial unit of SZ, dimensionless; as sampled, *SZCOLRAL* is actually the logarithm of the indicated retardation factor), *RHMU0* (scale factor used to represent uncertainty in chloride concentration in drift waters for relative humidities in the range [0, 0.2]; as sampled, *RHMU0* is actually the logarithm of the indicated scale factor), and *DSFLUX* (flux splitting factor for DS). Specifically, the positive effect associated with *INFIL* results from increasing water flux through the EBS; the negative effects associated with *SEEPPRM* and *ALPHAL* result from increasing water diversion around the EBS; the positive effects associated with *MICTC99* and *MICPU239* result from increasing the received dose for a given exposure level; and the remaining variables have very small effects that may be real or may be spurious.

The dominant effect of *PROBDSEF* is readily apparent in the scatterplot in Figure K5.7.1-2b. Further, the smaller effects of *SEEPUNC* and *INFIL* can be seen in the scatterplots in Figure K5.7.1-2b,c.

It may seen strange that several of the variables identified in the analysis with PRCCs (i.e., *SZFIPOVO*, *SZGWSPDM*, *THERMCON*) in Figure K5.7.1-1c do not appear in the regressions in Figure K5.7.1-2a. However, the times at which these variables have identifiable effects on *EXPDOSE* in Figure K5.7.1-1c are not the times at which the regressions in Figure K5.7.1-2a are performed.

Expected Dose to RMEI over [0, 1,000,000 yr]: *EXPDOSE*. The uncertainty and sensitivity analyses for expected dose to the RMEI (*EXPDOSE*, mrem/yr) over the time interval [0, 1,000,000 years] resulting from early DS failure are summarized in Figures K5.7.1-3 and K5.7.1-4. The time dependent results for *EXPDOSE* tend to decrease until about 200,000 yr and then level off (Figure K5.7.1-a,b). This decrease is probably due to the decay of ^{239}Pu, which has a half life of 24,100 yr. The values for *EXPDOSE* are bounded above by 0.01 mrem/yr and, after 200,000 yr, by 0.001 mrem/yr.

The sensitivity analyses for the time interval [0, 1,000,000 yr] are similar to those for the time interval [0, 20,000 yr]. Specifically, the sensitivity analysis with PRCCs for [0, 1,000,000 yr] in Figure K5.7.1-3c identifies the following variables as influencing the uncertainty in *EXPDOSE*:

PROBDSEF (probability that a randomly selected DS will experience an early failure), *INFIL* (infiltration level), *SEEPPRM* (mean fracture permeability in lithophysal rock units, m^2; as sampled, *SEEPPRM* is actually the logarithm of the indicated permeability), *SZFIPOVO* (flowing interval porosity in the volcanic unit of the SZ), *SEEPUNC* (pointer variable used to determine local seepage rates), and *SZGWSPDM* (groundwater specific discharge multiplier; as sampled, *SZGWSPDM* is actually the logarithm of the indicated multiplier). Similarly, the sensitivity analysis with PRCCs for [0, 20,000 yr] in Figure K5.7.1-1c identifies the following variables as influencing the uncertainty in *EXPDOSE*: *PROBDSEF*, *SZFIPOVO*, *SZGWSPDM*, *SEEPUNC*, *THERMCON* (host rock thermal conductivity level), and *INFIL*. For both time periods, *PROBDSEF* is the dominant contributor to the uncertainty in *EXPDOSE*, with the other variables making much smaller contributions to the uncertainty in *EXPDOSE*. The PRCC plots are constrained to contain a maximum of 6 variables. As a result, the slight differences in the variables shown in Figures K5.7.1-1c and K5.7.1-3c results from slight variations in the importance of individual variables over the time intervals under consideration.

More detailed sensitivity analyses for the time interval [0, 1,000,000 yr] are provided by the regressions in Figure K5.7.1-4a. As for the regressions in Figure K5.7.1-2a, the dominant variable is *PROBDSEF*. Specifically, the dominant effect of *PROBDSEF* on the uncertainty in *EXPDOSE* is indicated by R^2 values of 0.44, 0.51 and 0.48 for the regressions containing only *PROBDSEF* at 50,000, 200,000 and 500,000 yr. These values are lower than the corresponding R^2 values of 0.74, 0.76 and 0.69 obtained in the analyses in K5.7.1-2a at 3,000, 5,000 and 10,000 yr , which suggests that more variables are having small effects on the uncertainty in *EXPDOSE* at later times than is the case for the first 20,000 yr. This is borne out by the large number of variables indicated as having small effects on *EXPDOSE* in the regression analyses in Figure K5.7.1-4a. After *PROBDSEF*, the next most important variable in all three regressions is *INFIL*, with *EXPDOSE* tending to increase as *INFIL* increases as a result of increased water flow through the EBS and UZ. Together, *PROBDSEF* and *INFIL* result in regressions with R^2 values of 0.55, 0.60 and 0.61 at 50,000, 200,000 and 500,000 yr.

After *PROBDSEF* and *INFIL*, all three regressions select *SZGWSPDM*, *SEEPUNC* and *SEEPPRM* as the next three variables to add to the regression models, although not necessarily in the same order (Figure K5.7.1-4a). Addition of these three variables brings the R^2 values up to 0.74, 0.75 and 0.73 at 50,000, 200,000 and 500,000 yr. As previously discussed, *SZGWSPDM* has a positive effect on *EXPDOSE* as a result of speeding up flow in the SZ; *SEEPUNC* has a positive effect on *EXPDOSE* as a result of increasing water flow through the EBS; and *SEEPPRM* has a negative effect on *EXPDOSE* as a result of increasing water flow around the EBS and thus reducing water flow through the EBS.

After *PROBDSEF*, *INFIL*, *SZGWSPDM*, *SEEPUNC* and *SEEPPRM*, the regressions at 50,000, 200,000 and 500,000 yr add 9, 9 and 10 additional variables, respectively, and produce models with R^2 values of 0.84, 0.85 and 0.86 (Figure K5.7.1-4a). Thus, as noted earlier, a large number of variables are having small effects on the uncertainty in *EXPDOSE* at later times.

The dominant effect of *PROBDSEF* on the uncertainty in *EXPDOSE* can also been seen in the scatterplot in Figure K5.7.1-4b. In contrast, the much smaller effects of *INFIL* and *SZGWSPDM* on the uncertainty in *EXPDOSE* can been in the scatterplots in Figure K5.7.1-4c,d.

K5.7.2 Early Failure Scenario Classes: Expected Dose to Reasonably Maximally Exposed Individual from Early Waste Package Failure

Expected Dose to RMEI over [0, 20,000 yr]: *EXPDOSE*. The uncertainty and sensitivity analyses for expected dose to the RMEI (*EXPDOSE*, mrem/yr) over the time interval [0, 20,000 yr] resulting from early WP failure are summarized in Figures K5.7.2-1 and K5.7.2-2. There is a sharp peak in *EXPDOSE* between 1,000 and 2000 yr resulting from the release of ^{99}Tc from the failure of CDSP WPs (Figure K5.7.1-2a,b). At the time of this peak, maximum values for *EXPDOSE* are in the vicinity of 0.1 mrem/yr, although the values for most sample elements are considerably smaller. After this initial early peak, *EXPDOSE* has values in a range from approximately 10^{-5} to 10^{-3} mrem/yr until a time of about 10, 000 yr.

At 10,000 yr, there is a sharp jump in the values for *EXPDOSE* (Figure K5.7.1-2a,b). This jump results from the arrival of radionuclide releases at the location of the RMEI that result from the failure of CSNF WPs. The CSNF WPs are hotter than the CDSP WPs, with the result that releases from CSNF WPs are delayed until both the WP temperature falls below 100°C and the relative humidity interior to these packages reaches 95 percent, at which time diffusive transport begins. The jump in *EXPDOSE* between approximately 9000 and 14,000 yr results from the arrival of ^{99}Tc at the location of the RMEI. After this jump, the values for *EXPDOSE* again decrease as the pulse of ^{99}Tc passes.

This bimodal behavior of *EXPDOSE* with different peaks for the two waste types does not occur for early DS failure (compare Figures K5.7.1-1a,b and K5.7.2-2a,b). Early DS failure is assumed to result in WP failure only if the failed DS is experiencing dripping conditions; otherwise, there is no WP failure and hence no radionuclide release. Because all failed WPs are in dripping conditions, water flows into every failed WP as soon as WP temperature falls below 100°C and advective transport occurs immediately, with the result that there is little temporal variability in the start of radionuclide releases from the EBS for different WP types.

The PRCCs in Figure K5.7.2-1c indicate that the uncertainty in *EXPDOSE* is dominated by *PROBWPEF* (probability that a randomly selected WP will experience an early failure), with the value for *EXPDOSE* increasing as *PROBWPEF* increases. This effect results because increasing *PROBWPEF* increases the expected number of WPs that experience early failure and hence increases *EXPDOSE*. The PRCCs for *PROBWPEF* decrease in value over the period from approximately 9000 to 14,000 yr as a result of the noise introduced into the analysis as a result of the pulse releases arriving from the failed CSNF WPs.

In addition to *PROBWPEF*, smaller effects are indicated for *INFIL* (infiltration level), *THERMCON* (host rock thermal conductivity level), *SZFIPOVO* (flowing interval porosity in the volcanic unit of the SZ), *SZGWSPDM* (groundwater specific discharge multiplier; as sampled, *SZGWSPDM* is actually the logarithm of the indicated multiplier), and *DSNFMASS* (scale factor used to characterize uncertainty in the amount of DSNF contained in CDSP WPs) (Figure K5.7.2-1c). The effects of *INFIL*, *SZFIPOVO* and *SZGWSPDM* are the same as previously discussed in conjunction with Figure K5.7.1-1c. The effect of *THERMCON* is similar, although more pronounced. Increasing *THERMCON* leads to lower drift temperatures and earlier arrival of seepage waters, and thus to earlier beginning of diffusive transport. This effect is evident in the positive correlation between *THERMCON* and *EXPDOSE* between 0 yr and

1,500 yr. However, between 2,500 yr and 9,500 yr, the correlation becomes negative. This change in correlation results from the effect of temperature on waste form degradation. Increasing temperature increases the dissolution rate of the HLW in CDSP WPs (BSC 2004 ANL-EBS-MD-000016 REV 02, [DIRS 169988], Section 6.5.2.1). Consequently, as *THERMCON* increases, temperatures decrease and HLW degradation slows, resulting in less radionuclides available for mobilization and transport, and in turn reducing *EXPDOSE*. This pattern repeats for the CSNF waste, which starts diffusive transport at about 9,500 yr. The positive effect associated with *DSNFMASS* results from increasing the amount of ^{99}Tc in CDSP WPs and hence the dose from ^{99}Tc that results from the failure of these WPs.

More detailed sensitivity analyses for *EXPDOSE* are provided by the regression analyses in Figure K5.7.2-2a. The dominant effect of *PROBWPEF* on the uncertainty in *EXPDOSE* is indicated by R^2 values of 0.62, 0.79 and 0.47 for the regressions containing only *PROBWPEF* at 3,000, 5,000 and 10,000 yr.

As for the PRCCs for *PROBWPEF* in Figure K5.7.2-1c, the R^2 value for the regression at 10,000 years decreases in value as a result of the noise introduced into the analysis by the pulse releases arriving from the failed CSNF WPs over the period from approximately 9000 to 14,000 yr. Because of this noise, the final regression model at 10,000 contains only 5 variables and has an R^2 value of 0.67. However, a clearer view of what is driving the uncertainty in *EXPDOSE* at 10,000 yr is provided by the scatterplots in Figure K5.7.2-2b,c,d. Specifically, the uncertainty in *EXPDOSE* is still clearly dominated by *PROBWPEF* (Figure K5.7.2-2b), with smaller contributions to this uncertainty from *INFIL* (Figure K5.7.2-2c) and *THERMCON* (Figure K5.7.2-2d). The scatterplot for *PROBWPEF* (Figure K5.7-2b) shows an interesting pattern in that it contains two separate populations of points that each increase monotonically with *PROBWPEF*. The upper population of points consists of realizations in which the CSNF WPs in one or more percolation bins have begun diffusive transport (relative humidity interior to the WP exceeds 95 percent) by 10,000 yr. Because infiltration rates and temperatures vary between percolation bins, the time at which diffusive transport begins also varies, with most CSNF WPs beginning diffusive transport between 9,000 yr and 14,000 yr, whereas CDSP WPs begin diffusive transport between 500 yr and 3,000 yr. The differences are also apparent in Figure K5.7.2-1a as two jumps in expected dose corresponding to the occurrence of dose from each of the two WP types.

Figure K5.7.2-2c indicates that the expected dose at 10,000 yr decreases as *INFIL* increases. As *INFIL* increases, percolation rates tend to increase in most percolation bins, leading to earlier arrival of seepage into a drift. Because increased infiltration also leads to lower temperatures, and at lower drift temperatures, the difference in relative humidity on WPs of different temperatures becomes more pronounced, increasing infiltration results in the counter-intuitive effect that the warmer WPs (CSNF WPs) have lower relative humidity at higher values of infiltration. These lower values of relative humidity are less likely to permit diffusive transport, which in turn yields a negative relationship between *INFIL* and expected dose at 10,000 years. The relationship between infiltration, temperature and relative humidity is described and documented in (SNL 2007, DIRS [181383]).

Figure K5.7.2-2c indicates that expected dose at 10,000 yr increases as *THERMCON* (thermal conductivity) increases. This correlation is valid at 10,000 yr because at this time CSNF WPs are

just beginning diffusive transport, so the correlation indicates the positive relationship between *THERMCON* and *EXPDOSE* described above. If the correlation were to be performed at later times, after transport has begun, the relationship between *THERMCON* and *EXPDOSE* would be reversed, because at these times *THERMCON* is affecting waste degradation rates, as described above. .

In contrast, more informative results are given by the regression analyses at 3,000 and 5,000 years without the added need to examine scatterplots (Figure K5.7.2-2a). Specifically, both the indicated regressions select the following four variables after *PROBWPEF*: *MICTC99* (dose conversion factor for ^{99}Tc for modern interglacial climate, (rem/yr)/(pCi/L)), *MICC14* (dose conversion factor for ^{14}C for modern interglacial climate, (rem/yr)/(pCi/L)), *DSNFMASS*, and *UZFAG8* (fracture aperture for Group 8 rock units in UZ). Increasing *MICTC99* and *MICC14* has a positive effect on *EXPDOSE* that results from increasing the received dose for a given exposure level; increasing *DSNFMASS* has a positive effect on *EXPDOSE* that results from increasing the amount of ^{99}Tc in CDSP WPs and hence the dose from ^{99}Tc that results from the failure of these WPs; and increasing *UZFAG8* has a negative effect on *EXPDOSE* that results from decreasing the proportion of radionuclides moving through fractures in the UZ. Specifically, increasing *UZFAG8* increases the proportion of the interface area between the EBS and the UZ that consists of fractures, which increases the mass of radionuclides that diffuse into fractures in the UZ, where radionuclide movement is relatively rapid, and decreases the mass of radionuclides that diffuse into the surrounding rock matrix, where radionuclide movement is slower. Collectively, the inclusion of *MICTC99*, *MICC14*, *DSNFMASS* and *UZFAG8* increases the R^2 values for the two regressions to 0.75 and 0.87. After *MICTC99*, *MICC14*, *DSNFMASS* and *UZFAG8*, the regressions add an additional six variables that have small effects and result in final models that have R^2 values of 0.80 and 0.90. The regression models at 3,000 yr tend to have smaller R^2 values than the regression models at 5,000 yr because of the noise introduced by the arrival of the ^{99}Tc releases (i.e., compare the smoothness of the time-dependent releases at 3,000 and 5,000 yr in Figure K5.7.2-2a,b).

Expected Dose to RMEI over [0, 1,000,000 yr]: *EXPDOSE*. The uncertainty and sensitivity analyses for expected dose to the RMEI (*EXPDOSE*, mrem/yr) over the time interval [0, 1,000,000 yr] resulting from early WP failure are summarized in Figures K5.7.2-3 and K5.7.2-4.

Except for very early times, the values for *EXPDOSE* fall between 10^{-6} and 0.1 mrem/yr for the 0 to 1,000,000 yr time interval (Figure K5.7.2-3a). For most sample elements, the values for *EXPDOSE* monotonically decrease until about 300,000 yr, at which time they show a sharp increase in value as the result of the failure of the DSs from general corrosion. This failure allows seeping water to directly contact the failed WPs, and as a consequence, produces larger radionuclide releases from the failed WPs.

The single most important variable with respect to the uncertainty in *EXPDOSE* is *PROBWPEF* (probability that a randomly selected WP will experience an early failure), with the value for *EXPDOSE* increasing as *PROBWPEF* increases. This effect results because increasing *PROBWPEF* increases the expected number of WPs that experience early failure and hence

increases *EXPDOSE* (Figures K5.7.2-3c, K5.7.2-4a). The positive effect of *PROBWPEF* can be seen in the scatterplot in Figure K5.7.2-4b.

Prior to 300,000 yr, *ISCSNS* (pointer variable used to determine ionic strength in CSNF cell under vapor influx conditions) and *SZGWSPDM* (groundwater specific discharge multiplier; as sampled, *SZGWSPDM* is actually the logarithm of the indicated multiplier) also have significant positive effects on the uncertainty in *EXPDOSE* (Figures K5.7.2-3c, K5.7.2-4a). These effects result because increasing *ISCSNS* increases plutonium solubility, and increasing *SZGWSPDM* increases water flow in the SZ. After 300,000 yr, *INFIL* (infiltration level) and again *SZGWSPDM* are indicated as having positive effects on *EXPDOSE* (Figures K5.7.2-3c, K5.7.2-4a). These effects result because increasing *INFIL* increases water flow in the EBS and UZ, and increasing *SZGWSPDM* increases water flow in the SZ. After *PROBWPEF*, *ISCSNS*, *SZGWSPDM* and *INFIL*, the analyses identify a number of additional variables that have small effects on *EXPDOSE*.

K5.7.3 Early Failure Scenario Classes: Expected Dose to Reasonably Maximally Exposed Individual from Both Early Drip Shield Failure and Early Waste Package Failure

Expected Dose to RMEI over [0, 20,000 yr]: *EXPDOSE*. The uncertainty and sensitivity analyses for expected dose to the RMEI (*EXPDOSE*, mrem/yr) over the time interval [0, 20,000 yr] resulting from both early DS failure and early WP failure are summarized in Figures K5.7.3-1 and K5.7.3-2. Because the expected doses from early WP failure tend to be one or more orders of magnitude greater than the expected doses from early DS failure (i.e., compare the results in Figures K5.7.1-1a,b and K5.7.2-1a,b), the results in Figures K5.7.3-1 and K5.7.3-2 from both early DS failure and early WP failure are very similar to the results in Figures K5.7.2-1 and K5.7.2-2 for early WP failure alone. For this reason, the discussion associated with Figures K5.7.2-1 and K5.7.2-2 for early WP failure is also applicable to the results in Figures K5.7.3-1 and K5.7.3-2 for both early DS failure and early WP failure and will not be repeated.

Expected Dose to RMEI over [0, 1,000,000 yr]: *EXPDOSE*. The uncertainty and sensitivity analyses for expected dose to the RMEI (*EXPDOSE*, mrem/yr) over the time interval [0, 1,000,000 yr] resulting from both early DS failure and early WP failure are summarized in Figures K5.7.3-3 and K5.7.3-4. As for the 20,000 yr time period, the behavior of *EXPDOSE* for the combined releases from early DS failure and early WP failure is essentially the same as obtained for early WP failure alone (i.e., compare the results in Figures K5.7.1-3a,b and K5.7.2-3a,b). For this reason, the discussion associated with Figures K5.7.2-3 and K5.7.2-4 for early WP failure is also applicable to the results in Figures K5.7.3-3 and K5.7.3-4 for both early DS failure and early WP failure and will not be repeated.

K5.7.4 Early Failure Scenario Classes: Expected Dose to Reasonably Maximally Exposed Individual from Early Drip Shield Failure, Early Waste Package Failure, and Nominal Processes

Expected Dose to RMEI over [0, 20,000 yr]: *EXPDOSE*. Nominal processes cause no WP failures within the 0 to 20,000 yr time interval. As a result, the combined early DS failure and early WP failure results summarized in Figures K5.7.3-1 and K5.7.3-2 are the same as what would be obtained if (the nonexistent) releases from nominal processes were included in the analysis.

Expected Dose to RMEI over [0, 1,000,000 yr]: *EXPDOSE*. The uncertainty and sensitivity analyses for expected dose to the RMEI (*EXPDOSE*, mrem/yr) over the time interval [0, 1,000,000 yr] resulting from early DS failure, early WP failure and nominal process WP failure are summarized in Figures K5.7.4-1 and K5.7.4-2.

Prior to 200,000 yr, the value of *EXPDOSE* is determined by processes related to early DS failure and early WP failure. As a result, the regression at 50,000 yr in Figure K5.7.3-4a conditional on early DS failure and early WP failure is the same as the corresponding regression in Figure K5.7.4-2a conditional on early DS failure, early WP failure, and nominal process WP failure. By 200,000 yr, failures resulting from nominal processes are starting to occur. As a result, the regression at 200,000 yr in Figure K5.7.4-2a is slightly different from the corresponding regression in Figure K5.7.3-4a. For example, *WDGCA22* (temperature dependence associated with the general corrosion rate for alloy 22, K) now appears in the regression model. However, the regression model at 200,000 yr has a relatively low R^2 value of 0.51 as a result of the noisy behavior of the time-dependent values for *EXPDOSE* in the vicinity of 200,000 yr (Figure K5.7.4-1a,b). This noisy behavior creates patterns that the regression model cannot capture and results from *EXPDOSE* changing for individual sample elements from being dominated by effects associated with early DS and WP failures to effects associated with WP failures from nominal processes.

After 200,000 yr, the value of *EXPDOSE* is determined primarily by processes related to the failure of WPs from nominal processes (i.e., compare the post 200,000 yr results in Figure K5.7.3-3a,b for early DS and WP failure with the corresponding results in Figure K5.7.4-1a,b for all three failure processes). As a result, the regression at 500,000 yr in Figure K5.7.4-2a is very different from the regression at 500,000 yr in Figure K5.7.3-4a when only early DS and WP failures are considered in the definition of *EXPDOSE*. In particular, the dominant variable in the regression in Figure K5.7.3-4a when only early DS and WP failures are considered is *PROBWPEF* (probability that a randomly selected WP will experience an early failure). In contrast, the dominant variable in the regression in Figure K5.7.4-2a when all three failure processes are considered is *WDGCA22*, with a relatively small effect indicated for *PROBWPEF*. Specifically, the regression model containing only *WDGCA22* has an R^2 value of 0.78; in contrast, *PROBWPEF* is the fourth variable selected in the stepwise process and only increases the R^2 value from 0.83 to 0.84.

The dominant effect of *WDGCA22* can be seen in the scatterplot in Figure K5.7.4-2b, with *EXPDOSE* decreasing as *WDGCA22* increases. After *WDGCA22*, the regression at 500,000 yr in

Figure K5.7.4-2a selects *THERMCON* (host rock thermal conductivity level) and *WDNSCC* (stress corrosion cracking growth rate exponent) to add to the model. However, as can be seen in the scatterplots in Figure K5.7.4-2c,d, *THERMCON* and *WDNSCC* have relatively small effects on *EXPDOSE* and only increase the R^2 value from 0.78 for a model containing only *WDGCA22* to (i) 0.83 for a model containing *WDGCA22*, *THERMCON* and *WDNSCC* and (ii) 0.84 for a model containing *WDGCA22*, *THERMCON*, *WDNSCC* and *PROBWPEF*. After *WDGCA22*, *THERMCON*, *WDNSCC* and *PROBWPEF*, the regression analysis selects 9 additional variables that have small effects on *EXPDOSE* and produces a final model with an R^2 value of 0.88.

K6 IGNEOUS SCENARIO CLASSES

K6.1 Igneous Scenario Classes: Summary

The igneous scenario classes are defined on the basis of futures that involve one or more igneous events (Section J7). This section (Section K6) presents uncertainty and sensitivity analysis results for selected analysis outcomes associated with the igneous scenario classes (Table K6.1-1). The primary emphasis is on the igneous intrusive scenario class but expected dose results for igneous eruptive scenario class are also presented.

The primary results considered for the igneous intrusive scenario class are radionuclide movement from the EBS to the UZ (Table K6.1-2), radionuclide movement from the UZ to the SZ (Table K6.1-3), radionuclide movement in the SZ at the location of the RMEI (Table K6.1-4), dose to the RMEI from selected radionuclides (Table K6.1-5), and expected dose to the RMEI from all radionuclides (Table K6.1-6). High-level summaries of the uncertainty and sensitivity analysis results presented in this section are provided in Tables K6.1-2 to K6.1-6. Additional uncertainty analysis results are also available in Section J7.

From a regulatory perspective, expected dose to the RMEI (*EXPDOS*, mrem/yr) is the analysis outcome of greatest interest associated with the igneous scenario classes (Table K6.1-6). For the igneous intrusive scenario class, *EXPDOS* tends to monotonically increase over the time interval [0, 2×10^4 yr], and the range of possible values for *EXPDOS* at 10^4 yr is approximately [10^{-4}, 3 mrem/yr] (Figure K6.7.1-1). For the [0, 10^6 yr] time interval, *EXPDOS* tends to monotonically increase over the time interval [0, 10^5 yr], monotonically decrease over the time interval [10^5, 2×10^5 yr], and then monotonically increase over the time interval [2×10^5, 10^6 yr] (Figure K6.7.2-1). Over the time interval [0, 10^6 yr], the range of possible values for *EXPDOS* is approximately [10^{-4}, 100 mrem/yr]. The dominant variable with respect to the uncertainty associated with *EXPDOS* is *IGRATE* (rate of occurrence of igneous intrusive events, yr^{-1}) (Figures K6.7.1-1, K6.7.1-2, K6.7.2-1, K6.7.2-2). A smaller contribution to the uncertainty in *EXPDOS* are made by *SZGWSPDM* (groundwater specific discharge multiplier; as sampled, *SZGWSPDM* is actually the logarithm of the indicated multiplier) and a number of additional variables.

For the igneous eruptive scenario class, the possible values for *EXPDOS* fall in the interval [2×10^{-7}, 2×10^{-3} mrem/yr] for both the [0, 2×10^4 yr] and [0, 10^6 yr] time intervals (Figures K6.8.1-1, K6.8.2-1). The dominant variable with respect to the uncertainty in *EXPDOS* for the igneous eruptive scenario class is *IGERATE* (rate of occurrence of igneous eruptive

events, yr^{-1}; *IGERATE* = (0.29) (0.27) *IGRATE*, where 0.29 is the probability that an igneous intrusive event will have an eruptive component and 0.27 is the probability that the eruptive component of an igneous intrusive event will intercept waste) (Figures K6.8.1-1, K6.8.1-2, K6.8.2-1, K6.8.2-2).

K6.2 Igneous Intrusive Scenario Classes: Engineered Barrier System Conditions over the Time Interval [0, 1,000,000 yr] for an Event at 250 yr

This section discusses conditions in the EBS after an igneous intrusive event at 250 yr that damages all WPs in the repository. Similar conditions exist after igneous intrusive events at other times.

The EBS is assumed to rapidly cool after an igneous intrusive event. Specifically, the EBS is assumed to revert to temperature conditions consistent with heating from radioactive decay 250 yr after an igneous intrusive event (Figure K6.2-1). Consistent with this, the post 500 year results in Figure K6.2-1 are the same as the post 500 yr results in Figure K4.3-5. Similarly, the relative humidity conditions and the partial pressures for CO_2 in the EBS are assumed to revert to conditions consistent with heating from radioactive decay 250 yr after an igneous event. As a result, the post 500 yr relative humidity conditions and the partial pressures for CO_2 in the EBS are the same as the post 500 yr results in Figures K4.3-6 and K4.3-7.

After an igneous intrusion, the drift is assumed to be filled with basalt. In consistency with the assumption that the resultant basalt has properties similar to the host rock that surrounds the drift, seepage into the EBS (m^3/yr/WP) is determined by multiplying the percolation rate (m^3/m^2/yr) at the base on the PTn (an overlying rock formation) by the footprint area (m^2/WP) of the drift segment containing a WP (Section 6.5.1.1) (Figure K6.2-2). The seepage levels for CSNF and CDSP WPs in a given percolation bin are assumed to be the same. Further, all WPs are assumed to experience seepage (i.e., dripping conditions).

An igneous intrusion causes a change in chemical conditions in the EBS. As a result, the ionic strengths of EBS waters after an igneous intrusion (Figure K6.2-3) are different from the ionic strengths of EBS waters under nominal conditions (Figures K4.3-9 and K4.3-11). As indicated by the PRCCs in Figure K6.2-3e, the uncertainty in ionic strength (mol/kg) under dripping conditions in the invert for CSNF WPs (*ISCSINAD*) is completely dominated by *ISCSS* (pointer variable used to determine ionic strength in CSNF cell 1 under dripping conditions), with *ISCSINAD* increasing as *ISCSS* increases. Similarly, the PRCCs in Figure K6.2-3f indicate that the uncertainty in ionic strength (mol/kg) under dripping conditions in the invert for CDSP WPs (*ISCDINAD*) is completely dominated by *IS2MCOS* (pointer variable used to determine ionic strength in CDSP WP cell 1b under liquid influx conditions), with *ISCDINAD* increasing as *IS2MCOS* increases. As a reminder, all WPs are assumed to experience dripping conditions after an igneous event.

Because of the changed chemical conditions, the pH conditions of EBS waters after an igneous intrusion (Figure K6.2-4) are different from the pH conditions of EBS waters under nominal conditions (Figures K4.3-12 and K4.3-14). As indicated by the PRCCs in Figure K6.2-4e, the uncertainty in pH in the invert for CSNF WPs experiencing dripping conditions (*PHCSINAD*) is dominated by *PH2RGER* (error term in regression equation used to determine pH of corrosion

products domain), with *PHCSINAD* increasing as *PH2RGER* increases. Prior to 10,000 yr, a negative effect is indicated for *DELPPCO2* (scale factor used to incorporate uncertainty into the value for the partial pressure of CO_2). Smaller effects are indicated for several other variables, but it is *PH2RGER* that dominates the uncertainty in *PHCSINAD*. The PRCC analysis in Figure K6.2-4f for pH in the invert for CDSP WPs experiencing dripping conditions (*PHCDINAD*) is similar to the corresponding analysis for *PHCSINAD* in Figure K6.2-4e.

K6.3 Igneous Intrusive Scenario Classes: Release from Engineered Barrier System

K6.3.1 Igneous Intrusive Scenario Classes: Release from Engineered Barrier System over the Time Interval [0, 20,000 yr] for an Event at 10 yr

Movement of ^{239}Pu Irreversibly Attached to Glass/Waste Form (i.e., Ic) Colloids: *ESIC239* and *ESIC239C*. The uncertainty and sensitivity analyses for the time-dependent release rates (*ESIC239*, g/yr) and cumulative releases (*ESIC239C*, g) over the time interval [0, 20,000 yr] for the movement of ^{239}Pu irreversibly attached to glass/waste form (i.e., Ic) colloids from the EBS to the UZ resulting from an igneous intrusive event at 10 yr that destroys all WPs in the repository are summarized in Figures K6.3.1-1 and K6.3.1-2. Except for transient spikes in release rates before 1,000 yr, the release rates maintain steady values for each climate period.

As indicated by the PRCCs in Figure K6.3.1-1e,f and the regression analyses in Figure K6.3.1-2a,b, the dominant variables contributing to the uncertainty in *ESIC239* and *ESIC239C* are *CPUCOLWF* (maximum concentration of plutonium irreversibly attached to glass colloids, mol/L) and *INFIL* (infiltration level), with *ESIC239* and *ESIC239C* increasing as each of these variables increases. These effects result because increasing *CPUCOLWF* increases the amount of ^{239}Pu that can potentially be irreversibly attached to glass colloids and increasing *INFIL* increases water flow in the EBS and the UZ. The regression models for *ESIC239* and *ESIC239C* containing only *CPUCOLWF* have R^2 values of 0.63 or 0.64, and the models containing both *CPUCOLWF* and *INFIL* have R^2 values between 0.91 and 0.93 (Figure K6.3.1-2a,b). Thus, the uncertainty in *CPUCOLWF* and *INFIL* dominates the uncertainty in *ESIC239* and *ESIC239C*. In addition to *CPUCOLWF* and *INFIL*, the regression analyses indicate small effects for several additional variables. The dominant effects of *CPUCOLWF* and *INFIL* can be seen in the scatterplots in Figure K6.3.1-2c,d,e,f,g,h.

The PRCCs indicate effects for *THERMCON* (host rock thermal conductivity level) prior to 1,000 yr (Figure K6.3.1-1e,f). The effects associated with *THERMCON* result from an implementation error in the Goldsim component of the TSPA-LA Model that incorrectly allowed drift-wall condensation to occur after an igneous intrusion (Appendix P, Table P-6). When condensation occurs, water flow through the waste is increased by the condensation, resulting in the transient spikes in release rates evident in Figure K6.3.1-1a,c and also in the correlation of release rates and cumulative releases with *THERMCON*.

Movement of ^{239}Pu Irreversibly Attached to Ferrous (i.e., If) Colloids: *ESIF239* and *ESIF239C*. Uncertainty and sensitivity analyses for the movement of ^{239}Pu irreversibly attached to ferrous colloids are not presented due to an error in the GoldSim component of the TSPA-LA Model that affects the calculation of stability of ferrous colloids. Consequently,

Figure K6.3.1-3 and Figure K6.3.1-4 have been removed from this document. See Appendix P, Section P18, for a discussion of the error and the effect of the error on TSPA-LA Model results.

Movement of Dissolved ^{237}Np: *ESNP237* and *ESNP237C*. The uncertainty and sensitivity analyses for the time-dependent release rates (*ESNP237*, g/yr) and cumulative releases (*ESNP237C*, g) over the time interval [0, 20,000 yr] for the movement of dissolved ^{237}Np from the EBS to the UZ resulting from an igneous intrusive event at 10 yr that destroys all WPs in the repository are summarized in Figures K6.3.1-5 and K6.3.1-6.

As indicated by the PRCCs in Figure K6.3.1-5e,f and the regression analyses in Figure K6.3.1-6a,b, the most important variable with respect to the uncertainty in *ESNP237* and *ESNP237C* is *PHCSS* (pointer variable used to determine pH in CSNF cell 1 under liquid influx conditions), with *ESNP237* and *ESNP237C* tending to decrease as *PHCSS* increases. This effect results because increasing *PHCSS* reduces the solubility of neptunium in CSNF WPs. The five individual regressions containing only *PHCSS* have R^2 values between 0.27 or 0.3; thus, the uncertainty in *ESNP237* and *ESNP237C* is not dominated by *PHCSS*.

In addition to the effects associated with *PHCSS*, significant effects on the uncertainty in *ESNP237* and *ESNP237C* are indicated for *EP1NPO2* (scale factor used to incorporate uncertainty into NpO_2 solubility below 1 molal ionic strength; as sampled, *EP1NPO2* is actually the logarithm of the indicated scale factor), *EP1LOWAM* (scale factor used to incorporate uncertainty into americium solubility under low ionic strength conditions; as sampled, *EP1LOWAM* is actually the logarithm of the indicated scale factor), *CORRATSS* (corrosion rate for stainless steel, μm/yr), *INFIL* (infiltration level), and *DELPPCO2* (scale factor used to incorporate uncertainty into the value for the partial pressure of CO_2), and *EP1LOWNU* (scale factor used to incorporate uncertainty into uranium solubility under low ionic strength conditions for nominal and seismic conditions; as sampled, *EP1LOWNU* is actually the logarithm of the indicated scale factor; in the present analysis, *EP1LOWNU* was used instead of the corresponding and intended variable *EP1LOWOU* for igneous conditions; however, this has no effect on analysis outcomes as *EP1LOWNU* and *EP1LOWOU* are assigned the same distribution) (Figures K6.3.1-5e,f and K6.3.1-6a,b).

The indicated effects associated with *EP1NPO2*, *CORRATSS*, *INFIL* and *DELPPCO2* result because (i) increasing *EP1NPO2* increases the solubility of neptunium and hence the dissolved concentration ^{237}Np, (ii) increasing *CORRATSS* increases the corrosion rate of stainless steel and thus decreases the dissolved concentration ^{237}Np as a result of sorption on corrosion products, (iii) increasing *INFIL* increases water flow through the EBS and thus increases the rate at which ^{237}Np is transported out of the EBS, and (iv) increasing *DELPPCO2* increases the partial pressure of CO_2, which tends to increase the solubility of Np.

The positive effects for *EP1LOWAM* and *EP1LOWNU* result from increasing the amounts of uranium and americium that go into solution. In turn, this increases the amount sorbed uranium and americium and thus reduces the sorption sites available for the sorption of neptunium. This reduction in the number of sorption sites tends to increase the concentration of dissolved ^{237}Np and hence increase *ESNP237* and *ESNP237C*. It is also possible that the decay of ^{241}Am to

^{237}Np may have a positive effect on the amount of dissolved ^{237}Np and hence on *ESNP237* and *ESNP237C*.

The effects of *EP1NPO2*, *INFIL* and *PHCSS* on *ESNP237* and *ESNP237C* can be seen in the scatterplots in Figure K6.3.1-6c,d,e,f,g.

After *PHCSS*, *EP1NPO2*, *CORRATSS*, *EP1LOWAM*, *INFIL*, *DELPPCO2* and *EP1LOWNU*, the regression analyses select a number of additional variables that have small effects on *ESNP237* and *ESNP237C*. The final regression models for *ESNP237* and *ESNP237C* have R^2 values between 0.77 and 0.82 (Figure K6.3.1-6a,b). Thus, most of the uncertainty associated with *ESNP237* and *ESNP237C* is accounted for.

It is possible that some of the variables selected near the ends of the regression analyses for *ESNP237* and *ESNP237C* may be spurious (Figure K6.3.1-6a,b). For example, *WDCRCDEN* (scale factor to convert area on a WP experiencing stress corrosion cracking to a resultant diffusive area) should have no effect on *ESNP237* and *ESNP237C* for igneous intrusive events and thus its selection is most likely spurious as a result of a slight nonrandom pattern in the mapping between the sampled values for *WDCRCDEN* and the calculated values for *ESNP237* and *ESNP237C*. However, variables such as *WDCRCDEN* added near the end of a stepwise regression analysis have little effect on the final R^2 values. An occasional spurious variable near the end of a stepwise regression analysis will often occur when a large number of analyses with large numbers of sampled variables are being performed.

Movement of Dissolved ^{239}Pu: *ESPU239* and *ESPU239C*. The uncertainty and sensitivity analyses for the time-dependent release rates (*ESPU239*, g/yr) and cumulative releases (*ESPU239C*, g) over the time interval [0, 20,000 yr] for the movement of dissolved ^{239}Pu from the EBS to the UZ resulting from an igneous intrusive event at 10 yr that destroys all WPs in the repository are summarized in Figures K6.3.1-7 and K6.3.1-8.

The dominant contributors to the uncertainty in *ESPU239* and *ESPU239C* are *EP1LOWPU* (scale factor used to incorporate uncertainty into plutonium solubility under low ionic strength conditions; as sampled, *EP1LOWPU* is actually the logarithm of the indicated scale factor), *DELPPCO2* (scale factor used to incorporate uncertainty into the value for the partial pressure of CO_2), *INFIL* (infiltration level), and *PHCSS* (pointer variable used to determine pH in CSNF cell 1 under liquid influx conditions) (Figures K6.3.1-7e,f and K6.3.1-8a,b). The variables *EP1LOWPU*, *DELPPCO2* and *INFIL* have positive effects on *ESPU239* and *ESPU239C* because increasing *EP1LOWPU* increases plutonium solubility, increasing *DELPPCO2* increases the partial pressure of CO_2, which, although decreasing pH, also increases the solubility of Pu and thus has a net effect of increasing the amount of dissolved ^{239}Pu, and increasing *INFIL* increases water flow through the EBS. In contrast, increasing *PHCSS* has a negative effect on *ESPU239* and *ESPU239C* because increasing *PHCSS* increases pH, which (as long as pH is below about 9) tends to decrease Pu solubility. The regression models containing *EP1LOWPU*, *DELPPCO2*, *INFIL* and *PHCSS* have R^2 values between 0.75 and 0.90 (Figure K6.3.1-8a,b).

The effects of *EP1LOWPU*, *DELPPCO2* and *INFIL* on *ESPU239* and *ESPU239C* can be seen in the scatterplots in Figure K6.3.1-8c,d,e,f,g.

After *EP1LOWPU*, *DELPPCO2*, *INFIL* and *PHCSS*, the regression analyses select a number of additional variables that have small effects on *ESPU239* and *ESPU239C* and produce final models with R^2 values between 0.82 and 0.92 (Figure K6.3.1-8a,b). Thus, most of the uncertainty associated with *ESPU239* and *ESPU239C* is accounted for

Movement of Dissolved ^{99}Tc: *ESTC99* and *ESTC99C*. The uncertainty and sensitivity analyses for the time-dependent release rates (*ESTC99*, g/yr) and cumulative releases (*ESTC99C*, g) over the time interval [0, 20,000 yr] for the movement of dissolved ^{99}Tc from the EBS to the UZ resulting from an igneous intrusive event at 10 yr that destroys all WPs in the repository are summarized in Figures K6.3.1-9 and K6.3.1-10.

The release of ^{99}Tc from the EBS is very rapid (Figure K6.3.1-9a,b,c,d). As time progresses, the uncertainty in *ESTC99* is dominated by *HLWDRALK* (dissolution rate of HLW glass under alkaline conditions, g/m^2/d) (Figures K6.3.1-9e and K6.3.1-10a,c). The negative effect associated with *HLWDRALK* at later times results because increasing *HLWDRALK* increases dissolution rate of HLW glass and hence increases the rate of release of ^{99}Tc. This results in a negative effect on *ESTC99* at later times because increasing the amount of ^{99}Tc released at early times reduces the amount of ^{99}Tc that can be released at later times and, as a result, reduces *ESTC99* as time increases. However, further investigation of model results determined that the HLW degradation after an igneous intrusion was not implemented correctly (see Appendix P, Section P16). Consistent with TSPA-LA Model assumptions, the HLW should degrade completely and instantaneously at the time of the igneous intrusion. Thus, the sensitivity of *ESTC99* to uncertainty in *HLWDRALK*, while phenomenologically correct, appears in the model results due to an error in the TSPA-LA Model.

The uncertainty in *ESTC99C* is completely dominated by *CSNFMASS* (scale factor used to characterize uncertainty in amount of CSNF in CSNF WPs) (Figures K6.3.1-9f and K6.3.1-10b,f). The positive effect of *CSNFMASS* on *ESTC99C* results because increasing *CSNFMASS* increases the mass of ^{99}Tc present in the repository. The dominant effect of *CSNFMASS* results from the rapid and unimpeded transport of ^{99}Tc out of the EBS. Specifically, the only thing that determines how much ^{99}Tc is transported out of the EBS is how much ^{99}Tc is present in the repository. Because the uncertainty in this amount is dominated by *CSNFMASS*, the uncertainty in *ESTC99C* is also dominated by *CSNFMASS*. In contrast, *CSNFMASS* is not significant in the regression analyses for *ESTC99* (rate of ^{99}Tc transport) due to the numerical resolution of this highly transient quantity. Because the solubility of ^{99}Tc is not limited, all of the ^{99}Tc available from degraded waste is mobilized and transported from the EBS over a few timesteps after the intrusion. During this interval, the rate of transport should depend on the mass of ^{99}Tc present, because the solubility of ^{99}Tc is high enough that any ^{99}Tc released from the waste is dissolved and transported immediately. Although the transport of ^{99}Tc during this interval is sufficiently resolved numerically to estimate dose (see Section 7.3.3), it is not sufficiently resolved numerically that the sensitivity analysis reported in Figures K6.3.1-9 and K6.3.1-10 can determine the effect of *CSNFMASS* on *ESTC99* during the time of initial transport.

K6.3.2 Igneous Intrusive Scenario Classes: Release from Engineered Barrier System over the Time Interval [0, 1,000,000 yr] for an Event at 250 yr

For completeness, this section presents summaries of the uncertainty and sensitivity analyses for release from the EBS over the time interval [0, 1,000,000 yr] for an igneous intrusive event at 250 yr that destroys all WPs in the repository without discussion.

Movement of ^{239}Pu Irreversibly Attached to Glass/ Waste Form (i.e., Ic) Colloids: *ESIC239* and *ESIC239C*. The uncertainty and sensitivity analyses for the time-dependent release rates (*ESIC239*, g/yr) and cumulative releases (*ESIC239C*, g) over the time interval [0, 1,000,000 yr] for the movement of ^{239}Pu irreversibly attached to glass/ waste form (i.e., Ic) colloids from the EBS to the UZ resulting from an igneous intrusive event at 250 yr that destroys all WPs in the repository are summarized in Figure K6.3.2-1.

Movement of ^{239}Pu Irreversibly Attached to Ferrous (i.e., If) Colloids: *ESIF239* and *ESIF239C*. Uncertainty and sensitivity analyses for the movement of ^{239}Pu irreversibly attached to ferrous colloids are not presented due to an error in the GoldSim component of the TSPA-LA Model that affects the calculation of stability of ferrous colloids. Consequently, Figure K6.3.2-2 has been removed from this document. See Appendix P, Section P18, for a discussion of the error and the effect of the error on TSPA-LA Model results.

Movement of Dissolved ^{237}Np: *ESNP237* and *ESNP237C*. The uncertainty and sensitivity analyses for the time-dependent release rates (*ESNP237*, g/yr) and cumulative releases (*ESNP237C*, g) over the time interval [0, 1,000,000 yr] for the movement of dissolved ^{237}Np from the EBS to the UZ resulting from an igneous intrusive event at 250 yr that destroys all WPs in the repository are summarized in Figure K6.3.2-3.

Movement of Dissolved ^{239}Pu: *ESPU239* and *ESPU239C*. The uncertainty and sensitivity analyses for the time-dependent release rates (*ESPU239*, g/yr) and cumulative releases (*ESPU239C*, g) over the time interval [0, 1,000,000 yr] for the movement of dissolved ^{239}Pu from the EBS to the UZ resulting from an igneous intrusive event at 250 yr that destroys all WPs in the repository are summarized in Figure K6.3.2-4.

Movement of Dissolved ^{99}Tc: *ESTC99* and *ESTC99C*. The uncertainty and sensitivity analyses for the time-dependent release rates (*ESTC99*, g/yr) and cumulative releases (*ESTC99C*, g) over the time interval [0, 1,000,000 yr] for the movement of dissolved ^{99}Tc from the EBS to the UZ resulting from an igneous intrusive event at 250 yr that destroys all WPs in the repository are omitted because of the rapid depletion of the 99Tc inventory (see Figure K6.3.1-9a,c).

K6.4 Igneous Intrusive Scenario Classes: Release from Unsaturated Zone (UZ)

K6.4.1 Igneous Intrusive Scenario Classes: Release from Unsaturated Zone (UZ) over the Time Interval [0, 20,000 yr] for an Event at 10 yr

Movement of ^{239}Pu Irreversibly Attached to Slow (i.e., Ic) Colloids: *UZIC239* and *UZIC239C*. To understand the presented analyses for colloids in the UZ and SZ, it is necessary to realize that a reapportioning of colloids takes place upon entry into the UZ (Section 6.3.8.3, EBS Transport Submodel Outputs). The EBS release involves ^{239}Pu attached to Ic colloids (i.e., glass colloids for releases from CDSP WPs and waste form colloids for releases from CSNF WPs). Upon entry into the UZ, the ^{239}Pu irreversibly attached to glass/waste form (i.e., Ic) and ferrous (i.e., If) colloids in the EBS is reapportioned. Specifically, (i) Ic now designates slow moving colloids, (ii) If now designates fast moving colloids, and (iii) the total amount of ^{239}Pu attached to Ic and If colloids in the EBS is reapportioned so that 99.832 percent of the total ^{239}Pu is attached to slow colloids (i.e., the new Ic colloids) upon entry into the UZ and the remaining 0.168 percent is attached to fast colloids (i.e., the new If colloids) upon entry into the UZ. Because the mass of ^{239}Pu attached to glass/waste form colloids in the EBS is much greater than the mass of ^{239}Pu attached to ferrous colloids in the EBS, the mass of ^{239}Pu attached to slow colloids entering the UZ is effectively the same as the mass of ^{239}Pu attached to glass colloids leaving the EBS. However, because the mass of ^{239}Pu attached to glass/waste form colloids in the EBS is much greater than the mass of ^{239}Pu attached to ferrous colloids in the EBS, the indicated reapportioning results in the release of ^{239}Pu attached to fast colloids into the UZ having very different properties from the release of ^{239}Pu attached to ferrous colloids out of the EBS.

The uncertainty and sensitivity analyses for the time-dependent release rates (*UZIC239*, g/yr) and cumulative releases (*UZIC239C*, g) over the time interval [0, 20,000 yr] for the movement of ^{239}Pu irreversibly attached to slow (i.e., Ic) colloids from the UZ to the SZ resulting from an igneous intrusive event at 10 yr that destroys all WPs in the repository are summarized in Figures K6.4.1-1, K6.4.1-2 and K6.4.1-3. Transport through the UZ occurs relatively rapidly, with ^{239}Pu irreversibly attached to slow (i.e., Ic) colloids leaving the UZ within 2,000 yr after the intrusion for all sample elements (Figure K6.4.1-3).

With increasing time, most ^{239}Pu irreversibly attached to slow (i.e., Ic) colloids moves from the UZ to the SZ (Figure K6.4.1-3). As a result, the analyses for *UZIC239* and *UZIC239C* in Figures K6.4.1-1 and K6.4.1-2 are very similar to the analyses for *ESIC239* and *ESIC239C* in Figures K6.3.1-1 and K6.3.1-2. For example, *CPUCOLWF* (maximum concentration of plutonium irreversibly attached to glass colloids, mol/L) and *INFIL* (infiltration level) are the first two variables selected in the regression analyses for *ESIC239* and *ESIC239C* (Figure K6.3.1-2a,b) and also the first two variables selected in the regression analyses for *UZIC239* and *UZIC239C* (Figure K6.3.4-2a,b). The dominant effects of *CPUCOLWF* and *INFIL* on *UZIC239* and *UZIC239C* can be seen in the scatterplots in Figure K6.3.4-2c,d,f,g.

The only UZ parameter that has a noticeable effect on *UZIC239* and *UZIC239C* is *UZRCOL* (retardation coefficient for colloids in UZ), with *UZIC239* and *UZIC239C* tending to decrease as *UZRCOL* increases (Figures K6.4.1-1a,b and K6.4.1-2a,b). However, the effect of *UZRCOL* is

primarily to delay the movement of ^{239}Pu irreversibly attached to slow (i.e., Ic) colloids from the UZ to the SZ (i.e., compare Figure K6.4.1-3a and Figure K6.4.1-3d). This effect can also be seen in the decreasing importance of *UZRCOL* with increasing time in the regression analyses in Figure K6.4.1-2a,b.

Movement of ^{239}Pu Irreversibly Attached to Fast (i.e., If) Colloids: *UZIF239* and *UZIF239C*. The uncertainty and sensitivity analyses for the time-dependent release rates (*UZIF239*, g/yr) and cumulative releases (*UZIF239C*, g) over the time interval [0, 20,000 yr] for the movement of ^{239}Pu irreversibly attached to fast (i.e., If) colloids from the UZ to the SZ resulting from an igneous intrusive event at 10 yr that destroys all WPs in the repository are summarized in Figures K6.4.1-4, K6.4.1-5 and K6.4.1-6. Transport through the UZ happens within about 1,000 yr after the intrusion.

The ^{239}Pu irreversibly attached to fast (i.e., If) colloids moves rapidly from the UZ to the SZ (Figure K6.4.1-6). As discussed in conjunction with *UZIC239* and *UZIC239C*, the release into the UZ of ^{239}Pu irreversibly attached to fast (i.e., If) colloids is, in effect, defined by the release from the EBS of ^{239}Pu irreversibly attached to glass/waste form (i.e., Ic) colloids. As a result, the analyses for *UZIC239* and *UZIC239C* in Figures K6.4.1-4 and K6.4.1-5 are effectively the same as the analyses for *ESIC239* and *ESIC239C* in Figures K6.3.1-1 and K6.3.1-2.

Movement of Dissolved ^{237}Np: *UZNP237* and *UZNP237C*. The uncertainty and sensitivity analyses for the time-dependent release rates (*UZNP237*, g/yr) and cumulative releases (*UZNP237C*, g) over the time interval [0, 20,000 yr] for the movement of dissolved ^{237}Np from the UZ to the SZ resulting from an igneous intrusive event at 10 yr that destroys all WPs in the repository are summarized in Figures K6.4.1-7, K6.4.1-8 and K6.4.1-9. Transport through the UZ occurs relatively rapidly, with dissolved ^{237}Np leaving the UZ within 1,500 yr after the intrusion.

With increasing time, most dissolved ^{237}Np moves from the UZ to the SZ (Figure K6.4.1-9). As a result, the analyses for *UZNP237*and *UZNP237C* in Figures K6.4.1-7 and K6.4.1-8 are similar to the analyses for *ESNP237* and *ESNP237C* in Figures K6.3.1-5 and K6.3.1-6. For example, the first six or seven variables selected in the regression analyses for *ESNP237* and *ESNP237C* (Figure K6.3.1-6a,b) are generally the same as the first six or seven variables selected in the regression analyses for *UZNP237* and *UZNP237C* (Figure K6.4.1-8a,b), although the order of selection may vary slightly. As a result, the discussions for *ESNP237* and *ESNP237C* associated with Figures K6.3.1-5 and K6.3.1-6 also apply to *UZNP237* and *UZNP237C*.

Movement of Dissolved ^{239}Pu: *UZPU239* and *UZPU239C*. The uncertainty and sensitivity analyses for the time-dependent release rates (*UZPU239*, g/yr) and cumulative releases (*UZPU239C*, g) over the time interval [0, 20,000 yr] for the movement of dissolved ^{239}Pu from the UZ to the SZ resulting from an igneous intrusive event at 10 yr that destroys all WPs in the repository are summarized in Figures K6.4.1-10, K6.4.1-11 and K6.4.1-12. Transport through the UZ occurs relatively rapidly, with dissolved ^{239}Pu leaving the UZ within 2,000 yr after the intrusion.

With increasing time, most dissolved ^{239}Pu moves from the UZ to the SZ (Figure K6.4.1-12). As a result, the analyses for *UZPU239* and *UZPU239C* in Figures K6.4.1-10 and K6.4.1-11 are similar to the analyses for *ESPU239* and *ESPU239C* in Figures K6.3.1-7 and K6.3.1-8. For example, all six regression analyses for *ESPU239* and *ESPU239C* in Figure K6.3.1-8a,b and also all six regression analyses for *UZPU239* and *UZPU239C* in Figure K6.4.1-11a,b initially select the following three variables: *EP1LOWPU* (scale factor used to incorporate uncertainty into plutonium solubility under low ionic strength conditions; as sampled, *EP1LOWPU* is actually the logarithm of the indicated scale factor), *DELPPCO2* (scale factor used to incorporate uncertainty into the value for the partial pressure of CO_2), and *INFIL* (infiltration level).

In all the regression analyses for *ESPU239* and *ESPU239C*, the fourth selected variable is *PHCSS* (pointer variable used to determine pH in CSNF cell 1 under liquid influx conditions) (Figure K6.3.1-8a,b). In all the regression analyses for *UZPU239* and *UZPU239C* except the analysis for *UZPU239* at 10,000 yr, the fourth and fifth selected variables are *PHCSS* and *UZKDPUDT* (sorption coefficient for plutonium in devitrified tuff units of UZ, mL/g), although the order of selection varies in the individual analyses (Figure K6.4.1-11a,b). Further, *UZKDPUDT* is the sixth variable selected in the regression analysis for *UZPU239* at 10,000 yr. The presence of *UZKDPUDT* in the regression analyses for *UZPU239* and *UZPU239C* indicates that retardation in the UZ is having a negative effect on the rate of movement of dissolved ^{239}Pu through the UZ to the SZ. However, incremental R^2 values associated with the addition of *UZKDPUDT* to the individual regression models varies between 0.01 and 0.08, with the size of this increment decreasing with increasing time (Figure K6.4.1-11a,b). Thus, *UZKDPUDT* does not have a large effect on the uncertainty associated with *UZPU239* and *UZPU239C*.

Figure 6.4.1-12 compares the cumulative mass of ^{239}Pu released from the EBS to the UZ (*ESPU239C*, g) to the cumulative mass of ^{239}Pu released from the UZ to the SZ (*UZPU239C*, g) after an igneous intrusive event at 10 years. The separation of each point from the isoline indicates the proportion of ^{239}Pu released from the EBS that is still within the UZ, at several times (1,000 years, 3,000 years, 5,000 years and 10,000 years). At 10,000 years, most points lie remain below the isoline, indicating the reduction of ^{239}Pu by decay during transport in the UZ, and also the possibility that some ^{239}Pu is still in transit through the UZ. The few realizations with points above the isoline are those in which a substantial amount of ^{243}Am is released from the EBS into the UZ, and subsequently decays in the UZ to ^{239}Np and then to ^{239}Pu. Thus, in these realizations, because ^{239}Pu is being produced by decay in the UZ, more ^{239}Pu can be released from the UZ than is released into the UZ.

Overall, the sensitivity analyses for *UZPU239* and *UZPU239C* in Figures K6.4.1-10e,f and K6.4.1-11a,b are very similar to the sensitivity analyses for *ESPU239* and *ESPU239C* in Figures K6.3.1-7e,f and K6.3.1-8a,b. As a result, the discussions for *ESPU239* and *ESPU239C* associated with Figures K6.3.1-7 and K6.3.1-8 also apply to *UZPU239* and *UZPU239C*.

Movement of Dissolved ^{99}Tc: *UZTC99* and *UZTC99C*. The uncertainty and sensitivity analyses for the time-dependent release rates (*UZTC99*, g/yr) and cumulative releases (*UZTC99C*, g) over the time interval [0, 20,000 yr] for the movement of dissolved ^{99}Tc from the UZ to the SZ resulting from an igneous intrusive event at 10 yr that destroys all WPs in the

repository are summarized in Figures K6.4.1-13, K6.4.1-14 and K6.4.1-15. Transport through the UZ occurs rapidly, with ^{99}Tc leaving the UZ within 1,000 yr after the intrusion.

With increasing time, effectively all dissolved ^{99}Tc moves from the UZ to the SZ (Figure K6.4.1-15). However, the UZ does delay this movement (i.e., compare Figures K6.4.1-15a and K6.4.1-15d). This delay is more apparent for ^{99}Tc than the other radioactive species under consideration because of the very rapid release of ^{99}Tc from the EBS (i.e., compare Figures K6.4.1-15 with Figures K6.4.1-3, K6.4.1-6, K6.4.1-9 and K6.4.1-12).

As indicated by the PRCCs in Figure K6.4.1-13e,f and the regression analyses in Figure K6.4.1-14a,b, the dominant variables influencing the uncertainty in *UZTC99* and *UZTC99C* are *INFIL* (infiltration level) and *CSNFMASS* (scale factor used to characterize uncertainty in amount of CSNF in CSNF WPs). The variable *INFIL* has a complex pattern of effects on *UZTC99* and *UZTC99C*. For *UZTC99*, the effect of *INFIL* is positive at early times (Figure K6.4.1-13e) and then negative at later times (Figures K6.4.1-13e and K6.4.1-14a). This pattern results because increasing *INFIL* initially increases water flow in the EBS and UZ, which increases the movement of ^{99}Tc in the EBS and UZ. However, by increasing the early movement of ^{99}Tc in the EBS and UZ, increasing *INFIL* also reduces the amount of ^{99}Tc that can be released from the UZ to the SZ at later times. As a result, increasing *INFIL* has a negative effect on *UZTC99* at later times. In contrast, *INFIL* has a positive effect on *UZTC99C* at all times (Figures K6.4.1-13f and K6.4.1-14b) because *UZTC99C* is the cumulative release of ^{99}Tc from the UZ to the SZ. Increasing *CSNFMASS* has positive effect on both *UZTC99* and *UZTC99C*, which results from increasing the amount of ^{99}Tc placed in the repository (Figures K6.4.1-13e,f and K6.4.1-14a,b). Similar but smaller effects are also indicated for *HLWMASS* (scale factor used to characterize uncertainty in amount of HLW in CDSP WPs) and *DSNFMASS* (scale factor used to characterize uncertainty in amount of DSNF in CDSP WPs) for *UZTC99C* at 10,000 yr (Figure K6.4.1-14b).

The opposite effects of *INFIL* on *UZTC99* and *UZTC99C* at 10,000 yr can be seen in the scatterplots in Figure K6.4.1-14c,d,f,g, with *UZTC99* tending to decrease as *INFIL* increases and *UZTC99C* tending to increase as *INFIL* increases.

In addition to *INFIL* and *CSNFMASS*, a number of variables related to flow in the UZ have small effects on *UZTC99* and *UZTC99C*, with the effects of these variables tending to decrease with increasing time (Figures K6.4.1-13e,f and K6.4.1-14a,b). For example, the regression analysis for *UZTC99* at 3,000 yr selects the following four variables after *INFIL* and *CSNFMASS*: *UZTORRG3* (tortuosity in rock group 3 of the UZ; as sampled, *UZTORRG3* is the logarithm of the indicated tortuosity, m), *UZGAM* (parameter gamma in active fracture model, dimensionless), *UZFAG8* (fracture aperture for rock group 8 in UZ, m), and *UZFAG3* (fracture aperture for rock group 3 in UZ, m). As indicated by the PRCCs in Figure K6.4.1-13e, variables such as *UZTORRG3*, *UZGAM*, *UZFAG8* and *UZFAG3* tend to have temporally dependent effects on *UZTC99* that derive from the role that the individual variable plays on speeding up or slowing down the movement of ^{99}Tc in the UZ. However, as previously noted, these effects tend to diminish with time as a result of the essentially complete movement ^{99}Tc through the UZ. For example, adding *UZTORRG3*, *UZGAM*, *UZFAG8* and *UZFAG3* to the regression model for *UZTC99* at 3,000 yr increases the R^2 value from 0.78 for a model containing only *INFIL* and

CSNFMASS to 0.90 for a model containing *INFIL*, *CSNFMASS*, *UZTORRG3*, *UZGAM*, *UZFAG8* and *UZFAG3* (Figure K6.4.1-14a). In contrast, the regression analysis for *UZTC99* at 5000 yr initially selects *INFIL* and *CSNFMASS* and produces a model with an R^2 value of 0.78; then, only *UZTORRG3* and *UZGAM* are selected from the variables that affect ^{99}Tc movement in the UZ for a resultant model containing *INFIL*, *CSNFMASS*, *UZTORRG3* and *UZGAM* with an R^2 value of 0.79 (Figure K6.4.1-14a).

As previously noted, the uncertainty in *UZTC99C* is dominated by *INFIL* and *CSNFMASS*. Specifically, the regression model for *UZTC99C* at 3,000 yr containing only *INFIL* has an R^2 value of 0.59, and the regression models for *UZTC99C* at 5,000 and 10,000 yr containing only *CSNFMASS* have R^2 values of 0.62 and 0.84, and the corresponding models containing both *CSNFMASS* and *INFIL* have R^2 values of 0.90, 0.94 and 0.97 (Figure K6.4.1-14b). Further, there is an interesting pattern in the relationship between *UZTC99C, INFIL* and *CSNFMASS* (Figure K6.4.1-14f). Specifically, there are two linear relationships between *UZTC99C* and *CSNFMASS*, with the possibilities *INFIL* = 1 and *INFIL* = 2, 3 or 4 acting as switches between these two relationships. The role of *INFIL* as a switch occurs because the water flow for *INFIL* = 2, 3 or 4 is rapid enough that almost all the ^{99}Tc from the CSNF waste (comprising between 5.7×10^7 g and 8.8×10^7 g) is transported through the UZ by 10,000 yr, whereas for *INFIL* = 1 the transport of ^{99}Tc through the UZ is still in progress. For *INFIL* = 1 the average seepage rate (over all percolation bins) is about 0.55 m^3/yr/WP, whereas for *INFIL* = 2 the average seepage rate is about 1.24 m^3/yr/WP (Figure K6.2-2). The inventory of ^{99}Tc in CDSP WPs is much less, ranging between 2.5×10^6 g and 5.1×10^6 g.

K6.4.2 Igneous Intrusive Scenario Classes: Release from Unsaturated Zone (UZ) over the Time Interval [0, 1,000,000 yr] for an Event at 250 yr

Uncertainty and sensitivity analysis results for this case are not presented because of the relatively rapid transport of material through UZ (see Figures K6.4.1-3, K6.4.1-6, K6.4.1-9, K6.4.1-12 and K6.4.1-15).

K6.5 Igneous Intrusive Scenario Classes: Release from Saturated Zone (SZ)

K6.5.1 Igneous Intrusive Scenario Classes: Release from Saturated Zone (SZ) over the Time Interval [0, 20,000 yr] for an Event at 10 yr

Movement of ^{239}Pu Irreversibly Attached to Slow (i.e., Ic) Colloids: *SZIC239* and *SZIC239C*. The uncertainty and sensitivity analyses for the time-dependent release rates (*SZIC239*, g/yr) and cumulative releases (*SZIC239C*, g) over the time interval [0, 20,000 yr] for the movement of ^{239}Pu irreversibly attached to slow (i.e., Ic) colloids across a subsurface plane at the location of the RMEI resulting from an igneous intrusive event at 10 yr that destroys all WPs in the repository are summarized in Figures K6.5.1-1, K6.5.1-2 and K6.5.1-3. The delay in arrival of ^{239}Pu irreversibly attached to slow (i.e., Ic) colloids due to transport through the SZ is apparent in Figure K6.6.1-1(a), which shows that ^{239}Pu irreversibly attached to slow (i.e., Ic) colloids arrives at the RMEI location within 5,000 yr for many sample elements, but may be delayed out to and beyond 20,000 yr for some sample elements.

As indicated by the PRCCs in Figure K6.5.1-1e,f and the regression analyses in Figure K6.5.1-2a,b, the uncertainty in *SZIC239* and *SZIC239C* is dominated by *SZCOLRAL* (colloid retardation factor in alluvial unit of SZ; as sampled, *SZCOLRAL* is actually the logarithm of the indicated retardation factor), *SZFIPOVO* (flowing interval porosity in the volcanic unit of the SZ), *SZGWSPDM* (groundwater specific discharge multiplier; as sampled, *SZGWSPDM* is actually the logarithm of the indicated multiplier), and *CPUCOLWF* (concentration of irreversibly attached plutonium on stable glass colloids, mol/L). The negative effects associated with *SZCOLRAL* and *SZFIPOVO* result because increasing *SZCOLRAL* increases colloid retardation in the SZ and increasing *SZFIPOVO* slows water flow in the SZ. The positive effects associated with *SZGWSPDM* and *CPUCOLWF* result because increasing *SZGWSPDM* increases water flow in the SZ and increasing *CPUCOLWF* increases the amount of ^{239}Pu released from the EBS that is irreversibly attached to glass colloids. In addition to *SZCOLRAL*, *SZFIPOVO*, *SZGWSPDM* and *CPUCOLWF*, the analyses indicate a number of additional variables that have small effects on *SZIC239* and *SZIC239C*. Most of these additional variables relate to properties of the SZ. However, the final R^2 values in the regressions in Figure K6.5.1-2a,b are not very high (i.e., the range in R^2 values is 0.52 to 0.72).

The relatively low R^2 values result from the large number of sample elements for which *SZIC239* and *SZIC239C* are effectively zero (Figure K6.5.1-2f,g,h). These small values create a pattern that the regression models cannot effectively capture. As shown by the scatterplot in Figure K6.5.1-2f, the small values for *SZIC239* and *SZIC239C* tend to be associated with large values for *SZCOLRAL*, which indicates that the larger values for colloid retardation can result in no colloid transport through the SZ to the location of the RMEI. However, the extent of colloid retardation varies widely across the sample elements (Figure K6.5.1-3).

Movement of ^{239}Pu Irreversibly Attached to Fast (i.e., If) Colloids: SZ*IF239* and *SZIF239C*. The uncertainty and sensitivity analyses for the time-dependent release rates (*SZIF239*, g/yr) and cumulative releases (*SZIF239C*, g) over the time interval [0, 20,000 yr] for the movement of ^{239}Pu irreversibly attached to ferrous (i.e., If) colloids across a subsurface plane at the location of the RMEI resulting from an igneous intrusive event at 10 yr that destroys all WPs in the repository are summarized in Figures K6.5.1-4, K6.5.1-5 and K6.5.1-6. The relatively rapid transport through the SZ of ^{239}Pu irreversibly attached to fast (i.e., If) colloids is evident in Figure K6.6.1-3(a), which shows that ^{239}Pu irreversibly attached to fast colloids arrive at the RMEI location within 2,000 yr after the intrusion.

The uncertainty in *SZIF239* and *SZIF239C* is dominated by *CPUCOLWF* (concentration of irreversibly attached plutonium on stable glass colloids, mol/L) and *INFIL* (infiltration level) (Figures K6.5.1-4e,f and K6.5.1-5a,b,c,d,f,g). In particular, the interacting effects of *CPUCOLWF* and *INFIL* are particularly evident in the scatterplots in Figure K6.5.1-5c,f. The positive effect associated with *CPUCOLWF* results from increasing the amount of ^{239}Pu released from the EBS that is irreversibly attached to slow colloids, and the positive effect associated with *INFIL* results form increasing water flow in the EBS and UZ. Together, *CPUCOLWF* and *INFIL* result in regression models for *SZIF239* and *SZIF239C* with R^2 values between 0.87 and 0.93. After *CPUCOLWF* and *INFIL*, the analyses select several additional variables with small effects on *SZIF239* and *SZIF239C*. However, as indicated by the

scatterplots in Figure K6.5.1-5c,f, the uncertainty in *SZIF239* and *SZIF239C* is determined primarily by *CPUCOLWF* and *INFIL*.

As shown by the scatterplots in Figure K6.5.1-6, effectively all ^{239}Pu entering the SZ irreversibly attached to fast (i.e., If) colloids transports through the SZ to the location of the RMEI.

Movement of Dissolved ^{237}Np: *SZNP237* and *SZNP237C*. The uncertainty and sensitivity analyses for the time-dependent release rates (*SZNP237*, g/yr) and cumulative releases (*SZNP237C*, g) over the time interval [0, 20,000 yr] for the movement of dissolved ^{237}Np across a subsurface plane at the location of the RMEI resulting from an igneous intrusive event at 10 yr that destroys all WPs in the repository are summarized in Figures K6.5.1-7, K6.5.1-8 and K6.5.1-9. The delay in arrival of dissolved ^{237}Np due to transport through the SZ is apparent in Figure K6.5.1-9a, which shows that dissolved ^{237}Np arrives at the RMEI location within 5,000 yr for many sample elements, but may be delayed out to and beyond 20,000 yr for some sample elements.

As indicated by the PRCCs in Figure K6.5.1-7e,f and the regression analyses in Figure K6.5.1-8a,b, the uncertainty in *SZNP237*and *SZNP237C* is affected by a large number of variables. At 3000 yr, *SZGWSPDM* (groundwater specific discharge multiplier; as sampled, *SZGWSPDM* is actually the logarithm of the indicated multiplier) is the dominant variable affecting *SZNP237*and *SZNP237C*. Specifically, the regressions for *SZNP237*and *SZNP237C* at 3000 yr have R^2 values of 0.44 and 0.50 for models including only *SZGWSPDM*. However, the importance of *SZGWSPDM* diminishes with time. At 5000 yr, *SZGWSPDM* is the again the first variable selected in the regressions for *SZNP237*and *SZNP237C*, but the R^2 values are only 0.18 and 0.27. At 10,000 yr, *PHCSS* (pointer variable used to determine pH in CSNF cell 1 under liquid influx conditions) is the first variable selected in the regressions for *SZNP237*and *SZNP237C* but with R^2 values of only 0.21 and 0.22; in contrast, *SZGWSPDM* is now the fourth and third variable selected in the regressions for *SZNP237*and *SZNP237C*, respectively. This declining importance for *SZGWSPDM* results because *SZGWSPDM* affects the early arrival of ^{237}Np at the location of the RMEI but becomes less important with increasing time as additional variables start to affect the amount of ^{237}Np arriving at the location of the RMEI. Overall, the uncertainty in *SZNP237*and *SZNP237C* is determined by small effects associated with a large number of variables.

The analysis for *SZNP237C* at 10,000 yr is used as an example (Figure K6.5.1-8b). The first four variables selected in the regression analysis are *PHCSS*, *INFIL* (infiltration level), *SZGWSPDM*, and *SZFISPVO* (flowing interval spacing in volcanic unit of SZ, m). The negative effect associated with *PHCSS* results because increasing *PHCSS* increases pH, which (as long as pH is below about 9) tends to decrease Np solubility. The positive effects associated with the remaining variables result because (i) increasing *INFIL* increases water flow in the EBS and UZ and hence increases the release of ^{237}Np into the SZ, (ii) increasing *SZGWSPDM* increases water flow in the SZ, and (iii) increasing *SZFISPVO* decreases the diffusion of ^{237}Np from fractures in the volcanic unit of the SZ into the surrounding matrix. Together, these variables result in a model with an R^2 value of 0.56.

The next four variables selected are *EP1NPO2* (scale factor used to incorporate uncertainty into NpO_2 solubility below 1 molal ionic strength; as sampled, *EP1NPO2* is actually the logarithm of the indicated scale factor), *DELPPCO2* (scale factor used to incorporate uncertainty into the value for the partial pressure of CO_2), *EP1LOWAM* (scale factor used to incorporate uncertainty into americium solubility under low ionic strength conditions; as sampled, *EP1LOWAM* is actually the logarithm of the indicated scale factor), and *SZDIFCVO* (diffusion coefficient in fractured volcanic units, m^2/s) (Figure K6.5.1-8b). The positive effects associated with *EP1NPO2*, *DELPPCO2* and *EP1LOWAM* result from their influence on the amount of ^{237}Np that moves from the EBS (Section K6.3.1). The negative effect associated with *SZDIFCVO* results from increasing the amount of ^{237}Np that diffuses from fractures in the volcanic unit of the SZ to the surrounding matrix. The addition of these four variables raises the R^2 value for the model from 0.56 to 0.67.

After the first eight variables, the regression analysis selects the following six additional variables: *CORRATSS* (corrosion rate for stainless steel, μm/yr), *EP1LOWNU* (scale factor used to incorporate uncertainty into uranium solubility under low ionic strength conditions for nominal and seismic conditions; as sampled, *EP1LOWNU* is actually the logarithm of the indicated scale factor; in the present analysis, *EP1LOWNU* was used instead of the corresponding and intended variable *EP1LOWOU* for igneous conditions; however, this has no effect on analysis outcomes as *EP1LOWNU* and *EP1LOWOU* are assigned the same distribution), *COLGW* (concentration of groundwater colloids when colloids are stable, mg/L), *SZKDCSVO* (sorption coefficient for cesium in volcanic unit of SZ, mL/g), *SZKDNPVO* (sorption coefficient for neptunium in volcanic unit of SZ, mL/g), and *THERMCON* (host rock thermal conductivity level). The negative and positive effects of *CORRATSS* and *EP1LOWNU*, respectively, result from their influence on the amount of ^{237}Np that moves from the EBS (Section K6.3.1). The negative effect associated with *SZKDNPVO* results from its role in slowing the movement of ^{237}Np in the SZ. The small indicated effects associated with *COLGW*, *SZKDCSVO* and *THERMCON* are probably spurious. The model containing all 14 variables has an R^2 value of 0.74. Elimination of the three possibly spurious variables reduces the R^2 value to 0.72, which is only slightly higher than the R^2 value of 0.67 obtained with the first eight variables. The relatively low R^2 value for the final model is resulting from the large number of variables that have relatively small effects on *SZNP237C*.

The same general pattern of effects observed for *SZNP237C* at 10,000 yr also holds for *SZNP237*and *SZNP237C* at other times (Figure K6.5.1-8a,b).

As indicated by the scatterplots in Figure K6.5.1-9, substantial hold up of ^{237}Np occurs in the SZ.

Movement of Dissolved ^{239}Pu: *SZPU239* and *SZPU239C*. The uncertainty and sensitivity analyses for the time-dependent release rates (*SZPU239*, g/yr) and cumulative releases (*SZPU239C*, g) over the time interval [0, 20,000 yr] for the movement of dissolved ^{239}Pu across a subsurface plane at the location of the RMEI resulting from an igneous intrusive event at 10 yr that destroys all WPs in the repository are summarized in Figures K6.5.1-10, K6.5.1-11 and K6.5.1-12.

For many sample elements, there is no significant movement of ^{239}Pu through the SZ to the location of the RMEI (Figure K6.5.1-12). In particular, the uncertainty in whether or not significant movement of ^{239}Pu through the SZ to the location of the RMEI occurs is dominated by *SZGWSPDM* (groundwater specific discharge multiplier; as sampled, *SZGWSPDM* is actually the logarithm of the indicated multiplier), with no significant movement occurring when *SZGWSPDM* is less than 0 and often no significant movement occurring when *SZGWSPDM* is less than 0.5 (Figure K6.5.1-11f).

The PRCCs in Figure K6.5.1-10e,f and the regression analyses in Figure K6.5.1-11a,b are hindered in their effectiveness by the large number of effectively zero values for *SZPU239* and *SZPU239C*. However, the source of the uncertainty associated with *SZPU239* and *SZPU239C* is clearly revealed by the scatterplot in Figure K6.5.1-11f. Specifically, smaller values for *SZGWSPDM* result in no significant movement of ^{239}Pu through the SZ to the location of the RMEI, and when significant movement does occur, the values for *SZPU239* and *SZPU239C* tend to increase as *SZGWSPDM* increases.

The extensive retardation of ^{239}Pu in the SZ can also be seen in Figure K6.5.1-12.

Movement of Dissolved ^{99}Tc: *SZTC99* and *SZTC99C*. The uncertainty and sensitivity analyses for the time-dependent release rates (*SZTC99*, g/yr) and cumulative releases (*SZTC99C*, g) over the time interval [0, 20,000 yr] for the movement of dissolved ^{99}Tc across a subsurface plane at the location of the RMEI resulting from an igneous intrusive event at 10 yr that destroys all WPs in the repository are summarized in Figures K6.5.1-13, K6.5.1-14 and K6.5.1-15.

The movement of ^{99}Tc through the SZ is rapid (Figure K6.5.1-13a,b,c,d). With the exception of a small jump associated with the climate change at 2,000 yr, *SZTC99* monotonically decreases with time from an initial high value.

The PRCCs for *SZTC99* are very choppy because of the noise introduced into the analysis by the particle tracking algorithm used for solution of the transport equations in the UZ (Figure K6.5.1-13e). However, as indicated by both the PRCCs in Figure K6.5.1-13e and the regression analyses in Figure K6.5.1-14a, the most important variable with respect to the uncertainty in *SZTC99* is *INFIL* (infiltration level), with *SZTC99* tending to increase with increasing values for *INFIL* at early times and to decrease with increasing values for *INFIL* at later times. This pattern of effects results because increasing *INFIL* increases the early release of ^{99}Tc and thus reduces the amount of ^{99}Tc available for release at later times. Similarly, *SZGWSPDM* (groundwater specific discharge multiplier; as sampled, *SZGWSPDM* is actually the logarithm of the indicated multiplier) has a positive effect on *SZTC99* at early times and a negative effect on *SZTC99*at later times as a result of increasing the rate of ^{99}Tc movement through the SZ at early times and thus reducing the amount of ^{99}Tc available for release at later times. The PRCCs indicate a positive effect for *THERMCON* (host rock thermal conductivity level) prior to 1,000 yr as result of its influence on repository cooling and the time at which radionuclide movement from the repository begins (Figure K6.5.1-13e); specifically, increasing *THERMCON* results in earlier radionuclide releases from the EBS. Similarly to *INFIL* and *SZGWSPDM*, *SZFISPVO* (flowing interval spacing in volcanic unit of SZ, m). has positive effect on *SZTC99* at early times and a negative effect at later times; again, this pattern results from

increasing the release of ^{99}Tc at early times and thus reducing the amount of ^{99}Tc available for release at later times. In contrast, *SZFIPOVO* (flowing interval porosity in the volcanic unit of the SZ) has the opposite pattern of effects, with increasing values for *SZFIPOVO* tending to decrease *SZTC99* at early times and increase *SZTC99* at later times. This pattern results because increasing *SZFIPOVO* slows water flow in the SZ, which reduces the release of ^{99}Tc at early times and thus results in larger values for *SZTC99* at later times. Further, *CSNFMASS* (scale factor used to characterize uncertainty in amount of CSNF in CSNF WPs) has a positive effect on *SZTC99* because of its role in defining the amount of ^{99}Tc in the repository.

The effects of *INFIL*, *SZGWSPDM* and *SZFISPVO* on *SZTC99* at 10,000 yr can be seen in the scatterplots in Figure K6.5.1-14c,d,e.

The PRCCs in Figure K6.5.1-13f indicate the same early time effects of *THERMCON* and *SZFIPOVO* on *SZTC99C* as previously discussed for *SZTC99*. Then, as time increases, the PRCCs indicate that the dominant variables are *CSNFMASS*, *SZGWSPDM INFIL* and *SZFISPVO*, with *SZTC99C* tending to increase as each of these variables increases. These effects result because (i) increasing *CSNFMASS* increases the amount of ^{99}Tc present in the repository, (ii) increasing *SZGWSPDM* increases water flow in the SZ, (iii) increasing *INFIL* increases the release of ^{99}Tc from the UZ to the SZ, and (iv) increasing *SZFISPVO* reduces the movement of ^{99}Tc from fractures in the volcanic unit of the SZ to the surrounding matrix. Similar effects are indicated in the regression analyses in Figure K6.5.1-14b. Specifically, the analyses for *SZTC99C* at 3000, 5000 and 10,000 yr all pick *CSNFMASS*, *SZGWSPDM*, *INFIL* and *SZFISPVO* as the first four variables, although not in the same order, and produce models with R^2 values of 0.75, 0.77 and 0.81, respectively. Thus, *CSNFMASS*, *SZGWSPDM*, *INFIL* and *SZFISPVO* give rise to most of the uncertainty in *SZTC99C*. The fifth variable selected in each of the regressions in Figure K6.5.1-14b is *SZDIFCVO* (diffusion coefficient in fractured volcanic units, m^2/s), with *SZTC99C* tending to decrease as *SZDIFCVO* increases. The negative effect associated with *SZDIFCVO* results from increasing the amount of ^{99}Tc that diffuses from fractures in the volcanic unit of the SZ to the surrounding matrix. The inclusion of *SZDIFCVO* increases the R^2 values to 0.80, 0.81 and 0.85 for the three regression models.

The dominant effects of *CSNFMASS*, *SZGWSPDM* and *INFIL* on *SZTC99C* at 10,000 yr can be seen in the scatterplots in Figure K6.5.1-14f,g,h.

As shown in Figure K6.5.1-15, there can be a substantial delay in the movement of ^{99}Tc in the SZ from the discharge location of the UZ to the location of the RMEI over time periods of 1,000 and 3000 yr. However, as the time period increases to 10,000 yr, substantial movement of ^{99}Tc to the location of the RMEI takes place.

K6.5.2 Igneous Intrusive Scenario Classes: Release from Saturated Zone (SZ) beyond 20,000 yr for an Event at 250 yr

For completeness, this section presents summaries of the uncertainty and sensitivity analyses for release from the SZ beyond 20,000 yr for an igneous intrusive event at 250 yr that destroys all WPs in the repository without discussion. Section K6.5.1 presents uncertainty and sensitivity analyses for release from the SZ over the time interval [0, 20,000 yr] for an intrusion that occurs

at 10 yr. The uncertainties affecting release from the SZ following an intrusion at 250 yr are similar to the uncertainties affecting release from the SZ following an intrusion at 10 yr.

Movement of ^{239}Pu Irreversibly Attached to Slow (i.e., Ic) Colloids: *SZIC239* and *SZIC239C*. The uncertainty and sensitivity analyses for the time-dependent release rates (*SZIC239*, g/yr) and cumulative releases (*SZIC239C*, g) over the time interval [0, 200,000 yr] for the movement of ^{239}Pu irreversibly attached to slow (i.e., Ic) colloids across a subsurface plane at the location of the RMEI resulting from an igneous intrusive event at 250 yr that destroys all WPs in the repository are summarized in Figure K6.5.2-1.

Movement of ^{239}Pu Irreversibly Attached to Fast (i.e., If) Colloids: SZ*IF239* and *SZIF239C*. The uncertainty and sensitivity analyses for the time-dependent release rates (*SZIF239*, g/yr) and cumulative releases (*SZIF239C*, g) over the time interval [0, 200,000 yr] for the movement of ^{239}Pu irreversibly attached to fast (i.e., If) colloids across a subsurface plane at the location of the RMEI resulting from an igneous intrusive event at 250 yr that destroys all WPs in the repository are summarized in Figure K6.5.2-2.

Movement of Dissolved ^{237}Np: *SZNP237* and *SZNP237C*. The uncertainty and sensitivity analyses for the time-dependent release rates (*SZNP237*, g/yr) and cumulative releases (*SZNP237C*, g) over the time interval [0, 1,000,000 yr] for the movement of dissolved ^{237}Np across a subsurface plane at the location of the RMEI resulting from an igneous intrusive event at 250 yr that destroys all WPs in the repository are summarized in Figure K6.5.2-3.

Movement of Dissolved ^{239}Pu: *SZPU239* and *SZPU239C*. The uncertainty and sensitivity analyses for the time-dependent release rates (*SZPU239*, g/yr) and cumulative releases (*SZPU239C*, g) over the time interval [0, 200,000 yr] for the movement of dissolved ^{239}Pu across a subsurface plane at the location of the RMEI resulting from an igneous intrusive event at 250 yr that destroys all WPs in the repository are summarized in Figure K6.5.2-4.

Movement of Dissolved ^{99}Tc: *SZTC99* and *SZTC99C*. The uncertainty and sensitivity analyses for the time-dependent release rates (*SZTC99*, g/yr) and cumulative releases (*SZTC99C*, g) over the time interval [0, 1,000,000 yr] for the movement of dissolved ^{99}Tc across a subsurface plane at the location of the RMEI resulting from an igneous intrusive event at 250 yr that destroys all WPs in the repository are omitted because of the rapid transport of ^{99}Tc through the repository system (see Figure K6.3.1-9a,c).

K6.6 Igneous Intrusive Scenario Classes: Dose to Reasonably Maximally Exposed Individual

This section presents analysis results for dose to the RMEI from individual radionuclides for the time intervals [0, 20,000 yr] and [0, 1,000,000 yr].

K6.6.1 Igneous Intrusive Scenario Classes: Dose to Reasonably Maximally Exposed Individual over the Time Interval [0, 20,000 yr] for an Event at 10 yr

Dose to RMEI from ^{239}Pu Irreversibly Attached to Slow (i.e., Ic) Colloids: *DOIC239*. The uncertainty and sensitivity analyses for dose to the RMEI (*DOIC239*, mrem/yr) over the time interval [0, 20,000 yr] for the movement of ^{239}Pu irreversibly attached to slow (i.e., Ic) colloids across a subsurface plane at the location of the RMEI resulting from an igneous intrusive event at 10 yr that destroys all WPs in the repository are summarized in Figures K6.6.1-1 and K6.6.1-2.

The uncertainty in *DOIC239* is dominated by the uncertainty in the groundwater concentration of ^{239}Pu irreversibly attached to slow (i.e., Ic) colloids at the location of the RMEI. This concentration is proportional to *SZIC239*. As shown by the scatterplot in Figure K6.6.1-2e, the uncertainty in *DOIC239* is small relative to the uncertainty in *SZIC239*. As a result, the sensitivity analyses for *DOIC239* in Figures K6.6.1-1 and K6.6.1-2 are very similar to the sensitivity analyses for *SZIC239* in Figures K6.5.1-1 and K6.5.1-2. Because of this similarity, the discussion of the sensitivity analyses for *SZIC239* is also applicable to the sensitivity analyses for *DOIC239*. For this reason, the sensitivity analyses for *DOIC239* will not be extensively discussed.

The similarity of the sensitivity analyses for *DOIC239* and *SZIC239* results because the impact of the uncertainty in the dose conversion factor *MICPU239* (dose conversion factor for ^{239}Pu for modern interglacial climate, (rem/yr)/(pCi/L)) is small relative to the impact of the uncertainty in other variables that effect *SZIC239* and hence *DOIC239*. For example, *MICPU239* is the sixth variable selected in the regression analysis for *DOIC239* at 10,000 yr and only raises the R^2 value from 0.50 to 0.52 (Figure K6.5.1-2a).

The regressions for *DOIC239* also indicate small effects for *MICI129* (dose conversion factor for ^{129}I for modern interglacial climate, (rem/yr)/(pCi/L)) and *MICCL36* (dose conversion factor for ^{36}Cl for modern interglacial climate, (rem/yr)/(pCi/L)) (Figure K6.5.1-2a). These selections are spurious and may result from underlying correlations involving *MICPU239*, *MICI129* and *MICCL36* that derive from the presence of common underlying variables in the determination of the uncertainty distributions used for dose conversion factors.

Dose to RMEI from ^{239}Pu Irreversibly Attached to Fast (i.e., If) Colloids: *DOIF239*. The uncertainty and sensitivity analyses for dose to the RMEI (*DOIF239*, mrem/yr) over the time interval [0, 20,000 yr] for the movement of ^{239}Pu irreversibly attached to fast (i.e., If) colloids across a subsurface plane at the location of the RMEI resulting from an igneous intrusive event at 10 yr that destroys all WPs in the repository are summarized in Figures K6.6.1-3 and K6.6.1-4.

Similarly to *DOIC239*, the uncertainty in *DOIF239* is dominated by the uncertainty in the groundwater concentration of ^{239}Pu irreversibly attached to fast (i.e., If) colloids at the location of the RMEI. This concentration is proportional to *SZIF239*. As shown by the scatterplot in Figure K6.6.1-4e, the uncertainty in *DOIF239* is small relative to the uncertainty in *SZIF239*. As a result, the sensitivity analyses for *DOIF239* in Figures K6.6.1-3 and K6.6.1-4 are very similar to the sensitivity analyses for *SZIF239* in Figures K6.5.1-4 and K6.5.1-5. Because of this similarity, the discussion of the sensitivity analyses for *SZIF239* is also applicable to the

sensitivity analyses for *DOIF239*. For this reason, the sensitivity analyses for *DOIF239* will not be extensively discussed.

The similarity of the sensitivity analyses for *DOIF239* and *SZIF239* results because the impact of the uncertainty in the dose conversion factor *MICPU239* (dose conversion factor for ^{239}Pu for modern interglacial climate, (rem/yr)/(pCi/L)) is small relative to the impact of the uncertainty in other variables that effect *SZIF239* and hence *DOIF239*. For example, *MICPU239* is the third variable selected in the regression analysis for *DOIF239* at 10,000 yr and raises the R^2 value from 0.81 to 0.91 (Figure K6.5.1-4a).

Dose to RMEI from Dissolved ^{237}Np: *DONP237*. The uncertainty and sensitivity analyses for dose to the RMEI (*DONP237*, mrem/yr) over the time interval [0, 20,000 yr] for the movement of dissolved ^{237}Np across a subsurface plane at the location of the RMEI resulting from an igneous intrusive event at 10 yr that destroys all WPs in the repository are summarized in Figures K6.6.1-5 and K6.6.1-6.

Similarly to *DOIC239* and *DOIF239*, the uncertainty in *DONP237* is dominated by the uncertainty in the groundwater concentration of dissolved ^{237}Np at the location of the RMEI. This concentration is proportional to *SZNP237*. As shown by the scatterplot in Figure K6.6.1-6e, the uncertainty in *DONP237* is small relative to the uncertainty in *SZNP237*. As a result, the sensitivity analyses for *DONP237* in Figures K6.6.1-5 and K6.6.1-6 are very similar to the sensitivity analyses for *SZNP237* in Figures K6.5.1-7 and K6.5.1-8. Because of this similarity, the discussion of the sensitivity analyses for *SZNP237* is also applicable to the sensitivity analyses for *DONP237*. For this reason, the sensitivity analyses for *DONP237* will not be extensively discussed.

The similarity of the sensitivity analyses for *DONP237* and *SZNP237* results because the impact of the uncertainty in the dose conversion factor *MICNP237* (dose conversion factor for ^{237}Np for modern interglacial climate, (rem/yr)/(pCi/L)) is small relative to the impact of the uncertainty in other variables that effect *SZNP237* and hence *DONP237*. For example, *MICNP237* is the seventh variable selected in the regression analysis for *DONP237*at 10,000 yr and only raises the R^2 value from 0.61 to 0.64 (Figure K6.5.1-6a).

The regressions for *DONP237* also indicate small effects for *MICTH229* (dose conversion factor for ^{229}Th for modern interglacial climate, (rem/yr)/(pCi/L)) at 3000 and 5000 yr (Figure K6.5.1-6a). These effects are spurious and result from underlying correlations involving *MICNP237* and *MICTH229* that derive from the presence of common underlying variables in the determination of the uncertainty distributions used for dose conversion factors.

Dose to RMEI from Dissolved ^{239}Pu: *DOPU239*. The uncertainty and sensitivity analyses for dose to the RMEI (*DOPU239*, mrem/yr) over the time interval [0, 20,000 yr] for the movement of dissolved ^{239}Pu across a subsurface plane at the location of the RMEI resulting from an igneous intrusive event at 10 yr that destroys all WPs in the repository are summarized in Figures K6.6.1-7 and K6.6.1-8.

The uncertainty in *DOPU239* is totally dominated by the uncertainty in *SZPU239* (Figure K6.6.1-8e). Therefore, the discussion associated with the sensitivity analyses for

SZPU239 presented in Figures K6.5.1-10 and K6.5.1-11 also applies to the sensitivity analyses for *DOPU239*. The appearance of *MICC14* (dose conversion factor for ^{14}C for modern interglacial climate, (rem/yr)/(pCi/L)) in the regression for *DOPU239* at 10,000 yr is spurious and results from the previously discussed correlations involving the dose conversion factors.

Dose to RMEI from Dissolved ^{99}Tc: *DOTC99*. The uncertainty and sensitivity analyses for dose to the RMEI (*DOTC99*, mrem/yr) over the time interval [0, 20,000 yr] for the movement of dissolved ^{99}Tc across a subsurface plane at the location of the RMEI resulting from an igneous intrusive event at 10 yr that destroys all WPs in the repository are summarized in Figures K6.6.1-9 and K6.6.1-10.

Unlike the other doses considered in this section, the uncertainty in *DOTC99* is not dominated by the corresponding radionuclide flux (i.e., *SZTC99*) at the location of the RMEI (Figure K6.6.1-10e). Because of this, *MICTC99* (dose conversion factor for ^{99}Tc for modern interglacial climate, (rem/yr)/(pCi/L)) is an important contributor to the uncertainty in *DOTC99* (Figures K6.6.1-9c and K6.6.1-10a). The important effect of *MICTC99* on the uncertainty in *DOTC99* is shown by *MICTC99* having the largest PRCC in Figure K6.6.1-9c and being the first variable selected in each of the regressions in Figure K6.6.1-10a.

K6.6.2 Igneous Intrusive Scenario Classes: Dose to Reasonably Maximally Exposed Individual over the Time Interval [0, 1,000,000 yr] for an Event at 250 yr

For completeness, this section presents summaries of the uncertainty and sensitivity analyses for dose to the RMEI over the time interval [0, 1,000,000 yr] for an igneous intrusive event at 250 yr that destroys all WPs in the repository without discussion.

Dose to RMEI from ^{239}Pu Irreversibly Attached to Slow (i.e., Ic) Colloids: *DOIC239*. The uncertainty and sensitivity analyses for dose to the RMEI (*DOIC239*, mrem/yr) over the time interval [0, 200,000 yr] for the movement of ^{239}Pu irreversibly attached to slow (i.e., Ic) colloids across a subsurface plane at the location of the RMEI resulting from an igneous intrusive event at 250 yr that destroys all WPs in the repository are summarized in Figure K6.6.2-1.

Dose to RMEI from ^{239}Pu Irreversibly Attached to Fast (i.e., If) Colloids: *DOIF239*. The uncertainty and sensitivity analyses for dose to the RMEI (*DOIF239*, mrem/yr) over the time interval [0, 200,000 yr] for the movement of ^{239}Pu irreversibly attached to fast (i.e., If) colloids across a subsurface plane at the location of the RMEI resulting from an igneous intrusive event at 250 yr that destroys all WPs in the repository are summarized in Figure K6.6.2-2.

Dose to RMEI from Dissolved ^{237}Np: *DONP237*. The uncertainty and sensitivity analyses for dose to the RMEI (*DONP237*, mrem/yr) over the time interval [0, 1,000,000 yr] for the movement of dissolved ^{237}Np across a subsurface plane at the location of the RMEI resulting from an igneous intrusive event at 250 yr that destroys all WPs in the repository are summarized in Figure K6.6.2-3.

Dose to RMEI from Dissolved ^{239}Pu: *DOPU239*. The uncertainty and sensitivity analyses for dose to the RMEI (*DOPU239*, mrem/yr) over the time interval [0, 200,000 yr] for the movement

of dissolved ^{239}Pu across a subsurface plane at the location of the RMEI resulting from an igneous intrusive event at 250 yr that destroys all WPs in the repository are summarized in Figure K6.6.2-4.

Dose to RMEI from Dissolved ^{99}Tc: *DOTC99*. The uncertainty and sensitivity analyses for dose to the RMEI (*DOTC99*, mrem/yr) over the time interval [0, 1,000,000 yr] for the movement of dissolved ^{99}Tc across a subsurface plane at the location of the RMEI resulting from an igneous intrusive event at 250 yr that destroys all WPs in the repository are omitted because of the rapid depletion of the ^{99}Tc inventory (see Figure K6.3.1-9a,c).

K6.7 Igneous Intrusive Scenario Classes: Expected Dose (*EXPDOSE*) to Reasonably Maximally Exposed Individual

This section presents analysis results for expected dose to the RMEI resulting from igneous intrusions over the time intervals [0, 20,000 yr] and [0, 1,000,000 yr].

K6.7.1 Igneous Intrusive Scenario Classes: Expected Dose (*EXPDOSE*) to Reasonably Maximally Exposed Individual over [0, 20,000 yr]

The uncertainty and sensitivity analyses for expected dose to the RMEI (*EXPDOSE*, mrem/yr) over the time interval [0, 20,000 yr] resulting from igneous intrusion are summarized in Figures K6.7.1-1 and K6.7.1-2. Initial transport to the location of the RMEI takes up to 2000 yr; after the earliest possible arrival time for released radionuclides at the location of the RMEI, *EXPDOSE* increases monotonically with time (Figure K6.7.1-1a,b). At 10,000 yr, the value for *EXPDOSE* falls between 10^{-4} and 1 mrem/yr for most sample elements, with a few sample elements having values for *EXPDOSE* between 1 and 10 mrem/yr.

The PRCCs in Figure K6.7.1-1c indicate that the uncertainty in *EXPDOSE* is dominated by *IGRATE* (rate of occurrence of igneous intrusive events, yr^{-1}), with the value for *EXPDOSE* increasing as *IGRATE* increases. This effect results because increasing *IGRATE* increases the probability that an igneous intrusive event will occur and hence increases *EXPDOSE*.

In addition to *IGRATE*, smaller effects are indicated for *SZGWSPDM* (groundwater specific discharge multiplier; as sampled, *SZGWSPDM* is actually the logarithm of the indicated multiplier), *SZFIPOVO* (flowing interval porosity in the volcanic unit of the SZ), *SZCOLRAL* (colloid retardation factor in alluvial unit of SZ, dimensionless; as sampled, *SZCOLRAL* is actually the logarithm of the indicated retardation factor), *INFIL* (infiltration level), and *SZDENAL* (density of alluvial unit of the SZ, kg/m^3) (Figure K6.7.1-1c). The variables *SZGWSPDM* and *INFIL* have positive effects on *EXPDOSE*, with these effects resulting because increasing *SZGWSPDM* increases water flow in the SZ and increasing *INFIL* increases water flow through the EBS and UZ. The variables *SZFIPOVO*, *SZCOLRAL* and *SZDENAL* have negative effects on *EXPDOSE*, with these effects resulting because increasing *SZFIPOVO* slows flow in the SZ and increasing *SZCOLRAL* and *SZDENAL* increases retardation in the alluvial unit of the SZ.

More detailed sensitivity analyses for *EXPDOSE* are provided by the regression analyses in Figure K6.7.1-2a. The dominant effect of *IGRATE* on the uncertainty in *EXPDOSE* is indicated

by R^2 values of 0.74, 0.80 and 0.78 for the regressions containing only *IGRATE* at 3000, 5000 and 10,000 yr. After *IGRATE*, the most important variable is *SZGWSPDM*. However the incremental effect associated with *SZGWSPDM* is small as the R^2 values for the regression models containing both *IGRATE* and *SZGWSPDM* are 0.79, 0.84 and 0.83.

After *IGRATE* and *SZGWSPDM*, all three regressions select *MICTC99* (dose conversion factor for ^{99}Tc for modern interglacial climate, (rem/yr)/(pCi/L)) and *INFIL* as the next two variables to include in the model, with *EXPDOSE* tending to increase as each of these variables increases (Figure K6.7.1-2a). These effects result because increasing *MICTC99* increases the received dose for a given exposure to ^{99}Tc and increasing *INFIL* increases water flow in the EBS and UZ. Inclusion of *IGRATE*, *SZGWSPDM*, *MICTC99* and *INFIL* in the regression models results in R^2 values of 0.86, 0.89 and 0.86. Thus, *IGRATE*, *SZGWSPDM*, *MICTC99* and *INFIL* account for most of the uncertainty in *EXPDOSE*, with the dominant contribution coming from *IGRATE*. After these four variables, the individual regressions pick an additional 10, 11 and 9 variables, respectively, that have small effects on *EXPDOSE* (Figure K6.7.1-2a). The final regressions have R^2 values of 0.91, 0.93 and 0.92, which indicates that most of the uncertainty in *EXPDOSE* is being accounted for.

The dominant effect of *IGRATE* on the uncertainty in *EXPDOSE* can be seen in the scatterplot in Figure K6.7.1-2b. The much smaller effects associated with *SZGWSPDM* and *MICTC99* can be seen in the scatterplots in Figure K6.7.1-2c,d.

K6.7.2 Igneous Intrusive Scenario Classes: Expected Dose (*EXPDOSE*) to Reasonably Maximally Exposed Individual over [0, 1,000,000 yr]

The uncertainty and sensitivity analyses for expected dose to the RMEI (*EXPDOSE*, mrem/yr) over the time interval [0, 1,000,000 yr] resulting from igneous intrusion are summarized in Figures K6.7.2-1 and K6.7.2-2. The values for *EXPDOSE* tend to increase until about 100,000 yr and then decrease until about 200,000 yr (Figure K6.7.2-1a,b). This behavior results because, with increasing time, more and more potential igneous intrusive events contribute to *EXPDOSE*. As a result, *EXPDOSE* initially increases with time. However, ^{239}Pu is an important contributor to *EXPDOSE* and has a half life of 24,100 yr. As a result, the contribution of ^{239}Pu to *EXPDOSE* declines after 100,000 yr and causes the drop in *EXPDOSE* between 100,000 and 200,000 yr. After 200,000 yr, *EXPDOSE* again increases due to the increasing number of potential igneous intrusions but without a significant contribution from ^{239}Pu.

The PRCCs in Figure K6.7.2-1c indicate that the uncertainty in *EXPDOSE* is dominated by *IGRATE* (rate of occurrence of igneous intrusive events, yr^{-1}), with the value for *EXPDOSE* increasing as *IGRATE* increases. This effect results because increasing *IGRATE* increases the probability that an igneous intrusive event will occur and hence increases *EXPDOSE*.

In addition to *IGRATE*, smaller effects are indicated for *SZGWSPDM* (groundwater specific discharge multiplier; as sampled, *SZGWSPDM* is actually the logarithm of the indicated multiplier), *SZFIPOVO* (flowing interval porosity in the volcanic unit of the SZ), *SZCOLRAL* (colloid retardation factor in alluvial unit of SZ; as sampled, *SZCOLRAL* is actually the logarithm of the indicated retardation factor), *EP1LOWPU* (scale factor used to represent

uncertainty in plutonium solubility in solutions below 1 molal ionic strength; as sampled, *EP1LOWPU* is actually the logarithm of the indicated scale factor) and *INFIL* (infiltration level) (Figure K6.7.2-1c). With the exception of *EP1LOWPU*, the preceding variables were also identified in the analysis in Figure K6.7.1-1c for the 0 to 20,000 yr time period. The variables *SZGWSPDM, EP1LOWPU* and *INFIL* have positive effects on *EXPDOSE*, with these effects resulting because increasing *SZGWSPDM* increases water flow in the SZ, increasing *EP1LOWPU* increases the solubility of plutonium, and increasing *INFIL* increases water flow through the EBS and UZ. The variables *SZFIPOVO* and *SZCOLRAL* have negative effects on *EXPDOSE*, with these effects resulting because increasing *SZFIPOVO* slows flow in the SZ and increasing *SZCOLRAL* increases retardation in the alluvial unit of the SZ. However, the negative effects associated with *SZFIPOVO* and *SZCOLRAL* occur prior to 200,000 yr, with the PRCCs indicating little effect for these variables on the uncertainty in *EXPDOSE* after this time.

More detailed sensitivity analyses for *EXPDOSE* are provided by the regression analyses in Figure K6.7.2-2a. The dominant effect of *IGRATE* on the uncertainty in *EXPDOSE* is indicated by R^2 values of 0.52, 0.55 and 0.59 for the regressions containing only *IGRATE* at 50,000, 200,000 and 500,000 yr. After *IGRATE*, the most important variable is *SZGWSPDM*. However the incremental effect associated with *SZGWSPDM* is moderate as the R^2 values for the regression models containing both *IGRATE* and *SZGWSPDM* are 0.69, 0.69 and 0.68.

The analyses at 50,000 and 200,000 yr then select *EP1LOWPU* and *INFIL* as the next two variables, and the analysis at 500,000 yr selects *INFIL* and flowing interval spacing in the volcanic unit of the SZ (*SZFISPVO*) as the next two variables (Figure K6.7.2-2a). The effects of *EP1LOWPU* and *INFIL* on *EXPDOSE* have already been discussed. The positive effect associated with *SZFISPVO* results from reducing the surface area associated with fractures in the volcanic unit of the SZ; in turn, this reduces radionuclide movement from fractures into the surrounding matrix and thus reduces radionuclide movement to the location of the RMEI. The regression models with the indicated variables now have R^2 values of 0.77, 0.76 and 0.75. After the first four variables, the individual regressions pick an additional 10, 9 and 10 variables, respectively, that have small effects on *EXPDOSE* (Figure K6.7-4a). The final regressions have R^2 values of 0.85, 0.85 and 0.84, which indicates that most of the uncertainty in *EXPDOSE* is being accounted for.

The dominant effect of *IGRATE* on the uncertainty in *EXPDOSE* can be seen in the scatterplot in Figure K6.7.2-2b. The much smaller effects associated with *SZGWSPDM* and *INFIL* can be seen in the scatterplots in Figure K6.7.2-2c,d.

K6.8 Igneous Eruptive Scenario Classes: Expected Dose (*EXPDOSE*) to Reasonably Maximally Exposed Individual

This section presents analysis results for expected dose to the RMEI resulting from igneous eruptions for the time intervals [0, 20,000 yr] and [0, 1,000,000 yr].

K6.8.1 Igneous Eruptive Scenario Classes: Expected Dose (*EXPDOSE*) to Reasonably Maximally Exposed Individual over [0, 20,000 yr]

The uncertainty and sensitivity analyses for expected dose to the RMEI (*EXPDOSE*, mrem/yr) over the time interval [0, 20,000 yr] resulting from igneous eruptive events are summarized in Figures K6.8.1-1 and K6.8.1-2. The values for *EXPDOSE* range between 10^{-7} and 10^{-3} mrem/yr and show a slight tendency to increase with time (Figure K6.8.1-1a,b). The relative flatness of *EXPDOSE* with time results from the rapid decrease of dose to the RMEI after individual eruptive events. As a result, *EXPDOSE* shows little increase with time as increasing numbers of potential eruptive events are included in its calculation.

The PRCCs in Figure K6.8.1-1c indicate that the uncertainty in *EXPDOSE* is dominated by *IGERATE* (rate of occurrence of igneous eruptive events, yr^{-1}; *IGERATE* = (0.28)(0.2968)*IGRATE*, where 0.28 is the probability that an igneous intrusive event will have an eruptive component, 0.2968 is the probability that the eruptive component of an igneous intrusive event will intercept waste, and *IGRATE* is the rate of occurrence (yr^{-1}) of igneous intrusive events), with the value for *EXPDOSE* increasing as *IGERATE* increases. This effect results because increasing *IGERATE* increases the probability that an igneous eruptive event will occur and hence increases *EXPDOSE*.

Smaller effects on *EXPDOSE* are indicated for *INHLTPV* (pointer variable for long-term inhalation dose), *DDIVIDE* (diffusivity of radionuclides in divides of the Fortymile Wash alluvial fan, cm^2/yr), *CSNFMASS* (scale factor used to characterize uncertainty in radionuclide content of CSNF, dimensionless), and *DASHAVG* (mass median ash particle diameter, cm) (Figure K6.8.1-1c). Increasing *INHLTPV* increases the BDCF for all radionuclides contributing to long-term inhalation dose. Increasing *DDIVIDE* increases the rate at which radionuclides diffuse downward and out of the biosphere and thus reduces *EXPDOSE*. Increasing *CSNFMASS* increases the mass of radionuclides intercepted by eruptive events. Increasing *DASHAVG* increases the fraction of ash mass consisting of larger ash particles, which in turn permits an increased fraction of the waste particles to be incorporated into ash particles and thus results in a larger fraction of the waste affected by the eruption being deposited in contaminated tephra.

More detailed sensitivity analyses for *EXPDOSE* are provided by the regression analyses in Figure K6.8.2-2a at 3000, 5000 and 10,000 yr. The three regression analyses are almost identical and each contains the following four variables in the same order: *IGERATE*, *INHLTPV*, *DDIVIDE*, *CSNFMASS*, and *DASHAVG*. The dominant effect of *IGERATE* on the uncertainty in *EXPDOSE* is indicated by R^2 values of 0.76, 0.76 and 0.76 for the regressions containing only *IGERATE*. After *IGERATE*, the most important variable is *INHLTPV*. However the incremental effect associated with *INHLTPV*is significant as the R^2 value for the regression models containing both *IGERATE* and *DDIVIDE* is 0.91. Inclusion of *DDIVIDE*, *CSNFMASS* and *DASHAVG* in the regression models brings the final R^2 value up to 0.95.

The dominant effect of *IGERATE* on the uncertainty in *EXPDOSE* and the lesser effects of *INHLTPV* and *DDIVIDE* can be seen in the scatterplots in Figure K6.8.1-2b,c.d.

K6.8.2 Igneous Eruptive Scenario Classes: Expected Dose (*EXPDOSE*) to Reasonably Maximally Exposed Individual over [0, 1,000,000 yr]

The uncertainty and sensitivity analyses for expected dose to the RMEI (*EXPDOSE*, mrem/yr) over the time interval [0, 1,000,000 yr] resulting from igneous eruptive events are summarized in Figures K6.8.2-1 and K6.8.2-2. The values for *EXPDOSE* tend to increase up to 50,000 yr, then decrease up to 150,000 yr, and then slowly increase again (Figure K6.8.2-1a,b). This pattern results from an initial build up of the contribution of multiple possible igneous eruptive events over the first 50,000 yr to *EXPDOSE*. Then, *EXPDOSE* decreases up to about 150,000 yr because of the decay of radionuclides such as ^{239}Pu. After 150,000 yr, *EXPDOSE* increases again from the build up of the contributions of multiple possible igneous eruptive events. The relatively slow increase of *EXPDOSE* after 150,000 yr results from the rapid decrease of dose to the RMEI after individual eruptive events. Overall, the values for *EXPDOSE* are small and range between 10^{-7} and 10^{-3} mrem/yr (Figure K6.8.2-1a,b).

The PRCCs in Figure K6.8.2-1c indicate that the uncertainty in *EXPDOSE* is dominated by *IGERATE* (rate of occurrence of igneous eruptive events, yr^{-1}; *IGERATE* = (0.28)(0.2968)*IGRATE*, where 0.28 is the probability that an igneous intrusive event will have an eruptive component, 0.2968 is the probability that the eruptive component of an igneous intrusive event will intercept waste, and *IGRATE* is the rate of occurrence (yr^{-1}) of igneous intrusive events), with the value for *EXPDOSE* increasing as *IGERATE* increases. This effect results because increasing *IGERATE* increases the probability that an igneous eruptive event will occur and hence increases *EXPDOSE*.

Smaller effects on *EXPDOSE* are indicated for *INHLTPV* (pointer variable for long-term inhalation dose), *FRACCHNL* (fraction of Fortymile Wash alluvial fan subject to fluvial deposition), *DDIVIDE* (diffusivity of radionuclides in divides of the Fortymile Wash alluvial fan, cm^2/yr), *BTILLAGE* (depth of soil within which radionuclides contribute to dose from external exposure, m), and *CSNFMASS* (scale factor used to characterize uncertainty in radionuclide content of CSNF). Increasing *INHLTPV* increases the BDCF for all radionuclides contributing to long-term inhalation dose. Increasing *FRACCHNL* increases the area on which redistributed tephra is deposited. Within a relatively short time after an eruption, the radionuclide concentration in redistributed tephra in channels is much higher than in the surface soil layers on divides. As a consequence, increasing *FRACCHNL* has the effect of increasing the spatially-averaged radionuclide concentration at the RMEI location from all eruptions preceding a specific time *t*, and thus effectively increases *EXPDOSE* at time *t*. Increasing *DDIVIDE* increases the rate at which radionuclides diffuse downward past the tillage depth and out of the biosphere. Increasing *BTILLAGE* increases the depth to which radionuclides remain accessible to the biosphere through plant root uptake and other processes. Increasing *CSNFMASS* increases the mass of radionuclides intercepted by eruptive events.

The reduction in importance of *INHLTPV* after 50,000 yr is due to two factors: (i) the decay of ^{239}Pu, which is the primary radionuclide contributing to inhalation dose from igneous eruptive events during the first 100,000 years (Figure 8.2-10), and (ii) the reduction in contribution to annual dose from inhalation pathways. The dose from plutonium occurs primarily though the inhalation pathways (SNL 2007 [DIRS 177399], Table 6.14-2). The radionuclides considered for dose through inhalation pathways are limited to the resuspendable mass very near the surface

(i.e. within a depth defined by *RSUSTHIK*. Diffusion out of this depth is relatively rapid, hence the contribution from inhalation pathways to annual dose is reduced with time. The change in importance of *BTILLAGE* between 0 yr and 200,000 yr is due to the increasing importance of the external exposure pathway with time. The input variable *BTILLAGE* is used to estimate the mass of radionuclides below the near-surface layers of soil that contribute to annual dose from external exposure pathways (SNL 2007 [DIRS 177399], Section 6.4.1.1). Before 100,000 yr, ^{239}Pu and ^{240}Pu are the major contributors to dose from eruptive events. These radionuclides have relatively low rates of plant uptake, with the result that plutonium below the critical depth *RSUSTHIK* but within the tillage depth given by *BTILLAGE* contributes little to dose from external exposure, and thus has little effect on annual dose. After roughly 100,000 yr, the major contributor to annual dose is ^{226}Ra, which has a large contribution to dose from external exposure. The Biosphere Model conservatively assumes that all radionuclides down to the tillage depth (*BTILLAGE*) contribute to dose from external exposure. Thus, as ^{226}Ra becomes the dominant radionuclide, the influence of *BTILLAGE* increases. The change in importance of *FRACCHNL* parallels the change in importance of *BTILLAGE* because increasing the area on which redistributed tephra is deposited increases the mass of radionuclides in the soil down to the depth given by *BTILLAGE*.

More detailed sensitivity analyses for *EXPDOSE* are provided by the regression analyses in Figure K6.8.2-2a. The dominant effect of *IGERATE* on the uncertainty in *EXPDOSE* is indicated by R^2 values of 0.80, 0.86 and 0.86 for the regressions containing only *IGERATE* at 50,000, 200,000 and 500,000 yr.

After *IGERATE*, the regression for *EXPDOSE* at 50,000 yr selects *INHLTPV*, *DDIVIDE*, *CSNFMASS*, *FRACCHNL*, *DASHAVG*, *BTILLAGE*, *CRITSLOP* (critical gradient for tehpra mobilization from hillsides) and *DCHANL* (diffusivity of radionuclides in channels of the Fortymile Wash alluvial fan, cm^2/yr) and produces a final model with an R^2 values of 0.96 (Figure K6.8.2-2a). Thus, most of the uncertainty in *EXPDOSE* at 50,000 yr is being accounted for. The effects of *INHLTPV*, *DDIVIDE*, *CSNFMASS*, *FRACCHNL*, *DASHAVG* and *BTILLAGE* on the uncertainty in *EXPDOSE* have already been discussed. The small negative effect associated with *CRITSLOP* results because ash is mobilized from terrain at which the downhill gradient exceeds *CRITSLOP*; thus, increasing *CRITSLOP* decreases the area from which ash is mobilized and thus decreases the mass of radionuclides that are transported with the mobilized ash. The small negative effect associated with *DCHANL* results because increasing this diffusivity reduces the time required for radionuclides to diffuse down out of the biosphere.

The regressions for *EXPDOSE* at 200,000 and 500,000 yr are similar and select the following first five variables in the same order: *IGERATE*, *INHLTPV*, *BTILLAGE*, *FRACCHNL* and *CSNFMASS* (Figure K6.8.2-2a). With all five variables, the regression models have R^2 values of 0.95 and 0.96. Thus, the regression models at 200,000 and 500,000 yr are very successful in accounting for the uncertainty in *EXPDOSE*. The effects of *IGERATE*, *BTILLAGE*, *FRACCHNL*, *INHLTPV* and *CSNFMASS* on *EXPDOSE* have already been discussed. After *IGERATE*, *BTILLAGE*, *FRACCHNL*, *INHLTPV* and *CSNFMASS*, the regressions at 200,000 and 500,000 yr add several additional variables that have very small effects on *EXPDOSE* and end with R^2 values of 0.97 and 0.98.

The dominant effect of *IGERATE* on the uncertainty in *EXPDOSE* at 500,000 yr and the lesser effects of *BTILLAGE* and *FRACCHNL* can be seen in the scatterplots in Figure K6.8.2-2b,c.d.

K7 SEISMIC SCENARIO CLASSES

K7.1 Seismic Scenario Classes: Summary

The seismic scenario classes are defined on the basis of futures that involve one or more seismic events (Section J8). This section (Section K7) presents uncertainty and sensitivity analysis results for selected analysis outcomes associated with the seismic scenario classes (Table K7.1-1). The primary emphasis is on the seismic ground motion scenario class but expected dose results for the seismic fault displacement scenario class are also presented.

The primary results considered for the seismic ground motion scenario class for 20,000 yr are radionuclide movement from the EBS to the UZ (Table K7.1-2), radionuclide movement from the UZ to the SZ (Table K7.1-3), radionuclide movement in the SZ at the location of the RMEI (Table K7.1-4), dose to the RMEI from selected radionuclides (Table K7.1-5), and expected dose to the RMEI from all radionuclides (Table K7.1-6). High-level summaries of the uncertainty and sensitivity analysis results presented in this section are provided in Tables K7.1-2 to K7.1-6. Additional uncertainty analysis results are also available in Section J8.

The analysis of radionuclide movement considers releases following a seismic event at 200 years that causes a fractional damaged area of 10^{-6}(32.6 m^2) at 200 yr to all CDSP WPs in the repository. The variability in dose to the RMEI following seismic GM events at different times is shown in Figure J8.3-1. Because of the similarity in dose following events at different times, it is anticipated that sensitivity analysis results would be similar if different event times were to be considered. Figure J8.3-2 illustrates that dose to the RMEI changes in proportion to damaged area for damaged area within a range between has 10^{-7}(32.6 m^2) and 10^{-5}(32.6 m^2). A damaged area of 10^{-6}(32.6 m^2) was selected within this range. This damaged area is typical of the damaged area that may result from a seismic event that initially damages CDSP WPs (DTN: MO0708CDSPSEIS.000_R0 [DIRS183007], CDSP_Damage_Fraction_CDF.JNB).

From a regulatory perspective, expected dose to the RMEI (*EXPDOS*, mrem/yr) is the analysis outcome of greatest interest associated with the seismic scenario classes (Table K7.1-6). For the seismic ground motion scenario class, *EXPDOS* tends to monotonically increase over the time interval [0, 2×10^4 yr], with the value for *EXPDOSE* between 10^{-4} and 1 mrem/yr for most sample elements, with a few sample elements having values for *EXPDOSE* between 1 and 10 mrem/yr. (Figure K7.7.1-1). The uncertainty in *EXPDOSE* is dominated by the residual stress threshold *SCCTHRP* (as sampled, *SCCTHRP* is a percent of a base value of 351 MPa and is related to the stress corrosion cracking threshold, *SCCTHR*, by *SCCTHRP* = (*SCCTHR* × 100)/(351 MPa)), with the value for *EXPDOSE* decreasing as *SCCTHRP* increases.

For the [0, 10^6 yr] time interval, the sensitivity analysis considers only expected dose to the RMEI (*EXPDOS*, mrem/yr). The individual realizations of *EXPDOS* are noisy (Figure K7.7.2-1) due to the combination of nominal processes and seismic events in this scenario class, and the resultant use of a Monte Carlo method to evaluate expected dose. This noise propagates into the sensitivity analysis results and appears as time-dependent noise in the correlations between

EXPDOS and uncertain parameters. Over the time interval [0, 10^6 yr], the observed range of possible values for *EXPDOS* with the current sample size is approximately [10^{-4}, 70 mrem/yr]. Because the peak values of *EXPDOS* are associated with spikes, these values may not be representative of the peak values of *EXPDOS* that may result from an improved numerical calculation. The use of larger sample sizes in the integration over aleatory uncertainty (i.e., over seismic events and their associated properties) or the use of appropriate numerical smoothing techniques would reduce the noise in each individual realization and would produce smoother time-dependent results for *EXPDOS*. Despite the noise present in the individual realizations of expected dose, Figure 7.3.1-11 demonstrates that the distribution of uncertainty in expected dose is stable at the sample size used in the TSPA-LA analysis. Thus, the noise evident in *EXPDOS* affects the tails of the distribution of *EXPDOS* at each point in time, but does not influence the mean dose.

The dominant variables contributing to the uncertainty in *EXPDOS* for the seismic ground motion scenario class over the time interval [0, 10^6 yr] are *SCCTHRP* and *WDGCA22* (temperature dependence coefficient associated with the general corrosion rate for alloy 22, K) (Figures K7.7.1-1, K7.7.1-2, K7.7.2-1, K7.7.2-2). The effect associated with *SCCTHRP* results from its role in decreasing the stress level at which stress corrosion cracking will initiate after a seismic event. The 10^6 yr seismic analysis also includes WP thinning and failure due to nominal processes. The importance of *WDGCA22* results from its role in affecting general corrosion of alloy 22 and hence WP thinning, which in turn affects both WP failure caused by seismic events and WP failure from nominal processes. Prior to approximately 2×10^5 yr, *SCCTHRP* is the dominant variable affecting the uncertainty associated with *EXPDOS*; after 2×10^5 yr, *SCCTHRP* and *WDGCA22* are both important contributors to the uncertainty in *EXPDOS*. This analysis does not include the uncertainty in the seismic hazard curve; if included, this uncertainty would probably also be an important contributor to the uncertainty in *EXPDOS*.

The sensitivity analysis for the [0, 10^6 yr] time interval did not investigate radionuclide movement within the repository system. As described in Appendix J, Section J8.4, a Monte Carlo method is used to evaluate annual dose from the combined effects of nominal processes and seismic events for each combination of a sampled future and an LHS element. Figure J8.4-1 illustrates a few of the 9,000 annual dose histories calculated by the Monte Carlo technique. In the Monte Carlo analysis, the futures describing each sequence of seismic events are sampled independently for each LHS element in order to obtain a more stable estimate of the mean dose than would result if the same sampled futures were used for all LHS elements. As a consequence, the uncertainty analysis does not produce a set of results that are conditional on a common future. Hence, sensitivity analysis to determine the effects of epistemic uncertainty can be performed only on expected values of model outputs, where the expected values are averages of model output results for each epistemic sample. Sensitivity analyses are performed on expected dose to the RMEI. These analyses show that the uncertainty in expected dose to the RMEI is dominated by the uncertainty in two variables that determine when WPs fail: *SCCTHRP* and *WDGCA22*. As a result, it is anticipated that the uncertainty in the expected value of the rates of radionuclide movement would also be dominated by these same two variables as these variables determine the likelihood of releases from the WP.

For the seismic fault displacement scenario class, the possible values for *EXPDOS* fall in the interval [10^{-4}, 4 mrem/yr] over the [0, 10^6 yr] time interval (Figures K7.8.1-1, K7.8.2-1). Overall, the two most important variables with respect to the uncertainty in *EXPDOS* for the seismic fault displacement scenario class over the time interval [0, 10^6 yr] are *SZGWSPDM* (groundwater specific discharge multiplier; as sampled, *SZGWSPDM* is actually the logarithm of the indicated multiplier) and *INFIL* (infiltration level) (Figures K7.8.1-1, K7.8.1-2, K7.8.2-1, K7.8.2-2). At early times (e.g., prior to 2×10^4 yr), *MICTC99* (dose conversion factor for ^{99}Tc for modern interglacial climate, (rem/yr)/(pCi/L)) is also important but has limited effect on the uncertainty in *EXPDOS* at later times. However, no individual variable has a dominant effect on the uncertainty in *EXPDOS* for the seismic fault displacement scenario class. Similarly to the seismic ground motion scenario class, the uncertainty in the occurrence rate for the seismic fault displacement events is not included in the analysis. Movement of radionuclides through the repository system is not investigated for the seismic fault displacement scenario class.

K7.2 Seismic Ground Motion Scenario Classes: Engineered Barrier System Conditions over the Time Interval [0, 20,000 yr]

The environmental conditions in the barrier system for seismic ground motion events in the time interval [0, 20,000 yr] are the same as described in Section K4 for the nominal scenario class.

K7.3 Seismic Ground Motion Scenario Classes: Release from Engineered Barrier System over the Time Interval [0, 20,000 yr]

Movement of ^{239}Pu Irreversibly Attached to Glass (i.e., Ic) Colloids: *ESIC239* and *ESIC239C*. Uncertainty and sensitivity analyses for movement of ^{239}Pu irreversibly attached to glass colloids are not presented when transport is predominantly by diffusion due to an error in the GoldSim component of the TSPA-LA Model that affects the calculation of concentration of glass colloids when glass colloids are unstable. Consequently, Figure K7.3-1 and Figure K7.3-2 have been removed from this document. See Appendix P, Table P-6, for a discussion of the error and the effect of the error on TSPA-LA Model results.

Movement of ^{239}Pu Irreversibly Attached to Ferrous (i.e., If) Colloids: Uncertainty and sensitivity analyses for movement of ^{239}Pu irreversibly attached to ferrous colloids are not presented due to an error in the Goldsim component of the TSPA-LA Model that affects the calculation of stability of ferrous colloids. Consequently, Figure K7.3-3 and Figure K7.3-4 have been removed from this document. See Appendix P, Section P18, for a discussion of the error and the effect of the error on TSPA-LA Model results.

Movement of Dissolved ^{237}Np: *ESNP237* and *ESNP237C*. The uncertainty and sensitivity analyses for the time-dependent release rates (*ESNP237*, g/yr) and cumulative releases (*ESNP237C*, g) over the time interval [0, 20,000 yr] for the movement of dissolved ^{237}Np from the EBS to the UZ resulting from a seismically induced fractional damaged area of 10^{-6} (32.6 m^2) at 200 yr to all CDSP WPs in the repository are summarized in Figures K7.3-5 and K7.3-6.

The values for *ESNP237C* at 20,000 yr fall between 10^{-2} and 10^{1} g (Figure K7.3-5b). Thus, from a risk perspective, the values for *ESNP237* and *ESNP237C* for this analysis case are inconsequential because of their small sizes (i.e., the dose resulting from dissolved ^{237}Np is much less than the dose resulting from other radionuclides such as ^{99}Tc (Section 8.2.4.1)).As indicated by the PRCCs in Figure K7.3-5e,f, the uncertainty in *ESNP237* and *ESNP237C* at early times is affected by *THERMCON* (host rock thermal conductivity level) and *INFIL* (infiltration level). The positive effects associated with these two variables at early times result from their role in decreasing the time at which the EBS cools to the level at which radionuclide movement is possible. A very early effect is also indicated for *DIAMCOLL* (diameter of colloid particles, nm); however, this effect occurs during the early period when the results are very noisy and also include many zero values. As a result, the selection of *DIAMCOLL* is probably spurious. As time increases, *GOESITED* (density of sorption sites on goethite, sites/nm^2) is the only variable with large PRCCs. In particular, the negative PRCCs associated with *GOESITED* indicate that *ESNP237* and *ESNP237C* decrease as *GOESITED* increases. This effect results because increasing *GOESITED* increases the amount of ^{237}Np sorbed onto goethite and thus reduces the amount of dissolved ^{237}Np available for release from the EBS.

As shown in Figure K7.3-5a,c, the release rates of dissolved ^{237}Np after about 1,000 years generally evolve toward a steady state value as environmental conditions inside the WP evolve toward steady state. These environmental variables determine the solubility of ^{237}Np at each time. This evolution is apparent in the changing values of the PRCCs for *DELPPCO2* (scale factor used to incorporate uncertainty into the value for the partial pressure of CO_2) and *PH2MCOS* (pointer variable used to incorporate uncertainty into pH in cell 1b of CDSP WPs under liquid influx conditions). The steady state release rate is determine by the balance between waste form degradation and reversible sorption onto ferrous corrosion products as indicated by the PRCC for *GOESITED* (density of sorption sites on goethite, sites/nm^2). The effect of climate changes at 2,000 yr and 10,000 yr can also be observed in Figure K7.3-5a,c, where the assumption that climate change is instantaneous (Section 5.1.1) results in temporary jumps in release rates.

Overall, the absence of variables with large PRCCs in Figure K7.3-5e,f suggests that the uncertainty in *ESNP237* and *ESNP237C* is determined by small effects associated with a large number of individual variables. This is borne out by the regression analyses in Figure K7.3-6a,b. For example, the first variable selected in the individual regressions in Figure K7.3-6a,b is either *GOESITED* or *DELPPCO2* and the resultant regression model has an R^2 value between 0.13 and 0.24. Further, after the selection of six variables, the resultant regression models have R^2 values between 0.50 and 0.54, and the final regression models contain from 11 to 14 variables and have R^2 values between 0.60 and 0.64. Thus, the uncertainty in *ESNP237* and *ESNP237C* is affected by a large number of variables without being dominated by the uncertainty in a small number of variables.

As an example, the regression analysis for *ESNP237* at 10,000 yr will be discussed. The first six variables selected in the analysis are *GOESITED*, *EP1LOWNU* (scale factor used to incorporate uncertainty into uranium solubility under low ionic strength conditions for nominal and seismic conditions; as sampled, *EP1LOWNU* is actually the logarithm of the indicated scale factor; in the present analysis, *EP1LOWNU* was used instead of the corresponding and intended variable

EP1LOWOU for igneous conditions; however, this has no effect on analysis outcomes as *EP1LOWNU* and *EP1LOWOU* are assigned the same distribution), *DSNFMASS* (scale factor used to characterize uncertainty in amount of DSNF in CDSP WPs), *HFOSA* (hydrous ferrous oxide surface area, m^2/g), *GOESA* (specific surface area of goethite, m^2/g), and *IS2MCONS* (pointer variable used to determine ionic strength in 2MCO Cell i.e., Cell 1b, of CDSP WPs under nondripping conditions) (Figure K7.3-6a). Of the preceding variables, *GOESITED* and *HFOSA* have negative regression coefficients, and the remaining variables have positive regression coefficients. The negative effects associated with *GOESITED* and *HFOSA* result because increasing these variables increases the sorption of ^{237}Np onto stationary surfaces and thus reduces the amount of dissolved ^{237}Np available for release from the EBS. The positive effects associated with *EP1LOWNU*, *DSNFMASS*, *GOESA* and *IS2MCONS* result because (i) increasing *EP1LOWNU* increases the amount of dissolved uranium which in turn competes with ^{237}Np for sorption sites, with the result that the dissolved concentration of ^{237}Np increases because less ^{237}Np is sorbed onto stationary sites, (ii) increasing *DSNFMASS* increases the amount of DSNF in CDSP WPs, which in turn increases the amount of ^{237}Np available for release from the EBS, (iii) increasing *GOESA* increases the surface area of corrosion products, which increases the sorption of water onto the corrosion products, thereby increasing saturation of the corrosion products and facilitating transport, and (iv) increasing *IS2MCONS* increases ionic strength which in turn increases neptunium solubility. Together, *GOESITED*, *EP1LOWNU*, *DSNFMASS*, *HFOSA*, *GOESA* and *IS2MCONS* result in a regression model with an R^2 value of 0.54. For perspective, the scatterplots for *GOESITED*, *EP1LOWNU* and *DSNFMASS* are presented in Figure K7.3-6c,d,e.

The next six variables selected in the regression analysis for *ESNP237* at 10,000 years are *DELPPCO2*, *PH2MCONS* (pointer variable used to incorporate uncertainty into pH in cell 1b of CDSP WPs under vapor influx conditions), *CSRINDSA* (specific surface area of CSNF and DSNF degradation rind, m^2/g), *EP1NPO2* (scale factor used to incorporate uncertainty into NpO_2 solubility below 1 molal ionic strength; as sampled, *EP1NPO2* is actually the logarithm of the indicated scale factor), *GOERELAB* (fraction of total iron oxide that is goethite), and *HFOSITED* (sorption site density for hydrous ferric oxide, sites/nm^2) (Figure K7.3-6a). Of these variables, *DELPPCO2*, *CSRINDA, EP1NPO2* and *GOERELAB* have positive regression coefficients, and *PH2MCONS* and *HFOSITED* have negative regression coefficients. The positive effects associated with *DELPPCO2*, *CSRINDA, EP1NPO2* and *GOERELAB* result because (i) increasing *DELPPCO2* tends to increase the solubility of ^{237}Np, (ii) increasing *CSRINDA* increases water saturation in the degraded waste form, thus facilitating diffusive transport of dissolved species, (iii) increasing *EP1NPO2* increases the solubility of neptunium and thus increases the amount of dissolved ^{237}Np available for release from the EBS, and (iv) increasing *GOERELAB* increases the fraction of total iron oxide that is goethite, which generally results in a net decrease in the number of sorption sites on the corrosion products. The negative effects associated with *PH2MCONS* and *HFOSITED* result because (i) increasing *PH2MCONS* increases pH and thus generally decreases the solubility of neptunium in the commonly observed chemical environments, and (ii) increasing *HFOSITED* increases the number of sorption sites on corrosion products, which increases the sorption of ^{237}Np onto stationary surfaces and thus reduces the amount of dissolved ^{237}Np available for release from the EBS. The addition of *DELPPCO2*, *PH2MCONS*, *CSRINDSA*, *EP1NPO2*, *GOERELAB* and *HFOSITED* to the

regression model results in a final model containing twelve variables and having an R^2 value of 0.64 (Figure K7.3-6a).

The remaining five regression analyses in Figure K7.3-6a (i.e., for *ESNP237* at 3000 and 5000 years and *ESNP237C* at 3000, 5000 and 10,000 years) are generally similar to the regression analysis just discussed for *ESNP237* at 10,000 yr.

Movement of Dissolved ^{239}Pu: *ESPU239* and *ESPU239C*. The uncertainty and sensitivity analyses for the time-dependent release rates (*ESPU239*, g/yr) and cumulative releases (*ESPU239C*, g) over the time interval [0, 20,000 yr] for the movement of dissolved ^{239}Pu from the EBS to the UZ resulting from a seismically induced fractional damaged area of 10^{-6}(32.6 m^2) at 200 yr to all CDSP WPs in the repository are summarized in Figures K7.3-7 and K7.3-8.

The values for *ESPU239C* at 20,000 yr fall between 10^{-2} and 10^2 g (Figure K7.7-7b). Thus, from a risk perspective, the values for *ESPU239*and *ESPU239C* for this analysis case are inconsequential, because of their small sizes (i.e., the dose resulting from dissolved ^{239}Pu is much less than the dose resulting from other radionuclides such as ^{99}Tc (Section 8.2.4.1)). Similar to the evolution of the release rates of dissolved ^{237}Np (Figure K7.3.1-5a,c), the release rates of dissolved ^{239}Pu generally evolve toward a steady state value, as environmental conditions inside the WP evolve toward steady state. The effect of climate changes at 2,000 yr and 10,000 yr can also be observed in Figure K7.3-7a,c, where the assumption that climate change is instantaneous (Section 5.1.1) results in temporary jumps in release rates.

As indicated by the PRCCs in Figure K7.3-7e,f, the uncertainty in *ESPU239*and *ESPU239C* is dominated by *EP1LOWPU* (scale factor used to incorporate uncertainty into plutonium solubility under low ionic strength conditions; as sampled, *EP1LOWPU* is actually the logarithm of the indicated scale factor). Further, *EP1LOWPU* is the first variable selected in each of the regressions in Figure K7.3-8a,b, with the individual regressions containing only *EP1LOWPU* having R^2 values between 0.30 and 0.51. For both *ESPU239* and *ESPU239C*, the R^2 values increase with increasing time. Thus, the importance of *EP1LOWPU* with respect to the uncertainty in *ESPU239* and *ESPU239C* increases with time. The positive effects indicated for *EP1LOWPU* on *ESPU239* and *ESPU239C* result because increasing *EP1LOWPU* increases the solubility of plutonium and thus increases the amount of dissolved ^{239}Pu available to be released from the EBS.

After *EP1LOWPU*, the PRCCs in Figure K7.3-7e,f indicate effects for several additional variables. In particular, positive effects are indicated for *THERMCON* (host rock thermal conductivity level) and *INFIL* (infiltration level) at early times because of the influence that these two variables have on the cooling of the EBS and the resultant initiation of radionuclide movement. At later times, positive effects are indicated for *INFIL* and *DELPPCO2* (scale factor used to incorporate uncertainty into the value for the partial pressure of CO_2), and negative effects are indicated for *PH2MCONS* (pointer variable used to incorporate uncertainty into pH in cell 1b of CDSP WPs under vapor influx conditions) and *SEEPPRM* (fracture permeability in lithophysal rock units, m^2; as sampled, *SEEPPRM* is actually the logarithm of the indicated permeability) (Figure K7.3-7e,f). The positive effects associated with *INFIL* and *DELPPCO2* result because (i) increasing *INFIL* increases water movement in the EBS and (ii) increasing

DELPPCO2 increases the solubility of plutonium. The negative effects associated with *PH2MCONS* and *SEEPPRM* result because (i) increasing *PH2MCONS* increases pH and thus reduces the solubility of plutonium for most chemical conditions that are observed and (ii) increasing *SEEPPRM* increases water flow around the EBS and thus reduces water flow into the EBS.

The same pattern of effects is present in the regression analyses in Figure K7.3-8a,b. Specifically, the first three variables selected in all six regression analyses are *EP1LOWPU*, *DELPPCO2* and *INFIL*, with the resultant regression models having R^2 values between 0.57 and 0.65. Thus, these three variables are having a large influence on the uncertainty in *ESPU239* and *ESPU239C*. Further, *PH2MCONS* is the fourth variable selected in five of the six regressions and is the fifth variable selected in the remaining regression. More specifically, the next three variables selected after *EP1LOWPU*, *DELPPCO2* and *INFIL* in all six regressions are *PH2MCONS*, *SEEPPRM* and *GOESITED* (density of sorption sites on goethite, sites/nm^2). The inclusion of *PH2MCONS*, *SEEPPRM* and *GOESITED* in the regression models results in R^2 values between 0.72 and 0.75. Thus, these six variables can account for most of the uncertainty associated with *ESPU239*and *ESPU239C*. The effects of *EP1LOWPU*, *DELPPCO2*, *INFIL*, *PH2MCONS* and *SEEPPRM* on *ESPU239* and *ESPU239C* have already been discussed in conjunction with the PRCCs in Figure K7.3-7e,f. The negative effect associated with *GOESITED* results because increasing *GOESITED* increases the amount of plutonium sorbed to stationary surfaces and thus reduces the amount of dissolved ^{239}Pu available to be released from the EBS. After the first six variables, the individual regression analysis select a number of additional variables having small effects on *ESPU239* and *ESPU239C*. At completion, the individual regression models contain 11 or 12 variables and have R^2 values between 0.77 and 0.81.

For perspective, scatterplots showing the effects of *EP1LOWPU*, *DELPPCO2* and *INFIL* on *ESPU239* and *ESPU239C* at 10,000 yr are given in Figure K7.3-8c,d,e,f,g,h. The positive effects of *EP1LOWPU*, *DELPPCO2* and *INFIL* on *ESPU239* and *ESPU239C* can be seen in these plots.

Movement of Dissolved ^{99}Tc: *ESTC99* and *ESTC99C*. The uncertainty and sensitivity analyses for the time-dependent release rates (*ESTC99*, g/yr) and cumulative releases (*ESTC99C*, g) over the time interval [0, 20,000 yr] for the movement of dissolved ^{99}Tc from the EBS to the UZ resulting from a seismically induced fractional damaged area of 10^{-6} (32.6 m^2) at 200 yr to all CDSP WPs in the repository are summarized in Figures K7.3-9 and K7.3-10.

Unlike the results for the other two radioactive species (i.e., ^{237}Np and ^{239}Pu) used to illustrate the effects of seismic ground motion damage, substantial releases of ^{99}Tc from the EBS are observed. Specifically, the value for *ESTC99C* at 20,000 yr falls between 10^5 and 10^6 g (Figure K7.3-9b). As shown in Figure 8.2-12 and Figure J8.3-8, the release of dissolved ^{99}Tc from the repository results in the largest contribution to expected dose to the RMEI. As shown in Figure K7.3-9a,c, the values for *ESTC99* tend to decrease monotonically with time; however, this decrease is not nearly as rapid as is the case when the WP is destroyed (e.g., see Figures K5.3.3-5, K5.3.5-5). The less rapid release of ^{99}Tc following a seismic event results because the seismic event damages a relatively small area on each WP, which in turn limits the

rate of diffusion of ^{99}Tc from the interior of the WP. The spikes in release rates at 2,000 yr and 10,000 yr are due to climate change at these times.

The sensitivity analyses for *ESTC99* are discussed first. As shown by the PRCCs in Figure K7.3-9e, the uncertainty in *ESTC99* at early times is dominated by *THERMCON* (host rock thermal conductivity level) and *INFIL* (infiltration level). The positive effects associated with these two variables at early times results from their role in decreasing the time at which the EBS cools to the level at which radionuclide movement is possible. At later times, *THERMCON* and *INFIL* have a negative effect on *ESTC99* because the release of ^{99}Tc at early times reduces the amount of ^{99}Tc available to be released at later times. Higher values of *THERMCON* and *INFIL* generally correspond to more rapid cooling of the waste. Lower temperatures result in slower degradation of HLW and in corresponding less total ^{99}Tc released over 10,000 yr. Specifically, HLW contains almost all of the ^{99}Tc in CDSP WPs (between 2.5×10^6 g and 5.1×10^6 g). In contrast, the DSNF component of waste in CDSP WPs contains between 1.0×10^4 g and 6.0×10^4 g of ^{99}Tc. In addition, positive effects are indicated for *GOESA* (specific surface area of goethite, m^2/g), *HLWMASS* (scale factor used to characterize uncertainty in radionuclide content of HLW in CDSP WPs), and *HLWDRALK* (dissolution rate of HLW glass under alkaline conditions, $g/m^2/d$); and a negative effect is indicated for *CORRATSS* (stainless steel corrosion rate, μm/yr). The positive effects associated with *GOESA*, *HLWMASS* and *HLWDRALK* result because (i) increasing *GOESA* increases the saturation of the corrosion products, thereby facilitating diffusive transport, (ii) increasing *HLWMASS* increases the amount of ^{99}Tc in CDSP WPs, and (iii) increasing *HLWDRALK* increases the dissolution rate of HLW glass and thus accelerates the release of ^{99}Tc within CDSP WPs. The negative effect associated with *CORRATSS* results because increasing *CORRATSS* increases the amount of corrosion products in WPs, which in turn decreases the saturation of the corrosion products and hence slows the diffusion rate of ^{99}Tc out of damaged WPs.

More detailed sensitivity analysis results for *ESTC99* are provided by the regression analyses in Figure K7.3-10a. The three regressions all select *GOESA* first and then either *HLWDRALK* or *HLWMASS*. The regression models at 3000, 5000 and 10,000 yr with only *GOESA* have R^2 values of 0.18, 0.18 and 0.14, respectively, and the models with two variables have R^2 values of 0.37, 0.32 and 0.29. Thus, although important, the uncertainty in *GOESA, HLWDRALK* and *HLWMASS* does not dominate the uncertainty in *ESTC99*. The variables selected at steps 2 through 6 in the individual regression analyses are subsets of the variables *HLWDRALK*, *HLWMASS*, *CORRATSS*, *THERMCON*, *INFIL* and *DSNFMASS* (scale factor used to characterize uncertainty in amount of DSNF in CDSP WPs). With the exception of *DSNFMASS*, these variables were also identified as having similar effects in the analysis with PRCCs (see Figure K7.3-9e and associated discussion). Similarly to *HLWMASS*, the positive effect associated with *DSNFMASS* results from increasing the amount of ^{99}Tc in CDSP WPs. The regression models at 3000, 5000 and 10,000 yr with the first six variables have R^2 values of 0.65, 0.63 and 0.60, respectively; thus, the first six variables selected in the regression analyses account for over half the uncertainty associated with *ESTC99*. The final regressions for *ESTC99* at 3000, 5000 and 10,000 yr contain 12, 13 and 15 variables, respectively, and have R^2 values of 0.77, 0.78 and 0.78. However, variables selected near the end of the stepwise procedures that have small incremental effects on the cumulative R^2 values may be spurious. For example, the selection of

WDGCUA22 (pointer variable used to select the distribution of base corrosion rates of alloy 22 at 60 °C over the patches on WPs) in the regression analysis for *ESTC99* at 10,000 yr is spurious as this variable is not involved in the present analysis.

For perspective, scatterplots showing the effects of *GOESA*, *HLWMASS* and *CORRATSS* on *ESTC99* at 10,000 yr are given in Figure K7.3-10c,d,e. The positive effects of *GOESA* and *HLWMASS* and the negative effect of *CORRATSS* on *ESTC99* can be seen in these plots.

The sensitivity analyses for *ESTC99C* are now discussed. As shown by the PRCCs in Figure K7.3-9f, the uncertainty in *ESTC99C* at early times is dominated by *THERMCON* and *INFIL*. The positive effects associated with these two variables at early times results from their role in decreasing the time at which the EBS cools to the level at which radionuclide movement is possible. At later times, *THERMCON* and *INFIL* have a negative effect on *ESTC99C* because higher values of *THERMCON* and *INFIL* generally correspond to lower temperatures at late times. The lower temperatures result in slower degradation of HLW and in corresponding less total ^{99}Tc released over 10,000 yr. As previously noted, HLW contains almost all of the ^{99}Tc in CDSP WPs (between 2.5×10^6 g and 5.1×10^6 g). In contrast, the DSNF component of waste in CDSP WPs contains between 1.0×10^4 g and 6.0×10^4 g of ^{99}Tc. With increasing time, positive effects are indicated for *GOESA, DSNFMASS*, *HLWDRALK* and *HLWMASS*. As discussed in conjunction with *ESTC99*, the indicated positive effects result because (i) increasing *GOESA* increases the saturation of the corrosion products, thereby facilitating diffusive transport, (ii) increasing *DSNFMASS* and *HLWMASS* increases the amount of ^{99}Tc in CDSP WPs, and (iii) increasing *HLWDRALK* increases the dissolution of HLW glass and thus increases the release of ^{99}Tc within CDSP WPs.

More detailed sensitivity analysis results for *ESTC99C* are provided by the regression analyses in Figure K7.3-10b. The three regressions all sequentially select *GOESA*, *HLWDRALK*, *HLWMASS* and *DSNFMASS* as the first four variables for inclusion in the regression models. The resultant models at 3000, 5000 and 10,000 yr with all four variables have R^2 values of 0.60, 0.59 and 0.53, respectively; thus, the first four variables selected in the regression analyses account for slightly over half the uncertainty associated with *ESTC99C*. The positive effects of *GOESA*, *HLWDRALK*, *HLWMASS* and *DSNFMASS* on *ESTC99C* are the same as previously discussed in conjunction with the PRCCs in Figure K7.3-9f.

After *GOESA*, *HLWDRALK*, *HLWMASS* and *DSNFMASS*, the regression analyses for *ESTC99C* select a number of additional variables with small effects (Figure K7.3-10b). The analysis for *ESTC99C* at 10,000 yr will be discussed as an example. The next three variables selected after *GOESA*, *HLWDRALK*, *HLWMASS* and *DSNFMASS* are *CORRATSS*, *THERMCON* and *INFIL*, with all three variables having negative effects on *ESTC99C*. The negative effect associated with *CORRATSS* results because increasing *CORRATSS* increases the amount of corrosion products in WPs, which in turn slows the diffusion rate of ^{99}Tc diffuses out of damaged WPs. The negative effects associated with *THERMCON* and *INFIL* are the same as previously discussed in conjunction with the PRCCs in Figure K7.3-9f. Inclusion of *CORRATSS*, *THERMCON* and *INFIL* results in a regression model with seven variables and raises the R^2 value from 0.53 to 0.66. The remaining five variables selected in the regression analysis are *PH2DHLNS* (pointer variable used to determine pH in 2DHLW Cell, i.e., Cell 1, of CDSP WPs under vapor influx

conditions), *WFDEGEXF* (surface area exposure factor for amount of HLW glass contacted by water), *HLWDRACD* (dissolution rate of HLW glass under acidic conditions, g/m^2/d), *FHHISSCP* (Frenkel-Halsey-Hill water vapor adsorption isotherm parameter *s* for corrosion products), and *DIAMCOLL* (diameter of colloid particles, m). The negative effect associated with *PH2DHLNS* results because increasing pH decreases the degradation rate of DHLW in acidic conditions (BSC 2004 *Defense HLW Glass Degradation Model*, Section 8.1, [DIRS169988]) and thus decreases the mass of ^{99}Tc released within 20,000 yr**;** the positive effects associated with *WFDEGEXF* and *HLWDRACD* result from their role in increasing the degradation of HLW glass and hence the release of ^{99}Tc from HLW glass; and the negative effect associated with *FHHISSCP* results because increasing *FHHISSCP* decreases the number of monolayers of water adsorbed onto the corrosion products, thereby inhibiting transport (EBS Radionuclide Transport Abstraction, Equation 6.3.4.3.2-2, [DIRS177407]). The selection of *DIAMCOLL* as the last variable in the stepwise process is spurious.

For perspective, scatterplots showing the effects of *GOESA*, *HLWDRALK* and *HLWMASS* on *ESTC99C* at 10,000 yr are given in Figure K7.3-10f,g,h. The positive effects of *GOESA*, *HLWDRALK* and *HLWMASS* on *ESTC99C* can be seen in these plots.

K7.4 Seismic Ground Motion Scenario Classes: Release from Unsaturated Zone (UZ) over the Time Interval [0, 20,000 yr]

For completeness, this section presents summaries of the uncertainty and sensitivity analyses for release from the UZ to the SZ over the time interval [0, 20,000 yr] resulting from a seismically induced fractional damaged area of 10^{-6} (32.6 m^2) at 200 yr to all CDSP WPs in the repository without discussion.

Movement of ^{239}Pu Irreversibly Attached to Slow (i.e., Ic) Colloids: *UZIC239* and *UZIC239C*. The uncertainty and sensitivity analyses for the time-dependent release rates (*UZIC239*, g/yr) and cumulative releases (*UZIC239C*, g) over the time interval [0, 20,000 yr] for the movement of ^{239}Pu irreversibly attached to slow (i.e., Ic) colloids from the UZ to the SZ resulting from a seismically induced fractional damaged area of 10^{-6} (32.6 m^2) at 200 yr to all CDSP WPs in the repository are summarized in Figure K7.4-1.

Movement of ^{239}Pu Irreversibly Attached to Fast (i.e., If) Colloids: *UZIF239* and *UZIF239C*. The uncertainty and sensitivity analyses for the time-dependent release rates (*UZIF239*, g/yr) and cumulative releases (*UZIF239C*, g) over the time interval [0, 20,000 yr] for the movement of ^{239}Pu irreversibly attached to fast (i.e., If) colloids from the UZ to the SZ resulting from a seismically induced fractional damaged area of 10^{-6} (32.6 m^2) at 200 yr to all CDSP WPs in the repository are summarized in Figure K7.4-2.

Movement of Dissolved ^{237}Np: *UZNP237* and *UZNP237C*. The uncertainty and sensitivity analyses for the time-dependent release rates (*UZNP237*, g/yr) and cumulative releases (*UZNP237C*, g) over the time interval [0, 20,000 yr] for the movement of dissolved ^{237}Np from the UZ to the SZ resulting from a seismically induced fractional damaged area of 10^{-6} (32.6 m^2) at 200 yr to all CDSP WPs in the repository are summarized in Figure K7.4-3.

Movement of Dissolved ^{239}Pu: *UZPU239* and *UZPU239C*. The uncertainty and sensitivity analyses for the time-dependent release rates (*UZPU239*, g/yr) and cumulative releases (*UZPU239C*, g) over the time interval [0, 20,000 yr] for the movement of dissolved ^{239}Pu from the UZ to the SZ resulting from a seismically induced fractional damaged area of 10^{-6} (32.6 m^2) at 200 yr to all CDSP WPs in the repository are summarized in Figure K7.4-4.

Movement of Dissolved ^{99}Tc: *UZTC99* and *UZTC99C*. The uncertainty and sensitivity analyses for the time-dependent release rates (*UZTC99*, g/yr) and cumulative releases (*UZTC99C*, g) over the time interval [0, 20,000 yr] for the movement of dissolved ^{99}Tc from the UZ to the SZ resulting from a seismically induced fractional damaged area of 10^{-6} (32.6 m^2) at 200 yr to all CDSP WPs in the repository are summarized in Figures K7.4-5.

K7.5 Seismic Ground Motion Scenario Classes: Release from Saturated Zone (SZ) over the Time Interval [0, 20,000 yr]

For completeness, this section presents summaries of the uncertainty and sensitivity analyses for radionuclide movement across a subsurface plane at the location of the RMEI over the time interval [0, 20,000 yr] resulting from a seismically induced fractional damaged area of 10^{-6} (32.6 m^2) at 200 yr to all CDSP WPs in the repository without discussion.

Movement of ^{239}Pu Irreversibly Attached to Slow (i.e., Ic) Colloids: *SZIC239* and *SZIC239C*. The uncertainty and sensitivity analyses for the time-dependent release rates (*SZIC239*, g/yr) and cumulative releases (*SZIC239C*, g) over the time interval [0, 20,000 yr] for the movement of ^{239}Pu irreversibly attached to slow (i.e., Ic) colloids across a subsurface plane at the location of the RMEI resulting from a seismically induced fractional damaged area of 10^{-6} (32.6 m^2) at 200 yr to all CDSP WPs in the repository are summarized in Figure K7.5-1.

Movement of ^{239}Pu Irreversibly Attached to Fast (i.e., If) Colloids: *SZIF239* and *SZIF239C*. The uncertainty and sensitivity analyses for the time-dependent release rates (*SZIF239*, g/yr) and cumulative releases (*SZIF239C*, g) over the time interval [0, 20,000 yr] for the movement of ^{239}Pu irreversibly attached to fast (i.e., If) colloids across a subsurface plane at the location of the RMEI resulting from a seismically induced fractional damaged area of 10^{-6} (32.6 m^2) at 200 yr to all CDSP WPs in the repository are summarized in Figure K7.5-2.

Movement of Dissolved ^{237}Np: *SZNP237* and *SZNP237C*. The uncertainty and sensitivity analyses for the time-dependent release rates (*SZNP237*, g/yr) and cumulative releases (*SZNP237C*, g) over the time interval [0, 20,000 yr] for the movement of dissolved ^{237}Np across a subsurface plane at the location of the RMEI resulting from a seismically induced fractional damaged area of 10^{-6} (32.6 m^2) at 200 yr to all CDSP WPs in the repository are summarized in Figure K7.5-3.

Movement of Dissolved ^{239}Pu: *SZPU239* and *SZPU239C*. The uncertainty and sensitivity analyses for the time-dependent release rates (*SZPU239*, g/yr) and cumulative releases (*SZPU239C*, g) over the time interval [0, 20,000 yr] for the movement of dissolved ^{239}Pu across

a subsurface plane at the location of the RMEI resulting from a seismically induced fractional damaged area of 10^{-6} (32.6 m^2) at 200 yr to all CDSP WPs in the repository are summarized in Figure K7.5-4.

Movement of Dissolved ^{99}Tc: *SZTC99* and *SZTC99C*. The uncertainty and sensitivity analyses for the time-dependent release rates (*SZTC99*, g/yr) and cumulative releases (*SZTC99C*, g) over the time interval [0, 20,000 yr] for the movement of dissolved ^{99}Tc across a subsurface plane at the location of the RMEI resulting from a seismically induced fractional damaged area of 10^{-6} (32.6 m^2) at 200 yr to all CDSP WPs in the repository are summarized in Figure K7.5-5.

K7.6 Seismic Ground Motion Scenario Classes: Dose to Reasonably Maximally Exposed Individual over the Time Interval [0, 20,000 yr]

For completeness, this section presents summaries of the uncertainty and sensitivity analyses for dose to the RMEI over the time interval [0, 20,000 yr] for a seismically induced fractional damaged area of 10^{-6} (32.6 m^2) at 200 yr to all CDSP WPs in the repository without discussion.

Dose to RMEI from ^{239}Pu Irreversibly Attached to Slow (i.e., Ic) Colloids: *DOIC239*. The uncertainty and sensitivity analyses for dose to the RMEI (*DOIC239*, mrem/yr) over the time interval [0, 20,000 yr] for the movement of ^{239}Pu irreversibly attached to slow (i.e., Ic) colloids across a subsurface plane at the location of the RMEI resulting from a seismically induced fractional damaged area of 10^{-6} (32.6 m^2) at 200 yr to all CDSP WPs in the repository are summarized in Figure K7.6-1.

Dose to RMEI from ^{239}Pu Irreversibly Attached to Fast (i.e., Ic) Colloids: *DOIF239*. The uncertainty and sensitivity analyses for dose to the RMEI (*DOIF239*, mrem/yr) over the time interval [0, 20,000 yr] for the movement of ^{239}Pu irreversibly attached to fast (i.e., Ic) colloids across a subsurface plane at the location of the RMEI resulting from a seismically induced fractional damaged area of 10^{-6} (32.6 m^2) at 200 yr to all CDSP WPs in the repository are summarized in Figure K7.6-2.

Dose to RMEI from Dissolved ^{237}Np: *DONP237*. The uncertainty and sensitivity analyses for dose to the RMEI (*DONP237*, mrem/yr) over the time interval [0, 20,000 yr] for the movement of dissolved ^{237}Np across a subsurface plane at the location of the RMEI resulting from a seismically induced fractional damaged area of 10^{-6} (32.6 m^2) at 200 yr to all CDSP WPs in the repository are summarized in Figure K7.6-3.

Dose to RMEI from Dissolved ^{239}Pu: *DOPU239*. The uncertainty and sensitivity analyses for dose to the RMEI (*DOPU239*, mrem/yr) over the time interval [0, 20,000 yr] for the movement of dissolved ^{239}Pu across a subsurface plane at the location of the RMEI resulting from a seismically induced fractional damaged area of 10^{-6} (32.6 m^2) at 200 yr to all CDSP WPs in the repository are summarized in Figure K7.6-4.

Dose to RMEI from Dissolved ^{99}Tc: *DOTC99*. The uncertainty and sensitivity analyses for dose to the RMEI (*DOTC99*, mrem/yr) over the time interval [0, 20,000 yr] for the movement of dissolved ^{99}Tc across a subsurface plane at the location of the RMEI resulting from a seismically induced fractional damaged area of 10^{-6} (32.6 m^2) at 200 yr to all CDSP WPs in the repository are summarized in Figure K7.6-5.

K7.7 Seismic Ground Motion Scenario Classes: Expected Dose to Reasonably Maximally Exposed Individual

This section presents analysis results for expected dose to the RMEI resulting from seismic ground motion over the time intervals [0, 20,000 yr] and [0, 1,000,000 yr].

K7.7.1 Seismic Ground Motion Scenario Classes: Expected Dose (*EXPDOSE*) to Reasonably Maximally Exposed Individual over the Time Interval [0, 20,000 yr]

The uncertainty and sensitivity analyses for expected dose to the RMEI (*EXPDOSE*, mrem/yr) over the time interval [0, 20,000 yr] resulting from seismic ground motion events are summarized in Figures K7.7.1-1 and K7.7.1-2. After the earliest arrival of released radionuclides at the location of the RMEI, *EXPDOSE* increases monotonically with time (Figure K7.7-1a,b). At 10,000 yr, the value for *EXPDOSE* falls between 10^{-4} and 1 mrem/yr for most sample elements, with a few sample elements having values for *EXPDOSE* between 1 and 10 mrem/yr. Due to the use of the quadrature-based methods rather than Monte Carlo methods to evaluate expected dose to the RMEI over the time interval [0, 20,000 yr] (see Equations J8.3-8 and J8.3-13), the expected dose results in Figure 7.7.1-1a,b are relatively smooth.

The PRCCs in Figure K7.7.1-1c indicate that the uncertainty in *EXPDOSE* is dominated by residual stress threshold *SCCTHRP* (as sampled, *SCCTHRP* is a percent of a base value of 351 MPa and is related to the stress corrosion cracking threshold, *SCCTHR*, by *SCCTHRP* = (*SCCTHR* × 100)/(351 MPa)). The value for *EXPDOSE* decreases as *SCCTHRP* increases. This effect results because increasing *SCCTHRP* increases the stress required toinitiate stress corrosion cracking and thus decreases the probability that a given seismic ground motion event will cause WP damage.

In addition to *SCCTHRP*, smaller effects are indicated for *SZGWSPDM* (groundwater specific discharge multiplier; as sampled, *SZGWSPDM* is actually the logarithm of the indicated multiplier), *SZFIPOVO* (flowing interval porosity in the volcanic unit of the SZ), *INFIL* (infiltration level), *DSNFMASS* (scale factor used to characterize uncertainty in the radionuclide content of DSNF contained in CDSP WPs), and *WDCRCDEN* (scale factor to convert area on a WP experiencing stress corrosion cracking to a resultant diffusive area) (Figure K7.7.1-1c). The variables *SZGWSPDM*, *DSNFMASS* and *WDCRCDEN* have positive effects on *EXPDOSE*, with these effects resulting because (i) increasing *SZGWSPDM* increases water flow in the SZ, (ii) increasing *DSNFMASS* increases the amount of ^{99}Tc in CDSP WPs and hence the dose from ^{99}Tc that results from the failure of these WPs, and (iii) increasing *WDCRCDEN* increases the diffusive area on damaged WPs for a given seismic ground motion event. The variables *SZFIPOVO* and *INFIL* have effects prior to 5000 and 10,000 yr, respectively, but no indicated effects after these times. The negative effect for *SZFIPOVO* results from slowing water flow in the SZ and thus delaying the initial arrival of radionuclides at the location of the RMEI. In

contrast, the positive effect for *INFIL* results from accelerating the initial arrival of radionuclides at the location of the RMEI; specifically, increased values for *INFIL* result (i) in cooler conditions in the EBS, which contributes to earlier radionuclide releases and also (ii) in more water flux in the EBS and UZ, which contributes to more rapid radionuclide movement. Owing to the nature of the integration process that defines *EXPDOSE*, the indicated effects associated with *SZFIPOVO* and *INFIL* decrease and then disappear with increasing time.

More detailed sensitivity analyses for *EXPDOSE* are provided by the regression analyses in Figure K7.7.1-2a. The dominant effect of *SCCTHRP* on the uncertainty in *EXPDOSE* is indicated by R^2 values of 0.81, 0.86 and 0.87 for the regressions containing only *SCCTHRP* at 3,000, 5,000 and 10,000 yr. After *SCCTHRP*, the regressions select a large number of variables that have small effects on *EXPDOSE*. For example, the regression at 3000 yr then selects *SZGWSPDM*, *INFIL* and *MICTC99* (dose conversion factor for ^{99}Tc for modern interglacial climate, (rem/yr)/(pCi/L)) and produces a model with an R^2 value of 0.87; the regression at 5,000 yr then selects *MICTC99*, *DSNFMASS* and *MICC14* (dose conversion factor for ^{14}C for modern interglacial climate, (rem/yr)/(pCi/L)) and produces a model with an R^2 value of 0.90; and the regression at 10,000 yr then selects *MICTC99*, *DSNFMASS* and *HLWDRACD* (rate term for dissolution of HLW glass in CDSP WPs under low pH conditions, g/m^2/d) and produces a model with an R^2 value of 0.91. After the first four variables, the regressions at 3000, 5000 and 10,000 yr select an additional 12, 12 and 11 variables, respectively, and produce final models with R^2 values of 0.92, 0.94 and 0.95. Thus, the uncertainty in *EXPDOSE* is dominated by *SCCTHRP*, with small contributions to this uncertainty by many additional variables.

The doses that are integrated to obtain *EXPDOSE* arise primarily from ^{99}Tc (Figure 8.2-12(a), Figure J8.3-8). The importance of ^{99}Tc to *EXPDOSE* is also evident in the regression results at 10,000 yr (Figure K7.7.1-2a). Specifically, the three variables selected immediately after *SCCTHRP* (i.e., *MICTC99*, *DSNFMASS* and *HLWDRACD*) are variables that affect the dose received from ^{99}Tc. Specifically, increasing *MICTC99* increases the dose received from a fixed concentration of ^{99}Tc in groundwater; increasing *DSNFMASS* increases the mass of ^{99}Tc present to be released from the CDSP WPs; and increasing *HLWDRACD* increases the rate at which ^{99}Tc is released from the waste form.

The dominant effect of *SCCTHRP* on the uncertainty in *EXPDOSE* can be seen in the scatterplot in Figure K7.7.1-2b. The much smaller effects associated with *MICTC99* and *DSNFMASS* can be seen in the scatterplots in Figure K7.7.1-2c,d.

It is important to recognize that the results in Figures K7.7.1-1 and K7.7.1-2 reflect the sensitivity of *EXPDOSE* to the parameters that are treated as being uncertain in the TSPA-LA Model. Some important parameters and model inputs are not treated as being uncertain, but are instead represented by conservative, fixed values or by assumptions. The sensitivity of *EXPDOSE* to these parameters can be discussed qualitatively but can not be quantified. For example, the results in Figures K7.7.1-1 and K7.7.1-2 were generated with a fixed value for the seismic hazard curve, estimated as the mean of a distribution of possible seismic hazard curves. This mean seismic hazard curve underlies the probabilistic weightings of the seismic events that give rise to *EXPDOSE* through an integration process (Section 6.1.2.4). Significant uncertainty is associated with the definition of the mean seismic hazard curve (SNL 2007 [DIRS 176828],

Section 6.4.1). If the uncertainty associated with the seismic hazard curve was incorporated into the analysis, it is likely that this uncertainty would have a significant effect on the uncertainty associated with *EXPDOSE*. Including this uncertainty in the TSPA-LA Model would likely improve the estimated repository performance, because the mean seismic hazard curve typically lies above the 80th percentile of the distribution of seismic hazard curves. Including the uncertainty in the seismic hazard curve would reduce the frequency of damaging seismic events in most realizations, which would reduce releases from the repository and improve repository performance. Thus, the use of the mean seismic hazard curve results in conservative estimates of repository performance.

K7.7.2 Seismic Ground Motion Scenario Classes: Expected Dose (*EXPDOSE*) to Reasonably Maximally Exposed Individual over the Time Interval [0, 1,000,000 yr]

The uncertainty and sensitivity analyses for expected dose to the RMEI (*EXPDOSE*, mrem/yr) over the time interval [0, 1,000,000 yr] resulting from seismic ground motion are summarized in Figures K7.7.2-1 and K7.7.2-2.

The time-dependent values for *EXPDOSE* for the 1,000,000 yr period in Figure K7.7.2-1a,b are much choppier than the values for the 20,000 yr time period in Figure K7.7.1-1a,b. This difference results from the numerical procedures used over 20,000 yr and 1,000,000 yr, respectively, to evaluate the integrals that define *EXPDOSE*. Because the effects of the seismic ground motion events are relatively well behaved for the 20,000 yr time period, it is possible to use a quadrature procedure to evaluate *EXPDOSE* for this time period. This results in the relatively smooth time-dependent values for *EXPDOSE* in Figure K7.7.1-1a,b. In contrast, the effects of seismic ground motion events are much more complex for the 1,000,000 yr time period. As a result of this complexity, it is not possible to use a quadrature procedure to evaluate the defining integral for *EXPDOSE* over this longer time period. Instead, it was necessary to use a sampling-based (i.e., Monte Carlo) integration procedure to evaluate the defining integral for *EXPDOSE*. Specifically, 30 1,000,000 yr futures involving seismic ground motion events were randomly sampled for each LHS element and then the 30 time-dependent dose results associated with these futures were vertically averaged at each point in time to produce the estimated time-dependent value for *EXPDOSE* for each sample element. Because individual seismic ground motion events are discrete occurrences that initiate radionuclide releases that ultimately lead to doses to the RMEI, the time dependent doses associated with individual futures and their vertical averages to produce expected doses for individual LHS elements tend to be choppy. In addition, the progression of nominal processes and the occurrence of resultant DS and WP failures contribute to the complexity of the 1,000,000 yr dose calculations. The individual curves in Figure K7.7.2-1a,b would eventually converge to smooth curves if a sufficiently large number of futures was sampled for each LHS element, or if an appropriate kernel smoother was used on the time-dependent results for each LHS element. However, despite the lack of smoothness in the results presented in Figure 7.7.2-1a,b, the distribution of expected annual doses (*EXPDOSE*) is shown to be statistically stable (Section 7.3.1) by means of a replicated sampling procedure (Section J4.10). In addition, confidence intervals are computed which show that the mean annual dose is estimated with sufficient accuracy (Section 7.3.1).

Most values for *EXPDOSE* Figure K7.7.2-1a,b are less than 10 mrem/yr, with a few values between 10 and 100 mrem/yr. The largest values for *EXPDOSE* in Figure K7.7.2-1a,b are associated with peaks that derive form single seismic ground motion events. These peaks would go away if the sampling-based approximations to the integrals defining *EXPDOSE* were more fully converged.

Although the results in Figure K7.7.2-1a,b are choppy, insights can be gained from a careful examination. In particular, Figure K7.7.2-1b is more informative that Figure K7.7.2-1a because the time-dependent values for *EXPDOSE* for individual LHS elements are more distinct. Overall, there is a tendency for *EXPDOSE* to decrease up to about 200,000 yr, with this decrease resulting from the decay of ^{239}Pu and possibly other radionuclides. In this time period, the values of *EXPDOSE* derive from the occurrence of seismic ground motion events as the failure of WPs from nominal processes does not begin until about 200,000 yr. The dominance of seismic ground motion events is indicated by the importance of the residual stress threshold *SCCTHRP* (as sampled, *SCCTHRP* is a percent of a base value of 351 MPa and is related to the stress corrosion cracking threshold, *SCCTHR*, by *SCCTHRP* = (*SCCTHR* × 100)/(351 MPa)); specifically, the PRCCs in Figure K7.7.2-1c indicate that *SCCTHRP* dominates the uncertainty in *EXPDOSE* out to approximately 200,000 yr. This result is also indicated by the regression for *EXPDOSE* at 50,000 yr in Figure K7.7.2-2a, where *SCCTHRP* is the first variable selected in the analysis with an R^2 value of 0.71.

Between 200,000 and 300,000 yr, there is a jump in the values for *EXPDOSE* (Figure K7.7.2-1a,b). This increase in *EXPDOSE* (Figure K7.7.2-1a,b) occurs between 200,000 and 300,000 yr because of the conservative manner in which the interaction between corrosion processes and seismic events was implemented. As explained in Appendix P, Section P.3, the increase in *EXPDOSE* occurs when corrosion failures occur before seismic damage to CSNF WPs and before failure of the DS. The implementation results in a dramatic increase in the probability of seismic damage to CSNF WPs between 200,000 and 300,000 years for a minority of realizations, as is evident in Figure 8.1-5(b). Consistent with this, the PRCCs in Figure K7.7.2-1c indicate that the uncertainty in *EXPDOSE* becomes dominated by *WDGCA22* (temperature dependence coefficient associated with the general corrosion rate for alloy 22, K). Specifically, *WDGCA22* corresponds to a coefficient used to alter the general corrosion rate for alloy 22 as function of temperature, with the alloy 22 corrosion rate decreasing as *WDGCA22* increases. As indicated in Figures K4.2-2e,f and K4.5-1c, *WDGCA22* is the dominant variable with respect to the uncertainty associated with the failure of WPs from nominal processes. After 400,000 yr, the values for *EXPDOSE* tend to increase and beyond 700,000 years are somewhat smoother than at earlier times (Figure K7.7.2-1a,b). This smoothness results from an increasing dominance of nominal corrosion processes in the values for *EXPDOSE*.

In addition to *SCCTHRP* and *WDGCA22*, the PRCCs in Figure K7.7.2-1c indicate effects for several additional variables. However, the effects are small and the PRCCs are very choppy as a result of the choppiness in the values for *EXPDOSE*. Smoother results for *EXPDOSE* would result in smoother values for the PRCCs in Figure K7.7.2-1c.

More detailed sensitivity analyses for *EXPDOSE* are provided by the regression analyses in Figure K7.7.2-2a. Specifically, *SCCTHRP* is the dominant contributor to the uncertainty in *EXPDOSE* at 50,000 yr; *SCCTHRP* is the dominant contributor to the uncertainty in *EXPDOSE*

at 200,000 yr with a contribution from *WDGCA22*; and *WDGCA22* is the dominant contributor to the uncertainty in *EXPDOSE* at 500,000 yr with a contribution from *SCCTHRP*. The individual regressions then add several additional variables that have small effects on *EXPDOSE*. The final regression models 50,000, 200,000 and 500,000 yr have R^2 values of 0.79, 0.56 and 0.71, which are not particularly high. These values are probably due in part to the choppiness of the values for *EXPDOSE* (Figure K7.7.2-1a,b) and in part to the large number of processes that affect *EXPDOSE* for the 1,000,000 yr seismic ground motion calculation. .

For perspective, the scatterplots in Figure K7.7.2-2b,c,d show the effects of *WDGCA22*, *SCCTHRP* and *WDNSCC* (stress corrosion cracking growth rate exponent) at 500,000 yr. The negative effects of *WDGCA22* and *SCCTHRP* can be easily seen in the scatterplots in Figure K7.7.2-2b,c. The negative effect for *WDNSCC* is more subtle but still discernable in the scatterplot in Figure K7.7.2-2d.

As previously indicated in conjunction with Figures K7.7.1-1 and K7.7.1-2 for the 20,000 yr time period, it is important to recognize that the results in Figures K7.7.2-1 and K7.7.2-2 reflect the sensitivity of *EXPDOSE* for the 1,000,000 yr time period to those parameters that are treated as being uncertain in the TSPA-LA Model. Some important parameters and model inputs are not treated as being uncertain, but are instead represented by conservative, fixed values or by assumptions. The sensitivity of *EXPDOSE* to these parameters can be discussed qualitatively but can not be quantified. In particular, significant uncertainty is associated with the definition of the seismic hazard curve that underlies the occurrence of seismic events and the effects of seismic events. If the uncertainty associated with the seismic hazard curve was incorporated into the analysis, it is likely that this uncertainty would have a significant effect on the uncertainty associated with *EXPDOSE*.

K7.8 Seismic Fault Displacement Scenario Classes: Expected Dose (*EXPDOSE*) to Reasonably Maximally Exposed Individual

This section presents analysis results for expected dose to the RMEI resulting from seismic fault displacement over the time intervals [0, 20,000 yr] and [0, 1,000,000 yr].

K7.8.1 Seismic Fault Displacement Scenario Classes: Expected Dose (*EXPDOSE*) to Reasonably Maximally Exposed Individual over the Time Interval [0, 20,000 yr]

The uncertainty and sensitivity analyses for expected dose to the RMEI (*EXPDOSE*, mrem/yr) over the time interval [0, 20,000 yr] resulting from seismic fault displacement are summarized in Figures K7.8.1-1 and K7.8.1-2. After the earliest arrival time for released radionuclides at the location of the RMEI, *EXPDOSE* increases monotonically with time (Figure K7.8.1-1a,b). At 10,000 yr, the value for *EXPDOSE* falls between 10^{-4} and 10^{-2} mrem/yr for most sample elements, with two sample elements having values for *EXPDOSE* between 10^{-2} and 10^{-1} mrem/yr.

The PRCCs in Figure K7.8.1-1c indicate that the uncertainty in *EXPDOSE* is affected by the following variables: *SZGWSPDM* (groundwater specific discharge multiplier; as sampled, *SZGWSPDM* is actually the logarithm of the indicated multiplier), *SZFIPOVO* (flowing interval porosity in the volcanic unit of the SZ), *INFIL* (infiltration level), *SEEPUNC* (pointer variable

used to determine local seepage rates), *MICTC99* (dose conversion factor for ^{99}Tc for modern interglacial climate, (rem/yr)/(pCi/L)), and *SEEPPRM* (mean fracture permeability in lithophysal rock units, m^2; as sampled, *SEEPPRM* is actually the logarithm of the indicated permeability). The variables *SZGWSPDM*, *INFIL*, *SEEPUNC* and *MICTC99* have positive effects on *EXPDOSE*. Specifically, increasing *SZGWSPDM* increase water flow in the SZ; increasing *INFIL* increases water flow in the EBS and UZ; increasing *SEEPUNC* increases water flow in the EBS; and increasing *MICTC99* increases the received dose for a given exposure to ^{99}Tc. The variables *SZFIPOVO* and *SEEPPRM* have negative effects on *EXPDOSE*. The negative effect of *SZFIPOVO* takes place at early times because increasing *SZFIPOVO* tends to delay the time at which released radionuclides first reach the RMEI; the nature of the integration process that produces *EXPDOSE* reduces the importance of *SZFIPOVO* with increasing time. The negative effect of *SEEPPRM* results from increasing water flow around the EBS and hence reducing water flow through the EBS.

More detailed sensitivity analyses for *EXPDOSE* are provided by the regression analyses in Figure K7.8.1-2a at 3000, 5000 and 10,000 yr. The three regression analyses are similar and indicate that a large number of variables have small effects on *EXPDOSE*. However, no single variable dominates the uncertainty in *EXPDOSE*. For example, the first variables selected in the three regressions in Figure K7.8.1-2a have R^2 values of only 0.16, 0.16 and 0.21. The final regression models contain 14, 15 and 15 variables, respectively, and have R^2 values of 0.74, 0.75 and 0.67. The relatively low R^2 values probably results from the complex interaction of a large number of variables in determining the uncertainty in *EXPDOSE*.

For perspective, scatterplots are given in Figure K7.8.1-2b,c,d for the first three variables selected in the regression analysis for *EXPDOSE* at 10,000 yr in Figure K7.8.1-2a. Specifically, these variables are *MICTC99*, *SZGWSPDM* and *DTDRHUNC* (pointer variable for collapsed drift rubble thermal conductivity). The previously discussed positive effects associated with *MICTC99* and *SZGWSPDM* can be seen in the scatterplots in Figure K7.8.1-2b,c. A positive effect for *DTDRHUNC* can be seen in the scatterplot in Figure K7.8.1-2d. A value of 2 for *DTDRHUNC* corresponds to selecting a high thermal conductivity for the rubble surrounding packages affected by fault displacement. Higher values of thermal conductivity lead to more rapid cooling of the affected WPs (SNL 2007 [DIRS 181383], Figure 6.3-87[a]) and consequently to earlier occurrence of seepage, or earlier return of seepage if seepage had occurred prior to the fault displacement event. In Figure K7.8.1-2, results are shown following a seismic fault displacement at 200 years. In this case, the higher values of thermal conductivity lead to earlier occurrence of seepage, which leads to somewhat higher expected dose at 10,000 years, but the effect is relatively minor.

It is important to recognize that the results in Figures K7.8.1-1 and K7.8.1-2 reflect the sensitivity of *EXPDOSE* for the 20,000 yr time period to those parameters that are treated as being uncertain in the TSPA-LA Model. Some important parameters and model inputs are not treated was being uncertain, but are instead represented by conservative, fixed values or by assumptions. The sensitivity of *EXPDOSE* to these parameters can be discussed qualitatively but can not be quantified. In particular, the results in Figures K7.8.1-1 and K7.8.1-2 were generated without consideration of the uncertainty in the rate of occurrence of seismic fault displacement events. The rates of occurrence of seismic fault displacement events represent mean rates of

occurrence of various fault displacements, and these mean rates underlie the probabilistic weightings of the events that give rise to *EXPDOSE* through an integration process (Section 6.1.2.4). Significant uncertainty is associated with the definition of these rates of occurrence (SNL 2007 [DIRS 176828], Section 6.11.5). If the uncertainty associated with the rates of occurrence of seismic fault displacement events was incorporated into the analysis, this uncertainty would likely be a major contributor to the uncertainty associated with *EXPDOSE*. However, because seismic fault displacement events are not a major contributor to total expected dose when all sources of potential dose to the RMEI are considered (Figure 8.1-3), the use the mean rates yields an adequate estimate of *EXPDOSE* without adding unnecessary complexity to the calculation of *EXPDOSE*.

K7.8.2 Seismic Fault Displacement Scenario Classes: Expected Dose (*EXPDOSE*) to Reasonably Maximally Exposed Individual over the Time Interval [0, 1,000,000 yr]

The uncertainty and sensitivity analyses for expected dose to the RMEI (*EXPDOSE*, mrem/yr) over the time interval [0, 1,000,000 yr] resulting from seismic fault displacement are summarized in Figures K7.8.2-1 and K7.8.2-2. Many sample elements show a rise and then a decrease in *EXPDOSE* over the time interval [0, 200,000 yr] followed by a monotonic increase in *EXPDOSE* after 200,000 yr (Figure K7.8.2-1a,b). The rise and fall in *EXPDOSE* over the time interval [0, 200,000 yr] results from the decay of ^{239}Pu, which is an important contributor to dose but has a half-life of 24,100 yr. As a result, the contribution of ^{239}Pu to dose is initially high but decreases with time; by 200,000 yr, the ^{239}Pu inventory has been reduced by a factor of approximately $(1/2)^8$. The monotonic increase in *EXPDOSE* after 200,000 yr results from the inclusion of the effects of the increasing number of possible prior events with increasing time. As a reminder, *EXPDOSE* at a specific time is not the dose from a single prior event but rather is the expected dose from all possible prior events. Overall, the maximum value for *EXPDOSE* falls between 10^{-4} and 10^{-1} mrem/yr for most sample elements and has maximum values between 10^{-1} and 10^{0} mrem/yr for a few sample elements (Figure K7.8.2-1a).

The sensitivity analyses indicate that the two most important variables with respect to the uncertainty in *EXPDOSE* are *SZGWSPDM* (groundwater specific discharge multiplier; as sampled, *SZGWSPDM* is actually the logarithm of the indicated multiplier) and *INFIL* (infiltration level) (Figures K7.8.2-1c and K7.8.2-2a). Together, *SZGWSPDM* and *INFIL* result in regression models for *EXPDOSE* with R^2 values of 0.40, 0.31 and 0.31 at 50,000, 200,000 and 500,000 yr, respectively (Figure K7.8.2-2a). Thus, *SZGWSPDM* and *INFIL* are important contributors to the uncertainty in *EXPDOSE* but do not dominate this uncertainty. Rather, the regression analyses indicate that the uncertainty in *EXPDOSE* arises from the cumulative effects of a large number of individual variables. After *SZGWSPDM* and *INFIL*, all three regressions then select *WPFLUX* (WP flux splitting factor) and *EP1LOWPU* (scale factor used to incorporate uncertainty into plutonium solubility under low ionic strength conditions; as sampled, *EP1LOWPU* is actually the logarithm of the indicated scale factor). The positive effects associated with *WPFLUX* and *EP1LOWPU* result because increasing *WPFLUX* increases the fraction of seepage water falling on a WP that actually enters the WP and increasing *EP1LOWPU* increases the solubility of plutonium and thus the amount of dissolved plutonium (e.g., ^{239}Pu or ^{242}Pu) that is available for movement out of the EBS. The inclusion of *WPFLUX*

and *EP1LOWPU* results in regression models with four variables and R^2 values of 0.49, 0.45 and 0.45. The individual regression analyses in Figure K7.8.2-2a then continue, with each selecting a total of 16 variables and producing final models with R^2 values of 0.69, 0.68 and 0.69. The relatively low R^2 values result from the interacting effects of a large number of uncertain analysis inputs.

For perspective, scatterplots showing the effects of *INFIL*, *SZGWSPDM* and *EP1LOWPU* on *EXPDOSE* at 500,000 yr are given in Figure K7.8.2-2b,c,d. The positive effects of *INFIL*, *SZGWSPDM* and *EP1LOWPU* on *EXPDOSE* can be seen in these plots.

It is important to recognize that the results in Figures K7.8.2-1 and K7.8.2-2 reflect the sensitivity of *EXPDOSE* for the 20,000 yr time period to the parameters that are treated as being uncertain in the TSPA-LA Model. Some important parameters and model inputs are not treated as being uncertain, but are instead represented by conservative, fixed values or by assumptions. The sensitivity of *EXPDOSE* to these parameters can be discussed qualitatively but can not be quantified. For example, the results in Figures K7.8.2-1 and K7.8.2-2 were generated without consideration of the uncertainty in the rates of occurrence of seismic fault displacement events. The rates of occurrence of seismic fault displacement events represent mean rates of occurrence of various fault displacements, and these mean rates underlie the probabilistic weightings of the events that give rise to *EXPDOSE* through an integration process (Section 6.1.2.4). Significant uncertainty is associated with the definition of these rates of occurrence (SNL 2007 [DIRS 176828], Section 6.11.5). If the uncertainty associated with the rates of occurrence of seismic fault displacement events was incorporated into the analysis, this uncertainty would likely be a major contributor to the uncertainty associated with *EXPDOSE*. However, because seismic fault displacement events are not a major contributor to total expected dose when all sources of potential dose to the RMEI are considered (Figure 8.1-3), the use the mean rates yields an adequate estimate of *EXPDOSE* without adding unnecessary complexity to the calculation of *EXPDOSE*.

K8 ALL SCENARIO CLASSES: EXPECTED DOSE (*EXPDOSE*) TO REASONABLY MAXIMALLY EXPOSED INDIVIDUAL

This section presents analysis results for expected dose to the RMEI resulting from all scenario classes over the time intervals [0, 20,000 yr] and [0, 1,000,000 yr].

K8.1 All Scenario Classes: Expected Dose (*EXPDOSE*) to Reasonably Maximally Exposed Individual over the Time Interval [0, 20,000 yr]

The uncertainty and sensitivity analyses for expected dose to the RMEI (*EXPDOSE*, mrem/yr) over the time interval [0, 20,000 yr] resulting from all scenario classes are summarized in Figures K8.1-1 and K8.1-2. Initial transport to the location of the RMEI takes up to 2000 yr; after the earliest possible arrival time for released radionuclides at the location of the RMEI, *EXPDOSE* increases monotonically with time (Figure K8.1-1a,b). At 10,000 yr, the value for *EXPDOSE* falls between 10^{-3} and 3 mrem/yr. As indicated by Figure 8.1-3(a), the expected dose to the RMEI from all scenario classes is predominantly determined by the expected dose to the RMEI resulting from seismic ground motion and from igneous intrusion. However, for some sample elements, minor effects from early WP failures can be observed in Figure K8.1-1b, where

the initiation of transport from CNSF WPs after 9,000 yr produces spikes in the expected dose. In turn, these spikes result in minor variability in the PRCCs (Figure K8.1-1c).

The PRCCs in Figure K8.1-1c indicate that the three most important variables with respect to the uncertainty in *EXPDOSE* are *SCCTHRP* (residual stress threshold; as sampled, *SCCTHRP* is a percent of a base value of 351 MPa and is related to the stress corrosion cracking threshold, *SCCTHR*, by *SCCTHRP* = (*SCCTHR* × 100)/(351 MPa)), *IGRATE* (rate of occurrence of igneous intrusive events, yr^{-1}), and *SZGWSPDM* (groundwater specific discharge multiplier; as sampled, *SZGWSPDM* is actually the logarithm of the indicated multiplier). The negative effect associated with *SCCTHRP* results because increasing *SCCTHRP* results in WPs being more resistant to seismic ground motion damage; the positive effect associated with *IGRATE* results because increasing *IGRATE* increases the probability of occurrence for igneous events; and the positive effect associated with *SZGWSPDM* results because increasing *SZGWSPDM* increases water flow in the SZ.

After *SCCTHRP*, *IGRATE* and *SZGWSPDM*, smaller effects are indicated for *SZFIPOVO* (flowing interval porosity in the volcanic unit of the SZ), *INFIL* (infiltration level), and *HLWGRNDS* (specific surface area for rind on HLW glass) (Figure K8.1-1c). The negative effect associated with *SZFIPOVO* at early times results from initially slowing the movement of radioactive species in the SZ, and the positive effect associated with *INFIL* results from its role in both speeding the cooling of the repository and increasing water flow in the EBS and UZ. The small negative effect indicated for *HLWGRNDS* results because increasing HLW specific surface area increases the effective saturation of the rind on the HLW glass, which reduces the concentration of those radionuclides without saturation limits (such as ^{99}Tc), which in turn reduces the gradient for diffusion out of the waste form cell and thus reduces the rate of release and the consequent dose.

More detailed sensitivity analyses for *EXPDOSE* are provided by the regression analyses and associated scatterplots in Figure K8.1-2. Overall, the dominant variable with respect to the uncertainty in *EXPDOSE* is *SCCTHRP*. Specifically, the regressions containing only *SCCTHRP* have R^2 values of 0.55, 0.66 and 0.69 at 3000, 5000 and 10,000 yr, respectively (Figure K8.1-2a). After *SCCTHRP*, the next variable selected in all regressions is *IGRATE*, with the inclusion of *IGRATE* raising the cumulative R^2 values to 0.62, 0.73 and 0.73. Thus, the effect of *IGRATE* on *EXPDOSE* is not as great as the effect of *SCCTHRP*. In consistency with the analysis with PRCCs, *SZGWSPDM* is then the third or fourth variable selected in the three regressions analyses. The negative effect associated with *SCCTHRP* and the positive effects associated with *IGRATE* and *SZGWSPDM* can be seen in the scatterplots in Figure K8.1-2a,b,c. After *SCCTHRP*, *IGRATE* and *SZGWSPDM*, The regressions select a number of additional variables that have small effects on *EXPDOSE*. The final regression models have R^2 values of 0.80, 0.84 and 0.83, which indicates that they are reasonably successful in accounting for the uncertainty in *EXPDOSE*. However, as is always the case, some of the variables selected at the ends of individual regression analyses that have very small effects on cumulative R^2 values may be spurious.

It is important to recognize that the results in Figures K8.1-1 and K8.1-2 reflect the sensitivity of *EXPDOSE* for the 20,000 yr time period to those parameters that are treated as being uncertain in

the TSPA-LA Model. Where parameters and model inputs are not treated as being uncertain, but are instead represented by conservative, fixed values or by assumptions, the sensitivity of *EXPDOSE* to these parameters can be discussed qualitatively but can not be quantified. For example, significant uncertainty is associated with the definition of the seismic hazard curve that underlies the occurrence of seismic events and the effects of seismic events. If the uncertainty associated with the seismic hazard curve was incorporated into the analysis, it is likely that this uncertainty would have an effect on the uncertainty associated with *EXPDOSE*.

K8.2 All Scenario Classes: Expected Dose (*EXPDOSE*) to Reasonably Maximally Exposed Individual over the Time Interval [0, 1,000,000 yr]

The uncertainty and sensitivity analyses for expected dose to the RMEI (*EXPDOSE*, mrem/yr) over the time interval [0, 1,000,000 yr] resulting from all scenario classes are summarized in Figures K8.2-1 and K8.2-2. As indicated by Figure 8.1-3(b), the expected dose to the RMEI from all scenario classes is predominantly determined by the expected dose to the RMEI resulting from seismic ground motion and from igneous intrusion.

The time-dependent values for *EXPDOSE* appear somewhat choppy as a result of the sampling-based calculation of the combined doses that result from nominal processes and seismic ground motion events (Figure K7.7.2-1). Smoother results could be obtained by using a larger sample of aleatory futures for seismic ground motion events or possibly a more sophisticated integration procedure for the incorporation of such events. However, because the distribution of *EXPDOSE* has been shown to be statistically stable (Section 7.3.1.3), improved convergence or use of a better integration procedure would produce smoother estimates of expected dose, but would not produce results that differ statistically from those shown in Figure K8.2-1. Overall, most sample elements result in values for *EXPDOSE* in a range from 10^{-2} to 30 mrem/yr, with a few sample elements resulting in values for *EXPDOSE* between 30 and 100 mrem/yr. These sample elements with high values for *EXPDOSE* result from an unbounded range for the longitudinal dispersivity parameter (*LDISP* in Table K3-1) or from conservatism in the extent of seismic damage to WPs that have been breached by general corrosion processes. The sample element in which *EXPDOSE* approaches 100 mrem/yr involves an extreme value for the longitudinal dispersivity parameter (*LDISP*) that consequently produces unrealistically rapid transport of ^{226}Ra as described in Appendix P, Section P15. Other realizations in which *EXPDOSE* spikes above 30 mrem/yr result from the conservative manner in which WPs with corrosion failures are affected by seismic events (see Appendix P, Section P3, for details).

The PRCCs in Figure K8.2-1c indicate that the three most important variables with respect to the uncertainty in *EXPDOSE* are *IGRATE* (rate of occurrence of igneous intrusive events, yr^{-1}), *SZGWSPDM* (groundwater specific discharge multiplier; as sampled, *SZGWSPDM* is actually the logarithm of the indicated multiplier), and *WDGCA22* (temperature dependence coefficient associated with the general corrosion rate for alloy 22, K). The positive effect associated with *IGRATE* results because increasing *IGRATE* increases the probability of occurrence for seismic events; the positive effect associated with *SZGWSPDM* results because increasing *SZGWSPDM* increases water flow in the SZ; and the negative effect associated with *WDGCA22* results from its role in slowing the rate of general corrosion of alloy 22, which in turn delays and reduces WP failures due to both seismic ground motion events and general corrosion.

Smaller effects are indicated for *SZFIPOVO* (flowing interval porosity in the volcanic unit of the SZ), *EP1LOWPU* (scale factor used to incorporate uncertainty into plutonium solubility under low ionic strength conditions; as sampled, *EP1LOWPU* is actually the logarithm of the indicated scale factor), and *KDCSCOL* (distribution coefficient for reversible sorption of cesium on uranophane colloids, mL/g). The positive relationship between these variables and *EXPDOSE* at about 100,000 years indicates that the uncertainty in these variables contributes to some degree to uncertainty in *EXPDOSE*. However, in general the PRCCs for these variables do not indicate any meaningful relationship after about 100,000 years.

As previously indicated in conjunction with Figures K8.1-1 and K8.1-2 for the 20,000 yr time period, it is important to recognize that the results in Figures K8.2-1 and K8.2-2 reflect the sensitivity of *EXPDOSE* for the 1,000,000 yr time period to those parameters that are treated as being uncertain in the TSPA-LA Model. Some important parameters and model inputs are not treated as being uncertain, but are instead represented by conservative, fixed values or by assumptions. In particular, if the uncertainty associated with the seismic hazard curve was incorporated into the analysis, it is likely that this uncertainty would have an effect on the uncertainty associated with *EXPDOSE*.

K9 SUMMARY

This appendix documents results of uncertainty and sensitivity analyses for the TSPA-LA. Sensitivity analyses identify the contribution of uncertain model inputs to the uncertainty in model output. The analyses reported in this Appendix identify the dominant sources of uncertainty in total expected dose to the RMEI. For each scenario class, the analyses also investigate the sources of uncertainty in expected dose to the RMEI and in the movement of several key radionuclides (i.e., ^{239}Pu, both dissolved and sorbed to colloids, ^{237}Np, and ^{99}Tc). These radionuclides were chosen to illustrate a range of radionuclide behavior, including colloid-facilitated transport. In addition, for some of the scenario classes, the analyses investigate uncertainty in other process model results, such as the time of DS failure and the chemical environment in the drifts.

Table K9-1 summarizes sensitivity analysis results for total expected dose and expected dose by scenario class by listing the key uncertain inputs identified by the analysis. The key uncertain inputs in Table K9-1 are listed in decreasing order of importance, with the first listed input having the most effect on the output quantity. The key uncertain inputs are identified on the basis of sensitivity analysis results at roughly the time at which the mean of the output variable achieves its maximum value.

Generally, the uncertain inputs that predominantly determine uncertainty in expected dose for each scenario class are those inputs that describe the occurrence and extent of failure of EBS components. For the seismic ground motion scenario class, the key uncertain input is *SCCTHRP* (residual stress threshold; as sampled, *SCCTHRP* is a percent of a base value of 351 MPa and is related to the stress corrosion cracking threshold, *SCCTHR*, by *SCCTHRP* = (*SCCTHR* × 100)/(351 MPa)), which essentially determines the probability of damage to CDSP or CSNF WPs for each seismic event. For the igneous intrusive scenario class, the key uncertain input is *IGRATE* (rate of occurrence of igneous intrusive events, yr^{-1}). For the nominal scenario class the key uncertain input is *WDGCA22* (temperature dependence coefficient associated with

general corrosion rate for alloy 22, K), which essentially determines the uncertainty in the time and extent of general corrosion failures (both by stress-corrosion cracking and by patches). For the early failure scenario classes key uncertain inputs are *PROBWPEF* (probability that a randomly selected WP will experience an early failure) and *PROBDSEF* (probability that a randomly selected DS will experience an early failure). For the igneous eruptive scenario class the key uncertain input is *IGERATE* (rate of occurrence of igneous eruptive events, yr^{-1}). For the seismic fault displacement scenario class, no single input emerged as predominant. Rather, the analysis identified several uncertain inputs with moderately monotonic effect on the expected dose for the scenario class.

The sensitivity analysis confirms that uncertain inputs are propagated through the TSPA-LA Model and that the effects of uncertainty in these inputs are consistent with physical principles. The confirmation is demonstrated through causal explanations of the relationships between input and output variables. For example, where the analysis indicates a positive correlation between the input and output variables, the causal explanation illustrates the reasons why a positive correlation should be observed.

The final sensitivity analysis also identified a relatively small number of implementation errors present in the version of the TSPA-LA Model (v5.000) that was subject to analysis. These errors, along with others identified by check and review activities, are documented in Appendix P along with impact assessments investigating the effect of each error on the TSPA-LA Model v5.000 results. Although the errors do not significantly affect the output from the TSPA-LA Model, the errors influence the selection of uncertain input variables correlated to uncertainty in the transport of plutonium sorbed to certain colloids. As a consequence, the affected results were removed from the final version of Appendix K.

Table K3-1. High-Level Summary of Epistemically Uncertain Variables (i.e., elements of **e**) Considered in the TSPA-LA (Sensitivity Analysis Name)

NOTE: * indicates variable not considered in sensitivity analysis due to correlations.

ALPHAL. van Genuchten capillary strength parameter in lithophysal rock units (Pa). *Distribution:* Triangular. *Range:* -105 to 105. *Mean/Median/Mode:* 0. *TSPA-LA Name:* Alpha_Uncert_Lith_a. *Location in TSPA-LA:* Sections 6.3.3.1.2 and 6.3.3.1.3; Tables 6.3.3-1, 6.3.3-3 and 6.3.5-4.
ALPHANL*. van Genuchten capillary strength parameter in nonlithophysal rock units (Pa). *Distribution:* Triangular. *Range:* -105 to 105. *Mean/Median/Mode:* 0. *TSPA-LA Name:* Alpha_Uncert_NonLith_a*. *Location in TSPA-LA:* Section 6.3.3.1.2; Tables 6.3.3-1, 6.3.3-3 and 6.3.5-4.
ASHDENS. Tephra settled density (kg/m^3). *Distribution:* Truncated normal *Range:* 300 to 1,500. *Mean:* 1,000. *Standard Deviation:* 100. *TSPA-LA Name:* Ash_Density_a. *Location in TSPA-LA:* Table 6.5-5.
BCKALPHA. Natural background levels of alpha emitters in groundwater (pCi/L). *Distribution:* Truncated normal. *Range:* 0 to 0.71. *Mean/Median/Mode:* 0.5. *TSPA-LA Name:* Background_Alpha_a. *Location in TSPA-LA:* Sections 6.3.10.2, 6.3.11.2, and Table 6.3.10-6.
BCKRA226. Natural background levels of combined ^{226}Ra and ^{228}Ra in groundwater (pCi/L). *Distribution:* Truncated normal. *Range:* 0 to 0.71. *Mean/Median/Mode:* 0.5. *TSPA-LA Name:* Background_Ra226_Ra228_a. *Location in TSPA-LA:* Sections 6.3.10.2, 6.3.11.2, and Table 6.3.10-6.
BETA. Column diffusion constant (dimensionless). *Distribution:* Uniform. *Range:* 0.01 to 0.5. *TSPA-LA Name:* Beta_Dist_a. *Location in TSPA-LA:* Table 6.5-4.
BTILLAGE. Depth of soil within which radionuclides contribute to dose from external exposure (m). *Distribution:* Uniform. *Range:* 0.05 to 0.3. *TSPA-LA Name:* b_Tillage_a. *Location in TSPA-LA:* Table 6.5-5.
CFLUXOUT. Ratio of radionuclide mass associated with colloids (reversible and irreversible) to radionuclide mass associated with colloids and dissolved radionuclide mass (dimensionless). *Distribution:* Uniform. *Range:* 0.9 to 0.99. *TSPA-LA Name:* Target_Flux_Out_Ratio_a. *Location in TSPA-LA:* Table 6.3.7-65.
COLFEOCS. FeOx colloid concentration when carbon steel is corroding (mg/L). *Distribution:* Truncated log normal. *Range:* 0.3 to 30. *Mean:* 3.69. *Standard Deviation:* 2.79. *TSPA-LA Name:* Conc_Col_FeOx_CS_Sampled_a. *Location in TSPA-LA:* Table 6.3.7-65.
COLFEOSS. FeOx colloid concentration when degraded stainless steel is present, but no degrading carbon steel is present (mg/L). *Distribution:* Piecewise uniform. *Range:* 1.00E-03 to 3.00E+01. *TSPA-LA Name:* Conc_Col_FeOx_SS_Sampled_a. *Location in TSPA-LA:* Table 6.3.7-65.
COLGW. Concentration of groundwater colloids when colloids are stable (mg/L). *Distribution:* Piecewise uniform. *Range:* 0.001 to 200. *Median:* 0.1. *TSPA-LA Name:* Conc_Col_Gw_Sampled_a. *Location in TSPA-LA:* Table 6.3.7-66.
COLU. Concentration of uranophane colloids when colloids are stable (mg/L). *Distribution:* Piecewise uniform. *Range:* 0.001 to 200. *Median:* 0.1. *TSPA-LA Name:* Conc_Col_U_Sampled_a. *Location in TSPA-LA:* Table 6.3.7-64.
CORRATSS. Stainless steel corrosion rate (μm/yr). *Distribution:* Truncated log normal. *Range:* 0.01 to 0.51. *Mean/Median/Mode:* 0.267. *Standard Deviation:* 0.209. *TSPA-LA Name:* SS_Corrosion_Rate_a. *Location in TSPA-LA:* Tables 6.3.8-1 and 6.3.8-4.
CPUCOLCS. Concentration of irreversibly attached plutonium on CSNF colloids when colloids are stable (mol/L). *Distribution:* Piecewise uniform. *Range:* 1.00E-10 to 5.00E-06. *Median:* 1.00E-07. *TSPA-LA Name:* CPu_Col_CSNF_Sampled_a. *Location in TSPA-LA:* Section 6.3.7.6.2 and Table 6.3.7-63.
CPUCOLWF. Concentration of irreversibly attached plutonium on glass/waste form colloids when colloids are stable (mol/L). *Distribution:* Uniform. *Range:* 1.00E-11 to 1.00E-08. *TSPA-LA Name:* CPu_Col_Wf_Embed_Sampled_a. *Location in TSPA-LA:* Section 6.3.7.6.2 and Table 6.3.7-62.
CPUPERCS. Concentration of irreversibly attached plutonium per concentration of CSNF colloids ((mol/L)/(mg/L)). *Distribution:* Uniform. *Range:* 5.00E-07 to 1.00E-06. *TSPA-LA Name:* CPu_Per_CSNF_Embed_Col_a. *Location in TSPA-LA:* Section 6.3.7.6.2 and Table 6.3.7-63.
CPUPERWF. Concentration of irreversibly attached plutonium per concentration of waste form colloids ((mol/L)/(mg/L)). *Distribution:* Triangular. *Range:* 5.00E-09 to 2.5E-08. *Most Likely:* 2.00E-08. *TSPA-LA Name:* CPu_Per_WF_Embed_Col_a. *Location in TSPA-LA:* Section 6.3.7.6.2 and Table 6.3.7-62.

Table K3-1. High-Level Summary of Epistemically Uncertain Variables (i.e., elements of **e**) Considered in the TSPA-LA (Sensitivity Analysis Name) (Continued)

NOTE: * indicates variable not considered in sensitivity analysis due to correlations.

CR2O3SA. Specific surface area of Cr_2O_3 (m^2/g). *Distribution:* Uniform. *Range:* 1 to 20. *TSPA-LA Name:* Cr2O3_SA_a. *Location in TSPA-LA:* Table 6.3.8-4 and S_{CP} in Equation 6.3.8-19.
CRITSLOP. Critical gradient for tephra mobilization from hillslopes (dimensionless). *Distribution:* Uniform. *Range:* 0.21 to 0.47. *TSPA-LA Name:* Critical_Slope_a. *Location in TSPA-LA:* Table 6.5-5.
CSCORRAT. Carbon steel corrosion rate (μm/yr). *Distribution:* Truncated log normal. *Range:* 25 to 135. *Mean:* 78.5. *Standard Deviation:* 25. *TSPA-LA Name:* CS_Corrosion_Rate_a. *Location in TSPA-LA:* Tables 6.3.8-1 and 6.3.8-4.
CSNFMASS. Scale factor used to characterize uncertainty in radionuclide content of CSNF (dimensionless). *Distribution:* Uniform. *Range:* 0.85 to 1.4. *TSPA-LA Name:* CSNF_Mass_Uncert_a. *Location in TSPA-LA:* Sections 6.3.7.1.2, 6.3.7.1.3, and Table 6.3.7-7.
CSRINDDN. Grain density of CSNF rind (kg/m^3). *Distribution:* Uniform. *Range:* 5600 to 11500. *TSPA-LA Name:* Density_CSNF_Rind_a. *Location in TSPA-LA:* Table 6.3.8-4.
CSRINDPO. Porosity in CSNF rind (dimensionless). *Distribution:* Uniform. *Range:* 0.05 to 0.3. *TSPA-LA Name:* Rind_Porosity_CSNF_a. *Location in TSPA-LA:* Section 6.3.8.2.1 and Table 6.3.8-6.
CSRINDSA. Specific surface area of CSNF degradation rind (m^2/g). *Distribution:* Uniform. *Range:* 0.5 to 60. *TSPA-LA Name:* CSNF_Rind_SA_a. *Location in TSPA-LA:* Tables 6.3.8-2 and 6.3.8-4.
CSSPECSA. Logarithm of the effective specific surface area (m^2/mg) of the representative CSNF waste form (dimensionless). *Distribution:* Triangular. *Range:* -7.3 to -5.4. *Most Likely:* -6.7. *TSPA-LA Name:* Log_Specific_SA_CSNF_a. *Location in TSPA-LA:* Sections 6.3.7.4.1.2 and 6.3.7.4.1.3; Tables 6.3.7-30 and 6.3.7-31; and Equations 6.3.7-5 and 6.3.7-6.
CSWFA0AC. Correlated regression coefficient a0 in the abstracted rate model under acidic conditions (dimensionless). *Distribution:* Normal. *Mean/Median/Mode:* 0. *Standard Deviation:* 1. *TSPA-LA Name:* CSNF_WF_Uncert_a0_Acid_a. *Location in TSPA-LA:* Section 6.3.7.4.1.2; Equation 6.3.7-6.
CSWFA0AK. Correlated coefficient a0 in the abstracted rate model under alkaline conditions (dimensionless). *Distribution:* Normal. *Mean/Median/Mode:* 0. *Standard Deviation:* 1. *TSPA-LA Name:* CSNF_WF_Uncert_a0_Alk_a. *Location in TSPA-LA:* Section 6.3.7.4.1.2; Equation 6.3.7-5.
CSWFA1AK. Correlated coefficient a1 in the abstracted rate model under alkaline conditions (dimensionless). *Distribution:* Normal. *Mean/Median/Mode:* 0. *Standard Deviation:* 1. *TSPA-LA Name:* CSNF_WF_Uncert_a1_Alk_a. *Location in TSPA-LA:* Section 6.3.7.4.1.2 and Equation 6.3.7-5.
CSWFA2AK. Correlated coefficient a2 in the abstracted rate model under alkaline conditions (dimensionless). *Distribution:* Normal. *Mean/Median/Mode:* 0. *Standard Deviation:* 1. *TSPA-LA Name:* CSNF_WF_Uncert_a2_Alk_a. *Location in TSPA-LA:* Section 6.3.7.4.1.2 and Equation 6.3.7-5.
CSWFA3AK. Correlated coefficient a3 in the abstracted rate model under alkaline conditions (dimensionless). *Distribution:* Normal. *Mean/Median/Mode:* 0. *Standard Deviation:* 1. *TSPA-LA Name:* CSNF_WF_Uncert_a3_Alk_a. *Location in TSPA-LA:* Section 6.3.7.4.1.2 and Equation 6.3.7-5.
CSWFA4AC. Correlated coefficient a4 in the abstracted rate model under acid conditions (dimensionless). *Distribution:* Normal. *Mean/Median/Mode:* 0. *Standard Deviation:* 1. *TSPA-LA Name:* CSNF_WF_Uncert_a4_Acid_a. *Location in TSPA-LA :* Section 6.3.7.4.1.2 and Equation 6.3.7-6.
DASHAVG. Mass median ash particle diameter (cm). *Distribution:* Log triangular. *Range:* 0.001 to 0.1. *Mode:* 0.01. *TSPA-LA Name:* Dash_mean_a. *Location in TSPA-LA:* Table 6.5-4.
DASHSIG. Ash particle diameter standard deviation (log (cm)). *Distribution:* Uniform. *Range:* 0.301 to 0.903. *TSPA-LA Name:* Dash_sigma_a. *Location in TSPA-LA:* Table 6.5-4.
DCHANL. Diffusivity of radionuclides in channels of the Fortymile Wash fan (RMEI location) (cm^2/yr). *Distribution:* Uniform. *Range:* 0.035 to 0.266. *Mean:* 0.1505. *TSPA-LA Name:* D_Channels_a. *Location in TSPA-LA:* Table 6.5-5.
DDIVIDE. Diffusivity of radionuclides in divides of the Fortymile Wash fan (RMEI location) (cm^2/yr). *Distribution:* Uniform. *Range:* 0.001 to 0.095. *Mean* 0.048. *TSPA-LA Name:* D_Divides_a. *Location in TSPA-LA:* Table 6.5-5.

Table K3-1. High-Level Summary of Epistemically Uncertain Variables (i.e., elements of **e**) Considered in the TSPA-LA (Sensitivity Analysis Name) (Continued)

NOTE: * indicates variable not considered in sensitivity analysis due to correlations.

DELPPCO2. Selector variable for partial pressure of CO_2 (dimensionless). *Distribution:* Uniform. *Range:* -1 to 1. *TSPA-LA Name:* PCE_Delta_pCO2_a. *Location in TSPA-LA:* Sections 6.3.4.2 and 6.3.5.2.3; Table 6.3.5-4.
DIAMCOLL. Diameter of colloid particle (nm). *Distribution:* Uniform. *Range:* 50 to 300. *TSPA-LA Name:* Diameter_Colloid_a. *Location in TSPA-LA:* Tables 6.3.8-1 and 6.3.8-4.
DIFPATHL. Diffusive path length from waste package outer corrosion barrier to mid-point of invert (m). *Distribution:* Uniform. *Range:* 0.3 to 1.24. *TSPA-LA Name:* Diff_Path_Length_Invert_Top_a. *Location in TSPA-LA:* Section 6.3.8.2.4; Table 6.3.8-4.
DRAINDNS. Average drainage density for the Fortymile Wash drainage basin (1/km). *Distribution:* Uniform. *Range:* 20 to 33. *TSPA-LA Name:* Drainage_Density_a. *Location in TSPA-LA:* Table 6.5-5.
DSFLUX. Drip shield flux splitting factor (dimensionless). *Distribution:* Uniform. *Range:* 0 to 0.85. *TSPA-LA Name:* DS_Flux_Uncertainty_a. *Location in TSPA-LA:* Tables 6.3.6-1, 6.3.6-2 and 6.3.8-4; Sections 6.3.6.2 and 6.3.6.4.1; Equation 6.3.6-5.
DSNFMASS. Scale factor used to characterize uncertainty in radionuclide content of DSNF (dimensionless). *Distribution:* Triangular. *Range:* 0.45 to 2.9. *Most Likely:* 0.62. *TSPA-LA Name:* DSNF_Mass_Uncert_a. *Location in TSPA-LA:* Sections 6.3.7.1.2 and 6.3.7.1.3; Table 6.3.7-7.
DTDRHUNC. Selector variable used to determine the collapsed drift rubble thermal conductivity (dimensionless). *Distribution:* Discrete. *Range:* 1 to 2. *TSPA-LA Name:* dt_dRh_uncertainty. *Location in TSPA-LA:* Section 6.6.2.2.
DWCDISP. Selector variable used to determine the axial dispersion modeling case (dimensionless). *Distribution:* Discrete. *Range:* 0 to 1. *TSPA-LA Name:* DWC_Dispersivity_Cond_a. *Location in TSPA-LA:* Section 6.3.3.2.2; Table 6.3.3-5.
DWCSTERA. Multiplier for the standard deviation on the slope coefficient for determining the probability of condensation from percolation rate (dimensionless). *Distribution:* Normal. *Mean/Median/Mode:* 0. *Standard Deviation:* 1. *TSPA-LA Name:* DWC_Std_Error_a_a. *Location in TSPA-LA:* Section 6.3.3.2.2; Tables 6.3.3-4 and 6.3.3-5.
DWCSTERB. Multiplier for the standard deviation on the y-intercept coefficient for determining the probability of condensation from percolation rate (dimensionless). *Distribution:* Normal. *Mean/Median/Mode:* 0. *Standard Deviation:* 1. *TSPA-LA Name:* DWC_Std_Error_b_a. *Location in TSPA-LA:* Section 6.3.3.2.2; Tables 6.3.3-4 and 6.3.3-5.
DWCSTERC. Multiplier for the standard deviation on the slope coefficient for determining condensation rate from percolation rate (dimensionless). *Distribution:* Normal. *Mean/Median/Mode:* 0. *Standard Deviation:* 1. *TSPA-LA Name:* DWC_Std_Error_c_a. *Location in TSPA-LA:* Section 6.3.3.2.2; Tables 6.3.3-4 and 6.3.3-5.
DWCSTERD. Multiplier for the standard deviation on the y-intercept coefficient for determining the condensation rate from percolation rate (dimensionless). *Distribution:* Normal. *Mean/Median/Mode:* 0. *Standard Deviation:* 1. *TSPA-LA Name:* DWC_Std_Error_d_a. *Location in TSPA-LA:* Section 6.3.3.2.2; Tables 6.3.3-4 and 6.3.3-5.
DWCVENT. Selector variable specifying whether the ventilated or unventilated drip shield DWC modeling case is performed (dimensionless). *Distribution:* Discrete. *Range:* 0, 1. *TSPA-LA Name:* DWC_Ventilated_Cond_a. *Location in TSPA-LA:* Sections 6.3.3.2.2 and 6.3.3.2.3; Table 6.3.3-5.
EBSDIFCF. Exponential term representing uncertainty in the invert diffusion coefficient (dimensionless). *Distribution:* Truncated normal. *Range:* -0.621 to 0.687. *Mean:* 0.033. *Standard Deviation:* 0.218. *TSPA-LA Name:* Invert_Diff_Coeff_Uncert_a. *Location in TSPA-LA:* Section 6.3.8.2.4; Table 6.3.8-4; Equation 6.3.8-24.
EP1HINP2*. Logarithm of the scale factor used to characterize uncertainty in Np_2O_5 solubility for ionic strength values between 1 and 3 molal (dimensionless). *Distribution:* Truncated normal. *Range:* -1.7 to 1.7. *Mean:* 0. *Standard Deviation:* 0.85. *TSPA-LA Name:* Np2O5_Eps_1_high_a*. *Location in TSPA-LA:* Sections 6.3.7.5.1 and 6.3.7.5.2; Table 6.3.7-42; Equation 6.3.7-13a.
EP1HINPO2*. Logarithm of the scale factor used to characterize uncertainty in NpO_2 solubility at an ionic strength between 1 and 3 molal (dimensionless). *Distribution:* Truncated normal. *Range:* -1.34 to 1.34. *Mean:* 0. *Standard Deviation:* 0.67. *TSPA-LA Name:* NpO2_Eps_1_high_a*. *Location in TSPA-LA:* Sections 6.3.7.5.1, 6.3.7.5.2 and 6.3.7.5.3; Table 6.3.7-43; Equation 6.3.7-13a.

Table K3-1. High-Level Summary of Epistemically Uncertain Variables (i.e., elements of **e**) Considered in the TSPA-LA (Sensitivity Analysis Name) (Continued)

NOTE: * indicates variable not considered in sensitivity analysis due to correlations.

EP1HINU*. Logarithm of the scale factor used to characterize uncertainty in uranium solubility under nominal or seismic conditions at an ionic strength between 1and 3 molal (dimensionless). *Distribution:* Truncated normal. *Range:* -1.2 to 1.2. *Mean:* 0. *Standard Deviation:* 0.6. *TSPA-LA Name:* U_Eps_1_high_Nominal_a*. *Location in TSPA-LA:* Section 6.3.7.5.1, 6.3.7.5.2 and 6.3.7.5.3; Table 6.3.7-54; Equation 6.3.7-13a.
EP1HIOU*. Logarithm of the scale factor used to characterize uncertainty in uranium solubility under conditions other than nominal and seismic at an ionic strength between 1and 3 molal (dimensionless). *Distribution:* Truncated normal. *Range:* -1.2 to 1.2. *Mean:* 0. *Standard Deviation:* 0.6. *TSPA-LA Name:* U_Eps_1_high_Other_a*. *Location in TSPA-LA:* Sections 6.3.7.5.1, 6.3.7.5.2 and 6.3.7.5.3; Table 6.3.7-58; Equation 6.3.7-13a.
EP1HIPU*. Logarithm of the scale factor used to characterize uncertainty in plutonium solubility for ionic strength between 1 and 3 molal (dimensionless). *Distribution:* Truncated normal. *Range:* -1.52 to 1.52. *Mean:* 0. *Standard Deviation:* 0.76. *TSPA-LA Name:* Pu_Eps_1_high_a*. *Location in TSPA-LA:* Sections 6.3.7.5.1, 6.3.7.5.2 and 6.3.7.5.3; Table 6.3.7-44; Equation 6.3.7-13a.
EP1HISN*. Logarithm of the scale factor used to characterize uncertainty in tin solubility for high ionic strength conditions (dimensionless). *Distribution:* Truncated normal. *Range:* -1.08 to 1.08. *Mean:* 0. *Standard Deviation:* 0.54. *TSPA-LA Name:* Sn_Eps_high_a*. *Location in TSPA-LA:* Sections 6.3.7.5.2 and 6.3.7.5.3; Table 6.3.7-47; Equation 6.3.7-13a.
EP1HITH*. Logarithm of the scale factor used to characterize uncertainty in thorium solubility at ionic strength between 1 and 3 molal (dimensionless). *Distribution:* Truncated normal. *Range:* -1.52 to 1.52. *Mean:* 0. *Standard Deviation:* 0.76. *TSPA-LA Name:* Th_Eps_1_high_a*. *Location in TSPA-LA:* Sections 6.3.7.5.1, 6.3.7.5.2 and 6.3.7.5.3; Table 6.3.7-46; Equation 6.3.7-13a.
EP1LOWAM. Logarithm of the scale factor used to characterize uncertainty in americium solubility at an ionic strength below 1 molal (dimensionless). *Distribution:* Truncated normal. *Range:* -2 to 2. *Mean:* 0. *Standard Deviation:* 1. *TSPA-LA Name:* Am_Eps_1_low_a. *Location in TSPA-LA:* Sections 6.3.7.5.1, 6.3.7.5.2 and 6.3.7.5.3; Table 6.3.7-41; Equation 6.3.7-13a.
EP1LOWNU. Logarithm of the scale factor used to characterize uncertainty in uranium solubility under nominal or seismic conditions at an ionic strength below 1 molal (dimensionless). *Distribution:* Truncated normal. *Range:* -1 to 1. *Mean/Median/Mode:* 0. *Standard Deviation:* 0.5. *TSPA-LA Name:* U_Eps_1_low_Nominal_a. *Location in TSPA-LA:* Section 6.3.7.5.1, 6.3.7.5.2 and 6.3.7.5.3; Table 6.3.7-54; Equation 6.3.7-13a.
EP1LOWOU. Logarithm of the scale factor used to characterize uncertainty in uranium solubility under conditions other than nominal and seismic at an ionic strength below 1 molal (dimensionless). *Distribution:* Truncated normal. *Range:* -1 to 1. *Mean/Median/Mode:* 0. *Standard Deviation:* 0.5. *TSPA-LA Name:* U_Eps_1_low_Other_a. *Location in TSPA-LA:* Sections 6.3.7.5.1, 6.3.7.5.2 and 6.3.7.5.3; Table 6.3.7-58; Equation 6.3.7-13a.
EP1LOWPU. Logarithm of the scale factor used to characterize uncertainty in plutonium solubility at an ionic strength below 1 molal (dimensionless). *Distribution:* Truncated normal. *Range:* -1.4 to 1.4. *Mean/Median/Mode:* 0. *Standard Deviation:* 0.7. *TSPA-LA Name:* Pu_Eps_1_low_a. *Location in TSPA-LA:* Sections 6.3.7.5.1, 6.3.7.5.2 and 6.3.7.5.3; Table 6.3.7-44; Equation 6.3.7-13a.
EP1LOWSN. Logarithm of the scale factor used to characterize uncertainty in tin solubility for low ionic strength conditions (dimensionless). *Distribution:* Truncated normal. *Range:* -0.9 to 0.9. *Mean/Median/Mode:* 0. *Standard Deviation:* 0.45. *TSPA-LA Name:* Sn_Eps_low_a. *Location in TSPA-LA:* Sections 6.3.7.5.2 and 6.3.7.5.3; Table 6.3.7-47; Equation 6.3.7-13a.
EP1LOWTH. Logarithm of the scale factor used to characterize uncertainty in thorium solubility at an ionic strength below 1 molal (dimensionless). *Distribution:* Truncated normal. *Range:* -1.4 to 1.4. *Mean:* 0. *Standard Deviation:* 0.7. *TSPA-LA Name:* Th_Eps_1_low_a. *Location in TSPA-LA:* Sections 6.3.7.5.1, 6.3.7.5.2 and 6.3.7.5.3; Table 6.3.7-46; Equation 6.3.7-13a.
EP1NP2O5. Logarithm of the scale factor used to characterize uncertainty in Np_2O_5 solubility at an ionic strength below 1 molal (dimensionless). *Distribution:* Truncated normal. *Range:* -1.6 to 1.6. *Mean:* 0. *Standard Deviation:* 0.8. *TSPA-LA Name:* Np2O5_Eps_1_low_a. *Location in TSPA-LA:* Sections 6.3.7.5.1 and 6.3.7.5.2; Table 6.3.7-42; Equation 6.3.7-13a.
EP1NPO2. Logarithm of the scale factor used to characterize uncertainty in NpO_2 solubility at an ionic strength below 1 molal (dimensionless). *Distribution:* Truncated normal. *Range:* -1.2 to 1.2. *Mean:* 0. *Standard Deviation:* 0.6. *TSPA-LA Name:* NpO2_Eps_1_low_a. *Location in TSPA-LA:* Sections 6.3.7.5.1, 6.3.7.5.2 and 6.3.7.5.3; Table 6.3.7-43; Equation 6.3.7-13a.

Table K3-1. High-Level Summary of Epistemically Uncertain Variables (i.e., elements of **e**) Considered in the TSPA-LA (Sensitivity Analysis Name) (Continued)

NOTE: * indicates variable not considered in sensitivity analysis due to correlations.

EP1PA. Logarithm of the scale factor used to characterize uncertainty in protactinium solubility (dimensionless). *Distribution:* Uniform. *Range:* -4.42 to -0.05. *TSPA-LA Name:* Pa_Eps_1_a. *Location in TSPA-LA:* Sections 6.3.7.5.2 and 6.3.7.5.3; Table 6.3.7-45; Equation 6.3.7-13b.
EP2BCDHU*. Term associated with uncertainty in uranium solubility (controlled by boldwoodite saturation) due to variations in fluoride concentration for CDSP waste packages when ionic strength is greater than or equal to 0.004 molal and for the invert below CDSP waste packages (mg/L). *Distribution:* Triangular. *Range:* 0 to 272.3. *Most Likely:* 0. *TSPA-LA Name:* U_Eps_2_Boltwoodite_CDSP_Hig_a*. *Location in TSPA-LA:* Sections 6.3.7.5.1, 6.3.7.5.2 and 6.3.7.5.3; Table 6.3.7-58; Equation 6.3.7-13a.
EP2BCSHU*. Term associated with uncertainty in uranium solubility (controlled by boldwoodite saturation) due to variations in fluoride concentration for CSNF waste packages when ionic strength is greater than or equal to 0.2 molal and for the invert below CSNF waste packages (mg/L). *Distribution:* Triangular. *Range:* 0 to 57.01. *Most Likely:* 0. *TSPA-LA Name:* U_Eps_2_Boltwoodite_CSNF_Hig_a*. *Location in TSPA-LA:* Sections 6.3.7.5.1, 6.3.7.5.2 and 6.3.7.5.3; Table 6.3.7-58; Equation 6.3.7-13a.
EP2BLOWU*. Term associated with uncertainty in uranium solubility (controlled by boldwoodite saturation) due to variations in fluoride concentration for CDSP waste packages Cell 1a, Cell 1b when ionic strength is less than 0.004 molal, and CSNF waste packages when ionic strength is less than 0.2 molal (mg/L). *Distribution:* Triangular. *Range:* 0 to 6.13. *Most Likely:* 0. *TSPA-LA Name:* U_Eps_2_Boltwoodite_Glass_Lo_a*. *Location in TSPA-LA:* Sections 6.3.7.5.1, 6.3.7.5.2 and 6.3.7.5.3; Table 6.3.7-58; Equation 6.3.7-13a.
EP2CDNP2*. Term associated with uncertainty in Np_2O_5 solubility due to variations in fluoride concentration for CDSP waste packages when ionic strength is greater than or equal to 0.004 molal and for the invert below CDSP waste packages (mg/L). *Distribution:* Triangular. *Range:* 0 to 853. *Most Likely:* 0. *TSPA-LA Name:* Np2O5_Eps_2_CDSP_High_a*. *Location in TSPA-LA:* Sections 6.3.7.5.1 and 6.3.7.5.2; Table 6.3.7-42; Equation 6.3.7-13a.
EP2CDNPO2*. Term associated with uncertainty in NpO_2 solubility due to variations in fluoride concentration for CDSP waste packages when ionic strength is greater than or equal to 0.004 molal and for the invert below CDSP waste packages (mg/L). *Distribution:* Triangular. *Range:* 0 to 1093.5. *Most Likely:* 0. *TSPA-LA Name:* NpO2_Eps_2_CDSP_High_a*. *Location in TSPA-LA:* Sections 6.3.7.5.1, 6.3.7.5.2 and 6.3.7.5.3; Table 6.3.7-43; Equation 6.3.7-13a.
EP2CDPA*. Term associated with uncertainty in protactinium solubility due to variations in fluoride concentration for CDSP waste packages when ionic strength is greater than or equal to 0.004 molal and for the invert below CDSP waste packages (mg/L). *Distribution:* Triangular. *Range:* 0 to 853. *Most Likely:* 0. *TSPA-LA Name:* Pa_Eps_2_CDSP_High_a*. *Location in TSPA-LA:* Sections 6.3.7.5.2 and 6.3.7.5.3; Table 6.3.7-45; Equation 6.3.7-13b.
EP2CDPU*. Term associated with uncertainty in plutonium solubility due to variations in fluoride concentration for CDSP waste packages when ionic strength is greater than or equal to 0.004 molal and for the invert below CDSP waste packages (mg/L). *Distribution:* Triangular. *Range:* 0 to 5460. *Most Likely:* 0. *TSPA-LA Name:* Pu_Eps_2_CDSP_High_a*. *Location in TSPA-LA:* Sections 6.3.7.5.1, 6.3.7.5.2 and 6.3.7.5.3; Table 6.3.7-44; Equation 6.3.7-13a.
EP2CDTH*. Term associated with uncertainty in thorium solubility due to variations in fluoride concentration for CDSP waste packages when ionic strength is greater than or equal to 0.004 molal and for the invert below CDSP waste packages (mg/L). *Distribution:* Triangular. *Range:* 0 to 23723.2. *Most Likely:* 0. *TSPA-LA Name:* Th_Eps_2_CDSP_High_a*. *Location in TSPA-LA:* Sections 6.3.7.5.1, 6.3.7.5.2 and 6.3.7.5.3; Table 6.3.7-46; Equation 6.3.7-13a.
EP2CSHNU*. Term associated with uncertainty in uranium solubility (under nominal or seismic conditions) due to variations in fluoride concentration for CSNF waste packages when ionic strength is greater than or equal to 0.2 molal and for the invert below CSNF waste packages (mg/L). *Distribution:* Triangular. *Range:* 0 to 1361. *Most Likely:* 0. *TSPA-LA Name:* U_Eps_2_CSNF_High_Nominal_a*. *Location in TSPA-LA:* Section 6.3.7.5.1, 6.3.7.5.2 and 6.3.7.5.3; Table 6.3.7-54; Equation 6.3.7-13a.
EP2CSLNU*. Term associated with uncertainty in uranium solubility (under nominal or seismic conditions) due to variations in fluoride concentration for CSNF waste packages when ionic strength is less than 0.2 molal and for the invert below CSNF waste packages (mg/L). *Distribution:* Triangular. *Range:* 0 to 78. *Most Likely:* 0. *TSPA-LA Name:* U_Eps_2_CSNF_Low_Nominal_a*. *Location in TSPA-LA:* Section 6.3.7.5.1, 6.3.7.5.2 and 6.3.7.5.3; Table 6.3.7-54; Equation 6.3.7-13a.

Table K3-1. High-Level Summary of Epistemically Uncertain Variables (i.e., elements of **e**) Considered in the TSPA-LA (Sensitivity Analysis Name) (Continued)

NOTE: * indicates variable not considered in sensitivity analysis due to correlations.

EP2CSNP2*. Term associated with uncertainty in Np_2O_5 solubility due to variations in fluoride concentration for CSNF waste packages when ionic strength is greater than or equal to 0.2 molal and for the invert below CSNF waste packages (mg/L). *Distribution:* Triangular. *Range:* 0 to 197. *Most Likely:* 0. *TSPA-LA Name:* Np2O5_Eps_2_CSNF_High_a*. *Location in TSPA-LA:* Sections 6.3.7.5.1 and 6.3.7.5.2; Table 6.3.7-42; Equation 6.3.7-13a.
EP2CSNPO2*. Term associated with uncertainty in NpO_2 solubility due to variations in fluoride concentration for CSNF waste packages when ionic strength is greater than or equal to 0.2 molal and for the invert below CSNF waste packages (mg/L). *Distribution:* Triangular. *Range:* 0 to 255.8. *Most Likely:* 0. *TSPA-LA Name:* NpO2_Eps_2_CSNF_High_a*. *Location in TSPA-LA:* Sections 6.3.7.5.1, 6.3.7.5.2 and 6.3.7.5.3; Table 6.3.7-43; Equation 6.3.7-13a.
EP2CSPA*. Term associated with uncertainty in protactinium solubility due to variations in fluoride concentration for CSNF waste packages when ionic strength is greater than or equal to 0.2 molal and for the invert below CSNF waste packages (mg/L). *Distribution:* Triangular. *Range:* 0 to 197. *Most Likely:* 0. *TSPA-LA Name:* Pa_Eps_2_CSNF_High_a*. *Location in TSPA-LA:* Sections 6.3.7.5.2 and 6.3.7.5.3; Table 6.3.7-45; Equation 6.3.7-13b.
EP2CSPU*. Term associated with uncertainty in plutonium solubility due to variations in fluoride concentration for CSNF waste packages when ionic strength is greater than or equal to 0.2 molal and for the invert below CSNF waste packages (mg/L). *Distribution:* Triangular. *Range:* 0 to 1374. *Most Likely:* 0. *TSPA-LA Name:* Pu_Eps_2_CSNF_High_a*. *Location in TSPA-LA:* Sections 6.3.7.5.1, 6.3.7.5.2 and 6.3.7.5.3; Table 6.3.7-44; Equation 6.3.7-13a.
EP2CSTH*. Term associated with uncertainty in thorium solubility due to variations in fluoride concentration for CSNF waste packages when ionic strength is greater than or equal to 0.2 molal and for the invert below CSNF waste packages (mg/L). *Distribution:* Triangular. *Range:* 0 to 7848.3. *Most Likely:* 0. *TSPA-LA Name:* Th_Eps_2_CSNF_High_a*. *Location in TSPA-LA:* Sections 6.3.7.5.1, 6.3.7.5.2 and 6.3.7.5.3; Table 6.3.7-46; Equation 6.3.7-13a.
EP2HIAM*. Logarithm of the scale factor used to characterize uncertainty in americium solubility at ionic strength values between 1 and 3 molal (dimensionless). *Distribution:* Truncated normal. *Range:* -2.08 to 2.08. *Mean:* 0. *Standard Deviation:* 1.04. *TSPA-LA Name:* Am_Eps_1_high_a*. *Location in TSPA-LA:* Sections 6.3.7.5.1, 6.3.7.5.2 and 6.3.7.5.3; Equation 6.3.7-13a; Table 6.3.7-41.
EP2HICAM. Term associated with uncertainty in americium solubility due to variations in fluoride concentration for CSNF waste packages when ionic strength is greater than or equal to 0.2 molal and for the invert below CSNF waste packages (mg/L). *Distribution:* Triangular. *Range:* 0 to 109.03. *Most Likely:* 0. *TSPA-LA Name:* Am_Eps_2_CSNF_High_a. *Location in TSPA-LA:* Sections 6.3.7.5.2 and 6.3.7.5.3; Table 6.3.7-41; Equation 6.3.7-13a.
EP2HICDAM*. Term associated with uncertainty in americium solubility due to variations in fluoride concentration for CDSP waste packages when ionic strength is greater than or equal to 0.004 molal and for the invert below CDSP waste packages (mg/L). *Distribution:* Triangular. *Range:* 0 to 688.6. *Most Likely:* 0. *TSPA-LA Name:* Am_Eps_2_CDSP_High_a*. *Location in TSPA-LA:* Sections 6.3.7.5.2 and 6.3.7.5.3; Table 6.3.7-41; Equation 6.3.7-13a.
EP2LONP2*. Term associated with uncertainty in Np_2O_5 solubility due to variations in fluoride concentration for CDSP waste packages Cell 1a, Cell 1b when ionic strength is less than 0.004 molal, and CSNF waste packages when ionic strength is less than 0.2 molal (mg/L). *Distribution:* Triangular. *Range:* 0 to 11. *Most Likely:* 0. *TSPA-LA Name:* Np2O5_Eps_2_Glass_Low_a*. *Location in TSPA-LA:* Sections 6.3.7.5.1 and 6.3.7.5.2; Table 6.3.7-42; Equation 6.3.7-13a.
EP2LONPO2*. Term associated with uncertainty in NpO_2 solubility due to variations in fluoride concentration for CDSP waste packages Cell 1a, Cell 1b when ionic strength is less than 0.004 molal, and CSNF waste packages when ionic strength is less than 0.2 molal (mg/L). *Distribution:* Triangular. *Range:* 0 to 14.1. *Most Likely:* 0. *TSPA-LA Name:* NpO2_Eps_2_Glass_Low_a*. *Location in TSPA-LA:* Sections 6.3.7.5.1, 6.3.7.5.2 and 6.3.7.5.3; Table 6.3.7-43; Equation 6.3.7-13a.

Table K3-1. High-Level Summary of Epistemically Uncertain Variables (i.e., elements of **e**) Considered in the TSPA-LA (Sensitivity Analysis Name) (Continued)

NOTE: * indicates variable not considered in sensitivity analysis due to correlations.

EP2LOPA*. Term associated with uncertainty in protactinium solubility due to variations in fluoride concentration for CDSP waste packages Cell 1a, Cell 1b when ionic strength is less than 0.004 molal, and CSNF waste packages when ionic strength is less than 0.2 molal (mg/L). *Distribution:* Triangular. *Range:* 0 to 11. *Most Likely:* 0. *TSPA-LA Name:* Pa_Eps_2_Glass_Low_a*. *Location in TSPA-LA:* Sections 6.3.7.5.2 and 6.3.7.5.3; Table 6.3.7-45; Equation 6.3.7-13b.
EP2LOWAM*. Term associated with uncertainty in americium solubility due to variations in fluoride concentration for CDSP waste packages Cell 1a, Cell 1b when ionic strength is less than 0.004 molal, and CSNF waste packages when ionic strength is less than 0.2 molal (mg/L). *Distribution:* Triangular. *Range:* 0 to 4.42. *Most Likely:* 0. *TSPA-LA Name:* Am_Eps_2_Glass_Low_a*. *Location in TSPA-LA:* Sections 6.3.7.5.2 and 6.3.7.5.3; Table 6.3.7-41; Equation 6.3.7-13a.
EP2LOWPU*. Term associated with uncertainty in plutonium solubility due to variations in fluoride concentration for CDSP waste packages Cell 1a, Cell 1b when ionic strength is less than 0.004 molal, and CSNF waste packages when ionic strength is less than 0.2 molal (mg/L). *Distribution:* Triangular. *Range:* 0 to 79. *Most Likely:* 0. *TSPA-LA Name:* Pu_Eps_2_Glass_Low_a*. *Location in TSPA-LA:* Sections 6.3.7.5.1, 6.3.7.5.2 and 6.3.7.5.3; Table 6.3.7-44; Equation 6.3.7-13a.
EP2LOWTH*. Term associated with uncertainty in thorium solubility due to variations in fluoride concentration for CDSP waste packages Cell 1a, Cell 1b when ionic strength is less than 0.004 molal, and CSNF waste packages when ionic strength is less than 0.2 molal (mg/L). *Distribution:* Triangular. *Range:* 0 to 626.2. *Most Likely:* 0. *TSPA-LA Name:* Th_Eps_2_Glass_Low_a*. *Location in TSPA-LA:* Sections 6.3.7.5.1, 6.3.7.5.2 and 6.3.7.5.3; Table 6.3.7-46; Equation 6.3.7-13a.
EP2SCDHU*. Term associated with uncertainty in uranium solubility (controlled by schoepite saturation) due to variations in fluoride concentration for CDSP waste packages when ionic strength is greater than or equal to 0.004 molal and for the invert below CDSP waste packages (mg/L). *Distribution:* Triangular. *Range:* 0 to 5385. *Most Likely:* 0. *TSPA-LA Name:* U_Eps_2_Schoepite_CDSP_High_a*. *Location in TSPA-LA:* Sections 6.3.7.5.1, 6.3.7.5.2 and 6.3.7.5.3; Table 6.3.7-58; Equation 6.3.7-13a.
EP2SCSHU*. Term associated with uncertainty in uranium solubility (controlled by schoepite saturation) due to variations in fluoride concentration for CSNF waste packages when ionic strength is greater than or equal to 0.2 molal and for the invert below CSNF waste packages (mg/L). *Distribution:* Triangular. *Range:* 0 to 1361. *Most Likely:* 0. *TSPA-LA Name:* U_Eps_2_Schoepite_CSNF_High_a*. *Location in TSPA-LA:* Sections 6.3.7.5.1, 6.3.7.5.2 and 6.3.7.5.3; Table 6.3.7-58; Equation 6.3.7-13a.
EP2SLOWU*. Term associated with uncertainty in uranium solubility (controlled by schoepite saturation) due to variations in fluoride concentration for CDSP waste packages Cell 1a, Cell 1b when ionic strength is less than 0.004 molal, and CSNF waste packages when ionic strength is less than 0.2 molal (mg/L). *Distribution:* Triangular. *Range:* 0 to 78. *Most Likely:* 0. *TSPA-LA Name:* U_Eps_2_Schoepite_Glass_Low_a*. *Location in TSPA-LA:* Sections 6.3.7.5.1, 6.3.7.5.2 and 6.3.7.5.3; Table 6.3.7-58; Equation 6.3.7-13a.
FHHISKCP. Frenkel Halsey Hill water vapor adsorption isotherm parameter, *k*, for corrosion products (dimensionless). *Distribution:* Uniform. *Range:* 1.048 to 1.370 (see additional information). *TSPA-LA Name:* FHH_Isotherm_k_CP_a. *Location in TSPA-LA:* Table 6.3.8-4.
FHHISKCS. Frenkel Halsey Hill water vapor adsorption isotherm parameter, *k*, for CSNF rind (dimensionless). *Distribution:* Uniform. *Range:* 1.606 to 8.215. *TSPA-LA Name:* FHH_Isotherm_k_CSNF_Rind_a. *Location in TSPA-LA:* Table 6.3.8-4.
FHHISSCP. Frenkel Halsey Hill water vapor adsorption isotherm parameter, *s*, for corrosion products (dimensionless). *Distribution:* Uniform. *Range:* 1.525 to 1.852 (see additional information). *TSPA-LA Name:* FHH_Isotherm_s_CP_a. *Location in TSPA-LA:* Table 6.3.8-4.
FHHISSCS. Frenkel Halsey Hill water vapor adsorption isotherm parameter, *s*, for CSNF rind (dimensionless). *Distribution:* Uniform. *Range:* 1.656 to 3.038. *TSPA-LA Name:* FHH_Isotherm_s_CSNF_Rind_a. *Location in TSPA-LA:* Table 6.3.8-4.
FRACCHNL. Fraction of the RMEI location subject to fluvial deposition (dimensionless). *Distribution:* Uniform. *Range:* 0.088 to 0.54. *TSPA-LA Name:* Fraction_Channel_a. *Location in TSPA-LA:* Table 6.5-5.
FWDRAT. Default forward rate constant for irreversible sorption of plutonium and americium ($m^3/m^2/yr$). *Distribution:* Log uniform. *Range:* 0.002 to 0.05. *TSPA-LA Name:* Default_Fwd_Rate_Const_a. *Location in TSPA-LA:* Table 6.3.7-65.

Table K3-1. High-Level Summary of Epistemically Uncertain Variables (i.e., elements of **e**) Considered in the TSPA-LA (Sensitivity Analysis Name) (Continued)

NOTE: * indicates variable not considered in sensitivity analysis due to correlations.

GOERELAB. Fraction of total iron oxide that is goethite (dimensionless). *Distribution:* Uniform. *Range:* 0.45 to 0.8. *TSPA-LA Name:* Relative_Abundance_Goethite_a. *Location in TSPA-LA:* Section 6.3.8.2.3; Table 6.3.8-4.
GOESA. Specific surface area of goethite (m^2/g). *Distribution:* Truncated log normal. *Range:* 14.7 to 110. *Mean:* 51.42. *Standard Deviation:* 30.09. *TSPA-LA Name:* Goethite_SA_a. *Location in TSPA-LA:* Table 6.3.8-4; S_{CP} in Equation 6.3.8-19.
GOESITED. Density of sorption sites on goethite ($1/nm^2$). *Distribution:* Discrete. *Range:* 1.02 to 8.59. *TSPA-LA Name:* Goethite_Site_Density_a. *Location in TSPA-LA:* Table 6.3.8-3.
GP1NO3. Ratio of Cl to NO_3 (Cl:N) in Group 1 pore waters (dimensionless). *Distribution:* Discrete. *Range:* 0.783 to 6.1213. *TSPA-LA Name:* PCE_Gp1_Cl_NO3_CDF_a. *Location in TSPA-LA:* Section 6.3.4.3.2.
GP2NO3. Ratio of Cl to NO_3 (Cl:N) in Group 2 pore waters (dimensionless). *Distribution:* Discrete. *Range:* 2.359 to 3.187. *TSPA-LA Name:* PCE_Gp2_Cl_NO3_CDF_a. *Location in TSPA-LA:* Section 6.3.4.3.2.
GP3NO3. Ratio of Cl to NO_3 (Cl:N) in Group 3 pore waters (dimensionless). *Distribution:* Discrete. *Range:* 9.7782 to 64.128. *TSPA-LA Name:* PCE_Gp3_Cl_NO3_CDF_a. *Location in TSPA-LA:* Section 6.3.4.3.2.
GP4NO3. Ratio of Cl to NO_3 (Cl:N) in Group 4 pore waters (dimensionless). *Distribution:* Discrete. *Range:* 4.4485 to 8.2119. *TSPA-LA Name:* PCE_Gp4_Cl_NO3_CDF_a. *Location in TSPA-LA:* Section 6.3.4.3.2.
HFOSA. Hydrous ferric oxide (HFO) surface area (m^2/g). *Distribution:* Truncated log normal. *Range:* 68 to 600. *Mean:* 275.6. *Standard Deviation:* 113.4. *TSPA-LA Name:* HFO_SA_a. *Location in TSPA-LA:* Table 6.3.8-4; S_{CP} in Equation 6.3.8-19.
HFOSITED. Sorption site density for hydrous ferric oxide (HFO) ($1/nm^2$). *Distribution:* Discrete. *Range:* 0.56 to 5.65. *TSPA-LA Name:* HFO_Site_Density_a. *Location in TSPA-LA:* Table 6.3.8-3.
HLWDRACD. Effective rate coefficient (affinity term) for the dissolution of HLW glass in CDSP waste packages under low pH conditions ($g/(m^2 d)$). *Distribution:* Triangular. *Range:* 8.41E+03 to 1.15E+07. *Mode:* 8.41E+03. *TSPA-LA Name:* HLW_Diss_kE_Acidic_a. *Location in TSPA-LA:* Sections 6.3.7.4.3.2 and 6.3.7.4.3.3; Table 6.3.7-32; Equation 6.3.7-8.
HLWDRALK. Effective rate coefficient (affinity term) for the dissolution of HLW glass in CDSP waste packages under high pH conditions ($g/(m^2 d)$). *Distribution:* Triangular. *Range:* 2.82E+01 to 3.47E+04. *Mode:* 2.82E+01. *TSPA-LA Name:* HLW_Diss_kE_Alkaline_a. *Location in TSPA-LA:* Sections 6.3.7.4.3.2 and 6.3.7.4.3.3; Table 6.3.7-32; Equation 6.3.7-8.
HLWGRNDS. Specific surface area of HLWG degradation rind (m^2/g). *Distribution:* Uniform. *Range:* 10 to 38. *TSPA-LA Name:* HLWG_Rind_SA_a. *Location in TSPA-LA:* Table 6.3.8-4.
HLWMASS. Scale factor used to characterize uncertainty in radionuclide content of HLW glass (dimensionless). *Distribution:* Triangular. *Range:* 0.7 to 1.5. *Most Likely:* 1. *TSPA-LA Name:* HLW_Mass_Uncert_a. *Location in TSPA-LA:* Sections 6.3.7.1.2 and 6.3.7.1.3; Table 6.3.7-7.
IGERATE. Frequency of occurrence of volcanic eruptive events (yr^{-1}). *Calculated by:* Igneous_Event_Prob_a x 0.083. *Range:* 0 to 6.44E-08. *TSPA-LA Name:* IGERATE. *Location in TSPA-LA:* Section 6.5.2.1.1; Appendix J; Equation J7.5-3.
IGRATE. Frequency of intersection of the repository footprint by a volcanic event (yr^{-1}). *Distribution:* Piecewise uniform. *Range:* 0 to 7.76E-07. *TSPA-LA Name:* Igneous_Event_Prob_a. *Location in TSPA-LA:* Table 6.5-2.
ILTAC227. Volcanic Biosphere Dose Conversion Factor (BDCF) component for long-term inhalation of ^{227}Ac in modern interglacial climate ((Sv/yr)/(Bq/kg)). *Distribution:* Discrete. *Range:* 1.53E-07 to 4.5E-06. *Mean:* 9.0E-07. *Standard Deviation:* 5.75E-07. *TSPA-LA Name:* DE_BDCF_Inh_LT_Ac227. *Location in TSPA-LA:* Sections 6.3.11.1 and 6.3.11.2; Equation 6.3.11-4.
ILTAM241. Volcanic Biosphere Dose Conversion Factor (BDCF) component for long-term inhalation of ^{241}Am in modern interglacial climate ((Sv/yr)/(Bq/kg)). *Distribution:* Discrete. *Range:* 8.45E-08 to 2.48E-06. *Mean:* 4.96E-07. *Standard Deviation:* 3.17E-07. *TSPA-LA Name:* DE_BDCF_Inh_LT_Am241. *Location in TSPA-LA:* Sections 6.3.11.1 and 6.3.11.2; Equation 6.3.11-4.
ILTAM243. Volcanic Biosphere Dose Conversion Factor (BDCF) component for long-term inhalation of ^{243}Am in modern interglacial climate ((Sv/yr)/(Bq/kg)). *Distribution:* Discrete. *Range:* 8.38E-08 to 2.46E-06. *Mean:* 4.93E-07. *Standard Deviation:* 3.15E-07. *TSPA-LA Name:* DE_BDCF_Inh_LT_Am243. *Location in TSPA-LA:* Sections 6.3.11.1 and 6.3.11.2; Equation 6.3.11-4.

Table K3-1. High-Level Summary of Epistemically Uncertain Variables (i.e., elements of **e**) Considered in the TSPA-LA (Sensitivity Analysis Name) (Continued)

NOTE: * indicates variable not considered in sensitivity analysis due to correlations.

ILTCS137. Volcanic Biosphere Dose Conversion Factor (BDCF) component for long-term inhalation of ^{137}Cs in modern interglacial climate ((Sv/yr)/(Bq/kg)). *Distribution:* Discrete. *Range:* 3.43E-11 to 1.01E-09. *Mean:* 2.02E-10. *Standard Deviation:* 1.29E-10. *TSPA-LA Name:* DE_BDCF_Inh_LT_Cs137. *Location in TSPA-LA:* Sections 6.3.11.1 and 6.3.11.2; Equation 6.3.11-4.
ILTI129. Volcanic Biosphere Dose Conversion Factor (BDCF) component for long-term inhalation of ^{129}I in modern interglacial climate ((Sv/yr)/(Bq/kg)). *Distribution:* Discrete. *Range:* 3.15E-11 to 9.23E-10. *Mean:* 1.85E-10. *Standard Deviation:* 1.18E-10. *TSPA-LA Name:* DE_BDCF_Inh_LT_I129. *Location in TSPA-LA:* Sections 6.3.11.1 and 6.3.11.2; Equation 6.3.11-4.
ILTNP237. Volcanic Biosphere Dose Conversion Factor (BDCF) component for long-term inhalation of ^{237}Np in modern interglacial climate ((Sv/yr)/(Bq/kg)). *Distribution:* Discrete. *Range:* 4.35E-08 to 1.28E-06. *Mean:* 2.56E-07. *Standard Deviation:* 1.63E-07. *TSPA-LA Name:* DE_BDCF_Inh_LT_Np237. *Location in TSPA-LA:* Sections 6.3.11.1 and 6.3.11.2; Equation 6.3.11-4.
ILTPA231. Volcanic Biosphere Dose Conversion Factor (BDCF) component for long-term inhalation of ^{231}Pa in modern interglacial climate ((Sv/yr)/(Bq/kg)). *Distribution:* Discrete. *Range:* 2.02E-07 to 5.92E-06. *Mean:* 1.18E-06. *Standard Deviation:* 7.56E-07. *TSPA-LA Name:* DE_BDCF_Inh_LT_Pa231. *Location in TSPA-LA:* Sections 6.3.11.1 and 6.3.11.2; Equation 6.3.11-4.
ILTPU238. Volcanic Biosphere Dose Conversion Factor (BDCF) component for long-term inhalation of ^{238}Pu in modern interglacial climate ((Sv/yr)/(Bq/kg)). *Distribution:* Discrete. *Range:* 9.46E-08 to 2.78E-06. *Mean:* 5.56E-07. *Standard Deviation:* 3.55E-07. *TSPA-LA Name:* DE_BDCF_Inh_LT_Pu238. *Location in TSPA-LA:* Sections 6.3.11.1 and 6.3.11.2; Equation 6.3.11-4.
ILTPU239. Volcanic Biosphere Dose Conversion Factor (BDCF) component for long-term inhalation of ^{239}Pu in modern interglacial climate ((Sv/yr)/(Bq/kg)). *Distribution:* Discrete. *Range:* 1.04E-07 to 3.06E-06. *Mean:* 6.12E-07. *Standard Deviation:* 3.91E-07. *TSPA-LA Name:* DE_BDCF_Inh_LT_Pu239. *Location in TSPA-LA:* Sections 6.3.11.1 and 6.3.11.2; Equation 6.3.11-4.
ILTPU240. Volcanic Biosphere Dose Conversion Factor (BDCF) component for long-term inhalation of ^{240}Pu in modern interglacial climate ((Sv/yr)/(Bq/kg)). *Distribution:* Discrete. *Range:* 1.04E-07 to 3.06E-06. *Mean:* 6.12E-07. *Standard Deviation:* 3.91E-07. *TSPA-LA Name:* DE_BDCF_Inh_LT_Pu240. *Location in TSPA-LA:* Sections 6.3.11.1 and 6.3.11.2; Equation 6.3.11-4.
ILTPU242. Volcanic Biosphere Dose Conversion Factor (BDCF) component for long-term inhalation of ^{242}Pu in modern interglacial climate ((Sv/yr)/(Bq/kg)). *Distribution:* Discrete. *Range:* 9.90E-08 to 2.91E-06. *Mean:* 5.82E-07. *Standard Deviation:* 3.72E-07. *TSPA-LA Name:* DE_BDCF_Inh_LT_Pu242. *Location in TSPA-LA:* Sections 6.3.11.1 and 6.3.11.2; Equation 6.3.11-4.
ILTRA226. Volcanic Biosphere Dose Conversion Factor (BDCF) component for long-term inhalation of ^{226}Ra and ^{210}Pb in modern interglacial climate ((Sv/yr)/(Bq/kg)). *Distribution:* Discrete. *Range:* 1.71E-08 to 5.03E-07. *Mean:* 1.01E-07. *Standard Deviation:* 6.43E-08. *TSPA-LA Name:* DE_BDCF_ILT_Ra226_Pb210. *Location in TSPA-LA:* Sections 6.3.11.1 and 6.3.11.2; Equation 6.3.11-4.
ILTRA228. Volcanic Biosphere Dose Conversion Factor (BDCF) component for long-term inhalation of ^{228}Ra in modern interglacial climate ((Sv/yr)/(Bq/kg)). *Distribution:* Discrete. *Range:* 1.40E-08 to 4.12E-07. *Mean:* 8.24E-08. *Standard Deviation:* 5.27E-08. *TSPA-LA Name:* DE_BDCF_Inh_LT_Ra228. *Location in TSPA-LA:* Sections 6.3.11.1 and 6.3.11.2; Equation 6.3.11-4.
ILTSN126. Volcanic Biosphere Dose Conversion Factor (BDCF) component for long-term inhalation of ^{126}Sn in modern interglacial climate ((Sv/yr)/(Bq/kg)). *Distribution:* Discrete. *Range:* 1.36E-10 to 4.00E-09. *Mean:* 8.0E-10. *Standard Deviation:* 5.11E-10. *TSPA-LA Name:* DE_BDCF_Inh_LT_Sn126. *Location in TSPA-LA:* Sections 6.3.11.1 and 6.3.11.2; Equation 6.3.11-4.
ILTSR90. Volcanic Biosphere Dose Conversion Factor (BDCF) component for long-term inhalation of ^{90}Sr in modern interglacial climate ((Sv/yr)/(Bq/kg)). *Distribution:* Discrete. *Range:* 1.39E-10 to 4.08E-09. *Mean:* 8.16E-10. *Standard Deviation:* 5.21E-10. *TSPA-LA Name:* DE_BDCF_Inh_LT_Sr90. *Location in TSPA-LA:* Sections 6.3.11.1 and 6.3.11.2; Equation 6.3.11-4.
ILTTC99. Volcanic Biosphere Dose Conversion Factor (BDCF) component for long-term inhalation of ^{99}Tc in modern interglacial climate ((Sv/yr)/(Bq/kg)). *Distribution:* Discrete. *Range:* 1.17E-11 to 3.42E-10. *Mean:* 6.84E-11. *Standard Deviation:* 4.37E-11. *TSPA-LA Name:* DE_BDCF_Inh_LT_Tc99. *Location in TSPA-LA:* Sections 6.3.11.1 and 6.3.11.2; Equation 6.3.11-4.

Table K3-1. High-Level Summary of Epistemically Uncertain Variables (i.e., elements of **e**) Considered in the TSPA-LA (Sensitivity Analysis Name) (Continued)

NOTE: * indicates variable not considered in sensitivity analysis due to correlations.

ILTTH229. Volcanic Biosphere Dose Conversion Factor (BDCF) component for long-term inhalation of ^{229}Th in modern interglacial climate ((Sv/yr)/(Bq/kg)). *Distribution:* Discrete. *Range:* 2.24E-07 to 6.57E-06. *Mean:* 1.31E-06. *Standard Deviation:* 8.39E-07. *TSPA-LA Name:* DE_BDCF_Inh_LT_Th229. *Location in TSPA-LA:* Sections 6.3.11.1 and 6.3.11.2; Equation 6.3.11-4.
ILTTH230. Volcanic Biosphere Dose Conversion Factor (BDCF) component for long-term inhalation of ^{230}Th in modern interglacial climate ((Sv/yr)/(Bq/kg)). *Distribution:* Discrete. *Range:* 8.94E-08 to 2.62E-06. *Mean:* 5.25E-07. *Standard Deviation:* 3.35E-07. *TSPA-LA Name:* DE_BDCF_Inh_LT_Th230. *Location in TSPA-LA:* Sections 6.3.11.1 and 6.3.11.2; Equation 6.3.11-4.
ILTTH232. Volcanic Biosphere Dose Conversion Factor (BDCF) component for long-term inhalation of ^{232}Th in modern interglacial climate ((Sv/yr)/(Bq/kg)). *Distribution:* Discrete. *Range:* 9.64E-08 to 2.83E-06. *Mean:* 5.66E-07. *Standard Deviation:* 3.62E-07. *TSPA-LA Name:* DE_BDCF_Inh_LT_Th232. *Location in TSPA-LA:* Sections 6.3.11.1 and 6.3.11.2; Equation 6.3.11-4.
ILTU233. Volcanic Biosphere Dose Conversion Factor (BDCF) component for long-term inhalation of ^{233}U in modern interglacial climate ((Sv/yr)/(Bq/kg)). *Distribution:* Discrete. *Range:* 8.40E-09 to 2.47E-07. *Mean:* 4.94E-08. *Standard Deviation:* 3.15E-08. *TSPA-LA Name:* DE_BDCF_Inh_LT_U233. *Location in TSPA-LA:* Sections 6.3.11.1 and 6.3.11.2; Equation 6.3.11-4.
ILTU234. Volcanic Biosphere Dose Conversion Factor (BDCF) component for long-term inhalation of ^{234}U in modern interglacial climate ((Sv/yr)/(Bq/kg)). *Distribution:* Discrete. *Range:* 8.23E-09 to 2.42E-07. *Mean:* 4.84E-08. *Standard Deviation:* 3.09E-08. *TSPA-LA Name:* DE_BDCF_Inh_LT_U234. *Location in TSPA-LA:* Sections 6.3.11.1 and 6.3.11.2; Equation 6.3.11-4.
ILTU238. Volcanic Biosphere Dose Conversion Factor (BDCF) component for long-term inhalation of ^{238}U in modern interglacial climate ((Sv/yr)/(Bq/kg)). *Distribution:* Discrete. *Range:* 7.05E-09 to 2.07E-07. *Mean:* 4.14E-08. *Standard Deviation:* 2.65E-08. *TSPA-LA Name:* DE_BDCF_Inh_LT_U238. *Location in TSPA-LA:* Sections 6.3.11.1 and 6.3.11.2; Equation 6.3.11-4.
INFIL. Pointer variable for determining infiltration conditions: 10th, 30th, 50th or 90th percentile infiltration scenario (dimensionless). *Distribution:* Discrete. *Range:* 1 to 4. *TSPA-LA Name:* Infiltration_Scenario_a. *Location in TSPA-LA:* Section 6.3.1.2; Tables 6.3.1-2 and 6.3.5-4.
INGAC227. Volcanic Biosphere Dose Conversion Factor (BDCF) component for radon, external exposure and ingestion of ^{227}Ac in modern interglacial climate ((Sv/yr)/(Bq/m^2)). *Distribution:* Discrete. *Range:* 5.78E-09 to 7.76E-09. *Mean:* 6.16E-09. *Standard Deviation:* 1.8E-10. *TSPA-LA Name:* DE_BDCF_Ing_Exp_Radon_Ac227. *Location in TSPA-LA:* Sections 6.3.11.1 and 6.3.11.2; Equation 6.3.11-4.
INGAM241. Volcanic Biosphere Dose Conversion Factor (BDCF) component for radon, external exposure and ingestion of ^{241}Am in modern interglacial climate ((Sv/yr)/(Bq/m^2)). *Distribution:* Discrete. *Range:* 1.86E-10 to 1.00E-09. *Mean:* 2.51E-10. *Standard Deviation:* 7.00E-11. *TSPA-LA Name:* DE_BDCF_Ing_Exp_Radon_Am241. *Location in TSPA-LA:* Sections 6.3.11.1 and 6.3.11.2; Equation 6.3.11-4.
INGAM243. Volcanic Biosphere Dose Conversion Factor (BDCF) component for radon, external exposure and ingestion of ^{243}Am in modern interglacial climate ((Sv/yr)/(Bq/m^2)). *Distribution:* Discrete. *Range:* 2.51E-09 to 3.42E-09. *Mean:* 2.67E-09. *Standard Deviation:* 8.02E-11. *TSPA-LA Name:* DE_BDCF_Ing_Exp_Radon_Am243. *Location in TSPA-LA:* Sections 6.3.11.1 and 6.3.11.2; Equation 6.3.11-4.
INGCS137. Volcanic Biosphere Dose Conversion Factor (BDCF) component for radon, external exposure and ingestion of ^{137}Cs in modern interglacial climate ((Sv/yr)/(Bq/m^2)). *Distribution:* Discrete. *Range:* 6.75E-09 to 8.48E-09. *Mean:* 7.17E-09. *Standard Deviation:* 1.55E-10. *TSPA-LA Name:* DE_BDCF_Ing_Exp_Radon_Cs137. *Location in TSPA-LA:* Sections 6.3.11.1 and 6.3.11.2; Equation 6.3.11-4.
INGI129. Volcanic Biosphere Dose Conversion Factor (BDCF) component for radon, external exposure and ingestion of ^{129}I in modern interglacial climate ((Sv/yr)/(Bq/m^2)). *Distribution:* Discrete. *Range:* 1.39E-10 to 2.86E-08. *Mean:* 1.26E-09. *Standard Deviation:* 2.59E-09. *TSPA-LA Name:* DE_BDCF_Ing_Exp_Radon_I129. *Location in TSPA-LA:* Sections 6.3.11.1 and 6.3.11.2; Equation 6.3.11-4.
INGNP237. Volcanic Biosphere Dose Conversion Factor (BDCF) component for radon, external exposure and ingestion of ^{237}Np in modern interglacial climate ((Sv/yr)/(Bq/m^2)). *Distribution:* Discrete. *Range:* 2.62E-09 to 1.2E-08. *Mean:* 2.98E-09. *Standard Deviation:* 6.36E-10. *TSPA-LA Name:* DE_BDCF_Ing_Exp_Radon_Np237. *Location in TSPA-LA:* Sections 6.3.11.1 and 6.3.11.2; Equation 6.3.11-4.

Table K3-1. High-Level Summary of Epistemically Uncertain Variables (i.e., elements of **e**) Considered in the TSPA-LA (Sensitivity Analysis Name) (Continued)

NOTE: * indicates variable not considered in sensitivity analysis due to correlations.

INGPA231. Volcanic Biosphere Dose Conversion Factor (BDCF) component for radon, external exposure and ingestion of ^{231}Pa in modern interglacial climate ((Sv/yr)/(Bq/m^2)). *Distribution:* Discrete. *Range:* 5.02E-10 to 4.56E-09. *Mean:* 7.14E-10. *Standard Deviation:* 2.92E-10. *TSPA-LA Name:* DE_BDCF_Ing_Exp_Radon_Pa231. *Location in TSPA-LA:* Sections 6.3.11.1 and 6.3.11.2; Equation 6.3.11-4.
INGPU238. Volcanic Biosphere Dose Conversion Factor (BDCF) component for radon, external exposure and ingestion of ^{238}Pu in modern interglacial climate ((Sv/yr)/(Bq/m^2)). *Distribution:* Discrete. *Range:* 1.33E-11 to 9.18E-10. *Mean:* 7.78E-11. *Standard Deviation:* 7.72E-11. *TSPA-LA Name:* DE_BDCF_Ing_Exp_Radon_Pu238. *Location in TSPA-LA:* Sections 6.3.11.1 and 6.3.11.2; Equation 6.3.11-4.
INGPU239. Volcanic Biosphere Dose Conversion Factor (BDCF) component for radon, external exposure and ingestion of ^{239}Pu in modern interglacial climate ((Sv/yr)/(Bq/m^2)). *Distribution:* Discrete. *Range:* 1.40E-11 to 1.01E-09. *Mean:* 8.49E-11. *Standard Deviation:* 8.5E-11. *TSPA-LA Name:* DE_BDCF_Ing_Exp_Radon_Pu239. *Location in TSPA-LA:* Sections 6.3.11.1 and 6.3.11.2; Equation 6.3.11-4.
INGPU240. Volcanic Biosphere Dose Conversion Factor (BDCF) component for radon, external exposure and ingestion of ^{240}Pu in modern interglacial climate ((Sv/yr)/(Bq/m^2)). *Distribution:* Discrete. *Range:* 1.42E-11 to 1.01E-09. *Mean:* 8.52E-11. *Standard Deviation:* 8.5E-11. *TSPA-LA Name:* DE_BDCF_Ing_Exp_Radon_Pu240. *Location in TSPA-LA:* Sections 6.3.11.1 and 6.3.11.2; Equation 6.3.11-4.
INGPU242. Volcanic Biosphere Dose Conversion Factor (BDCF) component for radon, external exposure and ingestion of ^{242}Pu in modern interglacial climate ((Sv/yr)/(Bq/m^2)). *Distribution:* Discrete. *Range:* 1.31E-11 to 9.57E-10. *Mean:* 8.04E-11. *Standard Deviation:* 8.06E-11. *TSPA-LA Name:* DE_BDCF_Ing_Exp_Radon_Pu242. *Location in TSPA-LA:* Sections 6.3.11.1 and 6.3.11.2; Equation 6.3.11-4.
INGRA226. Volcanic Biosphere Dose Conversion Factor (BDCF) component for radon, external exposure and ingestion of ^{226}Ra and ^{210}Pb in modern interglacial climate ((Sv/yr)/(Bq/m^2)). *Distribution:* Discrete. *Range:* 3.07E-08 to 9.43E-08. *Mean:* 3.52E-08. *Standard Deviation:* 3.45E-09. *TSPA-LA Name:* DE_BDCF_IER_Ra226_Pb210. *Location in TSPA-LA:* Sections 6.3.11.1 and 6.3.11.2; Equation 6.3.11-4.
INGRA228. Volcanic Biosphere Dose Conversion Factor (BDCF) component for radon, external exposure and ingestion of ^{228}Ra in modern interglacial climate ((Sv/yr)/(Bq/m^2)). *Distribution:* Discrete. *Range:* 1.17E-08 to 2.62E-08. *Mean:* 1.27E-08. *Standard Deviation:* 7.44E-10. *TSPA-LA Name:* DE_BDCF_Ing_Exp_Radon_Ra228. *Location in TSPA-LA:* Sections 6.3.11.1 and 6.3.11.2; Equation 6.3.11-4.
INGSN126. Volcanic Biosphere Dose Conversion Factor (BDCF) component for radon, external exposure and ingestion of ^{126}Sn in modern interglacial climate ((Sv/yr)/(Bq/m^2)). *Distribution:* Discrete. *Range:* 2.38E-08 to 2.79E-08. *Mean:* 2.54E-08. *Standard Deviation:* 4.41E-10. *TSPA-LA Name:* DE_BDCF_Ing_Exp_Radon_Sn126. *Location in TSPA-LA:* Sections 6.3.11.1 and 6.3.11.2; Equation 6.3.11-4.
INGSR90. Volcanic Biosphere Dose Conversion Factor (BDCF) component for radon, external exposure and ingestion of ^{90}Sr in modern interglacial climate ((Sv/yr)/(Bq/m^2)). *Distribution:* Discrete. *Range:* 1.44E-09 to 6.10E-09. *Mean:* 1.81E-09. *Standard Deviation:* 3.67E-10. *TSPA-LA Name:* DE_BDCF_Ing_Exp_Radon_Sr90. *Location in TSPA-LA:* Sections 6.3.11.1 and 6.3.11.2; Equation 6.3.11-4.
INGTC99. Volcanic Biosphere Dose Conversion Factor (BDCF) component for radon, external exposure and ingestion of ^{99}Tc in modern interglacial climate ((Sv/yr)/(Bq/m^2)). *Distribution:* Discrete. *Range:* 5.08E-12 to 8.95E-09. *Mean:* 2.72E-10. *Standard Deviation:* 5.16E-10. *TSPA-LA Name:* DE_BDCF_Ing_Exp_Radon_Tc99. *Location in TSPA-LA:* Sections 6.3.11.1 and 6.3.11.2; Equation 6.3.11-4.
INGTH229. Volcanic Biosphere Dose Conversion Factor (BDCF) component for radon, external exposure and ingestion of ^{229}Th in modern interglacial climate ((Sv/yr)/(Bq/m^2)). *Distribution:* Discrete. *Range:* 4.33E-09 to 7.02E-09. *Mean:* 4.69E-09. *Standard Deviation:* 2.4E-10. *TSPA-LA Name:* DE_BDCF_Ing_Exp_Radon_Th229. *Location in TSPA-LA:* Sections 6.3.11.1 and 6.3.11.2; Equation 6.3.11-4.
INGTH230. Volcanic Biosphere Dose Conversion Factor (BDCF) component for radon, external exposure and ingestion of ^{230}Th in modern interglacial climate ((Sv/yr)/(Bq/m^2)). *Distribution:* Discrete. *Range:* 1.92E-11 to 8.68E-10. *Mean:* 8.51E-11. *Standard Deviation:* 7.82E-11. *TSPA-LA Name:* DE_BDCF_Ing_Exp_Radon_Th230. *Location in TSPA-LA:* Sections 6.3.11.1 and 6.3.11.2; Equation 6.3.11-4.
INGTH232. Volcanic Biosphere Dose Conversion Factor (BDCF) component for radon, external exposure and ingestion of ^{232}Th in modern interglacial climate ((Sv/yr)/(Bq/m^2)). *Distribution:* Discrete. *Range:* 1.72E-11 to 9.34E-10. *Mean:* 8.83E-11. *Standard Deviation:* 8.44E-11. *TSPA-LA Name:* DE_BDCF_Ing_Exp_Radon_Th232. *Location in TSPA-LA:* Sections 6.3.11.1 and 6.3.11.2; Equation 6.3.11-4.

Table K3-1. High-Level Summary of Epistemically Uncertain Variables (i.e., elements of **e**) Considered in the TSPA-LA (Sensitivity Analysis Name) (Continued)

NOTE: * indicates variable not considered in sensitivity analysis due to correlations.

INGU233. Volcanic Biosphere Dose Conversion Factor (BDCF) component for radon, external exposure and ingestion of ^{233}U in modern interglacial climate ((Sv/yr)/(Bq/m^2)). *Distribution:* Discrete. *Range:* 1.31E-11 to 9.04E-10. *Mean:* 6.48E-11. *Standard Deviation:* 6.12E-11. *TSPA-LA Name:* DE_BDCF_Ing_Exp_Radon_U233. *Location in TSPA-LA:* Sections 6.3.11.1 and 6.3.11.2; Equation 6.3.11-4.
INGU234. Volcanic Biosphere Dose Conversion Factor (BDCF) component for radon, external exposure and ingestion of ^{234}U in modern interglacial climate ((Sv/yr)/(Bq/m^2)). *Distribution:* Discrete. *Range:* 9.60E-12 to 8.7E-10. *Mean:* 5.96E-11. *Standard Deviation:* 5.9E-11. *TSPA-LA Name:* DE_BDCF_Ing_Exp_Radon_U234. *Location in TSPA-LA:* Sections 6.3.11.1 and 6.3.11.2; Equation 6.3.11-4.
INGU238. Volcanic Biosphere Dose Conversion Factor (BDCF) component for radon, external exposure and ingestion of ^{238}U in modern interglacial climate ((Sv/yr)/(Bq/m^2)). *Distribution:* Discrete. *Range:* 1.52E-09 to 2.41E-09. *Mean:* 1.62E-09. *Standard Deviation:* 6.16E-11. *TSPA-LA Name:* DE_BDCF_Ing_Exp_Radon_U238. *Location in TSPA-LA:* Sections 6.3.11.1 and 6.3.11.2; Equation 6.3.11-4.
INHLTPV. Pointer variable for long-term inhalation dose conversion factor for volcanic ash exposure (dimensionless). *Distribution:* Discrete. *Range:* 1 to 300. *TSPA-LA Name:* BDCF_Inh_LT. *Location in TSPA-LA:* Section 6.3.11; Equation 6.3.11-4.
INHSTPV. Pointer variable for short-term inhalation dose conversion factor for volcanic ash exposure (dimensionless). *Distribution:* Discrete. *Range:* 1 to 300. *TSPA-LA Name:* BDCF_Inh_ShT. *Location in TSPA-LA:* Section 6.3.11; Equation 6.3.11-4.
INRFRCCS. The initial release fraction of ^{137}Cs in a CSNF waste package (dimensionless). *Distribution:* Triangular. *Range:* 0.0039 to 0.1106. *Mode:* 0.0363. *TSPA-LA Name:* Initial_Release_Frac_Cs_a. *Location in TSPA-LA:* Sections 6.3.7.4.1.2 and 6.3.7.4.1.3; Table 6.3.7-29.
INRFRCI. The initial release fraction of ^{129}I in a CSNF waste package (dimensionless). *Distribution:* Triangular. *Range:* 0.0204 to 0.2675. *Mode:* 0.1124. *TSPA-LA Name:* Initial_Release_Frac_I_a. *Location in TSPA-LA:* Sections 6.3.7.4.1.2 and 6.3.7.4.1.3; Table 6.3.7-29.
INRFRCSR. The initial release fraction of ^{90}Sr in a CSNF waste package (dimensionless). *Distribution:* Triangular. *Range:* 0.0002 to 0.0025. *Mode:* 0.0009. *TSPA-LA Name:* Initial_Release_Frac_Sr_a. *Location in TSPA-LA:* Sections 6.3.7.4.1.2 and 6.3.7.4.1.3; Table 6.3.7-29.
INRFRCTC. The initial release fraction of ^{99}Tc in a CSNF waste package (dimensionless). *Distribution:* Triangular. *Range:* 0.0001 to 0.0026. *Mode:* 0.001. *TSPA-LA Name:* Initial_Release_Frac_Tc_a. *Location in TSPA-LA:* Sections 6.3.7.4.1.2 and 6.3.7.4.1.3; Table 6.3.7-29.
IS2DHLNS. Pointer variable used to determine ionic strength for 2DHLW Cell (Cell 1a) of CDSP waste packages under vapor influx conditions (dimensionless). *Distribution:* Uniform. *Range:* 0 to 1. *TSPA-LA Name:* Inpkg_IStr_2DHLW_NS_Rand_a. *Location in TSPA-LA:* Section 6.3.7.2.2 Part III.
IS2DHLS. Pointer variable used to determine ionic strength for 2DHLW Cell (Cell 1a) of CDSP waste packages under liquid influx conditions (dimensionless). *Distribution:* Uniform. *Range:* 0 to 1. *TSPA-LA Name:* Inpkg_IStr_2DHLW_S_Rand_a. *Location in TSPA-LA:* Section 6.3.7.2.2 Part III.
IS2MCONS. Pointer variable used to determine ionic strength for 2MCO Cell (Cell 1b) of CDSP waste packages under vapor influx conditions (dimensionless). *Distribution:* Uniform. *Range:* 0 to 1. *TSPA-LA Name:* Inpkg_IStr_2MCO_NS_Rand_a. *Location in TSPA-LA:* Section 6.3.7.2.2 Part III.
IS2MCOS. Pointer variable used to determine ionic strength for 2MCO Cell (Cell 1b) of CDSP waste packages under liquid influx conditions (dimensionless). *Distribution:* Uniform. *Range:* 0 to 1. *TSPA-LA Name:* Inpkg_IStr_2MCO_S_Rand_a. *Location in TSPA-LA:* Section 6.3.7.2.2 Part III.
ISCSNS. Pointer variable used to determine ionic strength for CSNF Cell under vapor influx conditions (dimensionless). *Distribution:* Uniform. *Range:* 0 to 1. *TSPA-LA Name:* Inpkg_IStr_CSNF_NS_Rand_a. *Location in TSPA-LA:* Section 6.3.7.2.2 Part III.
ISCSS. Pointer variable used to determine ionic strength for CSNF Cell under liquid influx conditions (dimensionless). *Distribution:* Uniform. *Range:* 0 to 1. *TSPA-LA Name:* Inpkg_IStr_CSNF_S_Rand_a. *Location in TSPA-LA:* Section 6.3.7.2.2 Part III.
ISTAC227. Volcanic Biosphere Dose Conversion Factor (BDCF) component for short-term inhalation of ^{227}Ac in modern interglacial climate ((Sv/yr)/(Bq/kg)). *Distribution:* Discrete. *Range:* 8.47E-08 to 2.14E-06. *Mean:* 5.85E-07. *Standard Deviation:* 3.32E-07. *TSPA-LA Name:* DE_BDCF_Inh_ShT_Ac227. *Location in TSPA-LA:* Sections 6.3.11.1 and 6.3.11.2; Equation 6.3.11-4.

Table K3-1. High-Level Summary of Epistemically Uncertain Variables (i.e., elements of **e**) Considered in the TSPA-LA (Sensitivity Analysis Name) (Continued)

NOTE: * indicates variable not considered in sensitivity analysis due to correlations.

ISTAM241. Volcanic Biosphere Dose Conversion Factor (BDCF) component for short-term inhalation of ^{241}Am in modern interglacial climate ((Sv/yr)/(Bq/kg)). *Distribution:* Discrete. *Range:* 4.67E-08 to 1.18E-06. *Mean:* 3.23E-07. *Standard Deviation:* 1.83E-07. *TSPA-LA Name:* DE_BDCF_Inh_ShT_Am241. *Location in TSPA-LA:* Sections 6.3.11.1 and 6.3.11.2; Equation 6.3.11-4.
ISTAM243. Volcanic Biosphere Dose Conversion Factor (BDCF) component for short-term inhalation of ^{243}Am in modern interglacial climate ((Sv/yr)/(Bq/kg)). *Distribution:* Discrete. *Range:* 4.64E-08 to 1.17E-06. *Mean:* 3.2E-07. *Standard Deviation:* 1.82E-07. *TSPA-LA Name:* DE_BDCF_Inh_ShT_Am243. *Location in TSPA-LA:* Sections 6.3.11.1 and 6.3.11.2; Equation 6.3.11-4.
ISTCS137. Volcanic Biosphere Dose Conversion Factor (BDCF) component for short-term inhalation of ^{137}Cs in modern interglacial climate ((Sv/yr)/(Bq/kg)). *Distribution:* Discrete. *Range:* 1.90E-11 to 4.80E-10. *Mean:* 1.31E-10. *Standard Deviation:* 7.44E-11. *TSPA-LA Name:* DE_BDCF_Inh_ShT_Cs137. *Location in TSPA-LA:* Sections 6.3.11.1 and 6.3.11.2; Equation 6.3.11-4.
ISTI129. Volcanic Biosphere Dose Conversion Factor (BDCF) component for short-term inhalation of ^{129}I in modern interglacial climate ((Sv/yr)/(Bq/kg)). *Distribution:* Discrete. *Range:* 1.74E-11 to 4.40E-10. *Mean:* 1.2E-10. *Standard Deviation:* 6.81E-11. *TSPA-LA Name:* DE_BDCF_Inh_ShT_I129. *Location in TSPA-LA:* Sections 6.3.11.1 and 6.3.11.2; Equation 6.3.11-4.
ISTNP237. Volcanic Biosphere Dose Conversion Factor (BDCF) component for short-term inhalation of ^{237}Np in modern interglacial climate ((Sv/yr)/(Bq/kg)). *Distribution:* Discrete. *Range:* 2.41E-08 to 6.08E-07. *Mean:* 1.66E-07. *Standard Deviation:* 9.43E-08. *TSPA-LA Name:* DE_BDCF_Inh_ShT_Np237. *Location in TSPA-LA:* Sections 6.3.11.1 and 6.3.11.2; Equation 6.3.11-4.
ISTPA231. Volcanic Biosphere Dose Conversion Factor (BDCF) component for short-term inhalation of ^{231}Pa in modern interglacial climate ((Sv/yr)/(Bq/kg)). *Distribution:* Discrete. *Range:* 1.11E-07 to 2.82E-06. *Mean:* 7.7E-07. *Standard Deviation:* 4.37E-07. *TSPA-LA Name:* DE_BDCF_Inh_ShT_Pa231. *Location in TSPA-LA:* Sections 6.3.11.1 and 6.3.11.2; Equation 6.3.11-4.
ISTPU238. Volcanic Biosphere Dose Conversion Factor (BDCF) component for short-term inhalation of ^{238}Pu in modern interglacial climate ((Sv/yr)/(Bq/kg)). *Distribution:* Discrete. *Range:* 5.23E-08 to 1.32E-06. *Mean:* 3.61E-07. *Standard Deviation:* 2.05E-07. *TSPA-LA Name:* DE_BDCF_Inh_ShT_Pu238. *Location in TSPA-LA:* Sections 6.3.11.1 and 6.3.11.2; Equation 6.3.11-4.
ISTPU239. Volcanic Biosphere Dose Conversion Factor (BDCF) component for short-term inhalation of ^{239}Pu in modern interglacial climate ((Sv/yr)/(Bq/kg)). *Distribution:* Discrete. *Range:* 5.76E-08 to 1.46E-06. *Mean:* 3.98E-07. *Standard Deviation:* 2.26E-07. *TSPA-LA Name:* DE_BDCF_Inh_ShT_Pu239. *Location in TSPA-LA:* Sections 6.3.11.1 and 6.3.11.2; Equation 6.3.11-4.
ISTPU240. Volcanic Biosphere Dose Conversion Factor (BDCF) component for short-term inhalation of ^{240}Pu in modern interglacial climate ((Sv/yr)/(Bq/kg)). *Distribution:* Discrete. *Range:* 5.76E-08 to 1.46E-06. *Mean:* 3.98E-07. *Standard Deviation:* 2.26E-07. *TSPA-LA Name:* DE_BDCF_Inh_ShT_Pu240. *Location in TSPA-LA:* Sections 6.3.11.1 and 6.3.11.2; Equation 6.3.11-4.
ISTPU242. Volcanic Biosphere Dose Conversion Factor (BDCF) component for short-term inhalation of ^{242}Pu in modern interglacial climate ((Sv/yr)/(Bq/kg)). *Distribution:* Discrete. *Range:* 5.47E-08 to 1.38E-06. *Mean:* 3.78E-07. *Standard Deviation:* 2.14E-07. *TSPA-LA Name:* DE_BDCF_Inh_ShT_Pu242. *Location in TSPA-LA:* Sections 6.3.11.1 and 6.3.11.2; Equation 6.3.11-4.
ISTRA226. Volcanic Biosphere Dose Conversion Factor (BDCF) component for short-term inhalation of ^{226}Ra and ^{210}Pb in modern interglacial climate ((Sv/yr)/(Bq/kg)). *Distribution:* Discrete. *Range:* 9.47E-09 to 2.39E-07. *Mean:* 6.54E-08. *Standard Deviation:* 3.71E-08. *TSPA-LA Name:* DE_BDCF_IST_Ra226_Pb210. *Location in TSPA-LA:* Sections 6.3.11.1 and 6.3.11.2; Equation 6.3.11-4.
ISTRA228. Volcanic Biosphere Dose Conversion Factor (BDCF) component for short-term inhalation of ^{228}Ra in modern interglacial climate ((Sv/yr)/(Bq/kg)). *Distribution:* Discrete. *Range:* 7.76E-09 to 1.96E-07. *Mean:* 5.36E-08. *Standard Deviation:* 3.04E-08. *TSPA-LA Name:* DE_BDCF_Inh_ShT_Ra228. *Location in TSPA-LA:* Sections 6.3.11.1 and 6.3.11.2; Equation 6.3.11-4.
ISTSN126. Volcanic Biosphere Dose Conversion Factor (BDCF) component for short-term inhalation of ^{126}Sn in modern interglacial climate ((Sv/yr)/(Bq/kg)). *Distribution:* Discrete. *Range:* 7.53E-11 to 1.90E-09. *Mean:* 5.2E-10. *Standard Deviation:* 2.95E-10. *TSPA-LA Name:* DE_BDCF_Inh_ShT_Sn126. *Location in TSPA-LA:* Sections 6.3.11.1 and 6.3.11.2; Equation 6.3.11-4.

Table K3-1. High-Level Summary of Epistemically Uncertain Variables (i.e., elements of **e**) Considered in the TSPA-LA (Sensitivity Analysis Name) (Continued)

NOTE: * indicates variable not considered in sensitivity analysis due to correlations.

ISTSR90. Volcanic Biosphere Dose Conversion Factor (BDCF) component for short-term inhalation of ^{90}Sr in modern interglacial climate ((Sv/yr)/(Bq/kg)). *Distribution:* Discrete. *Range:* 7.68E-11 to 1.94E-09. *Mean:* 5.3E-10. *Standard Deviation:* 3.01E-10. *TSPA-LA Name:* DE_BDCF_Inh_ShT_Sr90. *Location in TSPA-LA:* Sections 6.3.11.1 and 6.3.11.2; Equation 6.3.11-4.
ISTTC99. Volcanic Biosphere Dose Conversion Factor (BDCF) component for short-term inhalation of ^{99}Tc in modern interglacial climate ((Sv/yr)/(Bq/kg)). *Distribution:* Discrete. *Range:* 6.44E-12 to 1.63E-10. *Mean:* 4.45E-11. *Standard Deviation:* 2.52E-11. *TSPA-LA Name:* DE_BDCF_Inh_ShT_Tc99. *Location in TSPA-LA:* Sections 6.3.11.1 and 6.3.11.2; Equation 6.3.11-4.
ISTTH229. Volcanic Biosphere Dose Conversion Factor (BDCF) component for short-term inhalation of ^{229}Th in modern interglacial climate ((Sv/yr)/(Bq/kg)). *Distribution:* Discrete. *Range:* 1.24E-07 to 3.13E-06. *Mean:* 8.54E-07. *Standard Deviation:* 4.84E-07. *TSPA-LA Name:* DE_BDCF_Inh_ShT_Th229. *Location in TSPA-LA:* Sections 6.3.11.1 and 6.3.11.2; Equation 6.3.11-4.
ISTTH230. Volcanic Biosphere Dose Conversion Factor (BDCF) component for short-term inhalation of ^{230}Th in modern interglacial climate ((Sv/yr)/(Bq/kg)). *Distribution:* Discrete. *Range:* 4.94E-08 to 1.25E-06. *Mean:* 3.41E-07. *Standard Deviation:* 1.94E-07. *TSPA-LA Name:* DE_BDCF_Inh_ShT_Th230. *Location in TSPA-LA:* Sections 6.3.11.1 and 6.3.11.2; Equation 6.3.11-4.
ISTTH232. Volcanic Biosphere Dose Conversion Factor (BDCF) component for short-term inhalation of ^{232}Th in modern interglacial climate ((Sv/yr)/(Bq/kg)). *Distribution:* Discrete. *Range:* 5.33E-08 to 1.35E-06. *Mean:* 3.68E-07. *Standard Deviation:* 2.09E-07. *TSPA-LA Name:* DE_BDCF_Inh_ShT_Th232. *Location in TSPA-LA:* Sections 6.3.11.1 and 6.3.11.2; Equation 6.3.11-4.
ISTU233. Volcanic Biosphere Dose Conversion Factor (BDCF) component for short-term inhalation of ^{233}U in modern interglacial climate ((Sv/yr)/(Bq/kg)). *Distribution:* Discrete. *Range:* 4.65E-09 to 1.17E-07. *Mean:* 3.21E-08. *Standard Deviation:* 1.82E-08. *TSPA-LA Name:* DE_BDCF_Inh_ShT_U233. *Location in TSPA-LA:* Sections 6.3.11.1 and 6.3.11.2; Equation 6.3.11-4.
ISTU234. Volcanic Biosphere Dose Conversion Factor (BDCF) component for short-term inhalation of ^{234}U in modern interglacial climate ((Sv/yr)/(Bq/kg)). *Distribution:* Discrete. *Range:* 4.55E-09 to 1.15E-07. *Mean:* 3.15E-08. *Standard Deviation:* 1.78E-08. *TSPA-LA Name:* DE_BDCF_Inh_ShT_U234. *Location in TSPA-LA:* Sections 6.3.11.1 and 6.3.11.2; Equation 6.3.11-4.
ISTU238. Volcanic Biosphere Dose Conversion Factor (BDCF) component for short-term inhalation of ^{238}U in modern interglacial climate ((Sv/yr)/(Bq/kg)). *Distribution:* Discrete. *Range:* 3.90E-09 to 9.85E-08. *Mean:* 2.69E-08. *Standard Deviation:* 1.53E-08. *TSPA-LA Name:* DE_BDCF_Inh_ShT_U238. *Location in TSPA-LA:* Sections 6.3.11.1 and 6.3.11.2; Equation 6.3.11-4.
KDAMCOL. Distribution coefficient for reversible sorption of americium onto uranophane colloids (mL/g). *Distribution:* Log uniform. *Range:* 5 to 1.00E+04. *TSPA-LA Name:* Kd_Am_Rev_U_Col_a. *Location in TSPA-LA:* Sections 6.3.7.6.2 and 6.3.7.6.3; Equation 6.3.7-20; Table 6.3.7-64.
KDAMSMEC. Distribution coefficient for reversible sorption of americium to waste form (smectite) colloids (mL/g). *Distribution:* Piecewise uniform. *Range:* 1.00E+04 to 1.00E+07. *TSPA-LA Name:* Kd_Am_Rev_Smectite_a. *Location in TSPA-LA:* Sections 6.3.7.6.2 and 6.3.7.6.3; Equation 6.3.7-20; Tables 6.3.7-62 and 6.3.7-66.
KDCSCOL. Distribution coefficient for reversible sorption of cesium onto uranophane colloids (mL/g). *Distribution:* Log uniform. *Range:* 10 to 1000. *TSPA-LA Name:* Kd_Cs_Rev_U_Col_a. *Location in TSPA-LA:* Sections 6.3.7.6.2 and 6.3.7.6.3; Equation 6.3.7-20; Table 6.3.7-64.
KDCSSMEC. Distribution coefficient for reversible sorption of cesium to waste form (smectite) colloids (mL/g). *Distribution:* Piecewise uniform. *Range:* 50 to 5000. *TSPA-LA Name:* Kd_Cs_Rev_Smectite_a. *Location in TSPA-LA:* Sections 6.3.7.6.2 and 6.3.7.6.3; Equation 6.3.7-20; Tables 6.3.7-62 and 6.3.7-66.
KDNPCOL. Distribution coefficient for reversible sorption of neptunium onto uranophane colloids (mL/g). *Distribution:* Log uniform. *Range:* 1 to 500. *TSPA-LA Name:* Kd_Np_Rev_U_Col_a. *Location in TSPA-LA:* Sections 6.3.7.6.2 and 6.3.7.6.3; Equation 6.3.7-20; Table 6.3.7-64.
KDNPSMEC. Distribution coefficient for reversible sorption of neptunium to waste form (smectite) colloids (mL/g). *Distribution:* Log uniform. *Range:* 10 to 500. *TSPA-LA Name:* Kd_Np_Rev_Smectite_a. *Location in TSPA-LA:* Sections 6.3.7.6.2 and 6.3.7.6.3; Equation 6.3.7-20; Tables 6.3.7-62 and 6.3.7-66.

Table K3-1. High-Level Summary of Epistemically Uncertain Variables (i.e., elements of **e**) Considered in the TSPA-LA (Sensitivity Analysis Name) (Continued)

NOTE: * indicates variable not considered in sensitivity analysis due to correlations.

KDPACOL. Distribution coefficient for reversible sorption of protactinium onto uranophane colloids (mL/g). *Distribution:* Log uniform. *Range:* 5 to 1.00E+04. *TSPA-LA Name:* Kd_Pa_Rev_U_Col_a. *Location in TSPA-LA:* Sections 6.3.7.6.2 and 6.3.7.6.3; Equation 6.3.7-20; Table 6.3.7-64.
KDPASMEC. Distribution coefficient for reversible sorption of protactinium to waste form (smectite) colloids (mL/g). *Distribution:* Piecewise uniform. *Range:* 1.00E+04 to 1.00E+07. *TSPA-LA Name:* Kd_Pa_Rev_Smectite_a. *Location in TSPA-LA:* Sections 6.3.7.6.2 and 6.3.7.6.3; Equation 6.3.7-20; Tables 6.3.7-62 and 6.3.7-66.
KDPUCOL. Distribution coefficient for reversible sorption of plutonium onto uranophane colloids (mL/g). *Distribution:* Log uniform. *Range:* 5 to 1.00E+04. *TSPA-LA Name:* Kd_Pu_Rev_U_Col_a. *Location in TSPA-LA:* Sections 6.3.7.6.2 and 6.3.7.6.3; Equation 6.3.7-20; Table 6.3.7-64.
KDPUSMEC. Distribution coefficient for reversible sorption of plutonium to waste form (smectite) colloids (mL/g). *Distribution:* Piecewise uniform. *Range:* 1.00E+03 to 1.00E+05. *TSPA-LA Name:* Kd_Pu_Rev_Smectite_a. *Location in TSPA-LA:* Sections 6.3.7.6.2 and 6.3.7.6.3; Equation 6.3.7-20; Tables 6.3.7-62 and 6.3.7-66.
KDRACOL. Distribution coefficient for reversible sorption of radium onto uranophane colloids (mL/g). *Distribution:* Log uniform. *Range:* 10 to 1000. *TSPA-LA Name:* Kd_Ra_Rev_U_Col_a. *Location in TSPA-LA:* Sections 6.3.7.6.2 and 6.3.7.6.3; Equation 6.3.7-20; Table 6.3.7-64.
KDRASMEC. Distribution coefficient for reversible sorption of radium to waste form (smectite) colloids (mL/g). *Distribution:* Log uniform. *Range:* 100 to 5000. *TSPA-LA Name:* Kd_Ra_Rev_Smectite_a. *Location in TSPA-LA:* Sections 6.3.7.6.2 and 6.3.7.6.3; Equation 6.3.7-20; Tables 6.3.7-62 and 6.3.7-66.
KDSNCOL. Distribution coefficient for reversible sorption of tin onto uranophane colloids (mL/g). *Distribution:* Log uniform. *Range:* 1 to 100. *TSPA-LA Name:* Kd_Sn_Rev_U_Col_a. *Location in TSPA-LA:* Sections 6.3.7.6.2 and 6.3.7.6.3; Equation 6.3.7-20; Table 6.3.7-64.
KDSNSMEC. Distribution coefficient for reversible sorption of tin to waste form (smectite) colloids (mL/g). *Distribution:* Log uniform. *Range:* 1.00E+05 to 1.00E+06. *TSPA-LA Name:* Kd_Sn_Rev_Smectite_a. *Location in TSPA-LA:* Sections 6.3.7.6.2 and 6.3.7.6.3; Equation 6.3.7-20; Tables 6.3.7-62 and 6.3.7-66.
KDTHCOL. Distribution coefficient for reversible sorption of thorium onto uranophane colloids (mL/g). *Distribution:* Log uniform. *Range:* 5 to 1.00E+04. *TSPA-LA Name:* Kd_Th_Rev_U_Col_a. *Location in TSPA-LA:* Sections 6.3.7.6.2 and 6.3.7.6.3; Equation 6.3.7-20; Table 6.3.7-64.
KDTHSMEC. Distribution coefficient for reversible sorption of thorium to waste form (smectite) colloids (mL/g). *Distribution:* Piecewise uniform. *Range:* 1.00E+04 to 1.00E+07. *TSPA-LA Name:* Kd_Th_Rev_Smectite_a. *Location in TSPA-LA:* Sections 6.3.7.6.2 and 6.3.7.6.3; Equation 6.3.7-20; Tables 6.3.7-62 and 6.3.7-66.
KDUSMEC. Distribution coefficient for reversible sorption of uranium to waste form (smectite) colloids (mL/g). *Distribution:* Log uniform. *Range:* 5.00E+02 to 5.00E+04. *TSPA-LA Name:* Kd_U_Rev_Smectite_a. *Location in TSPA-LA:* Sections 6.3.7.6.2 and 6.3.7.6.3; Equation 6.3.7-20; Tables 6.3.7-62 and 6.3.7-66.
LDIVIDE. Depth of permeable soil on divides of the Fortymile Wash fan (RMEI location) (cm). *Distribution:* Uniform. *Range:* 102 to 140. *TSPA-LA Name:* L_Divides_a. *Location in TSPA-LA:* Table 6.5-5.
MASSDCRS. Mass loading decrease rate constant (1/yr). *Distribution:* Triangular. *Range:* 0.125 to 1. *Mode:* 0.2. *TSPA-LA Name:* Mass_Decrease_Const_GE10_a. *Location in TSPA-LA:* Equation 6.3.11-5.
MICAC227. Groundwater Biosphere Dose Conversion Factor (BDCF) for ^{227}Ac in modern interglacial climate ((Sv/year)/(Bq/m^3)). *Distribution:* Discrete. *Range:* 4.08E-07 to 4.32E-06. *Mean:* 1.3E-06. *Standard Deviation:* 5.28E-07. *TSPA-LA Name:* GW_BDCF_MIC_Ac227. *Location in TSPA-LA:* Sections 6.3.11.2 and 6.3.11.3; Table 6.3.11-3.
MICAM241. Groundwater Biosphere Dose Conversion Factor (BDCF) for ^{241}Am in modern interglacial climate ((Sv/year)/(Bq/m^3)). *Distribution:* Discrete. *Range:* 2.16E-07 to 3.30E-06. *Mean:* 8.34E-07. *Standard Deviation:* 4.03E-07. *TSPA-LA Name:* GW_BDCF_MIC_Am241. *Location in TSPA-LA:* Sections 6.3.11.2 and 6.3.11.3; Table 6.3.11-3.
MICAM243. Groundwater Biosphere Dose Conversion Factor (BDCF) for ^{243}Am in modern interglacial climate ((Sv/year)/(Bq/m^3)). *Distribution:* Discrete. *Range:* 2.21E-07 to 3.37E-06. *Mean:* 8.88E-07. *Standard Deviation:* 4.12E-07. *TSPA-LA Name:* GW_BDCF_MIC_Am243. *Location in TSPA-LA:* Sections 6.3.11.2 and 6.3.11.3; Table 6.3.11-3.

Table K3-1. High-Level Summary of Epistemically Uncertain Variables (i.e., elements of **e**) Considered in the TSPA-LA (Sensitivity Analysis Name) (Continued)

NOTE: * indicates variable not considered in sensitivity analysis due to correlations.

MICC14. Groundwater Biosphere Dose Conversion Factor (BDCF) for ^{14}C in modern interglacial climate ((Sv/year)/(Bq/m^3)). *Distribution:* Discrete. *Range:* 7.18E-10 to 2.56E-08. *Mean:* 1.93E-09. *Standard Deviation:* 1.85E-09. *TSPA-LA Name:* GW_BDCF_MIC_C14. *Location in TSPA-LA:* Sections 6.3.11.2 and 6.3.11.3; Table 6.3.11-3.
MICCl36. Groundwater Biosphere Dose Conversion Factor (BDCF) for ^{36}Cl in modern interglacial climate ((Sv/year)/(Bq/m^3)). *Distribution:* Discrete. *Range:* 1.28E-09 to 3.00E-07. *Mean:* 8.09E-09. *Standard Deviation:* 1.41E-08. *TSPA-LA Name:* GW_BDCF_MIC_Cl36. *Location in TSPA-LA:* Sections 6.3.11.2 and 6.3.11.3; Table 6.3.11-3.
MICCS135. Groundwater Biosphere Dose Conversion Factor (BDCF) for ^{135}Cs in modern interglacial climate ((Sv/year)/(Bq/m^3)). *Distribution:* Discrete. *Range:* 3.1E-09 to 8.48E-08. *Mean:* 1.45E-08. *Standard Deviation:* 1.02E-08. *TSPA-LA Name:* GW_BDCF_MIC_Cs135. *Location in TSPA-LA:* Sections 6.3.11.2 and 6.3.11.3; Table 6.3.11-3.
MICCS137. Groundwater Biosphere Dose Conversion Factor (BDCF) for ^{137}Cs in modern interglacial climate ((Sv/year)/(Bq/m^3)). *Distribution:* Discrete. *Range:* 3.87E-08 to 4.56E-07. *Mean:* 1.30E-07. *Standard Deviation:* 6.33E-08. *TSPA-LA Name:* GW_BDCF_MIC_Cs137. *Location in TSPA-LA:* Sections 6.3.11.2 and 6.3.11.3; Table 6.3.11-3.
MICI129. Groundwater Biosphere Dose Conversion Factor (BDCF) for ^{129}I in modern interglacial climate ((Sv/year)/(Bq/m^3)). *Distribution:* Discrete. *Range:* 8.59E-08 to 1.13E-06. *Mean:* 1.29E-07. *Standard Deviation:* 5.28E-08. *TSPA-LA Name:* GW_BDCF_MIC_I129. *Location in TSPA-LA:* Sections 6.3.11.2 and 6.3.11.3; Table 6.3.11-3.
MICNP237. Groundwater Biosphere Dose Conversion Factor (BDCF) for ^{237}Np in modern interglacial climate ((Sv/year)/(Bq/m^3)). *Distribution:* Discrete. *Range:* 1.06E-07 to 8.05E-07. *Mean:* 2.74E-07. *Standard Deviation:* 9.70E-08. *TSPA-LA Name:* GW_BDCF_MIC_Np237. *Location in TSPA-LA:* Sections 6.3.11.2 and 6.3.11.3; Table 6.3.11-3.
MICPA231. Groundwater Biosphere Dose Conversion Factor (BDCF) for ^{231}Pa in modern interglacial climate ((Sv/year)/(Bq/m^3)). *Distribution:* Discrete. *Range:* 6.58E-07 to 8.56E-06. *Mean:* 2.44E-06. *Standard Deviation:* 1.02E-06. *TSPA-LA Name:* GW_BDCF_MIC_Pa231. *Location in TSPA-LA:* Sections 6.3.11.2 and 6.3.11.3; Table 6.3.11-3.
MICPU238. Groundwater Biosphere Dose Conversion Factor (BDCF) for ^{238}Pu in modern interglacial climate ((Sv/year)/(Bq/m^3)). *Distribution:* Discrete. *Range:* 2.61E-07 to 2.09E-006. *Mean:* 7.61E-07. *Standard Deviation:* 2.78E-07. *TSPA-LA Name:* GW_BDCF_MIC_Pu238. *Location in TSPA-LA:* Sections 6.3.11.2 and 6.3.11.3; Table 6.3.11-3.
MICPU239. Groundwater Biosphere Dose Conversion Factor (BDCF) for ^{239}Pu in modern interglacial climate ((Sv/year)/(Bq/m^3)). *Distribution:* Discrete. *Range:* 3.49E-07 to 2.93E-06. *Mean:* 9.55E-07. *Standard Deviation:* 3.37E-07. *TSPA-LA Name:* GW_BDCF_MIC_Pu239. *Location in TSPA-LA:* Sections 6.3.11.2 and 6.3.11.3; Table 6.3.11-3.
MICPU240. Groundwater Biosphere Dose Conversion Factor (BDCF) for ^{240}Pu in modern interglacial climate ((Sv/year)/(Bq/m^3)). *Distribution:* Discrete. *Range:* 3.47E-07 to 2.90E-06. *Mean:* 9.51E-07. *Standard Deviation:* 3.35E-07. *TSPA-LA Name:* GW_BDCF_MIC_Pu240. *Location in TSPA-LA:* Sections 6.3.11.2 and 6.3.11.3; Table 6.3.11-3.
MICRA226. Groundwater Biosphere Dose Conversion Factor (BDCF) for ^{210}Pb summed into ^{226}Ra in modern interglacial climate ((Sv/year)/(Bq/m^3)). *Distribution:* Discrete. *Range:* 2.90E-06 to 2.82E-05. *Mean:* 6.52E-06. *Standard Deviation:* 2.58E-06. *TSPA-LA Name:* GW_BDCF_MIC_Ra226_Pb210. *Location in TSPA-LA:* Sections 6.3.11.2 and 6.3.11.3; Table 6.3.11-3.
MICSE79. Groundwater Biosphere Dose Conversion Factor (BDCF) for ^{79}Se in modern interglacial climate. ((Sv/year)/(Bq/m^3)). *Distribution:* Discrete. *Range:* 3.62E-09 to 1.51E-06. *Mean:* 2.42E-08. *Standard Deviation:* 7.48E-08. *TSPA-LA Name:* GW_BDCF_MIC_Se79. *Location in TSPA-LA:* Sections 6.3.11.2 and 6.3.11.3; Table-6.3.11-3.
MICSN126. Groundwater Biosphere Dose Conversion Factor (BDCF) for ^{126}Sn in modern interglacial climate ((Sv/year)/(Bq/m^3)). *Distribution:* Discrete. *Range:* 8.92E-08 to 1.68E-06. *Mean:* 4.33E-07. *Standard Deviation:* 2.39E-07. *TSPA-LA Name:* GW_BDCF_MIC_Sn126. *Location in TSPA-LA:* Sections 6.3.11.2 and 6.3.11.3; Table 6.3.11-3.

Table K3-1. High-Level Summary of Epistemically Uncertain Variables (i.e., elements of **e**) Considered in the TSPA-LA (Sensitivity Analysis Name) (Continued)

NOTE: * indicates variable not considered in sensitivity analysis due to correlations.

MICSR90. Groundwater Biosphere Dose Conversion Factor (BDCF) for ^{90}Sr in modern interglacial climate ((Sv/year)/(Bq/m^3)). *Distribution:* Discrete. *Range:* 2.51E-08 to 8.60E-08. *Mean:* 3.43E-08. *Standard Deviation:* 6.59E-09. *TSPA-LA Name:* GW_BDCF_MIC_Sr90. *Location in TSPA-LA:* Sections 6.3.11.2 and 6.3.11.3; Table 6.3.11-3.
MICTC99. Groundwater Biosphere Dose Conversion Factor (BDCF) for ^{99}Tc in modern interglacial climate ((Sv/year)/(Bq/m^3)). *Distribution:* Discrete. *Range:* 5.28E-10 to 2.85E-08. *Mean:* 1.12E-09. *Standard Deviation:* 1.26E-09. *TSPA-LA Name:* GW_BDCF_MIC_Tc99. *Location in TSPA-LA:* Sections 6.3.11.2 and 6.3.11.3; Table-6.3.11-3.
MICTH229. Groundwater Biosphere Dose Conversion Factor (BDCF) for ^{229}Th in modern interglacial climate ((Sv/year)/(Bq/m^3)). *Distribution:* Discrete. *Range:* 7.43E-07 to 8.05E-06. *Mean:* 2.58E-06. *Standard Deviation:* 1.03E-06. *TSPA-LA Name:* GW_BDCF_MIC_Th229. *Location in TSPA-LA:* Sections 6.3.11.2 and 6.3.11.3; Table 6.3.11-3.
MICU232. Groundwater Biosphere Dose Conversion Factor (BDCF) for 232U in modern interglacial climate ((Sv/year)/(Bq/m^3)). *Distribution:* Discrete. *Range:* 2.87E-07 to 1.86E-06. *Mean:* 6.04E-07. *Standard Deviation:* 2.17E-07. *TSPA-LA Name:* GW_BDCF_MIC_U232. *Location in TSPA-LA:* Sections 6.3.11.2 and 6.3.11.3; Table 6.3.11-3.
MICU233. Groundwater Biosphere Dose Conversion Factor (BDCF) for ^{233}U in modern interglacial climate ((Sv/year)/(Bq/m^3)). *Distribution:* Discrete. *Range:* 4.13E-08 to 3.13E-07. *Mean:* 8.97E-08. *Standard Deviation:* 3.35E-08. *TSPA-LA Name:* GW_BDCF_MIC_U233. *Location in TSPA-LA:* Sections 6.3.11.2 and 6.3.11.3; Table 6.3.11-3.
MICU234. Groundwater Biosphere Dose Conversion Factor (BDCF) for ^{234}U in modern interglacial climate ((Sv/year)/(Bq/m^3)). *Distribution:* Discrete. *Range:* 3.96E-08 to 2.20E-07. *Mean:* 8.19E-08. *Standard Deviation:* 2.81E-08. *TSPA-LA Name:* GW_BDCF_MIC_U234. *Location in TSPA-LA:* Sections 6.3.11.2 and 6.3.11.3; Table 6.3.11-3.
MICU238. Groundwater Biosphere Dose Conversion Factor (BDCF) for ^{238}U in modern interglacial climate ((Sv/year)/(Bq/m^3)). *Distribution:* Discrete. *Range:* 3.85E-08 to 2.07E-07. *Mean:* 7.87E-08. *Standard Deviation:* 2.62E-08. *TSPA-LA Name:* GW_BDCF_MIC_U238. *Location in TSPA-LA:* Sections 6.3.11.2 and 6.3.11.3; Table 6.3.11-3.
NIOSA. Specific surface area of NiO (m^2/g). *Distribution:* Uniform. *Range:* 1 to 30. *TSPA-LA Name:* NiO_SA_a. *Location in TSPA-LA:* Table 6.3.8-4; S_{CP} in Equation 6.3.8-19.
PH2DHLNS. Pointer variable used to determine pH in 2DHLW Cell (Cell 1a) of CDSP waste packages under vapor influx conditions (dimensionless). *Distribution:* Uniform. *Range:* 0 to 1. *TSPA-LA Name:* Inpkg_pH_2DHLW_NS_Rand_a. *Location in TSPA-LA:* Section 6.3.7.2.2 Part IV.
PH2DHLS. Pointer variable used to determine pH in 2DHLW Cell (Cell 1a) of CDSP waste packages under liquid influx conditions (dimensionless). *Distribution:* Uniform. *Range:* 0 to 1. *TSPA-LA Name:* Inpkg_pH_2DHLW_S_Rand_a. *Location in TSPA-LA:* Section 6.3.7.2.2 Part IV.
PH2MCONS. Pointer variable used to determine pH in 2MCO Cell (Cell 1b) of CDSP waste packages under vapor influx conditions (dimensionless). *Distribution:* Uniform. *Range:* 0 to 1. *TSPA-LA Name:* Inpkg_pH_2MCO_NS_Rand_a. *Location in TSPA-LA:* Section 6.3.7.2.2 Part IV.
PH2MCOS. Pointer variable used to determine pH in 2MCO Cell (Cell 1b) of CDSP waste packages under liquid influx conditions (dimensionless). *Distribution:* Uniform. *Range:* 0 to 1. *TSPA-LA Name:* Inpkg_pH_2MCO_S_Rand_a. *Location in TSPA-LA:* Section 6.3.7.2.2 Part IV.
PH2RGER. Error term in regression equation for pH of corrosion products domain (dimensionless). *Distribution:* Truncated normal. *Range:* -0.64 to 0.64. *Mean/Median/Mode:* 0. *Standard Deviation:* 0.32. *TSPA-LA Name:* pH_Cell2_Regression_Error_a. *Location in TSPA-LA:* Equation 6.3.8-27.
PHCSNS. Pointer variable used to determine pH in CSNF Cell1 under vapor influx conditions (dimensionless). *Distribution:* Uniform. *Range:* 0 to 1. *TSPA-LA Name:* Inpkg_pH_CSNF_NS_Rand_a. *Location in TSPA-LA:* Section 6.3.7.2.2 Part IV.
PHCSS. Pointer variable used to determine pH in CSNF Cell1 under liquid influx conditions (dimensionless). *Distribution:* Uniform. *Range:* 0 to 1. *TSPA-LA Name:* Inpkg_pH_CSNF_S_Rand_a. *Location in TSPA-LA:* Section 6.3.7.2.2 Part IV.

Table K3-1. High-Level Summary of Epistemically Uncertain Variables (i.e., elements of **e**) Considered in the TSPA-LA (Sensitivity Analysis Name) (Continued)

NOTE: * indicates variable not considered in sensitivity analysis due to correlations.

PROBDSEF. Probability for undetected defects in drip shields (dimensionless). *Distribution:* Log-normal. *Median:* 4.3E-07. *Error Factor:* 14. *TSPA-LA Name:* UNC_DS_EF_conv_from_ln. *Location in TSPA-LA:* Section 6.4.1; Tables 6.4-1 and 6.4-2.
PROBWPEF. Probability for the undetected defects in waste packages (dimensionless). *Distribution:* Log-normal. *Median:* 4.14E-05. *Error Factor:* 8.17. *TSPA-LA Name:* UNC_WP_EF_conv_from_ln. *Location in TSPA-LA:* Section 6.4.2; Tables 6.4-1 and 6.4-2.
RHI85. The in-drift precipitated/salts (IDPS) process model uncertainty factor for the logarithm of the ionic strength of the in-drift waters at high relative humidity (≥85%) (log molal). *Distribution:* Triangular. *Range:* -0.1 to 0.1. *Mean/Median/Mode:* 0. *TSPA-LA Name:* PCE_I_Uncert_RH_85_100_a. *Location in TSPA-LA:* Section 6.4.1; Tables 6.4-1 and 6.4-2; Figure 6.4-4.
RHMU0. The IDPS process model uncertainty factor for the logarithm of the chloride concentration of the in-drift waters at relative humidity ≤20% (dimensionless). *Distribution:* Triangular. *Range:* -0.7 to 0.7. *Most Likely:* 0. *TSPA-LA Name:* PCE_Cl_MU_RH_0_20_a. *Location in TSPA-LA:* Sections 6.3.4, 6.3.4.2, 6.3.4.3.1, 6.3.4.3.2 and 6.3.5.2.3; Tables 6.3.4-2, 6.3.4-3 and 6.3.5-4.
RHMU20. The IDPS process model uncertainty factor for the logarithm of the chloride concentration of the in-drift waters at relative humidity >20 and ≤40% (dimensionless). *Distribution:* Triangular. *Range:* -0.5 to 0.5. *Most Likely:* 0. *TSPA-LA Name:* PCE_Cl_MU_RH_20_40_a. *Location in TSPA-LA:* Sections 6.3.4, 6.3.4.2, 6.3.4.3.1, 6.3.4.3.2 and 6.3.5.2.3; Tables 6.3.4-2, 6.3.4-3 and 6.3.5-4.
RHMU40. The IDPS process model uncertainty factor for the logarithm of the chloride concentration of the in-drift waters at relative humidity >40 and ≤65% (dimensionless). *Distribution:* Triangular. *Range:* -0.4 to 0.4. *Most Likely:* 0. *TSPA-LA Name:* PCE_Cl_MU_RH_40_65_a. *Location in TSPA-LA:* Sections 6.3.4, 6.3.4.2, 6.3.4.3.1, 6.3.4.3.2 and 6.3.5.2.3; Tables 6.3.4-2, 6.3.4-3 and 6.3.5-4.
RHMU65. The IDPS process model uncertainty factor for the logarithm of the chloride concentration of the in-drift waters at relative humidity >65 and ≤85% (dimensionless). *Distribution:* Triangular. *Range:* -0.1 to 0.1. *Most Likely:* 0. *TSPA-LA Name:* PCE_Cl_MU_RH_65_85_a. *Location in TSPA-LA:* Sections 6.3.4, 6.3.4.2, 6.3.4.3.1, 6.3.4.3.2 and 6.3.5.2.3; Tables 6.3.4-2, 6.3.4-3 and 6.3.5-4.
RHMU85*. The IDPS process model uncertainty factor for the logarithm of the chloride concentration of the in-drift waters at relative humidity >85% (dimensionless). *Distribution:* Triangular. *Range:* 0 to 0. *Most Likely:* 0. *TSPA-LA Name:* PCE_Cl_MU_RH_85_100_a*. *Location in TSPA-LA:* Sections 6.3.4, 6.3.4.2, 6.3.4.3.1, 6.3.4.3.2 and 6.3.5.2.3; Tables 6.3.4-2, 6.3.4-3 and 6.3.5-4.
RHMUN40. The IDPS process model uncertainty factor for the logarithm of the chloride + nitrate concentration of the in-drift waters at relative humidity >40% and ≤65% (dimensionless). *Distribution:* Triangular. *Range:* -0.57 to 0.57. *Most Likely:* 0. *TSPA-LA Name:* PCE_Cl_N_MU_RH_40_65_a. *Location in TSPA-LA:* Sections 6.3.4.3.2 and 6.3.5.2.3; Tables 6.3.4-2, 6.3.4-3 and 6.3.5-4.
RHMUN65. The IDPS process model uncertainty factor for the logarithm of the chloride + nitrate concentration of the in-drift waters at relative humidity >65% and ≤85% (dimensionless). *Distribution:* Triangular. *Range:* -0.22 to 0.22. *Most Likely:* 0. *TSPA-LA Name:* PCE_Cl_N_MU_RH_65_85_a. *Location in TSPA-LA:* Sections 6.3.4.3.2 and 6.3.5.2.3; Tables 6.3.4-2, 6.3.4-3 and 6.3.5-4.
RHMUN85*. The IDPS process model uncertainty factor for the logarithm of the chloride + nitrate concentration of the in-drift waters at relative humidity >85% (dimensionless). *Distribution:* Triangular. *Range:* 0 to 0. *Most Likely:* 0. *TSPA-LA Name:* PCE_Cl_N_MU_RH_85_100_a*. *Location in TSPA-LA:* Sections 6.3.4.3.2 and 6.3.5.2.3; Tables 6.3.4-2, 6.3.4-3 and 6.3.5-4.
RHMUNO0. The IDPS process model uncertainty factor for the logarithm of the chloride to nitrate ratio of the in-drift waters at relative humidity ≤20% (dimensionless). *Distribution:* Triangular. *Range:* -1.4 to 1.4. *Most Likely:* 0. *TSPA-LA Name:* PCE_Cl_NO3_MU_RH_0_20_a. *Location in TSPA-LA:* Sections 6.3.4.3.1, 6.3.4.3.2 and 6.3.5.2.3; Tables 6.3.4-2, 6.3.4-3 and 6.3.5-4.
RHMUNO20. The IDPS process model uncertainty factor for the logarithm of the chloride to nitrate ratio of the in-drift waters at relative humidity >20% and ≤65% (dimensionless). *Distribution:* Triangular. *Range:* -0.5 to 0.5. *Most Likely:* 0. *TSPA-LA Name:* PCE_Cl_NO3_MU_RH_20_65_a. *Location in TSPA-LA:* Sections 6.3.4.3.1, 6.3.4.3.2 and 6.3.5.2.3; Tables 6.3.4-2, 6.3.4-3 and 6.3.5-4.

Table K3-1. High-Level Summary of Epistemically Uncertain Variables (i.e., elements of **e**) Considered in the TSPA-LA (Sensitivity Analysis Name) (Continued)

NOTE: * indicates variable not considered in sensitivity analysis due to correlations.

RHMUNO65. The IDPS process model uncertainty factor for the logarithm of the chloride to nitrate ratio of the in-drift waters at relative humidity >65% and ≤85% (dimensionless). *Distribution:* Triangular. *Range:* -0.2 to 0.2. *Most Likely:* 0. *TSPA-LA Name:* PCE_Cl_NO3_MU_RH_65_85_a. *Location in TSPA-LA:* Sections 6.3.4.3.1, 6.3.4.3.2 and 6.3.5.2.3; Tables 6.3.4-2, 6.3.4-3 and 6.3.5-4.
RHMUNO85*. The IDPS process model uncertainty factor for the logarithm of the chloride to nitrate ratio of the in-drift waters at low relative humidity >85% (dimensionless). *Distribution:* Triangular. *Range:* 0 to 0. *Most Likely:* 0. *TSPA-LA Name:* PCE_Cl_NO3_MU_RH_85_100_a*. *Location in TSPA-LA:* Sections 6.3.4.3.1, 6.3.4.3.2 and 6.3.5.2.3; Tables 6.3.4-2, 6.3.4-3 and 6.3.5-4.
RHPH0. The IDPS process model uncertainty factor for the pH of the in-drift waters at relative humidity ≤65% (dimensionless). *Distribution:* Triangular. *Range:* -2 to 2. *Most Likely:* 0. *TSPA-LA Name:* PCE_pH_Uncert_RH_0_65_a. *Location in TSPA-LA:* Table 6.3.5-4.
RHPH65. The IDPS process model uncertainty factor for the pH of the in-drift waters at relative humidity >65 and ≤75% (dimensionless). *Distribution:* Triangular. *Range:* -1 to 1. *Most Likely:* 0. *TSPA-LA Name:* PCE_pH_Uncert_RH_65_75_a. *Location in TSPA-LA:* Table 6.3.5-4.
RHPH75. The IDPS process model uncertainty factor for the pH of the in-drift waters at relative humidity >75% (dimensionless). *Distribution:* Discrete. *Range:* -0.3123 to 0.4288. *TSPA-LA Name:* PCE_pH_Uncert_RH_75_100_a. *Location in TSPA-LA:* Table 6.3.5-4.
RSUSTHIK. Thickness of combined ash/soil mixture available for resuspension (m). *Distribution:* Uniform. *Range:* 0.001 to 0.003. *Mean/Median/Mode:* 0.002. *TSPA-LA Name:* Resuspension_Thickness_a. *Location in TSPA-LA:* Equation 6.3.11-6.
RUBMAXL. Volume of lithophysal rock that must fall to fill the drift (m^3/m). *Distribution:* Uniform. *Range:* 30 to 120. *TSPA-LA Name:* Vol_Rubble_Max_Lith_a. *Location in TSPA-LA:* Sections 6.3.5.2.3 and 6.6.3.1; Tables 6.3.5-4 and 6.6-2.
RUBMAXNL. Volume of nonlithophysal rock that must fall to fill the drift (m^3/m). *Distribution:* Uniform. *Range:* 30 to 120. *TSPA-LA Name:* Vol_Rubble_Max_NonLith_a. *Location in TSPA-LA:* Section 6.3.5.2.3 and 6.6.3.1; Tables 6.3.5-4 and 6.6-2.
SC_DPTH. Scour depth in Fortymile Wash at the fan apex (cm). *Distribution:* Uniform. *Range:* 73 to 122. *TSPA-LA Name:* Scour_Depth_a. *Location in TSPA-LA:* Table 6.5-5.
SCCTHR. Stress threshold for stress corrosion cracking (MPa). *Distribution:* Uniform. *Range:* 315.9 to 368.55. *TSPA-LA Name:* Stress_Thresh_SCC_a. *Location in TSPA-LA:* Table 6.3.5-3.
SCCTHRP. Residual stress threshold for SCC nucleation of Alloy 22 (as a percentage of yield strength in MPa) (dimensionless). *Distribution:* Uniform. *Range:* 90 to 105. *TSPA-LA Name:* Stress_Thresh_A22_a. *Location in TSPA-LA:* Section 6.6.1.3.7; Table 6.6-2.
SCHOBOLT. Fractional value used to interpolate between Schoepite and Boltwoodite look-up tables (dimensionless). *Distribution:* Uniform. *Range:* 0 to 1. *TSPA-LA Name:* Schoepite_Boltwoodite_Interp_a. *Location in TSPA-LA:* Table 6.3.7-58.
SEEPCON*. Pointer variable to determine the seepage/condensation regime for the first failed waste package in a percolation subregion (dimensionless). *Distribution:* Uniform. *Range:* 0 to 1. *TSPA-LA Name:* Seepage_Condensation_Prob_a*.
SEEPPRM. Logarithm of the mean fracture permeability in lithophysal rock units (dimensionless). *Distribution:* Triangular. *Range:* -0.92 to 0.92. *Mode:* 0. *TSPA-LA Name:* LogK_Uncert_Lith_a. *Location in TSPA-LA:* Sections 6.3.5.2.3, 6.3.3.1.2 and 6.3.3.1.3; Tables 6.3.5-4, 6.3.3-2 and 6.3.3-3.
SEEPPRMN. Logarithm of the mean fracture permeability in non-lithophysal rock units (dimensionless). *Distribution:* Triangular. *Range:* -0.68 to 0.68. *Mode:* 0. *TSPA-LA Name:* LogK_Uncert_NonLith_a. *Location in TSPA-LA:* Sections 6.3.5.2.3, 6.3.3.1.2 and 6.3.3.1.3; Tables 6.3.5-4, 6.3.3-2 and 6.3.3-3.
SEEPUNC. Uncertainty factor to account for small-scale heterogeneity in fracture permeability (dimensionless). *Distribution:* Uniform. *Range:* 0 to 1. *TSPA-LA Name:* Seepage_Uncertainty_a. *Location in TSPA-LA:* Section 6.3.3.1.2; Tables 6.3.3-3 and 6.3.5-4.
SEEPWAT. Pointer variable used to select which seepage water type in used in the physical and chemical environment (P&CE) submodel calculations (dimensionless). *Distribution:* Discrete. *Range:* 1 to 4. *TSPA-LA Name:* Seepage_Water_Type_a. *Location in TSPA-LA:* Table 6.3.5-4.

Table K3-1. High-Level Summary of Epistemically Uncertain Variables (i.e., elements of **e**) Considered in the TSPA-LA (Sensitivity Analysis Name) (Continued)

NOTE: * indicates variable not considered in sensitivity analysis due to correlations.

SMECSA. Specific surface area for smectite colloids (m^2/g). *Distribution:* Uniform. *Range:* 10 to 100. *TSPA-LA Name:* Specific_SA_Smectite_Col_a. *Location in TSPA-LA:* Table 6.3.7-62.
SOILDENS. Density of surface soil correlated with the volcanic BDCFs (kg/m^3). *Distribution:* Triangular. *Range:* 1300 to 1700. *Mean/Median/Mode:* 1500. *TSPA-LA Name:* Soil_Density_a. *Location in TSPA-LA:* Equation 6.3.11-6.
SZCOLRAL. Logarithm of colloid retardation factor in alluvium (dimensionless). *Distribution:* Piecewise uniform. *Range:* 0.903 to 3.715. *TSPA-LA Name:* CORAL. *Location in TSPA-LA:* Sections 6.3.10.1, 6.3.10.2 and 6.3.10.4.2; Table 6.3.10-2.
SZCOLRVO. Logarithm of colloid retardation factor in volcanic units (dimensionless). *Distribution:* Piecewise uniform. *Range:* 0.778 to 2.903. *TSPA-LA Name:* CORVO. *Location in TSPA-LA:* Sections 6.3.10.1, 6.3.10.2 and 6.3.10.4.2; Table 6.3.10-2.
SZCONCOL. Logarithm of ambient concentration of colloids in groundwater (g/mL). *Distribution:* Piecewise uniform. *Range:* -9 to -3.6. *TSPA-LA Name:* Conc_Col. *Location in TSPA-LA:* Table 6.3.10-2.
SZDENAL. Bulk density of alluvium (kg/m^3). *Distribution:* Normal. *Mean/Median/Mode:* 1910. *Standard Deviation:* 78. *TSPA-LA Name:* Alluvium_Density. *Location in TSPA-LA:* Table 6.3.10-2.
SZDIFCVO. Logarithm of effective diffusion coefficient in fractured volcanic units (m^2/s). *Distribution:* Piecewise uniform. *Range:* -11.3 to -9.3. *TSPA-LA Name:* DCVO. *Location in TSPA-LA:* Sections 6.3.10.2 and 6.3.10.5; Table 6.3.10-2.
SZFIPOVO. Logarithm of flowing interval porosity in volcanic units (dimensionless). *Distribution:* Piecewise uniform. *Range:* -5 to -1. *Mean/Median/Mode:* -3. *TSPA-LA Name:* FPVO. *Location in TSPA-LA:* Table 6.3.10-2.
SZFISPVO. Flowing interval spacing in fractured volcanic units (m). *Distribution:* Piecewise uniform. *Range:* 1.86 to 80. *TSPA-LA Name:* FISVO. *Location in TSPA-LA:* Section 6.3.10.5; Table 6.3.10-2.
SZGWSPDM. Logarithm of the scale factor used to characterize uncertainty in groundwater specific discharge (dimensionless). *Distribution:* Piecewise uniform. *Range:* -0.951 to 0.951. *TSPA-LA Name:* GWSPD. *Location in TSPA-LA:* Section 6.3.10.2; Table 6.3.10-2.
SZKDAMAL. Americium sorption coefficient in alluvium (mL/g). *Distribution:* Truncated normal. *Range:* 1000 to 10000. *Mean/Median/Mode:* 5500. *Standard Deviation:* 1500. *TSPA-LA Name:* Kd_Am_Al. *Location in TSPA-LA:* Section 6.3.10.2; Table 6.3.10-2.
SZKDAMCO. Americium sorption coefficient onto smectite colloids (mL/g). *Distribution:* Piecewise uniform. *Range:* 1.00E+04 to 1.00E+07. *TSPA-LA Name:* Kd_Am_Col. *Location in TSPA-LA:* Section 6.3.10.2; Table 6.3.10-2.
SZKDAMVO. Americium sorption coefficient in volcanic units (mL/g). *Distribution:* Truncated normal. *Range:* 1000 to 10000. *Mean/Median/Mode:* 5500. *Standard Deviation:* 1500. *TSPA-LA Name:* Kd_Am_Vo. *Location in TSPA-LA:* Section 6.3.10.2; Table 6.3.10-2.
SZKDCSAL. Cesium sorption coefficient in alluvium (mL/g). *Distribution:* Truncated normal. *Range:* 100 to 1000. *Mean/Median/Mode:* 728. *Standard Deviation:* 464. *TSPA-LA Name:* Kd_Cs_Al. *Location in TSPA-LA:* Section 6.3.10.2; Table 6.3.10-2.
SZKDCSCO. Cesium sorption coefficient onto smectite colloids (mL/g). *Distribution:* Piecewise uniform. *Range:* 50 to 5000. *TSPA-LA Name:* Kd_Cs_Col. *Location in TSPA-LA:* Section 6.3.10.2; Table 6.3.10-2.
SZKDCSVO. Cesium sorption coefficient in volcanic units (mL/g). *Distribution:* Piecewise uniform. *Range:* 100 to 6783. *TSPA-LA Name:* Kd_Cs_Vo. *Location in TSPA-LA:* Section 6.3.10.2; Table 6.3.10-2.
SZKDNPAL. Neptunium sorption coefficient in alluvium (mL/g). *Distribution:* Piecewise uniform. *Range:* 1.8 to 13. *TSPA-LA Name:* Kd_Np_Al. *Location in TSPA-LA:* Section 6.3.10.2; Table 6.3.10-2.
SZKDNPVO. Neptunium sorption coefficient in volcanic units (mL/g). *Distribution:* Piecewise uniform. *Range:* 0 to 6. *TSPA-LA Name:* Kd_Np_Vo. *Location in TSPA-LA:* Section 6.3.10.2; Table 6.3.10-2.
SZKDPUAL. Plutonium sorption coefficient in alluvium (mL/g). *Distribution:* Beta. *Range:* 50 to 300. *Mean/Median/Mode:* 100. *Standard Deviation:* 15. *TSPA-LA Name:* Kd_Pu_Al. *Location in TSPA-LA:* Section 6.3.10.2; Table 6.3.10-2.

Table K3-1. High-Level Summary of Epistemically Uncertain Variables (i.e., elements of **e**) Considered in the TSPA-LA (Sensitivity Analysis Name) (Continued)

NOTE: * indicates variable not considered in sensitivity analysis due to correlations.

SZKDPUCO. Plutonium sorption coefficient onto smectite colloids (mL/g). *Distribution:* Piecewise uniform. *Range:* 1.00E+03 to 1.00E+05. *TSPA-LA Name:* Kd_Pu_Col. *Location in TSPA-LA:* Section 6.3.10.2; Table 6.3.10-2.
SZKDPUVO. Plutonium sorption coefficient in volcanic units (mL/g). *Distribution:* Piecewise uniform. *Range:* 10 to 300. *TSPA-LA Name:* Kd_Pu_Vo. *Location in TSPA-LA:* Section 6.3.10.2; Table 6.3.10-2.
SZKDRAAL. Radium sorption coefficient in alluvium (mL/g). *Distribution:* Uniform. *Range:* 100 to 1000. *TSPA-LA Name:* Kd_Ra_Al. *Location in TSPA-LA:* Section 6.3.10.2; Table 6.3.10-2.
SZKDRAVO*. Radium sorption coefficient in volcanic units (mL/g). *Distribution:* Uniform. *Range:* 100 to 1000. *TSPA-LA Name:* Kd_Ra_Vo*. *Location in TSPA-LA:* Section 6.3.10.2; Table 6.3.10-2.
SZKDSEAL. Selenium sorption coefficient in alluvium (mL/g). *Distribution:* Truncated log normal. *Range:* 1 to 50. *Mean/Median/Mode:* 14. *Standard Deviation:* 11.2. *TSPA-LA Name:* Kd_Se_Al. *Location in TSPA-LA:* Section 6.3.10.2; Table 6.3.10-2.
SZKDSEVO. Selenium sorption coefficient in volcanic units (mL/g). *Distribution:* Truncated log normal. *Range:* 1 to 50. *Mean/Median/Mode:* 14. *Standard Deviation:* 11.2. *TSPA-LA Name:* Kd_Se_Vo. *Location in TSPA-LA:* Section 6.3.10.2; Table 6.3.10-2.
SZKDSNAL. Tin sorption coefficient in alluvium (mL/g). *Distribution:* Log uniform. *Range:* 1.00E+02 to 1.00E+05. *TSPA-LA Name:* Kd_Sn_Al. *Location in TSPA-LA:* Section 6.3.10.2; Table 6.3.10-2.
SZKDSNCO. Tin sorption coefficient onto smectite colloids (mL/g). *Distribution:* Log uniform. *Range:* 1.00E+05 to 1.00E+06. *TSPA-LA Name:* Kd_Sn_Col. *Location in TSPA-LA:* Section 6.3.10.2; Table 6.3.10-2.
SZKDSNVO. Tin sorption coefficient in volcanic units (mL/g). *Distribution:* Log uniform. *Range:* 1.00E+02 to 1.00E+05. *TSPA-LA Name:* Kd_Sn_Vo. *Location in TSPA-LA:* Section 6.3.10.2; Table 6.3.10-2.
SZKDSRAL. Strontium sorption coefficient in alluvium (mL/g). *Distribution:* Uniform. *Range:* 20 to 400. *TSPA-LA Name:* Kd_Sr_Al. *Location in TSPA-LA:* Section 6.3.10.2; Table 6.3.10-2.
SZKDSRVO. Strontium sorption coefficient in volcanic units (mL/g). *Distribution:* Uniform. *Range:* 20 to 400. *TSPA-LA Name:* Kd_Sr_Vo. *Location in TSPA-LA:* Section 6.3.10.2; Table 6.3.10-2.
SZKDUAL. Uranium sorption coefficient in alluvium (mL/g). *Distribution:* Piecewise uniform. *Range:* 1.7 to 8.9. *TSPA-LA Name:* Kd_U_Al. *Location in TSPA-LA:* Section 6.3.10.2; Table 6.3.10-2.
SZKDUVO. Uranium sorption coefficient in volcanic units (mL/g). *Distribution:* Piecewise uniform. *Range:* 0 to 20. *TSPA-LA Name:* Kd_U_Vo. *Location in TSPA-LA:* Section 6.3.10.2; Table 6.3.10-2.
SZLODISP. Logarithm of longitudinal dispersivity (m). *Distribution:* Right-truncated normal. *Range*: $-\infty$ to 3.5. Mean: 2.0. *Standard Deviation:* 0.75. *TSPA-LA Name:* LDISP. *Location in TSPA-LA:* Section 6.3.10.2; Table 6.3.10-2.
SZPORSAL. Effective porosity in shallow alluvium (dimensionless). *Distribution:* Truncated normal. *Range:* 0 to 0.3. *Mean:* 0.18. *Standard Deviation:* 0.051. *TSPA-LA Name:* NVF26. *Location in TSPA-LA:* Table 6.3.10-2.
SZPORUAL. Effective porosity in undifferentiated alluvium (valley fill) (dimensionless). *Distribution:* Truncated normal. *Range:* 0 to 0.3. *Mean:* 0.18. *Standard Deviation:* 0.051. *TSPA-LA Name:* NVF11. *Location in TSPA-LA:* Table 6.3.10-2.
SZRAHAVO. Ratio of horizontal anisotropy (north-south over east-west) in the permeability of the SZ volcanic units (dimensionless). *Distribution:* Piecewise uniform. *Range:* 0.05 to 20. *TSPA-LA Name:* HAVO. *Location in TSPA-LA:* Sections 6.3.10.2 and 6.3.10.5; Table 6.3.10-2.
SZSREG1X. Relative x location of point source in source region 1 (dimensionless). *Distribution:* Uniform. *Range:* 0 to 1. *TSPA-LA Name:* SRC1X. *Location in TSPA-LA:* Section 6.3.10.2; Table 6.3.10-2.
SZSREG1Y. Relative y location of point source in source region 1 (dimensionless). *Distribution:* Uniform. *Range:* 0 to 1. *TSPA-LA Name:* SRC1Y. *Location in TSPA-LA:* Section 6.3.10.2; Table 6.3.10-2.
SZSREG2X. Relative x location of point source in source region 2 (dimensionless). *Distribution:* Uniform. *Range:* 0 to 1. *TSPA-LA Name:* SRC2X. *Location in TSPA-LA:* Section 6.3.10.2; Table 6.3.10-2.
SZSREG2Y. Relative y location of point source in source region 2 (dimensionless). *Distribution:* Uniform. *Range:* 0 to 1. *TSPA-LA Name:* SRC2Y. *Location in TSPA-LA:* Section 6.3.10.2; Table 6.3.10-2.
SZSREG3X. Relative x location of point source in source region 3 (dimensionless). *Distribution:* Uniform. *Range:* 0 to 1. *TSPA-LA Name:* SRC3X. *Location in TSPA-LA:* Section 6.3.10.2; Table 6.3.10-2.

Table K3-1. High-Level Summary of Epistemically Uncertain Variables (i.e., elements of **e**) Considered in the TSPA-LA (Sensitivity Analysis Name) (Continued)

NOTE: * indicates variable not considered in sensitivity analysis due to correlations.

SZSREG3Y. Relative y location of point source in source region 3 (dimensionless). *Distribution:* Uniform. *Range:* 0 to 1. *TSPA-LA Name:* SRC3Y. *Location in TSPA-LA:* Section 6.3.10.2; Table 6.3.10-2.
SZSREG4X. Relative x location of point source in source region 4 (dimensionless). *Distribution:* Uniform. *Range:* 0 to 1. *TSPA-LA Name:* SRC4X. *Location in TSPA-LA:* Section 6.3.10.2; Table 6.3.10-2.
SZSREG4Y. Relative y location of point source in source region 4 (dimensionless). *Distribution:* Uniform. *Range:* 0 to 1. *TSPA-LA Name:* SRC4Y. *Location in TSPA-LA:* Section 6.3.10.2; Table 6.3.10-2.
SZWBNDAL. Northwestern boundary of alluvial uncertainty zone (dimensionless). *Distribution:* Uniform. *Range:* 0 to 1. *TSPA-LA Name:* FPLANW. *Location in TSPA-LA:* Section 6.3.10.2; Table 6.3.10-2.
THERMCON. Selector variable for one of three host-rock thermal conductivity scenarios (low, mean, and high) (dimensionless). *Distribution:* Discrete. *Range:* 1 to 3. *TSPA-LA Name:* Thermal_Conductivity_Uncert_a. *Location in TSPA-LA:* Sections 6.3.2.2, 6.3.2.3, 6.3.5.1.3, 6.3.5.2.3 and 6.6.2.2; Tables 6.3.2-1, 6.3.2-3 and 6.3.5-4.
UZCOKDAM. Colloid sorption coefficient for americium (mg/mg). *Calculated by:* Colloidal_Kd_Am_uz*Colloidal_Concentration_uz. *TSPA-LA Name:* Colloidal_Kc_Am_UZP. *Location in TSPA-LA:* Section 6.3.9.2.
UZCOKDCS. Colloid sorption coefficient for cesium (mg/mg). *Calculated by:* Colloidal_Kd_Cs_uz*Colloidal_Concentration_uz. *TSPA-LA Name:* Colloidal_Kc_Cs_UZP. *Location in TSPA-LA:* Section 6.3.9.2.
UZCOKDPA. Colloid sorption coefficient for protactinium (mg/mg). *Calculated by:* Colloidal_Kd_Am_uz*Colloidal_Concentration_uz. *TSPA-LA Name:* Colloidal_Kc_Pa_UZP. *Location in TSPA-LA:* Section 6.3.9.2.
UZCOKDPU. Colloid sorption coefficient for plutonium (mg/mg). *Calculated by:* Colloidal_Kd_Pu_uz*Colloidal_Concentration_uz. *TSPA-LA Name:* Colloidal_Kc_Pu_UZP. *Location in TSPA-LA:* Section 6.3.9.2.
UZCOKDSN. Colloid sorption coefficient for tin (mg/mg). *Calculated by:* Colloidal_Kd_Sn_uz*Colloidal_Concentration_uz. *TSPA-LA Name:* Colloidal_Kc_Sn_UZP. *Location in TSPA-LA:* Section 6.3.9.2.
UZCOKDTH. Colloid sorption coefficient for thorium (mg/mg). *Calculated by:* Calculated by Colloidal_Kd_Am_uz*Colloidal_Concentration_uz. *TSPA-LA Name:* Colloidal_Kc_Th_UZP. *Location in TSPA-LA:* Section 6.3.9.2.
UZFAG1. Fracture aperture for group 1 rock unit (chnf) (m). *Calculated by:* Por_group1_a/ff_group1_a. *TSPA-LA Name:* fa_group1_a. *Location in TSPA-LA:* Section 6.3.9.2; Equation 6.3.9-2; Fracture porosity values and frequency values are shown in Tables 6.3.9-6 and 6.3.9-7.
UZFAG2. Fracture aperture for group 2 rock unit (tswf) (m). *Calculated by:* Por_group2_a/ff_group2_a. *TSPA-LA Name:* fa_group2_a. *Location in TSPA-LA:* Section 6.3.9.2; Equation 6.3.9-2; Fracture porosity values and frequency values are shown in Tables 6.3.9-6 and 6.3.9-7.
UZFAG3. Fracture aperture for group 3 rock units (ch[2,3,4,5]fz, pcf[2,5]z, pp4fz, pp1fz, bf2fz, tr2fz) (m). *Calculated by:* Por_group3_a/ff_group3_a. *TSPA-LA Name:* fa_group3_a. *Location in TSPA-LA:* Section 6.3.9.2; Equation 6.3.9-2; Fracture porosity values and frequency values are shown in Tables 6.3.9-6 and 6.3.9-7.
UZFAG4. Fracture aperture for group 4 rock units (pp3fd, pp2fd, bf3fd, tr3fd) (m). *Calculated by:* Por_group4_a/ff_group4_a. *TSPA-LA Name:* fa_group4_a. *Location in TSPA-LA:* Section 6.3.9.2; Equation 6.3.9-2; Fracture porosity values and frequency values are shown in Tables 6.3.9-6 and 6.3.9-7.
UZFAG5. Fracture aperture for group 5 rock units (ch1fz, pcf1z, ch6fz, pcf6z) (m). *Calculated by:* Por_group5_a/ff_group5_a. *TSPA-LA Name:* fa_group5_a. *Location in TSPA-LA:* Section 6.3.9.2; Equation 6.3.9-2; Fracture porosity values and frequency values are shown in Tables 6.3.9-6 and 6.3.9-7.
UZFAG6. Fracture aperture for group 6 rock units (ch[1,2,3,4,5,6]fv) (m). *Calculated by:* Por_group6_a/ff_group6_a. *TSPA-LA Name:* fa_group6_a. *Location in TSPA-LA:* Section 6.3.9.2; Equation 6.3.9-2; Fracture porosity values and frequency values are shown in Tables 6.3.9-6 and 6.3.9-7.
UZFAG7. Fracture aperture for group 7 rock units (tswf9, pcf39, tswfv, tswfz) (m). *Calculated by:* Por_group7_a/ff_group7_a. *TSPA-LA Name:* fa_group7_a. *Location in TSPA-LA:* Section 6.3.9.2; Equation 6.3.9-2; Fracture porosity values and frequency values are shown in Tables 6.3.9-6 and 6.3.9-7.

Table K3-1. High-Level Summary of Epistemically Uncertain Variables (i.e., elements of **e**) Considered in the TSPA-LA (Sensitivity Analysis Name) (Continued)

NOTE: * indicates variable not considered in sensitivity analysis due to correlations.

UZFAG8. Fracture aperture for group 8 rock units (tswf[4,5], tswf[6,7], tswf8, pcf38) (m). *Calculated by:* Por_group8_a/ff_group8_a. *TSPA-LA Name:* fa_group8_a. *Location in TSPA-LA:* Section 6.3.9.2; Equation 6.3.9-2; Fracture porosity values and frequency values are shown in Tables 6.3.9-6 and 6.3.9-7.
UZFAG9. Fracture aperture for group 9 rock units (tswf3) (m). *Calculated by:* Por_group9_a/ff_group9_a. *TSPA-LA Name:* fa_group9_a. *Location in TSPA-LA:* Section 6.3.9.2; Equation 6.3.9-2; Fracture porosity values and frequency values are shown in Tables 6.3.9-6 and 6.3.9-7.
UZGAM. Active fracture model (AFM) Gamma parameter (dimensionless). *Distribution:* Uniform. *Range:* 0.2 to 0.6. *TSPA-LA Name:* Gamma_AFM_a. *Location in TSPA-LA:* Sections 6.3.9.2, 6.3.9.3 and 6.3.9.4.1; Table 6.3.9-5.
UZKDAMDT. Sorption coefficient of americium in devitrified tuff units of UZ (mL/g). *Distribution:* Truncated normal. *Range:* 1000 to 10000. *Mean:* 5500. *Standard Deviation:* 1500. *TSPA-LA Name:* KdAm_Devit_a. *Location in TSPA-LA:* Sections 6.3.9.2 and 6.3.9.3; Equation 6.3.9-3; Table 6.3.9-2.
UZKDAMVT*. Sorption coefficient of americium in vitrified tuff units of UZ (mL/g). *Distribution:* Piecewise uniform. *Range:* 100 to 1000. *Median:* 400. *TSPA-LA Name:* KdAm_Vit_a*. *Location in TSPA-LA:* Sections 6.3.9.2 and 6.3.9.3; Equation 6.3.9-3; Table 6.3.9-2.
UZKDAMZT*. Sorption coefficient of americium in zeolitic tuff units of UZ (mL/g). *Distribution:* Truncated normal. *Range:* 1000 to 10000. *Mean:* 5500. *Standard Deviation:* 1500. *TSPA-LA Name:* KdAm_Zeo_a*. *Location in TSPA-LA:* Sections 6.3.9.2 and 6.3.9.3; Equation 6.3.9-3; Table 6.3.9-2.
UZKDCSDT. Sorption coefficient of cesium in devitrified tuff units of UZ (mL/g). *Distribution:* Uniform. *Range:* 1 to 15. *TSPA-LA Name:* KdCs_Devit_a. *Location in TSPA-LA:* Sections 6.3.9.2 and 6.3.9.3; Equation 6.3.9-3; Table 6.3.9-2.
UZKDCSVT*. Sorption coefficient of cesium in vitrified tuff units of UZ (mL/g). *Distribution:* Piecewise uniform. *Range:* 0 to 100. *Median:* 2. *TSPA-LA Name:* KdCs_Vit_a*. *Location in TSPA-LA:* Sections 6.3.9.2 and 6.3.9.3; Equation 6.3.9-3; Table 6.3.9-2.
UZKDCSZT. Sorption coefficient for cesium in zeolitic tuff units of UZ (mL/g). *Distribution:* Piecewise uniform. *Range:* 425 to 20000. *Median:* 5,000. *TSPA-LA Name:* KdCs_Zeo_a. *Location in TSPA-LA:* Sections 6.3.9.2 and 6.3.9.3; Equation 6.3.9-3; Table 6.3.9-2.
UZKDNPDT. Sorption coefficient for neptunium in devitrified tuff units of UZ (mL/g). *Distribution:* Piecewise uniform. *Range:* 0 to 6. *Median:* 0.5. *TSPA-LA Name:* KdNp_Devit_a. *Location in TSPA-LA:* Sections 6.3.9.2 and 6.3.9.3; Equation 6.3.9-3; Table 6.3.9-2.
UZKDNPVT*, Sorption coefficient for neptunium in vitrified tuff units of UZ (mL/g). *Distribution:* Piecewise uniform. *Range:* 0 to 3. *Median:* 1. *TSPA-LA Name:* KdNp_Vit_a*. *Location in TSPA-LA:* Sections 6.3.9.2 and 6.3.9.3; Equation 6.3.9-3; Table 6.3.9-2.
UZKDNPZT*. Sorption coefficient for neptunium in zeolitic tuff units of UZ (mL/g). *Distribution:* Piecewise uniform. *Range:* 0 to 6. *Median:* 0.5. *TSPA-LA Name:* KdNp_Zeo_a*. *Location in TSPA-LA:* Sections 6.3.9.2 and 6.3.9.3; Equation 6.3.9-3; Table 6.3.9-2.
UZKDPADT. Sorption coefficient for protactinium in devitrified tuff units of UZ (mL/g). *Distribution:* Truncated normal. *Range:* 1000 to 10000. *Mean:* 5500. *Standard Deviation:* 1500. *TSPA-LA Name:* KdPa_Devit_a. *Location in TSPA-LA:* Sections 6.3.9.2 and 6.3.9.3; Equation 6.3.9-3; Table 6.3.9-2.
UZKDPAVT*. Sorption coefficient for protactinium in vitrified tuff units of UZ (mL/g). *Distribution:* Truncated normal. *Range:* 1000 to 10000. *Mean:* 5500. *Standard Deviation:* 1500. *TSPA-LA Name:* KdPa_Vit_a*. *Location in TSPA-LA:* Sections 6.3.9.2 and 6.3.9.3; Equation 6.3.9-3; Table 6.3.9-2.
UZKDPAZT*. Sorption coefficient for protactinium in zeolitic tuff units of UZ (mL/g). *Distribution:* Truncated normal. *Range:* 1000 to 10000. *Mean:* 5500. *Standard Deviation:* 1500. *TSPA-LA Name:* KdPa_Zeo_a*. *Location in TSPA-LA:* Sections 6.3.9.2 and 6.3.9.3; Equation 6.3.9-3; Table 6.3.9-2.
UZKDPUDT. Sorption coefficient for plutonium in devitrified tuff units of UZ (mL/g). *Distribution:* Piecewise uniform. *Range:* 10 to 200. *Median:* 70. *TSPA-LA Name:* KdPu_Devit_a. *Location in TSPA-LA:* Sections 6.3.9.2 and 6.3.9.3; Equation 6.3.9-3; Table 6.3.9-2.
UZKDPUVT*. Sorption coefficient for plutonium in vitrified tuff units of UZ (mL/g). *Distribution:* Piecewise uniform. *Range:* 10 to 200. *Median:* 100. *TSPA-LA Name:* KdPu_Vit_a*. *Location in TSPA-LA:* Sections 6.3.9.2 and 6.3.9.3; Equation 6.3.9-3; Table 6.3.9-2.

Table K3-1. High-Level Summary of Epistemically Uncertain Variables (i.e., elements of **e**) Considered in the TSPA-LA (Sensitivity Analysis Name) (Continued)

NOTE: * indicates variable not considered in sensitivity analysis due to correlations.

UZKDPUZT*. Sorption coefficient for plutonium in zeolitic tuff units of UZ (mL/g). *Distribution:* Piecewise uniform. *Range:* 10 to 200. *Median:* 100. *TSPA-LA Name:* KdPu_Zeo_a*. *Location in TSPA-LA:* Sections 6.3.9.2 and 6.3.9.3; Equation 6.3.9-3; Table 6.3.9-2.
UZKDRADT*. Sorption coefficient for radium in devitrified tuff units of UZ (mL/g). *Distribution:* Uniform. *Range:* 100 to 1000. *TSPA-LA Name:* KdRa_Devit_a*. *Location in TSPA-LA:* Sections 6.3.9.2 and 6.3.9.3; Equation 6.3.9-3; Table 6.3.9-2.
UZKDRAVT*. Sorption coefficient for radium in vitrified tuff units of UZ (mL/g). *Distribution:* Uniform. *Range:* 50 to 600. *TSPA-LA Name:* KdRa_Vit_a*. *Location in TSPA-LA:* Sections 6.3.9.2 and 6.3.9.3; Equation 6.3.9-3; Table 6.3.9-2.
UZKDRAZT*. Sorption coefficient for radium in zeolitic tuff units of UZ (mL/g). *Distribution:* Uniform. *Range:* 1000 to 5000. *TSPA-LA Name:* KdRa_Zeo_a*. *Location in TSPA-LA:* Sections 6.3.9.2 and 6.3.9.3; Equation 6.3.9-3; Table 6.3.9-2.
UZKDSEDT. Sorption coefficient for selenium in devitrified tuff units of UZ (mL/g). *Distribution:* Truncated log normal. *Range:* 1 to 50. *Mean:* 14. *Standard Deviation:* 11.2. *TSPA-LA Name:* KdSe_Devit_a. *Location in TSPA-LA:* Sections 6.3.9.2 and 6.3.9.3; Equation 6.3.9-3; Table 6.3.9-2.
UZKDSEVT*. Sorption coefficient for selenium in vitrified tuff units of UZ (mL/g). *Distribution:* Truncated log normal. *Range:* 0 to 25. *Mean:* 8.6. *Standard Deviation:* 7.9. *TSPA-LA Name:* KdSe_Vit_a*. *Location in TSPA-LA:* Sections 6.3.9.2 and 6.3.9.3; Equation 6.3.9-3; Table 6.3.9-2.
UZKDSEZT*. Sorption coefficient for selenium in zeolitic tuff units of UZ (mL/g). *Distribution:* Truncated log normal. *Range:* 1 to 35. *Mean:* 14.3. *Standard Deviation:* 7.9. *TSPA-LA Name:* KdSe_Zeo_a*. *Location in TSPA-LA:* Sections 6.3.9.2 and 6.3.9.3; Equation 6.3.9-3; Table 6.3.9-2.
UZKDSNDT. Sorption coefficient for tin in devitrified tuff units of UZ (mL/g). *Distribution:* Log-uniform. *Range:* 100 to 100000. *TSPA-LA Name:* KdSn_Devit_a. *Location in TSPA-LA:* Sections 6.3.9.2 and 6.3.9.3; Equation 6.3.9-3; Table 6.3.9-2.
UZKDSNVT*. Sorption coefficient for tin in vitrified tuff units of UZ (mL/g). *Distribution:* Log-uniform. *Range:* 100 to 5000. *TSPA-LA Name:* KdSn_Vit_a*. *Location in TSPA-LA:* Sections 6.3.9.2 and 6.3.9.3; Equation 6.3.9-3; Table 6.3.9-2.
UZKDSNZT*. Sorption coefficient for tin in zeolitic tuff units of UZ (mL/g). *Distribution:* Log-uniform. *Range:* 100 to 5000. *TSPA-LA Name:* KdSn_Zeo_a*. *Location in TSPA-LA:* Sections 6.3.9.2 and 6.3.9.3; Equation 6.3.9-3; Table 6.3.9-2.
UZKDSRDT. Sorption coefficient for strontium in devitrified tuff units of UZ (mL/g). *Distribution:* Uniform. *Range:* 10 to 70. *TSPA-LA Name:* KdSr_Devit_a. *Location in TSPA-LA:* Sections 6.3.9.2 and 6.3.9.3; Equation 6.3.9-3; Table 6.3.9-2.
UZKDSRVT*. Sorption coefficient for strontium in vitrified tuff units of UZ (mL/g). *Distribution:* Uniform. *Range:* 0 to 50. *TSPA-LA Name:* KdSr_Vit_a*. *Location in TSPA-LA:* Sections 6.3.9.2 and 6.3.9.3; Equation 6.3.9-3; Table 6.3.9-2.
UZKDSRZT*. Sorption coefficient for strontium in zeolitic tuff units of UZ (mL/g). *Distribution:* Uniform. *Range:* 50 to 2000. *TSPA-LA Name:* KdSr_Zeo_a*. *Location in TSPA-LA:* Sections 6.3.9.2 and 6.3.9.3; Equation 6.3.9-3; Table 6.3.9-2.
UZKDTHDT. Sorption coefficient for thorium in devitrified tuff units of UZ (mL/g). *Distribution:* Uniform. *Range:* 1000 to 10000. *TSPA-LA Name:* KdTh_Devit_a. *Location in TSPA-LA:* Sections 6.3.9.2 and 6.3.9.3; Equation 6.3.9-3; Table 6.3.9-2.
UZKDTHVT*. Sorption coefficient for thorium in vitrified tuff units of UZ (mL/g). *Distribution:* Uniform. *Range:* 1000 to 10000. *TSPA-LA Name:* KdTh_Vit_a*. *Location in TSPA-LA:* Sections 6.3.9.2 and 6.3.9.3; Equation 6.3.9-3; Table 6.3.9-2.
UZKDTHZT*. Sorption coefficient for thorium in zeolitic tuff units of UZ (mL/g). *Distribution:* Uniform. *Range:* 1000 to 30000. *TSPA-LA Name:* KdTh_Zeo_a*. *Location in TSPA-LA:* Sections 6.3.9.2 and 6.3.9.3; Equation 6.3.9-3; Table 6.3.9-2.
UZKDUDT. Sorption coefficient for uranium in devitrified tuff units of UZ (mL/g). *Distribution:* Piecewise uniform. *Range:* 0 to 4. *Median:* 0.2. *TSPA-LA Name:* KdU_Devit_a. *Location in TSPA-LA:* Sections 6.3.9.2 and 6.3.9.3; Equation 6.3.9-3; Table 6.3.9-2.

Table K3-1. High-Level Summary of Epistemically Uncertain Variables (i.e., elements of **e**) Considered in the TSPA-LA (Sensitivity Analysis Name) (Continued)

NOTE: * indicates variable not considered in sensitivity analysis due to correlations.

UZKDUVT*. Sorption coefficient for uranium in vitrified tuff units of UZ (mL/g). *Distribution:* Piecewise uniform. *Range:* 0 to 3. *Median:* 0.2. *TSPA-LA Name:* KdU_Vit_a*. *Location in TSPA-LA:* Sections 6.3.9.2 and 6.3.9.3; Equation 6.3.9-3; Table 6.3.9-2.
UZKDUZT*. Sorption coefficient for uranium in zeolitic tuff units of UZ (mL/g). *Distribution:* Piecewise uniform. *Range:* 0 to 30. *Median:* 0.5. *TSPA-LA Name:* KdU_Zeo_a*. *Location in TSPA-LA:* Sections 6.3.9.2 and 6.3.9.3; Equation 6.3.9-3; Table 6.3.9-2.
UZRCOL. Colloid retardation factor (dimensionless). *Distribution:* Piecewise uniform. *Range:* 6 to 799.83. *TSPA-LA Name:* Colloidal_Retard_Factor_dist_a. *Location in TSPA-LA:* Sections 6.3.9.2 and 6.3.9.3; Table 6.3.9-12.
UZTORRG1. Logarithm of the tortuosity in rock group 1 (dimensionless). *Distribution:* Left truncated normal. *Range*: 0 to ∞. *Mean:* -1.15. *Standard Deviation:* 0.29. *TSPA-LA Name:* UZ_Tortuosity_RG1. *Location in TSPA-LA:* Section 6.3.9.2; Table 6.3.9-4.
UZTORRG2. Logarithm of the tortuosity in rock group 2 (dimensionless). *Distribution:* Left truncated normal. *Range*: 0 to ∞. *Mean:* -3.62. *Standard Deviation:* 0.29. *TSPA-LA Name:* UZ_Tortuosity_RG2. *Location in TSPA-LA:* Section 6.3.9.2; Table 6.3.9-4.
UZTORRG3. Logarithm of the tortuosity in rock group 3 (dimensionless). *Distribution:* Left truncated normal. *Range*: 0 to ∞. *Mean:* -1.84. *Standard Deviation:* 0.29. *TSPA-LA Name:* UZ_Tortuosity_RG3. *Location in TSPA-LA:* Section 6.3.9.2; Table 6.3.9-4.
WATRCKIN. Parameter used to correlate WRIP_beta so that it resamples at the same probability level throughout a realization (dimensionless). *Distribution:* Uniform. *Range:* 0 to 1. *TSPA-LA Name:* WRIP_beta_rand_a. *Location in TSPA-LA:* Section 6.3.4.2; Table 6.3.4-1.
WDCRCDEN. Ratio of SCC area to unit of seismic damaged area for a waste package (dimensionless). *Distribution:* Uniform. *Range:* 0.00327 to 0.0131. *TSPA-LA Name:* WP_Crack_Area_Density_a. *Location in TSPA-LA:* Table 6.6-2.
WDDEFCNT. Flaw density parameter (flaws per mm^3 of weld) (dimensionless). *Distribution:* Gamma. *Mean:* 4.529E-07. *Standard Deviation:* 1.654E-07. *TSPA-LA Name:* Defect_Count_a. *Location in TSPA-LA:* Section 6.3.5.1.2; Table 6.3.5-3.
WDDEFSZE. Flaw size parameter (flaw size per mm of weld) (dimensionless). *Distribution:* Gamma. *Mean:* 0.2205. *Standard Deviation:* 0.0833. *TSPA-LA Name:* Defect_Size_a. *Location in TSPA-LA:* Section 6.3.5.1.2; Table 6.3.5-3; Equation 6.3.5-10.
WDDSAGGC. Topside general corrosion rate of the drip shield (nm/yr). *Distribution:* Normal. *Mean:* 46.067. *Standard Deviation:* 1.187. *TSPA-LA Name:* WDDSAggrGC_Mean_a. *Location in TSPA-LA:* Sections 6.3.5.1.2 and 6.3.5.1.3; Table 6.3.5-3.
WDDSBEGC. Underside general corrosion rate of the drip shield (mm/yr). *Distribution:* Normal. *Mean:* 5.15E-06. *Standard Deviation:* 8.31E-07. *TSPA-LA Name:* WDDSBenignGC_Mean_a. *Location in TSPA-LA:* Sections 6.3.5.1.2 and 6.3.5.1.3; Table 6.3.5-3.
WDDSGC29. General corrosion rate ratio for drip shield support material (ratio of Titanium Grade 29 to Titanium Grade 7) (dimensionless). *Distribution:* Discrete. *Range:* 1 to 6.6786. *TSPA-LA Name:* WDDSGC_29_a. *Location in TSPA-LA:* Section 6.3.5.1.2.
WDGCA22. Temperature dependent slope term of Alloy 22 general corrosion rate (K). *Distribution:* Truncated normal. *Range:* 666 to 7731. *Mean:* 4905. *Standard Deviation:* 1413. *TSPA-LA Name:* C1_GenCorr_A22_a. *Location in TSPA-LA:* Sections 6.3.5.1.2 and 6.3.5.1.3; Tables 6.3.5-3 and 6.3.5-4; Equation 6.3.5-4.
WDGCUA22. Variable for selecting distribution for general corrosion rate (low, medium, or high) (dimensionless). *Distribution:* Discrete. *Range:* 1 to 3. *TSPA-LA Name:* GC_ULevel_A22_a. *Location in TSPA-LA:* Table 6.3.5-4.
WDLCRATE. Crevice corrosion (localized corrosion) propagation rate (mm/yr). *Distribution:* Log uniform. *Range:* 0.0127 to 1.27. *TSPA-LA Name:* LC_rate_a. *Location in TSPA-LA:* Sections 6.3.5.2.1, 6.3.5.2.2, 6.3.5.2.3, 6.3.5.3.2 and 6.3.5.4; Table 6.3.5-4.
WDMICRHT. Relative humidity threshold for initiating microbially induced corrosion (dimensionless). *Distribution:* Uniform. *Range:* 0.75 to 0.9. *TSPA-LA Name:* MIC_RHThresh_a. *Location in TSPA-LA:* Sections 6.3.5.1.2 and 6.3.5.1.3; Tables 6.3.5-3 and 6.3.5-4.

Table K3-1. High-Level Summary of Epistemically Uncertain Variables (i.e., elements of **e**) Considered in the TSPA-LA (Sensitivity Analysis Name) (Continued)

NOTE: * indicates variable not considered in sensitivity analysis due to correlations.

WDNSCC. Stress corrosion cracking growth rate exponent (repassivation slope) (dimensionless). *Distribution:* Truncated normal. *Range:* 0.935 to 1.395. *Mean:* 1.165. *Standard Deviation:* 0.115. *TSPA-LA Name:* n_SCC_a. *Location in TSPA-LA:* Sections 6.3.5.1.2 and 6.3.5.4; Table 6.3.5-3; Equations 6.3.5-13 and 6.3.5-14.
WDZOLID. Deviation from median yield strength range for outer lid (dimensionless). *Distribution:* Truncated normal. *Range:* -3 to 3. *Mean/Median/Mode:* 0. *Standard Deviation:* 1. *TSPA-LA Name:* z_OL_a. *Location in TSPA-LA:* Sections 6.3.5.1.2 and 6.3.5.1.3; Table 6.3.5-3.
WFDEGEXF. The surface area exposure factor for the amount of HLW glass contacted by water (dimensionless). *Distribution:* Triangular. *Range:* 4 to 17. *Mode:* 4. *TSPA-LA Name:* Exposure_Factor_a. *Location in TSPA-LA:* Sections 6.3.7.4.3.2 and 6.3.7.4.3.3; Equation 6.3.7-9; Table 6.3.7-32.
WPFLUX. Waste package flux splitting factor (dimensionless). *Distribution:* Uniform. *Range:* 0 to 2.41. *TSPA-LA Name:* WP_Flux_Uncertainty_a. *Location in TSPA-LA:* Sections 6.3.6.1, 6.3.6.2 and 6.3.6.3; Tables 6.3.6-1, 6.3.6-2 and 6.3.8-4; Equation 6.3.6-6.

Table K3-2. High-Level Summary of Epistemically Uncertain Variables (i.e., elements of **e**) Considered in the TSPA-LA (TSPA Parameter Name)

NOTE: * indicates variable not considered in sensitivity analysis due to correlations.

Alluvium_Density - Bulk density of alluvium (kg/m^3). *Distribution:* Normal. *Mean/Median/Mode:* 1910. *Standard Deviation:* 78. *Sensitivity Name:* SZDENAL. *Location in TSPA-LA:* Table 6.3.10-2.
Alpha_Uncert_Lith_a - van Genuchten capillary strength parameter in lithophysal rock units (Pa). *Distribution:* Triangular. *Range:* -105 to 105. *Mean/Median/Mode:* 0. *Sensitivity Name:* ALPHAL. *Location in TSPA-LA:* Sections 6.3.3.1.2 and 6.3.3.1.3; Tables 6.3.3-1, 6.3.3-3 and 6.3.5-4.
Alpha_Uncert_NonLith_a* - van Genuchten capillary strength parameter in nonlithophysal rock units (Pa). *Distribution:* Triangular. *Range:* -105 to 105. *Mean/Median/Mode:* 0. *Sensitivity Name:* ALPHANL*. *Location in TSPA-LA:* Section 6.3.3.1.2; Tables 6.3.3-1, 6.3.3-3 and 6.3.5-4.
Am_Eps_1_high_a* - Logarithm of the scale factor used to characterize uncertainty in americium solubility at ionic strength values between 1 and 3 molal (dimensionless). *Distribution:* Truncated normal. *Range:* -2.08 to 2.08. *Mean:* 0. *Standard Deviation:* 1.04. *Sensitivity Name:* EP2HIAM*. *Location in TSPA-LA:* Sections 6.3.7.5.1, 6.3.7.5.2 and 6.3.7.5.3; Equation 6.3.7-13a; Table 6.3.7-41.
Am_Eps_1_low_a - Logarithm of the scale factor used to characterize uncertainty in americium solubility at an ionic strength below 1 molal (dimensionless). *Distribution:* Truncated normal. *Range:* -2 to 2. *Mean:* 0. *Standard Deviation:* 1. *Sensitivity Name:* EP1LOWAM. *Location in TSPA-LA:* Sections 6.3.7.5.1, 6.3.7.5.2 and 6.3.7.5.3; Table 6.3.7-41; Equation 6.3.7-13a.
Am_Eps_2_CDSP_High_a* - Term associated with uncertainty in americium solubility due to variations in fluoride concentration for CDSP waste packages when ionic strength is greater than or equal to 0.004 molal and for the invert below CDSP waste packages (mg/L). *Distribution:* Triangular. *Range:* 0 to 688.6. *Most Likely:* 0. *Sensitivity Name:* EP2HICDAM*. *Location in TSPA-LA:* Sections 6.3.7.5.2 and 6.3.7.5.3; Table 6.3.7-41; Equation 6.3.7-13a.
Am_Eps_2_CSNF_High_a - Term associated with uncertainty in americium solubility due to variations in fluoride concentration for CSNF waste packages when ionic strength is greater than or equal to 0.2 molal and for the invert below CSNF waste packages (mg/L). *Distribution:* Triangular. *Range:* 0 to 109.03. *Most Likely:* 0. *Sensitivity Name:* EP2HICAM. *Location in TSPA-LA:* Sections 6.3.7.5.2 and 6.3.7.5.3; Table 6.3.7-41; Equation 6.3.7-13a.
Am_Eps_2_Glass_Low_a* - Term associated with uncertainty in americium solubility due to variations in fluoride concentration for CDSP waste packages Cell 1a, Cell 1b when ionic strength is less than 0.004 molal, and CSNF waste packages when ionic strength is less than 0.2 molal (mg/L). *Distribution:* Triangular. *Range:* 0 to 4.42. *Most Likely:* 0. *Sensitivity Name:* EP2LOWAM*. *Location in TSPA-LA:* Sections 6.3.7.5.2 and 6.3.7.5.3; Table 6.3.7-41; Equation 6.3.7-13a.
Ash_Density_a - Tephra settled density (kg/m^3). *Distribution:* Truncated normal. *Range:* 300 to 1500. *Mean:* 1000. *Standard Deviation:* 100. *Sensitivity Name:* ASHDENS. *Location in TSPA-LA:* Table 6.5-5.
b_Tillage_a - Depth of soil within which radionuclides contribute to dose from external exposure (m). *Distribution:* Uniform. *Range:* 0.05 to 0.3. *Sensitivity Name:* BTILLAGE. *Location in TSPA-LA:* Table 6.5-5.
Background_Alpha_a - Natural background levels of alpha emitters in groundwater (pCi/L). *Distribution:* Truncated normal. *Range:* 0 to 0.71. *Mean/Median/Mode:* 0.5. *Sensitivity Name:* BCKALPHA. *Location in TSPA-LA:* Sections 6.3.10.2 and 6.3.11.2; Table 6.3.10-6.
Background_Ra226_Ra228_a - Natural background levels of combined ^{226}Ra and ^{228}Ra in groundwater (pCi/L). *Distribution:* Truncated normal. *Range:* 0 to 0.71. *Mean/Median/Mode:* 0.5. *Sensitivity Name:* BCKRA226. *Location in TSPA-LA:* Sections 6.3.10.2 and 6.3.11.2; Table 6.3.10-6.
BDCF_Inh_LT - Pointer variable for long-term inhalation dose conversion factor for volcanic ash exposure (dimensionless). *Distribution:* Discrete. *Range:* 1 to 300. *Sensitivity Name:* INHLTPV. *Location in TSPA-LA:* Section 6.3.11; Equation 6.3.11-4.
BDCF_Inh_ShT - Pointer variable for short-term inhalation dose conversion factor for volcanic ash exposure (dimensionless). *Distribution:* Discrete. *Range:* 1 to 300. *Sensitivity Name:* INHSTPV. *Location in TSPA-LA:* Section 6.3.11; Equation 6.3.11-4.
Beta_Dist_a - Column diffusion constant (dimensionless). *Distribution:* Uniform. *Range:* 0.01 to 0.5. *Sensitivity Name:* BETA. *Location in TSPA-LA:* Table 6.5-4.
C1_GenCorr_A22_a - Temperature dependent slope term of Alloy 22 general corrosion rate (K). *Distribution:* Truncated normal. *Range:* 666 to 7731. *Mean:* 4905. *Standard Deviation:* 1413. *Sensitivity Name:* WDGCA22. *Location in TSPA-LA:* Sections 6.3.5.1.2 and 6.3.5.1.3; Tables 6.3.5-3 and 6.3.5-4; Equation 6.3.5-4.

Table K3-2. High-Level Summary of Epistemically Uncertain Variables (i.e., elements of **e**) Considered in the TSPA-LA (TSPA Parameter Name) (Continued)

NOTE: * indicates variable not considered in sensitivity analysis due to correlations.

Colloidal_Kc_Am_UZP - Colloid sorption coefficient for americium (mg/mg). *Calculated by:* Colloidal_Kd_Am_uz*Colloidal_Concentration_uz. *Sensitivity Name:* UZCOKDAM. *Location in TSPA-LA:* Section 6.3.9.2.
Colloidal_Kc_Cs_UZP - Colloid sorption coefficient for cesium (mg/mg). *Calculated by:* Colloidal_Kd_Cs_uz*Colloidal_Concentration_uz. *Sensitivity Name:* UZCOKDCS. *Location in TSPA-LA:* Section 6.3.9.2.
Colloidal_Kc_Pa_UZP - Colloid sorption coefficient for protactinium (mg/mg). *Calculated by:* Colloidal_Kd_Am_uz*Colloidal_Concentration_uz. *Sensitivity Name:* UZCOKDPA. *Location in TSPA-LA:* Section 6.3.9.2.
Colloidal_Kc_Pu_UZP - Colloid sorption coefficient for plutonium (mg/mg). *Calculated by:* Colloidal_Kd_Pu_uz*Colloidal_Concentration_uz. *Sensitivity Name:* UZCOKDPU. *Location in TSPA-LA:* Section 6.3.9.2.
Colloidal_Kc_Sn_UZP - Colloid sorption coefficient for tin (mg/mg). *Calculated by:* Colloidal_Kd_Sn_uz*Colloidal_Concentration_uz. *Sensitivity Name:* UZCOKDSN. *Location in TSPA-LA:* Section 6.3.9.2.
Colloidal_Kc_Th_UZP - Colloid sorption coefficient for thorium (mg/mg). *Calculated by:* Calculated by Colloidal_Kd_Am_uz*Colloidal_Concentration_uz. *Sensitivity Name:* UZCOKDTH. *Location in TSPA-LA:* Section 6.3.9.2.
Colloidal_Retard_Factor_dist_a - Colloid retardation factor (dimensionless). *Distribution:* Piecewise uniform. *Range:* 6 to 799.83. *Sensitivity Name:* UZRCOL. *Location in TSPA-LA:* Sections 6.3.9.2 and 6.3.9.3; Table 6.3.9-12.
Conc_Col – Logarithm of ambient concentration of colloids in groundwater (g/mL). *Distribution:* Piecewise uniform. *Range:* -9 to -3.6. *Sensitivity Name:* SZCONCOL. *Location in TSPA-LA:* Table 6.3.10-2.
Conc_Col_FeOx_CS_Sampled_a - FeOx colloid concentration when carbon steel is corroding (mg/L). *Distribution:* Truncated log normal. *Range:* 0.3 to 30. *Mean:* 3.69. *Standard Deviation:* 2.79. *Sensitivity Name:* COLFEOCS. *Location in TSPA-LA:* Table 6.3.7-65.
Conc_Col_FeOx_SS_Sampled_a - FeOx colloid concentration when degraded stainless steel is present, but no degrading carbon steel is present (mg/L). *Distribution:* Piecewise uniform. *Range:* 1.00E-03 to 3.00E+01. *Sensitivity Name:* COLFEOSS. *Location in TSPA-LA:* Table 6.3.7-65.
Conc_Col_Gw_Sampled_a - Concentration of groundwater colloids when colloids are stable (mg/L). *Distribution:* Piecewise uniform. *Range:* 0.001 to 200. *Median:* 0.1. *Sensitivity Name:* COLGW. *Location in TSPA-LA:* Table 6.3.7-66.
Conc_Col_U_Sampled_a - Concentration of uranophane colloids when colloids are stable (mg/L). *Distribution:* Piecewise uniform. *Range:* 0.001 to 200. *Median:* 0.1. *Sensitivity Name:* COLU. *Location in TSPA-LA:* Table 6.3.7-64.
CORAL – Logarithm of colloid retardation factor in alluvium (dimensionless). *Distribution:* Piecewise uniform. *Range:* 0.903 to 3.715. *Sensitivity Name:* SZCOLRAL. *Location in TSPA-LA:* Sections 6.3.10.1, 6.3.10.2 and 6.3.10.4.2; Table 6.3.10-2.
CORVO – Logarithm of colloid retardation factor in volcanic units (dimensionless). *Distribution:* Piecewise uniform. *Range:* 0.778 to 2.903. *Sensitivity Name:* SZCOLRVO. *Location in TSPA-LA:* Sections 6.3.10.1, 6.3.10.2 and 6.3.10.4.2; Table 6.3.10-2.
CPu_Col_CSNF_Sampled_a Concentration of irreversibly attached plutonium on CSNF colloids when colloids are stable (mol/L). *Distribution:* Piecewise uniform. *Range:* 1.00E-10 to 5.00E-06. *Median:* 1.00E-07. *Sensitivity Name:* CPUCOLCS. *Location in TSPA-LA:* Section 6.3.7.6.2; Table 6.3.7-63.
CPu_Col_Wf_Embed_Sampled_a - Concentration of irreversibly attached plutonium on glass/waste form colloids when colloids are stable (mol/L). *Distribution:* Uniform. *Range:* 1.00E-11 to 1.00E-08. *Sensitivity Name:* CPUCOLWF. *Location in TSPA-LA:* Section 6.3.7.6.2; Table 6.3.7-62.
CPu_Per_CSNF_Embed_Col_a - Concentration of irreversibly attached plutonium per concentration of CSNF colloids ((mol/L)/(mg/L)). *Distribution:* Uniform. *Range:* 5.00E-07 to 1.00E-06. *Sensitivity Name:* CPUPERCS. *Location in TSPA-LA:* Section 6.3.7.6.2; Table 6.3.7-63.

Table K3-2. High-Level Summary of Epistemically Uncertain Variables (i.e., elements of **e**) Considered in the TSPA-LA (TSPA Parameter Name) (Continued)

NOTE: * indicates variable not considered in sensitivity analysis due to correlations.

CPu_Per_WF_Embed_Col_a - Concentration of irreversibly attached plutonium per concentration of waste form colloids ((mol/L)/(mg/L)). *Distribution:* Triangular. *Range:* 5.00E-09 to 2.5E-08. *Most Likely:* 2.00E-08. *Sensitivity Name:* CPUPERWF. *Location in TSPA-LA:* Section 6.3.7.6.2; Table 6.3.7-62.
Cr2O3_SA_a - Specific surface area of Cr_2O_3 (m^2/g). *Distribution:* Uniform. *Range:* 1 to 20. *Sensitivity Name:* CR2O3SA. *Location in TSPA-LA:* Table 6.3.8-4, S_{CP} in Equation 6.3.8-19.
Critical_Slope_a - Critical gradient for tephra mobilization from hillslopes (dimensionless). *Distribution:* Uniform. *Range:* 0.21 to 0.47. *Sensitivity Name:* CRITSLOP. *Location in TSPA-LA:* Table 6.5-5.
CS_Corrosion_Rate_a - Carbon steel corrosion rate (□m/yr). *Distribution:* Truncated log normal. *Range:* 25 to 135. *Mean:* 78.5. *Standard Deviation:* 25. *Sensitivity Name:* CSCORRAT. *Location in TSPA-LA:* Tables 6.3.8-1 and 6.3.8-4.
CSNF_Mass_Uncert_a - Scale factor used to characterize uncertainty in radionuclide content of CSNF (dimensionless). *Distribution:* Uniform. *Range:* 0.85 to 1.4. *Sensitivity Name:* CSNFMASS. *Location in TSPA-LA:* Sections 6.3.7.1.2 and 6.3.7.1.3; Table 6.3.7-7.
CSNF_Rind_SA_a - Specific surface area of CSNF degradation rind (m^2/g). *Distribution:* Uniform. *Range:* 0.5 to 60. *Sensitivity Name:* CSRINDSA. *Location in TSPA-LA:* Tables 6.3.8-2 and 6.3.8-4.
CSNF_WF_Uncert_a0_Acid_a - Correlated regression coefficient a0 in the abstracted rate model under acidic conditions (dimensionless). *Distribution:* Normal. *Mean/Median/Mode:* 0. *Standard Deviation:* 1. *Sensitivity Name:* CSWFA0AC. *Location in TSPA-LA:* Section 6.3.7.4.1.2; Equation 6.3.7-6.
CSNF_WF_Uncert_a0_Alk_a - Correlated coefficient a0 in the abstracted rate model under alkaline conditions (dimensionless). *Distribution:* Normal. *Mean/Median/Mode:* 0. *Standard Deviation:* 1. *Sensitivity Name:* CSWFA0AK. *Location in TSPA-LA:* Section 6.3.7.4.1.2; Equation 6.3.7-5.
CSNF_WF_Uncert_a1_Alk_a - Correlated coefficient a1 in the abstracted rate model under alkaline conditions (dimensionless). *Distribution:* Normal. *Mean/Median/Mode:* 0. *Standard Deviation:* 1. *Sensitivity Name:* CSWFA1AK. *Location in TSPA-LA:* Section 6.3.7.4.1.2; Equation 6.3.7-5.
CSNF_WF_Uncert_a2_Alk_a - Correlated coefficient a2 in the abstracted rate model under alkaline conditions (dimensionless). *Distribution:* Normal. *Mean/Median/Mode:* 0. *Standard Deviation:* 1. *Sensitivity Name:* CSWFA2AK. *Location in TSPA-LA:* Section 6.3.7.4.1.2; Equation 6.3.7-5.
CSNF_WF_Uncert_a3_Alk_a - Correlated coefficient a3 in the abstracted rate model under alkaline conditions (dimensionless). *Distribution:* Normal. *Mean/Median/Mode:* 0. *Standard Deviation:* 1. *Sensitivity Name:* CSWFA3AK. *Location in TSPA-LA:* Section 6.3.7.4.1.2; Equation 6.3.7-5.
CSNF_WF_Uncert_a4_Acid_a - Correlated coefficient a4 in the abstracted rate model under acid conditions (dimensionless). *Distribution:* Normal. *Mean/Median/Mode:* 0. *Standard Deviation:* 1. *Sensitivity Name:* CSWFA4AC. *Location in TSPA-LA:* Section 6.3.7.4.1.2; Equation 6.3.7-6.
D_Channels_a - Diffusivity of radionuclides in channels of the Fortymile Wash fan (RMEI location) (cm^2/yr). *Distribution:* Uniform. *Range:* 0.035 to 0.266. *Mean:* 0.1505. *Sensitivity Name:* DCHANL. *Location in TSPA-LA:* Table 6.5-5.
D_Divides_a - Diffusivity of radionuclides in divides of the Fortymile Wash fan (RMEI location) (cm^2/yr). *Distribution:* Uniform. *Range:* 0.001 to 0.095. *Mean* 0.048. *Sensitivity Name:* DDIVIDE. *Location in TSPA-LA:* Table 6.5-5.
Dash_mean_a - Mass median ash particle diameter (cm). *Distribution:* Log triangular. *Range:* 0.001 to 0.1. *Mode:* 0.01. *Sensitivity Name:* DASHAVG. *Location in TSPA-LA:* Table 6.5-4.
Dash_sigma_a - Ash particle diameter standard deviation (log (cm)). *Distribution:* Uniform. *Range:* 0.301 to 0.903. *Sensitivity Name:* DASHSIG. *Location in TSPA-LA:* Table 6.5-4.
DCVO – Logarithm of effective diffusion coefficient in fractured volcanic units (m^2/s). *Distribution:* Piecewise uniform. *Range:* -11.3 to -9.3. *Sensitivity Name:* SZDIFCVO. *Location in TSPA-LA:* Sections 6.3.10.2 and 6.3.10.5; Table 6.3.10-2.
DE_BDCF_IER_Ra226_Pb210 - Volcanic Biosphere Dose Conversion Factor (BDCF) component for radon, external exposure and ingestion of ^{226}Ra and ^{210}Pb in modern interglacial climate ((Sv/yr)/(Bq/m^2)). *Distribution:* Discrete. *Range:* 3.07E-08 to 9.43E-08. *Mean:* 3.52E-08. *Standard Deviation:* 3.45E-09. *Sensitivity Name:* INGRA226. *Location in TSPA-LA:* Sections 6.3.11.1 and 6.3.11.2; Equation 6.3.11-4.

Table K3-2. High-Level Summary of Epistemically Uncertain Variables (i.e., elements of **e**) Considered in the TSPA-LA (TSPA Parameter Name) (Continued)

NOTE: * indicates variable not considered in sensitivity analysis due to correlations.

DE_BDCF_ILT_Ra226_Pb210 - Volcanic Biosphere Dose Conversion Factor (BDCF) component for long-term inhalation of ^{226}Ra and ^{210}Pb in modern interglacial climate ((Sv/yr)/(Bq/kg)). *Distribution:* Discrete. *Range:* 1.71E-08 to 5.03E-07. *Mean:* 1.01E-07. *Standard Deviation:* 6.43E-08. *Sensitivity Name:* ILTRA226. *Location in TSPA-LA:* Sections 6.3.11.1 and 6.3.11.2; Equation 6.3.11-4.
DE_BDCF_Ing_Exp_Radon_Ac227 - Volcanic Biosphere Dose Conversion Factor (BDCF) component for radon, external exposure and ingestion of ^{227}Ac in modern interglacial climate ((Sv/yr)/(Bq/m^2)). *Distribution:* Discrete. *Range:* 5.78E-09 to 7.76E-09. *Mean:* 6.16E-09. *Standard Deviation:* 1.8E-10. *Sensitivity Name:* INGAC227. *Location in TSPA-LA:* Sections 6.3.11.1 and 6.3.11.2; Equation 6.3.11-4.
DE_BDCF_Ing_Exp_Radon_Am241 - Volcanic Biosphere Dose Conversion Factor (BDCF) component for radon, external exposure and ingestion of ^{241}Am in modern interglacial climate ((Sv/yr)/(Bq/m^2)). *Distribution:* Discrete. *Range:* 1.86E-10 to 1.00E-09. *Mean:* 2.51E-10. *Standard Deviation:* 7.00E-11. *Sensitivity Name:* INGAM241. *Location in TSPA-LA:* Sections 6.3.11.1 and 6.3.11.2; Equation 6.3.11-4.
DE_BDCF_Ing_Exp_Radon_Am243 - Volcanic Biosphere Dose Conversion Factor (BDCF) component for radon, external exposure and ingestion of ^{243}Am in modern interglacial climate ((Sv/yr)/(Bq/m^2)). *Distribution:* Discrete. *Range:* 2.51E-09 to 3.42E-09. *Mean:* 2.67E-09. *Standard Deviation:* 8.02E-11. *Sensitivity Name:* INGAM243. *Location in TSPA-LA:* Sections 6.3.11.1 and 6.3.11.2; Equation 6.3.11-4.
DE_BDCF_Ing_Exp_Radon_Cs137 - Volcanic Biosphere Dose Conversion Factor (BDCF) component for radon, external exposure and ingestion of ^{137}Cs in modern interglacial climate ((Sv/yr)/(Bq/m^2)). *Distribution:* Discrete. *Range:* 6.75E-09 to 8.48E-09. *Mean:* 7.17E-09. *Standard Deviation:* 1.55E-10. *Sensitivity Name:* INGCS137. *Location in TSPA-LA:* Sections 6.3.11.1 and 6.3.11.2; Equation 6.3.11-4.
DE_BDCF_Ing_Exp_Radon_I129 - Volcanic Biosphere Dose Conversion Factor (BDCF) component for radon, external exposure and ingestion of ^{129}I in modern interglacial climate ((Sv/yr)/(Bq/m^2)). *Distribution:* Discrete. *Range:* 1.39E-10 to 2.86E-08. *Mean:* 1.26E-09. *Standard Deviation:* 2.59E-09. *Sensitivity Name:* INGI129. *Location in TSPA-LA:* Sections 6.3.11.1 and 6.3.11.2; Equation 6.3.11-4.
DE_BDCF_Ing_Exp_Radon_Np237 - Volcanic Biosphere Dose Conversion Factor (BDCF) component for radon, external exposure and ingestion of ^{237}Np in modern interglacial climate ((Sv/yr)/(Bq/m^2)). *Distribution:* Discrete. *Range:* 2.62E-09 to 1.2E-08. *Mean:* 2.98E-09. *Standard Deviation:* 6.36E-10. *Sensitivity Name:* INGNP237. *Location in TSPA-LA:* Sections 6.3.11.1 and 6.3.11.2; Equation 6.3.11-4.
DE_BDCF_Ing_Exp_Radon_Pa231 - Volcanic Biosphere Dose Conversion Factor (BDCF) component for radon, external exposure and ingestion of ^{231}Pa in modern interglacial climate ((Sv/yr)/(Bq/m^2)). *Distribution:* Discrete. *Range:* 5.02E-10 to 4.56E-09. *Mean:* 7.14E-10. *Standard Deviation:* 2.92E-10. *Sensitivity Name:* INGPA231. *Location in TSPA-LA:* Sections 6.3.11.1 and 6.3.11.2; Equation 6.3.11-4.
DE_BDCF_Ing_Exp_Radon_Pu238 - Volcanic Biosphere Dose Conversion Factor (BDCF) component for radon, external exposure and ingestion of ^{238}Pu in modern interglacial climate ((Sv/yr)/(Bq/m^2)). *Distribution:* Discrete. *Range:* 1.33E-11 to 9.18E-10. *Mean:* 7.78E-11. *Standard Deviation:* 7.72E-11. *Sensitivity Name:* INGPU238. *Location in TSPA-LA:* Sections 6.3.11.1 and 6.3.11.2; Equation 6.3.11-4.
DE_BDCF_Ing_Exp_Radon_Pu239 - Volcanic Biosphere Dose Conversion Factor (BDCF) component for radon, external exposure and ingestion of ^{239}Pu in modern interglacial climate ((Sv/yr)/(Bq/m^2)). *Distribution:* Discrete. *Range:* 1.40E-11 to 1.01E-09. *Mean:* 8.49E-11. *Standard Deviation:* 8.5E-11. *Sensitivity Name:* INGPU239. *Location in TSPA-LA:* Sections 6.3.11.1 and 6.3.11.2; Equation 6.3.11-4.
DE_BDCF_Ing_Exp_Radon_Pu240 - Volcanic Biosphere Dose Conversion Factor (BDCF) component for radon, external exposure and ingestion of ^{240}Pu in modern interglacial climate ((Sv/yr)/(Bq/m^2)). *Distribution:* Discrete. *Range:* 1.42E-11 to 1.01E-09. *Mean:* 8.52E-11. *Standard Deviation:* 8.5E-11. *Sensitivity Name:* INGPU240. *Location in TSPA-LA:* Sections 6.3.11.1 and 6.3.11.2; Equation 6.3.11-4.
DE_BDCF_Ing_Exp_Radon_Pu242 - Volcanic Biosphere Dose Conversion Factor (BDCF) component for radon, external exposure and ingestion of ^{242}Pu in modern interglacial climate ((Sv/yr)/(Bq/m^2)). *Distribution:* Discrete. *Range:* 1.31E-11 to 9.57E-10. *Mean:* 8.04E-11. *Standard Deviation:* 8.06E-11. *Sensitivity Name:* INGPU242. *Location in TSPA-LA:* Sections 6.3.11.1 and 6.3.11.2; Equation 6.3.11-4.
DE_BDCF_Ing_Exp_Radon_Ra228 - Volcanic Biosphere Dose Conversion Factor (BDCF) component for radon, external exposure and ingestion of ^{228}Ra in modern interglacial climate ((Sv/yr)/(Bq/m^2)). *Distribution:* Discrete. *Range:* 1.17E-08 to 2.62E-08. *Mean:* 1.27E-08. *Standard Deviation:* 7.44E-10. *Sensitivity Name:* INGRA228. *Location in TSPA-LA:* Sections 6.3.11.1 and 6.3.11.2; Equation 6.3.11-4.

Table K3-2. High-Level Summary of Epistemically Uncertain Variables (i.e., elements of **e**) Considered in the TSPA-LA (TSPA Parameter Name) (Continued)

NOTE: * indicates variable not considered in sensitivity analysis due to correlations.

DE_BDCF_Ing_Exp_Radon_Sn126 - Volcanic Biosphere Dose Conversion Factor (BDCF) component for radon, external exposure and ingestion of ^{126}Sn in modern interglacial climate ((Sv/yr)/(Bq/m^2)). *Distribution:* Discrete. *Range:* 2.38E-08 to 2.79E-08. *Mean:* 2.54E-08. *Standard Deviation:* 4.41E-10. *Sensitivity Name:* INGSN126. *Location in TSPA-LA:* Sections 6.3.11.1 and 6.3.11.2; Equation 6.3.11-4.
DE_BDCF_Ing_Exp_Radon_Sr90 - Volcanic Biosphere Dose Conversion Factor (BDCF) component for radon, external exposure and ingestion of ^{90}Sr in modern interglacial climate ((Sv/yr)/(Bq/m^2)). *Distribution:* Discrete. *Range:* 1.44E-09 to 6.10E-09. *Mean:* 1.81E-09. *Standard Deviation:* 3.67E-10. *Sensitivity Name:* INGSR90. *Location in TSPA-LA:* Sections 6.3.11.1 and 6.3.11.2; Equation 6.3.11-4.
DE_BDCF_Ing_Exp_Radon_Tc99 - Volcanic Biosphere Dose Conversion Factor (BDCF) component for radon, external exposure and ingestion of ^{99}Tc in modern interglacial climate ((Sv/yr)/(Bq/m^2)). *Distribution:* Discrete. *Range:* 5.08E-12 to 8.95E-09. *Mean:* 2.72E-10. *Standard Deviation:* 5.16E-10. *Sensitivity Name:* INGTC99. *Location in TSPA-LA:* Sections 6.3.11.1 and 6.3.11.2; Equation 6.3.11-4.
DE_BDCF_Ing_Exp_Radon_Th229 - Volcanic Biosphere Dose Conversion Factor (BDCF) component for radon, external exposure and ingestion of ^{229}Th in modern interglacial climate ((Sv/yr)/(Bq/m^2)). *Distribution:* Discrete. *Range:* 4.33E-09 to 7.02E-09. *Mean:* 4.69E-09. *Standard Deviation:* 2.4E-10. *Sensitivity Name:* INGTH229. *Location in TSPA-LA:* Sections 6.3.11.1 and 6.3.11.2; Equation 6.3.11-4.
DE_BDCF_Ing_Exp_Radon_Th230 - Volcanic Biosphere Dose Conversion Factor (BDCF) component for radon, external exposure and ingestion of ^{230}Th in modern interglacial climate ((Sv/yr)/(Bq/m^2)). *Distribution:* Discrete. *Range:* 1.92E-11 to 8.68E-10. *Mean:* 8.51E-11. *Standard Deviation:* 7.82E-11. *Sensitivity Name:* INGTH230. *Location in TSPA-LA:* Sections 6.3.11.1 and 6.3.11.2; Equation 6.3.11-4.
DE_BDCF_Ing_Exp_Radon_Th232 - Volcanic Biosphere Dose Conversion Factor (BDCF) component for radon, external exposure and ingestion of ^{232}Th in modern interglacial climate ((Sv/yr)/(Bq/m^2)). *Distribution:* Discrete. *Range:* 1.72E-11 to 9.34E-10. *Mean:* 8.83E-11. *Standard Deviation:* 8.44E-11. *Sensitivity Name:* INGTH232. *Location in TSPA-LA:* Sections 6.3.11.1 and 6.3.11.2; Equation 6.3.11-4.
DE_BDCF_Ing_Exp_Radon_U233 - Volcanic Biosphere Dose Conversion Factor (BDCF) component for radon, external exposure and ingestion of ^{233}U in modern interglacial climate ((Sv/yr)/(Bq/m^2)). *Distribution:* Discrete. *Range:* 1.31E-11 to 9.04E-10. *Mean:* 6.48E-11. *Standard Deviation:* 6.12E-11. *Sensitivity Name:* INGU233. *Location in TSPA-LA:* Sections 6.3.11.1 and 6.3.11.2; Equation 6.3.11-4.
DE_BDCF_Ing_Exp_Radon_U234 - Volcanic Biosphere Dose Conversion Factor (BDCF) component for radon, external exposure and ingestion of ^{234}U in modern interglacial climate ((Sv/yr)/(Bq/m^2)). *Distribution:* Discrete. *Range:* 9.60E-12 to 8.7E-10. *Mean:* 5.96E-11. *Standard Deviation:* 5.9E-11. *Sensitivity Name:* INGU234. *Location in TSPA-LA:* Sections 6.3.11.1 and 6.3.11.2; Equation 6.3.11-4.
DE_BDCF_Ing_Exp_Radon_U238 - Volcanic Biosphere Dose Conversion Factor (BDCF) component for radon, external exposure and ingestion of ^{238}U in modern interglacial climate ((Sv/yr)/(Bq/m^2)). *Distribution:* Discrete. *Range:* 1.52E-09 to 2.41E-09. *Mean:* 1.62E-09. *Standard Deviation:* 6.16E-11. *Sensitivity Name:* INGU238. *Location in TSPA-LA:* Sections 6.3.11.1 and 6.3.11.2; Equation 6.3.11-4.
DE_BDCF_Inh_LT_Ac227 - Volcanic Biosphere Dose Conversion Factor (BDCF) component for long-term inhalation of ^{227}Ac in modern interglacial climate ((Sv/yr)/(Bq/kg)). *Distribution:* Discrete. *Range:* 1.53E-07 to 4.5E-06. *Mean:* 9.0E-07. *Standard Deviation:* 5.75E-07. *Sensitivity Name:* ILTAC227. *Location in TSPA-LA:* Sections 6.3.11.1 and 6.3.11.2; Equation 6.3.11-4.
DE_BDCF_Inh_LT_Am241 - Volcanic Biosphere Dose Conversion Factor (BDCF) component for long-term inhalation of ^{241}Am in modern interglacial climate ((Sv/yr)/(Bq/kg)). *Distribution:* Discrete. *Range:* 8.45E-08 to 2.48E-06. *Mean:* 4.96E-07. *Standard Deviation:* 3.17E-07. *Sensitivity Name:* ILTAM241. *Location in TSPA-LA:* Sections 6.3.11.1 and 6.3.11.2; Equation 6.3.11-4.
DE_BDCF_Inh_LT_Am243 - Volcanic Biosphere Dose Conversion Factor (BDCF) component for long-term inhalation of ^{243}Am in modern interglacial climate ((Sv/yr)/(Bq/kg)). *Distribution:* Discrete. *Range:* 8.38E-08 to 2.46E-06. *Mean:* 4.93E-07. *Standard Deviation:* 3.15E-07. *Sensitivity Name:* ILTAM243. *Location in TSPA-LA:* Sections 6.3.11.1 and 6.3.11.2; Equation 6.3.11-4.
DE_BDCF_Inh_LT_Cs137 - Volcanic Biosphere Dose Conversion Factor (BDCF) component for long-term inhalation of ^{137}Cs in modern interglacial climate ((Sv/yr)/(Bq/kg)). *Distribution:* Discrete. *Range:* 3.43E-11 to 1.01E-09. *Mean:* 2.02E-10. *Standard Deviation:* 1.29E-10. *Sensitivity Name:* ILTCS137. *Location in TSPA-LA:* Sections 6.3.11.1 and 6.3.11.2; Equation 6.3.11-4.

Table K3-2. High-Level Summary of Epistemically Uncertain Variables (i.e., elements of **e**) Considered in the TSPA-LA (TSPA Parameter Name) (Continued)

NOTE: * indicates variable not considered in sensitivity analysis due to correlations.

DE_BDCF_Inh_LT_I129 - Volcanic Biosphere Dose Conversion Factor (BDCF) component for long-term inhalation of ^{129}I in modern interglacial climate ((Sv/yr)/(Bq/kg)). *Distribution:* Discrete. *Range:* 3.15E-11 to 9.23E-10. *Mean:* 1.85E-10. *Standard Deviation:* 1.18E-10. *Sensitivity Name:* ILTI129. *Location in TSPA-LA:* Sections 6.3.11.1 and 6.3.11.2; Equation 6.3.11-4.
DE_BDCF_Inh_LT_Np237 - Volcanic Biosphere Dose Conversion Factor (BDCF) component for long-term inhalation of ^{237}Np in modern interglacial climate ((Sv/yr)/(Bq/kg)). *Distribution:* Discrete. *Range:* 4.35E-08 to 1.28E-06. *Mean:* 2.56E-07. *Standard Deviation:* 1.63E-07. *Sensitivity Name:* ILTNP237. *Location in TSPA-LA:* Sections 6.3.11.1 and 6.3.11.2; Equation 6.3.11-4.
DE_BDCF_Inh_LT_Pa231 - Volcanic Biosphere Dose Conversion Factor (BDCF) component for long-term inhalation of ^{231}Pa in modern interglacial climate ((Sv/yr)/(Bq/kg)). *Distribution:* Discrete. *Range:* 2.02E-07 to 5.92E-06. *Mean:* 1.18E-06. *Standard Deviation:* 7.56E-07. *Sensitivity Name:* ILTPA231. *Location in TSPA-LA:* Sections 6.3.11.1 and 6.3.11.2; Equation 6.3.11-4.
DE_BDCF_Inh_LT_Pu238 - Volcanic Biosphere Dose Conversion Factor (BDCF) component for long-term inhalation of ^{238}Pu in modern interglacial climate ((Sv/yr)/(Bq/kg)). *Distribution:* Discrete. *Range:* 9.46E-08 to 2.78E-06. *Mean:* 5.56E-07. *Standard Deviation:* 3.55E-07. *Sensitivity Name:* ILTPU238. *Location in TSPA-LA:* Sections 6.3.11.1 and 6.3.11.2; Equation 6.3.11-4.
DE_BDCF_Inh_LT_Pu239 - Volcanic Biosphere Dose Conversion Factor (BDCF) component for long-term inhalation of ^{239}Pu in modern interglacial climate ((Sv/yr)/(Bq/kg)). *Distribution:* Discrete. *Range:* 1.04E-07 to 3.06E-06. *Mean:* 6.12E-07. *Standard Deviation:* 3.91E-07. *Sensitivity Name:* ILTPU239. *Location in TSPA-LA:* Sections 6.3.11.1 and 6.3.11.2; Equation 6.3.11-4.
DE_BDCF_Inh_LT_Pu240 - Volcanic Biosphere Dose Conversion Factor (BDCF) component for long-term inhalation of ^{240}Pu in modern interglacial climate ((Sv/yr)/(Bq/kg)). *Distribution:* Discrete. *Range:* 1.04E-07 to 3.06E-06. *Mean:* 6.12E-07. *Standard Deviation:* 3.91E-07. *Sensitivity Name:* ILTPU240. *Location in TSPA-LA:* Sections 6.3.11.1 and 6.3.11.2; Equation 6.3.11-4.
DE_BDCF_Inh_LT_Pu242 - Volcanic Biosphere Dose Conversion Factor (BDCF) component for long-term inhalation of ^{242}Pu in modern interglacial climate ((Sv/yr)/(Bq/kg)). *Distribution:* Discrete. *Range:* 9.90E-08 to 2.91E-06. *Mean:* 5.82E-07. *Standard Deviation:* 3.72E-07. *Sensitivity Name:* ILTPU242. *Location in TSPA-LA:* Sections 6.3.11.1 and 6.3.11.2; Equation 6.3.11-4.
DE_BDCF_Inh_LT_Ra228 - Volcanic Biosphere Dose Conversion Factor (BDCF) component for long-term inhalation of ^{228}Ra in modern interglacial climate ((Sv/yr)/(Bq/kg)). *Distribution:* Discrete. *Range:* 1.40E-08 to 4.12E-07. *Mean:* 8.24E-08. *Standard Deviation:* 5.27E-08. *Sensitivity Name:* ILTRA228. *Location in TSPA-LA:* Sections 6.3.11.1 and 6.3.11.2; Equation 6.3.11-4.
DE_BDCF_Inh_LT_Sn126 - Volcanic Biosphere Dose Conversion Factor (BDCF) component for long-term inhalation of ^{126}Sn in modern interglacial climate ((Sv/yr)/(Bq/kg)). *Distribution:* Discrete. *Range:* 1.36E-10 to 4.00E-09. *Mean:* 8.0E-10. *Standard Deviation:* 5.11E-10. *Sensitivity Name:* ILTSN126. *Location in TSPA-LA:* Sections 6.3.11.1 and 6.3.11.2; Equation 6.3.11-4.
DE_BDCF_Inh_LT_Sr90 - Volcanic Biosphere Dose Conversion Factor (BDCF) component for long-term inhalation of ^{90}Sr in modern interglacial climate ((Sv/yr)/(Bq/kg)). *Distribution:* Discrete. *Range:* 1.39E-10 to 4.08E-09. *Mean:* 8.16E-10. *Standard Deviation:* 5.21E-10. *Sensitivity Name:* ILTSR90. *Location in TSPA-LA:* Sections 6.3.11.1 and 6.3.11.2; Equation 6.3.11-4.
DE_BDCF_Inh_LT_Tc99 - Volcanic Biosphere Dose Conversion Factor (BDCF) component for long-term inhalation of ^{99}Tc in modern interglacial climate ((Sv/yr)/(Bq/kg)). *Distribution:* Discrete. *Range:* 1.17E-11 to 3.42E-10. *Mean:* 6.84E-11. *Standard Deviation:* 4.37E-11. *Sensitivity Name:* ILTTC99. *Location in TSPA-LA:* Sections 6.3.11.1 and 6.3.11.2; Equation 6.3.11-4.
DE_BDCF_Inh_LT_Th229 - Volcanic Biosphere Dose Conversion Factor (BDCF) component for long-term inhalation of ^{229}Th in modern interglacial climate ((Sv/yr)/(Bq/kg)). *Distribution:* Discrete. *Range:* 2.24E-07 to 6.57E-06. *Mean:* 1.31E-06. *Standard Deviation:* 8.39E-07. *Sensitivity Name:* ILTTH229. *Location in TSPA-LA:* Sections 6.3.11.1 and 6.3.11.2; Equation 6.3.11-4.
DE_BDCF_Inh_LT_Th230 - Volcanic Biosphere Dose Conversion Factor (BDCF) component for long-term inhalation of ^{230}Th in modern interglacial climate ((Sv/yr)/(Bq/kg)). *Distribution:* Discrete. *Range:* 8.94E-08 to 2.62E-06. *Mean:* 5.25E-07. *Standard Deviation:* 3.35E-07. *Sensitivity Name:* ILTTH230. *Location in TSPA-LA:* Sections 6.3.11.1 and 6.3.11.2; Equation 6.3.11-4.

Table K3-2. High-Level Summary of Epistemically Uncertain Variables (i.e., elements of **e**) Considered in the TSPA-LA (TSPA Parameter Name) (Continued)

NOTE: * indicates variable not considered in sensitivity analysis due to correlations.

DE_BDCF_Inh_LT_Th232 - Volcanic Biosphere Dose Conversion Factor (BDCF) component for long-term inhalation of ^{232}Th in modern interglacial climate ((Sv/yr)/(Bq/kg)). *Distribution:* Discrete. *Range:* 9.64E-08 to 2.83E-06. *Mean:* 5.66E-07. *Standard Deviation:* 3.62E-07. *Sensitivity Name:* ILTTH232. *Location in TSPA-LA:* Sections 6.3.11.1 and 6.3.11.2; Equation 6.3.11-4.
DE_BDCF_Inh_LT_U233 - Volcanic Biosphere Dose Conversion Factor (BDCF) component for long-term inhalation of ^{233}U in modern interglacial climate ((Sv/yr)/(Bq/kg)). *Distribution:* Discrete. *Range:* 8.40E-09 to 2.47E-07. *Mean:* 4.94E-08. *Standard Deviation:* 3.15E-08. *Sensitivity Name:* ILTU233. *Location in TSPA-LA:* Sections 6.3.11.1 and 6.3.11.2; Equation 6.3.11-4.
DE_BDCF_Inh_LT_U234 - Volcanic Biosphere Dose Conversion Factor (BDCF) component for long-term inhalation of ^{234}U in modern interglacial climate ((Sv/yr)/(Bq/kg)). *Distribution:* Discrete. *Range:* 8.23E-09 to 2.42E-07. *Mean:* 4.84E-08. *Standard Deviation:* 3.09E-08. *Sensitivity Name:* ILTU234. *Location in TSPA-LA:* Sections 6.3.11.1 and 6.3.11.2; Equation 6.3.11-4.
DE_BDCF_Inh_LT_U238 - Volcanic Biosphere Dose Conversion Factor (BDCF) component for long-term inhalation of ^{238}U in modern interglacial climate ((Sv/yr)/(Bq/kg)). *Distribution:* Discrete. *Range:* 7.05E-09 to 2.07E-07. *Mean:* 4.14E-08. *Standard Deviation:* 2.65E-08. *Sensitivity Name:* ILTU238. *Location in TSPA-LA:* Sections 6.3.11.1 and 6.3.11.2; Equation 6.3.11-4.
DE_BDCF_Inh_ShT_Ac227 - Volcanic Biosphere Dose Conversion Factor (BDCF) component for short-term inhalation of ^{227}Ac in modern interglacial climate ((Sv/yr)/(Bq/kg)). *Distribution:* Discrete. *Range:* 8.47E-08 to 2.14E-06. *Mean:* 5.85E-07. *Standard Deviation:* 3.32E-07. *Sensitivity Name:* ISTAC227. *Location in TSPA-LA:* Sections 6.3.11.1 and 6.3.11.2; Equation 6.3.11-4.
DE_BDCF_Inh_ShT_Am241 - Volcanic Biosphere Dose Conversion Factor (BDCF) component for short-term inhalation of ^{241}Am in modern interglacial climate ((Sv/yr)/(Bq/kg)). *Distribution:* Discrete. *Range:* 4.67E-08 to 1.18E-06. *Mean:* 3.23E-07. *Standard Deviation:* 1.83E-07. *Sensitivity Name:* ISTAM241. *Location in TSPA-LA:* Sections 6.3.11.1 and 6.3.11.2; Equation 6.3.11-4.
DE_BDCF_Inh_ShT_Am243 - Volcanic Biosphere Dose Conversion Factor (BDCF) component for short-term inhalation of ^{243}Am in modern interglacial climate ((Sv/yr)/(Bq/kg)). *Distribution:* Discrete. *Range:* 4.64E-08 to 1.17E-06. *Mean:* 3.2E-07. *Standard Deviation:* 1.82E-07. *Sensitivity Name:* ISTAM243. *Location in TSPA-LA:* Sections 6.3.11.1 and 6.3.11.2; Equation 6.3.11-4.
DE_BDCF_Inh_ShT_Cs137 - Volcanic Biosphere Dose Conversion Factor (BDCF) component for short-term inhalation of ^{137}Cs in modern interglacial climate ((Sv/yr)/(Bq/kg)). *Distribution:* Discrete. *Range:* 1.90E-11 to 4.80E-10. *Mean:* 1.31E-10. *Standard Deviation:* 7.44E-11. *Sensitivity Name:* ISTCS137. *Location in TSPA-LA:* Sections 6.3.11.1 and 6.3.11.2; Equation 6.3.11-4.
DE_BDCF_Inh_ShT_I129 - Volcanic Biosphere Dose Conversion Factor (BDCF) component for short-term inhalation of ^{129}I in modern interglacial climate ((Sv/yr)/(Bq/kg)). *Distribution:* Discrete. *Range:* 1.74E-11 to 4.40E-10. *Mean:* 1.2E-10. *Standard Deviation:* 6.81E-11. *Sensitivity Name:* ISTI129. *Location in TSPA-LA:* Sections 6.3.11.1 and 6.3.11.2; Equation 6.3.11-4.
DE_BDCF_Inh_ShT_Np237 - Volcanic Biosphere Dose Conversion Factor (BDCF) component for short-term inhalation of ^{237}Np in modern interglacial climate ((Sv/yr)/(Bq/kg)). *Distribution:* Discrete. *Range:* 2.41E-08 to 6.08E-07. *Mean:* 1.66E-07. *Standard Deviation:* 9.43E-08. *Sensitivity Name:* ISTNP237. *Location in TSPA-LA:* Sections 6.3.11.1 and 6.3.11.2; Equation 6.3.11-4.
DE_BDCF_Inh_ShT_Pa231 - Volcanic Biosphere Dose Conversion Factor (BDCF) component for short-term inhalation of ^{231}Pa in modern interglacial climate ((Sv/yr)/(Bq/kg)). *Distribution:* Discrete. *Range:* 1.11E-07 to 2.82E-06. *Mean:* 7.7E-07. *Standard Deviation:* 4.37E-07. *Sensitivity Name:* ISTPA231. *Location in TSPA-LA:* Sections 6.3.11.1 and 6.3.11.2; Equation 6.3.11-4.
DE_BDCF_Inh_ShT_Pu238 - Volcanic Biosphere Dose Conversion Factor (BDCF) component for short-term inhalation of ^{238}Pu in modern interglacial climate ((Sv/yr)/(Bq/kg)). *Distribution:* Discrete. *Range:* 5.23E-08 to 1.32E-06. *Mean:* 3.61E-07. *Standard Deviation:* 2.05E-07. *Sensitivity Name:* ISTPU238. *Location in TSPA-LA:* Sections 6.3.11.1 and 6.3.11.2; Equation 6.3.11-4.
DE_BDCF_Inh_ShT_Pu239 - Volcanic Biosphere Dose Conversion Factor (BDCF) component for short-term inhalation of ^{239}Pu in modern interglacial climate ((Sv/yr)/(Bq/kg)). *Distribution:* Discrete. *Range:* 5.76E-08 to 1.46E-06. *Mean:* 3.98E-07. *Standard Deviation:* 2.26E-07. *Sensitivity Name:* ISTPU239. *Location in TSPA-LA:* Sections 6.3.11.1 and 6.3.11.2; Equation 6.3.11-4.

Table K3-2. High-Level Summary of Epistemically Uncertain Variables (i.e., elements of **e**) Considered in the TSPA-LA (TSPA Parameter Name) (Continued)

NOTE: * indicates variable not considered in sensitivity analysis due to correlations.

DE_BDCF_Inh_ShT_Pu240 - Volcanic Biosphere Dose Conversion Factor (BDCF) component for short-term inhalation of ^{240}Pu in modern interglacial climate ((Sv/yr)/(Bq/kg)). *Distribution:* Discrete. *Range:* 5.76E-08 to 1.46E-06. *Mean:* 3.98E-07. *Standard Deviation:* 2.26E-07. *Sensitivity Name:* ISTPU240. *Location in TSPA-LA:* Sections 6.3.11.1 and 6.3.11.2; Equation 6.3.11-4.
DE_BDCF_Inh_ShT_Pu242 - Volcanic Biosphere Dose Conversion Factor (BDCF) component for short-term inhalation of ^{242}Pu in modern interglacial climate ((Sv/yr)/(Bq/kg)). *Distribution:* Discrete. *Range:* 5.47E-08 to 1.38E-06. *Mean:* 3.78E-07. *Standard Deviation:* 2.14E-07. *Sensitivity Name:* ISTPU242. *Location in TSPA-LA:* Sections 6.3.11.1 and 6.3.11.2; Equation 6.3.11-4.
DE_BDCF_Inh_ShT_Ra228 - Volcanic Biosphere Dose Conversion Factor (BDCF) component for short-term inhalation of ^{228}Ra in modern interglacial climate ((Sv/yr)/(Bq/kg)). *Distribution:* Discrete. *Range:* 7.76E-09 to 1.96E-07. *Mean:* 5.36E-08. *Standard Deviation:* 3.04E-08. *Sensitivity Name:* ISTRA228. *Location in TSPA-LA:* Sections 6.3.11.1 and 6.3.11.2; Equation 6.3.11-4.
DE_BDCF_Inh_ShT_Sn126 - Volcanic Biosphere Dose Conversion Factor (BDCF) component for short-term inhalation of ^{126}Sn in modern interglacial climate ((Sv/yr)/(Bq/kg)). *Distribution:* Discrete. *Range:* 7.53E-11 to 1.90E-09. *Mean:* 5.2E-10. *Standard Deviation:* 2.95E-10. *Sensitivity Name:* ISTSN126. *Location in TSPA-LA:* Sections 6.3.11.1 and 6.3.11.2; Equation 6.3.11-4.
DE_BDCF_Inh_ShT_Sr90 - Volcanic Biosphere Dose Conversion Factor (BDCF) component for short-term inhalation of ^{90}Sr in modern interglacial climate ((Sv/yr)/(Bq/kg)). *Distribution:* Discrete. *Range:* 7.68E-11 to 1.94E-09. *Mean:* 5.3E-10. *Standard Deviation:* 3.01E-10. *Sensitivity Name:* ISTSR90. *Location in TSPA-LA:* Sections 6.3.11.1 and 6.3.11.2; Equation 6.3.11-4.
DE_BDCF_Inh_ShT_Tc99 - Volcanic Biosphere Dose Conversion Factor (BDCF) component for short-term inhalation of ^{99}Tc in modern interglacial climate ((Sv/yr)/(Bq/kg)). *Distribution:* Discrete. *Range:* 6.44E-12 to 1.63E-10. *Mean:* 4.45E-11. *Standard Deviation:* 2.52E-11. *Sensitivity Name:* ISTTC99. *Location in TSPA-LA:* Sections 6.3.11.1 and 6.3.11.2; Equation 6.3.11-4.
DE_BDCF_Inh_ShT_Th229 - Volcanic Biosphere Dose Conversion Factor (BDCF) component for short-term inhalation of ^{229}Th in modern interglacial climate ((Sv/yr)/(Bq/kg)). *Distribution:* Discrete. *Range:* 1.24E-07 to 3.13E-06. *Mean:* 8.54E-07. *Standard Deviation:* 4.84E-07. *Sensitivity Name:* ISTTH229. *Location in TSPA-LA:* Sections 6.3.11.1 and 6.3.11.2; Equation 6.3.11-4.
DE_BDCF_Inh_ShT_Th230 - Volcanic Biosphere Dose Conversion Factor (BDCF) component for short-term inhalation of ^{230}Th in modern interglacial climate ((Sv/yr)/(Bq/kg)). *Distribution:* Discrete. *Range:* 4.94E-08 to 1.25E-06. *Mean:* 3.41E-07. *Standard Deviation:* 1.94E-07. *Sensitivity Name:* ISTTH230. *Location in TSPA-LA:* Sections 6.3.11.1 and 6.3.11.2; Equation 6.3.11-4.
DE_BDCF_Inh_ShT_Th232 - Volcanic Biosphere Dose Conversion Factor (BDCF) component for short-term inhalation of ^{232}Th in modern interglacial climate ((Sv/yr)/(Bq/kg)). *Distribution:* Discrete. *Range:* 5.33E-08 to 1.35E-06. *Mean:* 3.68E-07. *Standard Deviation:* 2.09E-07. *Sensitivity Name:* ISTTH232. *Location in TSPA-LA:* Sections 6.3.11.1 and 6.3.11.2; Equation 6.3.11-4.
DE_BDCF_Inh_ShT_U233 - Volcanic Biosphere Dose Conversion Factor (BDCF) component for short-term inhalation of ^{233}U in modern interglacial climate ((Sv/yr)/(Bq/kg)). *Distribution:* Discrete. *Range:* 4.65E-09 to 1.17E-07. *Mean:* 3.21E-08. *Standard Deviation:* 1.82E-08. *Sensitivity Name:* ISTU233. *Location in TSPA-LA:* Sections 6.3.11.1 and 6.3.11.2; Equation 6.3.11-4.
DE_BDCF_Inh_ShT_U234 - Volcanic Biosphere Dose Conversion Factor (BDCF) component for short-term inhalation of ^{234}U in modern interglacial climate ((Sv/yr)/(Bq/kg)). *Distribution:* Discrete. *Range:* 4.55E-09 to 1.15E-07. *Mean:* 3.15E-08. *Standard Deviation:* 1.78E-08. *Sensitivity Name:* ISTU234. *Location in TSPA-LA:* Sections 6.3.11.1 and 6.3.11.2; Equation 6.3.11-4.
DE_BDCF_Inh_ShT_U238 - Volcanic Biosphere Dose Conversion Factor (BDCF) component for short-term inhalation of ^{238}U in modern interglacial climate ((Sv/yr)/(Bq/kg)). *Distribution:* Discrete. *Range:* 3.90E-09 to 9.85E-08. *Mean:* 2.69E-08. *Standard Deviation:* 1.53E-08. *Sensitivity Name:* ISTU238. *Location in TSPA-LA:* Sections 6.3.11.1 and 6.3.11.2; Equation 6.3.11-4.
DE_BDCF_IST_Ra226_Pb210 - Volcanic Biosphere Dose Conversion Factor (BDCF) component for short-term inhalation of ^{226}Ra and ^{210}Pb in modern interglacial climate ((Sv/yr)/(Bq/kg)). *Distribution:* Discrete. *Range:* 9.47E-09 to 2.39E-07. *Mean:* 6.54E-08. *Standard Deviation:* 3.71E-08. *Sensitivity Name:* ISTRA226. *Location in TSPA-LA:* Sections 6.3.11.1 and 6.3.11.2; Equation 6.3.11-4.

Table K3-2. High-Level Summary of Epistemically Uncertain Variables (i.e., elements of **e**) Considered in the TSPA-LA (TSPA Parameter Name) (Continued)

NOTE: * indicates variable not considered in sensitivity analysis due to correlations.

Default_Fwd_Rate_Const_a - Default forward rate constant for irreversible sorption of plutonium and americium ($m^3/m^2/yr$). *Distribution:* Log uniform. *Range:* 0.002 to 0.05. *Sensitivity Name:* FWDRAT. *Location in TSPA-LA:* Table 6.3.7-65.
Defect_Count_a - Flaw density parameter (flaws per mm^3 of weld) (dimensionless). *Distribution:* Gamma. *Mean:* 4.529E-07. *Standard Deviation:* 1.654E-07. *Sensitivity Name:* WDDEFCNT. *Location in TSPA-LA:* Section 6.3.5.1.2; Table 6.3.5-3.
Defect_Size_a - Flaw size parameter (flaw size per mm of weld) (dimensionless). *Distribution:* Gamma. *Mean:* 0.2205. *Standard Deviation:* 0.0833. *Sensitivity Name:* WDDEFSZE. *Location in TSPA-LA:* Section 6.3.5.1.2; Table 6.3.5-3; Equation 6.3.5-10.
Density_CSNF_Rind_a - Grain density of CSNF rind (kg/m^3). *Distribution:* Uniform. *Range:* 5600 to 11500. *Sensitivity Name:* CSRINDDN. *Location in TSPA-LA:* Table 6.3.8-4.
Diameter_Colloid_a - Diameter of colloid particle (nm). *Distribution:* Uniform. *Range:* 50 to 300. *Sensitivity Name:* DIAMCOLL. *Location in TSPA-LA:* Tables 6.3.8-1 and 6.3.8-4.
Diff_Path_Length_Invert_Top_a - Diffusive path length from waste package outer corrosion barrier to mid-point of invert (m). *Distribution:* Uniform. *Range:* 0.3 to 1.24. *Sensitivity Name:* DIFPATHL. *Location in TSPA-LA:* Section 6.3.8.2.4; Table 6.3.8-4.
Drainage_Density_a - Average drainage density for the Fortymile Wash drainage basin (1/km). *Distribution:* Uniform. *Range:* 20 to 33. *Sensitivity Name:* DRAINDNS. *Location in TSPA-LA:* Table 6.5-5.
DS_Flux_Uncertainty_a - Drip shield flux splitting factor (dimensionless). *Distribution:* Uniform. *Range:* 0 to 0.85. *Sensitivity Name:* DSFLUX. *Location in TSPA-LA:* Tables 6.3.6-1, 6.3.6-2 and 6.3.8-4; Sections 6.3.6.2 and 6.3.6.4.1; Equation 6.3.6-5.
DSNF_Mass_Uncert_a - Scale factor used to characterize uncertainty in radionuclide content of DSNF (dimensionless). *Distribution:* Triangular. *Range:* 0.45 to 2.9. *Most Likely:* 0.62. *Sensitivity Name:* DSNFMASS. *Location in TSPA-LA:* Sections 6.3.7.1.2 and 6.3.7.1.3; Table 6.3.7-7.
dt_dRh_uncertainty - Selector variable used to determine the collapsed drift rubble thermal conductivity (dimensionless). *Distribution:* Discrete. *Range:* 1 to 2. *Sensitivity Name:* DTDRHUNC. *Location in TSPA-LA:* Section 6.6.2.2.
DWC_Dispersivity_Cond_a - Selector variable used to determine the axial dispersion modeling case (dimensionless). *Distribution:* Discrete. *Range:* 0 to 1. *Sensitivity Name:* DWCDISP. *Location in TSPA-LA:* Section 6.3.3.2.2; Table 6.3.3-5.
DWC_Std_Error_a_a - Multiplier for the standard deviation on the slope coefficient for determining the probability of condensation from percolation rate (dimensionless). *Distribution:* Normal. *Mean/Median/Mode:* 0. *Standard Deviation:* 1. *Sensitivity Name:* DWCSTERA. *Location in TSPA-LA:* Section 6.3.3.2.2; Tables 6.3.3-4 and 6.3.3-5.
DWC_Std_Error_b_a - Multiplier for the standard deviation on the y-intercept coefficient for determining the probability of condensation from percolation rate (dimensionless). *Distribution:* Normal. *Mean/Median/Mode:* 0. *Standard Deviation:* 1. *Sensitivity Name:* DWCSTERB. *Location in TSPA-LA:* Section 6.3.3.2.2; Tables 6.3.3-4 and 6.3.3-5.
DWC_Std_Error_c_a - Multiplier for the standard deviation on the slope coefficient for determining condensation rate from percolation rate (dimensionless). *Distribution:* Normal. *Mean/Median/Mode:* 0. *Standard Deviation:* 1. *Sensitivity Name:* DWCSTERC. *Location in TSPA-LA:* Section 6.3.3.2.2; Tables 6.3.3-4 and 6.3.3-5.
DWC_Std_Error_d_a - Multiplier for the standard deviation on the y-intercept coefficient for determining the condensation rate from percolation rate (dimensionless). *Distribution:* Normal. *Mean/Median/Mode:* 0. *Standard Deviation:* 1. *Sensitivity Name:* DWCSTERD. *Location in TSPA-LA:* Section 6.3.3.2.2; Tables 6.3.3-4 and 6.3.3-5.
DWC_Ventilated_Cond_a - Selector variable specifying whether the ventilated or unventilated drip shield DWC modeling case is performed (dimensionless). *Distribution:* Discrete. *Range:* 0, 1. *Sensitivity Name:* DWCVENT. *Location in TSPA-LA:* Sections 6.3.3.2.2 and 6.3.3.2.3; Table 6.3.3-5.
Exposure_Factor_a - The surface area exposure factor for the amount of HLW glass contacted by water (dimensionless). *Distribution:* Triangular. *Range:* 4 to 17. *Mode:* 4. *Sensitivity Name:* WFDEGEXF. *Location in TSPA-LA:* Sections 6.3.7.4.3.2 and 6.3.7.4.3.3; Equation 6.3.7-9; Table 6.3.7-32.

Table K3-2. High-Level Summary of Epistemically Uncertain Variables (i.e., elements of **e**) Considered in the TSPA-LA (TSPA Parameter Name) (Continued)

NOTE: * indicates variable not considered in sensitivity analysis due to correlations.

fa_group1_a - Fracture aperture for group 1 rock unit (chnf) (m). *Calculated by:* Por_group1_a/ff_group1_a. *Sensitivity Name:* UZFAG1. *Location in TSPA-LA:* Section 6.3.9.2; Equation 6.3.9-2; Fracture porosity values and frequency values are shown in Tables 6.3.9-6 and 6.3.9-7.
fa_group2_a - Fracture aperture for group 2 rock unit (tswf) (m). *Calculated by:* Por_group2_a/ff_group2_a. *Sensitivity Name:* UZFAG2. *Location in TSPA-LA:* Section 6.3.9.2; Equation 6.3.9-2; Fracture porosity values and frequency values are shown in Tables 6.3.9-6 and 6.3.9-7.
fa_group3_a - Fracture aperture for group 3 rock units (ch[2,3,4,5]fz, pcf[2,5]z, pp4fz, pp1fz, bf2fz, tr2fz) (m). *Calculated by:* Por_group3_a/ff_group3_a. *Sensitivity Name:* UZFAG3. *Location in TSPA-LA:* Section 6.3.9.2; Equation 6.3.9-2; Fracture porosity values and frequency values are shown in Tables 6.3.9-6 and 6.3.9-7.
fa_group4_a - Fracture aperture for group 4 rock units (pp3fd, pp2fd, bf3fd, tr3fd) (m). *Calculated by:* Por_group4_a/ff_group4_a. *Sensitivity Name:* UZFAG4. *Location in TSPA-LA:* Section 6.3.9.2; Equation 6.3.9-2; Fracture porosity values and frequency values are shown in Tables 6.3.9-6 and 6.3.9-7.
fa_group5_a - Fracture aperture for group 5 rock units (ch1fz, pcf1z, ch6fz, pcf6z) (m). *Calculated by:* Por_group5_a/ff_group5_a. *Sensitivity Name:* UZFAG5. *Location in TSPA-LA:* Section 6.3.9.2; Equation 6.3.9-2; Fracture porosity values and frequency values are shown in Tables 6.3.9-6 and 6.3.9-7.
fa_group6_a - Fracture aperture for group 6 rock units (ch[1,2,3,4,5,6]fv) (m). *Calculated by:* Por_group6_a/ff_group6_a. *Sensitivity Name:* UZFAG6. *Location in TSPA-LA:* Section 6.3.9.2; Equation 6.3.9-2; Fracture porosity values and frequency values are shown in Tables 6.3.9-6 and 6.3.9-7.
fa_group7_a - Fracture aperture for group 7 rock units (tswf9, pcf39, tswfv, tswfz) (m). *Calculated by:* Por_group7_a/ff_group7_a. *Sensitivity Name:* UZFAG7. *Location in TSPA-LA:* Section 6.3.9.2; Equation 6.3.9-2; Fracture porosity values and frequency values are shown in Tables 6.3.9-6 and 6.3.9-7.
fa_group8_a - Fracture aperture for group 8 rock units (tswf[4,5], tswf[6,7], tswf8, pcf38) (m). *Calculated by:* Por_group8_a/ff_group8_a. *Sensitivity Name:* UZFAG8. *Location in TSPA-LA:* Section 6.3.9.2; Equation 6.3.9-2; Fracture porosity values and frequency values are shown in Tables 6.3.9-6 and 6.3.9-7.
fa_group9_a - Fracture aperture for group 9 rock units (tswf3) (m). *Calculated by:* Por_group9_a/ff_group9_a. *Sensitivity Name:* UZFAG9. *Location in TSPA-LA:* Section 6.3.9.2; Equation 6.3.9-2; Fracture porosity values and frequency values are shown in Tables 6.3.9-6 and 6.3.9-7.
FHH_Isotherm_k_CP_a - Frenkel Halsey Hill water vapor adsorption isotherm parameter, *k*, for corrosion products (dimensionless). *Distribution:* Uniform. *Range:* 1.048 to 1.370 (see additional information). *Sensitivity Name:* FHHISKCP. *Location in TSPA-LA:* Table 6.3.8-4.
FHH_Isotherm_k_CSNF_Rind_a - Frenkel Halsey Hill water vapor adsorption isotherm parameter, *k*, for CSNF rind (dimensionless). *Distribution:* Uniform. *Range:* 1.606 to 8.215. *Sensitivity Name:* FHHISKCS. *Location in TSPA-LA:* Table 6.3.8-4.
FHH_Isotherm_s_CP_a - Frenkel Halsey Hill water vapor adsorption isotherm parameter, *s*, for corrosion products (dimensionless). *Distribution:* Uniform. *Range:* 1.525 to 1.852 (see additional information). *Sensitivity Name:* FHHISSCP. *Location in TSPA-LA:* Table 6.3.8-4.
FHH_Isotherm_s_CSNF_Rind_a - Frenkel Halsey Hill water vapor adsorption isotherm parameter, *s*, for CSNF rind (dimensionless). *Distribution:* Uniform. *Range:* 1.656 to 3.038. *Sensitivity Name:* FHHISSCS. *Location in TSPA-LA:* Table 6.3.8-4.
FISVO - Flowing interval spacing in fractured volcanic units (m). *Distribution:* Piecewise uniform. *Range:* 1.86 to 80. *Sensitivity Name:* SZFISPVO. *Location in TSPA-LA:* Section 6.3.10.5; Table 6.3.10-2.
FPLANW - Northwestern boundary of alluvial uncertainty zone (dimensionless). *Distribution:* Uniform. *Range:* 0 to 1. *Sensitivity Name:* SZWBNDAL. *Location in TSPA-LA:* Section 6.3.10.2; Table 6.3.10-2.
FPVO – Logarithm of flowing interval porosity in volcanic units (dimensionless). *Distribution:* Piecewise uniform. *Range:* -5 to -1. *Mean/Median/Mode:* -3. *Sensitivity Name:* SZFIPOVO. *Location in TSPA-LA:* Table 6.3.10-2.
Fraction_Channel_a - Fraction of the RMEI location subject to fluvial deposition (dimensionless). *Distribution:* Uniform. *Range:* 0.088 to 0.54. *Sensitivity Name:* FRACCHNL. *Location in TSPA-LA:* Table 6.5-5.
Gamma_AFM_a - Active fracture model (AFM) Gamma parameter (dimensionless). *Distribution:* Uniform. *Range:* 0.2 to 0.6. *Sensitivity Name:* UZGAM. *Location in TSPA-LA:* Sections 6.3.9.2, 6.3.9.3 and 6.3.9.4.1; Table 6.3.9-5.

Table K3-2. High-Level Summary of Epistemically Uncertain Variables (i.e., elements of **e**) Considered in the TSPA-LA (TSPA Parameter Name) (Continued)

NOTE: * indicates variable not considered in sensitivity analysis due to correlations.

GC_ULevel_A22_a - Variable for selecting distribution for general corrosion rate (low, medium, or high) (dimensionless). *Distribution:* Discrete. *Range:* 1 to 3. *Sensitivity Name:* WDGCUA22. *Location in TSPA-LA:* Table 6.3.5-4.
Goethite_SA_a - Specific surface area of goethite (m^2/g). *Distribution:* Truncated log normal. *Range:* 14.7 to 110. *Mean:* 51.42. *Standard Deviation:* 30.09. *Sensitivity Name:* GOESA. *Location in TSPA-LA:* Table 6.3.8-4; S_{CP} in Equation 6.3.8-19.
Goethite_Site_Density_a - Density of sorption sites on goethite (1/nm^2). *Distribution:* Discrete. *Range:* 1.02 to 8.59. *Sensitivity Name:* GOESITED. *Location in TSPA-LA:* Table 6.3.8-3.
GW_BDCF_MIC_Ac227 - Groundwater Biosphere Dose Conversion Factor (BDCF) for ^{227}Ac in modern interglacial climate ((Sv/year)/(Bq/m^3)). *Distribution:* Discrete. *Range:* 4.08E-07 to 4.32E-06. *Mean:* 1.3E-06. *Standard Deviation:* 5.28E-07. *Sensitivity Name:* MICAC227. *Location in TSPA-LA:* Sections 6.3.11.2 and 6.3.11.3; Table 6.3.11-3.
GW_BDCF_MIC_Am241 - Groundwater Biosphere Dose Conversion Factor (BDCF) for ^{241}Am in modern interglacial climate ((Sv/year)/(Bq/m^3)). *Distribution:* Discrete. *Range:* 2.16E-07 to 3.30E-06. *Mean:* 8.34E-07. *Standard Deviation:* 4.03E-07. *Sensitivity Name:* MICAM241. *Location in TSPA-LA:* Sections 6.3.11.2 and 6.3.11.3; Table 6.3.11-3.
GW_BDCF_MIC_Am243 - Groundwater Biosphere Dose Conversion Factor (BDCF) for ^{243}Am in modern interglacial climate ((Sv/year)/(Bq/m^3)). *Distribution:* Discrete. *Range:* 2.21E-07 to 3.37E-06. *Mean:* 8.88E-07. *Standard Deviation:* 4.12E-07. *Sensitivity Name:* MICAM243. *Location in TSPA-LA:* Sections 6.3.11.2 and 6.3.11.3; Table 6.3.11-3.
GW_BDCF_MIC_C14 - Groundwater Biosphere Dose Conversion Factor (BDCF) for ^{14}C in modern interglacial climate ((Sv/year)/(Bq/m^3)). *Distribution:* Discrete. *Range:* 7.18E-10 to 2.56E-08. *Mean:* 1.93E-09. *Standard Deviation:* 1.85E-09. *Sensitivity Name:* MICC14. *Location in TSPA-LA:* Sections 6.3.11.2 and 6.3.11.3; Table 6.3.11-3.
GW_BDCF_MIC_Cl36 - Groundwater Biosphere Dose Conversion Factor (BDCF) for ^{36}Cl in modern interglacial climate ((Sv/year)/(Bq/m^3)). *Distribution:* Discrete. *Range:* 1.28E-09 to 3.00E-07. *Mean:* 8.09E-09. *Standard Deviation:* 1.41E-08. *Sensitivity Name:* MICCl36. *Location in TSPA-LA:* Sections 6.3.11.2 and 6.3.11.3; Table 6.3.11-3.
GW_BDCF_MIC_Cs135 - Groundwater Biosphere Dose Conversion Factor (BDCF) for ^{135}Cs in modern interglacial climate ((Sv/year)/(Bq/m^3)). *Distribution:* Discrete. *Range:* 3.1E-09 to 8.48E-08. *Mean:* 1.45E-08. *Standard Deviation:* 1.02E-08. *Sensitivity Name:* MICCS135. *Location in TSPA-LA:* Sections 6.3.11.2 and 6.3.11.3; Table 6.3.11-3.
GW_BDCF_MIC_Cs137 - Groundwater Biosphere Dose Conversion Factor (BDCF) for ^{137}Cs in modern interglacial climate ((Sv/year)/(Bq/m^3)). *Distribution:* Discrete. *Range:* 3.87E-08 to 4.56E-07. *Mean:* 1.30E-07. *Standard Deviation:* 6.33E-08. *Sensitivity Name:* MICCS137. *Location in TSPA-LA:* Sections 6.3.11.2 and 6.3.11.3; Table 6.3.11-3.
GW_BDCF_MIC_I129 - Groundwater Biosphere Dose Conversion Factor (BDCF) for ^{129}I in modern interglacial climate ((Sv/year)/(Bq/m^3)). *Distribution:* Discrete. *Range:* 8.59E-08 to 1.13E-06. *Mean:* 1.29E-07. *Standard Deviation:* 5.28E-08. *Sensitivity Name:* MICI129. *Location in TSPA-LA:* Sections 6.3.11.2 and 6.3.11.3; Table 6.3.11-3.
GW_BDCF_MIC_Np237 - Groundwater Biosphere Dose Conversion Factor (BDCF) for ^{237}Np in modern interglacial climate ((Sv/year)/(Bq/m^3)). *Distribution:* Discrete. *Range:* 1.06E-07 to 8.05E-07. *Mean:* 2.74E-07. *Standard Deviation:* 9.70E-08. *Sensitivity Name:* MICNP237. *Location in TSPA-LA:* Sections 6.3.11.2 and 6.3.11.3; Table 6.3.11-3.
GW_BDCF_MIC_Pa231 - Groundwater Biosphere Dose Conversion Factor (BDCF) for ^{231}Pa in modern interglacial climate ((Sv/year)/(Bq/m^3)). *Distribution:* Discrete. *Range:* 6.58E-07 to 8.56E-06. *Mean:* 2.44E-06. *Standard Deviation:* 1.02E-06. *Sensitivity Name:* MICPA231. *Location in TSPA-LA:* Sections 6.3.11.2 and 6.3.11.3; Table 6.3.11-3.
GW_BDCF_MIC_Pu238 - Groundwater Biosphere Dose Conversion Factor (BDCF) for ^{238}Pu in modern interglacial climate ((Sv/year)/(Bq/m^3)). *Distribution:* Discrete. *Range:* 2.61E-07 to 2.09E-006. *Mean:* 7.61E-07. *Standard Deviation:* 2.78E-07. *Sensitivity Name:* MICPU238. *Location in TSPA-LA:* Sections 6.3.11.2 and 6.3.11.3; Table 6.3.11-3.

Table K3-2. High-Level Summary of Epistemically Uncertain Variables (i.e., elements of **e**) Considered in the TSPA-LA (TSPA Parameter Name) (Continued)

NOTE: * indicates variable not considered in sensitivity analysis due to correlations.

GW_BDCF_MIC_Pu239 - Groundwater Biosphere Dose Conversion Factor (BDCF) for ^{239}Pu in modern interglacial climate ((Sv/year)/(Bq/m^3)). *Distribution:* Discrete. *Range:* 3.49E-07 to 2.93E-06. *Mean:* 9.55E-07. *Standard Deviation:* 3.37E-07. *Sensitivity Name:* MICPU239. *Location in TSPA-LA:* Sections 6.3.11.2 and 6.3.11.3; Table 6.3.11-3.
GW_BDCF_MIC_Pu240 - Groundwater Biosphere Dose Conversion Factor (BDCF) for ^{240}Pu in modern interglacial climate ((Sv/year)/(Bq/m^3)). *Distribution:* Discrete. *Range:* 3.47E-07 to 2.90E-06. *Mean:* 9.51E-07. *Standard Deviation:* 3.35E-07. *Sensitivity Name:* MICPU240. *Location in TSPA-LA:* Sections 6.3.11.2 and 6.3.11.3; Table 6.3.11-3.
GW_BDCF_MIC_Ra226_Pb210 - Groundwater Biosphere Dose Conversion Factor (BDCF) for ^{210}Pb summed into ^{226}Ra in modern interglacial climate ((Sv/year)/(Bq/m^3)). *Distribution:* Discrete. *Range:* 2.90E-06 to 2.82E-05. *Mean:* 6.52E-06. *Standard Deviation:* 2.58E-06. *Sensitivity Name:* MICRA226. *Location in TSPA-LA:* Sections 6.3.11.2 and 6.3.11.3; Table 6.3.11-3.
GW_BDCF_MIC_Se79 - Groundwater Biosphere Dose Conversion Factor (BDCF) for ^{79}Se in modern interglacial climate ((Sv/year)/(Bq/m^3)). *Distribution:* Discrete. *Range:* 3.62E-09 to 1.51E-06. *Mean:* 2.42E-08. *Standard Deviation:* 7.48E-08. *Sensitivity Name:* MICSE79. *Location in TSPA-LA:* Sections 6.3.11.2 and 6.3.11.3; Table 6.3.11-3.
GW_BDCF_MIC_Sn126 - Groundwater Biosphere Dose Conversion Factor (BDCF) for ^{126}Sn in modern interglacial climate ((Sv/year)/(Bq/m^3)). *Distribution:* Discrete. *Range:* 8.92E-08 to 1.68E-06. *Mean:* 4.33E-07. *Standard Deviation:* 2.39E-07. *Sensitivity Name:* MICSN126. *Location in TSPA-LA:* Sections 6.3.11.2 and 6.3.11.3; Table 6.3.11-3.
GW_BDCF_MIC_Sr90 - Groundwater Biosphere Dose Conversion Factor (BDCF) for ^{90}Sr in modern interglacial climate ((Sv/year)/(Bq/m^3)). *Distribution:* Discrete. *Range:* 2.51E-08 to 8.60E-08. *Mean:* 3.43E-08. *Standard Deviation:* 6.59E-09. *Sensitivity Name:* MICSR90. *Location in TSPA-LA:* Sections 6.3.11.2 and 6.3.11.3; Table 6.3.11-3.
GW_BDCF_MIC_Tc99 - Groundwater Biosphere Dose Conversion Factor (BDCF) for ^{99}Tc in modern interglacial climate ((Sv/year)/(Bq/m^3)). *Distribution:* Discrete. *Range:* 5.28E-10 to 2.85E-08. *Mean:* 1.12E-09. *Standard Deviation:* 1.26E-09. *Sensitivity Name:* MICTC99. *Location in TSPA-LA:* Sections 6.3.11.2 and 6.3.11.3; Table 6.3.11-3.
GW_BDCF_MIC_Th229 - Groundwater Biosphere Dose Conversion Factor (BDCF) for ^{229}Th in modern interglacial climate ((Sv/year)/(Bq/m^3)). *Distribution:* Discrete. *Range:* 7.43E-07 to 8.05E-06. *Mean:* 2.58E-06. *Standard Deviation:* 1.03E-06. *Sensitivity Name:* MICTH229. *Location in TSPA-LA:* Sections 6.3.11.2 and 6.3.11.3; Table 6.3.11-3.
GW_BDCF_MIC_U232 - Groundwater Biosphere Dose Conversion Factor (BDCF) for 232U in modern interglacial climate ((Sv/year)/(Bq/m^3)). *Distribution:* Discrete. *Range:* 2.87E-07 to 1.86E-06. *Mean:* 6.04E-07. *Standard Deviation:* 2.17E-07. *Sensitivity Name:* MICU232. *Location in TSPA-LA:* Sections 6.3.11.2 and 6.3.11.3; Table 6.3.11-3.
GW_BDCF_MIC_U233 - Groundwater Biosphere Dose Conversion Factor (BDCF) for ^{233}U in modern interglacial climate ((Sv/year)/(Bq/m^3)). *Distribution:* Discrete. *Range:* 4.13E-08 to 3.13E-07. *Mean:* 8.97E-08. *Standard Deviation:* 3.35E-08. *Sensitivity Name:* MICU233. *Location in TSPA-LA:* Sections 6.3.11.2 and 6.3.11.3; Table 6.3.11-3.
GW_BDCF_MIC_U234 - Groundwater Biosphere Dose Conversion Factor (BDCF) for ^{234}U in modern interglacial climate ((Sv/year)/(Bq/m^3)). *Distribution:* Discrete. *Range:* 3.96E-08 to 2.20E-07. *Mean:* 8.19E-08. *Standard Deviation:* 2.81E-08. *Sensitivity Name:* MICU234. *Location in TSPA-LA:* Sections 6.3.11.2 and 6.3.11.3; Table 6.3.11-3.
GW_BDCF_MIC_U238 - Groundwater Biosphere Dose Conversion Factor (BDCF) for ^{238}U in modern interglacial climate ((Sv/year)/(Bq/m^3)). *Distribution:* Discrete. *Range:* 3.85E-08 to 2.07E-07. *Mean:* 7.87E-08. *Standard Deviation:* 2.62E-08. *Sensitivity Name:* MICU238. *Location in TSPA-LA:* Sections 6.3.11.2 and 6.3.11.3; Table 6.3.11-3.
GWSPD - Logarithm of the scale factor used to characterize uncertainty in groundwater specific discharge (dimensionless). *Distribution:* Piecewise uniform. *Range:* -0.951 to 0.951. *Sensitivity Name:* SZGWSPDM. *Location in TSPA-LA:* Section 6.3.10.2; Table 6.3.10-2.

Table K3-2. High-Level Summary of Epistemically Uncertain Variables (i.e., elements of **e**) Considered in the TSPA-LA (TSPA Parameter Name) (Continued)

NOTE: * indicates variable not considered in sensitivity analysis due to correlations.

HAVO - Ratio of horizontal anisotropy (north-south over east-west) in the permeability of the SZ volcanic units (dimensionless). *Distribution:* Piecewise uniform. *Range:* 0.05 to 20. *Sensitivity Name:* SZRAHAVO. *Location in TSPA-LA:* Sections 6.3.10.2 and 6.3.10.5; Table 6.3.10-2.
HFO_SA_a - Hydrous ferric oxide (HFO) surface area (m^2/g). *Distribution:* Truncated log normal. *Range:* 68 to 600. *Mean:* 275.6. *Standard Deviation:* 113.4. *Sensitivity Name:* HFOSA. *Location in TSPA-LA:* Table 6.3.8-4; S_{CP} in Equation 6.3.8-19.
HFO_Site_Density_a - Sorption site density for hydrous ferric oxide (HFO) (1/nm^2). *Distribution:* Discrete. *Range:* 0.56 to 5.65. *Sensitivity Name:* HFOSITED. *Location in TSPA-LA:* Table 6.3.8-3.
HLW_Diss_kE_Acidic_a - Effective rate coefficient (affinity term) for the dissolution of HLW glass in CDSP waste packages under low pH conditions (g/(m^2d)). *Distribution:* Triangular. *Range:* 8.41E+03 to 1.15E+07. *Mode:* 8.41E+03. *Sensitivity Name:* HLWDRACD. *Location in TSPA-LA:* Sections 6.3.7.4.3.2 and 6.3.7.4.3.3; Table 6.3.7-32; Equation 6.3.7-8.
HLW_Diss_kE_Alkaline_a - Effective rate coefficient (affinity term) for the dissolution of HLW glass in CDSP waste packages under high pH conditions (g/(m^2d)). *Distribution:* Triangular. *Range:* 2.82E+01 to 3.47E+04. *Mode:* 2.82E+01. *Sensitivity Name:* HLWDRALK. *Location in TSPA-LA:* Sections 6.3.7.4.3.2 and 6.3.7.4.3.3; Table 6.3.7-32; Equation 6.3.7-8.
HLW_Mass_Uncert_a - Scale factor used to characterize uncertainty in radionuclide content of HLW glass (dimensionless). *Distribution:* Triangular. *Range:* 0.7 to 1.5. *Most Likely:* 1. *Sensitivity Name:* HLWMASS. *Location in TSPA-LA:* Sections 6.3.7.1.2 and 6.3.7.1.3; Table 6.3.7-7.
HLWG_Rind_SA_a - Specific surface area of HLWG degradation rind (m^2/g). *Distribution:* Uniform. *Range:* 10 to 38. *Sensitivity Name:* HLWGRNDS. *Location in TSPA-LA:* Table 6.3.8-4.
IGERATE - Frequency of occurrence of volcanic eruptive events (yr^{-1}). *Calculated by:* Igneous_Event_Prob_a x 0.083. *Range:* 0 to 6.44E-08. *Sensitivity Name:* IGERATE. *Location in TSPA-LA:* Section 6.5.2.1.1; Appendix J; Equation J7.5-3.
Igneous_Event_Prob_a - Frequency of intersection of the repository footprint by a volcanic event (yr^{-1}). *Distribution:* Piecewise uniform. *Range:* 0 to 7.76E-07. *Sensitivity Name:* IGRATE. *Location in TSPA-LA:* Table 6.5-2.
Infiltration_Scenario_a - Pointer variable for determining infiltration conditions: 10th, 30th, 50th or 90th percentile infiltration scenario (dimensionless). *Distribution:* Discrete. *Range:* 1 to 4. *Sensitivity Name:* INFIL. *Location in TSPA-LA:* Section 6.3.1.2; Tables 6.3.1-2 and 6.3.5-4.
Initial_Release_Frac_Cs_a - The initial release fraction of ^{137}Cs in a CSNF waste package (dimensionless). *Distribution:* Triangular. *Range:* 0.0039 to 0.1106. *Mode:* 0.0363. *Sensitivity Name:* INRFRCCS. *Location in TSPA-LA:* Sections 6.3.7.4.1.2 and 6.3.7.4.1.3; Table 6.3.7-29.
Initial_Release_Frac_I_a - The initial release fraction of ^{129}I in a CSNF waste package (dimensionless). *Distribution:* Triangular. *Range:* 0.0204 to 0.2675. *Mode:* 0.1124. *Sensitivity Name:* INRFRCI. *Location in TSPA-LA:* Sections 6.3.7.4.1.2 and 6.3.7.4.1.3; Table 6.3.7-29.
Initial_Release_Frac_Sr_a - The initial release fraction of ^{90}Sr in a CSNF waste package (dimensionless). *Distribution:* Triangular. *Range:* 0.0002 to 0.0025. *Mode:* 0.0009. *Sensitivity Name:* INRFRCSR. *Location in TSPA-LA:* Sections 6.3.7.4.1.2 and 6.3.7.4.1.3; Table 6.3.7-29.
Initial_Release_Frac_Tc_a - The initial release fraction of ^{99}Tc in a CSNF waste package (dimensionless). *Distribution:* Triangular. *Range:* 0.0001 to 0.0026. *Mode:* 0.001. *Sensitivity Name:* INRFRCTC. *Location in TSPA-LA:* Sections 6.3.7.4.1.2 and 6.3.7.4.1.3; Table 6.3.7-29.
Inpkg_IStr_2DHLW_NS_Rand_a - Pointer variable used to determine ionic strength for 2DHLW Cell (Cell 1a) of CDSP waste packages under vapor influx conditions (dimensionless). *Distribution:* Uniform. *Range:* 0 to 1. *Sensitivity Name:* IS2DHLNS. *Location in TSPA-LA:* Section 6.3.7.2.2 Part III.
Inpkg_IStr_2DHLW_S_Rand_a - Pointer variable used to determine ionic strength for 2DHLW Cell (Cell 1a) of CDSP waste packages under liquid influx conditions (dimensionless). *Distribution:* Uniform. *Range:* 0 to 1. *Sensitivity Name:* IS2DHLS. *Location in TSPA-LA:* Section 6.3.7.2.2 Part III.
Inpkg_IStr_2MCO_NS_Rand_a - Pointer variable used to determine ionic strength for 2MCO Cell (Cell 1b) of CDSP waste packages under vapor influx conditions (dimensionless). *Distribution:* Uniform. *Range:* 0 to 1. *Sensitivity Name:* IS2MCONS. *Location in TSPA-LA:* Section 6.3.7.2.2 Part III.

Table K3-2. High-Level Summary of Epistemically Uncertain Variables (i.e., elements of **e**) Considered in the TSPA-LA (TSPA Parameter Name) (Continued)

NOTE: * indicates variable not considered in sensitivity analysis due to correlations.

lnpkg_IStr_2MCO_S_Rand_a - Pointer variable used to determine ionic strength for 2MCO Cell (Cell 1b) of CDSP waste packages under liquid influx conditions (dimensionless). *Distribution:* Uniform. *Range:* 0 to 1. *Sensitivity Name:* IS2MCOS. *Location in TSPA-LA:* Section 6.3.7.2.2 Part III.
lnpkg_IStr_CSNF_NS_Rand_a - Pointer variable used to determine ionic strength for CSNF Cell under vapor influx conditions (dimensionless). *Distribution:* Uniform. *Range:* 0 to 1. *Sensitivity Name:* ISCSNS. *Location in TSPA-LA:* Section 6.3.7.2.2 Part III.
lnpkg_IStr_CSNF_S_Rand_a - Pointer variable used to determine ionic strength for CSNF Cell under liquid influx conditions (dimensionless). *Distribution:* Uniform. *Range:* 0 to 1. *Sensitivity Name:* ISCSS. *Location in TSPA-LA:* Section 6.3.7.2.2 Part III.
lnpkg_pH_2DHLW_NS_Rand_a - Pointer variable used to determine pH in 2DHLW Cell (Cell 1a) of CDSP waste packages under vapor influx conditions (dimensionless). *Distribution:* Uniform. *Range:* 0 to 1. *Sensitivity Name:* PH2DHLNS. *Location in TSPA-LA:* Section 6.3.7.2.2 Part IV.
lnpkg_pH_2DHLW_S_Rand_a - Pointer variable used to determine pH in 2DHLW Cell (Cell 1a) of CDSP waste packages under liquid influx conditions (dimensionless). *Distribution:* Uniform. *Range:* 0 to 1. *Sensitivity Name:* PH2DHLS. *Location in TSPA-LA:* Section 6.3.7.2.2 Part IV.
lnpkg_pH_2MCO_NS_Rand_a - Pointer variable used to determine pH in 2MCO Cell (Cell 1b) of CDSP waste packages under vapor influx conditions (dimensionless). *Distribution:* Uniform. *Range:* 0 to 1. *Sensitivity Name:* PH2MCONS. *Location in TSPA-LA:* Section 6.3.7.2.2 Part IV.
lnpkg_pH_2MCO_S_Rand_a - Pointer variable used to determine pH in 2MCO Cell (Cell 1b) of CDSP waste packages under liquid influx conditions (dimensionless). *Distribution:* Uniform. *Range:* 0 to 1. *Sensitivity Name:* PH2MCOS. *Location in TSPA-LA:* Section 6.3.7.2.2 Part IV.
lnpkg_pH_CSNF_NS_Rand_a - Pointer variable used to determine pH in CSNF Cell1 under vapor influx conditions (dimensionless). *Distribution:* Uniform. *Range:* 0 to 1. *Sensitivity Name:* PHCSNS. *Location in TSPA-LA:* Section 6.3.7.2.2 Part IV.
lnpkg_pH_CSNF_S_Rand_a - Pointer variable used to determine pH in CSNF Cell1 under liquid influx conditions (dimensionless). *Distribution:* Uniform. *Range:* 0 to 1. *Sensitivity Name:* PHCSS. *Location in TSPA-LA:* Section 6.3.7.2.2 Part IV.
Invert_Diff_Coeff_Uncert_a - Exponential term representing uncertainty in the invert diffusion coefficient (dimensionless). *Distribution:* Truncated normal. *Range:* -0.621 to 0.687. *Mean:* 0.033. *Standard Deviation:* 0.218. *Sensitivity Name:* EBSDIFCF. *Location in TSPA-LA:* Section 6.3.8.2.4; Table 6.3.8-4; Equation 6.3.8-24.
Kd_Am_Al - Americium sorption coefficient in alluvium (mL/g). *Distribution:* Truncated normal. *Range:* 1000 to 10000. *Mean/Median/Mode:* 5500. *Standard Deviation:* 1500. *Sensitivity Name:* SZKDAMAL. *Location in TSPA-LA:* Section 6.3.10.2; Table 6.3.10-2.
Kd_Am_Col - Americium sorption coefficient onto smectite colloids (mL/g). *Distribution:* Piecewise uniform. *Range:* 1.00E+04 to 1.00E+07. *Sensitivity Name:* SZKDAMCO. *Location in TSPA-LA:* Section 6.3.10.2; Table 6.3.10-2.
Kd_Am_Rev_Smectite_a - Distribution coefficient for reversible sorption of americium to waste form (smectite) colloids (mL/g). *Distribution:* Piecewise uniform. *Range:* 1.00E+04 to 1.00E+07. *Sensitivity Name:* KDAMSMEC. *Location in TSPA-LA:* Sections 6.3.7.6.2 and 6.3.7.6.3; Equation 6.3.7-20; Tables 6.3.7-62 and 6.3.7-66.
Kd_Am_Rev_U_Col_a - Distribution coefficient for reversible sorption of americium onto uranophane colloids (mL/g). *Distribution:* Log uniform. *Range:* 5 to 1.00E+04. *Sensitivity Name:* KDAMCOL. *Location in TSPA-LA:* Sections 6.3.7.6.2 and 6.3.7.6.3; Equation 6.3.7-20; Table 6.3.7-64.
Kd_Am_Vo - Americium sorption coefficient in volcanic units (mL/g). *Distribution:* Truncated normal. *Range:* 1000 to 10000. *Mean/Median/Mode:* 5500. *Standard Deviation:* 1500. *Sensitivity Name:* SZKDAMVO. *Location in TSPA-LA:* Section 6.3.10.2; Table 6.3.10-2.
Kd_Cs_Al - Cesium sorption coefficient in alluvium (mL/g). *Distribution:* Truncated normal. *Range:* 100 to 1000. *Mean/Median/Mode:* 728. *Standard Deviation:* 464. *Sensitivity Name:* SZKDCSAL. *Location in TSPA-LA:* Section 6.3.10.2; Table 6.3.10-2.
Kd_Cs_Col - Cesium sorption coefficient onto smectite colloids (mL/g). *Distribution:* Piecewise uniform. *Range:* 50 to 5000. *Sensitivity Name:* SZKDCSCO. *Location in TSPA-LA:* Section 6.3.10.2; Table 6.3.10-2.

Table K3-2. High-Level Summary of Epistemically Uncertain Variables (i.e., elements of **e**) Considered in the TSPA-LA (TSPA Parameter Name) (Continued)

NOTE: * indicates variable not considered in sensitivity analysis due to correlations.

Kd_Cs_Rev_Smectite_a - Distribution coefficient for reversible sorption of cesium to waste form (smectite) colloids (mL/g). *Distribution:* Piecewise uniform. *Range:* 50 to 5000. *Sensitivity Name:* KDCSSMEC. *Location in TSPA-LA:* Sections 6.3.7.6.2 and 6.3.7.6.3; Equation 6.3.7-20; Tables 6.3.7-62 and 6.3.7-66.
Kd_Cs_Rev_U_Col_a - Distribution coefficient for reversible sorption of cesium onto uranophane colloids (mL/g). *Distribution:* Log uniform. *Range:* 10 to 1000. *Sensitivity Name:* KDCSCOL. *Location in TSPA-LA:* Sections 6.3.7.6.2 and 6.3.7.6.3; Equation 6.3.7-20; Table 6.3.7-64.
Kd_Cs_Vo - Cesium sorption coefficient in volcanic units (mL/g). *Distribution:* Piecewise uniform. *Range:* 100 to 6783. *Sensitivity Name:* SZKDCSVO. *Location in TSPA-LA:* Section 6.3.10.2; Table 6.3.10-2.
Kd_Np_Al - Neptunium sorption coefficient in alluvium (mL/g). *Distribution:* Piecewise uniform. *Range:* 1.8 to 13. *Sensitivity Name:* SZKDNPAL. *Location in TSPA-LA:* Section 6.3.10.2; Table 6.3.10-2.
Kd_Np_Rev_Smectite_a - Distribution coefficient for reversible sorption of neptunium to waste form (smectite) colloids (mL/g). *Distribution:* Log uniform. *Range:* 10 to 500. *Sensitivity Name:* KDNPSMEC. *Location in TSPA-LA:* Sections 6.3.7.6.2 and 6.3.7.6.3; Equation 6.3.7-20; Tables 6.3.7-62 and 6.3.7-66.
Kd_Np_Rev_U_Col_a - Distribution coefficient for reversible sorption of neptunium onto uranophane colloids (mL/g). *Distribution:* Log uniform. *Range:* 1 to 500. *Sensitivity Name:* KDNPCOL. *Location in TSPA-LA:* Sections 6.3.7.6.2 and 6.3.7.6.3; Equation 6.3.7-20; Table 6.3.7-64.
Kd_Np_Vo - Neptunium sorption coefficient in volcanic units (mL/g). *Distribution:* Piecewise uniform. *Range:* 0 to 6. *Sensitivity Name:* SZKDNPVO. *Location in TSPA-LA:* Section 6.3.10.2; Table 6.3.10-2.
Kd_Pa_Rev_Smectite_a - Distribution coefficient for reversible sorption of protactinium to waste form (smectite) colloids (mL/g). *Distribution:* Piecewise uniform. *Range:* 1.00E+04 to 1.00E+07. *Sensitivity Name:* KDPASMEC. *Location in TSPA-LA:* Sections 6.3.7.6.2 and 6.3.7.6.3; Equation 6.3.7-20; Tables 6.3.7-62 and 6.3.7-66.
Kd_Pa_Rev_U_Col_a - Distribution coefficient for reversible sorption of protactinium onto uranophane colloids (mL/g). *Distribution:* Log uniform. *Range:* 5 to 1.00E+04. *Sensitivity Name:* KDPACOL. *Location in TSPA-LA:* Sections 6.3.7.6.2 and 6.3.7.6.3; Equation 6.3.7-20; Table 6.3.7-64.
Kd_Pu_Al - Plutonium sorption coefficient in alluvium (mL/g). *Distribution:* Beta. *Range:* 50 to 300. *Mean/Median/Mode:* 100. *Standard Deviation:* 15. *Sensitivity Name:* SZKDPUAL. *Location in TSPA-LA:* Section 6.3.10.2; Table 6.3.10-2.
Kd_Pu_Col - Plutonium sorption coefficient onto smectite colloids (mL/g). *Distribution:* Piecewise uniform. *Range:* 1.00E+03 to 1.00E+05. *Sensitivity Name:* SZKDPUCO. *Location in TSPA-LA:* Section 6.3.10.2; Table 6.3.10-2.
Kd_Pu_Rev_Smectite_a - Distribution coefficient for reversible sorption of plutonium to waste form (smectite) colloids (mL/g). *Distribution:* Piecewise uniform. *Range:* 1.00E+03 to 1.00E+05. *Sensitivity Name:* KDPUSMEC. *Location in TSPA-LA:* Sections 6.3.7.6.2 and 6.3.7.6.3; Equation 6.3.7-20; Tables 6.3.7-62 and 6.3.7-66.
Kd_Pu_Rev_U_Col_a - Distribution coefficient for reversible sorption of plutonium onto uranophane colloids (mL/g). *Distribution:* Log uniform. *Range:* 5 to 1.00E+04. *Sensitivity Name:* KDPUCOL. *Location in TSPA-LA:* Sections 6.3.7.6.2 and 6.3.7.6.3; Equation 6.3.7-20; Table 6.3.7-64.
Kd_Pu_Vo - Plutonium sorption coefficient in volcanic units (mL/g). *Distribution:* Piecewise uniform. *Range:* 10 to 300. *Sensitivity Name:* SZKDPUVO. *Location in TSPA-LA:* Section 6.3.10.2; Table 6.3.10-2.
Kd_Ra_Al - Radium sorption coefficient in alluvium (mL/g). *Distribution:* Uniform. *Range:* 100 to 1000. *Sensitivity Name:* SZKDRAAL. *Location in TSPA-LA:* Section 6.3.10.2; Table 6.3.10-2.
Kd_Ra_Rev_Smectite_a - Distribution coefficient for reversible sorption of radium to waste form (smectite) colloids (mL/g). *Distribution:* Log uniform. *Range:* 100 to 5000. *Sensitivity Name:* KDRASMEC. *Location in TSPA-LA:* Sections 6.3.7.6.2 and 6.3.7.6.3; Equation 6.3.7-20; Tables 6.3.7-62 and 6.3.7-66.
Kd_Ra_Rev_U_Col_a - Distribution coefficient for reversible sorption of radium onto uranophane colloids (mL/g). *Distribution:* Log uniform. *Range:* 10 to 1000. *Sensitivity Name:* KDRACOL. *Location in TSPA-LA:* Sections 6.3.7.6.2 and 6.3.7.6.3; Equation 6.3.7-20; Table 6.3.7-64.
Kd_Ra_Vo* - Radium sorption coefficient in volcanic units (mL/g). *Distribution:* Uniform. *Range:* 100 to 1000. *Sensitivity Name:* SZKDRAVO*. *Location in TSPA-LA:* Section 6.3.10.2; Table 6.3.10-2.
Kd_Se_Al - Selenium sorption coefficient in alluvium (mL/g). *Distribution:* Truncated log normal. *Range:* 1 to 50. *Mean/Median/Mode:* 14. *Standard Deviation:* 11.2. *Sensitivity Name:* SZKDSEAL. *Location in TSPA-LA:* Section 6.3.10.2; Table 6.3.10-2.

Table K3-2. High-Level Summary of Epistemically Uncertain Variables (i.e., elements of **e**) Considered in the TSPA-LA (TSPA Parameter Name) (Continued)

NOTE: * indicates variable not considered in sensitivity analysis due to correlations.

Kd_Se_Vo - Selenium sorption coefficient in volcanic units (mL/g). *Distribution:* Truncated log normal. *Range:* 1 to 50. *Mean/Median/Mode:* 14. *Standard Deviation:* 11.2. *Sensitivity Name:* SZKDSEVO. *Location in TSPA-LA:* Section 6.3.10.2; Table 6.3.10-2.
Kd_Sn_Al - Tin sorption coefficient in alluvium (mL/g). *Distribution:* Log uniform. *Range:* 1.00E+02 to 1.00E+05. *Sensitivity Name:* SZKDSNAL. *Location in TSPA-LA:* Section 6.3.10.2; Table 6.3.10-2.
Kd_Sn_Col - Tin sorption coefficient onto smectite colloids (mL/g). *Distribution:* Log uniform. *Range:* 1.00E+05 to 1.00E+06. *Sensitivity Name:* SZKDSNCO. *Location in TSPA-LA:* Section 6.3.10.2; Table 6.3.10-2.
Kd_Sn_Rev_Smectite_a - Distribution coefficient for reversible sorption of tin to waste form (smectite) colloids (mL/g). *Distribution:* Log uniform. *Range:* 1.00E+05 to 1.00E+06. *Sensitivity Name:* KDSNSMEC. *Location in TSPA-LA:* Sections 6.3.7.6.2 and 6.3.7.6.3; Equation 6.3.7-20; Tables 6.3.7-62 and 6.3.7-66.
Kd_Sn_Rev_U_Col_a - Distribution coefficient for reversible sorption of tin onto uranophane colloids (mL/g). *Distribution:* Log uniform. *Range:* 1 to 100. *Sensitivity Name:* KDSNCOL. *Location in TSPA-LA:* Sections 6.3.7.6.2 and 6.3.7.6.3; Equation 6.3.7-20; Table 6.3.7-64.
Kd_Sn_Vo - Tin sorption coefficient in volcanic units (mL/g). *Distribution:* Log uniform. *Range:* 1.00E+02 to 1.00E+05. *Sensitivity Name:* SZKDSNVO. *Location in TSPA-LA:* Section 6.3.10.2; Table 6.3.10-2.
Kd_Sr_Al - Strontium sorption coefficient in alluvium (mL/g). *Distribution:* Uniform. *Range:* 20 to 400. *Sensitivity Name:* SZKDSRAL. *Location in TSPA-LA:* Section 6.3.10.2; Table 6.3.10-2.
Kd_Sr_Vo - Strontium sorption coefficient in volcanic units (mL/g). *Distribution:* Uniform. *Range:* 20 to 400. *Sensitivity Name:* SZKDSRVO. *Location in TSPA-LA:* Section 6.3.10.2; Table 6.3.10-2.
Kd_Th_Rev_Smectite_a - Distribution coefficient for reversible sorption of thorium to waste form (smectite) colloids (mL/g). *Distribution:* Piecewise uniform. *Range:* 1.00E+04 to 1.00E+07. *Sensitivity Name:* KDTHSMEC. *Location in TSPA-LA:* Sections 6.3.7.6.2 and 6.3.7.6.3; Equation 6.3.7-20; Tables 6.3.7-62 and 6.3.7-66.
Kd_Th_Rev_U_Col_a - Distribution coefficient for reversible sorption of thorium onto uranophane colloids (mL/g). *Distribution:* Log uniform. *Range:* 5 to 1.00E+04. *Sensitivity Name:* KDTHCOL. *Location in TSPA-LA:* Sections 6.3.7.6.2 and 6.3.7.6.3; Equation 6.3.7-20; Table 6.3.7-64.
Kd_U_Al - Uranium sorption coefficient in alluvium (mL/g). *Distribution:* Piecewise uniform. *Range:* 1.7 to 8.9. *Sensitivity Name:* SZKDUAL. *Location in TSPA-LA:* Section 6.3.10.2; Table 6.3.10-2.
Kd_U_Rev_Smectite_a - Distribution coefficient for reversible sorption of uranium to waste form (smectite) colloids (mL/g). *Distribution:* Log uniform. *Range:* 5.00E+02 to 5.00E+04. *Sensitivity Name:* KDUSMEC. *Location in TSPA-LA:* Sections 6.3.7.6.2 and 6.3.7.6.3; Equation 6.3.7-20; Tables 6.3.7-62 and 6.3.7-66.
Kd_U_Vo - Uranium sorption coefficient in volcanic units (mL/g). *Distribution:* Piecewise uniform. *Range:* 0 to 20. *Sensitivity Name:* SZKDUVO. *Location in TSPA-LA:* Section 6.3.10.2; Table 6.3.10-2.
KdAm_Devit_a - Sorption coefficient of americium in devitrified tuff units of UZ (mL/g). *Distribution:* Truncated normal. *Range:* 1000 to 10000. *Mean:* 5500. *Standard Deviation:* 1500. *Sensitivity Name:* UZKDAMDT. *Location in TSPA-LA:* Sections 6.3.9.2 and 6.3.9.3; Equation 6.3.9-3; Table 6.3.9-2.
KdAm_Vit_a* - Sorption coefficient of americium in vitrified tuff units of UZ (mL/g). *Distribution:* Piecewise uniform. *Range:* 100 to 1000. *Median:* 400. *Sensitivity Name:* UZKDAMVT*. *Location in TSPA-LA:* Sections 6.3.9.2 and 6.3.9.3; Equation 6.3.9-3; Table 6.3.9-2.
KdAm_Zeo_a* - Sorption coefficient of americium in zeolitic tuff units of UZ (mL/g). *Distribution:* Truncated normal. *Range:* 1000 to 10000. *Mean:* 5500. *Standard Deviation:* 1500. *Sensitivity Name:* UZKDAMZT*. *Location in TSPA-LA:* Sections 6.3.9.2 and 6.3.9.3; Equation 6.3.9-3; Table 6.3.9-2.
KdCs_Devit_a - Sorption coefficient of cesium in devitrified tuff units of UZ (mL/g). *Distribution:* Uniform. *Range:* 1 to 15. *Sensitivity Name:* UZKDCSDT. *Location in TSPA-LA:* Sections 6.3.9.2 and 6.3.9.3; Equation 6.3.9-3; Table 6.3.9-2.
KdCs_Vit_a* - Sorption coefficient of cesium in vitrified tuff units of UZ (mL/g). *Distribution:* Piecewise uniform. *Range:* 0 to 100. *Median:* 2. *Sensitivity Name:* UZKDCSVT*. *Location in TSPA-LA:* Sections 6.3.9.2 and 6.3.9.3; Equation 6.3.9-3; Table 6.3.9-2.
KdCs_Zeo_a - Sorption coefficient for cesium in zeolitic tuff units of UZ (mL/g). *Distribution:* Piecewise uniform. *Range:* 425 to 20000. *Median:* 5,000. *Sensitivity Name:* UZKDCSZT. *Location in TSPA-LA:* Sections 6.3.9.2 and 6.3.9.3; Equation 6.3.9-3; Table 6.3.9-2.

Table K3-2. High-Level Summary of Epistemically Uncertain Variables (i.e., elements of **e**) Considered in the TSPA-LA (TSPA Parameter Name) (Continued)

NOTE: * indicates variable not considered in sensitivity analysis due to correlations.

KdNp_Devit_a - Sorption coefficient for neptunium in devitrified tuff units of UZ (mL/g). *Distribution:* Piecewise uniform. *Range:* 0 to 6. *Median:* 0.5. *Sensitivity Name:* UZKDNPDT. *Location in TSPA-LA:* Sections 6.3.9.2 and 6.3.9.3; Equation 6.3.9-3; Table 6.3.9-2.
KdNp_Vit_a* - Sorption coefficient for neptunium in vitrified tuff units of UZ (mL/g). *Distribution:* Piecewise uniform. *Range:* 0 to 3. *Median:* 1. *Sensitivity Name:* UZKDNPVT*, *Location in TSPA-LA:* Sections 6.3.9.2 and 6.3.9.3; Equation 6.3.9-3; Table 6.3.9-2.
KdNp_Zeo_a* - Sorption coefficient for neptunium in zeolitic tuff units of UZ (mL/g). *Distribution:* Piecewise uniform. *Range:* 0 to 6. *Median:* 0.5. *Sensitivity Name:* UZKDNPZT*. *Location in TSPA-LA:* Sections 6.3.9.2 and 6.3.9.3; Equation 6.3.9-3; Table 6.3.9-2.
KdPa_Devit_a - Sorption coefficient for protactinium in devitrified tuff units of UZ (mL/g). *Distribution:* Truncated normal. *Range:* 1000 to 10000. *Mean:* 5500. *Standard Deviation:* 1500. *Sensitivity Name:* UZKDPADT. *Location in TSPA-LA:* Sections 6.3.9.2 and 6.3.9.3; Equation 6.3.9-3; Table 6.3.9-2.
KdPa_Vit_a* - Sorption coefficient for protactinium in vitrified tuff units of UZ (mL/g). *Distribution:* Truncated normal. *Range:* 1000 to 10000. *Mean:* 5500. *Standard Deviation:* 1500. *Sensitivity Name:* UZKDPAVT*. *Location in TSPA-LA:* Sections 6.3.9.2 and 6.3.9.3; Equation 6.3.9-3; Table 6.3.9-2.
KdPa_Zeo_a* - Sorption coefficient for protactinium in zeolitic tuff units of UZ (mL/g). *Distribution:* Truncated normal. *Range:* 1000 to 10000. *Mean:* 5500. *Standard Deviation:* 1500. *Sensitivity Name:* UZKDPAZT*. *Location in TSPA-LA:* Sections 6.3.9.2 and 6.3.9.3; Equation 6.3.9-3; Table 6.3.9-2.
KdPu_Devit_a - Sorption coefficient for plutonium in devitrified tuff units of UZ (mL/g). *Distribution:* Piecewise uniform. *Range:* 10 to 200. *Median:* 70. *Sensitivity Name:* UZKDPUDT. *Location in TSPA-LA:* Sections 6.3.9.2 and 6.3.9.3; Equation 6.3.9-3; Table 6.3.9-2.
KdPu_Vit_a* - Sorption coefficient for plutonium in vitrified tuff units of UZ (mL/g). *Distribution:* Piecewise uniform. *Range:* 10 to 200. *Median:* 100. *Sensitivity Name:* UZKDPUVT*. *Location in TSPA-LA:* Sections 6.3.9.2 and 6.3.9.3; Equation 6.3.9-3; Table 6.3.9-2.
KdPu_Zeo_a* - Sorption coefficient for plutonium in zeolitic tuff units of UZ (mL/g). *Distribution:* Piecewise uniform. *Range:* 10 to 200. *Median:* 100. *Sensitivity Name:* UZKDPUZT*. *Location in TSPA-LA:* Sections 6.3.9.2 and 6.3.9.3; Equation 6.3.9-3; Table 6.3.9-2.
KdRa_Devit_a* - Sorption coefficient for radium in devitrified tuff units of UZ (mL/g). *Distribution:* Uniform. *Range:* 100 to 1000. *Sensitivity Name:* UZKDRADT*. *Location in TSPA-LA:* Sections 6.3.9.2 and 6.3.9.3; Equation 6.3.9-3; Table 6.3.9-2.
KdRa_Vit_a* - Sorption coefficient for radium in vitrified tuff units of UZ (mL/g). *Distribution:* Uniform. *Range:* 50 to 600. *Sensitivity Name:* UZKDRAVT*. *Location in TSPA-LA:* Sections 6.3.9.2 and 6.3.9.3; Equation 6.3.9-3; Table 6.3.9-2.
KdRa_Zeo_a* - Sorption coefficient for radium in zeolitic tuff units of UZ (mL/g). *Distribution:* Uniform. *Range:* 1000 to 5000. *Sensitivity Name:* UZKDRAZT*. *Location in TSPA-LA:* Sections 6.3.9.2 and 6.3.9.3; Equation 6.3.9-3; Table 6.3.9-2.
KdSe_Devit_a - Sorption coefficient for selenium in devitrified tuff units of UZ (mL/g). *Distribution:* Truncated log normal. *Range:* 1 to 50. *Mean:* 14. *Standard Deviation:* 11.2. *Sensitivity Name:* UZKDSEDT. *Location in TSPA-LA:* Sections 6.3.9.2 and 6.3.9.3; Equation 6.3.9-3; Table 6.3.9-2.
KdSe_Vit_a* - Sorption coefficient for selenium in vitrified tuff units of UZ (mL/g). *Distribution:* Truncated log normal. *Range:* 0 to 25. *Mean:* 8.6. *Standard Deviation:* 7.9. *Sensitivity Name:* UZKDSEVT*. *Location in TSPA-LA:* Sections 6.3.9.2 and 6.3.9.3; Equation 6.3.9-3; Table 6.3.9-2.
KdSe_Zeo_a* - Sorption coefficient for selenium in zeolitic tuff units of UZ (mL/g). *Distribution:* Truncated log normal. *Range:* 1 to 35. *Mean:* 14.3. *Standard Deviation:* 7.9. *Sensitivity Name:* UZKDSEZT*. *Location in TSPA-LA:* Sections 6.3.9.2 and 6.3.9.3; Equation 6.3.9-3; Table 6.3.9-2.
KdSn_Devit_a - Sorption coefficient for tin in devitrified tuff units of UZ (mL/g). *Distribution:* Log-uniform. *Range:* 100 to 100000. *Sensitivity Name:* UZKDSNDT. *Location in TSPA-LA:* Sections 6.3.9.2 and 6.3.9.3; Equation 6.3.9-3; Table 6.3.9-2.
KdSn_Vit_a* - Sorption coefficient for tin in vitrified tuff units of UZ (mL/g). *Distribution:* Log-uniform. *Range:* 100 to 5000. *Sensitivity Name:* UZKDSNVT*. *Location in TSPA-LA:* Sections 6.3.9.2 and 6.3.9.3; Equation 6.3.9-3; Table 6.3.9-2.

Table K3-2. High-Level Summary of Epistemically Uncertain Variables (i.e., elements of **e**) Considered in the TSPA-LA (TSPA Parameter Name) (Continued)

NOTE: * indicates variable not considered in sensitivity analysis due to correlations.

KdSn_Zeo_a* - Sorption coefficient for tin in zeolitic tuff units of UZ (mL/g). *Distribution:* Log-uniform. *Range:* 100 to 5000. *Sensitivity Name:* UZKDSNZT*. *Location in TSPA-LA:* Sections 6.3.9.2 and 6.3.9.3; Equation 6.3.9-3; Table 6.3.9-2.
KdSr_Devit_a - Sorption coefficient for strontium in devitrified tuff units of UZ (mL/g). *Distribution:* Uniform. *Range:* 10 to 70. *Sensitivity Name:* UZKDSRDT. *Location in TSPA-LA:* Sections 6.3.9.2 and 6.3.9.3; Equation 6.3.9-3; Table 6.3.9-2.
KdSr_Vit_a* - Sorption coefficient for strontium in vitrified tuff units of UZ (mL/g). *Distribution:* Uniform. *Range:* 0 to 50. *Sensitivity Name:* UZKDSRVT*. *Location in TSPA-LA:* Sections 6.3.9.2 and 6.3.9.3; Equation 6.3.9-3; Table 6.3.9-2.
KdSr_Zeo_a* - Sorption coefficient for strontium in zeolitic tuff units of UZ (mL/g). *Distribution:* Uniform. *Range:* 50 to 2000. *Sensitivity Name:* UZKDSRZT*. *Location in TSPA-LA:* Sections 6.3.9.2 and 6.3.9.3; Equation 6.3.9-3; Table 6.3.9-2.
KdTh_Devit_a - Sorption coefficient for thorium in devitrified tuff units of UZ (mL/g). *Distribution:* Uniform. *Range:* 1000 to 10000. *Sensitivity Name:* UZKDTHDT. *Location in TSPA-LA:* Sections 6.3.9.2 and 6.3.9.3; Equation 6.3.9-3; Table 6.3.9-2.
KdTh_Vit_a* - Sorption coefficient for thorium in vitrified tuff units of UZ (mL/g). *Distribution:* Uniform. *Range:* 1000 to 10000. *Sensitivity Name:* UZKDTHVT*. *Location in TSPA-LA:* Sections 6.3.9.2 and 6.3.9.3; Equation 6.3.9-3; Table 6.3.9-2.
KdTh_Zeo_a* - Sorption coefficient for thorium in zeolitic tuff units of UZ (mL/g). *Distribution:* Uniform. *Range:* 1000 to 30000. *Sensitivity Name:* UZKDTHZT*. *Location in TSPA-LA:* Sections 6.3.9.2 and 6.3.9.3; Equation 6.3.9-3; Table 6.3.9-2.
KdU_Devit_a - Sorption coefficient for uranium in devitrified tuff units of UZ (mL/g). *Distribution:* Piecewise uniform. *Range:* 0 to 4. *Median:* 0.2. *Sensitivity Name:* UZKDUDT. *Location in TSPA-LA:* Sections 6.3.9.2 and 6.3.9.3; Equation 6.3.9-3; Table 6.3.9-2.
KdU_Vit_a* - Sorption coefficient for uranium in vitrified tuff units of UZ (mL/g). *Distribution:* Piecewise uniform. *Range:* 0 to 3. *Median:* 0.2. *Sensitivity Name:* UZKDUVT*. *Location in TSPA-LA:* Sections 6.3.9.2 and 6.3.9.3; Equation 6.3.9-3; Table 6.3.9-2.
KdU_Zeo_a* - Sorption coefficient for uranium in zeolitic tuff units of UZ (mL/g). *Distribution:* Piecewise uniform. *Range:* 0 to 30. *Median:* 0.5. *Sensitivity Name:* UZKDUZT*. *Location in TSPA-LA:* Sections 6.3.9.2 and 6.3.9.3; Equation 6.3.9-3; Table 6.3.9-2.
L_Divides_a - Depth of permeable soil on divides of the Fortymile Wash fan (RMEI location) (cm). *Distribution:* Uniform. *Range:* 102 to 140. *Sensitivity Name:* LDIVIDE. *Location in TSPA-LA:* Table 6.5-5.
LC_rate_a - Crevice corrosion (localized corrosion) propagation rate (mm/yr). *Distribution:* Log uniform. *Range:* 0.0127 to 1.27. *Sensitivity Name:* WDLCRATE. *Location in TSPA-LA:* Sections 6.3.5.2.1, 6.3.5.2.2, 6.3.5.2.3, 6.3.5.3.2 and 6.3.5.4; Table 6.3.5-4.
LDISP – Logarithm of longitudinal dispersivity (m). *Distribution:* Right truncated normal. *Range*: $-\infty$ to 3.5. *Mean:* 2.0. *Standard Deviation:* 0.75. *Sensitivity Name:* SZLODISP. *Location in TSPA-LA:* Section 6.3.10.2; Table 6.3.10-2.
Log_Specific_SA_CSNF_a - Logarithm of the effective specific surface area (m^2/mg) of the representative CSNF waste form (dimensionless). *Distribution:* Triangular. *Range:* -7.3 to -5.4. *Most Likely:* -6.7. *Sensitivity Name:* CSSPECSA. *Location in TSPA-LA:* Sections 6.3.7.4.1.2 and 6.3.7.4.1.3; Tables 6.3.7-30 and 6.3.7-31; Equations 6.3.7-5 and 6.3.7-6.
LogK_Uncert_Lith_a - Logarithm of the mean fracture permeability in lithophysal rock units (dimensionless). *Distribution:* Triangular. *Range:* -0.92 to 0.92. *Mode:* 0. *Sensitivity Name:* SEEPPRM. *Location in TSPA-LA:* Sections 6.3.5.2.3, 6.3.3.1.2 and 6.3.3.1.3; Tables 6.3.5-4, 6.3.3-2 and 6.3.3-3.
LogK_Uncert_NonLith_a - Logarithm of the mean fracture permeability in non-lithophysal rock units (dimensionless). *Distribution:* Triangular. *Range:* -0.68 to 0.68. *Mode:* 0. *Sensitivity Name:* SEEPPRMN. *Location in TSPA-LA:* Sections 6.3.5.2.3, 6.3.3.1.2 and 6.3.3.1.3; Tables 6.3.5-4, 6.3.3-2 and 6.3.3-3.
Mass_Decrease_Const_GE10_a - Mass loading decrease rate constant (1/yr). *Distribution:* Triangular. *Range:* 0.125 to 1. *Mode:* 0.2. *Sensitivity Name:* MASSDCRS. *Location in TSPA-LA:* Equation 6.3.11-5.

Table K3-2. High-Level Summary of Epistemically Uncertain Variables (i.e., elements of **e**) Considered in the TSPA-LA (TSPA Parameter Name) (Continued)

NOTE: * indicates variable not considered in sensitivity analysis due to correlations.

MIC_RHThresh_a - Relative humidity threshold for initiating microbially induced corrosion (dimensionless). *Distribution:* Uniform. *Range:* 0.75 to 0.9. *Sensitivity Name:* WDMICRHT. *Location in TSPA-LA:* Sections 6.3.5.1.2 and 6.3.5.1.3; Tables 6.3.5-3 and 6.3.5-4.
n_SCC_a - Stress corrosion cracking growth rate exponent (repassivation slope) (dimensionless). *Distribution:* Truncated normal. *Range:* 0.935 to 1.395. *Mean:* 1.165. *Standard Deviation:* 0.115. *Sensitivity Name:* WDNSCC. *Location in TSPA-LA:* Sections 6.3.5.1.2 and 6.3.5.4; Table 6.3.5-3; Equations 6.3.5-13 and 6.3.5-14.
NiO_SA_a - Specific surface area of NiO (m^2/g). *Distribution:* Uniform. *Range:* 1 to 30. *Sensitivity Name:* NIOSA. *Location in TSPA-LA:* Table 6.3.8-4; S_{CP} in Equation 6.3.8-19.
Np2O5_Eps_1_high_a* - Logarithm of the scale factor used to characterize uncertainty in Np_2O_5 solubility for ionic strength values between 1 and 3 molal (dimensionless). *Distribution:* Truncated normal. *Range:* -1.7 to 1.7. *Mean:* 0. *Standard Deviation:* 0.85. *Sensitivity Name:* EP1HINP2*. *Location in TSPA-LA:* Sections 6.3.7.5.1 and 6.3.7.5.2; Table 6.3.7-42; Equation 6.3.7-13a.
Np2O5_Eps_1_low_a - Logarithm of the scale factor used to characterize uncertainty in Np_2O_5 solubility at an ionic strength below 1 molal (dimensionless). *Distribution:* Truncated normal. *Range:* -1.6 to 1.6. *Mean:* 0. *Standard Deviation:* 0.8. *Sensitivity Name:* EP1NP2O5. *Location in TSPA-LA:* Sections 6.3.7.5.1 and 6.3.7.5.2; Table 6.3.7-42; Equation 6.3.7-13a.
Np2O5_Eps_2_CDSP_High_a* - Term associated with uncertainty in Np_2O_5 solubility due to variations in fluoride concentration for CDSP waste packages when ionic strength is greater than or equal to 0.004 molal and for the invert below CDSP waste packages (mg/L). *Distribution:* Triangular. *Range:* 0 to 853. *Most Likely:* 0. *Sensitivity Name:* EP2CDNP2*. *Location in TSPA-LA:* Sections 6.3.7.5.1 and 6.3.7.5.2; Table 6.3.7-42; Equation 6.3.7-13a.
Np2O5_Eps_2_CSNF_High_a* - Term associated with uncertainty in Np_2O_5 solubility due to variations in fluoride concentration for CSNF waste packages when ionic strength is greater than or equal to 0.2 molal and for the invert below CSNF waste packages (mg/L). *Distribution:* Triangular. *Range:* 0 to 197. *Most Likely:* 0. *Sensitivity Name:* EP2CSNP2*. *Location in TSPA-LA:* Sections 6.3.7.5.1 and 6.3.7.5.2; Table 6.3.7-42; Equation 6.3.7-13a.
Np2O5_Eps_2_Glass_Low_a* - Term associated with uncertainty in Np_2O_5 solubility due to variations in fluoride concentration for CDSP waste packages Cell 1a, Cell 1b when ionic strength is less than 0.004 molal, and CSNF waste packages when ionic strength is less than 0.2 molal (mg/L). *Distribution:* Triangular. *Range:* 0 to 11. *Most Likely:* 0. *Sensitivity Name:* EP2LONP2*. *Location in TSPA-LA:* Sections 6.3.7.5.1 and 6.3.7.5.2; Table 6.3.7-42; Equation 6.3.7-13a.
NpO2_Eps_1_high_a* - Logarithm of the scale factor used to characterize uncertainty in NpO_2 solubility at an ionic strength between 1 and 3 molal (dimensionless). *Distribution:* Truncated normal. *Range:* -1.34 to 1.34. *Mean:* 0. *Standard Deviation:* 0.67. *Sensitivity Name:* EP1HINPO2*. *Location in TSPA-LA:* Sections 6.3.7.5.1, 6.3.7.5.2 and 6.3.7.5.3; Table 6.3.7-43; Equation 6.3.7-13a.
NpO2_Eps_1_low_a - Logarithm of the scale factor used to characterize uncertainty in NpO_2 solubility at an ionic strength below 1 molal (dimensionless). *Distribution:* Truncated normal. *Range:* -1.2 to 1.2. *Mean:* 0. *Standard Deviation:* 0.6. *Sensitivity Name:* EP1NPO2. *Location in TSPA-LA:* Sections 6.3.7.5.1, 6.3.7.5.2 and 6.3.7.5.3; Table 6.3.7-43; Equation 6.3.7-13a.
NpO2_Eps_2_CDSP_High_a* - Term associated with uncertainty in NpO_2 solubility due to variations in fluoride concentration for CDSP waste packages when ionic strength is greater than or equal to 0.004 molal and for the invert below CDSP waste packages (mg/L). *Distribution:* Triangular. *Range:* 0 to 1093.5. *Most Likely:* 0. *Sensitivity Name:* EP2CDNPO2*. *Location in TSPA-LA:* Sections 6.3.7.5.1, 6.3.7.5.2 and 6.3.7.5.3; Table 6.3.7-43; Equation 6.3.7-13a.
NpO2_Eps_2_CSNF_High_a* - Term associated with uncertainty in NpO_2 solubility due to variations in fluoride concentration for CSNF waste packages when ionic strength is greater than or equal to 0.2 molal and for the invert below CSNF waste packages (mg/L). *Distribution:* Triangular. *Range:* 0 to 255.8. *Most Likely:* 0. *Sensitivity Name:* EP2CSNPO2*. *Location in TSPA-LA:* Sections 6.3.7.5.1, 6.3.7.5.2 and 6.3.7.5.3; Table 6.3.7-43; Equation 6.3.7-13a.
NpO2_Eps_2_Glass_Low_a* - Term associated with uncertainty in NpO_2 solubility due to variations in fluoride concentration for CDSP waste packages Cell 1a, Cell 1b when ionic strength is less than 0.004 molal, and CSNF waste packages when ionic strength is less than 0.2 molal (mg/L). *Distribution:* Triangular. *Range:* 0 to 14.1. *Most Likely:* 0. *Sensitivity Name:* EP2LONPO2*. *Location in TSPA-LA:* Sections 6.3.7.5.1, 6.3.7.5.2 and 6.3.7.5.3; Table 6.3.7-43; Equation 6.3.7-13a.

Table K3-2. High-Level Summary of Epistemically Uncertain Variables (i.e., elements of **e**) Considered in the TSPA-LA (TSPA Parameter Name) (Continued)

NOTE: * indicates variable not considered in sensitivity analysis due to correlations.

NVF11 - Effective porosity in undifferentiated alluvium (valley fill) (dimensionless). *Distribution:* Truncated normal. *Range:* 0 to 0.3. *Mean:* 0.18. *Standard Deviation:* 0.051. *Sensitivity Name:* SZPORUAL. *Location in TSPA-LA:* Table 6.3.10-2.
NVF26 - Effective porosity in shallow alluvium (dimensionless). *Distribution:* Truncated normal. *Range:* 0 to 0.3. *Mean:* 0.18. *Standard Deviation:* 0.051. *Sensitivity Name:* SZPORSAL. *Location in TSPA-LA:* Table 6.3.10-2.
Pa_Eps_1_a - Logarithm of the scale factor used to characterize uncertainty in protactinium solubility (dimensionless). *Distribution:* Uniform. *Range:* -4.42 to -0.05. *Sensitivity Name:* EP1PA. *Location in TSPA-LA:* Sections 6.3.7.5.2 and 6.3.7.5.3; Table 6.3.7-45; Equation 6.3.7-13b.
Pa_Eps_2_CDSP_High_a* - Term associated with uncertainty in protactinium solubility due to variations in fluoride concentration for CDSP waste packages when ionic strength is greater than or equal to 0.004 molal and for the invert below CDSP waste packages (mg/L). *Distribution:* Triangular. *Range:* 0 to 853. *Most Likely:* 0. *Sensitivity Name:* EP2CDPA*. *Location in TSPA-LA:* Sections 6.3.7.5.2 and 6.3.7.5.3; Table 6.3.7-45; Equation 6.3.7-13b.
Pa_Eps_2_CSNF_High_a* - Term associated with uncertainty in protactinium solubility due to variations in fluoride concentration for CSNF waste packages when ionic strength is greater than or equal to 0.2 molal and for the invert below CSNF waste packages (mg/L). *Distribution:* Triangular. *Range:* 0 to 197. *Most Likely:* 0. *Sensitivity Name:* EP2CSPA*. *Location in TSPA-LA:* Sections 6.3.7.5.2 and 6.3.7.5.3; Table 6.3.7-45; Equation 6.3.7-13b.
Pa_Eps_2_Glass_Low_a* - Term associated with uncertainty in protactinium solubility due to variations in fluoride concentration for CDSP waste packages Cell 1a, Cell 1b when ionic strength is less than 0.004 molal, and CSNF waste packages when ionic strength is less than 0.2 molal (mg/L). *Distribution:* Triangular. *Range:* 0 to 11. *Most Likely:* 0. *Sensitivity Name:* EP2LOPA*. *Location in TSPA-LA:* Sections 6.3.7.5.2 and 6.3.7.5.3; Table 6.3.7-45; Equation 6.3.7-13b.
PCE_CI_MU_RH_0_20_a - The IDPS process model uncertainty factor for the logarithm of the chloride concentration of the in-drift waters at relative humidity ≤20% (dimensionless). *Distribution:* Triangular. *Range:* -0.7 to 0.7. *Most Likely:* 0. *Sensitivity Name:* RHMU0. *Location in TSPA-LA:* Sections 6.3.4, 6.3.4.2, 6.3.4.3.1, 6.3.4.3.2 and 6.3.5.2.3; Tables 6.3.4-2, 6.3.4-3 and 6.3.5-4.
PCE_CI_MU_RH_20_40_a - The IDPS process model uncertainty factor for the logarithm of the chloride concentration of the in-drift waters at relative humidity >20 and ≤40% (dimensionless). *Distribution:* Triangular. *Range:* -0.5 to 0.5. *Most Likely:* 0. *Sensitivity Name:* RHMU20. *Location in TSPA-LA:* Sections 6.3.4, 6.3.4.2, 6.3.4.3.1, 6.3.4.3.2 and 6.3.5.2.3; Tables 6.3.4-2, 6.3.4-3 and 6.3.5-4.
PCE_CI_MU_RH_40_65_a – The IDPS process model uncertainty factor for the logarithm of the chloride concentration of the in-drift waters at relative humidity >40 and ≤65% (dimensionless). *Distribution:* Triangular. *Range:* -0.4 to 0.4. *Most Likely:* 0. *Sensitivity Name:* RHMU40. *Location in TSPA-LA:* Sections 6.3.4, 6.3.4.2, 6.3.4.3.1, 6.3.4.3.2 and 6.3.5.2.3; Tables 6.3.4-2, 6.3.4-3 and 6.3.5-4.
PCE_CI_MU_RH_65_85_a - The IDPS process model uncertainty factor for the logarithm of the chloride concentration of the in-drift waters at relative humidity >65 and ≤85% (dimensionless). *Distribution:* Triangular. *Range:* -0.1 to 0.1. *Most Likely:* 0. *Sensitivity Name:* RHMU65. *Location in TSPA-LA:* Sections 6.3.4, 6.3.4.2, 6.3.4.3.1, 6.3.4.3.2 and 6.3.5.2.3; Tables 6.3.4-2, 6.3.4-3 and 6.3.5-4.
PCE_CI_MU_RH_85_100_a* - The IDPS process model uncertainty factor for the logarithm of the chloride concentration of the in-drift waters at relative humidity >85% (dimensionless). *Distribution:* Triangular. *Range:* 0 to 0. *Most Likely:* 0. *Sensitivity Name:* RHMU85*. *Location in TSPA-LA:* Sections 6.3.4, 6.3.4.2, 6.3.4.3.1, 6.3.4.3.2 and 6.3.5.2.3; Tables 6.3.4-2, 6.3.4-3 and 6.3.5-4.
PCE_CI_N_MU_RH_40_65_a - The IDPS process model uncertainty factor for the logarithm of the chloride + nitrate concentration of the in-drift waters at relative humidity >40% and ≤65% (dimensionless). *Distribution:* Triangular. *Range:* -0.57 to 0.57. *Most Likely:* 0. *Sensitivity Name:* RHMUN40. *Location in TSPA-LA:* Sections 6.3.4.3.2 and 6.3.5.2.3; Tables 6.3.4-2, 6.3.4-3 and 6.3.5-4.
PCE_CI_N_MU_RH_65_85_a - The IDPS process model uncertainty factor for the logarithm of the chloride + nitrate concentration of the in-drift waters at relative humidity >65% and ≤85% (dimensionless). *Distribution:* Triangular. *Range:* -0.22 to 0.22. *Most Likely:* 0. *Sensitivity Name:* RHMUN65. *Location in TSPA-LA:* Sections 6.3.4.3.2 and 6.3.5.2.3; Tables 6.3.4-2, 6.3.4-3 and 6.3.5-4.

Table K3-2. High-Level Summary of Epistemically Uncertain Variables (i.e., elements of **e**) Considered in the TSPA-LA (TSPA Parameter Name) (Continued)

NOTE: * indicates variable not considered in sensitivity analysis due to correlations.

PCE_Cl_N_MU_RH_85_100_a* - The in-drift precipitates/salts (IDPS) process model uncertainty factor for the logarithm of the chloride + nitrate concentration of the in-drift waters at relative humidity >85% (dimensionless). *Distribution:* Triangular. *Range:* 0 to 0. *Most Likely:* 0. *Sensitivity Name:* RHMUN85*. *Location in TSPA-LA:* Sections 6.3.4.3.2 and 6.3.5.2.3; Tables 6.3.4-2, 6.3.4-3 and 6.3.5-4.
PCE_Cl_NO3_MU_RH_0_20_a - The IDPS process model uncertainty factor for the logarithm of the chloride to nitrate ratio of the in-drift waters at relative humidity ≤20% (dimensionless). *Distribution:* Triangular. *Range:* -1.4 to 1.4. *Most Likely:* 0. *Sensitivity Name:* RHMUNO0. *Location in TSPA-LA:* Sections 6.3.4.3.1, 6.3.4.3.2 and 6.3.5.2.3; Tables 6.3.4-2, 6.3.4-3 and 6.3.5-4.
PCE_Cl_NO3_MU_RH_20_65_a - The IDPS process model uncertainty factor for the logarithm of the chloride to nitrate ratio of the in-drift waters at relative humidity >20% and ≤65% (dimensionless). *Distribution:* Triangular. *Range:* -0.5 to 0.5. *Most Likely:* 0. *Sensitivity Name:* RHMUNO20. *Location in TSPA-LA:* Sections 6.3.4.3.1, 6.3.4.3.2 and 6.3.5.2.3; Tables 6.3.4-2, 6.3.4-3 and 6.3.5-4.
PCE_Cl_NO3_MU_RH_65_85_a – The IDPS process model uncertainty factor for the logarithm of the chloride to nitrate ratio of the in-drift waters at relative humidity >65% and ≤85% (dimensionless). *Distribution:* Triangular. *Range:* -0.2 to 0.2. *Most Likely:* 0. *Sensitivity Name:* RHMUNO65. *Location in TSPA-LA:* Sections 6.3.4.3.1, 6.3.4.3.2 and 6.3.5.2.3; Tables 6.3.4-2, 6.3.4-3 and 6.3.5-4.
PCE_Cl_NO3_MU_RH_85_100_a* - The IDPS process model uncertainty factor for the logarithm of the chloride to nitrate ratio of the in-drift waters at low relative humidity >85% (dimensionless). *Distribution:* Triangular. *Range:* 0 to 0. *Most Likely:* 0. *Sensitivity Name:* RHMUNO85*. *Location in TSPA-LA:* Sections 6.3.4.3.1, 6.3.4.3.2 and 6.3.5.2.3; Tables 6.3.4-2, 6.3.4-3 and 6.3.5-4.
PCE_Delta_pCO2_a - Selector variable for partial pressure of CO_2 (dimensionless). *Distribution:* Uniform. *Range:* -1 to 1. *Sensitivity Name:* DELPPCO2. *Location in TSPA-LA:* Sections 6.3.4.2 and 6.3.5.2.3; Table 6.3.5-4.
PCE_Gp1_Cl_NO3_CDF_a - Ratio of Cl to NO_3 (Cl:N) in Group 1 pore waters (dimensionless). *Distribution:* Discrete. *Range:* 0.783 to 6.1213. *Sensitivity Name:* GP1NO3. *Location in TSPA-LA:* Section 6.3.4.3.2.
PCE_Gp2_Cl_NO3_CDF_a - Ratio of Cl to NO_3 (Cl:N) in Group 2 pore waters (dimensionless). *Distribution:* Discrete. *Range:* 2.359 to 3.187. *Sensitivity Name:* GP2NO3. *Location in TSPA-LA:* Section 6.3.4.3.2.
PCE_Gp3_Cl_NO3_CDF_a - Ratio of Cl to NO_3 (Cl:N) in Group 3 pore waters (dimensionless). *Distribution:* Discrete. *Range:* 9.7782 to 64.128. *Sensitivity Name:* GP3NO3. *Location in TSPA-LA:* Section 6.3.4.3.2.
PCE_Gp4_Cl_NO3_CDF_a - Ratio of Cl to NO_3 (Cl:N) in Group 4 pore waters (dimensionless). *Distribution:* Discrete. *Range:* 4.4485 to 8.2119. *Sensitivity Name:* GP4NO3. *Location in TSPA-LA:* Section 6.3.4.3.2.
PCE_I_Uncert_RH_85_100_a - The IDPS process model uncertainty factor for the logarithm of the ionic strength of the in-drift waters at high relative humidity (≥85%) (log molal). *Distribution:* Triangular. *Range:* -0.1 to 0.1. *Mean/Median/Mode:* 0. *Sensitivity Name:* RHI85. *Location in TSPA-LA:* Section 6.4.1; Tables 6.4-1 and 6.4-2; Figure 6.4-4.
PCE_pH_Uncert_RH_0_65_a - The IDPS process model uncertainty factor for the pH of the in-drift waters at relative humidity ≤65% (dimensionless). *Distribution:* Triangular. *Range:* -2 to 2. *Most Likely:* 0. *Sensitivity Name:* RHPH0. *Location in TSPA-LA:* Table 6.3.5-4.
PCE_pH_Uncert_RH_65_75_a - The IDPS process model uncertainty factor for the pH of the in-drift waters at relative humidity >65 and ≤75% (dimensionless). *Distribution:* Triangular. *Range:* -1 to 1. *Most Likely:* 0. *Sensitivity Name:* RHPH65. *Location in TSPA-LA:* Table 6.3.5-4
PCE_pH_Uncert_RH_75_100_a - The IDPS process model uncertainty factor for the pH of the in-drift waters at relative humidity >75% (dimensionless). *Distribution:* Discrete. *Range:* -0.3123 to 0.4288. *Sensitivity Name:* RHPH75. *Location in TSPA-LA:* Table 6.3.5-4
pH_Cell2_Regression_Error_a - Error term in regression equation for pH of corrosion products domain (dimensionless). *Distribution:* Truncated normal. *Range:* -0.64 to 0.64. *Mean/Median/Mode:* 0. *Standard Deviation:* 0.32. *Sensitivity Name:* PH2RGER. *Location in TSPA-LA:* Equation 6.3.8-27.
Pu_Eps_1_high_a* - Logarithm of the scale factor used to characterize uncertainty in plutonium solubility for ionic strength between 1 and 3 molal (dimensionless). *Distribution:* Truncated normal. *Range:* -1.52 to 1.52. *Mean:* 0. *Standard Deviation:* 0.76. *Sensitivity Name:* EP1HIPU*. *Location in TSPA-LA:* Sections 6.3.7.5.1, 6.3.7.5.2 and 6.3.7.5.3; Table 6.3.7-44; Equation 6.3.7-13a.

Table K3-2. High-Level Summary of Epistemically Uncertain Variables (i.e., elements of **e**) Considered in the TSPA-LA (TSPA Parameter Name) (Continued)

NOTE: * indicates variable not considered in sensitivity analysis due to correlations.

Pu_Eps_1_low_a - Logarithm of the scale factor used to characterize uncertainty in plutonium solubility at an ionic strength below 1 molal (dimensionless). *Distribution:* Truncated normal. *Range:* -1.4 to 1.4. *Mean/Median/Mode:* 0. *Standard Deviation:* 0.7. *Sensitivity Name:* EP1LOWPU. *Location in TSPA-LA:* Sections 6.3.7.5.1, 6.3.7.5.2 and 6.3.7.5.3; Table 6.3.7-44; Equation 6.3.7-13a.
Pu_Eps_2_CDSP_High_a* - Term associated with uncertainty in plutonium solubility due to variations in fluoride concentration for CDSP waste packages when ionic strength is greater than or equal to 0.004 molal and for the invert below CDSP waste packages (mg/L). *Distribution:* Triangular. *Range:* 0 to 5460. *Most Likely:* 0. *Sensitivity Name:* EP2CDPU*. *Location in TSPA-LA:* Sections 6.3.7.5.1, 6.3.7.5.2 and 6.3.7.5.3; Table 6.3.7-44; Equation 6.3.7-13a.
Pu_Eps_2_CSNF_High_a* - Term associated with uncertainty in plutonium solubility due to variations in fluoride concentration for CSNF waste packages when ionic strength is greater than or equal to 0.2 molal and for the invert below CSNF waste packages (mg/L). *Distribution:* Triangular. *Range:* 0 to 1374. *Most Likely:* 0. *Sensitivity Name:* EP2CSPU*. *Location in TSPA-LA:* Sections 6.3.7.5.1, 6.3.7.5.2 and 6.3.7.5.3; Table 6.3.7-44; Equation 6.3.7-13a.
Pu_Eps_2_Glass_Low_a* - Term associated with uncertainty in plutonium solubility due to variations in fluoride concentration for CDSP waste packages Cell 1a, Cell 1b when ionic strength is less than 0.004 molal, and CSNF waste packages when ionic strength is less than 0.2 molal (mg/L). *Distribution:* Triangular. *Range:* 0 to 79. *Most Likely:* 0. *Sensitivity Name:* EP2LOWPU*. *Location in TSPA-LA:* Sections 6.3.7.5.1, 6.3.7.5.2 and 6.3.7.5.3; Table 6.3.7-44; Equation 6.3.7-13a.
Relative_Abundance_Goethite_a - Fraction of total iron oxide that is goethite (dimensionless). *Distribution:* Uniform. *Range:* 0.45 to 0.8. *Sensitivity Name:* GOERELAB. *Location in TSPA-LA:* Section 6.3.8.2.3; Table 6.3.8-4.
Resuspension_Thickness_a - Thickness of combined ash/soil mixture available for resuspension (m). *Distribution:* Uniform. *Range:* 0.001 to 0.003. *Mean/Median/Mode:* 0.002. *Sensitivity Name:* RSUSTHIK. *Location in TSPA-LA:* Equation 6.3.11-6.
Rind_Porosity_CSNF_a - Porosity in CSNF rind (dimensionless). *Distribution:* Uniform. *Range:* 0.05 to 0.3. *Sensitivity Name:* CSRINDPO. *Location in TSPA-LA:* Section 6.3.8.2.1; Table 6.3.8-6.
Schoepite_Boltwoodite_Interp_a - Fractional value used to interpolate between Schoepite and Boltwoodite look-up tables (dimensionless). *Distribution:* Uniform. *Range:* 0 to 1. *Sensitivity Name:* SCHOBOLT. *Location in TSPA-LA:* Table 6.3.7-58.
Scour_Depth_a - Scour depth in Fortymile Wash at the fan apex (cm). *Distribution:* Uniform. *Range:* 73 to 122. *Sensitivity Name:* SC_DPTH. *Location in TSPA-LA:* Table 6.5-5.
Seepage_Condensation_Prob_a* - Pointer variable to determine the seepage/condensation regime for the first failed waste package in a percolation subregion (dimensionless). *Distribution:* Uniform. *Range:* 0 to 1. *Sensitivity Name:* SEEPCON*.
Seepage_Uncertainty_a - Uncertainty factor to account for small-scale heterogeneity in fracture permeability (dimensionless). *Distribution:* Uniform. *Range:* 0 to 1. *Sensitivity Name:* SEEPUNC. *Location in TSPA-LA:* Section 6.3.3.1.2; Tables 6.3.3-3 and 6.3.5-4.
Seepage_Water_Type_a - Pointer variable used to select which seepage water type in used in the physical and chemical environment (P&CE) submodel calculations (dimensionless). *Distribution:* Discrete. *Range:* 1 to 4. *Sensitivity Name:* SEEPWAT. *Location in TSPA-LA:* Table 6.3.5-4.
Sn_Eps_high_a* - Logarithm of the scale factor used to characterize uncertainty in tin solubility for high ionic strength conditions (dimensionless). *Distribution:* Truncated normal. *Range:* -1.08 to 1.08. *Mean:* 0. *Standard Deviation:* 0.54. *Sensitivity Name:* EP1HISN*. *Location in TSPA-LA:* Sections 6.3.7.5.2 and 6.3.7.5.3; Table 6.3.7-47; Equation 6.3.7-13a.
Sn_Eps_low_a - Logarithm of the scale factor used to characterize uncertainty in tin solubility for low ionic strength conditions (dimensionless). *Distribution:* Truncated normal. *Range:* -0.9 to 0.9. *Mean/Median/Mode:* 0. *Standard Deviation:* 0.45. *Sensitivity Name:* EP1LOWSN. *Location in TSPA-LA:* Sections 6.3.7.5.2 and 6.3.7.5.3; Table 6.3.7-47; Equation 6.3.7-13a.
Soil_Density_a - Density of surface soil correlated with the volcanic BDCFs (kg/m^3). *Distribution:* Triangular. *Range:* 1300 to 1700. *Mean/Median/Mode:* 1500. *Sensitivity Name:* SOILDENS. *Location in TSPA-LA:* Equation 6.3.11-6.

Table K3-2. High-Level Summary of Epistemically Uncertain Variables (i.e., elements of **e**) Considered in the TSPA-LA (TSPA Parameter Name) (Continued)

NOTE: * indicates variable not considered in sensitivity analysis due to correlations.

Specific_SA_Smectite_Col_a - Specific surface area for smectite colloids (m^2/g). *Distribution:* Uniform. *Range:* 10 to 100. *Sensitivity Name:* SMECSA. *Location in TSPA-LA:* Table 6.3.7-62.
SRC1X - Relative x location of point source in source region 1 (dimensionless). *Distribution:* Uniform. *Range:* 0 to 1. *Sensitivity Name:* SZSREG1X. *Location in TSPA-LA:* Section 6.3.10.2; Table 6.3.10-2.
SRC1Y - Relative y location of point source in source region 1 (dimensionless). *Distribution:* Uniform. *Range:* 0 to 1. *Sensitivity Name:* SZSREG1Y. *Location in TSPA-LA:* Section 6.3.10.2; Table 6.3.10-2.
SRC2X - Relative x location of point source in source region 2 (dimensionless). *Distribution:* Uniform. *Range:* 0 to 1. *Sensitivity Name:* SZSREG2X. *Location in TSPA-LA:* Section 6.3.10.2; Table 6.3.10-2.
SRC2Y - Relative y location of point source in source region 2 (dimensionless). *Distribution:* Uniform. *Range:* 0 to 1. *Sensitivity Name:* SZSREG2Y. *Location in TSPA-LA:* Section 6.3.10.2; Table 6.3.10-2.
SRC3X - Relative x location of point source in source region 3 (dimensionless). *Distribution:* Uniform. *Range:* 0 to 1. *Sensitivity Name:* SZSREG3X. *Location in TSPA-LA:* Section 6.3.10.2; Table 6.3.10-2.
SRC3Y - Relative y location of point source in source region 3 (dimensionless). *Distribution:* Uniform. *Range:* 0 to 1. *Sensitivity Name:* SZSREG3Y. *Location in TSPA-LA:* Section 6.3.10.2; Table 6.3.10-2.
SRC4X - Relative x location of point source in source region 4 (dimensionless). *Distribution:* Uniform. *Range:* 0 to 1. *Sensitivity Name:* SZSREG4X. *Location in TSPA-LA:* Section 6.3.10.2; Table 6.3.10-2.
SRC4Y - Relative y location of point source in source region 4 (dimensionless). *Distribution:* Uniform. *Range:* 0 to 1. *Sensitivity Name:* SZSREG4Y. *Location in TSPA-LA:* Section 6.3.10.2; Table 6.3.10-2.
SS_Corrosion_Rate_a - Stainless steel corrosion rate (□m/yr). *Distribution:* Truncated log normal. *Range:* 0.01 to 0.51. *Mean/Median/Mode:* 0.267. *Standard Deviation:* 0.209. *Sensitivity Name:* CORRATSS. *Location in TSPA-LA:* Tables 6.3.8-1 and 6.3.8-4.
Stress_Thresh_A22_a - Residual stress threshold for SCC nucleation of Alloy 22 (as a percentage of yield strength in MPa) (dimensionless). *Distribution:* Uniform. *Range:* 90 to 105. *Sensitivity Name:* SCCTHRP. *Location in TSPA-LA:* Section 6.6.1.3.7; Table 6.6-2.
Stress_Thresh_SCC_a - Stress threshold for stress corrosion cracking (MPa). *Distribution:* Uniform. *Range:* 315.9 to 368.55. *Sensitivity Name:* SCCTHR. *Location in TSPA-LA:* Table 6.3.5-3.
Target_Flux_Out_Ratio_a - Ratio of radionuclide mass associated with colloids (reversible and irreversible) to radionuclide mass associated with colloids and dissolved radionuclide mass (dimensionless). *Distribution:* Uniform. *Range:* 0.9 to 0.99. *Sensitivity Name:* CFLUXOUT. *Location in TSPA-LA:* Table 6.3.7-65.
Th_Eps_1_high_a* - Logarithm of the scale factor used to characterize uncertainty in thorium solubility at ionic strength between 1 and 3 molal (dimensionless). *Distribution:* Truncated normal. *Range:* -1.52 to 1.52. *Mean:* 0. *Standard Deviation:* 0.76. *Sensitivity Name:* EP1HITH*. *Location in TSPA-LA:* Sections 6.3.7.5.1, 6.3.7.5.2 and 6.3.7.5.3; Table 6.3.7-46; Equation 6.3.7-13a.
Th_Eps_1_low_a - Logarithm of the scale factor used to characterize uncertainty in thorium solubility at an ionic strength below 1 molal (dimensionless). *Distribution:* Truncated normal. *Range:* -1.4 to 1.4. *Mean:* 0. *Standard Deviation:* 0.7. *Sensitivity Name:* EP1LOWTH. *Location in TSPA-LA:* Sections 6.3.7.5.1, 6.3.7.5.2 and 6.3.7.5.3; Table 6.3.7-46; Equation 6.3.7-13a.
Th_Eps_2_CDSP_High_a* - Term associated with uncertainty in thorium solubility due to variations in fluoride concentration for CDSP waste packages when ionic strength is greater than or equal to 0.004 molal and for the invert below CDSP waste packages (mg/L). *Distribution:* Triangular. *Range:* 0 to 23723.2. *Most Likely:* 0. *Sensitivity Name:* EP2CDTH*. *Location in TSPA-LA:* Sections 6.3.7.5.1, 6.3.7.5.2 and 6.3.7.5.3; Table 6.3.7-46; Equation 6.3.7-13a.
Th_Eps_2_CSNF_High_a* - Term associated with uncertainty in thorium solubility due to variations in fluoride concentration for CSNF waste packages when ionic strength is greater than or equal to 0.2 molal and for the invert below CSNF waste packages (mg/L). *Distribution:* Triangular. *Range:* 0 to 7848.3. *Most Likely:* 0. *Sensitivity Name:* EP2CSTH*. *Location in TSPA-LA:* Sections 6.3.7.5.1, 6.3.7.5.2 and 6.3.7.5.3; Table 6.3.7-46; Equation 6.3.7-13a.

Table K3-2. High-Level Summary of Epistemically Uncertain Variables (i.e., elements of **e**) Considered in the TSPA-LA (TSPA Parameter Name) (Continued)

NOTE: * indicates variable not considered in sensitivity analysis due to correlations.

Th_Eps_2_Glass_Low_a* - Term associated with uncertainty in thorium solubility due to variations in fluoride concentration for CDSP waste packages Cell 1a, Cell 1b when ionic strength is less than 0.004 molal, and CSNF waste packages when ionic strength is less than 0.2 molal (mg/L). *Distribution:* Triangular. *Range:* 0 to 626.2. *Most Likely:* 0. *Sensitivity Name:* EP2LOWTH*. *Location in TSPA-LA:* Sections 6.3.7.5.1, 6.3.7.5.2 and 6.3.7.5.3; Table 6.3.7-46; Equation 6.3.7-13a.
Thermal_Conductivity_Uncert_a - Selector variable for one of three host-rock thermal conductivity scenarios (low, mean, and high) (dimensionless). *Distribution:* Discrete. *Range:* 1 to 3. *Sensitivity Name:* THERMCON. *Location in TSPA-LA:* Sections 6.3.2.2, 6.3.2.3, 6.3.5.1.3, 6.3.5.2.3 and 6.6.2.2; Tables 6.3.2-1, 6.3.2-3 and 6.3.5-4.
U_Eps_1_high_Nominal_a* - Logarithm of the scale factor used to characterize uncertainty in uranium solubility under nominal or seismic conditions at an ionic strength between 1and 3 molal (dimensionless). *Distribution:* Truncated normal. *Range:* -1.2 to 1.2. *Mean:* 0. *Standard Deviation:* 0.6. *Sensitivity Name:* EP1HINU*. *Location in TSPA-LA:* Section 6.3.7.5.1, 6.3.7.5.2 and 6.3.7.5.3; Table 6.3.7-54; Equation 6.3.7-13a.
U_Eps_1_high_Other_a* - Logarithm of the scale factor used to characterize uncertainty in uranium solubility under conditions other than nominal and seismic at an ionic strength between 1and 3 molal (dimensionless). *Distribution:* Truncated normal. *Range:* -1.2 to 1.2. *Mean:* 0. *Standard Deviation:* 0.6. *Sensitivity Name:* EP1HIOU*. *Location in TSPA-LA:* Sections 6.3.7.5.1, 6.3.7.5.2 and 6.3.7.5.3; Table 6.3.7-58; Equation 6.3.7-13a.
U_Eps_1_low_Nominal_a - Logarithm of the scale factor used to characterize uncertainty in uranium solubility under nominal or seismic conditions at an ionic strength below 1 molal (dimensionless). *Distribution:* Truncated normal. *Range:* -1 to 1. *Mean/Median/Mode:* 0. *Standard Deviation:* 0.5. *Sensitivity Name:* EP1LOWNU. *Location in TSPA-LA:* Section 6.3.7.5.1, 6.3.7.5.2 and 6.3.7.5.3; Table 6.3.7-54; Equation 6.3.7-13a.
U_Eps_1_low_Other_a - Logarithm of the scale factor used to characterize uncertainty in uranium solubility under conditions other than nominal and seismic at an ionic strength below 1 molal (dimensionless). *Distribution:* Truncated normal. *Range:* -1 to 1. *Mean/Median/Mode:* 0. *Standard Deviation:* 0.5. *Sensitivity Name:* EP1LOWOU. *Location in TSPA-LA:* Sections 6.3.7.5.1, 6.3.7.5.2 and 6.3.7.5.3; Table 6.3.7-58; Equation 6.3.7-13a.
U_Eps_2_Boltwoodite_CDSP_Hig_a* - Term associated with uncertainty in uranium solubility (controlled by boldwoodite saturation) due to variations in fluoride concentration for CDSP waste packages when ionic strength is greater than or equal to 0.004 molal and for the invert below CDSP waste packages (mg/L). *Distribution:* Triangular. *Range:* 0 to 272.3. *Most Likely:* 0. *Sensitivity Name:* EP2BCDHU*. *Location in TSPA-LA:* Sections 6.3.7.5.1, 6.3.7.5.2 and 6.3.7.5.3; Table 6.3.7-58; Equation 6.3.7-13a.
U_Eps_2_Boltwoodite_CSNF_Hig_a* - Term associated with uncertainty in uranium solubility (controlled by boldwoodite saturation) due to variations in fluoride concentration for CSNF waste packages when ionic strength is greater than or equal to 0.2 molal and for the invert below CSNF waste packages (mg/L). *Distribution:* Triangular. *Range:* 0 to 57.01. *Most Likely:* 0. *Sensitivity Name:* EP2BCSHU*. *Location in TSPA-LA:* Sections 6.3.7.5.1, 6.3.7.5.2 and 6.3.7.5.3; Table 6.3.7-58; Equation 6.3.7-13a.
U_Eps_2_Boltwoodite_Glass_Lo_a* - Term associated with uncertainty in uranium solubility (controlled by boldwoodite saturation) due to variations in fluoride concentration for CDSP waste packages Cell 1a, Cell 1b when ionic strength is less than 0.004 molal, and CSNF waste packages when ionic strength is less than 0.2 molal (mg/L). *Distribution:* Triangular. *Range:* 0 to 6.13. *Most Likely:* 0. *Sensitivity Name:* EP2BLOWU*. *Location in TSPA-LA:* Sections 6.3.7.5.1, 6.3.7.5.2 and 6.3.7.5.3; Table 6.3.7-58; Equation 6.3.7-13a.
U_Eps_2_CSNF_High_Nominal_a* - Term associated with uncertainty in uranium solubility (under nominal or seismic conditions) due to variations in fluoride concentration for CSNF waste packages when ionic strength is greater than or equal to 0.2 molal and for the invert below CSNF waste packages (mg/L). *Distribution:* Triangular. *Range:* 0 to 1361. *Most Likely:* 0. *Sensitivity Name:* EP2CSHNU*. *Location in TSPA-LA:* Section 6.3.7.5.1, 6.3.7.5.2 and 6.3.7.5.3; Table 6.3.7-54; Equation 6.3.7-13a.
U_Eps_2_CSNF_Low_Nominal_a* - Term associated with uncertainty in uranium solubility (under nominal or seismic conditions) due to variations in fluoride concentration for CSNF waste packages when ionic strength is less than 0.2 molal and for the invert below CSNF waste packages (mg/L). *Distribution:* Triangular. *Range:* 0 to 78. *Most Likely:* 0. *Sensitivity Name:* EP2CSLNU*. *Location in TSPA-LA:* Section 6.3.7.5.1, 6.3.7.5.2 and 6.3.7.5.3; Table 6.3.7-54; Equation 6.3.7-13a.

Table K3-2. High-Level Summary of Epistemically Uncertain Variables (i.e., elements of **e**) Considered in the TSPA-LA (TSPA Parameter Name) (Continued)

NOTE: * indicates variable not considered in sensitivity analysis due to correlations.

U_Eps_2_Schoepite_CDSP_High_a* - Term associated with uncertainty in uranium solubility (controlled by schoepite saturation) due to variations in fluoride concentration for CDSP waste packages when ionic strength is greater than or equal to 0.004 molal and for the invert below CDSP waste packages (mg/L). *Distribution:* Triangular. *Range:* 0 to 5385. *Most Likely:* 0. *Sensitivity Name:* EP2SCDHU*. *Location in TSPA-LA:* Sections 6.3.7.5.1, 6.3.7.5.2 and 6.3.7.5.3; Table 6.3.7-58; Equation 6.3.7-13a.
U_Eps_2_Schoepite_CSNF_High_a* - Term associated with uncertainty in uranium solubility (controlled by schoepite saturation) due to variations in fluoride concentration for CSNF waste packages when ionic strength is greater than or equal to 0.2 molal and for the invert below CSNF waste packages (mg/L). *Distribution:* Triangular. *Range:* 0 to 1361. *Most Likely:* 0. *Sensitivity Name:* EP2SCSHU*. *Location in TSPA-LA:* Sections 6.3.7.5.1, 6.3.7.5.2 and 6.3.7.5.3; Table 6.3.7-58; Equation 6.3.7-13a.
U_Eps_2_Schoepite_Glass_Low_a* - Term associated with uncertainty in uranium solubility (controlled by schoepite saturation) due to variations in fluoride concentration for CDSP waste packages Cell 1a, Cell 1b when ionic strength is less than 0.004 molal, and CSNF waste packages when ionic strength is less than 0.2 molal (mg/L). *Distribution:* Triangular. *Range:* 0 to 78. *Most Likely:* 0. *Sensitivity Name:* EP2SLOWU*. *Location in TSPA-LA:* Sections 6.3.7.5.1, 6.3.7.5.2 and 6.3.7.5.3; Table 6.3.7-58; Equation 6.3.7-13a.
UNC_DS_EF_conv_from_In - Probability for undetected defects in drip shields (dimensionless). *Distribution:* Log-normal. *Median:* 4.3E-07. *Error Factor:* 14. *Sensitivity Name:* PROBDSEF. *Location in TSPA-LA:* Section 6.4.1; Tables 6.4-1 and 6.4-2.
UNC_WP_EF_conv_from_In - Probability for the undetected defects in waste packages (dimensionless). *Distribution:* Log-normal. *Median:* 4.14E-05. *Error Factor:* 8.17. *Sensitivity Name:* PROBWPEF. *Location in TSPA-LA:* Section 6.4.2; Tables 6.4-1 and 6.4-2.
UZ_Tortuosity_RG1 - Logarithm of the tortuosity in rock group 1 (dimensionless). *Distribution:* Left truncated normal. *Range*: 0 to ∞. *Mean:* -1.15. *Standard Deviation:* 0.29. *Sensitivity Name:* UZTORRG1. *Location in TSPA-LA:* Section 6.3.9.2; Table 6.3.9-4.
UZ_Tortuosity_RG2 - Logarithm of the tortuosity in rock group 2 (dimensionless). *Distribution:* Left truncated normal. *Range*: 0 to ∞. *Mean:* -1.57. *Standard Deviation:* 0.29. *Sensitivity Name:* UZTORRG2. *Location in TSPA-LA:* Section 6.3.9.2; Table 6.3.9-4.
UZ_Tortuosity_RG3 - Logarithm of the tortuosity in rock group 3 (dimensionless). *Distribution:* Left truncated normal. *Range*: 0 to ∞. *Mean:* -1.84. *Standard Deviation:* 0.29. *Sensitivity Name:* UZTORRG3. *Location in TSPA-LA:* Section 6.3.9.2; Table 6.3.9-4.
Vol_Rubble_Max_Lith_a - Volume of lithophysal rock that must fall to fill the drift (m^3/m). *Distribution:* Uniform. *Range:* 30 to 120. *Sensitivity Name:* RUBMAXL. *Location in TSPA-LA:* Sections 6.3.5.2.3 and 6.6.3.1; Tables 6.3.5-4 and 6.6-2.
Vol_Rubble_Max_NonLith_a - Volume of nonlithophysal rock that must fall to fill the drift (m^3/m). *Distribution:* Uniform. *Range:* 30 to 120. *Sensitivity Name:* RUBMAXNL. *Location in TSPA-LA:* Section 6.3.5.2.3 and 6.6.3.1; Tables 6.3.5-4 and 6.6-2.
WDDSAggrGC_Mean_a - Topside general corrosion rate of the drip shield (nm/yr). *Distribution:* Normal. *Mean:* 46.067. *Standard Deviation:* 1.187. *Sensitivity Name:* WDDSAGGC. *Location in TSPA-LA:* Sections 6.3.5.1.2 and 6.3.5.1.3; Table 6.3.5-3.
WDDSBenignGC_Mean_a - Underside general corrosion rate of the drip shield (mm/yr). *Distribution:* Normal. *Mean:* 5.15E-06. *Standard Deviation:* 8.31E-07. *Sensitivity Name:* WDDSBEGC. *Location in TSPA-LA:* Sections 6.3.5.1.2 and 6.3.5.1.3; Table 6.3.5-3.
WDDSGC_29_a - General corrosion rate ratio for drip shield support material (ratio of Titanium Grade 29 to Titanium Grade 7) (dimensionless). *Distribution:* Discrete. *Range:* 1 to 6.6786. *Sensitivity Name:* WDDSGC29. *Location in TSPA-LA:* Section 6.3.5.1.2.
WP_Crack_Area_Density_a - Ratio of SCC crack area to unit of seismic damaged area for a waste package (dimensionless). *Distribution:* Uniform. *Range:* 0.00327 to 0.0131. *Sensitivity Name:* WDCRCDEN. *Location in TSPA-LA:* Table 6.6-2.
WP_Flux_Uncertainty_a - Waste package flux splitting factor (dimensionless). *Distribution:* Uniform. *Range:* 0 to 2.41. *Sensitivity Name:* WPFLUX. *Location in TSPA-LA:* Sections 6.3.6.1, 6.3.6.2 and 6.3.6.3; Tables 6.3.6-1, 6.3.6-2 and 6.3.8-4; Equation 6.3.6-6.

Table K3-2. High-Level Summary of Epistemically Uncertain Variables (i.e., elements of **e**) Considered in the TSPA-LA (TSPA Parameter Name) (Continued)

NOTE: * indicates variable not considered in sensitivity analysis due to correlations.

WRIP_beta_rand_a - Parameter used to correlate WRIP_beta so that it resamples at the same probability level throughout a realization (dimensionless). *Distribution:* Uniform. *Range:* 0 to 1. *Sensitivity Name:* WATRCKIN. *Location in TSPA-LA:* Section 6.3.4.2; Table 6.3.4-1.
z_OL_a - Deviation from median yield strength range for outer lid (dimensionless). *Distribution:* Truncated normal. *Range:* -3 to 3. *Mean/Median/Mode:* 0. *Standard Deviation:* 1. *Sensitivity Name:* WDZOLID. *Location in TSPA-LA:* Sections 6.3.5.1.2 and 6.3.5.1.3; Table 6.3.5-3.

Table K3-3. Detailed Summary of Epistemically Uncertain Variables (i.e., elements of **e**) Considered in the TSPA-LA (TSPA Parameter Name)

NOTE: * indicates variable not considered in sensitivity analysis due to correlations.

Alluvium_Density - Bulk density of alluvium (kg/m^3). *Distribution:* Normal. *Mean/Median/Mode:* 1910. *Standard Deviation:* 78. *Additional Information:* The volcanic fracture porosity, volcanic matrix porosity and volcanic density are constants, while alluvium density (i.e., bulk density of alluvium) is a stochastic parameter. These parameters are provided to the TSPA-LA Model to use in the one-dimensional simulations. The alluvium density is used in the calculation of the retardation of sorbing radionuclides. The dry bulk density of alluvium is a flow and transport parameter that is not radionuclide specific. It is related to the matrix retardation coefficient and is used in the computation of the retardation of sorbing radionuclides for irreversible colloidal transport. To treat the one- and three-dimensional transport through the SZ consistently, the sampled values used to generate the saturated zone breakthrough curves are also used in the TSPA-LA Model. These values are tabulated as 200 sets of values for the SZ parameters, accounting for appropriate correletions, and are entered into the TSPA model as a table of 200 values for each parameter. The TSPA-LA Model selects values from this table using the Goldsim variable SZ_index_a. *Sensitivity Name:* SZDENAL. *Location in TSPA-LA:* Table 6.3.10-2. *DTN:* SN0702PASZFTMA.002_R1 [DIRS 183471]. *References: Saturated Zone Flow and Transport Model Abstraction* (SNL 2008 [DIRS 183750], Section 6.5.2.7; Tables 6-8, 7-1[a] and A-1[a]; Figure 6-17).
Alpha_Uncert_Lith_a - van Genuchten capillary strength parameter in lithophysal rock units (Pa). *Distribution:* Triangular. *Range:* -105 to 105. *Mean/Median/Mode:* 0. *Correlation:* Correlated with Alpha_Uncert_NonLith_a. *Symbol:* 1/α. *Additional Information:* The van Genuchten capillary-strength parameter characterizes the strength of the fracture network to retain the water within the formation, reducing or preventing seepage. The values of local percolation flux, the sampled values of local permeability, and capillary strength parameters are used to interpolate from the look-up tables for the mean seepage rate into a 5.1-m-long drift section and the seepage rate standard deviation. The value of standard deviation is used to account for uncertainty in the estimation of seepage rates. Recorded in TSPA Input Database as three constants: Alpha_Uncert_A_min (minimum), Alpha_Uncert_A_mode (mode), and Alpha_Uncert_A_max (maximum). *Sensitivity Name:* ALPHAL. *Location in TSPA-LA:* Sections 6.3.3.1.2 and 6.3.3.1.3; Tables 6.3.3-1, 6.3.3-3 and 6.3.5-4. *DTN:* LB0407AMRU0120.001_R0 [DIRS 173280]. *References: Abstraction of Drift Seepage* (SNL 2007, DIRS [181244], Sections 6.3[a] and 6.6[a]; Figures 6-1[a], 6-12[a], 6-20[a] and 7-4[a]).
Alpha_Uncert_NonLith_a*. van Genuchten capillary strength parameter in nonlithophysal rock units (Pa). *Distribution:* Triangular. *Range:* -105 to 105. *Mean/Median/Mode:* 0. *Correlation:* Correlated to Alpha_Uncert_Lith_a. *Symbol:* 1/α. *Additional Information:* See Alpha_Uncert_Lith_a. This parameter is used to select the mean and standard deviation of seepage flow, from their respective response surfaces. Recorded in TSPA Input Database as three constants: Alpha_Uncert_A_min (minimum), Alpha_Uncert_A_mode (mode), and Alpha_Uncert_A_max (maximum). *Sensitivity Name:* ALPHANL*. *Location in TSPA-LA:* Section 6.3.3.1.2; Tables 6.3.3-1, 6.3.3-3 and 6.3.5-4. *DTN:* LB0407AMRU0120.001_R0 [DIRS 173280]. *References: Abstraction of Drift Seepage* (SNL 2007 [DIRS 181244], Sections 6.3[a] and 6.6[a]; Figures 6-1[a], 6-12[a], 6-20[a] and 7-4[a]).
Am_Eps_1_high_a*. Logarithm of the scale factor used to characterize uncertainty in americium solubility at ionic strength values between 1 and 3 molal (dimensionless). *Distribution:* Truncated normal. *Range:* -2.08 to 2.08. *Mean:* 0. *Standard Deviation:* 1.04. *Correlation:* Correlated to Am_Eps_1_low_a with a correlation factor of 1. *Symbol:* ε_1. *Additional Information:* See Am_Eps_1_low_a. *Sensitivity Name:* EP2HIAM*. *Location in TSPA-LA:* Sections 6.3.7.5.1, 6.3.7.5.2 and 6.3.7.5.3; Equation 6.3.7-13a; Table 6.3.7-41. *DTN:* MO0702PADISCON.001_R0 [DIRS 179358], Tables 8 & 19. *References: Dissolved Concentration Limits of Elements with Radioactive Isotopes* (SNL 2007 [DIRS 177418], Sections 6.9 and 8.1.2; Equations 6.9-1 and 8-1; Table 6.9-4).
Am_Eps_1_low_a. Logarithm of the scale factor used to characterize uncertainty in americium solubility at an ionic strength below 1 molal (dimensionless). *Distribution:* Truncated normal. *Range:* -2 to 2. *Mean:* 0. *Standard Deviation:* 1. *Correlation:* Correlated to Am_Eps_1_high_a with a correlation factor of 1. *Symbol:* ε_1. *Additional Information:* This is an exponential term associated with uncertainty in americium solubility (log k) below 1 molal ionic strength. Am_Eps_1_low defines uncertainty in the log K of the solubility limit for ionic strengths below 1 molal. Am_Eps_1_high defines log K uncertainty for ionic strength values between 1 and 3 molal. This parameter is referred to as ε_1 in the referenced. This parameter is used in calculation as: [Pu, Np, U, Am, Th, and Sn] = 10^S* 10^ε_1+ (ε_2 • N). *Sensitivity Name:* EP1LOWAM. *Location in TSPA-LA:* Sections 6.3.7.5.1, 6.3.7.5.2 and 6.3.7.5.3; Table 6.3.7-41; Equation 6.3.7-13a. *DTN:* MO0702PADISCON.001_R0 [DIRS 179358], Tables 8 & 19. *References: Dissolved Concentration Limits of Elements with Radioactive Isotopes* (SNL 2007 [DIRS 177418], Sections 6.9 and 8.1.2; Equations 6.9-1 and 8.1; Table 6.9-4).

Table K3-3. Detailed Summary of Epistemically Uncertain Variables (i.e., elements of **e**) Considered in the TSPA-LA (TSPA Parameter Name) (Continued)

NOTE: * indicates variable not considered in sensitivity analysis due to correlations.

Am_Eps_2_CDSP_High_a*. Term associated with uncertainty in americium solubility due to variations in fluoride concentration for CDSP waste packages when ionic strength is greater than or equal to 0.004 molal and for the invert below CDSP waste packages (mg/L). *Distribution:* Triangular. *Range:* 0 to 688.6. *Most Likely:* 0. *Correlation:* Correlated to Am_Eps_2_CSNF_High_a. *Symbol:* $\varepsilon_2^{\text{CDSP-F-high}}$, $\varepsilon_2^{\text{CDSP-invert}}$. *Additional Information:* See Am_Eps_2_CSNF_High_a. *Sensitivity Name:* EP2HICDAM*. *Location in TSPA-LA:* Sections 6.3.7.5.2 and 6.3.7.5.3; Table 6.3.7-41; Equation 6.3.7-13a. *DTN:* MO0702PAFLUORI.000_R1 [DIRS 181219], Table 13. *References: Dissolved Concentration Limits of Elements with Radioactive Isotopes* (SNL 2007 [DIRS 177418], Sections 6.9 and 8.1.2; Equations 6.9-1 and 8.1; Tables 6.9-4 and 8-2).
Am_Eps_2_CSNF_High_a. Term associated with uncertainty in americium solubility due to variations in fluoride concentration for CSNF waste packages when ionic strength is greater than or equal to 0.2 molal and for the invert below CSNF waste packages (mg/L). *Distribution:* Triangular. *Range:* 0 to 109.03. *Most Likely:* 0. *Correlation:* Correlated to all other Eps_2 parameters. *Symbol:* $\varepsilon_2^{\text{CSNF-high}}$, $\varepsilon_2^{\text{CSNF-invert}}$. *Additional Information:* The range of fluoride uncertainty for a given TSPA-LA run depends on the type of waste package being considered and the pH. This pH dependence can be implemented into the TSPA model through the use of a multiplication factor that is a function of pH. In TSPA-LA, the fluoride uncertainty for the actinides should be perfectly correlated during sampling. This parameter is calculated from the difference in base solubility (in mg/L). This parameter is referred to as ε_2 in the referenced AMR. *Sensitivity Name:* EP2HICAM. *Location in TSPA-LA:* Sections 6.3.7.5.2 and 6.3.7.5.3; Table 6.3.7-41; Equation 6.3.7-13a. *DTN:* MO0702PAFLUORI.000_R1 [DIRS 181219], Table 13. *References: Dissolved Concentration Limits of Elements with Radioactive Isotopes* (SNL 2007 [DIRS 177418], Sections 6.9 and 8.1.2; Equations 6.9-1 and 8.1; Tables 6.9-4 and 8-2).
Am_Eps_2_Glass_Low_a*. Term associated with uncertainty in americium solubility due to variations in fluoride concentration for CDSP waste packages Cell 1a, Cell 1b when ionic strength is less than 0.004 molal, and CSNF waste packages when ionic strength is less than 0.2 molal (mg/L). *Distribution:* Triangular. *Range:* 0 to 4.42. *Most Likely:* 0. *Correlation:* Correlated to Am_Eps_2_CSNF_High_a. *Symbol:* $\varepsilon_2^{\text{CSNF-low}}$, $\varepsilon_2^{\text{CDSP-Glass}}$, $\varepsilon_2^{\text{CDSP-F-low}}$. *Additional Information:* See Am_Eps_2_CSNF_High_a. *Sensitivity Name:* EP2LOWAM*. *Location in TSPA-LA:* Sections 6.3.7.5.2 and 6.3.7.5.3; Table 6.3.7-41; Equation 6.3.7-13a. *DTN:* MO0702PAFLUORI.000_R1 [DIRS 181219], Table 13. *References: Dissolved Concentration Limits of Elements with Radioactive Isotopes* (SNL 2007 [DIRS 177418], Sections 6.9 and 8.1.2; Equations 6.9-1 and 8.1; Tables 6.9-4 and 8-2).
Ash_Density_a. Tephra settled density (kg/m^3). *Distribution:* Truncated normal. *Range:* 300 to 1500. *Mean:* 1000. *Standard Deviation:* 100. *Symbol:* ψ_s. *Additional Information:* The ash settled density is the bulk density of the ash that settles on the ground after an eruption. Areal densities can be converted to deposit thickness by dividing the areal density by the value of settled (deposit) density. There are two reasonable ways of treating deposit density in TSPA calculations: 1) simply use 1,000 kg/m^3, or 2) use a sample from a normal distribution. Uncertainties are due to a lack of published data. *Sensitivity Name:* ASHDENS. *Location in TSPA-LA:* Table 6.5-5. *DTN:* LA0612DK831811.001_R1 [DIRS 179987]. *References: Characterize Eruptive Processes at Yucca Mountain, Nevada* (SNL 2007 [DIRS 174260], Table 7-1).
b_Tillage_a. Depth of soil within which radionuclides contribute to dose from external exposure (m). *Distribution:* Uniform. *Range:* 0.05 to 0.3. *Additional Information:* The tillage depth is a biosphere model parameter that is also provided as input to the TSPA model to allow calculation of soil depth-integrated radionuclide concentration per unit surface area of the soil. The time-dependent areal radionuclide concentration in surface soil represents radionuclide activity integrated over the tillage depth. All crop roots are considered to be in the soil layer extending down to the tilling depth. For many crops, the root systems can extend to below the tillage depth. This approach effectively assumes (conservatively) that all roots, the source of radionuclide uptake for plants, are exposed to a radionuclide concentration as calculated for the tillage region. Recorded as b_tillage_a in the TSPA Input Database as a table of values presampled in the Biosphere model. Values for the TSPA-LA Model selected from b_tillage_a by the parameter Bio_Index. *Sensitivity Name:* BTILLAGE. *Location in TSPA-LA:* Table 6.5-5. *DTN:* MO0702PAVBPDCF.000_R0 [DIRS 179330]. *References: Biosphere Model Report* (SNL 2007 [DIRS 177399], Sections 6.3.1.6, 6.3.2.2, 6.3.2.6, 6.4.1, 6.4.2.1, 6.5.1 and 7.4.2; Equation 6.5.1-2; Tables 6.6-3 and 6.7-1).

Table K3-3. Detailed Summary of Epistemically Uncertain Variables (i.e., elements of **e**) Considered in the TSPA-LA (TSPA Parameter Name) (Continued)

NOTE: * indicates variable not considered in sensitivity analysis due to correlations.

Background_Alpha_a. Natural background levels of alpha emitters in groundwater (pCi/L). *Distribution:* Truncated normal. *Range:* 0 to 0.71. *Mean/Median/Mode:* 0.5. *Additional Information:* Inputs to the Biosphere Model include background concentrations of ^{226}Ra and ^{228}Ra and alpha emitters in the groundwater. To demonstrate compliance with 10 CFR 63.331 natural background concentrations of ^{226}Ra, ^{228}Ra and alpha emitters will be included in the groundwater protection calculations. The values used in the TSPA-LA model are the means of the natural background distributions calculated in the *Saturated Zone Flow and Transport Model Abstraction*. The mean values are used so that variations in the groundwater protection calculations will reflect variations in releases from the repository and not be masked by variation in the natural background distributions. *Sensitivity Name:* BCKALPHA. *Location in TSPA-LA:* Sections 6.3.10.2 and 6.3.11.2; Table 6.3.10-6. *Output DTN:* MO0708TSPAGENT.000_R0 [DIRS 183000].
Background_Ra226_Ra228_a. Natural background levels of combined ^{226}Ra and ^{228}Ra in groundwater (pCi/L). *Distribution:* Truncated normal. *Range:* 0 to 0.71. *Mean/Median/Mode:* 0.5. *Additional Information:* See Background_Alpha_a. *Sensitivity Name:* BCKRA226. *Location in TSPA-LA:* Sections 6.3.10.2 and 6.3.11.2; Table 6.3.10-6. *Output DTN:* MO0708TSPAGENT.000_R0 [DIRS 183000].
BDCF_Inh_LT. Pointer variable for long-term inhalation dose conversion factor for volcanic ash exposure (dimensionless). *Distribution:* Discrete. *Range:* 1 to 300. *Symbol:* $BDCF_{inh,p,i}$ *Additional Information:* This is the vector of values for each radionuclide, selected from the pre-sampled BDCFs by Bio_Index. This pointer variable selects a value for each radionuclide, and the values for each radionuclide are correlated with a coefficient of 1. The minimum value of this variable (1) is associated with the lowest value of the BDCF set. The highest value (300) is associated with the highest value of the BDCF set. *Sensitivity Name:* INHLTPV. *Location in TSPA-LA:* Section 6.3.11; Equation 6.3.11-4. *DTN:* MO0702PAVBPDCF.000 _R0 [DIRS 179330]. *References: Biosphere Model Report* (SNL 2007 [DIRS 177399], Sections 6.12.2 and 6.14.5; Table 6.12-2; Figure 6.14-2).
BDCF_Inh_ShT. Pointer variable for short-term inhalation dose conversion factor for volcanic ash exposure (dimensionless). *Distribution:* Discrete. *Range:* 1 to 300. *Symbol:* $BDCF_{inh,v,i}$ *Additional Information:* See BDCF_Inh_ShT. *Sensitivity Name:* INHSTPV. *Location in TSPA-LA:* Section 6.3.11; Equation 6.3.11-4. *DTN:* MO0702PAVBPDCF.000 _R0 [DIRS 179330]. *References: Biosphere Model Report* (SNL 2007 [DIRS 177399], Sections 6.12.2 and 6.14.5; Table 6.12-2; Figure 6.14-2).
Beta_Dist_a. Column diffusion constant (dimensionless). *Distribution:* Uniform. *Range:* 0.01 to 0.5. *Symbol:* β_c. *Additional Information:* This parameter affects the distribution of particles vertically in the ash column and helps determine where particles exit the column. ASHPLUME takes a beta value and determines the vertical profile of particle sizes in the erupted column that will then be transported down wind. The larger beta becomes, the more the particle distribution becomes skewed towards the top of the column. A value of 0.5 generates a column particle distribution that contains very few particles in the lower 70% of the column, whereas a beta value of 0.01 gives an upwardly decreasing distribution that contains the most particles lower in the column. The beta parameter is related to the buoyancy of particles in the eruptive column and determines how high most particles will travel before exiting the column. Based on comparisons of modeled and observed tephra distributions, beta values of 0.5 or greater are not representative of typical eruptions. Uncertainty in this value originates from the relationship between the mathematical coefficient and physical processes. *Sensitivity Name:* BETA. *Location in TSPA-LA:* Table 6.5-4. *DTN:* LA0702PADE03GK.002_R1 [DIRS 179980]. *References: Atmospheric Dispersal and Deposition of Tephra from a Potential Volcanic Eruption at Yucca Mountain, Nevada* (SNL 2007 [DIRS 177431], Sections 6.5.2.3, 7.2 and 8.2; Tables 4-1, 6-3, 8-2, C-1, C-5 and J-1; Figure C-4).
C1_GenCorr_A22_a. Temperature dependent slope term of Alloy 22 general corrosion rate (K). *Distribution:* Truncated normal. *Range:* 666 to 7731. *Mean:* 4905. *Standard Deviation:* 1413. *Symbol:* C_1. *Additional Information:* The temperature-dependence term represents the effect of temperature on corrosion rates of Alloy 22 based on polarization resistance measurements using a wide variety of specimen configurations, metallurgical conditions, and exposure environments (i.e., water chemistries). Truncation of the C_1 distribution at +2/-3 standard deviations is appropriate given that the resulting range in apparent activation energies spans a large range of values from extremely low temperature dependence to a high temperature dependence. The entire variance in the temperature dependence term is due to uncertainty. The higher the value of C_1, the greater the dependence of general corrosion rate on temperature. *Sensitivity Name:* WDGCA22. *Location in TSPA-LA:* Sections 6.3.5.1.2 and 6.3.5.1.3; Tables 6.3.5-3 and 6.3.5-4; Equation 6.3.5-4. *DTN:* MO0703PAGENCOR.001_R4 [DIRS 182029]. *References: General Corrosion and Localized Corrosion of the Waste Package Outer Barrier* (SNL 2007 [DIRS 178519], Sections 6.4.3 and 6.4.3.4).

Table K3-3. Detailed Summary of Epistemically Uncertain Variables (i.e., elements of **e**) Considered in the TSPA-LA (TSPA Parameter Name) (Continued)

NOTE: * indicates variable not considered in sensitivity analysis due to correlations.

Colloidal_Kc_Am_UZP. Colloid sorption coefficient for americium (mg/mg). *Calculated by:* Colloidal_Kd_Am_uz*Colloidal_Concentration_uz. *Correlation:* Correlated to Colloidal_Kc_Pa_UZP and Colloidal_Kc_Th_UZP with a correlation coefficient of 1. *Symbol:* K_c. *Additional Information:* Selector elements for colloidal K_cs. For colloid-facilitated radionuclide transport in which radionuclides are reversibly attached to colloids, a partition coefficient is defined to represent the potential for enhanced migration of radionuclides in association with colloids. For reversible radionuclide sorption on the colloids, the K_c values are calculated by multiplying a radionuclide's sorption coefficient for a species onto a colloid, K_d, by the colloid concentrations in the water. Used in FEHM as an input parameter for calculating the retardation factors for colloid facilitated radionuclide transport in the media. To address the uncertainty of colloid concentration on colloid facilitated transport, the colloid concentration is sampled at run time and provided to FEHM for the calculation of K_c. See Conc_Col_Gw_Sampled_a and Kd_Am_Col. *Sensitivity Name:* UZCOKDAM. *Location in TSPA-LA:* Section 6.3.9.2. *DTN:* LA0701PANS02BR.003_R2 [DIRS 180497] for Kds. *References: Particle Tracking Model and Abstraction of Transport Processes Addendum 002* (SNL 2008 [DIRS 184748], Sections 6.5.12 and 6.5.13; Tables 6.6.1-1 and 6-22).
Colloidal_Kc_Cs_UZP. Colloid sorption coefficient for cesium (mg/mg). *Calculated by:* Colloidal_Kd_Cs_uz*Colloidal_Concentration_uz. *Symbol:* K_c. *Additional Information:* Selector elements for colloidal K_cs. For colloid-facilitated radionuclide transport in which radionuclides are reversibly attached to colloids, a partition coefficient is defined to represent the potential for enhanced migration of radionuclides in association with colloids. For reversible radionuclide sorption on the colloids, the K_c values are calculated by multiplying a radionuclide's sorption coefficient for a species onto a colloid, K_d, by the colloid concentrations in the water. Used in FEHM as an input parameter for calculating the retardation factors for colloid facilitated radionuclide transport in the media. To address the uncertainty of colloid concentration on colloid facilitated transport, the colloid concentration is sampled at run time and provided to FEHM for the calculation of K_c. See Conc_Col_Gw_Sampled_a and Kd_Cs_Col. *Sensitivity Name:* UZCOKDCS. *Location in TSPA-LA:* Section 6.3.9.2. *DTN:* LA0701PANS02BR.003_R2 [DIRS 180497] for Kds. *References: Particle Tracking Model and Abstraction of Transport Processes Addendum 002* (SNL 2008 [DIRS 184748], Sections 6.5.12 and 6.5.13; Tables 6.6.1-1 and 6-22).
Colloidal_Kc_Pa_UZP. Colloid sorption coefficient for protactinium (mg/mg). *Calculated by:* Colloidal_Kd_Am_uz*Colloidal_Concentration_uz. *Correlation:* Correlated to Colloidal_Kc_Am_UZP and Colloidal_Kc_Th_UZP with a correlation coefficient of 1. *Symbol:* K_c. *Additional Information:* Selector elements for colloidal K_cs. For colloid-facilitated radionuclide transport in which radionuclides are reversibly attached to colloids, a partition coefficient is defined to represent the potential for enhanced migration of radionuclides in association with colloids. For reversible radionuclide sorption on the colloids, the K_c values are calculated by multiplying a radionuclide's sorption coefficient for a species onto a colloid, K_d, by the colloid concentrations in the water. Used in FEHM as an input parameter for calculating the retardation factors for colloid facilitated radionuclide transport in the media. To address the uncertainty of colloid concentration on colloid facilitated transport, the colloid concentration is sampled at run time and provided to FEHM for the calculation of K_c. See Conc_Col_Gw_Sampled_a and Kd_Am_Col. *Sensitivity Name:* UZCOKDPA. *Location in TSPA-LA:* Section 6.3.9.2. *DTN:* LA0701PANS02BR.003_R2 [DIRS 180497] for Kds. *References: Particle Tracking Model and Abstraction of Transport Processes Addendum 002* (SNL 2008 [DIRS 184748], Sections 6.5.12; Tables 6.6.1-1 and 6-22).
Colloidal_Kc_Pu_UZP. Colloid sorption coefficient for plutonium (mg/mg). *Calculated by:* Colloidal_Kd_Pu_uz*Colloidal_Concentration_uz. *Symbol:* K_c. *Additional Information:* Selector elements for colloidal K_cs. For colloid-facilitated radionuclide transport in which radionuclides are reversibly attached to colloids, a partition coefficient is defined to represent the potential for enhanced migration of radionuclides in association with colloids. For reversible radionuclide sorption on the colloids, the K_c values are calculated by multiplying a radionuclide's sorption coefficient for a species onto a colloid, K_d, by the colloid concentrations in the water. Used in FEHM as an input parameter for calculating the retardation factors for colloid facilitated radionuclide transport in the media. To address the uncertainty of colloid concentration on colloid facilitated transport, the colloid concentration is sampled at run time and provided to FEHM for the calculation of K_c. See Conc_Col_Gw_Sampled_a and Kd_Pu_Col. *Sensitivity Name:* UZCOKDPU. *Location in TSPA-LA:* Section 6.3.9.2. *DTN:* LA0701PANS02BR.003_R2 [DIRS 180497] for Kds. *References: Particle Tracking Model and Abstraction of Transport Processes Addendum 002* (SNL 2008 [DIRS 184748], Sections 6.5.12 and 6.5.13; Tables 6.6.1-1 and 6-22).

Table K3-3. Detailed Summary of Epistemically Uncertain Variables (i.e., elements of **e**) Considered in the TSPA-LA (TSPA Parameter Name) (Continued)

NOTE: * indicates variable not considered in sensitivity analysis due to correlations.

Colloidal_Kc_Sn_UZP. Colloid sorption coefficient for tin (mg/mg). *Calculated by:* Colloidal_Kd_Sn_uz*Colloidal_Concentration_uz. *Symbol:* K_c. *Additional Information:* Selector elements for colloidal K_cs. For colloid-facilitated radionuclide transport in which radionuclides are reversibly attached to colloids, a partition coefficient is defined to represent the potential for enhanced migration of radionuclides in association with colloids. For reversible radionuclide sorption on the colloids, the Kc values are calculated by multiplying a radionuclide's sorption coefficient for a species onto a colloid, Kd, by the colloid concentrations in the water. Used in FEHM as an input parameter for calculating the retardation factors for colloid facilitated radionuclide transport in the media. To address the uncertainty of colloid concentration on colloid facilitated transport, the colloid concentration is sampled at run time and provided to FEHM for the calculation of Kc. See Conc_Col_Gw_Sampled_a and Kd_Sn_Col. *Sensitivity Name:* UZCOKDSN. *Location in TSPA-LA:* Section 6.3.9.2. *DTN:* LA0701PANS02BR.003_R2 [DIRS 180497] for Kds. *References: Particle Tracking Model and Abstraction of Transport Processes Addendum 002* (SNL 2008 [DIRS 184748], Sections 6.5.12 and 6.5.13; Tables 6.6.1-1 and 6-22).
Colloidal_Kc_Th_UZP. Colloid sorption coefficient for thorium (mg/mg). *Calculated by:* Calculated by Colloidal_Kd_Am_uz*Colloidal_Concentration_uz. *Correlation:* Correlated to Colloidal_Kc_Am_UZP and Colloidal_Kc_Pa_UZP with a correlation coefficient of 1. *Symbol:* K_c. *Additional Information:* Selector elements for colloidal K_cs. For colloid-facilitated radionuclide transport in which radionuclides are reversibly attached to colloids, a partition coefficient is defined to represent the potential for enhanced migration of radionuclides in association with colloids. For reversible radionuclide sorption on the colloids, the K_c values are calculated by multiplying a radionuclide's sorption coefficient for a species onto a colloid, K_d, by the colloid concentrations in the water. Used in FEHM as an input parameter for calculating the retardation factors for colloid facilitated radionuclide transport in the media. To address the uncertainty of colloid concentration on colloid facilitated transport, the colloid concentration is sampled at run time and provided to FEHM for the calculation of K_c. See Conc_Col_Gw_Sampled_a and Kd_Am_Col. *Sensitivity Name:* UZCOKDTH. *Location in TSPA-LA:* Section 6.3.9.2. *DTN:* LA0701PANS02BR.003_R2 [DIRS 180497] for Kds. *References: Particle Tracking Model and Abstraction of Transport Processes Addendum 002* (SNL 2008 [DIRS 184748], Sections 6.5.12; Tables 6.6.1-1 and 6-22).
Colloidal_Retard_Factor_dist_a. Colloid retardation factor (dimensionless). *Distribution:* Piecewise uniform. *Range:* 6 to 799.83. *Symbol:* R_{coll}. *Additional Information:* The colloid retardation factor is used in the TSPA LA Model to simulate the impact of reversible filtration on colloids in the fractured media with respect to radionuclides irreversibly sorbed onto colloids. In TSPA-LA calculations, to investigate the uncertainty of colloid retardation factors on radionuclide transport, colloid retardation factors are sampled for each realization at run time. The colloid retardation factor is used by FEHM in simulating the effects of colloid retardation in fractured rock on colloid-facilitated radionuclide transport. *Sensitivity Name:* UZRCOL. *Location in TSPA-LA:* Sections 6.3.9.2 and 6.3.9.3; Table 6.3.9-12. *DTN:* LA0701PANS02BR.003_R2 [DIRS 180497], Table 5.doc. *References: Particle Tracking Model and Abstraction of Transport Processes Addendum 002* (SNL 2008 [DIRS 184748], Sections 4.1.9, 6.5.13 and 6.8.2.2; Table 8-2; Figures 6.8.2-23 and 6.8.2-24).
Conc_Col. Logarithm of ambient concentration of colloids in groundwater (g/mL). *Distribution:* Piecewise uniform. *Range:* -9 to -3.6. *Symbol:* C_{coll}. *Additional Information:* This parameter is used to calculate the retardation of radionuclides in colloidal transport. To treat the one- and three-dimensional transport through the SZ consistently, the sampled values used to generate the saturated zone breakthrough curves are also used in the TSPA-LA Model. These values are tabulated as 200 sets of values for the SZ parameters, accounting for appropriate correletions, and are entered into the TSPA model as a table of 200 values for each parameter. The TSPA-LA Model selects values from this table using the Goldsim variable SZ_index_a. *Sensitivity Name:* SZCONCOL. *Location in TSPA-LA:* Table 6.3.10-2. *DTN:* SN0702PASZFTMA.002_R1 [DIRS 183471]. *References: Saturated Zone Flow and Transport Model Abstraction* (SNL 2008 [DIRS 183750], Sections 6.3.1, 6.5.1.1 and 6.5.2.12; Tables 4-3, 6-8, A-1[a] and B-1; Equation 6-4).

Table K3-3. Detailed Summary of Epistemically Uncertain Variables (i.e., elements of **e**) Considered in the TSPA-LA (TSPA Parameter Name) (Continued)

NOTE: * indicates variable not considered in sensitivity analysis due to correlations.

Conc_Col_FeOx_CS_Sampled_a. FeOx colloid concentration when carbon steel is corroding (mg/L). *Distribution:* Truncated log normal. *Range:* 0.3 to 30. *Mean:* 3.69. *Standard Deviation:* 2.79. *Additional Information:* Iron oxyhydroxide colloids would be expected to form as a result of corrosion of the waste package and associated engineered barrier system components. The input data from carbon steel corrosion are short term tests with a less durable material; therefore, these are believed to be much higher than what will occur in the long term. Few peer-reviewed publications present information on iron oxide–oxyhydroxide colloid concentrations as a function of aqueous chemistry, therefore there is uncertainty in the amount of colloids produced from steel corrosion. The range of values for maximum iron oxide–oxyhydroxide colloids concentration was chosen so that it was greater than iron oxyhydroxide colloid levels found in groundwater, but high enough to reflect the masses of corroded ferrous metal anticipated in the repository. *Sensitivity Name:* COLFEOCS. *Location in TSPA-LA:* Table 6.3.7-65. *DTN:* MO0701PAIRONCO.000_R1 [DIRS 180440]. *References: Waste Form and In-Drift Colloids-Associated Radionuclide Concentrations: Abstraction and Summary* (SNL 2007 [DIRS 177423], Sections 6.3.2, 6.3.8, 6.5.1.4, 6.5.2, 6.3.12.1 and 6.6.5; Equations 6-13 and 6-15; Figure 6-20; Table 6-24).
Conc_Col_FeOx_SS_Sampled_a. FeOx colloid concentration when degraded stainless steel is present, but no degrading carbon steel is present (mg/L). *Distribution:* Piecewise uniform. *Range:* 1.00E-03 to 3.00E+01. *Additional Information:* The assessment of colloid concentrations from stainless steel is subjective as there is insufficient data available to make a reliable analysis. As stainless steel is less corrosive than carbon steel, the overall colloid mass distribution was reduced compared to carbon steel. *Sensitivity Name:* COLFEOSS. *Location in TSPA-LA:* Table 6.3.7-65. *DTN:* MO0701PAIRONCO.000_R1 [DIRS 180440]. *References: Waste Form and In-Drift Colloids-Associated Radionuclide Concentrations: Abstraction and Summary* (SNL 2007 [DIRS 177423], Sections 6.3.2, 6.3.8, 6.5.1.4, 6.5.2 and 6.6.5; Figure 6-21; Tables 6-11 and 6-24).
Conc_Col_Gw_Sampled_a. Concentration of groundwater colloids when colloids are stable (mg/L). *Distribution:* Piecewise uniform. *Range:* 0.001 to 200. *Median:* 0.1. *Additional Information:* At Yucca Mountain, inorganic groundwater colloids, primarily consisting of clay, silica, and iron oxyhydroxides, may be transported in seepage water into the repository from the vadose zone above it or may be formed due to changes in chemical conditions near the repository. Pseudocolloids may form due to the sorption onto these natural colloids of radionuclides mobilized from degradation of the waste form. Pseudocolloids thus formed in the waste and engineered barrier system may influence radionuclide transport. Several factors contribute to uncertainty in the concentrations of colloids in the groundwater samples used to establish parameters for use in the TSPA analysis including (1) field sampling techniques, including differences in pumping rates at each well during extraction of the water samples, (2) other unknown factors affecting the quantities of particles suspended in the water samples, including the types of additives introduced in the wells during the drilling process itself, and (3) errors inherent to the laboratory methods used to measure the quantities of colloids suspended in the water samples (e.g., filter ripening, interference and detection limitations for dynamic light scattering measurement techniques). A cumulative distribution function was developed to accommodate the variable colloid concentrations and the uncertainty in groundwater sample collection. This allowed for stochastic sampling, including high concentrations (i.e., ~100 mg/L) in at least 2% of the model iterations, while probabilistically allowing for the selection of lower mass concentrations (0.001 mg/L to 1.0 mg/L) 75% of the time. *Sensitivity Name:* COLGW. *Location in TSPA-LA:* Table 6.3.7-66. *DTN:* MO0701PAGROUND.000_R0 [DIRS 179310]. *References: Waste Form and In-Drift Colloids-Associated Radionuclide Concentrations: Abstraction and Summary* (SNL 2007 [DIRS 177423], Sections 6.3.1, 6.3.9, 6.3.11, 6.3.12, 6.5.1.5, 6.5.1.6, 6.5.3, 6.6.6, 7.1.4, 8.1 and Appendix I; Figures 6-22 and 6-24; Tables 6-13, 6-24, 7-1 and I-1).
Conc_Col_U_Sampled_a. Concentration of uranophane colloids when colloids are stable (mg/L). *Distribution:* Piecewise uniform. *Range:* 0.001 to 200. *Median:* 0.1. *Symbol:* $m_{coll,Uranophane,sampled}$. *Additional Information:* The selection of this distribution was based on comparison with commonly observed colloid population distributions of groundwater colloids that are dominated by smectite clay particles. To estimate the uncertainty, it is therefore recommended that the uranophane colloids have a distribution identical to that of the groundwater colloids because the dominant interfacial phase in the groundwater (smectite clay) has surface electrical properties that are similar to uranophane. As the K_d values for the uranophane are low, the probability of radionuclide transport, other than uranium, associated with these colloids is low. *Sensitivity Name:* COLU. *Location in TSPA-LA:* Table 6.3.7-64. *DTN:* MO0701PACSNFCP.000_R1 [DIRS 180439]. *References: Waste Form and In-Drift Colloids-Associated Radionuclide Concentrations: Abstraction and Summary* (SNL 2007 [DIRS 177423], Sections 5.6, 6.3.1, 6.3.2.5, 6.3.2.6, 6.5.1.3, 6.5.1.6, 6.5.2.1, 6.6.4 and 7.1.3; Figures 6-15, 6-28, 6-29 and 6-39; Tables 6-8 and 6-24).

Table K3-3. Detailed Summary of Epistemically Uncertain Variables (i.e., elements of **e**) Considered in the TSPA-LA (TSPA Parameter Name) (Continued)

NOTE: * indicates variable not considered in sensitivity analysis due to correlations.

CORAL. Logarithm of colloid retardation factor in alluvium (dimensionless). *Distribution:* Piecewise uniform. *Range:* 0.903 to 3.715. *Symbol:* R. *Additional Information:* This parameter specifies the retardation of colloids with irreversibly sorbed radionuclides in the alluvium. To treat the one- and three-dimensional transport through the SZ consistently, the sampled values used to generate the saturated zone breakthrough curves are also used in the TSPA-LA Model. These values are tabulated as 200 sets of values for the SZ parameters, accounting for appropriate correletions, and are entered into the TSPA model as a table of 200 values for each parameter. The TSPA-LA Model selects values from this table using the Goldsim variable SZ_index_a. *Sensitivity Name:* SZCOLRAL. *Location in TSPA-LA:* Sections 6.3.10.1, 6.3.10.2 and 6.3.10.4.2; Table 6.3.10-2. *DTN:* SN0702PASZFTMA.002_R1 [DIRS 183471]. *References: Saturated Zone Flow and Transport Model Abstraction* (SNL 2008 [DIRS 183750], Sections 6.3.1, 6.5.1.1 and 6.5.2.11; Tables 4-3, 6-8, A-1[a] and B-1; Equations 6-2 and 6-10; Figure 6-22).
CORVO. Logarithm of colloid retardation factor in volcanic units (dimensionless). *Distribution:* Piecewise uniform. *Range:* 0.778 to 2.903. *Symbol:* R. *Additional Information:* This parameter specifies retardation of colloids with irreversibly sorbed radionuclides in the volcanic units. To treat the one- and three-dimensional transport through the SZ consistently, the sampled values used to generate the saturated zone breakthrough curves are also used in the TSPA-LA Model. These values are tabulated as 200 sets of values for the SZ parameters, accounting for appropriate correletions, and are entered into the TSPA model as a table of 200 values for each parameter. The TSPA-LA Model selects values from this table using the Goldsim variable SZ_index_a. *Sensitivity Name:* SZCOLRVO. *Location in TSPA-LA:* Sections 6.3.10.1, 6.3.10.2 and 6.3.10.4.2; Table 6.3.10-2. *DTN:* SN0702PASZFTMA.002_R1 [DIRS 183471]. *References: Saturated Zone Flow and Transport Model Abstraction* (SNL 2008 [DIRS 183750], Sections 6.3.1, 6.5.1.1 and 6.5.2.11; Tables 4-3, 6-8, A-1[a] and B-1; Equations 6-2 and 6-10; Figure 6-22).
CPu_Col_CSNF_Sampled_a. Concentration of irreversibly attached plutonium on CSNF colloids when colloids are stable (mol/L). *Distribution:* Piecewise uniform. *Range:* 1.00E-10 to 5.00E-06. *Median:* 1.00E-07. *Symbol:* $C_{RN,coll,SNF,embed,sampled}$. *Additional Information:* This model looks exclusively at the irreversible attachment of radionuclides to CSNF colloids. The radionuclides Pu and Am are modeled as irreversibly embedded within CSNF colloids. An empirical cumulative distribution function was developed to accommodate the variable plutonium colloid concentrations and the uncertainty in testing configurations for CSNF corrosion tests. It is reasonable to assume that these CSNF plutonium colloid concentrations will persist for 1 Ma, if CSNF is still present and undergoing weathering, and the solution conditions are suitable for stable colloids. It is conservative to assume these colloids persist at late times after all waste forms are degraded and the initially suspended colloids are washed away. *Sensitivity Name:* CPUCOLCS. *Location in TSPA-LA:* Section 6.3.7.6.2; Table 6.3.7-63. *DTN:* MO0701PACSNFCP.000_R1 [DIRS 180439]. *References: Waste Form and In-Drift Colloids-Associated Radionuclide Concentrations: Abstraction and Summary* (SNL 2007 [DIRS 177423], Sections 6.3.1, 6.3.2.4, 6.3.4, 6.5, 6.5.1.2 and 6.6.3, Tables 6-6, 6-24 and 8-1, Figures 6-10, 6-28, 6-29 and 6-31).
CPu_Col_Wf_Embed_Sampled_a. Concentration of irreversibly attached plutonium on glass/waste form colloids when colloids are stable (mol/L). *Distribution:* Uniform. *Range:* 1.00E-11 to 1.00E-08. *Symbol:* $C_{RN,coll,DHLWG,embed,sampled}$. *Additional Information:* To obtain the plutonium concentration associated with DHLWG colloids, a range is sampled uniformly. Colloids from the corrosion of DHLWG are modeled as smectite particles with irreversibly associated (embedded) Pu and Am. In the case of DHLWG, modeling americium and plutonium as irreversible colloids is conservative and bounding. *Sensitivity Name:* CPUCOLWF. *Location in TSPA-LA:* Section 6.3.7.6.2; Table 6.3.7-62. *DTN:* MO0701PAGLASWF.000_R1 [DIRS 180393]. *References: Waste Form and In-Drift Colloids-Associated Radionuclide Concentrations: Abstraction and Summary* (SNL 2007 [DIRS 177423], Sections 6.3.1, 6.3.2.2, 6.3.3, 6.4.2, 6.5.1.1, 6.5.1.6, 6.5.2 and 6.6.2; Figures 6-6, 6-7, 6-18 and 6-28 to 6-31; Tables 6-4, 6-5, 6-24 and 8-1).
CPu_Per_CSNF_Embed_Col_a. Concentration of irreversibly attached plutonium per concentration of CSNF colloids ((mol/L)/(mg/L)). *Distribution:* Uniform. *Range:* 5.00E-07 to 1.00E-06. *Symbol:* $C_{coll,SNF,uniform}$. *Additional Information:* See CPu_Col_CSNF_Sampled_a. *Sensitivity Name:* CPUPERCS. *Location in TSPA-LA:* Section 6.3.7.6.2; Table 6.3.7-63. *DTN:* MO0701PACSNFCP.000_R1 [DIRS 180439]. *References: Waste Form and In-Drift Colloids-Associated Radionuclide Concentrations: Abstraction and Summary* (SNL 2007 [DIRS 177423], Table 6-24).
CPu_Per_WF_Embed_Col_a. Concentration of irreversibly attached plutonium per concentration of waste form colloids ((mol/L)/(mg/L)). *Distribution:* Triangular. *Range:* 5.00E-09 to 2.5E-08. *Most Likely:* 2.00E-08. *Symbol:* $C_{coll,DHLWG,sampled}$. *Additional Information:* See CPu_Col_CSNF_Sampled_a. *Sensitivity Name:* CPUPERWF. *Location in TSPA-LA:* Section 6.3.7.6.2; Table 6.3.7-62. *DTN:* MO0701PAGLASWF.000_R1 [DIRS 180393]. *References: Waste Form and In-Drift Colloids-Associated Radionuclide Concentrations: Abstraction and Summary* (MDL-EBS-PA-000004 REV 03, SNL 2007 [DIRS 177423], Figure 6-6; Table 6-24).

Table K3-3. Detailed Summary of Epistemically Uncertain Variables (i.e., elements of **e**) Considered in the TSPA-LA (TSPA Parameter Name) (Continued)

NOTE: * indicates variable not considered in sensitivity analysis due to correlations.

Cr2O3_SA_a. Specific surface area of Cr_2O_3 (m^2/g). *Distribution:* Uniform. *Range:* 1 to 20. *Symbol:* S_{CrOx}. *Additional Information:* For the water saturation calculation, the solid density of each of the four corrosion product components is multiplied by its respective specific surface area. *Sensitivity Name:* CR2O3SA. *Location in TSPA-LA:* Table 6.3.8-4, S_{CP} in Equation 6.3.8-19. *DTN:* SN0703PAEBSRTA.001_R3 [DIRS 183217]. *References: EBS Radionuclide Transport Abstraction* (ANL-WIS-PA-000001 REV 03, SNL 2007 [DIRS 177407], Sections 6.3.4.3.3 and 6.5.2.2.1; Tables 4.1-19, 6.3-7, and 8.2-4).
Critical_Slope_a. Critical gradient for tephra mobilization from hillslopes (dimensionless). *Distribution:* Uniform. *Range:* 0.21 to 0.47. *Symbol:* S. *Additional Information:* The critical slope is reported as a fraction of the vertical change in elevation over the horizontal change in distance and is dimensionless. It represents the steepest stable slope for tephra-blanketed hillslopes. The waste-contaminated tephra is mobilized from slopes greater than a specified critical slope. As the critical slope increases, the predicted mass of ash/fuel mobilized decreases. Capturing the lower bound of the critical slope is thus necessary to assure reasonable and conservative results. *Sensitivity Name:* CRITSLOP. *Location in TSPA-LA:* Table 6.5-5. *DTN:* MO0702PAFARDAT.001_R3 [DIRS 182578]. *References: Redistribution of Tephra and Waste by Geomorphic Processes Following a Potential Volcanic Eruption at Yucca Mountain, Nevada* (SNL 2007 [DIRS 179347], Sections 6.2.1, 6.3.2, 6.3.3, 6.5.2, 6.6.1 and 6.6.3; Tables 4.1-3, 6.4-1, 6.5.2-1 and 6.5.10-1; Figures 6.3.3-9 and 6.6.1-1).
CS_Corrosion_Rate_a. Carbon steel corrosion rate (μm/yr). *Distribution:* Truncated log normal. *Range:* 25 to 135. *Mean:* 78.5. *Standard Deviation:* 25. *Symbol:* r_{CS}. *Additional Information:* Carbon-steel corrosion rate is used in computing the mass of stationary corrosion products in the waste package. The corrosion rates for Carbon Steel A516 are known with some uncertainty. From these rates and the thicknesses of the steel components, the lifetime of each type of steel is computed. The extent of corrosion, specifically, the mass of corrosion products, is interpolated over the lifetime of each type of steel. *Sensitivity Name:* CSCORRAT. *Location in TSPA-LA:* Tables 6.3.8-1 and 6.3.8-4. *DTN:* SN0703PAEBSRTA.001_R3 [DIRS 183217]. *References: EBS Radionuclide Transport Abstraction* (SNL 2007 [DIRS 177407], Sections 6.3.4.3.4.3, 6.5.2.2.1 and Appendix F; Tables 4.1-1, 6.5-7, 8.2-4 and 8.2-7; Equation 6.5.2.2.1-1).
CSNF_Mass_Uncert_a. Scale factor used to characterize uncertainty in radionuclide content of CSNF (dimensionless). *Distribution:* Uniform. *Range:* 0.85 to 1.4. *Additional Information:* The sampled multiplier is applied to the nominal CSNF values for all radionuclides except ^{238}U. A radionuclide mass uncertainty multiplier is selected at the beginning of each realization and applied to each waste package that is assumed breached. The selected uncertainty multiplier is held constant during each realization run. CSNF, DSNF, and HLW glass each have their own uncertainty multiplier assigned at the beginning of each realization. *Sensitivity Name:* CSNFMASS. *Location in TSPA-LA:* Sections 6.3.7.1.2 and 6.3.7.1.3; Table 6.3.7-7. *DTN:* SN0310T0505503.004_R0 [DIRS 168761]. *References: Initial Radionuclides Inventory* (SNL 2007 [DIRS 180472], Section 6.6.1, 6.7 and 7; Table 7-2),
CSNF_Rind_SA_a. Specific surface area of CSNF degradation rind (m^2/g). *Distribution:* Uniform. *Range:* 0.5 to 60. *Symbol:* $s_{r,n}$ or s_{rind}. *Additional Information:* See Density_CSNF_Rind_a. The scatter in the data and use of several different materials lead to a range and distribution of parameter values for the FHH isotherm. The specific surface area is a sampled parameter, with a range given by the range of values for the surrogate materials used to generate the FHH adsorption isotherm. While the specific surface area does not necessarily affect the adsorption isotherm, the water saturation is directly proportional to specific surface area. The use of surrogate material properties, where both specific surface area and density are higher than the values estimated for schoepite and CSNF, will result in overestimating water saturation in and releases of radionuclides from the CSNF rind. Sampling from the range and distribution for rind specific surface area given above will enable TSPA to evaluate the sensitivity of estimates for releases of radionuclides to this parameter. To capture this large uncertainty, the specific surface area and density of the rind materials, as well as the porosity, will be sampled from uniform distributions over the ranges of the surrogate material properties. *Sensitivity Name:* CSRINDSA. *Location in TSPA-LA:* Tables 6.3.8-2 and 6.3.8-4. *DTN:* SN0703PAEBSRTA.001_R3 [DIRS 183217]. *References: EBS Radionuclide Transport Abstraction* (SNL 2007 [DIRS 177407], Section 6.3.4.6.1; Equation 6.3.4.6.1-4; Tables 6.5-9, 8.2-4 and 8.2-7).

Table K3-3. Detailed Summary of Epistemically Uncertain Variables (i.e., elements of **e**) Considered in the TSPA-LA (TSPA Parameter Name) (Continued)

NOTE: * indicates variable not considered in sensitivity analysis due to correlations.

CSNF_WF_Uncert_a0_Acid_a. Correlated regression coefficient a0 in the abstracted rate model under acidic conditions (dimensionless). *Distribution:* Normal. *Mean/Median/Mode:* 0. *Standard Deviation:* 1. *Additional Information:* The CSNF WF degradation rate is modeled with a regression model for the degradation rate with uncertain coefficients. The uncertainty in the regression coefficients is sampled by generating vectors from a multivariate normal population with a specified covariance matrix. For the acid-side determination, a random vector is comprised of sampled values for CSNF_WF_Uncert_a0_Acid_a and CSNF_WF_Uncert_a4_Acid_a. The uncertainty in the abstracted rate expression coefficients a0 and a4 is correlated as defined by a covariance matrix. The TSPA implementation of the covariance matrix utilizes the Cholesky Factorization of the covariance matrix and each realization of the random vector to compute the correlated coefficients a0 and a4 for each realization. *Sensitivity Name:* CSWFA0AC. *Location in TSPA-LA:* Section 6.3.7.4.1.2; Equation 6.3.7-6. *References: CSNF Waste Form Degradation: Summary Abstraction* (BSC 2004 [DIRS 169987], Sections 6.4.1.3 and 8.1; Equation 11).
CSNF_WF_Uncert_a0_Alk_a. Correlated coefficient a0 in the abstracted rate model under alkaline conditions (dimensionless). *Distribution:* Normal. *Mean/Median/Mode:* 0. *Standard Deviation:* 1. *Additional Information:* The CSNF WF degradation rate is modeled with a regression model for the degradation rate with uncertain coefficients. The uncertainty in the regression coefficients is sampled by generating vectors from a multivariate normal population with a specified covariance matrix. For the alkaline-side determination, the random vector is comprised of sampled values for CSNF_WF_Uncert_a0_Alk_a, CSNF_WF_Uncert_a1_Alk_a, CSNF_WF_Uncert_a2_Alk_a and CSNF_WF_Uncert_a3_Alk_a. The uncertainty in the abstracted rate expression coefficients a0, a1, a2, and a3 is correlated as defined by a covariance matrix. The TSPA implementation of the covariance matrix utilizes the Cholesky Factorization of the covariance matrix and each realization of the random vector to compute the correlated coefficients a0, a1, a2, and a3 for each realization. *Sensitivity Name:* CSWFA0AK. *Location in TSPA-LA:* Section 6.3.7.4.1.2; Equation 6.3.7-5. *References: CSNF Waste Form Degradation: Summary Abstraction* (BSC 2004 [DIRS 169987], Sections 6.4.1.2 and 8.1; Equation 10).
CSNF_WF_Uncert_a1_Alk_a. Correlated coefficient a1 in the abstracted rate model under alkaline conditions (dimensionless). *Distribution:* Normal. *Mean/Median/Mode:* 0. *Standard Deviation:* 1. *Additional Information:* See CSNF_WF_Uncert_a0_Alk_a. *Sensitivity Name:* CSWFA1AK. *Location in TSPA-LA:* Section 6.3.7.4.1.2; Equation 6.3.7-5. *References: CSNF Waste Form Degradation: Summary Abstraction* (BSC 2004 [DIRS 169987], Sections 6.4.1.2 and 8.1; Equation 10).
CSNF_WF_Uncert_a2_Alk_a. Correlated coefficient a2 in the abstracted rate model under alkaline conditions (dimensionless). *Distribution:* Normal. *Mean/Median/Mode:* 0. *Standard Deviation:* 1. *Additional Information:* See CSNF_WF_Uncert_a0_Alk_a. *Sensitivity Name:* CSWFA2AK. *Location in TSPA-LA:* Section 6.3.7.4.1.2; Equation 6.3.7-5. *References: CSNF Waste Form Degradation: Summary Abstraction* (BSC 2004 [DIRS 169987], Sections 6.4.1.2 and 8.1; Equation 10).
CSNF_WF_Uncert_a3_Alk_a. Correlated coefficient a3 in the abstracted rate model under alkaline conditions (dimensionless). *Distribution:* Normal. *Mean/Median/Mode:* 0. *Standard Deviation:* 1. *Additional Information:* See CSNF_WF_Uncert_a0_Alk_a. *Sensitivity Name:* CSWFA3AK. *Location in TSPA-LA:* Section 6.3.7.4.1.2; Equation 6.3.7-5. *References: CSNF Waste Form Degradation: Summary Abstraction* (BSC 2004 [DIRS 169987], Sections 6.4.1.2 and 8.1; Equation 10).
CSNF_WF_Uncert_a4_Acid_a. Correlated coefficient a4 in the abstracted rate model under acid conditions (dimensionless). *Distribution:* Normal. *Mean/Median/Mode:* 0. *Standard Deviation:* 1. *Additional Information:* See CSNF_WF_Uncert_a0_Acid_a. *Sensitivity Name:* CSWFA4AC. *Location in TSPA-LA:* Section 6.3.7.4.1.2; Equation 6.3.7-6. *References: CSNF Waste Form Degradation: Summary Abstraction* (BSC 2004 [DIRS 169987], Sections 6.4.1.3 and 8.1; Equation 11).
D_Channels_a. Diffusivity of radionuclides in channels of the Fortymile Wash fan (RMEI location) (cm^2/yr). *Distribution:* Uniform. *Range:* 0.035 to 0.266. *Mean:* 0.1505. *Symbol:* D_c. *Additional Information:* The uncertainty distribution for this parameter is based on measured ^{137}Cs profiles from channels and young terraces of the upper Fortymile Wash alluvial fan. The diffusivity model is used to calculate the waste concentration profile over time in the RMEI domain. As the diffusivity parameter increases, the rate of diffusion into the soil increases, decreasing the near surface contamination (and thus the calculated dose) at a more rapid rate. Capturing the low end of the diffusivity range is thus critical to assure reasonable and conservative results. *Sensitivity Name:* DCHANL. *Location in TSPA-LA:* Table 6.5-5. *DTN:* MO0702PAFARDAT.001_R3 [DIRS 182578]. *References: Redistribution of Tephra and Waste by Geomorphic Processes Following a Potential Volcanic Eruption at Yucca Mountain, Nevada* (SNL 2007 [DIRS 179347], Sections 6.5.8.2, 6.6.2 and 7.1.3; Tables 6.4-1, 6.5.8-2 and 6.6.2-1).

Table K3-3. Detailed Summary of Epistemically Uncertain Variables (i.e., elements of **e**) Considered in the TSPA-LA (TSPA Parameter Name) (Continued)

NOTE: * indicates variable not considered in sensitivity analysis due to correlations.

D_Divides_a. Diffusivity of radionuclides in divides of the Fortymile Wash fan (RMEI location) (cm^2/yr). *Distribution:* Uniform. *Range:* 0.001 to 0.095. *Mean* 0.048. *Symbol:* D_d. *Additional Information:* The uncertainty distribution for this parameter is based on measured ^{137}Cs profiles from interchannel divides (assumed to be older than 10,000 yr) on the upper Fortymile Wash alluvial fan. The diffusivity model is used to calculate the waste concentration profile over time in the RMEI domain. As the diffusivity parameter increases, the rate of diffusion into the soil increases, decreasing the near surface contamination (and thus the calculated dose) at a more rapid rate. Capturing the low end of the diffusivity range is thus critical to assure reasonable and conservative results. *Sensitivity Name:* DDIVIDE. *Location in TSPA-LA:* Table 6.5-5. *DTN:* MO0702PAFARDAT.001_R3 [DIRS 182578]. *References: Redistribution of Tephra and Waste by Geomorphic Processes Following a Potential Volcanic Eruption at Yucca Mountain, Nevada* (SNL 2007 [DIRS 179347], Sections 6.5.8.1, 6.6.2 and 7.1.3; Tables 6.4-1, 6.5.8-1 and 6.6.2-1).
Dash_mean_a. Mass median ash particle diameter (cm). *Distribution:* Log triangular. *Range:* 0.001 to 0.1. *Mode:* 0.01. *Symbol:* d. *Additional Information:* The ash particle diameter is defined within the ASHPLUME model by two parameters: the mean ash particle diameter and the ash particle diameter standard deviation. The mode honors the frequency of values near this value in samples from Lathrop Wells volcano, while the tails honor the variability in mean grain size observed at historical violent Strombolian eruptions. The size distribution of ash particles transported by the ASHPLUME code is generally much larger than the particle size used to calculate the inhalation BDCFs. Tephra concentrations show strong sensitivity (factor of 35) to mean ash particle diameter, and fuel concentrations show small sensitivity (factor of 2) to two orders of magnitude variation in mean ash particle diameter. *Sensitivity Name:* DASHAVG. *Location in TSPA-LA:* Table 6.5-4. *DTN:* LA0702PADE03GK.002_R1 [DIRS 179980]. *References: Atmospheric Dispersal and Deposition of Tephra from a Potential Volcanic Eruption at Yucca Mountain, Nevada* (SNL 2007 [DIRS 177431], Sections 6.5.2.4, 7.2, 7.7 and Appendix C; Tables 4-1, 6-3, 8-2 and C-3; Figure C-2).
Dash_sigma_a. Ash particle diameter standard deviation (log (cm)). *Distribution:* Uniform. *Range:* 0.301 to 0.903. *Symbol:* σ_d. *Additional Information:* The ash particle diameter is defined within the ASHPLUME model by two parameters: the mean ash particle diameter and the ash particle diameter standard deviation. The upper and lower bounds of the range were chosen based on scientific judgment to bracket the sparse observations, and the uniform distribution reflects sparseness of the data and the equal likelihood of any value within the range. *Sensitivity Name:* DASHSIG. *Location in TSPA-LA:* Table 6.5-4. *DTN:* LA0702PADE03GK.002_R1 [DIRS 179980]. *References:* Atmospheric Dispersal and Deposition of Tephra from a Potential Volcanic Eruption at Yucca Mountain, Nevada (MDL-MGR-GS-000002 REV 03, SNL 2007 [DIRS 177431], Section 6.5.2.5, 7.2 and Appendix C; Tables 4-1, 6-3, 8-2 and C-4; Figure C-3).
DCVO. Logarithm of effective diffusion coefficient in fractured volcanic units (m^2/s). *Distribution:* Piecewise uniform. *Range:* -11.3 to -9.3. *Symbol:* D_e. *Additional Information:* The uncertain input parameters influencing matrix diffusion include effective diffusion coefficient (DCVO), flowing interval spacing (FISVO), and flowing interval porosity (FPVO). For the SZ 1-D transport model the matrix diffusion coefficient for those radionuclides that do experience matrix diffusion is implemented by calculating an effective tortuosity, based on the sampled value of effective diffusion coefficient and the free water diffusion coefficient. To treat the one- and three-dimensional transport through the SZ consistently, the sampled values used to generate the saturated zone breakthrough curves are also used in the TSPA-LA Model. These values are tabulated as 200 sets of values for the SZ parameters, accounting for appropriate correletions, and are entered into the TSPA model as a table of 200 values for each parameter. The TSPA-LA Model selects values from this table using the Goldsim variable SZ_index_a. *Sensitivity Name:* SZDIFCVO. *Location in TSPA-LA:* Sections 6.3.10.2 and 6.3.10.5; Table 6.3.10-2. *DTN:* SN0702PASZFTMA.002_R1 [DIRS 183471]. *References: Saturated Zone Flow and Transport Model Abstraction* (SNL 2008 [DIRS 183750], Section 6.5.2.6; Tables 6-8, B-1, 7-1[a], A-1[a], B-2[a],; Equations 6-15 and 6-17; Figures 6-14 and 6-15).
DE_BDCF_IER_Ra226_Pb210. Volcanic Biosphere Dose Conversion Factor (BDCF) component for radon, external exposure and ingestion of ^{226}Ra and ^{210}Pb in modern interglacial climate ((Sv/yr)/(Bq/m^2)). *Distribution:* Discrete. *Range:* 3.07E-08 to 9.43E-08. *Mean:* 3.52E-08. *Standard Deviation:* 3.45E-09. *Symbol:* $BDCF_{ext,ing,Rn,i}$. *Additional Information:* See DE_BDCF_Inh_LT_Ac227. *Sensitivity Name:* INGRA226. *Location in TSPA-LA:* Sections 6.3.11.1 and 6.3.11.2; Equation 6.3.11-4. *DTN:* MO0702PAVBPDCF.000_R0 [DIRS 179330]. *References: Biosphere Model Report* SNL 2007 [DIRS 177399], Sections 6.12.2 and 6.12.3; Table 6.12-4; Equation 6.12-1).

Table K3-3. Detailed Summary of Epistemically Uncertain Variables (i.e., elements of **e**) Considered in the TSPA-LA (TSPA Parameter Name) (Continued)

NOTE: * indicates variable not considered in sensitivity analysis due to correlations.

DE_BDCF_ILT_Ra226_Pb210. Volcanic Biosphere Dose Conversion Factor (BDCF) component for long-term inhalation of ^{226}Ra and ^{210}Pb in modern interglacial climate ((Sv/yr)/(Bq/kg)). *Distribution:* Discrete. *Range:* 1.71E-08 to 5.03E-07. *Mean:* 1.01E-07. *Standard Deviation:* 6.43E-08. *Symbol:* $BDCF_{inh,p,i}$. *Additional Information:* See DE_BDCF_Inh_LT_Ac227. *Sensitivity Name:* ILTRA226. *Location in TSPA-LA:* Sections 6.3.11.1 and 6.3.11.2; Equation 6.3.11-4. *DTN:* MO0702PAVBPDCF.000_R0 [DIRS 179330]. *References: Biosphere Model Report* (SNL 2007 [DIRS 177399], Sections 6.12.2 and 6.12.3; Table 6.12-3; Equation 6.12-1).
DE_BDCF_Ing_Exp_Radon_Ac227. Volcanic Biosphere Dose Conversion Factor (BDCF) component for radon, external exposure and ingestion of ^{227}Ac in modern interglacial climate ((Sv/yr)/(Bq/m^2)). *Distribution:* Discrete. *Range:* 5.78E-09 to 7.76E-09. *Mean:* 6.16E-09. *Standard Deviation:* 1.8E-10. *Symbol:* $BDCF_{ext,ing,Rn,i}$. *Additional Information:* See DE_BDCF_Inh_LT_Ac227. *Sensitivity Name:* INGAC227. *Location in TSPA-LA:* Sections 6.3.11.1 and 6.3.11.2; Equation 6.3.11-4. *DTN:* MO0702PAVBPDCF.000_R0 [DIRS 179330]. *References: Biosphere Model Report* (MDL-MGR-MD-000001, SNL 2007 [DIRS 177399], Sections 6.12.2 and 6.12.3; Table 6.12-4; Equation 6.12-1).
DE_BDCF_Ing_Exp_Radon_Am241. Volcanic Biosphere Dose Conversion Factor (BDCF) component for radon, external exposure and ingestion of ^{241}Am in modern interglacial climate ((Sv/yr)/(Bq/m^2)). *Distribution:* Discrete. *Range:* 1.86E-10 to 1.00E-09. *Mean:* 2.51E-10. *Standard Deviation:* 7.00E-11. *Symbol:* $BDCF_{ext,ing,Rn,i}$. *Additional Information:* See DE_BDCF_Inh_LT_Ac227. *Sensitivity Name:* INGAM241. *Location in TSPA-LA:* Sections 6.3.11.1 and 6.3.11.2; Equation 6.3.11-4. *DTN:* MO0702PAVBPDCF.000_R0 [DIRS 179330]. *References: Biosphere Model Report* (MDL-MGR-MD-000001, SNL 2007 [DIRS 177399], Sections 6.12.2 and 6.12.3; Table 6.12-4; Equation 6.12-1).
DE_BDCF_Ing_Exp_Radon_Am243. Volcanic Biosphere Dose Conversion Factor (BDCF) component for radon, external exposure and ingestion of ^{243}Am in modern interglacial climate ((Sv/yr)/(Bq/m^2)). *Distribution:* Discrete. *Range:* 2.51E-09 to 3.42E-09. *Mean:* 2.67E-09. *Standard Deviation:* 8.02E-11. *Symbol:* $BDCF_{ext,ing,Rn,i}$. *Additional Information:* See DE_BDCF_Inh_LT_Ac227. *Sensitivity Name:* INGAM243. *Location in TSPA-LA:* Sections 6.3.11.1 and 6.3.11.2; Equation 6.3.11-4. *DTN:* MO0702PAVBPDCF.000_R0 [DIRS 179330]. *References: Biosphere Model Report* (SNL 2007 [DIRS 177399], Sections 6.12.2 and 6.12.3; Table 6.12-4; Equation 6.12-1).
DE_BDCF_Ing_Exp_Radon_Cs137. Volcanic Biosphere Dose Conversion Factor (BDCF) component for radon, external exposure and ingestion of ^{137}Cs in modern interglacial climate ((Sv/yr)/(Bq/m^2)). *Distribution:* Discrete. *Range:* 6.75E-09 to 8.48E-09. *Mean:* 7.17E-09. *Standard Deviation:* 1.55E-10. *Symbol:* $BDCF_{ext,ing,Rn,i}$. *Additional Information:* See DE_BDCF_Inh_LT_Ac227. *Sensitivity Name:* INGCS137. *Location in TSPA-LA:* Sections 6.3.11.1 and 6.3.11.2; Equation 6.3.11-4. *DTN:* MO0702PAVBPDCF.000_R0 [DIRS 179330]. *References: Biosphere Model Report* (SNL 2007 [DIRS 177399], Sections 6.12.2 and 6.12.3; Table 6.12-4; Equation 6.12-1).
DE_BDCF_Ing_Exp_Radon_I129. Volcanic Biosphere Dose Conversion Factor (BDCF) component for radon, external exposure and ingestion of ^{129}I in modern interglacial climate ((Sv/yr)/(Bq/m^2)). *Distribution:* Discrete. *Range:* 1.39E-10 to 2.86E-08. *Mean:* 1.26E-09. *Standard Deviation:* 2.59E-09. *Symbol:* $BDCF_{ext,ing,Rn,i}$. *Additional Information:* See DE_BDCF_Inh_LT_Ac227. *Sensitivity Name:* INGI129. *Location in TSPA-LA:* Sections 6.3.11.1 and 6.3.11.2; Equation 6.3.11-4. *DTN:* MO0702PAVBPDCF.000_R0 [DIRS 179330]. *References: Biosphere Model Report* (SNL 2007 [DIRS 177399], Sections 6.12.2 and 6.12.3; Table 6.12-4; Equation 6.12-1).
DE_BDCF_Ing_Exp_Radon_Np237. Volcanic Biosphere Dose Conversion Factor (BDCF) component for radon, external exposure and ingestion of ^{237}Np in modern interglacial climate ((Sv/yr)/(Bq/m^2)). *Distribution:* Discrete. *Range:* 2.62E-09 to 1.2E-08. *Mean:* 2.98E-09. *Standard Deviation:* 6.36E-10. *Symbol:* $BDCF_{ext,ing,Rn,i}$. *Additional Information:* See DE_BDCF_Inh_LT_Ac227. *Sensitivity Name:* INGNP237. *Location in TSPA-LA:* Sections 6.3.11.1 and 6.3.11.2; Equation 6.3.11-4. *DTN:* MO0702PAVBPDCF.000_R0 [DIRS 179330]. *References: Biosphere Model Report* (SNL 2007 [DIRS 177399], Sections 6.12.2 and 6.12.3; Table 6.12-4; Equation 6.12-1).
DE_BDCF_Ing_Exp_Radon_Pa231. Volcanic Biosphere Dose Conversion Factor (BDCF) component for radon, external exposure and ingestion of ^{231}Pa in modern interglacial climate ((Sv/yr)/(Bq/m^2)). *Distribution:* Discrete. *Range:* 5.02E-10 to 4.56E-09. *Mean:* 7.14E-10. *Standard Deviation:* 2.92E-10. *Symbol:* $BDCF_{ext,ing,Rn,i}$. *Additional Information:* See DE_BDCF_Inh_LT_Ac227. *Sensitivity Name:* INGPA231. *Location in TSPA-LA:* Sections 6.3.11.1 and 6.3.11.2; Equation 6.3.11-4. *DTN:* MO0702PAVBPDCF.000_R0 [DIRS 179330]. *References: Biosphere Model Report* (SNL 2007 [DIRS 177399], Sections 6.12.2 and 6.12.3; Table 6.12-4; Equation 6.12-1).

Table K3-3. Detailed Summary of Epistemically Uncertain Variables (i.e., elements of **e**) Considered in the TSPA-LA (TSPA Parameter Name) (Continued)

NOTE: * indicates variable not considered in sensitivity analysis due to correlations.

DE_BDCF_Ing_Exp_Radon_Pu238. Volcanic Biosphere Dose Conversion Factor (BDCF) component for radon, external exposure and ingestion of ^{238}Pu in modern interglacial climate ((Sv/yr)/(Bq/m^2)). *Distribution:* Discrete. *Range:* 1.33E-11 to 9.18E-10. *Mean:* 7.78E-11. *Standard Deviation:* 7.72E-11. *Symbol:* $BDCF_{ext,ing,Rn,i}$. *Additional Information:* See DE_BDCF_Inh_LT_Ac227. *Sensitivity Name:* INGPU238. *Location in TSPA-LA:* Sections 6.3.11.1 and 6.3.11.2; Equation 6.3.11-4. *DTN:* MO0702PAVBPDCF.000_R0 [DIRS 179330]. *References:* *Biosphere Model Report* (SNL 2007 [DIRS 177399], Sections 6.12.2 and 6.12.3; Table 6.12-4; Equation 6.12-1).
DE_BDCF_Ing_Exp_Radon_Pu239. Volcanic Biosphere Dose Conversion Factor (BDCF) component for radon, external exposure and ingestion of ^{239}Pu in modern interglacial climate ((Sv/yr)/(Bq/m^2)). *Distribution:* Discrete. *Range:* 1.40E-11 to 1.01E-09. *Mean:* 8.49E-11. *Standard Deviation:* 8.5E-11. *Symbol:* $BDCF_{ext,ing,Rn,i}$. *Additional Information:* See DE_BDCF_Inh_LT_Ac227. *Sensitivity Name:* INGPU239. *Location in TSPA-LA:* Sections 6.3.11.1 and 6.3.11.2; Equation 6.3.11-4. *DTN:* MO0702PAVBPDCF.000_R0 [DIRS 179330]. *References:* *Biosphere Model Report* (SNL 2007 [DIRS 177399], Sections 6.12.2 and 6.12.3; Table 6.12-4; Equation 6.12-1).
DE_BDCF_Ing_Exp_Radon_Pu240. Volcanic Biosphere Dose Conversion Factor (BDCF) component for radon, external exposure and ingestion of ^{240}Pu in modern interglacial climate ((Sv/yr)/(Bq/m^2)). *Distribution:* Discrete. *Range:* 1.42E-11 to 1.01E-09. *Mean:* 8.52E-11. *Standard Deviation:* 8.5E-11. *Symbol:* $BDCF_{ext,ing,Rn,i}$. *Additional Information:* See DE_BDCF_Inh_LT_Ac227. *Sensitivity Name:* INGPU240. *Location in TSPA-LA:* Sections 6.3.11.1 and 6.3.11.2; Equation 6.3.11-4. *DTN:* MO0702PAVBPDCF.000_R0 [DIRS 179330]. *References:* *Biosphere Model Report* (SNL 2007 [DIRS 177399], Sections 6.12.2 and 6.12.3; Table 6.12-4; Equation 6.12-1).
DE_BDCF_Ing_Exp_Radon_Pu242. Volcanic Biosphere Dose Conversion Factor (BDCF) component for radon, external exposure and ingestion of ^{242}Pu in modern interglacial climate ((Sv/yr)/(Bq/m^2)). *Distribution:* Discrete. *Range:* 1.31E-11 to 9.57E-10. *Mean:* 8.04E-11. *Standard Deviation:* 8.06E-11. *Symbol:* $BDCF_{ext,ing,Rn,i}$. *Additional Information:* See DE_BDCF_Inh_LT_Ac227. *Sensitivity Name:* INGPU242. *Location in TSPA-LA:* Sections 6.3.11.1 and 6.3.11.2; Equation 6.3.11-4. *DTN:* MO0702PAVBPDCF.000_R0 [DIRS 179330]. *References:* *Biosphere Model Report* (SNL 2007 [DIRS 177399], Sections 6.12.2 and 6.12.3; Table 6.12-4; Equation 6.12-1).
DE_BDCF_Ing_Exp_Radon_Ra228. Volcanic Biosphere Dose Conversion Factor (BDCF) component for radon, external exposure and ingestion of ^{228}Ra in modern interglacial climate ((Sv/yr)/(Bq/m^2)). *Distribution:* Discrete. *Range:* 1.17E-08 to 2.62E-08. *Mean:* 1.27E-08. *Standard Deviation:* 7.44E-10. *Symbol:* $BDCF_{ext,ing,Rn,i}$. *Additional Information:* See DE_BDCF_Inh_LT_Ac227. *Sensitivity Name:* INGRA228. *Location in TSPA-LA:* Sections 6.3.11.1 and 6.3.11.2; Equation 6.3.11-4. *DTN:* MO0702PAVBPDCF.000_R0 [DIRS 179330]. *References:* *Biosphere Model Report* (SNL 2007 [DIRS 177399], Sections 6.12.2 and 6.12.3; Table 6.12-4; Equation 6.12-1).
DE_BDCF_Ing_Exp_Radon_Sn126. Volcanic Biosphere Dose Conversion Factor (BDCF) component for radon, external exposure and ingestion of ^{126}Sn in modern interglacial climate ((Sv/yr)/(Bq/m^2)). *Distribution:* Discrete. *Range:* 2.38E-08 to 2.79E-08. *Mean:* 2.54E-08. *Standard Deviation:* 4.41E-10. *Symbol:* $BDCF_{ext,ing,Rn,i}$. *Additional Information:* See DE_BDCF_Inh_LT_Ac227. *Sensitivity Name:* INGSN126. *Location in TSPA-LA:* Sections 6.3.11.1 and 6.3.11.2; Equation 6.3.11-4. *DTN:* MO0702PAVBPDCF.000_R0 [DIRS 179330]. *References:* *Biosphere Model Report* (SNL 2007 [DIRS 177399], Sections 6.12.2 and 6.12.3; Table 6.12-4; Equation 6.12-1).
DE_BDCF_Ing_Exp_Radon_Sr90. Volcanic Biosphere Dose Conversion Factor (BDCF) component for radon, external exposure and ingestion of ^{90}Sr in modern interglacial climate ((Sv/yr)/(Bq/m^2)). *Distribution:* Discrete. *Range:* 1.44E-09 to 6.10E-09. *Mean:* 1.81E-09. *Standard Deviation:* 3.67E-10. *Symbol:* $BDCF_{ext,ing,Rn,i}$. *Additional Information:* See DE_BDCF_Inh_LT_Ac227. *Sensitivity Name:* INGSR90. *Location in TSPA-LA:* Sections 6.3.11.1 and 6.3.11.2; Equation 6.3.11-4. *DTN:* MO0702PAVBPDCF.000_R0 [DIRS 179330]. *References:* *Biosphere Model Report* (SNL 2007 [DIRS 177399], Sections 6.12.2 and 6.12.3; Table 6.12-4; Equation 6.12-1).
DE_BDCF_Ing_Exp_Radon_Tc99. Volcanic Biosphere Dose Conversion Factor (BDCF) component for radon, external exposure and ingestion of ^{99}Tc in modern interglacial climate ((Sv/yr)/(Bq/m^2)). *Distribution:* Discrete. *Range:* 5.08E-12 to 8.95E-09. *Mean:* 2.72E-10. *Standard Deviation:* 5.16E-10. *Symbol:* $BDCF_{ext,ing,Rn,i}$. *Additional Information:* See DE_BDCF_Inh_LT_Ac227. *Sensitivity Name:* INGTC99. *Location in TSPA-LA:* Sections 6.3.11.1 and 6.3.11.2; Equation 6.3.11-4. *DTN:* MO0702PAVBPDCF.000_R0 [DIRS 179330]. *References:* *Biosphere Model Report* (SNL 2007 [DIRS 177399], Sections 6.12.2 and 6.12.3; Table 6.12-4; Equation 6.12-1).
DE_BDCF_Ing_Exp_Radon_Th229. Volcanic Biosphere Dose Conversion Factor (BDCF) component for radon, external exposure and ingestion of ^{229}Th in modern interglacial climate ((Sv/yr)/(Bq/m^2)). *Distribution:* Discrete. *Range:* 4.33E-09 to 7.02E-09. *Mean:* 4.69E-09. *Standard Deviation:* 2.4E-10. *Symbol:* $BDCF_{ext,ing,Rn,i}$. *Additional Information:* See DE_BDCF_Inh_LT_Ac227. *Sensitivity Name:* INGTH229. *Location in TSPA-LA:* Sections 6.3.11.1 and 6.3.11.2; Equation 6.3.11-4. *DTN:* MO0702PAVBPDCF.000_R0 [DIRS 179330]. *References:* *Biosphere Model Report* (SNL 2007 [DIRS 177399], Sections 6.12.2 and 6.12.3; Table 6.12-4; Equation 6.12-1).

Table K3-3. Detailed Summary of Epistemically Uncertain Variables (i.e., elements of **e**) Considered in the TSPA-LA (TSPA Parameter Name) (Continued)

NOTE: * indicates variable not considered in sensitivity analysis due to correlations.

DE_BDCF_Ing_Exp_Radon_Th230. Volcanic Biosphere Dose Conversion Factor (BDCF) component for radon, external exposure and ingestion of ^{230}Th in modern interglacial climate ((Sv/yr)/(Bq/m^2)). *Distribution:* Discrete. *Range:* 1.92E-11 to 8.68E-10. *Mean:* 8.51E-11. *Standard Deviation:* 7.82E-11. *Symbol:* $BDCF_{ext,ing,Rn,i}$. *Additional Information:* See DE_BDCF_Inh_LT_Ac227. *Sensitivity Name:* INGTH230. *Location in TSPA-LA:* Sections 6.3.11.1 and 6.3.11.2; Equation 6.3.11-4. *DTN:* MO0702PAVBPDCF.000_R0 [DIRS 179330]. *References: Biosphere Model Report* (SNL 2007 [DIRS 177399], Sections 6.12.2 and 6.12.3; Table 6.12-4; Equation 6.12-1).
DE_BDCF_Ing_Exp_Radon_Th232. Volcanic Biosphere Dose Conversion Factor (BDCF) component for radon, external exposure and ingestion of ^{232}Th in modern interglacial climate ((Sv/yr)/(Bq/m^2)). *Distribution:* Discrete. *Range:* 1.72E-11 to 9.34E-10. *Mean:* 8.83E-11. *Standard Deviation:* 8.44E-11. *Symbol:* $BDCF_{ext,ing,Rn,i}$. *Additional Information:* See DE_BDCF_Inh_LT_Ac227. *Sensitivity Name:* INGTH232. *Location in TSPA-LA:* Sections 6.3.11.1 and 6.3.11.2; Equation 6.3.11-4. *DTN:* MO0702PAVBPDCF.000_R0 [DIRS 179330]. *References: Biosphere Model Report* (MDL-MGR-MD-000001, SNL 2007 [DIRS 177399], Sections 6.12.2 and 6.12.3; Table 6.12-4; Equation 6.12-1).
DE_BDCF_Ing_Exp_Radon_U233. Volcanic Biosphere Dose Conversion Factor (BDCF) component for radon, external exposure and ingestion of ^{233}U in modern interglacial climate ((Sv/yr)/(Bq/m^2)). *Distribution:* Discrete. *Range:* 1.31E-11 to 9.04E-10. *Mean:* 6.48E-11. *Standard Deviation:* 6.12E-11. *Symbol:* $BDCF_{ext,ing,Rn,i}$. *Additional Information:* See DE_BDCF_Inh_LT_Ac227. *Sensitivity Name:* INGU233. *Location in TSPA-LA:* Sections 6.3.11.1 and 6.3.11.2; Equation 6.3.11-4. *DTN:* MO0702PAVBPDCF.000_R0 [DIRS 179330]. *References: Biosphere Model Report* (MDL-MGR-MD-000001, SNL 2007 [DIRS 177399], Sections 6.12.2 and 6.12.3; Table 6.12-4; Equation 6.12-1).
DE_BDCF_Ing_Exp_Radon_U234. Volcanic Biosphere Dose Conversion Factor (BDCF) component for radon, external exposure and ingestion of ^{234}U in modern interglacial climate ((Sv/yr)/(Bq/m^2)). *Distribution:* Discrete. *Range:* 9.60E-12 to 8.7E-10. *Mean:* 5.96E-11. *Standard Deviation:* 5.9E-11. *Symbol:* $BDCF_{ext,ing,Rn,i}$. *Additional Information:* See DE_BDCF_Inh_LT_Ac227. *Sensitivity Name:* INGU234. *Location in TSPA-LA:* Sections 6.3.11.1 and 6.3.11.2; Equation 6.3.11-4. *DTN:* MO0702PAVBPDCF.000_R0 [DIRS 179330]. *References: Biosphere Model Report* (MDL-MGR-MD-000001, SNL 2007 [DIRS 177399], Sections 6.12.2 and 6.12.3; Table 6.12-4; Equation 6.12-1).
DE_BDCF_Ing_Exp_Radon_U238. Volcanic Biosphere Dose Conversion Factor (BDCF) component for radon, external exposure and ingestion of ^{238}U in modern interglacial climate ((Sv/yr)/(Bq/m^2)). *Distribution:* Discrete. *Range:* 1.52E-09 to 2.41E-09. *Mean:* 1.62E-09. *Standard Deviation:* 6.16E-11. *Symbol:* $BDCF_{ext,ing,Rn,i}$. *Additional Information:* See DE_BDCF_Inh_LT_Ac227. *Sensitivity Name:* INGU238. *Location in TSPA-LA:* Sections 6.3.11.1 and 6.3.11.2; Equation 6.3.11-4. *DTN:* MO0702PAVBPDCF.000_R0 [DIRS 179330]. *References: Biosphere Model Report* (MDL-MGR-MD-000001, SNL 2007 [DIRS 177399], Sections 6.12.2 and 6.12.3; Table 6.12-4; Equation 6.12-1).

Table K3-3. Detailed Summary of Epistemically Uncertain Variables (i.e., elements of **e**) Considered in the TSPA-LA (TSPA Parameter Name) (Continued)

NOTE: * indicates variable not considered in sensitivity analysis due to correlations.

DE_BDCF_Inh_LT_Ac227. Volcanic Biosphere Dose Conversion Factor (BDCF) component for long-term inhalation of ^{227}Ac in modern interglacial climate ((Sv/yr)/(Bq/kg)). *Distribution:* Discrete. *Range:* 1.53E-07 to 4.5E-06. *Mean:* 9.0E-07. *Standard Deviation:* 5.75E-07. *Symbol:* $BDCF_{inh,p,i}$. *Additional Information:* Volcanic BDCFs consist of three BDCF components for each primary radionuclide. The first component, called the ingestion component, $BDCF_{ext,ing,Rn,i}$, accounts for exposure to sources external to the body, ingestion, and inhalation of radon decay products. This component is numerically equal to the annual dose to the RMEI from these exposure pathways per unit of areal radionuclide concentration in the soil (Sv/yr per Bq/m^2). The second and third BDCF components, called the short-term and the long-term inhalation BDCF components, account for inhaling airborne particulates. The short-term inhalation component, $BDCF_{inh,v,i}$, is numerically equal to the early-time increase in inhalation dose (over and above the long-term inhalation dose described by the long-term inhalation BDCF component) during the first year following a volcanic eruption per unit of radionuclide concentration in the soil layer that can become resuspended (Sv/yr per Bq/kg). This term is used together with the time function, representing the decrease of the airborne particulate concentration with time, to calculate short-term increase in inhalation exposure due to elevated levels of airborne particulate matter after a volcanic eruption, relative to the conditions existing before and long after an eruption. With time, mass loading returns to the pre-eruption level. These exposure conditions are described by the long-term inhalation BDCF, $BDCF_{inh,p,i}$, which accounts for inhalation of resuspended particulates under nominal conditions, i.e., when the mass loading is not elevated as the result of volcanic eruption. This component is numerically equal to the annual dose to the RMEI from inhaling particulates at the nominal concentration in the air, per unit of radionuclide concentration in the soil that can be resuspended (Sv/yr per Bq/kg). To account for correlations between parameters used to compute BDCFs, the Biosphere Model generates a table of 1,000 sets of values for each BDCF. These values are entered into the TSPA Input Database as a table of 1,000 values for each parameter. The TSPA-LA Model selects values from this table using the Goldsim variable Bio_index_a. *Sensitivity Name:* ILTAC227. *Location in TSPA-LA:* Sections 6.3.11.1 and 6.3.11.2; Equation 6.3.11-4. *DTN:* MO0702PAVBPDCF.000_R0 [DIRS 179330]. *References: Biosphere Model Report* (MDL-MGR-MD-000001, SNL 2007 [DIRS 177399], Sections 6.12.2 and 6.12.3; Table 6.12-3; Equation 6.12-1).
DE_BDCF_Inh_LT_Am241. Volcanic Biosphere Dose Conversion Factor (BDCF) component for long-term inhalation of ^{241}Am in modern interglacial climate ((Sv/yr)/(Bq/kg)). *Distribution:* Discrete. *Range:* 8.45E-08 to 2.48E-06. *Mean:* 4.96E-07. *Standard Deviation:* 3.17E-07. *Symbol:* $BDCF_{inh,p,i}$. *Additional Information:* See DE_BDCF_Inh_LT_Ac227. *Sensitivity Name:* ILTAM241. *Location in TSPA-LA:* Sections 6.3.11.1 and 6.3.11.2; Equation 6.3.11-4. *DTN:* MO0702PAVBPDCF.000_R0 [DIRS 179330]. *References: Biosphere Model Report* (MDL-MGR-MD-000001, SNL 2007 [DIRS 177399], Sections 6.12.2 and 6.12.3; Table 6.12-3; Equation 6.12-1).
DE_BDCF_Inh_LT_Am243. Volcanic Biosphere Dose Conversion Factor (BDCF) component for long-term inhalation of ^{243}Am in modern interglacial climate ((Sv/yr)/(Bq/kg)). *Distribution:* Discrete. *Range:* 8.38E-08 to 2.46E-06. *Mean:* 4.93E-07. *Standard Deviation:* 3.15E-07. *Symbol:* $BDCF_{inh,p,i}$. *Additional Information:* See DE_BDCF_Inh_LT_Ac227. *Sensitivity Name:* ILTAM243. *Location in TSPA-LA:* Sections 6.3.11.1 and 6.3.11.2; Equation 6.3.11-4. *DTN:* MO0702PAVBPDCF.000_R0 [DIRS 179330]. *References: Biosphere Model Report* (SNL 2007 [DIRS 177399], Sections 6.12.2 and 6.12.3; Table 6.12-3; Equation 6.12-1).
DE_BDCF_Inh_LT_Cs137. Volcanic Biosphere Dose Conversion Factor (BDCF) component for long-term inhalation of ^{137}Cs in modern interglacial climate ((Sv/yr)/(Bq/kg)). *Distribution:* Discrete. *Range:* 3.43E-11 to 1.01E-09. *Mean:* 2.02E-10. *Standard Deviation:* 1.29E-10. *Symbol:* $BDCF_{inh,p,i}$. *Additional Information:* See DE_BDCF_Inh_LT_Ac227. *Sensitivity Name:* ILTCS137. *Location in TSPA-LA:* Sections 6.3.11.1 and 6.3.11.2; Equation 6.3.11-4. *DTN:* MO0702PAVBPDCF.000_R0 [DIRS 179330]. *References: Biosphere Model Report* (SNL 2007 [DIRS 177399], Sections 6.12.2 and 6.12.3; Table 6.12-3; Equation 6.12-1).
DE_BDCF_Inh_LT_I129. Volcanic Biosphere Dose Conversion Factor (BDCF) component for long-term inhalation of ^{129}I in modern interglacial climate ((Sv/yr)/(Bq/kg)). *Distribution:* Discrete. *Range:* 3.15E-11 to 9.23E-10. *Mean:* 1.85E-10. *Standard Deviation:* 1.18E-10. *Symbol:* $BDCF_{inh,p,i}$. *Additional Information:* See DE_BDCF_Inh_LT_Ac227. *Sensitivity Name:* ILTI129. *Location in TSPA-LA:* Sections 6.3.11.1 and 6.3.11.2; Equation 6.3.11-4. *DTN:* MO0702PAVBPDCF.000_R0 [DIRS 179330]. *References: Biosphere Model Report* (SNL 2007 [DIRS 177399], Sections 6.12.2 and 6.12.3; Table 6.12-3; Equation 6.12-1).
DE_BDCF_Inh_LT_Np237. Volcanic Biosphere Dose Conversion Factor (BDCF) component for long-term inhalation of ^{237}Np in modern interglacial climate ((Sv/yr)/(Bq/kg)). *Distribution:* Discrete. *Range:* 4.35E-08 to 1.28E-06. *Mean:* 2.56E-07. *Standard Deviation:* 1.63E-07. *Symbol:* $BDCF_{inh,p,i}$. *Additional Information:* See DE_BDCF_Inh_LT_Ac227. *Sensitivity Name:* ILTNP237. *Location in TSPA-LA:* Sections 6.3.11.1 and 6.3.11.2; Equation 6.3.11-4. *DTN:* MO0702PAVBPDCF.000_R0 [DIRS 179330]. *References: Biosphere Model Report* (SNL 2007 [DIRS 177399], Sections 6.12.2 and 6.12.3; Table 6.12-3; Equation 6.12-1).

Table K3-3. Detailed Summary of Epistemically Uncertain Variables (i.e., elements of **e**) Considered in the TSPA-LA (TSPA Parameter Name) (Continued)

NOTE: * indicates variable not considered in sensitivity analysis due to correlations.

DE_BDCF_Inh_LT_Pa231. Volcanic Biosphere Dose Conversion Factor (BDCF) component for long-term inhalation of ^{231}Pa in modern interglacial climate ((Sv/yr)/(Bq/kg)). *Distribution:* Discrete. *Range:* 2.02E-07 to 5.92E-06. *Mean:* 1.18E-06. *Standard Deviation:* 7.56E-07. *Symbol:* $BDCF_{inh,p,i}$. *Additional Information:* See DE_BDCF_Inh_LT_Ac227. *Sensitivity Name:* ILTPA231. *Location in TSPA-LA:* Sections 6.3.11.1 and 6.3.11.2; Equation 6.3.11-4. *DTN:* MO0702PAVBPDCF.000_R0 [DIRS 179330]. *References: Biosphere Model Report* (SNL 2007 [DIRS 177399], Sections 6.12.2 and 6.12.3; Table 6.12-3; Equation 6.12-1).
DE_BDCF_Inh_LT_Pu238. Volcanic Biosphere Dose Conversion Factor (BDCF) component for long-term inhalation of ^{238}Pu in modern interglacial climate ((Sv/yr)/(Bq/kg)). *Distribution:* Discrete. *Range:* 9.46E-08 to 2.78E-06. *Mean:* 5.56E-07. *Standard Deviation:* 3.55E-07. *Symbol:* $BDCF_{inh,p,i}$. *Additional Information:* See DE_BDCF_Inh_LT_Ac227. *Sensitivity Name:* ILTPU238. *Location in TSPA-LA:* Sections 6.3.11.1 and 6.3.11.2; Equation 6.3.11-4. *DTN:* MO0702PAVBPDCF.000_R0 [DIRS 179330]. *References: Biosphere Model Report* (SNL 2007 [DIRS 177399], Sections 6.12.2 and 6.12.3; Table 6.12-3; Equation 6.12-1).
DE_BDCF_Inh_LT_Pu239. Volcanic Biosphere Dose Conversion Factor (BDCF) component for long-term inhalation of ^{239}Pu in modern interglacial climate ((Sv/yr)/(Bq/kg)). *Distribution:* Discrete. *Range:* 1.04E-07 to 3.06E-06. *Mean:* 6.12E-07. *Standard Deviation:* 3.91E-07. *Symbol:* $BDCF_{inh,p,i}$. *Additional Information:* See DE_BDCF_Inh_LT_Ac227. *Sensitivity Name:* ILTPU239. *Location in TSPA-LA:* Sections 6.3.11.1 and 6.3.11.2; Equation 6.3.11-4. *DTN:* MO0702PAVBPDCF.000_R0 [DIRS 179330]. *References: Biosphere Model Report* (SNL 2007 [DIRS 177399], Sections 6.12.2 and 6.12.3; Table 6.12-3; Equation 6.12-1).
DE_BDCF_Inh_LT_Pu240. Volcanic Biosphere Dose Conversion Factor (BDCF) component for long-term inhalation of ^{240}Pu in modern interglacial climate ((Sv/yr)/(Bq/kg)). *Distribution:* Discrete. *Range:* 1.04E-07 to 3.06E-06. *Mean:* 6.12E-07. *Standard Deviation:* 3.91E-07. *Symbol:* $BDCF_{inh,p,i}$. *Additional Information:* See DE_BDCF_Inh_LT_Ac227. *Sensitivity Name:* ILTPU240. *Location in TSPA-LA:* Sections 6.3.11.1 and 6.3.11.2; Equation 6.3.11-4. *DTN:* MO0702PAVBPDCF.000_R0 [DIRS 179330]. *References: Biosphere Model Report* (SNL 2007 [DIRS 177399], Sections 6.12.2 and 6.12.3; Table 6.12-3; Equation 6.12-1).
DE_BDCF_Inh_LT_Pu242. Volcanic Biosphere Dose Conversion Factor (BDCF) component for long-term inhalation of ^{242}Pu in modern interglacial climate ((Sv/yr)/(Bq/kg)). *Distribution:* Discrete. *Range:* 9.90E-08 to 2.91E-06. *Mean:* 5.82E-07. *Standard Deviation:* 3.72E-07. *Symbol:* $BDCF_{inh,p,i}$. *Additional Information:* See DE_BDCF_Inh_LT_Ac227. *Sensitivity Name:* ILTPU242. *Location in TSPA-LA:* Sections 6.3.11.1 and 6.3.11.2; Equation 6.3.11-4. *DTN:* MO0702PAVBPDCF.000_R0 [DIRS 179330]. *References: Biosphere Model Report* (SNL 2007 [DIRS 177399], Sections 6.12.2 and 6.12.3; Table 6.12-3; Equation 6.12-1).
DE_BDCF_Inh_LT_Ra228. Volcanic Biosphere Dose Conversion Factor (BDCF) component for long-term inhalation of ^{228}Ra in modern interglacial climate ((Sv/yr)/(Bq/kg)). *Distribution:* Discrete. *Range:* 1.40E-08 to 4.12E-07. *Mean:* 8.24E-08. *Standard Deviation:* 5.27E-08. *Symbol:* $BDCF_{inh,p,i}$. *Additional Information:* See DE_BDCF_Inh_LT_Ac227. *Sensitivity Name:* ILTRA228. *Location in TSPA-LA:* Sections 6.3.11.1 and 6.3.11.2; Equation 6.3.11-4. *DTN:* MO0702PAVBPDCF.000_R0 [DIRS 179330]. *References: Biosphere Model Report* (SNL 2007 [DIRS 177399], Sections 6.12.2 and 6.12.3; Table 6.12-3; Equation 6.12-1).
DE_BDCF_Inh_LT_Sn126. Volcanic Biosphere Dose Conversion Factor (BDCF) component for long-term inhalation of ^{126}Sn in modern interglacial climate ((Sv/yr)/(Bq/kg)). *Distribution:* Discrete. *Range:* 1.36E-10 to 4.00E-09. *Mean:* 8.0E-10. *Standard Deviation:* 5.11E-10. *Symbol:* $BDCF_{inh,p,i}$. *Additional Information:* See DE_BDCF_Inh_LT_Ac227. *Sensitivity Name:* ILTSN126. *Location in TSPA-LA:* Sections 6.3.11.1 and 6.3.11.2; Equation 6.3.11-4. *DTN:* MO0702PAVBPDCF.000_R0 [DIRS 179330]. *References: Biosphere Model Report* (SNL 2007 [DIRS 177399], Sections 6.12.2 and 6.12.3; Table 6.12-3; Equation 6.12-1).
DE_BDCF_Inh_LT_Sr90. Volcanic Biosphere Dose Conversion Factor (BDCF) component for long-term inhalation of ^{90}Sr in modern interglacial climate ((Sv/yr)/(Bq/kg)). *Distribution:* Discrete. *Range:* 1.39E-10 to 4.08E-09. *Mean:* 8.16E-10. *Standard Deviation:* 5.21E-10. *Symbol:* $BDCF_{inh,p,i}$. *Additional Information:* See DE_BDCF_Inh_LT_Ac227. *Sensitivity Name:* ILTSR90. *Location in TSPA-LA:* Sections 6.3.11.1 and 6.3.11.2; Equation 6.3.11-4. *DTN:* MO0702PAVBPDCF.000_R0 [DIRS 179330]. *References: Biosphere Model Report* (SNL 2007 [DIRS 177399], Sections 6.12.2 and 6.12.3; Table 6.12-3; Equation 6.12-1).
DE_BDCF_Inh_LT_Tc99. Volcanic Biosphere Dose Conversion Factor (BDCF) component for long-term inhalation of ^{99}Tc in modern interglacial climate ((Sv/yr)/(Bq/kg)). *Distribution:* Discrete. *Range:* 1.17E-11 to 3.42E-10. *Mean:* 6.84E-11. *Standard Deviation:* 4.37E-11. *Symbol:* $BDCF_{inh,p,i}$. *Additional Information:* See DE_BDCF_Inh_LT_Ac227. *Sensitivity Name:* ILTTC99. *Location in TSPA-LA:* Sections 6.3.11.1 and 6.3.11.2; Equation 6.3.11-4. *DTN:* MO0702PAVBPDCF.000_R0 [DIRS 179330]. *References: Biosphere Model Report* (SNL 2007 [DIRS 177399], Sections 6.12.2 and 6.12.3; Table 6.12-3; Equation 6.12-1).

Table K3-3. Detailed Summary of Epistemically Uncertain Variables (i.e., elements of **e**) Considered in the TSPA-LA (TSPA Parameter Name) (Continued)

NOTE: * indicates variable not considered in sensitivity analysis due to correlations.

DE_BDCF_Inh_LT_Th229. Volcanic Biosphere Dose Conversion Factor (BDCF) component for long-term inhalation of ^{229}Th in modern interglacial climate ((Sv/yr)/(Bq/kg)). *Distribution:* Discrete. *Range:* 2.24E-07 to 6.57E-06. *Mean:* 1.31E-06. *Standard Deviation:* 8.39E-07. *Symbol:* $BDCF_{inh,p,i}$. *Additional Information:* See DE_BDCF_Inh_LT_Ac227. *Sensitivity Name:* ILTTH229. *Location in TSPA-LA:* Sections 6.3.11.1 and 6.3.11.2; Equation 6.3.11-4. *DTN:* MO0702PAVBPDCF.000_R0 [DIRS 179330]. *References: Biosphere Model Report* (SNL 2007 [DIRS 177399], Sections 6.12.2 and 6.12.3; Table 6.12-3; Equation 6.12-1).
DE_BDCF_Inh_LT_Th230. Volcanic Biosphere Dose Conversion Factor (BDCF) component for long-term inhalation of ^{230}Th in modern interglacial climate ((Sv/yr)/(Bq/kg)). *Distribution:* Discrete. *Range:* 8.94E-08 to 2.62E-06. *Mean:* 5.25E-07. *Standard Deviation:* 3.35E-07. *Symbol:* $BDCF_{inh,p,i}$. *Additional Information:* See DE_BDCF_Inh_LT_Ac227. *Sensitivity Name:* ILTTH230. *Location in TSPA-LA:* Sections 6.3.11.1 and 6.3.11.2; Equation 6.3.11-4. *DTN:* MO0702PAVBPDCF.000_R0 [DIRS 179330]. *References: Biosphere Model Report* (SNL 2007 [DIRS 177399], Sections 6.12.2 and 6.12.3; Table 6.12-3; Equation 6.12-1).
DE_BDCF_Inh_LT_Th232. Volcanic Biosphere Dose Conversion Factor (BDCF) component for long-term inhalation of ^{232}Th in modern interglacial climate ((Sv/yr)/(Bq/kg)). *Distribution:* Discrete. *Range:* 9.64E-08 to 2.83E-06. *Mean:* 5.66E-07. *Standard Deviation:* 3.62E-07. *Symbol:* $BDCF_{inh,p,i}$. *Additional Information:* See DE_BDCF_Inh_LT_Ac227. *Sensitivity Name:* ILTTH232. *Location in TSPA-LA:* Sections 6.3.11.1 and 6.3.11.2; Equation 6.3.11-4. *DTN:* MO0702PAVBPDCF.000_R0 [DIRS 179330]. *References: Biosphere Model Report* (SNL 2007 [DIRS 177399], Sections 6.12.2 and 6.12.3; Table 6.12-3; Equation 6.12-1).
DE_BDCF_Inh_LT_U233. Volcanic Biosphere Dose Conversion Factor (BDCF) component for long-term inhalation of ^{233}U in modern interglacial climate ((Sv/yr)/(Bq/kg)). *Distribution:* Discrete. *Range:* 8.40E-09 to 2.47E-07. *Mean:* 4.94E-08. *Standard Deviation:* 3.15E-08. *Symbol:* $BDCF_{inh,p,i}$. *Additional Information:* See DE_BDCF_Inh_LT_Ac227. *Sensitivity Name:* ILTU233. *Location in TSPA-LA:* Sections 6.3.11.1 and 6.3.11.2; Equation 6.3.11-4. *DTN:* MO0702PAVBPDCF.000_R0 [DIRS 179330]. *References: Biosphere Model Report* (SNL 2007 [DIRS 177399], Sections 6.12.2 and 6.12.3; Table 6.12-3; Equation 6.12-1).
DE_BDCF_Inh_LT_U234. Volcanic Biosphere Dose Conversion Factor (BDCF) component for long-term inhalation of ^{234}U in modern interglacial climate ((Sv/yr)/(Bq/kg)). *Distribution:* Discrete. *Range:* 8.23E-09 to 2.42E-07. *Mean:* 4.84E-08. *Standard Deviation:* 3.09E-08. *Symbol:* $BDCF_{inh,p,i}$. *Additional Information:* See DE_BDCF_Inh_LT_Ac227. *Sensitivity Name:* ILTU234. *Location in TSPA-LA:* Sections 6.3.11.1 and 6.3.11.2; Equation 6.3.11-4. *DTN:* MO0702PAVBPDCF.000_R0 [DIRS 179330]. *References: Biosphere Model Report* (SNL 2007 [DIRS 177399], Sections 6.12.2 and 6.12.3; Table 6.12-3; Equation 6.12-1).
DE_BDCF_Inh_LT_U238. Volcanic Biosphere Dose Conversion Factor (BDCF) component for long-term inhalation of ^{238}U in modern interglacial climate ((Sv/yr)/(Bq/kg)). *Distribution:* Discrete. *Range:* 7.05E-09 to 2.07E-07. *Mean:* 4.14E-08. *Standard Deviation:* 2.65E-08. *Symbol:* $BDCF_{inh,p,i}$. *Additional Information:* See DE_BDCF_Inh_LT_Ac227. *Sensitivity Name:* ILTU238. *Location in TSPA-LA:* Sections 6.3.11.1 and 6.3.11.2; Equation 6.3.11-4. *DTN:* MO0702PAVBPDCF.000_R0 [DIRS 179330]. *References: Biosphere Model Report* (SNL 2007 [DIRS 177399], Sections 6.12.2 and 6.12.3; Table 6.12-3; Equation 6.12-1).
DE_BDCF_Inh_ShT_Ac227. Volcanic Biosphere Dose Conversion Factor (BDCF) component for short-term inhalation of ^{227}Ac in modern interglacial climate ((Sv/yr)/(Bq/kg)). *Distribution:* Discrete. *Range:* 8.47E-08 to 2.14E-06. *Mean:* 5.85E-07. *Standard Deviation:* 3.32E-07. *Symbol:* $BDCF_{inh,v,i}$. *Additional Information:* See DE_BDCF_Inh_LT_Ac227. *Sensitivity Name:* ISTAC227. *Location in TSPA-LA:* Sections 6.3.11.1 and 6.3.11.2; Equation 6.3.11-4. *DTN:* MO0702PAVBPDCF.000_R0 [DIRS 179330]. *References: Biosphere Model Report* (SNL 2007 [DIRS 177399], Sections 6.12.2 and 6.12.3; Table 6.12-2; Equation 6.12-1).
DE_BDCF_Inh_ShT_Am241. Volcanic Biosphere Dose Conversion Factor (BDCF) component for short-term inhalation of ^{241}Am in modern interglacial climate ((Sv/yr)/(Bq/kg)). *Distribution:* Discrete. *Range:* 4.67E-08 to 1.18E-06. *Mean:* 3.23E-07. *Standard Deviation:* 1.83E-07. *Symbol:* $BDCF_{inh,v,i}$. *Additional Information:* See DE_BDCF_Inh_LT_Ac227. *Sensitivity Name:* ISTAM241. *Location in TSPA-LA:* Sections 6.3.11.1 and 6.3.11.2; Equation 6.3.11-4. *DTN:* MO0702PAVBPDCF.000_R0 [DIRS 179330]. *References: Biosphere Model Report* (SNL 2007 [DIRS 177399], Sections 6.12.2 and 6.12.3; Table 6.12-2; Equation 6.12-1).
DE_BDCF_Inh_ShT_Am243. Volcanic Biosphere Dose Conversion Factor (BDCF) component for short-term inhalation of ^{243}Am in modern interglacial climate ((Sv/yr)/(Bq/kg)). *Distribution:* Discrete. *Range:* 4.64E-08 to 1.17E-06. *Mean:* 3.2E-07. *Standard Deviation:* 1.82E-07. *Symbol:* $BDCF_{inh,v,i}$. *Additional Information:* See DE_BDCF_Inh_LT_Ac227. *Sensitivity Name:* ISTAM243. *Location in TSPA-LA:* Sections 6.3.11.1 and 6.3.11.2; Equation 6.3.11-4. *DTN:* MO0702PAVBPDCF.000_R0 [DIRS 179330]. *References: Biosphere Model Report* (SNL 2007 [DIRS 177399], Sections 6.12.2 and 6.12.3; Table 6.12-2; Equation 6.12-1).

Table K3-3. Detailed Summary of Epistemically Uncertain Variables (i.e., elements of **e**) Considered in the TSPA-LA (TSPA Parameter Name) (Continued)

NOTE: * indicates variable not considered in sensitivity analysis due to correlations.

DE_BDCF_Inh_ShT_Cs137. Volcanic Biosphere Dose Conversion Factor (BDCF) component for short-term inhalation of ^{137}Cs in modern interglacial climate ((Sv/yr)/(Bq/kg)). *Distribution:* Discrete. *Range:* 1.90E-11 to 4.80E-10. *Mean:* 1.31E-10. *Standard Deviation:* 7.44E-11. *Symbol:* $BDCF_{inh,v,i}$. *Additional Information:* See DE_BDCF_Inh_LT_Ac227. *Sensitivity Name:* ISTCS137. *Location in TSPA-LA:* Sections 6.3.11.1 and 6.3.11.2; Equation 6.3.11-4. *DTN:* MO0702PAVBPDCF.000_R0 [DIRS 179330]. *References: Biosphere Model Report* (SNL 2007 [DIRS 177399], Sections 6.12.2 and 6.12.3; Table 6.12-2; Equation 6.12-1).
DE_BDCF_Inh_ShT_I129. Volcanic Biosphere Dose Conversion Factor (BDCF) component for short-term inhalation of ^{129}I in modern interglacial climate ((Sv/yr)/(Bq/kg)). *Distribution:* Discrete. *Range:* 1.74E-11 to 4.40E-10. *Mean:* 1.2E-10. *Standard Deviation:* 6.81E-11. *Symbol:* $BDCF_{inh,v,i}$. *Additional Information:* See DE_BDCF_Inh_LT_Ac227. *Sensitivity Name:* ISTI129. *Location in TSPA-LA:* Sections 6.3.11.1 and 6.3.11.2; Equation 6.3.11-4. *DTN:* MO0702PAVBPDCF.000_R0 [DIRS 179330]. *References: Biosphere Model Report* (SNL 2007 [DIRS 177399], Sections 6.12.2 and 6.12.3; Table 6.12-2; Equation 6.12-1).
DE_BDCF_Inh_ShT_Np237. Volcanic Biosphere Dose Conversion Factor (BDCF) component for short-term inhalation of ^{237}Np in modern interglacial climate ((Sv/yr)/(Bq/kg)). *Distribution:* Discrete. *Range:* 2.41E-08 to 6.08E-07. *Mean:* 1.66E-07. *Standard Deviation:* 9.43E-08. *Symbol:* $BDCF_{inh,v,i}$. *Additional Information:* See DE_BDCF_Inh_LT_Ac227. *Sensitivity Name:* ISTNP237. *Location in TSPA-LA:* Sections 6.3.11.1 and 6.3.11.2; Equation 6.3.11-4. *DTN:* MO0702PAVBPDCF.000_R0 [DIRS 179330]. *References: Biosphere Model Report* (SNL 2007 [DIRS 177399], Sections 6.12.2 and 6.12.3; Table 6.12-2; Equation 6.12-1).
DE_BDCF_Inh_ShT_Pa231. Volcanic Biosphere Dose Conversion Factor (BDCF) component for short-term inhalation of ^{231}Pa in modern interglacial climate ((Sv/yr)/(Bq/kg)). *Distribution:* Discrete. *Range:* 1.11E-07 to 2.82E-06. *Mean:* 7.7E-07. *Standard Deviation:* 4.37E-07. *Symbol:* $BDCF_{inh,v,i}$. *Additional Information:* See DE_BDCF_Inh_LT_Ac227. *Sensitivity Name:* ISTPA231. *Location in TSPA-LA:* Sections 6.3.11.1 and 6.3.11.2; Equation 6.3.11-4. *DTN:* MO0702PAVBPDCF.000_R0 [DIRS 179330]. *References: Biosphere Model Report* (SNL 2007 [DIRS 177399], Sections 6.12.2 and 6.12.3; Table 6.12-2; Equation 6.12-1).
DE_BDCF_Inh_ShT_Pu238. Volcanic Biosphere Dose Conversion Factor (BDCF) component for short-term inhalation of ^{238}Pu in modern interglacial climate ((Sv/yr)/(Bq/kg)). *Distribution:* Discrete. *Range:* 5.23E-08 to 1.32E-06. *Mean:* 3.61E-07. *Standard Deviation:* 2.05E-07. *Symbol:* $BDCF_{inh,v,i}$. *Additional Information:* See DE_BDCF_Inh_LT_Ac227. *Sensitivity Name:* ISTPU238. *Location in TSPA-LA:* Sections 6.3.11.1 and 6.3.11.2; Equation 6.3.11-4. *DTN:* MO0702PAVBPDCF.000_R0 [DIRS 179330]. *References: Biosphere Model Report* (SNL 2007 [DIRS 177399], Sections 6.12.2 and 6.12.3; Table 6.12-2; Equation 6.12-1).
DE_BDCF_Inh_ShT_Pu239. Volcanic Biosphere Dose Conversion Factor (BDCF) component for short-term inhalation of ^{239}Pu in modern interglacial climate ((Sv/yr)/(Bq/kg)). *Distribution:* Discrete. *Range:* 5.76E-08 to 1.46E-06. *Mean:* 3.98E-07. *Standard Deviation:* 2.26E-07. *Symbol:* $BDCF_{inh,v,i}$. *Additional Information:* See DE_BDCF_Inh_LT_Ac227. *Sensitivity Name:* ISTPU239. *Location in TSPA-LA:* Sections 6.3.11.1 and 6.3.11.2; Equation 6.3.11-4. *DTN:* MO0702PAVBPDCF.000_R0 [DIRS 179330]. *References: Biosphere Model Report* (SNL 2007 [DIRS 177399], Sections 6.12.2 and 6.12.3; Table 6.12-2; Equation 6.12-1).
DE_BDCF_Inh_ShT_Pu240. Volcanic Biosphere Dose Conversion Factor (BDCF) component for short-term inhalation of ^{240}Pu in modern interglacial climate ((Sv/yr)/(Bq/kg)). *Distribution:* Discrete. *Range:* 5.76E-08 to 1.46E-06. *Mean:* 3.98E-07. *Standard Deviation:* 2.26E-07. *Symbol:* $BDCF_{inh,v,i}$. *Additional Information:* See DE_BDCF_Inh_LT_Ac227. *Sensitivity Name:* ISTPU240. *Location in TSPA-LA:* Sections 6.3.11.1 and 6.3.11.2; Equation 6.3.11-4. *DTN:* MO0702PAVBPDCF.000_R0 [DIRS 179330]. *References: Biosphere Model Report* (SNL 2007 [DIRS 177399], Sections 6.12.2 and 6.12.3; Table 6.12-2; Equation 6.12-1).
DE_BDCF_Inh_ShT_Pu242. Volcanic Biosphere Dose Conversion Factor (BDCF) component for short-term inhalation of ^{242}Pu in modern interglacial climate ((Sv/yr)/(Bq/kg)). *Distribution:* Discrete. *Range:* 5.47E-08 to 1.38E-06. *Mean:* 3.78E-07. *Standard Deviation:* 2.14E-07. *Symbol:* $BDCF_{inh,v,i}$. *Additional Information:* See DE_BDCF_Inh_LT_Ac227. *Sensitivity Name:* ISTPU242. *Location in TSPA-LA:* Sections 6.3.11.1 and 6.3.11.2; Equation 6.3.11-4. *DTN:* MO0702PAVBPDCF.000_R0 [DIRS 179330]. *References: Biosphere Model Report* (SNL 2007 [DIRS 177399], Sections 6.12.2 and 6.12.3; Table 6.12-2; Equation 6.12-1).
DE_BDCF_Inh_ShT_Ra228. Volcanic Biosphere Dose Conversion Factor (BDCF) component for short-term inhalation of ^{228}Ra in modern interglacial climate ((Sv/yr)/(Bq/kg)). *Distribution:* Discrete. *Range:* 7.76E-09 to 1.96E-07. *Mean:* 5.36E-08. *Standard Deviation:* 3.04E-08. *Symbol:* $BDCF_{inh,v,i}$. *Additional Information:* See DE_BDCF_Inh_LT_Ac227. *Sensitivity Name:* ISTRA228. *Location in TSPA-LA:* Sections 6.3.11.1 and 6.3.11.2; Equation 6.3.11-4. *DTN:* MO0702PAVBPDCF.000_R0 [DIRS 179330]. *References: Biosphere Model Report* (SNL 2007 [DIRS 177399], Sections 6.12.2 and 6.12.3; Table 6.12-2; Equation 6.12-1).

Table K3-3. Detailed Summary of Epistemically Uncertain Variables (i.e., elements of **e**) Considered in the TSPA-LA (TSPA Parameter Name) (Continued)

NOTE: * indicates variable not considered in sensitivity analysis due to correlations.

DE_BDCF_Inh_ShT_Sn126. Volcanic Biosphere Dose Conversion Factor (BDCF) component for short-term inhalation of ^{126}Sn in modern interglacial climate ((Sv/yr)/(Bq/kg)). *Distribution:* Discrete. *Range:* 7.53E-11 to 1.90E-09. *Mean:* 5.2E-10. *Standard Deviation:* 2.95E-10. *Symbol:* $BDCF_{inh,v,i}$. *Additional Information:* See DE_BDCF_Inh_LT_Ac227. *Sensitivity Name:* ISTSN126. *Location in TSPA-LA:* Sections 6.3.11.1 and 6.3.11.2; Equation 6.3.11-4. *DTN:* MO0702PAVBPDCF.000_R0 [DIRS 179330]. *References: Biosphere Model Report* (SNL 2007 [DIRS 177399], Sections 6.12.2 and 6.12.3; Table 6.12-2; Equation 6.12-1).
DE_BDCF_Inh_ShT_Sr90. Volcanic Biosphere Dose Conversion Factor (BDCF) component for short-term inhalation of ^{90}Sr in modern interglacial climate ((Sv/yr)/(Bq/kg)). *Distribution:* Discrete. *Range:* 7.68E-11 to 1.94E-09. *Mean:* 5.3E-10. *Standard Deviation:* 3.01E-10. *Symbol:* $BDCF_{inh,v,i}$. *Additional Information:* See DE_BDCF_Inh_LT_Ac227. *Sensitivity Name:* ISTSR90. *Location in TSPA-LA:* Sections 6.3.11.1 and 6.3.11.2; Equation 6.3.11-4. *DTN:* MO0702PAVBPDCF.000_R0 [DIRS 179330]. *References: Biosphere Model Report* (SNL 2007 [DIRS 177399], Sections 6.12.2 and 6.12.3; Table 6.12-2; Equation 6.12-1).
DE_BDCF_Inh_ShT_Tc99. Volcanic Biosphere Dose Conversion Factor (BDCF) component for short-term inhalation of ^{99}Tc in modern interglacial climate ((Sv/yr)/(Bq/kg)). *Distribution:* Discrete. *Range:* 6.44E-12 to 1.63E-10. *Mean:* 4.45E-11. *Standard Deviation:* 2.52E-11. *Symbol:* $BDCF_{inh,v,i}$. *Additional Information:* See DE_BDCF_Inh_LT_Ac227. *Sensitivity Name:* ISTTC99. *Location in TSPA-LA:* Sections 6.3.11.1 and 6.3.11.2; Equation 6.3.11-4. *DTN:* MO0702PAVBPDCF.000_R0 [DIRS 179330]. *References: Biosphere Model Report* (SNL 2007 [DIRS 177399], Sections 6.12.2 and 6.12.3; Table 6.12-2; Equation 6.12-1).
DE_BDCF_Inh_ShT_Th229. Volcanic Biosphere Dose Conversion Factor (BDCF) component for short-term inhalation of ^{229}Th in modern interglacial climate ((Sv/yr)/(Bq/kg)). *Distribution:* Discrete. *Range:* 1.24E-07 to 3.13E-06. *Mean:* 8.54E-07. *Standard Deviation:* 4.84E-07. *Symbol:* $BDCF_{inh,v,i}$. *Additional Information:* See DE_BDCF_Inh_LT_Ac227. *Sensitivity Name:* ISTTH229. *Location in TSPA-LA:* Sections 6.3.11.1 and 6.3.11.2; Equation 6.3.11-4. *DTN:* MO0702PAVBPDCF.000_R0 [DIRS 179330]. *References: Biosphere Model Report* (SNL 2007 [DIRS 177399], Sections 6.12.2 and 6.12.3; Table 6.12-2; Equation 6.12-1).
DE_BDCF_Inh_ShT_Th230. Volcanic Biosphere Dose Conversion Factor (BDCF) component for short-term inhalation of ^{230}Th in modern interglacial climate ((Sv/yr)/(Bq/kg)). *Distribution:* Discrete. *Range:* 4.94E-08 to 1.25E-06. *Mean:* 3.41E-07. *Standard Deviation:* 1.94E-07. *Symbol:* $BDCF_{inh,v,i}$. *Additional Information:* See DE_BDCF_Inh_LT_Ac227. *Sensitivity Name:* ISTTH230. *Location in TSPA-LA:* Sections 6.3.11.1 and 6.3.11.2; Equation 6.3.11-4. *DTN:* MO0702PAVBPDCF.000_R0 [DIRS 179330]. *References: Biosphere Model Report* (SNL 2007 [DIRS 177399], Sections 6.12.2 and 6.12.3; Table 6.12-2; Equation 6.12-1).
DE_BDCF_Inh_ShT_Th232. Volcanic Biosphere Dose Conversion Factor (BDCF) component for short-term inhalation of ^{232}Th in modern interglacial climate ((Sv/yr)/(Bq/kg)). *Distribution:* Discrete. *Range:* 5.33E-08 to 1.35E-06. *Mean:* 3.68E-07. *Standard Deviation:* 2.09E-07. *Symbol:* $BDCF_{inh,v,i}$. *Additional Information:* See DE_BDCF_Inh_LT_Ac227. *Sensitivity Name:* ISTTH232. *Location in TSPA-LA:* Sections 6.3.11.1 and 6.3.11.2; Equation 6.3.11-4. *DTN:* MO0702PAVBPDCF.000_R0 [DIRS 179330]. *References: Biosphere Model Report* (SNL 2007 [DIRS 177399], Sections 6.12.2 and 6.12.3; Table 6.12-2; Equation 6.12-1).
DE_BDCF_Inh_ShT_U233. Volcanic Biosphere Dose Conversion Factor (BDCF) component for short-term inhalation of ^{233}U in modern interglacial climate ((Sv/yr)/(Bq/kg)). *Distribution:* Discrete. *Range:* 4.65E-09 to 1.17E-07. *Mean:* 3.21E-08. *Standard Deviation:* 1.82E-08. *Symbol:* $BDCF_{inh,v,i}$. *Additional Information:* See DE_BDCF_Inh_LT_Ac227. *Sensitivity Name:* ISTU233. *Location in TSPA-LA:* Sections 6.3.11.1 and 6.3.11.2; Equation 6.3.11-4. *DTN:* MO0702PAVBPDCF.000_R0 [DIRS 179330]. *References: Biosphere Model Report* (SNL 2007 [DIRS 177399], Sections 6.12.2 and 6.12.3; Table 6.12-2; Equation 6.12-1).
DE_BDCF_Inh_ShT_U234. Volcanic Biosphere Dose Conversion Factor (BDCF) component for short-term inhalation of ^{234}U in modern interglacial climate ((Sv/yr)/(Bq/kg)). *Distribution:* Discrete. *Range:* 4.55E-09 to 1.15E-07. *Mean:* 3.15E-08. *Standard Deviation:* 1.78E-08. *Symbol:* $BDCF_{inh,v,i}$. *Additional Information:* See DE_BDCF_Inh_LT_Ac227. *Sensitivity Name:* ISTU234. *Location in TSPA-LA:* Sections 6.3.11.1 and 6.3.11.2; Equation 6.3.11-4. *DTN:* MO0702PAVBPDCF.000_R0 [DIRS 179330]. *References: Biosphere Model Report* (SNL 2007 [DIRS 177399], Sections 6.12.2 and 6.12.3; Table 6.12-2; Equation 6.12-1).
DE_BDCF_Inh_ShT_U238. Volcanic Biosphere Dose Conversion Factor (BDCF) component for short-term inhalation of ^{238}U in modern interglacial climate ((Sv/yr)/(Bq/kg)). *Distribution:* Discrete. *Range:* 3.90E-09 to 9.85E-08. *Mean:* 2.69E-08. *Standard Deviation:* 1.53E-08. *Symbol:* $BDCF_{inh,v,i}$. *Additional Information:* See DE_BDCF_Inh_LT_Ac227. *Sensitivity Name:* ISTU238. *Location in TSPA-LA:* Sections 6.3.11.1 and 6.3.11.2; Equation 6.3.11-4. *DTN:* MO0702PAVBPDCF.000_R0 [DIRS 179330]. *References: Biosphere Model Report* (SNL 2007 [DIRS 177399], Sections 6.12.2 and 6.12.3; Table 6.12-2; Equation 6.12-1).

Table K3-3. Detailed Summary of Epistemically Uncertain Variables (i.e., elements of **e**) Considered in the TSPA-LA (TSPA Parameter Name) (Continued)

NOTE: * indicates variable not considered in sensitivity analysis due to correlations.

DE_BDCF_IST_Ra226_Pb210. Volcanic Biosphere Dose Conversion Factor (BDCF) component for short-term inhalation of ^{226}Ra and ^{210}Pb in modern interglacial climate ((Sv/yr)/(Bq/kg)). *Distribution:* Discrete. *Range:* 9.47E-09 to 2.39E-07. *Mean:* 6.54E-08. *Standard Deviation:* 3.71E-08. *Symbol:* $BDCF_{inh,v,i}$. *Additional Information:* See DE_BDCF_Inh_LT_Ac227. *Sensitivity Name:* ISTRA226. *Location in TSPA-LA:* Sections 6.3.11.1 and 6.3.11.2; Equation 6.3.11-4. *DTN:* MO0702PAVBPDCF.000_R0 [DIRS 179330]. *References: Biosphere Model Report* (SNL 2007 [DIRS 177399], Sections 6.12.2 and 6.12.3; Table 6.12-2; Equation 6.12-1).
Default_Fwd_Rate_Const_a. Default forward rate constant for irreversible sorption of plutonium and americium ($m^3/m^2/yr$). *Distribution:* Log uniform. *Range:* 0.002 to 0.05. *Symbol:* k. *Additional Information:* A sampled parameter that defines the default forward rate constant for irreversible sorption of Pu and Am onto iron oxyhydroxide colloids and stationary corrosion products for zero or near zero advective flux conditions. The log-uniform distribution and range used for sampling Default_Fwd_Rate_Const_a is from the *Waste Form and In-Drift Colloids-Associated Radionuclide Concentrations: Abstraction and Summary* (SNL 2007 [DIRS 177423], Sections 6.3.12.2). Recorded in TSPA Input Database as Max_Default_Fwd_Rate_Const and Min_Default_Fwd_Rate_Const. *Sensitivity Name:* FWDRAT. *Location in TSPA-LA:* Table 6.3.7-65. *DTN:* MO0701PAIRONCO.000_R1 [DIRS 180440]. *References: Waste Form and In-Drift Colloids-Associated Radionuclide Concentrations: Abstraction and Summary* (SNL 2007 [DIRS 177423], Sections 6.3.12.2, 6.5.1.4 and 8.1; Equations 6-18 and 6-19; Table 6-24).
Defect_Count_a. Flaw density parameter (flaws per mm^3 of weld) (dimensionless). *Distribution:* Gamma. *Mean:* 4.529E-07. *Standard Deviation:* 1.654E-07. *Symbol:* λ_c. *Additional Information:* This parameter is used to compute the cumulative probability of a manufacturing defect based on the probability for the nondetection of weld flaws. Inputs to this calculation are the weld thickness, the weld volume, the defect fraction considered, a detection threshold, a characteristic flaw size, a shape factor, a defect count parameter, and a defect size parameter. The variation in the number of weld defects parameter is a function of the flaw size and count parameters that are sampled as uncertain for each realization. *Sensitivity Name:* WDDEFCNT. *Location in TSPA-LA:* Section 6.3.5.1.2; Table 6.3.5-3. *DTN:* MO0701PASHIELD.000_R2 [DIRS 180508]. *References: Analysis of Mechanisms for Early Waste Package / Drip Shield Failure* (SNL 2007 [DIRS 178765], Sections 6.3.1.3, 6.3.1.8 and A.3; Figure 6-4; Tables 6-4 and 7-1; Equations 11, 12 and 23).
Defect_Size_a. Flaw size parameter (flaw size per mm of weld) (dimensionless). *Distribution:* Gamma. *Mean:* 0.2205. *Standard Deviation:* 0.0833. *Symbol:* λ_s. *Additional Information:* See Defect_Count_a. The variation in weld flaw sizes is expressed as aleatory uncertainty at the WP level, given by a CDF dependent on an uncertain flaw size parameter that is sampled for each realization. *Sensitivity Name:* WDDEFSZE. *Location in TSPA-LA:* Section 6.3.5.1.2; Table 6.3.5-3; Equation 6.3.5-10. *DTN:* MO0701PASHIELD.000_R2 [DIRS 180508]. *References: Analysis of Mechanisms for Early Waste Package / Drip Shield Failure* (SNL 2007 [DIRS 178765], Sections 6.3.1.2 and A.2; Table 7-1; Equations 5 to 7).
Density_CSNF_Rind_a. Grain density of CSNF rind (kg/m^3). *Distribution:* Uniform. *Range:* 5600 to 11500. *Symbol:* ρ_r. *Additional Information:* The water saturation in waste form rind (for CSNF and HLWG waste forms) is dependent on the relative humidity, which varies over time, on the rind specific surface area and on the rind grain density. Density_CSNF_Rind_a is a sampled parameter whose range covers the range of values obtained from the literature for the surrogate materials used to create the adsorption isotherm. Sparse data do not show any trends to justify any distribution except uniform. To capture this large uncertainty, the specific surface area and density of the rind materials, as well as the porosity, will be sampled from uniform distributions over the ranges of the surrogate material properties. *Sensitivity Name:* CSRINDDN. *Location in TSPA-LA:* Table 6.3.8-4. *DTN:* SN0703PAEBSRTA.001_R3 [DIRS 183217]. *References: EBS Radionuclide Transport Abstraction* (SNL 2007 [DIRS 177407], Section 6.5.2.2.2.1; Equation 6.5.2.2.2.1-1; Tables 6.5-9 and 8.2-4).
Diameter_Colloid_a. Diameter of colloid particle (nm). *Distribution:* Uniform. *Range:* 50 to 300. *Symbol:* d_{coll}. *Additional Information:* The effect of colloid particle size, and thus the colloid diffusion coefficient, on releases of radionuclides from the EBS can be evaluated by sampling on the colloid particle size in TSPA. Because transport associated with individual colloid particles cannot be modeled in TSPA, a representative value of the colloid size is chosen from the population of colloid particles. This representative value is expected to be uncertain and can be represented by an epistemic uncertainty distribution that will be sampled in TSPA. The uncertainty range in the representative value is going to be narrower than the size range in the colloid population. At the same time, the representative value must be representative of all three types of colloids that are considered in the EBS transport model. For each TSPA realization, a single size (diameter) is sampled. *Sensitivity Name:* DIAMCOLL. *Location in TSPA-LA:* Tables 6.3.8-1 and 6.3.8-4. *DTN:* SN0703PAEBSRTA.001_R3 [DIRS 183217]. *References: EBS Radionuclide Transport Abstraction* (SNL 2007 [DIRS 177407], Section 6.3.4.4; Equation 6.3.4.4-1; Tables 8.2-4 and 8.2-7).

Table K3-3. Detailed Summary of Epistemically Uncertain Variables (i.e., elements of **e**) Considered in the TSPA-LA (TSPA Parameter Name) (Continued)

NOTE: * indicates variable not considered in sensitivity analysis due to correlations.

Diff_Path_Length_Invert_Top_a. Diffusive path length from waste package outer corrosion barrier to mid-point of invert (m). *Distribution:* Uniform. *Range:* 0.3 to 1.24. *Additional Information:* The lower end of the range is the distance from the center of the invert to the top of the invert; the upper end is the distance from the center of the invert up to a representative breach location up the side of the waste package. Uncertainty in breach locations in different waste packages over time precludes defining any distribution other than uniform. *Sensitivity Name:* DIFPATHL. *Location in TSPA-LA:* Section 6.3.8.2.4; Table 6.3.8-4. *DTN:* SN0703PAEBSRTA.001_R3 [DIRS 183217]. *References: EBS Radionuclide Transport Abstraction* (SNL 2007 [DIRS 177407], Table 8.2-4).
Drainage_Density_a. Average drainage density for the Fortymile Wash drainage basin (1/km). *Distribution:* Uniform. *Range:* 20 to 33. *Symbol:* X. *Additional Information:* The drainage density is the ratio of the total length of all channels within a drainage basin to the area of that basin. The drainage density parameter is used to define the channel system in the Fortymile Wash drainage basin. Since the drainage density parameter influences the amount of tephra that may be mobilized, it is important to define this parameter in such a way that adequately addresses the uncertainty in the extent of channels and their ability to redistribute and transport tephra. The value of the drainage density that yields the lowest value for the average distance between the observed and predicted channel heads is considered the optimal value for the drainage density input into the tephra redistribution model. This parameter is used in order to distinguish hillslopes from channels within the FAR software code. *Sensitivity Name:* DRAINDNS. *Location in TSPA-LA:* Table 6.5-5. *DTN:* MO0702PAFARDAT.001_R3 [DIRS 182578]. *References: Redistribution of Tephra and Waste by Geomorphic Processes Following a Potential Volcanic Eruption at Yucca Mountain, Nevada* (SNL 2007 [DIRS 179347], Sections 6.2.1, 6.3.2, 6.5.3, 6.6.1, 6.6.3, 7.2.4 and 8.1; Figures 6.3.3-9 and 6.6.1-1; Table 6.5.3-1).
DS_Flux_Uncertainty_a. Drip shield flux splitting factor (dimensionless). *Distribution:* Uniform. *Range:* 0 to 0.85. *Symbol:* f'_{DS}. *Additional Information:* Uncertainty in the drip shield flux splitting algorithm is given by DS_Flux_Uncertainty_a. The range is derived from analyses of breached drip shield experimental results. There is insufficient data to show trends on which to base any distribution other than uniform. *Sensitivity Name:* DSFLUX. *Location in TSPA-LA:* Tables 6.3.6-1, 6.3.6-2 and 6.3.8-4; Sections 6.3.6.2 and 6.3.6.4.1; Equation 6.3.6-5. *DTN:* SN0703PAEBSRTA.001_R3 [DIRS 183217]. *References: EBS Radionuclide Transport Abstraction* (SNL 2007 [DIRS 177407], Sections 6.3.1.1, 6.3.2.4, 6.5.1.1.1, 6.5.1.1.2.4, 7.1.1.1, Appendix C and Appendix E; Tables 6.3-1, 7.1-7, 8.1-1 and 8.2-4; Equations 6.3.2.4-2, 6.5.1.1.2.4-2 and 6.5.1.1.2.4-3).
DSNF_Mass_Uncert_a. Scale factor used to characterize uncertainty in radionuclide content of DSNF (dimensionless). *Distribution:* Triangular. *Range:* 0.45 to 2.9. *Most Likely:* 0.62. *Additional Information:* See CSNF_Mass_Uncert_a. *Sensitivity Name:* DSNFMASS. *Location in TSPA-LA:* Sections 6.3.7.1.2 and 6.3.7.1.3; Table 6.3.7-7. *DTN:* SN0310T0505503.004_R0 [DIRS 168761]. *References: Initial Radionuclides Inventory* (SNL 2007 [DIRS 180472], Sections 6.6.2, 6.7 and 7; Table 7-2),
dt_dRh_uncertainty. Selector variable used to determine the collapsed drift rubble thermal conductivity (dimensionless). *Distribution:* Discrete. *Range:* 1 to 2. *Additional Information:* There is epistemic uncertainty in the thermal conductivity (K_{th}) of the rubble resulting from a seismic event. A value of 1 indicates the low K_{th} case, while a value of 2 indicates the high K_{th} case. Neither the high-K_{th} case nor low-K_{th} case is more or less likely to be the appropriate value to be applied for effective thermal conductivity of the host-rock rubble. As a result of this argument, each alternative, the high- and low-K_{th} cases, can be assigned the same probability (of 50 percent). *Sensitivity Name:* DTDRHUNC. *Location in TSPA-LA:* Section 6.6.2.2. *DTN:* MO0505SPAROCKM.000_R0 [DIRS 173893]. *References: Multiscale Thermohydrologic Model* (SNL 2007 [DIRS 181383], Sections 6.2.10.3, 6.3.7 and 6.3.17[a]).
DWC_Dispersivity_Cond_a. Selector variable used to determine the axial dispersion modeling case (dimensionless). *Distribution:* Discrete. *Range:* 0 to 1. *Additional Information:* This TSPA implementation parameter specifies whether the high dispersivity (DWC_Dispersivity_Cond_a = 1) or low dispersivity (DWC_Dispersivity_Cond_a = 0) modeling case is used to calculate drift-wall condensation. The probability of encountering each of the two modeling cases is 0.5. *Sensitivity Name:* DWCDISP. *Location in TSPA-LA:* Section 6.3.3.2.2; Table 6.3.3-5. *References: In Drift Natural Convection and Condensation* (SNL 2007 [DIRS 181648], Sections 6.1 [a], 6.1.3[a], Appendix A[a] and B[a]; Tables 6-2[a] and 6-3[a].

Table K3-3. Detailed Summary of Epistemically Uncertain Variables (i.e., elements of **e**) Considered in the TSPA-LA (TSPA Parameter Name) (Continued)

NOTE: * indicates variable not considered in sensitivity analysis due to correlations.

DWC_Std_Error_a_a. Multiplier for the standard deviation on the slope coefficient for determining the probability of condensation from percolation rate (dimensionless). *Distribution:* Normal. *Mean/Median/Mode:* 0. *Standard Deviation:* 1. *Additional Information:* The standard errors applied to the coefficients used in the correlation between the percolation rate and the condensation rate/probability for the four drift wall condensation (DWC) modeling cases (high and low dispersivity, ventilated or unventilated drip shields) are applied as the product of the sampled value from a truncated normal distribution and the value of the standard error specifically defined for each modeling case. A unique distribution is sampled for the slope and y-intercept for both the condensation rate and probability. The standard errors can be used as uncertainty ranges around the slope and intercept parameters. Sampling for the standard error values should be independent. *Sensitivity Name:* DWCSTERA. *Location in TSPA-LA:* Section 6.3.3.2.2; Tables 6.3.3-4 and 6.3.3-5. *References: In Drift Natural Convection and Condensation* (SNL 2007 [DIRS 181648], Sections 6.1.3 [a], Appendix A[a] and B[a]; Tables A-1[a] to A-3[a] and B-1[a] to B-3[a]).
DWC_Std_Error_b_a. Multiplier for the standard deviation on the y-intercept coefficient for determining the probability of condensation from percolation rate (dimensionless). *Distribution:* Normal. *Mean/Median/Mode:* 0. *Standard Deviation:* 1. *Additional Information:* See DWC_Std_Error_a_a. *Sensitivity Name:* DWCSTERB. *Location in TSPA-LA:* Section 6.3.3.2.2; Tables 6.3.3-4 and 6.3.3-5. *References:* In Drift Natural Convection and Condensation (MDL-EBS-MD-000001 REV 00 AD 01, SNL 2007 [DIRS 181648], Section 6.1.3 [a], Appendix A[a] and B[a]; Tables A-1[a] to A-3[a] and B-1[a] to B-3[a]).
DWC_Std_Error_c_a. Multiplier for the standard deviation on the slope coefficient for determining condensation rate from percolation rate (dimensionless). *Distribution:* Normal. *Mean/Median/Mode:* 0. *Standard Deviation:* 1. *Additional Information:* See DWC_Std_Error_a_a. *Sensitivity Name:* DWCSTERC. *Location in TSPA-LA:* Section 6.3.3.2.2; Tables 6.3.3-4 and 6.3.3-5. *References: In Drift Natural Convection and Condensation* (SNL 2007 [DIRS 181648], Sections 6.1.3[a], Appendix A[a] and B [a]; Tables A-1[a] to A-3[a] and B-1[a] to B-3[a]).
DWC_Std_Error_d_a. Multiplier for the standard deviation on the y-intercept coefficient for determining the condensation rate from percolation rate (dimensionless). *Distribution:* Normal. *Mean/Median/Mode:* 0. *Standard Deviation:* 1. *Additional Information:* See DWC_Std_Error_a_a. *Sensitivity Name:* DWCSTERD. *Location in TSPA-LA:* Section 6.3.3.2.2; Tables 6.3.3-4 and 6.3.3-5. *References:* I*n Drift Natural Convection and Condensation* (SNL 2007 [DIRS 181648], Sections 6.1.3[a], Appendix A[a] and B [a]; Tables A-1[a] to A-3[a] and B-1[a] to B-3[a]).
DWC_Ventilated_Cond_a. Selector variable specifying whether the ventilated or unventilated drip shield DWC modeling case is performed (dimensionless). *Distribution:* Discrete. *Range:* 0, 1. *Additional Information:* This TSPA implementation parameter specifies whether the ventilated drip shield (DWC_Ventilated_Cond_a = 1) or unventilated drip shield (DWC_Ventilated_Cond_a = 0) modeling case is used to calculate drift-wall condensation. The probability of encountering each of the two modeling cases is 0.5. *Sensitivity Name:* DWCVENT. *Location in TSPA-LA:* Sections 6.3.3.2.2 and 6.3.3.2.3; Table 6.3.3-5. *References:* I*n Drift Natural Convection and Condensation* (SNL 2007 [DIRS 181648], Sections 6.1.2[a], 6.1.3 [a], Appendix A[a] and B [a]; Tables 6-2[a], 6-3[a] and 8-1[a]).
Exposure_Factor_a. The surface area exposure factor for the amount of HLW glass contacted by water (dimensionless). *Distribution:* Triangular. *Range:* 4 to 17. *Mode:* 4. *Symbol:* $f_{exposure}$. *Additional Information:* The exposure factor is used to account for several uncertainties regarding the glass surface area that is used to calculate the glass degradation rate and, ultimately, the radionuclide release rate. The upper limit of the range represents the case where glass in cracks has the same reactivity as glass at free surfaces. The lower limit of the range accounts for the limited access of water to glass in interior cracks and the lower reactivity of glass in the cracks. The exposure factor accounts for the thermal cracking anticipated for all glass and impact cracking anticipated for about 1% of the glass. *Sensitivity Name:* WFDEGEXF. *Location in TSPA-LA:* Sections 6.3.7.4.3.2 and 6.3.7.4.3.3; Equation 6.3.7-9; Table 6.3.7-32. *DTN:* MO0502ANLGAMR1.016_R0 [DIRS 172830]. *References: Defense HLW Glass Degradation Model* (BSC 2004 [DIRS 169988], Sections 4.1, 6.5.4, 6.6, 6.7, 6.8.1, 6.8.5, 8.1 and 8.2.1; Equations 44, 45, 48 and 49; Tables 6-14 and 8-1).

Table K3-3. Detailed Summary of Epistemically Uncertain Variables (i.e., elements of **e**) Considered in the TSPA-LA (TSPA Parameter Name) (Continued)

NOTE: * indicates variable not considered in sensitivity analysis due to correlations.

fa_group1_a. Fracture aperture for group 1 rock unit (chnf) (m). *Calculated by:* Por_group1_a/ff_group1_a. *Symbol:* 2b. *Additional Information:* This is the ratio of porosity (Por_group#_a) to fracture frequency (ff_group#_a). There is only one standard deviation for fracture porosity, so the other groups are assigned a fracture porosity standard deviation such that the ratio of the standard deviation to the mean is constant for all the groups. This is based on the relationship between fracture frequency and the standard deviation of fracture frequency found for model units above the proposed repository. In this way, the mean and standard deviation for each parameter in each group were computed. As porosity must lie within the finite range of 0 to 1, a beta distribution with these bounds is suitable for studying the influence of porosity uncertainty on radionuclide transport. The logarithm of the fracture frequency has a normal distribution with a mean of.2.33 and a standard deviation of 0.724. The fracture porosity has beta distribution with a minimum of 0, a maximum of 1, a mean of 0.001 and a standard deviation of 0.000309. *Sensitivity Name:* UZFAG1. *Location in TSPA-LA:* Section 6.3.9.2; Equation 6.3.9-2; Fracture porosity values and frequency values are shown in Tables 6.3.9-6 and 6.3.9-7. *DTN:* Fracture frequency, porosity and aperture found in: LA0701PANS02BR.003_R2 [DIRS 180497], Table 1.doc. *References: Particle Tracking Model and Abstraction of Transport Processes Addendum 002* (SNL 2008 [DIRS 184748], Sections 4.1.2 and 6.5.7; Tables 6.6.1-1, 7-1 and 8-2).
fa_group2_a. Fracture aperture for group 2 rock unit (tswf) (m). *Calculated by:* Por_group2_a/ff_group2_a. *Symbol:* 2b. *Additional Information:* See fa_group1_a. The logarithm of the fracture frequency has a normal distribution with a mean of 0.296 and a standard deviation of 0.724. The fracture porosity has a beta distribution with a minimum of 0, a maximum of 1, a mean of 0.025 and a standard deviation of 0.00725. *Sensitivity Name:* UZFAG2. *Location in TSPA-LA:* Section 6.3.9.2; Equation 6.3.9-2; Fracture porosity values and frequency values are shown in Tables 6.3.9-6 and 6.3.9-7. *DTN:* Fracture frequency, porosity and aperture found in: LA0701PANS02BR.003_R2 [DIRS 180497], Table 1.doc. *References: Particle Tracking Model and Abstraction of Transport Processes Addendum 002* (SNL 2008 [DIRS 184748], Sections 4.1.2 and 6.5.7; Tables 6.6.1-1, 7-1 and 8-2).
fa_group3_a. Fracture aperture for group 3 rock units (ch[2,3,4,5]fz, pcf[2,5]z, pp4fz, pp1fz, bf2fz, tr2fz) (m). *Calculated by:* Por_group3_a/ff_group3_a. *Symbol:* 2b. *Additional Information:* See fa_group1_a. The logarithm of the fracture frequency has a normal distribution with a mean of -2.23 and a standard deviation of 0.724. The fracture porosity has a beta distribution with a minimum of 0, a maximum of 1, a mean of 0.00037 and a standard deviation of 0.000109. *Sensitivity Name:* UZFAG3. *Location in TSPA-LA:* Section 6.3.9.2; Equation 6.3.9-2; Fracture porosity values and frequency values are shown in Tables 6.3.9-6 and 6.3.9-7. *DTN:* Fracture frequency, porosity and aperture found in: LA0701PANS02BR.003_R2 [DIRS 180497], Table 1.doc. *References: Particle Tracking Model and Abstraction of Transport Processes Addendum 002* (SNL 2008 [DIRS 184748], Sections 4.1.2 and 6.5.7; Tables 6.6.1-1, 7-1 and 8-2).
fa_group4_a. Fracture aperture for group 4 rock units (pp3fd, pp2fd, bf3fd, tr3fd) (m). *Calculated by:* Por_group4_a/ff_group4_a. *Symbol:* 2b. *Additional Information:* See fa_group1_a. The logarithm of the fracture frequency has a normal distribution with a mean of -1.87 and a standard deviation of 0.724. The fracture porosity has a beta distribution with a minimum of 0, a maximum of 1, a mean of 0.00097 and a standard deviation of 0.000285. *Sensitivity Name:* UZFAG4. *Location in TSPA-LA:* Section 6.3.9.2; Equation 6.3.9-2; Fracture porosity values and frequency values are shown in Tables 6.3.9-6 and 6.3.9-7. *DTN:* Fracture frequency, porosity and aperture found in: LA0701PANS02BR.003_R2 [DIRS 180497], Table 1.doc. *References: Particle Tracking Model and Abstraction of Transport Processes Addendum 002* (SNL 2008 [DIRS 184748], Sections 4.1.2 and 6.5.7; Tables 6.6.1-1, 7-1 and 8-2).
fa_group5_a. Fracture aperture for group 5 rock units (ch1fz, pcf1z, ch6fz, pcf6z) (m). *Calculated by:* Por_group5_a/ff_group5_a. *Symbol:* 2b. *Additional Information:* See fa_group1_a. The logarithm of the fracture frequency has a normal distribution with a mean of -3.48 and a standard deviation of 0.724. The fracture porosity has a beta distribution with a minimum of 0, a maximum of 1, a mean of 0.00016 and a standard deviation of 4.71E-05. *Sensitivity Name:* UZFAG5. *Location in TSPA-LA:* Section 6.3.9.2; Equation 6.3.9-2; Fracture porosity values and frequency values are shown in Tables 6.3.9-6 and 6.3.9-7. *DTN:* Fracture frequency, porosity and aperture found in: LA0701PANS02BR.003_R2 [DIRS 180497], Table 1.doc. *References: Particle Tracking Model and Abstraction of Transport Processes Addendum 002* (SNL 2008 [DIRS 184748], Sections 4.1.2 and 6.5.7; Tables 6.6.1-1, 7-1 and 8-2).

Table K3-3. Detailed Summary of Epistemically Uncertain Variables (i.e., elements of **e**) Considered in the TSPA-LA (TSPA Parameter Name) (Continued)

NOTE: * indicates variable not considered in sensitivity analysis due to correlations.

fa_group6_a. Fracture aperture for group 6 rock units (ch[1,2,3,4,5,6]fv) (m). *Calculated by:* Por_group6_a/ff_group6_a. *Symbol:* 2b. *Additional Information:* See fa_group1_a. The logarithm of the fracture frequency has a normal distribution with a mean of -2.38 and a standard deviation of 0.724. The fracture porosity has a beta distribution with a minimum of 0, a maximum of 1, a mean of 0.00069 and a standard deviation of 0.000203. *Sensitivity Name:* UZFAG6. *Location in TSPA-LA:* Section 6.3.9.2; Equation 6.3.9-2; Fracture porosity values and frequency values are shown in Tables 6.3.9-6 and 6.3.9-7. *DTN:* Fracture frequency, porosity and aperture found in: LA0701PANS02BR.003_R2 [DIRS 180497], Table 1.doc. *References: Particle Tracking Model and Abstraction of Transport Processes Addendum 002* (SNL 2008 [DIRS 184748], Sections 4.1.2 and 6.5.7; Tables 6.6.1-1, 7-1 and 8-2).
fa_group7_a. Fracture aperture for group 7 rock units (tswf9, pcf39, tswfv, tswfz) (m). *Calculated by:* Por_group7_a/ff_group7_a. *Symbol:* 2b. *Additional Information:* See fa_group1_a. The logarithm of the fracture frequency has a normal distribution with a mean of -0.303 and a standard deviation of 0.724. The fracture porosity has a beta distribution with a minimum of 0, a maximum of 1, a mean of 0.0043 and a standard deviation of 0.00126. *Sensitivity Name:* UZFAG7. *Location in TSPA-LA:* Section 6.3.9.2; Equation 6.3.9-2; Fracture porosity values and frequency values are shown in Tables 6.3.9-6 and 6.3.9-7. *DTN:* Fracture frequency, porosity and aperture found in: LA0701PANS02BR.003_R2 [DIRS 180497], Table 1.doc. *References: Particle Tracking Model and Abstraction of Transport Processes Addendum 002* (SNL 2008 [DIRS 184748], Sections 4.1.2 and 6.5.7; Tables 6.6.1-1, 7-1 and 8-2).
fa_group8_a. Fracture aperture for group 8 rock units (tswf[4,5], tswf[6,7], tswf8, pcf38) (m). *Calculated by:* Por_group8_a/ff_group8_a. *Symbol:* 2b. *Additional Information:* See fa_group1_a. The logarithm of the fracture frequency has a normal distribution with a mean of 1.12 and a standard deviation of 0.724. The fracture porosity has a beta distribution with a minimum of 0, a maximum of 1, a mean of 0.0105 and a standard deviation of 0.0031. *Sensitivity Name:* UZFAG8. *Location in TSPA-LA:* Section 6.3.9.2; Equation 6.3.9-2; Fracture porosity values and frequency values are shown in Tables 6.3.9-6 and 6.3.9-7. *DTN:* Fracture frequency, porosity and aperture found in: LA0701PANS02BR.003_R2 [DIRS 180497], Table 1.doc. *References: Particle Tracking Model and Abstraction of Transport Processes Addendum 002* (SNL 2008 [DIRS 184748], Sections 4.1.2 and 6.5.7; Tables 6.6.1-1, 7-1 and 8-2).
fa_group9_a. Fracture aperture for group 9 rock units (tswf3) (m). *Calculated by:* Por_group9_a/ff_group9_a. *Symbol:* 2b. *Additional Information:* See fa_group1_a. Group 9 (tswf3) has its own standard deviation for fracture frequency, which is used. As porosity must lie within the finite range of 0 to 1, a beta distribution with these bounds is suitable for studying the influence of porosity uncertainty on radionuclide transport. The logarithm of the fracture frequency has a normal distribution with a mean of -0.692 and a standard deviation of 0.981. The fracture porosity has a beta distribution with a minimum of 0, a maximum of 1, a mean of 0.0058 and a standard deviation of 0.00171. *Sensitivity Name:* UZFAG9. *Location in TSPA-LA:* Section 6.3.9.2; Equation 6.3.9-2; Fracture porosity values and frequency values are shown in Tables 6.3.9-6 and 6.3.9-7. *DTN:* Fracture frequency, porosity and aperture found in: LA0701PANS02BR.003_R2 [DIRS 180497], Table 1.doc. *References: Particle Tracking Model and Abstraction of Transport Processes Addendum 002* (SNL 2008 [DIRS 184748], Sections 4.1.2 and 6.5.7; Tables 6.6.1-1, 7-1 and 8-2).
FHH_Isotherm_k_CP_a. Frenkel Halsey Hill water vapor adsorption isotherm parameter, *k*, for corrosion products (dimensionless). *Distribution:* Uniform. *Range:* 1.048 to 1.370 (see additional information). *Symbol:* k_{CP}. *Additional Information: k* and *s* are parameters that in principle are calculable from properties of the absorbent and substrate but in practice are empirical. Because the adsorption isotherms for each corrosion product component (goethite, HFO, and chromium and nickel oxides) overlap and include uncertainty, data for all the components are lumped together to form a single isotherm, with the uncertainty accounted for using a range and uniform distribution for the corrosion product FHH parameters. Analysis of available water vapor adsorption isotherm data fit to the FHH function for the isotherm produced a mean and standard deviation for parameter *k*. A uniform distribution is used due to lack of trends in the empirical data to suggest any other distributions. In the TSPA-LA Model the incorrect range of values was used for this parameter. The correct range is 1.030 to 1.326. See Appendix P, Table P-6 for a discussion of the effects of this error. *Sensitivity Name:* FHHISKCP. *Location in TSPA-LA:* Table 6.3.8-4. *DTN:* SN0703PAEBSRTA.001_R3 [DIRS 183217]. *References: EBS Radionuclide Transport Abstraction* (ANL-WIS-PA-000001 REV 03, SNL 2007 [DIRS 177407], Sections 6.3.4.3.2 and 6.5.2.2.1; Tables 6.5-7 and 8.2-4; Equations 6.3.4.3.2-1 to 6.3.4.3.2-3).

Table K3-3. Detailed Summary of Epistemically Uncertain Variables (i.e., elements of **e**) Considered in the TSPA-LA (TSPA Parameter Name) (Continued)

NOTE: * indicates variable not considered in sensitivity analysis due to correlations.

FHH_Isotherm_k_CSNF_Rind_a. Frenkel Halsey Hill water vapor adsorption isotherm parameter, *k*, for CSNF rind (dimensionless). *Distribution:* Uniform. *Range:* 1.606 to 8.215. *Symbol:* k_{rind}. *Additional Information:* The water adsorption isotherm for waste form rind is of the same functional form as for corrosion products. The CSNF rind saturation calculation uses the FHH adsorption isotherm (a function of relative humidity). Uncertainty is accounted for using a range and uniform distribution for the CSNF rind FHH empirical parameters, *k* and *s*. See FHH_Isotherm_k_CP_a. *Sensitivity Name:* FHHISKCS. *Location in TSPA-LA:* Table 6.3.8-4. *DTN:* SN0703PAEBSRTA.001_R3 [DIRS 183217]. *References: EBS Radionuclide Transport Abstraction* (SNL 2007 [DIRS 177407], Sections 6.3.4.6.1 and 6.5.2.2.2; Tables 6.5-9 and 8.2-4; Equations 6.3.4.6.1-1 to 6.3.4.6.1-3).
FHH_Isotherm_s_CP_a. Frenkel Halsey Hill water vapor adsorption isotherm parameter, *s*, for corrosion products (dimensionless). *Distribution:* Uniform. *Range:* 1.525 to 1.852 (see additional information). *Symbol:* s_{CP}. *Additional Information:* See FHH_Isotherm_k_CP_a. Analysis of available water vapor adsorption isotherm data fit to FHH functional for of the isotherm produced a mean and standard deviation for parameter *s*. In the TSPA-LA Model the incorrect range of values was used for this parameter. The correct range is 1.493 to 1.799. See Appendix P, Table P-6, for a discussion of the effects of this error. *Sensitivity Name:* FHHISSCP. *Location in TSPA-LA:* Table 6.3.8-4. *DTN:* SN0703PAEBSRTA.001_R3 [DIRS 183217]. *References: EBS Radionuclide Transport Abstraction* (SNL 2007 [DIRS 177407], Sections 6.3.4.3.2 and 6.5.2.2.1; Tables 6.5-7 and 8.2-4; Equations 6.3.4.3.2-1 to 6.3.4.3.2-3).
FHH_Isotherm_s_CSNF_Rind_a. Frenkel Halsey Hill water vapor adsorption isotherm parameter, *s*, for CSNF rind (dimensionless). *Distribution:* Uniform. *Range:* 1.656 to 3.038. *Symbol:* s_{rind}. *Additional Information:* See FHH_Isotherm_k_CSNF_Rind_a. *Sensitivity Name:* FHHISSCS. *Location in TSPA-LA:* Table 6.3.8-4. *DTN:* SN0703PAEBSRTA.001_R3 [DIRS 183217]. *References: EBS Radionuclide Transport Abstraction* (SNL 2007 [DIRS 177407], Sections 6.3.4.6.1 and 6.5.2.2.2; Tables 6.5-9 and 8.2-4; Equations 6.3.4.6.1-1 to 6.3.4.6.1-3).
FISVO. Flowing interval spacing in fractured volcanic units (m). *Distribution:* Piecewise uniform. *Range:* 1.86 to 80. *Additional Information:* The uncertain input parameters influencing matrix diffusion in the SZ Flow and Transport Model Submodel include effective diffusion coefficient, flowing interval spacing, and flowing interval porosity. The flowing interval spacing and flowing interval porosity are used to define the effective area to flow in the fractured volcanic units. To treat the one- and three-dimensional transport through the SZ consistently, the sampled values used to generate the saturated zone breakthrough curves are also used in the TSPA-LA Model. These values are tabulated as 200 sets of values for the SZ parameters, accounting for appropriate correletions, and are entered into the TSPA model as a table of 200 values for each parameter. The TSPA-LA Model selects values from this table using the Goldsim variable SZ_index_a. *Sensitivity Name:* SZFISPVO. *Location in TSPA-LA:* Section 6.3.10.5; Table 6.3.10-2. *DTN:* SN0702PASZFTMA.002_R1 [DIRS 183471]. *References: Saturated Zone Flow and Transport Model Abstraction* (SNL 2008 [DIRS 183750], Sections 6.5.1.2, 6.5.2.3[a] B-2[a], 7-1[b], and A-1[b]; Tables 4-3, 6-7[a], 6-8, 7-1[a], A-1[a] and B-1; Figure 6-5[a]).
FPLANW. Northwestern boundary of alluvial uncertainty zone (dimensionless). *Distribution:* Uniform. *Range:* 0 to 1. *Additional Information:* This parameter is used to determine the lengths of the flow paths in the volcanic units and alluvium. Implemented as a uniform distribution where a value of 0.0 corresponds to the minimum extent of the uncertainty zone, and 1.0 corresponds to the maximum extent of the uncertainty zone in a westerly direction. FPLANW defines the location where the pathlines may cross from the fracture-dominated flow in the volcanic units to the higher-porosity alluvium. To treat the one- and three-dimensional transport through the SZ consistently, the sampled values used to generate the saturated zone breakthrough curves are also used in the TSPA-LA Model. These values are tabulated as 200 sets of values for the SZ parameters, accounting for appropriate correletions, and are entered into the TSPA model as a table of 200 values for each parameter. The TSPA-LA Model selects values from this table using the Goldsim variable SZ_index_a. *Sensitivity Name:* SZWBNDAL. *Location in TSPA-LA:* Section 6.3.10.2; Table 6.3.10-2. *DTN:* SN0702PASZFTMA.002_R1 [DIRS 183471]. *References: Saturated Zone Flow and Transport Model Abstraction* (SNL 2008 [DIRS 183750], Sections 6.5.1.2[a] and 6.5.2.2[a]; Tables 6-7[a], 7-1[a] and A-1[a]).

Table K3-3. Detailed Summary of Epistemically Uncertain Variables (i.e., elements of **e**) Considered in the TSPA-LA (TSPA Parameter Name) (Continued)

NOTE: * indicates variable not considered in sensitivity analysis due to correlations.

FPVO. Logarithm of lowing interval porosity in volcanic units (dimensionless). *Distribution:* Piecewise uniform. *Range:* -5 to -1. *Median:* -3. *Additional Information:* The flowing interval spacing and flowing interval porosity are used to define the effective area to flow in the fractured volcanic units. To treat the one- and three-dimensional transport through the SZ consistently, the sampled values used to generate the saturated zone breakthrough curves are also used in the TSPA-LA Model. These values are tabulated as 200 sets of values for the SZ parameters, accounting for appropriate correletions, and are entered into the TSPA model as a table of 200 values for each parameter. The TSPA-LA Model selects values from this table using the Goldsim variable SZ_index_a. *Sensitivity Name:* SZFIPOVO. *Location in TSPA-LA:* Table 6.3.10-2. *DTN:* SN0702PASZFTMA.002_R1 [DIRS 183471]. *References: Saturated Zone Flow and Transport Model Abstraction* (SNL 2008 [DIRS 183750], Sections 6.5.1.1, 6.5.1.2, 6.5.2.5, 6.5.2.15, B-2[a], 7-1[b], and A-1[b]; Tables 6-8, 7-1[a], A-1[a] and B-1).
Fraction_Channel_a. Fraction of the RMEI location subject to fluvial deposition (dimensionless). *Distribution:* Uniform. *Range:* 0.09 to 0.54. *Symbol:* F. *Additional Information:* The concentrations on divides and channels are combined using the weighting factor for the fraction of the alluvial fan composed of channels to yield one concentration for the resuspendable surface layer and one concentration for the tillage depth for use by the Volcanic Ash Exposure Submodel in dose calculations. The fraction of the Fortymile Wash alluvial fan area is estimated by measuring the fractional area of the current fan that has been active over the past 10,000 years. *Sensitivity Name:* FRACCHNL. *Location in TSPA-LA:* Table 6.5-5. *DTN:* MO0702PAFARDAT.001_R3 [DIRS 182578]. *References: Redistribution of Tephra and Waste by Geomorphic Processes Following a Potential Volcanic Eruption at Yucca Mountain, Nevada* (SNL 2007 [DIRS 179347], Section 6.3.2, 6.5.4.2 and 7.1.3; Tables 6.4-1 and 6.5.10-1).
Gamma_AFM_a. Active fracture model (AFM) Gamma parameter (dimensionless). *Distribution:* Uniform. *Range:* 0.2 to 0.6. *Additional Information:* The parameter will be sampled from a range to incorporate this uncertainty into the model. Process flow model results have demonstrated that the AFM parameters have very little influence on the relevant flow model parameters for transport, namely the fluid saturations and flow rates in the fracture and matrix continua. Smaller values of the gamma parameter reduce the effective size of the matrix block, and therefore increase the strength of the fracture-matrix flux term. A single, uncertain value of gamma will be provided for rock units below the repository. A reasonable upper bound is the value used in the development of the flow model, approximately 0.6. A range that extends down to 0.2 provides an overall range that is equally distributed above and below the nominal value of 0.4. With no additional information available to define this parameter uncertainty distribution, the parameter will be sampled from a uniform distribution from 0.2 to 0.6. This range is consistent with the available data, and maintains the model within a range in which preferential flow through a subset of fractures will occur for all realizations. *Sensitivity Name:* UZGAM. *Location in TSPA-LA:* Sections 6.3.9.2, 6.3.9.3 and 6.3.9.4.1; Table 6.3.9-5. *DTN:* LA0701PANS02BR.003_R2 [DIRS 180497], Readme.doc. *References: Particle Tracking Model and Abstraction of Transport Processes Addendum 002* (SNL 2008 [DIRS 184748], Section 6.5.6; Tables 6.6.1-1 and 8-2).
GC_ULevel_A22_a. Variable for selecting distribution for general corrosion rate (low, medium, or high) (dimensionless). *Distribution:* Discrete. *Range:* 1 to 3. *Additional Information:* In TSPA, the low, medium, and high general corrosion rate distribution for Alloy 22 is randomly selected in such a way that the low and high general corrosion rate distributions are each used for 5% of realizations and the medium general corrosion rate distribution is used for the remaining 90% of realizations. *Sensitivity Name:* WDGCUA22. *Location in TSPA-LA:* Table 6.3.5-4. *DTN:* MO0703PAGENCOR.001_R4 [DIRS 182029]. *References: General Corrosion and Localized Corrosion of the Waste Package Outer Barrier* (SNL 2007 [DIRS 178519], Sections 6.4.3 and 6.4.3.3; Table 6-7; Figure 6-23).
Goethite_SA_a. Specific surface area of goethite (m^2/g). *Distribution:* Truncated log normal. *Range:* 14.7 to 110. *Mean:* 51.42. *Standard Deviation:* 30.09. *Symbol:* S_G. *Additional Information:* For the water saturation calculation, the solid density of each of the four corrosion product components is multiplied by its respective specific surface area. Specific surface areas for goethite and HFO are used for the competitive radionuclide sorption model as well as for the water sorption and saturation model. *Sensitivity Name:* GOESA. *Location in TSPA-LA:* Table 6.3.8-4; S_{CP} in Equation 6.3.8-19. *DTN:* SN0703PAEBSRTA.001_R3 [DIRS 183217]. *References: EBS Radionuclide Transport Abstraction* (SNL 2007 [DIRS 177407], Sections 4.1.2, 6.3.4.2.3.1, 6.3.4.3.3, 6.5.2.2.1, J.6.3 and Appendix K; Equation 6.3.4.2.3.1-1; Tables 4.1-12, 4.1-19, 6.3-7, 6.5-7 and 8.2-4).
Goethite_Site_Density_a. Density of sorption sites on goethite ($1/nm^2$). *Distribution:* Discrete. *Range:* 1.02 to 8.59. *Symbol:* $N_{S,G}$. *Additional Information:* Range and distribution are those of the input data and adequately capture the behavior of the parameter without further analysis. *Sensitivity Name:* GOESITED. *Location in TSPA-LA:* Table 6.3.8-3. *DTN:* SN0703PAEBSRTA.001_R3 [DIRS 183217]. *References: EBS Radionuclide Transport Abstraction* (SNL 2007 [DIRS 177407], Sections 4.1.2, 6.3.4.2.3.1, J.6.3 and J.6.5.1; Equation 6.3.4.2.3.1-1; Tables 4.1-12, 6.3-4, 6.3-5 and 8.2-2).

Table K3-3. Detailed Summary of Epistemically Uncertain Variables (i.e., elements of **e**) Considered in the TSPA-LA (TSPA Parameter Name) (Continued)

NOTE: * indicates variable not considered in sensitivity analysis due to correlations.

GW_BDCF_MIC_Ac227. Groundwater Biosphere Dose Conversion Factor (BDCF) for ^{227}Ac in modern interglacial climate ((Sv/year)/(Bq/m^3)). *Distribution:* Discrete. *Range:* 4.08E-07 to 4.32E-06. *Mean:* 1.3E-06. *Standard Deviation:* 5.28E-07. *Additional Information:* The groundwater BDCFs predict, in a stochastic manner to allow for parametric uncertainty, the annual dose (Sv/yr) to the reasonably maximally exposed individual for a unit activity concentration (1 Bq/m^3) in the groundwater for each radionuclide considered by TSPA. BDCFs were developed for three climate states: the present-day climate, monsoon climate, and glacial transition climate. Some BDCFs include contributions from their short-lived decay products. To account for correlations between parameters used to compute BDCFs, the Biosphere Model generates a table of 1,000 sets of values for each BDCF. These values are entered into the TSPA Input Database as a table of 1,000 values for each parameter. The TSPA-LA Model selects values from this table using the Goldsim variable Bio_index_a. *Sensitivity Name:* MICAC227. *Location in TSPA-LA:* Sections 6.3.11.2 and 6.3.11.3; Table 6.3.11-3. *DTN:* MO0702PAGBDCFS.001_R0 [DIRS 179327]. *References: Biosphere Model Report* (SNL 2007 [DIRS 177399], Sections 1, 6.1, 6.4, 6.4.10, 6.8.10, 6.11 and 6.13; Equations 6.4.10-2, 6.4.10-4, 6.2.10-5 and 6.11-5; Tables 6.11-8 and 6.11-12).
GW_BDCF_MIC_Am241. Groundwater Biosphere Dose Conversion Factor (BDCF) for ^{241}Am in modern interglacial climate ((Sv/year)/(Bq/m^3)). *Distribution:* Discrete. *Range:* 2.16E-07 to 3.30E-06. *Mean:* 8.34E-07. *Standard Deviation:* 4.03E-07. *Additional Information:* See GW_BDCF_MIC_Ac227. *Sensitivity Name:* MICAM241. *Location in TSPA-LA:* Sections 6.3.11.2 and 6.3.11.3; Table 6.3.11-3. *DTN:* MO0702PAGBDCFS.001_R0 [DIRS 179327]. *References: Biosphere Model Report* (SNL 2007 [DIRS 177399], Sections 1, 6.1, 6.4, 6.4.10, 6.8.10, 6.11 and 6.13; Equations 6.4.10-2, 6.4.10-4, 6.2.10-5 and 6.11-5; Tables 6.11-8 and 6.11-12).
GW_BDCF_MIC_Am243. Groundwater Biosphere Dose Conversion Factor (BDCF) for ^{243}Am in modern interglacial climate ((Sv/year)/(Bq/m^3)). *Distribution:* Discrete. *Range:* 2.21E-07 to 3.37E-06. *Mean:* 8.88E-07. *Standard Deviation:* 4.12E-07. *Additional Information:* See GW_BDCF_MIC_Ac227. *Sensitivity Name:* MICAM243. *Location in TSPA-LA:* Sections 6.3.11.2 and 6.3.11.3; Table 6.3.11-3. *DTN:* MO0702PAGBDCFS.001_R0 [DIRS 179327]. *References: Biosphere Model Report* (SNL 2007 [DIRS 177399], Sections 1, 6.1, 6.4, 6.4.10, 6.8.10, 6.11 and 6.13; Equations 6.4.10-2, 6.4.10-4, 6.2.10-5 and 6.11-5; Tables 6.11-8 and 6.11-12).
GW_BDCF_MIC_C14. Groundwater Biosphere Dose Conversion Factor (BDCF) for ^{14}C in modern interglacial climate ((Sv/year)/(Bq/m^3)). *Distribution:* Discrete. *Range:* 7.18E-10 to 2.56E-08. *Mean:* 1.93E-09. *Standard Deviation:* 1.85E-09. *Additional Information:* See GW_BDCF_MIC_Ac227. *Sensitivity Name:* MICC14. *Location in TSPA-LA:* Sections 6.3.11.2 and 6.3.11.3; Table 6.3.11-3. *DTN:* MO0702PAGBDCFS.001_R0 [DIRS 179327]. *References: Biosphere Model Report* (SNL 2007 [DIRS 177399], Sections 1, 6.1, 6.4, 6.4.10, 6.8.10, 6.11 and 6.13; Equations 6.4.10-2, 6.4.10-4, 6.2.10-5 and 6.11-5; Tables 6.11-8 and 6.11-12).
GW_BDCF_MIC_Cl36. Groundwater Biosphere Dose Conversion Factor (BDCF) for ^{36}Cl in modern interglacial climate ((Sv/year)/(Bq/m^3)). *Distribution:* Discrete. *Range:* 1.28E-09 to 3.00E-07. *Mean:* 8.09E-09. *Standard Deviation:* 1.41E-08. *Additional Information:* See GW_BDCF_MIC_Ac227. *Sensitivity Name:* MICCl36. *Location in TSPA-LA:* Sections 6.3.11.2 and 6.3.11.3; Table 6.3.11-3. *DTN:* MO0702PAGBDCFS.001_R0 [DIRS 179327]. *References: Biosphere Model Report* (SNL 2007 [DIRS 177399], Sections 1, 6.1, 6.4, 6.4.10, 6.8.10, 6.11 and 6.13; Equations 6.4.10-2, 6.4.10-4, 6.2.10-5 and 6.11-5; Tables 6.11-8 and 6.11-12).
GW_BDCF_MIC_Cs135. Groundwater Biosphere Dose Conversion Factor (BDCF) for ^{135}Cs in modern interglacial climate ((Sv/year)/(Bq/m^3)). *Distribution:* Discrete. *Range:* 3.1E-09 to 8.48E-08. *Mean:* 1.45E-08. *Standard Deviation:* 1.02E-08. *Additional Information:* See GW_BDCF_MIC_Ac227. *Sensitivity Name:* MICCS135. *Location in TSPA-LA:* Sections 6.3.11.2 and 6.3.11.3; Table 6.3.11-3. *DTN:* MO0702PAGBDCFS.001_R0 [DIRS 179327]. *References: Biosphere Model Report* (SNL 2007 [DIRS 177399], Sections 1, 6.1, 6.4, 6.4.10, 6.8.10, 6.11 and 6.13; Equations 6.4.10-2, 6.4.10-4, 6.2.10-5 and 6.11-5; Tables 6.11-8 and 6.11-12).
GW_BDCF_MIC_Cs137. Groundwater Biosphere Dose Conversion Factor (BDCF) for ^{137}Cs in modern interglacial climate ((Sv/year)/(Bq/m^3)). *Distribution:* Discrete. *Range:* 3.87E-08 to 4.56E-07. *Mean:* 1.30E-07. *Standard Deviation:* 6.33E-08. *Additional Information:* See GW_BDCF_MIC_Ac227. *Sensitivity Name:* MICCS137. *Location in TSPA-LA:* Sections 6.3.11.2 and 6.3.11.3; Table 6.3.11-3. *DTN:* MO0702PAGBDCFS.001_R0 [DIRS 179327]. *References: Biosphere Model Report* (SNL 2007 [DIRS 177399], Sections 1, 6.1, 6.4, 6.4.10, 6.8.10, 6.11 and 6.13; Equations 6.4.10-2, 6.4.10-4, 6.2.10-5 and 6.11-5; Tables 6.11-8 and 6.11-12).

Table K3-3. Detailed Summary of Epistemically Uncertain Variables (i.e., elements of **e**) Considered in the TSPA-LA (TSPA Parameter Name) (Continued)

NOTE: * indicates variable not considered in sensitivity analysis due to correlations.

GW_BDCF_MIC_I129. Groundwater Biosphere Dose Conversion Factor (BDCF) for ^{129}I in modern interglacial climate ((Sv/year)/(Bq/m^3)). *Distribution:* Discrete. *Range:* 8.59E-08 to 1.13E-06. *Mean:* 1.29E-07. *Standard Deviation:* 5.28E-08. *Additional Information:* See GW_BDCF_MIC_Ac227. *Sensitivity Name:* MICI129. *Location in TSPA-LA:* Sections 6.3.11.2 and 6.3.11.3; Table 6.3.11-3. *DTN:* MO0702PAGBDCFS.001_R0 [DIRS 179327]. *References: Biosphere Model Report* (SNL 2007 [DIRS 177399], Sections 1, 6.1, 6.4, 6.4.10, 6.8.10, 6.11 and 6.13; Equations 6.4.10-2, 6.4.10-4, 6.2.10-5 and 6.11-5; Tables 6.11-8 and 6.11-12).
GW_BDCF_MIC_Np237. Groundwater Biosphere Dose Conversion Factor (BDCF) for ^{237}Np in modern interglacial climate ((Sv/year)/(Bq/m^3)). *Distribution:* Discrete. *Range:* 1.06E-07 to 8.05E-07. *Mean:* 2.74E-07. *Standard Deviation:* 9.70E-08. *Additional Information:* See GW_BDCF_MIC_Ac227. *Sensitivity Name:* MICNP237. *Location in TSPA-LA:* Sections 6.3.11.2 and 6.3.11.3; Table 6.3.11-3. *DTN:* MO0702PAGBDCFS.001_R0 [DIRS 179327]. *References: Biosphere Model Report* (SNL 2007 [DIRS 177399], Sections 1, 6.1, 6.4, 6.4.10, 6.8.10, 6.11 and 6.13; Equations 6.4.10-2, 6.4.10-4, 6.2.10-5 and 6.11-5; Tables 6.11-8 and 6.11-12).
GW_BDCF_MIC_Pa231. Groundwater Biosphere Dose Conversion Factor (BDCF) for ^{231}Pa in modern interglacial climate ((Sv/year)/(Bq/m^3)). *Distribution:* Discrete. *Range:* 6.58E-07 to 8.56E-06. *Mean:* 2.44E-06. *Standard Deviation:* 1.02E-06. *Additional Information:* See GW_BDCF_MIC_Ac227. *Sensitivity Name:* MICPA231. *Location in TSPA-LA:* Sections 6.3.11.2 and 6.3.11.3; Table 6.3.11-3. *DTN:* MO0702PAGBDCFS.001_R0 [DIRS 179327]. *References: Biosphere Model Report* (SNL 2007 [DIRS 177399], Sections 1, 6.1, 6.4, 6.4.10, 6.8.10, 6.11 and 6.13; Equations 6.4.10-2, 6.4.10-4, 6.2.10-5 and 6.11-5; Tables 6.11-8 and 6.11-12).
GW_BDCF_MIC_Pu238. Groundwater Biosphere Dose Conversion Factor (BDCF) for ^{238}Pu in modern interglacial climate ((Sv/year)/(Bq/m^3)). *Distribution:* Discrete. *Range:* 2.61E-07 to 2.09E-006. *Mean:* 7.61E-07. *Standard Deviation:* 2.78E-07. *Additional Information:* See GW_BDCF_MIC_Ac227. *Sensitivity Name:* MICPU238. *Location in TSPA-LA:* Sections 6.3.11.2 and 6.3.11.3; Table 6.3.11-3. *DTN:* MO0702PAGBDCFS.001_R0 [DIRS 179327]. *References: Biosphere Model Report* (SNL 2007 [DIRS 177399], Sections 1, 6.1, 6.4, 6.4.10, 6.8.10, 6.11 and 6.13; Equations 6.4.10-2, 6.4.10-4, 6.2.10-5 and 6.11-5; Tables 6.11-8 and 6.11-12).
GW_BDCF_MIC_Pu239. Groundwater Biosphere Dose Conversion Factor (BDCF) for ^{239}Pu in modern interglacial climate ((Sv/year)/(Bq/m^3)). *Distribution:* Discrete. *Range:* 3.49E-07 to 2.93E-06. *Mean:* 9.55E-07. *Standard Deviation:* 3.37E-07. *Additional Information:* See GW_BDCF_MIC_Ac227. *Sensitivity Name:* MICPU239. *Location in TSPA-LA:* Sections 6.3.11.2 and 6.3.11.3; Table 6.3.11-3. *DTN:* MO0702PAGBDCFS.001_R0 [DIRS 179327]. *References: Biosphere Model Report* (SNL 2007 [DIRS 177399], Sections 1, 6.1, 6.4, 6.4.10, 6.8.10, 6.11 and 6.13; Equations 6.4.10-2, 6.4.10-4, 6.2.10-5 and 6.11-5; Tables 6.11-8 and 6.11-12).
GW_BDCF_MIC_Pu240. Groundwater Biosphere Dose Conversion Factor (BDCF) for ^{240}Pu in modern interglacial climate ((Sv/year)/(Bq/m^3)). *Distribution:* Discrete. *Range:* 3.47E-07 to 2.90E-06. *Mean:* 9.51E-07. *Standard Deviation:* 3.35E-07. *Additional Information:* See GW_BDCF_MIC_Ac227. *Sensitivity Name:* MICPU240. *Location in TSPA-LA:* Sections 6.3.11.2 and 6.3.11.3; Table 6.3.11-3. *DTN:* MO0702PAGBDCFS.001_R0 [DIRS 179327]. *References: Biosphere Model Report* (SNL 2007 [DIRS 177399], Sections 1, 6.1, 6.4, 6.4.10, 6.8.10, 6.11 and 6.13; Equations 6.4.10-2, 6.4.10-4, 6.2.10-5 and 6.11-5; Tables 6.11-8 and 6.11-12).
GW_BDCF_MIC_Ra226_Pb210. Groundwater Biosphere Dose Conversion Factor (BDCF) for ^{210}Pb summed into ^{226}Ra in modern interglacial climate ((Sv/year)/(Bq/m^3)). *Distribution:* Discrete. *Range:* 2.90E-06 to 2.82E-05. *Mean:* 6.52E-06. *Standard Deviation:* 2.58E-06. *Additional Information:* BDCF sums were produced for the three primary radionuclides, ^{226}Ra, ^{232}Th and ^{232}U, to include the contribution from their long-lived decay products, which themselves are primary radionuclides, in the case the concentrations of these decay products were not calculated in the TSPA model. BDCFs sums included the following radionuclides: ^{226}Ra + ^{210}Pb; ^{232}Th + ^{228}Ra + ^{228}Th; and ^{232}U + ^{228}Th, assuming radioactive equilibrium with a parent radionuclide. Also see GW_BDCF_MIC_Ac227. *Sensitivity Name:* MICRA226. *Location in TSPA-LA:* Sections 6.3.11.2 and 6.3.11.3; Table 6.3.11-3. *DTN:* MO0702PAGBDCFS.001_R0 [DIRS 179327]. *References: Biosphere Model Report* (SNL 2007 [DIRS 177399], Sections 1, 6.1, 6.4, 6.4.10, 6.8.10, 6.11 and 6.13; Equations 6.4.10-2, 6.4.10-4, 6.2.10-5 and 6.11-5; Tables 6.11-8 and 6.11-12).
GW_BDCF_MIC_Se79. Groundwater Biosphere Dose Conversion Factor (BDCF) for ^{79}Se in modern interglacial climate. ((Sv/year)/(Bq/m^3)). *Distribution:* Discrete. *Range:* 3.62E-09 to 1.51E-06. *Mean:* 2.42E-08. *Standard Deviation:* 7.48E-08. *Additional Information:* See GW_BDCF_MIC_Ac227. *Sensitivity Name:* MICSE79. *Location in TSPA-LA:* Sections 6.3.11.2 and 6.3.11.3; Table 6.3.11-3. *DTN:* MO0702PAGBDCFS.001_R0 [DIRS 179327]. *References: Biosphere Model Report* (SNL 2007 [DIRS 177399], Sections 1, 6.1, 6.4, 6.4.10, 6.8.10, 6.11 and 6.13; Equations 6.4.10-2, 6.4.10-4, 6.2.10-5 and 6.11-5; Tables 6.11-8 and 6.11-12).

Table K3-3. Detailed Summary of Epistemically Uncertain Variables (i.e., elements of **e**) Considered in the TSPA-LA (TSPA Parameter Name) (Continued)

NOTE: * indicates variable not considered in sensitivity analysis due to correlations.

GW_BDCF_MIC_Sn126. Groundwater Biosphere Dose Conversion Factor (BDCF) for ^{126}Sn in modern interglacial climate ((Sv/year)/(Bq/m^3)). *Distribution:* Discrete. *Range:* 8.92E-08 to 1.68E-06. *Mean:* 4.33E-07. *Standard Deviation:* 2.39E-07. *Additional Information:* See GW_BDCF_MIC_Ac227. *Sensitivity Name:* MICSN126. *Location in TSPA-LA:* Sections 6.3.11.2 and 6.3.11.3; Table 6.3.11-3. *DTN:* MO0702PAGBDCFS.001_R0 [DIRS 179327]. *References: Biosphere Model Report* (SNL 2007 [DIRS 177399], Sections 1, 6.1, 6.4, 6.4.10, 6.8.10, 6.11 and 6.13; Equations 6.4.10-2, 6.4.10-4, 6.2.10-5 and 6.11-5; Tables 6.11-8 and 6.11-12).
GW_BDCF_MIC_Sr90. Groundwater Biosphere Dose Conversion Factor (BDCF) for ^{90}Sr in modern interglacial climate ((Sv/year)/(Bq/m^3)). *Distribution:* Discrete. *Range:* 2.51E-08 to 8.60E-08. *Mean:* 3.43E-08. *Standard Deviation:* 6.59E-09. *Additional Information:* See GW_BDCF_MIC_Ac227. *Sensitivity Name:* MICSR90. *Location in TSPA-LA:* Sections 6.3.11.2 and 6.3.11.3; Table 6.3.11-3. *DTN:* MO0702PAGBDCFS.001_R0 [DIRS 179327]. *References: Biosphere Model Report* (SNL 2007 [DIRS 177399], Sections 1, 6.1, 6.4, 6.4.10, 6.8.10, 6.11 and 6.13; Equations 6.4.10-2, 6.4.10-4, 6.2.10-5 and 6.11-5; Tables 6.11-8 and 6.11-12).
GW_BDCF_MIC_Tc99. Groundwater Biosphere Dose Conversion Factor (BDCF) for ^{99}Tc in modern interglacial climate ((Sv/year)/(Bq/m^3)). *Distribution:* Discrete. *Range:* 5.28E-10 to 2.85E-08. *Mean:* 1.12E-09. *Standard Deviation:* 1.26E-09. *Additional Information:* See GW_BDCF_MIC_Ac227. *Sensitivity Name:* MICTC99. *Location in TSPA-LA:* Sections 6.3.11.2 and 6.3.11.3; Table 6.3.11-3. *DTN:* MO0702PAGBDCFS.001_R0 [DIRS 179327]. *References: Biosphere Model Report* (SNL 2007 [DIRS 177399], Sections 1, 6.1, 6.4, 6.4.10, 6.8.10, 6.11 and 6.13; Equations 6.4.10-2, 6.4.10-4, 6.2.10-5 and 6.11-5; Tables 6.11-8 and 6.11-12).
GW_BDCF_MIC_Th229. Groundwater Biosphere Dose Conversion Factor (BDCF) for ^{229}Th in modern interglacial climate ((Sv/year)/(Bq/m^3)). *Distribution:* Discrete. *Range:* 7.43E-07 to 8.05E-06. *Mean:* 2.58E-06. *Standard Deviation:* 1.03E-06. *Additional Information:* See GW_BDCF_MIC_Ac227. *Sensitivity Name:* MICTH229. *Location in TSPA-LA:* Sections 6.3.11.2 and 6.3.11.3; Table 6.3.11-3. *DTN:* MO0702PAGBDCFS.001_R0 [DIRS 179327]. *References: Biosphere Model Report* (MDL-MGR-MD-000001 REV 02, SNL 2007 [DIRS 177399], Sections 1, 6.1, 6.4, 6.4.10, 6.8.10, 6.11 and 6.13; Equations 6.4.10-2, 6.4.10-4, 6.2.10-5 and 6.11-5; Tables 6.11-8 and 6.11-12).
GW_BDCF_MIC_U232. Groundwater Biosphere Dose Conversion Factor (BDCF) for 232U in modern interglacial climate ((Sv/year)/(Bq/m^3)). *Distribution:* Discrete. *Range:* 2.87E-07 to 1.86E-06. *Mean:* 6.04E-07. *Standard Deviation:* 2.17E-07. *Additional Information:* See GW_BDCF_MIC_Ac227. *Sensitivity Name:* MICU232. *Location in TSPA-LA:* Sections 6.3.11.2 and 6.3.11.3; Table 6.3.11-3. *DTN:* MO0702PAGBDCFS.001_R0 [DIRS 179327]. *References: Biosphere Model Report* (SNL 2007 [DIRS 177399], Sections 1, 6.1, 6.4, 6.4.10, 6.8.10, 6.11 and 6.13; Equations 6.4.10-2, 6.4.10-4, 6.2.10-5 and 6.11-5; Tables 6.11-8 and 6.11-12).
GW_BDCF_MIC_U233. Groundwater Biosphere Dose Conversion Factor (BDCF) for ^{233}U in modern interglacial climate ((Sv/year)/(Bq/m^3)). *Distribution:* Discrete. *Range:* 4.13E-08 to 3.13E-07. *Mean:* 8.97E-08. *Standard Deviation:* 3.35E-08. *Additional Information:* See GW_BDCF_MIC_Ac227. *Sensitivity Name:* MICU233. *Location in TSPA-LA:* Sections 6.3.11.2 and 6.3.11.3; Table 6.3.11-3. *DTN:* MO0702PAGBDCFS.001_R0 [DIRS 179327]. *References: Biosphere Model Report* (SNL 2007 [DIRS 177399], Sections 1, 6.1, 6.4, 6.4.10, 6.8.10, 6.11 and 6.13; Equations 6.4.10-2, 6.4.10-4, 6.2.10-5 and 6.11-5; Tables 6.11-8 and 6.11-12).
GW_BDCF_MIC_U234. Groundwater Biosphere Dose Conversion Factor (BDCF) for ^{234}U in modern interglacial climate ((Sv/year)/(Bq/m^3)). *Distribution:* Discrete. *Range:* 3.96E-08 to 2.20E-07. *Mean:* 8.19E-08. *Standard Deviation:* 2.81E-08. *Additional Information:* See GW_BDCF_MIC_Ac227. *Sensitivity Name:* MICU234. *Location in TSPA-LA:* Sections 6.3.11.2 and 6.3.11.3; Table 6.3.11-3. *DTN:* MO0702PAGBDCFS.001_R0 [DIRS 179327]. *References: Biosphere Model Report* (SNL 2007 [DIRS 177399], Sections 1, 6.1, 6.4, 6.4.10, 6.8.10, 6.11 and 6.13; Equations 6.4.10-2, 6.4.10-4, 6.2.10-5 and 6.11-5; Tables 6.11-8 and 6.11-12).
GW_BDCF_MIC_U238. Groundwater Biosphere Dose Conversion Factor (BDCF) for ^{238}U in modern interglacial climate ((Sv/year)/(Bq/m^3)). *Distribution:* Discrete. *Range:* 3.85E-08 to 2.07E-07. *Mean:* 7.87E-08. *Standard Deviation:* 2.62E-08. *Additional Information:* See GW_BDCF_MIC_Ac227. *Sensitivity Name:* MICU238. *Location in TSPA-LA:* Sections 6.3.11.2 and 6.3.11.3; Table 6.3.11-3. *DTN:* MO0702PAGBDCFS.001_R0 [DIRS 179327]. *References: Biosphere Model Report* (SNL 2007 [DIRS 177399], Sections 1, 6.1, 6.4, 6.4.10, 6.8.10, 6.11 and 6.13; Equations 6.4.10-2, 6.4.10-4, 6.2.10-5 and 6.11-5; Tables 6.11-8 and 6.11-12).

Table K3-3. Detailed Summary of Epistemically Uncertain Variables (i.e., elements of **e**) Considered in the TSPA-LA (TSPA Parameter Name) (Continued)

NOTE: * indicates variable not considered in sensitivity analysis due to correlations.

GWSPD. Logarithm of the scale factor used to characterize uncertainty in groundwater specific discharge (dimensionless). *Distribution:* Piecewise uniform. *Range:* -0.951 to 0.951. *Additional Information:* Uncertainty exists in the groundwater specific discharge in the SZ. The uncertainty is captured by the groundwater specific discharge multiplier. The uncertainty in GWSPD is applied to all of the climate states. To treat the one- and three-dimensional transport through the SZ consistently, the sampled values used to generate the saturated zone breakthrough curves are also used in the TSPA-LA Model. These values are tabulated as 200 sets of values for the SZ parameters, accounting for appropriate correletions, and are entered into the TSPA model as a table of 200 values for each parameter. The TSPA-LA Model selects values from this table using the Goldsim variable SZ_index_a. *Sensitivity Name:* SZGWSPDM. *Location in TSPA-LA:* Section 6.3.10.2; Table 6.3.10-2. *DTN:* SN0702PASZFTMA.002_R1 [DIRS 183471]. *References: Saturated Zone Flow and Transport Model Abstraction* (SNL 2008 [DIRS 183750], Sections 6.5.1.2[a], 6.5.2.1[a], 6.5.3[a] and 8.1[a]; Tables 6-7[a], 7-1[a] and A-1[a]; Figure 6-2[a]).
HAVO. Ratio of horizontal anisotropy (north-south over east-west) in the permeability of the SZ volcanic units (dimensionless). *Distribution:* Piecewise uniform. *Range:* 0.05 to 20. *Additional Information:* The average specific discharge varies as a function of the horizontal anisotropy. The values of flow path lengths are given for each of the four source regions beneath the repository, as functions of the parameter HAVO. To treat the one- and three-dimensional transport through the SZ consistently, the sampled values used to generate the saturated zone breakthrough curves are also used in the TSPA-LA Model. These values are tabulated as 200 sets of values for the SZ parameters, accounting for appropriate correletions, and are entered into the TSPA model as a table of 200 values for each parameter. The TSPA-LA Model selects values from this table using the Goldsim variable SZ_index_a. *Sensitivity Name:* SZRAHAVO. *Location in TSPA-LA:* Sections 6.3.10.2 and 6.3.10.5; Table 6.3.10-2. *DTN:* SN0702PASZFTMA.002_R1 [DIRS 183471]. *References: Saturated Zone Flow and Transport Model Abstraction* (SNL 2008 [DIRS 183750], Sections 6.4, 6.5.1.2[a], 6.5.2.1 and 6.5.2.10; Tables 4-3, 6-5[a], 6-6[a], 6-8, 7-1[a] and A-1[a]; Figure 6-5[a]).
HFO_SA_a. Hydrous ferric oxide (HFO) surface area (m^2/g). *Distribution:* Truncated log normal. *Range:* 68 to 600. *Mean:* 275.6. *Standard Deviation:* 113.4. *Symbol:* s_{HFO}. *Additional Information:* See Goethite_SA_a. *Sensitivity Name:* HFOSA. *Location in TSPA-LA:* Table 6.3.8-4; S_{CP} in Equation 6.3.8-19. *DTN:* SN0703PAEBSRTA.001_R3 [DIRS 183217]. *References: EBS Radionuclide Transport Abstraction* (SNL 2007 [DIRS 177407], Sections 4.1.2, 6.3.4.2.3.1, 6.3.4.3.3, 6.5.2.2.1 and Appendix K; Equation 6.3.4.2.3.1-1; Tables 4.1-14, 4.1-19, 6.3-7, 6.5-7 and 8.2-4).
HFO_Site_Density_a. Sorption site density for hydrous ferric oxide (HFO) ($1/nm^2$). *Distribution:* Discrete. *Range:* 0.56 to 5.65. *Symbol:* $N_{S,HFO}$. *Additional Information:* The sorption density and specific surface area data for goethite and for HFO were compiled from many laboratory studies mainly addressing the single metal sorption from aqueous solutions. The sorption density data for HFO were compiled from Dzombak and Morel (1990 [DIRS 105483]), which is widely referenced in the sorption modeling literature. *Sensitivity Name:* HFOSITED. *Location in TSPA-LA:* Table 6.3.8-3. *DTN:* SN0703PAEBSRTA.001_R3 [DIRS 183217]. *References: EBS Radionuclide Transport Abstraction* (SNL 2007 [DIRS 177407], Sections 4.1.2 and 6.3.4.2.3.1; Equation 6.3.4.2.3.1-1; Tables 4.1-13, 6.3-6 and 8.2-2).
HLW_Diss_kE_Acidic_a. Effective rate coefficient (affinity term) for the dissolution of HLW glass in CDSP waste packages under low pH conditions ($g/(m^2 d)$). *Distribution:* Triangular. *Range:* 8.41E+03 to 1.15E+07. *Mode:* 8.41E+03. *Symbol:* k_{E_acid}, k_{E_acidic}, k_E. *Additional Information:* HLW_Diss_kE_Acidic_a and HLW_Diss_kE_Alkaline_a define the uncertain parameters for k_{eff} in the rate equation under acidic and alkaline conditions, respectively. *Sensitivity Name:* HLWDRACD. *Location in TSPA-LA:* Sections 6.3.7.4.3.2 and 6.3.7.4.3.3; Table 6.3.7-32; Equation 6.3.7-8. *DTN:* MO0502ANLGAMR1.016_R0 [DIRS 172830]. *References: Defense HLW Glass Degradation Model* (BSC 2004 [DIRS 169988], Sections 6.5.1, 6.5.2.5, 6.5.2.6, 6.6, 6.7, 8.1 and 8.2.2; Equations 13, 31, 32 and 50; Tables 6-14 and 8-1).
HLW_Diss_kE_Alkaline_a. Effective rate coefficient (affinity term) for the dissolution of HLW glass in CDSP waste packages under high pH conditions ($g/(m^2 d)$). *Distribution:* Triangular. *Range:* 2.82E+01 to 3.47E+04. *Mode:* 2.82E+01. *Symbol:* $k_{E_alkaline}$, k_E. *Additional Information:* See HLW_Diss_kE_Acidic_a. *Sensitivity Name:* HLWDRALK. *Location in TSPA-LA:* Sections 6.3.7.4.3.2 and 6.3.7.4.3.3; Table 6.3.7-32; Equation 6.3.7-8. *DTN:* MO0502ANLGAMR1.016_R0 [DIRS 172830]. *References: Defense HLW Glass Degradation Model* (BSC 2004 [DIRS 169988], Sections 6.4.2, 6.5.1, 6.5.2.4, 6.5.2.6, 6.6, 6.7, 8.1 and 8.2.2; Equations 13 and 51; Tables 6-14 and 8-1).

Table K3-3. Detailed Summary of Epistemically Uncertain Variables (i.e., elements of **e**) Considered in the TSPA-LA (TSPA Parameter Name) (Continued)

NOTE: * indicates variable not considered in sensitivity analysis due to correlations.

HLW_Mass_Uncert_a. Scale factor used to characterize uncertainty in radionuclide content of HLW glass (dimensionless). *Distribution:* Triangular. *Range:* 0.7 to 1.5. *Most Likely:* 1. *Additional Information:* See CSNF_Mass_Uncert_a. *Sensitivity Name:* HLWMASS. *Location in TSPA-LA:* Sections 6.3.7.1.2 and 6.3.7.1.3; Table 6.3.7-7. *DTN:* SN0310T0505503.004_R0 [DIRS 168761]. *References: Initial Radionuclides Inventory* (SNL 2007 [DIRS 180472], Sections 6.6.3, 6.7 and 7; Table 7-2),
HLWG_Rind_SA_a. Specific surface area of HLWG degradation rind (m^2/g). *Distribution:* Uniform. *Range:* 10 to 38. *Symbol:* S_{HLWG}. *Additional Information:* See Density_CSNF_Rind_a. The HLW glass rind specific surface area is a new sampled parameter whose range is based on that of kaolinite, since glass degradation products are clay-like in nature. *Sensitivity Name:* HLWGRNDS. *Location in TSPA-LA:* Table 6.3.8-4. *DTN:* SN0703PAEBSRTA.001_R3 [DIRS 183217]. *References: EBS Radionuclide Transport Abstraction* (SNL 2007 [DIRS 177407], Sections 6.3.4.6.2, 6.5.2.2.2 and 6.5.2.2.2.2; Equation 6.3.4.6.2-2; Tables 6.5-9 and 8.2-4).
IGERATE. Frequency of occurrence of volcanic eruptive events (yr^{-1}). *Calculated by:* Igneous_Event_Prob_a x 0.083. *Range:* 0 to 6.44E-08. *Correlation:* Correlated to Igneous_Event_Prob_a with a correlation coefficient of 1. *Additional Information:* Volcanic eruptive events may occur in conjunction with an igneous intrusion event. The frequency of eruptive events that intersect waste is estimated as described in Appendix J, Equation J7.5-3. *Sensitivity Name:* IGERATE. *Location in TSPA-LA:* Section 6.5.2.1.1; Appendix J; Equation J7.5-3. *Output DTN:* MO0708TSPAGENT.000_R0 [DIRS 183000]. *References: Number of Waste Packages Hit by Igneous Events* (SNL 2007 [DIRS 177432], Table 6-5; Figure 7-2).
Igneous_Event_Prob_a. Frequency of intersection of the repository footprint by a volcanic event (yr^{-1}). *Distribution:* Piecewise uniform. *Range:* 0 to 7.76E-07. *Additional Information:* The probability of an igneous event is the annual frequency of an intersection of the repository by a volcanic dike. The parameter Igneous_Event_Prob_a is used in the TSPA model to determine the probability of an igneous event intersecting the repository footprint. An igneous event includes an intrusion by magma and may also include eruptive conduits intersecting the repository. Igneous_Event_Prob_a is treated as an epistemic uncertainty and is sampled from the distribution for each TSPA model realization. The resulting value is used as the annual frequency of igneous events in the calculation of expected value of dose resulting from igneous intrusion and igneous eruptive events. *Sensitivity Name:* IGRATE. *Location in TSPA-LA:* Table 6.5-2. *DTN:* LA0307BY831811.001_R0 [DIRS 164713], output data file PVHA-4PA.DST. *References: Characterize Framework for Igneous Activity at Yucca Mountain, Nevada* (BSC 2004 [DIRS 169989], Sections 6.1, 6.1.1, 6.3, 6.3.1.5, 6.3.1.8, 6.4.2, 6.5, 6.5.1.1, 6.5.2.1 and Appendix A; Figures 6-8, 6-23 and 6-24; Tables 6-5 and 7-1).
Infiltration_Scenario_a. Pointer variable for determining infiltration conditions: 10th, 30th, 50th or 90th percentile infiltration scenario (dimensionless). *Distribution:* Discrete. *Range:* 1 to 4. *Additional Information:* This parameter provides the weighting factors for the three infiltration scenarios used in the TSPA-LA analysis. The parameters contained within the TSPA parameter of Infiltration_Scenario_a correspond to infiltration uncertainty scenarios 1 through 4, going from the lowest infiltration scenario to the highest infiltration scenario. The use of the different percentile infiltration values is intended to cover the uncertainties associated with the infiltration for each climate. The two future climatic scenarios, the monsoon and glacial-transition periods, are used to account for possible climate-induced changes in precipitation and net infiltration. *Sensitivity Name:* INFIL. *Location in TSPA-LA:* Section 6.3.1.2; Tables 6.3.1-2 and 6.3.5-4. *DTN:* LB0701PAWFINFM.001_R0 [DIRS 179283]. *References: UZ Flow Models and Submodels* (SNL 2007 [DIRS 184614], Sections 6.1.4, 6.2.3, 6.2.5, 6.3.4, 6.6.1, 6.8.4 and 6.10.1; Tables 6.1-2 and 6.1-3).
Initial_Release_Frac_Cs_a. The initial release fraction of ^{137}Cs in a CSNF waste package (dimensionless). *Distribution:* Triangular. *Range:* 0.0039 to 0.1106. *Mode:* 0.0363. *Symbol:* f_i. *Additional Information:* Only a fraction of the inventory is immediately available for release upon the failure of the cladding within a failed waste package. Furthermore, only Cs, I, Tc and Sr are immediately available for release. The initial release fraction is set at the beginning of each realization and held constant during each realization. *Sensitivity Name:* INRFRCCS. *Location in TSPA-LA:* Sections 6.3.7.4.1.2 and 6.3.7.4.1.3; Table 6.3.7-29. *DTN:* MO0404ANLSF001.001R0 [DIRS 169007]. *References: CSNF Waste Form Degradation: Summary Abstraction* (BSC 2004 [DIRS 169987], Sections 1, 4.1.1, 6.3, 7.1.1 and 8.2; Equations 1 and 3; Tables 6-3, 7-2, 7-3, 8-1 and 8-4).
Initial_Release_Frac_I_a. The initial release fraction of ^{129}I in a CSNF waste package (dimensionless). *Distribution:* Triangular. *Range:* 0.0204 to 0.2675. *Mode:* 0.1124. *Symbol:* f_i. *Additional Information:* See Initial_Release_Frac_Cs_a. *Sensitivity Name:* INRFRCI. *Location in TSPA-LA:* Sections 6.3.7.4.1.2 and 6.3.7.4.1.3; Table 6.3.7-29. *DTN:* MO0404ANLSF001.001_R0 [DIRS 169007]. *References: CSNF Waste Form Degradation: Summary Abstraction* (BSC 2004 [DIRS 169987], Sections 1, 4.1.1, 6.3, 7.1.1 and 8.2; Equations 1 and 3; Tables 6-3, 7-2, 7-3, 8-1 and 8-4).

Table K3-3. Detailed Summary of Epistemically Uncertain Variables (i.e., elements of **e**) Considered in the TSPA-LA (TSPA Parameter Name) (Continued)

NOTE: * indicates variable not considered in sensitivity analysis due to correlations.

Initial_Release_Frac_Sr_a. The initial release fraction of ^{90}Sr in a CSNF waste package (dimensionless). *Distribution:* Triangular. *Range:* 0.0002 to 0.0025. *Mode:* 0.0009. *Symbol:* f_i. *Additional Information:* See Initial_Release_Frac_Cs_a. *Sensitivity Name:* INRFRCSR. *Location in TSPA-LA:* Sections 6.3.7.4.1.2 and 6.3.7.4.1.3; Table 6.3.7-29. *DTN:* MO0404ANLSF001.001_R0 [DIRS 169007]. *References: CSNF Waste Form Degradation: Summary Abstraction* (BSC 2004 [DIRS 169987], Sections 1, 4.1.1, 6.3, 7.1.1 and 8.2; Equations 1 and 3; Tables 6-3, 7-2, 7-3, 8-1 and 8-4).
Initial_Release_Frac_Tc_a. The initial release fraction of ^{99}Tc in a CSNF waste package (dimensionless). *Distribution:* Triangular. *Range:* 0.0001 to 0.0026. *Mode:* 0.001. *Symbol:* f_i. *Additional Information:* See Initial_Release_Frac_Cs_a. *Sensitivity Name:* INRFRCTC. *Location in TSPA-LA:* Sections 6.3.7.4.1.2 and 6.3.7.4.1.3; Table 6.3.7-29. *DTN:* MO0404ANLSF001.001_R0 [DIRS 169007]. *References: CSNF Waste Form Degradation: Summary Abstraction* (BSC 2004 [DIRS 169987], Sections 1, 4.1.1, 6.3, 7.1.1 and 8.2; Equations 1 and 3; Tables 6-3, 7-2, 7-3, 8-1 and 8-4).
Inpkg_IStr_2DHLW_NS_Rand_a. Pointer variable used to determine ionic strength for 2DHLW Cell (Cell 1a) of CDSP waste packages under vapor influx conditions (dimensionless). *Distribution:* Uniform. *Range:* 0 to 1. *Additional Information:* The parameter Inpkg_IStr_2DHLW_NS_Rand_a selects a percentile for the distribution of uncertainty in ionic strength in DHLW waste packages for vapor influx conditions. In the vapor influx environment, the distribution of uncertainty the ionic strength is a log-triangular distribution with vertices that are a function of the vapor flux rate through the failed waste package. The vapor flux rate into the failed waste package is sampled by IPC_NDB_Vapor_Flux_a. *Sensitivity Name:* IS2DHLNS. *Location in TSPA-LA:* Section 6.3.7.2.2 Part III. *DTN:* SN0702PAIPC1CA.001_R2 [DIRS 180451], Spreadsheet: Abstr 2DHLW No Drip Ion Str.xls. *References: In-Package Chemistry Abstraction* (SNL 2007 [DIRS 180506], Sections 6.5.2[a], 6.10.8.2[a], 6.10.9.3[a] and 8.2.2[a]).
Inpkg_IStr_2DHLW_S_Rand_a. Pointer variable used to determine ionic strength for 2DHLW Cell (Cell 1a) of CDSP waste packages under liquid influx conditions (dimensionless). *Distribution:* Uniform. *Range:* 0 to 1. *Additional Information:* The parameter Inpkg_IStr_2DHLW_S_Rand_a selects a percentile for the distribution of uncertainty in ionic strength in DHLW waste packages for liquid influx conditions. Under liquid influx conditions, the distribution of uncertainty the ionic strength is a log-triangular distribution the vertices of which are a function of the flow rate through the failed waste package and hence may change with time. *Sensitivity Name:* IS2DHLS. *Location in TSPA-LA:* Section 6.3.7.2.2 Part III. *DTN:* SN0702PAIPC1CA.001_R2 [DIRS 180451], Spreadsheet: Abstr 2DHLW Seepage Ion Str 2.xls. *References: In-Package Chemistry Abstraction* (SNL 2007 [DIRS 180506], Sections 6.5.1[a], 6.10.2[a], 6.10.9.2[a] and 8.2.2[a]).
Inpkg_IStr_2MCO_NS_Rand_a. Pointer variable used to determine ionic strength for 2MCO Cell (Cell 1b) of CDSP waste packages under vapor influx conditions (dimensionless). *Distribution:* Uniform. *Range:* 0 to 1. *Additional Information:* See Inpkg_IStr_2DHLW_NS_Rand_a. *Sensitivity Name:* IS2MCONS. *Location in TSPA-LA:* Section 6.3.7.2.2 Part III. *DTN:* SN0702PAIPC1CA.001_R2 [DIRS 180451], Spreadsheet: Abstr 2MCO No Drip Ion Str.xls. *References: In-Package Chemistry Abstraction* (SNL 2007 [DIRS 180506], Sections 6.5.2[a], 6.10.8.2[a], 6.10.9.3[a] and 8.2.2[a]).
Inpkg_IStr_2MCO_S_Rand_a. Pointer variable used to determine ionic strength for 2MCO Cell (Cell 1b) of CDSP waste packages under liquid influx conditions (dimensionless). *Distribution:* Uniform. *Range:* 0 to 1. *Additional Information:* See Inpkg_IStr_2DHLW_S_Rand_a. *Sensitivity Name:* IS2MCOS. *Location in TSPA-LA:* Section 6.3.7.2.2 Part III. *DTN:* SN0702PAIPC1CA.001_R2 [DIRS 180451], Spreadsheet: Abstr 2MCO Seepage Ion Str 2.xls. *References: In-Package Chemistry Abstraction* (SNL 2007 [DIRS 180506], Sections 6.5.1[a], 6.10.2[a], 6.10.9.2[a] and 8.2.2[a]).
Inpkg_IStr_CSNF_NS_Rand_a. Pointer variable used to determine ionic strength for CSNF Cell under vapor influx conditions (dimensionless). *Distribution:* Uniform. *Range:* 0 to 1. *Additional Information:* See discussion forInpkg_IStr_2DHLW_NS_Rand_a. *Sensitivity Name:* ISCSNS. *Location in TSPA-LA:* Section 6.3.7.2.2 Part III. *DTN:* SN0702PAIPC1CA.001_R2 [DIRS 180451], Spreadsheet: Abstr CSNF No Drip Ion Str.xls. *References: In-Package Chemistry Abstraction* (SNL 2007 [DIRS 180506], Sections 6.5.2[a], 6.10.8.2[a], 6.10.9.3[a] and 8.2.2[a]).
Inpkg_IStr_CSNF_S_Rand_a. Pointer variable used to determine ionic strength for CSNF Cell under liquid influx conditions (dimensionless). *Distribution:* Uniform. *Range:* 0 to 1. *Additional Information:* See Inpkg_IStr_2DHLW_S_Rand_a. *Sensitivity Name:* ISCSS. *Location in TSPA-LA:* Section 6.3.7.2.2 Part III. *DTN:* SN0702PAIPC1CA.001_R2 [DIRS 180451], Spreadsheet: Abstr CSNF Seepage Ion Str 2.xls. *References: In-Package Chemistry Abstraction* (SNL 2007 [DIRS 180506], Sections 6.5.1[a], 6.10.2[a], 6.10.9.2[a] and 8.2.2[a]).

Table K3-3. Detailed Summary of Epistemically Uncertain Variables (i.e., elements of **e**) Considered in the TSPA-LA (TSPA Parameter Name) (Continued)

NOTE: * indicates variable not considered in sensitivity analysis due to correlations.

lnpkg_pH_2DHLW_NS_Rand_a. Pointer variable used to determine pH in 2DHLW Cell (Cell 1a) of CDSP waste packages under vapor influx conditions (dimensionless). *Distribution:* Uniform. *Range:* 0 to 1. *Additional Information:* The TSPA implementation of the pH abstraction is discretized into three models, one for CSNF waste packages and two for CDSP waste packages (DHLW and 2MCO). The pH is a function of pCO_2 and the logarithm of ionic strength in the package. Two dimensional look-up tables provide values for the maximum and minimum pH as a function of pCO_2 and the logarithm of ionic strength, for three waste types (DHLW, 2MCO and CSNF) and for liquid influx and vapor influx conditions. Linear interpolation is used to determine maximum and minimum pH. Then, a sampled value between 0 and 1 selects a pH value between the minimum and maximum pH values, using linear interpolation between the minimum and the maximum. The pH selection is performed within each percolation subregion environment. The parameter lnpkg_pH_2DHLW_NS_Rand_a selects the value between 0 and 1 that is used to determine pH for DHLW waste packages in vapor influx conditions. *Sensitivity Name:* PH2DHLNS. *Location in TSPA-LA:* Section 6.3.7.2.2 Part IV. *DTN:* SN0702PAIPC1CA.001_R2 [DIRS 180451], Spreadsheet: Abstr 2DHLW No Drip pH.xls. *References: In-Package Chemistry Abstraction* (SNL 2007 [DIRS 180506], Sections 6.3.4[a], 6.10.1[a] and 8.2.1[a]).
lnpkg_pH_2DHLW_S_Rand_a. Pointer variable used to determine pH in 2DHLW Cell (Cell 1a) of CDSP waste packages under liquid influx conditions (dimensionless). *Distribution:* Uniform. *Range:* 0 to 1. *Additional Information:* See lnpkg_pH_2DHLW_NS_Rand_a. *Sensitivity Name:* PH2DHLS. *Location in TSPA-LA:* Section 6.3.7.2.2 Part IV. *DTN:* SN0702PAIPC1CA.001_R2 [DIRS 180451], Spreadsheet: Abstr 2DHLW Seepage pH.xls. *References: In-Package Chemistry Abstraction* (SNL 2007 [DIRS 180506], Sections 6.3.4[a], 6.10.1[a] and 8.2.1[a]).
lnpkg_pH_2MCO_NS_Rand_a. Pointer variable used to determine pH in 2MCO Cell (Cell 1b) of CDSP waste packages under vapor influx conditions (dimensionless). *Distribution:* Uniform. *Range:* 0 to 1. *Additional Information:* See lnpkg_pH_2DHLW_NS_Rand_a. *Sensitivity Name:* PH2MCONS. *Location in TSPA-LA:* Section 6.3.7.2.2 Part IV. *DTN:* SN0702PAIPC1CA.001_R2 [DIRS 180451], Spreadsheet: Abstr 2MCO No Drip pH.xls. *References: In-Package Chemistry Abstraction* (SNL 2007 [DIRS 180506], Sections 6.3.4[a], 6.10.1[a] and 8.2.1[a]).
lnpkg_pH_2MCO_S_Rand_a. Pointer variable used to determine pH in 2MCO Cell (Cell 1b) of CDSP waste packages under liquid influx conditions (dimensionless). *Distribution:* Uniform. *Range:* 0 to 1. *Additional Information:* See lnpkg_pH_2DHLW_NS_Rand_a. *Sensitivity Name:* PH2MCOS. *Location in TSPA-LA:* Section 6.3.7.2.2 Part IV. *DTN:* SN0702PAIPC1CA.001_R2 [DIRS 180451], Spreadsheet: Abstr 2MCO Seepage pH.xls. *References: In-Package Chemistry Abstraction* (SNL 2007 [DIRS 180506], Sections 6.3.4[a], 6.10.1[a] and 8.2.1[a]; Table 6-21[a]).
lnpkg_pH_CSNF_NS_Rand_a. Pointer variable used to determine pH in CSNF Cell1 under vapor influx conditions (dimensionless). *Distribution:* Uniform. *Range:* 0 to 1. *Additional Information:* See lnpkg_pH_2DHLW_NS_Rand_a. *Sensitivity Name:* PHCSNS. *Location in TSPA-LA:* Section 6.3.7.2.2 Part IV. *DTN:* SN0702PAIPC1CA.001_R2 [DIRS 180451], Spreadsheet: Abstr CSNF No Drip pH.xls. *References: In-Package Chemistry Abstraction* (SNL 2007 [DIRS 180506], Sections 6.3.4[a], 6.10.1[a] and 8.2.1[a]).
lnpkg_pH_CSNF_S_Rand_a. Pointer variable used to determine pH in CSNF Cell1 under liquid influx conditions (dimensionless). *Distribution:* Uniform. *Range:* 0 to 1. *Additional Information:* See lnpkg_pH_2DHLW_NS_Rand_a. *Sensitivity Name:* PHCSS. *Location in TSPA-LA:* Section 6.3.7.2.2 Part IV. *DTN:* SN0702PAIPC1CA.001_R2 [DIRS 180451], Spreadsheet: Abstr CSNF Seepage pH.xls. *References: In-Package Chemistry Abstraction* (SNL 2007 [DIRS 180506], Sections 6.3.4[a], 6.10.1[a] and 8.2.1[a]).
Invert_Diff_Coeff_Uncert_a. Exponential term representing uncertainty in the invert diffusion coefficient (dimensionless). *Distribution:* Truncated normal. *Range:* -0.621 to 0.687. *Mean:* 0.033. *Standard Deviation:* 0.218. *Symbol:* ND. *Additional Information:* ND is in the exponent because the residuals are calculated in the log-log space of the statistical fit. This statistical fit is the submodel for the invert diffusion coefficient to be used for the TSPA. The uncertainty in the invert diffusion coefficient ranges over a factor of 20 and essentially encompasses the variable breakthrough times that could occur from including the longitudinal dispersion. *Sensitivity Name:* EBSDIFCF. *Location in TSPA-LA:* Section 6.3.8.2.4; Table 6.3.8-4; Equation 6.3.8-24. *DTN:* SN0703PAEBSRTA.001_R3 [DIRS 183217]. *References: EBS Radionuclide Transport Abstraction* (SNL 2007 [DIRS 177407], Sections 6.3.1.2, 6.3.4.1.1, 7.2.2 and Appendix G; Table 8.2-4; Equation 6.3.4.1.1-22).

Table K3-3. Detailed Summary of Epistemically Uncertain Variables (i.e., elements of **e**) Considered in the TSPA-LA (TSPA Parameter Name) (Continued)

NOTE: * indicates variable not considered in sensitivity analysis due to correlations.

Kd_Am_Al. Americium sorption coefficient in alluvium (mL/g). *Distribution:* Truncated normal. *Range:* 1000 to 10000. *Mean/Median/Mode:* 5500. *Standard Deviation:* 1500. *Correlation:* See SN0702PASZFTMA.001 [DIRS 179504]. *Additional Information:* A linear, equilibrium, sorption coefficient, K_d, is considered appropriate for the radionuclides that exhibit sorption during transport because of experimental observations that establish the adequacy of this approach. The K_d model also depends on chemical equilibrium between the aqueous phase and sorbed phase of a given species. The K_d model determines transport retardation. To treat the one- and three-dimensional transport through the SZ consistently, the sampled values used to generate the saturated zone breakthrough curves are also used in the TSPA-LA Model. These values are tabulated as 200 sets of values for the SZ parameters, accounting for appropriate correletions, and are entered into the TSPA model as a table of 200 values for each parameter. The TSPA-LA Model selects values from this table using the Goldsim variable SZ_index_a. *Sensitivity Name:* SZKDAMAL. *Location in TSPA-LA:* Section 6.3.10.2; Table 6.3.10-2. *DTN:* SN0702PASZFTMA.002_R1 [DIRS 183471]. *References: Saturated Zone Flow and Transport Model Abstraction* (SNL 2008 [DIRS 183750], Sections 6.3.1, 6.5.1.1, 6.5.1.2 and 6.5.2.8; Tables 4-3, 6-8, A-1[a] and B-1; Equations 6-2, 6-3 and 6-26).
Kd_Am_Col. Americium sorption coefficient onto smectite colloids (mL/g). *Distribution:* Piecewise uniform. *Range:* 1.00E+04 to 1.00E+07. *Additional Information:* In addition to the transport of radionuclides as solutes in groundwater, radionuclides may also be sorbed onto colloids and travel through the SZ to the accessible environment. The radionuclides may be reversibly or irreversibly sorbed onto colloids. A retardation factor is established for radionuclides that are irreversibly sorbed onto colloids. Implied in the use of a retardation factor to describe colloid transport is that colloid filtration and detachment rates are fast relative to groundwater transport times through the system. In addition, a small fraction of colloids, also called the "fast fraction," is transported unretarded through the SZ, based on groundwater transport times. Radionuclides that are reversibly sorbed onto colloids are in equilibrium with the aqueous phase and the geologic medium. In this mode of transport, the effective retardation of these radionuclides during transport in the SZ depends on the sorption of radionuclides to colloids, the concentration of colloids in the groundwater, and the sorption coefficient of the radionuclide onto the geologic medium. To treat the one- and three-dimensional transport through the SZ consistently, the sampled values used to generate the saturated zone breakthrough curves are also used in the TSPA-LA Model. These values are tabulated as 200 sets of values for the SZ parameters, accounting for appropriate correletions, and are entered into the TSPA model as a table of 200 values for each parameter. The TSPA-LA Model selects values from this table using the Goldsim variable SZ_index_a. *Sensitivity Name:* SZKDAMCO. *Location in TSPA-LA:* Section 6.3.10.2; Table 6.3.10-2. *DTN:* SN0702PASZFTMA.002_R1 [DIRS 183471]. *References: Saturated Zone Flow and Transport Model Abstraction* (SNL 2008 [DIRS 183750], Sections 6.5.1.1, 6.5.1.2, 6.5.2.8 and 6.5.2.12; Tables 4-3, 6-8, A-1[a] and B-1; Equations 6-4 and 6-26; Figure 6-24).
Kd_Am_Rev_Smectite_a. Distribution coefficient for reversible sorption of americium to waste form (smectite) colloids (mL/g). *Distribution:* Piecewise uniform. *Range:* 1.00E+04 to 1.00E+07. *Symbol:* $Kd_{,Am,coll,wf}$. *Additional Information:* K_d value for combined adsorption and desorption of americium on waste form, iron oxide–oxyhydroxide, and groundwater colloids. This value is used to determine effective reversibility of the radionuclides on colloids according to the relationship: $RN_{adsorbed/desorbed} = RN_{dissolved} \times K_{d,RN} \times M_{colloid}$, where RN = radionuclide, $K_{d,RN}$ = sorption coefficient (ml/g) for radionuclide RN, and $M_{colloid}$ = concentration of colloids in moles/L. *Sensitivity Name:* KDAMSMEC. *Location in TSPA-LA:* Sections 6.3.7.6.2 and 6.3.7.6.3; Equation 6.3.7-20; Tables 6.3.7-62 and 6.3.7-66. *DTN:* MO0701PASORPTN.000_R1 [DIRS 180391]. *References: Waste Form and In-Drift Colloids-Associated Radionuclide Concentrations: Abstraction and Summary* (SNL 2007 [DIRS 177423], Sections 4.1.1, 6.3.2.2, 6.3.12.1 and 6.6.8; Equations 6-13 and 6-15; Figure 6-24c; Tables 6-15 and 6-24).
Kd_Am_Rev_U_Col_a. Distribution coefficient for reversible sorption of americium onto uranophane colloids (mL/g). *Distribution:* Log uniform. *Range:* 5 to 1.00E+04. *Symbol:* $Kd_{Am,coll,uranophane}$. *Additional Information:* K_d is an equilibrium sorption coefficient used to approximate the partitioning of dissolved radionuclide between colloids and fluid. Values are based on analogue sorption studies on closely related phases. Reversible sorption is calculated from the sampled mass concentration of uranophane colloids, K_d values describing the distribution of radionuclides between the fluid and the U(VI) phase (uranophane) colloids, and the dissolved concentration of radionuclides as calculated by the TSPA-LA model. *Sensitivity Name:* KDAMCOL. *Location in TSPA-LA:* Sections 6.3.7.6.2 and 6.3.7.6.3; Equation 6.3.7-20; Table 6.3.7-64. *DTN:* MO0701PACSNFCP.000_R1 [DIRS 180439]. *References: Waste Form and In-Drift Colloids-Associated Radionuclide Concentrations: Abstraction and Summary* (SNL 2007 [DIRS 177423], Sections 4.1.1, 6.3.2.2, 6.3.2.6, 6.3.12.1, 6.5.1.3, 6.6.4 and 6.6.8; Equations 6-13 and 6-15; Tables 6-9 and 6-24).

Table K3-3. Detailed Summary of Epistemically Uncertain Variables (i.e., elements of **e**) Considered in the TSPA-LA (TSPA Parameter Name) (Continued)

NOTE: * indicates variable not considered in sensitivity analysis due to correlations.

Kd_Am_Vo. Americium sorption coefficient in volcanic units (mL/g). *Distribution:* Truncated normal. *Range:* 1000 to 10000. *Mean/Median/Mode:* 5500. *Standard Deviation:* 1500. *Correlation:* See SN0702PASZFTMA.001 [DIRS 179504]. *Additional Information:* A linear equilibrium sorption coefficient, K_d, is considered appropriate for the radionuclides that exhibit sorption during transport because of experimental observations that establish the adequacy of this approach. The K_d model also depends on chemical equilibrium between the aqueous phase and sorbed phase of a given species. The K_d model determines transport retardation. To treat the one- and three-dimensional transport through the SZ consistently, the sampled values used to generate the saturated zone breakthrough curves are also used in the TSPA-LA Model. These values are tabulated as 200 sets of values for the SZ parameters, accounting for appropriate correletions, and are entered into the TSPA model as a table of 200 values for each parameter. The TSPA-LA Model selects values from this table using the Goldsim variable SZ_index_a. *Sensitivity Name:* SZKDAMVO. *Location in TSPA-LA:* Section 6.3.10.2; Table 6.3.10-2. *DTN:* SN0702PASZFTMA.002_R1 [DIRS 183471]. *References: Saturated Zone Flow and Transport Model Abstraction* (SNL 2008 [DIRS 183750], Sections 6.3.1, 6.5.1.1, 6.5.1.2 and 6.5.2.8; Tables 4-3, 6-8, A-1[a] and B-1; Equations 6-2, 6-3 and 6-26).
Kd_Cs_Al. Cesium sorption coefficient in alluvium (mL/g). *Distribution:* Truncated normal. *Range:* 100 to 1000. *Mean/Median/Mode:* 728. *Standard Deviation:* 464. *Correlation:* See SN0702PASZFTMA.001 [DIRS 179504]. *Additional Information:* See Kd_Am_Al. *Sensitivity Name:* SZKDCSAL. *Location in TSPA-LA:* Section 6.3.10.2; Table 6.3.10-2. *DTN:* SN0702PASZFTMA.002_R1 [DIRS 183471]. *References: Saturated Zone Flow and Transport Model Abstraction* (SNL 2008 [DIRS 183750], Sections 6.3.1, 6.5.1.1, 6.5.1.2 and 6.5.2.8; Tables 4-3, 6-8, A-1[a] and B-1; Equations 6-2, 6-3 and 6-26).
Kd_Cs_Col. Cesium sorption coefficient onto smectite colloids (mL/g). *Distribution:* Piecewise uniform. *Range:* 50 to 5000. *Additional Information:* See Kd_Am_Col. *Sensitivity Name:* SZKDCSCO. *Location in TSPA-LA:* Section 6.3.10.2; Table 6.3.10-2. *DTN:* SN0702PASZFTMA.002_R1 [DIRS 183471]. *References: Saturated Zone Flow and Transport Model Abstraction* (SNL 2008 [DIRS 183750], Sections 6.5.1.1, 6.5.1.2, 6.5.2.8, 6.5.2.12 and 6.5.4.2[a]; Tables 4-3[a], 6-7[a], A-1[a] and B-1; Equations 6-4 and 6-26; Figure 6-25).
Kd_Cs_Rev_Smectite_a. Distribution coefficient for reversible sorption of cesium to waste form (smectite) colloids (mL/g). *Distribution:* Piecewise uniform. *Range:* 50 to 5000. *Symbol:* $Kd_{Cs,coll,wf}$. *Additional Information:* See Kd_Am_Rev_Smectite_a. *Sensitivity Name:* KDCSSMEC. *Location in TSPA-LA:* Sections 6.3.7.6.2 and 6.3.7.6.3; Equation 6.3.7-20; Tables 6.3.7-62 and 6.3.7-66. *DTN:* MO0701PASORPTN.000_R1 [DIRS 180391]. *References: Waste Form and In-Drift Colloids-Associated Radionuclide Concentrations: Abstraction and Summary* (SNL 2007 [DIRS 177423], Sections 4.1.1, 6.3.2.2, 6.3.12.1 and 6.6.8; Equations 6-13 and 6-15; Figure 6-24b; Tables 6-15 and 6-24).
Kd_Cs_Rev_U_Col_a. Distribution coefficient for reversible sorption of cesium onto uranophane colloids (mL/g). *Distribution:* Log uniform. *Range:* 10 to 1000. *Symbol:* $Kd_{Cs,coll,uranophane}$. *Additional Information:* See Kd_Am_Rev_U_Col_a. *Sensitivity Name:* KDCSCOL. *Location in TSPA-LA:* Sections 6.3.7.6.2 and 6.3.7.6.3; Equation 6.3.7-20; Table 6.3.7-64. *DTN:* MO0701PACSNFCP.000_R1 [DIRS 180439]. *References: Waste Form and In-Drift Colloids-Associated Radionuclide Concentrations: Abstraction and Summary* (SNL 2007 [DIRS 177423], Sections 4.1.1, 6.3.2.2, 6.3.2.6, 6.3.12.1, 6.5.1.3, 6.6.4 and 6.6.8; Equations 6-13 and 6-15; Tables 6-9 and 6-24).
Kd_Cs_Vo. Cesium sorption coefficient in volcanic units (mL/g). *Distribution:* Piecewise uniform. *Range:* 100 to 6783. *Correlation:* See SN0702PASZFTMA.001 [DIRS 179504]. *Additional Information:* See Kd_Am_Vo. *Sensitivity Name:* SZKDCSVO. *Location in TSPA-LA:* Section 6.3.10.2; Table 6.3.10-2. *DTN:* SN0702PASZFTMA.002_R1 [DIRS 183471]. *References: Saturated Zone Flow and Transport Model Abstraction* (SNL 2008 [DIRS 183750], Sections 6.3.1, 6.5.1.1, 6.5.1.2 and 6.5.2.8; Tables 4-3, 6-8, A-1[a] and B-1; Equations 6-2, 6-3 and 6-26).
Kd_Np_Al. Neptunium sorption coefficient in alluvium (mL/g). *Distribution:* Piecewise uniform. *Range:* 1.8 to 13. *Correlation:* See SN0702PASZFTMA.001 [DIRS 179504]. *Additional Information:* See Kd_Am_Al. *Sensitivity Name:* SZKDNPAL. *Location in TSPA-LA:* Section 6.3.10.2; Table 6.3.10-2. *DTN:* SN0702PASZFTMA.002_R1 [DIRS 183471]. *References: Saturated Zone Flow and Transport Model Abstraction* (SNL 2008 [DIRS 183750], Sections 6.3.1, 6.5.1.1, 6.5.1.2, 6.5.2.8 and 8.1; Tables 4-3, 6-8, 7-1[a], A-1[a] and B-1; Equations 6-2, 6-3 and 6-26).

Table K3-3. Detailed Summary of Epistemically Uncertain Variables (i.e., elements of **e**) Considered in the TSPA-LA (TSPA Parameter Name) (Continued)

NOTE: * indicates variable not considered in sensitivity analysis due to correlations.

Kd_Np_Rev_Smectite_a. Distribution coefficient for reversible sorption of neptunium to waste form (smectite) colloids (mL/g). *Distribution:* Log uniform. *Range:* 10 to 500. *Symbol:* $Kd_{Np,coll,smectite}$. *Additional Information:* See Kd_Am_Rev_Smectite_a. *Sensitivity Name:* KDNPSMEC. *Location in TSPA-LA:* Sections 6.3.7.6.2 and 6.3.7.6.3; Equation 6.3.7-20; Tables 6.3.7-62 and 6.3.7-66. *DTN:* MO0701PAKDSUNP.000_R1 [DIRS 180392]. *References: Waste Form and In-Drift Colloids-Associated Radionuclide Concentrations: Abstraction and Summary* (SNL 2007 [DIRS 177423], Sections 4.1.1, 6.3.2.2, 6.3.12.1 and 6.6.8; Equations 6-13 and 6-15; Figure 6-24a; Tables 6-15 and 6-24).
Kd_Np_Rev_U_Col_a. Distribution coefficient for reversible sorption of neptunium onto uranophane colloids (mL/g). *Distribution:* Log uniform. *Range:* 1 to 500. *Symbol:* $Kd_{Np,coll,uranophane}$. *Additional Information:* See Kd_Am_Rev_U_Col_a. In the TSPA-LA Model the lower bound for this parameter was entered erroneously as 1. The correct lower bound is 10. See Appendix P, Table P-6, for a discussion of the effect of this error. *Sensitivity Name:* KDNPCOL. *Location in TSPA-LA:* Sections 6.3.7.6.2 and 6.3.7.6.3; Equation 6.3.7-20; Table 6.3.7-64. *DTN:* MO0701PACSNFCP.000_R1 [DIRS 180439]. *References: Waste Form and In-Drift Colloids-Associated Radionuclide Concentrations: Abstraction and Summary* (SNL 2007 [DIRS 177423], Sections 4.1.1, 6.3.2.2, 6.3.2.6, 6.3.12.1, 6.5.1.3, 6.6.4 and 6.6.8; Equations 6-13 and 6-15; Tables 6-9 and 6-24).
Kd_Np_Vo. Neptunium sorption coefficient in volcanic units (mL/g). *Distribution:* Piecewise uniform. *Range:* 0 to 6. *Correlation:* See SN0702PASZFTMA.001 [DIRS 179504]. *Additional Information:* See Kd_Am_Vo. *Sensitivity Name:* SZKDNPVO. *Location in TSPA-LA:* Section 6.3.10.2; Table 6.3.10-2. *DTN:* SN0702PASZFTMA.002_R1 [DIRS 183471]. *References: Saturated Zone Flow and Transport Model Abstraction* (SNL 2008 [DIRS 183750], Sections 6.3.1, 6.5.1.1, 6.5.1.2, 6.5.2.8 and 8.1; Tables 4-3, 6-8, 7-1[a], A-1[a] and B-1; Equations 6-2, 6-3 and 6-26).
Kd_Pa_Rev_Smectite_a. Distribution coefficient for reversible sorption of protactinium to waste form (smectite) colloids (mL/g). *Distribution:* Piecewise uniform. *Range:* 1.00E+04 to 1.00E+07. *Symbol:* $Kd_{Pa,coll,wf}$. *Additional Information:* See Kd_Am_Rev_Smectite_a. *Sensitivity Name:* KDPASMEC. *Location in TSPA-LA:* Sections 6.3.7.6.2 and 6.3.7.6.3; Equation 6.3.7-20; Tables 6.3.7-62 and 6.3.7-66. *DTN:* MO0701PASORPTN.000_R1 [DIRS 180391]. *References: Waste Form and In-Drift Colloids-Associated Radionuclide Concentrations: Abstraction and Summary* (SNL 2007 [DIRS 177423], Sections 4.1.1, 6.3.2.2, 6.3.12.1 and 6.6.8; Equations 6-13 and 6-15; Figure 6-24c; Tables 6-15 and 6-24).
Kd_Pa_Rev_U_Col_a. Distribution coefficient for reversible sorption of protactinium onto uranophane colloids (mL/g). *Distribution:* Log uniform. *Range:* 5 to 1.00E+04. *Symbol:* $Kd_{Pa,coll,uranophane}$. *Additional Information:* See Kd_Am_Rev_U_Col_a. *Sensitivity Name:* KDPACOL. *Location in TSPA-LA:* Sections 6.3.7.6.2 and 6.3.7.6.3; Equation 6.3.7-20; Table 6.3.7-64. *DTN:* MO0701PACSNFCP.000_R1 [DIRS 180439]. *References: Waste Form and In-Drift Colloids-Associated Radionuclide Concentrations: Abstraction and Summary* (SNL 2007 [DIRS 177423], Sections 4.1.1, 6.3.2.2, 6.3.2.6, 6.3.12.1, 6.5.1.3, 6.6.4 and 6.6.8; Equations 6-13 and 6-15; Tables 6-9 and 6-24).
Kd_Pu_Al. Plutonium sorption coefficient in alluvium (mL/g). *Distribution:* Beta. *Range:* 50 to 300. *Mean/Median/Mode:* 100. *Standard Deviation:* 15. *Correlation:* See SN0702PASZFTMA.001 [DIRS 179504]. *Additional Information:* See Kd_Am_Al. *Sensitivity Name:* SZKDPUAL. *Location in TSPA-LA:* Section 6.3.10.2; Table 6.3.10-2. *DTN:* SN0702PASZFTMA.002_R1 [DIRS 183471]. *References: Saturated Zone Flow and Transport Model Abstraction* (SNL 2008 [DIRS 183750], Sections 6.3.1, 6.5.1.1, 6.5.1.2, 6.5.2.8 and 8.1; Tables 4-3, 6-8, A-1[a] and B-1; Equations 6-2, 6-3 and 6-26).
Kd_Pu_Col. Plutonium sorption coefficient onto smectite colloids (mL/g). *Distribution:* Piecewise uniform. *Range:* 1.00E+03 to 1.00E+05. *Additional Information:* See Kd_Am_Col. *Sensitivity Name:* SZKDPUCO. *Location in TSPA-LA:* Section 6.3.10.2; Table 6.3.10-2. *DTN:* SN0702PASZFTMA.002_R1 [DIRS 183471]. *References: Saturated Zone Flow and Transport Model Abstraction* (SNL 2008 [DIRS 183750], Sections 6.5.1.1, 6.5.1.2, 6.5.2.8, 6.5.2.12 and 6.5.4.2[a]; Tables 4-3[a], 6-7[a], A-1[a] and B-1; Equations 6-4 and 6-26; Figure 6-23).
Kd_Pu_Rev_Smectite_a. Distribution coefficient for reversible sorption of plutonium to waste form (smectite) colloids (mL/g). *Distribution:* Piecewise uniform. *Range:* 1.00E+03 to 1.00E+05. *Symbol:* $Kd_{Pu,coll,wf}$. *Additional Information:* See Kd_Am_Rev_Smectite_a. *Sensitivity Name:* KDPUSMEC. *Location in TSPA-LA:* Sections 6.3.7.6.2 and 6.3.7.6.3; Equation 6.3.7-20; Tables 6.3.7-62 and 6.3.7-66. *DTN:* MO0701PASORPTN.000_R1 [DIRS 180391]. *References: Waste Form and In-Drift Colloids-Associated Radionuclide Concentrations: Abstraction and Summary* (SNL 2007 [DIRS 177423], Sections 4.1.1, 6.3.2.2, 6.3.12.1 and 6.6.8; Equations 6-13 and 6-15; Figure 6-24c; Tables 6-15 and 6-24).

Table K3-3. Detailed Summary of Epistemically Uncertain Variables (i.e., elements of **e**) Considered in the TSPA-LA (TSPA Parameter Name) (Continued)

NOTE: * indicates variable not considered in sensitivity analysis due to correlations.

Kd_Pu_Rev_U_Col_a. Distribution coefficient for reversible sorption of plutonium onto uranophane colloids (mL/g). *Distribution:* Log uniform. *Range:* 5 to 1.00E+04. *Symbol:* $Kd_{Pu,coll,uranophane}$. *Additional Information:* See Kd_Am_Rev_U_Col_a. *Sensitivity Name:* KDPUCOL. *Location in TSPA-LA:* Sections 6.3.7.6.2 and 6.3.7.6.3; Equation 6.3.7-20; Table 6.3.7-64. *DTN:* MO0701PACSNFCP.000_R1 [DIRS 180439]. *References: Waste Form and In-Drift Colloids-Associated Radionuclide Concentrations: Abstraction and Summary* (SNL 2007 [DIRS 177423], Sections 4.1.1, 6.3.2.2, 6.3.2.6, 6.3.12.1, 6.5.1.3, 6.6.4 and 6.6.8; Equations 6-13 and 6-15; Tables 6-9 and 6-24).
Kd_Pu_Vo. Plutonium sorption coefficient in volcanic units (mL/g). *Distribution:* Piecewise uniform. *Range:* 10 to 300. *Correlation:* See SN0702PASZFTMA.001 [DIRS 179504]. *Additional Information:* See Kd_Am_Vo. *Sensitivity Name:* SZKDPUVO. *Location in TSPA-LA:* Section 6.3.10.2; Table 6.3.10-2. *DTN:* SN0702PASZFTMA.002_R1 [DIRS 183471]. *References: Saturated Zone Flow and Transport Model Abstraction* (SNL 2008 [DIRS 183750], Sections 6.3.1, 6.5.1.1, 6.5.1.2 and 6.5.2.8; Tables 4-3, 6-8, A-1[a] and B-1; Equations 6-2, 6-3 and 6-26).
Kd_Ra_Al. Radium sorption coefficient in alluvium (mL/g). *Distribution:* Uniform. *Range:* 100 to 1000. *Correlation:* See SN0702PASZFTMA.001 [DIRS 179504]. *Additional Information:* See Kd_Am_Al. *Sensitivity Name:* SZKDRAAL. *Location in TSPA-LA:* Section 6.3.10.2; Table 6.3.10-2. *DTN:* SN0702PASZFTMA.002_R1 [DIRS 183471]. *References: Saturated Zone Flow and Transport Model Abstraction* (SNL 2008 [DIRS 183750], Sections 6.3.1, 6.5.1.1, 6.5.1.2 and 6.5.2.8; Tables 4-3, 6-8, A-1[a] and B-1; Equations 6-2, 6-3 and 6-26).
Kd_Ra_Rev_Smectite_a. Distribution coefficient for reversible sorption of radium to waste form (smectite) colloids (mL/g). *Distribution:* Log uniform. *Range:* 100 to 5000. *Symbol:* $Kd_{Ra,coll,smectite}$. *Additional Information:* See Kd_Am_Rev_Smectite_a. Waste glass derived smectite colloids, corrosion-generated colloids, and seepage water–groundwater colloids may become pseudocolloids through reversible sorption of aqueous radionuclides onto them. *Sensitivity Name:* KDRASMEC. *Location in TSPA-LA:* Sections 6.3.7.6.2 and 6.3.7.6.3; Equation 6.3.7-20; Tables 6.3.7-62 and 6.3.7-66. *DTN:* MO0701PAKDSUNP.000_R1 [DIRS 180392]. *References: Waste Form and In-Drift Colloids-Associated Radionuclide Concentrations: Abstraction and Summary* (SNL 2007 [DIRS 177423], Sections 4.1.1, 6.3.2.2, 6.3.12.1 and 6.6.8; Equations 6-13 and 6-15; Figure 6-24b; Tables 6-15 and 6-24).
Kd_Ra_Rev_U_Col_a. Distribution coefficient for reversible sorption of radium onto uranophane colloids (mL/g). *Distribution:* Log uniform. *Range:* 10 to 1000. *Symbol:* $Kd_{Ra,coll,uranophane}$. *Additional Information:* See Kd_Am_Rev_U_Col_a. *Sensitivity Name:* KDRACOL. *Location in TSPA-LA:* Sections 6.3.7.6.2 and 6.3.7.6.3; Equation 6.3.7-20; Table 6.3.7-64. *DTN:* MO0701PACSNFCP.000_R1 [DIRS 180439]. *References: Waste Form and In-Drift Colloids-Associated Radionuclide Concentrations: Abstraction and Summary* (SNL 2007 [DIRS 177423], Sections 4.1.1, 6.3.2.2, 6.3.2.6, 6.3.12.1, 6.5.1.3, 6.6.4 and 6.6.8; Equations 6-13 and 6-15; Tables 6-9 and 6-24).
Kd_Ra_Vo*. Radium sorption coefficient in volcanic units (mL/g). *Distribution:* Uniform. *Range:* 100 to 1000. *Correlation:* See SN0702PASZFTMA.001 [DIRS 179504]. *Additional Information:* See Kd_Am_Vo. *Sensitivity Name:* SZKDRAVO*. *Location in TSPA-LA:* Section 6.3.10.2; Table 6.3.10-2. *DTN:* SN0702PASZFTMA.002_R1 [DIRS 183471]. *References: Saturated Zone Flow and Transport Model Abstraction* (SNL 2008 [DIRS 183750], Sections 6.3.1, 6.5.1.1, 6.5.1.2 and 6.5.2.8; Tables 4-3, 6-8, A-1[a] and B-1; Equations 6-2, 6-3 and 6-26).
Kd_Se_Al. Selenium sorption coefficient in alluvium (mL/g). *Distribution:* Truncated log normal. *Range:* 1 to 50. *Mean/Median/Mode:* 14. *Standard Deviation:* 11.2. *Correlation:* See SN0702PASZFTMA.001 [DIRS 179504]. *Additional Information:* See Kd_Am_Al. Two new nuclides have been added, namely radionuclide tin reversibly attached to colloids and sorbing radionuclide selenium. Uncertainty distributions for sorption coefficients of selenium and tin have recently been developed based on the need to simulate the migration of associated radionuclides in the TSPA model. *Sensitivity Name:* SZKDSEAL. *Location in TSPA-LA:* Section 6.3.10.2; Table 6.3.10-2. *DTN:* SN0702PASZFTMA.002_R1 [DIRS 183471]. *References: Saturated Zone Flow and Transport Model Abstraction* (SNL 2008 [DIRS 183750], Sections 6.5.3[a] and 8.1[a]; Tables 4-3[a], 6-7[a] and A-1[a]).
Kd_Se_Vo. Selenium sorption coefficient in volcanic units (mL/g). *Distribution:* Truncated log normal. *Range:* 1 to 50. *Mean/Median/Mode:* 14. *Standard Deviation:* 11.2. *Correlation:* See SN0702PASZFTMA.001 [DIRS 179504]. *Additional Information:* See Kd_Am_Vo. Two new nuclides have been added, namely radionuclide tin reversibly attached to colloids and sorbing radionuclide selenium. Uncertainty distributions for sorption coefficients of selenium and tin have recently been developed based on the need to simulate the migration of associated radionuclides in the TSPA model. *Sensitivity Name:* SZKDSEVO. *Location in TSPA-LA:* Section 6.3.10.2; Table 6.3.10-2. *DTN:* SN0702PASZFTMA.002_R1 [DIRS 183471]. *References: Saturated Zone Flow and Transport Model Abstraction* (SNL 2008 [DIRS 183750], Sections 6.5.3[a] and 8.1[a]; Tables 4-3[a], 6-7[a] and A-1[a]).

Table K3-3. Detailed Summary of Epistemically Uncertain Variables (i.e., elements of **e**) Considered in the TSPA-LA (TSPA Parameter Name) (Continued)

NOTE: * indicates variable not considered in sensitivity analysis due to correlations.

Kd_Sn_Al. Tin sorption coefficient in alluvium (mL/g). *Distribution:* Log uniform. *Range:* 1.00E+02 to 1.00E+05. *Correlation:* See SN0702PASZFTMA.001 [DIRS 179504]. *Additional Information:* See Kd_Am_Al. Two new nuclides have been added, namely radionuclide tin reversibly attached to colloids and sorbing radionuclide selenium. Uncertainty distributions for sorption coefficients of selenium and tin have recently been developed based on the need to simulate the migration of associated radionuclides in the TSPA model. *Sensitivity Name:* SZKDSNAL. *Location in TSPA-LA:* Section 6.3.10.2; Table 6.3.10-2. *DTN:* SN0702PASZFTMA.002_R1 [DIRS 183471]. *References: Saturated Zone Flow and Transport Model Abstraction* (SNL 2008 [DIRS 183750], Sections 6.5.3[a] and 8.1[a]; Tables 4-3[a], 6-7[a] and A-1[a]).
Kd_Sn_Col. Tin sorption coefficient onto smectite colloids (mL/g). *Distribution:* Log uniform. *Range:* 1.00E+05 to 1.00E+06. *Additional Information:* See Kd_Am_Col. Two new nuclides have been added, namely radionuclide tin reversibly attached to colloids and sorbing radionuclide selenium. Uncertainty distributions for sorption coefficients of selenium and tin have recently been developed based on the need to simulate the migration of associated radionuclides in the TSPA model. *Sensitivity Name:* SZKDSNCO. *Location in TSPA-LA:* Section 6.3.10.2; Table 6.3.10-2. *DTN:* SN0702PASZFTMA.002_R1 [DIRS 183471]. *References: Saturated Zone Flow and Transport Model Abstraction* (SNL 2008 [DIRS 183750], Sections 6.5.2.4[a], 6.5.3[a] and 8.1[a]; Tables 4-3[a], 6-7[a] and A-1[a]).
Kd_Sn_Rev_Smectite_a. Distribution coefficient for reversible sorption of tin to waste form (smectite) colloids (mL/g). *Distribution:* Log uniform. *Range:* 1.00E+05 to 1.00E+06. *Symbol:* $Kd_{Sn,coll,smectite}$. *Additional Information:* See Kd_Am_Rev_Smectite_a. Waste glass derived smectite colloids, corrosion-generated colloids, and seepage water–groundwater colloids may become pseudocolloids through reversible sorption of aqueous radionuclides onto them. *Sensitivity Name:* KDSNSMEC. *Location in TSPA-LA:* Sections 6.3.7.6.2 and 6.3.7.6.3; Equation 6.3.7-20; Tables 6.3.7-62 and 6.3.7-66. *DTN:* MO0701PAKDSUNP.000_R1 [DIRS 180392]. *References: Waste Form and In-Drift Colloids-Associated Radionuclide Concentrations: Abstraction and Summary* (SNL 2007 [DIRS 177423], Sections 4.1.1, 6.3.2.2, 6.3.12.1 and 6.6.8; Equations 6-13 and 6-15; Figure 6-24b; Tables 6-15 and 6-24).
Kd_Sn_Rev_U_Col_a. Distribution coefficient for reversible sorption of tin onto uranophane colloids (mL/g). *Distribution:* Log uniform. *Range:* 1 to 100. *Symbol:* $Kd_{Sn,coll,uranophane}$. *Additional Information:* See Kd_Am_Rev_U_Col_a. *Sensitivity Name:* KDSNCOL. *Location in TSPA-LA:* Sections 6.3.7.6.2 and 6.3.7.6.3; Equation 6.3.7-20; Table 6.3.7-64. *DTN:* MO0701PACSNFCP.000_R1 [DIRS 180439]. *References: Waste Form and In-Drift Colloids-Associated Radionuclide Concentrations: Abstraction and Summary* (SNL 2007 [DIRS 177423], Sections 4.1.1, 6.3.2.2, 6.3.2.6, 6.3.12.1, 6.5.1.3, 6.6.4 and 6.6.8; Equations 6-13 and 6-15; Tables 6-9 and 6-24).
Kd_Sn_Vo. Tin sorption coefficient in volcanic units (mL/g). *Distribution:* Log uniform. *Range:* 1.00E+02 to 1.00E+05. *Correlation:* See SN0702PASZFTMA.001 [DIRS 179504]. *Additional Information:* See Kd_Am_Vo. Two new nuclides have been added, namely radionuclide tin reversibly attached to colloids and sorbing radionuclide selenium. Uncertainty distributions for sorption coefficients of selenium and tin have recently been developed based on the need to simulate the migration of associated radionuclides in the TSPA model. *Sensitivity Name:* SZKDSNVO. *Location in TSPA-LA:* Section 6.3.10.2; Table 6.3.10-2. *DTN:* SN0702PASZFTMA.002_R1 [DIRS 183471]. *References: Saturated Zone Flow and Transport Model Abstraction* (SNL 2008 [DIRS 183750], Sections 6.5.3[a] and 8.1[a]; Tables 4-3[a], 6-7[a] and A-1[a]).
Kd_Sr_Al. Strontium sorption coefficient in alluvium (mL/g). *Distribution:* Uniform. *Range:* 20 to 400. *Correlation:* See SN0702PASZFTMA.001 [DIRS 179504]. *Additional Information:* See Kd_Am_Al. *Sensitivity Name:* SZKDSRAL. *Location in TSPA-LA:* Section 6.3.10.2; Table 6.3.10-2. *DTN:* SN0702PASZFTMA.002_R1 [DIRS 183471]. *References: Saturated Zone Flow and Transport Model Abstraction* (SNL 2008 [DIRS 183750], Sections 6.3.1, 6.5.1.1, 6.5.1.2 and 6.5.2.8; Tables 4-3, 6-8, A-1[a] and B-1; Equations 6-2, 6-3 and 6-26).
Kd_Sr_Vo. Strontium sorption coefficient in volcanic units (mL/g). *Distribution:* Uniform. *Range:* 20 to 400. *Correlation:* See SN0702PASZFTMA.001 [DIRS 179504]. *Additional Information:* See Kd_Am_Vo. *Sensitivity Name:* SZKDSRVO. *Location in TSPA-LA:* Section 6.3.10.2; Table 6.3.10-2. *DTN:* SN0702PASZFTMA.002_R1 [DIRS 183471]. *References: Saturated Zone Flow and Transport Model Abstraction* (SNL 2008 [DIRS 183750], Sections 6.3.1, 6.5.1.1, 6.5.1.2 and 6.5.2.8; Tables 4-3, 6-8, A-1[a] and B-1; Equations 6-2, 6-3 and 6-26).

Table K3-3. Detailed Summary of Epistemically Uncertain Variables (i.e., elements of **e**) Considered in the TSPA-LA (TSPA Parameter Name) (Continued)

NOTE: * indicates variable not considered in sensitivity analysis due to correlations.

Kd_Th_Rev_Smectite_a. Distribution coefficient for reversible sorption of thorium to waste form (smectite) colloids (mL/g). *Distribution:* Piecewise uniform. *Range:* 1.00E+04 to 1.00E+07. *Symbol:* $Kd_{Th,coll,wf}$. *Additional Information:* See Kd_Am_Rev_Smectite_a. *Sensitivity Name:* KDTHSMEC. *Location in TSPA-LA:* Sections 6.3.7.6.2 and 6.3.7.6.3; Equation 6.3.7-20; Tables 6.3.7-62 and 6.3.7-66. *DTN:* MO0701PASORPTN.000_R1 [DIRS 180391]. *References: Waste Form and In-Drift Colloids-Associated Radionuclide Concentrations: Abstraction and Summary* (SNL 2007 [DIRS 177423], Sections 4.1.1, 6.3.2.2, 6.3.12.1 and 6.6.8; Equations 6-13 and 6-15; Figure 6-24c; Tables 6-15 and 6-24).
Kd_Th_Rev_U_Col_a. Distribution coefficient for reversible sorption of thorium onto uranophane colloids (mL/g). *Distribution:* Log uniform. *Range:* 5 to 1.00E+04. *Symbol:* $Kd_{Th,coll,uranophane}$. *Additional Information:* See Kd_Am_Rev_U_Col_a. *Sensitivity Name:* KDTHCOL. *Location in TSPA-LA:* Sections 6.3.7.6.2 and 6.3.7.6.3; Equation 6.3.7-20; Table 6.3.7-64. *DTN:* MO0701PACSNFCP.000_R1 [DIRS 180439]. *References: Waste Form and In-Drift Colloids-Associated Radionuclide Concentrations: Abstraction and Summary* (SNL 2007 [DIRS 177423], Sections 4.1.1, 6.3.2.2, 6.3.2.6, 6.3.12.1, 6.5.1.3, 6.6.4 and 6.6.8; Equations 6-13 and 6-15; Tables 6-9 and 6-24).
Kd_U_Al. Uranium sorption coefficient in alluvium (mL/g). *Distribution:* Piecewise uniform. *Range:* 1.7 to 8.9. *Correlation:* See SN0702PASZFTMA.001 [DIRS 179504]. *Additional Information:* See Kd_Am_Al. *Sensitivity Name:* SZKDUAL. *Location in TSPA-LA:* Section 6.3.10.2; Table 6.3.10-2. *DTN:* SN0702PASZFTMA.002_R1 [DIRS 183471]. *References: Saturated Zone Flow and Transport Model Abstraction* (SNL 2008 [DIRS 183750], Sections 6.3.1, 6.5.1.1, 6.5.1.2 and 6.5.2.8; Tables 4-3, 6-8, A-1[a] and B-1; Equations 6-2, 6-3 and 6-26).
Kd_U_Rev_Smectite_a. Distribution coefficient for reversible sorption of uranium to waste form (smectite) colloids (mL/g). *Distribution:* Log uniform. *Range:* 5.00E+02 to 5.00E+04. *Symbol:* $Kd_{U,coll,smectite}$. *Additional Information:* See Kd_Am_Rev_Smectite_a. Waste glass derived smectite colloids, corrosion-generated colloids, and seepage water–groundwater colloids may become pseudocolloids through reversible sorption of aqueous radionuclides onto them. *Sensitivity Name:* KDUSMEC. *Location in TSPA-LA:* Sections 6.3.7.6.2 and 6.3.7.6.3; Equation 6.3.7-20; Tables 6.3.7-62 and 6.3.7-66. *DTN:* MO0701PAKDSUNP.000_R1 [DIRS 180392]. *References: Waste Form and In-Drift Colloids-Associated Radionuclide Concentrations: Abstraction and Summary* (SNL 2007 [DIRS 177423], Section 4.1.1, 6.3.2.2, 6.3.12.1 and 6.6.8; Equations 6-13 and 6-15; Figure 6-24a; Tables 6-15 and 6-24).
Kd_U_Vo. Uranium sorption coefficient in volcanic units (mL/g). *Distribution:* Piecewise uniform. *Range:* 0 to 20. *Correlation:* See SN0702PASZFTMA.001 [DIRS 179504]. *Additional Information:* See Kd_Am_Vo. *Sensitivity Name:* SZKDUVO. *Location in TSPA-LA:* Section 6.3.10.2; Table 6.3.10-2. *DTN:* SN0702PASZFTMA.002_R1 [DIRS 183471]. *References: Saturated Zone Flow and Transport Model Abstraction* (SNL 2008 [DIRS 183750], Sections 6.3.1, 6.5.1.1, 6.5.1.2 and 6.5.2.8; Tables 4-3, 6-8, A-1[a] and B-1; Equations 6-2, 6-3 and 6-26).
KdAm_Devit_a. Sorption coefficient of americium in devitrified tuff units of UZ (mL/g). *Distribution:* Truncated normal. *Range:* 1000 to 10000. *Mean:* 5500. *Standard Deviation:* 1500. *Correlation:* See *Radionuclide Transport Models Under Ambient Conditions* (SNL 2007 [DIRS 177396], Appendix B[a], Table B-2[a]). *Additional Information:* The matrix K_d adsorption coefficient is used in conjunction with bulk density, matrix porosity, and matrix saturation to derive the retardation coefficient used to determine the effective transport rate for sorbed species. A correlated set of K_ds are generated for radionuclides transported through the different rock types (zeolitic, vitric and devitrified tuffs) in the UZ. The generated set of Kds is used in the FEHM external input file and by the EBS model to describe radionuclide concentrations at the contact between the EBS-invert and the UZ. Recorded in the TSPA Input Database as four constants: UZ_Kd_Am_D_max, UZ_Kd_Am_D_mean, UZ_Kd_Am_D_SD, and UZ_Kd_Am_D_min. *Sensitivity Name:* UZKDAMDT. *Location in TSPA-LA:* Sections 6.3.9.2 and 6.3.9.3; Equation 6.3.9-3; Table 6.3.9-2. *DTN(s):* UZ_Kd_Am_D_max, UZ_Kd_Am_D_mean, UZ_Kd_Am_D_SD, and UZ_Kd_Am_D_min found in LA0408AM831341.001_R0 [DIRS 171584]. Kd values found in MO0506SPAROCKU.000 [DIRS 173958], Table 1. *References: Radionuclide Transport Models Under Ambient Conditions* (SNL 2007 [DIRS 177396], Sections 6.5 and A8.1; Table 6-1[a]).
KdAm_Vit_a*. Sorption coefficient of americium in vitrified tuff units of UZ (mL/g). *Distribution:* Piecewise uniform. *Range:* 100 to 1000. *Median:* 400. *Correlation:* See *Radionuclide Transport Models Under Ambient Conditions* (SNL 2007 [DIRS 177396], Appendix B[a], Table B-2[a]). *Additional Information:* See KdAm_Devit_a. Recorded in the TSPA Input Database as three constants: UZ_Kd_Am_V_c1, UZ_Kd_Am_V_c2, UZ_Kd_Am_V_c3. *Sensitivity Name:* UZKDAMVT*. *Location in TSPA-LA:* Sections 6.3.9.2 and 6.3.9.3; Equation 6.3.9-3; Table 6.3.9-2. *DTN(s):* UZ_Kd_Am_V_c1, UZ_Kd_Am_V_c2 and UZ_Kd_Am_V_c3 found in LA0408AM831341.001_R0 [DIRS 171584]. Kd values found in MO0506SPAROCKU.000 [DIRS 173958], Table 1.. *References: Radionuclide Transport Models Under Ambient Conditions* (SNL 2007 [DIRS 177396], Sections 6.5 and A8.1; Table 6-1[a]).

Table K3-3. Detailed Summary of Epistemically Uncertain Variables (i.e., elements of **e**) Considered in the TSPA-LA (TSPA Parameter Name) (Continued)

NOTE: * indicates variable not considered in sensitivity analysis due to correlations.

KdAm_Zeo_a*. Sorption coefficient of americium in zeolitic tuff units of UZ (mL/g). *Distribution:* Truncated normal. *Range:* 1000 to 10000. *Mean:* 5500. *Standard Deviation:* 1500. *Correlation:* See *Radionuclide Transport Models Under Ambient Conditions* (SNL 2007 [DIRS 177396], Appendix B[a], Table B-2[a]). *Additional Information:* See KdAm_Devit_a. Recorded in the TSPA Input Database as four constants: UZ_Kd_Am_Z_max, UZ_Kd_Am_Z_mean, UZ_Kd_Am_Z_SD, and UZ_Kd_Am_Z_min. *Sensitivity Name:* UZKDAMZT*. *Location in TSPA-LA:* Sections 6.3.9.2 and 6.3.9.3; Equation 6.3.9-3; Table 6.3.9-2. *DTN(s):* UZ_Kd_Am_Z_max, UZ_Kd_Am_Z_mean, UZ_Kd_Am_Z_SD, and UZ_Kd_Am_Z_min found in LA0408AM831341.001_R0 [DIRS 171584]. Kd values found in MO0506SPAROCKU.000 [DIRS 173958], Table 1. *References: Radionuclide Transport Models Under Ambient Conditions* (SNL 2007 [DIRS 177396], Sections 6.5 and A8.1; Table 6-1[a]).
KdCs_Devit_a. Sorption coefficient of cesium in devitrified tuff units of UZ (mL/g). *Distribution:* Uniform. *Range:* 1 to 15. *Correlation:* See *Radionuclide Transport Models Under Ambient Conditions* (SNL 2007 [DIRS 177396], Appendix B[a], Table B-2[a]). *Additional Information:* See KdAm_Devit_a. Recorded in the TSPA Input Database as UZ_Kd_Cs_D_max and UZ_Kd_Cs_D_min. *Sensitivity Name:* UZKDCSDT. *Location in TSPA-LA:* Sections 6.3.9.2 and 6.3.9.3; Equation 6.3.9-3; Table 6.3.9-2. *DTN(s):* UZ_Kd_Cs_D_max and UZ_Kd_Cs_D_min found in LA0408AM831341.001_R0 [DIRS 171584]. Kd values found in MO0506SPAROCKU.000 [DIRS 173958], Table 1. *References: Radionuclide Transport Models Under Ambient Conditions* (SNL 2007 [DIRS 177396], Section 6.5; Table 6-1[a]).
KdCs_Vit_a*. Sorption coefficient of cesium in vitrified tuff units of UZ (mL/g). *Distribution:* Piecewise uniform. *Range:* 0 to 100. *Median:* 2. *Correlation:* See *Radionuclide Transport Models Under Ambient Conditions* (SNL 2007 [DIRS 177396], Appendix B[a], Table B-2[a]). *Additional Information:* See KdAm_Devit_a. Recorded in the TSPA Input Database as three constants: UZ_Kd_Cs_V_c1, UZ_Kd_Cs_V_c2, and UZ_Kd_Cs_V_c3. *Sensitivity Name:* UZKDCSVT*. *Location in TSPA-LA:* Sections 6.3.9.2 and 6.3.9.3; Equation 6.3.9-3; Table 6.3.9-2. *DTN(s):* UZ_Kd_Cs_V_c1, UZ_Kd_Cs_V_c2, and UZ_Kd_Cs_V_c3 found in LA0408AM831341.001_R0 [DIRS 171584]. Kd values found in MO0506SPAROCKU.000 [DIRS 173958], Table 1. *References: Radionuclide Transport Models Under Ambient Conditions* (SNL 2007 [DIRS 177396], Section 6.5; Table 6-1[a]).
KdCs_Zeo_a. Sorption coefficient for cesium in zeolitic tuff units of UZ (mL/g). *Distribution:* Piecewise uniform. *Range:* 425 to 20000. *Median:* 5,000. *Correlation:* See *Radionuclide Transport Models Under Ambient Conditions* (SNL 2007 [DIRS 177396], Appendix B[a], Table B-2[a]). *Additional Information:* See KdAm_Devit_a. Recorded in the TSPA Input Database as three constants: UZ_Kd_Cs_Z_c1, UZ_Kd_Cs_Z_c2, and UZ_Kd_Cs_Z_c3. *Sensitivity Name:* UZKDCSZT. *Location in TSPA-LA:* Sections 6.3.9.2 and 6.3.9.3; Equation 6.3.9-3; Table 6.3.9-2. *DTN(s): UZ_Kd_Cs_Z_c1, UZ_Kd_Cs_Z_c2, and UZ_Kd_Cs_Z_c3 found in LA0408AM831341.001_R0 [DIRS 171584]. Kd values found in MO0506SPAROCKU.000 [DIRS 173958], Table 1. References: Radionuclide Transport Models Under Ambient Conditions* (SNL 2007 [DIRS 177396], Section 6.5; Table 6-1[a]).
KdNp_Devit_a. Sorption coefficient for neptunium in devitrified tuff units of UZ (mL/g). *Distribution:* Piecewise uniform. *Range:* 0 to 6. *Median:* 0.5. *Correlation:* See *Radionuclide Transport Models Under Ambient Conditions* (SNL 2007 [DIRS 177396], Appendix B[a], Table B-2[a]). *Additional Information:* See KdAm_Devit_a. Recorded in the TSPA Input Database as three constants: UZ_Kd_Np_D_c1, UZ_Kd_Np_D_c2, and UZ_Kd_Np_D_c3. *Sensitivity Name:* UZKDNPDT. *Location in TSPA-LA:* Sections 6.3.9.2 and 6.3.9.3; Equation 6.3.9-3; Table 6.3.9-2. *DTN(s):* UZ_Kd_Np_D_c1, UZ_Kd_Np_D_c2, and UZ_Kd_Np_D_c3 found in LA0408AM831341.001_R0 [DIRS 171584]. Kd values found in MO0506SPAROCKU.000 [DIRS 173958], Table 1. *References: Radionuclide Transport Models Under Ambient Conditions* (SNL 2007 [DIRS 177396], Section 6.5; Table 6-1[a]).
KdNp_Vit_a*. Sorption coefficient for neptunium in vitrified tuff units of UZ (mL/g). *Distribution:* Piecewise uniform. *Range:* 0 to 3. *Median:* 1. *Correlation:* See *Radionuclide Transport Models Under Ambient Conditions* (SNL 2007 [DIRS 177396], Appendix B[a], Table B-2[a]). *Additional Information:* See KdAm_Devit_a. Recorded in the TSPA Input Database as three constants: UZ_Kd_Np_V_c1, UZ_Kd_Np_V_c2, and UZ_Kd_Np_V_c3. *Sensitivity Name:* UZKDNPVT*, *Location in TSPA-LA:* Sections 6.3.9.2 and 6.3.9.3; Equation 6.3.9-3; Table 6.3.9-2. *DTN(s):* UZ_Kd_Np_V_c1, UZ_Kd_Np_V_c2, and UZ_Kd_Np_V_c3 found in LA0408AM831341.001_R0 [DIRS 171584]. Kd values found in MO0506SPAROCKU.000 [DIRS 173958], Table 1. *References: Radionuclide Transport Models Under Ambient Conditions* (SNL 2007 [DIRS 177396], Section 6.5; Table 6-1[a]).

Table K3-3. Detailed Summary of Epistemically Uncertain Variables (i.e., elements of **e**) Considered in the TSPA-LA (TSPA Parameter Name) (Continued)

NOTE: * indicates variable not considered in sensitivity analysis due to correlations.

KdNp_Zeo_a*. Sorption coefficient for neptunium in zeolitic tuff units of UZ (mL/g). *Distribution:* Piecewise uniform. *Range:* 0 to 6. *Median:* 0.5. *Correlation:* See *Radionuclide Transport Models Under Ambient Conditions* (SNL 2007 [DIRS 177396], Appendix B[a], Table B-2[a]). *Additional Information:* See KdAm_Devit_a. Recorded in the TSPA Input Database as three constants: UZ_Kd_Np_Z_c1, UZ_Kd_Np_Z_c2, and UZ_Kd_Np_Z_c3. *Sensitivity Name:* UZKDNPZT*. *Location in TSPA-LA:* Sections 6.3.9.2 and 6.3.9.3; Equation 6.3.9-3; Table 6.3.9-2. *DTN(s):* UZ_Kd_Np_Z_c1, UZ_Kd_Np_Z_c2, and UZ_Kd_Np_Z_c3 found in LA0408AM831341.001_R0 [DIRS 171584]. Kd values found in MO0506SPAROCKU.000 [DIRS 173958], Table 1. *References: Radionuclide Transport Models Under Ambient Conditions* (SNL 2007 [DIRS 177396], Section 6.5; Table 6-1[a]).
KdPa_Devit_a. Sorption coefficient for protactinium in devitrified tuff units of UZ (mL/g). *Distribution:* Truncated normal. *Range:* 1000 to 10000. *Mean:* 5500. *Standard Deviation:* 1500. *Correlation:* See *Radionuclide Transport Models Under Ambient Conditions* (SNL 2007 [DIRS 177396], Appendix B[a], Table B-2[a]). *Additional Information:* See KdAm_Devit_a. Recorded in the TSPA Input Database as four constants: UZ_Kd_Pa_D_max, UZ_Kd_Pa_D_mean, UZ_Kd_Pa_D_SD, and UZ_Kd_Pa_D_min. *Sensitivity Name:* UZKDPADT. *Location in TSPA-LA:* Sections 6.3.9.2 and 6.3.9.3; Equation 6.3.9-3; Table 6.3.9-2. *DTN(s):* UZ_Kd_Pa_D_max, UZ_Kd_Pa_D_mean, UZ_Kd_Pa_D_SD, and UZ_Kd_Pa_D_min found in LA0408AM831341.001_R0 [DIRS 171584]. Kd values found in MO0506SPAROCKU.000 [DIRS 173958], Table 1. *References: Radionuclide Transport Models Under Ambient Conditions* (SNL 2007 [DIRS 177396], Section 6.5; Table 6-1[a]).
KdPa_Vit_a*. Sorption coefficient for protactinium in vitrified tuff units of UZ (mL/g). *Distribution:* Truncated normal. *Range:* 1000 to 10000. *Mean:* 5500. *Standard Deviation:* 1500. *Correlation:* See *Radionuclide Transport Models Under Ambient Conditions* (SNL 2007 [DIRS 177396], Appendix B[a], Table B-2[a]). *Additional Information:* See KdAm_Devit_a. Recorded in the TSPA Input Database as four constants: UZ_Kd_Pa_V_max, UZ_Kd_Pa_V_mean, UZ_Kd_Pa_V_SD, and UZ_Kd_Pa_V_min. *Sensitivity Name:* UZKDPAVT*. *Location in TSPA-LA:* Sections 6.3.9.2 and 6.3.9.3; Equation 6.3.9-3; Table 6.3.9-2. *DTN(s):* UZ_Kd_Pa_V_max, UZ_Kd_Pa_V_mean, UZ_Kd_Pa_V_SD, and UZ_Kd_Pa_V_min found in LA0408AM831341.001_R0 [DIRS 171584]. Kd values found in MO0506SPAROCKU.000 [DIRS 173958], Table 1. *References: Radionuclide Transport Models Under Ambient Conditions* (SNL 2007 [DIRS 177396], Section 6.5; Table 6-1[a]).
KdPa_Zeo_a*. Sorption coefficient for protactinium in zeolitic tuff units of UZ (mL/g). *Distribution:* Truncated normal. *Range:* 1000 to 10000. *Mean:* 5500. *Standard Deviation:* 1500. *Correlation:* See *Radionuclide Transport Models Under Ambient Conditions* (SNL 2007 [DIRS 177396], Appendix B[a], Table B-2[a]). *Additional Information:* See KdAm_Devit_a. Recorded in the TSPA Input Database as four constants: UZ_Kd_Pa_Z_max, UZ_Kd_Pa_Z_mean, UZ_Kd_Pa_Z_SD, and UZ_Kd_Pa_Z_min. *Sensitivity Name:* UZKDPAZT*. *Location in TSPA-LA:* Sections 6.3.9.2 and 6.3.9.3; Equation 6.3.9-3; Table 6.3.9-2. *DTN(s):* UZ_Kd_Pa_Z_max, UZ_Kd_Pa_Z_mean, UZ_Kd_Pa_Z_SD, and UZ_Kd_Pa_Z_min found in LA0408AM831341.001_R0 [DIRS 171584]. Kd values found in MO0506SPAROCKU.000 [DIRS 173958], Table 1. *References: Radionuclide Transport Models Under Ambient Conditions* (SNL 2007 [DIRS 177396], Section 6.5; Table 6-1[a]).
KdPu_Devit_a. Sorption coefficient for plutonium in devitrified tuff units of UZ (mL/g). *Distribution:* Piecewise uniform. *Range:* 10 to 200. *Median:* 70. *Correlation:* See *Radionuclide Transport Models Under Ambient Conditions* (SNL 2007 [DIRS 177396], Appendix B[a], Table B-2[a]). *Additional Information:* See KdAm_Devit_a. Recorded in the TSPA Input Database as three constants: UZ_Kd_Pu_D_c1, UZ_Kd_Pu_D_c2, and UZ_Kd_Pu_D_c3. *Sensitivity Name:* UZKDPUDT. *Location in TSPA-LA:* Sections 6.3.9.2 and 6.3.9.3; Equation 6.3.9-3; Table 6.3.9-2. *DTN(s):* UZ_Kd_Pu_D_c1, UZ_Kd_Pu_D_c2, and UZ_Kd_Pu_D_c3 found in LA0408AM831341.001_R0 [DIRS 171584]. Kd values found in MO0506SPAROCKU.000 [DIRS 173958], Table 1. *References: Radionuclide Transport Models Under Ambient Conditions* (SNL 2007 [DIRS 177396], Section 6.5; Table 6-1[a]).
KdPu_Vit_a*. Sorption coefficient for plutonium in vitrified tuff units of UZ (mL/g). *Distribution:* Piecewise uniform. *Range:* 10 to 200. *Median:* 100. *Correlation:* See *Radionuclide Transport Models Under Ambient Conditions* (SNL 2007 [DIRS 177396], Appendix B[a], Table B-2[a]). *Additional Information:* See KdAm_Devit_a. Recorded in the TSPA Input Database as three constants: UZ_Kd_Pu_V_c1, UZ_Kd_Pu_V_c2, and UZ_Kd_Pu_V_c3. *Sensitivity Name:* UZKDPUVT*. *Location in TSPA-LA:* Sections 6.3.9.2 and 6.3.9.3; Equation 6.3.9-3; Table 6.3.9-2. *DTN(s):* UZ_Kd_Pu_V_c1, UZ_Kd_Pu_V_c2, and UZ_Kd_Pu_V_c3 found in LA0408AM831341.001_R0 [DIRS 171584]. Kd values found in MO0506SPAROCKU.000 [DIRS 173958], Table 1. *References: Radionuclide Transport Models Under Ambient Conditions* (SNL 2007 [DIRS 177396], Section 6.5; Table 6-1[a]).

Table K3-3. Detailed Summary of Epistemically Uncertain Variables (i.e., elements of **e**) Considered in the TSPA-LA (TSPA Parameter Name) (Continued)

NOTE: * indicates variable not considered in sensitivity analysis due to correlations.

KdPu_Zeo_a*. Sorption coefficient for plutonium in zeolitic tuff units of UZ (mL/g). *Distribution:* Piecewise uniform. *Range:* 10 to 200. *Median:* 100. *Correlation:* See *Radionuclide Transport Models Under Ambient Conditions* (SNL 2007 [DIRS 177396], Appendix B[a], Table B-2[a]). *Additional Information:* See KdAm_Devit_a. Recorded in the TSPA Input Database as three constants: UZ_Kd_Pu_Z_c1, UZ_Kd_Pu_Z_c2, and UZ_Kd_Pu_Z_c3. *Sensitivity Name:* UZKDPUZT*. *Location in TSPA-LA:* Sections 6.3.9.2 and 6.3.9.3; Equation 6.3.9-3; Table 6.3.9-2. *DTN(s):* UZ_Kd_Pu_Z_c1, UZ_Kd_Pu_Z_c2, and UZ_Kd_Pu_Z_c3 found in LA0408AM831341.001_R0 [DIRS 171584]. Kd values found in MO0506SPAROCKU.000 [DIRS 173958], Table 1. *References: Radionuclide Transport Models Under Ambient Conditions* (SNL 2007 [DIRS 177396], Section 6.5; Table 6-1[a]).
KdRa_Devit_a*. Sorption coefficient for radium in devitrified tuff units of UZ (mL/g). *Distribution:* Uniform. *Range:* 100 to 1000. *Correlation:* See *Radionuclide Transport Models Under Ambient Conditions* (SNL 2007 [DIRS 177396], Appendix B[a], Table B-2[a]). *Additional Information:* See KdAm_Devit_a. Recorded in the TSPA Input Database as UZ_Kd_Ra_D_max and UZ_Kd_Ra_D_min. *Sensitivity Name:* UZKDRADT*. *Location in TSPA-LA:* Sections 6.3.9.2 and 6.3.9.3; Equation 6.3.9-3; Table 6.3.9-2. *DTN(s):* UZ_Kd_Ra_D_max and UZ_Kd_Ra_D_min found in LA0408AM831341.001_R0 [DIRS 171584]. Kd values found in MO0506SPAROCKU.000 [DIRS 173958], Table 1. *References: Radionuclide Transport Models Under Ambient Conditions* (SNL 2007 [DIRS 177396], Section 6.5; Table 6-1[a]).
KdRa_Vit_a*. Sorption coefficient for radium in vitrified tuff units of UZ (mL/g). *Distribution:* Uniform. *Range:* 50 to 600. *Correlation:* See *Radionuclide Transport Models Under Ambient Conditions* (SNL 2007 [DIRS 177396], Appendix B[a], Table B-2[a]). *Additional Information:* See KdAm_Devit_a. Recorded in the TSPA Input Database as UZ_Kd_Ra_V_max and UZ_Kd_Ra_V_min. *Sensitivity Name:* UZKDRAVT*. *Location in TSPA-LA:* Sections 6.3.9.2 and 6.3.9.3; Equation 6.3.9-3; Table 6.3.9-2. *DTN(s):* UZ_Kd_Ra_V_max and UZ_Kd_Ra_V_min found in LA0408AM831341.001_R0 [DIRS 171584]. Kd values found in MO0506SPAROCKU.000 [DIRS 173958], Table 1. *References: Radionuclide Transport Models Under Ambient Conditions* (SNL 2007 [DIRS 177396], Section 6.5; Table 6-1[a]).
KdRa_Zeo_a*. Sorption coefficient for radium in zeolitic tuff units of UZ (mL/g). *Distribution:* Uniform. *Range:* 1000 to 5000. *Correlation:* See *Radionuclide Transport Models Under Ambient Conditions* (SNL 2007 [DIRS 177396], Appendix B[a], Table B-2[a]). *Additional Information:* See KdAm_Devit_a. Recorded in the TSPA Input Database as UZ_Kd_Ra_Z_max and UZ_Kd_Ra_Z_min. *Sensitivity Name:* UZKDRAZT*. *Location in TSPA-LA:* Sections 6.3.9.2 and 6.3.9.3; Equation 6.3.9-3; Table 6.3.9-2. *DTN(s):* UZ_Kd_Ra_Z_max and UZ_Kd_Ra_Z_min found in LA0408AM831341.001_R0 [DIRS 171584]. Kd values found in MO0506SPAROCKU.000 [DIRS 173958], Table 1. *References: Radionuclide Transport Models Under Ambient Conditions* (SNL 2007 [DIRS 177396], Section 6.5; Table 6-1[a]).
KdSe_Devit_a. Sorption coefficient for selenium in devitrified tuff units of UZ (mL/g). *Distribution:* Truncated log normal. *Range:* 1 to 50. *Mean:* 14. *Standard Deviation:* 11.2. *Correlation:* See *Radionuclide Transport Models Under Ambient Conditions* (SNL 2007 [DIRS 177396], Appendix B[a], Table B-2[a]). *Additional Information:* See KdAm_Devit_a. Recorded in the TSPA Input Database as four constants: UZ_Kd_Se_D_max, UZ_Kd_Se_D_mean, UZ_Kd_Se_D_SD, and UZ_Kd_Se_D_min. *Sensitivity Name:* UZKDSEDT. *Location in TSPA-LA:* Sections 6.3.9.2 and 6.3.9.3; Equation 6.3.9-3; Table 6.3.9-2. *DTN:* UZ_Kd_Se_D_max, UZ_Kd_Se_D_mean, UZ_Kd_Se_D_SD, and UZ_Kd_Se_D_min found in LB0701PAKDSESN.001_R0 [DIRS 179299]. *References: Radionuclide Transport Models Under Ambient Conditions* (SNL 2007 [DIRS 177396], Sections 6.5 and A8.10; Table 6-3; Figure A-73).
KdSe_Vit_a*. Sorption coefficient for selenium in vitrified tuff units of UZ (mL/g). *Distribution:* Truncated log normal. *Range:* 0 to 25. *Mean:* 8.6. *Standard Deviation:* 7.9. *Correlation:* See *Radionuclide Transport Models Under Ambient Conditions* (SNL 2007 [DIRS 177396], Appendix B[a], Table B-2[a]). *Additional Information:* See KdAm_Devit_a. Recorded in the TSPA Input Database as four constants: UZ_Kd_Se_V_max, UZ_Kd_Se_V_mean, UZ_Kd_Se_V_SD, UZ_Kd_Se_V_min, and UZ_Kd_Se_V_min_5004. *Sensitivity Name:* UZKDSEVT*. *Location in TSPA-LA:* Sections 6.3.9.2 and 6.3.9.3; Equation 6.3.9-3; Table 6.3.9-2. *DTN:* UZ_Kd_Se_V_max, UZ_Kd_Se_V_mean, UZ_Kd_Se_V_SD, UZ_Kd_Se_V_min, and UZ_Kd_Se_V_min_5004 found in LB0701PAKDSESN.001_R0 [DIRS 179299]. *References: Radionuclide Transport Models Under Ambient Conditions* (SNL 2007 [DIRS 177396], Section 6.5; Table 6-1[a]).

Table K3-3. Detailed Summary of Epistemically Uncertain Variables (i.e., elements of **e**) Considered in the TSPA-LA (TSPA Parameter Name) (Continued)

NOTE: * indicates variable not considered in sensitivity analysis due to correlations.

KdSe_Zeo_a*. Sorption coefficient for selenium in zeolitic tuff units of UZ (mL/g). *Distribution:* Truncated log normal. *Range:* 1 to 35. *Mean:* 14.3. *Standard Deviation:* 7.9. *Correlation:* See *Radionuclide Transport Models Under Ambient Conditions* (SNL 2007 [DIRS 177396], Appendix B[a], Table B-2[a]). *Additional Information:* See KdAm_Devit_a. Recorded in the TSPA Input Database as four constants: UZ_Kd_Se_Z_max, UZ_Kd_Se_Z_mean, UZ_Kd_Se_Z_SD, and UZ_Kd_Se_Z_min. *Sensitivity Name:* UZKDSEZT*. *Location in TSPA-LA:* Sections 6.3.9.2 and 6.3.9.3; Equation 6.3.9-3; Table 6.3.9-2. *DTN:* UZ_Kd_Se_Z_max, UZ_Kd_Se_Z_mean, UZ_Kd_Se_Z_SD, and UZ_Kd_Se_Z_min found in LB0701PAKDSESN.001_R0 [DIRS 179299]. *References: Radionuclide Transport Models Under Ambient Conditions* (SNL 2007 [DIRS 177396], Section 6.5; Table 6-1[a]).
KdSn_Devit_a. Sorption coefficient for tin in devitrified tuff units of UZ (mL/g). *Distribution:* Log-uniform. *Range:* 100 to 100000. *Correlation:* See *Radionuclide Transport Models Under Ambient Conditions* (SNL 2007 [DIRS 177396], Appendix B[a], Table B-2[a]). *Additional Information:* See KdAm_Devit_a. See discussion for KdAm_Devit_a. Recorded in the TSPA Input Database as four constants: UZ_Kd_Sn_D_min and UZ_Kd_Sn_D_max. *Sensitivity Name:* UZKDSNDT. *Location in TSPA-LA:* Sections 6.3.9.2 and 6.3.9.3; Equation 6.3.9-3; Table 6.3.9-2. *DTN:* UZ_Kd_Sn_D_min and UZ_Kd_Sn_D_max found in LB0701PAKDSESN.001_R0 [DIRS 179299]. *References: Radionuclide Transport Models Under Ambient Conditions* (SNL 2007 [DIRS 177396], Section 6.5; Table 6-1[a]).
KdSn_Vit_a*. Sorption coefficient for tin in vitrified tuff units of UZ (mL/g). *Distribution:* Log-uniform. *Range:* 100 to 5000. *Correlation:* See *Radionuclide Transport Models Under Ambient Conditions* (SNL 2007 [DIRS 177396], Appendix B[a], Table B-2[a]). *Additional Information:* See KdAm_Devit_a. Recorded in the TSPA Input Database as four constants: UZ_Kd_Sn_V_min and UZ_Kd_Sn_V_max. *Sensitivity Name:* UZKDSNVT*. *Location in TSPA-LA:* Sections 6.3.9.2 and 6.3.9.3; Equation 6.3.9-3; Table 6.3.9-2. *DTN:* UZ_Kd_Sn_V_min and UZ_Kd_Sn_V_max found in LB0701PAKDSESN.001_R0 [DIRS 179299]. *References: Radionuclide Transport Models Under Ambient Conditions* (SNL 2007 [DIRS 177396], Section 6.5; Table 6-1[a]).
KdSn_Zeo_a*. Sorption coefficient for tin in zeolitic tuff units of UZ (mL/g). *Distribution:* Log-uniform. *Range:* 100 to 5000. *Correlation:* See *Radionuclide Transport Models Under Ambient Conditions* (SNL 2007 [DIRS 177396], Appendix B[a], Table B-2[a]). *Additional Information:* See KdAm_Devit_a. Recorded in the TSPA Input Database as four constants: UZ_Kd_Sn_Z_min and UZ_Kd_Sn_Z_max. *Sensitivity Name:* UZKDSNZT*. *Location in TSPA-LA:* Sections 6.3.9.2 and 6.3.9.3; Equation 6.3.9-3; Table 6.3.9-2. *DTN:* UZ_Kd_Sn_Z_min and UZ_Kd_Sn_Z_max found in LB0701PAKDSESN.001_R0 [DIRS 179299]. *References: Radionuclide Transport Models Under Ambient Conditions* (SNL 2007 [DIRS 177396], Section 6.5; Table 6-1[a]).
KdSr_Devit_a. Sorption coefficient for strontium in devitrified tuff units of UZ (mL/g). *Distribution:* Uniform. *Range:* 10 to 70. *Correlation:* See *Radionuclide Transport Models Under Ambient Conditions* (SNL 2007 [DIRS 177396], Appendix B[a], Table B-2[a]). *Additional Information:* See KdAm_Devit_a. Recorded in the TSPA Input Database as four constants: UZ_Kd_Sr_D_max and UZ_Kd_Sr_D_min. *Sensitivity Name:* UZKDSRDT. *Location in TSPA-LA:* Sections 6.3.9.2 and 6.3.9.3; Equation 6.3.9-3; Table 6.3.9-2. *DTN:* UZ_Kd_Sr_D_max and UZ_Kd_Sr_D_min found in LA0408AM831341.001_R0 [DIRS 171584]. *References: Radionuclide Transport Models Under Ambient Conditions* (SNL 2007 [DIRS 177396], Section 6.5; Table 6-1[a]).
KdSr_Vit_a*. Sorption coefficient for strontium in vitrified tuff units of UZ (mL/g). *Distribution:* Uniform. *Range:* 0 to 50. *Correlation:* See *Radionuclide Transport Models Under Ambient Conditions* (SNL 2007 [DIRS 177396], Appendix B[a], Table B-2[a]). *Additional Information:* See KdAm_Devit_a. Recorded in the TSPA Input Database as four constants: UZ_Kd_Sr_V_max and UZ_Kd_Sr_V_min. *Sensitivity Name:* UZKDSRVT*. *Location in TSPA-LA:* Sections 6.3.9.2 and 6.3.9.3; Equation 6.3.9-3; Table 6.3.9-2. *DTN:* UZ_Kd_Sr_V_max and UZ_Kd_Sr_V_min found in LA0408AM831341.001_R0 [DIRS 171584]. *References: Radionuclide Transport Models Under Ambient Conditions* (SNL 2007 [DIRS 177396], Section 6.5; Table 6-1[a]).
KdSr_Zeo_a*. Sorption coefficient for strontium in zeolitic tuff units of UZ (mL/g). *Distribution:* Uniform. *Range:* 50 to 2000. *Correlation:* See *Radionuclide Transport Models Under Ambient Conditions* (SNL 2007 [DIRS 177396], Appendix B[a], Table B-2[a]). *Additional Information:* See KdAm_Devit_a. Recorded in the TSPA Input Database as four constants: UZ_Kd_Sr_Z_max and UZ_Kd_Sr_Z_min. *Sensitivity Name:* UZKDSRZT*. *Location in TSPA-LA:* Sections 6.3.9.2 and 6.3.9.3; Equation 6.3.9-3; Table 6.3.9-2. *DTN:* UZ_Kd_Sr_Z_max and UZ_Kd_Sr_Z_min found in LA0408AM831341.001_R0 [DIRS 171584]. *References: Radionuclide Transport Models Under Ambient Conditions* (SNL 2007 [DIRS 177396], Section 6.5; Table 6-1[a]).

Table K3-3. Detailed Summary of Epistemically Uncertain Variables (i.e., elements of **e**) Considered in the TSPA-LA (TSPA Parameter Name) (Continued)

NOTE: * indicates variable not considered in sensitivity analysis due to correlations.

KdTh_Devit_a. Sorption coefficient for thorium in devitrified tuff units of UZ (mL/g). *Distribution:* Uniform. *Range:* 1000 to 10000. *Correlation:* See *Radionuclide Transport Models Under Ambient Conditions* (SNL 2007 [DIRS 177396], Appendix B[a], Table B-2[a]). *Additional Information:* See KdAm_Devit_a. Recorded in the TSPA Input Database as four constants: UZ_Kd_Th_D_max and UZ_Kd_Th_D_min. *Sensitivity Name:* UZKDTHDT. *Location in TSPA-LA:* Sections 6.3.9.2 and 6.3.9.3; Equation 6.3.9-3; Table 6.3.9-2. *DTN:* UZ_Kd_Th_D_max and UZ_Kd_Th_D_min found in LA0408AM831341.001_R0 [DIRS 171584]. *References: Radionuclide Transport Models Under Ambient Conditions* (SNL 2007 [DIRS 177396], Section 6.5; Table 6-1[a]).
KdTh_Vit_a*. Sorption coefficient for thorium in vitrified tuff units of UZ (mL/g). *Distribution:* Uniform. *Range:* 1000 to 10000. *Correlation:* See *Radionuclide Transport Models Under Ambient Conditions* (SNL 2007 [DIRS 177396], Appendix B[a], Table B-2[a]). *Additional Information:* See KdAm_Devit_a. Recorded in the TSPA Input Database as four constants: UZ_Kd_Th_V_max and UZ_Kd_Th_V_min. *Sensitivity Name:* UZKDTHVT*. *Location in TSPA-LA:* Sections 6.3.9.2 and 6.3.9.3; Equation 6.3.9-3; Table 6.3.9-2. *DTN:* UZ_Kd_Th_V_max and UZ_Kd_Th_V_min found in LA0408AM831341.001_R0 [DIRS 171584]. *References: Radionuclide Transport Models Under Ambient Conditions* (SNL 2007 [DIRS 177396], Section 6.5; Table 6-1[a]).
KdTh_Zeo_a*. Sorption coefficient for thorium in zeolitic tuff units of UZ (mL/g). *Distribution:* Uniform. *Range:* 1000 to 30000. *Correlation:* See *Radionuclide Transport Models Under Ambient Conditions* (SNL 2007 [DIRS 177396], Appendix B[a], Table B-2[a]). *Additional Information:* See KdAm_Devit_a. Recorded in the TSPA Input Database as four constants: UZ_Kd_Th_Z_max and UZ_Kd_Th_Z_min. *Sensitivity Name:* UZKDTHZT*. *Location in TSPA-LA:* Sections 6.3.9.2 and 6.3.9.3; Equation 6.3.9-3; Table 6.3.9-2. *DTN:* UZ_Kd_Th_Z_max and UZ_Kd_Th_Z_min found in LA0408AM831341.001_R0 [DIRS 171584]. *References: Radionuclide Transport Models Under Ambient Conditions* (SNL 2007 [DIRS 177396], Section 6.5; Table 6-1[a]).
KdU_Devit_a. Sorption coefficient for uranium in devitrified tuff units of UZ (mL/g). *Distribution:* Piecewise uniform. *Range:* 0 to 4. *Median:* 0.2. *Correlation:* See *Radionuclide Transport Models Under Ambient Conditions* (SNL 2007 [DIRS 177396], Appendix B[a], Table B-2[a]). *Additional Information:* See KdAm_Devit_a. Recorded in the TSPA Input Database as four constants: UZ_Kd_U_D_c1, UZ_Kd_U_D_c2 and UZ_Kd_U_D_c3. *Sensitivity Name:* UZKDUDT. *Location in TSPA-LA:* Sections 6.3.9.2 and 6.3.9.3; Equation 6.3.9-3; Table 6.3.9-2. *DTN:* UZ_Kd_U_D_c1, UZ_Kd_U_D_c2 and UZ_Kd_U_D_c3 found in LA0408AM831341.001_R0 [DIRS 171584]. *References: Radionuclide Transport Models Under Ambient Conditions* (SNL 2007 [DIRS 177396], Section 6.5; Table 6-1[a]).
KdU_Vit_a*. Sorption coefficient for uranium in vitrified tuff units of UZ (mL/g). *Distribution:* Piecewise uniform. *Range:* 0 to 3. *Median:* 0.2. *Correlation:* See *Radionuclide Transport Models Under Ambient Conditions* (SNL 2007 [DIRS 177396], Appendix B[a], Table B-2[a]). *Additional Information:* See KdAm_Devit_a. Recorded in the TSPA Input Database as four constants: UZ_Kd_U_V_c1, UZ_Kd_U_V_c2 and UZ_Kd_U_V_c3. *Sensitivity Name:* UZKDUVT*. *Location in TSPA-LA:* Sections 6.3.9.2 and 6.3.9.3; Equation 6.3.9-3; Table 6.3.9-2. *DTN:* UZ_Kd_U_V_c1, UZ_Kd_U_V_c2 and UZ_Kd_U_V_c3 found in LA0408AM831341.001_R0 [DIRS 171584]. *References: Radionuclide Transport Models Under Ambient Conditions* (SNL 2007 [DIRS 177396], Section 6.5; Table 6-1[a]).
KdU_Zeo_a*. Sorption coefficient for uranium in zeolitic tuff units of UZ (mL/g). *Distribution:* Piecewise uniform. *Range:* 0 to 30. *Median:* 0.5. *Correlation:* See *Radionuclide Transport Models Under Ambient Conditions* (SNL 2007 [DIRS 177396], Appendix B[a], Table B-2[a]). *Additional Information:* See KdAm_Devit_a. Recorded in the TSPA Input Database as four constants: UZ_Kd_U_V_c1, UZ_Kd_U_V_c2, UZ_Kd_U_V_c3 and UZ_Kd_U_V_c3_5004. *Sensitivity Name:* UZKDUZT*. *Location in TSPA-LA:* Sections 6.3.9.2 and 6.3.9.3; Equation 6.3.9-3; Table 6.3.9-2. *DTN:* UZ_Kd_U_V_c1, UZ_Kd_U_V_c2, UZ_Kd_U_V_c3 and UZ_Kd_U_V_c3_5004 found in LA0408AM831341.001_R0 [DIRS 171584]. *References: Radionuclide Transport Models Under Ambient Conditions* (SNL 2007 [DIRS 177396], Section 6.5; Table 6-1[a]).

Table K3-3. Detailed Summary of Epistemically Uncertain Variables (i.e., elements of **e**) Considered in the TSPA-LA (TSPA Parameter Name) (Continued)

NOTE: * indicates variable not considered in sensitivity analysis due to correlations.

L_Divides_a. Depth of permeable soil on divides of the Fortymile Wash fan (RMEI location) (cm). *Distribution:* Uniform. *Range:* 102 to 140. *Symbol:* L_d. *Additional Information:* This parameter is constrained using field measurements from soil pits dug into inter-channel divides of the Fortymile Wash alluvial fan. Permeable soil depths were measured at several locations on the Fortymile Wash alluvial fan. The model uses a different depth for each of the two sub-domains in the RMEI location (channels and divides). As the permeable depth increases, the mass of radionuclides that will diffuse into the soil over time (and thus move below the biosphere depth) increases. Capturing the lower bound of the possible permeable depth is necessary to assure conservative model results. The permeable depth in the channel subdomain was inferred from the measurements made on the divides. *Sensitivity Name:* LDIVIDE. *Location in TSPA-LA:* Table 6.5-5. *DTN:* MO0702PAFARDAT.001_R3 [DIRS 182578]. *References: Redistribution of Tephra and Waste by Geomorphic Processes Following a Potential Volcanic Eruption at Yucca Mountain, Nevada* (SNL 2007 [DIRS 179347], Section 6.3.2, 6.5.5.1 and 7.1.3; Tables 4.1-4, 6.4-1 and 6.5.5-1).
LC_rate_a. Crevice corrosion (localized corrosion) propagation rate (mm/yr). *Distribution:* Log uniform. *Range:* 0.0127 to 1.27. *Additional Information:* Localized corrosion rate or crevice corrosion propagation rate. The crevice corrosion penetration model assumes that, when it occurs, crevice corrosion propagates at a (time-independent) constant rate. Variation in this parameter values is attributed to uncertainty. *Sensitivity Name:* WDLCRATE. *Location in TSPA-LA:* Sections 6.3.5.2.1, 6.3.5.2.2, 6.3.5.2.3, 6.3.5.3.2 and 6.3.5.4; Table 6.3.5-4. *DTN:* MO0703PAGENCOR.001_R4 [DIRS 182029]. *References: General Corrosion and Localized Corrosion of Waste Package Outer Barrier* (SNL 2007 [DIRS 178519], Sections 6.4.4.7 and 7.2.5; Table 8-3).
LDISP. Logarithm of longitudinal dispersivity (m). *Distribution:* Right truncated normal. *Range*: $-\infty$ to 3.5. *Mean:* 2.0. *Standard Deviation:* 0.75. *Symbol:* α_L. *Additional Information:* Represents variation in the longitudinal dispersivity of all the saturated zone units. Longitudinal dispersivity will be important only at the leading edge of the advancing plume; transverse dispersivity (horizontal transverse and vertical transverse) is the strongest control on plume spreading and possible dilution within the aquifer. To treat the one- and three-dimensional transport through the SZ consistently, the sampled values used to generate the saturated zone breakthrough curves are also used in the TSPA-LA Model. These values are tabulated as 200 sets of values for the SZ parameters, accounting for appropriate correletions, and are entered into the TSPA model as a table of 200 values for each parameter. The TSPA-LA Model selects values from this table using the Goldsim variable SZ_index_a. *Sensitivity Name:* SZLODISP. *Location in TSPA-LA:* Section 6.3.10.2; Table 6.3.10-2. *DTN:* SN0702PASZFTMA.002_R1 [DIRS 183471]. *References: Saturated Zone Flow and Transport Model Abstraction* (SNL 2008 [DIRS 183750], Sections 6.3.1 and 6.5.2.9; Tables 4-3, 6-8, 7-1[a], A-1[a] and B-1; Equations 6-27 to 6-29; Figures 6-18 and 6-19).
Log_Specific_SA_CSNF_a. Logarithm of the effective specific surface area (m^2/mg) of the representative CSNF waste form (dimensionless). *Distribution:* Triangular. *Range:* -7.3 to -5.4. *Most Likely:* -6.7. *Symbol:* $Log_{10}(A)$. *Additional Information:* The radionuclide release rate form the CSNF matrix under alkaline conditions (pH ≥ 6.8) is modeled as the fractional matrix dissolution rate (d^{-1}) which has the following mathematical form: Log (F) = Log (A) + a0 + a1 * IT + a2 * pCO_3 + a3 * pO_2. Where Log (F) = Base 10 log of the fractional dissolution rate of the fuel (d^{-1}), IT = Inverse temperature (K^{-1}), pCO_3 = Negative base 10 log of total carbonate (molar). pO_2 = Negative base 10 log of oxygen pressure (atmospheres), Log (A) = Base 10 log of the fuel effective specific surface area (m^2/mg), and a0, a1, a2, a3 = Regression parameters for the dissolution rate per unit area. *Sensitivity Name:* CSSPECSA. *Location in TSPA-LA:* Sections 6.3.7.4.1.2 and 6.3.7.4.1.3; Tables 6.3.7-30 and 6.3.7-31; Equations 6.3.7-5 and 6.3.7-6. *DTN:* MO0404ANLSF001.001_R0 [DIRS 169007]. *References: CSNF Waste Form Degradation: Summary Abstraction* (BSC 2004 [DIRS 169987], Sections 4.1.3, 5.2, 6.2.2.3, 6.4.1, 8.1 and 8.2; Equations 13 and 14; Tables 8-2 and 8-3).
LogK_Uncert_Lith_a. Logarithm of the mean fracture permeability in lithophysal rock units (dimensionless). *Distribution:* Triangular. *Range:* -0.92 to 0.92. *Mode:* 0. *Symbol:* log k. *Additional Information:* Ambient seepage is a function of three key parameters: capillary strength, permeability, and percolation flux. The ambient seepage results derived from the seepage model for performance assessment provide the basis for the quantitative evaluation of seepage as a function of these key hydrological properties. The log(k) is used to select the mean and standard deviation of seepage flow. The units for the value of k must be m^2 prior to calculating the logarithm. *Sensitivity Name:* SEEPPRM. *Location in TSPA-LA:* Sections 6.3.5.2.3, 6.3.3.1.2 and 6.3.3.1.3; Tables 6.3.5-4, 6.3.3-2 and 6.3.3-3. *DTN:* LB0407AMRU0120.001_R0 [DIRS 173280], *Summary_seepage_abstraction.doc. References: Abstraction of Drift Seepage* (SNL 2007 [DIRS 181244], Section 6.6.3).

Table K3-3. Detailed Summary of Epistemically Uncertain Variables (i.e., elements of **e**) Considered in the TSPA-LA (TSPA Parameter Name) (Continued)

NOTE: * indicates variable not considered in sensitivity analysis due to correlations.

LogK_Uncert_NonLith_a. Logarithm of the mean fracture permeability in non-lithophysal rock units (dimensionless). *Distribution:* Triangular. *Range:* -0.68 to 0.68. *Mode:* 0. *Symbol:* log k. *Additional Information:* See LogK_Uncert_Lith_a. *Sensitivity Name:* SEEPPRMN. *Location in TSPA-LA:* Sections 6.3.5.2.3, 6.3.3.1.2 and 6.3.3.1.3; Tables 6.3.5-4, 6.3.3-2 and 6.3.3-3. *DTN:* LB0407AMRU0120.001_R0 [DIRS 173280], *Summary_seepage_abstraction.doc. References: Abstraction of Drift Seepage* (SNL 2007 [DIRS 181244], Section 6.6.3).
Mass_Decrease_Const_GE10_a. Mass loading decrease rate constant (1/yr). *Distribution:* Triangular. *Range:* 0.125 to 1. *Mode:* 0.2. *Symbol:* λ. *Additional Information:* Mass loading decreases exponentially with time after the eruption. The mass loading decrease rate constant depends on the ash thickness. Selected distribution is based in part on the influence of ash redistribution on changes in mass loading through time. The ash redistribution model considers the interchannel divides separately from the distributary channels that carry redistributed ash. These areas can have a different thickness of ash or ash mixed with soil, and thus different mass loading decrease rate constants. To account for these differences, it is recommended that the mass loading decrease rate constant used in the TSPA model is that for the greater of the contaminated soil thickness in the distributary channels and interchannel divides. Because the thickness of the redistributed ash in the channels is likely to be greater than the threshold depth of 10 mm, it is reasonable to always use the mass loading decrease rate constant for the thicker contaminated layer. *Sensitivity Name:* MASSDCRS. *Location in TSPA-LA:* Equation 6.3.11-5. *DTN:* MO0702PAVBPDCF.000_R0 [DIRS 179330]. *References: Biosphere Model Report* (SNL 2007 [DIRS 177399], Section 6.12.3; Tables 6.6-3 and 6.7-1; Equation 6.12-3).
MIC_RHThresh_a. Relative humidity threshold for initiating microbially induced corrosion (dimensionless). *Distribution:* Uniform. *Range:* 0.75 to 0.9. *Additional Information:* MIC effects are applied when the relative humidity at the waste package surface is greater than a threshold relative humidity sampled from a uniform distribution between 75% and 90%. A uniform distribution has been chosen for the MIC relative humidity threshold because this statistical distribution is recommended when the upper and lower bounds of the distribution are reasonably well known, but only a low state of knowledge exists about how the MIC relative humidity threshold varies between these bounds. Consistent with the aforementioned low state of knowledge, the variation in the MIC relative humidity threshold is considered solely due to uncertainty. *Sensitivity Name:* WDMICRHT. *Location in TSPA-LA:* Sections 6.3.5.1.2 and 6.3.5.1.3; Tables 6.3.5-3 and 6.3.5-4. *DTN:* MO0703PAGENCOR.001_R4 [DIRS 182029]. *References: General Corrosion and Localized Corrosion of Waste Package Outer Barrier* (SNL 2007 [DIRS 178519], Sections 1.2, 4.1.1.7, 6.3.3, 6.4.5.1 and 8.2; Table 8-1).
n_SCC_a. Stress corrosion cracking growth rate exponent (repassivation slope) (dimensionless). *Distribution:* Truncated normal. *Range:* 0.935 to 1.395. *Mean:* 1.165. *Standard Deviation:* 0.115. *Symbol:* n. *Additional Information:* The threshold stress intensity factor is a function of the repassivation slope and mean general corrosion rate. Crack growth velocity is a function of the stress-intensity factor and repassivation slope. Uncertainty in the crack growth and in the stress-intensity factor threshold is represented by the uncertainty in the repassivation slope. The repassivation slope is sampled once for every realization in the TSPA model. *Sensitivity Name:* WDNSCC. *Location in TSPA-LA:* Sections 6.3.5.1.2 and 6.3.5.4; Table 6.3.5-3; Equations 6.3.5-13 and 6.3.5-14. *DTN:* MO0702PASTRESS.002_R2 [DIRS 180514], File: Model Output DTN.doc. *References: Stress Corrosion Cracking of Waste Package Outer Barrier and Drip Shield Materials* (SNL 2007 [DIRS 181953], Sections 6.4.4.4, 8.4.2.3 and 8.4.3; Tables 6-7, 8-1, 8-5, 8-6 and 8-15; Equations 4, 5, 70 and 71).
NiO_SA_a. Specific surface area of NiO (m^2/g). *Distribution:* Uniform. *Range:* 1 to 30. *Symbol:* S_{NiO}. *Additional Information:* See Cr2O3_SA_a. The properties of hematite (Fe_2O_3), goethite (FeOOH), hydrous ferric oxide (HFO), Cr_2O_3, and NiO are used for calculating the amount of water adsorbed onto stationary corrosion product surfaces. *Sensitivity Name:* NIOSA. *Location in TSPA-LA:* Table 6.3.8-4; S_{CP} in Equation 6.3.8-19. *DTN:* SN0703PAEBSRTA.001_R3 [DIRS 183217]. *References: EBS Radionuclide Transport Abstraction* (SNL 2007 [DIRS 177407], Sections 6.3.4.3.3 and 6.5.2.2; Tables 6.5-7 and 8.2-4).
Np2O5_Eps_1_high_a*. Logarithm of the scale factor used to characterize uncertainty in Np_2O_5 solubility for ionic strength values between 1 and 3 molal (dimensionless). *Distribution:* Truncated normal. *Range:* -1.7 to 1.7. *Mean:* 0. *Standard Deviation:* 0.85. *Correlation:* Correlated to Np2O5_Eps_1_low_a. *Symbol:* ε_1. *Additional Information:* See Am_Eps_1_low_a. *Sensitivity Name:* EP1HINP2*. *Location in TSPA-LA:* Sections 6.3.7.5.1 and 6.3.7.5.2; Table 6.3.7-42; Equation 6.3.7-13a. *DTN: MO0702PADISCON.001_R0* [DIRS 179358], Tables 3 & 19. *References: Dissolved Concentration Limits of Elements with Radioactive Isotopes* (SNL 2007 [DIRS 177418], Sections 6.6 and 8.1.2; Equations 6.6-5 and 8-1; Table 6.6-11).

Table K3-3. Detailed Summary of Epistemically Uncertain Variables (i.e., elements of **e**) Considered in the TSPA-LA (TSPA Parameter Name) (Continued)

NOTE: * indicates variable not considered in sensitivity analysis due to correlations.

Np2O5_Eps_1_low_a. Logarithm of the scale factor used to characterize uncertainty in Np_2O_5 solubility at an ionic strength below 1 molal (dimensionless). *Distribution:* Truncated normal. *Range:* -1.6 to 1.6. *Mean:* 0. *Standard Deviation:* 0.8. *Correlation:* Correlated to Np2O5_Eps_1_high_a with a correlation factor of 1. *Symbol:* ε_1. *Additional Information:* See Am_Eps_1_low_a. This model is applied only in the invert. *Sensitivity Name:* EP1NP2O5. *Location in TSPA-LA:* Sections 6.3.7.5.1 and 6.3.7.5.2; Table 6.3.7-42; Equation 6.3.7-13a. *DTN: MO0702PADISCON.001_R0* [DIRS 179358], Tables 3 & 19. *References: Dissolved Concentration Limits of Elements with Radioactive Isotopes* (SNL 2007 [DIRS 177418], Sections 6.6 and 8.1.2; Equations 6.6-5 and 8-1; Table 6.6-11).
Np2O5_Eps_2_CDSP_High_a*. Term associated with uncertainty in Np_2O_5 solubility due to variations in fluoride concentration for CDSP waste packages when ionic strength is greater than or equal to 0.004 molal and for the invert below CDSP waste packages (mg/L). *Distribution:* Triangular. *Range:* 0 to 853. *Most Likely:* 0. *Correlation:* Correlated to Am_Eps_2_CSNF_High_a. *Symbol:* $\varepsilon_2^{\text{CDSP-F-high}}$, $\varepsilon_2^{\text{CDSP-invert}}$. *Additional Information:* See Am_Eps_2_CSNF_High_a. *Sensitivity Name:* EP2CDNP2*. *Location in TSPA-LA:* Sections 6.3.7.5.1 and 6.3.7.5.2; Table 6.3.7-42; Equation 6.3.7-13a. *DTN:* MO0702PAFLUORI.000_R1 [DIRS 181219], Table 5. *References: Dissolved Concentration Limits of Elements with Radioactive Isotopes* (SNL 2007 [DIRS 177418], Sections 6.6 and 8.1.2; Equations 6.6-5 and 8-1; Table 6.6-11).
Np2O5_Eps_2_CSNF_High_a*. Term associated with uncertainty in Np_2O_5 solubility due to variations in fluoride concentration for CSNF waste packages when ionic strength is greater than or equal to 0.2 molal and for the invert below CSNF waste packages (mg/L). *Distribution:* Triangular. *Range:* 0 to 197. *Most Likely:* 0. *Correlation:* Correlated to Am_Eps_2_CSNF_High_a. *Symbol:* $\varepsilon_2^{\text{CSNF-high}}$, $\varepsilon_2^{\text{CSNF-invert}}$. *Additional Information:* See Am_Eps_2_CSNF_High_a. *Sensitivity Name:* EP2CSNP2*. *Location in TSPA-LA:* Sections 6.3.7.5.1 and 6.3.7.5.2; Table 6.3.7-42; Equation 6.3.7-13a. *DTN:* MO0702PAFLUORI.000_R1 [DIRS 181219], Table 5. *References: Dissolved Concentration Limits of Elements with Radioactive Isotopes* (SNL 2007 [DIRS 177418], Sections 6.6 and 8.1.2; Equations 6.6-5 and 8-1; Table 6.6-11).
Np2O5_Eps_2_Glass_Low_a*. Term associated with uncertainty in Np_2O_5 solubility due to variations in fluoride concentration for CDSP waste packages Cell 1a, Cell 1b when ionic strength is less than 0.004 molal, and CSNF waste packages when ionic strength is less than 0.2 molal (mg/L). *Distribution:* Triangular. *Range:* 0 to 11. *Most Likely:* 0. *Correlation:* Correlated to Am_Eps_2_CSNF_High_a. *Symbol:* $\varepsilon_2^{\text{CSNF-low}}$, $\varepsilon_2^{\text{CDSP-Glass}}$, $\varepsilon_2^{\text{CDSP-F-low}}$. *Additional Information:* See Am_Eps_2_CSNF_High_a. *Sensitivity Name:* EP2LONP2*. *Location in TSPA-LA:* Sections 6.3.7.5.1 and 6.3.7.5.2; Table 6.3.7-42; Equation 6.3.7-13a. *DTN:* MO0702PAFLUORI.000_R1 [DIRS 181219], Table 5. *References: Dissolved Concentration Limits of Elements with Radioactive Isotopes* (SNL 2007 [DIRS 177418], Sections 6.6 and 8.1.2; Equations 6.6-5 and 8-1; Table 6.6-11).
NpO2_Eps_1_high_a*. Logarithm of the scale factor used to characterize uncertainty in NpO_2 solubility at an ionic strength between 1 and 3 molal (dimensionless). *Distribution:* Truncated normal. *Range:* -1.34 to 1.34. *Mean:* 0. *Standard Deviation:* 0.67. *Correlation:* Correlated to NpO2_Eps_1_low_a. *Symbol:* ε_1. *Additional Information:* See Am_Eps_1_low_a. *Sensitivity Name:* EP1HINPO2*. *Location in TSPA-LA:* Sections 6.3.7.5.1, 6.3.7.5.2 and 6.3.7.5.3; Table 6.3.7-43; Equation 6.3.7-13a. *DTN: MO0702PADISCON.001_R0* [DIRS 179358], Tables 2 & 19. *References: Dissolved Concentration Limits of Elements with Radioactive Isotopes* (SNL 2007 [DIRS 177418], Sections 6.6 and 8.1.2; Equations 6.6-2 and 8-1; Table 6.6-5).
NpO2_Eps_1_low_a. Logarithm of the scale factor used to characterize uncertainty in NpO_2 solubility at an ionic strength below 1 molal (dimensionless). *Distribution:* Truncated normal. *Range:* -1.2 to 1.2. *Mean:* 0. *Standard Deviation:* 0.6. *Correlation:* Correlated to NpO2_Eps_1_high_a with a correlation factor of 1. *Symbol:* ε_1. *Additional Information:* See Am_Eps_1_low_a. This model is applied only within the waste package. *Sensitivity Name:* EP1NPO2. *Location in TSPA-LA:* Sections 6.3.7.5.1, 6.3.7.5.2 and 6.3.7.5.3; Table 6.3.7-43; Equation 6.3.7-13a. *DTN: MO0702PADISCON.001_R0* [DIRS 179358], Tables 2 & 19. *References: Dissolved Concentration Limits of Elements with Radioactive Isotopes* (SNL 2007 [DIRS 177418], Sections 6.6 and 8.1.2; Equations 6.6-2 and 8-1; Table 6.6-5).
NpO2_Eps_2_CDSP_High_a*. Term associated with uncertainty in NpO_2 solubility due to variations in fluoride concentration for CDSP waste packages when ionic strength is greater than or equal to 0.004 molal and for the invert below CDSP waste packages (mg/L). *Distribution:* Triangular. *Range:* 0 to 1093.5. *Most Likely:* 0. *Correlation:* Correlated to Am_Eps_2_CSNF_High_a. *Symbol:* $\varepsilon_2^{\text{CDSP-F-high}}$, $\varepsilon_2^{\text{CDSP-invert}}$. *Additional Information:* See Am_Eps_2_CSNF_High_a. *Sensitivity Name:* EP2CDNPO2*. *Location in TSPA-LA:* Sections 6.3.7.5.1, 6.3.7.5.2 and 6.3.7.5.3; Table 6.3.7-43; Equation 6.3.7-13a. *DTN:* MO0702PAFLUORI.000_R1 [DIRS 181219], Table 3. *References: Dissolved Concentration Limits of Elements with Radioactive Isotopes* (SNL 2007 [DIRS 177418], Sections 6.6 and 8.1.2; Equations 6.6-2 and 8-1; Table 6.6-5).

Table K3-3. Detailed Summary of Epistemically Uncertain Variables (i.e., elements of **e**) Considered in the TSPA-LA (TSPA Parameter Name) (Continued)

NOTE: * indicates variable not considered in sensitivity analysis due to correlations.

NpO2_Eps_2_CSNF_High_a*. Term associated with uncertainty in NpO_2 solubility due to variations in fluoride concentration for CSNF waste packages when ionic strength is greater than or equal to 0.2 molal and for the invert below CSNF waste packages (mg/L). *Distribution:* Triangular. *Range:* 0 to 255.8. *Most Likely:* 0. *Correlation:* Correlated to Am_Eps_2_CSNF_High_a. *Symbol:* $\varepsilon_2^{CSNF\text{-}high}$, $\varepsilon_2^{CSNF\text{-}invert}$. *Additional Information:* See Am_Eps_2_CSNF_High_a. *Sensitivity Name:* EP2CSNPO2*. *Location in TSPA-LA:* Sections 6.3.7.5.1, 6.3.7.5.2 and 6.3.7.5.3; Table 6.3.7-43; Equation 6.3.7-13a. *DTN:* MO0702PAFLUORI.000_R1 [DIRS 181219], Table 3. *References: Dissolved Concentration Limits of Elements with Radioactive Isotopes* (SNL 2007 [DIRS 177418], Sections 6.6 and 8.1.2; Equations 6.6-2 and 8-1; Table 6.6-5).
NpO2_Eps_2_Glass_Low_a*. Term associated with uncertainty in NpO_2 solubility due to variations in fluoride concentration for CDSP waste packages Cell 1a, Cell 1b when ionic strength is less than 0.004 molal, and CSNF waste packages when ionic strength is less than 0.2 molal (mg/L). *Distribution:* Triangular. *Range:* 0 to 14.1. *Most Likely:* 0. *Correlation:* Correlated to Am_Eps_2_CSNF_High_a. *Symbol:* $\varepsilon_2^{CSNF\text{-}low}$, $\varepsilon_2^{CDSP\text{-}Glass}$, $\varepsilon_2^{CDSP\text{-}F\text{-}low}$. *Additional Information:* See Am_Eps_2_CSNF_High_a. *Sensitivity Name:* EP2LONPO2*. *Location in TSPA-LA:* Sections 6.3.7.5.1, 6.3.7.5.2 and 6.3.7.5.3; Table 6.3.7-43; Equation 6.3.7-13a. *DTN:* MO0702PAFLUORI.000_R1 [DIRS 181219], Table 3. *References: Dissolved Concentration Limits of Elements with Radioactive Isotopes* (SNL 2007 [DIRS 177418], Sections 6.6 and 8.1.2; Equations 6.6-2 and 8-1; Table 6.6-5).
NVF11. Effective porosity in undifferentiated alluvium (valley fill) (dimensionless). *Distribution:* Truncated normal. *Range:* 0 to 0.3. *Mean:* 0.18. *Standard Deviation:* 0.051. *Additional Information:* See NVF26. *Sensitivity Name:* SZPORUAL. *Location in TSPA-LA:* Table 6.3.10-2. *DTN:* SN0702PASZFTMA.002_R1 [DIRS 183471]. *References: Saturated Zone Flow and Transport Model Abstraction* (SNL 2008 [DIRS 183750], Sections 6.5.2.3 and 6.5.2.14; Tables 7-1[a] and A-1[a]; Figures 6-9 and 6-10).
NVF26. Effective porosity in shallow alluvium (dimensionless). *Distribution:* Truncated normal. *Range:* 0 to 0.3. *Mean:* 0.18. *Standard Deviation:* 0.051. *Additional Information:* In the porous media of the alluvium, sorption is conceptualized to occur in that portion of the aquifer corresponding to the effective porosity of the alluvium. The effective porosity is defined as the fraction of the total volume of the medium through which significant groundwater flow occurs. The effective porosity parameter in the alluvium is used to correctly calculate the pore velocity of groundwater. Effective porosity is important for determining the average linear groundwater velocities used in the simulation of radionuclide transport. Groundwater velocities are rendered more accurate when dead-end pores are eliminated from consideration because they do not transmit water. The effective porosity results from that elimination. To treat the one- and three-dimensional transport through the SZ consistently, the sampled values used to generate the saturated zone breakthrough curves are also used in the TSPA-LA Model. These values are tabulated as 200 sets of values for the SZ parameters, accounting for appropriate correletions, and are entered into the TSPA model as a table of 200 values for each parameter. The TSPA-LA Model selects values from this table using the Goldsim variable SZ_index_a. Parameters NVF26 and NVF11 are new names for parameters NVF19 and NVF7. *Sensitivity Name:* SZPORSAL. *Location in TSPA-LA:* Table 6.3.10-2. *DTN:* SN0702PASZFTMA.002_R1 [DIRS 183471]. *References: Saturated Zone Flow and Transport Model Abstraction* (SNL 2008 [DIRS 183750], Sections 6.5.2.3 and 6.5.2.14; Tables 7-1[a] and A-1[a]; Figures 6-9 and 6-10).
Pa_Eps_1_a. Logarithm of the scale factor used to characterize uncertainty in protactinium solubility (dimensionless). *Distribution:* Uniform. *Range:* -4.42 to -0.05. *Symbol:* ε_1. *Additional Information:* This defines uncertainty in the choice of an analogue for protactinium solubilities. The uncertainty range for protactinium solubility is taken as the difference between the solubilities of neptunium and thorium. For protactinium, no multiplication factor is used in conjunction with □2. *Sensitivity Name:* EP1PA. *Location in TSPA-LA:* Sections 6.3.7.5.2 and 6.3.7.5.3; Table 6.3.7-45; Equation 6.3.7-13b. *DTN: MO0702PADISCON.001_R0*_R0 [DIRS 179358], Tables 9 & 19. *References: Dissolved Concentration Limits of Elements with Radioactive Isotopes* (SNL 2007 [DIRS 177418], Sections 6.11 and 8.1.2; Equations 6.11-2 and 8-2; Table 6.11-4).
Pa_Eps_2_CDSP_High_a*. Term associated with uncertainty in protactinium solubility due to variations in fluoride concentration for CDSP waste packages when ionic strength is greater than or equal to 0.004 molal and for the invert below CDSP waste packages (mg/L). *Distribution:* Triangular. *Range:* 0 to 853. *Most Likely:* 0. *Correlation:* Correlated to Am_Eps_2_CSNF_High_a. *Symbol:* $\varepsilon_2^{CDSP\text{-}F\text{-}high}$, $\varepsilon_2^{CDSP\text{-}invert}$. *Additional Information:* See Am_Eps_2_CSNF_High_a. *Sensitivity Name:* EP2CDPA*. *Location in TSPA-LA:* Sections 6.3.7.5.2 and 6.3.7.5.3; Table 6.3.7-45; Equation 6.3.7-13b. *DTN:* MO0702PAFLUORI.000_R1 [DIRS 181219], Table 15. *References: Dissolved Concentration Limits of Elements with Radioactive Isotopes* (SNL 2007 [DIRS 177418], Sections 6.11 and 8.1.2; Equations 6.11-2 and 8-2; Table 6.11-4).

Table K3-3. Detailed Summary of Epistemically Uncertain Variables (i.e., elements of **e**) Considered in the TSPA-LA (TSPA Parameter Name) (Continued)

NOTE: * indicates variable not considered in sensitivity analysis due to correlations.

Pa_Eps_2_CSNF_High_a*. Term associated with uncertainty in protactinium solubility due to variations in fluoride concentration for CSNF waste packages when ionic strength is greater than or equal to 0.2 molal and for the invert below CSNF waste packages (mg/L). *Distribution:* Triangular. *Range:* 0 to 197. *Most Likely:* 0. *Correlation:* Correlated to Am_Eps_2_CSNF_High_a. *Symbol:* $\varepsilon_2^{\text{CSNF-high}}$, $\varepsilon_2^{\text{CSNF-invert}}$. *Additional Information:* See Am_Eps_2_CSNF_High_a. *Sensitivity Name:* EP2CSPA*. *Location in TSPA-LA:* Sections 6.3.7.5.2 and 6.3.7.5.3; Table 6.3.7-45; Equation 6.3.7-13b. *DTN:* MO0702PAFLUORI.000_R1 [DIRS 181219], Table 15. *References: Dissolved Concentration Limits of Elements with Radioactive Isotopes* (SNL 2007 [DIRS 177418], Sections 6.11 and 8.1.2; Equations 6.11-2 and 8-2; Table 6.11-4).
Pa_Eps_2_Glass_Low_a*. Term associated with uncertainty in protactinium solubility due to variations in fluoride concentration for CDSP waste packages Cell 1a, Cell 1b when ionic strength is less than 0.004 molal, and CSNF waste packages when ionic strength is less than 0.2 molal (mg/L). *Distribution:* Triangular. *Range:* 0 to 11. *Most Likely:* 0. *Correlation:* Correlated to Am_Eps_2_CSNF_High_a. *Symbol:* $\varepsilon_2^{\text{CSNF-low}}$, $\varepsilon_2^{\text{CDSP-Glass}}$, $\varepsilon_2^{\text{CDSP-F-low}}$. *Additional Information:* See Am_Eps_2_CSNF_High_a. *Sensitivity Name:* EP2LOPA*. *Location in TSPA-LA:* Sections 6.3.7.5.2 and 6.3.7.5.3; Table 6.3.7-45; Equation 6.3.7-13b. *DTN:* MO0702PAFLUORI.000_R1 [DIRS 181219], Table 15. *References: Dissolved Concentration Limits of Elements with Radioactive Isotopes* (SNL 2007 [DIRS 177418], Sections 6.11 and 8.1.2; Equations 6.11-2 and 8-2; Table 6.11-4).
PCE_Cl_MU_RH_0_20_a. The in-drift precipitated/salts (IDPS) process model uncertainty factor for the logarithm of the chloride concentration of the in-drift waters at relative humidity ≤20% (dimensionless). *Distribution:* Triangular. *Range:* -0.7 to 0.7. *Most Likely:* 0. *Additional Information:* The P&CE seepage dilution/evaporation abstraction instructs TSPA to apply IDPS uncertainties on key chemical parameters. IDPS uncertainty factors for the Cl, N, Cl:N, and I of in-drift water are used directly by the P&CE abstraction models. Four values are extracted from the seepage evaporation/dilution lookup tables: pH, I, Cl, and N. Cl, N, and Cl:N are assumed to be correlated. The P&CE abstraction models use the molal concentrations of Cl and N to represent Cl^- and NO_3^- concentrations. *Sensitivity Name:* RHMU0. *Location in TSPA-LA:* Sections 6.3.4, 6.3.4.2, 6.3.4.3.1, 6.3.4.3.2 and 6.3.5.2.3; Tables 6.3.4-2, 6.3.4-3 and 6.3.5-4. *DTN:* SN0703PAEBSPCE.007_R2 [DIRS 184141]. *References: Engineered Barrier System: Physical and Chemical Environment* (SNL 2007 [DIRS 177412], Sections 4.1.17.1 and 6.12.3; Tables 4.1-10 and 6.12-1; Figure 6.6-18).
PCE_Cl_MU_RH_20_40_a. The IDPS process model uncertainty factor for the logarithm of the chloride concentration of the in-drift waters at relative humidity >20 and ≤40% (dimensionless). *Distribution:* Triangular. *Range:* -0.5 to 0.5. *Most Likely:* 0. *Additional Information:* See PCE_Cl_MU_RH_0_20_a. *Sensitivity Name:* RHMU20. *Location in TSPA-LA:* Sections 6.3.4, 6.3.4.2, 6.3.4.3.1, 6.3.4.3.2 and 6.3.5.2.3; Tables 6.3.4-2, 6.3.4-3 and 6.3.5-4. *DTN:* SN0703PAEBSPCE.007_R2 [DIRS 184141]. *References: Engineered Barrier System: Physical and Chemical Environment* (SNL 2007 [DIRS 177412], Sections 4.1.17.1 and 6.12.3; Tables 4.1-10 and 6.12-1; Figure 6.6-18).
PCE_Cl_MU_RH_40_65_a. The IDPS process model uncertainty factor for the logarithm of the chloride concentration of the in-drift waters at relative humidity >40 and ≤65% (dimensionless). *Distribution:* Triangular. *Range:* -0.4 to 0.4. *Most Likely:* 0. *Additional Information:* See PCE_Cl_MU_RH_0_20_a. *Sensitivity Name:* RHMU40. *Location in TSPA-LA:* Sections 6.3.4, 6.3.4.2, 6.3.4.3.1, 6.3.4.3.2 and 6.3.5.2.3; Tables 6.3.4-2, 6.3.4-3 and 6.3.5-4. *DTN:* SN0703PAEBSPCE.007_R2 [DIRS 184141]. *References: Engineered Barrier System: Physical and Chemical Environment* (SNL 2007 [DIRS 177412], Sections 4.1.17.1 and 6.12.3; Tables 4.1-10 and 6.12-1; Figure 6.6-18).
PCE_Cl_MU_RH_65_85_a. The IDPS process model uncertainty factor for the logarithm of the chloride concentration of the in-drift waters at relative humidity >65 and ≤85% (dimensionless). *Distribution:* Triangular. *Range:* -0.1 to 0.1. *Most Likely:* 0. *Additional Information:* See PCE_Cl_MU_RH_0_20_a. *Sensitivity Name:* RHMU65. *Location in TSPA-LA:* Sections 6.3.4, 6.3.4.2, 6.3.4.3.1, 6.3.4.3.2 and 6.3.5.2.3; Tables 6.3.4-2, 6.3.4-3 and 6.3.5-4. *DTN:* SN0703PAEBSPCE.007_R2 [DIRS 184141]. *References: Engineered Barrier System: Physical and Chemical Environment* (SNL 2007 [DIRS 177412], Sections 4.1.17.1 and 6.12.3; Tables 4.1-10 and 6.12-1; Figure 6.6-18).
PCE_Cl_MU_RH_85_100_a*. The IDPS process model uncertainty factor for the logarithm of the chloride concentration of the in-drift waters at relative humidity >85% (dimensionless). *Distribution:* Triangular. *Range:* 0 to 0. *Most Likely:* 0. *Additional Information:* See PCE_Cl_MU_RH_0_20_a. *Sensitivity Name:* RHMU85*. *Location in TSPA-LA:* Sections 6.3.4, 6.3.4.2, 6.3.4.3.1, 6.3.4.3.2 and 6.3.5.2.3; Tables 6.3.4-2, 6.3.4-3 and 6.3.5-4. *DTN:* SN0703PAEBSPCE.007_R2 [DIRS 184141]. *References: Engineered Barrier System: Physical and Chemical Environment* (SNL 2007 [DIRS 177412], Sections 4.1.17.1 and 6.12.3; Tables 4.1-10 and 6.12-1; Figure 6.6-18).

Table K3-3. Detailed Summary of Epistemically Uncertain Variables (i.e., elements of **e**) Considered in the TSPA-LA (TSPA Parameter Name) (Continued)

NOTE: * indicates variable not considered in sensitivity analysis due to correlations.

PCE_Cl_N_MU_RH_40_65_a. The IDPS process model uncertainty factor for the logarithm of the chloride + nitrate concentration of the in-drift waters at relative humidity >40% and ≤65% (dimensionless). *Distribution:* Triangular. *Range:* -0.57 to 0.57. *Most Likely:* 0. *Additional Information:* The P&CE seepage dilution/evaporation abstraction instructs TSPA to apply IDPS uncertainties on key chemical parameters. The uncertainty associated with Cl+N is calculated assuming linear combinations of the uncertainties on Cl and N provided by the IDPS model. Four values are extracted from the seepage evaporation/dilution lookup tables: pH, I, Cl, and N. .The P&CE abstraction models use the molal concentrations of Cl and N to represent Cl^- and NO_3^- concentrations. In the event of no salt separation, take the Cl+N concentrations from the lookup tables, sample the [Cl+N] uncertainty using the appropriate relative humidity range by applying a triangular distribution, and calculate ([Cl+N] + uncertainty). *Sensitivity Name:* RHMUN40. *Location in TSPA-LA:* Sections 6.3.4.3.2 and 6.3.5.2.3; Tables 6.3.4-2, 6.3.4-3 and 6.3.5-4. *DTN:* SN0703PAEBSPCE.007_R2 [DIRS 184141], Spreadsheet: PCE_IDPS_Uncertainties.xls. *References: Engineered Barrier System: Physical and Chemical Environment* (SNL 2007 [DIRS 177412], Sections 4.1.17.1 and 6.12.3; Tables 4.1-10 and 6.12-1; Figure 6.6-18).
PCE_Cl_N_MU_RH_65_85_a. The IDPS process model uncertainty factor for the logarithm of the chloride + nitrate concentration of the in-drift waters at relative humidity >65% and ≤85% (dimensionless). *Distribution:* Triangular. *Range:* -0.22 to 0.22. *Most Likely:* 0. *Additional Information:* See PCE_Cl_N_MU_RH_40_65_a. *Sensitivity Name:* RHMUN65. *Location in TSPA-LA:* Sections 6.3.4.3.2 and 6.3.5.2.3; Tables 6.3.4-2, 6.3.4-3 and 6.3.5-4. *DTN:* SN0703PAEBSPCE.007_R2 [DIRS 184141], Spreadsheet: PCE_IDPS_Uncertainties.xls. *References: Engineered Barrier System: Physical and Chemical Environment* (SNL 2007 [DIRS 177412], Sections 4.1.17.1 and 6.12.3; Tables 4.1-10 and 6.12-1; Figure 6.6-18).
PCE_Cl_N_MU_RH_85_100_a*. The IDPS process model uncertainty factor for the logarithm of the chloride + nitrate concentration of the in-drift waters at relative humidity >85% (dimensionless). *Distribution:* Triangular. *Range:* 0 to 0. *Most Likely:* 0. *Additional Information:* See PCE_Cl_N_MU_RH_40_65_a. *Sensitivity Name:* RHMUN85*. *Location in TSPA-LA:* Sections 6.3.4.3.2 and 6.3.5.2.3; Tables 6.3.4-2, 6.3.4-3 and 6.3.5-4. *DTN:* SN0703PAEBSPCE.007_R2 [DIRS 184141], Spreadsheet: PCE_IDPS_Uncertainties.xls. *References: Engineered Barrier System: Physical and Chemical Environment* (SNL 2007 [DIRS 177412], Sections 4.1.17.1 and 6.12.3; Tables 4.1-10 and 6.12-1; Figure 6.6-18).
PCE_Cl_NO3_MU_RH_0_20_a. The IDPS process model uncertainty factor for the logarithm of the chloride to nitrate ratio of the in-drift waters at relative humidity ≤20% (dimensionless). *Distribution:* Triangular. *Range:* -1.4 to 1.4. *Most Likely:* 0. *Additional Information:* See PCE_Cl_MU_RH_0_20_a. *Sensitivity Name:* RHMUNO0. *Location in TSPA-LA:* Sections 6.3.4.3.1, 6.3.4.3.2 and 6.3.5.2.3; Tables 6.3.4-2, 6.3.4-3 and 6.3.5-4. *DTN:* SN0703PAEBSPCE.007_R2 [DIRS 184141], Spreadsheet: PCE_IDPS_Uncertainties.xls. *References: Engineered Barrier System: Physical and Chemical Environment* (SNL 2007 [DIRS 177412], Sections 4.1.17.1 and 6.12.3; Tables 4.1-10 and 6.12-1; Figure 6.6-18).
PCE_Cl_NO3_MU_RH_20_65_a. The IDPS process model uncertainty factor for the logarithm of the chloride to nitrate ratio of the in-drift waters at relative humidity >20% and ≤65% (dimensionless). *Distribution:* Triangular. *Range:* -0.5 to 0.5. *Most Likely:* 0. *Additional Information:* See PCE_Cl_MU_RH_0_20_a. *Sensitivity Name:* RHMUNO20. *Location in TSPA-LA:* Sections 6.3.4.3.1, 6.3.4.3.2 and 6.3.5.2.3; Tables 6.3.4-2, 6.3.4-3 and 6.3.5-4. *DTN:* SN0703PAEBSPCE.007_R2 [DIRS 184141], Spreadsheet: PCE_IDPS_Uncertainties.xls. *References: Engineered Barrier System: Physical and Chemical Environment* (SNL 2007 [DIRS 177412], Sections 4.1.17.1 and 6.12.3; Tables 4.1-10 and 6.12-1; Figure 6.6-18).
PCE_Cl_NO3_MU_RH_65_85_a. The IDPS process model uncertainty factor for the logarithm of the chloride to nitrate ratio of the in-drift waters at relative humidity >65% and ≤85% (dimensionless). *Distribution:* Triangular. *Range:* -0.2 to 0.2. *Most Likely:* 0. *Additional Information:* See PCE_Cl_MU_RH_0_20_a. *Sensitivity Name:* RHMUNO65. *Location in TSPA-LA:* Sections 6.3.4.3.1, 6.3.4.3.2 and 6.3.5.2.3; Tables 6.3.4-2, 6.3.4-3 and 6.3.5-4. *DTN:* SN0703PAEBSPCE.007_R2 [DIRS 184141], Spreadsheet: PCE_IDPS_Uncertainties.xls. *References: Engineered Barrier System: Physical and Chemical Environment* (SNL 2007 [DIRS 177412], Sections 4.1.17.1 and 6.12.3; Tables 4.1-10 and 6.12-1; Figure 6.6-18).
PCE_Cl_NO3_MU_RH_85_100_a*. The IDPS process model uncertainty factor for the logarithm of the chloride to nitrate ratio of the in-drift waters at low relative humidity >85% (dimensionless). *Distribution:* Triangular. *Range:* 0 to 0. *Most Likely:* 0. *Additional Information:* See PCE_Cl_MU_RH_0_20_a. *Sensitivity Name:* RHMUNO85*. *Location in TSPA-LA:* Sections 6.3.4.3.1, 6.3.4.3.2 and 6.3.5.2.3; Tables 6.3.4-2, 6.3.4-3 and 6.3.5-4. *DTN:* SN0703PAEBSPCE.007_R2 [DIRS 184141], Spreadsheet: PCE_IDPS_Uncertainties.xls. *References: Engineered Barrier System: Physical and Chemical Environment* (SNL 2007 [DIRS 177412], Sections 4.1.17.1 and 6.12.3; Tables 4.1-10 and 6.12-1; Figure 6.6-18).

Table K3-3. Detailed Summary of Epistemically Uncertain Variables (i.e., elements of **e**) Considered in the TSPA-LA (TSPA Parameter Name) (Continued)

NOTE: * indicates variable not considered in sensitivity analysis due to correlations.

PCE_Delta_pCO2_a. Selector variable for partial pressure of CO_2 (dimensionless). *Distribution:* Uniform. *Range:* -1 to 1. *Additional Information:* Calculating the pCO_2 in the drift is difficult because it is the result of competing processes such as degassing, precipitation, and diffusion and advection of gas in the fractures. The minimum potential pCO_2 is calculated from the bounding case of high gas flow through fractures. The maximum potential pCO_2 could occur if the drift were a completely closed system and the water moved down through the temperature field without degassing. TSPA uses this uniform stochastic variable to choose which case to use in each realization. A negative value of the variable implies using the minimum pCO_2 case and a positive value implies the maximum pCO_2 case. The actual pCO_2 in the drift is calculated by scaling between ambient (0.001 bars) and the minimum or maximum, using the absolute value of PCE_Delta_pCO2_a as the scaling factor. This scaling accounts for the uncertainty in the in-drift pCO_2. pCO_2 is determined at the beginning of each TSPA realization. *Sensitivity Name:* DELPPCO2. *Location in TSPA-LA:* Sections 6.3.4.2 and 6.3.5.2.3; Table 6.3.5-4. *References: Engineered Barrier System: Physical and Chemical Environment* (SNL 2007 [DIRS 177412], Sections 6.1, 6.7.2, 6.9.1, 6.12.2.1, 6.12.4.2, 6.13, 6.15.1, 7.1.2.2, 7.1.3.3, 7.1.4.2 and 7.2.3).
PCE_Gp1_Cl_NO3_CDF_a. Ratio of Cl to NO_3 (Cl:N) in Group 1 pore waters (dimensionless). *Distribution:* Discrete. *Range:* 0.783 to 6.1213. *Additional Information:* Elemental ratios such as Cl:N are important in assessing the potential for localized corrosion of the waste package in the EBS environment. The localized corrosion model is one of the most important downstream models, and it is based on an empirical fit to the pH, temperature, chloride concentration, and Cl:N values of the solutions used in the corrosion experiments. There is uncertainty associated with the distribution of Cl:N ratios among all the available waters. *Sensitivity Name:* GP1NO3. *Location in TSPA-LA:* Section 6.3.4.3.2. *DTN:* SN0703PAEBSPCE.007_R2 [DIRS 184141], Spreadsheet Cl_NO3_CDFs.xls. *References: Engineered Barrier System: Physical and Chemical Environment* (SNL 2007 [DIRS 177412], Sections 4.1.2, 4.1.17.1, 6.12.2.1 and 6.12.3; Tables 4.1-1, 4.1-4, 4.1-10 and 6.12-1; Figure 6.6-18).
PCE_Gp2_Cl_NO3_CDF_a. Ratio of Cl to NO_3 (Cl:N) in Group 2 pore waters (dimensionless). *Distribution:* Discrete. *Range:* 2.359 to 3.187. *Additional Information:* See PCE_Gp1_Cl_NO3_CDF_a. *Sensitivity Name:* GP2NO3. *Location in TSPA-LA:* Section 6.3.4.3.2. *DTN:* SN0703PAEBSPCE.007_R2 [DIRS 184141], Spreadsheet Cl_NO3_CDFs.xls. *References: Engineered Barrier System: Physical and Chemical Environment* (SNL 2007 [DIRS 177412], Sections 4.1.2, 4.1.17.1, 6.12.2.1 and 6.12.3, Tables 4.1-1, 4.1-4, 4.1-10 and 6.12-1, Figure 6.6-18).
PCE_Gp3_Cl_NO3_CDF_a. Ratio of Cl to NO_3 (Cl:N) in Group 3 pore waters (dimensionless). *Distribution:* Discrete. *Range:* 9.7782 to 64.128. *Additional Information:* See PCE_Gp1_Cl_NO3_CDF_a. *Sensitivity Name:* GP3NO3. *Location in TSPA-LA:* Section 6.3.4.3.2. *DTN:* SN0703PAEBSPCE.007_R2 [DIRS 184141], Spreadsheet Cl_NO3_CDFs.xls. *References: Engineered Barrier System: Physical and Chemical Environment* (SNL 2007 [DIRS 177412], Sections 4.1.2, 4.1.17.1, 6.12.2.1 and 6.12.3; Tables 4.1-1, 4.1-4, 4.1-10 and 6.12-1; Figure 6.6-18).
PCE_Gp4_Cl_NO3_CDF_a. Ratio of Cl to NO_3 (Cl:N) in Group 4 pore waters (dimensionless). *Distribution:* Discrete. *Range:* 4.4485 to 8.2119. *Additional Information:* See PCE_Gp1_Cl_NO3_CDF_a. *Sensitivity Name:* GP4NO3. *Location in TSPA-LA:* Section 6.3.4.3.2. *DTN:* SN0703PAEBSPCE.007_R2 [DIRS 184141], Spreadsheet Cl_NO3_CDFs.xls *References: Engineered Barrier System: Physical and Chemical Environment* (SNL 2007 [DIRS 177412], Sections 4.1.2, 4.1.17.1, 6.12.2.1 and 6.12.3; Tables 4.1-1, 4.1-4, 4.1-10 and 6.12-1; Figure 6.6-18).
PCE_I_Uncert_RH_85_100_a. The IDPS process model uncertainty factor for the logarithm of the ionic strength of the in-drift waters at high relative humidity (≥85%) (log molal). *Distribution:* Triangular. *Range:* -0.1 to 0.1. *Mean/Median/Mode:* 0. *Additional Information:* IDPS uncertainty factors for the Cl, N, Cl:N, and I of in-drift water are used directly by the Physical and Chemical Environment (P&CE) abstraction models. Four values are extracted from the seepage evaporation/dilution lookup tables. No uncertainty is associated with the ionic strength below 85 percent relative humidity from the lookup tables because the ionic strength is not used by TSPA at these concentrations. Between 85 percent and 100 percent relative humidity the ionic strength is adjusted for uncertainty by applying a triangular distribution. Between 100 and 95 percent relative humidity in the drift, the ionic strength of the evaporating solutions exceeds 1 molal. At the lower relative humidity conditions, concentrations of well over 10 molal are possible. The key chemical parameters that are provided to TSPA-LA by the P&CE dilution/evaporation abstraction model are pH, ionic strength, Cl^- and NO_3^- as a function of relative humidity. *Sensitivity Name:* RHI85. *Location in TSPA-LA:* Section 6.4.1; Tables 6.4-1 and 6.4-2; Figure 6.4-4. *DTN:* SN0703PAEBSPCE.007_R2 [DIRS 184141]. *References: Engineered Barrier System: Physical and Chemical Environment* (SNL 2007 [DIRS 177412], Sections 4.1.17.1, 6.2.1.1.2, 6.12.3 and 6.13.3; Tables 4.1-10, 6.9-1 and 6.12-1; Equation 6.2-8).

Table K3-3. Detailed Summary of Epistemically Uncertain Variables (i.e., elements of **e**) Considered in the TSPA-LA (TSPA Parameter Name) (Continued)

NOTE: * indicates variable not considered in sensitivity analysis due to correlations.

PCE_pH_Uncert_RH_0_65_a. The IDPS process model uncertainty factor for the pH of the in-drift waters at relative humidity ≤65% (dimensionless). *Distribution:* Triangular. *Range:* -2 to 2. *Most Likely:* 0. *Additional Information:* The uncertainties for pH represent uncertainties in the evaporative evolution of pH in unbuffered systems. The uncertainty in pH may be reduced by considering pH buffering reactions in specific systems. The pH value is taken directly from the lookup tables and is adjusted by the uncertainties using a triangular distribution for relative humidity values below 75 percent. The IDPS process model provides feeds to the P&CE model, which in turn provides water chemistries, including pH, for evaluating the occurrence of localized corrosion of the waste package outer barrier and the solubility of radionuclides in the invert. Included in the IDPS feeds are estimated model uncertainties in water compositional parameters, including the predicted pH. *Sensitivity Name:* RHPH0. *Location in TSPA-LA:* Table 6.3.5-4. *DTN:* SN0703PAEBSPCE.007_R2 [DIRS 184141], Spreadsheet: PCE_IDPS_Uncertainties.xls. *References: Engineered Barrier System: Physical and Chemical Environment* (SNL 2007 [DIRS 177412], Sections 4.1.17.1, 6.9.5, 6.12.3 and 6.13; Tables 4.1-11, 6.12-2 and 7.2-1; Figures 6.9-1 and 6.9-3).
PCE_pH_Uncert_RH_65_75_a. The IDPS process model uncertainty factor for the pH of the in-drift waters at relative humidity >65 and ≤75% (dimensionless). *Distribution:* Triangular. *Range:* -1 to 1. *Most Likely:* 0. *Additional Information:* See PCE_pH_Uncert_RH_0_65_a. *Sensitivity Name:* RHPH65. *Location in TSPA-LA:* Table 6.3.5-4 *DTN:* SN0703PAEBSPCE.007_R2 [DIRS 184141], Spreadsheet: PCE_IDPS_Uncertainties.xls. *References: Engineered Barrier System: Physical and Chemical Environment* (SNL 2007 [DIRS 177412], Sections 4.1.17.1, 6.9.5, 6.12.3 and 6.13; Tables 4.1-11, 6.12-2 and 7.2-1; Figures 6.9-1 and 6.9-3).
PCE_pH_Uncert_RH_75_100_a. The IDPS process model uncertainty factor for the pH of the in-drift waters at relative humidity >75% (dimensionless). *Distribution:* Discrete. *Range:* -0.3123 to 0.4288. *Additional Information:* See PCE_pH_Uncert_RH_0_65_a. Between 100 perecent to 75 percent relative humidity, pH uncertainties are sampled from a discrete CDF. *Sensitivity Name:* RHPH75. *Location in TSPA-LA:* Table 6.3.5-4 *DTN:* SN0703PAEBSPCE.007_R2 [DIRS 184141], Spreadsheet: Re-evaluation of pH uncertainty.xls, tab: CDF of pH uncertainty. *References: Engineered Barrier System: Physical and Chemical Environment* (SNL 2007 [DIRS 177412], Sections 4.1.17.1, 6.9.5, 6.12.3 and 6.13; Tables 4.1-11, 6.12-2 and 7.2-1; Figures 6.9-1 and 6.9-3).
pH_Cell2_Regression_Error_a. Error term in regression equation for pH of corrosion products domain (dimensionless). *Distribution:* Truncated normal. *Range:* -0.64 to 0.64. *Mean/Median/Mode:* 0. *Standard Deviation:* 0.32. *Symbol:* E. *Additional Information:* The pH for the corrosion products domain (Cell 2) is computed by applying the following equation: $pH = 4.5342 + 0.6132\ pCO_2 - 0.3805\ \log_{10}[U] - 0.0254\ (\log_{10}[U])^2 + E$, where E is the error term (pH_Cell2_Regression_Error_a). *Sensitivity Name:* PH2RGER. *Location in TSPA-LA:* Equation 6.3.8-27. *DTN:* SN0703PAEBSRTA.001_R3 [DIRS 183217]. *References: EBS Radionuclide Transport Abstraction* (SNL 2007 [DIRS 177407], Sections 6.5.2.4.5 and 6.5.2.4.6; Equation 6.5.2.4.6-2).
Pu_Eps_1_high_a*. Logarithm of the scale factor used to characterize uncertainty in plutonium solubility for ionic strength between 1 and 3 molal (dimensionless). *Distribution:* Truncated normal. *Range:* -1.52 to 1.52. *Mean:* 0. *Standard Deviation:* 0.76. *Correlation:* Correlated to Pu_Eps_1_low_a with a correlation factor of 1. *Symbol:* ε_1. *Additional Information:* See Am_Eps_1_low_a. *Sensitivity Name:* EP1HIPU*. *Location in TSPA-LA:* Sections 6.3.7.5.1, 6.3.7.5.2 and 6.3.7.5.3; Table 6.3.7-44; Equation 6.3.7-13a. *DTN: MO0702PADISCON.001_R0* [DIRS 179358], Tables 1 & 19. *References: Dissolved Concentration Limits of Elements with Radioactive Isotopes* (SNL 2007 [DIRS 177418], Sections 6.5 and 8.1.2; Equations 6.5-1, 6.5-2 and 8.1; Table 6.5-5).
Pu_Eps_1_low_a. Logarithm of the scale factor used to characterize uncertainty in plutonium solubility at an ionic strength below 1 molal (dimensionless). *Distribution:* Truncated normal. *Range:* -1.4 to 1.4. *Mean/Median/Mode:* 0. *Standard Deviation:* 0.7. *Correlation:* Correlated to Pu_Eps_1_high_a with a correlation factor of 1. *Symbol:* ε_1. *Additional Information:* See Am_Eps_1_low_a. *Sensitivity Name:* EP1LOWPU. *Location in TSPA-LA:* Sections 6.3.7.5.1, 6.3.7.5.2 and 6.3.7.5.3; Table 6.3.7-44; Equation 6.3.7-13a. *DTN: MO0702PADISCON.001_R0* [DIRS 179358], Tables 1 & 19. *References: Dissolved Concentration Limits of Elements with Radioactive Isotopes* (SNL 2007 [DIRS 177418], Sections 6.5 and 8.1.2; Equations 6.5-1, 6.5-2 and 8-1; Table 6.5-5).
Pu_Eps_2_CDSP_High_a*. Term associated with uncertainty in plutonium solubility due to variations in fluoride concentration for CDSP waste packages when ionic strength is greater than or equal to 0.004 molal and for the invert below CDSP waste packages (mg/L). *Distribution:* Triangular. *Range:* 0 to 5460. *Most Likely:* 0. *Correlation:* Correlated to Am_Eps_2_CSNF_High_a. *Symbol:* $\varepsilon_2^{\text{CDSP-F-high}}$, $\varepsilon_2^{\text{CDSP-invert}}$. *Additional Information:* See Am_Eps_2_CSNF_High_a. *Sensitivity Name:* EP2CDPU*. *Location in TSPA-LA:* Sections 6.3.7.5.1, 6.3.7.5.2 and 6.3.7.5.3; Table 6.3.7-44; Equation 6.3.7-13a. *DTN:* MO0702PAFLUORI.000_R1 [DIRS 181219], Table 1. *References: Dissolved Concentration Limits of Elements with Radioactive Isotopes* (SNL 2007 [DIRS 177418], Sections 6.5 and 8.1.2; Equations 6.5-1, 6.5-2 and 8-1; Table 6.5-5).

Table K3-3. Detailed Summary of Epistemically Uncertain Variables (i.e., elements of **e**) Considered in the TSPA-LA (TSPA Parameter Name) (Continued)

NOTE: * indicates variable not considered in sensitivity analysis due to correlations.

Pu_Eps_2_CSNF_High_a*. Term associated with uncertainty in plutonium solubility due to variations in fluoride concentration for CSNF waste packages when ionic strength is greater than or equal to 0.2 molal and for the invert below CSNF waste packages (mg/L). *Distribution:* Triangular. *Range:* 0 to 1374. *Most Likely:* 0. *Correlation:* Correlated to Am_Eps_2_CSNF_High_a. *Symbol:* $\varepsilon_2^{\text{CSNF-high}}$, $\varepsilon_2^{\text{CSNF-invert}}$. *Additional Information:* See Am_Eps_2_CSNF_High_a. *Sensitivity Name:* EP2CSPU*. *Location in TSPA-LA:* Sections 6.3.7.5.1, 6.3.7.5.2 and 6.3.7.5.3; Table 6.3.7-44; Equation 6.3.7-13a. *DTN:* MO0702PAFLUORI.000_R1 [DIRS 181219], Table 1. *References: Dissolved Concentration Limits of Elements with Radioactive Isotopes* (SNL 2007 [DIRS 177418], Sections 6.5 and 8.1.2; Equations 6.5-1, 6.5-2 and 8-1; Table 6.5-5).
Pu_Eps_2_Glass_Low_a*. Term associated with uncertainty in plutonium solubility due to variations in fluoride concentration for CDSP waste packages Cell 1a, Cell 1b when ionic strength is less than 0.004 molal, and CSNF waste packages when ionic strength is less than 0.2 molal (mg/L). *Distribution:* Triangular. *Range:* 0 to 79. *Most Likely:* 0. *Correlation:* Correlated to Am_Eps_2_CSNF_High_a. *Symbol:* $\varepsilon_2^{\text{CSNF-low}}$, $\varepsilon_2^{\text{CDSP-Glass}}$, $\varepsilon_2^{\text{CDSP-F-low}}$. *Additional Information:* See Am_Eps_2_CSNF_High_a. *Sensitivity Name:* EP2LOWPU*. *Location in TSPA-LA:* Sections 6.3.7.5.1, 6.3.7.5.2 and 6.3.7.5.3; Table 6.3.7-44; Equation 6.3.7-13a. *DTN:* MO0702PAFLUORI.000_R1 [DIRS 181219], Table 1. *References: Dissolved Concentration Limits of Elements with Radioactive Isotopes* (SNL 2007 [DIRS 177418], Sections 6.5 and 8.1.2; Equations 6.5-1, 6.5-2 and 8-1; Table 6.5-5).
Relative_Abundance_Goethite_a. Fraction of total iron oxide that is goethite (dimensionless). *Distribution:* Uniform. *Range:* 0.45 to 0.8. *Additional Information:* Mass fraction of iron oxide that is goethite. The relative abundance of goethite and hydrous ferric oxide (HFO) is uncertain and affects the sorption sites per unit water volume for both the stationary corrosion products and iron oxyhydroxide colloids. A uniform distribution is used due to lack of data. *Sensitivity Name:* GOERELAB. *Location in TSPA-LA:* Section 6.3.8.2.3; Table 6.3.8-4. *DTN:* SN0703PAEBSRTA.001_R3 [DIRS 183217]. *References: EBS Radionuclide Transport Abstraction* (SNL 2007 [DIRS 177407], Sections 6.3.4.2.3.1 and 6.5.2.4.1; Tables 6.3-5, 6.5-7 and 8.2-4).
Resuspension_Thickness_a. Thickness of combined ash/soil mixture available for resuspension (m). *Distribution:* Uniform. *Range:* 0.001 to 0.003. *Mean/Median/Mode:* 0.002. *Symbol:* d_c. *Additional Information:* This parameter is also known as the critical depth, which the depth of surface soil layer that is available for resuspension. This thin top layer of the surface soil is assumed to always have radionuclide concentrations at equilibrium. Radionuclide concentration in this layer, with dimensions of activity per unit mass, is calculated outside the biosphere model and is the source term for the dose calculations. The mass radionuclide concentration in the resuspendable layer of soil for noncultivated land is used to calculate the radionuclide concentration in air, which then is used to estimate the human inhalation dose. *Sensitivity Name:* RSUSTHIK. *Location in TSPA-LA:* Equation 6.3.11-6. *DTN:* MO0702PAVBPDCF.000_R0 [DIRS 179330]. *References: Biosphere Model Report* (SNL 2007 [DIRS 177399], Equations 6.4.1-6, 6.4.1-29, 6.4.1-30, 6.4.1-32 and 6.12-2).
Rind_Porosity_CSNF_a. Porosity in CSNF rind (dimensionless). *Distribution:* Uniform. *Range:* 0.05 to 0.3. *Additional Information:* In addition to the adsorption isotherm, the density of rind solids, the rind specific surface area, and the rind porosity are needed to evaluate the water saturation. *Sensitivity Name:* CSRINDPO. *Location in TSPA-LA:* Section 6.3.8.2.1; Table 6.3.8-6. *DTN:* MO0411SPACLDDG.003_R1 [DIRS 180755]. *References: Cladding Degradation Summary for LA* (SNL 2007 [DIRS 180616], Section 6.5; Table 7-1[a]).
Schoepite_Boltwoodite_Interp_a. Fractional value used to interpolate between Schoepite and Boltwoodite look-up tables (dimensionless). *Distribution:* Uniform. *Range:* 0 to 1. *Additional Information:* This parameter was developed by TSPA and is used in the TSPA-LA Model to determine the fractional value that is used to interpolate between schoepite and Na-Boltwoodite look-up tables. This fractional value is sampled at the beginning of a realization and is used for the entire pH and log fCO_2 range throughout an entire realization. *Sensitivity Name:* SCHOBOLT. *Location in TSPA-LA:* Table 6.3.7-58. *DTN:* MO0702PADISCON.001_R0 [DIRS 179358]. *References: Dissolved Concentration Limits of Elements with Radioactive Isotopes* (SNL 2007 [DIRS 177418]).

Table K3-3. Detailed Summary of Epistemically Uncertain Variables (i.e., elements of **e**) Considered in the TSPA-LA (TSPA Parameter Name) (Continued)

NOTE: * indicates variable not considered in sensitivity analysis due to correlations.

Scour_Depth_a. Scour depth in Fortymile Wash at the fan apex (cm). *Distribution:* Uniform. *Range:* 73 to 122. *Symbol:* H. *Additional Information:* This parameter represents an effective scour depth within the channels at and below the apex of the Fortymile Wash alluvial fan. This input parameter is used as an estimate of the tephra mixing depth at the RMEI location and as a calibration for scour depth estimated throughout the upper drainage basin. The depth to which tephra and channel sediment are mixed is the scour depth. The ratio of the tephra thickness to the scour depth at the fan apex, just upstream from the RMEI location, is used as the fraction of channel-bed material composed of tephra when the redistributed tephra and waste reach the RMEI location. The scour depth at the fan apex is directly proportional to the amount of dilution (and to initial waste concentration) predicted in the channel domain by the model. In the upper drainage domain, as the scour depth across the grid increases (e.g., due to larger flood events) the amount of dilution will increase and the waste concentration within the channels of the upper drainage basin domain will tend to decrease. The concentration calculated at the fan apex is applied (in addition to direct deposition) throughout the RMEI channel subdomain, so a decrease in concentration will translate into a lower dose rate. Therefore, it is especially important to capture the lower end of the scour depth range. The greater the scour depth the greater the overall mass stored in the channels, and the higher the potential associated dose. As the scour depth increases, the normalized concentration increases. Deeper scour depth results in a lower initial concentration, and slower diffusion into the medium. At equilibrium conditions, the competing effects of scour depth on the lower and upper drainage basins cancel each other out, and the resulting concentration in the channel is independent of scour depth. Thus scour depth only influences the dose for non-equilibrium times. Until the concentration equilibrates, the calculated concentrations in the channels will be higher for shallower scour depths, making it essential to capture the lower bound of scour depth range. *Sensitivity Name:* SC_DPTH. *Location in TSPA-LA:* Table 6.5-5. *DTN:* MO0704PASCOURD.000_R1 [DIRS 182149]. *References: Redistribution of Tephra and Waste by Geomorphic Processes Following a Potential Volcanic Eruption at Yucca Mountain, Nevada* (SNL 2007 [DIRS 179347], Sections 6.2.2, 6.3.2, 6.5.6, 6.6.1 and 7.1.3; Figure 6.6.1-1; Tables 6.4-1 and 6.5.6-1).
Seepage_Condensation_Prob_a*. Pointer variable to determine the seepage/condensation regime for the first failed waste package in a percolation subregion (dimensionless). *Distribution:* Uniform. *Range:* 0 to 1. *Additional Information:* Parameter determined within TSPA. *Sensitivity Name:* SEEPCON*. *Output DTN:* MO0708TSPAGENT.000_R0 [DIRS 183000].
Seepage_Uncertainty_a. Uncertainty factor to account for small-scale heterogeneity in fracture permeability (dimensionless). *Distribution:* Uniform. *Range:* 0 to 1. *Additional Information:* At each location in the UZ flow grid, the Seepage Model for PA (SMPA) computes a distribution of seepage rates - at this stage the uncertainty arises from small-scale parameters (capillary strength and permeability). Once the distributions are known at each location, Seepage_Uncertainty_a determines the actual seepage value. The percentile indicated by the sampled value of Seepage_Uncertainty_a is applied to all grid locations. Ambient seepage is derived in a random process using predictive seepage simulations that provide seepage results as a function of the seepage-relevant parameters. For a particular set of these parameters, randomly sampled from the respective distributions, the mean seepage rate and its inherent estimation uncertainty, expressed by the standard deviation over the 20 realizations conducted, are linearly interpolated between the table values. The standard deviation is used to define a uniform uncertainty distribution. A seepage uncertainty value is then randomly sampled from this distribution and used to adjust the mean seepage values, giving the final ambient seepage rate for the considered parameter set. Conducting this procedure over a large number of random parameter sets results in the final distribution of ambient seepage. *Sensitivity Name:* SEEPUNC. *Location in TSPA-LA:* Section 6.3.3.1.2; Tables 6.3.3-3 and 6.3.5-4. *DTN:* LB0407AMRU0120.001_R0 [DIRS 173280]. *References: Abstraction of Drift Seepage* (SNL 2007 [DIRS 181244], Sections 6.5.1.3, 6.5.2.2, 6.8 and 8.1; Tables 6.8-3 and 6-12[a]).
Seepage_Water_Type_a. Pointer variable used to select which seepage water type in used in the physical and chemical environment (P&CE) submodel calculations (dimensionless). *Distribution:* Discrete. *Range:* 1 to 4. *Additional Information:* This parameter randomly selects which seepage water type is used in P&CE submodel calculations. The starting water type determines which CO_2 profile and which P&CE Water Bin map is used in the TSPA chemical environment calculations. *Sensitivity Name:* SEEPWAT. *Location in TSPA-LA:* Table 6.3.5-4. *References: Engineered Barrier System: Physical and Chemical Environment* (SNL 2007 [DIRS 177412], Sections 5.2.2, 6.3, 6.6, 6.6.5, 6.9, 6.12.3 and 6.15.1; Tables 6.13-5).

Table K3-3. Detailed Summary of Epistemically Uncertain Variables (i.e., elements of **e**) Considered in the TSPA-LA (TSPA Parameter Name) (Continued)

NOTE: * indicates variable not considered in sensitivity analysis due to correlations.

Sn_Eps_high_a*. Logarithm of the scale factor used to characterize uncertainty in tin solubility for high ionic strength conditions (dimensionless). *Distribution:* Truncated normal. *Range:* -1.08 to 1.08. *Mean:* 0. *Standard Deviation:* 0.54. *Correlation:* Correlated to Sn_Eps_low_a with a correlation factor of 1. *Symbol:* ε_1. *Additional Information:* See Am_Eps_1_low_a. *Sensitivity Name:* EP1HISN*. *Location in TSPA-LA:* Sections 6.3.7.5.2 and 6.3.7.5.3; Table 6.3.7-47; Equation 6.3.7-13a. *DTN:* MO0702PADISCON.001_R0 [DIRS 179358], Tables 16 & 19. *References: Dissolved Concentration Limits of Elements with Radioactive Isotopes* (SNL 2007 [DIRS 177418], Sections 6.19 and 8.1.2; Equations 6.19-12 and 8-1; Table 6.19-5).
Sn_Eps_low_a. Logarithm of the scale factor used to characterize uncertainty in tin solubility for low ionic strength conditions (dimensionless). *Distribution:* Truncated normal. *Range:* -0.9 to 0.9. *Mean/Median/Mode:* 0. *Standard Deviation:* 0.45. *Correlation:* Correlated to Sn_Eps_high_a with a correlation factor of 1. *Symbol:* ε_1. *Additional Information:* See Am_Eps_1_low_a. *Sensitivity Name:* EP1LOWSN. *Location in TSPA-LA:* Sections 6.3.7.5.2 and 6.3.7.5.3; Table 6.3.7-47; Equation 6.3.7-13a. *DTN:* MO0702PADISCON.001_R0 [DIRS 179358], Tables 16 & 19. *References: Dissolved Concentration Limits of Elements with Radioactive Isotopes* (SNL 2007 [DIRS 177418], Sections 6.19 and 8.1.2; Equations 6.19-12 and 8-1; Table 6.19-5).
Soil_Density_a. Density of surface soil correlated with the volcanic BDCFs (kg/m^3). *Distribution:* Triangular. *Range:* 1300 to 1700. *Mean/Median/Mode:* 1500. *Additional Information:* In the channels, where the ash is mixed with soil and diluted, the density of resuspendable layer, ρ_c, can be approximated by the density of soil, ρ_s. The waste volumetric concentration can be converted to waste mass concentration in the soil by dividing it by the density of the resuspendable layer, ρ_c. In the interchannel divides, the density of the resuspendable layer, ρ_c, can be calculated from the known tephra thickness, d_a, and density, ρ_a, and surface soil density, ρ_s. Provided to TSPA-LA as a table of 1000 values sampled in correlation with the volcanic BDCFs. *Sensitivity Name:* SOILDENS. *Location in TSPA-LA:* Equation 6.3.11-6. *DTN:* MO0702PAVBPDCF.000_R0 [DIRS 179330]. *References: Biosphere Model Report* (SNL 2007 [DIRS 177399], Sections 6.4.1.1, 6.5.1.1 and 6.12.3; Equations 6.4.1-6, 6.5.1-2 and 6.13-2; Tables 6.6.3 and 6.8-2);).
Specific_SA_Smectite_Col_a. Specific surface area for smectite colloids (m^2/g). *Distribution:* Uniform. *Range:* 10 to 100. *Symbol:* $SA_{Smectite,\ coll}$. *Additional Information:* The surface area and site density values provide a means for limiting total sorption. Available surface area will depend on conditions of secondary mineral precipitation that depend on multiple factors. *Sensitivity Name:* SMECSA. *Location in TSPA-LA:* Table 6.3.7-62. *DTN:* MO0701PAGLASWF.000_R1 [DIRS 180393]. *References: Waste Form and In-Drift Colloids-Associated Radionuclide Concentrations: Abstraction and Summary* (SNL 2007 [DIRS 177423], Section 6.3.2.4.1; Table 6-24).
SRC1X. Relative x location of point source in source region 1 (dimensionless). *Distribution:* Uniform. *Range:* 0 to 1. *Additional Information:* This parameter is used to determine the point source locations for three dimensional discharge from the unsaturated zone to the saturated zone. Point source locations are directly correlated to the saturated zone breakthrough curves. The parameter values are drawn from an independent, uniform distribution and tabulated into a one-dimensional look-up table of 200 random values for input to the TSPA model. The result is a randomly located point source within each of the four source regions for each realization of the SZ flow and transport abstraction model. To treat the one- and three-dimensional transport through the SZ consistently, the sampled values used to generate the saturated zone breakthrough curves are also used in the TSPA-LA Model. These values are tabulated as 200 sets of values for the SZ parameters, accounting for appropriate correletions, and are entered into the TSPA model as a table of 200 values for each parameter. The TSPA-LA Model selects values from this table using the Goldsim variable SZ_index_a. *Sensitivity Name:* SZSREG1X. *Location in TSPA-LA:* Section 6.3.10.2; Table 6.3.10-2. *DTN:* SN0702PASZFTMA.002_R1 [DIRS 183471]. *References: Saturated Zone Flow and Transport Model Abstraction* (SNL 2008 [DIRS 183750], Sections 6.5.2.13 and 7.4.2[a]; Tables 6-8, A-1[a] and B-1).
SRC1Y. Relative y location of point source in source region 1 (dimensionless). *Distribution:* Uniform. *Range:* 0 to 1. *Additional Information:* See SRC1X. *Sensitivity Name:* SZSREG1Y. *Location in TSPA-LA:* Section 6.3.10.2; Table 6.3.10-2. *DTN:* SN0702PASZFTMA.002_R1 [DIRS 183471]. *References: Saturated Zone Flow and Transport Model Abstraction* (SNL 2008 [DIRS 183750], Sections 6.5.2.13 and 7.4.2[a]; Tables 6-8, A-1[a] and B-1).
SRC2X. Relative x location of point source in source region 2 (dimensionless). *Distribution:* Uniform. *Range:* 0 to 1. *Additional Information:* See SRC1X. *Sensitivity Name:* SZSREG2X. *Location in TSPA-LA:* Section 6.3.10.2; Table 6.3.10-2. *DTN:* SN0702PASZFTMA.002_R1 [DIRS 183471]. *References: Saturated Zone Flow and Transport Model Abstraction* (SNL 2008 [DIRS 183750], Sections 6.5.2.13 and 7.4.2[a]; Tables 6-8, A-1[a] and B-1).

Table K3-3. Detailed Summary of Epistemically Uncertain Variables (i.e., elements of **e**) Considered in the TSPA-LA (TSPA Parameter Name) (Continued)

NOTE: * indicates variable not considered in sensitivity analysis due to correlations.

SRC2Y. Relative y location of point source in source region 2 (dimensionless). *Distribution:* Uniform. *Range:* 0 to 1. *Additional Information:* See SRC1X. *Sensitivity Name:* SZSREG2Y. *Location in TSPA-LA:* Section 6.3.10.2; Table 6.3.10-2. *DTN:* SN0702PASZFTMA.002_R1 [DIRS 183471]. *References: Saturated Zone Flow and Transport Model Abstraction* (SNL 2008 [DIRS 183750], Sections 6.5.2.13 and 7.4.2[a]; Tables 6-8, A-1[a] and B-1).
SRC3X. Relative x location of point source in source region 3 (dimensionless). *Distribution:* Uniform. *Range:* 0 to 1. *Additional Information:* See SRC1X. *Sensitivity Name:* SZSREG3X. *Location in TSPA-LA:* Section 6.3.10.2; Table 6.3.10-2. *DTN:* SN0702PASZFTMA.002_R1 [DIRS 183471]. *References: Saturated Zone Flow and Transport Model Abstraction* (SNL 2008 [DIRS 183750], Sections 6.5.2.13 and 7.4.2[a]; Tables 6-8, A-1[a] and B-1).
SRC3Y. Relative y location of point source in source region 3 (dimensionless). *Distribution:* Uniform. *Range:* 0 to 1. *Additional Information:* See SRC1X. *Sensitivity Name:* SZSREG3Y. *Location in TSPA-LA:* Section 6.3.10.2; Table 6.3.10-2. *DTN:* SN0702PASZFTMA.002_R1 [DIRS 183471]. *References: Saturated Zone Flow and Transport Model Abstraction* (SNL 2008 [DIRS 183750], Sections 6.5.2.13 and 7.4.2[a]; Tables 6-8, A-1[a] and B-1).
SRC4X. Relative x location of point source in source region 4 (dimensionless). *Distribution:* Uniform. *Range:* 0 to 1. *Additional Information:* See SRC1X. *Sensitivity Name:* SZSREG4X. *Location in TSPA-LA:* Section 6.3.10.2; Table 6.3.10-2. *DTN:* SN0702PASZFTMA.002_R1 [DIRS 183471]. *References: Saturated Zone Flow and Transport Model Abstraction* (SNL 2008 [DIRS 183750], Sections 6.5.2.13 and 7.4.2[a]; Tables 6-8, A-1[a] and B-1).
SRC4Y. Relative y location of point source in source region 4 (dimensionless). *Distribution:* Uniform. *Range:* 0 to 1. *Additional Information:* See SRC1X. *Sensitivity Name:* SZSREG4Y. *Location in TSPA-LA:* Section 6.3.10.2; Table 6.3.10-2. *DTN:* SN0702PASZFTMA.002_R1 [DIRS 183471]. *References: Saturated Zone Flow and Transport Model Abstraction* (SNL 2008 [DIRS 183750], Sections 6.5.2.13 and 7.4.2[a]; Tables 6-8, A-1[a] and B-1).
SS_Corrosion_Rate_a. Stainless steel corrosion rate (μm/yr). *Distribution:* Truncated log normal. *Range:* 0.01 to 0.51. *Mean/Median/Mode:* 0.267. *Standard Deviation:* 0.209. *Symbol:* r_{SS}. *Additional Information:* This value is used for computing the mass of stationary corrosion products in the waste package. To characterize the uncertainty in stainless steel corrosion rates, a truncated lognormal distribution was developed applying Bayesian updating. The lower bound was chosen to be the approximate mean general corrosion rate of Alloy 22 on the basis that Stainless Steel Type 316 is recognized to corrode faster than Alloy 22. The upper bound is chosen the largest measured rate so as not to extend the already high rates any higher. From these rates and the thicknesses of the steel components, the lifetime of each type of steel is computed. The extent of corrosion, specifically, the mass of corrosion products, is interpolated over the lifetime of each type of steel. Although this interpolation provides a reasonable means for approximating the mass of corrosion product in the interior of a waste package over time as it degrades, there is still uncertainty as to the actual mass of corrosion product. *Sensitivity Name:* CORRATSS. *Location in TSPA-LA:* Tables 6.3.8-1 and 6.3.8-4. *DTN:* SN0703PAEBSRTA.001_R3 [DIRS 183217]. *References: EBS Radionuclide Transport Abstraction*, (SNL 2007 [DIRS 177407], Sections 6.3.4.3.4.3, 6.5.2.2.1 and Appendix F; Tables 4.1-1, 6.5-7, 8.2-4 and 8.2-7; Equation 6.5.2.2.1-2).
Stress_Thresh_A22_a. Residual stress threshold for SCC nucleation of Alloy 22 (as a percentage of yield strength in MPa) (dimensionless). *Distribution:* Uniform. *Range:* 90 to 105. *Correlation:* Correlated to Stress_Thresh_SCC_a with a correlation factor of 1. *Additional Information:* The threshold stress (Stress_Thresh_A22) is taken to be 90% to 105% of the yield strength. Inputs to the slip dissolution mechanism include threshold stress, threshold stress intensity factor, an incipient crack size, and crack-growth-rate parameters. *Sensitivity Name:* SCCTHRP. *Location in TSPA-LA:* Section 6.6.1.3.7; Table 6.6-2. *DTN:* MO070PASTRESS.002_R2 [DIRS 180514]. *References:* Stress Corrosion Cracking of Waste Package Outer Barrier and Drip Shield Materials (SNL 2007 [DIRS 181953], Sections 6.1.1, 6.2.2, and 8.1.1; Tables 6-3, 8-3 and 8-15).
Stress_Thresh_SCC_a. Stress threshold for stress corrosion cracking (MPa). *Distribution:* Uniform. *Range:* 315.9 to 368.55. *Additional Information:* See Stress_Thresh_A22. *Sensitivity Name:* SCCTHR. *Location in TSPA-LA:* Table 6.3.5-3. *DTN:* MO0702PASTRESS.002_R2 [DIRS 180514]. *References:* Stress Corrosion Cracking of Waste Package Outer Barrier and Drip Shield Materials (SNL 2007 [DIRS 181953], Sections 6.1.1, 6.2.2, and 8.1.1; Tables 6-3, 8-3 and 8-15).

Table K3-3. Detailed Summary of Epistemically Uncertain Variables (i.e., elements of **e**) Considered in the TSPA-LA (TSPA Parameter Name) (Continued)

NOTE: * indicates variable not considered in sensitivity analysis due to correlations.

Target_Flux_Out_Ratio_a. Ratio of radionuclide mass associated with colloids (reversible and irreversible) to radionuclide mass associated with colloids and dissolved radionuclide mass (dimensionless). *Distribution:* Uniform. *Range:* 0.9 to 0.99. *Symbol:* F_{RN}. *Additional Information:* The target flux out ratio is a parameter used in the TSPA model calculation of irreversible sorption of Pu and Am onto iron oxyhydroxide colloids in the waste package. This is one of three parameters used to describe limits on the formation of colloids. F_{RN} is defined as: (RN reversibly sorbed to iron oxyhydroxide + RN irreversibly sorbed to iron oxyhydroxide)/(RN reversibly sorbed to iron oxyhydroxide + RN irreversibly sorbed to iron oxyhydroxide + dissolved RN). Can also be written as (concentration of Pu/Am on colloids / (concentration of Pu/Am on colloids + concentration of Pu/Am in water)). *Sensitivity Name:* CFLUXOUT. *Location in TSPA-LA:* Table 6.3.7-65. *DTN:* MO0701PAIRONCO.000_R1 [DIRS 180440]. *References: EBS Radionuclide Transport Abstraction* (SNL 2007 [DIRS 177407], Equations B-27 to B-30); *Waste Form and In-Drift Colloids-Associated Radionuclide Concentrations: Abstraction and Summary* (SNL 2007 [DIRS 177423], Sections 6.3.12.2 and 8.1; Table 6-24).
Th_Eps_1_high_a*. Logarithm of the scale factor used to characterize uncertainty in thorium solubility at ionic strength between 1 and 3 molal (dimensionless). *Distribution:* Truncated normal. *Range:* -1.52 to 1.52. *Mean:* 0. *Standard Deviation:* 0.76. *Correlation:* Correlated to Th_Eps_1_low_a with a correlation factor of 1. *Symbol:* ε_1. *Additional Information:* See Am_Eps_1_low_a. *Sensitivity Name:* EP1HITH*. *Location in TSPA-LA:* Sections 6.3.7.5.1, 6.3.7.5.2 and 6.3.7.5.3; Table 6.3.7-46; Equation 6.3.7-13a. *DTN:* MO0702PADISCON.001_R0 [DIRS 179358], Tables 7 & 19. *References: Dissolved Concentration Limits of Elements with Radioactive Isotopes* (SNL 2007 [DIRS 177418], Sections 6.8 and 8.1.2; Equations 6.8-2 and 8-1; Table 6.8-4).
Th_Eps_1_low_a. Logarithm of the scale factor used to characterize uncertainty in thorium solubility at an ionic strength below 1 molal (dimensionless). *Distribution:* Truncated normal. *Range:* -1.4 to 1.4. *Mean:* 0. *Standard Deviation:* 0.7. *Correlation:* Correlated to Th_Eps_1_high_a with a correlation factor of 1. *Symbol:* ε_1. *Additional Information:* See Am_Eps_1_low_a. *Sensitivity Name:* EP1LOWTH. *Location in TSPA-LA:* Sections 6.3.7.5.1, 6.3.7.5.2 and 6.3.7.5.3; Table 6.3.7-46; Equation 6.3.7-13a. *DTN:* MO0702PADISCON.001_R0 [DIRS 179358], Tables 7 & 19. *References: Dissolved Concentration Limits of Elements with Radioactive Isotopes* (SNL 2007 [DIRS 177418], Sections 6.8 and 8.1.2; Equations 6.8-2 and 8-1; Table 6.8-4).
Th_Eps_2_CDSP_High_a*. Term associated with uncertainty in thorium solubility due to variations in fluoride concentration for CDSP waste packages when ionic strength is greater than or equal to 0.004 molal and for the invert below CDSP waste packages (mg/L). *Distribution:* Triangular. *Range:* 0 to 23723.2. *Most Likely:* 0. *Correlation:* Correlated to Am_Eps_2_CSNF_High_a. *Symbol:* $\varepsilon_2^{\text{CDSP-F-high}}$, $\varepsilon_2^{\text{CDSP-invert}}$. *Additional Information:* See Am_Eps_2_CSNF_High_a. *Sensitivity Name:* EP2CDTH*. *Location in TSPA-LA:* Sections 6.3.7.5.1, 6.3.7.5.2 and 6.3.7.5.3; Table 6.3.7-46; Equation 6.3.7-13a. *DTN:* MO0702PAFLUORI.000_R1 [DIRS 181219], Table 11. *References: Dissolved Concentration Limits of Elements with Radioactive Isotopes* (SNL 2007 [DIRS 177418], Sections 6.8 and 8.1.2; Equations 6.8-2 and 8.1; Table 6.8-4).
Th_Eps_2_CSNF_High_a*. Term associated with uncertainty in thorium solubility due to variations in fluoride concentration for CSNF waste packages when ionic strength is greater than or equal to 0.2 molal and for the invert below CSNF waste packages (mg/L). *Distribution:* Triangular. *Range:* 0 to 7848.3. *Most Likely:* 0. *Correlation:* Correlated to Am_Eps_2_CSNF_High_a. *Symbol:* $\varepsilon_2^{\text{CSNF-high}}$, $\varepsilon_2^{\text{CSNF-invert}}$. *Additional Information:* See Am_Eps_2_CSNF_High_a. *Sensitivity Name:* EP2CSTH*. *Location in TSPA-LA:* Sections 6.3.7.5.1, 6.3.7.5.2 and 6.3.7.5.3; Table 6.3.7-46; Equation 6.3.7-13a. *DTN:* MO0702PAFLUORI.000_R1 [DIRS 181219], Table 11. *References: Dissolved Concentration Limits of Elements with Radioactive Isotopes* (SNL 2007 [DIRS 177418], Sections 6.8 and 8.1.2; Equations 6.8-2 and 8.1; Table 6.8-4).
Th_Eps_2_Glass_Low_a*. Term associated with uncertainty in thorium solubility due to variations in fluoride concentration for CDSP waste packages Cell 1a, Cell 1b when ionic strength is less than 0.004 molal, and CSNF waste packages when ionic strength is less than 0.2 molal (mg/L). *Distribution:* Triangular. *Range:* 0 to 626.2. *Most Likely:* 0. *Correlation:* Correlated to Am_Eps_2_CSNF_High_a. *Symbol:* $\varepsilon_2^{\text{CSNF-low}}$, $\varepsilon_2^{\text{CDSP-Glass}}$, $\varepsilon_2^{\text{CDSP-F-low}}$. *Additional Information:* See Am_Eps_2_CSNF_High_a. *Sensitivity Name:* EP2LOWTH*. *Location in TSPA-LA:* Sections 6.3.7.5.1, 6.3.7.5.2 and 6.3.7.5.3; Table 6.3.7-46; Equation 6.3.7-13a. *DTN:* MO0702PAFLUORI.000_R1 [DIRS 181219], Table 11. *References: Dissolved Concentration Limits of Elements with Radioactive Isotopes* (SNL 2007 [DIRS 177418], Sections 6.8 and 8.1.2; Equations 6.8-2 and 8.1; Table 6.8-4).

Table K3-3. Detailed Summary of Epistemically Uncertain Variables (i.e., elements of **e**) Considered in the TSPA-LA (TSPA Parameter Name) (Continued)

NOTE: * indicates variable not considered in sensitivity analysis due to correlations.

Thermal_Conductivity_Uncert_a. Selector variable for one of three host-rock thermal conductivity scenarios (low, mean, and high) (dimensionless). *Distribution:* Discrete. *Range:* 1 to 3. *Additional Information:* The thermal conductivity uncertainty model provides a discrete distribution between the three conductivity scenarios: Low, Mean, and High thermal conductivity. The three probability weightings for thermal conductivity uncertainty and the three probability weightings for infiltration scenario uncertainty are used to determine the aggregate probability weightings for the five MSTHM Process Model data sets provided as input to the TSPA LA Model. *Sensitivity Name:* THERMCON. *Location in TSPA-LA:* Sections 6.3.2.2, 6.3.2.3, 6.3.5.1.3, 6.3.5.2.3 and 6.6.2.2; Tables 6.3.2-1, 6.3.2-3 and 6.3.5-4. *DTN:* LL0703PA026MST.013_R0 [DIRS 179981]. *References: Multiscale Thermohydrologic Model* (SNL 2007 [DIRS 181383], Sections 6.2.13.3[a], 6.3.4[a] and 6.3.16[a]; Tables 6.3-47[a], 6.3-48[a]).
U_Eps_1_high_Nominal_a*. Logarithm of the scale factor used to characterize uncertainty in uranium solubility under nominal or seismic conditions at an ionic strength between 1and 3 molal (dimensionless). *Distribution:* Truncated normal. *Range:* -1.2 to 1.2. *Mean:* 0. *Standard Deviation:* 0.6. *Correlation:* Correlated to U_Eps_1_low_Nominal_a. *Symbol:* ε_1. *Additional Information:* There are two uranium solubility models: one for CSNF waste packages in nominal and seismic scenarios, and another for CDSP waste packages in all scenarios, CSNF packages breached during an igneous intrusion, and the invert. See Am_Eps_1_low_a. *Sensitivity Name:* EP1HINU*. *Location in TSPA-LA:* Section 6.3.7.5.1, 6.3.7.5.2 and 6.3.7.5.3; Table 6.3.7-54; Equation 6.3.7-13a. *DTN:* MO0702PADISCON.001_R0 [DIRS 179358], Tables 4 & 19. *References: Dissolved Concentration Limits of Elements with Radioactive Isotopes* (SNL 2007 [DIRS 177418], Sections 6.7 and 8.1.2; Equations 6.7-4 and 8.1; Table 6.7-9).
U_Eps_1_high_Other_a*. Logarithm of the scale factor used to characterize uncertainty in uranium solubility under conditions other than nominal and seismic at an ionic strength between 1and 3 molal (dimensionless). *Distribution:* Truncated normal. *Range:* -1.2 to 1.2. *Mean:* 0. *Standard Deviation:* 0.6. *Correlation:* Correlated to U_Eps_1_low_Other_a. *Symbol:* ε_1. *Additional Information:* This is the exponential term associated with uncertainty in uranium solubility below 1 molal ionic strength under conditions of igneous intrusion, all scenarios, and in the invert. Used for CDSP fuel types (all scenarios), CSNF fuel in the igneous scenario and all invert locations. See U_Eps_1_low_Nominal_a. *Sensitivity Name:* EP1HIOU*. *Location in TSPA-LA:* Sections 6.3.7.5.1, 6.3.7.5.2 and 6.3.7.5.3; Table 6.3.7-58; Equation 6.3.7-13a. *DTN:* MO0702PADISCON.001_R0 [DIRS 179358], Tables 5, 6 and 19. *References: Dissolved Concentration Limits of Elements with Radioactive Isotopes* (SNL 2007 [DIRS 177418], Sections 6.7 and 8.1.2; Equations 6.7-4 and 8.1; Table 6.7-11).
U_Eps_1_low_Nominal_a. Logarithm of the scale factor used to characterize uncertainty in uranium solubility under nominal or seismic conditions at an ionic strength below 1 molal (dimensionless). *Distribution:* Truncated normal. *Range:* -1 to 1. *Mean/Median/Mode:* 0. *Standard Deviation:* 0.5. *Correlation:* Correlated to U_Eps_1_high_Nominal_a with a correlation factor of 1. *Symbol:* ε_1. *Additional Information:* There are two uranium solubility models: one for CSNF waste packages in nominal and seismic scenarios, and another for CDSP waste packages in all scenarios, CSNF packages breached during an igneous intrusion, and the invert. See Am_Eps_1_low_a. *Sensitivity Name:* EP1LOWNU. *Location in TSPA-LA:* Section 6.3.7.5.1, 6.3.7.5.2 and 6.3.7.5.3; Table 6.3.7-54; Equation 6.3.7-13a. *DTN:* MO0702PADISCON.001_R0 [DIRS 179358], Tables 4 & 19. *References: Dissolved Concentration Limits of Elements with Radioactive Isotopes* (SNL 2007 [DIRS 177418], Sections 6.7 and 8.1.2; Equations 6.7-4 and 8-1; Table 6.7-9).
U_Eps_1_low_Other_a. Logarithm of the scale factor used to characterize uncertainty in uranium solubility under conditions other than nominal and seismic at an ionic strength below 1 molal (dimensionless). *Distribution:* Truncated normal. *Range:* -1 to 1. *Mean/Median/Mode:* 0. *Standard Deviation:* 0.5. *Correlation:* Correlated to U_Eps_1_high_Nominal_a with a correlation factor of 1. *Symbol:* ε_1. *Additional Information:* This is the exponential term associated with uncertainty in uranium solubility below 1 molal ionic strength under conditions of igneous intrusion, all scenarios, and in the invert. Used for CDSP fuel types (all scenarios), CSNF fuel in the igneous scenario and all invert locations. See U_Eps_1_low_Nominal_a. *Sensitivity Name:* EP1LOWOU. *Location in TSPA-LA:* Sections 6.3.7.5.1, 6.3.7.5.2 and 6.3.7.5.3; Table 6.3.7-58; Equation 6.3.7-13a. *DTN:* MO0702PADISCON.001_R0 [DIRS 179358], Tables 5, 6 and 19. *References: Dissolved Concentration Limits of Elements with Radioactive Isotopes* (SNL 2007 [DIRS 177418], Sections 6.7 and 8.1.2; Equations 6.7-4 and 8-1; Table 6.7-11).

Table K3-3. Detailed Summary of Epistemically Uncertain Variables (i.e., elements of **e**) Considered in the TSPA-LA (TSPA Parameter Name) (Continued)

NOTE: * indicates variable not considered in sensitivity analysis due to correlations.

U_Eps_2_Boltwoodite_CDSP_High_a*. Term associated with uncertainty in uranium solubility (controlled by boldwoodite saturation) due to variations in fluoride concentration for CDSP waste packages when ionic strength is greater than or equal to 0.004 molal and for the invert below CDSP waste packages (mg/L). *Distribution:* Triangular. *Range:* 0 to 272.3. *Most Likely:* 0. *Correlation:* Correlated to Am_Eps_2_CSNF_High_a. *Symbol:* $\varepsilon_2^{\text{CDSP-F-high}}$, $\varepsilon_2^{\text{CDSP-invert}}$. *Additional Information:* See Am_Eps_2_CSNF_High_a. *Sensitivity Name:* EP2BCDHU*. *Location in TSPA-LA:* Sections 6.3.7.5.1, 6.3.7.5.2 and 6.3.7.5.3; Table 6.3.7-58; Equation 6.3.7-13a. *DTN:* MO0702PAFLUORI.000_R1 [DIRS 181219], Table 9. *References: Dissolved Concentration Limits of Elements with Radioactive Isotopes* (SNL 2007 [DIRS 177418], Sections 6.7 and 8.1.2; Equations 6.7-4 and 8-1; Table 6.7-11).
U_Eps_2_Boltwoodite_CSNF_High_a*. Term associated with uncertainty in uranium solubility (controlled by boldwoodite saturation) due to variations in fluoride concentration for CSNF waste packages when ionic strength is greater than or equal to 0.2 molal and for the invert below CSNF waste packages (mg/L). *Distribution:* Triangular. *Range:* 0 to 57.01. *Most Likely:* 0. *Correlation:* Correlated to Am_Eps_2_CSNF_High_a. *Symbol:* $\varepsilon_2^{\text{CSNF-high}}$, $\varepsilon_2^{\text{CSNF-invert}}$. *Additional Information:* See Am_Eps_2_CSNF_High_a. *Sensitivity Name:* EP2BCSHU*. *Location in TSPA-LA AMR:* Sections 6.3.7.5.1, 6.3.7.5.2 and 6.3.7.5.3; Table 6.3.7-58; Equation 6.3.7-13a. *DTN:* MO0702PAFLUORI.000_R1 [DIRS 181219], Table 9. *References: Dissolved Concentration Limits of Elements with Radioactive Isotopes* (ANL-WIS-MD-000010 REV 06 [DIRS 177418], Sections 6.7 and 8.1.2; Equations 6.7-4 and 8-1; Table 6.7-11).
U_Eps_2_Boltwoodite_Glass_Low_a*. Term associated with uncertainty in uranium solubility (controlled by boldwoodite saturation) due to variations in fluoride concentration for CDSP waste packages Cell 1a, Cell 1b when ionic strength is less than 0.004 molal, and CSNF waste packages when ionic strength is less than 0.2 molal (mg/L). *Distribution:* Triangular. *Range:* 0 to 6.13. *Most Likely:* 0. *Correlation:* Correlated to Am_Eps_2_CSNF_High_a. *Symbol:* $\varepsilon_2^{\text{CSNF-low}}$, $\varepsilon_2^{\text{CDSP-Glass}}$, $\varepsilon_2^{\text{CDSP-F-low}}$. *Additional Information:* See Am_Eps_2_CSNF_High_a. *Sensitivity Name:* EP2BLOWU*. *Location in TSPA-LA:* Sections 6.3.7.5.1, 6.3.7.5.2 and 6.3.7.5.3; Table 6.3.7-58; Equation 6.3.7-13a. *DTN:* MO0702PAFLUORI.000_R1 [DIRS 181219], Table 9. *References: Dissolved Concentration Limits of Elements with Radioactive Isotopes* (SNL 2007 [DIRS 177418], Sections 6.7 and 8.1.2; Equations 6.7-4 and 8-1; Table 6.7-11).
U_Eps_2_CSNF_High_Nominal_a*. Term associated with uncertainty in uranium solubility (under nominal or seismic conditions) due to variations in fluoride concentration for CSNF waste packages when ionic strength is greater than or equal to 0.2 molal and for the invert below CSNF waste packages (mg/L). *Distribution:* Triangular. *Range:* 0 to 1361. *Most Likely:* 0. *Correlation:* Correlated to Am_Eps_2_CSNF_High_a. *Symbol:* $\varepsilon_2^{\text{CSNF-high}}$, $\varepsilon_2^{\text{CSNF-invert}}$. *Additional Information:* See Am_Eps_2_CSNF_High_a. *Sensitivity Name:* EP2CSHNU*. *Location in TSPA-LA:* Section 6.3.7.5.1, 6.3.7.5.2 and 6.3.7.5.3; Table 6.3.7-54; Equation 6.3.7-13a. *DTN:* MO0702PAFLUORI.000_R1 [DIRS 181219], Table 7. *References: Dissolved Concentration Limits of Elements with Radioactive Isotopes* (SNL 2007 [DIRS 177418], Sections 6.7 and 8.1.2; Equations 6.7-4 and 8-1; Table 6.7-9).
U_Eps_2_CSNF_Low_Nominal_a*. Term associated with uncertainty in uranium solubility (under nominal or seismic conditions) due to variations in fluoride concentration for CSNF waste packages when ionic strength is less than 0.2 molal and for the invert below CSNF waste packages (mg/L). *Distribution:* Triangular. *Range:* 0 to 78. *Most Likely:* 0. *Correlation:* Correlated to Am_Eps_2_CSNF_High_a. *Symbol:* $\varepsilon_2^{\text{CSNF-low}}$. *Additional Information:* See Am_Eps_2_CSNF_High_a. *Sensitivity Name:* EP2CSLNU*. *Location in TSPA-LA:* Section 6.3.7.5.1, 6.3.7.5.2 and 6.3.7.5.3; Table 6.3.7-54; Equation 6.3.7-13a. *DTN:* MO0702PAFLUORI.000_R1 [DIRS 181219], Table 7. *References: Dissolved Concentration Limits of Elements with Radioactive Isotopes* (SNL 2007 [DIRS 177418], Sections 6.7 and 8.1.2; Equations 6.7-4 and 8-1; Table 6.7-9).
U_Eps_2_Schoepite_CDSP_High_a*. Term associated with uncertainty in uranium solubility (controlled by schoepite saturation) due to variations in fluoride concentration for CDSP waste packages when ionic strength is greater than or equal to 0.004 molal and for the invert below CDSP waste packages (mg/L). *Distribution:* Triangular. *Range:* 0 to 5,385. *Most Likely:* 0. *Correlation:* Correlated to Am_Eps_2_CSNF_High_a. *Symbol:* $\varepsilon_2^{\text{CDSP-F-high}}$, $\varepsilon_2^{\text{CDSP-invert}}$. *Additional Information:* See Am_Eps_2_CSNF_High_a. *Sensitivity Name:* EP2SCDHU*. *Location in TSPA-LA:* Sections 6.3.7.5.1, 6.3.7.5.2 and 6.3.7.5.3; Table 6.3.7-58; Equation 6.3.7-13a. *DTN:* MO0702PAFLUORI.000_R1 [DIRS 181219], Table 9. *References: Dissolved Concentration Limits of Elements with Radioactive Isotopes* (SNL 2007 [DIRS 177418], Sections 6.7 and 8.1.2; Equations 6.7-4 and 8-1; Table 6.7-11).

Table K3-3. Detailed Summary of Epistemically Uncertain Variables (i.e., elements of **e**) Considered in the TSPA-LA (TSPA Parameter Name) (Continued)

NOTE: * indicates variable not considered in sensitivity analysis due to correlations.

U_Eps_2_Schoepite_CSNF_High_a*. Term associated with uncertainty in uranium solubility (controlled by schoepite saturation) due to variations in fluoride concentration for CSNF waste packages when ionic strength is greater than or equal to 0.2 molal and for the invert below CSNF waste packages (mg/L). *Distribution:* Triangular. *Range:* 0 to 1,361. *Most Likely:* 0. *Correlation:* Correlated to m_Eps_2_CSNF_High_a. *Symbol:* $\varepsilon_2^{\text{CSNF-high}}$, $\varepsilon_2^{\text{CSNF-invert}}$. *Additional Information:* See Am_Eps_2_CSNF_High_a. *Sensitivity Name:* EP2SCSHU*. *Location in TSPA-LA:* Sections 6.3.7.5.1, 6.3.7.5.2 and 6.3.7.5.3; Table 6.3.7-58; Equation 6.3.7-13a. *DTN:* MO0702PAFLUORI.000_R1 [DIRS 181219], Table 9. *References: Dissolved Concentration Limits of Elements with Radioactive Isotopes* (SNL 2007 [DIRS 177418], Sections 6.7 and 8.1.2; Equations 6.7-4 and 8-1; Table 6.7-11).
U_Eps_2_Schoepite_Glass_Low_a*. Term associated with uncertainty in uranium solubility (controlled by schoepite saturation) due to variations in fluoride concentration for CDSP waste packages Cell 1a, Cell 1b when ionic strength is less than 0.004 molal, and CSNF waste packages when ionic strength is less than 0.2 molal (mg/L). *Distribution:* Triangular. *Range:* 0 to 78. *Most Likely:* 0. *Correlation:* Correlated to Am_Eps_2_CSNF_High_a. *Symbol:* $\varepsilon_2^{\text{CSNF-low}}$, $\varepsilon_2^{\text{CDSP-Glass}}$, $\varepsilon_2^{\text{CDSP-F-low}}$. *Additional Information:* See Am_Eps_2_CSNF_High_a. *Sensitivity Name:* EP2SLOWU*. *Location in TSPA-LA:* Sections 6.3.7.5.1, 6.3.7.5.2 and 6.3.7.5.3; Table 6.3.7-58; Equation 6.3.7-13a. *DTN:* MO0702PAFLUORI.000_R1 [DIRS 181219], Table 9. *References: Dissolved Concentration Limits of Elements with Radioactive Isotopes* (SNL 2007 [DIRS 177418], Sections 6.7 and 8.1.2; Equations 6.7-4 and 8-1; Table 6.7-11).
UNC_DS_EF_conv_from_ln. Probability for undetected defects in drip shields (dimensionless). *Distribution:* Log-normal. *Median:* 4.3E-07. *Error Factor:* 14., *Additional Information:* For TSPA purposes, this distribution is the probability that a drip shield will fail soon after emplacement. The mechanisms of early failure implementation consists of specifying the likelihood (probability) that waste packages and drip shields can be considered as potentially subject to early failure (i.e., have undetected defects). Computed from TSPA Input Database parameter UNC_DS_EF by UNC_DS_EF_conv_from_ln = exp(UNC_DS_EF). *Sensitivity Name:* PROBDSEF. *Location in TSPA-LA:* Section 6.4.1; Tables 6.4-1 and 6.4-2. *DTN:* MO0701PASHIELD.000_R2 [DIRS 180508]. *References:* Analysis of Mechanisms for Early Waste Package / Drip Shield Failure (SNL 2007 [DIRS 178765], Sections 6.4, 6.5 and 7.1; Tables 6-10 and 7-1; Figure 6-21).
UNC_WP_EF_conv_from_ln. Probability for the undetected defects in waste packages (dimensionless). *Distribution:* Log-normal. *Median:* 4.14E-05. *Error Factor:* 8.17. *Additional Information:* For TSPA purposes, this distribution is the probability that a waste package will fail soon after emplacement. The mechanisms of early failure implementation consists of specifying the likelihood (probability) that waste packages and drip shields can be considered as potentially subject to early failure (i.e., have undetected defects). Computed from TSPA Input Database parameter UNC_WP_EF by UNC_WP_EF_conv_from_ln = exp(UNC_WP_EF). *Sensitivity Name:* PROBWPEF. *Location in TSPA-LA:* Section 6.4.2; Tables 6.4-1 and 6.4-2. *DTN:* MO0701PASHIELD.000_R2 [DIRS 180508]. *References:* Analysis of Mechanisms for Early Waste Package / Drip Shield Failure (SNL 2007 [DIRS 178765], Sections 6.3, 6.5 and 7.1; Tables 6-9 and 7-1; Figure 6-20).
UZ_Tortuosity_RG1. Logarithm of the tortuosity in rock group 1 (dimensionless). *Distribution:* Left truncated normal. *Range*: 0 to ∞. *Mean:* -1.15. *Standard Deviation:* 0.29. *Additional Information:* The tortuosity is computed from water content and base 10 log of the effective permeability. The uncertainty is implemented in the TSPA-LA Model for each rock group by selecting a standard normal random number and adding the product of the standard normal random number and standard deviation (in log10 space) to the log10 value of the mean tortuosity, taking the antilog of the value to derive the tortuosity for the present realization and multiplying each element-specific free-water diffusion coefficient by the tortuosity to derive 15 element-specific effective diffusion coefficients. In the UZ transport abstraction model, there are three tortuosity coefficient distributions for the three rock types (groups of layers with similar properties) specified in the compliance model. The range of tortuosity values is subdivided into three subranges called tortuosity rock groups, based on the tortuosity characteristics of the rock types in the unsaturated zone. Recorded in TSPA Input Database as UZDC_Mean_RG1 (mean) and UZ_DC_SD_RG1 (standard deviation). *Sensitivity Name:* UZTORRG1. *Location in TSPA-LA:* Section 6.3.9.2; Table 6.3.9-4. *DTN:* LB0702PAUZMTDF.001_R1 [DIRS 180776]. *References: Particle Tracking Model and Abstraction of Transport Processes Addendum 002* (SNL 2008 [DIRS 184748], Sections 4.1.4, 6.5.5 and Appendix A; Equation 6.5.5-1; Table 6.5.5-1).

Table K3-3. Detailed Summary of Epistemically Uncertain Variables (i.e., elements of **e**) Considered in the TSPA-LA (TSPA Parameter Name) (Continued)

NOTE: * indicates variable not considered in sensitivity analysis due to correlations.

UZ_Tortuosity_RG2. Logarithm of the tortuosity in rock group 2 (dimensionless). *Distribution:* Left truncated normal. *Range*: 0 to ∞. *Mean:* -1.57. *Standard Deviation:* 0.29. *Additional Information:* See UZ_Tortuosity_RG1. Recorded in TSPA Input Database as UZDC_Mean_RG2 (mean) and UZ_DC_SD_RG2 (standard deviation). *Sensitivity Name:* UZTORRG2. *Location in TSPA-LA:* Section 6.3.9.2; Table 6.3.9-4. *DTN:* LB0702PAUZMTDF.001_R1 [DIRS 180776]. *References: Particle Tracking Model and Abstraction of Transport Processes Addendum 002* (SNL 2008 [DIRS 184748], Sections 4.1.4, 6.5.5 and Appendix A; Equation 6.5.5-1; Table 6.5.5-1).
UZ_Tortuosity_RG3. Logarithm of the tortuosity in rock group 3 (dimensionless). *Distribution:* Left truncated normal. *Range*: 0 to ∞. *Mean:* -1.84. *Standard Deviation:* 0.29. *Additional Information:* See UZ_Tortuosity_RG1. Recorded in TSPA Input Database as UZDC_Mean_RG3 (mean) and UZ_DC_SD_RG3 (standard deviation). *Sensitivity Name:* UZTORRG3. *Location in TSPA-LA:* Section 6.3.9.2; Table 6.3.9-4. *DTN:* LB0702PAUZMTDF.001_R1 [DIRS 180776]. *References: Particle Tracking Model and Abstraction of Transport Processes Addendum 002* (SNL 2008 [DIRS 184748], Sections 4.1.4, 6.5.5 and Appendix A; Equation 6.5.5-1; Table 6.5.5-1).
Vol_Rubble_Max_Lith_a. Volume of lithophysal rock that must fall to fill the drift (m^3/m). *Distribution:* Uniform. *Range:* 30 to 120. *Additional Information:* This parameter represents epistemic uncertainty and spatial variability within the lithophysal zones. This distribution is sampled once per realization to determine the volume of intact lithophysal rock corresponding to complete drift collapse. A uniform distribution is appropriate here because the end points of the range are known, but the distribution of values within the range is not known. *Sensitivity Name:* RUBMAXL. *Location in TSPA-LA:* Sections 6.3.5.2.3 and 6.6.3.1; Tables 6.3.5-4 and 6.6-2. *DTN:* MO0703PASEISDA.002_R4 [DIRS 183156]. *References: Seismic Consequence Abstraction* (SNL 2007 [DIRS 176828], Sections 6.7.1 and 6.12.2; Tables 4-1, 6-28, 6-30, 6-32 and 6-88; Figures 6-52 to 6-54 and 6-57; Equations 5.3-1 and 6.7-2).
Vol_Rubble_Max_NonLith_a. Volume of nonlithophysal rock that must fall to fill the drift (m^3/m). *Distribution:* Uniform. *Range:* 30 to 120. *Additional Information:* See Vol_Rubble_Max_Lith_a. This parameter represents epistemic uncertainty and spatial variability within the nonlithophysal zones. *Sensitivity Name:* RUBMAXNL. *Location in TSPA-LA:* Section 6.3.5.2.3 and 6.6.3.1; Tables 6.3.5-4 and 6.6-2. *DTN:* MO0703PASEISDA.002_R4 [DIRS 183156]. *References: Seismic Consequence Abstraction* (SNL 2007 [DIRS 176828], Sections 6.7.2 and 6.12.2; Tables 6-31, 6-32 and 6-88; Figures 6-58 to 6-61; Equation 5.3-1).
WDDSAggrGC_Mean_a. Topside general corrosion rate of the drip shield (nm/yr). *Distribution:* Normal. *Mean:* 46.067. *Standard Deviation:* 1.187. *Additional Information:* The corrosion of the underside surface of the drip shield is more likely to be dry oxidation and humid-air corrosion, while the topside surface of the drip shield is more likely to undergo dry oxidation, humid-air and aqueous-phase corrosion. The topside surfaces that are subject to seepage dripping may be exposed to more aggressive chemical environment and conditions than those not subject to seepage dripping. The underside surfaces, where seepage cannot physically contact and dust cannot settle and accumulate, are not expected to be exposed to seepage water, and therefore corrosion will proceed under benign conditions. For the modeling purpose, the entire variation in the data is assumed to be due to the variability in the corrosion process. The resulting normal probability model represents the variability in the drip shield general corrosion rates for the aggressive conditions. The variability in the general corrosion rate is likely due to the randomness of the corrosion process under the conditions in the exposure environment. Recorded in the TSPA Input Database as two constants: WDDSAggrGC_Uncert_Mean and WDDSAggrGC_Uncert_SD. *Sensitivity Name:* WDDSAGGC. *Location in TSPA-LA:* Sections 6.3.5.1.2 and 6.3.5.1.3; Table 6.3.5-3. *DTN:* SN0704PADSGCMT.001_R2 [DIRS 182122]. *References: General Corrosion and Localized Corrosion of the Drip Shield* (SNL 2007 [DIRS 180778], Sections 1.3[a], 6.1.6.2[a] and 8.1[a]; Table 8-1[a]).
WDDSBenignGC_Mean_a. Underside general corrosion rate of the drip shield (mm/yr). *Distribution:* Normal. *Mean:* 5.15E-06. *Standard Deviation:* 8.31E-07. *Additional Information:* The description of the general corrosion model for the benign condition is split into two parts. First is the characterization and quantification of the uncertainty in the general corrosion model for the benign environmental condition. Second is the description of the corrosion rate variability model that represents the data. The variability in the general corrosion rate for the benign condition is due mainly to the randomness of the corrosion process under the conditions in the exposure environment. The experimental variability (e.g., variations in sample preparation and cleaning) also contributes to the variability in the corrosion rate. *Sensitivity Name:* WDDSBEGC. *Location in TSPA-LA:* Sections 6.3.5.1.2 and 6.3.5.1.3; Table 6.3.5-3. *DTN:* SN0704PADSGCMT.001_R2 [DIRS 182122]. *References: General Corrosion and Localized Corrosion of the Drip Shield* (SNL 2007 [DIRS 180778], Sections 1.3[a], 6.1.7.1[a] and 8.1[a]; Table 8-1[a]).

Table K3-3. Detailed Summary of Epistemically Uncertain Variables (i.e., elements of **e**) Considered in the TSPA-LA (TSPA Parameter Name) (Continued)

NOTE: * indicates variable not considered in sensitivity analysis due to correlations.

WDDSGC_29_a. General corrosion rate ratio for drip shield support material (ratio of Titanium Grade 29 to Titanium Grade 7) (dimensionless). *Distribution:* Discrete. *Range:* 1 to 6.6786. *Additional Information:* The general corrosion rate of Titanium Grade 29 is the value of Titanium Grade 7 multiplied by sampled value from the rate ratio distribution. For each realization of the TSPA-LA model, one general corrosion rate ratio is sampled from the distribution for general corrosion rate ratio, and one general corrosion rate for Titanium Grade 7 is sampled from the topside surface distribution of general corrosion rates of Titanium Grade 7 for an aggressive condition. In this way, the corrosion rate of the Titanium Grade 29 components will conservatively be independent of whether they are on the inside or outside of the drip shield Titanium Grade 7 plates. Only one sampled value of the general corrosion rate ratio is used per realization, assuming that the ratio is constant for the entire simulation period. *Sensitivity Name:* WDDSGC29. *Location in TSPA-LA:* Section 6.3.5.1.2. *DTN:* SN0704PADSGCMT.002_R1 [DIRS 182188]. *References: General Corrosion and Localized Corrosion of the Drip Shield* (SNL 2007 [DIRS 180778], Sections 6.2.2[a], 6.2.3[a] and 8.1[a]; Tables 6-8[a] and 8-1[a]; Figure 6-21[a]).
WP_Crack_Area_Density_a. Ratio of SCC crack area to unit of seismic damaged area for a waste package (dimensionless). *Distribution:* Uniform. *Range:* 0.00327 to 0.0131. *Additional Information:* WP_Crack_Area_Density_a is a scaling factor applied to the seismically damaged area to obtain the total area of the crack network. The use of a uniform distribution is reasonable as it accurately reflects the lack of knowledge of the exact value of the crack area density. *Sensitivity Name:* WDCRCDEN. *Location in TSPA-LA:* Table 6.6-2. *DTN:* MO0702PASTRESS.002_R2 [DIRS 180514]. *References: Stress Corrosion Cracking of Waste Package Outer Barrier and Drip Shield Materials* (SNL 2007 [DIRS 181953], Sections 6.7.2 to 6.7.4, 8.4.2.4 and 8.4.3; Tables 6-18, 8-1 and 8-15; Equations 32 and 73).
WP_Flux_Uncertainty_a. Waste package flux splitting factor (dimensionless). *Distribution:* Uniform. *Range:* 0 to 2.41. *Symbol:* f'_{WP}. *Additional Information:* See DS_Flux_Uncertainty_a. Uncertainty in the waste package flux splitting algorithm is given by WP_Flux_Uncertainty_a. As with the corresponding factor f_{DS} for the drip shield, bounds can be established for f_{WP} based on the dimensions of the patches, the waste package and the uncertain rivulet spread angle. A lower bound of zero is necessary to account for the possibility that seepage through the drip shield is completely diverted by an intact portion of the waste package outer corrosion barrier. An upper bound on f_{WP} is developed based on results of the breached drip shield experiments. The range for f_{WP} based entirely on experimental results is used in TSPA. *Sensitivity Name:* WPFLUX. *Location in TSPA-LA:* Sections 6.3.6.1, 6.3.6.2 and 6.3.6.3; Tables 6.3.6-1, 6.3.6-2 and 6.3.8-4; Equation 6.3.6-6. *DTN:* SN0703PAEBSRTA.001_R3 [DIRS 183217]. *References: EBS Radionuclide Transport Abstraction* (SNL 2007 [DIRS 177407], Sections 6.3.3.2.5, 6.5.1.1.3, 7.1.1.2, Appendix D and Appendix E; Tables 6.3-1, 7.1-12, 8.1-1 and 8.2-4; Equations 6.3.3.2.5 and 6.5.1.1.3).
WRIP_beta_rand_a. Parameter used to correlate WRIP_beta so that it resamples at the same probability level throughout a realization (dimensionless). *Distribution:* Uniform. *Range:* 0 to 1. *Additional Information:* The WRIP is sampled from beta distribution. WRIP_beta is sampled at every time step and perfectly correlated with WRIP_beta_rand_a. The WRIP value in the look-up table does not contain any uncertainty. It is specified as the mean of a beta distribution with a maximum equal to 2.838 times the mean, the minimum equal to 0.2039 times the mean, and the standard deviation equal to 0.4251 times the mean. This uncertainty accounts for uncertainty in the feldspar dissolution rate. This parameter is determined within TSPA. *Sensitivity Name:* WATRCKIN. *Location in TSPA-LA:* Section 6.3.4.2; Table 6.3.4-1. Output *DTN:* MO0708TSPAGENT.000_R0 [DIRS 183000].
z_OL_a. Deviation from median yield strength range for outer lid (dimensionless). *Distribution:* Truncated normal. *Range:* -3 to 3. *Mean/Median/Mode:* 0. *Standard Deviation:* 1. *Symbol:* z. *Additional Information:* Stress and stress-intensity factor profile model output parameters are to be used as inputs into the TSPA model. These parameters include the stress intensity versus depth for outer lid, the outer lid stress coefficients, the outer lid yield strength scaling factor, the uncertain deviation from median yield strength range for outer lid, the number of angles at which the stress intensity factor for the outer lid will be evaluated by SCCD, and the amplitude of the stress variation with angle for the outer lid. *Sensitivity Name:* WDZOLID. *Location in TSPA-LA:* Sections 6.3.5.1.2 and 6.3.5.1.3; Table 6.3.5-3. *DTN:* MO0702PASTRESS.002_R2 [DIRS 180514]. *References: Stress Corrosion Cracking of Waste Package Outer Barrier and Drip Shield Materials* (SNL 2007 [DIRS 181953], Sections 6.5.6.5 and 8.4.2.2; Table 8-15; Equation 67).

INTENTIONALLY LEFT BLANK

Table K3-4. Alphabetic Listing of the Various TSPA-LA Model Results Considered in Uncertainty and Sensitivity Analyses for Nominal (N), Drip Shield Early Failure (ED), Waste Package Early Failure (EW), Igneous Intrusive (II), Igneous Eruptive (IE), Seismic Ground Motion (SG), and Seismic Fault Displacement (SF) Modeling Cases in Appendix K4, K5, K6, and K7

Output Variable	Definition
BACDFLAD	Average breached area (m^2) on failed CDSP WPs under dripping conditions
BACDFLND	Average breached area (m^2) on failed CDSP WPs under nondripping conditions
BACSFLAD	Average breached area (m^2) on failed CSNF WPs under dripping conditions
BACSFLND	Average breached area (m^2) on failed CSNF WPs under nondripping conditions
DOIC239	Dose to RMEI (mrem/yr) from ^{239}Pu irreversibly attached to slow (i.e., Ic) colloids
DOIF239	Dose to RMEI (mrem/yr) from ^{239}Pu irreversibly attached to fast (i.e., If) colloids
DONP237	Dose to RMEI (mrem/yr) from dissolved ^{237}Np
DOPU239	Dose to RMEI (mrem/yr) from dissolved ^{239}Pu
DOSTOT	Dose to RMEI (mrem/yr) from all radioactive species
DOTC99	Dose to RMEI (mrem/yr) from dissolved ^{99}Tc
DSFLTM	Drip Shield failure time (yr)
ESFA239C	Cumulative release (g) for the movement of ^{239}Pu irreversibly attached to fast (i.e., If) colloids from the EBS to the UZ
ESIC239	Release rate (g/yr) for the movement of ^{239}Pu irreversibly attached to waste form (i.e., Ic) colloids from the EBS to the UZ
ESIC239C	Cumulative release (g) for the movement of ^{239}Pu irreversibly attached to waste form (i.e., Ic) colloids from the EBS to the UZ
ESIF239	Release rate (g/yr) for the movement of ^{239}Pu irreversibly attached to ferrous (i.e., If) colloids from the EBS to the UZ
ESIF239C	Cumulative release (g) for the movement of ^{239}Pu irreversibly attached to ferrous (i.e., If) colloids from the EBS to the UZ
ESNP237	Release rate (g/yr) for the movement of dissolved ^{237}Np from the EBS to the UZ
ESNP237C	Cumulative release (g) for the movement of dissolved ^{237}Np from the EBS to the UZ
ESPU239	Release rate (g/yr) for the movement of dissolved ^{239}Pu from the EBS to the UZ
ESPU239C	Cumulative release (g) for the movement of dissolved ^{239}Pu from the EBS to the UZ
ESSL239C	Cumulative release (g) for the movement of ^{239}Pu irreversibly attached to slow colloids from the EBS to the UZ

Table K3-4. Alphabetic Listing of the Various TSPA-LA Model Results Considered in Uncertainty and Sensitivity Analyses for Nominal (N), Drip Shield Early Failure (ED), Waste Package Early Failure (EW), Igneous Intrusive (II), Igneous Eruptive (IE), Seismic Ground Motion (SG), and Seismic Fault Displacement (SF) Modeling Cases in Appendix K4, K5, K6, and K7 (Continued)

Output Variable	Definition
ESTC99	Release rate (g/yr) for the movement of dissolved ^{99}Tc from the EBS to the UZ
ESTC99C	Cumulative release (g) for the movement of dissolved ^{99}Tc from the EBS to the UZ
EXPDOSE	Expected dose to RMEI (mrem/yr) from all radioactive species
ISCDINAD	Ionic strength (molal) in the invert beneath the WP for CDSP WPs under dripping conditions
ISCDINND	Ionic strength (molal) in the invert beneath the WP for CDSP WPs under nondripping conditions
ISCSINAD	Ionic strength (molal) in the invert beneath the WP for CSNF WPs under dripping conditions
ISCSINND	Ionic strength (molal) in the invert beneath the WP for CSNF WPs under nondripping conditions
NCDFL	Number of failed CDSP WPs
NCDFLAD	Number of failed CDSP WPs under dripping conditions
NCDFLND	Number of failed CDSP WPs under nondripping conditions
NCSFL	Number of failed CSNF WPs
NCSFLAD	Number of failed CSNF WPs under dripping conditions
NCSFLND	Number of failed CSNF WPs under nondripping conditions
PCO2CDIA	Partial pressure of CO_2 (bars) in the invert for CDSP WPs under dripping conditions
PCO2CDIN	Partial pressure of CO_2 (bars) in the invert for CDSP WPs under nondripping conditions
PCO2CSIA	Partial pressure of CO_2 (bars) in the invert for CSNF WPs under dripping conditions
PCO2CSIN	Partial pressure of CO_2 (bars) in the invert for CSNF WPs under nondripping conditions
PHCDINAD	pH in the invert beneath the WP for CDSP WPs under dripping conditions
PHCDINND	pH in the invert beneath the WP for CDSP WPs under nondripping conditions
PHCSINAD	pH in the invert beneath the WP for CSNF WPs under dripping conditions
PHCSINND	pH in the invert beneath the WP for CSNF WPs under nondripping conditions
RHCDINV	Relative humidity for CDSP WPs in the invert beneath the WP

Table K3-4. Alphabetic Listing of the Various TSPA-LA Model Results Considered in Uncertainty and Sensitivity Analyses for Nominal (N), Drip Shield Early Failure (ED), Waste Package Early Failure (EW), Igneous Intrusive (II), Igneous Eruptive (IE), Seismic Ground Motion (SG), and Seismic Fault Displacement (SF) Modeling Cases in Appendix K4, K5, K6, and K7 (Continued)

Output Variable	Definition
RHCDWP	Relative humidity for CDSP WPs on the WP
RHCSINV	Relative humidity for CSNF WPs in the invert beneath the WP
RHCSWP	Relative humidity for CSNF WPs on the WP
SPRATECD	Seepage rate (m^3/yr/WP) into the repository above CDSP WPs
SPRATECS	Seepage rate (m^3/yr/WP) into the repository above CSNF WPs
SZIC239	Release rate (g/yr) for the movement of ^{239}Pu irreversibly attached to slow (i.e., Ic) colloids across a subsurface plane at the location of the RMEI
SZIC239C	Cumulative release (g) for the movement of ^{239}Pu irreversibly attached to slow (i.e., Ic) colloids across a subsurface plane at the location of the RMEI
SZIF239	Release rate (g/yr) for the movement of ^{239}Pu irreversibly attached to fast (i.e., If) colloids across a subsurface plane at the location of the RMEI
SZIF239C	Cumulative release (g) for the movement of ^{239}Pu irreversibly attached to fast (i.e., If) colloids across a subsurface plane at the location of the RMEI
SZNP237	Release rate (g/yr) for the movement of dissolved ^{237}Np across a subsurface plane at the location of the RMEI
SZNP237C	Cumulative release (g) for the movement of dissolved ^{237}Np across a subsurface plane at the location of the RMEI
SZPU239	Release rate (g/yr) for the movement of dissolved ^{239}Pu across a subsurface plane at the location of the RMEI
SZPU239C	Cumulative release (g) for the movement of dissolved ^{239}Pu across a subsurface plane at the location of the RMEI
SZTC99	Release rate (g/yr) for the movement of dissolved ^{99}Tc across a subsurface plane at the location of the RMEI
SZTC99C	Cumulative release (g) for the movement of dissolved ^{99}Tc across a subsurface plane at the location of the RMEI
TMPCDINV	Drift temperature (C) for CDSP WPs in the invert beneath the WP
TMPCDWL	Drift temperature (C) for CDSP WPs at the drift wall
TMPCDWP	Drift temperature (C) for CDSP WPs on the WP
TMPCSINV	Drift temperature (C) for CSNF WPs in the invert beneath the WP
TMPCSWL	Drift temperature (C) for CSNF WPs at the drift wall
TMPCSWP	Drift temperature (C) for CSNF WPs on the WP
UZIC239	Release rate (g/yr) for the movement of ^{239}Pu irreversibly attached to slow (i.e., Ic) colloids from the UZ to the SZ

Table K3-4. Alphabetic Listing of the Various TSPA-LA Model Results Considered in Uncertainty and Sensitivity Analyses for Nominal (N), Drip Shield Early Failure (ED), Waste Package Early Failure (EW), Igneous Intrusive (II), Igneous Eruptive (IE), Seismic Ground Motion (SG), and Seismic Fault Displacement (SF) Modeling Cases in Appendix K4, K5, K6, and K7 (Continued)

Output Variable	Definition
UZIC239C	Cumulative release (g) for the movement of ^{239}Pu irreversibly attached to slow (i.e., Ic) colloids from the UZ to the SZ
UZIF239	Release rate (g/yr) for the movement of ^{239}Pu irreversibly attached to fast (i.e., If) colloids from the UZ to the SZ
UZIF239C	Cumulative release (g) for the movement of ^{239}Pu irreversibly attached to fast (i.e., If) colloids from the UZ to the SZ
UZNP237	Release rate (g/yr) for the movement of dissolved ^{237}Np from the UZ to the SZ
UZNP237C	Cumulative release (g) for the movement of dissolved ^{237}Np from the UZ to the SZ
UZPU239	Release rate (g/yr) for the movement of dissolved ^{239}Pu from the UZ to the SZ
UZPU239C	Cumulative release (g) for the movement of dissolved ^{239}Pu from the UZ to the SZ
UZTC99	Release rate (g/yr) for the movement of dissolved ^{99}Tc from the UZ to the SZ
UZTC99C	Cumulative release (g) for the movement of dissolved ^{99}Tc from the UZ to the SZ

Table K4.1-1. Summary of TSPA-LA Model Results Considered in Uncertainty and Sensitivity Analyses for the Nominal Scenario Class

BACSFLAD	Average breached area (m^2) on failed CSNF WPs under dripping conditions (Figures K.4.2-6, K.4.2-7)
BACSFLND	Average breached area (m^2) on failed CSNF WPs under nondripping conditions (Figures K.4.2-6, K.4.2-7)
DOSTOT	Dose to RMEI (mrem/yr) from all radioactive species (Figure K.4.5-1, K.4.5-2, K.4.5-3)
DSFLTM	Drip Shield failure time (yr) (Figure K.4.2-1)
ESNP237	Release rate (g/yr) for the movement of dissolved ^{237}Np from the EBS to the UZ (Figures K.4.4-1, K.4.4-2)
ESNP237C	Cumulative release (g) for the movement of dissolved ^{237}Np from the EBS to the UZ (Figures K.4.4-1, K.4.4-2)
ISCDINAD	Ionic strength (molal) in the invert beneath the WP for CDSP WPs under dripping conditions (Figure K.4.3-10)
ISCDINND	Ionic strength (molal) in the invert beneath the WP for CDSP WPs under nondripping conditions (Figure K.4.3-10)
ISCSINAD	Ionic strength (molal) in the invert beneath the WP for CSNF WPs under dripping conditions (Figures K.4.3-9, K.4.3-11)
ISCSINND	Ionic strength (molal) in the invert beneath the WP for CSNF WPs under nondripping conditions (Figure K.4.3-9)
NCDFL	Number of failed CDSP WPs (Figure K.4.2-2)
NCSFL	Number of failed CSNF WPs (Figures K.2-1, K.4.2-3)
NCSFLAD	Number of failed CSNF WPs under dripping conditions (Figures K.4.2-4, K.4.2-5)
NCSFLND	Number of failed CSNF WPs under nondripping conditions (Figures K.4.2-4, K.4.2-5)
PCO2CDIA	Partial pressure of CO_2 (bars) in the invert for CDSP WPs under dripping conditions (Figure K.4.3-7)
PCO2CSIA	Partial pressure of CO_2 (bars) in the invert for CSNF WPs under dripping conditions (Figures K.4.3-7, K.4.3-8)
PHCDINAD	pH in the invert beneath the WP for CDSP WPs under dripping conditions (Figure K.4.3-14)
PHCDINND	pH in the invert beneath the WP for CDSP WPs under nondripping conditions (Figure K.4.3-14)
PHCSINAD	pH in the invert beneath the WP for CSNF WPs under dripping conditions (Figures K.4.3-12, K.4.3-13)
PHCSINND	pH in the invert beneath the WP for CSNF WPs under nondripping conditions (Figures K.4.3-12, K.4.3-13)
RHCDINV	Relative humidity for CDSP WPs in the invert beneath the WP (Figure K.4.3-6)

Table K4.1-1. Summary of TSPA-LA Model Results Considered in Uncertainty and Sensitivity Analyses for the Nominal Scenario Class (Continued)

RHCDWP	Relative humidity for CDSP WPs on the WP (Figure K.4.3-6)
RHCSINV	Relative humidity for CSNF WPs in the invert beneath the WP (Figure K.4.3-6)
RHCSWP	Relative humidity for CSNF WPs on the WP (Figure K.4.3-6)
SPRATECD	Seepage rate (m^3/yr/WP) into the repository above CDSP WPs (Figures K.4.3-1, K.4.3-4)
SPRATECS	Seepage rate (m^3/yr/WP) into the repository above CSNF WPs (Figures K.4.3-1, K.4.3-2, K.4.3-3)
TMPCDINV	Drift temperature (C) for CDSP WPs in the invert beneath the WP (Figure K.4.3-5)
TMPCDWL	Drift temperature (C) for CDSP WPs at the drift wall (Figure K.4.3-5)
TMPCDWP	Drift temperature (C) for CDSP WPs on the WP (Figure K.4.3-5)
TMPCSINV	Drift temperature (C) for CSNF WPs in the invert beneath the WP (Figure K.4.3-5)
TMPCSWL	Drift temperature (C) for CSNF WPs at the drift wall (Figure K.4.3-5)
TMPCSWP	Drift temperature (C) for CSNF WPs on the WP (Figure K.4.3-5)

Table K5.1-1. Summary of TSPA-LA Model Results Considered in Uncertainty and Sensitivity Analyses for the Early Failure Scenario Classes

Output Variable	Definition
DOIC239	Dose to RMEI (mrem/yr) from ^{239}Pu irreversibly attached to slow (i.e., Ic) colloids (Figure K.5.6.1-1)
DOIF239	Dose to RMEI (mrem/yr) from ^{239}Pu irreversibly attached to fast (i.e., If) colloids (Figure K.5.6.1-2)
DONP237	Dose to RMEI (mrem/yr) from dissolved ^{237}Np (Figure K.5.6.1-3)
DOPU239	Dose to RMEI (mrem/yr) from dissolved ^{239}Pu (Figure K.5.6.1-4)
DOTC99	Dose to RMEI (mrem/yr) from dissolved ^{99}Tc (Figure K.5.6.1-5)
ESFA239C	Cumulative release (g) for the movement of ^{239}Pu irreversibly attached to fast (i.e., If) colloids from the EBS to the UZ (Figure K.5.4.1-6)
ESIC239	Release rate (g/yr) for the movement of ^{239}Pu irreversibly attached to waste form (i.e., Ic) colloids from the EBS to the UZ (Figures K.5.3.1-1, K.5.3.1-2, K.5.3.2-1, K.5.3.3-1, K.5.3.5-1)
ESIC239C	Cumulative release (g) for the movement of ^{239}Pu irreversibly attached to waste form (i.e., Ic) colloids from the EBS to the UZ (Figures K.5.3.1-1, K.5.3.1-2, K.5.3.2-1, K.5.3.3-1, K.5.3.5-1)
ESIF239	Release rate (g/yr) for the movement of ^{239}Pu irreversibly attached to ferrous (i.e., If) colloids from the EBS to the UZ (Figures K.5.3.1-3, K.5.3.1-4, K.5.3.2-2, K.5.3.3-2, K.5.3.5-2)
ESIF239C	Cumulative release (g) for the movement of ^{239}Pu irreversibly attached to ferrous (i.e., If) colloids from the EBS to the UZ (Figures K.5.3.1-3, K.5.3.1-4, K.5.3.2-2, K.5.3.3-2, K.5.3.5-2)
ESNP237	Release rate (g/yr) for the movement of dissolved ^{237}Np from the EBS to the UZ (Figures K.5.3.1-5, K.5.3.1-6, K.5.3.2-3, K.5.3.3-3, K.5.3.5-3, K.5.3.7-1, K.5.3.8-1, K.5.3.9-1, K.5.3.10-1, K.5.3.11-1, K.5.3.12-1)
ESNP237C	Cumulative release (g) for the movement of dissolved ^{237}Np from the EBS to the UZ (Figures K.5.3.1-5, K.5.3.1-6, K.5.3.2-3, K.5.3.3-3, K.5.3.5-3, K.5.3.7-1, K.5.3.8-1, K.5.3.9-1, K.5.3.10-1, K.5.3.11-1, K.5.3.12-1, K.5.4.1-9)
ESPU239	Release rate (g/yr) for the movement of dissolved ^{239}Pu from the EBS to the UZ (Figures K.5.3.1-7, K.5.3.1-8, K.5.3.2-4, K.5.3.3-4, K.5.3.5-4, K.5.3.7-2, K.5.3.8-2, K.5.3.9-2, K.5.3.10-2, K.5.3.11-2, K.5.3.12-2)
ESPU239C	Cumulative release (g) for the movement of dissolved ^{239}Pu from the EBS to the UZ (Figures K.5.3.1-7, K.5.3.1-8, K.5.3.2-4, K.5.3.3-4, K.5.3.5-4, K.5.3.7-2, K.5.3.8-2, K.5.3.9-2, K.5.3.10-2, K.5.3.11-2, K.5.3.12-2, K.5.4.1-12)
ESSL239C	Cumulative release (g) for the movement of ^{239}Pu irreversibly attached to slow colloids from the EBS to the UZ (Figure K.5.4.1-3)
ESTC99	Release rate (g/yr) for the movement of dissolved ^{99}Tc from the EBS to the UZ (Figures K.5.3.1-9, K.5.3.1-10, K.5.3.2-5, K.5.3.3-5, K.5.3.5-5)
ESTC99C	Cumulative release (g) for the movement of dissolved ^{99}Tc from the EBS to the UZ (Figures K.5.3.1-9, K.5.3.1-10, K.5.3.2-5, K.5.3.3-5, K.5.3.5-5, K.5.4.1-15)
EXPDOSE	Expected dose to RMEI (mrem/yr) from all radioactive species (Figure K.5.7.1-1, K.5.7.1-2, K.5.7.1-3, K.5.7.1-4, K.5.7.2-1, K.5.7.2-2, K.5.7.2-3, K.5.7.2-4, K.5.7.3-1, K.5.7.3-2, K.5.7.3-3, K.5.7.3-4, K.5.7.4-1, K.5.7.4-2)
ISCDINAD	Ionic strength (molal) in the invert beneath the WP for CDSP WPs under dripping conditions (Figure K.5.2-1)
ISCSINAD	Ionic strength (molal) in the invert beneath the WP for CSNF WPs under dripping conditions (Figure K.5.2-1)

Table K5.1-1. Summary of TSPA-LA Model Results Considered in Uncertainty and Sensitivity Analyses for the Early Failure Scenario Classes (Continued)

Output Variable	Definition
PHCDINAD	pH in the invert beneath the WP for CDSP WPs under dripping conditions (Figure K.5.2-2)
PHCSINAD	pH in the invert beneath the WP for CSNF WPs under dripping conditions (Figure K.5.2-2)
SZIC239	Release rate (g/yr) for the movement of ^{239}Pu irreversibly attached to slow (i.e., Ic) colloids across a subsurface plane at the location of the RMEI (Figure K.5.5.1-1)
SZIC239C	Cumulative release (g) for the movement of ^{239}Pu irreversibly attached to slow (i.e., Ic) colloids across a subsurface plane at the location of the RMEI (Figure K.5.5.1-1)
SZIF239	Release rate (g/yr) for the movement of ^{239}Pu irreversibly attached to fast (i.e., If) colloids across a subsurface plane at the location of the RMEI (Figure K.5.5.1-2)
SZIF239C	Cumulative release (g) for the movement of ^{239}Pu irreversibly attached to fast (i.e., If) colloids across a subsurface plane at the location of the RMEI (Figure K.5.5.1-2)
SZNP237	Release rate (g/yr) for the movement of dissolved ^{237}Np across a subsurface plane at the location of the RMEI (Figure K.5.5.1-3)
SZNP237C	Cumulative release (g) for the movement of dissolved ^{237}Np across a subsurface plane at the location of the RMEI (Figure K.5.5.1-3)
SZPU239	Release rate (g/yr) for the movement of dissolved ^{239}Pu across a subsurface plane at the location of the RMEI (Figure K.5.5.1-4)
SZPU239C	Cumulative release (g) for the movement of dissolved ^{239}Pu across a subsurface plane at the location of the RMEI (Figure K.5.5.1-4)
SZTC99	Release rate (g/yr) for the movement of dissolved ^{99}Tc across a subsurface plane at the location of the RMEI (Figure K.5.5.1-5)
SZTC99C	Cumulative release (g) for the movement of dissolved ^{99}Tc across a subsurface plane at the location of the RMEI (Figure K.5.5.1-5)
UZIC239	Release rate (g/yr) for the movement of ^{239}Pu irreversibly attached to slow (i.e., Ic) colloids from the UZ to the SZ (Figures K.5.4.1-1, K.5.4.1-2)
UZIC239C	Cumulative release (g) for the movement of ^{239}Pu irreversibly attached to slow (i.e., Ic) colloids from the UZ to the SZ (Figures K.5.4.1-1, K.5.4.1-2, K.5.4.1-3)
UZIF239	Release rate (g/yr) for the movement of ^{239}Pu irreversibly attached to fast (i.e., If) colloids from the UZ to the SZ (Figures K.5.4.1-4, K.5.4.1-5)
UZIF239C	Cumulative release (g) for the movement of ^{239}Pu irreversibly attached to fast (i.e., If) colloids from the UZ to the SZ (Figures K.5.4.1-4, K.5.4.1-5, K.5.4.1-6)
UZNP237	Release rate (g/yr) for the movement of dissolved ^{237}Np from the UZ to the SZ (Figures K.5.4.1-7, K.5.4.1-8)
UZNP237C	Cumulative release (g) for the movement of dissolved ^{237}Np from the UZ to the SZ (Figures K.5.4.1-7, K.5.4.1-8, K.5.4.1-9)
UZPU239	Release rate (g/yr) for the movement of dissolved ^{239}Pu from the UZ to the SZ (Figures K.5.4.1-10, K.5.4.1-11)
UZPU239C	Cumulative release (g) for the movement of dissolved ^{239}Pu from the UZ to the SZ (Figures K.5.4.1-10, K.5.4.1-11, K.5.4.1-12)

Table K5.1-1. Summary of TSPA-LA Model Results Considered in Uncertainty and Sensitivity Analyses for the Early Failure Scenario Classes (Continued)

Output Variable	Definition
UZTC99	Release rate (g/yr) for the movement of dissolved ^{99}Tc from the UZ to the SZ (Figures K.5.4.1-13, K.5.4.1-14)
UZTC99C	Cumulative release (g) for the movement of dissolved ^{99}Tc from the UZ to the SZ (Figures K.5.4.1-13, K.5.4.1-14, K.5.4.1-15)

Table K5.1-2 Summary of Uncertainty and Sensitivity Analysis Results for the Early Failure Scenario Class for Release from the Engineered Barrier System

Output Variable[a]	Time Interval[b]	Range[c]	Dominant Input Variable[d]	Figures[e]
Time-Dependent Release Rate (*ESIC239*, g/yr) and Cumulative Release (*ESIC239C*, g) for ^{239}Pu Irreversibly Attached to Waste Form Colloids				
Early DS Failure Above a CDSP WP Under Dripping Conditions				
ESIC239	[0, 10^4, 2 × 10^4 yr]	[2 × 10^{-7}, 10^{-3} g/yr]	*INFIL*(+) *CPUCOLWF*(+) *SEEPPRM*(–)	K5.3.1-1 K5.3.1-2
ESIC239C	[0, 10^4, 2 × 10^4 yr]	[3 × 10^{-3}, 10 g]	*CPUCOLWF*(+) *INFIL*(+) *SEEPPRM*(–)	K5.3.1-1 K5.3.1-2
Early DS Failure Above a CSNF WP Under Dripping Conditions				
ESIC239	[0, 10^4, 2 × 10^4 yr]	[3 × 10^{-11}, 10^{-8} g/yr]	*INFIL*(+)	K5.3.2-1
ESIC239C	[0, 10^4, 2 × 10^4 yr]	[3 × 10^{-7}, 10^{-1} g]	*INFIL*(+)	K5.3.2-1
Early CDSP WP Failure Under Dripping Conditions				
ESIC239	[0, 10^4, 2 × 10^4 yr]	Results removed due to model error		K5.3.3-1
ESIC239C	[0, 10^4, 2 × 10^4 yr]	Results removed due to model error		K5.3.3-1
Early CSNF WP Failure Under Dripping Conditions				
ESIC239	[0, 1.5 × 10^4, 2 × 10^4 yr]	Results removed due to model error		K5.3.5-1
ESIC239C	[0, 1.5 × 10^4, 2 × 10^4 yr]	Results removed due to model error		K5.3.5-1
Comment: *ESIC239* is zero prior to 10^4 yr.				
Time-Dependent Release Rate (*ESIF239*, g/yr) and Cumulative Release (*ESIF239C*, g) for ^{239}Pu Irreversibly Attached to Ferrous Colloids				
Early DS Failure Above a CDSP WP Under Dripping Conditions				
ESIF239	[0, 10^4, 2 × 10^4 yr]	Results removed due to model error		K5.3.1-3 K5.3.1-4
ESIF239C	[0, 10^4, 2 × 10^4 yr]	Results removed due to model error		K5.3.1-3 K5.3.1-4

Table K5.1-2 Summary of Uncertainty and Sensitivity Analysis Results for the Early Failure Scenario Class for Release from the Engineered Barrier System (Continued)

Variable[a]	Time Interval[b]	Range[c]	Dominant Input Variables[d]	Figures[e]
Early DS Failure Above a CSNF WP Under Dripping Conditions				
ESIF239	[0, 10^4, 2 × 10^4 yr]	Results removed due to model error		K5.3.2-2
ESIF239C	[0, 10^4, 2 × 10^4 yr]	Results removed due to model error		K5.3.2-2
Early CDSP WP Failure Under Dripping Conditions				
ESIF239	[0, 10^4, 2 × 10^4 yr]	Results removed due to model error		K5.3.3-2
ESIF239C	[0, 10^4, 2 × 10^4 yr]	Results removed due to model error		K5.3.2-2
Early CSNF WP Failure Under Dripping Conditions				
ESIF239	[0, 1.5 × 10^4, 2 × 10^4 yr]	Results removed due to model error		K5.3.5-2
ESIF239C	[0, 1.5 × 10^4, 2 × 10^4 yr]	Results removed due to model error		K5.3.5-2
Comment: *ESIF239* zero prior to 10^4 yr and values for some sample elements remain zero after 10^4 yr.				
Time-Dependent Release Rate (*ESNP237*, g/yr) and Cumulative Release (*ESNP237C*, g) for Dissolved ^{237}Np				
Early DS Failure Above a CDSP WP Under Dripping Conditions				
ESNP237	[0, 10^4, 2 × 10^4 yr]	[3 × 10^{-6}, 10^{-2} g/yr]	*INFIL*(+) *GOESITED*(–) *DSNFMASS*(+) *HFOSA*(–)	K5.3.1-5 K5.3.1-6
ESNP237C	[0, 10^4, 2 × 10^4 yr]	[2 × 10^{-2}, 10^2 g]	*DELPPCO2*(+) *PH2MCOS*(–) *INFIL*(+) *GOESITED*(–)	K5.3.1-5 K5.3.1-6
ESNP237	[0, 5 × 10^5, 10^6 yr]	[10^{-5}, 3 × 10^{-4} g/yr]	*GOESITED*(–) *INFIL*(+) *DSNFMASS*(+) *HFOSA*(–)	K5.3.7-1
ESNP237C	[0, 5 × 10^5, 10^6, yr]	[6, 800 g]	*GOESITED*(–) *INFIL*(+) *DSNFMASS*(+) *HFOSA*(–)	K5.3.7-1
Comment: Many variables have small effects on *ESNP237* and *ESNP237C*; see Figure K5.3.1-6				
Early DS Failure Above a CSNF WP Under Dripping Conditions				
ESNP237	[0, 10^4, 2 × 10^4 yr]	[7 × 10^{-7}, 10^{-1} g/yr]	*PHCSS*(–) *CORRATSS*(–) *INFIL*(+) *EP1NPO2*(+)	K5.3.2-3

Table K5.1-2 Summary of Uncertainty and Sensitivity Analysis Results for the Early Failure Scenario Class for Release from the Engineered Barrier System (Continued)

Variable[a]	Time Interval[b]	Range[c]	Dominant Input Variables[d]	Figures[e]
ESNP237C	[0, 10^4, 2 × 10^4 yr]	[8 × 10^{-3}, 4 × 10^3 g]	*PHCSS*(–) *INFIL*(+) *EP1NPO2*(+) *EP1LOWAM*(+) *CORRATSS*(–)	K5.3.2-3
ESNP237	[0, 5 × 10^5, 10^6 yr]	[7 × 10^{-5}, 2 × 10^{-2} g/yr]	*GOESITED*(–) *INFIL*(+) *PHCSS*(+)	K5.3.8-1
ESNP237C	[0, 5 × 10^5, 10^6, yr]	[10, 2 × 10^4 g]	*INFIL*(+) *GOESITED*(–)	K5.3.8-1
Early CDSP WP Failure Under Dripping Conditions				
ESNP237	[0, 10^4, 2 × 10^4 yr]	[10^{-7}, 2 × 10^{-2} g/yr]	*GOESITED*(–) *EBSDIFCF*(+)	K5.3.3-3
ESNP237C	[0, 10^4, 2 × 10^4 yr]	[4 × 10^{-3}, 7 g]	*GOESITED*(–) *DELPPCO2*(+) *PH2MCONS*(–) *INFIL*(+)	K5.3.3-3
ESNP237	[0, 5 × 10^5, 10^6 yr]	[8 × 10^{-6}, 10^{-3} g/yr]	*GOESITED*(–) *INFIL*(+)	K5.3.9-1
ESNP237C	[0, 5 × 10^5, 10^6, yr]	[2, 500 g]	*INFIL*(+) *GOESITED*(–) *HFOSA*(–)	K5.3.9-1
Early CSNF WP Failure Under Dripping Conditions				
ESNP237	[0, 1.5 × 10^4, 2 × 10^4 yr]	[0, 1 g/yr]	*INFIL*(–) *ISCSNS*(+)	K5.3.5-3
ESNP237C	[0, 1.5 × 10^4, 2 × 10^4 yr]	[0, 7 × 10^3, 7 g]	*INFIL*(–) *ISCSNS*(+)	K5.3.5-3
ESNP237	[0, 5 × 10^5, 10^6 yr]	[4 × 10^{-5}, 4 × 10^{-2} g/yr]	*GOESITED*(–) *INFIL*(+)	K5.3.11-1
ESNP237C	[0, 5 × 10^5, 10^6, yr]	[2, 2 × 10^4 g]	*ISCSNS*(+) *GOESITED*(–)	K5.3.11-1
Early CDSP WP Failure Under Nondripping Conditions				
ESNP237	[0, 5 × 10^5, 10^6 yr]	[10^{-7}, 2 × 10^{-5} g/yr]	*GOESITED*(–) *HFOSA*(–) *DSNFMASS*(+)	K5.3.10-1
ESNP237C	[0, 5 × 10^5, 10^6 yr]	[7 × 10^{-2}, 10 g]	*GOESITED*(–) *HFOSA*(–) *DSNFMASS*(+)	K5.3.10-1
Early CSNF WP Failure Under Nondripping Conditions				
ESNP237	[0, 5 × 10^5, 10^6 yr]	[10^{-7}, 8 × 10^{-3} g/yr]	*ISCSNS*(+)	K5.3.12-1

Table K5.1-2 Summary of Uncertainty and Sensitivity Analysis Results for the Early Failure Scenario Class for Release from the Engineered Barrier System (Continued)

Variable[a]	Time Interval[b]	Range[c]	Dominant Input Variables[d]	Figures[e]
			GOESITED(–)	
ESNP237C	[0, 5×10^5, 10^6 yr]	[10^{-1}, 7×10^3 g]	*ISCSNS*(+) *GOESITED*(–)	K5.3.12-1
Time-Dependent Release Rate (*ESPU239*, g/yr) and Cumulative Release (*ESPU239C*, g) for Dissolved ^{239}Pu				
Early DS Failure Above a CDSP WP Under Dripping Conditions				
ESPU239	[0, 10^4, 2×10^4 yr]	[2×10^{-7}, 2×10^{-2} g/yr]	*EP1LOWPU*(+) *INFIL*(+) *DELPPCO2*(+)	K5.3.1-7 K5.3.1-8
ESPU239C	[0, 10^4, 2×10^4 yr]	[10^{-3}, 300 g]	*EP1LOWPU*(+) *INFIL*(+) *DELPPCO2*(+)	K5.3.1-7 K5.3.1-8
ESPU239	[0, 10^5, 2×10^5 yr]	[4×10^{-6}, 5×10^{-3} g/yr]	*EP1LOWPU*(+) *INFIL*(+) *GOESITED*(–)	K5.3.7-2
ESPU239C	[0, 10^5, 2×10^5, yr]	[0.5, 3×10^3 g]	*EP1LOWPU*(+) *INFIL*(+) *GOESITED*(+)	K5.3.7-2
Early DS Failure Above a CSNF WP Under Dripping Conditions				
ESPU239	[0, 10^4, 2×10^4 yr]	[4×10^{-7}, 3×10^{-2} g/yr]	*EP1LOWPU*(+) *INFIL*(+) *DELPPCO2*(+) *PHCSS*(–)	K5.3.2-4
ESPU239C	[0, 10^4, 2×10^4 yr]	[3×10^{-3}, 200 g]	*INFIL*(+) *EP1LOWPU*(+) *DELPPCO2*(+) *PHCSS*(–)	K5.3.2-4
ESPU239	[0, 10^5, 2×10^5 yr]	[3×10^{-6}, 10^{-2} g/yr]	*EP1LOWPU*(+) *INFIL*(+) *GOESITED*(–) *PHCSS*(–)	K5.3.8-2
ESPU239C	[0, 10^5, 2×10^5, yr]	[0.8, 4×10^4 g/yr]	*EP1LOWPU*(+) *INFIL*(+) *PHCSS*(–) *DELPPCO2*(+)	K5.3.8-2
Early CDSP WP Failure Under Dripping Conditions				
ESPU239	[0, 10^4, 2×10^4 yr]	[10^{-7}, 2×10^{-2} g/yr]	*EP1LOWPU*(+) *INFIL*(+) *DELPPCO2*(+) *PH2MCONS*(–)	K5.3.3-4
ESPU239C	[0, 10^4, 2×10^4 yr]	[3×10^{-4}, 100 g]	*EP1LOWPU*(+) *DELPPCO2*(+)	K5.3.3-4

Table K5.1-2 Summary of Uncertainty and Sensitivity Analysis Results for the Early Failure Scenario Class for Release from the Engineered Barrier System (Continued)

Variable[a]	Time Interval[b]	Range[c]	Dominant Input Variables[d]	Figures[e]
			INFIL(+) *PH2MCONS*(–)	
ESPU239	[0, 10^5, 2 × 10^5 yr]	[3 × 10^{-6}, 10^{-3} g/yr]	*EP1LOWPU*(+) *EBSDIFCF*(+) *GOESITED*(–) *INFIL*(+)	K5.3.9-2
ESPU239C	[0, 10^5, 2 × 10^5, yr]	[0.3, 10^3 g]	*EP1LOWPU*(+) *EBSDIFCF*(+) *DIFPATHL*(–) *INFIL*(+)	K5.3.9-2
Early CSNF WP Failure Under Dripping Conditions				
ESPU239	[0, 1.5 × 10^4, 2 × 10^4 yr]	[0, 2 × 10^{-2} g/yr]	*ISCSNS*(+) *INFIL*(–)	K5.3.5-4
ESPU239C	[0, .5 × 10^4, 2 × 10^4 yr]	[0, 100 g]	*ISCSNS*(+) *INFIL*(–)	K5.3.5-4
ESPU239	[0, 10^5, 2 × 10^5 yr]	[10^{-6}, 5 × 10^{-3} g/yr]	*EP1LOWPU*(+) *ISCSNS*(+) *PHCSNS*(–)	K5.3.11-2
ESPU239C	[0, 10^5, 2 × 10^5, yr]	[0.1, 10^3 g]	*EP1LOWPU*(+) *ISCSNS*(+) *PHCSNS*(–)	K5.3.11-2
Early CDSP WP Failure Under Nondripping Conditions				
ESPU239	[0, 10^5, 2 × 10^5 yr]	[2 × 10^{-8}, 7 × 10^{-5} g/yr]	*EP1LOWPU*(+) *EBSDIFCF*(+) *GOESITED*(–)	K5.3.10-2
ESPU239C	[0, 10^5, 2 × 10^5 yr]	[10^{-3}, 30 g]	*EP1LOWPU*(+) *EBSDIFCF*(+) *PH2MCONS*(–)	K5.3.10-2
Early CSNF WP Failure Under Nondripping Conditions				
ESPU239	[0, 10^5, 2 × 10^5 yr]	[2 × 10^{-8}, 8 × 10^{-5}]	*EP1LOWPU*(+) *ISCSNS*(+) *PHCSNS*(–)	K5.3.12-2
ESPU239C	[0, 10^5, 2 × 10^5 yr]	[10^{-3}, 20 g]	*EP1LOWPU*(+) *ISCSNS*(+) *PHCSNS*(–)	K5.3.12-2
Time-Dependent Release Rate (*ESTC99*, g/yr) and Cumulative Release (*ESTC99C*, g) for Dissolved ^{99}Tc				
Early DS Failure Above CDSP WP Under Dripping Conditions				
ESTC99	[0, 3 × 10^3, 2 × 10^4 yr]	[3 × 10^{-5}, 0.2 g/yr]	*HLWDRALK*(–) *WFDEGEXF*(–) *HLWDRACD*(+) *PH2DHLS*(–)	K5.3.1-9 K5.3.1-10

Table K5.1-2 Summary of Uncertainty and Sensitivity Analysis Results for the Early Failure Scenario Class for Release from the Engineered Barrier System (Continued)

Variable[a]	Time Interval[b]	Range[c]	Dominant Input Variables[d]	Figures[e]
ESTC99C	[0, 3×10^3, 2×10^4 yr]	[200, 1700 g]	*HLWDRALK*(+) *HLWMASS*(+) *WFDEGEXF*(+) *HLWDRACD*(+) *DSNFMASS*(+)	K5.3.1-9 K5.3.1-10
Note: Most ^{99}Tc released by 3000 yr after DS failure.				
Early DS Failure Above CSNF WP Under Dripping Conditions				
ESTC99	[0, 3×10^3, 2×10^4 yr]	[3×10^{-9}, 0.1 g/yr]	*INFIL*(–) *SEEPPRMN*(+)	K5.3.2-5
ESTC99C	[0, 3×10^3, 2×10^4 yr]	[6500, 10,600 g]	*CSNFMASS*(+)	K5.3.2-5
Note: Effectively all ^{99}Tc released by 1500 yr after DS failure.				
Early CDSP WP Failure Under Dripping Conditions				
ESTC99	[0, 3×10^3, 2×10^4 yr]	[7×10^{-6}, 0.3 g/yr]	*HLWDRALK*(–) *INFIL*(–) *WFDEGEXF*(–)	K5.3.3-5
ESTC99C	[0, 3×10^3, 2×10^4 yr]	[200, 1700 g]	*HLWDRALK*(+) *HLWMASS*(+) *DSNFMASS*(+) *WFDEGEXF*(+)	K5.3.3-5
NOTE: Most ^{99}Tc released by 3000 yr after WP failure.				
Early CSNF WP Failure Under Dripping Conditions				
Release rate *ESTC99* zero until after 10^4 yr; then, release very rapid (Figure K.5.3.5-5a). Nonzero values for *ESTC99C* rapidly approach an asymptote with values between 6200 and 10,300 g, which is approximately the same range (i.e., 6500 to 10,600 g) obtained for *ESTC99C* for early failure of a DS above a CSNF WP under dripping conditions.				

[a] Dependent variable under consideration.
[b] Time interval [t_1, t_2, t_3], where t_1 is initial or event time, t_2 is time at which variable range (Column c) and dominant input variables (Column d) are determined, and t_3 is the end time for the analysis.
[c] Range of values at time t_2.
[d] Dominant input variables at time t_2 with "+" and "–" indicating positive and negative effects respectively.
[e] Figures presenting detailed analyses.

Table K5.1-3 Summary of Uncertainty and Sensitivity Analysis Results for Radionuclide Movement from the UZ to the SZ Resulting from Early DS Failure Above a CDSP WP Under Dripping Conditions

Variable[a]	Time Interval[b]	Range[c]	Dominant Variables[d]	Figures[e]
Release Rate (*UZIC239*, g/yr) and Cumulative Release (*UZIC239C*, g) for ^{239}Pu Irreversibly Attached to Slow Colloids				
UZIC239	[0, 10^4, 2 × 10^4 yr]	[2 × 10^{-7}, 10^{-3} g/yr]	*INFIL*(+) *CPUCOLWF*(+)	K5.4.1-1 K5.4.1-2
UZIC239C	[0, 10^4, 2 × 10^4 yr]	[3 × 10^{-3}, 10 g]	*CPUCOLWF*(+) *INFIL*(+)	K5.4.1-1 K5.4.1-2 K5.4.1-3
Release Rate (*UZIF239*, g/yr) and cumulative release (*UZIF239C*, g) for ^{239}Pu Irreversibly Attached to Fast Colloids				
UZIF239	[0, 10^4, 2 × 10^4 yr]	[4 × 10^{-10}, 2 × 10^{-6} g/yr]	*INFIL*(+) *CPUCOLWF*(+)	K5.4.1-4 K5.4.1-5
UZIF239C	[0, 10^4, 2 × 10^4 yr]	[4 × 10^{-6}, 0.02 g]	*CPUCOLWF*(+) *INFIL*(+)	K5.4.1-4 K5.4.1-5 K5.4.1-6
Release Rate (*UZNP237*, g/yr) and cumulative release (*UZNP237C*, g) for Dissolved ^{237}Np				
UZNP237	[0, 10^4, 2 × 10^4 yr]	[2 × 10^{-6}, 0.01 g/yr]	*INFIL*(+) *GOESITED*(–) *DEPPCO2*(+) *DSNFMASS*(+)	K5.4.1-7 K5.4.1-8
UZNP237C	[0, 10^4, 2 × 10^4 yr]	[0.01, 100 g]	*DELPPCO2*(+) *INFIL*(+) *PH2MCOS*(–) *GOESITED*(–)	K5.4.1-7 K5.4.1-8 K5.4.1-9
Release Rate (*UZPU239*, g/yr) and cumulative release (*UZPUP239C*, g) for Dissolved ^{237}Np				
UZPU239	[0, 10^9, 2 × 10^4 yr]	[10^{-7}, 0.02 g/yr]	*EP1LOWPU*(+) *INFIL*(+) *DELPPCO2*(+) *UZKDPUDT*(–)	K5.4.1-10 K5.4.1-11
UZPU239C	[0, 10^4, 2 × 10^4 yr]	[3 × 10^{-4}, 100 g]	*INFIL*(+) *EP1LOWPU*(+) *DELPPCO2*(+) *UZKDPUDT*(–)	K5.4.1-10 K5.4.1-11 K5.4.1-12

Table K5.1-3 Summary of Uncertainty and Sensitivity Analysis Results for Radionuclide Movement from the UZ to the SZ Resulting from Early DS Failure Above a CDSP WP Under Dripping Conditions (Continued)

Variable[a]	Time Interval[b]	Range[c]	Dominant Variables[d]	Figures[e]
Release Rate (*UZTC99*, g/yr) and cumulative release (*UZTC99C*, g) for Dissolved ^{99}Tc				
UZTC99	[0, 3×10^3, 2×10^4 yr]	[0.01, 0.3 g/yr]	*INFIL*(–) *HLWMASS*(+) *HLWDRACD*(+)	K5.4.1-13 K5.4.1-14
UZTC99C	[0, 2×10^3, 2×10^4 yr]	[100, 1.5×10^3g]	*INFIL*(+) *HLWDRALK*(+) *HLWMASS*(+) *WFDEGEXF*(+) *HLWDRACD*(+) *DSNFMASS*(+)	K5.4.1-13 K5.4.1-14 K5.4.1-15

[a] Dependent variable under consideration.
[b] Time interval [t_1, t_2, t_3], where t_1 is initial or event time, t_2 is time at which variable range (Column c) and dominant input variables (Column d) are determined, and t_3 is the end time for the analysis.
[c] Range of values at time t_2.
[d] Dominant input variables at time t_2 with "+" and "–" indicating positive and negative effects respectively.
[e] Figures presenting detailed analyses.

Table K5.1-4 Summary of Uncertainty and Sensitivity Analysis Results for Radionuclide Movement in the SZ Across a Subsurface Plane at the Location of the RMEI Resulting from Early DS Failure Above a CDSP WP Under Dripping Conditions

Variable[a]	Time Interval[b]	Range[c]	Dominant Input Variables[d]	Figures[e]
Release Rate (*SZIC239*, g/yr) and cumulative release (*SZIC239C*, g) for ^{239}Pu Irreversibly Attached to Waste Form Colloids				
SZIC239	[0, 10^4, 2×10^4 yr]	[?, 10^{-3} g/yr]	*SZCOLRAL*(–) *SZGWSPDM*(+) *SZF1POVO*(–) *SZLODISP*(+) *CPUCOLWF*(+)	K5.5.1-1
SZIC239C	[0, 10^4, 2×10^4 yr]	[?, 8 g]	*SZCOLRAL*(–) *SZGWSPDM*(+) *SZF1POVO*(–) *SZLODISP*(+)	K5.5.1-1
Release Rate (*SZIF239*, g/yr) and cumulative release (*SZIF239C*, g) for ^{239}Pu Irreversibly Attached to Fast Colloids				
SZIF239	[0, 10^4, 2×10^4 yr]	[4×10^{-10}, 2×10^{-6} g/yr]	*CPUCOLWF*(+) *INFIL*(+) *SEEPPRM*(–)	K5.5.1-2
SZIF239C	[0, 10^4, 2×10^4 yr]	[4×10^{-6}, 0.02 g]	*CPUCOLWF*(+) *INFIL*(+)	K5.5.1-2
Release Rate (*SZNP237*, g/yr) and cumulative release (*SZNP237C*, g) for Dissolved ^{237}Np				
SZNP237	[0, 10^4, 2×10^4 yr]	[10^{-7}, 8×10^{-3} g/yr]	*DELPPCO2*(+) *HFOSA*(–) *GOESITED*(–) *SZGWSPDM*(+)	K5.5.1-3
SZNP237C	[0, 10^4, 2×10^4 yr]	[?, 100 g]	*DELPPCO2*(+) *SZGWSPDM*(+) *SZFISPVO*(+)	K5.5.1-3
Release Rate (*SZPU239*, g/yr) and cumulative release (*SZPU239C*, g) for Dissolved ^{239}Pu				
SZPU239	[0, 10^4, 2×10^4 yr]	[0, 8×10^{-3} g/yr]	*SZGWSPDM*(+) *SZFISPVO*(+) SZCONCOL(+)	K5.5.1-4
SZPU239C	[0, 10^4, 2×10^4 yr]	[0, 20 g]	*SZGWSPDM*(+) *SZFISPVO*(+) SZCONCOL(+)	K5.5.1-4

Table K5.1-4 Summary of Uncertainty and Sensitivity Analysis Results for Radionuclide Movement in the SZ Across a Subsurface Plane at the Location of the RMEI Resulting from Early DS Failure Above a CDSP WP Under Dripping Conditions (Continued)

Variable[a]	Time Interval[b]	Range[c]	Dominant Variables[d]	Figures[e]
Release Rate (*SZTC99*, g/yr) and cumulative release (*SZTC99C*, g) for Dissolved ^{99}Tc				
SZTC99	[0, 2×10^3, 2×10^4 yr]	[5×10^{-3}, 0.4 g/yr]	*INFIL*(–) *SZFISPVO*(–) *SZGWSPDM*(–)	K5.5.1-5
SZTC99C	[0, 2×10^3, 2×10^4 yr]	[?, 1.4×10^3g]	*SZGWSPDM*(+) *INFIL*(+) *SZFISPOVO*(–) *DSNFMASS*(+) *HLWMASS*(+)	K5.5.1-5

[a] Dependent variable under consideration.
[b] Time interval [t_1, t_2, t_3], where t_1 is initial or event time, t_2 is time at which variable range (Column c) and dominant input variables (Column d) are determined, and t_3 is the end time for the analysis.
[c] Range of values at time t_2.
[d] Dominant input variables at time t_2 with "+" and "–" indicating positive and negative effects respectively.
[e] Figures presenting detailed analyses.

Table K5.1-5 Summary of Uncertainty and Sensitivity Analysis Results for Dose to the RMEI from Selected Radionuclides Resulting from Early DS Failure Above a CDSP WP Under Dripping Conditions

Variable[a]	Time Interval[b]	Range[c]	Dominant Input Variables[d]	Figures[e]
Dose from ^{239}Pu Irreversibly Attached to Slow Colloids (*DOIC239*, mrem/yr)				
DOIC239	[0, 10^4, 2×10^4 yr]	[10^{-8}, 0.1 mrem/yr]	*SZCOLRAL*(–) *SZGWSPDM*(+) *SZFIPOVO*(–) *SZLODISP*(+) *CPUCOLWF*(+)	K5.6.1-1
Dose from ^{239}Pu Irreversibly Attached to Fast Colloids (*DOIF239*, mrem/yr)				
DOIF239	[0, 10^4, 2×10^4 yr]	[2×10^{-8}, 2×10^{-4} mrem/yr]	*CPUCOLWF*(+) *INFIL*(+) *MICPU239*(+)	K5.6.1-2
Dose from Dissolved ^{237}Np (*DONP237*, mrem/yr)				
DONP237	[0, 10^4, 2×10^4 yr]	[10^{-8}, 10^{-3} mrem/yr]	*DELPPCO2*(+) *HFOSA*(–) *SEEPWAT*(+) *SZGWSPDM*(+)	K5.6.1-3
Dose from Dissolved ^{239}Pu (*DOPU239*, mrem/yr)				
DOPU239	[0, 10^4, 2×10^4 yr]	[0, 0.4 mrem/yr]	*SZGWSPDM*(+) *SZFISPVO*(+) *SZCONCOL*(+)	K5.6.1-4
Dose from Dissolved ^{99}Tc (*DOTC99*, mrem/yr)				
DOTC99	[0, 3×10^3, 2×10^4 yr]	[5×10^{-5}, 0.06 mrem/yr]	*MICTC99*(+) *INFIL*(–) *SZFIPOVO*(+)	K5.6.1-5

[a] Dependent variable under consideration.
[b] Time interval [t_1, t_2, t_3], where t_1 is initial or event time, t_2 is time at which variable range (Column c) and dominant input variables (Column d) are determined, and t_3 is the end time for the analysis.
[c] Range of values at time t_2.
[d] Dominant input variables at time t_2 with "+" and "–" indicating positive and negative effects respectively.
[e] Figures presenting detailed analyses.

Table K5.1-6 Summary of Uncertainty and Sensitivity Analysis Results for Expected Dose to the RMEI (*EXPDOSE*, mrem/yr) Resulting from Early Failures

Variable[a]	Time Interval[b]	Range[c]	Dominant Input Variables[d]	Figures[e]
Expected Dose for Early DS Failures (*EXPDOSE*, mrem/yr)				
EXPDOSE	[0, 10^4, 2×10^4 yr]	[10^{-8}, 4×10^{-3} mrem/yr]	*PROBDSEF*(+) *SEEPUNC*(+)	K5.7.1-1 K5.7.1-2
EXPDOSE	[0, 5×10^5, 10^6 yr]	[10^{-8}, 8×10^{-4} mrem/yr]	*PROBDSEF*(+) *INFIL*(+) *SZGWSPDM*(+) *SEEPUNC*(+) *SEEPRM*(–)	K5.7.1-3 K5.7.1-4
Expected Dose for Early WP Failures (*EXPDOSE*, mrem/yr)				
EXPDOSE	[0, 10^4, 2×10^4 yr]	[3×10^{-6}, 0.5 mrem/yr]	*PROBWPEF*(+) *INFIL*(–) *THERMCON*(+)	K5.7.2-1 K5.7.2-2
EXPDOSE	[10, 5×10^5, 10^6 yr]	[10^{-6}, 0.08 mrem/yr]	*PROBWPEF*(+) *INFIL*(+) *SZGWSPDM*(+) *SEEPRM*(–)	K5.7.2-3 K5.7.2-4
Expected Dose from Both Early DS Failure and Early WP Failure (*EXPDOSE*, mrem/yr)				
EXPDOSE	[0, 10^4, 2×10^4 yr]	[4×10^{-6}, 0.5 mrem/yr]	*PROBWPEF*(+) *INFIL*(–) *THERMCON*(+) *PPOBDSEF*(+)	K5.7.3-1 K5.7.3-2
EXPDOSE	[0, 5×10^5, 10^6 yr]	[10^{-6}, 0.09 mrem/yr]	*PROBWPEF*(+) *INFIL*(+) *SZGWSPDM*(+) *SEEPUNC*(+)	K5.7.3-3 K5.7.3-4
Expected Dose from Early DS Failure, Early WP Failure and Nominal Process WP Failure (*EXPDOSE*, mrem/yr)				
EXPDOSE	[0, 5×10^5, 10^6 yr]	[10^{-6}, 7 mrem/yr]	*WDGCA22*(–)	K5.7.4-1 K5.7.4-2

[a] Dependent variable under consideration.
[b] Time interval [t_1, t_2, t_3], where t_1 is initial or event time, t_2 is time at which variable range (Column c) and dominant input variables (Column d) are determined, and t_3 is the end time for the analysis.
[c] Range of values at time t_2.
[d] Dominant input variables at time t_2 with "+" and "–" indicating positive and negative effects respectively.
[e] Figures presenting detailed analyses.

INTENTIONALLY LEFT BLANK

Table K6.1-1. Summary of TSPA-LA Model Results Considered in Uncertainty and Sensitivity Analyses for the Igneous Scenario Classes

Output Variable	Definition
DOIC239	Dose to RMEI (mrem/yr) from ^{239}Pu irreversibly attached to slow (i.e., Ic) colloids (Figures K.6.6.1-1, K.6.6.1-2, K.6.6.2-1)
DOIF239	Dose to RMEI (mrem/yr) from ^{239}Pu irreversibly attached to fast (i.e., If) colloids (Figures K.6.6.1-3, K.6.6.1-4, K.6.6.2-2)
DONP237	Dose to RMEI (mrem/yr) from dissolved ^{237}Np (Figures K.6.6.1-5, K.6.6.1-6, K.6.6.2-3)
DOPU239	Dose to RMEI (mrem/yr) from dissolved ^{239}Pu (Figures K.6.6.1-7, K.6.6.1-8, K.6.6.2-4)
DOTC99	Dose to RMEI (mrem/yr) from dissolved ^{99}Tc (Figures K.6.6.1-9, K.6.6.1-10)
ESFA239C	Cumulative release (g) for the movement of ^{239}Pu irreversibly attached to fast (i.e., If) colloids from the EBS to the UZ (Figure K.6.4.1-6)
ESIC239	Release rate (g/yr) for the movement of ^{239}Pu irreversibly attached to waste form (i.e., Ic) colloids from the EBS to the UZ (Figures K.6.3.1-1, K.6.3.1-2, K.6.3.2-1)
ESIC239C	Cumulative release (g) for the movement of ^{239}Pu irreversibly attached to waste form (i.e., Ic) colloids from the EBS to the UZ (Figures K.6.3.1-1, K.6.3.1-2, K.6.3.2-1)
ESIF239	Release rate (g/yr) for the movement of ^{239}Pu irreversibly attached to ferrous (i.e., If) colloids from the EBS to the UZ (Figures K.6.3.1-3, K.6.3.1-4, K.6.3.2-2)
ESIF239C	Cumulative release (g) for the movement of ^{239}Pu irreversibly attached to ferrous (i.e., If) colloids from the EBS to the UZ (Figures K.6.3.1-3, K.6.3.1-4, K.6.3.2-2)
ESNP237	Release rate (g/yr) for the movement of dissolved ^{237}Np from the EBS to the UZ (Figures K.6.3.1-5, K.6.3.1-6, K.6.3.2-3)
ESNP237C	Cumulative release (g) for the movement of dissolved ^{237}Np from the EBS to the UZ (Figures K.6.3.1-5, K.6.3.1-6, K.6.3.2-3, K.6.4.1-9)
ESPU239	Release rate (g/yr) for the movement of dissolved ^{239}Pu from the EBS to the UZ (Figures K.6.3.1-7, K.6.3.1-8, K.6.3.2-4)
ESPU239C	Cumulative release (g) for the movement of dissolved ^{239}Pu from the EBS to the UZ (Figures K.6.3.1-7, K.6.3.1-8, K.6.3.2-4, K.6.4.1-12)
ESSL239C	Cumulative release (g) for the movement of ^{239}Pu irreversibly attached to slow colloids from the EBS to the UZ (Figure K.6.4.1-3)
ESTC99	Release rate (g/yr) for the movement of dissolved ^{99}Tc from the EBS to the UZ (Figures K.6.3.1-9, K.6.3.1-10)
ESTC99C	Cumulative release (g) for the movement of dissolved ^{99}Tc from the EBS to the UZ (Figures K.6.3.1-9, K.6.3.1-10, K.6.4.1-15)
EXPDOSE	Expected dose to RMEI (mrem/yr) from all radioactive species (Figures K.6.7.1-1, K.6.7.1-2, K.6.7.2-1, K.6.7.2-2, K.6.8.1-1, K.6.8.1-2, K.6.8.2-1, K.6.8.2-2)
ISCDINAD	Ionic strength (molal) in the invert beneath the WP for CDSP WPs under dripping conditions (Figure K.6.2-3)
ISCSINAD	Ionic strength (molal) in the invert beneath the WP for CSNF WPs under dripping conditions (Figure K.6.2-3)

Table K6.1-1. Summary of TSPA-LA Model Results Considered in Uncertainty and Sensitivity Analyses for the Igneous Scenario Classes (Continued)

Output Variable	Definition
PHCDINAD	pH in the invert beneath the WP for CDSP WPs under dripping conditions (Figure K.6.2-4)
PHCSINAD	pH in the invert beneath the WP for CSNF WPs under dripping conditions (Figure K.6.2-4)
SPRATECS	Seepage rate (m^3/yr/WP) into the repository above CSNF WPs (Figure K.6.2-2)
SZIC239	Release rate (g/yr) for the movement of ^{239}Pu irreversibly attached to slow (i.e., Ic) colloids across a subsurface plane at the location of the RMEI (Figures K.6.5.1-1, K.6.5.1-2, K.6.5.2-1)
SZIC239C	Cumulative release (g) for the movement of ^{239}Pu irreversibly attached to slow (i.e., Ic) colloids across a subsurface plane at the location of the RMEI (Figures K.6.5.1-1, K.6.5.1-2, K.6.5.1-3, K.6.5.2-1)
SZIF239	Release rate (g/yr) for the movement of ^{239}Pu irreversibly attached to fast (i.e., If) colloids across a subsurface plane at the location of the RMEI (Figures K.6.5.1-4, K.6.5.1-5, K.6.5.2-2)
SZIF239C	Cumulative release (g) for the movement of ^{239}Pu irreversibly attached to fast (i.e., If) colloids across a subsurface plane at the location of the RMEI (Figures K.6.5.1-4, K.6.5.1-5, K.6.5.1-6, K.6.5.2-2)
SZNP237	Release rate (g/yr) for the movement of dissolved ^{237}Np across a subsurface plane at the location of the RMEI (Figures K.6.5.1-7, K.6.5.1-8, K.6.5.2-3)
SZNP237C	Cumulative release (g) for the movement of dissolved ^{237}Np across a subsurface plane at the location of the RMEI (Figures K.6.5.1-7, K.6.5.1-8, K.6.5.1-9, K.6.5.2-3)
SZPU239	Release rate (g/yr) for the movement of dissolved ^{239}Pu across a subsurface plane at the location of the RMEI (Figures K.6.5.1-10, K.6.5.1-11, K.6.5.2-4)
SZPU239C	Cumulative release (g) for the movement of dissolved ^{239}Pu across a subsurface plane at the location of the RMEI (Figures K.6.5.1-10, K.6.5.1-11, K.6.5.1-12, K.6.5.2-4)
SZTC99	Release rate (g/yr) for the movement of dissolved ^{99}Tc across a subsurface plane at the location of the RMEI (Figures K.6.5.1-13, K.6.5.1-14)
SZTC99C	Cumulative release (g) for the movement of dissolved ^{99}Tc across a subsurface plane at the location of the RMEI (Figures K.6.5.1-13, K.6.5.1-14, K.6.5.1-15)
TMPCDINV	Drift temperature (C) for CDSP WPs in the invert beneath the WP (Figure K.6.2-1)
TMPCDWL	Drift temperature (C) for CDSP WPs at the drift wall (Figure K.6.2-1)
TMPCDWP	Drift temperature (C) for CDSP WPs on the WP (Figure K.6.2-1)
TMPCSINV	Drift temperature (C) for CSNF WPs in the invert beneath the WP (Figure K.6.2-1)
TMPCSWL	Drift temperature (C) for CSNF WPs at the drift wall (Figure K.6.2-1)
TMPCSWP	Drift temperature (C) for CSNF WPs on the WP (Figure K.6.2-1)
UZIC239	Release rate (g/yr) for the movement of ^{239}Pu irreversibly attached to slow (i.e., Ic) colloids from the UZ to the SZ (Figures K.6.4.1-1, K.6.4.1-2)
UZIC239C	Cumulative release (g) for the movement of ^{239}Pu irreversibly attached to slow (i.e., Ic) colloids from the UZ to the SZ (Figures K.6.4.1-1, K.6.4.1-2, K.6.4.1-3,

Table K6.1-1. Summary of TSPA-LA Model Results Considered in Uncertainty and Sensitivity Analyses for the Igneous Scenario Classes (Continued)

Output Variable	Definition
	K.6.5.1-3)
UZIF239	Release rate (g/yr) for the movement of ^{239}Pu irreversibly attached to fast (i.e., If) colloids from the UZ to the SZ (Figures K.6.4.1-4, K.6.4.1-5)
UZIF239C	Cumulative release (g) for the movement of ^{239}Pu irreversibly attached to fast (i.e., If) colloids from the UZ to the SZ (Figures K.6.4.1-4, K.6.4.1-5, K.6.4.1-6, K.6.5.1-6)
UZNP237	Release rate (g/yr) for the movement of dissolved ^{237}Np from the UZ to the SZ (Figures K.6.4.1-7, K.6.4.1-8)
UZNP237C	Cumulative release (g) for the movement of dissolved ^{237}Np from the UZ to the SZ (Figures K.6.4.1-7, K.6.4.1-8, K.6.4.1-9, K.6.5.1-9)
UZPU239	Release rate (g/yr) for the movement of dissolved ^{239}Pu from the UZ to the SZ (Figures K.6.4.1-10, K.6.4.1-11)
UZPU239C	Cumulative release (g) for the movement of dissolved ^{239}Pu from the UZ to the SZ (Figures K.6.4.1-10, K.6.4.1-11, K.6.4.1-12, K.6.5.1-12)
UZTC99	Release rate (g/yr) for the movement of dissolved ^{99}Tc from the UZ to the SZ (Figures K.6.4.1-13, K.6.4.1-14)
UZTC99C	Cumulative release (g) for the movement of dissolved ^{99}Tc from the UZ to the SZ (Figures K.6.4.1-13, K.6.4.1-14, K.6.4.1-15, K.6.5.1-15)

Table K6.1-2 Summary of Uncertainty and Sensitivity Analysis Results for Radionuclide Movement from the EBS to the UZ Resulting from an Igneous Intrusive Event that Destroys All WPs in the Repository

Output Variable[a]	Time Interval[b]	Range[c]	Dominant Input Variables[d]	Figures[e]
Release Rate (*ESIC239*, g/yr) and Cumulative Release (*ESIC239C*, g) for ^{239}Pu Irreversibly Attached to WP Colloids				
ESIC239	[10, 10^4, 2×10^4 yr]	[9×10^{-3}, 20 g/yr]	*CPUCOLWF*(+) *INFIL*(+)	K6.3.1-1 K6.3.1-2
ESIC239C	[10, 10^4, 2×10^4 yr]	[80, 2×10^5 g]	*CPUCOLWF*(+) *INFIL*(+)	K6.3.1-1 K6.3.1-2
ESIC239	[250, 10^5, 2×10^5 yr]	[0.02, 10 g/yr]	*EP1LOWPU*(–) *CPUCOLWF*(+)	K6.3.2-1
ESIC239C	[250, 10^5, 2×10^5 yr]	[2×10^3, 10^6 g]	*CPUCOLWF*(+) *EP1LOWPU*(–)	K6.3.2-1
Release Rate (*ESIF239*, g/yr) and Cumulative Release (*ESIF239C*, g) for ^{239}Pu Irreversibly Attached to Ferrous Colloids				
ESIF239	[10, 10^4, 2×10^4 yr]	Results removed due to model error		K6.3.1-3 K6.3.1-4

Table K6.1-2 Summary of Uncertainty and Sensitivity Analysis Results for Radionuclide Movement from the EBS to the UZ Resulting from an Igneous Intrusive Event that Destroys All WPs in the Repository (Continued)

Ouput Variable[a]	Time Interval[b]	Range[c]	Dominant Input Variables[d]	Figures[e]
ESIF239C	[10, 10^4, 2 × 10^4 yr]	Results removed due to model error		K6.3.1-3 K6.3.1-4
ESIF239	[250, 10^5, 2 × 10^5 yr]	Results removed due to model error		K6.3.2-2
ESIF239C	[250, 10^5, 2 × 10^5 yr]	Results removed due to model error		K6.3.2-2
Release Rate (*ESNP237*, g/yr) and Cumulative Release (*ESNP237C*, g) of Dissolved ^{237}Np				
ESNP237	[10, 10^4, 2 × 10^4 yr]	[0.3, 4 × 10^3 g/yr]	*EP1NP02*(+) *PHCSS*(–) *INFIL*(+) *CORRATSS*(–)	K6.3.1-5 K6.3.1-6
ESNP237C	[10, 10^4, 2 × 10^4 yr]	[3 × 10^3, 8 × 10^7 g]	*PHCSS*(–) *INFIL*(+) *EP1NP02*(+) *DELPPC02*(+) *EP1LOWAM*(+)	K6.3.1-5 K6.3.1-6
ESNP237	[250, 5 × 10^5, 10^6 yr]	[3, 200 g/yr]	*EPINPO2*(–) *PHCSS*(+) *GOESITED*(–)	K6.3.2-3
ESNP237C	[250, 5 × 10^5, 10^6 yr]	[2 × 10^6, 10^8 g]	*GOESITED*(–) *INFIL*(+) *EP1NPO2*(+)	K6.3.2-3
Release Rate (*ESPU239*, g/yr) and Cumulative Release (*ESPU239C*, g) of Dissolved ^{239}Pu				
ESPU239	[10, 10^4, 2 × 10^4 yr]	[1, 2 × 10^3 g/yr]	*EP1LOWPU*(+) *INFIL*(+) *DELPPCO2*(+)	K6.3.1-7 K6.3.1-8
ESPU239C	[10, 10^4, 2 × 10^4 yr]	[7 × 10^3, 2 × 10^7 g]	*EP1LOWPU*(+) *INFIL*(+) *DELPPCO2*(+)	K6.3.1-7 K6.3.1-8
ESPU239	[250, 10^5, 2 × 10^5 yr]	[1, 300 g/yr]	*EP1LOWPU*(+) *GOESITED*(–) *INFIL*(+)	K6.3.2-4
ESPU239C	[250, 10^5, 2 × 10^5 yr]	[2 × 10^5, 10^8 g]	*EP1LOWPU*(+) *INFIL*(+) *DELPPCO2*(+)	K6.3.2-4
Release Rate (*ESTC99*, g/yr) and Cumulative Release (*ESTC99C*, g) of Dissolved ^{99}Tc				
ESTC99	[10, 3 × 10^3, 2 × 10^4 yr]	[10^{-3}, 200 g/yr]	*HLWDRALK*(–) *INFIL*(–)	K6.3.1-9 K6.3.1-10

Table K6.1-2 Summary of Uncertainty and Sensitivity Analysis Results for Radionuclide Movement from the EBS to the UZ Resulting from an Igneous Intrusive Event that Destroys All WPs in the Repository (Continued)

Ouput Variable[a]	Time Interval[b]	Range[c]	Dominant Input Variables[d]	Figures[e]
ESTC99C	[10, 3×10^3, 2×10^4 yr]	[5.6×10^7, 9.3×10^7 g]	*CSNFMASS*(+)	K6.3.1-9 K6.3.1-10

[a] Dependent variable under consideration.
[b] Time interval [t_1, t_2, t_3], where t_1 is initial or event time, t_2 is time at which variable range (Column c) and dominant input variables (Column d) are determined, and t_3 is the end time for the analysis.
[c] Range of values at time t_2.
[d] Dominant input variables at time t_2 with "+" and "–" indicating positive and negative effects, respectively.
[e] Figures presenting detailed analyses.

Table K6.1-3 Summary of Uncertainty and Sensitivity Analysis Results for Radionuclide Movement from the UZ to the SZ Resulting from an Igneous Intrusive Event that Destroys all WPs in the Repository.

Output Variable[a]	Time Interval[b]	Range[c]	Dominant Input Variables[d]	Figures[e]
Release Rate (*UZIC239*, g/yr) and Cumulative Release (*UZIC239C*, g) for ^{239}Pu Irreversibly Attached to Slow Colloids				
UZIC239	[10, 10^4, 2×10^4 yr]	[9×10^{-3}, 20 g/yr]	*CPUCOLWF*(+) *INFIL*(+)	K6.4.1-1 K6.4.1-2
UZIC239C	[10, 10^4, 2×10^4 yr]	[70, 2×10^5 g]	*CPUCOLWF*(+) *INFIL*(+)	K6.4.1-1 K6.4.1-2 K6.4.1-3
Release Rate (*UZIF239*, g/yr) and Cumulative Release (*UZIF239C*, g) for ^{239}Pu Irreversibly Attached to Slow Colloids				
UZIF239	[10, 10^4, 2×10^4 yr]	[10^{-5}, 0.02 g/yr]	*CPUCOLWF*(+) *INFIL*(+)	K6.4.1-4 K6.4.1-5
UZIF239C	[10, 10^4, 2×10^4 yr]	[0.1, 300 g]	*CPUCOLWF*(+) *INFIL*(+)	K6.4.1-4 K6.4.1-5 K6.4.1-6
Release Rate (*UZNP237*, g/yr) and Cumulative Release (*UZIF239C*, g) for Dissolved ^{237}Np				
UZNP237	[10, 10^4, 2×10^4 yr]	[0.2, 4×10^3 g/yr]	*PHCSS*(–) *INFIL*(+) *DELPPCO2*(+) *EP1LOWAM*(+) *EP1NPO2*(+)	K6.4.1-7 K6.4.1-8

Table K6.1-3 Summary of Uncertainty and Sensitivity Analysis Results for Radionuclide Movement from the UZ to the SZ Resulting from an Igneous Intrusive Event that Destroys all WPs in the Repository. (Continued)

Output Variable[a]	Time Interval[b]	Range[c]	Dominant Input Variables[d]	Figures[e]
UZNP237C	[10, 10^4, 2×10^4 yr]	[10^3, 8×10^7 g]	*PHCSS*(–) *INFIL*(+) *EP1NP02*(+) *EP1LOWAM*(+) *DELPPC02*(+)	K6.4.1-7 K6.4.1-8 K6.4.1-9
Release Rate (*UZPU239*, g/yr) and Cumulative Release (*UZPU239C*, g) for Dissolved ^{239}Pu				
UZPU239	[10, 10^4, 2×10^4 yr]	[0.5, 10^3 g/yr]	*EP1LOWPU*(+) *INFIL*(+) *DELPPCO2*(+)	K6.4.1-10 K6.4.1-11
UZPU239C	[10, 10^4, 2×10^4 yr]	[2×10^3, 10^7 g]	*EP1LOWPU*(+) *INFIL*(+) *DELPPCO2*(+)	K6.4.1-10 K6.4.1-11 K6.4.1-12
Release Rate (*UZTC99*, g/yr) and Cumulative Release (*UZTC99C*, g) for Dissolved ^{99}Tc				
UZTC99	[10, 3×10^3, 2×10^4 yr]	[200, 10^4 g/yr]	*INFIL*(–) *CSNFMASS*(+)	K6.4.1-13 K6.4.1-14
UZTC99C	[10, 3×10^3, 2×10^4 yr]	[4.8×10^7, 8.9×10^7 g]	*CSNFMASS*(+) *INFIL(+)*	K6.4.1-13 K6.4.1-14 K6.4.1-15

[a] Dependent variable under consideration.
[b] Time interval [t_1, t_2, t_3], where t_1 is initial or event time, t_2 is time at which variable range (Column c) and dominant input variables (Column d) are determined, and t_3 is the end time for the analysis.
[c] Range of values at time t_2.
[d] Dominant input variables at time t_2 with "+" and "–" indicating positive and negative effects, respectively.
[e] Figures presenting detailed analyses.

Table K6.1-4 Summary of Uncertainty and Sensitivity Analysis Results for Radionuclide Movement in the SZ Across a Subsurface Plane at the Location of the RMEI Resulting from an Igneous Intrusive Event That Destroys all WPs in the Repository.

Output Variable[a]	Time Interval[b]	Range[c]	Dominant Input Variables[d]	Figures[e]
Release Rate (*SZIC239*, g/yr) and Cumulative Release (*SZIC239C*, g) for ^{239}Pu Irreversibly Attached to Slow Colloids				
SZIC239	[10, 10^4, 2 × 10^4 yr]	[0, 10 g/yr]	*SZCOLRAL*(–) CPUCOLWF(+) *SZGWSPDM*(+) *SZFIPOVO*(–) *INFIL*(+)	K6.5.1-1 K6.5.1-2
SZIC239C	[10, 10^4, 2 × 10^4 yr]	[0, 10^5 g]	*SZCOLRAL*(–) *SZFIPOVO*(–) *SZGWSPDM*(+) CPUCOLWF(+) *INFIL*(+)	K6.5.1-1 K6.5.1-2 K6.5.1-3
SZIC239	[250, 10^5, 2 × 10^5 yr]	[10^{-3}, 10 g/yr]	CPUCOLWF(+) *EP1LOWPU*(–) *SZCOLRAL*(–)	K6.5.2-1
SZIC239C	[250, 10^5, 2 × 10^5 yr]	[10, 10^6 g]	*SZCOLRAL*(–) *CPUCOLWF*(+) *SZGWSPDM*(+) *INFIL*(+)	K6.5.2-1
Release Rate (*SZIF239*, g/yr) and Cumulative Release (*SZIF239C*, g) for ^{239}Pu Irreversibly Attached to Fast Colloids				
SZIF239	[10, 10^4, 2 × 10^4 yr]	[10^{-5}, 0.02 g/yr]	*CPUCOLWF*(+) *INFIL*(+)	K6.5.1-4 K6.5.1-5
SZIF239C	[10, 10^4, 2 × 10^4 yr]	[0.1, 200 g]	*CPUCOLWF*(+) *INFIL*(+)	K6.5.1-4 K6.5.1-5 K.6.5.1-6
SZIF239	[250, 10^5, 2 × 10^5 yr]	[3 × 10^{-5}, 0.02 g/yr]	*EP1LOWPU*(–) *CPUCOLWF*(+)	K6.5.2-2
SZIF239C	[250, 10^5, 2 × 10^5 yr]	[3, 2 × 10^3 g]	*CPUCOLWF*(+) *EP1LOWPU*(–) *INFIL*(+)	K6.5.2-2
Release Rate (*SZNP237*, g/yr) and Cumulative Release (*SZNP237C*, g) of Dissolved ^{237}Np				
SZNP237	[10, 10^4, 2 × 10^4 yr]	[0, 10^3 g/yr]	*PHCSS*(–) *INFIL*(+) *EP1NP02*(+) *SZGWSPDM*(+)	K6.5.1-7 K6.5.1-8
SZNP237C	[10, 10^4, 2 × 10^4 yr]	[10^{-8}, 3 × 10^7 g]	*PHCSS*(–) *INFIL*(+) *SZGWSPDM*(+) *SZFISPVO*(+)	K6.5.1-7 K6.5.1-8 K6.5.1-9

Table K6.1-4 Summary of Uncertainty and Sensitivity Analysis Results for Radionuclide Movement in the SZ Across a Subsurface Plane at the Location of the RMEI Resulting from an Igneous Intrusive Event That Destroys all WPs in the Repository. (Continued)

Output Variable[a]	Time Interval[b]	Range[c]	Dominant Input Variables[d]	Figures[e]
SZNP237	[250, 5 × 10^5, 10^6 yr]	[3, 300 g/yr]	*GOESITED*(–) *PHCSS*(+) *EP1NP02*(–)	K6.5.2-3
SZNP237C	[250, 5 × 10^5, 10^6 yr]	[10^6, 10^8 g]	*GOESITED*(–) *INFIL*(+) *EP1NP02*(+)	K6.5.2-3
Release Rate (*SZPU239*, g/yr) and Cumulative Release (*SZPU239C*, g) of Dissolved ^{239}Pu				
SZPU239	[10, 10^4, 2 × 10^4 yr]	[0, 800 g/yr]	*SZGWSPDM*(+) *SZFISPVO*(+) *SZKDPUVO*(–)	K6.5.1-10 K6.5.1-11
SZPU239C	[10, 10^4, 2 × 10^4 yr]	[0, 3 × 10^6 g]	*SZGWSPDM*(+) *INFIL*(+) *SZFISPVO*(+)	K6.5.1-10 K6.5.1-11 K6.5.1-12
SZPU239	[250, 10^5, 2 × 10^5 yr]	[10^{-3}, 100 g/yr]	*SZGWSPDM*(+) *EP1LOWPU*(+) *SZFISPVO*(+) *SZDIFCVO*(–)	K6.5.2-4
SZPU239C	[250, 10^5, 2 × 10^5 yr]	[100, 4 × 10^7 g]	*SZGWSPDM*(+) *SZFISPVO*(+) *SZDIFCVO*(–) *EP1LOWPU*(+)	K6.5.2-4
Release Rate (*SZTC99*, g/yr) and Cumulative Release (*SZTC99C*, g) for Dissolved ^{99}Tc				
SZTC99	[10, 3 × 10^3, 2 × 10^4 yr]	[300, 3 × 10^4 g/yr]	*INFIL*(–) *CNSFMASS*(+) *UZFAG8*(–) *SZFIPOVO*(+)	K6.5.1-13 K6.5.1-14
SZTC99C	[10, 3 × 10^3, 2 × 10^4 yr]	[1.8 × 10^7, 8.2 × 10^7g]	*INFIL(+)* *SZGWSPDM*(+) *SZFISPVO*(+) *CSNFMASS*(+) *SZDIFCVO*(–)	K6.5.1-13 K6.5.1-14 K6.4.1-15

[a] Dependent variable under consideration.
[b] Time interval [t_1, t_2, t_3], where t_1 is initial or event time, t_2 is time at which variable range (Column c) and dominant input variables (Column d) are determined, and t_3 is the end time for the analysis.
[c] Range of values at time t_2.
[d] Dominant input variables at time t_2 with "+" and "–" indicating positive and negative effects, respectively.
[e] Figures presenting detailed analyses.

Table K6.1-5 Summary of Uncertainty and Sensitivity Analysis Results for Dose to the RMEI from Selected Radionuclides Resulting from an Igneous Intrusive Event that Destroys All WPs in the Repository.

Output Variable[a]	Time Interval[b]	Range[c]	Dominant Input Variables[d]	Figures[e]
Dose from ^{239}Pu Irreversibly Attached to Slow Colloids (*DOIC239*, mrem/yr)				
DOIC239	[10, 10^4, 2 × 10^4 yr]	[0.1, 10^3 mrem/yr]	*SZCOLRAL*(–) *CPUCOLWF*(+) *SZGWSPDM*(+) *SZFIPOVO*(–) *INFIL*(+)	K6.6.1-1 K6.6.1-2
DOIC239	[250, 10^5, 2 × 10^5 yr]	[0.1, 500 mrem/yr]	*CPUCOLWF*(+) *EP1LOWPU*(–) *SZCOLRAL*(–)	K6.6.2-1
Dose from ^{239}Pu Irreversibly Attached to Fast Colloids (*DOIF239*, mrem/yr)				
DOIF239	[10, 10^4, 2 × 10^4 yr]	[10^{-3}, 2 mrem/yr]	*CPUCOLWF*(+) *INFIL*(+) *MICPU239*(+)	K6.6.1-3 K6.6.1-4
DOIF239	[250, 10^5, 2 × 10^5 yr]	[10^{-3}, 1 mrem/yr]	*EP1LOWPU*(–) *CPUCOLWF*(+) *MICPU239*(+)	K6.6.2-2
Dose from Dissolved ^{237}Np (*DONP237*, mrem/yr)				
DONP237	[10, 10^4, 2 × 10^4 yr]	[10^{-2}, 700 mrem/yr]	*PHCSS*(–) *INFIL*(+) *EP1NP02*(+) *SZGWSPDM*(+)	K6.6.1-5 K6.6.1-6
DONP237	[250, 5 × 10^5, 10^6 yr]	[0.6, 50 mrem/yr]	*PHCSS*(+) *GOESITED*(–) *INFIL*(+) *EP1NP02*(+)	K6.6.2-3
Dose from Dissolved ^{239}Pu (*DOPU239*, mrem/yr)				
DOPU239	[10, 10^4, 2 × 10^4 yr]	[0, 3 × 10^4 mrem/yr]	*SZGWSPDM*(+) *SZFISPVO*(+) *SCKDPUVO*(–)	K6.6.1-7 K6.6.1-8
DOPU239	[250, 10^5, 2 × 10^5 yr]	[1, 5 × 10^3 mrem/yr]	*SZGWSPDM*(+) *EP1LOWPU*(+) *SZFISPOV*(+) *SZDIFCVO*(–)	K6.6.1-9 K6.6.1-10

Table K6.1-5 Summary of Uncertainty and Sensitivity Analysis Results for Dose to the RMEI from Selected Radionuclides Resulting from an Igneous Intrusive Event that Destroys All WPs in the Repository. (Continued)

Output Variable[a]	Time Interval[b]	Range[c]	Dominant Input Variables[d]	Figures[e]
Dose from Dissolved ^{99}Tc (*DOTC99*, mrem/yr)				
DOTC99	[10, 3 × 10^3, 2 × 10^4 yr]	[4, 3 × 10^3 mrem/yr]	*MICTC99*(+) *INFIL*(+) *CSNFMASS*(+)	K6.6.1-9 K6.6.1-10

[a] Dependent variable under consideration.
[b] Time interval [t_1, t_2, t_3], where t_1 is initial or event time, t_2 is time at which variable range (Column c) and dominant input variables (Column d) are determined, and t_3 is the end time for the analysis.
[c] Range of values at time t_2.
[d] Dominant input variables at time t_2 with "+" and "–" indicating positive and negative effects, respectively.
[e] Figures presenting detailed analyses.

Table K6.1-6 Summary of Uncertainty and Sensitivity Analysis Results for Effected Dose to the RMEI (*EXPDOSE*, mrem/yr) Resulting from Igneous Events

Output Variable[a]	Time Interval[b]	Range[c]	Dominant Input Variables[d]	Figures[e]
Expected Dose for Igneous Intrusive Events (*EXPDOSE*, mrem/yr)				
EXPDOSE	[0, 10^4, 2 × 10^4 yr]	[10^{-4}, 3 mrem/yr]	*IGRATE*(+) *SZGWSPDM*(+)	K6.7.1-1 K6.7.1-2
EXPDOSE	[0, 5 × 10^5, 10^6 yr]	[2 × 10^{-3}, 100 mrem/yr]	*IGRATE*(+) *SZGWSPDM*(+) *INFIL*(+)	K6.7.2-1 K6.7.2-2
Expected Dose for Igneous Eruptive Events (*EXPDOSE*, mrem/yr)				
EXPDOSE	[0, 10^4, 2 × 10^4 yr]	[3 × 10^{-7}, 2 × 10^{-2} mrem/yr]	*IGERATE*(+) *INHLTPV*(+) *DDIVIDE*(-)	K6.8.1-1 K6.8.1-2
EXPDOSE	[0, 5 × 10^5, 10^6 yr]	[7 × 10^{-7}, 10^{-3} mrem/yr]	*IGERATE*(+) *BTILLAGE*(+)	K6.8.2-1 K6.8.2-2

[a] Dependent variable under consideration.
[b] Time interval [t_1, t_2, t_3], where t_1 is initial or event time, t_2 is time at which variable range (Column c) and dominant input variables (Column d) are determined, and t_3 is the end time for the analysis.
[c] Range of values at time t_2.
[d] Dominant input variables at time t_2 with "+" and "–" indicating positive and negative effects, respectively.
[e] Figures presenting detailed analyses.

Table K7.1-1. Summary of TSPA-LA Model Results Considered in Uncertainty and Sensitivity Analyses for the Seismic Scenario Classes

Ouput Variable	Definition
DOIC239	Dose to RMEI (mrem/yr) from ^{239}Pu irreversibly attached to slow (i.e., Ic) colloids (Figure K.7.6-1)
DOIF239	Dose to RMEI (mrem/yr) from ^{239}Pu irreversibly attached to fast (i.e., If) colloids (Figure K.7.6-2)
DONP237	Dose to RMEI (mrem/yr) from dissolved ^{237}Np (Figure K.7.6-3)
DOPU239	Dose to RMEI (mrem/yr) from dissolved ^{239}Pu (Figure K.7.6-4)
DOTC99	Dose to RMEI (mrem/yr) from dissolved ^{99}Tc (Figure K.7.6-5)
ESIC239	Release rate (g/yr) for the movement of ^{239}Pu irreversibly attached to waste form (i.e., Ic) colloids from the EBS to the UZ (Figures K.7.3-1, K.7.3-2)
ESIC239C	Cumulative release (g) for the movement of ^{239}Pu irreversibly attached to waste form (i.e., Ic) colloids from the EBS to the UZ (Figures K.7.3-1, K.7.3-2)
ESIF239	Release rate (g/yr) for the movement of ^{239}Pu irreversibly attached to ferrous (i.e., If) colloids from the EBS to the UZ (Figures K.7.3-3, K.7.3-4)
ESIF239C	Cumulative release (g) for the movement of ^{239}Pu irreversibly attached to ferrous (i.e., If) colloids from the EBS to the UZ (Figures K.7.3-3, K.7.3-4)
ESNP237	Release rate (g/yr) for the movement of dissolved ^{237}Np from the EBS to the UZ (Figures K.7.3-5, K.7.3-6)
ESNP237C	Cumulative release (g) for the movement of dissolved ^{237}Np from the EBS to the UZ (Figures K.7.3-5, K.7.3-6)
ESPU239	Release rate (g/yr) for the movement of dissolved ^{239}Pu from the EBS to the UZ (Figures K.7.3-7, K.7.3-8)
ESPU239C	Cumulative release (g) for the movement of dissolved ^{239}Pu from the EBS to the UZ (Figures K.7.3-7, K.7.3-8)
ESTC99	Release rate (g/yr) for the movement of dissolved ^{99}Tc from the EBS to the UZ (Figures K.7.3-9, K.7.3-10)
ESTC99C	Cumulative release (g) for the movement of dissolved ^{99}Tc from the EBS to the UZ (Figures K.7.3-9, K.7.3-10)
EXPDOSE	Expected dose to RMEI (mrem/yr) from all radioactive species (Figures K.7.7.1-1, K.7.7.1-2, K.7.7.2-1, K.7.7.2-2, K.7.8.1-1, K.7.8.1-2, K.7.8.2-1, K.7.8.2-2)
SZIC239	Release rate (g/yr) for the movement of ^{239}Pu irreversibly attached to slow (i.e., Ic) colloids across a subsurface plane at the location of the RMEI (Figure K.7.5-1)
SZIC239C	Cumulative release (g) for the movement of ^{239}Pu irreversibly attached to slow (i.e., Ic) colloids across a subsurface plane at the location of the RMEI (Figure K.7.5-1)
SZIF239	Release rate (g/yr) for the movement of ^{239}Pu irreversibly attached to fast (i.e., If) colloids across a subsurface plane at the location of the RMEI (Figure K.7.5-2)
SZIF239C	Cumulative release (g) for the movement of ^{239}Pu irreversibly attached to fast (i.e., If) colloids across a subsurface plane at the location of the RMEI (Figure K.7.5-2)

Table K7.1-1. Summary of TSPA-LA Model Results Considered in Uncertainty and Sensitivity Analyses for the Seismic Scenario Classes (Continued)

Output Variable	Definition
SZNP237	Release rate (g/yr) for the movement of dissolved ^{237}Np across a subsurface plane at the location of the RMEI (Figure K.7.5-3)
SZNP237C	Cumulative release (g) for the movement of dissolved ^{237}Np across a subsurface plane at the location of the RMEI (Figure K.7.5-3)
SZPU239	Release rate (g/yr) for the movement of dissolved ^{239}Pu across a subsurface plane at the location of the RMEI (Figure K.7.5-4)
SZPU239C	Cumulative release (g) for the movement of dissolved ^{239}Pu across a subsurface plane at the location of the RMEI (Figure K.7.5-4)
SZTC99	Release rate (g/yr) for the movement of dissolved ^{99}Tc across a subsurface plane at the location of the RMEI (Figure K.7.5-5)
SZTC99C	Cumulative release (g) for the movement of dissolved ^{99}Tc across a subsurface plane at the location of the RMEI (Figure K.7.5-5)
UZIC239	Release rate (g/yr) for the movement of ^{239}Pu irreversibly attached to slow (i.e., Ic) colloids from the UZ to the SZ (Figure K.7.4-1)
UZIC239C	Cumulative release (g) for the movement of ^{239}Pu irreversibly attached to slow (i.e., Ic) colloids from the UZ to the SZ (Figure K.7.4-1)
UZIF239	Release rate (g/yr) for the movement of ^{239}Pu irreversibly attached to fast (i.e., If) colloids from the UZ to the SZ (Figure K.7.4-2)
UZIF239C	Cumulative release (g) for the movement of ^{239}Pu irreversibly attached to fast (i.e., If) colloids from the UZ to the SZ (Figure K.7.4-2)
UZNP237	Release rate (g/yr) for the movement of dissolved ^{237}Np from the UZ to the SZ (Figure K.7.4-3)
UZNP237C	Cumulative release (g) for the movement of dissolved ^{237}Np from the UZ to the SZ (Figure K.7.4-3)
UZPU239	Release rate (g/yr) for the movement of dissolved ^{239}Pu from the UZ to the SZ (Figure K.7.4-4)
UZPU239C	Cumulative release (g) for the movement of dissolved ^{239}Pu from the UZ to the SZ (Figure K.7.4-4)
UZTC99	Release rate (g/yr) for the movement of dissolved ^{99}Tc from the UZ to the SZ (Figure K.7.4-5)
UZTC99C	Cumulative release (g) for the movement of dissolved ^{99}Tc from the UZ to the SZ (Figure K.7.4-5)

Table K7.1-2 Summary of Uncertainty and Sensitivity Analysis Results for Radionuclide Movement from the EBS to the UZ Resulting from a Seismically Induced Damaged Area of 10^{-6} (32.6 m^2) at 10 yrs to All CDSP WPs in the Repository

Output Variable[a]	Time Interval[b]	Range[c]	Dominant Input Variables[d]	Figures[e]
Release Rate (*ESIC239*, g/yr) and Cumulative Release (*ESIC239C*, g) for ^{239}Pu Irreversibly Attached to WP Colloids				
ESIC239	[10, 10^4, 2 × 10^4 yr]	Results removed due to model error		K7.3-1 K7.3-2
ESIC239C	[10, 10^4, 2 × 10^4 yr]	Results removed due to model error		K7.3-1 K7.3-2
Release Rate (*ESIF239*, g/yr) and Cumulative Release (*ESIF239C*, g) for ^{239}Pu Irreversibly Attached to Ferrous Colloids				
ESIF239	[10, 10^4, 2 × 10^4 yr]	Results removed due to model error		K7.3-3 K7.3-4
ESIF239C	[10, 10^4, 2 × 10^4 yr]	Results removed due to model error		K7.3-3 K7.3-4
Release Rate (*ESNP237*, g/yr) and Cumulative Release (*ESNP237C*, g) for Dissolved ^{237}Np				
ESNP237	[10, 10^4, 2 × 10^4 yr]	[4 × 10^{-7}, 7 × 10^{-4} g/yr]	*GOESITED*(–) *EP1LOWNU*(+) *DSNFMASS*(+) *HFOSA*(–)	K7.3-5 K7.3-6
ESNP237C	[10, 10^4, 2 × 10^4 yr]	[2 × 10^{-4}, 7 g]	*GOESITED*(–) *DSNFMASS*(+) *DELPPC02*(+) *HFOSA*(–) *PH2MCONS*(–) *EP1LOWNU*(+)	K7.3-5 K7.3-6
Release Rate (*ESPU239*, g/yr) and Cumulative Release (*ESPU239C*, g) for Dissolved ^{239}Pu				
ESPU239	[10, 10^4, 2 × 10^4 yr]	[4 × 10^{-8}, 10^{-2} g/yr]	*EP1LOWPU*(+) *DELPPCO2*(+) *INFIL*(+) *SEEPPRM*(–)	K7.3-7 K7.3-8
ESPU239C	[10, 10^4, 2 × 10^4 yr]	[10^{-4}, 50 g]	*EP1LOWPU*(+) *DELPPCO2*(+) *INFIL*(+) *PH2MCONS*(–)	K7.3-7 K7.3-8

Table K7.1-2 Summary of Uncertainty and Sensitivity Analysis Results for Radionuclide Movement from the EBS to the UZ Resulting from a Seismically Induced Damaged Area of 10^{-6} (32.6 m^2) at 10 yrs to All CDSP WPs in the Repository (Continued)

Output Variable[a]	Time Interval[b]	Range[c]	Dominant Input Variables[d]	Figures[e]
Release Rate (*ESTC99*, g/yr) and Cumulative Release (*ESTC99C*, g) for Dissolved ^{99}Tc				
ESTC99	[10, 2 × 10^3, 2 × 10^4 yr]	[8, 100 g/yr]	*GOESA*(+) *HLWDRALK*(+) *HLWMASS*(+) *THERMCON*(–) *DSNFMASS*(+) *INFIL*(+)	K7.3-9 K7.3-10
ESTC99C	[10, 2 × 10^3, 2 × 10^4 yr]	[2 × 10^4, 2 × 10^5 g]	*GOESA*(+) *HLWDRALK*(+) *HLWMASS*(+) *DSNFMASS*(+)	K7.3-9 K7.3-10

[a] Dependent variable under consideration.
[b] Time interval [t_1, t_2, t_3], where t_1 is initial or event time, t_2 is time at which variable range (Column c) and dominant input variables (Column d) are determined, and t_3 is the end time for the analysis.
[c] Range of values at time t_2.
[d] Dominant input variables at time t_2 with "+" and "–" indicating positive and negative effects respectively.
[e] Figures presenting detailed analyses.

Table K7.1-3 Summary of Uncertainty and Sensitivity Analysis Results for Radionuclide Movement from the UZS to the SZ Resulting from a Seismically Induced Damaged Area of 10^{-6} (32.6 m^2) at 10 yrs to All CDSP WPs in the Repository

Output Variable[a]	Time Interval[b]	Range[c]	Dominant Input Variables[d]	Figures[e]
Release Rate (*UZIC239*, g/yr) and Cumulative Release (*UZIC239C*, g) for ^{239}Pu Irreversibly Attached to Slow Colloids				
UZIC239	[10, 10^4, 2 × 10^4 yr]	[10^{-13}, 3 × 10^{-10} g/yr]	*EP1LOWPU*(+) *DIAMCOLL*(–) *PH2MCONS*(–)	K7.4-1
UZIC239C	[10, 10^4, 2 × 10^4 yr]	[3 × 10^{-10}, 2 × 10^{-6} g]	*EP1LOWPU*(+) *DIAMCOL*(–) *PH2MCONS*(–)	K7.4-1

Table K7.1-3 Summary of Uncertainty and Sensitivity Analysis Results for Radionuclide Movement from the UZS to the SZ Resulting from a Seismically Induced Damaged Area of 10^{-6} (32.6 m^2) at 10 yrs to All CDSP WPs in the Repository (Continued)

Output Variable[a]	Time Interval[b]	Range[c]	Dominant Input Variables[d]	Figures[e]
Release Rate (*UZIF239*, g/yr) and Cumulative Release (*UZIF239C*, g) for ^{239}Pu Irreversibly Attached to Fast Colloids				
UZIF239	[10, 10^4, 2×10^4 yr]	[2×10^{-16}, 6×10^{-13} g/yr]	*EP1LOWPU*(+) *PH2MCONS*(–) *DIAMCOLL*(–) *GOESA*(+)	K7.4-2
UZIF239C	[10, 10^4, 2×10^4 yr]	[10^{-12}, 3×10^{-9} g]	*EP1LOWPU*(+) *DIAMCOLL*(–) *PH2MCONS*(–)	K7.4-2
Release Rate (*UZNP237*, g/yr) and Cumulative Release (*UZNP237C*, g) for Dissolved ^{237}Np				
UZNP237	[10, 10^4, 2×10^4 yr]	[10^{-7}, 6×10^{-4} g/yr]	*GOESITED*(–) *DELPPCO2*(+) *PH2MCONS*(–)	K7.4-3
UZNP237C	[10, 10^4, 2×10^4 yr]	[4×10^{-4}, 5 g]	*GOESITED*(–) *DELPPC02*(+) *PH2MCONS*(–) *INFIL*(+)	K7.4-3
Release Rate (*UZPU239*, g/yr) and Cumulative Release (*UZPU239C*, g) for Dissolved ^{239}Pu				
UZPU239	[10, 10^4, 2×10^4 yr]	[2×10^{-5}, 4×10^{-3} g/yr]	*EP1LOWPU*(+) *DELPPCO2*(+) *INFIL*(+) *GOESA*(+) *PH2MCONS*(–)	K7.4-4
UZPU239C	[10, 10^4, 2×10^4 yr]	[5×10^{-5}, 20 g]	*EP1LOWPU*(+) *DELPPCO2*(+) *INFIL*(+) *PH2MCONS*(–) *GOESA*(+)	K7.4-4
Release Rate (*UZTC99*, g/yr) and Cumulative Release (*UZTC99C*, g) for Dissolved ^{99}Tc				
UZTC99	[10, 2×10^3, 2×10^4 yr]	[3, 80 g/yr]	*GOESA*(+) *HLWMASS*(+) *THERMCON*(–) *INFIL*(+) *SEEPPRM*(–)	K7.4-5

Table K7.1-3 Summary of Uncertainty and Sensitivity Analysis Results for Radionuclide Movement from the UZS to the SZ Resulting from a Seismically Induced Damaged Area of 10^{-6} (32.6 m^2) at 10 yrs to All CDSP WPs in the Repository (Continued)

Output Variable[a]	Time Interval[b]	Range[c]	Dominant Input Variables[d]	Figures[e]
UZTC99C	[10, 2×10^3, 2×10^4 yr]	[10^4, 10^5 g]	*INFIL*(+) *GOESA*(+) *HLWDRALK*(+) *SEEPPRM*(–) *DSNFMASS*(+)	K7.4-5

[a] Dependent variable under consideration.
[b] Time interval [t_1, t_2, t_3], where t_1 is initial or event time, t_2 is time at which variable range (Column c) and dominant input variables (Column d) are determined, and t_3 is the end time for the analysis.
[c] Range of values at time t_2.
[d] Dominant input variables at time t_2 with "+" and "–" indicating positive and negative effects respectively.
[e] Figures presenting detailed analyses.

Table K7.1-4 Summary of Uncertainty and Sensitivity Analysis Results for Radionuclide Movement in the SZ Across a Subsurface Plane at the Location of the RMEI Resulting from a Seismically Induced Damaged Area of 10^{-6} (32.6 m^2) at 10 yrs to All CDSP WPs in the Repository

Output Variable[a]	Time Interval[b]	Range[c]	Dominant Input Variables[d]	Figures[e]
Release Rate (*SZIC239*, g/yr) and Cumulative Release (*SZIC239C*, g) for ^{239}Pu Irreversibly Attached to Slow Colloids				
SZIC239	[10, 10^4, 2 × 10^4 yr]	[0, 2 × 10^{-10} g/yr]	*SZCOLRAL*(–) *SZGWSPDM*(+) *SZFIPOUO*(–) *GOESA*(+) *PH2MCONS*(–)	K7.5-1
SZIC239C	[10, 10^4, 2 × 10^4 yr]	[0, 10^{-6} g]	*SZCOLRAL*(–) *SZGWSPDM*(+) *SZFIPOUO*(–)	K7.5-1
Release Rate (*SZIF239*, g/yr) and Cumulative Release (*SZIF239C*, g) for ^{239}Pu Irreversibly Attached to Fast Colloids				
SZIF239	[10, 10^4, 2 × 10^4 yr]	[2 × 10^{-16}, 6 × 10^{-13} g/yr]	*EP1LOWPU*(+) *DIAMCOLL*(–) *PH2MCONS*(–)	K7.5-2
SZIF239C	[10, 10^4, 2 × 10^4 yr]	[10^{-12}, 2 × 10^{-9} g]	*DIAMCOLL*(–) *EP1LOWPU*(+)	K7.5-2
Release Rate (*SZNP237*, g/yr) and Cumulative Release (*SZNP237C*, g) for Dissolved ^{237}Np				
SZNP237	[10, 10^4, 2 × 10^4 yr]	[10^{-9}, 2 × 10^{-4} g/yr]	*SZGWSPDM*(+) *GOESITED*(–)	K7.5-3
SZNP237C	[10, 10^4, 2 × 10^4 yr]	[2 × 10^{-4}, 7 g]	*GOESITED*(–) *SZGWSPDM*(+)	K7.5-3
Release Rate (*SZPU239*, g/yr) and Cumulative Release (*SZPU239C*, g) for Dissolved ^{239}Pu				
SZPU239	[10, 10^4, 2 × 10^4 yr]	[0, 3 × 10^{-4} g/yr]	*SZGWSPDM*(+) SZFISPVO(+)	K7.5-4
SZPU239C	[10, 10^4, 2 × 10^4 yr]	[0, 1 g]	*SZGWSPDM*(+) *SZFISPVO*(+)	K7.5-4

Table K7.1-4 Summary of Uncertainty and Sensitivity Analysis Results for Radionuclide Movement in the SZ Across a Subsurface Plane at the Location of the RMEI Resulting from a Seismically Induced Damaged Area of 10^{-6} (32.6 m^2) at 10 yrs to All CDSP WPs in the Repository (Continued)

Output Variable[a]	Time Interval[b]	Range[c]	Dominant Input Variables[d]	Figures[e]
Release Rate (*SZTC99*, g/yr) and Cumulative Release (*SZTC99C*, g) for Dissolved ^{99}Tc				
SZTC99	[10, 2 × 10^3, 2 × 10^4 yr]	[1, 70 g/yr]	*SZGWSPDM*(+) *GOESA*(+) *INFIL*(+)	K7.5-5
SZTC99C	[10, 2 × 10^3, 2 × 10^4 yr]	[?,8 × 10^4 g]	*INFIL*(+) *SZGWSPDM*(+) *SZDIFCVO*(–) *SZFIPOVO*(–)	K7.5-5

[a] Dependent variable under consideration.
[b] Time interval [t_1, t_2, t_3], where t_1 is initial or event time, t_2 is time at which variable range (Column c) and dominant input variables (Column d) are determined, and t_3 is the end time for the analysis.
[c] Range of values at time t_2.
[d] Dominant input variables at time t_2 with "+" and "–" indicating positive and negative effects respectively.
[e] Figures presenting detailed analyses.

Table K7.1-5 Summary of Uncertainty and Sensitivity Analysis Results for Dose to the RMEI from Selected Radionuclides Resulting from a Seismically Induced Damaged Area of 10^{-6} (32.6 m^2) at 10 yrs to All CDSP WPs in the Repository.

Output Variable[a]	Time Interval[b]	Range[c]	Dominant Input Variables[d]	Figures[e]
Dose from ^{239}Pu Irreversibly Attached to Slow Colloids (*DOIC239*, mrem/yr)				
DOIC239	[10, 10^4, 2 × 10^4 yr]	[0, ? mrem/yr]	*SZCOLRAL*(–) *SZGWSPDM*(+) *SZFIPOVO*(–) *SZLODISP*(+) *PH2MCONS*(–)	K7.6-1
Dose from ^{239}Pu Irreversibly Attached to Fast Colloids (*DOIF239*, mrem/yr)				
DOIF239	[10, 10^4, 2 × 10^4 yr]	[0, 4 × 10^{-5} mrem/yr]	*EP1LOWPU*(+) *DIAMCOLL*(–) *SZGWSPDM*(+)	K7.6-2
Dose from Dissolved ^{237}Np (*DONP237*, mrem/yr)				
DONP237	[10, 10^4, 2 × 10^4 yr]	[0, 4 × 10^{-5} mrem/yr]	*SZGWSPDM(+)* *GOESITED*(–) *DSNFMASS*(+)	K7.6-3
Dose from Dissolved ^{239}Pu (*DOPU239*, mrem/yr)				
DOPU239	[10, 10^4, 2 × 10^4 yr]	[0, 0.02 mrem/yr]]	*SZGWSPDM*(+) *SZFISPVO*(+)	K7.6-4
Dose from Dissolved ^{99}Tc (*DOTC99*, mrem/yr)				
DOTC99	[10, 10^4, 2 × 10^4 yr]	[0, 6 mrem/yr]	*MICTC99*(+) *SZGWSPDM*(+) *GOESA*(+) *INFIL*(+)	K7.6-5

[a] Dependent variable under consideration.
[b] Time interval [t_1, t_2, t_3], where t_1 is initial or event time, t_2 is time at which variable range (Column c) and dominant input variables (Column d) are determined, and t_3 is the end time for the analysis.
[c] Range of values at time t_2.
[d] Dominant input variables at time t_2 with "+" and "–" indicating positive and negative effects respectively.
[e] Figures presenting detailed analyses.

Table K7.1-6 Summary of Uncertainty and Sensitivity Analysis Results for Expected Dose to the RMEI (*EXPD05*, mrem/yr) Resulting from Seismic Events

Output Variable[a]	Time Interval[b]	Range[c]	Dominant Input Variables[d]	Figures[e]
Expected Dose for Seismic Ground Motion Events (*EXPDOS*, mrem/yr)				
EXPDOS	[0, 10^4, 2 × 10^4 yr]	[8 × 10^{-7}, 3 mrem/yr]	*SCCTHRP*(–)	K7.7.1-1 K7.7.1-2
EXPDOS	[0, 5 × 10^5, 10^6 yr]	[10^{-3}, 9 mrem/yr]	*WDGCA22*(–) *SCCTHRP*(–)	K7.7.2-1 K7.7.2-2
Expected Dose for Seismic Fault Displacement Events (*EXPDOS*, mrem/yr)				
EXPDOS	[0, 10^4, 2 × 10^4 yr]	[5 × 10^{-5}, 0.04 mrem/yr]	*MICTC99*(+) *SZGWSPDM*(+) *DTDRHUNC*(+) *INFIL*(+) *SZFISPVO*(+)	K7.8.1-1 K7.8.1-2
EXPDOS	[10, 5 × 10^5, 10^6 yr]	[10^{-4}, 0.3 mrem/yr]	*INFIL*(+) *SZGWSPDM*(+) *EP1LOWPU*(+) *WPFLUX*(+) *GOESITED*(–)	K7.8.2-1 K7.8.2-2

[a] Dependent variable under consideration.
[b] Time interval [t_1, t_2, t_3], where t_1 is initial or event time, t_2 is time at which variable range (Column c) and dominant input variables (Column d) are determined, and t_3 is the end time for the analysis.
[c] Range of values at time t_2.
[d] Dominant input variables at time t_2 with "+" and "–" indicating positive and negative effects respectively.
[e] Figures presenting detailed analyses.

Table K9-1. Summary of Selected Sensitivity Analysis Results

Scenario Class	TSPA-LA Model Output (time of maximum mean value)	Key Uncertain Inputs[a]
Total System	Total expected dose 0 to 10,000 years (10,000 years)	Residual stress threshold for SCC (SCCTHRP) Frequency of occurrence of igneous events (IGRATE) Scale factor in ground water specific discharge (SZGWSPDM)
	Total expected dose 10,000 to 1,000,000 years (230,000 years)	Frequency of occurrence of igneous events (IGRATE) Residual stress threshold for SCC (SCCTHRP) General corrosion rate (Alloy 22) temperature dependence (WDGCA22) Scale factor in ground water specific discharge (SZGWSPDM)
Nominal	Expected dose resulting from corrosion processes (720,000 years)	General corrosion rate (Alloy 22) temperature dependence (WDGCA22) Deviation from median yield strength range for outer lid (WDZOLID)
Early Failure Waste Package	Expected dose resulting from early failure of waste packages over 20,000 years (12,000 years)	Probability of early failure per waste package (PROBWPEF) Pointer variable for infiltration scenario (INFIL) Selector for host-rock thermal conductivity scenario (THERMCON)
Early Failure Drip Shield	Expected dose resulting from early failure of drip shields over 20,000 years (2,000 years)	Probability of early failure per drip shield (PROBDSEF) Uncertainty factor accounting for small-scale heterogeneity in fracture permeability (SEEPUNC) Flowing interval porosity in volcanic units (SZFIPOVO)
Igneous Intrusive	Expected dose resulting from igneous intrusion over 20,000 years (20,000 years)	Frequency of occurrence of igneous events (IGRATE) Scale factor in ground water specific discharge (SZGWSPDM)
	Expected dose resulting from igneous intrusion over 1,000,000 years (1,000,000 years)	Frequency of occurrence of igneous events (IGRATE) Scale factor in ground water specific discharge (SZGWSPDM) Pointer variable for infiltration scenario (INFIL)
Igneous Eruptive	Expected dose resulting from volcanic eruption over 20,000 years (20,000 years)	Frequency of occurrence of volcanic eruptions (IGERATE) Pointer variable for long-term inhalation dose conversation factors for exposure to volcanic ash (INHLTPV) Diffusivity of radionuclides in divides (DDIVIDE)
	Expected dose resulting from volcanic eruption over 1,000,000 years (1,000,000 years)	Frequency of occurrence of volcanic eruptions (IGERATE) Depth of soil within which radionuclides affect the biosphere (BTILLAGE)

Table K9-1. Summary of Selected Sensitivity Analysis Results (Continued)

Scenario Class	TSPA-LA Model Output	Key Uncertain Inputs[a]
Seismic Ground Motion	Expected dose resulting from seismic ground motion over 20,000 years (20,000 years)	Residual stress threshold for SCC (SCCTHRP)
	Expected dose resulting from combination of seismic ground motion and corrosion processes over 1,000,000 years (230,000 years)	Residual stress threshold (SCCTHRP) General corrosion rate (Alloy 22) temperature dependence (WDGCA22)
Seismic Fault Displacement	Expected dose resulting from fault displacement over 20,000 years (20,000 years)	Groundwater biosphere dose conversion factor for ^{99}Tc (MICTC99) Scale factor in ground water specific discharge (SZGWSPDM)
	Expected dose resulting from fault displacement over 1,000,000 years (1,000,000 years)	Scale factor in ground water specific discharge (SZGWSPDM) Pointer variable for infiltration scenario (INFIL)

a. Name (in parentheses) is the variable name used in the sensitivity analyses (see Table K3-1).

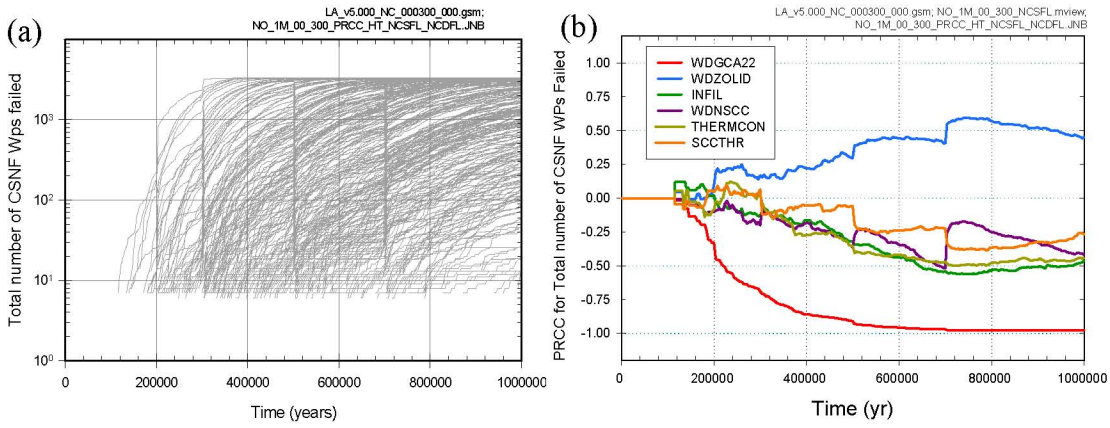

(c)

	NCSFL: 600K yr			NCSFL: 800K yr			NCSFL: 1M yr		
Step[a]	**Variable**[b]	**R^2** [c]	**SRRC**[d]	**Variable**	**R^2**	**SRRC**	**Variable**	**R^2**	**SRRC**
1	WDGCA22	0.86	-0.96	WDGCA22	0.90	-0.98	WDGCA22	0.91	-0.98
2	WDZOLID	0.88	0.13	WDZOLID	0.92	0.14	WDZOLID	0.92	0.10
3	INFIL	0.90	-0.15	INFIL	0.94	-0.13	INFIL	0.93	-0.12
4	THERMCON	0.91	-0.13	THERMCON	0.95	-0.11	THERMCON	0.94	-0.10
5	WDNSCC	0.92	-0.09	SCCTHR	0.95	-0.08	WDNSCC	0.95	-0.09
6	SCCTHR	0.93	-0.08	WDGCUA22	0.96	0.08	WDGCUA22	0.96	0.09
7	WDGCUA22	0.93	0.06	WDNSCC	0.96	-0.05	SCCTHR	0.96	-0.05
8	SEEPPRMN	0.93	0.06	PH2DHLNS	0.96	-0.03			

a: Steps in stepwise rank regression analysis
b: Variables listed in order of selection in stepwise regression
c: Cumulative R^2 value with entry of each variable into regression model
d: Standardized rank regression coefficients (SRRCs) in final regression model

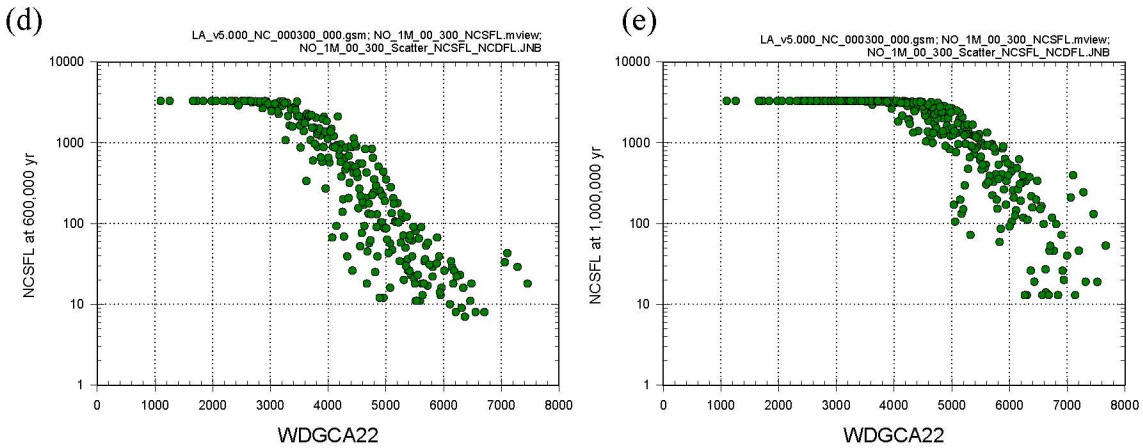

Source: Output DTNs: MO0709TSPAREGS.000 [DIRS 182976]; and MO0709TSPAPLOT.000 [DIRS 183010].

Figure K2-1. Illustration of uncertainty and sensitivity analysis results for time-dependent number of failed CSNF WPs in percolation bin 3 under nominal conditions: (a) *NCSFL* for all (i.e., 300) sample elements, (b) PRCCs for *NCSFL*, (c) stepwise rank regressions for *NCSFL* at 600,000, 800,000 and 1,000,000 years, and (d, e) scatterplots for (*WDGA22*, *NCSFL*) at 600,000 and 1,000,000 years.

(a)

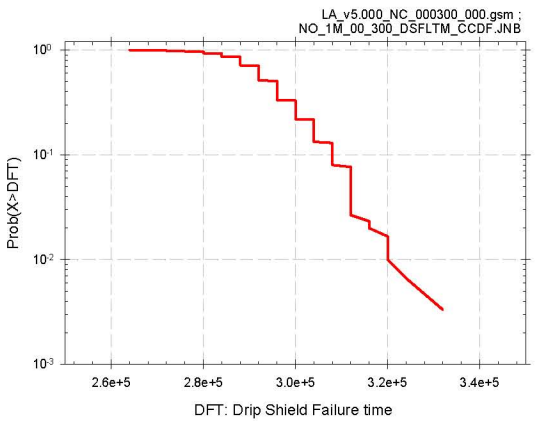

(b)

	DSFLTM		
Step[a]	Variable[b]	R^{2c}	SRRC[d]
1	WDDSAGGC	0.64	-0.82
2	WDDSBEGC	0.93	-0.54

a: Steps in stepwise rank regression analysis

b: Variables listed in order of selection in stepwise regression

c: Cumulative R^2 value with entry of each variable into regression model

d: Standardized rank regression coefficients (SRRCs) in final regression model

(c)

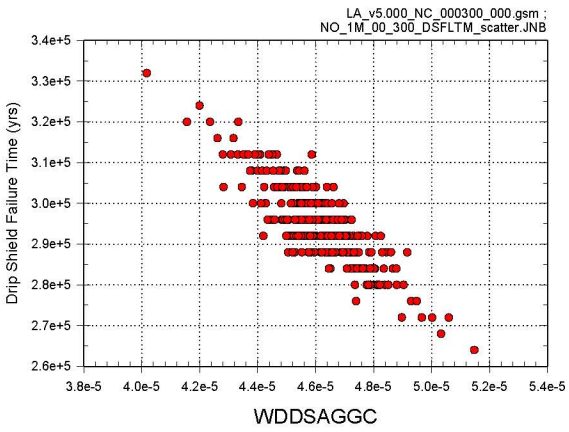

(d)

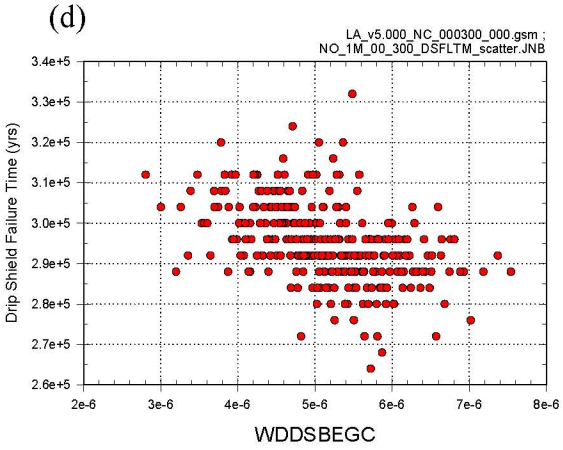

(e)

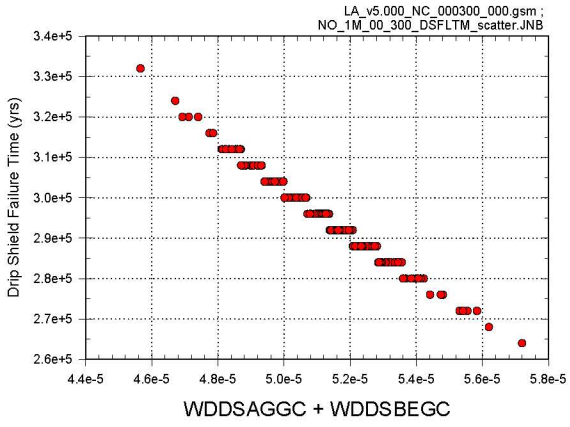

Source: Output DTNs: MO0709TSPAREGS.000 [DIRS 182976]; and MO0709TSPAPLOT.000 [DIRS 183010].

Figure K4.2-1. Uncertainty and sensitivity analysis results for DS failure time (*DSFLTM*, yr) under nominal conditions: (a) CCDF for *DSFLTM*, (b) Stepwise rank regression for *DSFLTM*, and (c,d,e) Selected scatterplots for *DSFLTM*.

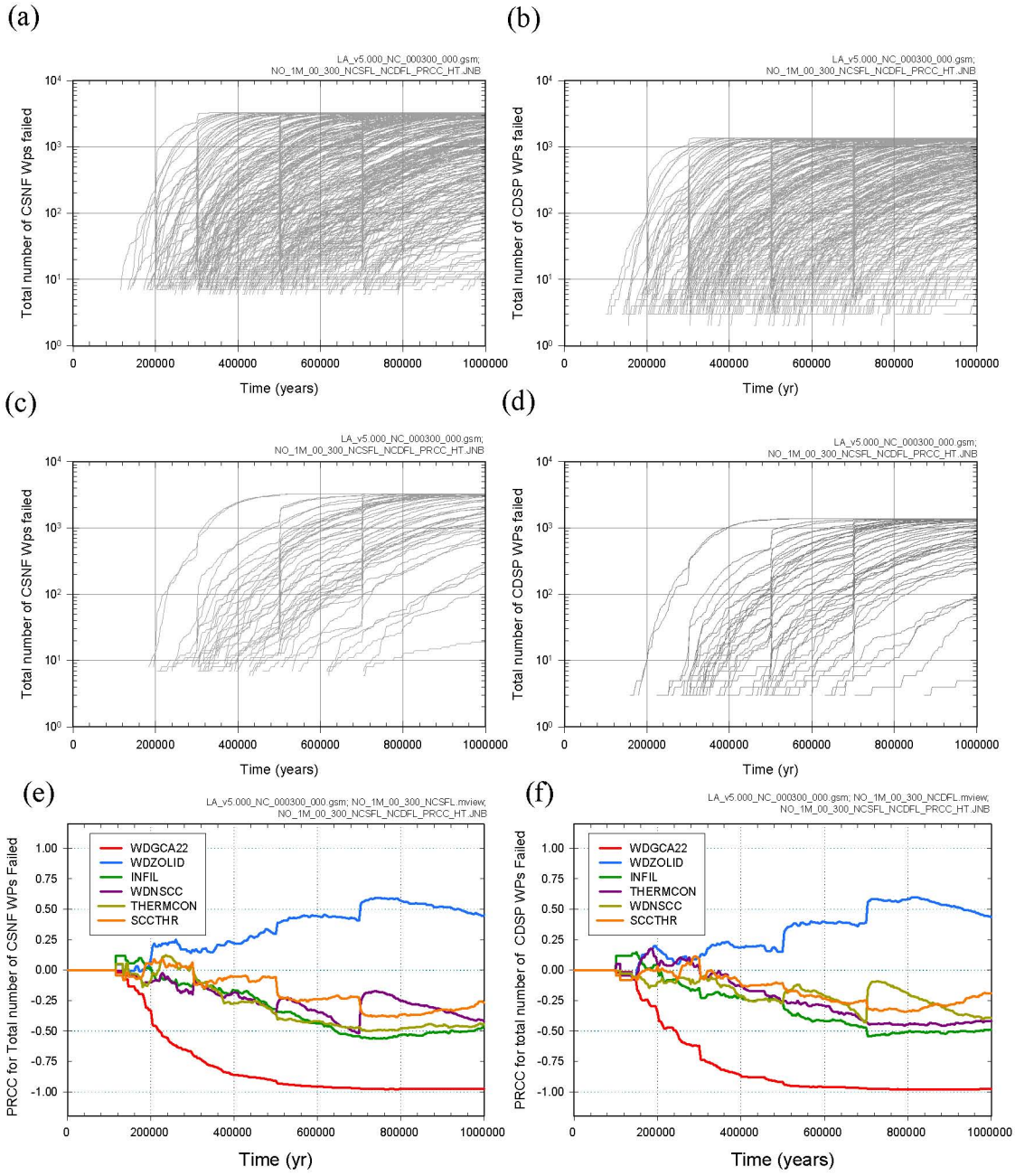

Source: Output DTNs: MO0709TSPAREGS.000 [DIRS 182976]; and MO0709TSPAPLOT.000 [DIRS 183010].

Figure K4.2-2. Time-dependent numbers of failed CSNF WPs (*NCSFL*) and failed CDSP WPs (*NCDFL*) in percolation bin 3 under nominal conditions: (a, b) *NCSFL* and *NCDFL* for all (i.e., 300) sample elements, (c, d) *NCSFL* and *NCDFL* for first 50 sample elements, and (e, f) PRCCs for *NCSFL* and *NCDFL*

(a)

	NCSFL: 600K yr			NCSFL: 800K yr			NCSFL: 1M yr		
Step[a]	**Variable[b]**	**R^{2c}**	**SRRC[d]**	**Variable**	**R^2**	**SRRC**	**Variable**	**R^2**	**SRRC**
1	WDGCA22	0.86	-0.96	WDGCA22	0.90	-0.98	WDGCA22	0.91	-0.98
2	WDZOLID	0.88	0.13	WDZOLID	0.92	0.14	WDZOLID	0.92	0.10
3	INFIL	0.90	-0.15	INFIL	0.94	-0.13	INFIL	0.93	-0.12
4	THERMCON	0.91	-0.13	THERMCON	0.95	-0.11	THERMCON	0.94	-0.10
5	WDNSCC	0.92	-0.09	SCCTHR	0.95	-0.08	WDNSCC	0.95	-0.09
6	SCCTHR	0.93	-0.08	WDGCUA22	0.96	0.08	WDGCUA22	0.96	0.09
7	WDGCUA22	0.93	0.06	WDNSCC	0.96	-0.05	SCCTHR	0.96	-0.05
8	SEEPPRMN	0.93	0.06	PH2DHLNS	0.96	-0.03			

a: Steps in stepwise rank regression analysis
b: Variables listed in order of selection in stepwise regression
c: Cumulative R^2 value with entry of each variable into regression model
d: Standardized rank regression coefficients (SRRCs) in final regression model

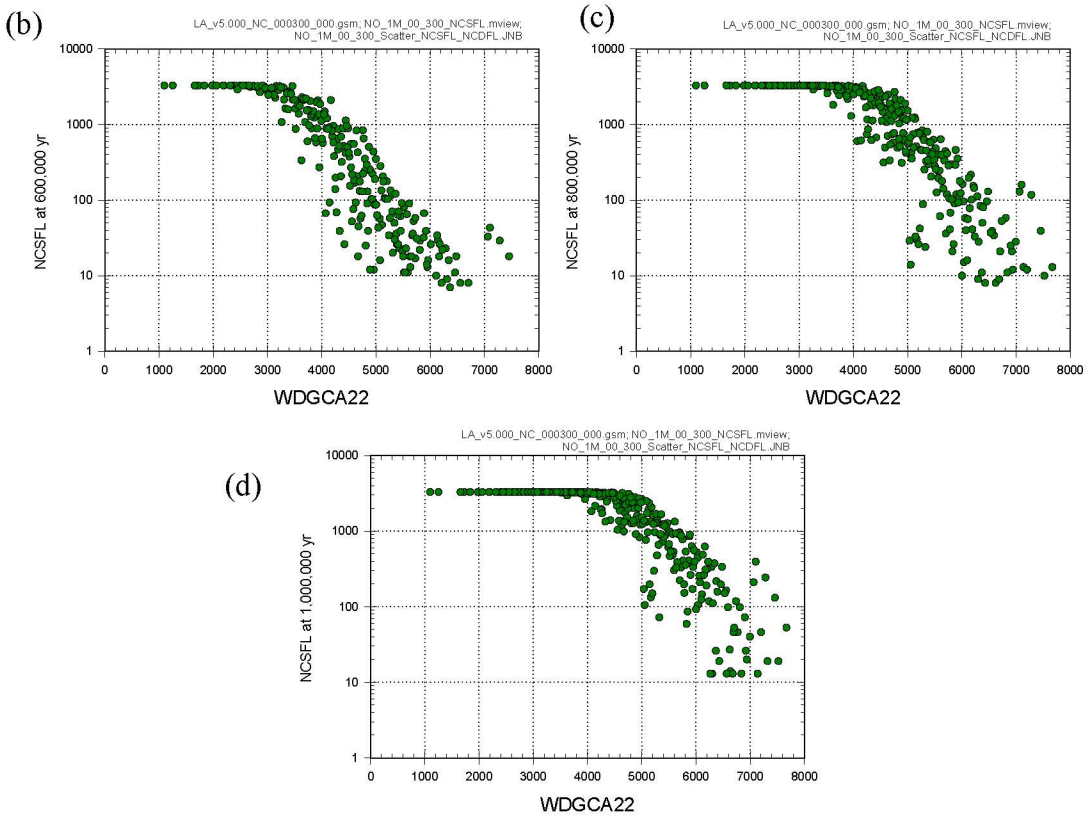

Source: Output DTNs: MO0709TSPAREGS.000 [DIRS 182976]; and MO0709TSPAPLOT.000 [DIRS 183010].

Figure K4.2-3. Stepwise rank regression analyses and selected scatterplots for number of failed CSNF WPs (*NCSFL*) in percolation bin 3 under nominal conditions: (a) Regressions for *NCSFL* at 6×10^5, 8×10^5 and 1×10^6 years, and (b, c, d) Scatterplots for *NCSFL* at 6×10^5, 8×10^5 and 1×10^6 years

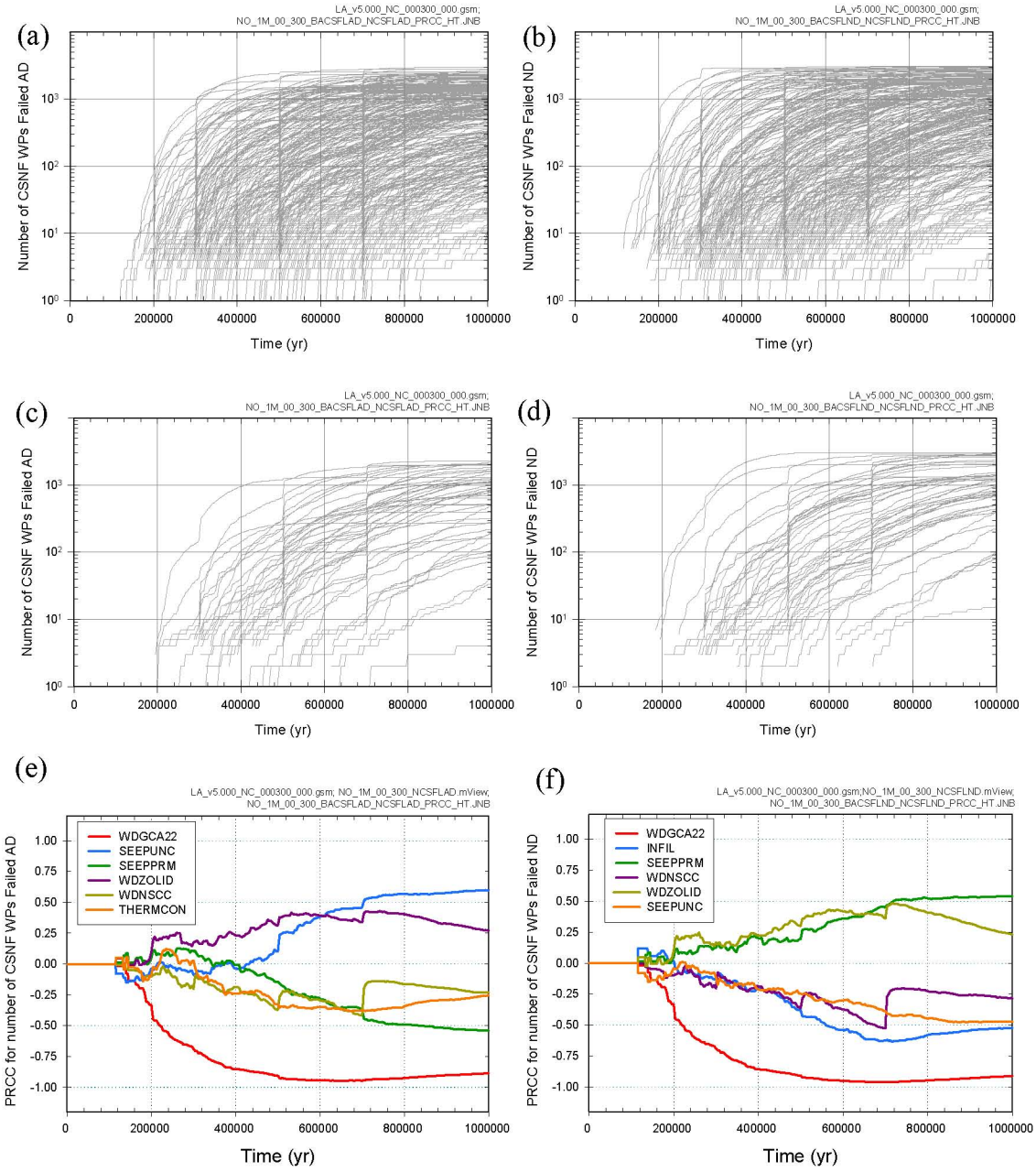

Source: Output DTNs: MO0709TSPAREGS.000 [DIRS 182976]; and MO0709TSPAPLOT.000 [DIRS 183010].

Figure K4.2-4. Time-dependent numbers of failed CSNF WPs experiencing dripping conditions (*NCSFLAD*) and nondripping conditions (*NCSFLND*) in percolation bin 3 under nominal conditions: (a, b) *NCSFLAD* and *NCSFLND* for all (i.e., 300) sample elements, (c, d) *NCSFLAD* and *NCSFLND* for first 50 sample elements, and (e, f) PRCCs for *NCSFLAD* and *NCSFLND*.

(a)

	NCSFLAD: 600K yr			NCSFLAD: 800K yr			NCSFLAD: 1M yr		
Step[a]	**Variable[b]**	**R^{2c}**	**SRRC[d]**	**Variable**	**R^2**	**SRRC**	**Variable**	**R^2**	**SRRC**
1	WDGCA22	0.82	-0.93	WDGCA22	0.73	-0.87	WDGCA22	0.62	-0.81
2	SEEPUNC	0.84	0.15	SEEPUNC	0.79	0.25	SEEPUNC	0.71	0.31
3	WDZOLID	0.86	0.13	SEEPPRM	0.82	-0.18	SEEPPRM	0.78	-0.26
4	THERMCON	0.87	-0.13	WDZOLID	0.85	0.15	ALPHAL	0.79	-0.15
5	SEEPPRM	0.88	-0.09	ALPHAL	0.86	-0.10	WDZOLID	0.81	0.10
6	SCCTHR	0.89	-0.08	THERMCON	0.87	-0.11	THERMCON	0.81	-0.08
7	INFIL	0.89	-0.09	SCCTHR	0.87	-0.08	WDNSCC	0.82	-0.07
8	WDNSCC	0.90	-0.07	WDGCUA22	0.88	0.07	GP1NO3	0.82	0.07
9	WDGCUA22	0.90	0.06						
10	ALPHAL	0.91	-0.06						

(b)

	NCSFLND: 600K yr			NCSFLND: 800K yr			NCSFLND: 1M yr		
Step[a]	**Variable[b]**	**R^{2c}**	**SRRC[d]**	**Variable**	**R^2**	**SRRC**	**Variable**	**R^2**	**SRRC**
1	WDGCA22	0.81	-0.94	WDGCA22	0.78	-0.92	WDGCA22	0.70	-0.87
2	INFIL	0.85	-0.21	INFIL	0.83	-0.24	INFIL	0.76	-0.25
3	WDZOLID	0.87	0.13	WDZOLID	0.85	0.14	SEEPPRM	0.80	0.23
4	THERMCON	0.89	-0.14	SEEPPRM	0.88	0.18	SEEPUNC	0.83	-0.18
5	WDNSCC	0.90	-0.11	SEEPUNC	0.89	-0.13	WDZOLID	0.85	0.11
6	SEEPPRM	0.90	0.11	THERMCON	0.90	-0.11	WDNSCC	0.86	-0.11
7	SEEPPRMN	0.91	0.07	SCCTHR	0.91	-0.07	THERMCON	0.87	-0.10
8	SEEPUNC	0.91	-0.07	WDGCUA22	0.91	0.08	WDGCUA22	0.88	0.08
9	SCCTHR	0.92	-0.07	ALPHAL	0.92	0.06	ALPHAL	0.88	0.07
10	WDGCUA22	0.92	0.07	WDNSCC	0.92	-0.06	SEEPPRMN	0.88	0.06
11				SEEPPRMN	0.92	0.06	KDSNCOL	0.89	0.05

a: Steps in stepwise rank regression analysis

b: Variables listed in order of selection in stepwise regression

c: Cumulative R^2 value with entry of each variable into regression model

d: Standardized rank regression coefficients (SRRCs) in final regression model

Source: Output DTNs: MO0709TSPAREGS.000 [DIRS 182976]; and MO0709TSPAPLOT.000 [DIRS 183010].

Figure K4.2-5. Stepwise rank regression analyses and selected scatterplots for numbers of failed CSNF WPs experiencing dripping conditions (*NCSFLAD*) and nondripping conditions (*NCSFLND*) in percolation bin 3 under nominal conditions: (a, b) Regressions for *NCSFLAD* and *NCSFLND* at 6×10^5, 8×10^5 and 1×10^6 years, and (c, d, e, f) Scatterplots for *NCSFLAD* and *NCSFLND* at 8×10^5 years, and (g, h) Scatterplots comparing *NCSFLAD* and *NCSFLND* at 6×10^5 and 8×10^5 years.

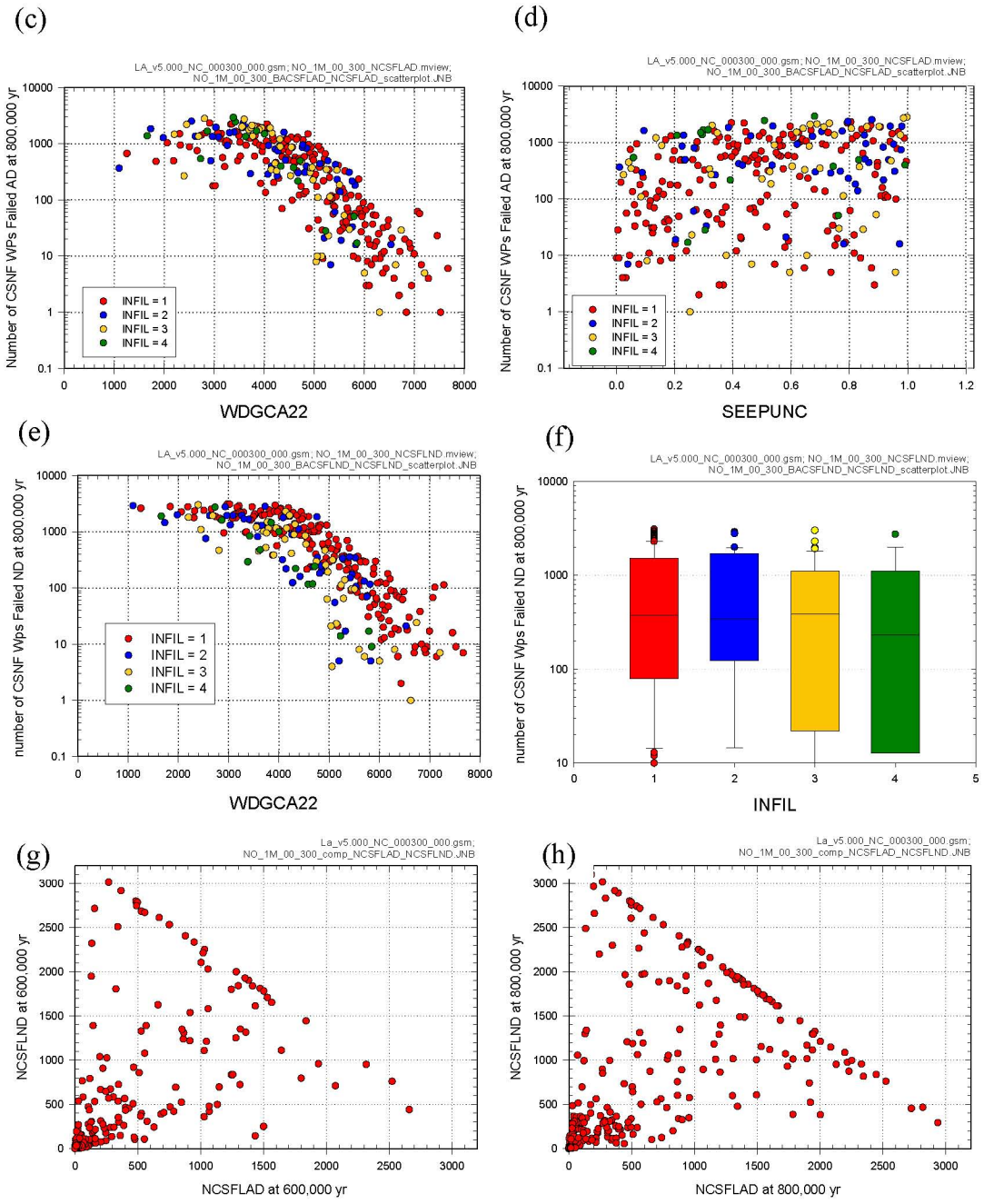

Source: Output DTNs: MO0709TSPAREGS.000 [DIRS 182976]; and MO0709TSPAPLOT.000 [DIRS 183010].

Note: In (f), the box extends from 0.25 to 0.75 quantile; lower and upper bar and whisker extend to 0.1 and 0.9 quantile, respectively; dots represent values outside 0.1 to 0.9 quantile range; median indicated by light horizontal line.

Figure K4.2-5. Stepwise rank regression analyses and selected scatterplots for numbers of failed CSNF WPs experiencing dripping conditions (*NCSFLAD*) and nondripping conditions (*NCSFLND*) in percolation bin 3 under nominal conditions: (a, b) Regressions for *NCSFLAD* and *NCSFLND* at 6×10^5, 8×10^5 and 1×10^6 years, and (c, d, e, f) Scatterplots for *NCSFLAD* and *NCSFLND* at 8×10^5 years, and (g, h) Scatterplots comparing *NCSFLAD* and *NCSFLND* at 6×10^5 and 8×10^5 years (continued).

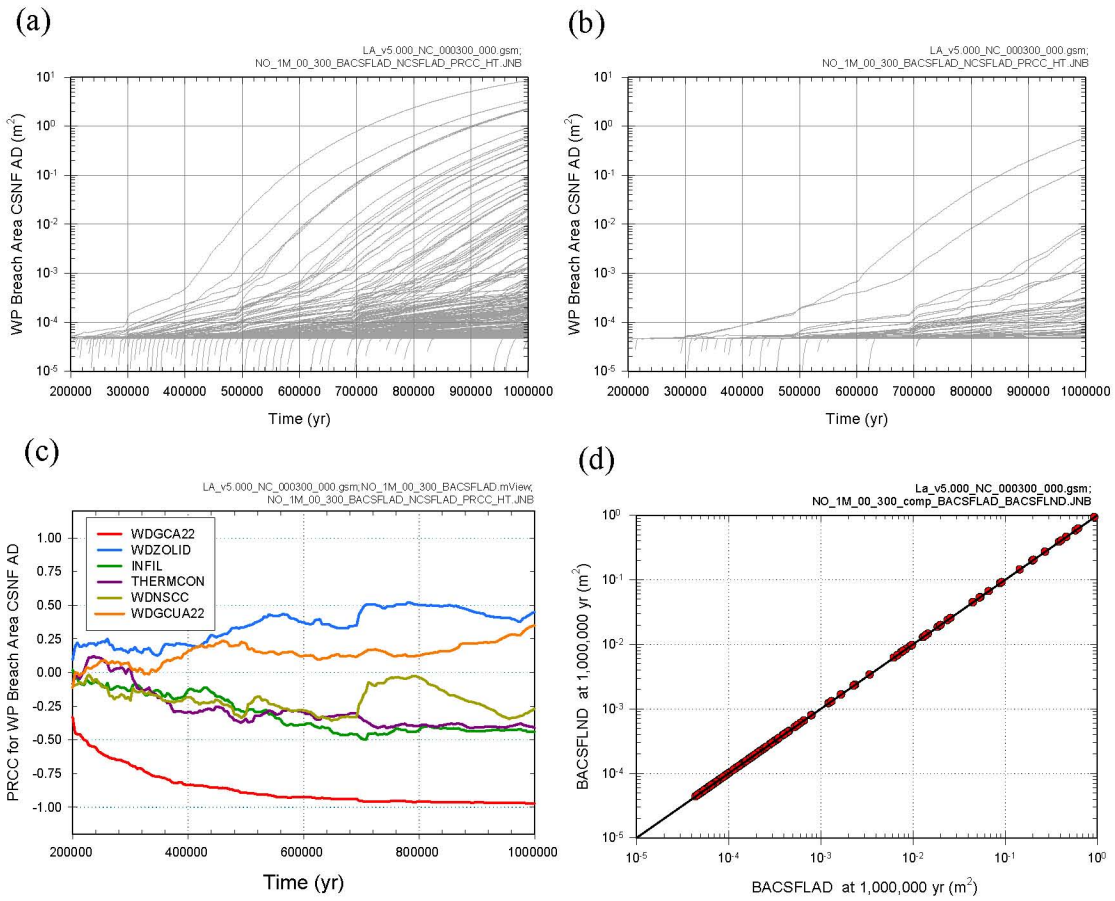

Source: Output DTNs: MO0709TSPAREGS.000 [DIRS 182976]; and MO0709TSPAPLOT.000 [DIRS 183010].

Figure K4.2-6. Time-dependent average breached area on failed CSNF WPs experiencing dripping conditions (*BACSFLAD*) and nondripping conditions (*BACSFLND*) in percolation bin 3 under nominal conditions: (a) *BACSFLAD* for all (i.e., 300) sample elements, (b) *BACSFLAD* for first 50 sample elements, (c) PRCCs for *BACSFLAD*, and (d) Scatterplot comparing *BACSFLAD* and *BACSFLND* at 1×10^6 years.

(a)

	BACSFLAD: 600K yr			BACSFLAD: 800K yr			BACSFLAD: 1M yr		
Step[a]	**Variable[b]**	**R^{2c}**	**SRRC[d]**	**Variable**	**R^2**	**SRRC**	**Variable**	**R^2**	**SRRC**
1	WDGCA22	0.81	-0.93	WDGCA22	0.86	-0.96	WDGCA22	0.91	-0.97
2	WDZOLID	0.83	0.14	WDZOLID	0.89	0.16	WDZOLID	0.92	0.10
3	INFIL	0.85	-0.15	INFIL	0.91	-0.14	INFIL	0.93	-0.12
4	THERMCON	0.87	-0.11	THERMCON	0.93	-0.13	THERMCON	0.94	-0.10
5	SCCTHR	0.87	-0.08	SCCTHR	0.93	-0.08	WDGCUA22	0.95	0.09
6	WDNSCC	0.88	-0.08	WDGCUA22	0.93	0.06	SCCTHR	0.95	-0.08
7							WDNSCC	0.96	-0.05

a: Steps in stepwise rank regression analysis

b: Variables listed in order of selection in stepwise regression

c: Cumulative R^2 value with entry of each variable into regression model

d: Standardized rank regression coefficients (SRRCs) in final regression model

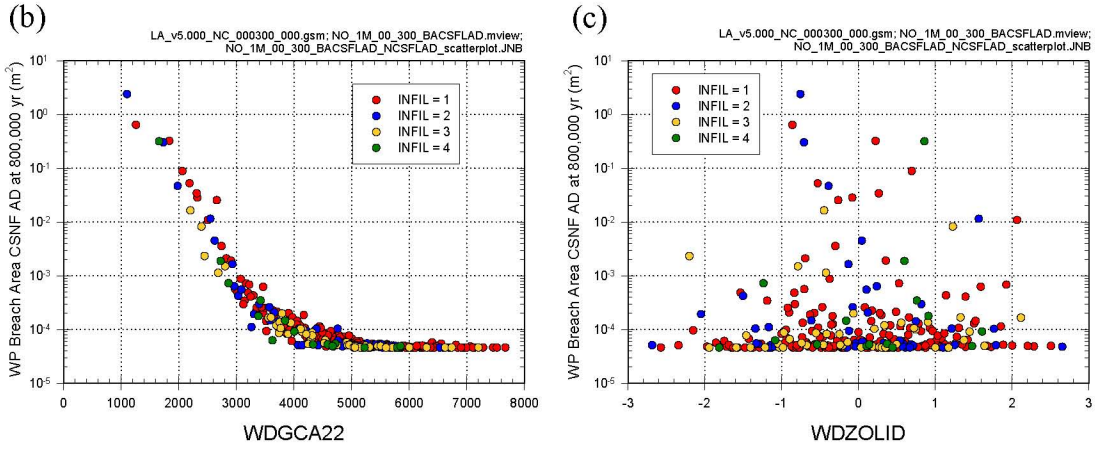

Source: Output DTNs: MO0709TSPAREGS.000 [DIRS 182976]; and MO0709TSPAPLOT.000 [DIRS 183010].

Figure K4.2-7. Stepwise rank regression analyses and selected scatterplots for average breached area on failed CSNF WPs experiencing dripping conditions (*BACSFLAD*) in percolation bin 3 under nominal conditions: (a) Regressions for *BACSFLAD* at 6×10^5, 8×10^5 and 1×10^6 years, and (b, c) Scatterplots for *BACSFLAD* and *NCSFLND* at 8×10^5 years.

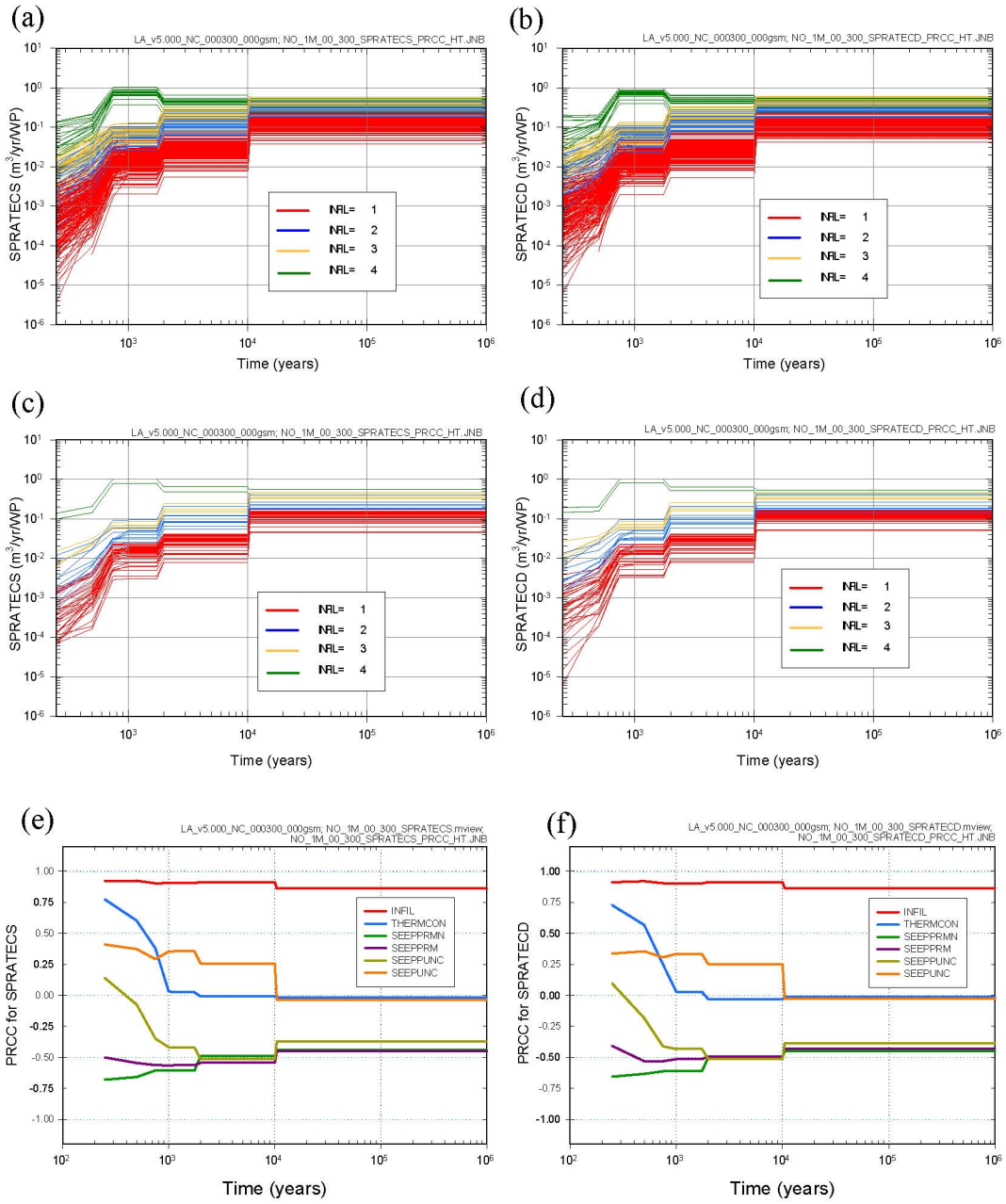

Source: Output DTNs: MO0709TSPAREGS.000 [DIRS 182976]; and MO0709TSPAPLOT.000 [DIRS 183010].

Figure K4.3-1. Time-dependent seepage rates (m^3/yr/WP) into the repository above CSNF WPs (*SPRATECS*) and CDSP WPs (*SPRATECD*) in percolation bin 3 under nominal conditions: (a, b) *SPRATECS* and *SPRATECD* for all (i.e., 300) sample elements, (c, d) *SPRATECS* and *SPRATECD* for first 50 sample elements, and (e, f) PRCCs for *SPRATECS* and *SPRATECD*.

(a)

	SPRATECS: 1K yr			SPRATECS: 50K yr			SPRATECS: 100K yr		
Step[a]	Variable[b]	R^{2c}	SRRC[d]	Variable	R^2	SRRC	Variable	R^2	SRRC
1	INFIL	0.67	0.83	INFIL	0.73	0.86	INFIL	0.68	0.85
2	SEEPPRMN	0.76	-0.28	ALPHAL	0.78	-0.23	ALPHAL	0.73	-0.23
3	ALPHAL	0.82	-0.26	SEEPPRM	0.83	-0.24	SEEPPRMN	0.77	-0.23
4	SEEPPRM	0.85	-0.19	SEEPPRMN	0.87	-0.21	SEEPPRM	0.81	-0.21
5	SEEPUNC	0.87	0.15	SEEPUNC	0.88	0.10	DIFPATHL	0.82	-0.07
6	INRFRCTC	0.88	0.06	DIFPATHL	0.89	-0.05			
7	CORRATSS	0.88	-0.05	INRFRCTC	0.89	0.05			

a: Steps in stepwise rank regression analysis
b: Variables listed in order of selection in stepwise regression
c: Cumulative R^2 value with entry of each variable into regression model
d: Standardized rank regression coefficients (SRRCs) in final regression model

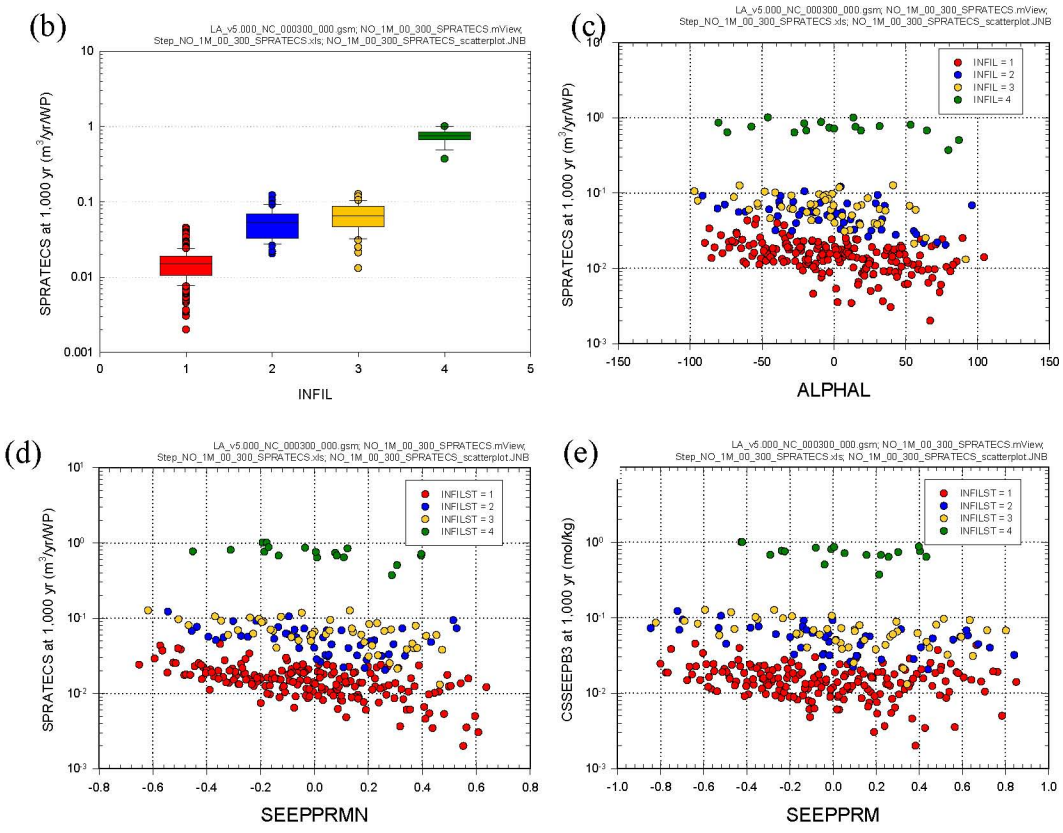

Source: Output DTNs: MO0709TSPAREGS.000 [DIRS 182976]; and MO0709TSPAPLOT.000 [DIRS 183010].

Note: In (b), the box extends from 0.25 to 0.75 quantile; lower and upper bar and whisker extend to 0.1 and 0.9 quantile, respectively; dots represent values outside 0.1 to 0.9 quantile range; median indicated by light horizontal line.

Figure K4.3-2. Stepwise rank regression analyses and selected scatterplots for seepage rate (m^3/yr/WP) into the repository above CSNF WPs (*SPRATECS*) in percolation bin 3 under nominal conditions: (a) Regressions for *SPRATECS* at 1000, 5000 and 100,000 years, and (b, c, d, e) Scatterplots for *SPRATECS* at 1000 years.

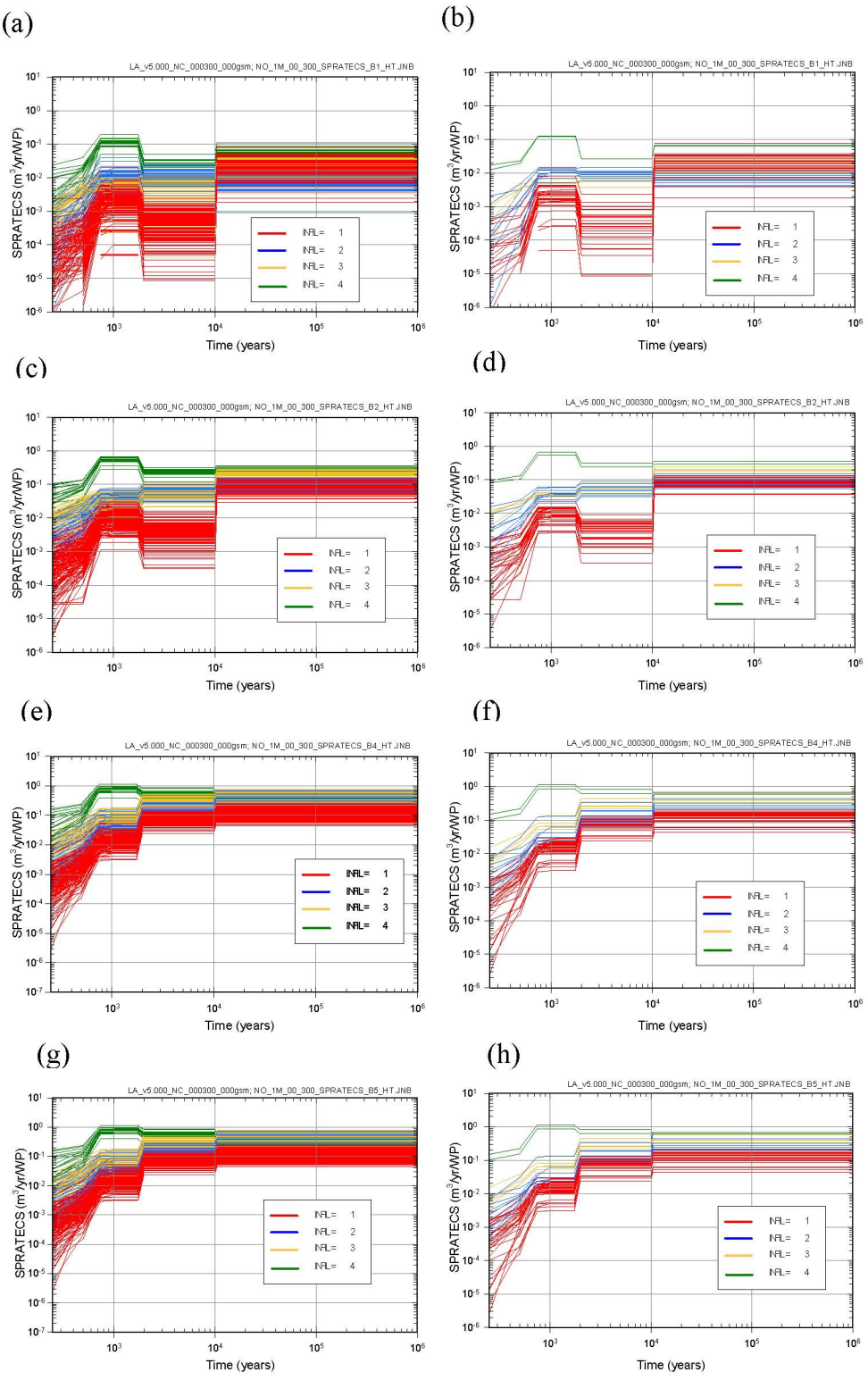

Source: Output DTN MO0709TSPAREGS.000: [DIRS 182976].

Figure K4.3-3. Time-dependent seepage rates (m^3/yr/WP) into the repository above CSNF WPs (*SPRATECS*) in percolation bins 1, 2, 4 and 5 under nominal conditions: (a, c, e, g) *SPRATECS* for all (i.e., 300) sample elements, and (b, d, f, h) *SPRATECS* for first 50 sample elements

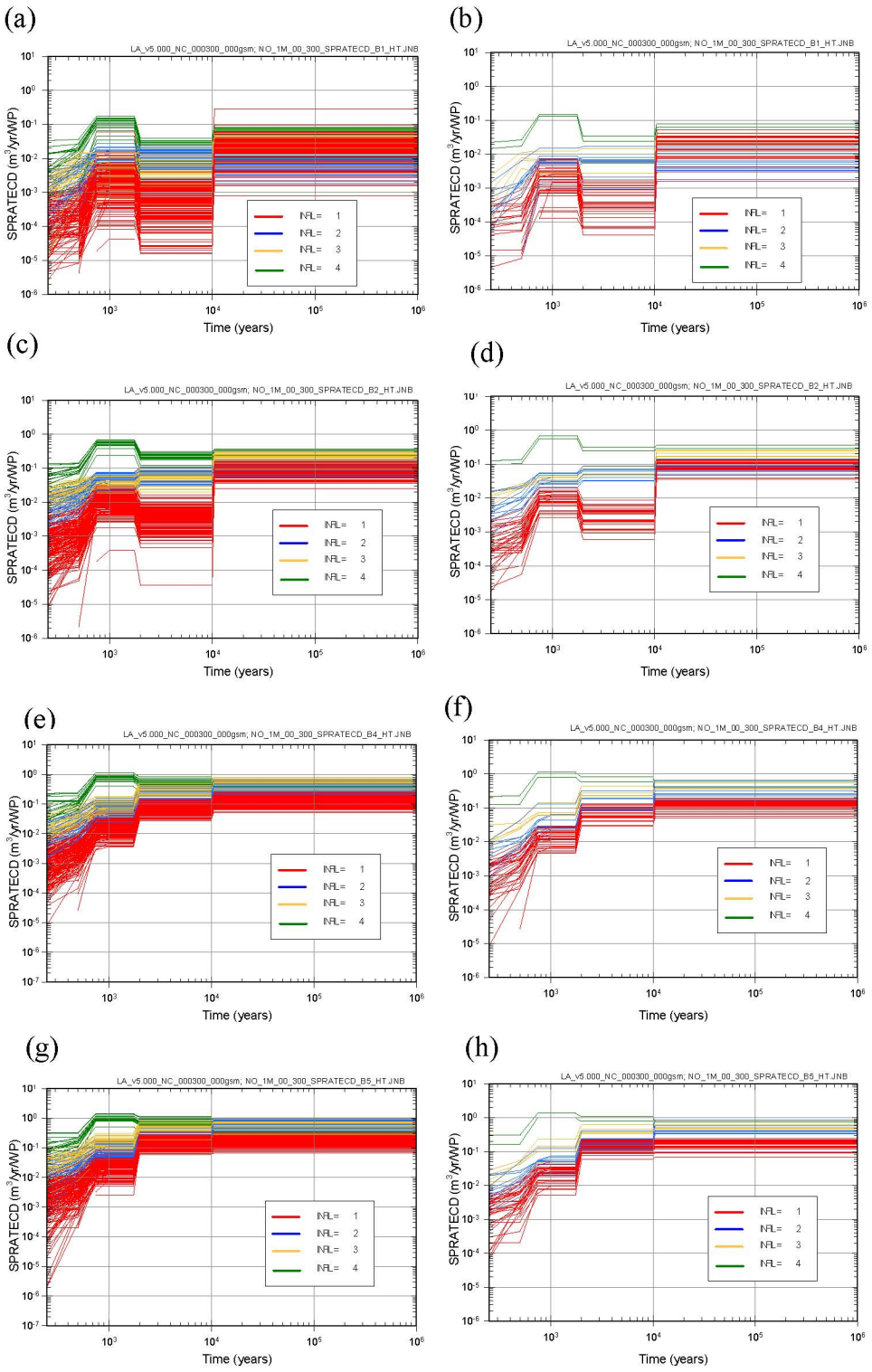

Source: Output DTN: MO0709TSPAREGS.000 [DIRS 182976].

Figure K4.3-4. Time-dependent seepage rates (m^3/yr/WP) into the repository above CDSP WPs (*SPRATECD*) in percolation bins 1, 2, 4 and 5 under nominal conditions: (a, c, e, g) *SPRATECD* for all (i.e., 300) sample elements, and (b, d, f, h) *SPRATECD* for first 50 sample elements

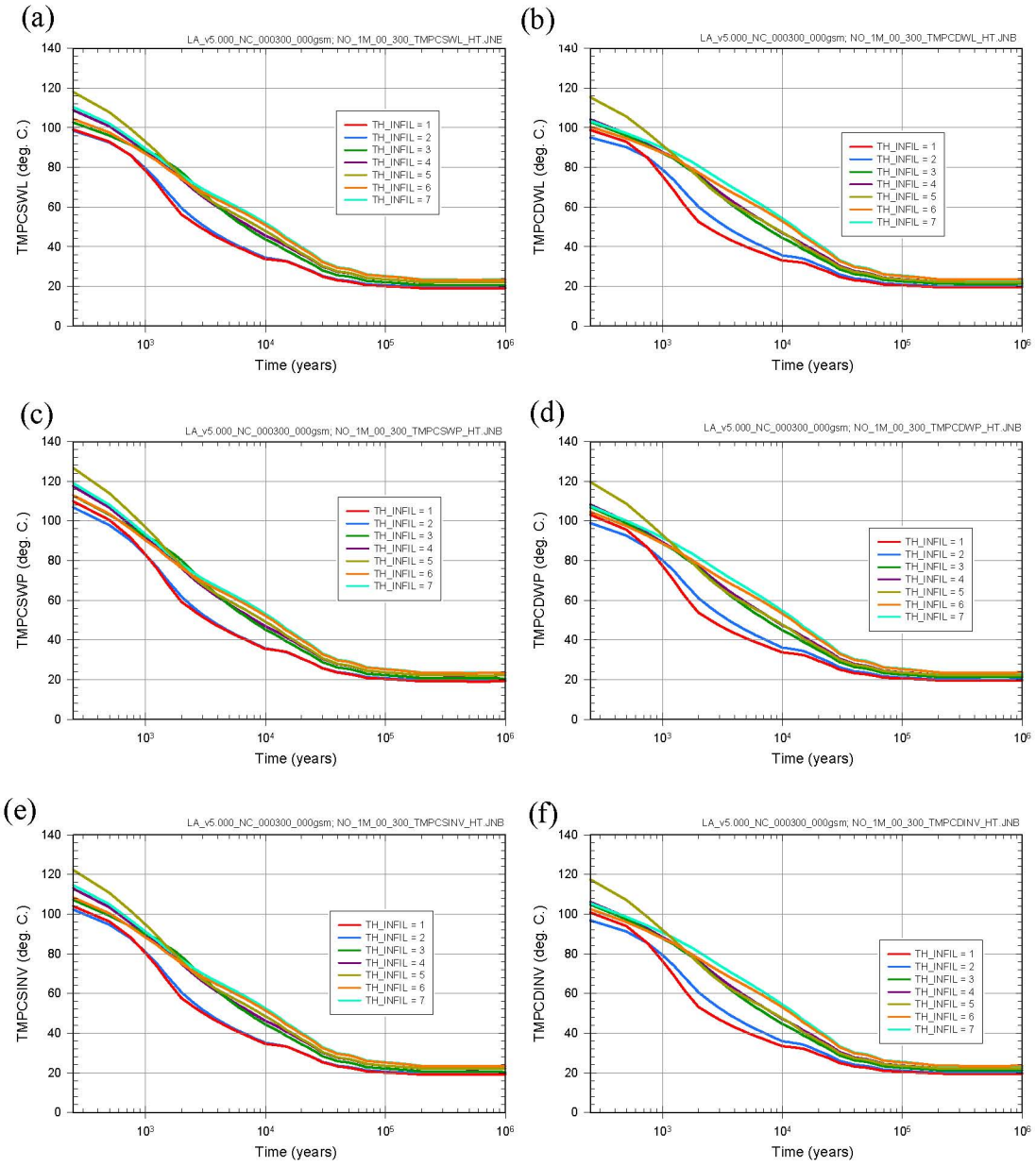

Source: Output DTN: MO0709TSPAREGS.000 [DIRS 182976].

Figure K4.3-5. Time-dependent temperatures in percolation bin 3 under nominal conditions for CSNF WPs at the drift wall (*TMPCSWL*), on the WP (*TMPCSWP*) and in the invert beneath the WP (*TMPCSINV*) and similarly for CDSP WPs at the drift wall (*TMPCDWL*), on the WP (*TMPCDWP*) and in the invert beneath the WP (*TMPCDINV*): (a, c, e) *TMPCSWL*, *TMPCSWP* and *TMPCSINV*, and (b, d, f) *TMPCDWL*, *TMPCDWP* and *TMPCDINV*

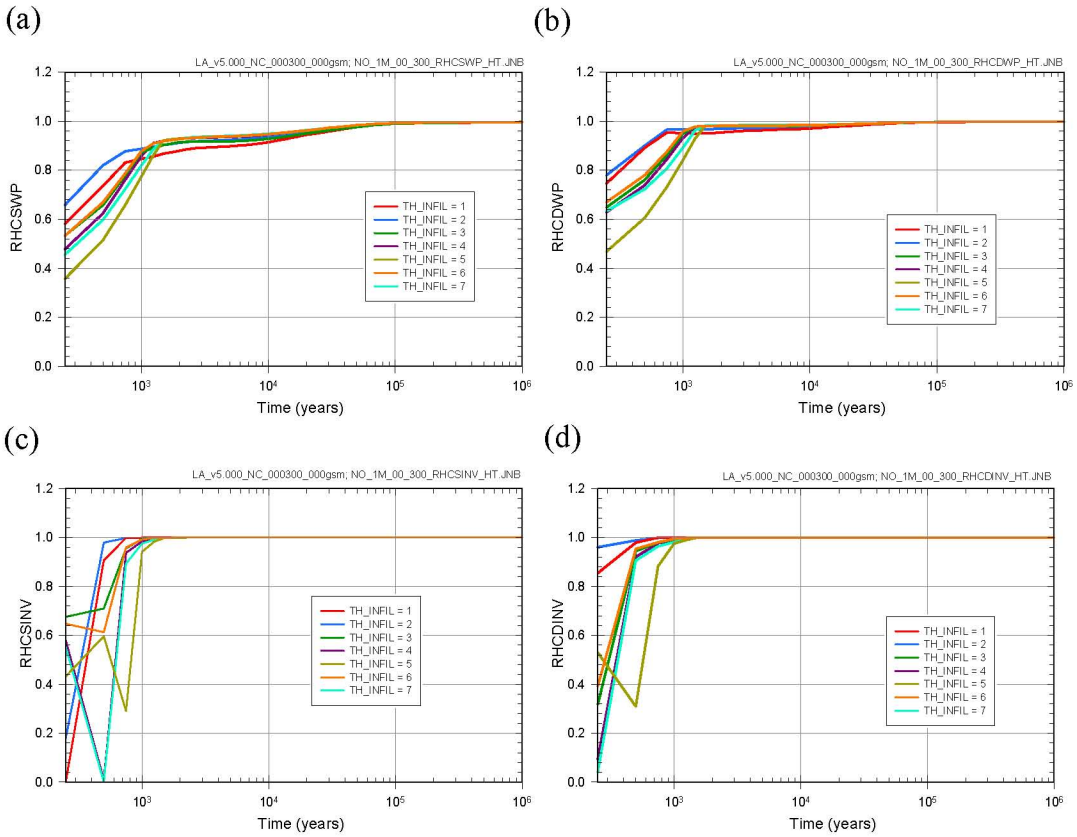

Source: Output DTN: MO0709TSPAREGS.000 [DIRS 182976].

Figure K4.3-6. Time-dependent relative humidities in percolation bin 3 under nominal conditions for CSNF WPs on the WP (*RHCSWP*) and in the invert beneath the WP (*RHCSINV*) and similarly for CDSP WPs on the WP (*RHCDWP*) and in the invert beneath the WP (*RHCDINV*): (a, c) *RHCSWP* and *RHCSINV*, and (b, d) *RHCDWP* and *RHCDINV*

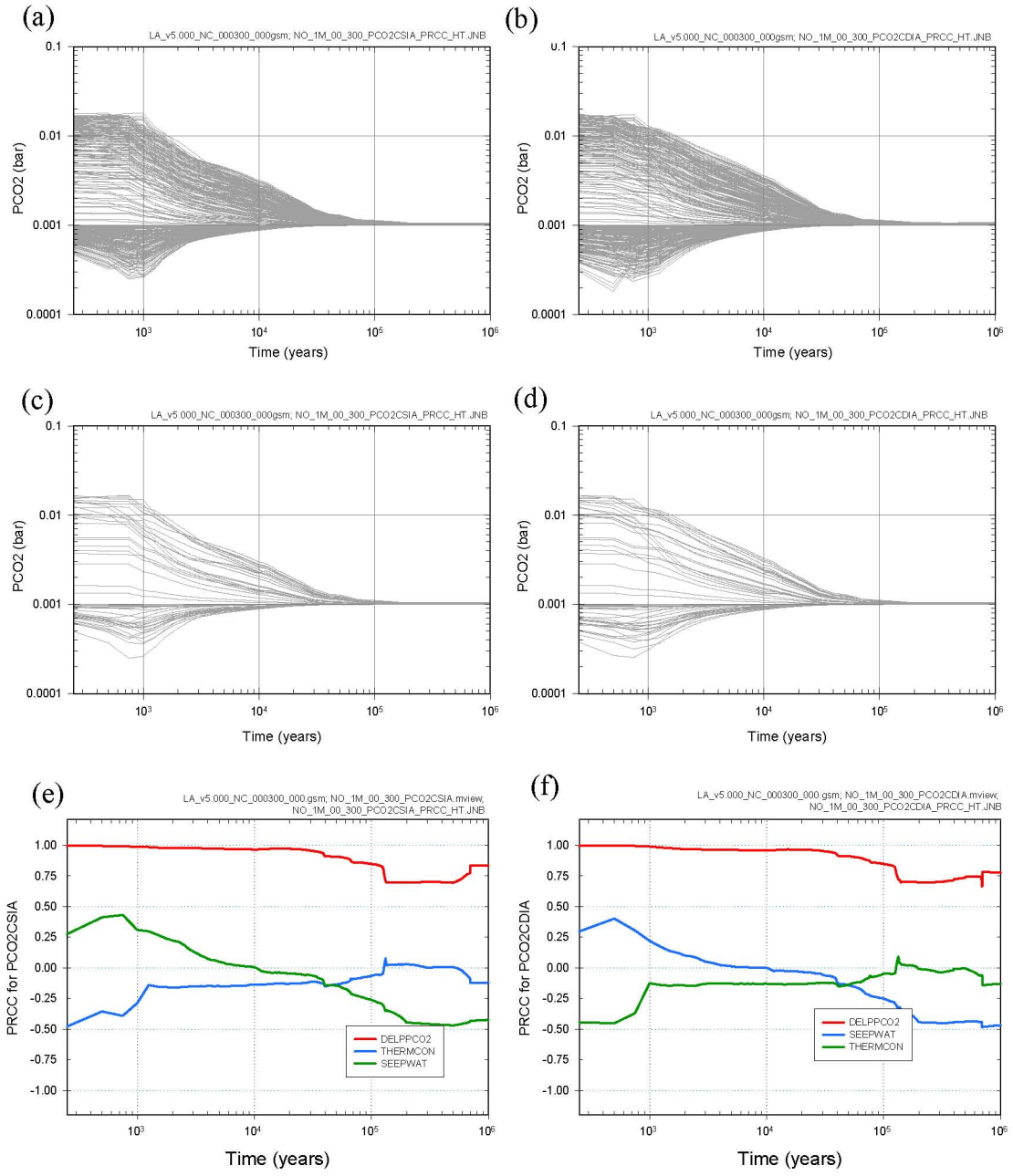

Source: Output DTNs: MO0709TSPAREGS.000 [DIRS 182976]; and MO0709TSPAPLOT.000 [DIRS 183010].

Figure K4.3-7. Time-dependent partial pressures for CO_2 (bars) in the invert for dripping conditions for CSNF WPs (*PCO2CSIA*) and CDSP WPs (*PCO2CDIA*) in percolation bin 3 under nominal conditions: (a, b) *PCO2CSIA* and *PCO2CDIA* for all (i.e., 300) sample elements, (c, d) *PCO2CSIA* and *PCO2CDIA* for first 50 sample elements, and (e, f) PRCCs for *PCO2CSIA* and *PCO2CDIA*

(a)

	PCO2CSIA: 1K yr			PCO2CSIA: 5K yr			PCO2CSIA: 10K yr		
Step[a]	**Variable[b]**	**R^{2c}**	**SRRC[d]**	**Variable**	**R^2**	**SRRC**	**Variable**	**R^2**	**SRRC**
1	DELPPCO2	0.97	0.99	DELPPCO2	0.94	0.97	DELPPCO2	0.92	0.96
2	SEEPWAT	0.97	0.05	WPFLUX	0.94	-0.06	WPFLUX	0.93	-0.06
3	THERMCON	0.98	-0.05	WDDSBEGC	0.94	0.05	WDDSBEGC	0.93	0.05
4				EP1LOWAM	0.94	0.04			

a: Steps in stepwise rank regression analysis
b: Variables listed in order of selection in stepwise regression
c: Cumulative R^2 value with entry of each variable into regression model
d: Standardized rank regression coefficients (SRRCs) in final regression model

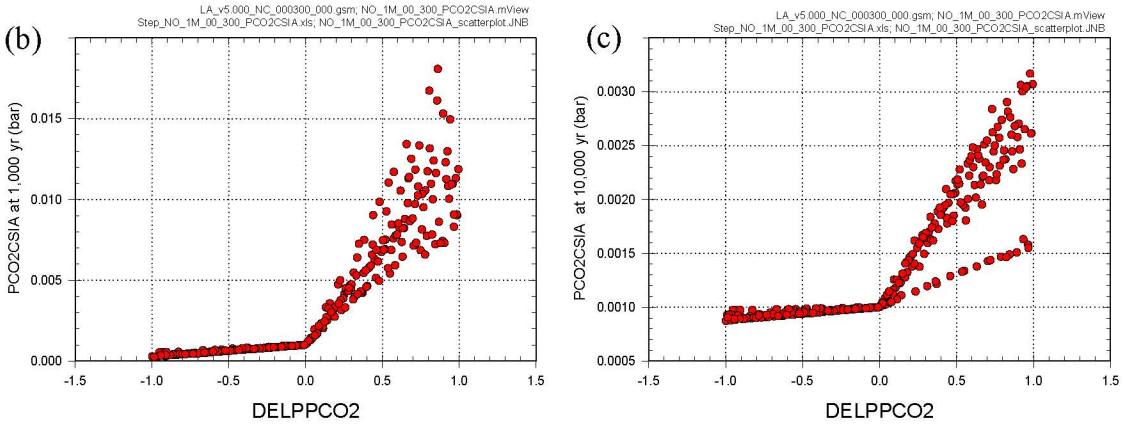

Source: Output DTNs: MO0709TSPAREGS.000 [DIRS 182976]; and MO0709TSPAPLOT.000 [DIRS 183010].

Figure K4.3-8. Stepwise rank regression analyses and selected scatterplots for CO_2 partial pressure (bars) in the invert under dripping conditions for CSNF WPs (*PCO2CSIA*) in percolation bin 3 under nominal conditions: (a) Regressions for *PCO2CSIA* at 1000, 5000 and 10,000 years, and (b, c) Scatterplots for *PCO2CSIA* at 1000 and 10,000 years.

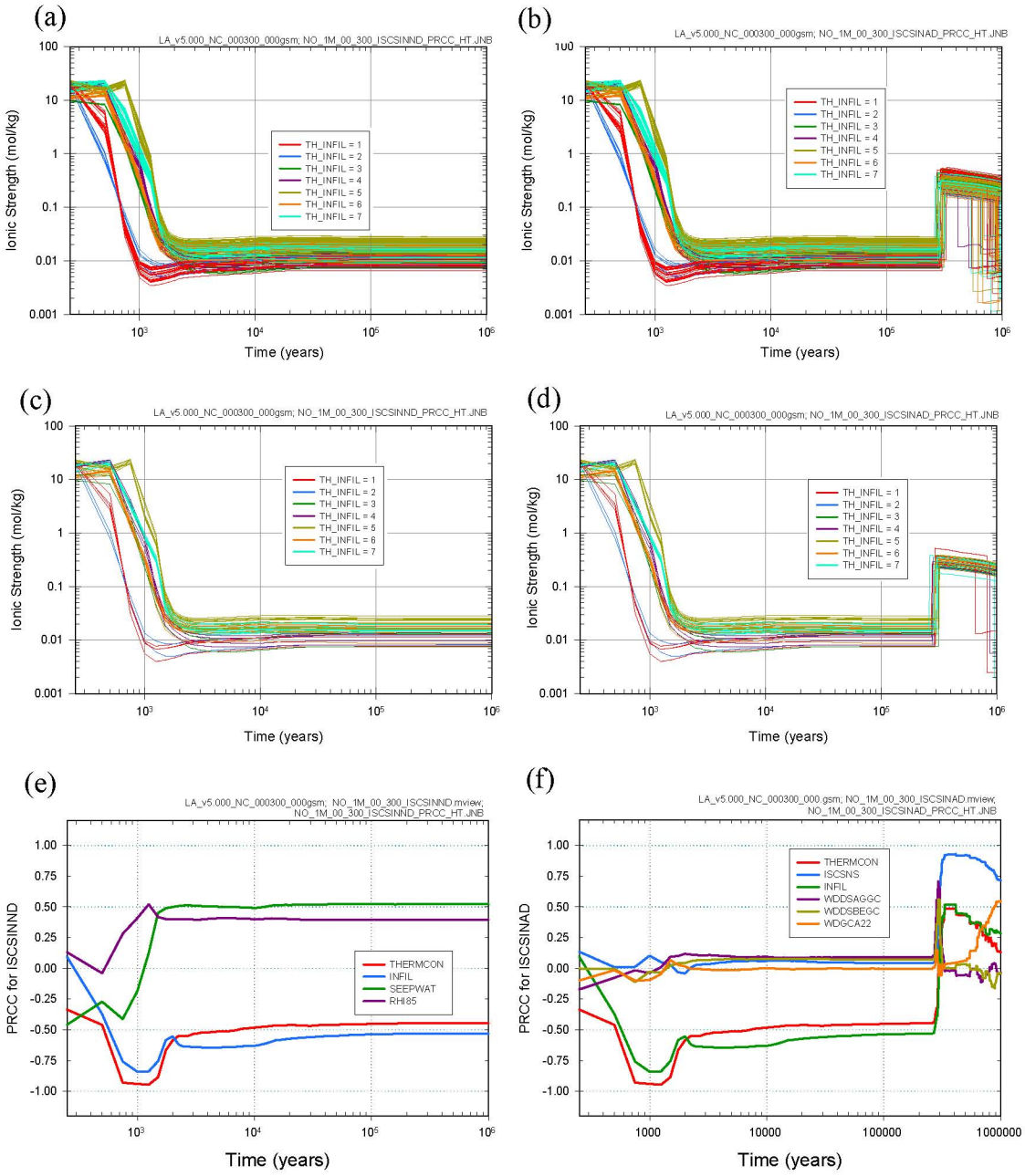

Source: Output DTNs: MO0709TSPAREGS.000 [DIRS 182976]; and MO0709TSPAPLOT.000 [DIRS 183010].

Figure K4.3-9. Time-dependent ionic strength (mol/kg) in the invert for CSNF WPs experiencing nondripping conditions (*ISCSINND*) and dripping conditions (*ISCSINAD*) in percolation bin 3 under nominal conditions: (a, b) *ISCSINND* and *ISCSINAD* for all (i.e., 300) sample elements, (c, d) *ISCSINND* and *ISCSINAD* for first 50 sample elements, and (e, f) PRCCs for *ISCSINND* and *ISCSINAD*.

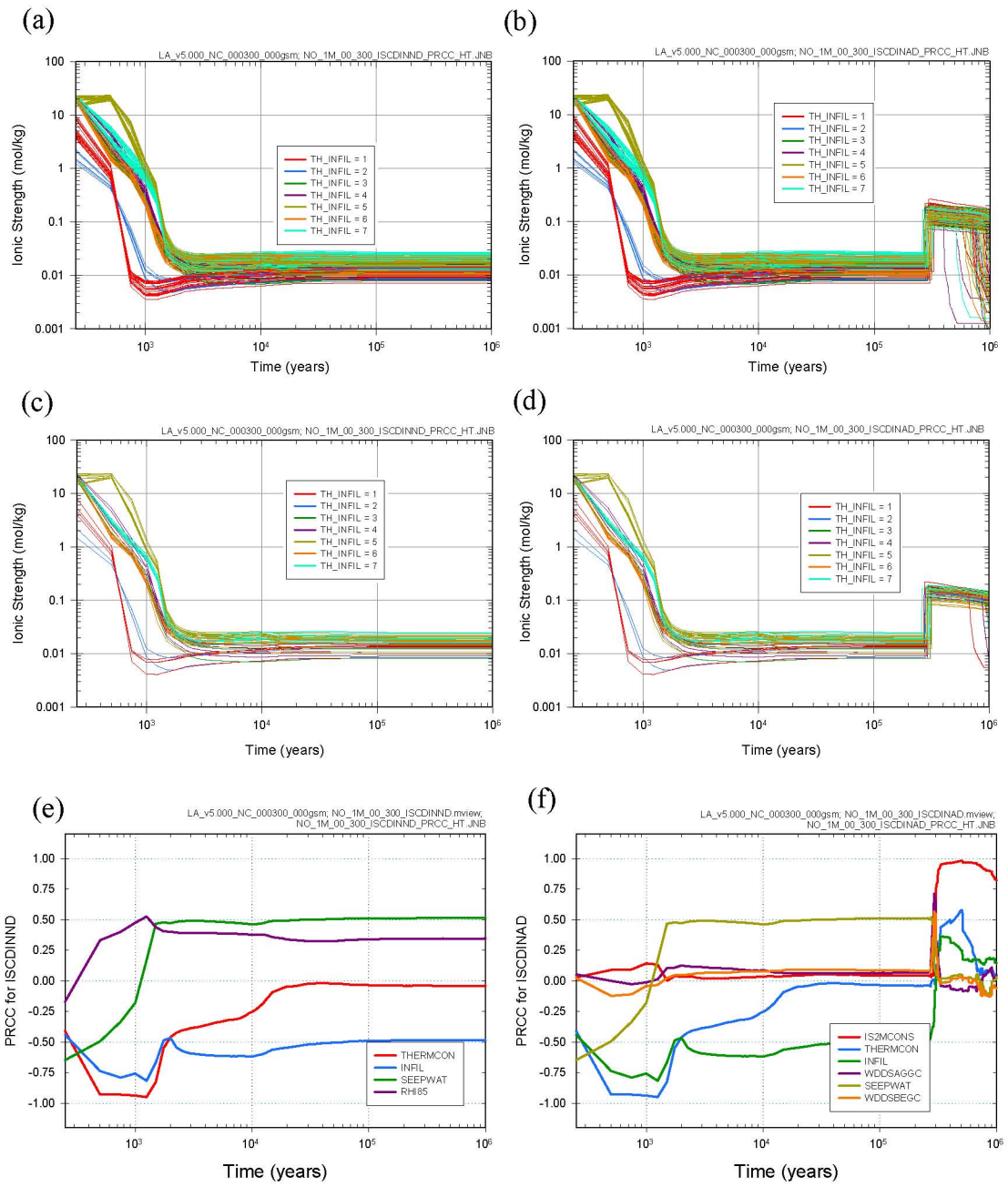

Source: Output DTNs: MO0709TSPAREGS.000 [DIRS 182976]; and MO0709TSPAPLOT.000 [DIRS 183010].

Figure K4.3-10. Time-dependent ionic strength (mol/kg) in the invert for CDSP WPs experiencing nondripping conditions (*ISCDINND*) and dripping conditions (*ISCDINAD*) in percolation bin 3 under nominal conditions: (a, b) *ISCDINND* and *ISCDINAD* for all (i.e., 300) sample elements, (c, d) *ISCDINND* and *ISCDINAD* for first 50 sample elements, and (e, f) PRCCs for *ISCDINND* and *ISCDINAD*.

(a)

	ISCSINAD: 1K yr			ISCSINAD: 50K yr			ISCSINAD: 500K yr		
Step[a]	**Variable[b]**	**R^{2c}**	**SRRC[d]**	**Variable**	**R^2**	**SRRC**	**Variable**	**R^2**	**SRRC**
1	THERMCON	0.65	-0.84	INFIL	0.21	-0.46	ISCSNS	0.80	0.90
2	INFIL	0.90	-0.49	THERMCON	0.40	-0.42	INFIL	0.85	0.23
3	RHI85	0.92	0.14	SEEPWAT	0.53	0.38	THERMCON	0.88	0.16
4	SEEPWAT	0.92	-0.06	RHI85	0.60	0.27	RUBMAXL	0.88	-0.05
5	DELPPCO2	0.92	0.05						
6	KDSNSMEC	0.92	0.04						

a: Steps in stepwise rank regression analysis
b: Variables listed in order of selection in stepwise regression
c: Cumulative R^2 value with entry of each variable into regression model
d: Standardized rank regression coefficients (SRRCs) in final regression model

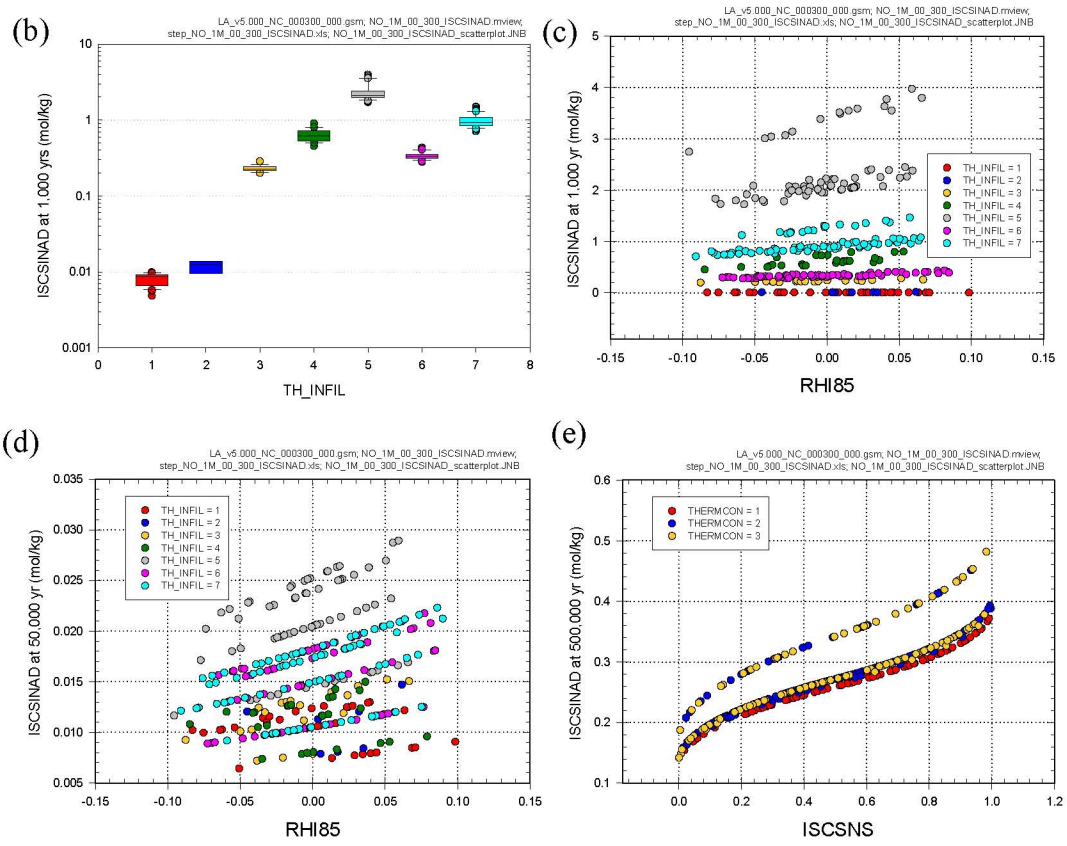

Source: Output DTNs: MO0709TSPAREGS.000 [DIRS 182976]; and MO0709TSPAPLOT.000 [DIRS 183010].

Note: In (b), the box extends from 0.25 to 0.75 quantile; lower and upper bar and whisker extend to 0.1 and 0.9 quantile, respectively; dots represent values outside 0.1 to 0.9 quantile range; median indicated by light horizontal line.

Figure K4.3-11. Stepwise rank regression analyses and selected scatterplots for ionic strength (mol/kg) in the invert for CSNF WPs experiencing dripping conditions (*ISCSINAD*) in percolation bin 3 under nominal conditions: (a) Regressions for *ISCSINAD* at 1000, 50,000 and 500,000 years, and (b, c, d) Scatterplots for *ISCSINAD* at 1000, 50,000 and 500,000 years.

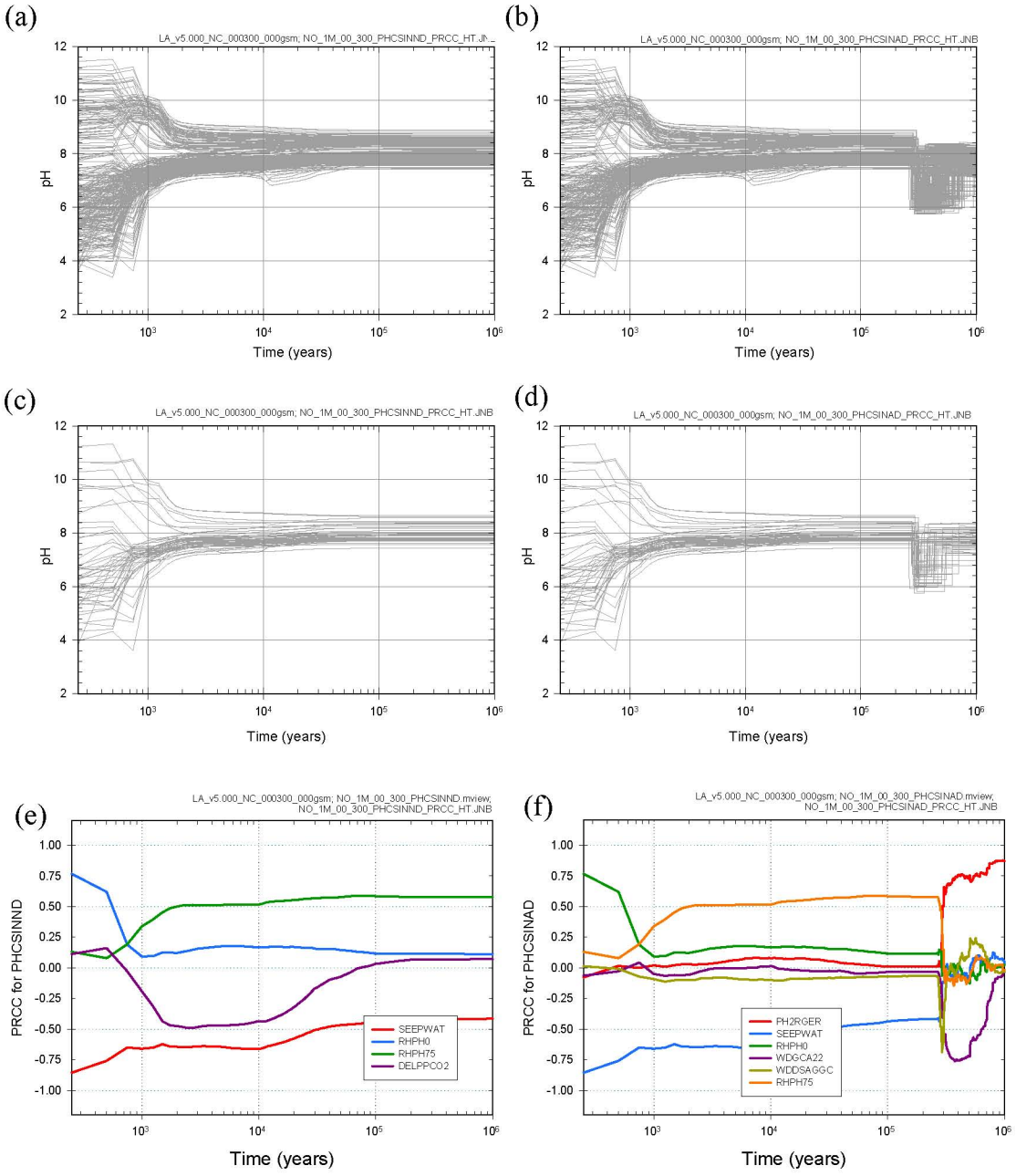

Source: Output DTNs: MO0709TSPAREGS.000 [DIRS 182976]; and MO0709TSPAPLOT.000 [DIRS 183010].

Figure K4.3-12. Time-dependent pH in the invert for CSNF WPs experiencing nondripping conditions (*PHCSINND*) and dripping conditions (*PHCSINAD*) in percolation bin 3 under nominal conditions: (a, b) *PHCSINND* and *PHCSINAD* for all (i.e., 300) sample elements, (c, d) *PHCSINND* and *PHCSINAD* for first 50 sample elements, and (e, f) PRCCs for *PHCSINND* and *PHCSINAD*.

(a)

	PHCSINND: 1K yr			PHCSINND: 50K yr			PHCSINND: 500K yr		
Step[a]	Variable[b]	R^{2c}	SRRC[d]	Variable	R^2	SRRC	Variable	R^2	SRRC
1	SEEPWAT	0.39	-0.61	RHPH75	0.27	0.51	RHPH75	0.28	0.51
2	RHPH75	0.44	0.21	SEEPWAT	0.42	-0.40	SEEPWAT	0.40	-0.36
3	DELPPCO2	0.46	-0.16	RHPH65	0.43	-0.13	RHPH65	0.41	-0.12
4	THERMCON	0.47	0.11	CPUCOLWF	0.45	-0.12			

(b)

	PHCSINAD: 1K yr			PHCSINAD: 50K yr			PHCSINAD: 500K yr		
Step[a]	Variable[b]	R^{2c}	SRRC[d]	Variable	R^2	SRRC	Variable	R^2	SRRC
1	SEEPWAT	0.39	-0.61	RHPH75	0.27	0.51	PH2RGER	0.29	0.58
2	RHPH75	0.44	0.21	SEEPWAT	0.42	-0.40	WDGCA22	0.60	-0.59
3	DELPPCO2	0.46	-0.16	RHPH65	0.43	-0.13	THERMCON	0.63	-0.18
4	THERMCON	0.47	0.11	CPUCOLWF	0.45	-0.12	WDZOLID	0.65	0.16
5							INFIL	0.67	-0.13
6							WDNSCC	0.68	-0.11
7							INRFRCI	0.69	0.09
8							WDGCUA22	0.70	0.08

a: Steps in stepwise rank regression analysis
b: Variables listed in order of selection in stepwise regression
c: Cumulative R^2 value with entry of each variable into regression model
d: Standardized rank regression coefficients (SRRCs) in final regression model

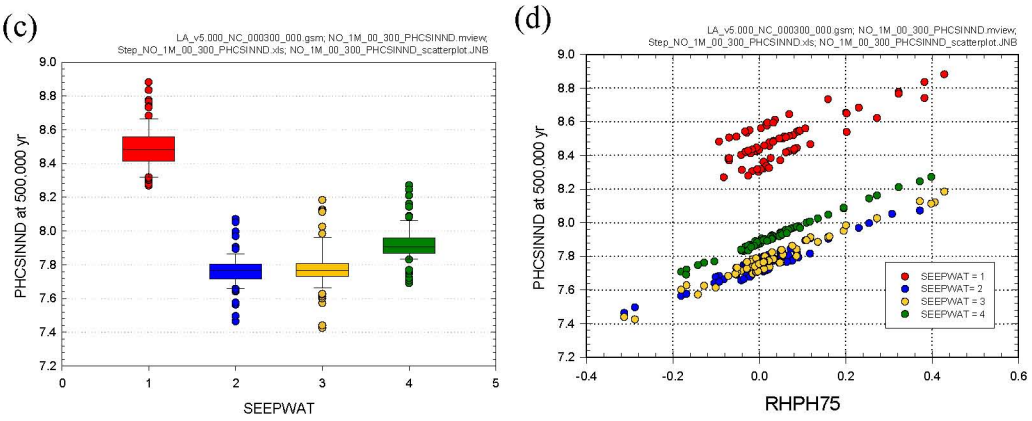

Source: Output DTNs: MO0709TSPAREGS.000 [DIRS 182976]; and MO0709TSPAPLOT.000 [DIRS 183010].

NOTE: In (c, e, g), the box extends from 0.25 to 0.75 quantile; lower and upper bar and whisker extend to 0.1 and 0.9 quantile, respectively; dots represent values outside 0.1 to 0.9 quantile range; median indicated by light horizontal line.

Figure K4.3-13. Stepwise rank regression analyses and selected scatterplots for pH in the invert for CSNF WPs experiencing nondripping conditions (*PHCSINND*) and dripping conditions (*PHCSINAD*) in percolation bin 3 under nominal conditions: (a, b) Regressions for *PHCSINND* and *PHCSINAD* at 1000, 50,000 and 500,000 years, and (c-j) Scatterplots for *PHCSINND* and *PHCSINAD* at 1000, 50,000 and 500,000 years.

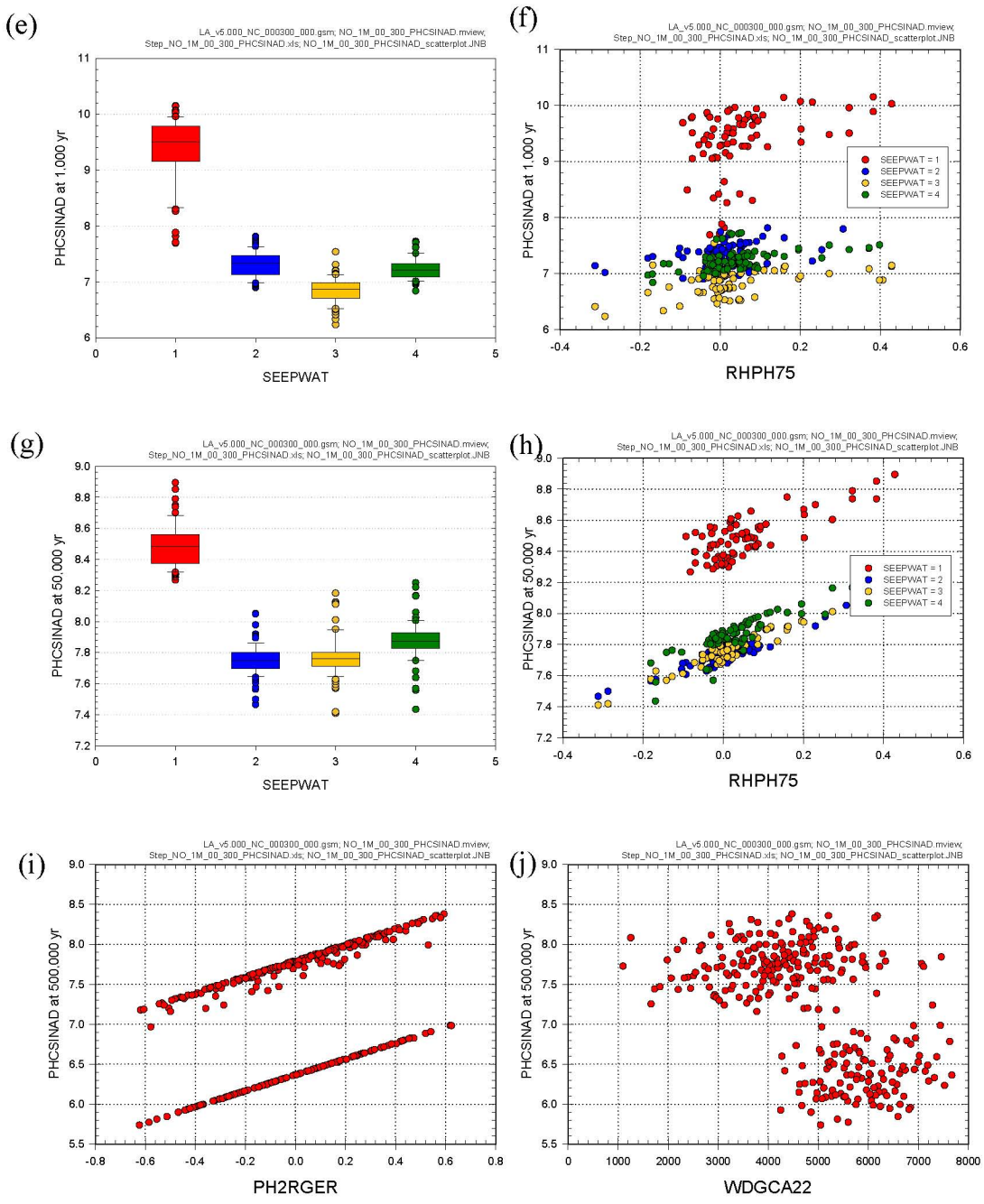

Source: Output DTNs: MO0709TSPAREGS.000 [DIRS 182976]; and MO0709TSPAPLOT.000 [DIRS 183010].

NOTE: In (c, e, g), the box extends from 0.25 to 0.75 quantile; lower and upper bar and whisker extend to 0.1 and 0.9 quantile, respectively; dots represent values outside 0.1 to 0.9 quantile range; median indicated by light horizontal line.

Figure K4.3-13. Stepwise rank regression analyses and selected scatterplots for pH in the invert for CSNF WPs experiencing nondripping conditions (*PHCSINND*) and dripping conditions (*PHCSINAD*) in percolation bin 3 under nominal conditions: (a, b) Regressions for *PHCSINND* and *PHCSINAD* at 1000, 50,000 and 500,000 years, and (c-j) Scatterplots for *PHCSINND* and *PHCSINAD* at 1000, 50,000 and 500,000 years (Continued).

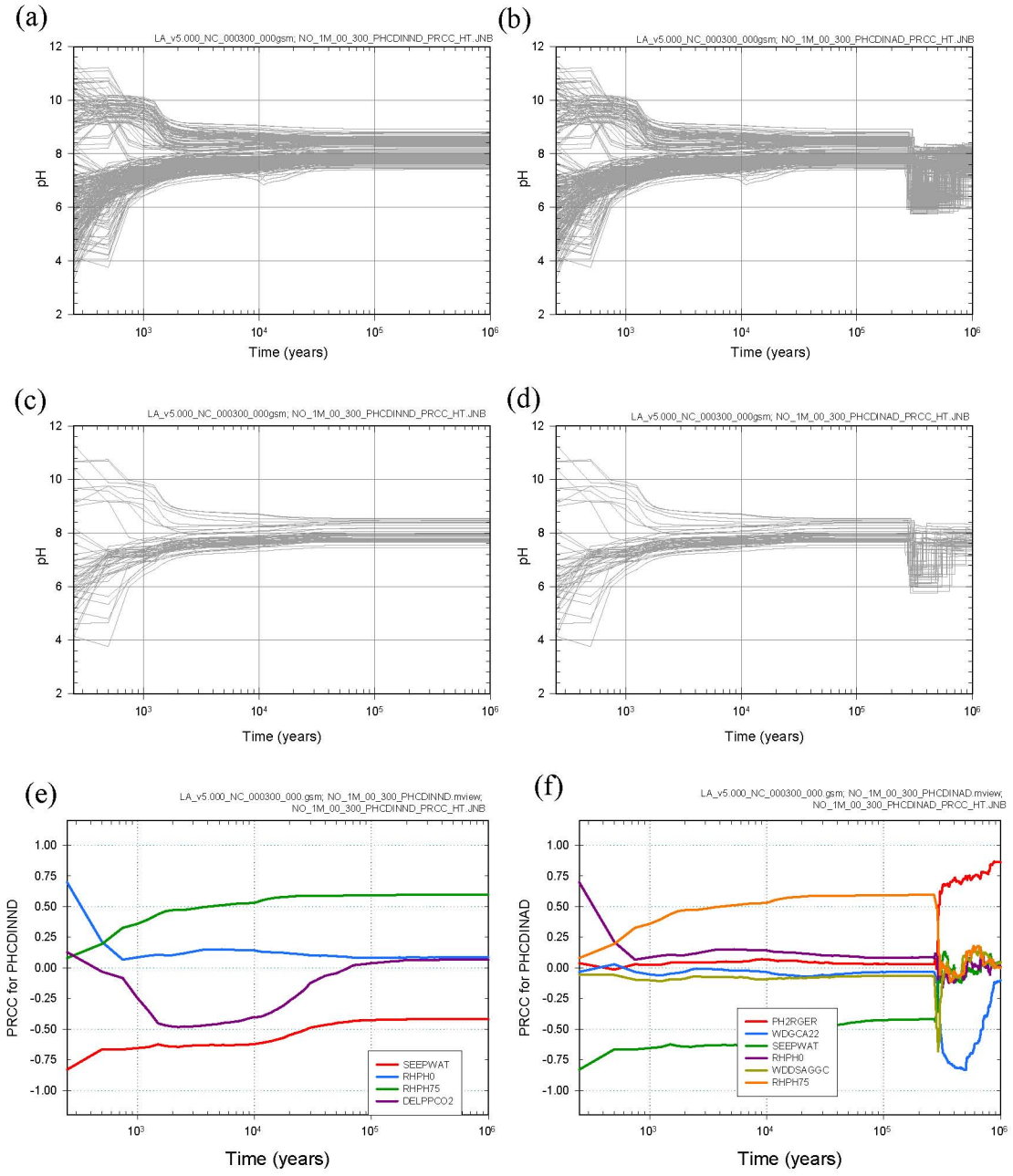

Source: Output DTNs: MO0709TSPAREGS.000 [DIRS 182976]; and MO0709TSPAPLOT.000 [DIRS 183010].

Figure K4.3-14. Time-dependent pH in the invert for CDSP WPs experiencing nondripping conditions (*PHCDINND*) and dripping conditions (*PHCDINAD*) in percolation bin 3 under nominal conditions: (a, b) *PHCDINND* and *PHCDINAD* for all (i.e., 300) sample elements, (c, d) *PHCDINND* and *PHCDINAD* for first 50 sample elements, and (e, f) PRCCS for *PHCDINND* and *PHCDINAD*.

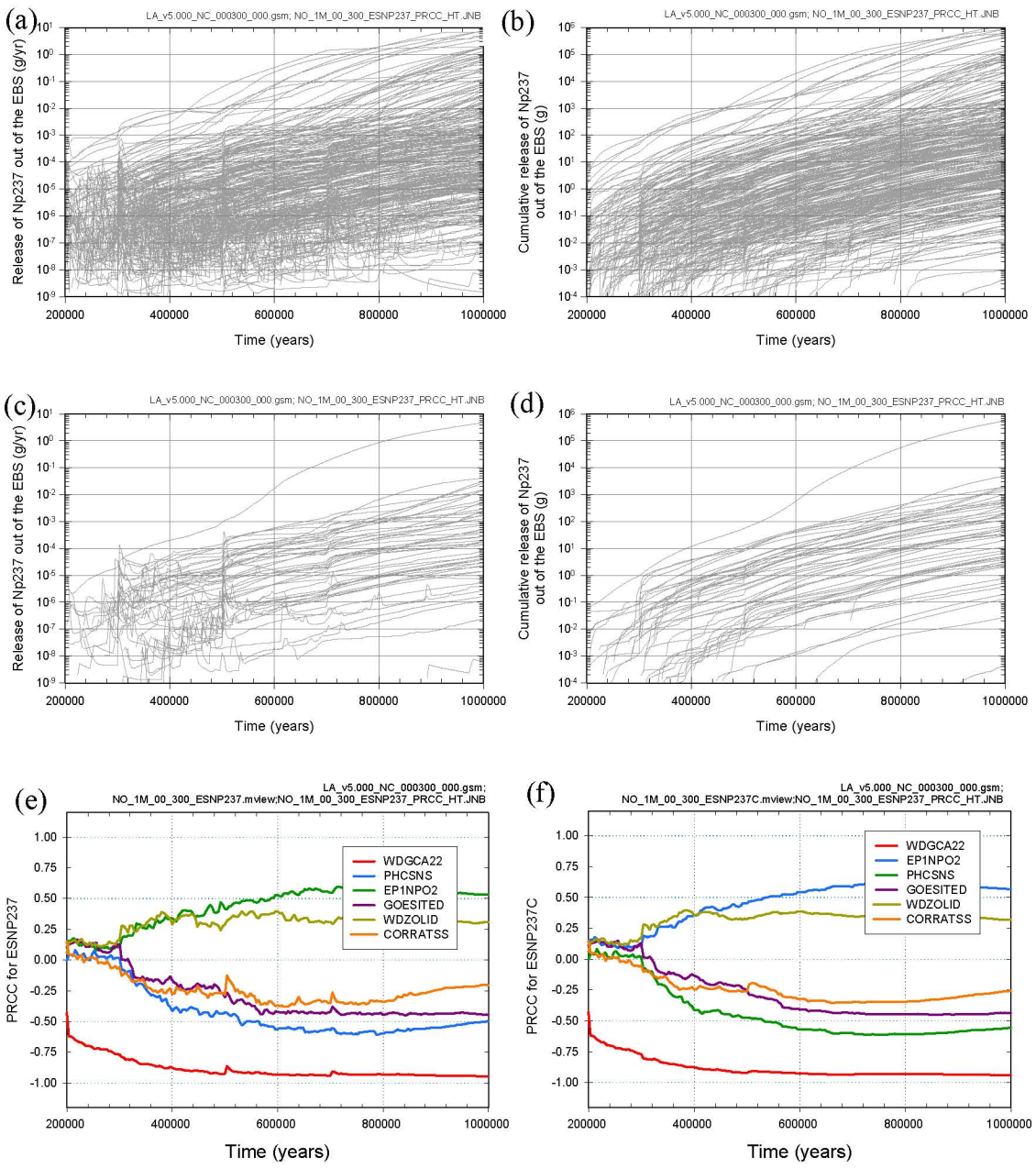

Source: Output DTNs: MO0709TSPAREGS.000 [DIRS 182976]; and MO0709TSPAPLOT.000 [DIRS 183010].

Figure K4.4-1. Time-dependent release rates (*ESNP237*, g/yr) and cumulative (i.e., integrated) releases (*ESNP237C*, g) for movement of dissolved ^{237}Np from the EBS to the UZ under nominal conditions: (a, b) *ESNP237* and *ESNP237C* for all (i.e., 300) sample elements, (c, d) *ESNP237* and *ESNP237C* for first 50 sample elements, and (e, f) PRCCs for *ESNP237* and *ESNP237C*.

(a)

	ESNP237: 400K yr			ESNP237: 600K yr			ESNP237: 800K yr		
Step[a]	Variable[b]	R^{2c}	SRRC[d]	Variable	R^2	SRRC	Variable	R^2	SRRC
1	WDGCA22	0.71	-0.83	WDGCA22	0.74	-0.83	WDGCA22	0.74	-0.83
2	PHCSNS	0.74	-0.16	PHCSNS	0.78	-0.21	EP1NPO2	0.79	0.21
3	WDZOLID	0.76	0.14	EP1NPO2	0.82	0.18	PHCSNS	0.82	-0.21
4	EP1NPO2	0.78	0.13	WDZOLID	0.84	0.12	WDZOLID	0.84	0.11
5	WDNSCC	0.79	-0.11	CORRATSS	0.85	-0.11	EP1LOWNU	0.85	0.09
6	THERMCON	0.80	-0.12	GOESITED	0.86	-0.11	GOESITED	0.87	-0.12
7	SCCTHR	0.81	-0.10	INFIL	0.87	-0.10	CORRATSS	0.87	-0.09
8	INFIL	0.82	-0.09	THERMCON	0.88	-0.10	INFIL	0.88	-0.10
9	WDGCUA22	0.82	0.07	EP1LOWNU	0.89	0.07	SCCTHR	0.89	-0.10
10	CORRATSS	0.83	-0.07	WDNSCC	0.89	-0.08	HFOSA	0.90	-0.09
11				HFOSA	0.90	-0.07	HFOSITED	0.90	-0.07
12				SCCTHR	0.90	-0.08	THERMCON	0.91	-0.07
13				WDGCUA22	0.91	0.07	GOERELAB	0.91	0.08
14				CR2O3SA	0.91	0.06	WDGCUA22	0.91	0.07
15				GOERELAB	0.91	0.05	WDNSCC	0.92	-0.06
16				HFOSITED	0.92	-0.05	DTDRHUNC	0.92	0.05

(b)

	ESNP237C: 400K yr			ESNP237C: 600K yr			ESNP237C: 800K yr		
Step[a]	Variable[b]	R^{2c}	SRRC[d]	Variable	R^2	SRRC	Variable	R^2	SRRC
1	WDGCA22	0.70	-0.82	WDGCA22	0.73	-0.82	WDGCA22	0.74	-0.82
2	PHCSNS	0.74	-0.16	PHCSNS	0.78	-0.22	PHCSNS	0.79	-0.22
3	WDZOLID	0.77	0.16	EP1NPO2	0.82	0.20	EP1NPO2	0.83	0.22
4	EP1NPO2	0.78	0.14	WDZOLID	0.84	0.12	WDZOLID	0.84	0.10
5	THERMCON	0.80	-0.12	CORRATSS	0.85	-0.10	GOESITED	0.86	-0.12
6	WDNSCC	0.81	-0.10	INFIL	0.86	-0.11	CORRATSS	0.87	-0.10
7	INFIL	0.82	-0.10	THERMCON	0.87	-0.10	EP1LOWNU	0.88	0.08
8	SCCTHR	0.83	-0.10	GOESITED	0.88	-0.10	INFIL	0.89	-0.10
9	WDGCUA22	0.83	0.07	WDNSCC	0.89	-0.07	SCCTHR	0.89	-0.10
10				SCCTHR	0.89	-0.08	HFOSA	0.90	-0.08
11				WDGCUA22	0.90	0.06	THERMCON	0.90	-0.07
12				HFOSA	0.90	-0.06	WDGCUA22	0.91	0.07
13				EP1LOWNU	0.90	0.06	WDNSCC	0.91	-0.07
14							GOERELAB	0.92	0.07
15							HFOSITED	0.92	-0.06
16							DTDRHUNC	0.92	0.05

a: Steps in stepwise rank regression analysis
b: Variables listed in order of selection in stepwise regression
c: Cumulative R^2 value with entry of each variable into regression model
d: Standardized rank regression coefficients (SRRCs) in final regression model

Source: Output DTNs: MO0709TSPAREGS.000 [DIRS 182976]; and MO0709TSPAPLOT.000 [DIRS 183010].

Figure K4.4-2. Stepwise rank regression analyses and selected scatterplots for release rates (*ESNP237*, g/yr) and cumulative (i.e., integrated) releases (*ESNP237C*, g) for movement of dissolved ^{237}Np from the EBS to the UZ under nominal conditions: (a, b) Regressions for *ESNP237* and *ESNP237C* at 400,000, 600,000 and 800,000 years, and (c-h) Scatterplots for *ESNP237* and *ESNP237C* at 800,000 years.

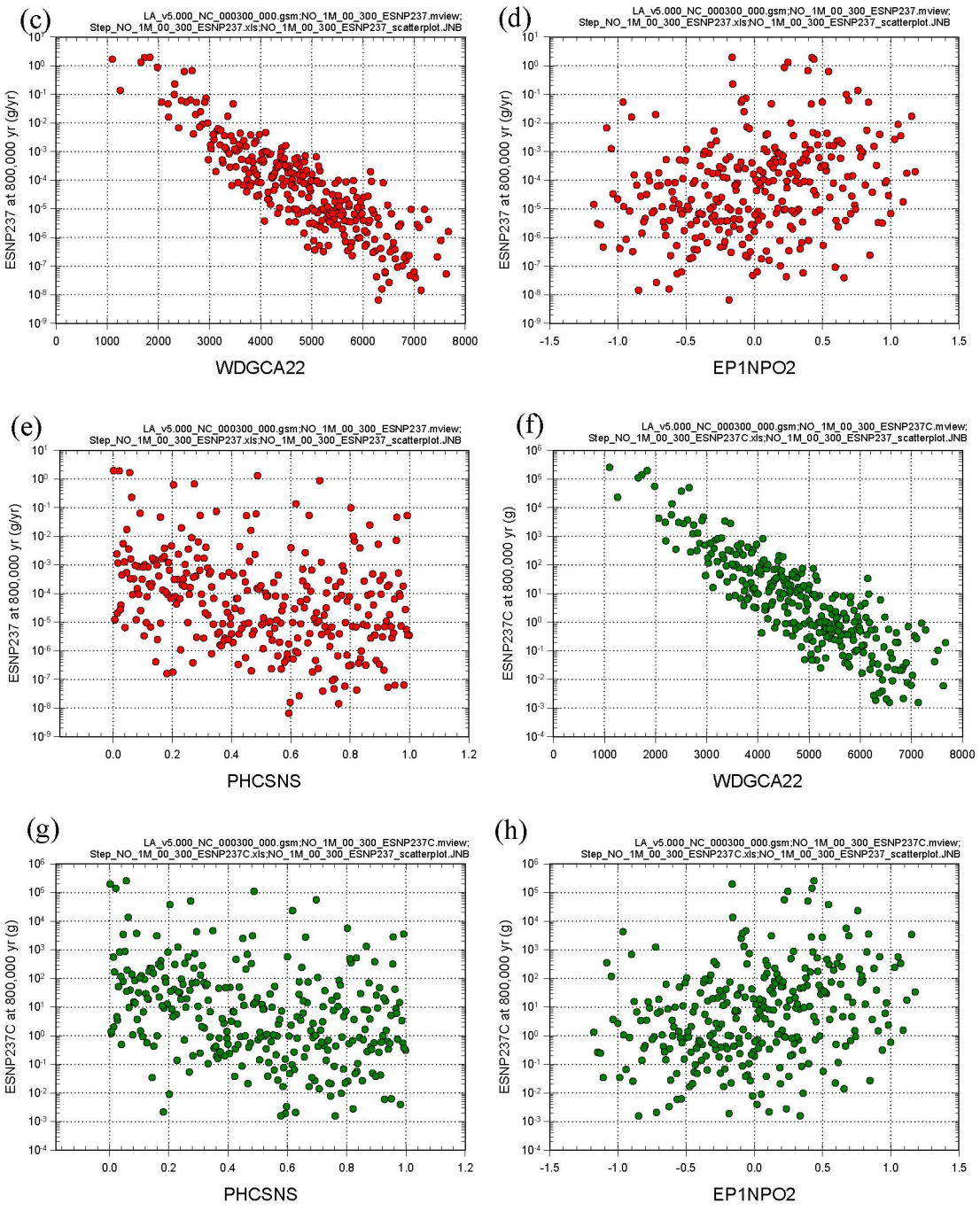

Source: Output DTNs: MO0709TSPAREGS.000 [DIRS 182976]; and MO0709TSPAPLOT.000 [DIRS 183010].

Figure K4.4-2. Stepwise rank regression analyses and selected scatterplots for release rates (*ESNP237*, g/yr) and cumulative (i.e., integrated) releases (*ESNP237C*, g) for movement of dissolved ^{237}Np from the EBS to the UZ under nominal conditions: (a, b) Regressions for *ESNP237* and *ESNP237C* at 400,000, 600,000 and 800,000 years, and (c-h) Scatterplots for *ESNP237* and *ESNP237C* at 800,000 Years (continued).

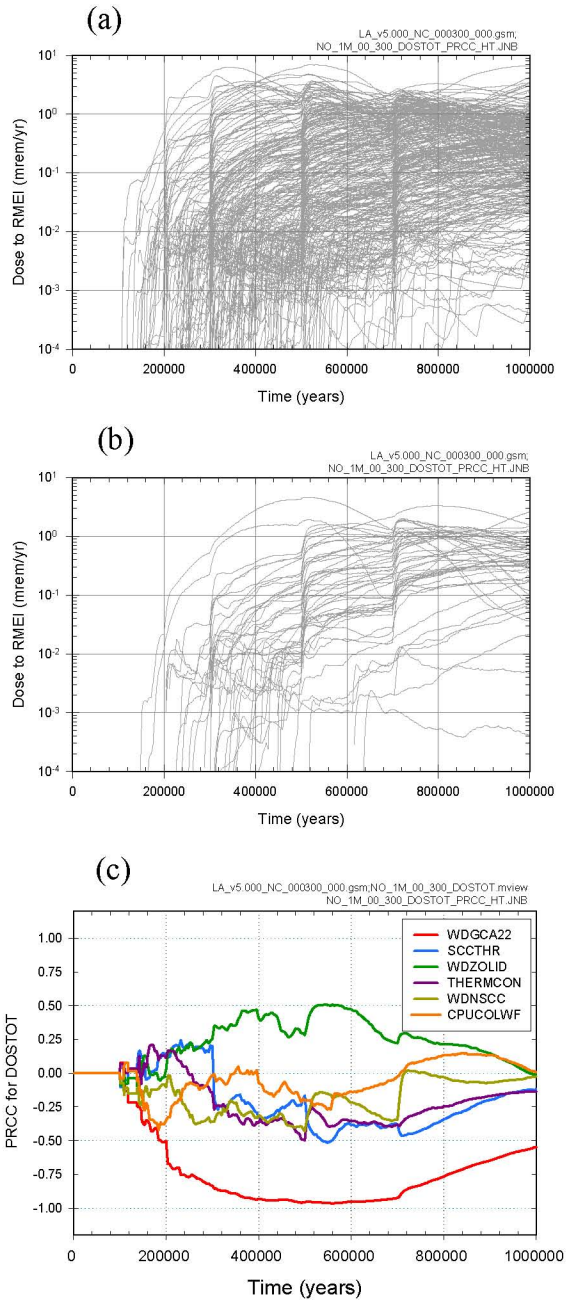

Source: Output DTNs: MO0709TSPAREGS.000 [DIRS 182976]; and MO0709TSPAPLOT.000 [DIRS 183010].

Figure K4.5-1. Dose to RMEI (*DOSTOT*, mrem/yr) for all radioactive species under nominal conditions: (a) *DOSTOT* for all (i.e., 300) sample elements, (b) *DOSTOT* for first 50 sample elements, and (c) PRCCs for *DOSTOT*.

(a)

	DOSTOT: 400K yr			DOSTOT: 600K yr			DOSTOT: 800K yr		
Step[a]	Variable[b]	R^{2c}	SRRC[d]	Variable	R^2	SRRC	Variable	R^2	SRRC
1	WDGCA22	0.77	-0.90	WDGCA22	0.84	-0.94	WDGCA22	0.60	-0.77
2	WDZOLID	0.80	0.16	WDZOLID	0.87	0.14	WDZOLID	0.62	0.16
3	WDNSCC	0.82	-0.12	THERMCON	0.88	-0.10	MICI129	0.63	0.11
4	THERMCON	0.83	-0.12	INFIL	0.89	-0.11	SZWBNDAL	0.65	-0.11
5	INFIL	0.84	-0.10	SCCTHR	0.90	-0.09	SCCTHR	0.65	-0.10
6	SCCTHR	0.85	-0.08	CORRATSS	0.90	-0.07			
7	WDGCUA22	0.85	0.07	WDNSCC	0.91	-0.08			
8	UZRCOL	0.86	-0.07	WDGCUA22	0.91	0.08			
9	CORRATSS	0.86	-0.06	MICTC99	0.92	0.07			
10				DTDRHUNC	0.92	0.05			
11				CSNFMASS	0.92	0.05			

a: Steps in stepwise rank regression analysis
b: Variables listed in order of selection in stepwise regression
c: Cumulative R^2 value with entry of each variable into regression model
d: Standardized rank regression coefficients (SRRCs) in final regression model

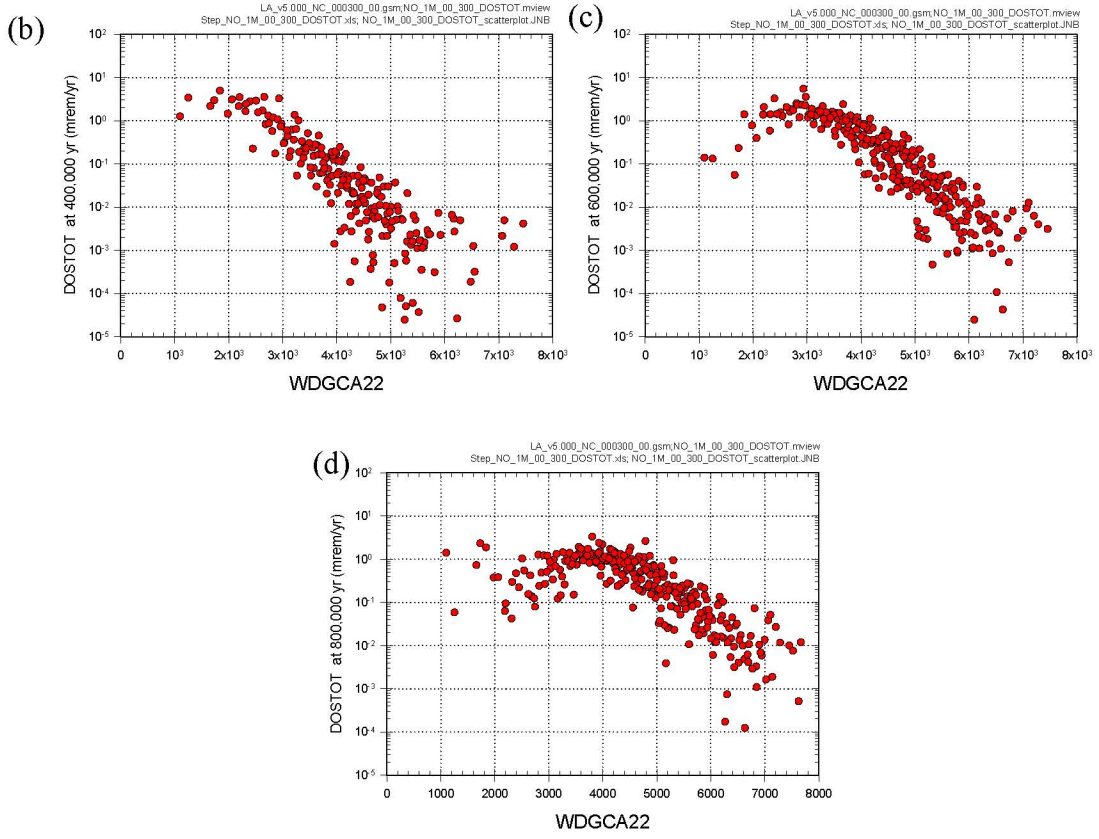

Source: Output DTNs: MO0709TSPAREGS.000 [DIRS 182976]; and MO0709TSPAPLOT.000 [DIRS 183010].

Figure K4.5-2. Stepwise rank regression analyses and selected scatterplots for dose to RMEI (*DOSTOT*, mrem/yr) for all radioactive species under nominal conditions: (a) Regressions for *DOSTOT* at 400,000, 600,000 and 800,000 years, and (b,c,d) Scatterplots for *DOSTOT* at 400,000, 600,000 and 800,000 years.

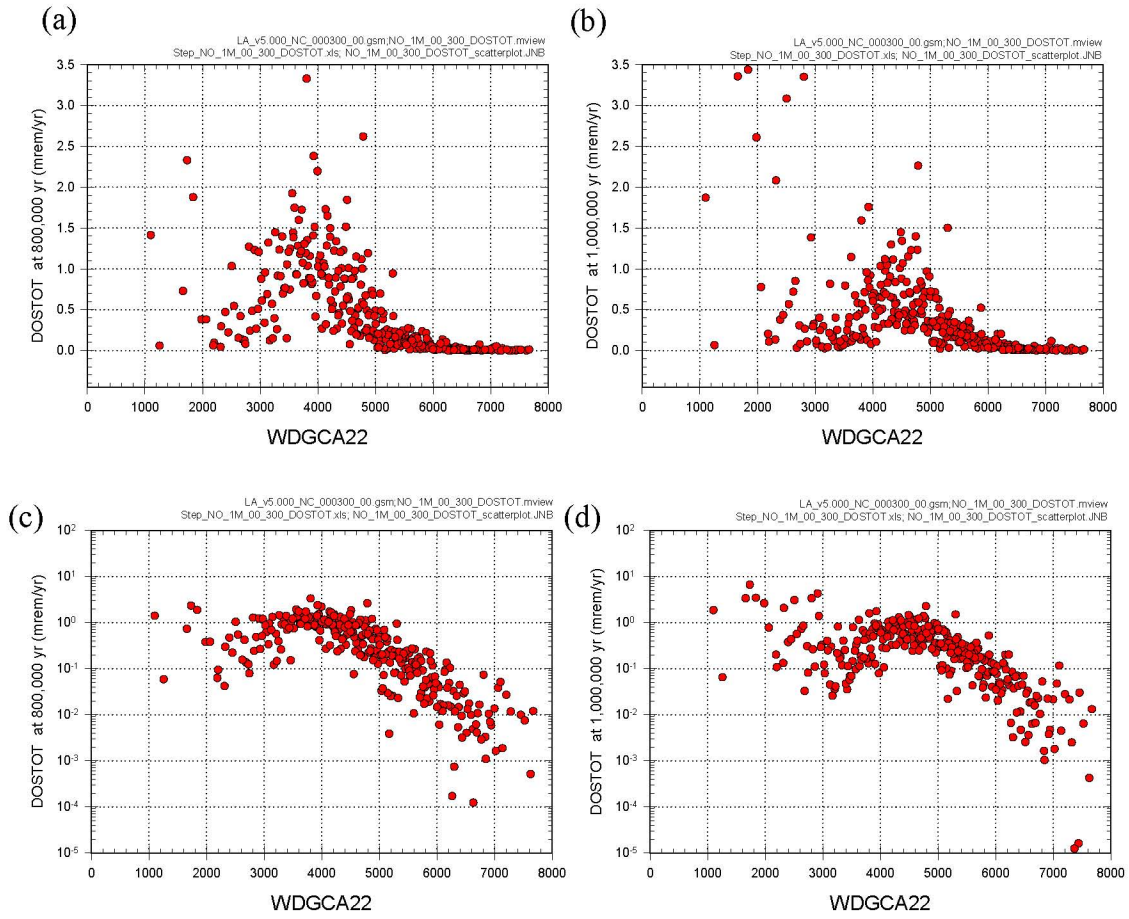

Source: Output DTNs: MO0709TSPAREGS.000 [DIRS 182976]; and MO0709TSPAPLOT.000 [DIRS 183010].

Figure K4.5-3. Selected scatterplots for dose to RMEI (*DOSTOT*, mrem/yr) for all radioactive species under nominal conditions at 800,000 and 1,000,000 years.

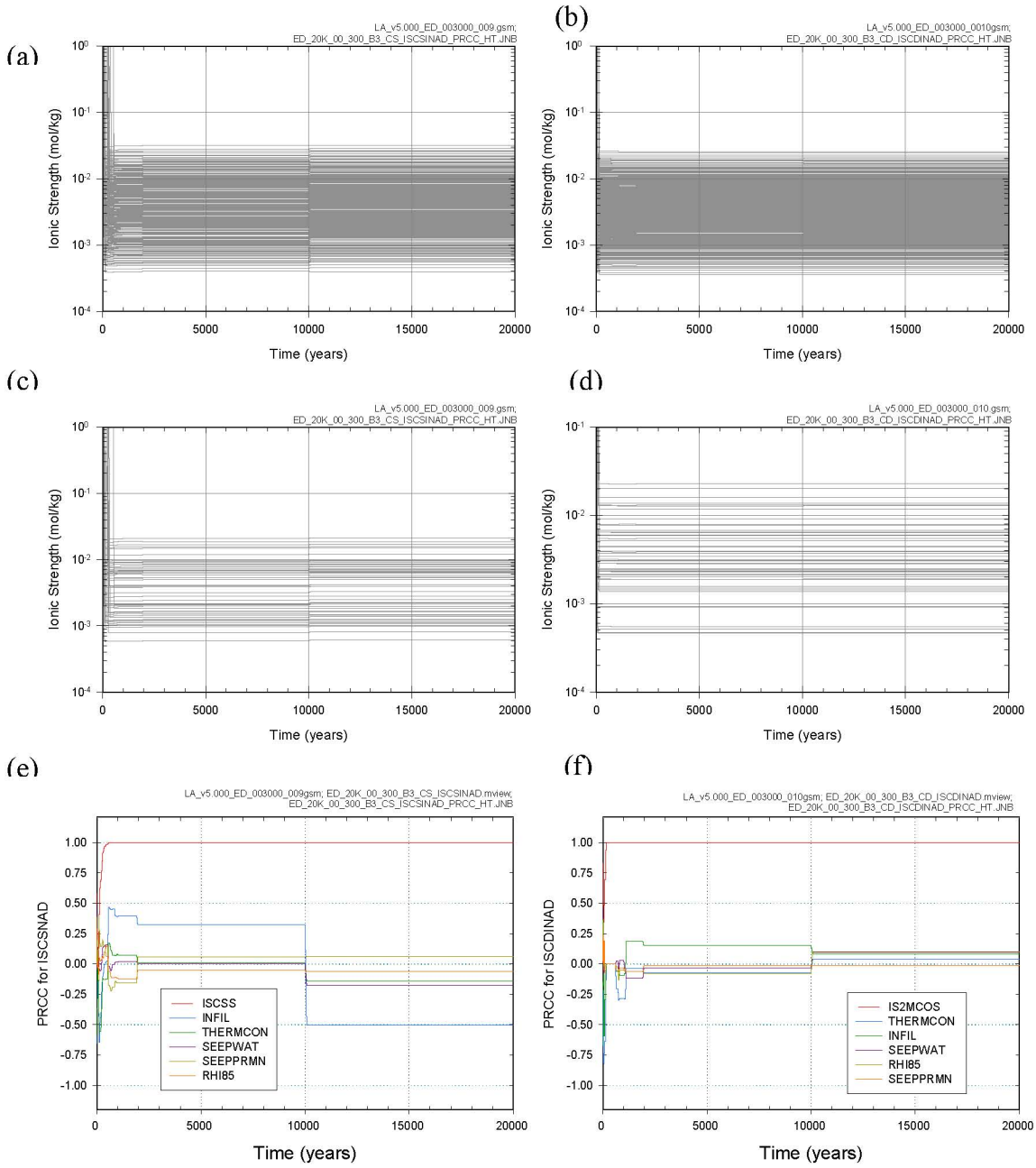

Source: Output DTNs: MO0709TSPASENS.000 [DIRS 183982]; and MO0709TSPAPLOT.000 [DIRS 183010].

Figure K5.2-1 Time-dependent ionic strength (mol/kg) in the invert for CSNF WPs (*ISCSINAD*) and CDSP WPs (*ISCDINAD*) experiencing an early drip shield failure under dripping conditions in percolation bin 3: (a, b) *ISCSINAD* and *ISCDINAD* for all (i.e., 300) sample elements, (c, d) *ISCSINAD* and *ISCDINAD* for first 50 sample elements, and (e, f) PRCCs for *ISCSINAD* and *ISCDINAD*

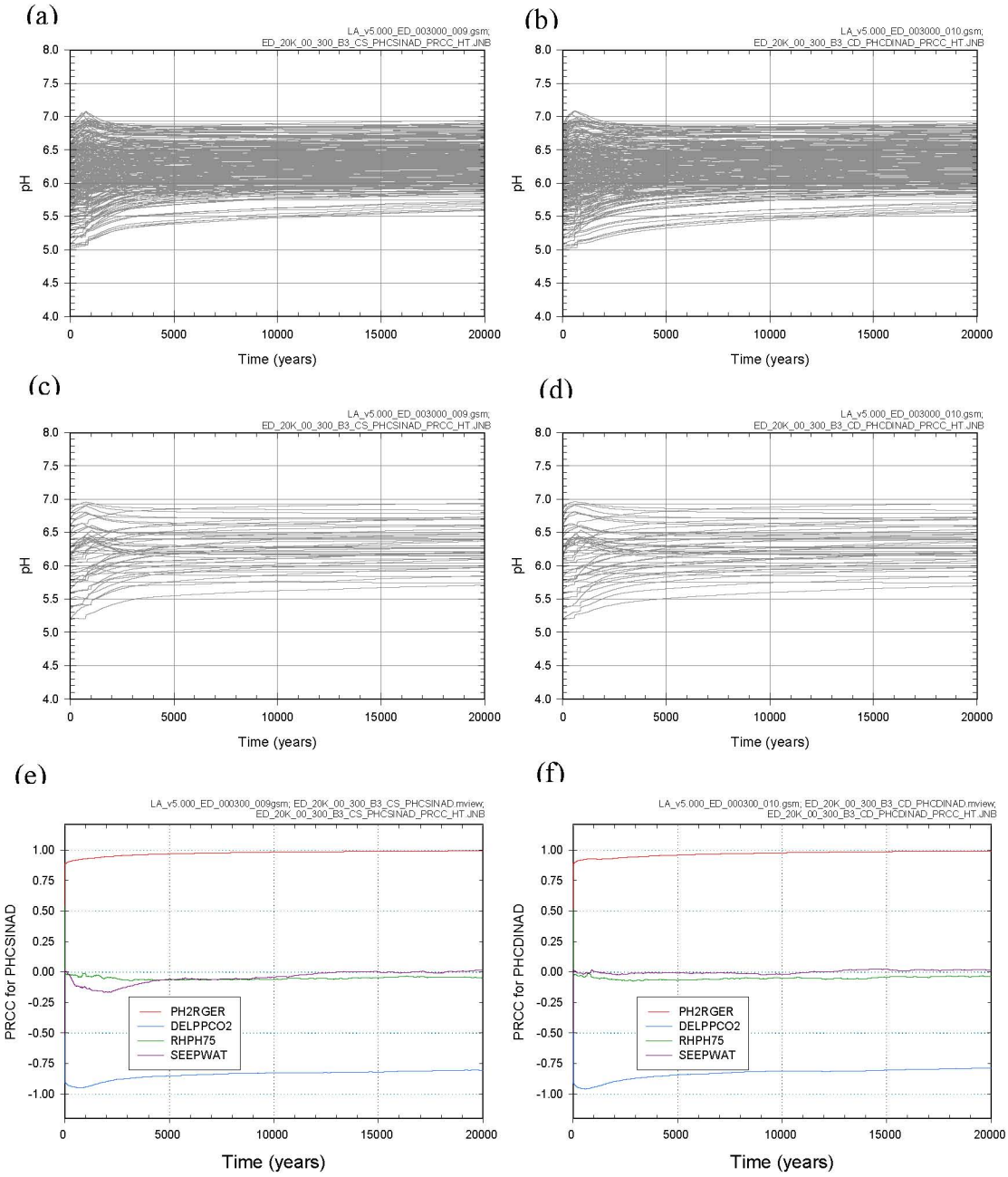

Source: Output DTNs: MO0709TSPAREGS.000 [DIRS 182976]; and MO0709TSPAPLOT.000 [DIRS 183010].

Figure K5.2-2 Time-dependent pH in the invert for CSNF WPs (*PHCSINAD*) and CDSP WPs (*PHCDINAD*) experiencing an early DS failure under dripping conditions in percolation bin 3: (a, b) *PHCSINAD* and *PHCDINAD* for all (i.e., 300) sample elements, (c, d) *PHCSINAD* and *PHCDINAD* for first 50 sample elements, and (e, f) PRCCs for *PHCSINAD* and *PHCDINAD*

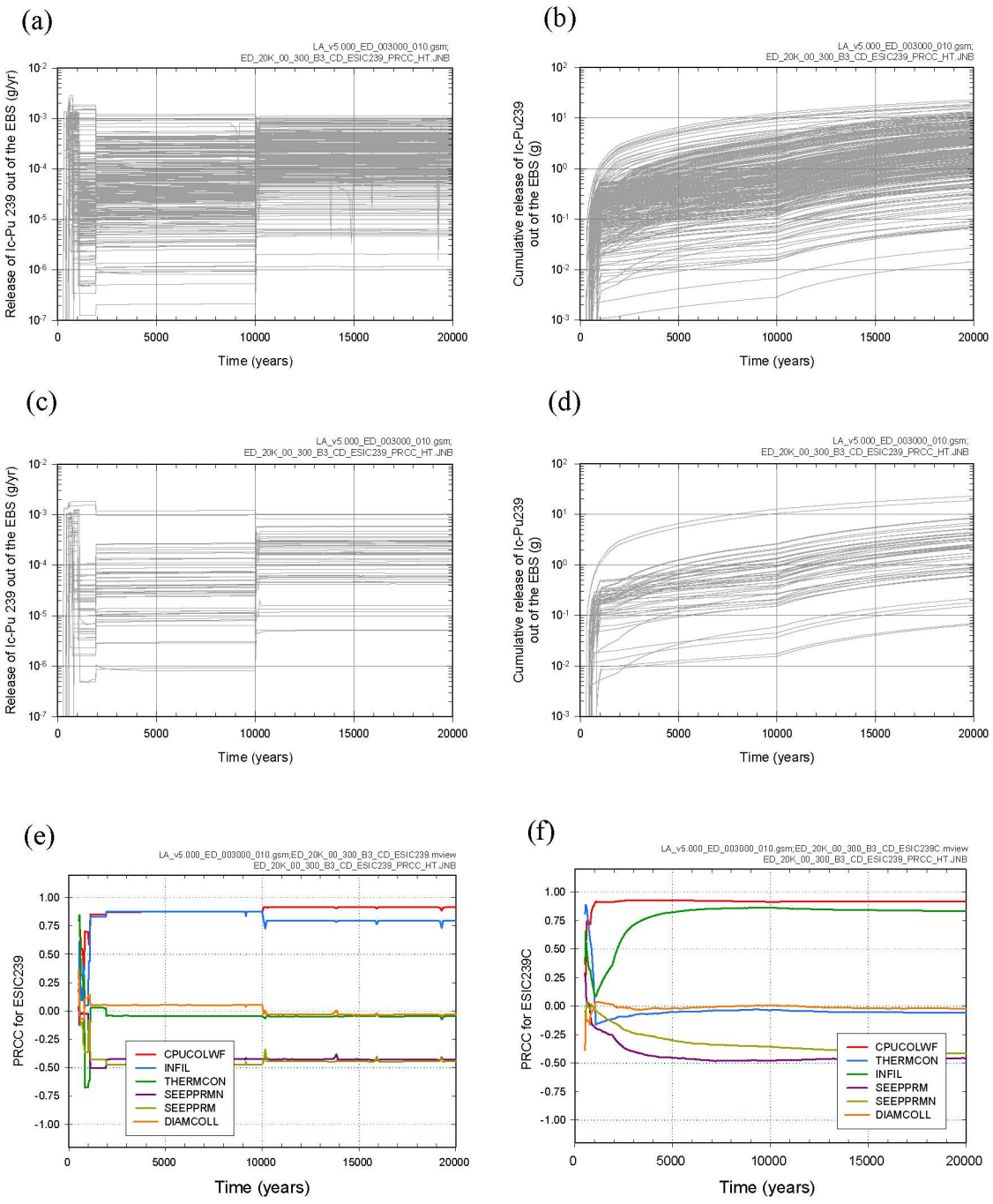

Source: Output DTNs: MO0709TSPAREGS.000 [DIRS 182976]; and MO0709TSPAPLOT.000 [DIRS 183010].

Figure K5.3.1-1. Time-dependent release rates (*ESIC239*, g/yr) and cumulative (i.e., integrated) releases (*ESIC239C*, g) over 20,000 years for the movement of ^{239}Pu irreversibly attached to glass/waste form colloids from the EBS to the UZ resulting from a single early DS failure above a CDSP WP in percolation bin 3 under dripping conditions: (a, b) *ESIC239* and *ESIC239C* for all (i.e., 300) sample elements, (c, d) *ESIC239* and *ESIC239C* for first 50 sample elements, and (e, f) PRCCs for *ESIC239* and *ESIC239C*.

(a)

	ESIC239: 3000 yr			ESIC239: 5000 yr			ESIC239: 10,000 yr		
Step[a]	Variable[b]	R^{2c}	SRRC[d]	Variable	R^2	SRRC	Variable	R^2	SRRC
1	INFIL	0.51	0.68	INFIL	0.51	0.67	INFIL	0.51	0.67
2	CPUCOLWF	0.83	0.58	CPUCOLWF	0.83	0.58	CPUCOLWF	0.83	0.58
3	SEEPPRM	0.86	-0.18	SEEPPRM	0.86	-0.18	SEEPPRM	0.86	-0.18
4	SEEPPRMN	0.88	-0.15	SEEPPRMN	0.88	-0.15	SEEPPRMN	0.88	-0.15
5	ALPHAL	0.90	-0.13	ALPHAL	0.90	-0.13	ALPHAL	0.90	-0.13
6	SEEPUNC	0.90	0.07	SEEPUNC	0.90	0.07	SEEPUNC	0.90	0.07
7	PHCSS	0.90	-0.05	PHCSS	0.90	-0.05	PHCSS	0.90	-0.05

(b)

	ESIC239C: 3000 yr			ESIC239C: 5000 yr			ESIC239C: 10,000 yr		
Step[a]	Variable[b]	R^{2c}	SRRC[c]	Variable	R^2	SRRC	Variable	R^2	SRRC
1	CPUCOLWF	0.68	0.79	CPUCOLWF	0.60	0.74	CPUCOLWF	0.52	0.69
2	INFIL	0.84	0.41	INFIL	0.86	0.52	INFIL	0.86	0.58
3	SEEPPRM	0.85	-0.12	SEEPPRM	0.87	-0.13	SEEPPRM	0.88	-0.15
4	SEEPPRMN	0.86	-0.09	SEEPPRMN	0.88	-0.09	SEEPPRMN	0.89	-0.10
5	ALPHAL	0.87	-0.07	ALPHAL	0.89	-0.08	ALPHAL	0.90	-0.10
6				KDPASMEC	0.89	0.06	SEEPUNC	0.90	0.06
7				CSNFMASS	0.90	0.05	KDPASMEC	0.91	0.05
8				KDAMCOL	0.90	-0.06	CSNFMASS	0.91	0.05
9				GOESA	0.90	-0.06	KDAMCOL	0.91	-0.06
10							RHMUNO20	0.91	-0.05

a: Steps in stepwise rank regression analysis
b: Variables listed in order of selection in stepwise regression
c: Cumulative R^2 value with entry of each variable into regression model
d: Standardized rank regression coefficients (SRRCs) in final regression model

Source: Output DTNs: MO0709TSPAREGS.000 [DIRS 182976]; and MO0709TSPAPLOT.000 [DIRS 183010].

NOTE: In (c, g), the box extends from 0.25 to 0.75 quantile; lower and upper bar and whisker extend to 0.1 and 0.9 quantile, respectively; dots represent values outside 0.1 to 0.9 quantile range; median indicated by light horizontal line.

Figure K5.3.1-2. Stepwise rank regression analyses and selected scatterplots for time-dependent release rates (*ESIC239*, g/yr) and cumulative (i.e., integrated) releases (*ESIC239C*, g) for the movement of ^{239}Pu irreversibly attached to glass/waste form colloids from the EBS to the UZ resulting from a single early DS failure above a CDSP WP in percolation bin 3 under dripping conditions : (a, b) Regressions for *ESIC239* and *ESIC239C* at 3000, 5000 and 10,000 years, and (c-h) Scatterplots for *ESIC239* and *ESIC239C* at 10,000 years.

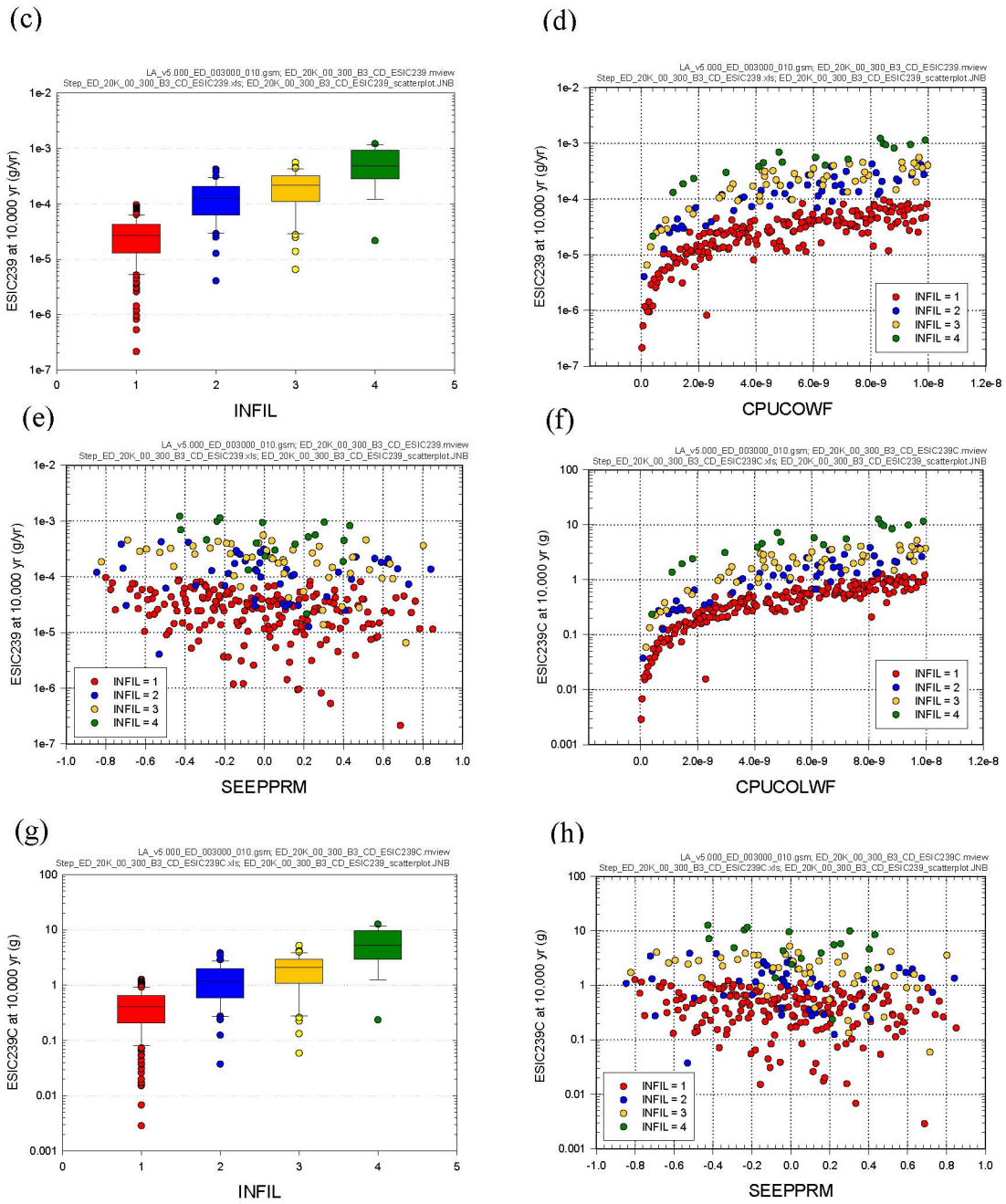

Source: Output DTNs: MO0709TSPAREGS.000 [DIRS 182976]; and MO0709TSPAPLOT.000 [DIRS 183010].

NOTE: In (c, g), the box extends from 0.25 to 0.75 quantile; lower and upper bar and whisker extend to 0.1 and 0.9 quantile, respectively; dots represent values outside 0.1 to 0.9 quantile range; median indicated by light horizontal line.

Figure K5.3.1-2. Stepwise rank regression analyses and selected scatterplots for time-dependent release rates (*ESIC239*, g/yr) and cumulative (i.e., integrated) releases (*ESIC239C*, g) for the movement of ^{239}Pu irreversibly attached to glass/waste form colloids from the EBS to the UZ resulting from a single early DS failure above a CDSP WP in percolation bin 3 under dripping conditions : (a, b) Regressions for *ESIC239* and *ESIC239C* at 3000, 5000 and 10,000 years, and (c-h) Scatterplots for *ESIC239* and *ESIC239C* at 10,000 years (continued).

Figure Removed. See discussion in Section K5.3.1.

Figure K5.3.1-3. Time-dependent release rates (*ESIF239*, g/yr) and cumulative (i.e., integrated) releases (*ESIF239C*, g) over 20,000 years for the movement of ^{239}Pu irreversibly attached to ferrous colloids from the EBS to the UZ resulting from a single early DS failure above a CDSP WP in percolation bin 3 under dripping conditions: (a, b) *ESIF239* and *ESIF239C* for all (i.e., 300) sample elements, (c, d) *ESIF239* and *ESIF239C* for first 50 sample elements, and (e, f) PRCCs for *ESIF239* and *ESIF239C*.

Figure Removed. See discussion in Section K5.3.1.

Figure K5.3.1-4. Stepwise rank regression analyses and selected scatterplots for time-dependent release rates (*ESIF239*, g/yr) and cumulative (i.e., integrated) releases (*ESIF239C*, g) for the movement of ^{239}Pu irreversibly attached to ferrous colloids from the EBS to the UZ resulting from a single early DS failure above a CDSP WP in percolation bin 3 under dripping conditions : (a, b) Regressions for *ESIF239* and *ESIF239C* at 3000, 5000 and 10,000 years, and (c-h) Scatterplots for *ESIF239* and *ESIF239C* at 10,000 years.

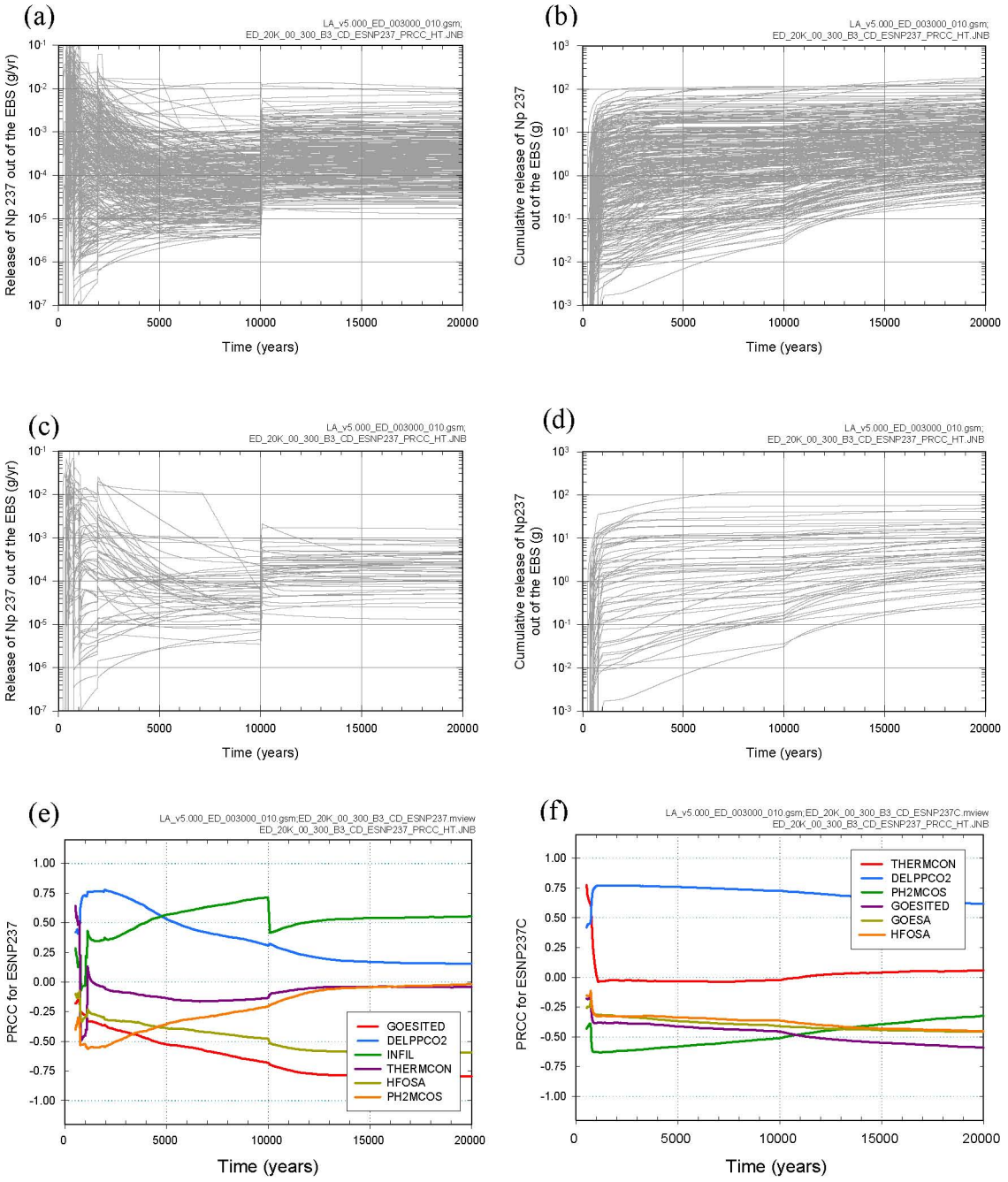

Source: Output DTNs: MO0709TSPAREGS.000 [DIRS 182976]; and MO0709TSPAPLOT.000 [DIRS 183010].

Figure K5.3.1-5. Time-dependent release rates (*ESNP237*, g/yr) and cumulative (i.e., integrated) releases (*ESNP2379C*, g) over 20,000 years for the movement of dissolved ^{237}Np from the EBS to the UZ resulting from a single early DS failure above a CDSP WP in percolation bin 3 under dripping conditions: (a, b) *ESNP237* and *ESNP237C* for all (i.e., 300) sample elements, (c, d) *ESNP237* and *ESNP237C* for first 50 sample elements, and (e, f) PRCCs for *ESNP237* and *ESNP237C*.

(a)

	ESNP237: 3000 yr			ESNP237: 5000 yr			ESNP237: 10,000 yr		
Step[a]	Variable[b]	R^{2c}	SRRC[d]	Variable	R^2	SRRC	Variable	R^2	SRRC
1	DELPPCO2	0.27	0.56	INFIL	0.18	0.45	INFIL	0.29	0.55
2	INFIL	0.37	0.29	DELPPCO2	0.29	0.35	GOESITED	0.43	-0.41
3	PH2MCOS	0.46	-0.32	GOESITED	0.37	-0.30	DSNFMASS	0.48	0.19
4	KDAMSMEC	0.50	0.17	PH2MCOS	0.41	-0.20	HFOSA	0.53	-0.31
5	GOESITED	0.54	-0.21	EP1LOWNU	0.44	0.18	EP1LOWNU	0.57	0.21
6	EP1LOWAM	0.57	0.19	HFOSA	0.47	-0.23	DELPPCO2	0.60	0.16
7	COLGW	0.60	0.16	IS2MCOS	0.51	0.18	IS2MCOS	0.63	0.15
8	HFOSA	0.61	-0.16	KDAMSMEC	0.54	0.15	GOESA	0.65	-0.15
9	IS2MCOS	0.63	0.14	DSNFMASS	0.57	0.13	ALPHAL	0.67	-0.14
10	GOESA	0.65	-0.14	SEEPPRMN	0.59	-0.15	GOERELAB	0.69	0.15
11	DSNFMASS	0.66	0.12	GOESA	0.60	-0.16	SEEPPRMN	0.70	-0.12
12	EP1LOWNU	0.67	0.10	EP1LOWAM	0.62	0.12	KDAMSMEC	0.72	0.11
13	SCHOBOLT	0.69	0.10	GOERELAB	0.63	0.12	HFOSITED	0.72	-0.09
14	WDCRCDEN	0.69	0.09	SCHOBOLT	0.65	0.11	PH2DHLS	0.73	-0.08
15	GOERELAB	0.70	0.09	WDNSCC	0.66	0.09			

(b)

	ESNP237C: 3000 yr			ESNP237C: 5000 yr			ESNP237C: 10,000 yr		
Step[a]	Variable[b]	R^{2c}	SRRC[c]	Variable	R^2	SRRC	Variable	R^2	SRRC
1	DELPPCO2	0.33	0.60	DELPPCO2	0.31	0.58	DELPPCO2	0.27	0.54
2	PH2MCOS	0.50	-0.41	PH2MCOS	0.47	-0.39	PH2MCOS	0.39	-0.35
3	EP1LOWAM	0.56	0.21	EP1LOWAM	0.52	0.20	INFIL	0.46	0.25
4	COLGW	0.61	0.23	COLGW	0.58	0.21	GOESITED	0.51	-0.24
5	KDAMSMEC	0.64	0.16	GOESITED	0.61	-0.20	KDAMSMEC	0.54	0.17
6	GOESITED	0.66	-0.18	KDAMSMEC	0.64	0.16	COLGW	0.58	0.20
7	GOESA	0.68	-0.13	INFIL	0.66	0.17	EP1LOWAM	0.61	0.19
8	INFIL	0.69	0.12	GOESA	0.67	-0.15	GOESA	0.63	-0.18
9	HFOSA	0.70	-0.11	DSNFMASS	0.69	0.13	DSNFMASS	0.65	0.15
10	EP1NPO2	0.71	0.11	WDCRCDEN	0.70	0.12	HFOSA	0.67	-0.16
11	WDCRCDEN	0.72	0.12	HFOSA	0.71	-0.12	WDCRCDEN	0.68	0.12
12	DSNFMASS	0.73	0.11	EP1NPO2	0.72	0.10	IS2MCOS	0.69	0.10
13				IS2MCOS	0.72	0.09	RHPH75	0.70	-0.09
14				GP2NO3	0.73	-0.09	GP2NO3	0.71	-0.09
15				RHPH75	0.74	-0.08	HFOSITED	0.71	-0.10
16							EP1NPO2	0.72	0.11

a: Steps in stepwise rank regression analysis
b: Variables listed in order of selection in stepwise regression
c: Cumulative R^2 value with entry of each variable into regression model
d: Standardized rank regression coefficients (SRRCs) in final regression model

Source: Output DTNs: MO0709TSPASENS.000 [DIRS 183982]; and MO0709TSPAPLOT.000 [DIRS 183010].

Figure K5.3.1-6. Stepwise rank regression analyses and selected scatterplots for time-dependent release rates (*ESNP237*, g/yr) and cumulative (i.e., integrated) releases (*ESNP237C*, g) for the movement of dissolved 237Np from the EBS to the UZ resulting from a single early DS failure above a CDSP WP in percolation bin 3 under dripping conditions: (a, b) Regressions for *ESNP237* and *ESNP237C* at 3000, 5000 and 10,000 years, and (c-h) Scatterplots for *ESNP237* and *ESNP237C* at 10,000 years.

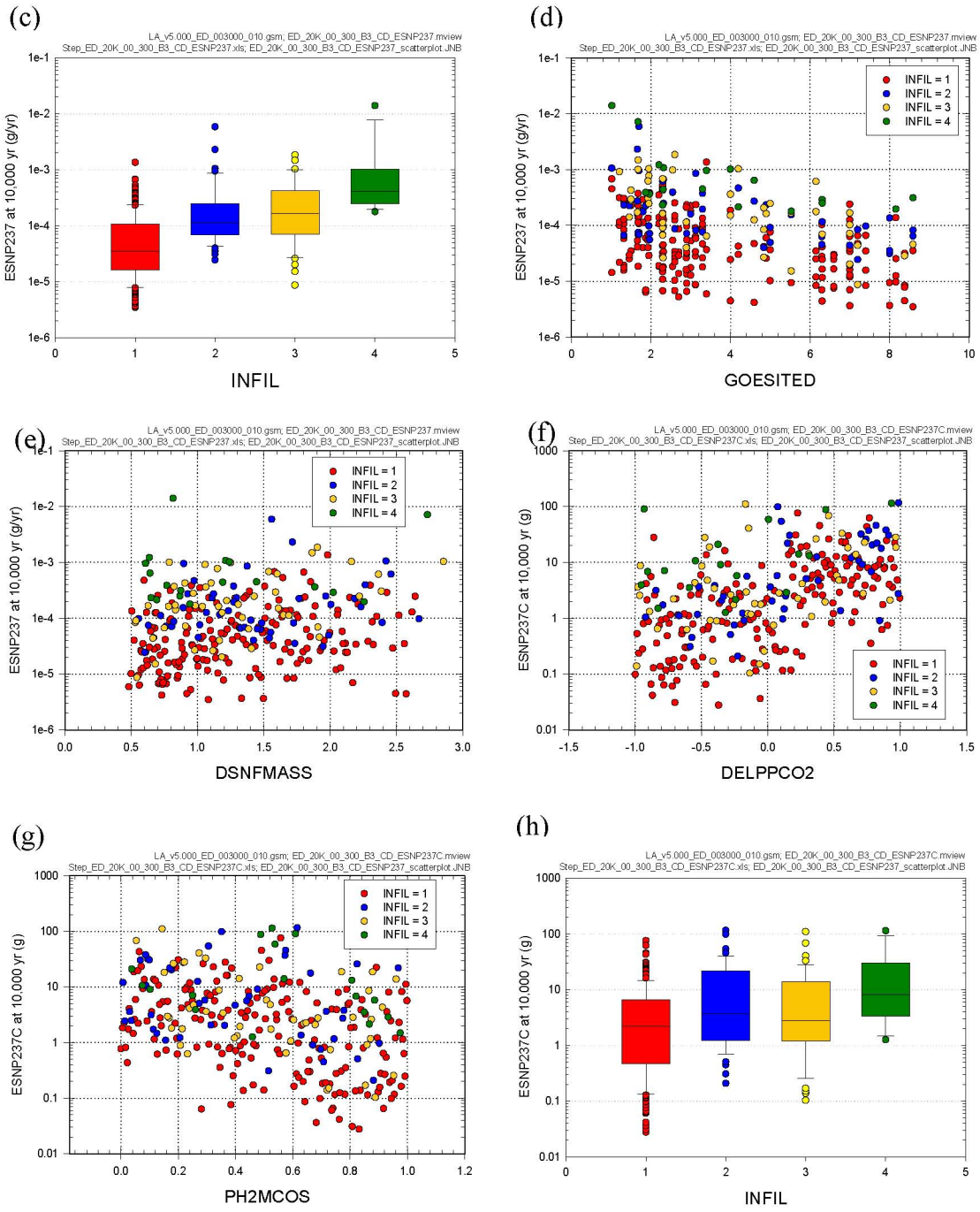

Source: Output DTNs: MO0709TSPASENS.000 [DIRS 183982]; and MO0709TSPAPLOT.000 [DIRS 183010].

NOTE: In (c, h), the box extends from 0.25 to 0.75 quantile; lower and upper bar and whisker extend to 0.1 and 0.9 quantile, respectively; dots represent values outside 0.1 to 0.9 quantile range; median indicated by light horizontal line.

Figure K5.3.1-6. Stepwise rank regression analyses and selected scatterplots for time-dependent release rates (*ESNP237*, g/yr) and cumulative (i.e., integrated) releases (*ESNP237C*, g) for the movement of dissolved 237Np from the EBS to the UZ resulting from a single early DS failure above a CDSP WP in percolation bin 3 under dripping conditions: (a, b) Regressions for *ESNP237* and *ESNP237C* at 3000, 5000 and 10,000 years, and (c-h) Scatterplots for *ESNP237* and *ESNP237C* at 10,000 years (continued).

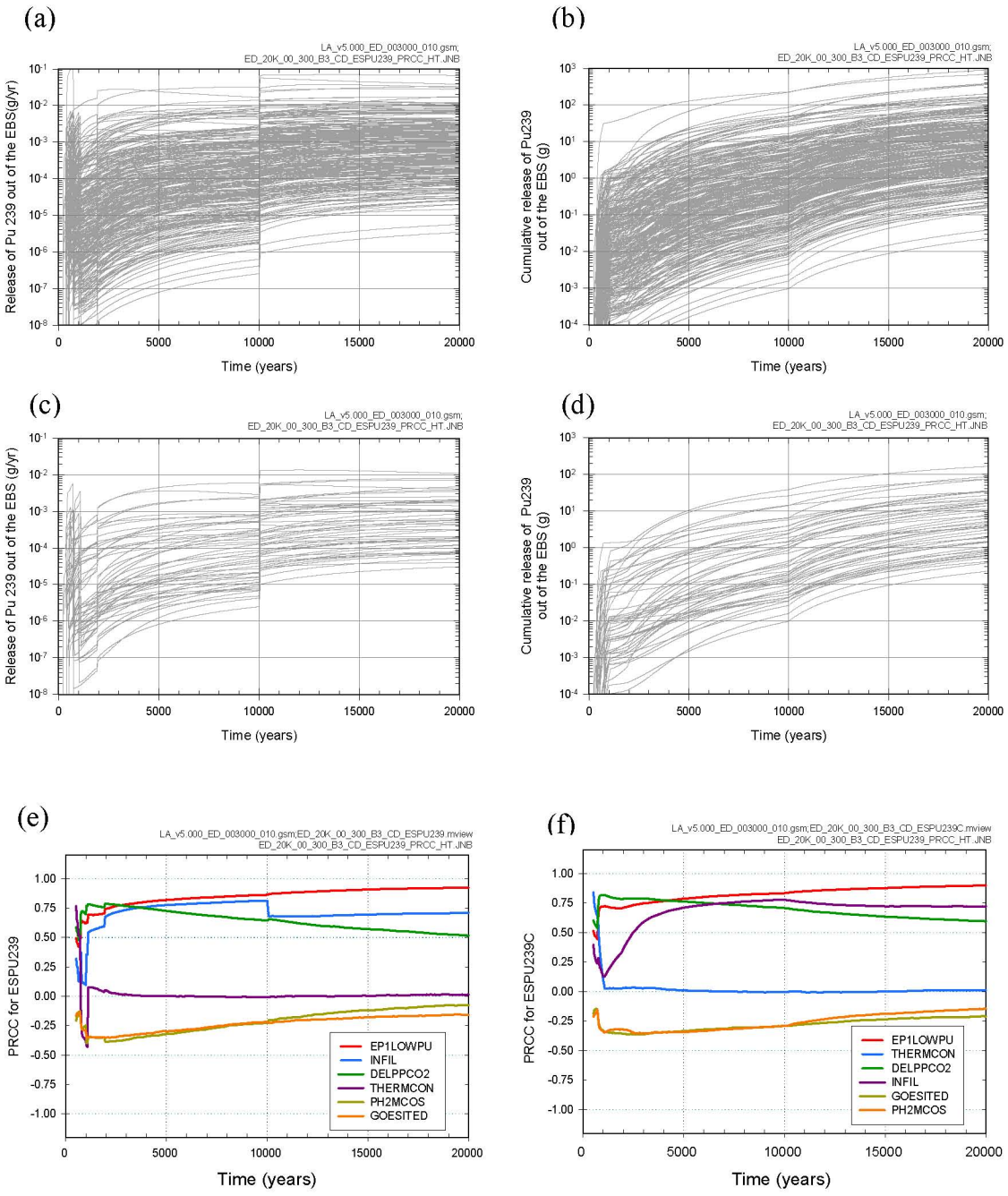

Source: Output DTNs: MO0709TSPAREGS.000 [DIRS 182976]; and MO0709TSPAPLOT.000 [DIRS 183010].

Figure K5.3.1-7. Time-dependent release rates (*ESPU239*, g/yr) and cumulative (i.e., integrated) releases (*ESPU239C*, g) over 20,000 years for the movement of dissolved ^{239}Pu from the EBS to the UZ resulting from a single early DS failure above a CDSP WP in percolation bin 3 under dripping conditions: (a, b) *ESPU239* and *ESPU239C* for all (i.e., 300) sample elements, (c, d) *ESPU239* and *ESPU239C* for first 50 sample elements, and (e, f) PRCCs for *ESPU239* and *ESPU239C*.

(a)

	ESPU239: 3000 yr			ESPU239: 5000 yr			ESPU239: 10,000 yr		
Step[a]	Variable[b]	R^{2c}	SRRC[d]	Variable	R^2	SRRC	Variable	R^2	SRRC
1	EP1LOWPU	0.25	0.51	EP1LOWPU	0.30	0.56	EP1LOWPU	0.38	0.63
2	DELPPCO2	0.48	0.51	INFIL	0.55	0.54	INFIL	0.68	0.56
3	INFIL	0.71	0.50	DELPPCO2	0.73	0.43	DELPPCO2	0.78	0.31
4	PH2MCOS	0.74	-0.16	GOESITED	0.75	-0.14	SEEPPRM	0.79	-0.12
5	GOESITED	0.76	-0.16	PH2MCOS	0.77	-0.13	SEEPPRMN	0.80	-0.08
6	GOESA	0.77	-0.10	SEEPPRM	0.78	-0.10	GOESITED	0.81	-0.10
7	SEEPPRM	0.77	-0.09	GOESA	0.79	-0.09	ALPHAL	0.82	-0.08
8	GP2NO3	0.78	-0.09	EBSDIFCF	0.79	0.12	EBSDIFCF	0.82	0.08
9	RHPH75	0.79	-0.09	GP2NO3	0.80	-0.09	PH2MCOS	0.83	-0.08
10	EBSDIFCF	0.79	0.11	RHPH75	0.81	-0.09	GP2NO3	0.84	-0.09
11	CPUCOLCS	0.80	-0.08	CPUCOLCS	0.81	-0.07	RHPH75	0.84	-0.08
12	HFOSA	0.81	-0.10	ALPHAL	0.82	-0.08	GOESA	0.85	-0.07
13	IS2MCOS	0.81	0.08	HFOSA	0.82	-0.08	DIFPATHL	0.85	-0.06
14	ALPHAL	0.82	-0.08	IS2MCOS	0.83	0.07			
15	EP1LOWNU	0.82	0.07	EP1LOWNU	0.83	0.07			

(b)

	ESPU239C: 3000 yr			ESPU239C: 5000 yr			ESPU239C: 10,000 yr		
Step[a]	Variable[b]	R^{2c}	SRRC[d]	Variable	R^2	SRRC	Variable	R^2	SRRC
1	DELPPCO2	0.28	0.59	EP1LOWPU	0.26	0.53	EP1LOWPU	0.33	0.58
2	EP1LOWPU	0.55	0.50	DELPPCO2	0.50	0.52	INFIL	0.58	0.53
3	INFIL	0.67	0.35	INFIL	0.71	0.47	DELPPCO2	0.74	0.40
4	PH2MCOS	0.71	-0.17	PH2MCOS	0.73	-0.15	GOESITED	0.76	-0.13
5	GOESITED	0.73	-0.18	GOESITED	0.75	-0.16	PH2MCOS	0.78	-0.12
6	GOESA	0.74	-0.11	GOESA	0.76	-0.10	SEEPPRM	0.79	-0.10
7	GP2NO3	0.75	-0.11	GP2NO3	0.77	-0.10	GOESA	0.79	-0.08
8	RHPH75	0.76	-0.09	RHPH75	0.78	-0.10	RHPH75	0.80	-0.10
9	HFOSA	0.77	-0.09	EBSDIFCF	0.79	0.11	GP2NO3	0.81	-0.09
10				HFOSA	0.79	-0.10	EBSDIFCF	0.81	0.11
11				IS2MCOS	0.80	0.08	ALPHAL	0.82	-0.08
12				CPUCOLCS	0.80	-0.07	HFOSA	0.82	-0.09
13				SEEPPRM	0.81	-0.08	EP1LOWNU	0.83	0.08
14				EP1LOWNU	0.81	0.08	IS2MCOS	0.84	0.08
15				ALPHAL	0.82	-0.07			

a: Steps in stepwise rank regression analysis
b: Variables listed in order of selection in stepwise regression
c: Cumulative R^2 value with entry of each variable into regression model
d: Standardized rank regression coefficients (SRRCs) in final regression model

Source: Output DTNs: MO0709TSPASENS.000 [DIRS 183982]; and MO0709TSPAPLOT.000 [DIRS 183010].

Figure K5.3.1-8. Stepwise rank regression analyses and selected scatterplots for time-dependent release rates (*ESPU239*, g/yr) and cumulative (i.e., integrated) releases (*ESPU239*, g) for the movement of dissolved ^{239}Pu from the EBS to the UZ resulting from a single early DS failure above a CDSP WP in percolation bin 3 under dripping conditions: (a, b) Regressions for *ESPU239* and *ESPU239C* at 3000, 5000 and 10,000 years, and (c-h) Scatterplots for *ESPU239* and *ESPU239C* at 10,000 years.

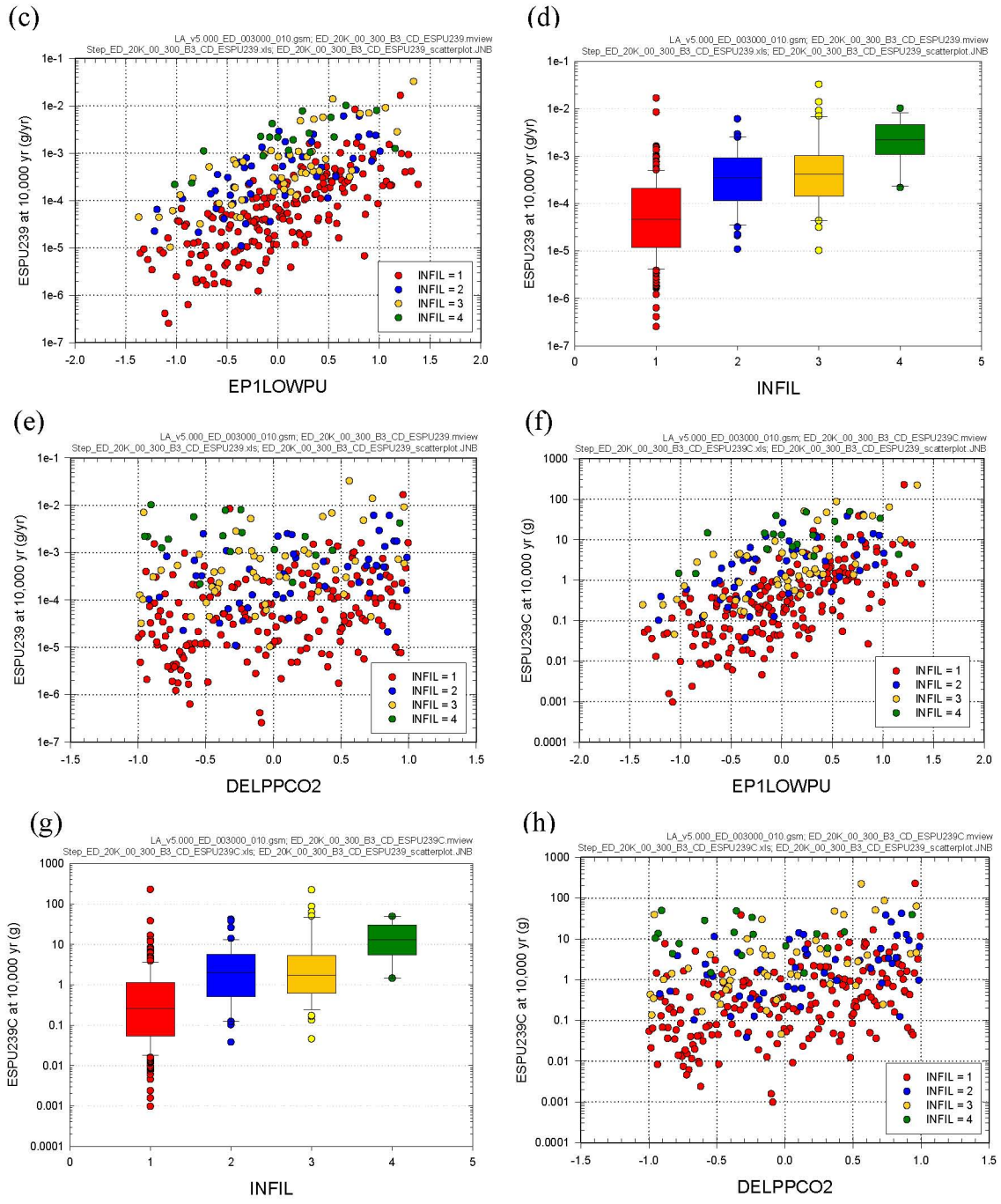

Source: Output DTNs: MO0709TSPASENS.000 [DIRS 183982]; and MO0709TSPAPLOT.000 [DIRS 183010].

NOTE: In (d, g), the box extends from 0.25 to 0.75 quantile; lower and upper bar and whisker extend to 0.1 and 0.9 quantile, respectively; dots represent values outside 0.1 to 0.9 quantile range; median indicated by light horizontal line.

Figure K5.3.1-8. Stepwise rank regression analyses and selected scatterplots for time-dependent release rates (*ESPU239*, g/yr) and cumulative (i.e., integrated) releases (*ESPU239*, g) for the movement of dissolved ^{239}Pu from the EBS to the UZ resulting from a single early DS failure above a CDSP WP in percolation bin 3 under dripping conditions: (a, b) Regressions for *ESPU239* and *ESPU239C* at 3000, 5000 and 10,000 years, and (c-h) Scatterplots for *ESPU239* and *ESPU239C* at 10,000 years (continued).

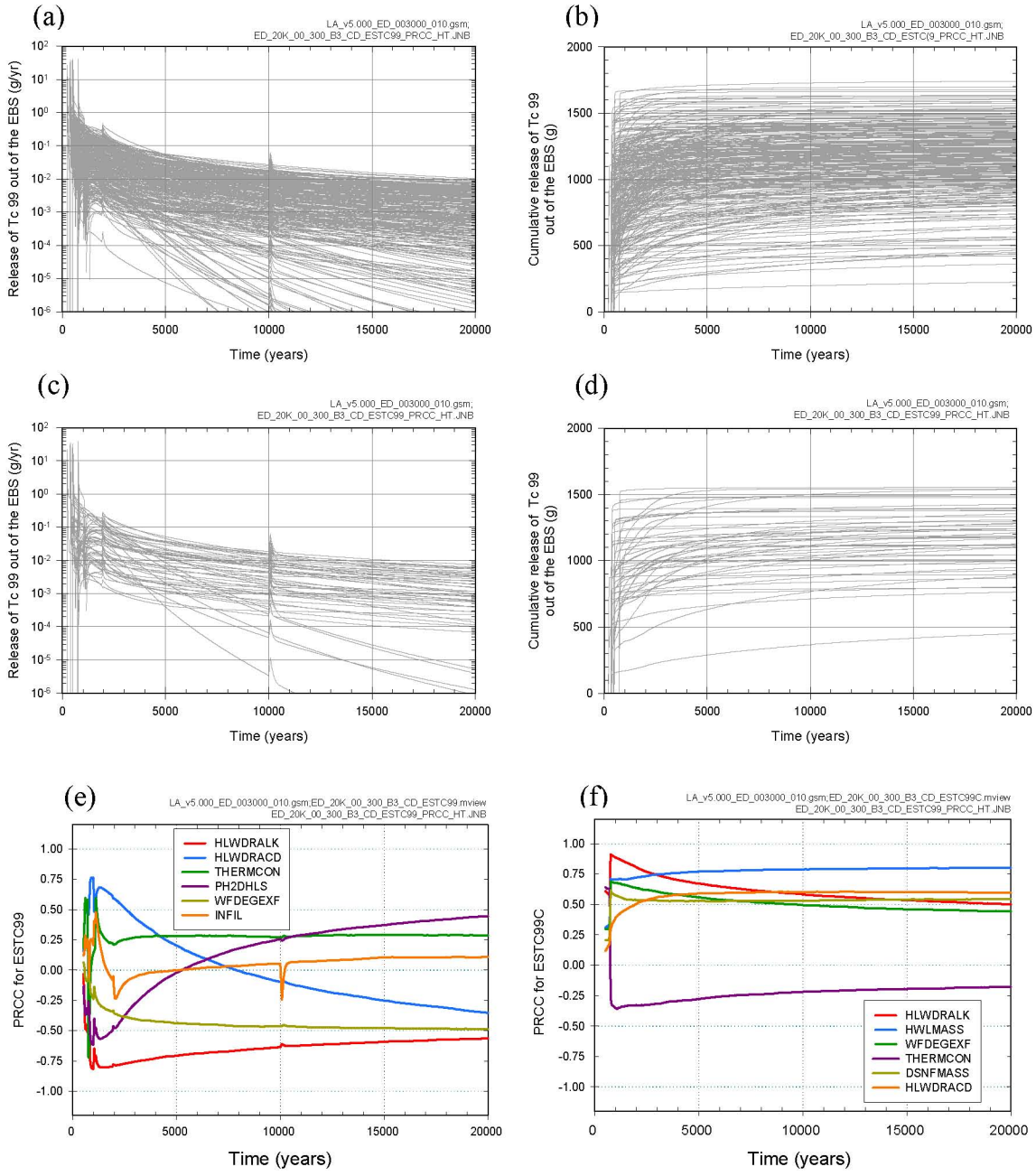

Source: Output DTNs: MO0709TSPASENS.000 [DIRS 183982]; and MO0709TSPAPLOT.000 [DIRS 183010].

Figure K5.3.1-9. Time-dependent release rates (*ESTC99*, g/yr) and cumulative (i.e., integrated) releases (*ESTC99C*, g) over 20,000 years for the movement of dissolved ^{99}Tc from the EBS to the UZ resulting from a single early DS failure above a CDSP WP in percolation bin 3 under dripping conditions: (a, b) *ESTC99* and *ESTC99C* for all (i.e., 300) sample elements, (c, d) *ESTC99* and *ESTC99C* for first 50 sample elements, and (e, f) PRCCs for *ESTC99* and *ESTC99C*.

(a)

	ESTC99: 3000 yr			ESTC99: 5000 yr			ESTC99: 10,000 yr		
Step[a]	Variable[b]	Rc^2	SRRC[c]	Variable	R^2	SRRC	Variable	R^2	SRRC
1	HLWDRALK	0.47	-0.70	HLWDRALK	0.44	-0.67	HLWDRALK	0.34	-0.59
2	WFDEGEXF	0.54	-0.28	WFDEGEXF	0.54	-0.32	WFDEGEXF	0.47	-0.35
3	HLWDRACD	0.59	0.24	THERMCON	0.56	0.15	THERMCON	0.50	0.16
4	PH2DHLS	0.61	-0.16	SEEPPRMN	0.58	0.12	PH2DHLS	0.53	0.15
5	THERMCON	0.63	0.14	RHMU20	0.59	-0.10	HLWDRACD	0.54	-0.10
6	SEEPPRMN	0.65	0.12				SEEPPRMN	0.55	0.10
7	GP4NO3	0.66	-0.10				GP4NO3	0.56	-0.10

(b)

	ESTC99C: 3000 yr			ESTC99C: 5000 yr			ESTC99C: 10,000 yr		
Step[a]	Variable[b]	R^{2c}	SRRC[d]	Variable	R^2	SRRC	Variable	R^2	SRRC
1	HLWDRALK	0.26	0.49	HLWMASS	0.29	0.54	HLWMASS	0.34	0.59
2	HLWMASS	0.49	0.49	HLWDRALK	0.46	0.41	HLWDRACD	0.46	0.34
3	WFDEGEXF	0.60	0.32	WFDEGEXF	0.56	0.29	DSNFMASS	0.57	0.33
4	HLWDRACD	0.68	0.28	HLWDRACD	0.66	0.32	HLWDRALK	0.66	0.33
5	DSNFMASS	0.76	0.30	DSNFMASS	0.74	0.30	WFDEGEXF	0.73	0.26
6	PH2DHLS	0.80	-0.21	PH2DHLS	0.79	-0.23	PH2DHLS	0.79	-0.25
7	THERMCON	0.82	-0.13	THERMCON	0.80	-0.12	THERMCON	0.80	-0.09
8	DELPPCO2	0.82	0.07	CSRINDPO	0.81	0.08	CSRINDPO	0.80	0.08
9	IPCNDMVF	0.83	0.07	IPCNDMVF	0.81	0.07	IPCNDMVF	0.81	0.08
10	CSRINDPO	0.83	0.07	DELPPCO2	0.82	0.07	CORRATSS	0.81	-0.08

a: Steps in stepwise rank regression analysis
b: Variables listed in order of selection in stepwise regression
c: Cumulative R^2 value with entry of each variable into regression model
d: Standardized rank regression coefficients (SRRCs) in final regression model

Source: Output DTNs: MO0709TSPASENS.000 [DIRS 183982]; and MO0709TSPAPLOT.000 [DIRS 183010].

Figure K5.3.1-10. Stepwise rank regression analyses and selected scatterplots for time-dependent release rates (*ESTC99*, g/yr) and cumulative (i.e., integrated) releases (*ESTC99*, g) for the movement of dissolved ^{99}Tc from the EBS to the UZ resulting from a single early DS failure above a CDSP WP in percolation bin 3 under dripping conditions: (a, b) Regressions for *ESTC99* and *ESTC99C* at 3000, 5000 and 10,000 years, and (c-h) Scatterplots for *ESTC99* and *ESTC99C* at 10,000 years.

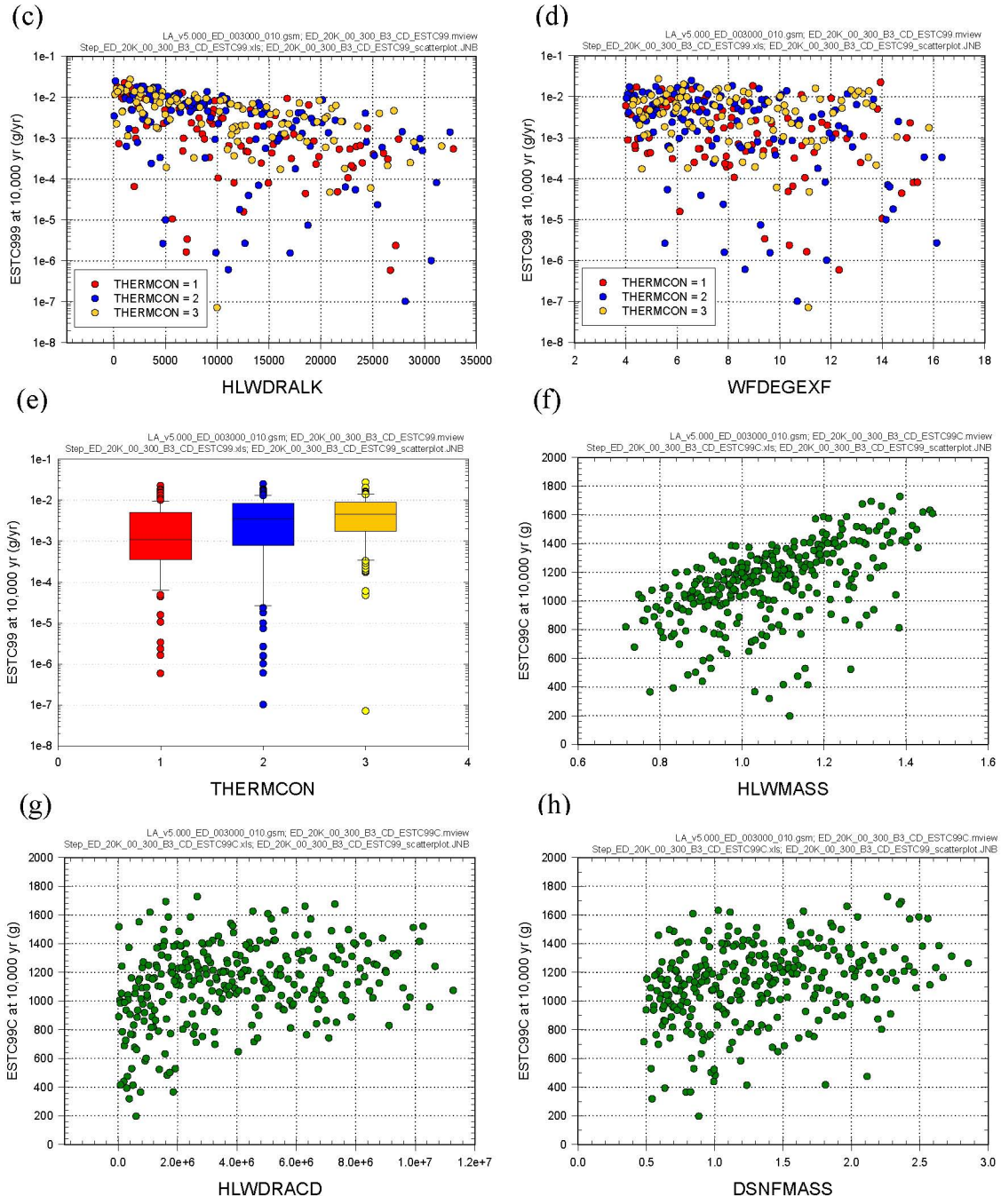

Source: Output DTNs: MO0709TSPASENS.000 [DIRS 183982]; and MO0709TSPAPLOT.000 [DIRS 183010].

NOTE: In (e), the box extends from 0.25 to 0.75 quantile; lower and upper bar and whisker extend to 0.1 and 0.9 quantile, respectively; dots represent values outside 0.1 to 0.9 quantile range; median indicated by light horizontal line.

Figure K5.3.1-10. Stepwise rank regression analyses and selected scatterplots for time-dependent release rates (*ESTC99*, g/yr) and cumulative (i.e., integrated) releases (*ESTC99*, g) for the movement of dissolved ^{99}Tc from the EBS to the UZ resulting from a single early DS failure above a CDSP WP in percolation bin 3 under dripping conditions: (a, b) Regressions for *ESTC99* and *ESTC99C* at 3000, 5000 and 10,000 years, and (c-h) Scatterplots for *ESTC99* and *ESTC99C* at 10,000 years. (Continued)

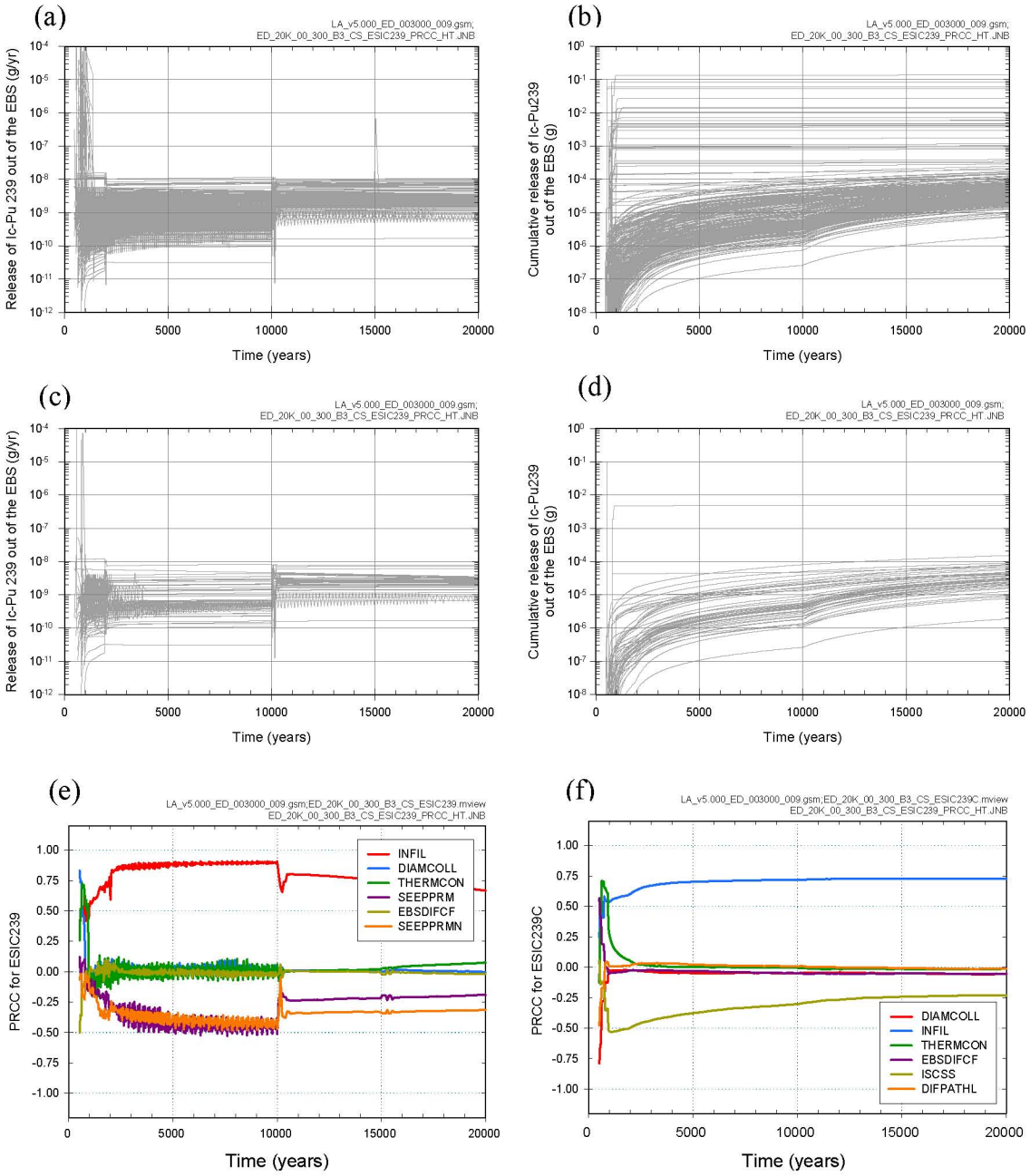

Source: Output DTNs: MO0709TSPASENS.000 [DIRS 183982]; and MO0709TSPAPLOT.000 [DIRS 183010].

Figure K5.3.2-1. Time-dependent release rates (*ESIC239*, g/yr) and cumulative (i.e., integrated) releases (*ESIC239C*, g) over 20,000 years for the movement of ^{239}Pu irreversibly attached to glass/waste form colloids from the EBS to the UZ resulting from a single early DS failure above a CSNF WP in percolation bin 3 under dripping conditions: (a, b) *ESIC239* and *ESIC239C* for all (i.e., 300) sample elements, (c, d) *ESIC239* and *ESIC239C* for first 50 sample elements, and (e, f) PRCCs for *ESIC239* and *ESIC239C*.

Figure Removed. See discussion in Section K5.3.2.

Figure K5.3.2-2. Time-dependent release rates (*ESIF239*, g/yr) and cumulative (i.e., integrated) releases (*ESIF239C*, g) over 20,000 years for the movement of ^{239}Pu irreversibly attached to ferrous colloids from the EBS to the UZ resulting from a single early DS failure above a CSNF WP in percolation bin 3 under dripping conditions: (a, b) *ESIF239* and *ESIF239C* for all (i.e., 300) sample elements, (c, d) *ESIF239* and *ESIF239C* for first 50 sample elements, and (e, f) PRCCs for *ESIF239* and *ESIF239C*.

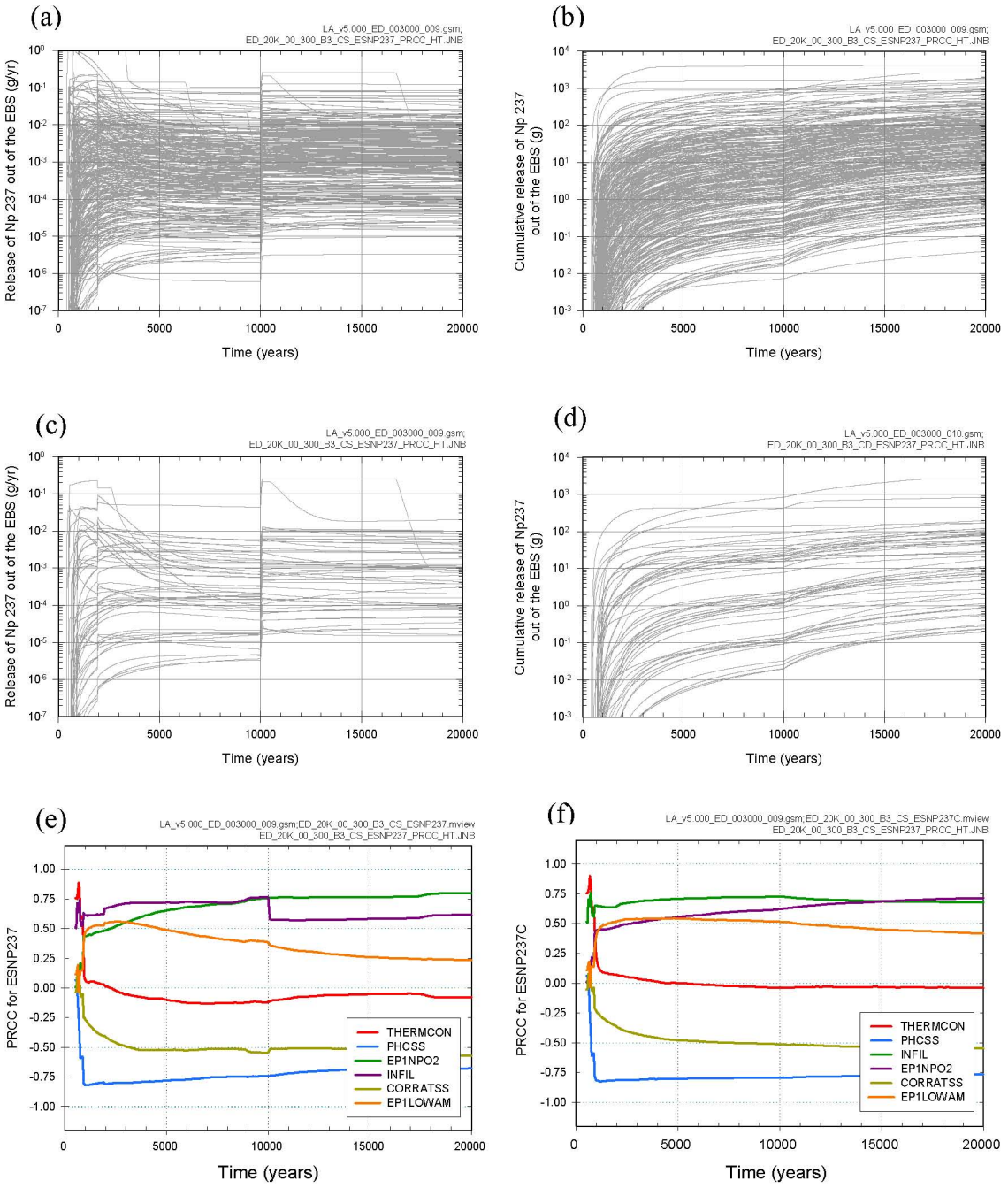

Source: Output DTNs: MO0709TSPASENS.000 [DIRS 183982]; and MO0709TSPAPLOT.000 [DIRS 183010].

Figure K5.3.2-3. Time-dependent release rates (*ESNP237*, g/yr) and cumulative (i.e., integrated) releases (*ESNP237C*, g) over 20,000 years for the movement of dissolved ^{237}Np from the EBS to the UZ resulting from a single early DS failure above a CNSF WP in percolation bin 3 under dripping conditions: (a, b) *ESNP237* and *ESNP237C* for all (i.e., 300) sample elements, (c, d) *ESNP237* and *ESNP237C* for first 50 sample elements, and (e, f) PRCCs for *ESNP237* and *ESNP237C*.

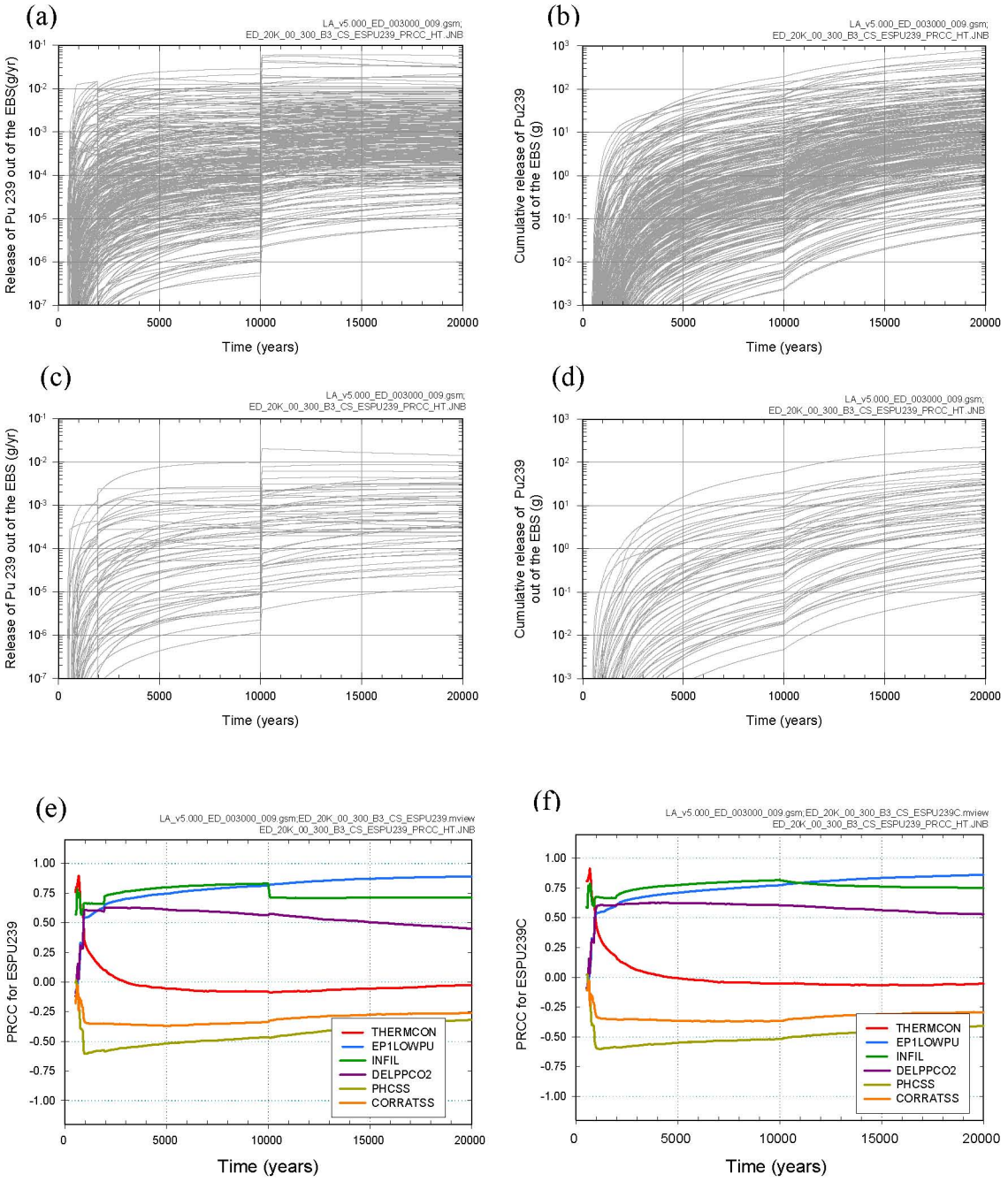

Source: Output DTNs: MO0709TSPASENS.000 [DIRS 183982]; and MO0709TSPAPLOT.000 [DIRS 183010].

Figure K5.3.2-4. Time-dependent release rates (*ESPU239*, g/yr) and cumulative (i.e., integrated) releases (*ESPU239C*, g) over 20,000 years for the movement of dissolved ^{239}Pu from the EBS to the UZ resulting from a single early DS failure above a CNSF WP in percolation bin 3 under dripping conditions: (a, b) *ESPU239* and *ESPU239C* for all (i.e., 300) sample elements, (c, d) *ESPU239* and *ESPU239C* for first 50 sample elements, and (e, f) PRCCs for *ESPU239* and *ESPU239C*.

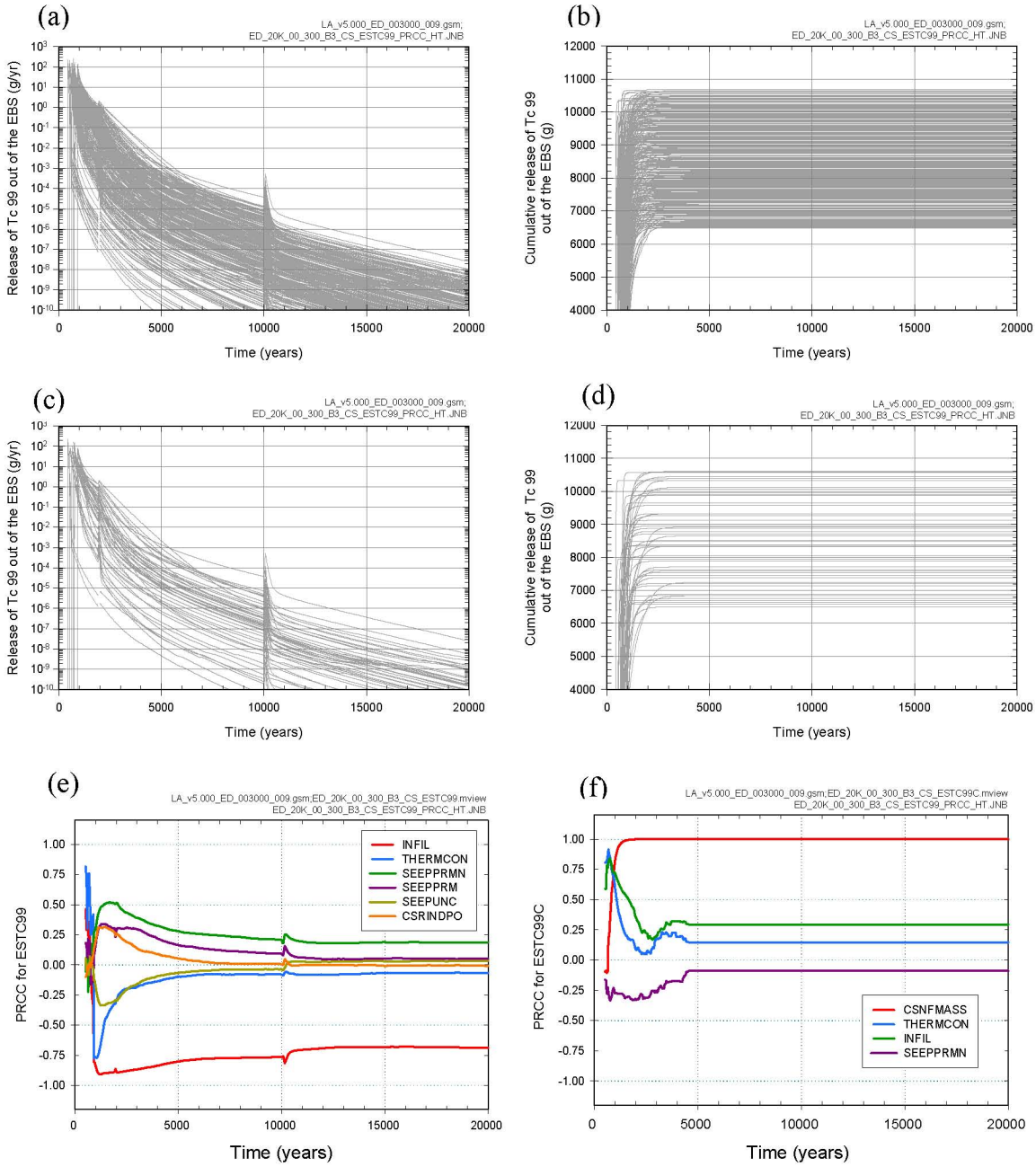

Source: Output DTNs: MO0709TSPASENS.000 [DIRS 183982]; and MO0709TSPAPLOT.000 [DIRS 183010].

Figure K5.3.2-5. Time-dependent release rates (*ESTC99*, g/yr) and cumulative (i.e., integrated) releases (*ESTC99C*, g) over 20,000 years for the movement of dissolved ^{99}Tc from the EBS to the UZ resulting from a single early DS failure above a CNSF WP in percolation bin 3 under dripping conditions: (a, b) *ESTC99* and *ESTC99C* for all (i.e., 300) sample elements, (c, d) *ESTC99* and *ESTC99C* for first 50 sample elements, and (e, f) PRCCs for *ESTC99* and *ESTC99C*.

Figure Removed. See discussion in Section K5.3.3.

Figure K5.3.3-1. Time-dependent release rates (*ESIC239*, g/yr) and cumulative (i.e., integrated) releases (*ESIC239C*, g) over 20,000 years for the movement of ^{239}Pu irreversibly attached to glass/waste form colloids from the EBS to the UZ resulting from the early failure of a CDSP WP in percolation bin 3 under dripping conditions: (a, b) *ESIC239* and *ESIC239C* for all (i.e., 300) sample elements, (c, d) *ESIC239* and *ESIC239C* for first 50 sample elements, and (e, f) PRCCs for *ESIC239* and *ESIC239C*.

Figure Removed. See Discussion in Section K5.3.3.

Figure K5.3.3-2. Time-dependent release rates (*ESIF239*, g/yr) and cumulative (i.e., integrated) releases (*ESIF239C*, g) over 20,000 years for the movement of ^{239}Pu irreversibly attached to ferrous colloids from the EBS to the UZ resulting from the early failure of a CDSP WP in percolation bin 3 under dripping conditions: (a, b) *ESIF239* and *ESIF239C* for all (i.e., 300) sample elements, (c, d) *ESIF239* and *ESIF239C* for first 50 sample elements, and (e, f) PRCCs for *ESIF239* and *ESIF239C*.

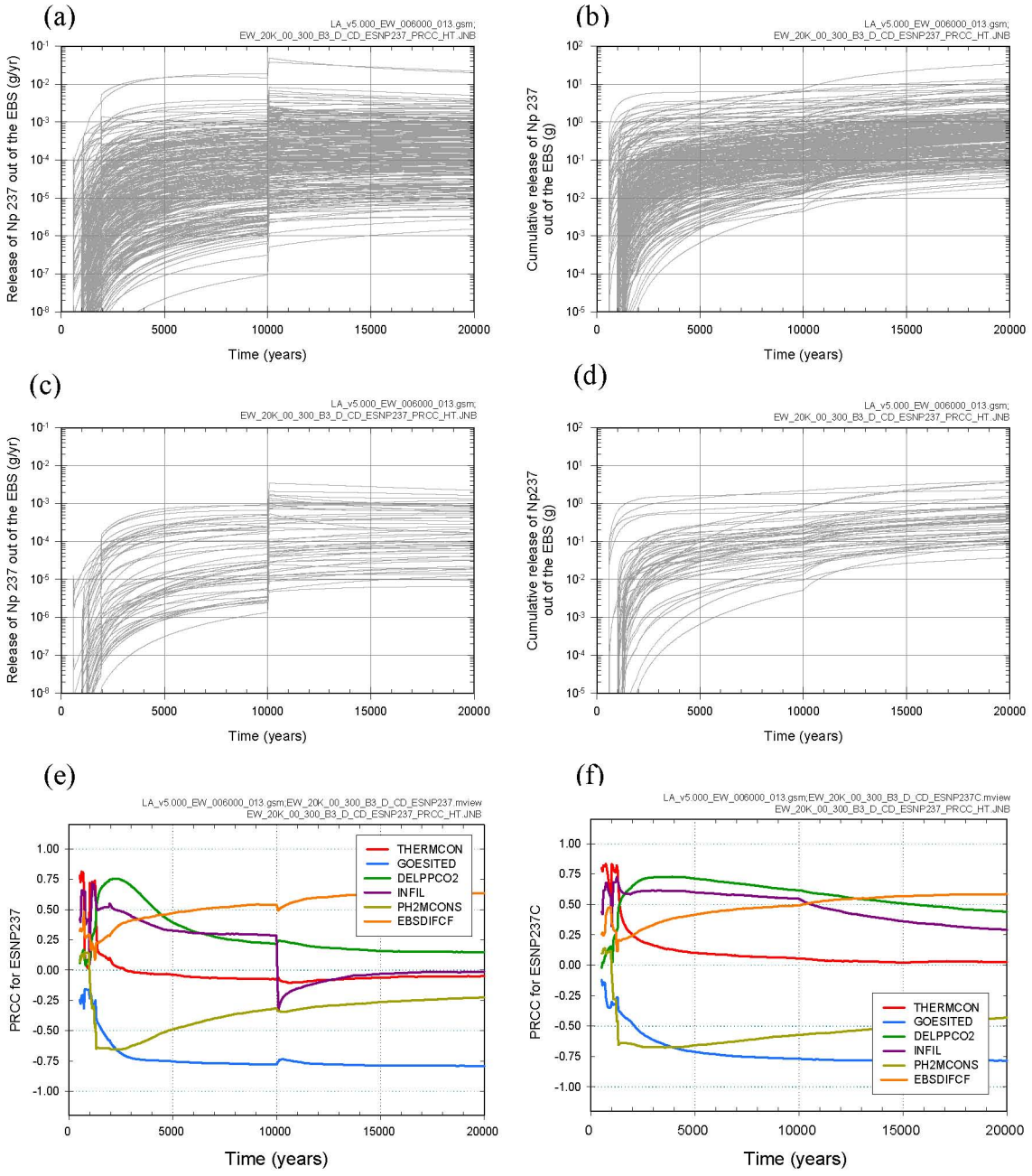

Source: Output DTNs: MO0709TSPASENS.000 [DIRS 183982]; and MO0709TSPAPLOT.000 [DIRS 183010].

Figure K5.3.3-3. Time-dependent release rates (*ESNP237*, g/yr) and cumulative (i.e., integrated) releases (*ESNP237C*, g) over 20,000 years for the movement of dissolved ^{237}Np from the EBS to the UZ resulting from the early failure of a CDSP WP in percolation bin 3 under dripping conditions: (a, b) *ESNP237* and *ESNP237C* for all (i.e., 300) sample elements, (c, d) *ESNP237* and *ESNP237C* for first 50 sample elements, and (e, f) PRCCs for *ESNP237* and *ESNP237C*.

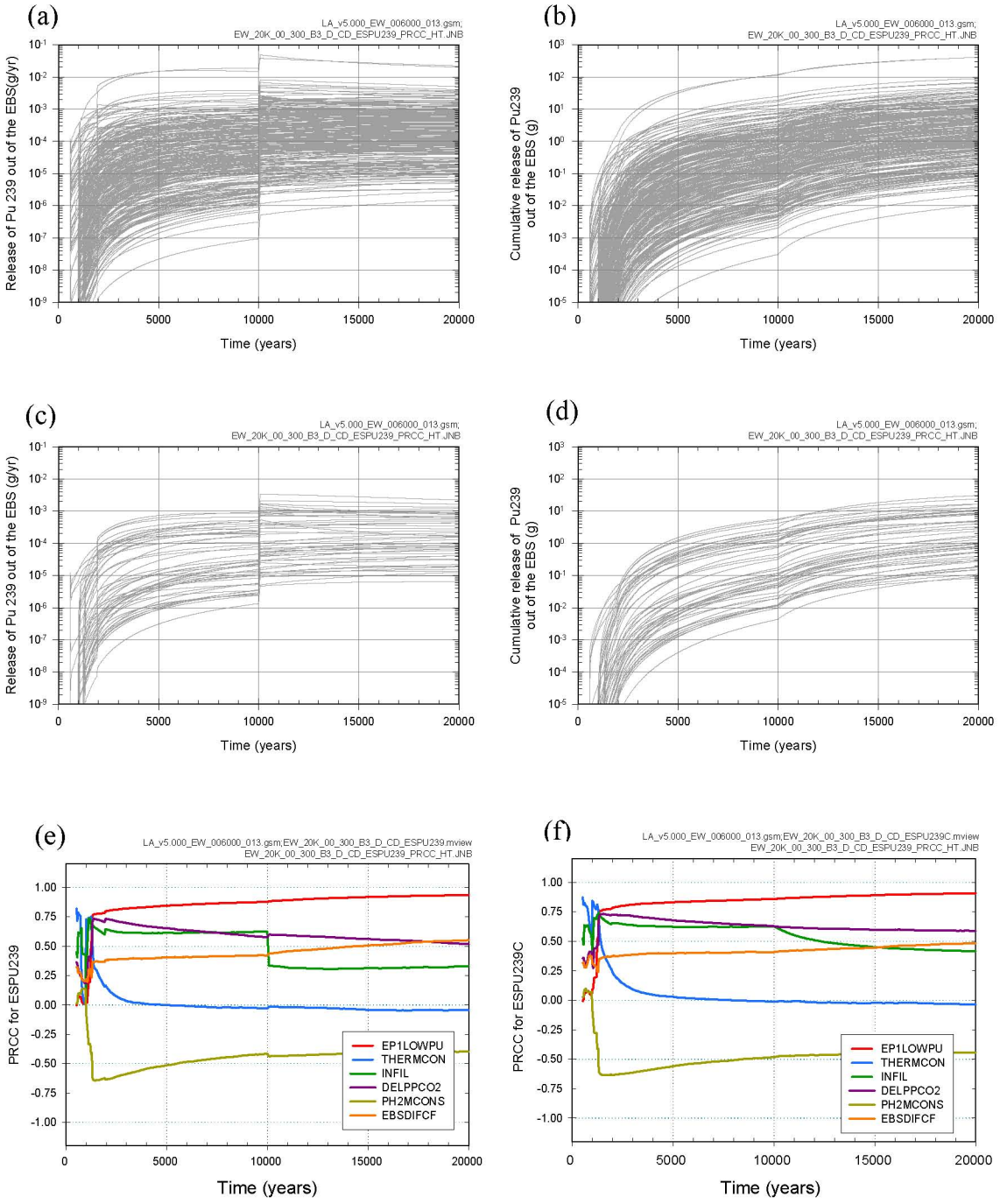

Source: Output DTNs: MO0709TSPASENS.000 [DIRS 183982]; and MO0709TSPAPLOT.000 [DIRS 183010].

Figure K5.3.3-4. Time-dependent release rates (*ESPU239*, g/yr) and cumulative (i.e., integrated) releases (*ESPU239C*, g) over 20,000 years for the movement of dissolved ^{239}Pu from the EBS to the UZ resulting from the early failure of a CDSP WP in percolation bin 3 under dripping conditions: (a, b) *ESPU239* and *ESPU239C* for all (i.e., 300) sample elements, (c, d) *ESPU239* and *ESPU239C* for first 50 sample elements, and (e, f) PRCCs for *ESPU239* and *ESPU239C*.

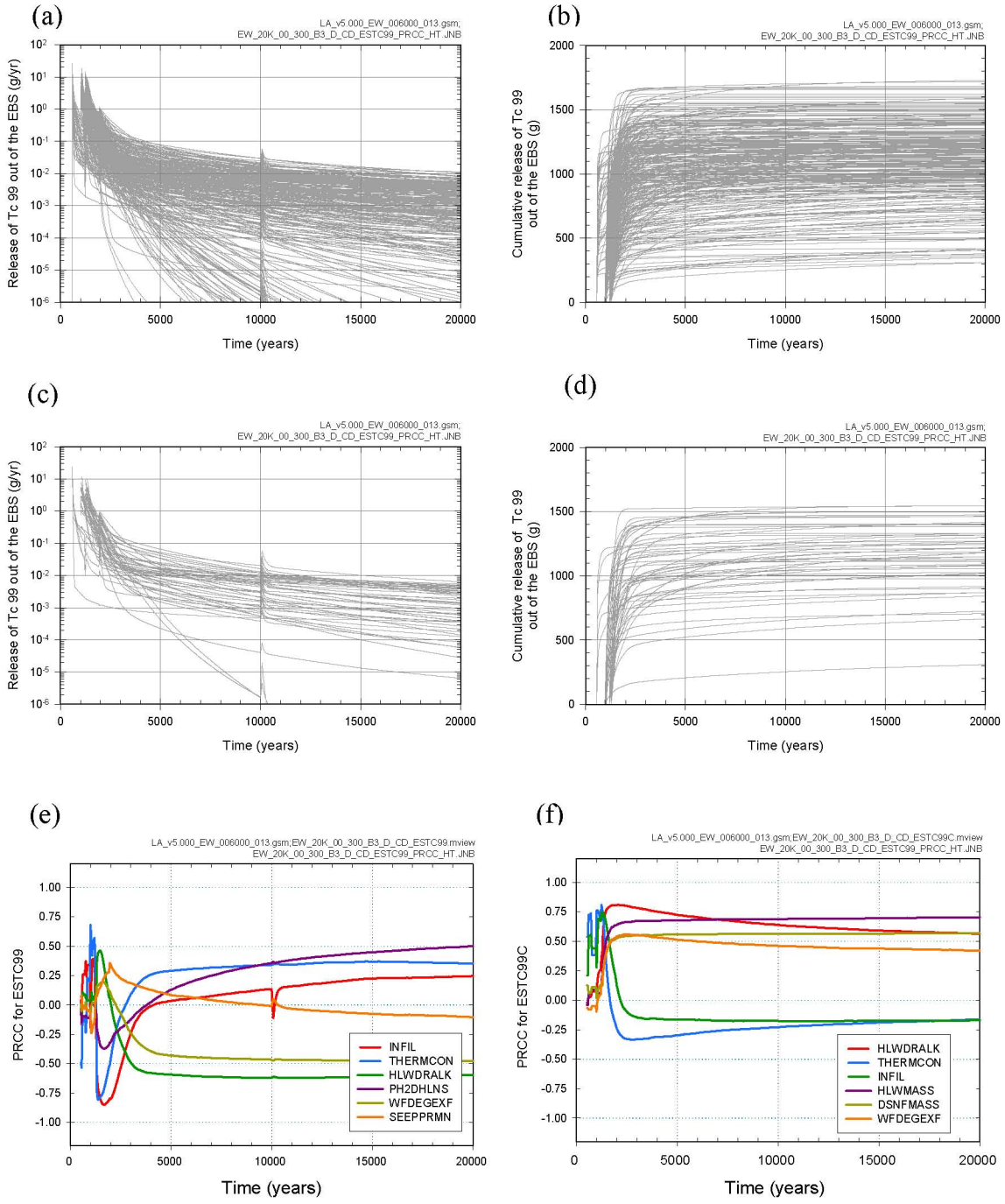

Source: Output DTNs: MO0709TSPASENS.000 [DIRS 183982]; and MO0709TSPAPLOT.000 [DIRS 183010].

Figure K5.3.3-5. Time-dependent release rates (*ESTC99*, g/yr) and cumulative (i.e., integrated) releases (*ESTC99C*, g) over 20,000 years for the movement of dissolved ^{99}Tc from the EBS to the UZ resulting from the early failure of a CDSP WP in percolation bin 3 under dripping conditions: (a, b) *ESTC99* and *ESTC99C* for all (i.e., 300) sample elements, (c, d) *ESTC99* and *ESTC99C* for first 50 sample elements, and (e, f) PRCCs for *ESTC99* and *ESTC99C*.

Figure Removed. See discussion in Section K5.3.5.

Figure K5.3.5-1. Time-dependent release rates (*ESIC239*, g/yr) and cumulative (i.e., integrated) releases (*ESIC239C*, g) over 20,000 years for the movement of ^{239}Pu irreversibly attached to glass/waste form colloids from the EBS to the UZ resulting from the early failure of a CSNF WP in percolation bin 3 under dripping conditions: (a, b) *ESIC239* and *ESIC239C* for all (i.e., 300) sample elements, (c, d) *ESIC239* and *ESIC239C* for first 50 sample elements, and (e, f) PRCCs for *ESIC239* and *ESIC239C*.

Figure Removed. See discussion in Section K5.3.5.

Figure K5.3.5-2. Time-dependent release rates (*ESIF239*, g/yr) and cumulative (i.e., integrated) releases (*ESIF239C*, g) over 20,000 years for the movement of ^{239}Pu irreversibly attached to ferrous colloids from the EBS to the UZ resulting from the early failure of a CSNF WP in percolation bin 3 under dripping conditions: (a, b) *ESIF239* and *ESIF239C* for all (i.e., 300) sample elements, (c, d) *ESIF239* and *ESIF239C* for first 50 sample elements, and (e, f) PRCCs for *ESIF239* and *ESIF239C*.

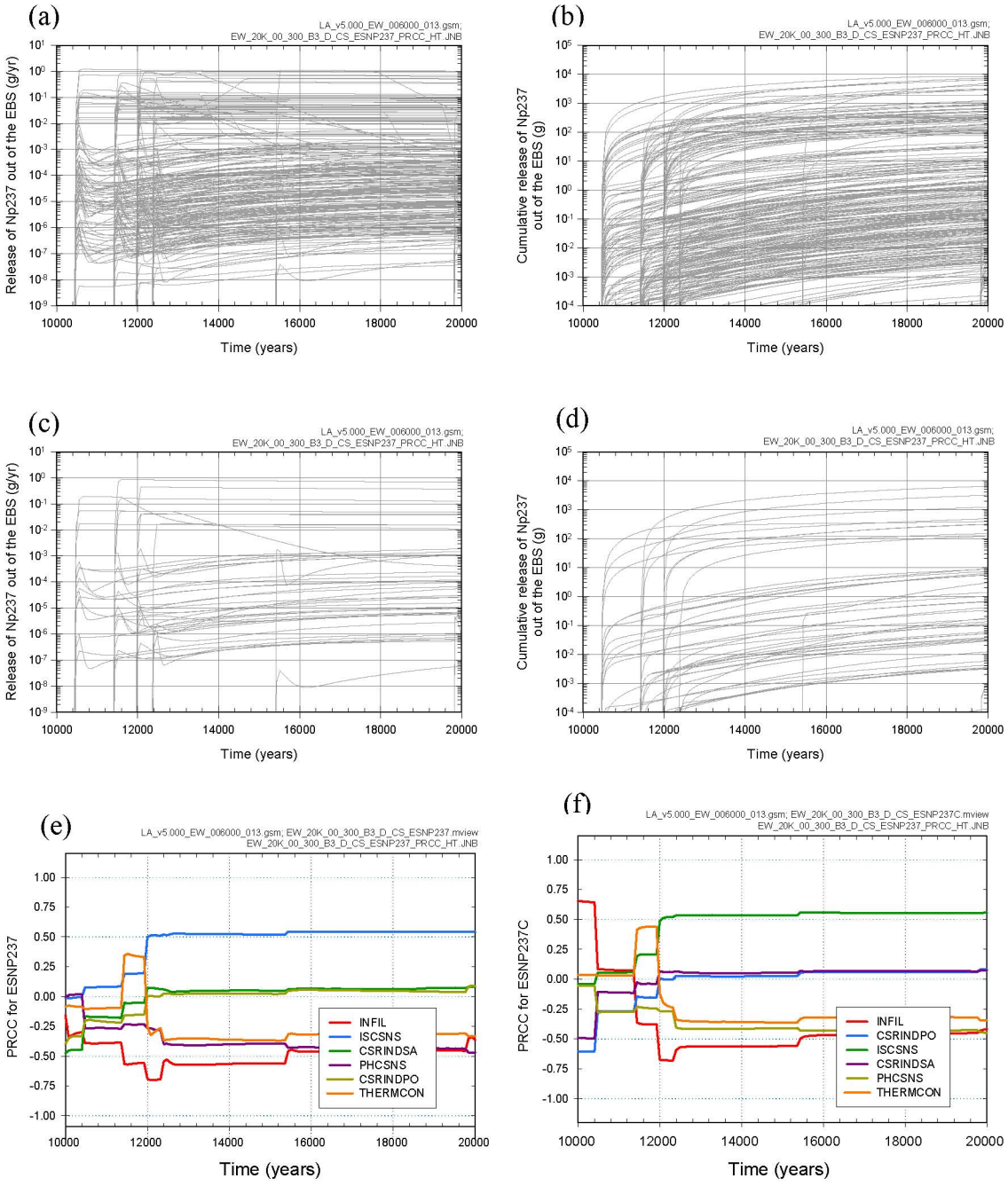

Source: Output DTNs: MO0709TSPASENS.000 [DIRS 183982]; and MO0709TSPAPLOT.000 [DIRS 183010].

Figure K5.3.5-3. Time-dependent release rates (*ESNP237*, g/yr) and cumulative (i.e., integrated) releases (*ESNP237C*, g) over 20,000 years for the movement of dissolved ^{237}Np from the EBS to the UZ resulting from the early failure of a CSNF WP in percolation bin 3 under dripping conditions: (a, b) *ESNP237* and *ESNP237C* for all (i.e., 300) sample elements, (c, d) *ESNP237* and *ESNP237C* for first 50 sample elements, and (e, f) PRCCs for *ESNP237* and *ESNP237C*.

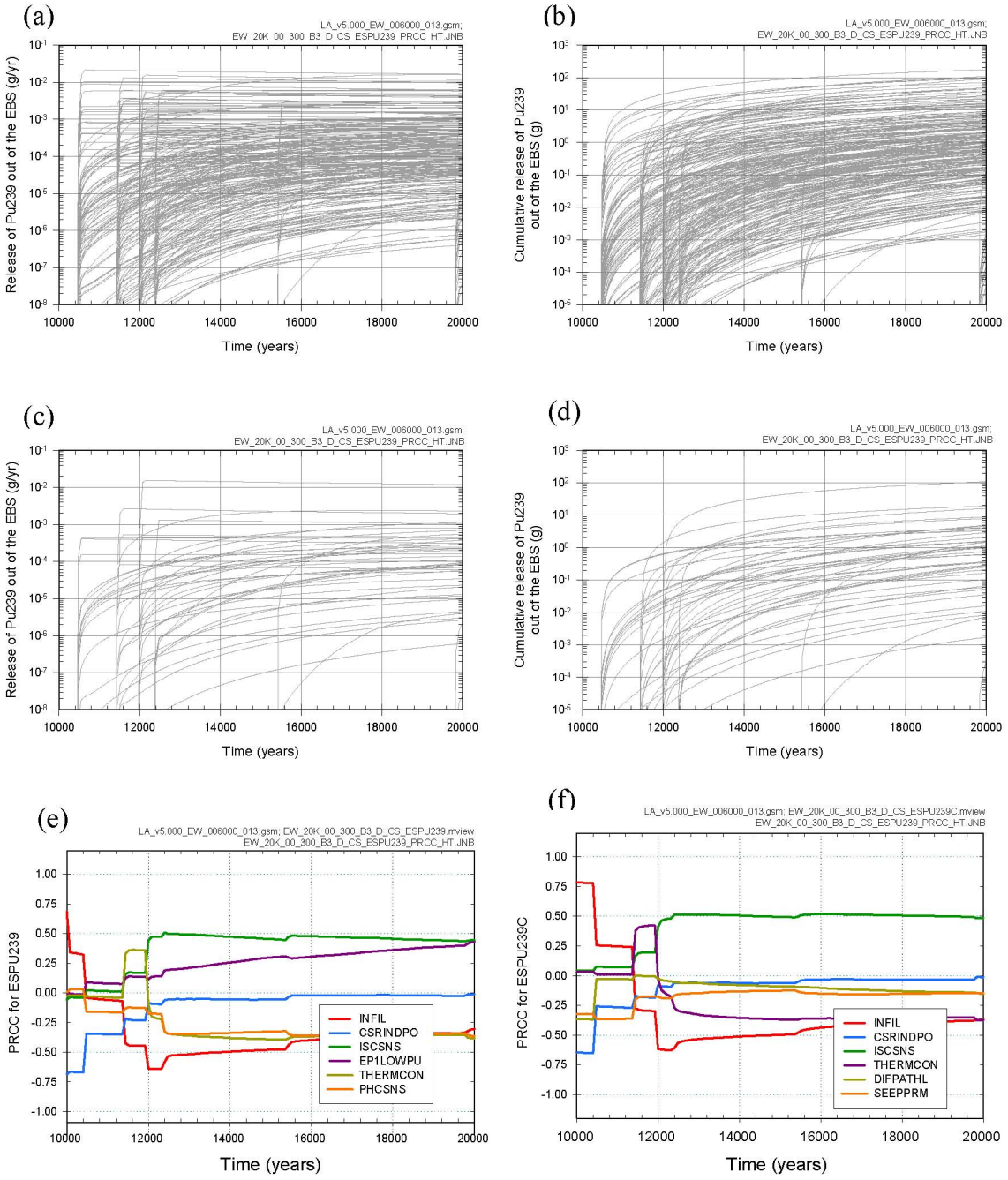

Source: Output DTNs: MO0709TSPASENS.000 [DIRS 183982]; and MO0709TSPAPLOT.000 [DIRS 183010].

Figure K5.3.5-4. Time-dependent release rates (*ESPU239*, g/yr) and cumulative (i.e., integrated) releases (*ESPU239C*, g) over 20,000 years for the movement of dissolved ^{239}Pu from the EBS to the UZ resulting from the early failure of a CSNF WP in percolation bin 3 under dripping conditions: (a, b) *ESPU239* and *ESPU239C* for all (i.e., 300) sample elements, (c, d) *ESPU239* and *ESPU239C* for first 50 sample elements, and (e, f) PRCCs for *ESPU239* and *ESPU239C*.

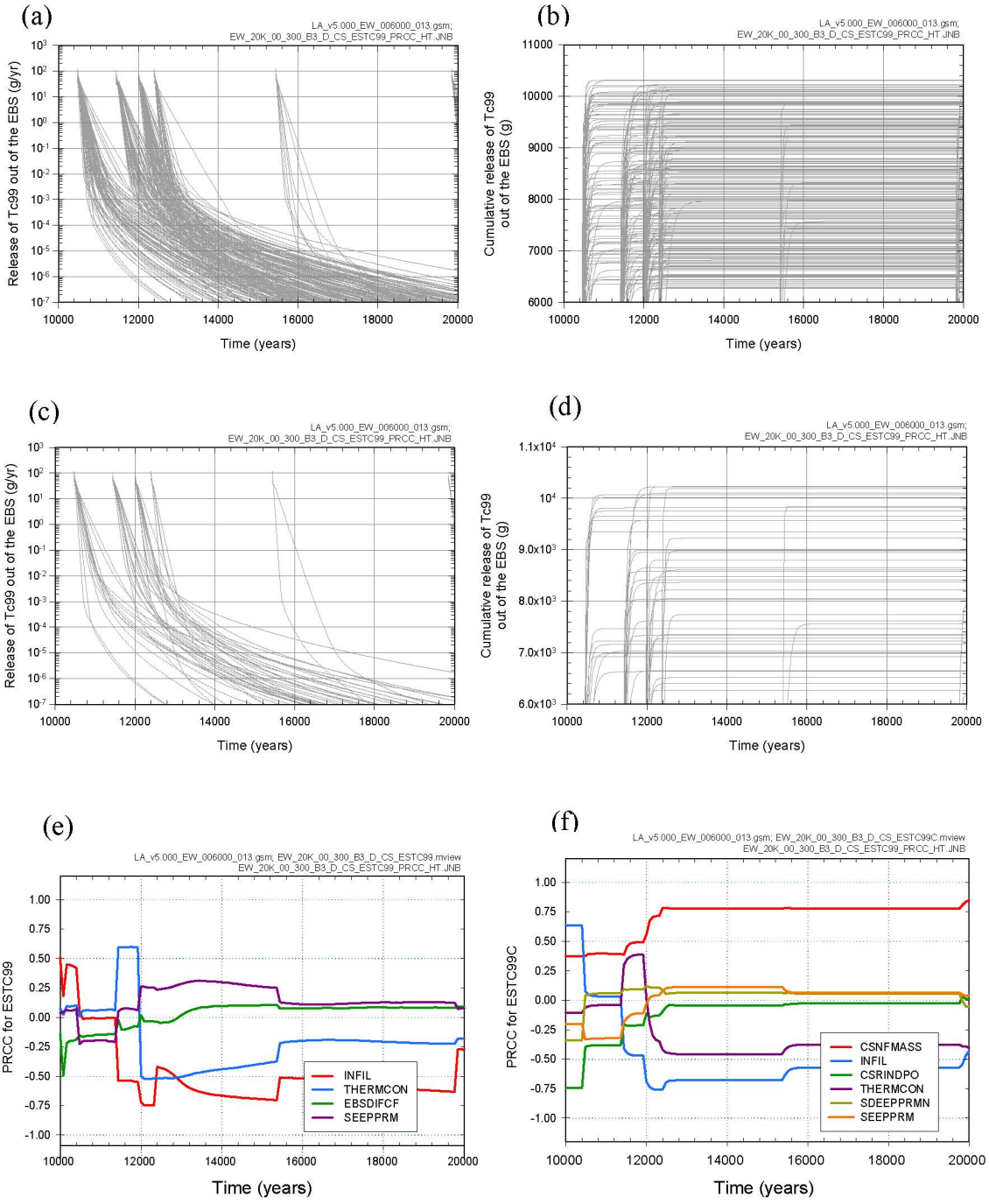

Source: Output DTNs: MO0709TSPASENS.000 [DIRS 183982]; and MO0709TSPAPLOT.000 [DIRS 183010].

Figure K5.3.5-5. Time-dependent release rates (*ESTC99*, g/yr) and cumulative (i.e., integrated) releases (*ESTC99C*, g) over 20,000 years for the movement of dissolved ^{99}Tc from the EBS to the UZ resulting from the early failure of a CSNF WP in percolation bin 3 under dripping conditions: (a, b) *ESTC99* and *ESTC99C* for all (i.e., 300) sample elements, (c, d) *ESTC99* and *ESTC99C* for first 50 sample elements, and (e, f) PRCCs for *ESTC99* and *ESTC99C*.

INTENTIONALLY LEFT BLANK

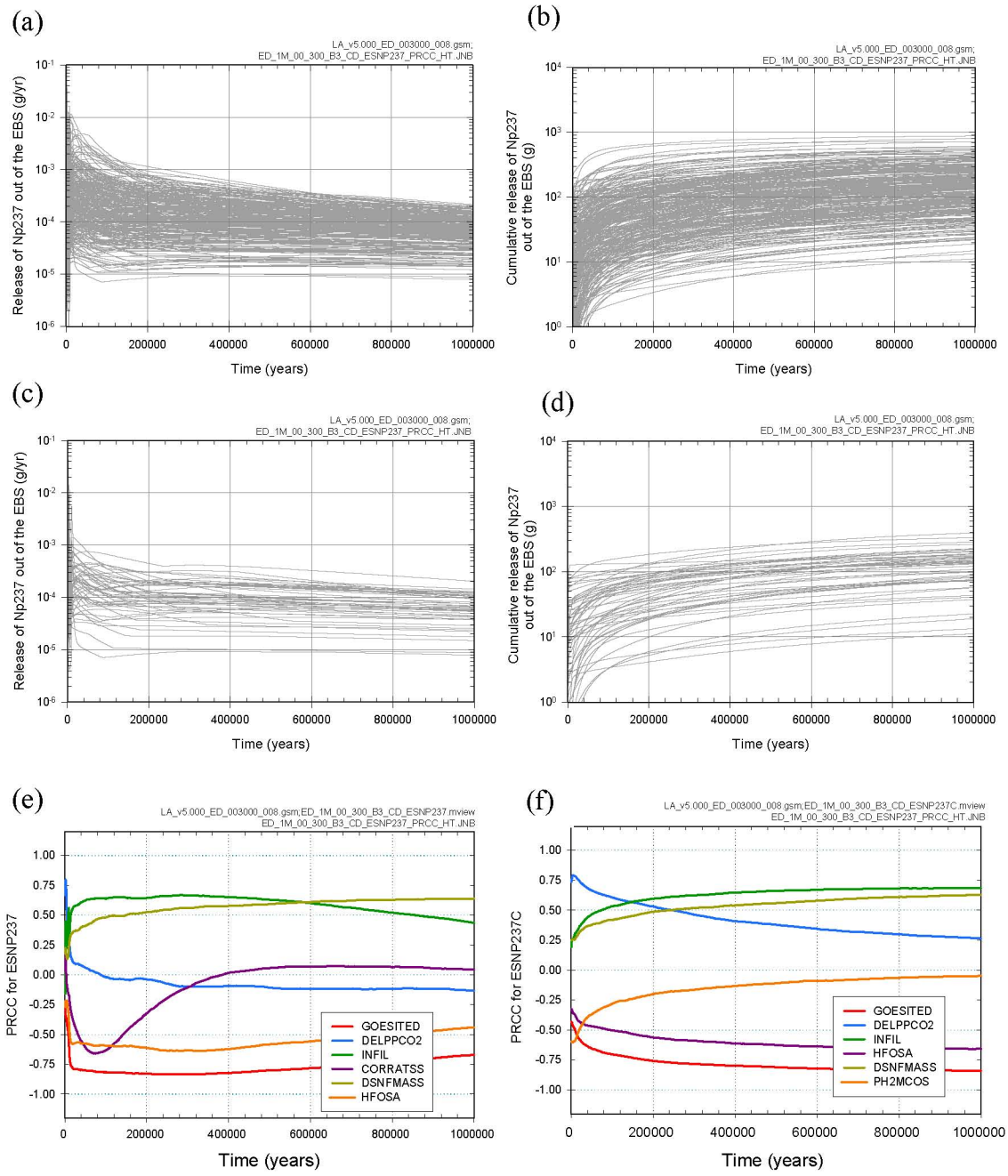

Source: Output DTNs: MO0709TSPAREGS.000 [DIRS 182976]; and MO0709TSPAPLOT.000 [DIRS 183010].

Figure K5.3.7-1. Time-dependent release rates (*ESNP237*, g/yr) and cumulative (i.e., integrated) releases (*ESNP237C*, g) over 1,000,000 years for the movement of dissolved ^{237}Np from the EBS to the UZ resulting from a single early DS failure above a CDSP WP in percolation bin 3 under dripping conditions: (a, b) *ESNP237* and *ESNP237C* for all (i.e., 300) sample elements, (c, d) *ESNP237* and *ESNP237C* for first 50 sample elements, and (e, f) PRCCs for *ESNP237* and *ESNP237C*

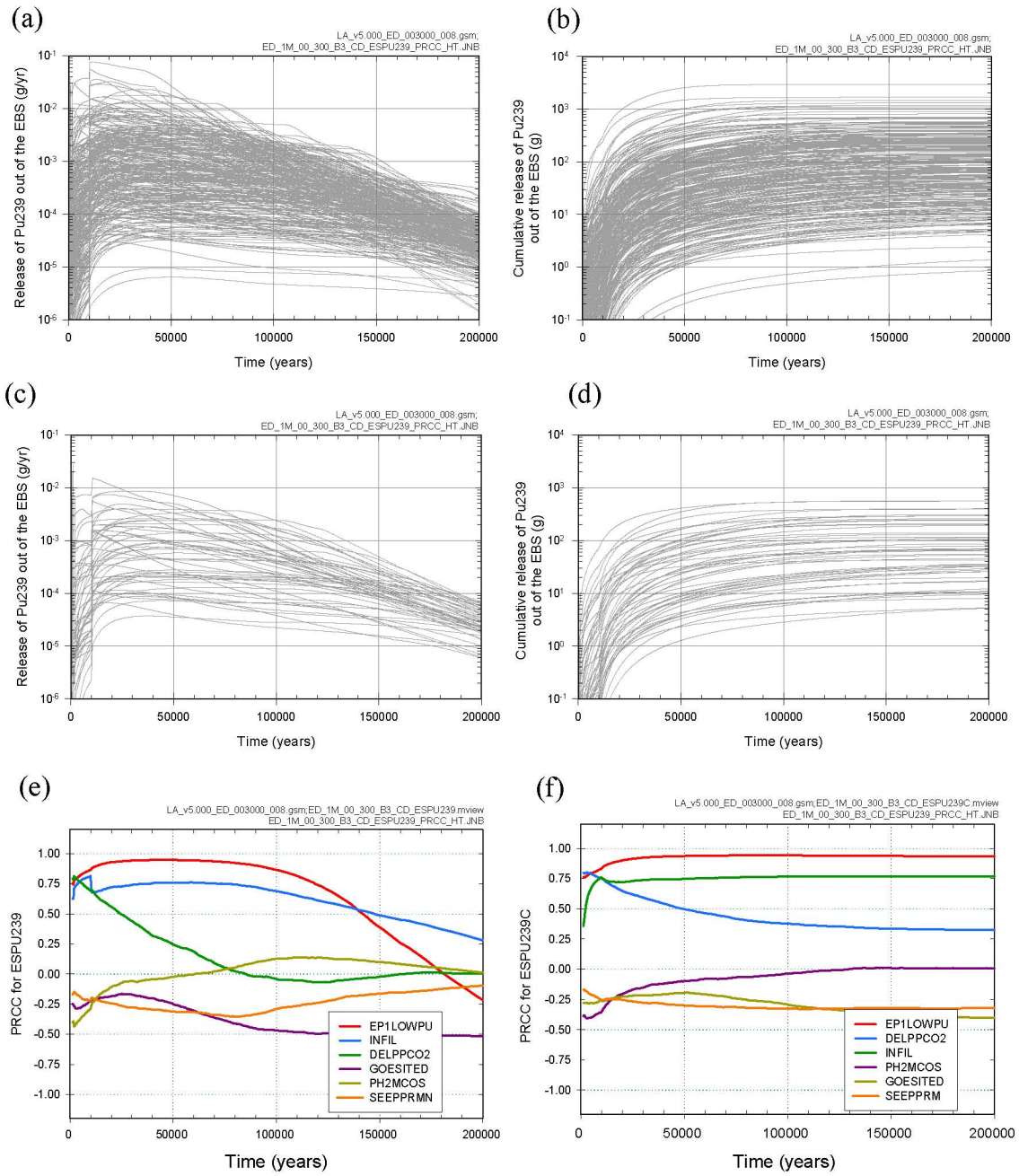

Source: Output DTNs: MO0709TSPAREGS.000 [DIRS 182976]; and MO0709TSPAPLOT.000 [DIRS 183010].

Figure K5.3.7-2. Time-dependent release rates (*ESPU239*, g/yr) and cumulative (i.e., integrated) releases (*ESPU239C*, g) over 200,000 years for the movement of dissolved ^{239}Pu from the EBS to the UZ resulting from a single early DS failure above a CDSP WP in percolation bin 3 under dripping conditions: (a, b) *ESPU239* and *ESPU239C* for all (i.e., 300) sample elements, (c, d) *ESPU239* and *ESPU239C* for first 50 sample elements, and (e, f) PRCCs for *ESPU239* and *ESPU239C*.

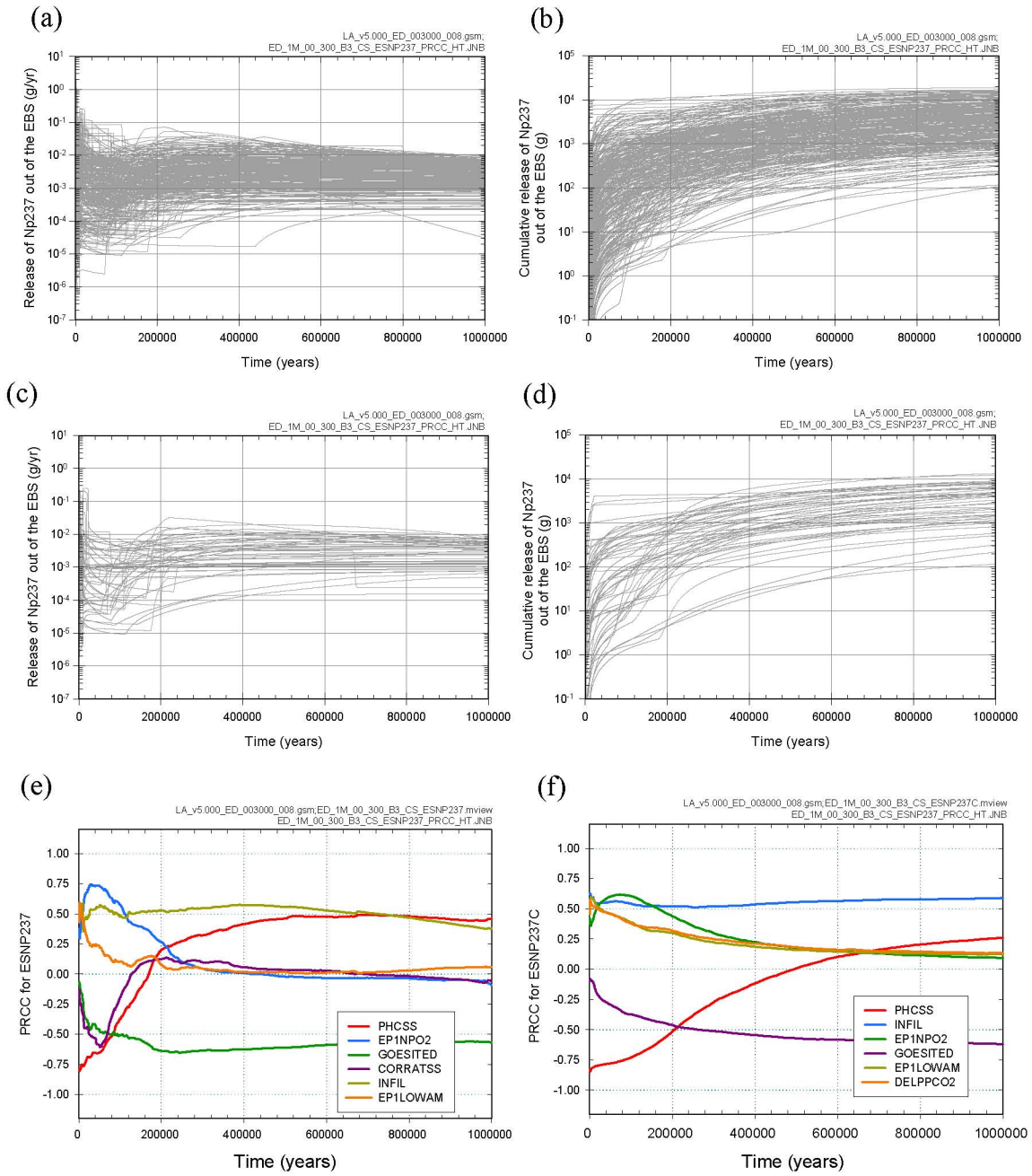

Source: Output DTNs: MO0709TSPAREGS.000 [DIRS 182976]; and MO0709TSPAPLOT.000 [DIRS 183010].

Figure K5.3.8-1. Time-dependent release rates (*ESNP237*, g/yr) and cumulative (i.e., integrated) releases (*ESNP237C*, g) over 1,000,000 years for the movement of dissolved ^{237}Np from the EBS to the UZ resulting from a single early DS failure above a CSNF WP in percolation bin 3 under dripping conditions: (a, b) *ESNP237* and *ESNP237C* for all (i.e., 300) sample elements, (c, d) *ESNP237* and *ESNP237C* for first 50 sample elements, and (e, f) PRCCs for *ESNP237* and *ESNP237C.*

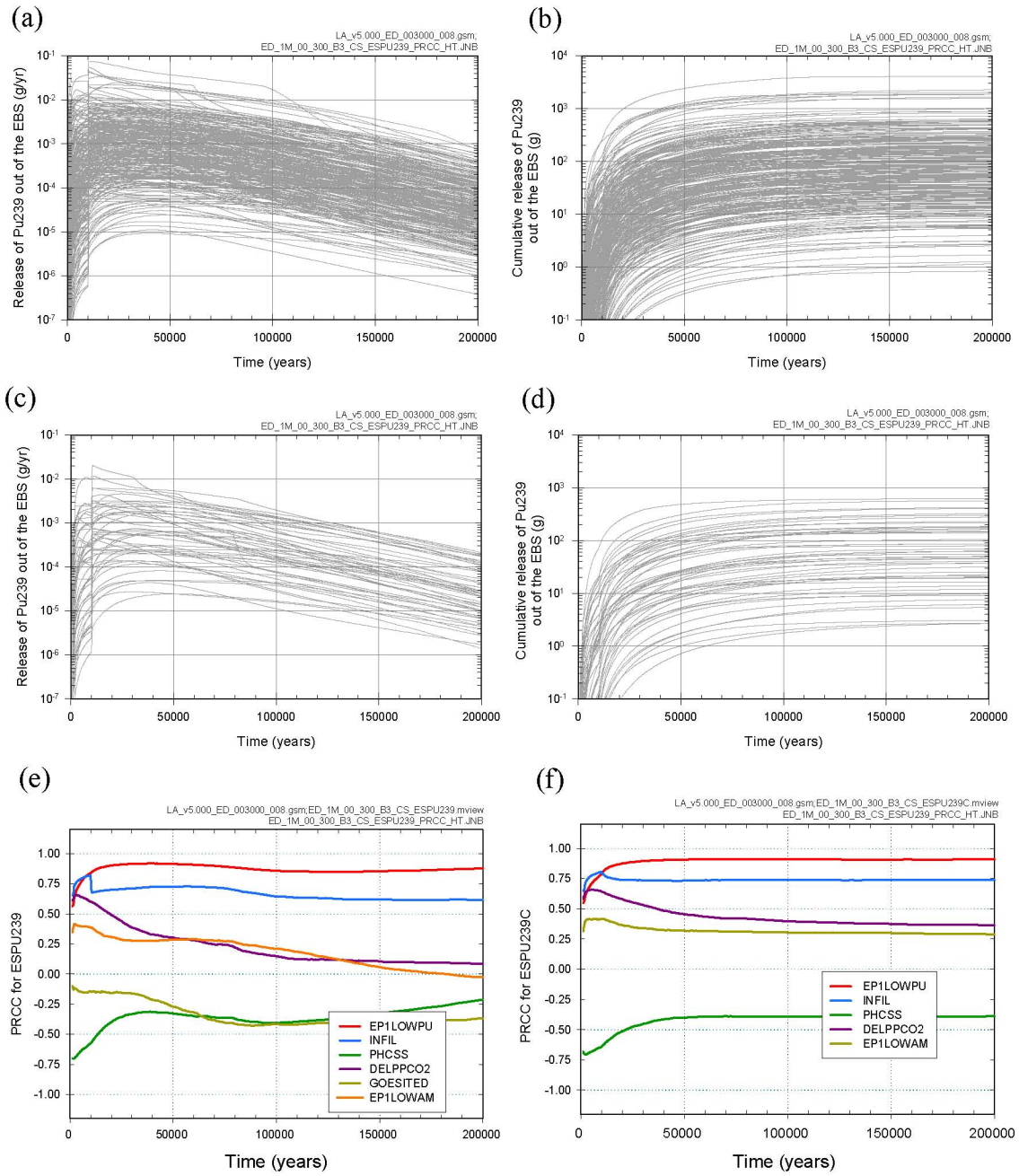

Source: Output DTNs: MO0709TSPAREGS.000 [DIRS 182976]; and MO0709TSPAPLOT.000 [DIRS 183010].

Figure K5.3.8-2. Time-dependent release rates (*ESPU239*, g/yr) and cumulative (i.e., integrated) releases (*ESPU239C*, g) over 200,000 years for the movement of dissolved ^{239}Pu from the EBS to the UZ resulting from a single early DS failure above a CSNF WP in percolation bin 3 under dripping conditions: (a, b) *ESPU239* and *ESPU239C* for all (i.e., 300) sample elements, (c, d) *ESPU239* and *ESPU239C* for first 50 sample elements, and (e, f) PRCCs for *ESPU239* and *ESPU239C*.

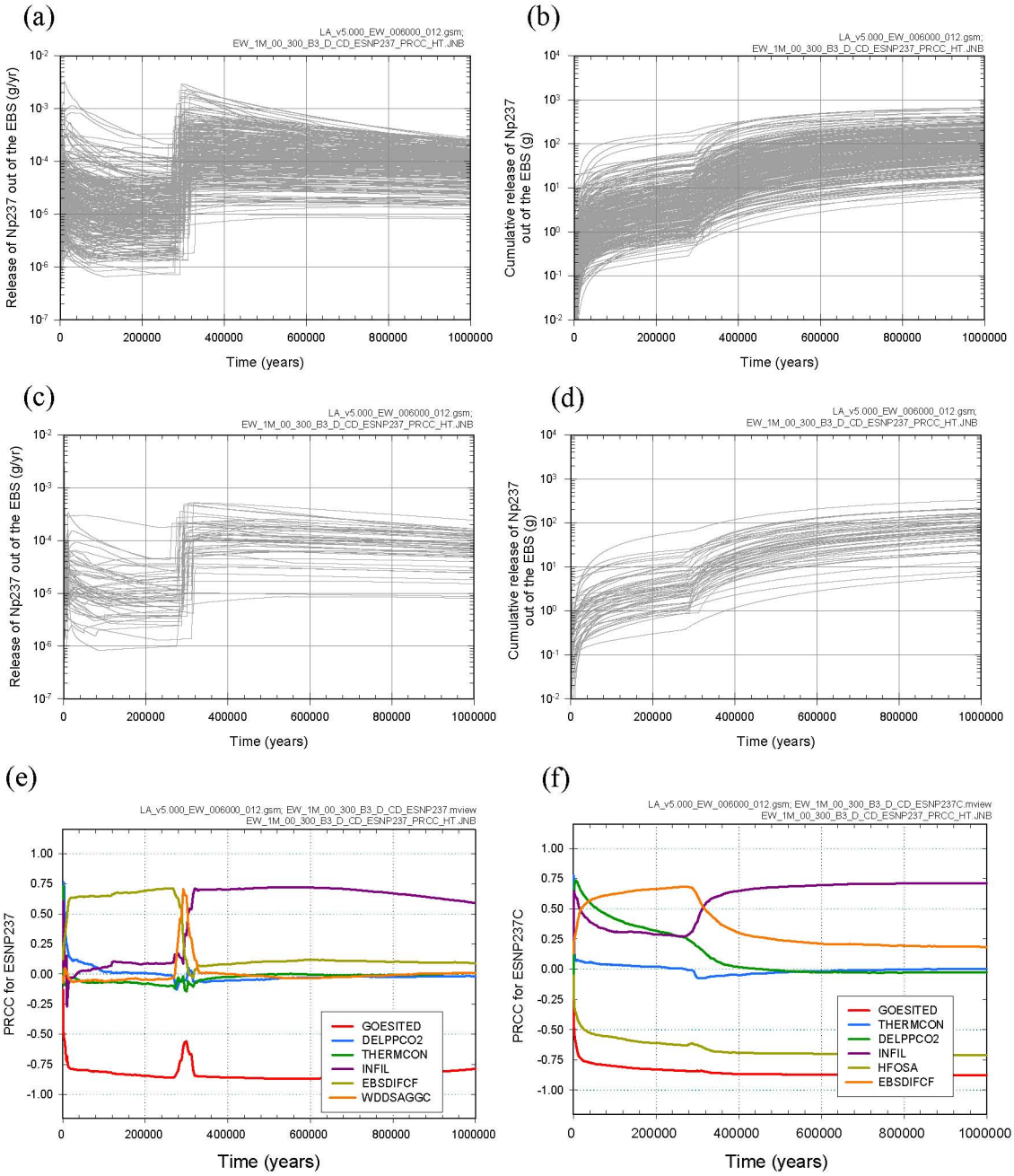

Source: Output DTNs: MO0709TSPAREGS.000 [DIRS 182976]; and MO0709TSPAPLOT.000 [DIRS 183010].

Figure K5.3.9-1. Time-dependent release rates (*ESNP237*, g/yr) and cumulative (i.e., integrated) releases (*ESNP237C*, g) over 1,000,000 years for the movement of dissolved ^{237}Np from the EBS to the UZ resulting from the early failure of a CDSP WP in percolation bin 3 under dripping conditions: (a, b) *ESNP237* and *ESNP237C* for all (i.e., 300) sample elements, (c, d) *ESNP237* and *ESNP237C* for first 50 sample elements, and (e, f) PRCCs for *ESNP237* and *ESNP237C.*

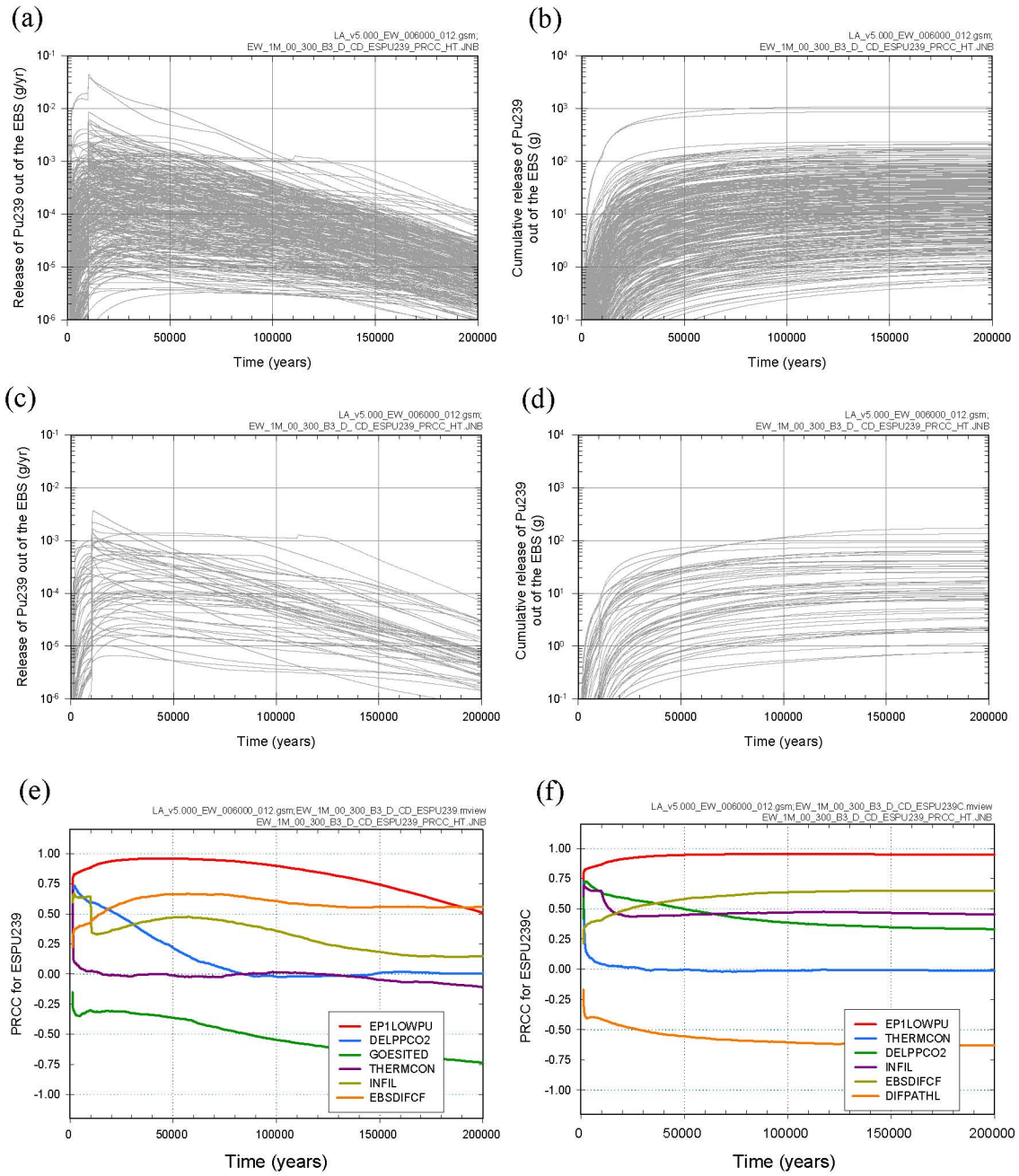

Source: Output DTNs: MO0709TSPAREGS.000 [DIRS 182976]; and MO0709TSPAPLOT.000 [DIRS 183010].

Figure K5.3.9-2. Time-dependent release rates (*ESPU239*, g/yr) and cumulative (i.e., integrated) releases (*ESPU239C*, g) over 200,000 years for the movement of dissolved ^{239}Pu from the EBS to the UZ resulting from the early failure of a CDSP WP in percolation bin 3 under dripping conditions: (a, b) *ESPU239* and *ESPU239C* for all (i.e., 300) sample elements, (c, d) *ESPU239* and *ESPU239C* for first 50 sample elements, and (e, f) PRCCs for *ESPU239* and *ESPU239C*.

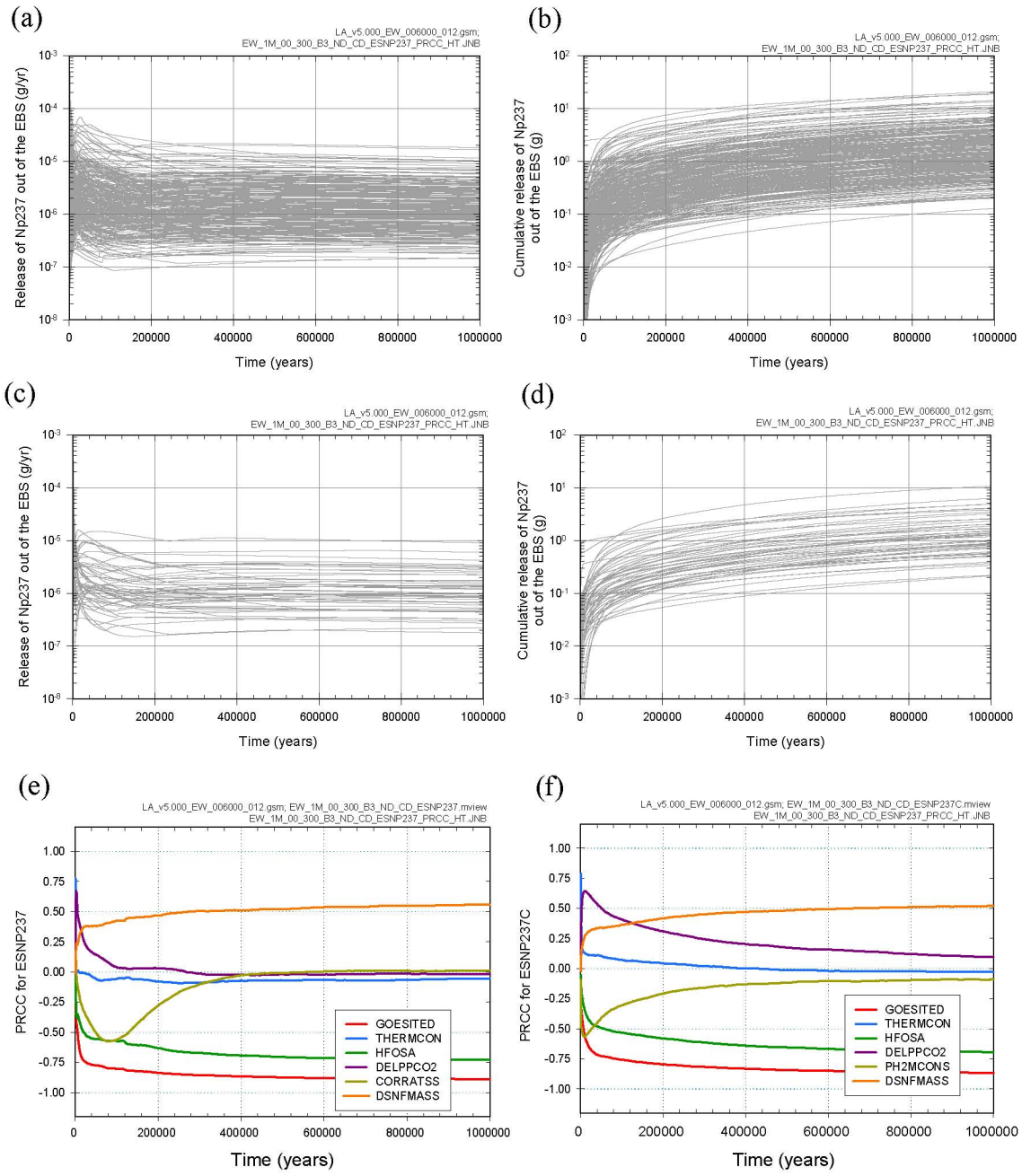

Source: Output DTNs: MO0709TSPAREGS.000 [DIRS 182976]; and MO0709TSPAPLOT.000 [DIRS 183010].

Figure K5.3.10-1. Time-dependent release rates (*ESNP237*, g/yr) and cumulative (i.e., integrated) releases (*ESNP237C*, g) over 1,000,000 years for the movement of dissolved ^{237}Np from the EBS to the UZ resulting from the early failure of a CDSP WP in percolation bin 3 under nondripping conditions: (a, b) *ESNP237* and *ESNP237C* for all (i.e., 300) sample elements, (c, d) *ESNP237* and *ESNP237C* for first 50 sample elements, and (e, f) PRCCs for *ESNP237* and *ESNP237C*.

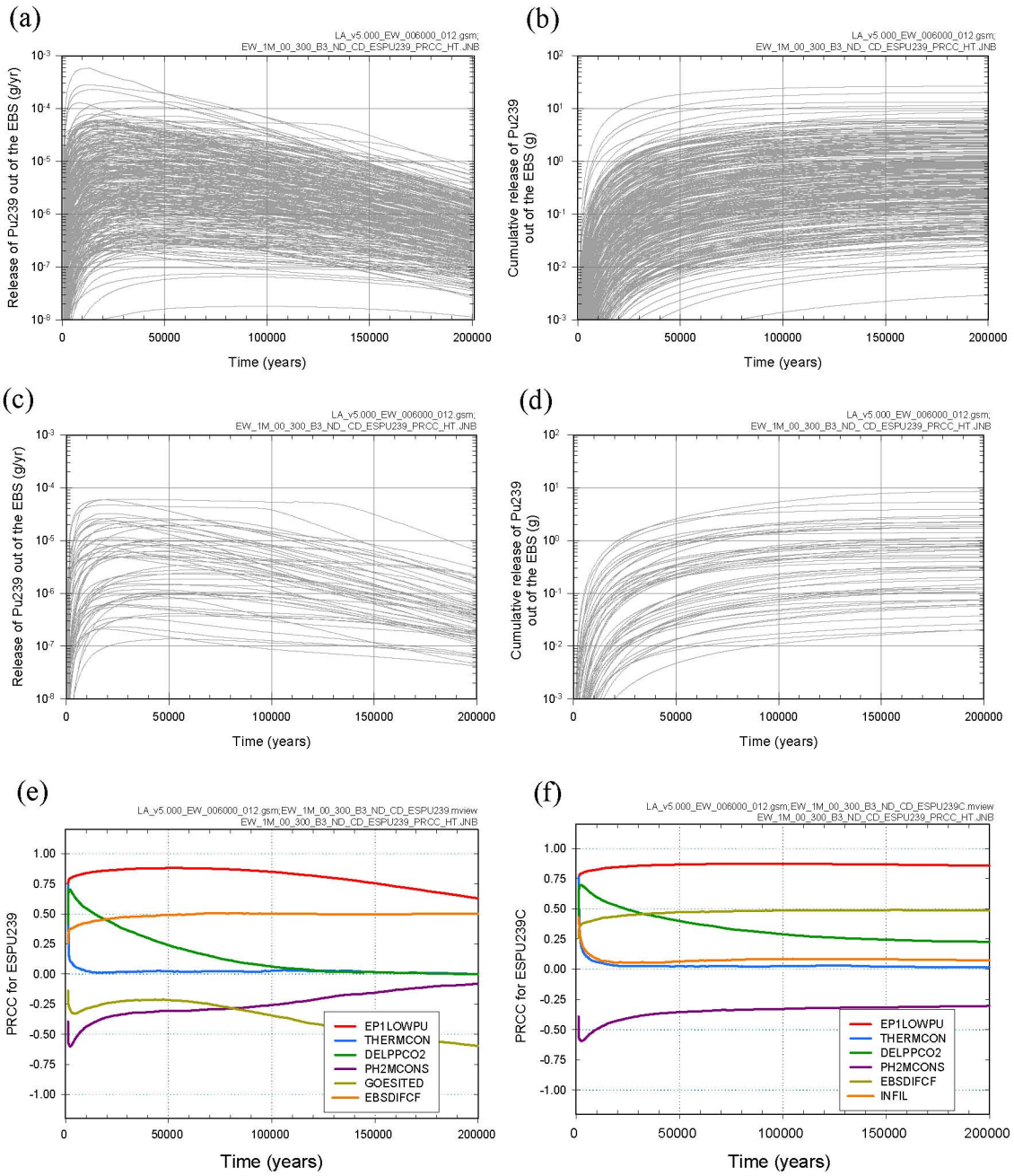

Source: Output DTNs: MO0709TSPAREGS.000 [DIRS 182976]; and MO0709TSPAPLOT.000 [DIRS 183010].

Figure K5.3.10-2. Time-dependent release rates (*ESPU239*, g/yr) and cumulative (i.e., integrated) releases (*ESPU239C*, g) over 200,000 years for the movement of dissolved ^{239}Pu from the EBS to the UZ resulting from the early failure of a CDSP WP in percolation bin 3 under nondripping conditions: (a, b) *ESPU239* and *ESPU239C* for all (i.e., 300) sample elements, (c, d) *ESPU239* and *ESPU239C* for first 50 sample elements, and (e, f) PRCCs for *ESPU239* and *ESPU239C*.

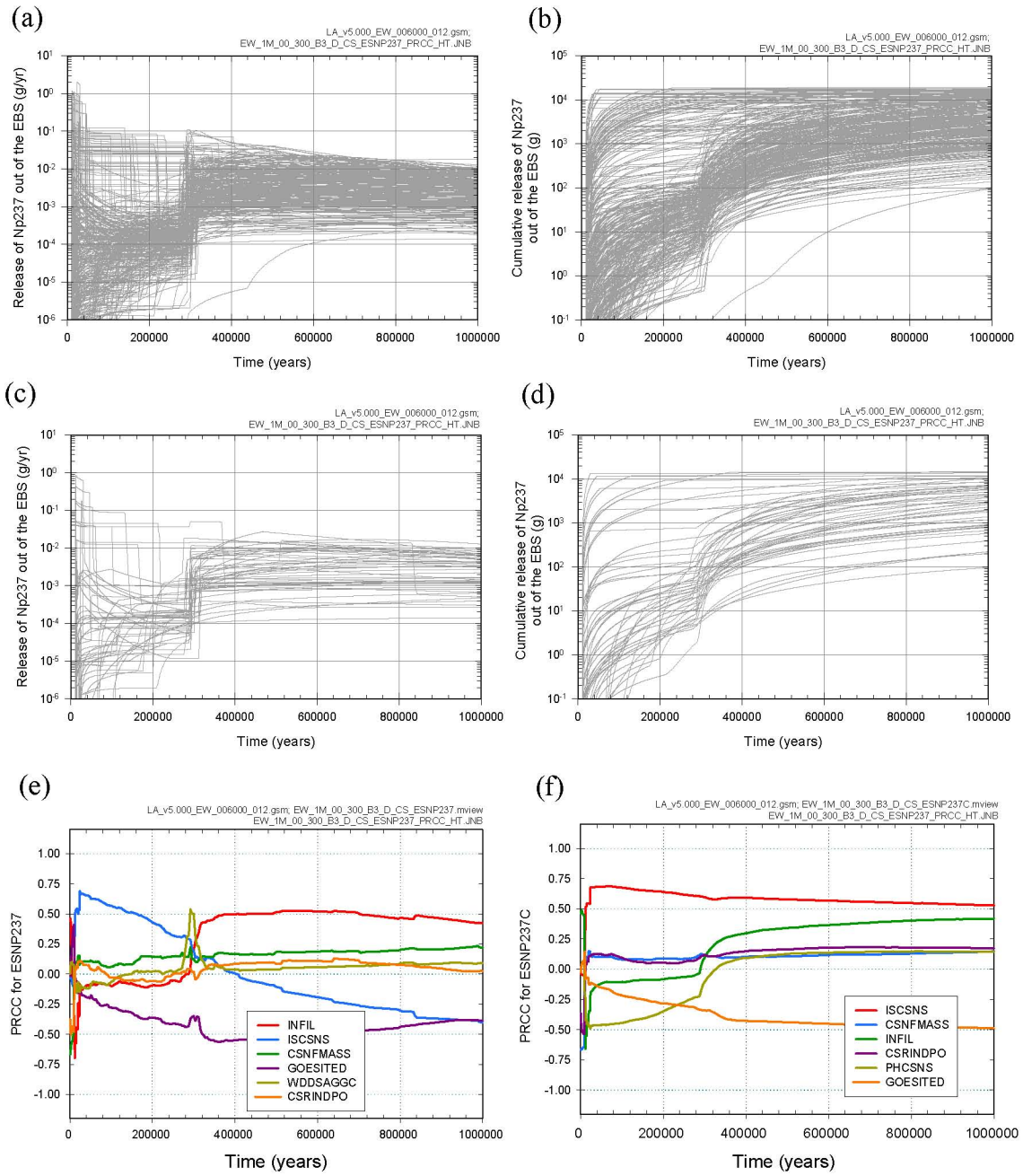

Source: Output DTNs: MO0709TSPAREGS.000 [DIRS 182976]; and MO0709TSPAPLOT.000 [DIRS 183010].

Figure K5.3.11-1. Time-dependent release rates (*ESNP237*, g/yr) and cumulative (i.e., integrated) releases (*ESNP237C*, g) over 1,000,000 years for the movement of dissolved ^{237}Np from the EBS to the UZ resulting from the early failure of a CSNF WP in percolation bin 3 under dripping conditions: (a, b) *ESNP237* and *ESNP237C* for all (i.e., 300) sample elements, (c, d) *ESNP237* and *ESNP237C* for first 50 sample elements, and (e, f) PRCCs for *ESNP237* and *ESNP237C*.

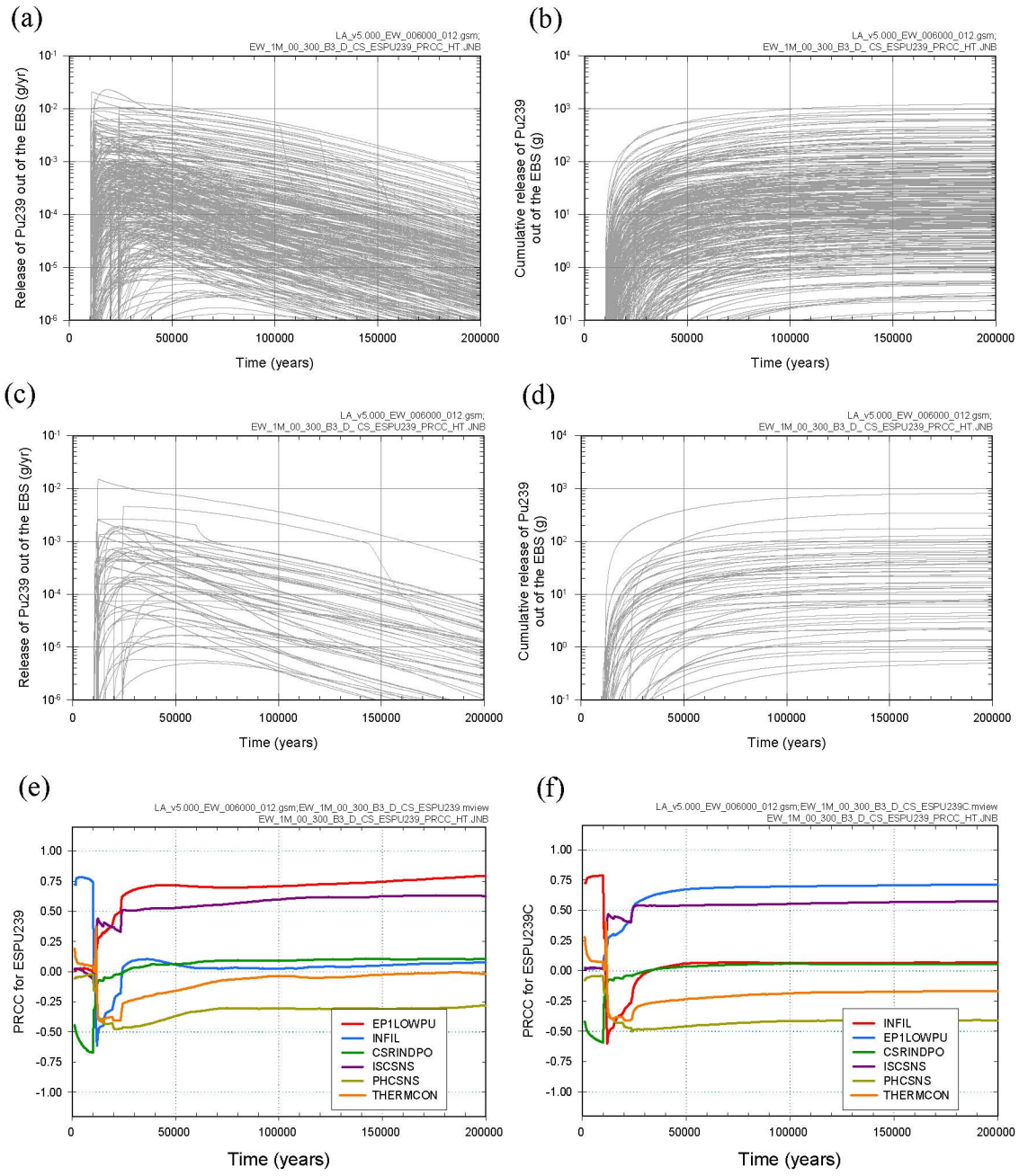

Source: Output DTNs: MO0709TSPAREGS.000 [DIRS 182976]; and MO0709TSPAPLOT.000 [DIRS 183010].

Figure K5.3.11-2. Time-dependent release rates (*ESPU239*, g/yr) and cumulative (i.e., integrated) releases (*ESPU239C*, g) over 200,000 years for the movement of dissolved ^{239}Pu from the EBS to the UZ resulting from the early failure of a CSNF WP in percolation bin 3 under dripping conditions: (a, b) *ESPU239* and *ESPU239C* for all (i.e., 300) sample elements, (c, d) *ESPU239* and *ESPU239C* for first 50 sample elements, and (e, f) PRCCs for *ESPU239* and *ESPU239C*

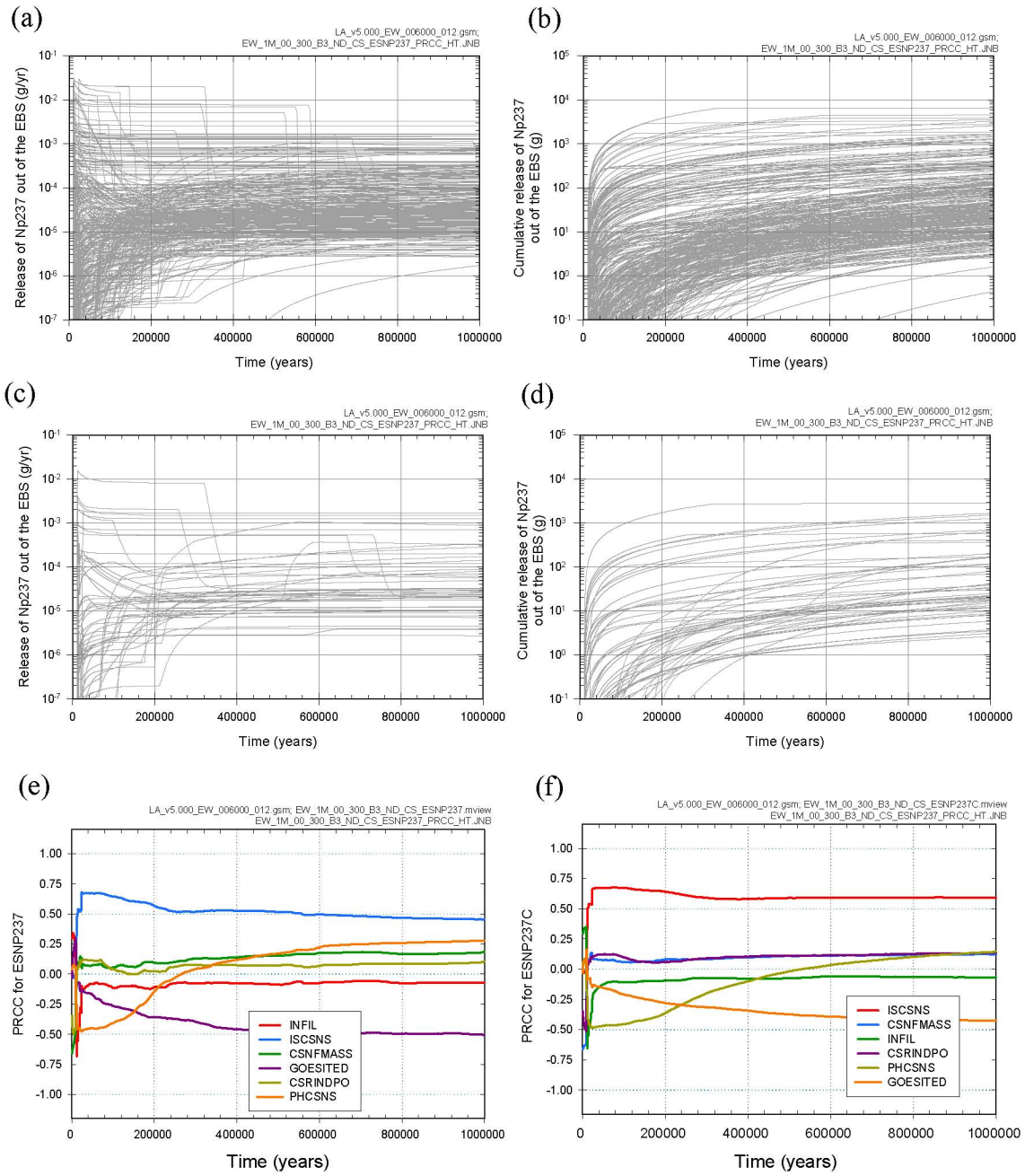

Source: Output DTNs: MO0709TSPAREGS.000 [DIRS 182976]; and MO0709TSPAPLOT.000 [DIRS 183010].

Figure K5.3.12-1. Time-dependent release rates (*ESNP237*, g/yr) and cumulative (i.e., integrated) releases (*ESNP237C*, g) over 1,000,000 years for the movement of dissolved ^{237}Np from the EBS to the UZ resulting from the early failure of a CSNF WP in percolation bin 3 under nondripping conditions: (a, b) *ESNP237* and *ESNP237C* for all (i.e., 300) sample elements, (c, d) *ESNP237* and *ESNP237C* for first 50 sample elements, and (e, f) PRCCs for *ESNP237* and *ESNP237C*.

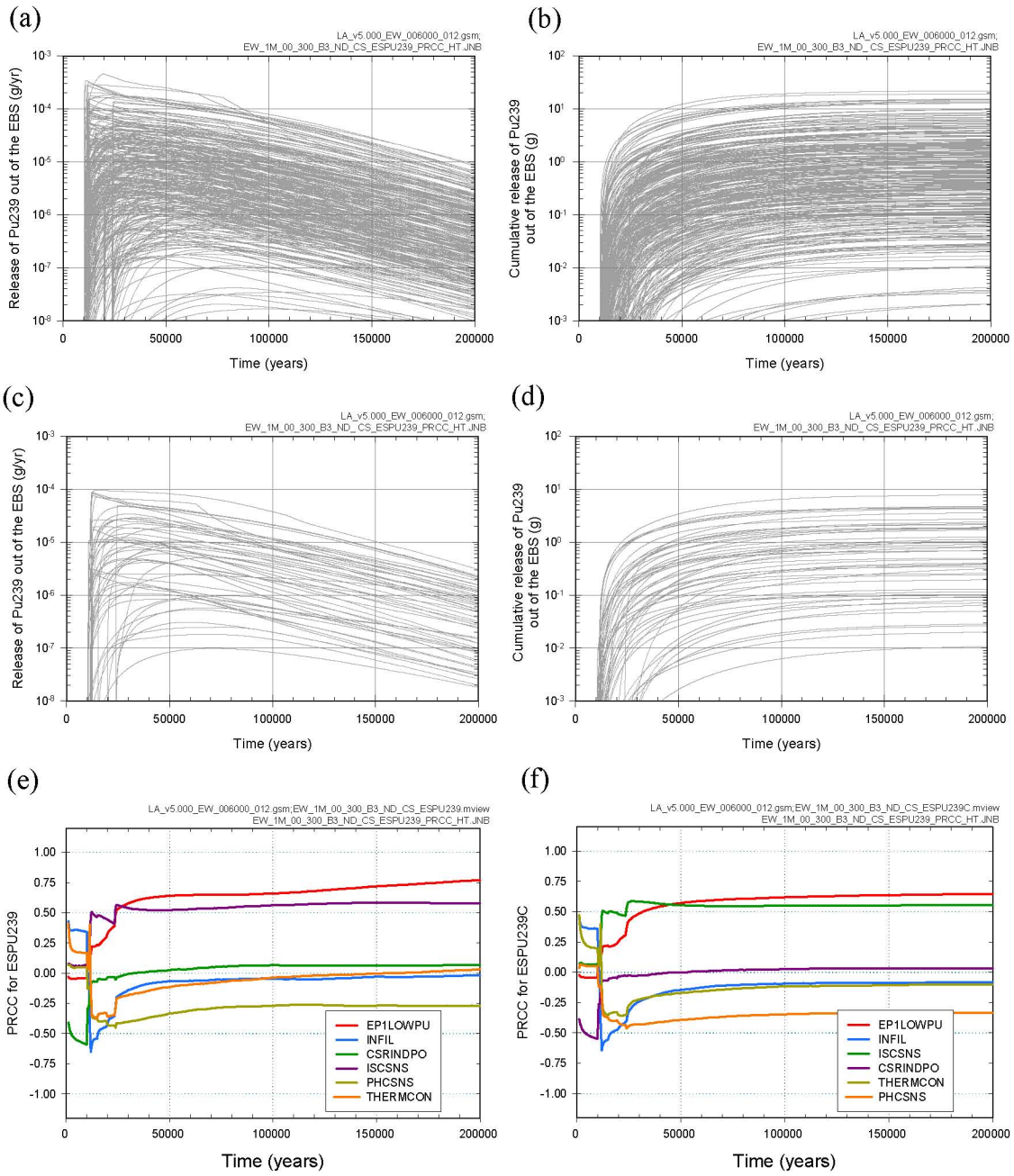

Source: Output DTNs: MO0709TSPAREGS.000 [DIRS 182976]; and MO0709TSPAPLOT.000 [DIRS 183010].

Figure K5.3.12-2. Time-dependent release rates (*ESPU239*, g/yr) and cumulative (i.e., integrated) releases (*ESPU239C*, g) over 200,000 years for the movement of dissolved ^{239}Pu from the EBS to the UZ resulting from the early failure of a CSNF WP in percolation bin 3 under nondripping conditions: (a, b) *ESPU239* and *ESPU239C* for all (i.e., 300) sample elements, (c, d) *ESPU239* and *ESPU239C* for first 50 sample elements, and (e, f) PRCCs for *ESPU239* and *ESPU239C*.

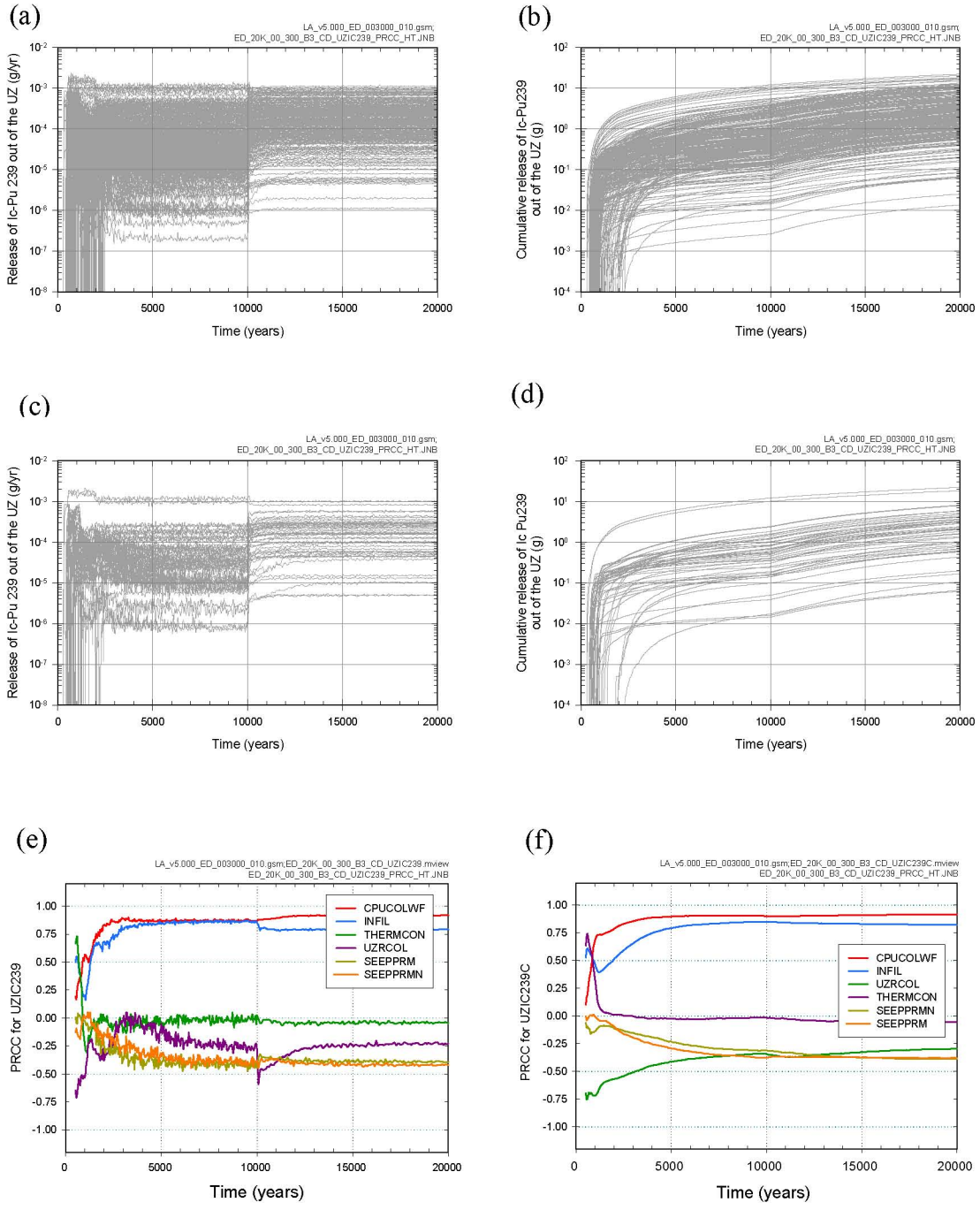

Source: Output DTNs: MO0709TSPASENS.000 [DIRS 183982]; and MO0709TSPAPLOT.000 [DIRS 183010].

Figure K5.4.1-1. Time-dependent release rates (*UZIC239*, g/yr) and cumulative (i.e., integrated) releases (*UZIC239C*, g) over 20,000 years for the movement of ^{239}Pu irreversibly attached to slow colloids from the UZ to the SZ resulting from a single early DS failure above a CDSP WP in percolation bin 3 under dripping conditions: (a, b) *UZIC239* and *UZIC239C* for all (i.e., 300) sample elements, (c, d) *UZIC239* and *UZIC239C* for first 50 sample elements, and (e, f) PRCCs for *UZIC239* and *UZIC239C*.

(a)

	UZIC239: 3000 yr			UZIC239: 5000 yr			UZIC239: 10,000 yr		
Step[a]	Variable[b]	R^{2c}	SRRC[d]	Variable	R^2	SRRC	Variable	R^2	SRRC
1	CPUCOLWF	0.48	0.64	INFIL	0.50	0.66	INFIL	0.51	0.68
2	INFIL	0.81	0.58	CPUCOLWF	0.82	0.58	CPUCOLWF	0.82	0.57
3	SEEPPRM	0.83	-0.15	SEEPPRM	0.85	-0.17	SEEPPRM	0.84	-0.18
4	ALPHAL	0.84	-0.11	SEEPPRMN	0.87	-0.14	SEEPPRMN	0.87	-0.15
5	SEEPPRMN	0.84	-0.09	ALPHAL	0.88	-0.11	ALPHAL	0.88	-0.12
6	SEEPUNC	0.85	0.07	SEEPUNC	0.88	0.07	SEEPUNC	0.89	0.08
7	CR2O3SA	0.85	-0.06	CORRATSS	0.89	-0.06	UZRCOL	0.89	-0.06
8	CORRATSS	0.86	-0.06	RUBMAXNL	0.89	-0.06	PHCSS	0.89	-0.06
9	CSNFMASS	0.86	0.06	PHCSS	0.89	-0.06	KDPASMEC	0.90	0.05

(b)

	UZIC239C: 3000 yr			UZIC239C: 5000 yr			UZIC239C: 10,000 yr		
Step[a]	Variable[b]	R^{2c}	SRRC[d]	Variable	R^2	SRRC	Variable	R^2	SRRC
1	CPUCOLWF	0.51	0.69	CPUCOLWF	0.53	0.70	CPUCOLWF	0.49	0.66
2	INFIL	0.73	0.48	INFIL	0.82	0.55	INFIL	0.85	0.60
3	UZRCOL	0.78	-0.22	UZRCOL	0.84	-0.13	SEEPPRM	0.86	-0.14
4	SEEPPRM	0.78	-0.09	SEEPPRM	0.85	-0.12	SEEPPRMN	0.88	-0.10
5	SEEPPRMN	0.79	-0.08	SEEPPRMN	0.86	-0.10	ALPHAL	0.89	-0.10
6	UZKDSRDT	0.79	0.07	ALPHAL	0.87	-0.08	UZRCOL	0.89	-0.08
7				KDPASMEC	0.87	0.06	SEEPUNC	0.90	0.06
8							KDPASMEC	0.90	0.06
9							CSNFMASS	0.90	0.05
10							KDAMCOL	0.90	-0.05

a: Steps in stepwise rank regression analysis
b: Variables listed in order of selection in stepwise regression
c: Cumulative R^2 value with entry of each variable into regression model
d: Standardized rank regression coefficients (SRRCs) in final regression model

Source: Output DTNs: MO0709TSPASENS.000 [DIRS 183982]; and MO0709TSPAPLOT.000 [DIRS 183010].

Figure K5.4.1-2. Stepwise rank regression analyses and selected scatterplots for time-dependent release rates (*UZIC239*, g/yr) and cumulative (i.e., integrated) releases (*UZIC239C*, g) for the movement of ^{239}Pu irreversibly attached to slow colloids from the UZ to the SZ resulting from a single early DS failure above a CDSP WP in percolation bin 3 under dripping conditions: (a, b) Regressions for *UZIC239* and *UZIC239C* at 3000, 5000 and 10,000 years, and (c-h) Scatterplots for *UZIC239* and *UZIC239C* at 10,000 years.

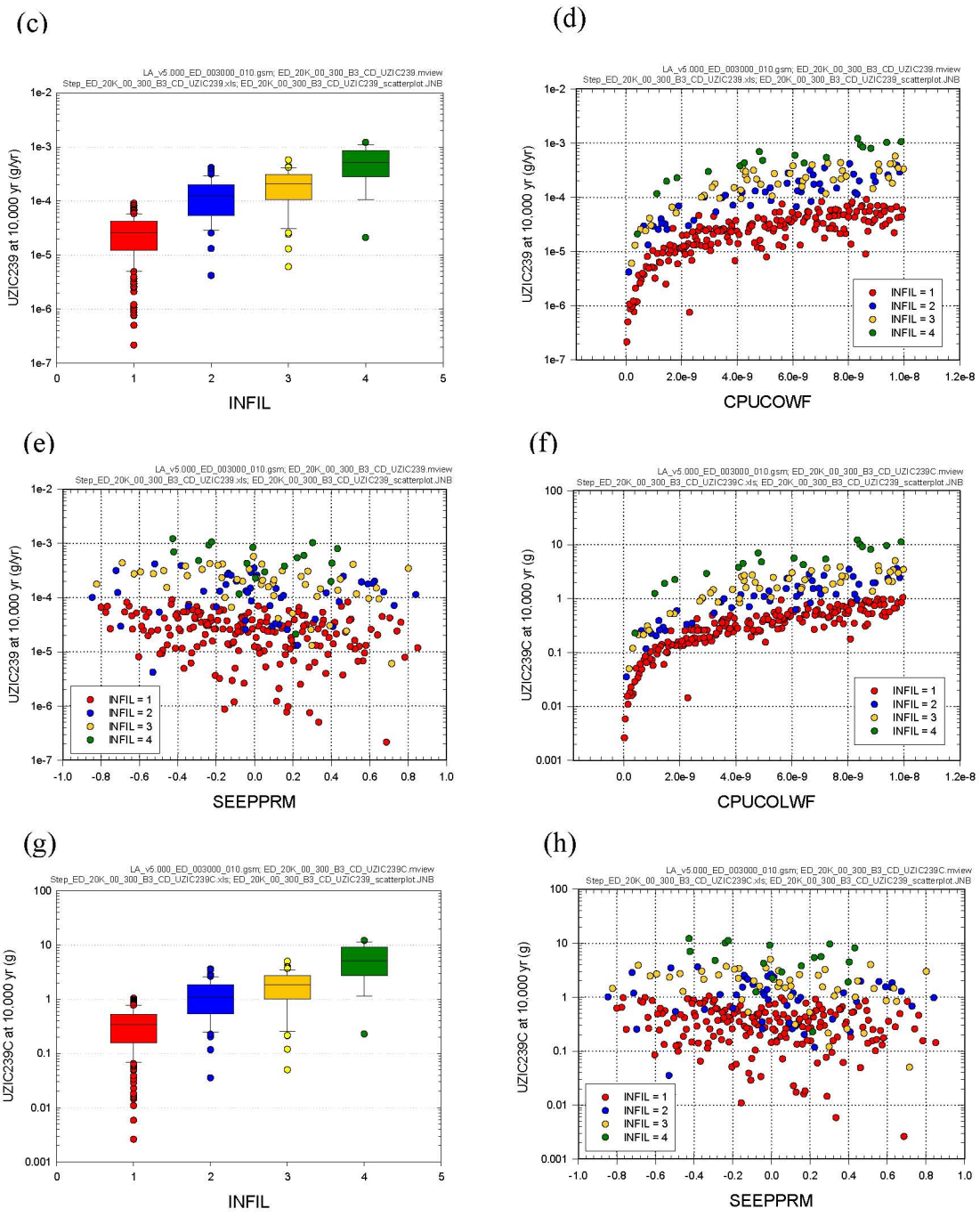

Source: Output DTNs: MO0709TSPASENS.000 [DIRS 183982]; and MO0709TSPAPLOT.000 [DIRS 183010].

NOTE: In (c, g), the box extends from 0.25 to 0.75 quantile; lower and upper bar and whisker extend to 0.1 and 0.9 quantile, respectively; dots represent values outside 0.1 to 0.9 quantile range; median indicated by light horizontal line.

Figure K5.4.1-2. Stepwise rank regression analyses and selected scatterplots for time-dependent release rates (*UZIC239*, g/yr) and cumulative (i.e., integrated) releases (*UZIC239C*, g) for the movement of ^{239}Pu irreversibly attached to slow colloids from the UZ to the SZ resulting from a single early DS failure above a CDSP WP in percolation bin 3 under dripping conditions: (a, b) Regressions for *UZIC239* and *UZIC239C* at 3000, 5000 and 10,000 years, and (c-h) Scatterplots for *UZIC239* and *UZIC239C* at 10,000 years (continued).

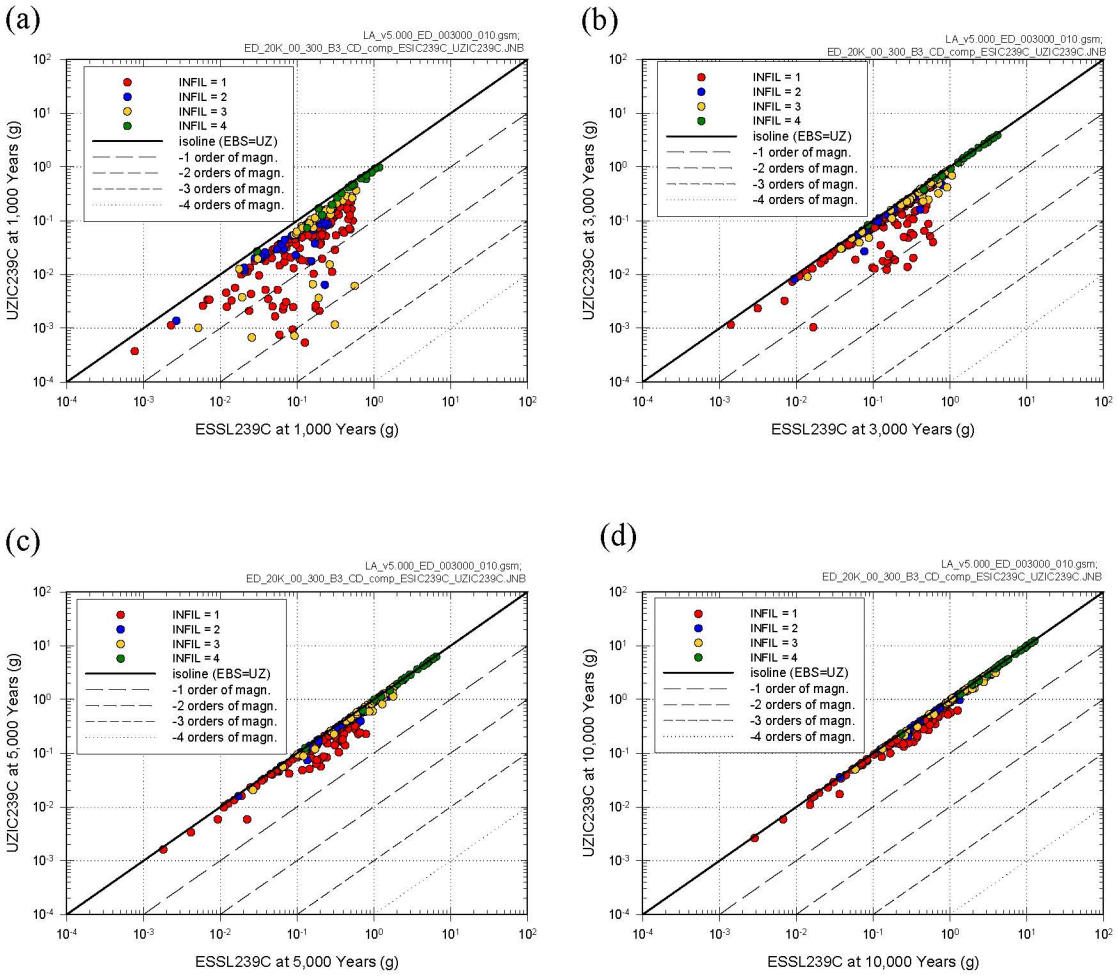

Source: Output DTN MO0709TSPASENS.000 [DIRS 183982].

Figure K5.4.1-3. Comparison of cumulative releases of ^{239}Pu irreversibly attached to slow colloids into the UZ (*ESSL239C*, g) and out of the UZ (*UZIC239C*, g) at (a) 1000 years, (b) 3000 years, (c) 5000 years and (d) 10,000 years for a single early DS failure above a CDSP WP in percolation bin 3 under dripping conditions.

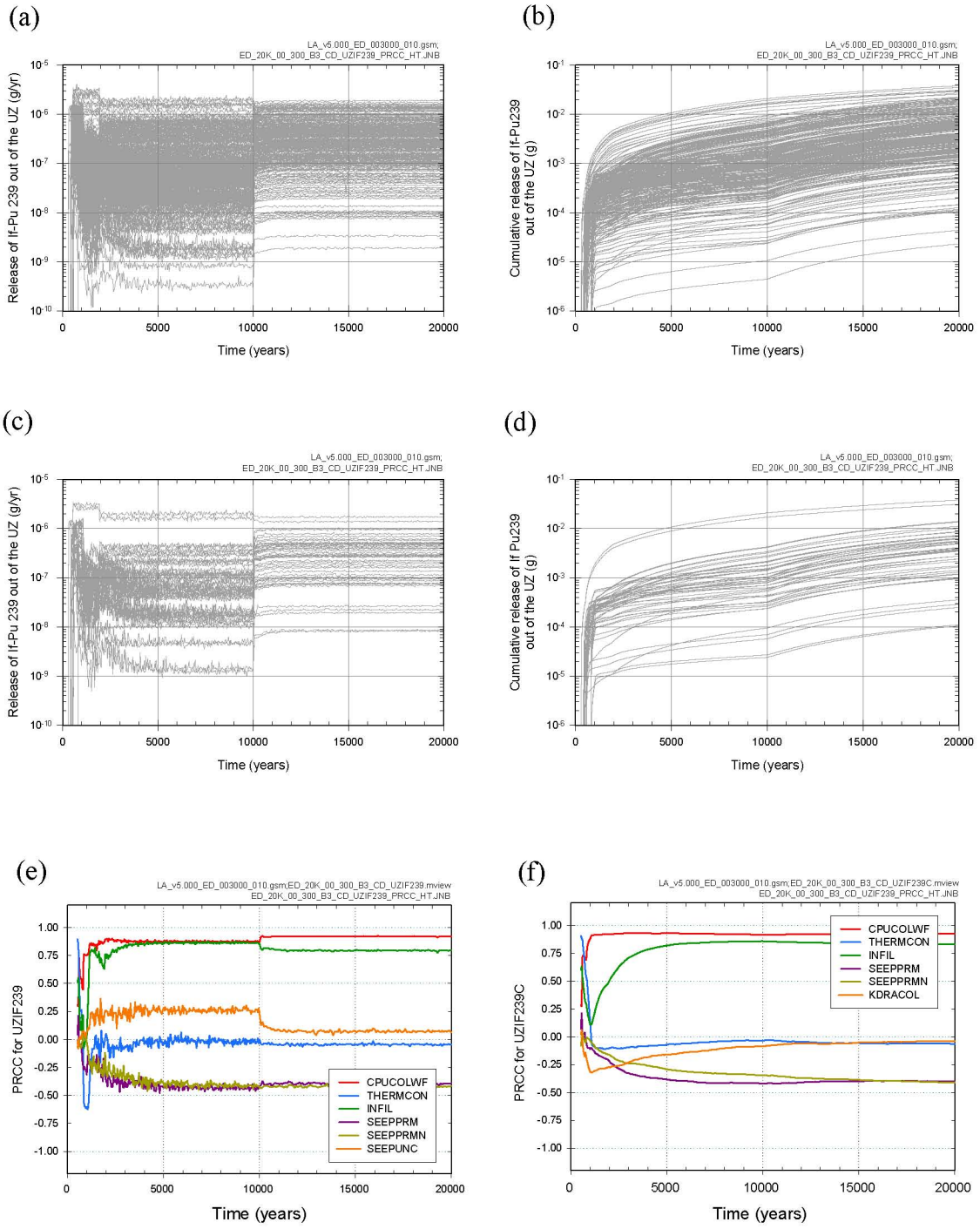

Source: Output DTNs: MO0709TSPASENS.000 [DIRS 183982]; and MO0709TSPAPLOT.000 [DIRS 183010].

Figure K5.4.1-4. Time-dependent release rates (*UZIF239*, g/yr) and cumulative (i.e., integrated) releases (*UZIF239C*, g) over 20,000 years for the movement of ^{239}Pu irreversibly attached to fast colloids from the UZ to the SZ resulting from a single early DS failure above a CDSP WP in percolation bin 3 under dripping conditions: (a, b) *UZIF239* and *UZIF239C* for all (i.e., 300) sample elements, (c, d) *UZIF239* and *UZIF239C* for first 50 sample elements, and (e, f) PRCCs for *UZIF239* and *UZIF239C*.

(a)

	UZIF239: 3000 yr			UZIF239: 5000 yr			UZIF239: 10,000 yr		
Step[a]	**Variable[b]**	**R^{2c}**	**SRRC[d]**	**Variable**	**R^2**	**SRRC**	**Variable**	**R^2**	**SRRC**
1	INFIL	0.46	0.63	INFIL	0.50	0.67	INFIL	0.50	0.67
2	CPUCOLWF	0.82	0.61	CPUCOLWF	0.83	0.58	CPUCOLWF	0.82	0.58
3	SEEPPRM	0.84	-0.16	SEEPPRM	0.85	-0.18	SEEPPRM	0.85	-0.18
4	SEEPPRMN	0.86	-0.14	SEEPPRMN	0.88	-0.14	SEEPPRMN	0.88	-0.16
5	ALPHAL	0.87	-0.10	ALPHAL	0.89	-0.11	ALPHAL	0.89	-0.13
6	SEEPUNC	0.87	0.07	SEEPUNC	0.89	0.07	SEEPUNC	0.90	0.07
7	KDPASMEC	0.88	0.06	PHCSS	0.89	-0.05			

(b)

	UZIF239C: 3000 yr			UZIF239C: 5000 yr			UZIF239C: 10,000 yr		
Step[a]	**Variable[b]**	**R^{2c}**	**SRRC[d]**	**Variable**	**R^2**	**SRRC**	**Variable**	**R^2**	**SRRC**
1	CPUCOLWF	0.67	0.79	CPUCOLWF	0.59	0.73	CPUCOLWF	0.51	0.68
2	INFIL	0.84	0.43	INFIL	0.86	0.54	INFIL	0.86	0.59
3	SEEPPRM	0.85	-0.11	SEEPPRM	0.87	-0.13	SEEPPRM	0.88	-0.15
4	SEEPPRMN	0.86	-0.09	SEEPPRMN	0.88	-0.10	SEEPPRMN	0.89	-0.10
5	ALPHAL	0.87	-0.07	ALPHAL	0.89	-0.08	ALPHAL	0.90	-0.10
6							SEEPUNC	0.90	0.06
7							KDPASMEC	0.91	0.05
8							CSNFMASS	0.91	0.05
9							KDAMCOL	0.91	-0.06
10							RHMUNO20	0.91	-0.05

a: Steps in stepwise rank regression analysis
b: Variables listed in order of selection in stepwise regression
c: Cumulative R^2 value with entry of each variable into regression model
d: Standardized rank regression coefficients (SRRCs) in final regression model

Source: Output DTNs: MO0709TSPASENS.000 [DIRS 183982]; and MO0709TSPAPLOT.000 [DIRS 183010].

Figure K 5.4.1-5 Stepwise rank regression analyses and selected scatterplots for time-dependent release rates (*UZIF239*, g/yr) and cumulative (i.e., integrated) releases (*UZIF239C*, g) for the movement of ^{239}Pu irreversibly attached to fast colloids from the UZ to the SZ resulting from a single early DS failure above a CDSP WP in percolation bin 3 under dripping conditions : (a, b) Regressions for *UZIF239* and *UZIF239C* at 3000, 5000 and 10,000 years, and (c-h) Scatterplots for *UZIF239* and *UZIF239C* at 10,000 years.

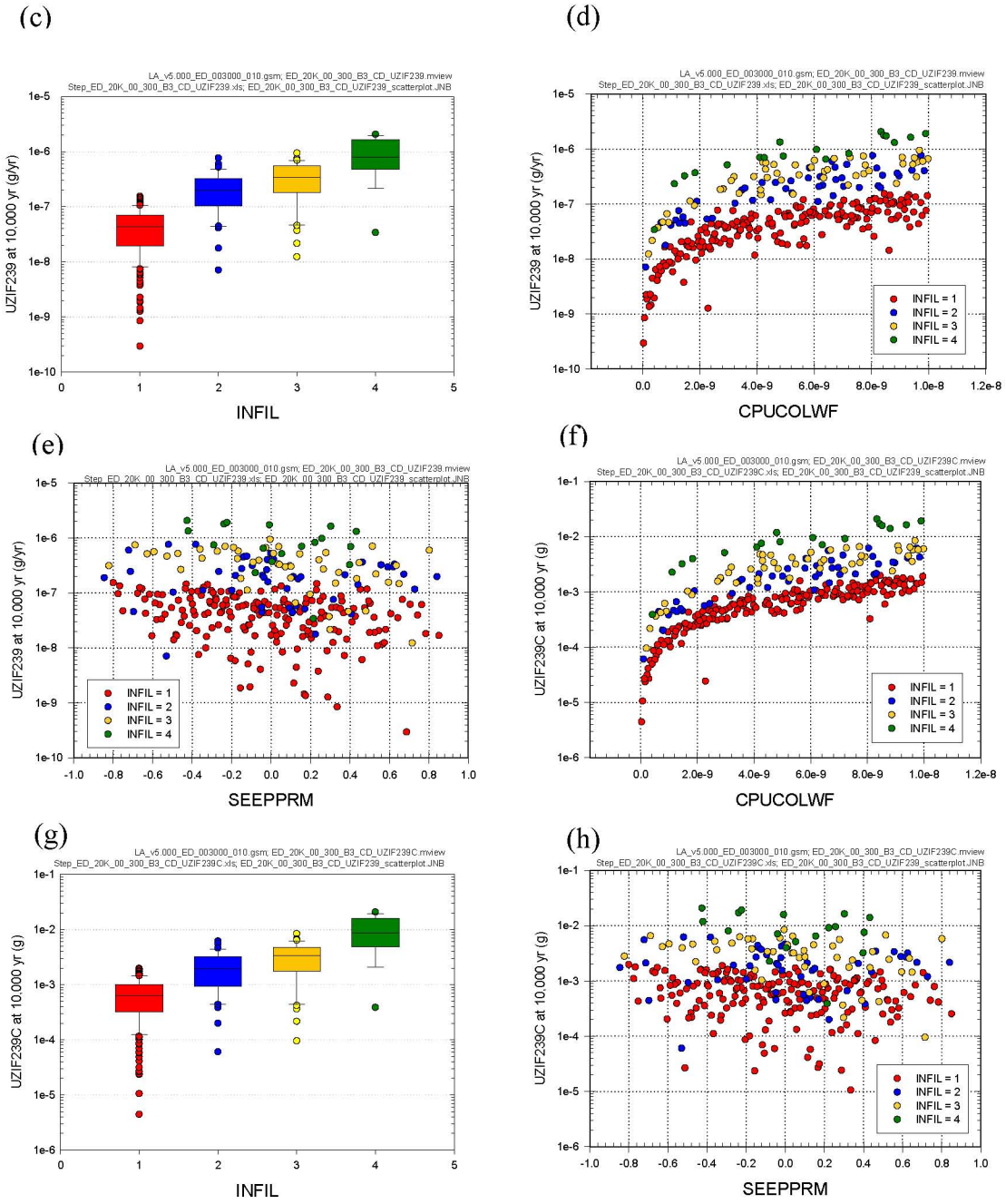

Source: Output DTNs: MO0709TSPASENS.000 [DIRS 183982]; and MO0709TSPAPLOT.000 [DIRS 183010].

NOTE: In (c, g), the box extends from 0.25 to 0.75 quantile; lower and upper bar and whisker extend to 0.1 and 0.9 quantile, respectively; dots represent values outside 0.1 to 0.9 quantile range; median indicated by light horizontal line.

Figure K 5.4.1-5. Stepwise rank regression analyses and selected scatterplots for time-dependent release rates (*UZIF239*, g/yr) and cumulative (i.e., integrated) releases (*UZIF239C*, g) for the movement of ^{239}Pu irreversibly attached to fast colloids from the UZ to the SZ resulting from a single early DS failure above a CDSP WP in percolation bin 3 under dripping conditions : (a, b) Regressions for *UZIF239* and *UZIF239C* at 3000, 5000 and 10,000 years, and (c-h) Scatterplots for *UZIF239* and *UZIF239C* at 10,000 years (continued).

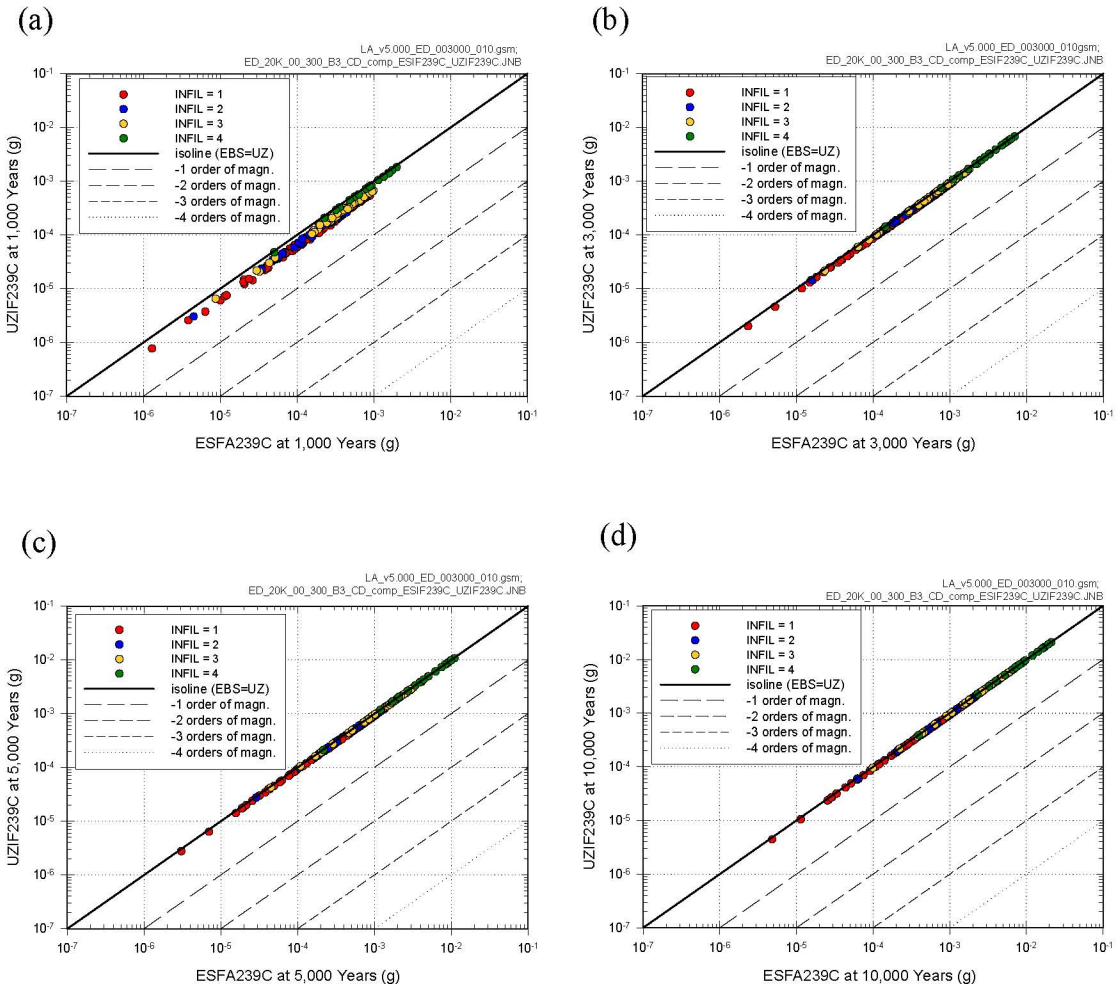

Source: Output DTN MO0709TSPASENS.000 [DIRS 183982].

Figure K5.4.1-6. Comparison of cumulative releases of ^{239}Pu irreversibly attached to fast colloids into the UZ (*ESFA239C*, g) and out of the UZ (*UZIF239C*, g) at (a) 1000 years, (b) 3000 years, (c) 5000 years and (d) 10,000 years for a single early DS failure above a CDSP WP in percolation bin 3 under dripping conditions.

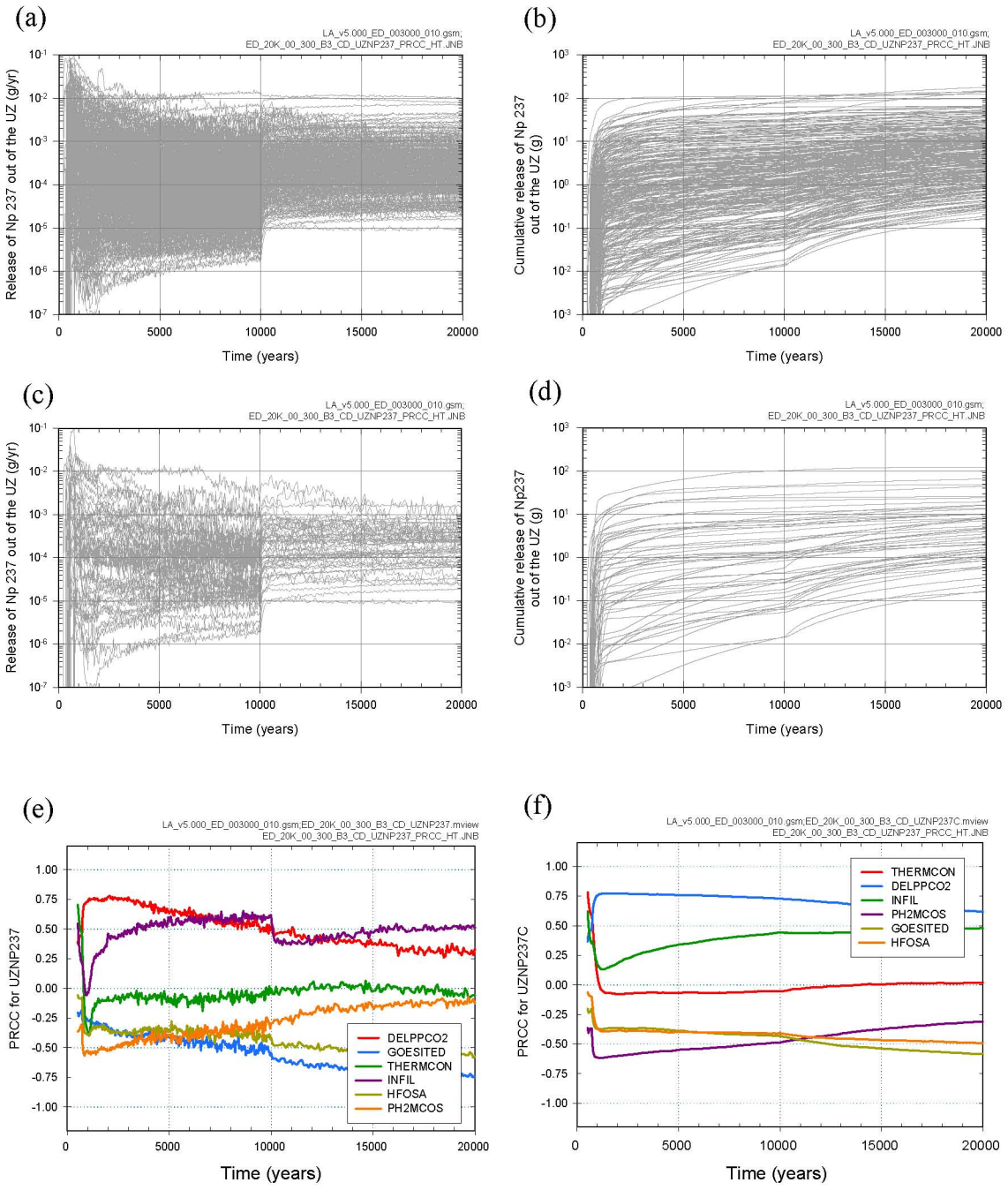

Source: Output DTNs: MO0709TSPASENS.000 [DIRS 183982]; and MO0709TSPAPLOT.000 [DIRS 183010].

Figure K5.4.1-7. Time-dependent release rates (*UZNP237*, g/yr) and cumulative (i.e., integrated) releases (*UZNP237C*, g) over 20,000 years for the movement of dissolved ^{237}Np from the UZ to the SZ resulting from a single early DS failure above a CDSP WP in percolation bin 3 under dripping conditions: (a, b) *UZNP237* and *UZNP237C* for all (i.e., 300) sample elements, (c, d) *UZNP237* and *UZNP237C* for first 50 sample elements, and (e, f) PRCCs for *UZNP237* and *UZNP237C*.

(a)

	UZNP237: 3000 yr			UZNP237: 5000 yr			UZNP237: 10,000 yr		
Step[a]	Variable[b]	R^{2c}	SRRC[d]	Variable	R^2	SRRC	Variable	R^2	SRRC
1	DELPPCO2	0.28	0.55	INFIL	0.20	0.43	INFIL	0.28	0.52
2	INFIL	0.42	0.33	DELPPCO2	0.38	0.43	GOESITED	0.36	-0.31
3	PH2MCOS	0.53	-0.33	PH2MCOS	0.45	-0.28	DELPPCO2	0.44	0.30
4	EP1LOWAM	0.57	0.19	GOESITED	0.49	-0.22	DSNFMASS	0.48	0.17
5	COLGW	0.60	0.18	KDAMSMEC	0.53	0.18	HFOSA	0.51	-0.22
6	KDAMSMEC	0.63	0.17	EP1LOWAM	0.55	0.17	KDAMSMEC	0.55	0.15
7	GOESITED	0.66	-0.18	DSNFMASS	0.57	0.14	PH2MCOS	0.57	-0.21
8	DSNFMASS	0.67	0.13	HFOSA	0.59	-0.17	IS2MCOS	0.59	0.14
9	HFOSA	0.69	-0.14	GOESA	0.61	-0.15	COLGW	0.60	0.14
10	GOESA	0.70	-0.13	COLGW	0.63	0.12	EP1LOWNU	0.62	0.12
11	WDCRCDEN	0.71	0.11	GOERELAB	0.64	0.11	GOESA	0.63	-0.13
12	IS2MCOS	0.72	0.09	HFOSITED	0.65	-0.10	GOERELAB	0.64	0.12
13	RHPH75	0.73	-0.08	IS2MCOS	0.66	0.11	EP1LOWAM	0.65	0.11
14	GOERELAB	0.73	0.08	EP1LOWNU	0.68	0.11	UZKDNPDT	0.67	-0.12
15				RHPH75	0.69	-0.10	CPUPERCS	0.67	-0.10
16							DWCSTERD	0.68	0.10

(b)

	UZNP237C: 3000 yr			UZNP237C: 5000 yr			UZNP237C: 10,000 yr		
Step[a]	Variable[b]	R^{2c}	SRRC[d]	Variable	R^2	SRRC	Variable	R^2	SRRC
1	DELPPCO2	0.30	0.58	DELPPCO2	0.29	0.57	DELPPCO2	0.25	0.53
2	PH2MCOS	0.46	-0.39	PH2MCOS	0.43	-0.38	INFIL	0.37	0.31
3	EP1LOWAM	0.53	0.21	INFIL	0.51	0.23	PH2MCOS	0.48	-0.33
4	COLGW	0.59	0.23	COLGW	0.55	0.22	GOESITED	0.52	-0.21
5	INFIL	0.61	0.17	EP1LOWAM	0.60	0.20	KDAMSMEC	0.56	0.17
6	GOESITED	0.64	-0.18	GOESITED	0.63	-0.18	COLGW	0.59	0.20
7	KDAMSMEC	0.67	0.16	KDAMSMEC	0.66	0.17	EP1LOWAM	0.62	0.18
8	GOESA	0.68	-0.13	GOESA	0.67	-0.14	DSNFMASS	0.64	0.14
9	UZKDNPDT	0.70	-0.11	UZKDNPDT	0.68	-0.11	GOESA	0.66	-0.15
10	HFOSA	0.71	-0.11	HFOSA	0.69	-0.13	HFOSA	0.67	-0.14
11	EP1NPO2	0.71	0.10	DSNFMASS	0.70	0.11	WDCRCDEN	0.68	0.12
12	WDCRCDEN	0.72	0.12	WDCRCDEN	0.72	0.13	UZKDNPDT	0.70	-0.12
13	DSNFMASS	0.73	0.10	EP1NPO2	0.72	0.09	IS2MCOS	0.71	0.10
14				IS2MCOS	0.73	0.09			

a: Steps in stepwise rank regression analysis
b: Variables listed in order of selection in stepwise regression
c: Cumulative R^2 value with entry of each variable into regression model
d: Standardized rank regression coefficients (SRRCs) in final regression model

Source: Output DTNs: MO0709TSPASENS.000 [DIRS 183982]; and MO0709TSPAPLOT.000 [DIRS 183010].

Figure K 5.4.1-8. Stepwise rank regression analyses and selected scatterplots for time-dependent release rates (*UZNP237*, g/yr) and cumulative (i.e., integrated) releases (*UZNP237C*, g) for the movement of dissolved ^{237}Np from the EBS to the UZ resulting from a single early DS failure above a CDSP WP in percolation bin 3 under dripping conditions: (a, b) Regressions for *UZNP237* and *UZNP237C* at 3000, 5000 and 10,000 years, and (c-h) Scatterplots for *UZNP237* and *UZNP237C* at 10,000 years.

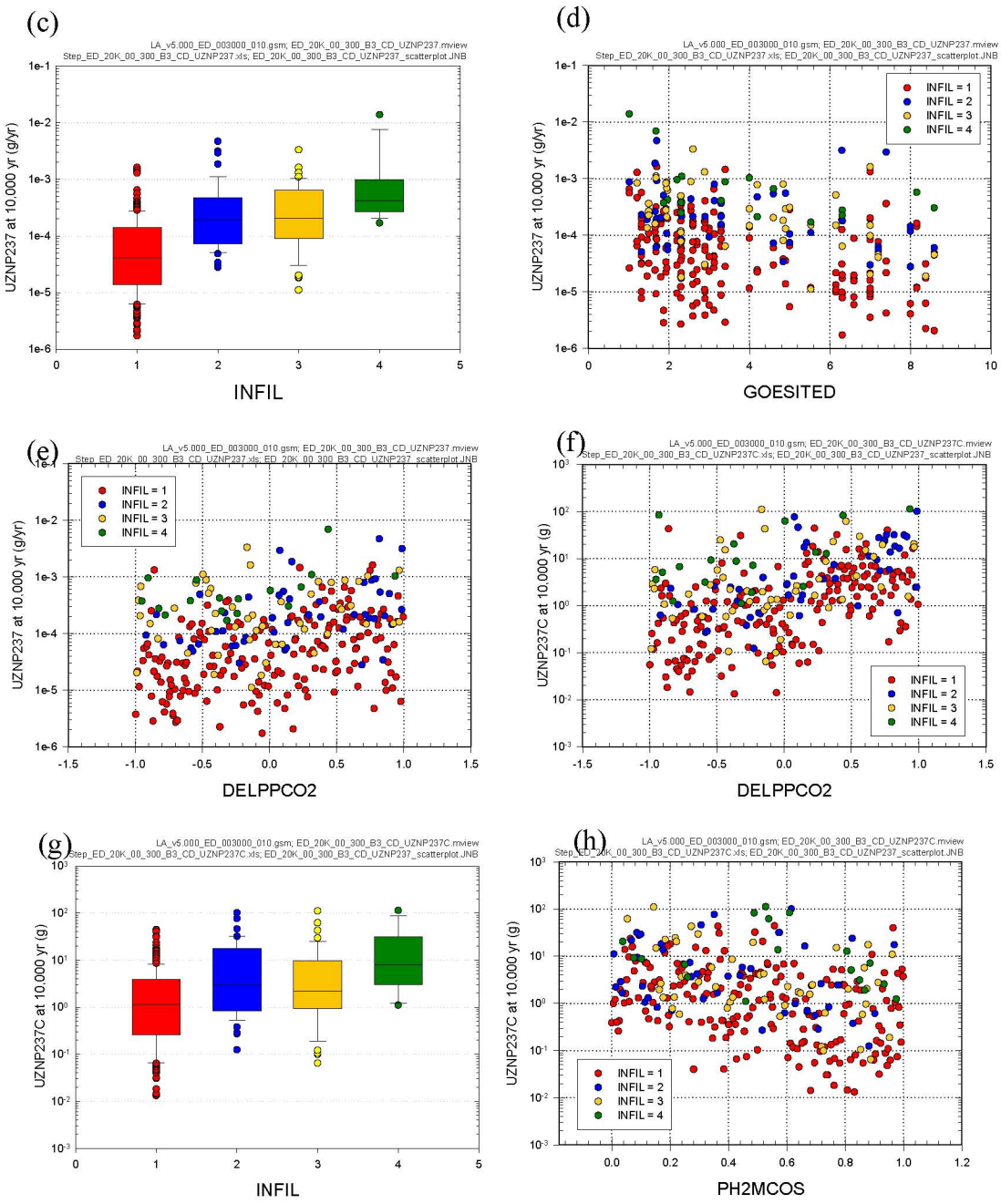

Source: Output DTNs: MO0709TSPASENS.000 [DIRS 183982]; and MO0709TSPAPLOT.000 [DIRS 183010].

NOTE: In (c, g), the box extends from 0.25 to 0.75 quantile; lower and upper bar and whisker extend to 0.1 and 0.9 quantile, respectively; dots represent values outside 0.1 to 0.9 quantile range; median indicated by light horizontal line.

Figure K5.4.1-8. Stepwise rank regression analyses and selected scatterplots for time-dependent release rates (*UZNP237*, g/yr) and cumulative (i.e., integrated) releases (*UZNP237C*, g) for the movement of dissolved ^{237}Np from the EBS to the UZ resulting from a single early DS failure above a CDSP WP in percolation bin 3 under dripping conditions: (a, b) Regressions for *UZNP237* and *UZNP237C* at 3000, 5000 and 10,000 years, and (c-h) Scatterplots for *UZNP237* and *UZNP237C* at 10,000 years (continued).

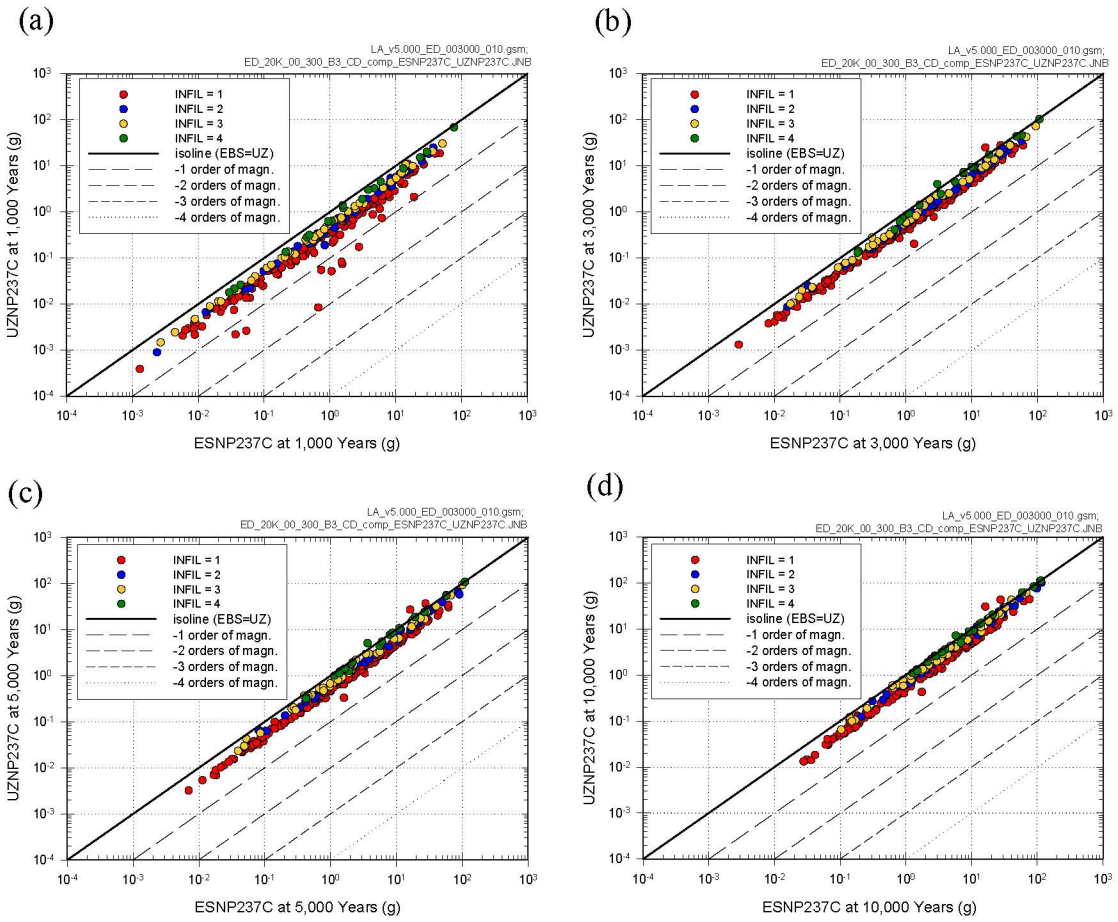

Source: Output DTN MO0709TSPASENS.000 [DIRS 183982].

Figure K5.4.1-9. Comparison of cumulative releases of dissolved ^{237}Np into the UZ (*ESNP237C*, g) and out of the UZ (*UZNP237C*, g) at (a) 1000 years, (b) 3000 years, (c) 5000 years and (d) 10,000 years for a single early DS failure above a CDSP WP in percolation bin 3 under dripping conditions.

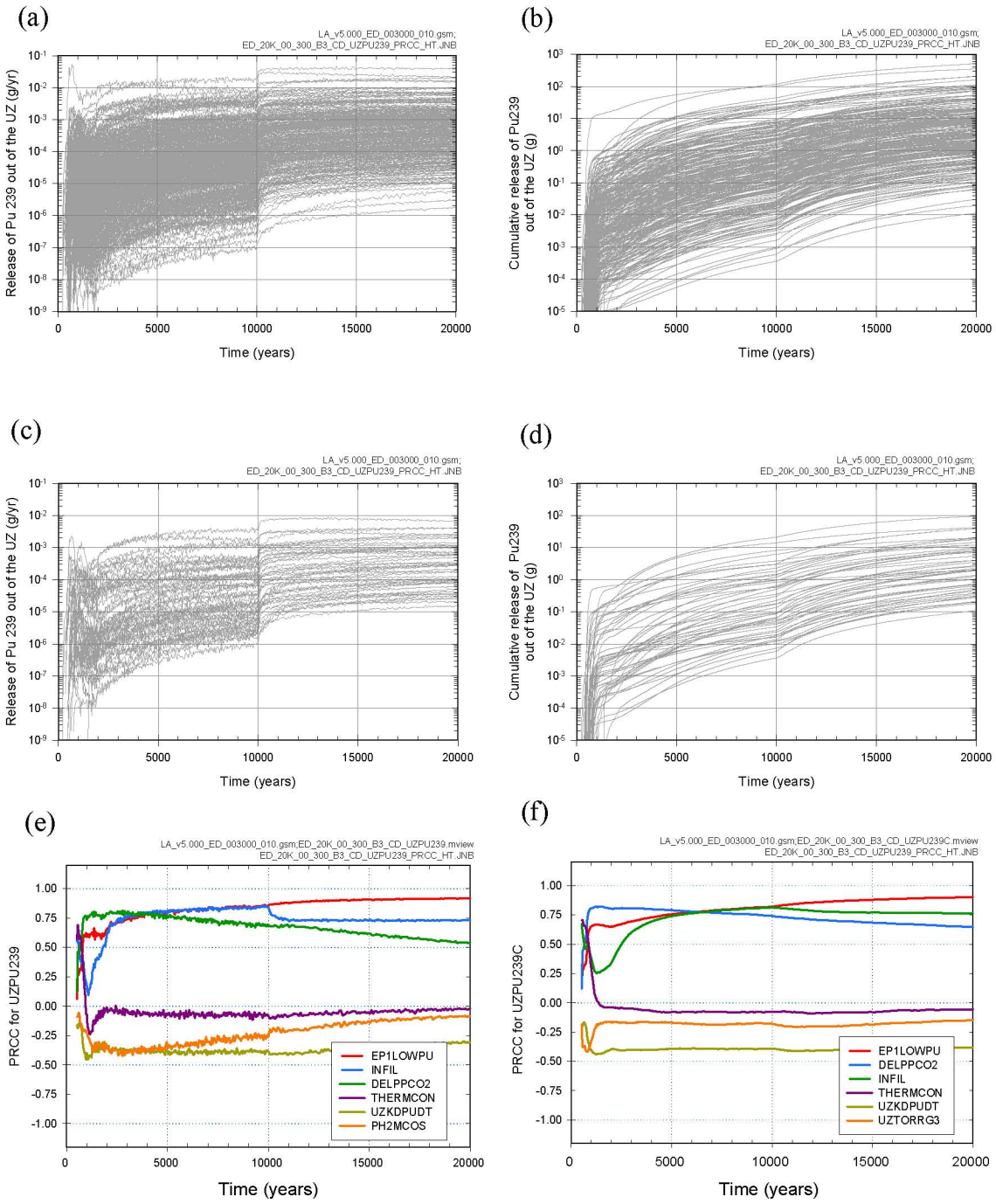

Source: Output DTNs: MO0709TSPASENS.000 [DIRS 183982]; and MO0709TSPAPLOT.000 [DIRS 183010].

Figure K5.4.1-10. Time-dependent release rates (*UZPU239*, g/yr) and cumulative (i.e., integrated) releases (*UZPU239C*, g) over 20,000 years for the movement of dissolved ^{239}Pu from the UZ to the SZ resulting from a single early DS failure above a CDSP WP in percolation bin 3 under dripping conditions: (a, b) *UZPU239* and *UZPU239C* for all (i.e., 300) sample elements, (c, d) *UZPU239* and *UZPU239C* for first 50 sample elements, and (e, f) PRCCs for *UZPU239* and *UZPU239C*.

(a)

	UZPU239: 3000 yr			UZPU239: 5000 yr			UZPU239: 10,000 yr		
Step[a]	Variable[b]	R^{2c}	SRRC[c]	Variable	R^2	SRRC	Variable	R^2	SRRC
1	INFIL	0.25	0.49	INFIL	0.30	0.56	EP1LOWPU	0.35	0.59
2	EP1LOWPU	0.46	0.47	EP1LOWPU	0.56	0.54	INFIL	0.68	0.59
3	DELPPCO2	0.68	0.50	DELPPCO2	0.73	0.43	DELPPCO2	0.78	0.32
4	UZKDPUDT	0.75	-0.31	UZKDPUDT	0.80	-0.25	UZKDPUDT	0.83	-0.21
5	PH2MCOS	0.78	-0.17	PH2MCOS	0.81	-0.12	PH2MCOS	0.84	-0.08
6	GOESITED	0.79	-0.12	GOESITED	0.83	-0.12	SEEPPRM	0.85	-0.11
7	GOESA	0.80	-0.10	EBSDIFCF	0.83	0.09	EBSDIFCF	0.85	0.08
8	SCHOBOLT	0.81	0.09	HFOSA	0.84	-0.09	ALPHAL	0.86	-0.08
9	HFOSA	0.81	-0.10	SCHOBOLT	0.84	0.07	GOESITED	0.87	-0.08
10	EBSDIFCF	0.82	0.08	GOESA	0.85	-0.07	EP1LOWNU	0.87	0.08
11	IS2MCOS	0.82	0.08	IS2MCOS	0.85	0.07	SCHOBOLT	0.87	0.07
12	EP1LOWNU	0.83	0.09	DIFPATHL	0.86	-0.07	HFOSA	0.88	-0.07
13	EP1LOWAM	0.83	0.08	EP1LOWNU	0.86	0.08	IS2MCOS	0.88	0.06
14	SEEPPRM	0.84	-0.09	SEEPPRM	0.87	-0.08	DIFPATHL	0.89	-0.07
15	FWDRAT	0.84	0.07	ALPHAL	0.87	-0.08	WDGCUA22	0.89	-0.06
16	COLGW	0.85	0.07	CPUCOLCS	0.87	-0.06	SEEPPRMN	0.89	-0.07

(b)

	UZPU239C: 3000 yr			UZPU239C: 5000 yr			UZPU239C: 10,000 yr		
Step[a]	Variable[b]	R^{2c}	SRRC[d]	Variable	R^2	SRRC	Variable	R^2	SRRC
1	DELPPCO2	0.25	0.58	EP1LOWPU	0.24	0.50	INFIL	0.31	0.55
2	EP1LOWPU	0.48	0.47	INFIL	0.46	0.48	EP1LOWPU	0.59	0.56
3	INFIL	0.64	0.37	DELPPCO2	0.68	0.51	DELPPCO2	0.73	0.40
4	UZKDPUDT	0.73	-0.28	UZKDPUDT	0.76	-0.26	UZKDPUDT	0.80	-0.24
5	PH2MCOS	0.75	-0.16	PH2MCOS	0.78	-0.15	PH2MCOS	0.81	-0.11
6	GOESITED	0.77	-0.14	GOESITED	0.80	-0.13	GOESITED	0.82	-0.11
7	GOESA	0.78	-0.10	GOESA	0.81	-0.09	SEEPPRM	0.83	-0.09
8	SCHOBOLT	0.79	0.09	SCHOBOLT	0.81	0.09	GOESA	0.84	-0.07
9	HFOSA	0.79	-0.09	HFOSA	0.82	-0.10	SCHOBOLT	0.84	0.08
10	EP1LOWNU	0.80	0.07	EP1LOWNU	0.82	0.08	EBSDIFCF	0.85	0.08
11	COLGW	0.80	0.07	EBSDIFCF	0.83	0.08	EP1LOWNU	0.85	0.09
12				IS2MCOS	0.83	0.07	HFOSA	0.86	-0.08
13							ALPHAL	0.86	-0.07
14							IS2MCOS	0.87	0.07
15							DIFPATHL	0.87	-0.07
16							WDGCUA22	0.87	-0.06

a: Steps in stepwise rank regression analysis
b: Variables listed in order of selection in stepwise regression
c: Cumulative R^2 value with entry of each variable into regression model
d: Standardized rank regression coefficients (SRRCs) in final regression model

Source: Output DTNs: MO0709TSPASENS.000 [DIRS 183982]; and MO0709TSPAPLOT.000 [DIRS 183010].

Figure K5.4.1-11. Stepwise rank regression analyses and selected scatterplots for time-dependent release rates (*UZPU239*, g/yr) and cumulative (i.e., integrated) releases (*UZPU239*, g) for the movement of dissolved ^{239}Pu from the UZ to the SZ resulting from a single early DS failure above a CDSP WP in percolation bin 3 under dripping conditions: (a, b) Regressions for *UZPU239* and *UZPU239C* at 3000, 5000 and 10,000 years, and (c-h) Scatterplots for *UZPU239* and *UZPU239C* at 10,000 years.

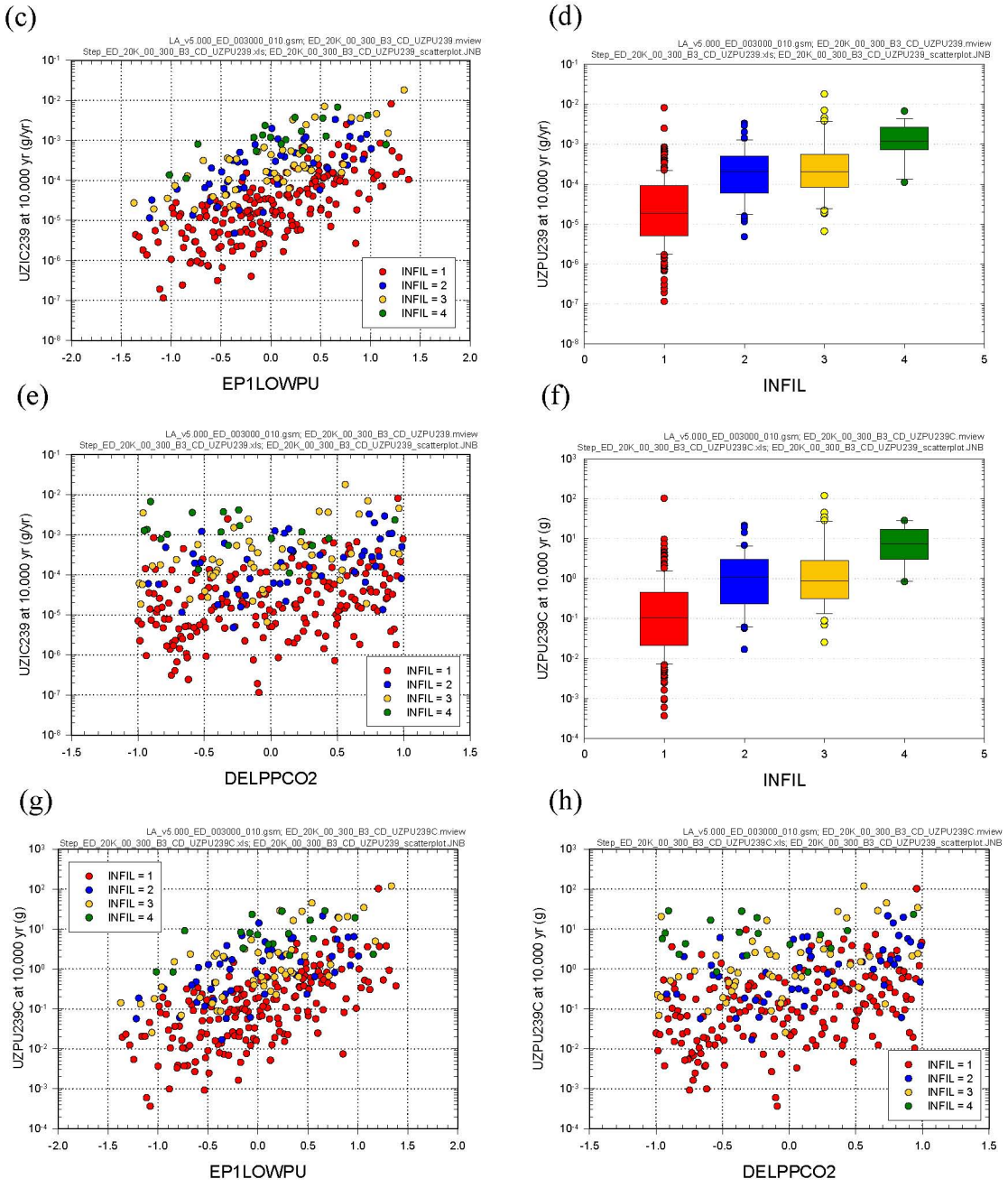

Source: Output DTNs: MO0709TSPASENS.000 [DIRS 183982]; and MO0709TSPAPLOT.000 [DIRS 183010].

NOTE: In (d, f), the box extends from 0.25 to 0.75 quantile; lower and upper bar and whisker extend to 0.1 and 0.9 quantile, respectively; dots represent values outside 0.1 to 0.9 quantile range; median indicated by light horizontal line.

Figure K5.4.1-11 Stepwise rank regression analyses and selected scatterplots for time-dependent release rates (*UZPU239*, g/yr) and cumulative (i.e., integrated) releases (*UZPU239*, g) for the movement of dissolved ^{239}Pu from the UZ to the SZ resulting from a single early DS failure above a CDSP WP in percolation bin 3 under dripping conditions: (a, b) Regressions for *UZPU239* and *UZPU239C* at 3000, 5000 and 10,000 years, and (c-h) Scatterplots for *UZPU239* and *UZPU239C* at 10,000 years (continued).

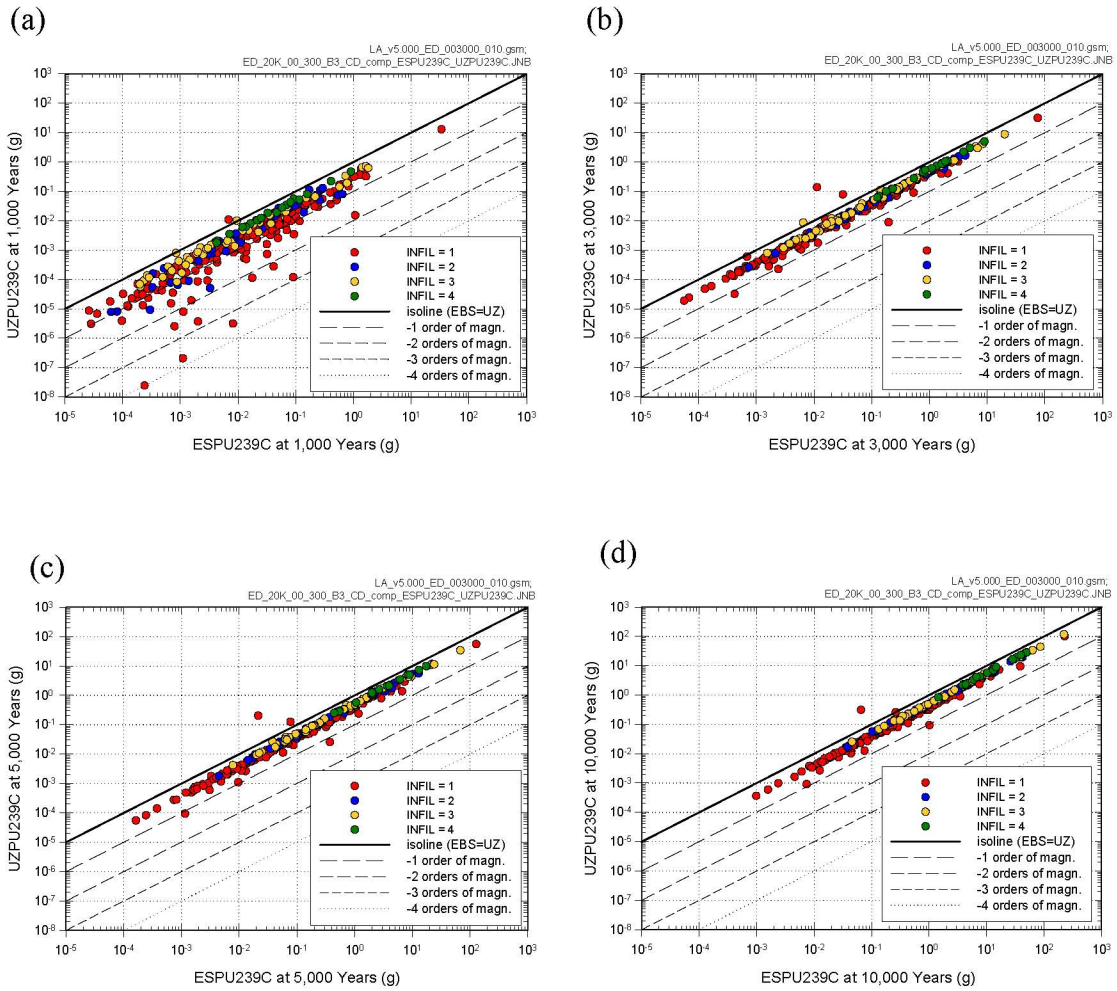

Source: Output DTN MO0709TSPASENS.000 [DIRS 183982].

Figure K5.4.1-12. Comparison of cumulative releases of dissolved ^{239}Pu into the UZ (*ESPU239C*, g) and out of the UZ (*UZPU239C*, g) at (a) 1000 years, (b) 3000 years, (c) 5000 years and (d) 10,000 years for a single early DS failure above a CDSP WP in percolation bin 3 under dripping conditions.

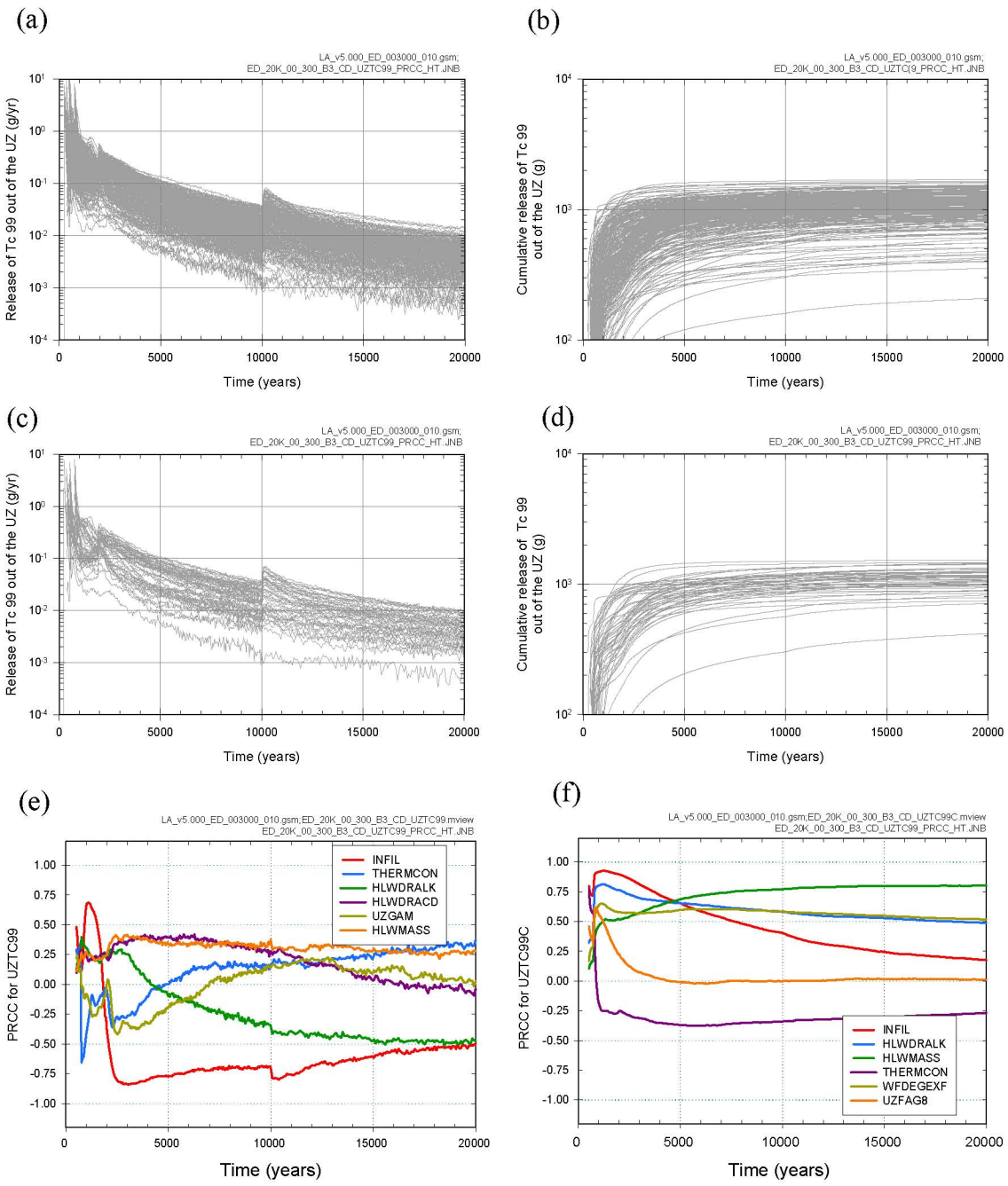

Source: Output DTNs: MO0709TSPASENS.000 [DIRS 183982]; and MO0709TSPAPLOT.000 [DIRS 183010].

Figure K5.4.1-13. Time-dependent release rates (*UZTC99*, g/yr) and cumulative (i.e., integrated) releases (*UZTC99C*, g) over 20,000 years for the movement of dissolved ^{99}Tc from the UZ to the SZ resulting from a single early DS failure above a CDSP WP in percolation bin 3 under dripping conditions: (a, b) *UZTC99* and *UZTC99C* for all (i.e., 300) sample elements, (c, d) *UZTC99* and *UZTC99C* for first 50 sample elements, and (e, f) PRCCs for *UZTC99* and *UZTC99C*.

(a)

	UZTC99: 3000 yr			UZTC99: 5000 yr			UZTC99: 10,000 yr		
Step[a]	Variable[b]	R^{2c}	SRRC[d]	Variable	R^2	SRRC	Variable	R^2	SRRC
1	INFIL	0.59	-0.79	INFIL	0.58	-0.76	INFIL	0.46	-0.64
2	HLWMASS	0.64	0.22	HLWDRACD	0.62	0.21	HLWDRALK	0.51	-0.25
3	HLWDRACD	0.69	0.19	HLWMASS	0.66	0.19	HLWMASS	0.55	0.20
4	UZTORRG3	0.71	0.15	PH2DHLS	0.67	-0.12	HLWDRACD	0.57	0.16
5	PH2DHLS	0.73	-0.18	UZFAG1	0.68	0.09	UZTORRG3	0.58	-0.11
6	HLWDRALK	0.75	0.11				GP4NO3	0.60	-0.13
7	UZFAG8	0.76	-0.12				UZGAM	0.61	0.12
8	DSNFMASS	0.77	0.10				UZFAG8	0.62	0.11
9	WFDEGEXF	0.78	0.10						
10	UZGAM	0.79	-0.11						
11	THERMCON	0.80	-0.09						
12	UZFAG3	0.80	0.10						
13	RUBMAXNL	0.81	0.07						

(b)

	UZTC99C: 3000 yr			UZTC99C: 5000 yr			UZTC99C: 10,000 yr		
Step[a]	Variable[b]	R^{2c}	SRRC[d]	Variable	R^2	SRRC	Variable	R^2	SRRC
1	INFIL	0.33	0.58	HLWDRALK	0.20	0.41	HLWMASS	0.30	0.57
2	HLWDRALK	0.52	0.42	HLWMASS	0.36	0.47	HLWDRALK	0.43	0.34
3	HLWMASS	0.63	0.34	INFIL	0.53	0.38	HLWDRACD	0.53	0.33
4	WFDEGEXF	0.69	0.24	WFDEGEXF	0.61	0.28	DSNFMASS	0.63	0.31
5	HLWDRACD	0.74	0.22	HLWDRACD	0.69	0.28	WFDEGEXF	0.71	0.26
6	DSNFMASS	0.79	0.23	DSNFMASS	0.76	0.27	PH2DHLS	0.77	-0.23
7	PH2DHLS	0.81	-0.15	PH2DHLS	0.79	-0.19	INFIL	0.79	0.17
8	THERMCON	0.82	-0.11	THERMCON	0.81	-0.13	THERMCON	0.81	-0.11
9	IPCNDMVF	0.83	0.07	IPCNDMVF	0.82	0.09	IPCNDMVF	0.81	0.10
10				DELPPCO2	0.82	0.07	CSRINDPO	0.82	0.09
11							CORRATSS	0.82	-0.08
12							UZFAG4	0.83	0.07

a: Steps in stepwise rank regression analysis
b: Variables listed in order of selection in stepwise regression
c: Cumulative R^2 value with entry of each variable into regression model
d: Standardized rank regression coefficients (SRRCs) in final regression model

Source: Output DTNs: MO0709TSPASENS.000 [DIRS 183982]; and MO0709TSPAPLOT.000 [DIRS 183010].

Figure K5.4.1-14. Stepwise rank regression analyses and selected scatterplots for time-dependent release rates (*UZTC99*, g/yr) and cumulative (i.e., integrated) releases (*UZTC99*, g) for the movement of dissolved ^{99}Tc from the UZ to the SZ resulting from a single early DS failure above a CDSP WP in percolation bin 3 under dripping conditions: (a, b) Regressions for *UZTC99* and *UZTC99C* at 3000, 5000 and 10,000 years, and (c-h) Scatterplots for *UZTC99* and *UZTC99C* at 10,000 years.

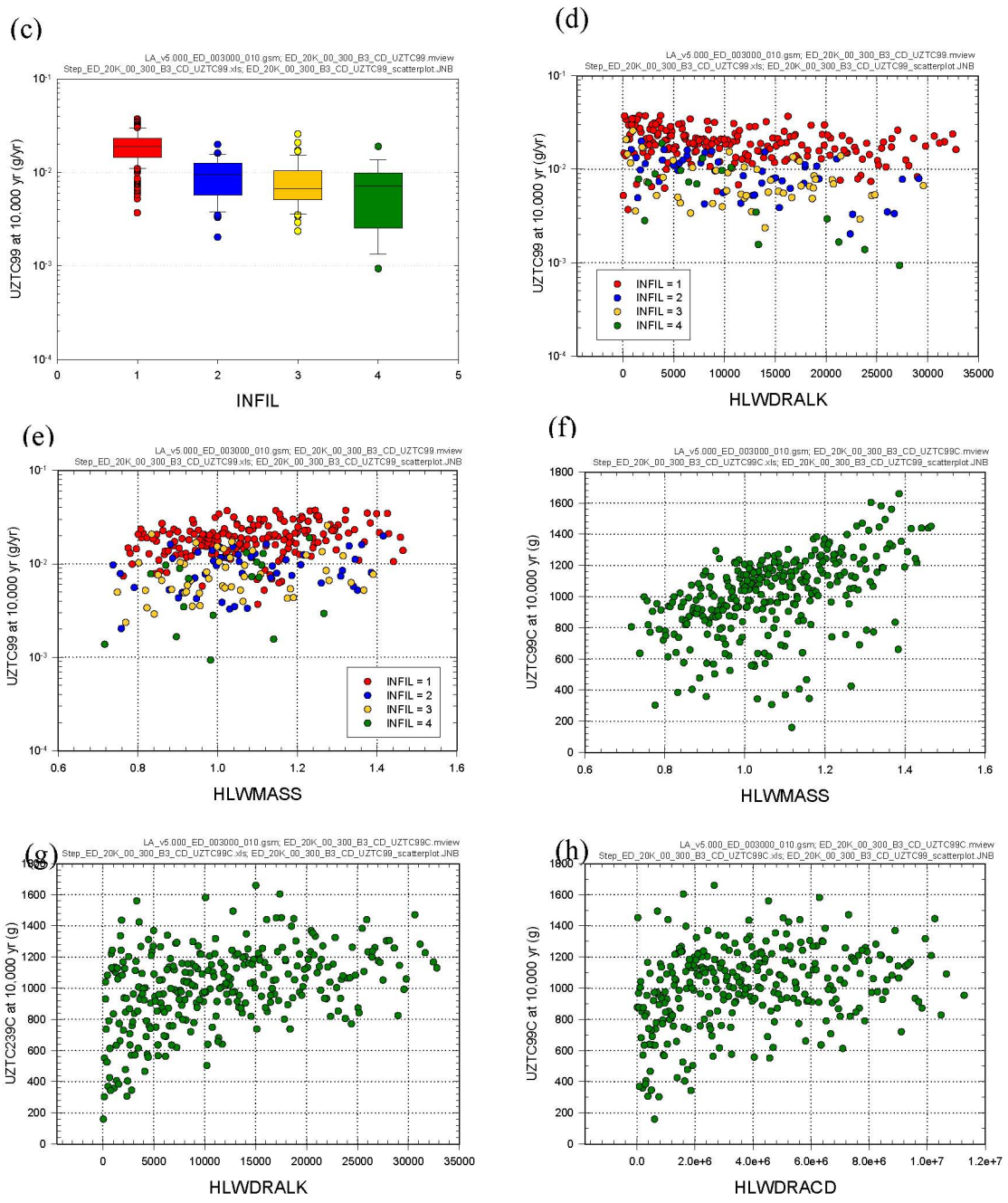

Source: Output DTNs: MO0709TSPASENS.000 [DIRS 183982]; and MO0709TSPAPLOT.000 [DIRS 183010].

NOTE: In (c), the box extends from 0.25 to 0.75 quantile; lower and upper bar and whisker extend to 0.1 and 0.9 quantile, respectively; dots represent values outside 0.1 to 0.9 quantile range; median indicated by light horizontal line.

Figure K5.4.1-14. Stepwise rank regression analyses and selected scatterplots for time-dependent release rates (*UZTC99*, g/yr) and cumulative (i.e., integrated) releases (*UZTC99*, g) for the movement of dissolved ^{99}Tc from the UZ to the SZ resulting from a single early DS failure above a CDSP WP in percolation bin 3 under dripping conditions: (a, b) Regressions for *UZTC99* and *UZTC99C* at 3000, 5000 and 10,000 years, and (c-h) Scatterplots for *UZTC99* and *UZTC99C* at 10,000 years (continued).

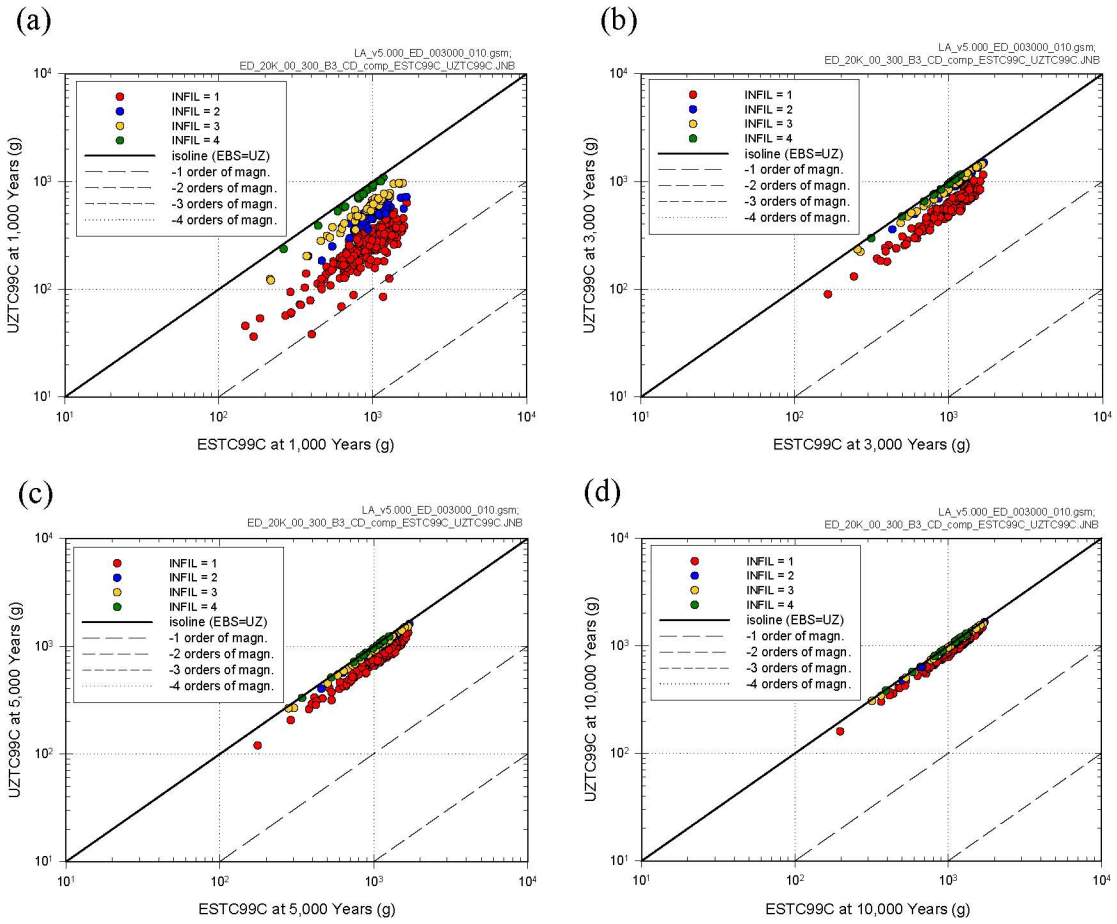

Source: Output DTN MO0709TSPASENS.000 [DIRS 183982].

Figure K5.4.1-15. Comparison of cumulative releases of dissolved ^{99}Tc into the UZ (*ESTC99C*, g) and out of the UZ (*UZTC99C*, g) at (a) 1000 years, (b) 3000 years, (c) 5000 years and (d) 10,000 years for a single early DS failure above a CDSP WP in percolation bin 3 under dripping conditions.

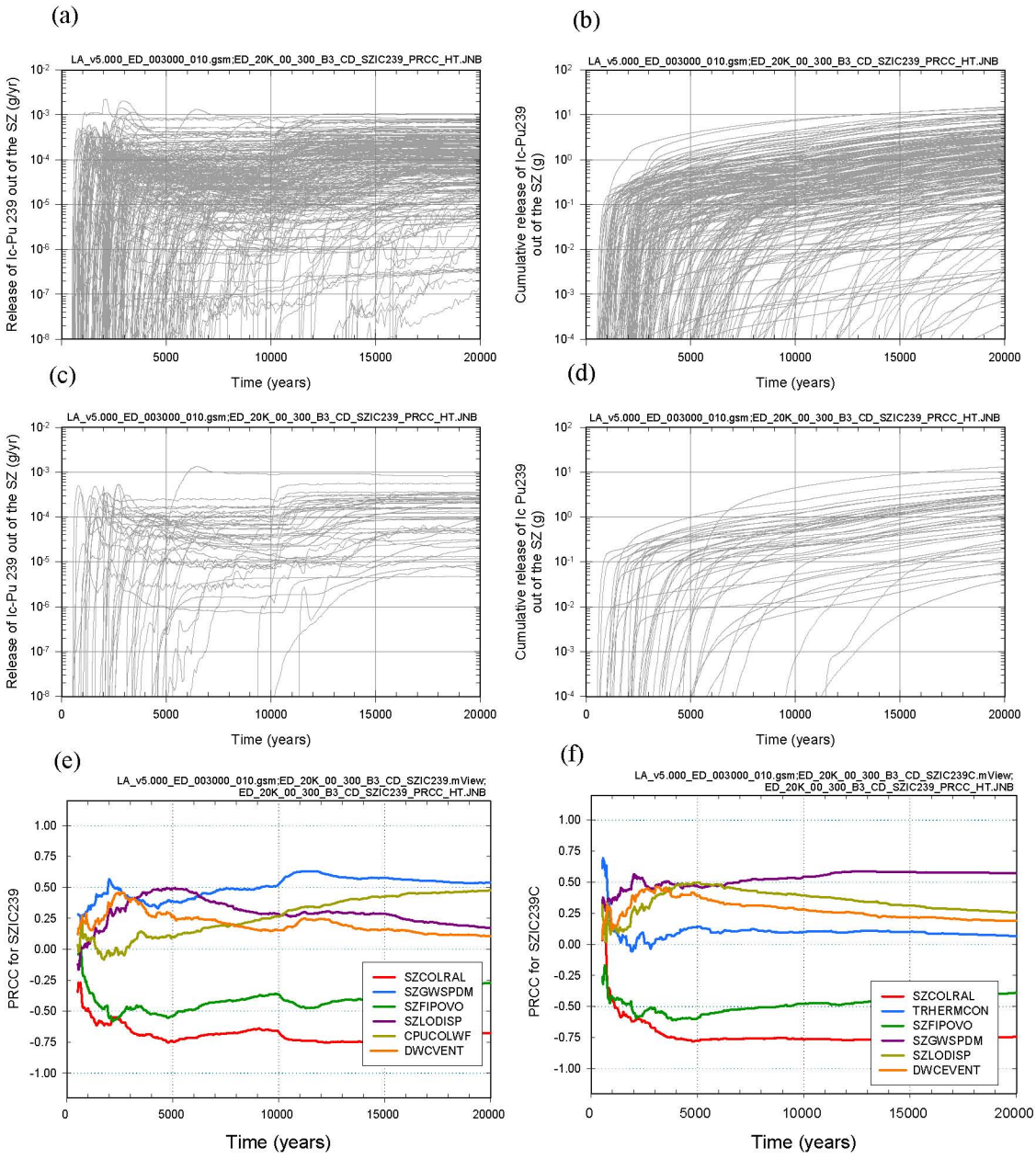

Source: Output DTNs: MO0709TSPASENS.000 [DIRS 183982]; and MO0709TSPAPLOT.000 [DIRS 183010].

Figure K5.5.1-1. Time-dependent release rates (*SZIC239*, g/yr) and cumulative (i.e., integrated) releases (*SZIC239C*, g) over 20,000 years for the movement of ^{239}Pu irreversibly attached to slow colloids across a subsurface plane at the location of the RMEI resulting from a single early DS failure above a CDSP WP in percolation bin 3 under dripping conditions: (a, b) *SZIC239* and *SZIC239C* for all (i.e., 300) sample elements, (c, d) *SZIC239* and *SZIC239C* for first 50 sample elements, and (e, f) PRCCs for *SZIC239* and *SZIC239C*.

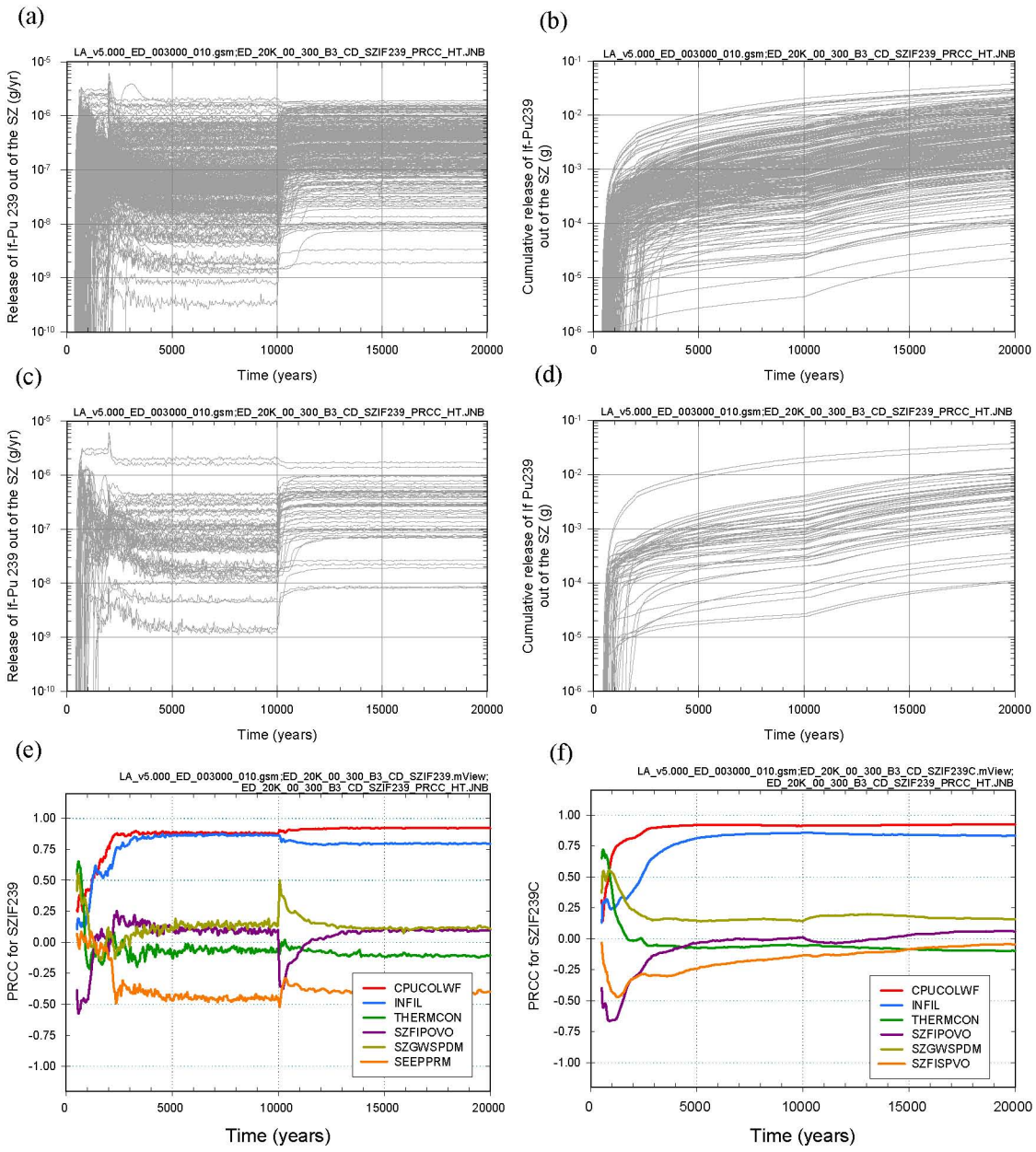

Source: Output DTNs: MO0709TSPASENS.000 [DIRS 183982]; and MO0709TSPAPLOT.000 [DIRS 183010].

Figure K5.5.1-2. Time-dependent release rates (*SZIF239*, g/yr) and cumulative (i.e., integrated) releases (*SZIF239C*, g) over 20,000 years for the movement of ^{239}Pu irreversibly attached to fast colloids across a subsurface plane at the location of the RMEI resulting from a single early DS failure above a CDSP WP in percolation bin 3 under dripping conditions: (a, b) *SZIF239* and *SZIF239C* for all (i.e., 300) sample elements, (c, d) *SZIF239* and *SZIF239C* for first 50 sample elements, and (e, f) PRCCs for *SZIF239* and *SZIF239C*.

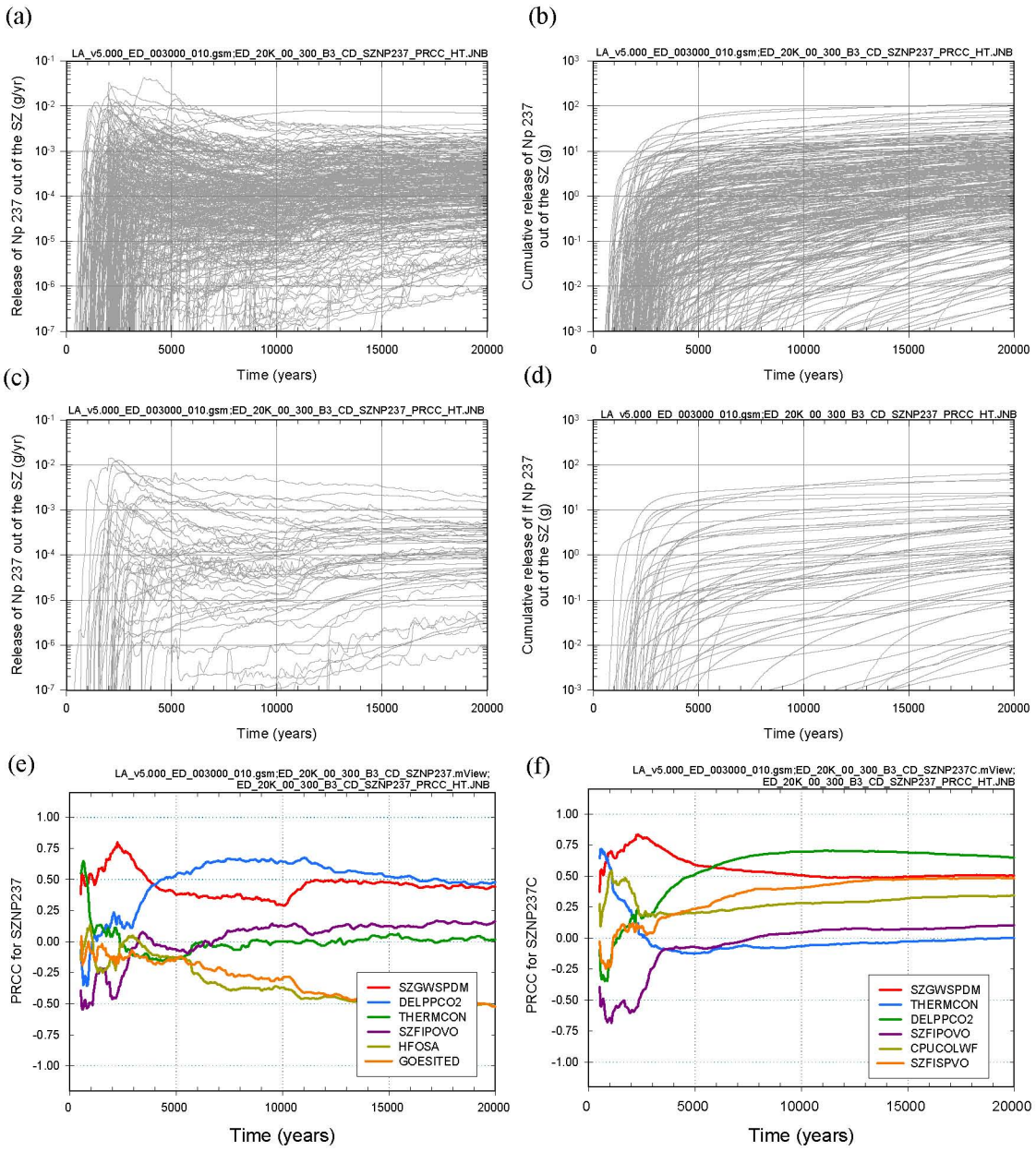

Source: Output DTNs: MO0709TSPASENS.000 [DIRS 183982]; and MO0709TSPAPLOT.000 [DIRS 183010].

Figure K5.5.1-3. Time-dependent release rates (*SZNP237*, g/yr) and cumulative (i.e., integrated) releases (*SZNP237C*, g) over 20,000 years for the movement of dissolved ^{237}Np across a subsurface plane at the location of the RMEI resulting from a single early DS failure above a CDSP WP in percolation bin 3 under dripping conditions: (a, b) *SZNP237* and *SZNP237C* for all (i.e., 300) sample elements, (c, d) *SZNP237* and *SZNP237C* for first 50 sample elements, and (e, f) PRCCs for *SZNP237* and *SZNP237C*.

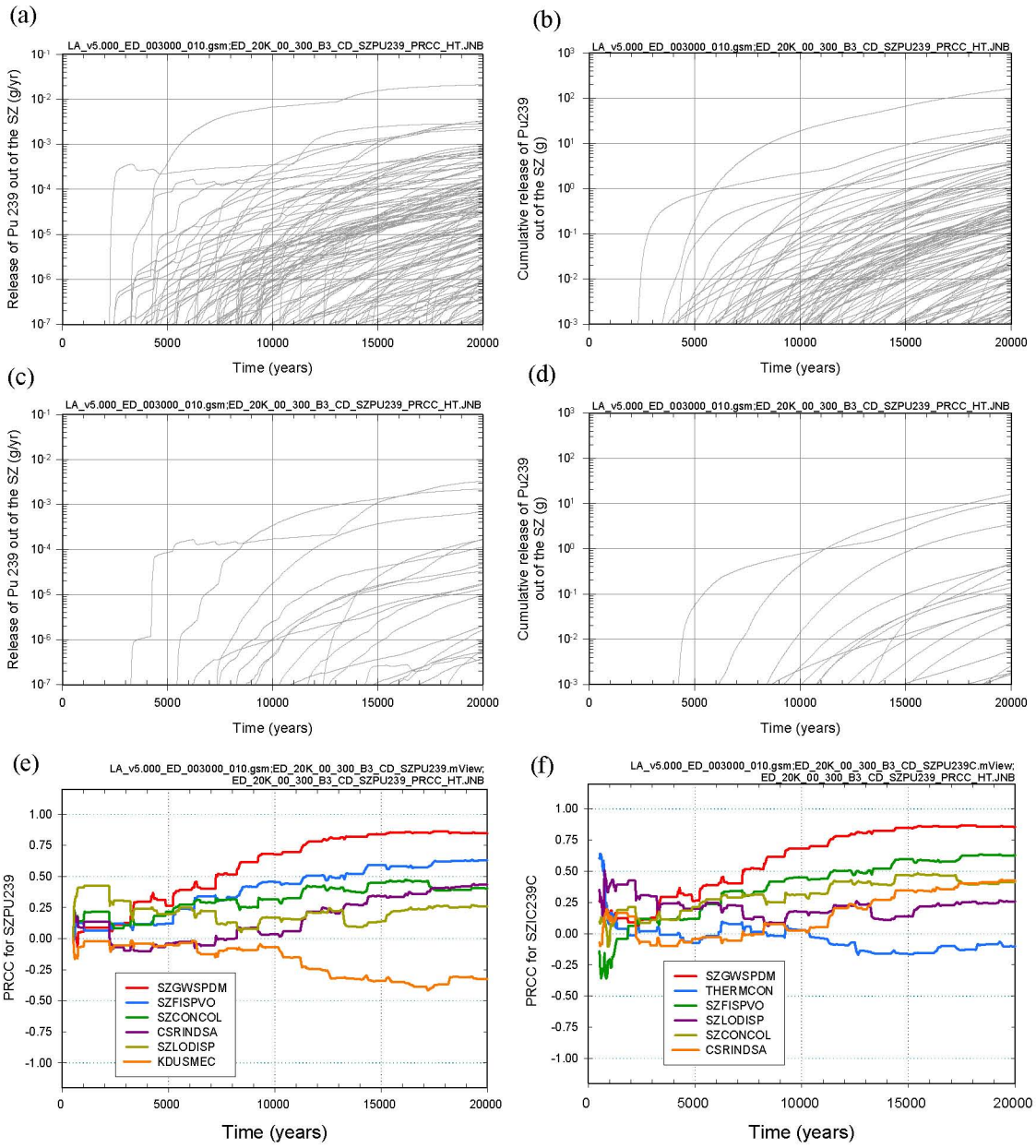

Source: Output DTNs: MO0709TSPASENS.000 [DIRS 183982]; and MO0709TSPAPLOT.000 [DIRS 183010].

Figure K5.5.1-4. Time-dependent release rates (*SZPU239*, g/yr) and cumulative (i.e., integrated) releases (*SZPU239C*, g) over 20,000 years for the movement of dissolved ^{239}Pu across a subsurface plane at the location of the RMEI resulting from a single early DS failure above a CDSP WP in percolation bin 3 under dripping conditions: (a, b) *SZPU239* and *SZPU239C* for all (i.e., 300) sample elements, (c, d) *SZPU239* and *SZPU239C* for first 50 sample elements, and (e, f) PRCCs for *SZPU239* and *SZPU239C*.

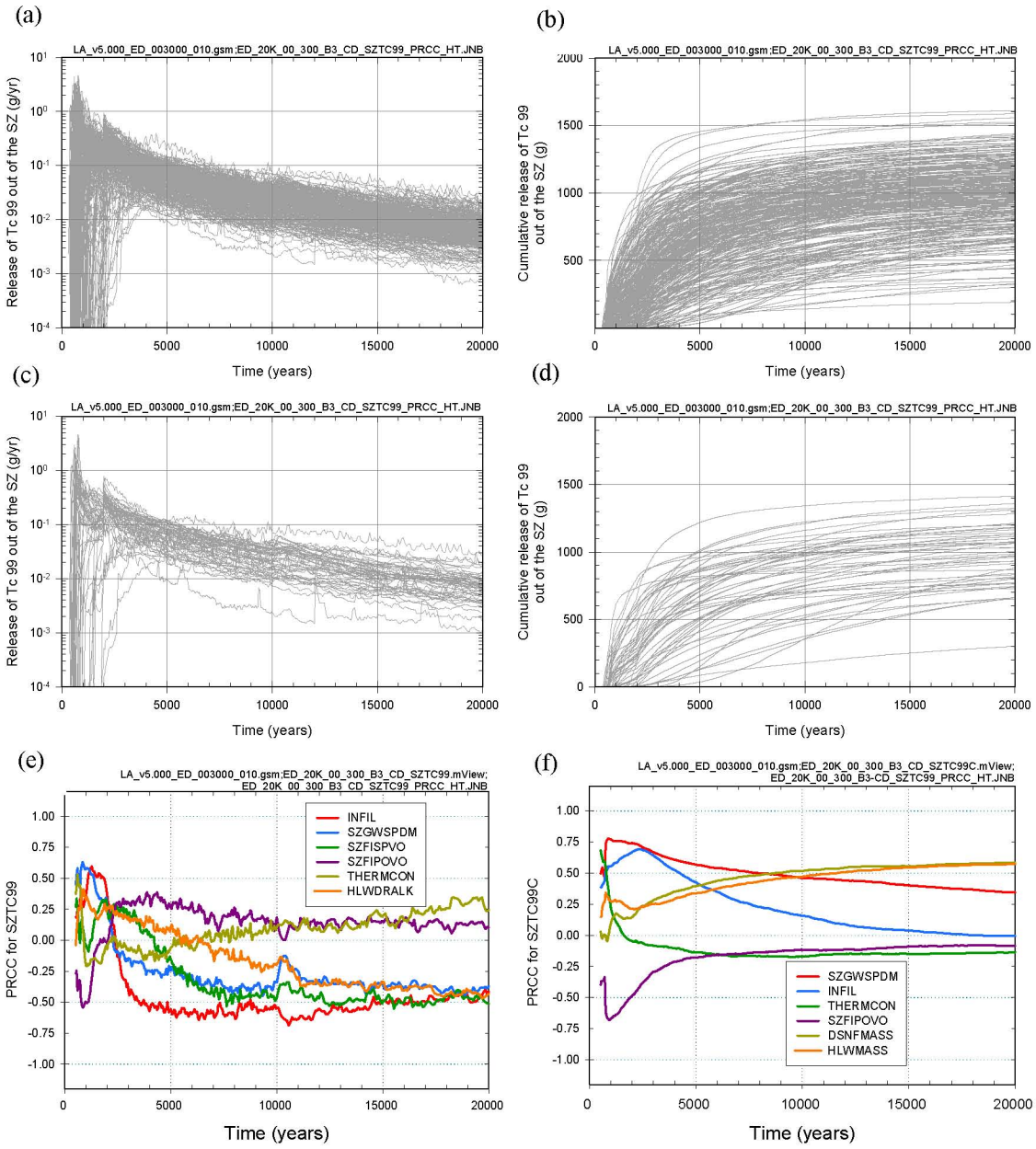

Source: Output DTNs: MO0709TSPASENS.000 [DIRS 183982]; and MO0709TSPAPLOT.000 [DIRS 183010].

Figure K5.5.1-5. Time-dependent release rates (*SZTC99*, g/yr) and cumulative (i.e., integrated) releases (*SZTC99C*, g) over 20,000 years for the movement of dissolved ^{99}Tc across a subsurface plane at the location of the RMEI resulting from a single early DS failure above a CDSP WP in percolation bin 3 under dripping conditions: (a, b) *SZTC99* and *SZTC99C* for all (i.e., 300) sample elements, (c, d) *SZTC99* and *SZTC99C* for first 50 sample elements, and (e, f) PRCCs for *SZTC99* and *SZTC99C*.

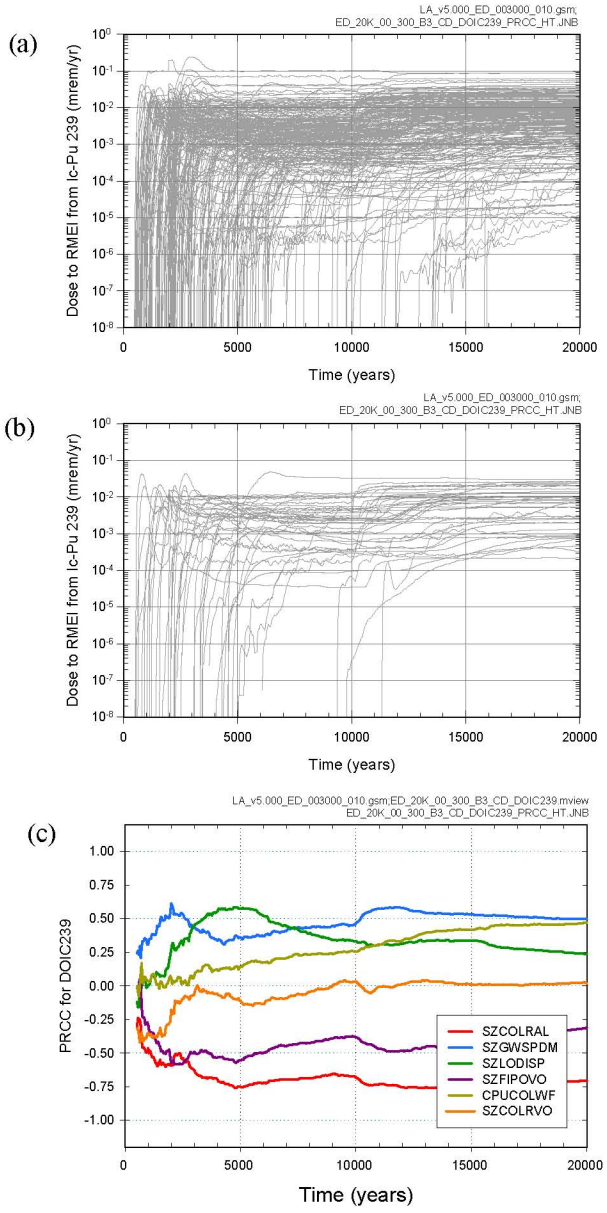

Source: Output DTNs: MO0709TSPASENS.000 [DIRS 183982]; and MO0709TSPAPLOT.000 [DIRS 183010].

Figure K5.6.1-1. Time-dependent dose to the RMEI (*DOIC239*, mrem/yr) over 20,000 years for the movement of ^{239}Pu irreversibly attached to slow colloids across a subsurface plane at the location of the RMEI resulting from a single early DS failure above a CDSP WP in percolation bin 3 under dripping conditions: (a) *DOIC239* for all (i.e., 300) sample elements, (b) *DOIC239* for first 50 sample elements, and (c) PRCCs for *DOIC239*.

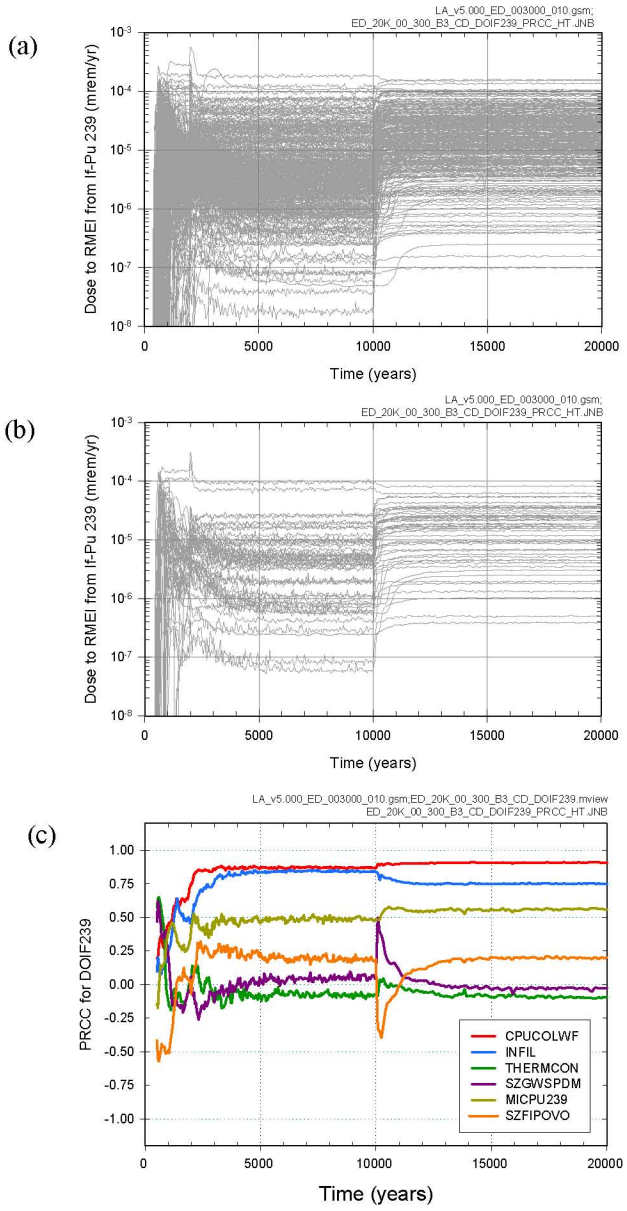

Source: Output DTNs: MO0709TSPASENS.000 [DIRS 183982]; and MO0709TSPAPLOT.000 [DIRS 183010].

Figure K5.6.1-2. Time-dependent dose to the RMEI (*DOIF239*, mrem/yr) over 20,000 years for the movement of ^{239}Pu irreversibly attached to fast colloids across a subsurface plane at the location of the RMEI resulting from a single early DS failure above a CDSP WP in percolation bin 3 under dripping conditions: (a) *DOIF239* for all (i.e., 300) sample elements, (b) *DOIF239* for first 50 sample elements, and (c) PRCCs for *DOIF239*.

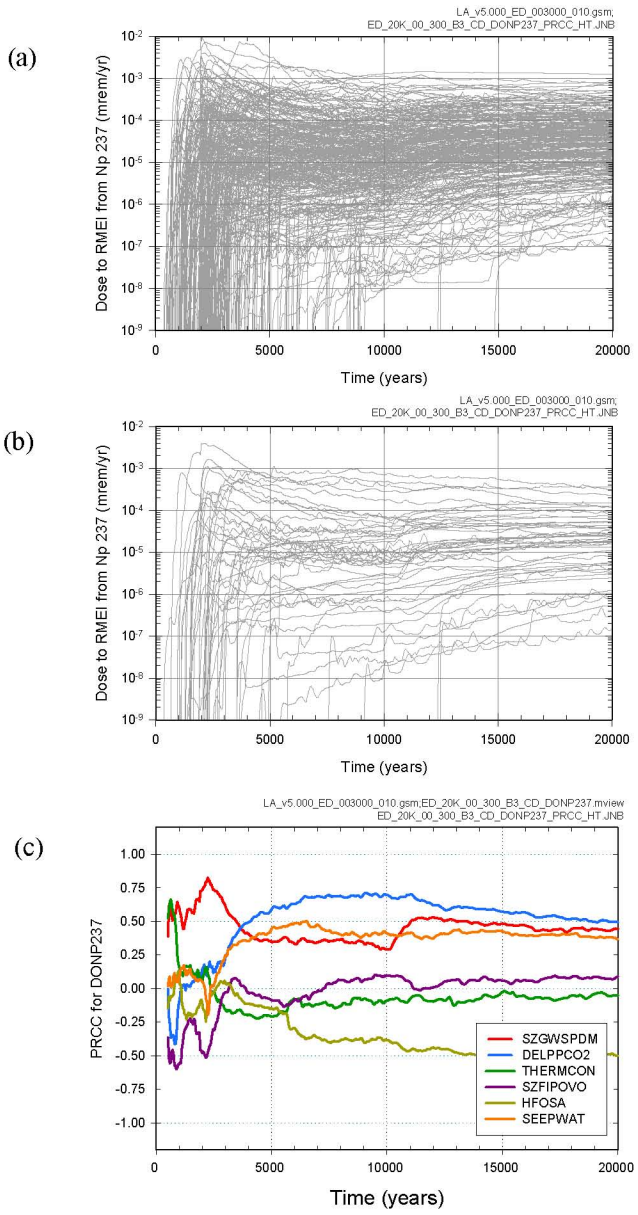

Source: Output DTNs: MO0709TSPASENS.000 [DIRS 183982]; and MO0709TSPAPLOT.000 [DIRS 183010].

Figure K5.6.1-3. Time-dependent dose to the RMEI (*DONP237*, mrem/yr) over 20,000 years for the movement of dissolved ^{237}Np across a subsurface plane at the location of the RMEI resulting from a single early DS failure above a CDSP WP in percolation bin 3 under dripping conditions: (a) *DONP237*for all (i.e., 300) sample elements, (b) *DONP237*for first 50 sample elements, and (c) PRCCs for *DONP237*.

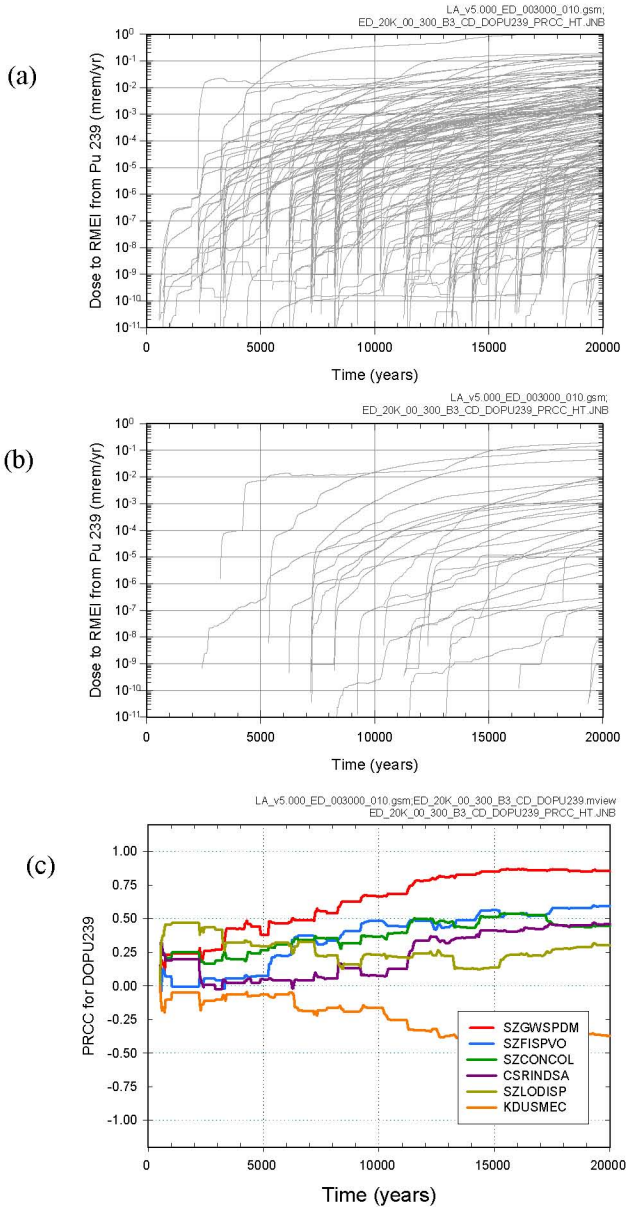

Source: Output DTNs: MO0709TSPASENS.000 [DIRS 183982]; and MO0709TSPAPLOT.000 [DIRS 183010].

Figure K5.6.1-4. Time-dependent dose to the RMEI (*DOPU239*, mrem/yr) over 20,000 years for the movement of dissolved ^{239}Pu across a subsurface plane at the location of the RMEI resulting from a single early DS failure above a CDSP WP in percolation bin 3 under dripping conditions: (a) *DOPU239* for all (i.e., 300) sample elements, (b) *DOPU239* for first 50 sample elements, and (c) PRCCs for *DOPU239*.

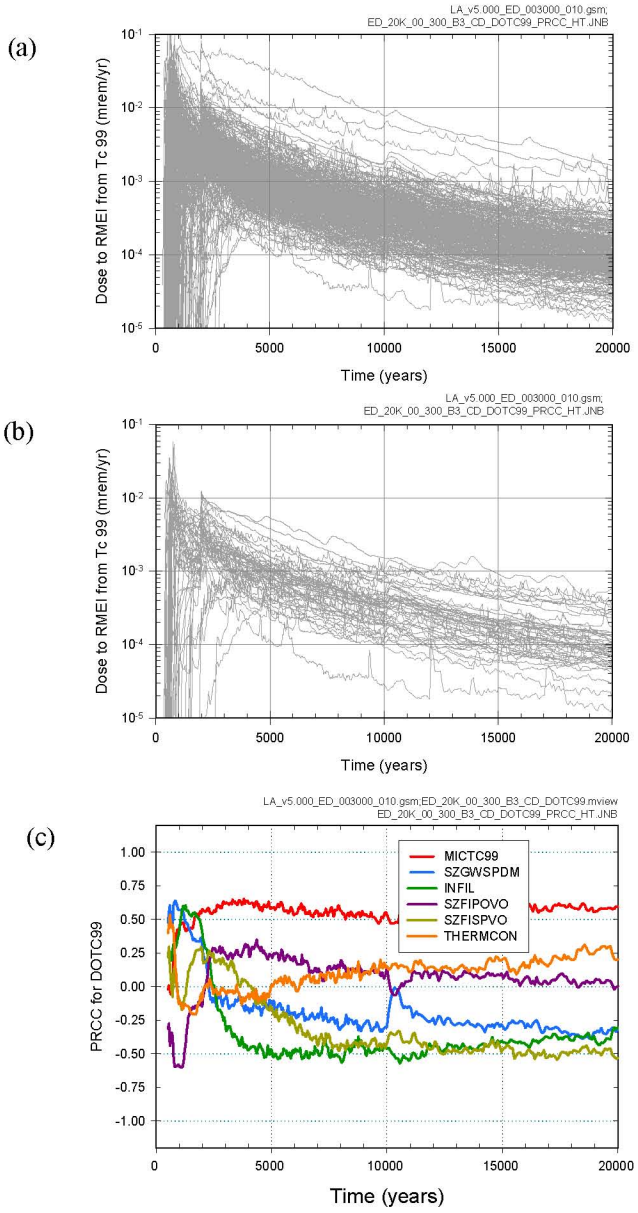

Source: Output DTNs: MO0709TSPASENS.000 [DIRS 183982]; and MO0709TSPAPLOT.000 [DIRS 183010].

Figure K5.6.1-5. Time-dependent dose to the RMEI (*DOTC99*, mrem/yr) over 20,000 years for the movement of dissolved ^{99}Tc across a subsurface plane at the location of the RMEI resulting from a single early DS failure above a CDSP WP in percolation bin 3 under dripping conditions: (a) *DOTC99* for all (i.e., 300) sample elements, (b) *DOTC99* for first 50 sample elements, and (c) PRCCs for *DOTC99*.

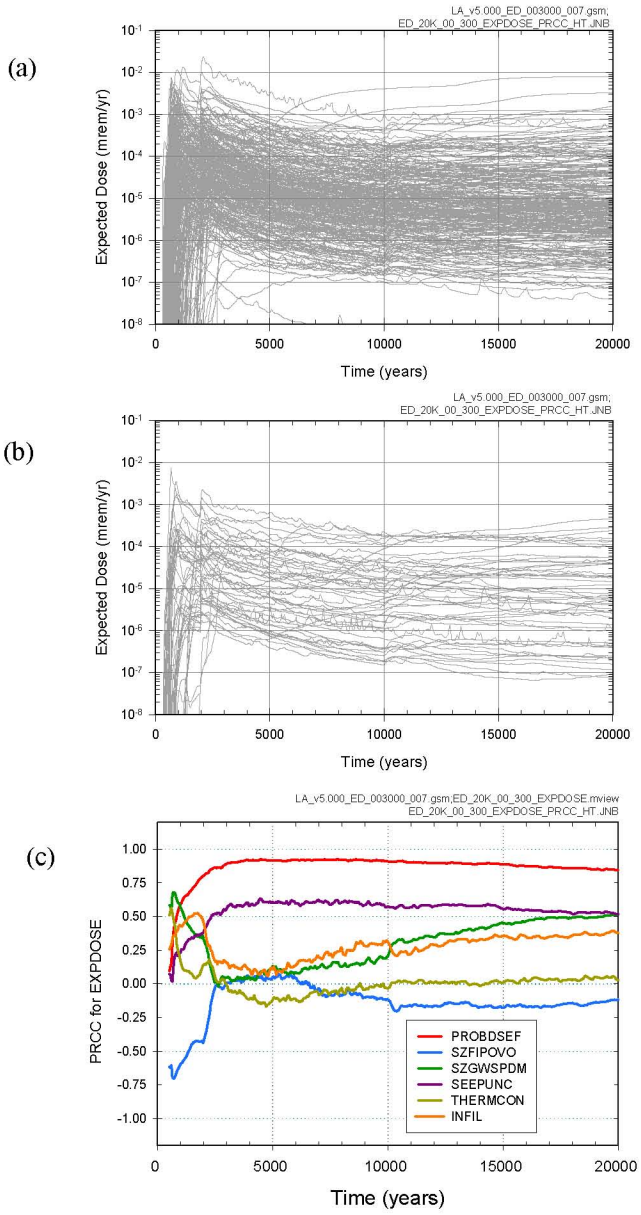

Source: Output DTNs: MO0709TSPAREGS.000 [DIRS 182976]; and MO0709TSPAPLOT.000 [DIRS 183010].

Figure K5.7.1-1. Expected dose to RMEI (*EXPDOSE*, mrem/yr) over [0, 20,000 yr] for all radioactive species resulting from early DS failure: (a) *EXPDOSE* for all (i.e., 300) sample elements, (b) *EXPDOSE* for first 50 sample elements, and (c) PRCCs for *EXPDOSE*.

(a)

	EXPDOSE: 3000 yr			EXPDOSE: 5000 yr			EXPDOSE: 10,000 yr		
Step[a]	Variable[b]	R^{2c}	SRRC[d]	Variable	R^2	SRRC	Variable	R^2	SRRC
1	PROBDSEF	0.74	0.83	PROBDSEF	0.76	0.84	PROBDSEF	0.69	0.81
2	SEEPUNC	0.79	0.22	SEEPUNC	0.82	0.23	SEEPUNC	0.75	0.22
3	SEEPPRM	0.82	-0.20	SEEPPRM	0.84	-0.18	INFIL	0.77	0.17
4	MICTC99	0.85	0.16	MICTC99	0.86	0.13	SEEPPRM	0.80	-0.19
5	ALPHAL	0.86	-0.06	ALPHAL	0.87	-0.09	ALPHAL	0.82	-0.11
6	INFIL	0.87	0.07	MICAM243	0.88	0.09	MICTC99	0.83	0.10
7	UZFAG8	0.87	-0.06	INFIL	0.88	0.06	MICPU239	0.84	0.09
8	CSNFMASS	0.87	0.07	COLGW	0.88	0.06	PHCSS	0.85	-0.07
9	GP4NO3	0.88	0.06	CSRINDPO	0.89	-0.06	CPUCOLWF	0.85	0.07
10	MICNP237	0.88	0.06	KDRASMEC	0.89	0.05	SZCOLRAL	0.86	-0.07
11							RHMU0	0.86	0.06
12							DSFLUX	0.86	-0.06

a: Steps in stepwise rank regression analysis
b: Variables listed in order of selection in stepwise regression
c: Cumulative R^2 value with entry of each variable into regression model
d: Standardized rank regression coefficients (SRRCs) in final regression model

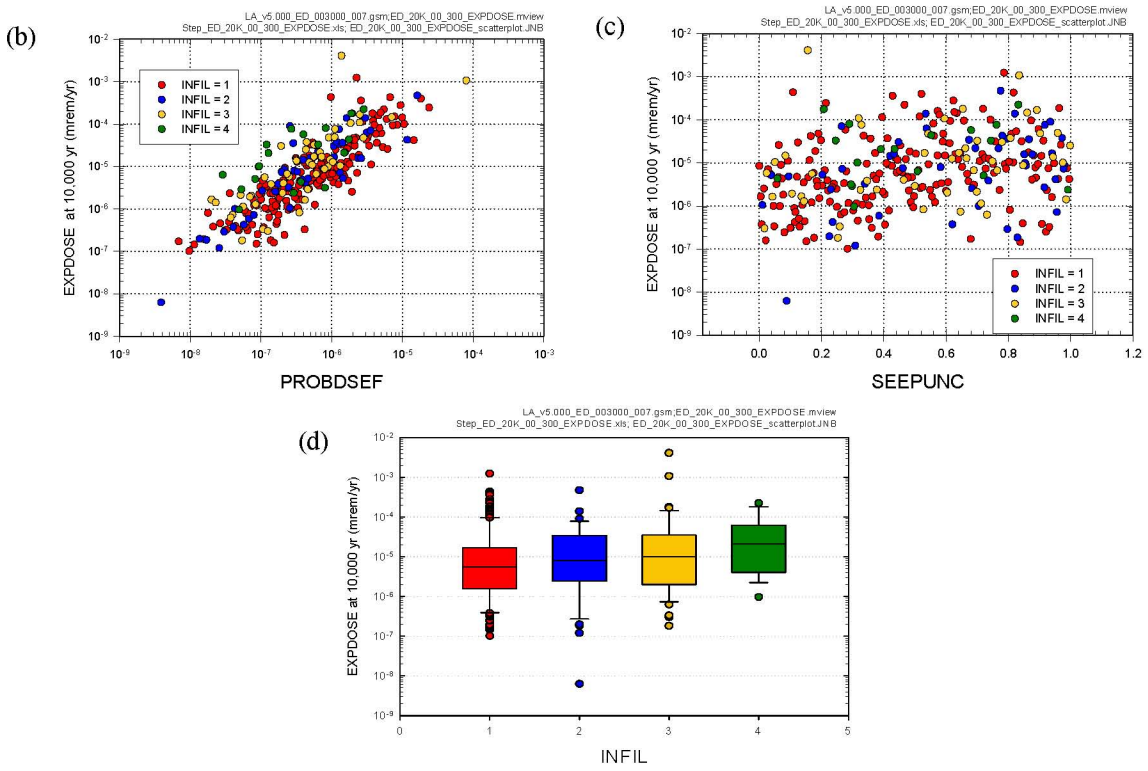

Source: Output DTNs: MO0709TSPAREGS.000 [DIRS 182976]; and MO0709TSPAPLOT.000 [DIRS 183010].

NOTE: In (d), the box extends from 0.25 to 0.75 quantile; lower and upper bar and whisker extend to 0.1 and 0.9 quantile, respectively; dots represent values outside 0.1 to 0.9 quantile range; median indicated by light horizontal line.

Figure K5.7.1-2. Stepwise rank regression analyses and selected scatterplots for expected dose to RMEI (*EXPDOSE*, mrem/yr) over [0, 20,000 yr] for all radioactive species resulting from early DS failure: (a) Regressions for *EXPDOSE* at 3000, 5000 and 10,000 years, and (b,c,d) Scatterplots for *EXPDOSE* at 10,000 years.

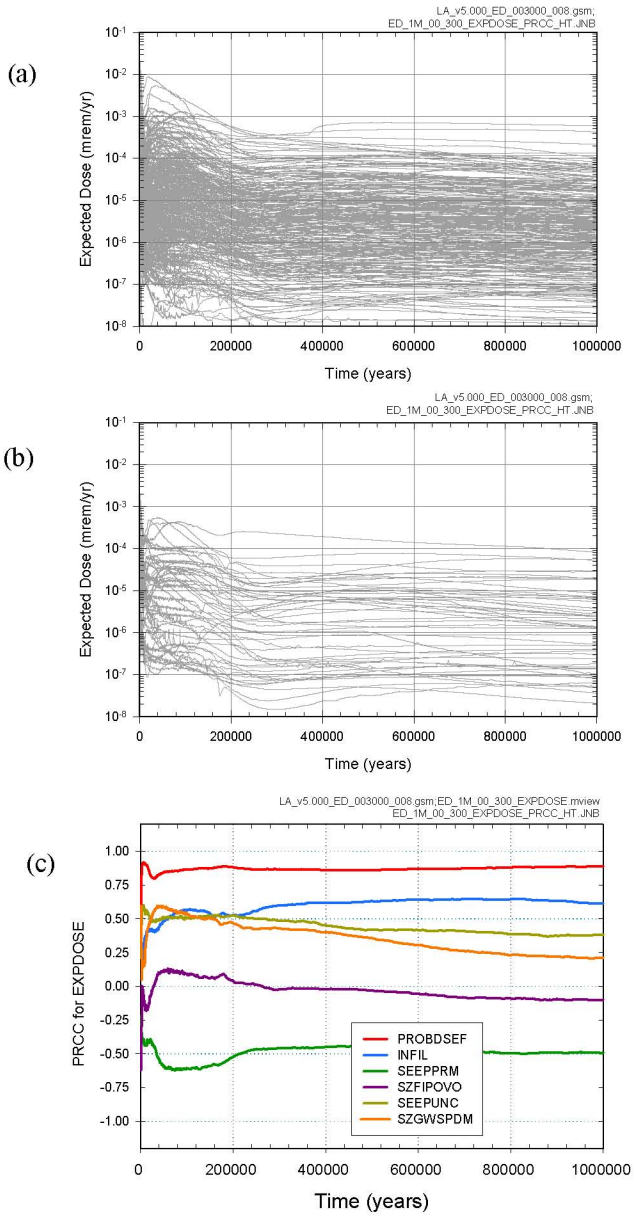

Source: Output DTNs: MO0709TSPAREGS.000 [DIRS 182976]; and MO0709TSPAPLOT.000 [DIRS 183010].

Figure K5.7.1-3. Expected dose to RMEI (*EXPDOSE*, mrem/yr) over [0, 1,000,000 yr] for all radioactive species resulting from early DS failure: (a) *EXPDOSE* for all (i.e., 300) sample elements, (b) *EXPDOSE* for first 50 sample elements, and (c) PRCCs for *EXPDOSE*.

(a)

	EXPDOSE: 50,000 yr			EXPDOSE: 200,000 yr			EXPDOSE: 500,000 yr		
Step[a]	**Variable[b]**	**R^{2c}**	**SRRC[d]**	**Variable**	**R^2**	**SRRC**	**Variable**	**R^2**	**SRRC**
1	PROBDSEF	0.44	0.68	PROBDSEF	0.51	0.73	PROBDSEF	0.48	0.70
2	INFIL	0.55	0.30	INFIL	0.60	0.27	INFIL	0.61	0.31
3	SZGWSPDM	0.65	0.32	SZGWSPDM	0.66	0.23	SZGWSPDM	0.65	0.19
4	SEEPPRM	0.70	-0.24	SEEPUNC	0.71	0.24	SEEPUNC	0.69	0.20
5	SEEPUNC	0.74	0.21	SEEPPRM	0.75	-0.21	SEEPPRM	0.73	-0.20
6	EP1LOWPU	0.77	0.17	MICPU239	0.77	0.14	EP1LOWPU	0.76	0.16
7	MICPU239	0.79	0.14	EP1LOWPU	0.78	0.14	GOESITED	0.77	-0.12
8	PHCSS	0.80	-0.08	GOESITED	0.79	-0.10	MICPU239	0.79	0.12
9	ALPHAL	0.80	-0.10	ALPHAL	0.80	-0.13	ALPHAL	0.80	-0.13
10	SZFISPVO	0.81	0.12	SZCONCOL	0.81	0.10	SZFISPVO	0.81	0.13
11	SZDIFCVO	0.82	-0.09	SZFISPVO	0.82	0.11	PHCSS	0.82	0.10
12	SZCOLRAL	0.82	-0.08	HFOSA	0.83	-0.09	EP1LOWNU	0.83	0.12
13	CPUCOLWF	0.83	0.09	SZDIFCVO	0.84	-0.10	SZDIFCVO	0.84	-0.08
14	HFOSA	0.83	-0.07	EP1LOWNU	0.85	0.08	HFOSA	0.85	-0.09
15	SEEPPRMN	0.84	-0.07	SZKDAMCO	0.85	0.07	MICSN126	0.85	0.07
16							SZCONCOL	0.86	0.07

a: Steps in stepwise rank regression analysis
b: Variables listed in order of selection in stepwise regression
c: Cumulative R^2 value with entry of each variable into regression model
d: Standardized rank regression coefficients (SRRCs) in final regression model

Source: Output DTNs: MO0709TSPAREGS.000 [DIRS 182976]; and MO0709TSPAPLOT.000 [DIRS 183010].

Figure K5.7.1-4. Stepwise rank regression analyses and selected scatterplots for expected dose to RMEI (*EXPDOSE*, mrem/yr) over [0, 1,000,000 yr] for all radioactive species resulting from early DS failure: (a) Regressions for *EXPDOSE* at 50,000, 200,000 and 500,000 years, and (b,c,d) Scatterplots for *EXPDOSE* at 500,000 years.

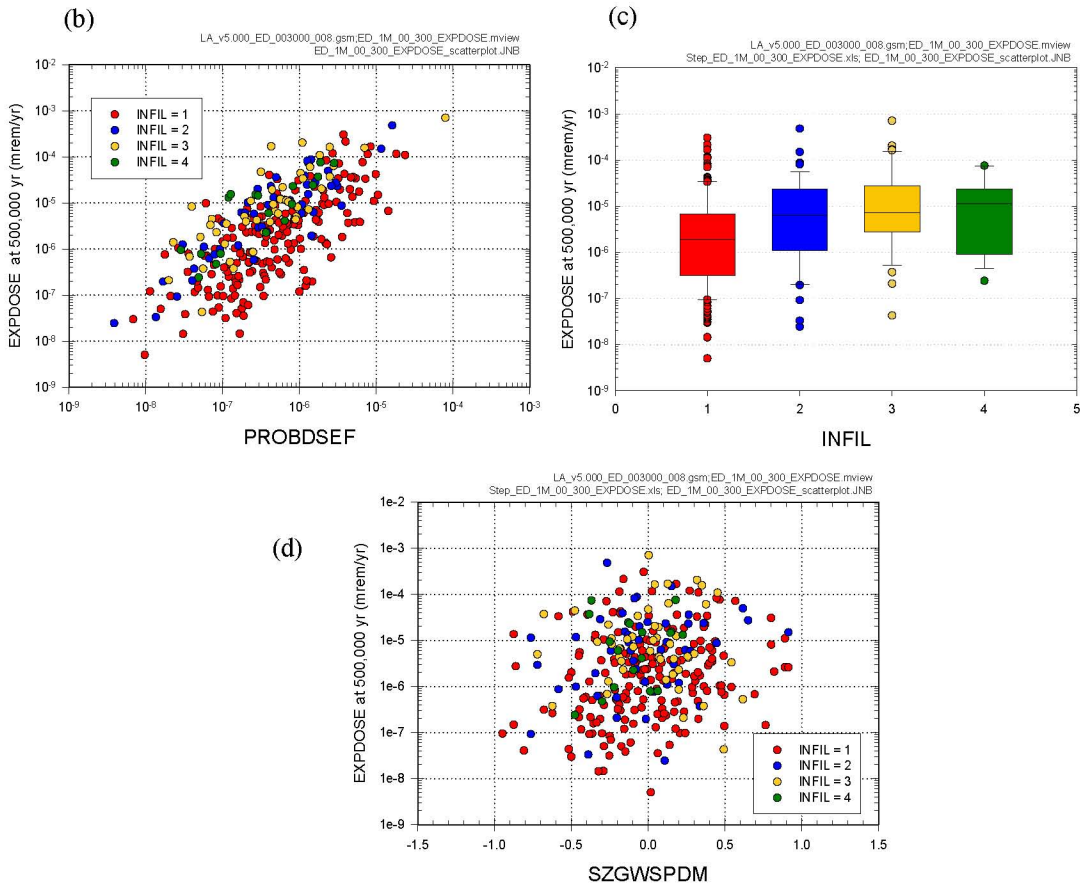

Source: Output DTNs: MO0709TSPAREGS.000 [DIRS 182976]; and MO0709TSPAPLOT.000 [DIRS 183010].

NOTE: In (c), the box extends from 0.25 to 0.75 quantile; lower and upper bar and whisker extend to 0.1 and 0.9 quantile, respectively; dots represent values outside 0.1 to 0.9 quantile range; median indicated by light horizontal line.

Figure K5.7.1-4. Stepwise rank regression analyses and selected scatterplots for expected dose to RMEI (*EXPDOSE*, mrem/yr) over [0, 1,000,000 yr] for all radioactive species resulting from early DS failure: (a) Regressions for *EXPDOSE* at 50,000, 200,000 and 500,000 years, and (b,c,d) Scatterplots for *EXPDOSE* at 500,000 years (continued).

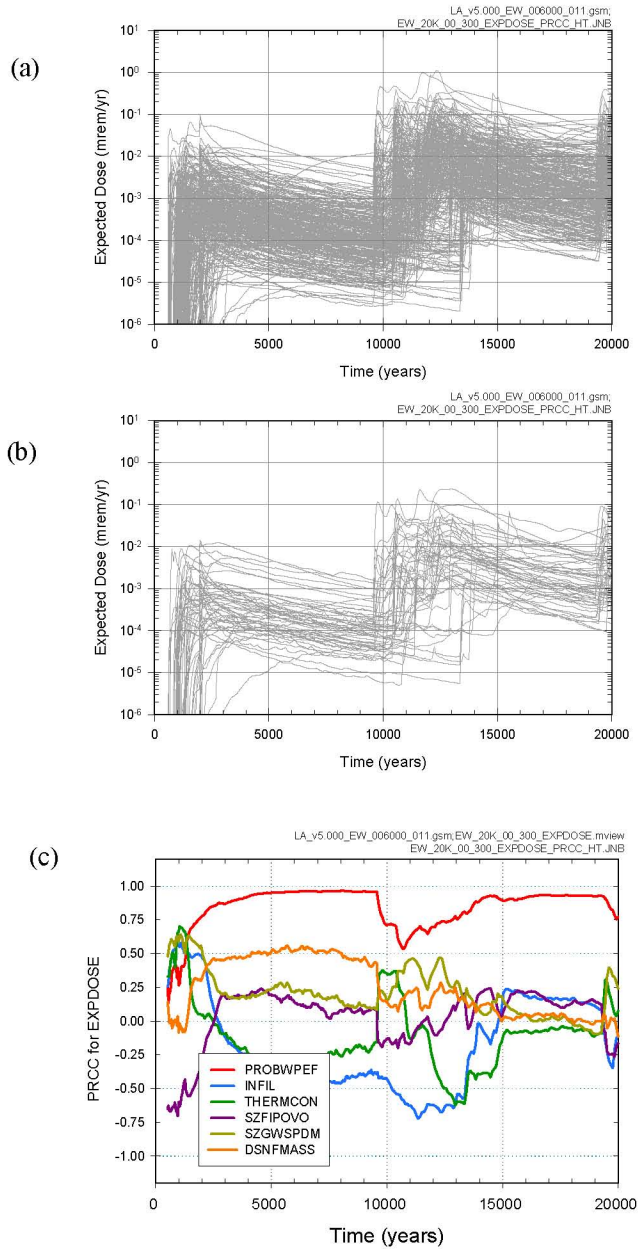

Source: Output DTNs: MO0709TSPAREGS.000 [DIRS 182976]; and MO0709TSPAPLOT.000 [DIRS 183010].

Figure K5.7.2-1. Expected dose to RMEI (*EXPDOSE*, mrem/yr) over [0, 20,000 yr] for all radioactive species resulting from early WP failure: (a) *EXPDOSE* for all (i.e., 300) sample elements, (b) *EXPDOSE* for first 50 sample elements, and (c) PRCCs for *EXPDOSE*.

(a)

	EXPDOSE: 3000 yr			EXPDOSE: 5000 yr			EXPDOSE: 10,000 yr		
Step[a]	Variable[b]	R^{2c}	SRRC[d]	Variable	R^2	SRRC	Variable	R^2	SRRC
1	PROBWPEF	0.62	0.76	PROBWPEF	0.79	0.87	PROBWPEF	0.47	0.68
2	MICTC99	0.68	0.23	MICTC99	0.82	0.19	INFIL	0.56	-0.31
3	MICC14	0.71	0.17	MICC14	0.84	0.14	THERMCON	0.64	0.28
4	DSNFMASS	0.73	0.17	DSNFMASS	0.87	0.16	MICTC99	0.66	0.15
5	UZFAG8	0.75	-0.13	UZFAG8	0.87	-0.10	EP1LOWPU	0.67	0.10
6	SZFISPVO	0.76	0.12	HLWDRACD	0.88	0.08			
7	HLWDRACD	0.77	0.08	INFIL	0.89	-0.09			
8	UZTORRG3	0.78	0.10	HLWDRALK	0.89	0.07			
9	SZGWSPDM	0.79	0.09	PH2DHLNS	0.90	-0.07			
10	SZDIFCVO	0.79	-0.08	THERMCON	0.90	-0.06			
11	UZGAM	0.80	-0.07	UZGAM	0.90	-0.06			

a: Steps in stepwise rank regression analysis
b: Variables listed in order of selection in stepwise regression
c: Cumulative R^2 value with entry of each variable into regression model
d: Standardized rank regression coefficients (SRRCs) in final regression model

(b)

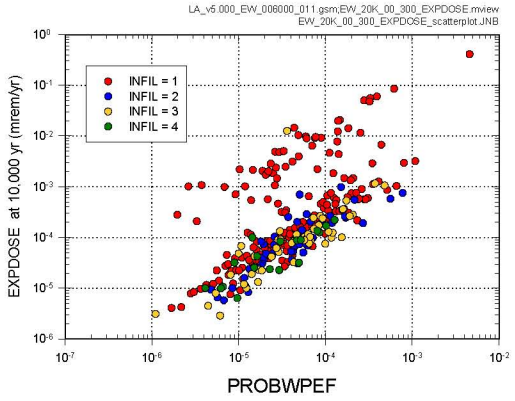

(c)

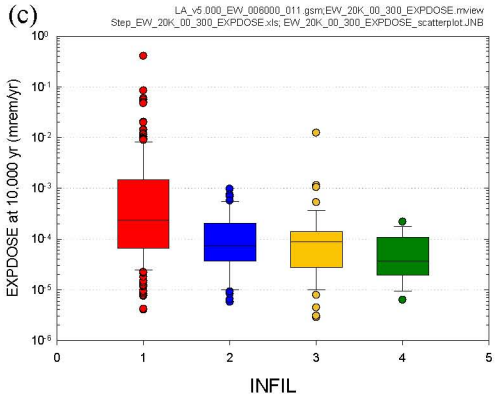

(d)

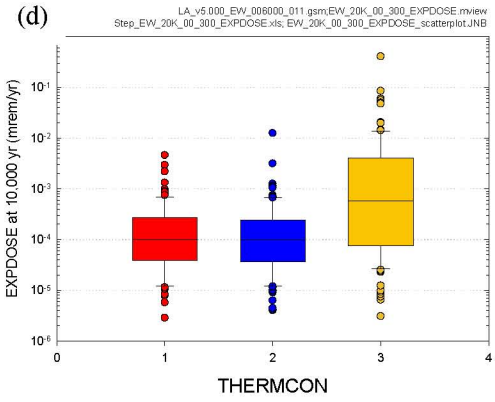

Source: Output DTNs: MO0709TSPAREGS.000 [DIRS 182976]; and MO0709TSPAPLOT.000 [DIRS 183010].

NOTE: In (c,d), the box extends from 0.25 to 0.75 quantile; lower and upper bar and whisker extend to 0.1 and 0.9 quantile, respectively; dots represent values outside 0.1 to 0.9 quantile range; median indicated by light horizontal line.

Figure K5.7.2-2. Stepwise rank regression analyses and selected scatterplots for expected dose to RMEI (*EXPDOSE*, mrem/yr) over [0, 20,000 yr] for all radioactive species resulting from early WP failure: (a) Regressions for *EXPDOSE* at 3000, 5000 and 10,000 years, and (b,c,d) Scatterplots for *EXPDOSE* at 10,000 years.

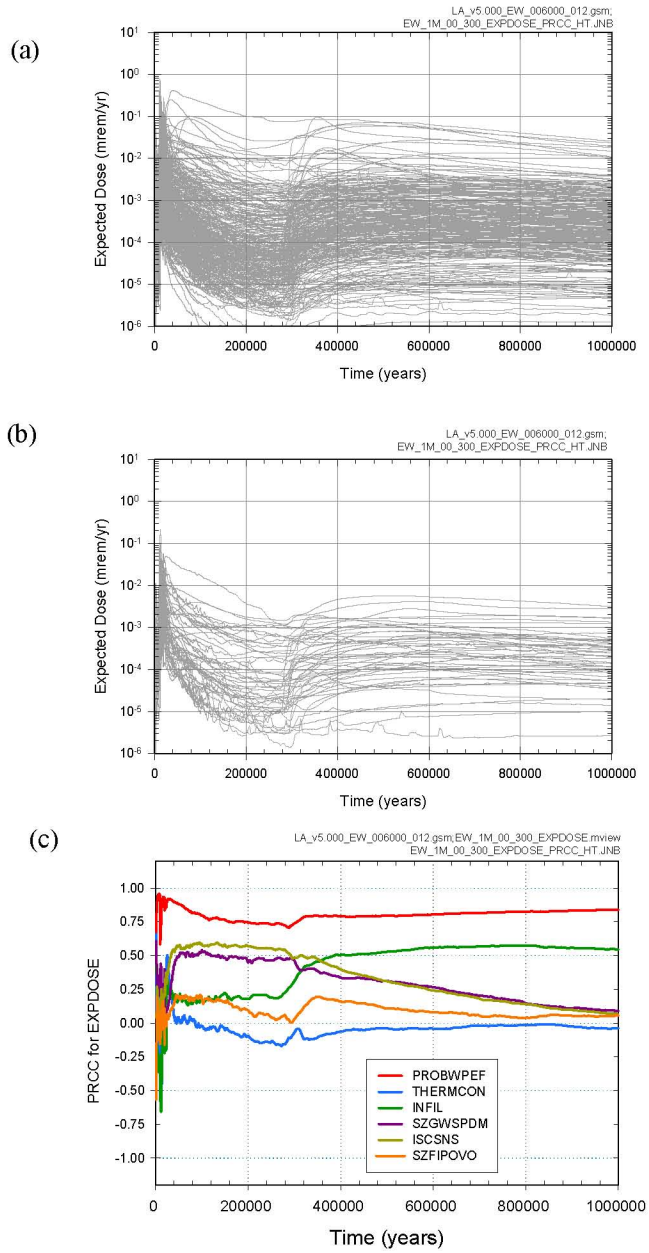

Source: Output DTNs: MO0709TSPAREGS.000 [DIRS 182976]; and MO0709TSPAPLOT.000 [DIRS 183010].

Figure K5.7.2-3. Expected dose to RMEI (*EXPDOSE*, mrem/yr) over [0, 1,000,000 yr] for all radioactive species resulting from early WP failure: (a) *EXPDOSE* for all (i.e., 300) sample elements, (b) *EXPDOSE* for first 50 sample elements, and (c) PRCCs for *EXPDOSE*.

(a)

	EXPDOSE: 50,000 yr			EXPDOSE: 200,000 yr			EXPDOSE: 500,000 yr		
Step[a]	**Variable[b]**	**R^{2c}**	**SRRC[d]**	**Variable**	**R^2**	**SRRC**	**Variable**	**R^2**	**SRRC**
1	PROBWPEF	0.58	0.78	PROBWPEF	0.35	0.60	PROBWPEF	0.35	0.66
2	ISCSNS	0.65	0.26	ISCSNS	0.48	0.37	INFIL	0.48	0.31
3	SZGWSPDM	0.71	0.22	SZGWSPDM	0.55	0.24	SZGWSPDM	0.53	0.21
4	EP1LOWPU	0.73	0.14	EP1LOWPU	0.57	0.15	SEEPPRM	0.57	-0.21
5	MICTC99	0.74	0.09	SZFISPVO	0.59	0.17	SEEPUNC	0.60	0.18
6	COLU	0.75	0.10	SZDIFCVO	0.61	-0.15	EP1LOWPU	0.62	0.17
7	SZFISPVO	0.76	0.11	IGRATE	0.62	0.12	ALPHAL	0.65	-0.20
8	SZDIFCVO	0.76	-0.10	SEEPUNC	0.63	0.10	EP1LOWNU	0.68	0.18
9	IGRATE	0.77	0.09	DIFPATHL	0.64	-0.11	SZFISPVO	0.70	0.17
10	MICPU239	0.78	0.09	GOESITED	0.65	-0.10	MICNP237	0.71	0.13
11				RHMU40	0.66	-0.10	SZDIFCVO	0.73	-0.11
12							GOESITED	0.74	-0.11
13							HFOSA	0.75	-0.10
14							SZCONCOL	0.75	0.10
15							ISCSNS	0.76	0.10
16							COLGW	0.77	0.09

a: Steps in stepwise rank regression analysis
b: Variables listed in order of selection in stepwise regression
c: Cumulative R^2 value with entry of each variable into regression model
d: Standardized rank regression coefficients (SRRCs) in final regression model

Source: Output DTNs: MO0709TSPAREGS.000 [DIRS 182976]; and MO0709TSPAPLOT.000 [DIRS 183010].

Figure K5.7.2-4. Stepwise rank regression analyses and selected scatterplots for expected dose to RMEI (*EXPDOSE*, mrem/yr) over [0, 1,000,000 yr] for all radioactive species resulting from early WP failure: (a) Regressions for *EXPDOSE* at 50,000, 200,000 and 500,000 years, and (b,c,d) Scatterplots for *EXPDOSE* at 500,000 years.

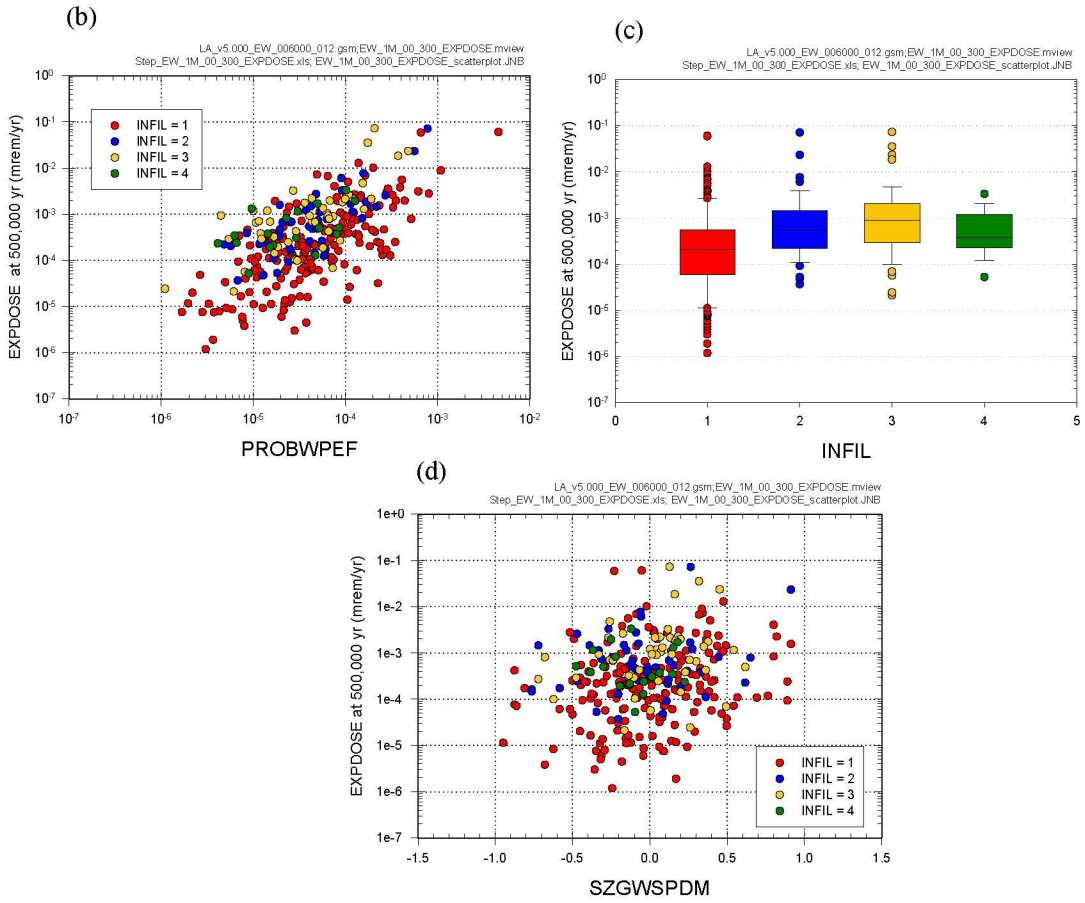

Source: Output DTNs: MO0709TSPAREGS.000 [DIRS 182976]; and MO0709TSPAPLOT.000 [DIRS 183010].

NOTE: In (c), the box extends from 0.25 to 0.75 quantile; lower and upper bar and whisker extend to 0.1 and 0.9 quantile, respectively; dots represent values outside 0.1 to 0.9 quantile range; median indicated by light horizontal line.

Figure K5.7.2-4. Stepwise rank regression analyses and selected scatterplots for expected dose to RMEI (*EXPDOSE*, mrem/yr) over [0, 1,000,000 yr] for all radioactive species resulting from early WP failure: (a) Regressions for *EXPDOSE* at 50,000, 200,000 and 500,000 years, and (b,c,d) Scatterplots for *EXPDOSE* at 500,000 years (continued).

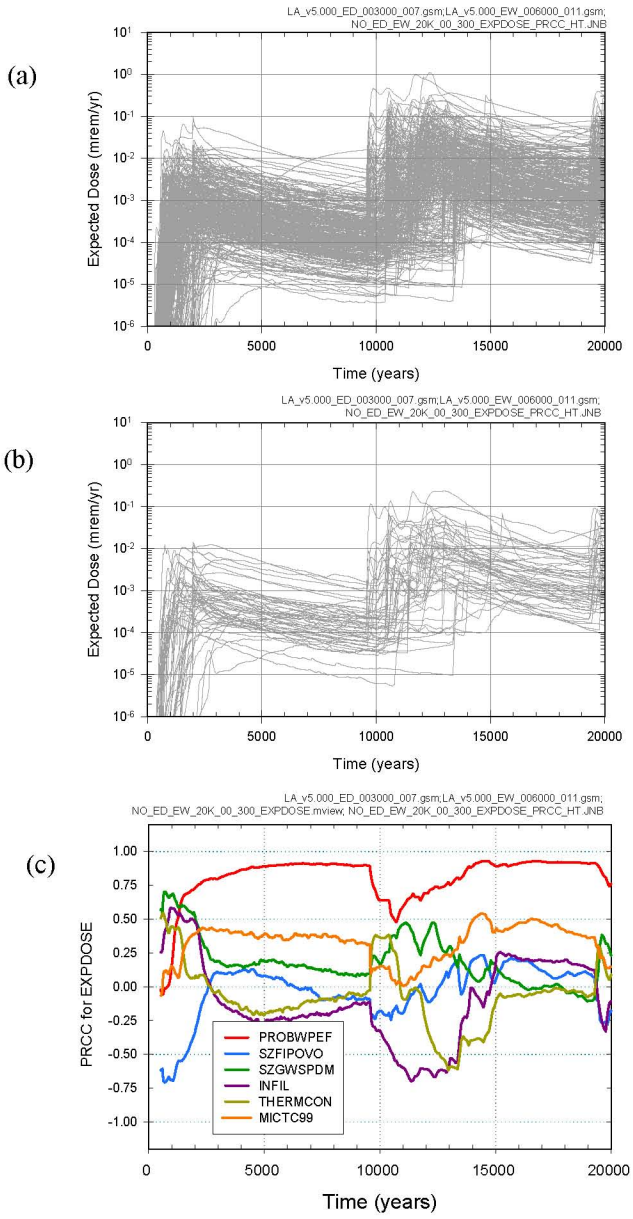

Source: Output DTNs: MO0709TSPAREGS.000 [DIRS 182976]; and MO0709TSPAPLOT.000 [DIRS 183010].

Figure K5.7.3-1. Expected dose to RMEI (*EXPDOSE*, mrem/yr) over [0, 20,000 yr] for all radioactive species resulting from both early DS failure and early WP failure: (a) *EXPDOSE* for all (i.e., 300) sample elements, (b) *EXPDOSE* for first 50 sample elements, and (c) PRCCs for *EXPDOSE*.

(a)

	EXPDOSE: 3000 yr			EXPDOSE: 5000 yr			EXPDOSE: 10,000 yr		
Step[a]	**Variable[b]**	**R^{2c}**	**SRRC[d]**	**Variable**	**R^2**	**SRRC**	**Variable**	**R^2**	**SRRC**
1	PROBWPEF	0.49	0.69	PROBWPEF	0.64	0.78	PROBWPEF	0.39	0.62
2	MICTC99	0.57	0.23	MICTC99	0.70	0.22	INFIL	0.48	-0.26
3	PROBDSEF	0.61	0.20	PROBDSEF	0.74	0.20	THERMCON	0.55	0.28
4	UZFAG8	0.63	-0.15	DSNFMASS	0.76	0.15	PROBDSEF	0.59	0.20
5	DSNFMASS	0.65	0.15	MICC14	0.78	0.12	MICTC99	0.61	0.14
6	MICC14	0.67	0.16	UZFAG8	0.79	-0.09			
7	HLWDRACD	0.68	0.09	HLWDRACD	0.79	0.08			
8	UZGAM	0.69	-0.09	CSRINDDN	0.80	-0.08			
9	SZGWSPDM	0.70	0.11	INFIL	0.80	-0.08			
10	SEEPUNC	0.71	0.11	THERMCON	0.81	-0.09			
11	IS2DHLNS	0.72	-0.09	UZGAM	0.81	-0.08			
12				HLWMASS	0.82	0.07			
13				RHMUNO0	0.82	0.08			
14				KDAMCOL	0.83	-0.07			
15				UZFAG9	0.83	0.07			

a: Steps in stepwise rank regression analysis
b: Variables listed in order of selection in stepwise regression
c: Cumulative R^2 value with entry of each variable into regression model
d: Standardized rank regression coefficients (SRRCs) in final regression model

Source: Output DTNs: MO0709TSPAREGS.000 [DIRS 182976]; and MO0709TSPAPLOT.000 [DIRS 183010].

Figure K5.7.3-2. Stepwise rank regression analyses and selected scatterplots for expected dose to RMEI (*EXPDOSE*, mrem/yr) over [0, 20,000 yr] for all radioactive species resulting from both early DS failure and early WP failure: (a) Regressions for *EXPDOSE* at 3000, 5000 and 10,000 years, and (b,c,d) Scatterplots for *EXPDOSE* at 10,000 years.

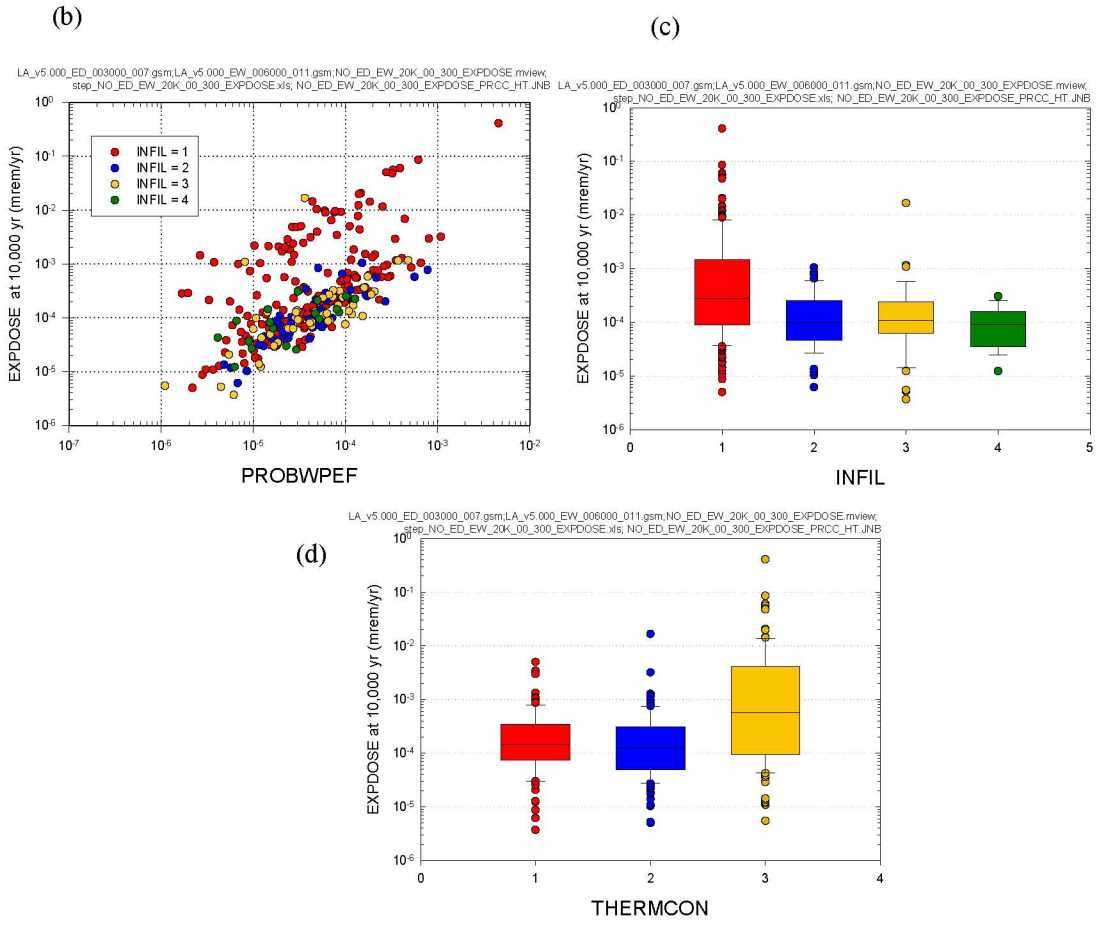

Source: Output DTNs: MO0709TSPAREGS.000 [DIRS 182976]; and MO0709TSPAPLOT.000 [DIRS 183010].

Notes: In (c,d), the box extends from 0.25 to 0.75 quantile; lower and upper bar and whisker extend to 0.1 and 0.9 quantile, respectively; dots represent values outside 0.1 to 0.9 quantile range; median indicated by light horizontal line

Figure K5.7.3-2. Stepwise rank regression analyses and selected scatterplots for expected dose to RMEI (*EXPDOSE*, mrem/yr) over [0, 20,000 yr] for all radioactive species resulting from both early DS failure and early WP failure: (a) Regressions for *EXPDOSE* at 3000, 5000 and 10,000 years, and (b,c,d) Scatterplots for *EXPDOSE* at 10,000 years (continued).

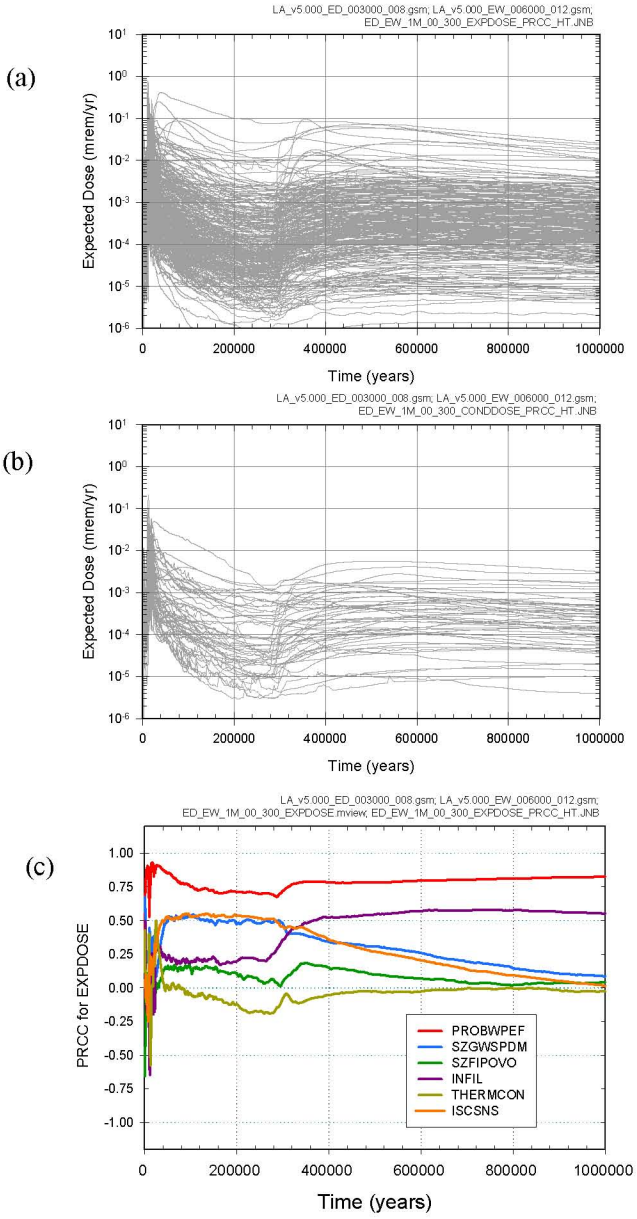

Source: Output DTNs: MO0709TSPAREGS.000 [DIRS 182976]; and MO0709TSPAPLOT.000 [DIRS 183010].

Figure K5.7.3-3. Expected dose to RMEI (*EXPDOSE*, mrem/yr) over [0, 1,000,000 yr] for all radioactive species resulting from both early DS failure and early WP failure: (a) *EXPDOSE* for all (i.e., 300) sample elements, (b) *EXPDOSE* for first 50 sample elements, and (c) PRCCs for *EXPDOSE*.

(a)

	EXPDOSE: 50K yr			EXPDOSE: 200K yr			EXPDOSE: 500K yr		
Step[a]	**Variable[b]**	**R^{2c}**	**SRRC[d]**	**Variable**	**R^2**	**SRRC**	**Variable**	**R^2**	**SRRC**
1	PROBWPEF	0.51	0.73	PROBWPEF	0.27	0.56	PROBWPEF	0.32	0.64
2	SZGWSPDM	0.59	0.27	ISCSNS	0.39	0.37	INFIL	0.46	0.32
3	ISCSNS	0.66	0.26	SZGWSPDM	0.47	0.26	SZGWSPDM	0.51	0.22
4	EP1LOWPU	0.68	0.12	SEEPUNC	0.50	0.17	SEEPUNC	0.55	0.20
5	SEEPUNC	0.69	0.11	PROBDSEF	0.52	0.16	SEEPPRM	0.58	-0.22
6	MICNP237	0.70	0.12	EP1LOWPU	0.54	0.15	ALPHAL	0.61	-0.20
7	SZKDSRAL	0.72	0.12	SEEPPRM	0.56	-0.13	EP1LOWPU	0.64	0.17
8	DTDRHUNC	0.73	0.11	SZFISPVO	0.58	0.17	EP1LOWNU	0.67	0.18
9	HFOSA	0.73	-0.10	SZDIFCVO	0.60	-0.16	SZFISPVO	0.69	0.16
10				EP1LOWNU	0.61	0.11	MICNP237	0.70	0.13
11				ALPHAL	0.62	-0.11	SZDIFCVO	0.71	-0.11
12				HFOSA	0.63	-0.11	ISCSNS	0.72	0.10
13				IGRATE	0.63	0.11	GOESITED	0.73	-0.11
14				MICPU239	0.64	0.10	HFOSA	0.74	-0.11
15							SZCONCOL	0.75	0.09
16							COLGW	0.76	0.09

a: Steps in stepwise rank regression analysis
b: Variables listed in order of selection in stepwise regression
c: Cumulative R^2 value with entry of each variable into regression model
d: Standardized rank regression coefficients (SRRCs) in final regression model

Source: Output DTNs: MO0709TSPAREGS.000 [DIRS 182976]; and MO0709TSPAPLOT.000 [DIRS 183010].

Figure K5.7.3-4. Stepwise rank regression analyses and selected scatterplots for expected dose to RMEI (*EXPDOSE*, mrem/yr) over [0, 1,000,000 yr] for all radioactive species resulting from both early DS failure and early WP failure: (a) Regressions for *EXPDOSE* at 50,000, 200,000 and 500,000 years, and (b,c,d) Scatterplots for *EXPDOSE* at 500,000 years.

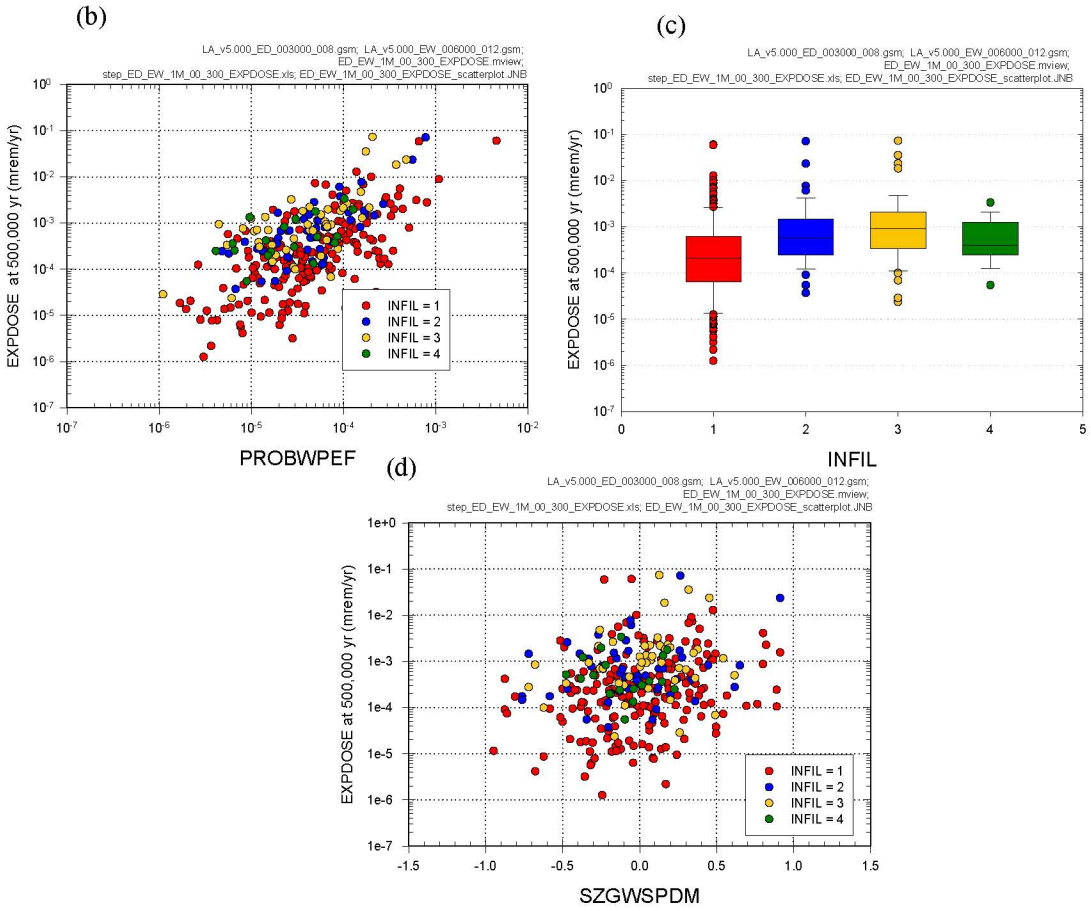

Source: Output DTNs: MO0709TSPAREGS.000 [DIRS 182976]; and MO0709TSPAPLOT.000 [DIRS 183010].

NOTE: In (c), the box extends from 0.25 to 0.75 quantile; lower and upper bar and whisker extend to 0.1 and 0.9 quantile, respectively; dots represent values outside 0.1 to 0.9 quantile range; median indicated by light horizontal line.

Figure K5.7.3-4. Stepwise rank regression analyses and selected scatterplots for expected dose to RMEI (*EXPDOSE*, mrem/yr) over [0, 1,000,000 yr] for all radioactive species resulting from both early DS failure and early WP failure: (a) Regressions for *EXPDOSE* at 50,000, 200,000 and 500,000 years, and (b,c,d) Scatterplots for *EXPDOSE* at 500,000 years (continued).

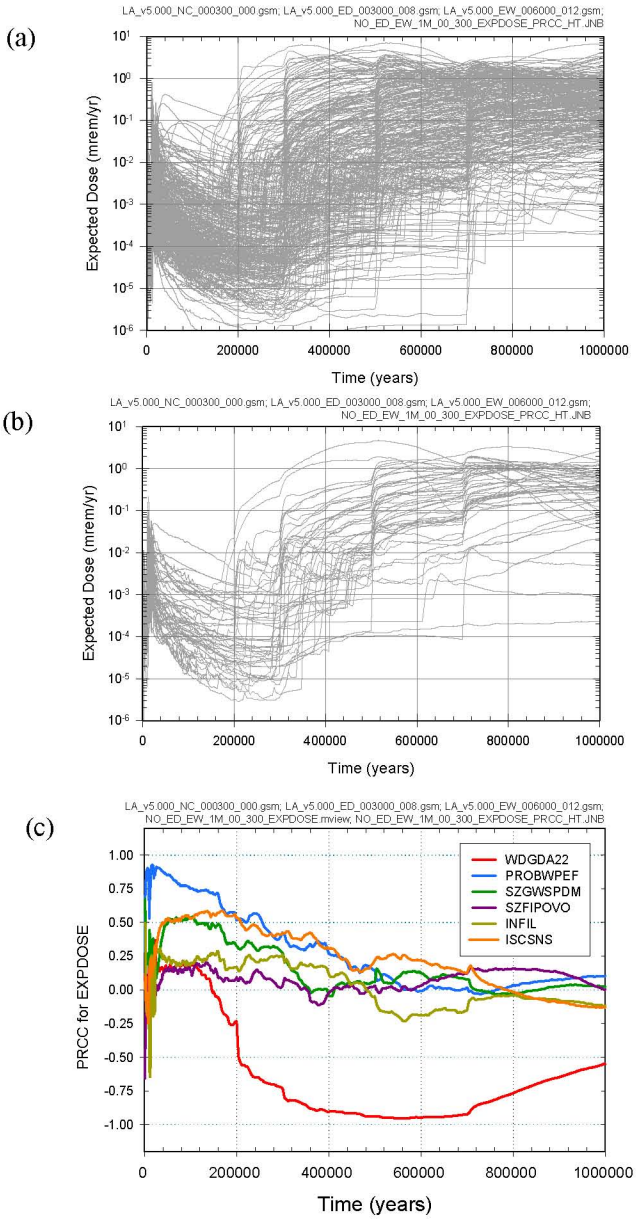

Source: Output DTNs: MO0709TSPAREGS.000 [DIRS 182976]; and MO0709TSPAPLOT.000 [DIRS 183010].

Figure K5.7.4-1. Expected dose to RMEI (*EXPDOSE*, mrem/yr) over [0, 1,000,000 yr] for all radioactive species resulting from early DS failure, early WP failure and nominal process WP failure: (a) *EXPDOSE* for all (i.e., 300) sample elements, (b) *EXPDOSE* for first 50 sample elements, and (c) PRCCs for *EXPDOSE*

(a)

	EXPDOSE: 50K yr			EXPDOSE: 200K yr			EXPDOSE: 500K yr		
Step[a]	**Variable[b]**	**R^{2c}**	**SRRC[d]**	**Variable**	**R^2**	**SRRC**	**Variable**	**R^2**	**SRRC**
1	PROBWPEF	0.51	0.73	PROBWPEF	0.19	0.46	WDGCA22	0.78	-0.89
2	SZGWSPDM	0.59	0.27	ISCSNS	0.31	0.32	WDNSCC	0.81	-0.18
3	ISCSNS	0.66	0.26	SZGWSPDM	0.37	0.26	THERMCON	0.83	-0.14
4	EP1LOWPU	0.68	0.12	WDGCA22	0.42	-0.22	PROBWPEF	0.84	0.10
5	SEEPUNC	0.69	0.11	PROBDSEF	0.44	0.13	WDGCUA22	0.85	0.10
6	MICNP237	0.70	0.12	INRFRCTC	0.46	0.13	WDZOLID	0.86	0.08
7	SZKDSRAL	0.72	0.12	SZSREG3Y	0.48	-0.16	MICNP237	0.86	0.06
8	DTDRHUNC	0.73	0.11	INRFRCSR	0.49	-0.14	CORRATSS	0.87	-0.07
9	HFOSA	0.73	-0.10	SEEPUNC	0.51	0.12	MICI129	0.87	0.07
10							KDRACOL	0.88	-0.06
11							CSNFMASS	0.88	0.06
12							CPUPERCS	0.88	-0.06
13							SZGWSPDM	0.88	0.06

a: Steps in stepwise rank regression analysis
b: Variables listed in order of selection in stepwise regression
c: Cumulative R^2 value with entry of each variable into regression model
d: Standardized rank regression coefficients (SRRCs) in final regression model

Source: Output DTNs: MO0709TSPAREGS.000 [DIRS 182976]; and MO0709TSPAPLOT.000 [DIRS 183010].

Figure K5.7.4-2. Stepwise rank regression analyses and selected scatterplots for expected dose to RMEI (*EXPDOSE*, mrem/yr) over [0, 1,000,000 yr] for all radioactive species resulting from early DS failure, early WP failure and nominal process WP failure: (a) Regressions for *EXPDOSE* at 50,000, 200,000 and 500,000 years, and (b,c,d) Scatterplots for *EXPDOSE* at 500,000 years.

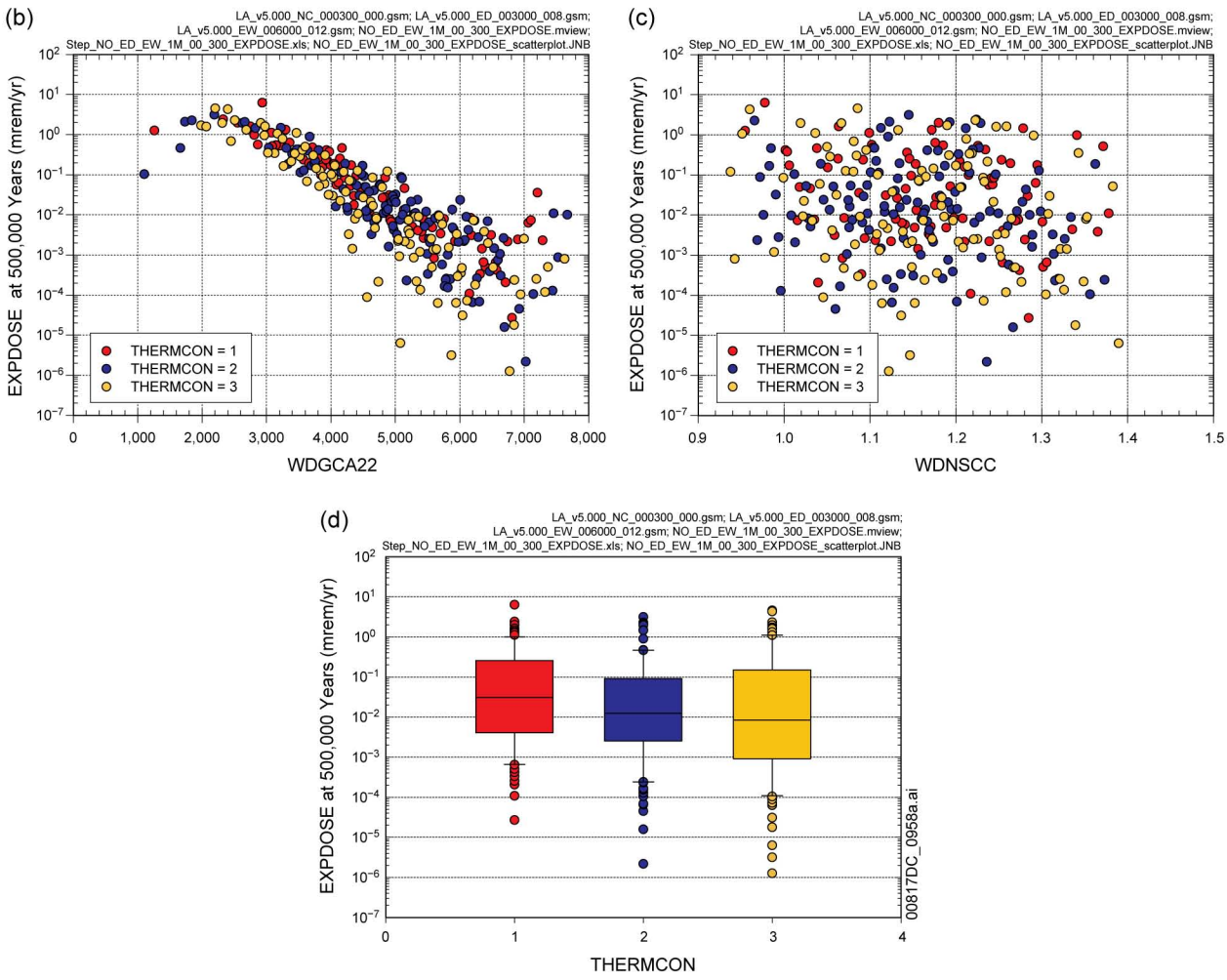

Source: Output DTNs: MO0709TSPAREGS.000 [DIRS 182976]; and MO0709TSPAPLOT.000 [DIRS 183010].

NOTE: In (d), the box extends from 0.25 to 0.75 quantile; lower and upper bar and whisker extend to 0.1 and 0.9 quantile, respectively; dots represent values outside 0.1 to 0.9 quantile range; median indicated by light horizontal line.

Figure K5.7.4-2. Stepwise rank regression analyses and selected scatterplots for expected dose to RMEI (*EXPDOSE*, mrem/yr) over [0, 1,000,000 yr] for all radioactive species resulting from early DS failure, early WP failure and nominal process WP failure: (a) Regressions for *EXPDOSE* at 50,000, 200,000 and 500,000 years, and (b,c,d) Scatterplots for *EXPDOSE* at 500,000 years (continued).

INTENTIONALLY LEFT BLANK

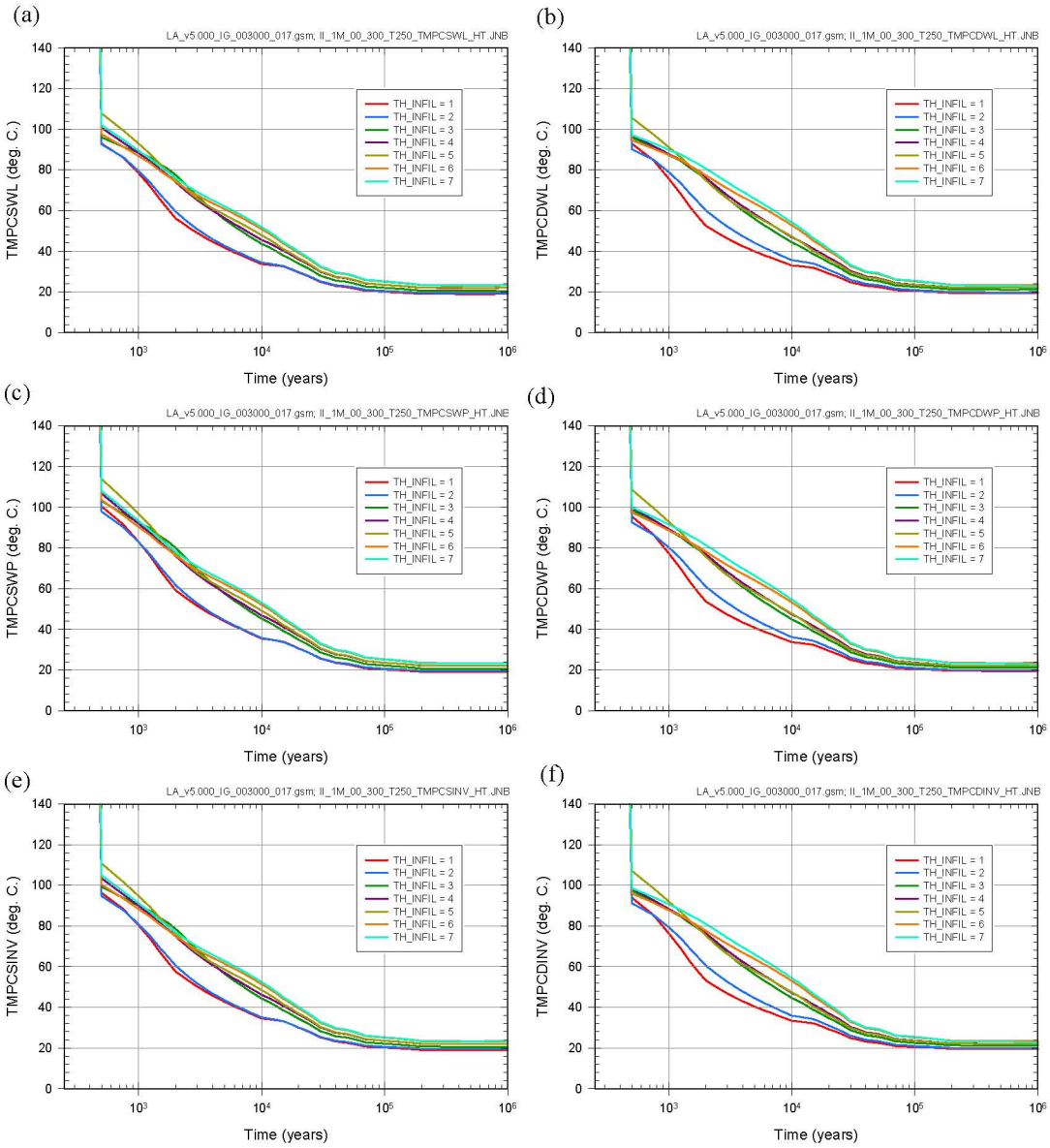

Source: Output DTN: MO0709TSPAREGS.000 [DIRS 182976].

Figure K6.2-1. Time-dependent temperatures in percolation bin 3 for CSNF WPs at the drift wall (*TMPCSWL*), on the WP (*TMPCSWP*) and in the invert beneath the WP (*TMPCSINV*) and similarly for CDSP WPs at the drift wall (*TMPCDWL*), on the WP (*TMPCDWP*) and in the invert beneath the WP (*TMPCDINV*) resulting from an igneous intrusive event at 250 years that destroys all WPs in the repository: (a, c, e) *TMPCSWL*, *TMPCSWP* and *TMPCSINV*, and (b, d, f) *TMPCDWL*, *TMPCDWP* and *TMPCDINV*

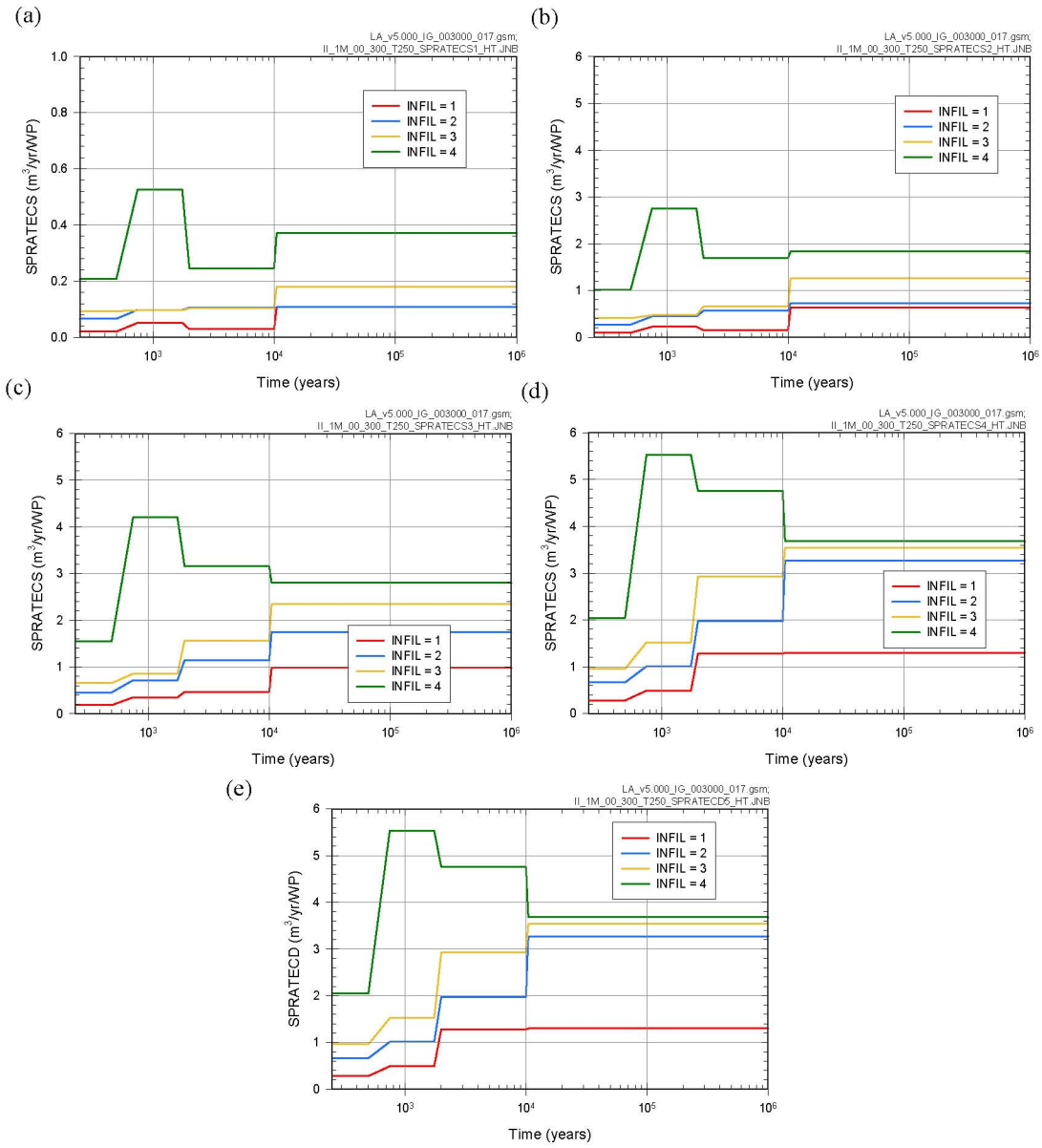

Source: Output DTN: MO0709TSPAREGS.000 [DIRS 182976].

Figure K6.2-2. Time-dependent seepage rates (m^3/yr/WP) into the repository above CSNF WPs (*SPRATECS*) resulting from an igneous intrusive event at 250 years that destroys all WPs in the repository: (a) Bin 1, (b) Bin 2, (c) Bin 3, (d) Bin 4, and (e) Bin 5.

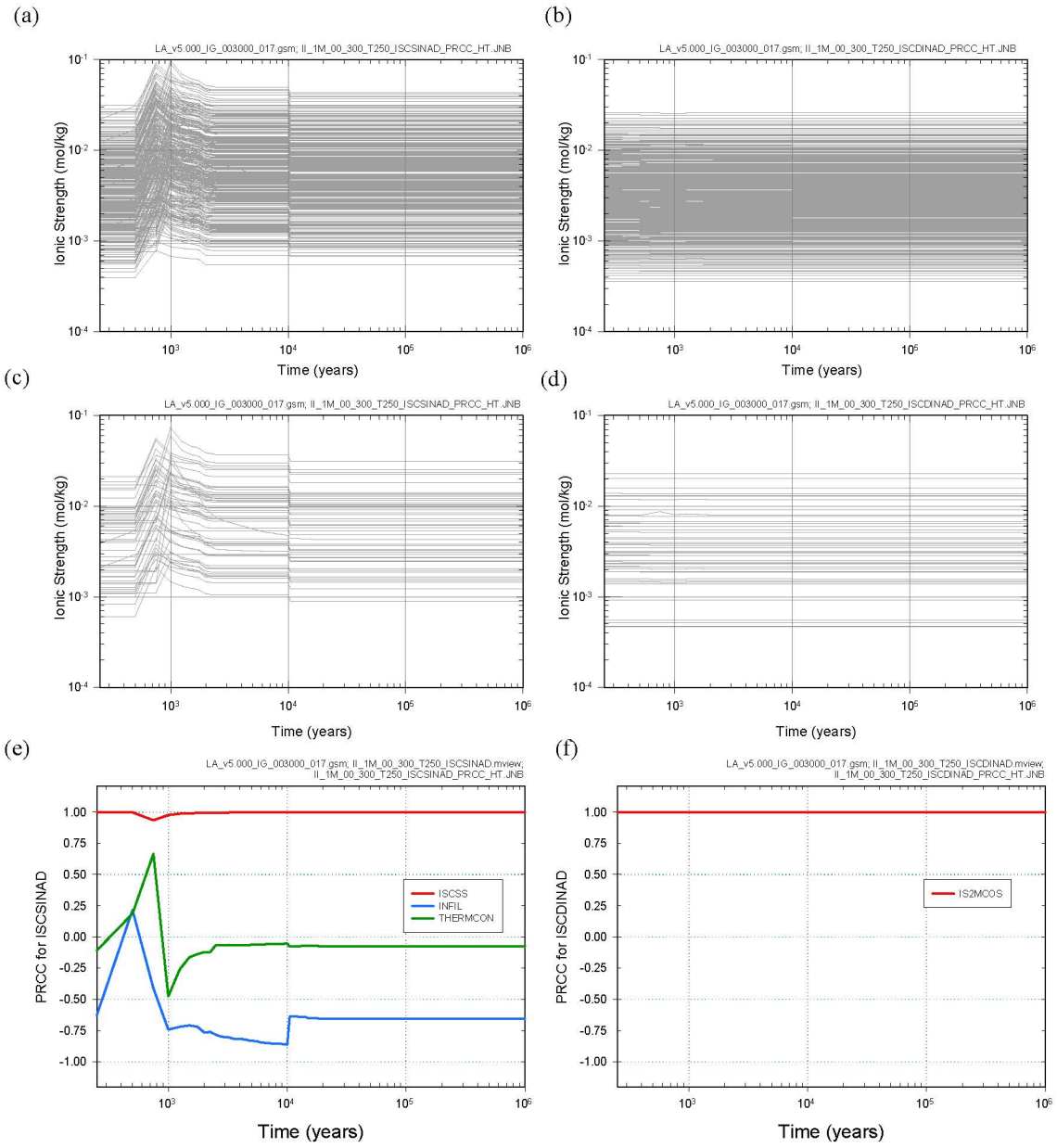

Source: Output DTNs: MO0709TSPAREGS.000 [DIRS 182976]; and MO0709TSPAPLOT.000 [DIRS 183010].

Figure K6.2-3. Time-dependent ionic strength (mol/kg) under dripping conditions in the invert for CSNF WPs (*ISCSINAD*) and CDSP WPs (*ISCDINAD*) in percolation bin 3 resulting from an igneous intrusive event at 250 years that destroys all WPs in the repository: (a, b) *ISCSINAD* and *ISCDINAD* for all (i.e., 300) sample elements, (c, d) *ISCSINAD* and *ISCDINAD* for first 50 sample elements, and (e, f) PRCCs for *ISCSINAD* and *ISCDINAD*

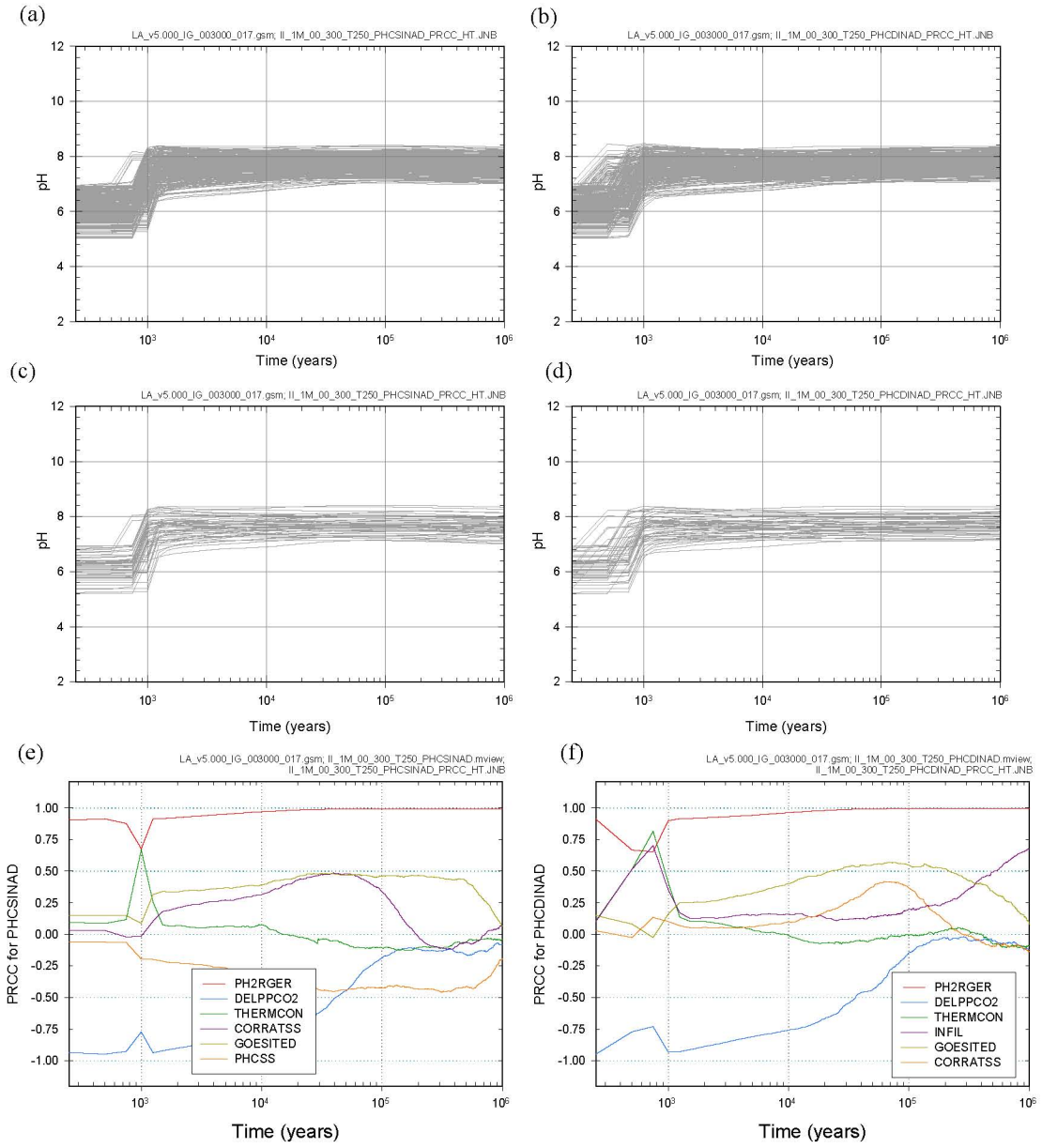

Source: Output DTNs: MO0709TSPAREGS.000 [DIRS 182976]; and MO0709TSPAPLOT.000 [DIRS 183010].

Figure K6.2-4. Time-dependent pH under dripping conditions in the invert for CSNF WPs (*PHCSINAD*) and CDSP WPs (*PHCDINAD*) in percolation bin 3 resulting from an igneous intrusive event at 250 years that destroys all WPs in the repository: (a, b) *PHCSINAD* and *PHCDINAD* for all (i.e., 300) sample elements, (c, d) *PHCSINAD* and *PHCDINAD* for first 50 sample elements, and (e, f) PRCCs for *PHCSINAD* and *PHCDINAD*

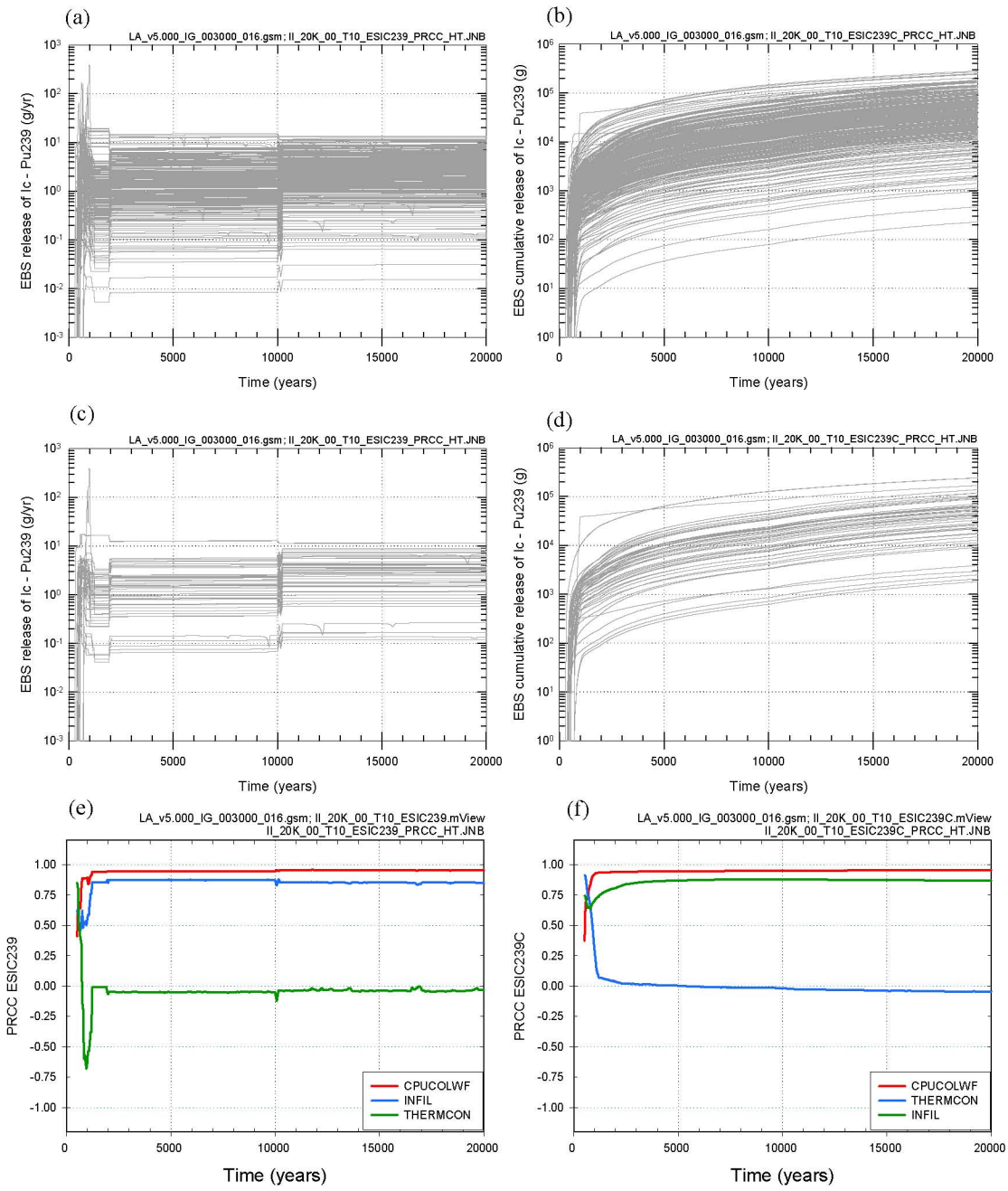

Source: Output DTNs: MO0709TSPAREGS.000 [DIRS 182976]; and MO0709TSPAPLOT.000 [DIRS 183010].

Figure K6.3.1-1. Time-dependent release rates (*ESIC239*, g/yr) and cumulative (i.e., integrated) releases (*ESIC239C*, g) over 20,000 years for the movement of ^{239}Pu irreversibly attached to glass/ waste form colloids from the EBS to the UZ resulting from an igneous intrusive event at 10 years that destroys all WPs in the repository: (a, b) *ESIC239* and *ESIC239C* for all (i.e., 300) sample elements, (c, d) *ESIC239* and *ESIC239C* for first 50 sample elements, and (e, f) PRCCs for *ESIC239* and *ESIC239C*

(a)

	ESIC239: 3000 yr			ESIC239: 5000 yr			ESIC239: 10,000 yr		
Step[a]	**Variable[b]**	**R^{2c}**	**SRRC[d]**	**Variable**	**R^2**	**SRRC**	**Variable**	**R^2**	**SRRC**
1	CPUCOLWF	0.64	0.75	CPUCOLWF	0.64	0.75	CPUCOLWF	0.64	0.75
2	INFIL	0.93	0.54	INFIL	0.93	0.54	INFIL	0.93	0.54
3	DIFPATHL	0.93	0.04	DIFPATHL	0.93	0.04	DIFPATHL	0.93	0.04

(b)

	ESIC239C: 3000 yr			ESIC239C: 5000 yr			ESIC239C: 10,000 yr		
Step[a]	**Variable[b]**	**R^{2c}**	**SRRC[d]**	**Variable**	**R^2**	**SRRC**	**Variable**	**R^2**	**SRRC**
1	CPUCOLWF	0.64	0.75	CPUCOLWF	0.63	0.75	CPUCOLWF	0.64	0.75
2	INFIL	0.90	0.52	INFIL	0.92	0.54	INFIL	0.93	0.54
3	DWCSTERB	0.91	-0.06	DWCSTERB	0.92	-0.06	DWCSTERB	0.93	-0.05
4	DELPPCO2	0.91	0.06	DELPPCO2	0.92	0.05	DELPPCO2	0.93	0.04
5	RUBMAXL	0.91	-0.05	RUBMAXL	0.92	-0.05	RUBMAXL	0.93	-0.04

a: Steps in stepwise rank regression analysis
b: Variables listed in order of selection in stepwise regression
c: Cumulative R^2 value with entry of each variable into regression model
d: Standardized rank regression coefficients (SRRCs) in final regression model

Source: Output DTNs: MO0709TSPAREGS.000 [DIRS 182976]; and MO0709TSPAPLOT.000 [DIRS 183010].

Figure K6.3.1-2. Stepwise rank regression analyses and selected scatterplots for time-dependent release rates (*ESIC239*, g/yr) and cumulative (i.e., integrated) releases (*ESIC239C*, g) for the movement of ^{239}Pu irreversibly attached to glass/ waste form colloids from the EBS to the UZ resulting from an igneous intrusive event at 10 years that destroys all WPs in the repository: (a, b) Regressions for *ESIC239* and *ESIC239C* at 3000, 5000 and 10,000 years, and (c-h) Scatterplots for *ESIC239* and *ESIC239C* at 10,000 years

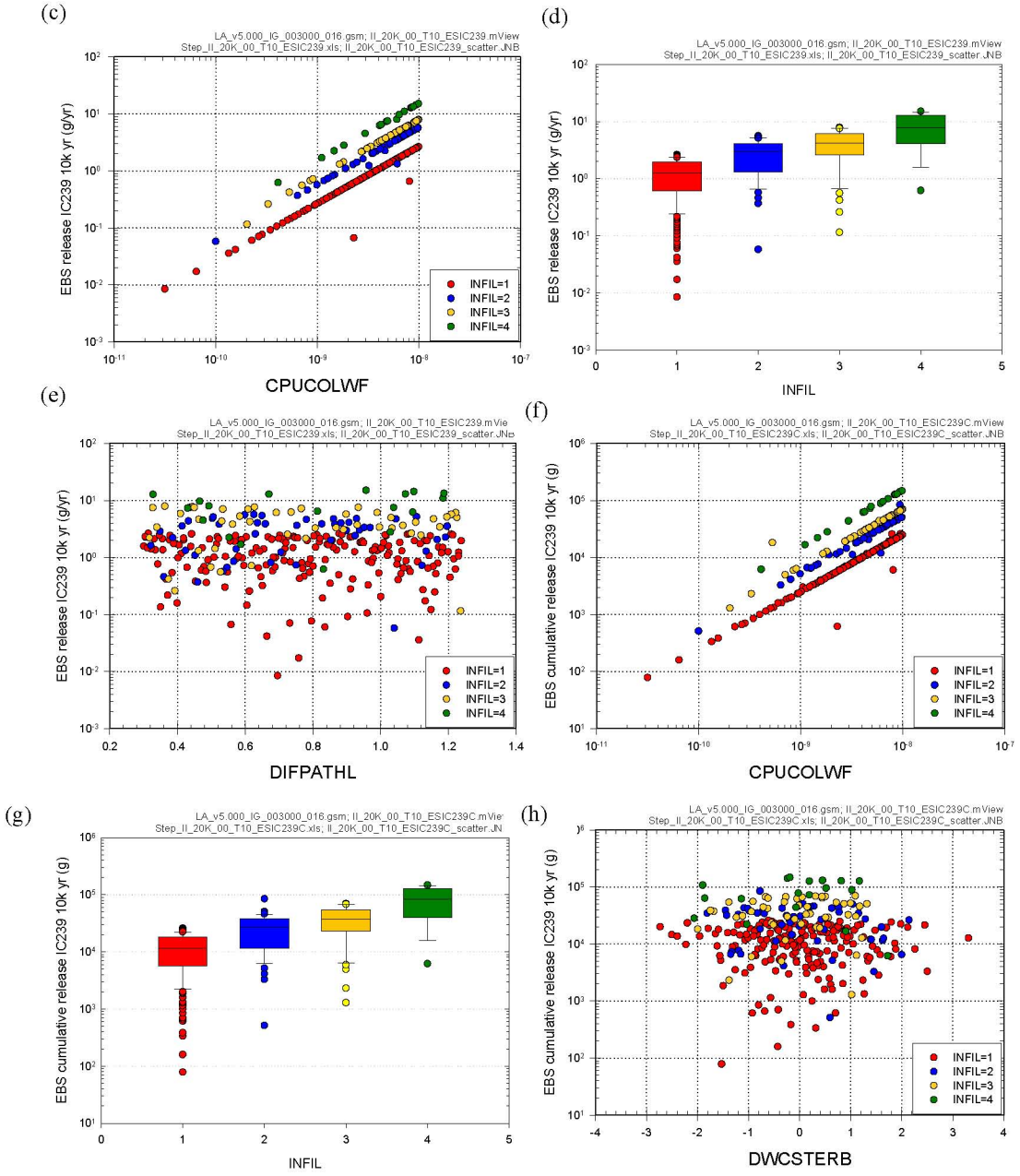

Source: Output DTNs: MO0709TSPAREGS.000 [DIRS 182976]; and MO0709TSPAPLOT.000 [DIRS 183010].

NOTE: In (d,g), the box extends from 0.25 to 0.75 quantile; lower and upper bar and whisker extend to 0.1 and 0.9 quantile, respectively; dots represent values outside 0.1 to 0.9 quantile range; median indicated by light horizontal line.

Figure K.6.3.1-2. Stepwise rank regression analyses and selected scatterplots for time-dependent release rates (*ESIC239*, g/yr) and cumulative (i.e., integrated) releases (*ESIC239C*, g) for the movement of ^{239}Pu irreversibly attached to glass/waste form colloids from the EBS to the UZ resulting from an igneous intrusive event at 10 years that destroys all WPs in the repository: (a, b) Regressions for *ESIC239* and *ESIC239C* at 3000, 5000 and 10,000 years, and (c-h) Scatterplots for *ESIC239* and *ESIC239C* at 10,000 years (continued).

Figure Removed. See discussion in Section K6.3.1.

Figure K6.3.1-3. Time-dependent release rates (*ESIF239*, g/yr) and cumulative (i.e., integrated) releases (*ESIF239C*, g) over 20,000 years for the movement of ^{239}Pu irreversibly attached to ferrous colloids from the EBS to the UZ resulting from an igneous intrusive event at 10 years that destroys all WPs in the repository: (a, b) *ESIF239* and *ESIF239C* for all (i.e., 300) sample elements, (c, d) *ESIF239* and *ESIF239C* for first 50 sample elements, and (e, f) PRCCs for *ESIF239* and *ESIF239C*

Figure Removed. See discussion in Section K6.3.1.

Figure K6.3.1-4. Stepwise rank regression analyses and selected scatterplots for time-dependent release rates (*ESIF239*, g/yr) and cumulative (i.e., integrated) releases (*ESIF239C*, g) for the movement of ^{239}Pu irreversibly attached to ferrous colloids from the EBS to the UZ resulting from an igneous intrusive event at 10 years that destroys all WPs in the repository: (a, b) Regressions for *UZIF239* and *UZIF239C* at 3000, 5000 and 10,000 years, and (c-h) Scatterplots for *UZIF239* and *UZIF239C* at 10,000 years

Figure Removed. See discussion in Section K6.3.1.

Figure K6.3.1-4. Stepwise rank regression analyses and selected scatterplots for time-dependent release rates (*ESIF239*, g/yr) and cumulative (i.e., integrated) releases (*ESIF239C*, g) for the movement of ^{239}Pu irreversibly attached to ferrous colloids from the EBS to the UZ resulting from an igneous intrusive event at 10 years that destroys all WPs in the repository: (a, b) Regressions for *UZIF239* and *UZIF239C* at 3000, 5000 and 10,000 years, and (c-h) Scatterplots for *UZIF239* and *UZIF239C* at 10,000 years (continued)

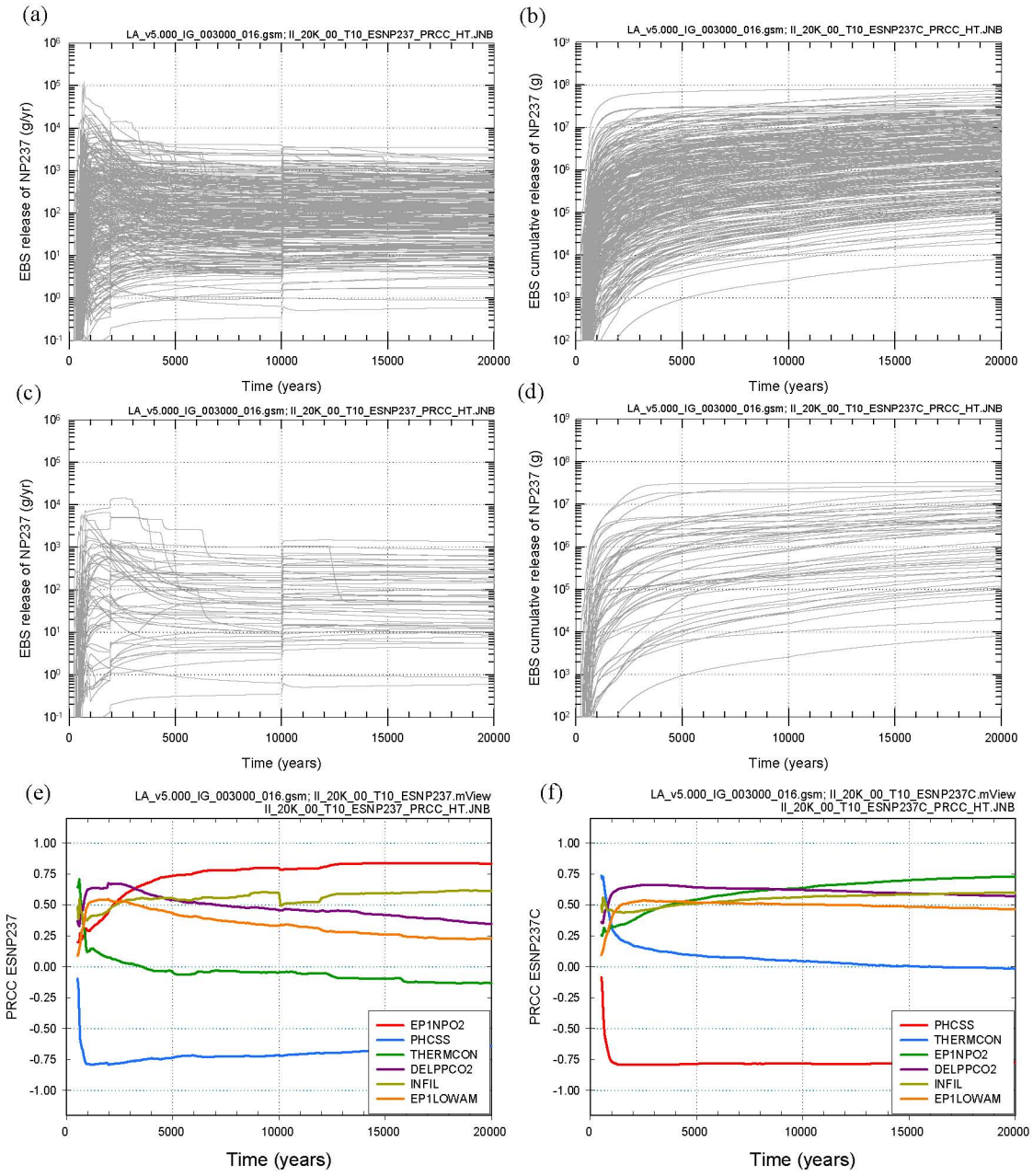

Source: Output DTNs: MO0709TSPAREGS.000 [DIRS 182976]; and MO0709TSPAPLOT.000 [DIRS 183010].

Figure K6.3.1-5. Time-dependent release rates (*ESNP237*, g/yr) and cumulative (i.e., integrated) releases (*ESNP237C*, g) over 20,000 years for the movement of dissolved ^{237}Np from the EBS to the UZ resulting from an igneous intrusive event at 10 years that destroys all WPs in the repository: (a, b) *ESNP237* and *ESNP237C* for all (i.e., 300) sample elements, (c, d) *ESNP237* and *ESNP237C* for first 50 sample elements, and (e, f) PRCCs for *ESNP237* and *ESNP237C*

(a)

	ESNP237: 3000 yr			ESNP237: 5000 yr			ESNP237: 10,000 yr		
Step[a]	Variable[b]	R^{2c}	SRRC[d]	Variable	R^2	SRRC	Variable	R^2	SRRC
1	PHCSS	0.32	-0.51	PHCSS	0.27	-0.46	EP1NPO2	0.27	0.54
2	INFIL	0.44	0.33	EP1NPO2	0.42	0.45	PHCSS	0.46	-0.44
3	DELPPCO2	0.51	0.31	INFIL	0.58	0.36	INFIL	0.63	0.38
4	EP1NPO2	0.59	0.30	CORRATSS	0.63	-0.20	CORRATSS	0.69	-0.22
5	EP1LOWAM	0.66	0.28	EP1LOWAM	0.67	0.22	GOESITED	0.72	-0.18
6	CORRATSS	0.71	-0.19	DELPPCO2	0.71	0.23	DELPPCO2	0.74	0.18
7	EP1LOWNU	0.73	0.14	EP1LOWNU	0.74	0.14	EP1LOWAM	0.77	0.15
8	GOESITED	0.74	-0.12	GOESITED	0.75	-0.14	EP1LOWNU	0.79	0.14
9	CSRINDPO	0.75	0.09	PH2RGER	0.76	-0.12	PH2RGER	0.80	-0.10
10	PH2RGER	0.76	-0.10	WDCRCDEN	0.77	0.10	WDCRCDEN	0.80	0.09
11	WDCRCDEN	0.77	0.10				HFOSA	0.81	-0.09
12	COLGW	0.78	0.08				GOERELAB	0.82	0.08

(b)

	ESNP237C: 3000 yr			ESNP237C: 5000 yr			ESNP237C: 10,000 yr		
Step[a]	Variable[b]	R^{2c}	SRRC[d]	Variable	R^2	SRRC	Variable	R^2	SRRC
1	PHCSS	0.39	-0.58	PHCSS	0.37	-0.56	PHCSS	0.34	-0.54
2	INFIL	0.49	0.30	INFIL	0.48	0.33	INFIL	0.48	0.34
3	DELPPCO2	0.58	0.34	DELPPCO2	0.56	0.32	EP1NPO2	0.56	0.32
4	EP1LOWAM	0.67	0.30	EP1LOWAM	0.64	0.29	DELPPCO2	0.62	0.28
5	EP1NPO2	0.69	0.18	EP1NPO2	0.69	0.24	EP1LOWAM	0.69	0.28
6	CORRATSS	0.72	-0.15	CORRATSS	0.72	-0.17	CORRATSS	0.73	-0.18
7	EP1LOWNU	0.73	0.10	EP1LOWNU	0.74	0.12	EP1LOWNU	0.75	0.14
8	GOESITED	0.74	-0.11	GOESITED	0.75	-0.11	GOESITED	0.76	-0.13
9	EP1NP2O5	0.75	0.12	CSRINDPO	0.76	0.08	PH2RGER	0.77	-0.11
10	CSRINDPO	0.76	0.08	PH2RGER	0.77	-0.10	WDCRCDEN	0.78	0.10
11	PH2RGER	0.77	-0.10	EP1NP2O5	0.77	0.10	EP1NP2O5	0.79	0.09
12	COLGW	0.78	0.08	WDCRCDEN	0.78	0.09	COLGW	0.79	0.09
13	WDCRCDEN	0.79	0.08	KDRACOL	0.79	-0.08	SEEPUNC	0.80	0.08
14	KDRACOL	0.79	-0.09	COLGW	0.79	0.08			

a: Steps in stepwise rank regression analysis
b: Variables listed in order of selection in stepwise regression
c: Cumulative R^2 value with entry of each variable into regression model
d: Standardized rank regression coefficients (SRRCs) in final regression model

Source: Output DTNs: MO0709TSPAREGS.000 [DIRS 182976]; and MO0709TSPAPLOT.000 [DIRS 183010].

Figure K6.3.1-6. Stepwise rank regression analyses and selected scatterplots for time-dependent release rates (*ESNP237*, g/yr) and cumulative (i.e., integrated) releases (*ES NP237C*, g) for the movement of dissolved ^{237}Np from the EBS to the UZ resulting from an igneous intrusive event at 10 years that destroys all WPs in the repository: (a, b) Regressions for *ESNP237* and *ESNP237C* at 3000, 5000 and 10,000 years, and (c-h) Scatterplots for *ESNP237* and *ESNP237C* at 10,000 years

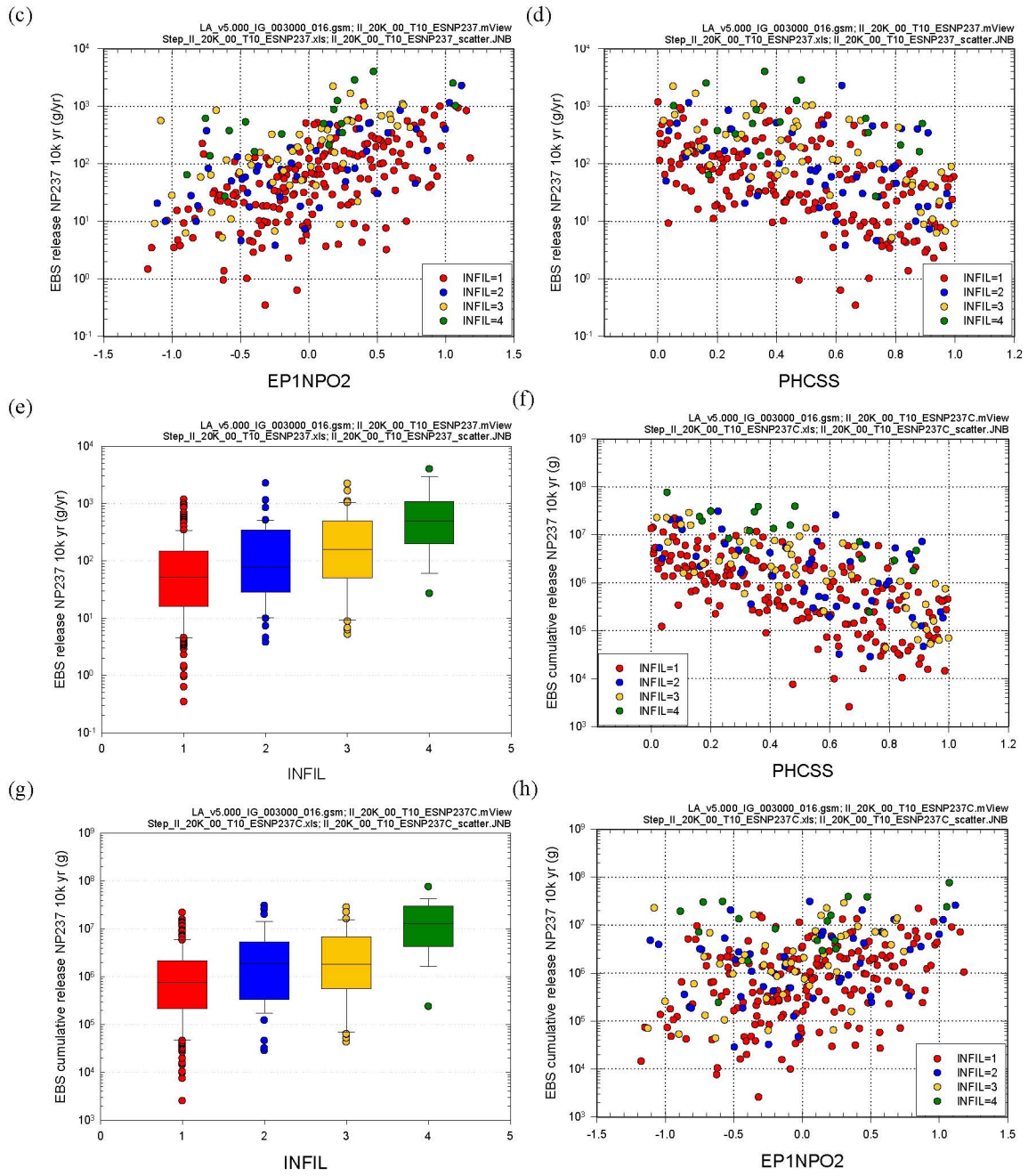

Source: Output DTNs: MO0709TSPAREGS.000 [DIRS 182976]; and MO0709TSPAPLOT.000 [DIRS 183010].

NOTE: In (e,g), the box extends from 0.25 to 0.75 quantile; lower and upper bar and whisker extend to 0.1 and 0.9 quantile, respectively; dots represent values outside 0.1 to 0.9 quantile range; median indicated by light horizontal line.

Figure K6.3.1-6. Stepwise rank regression analyses and selected scatterplots for time-dependent release rates (*ESNP237*, g/yr) and cumulative (i.e., integrated) releases (*ES NP237C*, g) for the movement of dissolved ^{237}Np from the EBS to the UZ resulting from an igneous intrusive event at 10 years that destroys all WPs in the repository: (a, b) Regressions for *ESNP237* and *ESNP237C* at 3000, 5000 and 10,000 years, and (c-h) Scatterplots for *ESNP237* and *ESNP237C* at 10,000 years (continued).

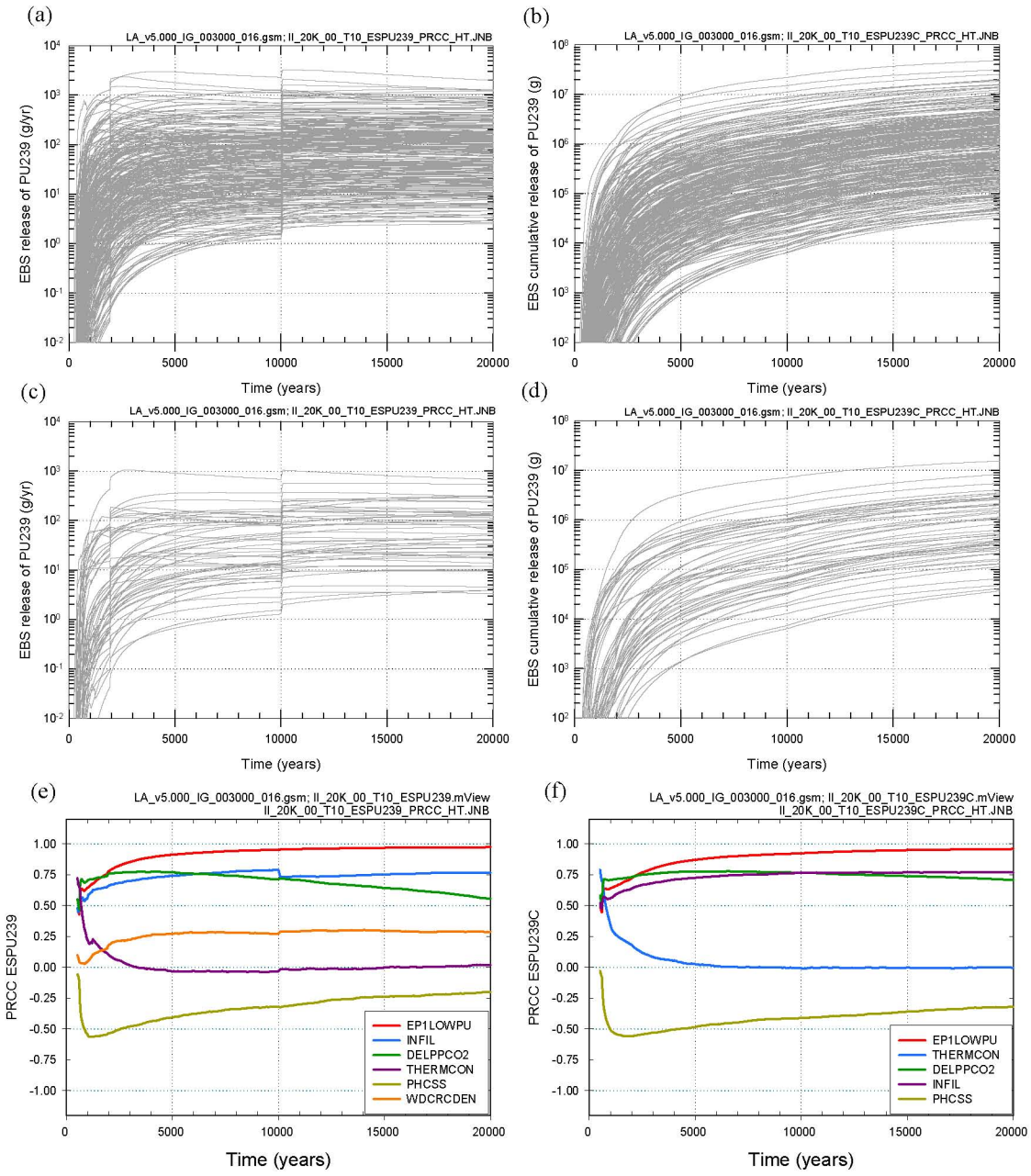

Source: Output DTNs: MO0709TSPAREGS.000 [DIRS 182976]; and MO0709TSPAPLOT.000 [DIRS 183010].]

Figure K6.3.1-7. Time-dependent release rates (*ESPU239*, g/yr) and cumulative (i.e., integrated) releases (*ESPU239C*, g) over 20,000 years for the movement of dissolved ^{239}Pu from the EBS to the UZ resulting from an igneous intrusive event at 10 years that destroys all WPs in the repository: (a, b) *ESPU239* and *ESPU239C* for all (i.e., 300) sample elements, (c, d) *ESPU239* and *ESPU239C* for first 50 sample elements, and (e, f) PRCCs for *ESPU239* and *ESPU239C*

(a)

	ESPU239: 3000 yr			ESPU239: 5000 yr			ESPU239: 10,000 yr		
Step[a]	Variable[b]	R^{2c}	SRRC[d]	Variable	R^2	SRRC	Variable	R^2	SRRC
1	EP1LOWPU	0.36	0.62	EP1LOWPU	0.50	0.72	EP1LOWPU	0.66	0.82
2	DELPPCO2	0.57	0.46	DELPPCO2	0.66	0.40	INFIL	0.80	0.39
3	INFIL	0.75	0.41	INFIL	0.83	0.40	DELPPCO2	0.89	0.29
4	PHCSS	0.80	-0.20	PHCSS	0.85	-0.14	PHCSS	0.90	-0.09
5	EP1LOWAM	0.81	0.13	EP1LOWAM	0.86	0.10	EP1LOWAM	0.91	0.06
6	GOESITED	0.82	-0.09	GOESITED	0.87	-0.08	GOESITED	0.91	-0.06
7	CORRATSS	0.83	-0.09	CORRATSS	0.87	-0.07	CORRATSS	0.91	-0.06
8	GP2NO3	0.83	-0.09	RHPH75	0.87	-0.07	RHPH75	0.92	-0.05
9	RHPH75	0.84	-0.08	GP2NO3	0.88	-0.07	GP2NO3	0.92	-0.04
10	COLGW	0.85	0.07	COLGW	0.88	0.06			
11	GP1NO3	0.85	-0.06						

(b)

	ESPU239C: 3000 yr			ESPU239C: 5000 yr			ESPU239C: 10,000 yr		
Step[a]	Variable[b]	R^{2c}	SRRC[d]	Variable	R^2	SRRC	Variable	R^2	SRRC
1	EP1LOWPU	0.28	0.54	EP1LOWPU	0.39	0.64	EP1LOWPU	0.53	0.74
2	DELPPCO2	0.49	0.47	DELPPCO2	0.58	0.44	INFIL	0.69	0.41
3	INFIL	0.68	0.42	INFIL	0.77	0.42	DELPPCO2	0.84	0.38
4	PHCSS	0.76	-0.25	PHCSS	0.81	-0.20	PHCSS	0.86	-0.14
5	EP1LOWAM	0.78	0.15	EP1LOWAM	0.83	0.12	EP1LOWAM	0.87	0.10
6	GOESITED	0.79	-0.10	GOESITED	0.83	-0.09	GOESITED	0.88	-0.08
7	GP2NO3	0.80	-0.11	GP2NO3	0.84	-0.08	CORRATSS	0.88	-0.07
8	CORRATSS	0.81	-0.09	CORRATSS	0.85	-0.08	GP2NO3	0.89	-0.07
9	RHPH75	0.81	-0.08	RHPH75	0.85	-0.08	RHPH75	0.89	-0.06
10	COLGW	0.82	0.08	COLGW	0.86	0.06	COLGW	0.90	0.06
11	GP1NO3	0.82	-0.07						

a: Steps in stepwise rank regression analysis
b: Variables listed in order of selection in stepwise regression
c: Cumulative R^2 value with entry of each variable into regression model
d: Standardized rank regression coefficients (SRRCs) in final regression model

Source: Output DTNs: MO0709TSPAREGS.000 [DIRS 182976]; and MO0709TSPAPLOT.000 [DIRS 183010].

Figure K6.3.1-8. Stepwise rank regression analyses and selected scatterplots for time-dependent release rates (*ESPU239*, g/yr) and cumulative (i.e., integrated) releases (*ESPU239*, g) for the movement of dissolved ^{239}Pu from the EBS to the UZ resulting from an igneous intrusive event at 10 years that destroys all WPs in the repository: (a, b) Regressions for *ESPU239* and *ESPU239C* at 3000, 5000 and 10,000 years, and (c-h) Scatterplots for *ESPU239* and *ESPU239C* at 10,000 years

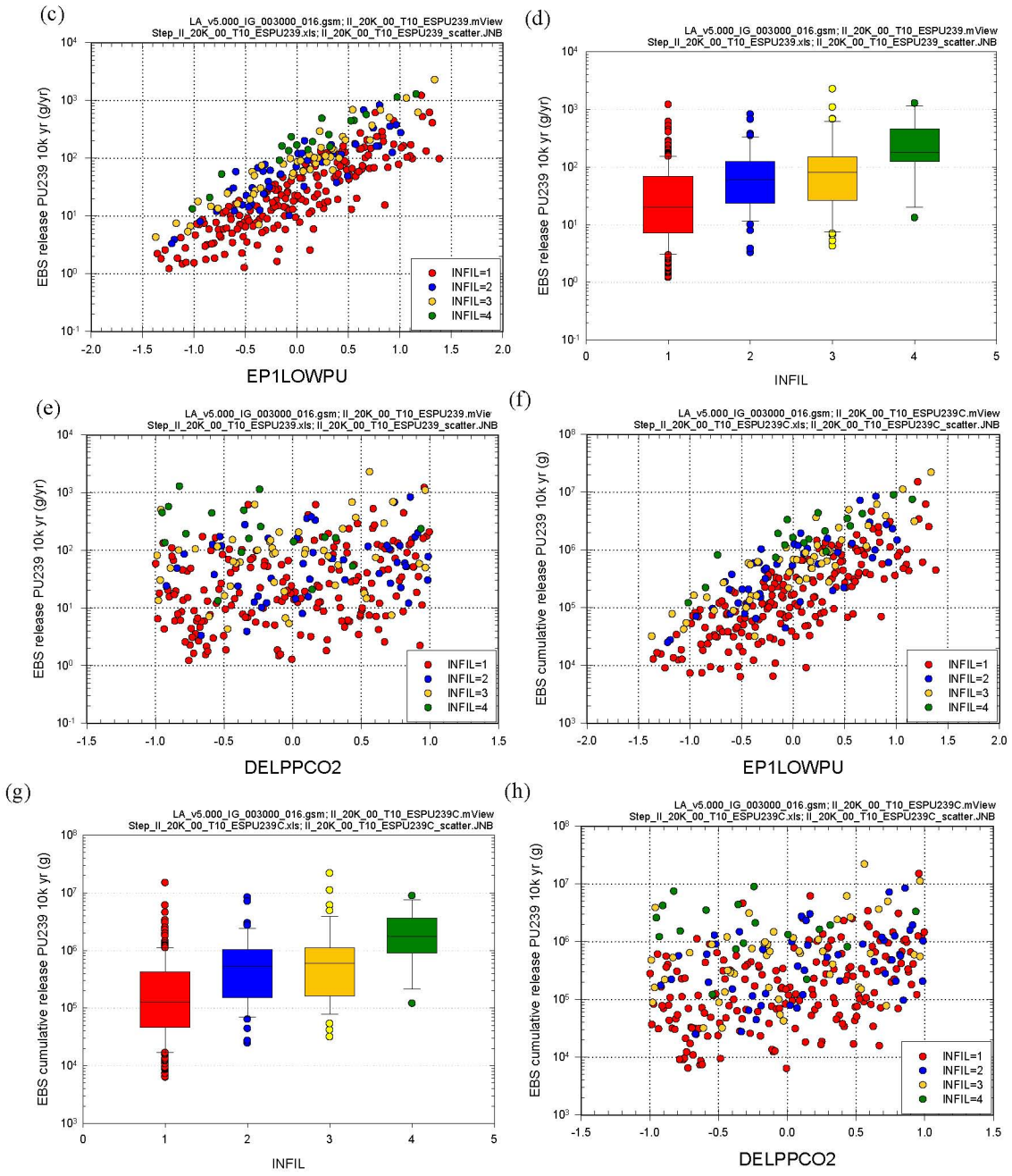

Source: Output DTNs: MO0709TSPAREGS.000 [DIRS 182976]; and MO0709TSPAPLOT.000 [DIRS 183010].

NOTE: In (c,g), the box extends from 0.25 to 0.75 quantile; lower and upper bar and whisker extend to 0.1 and 0.9 quantile, respectively; dots represent values outside 0.1 to 0.9 quantile range; median indicated by light horizontal line.

Figure K6.3.1-8. Stepwise rank regression analyses and selected scatterplots for time-dependent release rates (*ESPU239*, g/yr) and cumulative (i.e., integrated) releases (*ESPU239*, g) for the movement of dissolved ^{239}Pu from the EBS to the UZ resulting from an igneous intrusive event at 10 years that destroys all WPs in the repository: (a, b) Regressions for *ESPU239* and *ESPU239C* at 3000, 5000 and 10,000 years, and (c-h) Scatterplots for *ESPU239* and *ESPU239C* at 10,000 years (continued).

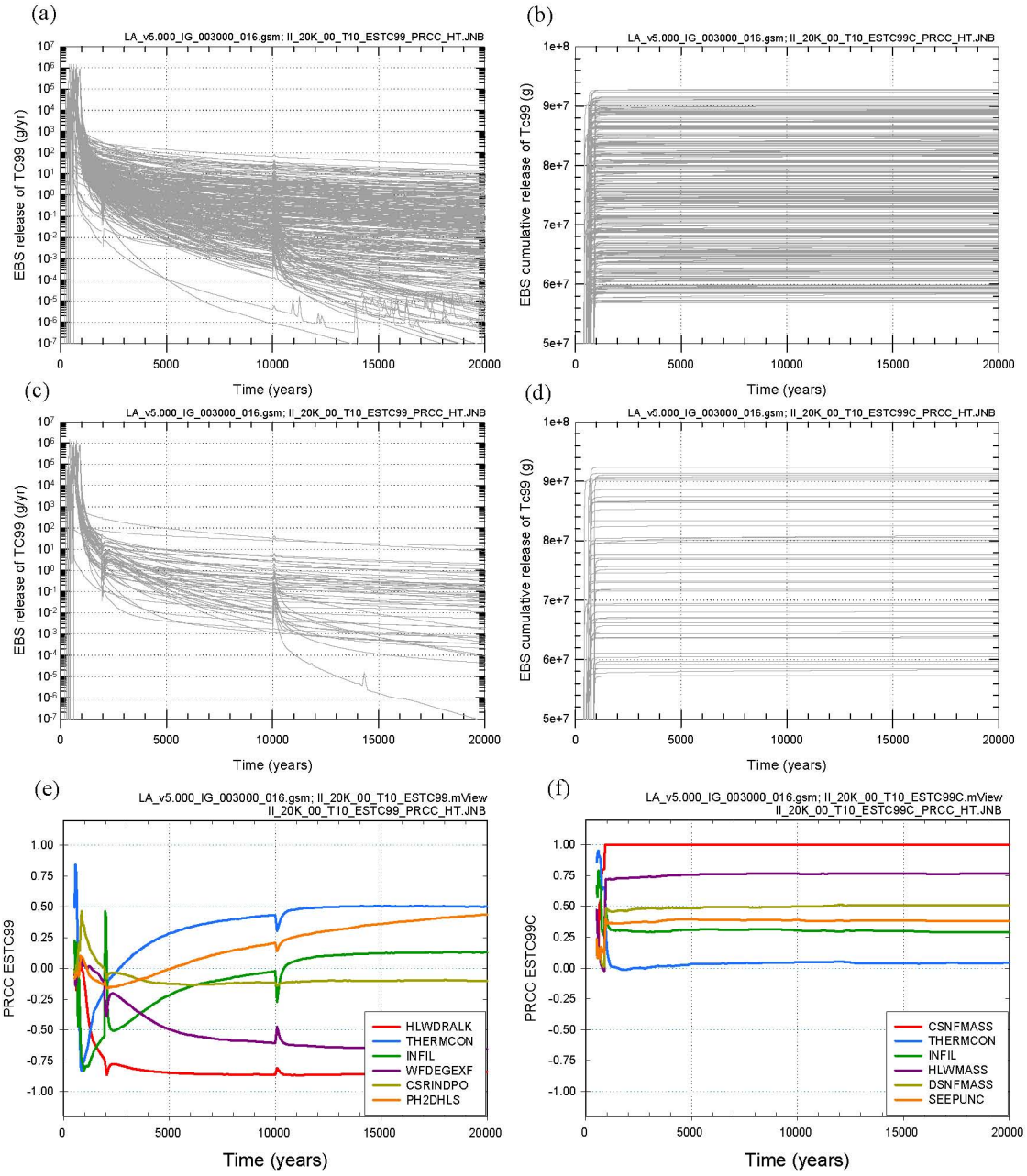

Source: Output DTNs: MO0709TSPAREGS.000 [DIRS 182976]; and MO0709TSPAPLOT.000 [DIRS 183010].

Figure K6.3.1-9. Time-dependent release rates (*ESTC99*, g/yr) and cumulative (i.e., integrated) releases (*ESTC99C*, g) over 20,000 years for the movement of dissolved ^{99}Tc from the EBS to the UZ resulting from an igneous intrusive event at 10 years that destroys all WPs in the repository: (a, b) *ESTC99* and *ESTC99C* for all (i.e., 300) sample elements, (c, d) *ESTC99* and *ESTC99C* for first 50 sample elements, and (e, f) PRCCs for *ESTC99* and *ESTC99C*.

(a)

	ESTC99: 3000 yr			ESTC99: 5000 yr			ESTC99: 10,000 yr		
Step[a]	Variable[b]	R^{2c}	SRRC[d]	Variable	R^2	SRRC	Variable	R^2	SRRC
1	HLWDRALK	0.55	-0.76	HLWDRALK	0.62	-0.81	HLWDRALK	0.59	-0.78
2	INFIL	0.64	-0.28	WFDEGEXF	0.72	-0.31	WFDEGEXF	0.72	-0.36
3	WFDEGEXF	0.67	-0.20	THERMCON	0.75	0.17	THERMCON	0.78	0.24
4	IS2DHLNS	0.68	-0.09	INFIL	0.76	-0.11	WDDSBEGC	0.79	0.09
5				WDDSBEGC	0.77	0.09	PH2DHLS	0.80	0.09
6				IS2DHLNS	0.77	-0.09	HLWDRACD	0.81	-0.08
7				IS2DHLS	0.78	-0.07			

(b)

	ESTC99C: 3000 yr			ESTC99C: 5000 yr			ESTC99C: 10,000 yr		
Step[a]	Variable[b]	R^{2c}	SRRC[d]	Variable	R^2	SRRC	Variable	R^2	SRRC
1	CSNFMASS	0.99	0.99	CSNFMASS	0.99	0.99	CSNFMASS	0.99	0.99
2	HLWMASS	1.00	0.05	HLWMASS	1.00	0.05	HLWMASS	1.00	0.05
3	DSNFMASS	1.00	0.02	DSNFMASS	1.00	0.02	DSNFMASS	1.00	0.02
4	SEEPUNC	1.00	0.02	SEEPUNC	1.00	0.02	SEEPUNC	1.00	0.02
5	HLWDRALK	1.00	0.02	HLWDRALK	1.00	0.01	SEEPPRM	1.00	-0.01
6	SEEPPRM	1.00	-0.01	SEEPPRM	1.00	-0.01	INFIL	1.00	0.01
7	INFIL	1.00	0.01	INFIL	1.00	0.01	HLWDRALK	1.00	0.01
8	PHCSNS	1.00	-0.01	INRFRCCS	1.00	-0.01	KDCSCOL	1.00	-0.01
9	INRFRCCS	1.00	-0.01	KDCSCOL	1.00	-0.01	INRFRCCS	1.00	-0.01
10	KDCSCOL	1.00	-0.01	PHCSNS	1.00	-0.01	ALPHAL	1.00	-0.01

a: Steps in stepwise rank regression analysis
b: Variables listed in order of selection in stepwise regression
c: Cumulative R^2 value with entry of each variable into regression model
d: Standardized rank regression coefficients (SRRCs) in final regression model

Source: Output DTNs: MO0709TSPAREGS.000 [DIRS 182976]; and MO0709TSPAPLOT.000 [DIRS 183010].

Figure K6.3.1-10. Stepwise rank regression analyses and selected scatterplots for time-dependent release rates (*ESTC99*, g/yr) and cumulative (i.e., integrated) releases (*ESTC99C*, g) for the movement of dissolved ^{99}Tc from the EBS to the UZ resulting from an igneous intrusive event at 10 years that destroys all WPs in the repository: (a, b) Regressions for *ESTC99* and *ESTC99C* at 3000, 5000 and 10,000 years, and (c-h) Scatterplots for *ESTC99* and *ESTC99C* at 10,000 years.

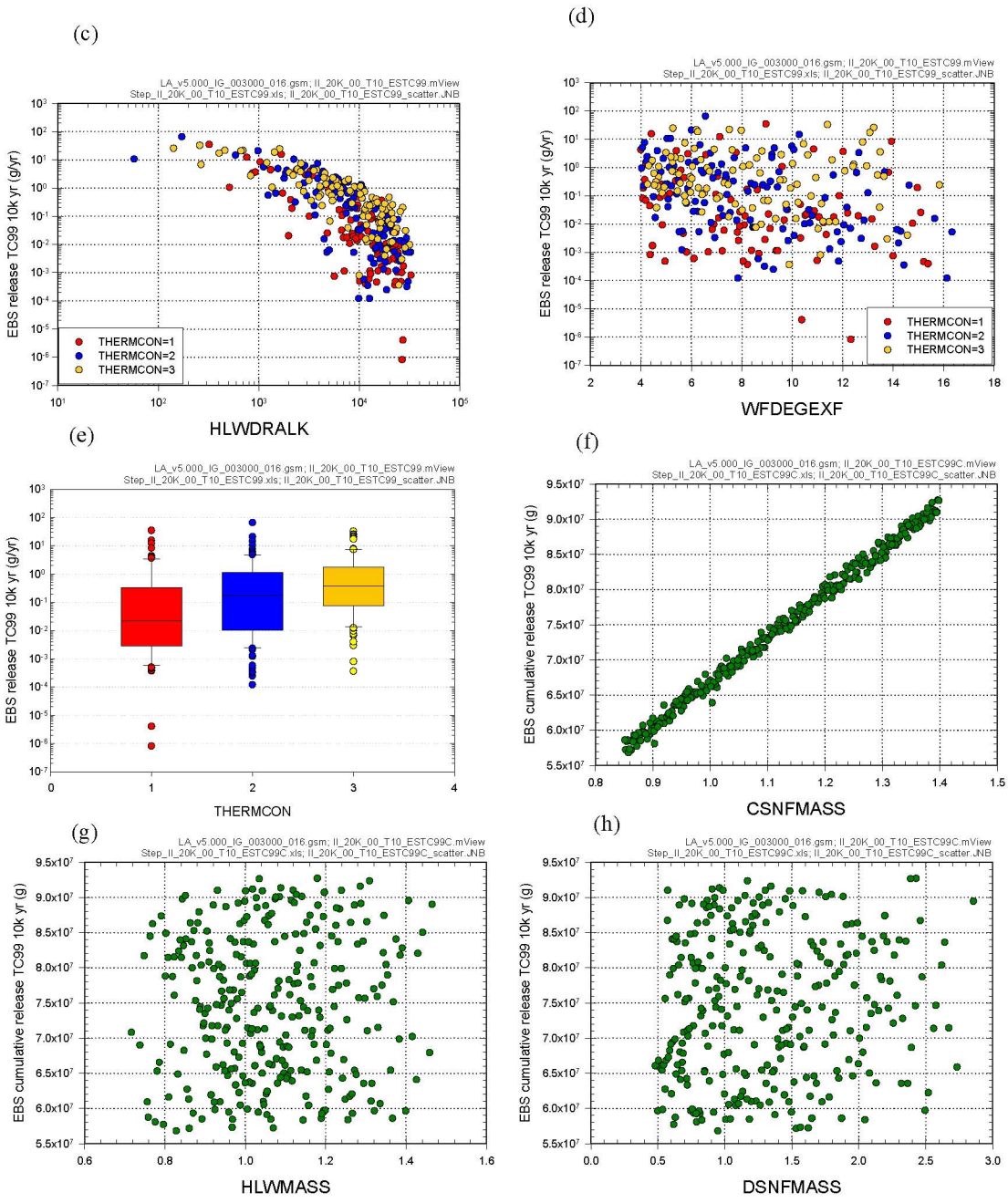

Source: Output DTNs: MO0709TSPAREGS.000 [DIRS 182976]; and MO0709TSPAPLOT.000 [DIRS 183010].

NOTE: In (e), the box extends from 0.25 to 0.75 quantile; lower and upper bar and whisker extend to 0.1 and 0.9 quantile, respectively; dots represent values outside 0.1 to 0.9 quantile range; median indicated by light horizontal line.

Figure K6.3.1-10. Stepwise rank regression analyses and selected scatterplots for time-dependent release rates (ESTC99, g/yr) and cumulative (i.e., integrated) releases (ESTC99C, g) for the movement of dissolved 99Tc from the EBS to the UZ resulting from an igneous intrusive event at 10 years that destroys all WPs in the repository: (a, b) Regressions for ESTC99 and ESTC99C at 3000, 5000 and 10,000 years, and (c-h) Scatterplots for *ESTC99* and *ESTC99C* at 10,000 years (continued).

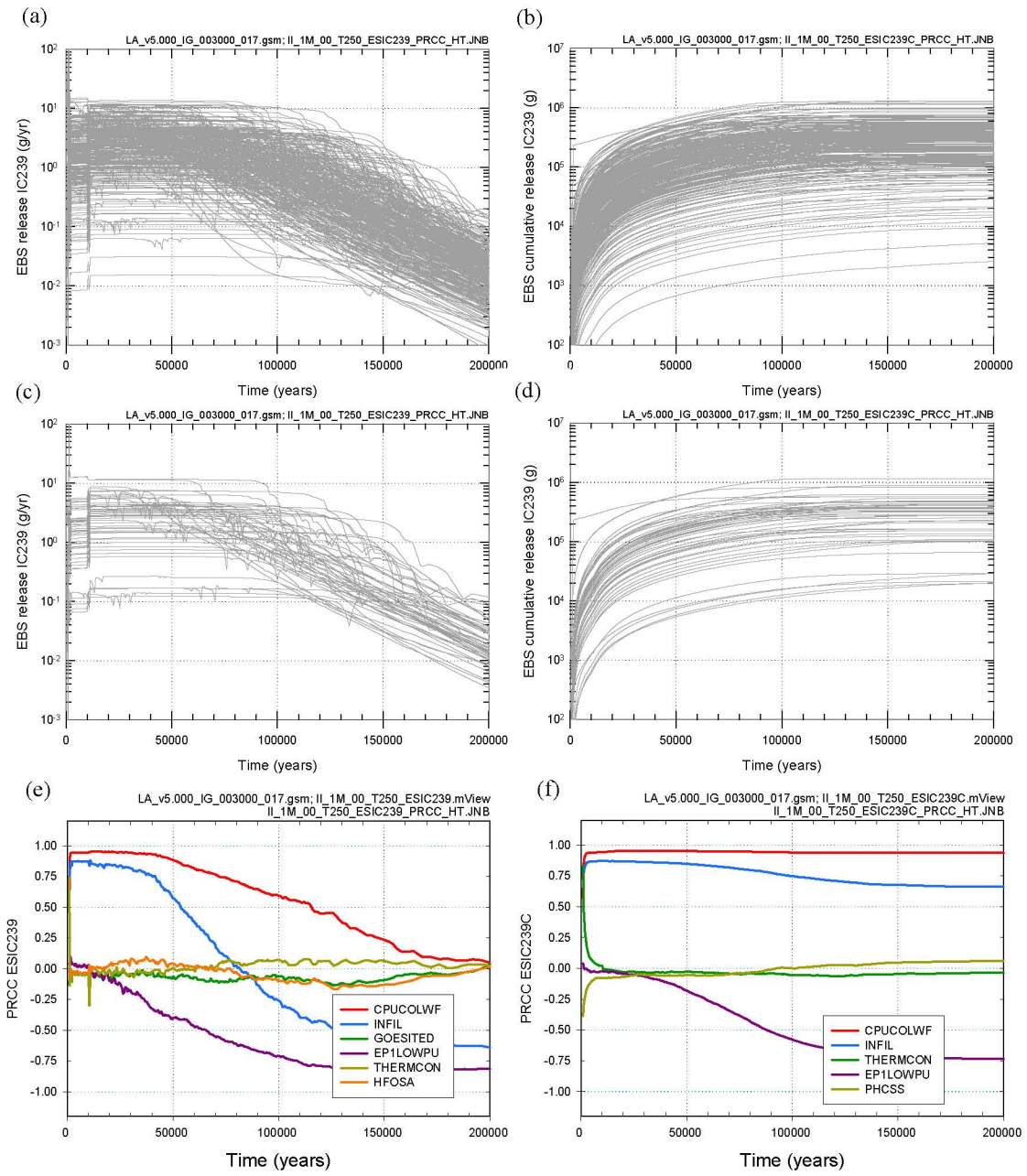

Source: Output DTNs: MO0709TSPAREGS.000 [DIRS 182976]; and MO0709TSPAPLOT.000 [DIRS 183010].

Figure K6.3.2-1. Time-dependent release rates (*ESIC239*, g/yr) and cumulative (i.e., integrated) releases (*ESIC239C*, g) over 200,000 years for the movement of ^{239}Pu irreversibly attached to glass/ waste form colloids from the EBS to the UZ resulting from an igneous intrusive event at 250 years that destroys all WPs in the repository: (a, b) *ESIC239* and *ESIC239C* for all (i.e., 300) sample elements, (c, d) *ESIC239* and *ESIC239C* for first 50 sample elements, and (e, f) PRCCs for *ESIC239* and *ESIC239C*.

Figure Removed. See discussion in Section K6.3.2.

Figure K6.3.2-2. Time-dependent release rates (*ESIF239*, g/yr) and cumulative (i.e., integrated) releases (*ESIF239C*, g) over 200,000 years for the movement of ^{239}Pu irreversibly attached to glass/ waste form colloids from the EBS to the UZ resulting from an igneous intrusive event at 250 years that destroys all WPs in the repository: (a, b) *ESIF239* and *ESIF239C* for all (i.e., 300) sample elements, (c, d) *ESIF239* and *ESIF239C* for first 50 sample elements, and (e, f) PRCCs for *ESIF239* and *ESIF239C*.

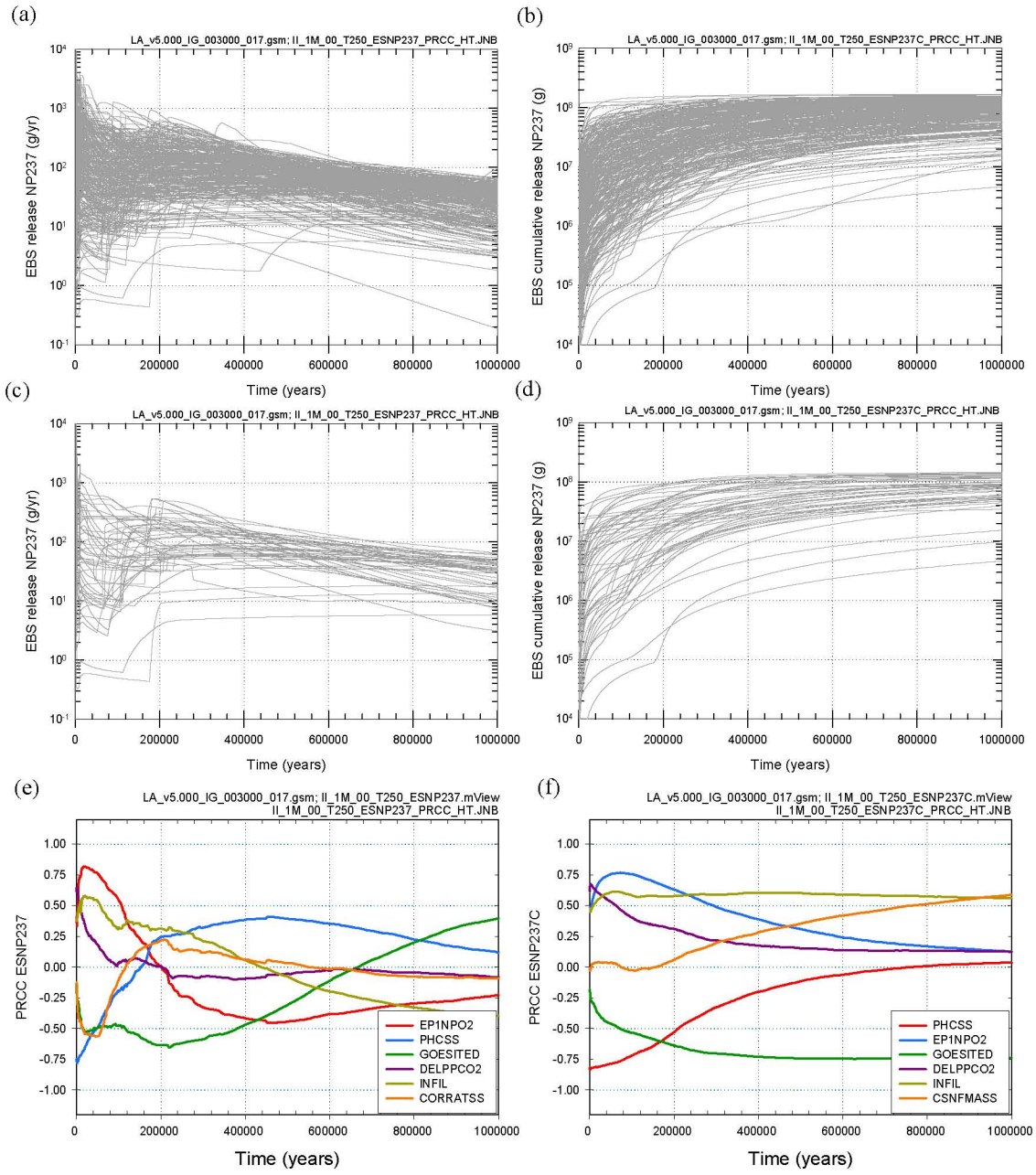

Source: Output DTNs: MO0709TSPAREGS.000 [DIRS 182976]; and MO0709TSPAPLOT.000 [DIRS 183010].

Figure K6.3.2-3. Time-dependent release rates (*ESNP237*, g/yr) and cumulative (i.e., integrated) releases (*ESNP237C*, g) over 1,000,000 years for the movement of dissolved ^{237}Np from the EBS to the UZ resulting from an igneous intrusive event at 250 years that destroys all WPs in the repository: (a, b) *ESNP237* and *ESNP237C* for all (i.e., 300) sample elements, (c, d) *ESNP237* and *ESNP237C* for first 50 sample elements, and (e, f) PRCCs for *ESNP237* and *ESNP237C*.

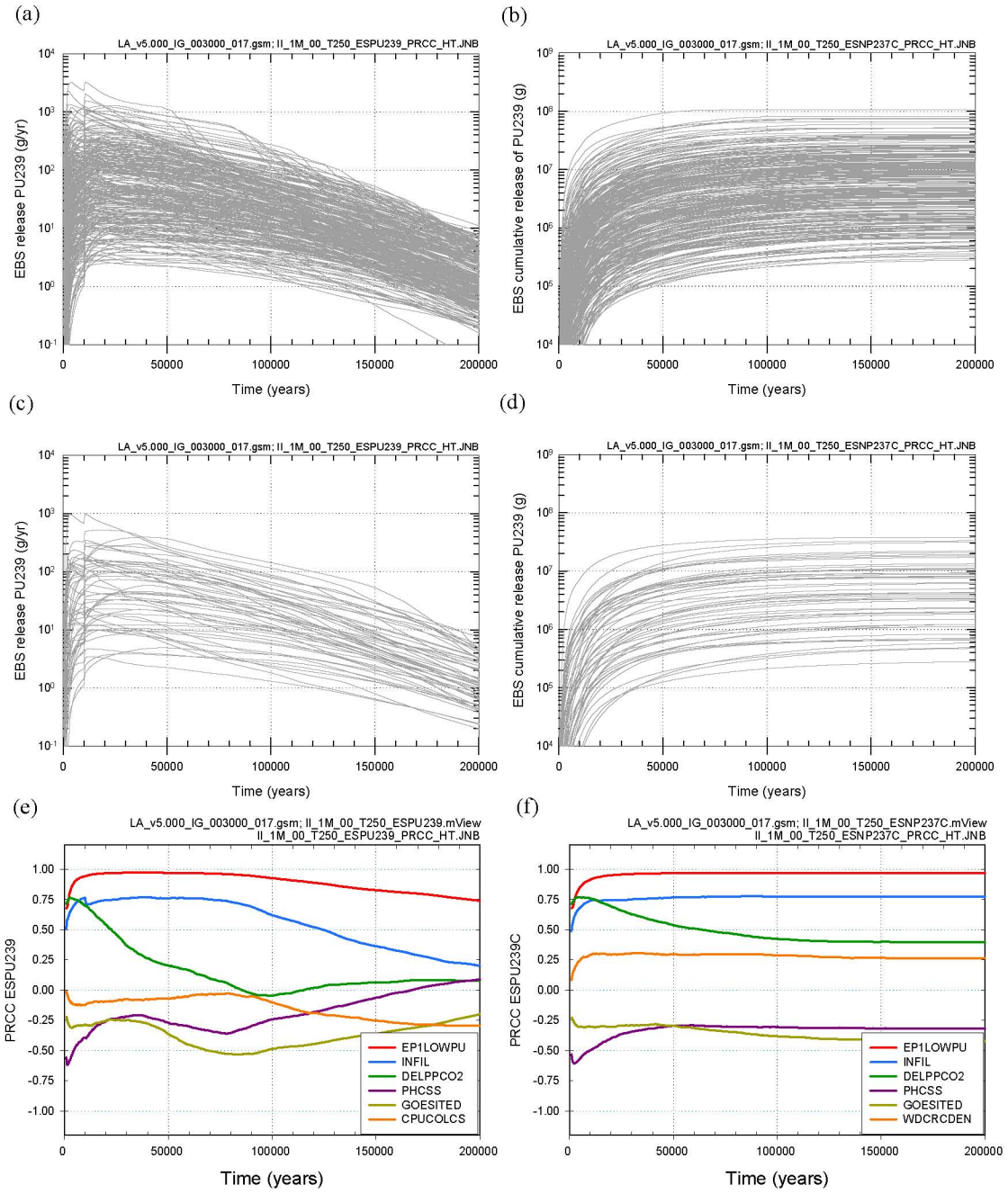

Source: Output DTNs: MO0709TSPAREGS.000 [DIRS 182976]; and MO0709TSPAPLOT.000 [DIRS 183010].

Figure K6.3.2-4. Time-dependent release rates (*ESPU239*, g/yr) and cumulative (i.e., integrated) releases (*ESPU239C*, g) over 200,000 years for the movement of dissolved ^{239}Pu from the EBS to the UZ resulting from an igneous intrusive event at 250 years that destroys all WPs in the repository: (a, b) *ESPU239* and *ESPU239C* for all (i.e., 300) sample elements, (c, d) *ESPU239* and *ESPU239C* for first 50 sample elements, and (e, f) PRCCs for *ESPU239* and *ESPU239C*.

INTENTIONALLY LEFT BLANK

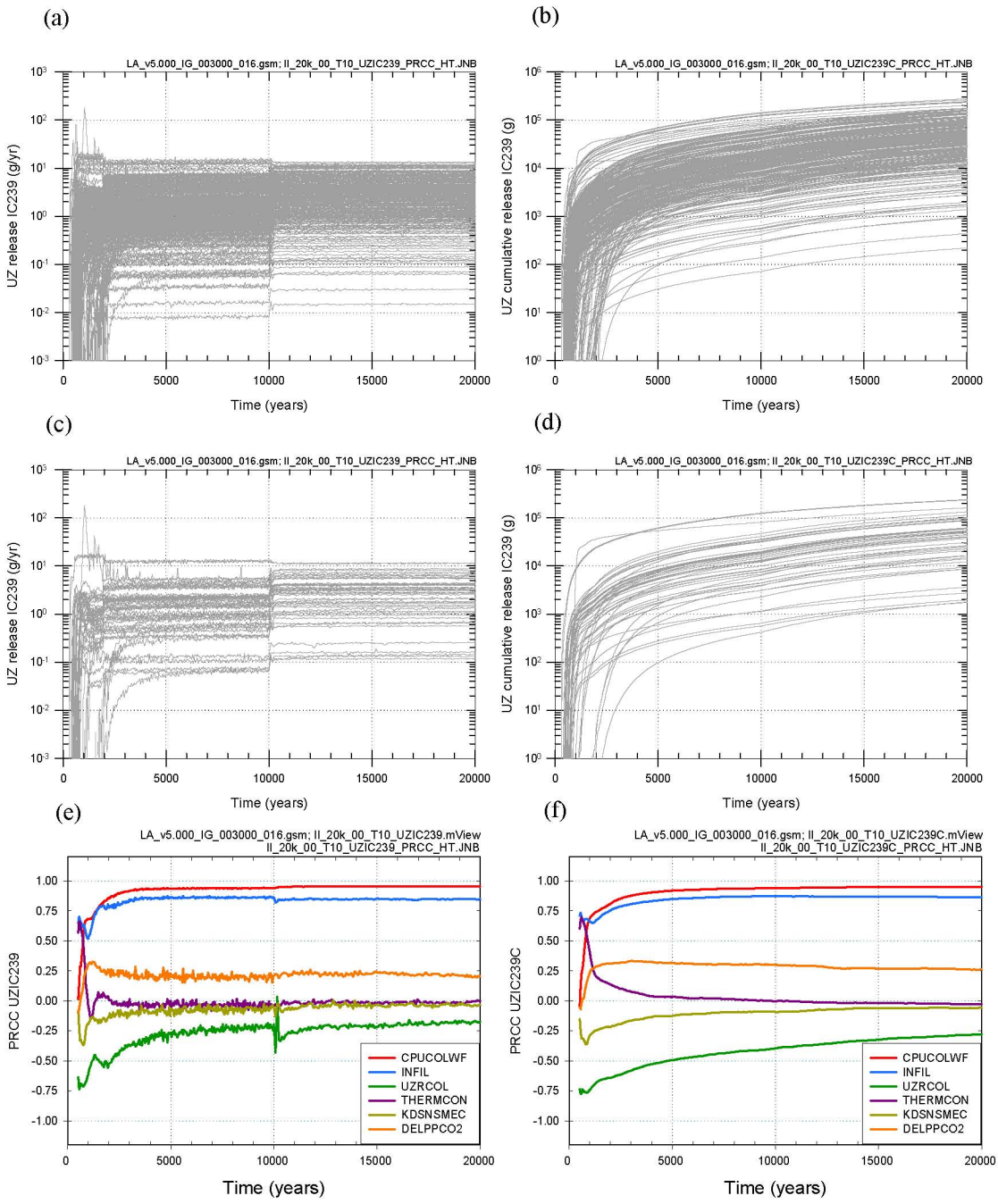

Source: Output DTNs: MO0709TSPAREGS.000 [DIRS 182976]; and MO0709TSPAPLOT.000 [DIRS 183010].

Figure K6.4.1-1. Time-dependent release rates (*UZIC239*, g/yr) and cumulative (i.e., integrated) releases (*UZIC239C*, g) over 20,000 years for the movement of ^{239}Pu irreversibly attached to slow colloids from the UZ to the SZ resulting from an igneous intrusive event at 10 years that destroys all WPs in the repository: (a, b) *UZIC239* and *UZIC239C* for all (i.e., 300) sample elements, (c, d) *UZIC239* and *UZIC239C* for first 50 sample elements, and (e, f) PRCCs for *UZIC239* and *UZIC239C*

(a)

	UZIC239: 3000 yr			UZIC239: 5000 yr			UZIC239: 10,000 yr		
Step[a]	**Variable[b]**	**R^{2c}**	**SRRC[d]**	**Variable**	**R^2**	**SRRC**	**Variable**	**R^2**	**SRRC**
1	CPUCOLWF	0.56	0.71	CPUCOLWF	0.61	0.73	CPUCOLWF	0.63	0.74
2	INFIL	0.89	0.57	INFIL	0.91	0.55	INFIL	0.92	0.54
3	UZRCOL	0.90	-0.10	UZRCOL	0.91	-0.06	DIFPATHL	0.92	0.05
4	DIFPATHL	0.90	0.05				DWCSTERB	0.92	-0.04

(b)

	UZIC239C: 3000 yr			UZIC239C: 5000 yr			UZIC239C: 10,000 yr		
Step[a]	**Variable[b]**	**R^{2c}**	**SRRC[d]**	**Variable**	**R^2**	**SRRC**	**Variable**	**R^2**	**SRRC**
1	CPUCOLWF	0.44	0.63	CPUCOLWF	0.53	0.69	CPUCOLWF	0.59	0.73
2	INFIL	0.79	0.59	INFIL	0.87	0.58	INFIL	0.91	0.56
3	UZRCOL	0.84	-0.23	UZRCOL	0.89	-0.15	UZRCOL	0.91	-0.10
4	DELPPCO2	0.85	0.09	DELPPCO2	0.89	0.07	DELPPCO2	0.92	0.05
5				DWCSTERB	0.90	-0.05	DWCSTERB	0.92	-0.05
6							KDSNCOL	0.92	-0.04

a: Steps in stepwise rank regression analysis
b: Variables listed in order of selection in stepwise regression
c: Cumulative R^2 value with entry of each variable into regression model
d: Standardized rank regression coefficients (SRRCs) in final regression model

Source: Output DTNs: MO0709TSPAREGS.000 [DIRS 182976]; and MO0709TSPAPLOT.000 [DIRS 183010].

Figure K6.4.1-2. Stepwise rank regression analyses and selected scatterplots for time-dependent release rates (*UZIC239*, g/yr) and cumulative (i.e., integrated) releases (*UZIC239C*, g) for the movement of ^{239}Pu irreversibly attached to slow colloids from the UZ to the SZ resulting from an igneous intrusive event at 10 years that destroys all WPs in the repository: (a, b) Regressions for *UZIC239* and *UZIC239C* at 3000, 5000 and 10,000 years, and (c-h) Scatterplots for *UZIC239* and *UZIC239C* at 10,000 years

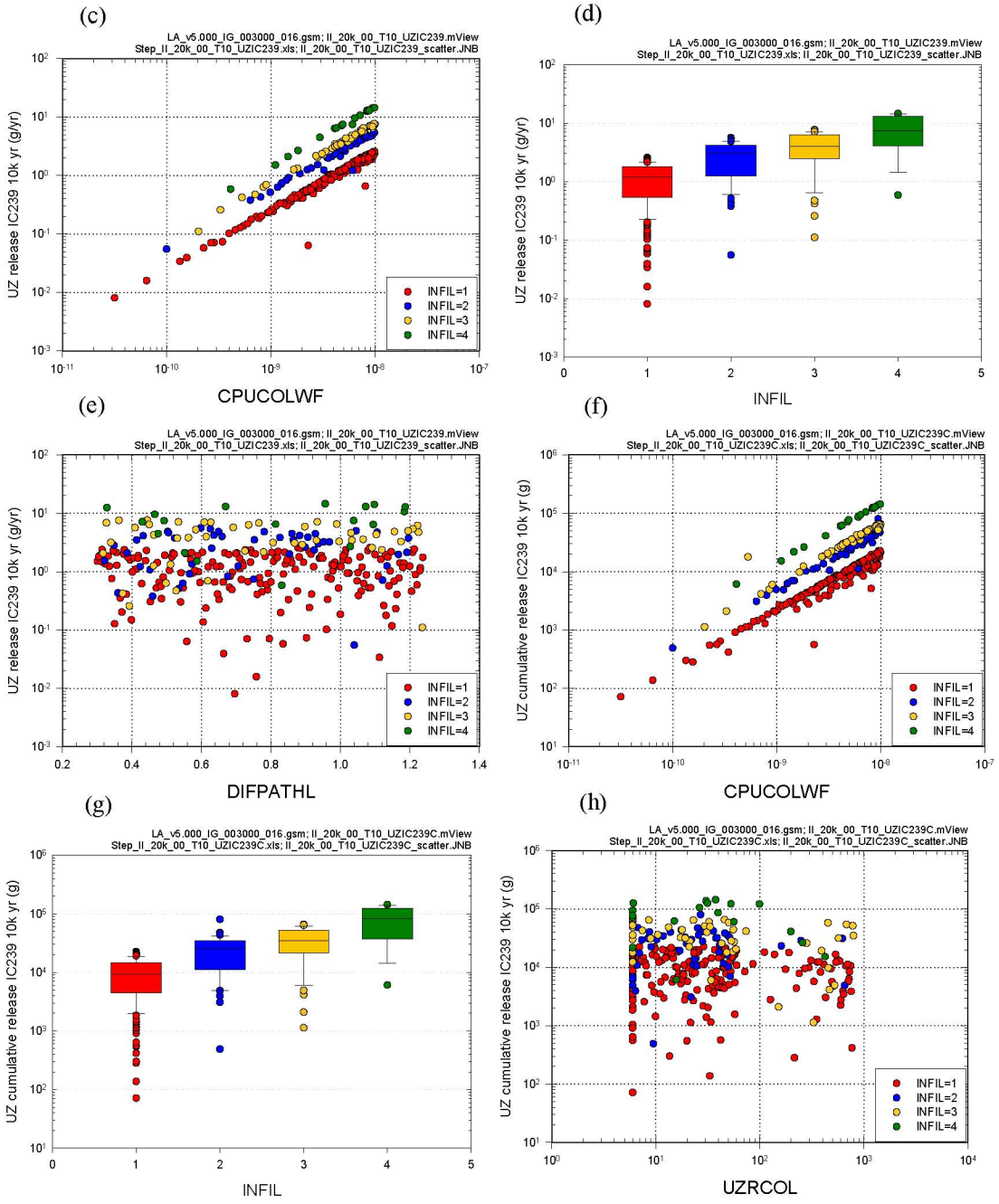

Source: Output DTNs: MO0709TSPAREGS.000 [DIRS 182976]; and MO0709TSPAPLOT.000 [DIRS 183010].

NOTE: In (g), the box extends from 0.25 to 0.75 quantile; lower and upper bar and whisker extend to 0.1 and 0.9 quantile, respectively; dots represent values outside 0.1 to 0.9 quantile range; median indicated by light horizontal line.

Figure K6.4.1-2. Stepwise rank regression analyses and selected scatterplots for time-dependent release rates (*UZIC239*, g/yr) and cumulative (i.e., integrated) releases (*UZIC239C*, g) for the movement of ^{239}Pu irreversibly attached to slow colloids from the UZ to the SZ resulting from an igneous intrusive event at 10 years that destroys all WPs in the repository: (a, b) Regressions for *UZIC239* and *UZIC239C* at 3000, 5000 and 10,000 years, and (c-h) Scatterplots for *UZIC239* and *UZIC239C* at 10,000 years (continued).

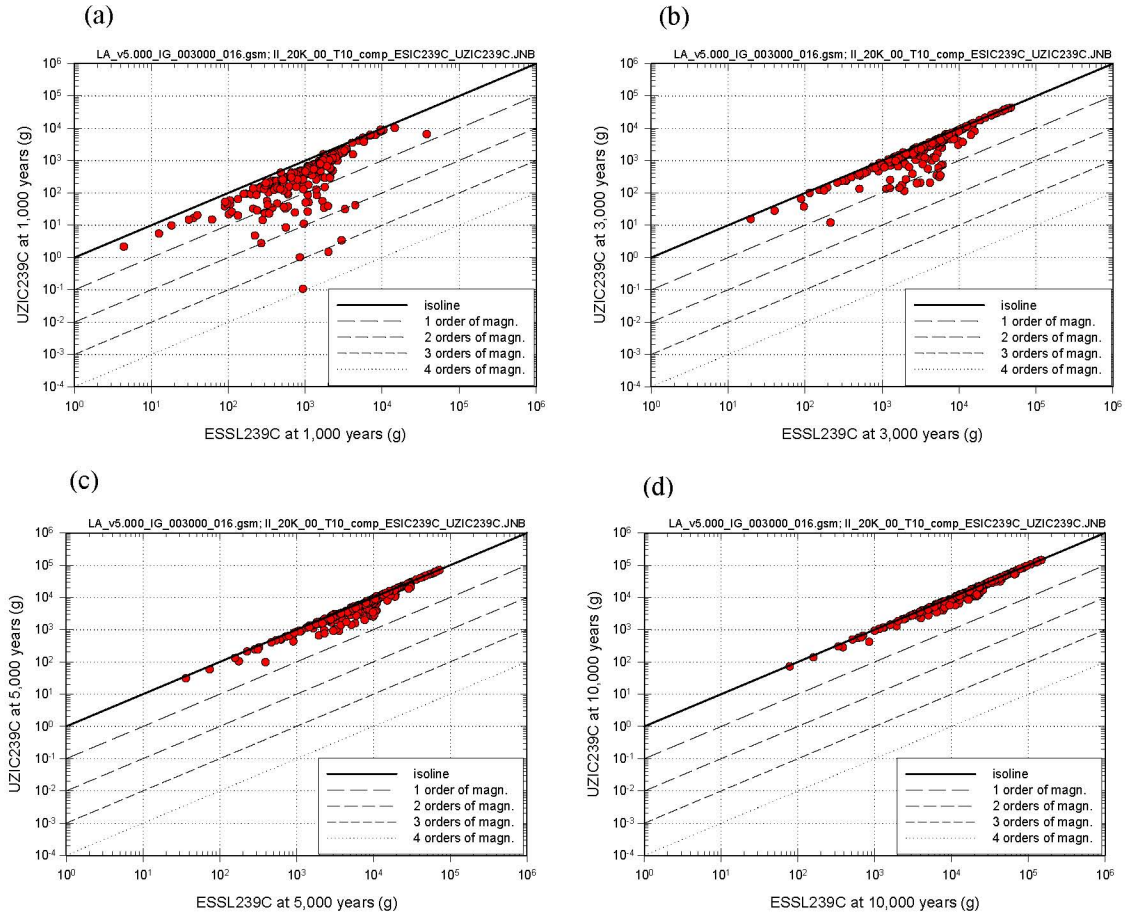

Source: Output DTN: MO0709TSPAREGS.000 [DIRS 182976].

Figure K6.4.1-3. Comparison of cumulative releases of ^{239}Pu irreversibly attached to slow colloids into the UZ (*ESSL239C*, g) and out of the UZ (*UZIC239C*, g) at (a) 1000 years, (b) 3000 years, (c) 5000 years and (d) 10,000 years for an igneous intrusive event at 10 years that destroys all WPs in the repository

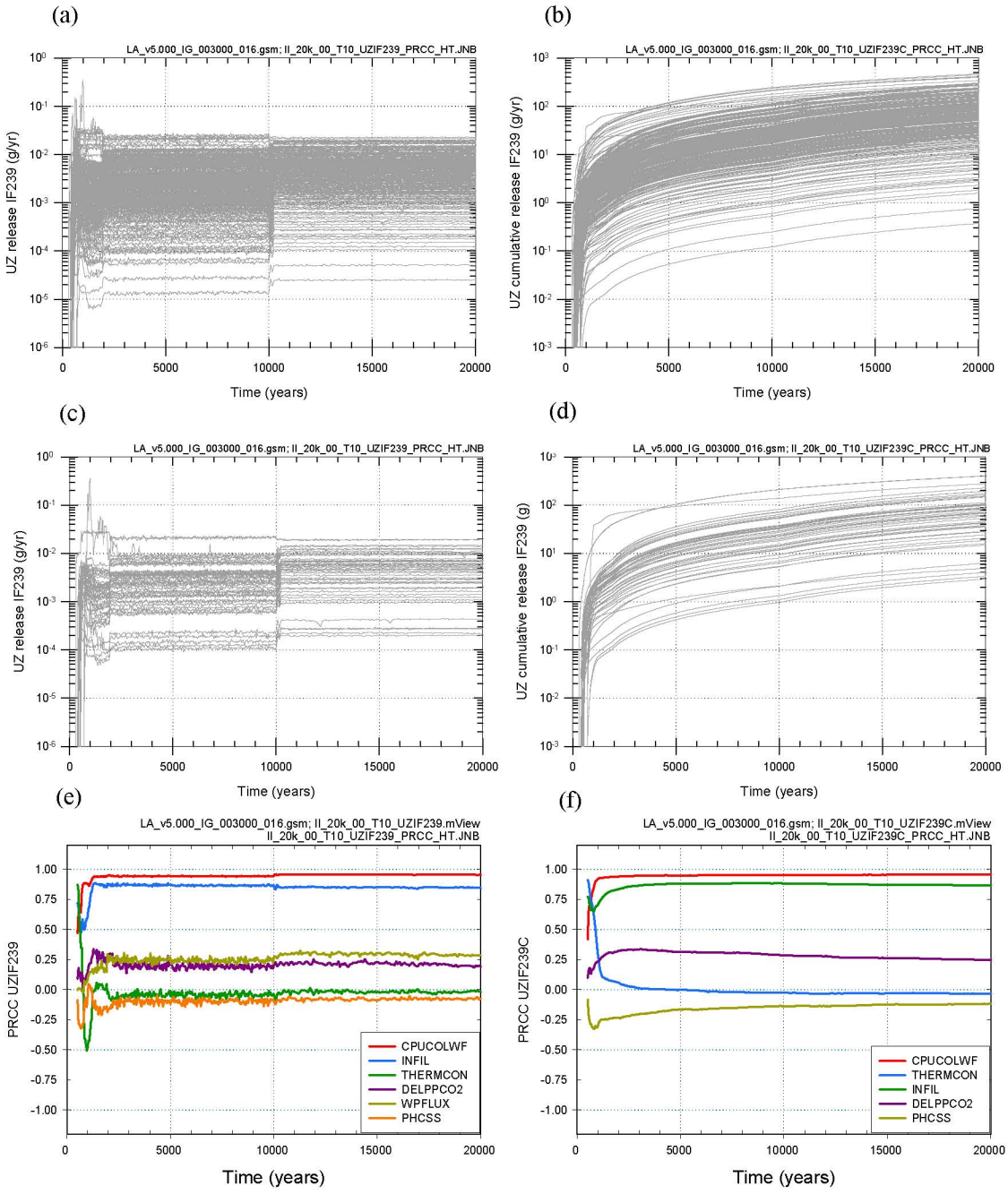

Source: Output DTNs: MO0709TSPAREGS.000 [DIRS 182976]; and MO0709TSPAPLOT.000 [DIRS 183010].

Figure K6.4.1-4. Time-dependent release rates (*UZIF239*, g/yr) and cumulative (i.e., integrated) releases (*UZIF239C*, g) over 20,000 years for the movement of ^{239}Pu irreversibly attached to fast colloids from the UZ to the SZ resulting from an igneous intrusive event at 10 years that destroys all WPs in the repository: (a, b) *UZIF239* and *UZIF239C* for all (i.e., 300) sample elements, (c, d) *UZIF239* and *UZIF239C* for first 50 sample elements, and (e, f) PRCCs for *UZIF239* and *UZIF239C*

(a)

	UZIF239: 3000 yr			UZIF239: 5000 yr			UZIF239: 10,000 yr		
Step[a]	**Variable[b]**	**R^{2c}**	**SRRC[d]**	**Variable**	**R^2**	**SRRC**	**Variable**	**R^2**	**SRRC**
1	CPUCOLWF	0.63	0.74	CPUCOLWF	0.63	0.74	CPUCOLWF	0.64	0.75
2	INFIL	0.92	0.55	INFIL	0.92	0.54	INFIL	0.92	0.54
3							DIFPATHL	0.93	0.04
4							WPFLUX	0.93	0.04

(b)

	UZIF239C: 3000 yr			UZIF239C: 5000 yr			UZIF239C: 10,000 yr		
Step[a]	**Variableb**	**R^{2c}**	**SRRC[d]**	**Variable**	**R^2**	**SRRC**	**Variable**	**R^2**	**SRRC**
1	CPUCOLWF	0.61	0.73	CPUCOLWF	0.61	0.73	CPUCOLWF	0.63	0.74
2	INFIL	0.90	0.55	INFIL	0.92	0.56	INFIL	0.93	0.55
3	DWCSTERB	0.91	-0.06	DWCSTERB	0.92	-0.06	DWCSTERB	0.93	-0.05
4	DELPPCO2	0.91	0.05	RUBMAXL	0.92	-0.05	RUBMAXL	0.93	-0.04
5	RUBMAXL	0.91	-0.04	DELPPCO2	0.92	0.05	DELPPCO2	0.93	0.04
6	THERMCON	0.92	0.05						
7	RHMUNO0	0.92	-0.05						

a: Steps in stepwise rank regression analysis
b: Variables listed in order of selection in stepwise regression
c: Cumulative R^2 value with entry of each variable into regression model
d: Standardized rank regression coefficients (SRRCs) in final regression model

Source: Output DTNs: MO0709TSPAREGS.000 [DIRS 182976]; and MO0709TSPAPLOT.000 [DIRS 183010].

Figure K6.4.1-5. Stepwise rank regression analyses and selected scatterplots for time-dependent release rates (*UZIF239*, g/yr) and cumulative (i.e., integrated) releases (*UZIF239C*, g) for the movement of ^{239}Pu irreversibly attached to fast colloids from the UZ to the SZ resulting from an igneous intrusive event at 10 years that destroys all WPs in the repository: (a, b) Regressions for *UZIF239* and *UZIF239C* at 3000, 5000 and 10,000 years, and (c-h) Scatterplots for *UZIF239* and *UZIF239C* at 10,000 years

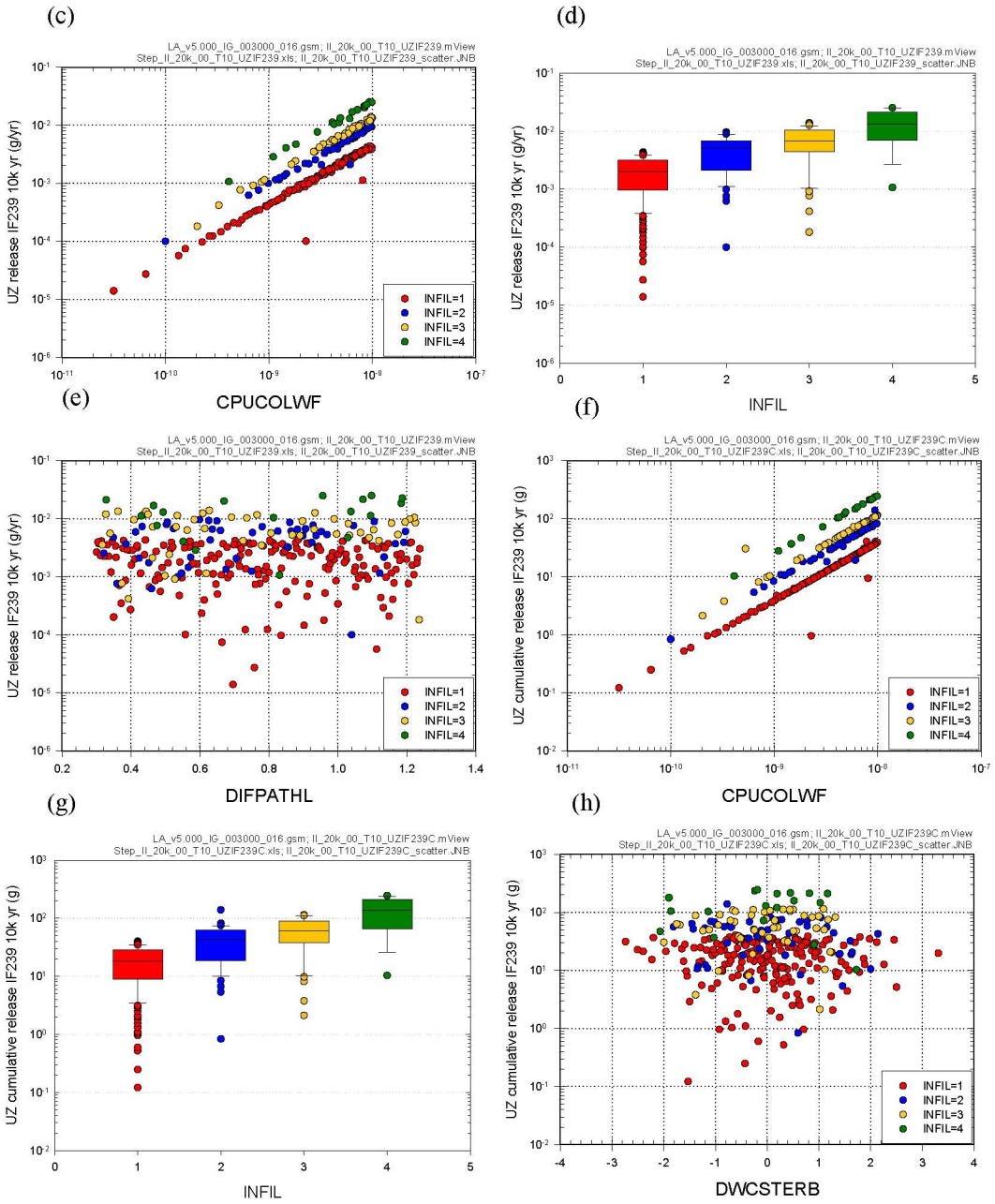

Source: Output DTNs: MO0709TSPAREGS.000 [DIRS 182976]; and MO0709TSPAPLOT.000 [DIRS 183010].

NOTE: In (d,g), the box extends from 0.25 to 0.75 quantile; lower and upper bar and whisker extend to 0.1 and 0.9 quantile, respectively; dots represent values outside 0.1 to 0.9 quantile range; median indicated by light horizontal line.

Figure K6.4.1-5. Stepwise rank regression analyses and selected scatterplots for time-dependent release rates (*UZIF239*, g/yr) and cumulative (i.e., integrated) releases (*UZIF239C*, g) for the movement of ^{239}Pu irreversibly attached to fast colloids from the UZ to the SZ resulting from an igneous intrusive event at 10 years that destroys all WPs in the repository: (a, b) Regressions for *UZIF239* and *UZIF239C* at 3000, 5000 and 10,000 years, and (c-h) Scatterplots for *UZIF239* and *UZIF239C* at 10,000 years (continued).

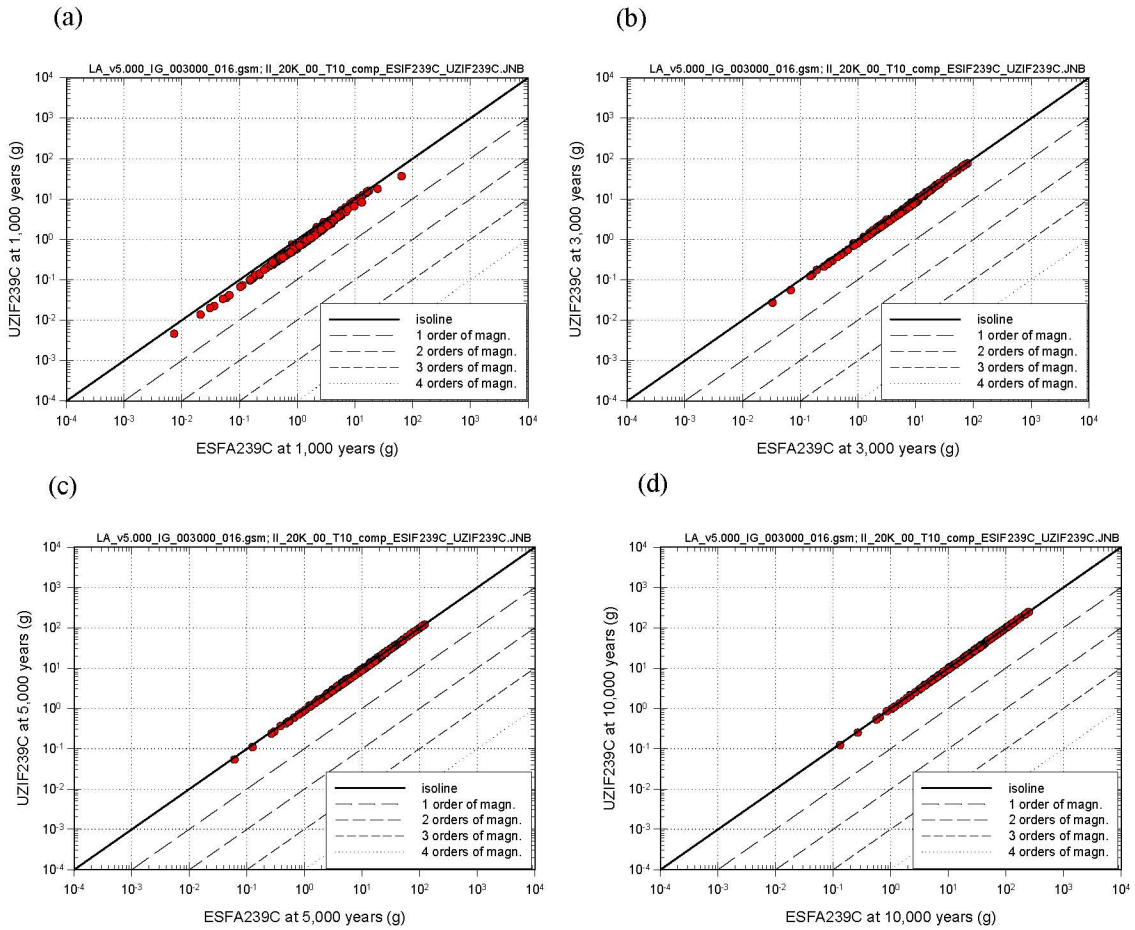

Source: Output DTN: MO0709TSPAREGS.000 [DIRS 182976].

Figure K6.4.1-6. Comparison of cumulative releases of ^{239}Pu irreversibly attached to fast colloids into the UZ (*ESFA239C*, g) and out of the UZ (*UZIF239C*, g) at (a) 1000 years, (b) 3000 years, (c) 5000 years and (d) 10,000 years for an igneous intrusive event at 10 years that destroys all WPs in the repository

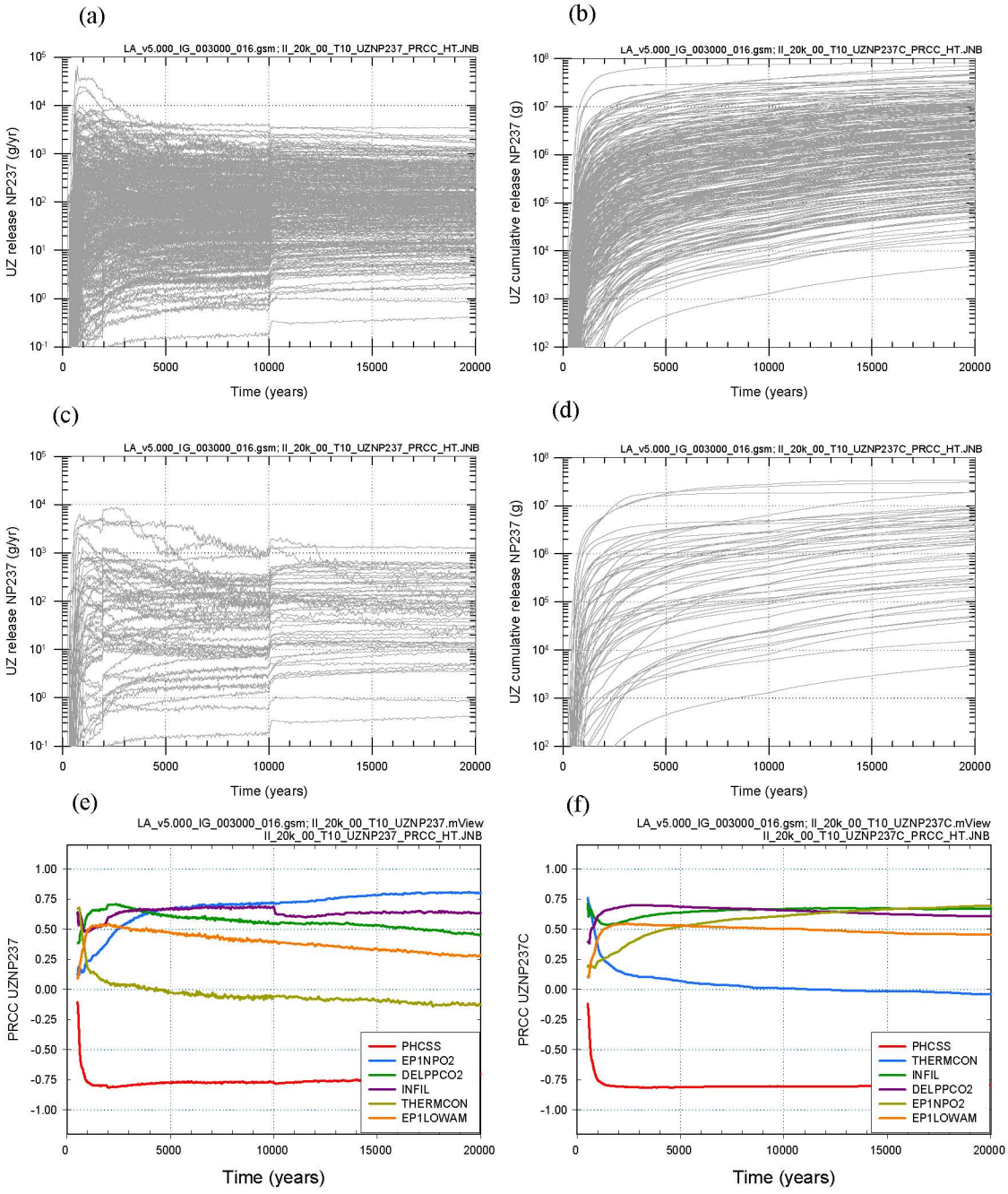

Source: Output DTNs: MO0709TSPAREGS.000 [DIRS 182976]; and MO0709TSPAPLOT.000 [DIRS 183010].

Figure K6.4.1-7. Time-dependent release rates (*UZNP237*, g/yr) and cumulative (i.e., integrated) releases (*UZNP237C*, g) over 20,000 years for the movement of dissolved ^{237}Np from the UZ to the SZ resulting from an igneous intrusive event at 10 years that destroys all WPs in the repository: (a, b) *UZNP237* and *UZNP237C* for all (i.e., 300) sample elements, (c, d) *UZNP237* and *UZNP237C* for first 50 sample elements, and (e, f) PRCCs for *UZNP237* and *UZNP237C*

(a)

	UZNP237: 3000 yr			UZNP237: 5000 yr			UZNP237: 10,000 yr		
Step[a]	Variable[b]	R^{2c}	SRRC[d]	Variable	R^2	SRRC	Variable	R^2	SRRC
1	PHCSS	0.31	-0.52	PHCSS	0.28	-0.50	PHCSS	0.27	-0.49
2	INFIL	0.49	0.39	INFIL	0.48	0.42	INFIL	0.46	0.42
3	DELPPCO2	0.56	0.31	EP1NPO2	0.59	0.38	EP1NPO2	0.63	0.45
4	EP1LOWAM	0.63	0.30	EP1LOWAM	0.64	0.25	CORRATSS	0.68	-0.19
5	EP1NPO2	0.69	0.26	DELPPCO2	0.69	0.25	EP1LOWAM	0.71	0.20
6	CORRATSS	0.73	-0.18	CORRATSS	0.73	-0.17	DELPPCO2	0.74	0.20
7	EP1LOWNU	0.74	0.11	EP1LOWNU	0.75	0.14	GOESITED	0.76	-0.16
8	COLGW	0.76	0.12	GOESITED	0.77	-0.14	EP1LOWNU	0.78	0.14
9	GOESITED	0.77	-0.11	PH2RGER	0.78	-0.09	PH2RGER	0.79	-0.10
10	WDCRCDEN	0.78	0.10	WDCRCDEN	0.79	0.10	GOERELAB	0.80	0.10
11	SEEPUNC	0.79	0.10	COLGW	0.79	0.10	WDCRCDEN	0.81	0.10
12	PH2RGER	0.79	-0.10	SEEPUNC	0.80	0.09	HFOSA	0.82	-0.08
13	EP1NP2O5	0.80	0.10	GOERELAB	0.81	0.08	COLGW	0.82	0.08
14	KDRACOL	0.80	-0.07	HFOSA	0.81	-0.07	SEEPUNC	0.83	0.08

(b)

	UZNP237C: 3000 yr			UZNP237C: 5000 yr			UZNP237C: 10,000 yr		
Step[a]	Variable[b]	R^{2c}	SRRC[d]	Variable	R^2	SRRC	Variable	R^2	SRRC
1	PHCSS	0.37	-0.56	PHCSS	0.35	-0.55	PHCSS	0.32	-0.53
2	INFIL	0.51	0.37	INFIL	0.51	0.38	INFIL	0.51	0.41
3	DELPPCO2	0.60	0.30	DELPPCO2	0.58	0.30	EP1NPO2	0.58	0.31
4	EP1LOWAM	0.68	0.29	EP1LOWAM	0.66	0.29	EP1LOWAM	0.64	0.27
5	EP1NPO2	0.70	0.16	EP1NPO2	0.70	0.23	DELPPCO2	0.70	0.27
6	CORRATSS	0.72	-0.13	CORRATSS	0.73	-0.15	CORRATSS	0.74	-0.17
7	GOESITED	0.74	-0.11	GOESITED	0.74	-0.12	EP1LOWNU	0.75	0.13
8	COLGW	0.75	0.11	EP1LOWNU	0.76	0.11	GOESITED	0.77	-0.13
9	KDAMSMEC	0.76	0.09	COLGW	0.77	0.11	COLGW	0.78	0.10
10	EP1NP2O5	0.77	0.09	EP1NP2O5	0.77	0.10	WDCRCDEN	0.79	0.10
11	EP1LOWNU	0.77	0.08	WDCRCDEN	0.78	0.09	PH2RGER	0.79	-0.10
12	CSRINDPO	0.78	0.08	PH2RGER	0.79	-0.09	EP1NP2O5	0.80	0.09
13				SEEPUNC	0.80	0.09	SEEPUNC	0.81	0.09
14				KDAMSMEC	0.80	0.07			

a: Steps in stepwise rank regression analysis
b: Variables listed in order of selection in stepwise regression
c: Cumulative R^2 value with entry of each variable into regression model
d: Standardized rank regression coefficients (SRRCs) in final regression model

Source: Output DTNs: MO0709TSPAREGS.000 [DIRS 182976]; and MO0709TSPAPLOT.000 [DIRS 183010].

Figure K6.4.1-8. Stepwise rank regression analyses and selected scatterplots for time-dependent release rates (*UZNP237*, g/yr) and cumulative (i.e., integrated) releases (*UZNP237C*, g) for the movement of dissolved ^{237}Np from the EBS to the UZ resulting from an igneous intrusive event at 10 years that destroys all WPs in the repository: (a, b) Regressions for *UZNP237* and *UZNP237C* at 3000, 5000 and 10,000 years, and (c-h) Scatterplots for *UZNP237* and *UZNP237C* at 10,000 years

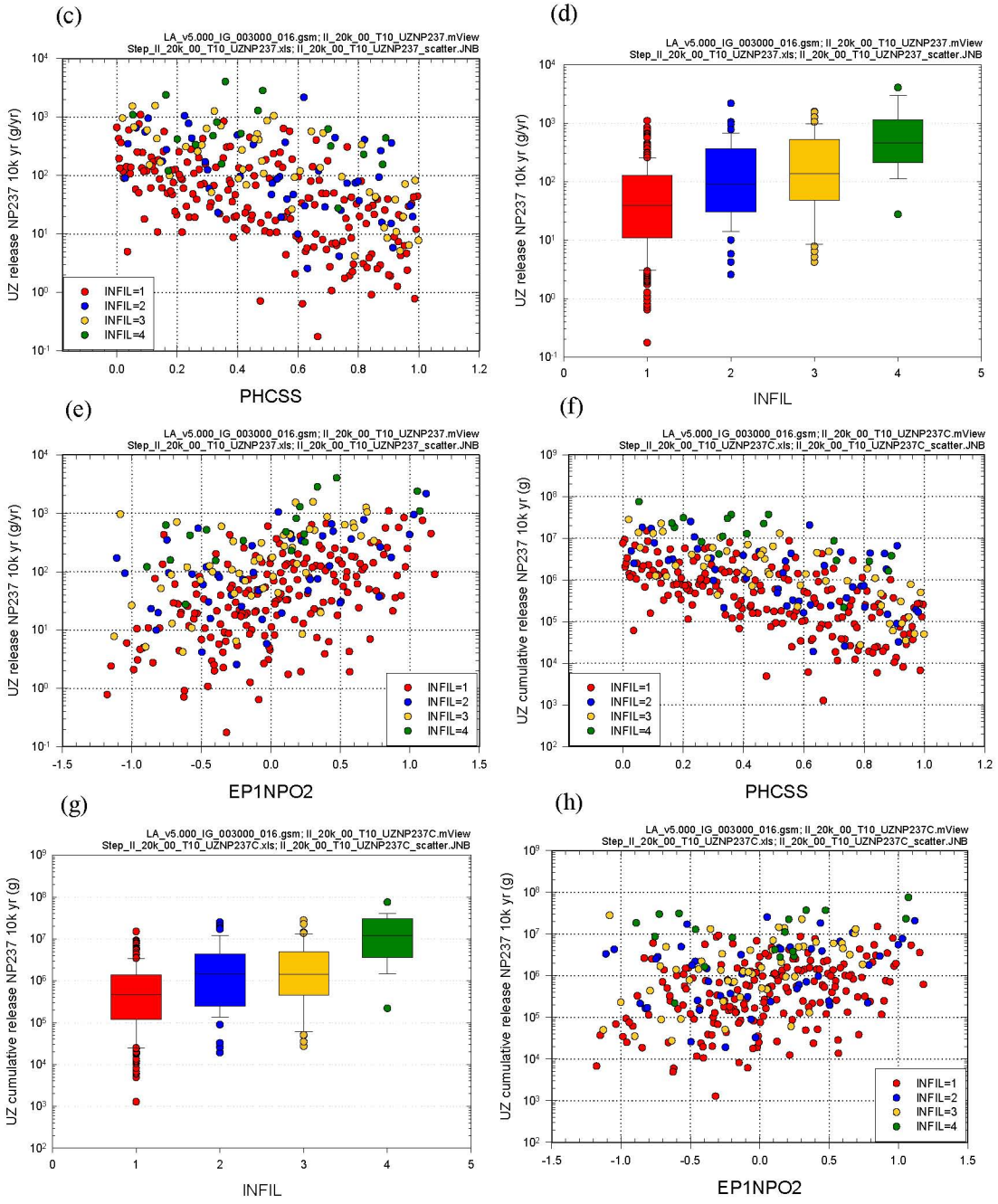

Source: Output DTNs: MO0709TSPAREGS.000 [DIRS 182976]; and MO0709TSPAPLOT.000 [DIRS 183010].

NOTE: In (d,g), the box extends from 0.25 to 0.75 quantile; lower and upper bar and whisker extend to 0.1 and 0.9 quantile, respectively; dots represent values outside 0.1 to 0.9 quantile range; median indicated by light horizontal line.

Figure K6.4.1-8. Stepwise rank regression analyses and selected scatterplots for time-dependent release rates (UZNP237, g/yr) and cumulative (i.e., integrated) releases (UZNP237C, g) for the movement of dissolved 237Np from the EBS to the UZ resulting from an igneous intrusive event at 10 years that destroys all WPs in the repository: (a, b) Regressions for UZNP237 and UZNP237C at 3000, 5000 and 10,000 years, and (c-h) Scatterplots for UZNP237 and UZNP237C at 10,000 years (continued).

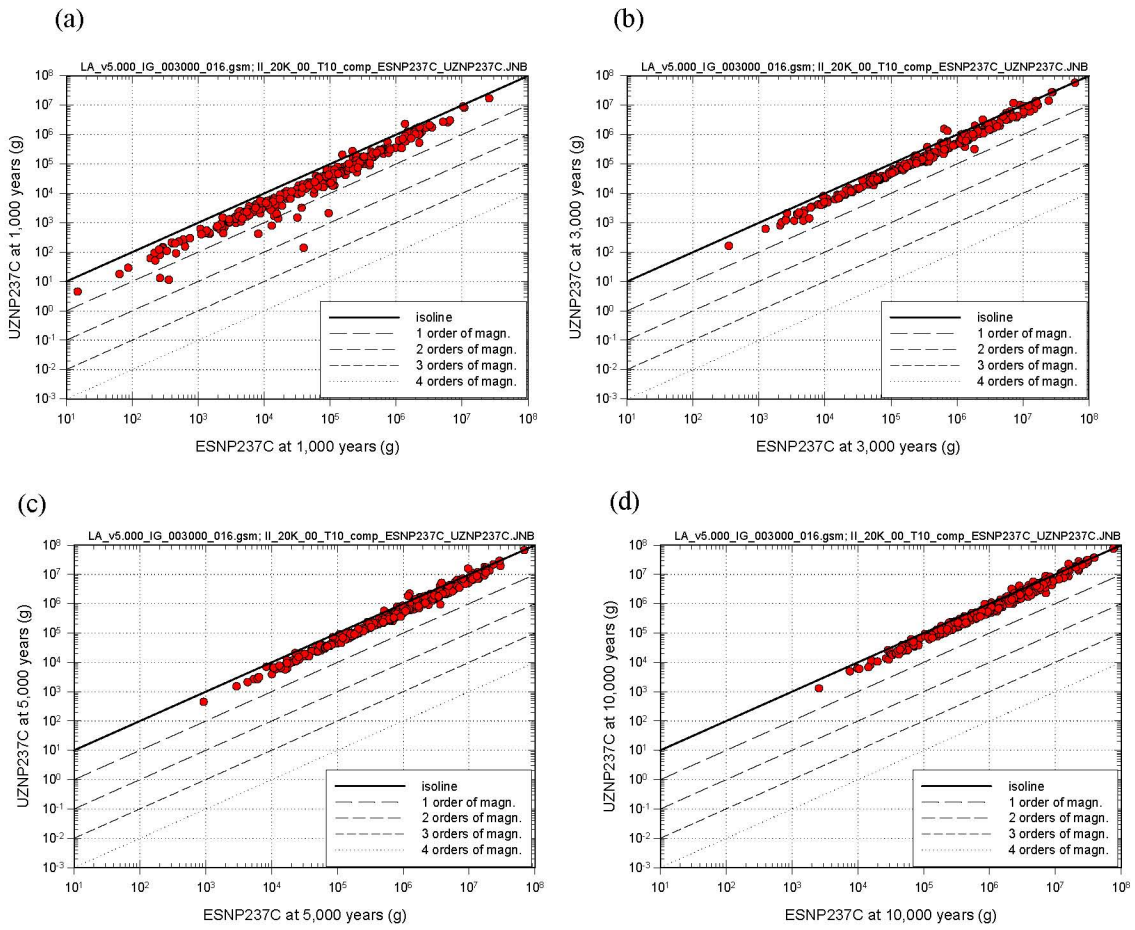

Source: Output DTN: MO0709TSPAREGS.000 [DIRS 182976].

Figure K6.4.1-9. Comparison of cumulative releases of dissolved ^{237}Np into the UZ (*ESNP237C*, g) and out of the UZ (*UZNP237C*, g) at (a) 1000 years, (b) 3000 years, (c) 5000 years and (d) 10,000 years for an igneous intrusive event at 10 years that destroys all WPs in the repository

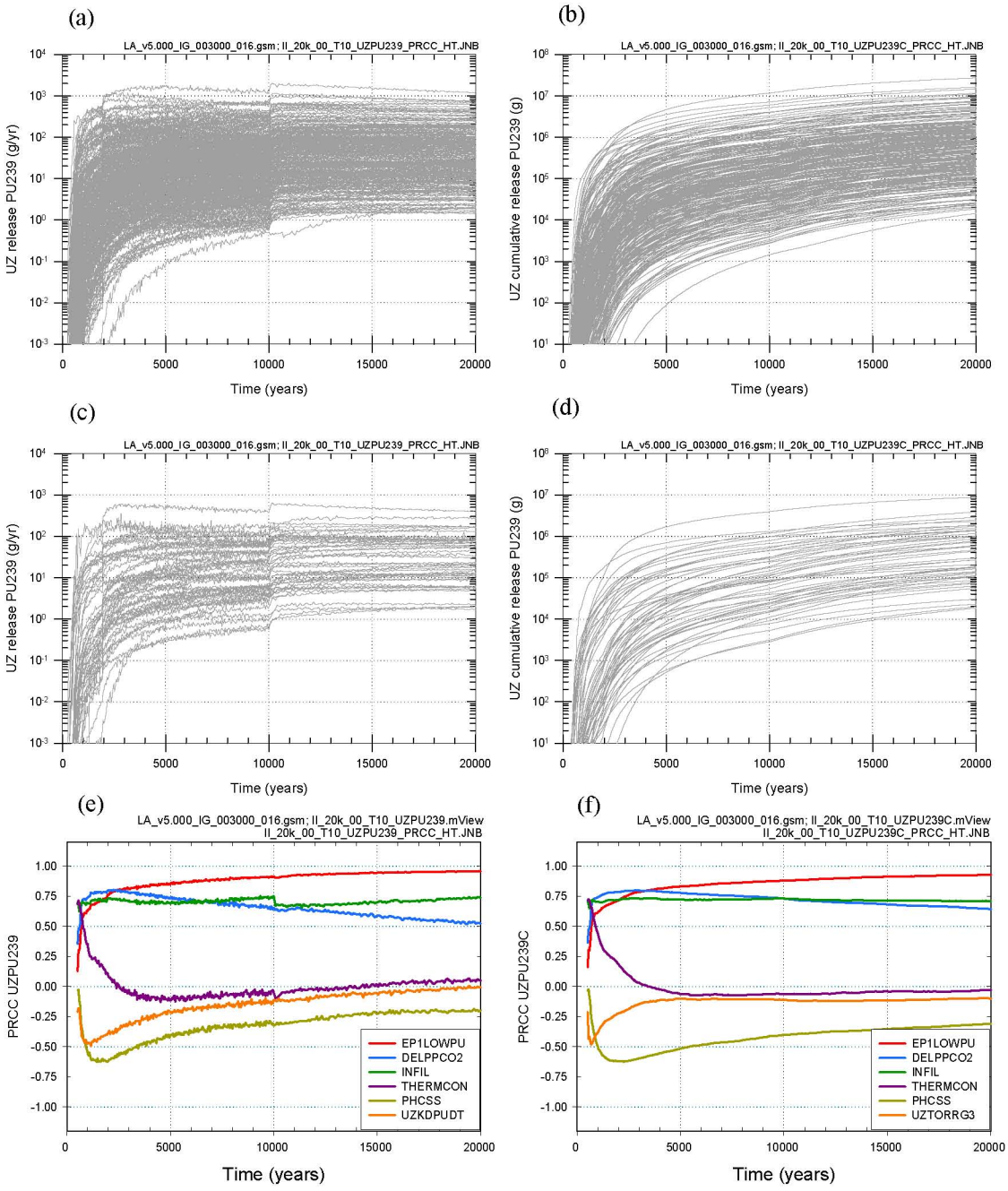

Source: Output DTNs: MO0709TSPAREGS.000 [DIRS 182976]; and MO0709TSPAPLOT.000 [DIRS 183010].

Figure K6.4.1-10. Time-dependent release rates (*UZPU239*, g/yr) and cumulative (i.e., integrated) releases (*UZPU239C*, g) over 20,000 years for the movement of dissolved ^{239}Pu from the UZ to the SZ resulting from an igneous intrusive event at 10 years that destroys all WPs in the repository: (a, b) *UZPU239* and *UZPU239C* for all (i.e., 300) sample elements, (c, d) *UZPU239* and *UZPU239C* for first 50 sample elements, and (e, f) PRCCs for *UZPU239* and *UZPU239C*

(a)

	UZPU239: 3000 yr			UZPU239: 5000 yr			UZPU239: 10,000 yr		
Step[a]	Variable[b]	R^{2c}	SRRC[d]	Variable	R^2	SRRC	Variable	R^2	SRRC
1	EP1LOWPU	0.30	0.56	EP1LOWPU	0.42	0.65	EP1LOWPU	0.58	0.76
2	INFIL	0.51	0.44	INFIL	0.61	0.43	INFIL	0.77	0.43
3	DELPPCO2	0.69	0.43	DELPPCO2	0.75	0.38	DELPPCO2	0.85	0.28
4	UZKDPUDT	0.74	-0.21	PHCSS	0.78	-0.14	PHCSS	0.86	-0.09
5	PHCSS	0.79	-0.19	UZKDPUDT	0.80	-0.13	COLGW	0.87	0.09
6	EP1LOWAM	0.81	0.15	COLGW	0.81	0.11	EP1LOWAM	0.87	0.08
7	COLGW	0.82	0.10	EP1LOWAM	0.82	0.11	UZKDPUDT	0.88	-0.06
8	CORRATSS	0.82	-0.08	CORRATSS	0.83	-0.08	WDCRCDEN	0.88	0.06
9	FHHISSCP	0.83	0.07	INRFRCTC	0.83	0.07	CORRATSS	0.88	-0.05

(b)

	UZPU239C: 3000 yr			UZPU239C: 5000 yr			UZPU239C: 10,000 yr		
Step[a]	Variable[b]	R^{2c}	SRRC[d]	Variable	R^2	SRRC	Variable	R^2	SRRC
1	EP1LOWPU	0.23	0.49	EP1LOWPU	0.33	0.58	EP1LOWPU	0.46	0.68
2	INFIL	0.45	0.45	INFIL	0.54	0.45	INFIL	0.66	0.44
3	DELPPCO2	0.63	0.45	DELPPCO2	0.71	0.42	DELPPCO2	0.78	0.36
4	UZKDPUDT	0.71	-0.23	UZKDPUDT	0.75	-0.20	PHCSS	0.81	-0.13
5	PHCSS	0.78	-0.23	PHCSS	0.79	-0.18	UZKDPUDT	0.82	-0.12
6	EP1LOWAM	0.80	0.15	EP1LOWAM	0.81	0.14	EP1LOWAM	0.83	0.11
7	COLGW	0.81	0.09	COLGW	0.82	0.10	COLGW	0.84	0.11
8	CORRATSS	0.82	-0.08	CORRATSS	0.83	-0.07	CORRATSS	0.85	-0.07
9	GP2NO3	0.82	-0.08						
10	GOESITED	0.83	-0.07						
11	GP1NO3	0.83	-0.09						
12	UZFAG8	0.84	0.08						
13	INRFRCTC	0.84	0.07						

a: Steps in stepwise rank regression analysis
b: Variables listed in order of selection in stepwise regression
c: Cumulative R^2 value with entry of each variable into regression model
d: Standardized rank regression coefficients (SRRCs) in final regression model

Source: Output DTNs: MO0709TSPAREGS.000 [DIRS 182976]; and MO0709TSPAPLOT.000 [DIRS 183010].

Figure K6.4.1-11. Stepwise rank regression analyses and selected scatterplots for time-dependent release rates (*UZPU239*, g/yr) and cumulative (i.e., integrated) releases (*UZPU239*, g) for the movement of dissolved ^{239}Pu from the UZ to the SZ resulting from an igneous intrusive event at 10 years that destroys all WPs in the repository: (a, b) Regressions for *UZPU239* and *UZPU239C* at 3000, 5000 and 10,000 years, and (c-h) Scatterplots for *UZPU239* and *UZPU239C* at 10,000 years

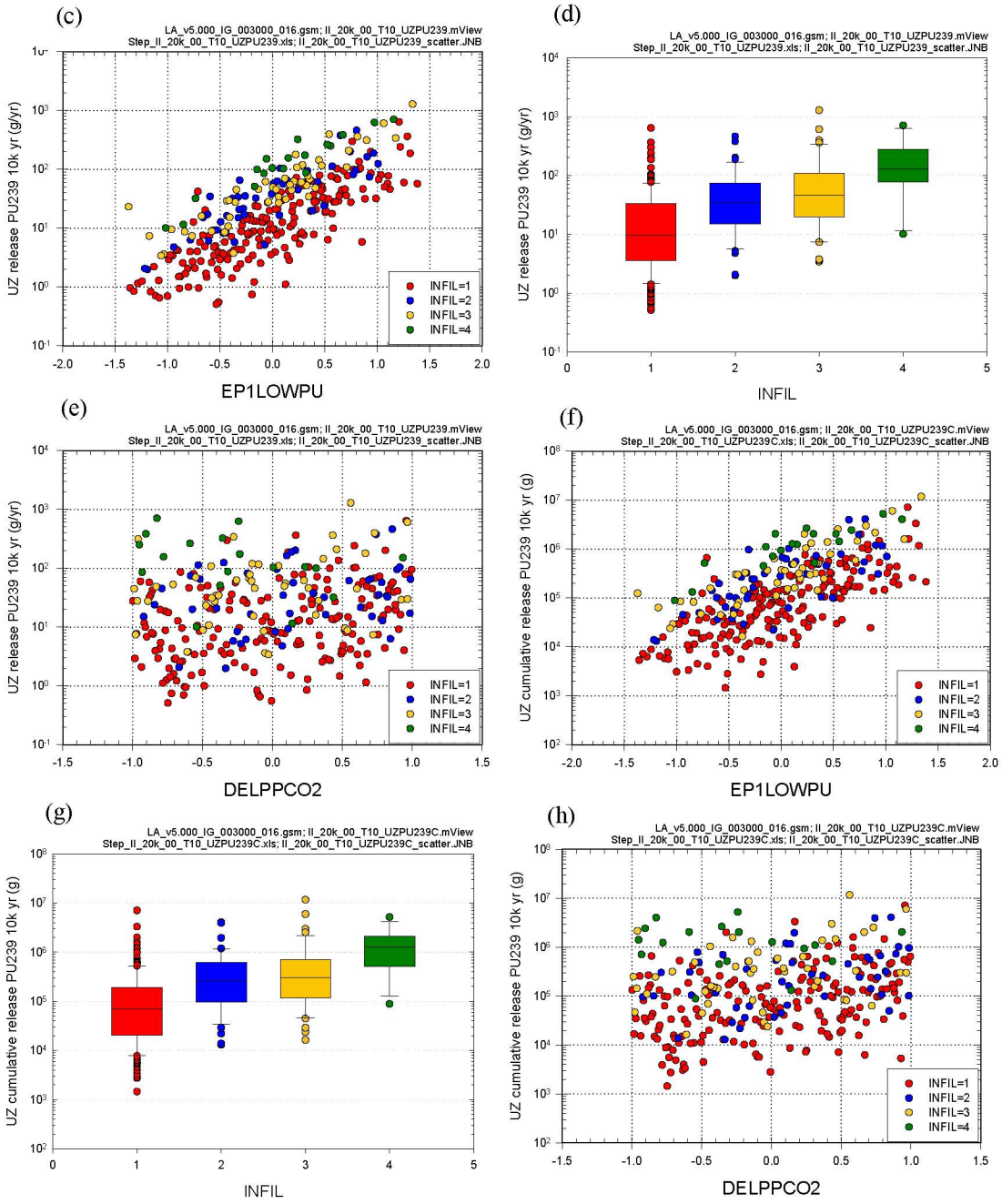

Source: Output DTNs: MO0709TSPAREGS.000 [DIRS 182976]; and MO0709TSPAPLOT.000 [DIRS 183010].

NOTE: In (d,g), the box extends from 0.25 to 0.75 quantile; lower and upper bar and whisker extend to 0.1 and 0.9 quantile, respectively; dots represent values outside 0.1 to 0.9 quantile range; median indicated by light horizontal line.

Figure K6.4.1-11. Stepwise rank regression analyses and selected scatterplots for time-dependent release rates (UZPU239, g/yr) and cumulative (i.e., integrated) releases (UZPU239, g) for the movement of dissolved 239Pu from the UZ to the SZ resulting from an igneous intrusive event at 10 years that destroys all WPs in the repository: (a, b) Regressions for UZPU239 and UZPU239C at 3000, 5000 and 10,000 years, and (c-h) Scatterplots for UZPU239 and UZPU239C at 10,000 years (continued).

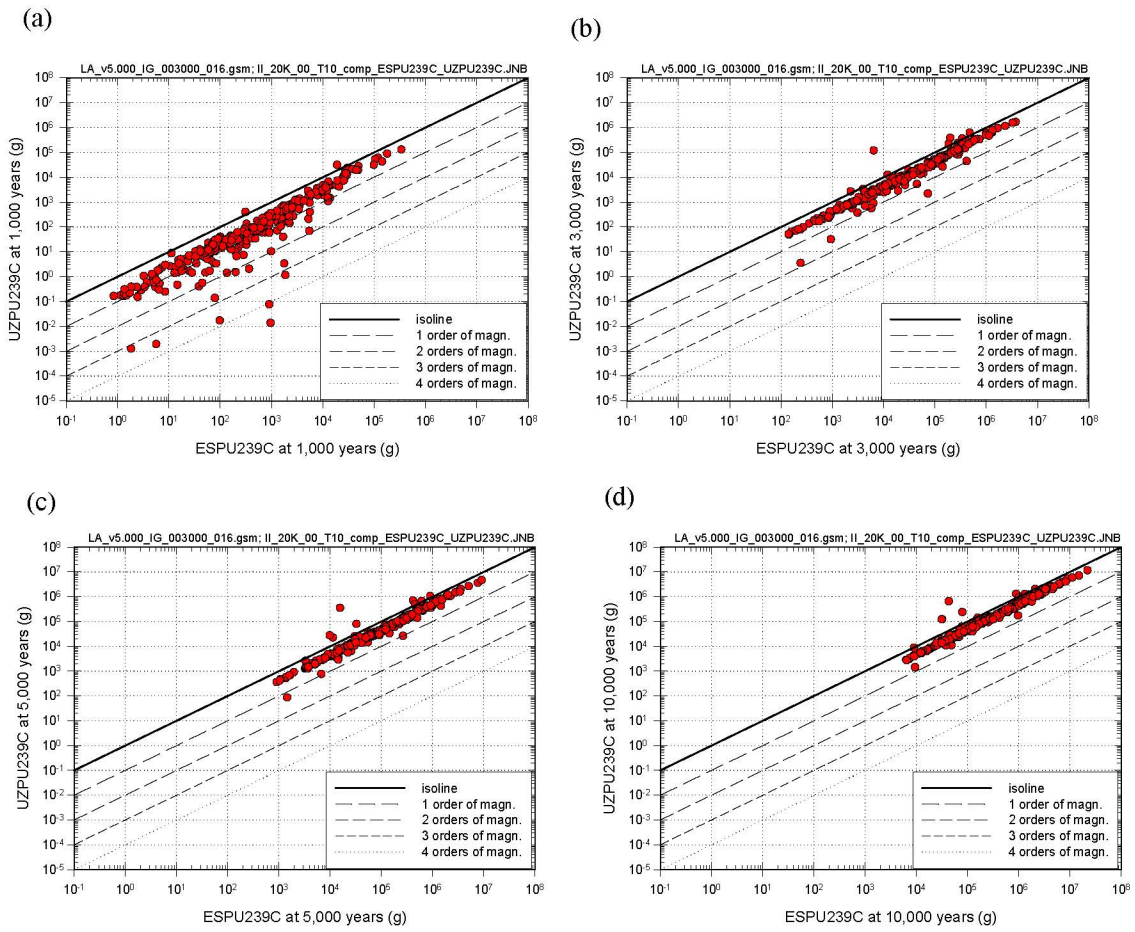

Source: Output DTN: MO0709TSPAREGS.000 [DIRS 182976].

Figure K6.4.1-12. Comparison of cumulative releases of dissolved ^{239}Pu into the UZ (*ESPU239C*, g) and out of the UZ (*UZPU239C*, g) at (a) 1000 years, (b) 3000 years, (c) 5000 years and (d) 10,000 years for an igneous intrusive event at 10 years that destroys all WPs in the repository

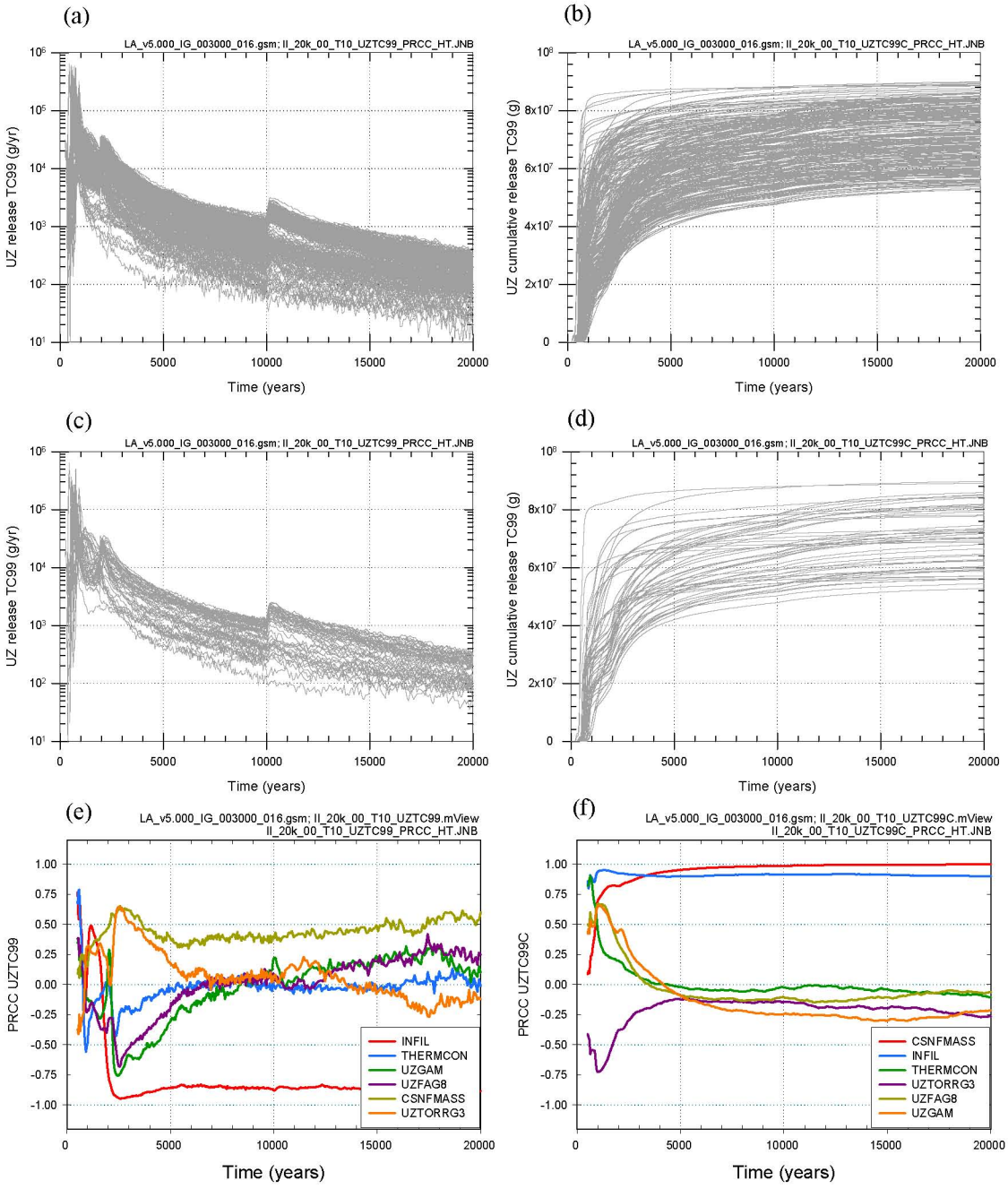

Source: Output DTNs: MO0709TSPAREGS.000 [DIRS 182976]; and MO0709TSPAPLOT.000 [DIRS 183010].

Figure K6.4.1-13. Time-dependent release rates (*UZTC99*, g/yr) and cumulative (i.e., integrated) releases (*UZTC99C*, g) over 20,000 years for the movement of dissolved ^{99}Tc from the UZ to the SZ resulting from an igneous intrusive event at 10 years that destroys all WPs in the repository: (a, b) *UZTC99* and *UZTC99C* for all (i.e., 300) sample elements, (c, d) *UZTC99* and *UZTC99C* for first 50 sample elements, and (e, f) PRCCs for *UZTC99* and *UZTC99C*

(a)

	UZTC99: 3000 yr			UZTC99: 5000 yr			UZTC99: 10,000 yr		
Step[a]	Variable[b]	R^{2c}	SRRC[d]	Variable	R^2	SRRC	Variable	R^2	SRRC
1	INFIL	0.71	-0.87	INFIL	0.70	-0.86	INFIL	0.67	-0.82
2	CSNFMASS	0.78	0.23	CSNFMASS	0.78	0.26	CSNFMASS	0.74	0.25
3	UZTORRG3	0.82	0.20	UZTORRG3	0.79	0.10	UZFAG5	0.75	-0.11
4	UZGAM	0.86	-0.21	UZGAM	0.79	-0.09	UZTORRG2	0.77	0.12
5	UZFAG8	0.89	-0.20	KDAMSMEC	0.80	-0.08	UZFAG3	0.78	-0.10
6	UZFAG3	0.90	0.08				UZGAM	0.79	0.10
7	THERMCON	0.90	-0.06				EP1NPO2	0.79	0.08
8	BCKALPHA	0.91	-0.07				UZFAG8	0.80	0.07
9	PH2MCOS	0.91	0.05				KDUSMEC	0.80	-0.07
10	KDNPSMEC	0.91	0.06						
11	RHMUN65	0.91	-0.05						
12	IS2MCONS	0.91	-0.05						
13	UZKDCSDT	0.92	-0.05						

(b)

	UZTC99C: 3000 yr			UZTC99C: 5000 yr			UZTC99C: 10,000 yr		
Step[a]	Variable[b]	R^{2c}	SRRC[d]	Variable	R^2	SRRC	Variable	R^2	SRRC
1	INFIL	0.59	0.74	CSNFMASS	0.62	0.76	CSNFMASS	0.84	0.89
2	CSNFMASS	0.90	0.56	INFIL	0.94	0.55	INFIL	0.97	0.37
3	UZTORRG3	0.91	-0.06	UZFAG3	0.94	0.08	HLWMASS	0.98	0.04
4	CSWFA3AK	0.91	0.05	RHMUNO0	0.94	-0.04	UZFAG3	0.98	0.03
5				KDAMSMEC	0.95	0.04	UZGAM	0.98	-0.03
6				GOERELAB	0.95	0.04	DSNFMASS	0.98	0.03
7							SEEPUNC	0.98	0.03
8							UZFAG8	0.98	-0.02

a: Steps in stepwise rank regression analysis
b: Variables listed in order of selection in stepwise regression
c: Cumulative R^2 value with entry of each variable into regression model
d: Standardized rank regression coefficients (SRRCs) in final regression model

Source: Output DTNs: MO0709TSPAREGS.000 [DIRS 182976]; and MO0709TSPAPLOT.000 [DIRS 183010].

Figure K6.4.1-14. Stepwise rank regression analyses and selected scatterplots for time-dependent release rates (*UZTC99*, g/yr) and cumulative (i.e., integrated) releases (*UZTC99*, g) for the movement of dissolved ^{99}Tc from the UZ to the SZ resulting from an igneous intrusive event at 10 years that destroys all WPs in the repository: (a, b) Regressions for *UZTC99* and *UZTC99C* at 3000, 5000 and 10,000 years, and (c-h) Scatterplots for *UZTC99* and *UZTC99C* at 10,000 years

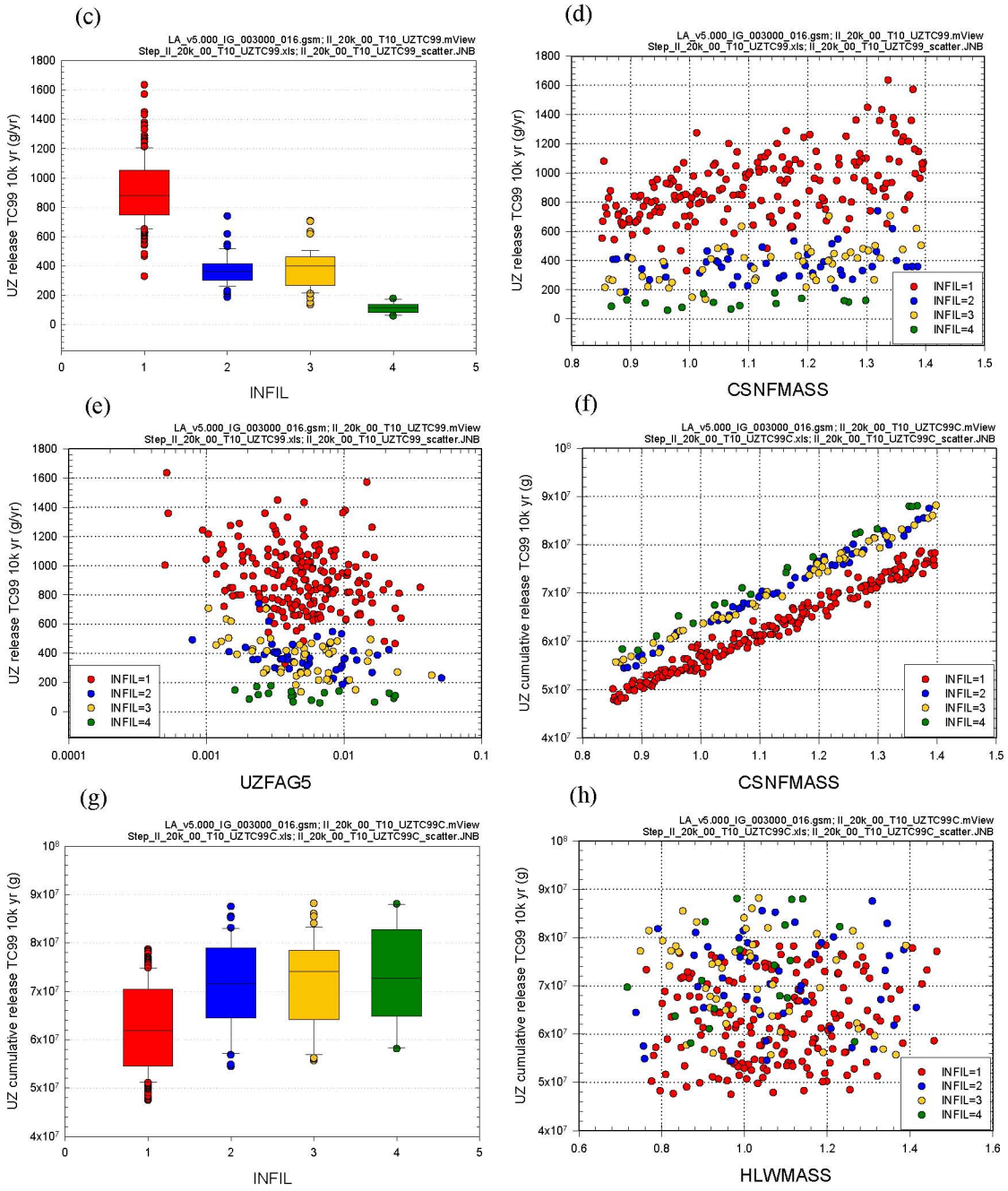

Source: Output DTNs: MO0709TSPAREGS.000 [DIRS 182976]; and MO0709TSPAPLOT.000 [DIRS 183010].

NOTE: In (c,g), the box extends from 0.25 to 0.75 quantile; lower and upper bar and whisker extend to 0.1 and 0.9 quantile, respectively; dots represent values outside 0.1 to 0.9 quantile range; median indicated by light horizontal line.

Figure K6.4.1-14. Stepwise rank regression analyses and selected scatterplots for time-dependent release rates (*UZTC99*, g/yr) and cumulative (i.e., integrated) releases (*UZTC99*, g) for the movement of dissolved ^{99}Tc from the UZ to the SZ resulting from an igneous intrusive event at 10 years that destroys all WPs in the repository: (a, b) Regressions for *UZTC99* and *UZTC99C* at 3000, 5000 and 10,000 years, and (c-h) Scatterplots for *UZTC99* and *UZTC99C* at 10,000 years (continued).

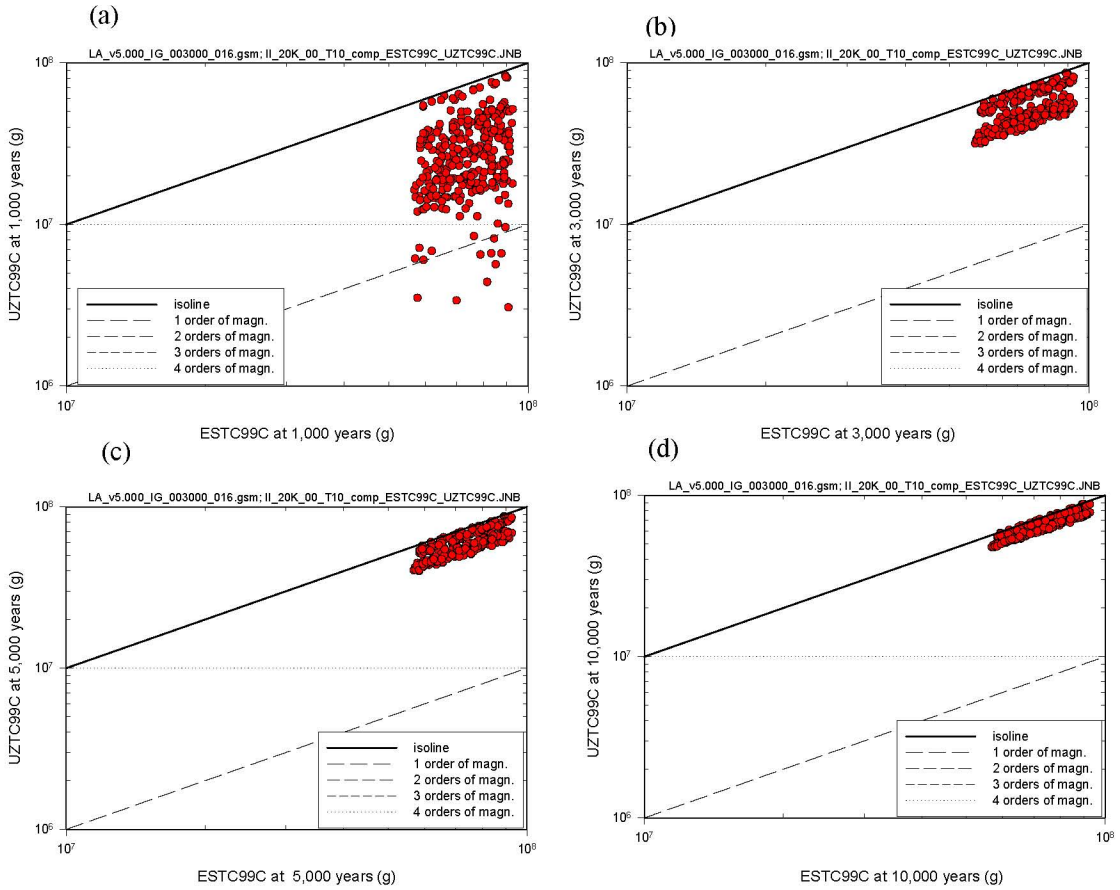

Source: Output DTN: MO0709TSPAREGS.000 [DIRS 182976].

Figure K6.4.1-15. Comparison of cumulative releases of dissolved ^{99}Tc into the UZ (*ESTC99C*, g) and out of the UZ (*UZTC99C*, g) at (a) 1000 years, (b) 3000 years, (c) 5000 years and (d) 10,000 years for an igneous intrusive event at 10 years that destroys all WPs in the repository

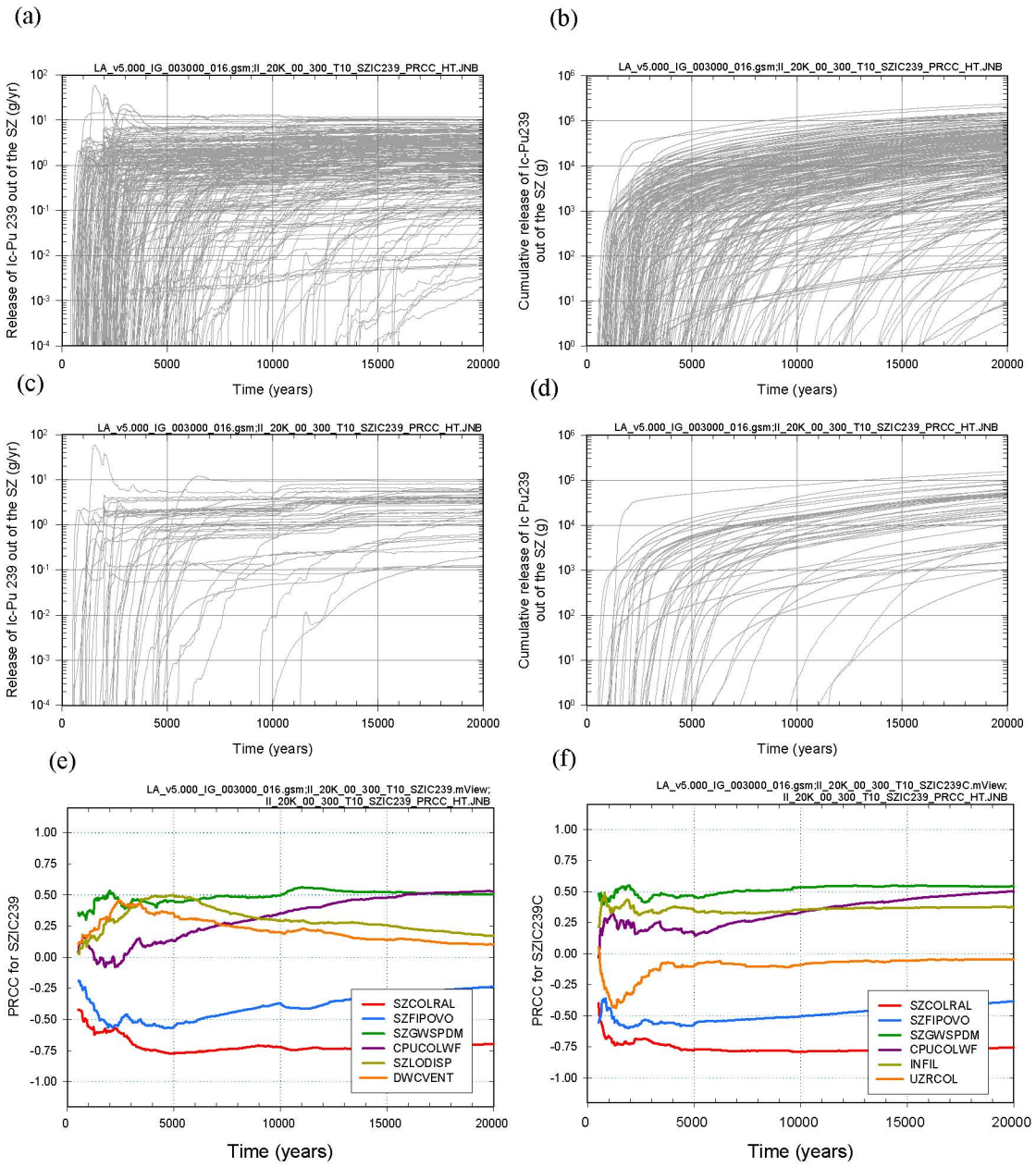

Source: Output DTNs: MO0709TSPAREGS.000 [DIRS 182976]; and MO0709TSPAPLOT.000 [DIRS 183010].

Figure K6.5.1-1. Time-dependent release rates (*SZIC239*, g/yr) and cumulative (i.e., integrated) releases (*SZIC239C*, g) over 20,000 years for the movement of ^{239}Pu irreversibly attached to slow colloids across a subsurface plane at the location of the RMEI resulting from an igneous intrusive event at 10 years that destroys all WPs in the repository: (a, b) *SZIC239* and *SZIC239C* for all (i.e., 300) sample elements, (c, d) *SZIC239* and *SZIC239C* for first 50 sample elements, and (e, f) PRCCs for *SZIC239* and *SZIC239C*

(a)

	SZIC239: 3,000 yr			SZIC239: 5,000 yr			SZIC239: 10,000 yr		
Step[a]	Variable[b]	R^{2c}	SRRC[d]	Variable	R^2	SRRC	Variable	R^2	SRRC
1	SZCOLRAL	0.26	-0.56	SZCOLRAL	0.32	-0.64	SZCOLRAL	0.26	-0.59
2	SZFIPOVO	0.38	-0.37	SZFIPOVO	0.44	-0.36	CPUCOLWF	0.35	0.28
3	SZGWSPDM	0.47	0.27	SZGWSPDM	0.52	0.30	SZGWSPDM	0.43	0.31
4	SZKDAMCO	0.49	0.16	CPUCOLWF	0.54	0.16	SZFIPOVO	0.48	-0.26
5	SZCOLRVO	0.51	-0.15	KDRASMEC	0.57	0.15	INFIL	0.53	0.20
6	INFIL	0.52	0.12	SZCOLRVO	0.59	-0.14	RUBMAXNL	0.55	-0.16
7				INFIL	0.60	0.12	SZSREG3Y	0.57	-0.13
8				UZFAG8	0.61	0.13	KDRASMEC	0.58	0.11
9				KDAMCOL	0.62	-0.13			
10				SZLODISP	0.63	0.11			
11				SZKDPUVO	0.64	0.11			

(b)

	SZIC239C: 3,000 yr			SZIC239C: 5,000 yr			SZIC239C: 10,000 yr		
Step[a]	Variable[b]	R^{2c}	SRRC[d]	Variable	R^2	SRRC	Variable	R^2	SRRC
1	SZCOLRAL	0.29	-0.59	SZCOLRAL	0.34	-0.66	SZCOLRAL	0.32	-0.66
2	SZFIPOVO	0.43	-0.36	SZFIPOVO	0.47	-0.37	SZFIPOVO	0.41	-0.32
3	SZGWSPDM	0.54	0.33	SZGWSPDM	0.57	0.33	SZGWSPDM	0.51	0.32
4	INFIL	0.58	0.21	INFIL	0.60	0.18	CPUCOLWF	0.57	0.24
5	CPUCOLWF	0.61	0.16	CPUCOLWF	0.63	0.15	INFIL	0.62	0.22
6	SZFISPVO	0.62	-0.13	SZCOLRVO	0.64	-0.13	RUBMAXNL	0.63	-0.12
7	SZKDAMCO	0.64	0.13	SZFISPVO	0.66	-0.12	SZSREG3Y	0.64	-0.10
8	SZCOLRVO	0.65	-0.11	SZLODISP	0.67	0.11	SZFISPVO	0.65	-0.10
9	SZLODISP	0.66	0.11	KDRASMEC	0.68	0.12	SZSREG4Y	0.66	0.11
10	UZRCOL	0.67	-0.09	UZFAG8	0.69	0.12	SZKDSEAL	0.67	-0.22
11	ISCSNS	0.68	0.09	SZKDPUVO	0.71	0.12	SZCOLRVO	0.68	-0.11
12				DWCVENT	0.71	0.11	KDRASMEC	0.69	0.12
13				KDAMCOL	0.72	-0.11	SZKDNPAL	0.70	0.16
14				PH2RGER	0.72	-0.10	SZKDPUVO	0.71	0.10
15				INRFRCSR	0.73	0.09	PHCSNS	0.72	-0.09

a: Steps in stepwise rank regression analysis
b: Variables listed in order of selection in stepwise regression
c: Cumulative R^2 value with entry of each variable into regression model
d: Standardized rank regression coefficients (SRRCs) in final regression model

Source: Output DTNs: MO0709TSPAREGS.000 [DIRS 182976]; and MO0709TSPAPLOT.000 [DIRS 183010].

Figure K6.5.1-2. Stepwise rank regression analyses and selected scatterplots for time-dependent release rates (*SZIC239*, g/yr) and cumulative (i.e., integrated) releases (*SZIC239C*, g) for the movement of ^{239}Pu irreversibly attached to slow colloids across a subsurface plane at the location of the RMEI resulting from an igneous intrusive event at 10 years that destroys all WPs in the repository: (a, b) Regressions for *SZIC239* and *SZIC239C* at 3000, 5000 and 10,000 years, and (c-h) Scatterplots for *SZIC239* and *SZIC239C* at 10,000 years

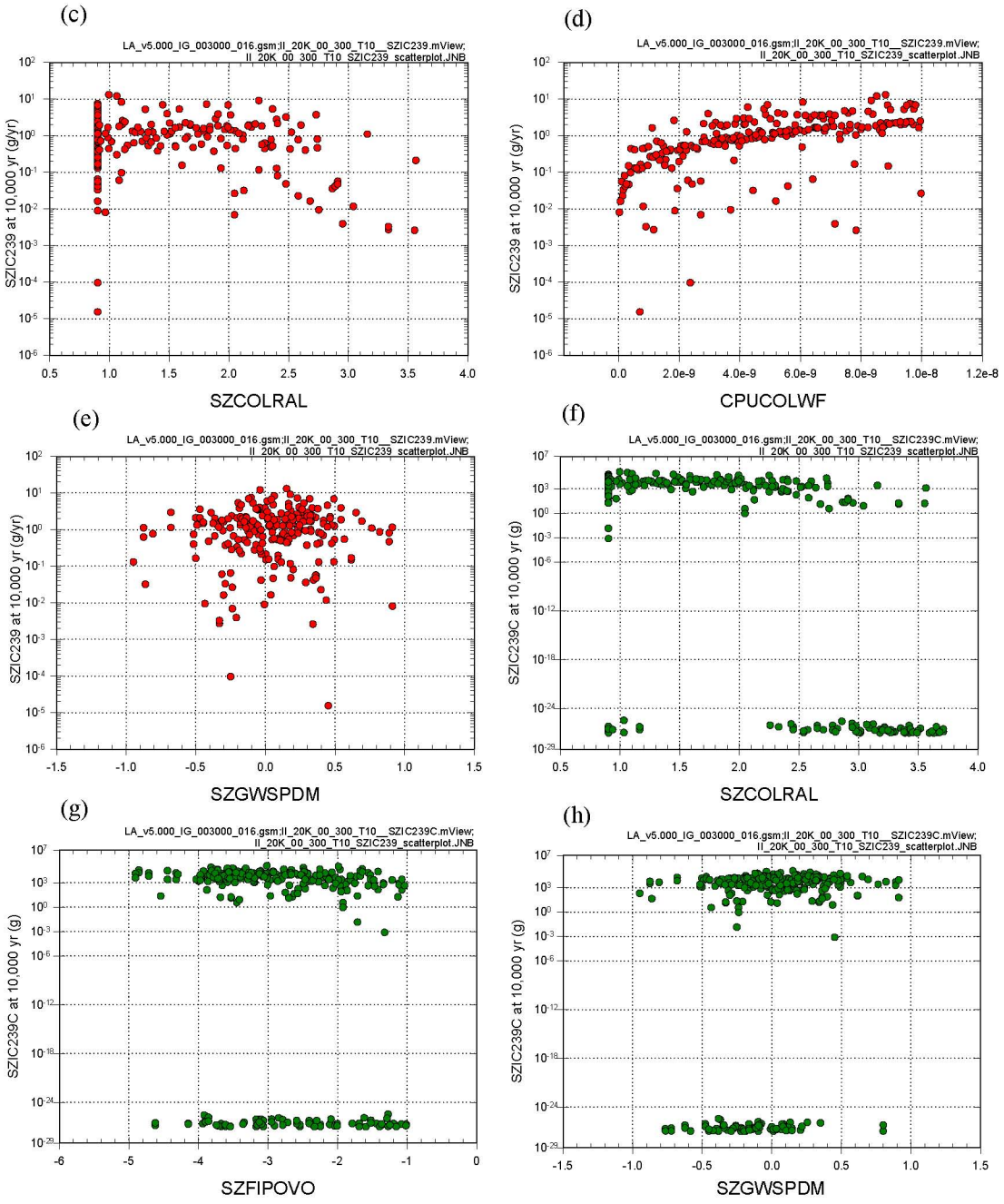

Source: Output DTNs: MO0709TSPAREGS.000 [DIRS 182976]; and MO0709TSPAPLOT.000 [DIRS 183010].

Figure K6.5.1-2. Stepwise rank regression analyses and selected scatterplots for time-dependent release rates (*SZIC239*, g/yr) and cumulative (i.e., integrated) releases (*SZIC239C*, g) for the movement of ^{239}Pu irreversibly attached to slow colloids across a subsurface plane at the location of the RMEI resulting from an igneous intrusive event at 10 years that destroys all WPs in the repository: (a, b) Regressions for *SZIC239* and *SZIC239C* at 3000, 5000 and 10,000 years, and (c-h) Scatterplots for *SZIC239* and *SZIC239C* at 10,000 years (continued).

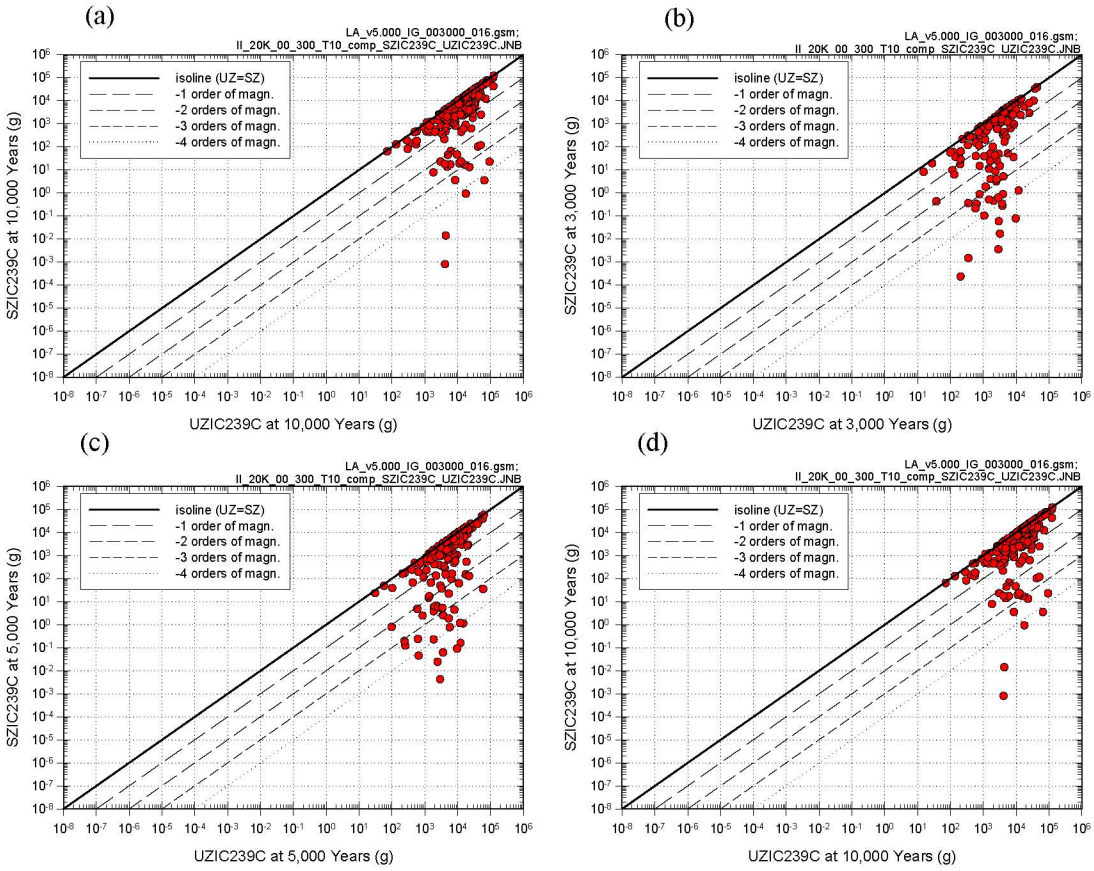

Source: Output DTN: MO0709TSPAREGS.000 [DIRS 182976].

Figure K6.5.1-3. Comparison of cumulative releases of ^{239}Pu irreversibly attached to slow colloids into the SZ (*UZIC239C*, g) and across a subsurface plane at the location of the RMEI (*SZIC239C*, g) at (a) 1000 years, (b) 3000 years, (c) 5000 years and (d) 10,000 years for an igneous intrusive event at 10 years that destroys all WPs in the repository

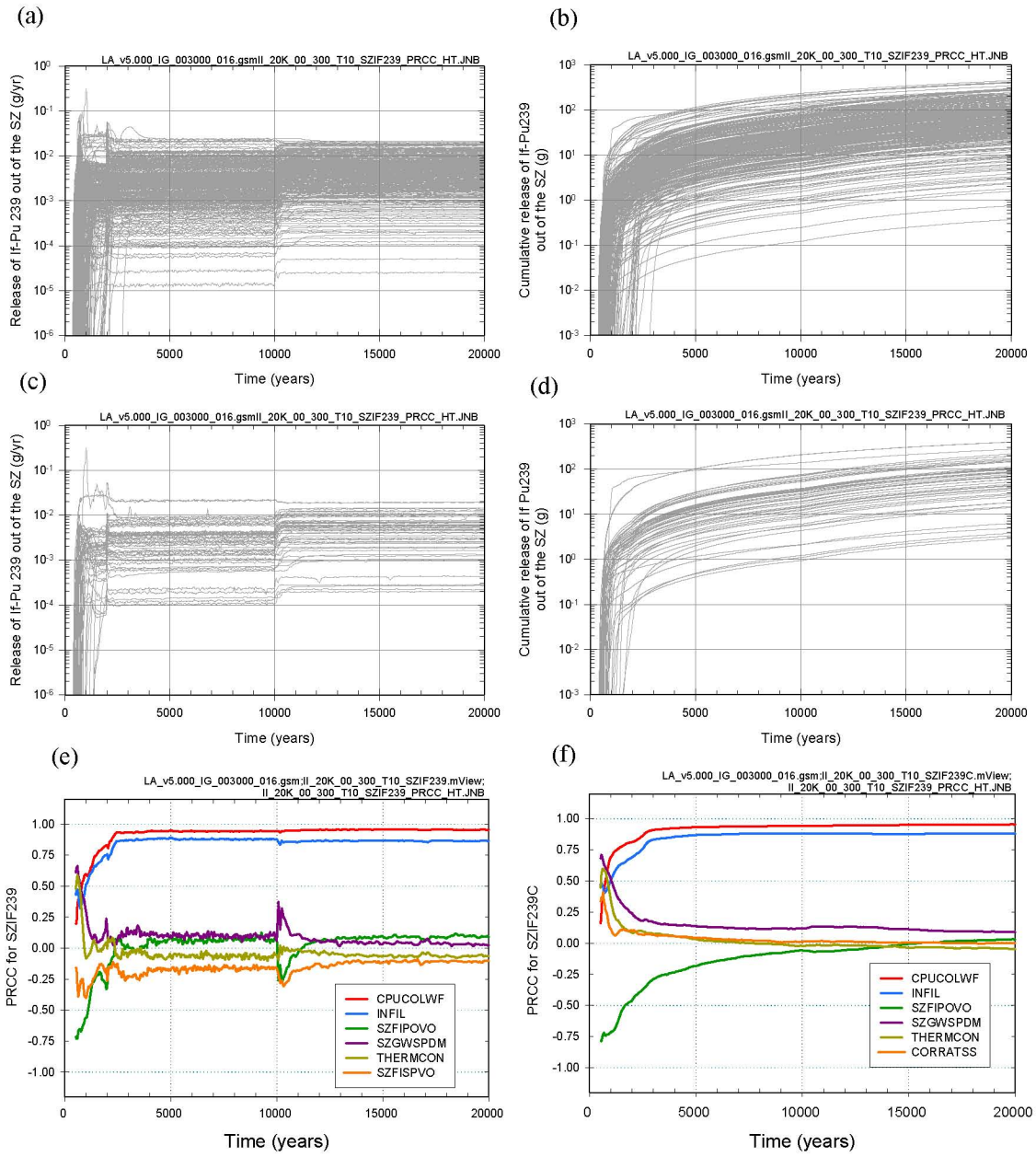

Source: Output DTNs: MO0709TSPAREGS.000 [DIRS 182976]; and MO0709TSPAPLOT.000 [DIRS 183010].

Figure K6.5.1-4. Time-dependent release rates (*SZIF239*, g/yr) and cumulative (i.e., integrated) releases (*SZIF239C*, g) over 20,000 years for the movement of ^{239}Pu irreversibly attached to fast colloids across a subsurface plane at the location of the RMEI resulting from an igneous intrusive event at 10 years that destroys all WPs in the repository: (a, b) *SZIF239* and *SZIF239C* for all (i.e., 300) sample elements, (c, d) *SZIF239* and *SZIF239C* for first 50 sample elements, and (e, f) PRCCs for *SZIF239* and *SZIF239C*

(a)

	SZIF239: 3,000 yr			SZIF239: 5,000 yr			SZIF239: 10,000 yr		
Step[a]	**Variable[b]**	**R^{2c}**	**SRRC[d]**	**Variable**	**R^2**	**SRRC**	**Variable**	**R^2**	**SRRC**
1	CPUCOLWF	0.62	0.73	CPUCOLWF	0.63	0.74	CPUCOLWF	0.64	0.75
2	INFIL	0.92	0.55	INFIL	0.93	0.55	INFIL	0.93	0.54
3	DWCSTERB	0.92	-0.04				DIFPATHL	0.93	0.04

(b)

	SZIF239C: 3,000 yr			SZIF239C: 5,000 yr			SZIF239C: 10,000 yr		
Step[a]	**Variable[b]**	**R^{2c}**	**SRRC[d]**	**Variable**	**R^2**	**SRRC**	**Variable**	**R^2**	**SRRC**
1	CPUCOLWF	0.58	0.70	CPUCOLWF	0.60	0.72	CPUCOLWF	0.62	0.74
2	INFIL	0.87	0.55	INFIL	0.91	0.56	INFIL	0.92	0.55
3	SZFIPOVO	0.88	-0.09	SZFIPOVO	0.91	-0.06	DELPPCO2	0.93	0.05
4	DELPPCO2	0.89	0.06	DELPPCO2	0.91	0.06	DWCSTERB	0.93	-0.05
5	THERMCON	0.89	0.06	DWCSTERB	0.92	-0.06	SZSREG4Y	0.93	0.05
6	UZKDPADT	0.89	0.05	RUBMAXL	0.92	-0.05	DWCSTERC	0.93	-0.04
7	DWCSTERB	0.89	-0.06	SZSREG4Y	0.92	0.05	KDAMCOL	0.93	-0.04
8	RHMUNO0	0.90	-0.05						
9	RUBMAXL	0.90	-0.05						
10	SZSREG4Y	0.90	0.05						

a: Steps in stepwise rank regression analysis
b: Variables listed in order of selection in stepwise regression
c: Cumulative R^2 value with entry of each variable into regression model
d: Standardized rank regression coefficients (SRRCs) in final regression model

Source: Output DTNs: MO0709TSPAREGS.000 [DIRS 182976]; and MO0709TSPAPLOT.000 [DIRS 183010].

Figure K6.5.1-5. Stepwise rank regression analyses and selected scatterplots for time-dependent release rates (*SZIF239*, g/yr) and cumulative (i.e., integrated) releases (*SZIF239C*, g) for the movement of ^{239}Pu irreversibly attached to fast colloids across a subsurface plane at the location of the RMEI resulting from an igneous intrusive event at 10 years that destroys all WPs in the repository: (a, b) Regressions for *SZIF239* and *SZIF239C* at 3000, 5000 and 10,000 years, and (c-h) Scatterplots for *SZIF239* and *SZIF239C* at 10,000 years

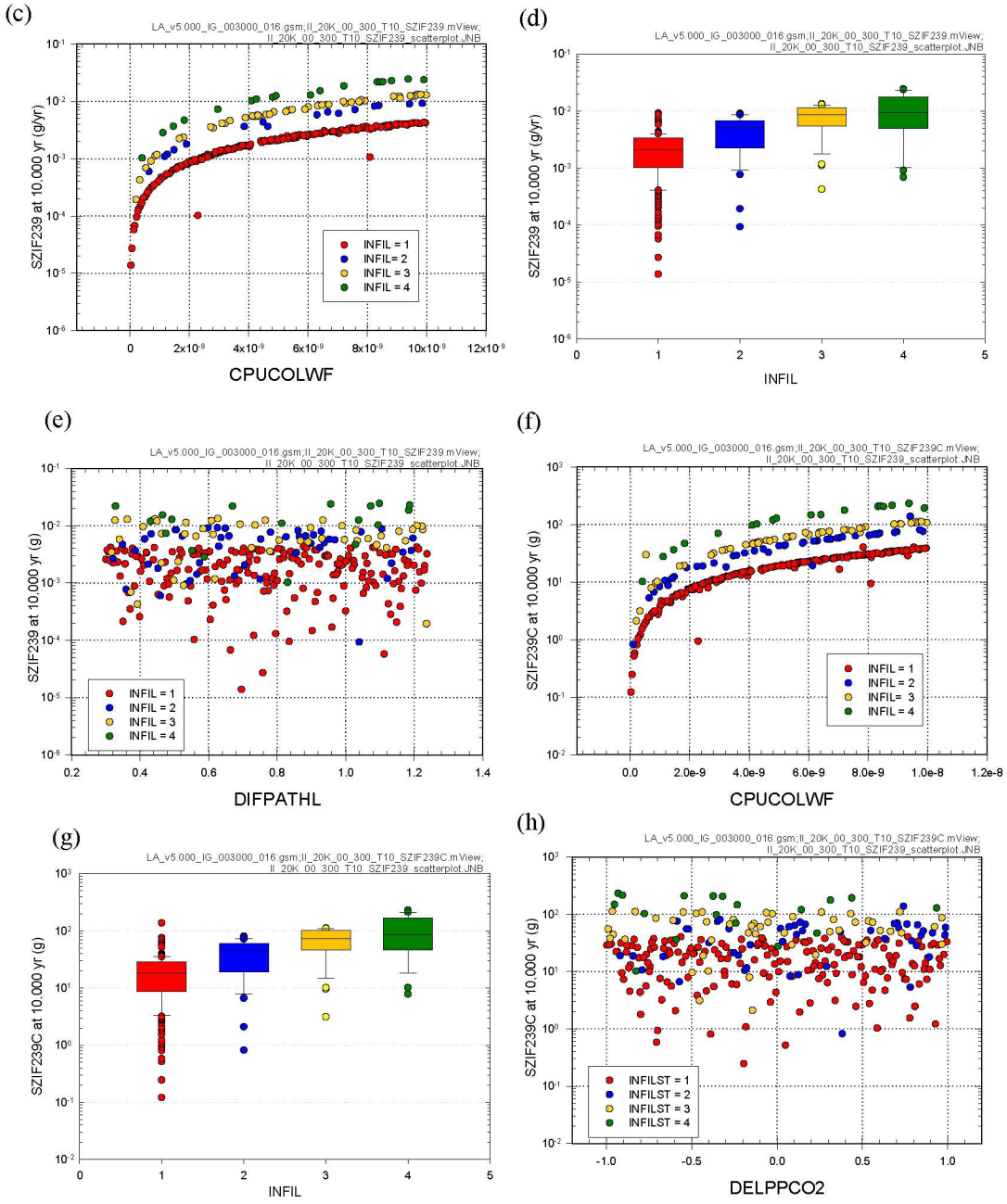

Source: Output DTNs: MO0709TSPAREGS.000 [DIRS 182976]; and MO0709TSPAPLOT.000 [DIRS 183010].

NOTE: In (d,g), the box extends from 0.25 to 0.75 quantile; lower and upper bar and whisker extend to 0.1 and 0.9 quantile, respectively; dots represent values outside 0.1 to 0.9 quantile range; median indicated by light horizontal line.

Figure K6.5.1-5. Stepwise rank regression analyses and selected scatterplots for time-dependent release rates (*SZIF239*, g/yr) and cumulative (i.e., integrated) releases (*SZIF239C*, g) for the movement of ^{239}Pu irreversibly attached to fast colloids across a subsurface plane at the location of the RMEI resulting from an igneous intrusive event at 10 years that destroys all WPs in the repository: (a, b) Regressions for *SZIF239* and *SZIF239C* at 3000, 5000 and 10,000 years, and (c-h) Scatterplots for *SZIF239* and *SZIF239C* at 10,000 years (continued).

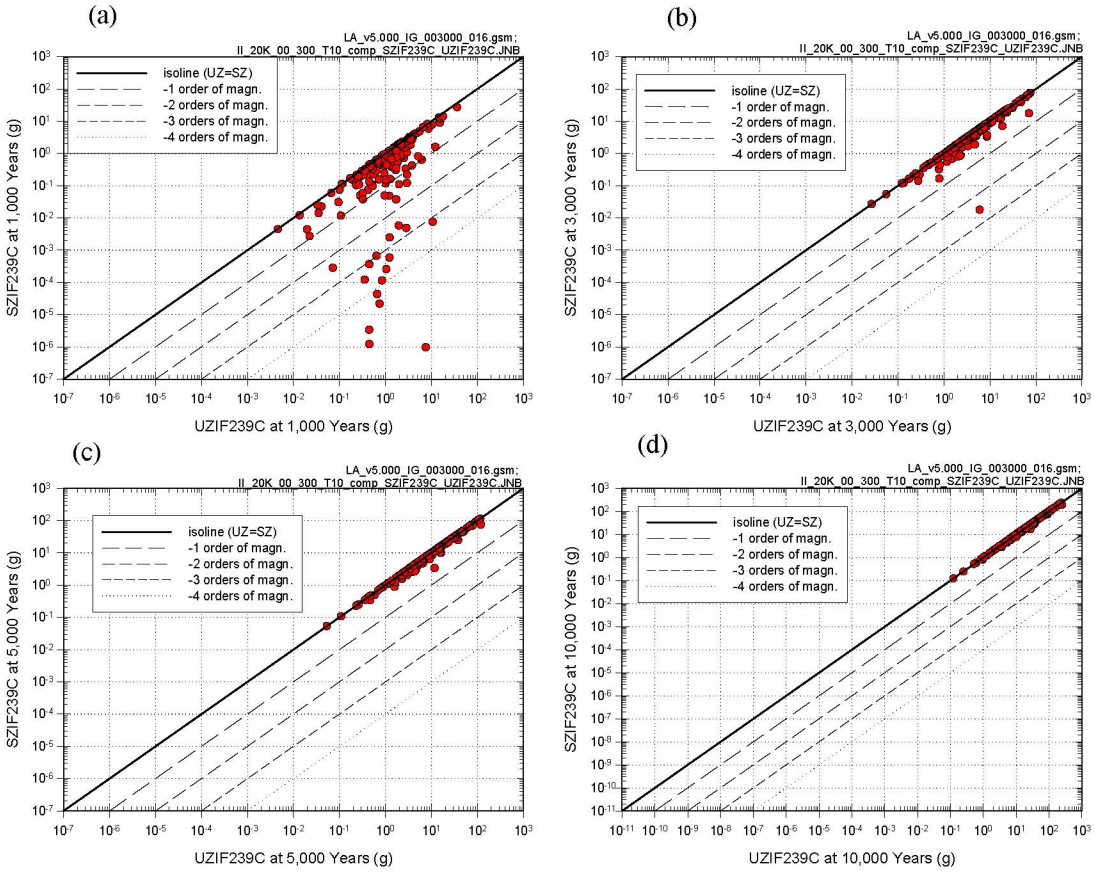

Source: Output DTN: MO0709TSPAREGS.000 [DIRS 182976].

Figure K6.5.1-6. Comparison of cumulative releases of ^{239}Pu irreversibly attached to fast colloids into the SZ (*UZIF239C*, g) and across a subsurface plane at the location of the RMEI (*SZIF239C*, g) at (a) 1000 years, (b) 3000 years, (c) 5000 years and (d) 10,000 years for an igneous intrusive event at 10 years that destroys all WPs in the repository

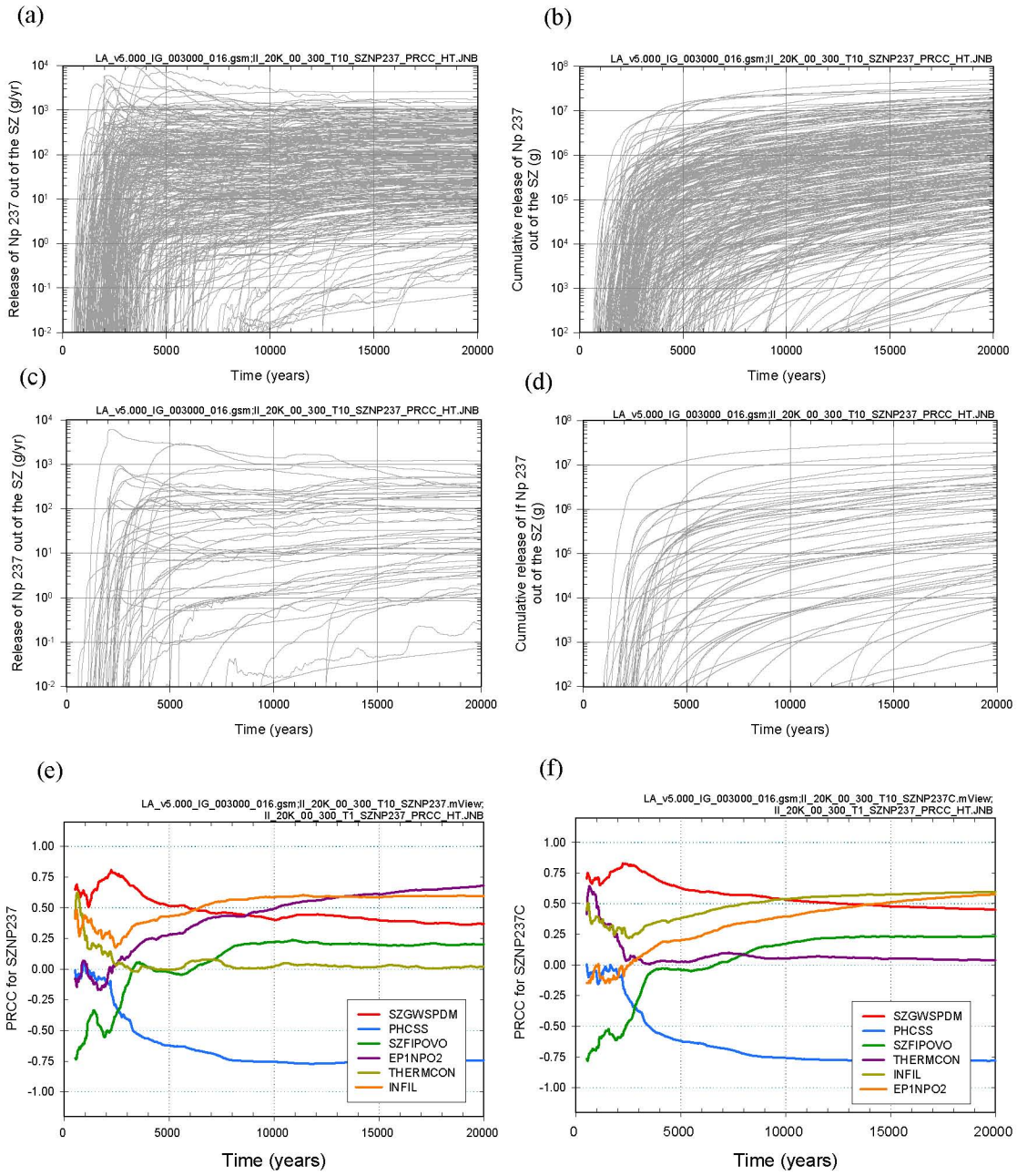

Source: Output DTNs: MO0709TSPAREGS.000 [DIRS 182976]; and MO0709TSPAPLOT.000 [DIRS 183010].

Figure K6.5.1-7. Time-dependent release rates (*SZNP237*, g/yr) and cumulative (i.e., integrated) releases (*SZNP237C*, g) over 20,000 years for the movement of dissolved ^{237}Np across a subsurface plane at the location of the RMEI resulting from an igneous intrusive event at 10 years that destroys all WPs in the repository: (a, b) *SZNP237* and *SZNP237C* for all (i.e., 300) sample elements, (c, d) *SZNP237* and *SZNP237C* for first 50 sample elements, and (e, f) PRCCs for *SZNP237* and *SZNP237C*

(a)

	SZNP237: 3,000 yr			SZNP237: 5,000 yr			SZNP237: 10,000 yr		
Step[a]	Variable[b]	R^{2c}	SRRC[d]	Variable	R^2	SRRC	Variable	R^2	SRRC
1	SZGWSPDM	0.44	0.68	SZGWSPDM	0.18	0.43	PHCSS	0.21	-0.40
2	PHCSS	0.50	-0.23	PHCSS	0.33	-0.37	INFIL	0.42	0.43
3	INFIL	0.54	0.17	INFIL	0.46	0.32	EP1NPO2	0.49	0.29
4	SZFIPOVO	0.58	-0.19	SZFISPVO	0.49	0.21	SZGWSPDM	0.55	0.25
5	SZKDSEAL	0.61	-0.17	SZDIFCVO	0.52	-0.21	CORRATSS	0.59	-0.17
6	SZFISPVO	0.63	0.16	EP1NPO2	0.54	0.15	SZFISPVO	0.62	0.22
7	SZDIFCVO	0.64	-0.14	DELPPCO2	0.56	0.15	DELPPCO2	0.65	0.17
8	SZPORUAL	0.66	-0.10	EP1LOWNU	0.57	0.13	EP1LOWAM	0.67	0.17
9	EP1LOWAM	0.67	0.12	EP1LOWAM	0.59	0.13	EP1LOWNU	0.69	0.14
10	WDGCA22	0.68	-0.11	SZKDCSVO	0.60	-0.10	SZDIFCVO	0.70	-0.14
11				HLWDRACD	0.61	-0.11	COLGW	0.71	0.11
12				SZKDUAL	0.62	-0.10	SZKDNPVO	0.72	-0.10

(b)

	SZNP237C: 3,000 yr			SZNP237C: 5,000 yr			SZNP237C: 10,000 yr		
Step[a]	Variable[b]	R^{2c}	SRRC[d]	Variable	R^2	SRRC	Variable	R^2	SRRC
1	SZGWSPDM	0.50	0.73	SZGWSPDM	0.27	0.53	PHCSS	0.22	-0.41
2	SZFIPOVO	0.55	-0.22	PHCSS	0.42	-0.37	INFIL	0.39	0.38
3	PHCSS	0.61	-0.21	INFIL	0.51	0.28	SZGWSPDM	0.51	0.35
4	INFIL	0.64	0.15	SZFISPVO	0.55	0.24	SZFISPVO	0.56	0.26
5	SZKDSEAL	0.67	-0.18	SZDIFCVO	0.59	-0.21	EP1NPO2	0.59	0.21
6	SZFISPVO	0.69	0.17	SZKDSEAL	0.61	-0.11	DELPPCO2	0.62	0.18
7	SZPORUAL	0.71	-0.11	EP1LOWAM	0.62	0.14	EP1LOWAM	0.65	0.18
8	SZDIFCVO	0.72	-0.13	DELPPCO2	0.64	0.14	SZDIFCVO	0.67	-0.18
9	EP1LOWAM	0.73	0.10	HLWDRACD	0.65	-0.10	CORRATSS	0.69	-0.13
10	WDGCA22	0.74	-0.10	SZFIPOVO	0.66	-0.11	EP1LOWNU	0.71	0.14
11	WDLCRATE	0.75	0.08	EP1NPO2	0.67	0.10	COLGW	0.72	0.11
12				EP1LOWNU	0.68	0.10	SZKDCSVO	0.73	-0.09
13				SZKDCSVO	0.69	-0.10	SZKDNPVO	0.74	-0.09
14							THERMCON	0.74	0.08

a: Steps in stepwise rank regression analysis
b: Variables listed in order of selection in stepwise regression
c: Cumulative R^2 value with entry of each variable into regression model
d: Standardized rank regression coefficients (SRRCs) in final regression model

Source: Output DTNs: MO0709TSPAREGS.000 [DIRS 182976]; and MO0709TSPAPLOT.000 [DIRS 183010].

Figure K6.5.1-8. Stepwise rank regression analyses and selected scatterplots for time-dependent release rates (*SZNP237*, g/yr) and cumulative (i.e., integrated) releases (*SZNP237C*, g) for the movement of dissolved ^{237}Np across a subsurface plane at the location of the RMEI resulting from an igneous intrusive event at 10 years that destroys all WPs in the repository: (a, b) Regressions for *SZNP237* and *SZNP237C* at 3000, 5000 and 10,000 years, and (c-h) Scatterplots for *SZNP237* and *SZNP237C* at 10,000 years

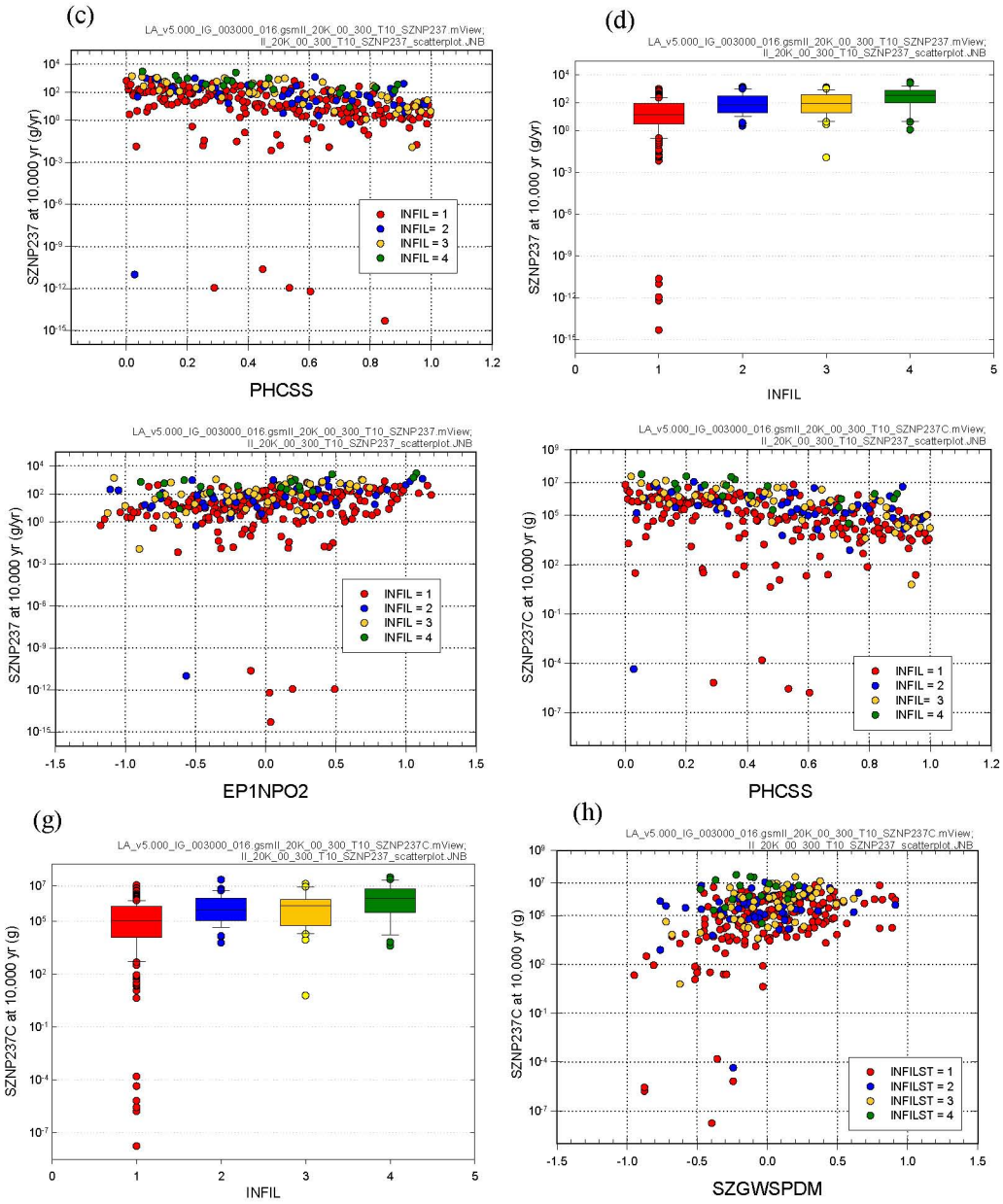

Source: Output DTNs: MO0709TSPAREGS.000 [DIRS 182976]; and MO0709TSPAPLOT.000 [DIRS 183010].

Note: In (d,g), the box extends from 0.25 to 0.75 quantile; lower and upper bar and whisker extend to 0.1 and 0.9 quantile, respectively; dots represent values outside 0.1 to 0.9 quantile range; median indicated by light horizontal line

Figure K6.5.1-8. Stepwise rank regression analyses and selected scatterplots for time-dependent release rates (*SZNP237*, g/yr) and cumulative (i.e., integrated) releases (*SZNP237C*, g) for the movement of dissolved ^{237}Np across a subsurface plane at the location of the RMEI resulting from an igneous intrusive event at 10 years that destroys all WPs in the repository: (a, b) Regressions for *SZNP237* and *SZNP237C* at 3000, 5000 and 10,000 years, and (c-h) Scatterplots for *SZNP237* and *SZNP237C* at 10,000 years (continued).

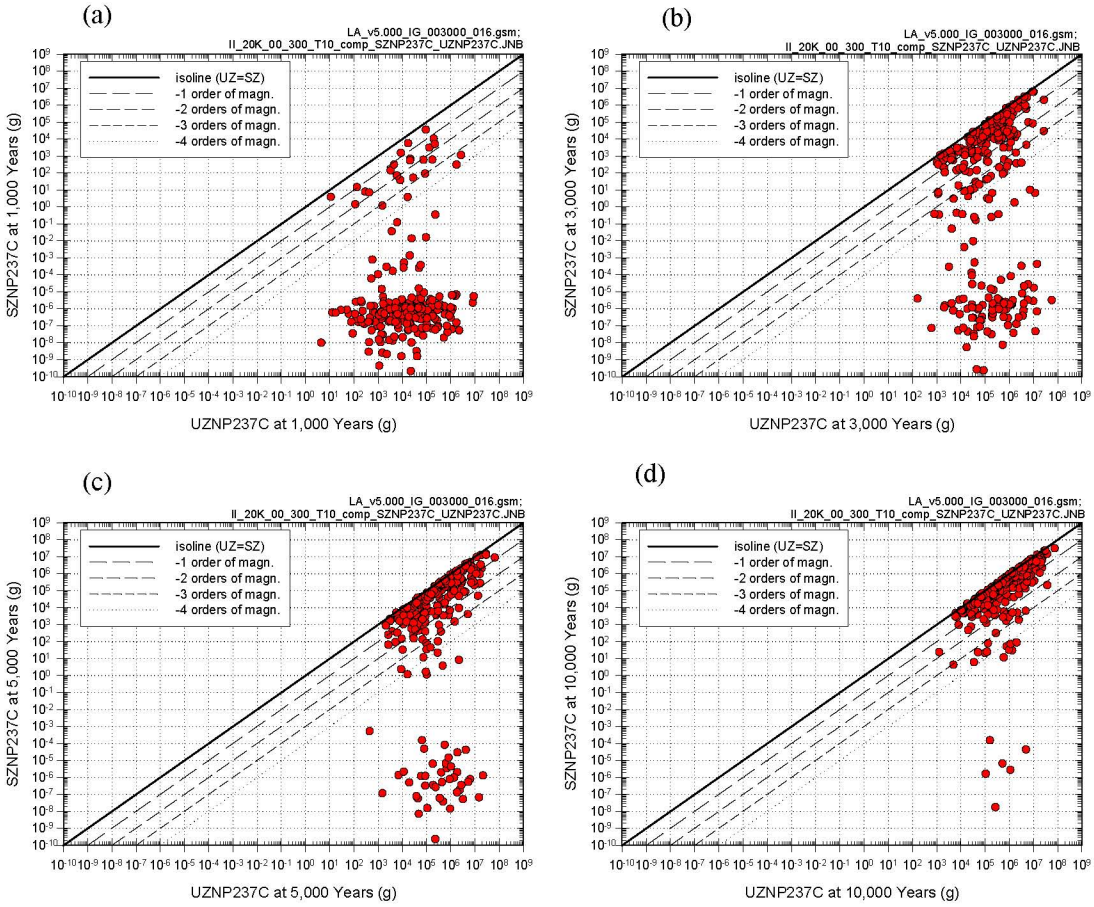

Source: Output DTN: MO0709TSPAREGS.000 [DIRS 182976].

Figure K6.5.1-9. Comparison of cumulative releases of dissolved ^{237}Np into the SZ (*UZNP237C*, g) and across a subsurface plane at the location of the RMEI (*SZNP237C*, g) at (a) 1000 years, (b) 3000 years, (c) 5000 years and (d) 10,000 years for an igneous intrusive event at 10 years that destroys all WPs in the repository

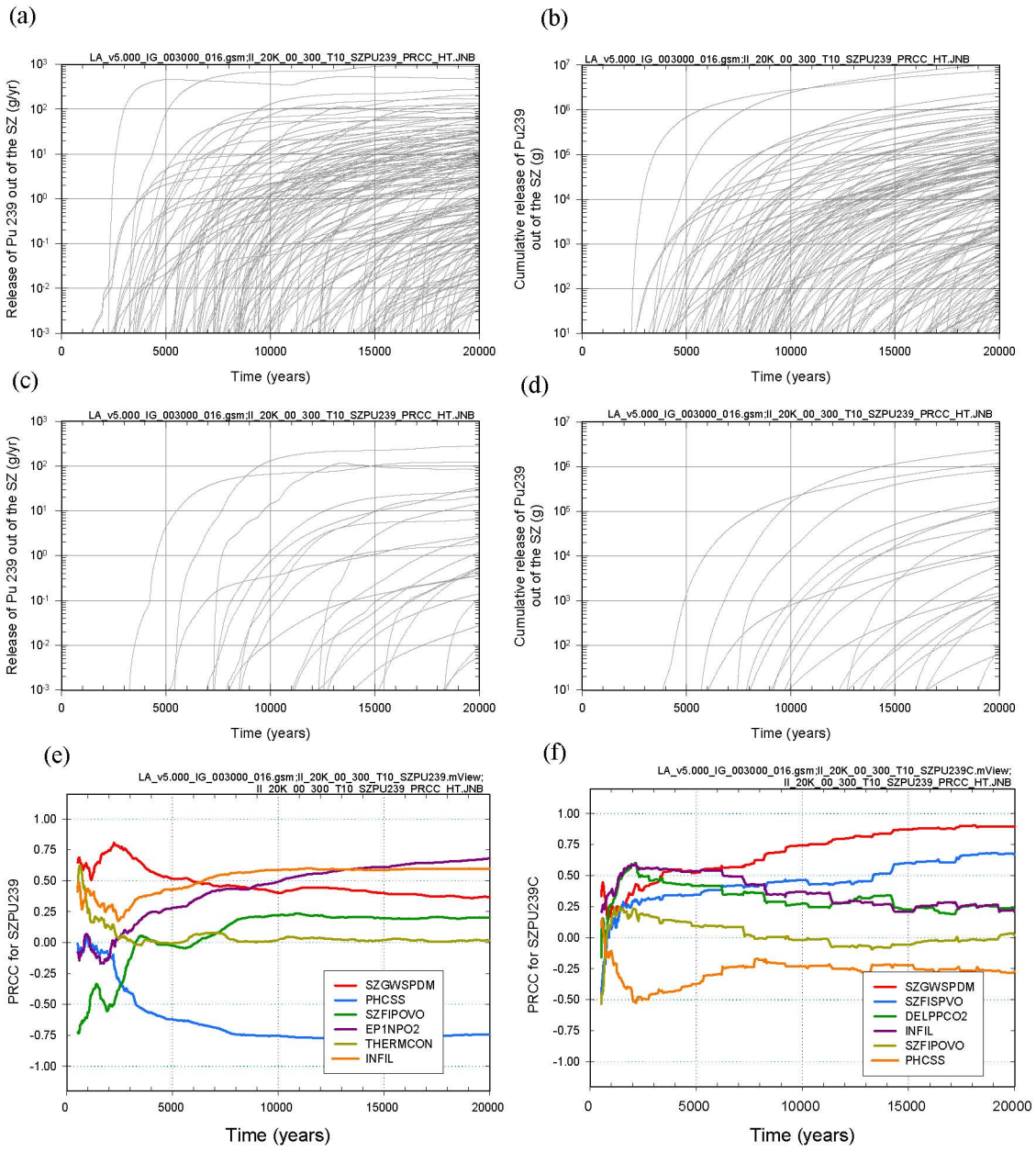

Source: Output DTNs: MO0709TSPAREGS.000 [DIRS 182976]; and MO0709TSPAPLOT.000 [DIRS 183010].

Figure K6.5.1-10. Time-dependent release rates (*SZPU239*, g/yr) and cumulative (i.e., integrated) releases (*SZPU239C*, g) over 20,000 years for the movement of dissolved ^{239}Pu across a subsurface plane at the location of the RMEI resulting from an igneous intrusive event at 10 years that destroys all WPs in the repository: (a, b) *SZPU239* and *SZPU239C* for all (i.e., 300) sample elements, (c, d) *SZPU239* and *SZPU239C* for first 50 sample elements, and (e, f) PRCCs for *SZPU239* and *SZPU239C*

(a)

	SZPU239: 3,000 yr			SZPU239: 5,000 yr			SZPU239: 10,000 yr		
Step[a]	Variable[b]	R^{2c}	SRRC[d]	Variable	R^2	SRRC	Variable	R^2	SRRC
1	SZGWSPDM	0.07	0.26	SZGWSPDM	0.13	0.36	SZGWSPDM	0.44	0.67
2	SZLODISP	0.11	0.20	SZLODISP	0.18	0.24	SZFISPVO	0.49	0.24
3	SZKDAMCO	0.13	0.14	SZPORUAL	0.21	-0.19	SZKDPUVO	0.53	-0.22
4				CSWFA1AK	0.24	-0.17	SZPORUAL	0.56	-0.16
5				SZKDAMCO	0.27	0.17	SZCONCOL	0.58	0.14
6				CPUPERCS	0.28	0.13	SZLODISP	0.60	0.13
7				SZKDCSCO	0.30	0.15	SZSREG1X	0.61	-0.12
8				SZKDPUVO	0.32	-0.15			
9				SZKDSNAL	0.34	-0.14			

(b)

	SZPU239C: 3,000 yr			SZPU239C: 5,000 yr			SZPU239C: 10,000 yr		
Step[a]	Variable[b]	R^{2c}	SRRC[d]	Variable	R^2	SRRC	Variable	R^2	SRRC
1	INFIL	0.18	0.42	SZGWSPDM	0.21	0.44	SZGWSPDM	0.43	0.62
2	SZGWSPDM	0.34	0.37	INFIL	0.37	0.38	INFIL	0.51	0.26
3	EP1LOWPU	0.42	0.31	EP1LOWPU	0.45	0.33	SZFISPVO	0.57	0.27
4	PHCSS	0.49	-0.20	PHCSS	0.49	-0.15	EP1LOWPU	0.60	0.24
5	DELPPCO2	0.54	0.25	DELPPCO2	0.51	0.19	SZKDPUVO	0.63	-0.17
6	UZKDPUDT	0.58	-0.19	SZKDAMCO	0.54	0.14	SZCONCOL	0.65	0.15
7	EP1LOWAM	0.60	0.14	UZKDPUDT	0.55	-0.14	SZPORUAL	0.66	-0.13
8	SZFISPVO	0.61	0.13	SZCONCOL	0.57	0.13	DELPPCO2	0.68	0.11
9	SZPORUAL	0.62	-0.12	SZFISPVO	0.59	0.13	SZLODISP	0.69	0.12
10	SZCONCOL	0.64	0.11	CORRATSS	0.60	-0.12	PHCSS	0.70	-0.12
11	CORRATSS	0.65	-0.12	EP1LOWAM	0.61	0.11	IS2MCONS	0.71	0.11
12	DWCSTERB	0.66	-0.10	SZKDPUVO	0.63	-0.12	SZDIFCVO	0.72	-0.10
13	SZKDPUVO	0.67	-0.09	SZPORUAL	0.64	-0.12	UZKDPUDT	0.73	-0.09
14	SZKDAMCO	0.68	0.11						
15	UZFAG8	0.69	0.10						

a: Steps in stepwise rank regression analysis
b: Variables listed in order of selection in stepwise regression
c: Cumulative R^2 value with entry of each variable into regression model
d: Standardized rank regression coefficients (SRRCs) in final regression model

Source: Output DTNs: MO0709TSPAREGS.000 [DIRS 182976]; and MO0709TSPAPLOT.000 [DIRS 183010].

Figure K6.5.1-11. Stepwise rank regression analyses and selected scatterplots for time-dependent release rates (*SZPU239*, g/yr) and cumulative (i.e., integrated) releases (*SZPU239C*, g) for the movement of dissolved ^{239}Pu across a subsurface plane at the location of the RMEI resulting from an igneous intrusive event at 10 years that destroys all WPs in the repository: (a, b) Regressions for *SZPU239* and *SZPU239C* at 3000, 5000 and 10,000 years, and (c-h) Scatterplots for *SZPU239* and *SZPU239C* at 10,000 years

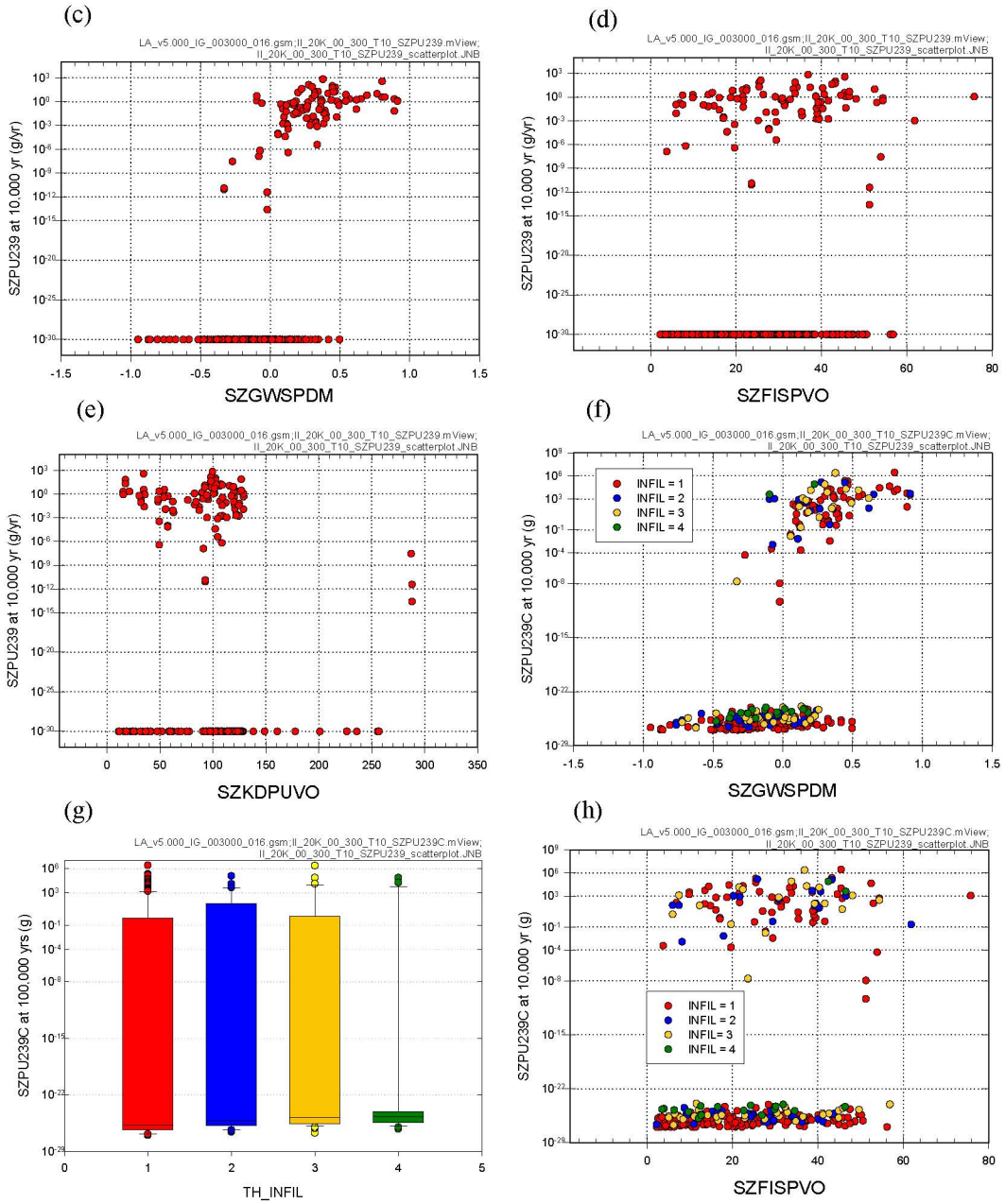

Source: Output DTNs: MO0709TSPAREGS.000 [DIRS 182976]; and MO0709TSPAPLOT.000 [DIRS 183010].

NOTE: In (g), the box extends from 0.25 to 0.75 quantile; lower and upper bar and whisker extend to 0.1 and 0.9 quantile, respectively; dots represent values outside 0.1 to 0.9 quantile range; median indicated by light horizontal line.

Figure K6.5.1-11. Stepwise rank regression analyses and selected scatterplots for time-dependent release rates (*SZPU239*, g/yr) and cumulative (i.e., integrated) releases (*SZPU239C*, g) for the movement of dissolved ^{239}Pu across a subsurface plane at the location of the RMEI resulting from an igneous intrusive event at 10 years that destroys all WPs in the repository: (a, b) Regressions for *SZPU239* and *SZPU239C* at 3000, 5000 and 10,000 years, and (c-h) Scatterplots for *SZPU239* and *SZPU239C* at 10,000 years (continued).

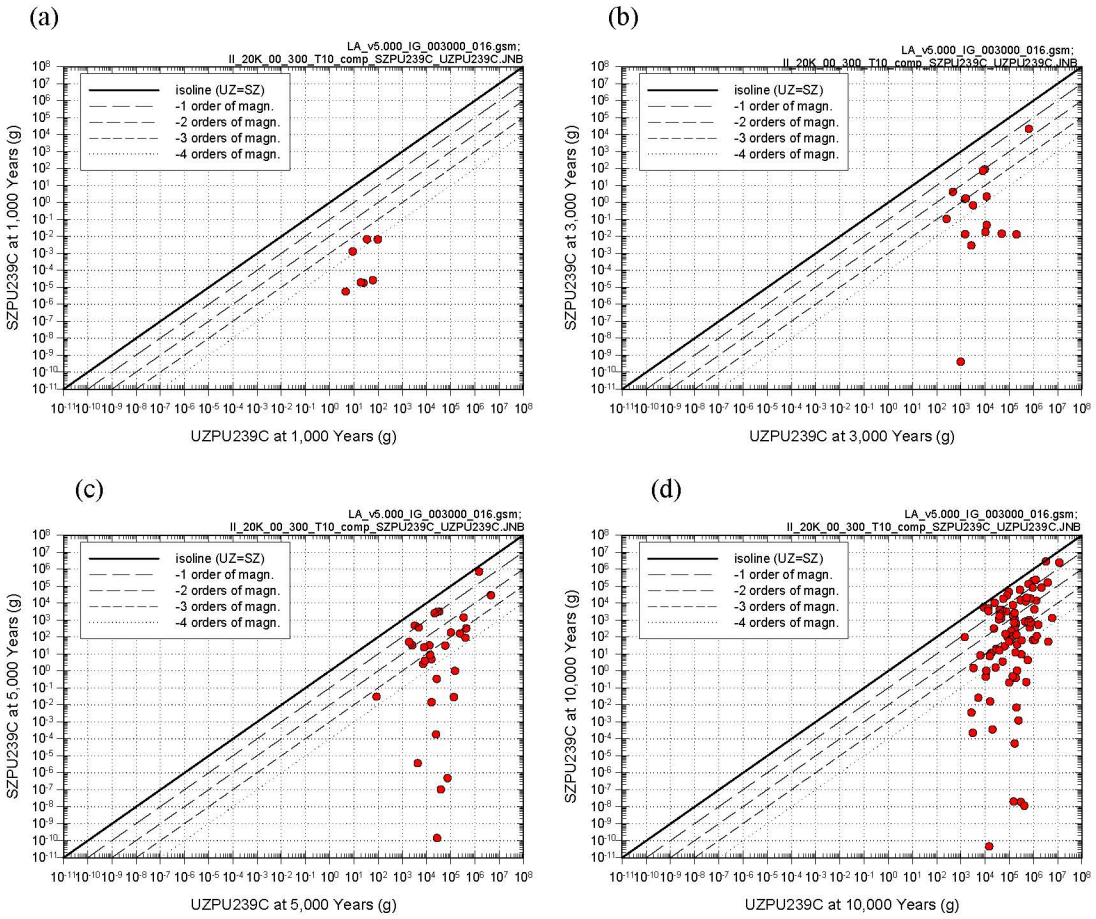

Source: Output DTN: MO0709TSPAREGS.000 [DIRS 182976].

Figure K6.5.1-12. Comparison of cumulative releases of dissolved ^{239}Pu into the SZ (*UZPU239C*, g) and across a subsurface plane at the location of the RMEI (*SZPU239C*, g) at (a) 1000 years, (b) 3000 years, (c) 5000 years and (d) 10,000 years for an igneous intrusive event at 10 years that destroys all WPs in the repository

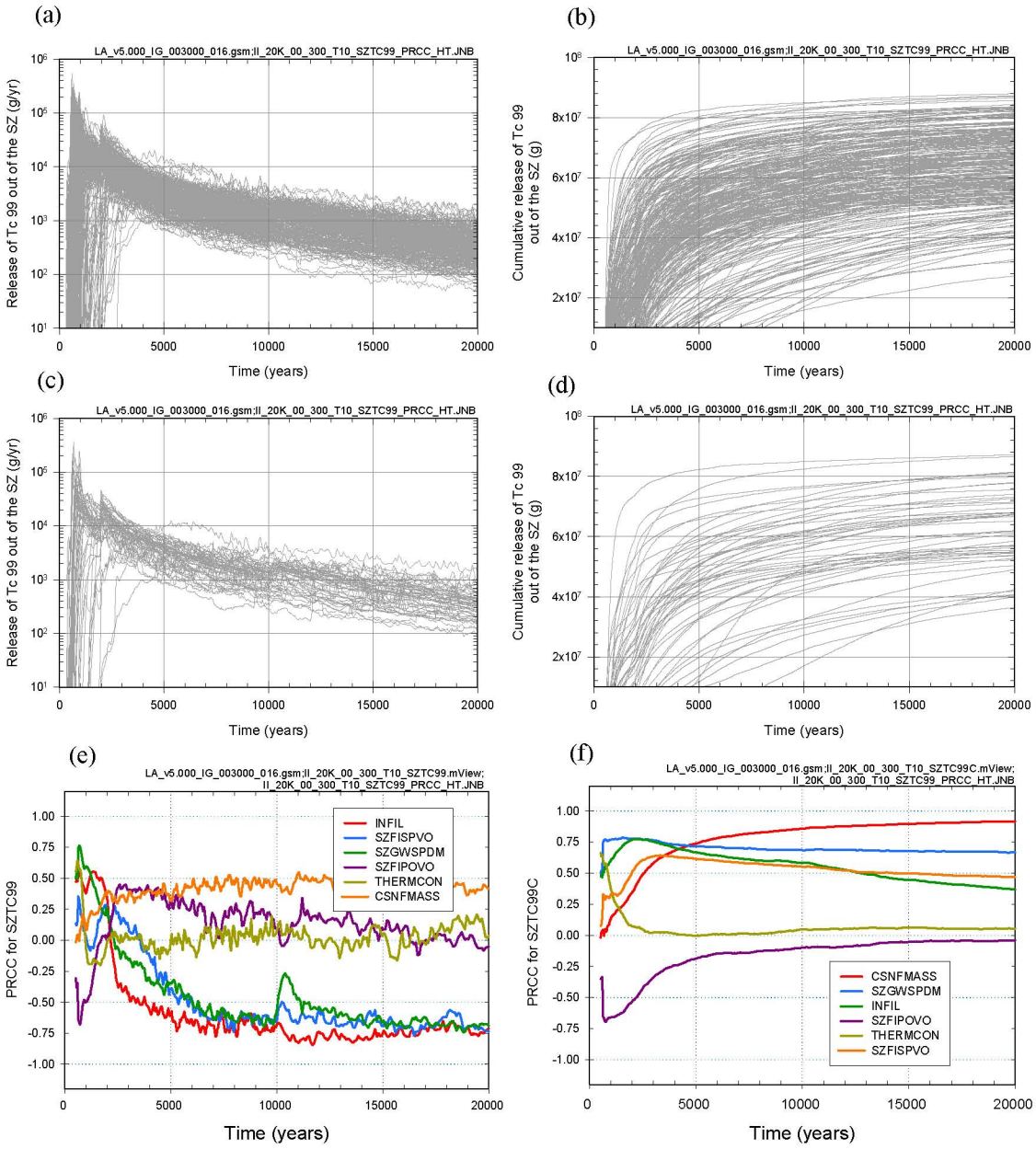

Source: Output DTNs: MO0709TSPAREGS.000 [DIRS 182976]; and MO0709TSPAPLOT.000 [DIRS 183010].

Figure K6.5.1-13. Time-dependent release rates (*SZTC99*, g/yr) and cumulative (i.e., integrated) releases (*SZTC99C*, g) over 20,000 years for the movement of dissolved ^{99}Tc across a subsurface plane at the location of the RMEI resulting from an igneous intrusive event at 10 years that destroys all WPs in the repository: (a, b) *SZTC99* and *SZTC99C* for all (i.e., 300) sample elements, (c, d) *SZTC99* and *SZTC99C* for first 50 sample elements, and (e, f) PRCCs for *SZTC99* and *SZTC99C*

(a)

	SZTC99: 3,000 yr			SZTC99: 5,000 yr			SZTC99: 10,000 yr		
Step[a]	Variable[b]	R^{2c}	SRRC[d]	Variable	R^2	SRRC	Variable	R^2	SRRC
1	INFIL	0.14	-0.41	INFIL	0.27	-0.53	INFIL	0.32	-0.57
2	CSNFMASS	0.26	0.33	SZGWSPDM	0.39	-0.34	SZGWSPDM	0.52	-0.41
3	UZFAG8	0.31	-0.24	CSNFMASS	0.46	0.26	SZFISPVO	0.60	-0.37
4	SZFIPOVO	0.36	0.26	SZFISPVO	0.52	-0.28	CSNFMASS	0.68	0.27
5	UZGAM	0.37	-0.17	SZDIFCVO	0.55	0.17	SZDIFCVO	0.70	0.17
6	SZGWSPDM	0.39	-0.16	SZFIPOVO	0.57	0.20	HLWDRACD	0.71	0.10
7	GP4NO3	0.42	0.15	UZFAG8	0.59	-0.15			
8				UZGAM	0.61	-0.14			
9				WDDEFSZE	0.62	0.11			
10				SZKDSNCO	0.63	0.10			
11				GP2NO3	0.64	-0.10			
12				DWCSTERC	0.64	0.10			

(b)

	SZTC99C: 3,000 yr			SZTC99C: 5,000 yr			SZTC99C: 10,000 yr		
Step[a]	Variable[b]	R^{2c}	SRRC[d]	Variable	R^2	SRRC	Variable	R^2	SRRC
1	INFIL	0.27	0.49	CSNFMASS	0.26	0.47	CSNFMASS	0.47	0.65
2	SZGWSPDM	0.54	0.51	SZGWSPDM	0.49	0.46	SZGWSPDM	0.64	0.40
3	SZFISPVO	0.66	0.36	INFIL	0.68	0.41	INFIL	0.75	0.30
4	CSNFMASS	0.75	0.31	SZFISPVO	0.77	0.35	SZFISPVO	0.81	0.29
5	SZDIFCVO	0.80	-0.25	SZDIFCVO	0.81	-0.24	SZDIFCVO	0.85	-0.21
6	SZFIPOVO	0.81	-0.12	HLWDRACD	0.82	-0.09	SEEPCOND	0.86	-0.06
7	HLWDRACD	0.82	-0.10	SZFIPOVO	0.83	-0.07			
8	SZRAHAVO	0.83	0.08	SZRAHAVO	0.83	0.07			

a: Steps in stepwise rank regression analysis
b: Variables listed in order of selection in stepwise regression
c: Cumulative R^2 value with entry of each variable into regression model
d: Standardized rank regression coefficients (SRRCs) in final regression model

Source: Output DTNs: MO0709TSPAREGS.000 [DIRS 182976]; and MO0709TSPAPLOT.000 [DIRS 183010].

Figure K6.5.1-14. Stepwise rank regression analyses and selected scatterplots for time-dependent release rates (*SZTC99*, g/yr) and cumulative (i.e., integrated) releases (*SZTC99C*, g) for the movement of dissolved ^{99}Tc across a subsurface plane at the location of the RMEI resulting from an igneous intrusive event at 10 years that destroys all WPs in the repository: (a, b) Regressions for *SZTC99* and *SZTC99C* at 3000, 5000 and 10,000 years, and (c-h) Scatterplots for *SZTC99* and *SZTC99C* at 10,000 years

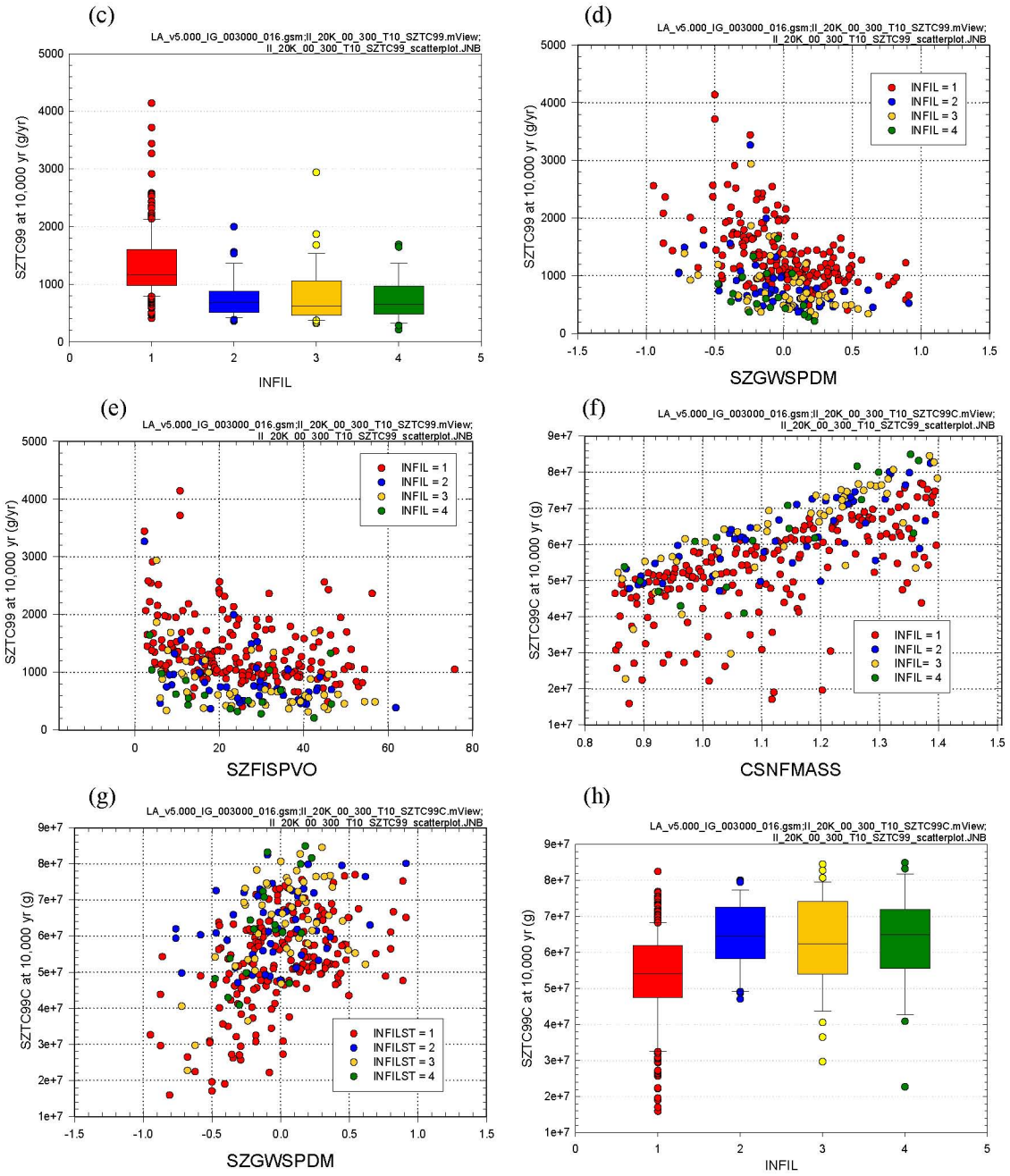

Source: Output DTNs: MO0709TSPAREGS.000 [DIRS 182976]; and MO0709TSPAPLOT.000 [DIRS 183010].

NOTE: In (c,h), the box extends from 0.25 to 0.75 quantile; lower and upper bar and whisker extend to 0.1 and 0.9 quantile, respectively; dots represent values outside 0.1 to 0.9 quantile range; median indicated by light horizontal line.

Figure K6.5.1-14. Stepwise rank regression analyses and selected scatterplots for time-dependent release rates (*SZTC99*, g/yr) and cumulative (i.e., integrated) releases (*SZTC99C*, g) for the movement of dissolved ^{99}Tc across a subsurface plane at the location of the RMEI resulting from an igneous intrusive event at 10 years that destroys all WPs in the repository: (a, b) Regressions for *SZTC99* and *SZTC99C* at 3000, 5000 and 10,000 years, and (c-h) Scatterplots for *SZTC99* and *SZTC99C* at 10,000 years (continued).

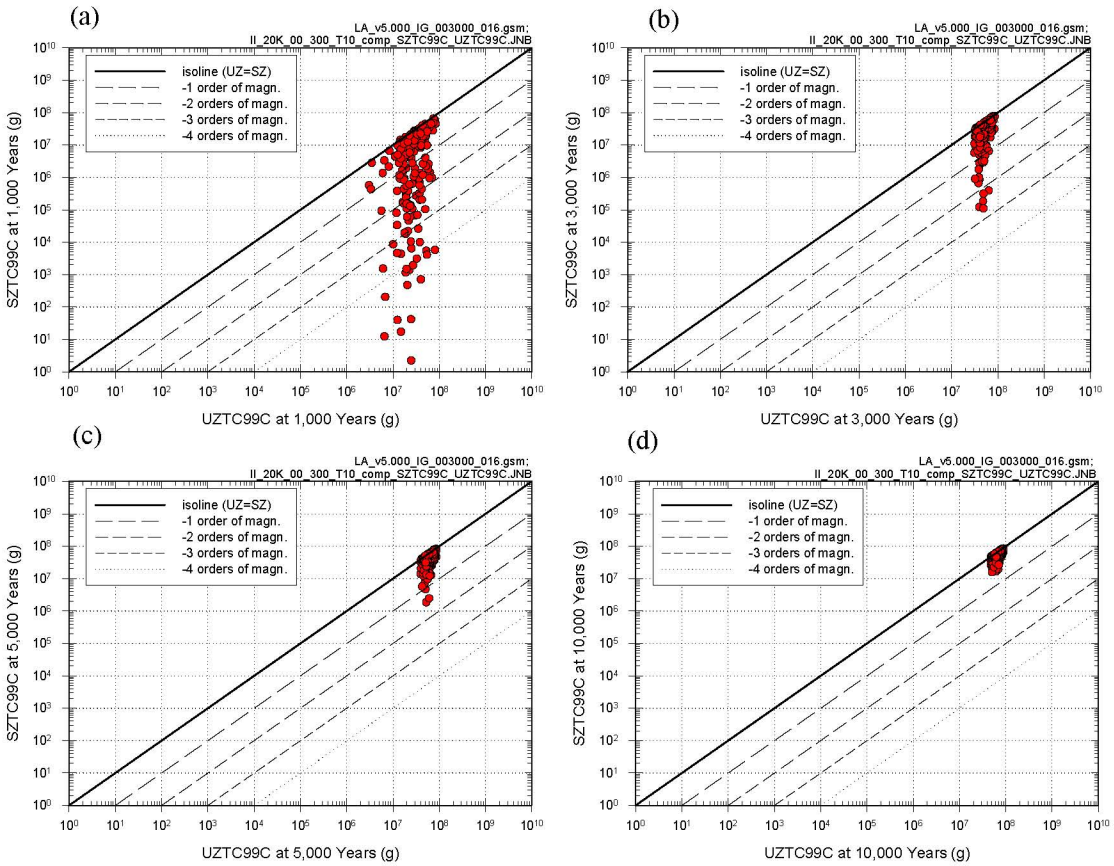

Source: Output DTN: MO0709TSPAREGS.000 [DIRS 182976].

Figure K6.5.1-15. Comparison of cumulative releases of dissolved ^{99}Tc into the SZ (*UZTC99C*, g) and across a subsurface plane at the location of the RMEI (*SZTC99C*, g) at (a) 1000 years, (b) 3000 years, (c) 5000 years and (d) 10,000 years for an igneous intrusive event at 10 years that destroys all WPs in the repository

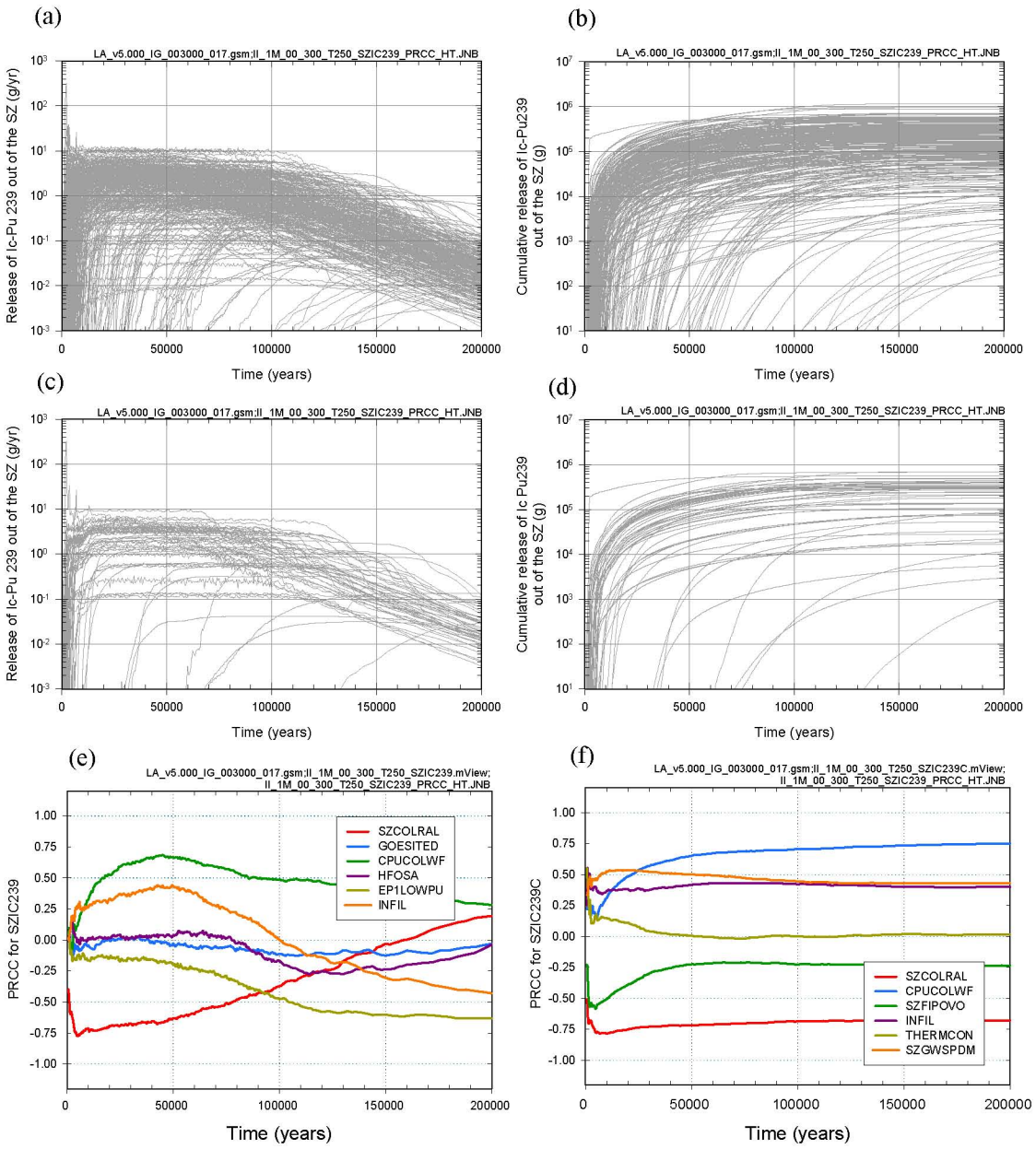

Source: Output DTNs: MO0709TSPAREGS.000 [DIRS 182976]; and MO0709TSPAPLOT.000 [DIRS 183010].

Figure K6.5.2-1. Time-dependent release rates (*SZIC239*, g/yr) and cumulative (i.e., integrated) releases (*SZIC239C*, g) over 200,000 years for the movement of ^{239}Pu irreversibly attached to slow colloids across a subsurface plane at the location of the RMEI resulting from an igneous intrusive event at 250 years that destroys all WPs in the repository: (a, b) *SZIC239* and *SZIC239C* for all (i.e., 300) sample elements, (c, d) *SZIC239* and *SZIC239C* for first 50 sample elements, and (e, f) PRCCs for *SZIC239* and *SZIC239C*

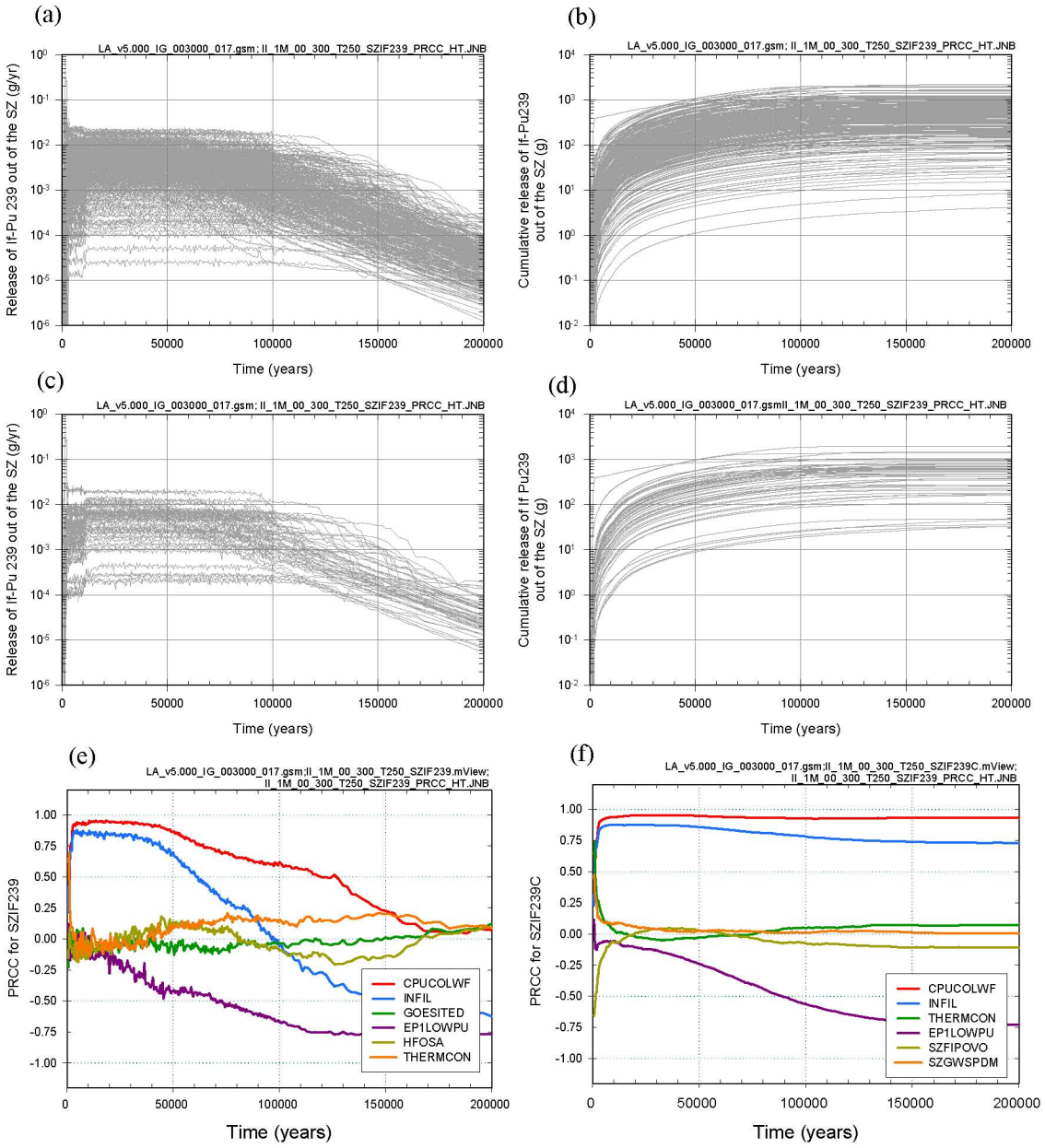

Source: Output DTNs: MO0709TSPAREGS.000 [DIRS 182976]; and MO0709TSPAPLOT.000 [DIRS 183010].

Figure K6.5.2-2. Time-dependent release rates (*SZIF239*, g/yr) and cumulative (i.e., integrated) releases (*SZIF239C*, g) over 200,000 years for the movement of ^{239}Pu irreversibly attached to fast colloids across a subsurface plane at the location of the RMEI resulting from an igneous intrusive event at 250 years that destroys all WPs in the repository: (a, b) *SZIF239* and *SZIF239C* for all (i.e., 300) sample elements, (c, d) *SZIF239* and *SZIF239C* for first 50 sample elements, and (e, f) PRCCs for *SZIF239* and *SZIF239C*

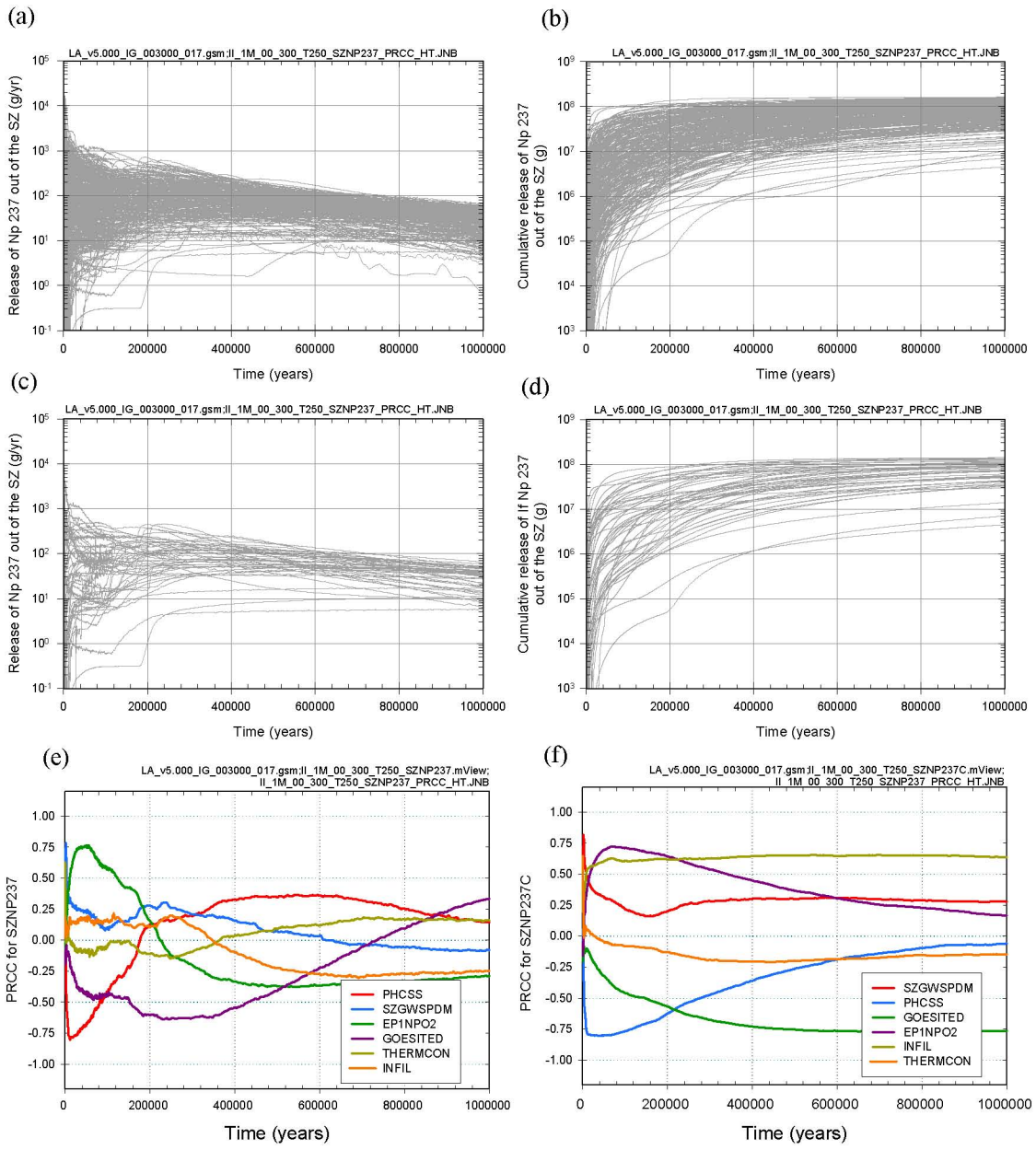

Source: Output DTNs: MO0709TSPAREGS.000 [DIRS 182976]; and MO0709TSPAPLOT.000 [DIRS 183010].

Figure K6.5.2-3. Time-dependent release rates (*SZNP237*, g/yr) and cumulative (i.e., integrated) releases (*SZNP237C*, g) over 1,000,000 years for the movement of dissolved ^{237}Np across a subsurface plane at the location of the RMEI resulting from an igneous intrusive event at 250 years that destroys all WPs in the repository: (a, b) *SZNP237* and *SZNP237C* for all (i.e., 300) sample elements, (c, d) *SZNP237* and *SZNP237C* for first 50 sample elements, and (e, f) PRCCs for *SZNP237* and *SZNP237C*

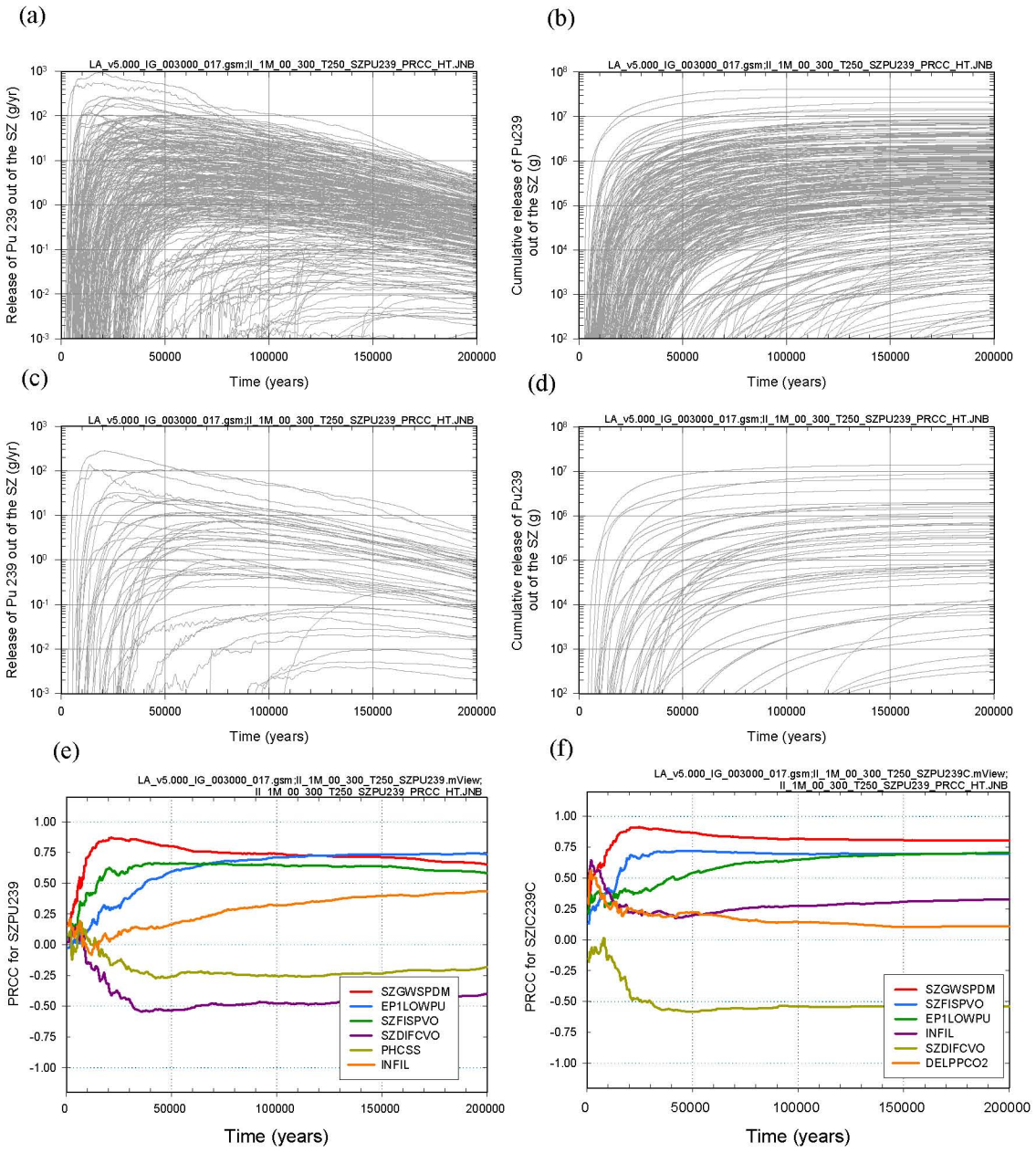

Source: Output DTNs: MO0709TSPAREGS.000 [DIRS 182976]; and MO0709TSPAPLOT.000 [DIRS 183010].

Figure K6.5.2-4. Time-dependent release rates (*SZPU239*, g/yr) and cumulative (i.e., integrated) releases (*SZPU239C*, g) over 200,000 years for the movement of dissolved ^{239}Pu across a subsurface plane at the location of the RMEI resulting from an igneous intrusive event at 250 years that destroys all WPs in the repository: (a, b) *SZPU239* and *SZPU239C* for all (i.e., 300) sample elements, (c, d) *SZPU239* and *SZPU239C* for first 50 sample elements, and (e, f) PRCCs for *SZPU239* and *SZPU239C*

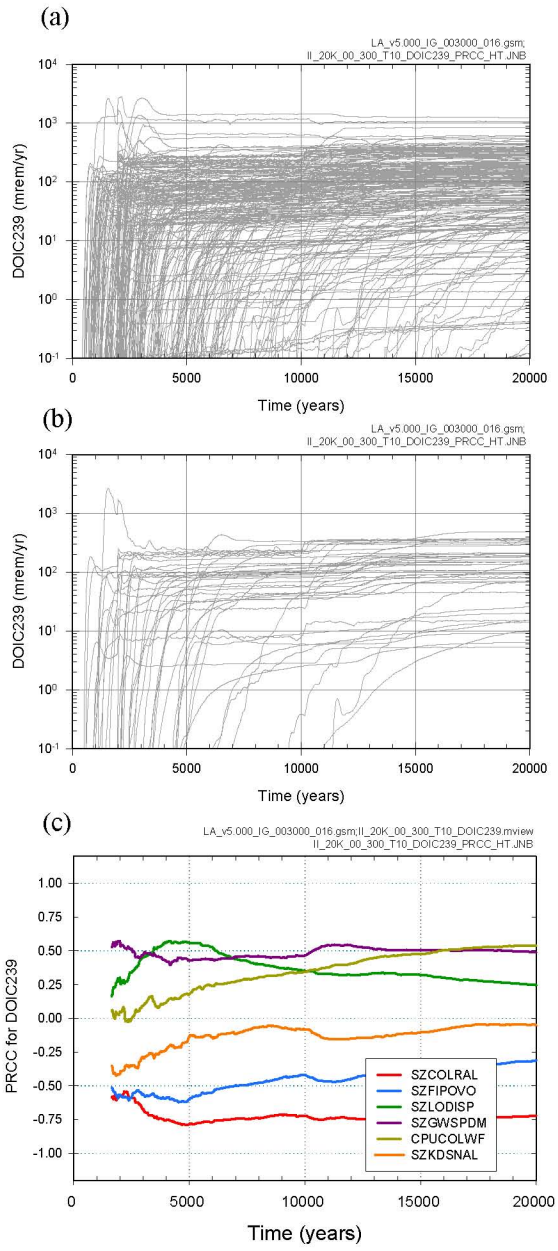

Source: Output DTNs: MO0709TSPAREGS.000 [DIRS 182976]; and MO0709TSPAPLOT.000 [DIRS 183010].

Figure K6.6.1-1. Time-dependent dose to the RMEI (*DOIC239*, mrem/yr) over 20,000 years for the movement of ^{239}Pu irreversibly attached to slow colloids across a subsurface plane at the location of the RMEI resulting from an igneous intrusive event at 10 years that destroys all WPs in the repository: (a) *DOIC239* for all (i.e., 300) sample elements, (b) *DOIC239* for first 50 sample elements, and (c) PRCCs for *DOIC239*

(a)

	DOIC239: 3000 yr			DOIC239: 5000 yr			DOIC239: 10,000 yr		
Step[a]	**Variable[b]**	**R^{2c}**	**SRRC[d]**	**Variable**	**R^2**	**SRRC**	**Variable**	**R^2**	**SRRC**
1	SZCOLRAL	0.26	-0.56	SZCOLRAL	0.32	-0.66	SZCOLRAL	0.26	-0.60
2	SZFIPOVO	0.39	-0.39	SZFIPOVO	0.44	-0.40	CPUCOLWF	0.33	0.26
3	SZGWSPDM	0.47	0.27	SZGWSPDM	0.51	0.28	SZGWSPDM	0.40	0.29
4	SZCOLRVO	0.49	-0.16	SZCOLRVO	0.53	-0.13	SZFIPOVO	0.45	-0.27
5	SZKDAMCO	0.51	0.17	INFIL	0.55	0.11	INFIL	0.50	0.18
6	INFIL	0.52	0.11	KDRASMEC	0.56	0.17	MICPU239	0.52	0.20
7	SZKDSRVO	0.53	0.11	CPUCOLWF	0.58	0.13	RUBMAXNL	0.55	-0.17
8	SZSREG1Y	0.55	0.11	RUBMAXNL	0.59	-0.10	SZSREG3Y	0.57	-0.11
9				MICPU239	0.61	0.16	KDRASMEC	0.58	0.12
10				UZFAG8	0.62	0.14	MICCL36	0.59	-0.12
11				MICI129	0.63	-0.12	SZKDPUVO	0.60	0.11
12				SZKDPUVO	0.64	0.11	SZKDSRAL	0.61	0.11
13				RHMUNO20	0.65	0.11	PH2MCONS	0.62	-0.10

a: Steps in stepwise rank regression analysis
b: Variables listed in order of selection in stepwise regression
c: Cumulative R^2 value with entry of each variable into regression model
d: Standardized rank regression coefficients (SRRCs) in final regression model

Source: Output DTNs: MO0709TSPAREGS.000 [DIRS 182976]; and MO0709TSPAPLOT.000 [DIRS 183010].

Figure K6.6.1-2. Stepwise rank regression analyses and selected scatterplots for time-dependent dose to the RMEI (*DOIC239*, mrem/yr) for the movement of ^{239}Pu irreversibly attached to slow colloids across a subsurface plane at the location of the RMEI (*SZIC239*, g/yr) resulting from an igneous intrusive event at 10 years that destroys all WPs in the repository: (a) Regressions for *DOIC239* at 3000, 5000 and 10,000 years, (b,c,d) Scatterplots for *DOIC239* at 10,000 years, and (e) Scatterplot comparing *SZIC239* and *DOIC239* at 10,000 years

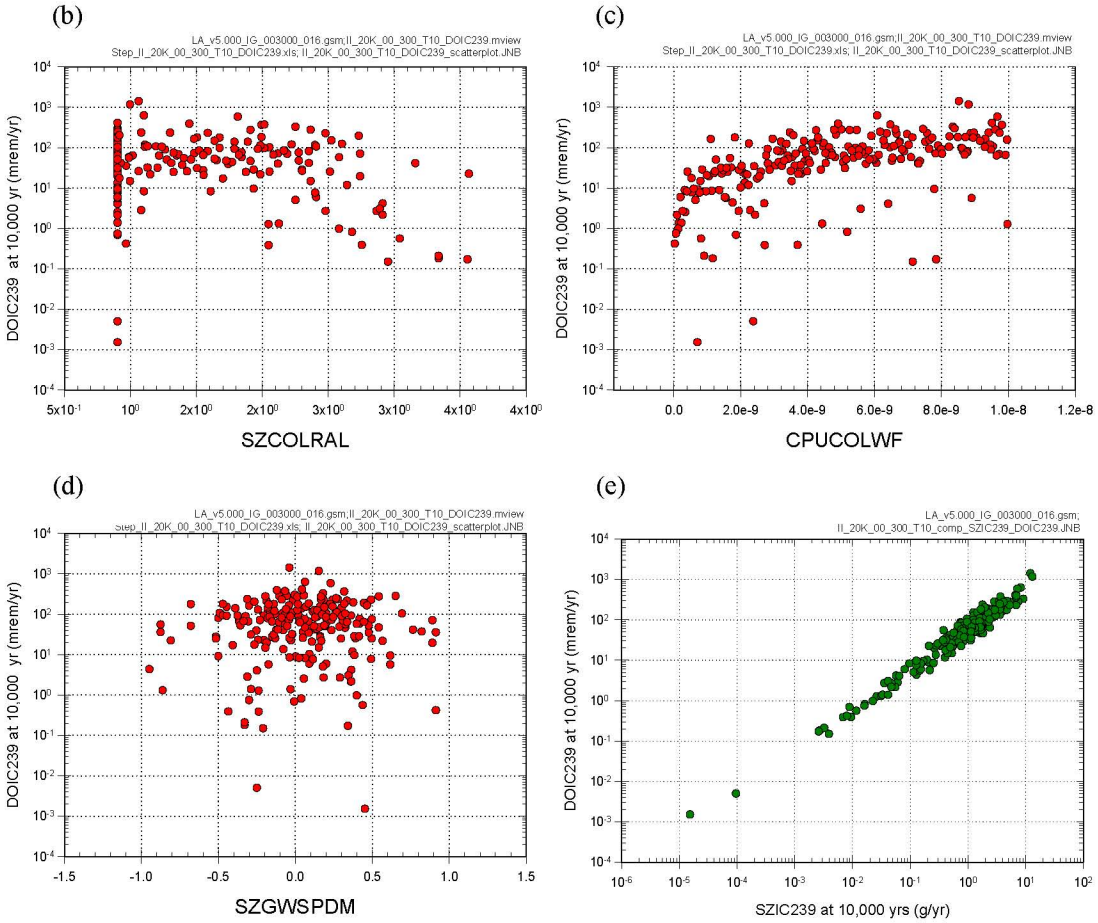

Source: Output DTNs: MO0709TSPAREGS.000 [DIRS 182976]; and MO0709TSPAPLOT.000 [DIRS 183010].

Figure K6.6.1-2. Stepwise rank regression analyses and selected scatterplots for time-dependent dose to the RMEI (*DOIC239*, mrem/yr) for the movement of ^{239}Pu irreversibly attached to slow colloids across a subsurface plane at the location of the RMEI (*SZIC239*, g/yr) resulting from an igneous intrusive event at 10 years that destroys all WPs in the repository: (a) Regressions for *DOIC239* at 3000, 5000 and 10,000 years, (b,c,d) Scatterplots for *DOIC239* at 10,000 years, and (e) Scatterplot comparing *SZIC239* and *DOIC239* at 10,000 years (continued)

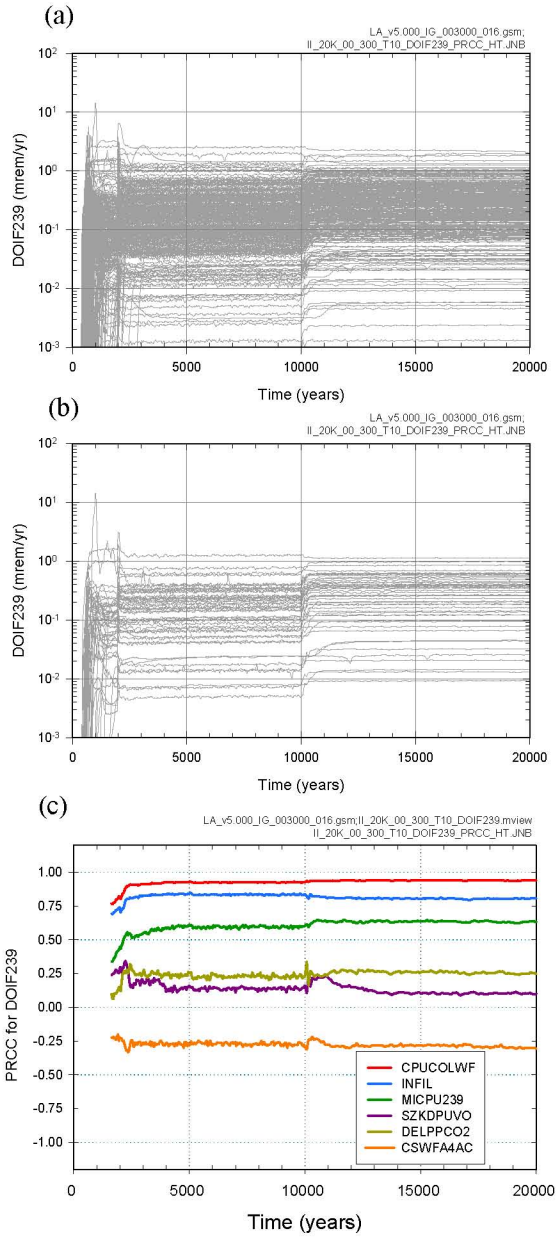

Source: Output DTNs: MO0709TSPAREGS.000 [DIRS 182976]; and MO0709TSPAPLOT.000 [DIRS 183010].

Figure K6.6.1-3. Time-dependent dose to the RMEI (*DOIF239*, mrem/yr) over 20,000 years for the movement of ^{239}Pu irreversibly attached to fast colloids across a subsurface plane at the location of the RMEI resulting from an igneous intrusive event at 10 years that destroys all WPs in the repository: (a) *DOIF239* for all (i.e., 300) sample elements, (b) *DOIF239* for first 50 sample elements, and (c) PRCCs for *DOIF239*

(a)

	DOIF239: 3000 yr			DOIF239: 5000 yr			DOIF239: 10,000 yr		
Step[a]	**Variable[b]**	**R^{2c}**	**SRRC[d]**	**Variable**	**R^2**	**SRRC**	**Variable**	**R^2**	**SRRC**
1	CPUCOLWF	0.52	0.69	CPUCOLWF	0.53	0.69	CPUCOLWF	0.54	0.70
2	INFIL	0.80	0.52	INFIL	0.81	0.51	INFIL	0.81	0.51
3	MICPU239	0.90	0.31	MICPU239	0.91	0.32	MICPU239	0.91	0.32
4	DWCSTERC	0.90	-0.05	DWCSTERC	0.92	-0.05	RUBMAXL	0.91	-0.04
5	DWCSTERB	0.91	-0.05	WPFLUX	0.92	0.05	DWCSTERC	0.92	-0.05
6	RUBMAXL	0.91	-0.05				WPFLUX	0.92	0.04

a: Steps in stepwise rank regression analysis
b: Variables listed in order of selection in stepwise regression
c: Cumulative R^2 value with entry of each variable into regression model
d: Standardized rank regression coefficients (SRRCs) in final regression model

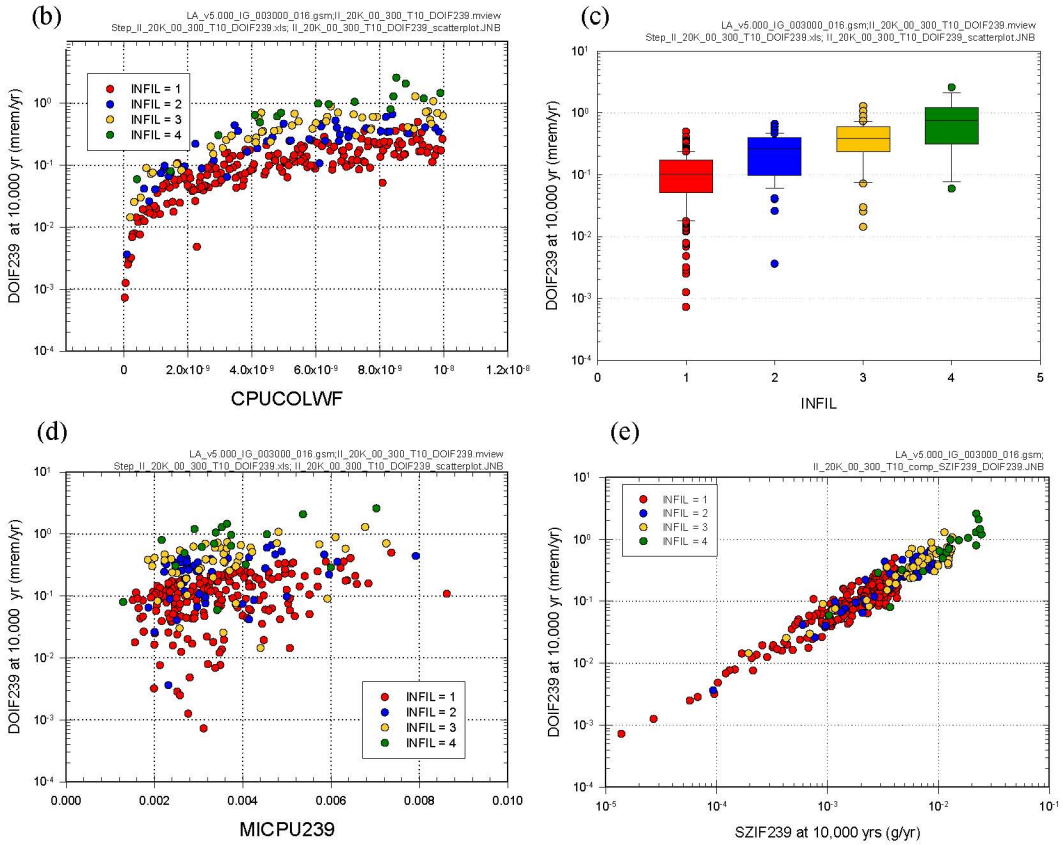

Source: Output DTNs: MO0709TSPAREGS.000 [DIRS 182976]; and MO0709TSPAPLOT.000 [DIRS 183010].

NOTE: In (c), the box extends from 0.25 to 0.75 quantile; lower and upper bar and whisker extend to 0.1 and 0.9 quantile, respectively; dots represent values outside 0.1 to 0.9 quantile range; median indicated by light horizontal line.

Figure K6.6.1-4. Stepwise rank regression analyses and selected scatterplots for time-dependent dose to the RMEI (*DOIF239*, mrem/yr) for the movement of ^{239}Pu irreversibly attached to fast colloids across a subsurface plane at the location of the RMEI (*SZIF239*, g/yr) resulting from an igneous intrusive event at 10 years that destroys all WPs in the repository: (a) Regressions for *DOIF239* at 3000, 5000 and 10,000 years, (b,c,d) Scatterplots for *DOIF239* at 10,000 years, and (e) Scatterplot comparing *SZIF239* and *DOIF239* at 10,000 years.

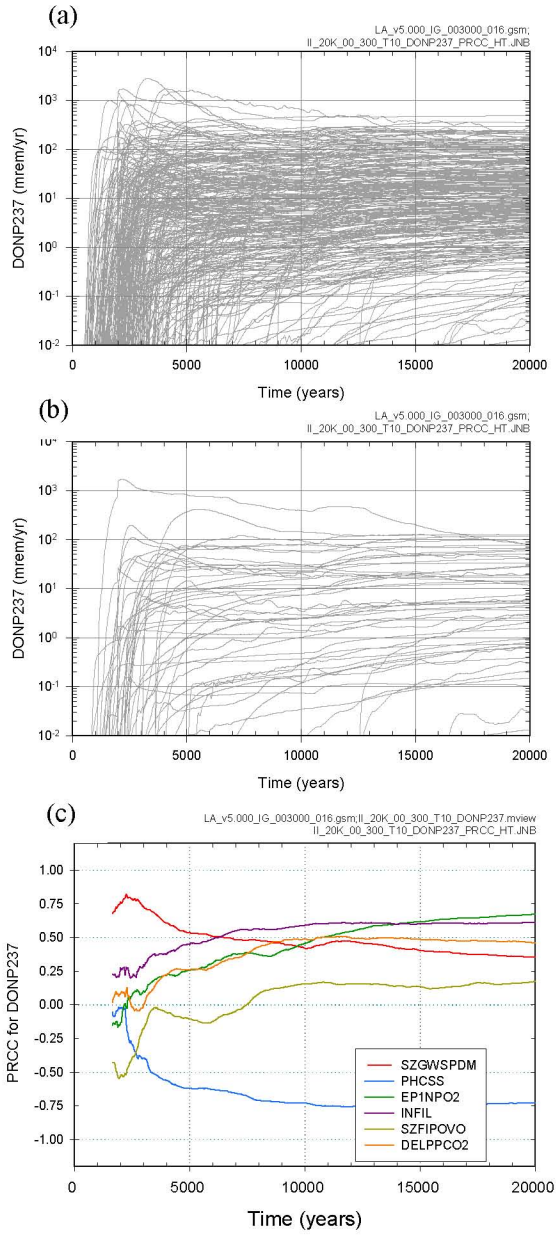

Source: Output DTNs: MO0709TSPAREGS.000 [DIRS 182976]; and MO0709TSPAPLOT.000 [DIRS 183010].

Figure K6.6.1-5. Time-dependent dose to the RMEI (*DONP237*, mrem/yr) over 20,000 years for the movement of dissolved ^{237}Np across a subsurface plane at the location of the RMEI resulting from an igneous intrusive event at 10 years that destroys all WPs in the repository: (a) *DONP237* for all (i.e., 300) sample elements, (b) *DONP237*for first 50 sample elements, and (c) PRCCs for *DONP237*

(a)

	DONP237: 3000 yr			DONP237: 5000 yr			DONP237: 10,000 yr		
Step[a]	**Variable[b]**	**R^{2c}**	**SRRC[d]**	**Variable**	**R^2**	**SRRC**	**Variable**	**R^2**	**SRRC**
1	SZGWSPDM	0.44	0.69	SZGWSPDM	0.18	0.44	PHCSS	0.19	-0.39
2	PHCSS	0.50	-0.23	PHCSS	0.33	-0.36	INFIL	0.40	0.42
3	INFIL	0.54	0.17	INFIL	0.45	0.32	EP1NPO2	0.47	0.29
4	SZFIPOVO	0.58	-0.19	SZFISPVO	0.48	0.21	SZGWSPDM	0.54	0.25
5	SZKDSEAL	0.60	-0.16	SZDIFCVO	0.51	-0.20	CORRATSS	0.58	-0.16
6	SZFISPVO	0.62	0.16	MICTH229	0.53	0.11	SZFISPVO	0.61	0.21
7	MICTH229	0.64	0.12	EP1LOWNU	0.55	0.14	MICNP237	0.64	0.17
8	SZDIFCVO	0.65	-0.14	DELPPCO2	0.57	0.14	DELPPCO2	0.66	0.16
9	WDGCA22	0.66	-0.11	EP1NPO2	0.58	0.14	EP1LOWAM	0.69	0.17
10	EP1LOWAM	0.68	0.11	SZKDUAL	0.59	-0.10	EP1LOWNU	0.70	0.14
11	SZPORUAL	0.69	-0.09	HLWDRACD	0.61	-0.12	SZDIFCVO	0.72	-0.12
12	WDLCRATE	0.69	0.09	EP1LOWAM	0.62	0.12	COLGW	0.73	0.11
13				SZKDCSVO	0.63	-0.10	SZKDNPVO	0.73	-0.09

a: Steps in stepwise rank regression analysis
b: Variables listed in order of selection in stepwise regression
c: Cumulative R^2 value with entry of each variable into regression model
d: Standardized rank regression coefficients (SRRCs) in final regression model

Source: Output DTNs: MO0709TSPAREGS.000 [DIRS 182976]; and MO0709TSPAPLOT.000 [DIRS 183010].

Figure K6.6.1-6. Stepwise rank regression analyses and selected scatterplots for time-dependent dose to the RMEI (*DONP237*, mrem/yr) for the movement of dissolved ^{237}Np across a subsurface plane at the location of the RMEI (*SZNP237*, g/yr) resulting from an igneous intrusive event at 10 years that destroys all WPs in the repository: (a) Regressions for *DONP237* at 3000, 5000 and 10,000 years, (b,c,d) Scatterplots for *DONP237* at 10,000 years, and (e) Scatterplot comparing *SZNP237* and *DONP237* at 10,000 years

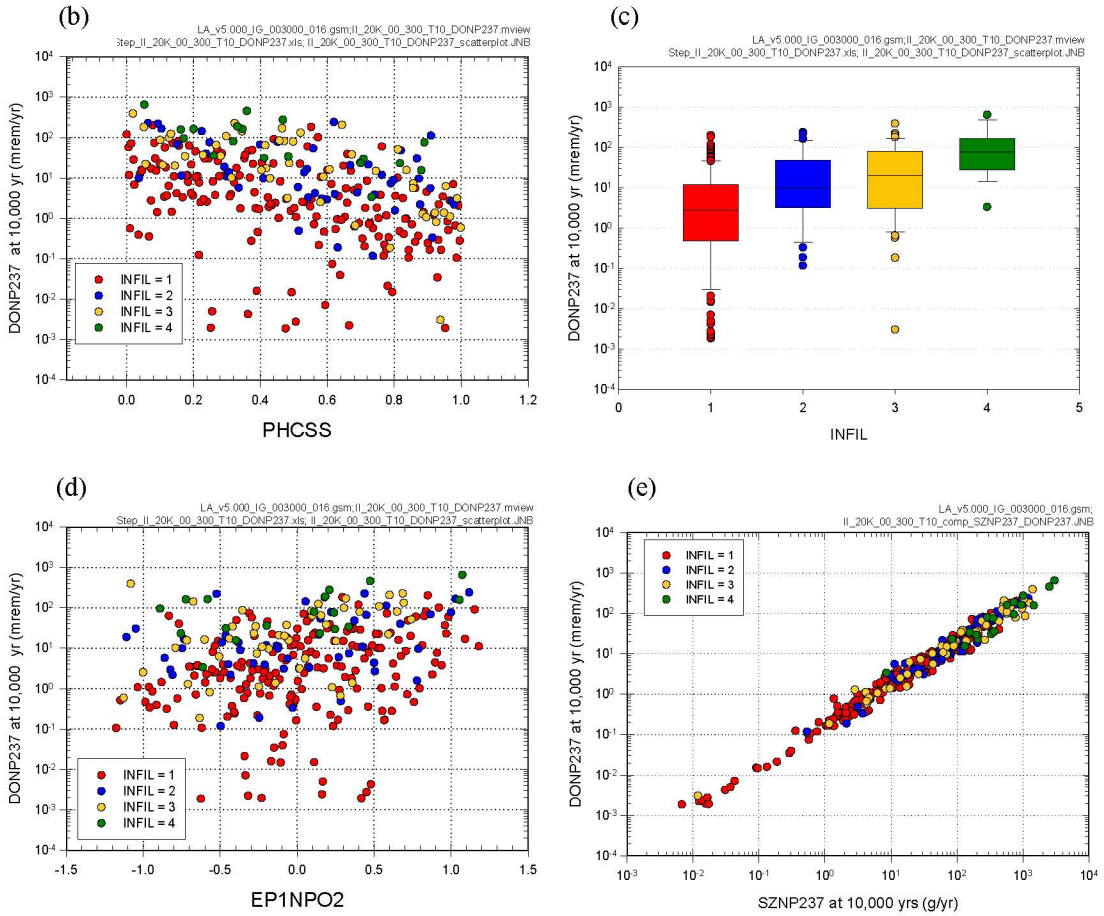

Source: Output DTNs: MO0709TSPAREGS.000 [DIRS 182976]; and MO0709TSPAPLOT.000 [DIRS 183010].

NOTE: In (c), the box extends from 0.25 to 0.75 quantile; lower and upper bar and whisker extend to 0.1 and 0.9 quantile, respectively; dots represent values outside 0.1 to 0.9 quantile range; median indicated by light horizontal line.

Figure K6.6.1-6. Stepwise rank regression analyses and selected scatterplots for time-dependent dose to the RMEI (*DONP237*, mrem/yr) for the movement of dissolved ^{237}Np across a subsurface plane at the location of the RMEI (*SZNP237*, g/yr) resulting from an igneous intrusive event at 10 years that destroys all WPs in the repository: (a) Regressions for *DONP237* at 3000, 5000 and 10,000 years, (b,c,d) Scatterplots for *DONP237* at 10,000 years, and (e) Scatterplot comparing *SZNP237* and *DONP237* at 10,000 years (continued).

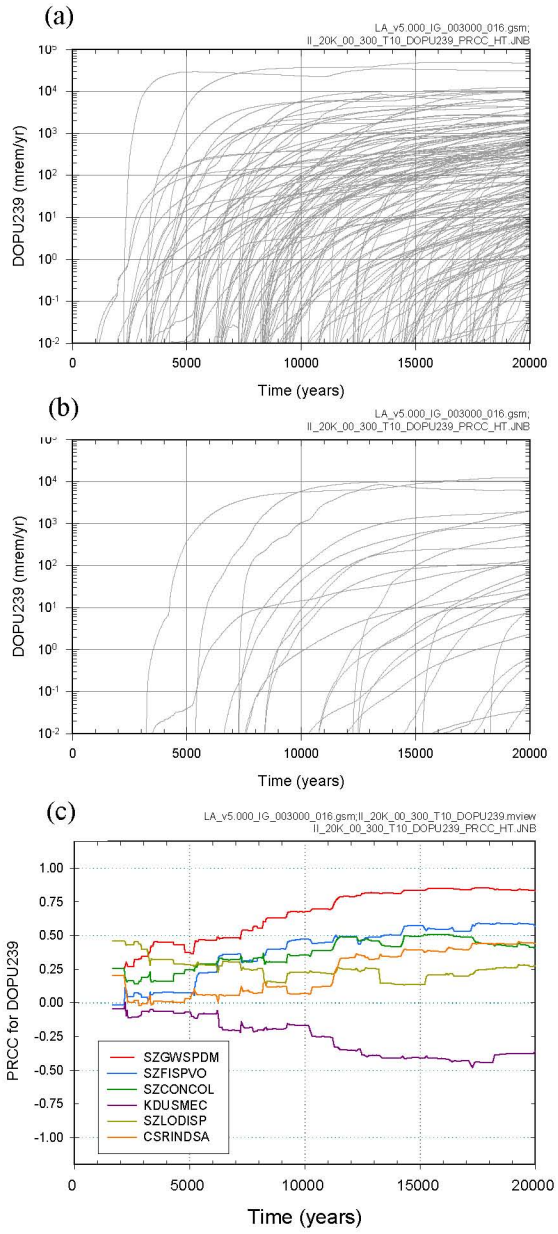

Source: Output DTNs: MO0709TSPAREGS.000 [DIRS 182976]; and MO0709TSPAPLOT.000 [DIRS 183010].

Figure K6.6.1-7. Time-dependent dose to the RMEI (*DOPU239*, mrem/yr) over 20,000 years for the movement of dissolved ^{239}Pu across a subsurface plane at the location of the RMEI resulting from an igneous intrusive event at 10 years that destroys all WPs in the repository: (a) *DOPU239* for all (i.e., 300) sample elements, (b) *DOPU239* for first 50 sample elements, and (c) PRCCs for *DOPU239*

(a)

	DOPU239: 3000 yr			DOPU239: 5000 yr			DOPU239: 10,000 yr		
Step[a]	**Variable[b]**	**R^{2c}**	**SRRC[d]**	**Variable**	**R^2**	**SRRC**	**Variable**	**R^2**	**SRRC**
1	SZGWSPDM	0.07	0.27	SZGWSPDM	0.12	0.35	SZGWSPDM	0.44	0.67
2	SZLODISP	0.11	0.23	SZLODISP	0.17	0.24	SZFISPVO	0.49	0.25
3	UZFAG9	0.13	0.16	SZKDCSCO	0.21	0.21	SZKDPUVO	0.53	-0.22
4	CSWFA1AK	0.15	-0.14	SZPORUAL	0.23	-0.16	SZPORUAL	0.55	-0.17
5				SZSREG1X	0.25	-0.17	SZCONCOL	0.58	0.14
6				SZKDPUVO	0.27	-0.19	SZLODISP	0.59	0.12
7				SZKDSNAL	0.30	-0.20	SZSREG1X	0.61	-0.12
8				DELPPCO2	0.32	-0.15	MICC14	0.62	-0.13
9				WDDSGC29	0.34	0.14	NIOSA	0.63	0.11
10				SZKDAMCO	0.36	0.13	CSRINDPO	0.64	0.10
11				CSWFA1AK	0.37	-0.13			

a: Steps in stepwise rank regression analysis
b: Variables listed in order of selection in stepwise regression
c: Cumulative R^2 value with entry of each variable into regression model
d: Standardized rank regression coefficients (SRRCs) in final regression model

Source: Output DTNs: MO0709TSPAREGS.000 [DIRS 182976]; and MO0709TSPAPLOT.000 [DIRS 183010].

Figure K6.6.1-8. Stepwise rank regression analyses and selected scatterplots for time-dependent dose to the RMEI (*DOPU239*, mrem/yr) for the movement of dissolved ^{239}Pu across a subsurface plane at the location of the RMEI (*SZPU239*, g/yr) resulting from an igneous intrusive event at 10 years that destroys all WPs in the repository: (a) Regressions for *DOPU239*at 3000, 5000 and 10,000 years, (b,c,d) Scatterplots for *DOPU239* at 10,000 years, and (e) Scatterplot comparing *SZPU239* and *DOPU239* at 10,000 years

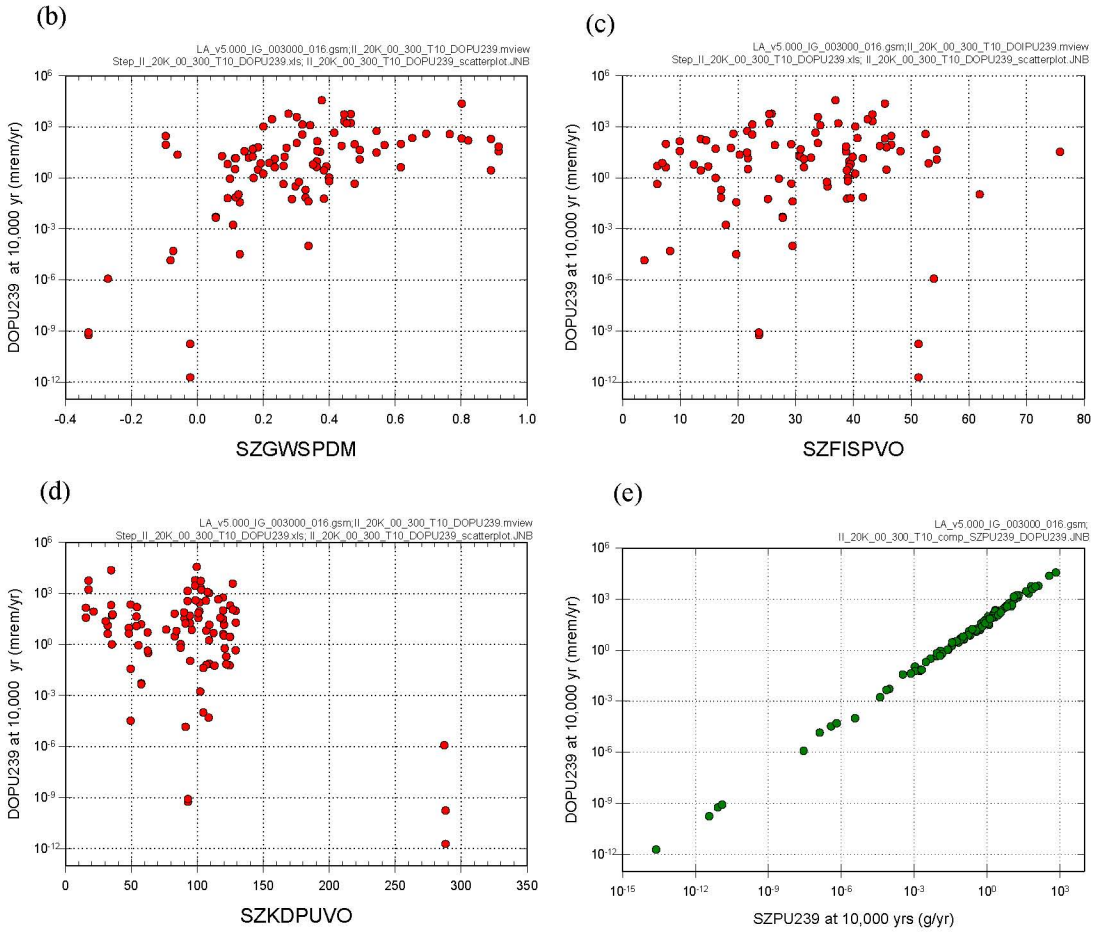

Source: Output DTNs: MO0709TSPAREGS.000 [DIRS 182976]; and MO0709TSPAPLOT.000 [DIRS 183010].

Figure K6.6.1-8. Stepwise rank regression analyses and selected scatterplots for time-dependent dose to the RMEI (*DOPU239*, mrem/yr) for the movement of dissolved ^{239}Pu across a subsurface plane at the location of the RMEI (*SZPU239*, g/yr) resulting from an igneous intrusive event at 10 years that destroys all WPs in the repository: (a) Regressions for *DOPU239*at 3000, 5000 and 10,000 years, (b,c,d) Scatterplots for *DOPU239* at 10,000 years, and (e) Scatterplot comparing *SZPU239* and *DOPU239* at 10,000 years (continued).

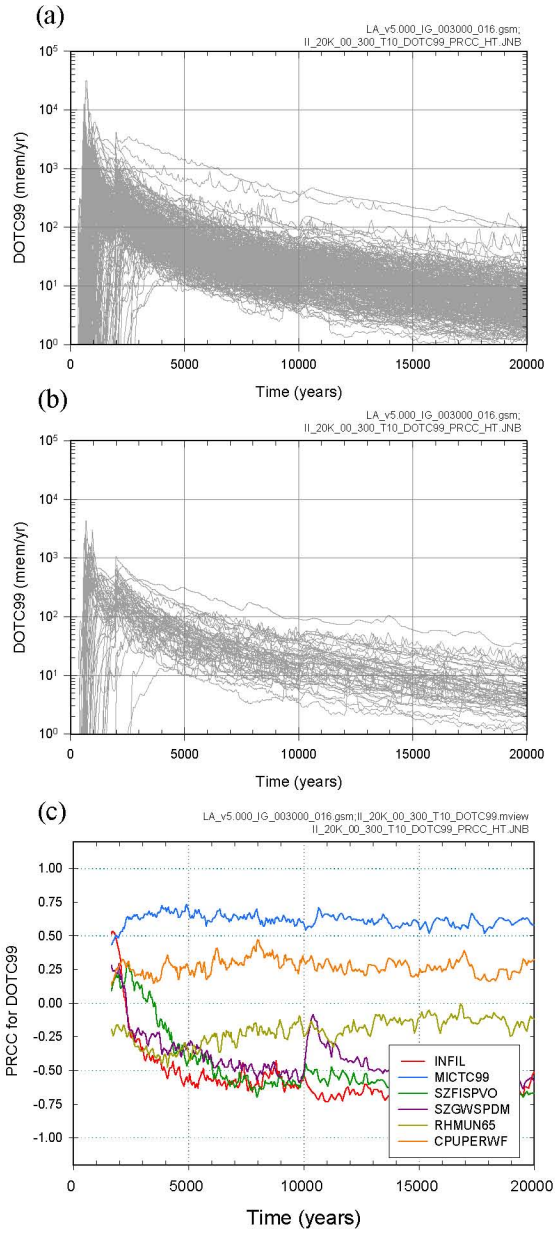

Source: Output DTNs: MO0709TSPAREGS.000 [DIRS 182976]; and MO0709TSPAPLOT.000 [DIRS 183010].

Figure K6.6.1-9. Time-dependent dose to the RMEI (*DOTC99*, mrem/yr) over 20,000 years for the movement of dissolved ^{99}Tc across a subsurface plane at the location of the RMEI resulting from an igneous intrusive event at 10 years that destroys all WPs in the repository: (a) *DOTC99* for all (i.e., 300) sample elements, (b) *DOTC99* for first 50 sample elements, and (c) PRCCs for *DOTC99*

(a)

	DOTC99: 3000 yr			DOTC99: 5000 yr			DOTC99: 10,000 yr		
Step[a]	**Variable[b]**	**R^{2c}**	**SRRC[d]**	**Variable**	**R^2**	**SRRC**	**Variable**	**R^2**	**SRRC**
1	MICTC99	0.39	0.64	MICTC99	0.35	0.61	MICTC99	0.29	0.57
2	INFIL	0.46	-0.28	INFIL	0.50	-0.39	INFIL	0.47	-0.43
3	CSNFMASS	0.52	0.24	SZGWSPDM	0.57	-0.26	SZGWSPDM	0.59	-0.33
4	UZFAG8	0.56	-0.21	CSNFMASS	0.61	0.21	SZFISPVO	0.64	-0.30
5	SZFIPOVO	0.58	0.19	SZFISPVO	0.64	-0.21	CSNFMASS	0.70	0.24
6	UZGAM	0.60	-0.14	SZDIFCVO	0.66	0.15	SZDIFCVO	0.72	0.13
7	SZGWSPDM	0.61	-0.11	SZFIPOVO	0.67	0.15	KDRACOL	0.73	0.09
8				UZFAG8	0.68	-0.11	SZCOLRVO	0.73	-0.08
9				UZGAM	0.69	-0.11			
10				IS2DHLNS	0.70	-0.09			

a: Steps in stepwise rank regression analysis
b: Variables listed in order of selection in stepwise regression
c: Cumulative R^2 value with entry of each variable into regression model
d: Standardized rank regression coefficients (SRRCs) in final regression model

Source: Output DTNs: MO0709TSPAREGS.000 [DIRS 182976]; and MO0709TSPAPLOT.000 [DIRS 183010].

Figure K6.6.1-10. Stepwise rank regression analyses and selected scatterplots for time-dependent dose to the RMEI (*DOTC99*, mrem/yr) for the movement of dissolved ^{99}Tc across a subsurface plane at the location of the RMEI (*SZTC99*, g/yr) resulting from an igneous intrusive event at 10 years that destroys all WPs in the repository: (a) Regressions for *DOTC99* at 3000, 5000 and 10,000 years, (b,c,d) Scatterplots for *DOTC99* at 10,000 years, and (e) Scatterplot comparing *SZTC99* and *DOTC99* at 10,000 years

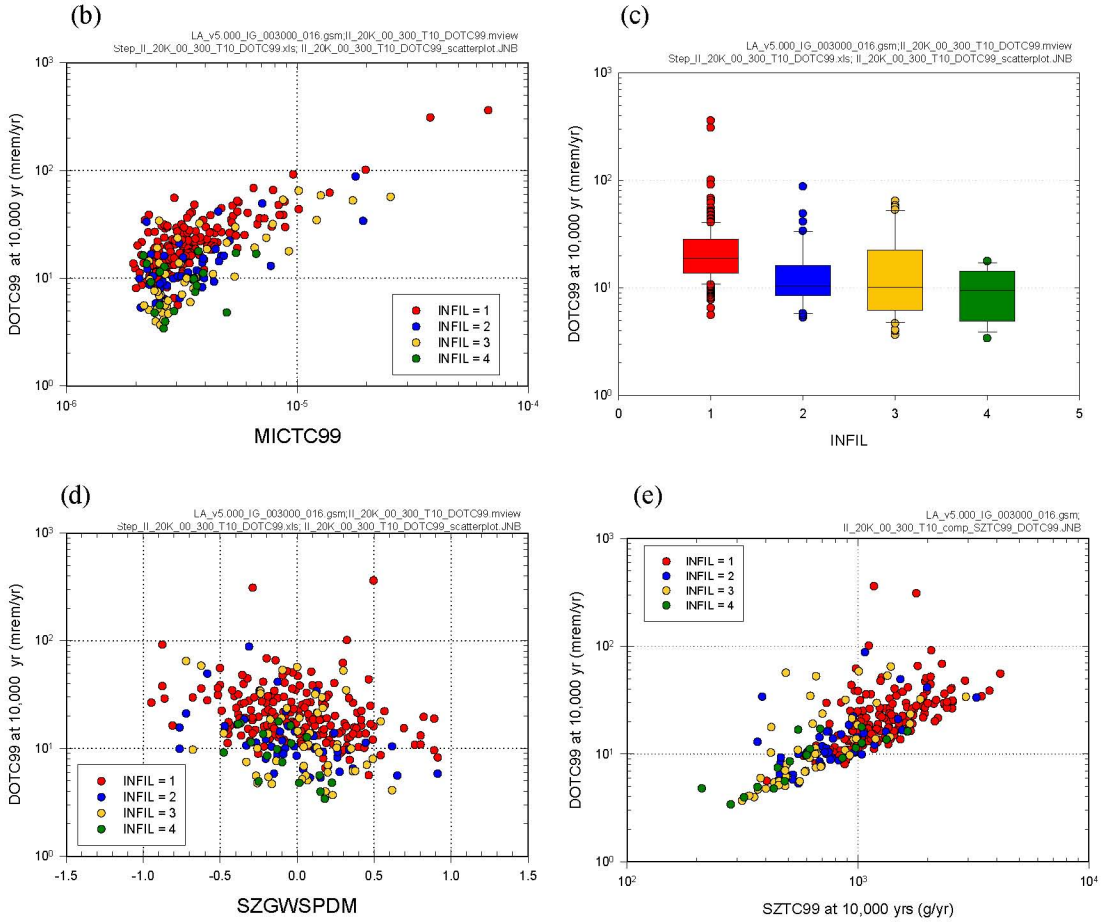

Source: Output DTNs: MO0709TSPAREGS.000 [DIRS 182976]; and MO0709TSPAPLOT.000 [DIRS 183010].

NOTE: In (c), the box extends from 0.25 to 0.75 quantile; lower and upper bar and whisker extend to 0.1 and 0.9 quantile, respectively; dots represent values outside 0.1 to 0.9 quantile range; median indicated by light horizontal line.

Figure K6.6.1-10. Stepwise rank regression analyses and selected scatterplots for time-dependent dose to the RMEI (*DOTC99*, mrem/yr) for the movement of dissolved ^{99}Tc across a subsurface plane at the location of the RMEI (*SZTC99*, g/yr) resulting from an igneous intrusive event at 10 years that destroys all WPs in the repository: (a) Regressions for *DOTC99* at 3000, 5000 and 10,000 years, (b,c,d) Scatterplots for *DOTC99* at 10,000 years, and (e) Scatterplot comparing *SZTC99* and *DOTC99* at 10,000 years (continued).

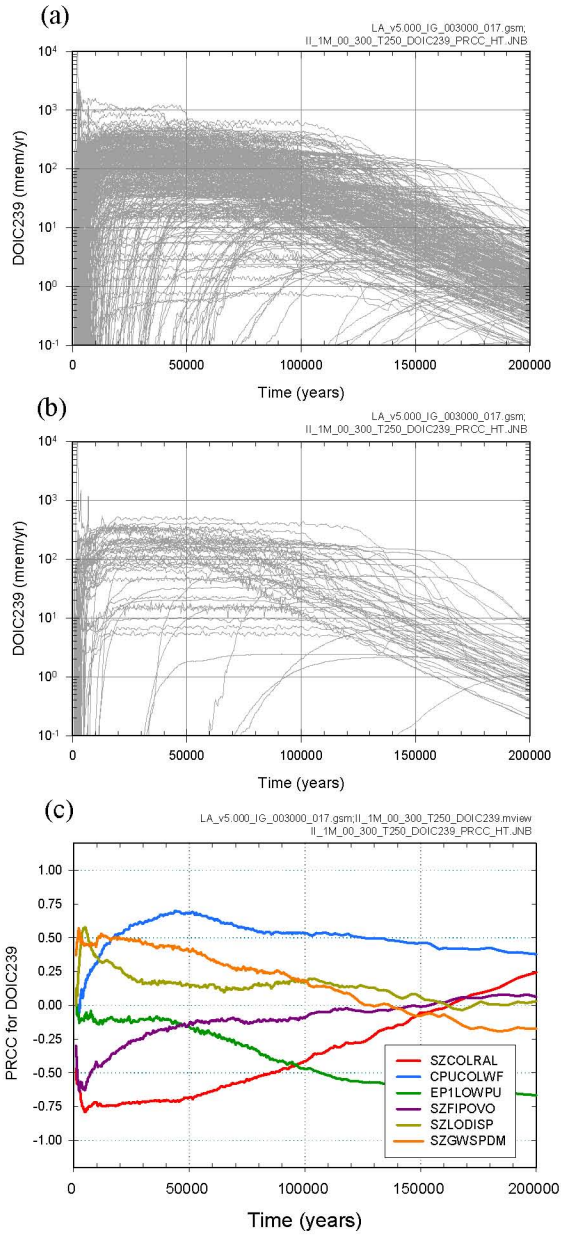

Source: Output DTNs: MO0709TSPAREGS.000 [DIRS 182976]; and MO0709TSPAPLOT.000 [DIRS 183010].

Figure K6.6.2-1. Time-dependent dose to the RMEI (*DOIC239*, mrem/yr) over 200,000 years for the movement of ^{239}Pu irreversibly attached to slow colloids across a subsurface plane at the location of the RMEI resulting from an igneous intrusive event at 250 years that destroys all WPs in the repository: (a) *DOIC239* for all (i.e., 300) sample elements, (b) *DOIC239* for first 50 sample elements, and (c) PRCCs for *DOIC239*

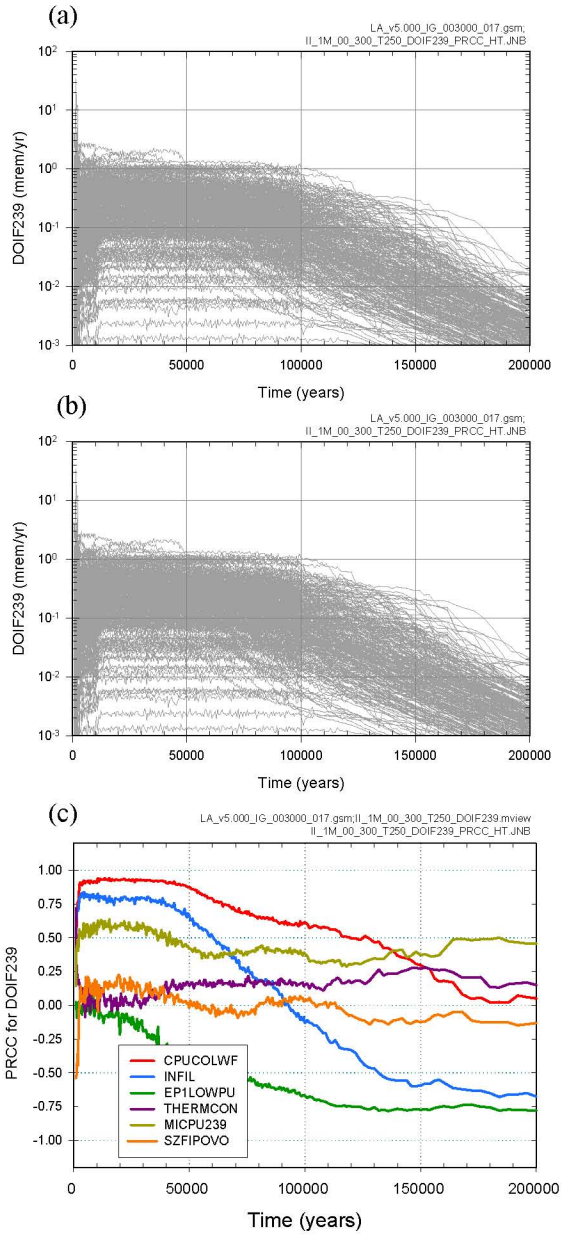

Source: Output DTNs: MO0709TSPAREGS.000 [DIRS 182976]; and MO0709TSPAPLOT.000 [DIRS 183010].

Figure K6.6.2-2. Time-dependent dose to the RMEI (*DOIF239*, mrem/yr) over 200,000 years for the movement of ^{239}Pu irreversibly attached to fast colloids across a subsurface plane at the location of the RMEI resulting from an igneous intrusive event at 250 years that destroys all WPs in the repository: (a) *DOIF239* for all (i.e., 300) sample elements, (b) *DOIF239* for first 50 sample elements, and (c) PRCCs for *DOIF239*

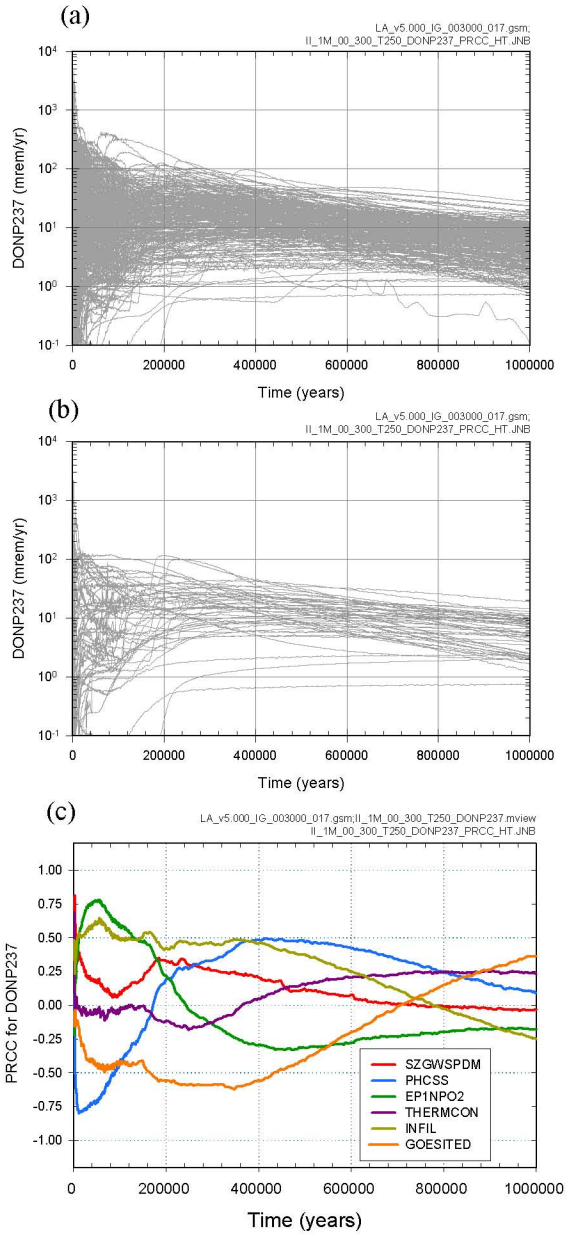

Source: Output DTNs: MO0709TSPAREGS.000 [DIRS 182976]; and MO0709TSPAPLOT.000 [DIRS 183010].

Figure K6.6.2-3. Time-dependent dose to the RMEI (*DONP237*, mrem/yr) over 1,000,000 years for the movement of dissolved ^{237}Np across a subsurface plane at the location of the RMEI resulting from an igneous intrusive event at 250 years that destroys all WPs in the repository: (a) *DONP237*for all (i.e., 300) sample elements, (b) *DONP237*for first 50 sample elements, and (c) PRCCs for *DONP237*

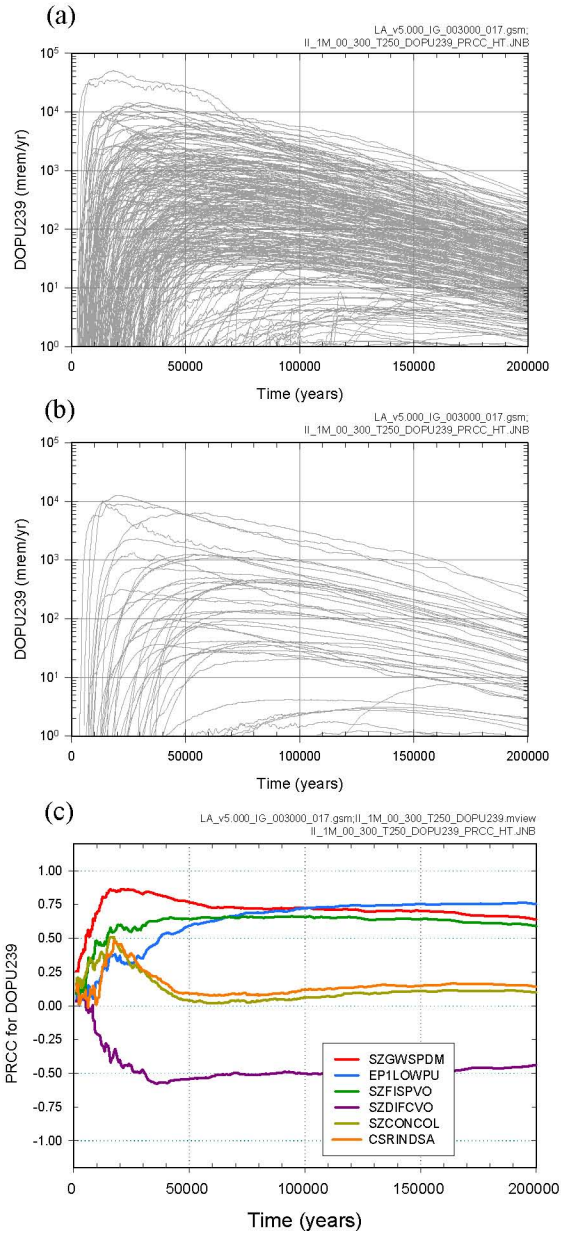

Source: Output DTNs: MO0709TSPAREGS.000 [DIRS 182976]; and MO0709TSPAPLOT.000 [DIRS 183010].

Figure K6.6.2-4. Time-dependent dose to the RMEI (*DOPU239*, mrem/yr) over 200,000 years for the movement of dissolved ^{239}Pu across a subsurface plane at the location of the RMEI resulting from an igneous intrusive event at 250 years that destroys all WPs in the repository: (a) *DOPU239* for all (i.e., 300) sample elements, (b) *DOPU239* for first 50 sample elements, and (c) PRCCs for *DOPU239*

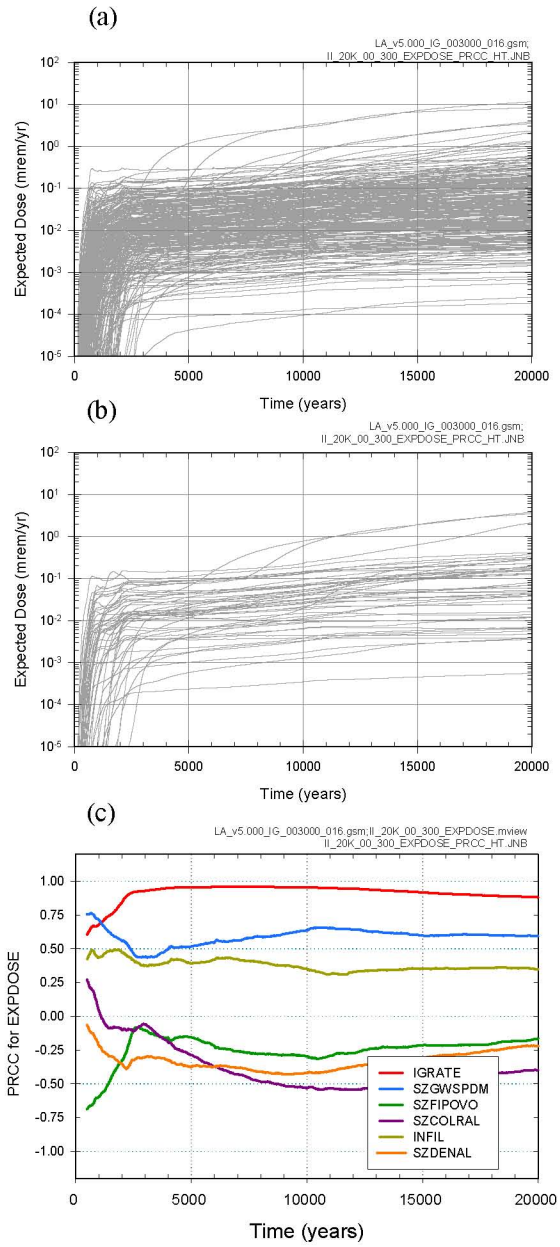

Source: Output DTNs: MO0709TSPAREGS.000 [DIRS 182976]; and MO0709TSPAPLOT.000 [DIRS 183010].

Figure K6.7.1-1. Expected dose to RMEI (*EXPDOSE*, mrem/yr) over [0, 20,000 yr] for all radioactive species resulting from igneous intrusion: (a) *EXPDOSE* for all (i.e., 300) sample elements, (b) *EXPDOSE* for first 50 sample elements, and (c) PRCCs for *EXPDOSE*

(a)

	EXPDOSE: 3000 yr			EXPDOSE: 5000 yr			EXPDOSE: 10,000 yr		
Step[a]	**Variable[b]**	**R^{2c}**	**SRRC[d]**	**Variable**	**R^2**	**SRRC**	**Variable**	**R^2**	**SRRC**
1	IGRATE	0.74	0.88	IGRATE	0.80	0.90	IGRATE	0.78	0.90
2	SZGWSPDM	0.79	0.21	SZGWSPDM	0.84	0.18	SZGWSPDM	0.83	0.21
3	INFIL	0.83	0.17	MICTC99	0.87	0.14	MICTC99	0.85	0.12
4	MICTC99	0.86	0.16	INFIL	0.89	0.16	INFIL	0.86	0.12
5	SZFISPVO	0.87	0.13	SZFISPVO	0.90	0.07	CPUCOLWF	0.87	0.10
6	CSNFMASS	0.88	0.09	MICC14	0.90	0.08	SZCOLRAL	0.88	-0.11
7	SZDIFCVO	0.88	-0.09	CSNFMASS	0.91	0.07	SZFISPVO	0.89	0.08
8	MICC14	0.89	0.08	SZFIPOVO	0.91	-0.06	MICPU239	0.90	0.09
9	SZCOLRVO	0.89	-0.06	MICNP237	0.92	0.07	SZFIPOVO	0.90	-0.08
10	MICNP237	0.90	0.07	SZCOLRAL	0.92	-0.07	SZDENAL	0.91	-0.08
11	SZSREG3Y	0.90	-0.05	SZDENAL	0.93	-0.06	EP1NPO2	0.91	0.06
12	SZFIPOVO	0.90	-0.05	CPUCOLWF	0.93	0.06	BCKRA226	0.91	-0.06
13	ISCSNS	0.90	0.05	KDPUSMEC	0.93	0.05	MICC14	0.92	0.05
14	KDSNCOL	0.91	0.05	BCKRA226	0.93	-0.05			
15				SZSREG3Y	0.93	-0.04			

a: Steps in stepwise rank regression analysis
b: Variables listed in order of selection in stepwise regression
c: Cumulative R^2 value with entry of each variable into regression model
d: Standardized rank regression coefficients (SRRCs) in final regression model

Source: Output DTNs: MO0709TSPAREGS.000 [DIRS 182976]; and MO0709TSPAPLOT.000 [DIRS 183010].

Figure K6.7.1-2. Stepwise rank regression analyses and selected scatterplots for expected dose to RMEI (*EXPDOSE*, mrem/yr) over [0, 20,000 yr] for all radioactive species resulting from igneous intrusion: (a) Regressions for *EXPDOSE* at 3000, 5000 and 10,000 years, and (b,c,d) Scatterplots for *EXPDOSE* at 10,000 years

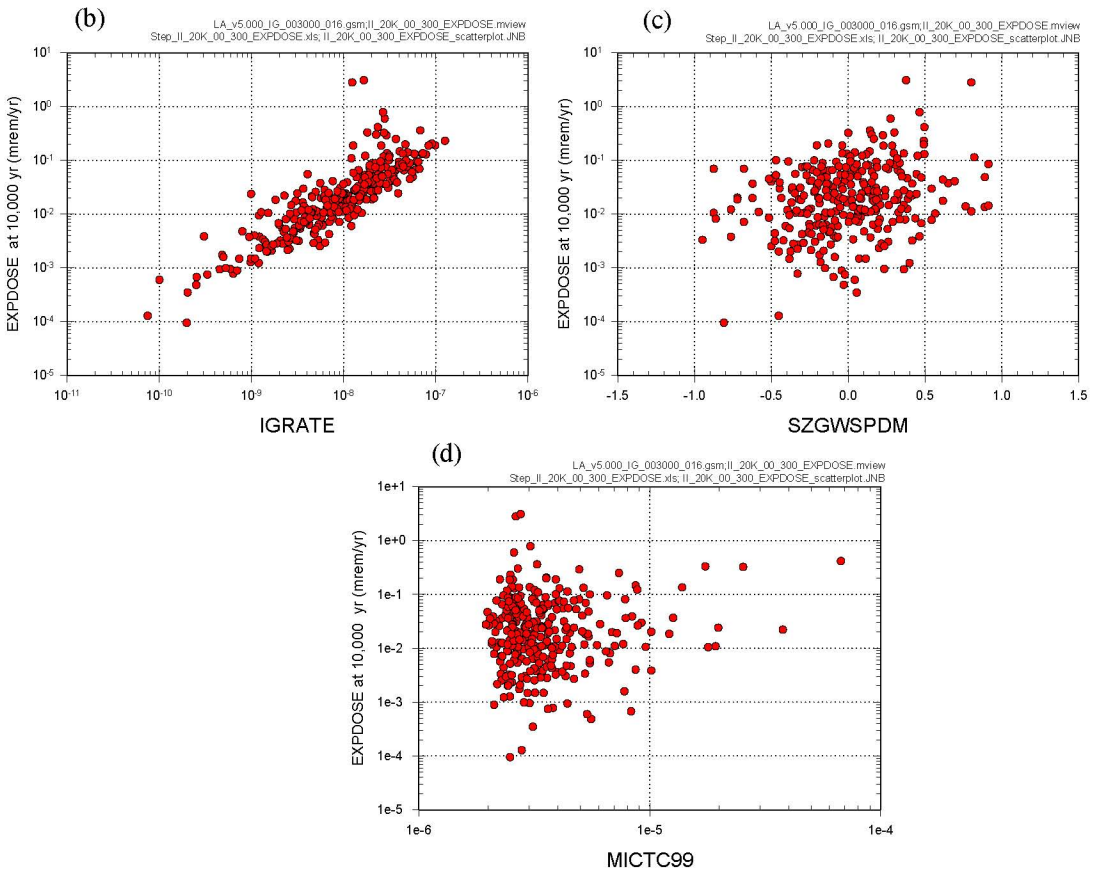

Source: Output DTNs: MO0709TSPAREGS.000 [DIRS 182976]; and MO0709TSPAPLOT.000 [DIRS 183010].

Figure K6.7.1-2. Stepwise rank regression analyses and selected scatterplots for expected dose to RMEI (*EXPDOSE*, mrem/yr) over [0, 20,000 yr] for all radioactive species resulting from igneous intrusion: (a) Regressions for *EXPDOSE* at 3000, 5000 and 10,000 years, and (b,c,d) Scatterplots for *EXPDOSE* at 10,000 years (continued).

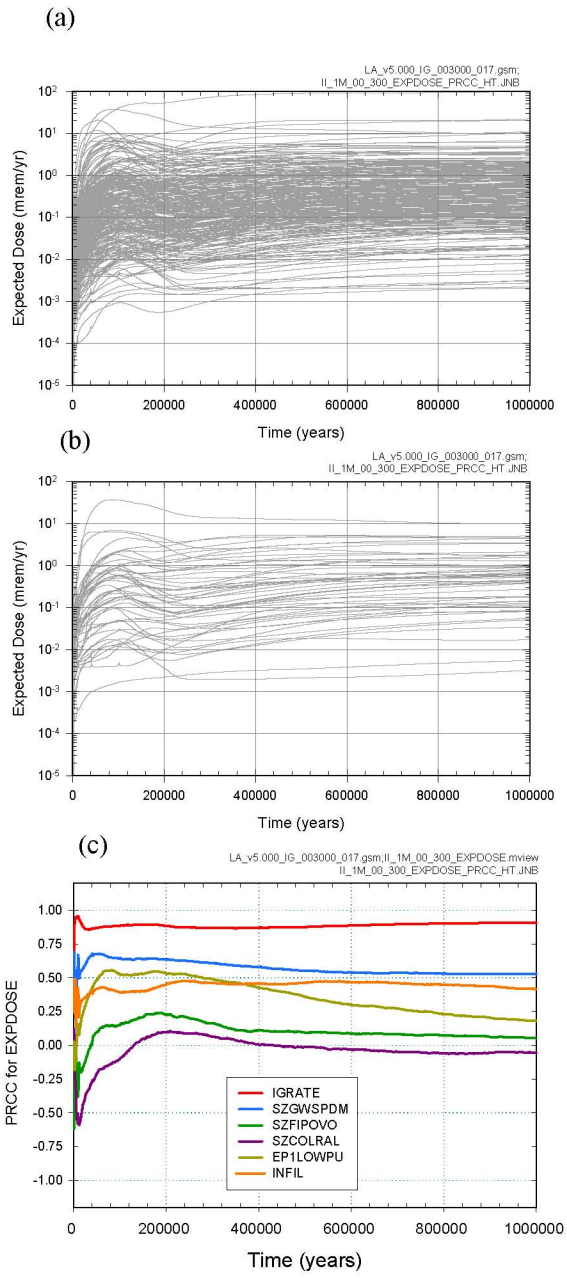

Source: Output DTNs: MO0709TSPAREGS.000 [DIRS 182976]; and MO0709TSPAPLOT.000 [DIRS 183010].

Figure K6.7.2-1. Expected dose to RMEI (*EXPDOSE*, mrem/yr) over [0, 1,000,000 yr] for all radioactive species resulting from igneous intrusion: (a) *EXPDOSE* for all (i.e., 300) sample elements, (b) *EXPDOSE* for first 50 sample elements, and (c) PRCCs for *EXPDOSE*

(a)

	EXPDOSE: 50,000 yr			EXPDOSE: 200,000 yr			EXPDOSE: 500,000 yr		
Step[a]	**Variable[b]**	**R^{2c}**	**SRRC[d]**	**Variable**	**R^2**	**SRRC**	**Variable**	**R^2**	**SRRC**
1	IGRATE	0.52	0.73	IGRATE	0.55	0.75	IGRATE	0.59	0.77
2	SZGWSPDM	0.69	0.39	SZGWSPDM	0.69	0.34	SZGWSPDM	0.68	0.30
3	EP1LOWPU	0.74	0.19	INFIL	0.73	0.19	INFIL	0.73	0.19
4	INFIL	0.77	0.18	EP1LOWPU	0.76	0.19	SZFISPVO	0.75	0.15
5	EP1NPO2	0.78	0.12	SZFISPVO	0.79	0.16	EP1LOWNU	0.77	0.13
6	CPUCOLWF	0.80	0.12	MICNP237	0.80	0.11	EP1LOWPU	0.79	0.15
7	MICNP237	0.81	0.12	EP1LOWNU	0.81	0.10	MICNP237	0.80	0.12
8	SZFISPVO	0.82	0.09	SZDIFCVO	0.82	-0.10	SZCONCOL	0.81	0.08
9	KDRASMEC	0.83	0.07	EP1NPO2	0.83	0.10	GOESITED	0.82	-0.09
10	EP2HICAM	0.84	0.07	SZCONCOL	0.83	0.08	SZDIFCVO	0.83	-0.09
11	SZKDSEAL	0.84	-0.12	GOESITED	0.84	-0.09	SZWBNDAL	0.83	-0.08
12	SZKDAMAL	0.84	0.08	HFOSA	0.85	-0.08	SZKDRAAL	0.84	-0.07
13	PH2RGER	0.85	-0.08	SZKDAMCO	0.85	0.07	KDPUSMEC	0.84	0.06
14	SZKDUVO	0.85	0.09				WDGCUA22	0.84	0.07

a: Steps in stepwise rank regression analysis
b: Variables listed in order of selection in stepwise regression
c: Cumulative R^2 value with entry of each variable into regression model
d: Standardized rank regression coefficients (SRRCs) in final regression model

Source: Output DTNs: MO0709TSPAREGS.000 [DIRS 182976]; and MO0709TSPAPLOT.000 [DIRS 183010].

Figure K6.7.2-2. Stepwise rank regression analyses and selected scatterplots for expected dose to RMEI (*EXPDOSE*, mrem/yr) over [0, 1,000,000 yr] for all radioactive species resulting from igneous intrusion: (a) Regressions for *EXPDOSE* at 50,000, 200,000 and 500,000 years, and (b,c,d) Scatterplots for *EXPDOSE* at 500,000 years

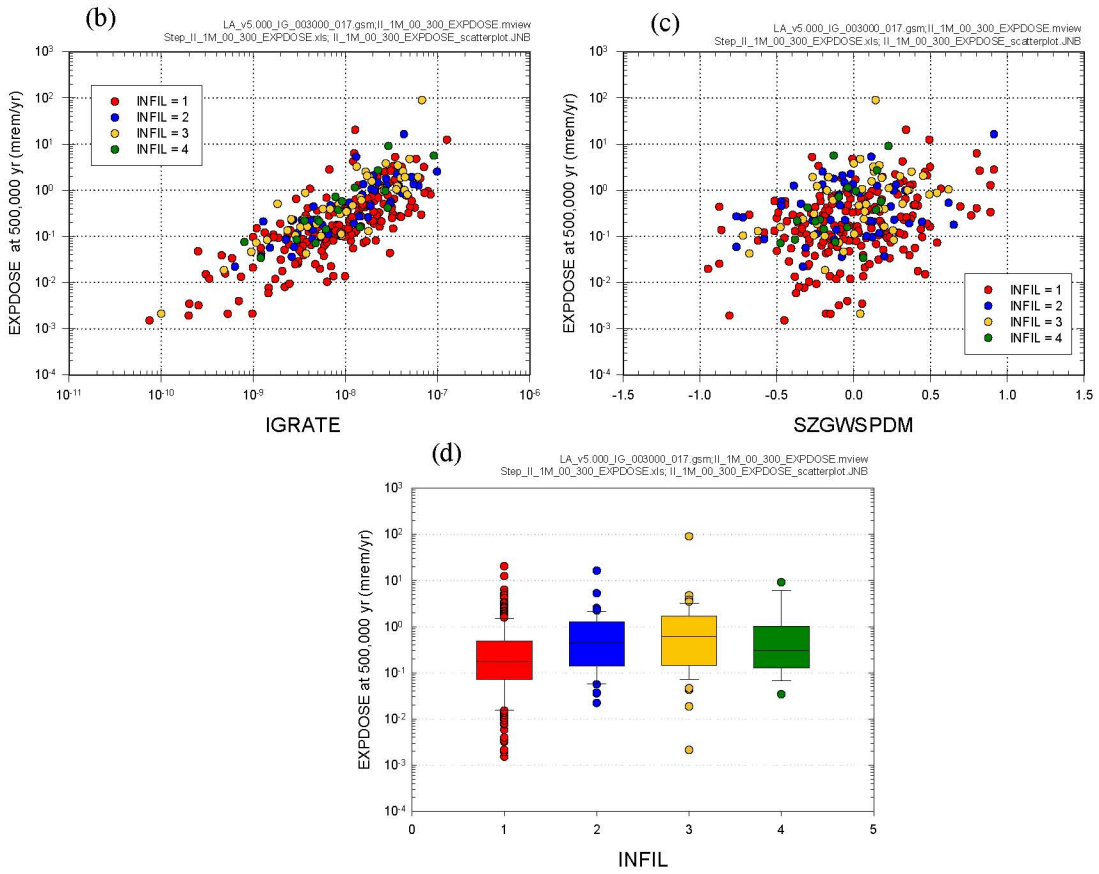

Source: Output DTNs: MO0709TSPAREGS.000 [DIRS 182976]; and MO0709TSPAPLOT.000 [DIRS 183010].

NOTE: In (d), the box extends from 0.25 to 0.75 quantile; lower and upper bar and whisker extend to 0.1 and 0.9 quantile, respectively; dots represent values outside 0.1 to 0.9 quantile range; median indicated by light horizontal line.

Figure K6.7.2-2. Stepwise rank regression analyses and selected scatterplots for expected dose to RMEI (*EXPDOSE*, mrem/yr) over [0, 1,000,000 yr] for all radioactive species resulting from igneous intrusion: (a) Regressions for *EXPDOSE* at 50,000, 200,000 and 500,000 years, and (b,c,d) Scatterplots for *EXPDOSE* at 500,000 years (continued).

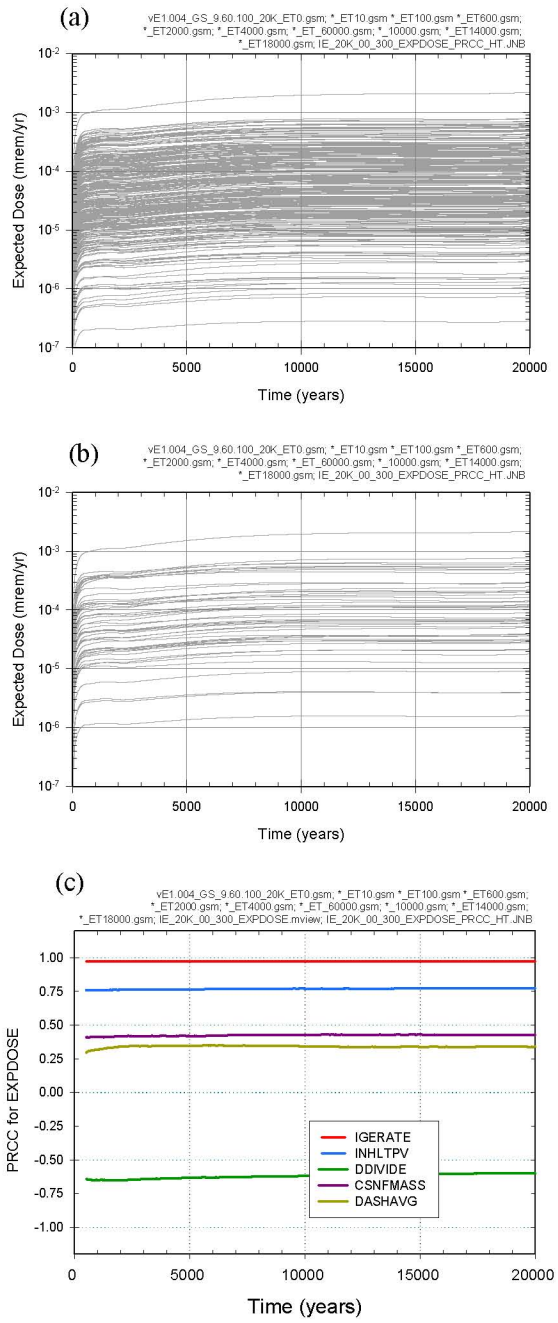

Source: Output DTNs: MO0709TSPAREGS.000 [DIRS 182976]; and MO0709TSPAPLOT.000 [DIRS 183010].

Figure K6.8.1-1. Expected dose to RMEI (*EXPDOSE*, mrem/yr) over [0, 20,000 yr] for all radioactive species resulting from igneous eruption: (a) *EXPDOSE* for all (i.e., 300) sample elements, (b) *EXPDOSE* for first 50 sample elements, and (c) PRCCs for *EXPDOSE*

(a)

	EXPDOSE: 3000 yr			EXPDOSE: 5000 yr			EXPDOSE: 10,000 yr		
Step[a]	Variable[b]	R^{2c}	SRRC[d]	Variable	R^2	SRRC	Variable	R^2	SRRC
1	IGERATE	0.76	0.87	IGERATE	0.76	0.87	IGERATE	0.76	0.87
2	INHLTPV	0.91	0.38	INHLTPV	0.91	0.38	INHLTPV	0.91	0.38
3	DDIVIDE	0.94	-0.17	DDIVIDE	0.94	-0.17	DDIVIDE	0.94	-0.16
4	CSNFMASS	0.95	0.10	CSNFMASS	0.95	0.10	CSNFMASS	0.95	0.10
5	DASHAVG	0.95	0.09	DASHAVG	0.95	0.09	DASHAVG	0.95	0.08

a: Steps in stepwise rank regression analysis
b: Variables listed in order of selection in stepwise regression
c: Cumulative R^2 value with entry of each variable into regression model
d: Standardized rank regression coefficients (SRRCs) in final regression model

(b)

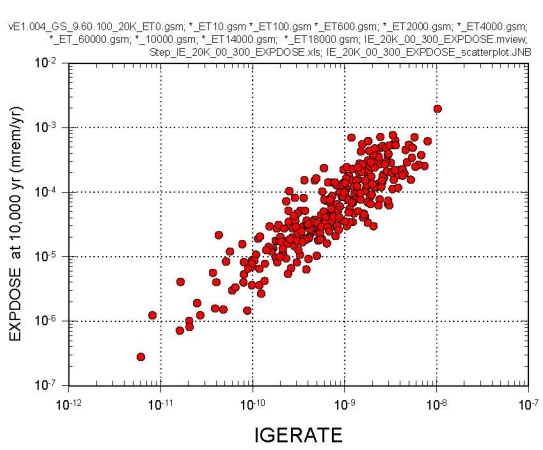

(c)

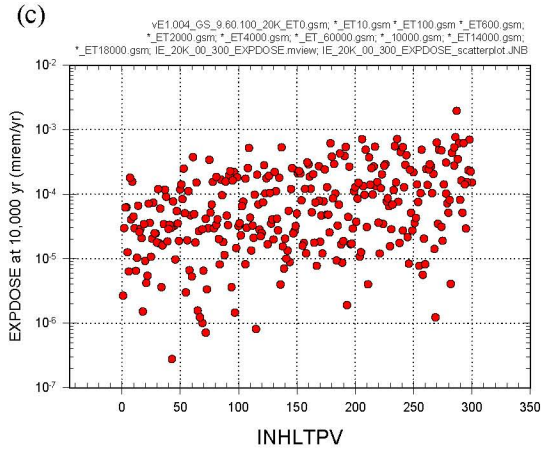

(d)

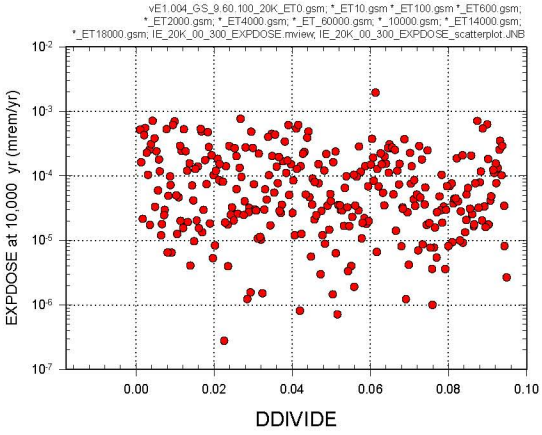

Source: Output DTNs: MO0709TSPAREGS.000 [DIRS 182976]; and MO0709TSPAPLOT.000 [DIRS 183010].

Figure K6.8.1-2. Stepwise rank regression analyses and selected scatterplots for expected dose to RMEI (*EXPDOSE*, mrem/yr) over [0, 20,000 yr] for all radioactive species resulting from igneous eruption: (a) Regressions for *EXPDOSE* at 3000, 5000 and 10,000 years, and (b,c,d) Scatterplots for *EXPDOSE* at 10,000 years

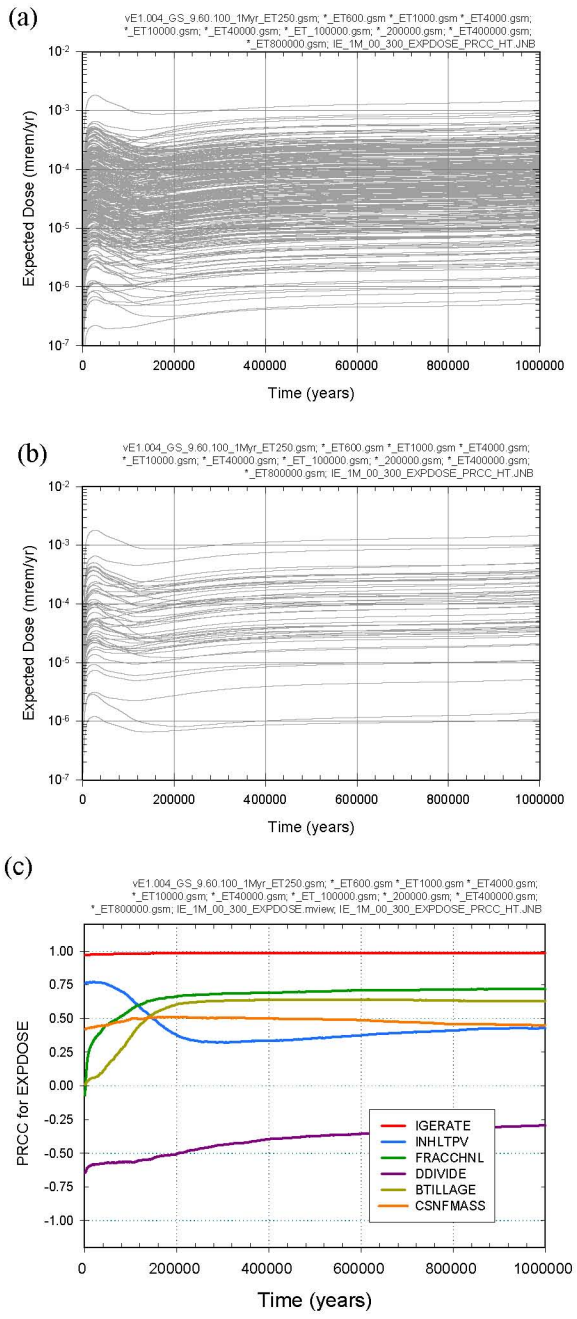

Source: Output DTNs: MO0709TSPAREGS.000 [DIRS 182976]; and MO0709TSPAPLOT.000 [DIRS 183010].

Figure K6.8.2-1. Expected dose to RMEI (*EXPDOSE*, mrem/yr) over [0, 1,000,000 yr] for all radioactive species resulting from igneous eruption: (a) *EXPDOSE* for all (i.e., 300) sample elements, (b) *EXPDOSE* for first 50 sample elements, and (c) PRCCs for *EXPDOSE*

(a)

	EXPDOSE: 50,000 yr			EXPDOSE: 200,000 yr			EXPDOSE: 500,000 yr		
Step[a]	**Variable[b]**	**R^{2c}**	**SRRC[d]**	**Variable**	**R^2**	**SRRC**	**Variable**	**R^2**	**SRRC**
1	IGERATE	0.80	0.88	IGERATE	0.86	0.89	IGERATE	0.86	0.89
2	INHLTPV	0.91	0.33	BTILLAGE	0.91	0.21	BTILLAGE	0.92	0.23
3	DDIVIDE	0.93	-0.13	FRACCHNL	0.93	0.15	FRACCHNL	0.94	0.16
4	CSNFMASS	0.94	0.09	INHLTPV	0.95	0.11	INHLTPV	0.96	0.10
5	FRACCHNL	0.95	0.10	CSNFMASS	0.96	0.09	CSNFMASS	0.96	0.09
6	DASHAVG	0.96	0.08	DDIVIDE	0.96	-0.09	CRITSLOP	0.97	-0.06
7	BTILLAGE	0.96	0.05	DASHAVG	0.97	0.07	DASHAVG	0.97	0.07
8	CRITSLOP	0.96	-0.05	CRITSLOP	0.97	-0.06	DDIVIDE	0.98	-0.06
9	DCHANL	0.96	-0.03	DCHANL	0.97	-0.03	DRAINDNS	0.98	0.03
10				DRAINDNS	0.97	0.03			

a: Steps in stepwise rank regression analysis
b: Variables listed in order of selection in stepwise regression
c: Cumulative R^2 value with entry of each variable into regression model
d: Standardized rank regression coefficients (SRRCs) in final regression model

(b)

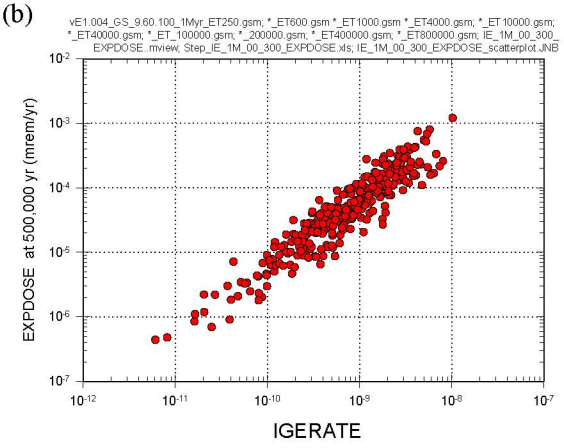

(c)

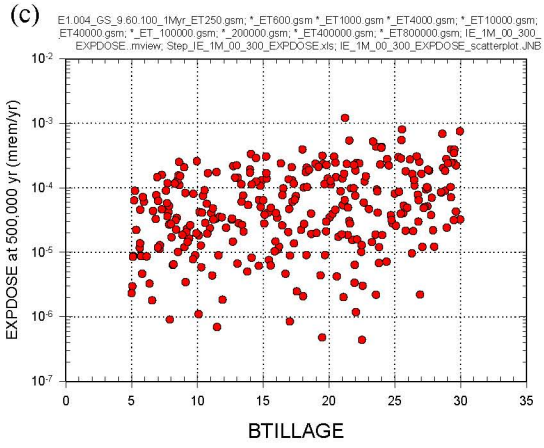

(d)

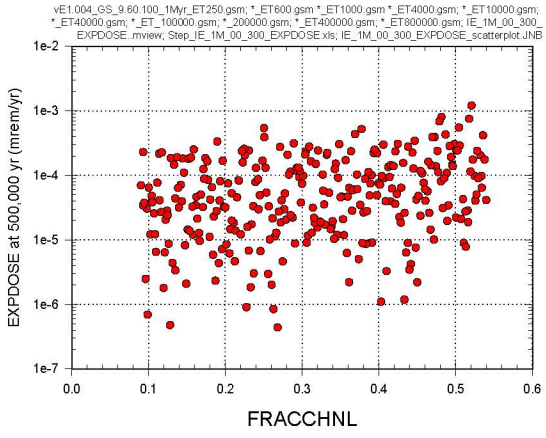

Source: Output DTNs: MO0709TSPAREGS.000 [DIRS 182976]; and MO0709TSPAPLOT.000 [DIRS 183010].

Figure K6.8.2-2. Stepwise rank regression analyses and selected scatterplots for expected dose to RMEI (*EXPDOSE*, mrem/yr) over [0, 1,000,000 yr] for all radioactive species resulting from igneous eruption: (a) Regressions for *EXPDOSE* at 50,000, 200,000 and 500,000 years, and (b,c,d) Scatterplots for *EXPDOSE* at 500,000 years

Figure Removed. See discussion in Section K7.3.

Figure K7.3-1. Time-dependent release rates (*ESIC239*, g/yr) and cumulative (i.e., integrated) releases (*ESIC239C*, g) over 20,000 years for the movement of ^{239}Pu irreversibly attached to glass colloids from the EBS to the UZ resulting from a seismically induced fractional damaged area of 10^{-6}(32.6 m^2) at 200 years to all CDSP WPs in the repository: (a, b) *ESIC239* and *ESIC239C* for all (i.e., 300) sample elements, (c, d) *ESIC239* and *ESIC239C* for first 50 sample elements, and (e, f) PRCCs for *ESIC239* and *ESIC239C*

Figure Removed. See discussion in Section K7.3.

Figure K7.3-2. Stepwise rank regression analyses and selected scatterplots for time-dependent release rates (*ESIC239*, g/yr) and cumulative (i.e., integrated) releases (*ESIC239C*, g) for the movement of ^{239}Pu irreversibly attached to glass colloids from the EBS to the UZ resulting from a seismically induced fractional damaged area of 10^{-6}(32.6 m^2) at 200 years to all CDSP WPs in the repository: (a, b) Regressions for *ESIC239* and *ESIC239C* at 3000, 5000 and 10,000 years, and (c-h) Scatterplots for *ESIC239* and *ESIC239C* at 10,000 years

Figure Removed. See discussion in Section K7.3.

Figure K7.3-3. Time-dependent release rates (*ESIF239*, g/yr) and cumulative (i.e., integrated) releases (*ESIF239C*, g) over 20,000 years for the movement of ^{239}Pu irreversibly attached to ferrous colloids from the EBS to the UZ resulting from a seismically induced fractional damaged area of 10^{-6}(32.6 m^2) at 200 years to all CDSP WPs in the repository: (a, b) *ESIF239* and *ESIF239C* for all (i.e., 300) sample elements, (c, d) *ESIC239* and *ESIC239C* for first 50 sample elements, and (e, f) PRCCs for *ESIF239* and *ESIF239C*

Figure Removed. See discussion in Section K7.3

Figure K7.3-4. Stepwise rank regression analyses and selected scatterplots for time-dependent release rates (*ESIF239*, g/yr) and cumulative (i.e., integrated) releases (*ESIF239C*, g) for the movement of ^{239}Pu irreversibly attached to ferrous colloids from the EBS to the UZ resulting from a seismically induced fractional damaged area of 10^{-6}(32.6 m^2) at 200 years to all CDSP WPs in the repository: (a, b) Regressions for *ESIF239* and *ESIF239C* at 3000, 5000 and 10,000 years, and (c-h) Scatterplots for *ESIF239* and *ESIF239C* at 10,000 years

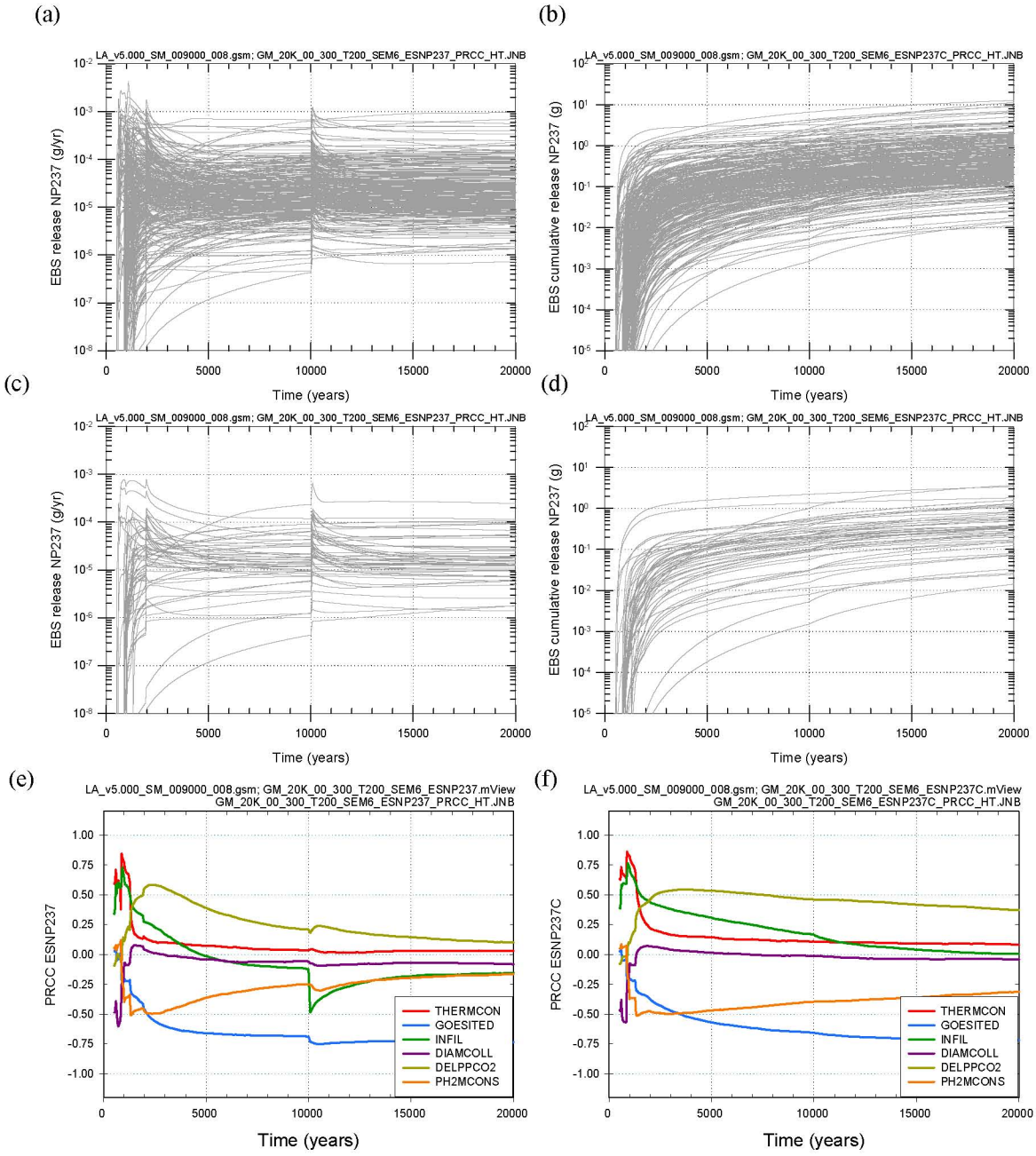

Source: Output DTNs: MO0709TSPASENS.000 [DIRS 183982]; and MO0709TSPAPLOT.000 [DIRS 183010].

Figure K7.3-5. Time-dependent release rates (*ESNP237*, g/yr) and cumulative (i.e., integrated) releases (*ESNP237C*, g) over 20,000 years for the movement of dissolved ^{237}Np from the EBS to the UZ resulting from a seismically induced fractional damaged area of 10^{-6}(32.6 m^2) at 200 years to all CDSP WPs in the repository: (a, b) *ESNP237* and *ESNP237C* for all (i.e., 300) sample elements, (c, d) *ESNP237* and *ESNP237C* for first 50 sample elements, and (e, f) PRCCs for *ESNP237* and *ESNP237C*

(a)

	ESNP237: 3000 yr			ESNP237: 5000 yr			ESNP237: 10,000 yr		
Step	**Variable[b]**	**R^{2c}**	**SRRC[d]**	**Variable**	**R^2**	**SRRC**	**Variable**	**R^2**	**SRRC**
1	GOESITED	0.14	-0.39	GOESITED	0.20	-0.46	GOESITED	0.24	-0.52
2	DELPPCO2	0.28	0.42	DSNFMASS	0.32	0.27	EP1LOWNU	0.34	0.32
3	PH2MCONS	0.39	-0.34	DELPPCO2	0.36	0.28	DSNFMASS	0.44	0.26
4	DSNFMASS	0.46	0.27	EP1LOWNU	0.41	0.23	HFOSA	0.50	-0.30
5	HFOSA	0.50	-0.20	HFOSA	0.46	-0.25	GOESA	0.52	0.15
6	INFIL	0.53	0.17	PH2MCONS	0.51	-0.24	IS2MCONS	0.54	0.13
7	GOESA	0.54	0.14	GOESA	0.53	0.15	DELPPCO2	0.56	0.14
8	CSRINDSA	0.56	0.13	EP1NPO2	0.55	0.16	PH2MCONS	0.58	-0.13
9	EP1NPO2	0.58	0.15	CSRINDSA	0.57	0.13	CSRINDSA	0.59	0.13
10	FHHISSCP	0.60	-0.14	IS2MCONS	0.58	0.11	EP1NPO2	0.61	0.15
11	EP1LOWNU	0.61	0.12	GOERELAB	0.59	0.11	GOERELAB	0.62	0.12
12				FHHISSCP	0.60	-0.10	HFOSITED	0.64	-0.12

(b)

	ESNP237C: 3000 yr			ESNP237C: 5000 yr			ESNP237C: 10,000 yr		
Step[a]	**Variable[b]**	**R^{2c}**	**SRRC[d]**	**Variable**	**R^2**	**SRRC**	**Variable**	**R^2**	**SRRC**
1	DELPPCO2	0.13	0.41	DELPPCO2	0.13	0.40	GOESITED	0.19	-0.45
2	PH2MCONS	0.27	-0.36	GOESITED	0.24	-0.35	DSNFMASS	0.29	0.25
3	INFIL	0.37	0.34	PH2MCONS	0.35	-0.32	DELPPCO2	0.36	0.33
4	GOESITED	0.45	-0.28	INFIL	0.42	0.26	HFOSA	0.40	-0.26
5	DSNFMASS	0.49	0.21	DSNFMASS	0.48	0.25	PH2MCONS	0.46	-0.24
6	HFOSA	0.51	-0.16	HFOSA	0.52	-0.20	EP1LOWNU	0.50	0.20
7	EP1NPO2	0.53	0.18	EP1NPO2	0.53	0.16	INFIL	0.52	0.14
8	FHHISSCP	0.55	-0.14	FHHISSCP	0.55	-0.13	GOESA	0.54	0.16
9	GOESA	0.57	0.14	GOESA	0.57	0.15	EP1NPO2	0.56	0.12
10	THERMCON	0.58	0.14	SEEPUNC	0.58	0.11	SEEPUNC	0.57	0.15
11	SEEPUNC	0.60	0.11	CSRINDSA	0.59	0.11	IS2MCONS	0.59	0.12
12	CSRINDSA	0.61	0.11	THERMCON	0.60	0.12	GOERELAB	0.60	0.12
13				EP1LOWNU	0.62	0.10	PHCSS	0.61	-0.10
14							KDUSMEC	0.62	0.10

a: Steps in stepwise rank regression analysis
b: Variables listed in order of selection in stepwise regression
c: Cumulative R^2 value with entry of each variable into regression model
d: Standardized rank regression coefficients (SRRCs) in final regression model

Source: Output DTNs: MO0709TSPASENS.000 [DIRS 183982]; and MO0709TSPAPLOT.000 [DIRS 183010].

Figure K7.3-6. Stepwise rank regression analyses and selected scatterplots for time-dependent release rates (*ESNP237*, g/yr) and cumulative (i.e., integrated) releases (*ES NP237C*, g) for the movement of dissolved ^{237}Np from the EBS to the UZ resulting from a seismically induced fractional damaged area of 10^{-6}(32.6 m^2) at 200 years to all CDSP WPs in the repository: (a, b) Regressions for *ESNP237* and *ESNP237C* at 3000, 5000 and 10,000 years, and (c-h) Scatterplots for *ESNP237* and *ESNP237C* at 10,000 years

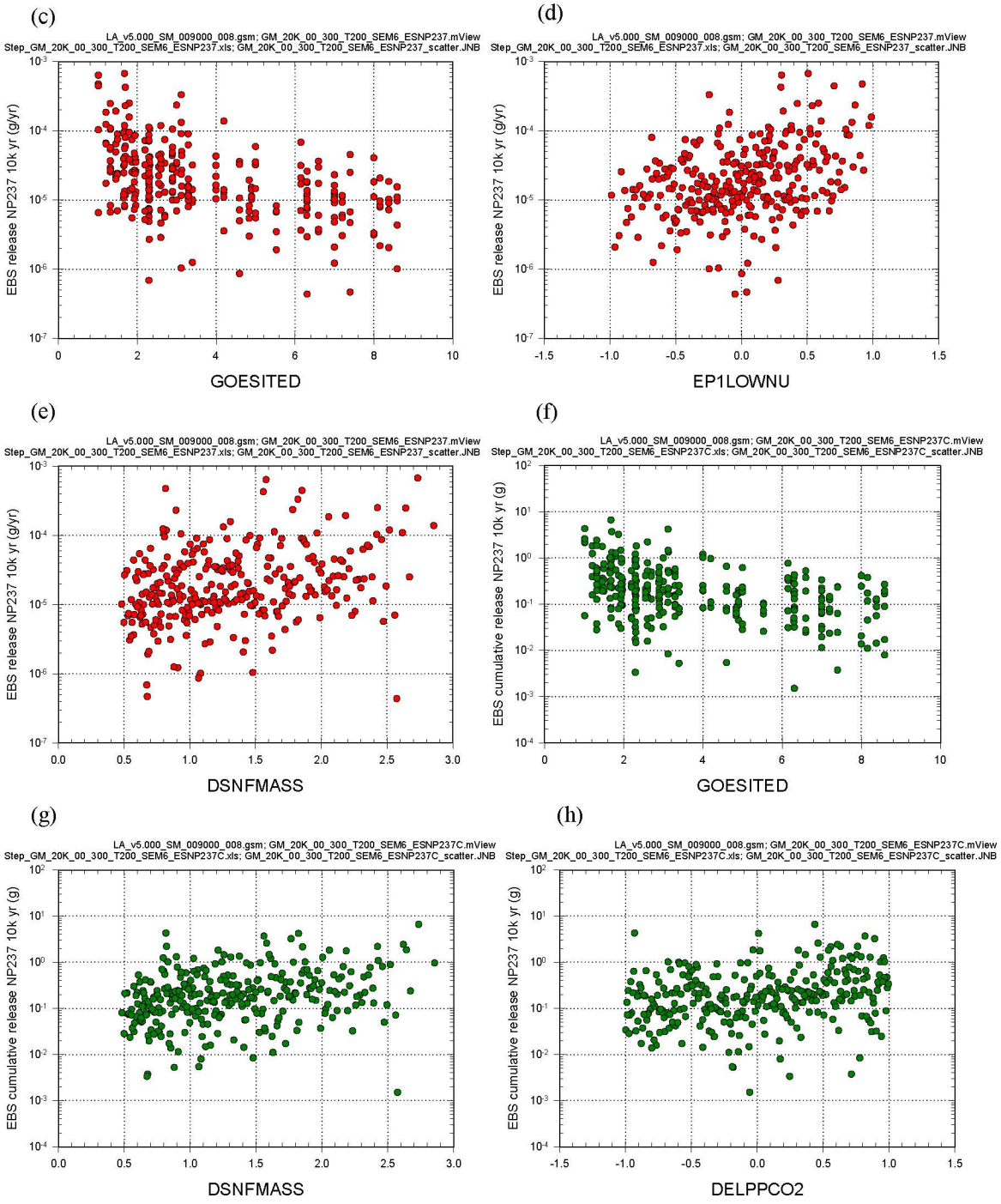

Source: Output DTNs: MO0709TSPASENS.000 [DIRS 183982]; and MO0709TSPAPLOT.000 [DIRS 183010].

Figure K7.3-6. Stepwise rank regression analyses and selected scatterplots for time-dependent release rates (*ESNP237*, g/yr) and cumulative (i.e., integrated) releases (*ES NP237C*, g) for the movement of dissolved ^{237}Np from the EBS to the UZ resulting froma seismically induced fractional damaged area of 10^{-6}(32.6 m^2) at 200 years to all CDSP WPs in the repository: (a, b) Regressions for *ESNP237* and *ESNP237C* at 3000, 5000 and 10,000 years, and (c-h) Scatterplots for *ESNP237* and *ESNP237C* at 10,000 years (continued)

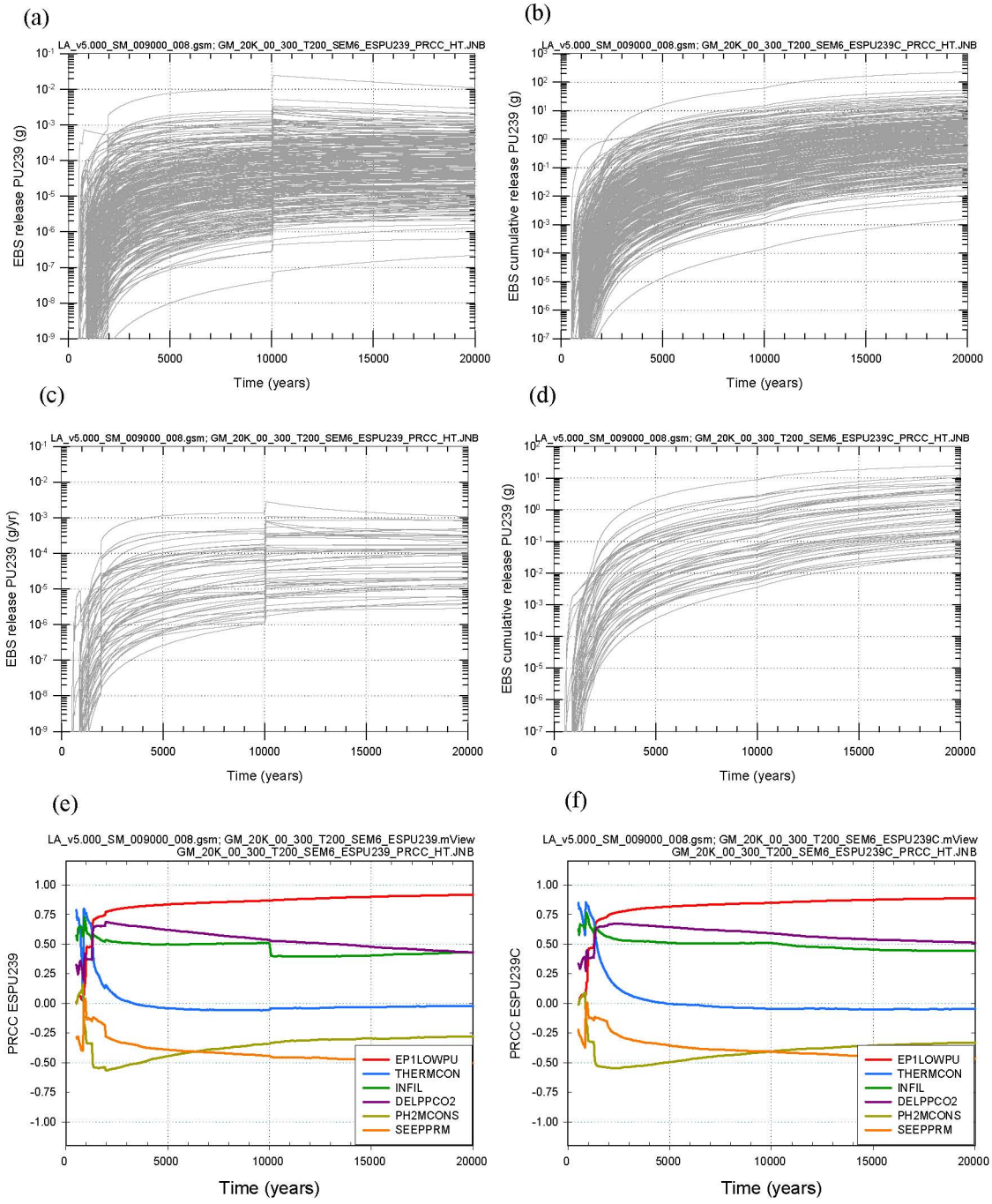

Source: Output DTNs: MO0709TSPASENS.000 [DIRS 183982]; and MO0709TSPAPLOT.000 [DIRS 183010].

Figure K7.3-7. Time-dependent release rates (*ESPU239*, g/yr) and cumulative (i.e., integrated) releases (*ESPU239C*, g) over 20,000 years for the movement of dissolved ^{239}Pu from the EBS to the UZ resulting from a seismically induced fractional damaged area of 10^{-6} (32.6 m^2) at 200 years to all CDSP WPs in the repository: (a, b) *ESPU239* and *ESPU239C* for all (i.e., 300) sample elements, (c, d) *ESPU239* and *ESPU239C* for first 50 sample elements, and (e, f) PRCCs for *ESPU239* and *ESPU239C*

(a)

	ESPU239: 3000 yr			ESPU239: 5000 yr			ESPU239: 10,000 yr		
Step[a]	Variable[b]	R^{2c}	SRRC[d]	Variable	R^2	SRRC	Variable	R^2	SRRC
1	EP1LOWPU	0.34	0.63	EP1LOWPU	0.41	0.67	EP1LOWPU	0.51	0.74
2	DELPPCO2	0.49	0.42	DELPPCO2	0.53	0.36	DELPPCO2	0.59	0.28
3	INFIL	0.58	0.29	INFIL	0.61	0.28	INFIL	0.65	0.26
4	PH2MCONS	0.67	-0.28	PH2MCONS	0.67	-0.23	SEEPPRM	0.70	-0.20
5	GOESITED	0.71	-0.19	SEEPPRM	0.71	-0.18	PH2MCONS	0.73	-0.16
6	SEEPPRM	0.73	-0.17	GOESITED	0.74	-0.17	GOESITED	0.75	-0.15
7	SEEPUNC	0.74	0.12	SEEPUNC	0.75	0.11	SEEPUNC	0.77	0.12
8	GOESA	0.75	0.10	GOESA	0.76	0.11	GOESA	0.78	0.12
9	GP2NO3	0.76	-0.08	GP2NO3	0.77	-0.10	GP2NO3	0.79	-0.09
10	IS2MCONS	0.77	0.08	ALPHAL	0.78	-0.08	ALPHAL	0.79	-0.08
11	ALPHAL	0.77	-0.08	RHPH75	0.78	-0.08	RHPH75	0.80	-0.08
12				CORRATSS	0.79	-0.08	CORRATSS	0.81	-0.08

(b)

	ESPU239C: 3000 yr			ESPU239C: 5000 yr			ESPU239C: 10,000 yr		
Step[a]	Variable[b]	R^{2c}	SRRC[d]	Variable	R^2	SRRC	Variable	R^2	SRRC
1	EP1LOWPU	0.30	0.59	EP1LOWPU	0.36	0.65	EP1LOWPU	0.45	0.69
2	DELPPCO2	0.46	0.44	DELPPCO2	0.50	0.40	DELPPCO2	0.55	0.33
3	INFIL	0.57	0.33	INFIL	0.59	0.30	INFIL	0.63	0.28
4	PH2MCONS	0.66	-0.30	PH2MCONS	0.67	-0.26	PH2MCONS	0.68	-0.20
5	GOESITED	0.70	-0.19	GOESITED	0.71	-0.18	SEEPPRM	0.72	-0.19
6	SEEPPRM	0.72	-0.16	SEEPPRM	0.73	-0.18	GOESITED	0.75	-0.16
7	GP2NO3	0.73	-0.09	SEEPUNC	0.75	0.12	SEEPUNC	0.76	0.11
8	CPUCOLCS	0.74	-0.09	GOESA	0.76	0.11	GOESA	0.77	0.11
9	SEEPUNC	0.75	0.11	GP2NO3	0.76	-0.09	GP2NO3	0.78	-0.10
10	IS2MCONS	0.76	0.10	ALPHAL	0.77	-0.08	ALPHAL	0.79	-0.08
11	GOESA	0.76	0.09	IS2MCONS	0.78	0.08	RHPH75	0.79	-0.08
12	ALPHAL	0.77	-0.08				CORRATSS	0.80	-0.08

a: Steps in stepwise rank regression analysis
b: Variables listed in order of selection in stepwise regression
c: Cumulative R^2 value with entry of each variable into regression model
d: Standardized rank regression coefficients (SRRCs) in final regression model

Source: Output DTNs: MO0709TSPASENS.000 [DIRS 183982]; and MO0709TSPAPLOT.000 [DIRS 183010].

Figure K7.3-8. Stepwise rank regression analyses and selected scatterplots for time-dependent release rates (*ESPU239*, g/yr) and cumulative (i.e., integrated) releases (*ESPU239*, g) for the movement of dissolved ^{239}Pu from the EBS to the UZ resulting from a seismically induced fractional damaged area of 10^{-6}(32.6 m^2) at 200 years to all CDSP WPs in the repository: (a, b) Regressions for *ESPU239* and *ESPU239C* at 3000, 5000 and 10,000 years, and (c-h) Scatterplots for *ESPU239* and *ESPU239C* at 10,000 years

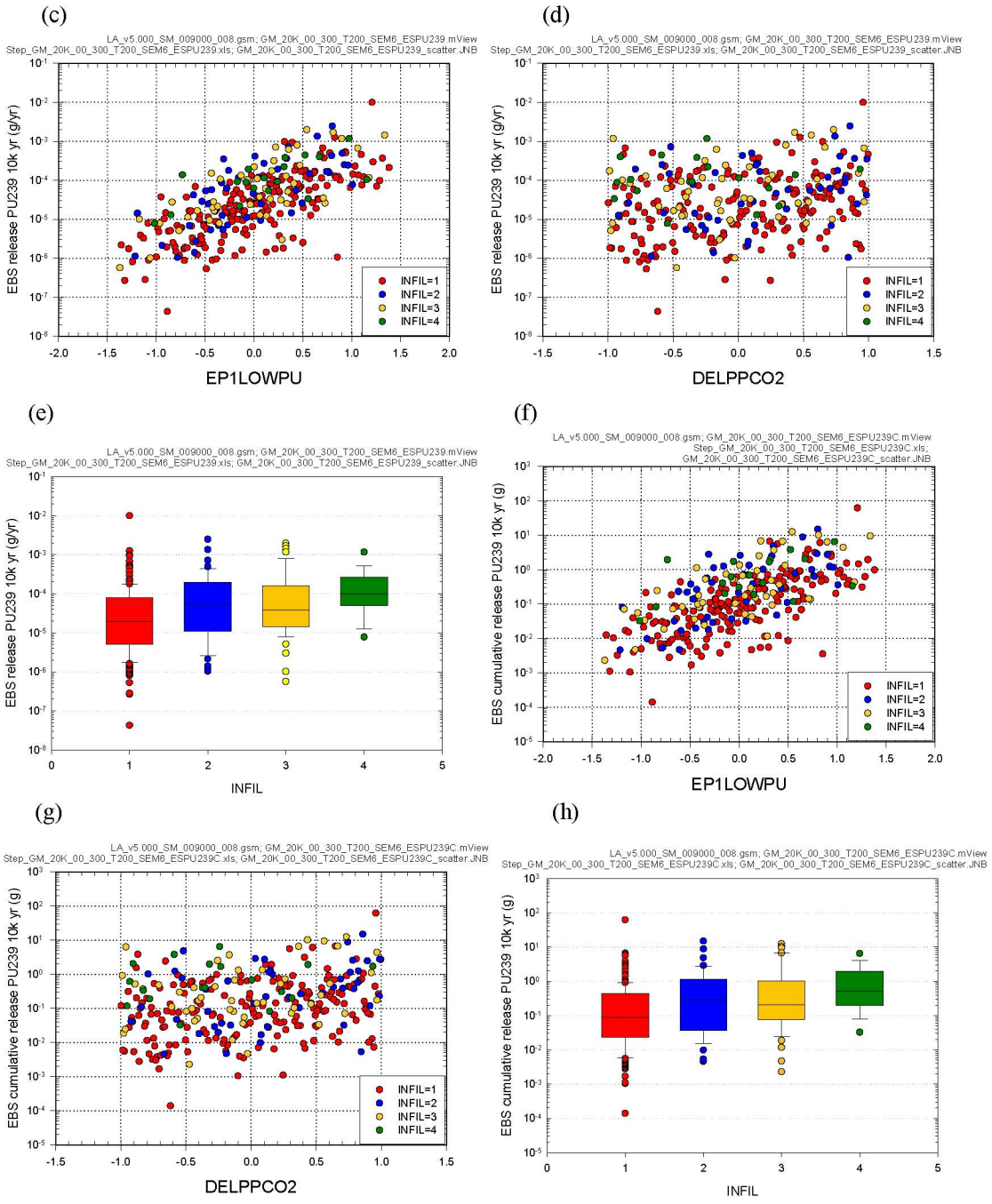

Source: Output DTNs: MO0709TSPASENS.000 [DIRS 183982]; and MO0709TSPAPLOT.000 [DIRS 183010].

NOTE: In (e,h), the box extends from 0.25 to 0.75 quantile; lower and upper bar and whisker extend to 0.1 and 0.9 quantile, respectively; dots represent values outside 0.1 to 0.9 quantile range; median indicated by light horizontal line.

Figure K7.3-8. Stepwise rank regression analyses and selected scatterplots for time-dependent release rates (*ESPU239*, g/yr) and cumulative (i.e., integrated) releases (*ESPU239*, g) for the movement of dissolved ^{239}Pu from the EBS to the UZ resulting from a seismically induced fractional damaged area of 10^{-6}(32.6 m^2) at 200 years to all CDSP WPs in the repository: (a, b) Regressions for *ESPU239* and *ESPU239C* at 3000, 5000 and 10,000 years, and (c-h) Scatterplots for *ESPU239* and *ESPU239C* at 10,000 years (continued).

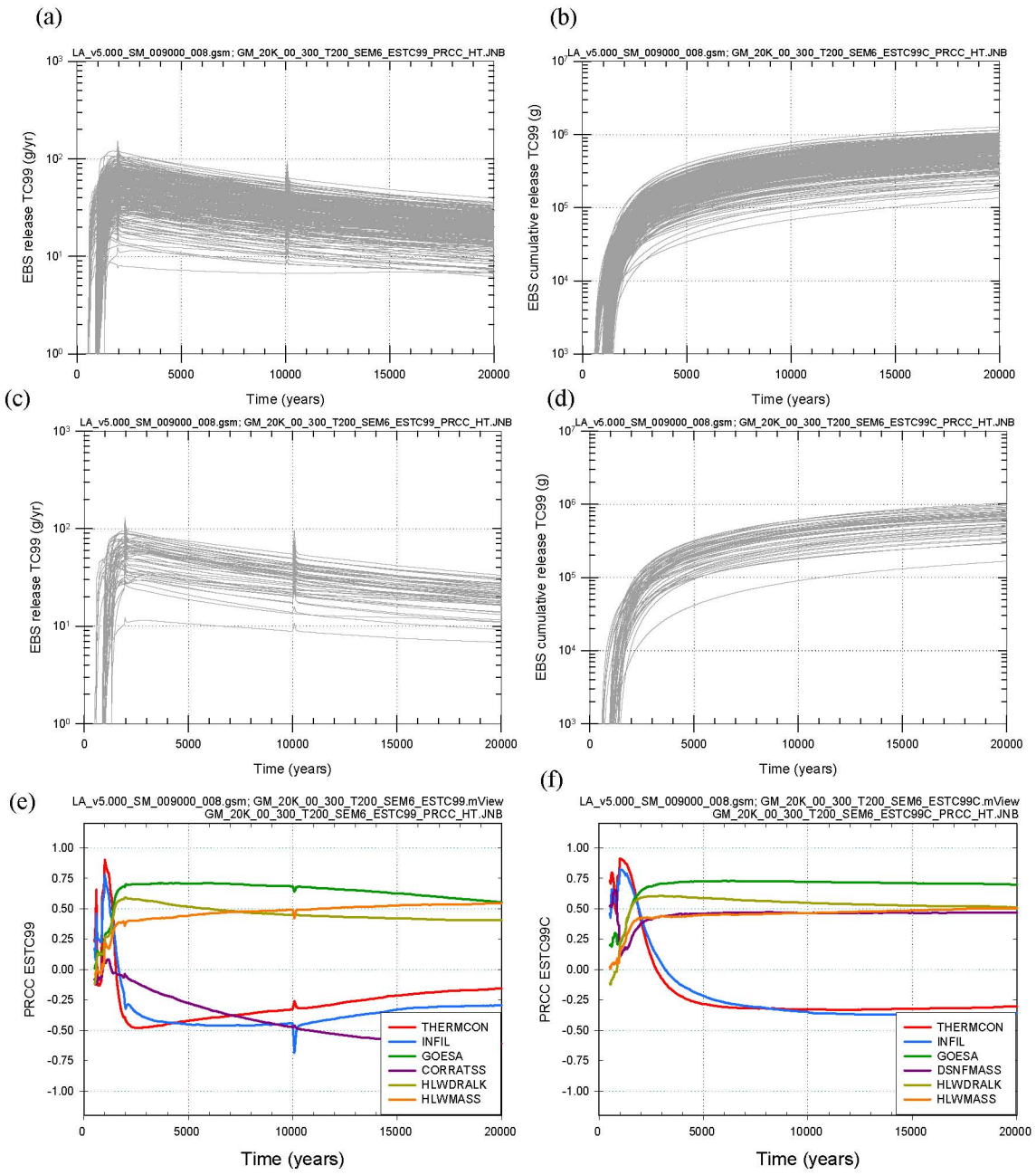

Source: Output DTNs: MO0709TSPASENS.000 [DIRS 183982]; and MO0709TSPAPLOT.000 [DIRS 183010].

Figure K7.3-9. Time-dependent release rates (*ESTC99*, g/yr) and cumulative (i.e., integrated) releases (*ESTC99C*, g) over 20,000 years for the movement of dissolved ^{99}Tc from the EBS to the UZ resulting from a seismically induced fractional damaged area of 10^{-6}(32.6 m^2) at 200 years to all CDSP WPs in the repository: (a, b) *ESTC99* and *ESTC99C* for all (i.e., 300) sample elements, (c, d) *ESTC99* and *ESTC99C* for first 50 sample elements, and (e, f) PRCCs for *ESTC99* and *ESTC99C*

(a)

	ESTC99: 3000 yr			ESTC99: 5000 yr			ESTC99: 10,000 yr		
Step[a]	Variable[b]	R^{2c}	SRRC[d]	Variable	R^2	SRRC	Variable	R^2	SRRC
1	GOESA	0.18	0.45	GOESA	0.18	0.46	GOESA	0.14	0.43
2	HLWDRALK	0.37	0.39	HLWDRALK	0.32	0.33	HLWMASS	0.29	0.33
3	HLWMASS	0.46	0.27	HLWMASS	0.43	0.29	CORRATSS	0.39	-0.30
4	THERMCON	0.55	-0.31	THERMCON	0.51	-0.29	HLWDRALK	0.49	0.29
5	DSNFMASS	0.60	0.28	INFIL	0.57	-0.28	INFIL	0.55	-0.26
6	INFIL	0.65	-0.25	DSNFMASS	0.63	0.28	THERMCON	0.60	-0.24
7	PH2DHLNS	0.69	-0.18	PH2DHLNS	0.67	-0.21	DSNFMASS	0.65	0.27
8	WFDEGEXF	0.71	0.16	CORRATSS	0.71	-0.17	PH2DHLNS	0.70	-0.23
9	HLWDRACD	0.73	0.13	WFDEGEXF	0.73	0.14	HLWDRACD	0.72	0.13
10	CORRATSS	0.75	-0.12	HLWDRACD	0.75	0.13	WFDEGEXF	0.74	0.13
11	FHHISSCP	0.76	-0.12	FHHISSCP	0.76	-0.12	FHHISSCP	0.75	-0.12
12	DIAMCOLL	0.77	-0.08	RUBMAXNL	0.77	0.08	RUBMAXNL	0.76	0.09
13				DIAMCOLL	0.78	-0.08	DIAMCOLL	0.77	-0.08
14							RHPH0	0.77	0.08
15							WDGCUA22	0.78	-0.08

(b)

	ESTC99C: 3000 yr			ESTC99C: 5000 yr			ESTC99C: 10,000 yr		
Step[a]	Variable[b]	R^{2c}	SRRC[d]	Variable	R^2	SRRC	Variable	R^2	SRRC
1	GOESA	0.22	0.49	GOESA	0.22	0.50	GOESA	0.20	0.48
2	HLWDRALK	0.45	0.44	HLWDRALK	0.43	0.42	HLWDRALK	0.37	0.37
3	HLWMASS	0.54	0.28	HLWMASS	0.53	0.30	HLWMASS	0.48	0.30
4	DSNFMASS	0.60	0.28	DSNFMASS	0.59	0.29	DSNFMASS	0.53	0.29
5	WFDEGEXF	0.64	0.21	WFDEGEXF	0.62	0.18	CORRATSS	0.58	-0.19
6	PH2DHLNS	0.66	-0.15	THERMCON	0.65	-0.16	THERMCON	0.62	-0.22
7	HLWDRACD	0.69	0.14	PH2DHLNS	0.67	-0.18	INFIL	0.66	-0.21
8	FHHISSCP	0.70	-0.12	HLWDRACD	0.70	0.14	PH2DHLNS	0.69	-0.20
9	WDGCUA22	0.71	-0.10	INFIL	0.71	-0.14	WFDEGEXF	0.72	0.16
10	SEEPPRM	0.71	-0.09	FHHISSCP	0.73	-0.12	HLWDRACD	0.74	0.13
11	EP1LOWTH	0.72	-0.09	CORRATSS	0.74	-0.11	FHHISSCP	0.75	-0.13
12							DIAMCOLL	0.76	-0.08

a: Steps in stepwise rank regression analysis
b: Variables listed in order of selection in stepwise regression
c: Cumulative R^2 value with entry of each variable into regression model
d: Standardized rank regression coefficients (SRRCs) in final regression model

Source: Output DTNs: MO0709TSPASENS.000 [DIRS 183982]; and MO0709TSPAPLOT.000 [DIRS 183010].

Figure K7.3-10. Stepwise rank regression analyses and selected scatterplots for time-dependent release rates (*ESTC99*, g/yr) and cumulative (i.e., integrated) releases (*ESTC99*, g) for the movement of dissolved ^{99}Tc from the EBS to the UZ resulting from a seismically induced fractional damaged area of 10^{-6}(32.6 m^2) at 200 years to all CDSP WPs in the repository: (a, b) Regressions for *ESTC99* and *ESTC99C* at 3000, 5000 and 10,000 years, and (c-h) Scatterplots for *ESTC99* and *ESTC99C* at 10,000 years

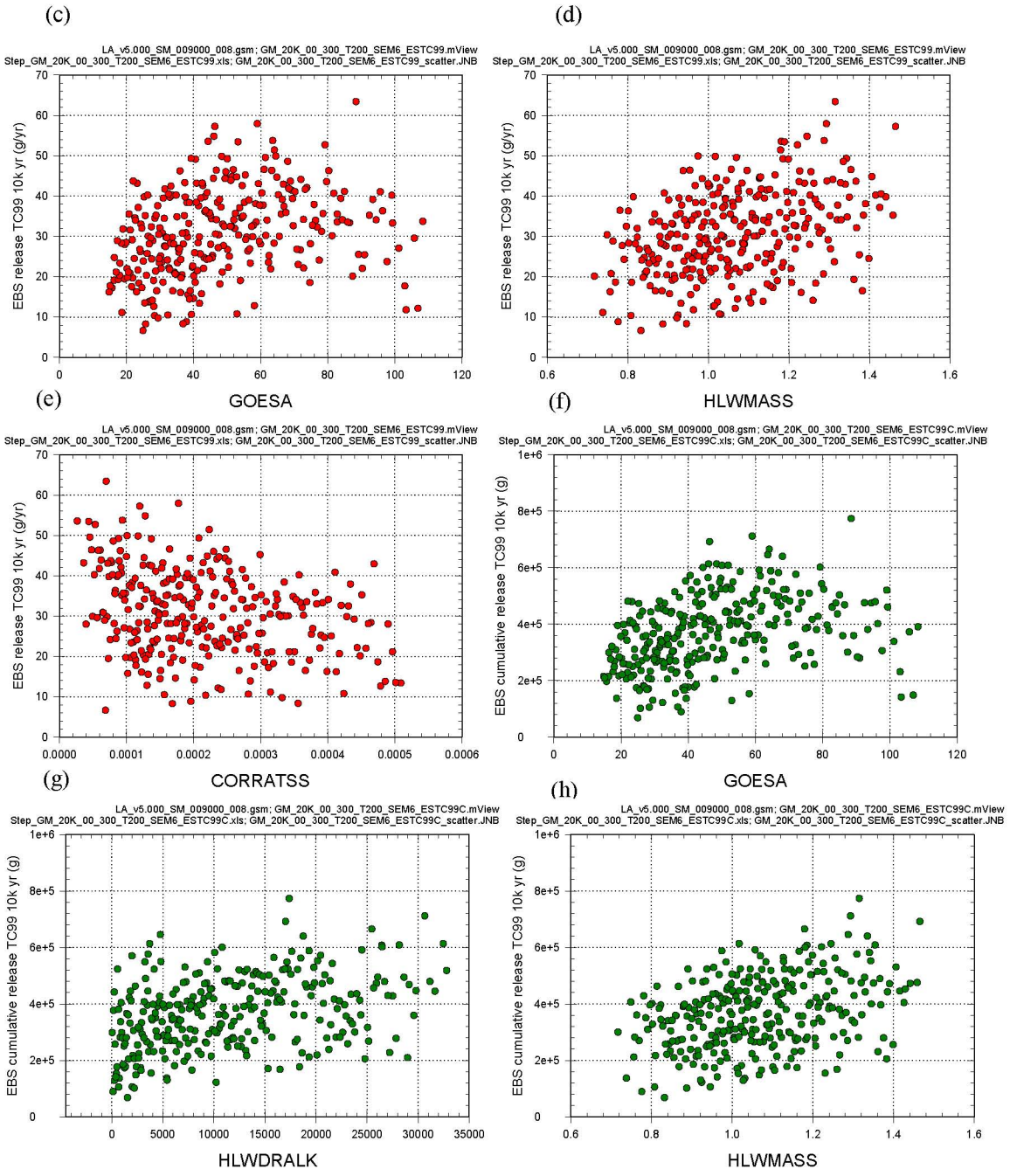

Source: Output DTNs: MO0709TSPASENS.000 [DIRS 183982]; and MO0709TSPAPLOT.000 [DIRS 183010].

Figure K7.3-10. Stepwise rank regression analyses and selected scatterplots for time-dependent release rates (*ESTC99*, g/yr) and cumulative (i.e., integrated) releases (*ESTC99*, g) for the movement of dissolved ^{99}Tc from the EBS to the UZ resulting from a seismically induced fractional damaged area of 10^{-6}(32.6 m^2) at 200 years to all CDSP WPs in the repository: (a, b) Regressions for *ESTC99* and *ESTC99C* at 3000, 5000 and 10,000 years, and (c-h) Scatterplots for *ESTC99* and *ESTC99C* at 10,000 years (continued)

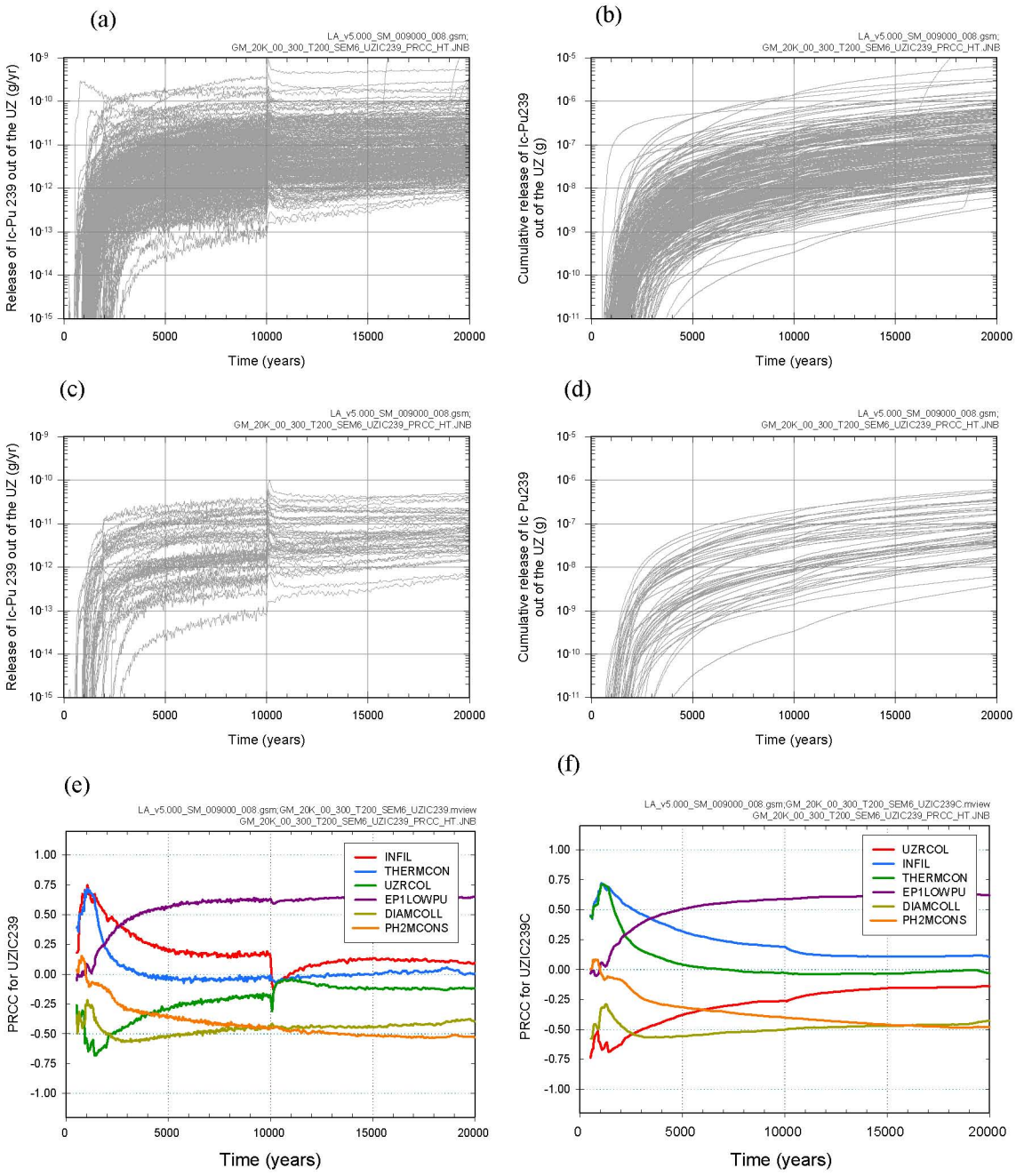

Source: Output DTNs: MO0709TSPASENS.000 [DIRS 183982]; and MO0709TSPAPLOT.000 [DIRS 183010].

Figure K7.4-1. Time-dependent release rates (*UZIC239*, g/yr) and cumulative (i.e., integrated) releases (*UZIC239C*, g) over 20,000 years for the movement of ^{239}Pu irreversibly attached to glass colloids from the UZ to the SZ resulting from a seismically induced fractional damaged area of 10^{-6}(32.6 m^2) at 200 years to all CDSP WPs in the repository: (a, b) *UZIC239* and *UZIC239C* for all (i.e., 300) sample elements, (c, d) *UZIC239* and *UZIC239C* for first 50 sample elements, and (e, f) PRCCs for *UZIC239* and *UZIC239C*

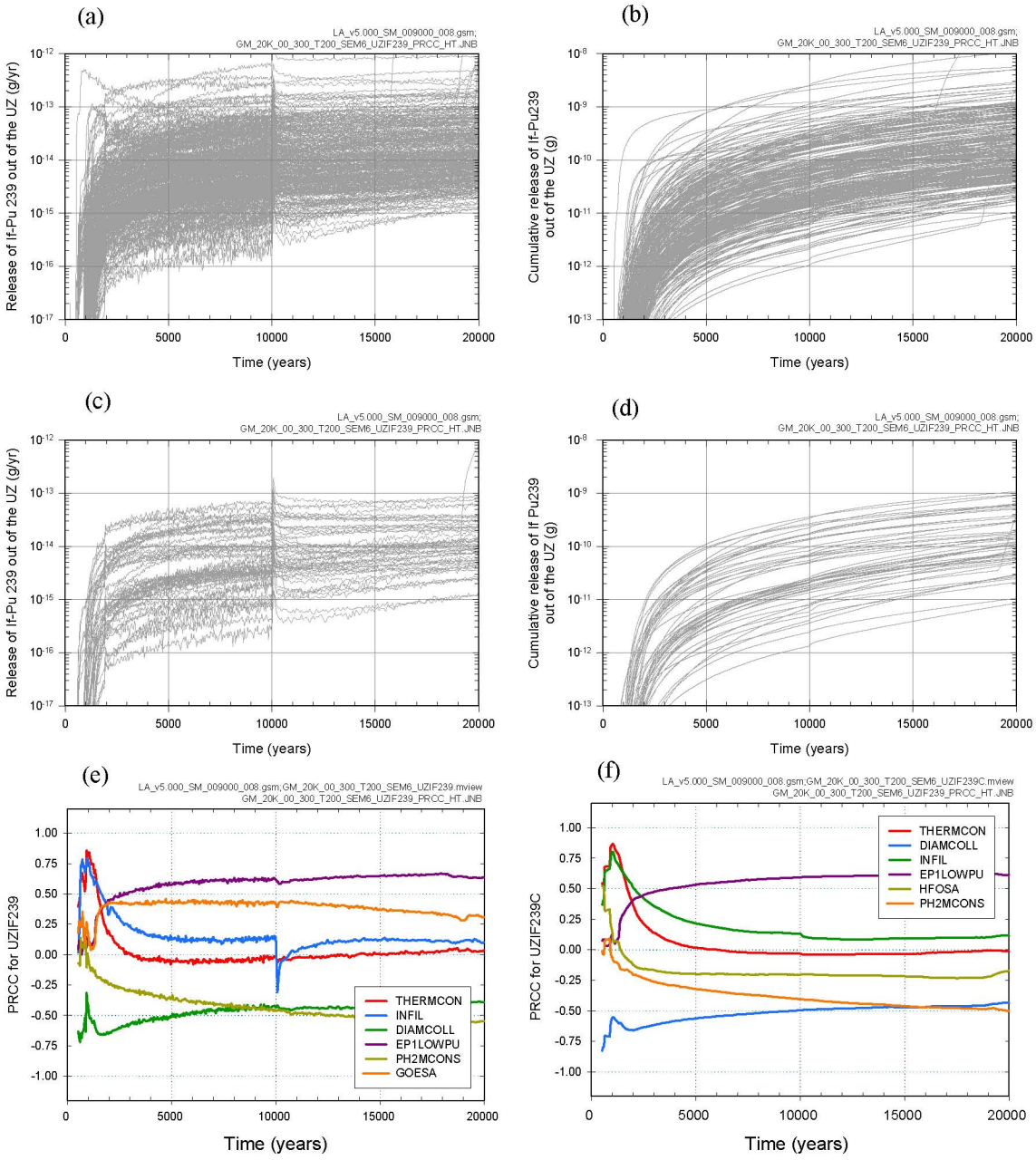

Source: Output DTNs: MO0709TSPASENS.000 [DIRS 183982]; and MO0709TSPAPLOT.000 [DIRS 183010].

Figure K7.4-2. Time-dependent release rates (*UZIF239*, g/yr) and cumulative (i.e., integrated) releases (*UZIF239C*, g) over 20,000 years for the movement of ^{239}Pu irreversibly attached to glass colloids from the UZ to the SZ resulting from a seismically induced fractional damaged area of 10^{-6}(32.6 m^2) at 200 years to all CDSP WPs in the repository: (a, b) *UZIF239* and *UZIF239C* for all (i.e., 300) sample elements, (c, d) *UZIC239* and *UZIC239C* for first 50 sample elements, and (e, f) PRCCs for *UZIF239* and *UZIF239C*

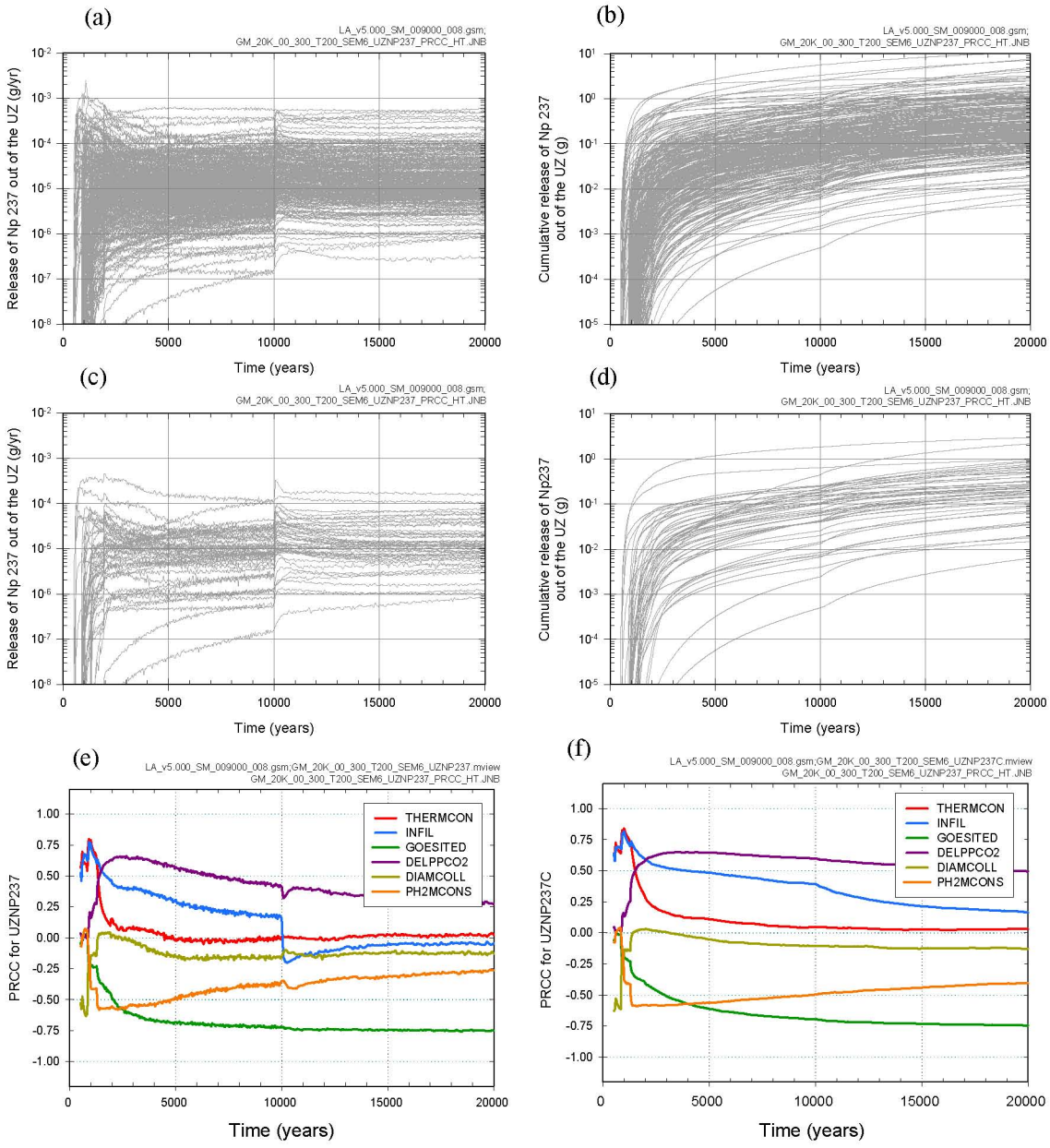

Source: Output DTNs: MO0709TSPASENS.000 [DIRS 183982]; and MO0709TSPAPLOT.000 [DIRS 183010].

Figure K7.4-3. Time-dependent release rates (*UZNP237*, g/yr) and cumulative (i.e., integrated) releases (*UZNP2379C*, g) over 20,000 years for the movement of dissolved ^{237}Np from the UZ to the SZ resulting from a seismically induced fractional damaged area of 10^{-6} (32.6 m^2) at 200 years to all CDSP WPs in the repository: (a, b) *UZNP237* and *UZNP237C* for all (i.e., 300) sample elements, (c, d) *UZNP237* and *UZNP237C* for first 50 sample elements, and (e, f) PRCCs for *UZNP237* and *UZNP237C*

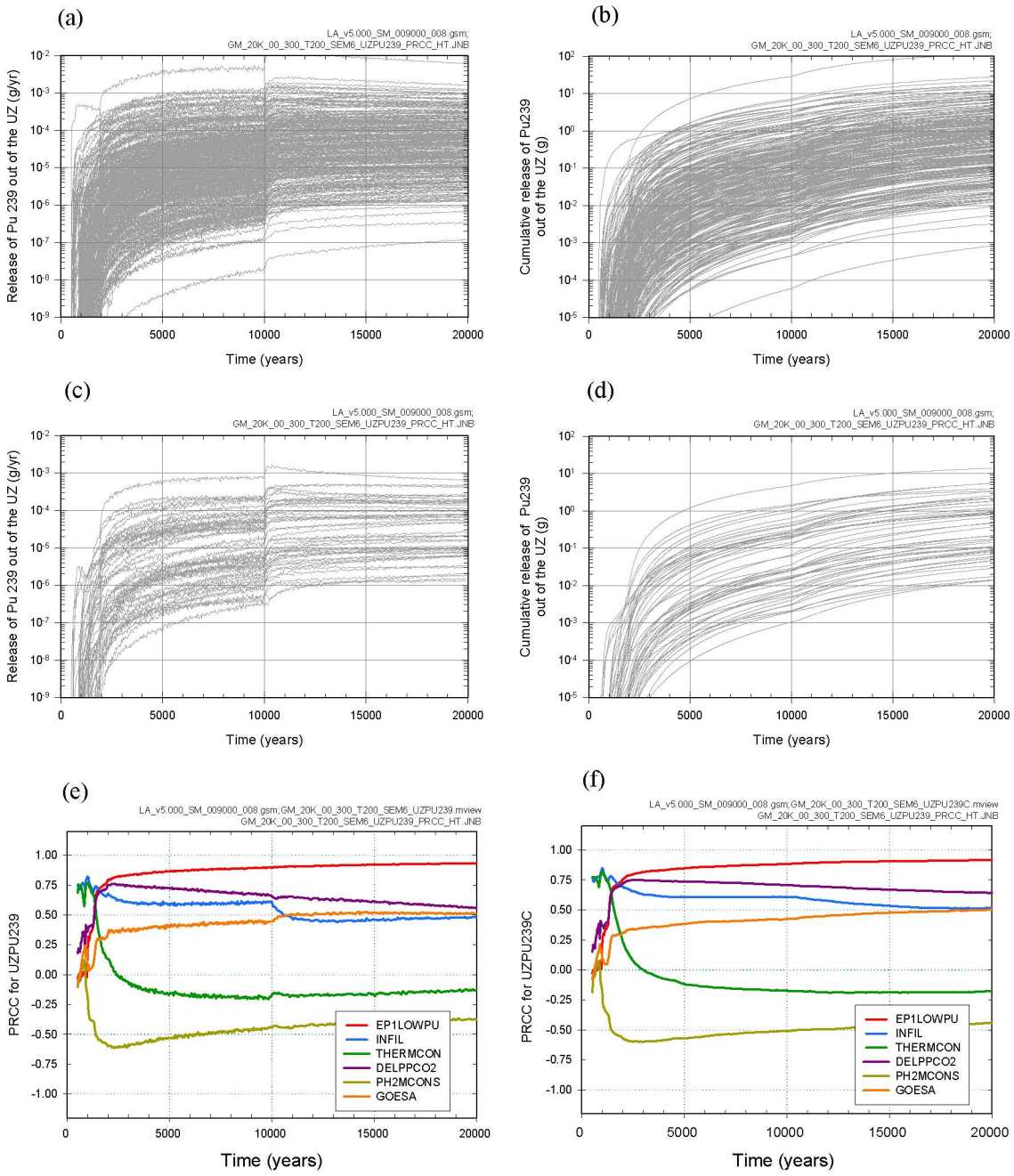

Source: Output DTNs: MO0709TSPASENS.000 [DIRS 183982]; and MO0709TSPAPLOT.000 [DIRS 183010].

Figure K7.4-4. Time-dependent release rates (*UZPU239*, g/yr) and cumulative (i.e., integrated) releases (*UZPU239C*, g) over 20,000 years for the movement of dissolved ^{239}Pu from the UZ to the SZ resulting from a seismically induced fractional damaged area of 10^{-6} (32.6 m^2) at 200 years to all CDSP WPs in the repository: (a, b) *UZPU239* and *UZPU239C* for all (i.e., 300) sample elements, (c, d) *UZPU239* and *UZPU239C* for first 50 sample elements, and (e, f) PRCCs for *UZPU239* and *UZPU239C*

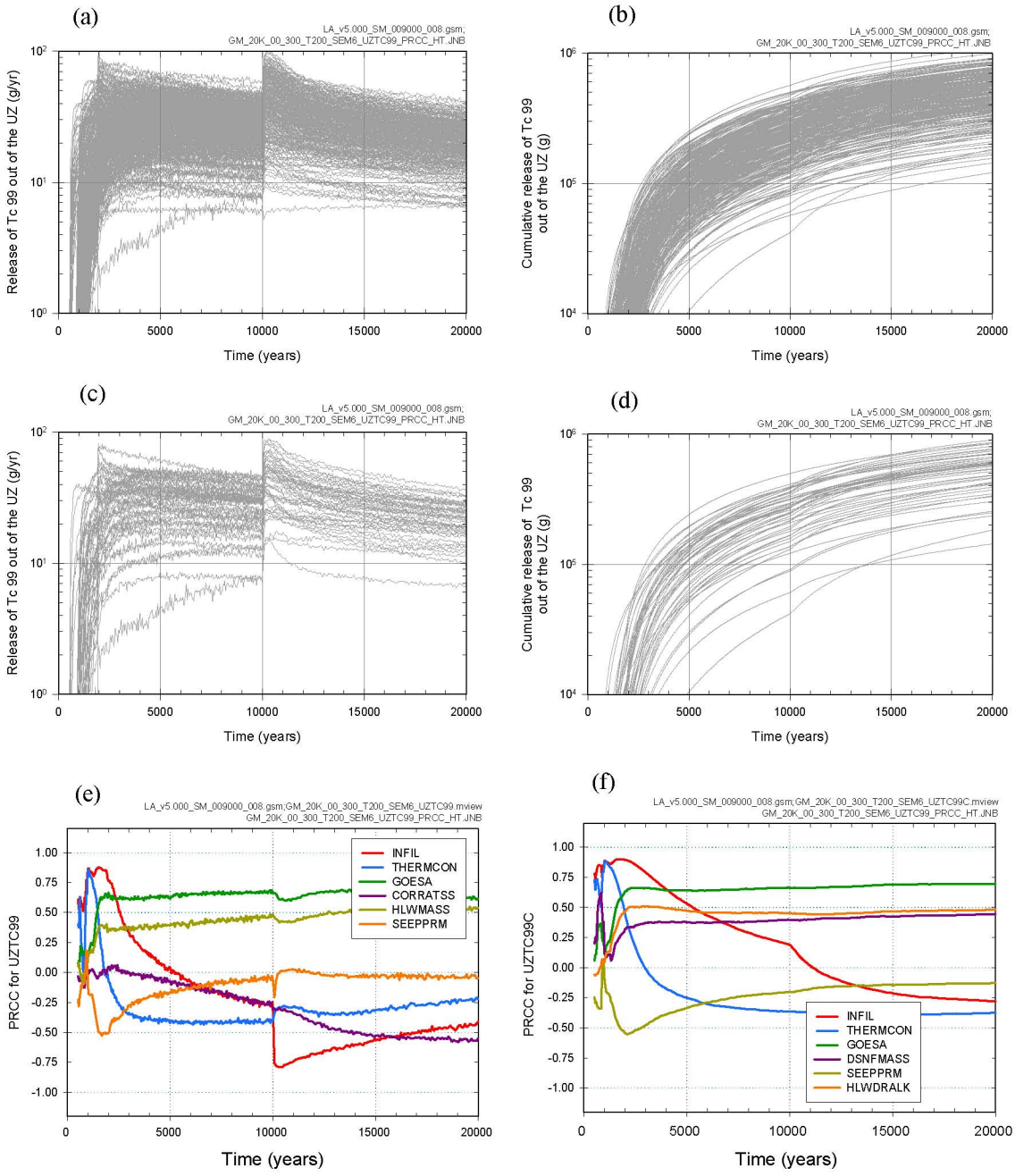

Source: Output DTNs: MO0709TSPASENS.000 [DIRS 183982]; and MO0709TSPAPLOT.000 [DIRS 183010].

Figure K7.4-5. Time-dependent release rates (*UZTC99*, g/yr) and cumulative (i.e., integrated) releases (*UZTC99C*, g) over 20,000 years for the movement of dissolved ^{99}Tc from the UZ to the SZ resulting from a seismically induced fractional damaged area of 10^{-6}(32.6 m^2) at 200 years to all CDSP WPs in the repository: (a, b) *UZTC99* and *UZTC99C* for all (i.e., 300) sample elements, (c, d) *UZTC99* and *UZTC99C* for first 50 sample elements, and (e, f) PRCCs for *UZTC99* and *UZTC99C*

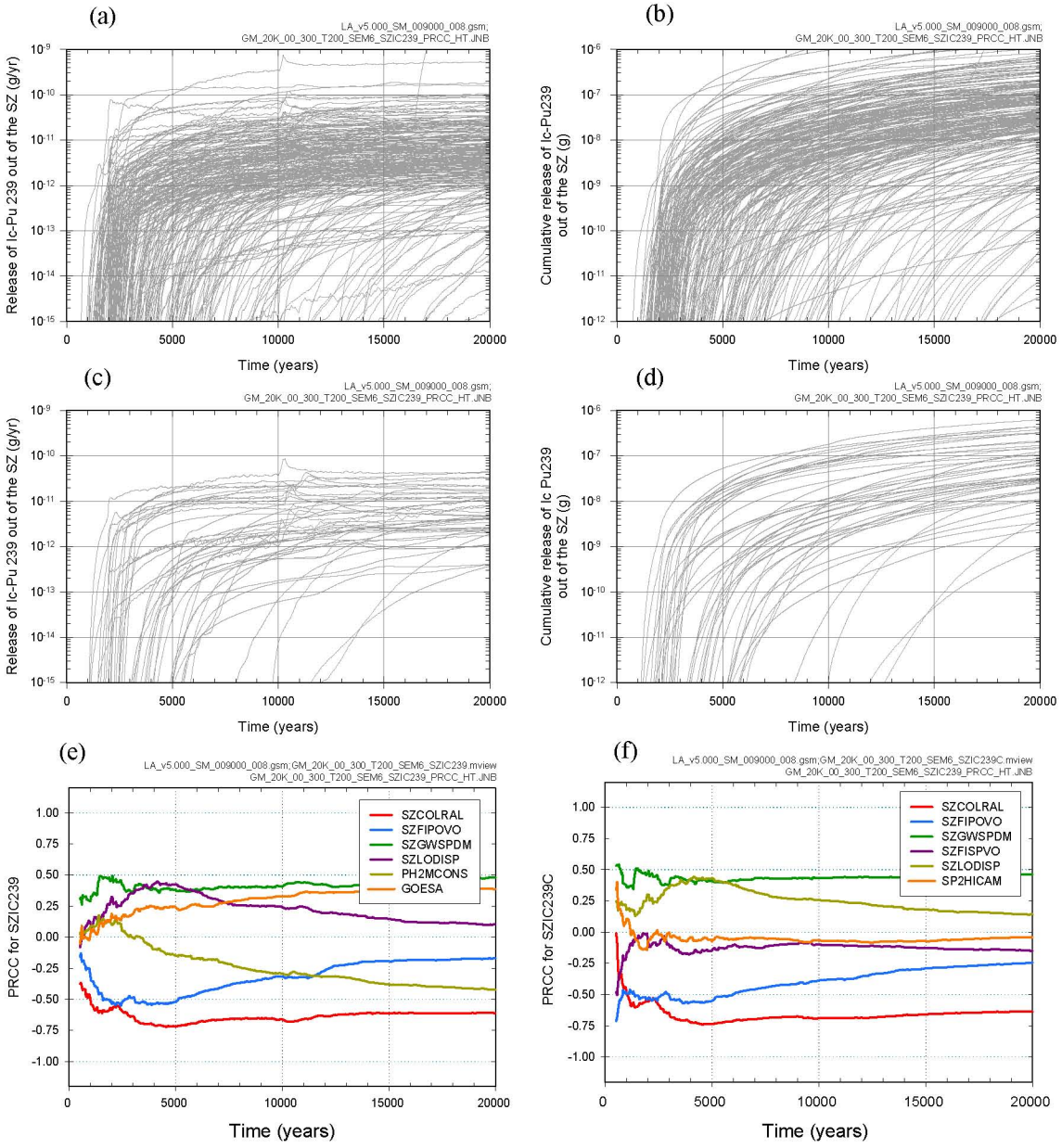

Source: Output DTNs: MO0709TSPASENS.000 [DIRS 183982]; and MO0709TSPAPLOT.000 [DIRS 183010].

Figure K7.5-1. Time-dependent release rates (*SZIC239*, g/yr) and cumulative (i.e., integrated) releases (*SZIC239C*, g) over 20,000 years for the movement of ^{239}Pu irreversibly attached to glass colloids across a subsurface plane at the location of the RMEI resulting from a seismically induced fractional damaged area of 10^{-6}(32.6 m^2) at 200 years to all CDSP WPs in the repository: (a, b) *SZIC239* and *SZIC239C* for all (i.e., 300) sample elements, (c, d) *SZIC239* and *SZIC239C* for first 50 sample elements, and (e, f) PRCCs for *SZIC239* and *SZIC239C*

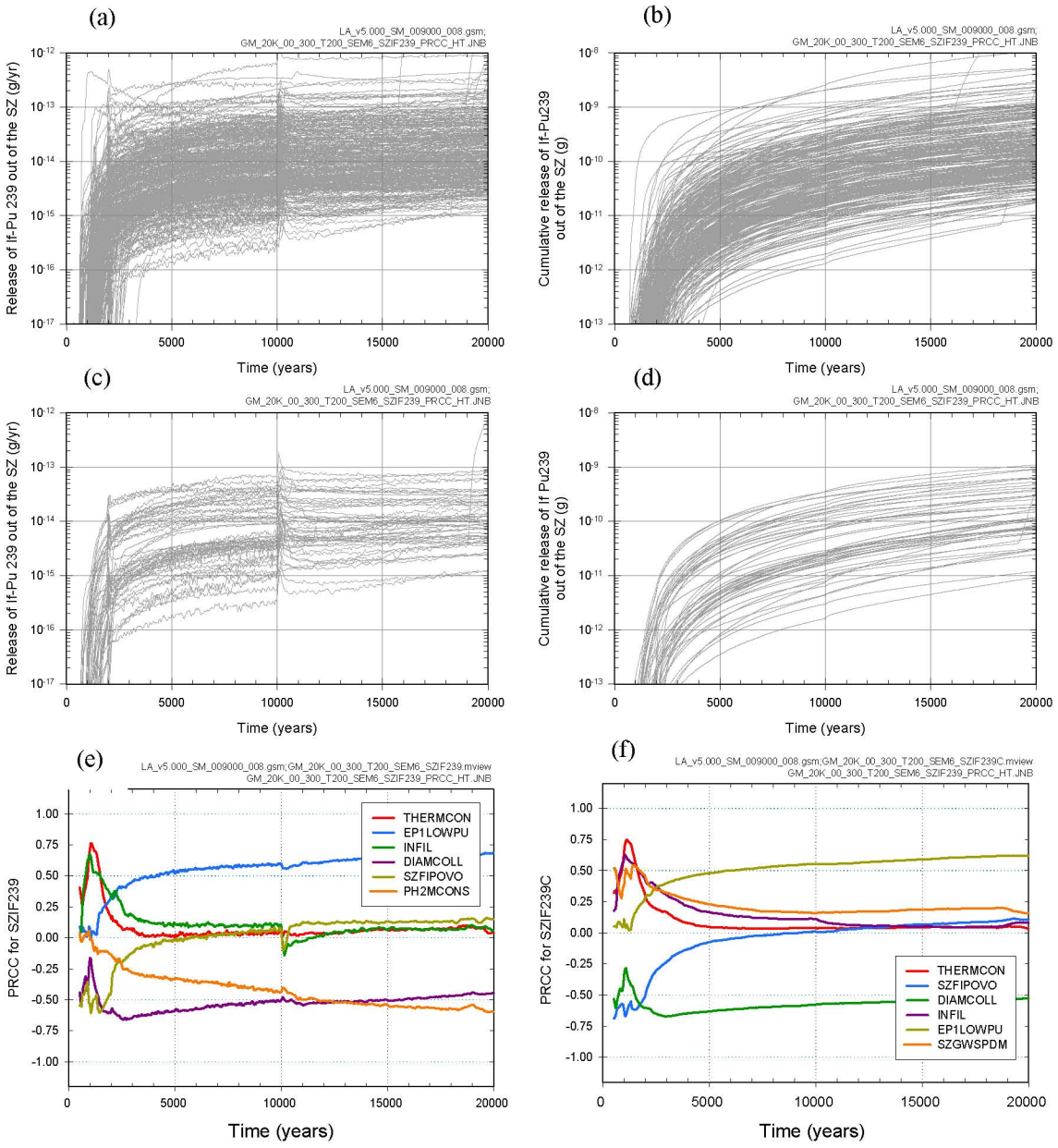

Source: Output DTNs: MO0709TSPASENS.000 [DIRS 183982]; and MO0709TSPAPLOT.000 [DIRS 183010].

Figure K7.5-2. Time-dependent release rates (*SZIF239*, g/yr) and cumulative (i.e., integrated) releases (*SZIF239C*, g) over 20,000 years for the movement of ^{239}Pu irreversibly attached to glass colloids across a subsurface plane at the location of the RMEI resulting from a seismically induced fractional damaged area of 10^{-6}(32.6 m^2) at 200 years to all CDSP WPs in the repository: (a, b) *SZIF239* and *SZIF239C* for all (i.e., 300) sample elements, (c, d) *SZIC239* and *SZIC239C* for first 50 sample elements, and (e, f) PRCCs for *SZIF239* and *SZIF239C*

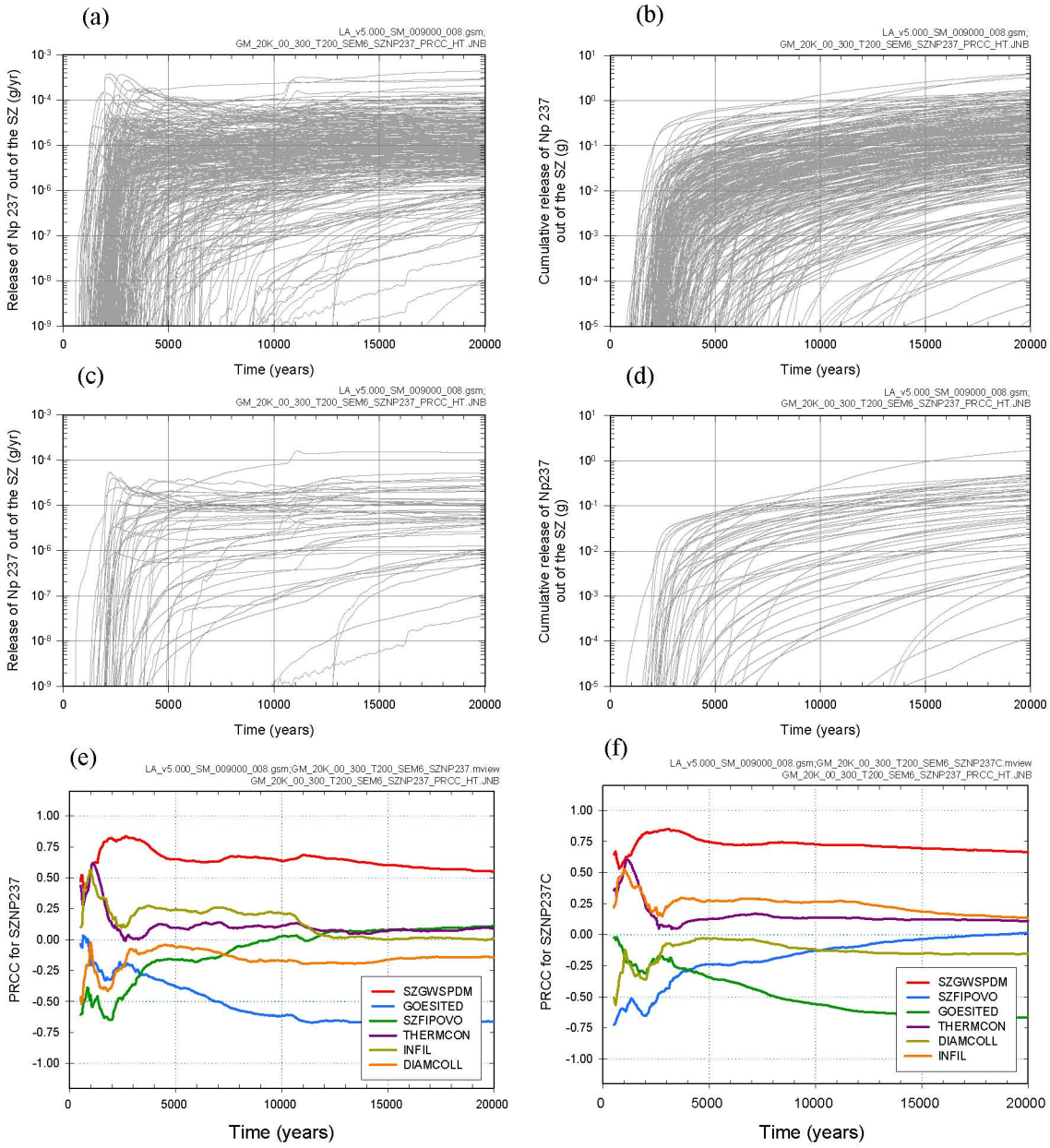

Source: Output DTNs: MO0709TSPASENS.000 [DIRS 183982]; and MO0709TSPAPLOT.000 [DIRS 183010].

Figure K7.5-3. Time-dependent release rates (*SZNP237*, g/yr) and cumulative (i.e., integrated) releases (*SZNP2379C*, g) over 20,000 years for the movement of dissolved ^{237}Np across a subsurface plane at the location of the RMEI resulting from a seismically induced fractional damaged area of 10^{-6}(32.6 m^2) at 200 years to all CDSP WPs in the repository: (a, b) *SZNP237* and *SZNP237C* for all (i.e., 300) sample elements, (c, d) *SZNP237* and *SZNP237C* for first 50 sample elements, and (e, f) PRCCs for *SZNP237* and *SZNP237C*

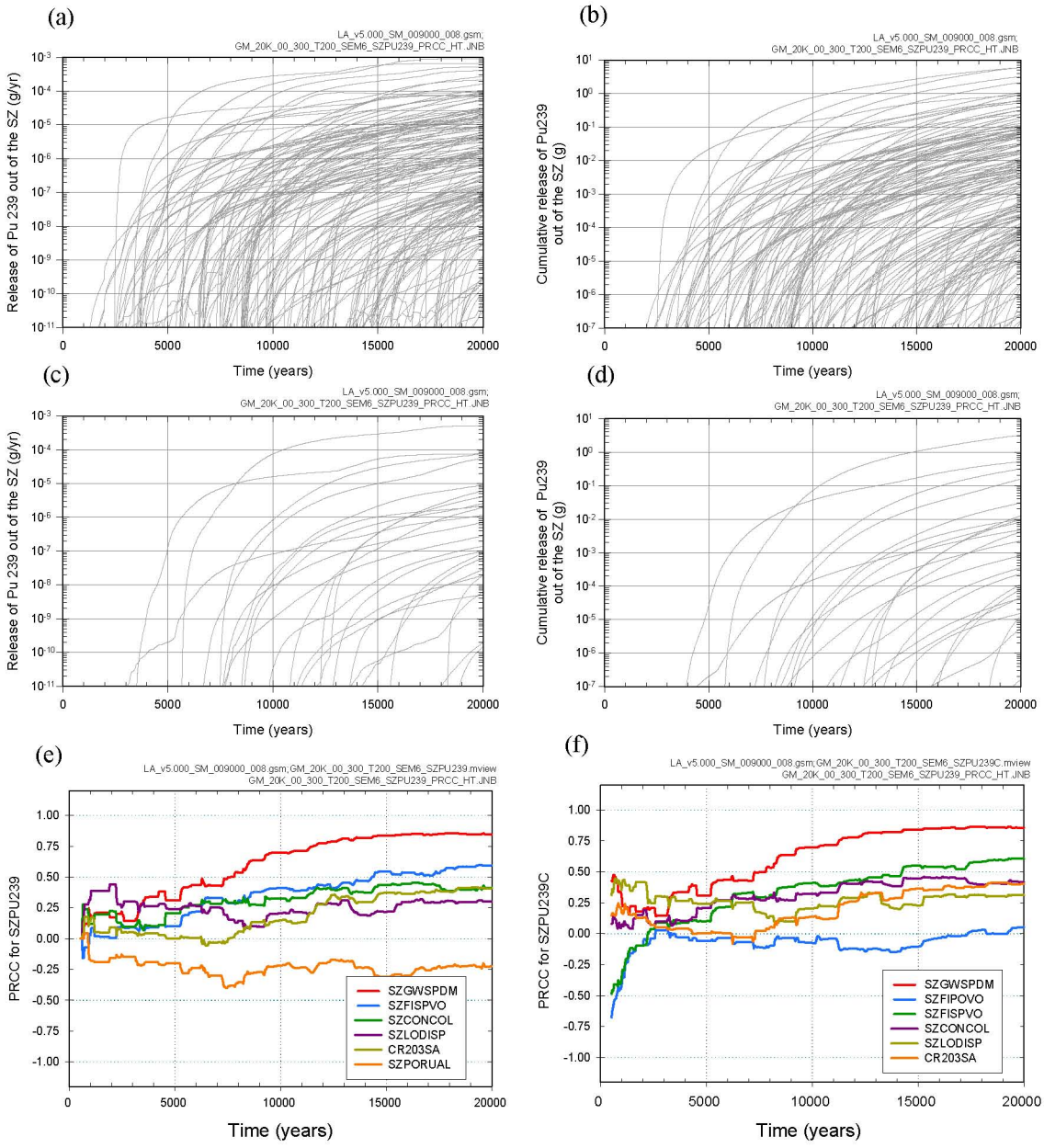

Source: Output DTNs: MO0709TSPASENS.000 [DIRS 183982]; and MO0709TSPAPLOT.000 [DIRS 183010].

Figure K7.5-4. Time-dependent release rates (*SZPU239*, g/yr) and cumulative (i.e., integrated) releases (*SZPU239C*, g) over 20,000 years for the movement of dissolved ^{239}Pu across a subsurface plane at the location of the RMEI resulting from a seismically induced fractional damaged area of 10^{-6}(32.6 m^2) at 200 years to all CDSP WPs in the repository: (a, b) *SZPU239* and *SZPU239C* for all (i.e., 300) sample elements, (c, d) *SZPU239* and *SZPU239C* for first 50 sample elements, and (e, f) PRCCs for *SZPU239* and *SZPU239C*

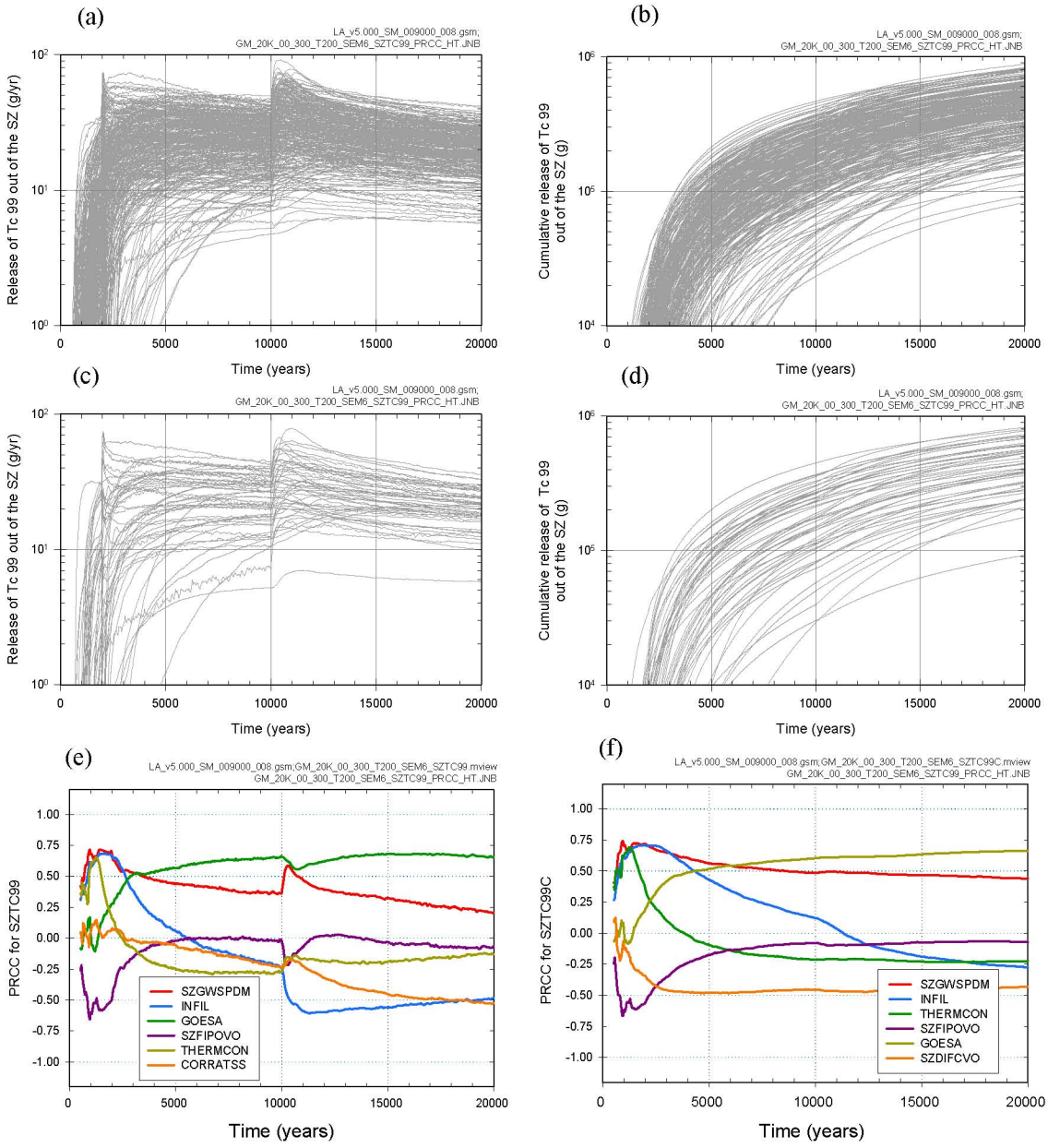

Source: Output DTNs: MO0709TSPASENS.000 [DIRS 183982]; and MO0709TSPAPLOT.000 [DIRS 183010].

Figure K7.5-5. Time-dependent release rates (*SZTC99*, g/yr) and cumulative (i.e., integrated) releases (*SZTC99C*, g) over 20,000 years for the movement of dissolved ^{99}Tc from across a subsurface plane at the location of the RMEI resulting from a seismically induced fractional damaged area of 10^{-6}(32.6 m^2) at 200 years to all CDSP WPs in the repository: (a, b) *SZTC99* and *SZTC99C* for all (i.e., 300) sample elements, (c, d) *SZTC99* and *SZTC99C* for first 50 sample elements, and (e, f) PRCCs for *SZTC99* and *SZTC99C*

INTENTIONALLY LEFT BLANK

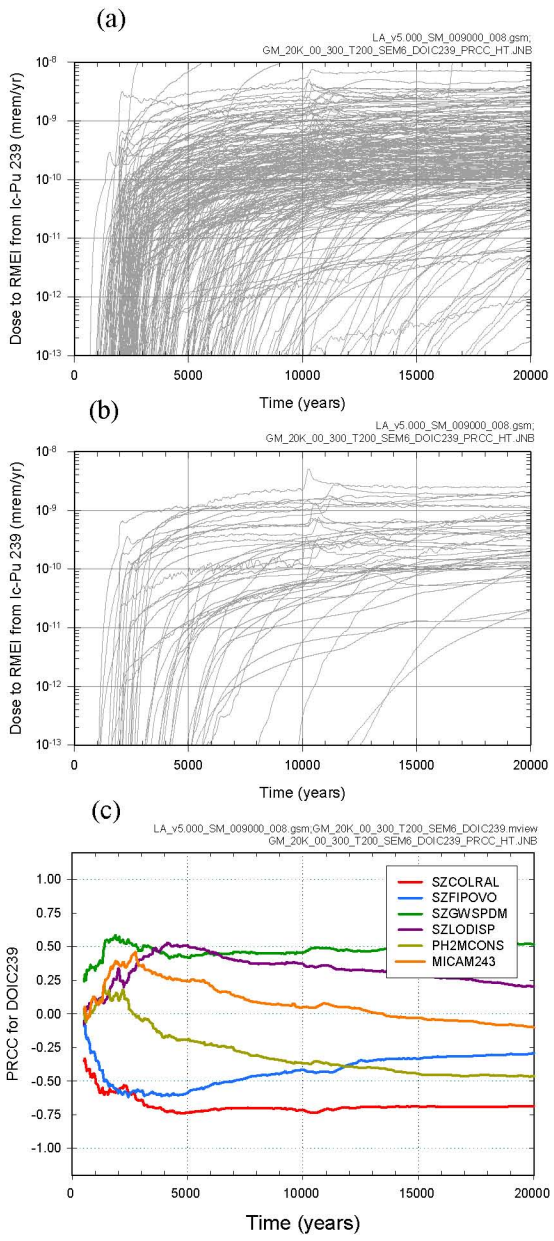

Source: Output DTNs: MO0709TSPASENS.000 [DIRS 183982]; and MO0709TSPAPLOT.000 [DIRS 183010].

Figure K.7.6-1. Time-dependent dose to the RMEI (*DOIC239*, mrem/yr) over 20,000 years for the movement of ^{239}Pu irreversibly attached to slow colloids across a subsurface plane at the location of the RMEI resulting from a seismically induced fractional damaged area of 10^{-6}(32.6 m^2) at 200 years to all CDSP WPs in the repository: (a) *DOIC239* for all (i.e., 300) sample elements, (b) *DOIC239* for first 50 sample elements, and (c) PRCCs for *DOIC239*

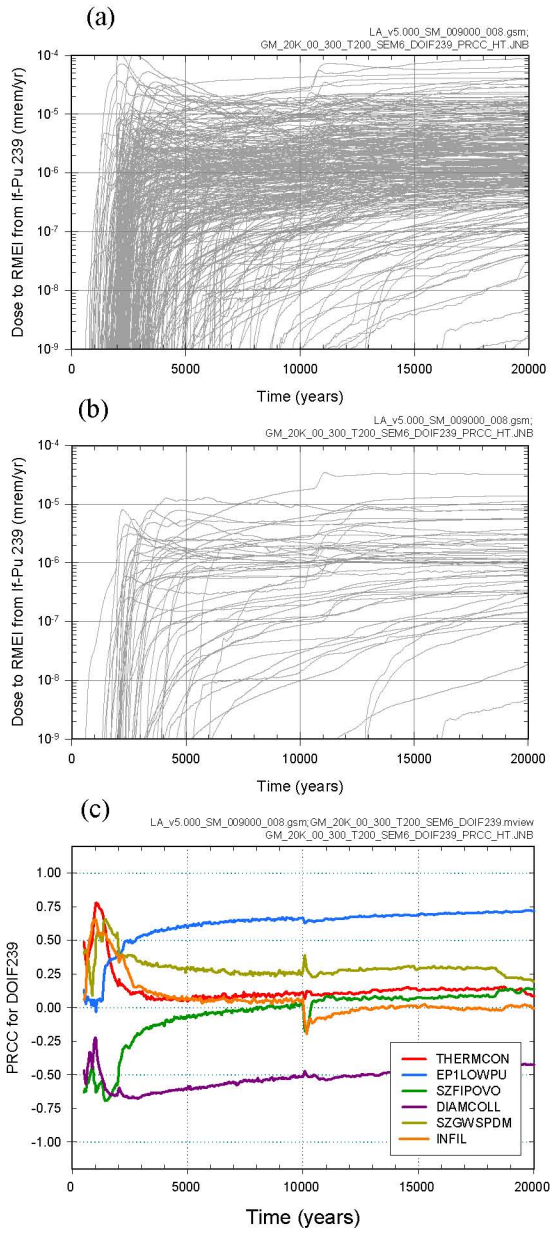

Source: Output DTNs: MO0709TSPASENS.000 [DIRS 183982]; and MO0709TSPAPLOT.000 [DIRS 183010].

Figure K.7.6-2. Time-dependent dose to the RMEI (*DOIF239*, mrem/yr) over 20,000 years for the movement of ^{239}Pu irreversibly attached to fast colloids across a subsurface plane at the location of the RMEI resulting from a seismically induced fractional damaged area of 10^{-6}(32.6 m^2) at 200 years to all CDSP WPs in the repository: (a) *DOIF239* for all (i.e., 300) sample elements, (b) *DOIF239* for first 50 sample elements, and (c) PRCCs for *DOIF239*

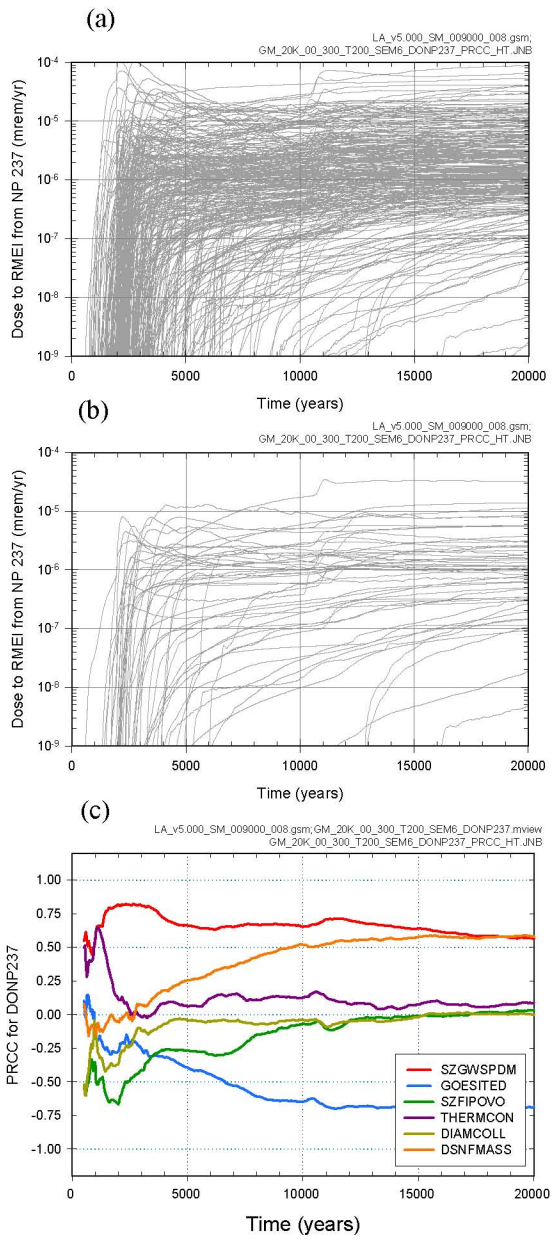

Source: Output DTNs: MO0709TSPASENS.000 [DIRS 183982]; and MO0709TSPAPLOT.000 [DIRS 183010].

Figure K.7.6-3. Time-dependent dose to the RMEI (*DONP237*, mrem/yr) over 20,000 years for the movement of dissolved ^{237}Np across a subsurface plane at the location of the RMEI resulting from a seismically induced fractional damaged area of 10^{-6}(32.6 m^2) at 200 years to all CDSP WPs in the repository: (a) *DONP237*for all (i.e., 300) sample elements, (b) *DONP237*for first 50 sample elements, and (c) PRCCs for *DONP237*

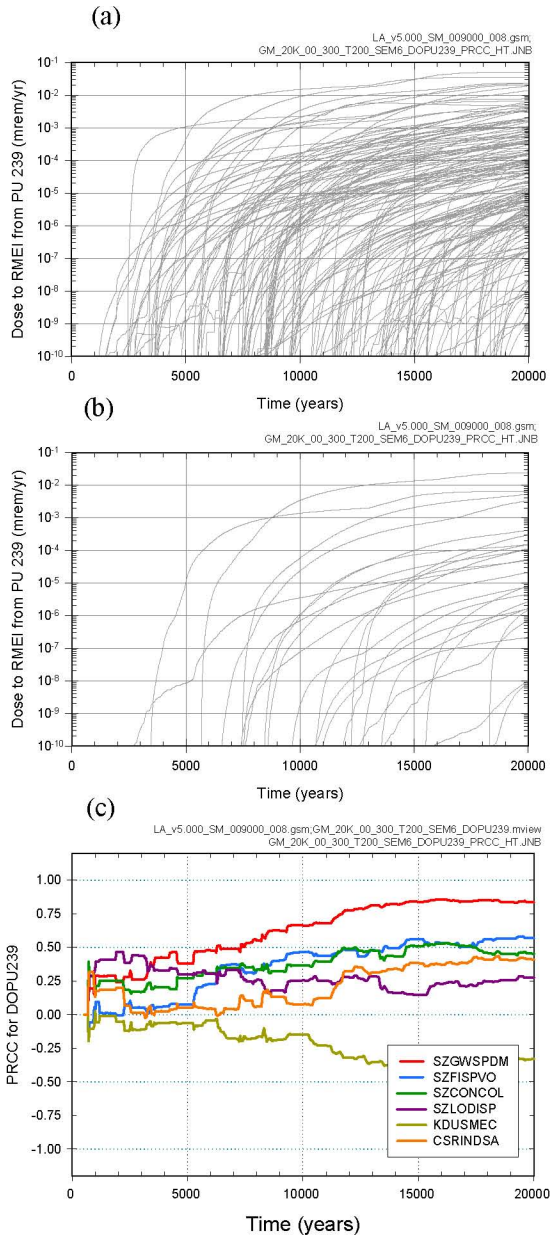

Source: Output DTNs: MO0709TSPASENS.000 [DIRS 183982]; and MO0709TSPAPLOT.000 [DIRS 183010].

Figure K.7.6-4. Time-dependent dose to the RMEI (*DOPU239*, mrem/yr) over 20,000 years for the movement of dissolved ^{239}Pu across a subsurface plane at the location of the RMEI resulting from a seismically induced fractional damaged area of 10^{-6}(32.6 m^2) at 200 years to all CDSP WPs in the repository: (a) *DOPU239* for all (i.e., 300) sample elements, (b) *DOPU239* for first 50 sample elements, and (c) PRCCs for *DOPU239*

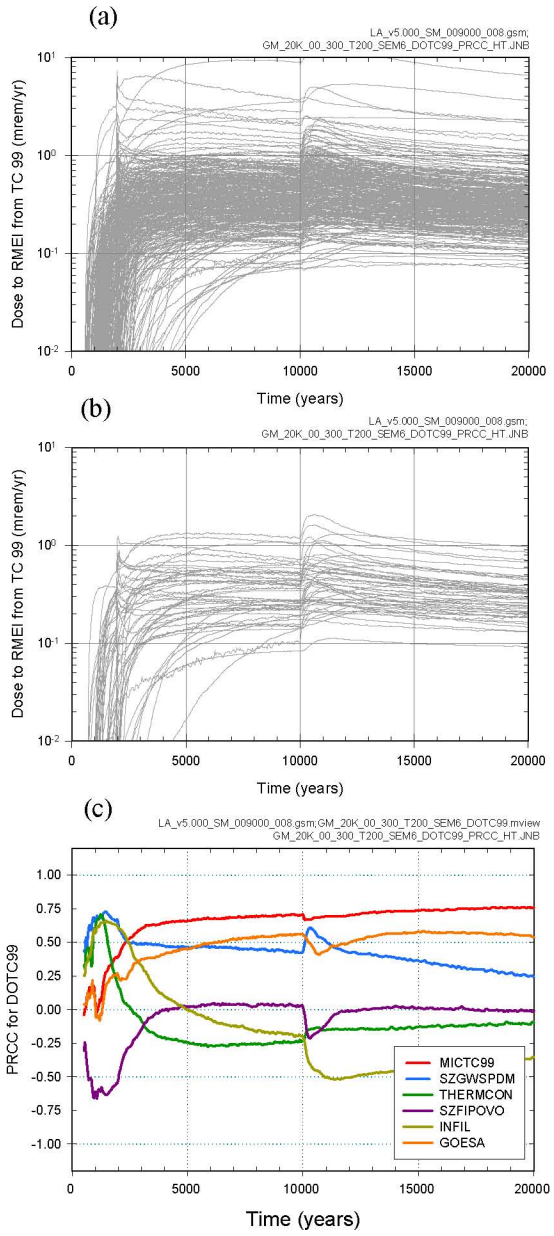

Source: Output DTNs: MO0709TSPASENS.000 [DIRS 183982]; and MO0709TSPAPLOT.000 [DIRS 183010].

Figure K.7.6-5. Time-dependent dose to the RMEI (*DOTC99*, mrem/yr) over 20,000 years for the movement of dissolved ^{99}Tc across a subsurface plane at the location of the RMEI resulting from a seismically induced fractional damaged area of 10^{-6}(32.6 m^2) at 200 years to all CDSP WPs in the repository: (a) *DOTC99*for all (i.e., 300) sample elements, (b) *DOTC99* for first 50 sample elements, and (c) PRCCs for *DOTC99*

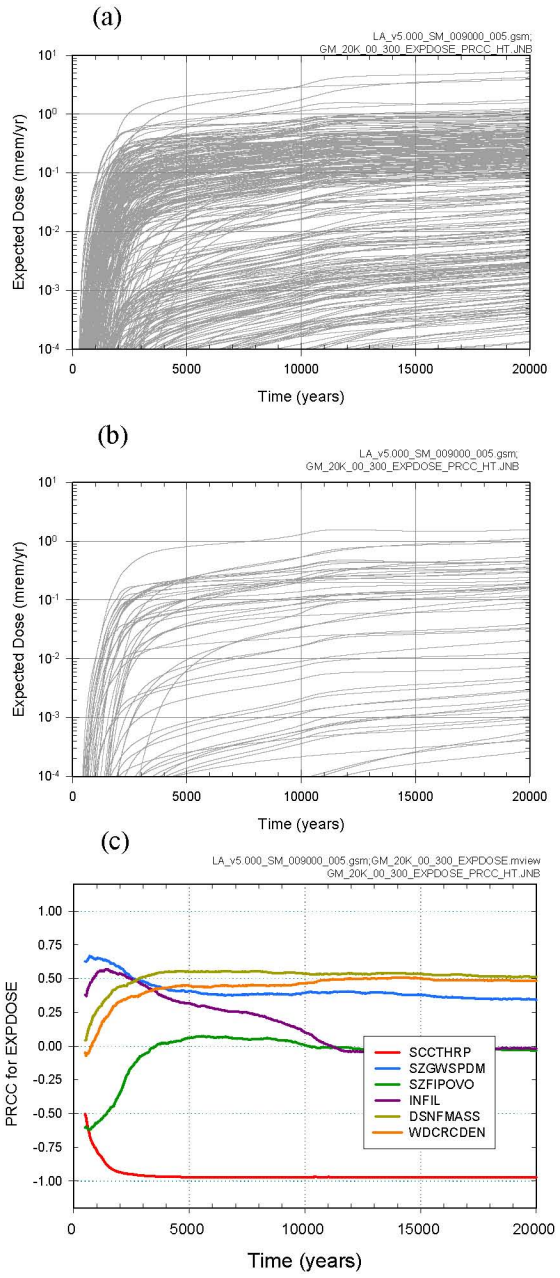

Source: Output DTNs: MO0709TSPAREGS.000 [DIRS 182976]; and MO0709TSPAPLOT.000 [DIRS 183010].

Figure K.7.7.1-1. Expected dose to RMEI (*EXPDOSE*, mrem/yr) over [0, 20,000 yr] for all radioactive species resulting from seismic ground motion: (a) *EXPDOSE* for all (i.e., 300) sample elements, (b) *EXPDOSE* for first 50 sample elements, and (c) PRCCs for *EXPDOSE*

(a)

	EXPDOSE: 3000 yr			EXPDOSE: 5000 yr			EXPDOSE: 10,000 yr		
Step[a]	**Variable[b]**	**R^{2c}**	**SRRC[d]**	**Variable**	**R^2**	**SRRC**	**Variable**	**R^2**	**SRRC**
1	SCCTHRP	0.81	-0.87	SCCTHRP	0.86	-0.91	SCCTHRP	0.87	-0.93
2	SZGWSPDM	0.83	0.16	MICTC99	0.88	0.09	MICTC99	0.89	0.12
3	INFIL	0.85	0.14	DSNFMASS	0.89	0.13	DSNFMASS	0.90	0.14
4	MICTC99	0.87	0.10	MICC14	0.90	0.10	HLWDRACD	0.91	0.09
5	DSNFMASS	0.87	0.12	SZGWSPDM	0.90	0.10	MICC14	0.92	0.08
6	MICC14	0.88	0.11	INFIL	0.91	0.07	WDCRCDEN	0.92	0.10
7	SZFISPVO	0.89	0.09	WDCRCDEN	0.92	0.09	SZGWSPDM	0.93	0.08
8	WDCRCDEN	0.90	0.08	HLWDRACD	0.92	0.07	PH2DHLNS	0.93	-0.07
9	SZDIFCVO	0.90	-0.07	SEEPUNC	0.93	0.06	WFDEGEXF	0.94	0.07
10	SEEPUNC	0.90	0.08	SZFISPVO	0.93	0.06	WDGCUA22	0.94	-0.05
11	GOESA	0.91	0.06	UZFAG8	0.93	-0.06	UZFAG8	0.94	-0.05
12	KDPUSMEC	0.91	0.06	WFDEGEXF	0.93	0.06	SEEPUNC	0.94	0.04
13	HLWDRACD	0.91	0.06	HLWDRALK	0.94	0.04	SZFISPVO	0.94	0.04
14	SZSREG4X	0.92	-0.06	KDUSMEC	0.94	0.04	HLWDRALK	0.95	0.04
15	SEEPPRM	0.92	-0.05	GOESA	0.94	0.04	UZGAM	0.95	-0.04
16	KDUSMEC	0.92	0.05	WDGCUA22	0.94	-0.04			

a: Steps in stepwise rank regression analysis
b: Variables listed in order of selection in stepwise regression
c: Cumulative R^2 value with entry of each variable into regression model
d: Standardized rank regression coefficients (SRRCs) in final regression model

Source: Output DTNs: MO0709TSPAREGS.000 [DIRS 182976]; and MO0709TSPAPLOT.000 [DIRS 183010].

Figure K.7.7.1-2. Stepwise rank regression analyses and selected scatterplots for expected dose to RMEI (*EXPDOSE*, mrem/yr) over [0, 20,000 yr] for all radioactive species resulting from seismic ground motion: (a) Regressions for *EXPDOSE* at 3000, 5000 and 10,000 years, and (b,c,d) Scatterplots for *EXPDOSE* at 10,000 years

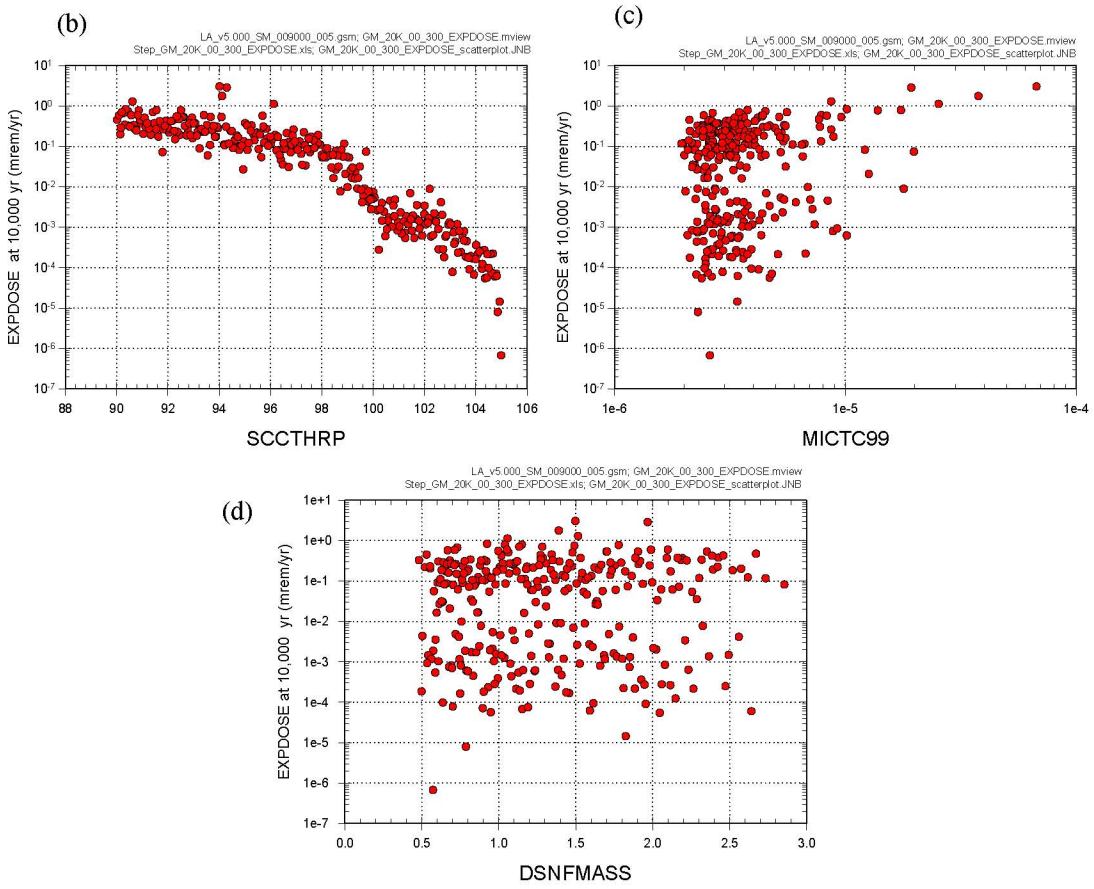

Source: Output DTNs: MO0709TSPAREGS.000 [DIRS 182976]; and MO0709TSPAPLOT.000 [DIRS 183010].

Figure K.7.7.1-2. Stepwise rank regression analyses and selected scatterplots for expected dose to RMEI (*EXPDOSE*, mrem/yr) over [0, 20,000 yr] for all radioactive species resulting from seismic ground motion: (a) Regressions for *EXPDOSE* at 3000, 5000 and 10,000 years, and (b,c,d) Scatterplots for *EXPDOSE* at 10,000 years (continued)

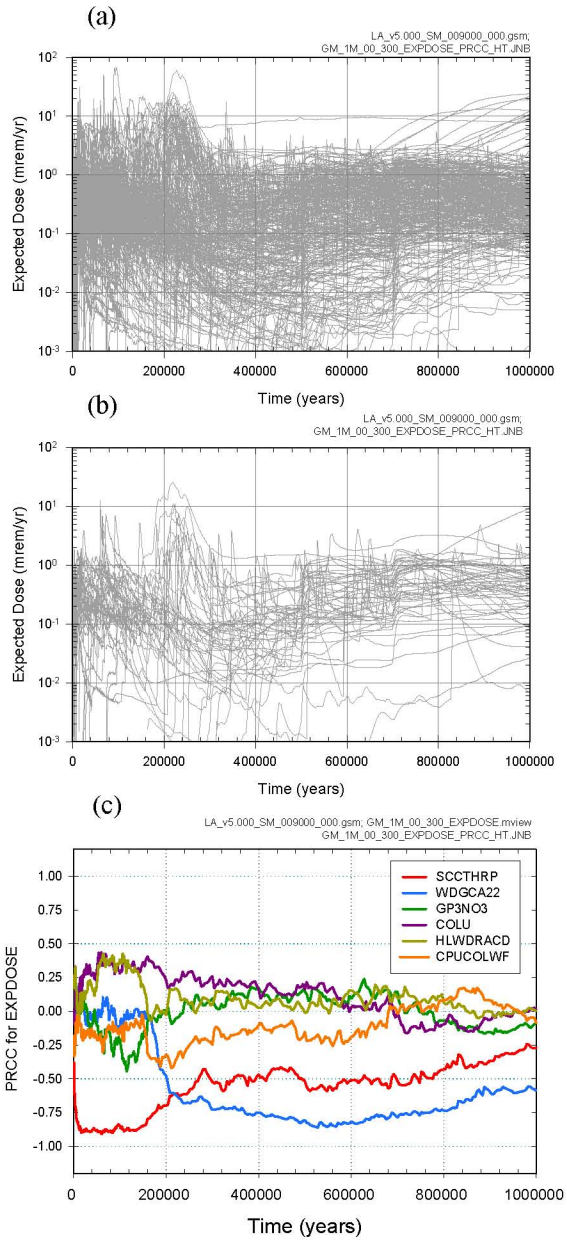

Source: OutputDTNs: MO0709TSPAREGS.000 [DIRS 182976]; and MO0709TSPAPLOT.000 [DIRS 183010].

Figure K.7.7.2-1. Expected dose to RMEI (*EXPDOSE*, mrem/yr) over [0, 1,000,000 yr] for all radioactive species resulting from seismic ground motion: (a) *EXPDOSE* for all (i.e., 300) sample elements, (b) *EXPDOSE* for first 50 sample elements, and (c) PRCCs for *EXPDOSE*

(a)

	EXPDOSE: 50,000 yr			EXPDOSE: 200,000 yr			EXPDOSE: 500,000 yr		
Step[a]	**Variable[b]**	**R^{2c}**	**SRRC[d]**	**Variable**	**R^2**	**SRRC**	**Variable**	**R^2**	**SRRC**
1	SCCTHRP	0.71	-0.85	SCCTHRP	0.47	-0.68	WDGCA22	0.45	-0.67
2	SZKDSEVO	0.73	-0.13	WDGCA22	0.53	-0.24	SCCTHRP	0.64	-0.40
3	CPUPERCS	0.74	0.11	MICTC99	0.55	0.12	WDNSCC	0.65	-0.15
4	MICTC99	0.75	0.10	SZKDAMAL	0.56	-0.11	SZGWSPDM	0.67	0.13
5	DSNFMASS	0.76	0.11				SZPORSAL	0.68	0.09
6	SEEPPRM	0.77	0.09				CORRATSS	0.69	-0.10
7	HLWDRACD	0.77	0.10				PH2DHLNS	0.70	0.10
8	KDAMCOL	0.78	-0.08				WDZOLID	0.71	0.09
9	SZLODISP	0.79	-0.08						

a: Steps in stepwise rank regression analysis
b: Variables listed in order of selection in stepwise regression
c: Cumulative R^2 value with entry of each variable into regression model
d: Standardized rank regression coefficients (SRRCs) in final regression model

Source: Output DTNs: MO0709TSPAREGS.000 [DIRS 182976]; and MO0709TSPAPLOT.000 [DIRS 183010].

Figure K.7.7.2-2. Stepwise rank regression analyses and selected scatterplots for expected dose to RMEI (*EXPDOSE*, mrem/yr) over [0, 1,000,000 yr] for all radioactive species resulting from seismic ground motion: (a) Regressions for *EXPDOSE* at 50,000, 200,000 and 500,000 years, and (b,c,d) Scatterplots for *EXPDOSE* at 500,000 years

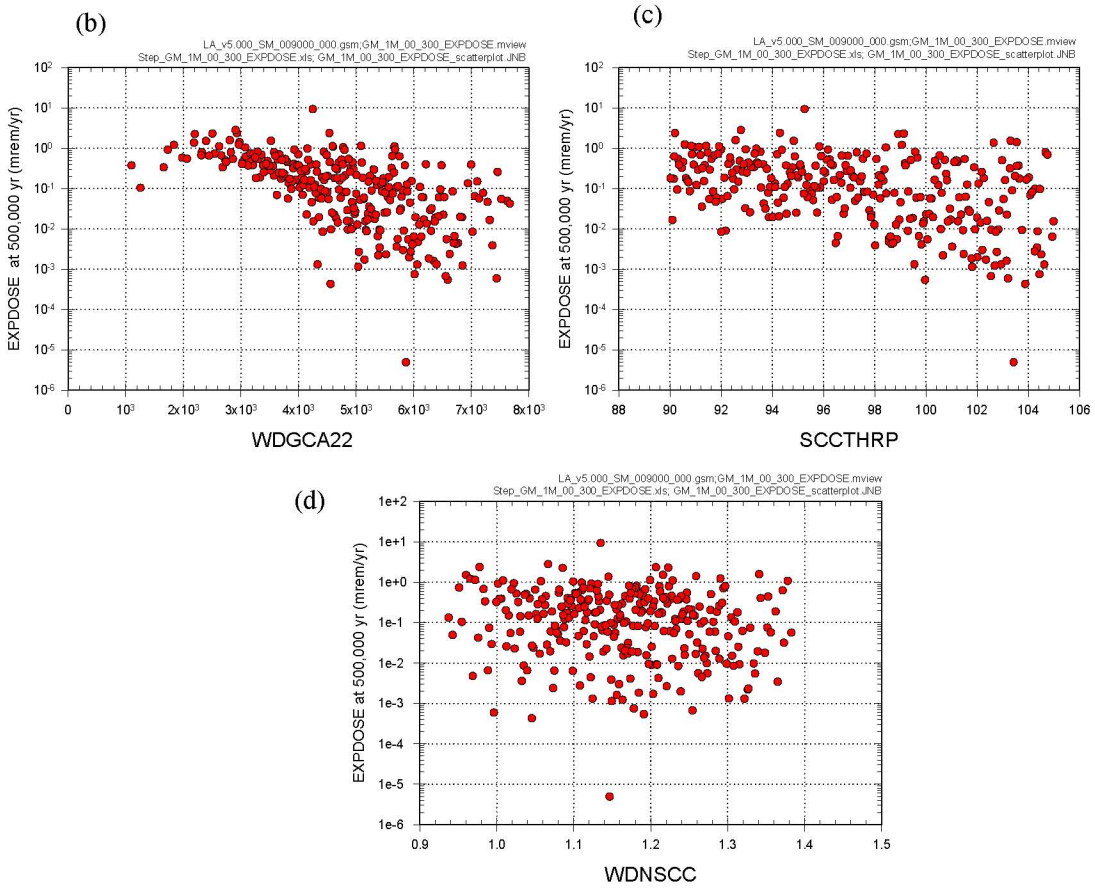

Source: Output DTNs: MO0709TSPAREGS.000 [DIRS 182976]; and MO0709TSPAPLOT.000 [DIRS 183010].

Figure K.7.7.2-2. Stepwise rank regression analyses and selected scatterplots for expected dose to RMEI (*EXPDOSE*, mrem/yr) over [0, 1,000,000 yr] for all radioactive species resulting from seismic ground motion: (a) Regressions for *EXPDOSE* at 50,000, 200,000 and 500,000 years, and (b,c,d) Scatterplots for *EXPDOSE* at 500,000 years (continued)

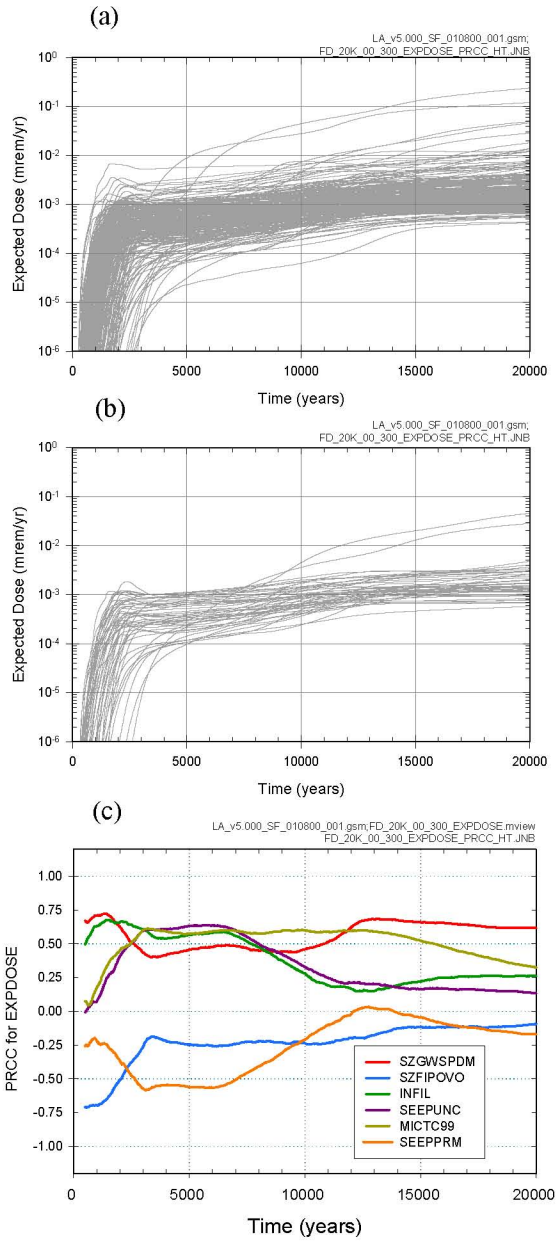

Source: Output DTNs: MO0709TSPAREGS.000 [DIRS 182976]; and MO0709TSPAPLOT.000 [DIRS 183010].

Figure K.7.8.1-1. Expected dose to RMEI (*EXPDOSE*, mrem/yr) over [0, 20,000 yr] for all radioactive species resulting from seismic fault displacement: (a) *EXPDOSE* for all (i.e., 300) sample elements, (b) *EXPDOSE* for first 50 sample elements, and (c) PRCCs for *EXPDOSE*

(a)

	EXPDOSE: 3000 yr			EXPDOSE: 5000 yr			EXPDOSE: 10,000 yr		
Step[a]	**Variable[b]**	**R^{2c}**	**SRRC[d]**	**Variable**	**R^2**	**SRRC**	**Variable**	**R^2**	**SRRC**
1	INFIL	0.16	0.40	MICTC99	0.16	0.39	MICTC99	0.21	0.44
2	MICTC99	0.30	0.36	INFIL	0.32	0.41	SZGWSPDM	0.30	0.32
3	SZGWSPDM	0.39	0.31	SEEPPRM	0.42	-0.30	DTDRHUNC	0.39	0.25
4	SEEPPRM	0.47	-0.27	SEEPUNC	0.49	0.30	INFIL	0.45	0.25
5	SEEPUNC	0.55	0.29	SZGWSPDM	0.57	0.26	SZFISPVO	0.49	0.23
6	CSSPECSA	0.60	0.22	CSSPECSA	0.61	0.22	SEEPPRM	0.52	-0.15
7	SZFISPVO	0.64	0.22	SZFISPVO	0.65	0.20	CSNFMASS	0.54	0.16
8	CSNFMASS	0.66	0.16	CSNFMASS	0.67	0.18	SZCOLRAL	0.56	-0.16
9	MICC14	0.68	0.14	ALPHAL	0.69	-0.16	SZDIFCVO	0.59	-0.16
10	SZDIFCVO	0.70	-0.15	MICC14	0.70	0.12	SZFIPOVO	0.61	-0.15
11	ALPHAL	0.71	-0.13	SZDIFCVO	0.71	-0.13	MICAM243	0.62	0.13
12	THERMCON	0.72	-0.09	SZFIPOVO	0.73	-0.10	CSSPECSA	0.63	0.13
13	SZFIPOVO	0.73	-0.09	SZCOLRAL	0.74	-0.11	CSWFA4AC	0.64	0.12
14	SZCOLRVO	0.74	-0.08	SZCOLRVO	0.74	-0.11	KDUSMEC	0.65	0.11
15				CSWFA4AC	0.75	0.09	INRFRCSR	0.66	0.10
16							ALPHAL	0.67	-0.10

a: Steps in stepwise rank regression analysis
b: Variables listed in order of selection in stepwise regression
c: Cumulative R^2 value with entry of each variable into regression model
d: Standardized rank regression coefficients (SRRCs) in final regression model

Source: Output DTNs: MO0709TSPAREGS.000 [DIRS 182976]; and MO0709TSPAPLOT.000 [DIRS 183010].

Figure K.7.8.1-2. Stepwise rank regression analyses and selected scatterplots for expected dose to RMEI (*EXPDOSE*, mrem/yr) over [0, 20,000 yr] for all radioactive species resulting from seismic fault displacement: (a) Regressions for *EXPDOSE* at 3000, 5000 and 10,000 years, and (b,c,d) Scatterplots for *EXPDOSE* at 10,000 years

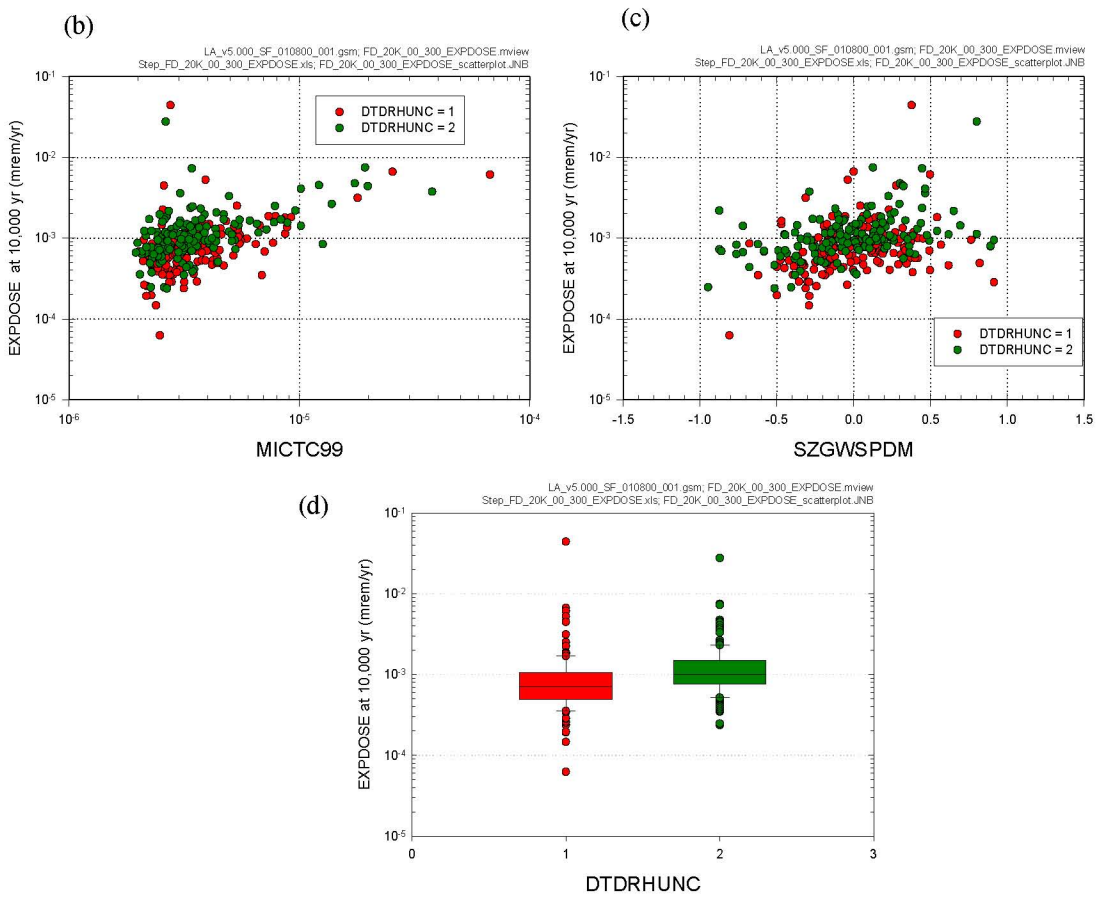

Source: Output DTNs: MO0709TSPAREGS.000 [DIRS 182976]; and MO0709TSPAPLOT.000 [DIRS 183010].

NOTE: In (d), the box extends from 0.25 to 0.75 quantile; lower and upper bar and whisker extend to 0.1 and 0.9 quantile, respectively; dots represent values outside 0.1 to 0.9 quantile range; median indicated by light horizontal line.

Figure K.7.8.1-2. Stepwise rank regression analyses and selected scatterplots for expected dose to RMEI (*EXPDOSE*, mrem/yr) over [0, 20,000 yr] for all radioactive species resulting from seismic fault displacement: (a) Regressions for *EXPDOSE* at 3000, 5000 and 10,000 years, and (b,c,d) Scatterplots for *EXPDOSE* at 10,000 years (continued).

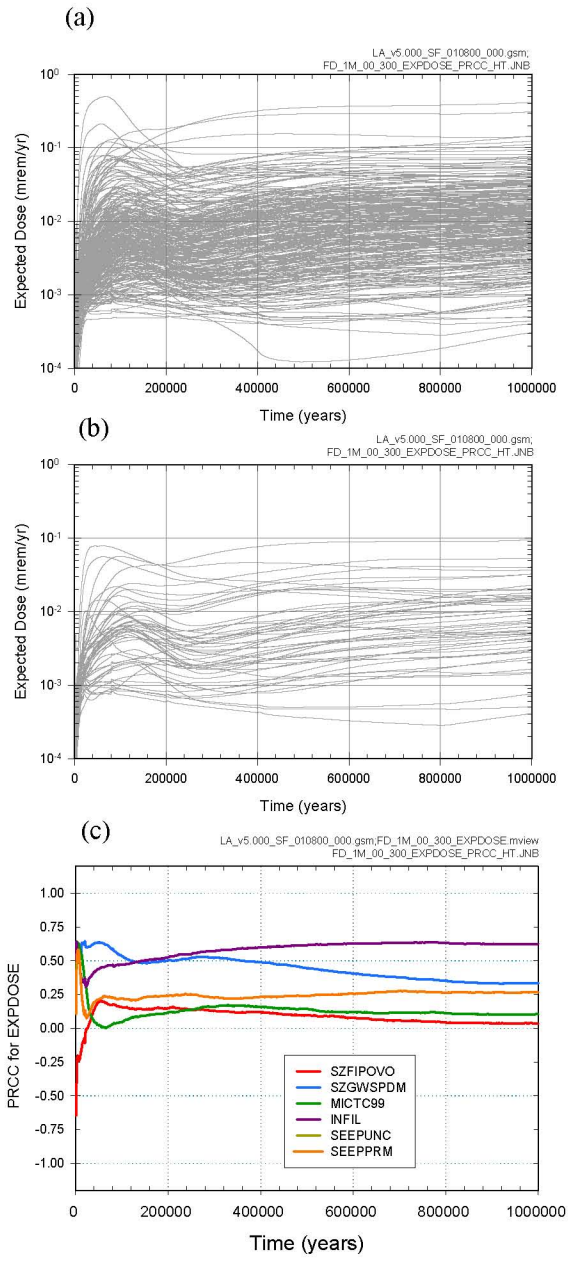

Source: Output DTNs: MO0709TSPAREGS.000 [DIRS 182976]; and MO0709TSPAPLOT.000 [DIRS 183010].

Figure K.7.8.2-1. Expected dose to RMEI (*EXPDOSE*, mrem/yr) over [0, 1,000,000 yr] for all radioactive species resulting from seismic fault displacement: (a) *EXPDOSE* for all (i.e., 300) sample elements, (b) *EXPDOSE* for first 50 sample elements, and (c) PRCCs for *EXPDOSE*

(a)

	EXPDOSE: 50,000 yr			EXPDOSE: 200,000 yr			EXPDOSE: 500,000 yr		
Step[a]	**Variable[b]**	**R^{2c}**	**SRRC[d]**	**Variable**	**R^2**	**SRRC**	**Variable**	**R^2**	**SRRC**
1	SZGWSPDM	0.28	0.51	SZGWSPDM	0.17	0.44	INFIL	0.16	0.39
2	INFIL	0.40	0.31	INFIL	0.31	0.34	SZGWSPDM	0.31	0.44
3	WPFLUX	0.45	0.23	WPFLUX	0.39	0.29	EP1LOWPU	0.39	0.30
4	EP1LOWPU	0.49	0.20	EP1LOWPU	0.45	0.25	WPFLUX	0.45	0.25
5	MICNP237	0.53	0.17	MICNP237	0.49	0.15	GOESITED	0.49	-0.16
6	CPUCOLWF	0.56	0.20	SZCONCOL	0.51	0.15	SZCONCOL	0.52	0.15
7	SEEPPRM	0.58	-0.18	SEEPPRM	0.54	-0.15	MICNP237	0.55	0.13
8	SZFISPVO	0.60	0.13	SZFISPVO	0.56	0.14	EP1LOWNU	0.57	0.18
9	SZCOLRAL	0.62	-0.13	SEEPUNC	0.58	0.14	SEEPUNC	0.59	0.15
10	MICTC99	0.63	0.11	EP1NPO2	0.59	0.13	SZFISPVO	0.61	0.12
11	HFOSA	0.65	-0.10	EP1LOWNU	0.61	0.13	HFOSA	0.63	-0.12
12	PHCSS	0.66	-0.13	SZDIFCVO	0.63	-0.15	SEEPPRM	0.64	-0.15
13	SZRAHAVO	0.67	0.10	SZKDAMCO	0.64	0.13	UZFAG4	0.66	-0.14
14	PH2RGER	0.68	-0.10	SZSREG1Y	0.66	0.14	KDPUSMEC	0.67	0.13
15	KDPUSMEC	0.69	0.10	MICAM243	0.67	0.11	MICRA226	0.68	0.11
16	SEEPUNC	0.69	0.10	GOESITED	0.68	-0.09	SZWBNDAL	0.69	-0.10

a: Steps in stepwise rank regression analysis
b: Variables listed in order of selection in stepwise regression
c: Cumulative R^2 value with entry of each variable into regression model
d: Standardized rank regression coefficients (SRRCs) in final regression model

Source: Output DTNs: MO0709TSPAREGS.000 [DIRS 182976]; and MO0709TSPAPLOT.000 [DIRS 183010].

Figure K.7.8.2-2. Stepwise rank regression analyses and selected scatterplots for expected dose to RMEI (*EXPDOSE*, mrem/yr) over [0, 1,000,000 yr] for all radioactive species resulting from seismic fault displacement: (a) Regressions for *EXPDOSE* at 50,000, 200,000 and 500,000 years, and (b,c,d) Scatterplots for *EXPDOSE* at 500,000 years

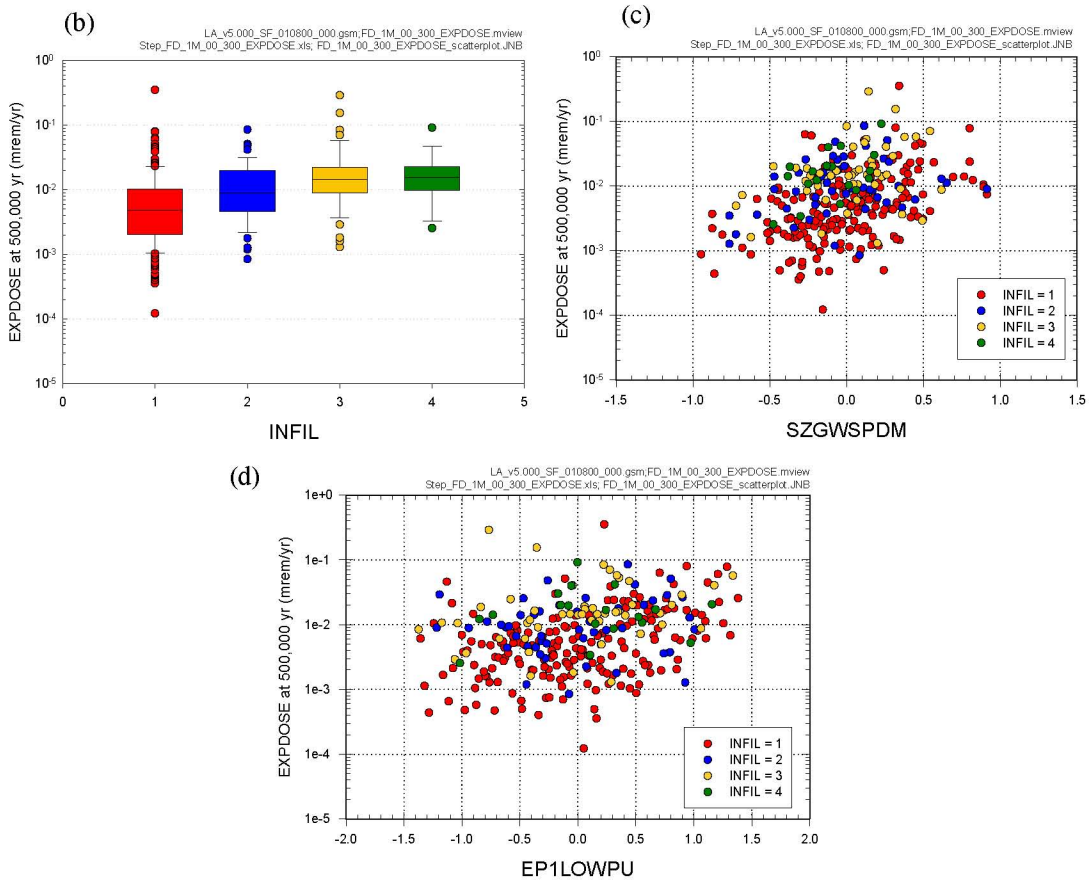

Source: Output DTNs: MO0709TSPAREGS.000 [DIRS 182976]; and MO0709TSPAPLOT.000 [DIRS 183010].

NOTE: In (b), the box extends from 0.25 to 0.75 quantile; lower and upper bar and whisker extend to 0.1 and 0.9 quantile, respectively; dots represent values outside 0.1 to 0.9 quantile range; median indicated by light horizontal line.

Figure K.7.8.2-2. Stepwise rank regression analyses and selected scatterplots for expected dose to RMEI (*EXPDOSE*, mrem/yr) over [0, 1,000,000 yr] for all radioactive species resulting from seismic fault displacement: (a) Regressions for *EXPDOSE* at 50,000, 200,000 and 500,000 years, and (b,c,d) Scatterplots for *EXPDOSE* at 500,000 years (continued).

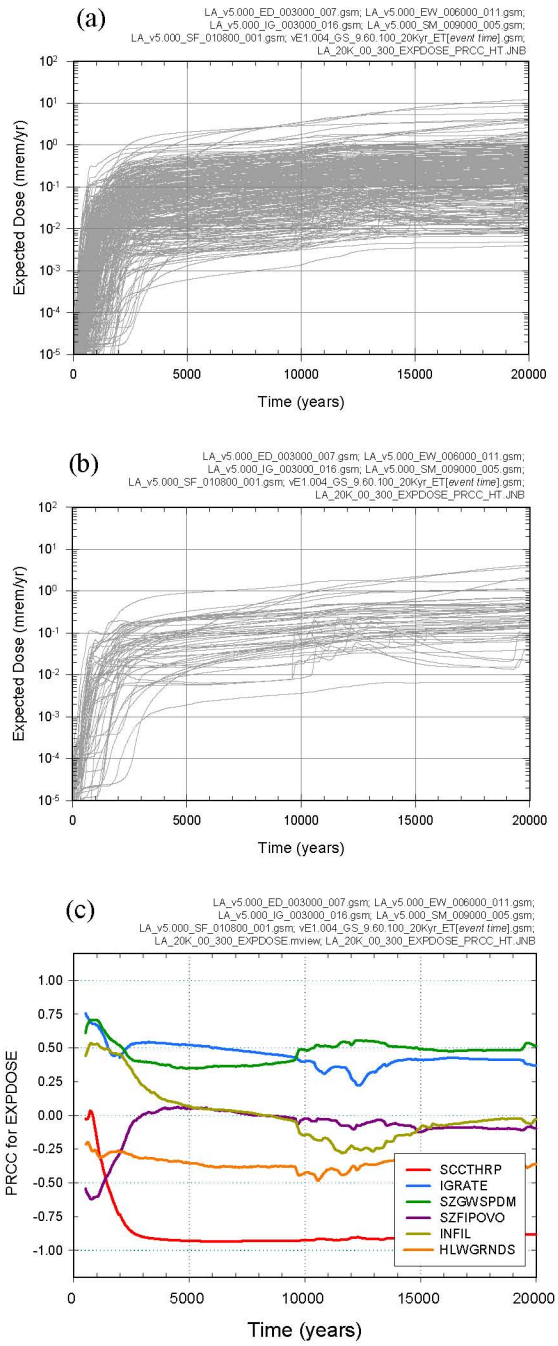

Source: Output DTNs: MO0709TSPAREGS.000 [DIRS 182976]; and MO0709TSPAPLOT.000 [DIRS 183010].

Figure K.8.1-1. Expected dose to RMEI (*EXPDOSE*, mrem/yr) over [0, 20,000 yr] for all scenario classes: (a) *EXPDOSE* for all (i.e., 300) sample elements, (b) *EXPDOSE* for first 50 sample elements, and (c) PRCCs for *EXPDOSE*

(a)

	EXPDOSE: 3000 yr			EXPDOSE: 5000 yr			EXPDOSE: 10,000 yr		
Step[a]	**Variable[b]**	**R^{2c}**	**SRRC[d]**	**Variable**	**R^2**	**SRRC**	**Variable**	**R^2**	**SRRC**
1	SCCTHRP	0.55	-0.71	SCCTHRP	0.66	-0.80	SCCTHRP	0.69	-0.82
2	IGRATE	0.62	0.29	IGRATE	0.72	0.25	IGRATE	0.73	0.22
3	SZGWSPDM	0.67	0.21	MICTC99	0.74	0.15	SZGWSPDM	0.76	0.17
4	INFIL	0.71	0.19	SZGWSPDM	0.77	0.14	MICTC99	0.78	0.14
5	MICTC99	0.73	0.16	MICC14	0.78	0.12	WFDEGEXF	0.79	0.11
6	MICC14	0.75	0.12	INFIL	0.80	0.12	MICC14	0.80	0.10
7	SZFISPVO	0.76	0.14	WFDEGEXF	0.81	0.10	UZGAM	0.81	-0.10
8	DSNFMASS	0.77	0.09	UZGAM	0.81	-0.10	WDGCUA22	0.81	-0.07
9	UZFAG8	0.77	-0.09	DSNFMASS	0.82	0.11	HLWGRNDS	0.82	-0.08
10	KDUSMEC	0.78	0.08	SZFISPVO	0.83	0.08	CSWFA0AC	0.82	-0.07
11	MICPA231	0.79	-0.08	UZFAG8	0.83	-0.09	UZFAG5	0.83	-0.07
12	WFDEGEXF	0.79	0.08	WDGCUA22	0.84	-0.07			
13	UZGAM	0.80	-0.08	WDCRCDEN	0.84	0.07			
14	SZDIFCVO	0.80	-0.08	WDZOLID	0.84	-0.07			

a: Steps in stepwise rank regression analysis
b: Variables listed in order of selection in stepwise regression
c: Cumulative R^2 value with entry of each variable into regression model
d: Standardized rank regression coefficients (SRRCs) in final regression model

Source: Output DTNs: MO0709TSPAREGS.000 [DIRS 182976]; and MO0709TSPAPLOT.000 [DIRS 183010].

Figure K.8.1.-2. Stepwise rank regression analyses and selected scatterplots for expected dose to RMEI (*EXPDOSE*, mrem/yr) over [0, 20,000 yr] for all scenario classes: (a) Regressions for *EXPDOSE* at 3000, 5000 and 10,000 years, and (b,c,d) Scatterplots for *EXPDOSE* at 10,000 years

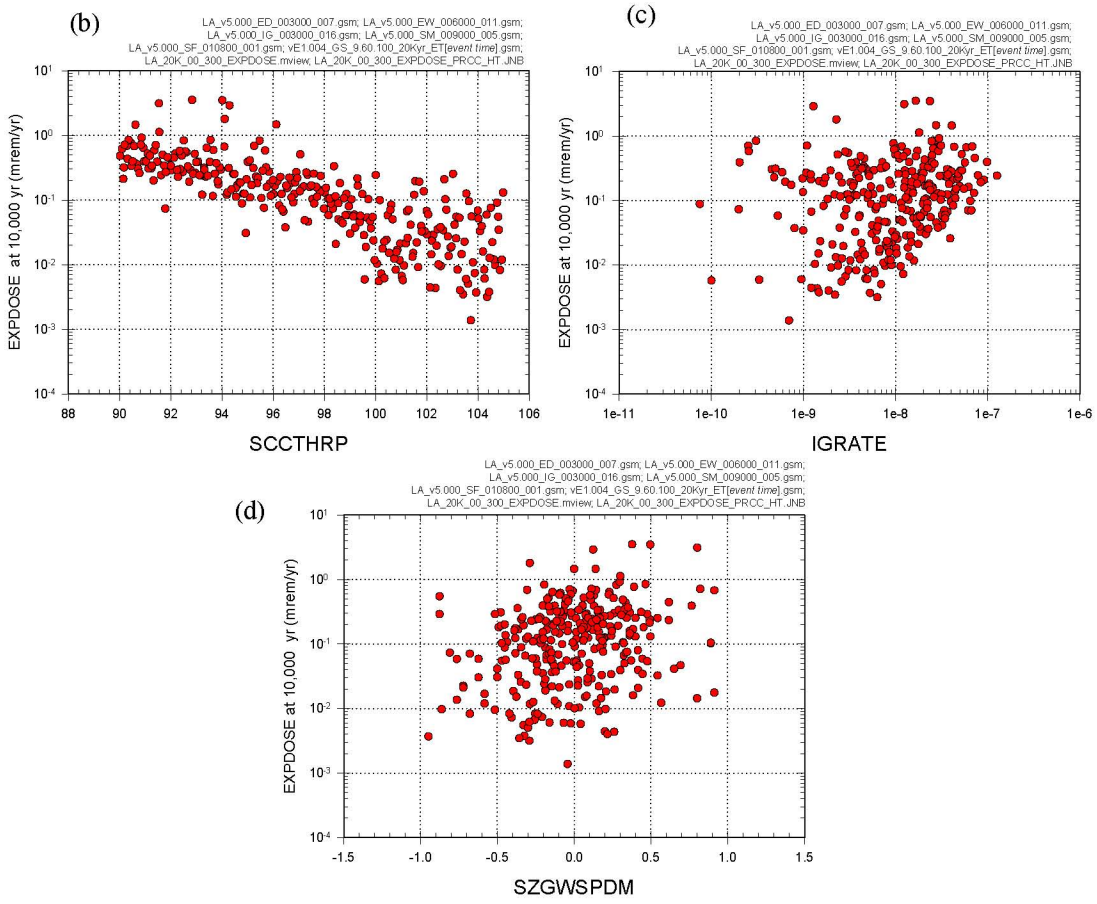

Source: Output DTNs: MO0709TSPAREGS.000 [DIRS 182976]; and MO0709TSPAPLOT.000 [DIRS 183010].

Figure K.8.1.-2. Stepwise rank regression analyses and selected scatterplots for expected dose to RMEI (*EXPDOSE*, mrem/yr) over [0, 20,000 yr] for all scenario classes: (a) Regressions for *EXPDOSE* at 3000, 5000 and 10,000 years, and (b,c,d) Scatterplots for *EXPDOSE* at 10,000 years (continued)

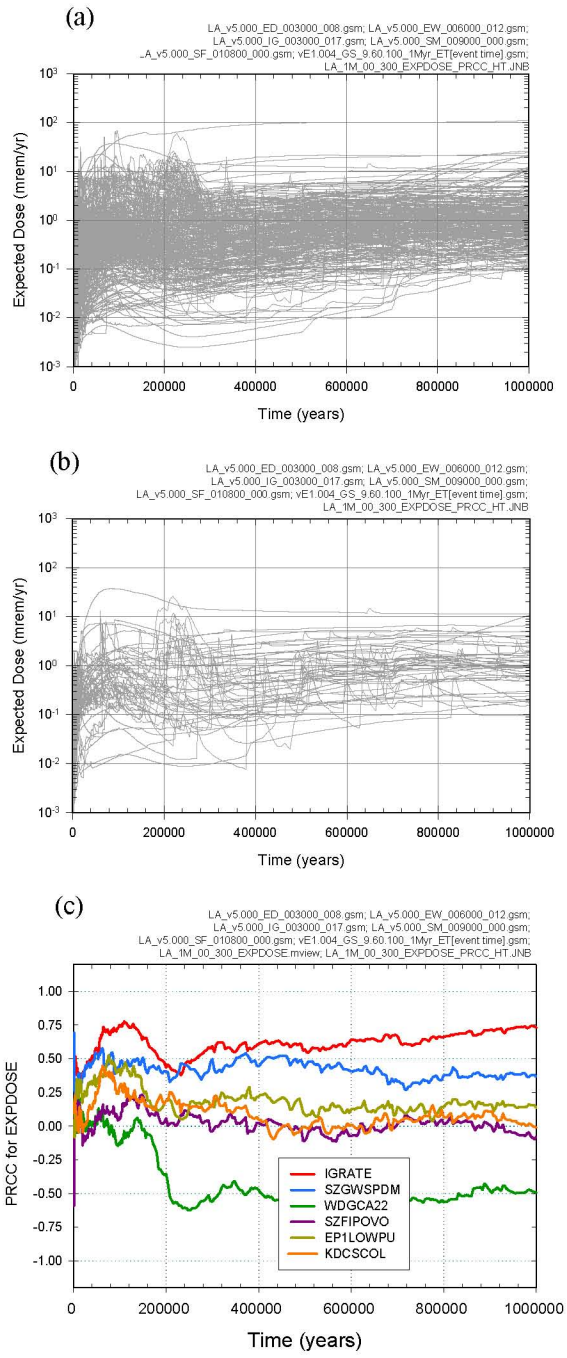

Source: Output DTNs: MO0709TSPAREGS.000 [DIRS 182976]; and MO0709TSPAPLOT.000 [DIRS 183010].

Figure K.8.2-1. Expected dose to RMEI (*EXPDOSE*, mrem/yr) over [0, 1,000,000 yr] for all scenario classes: (a) *EXPDOSE* for all (i.e., 300) sample elements, (b) *EXPDOSE* for first 50 sample elements, and (c) PRCCs for *EXPDOSE*

(a)

	50,000 Years			200,000 Years			500,000 Years		
Step[a]	Variable[b]	R^{2c}	SRRC[d]	Variable	R^2	SRRC	Variable	R^2	SRRC
1	SCCTHRP	0.31	-0.53	IGRATE	0.23	0.47	IGRATE	0.29	0.52
2	IGRATE	0.45	0.40	SCCTHRP	0.34	-0.28	WDGCA22	0.41	-0.31
3	SZGWSPDM	0.56	0.31	SZGWSPDM	0.43	0.29	SZGWSPDM	0.52	0.31
4	EP1LOWPU	0.59	0.17	WDGCA22	0.51	-0.30	EP1LOWNU	0.56	0.18
5	MICNP237	0.61	0.10	EP1LOWNU	0.53	0.15	MICNP237	0.59	0.18
6	INFIL	0.63	0.14	EP1LOWPU	0.55	0.14	SCCTHRP	0.61	-0.15
7	WFDEGEXF	0.64	0.11	MICSR90	0.56	0.13	SZCONCOL	0.63	0.13
8	EP1NPO2	0.65	0.12	SCHOBOLT	0.57	0.11	EP1LOWPU	0.64	0.14
9	MICTC99	0.67	0.11				SZFISPVO	0.66	0.14
10							SZDIFCVO	0.67	-0.12
11							RHMU20	0.68	0.10
12							SZKDSNAL	0.69	-0.10
13							INFIL	0.70	0.09
14							WDGCUA22	0.71	0.09

	126,000 Years			252,000 Years			1,000,000 Years		
Step[a]	Variable	R^{2c}	SRRC[d]	Variable	R^2	SRRC	Variable	R^2	SRRC
1	IGRATE	0.29	0.56	WDGCA22	0.23	-0.46	IGRATE	0.32	0.56
2	SCCTHRP	0.46	-0.38	IGRATE	0.37	0.37	WDGCA22	0.41	-0.27
3	SZGWSPDM	0.57	0.29	SZGWSPDM	0.44	0.22	SZGWSPDM	0.49	0.28
4	EP1LOWPU	0.61	0.18	SCCTHRP	0.48	-0.18	CSNFMASS	0.53	0.14
5	MICNP237	0.64	0.12	EP1LOWNU	0.52	0.18	SZCONCOL	0.55	0.15
6	INFIL	0.66	0.16	MICNP237	0.54	0.15	EP1LOWNU	0.57	0.16
7	MICSE79	0.67	0.11	SZFISPVO	0.56	0.15	MICNP237	0.59	0.14
8	SZDIFCVO	0.68	-0.13	EP1LOWPU	0.57	0.14	SZFISPVO	0.61	0.14
9	SZFISPVO	0.69	0.10	UZFAG6	0.59	0.14	SZDIFCVO	0.62	-0.13
10	EP1NPO2	0.70	0.11	SZKDCSVO	0.60	-0.13	SCCTHRP	0.63	-0.10
11	MICTC99	0.72	0.12	RHMU0	0.61	0.11			
12	SZKDSEAL	0.72	-0.08	WDZOLID	0.62	0.10			

a: Steps in stepwise rank regression analysis
b: Variables listed in order of selection in stepwise regression
c: Cumulative R^2 value with entry of each variable into regression model
d: Standardized rank regression coefficients (SRRCs) in final regression model

Source: Output DTNs: MO0709TSPAREGS.000 [DIRS 182976]; and MO0709TSPAPLOT.000 [DIRS 183010].

Figure K.8.2-2. Stepwise rank regression analyses and selected scatterplots for expected dose to RMEI (*EXPDOSE*, mrem/yr) over [0, 1,000,000 yr] for all scenario classes: (a) Regressions for *EXPDOSE* and (b,c,d) Scatterplots for *EXPDOSE* at 500,000 years

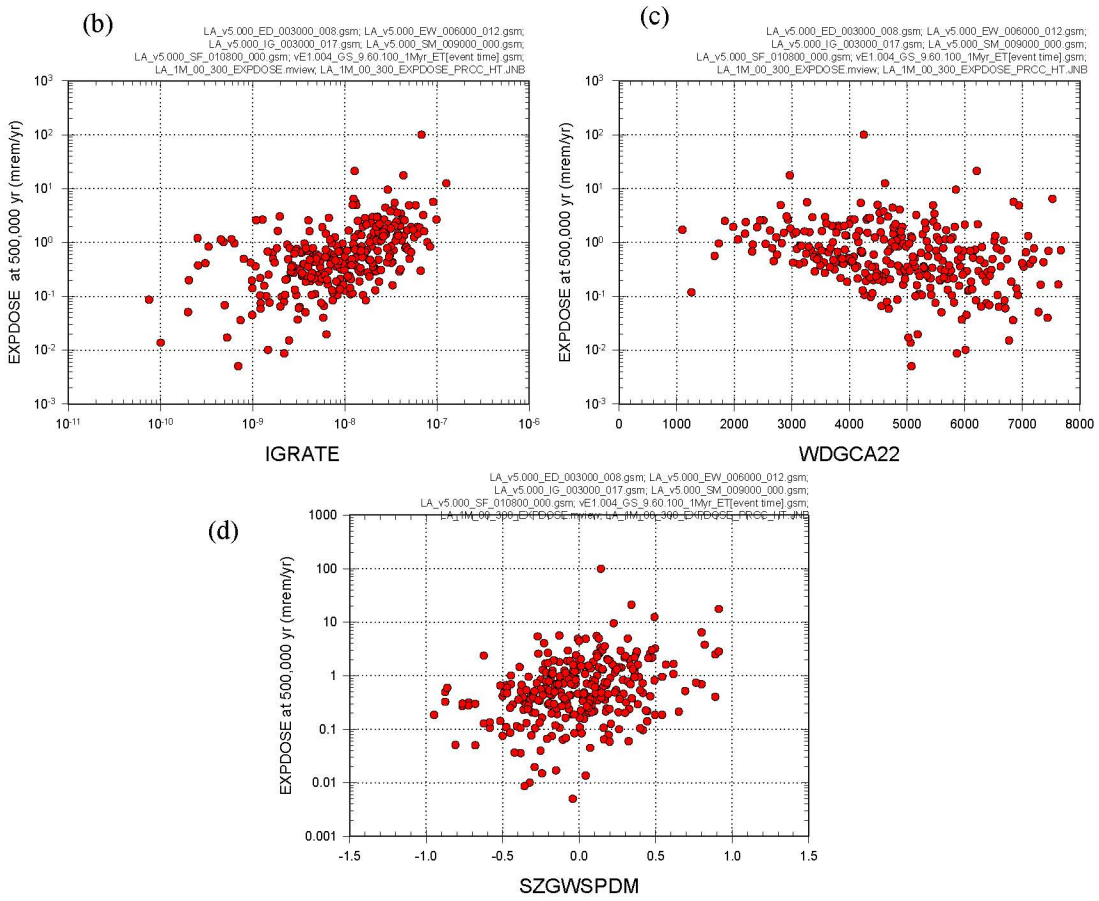

Source: Output DTNs: MO0709TSPAREGS.000 [DIRS 182976]; and MO0709TSPAPLOT.000 [DIRS 183010].

Figure K.8.2-2. Stepwise rank regression analyses and selected scatterplots for expected dose to RMEI (*EXPDOSE*, mrem/yr) over [0, 1,000,000 yr] for all scenario classes: (a) Regressions for *EXPDOSE* and (b,c,d) Scatterplots for *EXPDOSE* at 500,000 years (continued)

INTENTIONALLY LEFT BLANK

APPENDIX L
SIMPLIFIED TSPA

L1. INTRODUCTION

This appendix presents the Simplified Total System Performance Assessment (TSPA) Analysis to corroborate the Total System Performance Assessment for the License Application (TSPA-LA Model). The Simplified TSPA Analysis was developed as a stand-alone computer program written in FORTRAN 90 and compiled/linked using Compaq Visual Fortran as unqualified software. Unqualified software can be used to corroborate analysis or calculation results per Section 6.2.1M of SCI-PRO-006, *Model.*

This appendix is divided into two major sections. The first section presents the details of the Simplified TSPA Analysis. It discusses the approach taken for modeling each of the model areas included, the mathematical equations used in the FORTRAN computer program, and the input data used. The second section discusses the simulations that were conducted using this Simplified TSPA Analysis and discusses the results in comparison with the TSPA-LA Model.

L2. SIMPLIFIED TSPA MODELING APPROACH

The Simplified TSPA Analysis is a higher-level abstraction than the TSPA-LA Model. In general, it includes the same features, events, and processes (FEPs) that are considered in the TSPA, but the manner in which they are modeled is simpler. This simplification primarily involves removing a considerable amount of detail included in the TSPA-LA to capture spatial and temporal variability and treating the repository system with a more 'average' representation. In addition, process-level modeling results are further abstracted for inclusion in this Simplified TSPA instead of being directly included as in the TSPA-LA Model.

The Simplified TSPA Analysis has its bases in the process- and abstraction-level modeling captured in the supporting analysis and/or model reports. Thus, its technical bases are identical to those of the TSPA-LA Model. However, the Simplified TSPA is different from the TSPA-LA Model, both in its structure and computational method.

This section discusses each model area and how it is included in the Simplified TSPA.

L2.1. SEISMIC EVENTS

Seismic activity is modeled in *Seismic Consequence Abstraction* (SNL 2007 [DIRS 176828], Section 6.12.2) as a Poisson process with a mean frequency of 4.287×10^{-4} per year. This simplified model also assumes that seismic activity follows a Poisson process for those modeling cases that include seismic events. The probability of 'n' events occurring in a timestep is shown in Equation L-1.

$$P(n) = \frac{(\lambda \Delta t)^n e^{(-\lambda \Delta t)}}{n!} \qquad \text{(Eq. L-1)}$$

where

P(n) = the probability of 'n' events occurring during a timestep

λ = the mean frequency of the Poisson process, 4.287×10^{-4} per year

Δt = the timestep size (yr).

A random number (between 0 and 1) is drawn and compared to a cumulative probability distribution developed using Equation L-1 to determine whether 0, 1, 2, or 3 seismic events occur in a given timestep. No more than three events are assumed to occur because the probability of even three events occurring in a timestep becomes exceedingly small. For example, the probability of greater than three events occurring within a 1,000-year timestep is 0.0025. The use of a smaller timestep further reduces this probability.

The annual exceedance frequency, λ_j, is sampled for each seismic event that occurs during a timestep from a uniform distribution that varies from 10^{-8} per year and 4.287×10^{-4} per year (SNL 2007 [DIRS 176828], Section 6.12.2). The peak ground velocity (PGV) is then determined using the bounded hazard curve shown in Table L-1 for use in subsequent mechanical damage calculations. In addition, a random number is also drawn from a uniform distribution ranging from 0 to 1 for each seismic event that occurs for use in subsequent rock fall and mechanical damage calculations.

L2.2. ROCK FALL

The amount of rock that falls into the emplacement drifts is evaluated and modeled in *Seismic Consequence Abstraction* (SNL 2007 [DIRS 176828]). A similar approach is used in this simplified model.

For each seismic event, the probability of rock fall in the lithophysal and nonlithophysal zones is determined using Equation L-2 (SNL 2007 [DIRS 176828], Section 6.12.2). If the random number drawn for the seismic event, discussed above, is less than the calculated rock fall probability, then rock fall occurs.

$$P_{rockfall,Lith} = MIN(1.0, MAX(0.0, (1.288)PGV - 0.353)). \quad \text{(Eq. L-2)}$$

Seismic Consequence Abstraction (SNL 2007 [DIRS 176828]) treats the volume of rock that falls in a seismic event as a gamma distribution with the mean and variance of the distribution being functions of the PGV. This simplified model assumes that the volume of rock that falls is simply the mean value of the gamma distribution in order to model the 'average' evolution of the repository. For the lithophysal volume, an effective PGV for rock fall is used as shown in Equation L-3 (SNL 2007 [DIRS 176828], Section 6.12.2). The mean value of the gamma distributions, in terms of m^3 per meter of emplacement drift, is shown in Equations L-4 and L-5 for the lithophysal and nonlithophysal zones (SNL 2007 [DIRS 176828], Section 6.12.2):

$$PGV_{rf} = MAX(PGV, 0.4m/s) \quad \text{(Eq. L-3)}$$

$$\mu_{lith} = (20.307)\left(PGV_{rf}\right)^2 - (18.023)PGV_{rf} + 4.0102 \quad \text{(Eq. L-4)}$$

$$\mu_{non-lith} = (-0.0142)\left(PGV\right)^2 + (0.2064)PGV + 0.0387. \quad \text{(Eq. L-5)}$$

Rock fall accumulates within the drift in both the lithophysal and nonlithophysal zone and the maximum total rockfall volume of the two is assumed to be the total volume of rock in the drift. The fraction of the drift filled with fallen rock is then calculated as the ratio between the total volume of rock that has fallen and the total amount of rock required to fill the drift. The total amount of rock required to fill the drift is assumed to be a uniform distribution ranging between 30 m^3 per meter to 120 m^3 per meter of drift length (SNL 2007 [DIRS 176828], Section 6.12.2).

L2.3. CLIMATE

Future climate analyses were conducted that cover 10,000 years following closure of the repository and are documented in *Future Climate Analysis* (BSC 2004 [DIRS 170002]). Based on the results of this analysis, the present-day climate is assumed to occur for 600 years following repository closure. A monsoon climate then occurs until 2,000 years following repository closure. A glacial-transition climate then occurs until 10,000 years following repository closure.

A fourth climate state is assumed to occur beyond 10,000 years after repository closure. This climate state is assumed to be 'constant' with increased percolation flux through the repository as required by the NRC draft rule in 10 CFR 63.342(c) [DIRS 178394].

Changes from one climate state to another result in increased percolation fluxes across the repository horizon. This leads to higher seepage rates, a larger number of waste packages (WPs) that could potentially be contacted by seeping water (provided the drip shields [DSs] fail), and larger advective flow rates through any failed WPs and the invert. Increased percolation fluxes also correspond to faster groundwater flow rates in both the unsaturated zone (UZ) and saturated zone (SZ).

L2.4. INFILTRATION AND UNSATURATED ZONE FLOW ABOVE THE REPOSITORY

Infiltration rates over the surface of the repository for the present-day, monsoon, and glacial-transition climate states were presented in *Simulation of Net Infiltration for Present-Day and Potential Future Climates* (SNL 2007 [DIRS 182145]). Spatially varying infiltration rates, in the form of infiltration rate maps, were determined for four different infiltration uncertainty scenarios. These infiltration rate maps were used as boundary conditions in the modeling of groundwater flow through the UZ as discussed in *UZ Flow Models and Submodels* (SNL 2007 [DIRS 184614]).

The UZ Flow Model, discussed in detail in *UZ Flow Models and Submodels* (SNL 2007 [DIRS 184614]), produced flow field information for each infiltration uncertainty scenario for the present-day, monsoon, and glacial-transition climate states. A scaling technique was utilized to develop flow fields for the post-10,000-year climate. The flow field information was used to determine the spatial distribution of the percolation flux and the average percolation flux over the

repository area for each of the infiltration uncertainty scenarios and each climate state (DTN: SN0703PAEBSPCE.006_R2 [DIRS 181571]). These parameters were used in this simplified model. The distribution of percolation flux over the repository area is shown on Figure L-1 and the average percolation rates over the repository area for the different climate states and infiltration scenarios are shown in Table L-2.

Weighting factors were also developed for each of the infiltration scenarios in *UZ Flow Models and Submodels* (SNL 2007 [DIRS 184614]). These weighting factors are shown in Table L-2.

L2.5. EMPLACEMENT DRIFT SEEPAGE

The seepage model is described in detail in *Abstraction of Drift Seepage* (SNL 2007 [DIRS 181244]). The key factors that affect the seepage model are:

- **Local Percolation Flux**—The local percolation flux is represented by a two-dimensional map over the repository area. It is an output of the three-dimensional UZ Flow Model. The magnitude of the percolation flux depends on the infiltration rate at the repository surface. The percolation flux is spatially variable across the area of the repository.

- **Flow focusing**—Intermediate-scale heterogeneity may lead to focusing of flow on a scale smaller than the resolution of the three dimensional UZ Flow Model. This may increase the site-scale fluxes in some areas, while reducing them in other areas. The additional variability and uncertainty of percolation flux stemming from this effect can be accounted for by using appropriate flow focusing factors, to be multiplied with the percolation flux distribution from the three dimensional UZ Flow Model.

- **Capillary strength**—The local capillary-strength parameter ($1/\alpha$) of the fractured rock is one of the key parameters affecting the capillary barrier behavior at the drift crown. The larger this parameter, the stronger the capillary force, which holds water in the fractures and prevents it from seeping into the drift. A value of zero is the lower limit for the capillary-strength parameter, corresponding to a fractured rock with zero capillary forces.

- **Fracture permeability**—The second key parameter affecting the diversion of water around drifts is the tangential fracture permeability in the boundary layer near the drift wall. The larger this parameter, the more likely is the water-flow around the drift, and the less likely is seepage.

Seepage is modeled using a multi-dimensional response surface (in the form of a look-up table) that gives the seepage rate as a function of local percolation flux, capillary-strength, and fracture permeability. This simplified model utilizes the mean value for seepage rate from the response surfaces for:

- Noncollapsed drifts (DTN: LB0702PASEEP01.001_R0 [DIRS 179511])
- Collapsed drifts (DTN: LB0702PASEEP01.001_R0 [DIRS 179511]).

Abstraction of Drift Seepage (SNL 2007 [DIRS 181244]) provides ranges for the capillary strength and fracture permeability parameters. Table L-3 shows the ranges for the capillary-strength parameter and Table L-4 shows the ranges for the fracture permeability parameter for lithophysal and nonlithophysal units. The areal average fracture permeability is determined assuming 85 percent of the repository residing in lithophysal units and 15 percent in nonlithophysal units (SNL 2007 [DIRS 181244], Section 6.3.1). The distribution values for the areal average fracture permeability used in this simplified model are shown in Table L-4.

Abstraction of Drift Seepage (SNL 2007 [DIRS 181244], Section 6.7.1.1) also provides a probability distribution of the flow focusing factor to be applied at each location. The flow focusing factor probability distribution is shown in Table L-5 and is used in this simplified model.

This simplified approach determines the fraction of the repository area that is in a seeping environment (the seepage fraction) and the average seepage rate over this area. The repository is treated as a single 'region' with average seepage properties. The methodology used to calculate these 'repository average' properties is similar to that described in *Abstraction of Drift Seepage* (SNL 2007 [DIRS 181244], Section 6.5.1). The 'repository average' seepage properties are calculated for each climate state in the following manner.

- The infiltration scenario is sampled (10th, 30th, 50th, and 90th percentiles) based on the weighting factors shown in Table L-2.

- The percolation flux is determined for 100 discretized 'regions' for each climate state using the percolation flux distribution shown on Figure L-1 (DTN: SN0703PAEBSPCE.006_R2 [DIRS 181571]). Note that these 100 'regions' do not correspond to specific locations in the repository, but rather are regions that will experience a given percolation flux.

- The flow focusing factor is sampled from the distribution shown in Table L-5 for each of the 100 discretized 'regions' and multiplied by the corresponding percolation flux at that 'region.' This results in a localized spatially varying percolation flux distribution for 100 discretized 'regions' within the repository area.

- The uncertainty distributions for the capillary strength values are sampled (Table L-3 for capillary strength; Table L-4 for averaged values for fracture permeability).

- The spatial variability distributions for the capillary strength values are sampled at each 'node' (Table L-3 for capillary strength; Table L-4 for averaged values for fracture permeability).

- The resulting combination of local percolation flux, capillary strength, and fracture permeability are input to the intact and collapsed drift response surfaces to determine the seepage rate at each 'node' for intact and collapsed drift conditions.

- If the seepage rate for a 'node' is greater than zero, then that 'node' is considered to be seeping. The seepage fraction is simply the summation of the total number of seeping 'nodes' with each representing a fraction of 0.01.

- The seepage rate associated with each seeping 'node' is used to determine the average seepage rate using Equation L-6.

$$\overline{Q}_{Seep} = \frac{0.01 \sum_{i}^{N_{Seep}} Q_{Seep_i}}{F_{Seep}} \qquad \text{(Eq. L-6)}$$

where

$\overline{Q}_{Seep}$ = the average seepage rate (kg/yr) across the repository area experiencing seepage

Q_{Seep_i} = the seepage rate (kg/yr) for 'node' i that is experience seepage

F_{Seep} = the fraction of the repository area that is experiencing seepage.

Seepage fractions and average seepage rates are determined for each climate state for both intact and collapsed drift conditions. The effects of drift degradation are discussed in *Abstraction of Drift Seepage* (SNL 2007 [DIRS 181244], Section 6.2.2.1[a]) and the approach described there is also used in this simplified model to account for drift degradation. Rockfall volume, calculated in the simplified seismic model as discussed in Section L2.2, is used to determine both the seepage fraction and seepage rate as a function of the drift condition as follows:

- Use the intact drift seepage response surface to determine the seepage fraction and seepage rate for a rockfall volume less than 5 m^3 per meter of drift.

- Use the collapsed drift seepage response surface to determine the seepage fraction and seepage rate for a rockfall volume greater than or equal to 60 m^3 per meter of drift.

- Linear interpolate to determine the seepage fraction and seepage rate between results calculated using the collapsed and intact drift response surfaces for a rockfall volume greater than or equal to 5 m^3 per meter of drift and less than 60 m^3 per meter of drift. Increase the seepage rate by 20 percent to account for degraded drift conditions.

L2.6. IN-DRIFT ENVIRONMENT

L2.6.1 Waste Package Temperature

The *Multiscale Thermohydrologic Model* (SNL 2007 [DIRS 181383]) was used to calculate WP temperatures as a function of percolation flux, spatial location, and host rock thermal conductivity. Variability in the WP surface temperature exists due to WP location (edge effect), spatial variability in repository conditions (host rock properties and percolation flux), WP thermal output, and ventilation. The results show that the WP surface temperature is moderately sensitive to the infiltration rate, but quite sensitive to the host rock thermal conductivity. This

indicates that heat transfer within the repository and the resulting WP temperatures is dominated by conduction with thermal convection and radiation heat transfer being of lower significance.

Figure L-2 shows the commercial spent nuclear fuel (CSNF) and co-disposed (CDSP) WP temperature histories for the present-day, 10th percentile infiltration scenario, for the medium values of host rock thermal conductivity (Corroborative DTN: MO0708SIMPLIFI.000 [DIRS 182980]). The distributions of peak WP surface temperatures over the repository area for this case are shown on Figure L-3. It can be seen that the peak WP surface temperatures are approximately normally distributed across the repository area.

Figure L-4 shows the minimum and maximum temperature histories for the CSNF and CDSP WPs for low, medium, and high values of host rock thermal conductivity. Figure L-5 shows the average temperature profiles for the CSNF and CDSP WPs for low, medium, and high values of host rock thermal conductivity (Corroborative DTN: MO0708SIMPLIFI.000 [DIRS 182980]).

As discussed in Section L2.8, the general corrosion rate of the WP depends on the WP temperature through an Arrhenius relation. Over long time periods, the spatial variability in WP temperature translates to spatial variability in general corrosion penetration depths. This ultimately leads to WP failures occurring over a period of time, or temporal variability. Thus, it is necessary to capture the spatial variability in WP temperature since degradation of the WP plays an important role in the rate that radionuclides could be released from the engineered barrier system (EBS).

In order to capture spatial variability in WP temperature, this simplified model first samples the host-rock thermal conductivity with low, medium, and high each having equal probability (one-third). The range of temperatures across the repository area is then determined using the information on Figure L-4 for the 10th percentile infiltration scenario. As shown in Table L-2, this scenario is assumed to occur with a probability of over 60 percent. In addition, this infiltration scenario will result in higher WP temperatures than the other infiltration scenarios and will cause earlier WP failure because higher temperatures cause higher corrosion rates.

The temperature distribution across the repository area is assumed to vary according to a normal distribution with the minimum and maximums shown in L-2 assumed to represent the coolest and hottest 1 percent of the repository area. The WP surface temperature at each point in time across the repository horizon is then determined by interpolating over the temperature range shown on Figure L-4 using Equation L-7:

$$T_{wp}(t) = \frac{N^{-1}(\mathrm{P_A}) - z_{MIN}}{z_{MAX} - z_{MIN}} \left(T_{wp-MAX}(t) - T_{wp-MIN}(t)\right) + T_{wp-MIN}(t) \qquad \text{(Eq. L-7)}$$

where

$T_{wp,i}(t)$ = WP surface temperature at a location in the repository at time t (°C)

$T_{wp\text{-}MAX}$ = maximum WP surface temperature in the repository at time t (°C)

$T_{wp\text{-}MIN}$ = minimum WP surface temperature in the repository at time t (°C)

$N^{-1}(P_A)$ = value from the inverse of a cumulative normal distribution with a mean of 0 and a standard deviation of 1

P_A = cumulative area fraction (uniform distribution 0-1)

z_{MIN} = minimum value of a normal distribution with a mean of 0 and a standard deviation of 1 (-3.719)

z_{MAX} = maximum value of a normal distribution with a mean of 0 and a standard deviation of 1 (3.719).

As discussed in Section L.2.12, waste form degradation also depends on temperature. However, the intent of this simplified model is to evaluate repository performance under 'average' conditions and as such, the average WP temperature history is used to model waste form degradation. The average WP temperature is determined for a sampled value of the host rock thermal conductivity using Figure L-5.

L2.6.2 In-Drift Chemical Environment

The Simplified TSPA Analysis uses the CO_2 partial pressure to determine dissolved concentration limits and the total carbonate concentration used in the CSNF degradation submodel. The CO_2 partial pressure in the drift and invert is calculated in *Engineered Barrier System: Physical and Chemical Environment* (SNL 2007 [DIRS 177412]). The maximum CO_2 partial pressure was calculated for four different chemistries and degrees of rock-water reaction as a function of temperature. The results are shown on Figure L-6 (DTN: SN0701PAEBSPCE.002_R0 [DIRS 179425]) where the various lines correspond to different values of a water-rock interaction parameter that indicate the amount of feldspar dissolved in the water. The minimum value of the CO_2 partial pressure is also a function of temperature (SNL 2007 [DIRS 177412], Section 6.3.3.2.5).

The CO_2 partial pressure in the drift and the invert varies over the first few thousand years due to the thermal pulse, but thereafter tends to stabilize (SNL 2007 [DIRS 177412], Section 6.3.3.2.5). Rather than explicitly modeling the evolution of the CO_2 partial pressure over time, this simplified model assumes that the CO_2 partial pressure is equal to 10^{-2}. This is roughly equivalent to the maximum value of the CO_2 partial pressure for the various starting water chemistries and rock-water interactions at temperatures ranging from 80°C to 90°C.

Dissolved concentration limits tend to decrease with decreasing CO_2 partial pressure as shown in *Dissolved Concentration Limits of Elements with Radioactive Isotopes* (SNL 2007 [DIRS 177418]). Assuming a CO_2 partial pressure of 10^{-2} is conservative, in that it will result in larger concentrations of radionuclides in the EBS and consequently larger release rates. The degradation of CSNF, as discussed in Section L2.2, depends on the CO_2 partial pressure under acidic conditions. However, the CO_2 partial pressure is of much less significance that the specific surface area of the degrading UO_2 matrix and assuming a CO_2 partial pressure of 10^{-2} will have little effect on the degradation rate of CSNF under acidic conditions.

The O_2 partial pressure is assumed to equal 0.21 (SNL 2007 [DIRS 177412], Section 6.3.3.2.5), which further assumes that the air mass fraction in the drifts is 1 and that oxygen is not depleted through reactions with structural material in the emplacement drifts.

The pH in the invert affects the dissolved concentration limit as shown in *Dissolved Concentration Limits of Elements with Radioactive Isotopes* (SNL 2007 [DIRS 177418]). In a seeping environment with failed WPs and DSs, the invert pH is assumed to equal the in-package pH (SNL 2007 [DIRS 177412], Section 6.15.2). Otherwise, the invert pH is calculated for four different chemistries and degrees of rock-water reaction as a function of temperature and relative humidity in *Engineered Barrier System: Physical and Chemical Environment* (SNL 2007 [DIRS 177412]). The results indicate that as the relative humidity approaches 100 percent, the invert pH ranges from approximately 6 to 7 (based on the results in DTN: SN0701PAEBSPCE.001_R1 [DIRS 180523]). This simplified model thus assumes that the invert pH ranges uniformly from 6 to 7 in conditions where the DSs and WPs have not failed.

L2.7. DRIP SHIELD DEGRADATION

L2.7.1 Corrosion

Localized corrosion of the DS is excluded as a DS degradation mechanism (SNL 2007 [DIRS 179476], FEP Number 2.1.03.03.0B). DS general corrosion rate distributions are provided in *General and Localized Corrosion of the Drip Shield* (SNL 2007 [DIRS 180778]), based on weight loss and crevice corrosion specimens. DS corrosion rates were found to be both spatially variable and uncertain. However, *General and Localized Corrosion of the Drip Shield* (SNL 2007 [DIRS 180778], Section 8.1[a]) recommended that the DS corrosion rate be treated as uncertain with no variability in the TSPA-LA. Two uncertain mean corrosion rates, one for benign and one for aggressive conditions, are sampled independently and are used for the general corrosion of the DS. The distribution under aggressive conditions is applied to the top of all DSs, and the distribution for the less aggressive conditions is applied to the underside of all DSs. This simplified model uses this same approach for modeling general corrosion of the DS.

The DS general corrosion rate for aggressive conditions is represented in *General and Localized Corrosion of the Drip Shield* (SNL 2007 [DIRS 180778], Section 8.1[a]) as a student-t distribution with a mean of 46.1 nm/yr, a standard deviation of 1.19 nm/yr, and 5 degrees of freedom. This simplified analysis assumes a normal distribution with a mean of 46.1 nm/yr and a standard deviation of 1.19 nm/yr. Although these distributions are slightly different, the overall trend in DS performance will be similar.

The DS general corrosion rate for less aggressive conditions is represented in *General and Localized Corrosion of the Drip Shield* (SNL 2007 [DIRS 180778], Section 8.1[a]) as a normal distribution with a mean of 5.15 nm/yr and a standard deviation of 0.831 nm/yr. This distribution is used in this simplified model.

The corrosion rates for the DS tops and undersides are independently sampled, and the time that the DSs fail is calculated using Equation L-8. It is assumed that the entire DS surface is fully degraded.

$$t_{ds} = \frac{T_{ds}}{GC_{ds-os} + GC_{ds-us}} \qquad \text{(Eq. L-8)}$$

where

t_{ds} = the time that the DSs fail (year)

T_{ds} = DS thickness, 15 mm (BSC 2005 [DIRS 173303])

$GC_{ds\text{-}os}$ = sampled DS top surface general corrosion rate (mm/yr)

$GC_{ds\text{-}us}$ = sampled DS under side general corrosion rate (mm/yr).

The general corrosion rate of the DS frame thickness is determined by applying a factor to account for the increased general corrosion of Titanium Grade 29 (frame) as compared to Titanium Grade 7 (plates). This factor is uncertain and is shown in Table L-6 (DTN: SN0704PADSGCMT.002_R1 [DIRS 182188]).

L2.7.2 Mechanical Damage

Seismic Consequence Abstraction (SNL 2007 [DIRS 176828]) evaluated and developed approaches for modeling the effects of seismic events on the performance of the DS. It considered two modes of DS failure: rupture or tearing of the DS plates and buckling or collapse of the sides and/or top of the DS due to seismic events. Failure of the DS plates as a result of a seismic event renders the DS ineffective as a barrier to seepage. Buckling or collapse of the DS can result in the DS contacting the WP, influencing its response to seismic events. This effect on mechanical damage modeling of the WP is discussed later.

Before DS failure occurs due to either of the two failure modes discussed above, the DSs may accumulate damage from vibratory ground motion and from rockfall induced by vibratory ground motion. This is also evaluated in *Seismic Consequence Abstraction* (SNL 2007 [DIRS 176828]). Any such damage would result in an increased susceptibility to stress corrosion cracking (SCC). However, it is not expected that any water would be able to flow through such cracks and the DS would retain its effectiveness as a barrier to seepage (SNL 2007 [DIRS 179476], FEP Number 2.1.03.10.0B). Thus, this simplified model does not model the accumulation of damage to the DS surface due to seismic events.

This simplified model uses the same approach for modeling failure of the DS plates that is described in *Seismic Consequence Abstraction* (SNL 2007 [DIRS 176828], Section 6.12.2). The probability that the DS plates will fail in a seismic event or the plate fragility is shown in Table L-7 and is a function of the thickness of the plate (which degrades over time due to general corrosion), the amount of rock that has fallen into the drift, and the PGV associated with a seismic event.

When a seismic event occurs, the PGV associated with the seismic event, the current thickness of the DS plate, and the current amount of rock that has fallen into a drift are used to determine the probability that the DS plate will fail (linear interpolation). The DS plate is assumed to be failed if the random draw (Section L 2.1) associated with the seismic event is less than the calculated plate failure probability. If the DS plates fail, all DSs are assumed to no longer be a barrier to emplacement drift seepage.

This simplified model also uses the same approach for modeling failure of the DS structure due to buckling and/or collapse that is described in *Seismic Consequence Abstraction* (SNL 2007 [DIRS 176828], Section 6.12.2). The probability that the DS frame will fail in a seismic event, or due to the frame fragility, is shown in Table L-8. The frame fragility is a function of the thickness of the frame structure (which degrades over time due to general corrosion), the amount of rock that has fallen into the drift, and the PGV associated with a seismic event.

When a seismic event occurs, the PGV associated with the seismic event, the current thickness of the DS frame structure, and the current amount of rock that has fallen into a drift, are used to determine the probability that the DS plate will fail (linear interpolation). The DS frame structure is assumed to be failed if the random draw associated with the seismic event is less than the calculated plate failure probability. If the DS frame structure fails, all DSs are still assumed to be a barrier to emplacement drift seepage.

L2.8. WASTE PACKAGE DEGRADATION

L2.8.1 Corrosion

This simplified model considers two corrosion processes that can result in failure of the WPs, SCC and general corrosion. Localized corrosion (crevice corrosion and/or pitting) is not considered in this simplified model because these corrosion mechanisms are not expected to occur on the WP surface in the environment expected within the repository.

L2.8.1.1 General Corrosion

The base-case general corrosion model for the WP outer barrier is presented in *General Corrosion and Localized Corrosion of Waste Package Outer Barrier* (SNL 2007 [DIRS 178519], Section 8.2). The model is based on a temperature dependence of the corrosion process, represented by an activation energy using the natural logarithmic form of a modified Arrhenius relation as shown in Equation L-9:

$$\ln(R_T) = \ln(R_o) + C_1\left(\frac{1}{T} + \frac{1}{333.15}\right). \qquad \text{(Eq. L-9)}$$

R_T is the temperature-dependent general corrosion rate in nm/yr, T is temperature in Kelvin, and R_o and C_1 are uncertain constants. The temperature dependence term (C_1) was obtained from short-term polarization resistance data for Alloy 22 (UNS N06022) specimens tested for a range of sample configurations, metallurgical conditions, and exposure conditions. The temperature dependence term is represented as a truncated ($\pm 2\sigma$) normal distribution with a mean of 4,905°K and a standard deviation of 1,413°K (DTN: MO0703PAGENCOR.001_R4 [DIRS 182029]).

R_o is represented as a Weibull distribution shown in Equation L-10 (where p is the cumulative probability):

$$p = 1 - \exp\left[-\left(\frac{R_o}{s}\right)^b\right]. \qquad \text{(Eq. L-10)}$$

The Weibull scale and shape parameters are represented as a discrete probability distribution as shown in Table L-9. These parameters were determined from weight-loss data of 5-year exposed crevice specimens at 60°C and 90°C and were assumed to represent the distribution of long-term general corrosion rates of the WP outer barrier at 60°C (SNL 2007 [DIRS 178519], Section 8.2).

The WP outer barrier is subject to microbiologically influenced corrosion (MIC) when the relative humidity is equal to or greater than a relative humidity threshold that varies uniformly from 75 percent to 90 percent (SNL 2007 [DIRS 178519], Section 8.2). The effect of MIC on general corrosion of the WP outer barrier is treated as an enhancement factor applied to the general corrosion rate when the relative humidity threshold is exceeded. This MIC enhancement factor is represented as a uniform distribution ranging from 1 to 2 (DTN: MO0703PAGENCOR.001_R4 [DIRS 182029]).

This simplified model conservatively assumes a constant relative humidity threshold of 75 percent. Relative humidity histories (DTN: MO0506MWDPPMSV.000_R0 [DIRS 174806]) indicate that the time when the relative humidity exceeds a 75 percent threshold depends on the WP type and the host rock thermal conductivity. The time that the relative humidity exceeds a 75 percent threshold, where MIC is assumed to occur in this simplified model, is shown in Table L-10.

This simplified model assumes that the entire variance in R_o represents variability in the general corrosion process over the surface of the WP outer barrier, consistent with *General Corrosion and Localized Corrosion of Waste Package Outer Barrier* (SNL 2007 [DIRS 178519], Section 8.2). The general corrosion rate variability is applied among the modeled WPs and local areas on the surface of an individual WP. The entire variance in the temperature dependence term (C_1) is due to uncertainty, and the uncertainty is limited to ±2 standard deviations. The MIC enhancement factor is also due to uncertainty.

The simplified model calculates WP degradation due to general corrosion as discussed below. This approach captures spatial variability in general corrosion over the WP surface by discretizing the WP surface into 1,000 'locations' and spatial variability in the general corrosion rate across the repository area due to spatial variability in temperature by considering 100 'regions' as discussed in Section L2.6.1. The approach used in this simplified model is:

- The Weibull scale and shape parameters are sampled.
- The MIC enhancement factor is sampled.
- The MIC threshold time is determined for CSNF and CDSP WPs from Table L-10 for the sampled host rock thermal conductivity (low, medium, and high as discussed in Section L2.6.1).
- The general corrosion rate, R_o, on the WP outer surface is determined using an inversion of Equation L-10 for 1,000 'locations' on the WP surface.
- The general corrosion rate, R_o, is increased by the MIC enhancement factor at each 'location' on the WP surface.

- The temperature dependence term, C_1, is sampled.
- The repository is discretized into 100 'regions' and the WP temperature history for each of the 100 'regions' is calculated using Equation L-7.The temperature-dependent general corrosion rate, R_T, for each 'location' on the WP outer surface is determined using Equation L-9 for each of the 100 'regions.'
- The penetration depth is calculated for each 'location' on the WP outer surface and for each 'region' using numerical integration (trapezoidal rule with finely divided steps to ensure accuracy).
- The time that each 'location' on the WP outer surface and for each 'region' is determined when the penetration depth exceeds the thickness of the WP outer barrier, 25 mm (SNL 2007 [DIRS 177407], Section 4.1.1).

This approach results in a distribution of penetration times for each of 1,000 'locations' on the WP surface for each of 100 'regions' over the repository area. The initial general corrosion WP failure distribution (fraction of WPs failed as a function of time) is determined from the earliest time that a 'location' is penetrated in each 'region.' The fractional area breached on failed WPs is determined using Equation L-11:

$$\overline{F}_{WP-Area} = \frac{\sum_{i=1}^{N} F_{WP-Area,i}}{N} \qquad \text{(Eq. L-11)}$$

where

$\overline{F}_{WP-Area}$ = the average fraction of the WP surface area failed on all failed WPs

$F_{WP-Area,i}$ = the fraction of the WP surface area failed on all failed WPs in 'region' i

N = the total number of 'regions' with failed WPs.

L2.8.1.2 Stress Corrosion Cracking

SCC of the WP outer barrier is discussed in *Stress Corrosion Cracking of Waste Package Outer Barrier and Drip Shield Materials* (SNL 2007 [DIRS 181953]). The SCC model considers the initiation and propagation of cracks in the closure weld region of the WP outer barrier due to three factors present simultaneously: material susceptibility, critical environment, and static (or sustained) tensile stress. Crack initiation was evaluated and modeled for both weld flaws and incipient cracks. Crack propagation was modeled using the slip dissolution/film rupture model for the prediction of crack growth rate.

This simplified model considers SCC of the WP outer barrier closure lid weld regions. Incipient cracks are assumed to nucleate, grow, and immediately penetrate the thickness of the weld region when general corrosion has penetrated to the depth at which the hoop stress profile exceeds the threshold stress. Analyses presented in *Analysis of Mechanisms for Early Waste Package/Drip Shield Failure* (SNL 2007 [DIRS 178765], Section 6.3.1.9) indicated that over 80 percent of the

WPs will not experience any weld flaws. Since this simplified model evaluates the 'average' evolution of the repository it does not include weld flaws as locations where SCC can occur because only a limited number of WPs will have weld flaws. In addition, weld flaws are one of the factors that can lead to early WP failure as discussed in Section L2.8.2.

The hoop stress (σ in MPa) as a function of depth (x in mm) in the closure weld regions of the Alloy 22 WP outer barrier is given by a third-order polynomial regression as shown in Equation L-12 (SNL 2007 [DIRS 181953], Equation 22):

$$\sigma(x,\theta=0) = A_0 + A_1 x + A_2 x^2 + A_3 x^3 \quad \text{(Eq. L-12)}$$

where

σ = hoop stress as a function of depth, x, and at an angular position, θ, of 0

A_i = coefficients in third order polynomial (Table L-11).

The stress intensity factor (K_I in MPa) as a function of depth (x in mm) for the plasticity-burnished weld region was fit to a fourth-order polynomial regression as shown in Equation L-13. This regression was determined using the information for the laser peened WP outer closure weld region from *Stress Corrosion Cracking of the Drip Shield, the Waste Package Outer Barrier, and the Stainless Steel Structural Material* (SNL 2007 [DIRS 181953], Table 8-12):

$$K_I(x,\theta=0) = A_0 + A_1 x + A_2 x^2 + A_3 x^3 + A_4 x^4 \quad \text{(Eq. L-13)}$$

where

K_I = stress intensity factor as a function of depth, x, and at an angular position, θ, of 0

A_i = coefficients in fourth order polynomial (Table L-11).

The hoop stress varies with angle (θ) around the circumference of the Alloy 22 WP outer closure lid welds (θ = 0 point arbitrarily chosen) according to Equation L-14 (SNL 2007 [DIRS 181953], Table 8-1):

$$\sigma(x,\theta) = \sigma(x,\theta=0) - 17.2369\left(1-\cos(\theta)\right). \quad \text{(Eq. L-14)}$$

The stress intensity factor also varies with angle (θ) around the circumference of the Alloy 22 WP outer closure lid welds (θ = 0 point arbitrarily chosen) according to Equation L-15 (SNL 2007 [DIRS 181953], Table 8-1):

$$K_I(x,\theta) = K_I(x,\theta=0) \times \frac{\sigma(Thck,\theta)}{\sigma(Thck,0)} \quad \text{(Eq. L-15)}$$

where

$K_I(x, \theta)$ = stress intensity factor as a function of depth, x, and at angular position, θ

$K_I(x, \theta=0)$ = stress intensity factor as a function of depth, x, and at angular position of 0 (shown in Equation L-13)

$Thck$ = the thickness of the WP outer closure weld, 25 mm (SNL 2007 [DIRS 181953], Section 6.5.3.2).

The uncertainty in the stress and stress intensity factor profiles is treated through the use of a scaling factor, z, which is sampled from a normal distribution with a mean of zero and a standard deviation of 5 percent of the yield strength, with an upper-bound of 15 percent of the yield strength and a lower-bound of -15 percent of the yield strength (SNL 2007 [DIRS 181953], Table 8-1). The hoop stress as a function of depth, angle, and uncertainty is shown in Equation L-16 (SNL 2007 [DIRS 181953], Table 8-1):

$$\sigma(x, \theta, Z) = \sigma(x, \theta) \times \frac{\sigma(thck, \theta) + Z}{\sigma(thck, \theta)}. \quad \text{(Eq. L-16)}$$

The stress intensity factor as a function of depth, angle, and uncertainty is shown in Equation L-17 (SNL 2007 [DIRS 181953], Table 8-1):

$$K_I(x, \theta, Z) = K_I(x, \theta) \times \frac{\sigma(Thck, \theta) + Z}{\sigma(Thck, \theta)} = K_I(x, \theta = 0) \times \frac{\sigma(Thck, \theta) + Z}{\sigma(Thck, \theta = 0)}. \quad \text{(Eq. L-17)}$$

The threshold stress-intensity factor, $K_{I\text{-}SCC}$, is shown in Equation L-18 (SNL 2007 [DIRS 181953], Table 8-1):

$$K_{I-SCC} = \left(\frac{V_{gc}}{\overline{A}} \right)^{1/\overline{n}} \quad \text{(Eq. L-18)}$$

where

V_{gc} = crack growth velocity, 7.23 nm/yr (DTN: MO0702PASTRESS.002_R2 [DIRS 180514]).

The parameters $\overline{A}$ and $\overline{n}$ are functions of the repassivation slope, n, and given in Equation L-19 (SNL 2007 [DIRS 181953], Table 8-1). The repassivation slope, n, is represented by a truncated normal distribution (at ± 2 standard deviations) with a mean of 1.165 and a standard deviation of 0.115 (DTN: MO0702PASTRESS.002_R2 [DIRS 180514]):

$$\overline{A}(mm/s) = 7.8 \times 10^{-2} \, n^{3.6} \, (4.1 \times 10^{-14})^n$$
$$\overline{n} = 4n. \quad \text{(Eq. L-19)}$$

Cracks are assumed to nucleate when general corrosion has reduced the thickness of the WP outer barrier to a depth where the yield stress exceeds the threshold stress level. This threshold

stress is assumed in *Stress Corrosion Cracking of the Drip Shield, the Waste Package Outer Barrier, and the Stainless Steel Structural Material* (SNL 2007 [DIRS 181953], Table 8-1) to vary uniformly from 90 percent to 105 percent of the Alloy 22 yield stress, 351 MPa (DTN: MO0702PASTRESS.002_R2 [DIRS 180514]). This simplified model assumes that the threshold stress is 97.5 percent of the yield stress, the average of the range of uncertainty. Stress corrosion cracks can propagate when K_I exceeds $K_{I\text{-}SCC}$.

The depth where SCC can initiate and propagate in the WP outer closure weld is shown on Figure L-7 over the circumference of the weld region for various combinations of the repassivation slope, n, and the stress uncertainty scaling factor, 'Z', with the threshold stress at 90 percent of the yield stress (Corroborative DTN: MO0708SIMPLIFI.000 [DIRS 182980]). The solid lines show depths for mean values of 'n' at the extremes of 'Z' and at the mean values of 'Z' and the extremes of n. The dashed lines show depths for the extremes of both 'n' and 'Z'. Note that SCC does not either initiate or propagate at some locations along the circumference of the weld region for certain combinations of 'n' and 'Z' parameters. In addition, certain different combinations of 'n' and 'Z' parameters result in identical results.

The results shown on Figure L-7 indicate that the depths where SCC crack initiation and propagation can occur, range by a maximum of less than two millimeters along the circumference of the WP outer lid closure weld region. This simplified model uses an average depth where SCC crack initiation and propagation can occur as a function of the repassivation slope, n, and the stress uncertainty scaling factor, 'Z', shown in Table L-12. This average depth is computed for only those locations along the circumference of the closure weld where SCC cracks can initiate and propagate at some depth into the thickness of the closure weld region. This approach is a conservative and leads to the entire circumference of the closure weld region being susceptible to SCC at some point in time.

As stated above, incipient cracks are assumed to nucleate, grow, and immediately penetrate the thickness of the weld region when general corrosion has penetrated to the depth at which the hoop stress profile exceeds the threshold stress. The same method as discussed above is used to determine both the fraction of WPs initially failed due to SCC over time and the average fraction of 'locations' penetrated by SCC on WPs that have failed by SCC. The only difference being the penetration depth, which is determined by interpolating from Table L-12 for the sampled values of the repassivation slope, n, and the yield stress uncertainty 'Z'.

L2.8.2 Early Waste Package Failure

Analysis of Mechanisms for Early Waste Package/Drip Shield Failure (SNL 2007 [DIRS 178765], Section 6.3) identified several general types of manufacturing defects including weld flaws, base metal flaws, improper weld material, improper base metal, improper heat treatment, improper weld-flux material, poor weld-joint design, contamination, mislocated welds, missing welds, handling damage, and administrative or operational error.

Variation in the number of early failed WPs is expressed as variability deriving from a discrete Poisson distribution with an uncertain intensity parameter. The intensity parameter, or the probability that a single WP will experience early failure, is represented by a log-normal distribution. The intensity factor has a geometric mean of 4.14×0^{-5} and an error factor of 8.17

(DTN: MO0701PASHIELD.000_R2 [DIRS 180508]). This error factor translates into a geometric standard deviation of $8.17^{(1/1.645)}$. The base-10 logarithm of the intensity factor is thus represented as a normal distribution with a mean of -4.38 and a standard deviation of 0.55. This distribution is sampled and the inverse base-10 logarithm is taken to determine the intensity factor.

The realized value of the early failure intensity factor is multiplied by the number of CSNF and CDSP WPs to determine the Poisson λ for determining the number of CSNF and CDSP WP that experience early failure. The probability of having 0-5 early failed CSNF and CDSP WPs is determined using the Poisson distribution. A random number (0 to 1) is independently selected for the CSNF and CDSP WPs and compared to the early failure probability to yield the number of failed CSNF and CDSP WPs. The number of early failed CSNF and CDSP WPs is conservatively added to the total number of CSNF and CDSP WPs.

The entire WP surface is assumed to be affected by improper heat treatment and the entire surface of the WP is assumed to be lost upon failure of the WPs, because the affected area could be subjected to SCC and enhanced localized and general corrosion (SNL 2007 [DIRS 178765], Section 6.4.8). The entire surface area of the WP is assumed to be that of the CSNF WP (excluding the ends), 33.64 m^2 (DTN: SN0703PAEBSRTA.001_R3 [DIRS 183217]).

L2.8.3 Mechanical Damage

Seismic Consequence Abstraction (SNL 2007 [DIRS 176828]) evaluated and developed approaches for modeling the effects of seismic events on the performance of the WPs.

Failure of the DS changes the configuration of the EBS components. The configuration of the EBS and the mechanical response of the WPs to seismic events was defined in *Seismic Consequence Abstraction* (SNL 2007 [DIRS 176828]) for three states of the system: (1) the initial state, with an intact DS; (2) the final state, with the WPs surrounded by rubble after failure of the DS plates;, and (3) an intermediate state, where the legs of the DS have buckled, but the plates remain intact. This intermediate state can occur because the plastic load capacity of the plates is significantly greater than the plastic load capacity of the DS framework for a given reduction in thickness of the DS components from general corrosion.

While the DS is intact, the WPs are free to move and interact in response to vibratory ground motion. In this condition, end-to-end impacts between adjacent WP and impacts between the WP and its emplacement pallet may occur. The response of the WP for this initial state is assessed using the kinematic damage abstractions presented in *Seismic Consequence Abstraction* (SNL 2007 [DIRS 176828], Section 6.12.2) transportation, aging and disposal (TAD) bearing CSNF and CDSP WPs, respectively.

After the DS plates fail, rockfall can pass through the DS and surround the WP. The response for a WP was developed in *Seismic Consequence Abstraction* (SNL 2007 [DIRS 176828]) for a condition when the TAD-bearing CSNF and CDSP WPs are surrounded by rubble (i.e., the final state of the EBS).

After the DS framework buckles or collapses, the DS may be resting on top of the WP. The deformation and stresses in the Alloy 22 outer barrier of a TAD-bearing CSNF WP that is loaded by a collapsed DS was investigated with three-dimensional finite-element models (SNL 2007 [DIRS 176828], Section 6.9). Separate models represent the response of the TAD-bearing CSNF WP with intact or degraded internals.

This simplified model uses the abstractions developed in *Seismic Consequence Abstraction* (SNL 2007 [DIRS 176828], Section 6.12.2) to estimate WP damage as a result of seismic activity. WP damage is calculated using the same conceptual approach. However, it is conservatively assumed that the WP internals are degraded. This leads to higher probabilities that the WPs will fail than would be the case when the internals are intact.

Two key parameters used in this simplified WP mechanical degradation model are the residual stress threshold uncertainty (percentage of yield stress) and the thickness of the Alloy 22 WP outer barrier remaining. The residual stress threshold uncertainty is represented as a uniform distribution ranging from 90 percent to 105 percent (DTN: MO0702PASTRESS.002_R2 [DIRS 180514]).

The WP thickness remaining will vary across the WPs due to spatial variability in the repository temperature and across the WP surface due to spatial variability in general corrosion rates. However, this simplified analysis computes an average WP thickness remaining that is used on every WP.

Recall that the simplified general corrosion model presented above calculates the time that the penetration depth at each 'location' on the WP outer surface and for each of 100 'regions' exceeds the thickness of the WP outer barrier. These penetration times are used to determine an average general corrosion penetration time. The WP thickness remaining is simply calculated as the ratio of the simulation time and the average penetration time multiplied by the initial thickness of the WP outer barrier.

L2.8.3.1 Waste Package Surrounded By Rubble

As discussed in *Seismic Consequence Abstraction* (SNL 2007 [DIRS 176828], Section 6.12.2), the probability of rupture for a WP surrounded by rubble is zero for intact or degraded internals at all PGV levels and outer corrosion barrier (OCB) thicknesses that are relevant to 1,000,000 years. Table L-13 presents the probability of nonzero damaged area for the WP with degraded internals, surrounded by rubble. Note that these results are applicable to both the TAD-bearing CSNF and CDSP WPs. The PGV for the seismic event, the residual stress threshold, and the thickness of the WP outer barrier is used to determine the probability of nonzero damage area.

If the random number drawn for that seismic event is less than or equal to the probability of nonzero failure that is calculated, then the WPs are damaged by the seismic event and the damage area is calculated. All WPs are failed upon the first occurrence of damage (provided they have not already failed). The damaged area on the WP surface accumulates with each seismic event that causes damage.

The damage area for WPs surrounded by rubble developed in *Seismic Consequence Abstraction* (SNL 2007 [DIRS 176828], Section 6.12.2) is represented by a gamma distribution. However,

this simplified model assumes that the damage area is simply the mean of the gamma distribution (Table L-14) in order to model the 'average' evolution of WP when damaged by seismic events.

L2.8.3.2 Waste Package Free Movement

Seismic Consequence Abstraction (SNL 2007 [DIRS 176828], Section 6.12.2) presents an approach for determining whether TAD-bearing CSNF or CDSP WPs will rupture as a result of seismic events when they can freely move underneath the DS. This simplified model does not consider WP rupture when the WPs can move freely. Table L-15 shows the probability of TAD-bearing and CDSP WP rupture for a 17 mm thick WP outer barrier and for degraded WP internals. Table L-15 also shows the conditional probability associated with each PGV (probability that a seismic event will exceed that PGV level) and the expected number of events that would exceed that PGV level over a 1,000,000-year period. These results demonstrate that the likelihood of WP rupture over a million-year period is quite small and on the average, WPs will not rupture when they move freely underneath the DS.

Tables L-16 and L-17 present the probability of nonzero damaged area for the CSNF and CDSP WPs with intact and degraded internals that can move freely underneath the DS. Note that these results are applicable to both the TAD-bearing CSNF and CDSP WPs. The PGV for the seismic event, the residual stress threshold, and the thickness of the WP outer barrier is used to determine the probability of nonzero damage area.

If the random number drawn for that seismic event is less than or equal to the probability of nonzero failure that is calculated for intact WPs, then the WPs are damaged by the seismic event and the damage area is calculated. All WPs are failed upon the first occurrence of damage and the WP internals are assumed to be immediately degraded. Damage caused by subsequent seismic events is calculated using the probabilities of nonzero damage area in Tables L-16 and L-17 for degraded internals. The damaged area on the WP surface accumulates with each seismic event that causes damage due to free motion underneath the DS until the DS plates fail and the WPs are surrounded by rubble.

The damage area for TAD-bearing CSNF and CDSP WPs that move freely underneath the DS developed in *Seismic Consequence Abstraction* (SNL 2007 [DIRS 176828], Section 6.12.2), is represented by a gamma distribution. However, this simplified model assumes that the damage area is simply the mean of the gamma distribution, shown in Table L-18, in order to model the 'average' evolution of WP when damaged by seismic events.

L2.9. IN-PACKAGE CHEMISTRY

L2.9.1 In-Package pH

The in-package pH was evaluated in *In-Package Chemistry Abstraction* (SNL 2007 [DIRS 180506]) for both the CSNF and CDSP WPs under seeping and nonseeping (vapor influx) conditions. The in-package pH is a function of pCO_2, ionic strength. As discussed in Section L2.6.2, this simplified model assumes a pCO_2 of 0.01.

Under vapor influx and dripping conditions, the pH inside a breached CSNF WP ranges from approximately 5.5 to 7.5 for a medium ionic strength and a pCO_2 of 2.0. An order of magnitude

increase in the ionic strength yields a pH that ranges from 5.1 to 7.1 (DTN: SN0702PAIPC1CA.001_R2 [DIRS 180451]).

Under vapor influx and dripping conditions, the pH inside a breached CDSP WP and defense high-level waste (DHLW) canister ranges from approximately 5.5 to 8.2 for a medium ionic strength and a pCO_2 of 2.0. An order of magnitude increase in the ionic strength yields a pH that ranges from 5.1 to 9.0 (DTN: SN0702PAIPC1CA.001_R2 [DIRS 180451]).

Under vapor influx and dripping conditions, the pH inside a breached CDSP WP and U.S. Department of Energy (DOE) spent nuclear fuel (DSNF) canister ranges from approximately 5.5 to 7.5 for a medium ionic strength and a pCO_2 of 2.0. An order of magnitude increase in the ionic strength yields a pH that ranges from 5.1 to 7.2 (DTN: SN0702PAIPC1CA.001_R2 [DIRS 180451]).

Based on these results, this simplified model assumes the in-package chemistry ranges uniformly from 5 to 8 for both the CSNF and CDSP WPs under dripping and nondripping conditions. This sufficiently covers the range of uncertainty associated with the pH in both the CSNF and CDSP WPs for the purposes of this simplified model.

L2.9.2 In-Package Total Carbonate

The total carbonate was evaluated in *In-Package Chemistry Abstraction* (SNL 2007 [DIRS 180506], Section 8.1.3) and is a function of CO_2 partial pressure, in-package pH, and temperature as shown in Equation L-20:

$$\begin{aligned} \Sigma C &= pCO_2\left(10^{k_1} + 10^{(pH+k_1+k_2)} + 10^{(2\,pH+k_1+k_2+k_3)}\right) \\ Log\,k_1 &= 7\times10^{-5}\,T^2 - 0.0159T - 1.1023 \\ Log\,k_2 &= 5\times10^{-7}\,T^3 - 0.0002T^2 + 0.0132T - 6.5804 \\ Log\,k_3 &= -8\times10^{-5}\,T^2 + 0.0128T - 10.618 \end{aligned} \qquad \text{(Eq. L-20)}$$

where

pCO_2 = partial pressure of CO_2 in atmospheres, log[pCO_2]=-2.0 (Section L2.6.2)

pH = in-package pH

T = temperature (°C).

The degradation of the CSNF waste form depends on total carbonate as discussed in Section L2.12.1. This simplified model uses Equation L-20 to determine the total carbonate for the interior of all CSNF WPs with average CSNF WP temperature, discussed in Section L2.6.1, and the in-package pH, discussed in Section L2.9.1 as inputs.

L2.10. WASTE PACKAGE AND RADIONUCLIDE INVENTORY

The initial radionuclide and WP inventory is presented in *Initial Radionuclide Inventories* (SNL 2007 [DIRS 180472]). This simplified model includes a total of 11,629 WPs emplaced in

the repository of which 8,213 are CSNF WPs and 3,416 are CDSP WPs (DTN: MO0702PASTREAM.001_R0 [DIRS 179925]). The 413 WPs containing naval spent nuclear fuel are conservatively treated as CSNF.

The CSNF and CDSP WP inventories are further subdivided into those that reside in a seeping environment and those that do not. This subdivision is based on the seepage fraction for the long-term average climate state. Any WPs that experience early failure are assumed to reside in a seeping environment.

The radionuclide inventory per WP used in this simplified model is shown in Table L-19. Specific activities, molecular masses, half-lives, decay chains, and the manner in which each radionuclide is treated in this simplified model are also shown in Table L-19. Two additional 'species' are also included: 1,000 g/WP as a surrogate for the UO_2 matrix in CSNF WPs and 13,550 kg/WP as a surrogate for HLW glass in CDSP WPs. These are used in subsequent modeling of the degradation of the UO_2 matrix in the CSNF waste form and the HLW glass waste form.

The initial inventory values are adjusted by uncertainty multipliers shown in Table L-20 (DTN: SN0310T0505503.004_R0 [DIRS 168761]).

This simplified model accounts for radioactive decay and daughter product in-growth in the radionuclide inventory prior to exposure. A simple first-order chain decay model shown in Equation L-21 is used with subdivided timesteps to ensure accuracy. This is appropriate given the long half-lives of the radionuclides included in this simplified model. Note that this approach is conservative because it does not account for any daughter product decay during the timestep where they are formed.

$$Md_i = Md_{i-1}\, e^{-\lambda_d \Delta t_{sub}} + \frac{MMd}{MMp} Mp_{i-1} \left(1 - e^{-\lambda_p \Delta t_{sub}}\right) \qquad \text{(Eq. L-21)}$$

where

Md_i = mass of daughter radionuclide at current time sub-step i (gram per WP)

Md_{i-1} = mass of daughter radionuclide at previous time sub-step i-1 (gram per WP)

Mp_{i-1} = mass of parent radionuclide at previous time sub-step i-1 (gram per WP)

λ_p = decay constant of parent radionuclide (yr^{-1})

λ_d = decay constant of daughter radionuclide (yr^{-1})

MMp = molecular mass of parent radionuclide (g)

MMd = molecular mass of daughter radionuclide (g)

Δt = time sub-step size (yr).

L2.11. MASS EXPOSURE RATES

Radionuclides cannot be released from the EBS if they remain bound within the waste forms (or un-exposed). A radionuclide is considered to be exposed when it is made available for subsequent transport through the EBS. The rate that radionuclides are exposed depends on where they reside within the waste form. Radionuclides are contained in the waste form matrix for the CSNF, HLW, and DSNF waste forms. A fraction of the radionuclides reside in the fuel-clad gap and in grain boundary regions in CSNF and are assumed to be exposed instantaneously upon failure of the WP. In addition, it is conservatively assumed that the DSNF waste form degrades immediately upon WP failure, resulting in instantaneous exposure of the radionuclides. The approach for calculating mass exposure rates used in this simplified analysis is essentially identical to the approach used in the GoldSim software (GoldSim Technology Group 2007 [DIRS 183214], Appendix E).

The radionuclide exposure rate for those radionuclides in the CSNF fuel-clad gap and grain boundary region and those contained in the DSNF waste form is shown in Equation L-22:

$$e_{i,j}(t) = N_{wp} \bullet I_j(t) \bullet f_{wp}(t) \qquad \text{(Eq. L-22)}$$

where

$e_{i,j}(t)$ = the instantaneous exposure rate of radionuclide j at time t (g/yr)
N_{wp} = the number of WPs
I_j = the inventory of radionuclide j at time t (gram per WP)
$f_{wp}(t)$ = the WP fractional failure rate at time t (yr^{-1}).

The radionuclide exposure rate for those radionuclides bound in the CSNF and HLW glass matrix is shown in Equation L-23:

$$e_{b,j}(t) = N_{wp} \bullet M_s(t) \bullet k_s(t) \bullet I_j(t)$$
$$\frac{dM_s}{dt} = h(t) - M_s(t) \bullet k_s(t) \qquad \text{(Eq. L-23)}$$

where

$e_{b,j}(t)$ = the bound radionuclide exposure rate of radionuclide j at time t (g/yr)
N_{wp} = the number of WPs
$M_s(t)$ = the fraction of un-protected, but un-degraded matrix (unitless)
$k_s(t)$ = the fractional degradation rate of the waste matrix (yr^{-1})
$h(t)$ = the rate that the matrix becomes un-protected (yr^{-1})
I_j = the inventory of radionuclide j at time t (gram per WP).

The rate that the matrix becomes un-protected, h(t), depends on the number of barriers between the matrix and the repository environment. Both the CSNF and DHLW waste forms have additional barriers besides the Alloy 22 WP outer barrier. These barriers include the stainless steel WP inner barrier, cladding for CSNF, and canister for DHLW. However, no performance credit is ascribed to any of these barriers in relation to mass exposure in this simplified model and the rate that the matrix becomes unprotected, h(t), is simply the rate that the WPs fail, $f_{wp}(t)$.

If $f_{wp}(t)$ and $k_s(t)$ are constant, the equation for the fraction of un-protected, but un-degraded matrix is shown in Equation L-24 (GoldSim Technology Group 2007 [DIRS 183214], Appendix E):

$$M_s(t) = \frac{h}{k_s}\left(1 - e^{-k_s t}\right) + M_s(0)e^{-k_s t}. \qquad \text{(Eq. L-24)}$$

However, both $f_{wp}(t)$ and $k_s(t)$ vary over time but are assumed to be constant over a timestep. The fraction of mass un-protected, but un-degraded matrix is solved numerically using Equation L-25 (GoldSim Technology Group 2007 [DIRS 183214], Appendix E):

$$M_s(t) = \frac{h(t-\Delta t)}{k_s(t-\Delta t)}\left(1 - e^{-k_s \Delta t}\right) + M_s(t-\Delta t)e^{-k_s \Delta t}. \qquad \text{(Eq. L-25)}$$

L2.12. WASTE FORM DEGRADATION

L2.12.1 Commercial Spent Nuclear Fuel Waste Form Degradation

The CSNF waste form degradation model is developed in *CSNF Waste Form Degradation: Summary Abstraction* (BSC 2004 [DIRS 169987]). As discussed above, this model assumes instantaneous release of the fraction of radionuclides residing in either the fuel-clad gap or in the grain boundaries and a response surface for the degradation of the spent UO_2 matrix.

The release of the gap and grain-boundary inventories of cesium, iodine, and technetium is modeled as an instantaneous release of the fraction (f_i) of the total inventory of each of these elements estimated to be in the gap and grain-boundary regions. The instantaneous fractional releases for ^{135}Cs, ^{129}I, and ^{99}Tc are modeled as triangular distributions with the apex of the triangular probability distribution function located at the average release fractions shown in Table L-21 and spanning the range shown in the last row of this table for each element (DTN: MO0404ANLSF001.001_R0 [DIRS 169007]).

The CSNF waste form degradation model is shown in Equation L-26 (BSC 2004 [DIRS 169987], Section 8.1):

$$Log[k_{s-CSNF}] = Log(A) + a_0 + a_1 \bullet \frac{1}{T} + a_2 \bullet \Sigma C + a_3 \bullet pO_2 + a_4 \bullet pH \qquad \text{(Eq. L-26)}$$

where

$k_{s\text{-}CSNF}$	=	fractional degradation rate of the CSNF UO_2 matrix (d^{-1})
A	=	fuel effective specific surface area (m^2/d)
T	=	temperature (K)
ΣC	=	negative base 10 log of total carbonate (molal)
pO_2	=	negative base 10 log of oxygen pressure (atmospheres)
a_0, a_1, a_2, a_3, a_4	=	regression coefficients.

This model is used for both alkaline and acidic conditions with different regression coefficients. The expected values for each of these coefficients is shown in Table L-22 (DTN: MO0404ANLSF001.001_R0 [DIRS 169007]).

Uncertainties in the regression coefficients shown in Table L-22 are related through a Cholesky factorization method. Tables L-23 and L-24 show the covariance matrices for alkaline and acidic conditions, respectively. Note that coefficients a_1 and a_3 are identical for both alkaline and acidic conditions, and their values are determined using the covariance matrix shown in Table L-23.

The sampled value of the regression coefficients is determined using Equation L-27:

$$[a_n] = [CHO] \bullet [U] + [a_n^{expected}] \quad \text{(Eq. L-27)}$$

where

$[a_n]$	=	vector of regression coefficient (of length n)
$[U]$	=	vector of uncertainty coefficients (n values sampled from a normal distribution with a mean of 0 and a standard deviation of 1)
$[CHO]$	=	Cholesky factorization matrix (Tables L-23 and L-24)
$a_n^{expected}$	=	expected value of the regression coefficients (Table L-22).

Regression coefficients are sampled for each realization through the use of the covariance matrix. Fractional degradation rates are computed for both alkaline and acidic conditions and the maximum of the two is used for the CSNF waste form fractional degradation rate.

Figure L-8 (Corroborative DTN: MO0708SIMPLIFI.000 [DIRS 182980]) shows the CSNF waste form fractional degradation rate as a function of pH and temperature for the expected value of the coefficients in the CSNF degradation model shown in Table L-22. It can be seen that the CSNF waste form fully degrades in less than 1,000 years under expected repository conditions.

L2.12.2 Defense High-Level Waste Form Degradation

The DHLW glass waste form degradation model is developed in *Defense HLW Glass Degradation Model* (BSC 2004 [DIRS 169988]). This model is a simple model with the fractional degradation rate shown in Equation L-28 (BSC 2004 [DIRS 169988], Section 8.1):

$$k_{s-DHLW} = S \bullet f_{\exp} \bullet R_{alt} \qquad \text{(Eq. L-28)}$$

where

$k_{s\text{-}DLHW}$ = fractional degradation rate of DHLW glass (yr^{-1})
S = specific surface area (m^2/g)
f_{exp} = glass exposure factor
R_{alt} = glass alteration rate ($g/m^2/yr$).

The glass specific surface area, S, is constant at 2.7E-3 m^2/kg, and the glass exposure factor is a triangular distribution (minimum = 4, most probable value = 4, maximum = 17) (DTN: MO0502ANLGAMR1.016_R0 [DIRS 172830]). The glass alteration rate is shown in Equation L-29 (BSC 2004 [DIRS 169988], Section 8.1):

$$R_{alt} = k_g \times 10^{\eta \bullet pH} \times \exp\left(\frac{-E_a}{RT}\right) \qquad \text{(Eq. L-29)}$$

where

R_{alt} = glass alteration rate ($g/m^2/yr$)
k_g = forward glass dissolution rate ($g/m^2/yr$)
η = order of the reaction with respect to H^+
pH = in-package pH
E_a = activation energy for rate limiting step (kJ/mol)
R = gas constant, 8.314E-3 (kJ/mol/K)
T = temperature (K).

Separate sets of parameters are used for alkaline or acidic conditions. These parameters are provided in Table L-25 (DTN: MO0502ANLGAMR1.016_R0 [DIRS 172830]). Fractional degradation rates are calculated as a function of pH and temperature using both the alkaline and acidic parameters and the maximum is used as the fractional DHLW degradation rate.

Figure L-9 (Corroborative DTN: MO0708SIMPLIFI.000 [DIRS 182980]) shows the DHLW waste form fractional degradation rate as a function of pH and temperature for the expected value of the coefficients in the DHLW degradation model shown in Table L-25. It can be seen that the DHLW waste form degrades more slowly than the CSNF waste form.

L2.13. ENGINEERED BARRIER SYSTEM FLOW

The *EBS Radionuclide Abstraction* (SNL 2007 [DIRS 177407], Sections 6.3.2 and 6.3.3) describes the approach used in the TSPA-LA for determining the amount of water that flows through the engineered barriers.

This simplified model assumes that no water flows through either failed WPs or through the invert in regions of the repository that do not experience seepage. In those regions experiencing seepage, no flowing water is assumed to contact the surface of the WP when the DSs have not failed due to general corrosion. The DSs may experience SCC. However, it is not expected that any water would be able to flow through such cracks and the DS would retain its effectiveness as a barrier to seepage. Water is assumed to be diverted around the intact DSs and flow through the invert at a flow rate equal to the seepage rate. Water is assumed to contact the WP surface at a rate equal to the seepage rate when the DS fails due to general corrosion or due to plate failure due to a seismic event.

The WPs may experience SCC in the weld region and possibly due to seismic events. However, it is not expected that any water would be able to flow through such cracks and the WPs would retain their effectiveness as a barrier to seepage even if SCC occurs.

The fraction of drift seepage that enters a WP having general corrosion breaches underneath a failed DS is shown in Equation L-30 (SNL 2007 [DIRS 177407], Section 6.3.3.2.5):

$$F_{WP} = \min\left[\frac{N_P \frac{L_P}{2}}{L_{WP}} f'_{WP}, 1\right] \qquad \text{(Eq. L-30)}$$

where

F_{WP} = the fraction of drift seepage that enters a WP through general corrosion breaches

N_P = the number of patch penetrations on a failed WP

L_P = the length of a WP patch

L_{WP} = the total axial length of a WP

f'_{WP} = uncertainty factor for the fraction of rivulet flow that enters a breach, uniform distribution, 0-2.41 (DTN: SN0703PAEBSRTA.001_R3 [DIRS 183217]).

The approach for computing the fraction of seepage that flows through the WPs using Equation L-30 discretizes the surface of the WP into a number of patches over the WP surface in order to utilize computations from *WAPDEG Analysis of Waste Package and Drip Shield Degradation* (SNL 2007 [DIRS 177407]).

The number of patches failed can be expressed as the product of the fraction of the WP surface that is breached due to general corrosion and the total number of patches assumed in the discretization of the WP surface. The TSPA-LA Model discretizes the WP surface into approximately 1,400 patches each with an area of 23,150 mm^2 (Section 6.3.5.1.2). This gives a patch length, L_P, equal to 152.15 mm. The total axial length of a TAD-bearing WP, L_{WP}, is 5.691 m (DTN: SN0703PAEBSRTA.001_R3 [DIRS 183217]).

Figure L-10 shows fraction of seepage that would flow through a WP as a function of the fractional area of the WP surface penetrated by general corrosion and the uncertainty factor for rivulet flow, f'_{WP} (shown as percentiles of the uniform distribution). It can be seen that this approach results in a relatively small fraction of the WP surface needing to be breached by general corrosion to allow all of the drift seepage entering the WP. Based on these results, this simplified model assumes that all seepage that contacts the WP surface can flow through the WP upon initial failure by general corrosion.

L2.14. DISSOLVED CONCENTRATION LIMITS

Dissolved concentration limits (solubility limits) were determined in *Dissolved Concentration Limits of Radioactive Elements* (SNL 2007 [DIRS 177418]) as a function of geochemical conditions. The functional form for the dissolved concentration limits is shown in Equation L-31:

$$Log[SL] = S(pH, pCO_2) + \varepsilon_1 + Log[\varepsilon_2 \times N(pH)] \quad \text{(Eq. L-31)}$$

where

- $Log[SL]$ = the base-10 logarithm of the dissolved concentration limit, including uncertainty (solubility limits in mg/L)
- $S(pH,pCO_2)$ = the base-10 logarithm of the dissolved concentration limit as a function of pH and pCO_2
- ε_1 = uncertainty in the base-10 logarithm of the dissolved concentration limit due to uncertainties in the thermodynamic properties of both the controlling solid and significant dissolved species
- ε_2 = term for uncertainty in the base-10 logarithm of the dissolved concentration limit due to uncertainties in the fluoride concentration
- $N(pH)$ = multiplication term (function of pH) for uncertainty in the base-10 logarithm of the dissolved concentration limit due to uncertainties in the fluoride concentration.

As discussed in Section L.2.6.2, the pCO_2 is assumed to be constant at 0.01 and the pH in the EBS can vary from 5.0 to 8.0. The base-10 logarithm of the dissolved concentration limits as a function of pH at a pCO_2 of -2 are shown in Table L-24. These values are used in this simplified model. The dissolved concentration limit for U is assumed to be controlled by schoepite for pH<=6.75 and by Na-boltwoodite/$Na_4UO_2(CO_3)_3$ for pH>=7.75. The average in between the two is assumed to be the dissolved concentration limit. The dissolved concentration limits, not

accounting for uncertainty, used in this simplified model are shown on Figure L-11. The dissolved concentration limits shown in Table L-26 and on Figure L-11 show that uncertainty in the pH translates to a broad variation in the dissolved concentration limit, covering approximately two orders of magnitude over the pH range of 5 to 8.

The uncertainty terms are functions of the waste form type and the manner in which the WPs are breached (corrosion, seismic mechanical damage, or igneous intrusion). The dissolved concentration limit uncertainty terms used in this simplified model are shown in Table L-27. The ε_2 term for the CSNF and CDSP WPs is represented by a very skewed triangular distribution with minimums and best estimates of zero for all WP failure modes (DTN: MO0702PADISCON.001_R0 [DIRS 179358]). In addition, the N term, which is multiplied by the ε_2 term, has a maximum of 1 and minimums as low as 10^{-3} (depending on the pH) (DTN: MO0702PADISCON.001_R0 [DIRS 179358]). Given the skewness of the ε_2 triangular distribution, relatively low distribution maximums, and N values typically much less than 1, the contribution of fluoride uncertainty to the total uncertainty in the dissolved concentration limit will be small. Thus, this simplified model does not consider uncertainty in the fluoride concentration and the dissolved concentration limit is determined using Equation L-32 and the values in Tables L-26 and L-27.

$$Log[SL] = S(pH, pCO_2) + \varepsilon_1 \qquad \text{(Eq. L-32)}$$

Infinite solubility is assumed for carbon, chlorine, cesium, iodine, selenium, and technetium (SNL 2007 [DIRS 177418], Sections 6.14 to 6.17).

L2.15. RADIONUCLIDE TRANSPORT THROUGH THE ENGINEERED BARRIER SYSTEM

This simplified approach models the transport of dissolved radionuclides through the EBS via advective and diffusive transport mechanisms. The diffusive and advective conductance depends on the failure state of the EBS components (DS and WP) and the seepage environment (seeping or nonseeping). Colloid-facilitated radionuclide transport is not considered in this simplified model because past TSPA model results have demonstrated that colloid-facilitated radionuclide transport is not a significant contributor to overall repository performance.

The TSPA-LA Model incorporates radionuclide transport through the EBS by using a series of mixing cells to model one-dimensional transport via advective and diffusive processes. The governing equation is shown in Equation L-33 (GoldSim Technology Group 2007 [DIRS 183214], Appendix B):

$$\frac{dm}{dt} = -m\lambda + m_p\lambda_p \frac{MM}{MM_p} + \dot{m}_{in} - \dot{m}_{out} + S \qquad \text{(Eq. L-33)}$$

where

m = radionuclide mass in a cell

m_p = parent radionuclide mass in a cell

λ = radionuclide decay constant (yr^{-1})

λ_p = parent radionuclide decay constant (yr^{-1})

MM = molecular mass of radionuclide (g)

MM_p = molecular mass of parent radionuclide (g)

$\dot{m}_{in}$ = radionuclide mass flux into the cell (g/yr)

$\dot{m}_{out}$ = radionuclide mass flux out of cell (g/yr)

S = rate of direct radionuclide mass input from an external source, such as waste form degradation (g/yr).

The radionuclide mass flux into and out of a cell can be via advection, diffusion, or both. The advective mass flux from a cell is shown in Equation L-34. The advective 'direction' is always in the direction of the advective flow rate:

$$\dot{m}_{adv} = C\, q_{adv} \qquad \text{(Eq. L-34)}$$

where

$\dot{m}_{adv}$ = the advective radionuclide mass flux out of a cell (g/yr)

C = the dissolved radionuclide concentration in the cell (g/m^3)

q_{adv} = the advective flow rate out of the cell (m^3/yr).

The diffusive mass flux between two cells is shown in Equation L-35. The diffusive 'direction' depends on the concentration gradient between adjacent cells:

$$\dot{m}_{dif,i\to j} = D\left(C_i - C_j\right) \qquad \text{(Eq. L-35)}$$

where

$\dot{m}_{dif,i\to j}$ = the diffusive radionuclide mass flux between cells i and j (g/yr)

D = the diffusive conductance between cells i and j (m^3/yr)

C = the dissolved radionuclide concentration in cells i and j (g/m^3).

The diffusive conductance is shown in Equation L-36:

$$D = \frac{A_d}{\frac{L_i}{Deff_i} + \frac{L_j}{Deff_j}} \qquad \text{(Eq. L-36)}$$

where

A_d = the diffusive area between cells i and j (m^2)

L = the diffusive length in cells i and j (m)

$Deff$ = the effective diffusion coefficient in cells i and j (m^2/yr).

The dissolved radionuclide concentration may be constrained by the dissolved concentration limit (solubility limit). For those radionuclides that are not constrained by a dissolved concentration limit, the radionuclide concentration in a cell is given by the radionuclide mass in the cell divided by the fluid volume. For those radionuclides that are constrained by a dissolved concentration limit, the radionuclide concentration in the cell is the minimum of either the radionuclide mass in the cell divided by the fluid volume or the dissolved concentration limit. This is shown in Equation L-37:

$$\text{No Solubility Constraint} \quad C = \frac{M}{V}$$

$$\text{Solubility Constraint} \quad C = \min\left(\frac{M}{V}, S_L\right) \qquad \text{(Eq. L-37)}$$

where

C = the dissolved radionuclide concentration in a cell (g/m^3)

M = the radionuclide mass in the cell (g)

V = the fluid volume in the cell (m^3)

S_L = the dissolved concentration limit (g/m^3).

The EBS radionuclide transport model used in the TSPA-LA is detailed in *EBS Radionuclide Transport Abstraction* (SNL 2007 [DIRS 177407]). The TSPA-LA discretizes the repository into six regions to account for spatial variability in the repository environment. Within each region there are four networks of cells that represent the CSNF and CDSP WPs in seeping and nonseeping environments. A cell network is shown schematically on Figure L-12. Diffusive links are present in all cell networks whereas advective links are present only in those networks representing seeping environments. A total of 24 cell networks is established. Applying the above equations to each cell, results in a series of coupled differential equations that must be solved numerically at each timestep to determine the radionuclide mass in each cell.

This simplified model represents repository average conditions. A much simpler network of cells is used as shown on Figure L-13. There are two cell networks for each of the CSNF and CDSP WPs; one for those WPs that experience seepage and one for those WPs that do not experience seepage. CSNF and CDSP WPs that experience early failure are assumed to always experience seepage.

In the nonseeping environment, radionuclide transport is via diffusion only. In the seeping environment, radionuclide transport is via diffusion and advection.

In addition, the governing series of differential equation is not solved explicitly at each timestep. Rather, an approximate solution is used as outlined below. This approximation is applied to each cell progressing from the waste form cell to the corrosion product cell to the invert cell. Radionuclide sorption onto degraded materials within the EBS is conservatively not considered in this simplified model.

- Radionuclide mass is added to the cell from either degradation of the waste form or from an 'up-stream' cell.
- A fraction of the radionuclide mass within a cell in the no-seeping network is moved to the corresponding cell in the seeping network as a result of changes in the seepage fraction that occur when the climate state changes.
- The radionuclide mass is updated over the length of the timestep due to radioactive decay and daughter product in-growth. The technique used to update the radionuclide inventory per WP discussed above is used.
- The dissolved radionuclide concentration is determined in each cell using Equation L-37.
- The diffusive conductance (Equation L-36) and, for the seeping environment, the advective flow rate is determined. The total conductance is then determined.
- The total conductance and the dissolved radionuclide concentration in the cell is used to calculate the mass of each radionuclide that is passed to the 'down-stream' cell. If the radionuclide mass calculated to be passed to the 'down-stream' cell exceeds the radionuclide mass in the cell, then the radionuclide mass to be passed is set equal to the radionuclide mass in the cell.
- 'Back diffusion' is not allowed when the concentration of a 'down-stream' cell exceeds that of the 'up-stream' cell.

This approximate approach is essentially an explicit-in-time solution of Equation L-33.

L2.15.1 Corrosion Product Mass and Pore Volume in Waste Form and Corrosion Product Mixing Cells

The mixing cells contain corrosion product and water in the corrosion product void space from the degradation of (SNL 2007 [DIRS 177407], Section 6.5.3.4):

- CSNF waste form cell: basket tubes and absorber plates
- CDSP waste form cell: five DHLW canisters and one DSNF canister
- CSNF corrosion product cell: guide assembly, TAD canister, and inner vessel
- CDSP corrosion product cell: divider plate, inner brackets, support tube, and inner vessel.

This simplified analysis calculates the average mass of corrosion product in failed WPs using the same approach described in *EBS Radionuclide Transport Abstraction* (SNL 2007 [DIRS 177407], Section 6.5.3.4). The corrosion of both carbon and stainless steel is considered. Four corrosion products are also modeled; goethite, ferrihydrite (HFO), chromium oxides, and nickel oxides. The total mass of each corrosion product in each cell is determined using Equation L-38 (SNL 2007 [DIRS 177407], Equation 8-4):

$$m_{CPm,CS,n}(t) = \begin{cases} \left(\frac{\bar{t}}{t_{LCS,n}}\right) f_{CS} f_{GHFO} \omega_{CS,m} \frac{M_{CPm}}{\alpha_{CPm} M_m} m_{s,n}, & \bar{t} \le t_{LCS,n} \\ f_{CS} f_{GHFO} \omega_{CS,m} \frac{M_{CPm}}{\alpha_{CPm} M_m} m_{s,n}, & \bar{t} > t_{LCS,n} \end{cases}$$

$$m_{CPm,SS,n}(t) = \begin{cases} \left(\frac{\bar{t}}{t_{LSS,n}}\right)(1 - f_{CS}) f_{GHFO} \omega_{SS,m} \frac{M_{CPm}}{\alpha_{CPm} M_m} m_{s,n}, & \bar{t} \le t_{LSS,n} \\ (1 - f_{CS}) f_{GHFO} \omega_{SS,m} \frac{M_{CPm}}{\alpha_{CPm} M_m} m_{s,n}, & \bar{t} > t_{LSS,n} \end{cases} \quad \text{(Eq. L-38)}$$

where

$m_{CP,n}$ = total mass of corrosion products in cell 'n' (n is either CSNF waste form, CDSP waste form, CSNF corrosion product, or CDSP corrosion product cells) [kg]

$m_{CPm,CS,n}$ = mass of corrosion product m in cell 'n' from corrosion of carbon steel [kg]

$m_{CPm,SS,n}$ = mass of corrosion product m in cell 'n' from corrosion of stainless steel [kg]

$\bar{t}$ = average WP failure time [yr]

$t_{LCS,n}$ = lifetime of carbon steel in cell 'n' [yr]

$t_{LSS,n}$ = lifetime of stainless steel in cell 'n' [yr]

f_{CS} = fraction of carbon steel in steel mass [dimensionless]

$\omega_{CS,m}$ = mass fraction of metal *m* in carbon steel [dimensionless]

$\omega_{SS,m}$ = mass fraction of metal *m* in stainless steel [dimensionless]

M_m = atomic weight of metal *m* [kg mol^{-1}]

M_{CPm} = molecular weight of corrosion products from corrosion of metal *m* [kg mol^{-1}]

$\alpha_{CP,m}$ = stoichiometric coefficient for conversion of metal *m* to corrosion products from corrosion of metal *m* [mol *m* mol^{-1} *CPm*]

$m_{s,n}$ = total mass of steel in cell 'n' [kg].

The mass of corrosion products in breached WPs is calculated using the average WP failure time, shown as Equation L-39 (Section 6.3.7.2.3). The average WP failure time for those WPs that fail early (initially) is simply the time since repository closure:

$$\bar{t} = \frac{\left(N_{WP\,Failed}^{new} \times \frac{1}{2}\Delta t\right) + \left(N_{WP\,Failed}^{prev} \times (\bar{t}^{\,prev} + \Delta t)\right)}{N_{WP\,Failed}^{new} + N_{WP\,Failed}^{prev}} \qquad \text{(Eq. L-39)}$$

where

$\bar{t}$ = average WP failure time [yr]

$N_{WPFailed}^{New}$ = the number of new failures in the current timestep

$N_{WPFailed}^{prev}$ = the number of total failures in the previous timestep

Δt = the timestep length [yr].

The lifetime of carbon steel in cell 'n' is shown in Equation L-40 (SNL 2007 [DIRS 177407], Equation 8-4):

$$t_{LCS,n} = \frac{1000\, t_{max,CS,n}}{2 r_{CS}}$$

$$t_{LSS,n} = \frac{1000\, t_{max,SS,n}}{2 r_{SS}} \qquad \text{(Eq. L-40)}$$

where

r_{CS} = rate of corrosion of carbon steel [$\mu m\ yr^{-1}$]

r_{SS} = rate of corrosion of stainless steel [$\mu m\ yr^{-1}$]

$t_{max,CS,n}$ = maximum thickness of carbon steel in cell 'n' [m]

$t_{max,SS,n}$ = maximum thickness of stainless steel in cell 'n' [m].

The carbon steel corrosion rate, r_{CS}, is represented as a truncated log-normal distribution (μ = 78.5 $\mu m\ yr^{-1}$; σ = 25.0 $\mu m\ yr^{-1}$; minimum = 25.0 $\mu m\ yr^{-1}$; maximum =1,35.0 $\mu m\ yr^{-1}$) and the stainless steel corrosion rate, r_{SS}, is represented as a truncated log-normal distribution (μ = 0.267 $\mu m\ yr^{-1}$, σ = 0.209 $\mu m\ yr^{-1}$, minimum = 0.01 $\mu m\ yr^{-1}$, and maximum = 0.51 $\mu m\ yr^{-1}$) (DTN: SN0703PAEBSRTA.001_R3 [DIRS 183217]).

The parameter f_{GHFO} is shown in Equation L-41 (SNL 2007 [DIRS 177407], Equation 8-4):

$$f_{GHFO} = \begin{cases} \omega_G, & \text{for goethite} \\ (1-\omega_G), & \text{for HFO} \\ 1.0, & \text{for NiO and } Cr_2O_3 \end{cases} \quad \text{(Eq. L-41)}$$

where

ω_{Gn} = mass fraction of goethite in iron corrosion products, uniform distribution (0.45 - 0.80) (DTN: SN0703PAEBSRTA.001_R3 [DIRS 183217]).

The pore volume in the corrosion product is calculated for each cell using Equation L-42:

$$PV_{CP,n} = \frac{\phi_{CP}}{1-\phi_{CP}} V_{CP,n} = \frac{\phi_{CP}}{1-\phi_{CP}} \sum_{CPm} \left(m_{CPm,CS,n} + m_{CPm,SS,n} \right) / \rho_{CPm} \quad \text{(Eq. L-42)}$$

where

$PV_{CP,n}$ = pore volume of the corrosion product in cell 'n' (m^3)

$V_{CP,n}$ = volume of the corrosion product in cell 'n' (m^3)

ϕ_{CP} = porosity of corrosion product, 0.4 (DTN: SN0703PAEBSRTA.001_R3 [DIRS 183217])

ρ_{CPm} = density of corrosion product m (kg/m^3).

The parameters used to calculate the mass of each corrosion product and the total volume of water in the corrosion product for each cell are shown in Tables L-28 through L-30 (DTN: SN0703PAEBSRTA.001_R3 [DIRS 183217]).

L2.15.2 Commercial Spent Nuclear Fuel Waste Form Cell Parameters

The CSNF waste form cell contains the rind from reacted CSNF rods and corrosion product from degradation of the Stainless Steel Type 316 basket tubes and Borated Stainless Steel Type 304B4 absorber plates (SNL 2007 [DIRS 177407], Section 6.5.2.1.1). The volume of water in the CSNF waste form cell is the sum of the pore volume of the degraded UO_2 matrix and the pore volume of the corrosion product as shown in Equation L-43. This assumes that both the degraded UO_2 matrix and the corrosion product are fully saturated. The pore volume of the corrosion product is calculated using the approach described above:

$$PV_{CSNF-WF} = \phi_{rind} V_{rind} + PV_{CP,CSNF-WF} \quad \text{(Eq. L-43)}$$

where

$PV_{CSNF\text{-}WF}$ = pore volume of the CSNF waste form mixing cell (m^3)

$V_{rind\text{-}CSNF}$ = volume of reacted CSNF rind (m^3)

$PV_{CP,CSNF\text{-}WF}$ = pore volume of corrosion product in CSNF waste form (m^3)

ϕ_{rind} = porosity of the CSNF schoepite rind, uniform distribution: 0.05 to 0.30 (DTN: MO0411SPACLDDG.003_R1 [DIRS 180755]).

Models for the corrosion of the CSNF UO_2 matrix, and the subsequent rind volume, are described in *Cladding Degradation Summary for LA* (SNL 2007 [DIRS 180616]). The volume of the reacted CSNF rind is shown in Equation L-44 (SNL 2007 [DIRS 180616], Equation 6-7):

$$V_{rind-CSNF} = V_i \cdot VM \cdot F_{cor} \quad \text{(Eq. L-44)}$$

where

V_i = initial volume of CSNF UO_2 pellets per WP (m^2)

VM = volume increase due to UO_2 alteration to schoepite

F_{cor} = fraction of UO_2 altered to schoepite.

The initial volume of CSNF UO_2 pellets per WP is shown in Equation L-45 (SNL 2007 [DIRS 180616], Equation 6-4):

$$V_I = N_R \cdot L_R \cdot \pi/4 \cdot D_R^2 \quad \text{(Eq. L-45)}$$

where

L_R = fuel rod length, 3.66 m (DTN: MO0411SPACLDDG.003_R1 [DIRS 180755])

D_R = diameter of the fuel pellets, 0.819 cm (DTN: MO0411SPACLDDG.003_R1 [DIRS 180755])

N_R = total number of fuel rods failed in a WP, 5,544 (DTN: MO0411SPACLDDG.003_R1 [DIRS 180755]).

The volume increase due to the UO_2 alteration to schoepite is shown in Equation L-46 (SNL 2007 [DIRS 180616], Equation 6-3):

$$VM = \frac{MW_{schoepite}}{MW_{UO_2}} \frac{\rho_{UO_2}}{(1-\phi_{schoepite})\rho_{schoepite}} \quad \text{(Eq. L-46)}$$

where

$MW_{schoepite}$ = the molecular weight of schoepite, 322.1 g (DTN: MO0411SPACLDDG.003_R1 [DIRS 180755])

MW_{UO2} = the molecular weight of UO_2, 270 g (DTN: MO0411SPACLDDG.003_R1 [DIRS 180755])

$\rho_{schoepite}$ = the density of schoepite, 4.83 g/cm^3 (DTN: MO0411SPACLDDG.003_R1 [DIRS 180755])

ρ_{UO2} = the density of UO_2, 10.97 g/cm^3 (DTN: MO0411SPACLDDG.003_R1 [DIRS 180755])

$\phi_{schoepite}$ = the porosity of schoepite, uniform distribution: 0.05 to 0.30 (DTN: MO0411SPACLDDG.003_R1 [DIRS 180755]).

The fraction of UO_2 altered to schoepite is determined as an average over the total number of WPs that have failed in each region according to Equation L-47. This simplified model ascribes no barrier capability to the clad and the number of failed CSNF rods per WP equals the number of fuel rods in a WP:

$$F_{cor,j} = \frac{\frac{\Sigma M_{r,j}}{NF_{wp,j}}}{M_t} \qquad \text{(Eq. L-47)}$$

where

$F_{cor,j}$ = fraction of UO_2 altered to schoepite in region j (seeping or nonseeping)

$\Sigma M_{r,j}$ = total mass of UO_2 released from the waste form in region j

$NF_{wp,j}$ = number of failed CSNF WPs in region j

M_t = total mass of UO_2 per WP.

The total mass of UO_2 per WP, M_t, is set as a surrogate at 10^3 grams in the CSNF inventory as a nonradioactive species. The cumulative release is tracked over time and the numerator of Equation L-47 coverts this to an average mass of UO_2 (surrogate) released per failed fuel rod. The denominator is the total mass of UO_2 (surrogate) in a fuel rod.

The diffusion path length is equal to the inner radius of the TAD canister, 0.819 m (DTN: SN0703PAEBSRTA.001_R3 [DIRS 183217]). The diffusive area is equal to the surface area of a cylinder with a radius of half the TAD canister inner radius, and a length equal to the length of the fuel basket tubes (excluding the ends), 12.5 m^2 (DTN: SN0703PAEBSRTA.001_R3 [DIRS 183217]).

The effective diffusion coefficient in the CSNF rind is shown in Equation L-48 (SNL 2007 [DIRS 177407], Table 8.2-1):

$$\phi_{eff} S_w D_{CSNF,j} = \phi_{eff}^{1.3} S_w^{2} D_{0,j} \qquad \text{(Eq. L-48)}$$

where

$D_{CSNF,,j}$ = effective diffusion coefficient for radionuclide j in CSNF waste form cell (m^2/s)

$D_{0,,j}$ = free water diffusion coefficient for radionuclide j (m^2/s)

ϕ_{eff} = effective porosity of CSNF waste form cell

S_w = water saturation, 1 (SNL 2007 [DIRS 177407], Table 8.2-1).

The effective porosity of the CSNF waste form cell is shown in Equation L-49:

$$\phi_{CSNF-WF} = \frac{PV_{CSNF-WF}}{V_{rind-CSNF} + V_{CP,CSNF-WF}} \quad \text{(Eq. L-49)}$$

where

$PV_{CSNF\text{-}WF}$ = pore volume of the CSNF waste form mixing cell (m^3)

$V_{rind\text{-}CSNF}$ = volume of reacted CSNF rind in the waste form mixing cell (m^3)

$V_{CP,CSNF\text{-}WF}$ = volume of corrosion product in the CSNF waste form mixing cell (m^3).

The free diffusion coefficients for the species considered in this simplified model are shown in Table L-31. This simplified model first calculates an overall effective diffusion coefficient using the self-diffusion coefficient of water, 2.299×10^{-9} m^2/s. The diffusion coefficient for each radionuclide is then adjusted using the ratio of the free water diffusion coefficients shown in Table L-31 and self-diffusion coefficient of water.

L2.15.3 CDSP Waste Form Cell Parameters

The CDSP waste form cell contains the degraded DHLW glass and corrosion product from the degradation of the DHLW and DSNF canisters. This is a simpler representation of the CDSP waste form than is modeled in *EBS Radionuclide Transport Abstraction* (SNL 2007 [DIRS 177407]), where the DHLW and DSNF are each represented as a waste form cell.

The volume of water in the CDSP waste form cell is the sum of the pore volume of the degraded DHLW glass and the pore volume of the corrosion as shown in Equation L-50. This assumes that both the degraded DHLW glass and the corrosion product are fully saturated. The pore volume of the degraded DSNF is not included in the total pore volume. The pore volume of the corrosion product is calculated using the approach described above.

$$PV_{CDSP-WF} = PV_{glass} + PV_{CP,CDSP-WF} \quad \text{(Eq. L-50)}$$

where

$PV_{CDSP\text{-}WF}$ = pore volume of the CDSP waste form mixing cell (m^3)

PV_{glass} = volume of reacted DHLW glass (m^3)

$PV_{CP,CDSP\text{-}WF}$ = pore volume of corrosion product in CDSP waste form (m^3).

Models for the corrosion of the DHLW glass matrix, and the subsequent rind volume, are described in *Defense HLW Glass Degradation Model* (BSC 2004 [DIRS 169988]). The total volume and pore volume in the glass alteration layer is calculated using Equation L-51 (BSC 2005 [DIRS 169988], Section 8.1, Equations 54 and 55):

$$V_{glass} = 3.7 \times 10^{-4} \Sigma M_t$$
$$PV_{glass} = 6.3 \times 10^{-5} \Sigma M_t \quad \text{(Eq. L-51)}$$

where

V_{glass} = volume of the DHLW glass alteration layer (m^3)

PV_{glass} = pore volume of the DHLW glass alteration layer (m^3)

ΣM_t = total mass of altered DHLW glass (kg).

The total mass of altered DHLW glass is determined as an average over the total number of WPs that have failed in a region according to Equation L-52:

$$\Sigma M_{t,j} = \frac{\Sigma M_{ga,j}}{NF_{wp,j} \cdot N_{can}} \quad \text{(Eq. L-52)}$$

where

$\Sigma M_{t,j}$ = total mass of altered DHLW glass in region j (seeping or nonseeping environment) (kg)

$\Sigma M_{ga,j}$ = total mass of glass altered in region j

$NF_{wp,j}$ = number of failed CDSP WPs in region j

N_{can} = number of DHLW canisters per WP, 5 (DTN: SN0703PAEBSRTA.001_R3 [DIRS 183217]).

The initial mass of glass per canister, M_{gi}, is set as a surrogate at 2,710 kg in the DHLW inventory as a nonradioactive species. The cumulative release, $\Sigma M_{ga,j}$, is tracked over time for each region and Equation L-52 converts this to an average mass of glass altered per canister in the failed WPs.

The diffusion path length is equal to the radius of the inner vessel of the 5-DHLW/DOE Long WP, 0.941 m (DTN: MO0411SPACLDDG.003_R1 [DIRS 180755]). The diffusive area is equal to the surface area of a cylinder with a radius equal to half the radius of the inner vessel of

the 5-DHLW/DOE Long WP and a length of the inner vessel of that WP, 13.7 m^2 (DTN: SN0703PAEBSRTA.001_R3 [DIRS 183217]).

The diffusion coefficient in the altered glass is shown in Equation L-53 (SNL 2007 [DIRS 177407], Table 8.2-1):

$$\phi_{eff} S_w D_{HLW,j} = \phi_{eff}^{1.3} S_w^2 D_{0,j} \quad \text{(Eq. L-53)}$$

where

$D_{HLW,j}$ = effective diffusion coefficient for radionuclide j in the CDSP waste form (m^2/s)
$D_{0,j}$ = free water diffusion coefficient for radionuclide j (Table L-29) (m^2/s)
ϕ_{eff} = effective porosity of CDSP waste form cell
S_w = water saturation, 1 (SNL 2007 [DIRS 177407], Table 8.2-1).

The effective porosity of the CDSP waste form cell is shown in Equation L-54:

$$\phi_{CDSP-WF} = \frac{PV_{CDSP-WF}}{V_{glass} + V_{CP,CDSP-WF}} \quad \text{(Eq. L-54)}$$

where

$PV_{CDSP-WF}$ = pore volume of the CDSP waste form mixing cell (m^3)
V_{glass} = volume of reacted DHLW glass in the waste form mixing cell (m^3)
$V_{CP,CDSP-WF}$ = volume of corrosion product in the CDSP waste form mixing cell (m^3).

L2.15.4 Corrosion Product Cell Parameters

The volume of water in the CSNF and CDSP WP corrosion product cells, is the total pore volume of the degraded WP internals. This assumes that the corrosion products are fully saturated. The pore volume of the corrosion product is calculated using the approach described above.

The diffusive path length in the CSNF corrosion product cell excluding the outer barrier is the combined thickness of TAD and the inner vessel, 0.0914 m (DTN: SN0703PAEBSRTA.001_R3 [DIRS 183217]). The diffusive path length through the outer barrier of the CSNF corrosion product cell is the thickness of the WP outer barrier, 0.0302 m (DTN: SN0703PAEBSRTA.001_R3 [DIRS 183217]). This simplified model combines these into a total diffusion path length of 0.1216 m.

The diffusive area for the path through the outer barrier of the CSNF WP cell is the smaller of either the total area of all WP breaches or the surface area of a cylinder at the midpoint between the inner vessel outer surface and the outer surface of the CSNF WP outer barrier, 33.1 m^2 (DTN: SN0703PAEBSRTA.001_R3 [DIRS 183217]).

The diffusive path length in the CDSP corrosion product cell excluding the outer barrier is the thickness of inner vessel, 0.0508 m (DTN: MO0411SPACLDDG.003_R1 [DIRS 180755]). The diffusive path length through the CDSP outer barrier is given by the thickness of the WP outer barrier, 0.0302 m (DTN: SN0703PAEBSRTA.001_R3 [DIRS 183217]). This simplified model combines these into a total diffusion path length of 0.081 m.

The diffusive area for the path through the outer barrier of the CDSP WP is the smaller of either the total area of all WP breaches or the surface area of a cylinder at the midpoint between the inner vessel outer surface and the outer surface of the CSNF WP outer barrier, 33.1 m^2 (DTN: SN0703PAEBSRTA.001_R3 [DIRS 183217]).

The diffusive area for general corrosion breaches equals the product of the fraction of the WP that has failed due to general corrosion determined using Equation L-11 and the total area of the WP outer surface (33.1 m^2). The diffusive area for stress corrosion cracks in the outer weld region is determined using Equation L-55:

$$A_{D-SCC\ Weld} = F_{SCC\ Weld} N_{SCC\ Cracks} A_{SCC\ Crack} \quad \text{(Eq. L-55)}$$

where

$A_{D\text{-}SCC\ Weld}$ = diffusive area through SCC cracks in the closure weld region of the WP (m^2)

$F_{SCC\ Weld}$ = fractional area of the closure weld region that has experienced SCC penetration (calculated using Equation L-11)

$N_{SCC\ Cracks}$ = total number of SCC cracks that can ultimately penetrate the closure weld region

$A_{SCC\ Crack}$ = area of a single SCC crack opening (m^2).

The total number of SCC cracks that could ultimately penetrate the outer closure weld region, $N_{SCC\ Cracks}$, is determined from *WAPDEG Analysis of Waste Package and Drip Shield Degradation* (BSC 2004 [DIRS 169996], Section 6.3.2.1) and is equal to 192. The area of a single SCC crack opening, $A_{SCC\ Crack}$, is 7.682 mm^2 (DTN: SN0703PAEBSRTA.001_R3 [DIRS 183217]).

Determining the area of the WP outer barrier damaged due to seismic events is discussed in Section L2.8.3. The crack density in this area is represented as a uniform distribution with the bounds defined by Equation L-56 (SNL 2007 [DIRS 181953], Section 6.7.2):

$$\rho_{SEIS-SCC,Min} = \frac{\sqrt{3}}{2T_{WPOB}}$$
$$\rho_{SEIS-SCC,Max} = \frac{2}{\sqrt{3}T_{WPOB}} \quad \text{(Eq. L-56)}$$

where

$\rho_{SEIS\text{-}SCC,Min}$ = minimum SCC crack density (crack/m^2)

$\rho_{SEIS\text{-}SCC,Max}$ = maximum SCC crack density (crack/m^2)

T_{WPOB} = thickness of WP outer barrier (m).

The area of SCC cracks caused by seismic events is shown in Equation L-57 (SNL 2007 [DIRS 181953], Section 6.7.2):

$$A_{SEIS-SCC} = \frac{(2\pi T_{WPOB}^2)\sigma_{YS}}{E} \quad \text{(Eq. L-57)}$$

where

$A_{SEIS\text{-}SCC}$ = area of seismically induced SCC crack (m^2)

T_{WPOB} = thickness of WP outer barrier (m)

σ_{YS} = Alloy 22 yield stress, 403 MPa (DTN: MO0702PASTRESS.002_R2 [DIRS 180514])

E = Young's Modulus of Alloy 22, 206 GPa (DTN: MO0702PASTRESS.002_R2 [DIRS 180514]).

The diffusion coefficient in the corrosion product is shown in Equation L-58 (SNL 2007 [DIRS 177407], Table 8.2-1):

$$\phi_{CP} S_w D_{CP,j} = \phi_{CP}^{1.3} S_w^2 D_{0,j} \quad \text{(Eq. L-58)}$$

where

$D_{CP,j}$ = effective diffusion coefficient for radionuclide j in corrosion product (cm^2/s)

$D_{0,j}$ = free water diffusion coefficient for radionuclide j (Table L-29) (m^2/s)

ϕ_{CP} = porosity of corrosion product, 0.4 (DTN: SN0703PAEBSRTA.001_R3 [DIRS 183217])

S_w = water saturation in rind, 1 (SNL 2007 [DIRS 177407], Table 8.2-1).

L2.15.5 Invert Cell Parameters

The invert is modeled assuming it is comprised of crushed tuff. The mass of crushed tuff in the invert is calculated as the product of the invert volume, density of crushed tuff, and one-minus the invert porosity. The invert volume is equal to the length of the DS, 5.805 m; invert width, 4.7 m; and average thickness of the invert, 0.934 m (DTN: SN0703PAEBSRTA.001_R3 [DIRS 183217]). This results in an invert volume of 25.48 m^3. The invert porosity is 0.224 (DTN: SN0703PAEBSRTA.001_R3 [DIRS 183217]). The water volume in the invert is the

product of the total invert volume and the invert porosity, assuming that the invert is fully saturated. This gives an invert water volume of 3.1 m^3.

The invert diffusive area is assumed to equal the product of the invert length and width, 22.09 m^2. The diffusive path length in the invert is assumed to equal the average thickness of the invert, 0.934 m^2. The diffusion coefficient in the invert is shown in Equation L-59 (SNL 2007 [DIRS 177407], Table 8.2-7):

$$\phi_{Invert} S_w D_{Invert,j} = \phi_{Invert}^{1.863} S_w^{1.863} D_{0,j} 10^U \quad \text{(Eq. L-59)}$$

where

$D_{Invert,j}$ = effective diffusion coefficient for radionuclide j in the invert (cm^2/s)

$D_{0,j}$ = free water diffusion coefficient for radionuclide j (Table L-29) (m^2/s)

ϕ_{Invert} = porosity of corrosion product, 0.224 (DTN: SN0703PAEBSRTA.001_R3 [DIRS 183217])

S_w = water saturation in invert, assumed to be 1.

U = invert diffusion uncertainty factor, normal distribution with a mean of 0.033 and a standard deviation of 0.218

L2.16. RADIONUCLIDE TRANSPORT THROUGH THE NATURAL BARRIER SYSTEM

Modeling radionuclide transport in the UZ and SZ requires the use of complex three-dimensional models to accurately reflect the controlling processes and spatial variability in hydrologic properties. In order to model radionuclide transport it is first necessary to determine the rate and direction that groundwater flows in both the UZ and SZ. This is accomplished through the use of a dual permeability continuum approach in the UZ that is documented in *UZ Flow Models and Submodels* (SNL 2007 [DIRS 184614]) and an effective continuum approach in the SZ that is documented in *Saturated Zone Site-Scale Flow Model* (SNL 2007 [DIRS 177391]).

Several processes related to radionuclide transport within the natural system below the repository prevent or substantially reduce the movement of radionuclides from the repository to the accessible environment. These processes include matrix diffusion, radionuclide sorption, dispersion, and radionuclide decay along the transport pathway. The natural system below the repository alone can effectively isolate short lived and/or strongly-sorbing radionuclides from the environment. This barrier also reduces the movement of radionuclides that are long lived and non- or moderately-sorbing to the accessible environment.

Radionuclide transport modeling in the UZ is presented in *Radionuclide Transport Models Under Ambient Conditions* (SNL 2007 [DIRS 177396]) and *Particle Tracking Model and Abstraction of Transport Processes* (SNL 2008 [DIRS 184748]). Radionuclide transport modeling in the SZ is presented in *Site Scale Saturated Zone Transport* (SNL 2007 [DIRS 177392]) and *Saturated Zone Flow and Transport Model Abstraction* (SNL 2007 [DIRS 183750]).

L2.16.1 Radionuclide Transport in the Unsaturated Zone

The percentage of percolation flux in the rock matrix, fractures, and fault regions for the sixteen UZ flow fields (four infiltration scenarios; four climate states) considered in the TSPA-LA (SNL 2007 [DIRS 184614], Tables 6.6-2 and 6.6-3) indicates that a significant amount of the UZ percolation flux, both at the repository horizon and at the water table, flows in the fractures or in faults. The amount of flow in the fractures and faults is larger for higher infiltration rates and wetter climate states. Radionuclide breakthrough curves for Tc (nonsorbing), Np (moderately sorbing), and Pu (strongly sorbing) indicate that a significant fraction of these radionuclides is transported in fractures and faults from the repository horizon to the water table. This leads to the early arrival portion of the breakthrough curves. The fraction of radionuclides that is transported either partially or completely within the rock matrix leads to the later arrival portion of the breakthrough curves.

Based on these results, it can be concluded that a large fraction of any radionuclides being transported in the fractures or fault regions will traverse a hydrologic unit in the UZ within a single timestep used in this simplified model. It is therefore not necessary to reflect the breakthrough curve over the timestep for those radionuclides being transported in the fractures of a hydrologic unit in this simplified model. Rather, it is necessary to only determine the total amount of radionuclide mass that would traverse a unit during a single timestep. Radionuclide transport through the rock matrix is much slower with breakthrough occurring over many timesteps. It is necessary to reflect the breakthrough curve for those radionuclides transported in the rock matrix.

A simplified approach is used to model radionuclide transport in the UZ. The purpose of this simplified approach is to reflect the general behavior of the breakthrough curve, rather than the detailed behavior of groundwater flow and radionuclide transport within the UZ.

The UZ is represented by two 'regions' and three layers. The three layers represent the Topopah Spring, Calico Hills, and Prow Pass units, and the two 'regions' represent the area of the repository horizon that is and is not underlain by zeolitic rock. Average hydrologic properties are determined from the calibrated property sets contained in *Calibrated UZ Properties* (SNL 2007 [DIRS 179545]).

The EBS model presented above treats the repository as a single areal 'region' with discretization to account for seeping conditions and different waste forms only. A fraction of the entire mass flux out of the EBS is assumed to be released over the portion of the repository horizon underlain by zeolitic rock with the remaining fraction released over the portion of the repository not underlain by zeolitic rock. The interpreted extent of the vitric region in the various hydrologic units under the repository is given in *Development of Numerical Grids for UZ Flow and Transport* Modeling (BSC 2004 [DIRS 169855], Figures 6-7 and 6-8). It is assumed, based on these interpretations, that 70 percent of the area underlying the repository has zeolitic rock in the lower Topopah Spring and Calico Hills hydrologic units. Thus, 70 percent of the EBS releases are assumed to occur over the portion of the repository horizon underlain by zeolitic rock, with the remaining 30 percent assumed to be released over the portion of the repository not underlain by zeolitic rock.

The fraction of percolation flux flowing in the fractures and in the matrix is determined for each of the three layers by comparing the percolation flux to the saturated hydraulic conductivity using Equation L-60:

$$\begin{aligned} &\text{IF} \quad \phi > K_{sat} \quad \text{THEN} \quad F_{matrix} = \frac{K_{sat}}{\phi};\ F_{fracture} = \left(1 - \frac{K_{sat}}{\phi}\right) \\ &\text{ELSE} \qquad\qquad\qquad\quad F_{matrix} = 1; \qquad F_{fracture} = 0 \end{aligned} \qquad \text{(Eq. L-60)}$$

where

F_{matrix} = fraction of percolation flux flowing in the rock matrix

$F_{fracture}$ = fraction of percolation flux flowing in the rock fractures

ϕ = percolation flux (m/yr)

K_{sat} = matrix saturated hydraulic conductivity (m/yr).

The fraction of radionuclides transported in the matrix and the fractures of each layer are also determined using Equation L-60. The total release (matrix and fracture) from each layer is determined at each timestep and apportioned to the matrix and fracture 'columns' in the next layer. For example, a fraction of radionuclides exiting the fractures of one layer would be transported in the matrix of the next layer.

Interaction between radionuclides transported in the fractures and matrix, such as by matrix diffusion, is not considered in this simplified representation. This is a conservative approach since including matrix diffusion would result in radionuclide breakthrough being delayed. The approach being utilized herein (no fracture-matrix interaction) is conservative.

Radionuclides being transported in the fractures are assumed to migrate through a layer in a single timestep. Radionuclide transport in the matrix is modeled using a semi-analytic solution to the one-dimensional transport equation with radionuclide decay shown in Equation L-61 (Zheng and Bennett 1995 [DIRS 154702]). This simplified model does not include colloid facilitated transport in the UZ because past TSPA analysis results have shown that radionuclides transported on colloids do not contribute significantly to overall repository performance.

$$M(x,t) = \frac{x}{2\sqrt{\pi D'_x}} \sum_{i=1}^{NP} \Delta M_i \int_0^{t-t_i} \frac{1}{\xi^{\frac{3}{2}}} \exp\left[-\lambda\xi - \frac{(x - v'\xi)^2}{4D'_x \xi}\right] d\xi \qquad \text{(Eq. L-61)}$$

$$D'_x = \frac{\alpha_L v}{R}; \quad v' = \frac{v}{R}; \quad R = 1 + \rho K_d; \quad v = \frac{\phi}{\theta}$$

where

$M(x,t)$ = cumulative mass that has reached position x at time t (g)

ΔM_i = the radionuclide mass released into a layer over timestep i (g)

λ = decay constant (yr^{-1})

v = Groundwater velocity (m/yr)

α_L = longitudinal dispersivity (m)

R = retardation coefficient (unitless)

ρ = rock density (g/m^3)

K_d = distribution coefficient (m^3/g)

ϕ = Groundwater flux (m/yr)

θ = rock porosity (unitless)

NP = number of discrete steps (simulation time divided by the timestep size).

Equation L-61 is used to compute the total radionuclide mass that has been transported through the rock matrix to the bottom of each layer at each timestep where x is equal to the thickness of the layer. The integral is solved numerically using the trapezoidal rule with the overall timestep divided into five substeps to improve numerical accuracy. This numerical integration technique is appropriate for this simplified model because the breakthrough curves vary gradually over the timestep utilized. The numerical solution to Equation L-61 utilizing the trapezoidal numerical integration rule is given as Equation L-62:

$$M(T_{L,Unit,M},t_i)=\frac{T_L}{2\sqrt{\pi D'_x}}\frac{\Delta t}{2}\sum_{j=1}^{NP=t_i/\Delta t}\Delta M_{Unit,M}(t_i)\sum_{k=1}^{t_i-t_j/\Delta t}\left(f(\lambda,D'_x,t_{k-1})+f(\lambda,D'_x,t_k)\right)$$

$$f(\lambda,D'_x,t_k)=\frac{1}{t_k^{3/2}}\exp(-\lambda t_k-\frac{(T_L-v't_k)^2}{4D'_x t_k});\quad f(\lambda,D'_x,t_0)=0 \qquad \text{(Eq. L-62)}$$

$$t_k=k\Delta t$$

where

$M(T_{L,Unit,M},t_i)$ = cumulative mass that has exited the matrix at the bottom of a UZ layer at timestep t_i (g)

$\Delta M_{Unit,M}(t_i)$ = the mass that enters the matrix at the top of the UZ layer time over the timestep length (yr)

T_L = thickness of UZ layer (m)

Δt = timestep length (yr).

The mass that enters the top of each UZ layer in the matrix, $\Delta M_{Unit,M}(t_i)$, and the fractures, $\Delta M_{Unit,F}(t_i)$, is shown in Equation L-63:

Topopah Spring Zeolitic

$$\Delta M_{TSW-Z,M}(t_i) = F_{zeolitic}\, F_{TSW-Z,matrix}\, \Delta M_{EBS}(t_i) \quad Matrix$$
$$\Delta M_{TSW-Z,F}(t_i) = F_{zeolitic}\, F_{TSW-Z,fracture}\, \Delta M_{EBS}(t_i) \quad Fractures$$

Topopah Spring Vitric

$$\Delta M_{TSW-V,M}(t_i) = \left(1-F_{zeolitic}\right) F_{TSW-V,matrix}\, \Delta M_{EBS}(t_i) \quad Matrix$$
$$\Delta M_{TSW-V,F}(t_i) = \left(1-F_{zeolitic}\right) F_{TSW-V,fracture}\, \Delta M_{EBS}(t_i) \quad Fractures$$

Calico Hills Zeolitic

$$\Delta M_{CH-Z,M}(t_i) = F_{CH-Z,matrix}\, \Delta M(T_{L,TSW-Z}, t_i) \quad Matrix$$
$$\Delta M_{CH-Z,F}(t_i) = F_{CH-Z,fracture}\, \Delta M(T_{L,TSW-Z}, t_i) \quad Fractures$$

Calico Hills Vitric

$$\Delta M_{CH-V,M}(t_i) = F_{CH-V,matrix}\, \Delta M(T_{L,TSW-V}, t_i) \quad Matrix$$
$$\Delta M_{CH-V,F}(t_i) = F_{CH-V,fracture}\, \Delta M(T_{L,TSW-V}, t_i) \quad Fractures$$

Prow Pass

$$\Delta M_{PP,M}(t_i) = F_{PP,matrix}\left(\Delta M(T_{L,CH-Z}, t_i) + \Delta M(T_{L,CH-V}, t_i)\right) \quad Matrix \qquad \text{(Eq. L-63)}$$
$$\Delta M_{PP,F}(t_i) = F_{PP,fracture}\left(\Delta M(T_{L,CH-Z}, t_i) + \Delta M(T_{L,CH-V}, t_i)\right) \quad Fractures$$

where

$\Delta M_{Unit,,M/F}(t_i)$ = the mass entering the top of the unit in the matrix/fractures at timestep i (g)

$\Delta M_{EBS}(t_i)$ = the total mass exiting the EBS at timestep i (g)

$\Delta M(T_{L,Unit}, t_i)$ = the mass exiting the bottom of the unit in the matrix and fractures at timestep i (g)

$F_{zeolitic}$ = fraction of repository underlain by zeolitic rock (0.70 [see above])

$F_{Unit,matrix.fractures}$ = fraction of percolation flux flowing in the matrix/fractures of the unit (Equation L-59).

Radionuclide decay and daughter product in growth are modeled in the UZ matrix units by tracking the cumulative mass that exits the matrix for a parent radionuclide assuming no radioactive decay. It is assumed that the difference between the cumulative breakthrough of the parent without and with radioactive decay equals the mass of daughter product that built up during transit through that layer. This approach does not account for decay of the daughter radionuclide within the layer where it is formed. This approach is conservative as it leads to larger amounts of daughter product mass as compared to methods that allow for decay within the

layers. Thus, the radionuclide mass exiting the matrix at the bottom of each layer over a timestep, $\Delta M_{Unit,m}(T_L,t_i)$, is shown in Equation L-64:

No Parent

$$\Delta M(T_{L,Unit,m},t_i) = M(T_{L,Unit,m},t_i) - M(T_{L,Unit,m},t_{i-1})$$

Parent (Eq. L-64)

$$\Delta M(T_{L,Unit,m},t_i) = \left(M(T_{L,Unit,m},t_i) - M(T_{L,Unit,m},t_{i-1})\right) + \left[\left(MP_0(T_{L,Unit,m},t_i) - MP(T_{L,Unit,m},t_i)\right) - \left(MP_0(T_{L,Unit,m},t_{i-1}) - MP(T_{L,Unit,m},t_{i-1})\right)\right]$$

where

$MP(T_{L,Unit,m},t_i)$ = cumulative mass of parent radionuclide that has exited the matrix at the bottom of a UZ layer at timestep t_i (g)

$MP_0(T_{L,Unit,m},t_i)$ = cumulative mass of parent radionuclide that has exited the matrix at the bottom of a UZ layer at timestep t_i with no decay (g).

The total mass exiting the bottom of a unit is shown in Equation L-65 as the sum of the total mass exiting the matrix and fracture continua of each unit. Recall, radionuclide transport in the fractures is assumed to occur over one timestep and the mass exiting the fractures of a unit is simply equal to the mass entering the fractures. Note that daughter in-growth is not considered in the fracture continua given the relatively rapid transit times assumed.

$$\Delta M(T_{L,Unit},t_i) = \Delta M(T_{L,Unit,M},t_i) + \Delta M(T_{L,Unit,F},t_i) \quad \text{(Eq. L-65)}$$

where

$\Delta M(T_{L,Unit},t_i)$ = the mass exiting the bottom of the unit in the matrix and fractures at timestep i (g)

$\Delta M(T_{L,Unit,M},t_i)$ = the mass exiting the bottom of the unit in the matrix at timestep i (g)

$\Delta M(T_{L,Unit,F},t_i)$ = the mass exiting the bottom of the unit in the fractures at timestep i (g).

The average thickness for each layer was determined using unit contact information from *Development of Numerical Grids for UZ Flow and Transport Modeling* (BSC 20074 [DIRS 169855], Attachment II, Table II-1). The average thickness of the three layers used in this simplified model is shown in Table L-32 and was determined using the boreholes and contact information shown in Table L-33.

The average absolute matrix permeability in each layer is determined using Equation L-66:

$$\bar{k} = \frac{\sum_{i=1}^{NL} T_i}{\sum_{i=1}^{NL} \frac{T_i}{k_i}} \quad \text{(Eq. L-66)}$$

where

$\bar{k}$ = the average absolute matrix permeability in the layer (m^2)

T_i = the thickness of unit i in the layer (m)

k_i = the absolute matrix permeability of unit i in the layer (m^2).

The average relative permeability is determined using Equation L-67 (SNL 2007 [DIRS 184614], Appendix A, Equation A-9):

$$\bar{k}_r = \bar{k}\, S_E^{\frac{1}{2}} \left[1 - \left(1 - S_E^{\frac{1}{m}} \right)^m \right]^2 \quad \text{(Eq. L-67)}$$

where

$\bar{k}_r$ = the average relative matrix permeability in the layer (m^2)

$\bar{k}$ = the average absolute matrix permeability in the layer (m^2)

S_E = the effective matrix saturation (unitless)

m = Van Genuchten matrix parameter.

The effective saturation, S_E, is determined using Equation L-68:

$$S_E = \frac{S_M - S_R}{1 - S_R} \quad \text{(Eq. L-68)}$$

where

S_M = matrix saturation (unitless)

S_R = Residual matrix saturation (unitless).

The residual saturation, S_R, for each layer was determined from uncalibrated matrix properties provided in *UZ Flow Models and Submodels* (SNL 2007 [DIRS 184614], Section 4.1.2.1) using Equation L-69 and are shown in Table L-34.

$$\overline{S}_R = \frac{\sum_{i=1}^{NL} T_i S_{R,i}}{\sum_{i=1}^{NL} T_i} \quad \text{(Eq. L-69)}$$

where

$\overline{S}_R$ = the average residual saturation in the layer (m^2)

T_i = the thickness of unit i in the layer

$S_{R,i}$ = the residual saturation of unit i in the layer (m^2).

The van Genuchten matrix parameter, m, for each layer, was determined from calibrated matrix properties using Equation L-70 and is shown in Table L-35.

$$\overline{m} = \frac{\sum_{i=1}^{NL} T_i m_i}{\sum_{i=1}^{NL} T_i} \quad \text{(Eq. L-70)}$$

where

$\overline{m}$ = the average matrix van Genuchten parameter in the layer (m^2)

T_i = the thickness of unit i in the layer

m_i = the van Genuchten parameter m of unit i in the layer (m^2).

The matrix hydraulic conductivity is determined using Equation L-71:

$$K = \overline{k}_r \frac{\gamma}{\mu} \quad \text{(Eq. L-71)}$$

where

$\overline{k}_r$ = the average relative matrix permeability in the layer (m^2)

γ = the specific weight of water (9807 N/m^3)

μ = the dynamic viscosity of water (8.9×10^{-4} Pa·s).

The absolute permeability and Van Genuchten matrix parameter for each unit were obtained from *Calibrated UZ Properties* (SNL 2007 [DIRS 179545]), and the matrix saturation was estimated for each model layer from results shown in *UZ Flow Models and Submodels* (SNL 2007 [DIRS 184614]). These properties were used to calculate the effective saturation for each layer, the average layer relative permeability, and the layer average saturated hydraulic conductivities, which are shown in Table L-35.

The average porosity in each layer is determined using Equation L-72. The porosity of each unit was obtained from *Calibrated UZ Properties* (SNL 2007 [DIRS 179545]), and is shown in Table L-36.

$$\bar{\theta} = \frac{\sum_{i=1}^{NL} T_i \theta_i}{\sum_{i=1}^{NL} T_i} \qquad \text{(Eq. L-72)}$$

where

$\bar{\theta}$ = the average matrix porosity in the layer (m^2)

T_i = the thickness of unit i in the layer

θ_i = the matrix porosity of unit i in the layer (m^2).

Table L-37 shows the matrix and fracture percolation flux for each layer considered in this simplified model. The matrix and fracture percolation flux for each layer was determined using the average percolation flux for each climate state and infiltration scenario provided in Table L-2. The percolation flux in the matrix and fractures for each layer was then calculated using Equation L-60 and the layer average hydraulic conductivities provided in Table L-35 for each infiltration scenario.

Table L-38 shows the groundwater velocity in each layer and Table L-39 shows the time for flowing groundwater to traverse each layer. It can be seen from Table L-36 that the time to traverse a layer is much faster when groundwater is flowing in fractures as compared to when flowing in the matrix. Except for the present-day climate, low infiltration case, fracture travel times are significantly less than 500 years and are as small as tens of years or less. Thus, it is appropriate, and conservative, to assume that any radionuclides that are transported within the fractures immediately traverse a layer to the top of the underlying layer (or the interface with the SZ).

As discussed in *Radionuclide Transport Models Under Ambient Conditions* (SNL 2007 [DIRS 177396], Section 6.1.2.2), past analyses of UZ flow assumed that longitudinal dispersivity, α_L, values for both the fractures and matrix of all units had a mean of 20 meters and a standard deviation of 5 meters. This simplified model thus assumes that the longitudinal dispersivity, α_L, is normally distributed with a mean of 20 meters and a standard deviation of 5 meters.

The average density in each layer is determined using Equation L-73. The density of each unit was obtained from *Particle Tracking Model and Abstraction of Transport Processes* (SNL 2008 [DIRS 184748]) and is shown in Table L-40.

$$\overline{\rho} = \frac{\sum_{i=1}^{NL} T_i \rho_i}{\sum_{i=1}^{NL} T_i} \quad \text{(Eq. L-73)}$$

where

$\overline{\rho}$ = the average rock density in the layer (m^2)

T_i = the thickness of unit i in the layer

ρ_i = the rock density of unit i in the layer (m^2).

The distribution coefficients used for each layer used in this simplified model were obtained from *Particle Tracking Model and Abstraction of Transport Processes* (SNL 2008 [DIRS 184748]) and are shown in Table L-41.

L2.16.2 Radionuclide Transport in the Saturated Zone

Radionuclide transport in the SZ is also modeled using the semi-analytic solution to the one-dimensional transport equation with radionuclide decay that is used to model radionuclide transport in the UZ, shown in Equation L-61. The same numerical solution technique is utilized. This simplified model does not include colloid facilitated transport in the SZ because past TSPA analysis results have shown that radionuclides transported on colloids do not contribute significantly to overall repository performance.

The SZ is divided into three segments: (1) fractured-volcanic rock from underneath the repository to 5 km down gradient, (2) fractured-volcanic rock from 5 km to 13 km down gradient to the alluvium contact, and (3) alluvium to the 18 km compliance location. Radionuclides exiting the UZ enter the first segment.

If the groundwater transport time through a segment is less than the simulation timestep size, it is assumed that the radionuclides are immediately transported through that segment. If the groundwater transport time through a segment is greater than the simulation timestep, Equation L-74 is used to compute the total radionuclide mass that has been transported through the each segment of the SZ at each timestep. The integral is solved numerically using the trapezoidal rule. Given that radionuclide travel times in the SZ may be more rapid than those in the UZ matrix, the overall timestep is divided into 500 substeps for numerical accuracy.

$$M(T_{L,SZ-SEG}, t_i) = \frac{T_L}{2\sqrt{\pi D'_x}} \frac{\Delta t}{2} \sum_{j=1}^{NP=t_i/\Delta t} \Delta M_{SZ-SEG}(t_i) \sum_{k=1}^{t_i - t_j/\Delta t} \left(f(\lambda, D'_x, t_{k-1}) + f(\lambda, D'_x, t_k) \right)$$

$$f(\lambda, D'_x, t_k) = \frac{1}{t_k^{3/2}} \exp\left(-\lambda t_k - \frac{(T_L - v' t_k)^2}{4 D'_x t_k}\right); \quad f(\lambda, D'_x, t_0) = 0 \quad \text{(Eq. L-74)}$$

$$t_k = k\Delta t$$

where

$M(T_{L,SZ\text{-}SEG},t_i)$ = cumulative mass that has exited the SZ segment at timestep t_i (g)

$\Delta M_{SZ\text{-}SEGt,M}(t_i)$ = the mass that enters the SZ segment time over the timestep length (yr)

T_L = length of SZ segment (m)

Δt = timestep length (yr).

The mass that enters each SZ segment, $\Delta M_{SZ\text{-}SEG}(t_i)$, is shown in Equation L-75:

$$\begin{gathered}\text{SZ Segment 1}\\ \Delta M_{SZ-SEG1,M}(t_i)=\Delta M(T_{L,PP},t_i)\\ \text{SZ Segment 2}\\ \Delta M_{SZ-SEG2,M}(t_i)=\Delta M(T_{L,SZ-SEG1},t_i)\\ \text{SZ Segment 3}\\ \Delta M_{SZ-SEG3,M}(t_i)=\Delta M(T_{L,SZ-SEG2},t_i)\end{gathered} \qquad \text{(Eq. L-75)}$$

where

$\Delta M_{SZ\text{-}SEG}(t_i)$ = the mass entering the SZ segment at timestep i (g)

$\Delta M(T_{L,PP},t_i)$ = the mass exiting the bottom of the Prow Pass unit in the matrix and fractures at timestep i (g)

$\Delta M(T_{L,SZ\text{-}SEG},t_i)$ = the mass exiting the SZ segment at timestep i (g).

Radionuclide decay and daughter product in growth are modeled in the SZ segments by tracking the cumulative mass that exits the matrix for a parent radionuclide assuming no radioactive decay. It is assumed that the difference between the cumulative breakthrough of the parent without and with radioactive decay equals the mass of daughter product that built up during transit through that layer. This approach does not account for decay of the daughter radionuclide within the layer where it is formed. This approach is conservative as it leads to larger amounts of daughter product mass as compared to methods that allow for decay within the layers. Thus, the radionuclide mass exiting each SZ segment over a timestep, $\Delta M_{SZ\text{-}SEG}(T_L,t_i)$, is shown in Equation L-76:

$$\begin{gathered}\text{No Parent}\\ \Delta M(T_{L,SZ-SEG},t_i)=M(T_{L,SZ-SEG},t_i)-M(T_{L,SZ-SEG},t_{i-1})\\ \text{Parent}\\ \Delta M(T_{L,SZ-SEG},t_i)=\left(M(T_{L,SZ-SEG},t_i)-M(T_{L,SZ-SEG},t_{i-1})\right)+\\ \left[\left(MP_0(T_{L,SZ-SEG},t_i)-MP(T_{L,SZ-SEG},t_i)\right)-\left(MP_0(T_{L,SZ-SEG},t_{i-1})-MP(T_{L,SZ-SEG},t_{i-1})\right)\right]\end{gathered} \qquad \text{(Eq. L-76)}$$

where

$MP(T_{L,SZ\text{-}SEG}, t_i)$ = cumulative mass of parent radionuclide that has exited the SZ segment at timestep t_i (g)

$MP_0(T_{L,SZ\text{-}SEG}, t_i)$ = cumulative mass of parent radionuclide that has exited the SZ segment at timestep t_i with no decay (g).

The length of each segment is taken from the pipe length segments used in the one dimensional model developed in *Saturated Zone Flow and Transport Model Abstraction* (SNL 2007 [DIRS 183750], Section 6.5.1.2, Table 6-7). The pipe length segments used in the one dimensional model were determined for four source regions underneath the repository as a function of uncertainty in the horizontal anisotropy and in the contact between volcanic and alluvium units. The first pipe length segment is set at five kilometers.

The lengths of the second and third segments were determined by averaging the minimum and maximum values for each source region for a horizontal anisotropy of 5.0 (near the median of the uncertainty distribution). The length of the second segment is assumed to vary uniformly between 11 and 14 kilometers. The length of the third segment is assumed to vary uniformly between 2 and 5 kilometers, negatively correlated to the length of the second segment. For example, if the length of the second segment is 11 kilometers (the minimum), the length of the third segment is 5 kilometers (the maximum).

The specific discharge used in the one dimensional model developed in *Saturated Zone Flow and Transport Model Abstraction* (SNL 2007 [DIRS 183750], Section 6.5.1.2, Table 6-6) is also a function of uncertainty in the horizontal anisotropy as shown in Table L-42. The uncertainty distribution for the horizontal anisotropy is shown in Table L-43 (DTN: SN0302T0502203.001_R0 [DIRS 163563]). Additional uncertainty is applied to the average specific discharge through the use of a multiplication factor shown in Table L-44 (DTN: SN0702PASZFTMA.002_R1 [DIRS 183471]). The specific discharge values shown in Table L-44 are for the present-day climate state.

Saturated Zone Flow and Transport Model Abstraction (SNL 2007 [DIRS 183750], Section 6.5) applies an additional factor of 3.9 to the groundwater discharge for the glacial-transition climate state (DTN: SN0702PASZFTMA.002_R1 [DIRS 183471]). This factor is applied to all climate states in this simplified model. Applying this factor to the present-day and monsoon climate states is conservative because it leads to higher groundwater velocities. Application of this factor to the time period beyond 10,000 years is consistent with the approach being taken in the TSPA-LA.

The porosity in the fractured volcanic segments is assumed to be equal to the flowing interval porosity given in Table L-45 (SNL 2007 [DIRS 183750], Section 6.5.1.2, Table 6-8). The porosity of the alluvium is 0.30 (DTN: SN0702PASZFTMA.002_R1 [DIRS 183471]).

The logarithm of the longitudinal dispersivity is represented as a normal distribution with a mean of 2.0 and a standard deviation of 0.75 (DTN: MO0003SZFWTEEP.000_R0 [DIRS 148744]).

The average density of the fractured volcanic rock is 1,880 kg/m^3 (DTN: SN0702PASZFTMA.002_R1 [DIRS 183471]). The average density of the alluvium is 1,910 kg/m^3 (DTN: SN0310T0502103.009_R0 [DIRS 168763]).

The distribution coefficients used in this simplified model are shown in Table L-46.

L2.17. BIOSPHERE

The dose to the reasonably exposed maximally individual is calculated in this simplified model using Equation L-77:

$$D_T(t_i) = \sum_{j=1}^{NR} D_j(t_i)$$
$$D_j(t_i) = BDCF_j \frac{\dot{m}_{SZ,j}(t_i)}{Q_{well}} \qquad \text{(Eq. L-77)}$$

where

$D_{T,}(t_i)$ = total dose from NR radionuclides included in the simulation at timestep t_i (mrem/yr)

$D_{j,}(t_i)$ = dose from radionuclide j at timestep t_i (mrem/yr)

$BDCF_j$ = biosphere dose conversion factor for radionuclide j (mrem/yr per g/m^3)

$\dot{m}_{SZ,j}(t_i)$ = mass flux of radionuclide j crossing the 18 km boundary over timestep t_i (g/m^3)

Q_{well} = volumetric flow rate from the receptor wells, the representative volume of 3,000 acre-ft/yr).

The mass flux that crosses the 18 km boundary is determined from the cumulative mass that exits SZ segment three discussed above. As discussed above, radionuclide decay and daughter product in growth are modeled in the SZ segments by tracking the cumulative mass that exits the matrix for a parent radionuclide assuming no radioactive decay. It is assumed that the difference between the cumulative breakthrough of the parent through SZ segment three without and with radioactive decay equals the mass of daughter product that built up during transit through that layer. Thus, the mass flux exiting SZ segment three is shown in Equation L-78:

No Parent

$$\dot{m}_{SZ}(t_i) = \left(M(T_{L,SZ-SEG3}, t_i) - M(T_{L,SZ-SEG3}, t_{i-1})\right)/\Delta t$$

Parent

$$\dot{m}_{SZ}(t_i) = \left(M(T_{L,SZ-SEG3}, t_i) - M(T_{L,SZ-SEG3}, t_{i-1})\right)/\Delta t +$$
$$\left[\left(MP_0(T_{L,SZ-SEG3}, t_i) - MP(T_{L,SZ-SEG3}, t_i)\right) - \left(MP_0(T_{L,SZ-SEG3}, t_{i-1}) - MP(T_{L,SZ-SEG3}, t_{i-1})\right)\right]/\Delta t$$

(Eq. L-78)

where

$M(T_{L,SZ\text{-}SEG3}, t_i)$ = cumulative mass of radionuclide that has exited SZ segment three at timestep t_i (g)

$MP(T_{L,SZ\text{-}SEG3}, t_i)$ = cumulative mass of parent radionuclide that has exited SZ segment three at timestep t_i (g)

$MP_0(T_{L,SZ\text{-}SEG3}, t_i)$ = cumulative mass of parent radionuclide that has exited SZ segment three at timestep t_i with no decay (g).

The development of all-pathway biosphere dose conversion factors (BDCFs) is presented in *Biosphere Model Report* (SNL 2007 [DIRS 177399]). This simplified model uses the groundwater BDCFs for the present-day climate state, consistent with the approach taken in the TSPA-LA (Section 6.3.11.3). The BDCF probability distributions used in this simplified model are shown in Table L-47 (DTN: MO0702PAGBDCFS.001_R0 [DIRS 179327]). This simplified model assumes that:

- Ra^{226} and Pb^{210} are in radioactive equilibrium with Th^{230} at the receptor location
- Th^{228} and Ra^{228} are in radioactive equilibrium with Th^{232} at the receptor location
- Ac^{227} is in radioactive equilibrium with Pa^{231} at the receptor location.

L2.18. IGNEOUS INTRUSION MODELING CASE

This simplified model includes a simplified approach for evaluating the consequences of the igneous intrusion modeling case. In modeling cases where this is considered, it is assumed that a single igneous intrusion event occurs randomly over the duration of the simulation. The entire simplified model presented above is utilized with the following exceptions:

- WP and DS degradation due to general corrosion, SCC, and seismic induced mechanical damage is not considered.

- All WPs and DSs are assumed to fail completely when the intrusive event occurs.

- Collapsed drift seepage conditions are assumed to occur when the intrusive event occurs.

The simplified model then calculates a dose conditional on the occurrence of an igneous intrusion scenario. The probability-weighted dose is then calculated by multiplying the resultant conditional dose by the total probability of a single event occurring over the duration of the simulation. The mean frequency is 1.7×10^{-8} yr^{-1} (DTN: LA0307BY831811.001_R0 [DIRS 164713]), and in over 1,000,000 years the expected probability of a single event occurring is 0.017. The probability of two events is approximately 10^{-4} over 1,000,000 years.

L3. SIMULATIONS AND RESULTS

L3.1. SIMULATION METHODOLOGY AND APPROACH

The Simplified TSPA presented above was developed as a stand-alone computer program written in FORTRAN 90 and compiled/linked using Compaq Visual FORTRAN Professional Edition

Version 6.6.0 as unqualified software for execution on a personal computer using a Microsoft Windows operating system. The source code, input files, and output files for each modeling case are in corroborative DTN: MO0708SIMPLIFI.000 [DIRS 182980].

The Simplified TSPA was used to simulate four modeling cases that were analyzed using the TSPA-LA Model. These are:

- **Waste Package Early Failure Modeling Case**—This case evaluated repository performance considering only those WPs that experience early failure. In this case, no failure of the WPs is considered to occur due to general corrosion, SCC, or seismic mechanical damage. The number of early failures is determined using the approach described in Section L.2.8.2.

- **Nominal Modeling Case**—This case considered degradation of the WPs and DSs from corrosion processes only. Early WP failure was not considered in this case. Mechanical damage of the DS and WP was not considered in this case. Seismic induced rockfall and its subsequent effects on seepage were also not considered.

- **Seismic Ground Motion Modeling Case**—This modeling case considered degradation of the WPs and DSs from corrosion processes. The effects of ground motion were also considered, including mechanical damage to the WPs and DSs, and induced rockfall. Aleatory and epistemic uncertainties were both sampled randomly in each realization. Seismic events of varying magnitude were assumed to occur randomly following a Poisson process (Section L.2.1). The subsequent effects on rockfall, DS damage, and WP damage were then calculated.

- **Igneous Intrusion Modeling Case**—This case considered the degradation of the engineered barriers as a result of an intruding magma dike. Degradation of the WPs and DSs due to corrosion processes, seismic mechanical damage, and early WP failure were not considered. Aleatory and epistemic uncertainties were both randomly sampled in each realization. As discussed in Section L.2.18, a single igneous intrusion was assumed to occur randomly over the simulation period resulting in the failure of all DSs and WPs.

L3.2. SIMPLIFIED TSPA RESULTS

Further descriptions of the modeling cases simulated with this simplified model and the results can be found in Section 7.7.2.

Table L-1. Bounded Hazard Curve for Horizontal Peak Ground Velocity at the Emplacement Drifts

λ (1/yr)	PGV (m/s)
4.29 × 10-4	0.219
1.000 × 10-4	0.4019
3.826 × 10-5	0.6
1.919 × 10-5	0.8
9.955 × 10-6	1.05
6.682 × 10-6	1.2
3.812 × 10-6	1.4
2.136 × 10-6	1.6
1.288 × 10-6	1.8
8.755 × 10-7	2.0
6.399 × 10-7	2.2
4.518 × 10-7	2.44
3.504 × 10-7	2.6
2.507 × 10-7	2.8
1.731 × 10-7	3.0
1.137 × 10-7	3.2
7.168 × 10-8	3.4
4.362 × 10-8	3.6
2.508 × 10-8	3.8
1.319 × 10-8	4.0
5.967 × 10-9	4.20

Source: DTN: MO0501BPVELEMP.001_R0 [DIRS 172682].

Table L-2. Average Percolation Rate over the Repository Area

Infiltration Uncertainty Scenario (Percentile)	Climate State				Weighting Factor[b]
	Present-Day[a]	Monsoon[a]	Glacial Transition[a]	Post-10,000 Year[a]	
10th	2.73	6.14	8.66	15.82	0.6191
30th	7.34	12.01	18.07	24.79	0.1568
50th	11.16	13.81	22.12	31.49	0.1645
90th	25.10	68.78	42.34	45.87	0.0596

Sources: [a] DTN: SN0703PAEBSPCE.006_R2 [DIRS 181571]
[b] DTN: LB0701PAWFINFM.001_R0 [DIRS 179283].

Table L-3. Spatial Variability and Uncertainty Distributions for 1/α for Methods A, B, C, and D

1/α (Lithophysal Units)		*1*/α (Nonlithophysal Units)	
Spatial Variability Distribution	**Uncertainty Distribution**	**Spatial Variability Distribution**	**Uncertainty Distribution**
Uniform Distribution with Mean 591 Pa Lower Bound is 402 Pa Upper Bound is 780 Pa	Triangular Distribution with Mean 0 Lower Bound is - 105 Pa Upper Bound is + 105 Pa	Uniform Distribution with Mean 591 Pa Lower Bound is 402 Pa Upper Bound is 780 Pa	Triangular Distribution with Mean 0 Lower Bound is - 105 Pa Upper Bound is + 105 Pa

Source: DTN: LB0407AMRU0120.001_R0 [DIRS 173280].

Table L-4. Spatial Variability and Uncertainty Distributions Fracture Permeability (log (k [m2]))

Fracture Log (*k* [m^2]) (Lithophysal Units)		Fracture Log (*k* [m^2]) (Nonlithophysal Units)	
Spatial Variability Distribution	**Uncertainty Distribution**	**Spatial Variability Distribution**	**Uncertainty Distribution**
Log Normal Distribution with Mean - 11.5	Triangular Distribution with Mean 0	Log Normal Distribution with Mean - 12.2	Triangular Distribution with Mean 0
Standard Deviation 0.47	Lower Bound is - 0.92	Standard Deviation 0.34	Lower Bound is - 0.68
	Upper Bound is + 0.92		Upper Bound is + 0.68
Source: DTN: LB0407AMRU0120.001_R0 [DIRS 173280].			

Average Fracture Log (k [m^2]) (Lithophysal Units)	
Spatial Variability Distribution	**Uncertainty Distribution**
Log Normal Distribution with Mean - 11.6	Triangular Distribution with Mean 0
Standard Deviation 0.45	Lower/Upper Bounds are - 0.88/0.88

Table L-5. Flow Focusing Factor

Flow Focusing Factor	Cumulative Probability (%)
0.116	0
0.116	0.06
0.25	12.09
0.50	31.56
0.75	47.55
1.00	60.49
1.25	70.79
1.50	78.85
1.75	85.00
2.00	89.59
2.25	92.90
2.50	95.20
2.75	96.72
3.00	97.68
3.25	98.24
3.50	98.56
3.75	98.76
4.00	98.92
4.25	99.10
4.50	99.34
5.016	100.00

$y = -0.3137 x^4 + 5.4998 x^3 - 35.66 x^2 + 102.3 x - 11.434$

y = flow focusing factor

x = cumulative probability

valid for $0.116 < x < 0.5016$ and $0 \leq y \leq 1$

Source: SNL 2007 [DIRS 181244], Section 6.7.1.1.

Table L-6. Drip Shield General Corrosion Rate Ratio for Titanium Grade 29 Frame Material

Discrete Probability	Cumulative Probability	Ti-29/Ti-7 General Corrosion Rate Ratio
0.50000	0.50000	1.0000
0.11111	0.61111	1.1131
0.05556	0.66667	1.2522
0.02778	0.69445	1.3914
0.05556	0.75000	1.6697
0.11111	0.86111	2.0871
0.08333	0.94445	3.3393
0.02778	0.97222	4.1741
0.02778	1.00000	6.6786

Source: DTN: SN0704PADSGCMT.002_R1 [DIRS 182188].

Table L-7. Probability of Failure for the Drip Shield Plates

	Thickness of the Drip Shield Plate (mm)				
	0	2	5	10	15
PGV (m/s)	**Probability of Failure for 0% Rockfall Load (FDj = 0.0)**				
All Values	1	0	0	0	0
PGV (m/s)	**Probability of Failure for 10% Rockfall Load (FDj = 0.10)**				
0.2	1	0	0	0	0
0.4	1	0	0	0	0
1.05	1	0	0	0	0
2.44	1	0.006	0	0	0
4.07	1	0.036	0	0	0
PGV (m/s)	**Probability of Failure for 50% Rockfall Load (FDj = 0.50)**				
0.2	1	0	0	0	0
0.4	1	0.005	0	0	0
1.05	1	0.083	0.002	0	0
2.44	1	0.377	0.047	0.004	0
4.07	1	0.637	0.182	0.028	0.007
PGV (m/s)	**Probability of Failure for 100% Rockfall Load (FDj = 1.0)**				
0.2	1	0.027	0	0	0
0.4	1	0.093	0	0	0
1.05	1	0.390	0.030	0.001	0
2.44	1	0.765	0.268	0.047	0.013
4.07	1	0.912	0.557	0.186	0.073

Source: DTN: MO0703PASDSTAT.001_R3 [DIRS 183148].

NOTES: 1. Probabilities below 0.001 have been rounded down to 0.

2. Linear interpolate for given values of PGV, rock fall load, and drip shield thickness.

Table L-8. Probability of Failure for the Drip Shield Framework

	Reduction in Thickness of Framework Components (mm)				
	15	13	10	5	0
PGV (m/s)	**Probability of Failure for 0% Rockfall Load (FDj = 0.0)**				
All Values	1	0	0	0	0
PGV (m/s)	**Probability of Failure for 10% Rockfall Load (FDj = 0.10)**				
0.2	1	0	0	0	0
0.4	1	0	0	0	0
1.05	1	0.007	0	0	0
2.44	1	0.107	0.001	0	0
4.07	1	0.311	0.011	0	0
PGV (m/s)	**Probability of Failure for 50% Rockfall Load (FDj = 0.50)**				
0.2	1	0.048	0	0	0
0.4	1	0.192	0	0	0
1.05	1	0.635	0.025	0	0
2.44	1	0.929	0.230	0.029	0.006
4.07	1	0.985	0.502	0.127	0.039
PGV (m/s)	**Probability of Failure for 100% Rockfall Load (FDj = 1.0)**				
0.2	1	0.716	0.001	0	0
0.4	1	0.867	0.016	0	0
1.05	1	0.981	0.210	0.018	0.003
2.44	1	0.999	0.649	0.191	0.063
4.07	1	1.000	0.867	0.449	0.219

Source: DTN: MO0703PASDSTAT.001_R3 [DIRS 183148].

NOTES: 1. Probabilities below 0.001 have been rounded down to 0.

2. Linear interpolate for given values of PGV, rock fall load, and drip shield thickness.

Table L-9. Weibull Parameters for Alloy 22 Waste Package Outer Barrier General Corrosion

Probability	Weibull Scale Parameter, s (nm/yr)	Weibull Shape Parameter, b (unitless)
0.05	6.628	1.38
0.90	8.134	1.476
0.05	9.774	1.578

Source: DTN: MO0703PAGENCOR.001_R4 [DIRS 182029]

Table L-10. Time that Relative Humidity Exceeds 75 percent Threshold

Host Rock Thermal Conductivity	CSNF Waste Packages	CDSP Waste Packages
Low	950 years	700 years
Medium	850 years	500 years
High	600 years	400 years

Source: Determined from average bin WP relative humidity histories in DTN: MO0506MWDPPMSV.000_R0 [DIRS 174806].

Table L-11. Stress and Stress Intensity Factor Coefficients

Coefficient	Hoop Stress Outer Closure Lid Laser Peened[a]	K_I Outer Closure Lid Laser Peened[b]
A0	-519.127	-8.9124
A1	231.675	-9.4255
A2	-17.377	2.9749
A3	0.388	-0.1925
A4		0.0041

Source: [a] DTN: MO0702PASTRESS.002_R2 [DIRS 180514]
[b] Fitted from data in DTN: MO0702PASTRESS.002_R2 [DIRS 180514].

Table L-12. Average Depth Where SCC Cracks Can Initiate and Propagate

			Yield Stress Uncertainty (Z)												
			-15.0 %	**-12.5 %**	**-10.0 %**	**-7.5 %**	**-5.0 %**	**-2.5 %**	**0.0 %**	**2.5 %**	**5.0 %**	**7.5 %**	**10.0 %**	**12.5 %**	**15.0 %**
Repassivation Slope, n	-2 Standard Deviation	0.935	8.59	8.26	7.90	7.41	7.05	6.76	**6.52**	6.31	6.13	5.97	5.83	5.72	5.65
	5th percentile	0.976	8.59	8.26	7.90	7.41	7.05	6.76	**6.52**	6.31	6.13	5.97	5.84	5.74	5.68
	10th percentile	1.018	8.59	8.26	7.90	7.41	7.05	6.76	**6.52**	6.31	6.13	5.97	5.86	5.78	5.73
	15th percentile	1.046	8.59	8.26	7.90	7.41	7.05	6.76	**6.52**	6.31	6.13	5.98	5.88	5.81	5.78
	-1 Standard Deviation	1.050	8.59	8.26	7.90	7.41	7.05	6.76	**6.52**	6.31	6.13	5.98	5.88	5.81	5.78
	20th percentile	1.068	8.59	8.26	7.90	7.41	7.05	6.76	**6.52**	6.31	6.13	5.99	8.90	5.84	5.82
	30th percentile	1.105	8.59	8.26	7.90	7.41	7.05	6.76	**6.52**	6.31	6.14	6.03	5.95	5.92	5.90
	40th percentile	1.136	8.59	8.26	7.90	7.41	7.05	6.76	**6.52**	6.31	6.17	6.07	6.02	6.00	5.98
	Mean	1.165	**8.59**	**8.26**	**7.90**	**7.41**	**7.05**	**6.76**	**6.52**	**6.33**	**6.21**	**6.13**	**6.10**	**6.08**	**6.06**
	60th percentile	1.194	8.59	8.26	7.90	7.41	7.05	6.76	**6.52**	6.36	6.26	6.21	6.19	6.17	6.14
	70th percentile	1.225	8.59	8.26	7.90	7.41	7.05	6.76	**6.55**	6.42	6.35	6.32	6.29	6.26	6.24
	80th percentile	1.262	8.59	8.26	7.90	7.41	7.05	6.78	**6.62**	6.52	6.49	6.45	6.42	6.39	6.36
	1 Standard Deviation	1.280	8.59	8.26	7.90	7.41	7.05	6.81	**6.66**	6.80	6.53	6.53	6.49	6.46	6.43
	85th percentile	1.284	8.59	8.26	7.90	7.41	7.05	6.82	**6.67**	6.61	6.57	6.54	6.50	6.47	6.44
	90th percentile	1.312	8.59	8.26	7.90	7.41	7.08	6.88	**6.78**	6.73	6.69	6.65	6.61	6.52	6.55
	95th percentile	1.354	8.59	8.26	7.90	7.43	7.17	7.04	**6.98**	6.93	6.88	6.83	6.79	6.75	6.71
	2 Standard Deviation	1.395	8.59	8.26	7.92	7.53	7.32	7.25	**7.19**	7.13	7.08	7.03	6.98	7.02	6.89

Table L-13. Probability of Nonzero Damage for the Waste Package Surrounded by Rubble

	Residual Stress Threshold (% of Yield Strength)		
PGV Level (m/s)	**90%**	**100%**	**105%**
23-mm-Thick OCB with Degraded Internals			
0.40	0	0	0
1.05	0	0	0
2.44	0	0	0
4.07	0.294	0.118	0.059
17-mm-Thick OCB with Degraded Internals			
0.40	0	0	0
1.05	0	0	0
2.44	0.118	0	0
4.07	0.412	0.176	0.118

Source: DTN: MO0703PASDSTAT.001_R3 [DIRS 183148].

NOTES: 1. Linear interpolation for PGV and residual stress threshold.
2. If the thickness of the Alloy 22 outer barrier ≥ 23 mm, use the 23 mm thickness probabilities.
3. If the thickness is < 23 mm, calculate the probability using (interpolate for thickness between 17 mm and 23 mm, extrapolate for thickness less than 17 mm): $PD_{17\text{-}mm} + (PD_{23\text{-}mm} - PD_{17\text{-}mm})(t - 17\text{-mm})/(6\text{-mm})$.

Table L-14. Conditional Damaged Areas on the Waste Package Surrounded by Rubble

Waste Package Outer Barrier Thickness (mm)	State of Internals	Damage Area (m^2)
23	Degraded	$(0.0153492)(RST_i)^2 - 3.1814*RST_i + 165.834$
17	Degraded	$(0.0083948)(RST_i)^2 - 1.7755*RST_i + 94.0116$

Source: DTN: MO0703PASDSTAT.001_R3 [DIRS 183148].

NOTES: 1. Linear interpolation for PGV and residual stress threshold.
2. If the thickness of the Alloy 22 outer barrier ≥ 23 mm, use the 23 mm thickness probabilities.
3. If the thickness is < 23 mm, calculate the damage area using (interpolate for thickness between 17 mm and 23 mm, extrapolate for thickness less than 17 mm):
$DA_{17\text{-}mm} + (DA_{23\text{-}mm} - DA_{17\text{-}mm})(t - 17\text{-mm})/(6\text{-mm})$.

Table L-15. Probability of TAD-Bearing and CDSP Waste Package Rupture (17-mm-Thick Waste Package Outer Barrier, Degraded Internals)

PGV Level (m/s)	Conditional Probability of Exceedance[2]	Average Number of Events Expected over 1,000,000 Years having Larger PGV[3]	TAD-Bearing Waste Package[1]		CDSP Waste Package[1]	
			Probability of Incipient Rupture	Probability of Rupture	Probability of Incipient Rupture	Probability of Rupture
0.40	3.77×10^{-1}	~100	0	0	0	0
1.05	3.71×10^{-2}	~10	0.007	0	0	0
2.44	1.68×10^{-3}	~0.45	0.040	0	0.030	0
4.07	4.90×10^{-5}	~0.013	0.127	0.188	0.124	0.120

NOTES: 1. TAD-bearing WP information is derived from DTN: MO0703PASDSTAT.001_R3 [DIRS 183148].

2. Exceedance frequency for a given PGV from Table L-1 (λ) divided by the mean exceedance frequency (2.6909×10^{-4} yr^{-1}).

3. Conditional probability of exceedance x mean exceedance frequency (2.6909×10^{-4} yr^{-1}) x 1,000,000 years.

Table L-16. Probability of Nonzero Damage for the TAD-bearing Waste Package, Free Movement Underneath the Drip Shield

	Residual Stress Threshold (%)		
	90	**100**	**105**
***PGV* (m/s)**	**Probability of Nonzero Damage for 23-mm-Thick OCB with Intact Internals**		
0.2	0	0	0
0.4	0	0	0
1.05	0	0	0
2.44	0	0	0
4.07	0.118	0	0
***PGV* (m/s)**	**Probability of Nonzero Damage for 23-mm-Thick OCB with Degraded Internals**		
0.266	0	0	0
0.349	0.085	0	0
0.4	0.137	0.059	0
1.05	0.804	0.804	0.784
2.44	1	1	1
4.07	1	1	1
***PGV* (m/s)**	**Probability of Nonzero Damage for 17-mm-Thick OCB with Degraded Internals**		
0.280	0	0	0
0.351	0.081	0	0
0.4	0.137	0.059	0
1.05	0.882	0.843	0.804
2.44	1	1	1
4.07	1	1	1

Source: DTN: MO0703PASDSTAT.001_R3 [DIRS 183148].

NOTES: 1. Linear interpolation for PGV and residual stress threshold.

2. If the thickness of the Alloy 22 outer barrier ≥ 23 mm, use the 23 mm thickness probabilities.

3. If the thickness is < 23 mm, calculate the probability using (interpolate for thickness between 17 mm and 23 mm, extrapolate for thickness less than 17 mm): $PD_{17\text{-}mm} + (PD_{23\text{-}mm} - PD_{17\text{-}mm})(t - 17\text{-mm})/(6\text{-mm})$.

Table L-17. Probability of Nonzero Damage for the CDSP Waste Package, Free Movement Underneath the Drip Shield

	Residual Stress Threshold (%)		
	90	100	105
***PGV* (m/s)**	**Probability of Nonzero Damage for 23-mm-Thick OCB with Intact Internals**		
0.364	0	0	0
0.4	0.029	0	0
1.05	0.559	0	0
2.44	0.941	0.147	0
4.07	1	0.412	0
***PGV* (m/s)**	**Probability of Nonzero Damage for 23-mm-Thick OCB with Degraded Internals**		
0.238	0	0	0
0.285	0	0	0
0.364	0.060	0.060	0
0.4	0.088	0.088	0.029
1.05	0.588	0.588	0.559
2.44	0.941	0.941	0.941
4.07	1	1	1
***PGV* (m/s)**	**Probability of Nonzero Damage for 17-mm-Thick OCB with Degraded Internals**		
0.219	0	0	0
0.338	0.097	0	0
0.4	0.147	0.059	0
1.05	0.676	0.676	0.382
2.44	0.941	0.941	0.882
4.07	1	1	1

Source: DTN: MO0703PASDSTAT.001_R3 [DIRS 183148].

NOTES: 1. Linear interpolation for PGV and residual stress threshold.

2. If the thickness of the Alloy 22 outer barrier ≥ 23 mm, use the 23 mm thickness probabilities.

3. If the thickness is < 23 mm, calculate the probability using (interpolate for thickness between 17 mm and 23 mm, extrapolate for thickness less than 17 mm): $PD_{17\text{-}mm} + (PD_{23\text{-}mm} - PD_{17\text{-}mm})(t - 17\text{-mm})/(6\text{-mm})$.

Table L-18. Conditional Damage Area on TAD-bearing and CDSP Waste Packages When Damaged Due to Free Motion Underneath the Drip Shield

	Waste Package Outer Barrier Thickness (mm)	State of Internals	Damage Area (m^2)
TAD-Bearing Waste Packages		Intact	0.00408
	23	Degraded	$(0.1096 - 0.00664*(RSTi - 100))PGV^2 + (0.1722 - 0.01701*(RSTi - 100))PGV + 0.0828 - 0.00661*(RSTi - 100)$
	17	Degraded	$(0.1394 - 0.00838*(RSTi - 100))PGV^2 + (0.1649 - 0.02224*(RSTi - 100))PGV + 0.0766 - 0.00628*(RSTi - 100)$
CDSP Waste Packages		Intact	If $(RST \leq 100)$ $- 0.0033*(RSTi - 100)PGV^2 - 0.00567*(RSTi - 100)PGV - 0.0004*(RSTi - 100))+0.0061$ Else $-0.0012(RST-105)$
	23	Degraded	$(0.0637 - 0.0016*(RSTi - 100))PGV^2 + (0.2274 - 0.0277*(RSTi - 100))PGV + (-0.0144 + 0.0029*(RSTi - 100))$
	17	Degraded	$(0.0670 - 0.0011*(RSTi - 100))PGV^2 + (0.1879 - 0.0376*(RSTi - 100))PGV + (-0.0187 + 0.0034*(RSTi - 100))$

Source: DTN: MO0703PASDSTAT.001_R3 [DIRS 183148].

NOTES: 1. Linear interpolation for PGV and residual stress threshold.

2. If the thickness of the Alloy 22 outer barrier ≥ 23 mm, use the 23 mm thickness probabilities.

3. If the thickness is < 23 mm, calculate the damage area using (interpolate for thickness between 17 mm and 23 mm, extrapolate for thickness less than 17 mm):

$DA_{17\text{-}mm} + (DA2_{3\text{-}mm} - DA_{17\text{-}mm})$(t - 17-mm)/(6-mm).

Table L-19. Initial Radionuclide Inventory and Treatment

Radio-nuclide	Specific Activity (Ci/g)	Initial Inventory[1] CSNF w/MOX Added (g/WP)	Initial Inventory[1] DSNF (g/WP)	Initial Inventory[1] HLW w/LABS Added (g/WP)	Molecular Mass (g/mol)	Decay Constant (yr^{-1})	Half Life (yr)[1]	Treatment in Simplified Analyses[2]
^{227}Ac	7.23E+01	2.47E-06	1.22E-03	1.91E-04	227	3.18E-02	2.18E+01	Inventory fully decays, secular equilibrium with ^{231}Pa at well
^{241}Am	3.43E+00	8.20E+03	2.18E+02	6.53E+01	241	1.60E-03	4.33E+02	Inventory fully decays to ^{237}Np
^{243}Am	2.00E-01	1.29E+03	6.73E+00	5.75E-01	243	9.40E-05	7.37E+03	Inventory fully decays to ^{239}Pu
^{14}C	4.47E+00	1.38E+00	1.81E+00	0.00E+00	14	1.21E-04	5.72E+03	
^{36}Cl	3.30E-02	3.23E+00	4.23E+00	0.00E+00	36	2.30E-06	3.01E+05	
^{245}Cm	1.72E-01	1.89E+01	9.25E-02	5.43E-02	245	8.15E-05	8.50E+03	Inventory fully decays to ^{241}Pu
^{135}Cs	1.15E-03	4.43E+03	9.74E+01	1.27E+02	135	3.01E-07	2.30E+06	
^{137}Cs	8.68E+01	6.06E+03	9.72E+01	3.02E+02	137	2.31E-02	3.01E+01	Inventory fully decays
^{129}I	1.77E-04	1.76E+03	3.56E+01	7.27E+01	129	4.41E-08	1.57E+07	
^{237}Np	7.05E-04	4.59E+03	8.14E+01	1.00E+02	237	3.24E-07	2.14E+06	Parent of ^{233}U
^{231}Pa	4.72E-02	9.17E-03	2.14E+00	1.53E+00	231	2.11E-05	3.28E+04	Secular Equilibrium with ^{227}Ac at well
^{210}Pb	7.63E+01	1.13E-12	3.35E-07	3.40E-10	210	3.11E-02	2.23E+01	Inventory fully decays, secular equilibrium with ^{230}Th at well
^{238}Pu	1.71E+01	1.54E+03	1.25E+01	4.25E+01	238	7.90E-03	8.77E+01	Inventory fully decays to ^{234}U
^{239}Pu	6.21E-02	4.42E+04	2.21E+03	4.04E+03	239	2.88E-05	2.41E+04	Parent of ^{235}U
^{240}Pu	2.27E-01	2.13E+04	4.35E+02	3.56E+02	240	1.06E-04	6.56E+03	Parent of ^{236}U
^{241}Pu	1.03E+02	3.08E+03	2.92E+01	1.38E+01	241	4.81E-02	1.44E+01	Inventory fully decays to ^{237}Np
^{242}Pu	3.94E-03	5.45E+03	3.02E+01	9.98E+00	242	1.85E-06	3.75E+05	Parent of ^{238}U
^{226}Ra	9.89E-01	8.79E-11	4.57E-05	2.42E-05	226	4.33E-04	1.60E+03	Inventory fully decays, secular equilibrium with ^{230}Th at well
^{228}Ra	2.72E+02	5.89E-17	1.51E-05	6.00E-06	228	1.20E-01	5.76E+00	Inventory fully decays
^{79}Se	1.56E-02	4.24E+01	6.82E+00	7.01E+00	79	2.39E-06	2.90E+05	
^{126}Sn	1.23E-02	4.75E+02	9.40E+00	1.70E+01	126	3.01E-06	2.30E+05	
^{90}Sr	1.38E+02	2.53E+03	5.22E+01	1.74E+02	90	2.41E-02	2.88E+01	Inventory fully decays
^{99}Tc	1.70E-02	7.65E+03	1.58E+02	1.01E+03	99	3.25E-06	2.13E+05	
^{229}Th	2.14E-01	2.68E-09	3.24E-01	3.30E-03	229	9.50E-05	7.30E+03	
^{230}Th	2.06E-02	1.52E-01	1.18E-01	8.12E-04	230	9.19E-06	7.54E+04	Secular equilibrium with ^{226}Ra at well

Table L-19. Initial Radionuclide Inventory and Treatment (Continued)

Radio-nuclide	Specific Activity (Ci/g)	Initial Inventory[1] CSNF w/MOX Added (g/WP)	DSNF (g/WP)	HLW w/LABS Added (g/WP)	Molecular Mass (g/mol)	Decay Constant (yr^{-1})	Half Life (yr)[1]	Treatment in Simplified Analyses[2]
^{232}Th	1.10E-07	1.15E-06	2.17E+04	2.98E+04	232	4.95E-11	1.40E+10	
^{232}U	2.21E+01	1.02E-02	1.28E+00	4.08E-04	232	9.93E-03	6.98E+01	Inventory fully decays
^{233}U	9.63E-03	5.76E-02	5.38E+02	1.94E+01	233	4.35E-06	1.59E+05	Parent of ^{229}Th
^{234}U	6.21E-03	1.75E+03	4.73E+02	2.75E+01	234	2.82E-06	2.46E+05	Parent of ^{230}Th
^{235}U	2.16E-06	6.27E+04	2.51E+04	1.67E+03	235	9.85E-10	7.04E+08	Parent of ^{231}Pa
^{236}U	6.47E-05	3.85E+04	1.25E+03	5.99E+01	236	2.96E-08	2.34E+07	Parent of ^{232}Th
^{238}U	3.36E-07	7.90E+06	6.84E+05	2.38E+05	238	1.55E-10	4.47E+09	Parent of ^{234}U

Sources: 1. DTN: MO0702PASTREAM.001_R0 [DIRS 179925].
2. Decay series from *Initial Radionuclide Inventories* (SNL 2007 [DIRS 180472], Table 4-14).

Table L-20. Uncertainty Multipliers for Grams per Waste Package for Each Waste Type

	CSNF	Defense Spent Nuclear Fuel	HLW
Isotope	All except ^{238}U	All except ^{238}U	All
Distribution	Uniform	Triangular	Triangular
Minimum	0.85	0.45	0.70
Most Likely	N/A	0.62	1
Maximum	1.40	2.90	1.5

Source: DTN: SN0310T0505503.004_R0 [DIRS 168761].

Table L-21. Gap and Grain Boundary Fractions for CSNF Waste Forms

	Cs^{135}	I^{129}	Tc^{99}
Average Release Fraction (%)	3.63	11.24	0.1
Range (%)	0.39 – 11.06	2.04 – 26.75	0.01 – 0.26

Source: DTN: MO0404ANLSF001.001_R0 [DIRS 169007].

Table L-22. Coefficients in CSNF Degradation Rate Model

Coefficient	Acidic Conditions	Alkaline Conditions
Log(A)	Triangular Distribution (minimum = -7.3, expected value = -6.7, maximum = -5.4)	
a_0	4.705	6.6
a_1	-1093.826	-1093.823
a_2	-0.102	0
a_3	-0.388	-0.338
a_4	0	-0.34

Source: DTN: MO0404ANLSF001.001_R0 [DIRS 169007].

NOTE: The values for the regression coefficient are expected values.

Table L-23. CSNF Waste Form Degradation Covariance Matrix for Alkaline Conditions

	a_0	a_1	a_2	a_3
a_0	0.60095	0	0	0
a_1	-181.156	45.68717	0	0
a_2	-0.00834	-0.03852	0.02586	0
a_3	-0.00831	-0.0226	-0.03754	0.02659

Source: DTN: MO0404ANLSF001.001_R0 [DIRS 169007].

Table L-24. CSNF Waste Form Degradation Covariance Matrix for Acidic Conditions

	a_0	a_4
a_0	0.4475	0
a_4	-0.10475	0.03495

Source: DTN: MO0404ANLSF001.001_R0 [DIRS 169007].

Table L-25. DHLW Glass Degradation Parameters

Parameter	Alkaline Conditions	Acidic Conditions
k_g, forward glass dissolution rate ($g/m^2/day$)	Triangular Distribution	Triangular Distribution
	Minimum = 2.82×10^1	Minimum = 8.41×10^3
	Most Probable = 2.82×10^1	Most Probable = 8.41×10^3
	Maximum = 3.47×10^4	Maximum = 1.15×10^7
η, order of the reaction with respect to H+	0.49	-0.49
E_a, activation energy for rate limiting step (kJ/mol)	69	31

Source: DTN: MO0502ANLGAMR1.016_R0 [DIRS 172830].

Table L-26. Dissolved Concentration Limits (without Uncertainty)

pH	Base-10 Logarithm of the Dissolved Concentration Limit (mg/L)								
	NpO_2	Np_2O_5	Pa	Pu	Th	Sn	U (Schoepite)	U (Na-boltwoodite and $Na_4UO_2(CO_3)_3$	U[1]
4.00	2.05E+00	3.29E+00	3.29E+00	7.12E-01	1.14E+00	-2.39E+00	2.86E+00		2.86E+00
4.25	1.80E+00	3.03E+00	3.03E+00	4.12E-01	9.41E-01	-2.39E+00	2.33E+00		2.33E+00
4.50	1.55E+00	2.77E+00	2.77E+00	1.35E-01	7.42E-01	-2.39E+00	1.91E+00		1.91E+00
4.75	1.29E+00	2.52E+00	2.52E+00	-1.22E-01	3.82E-01	-2.39E+00	1.59E+00		1.59E+00
5.00	1.04E+00	2.26E+00	2.26E+00	-3.60E-01	-2.94E-01	-2.38E+00	1.31E+00		1.31E+00
5.25	7.94E-01	2.01E+00	2.01E+00	-5.75E-01	-1.20E+00	-2.38E+00	1.02E+00		1.02E+00
5.50	5.44E-01	1.76E+00	1.76E+00	-7.62E-01	-1.99E+00	-2.38E+00	7.55E-01		7.55E-01
5.75	2.94E-01	1.51E+00	1.51E+00	-9.17E-01	-2.13E+00	-2.38E+00	6.11E-01		6.11E-01
6.00	4.36E-02	1.26E+00	1.26E+00	-1.03E+00	-1.94E+00	-2.37E+00	6.30E-01		6.30E-01
6.25	-2.06E-01	1.01E+00	1.01E+00	-1.12E+00	-1.70E+00	-2.37E+00	7.66E-01		7.66E-01
6.50	-4.54E-01	7.62E-01	7.62E-01	-1.17E+00	-1.46E+00	-2.35E+00	9.70E-01		9.70E-01
6.75	-6.98E-01	5.17E-01	5.17E-01	-1.21E+00	-1.22E+00	-2.33E+00	1.22E+00	2.00E+00	1.61E+00
7.00	-9.24E-01	2.84E-01	2.84E-01	-1.23E+00	-9.69E-01	-2.29E+00	1.51E+00	1.82E+00	1.67E+00
7.25	-1.09E+00	8.83E-02	8.30E-02	-1.24E+00	-7.16E-01	-2.22E+00	1.89E+00	1.51E+00	1.70E+00
7.50	-1.09E+00	-1.94E-02	-1.94E-02	-1.24E+00	-4.60E-01	-2.12E+00	2.54E+00	1.55E+00	2.05E+00
7.75	-8.33E-01	8.77E-03	8.77E-03	-1.23E+00	-2.02E-01	-1.99E+00		1.98E+00	1.98E+00
8.00	-3.51E-01	1.71E-01	1.71E-01	-1.17E+00	5.91E-02	-1.82E+00		2.76E+00	2.76E+00
8.25	3.96E-01	4.49E-01	4.49E-01	-8.71E-01	3.23E-01	-1.62E+00		4.78E+00	4.78E+00
8.50	4.41E-01	1.00E+00	1.00E+00	1.11E+00	5.96E-01	-1.39E+00		4.78E+00	4.78E+00

Source: DTN: MO0702PADISCON.001_R0 [DIRS 179358]: column NpO_2 (Table 2); column Np_2O_5 (Table 3); column Pa (Table 9); column Pu (Table 1); column Th (Table 7); column Sn (Table 16); column U (Table 5); column U (Na-boltwoodite and $Na_4UO_2(CO_3)_3$ (Table 6).

NOTE: Dissolved concentration limit for U is controlled by schoepite for pH<=6.75 and by Na-boltwoodite, and $Na_4UO_2(CO_3)_3$ for pH>=7.75. In between, the average between the two is assumed to be the dissolved concentration limit.

Table L-27. Dissolved Concentration Limit Uncertainty Terms

Element	ε^1	
	μ	σ
NpO_2	0	0.6
Np_2O_5	0	0.8
Pa	-4.42[1]	-0.05[1]
Pu	0	1
Th	0	0.7
U	0	0.5
Sn	0	0.45

Source: DTN: MO0702PADISCON.001_R0 [DIRS 179358].

NOTE: [1]Uniform Distribution (min., max.).

Table L-28. Mixing Cell Steel Parameters Used in Calculation of Corrosion Product Mass and Volume of Water

		Waste Form Cell				Corrosion Product Cell			
Waste Form		m_s Mass of Steel (kg)	f_{CS} Fraction of Carbon Steel	$t_{max,CS}$ Maximum Thickness of Carbon Steel (mm)	$t_{max,SS}$ Maximum Thickness of Stainless Steel (mm)	m_s Mass of Steel (kg)	f_{CS} Fraction of Carbon Steel	$t_{max,CS}$ Maximum Thickness of Carbon Steel (mm)	$t_{max,SS}$ Maximum Thickness of Stainless Steel (mm)
CSNF		9,980	0	0	11.11	24,600	0	0	11.11
CD SP	DHLW	3,800	0	0	10.5	18,900	0.31	31.75	50.8
	DSNF	1,270	0.24	6.35	9.525				

Source: DTN: SN0703PAEBSRTA.001_R3 [DIRS 183217].

Table L-29. Metal Mass Fractions and Atomic Weights Used in Calculation of Corrosion Product Mass and Volume of Water

Metal	$\omega_{CS,m}$ Mass Fraction of Metal in Carbon Steel	$\omega_{SS,m}$ Mass Fraction of Metal in Stainless Steel	M_m Atomic Weight of Metal (kg/mol)
Fe	0.98	0.65	0.055847
Ni	0	0.12	0.05869
Cr	0	0.17	0.051996

Source: DTN: SN0703PAEBSRTA.001_R3 [DIRS 183217].

Table L-30. Properties of Corrosion Product Used in Calculation of Corrosion Product Mass and Volume of Water

Corrosion Product	$M_{CP,m}$ Molecular Weight of Corrosion Product (kg/mol)	$\alpha_{CP,m}$ Stoichiometric Coefficient	$\rho_{CP,m}$ Density of Corrosion Product (kg/m^3)
Goethite	0.088852	1 mol goethite/mol Fe	4,260
HFO	0.088852	1 mol HFO/mol Fe	3,960
NiO	0.074692	1 mol NiO/mol Ni	5,220
Cr_2O_3	0.151990	2 mol Cr_2O_3/mol Cr	6,720

Source: DTN: SN0703PAEBSRTA.001_R3 [DIRS 183217].

Table L-31. Free Water Diffusion Coefficients

Species	Free Water Diffusion Coefficient (m^2/s)
C	1.18×10^{-9}
Cs	2.06×10^{-9}
I	2.05×10^{-9}
Np	6.18×10^{-10}
Pa	6.04×10^{-10}
Pu	1.30×10^{-9}
Tc	1.95×10^{-9}
Th	5.97×10^{-10}
U	6.64×10^{-10}
Se	1.04×10^{-9}
Cl	2.03×10^{-9}
Sn	1.55×10^{-9}

Source: DTN: SN0703PAEBSRTA.001_R3 [DIRS 183217].

Table L-32. Calculation of Average Unsaturated Zone Layer Thickness

Unit	Average Thickness (m)	Simplified Model Layer	
		Layer Configuration	Thickness (m)
tsw31	2.0		
tsw32	42.5		
tsw33	78.6		
tsw34	34.7		
tsw35	102.4	TSW Layer = 1/2 tsw35+ tsw36+tsw37+ tsw38+tsw39	120
tsw36	31.3		
tsw37	15.7		
tsw38	15.5		
tsw39	6.7		
ch1	15.7	CH Layer = ch1+ch2+ch3+ ch4+ch5+ch6	111
ch2	19.3		
ch3	19.3		
ch4	19.3		
ch5	19.3		
ch6	18.0		
pp4	9.7	PP Layer = pp1+pp2+pp3+ pp4	81
pp3	19.1		
pp2	17.4		
pp1	34.5		
Total Depth (meters)			312

Source: BSC 2004 [DIRS 169855], Attachment II, Table II-1.

Table L-33. Layer Contact and Thickness from the GFM2000 Contact Information

Unit	USW H-4		USW H-5		USW G-1		USW G-4		USW H-1	
	GFM2000 Contact (m)[a]	Thick-ness (m)	GFM2000 Contact (m)[a]	Thick-ness (m)	GFM2000 Contact (m)[a]	Thick-ness (m)	GFM2000 Contact (m)[a]	Thick-ness (m)	GFM2000 Contact (m)[a]	Thick-ness (m)
tsw31	1,172.261	2.0	1,307.783	2.0	1,244.388	2.0	1,197.259	2.0	1,202.741	2.0
tsw32	1,170.261	36.1	1,305.783	40.0	1,242.388	49.2	1,195.259	47.2	1,200.741	51.3
tsw33	1,134.161	61.0	1,265.736	87.7	1,193.215	84.0	1,148.069	83.4	1,149.401	86.3
tsw34	1,073.201	38.7	1,178.021	30.5	1,109.192	31.0	1,064.668	30.5	1,063.142	33.2
tsw35	1,034.491	86.6	1,147.494	110.3	1,078.217	117.1	1,034.197	107.8	1,029.919	130.1
tsw36	947.928	40.2	1,037.192	26.9	961.1646	18.0	926.425	38.4	899.7696	17.5
tsw37	907.6944	20.1	1,010.321	13.4	943.1175	9.0	888.0687	19.2	882.2944	8.7
tsw38	887.576	7.3	996.8859	23.5	934.094	17.0	868.8906	8.8	873.5568	18.1
tsw39	880.2624	11.6	973.4256	4.0	917.0564	5.5	860.0588	2.5	855.4212	5.1
ch1	868.68	21.3	969.4739	10.1	911.5274	19.5	857.5441	17.0	850.331	5.7
ch2	847.344	19.4	959.3875	13.3	892.0233	23.5	840.5243	22.6	844.6008	22.6
ch3	827.913	19.4	946.072	13.3	868.4737	23.6	817.9547	22.6	821.9694	22.6
ch4	808.482	19.4	932.7565	13.3	844.8841	23.6	795.3852	22.6	799.338	22.6
ch5	789.051	19.4	919.441	13.3	821.3145	23.6	772.8157	22.6	776.7066	22.6
ch6	769.62	16.8	906.1255	19.8	797.7448	19.0	750.2462	17.4	754.072	18.0
pp4	752.865	10.7	886.3395	6.8	778.724	19.3	732.8007	2.2	736.092	5.5
pp3	742.188	11.7	879.5576	35.9	759.4007	5.2				
pp2			843.6558	13.7						
pp1			829.9347	54.3						
Water Table	730.5		775.6		754.2		730.6		730.6	

Table L-33. Layer Contact and Thickness from the GFM2000 Contact Information (Continued)

Unit	USW SD-9		USW SD-12		USW UZ-1/14		USW WT-2	
	GFM2000 Contact (m)[a]	Thick-ness (m)	GFM2000 Contact (m)[a]	Thick-ness (m)	GFM2000 Contact (m)[a]	Thick-ness (m)	GFM2000 Contact (m)[a]	Thick-ness (m)
tsw31	1,221.181	2.0	1,224.839	2.0	1,263.237	2.0	1,216.156	2.0
tsw32	1,219.181	53.3	1,222.839	32.1	1,261.237	43.7	1,214.156	29.4
tsw33	1,165.86	85.3	1,190.732	69.3	1,217.538	86.2	1,184.726	64.0
tsw34	1,080.516	35.3	1,121.421	37.5	1,131.36	34.4	1,120.757	41.3
tsw35	1,045.22	102.5	1,083.899	84.9	1,096.919	95.4	1,079.452	87.2
tsw36	942.7464	35.8	998.982	43.2	1,001.555	28.2	992.2496	33.7
tsw37	906.9832	17.9	955.7817	21.6	973.3775	14.1	958.5879	16.8
tsw38	889.1013	18.4	934.1815	9.1	959.2885	23.8	941.7571	13.5
tsw39	870.6917	2.2	925.068	9.0	935.5172	7.6	928.2658	12.4
ch1	868.4666	16.5	916.0764	22.6	927.9533	11.7	915.8546	17.0
ch2	851.9465	21.7	893.5212	14.3	916.2651	21.0	898.901	15.4
ch3	830.2676	21.7	879.1956	14.3	895.2167	21.0	883.5388	15.4
ch4	808.5887	21.7	864.87	14.3	874.1683	21.0	868.1765	15.4
ch5	786.9098	21.7	850.5444	14.3	853.1199	21.0	852.8143	15.4
ch6	765.2309	17.2	836.2188	14.9	832.0715	17.2	837.452	22.1
pp4	748.0706	14.6	821.3141	8.7	814.8519	19.8		0.0
pp3	733.4402	2.3	812.5968	33.5	795.0506	10.8	815.3688	34.1
pp2			779.0688	23.8	784.2032	5.2	781.2358	26.9
pp1			755.2944	25.3			754.3675	23.8
Water Table	731.1		730		779		730.6	

Source: BSC 2004 [DIRS 169855], Attachment II, Table II-1.

Table L-34. Layer Average Residual Saturation

Layer	Unit	Thickness (m)	Residual Saturation[1]	Average Residual Saturation[2]
TSW	tsw35	102.4	0.12	0.1
	tsw36	31.3	0.20	
	tsw37	15.7	0.20	
	tsw38	15.5	0.42	
	tsw39	6.7	0.36	
CH	Zeolitic		0.3	0.3
	Vitric		0.1	0.1
PP	pp4	9.7	0.29	0.1
	pp3	19.1	0.08	
	pp2	17.4	0.10	
	pp1	34.5	0.30	

Source: [1] Calibrated Unsaturated Zone Properties [DIRS 179545], Table 4-2.

[2] Average residual saturation calculated using Equation L-68 for TSW and PP layers.

Table L-35. Unsaturated Zone Layer Average Properties for Determination of Matrix Hydraulic Conductivity

10th Percentile Infiltration Scenario, Repository Underlain by Vitric Units tsw39 and Ch1-6											
Model Layer	Unit	Average Thick-ness (m)	Matrix Permeability (m^2)[a]	Van Genuchten m[a]	Layer Average Matrix Permeability (m^2)	Layer Average Van Genuchten m	Average Saturation[e]	Residual Saturation	Effective Saturation	Layer Average Matrix Relative Permeability (m^2)	Layer Average Matrix Hydraulic Conductivity (mm/yr)
TSW	tsw35	51.2	1.09E-17	0.216	5.09E-18	0.32	0.95	0.1	0.94	9.39E-19	3.27E-01
	tsw36	31.3	3.16E-18	0.442							
	tsw37	15.7	3.16E-18	0.442							
	tsw38	15.5	3.79E-18	0.286							
	tsw39	6.7	1.49E-13	0.293							
CH	ch1	15.7	2.21E-12	0.24	1.08E-12	0.17	0.7	0.1	0.67	2.13E-16	7.42E+01
	ch2	19.3	1.55E-12	0.158							
	ch3	19.3	1.55E-12	0.158							
	ch4	19.3	1.55E-12	0.158							
	ch5	19.3	1.55E-12	0.158							
	ch6	18.0	3.92E-13	0.147							
PP	pp4	9.7	3.01E-17	0.474	7.90E-17	0.34	0.8	0.1	0.78	2.62E-18	9.12E-01
	pp3	19.1	9.24E-14	0.407							
	pp2	17.4	1.68E-15	0.309							
	pp1	34.5	5.01E-17	0.272							

Table L-35. Unsaturated Zone Layer Average Properties for Determination of Matrix Hydraulic Conductivity (Continued)

30th Percentile Infiltration Scenario, Repository Underlain by Vitric Units tsw39 and Ch1-6											
Model Layer	**Unit**	**Average Thick-ness (m)**	**Matrix Permeability (m^2)[b]**	**Van Genuchten m[b]**	**Layer Average Matrix Permeability (m^2)**	**Layer Average Van Genuchten m**	**Average Saturation[e]**	**Residual Saturation**	**Effective Saturation**	**Layer Average Matrix Relative Permeability (m^2)**	**Layer Average Matrix Hydraulic Conductivity (mm/yr)**
TSW	tsw35	51.2	1.11E-17	0.216	5.81E-18	0.32	0.95	0.1	0.94	1.07E-18	3.73E-01
	tsw36	31.3	3.16E-18	0.442							
	tsw37	15.7	3.16E-18	0.442							
	tsw38	15.5	1.27E-17	0.286							
	tsw39	6.7	2.23E-13	0.293							
CH	ch1	15.7	2.59E-12	0.24	1.51E-12	0.17	0.7	0.1	0.67	2.98E-16	1.04E+02
	ch2	19.3	6.77E-11	0.158							
	ch3	19.3	6.77E-11	0.158							
	ch4	19.3	6.77E-11	0.158							
	ch5	19.3	6.77E-11	0.158							
	ch6	18.0	2.71E-13	0.147							
PP	pp4	9.7	3.51E-17	0.474	4.95E-17	0.34	0.8	0.1	0.78	1.65E-18	5.72E-01
	pp3	19.1	1.02E-13	0.407							
	pp2	17.4	1.69E-15	0.309							
	pp1	34.5	2.57E-17	0.272							

Table L-35. Unsaturated Zone Layer Average Properties for Determination of Matrix Hydraulic Conductivity (Continued)

50th Percentile Infiltration Scenario, Repository Underlain byVitric Units tsw39 and Ch1-6											
Model Layer	Unit	Average Thick-ness (m)	Matrix Permeability (m^2)[c]	Van Genuchten m[c]	Layer Average Matrix Permeability (m^2)	Layer Average Van Genuchten m	Average Saturation[e]	Residual Saturation	Effective Saturation	Layer Average Matrix Relative Permeability (m^2)	Layer Average Matrix Hydraulic Conductivity (mm/yr)
TSW	tsw35	51.2	1.94E-17	0.216	8.65E-18	0.32	0.95	0.1	0.94	1.60E-18	5.55E-01
	tsw36	31.3	4.45E-18	0.442							
	tsw37	15.7	4.45E-18	0.442							
	tsw38	15.5	2.16E-17	0.286							
	tsw39	6.7	2.24E-13	0.293							
CH	ch1	15.7	3.16E-12	0.24	2.47E-12	0.17	0.7	0.1	0.67	4.89E-16	1.70E+02
	ch2	19.3	1.58E-11	0.158							
	ch3	19.3	1.58E-11	0.158							
	ch4	19.3	1.58E-11	0.158							
	ch5	19.3	1.58E-11	0.158							
	ch6	18.0	5.14E-13	0.147							
PP	pp4	9.7	1.89E-17	0.474	4.31E-17	0.34	0.8	0.1	0.78	1.43E-18	4.98E-01
	pp3	19.1	1.79E-13	0.407							
	pp2	17.4	1.00E-15	0.309							
	pp1	34.5	2.57E-17	0.272							

Table L-35. Unsaturated Zone Layer Average Properties for Determination of Matrix Hydraulic Conductivity (Continued)

90th Percentile Infiltration Scenario, Repository Underlain by Vitric Units tsw39 and Ch1-6											
Model Layer	Unit	Average Thick-ness (m)	Matrix Permeability (m^2)[d]	Van Genuchten m[d]	Layer Average Matrix Permeability (m^2)	Layer Average Van Genuchten m	Average Saturation[e]	Residual Saturation	Effective Saturation	Layer Average Matrix Relative Permeability (m^2)	Layer Average Matrix Hydraulic Conductivity (mm/yr)
TSW	tsw35	51.2	7.54E-17	0.216	1.65E-17	0.32	0.95	0.1	0.94	3.05E-18	1.06E+00
	tsw36	31.3	7.50E-18	0.442							
	tsw37	15.7	7.50E-18	0.442							
	tsw38	15.5	4.40E-17	0.286							
	tsw39	6.7	2.24E-13	0.293							
CH	ch1	15.7	2.51E-12	0.240	1.80E-12	0.17	0.7	0.1	0.67	3.56E-16	1.24E+02
	ch2	19.3	3.16E-11	0.158							
	ch3	19.3	3.16E-11	0.158							
	ch4	19.3	3.16E-11	0.158							
	ch5	19.3	3.16E-11	0.158							
	ch6	18.0	3.40E-13	0.147							
PP	pp4	9.7	1.00E-17	0.474	4.78E-17	0.34	0.8	0.1	0.78	1.59E-18	5.52E-01
	pp3	19.1	1.71E-13	0.407							
	pp2	17.4	6.31E-16	0.309							
	pp1	34.5	5.01E-17	0.272							

Table L-35. Unsaturated Zone Layer Average Properties for Determination of Matrix Hydraulic Conductivity (Continued)

10th Percentile Infiltration Scenario, Repository Underlain by Zeolitic Units tsw39 and Ch1-6											
Model Layer	Unit	Average Thick-ness (m)	Matrix Permeability (m^2)[a]	Van Genuchten m[a]	Layer Average Matrix Permeability (m^2)	Layer Average Van Genuchten m	Average Saturation[e]	Residual Saturation	Effective Saturation	Layer Average Matrix Relative Permeability (m^2)	Layer Average Matrix Hydraulic Conductivity (mm/yr)
TSW	tsw35	51.2	1.09E-17	0.216	5.05E-18	0.30	0.95	0.1	0.94	8.48E-19	2.95E-01
	tsw36	31.3	3.16E-18	0.442							
	tsw37	15.7	3.16E-18	0.442							
	tsw38	15.5	3.79E-18	0.286							
	tsw39	6.7	3.50E-17	0.059							
CH	ch1	15.7	3.50E-17	0.349	2.98E-18	0.31	0.7	0.3	0.57	6.52E-21	2.27E-03
	ch2	19.3	5.20E-18	0.257							
	ch3	19.3	5.20E-18	0.257							
	ch4	19.3	5.20E-18	0.257							
	ch5	19.3	5.20E-18	0.257							
	ch6	18.0	8.20E-19	0.499							
PP	pp4	9.7	3.01E-17	0.474	7.90E-17	0.34	0.8	0.1	0.78	2.62E-18	9.12E-01
	pp3	19.1	9.24E-14	0.407							
	pp2	17.4	1.68E-15	0.309							
	pp1	34.5	5.01E-17	0.272							

Table L-35. Unsaturated Zone Layer Average Properties for Determination of Matrix Hydraulic Conductivity (Continued)

30th Percentile Infiltration Scenario, Repository Underlain by Zeolitic Units tsw39 and Ch1-6											
Model Layer	Unit	Average Thick-ness (m)	Matrix Permeability (m^2)[b]	Van Genuchten m[b]	Layer Average Matrix Permeability (m^2)	Layer Average Van Genuchten m	Average Saturation[e]	Residual Saturation	Effective Saturation	Layer Average Matrix Relative Permeability (m^2)	Layer Average Matrix Hydraulic Conductivity (mm/yr)
TSW	tsw35	51.2	1.11E-17	0.216	5.76E-18	0.30	0.95	0.1	0.94	9.68E-19	3.37E-01
	tsw36	31.3	3.16E-18	0.442							
	tsw37	15.7	3.16E-18	0.442							
	tsw38	15.5	1.27E-17	0.286							
	tsw39	6.7	3.50E-17	0.059							
CH	ch1	15.7	3.50E-17	0.349	2.98E-18	0.31	0.7	0.3	0.57	6.52E-21	2.27E-03
	ch2	19.3	5.20E-18	0.257							
	ch3	19.3	5.20E-18	0.257							
	ch4	19.3	5.20E-18	0.257							
	ch5	19.3	5.20E-18	0.257							
	ch6	18.0	8.20E-19	0.499							
PP	pp4	9.7	3.51E-17	0.474	4.95E-17	0.34	0.8	0.1	0.78	1.65E-18	5.72E-01
	pp3	19.1	1.02E-13	0.407							
	pp2	17.4	1.69E-15	0.309							
	pp1	34.5	2.57E-17	0.272							

Table L-35. Unsaturated Zone Layer Average Properties for Determination of Matrix Hydraulic Conductivity (Continued)

50th Percentile Infiltration Scenario, Repository Underlain by Zeolitic Units tsw39 and Ch1-6											
Model Layer	Unit	Average Thick-ness (m)	Matrix Permeability (m^2)[c]	Van Genuchten m^c	Layer Average Matrix Permeability (m^2)	Layer Average Van Genuchten m	Average Saturation[e]	Residual Saturation	Effective Saturation	Layer Average Matrix Relative Permeability (m^2)	Layer Average Matrix Hydraulic Conductivity (mm/yr)
TSW	tsw35	51.2	1.94E-17	0.216	8.53E-18	0.30	0.95	0.1	0.94	1.43E-18	4.99E-01
	tsw36	31.3	4.45E-18	0.442							
	tsw37	15.7	4.45E-18	0.442							
	tsw38	15.5	2.16E-17	0.286							
	tsw39	6.7	3.50E-17	0.059							
CH	ch1	15.7	3.50E-17	0.349	2.98E-18	0.31	0.7	0.3	0.57	6.52E-21	2.27E-03
	ch2	19.3	5.20E-18	0.257							
	ch3	19.3	5.20E-18	0.257							
	ch4	19.3	5.20E-18	0.257							
	ch5	19.3	5.20E-18	0.257							
	ch6	18.0	8.20E-19	0.499							
PP	pp4	9.7	1.89E-17	0.474	4.31E-17	0.34	0.8	0.1	0.78	1.43E-18	4.98E-01
	pp3	19.1	1.79E-13	0.407							
	pp2	17.4	1.00E-15	0.309							
	pp1	34.5	2.57E-17	0.272							

Table L-35. Unsaturated Zone Layer Average Properties for Determination of Matrix Hydraulic Conductivity (Continued)

90th Percentile Infiltration Scenario, Repository Underlain by Zeolitic Units tsw39 and Ch1-6											
Model Layer	Unit	Average Thick-ness (m)	Matrix Permeability (m^2)[d]	Van Genuchten m[d]	Layer Average Matrix Permeability (m^2)	Layer Average Van Genuchten m	Average Saturation[e]	Residual Saturation	Effective Saturation	Layer Average Matrix Relative Permeability (m^2)	Layer Average Matrix Hydraulic Conductivity (mm/yr)
TSW	tsw35	51.2	7.54E-17	0.216	1.61E-17	0.30	0.95	0.1	0.94	2.70E-18	9.40E-01
	tsw36	31.3	7.50E-18	0.442							
	tsw37	15.7	7.50E-18	0.442							
	tsw38	15.5	4.40E-17	0.286							
	tsw39	6.7	3.50E-17	0.059							
CH	ch1	15.7	3.50E-17	0.349	5.91E-18	0.20	0.7	0.3	0.57	6.79E-22	2.36E-04
	ch2	19.3	5.20E-18	0.240							
	ch3	19.3	5.20E-18	0.158							
	ch4	19.3	5.20E-18	0.158							
	ch5	19.3	5.20E-18	0.158							
	ch6	18.0	5.20E-18	0.158							
PP	pp4	9.7	1.00E-17	0.474	4.78E-17	0.34	0.8	0.1	0.78	1.59E-18	5.52E-01
	pp3	19.1	1.71E-13	0.407							
	pp2	17.4	6.31E-16	0.309							
	pp1	34.5	5.01E-17	0.272							

Sources: [a] DTN:LB0610UZDSCP10.001_R0 [DIRS 180502]
[b] DTN:LB0610UZDSCP30.001_R0 [DIRS 179180]
[c] DTN:LB0611UZDSCP50.001_R0 [DIRS 183948]
[d] DTN:LB0612UZD SCP90.001_R0 [DIRS 183949]
[e] Estimated from Calibrated UZ Properties, ANL-NBS-HS-000058 [DIRS 179545], Figures 6-1, 6-3, 6-5, and 6-9.

Table L-36. Unsaturated Zone Layer Average Matrix and Fracture Porosity

Model Layer	Unit	Thickness (m)	Matrix Porosity (Vitric tsw39 and Ch)[a]	Matrix Porosity (Zeolitic tsw39 and Ch)[a]	Fracture Porosity[b]	Layer Average Matrix Porosity (Vitric tsw39 and Ch)	Layer Average Matrix Porosity (Zeolitic tsw39 and Ch)	Layer Average Fracture Porosity
TSW	tsw35	102.42	1.31E-01	1.31E-01	9.60E-03	0.12	0.12	0.010
	tsw36	31.31	1.03E-01	1.03E-01	1.30E-02			
	tsw37	15.655	1.03E-01	1.03E-01	1.30E-02			
	tsw38	15.507	4.30E-02	4.30E-02	1.10E-02			
	tsw39	6.6511	2.29E-01	2.75E-01	4.30E-03			
CH	ch1	15.71	3.31E-01	2.85E-01	6.10E-04	0.34	0.31	0.001
	ch2	19.324	3.46E-01	3.22E-01	7.70E-04			
	ch3	19.328	3.46E-01	3.22E-01	7.70E-04			
	ch4	19.326	3.46E-01	3.22E-01	7.70E-04			
	ch5	19.326	3.46E-01	3.22E-01	7.70E-04			
	ch6	18.039	3.31E-01	2.71E-01	7.70E-04			
PP	pp4	9.736	3.21E-01	3.21E-01	3.70E-04	0.29	0.29	0.001
	pp3	19.091	3.18E-01	3.18E-01	9.70E-04			
	pp2	17.392	2.21E-01	2.21E-01	9.70E-04			
	pp1	34.466	2.97E-01	2.97E-01	3.70E-04			

Sources: [a]BSC 2004 [DIRS 169857], Table 4-2; DTN: LB0207REVUZPRP.002_R0 [DIRS 159672]
[b]BSC 2004 [DIRS 169857], Table 4-3; DTN: LB0205REVUZPRP.001_R0 [DIRS 159525] and DTN: LB0207REVUZPRP.001_R0 [DIRS 159526].

Table L-37. Unsaturated Zone Layer Fracture and Matrix Percolation Flux (mm/yr)

10th Percentile Infiltration Scenario									
Layer	Ksat	Present-Day		Monsoon		Glacial-Transition		Post-10,000 Year	
		Matrix Flux (mm/yr)	Fracture Flux (mm/yr)	Matrix Flux (mm/yr)	Fracture Flux (mm/yr)	Matrix Flux (mm/yr)	Fracture Flux (mm/yr)	Matrix Flux (mm/yr)	Fracture Flux (mm/yr)
TSW-Vitric	2.58E-01	0.33	2.40	0.33	5.81	0.33	8.33	0.33	15.49
TSW-Zeolitic	1.57E-01	0.29	2.44	0.29	5.85	0.29	8.37	0.29	15.53
CH-Vitric	6.29E+01	2.73	0.00	6.14	0.00	8.66	0.00	15.82	0.00
CH-Zeolitic	1.57E-03	0.00	2.73	0.00	6.14	0.00	8.66	0.00	15.82
PP	7.78E-01	0.91	1.82	0.91	5.23	0.91	7.75	0.91	14.91
30th Percentile Infiltration Scenario									
Layer	Ksat	Present-Day		Monsoon		Glacial-Transition		Post 10,000 Year	
		Matrix Flux (mm/yr)	Fracture Flux (mm/yr)	Matrix Flux (mm/yr)	Fracture Flux (mm/yr)	Matrix Flux (mm/yr)	Fracture Flux (mm/yr)	Matrix Flux (mm/yr)	Fracture Flux (mm/yr)
TSW-Vitric	2.94E-01	0.37	6.97	0.37	11.64	0.37	17.70	0.37	24.42
TSW-Zeolitic	1.80E-01	0.34	7.00	0.34	11.67	0.34	17.73	0.34	24.45
CH-Vitric	8.78E+01	7.34	0.00	12.01	0.00	18.07	0.00	24.79	0.00
CH-Zeolitic	1.57E-03	0.00	7.34	0.00	12.01	0.00	18.07	0.00	24.79
PP	4.88E-01	0.57	6.77	0.57	11.44	0.57	17.50	0.57	24.22
50th Percentile Infiltration Scenario									
Layer	Ksat	Present-Day		Monsoon		Glacial-Transition		Post 10,000 Year	
		Matrix Flux (mm/yr)	Fracture Flux (mm/yr)	Matrix Flux (mm/yr)	Fracture Flux (mm/yr)	Matrix Flux (mm/yr)	Fracture Flux (mm/yr)	Matrix Flux (mm/yr)	Fracture Flux (mm/yr)
TSW-Vitric	4.38E-01	0.56	10.60	0.56	13.25	0.56	21.56	0.56	30.93
TSW-Zeolitic	2.66E-01	0.50	10.66	0.50	13.31	0.50	21.62	0.50	30.99
CH-Vitric	1.44E+02	11.16	0.00	13.81	0.00	22.12	0.00	31.49	0.00
CH-Zeolitic	1.57E-03	0.00	11.16	0.00	13.81	0.00	22.12	0.00	31.49
PP	4.24E-01	0.50	10.66	0.50	13.31	0.50	21.62	0.50	30.99
90th Percentile Infiltration Scenario									
Layer	Ksat	Present-Day		Monsoon		Glacial-Transition		Post 10,000 Year	
		Matrix Flux (mm/yr)	Fracture Flux (mm/yr)	Matrix Flux (mm/yr)	Fracture Flux (mm/yr)	Matrix Flux (mm/yr)	Fracture Flux (mm/yr)	Matrix Flux (mm/yr)	Fracture Flux (mm/yr)
TSW-Vitric	8.35E-01	1.06	24.04	1.06	67.72	1.06	41.28	1.06	44.81
TSW-Zeolitic	5.02E-01	0.94	24.16	0.94	67.84	0.94	41.40	0.94	44.93
CH-Vitric	1.05E+02	25.10	0.00	68.78	0.00	42.34	0.00	45.87	0.00
CH-Zeolitic	1.20E-04	0.00	25.10	0.00	68.78	0.00	42.34	0.00	45.87
PP	4.71E-01	0.55	24.55	0.55	68.23	0.55	41.79	0.55	45.32

Table L-38. Unsaturated Zone Fracture and Matrix Groundwater Velocity

10th Percentile Infiltration Scenario										
Layer	Layer Average Matrix Porosity	Layer Average Fracture Porosity	Present-Day		Monsoon		Glacial-Transition		Post-10,000 Year	
			Matrix Velocity (mm/yr)	Fracture Velocity (mm/yr)	Matrix Velocity (mm/yr)	Fracture Velocity (mm/yr)	Matrix Velocity (mm/yr)	Fracture Velocity (mm/yr)	Matrix Velocity (mm/yr)	Fracture Velocity (mm/yr)
TSW-Vitric	0.12	9.95E-03	2.74E+00	2.42E+02	2.74E+00	5.84E+02	2.74E+00	8.37E+02	2.74E+00	1.56E+03
TSW-Zeolitic	0.12	9.95E-03	2.44E+00	2.45E+02	2.44E+00	5.87E+02	2.44E+00	8.41E+02	2.44E+00	1.56E+03
CH-Vitric	0.34	7.42E-04	8.00E+00		1.80E+01		2.54E+01		4.63E+01	
CH-Zeolitic	0.31	7.42E-04		3.68E+03		8.27E+03		1.17E+04		2.13E+04
PP	0.29	5.14E-04	3.16E+00	3.54E+03	3.16E+00	1.02E+04	3.16E+00	1.51E+04	3.16E+00	2.90E+04
30th Percentile Infiltration Scenario										
Layer	Layer Average Matrix Porosity	Layer Average Fracture Porosity	Present-Day		Monsoon		Glacial-Transition		Post-10,000 Year	
			Matrix Velocity (mm/yr)	Fracture Velocity (mm/yr)	Matrix Velocity (mm/yr)	Fracture Velocity (mm/yr)	Matrix Velocity (mm/yr)	Fracture Velocity (mm/yr)	Matrix Velocity (mm/yr)	Fracture Velocity (mm/yr)
TSW-Vitric	0.12	9.95E-03	3.13E+00	7.00E+02	3.13E+00	1.17E+03	3.13E+00	1.78E+03	3.13E+00	2.45E+03
TSW-Zeolitic	0.12	9.95E-03	2.78E+00	7.04E+02	2.78E+00	1.17E+03	2.78E+00	1.78E+03	2.78E+00	2.46E+03
CH-Vitric	0.34	7.42E-04	2.15E+01		3.52E+01		5.29E+01		7.26E+01	
CH-Zeolitic	0.31	7.42E-04		9.89E+03		1.62E+04		2.43E+04		3.34E+04
PP	0.29	5.14E-04	1.98E+00	1.32E+04	1.98E+00	2.23E+04	1.98E+00	3.41E+04	1.98E+00	4.71E+04

Table L-38. Unsaturated Zone Fracture and Matrix Groundwater Velocity (Continued)

50th Percentile Infiltration Scenario										
Layer	Layer Average Matrix Porosity	Layer Average Fracture Porosity	Present-Day		Monsoon		Glacial-Transition		Post-10,000 Year	
			Matrix Velocity (mm/yr)	Fracture Velocity (mm/yr)	Matrix Velocity (mm/yr)	Fracture Velocity (mm/yr)	Matrix Velocity (mm/yr)	Fracture Velocity (mm/yr)	Matrix Velocity (mm/yr)	Fracture Velocity (mm/yr)
TSW-Vitric	0.12	9.95E-03	4.66E+00	1.07E+03	4.66E+00	1.33E+03	4.66E+00	2.17E+03	4.66E+00	3.11E+03
TSW-Zeolitic	0.12	9.95E-03	4.12E+00	1.07E+03	4.12E+00	1.34E+03	4.12E+00	2.17E+03	4.12E+00	3.11E+03
CH-Vitric	0.34	7.42E-04	3.27E+01		4.04E+01		6.48E+01		9.22E+01	
CH-Zeolitic	0.31	7.42E-04		1.50E+04		1.86E+04		2.98E+04		4.24E+04
PP	0.29	5.14E-04	1.73E+00	2.08E+04	1.73E+00	2.59E+04	1.73E+00	4.21E+04	1.73E+00	6.03E+04
90th Percentile Infiltration Scenario										
Layer	Layer Average Matrix Porosity	Layer Average Fracture Porosity	Present-Day		Monsoon		Glacial-Transition		Post-10,000 Year	
			Matrix Velocity (mm/yr)	Fracture Velocity (mm/yr)	Matrix Velocity (mm/yr)	Fracture Velocity (mm/yr)	Matrix Velocity (mm/yr)	Fracture Velocity (mm/yr)	Matrix Velocity (mm/yr)	Fracture Velocity (mm/yr)
TSW-Vitric	0.12	9.95E-03	8.89E+00	2.42E+03	8.89E+00	6.81E+03	8.89E+00	4.15E+03	8.89E+00	4.50E+03
TSW-Zeolitic	0.12	9.95E-03	7.77E+00	2.43E+03	7.77E+00	6.82E+03	7.77E+00	4.16E+03	7.77E+00	4.51E+03
CH-Vitric	0.34	7.42E-04	7.35E+01		2.01E+02		1.24E+02		1.34E+02	
CH-Zeolitic	0.31	7.42E-04		3.38E+04		9.26E+04		5.70E+04		6.18E+04
PP	0.29	5.14E-04	1.91E+00	4.78E+04	1.91E+00	1.33E+05	1.91E+00	8.14E+04	1.91E+00	8.82E+04

Table L-39. Unsaturated Zone Layer Groundwater Travel Times (yr)

Layer	Average Layer Thick-ness (m)	Present-Day		Monsoon		Glacial-Transition		Post-10,000 Year	
		Matrix Travel Time (yr)	Fracture Travel Time (yr)	Matrix Travel Time (yr)	Fracture Travel Time (yr)	Matrix Travel Time (yr)	Fracture Travel Time (yr)	Matrix Travel Time (yr)	Fracture Travel Time (yr)
10th Percentile Infiltration Scenario									
TSW-Vitric	120	43,902	498	43,902	206	43,902	144	43,902	77
TSW-Zeolitic	120	49,343	492	49,343	205	49,343	143	49,343	77
CH-Vitric	111	13,889		6,176		4,379		2,397	
CH-Zeolitic	111		30		13		10		5
PP	81	25,511	23	25,511	8	25,511	5	25,511	3
30th Percentile Infiltration Scenario									
TSW-Vitric	120	38,416	172	38,416	103	38,416	68	38,416	49
TSW-Zeolitic	120	43,227	171	43,227	103	43,227	68	43,227	49
CH-Vitric	111	5,166		3,157		2,098		1,530	
CH-Zeolitic	111		11		7		5		3
PP	81	40,662	6	40,662	4	40,662	2	40,662	2
50th Percentile Infiltration Scenario									
TSW-Vitric	120	25,822	113	25,822	90	25,822	56	25,822	39
TSW-Zeolitic	120	29,184	112	29,184	90	29,184	55	29,184	39
CH-Vitric	111	3,398		2,746		1,714		1,204	
CH-Zeolitic	111		7		6		4		3
PP	81	46,773	4	46,773	3	46,773	2	46,773	1
90th Percentile Infiltration Scenario									
TSW-Vitric	120	13,538	50	13,538	18	13,538	29	13,538	27
TSW-Zeolitic	120	15,488	50	15,488	18	15,488	29	15,488	27
CH-Vitric	111	1,511		551		896		827	
CH-Zeolitic	111		3		1		2		2
PP	81	42,167	2	42,167	1	42,167	1	42,167	1

Table L-40. Unsaturated Zone Layer Average Rock Density

Layer	Unit	Thickness (m)	Density (kg/m^3)[a]	Layer Average Matrix Density (Vitric tsw39 and Ch)
TSW	tsw35	102.4	1.98E+03	2067.8
	tsw36	31.3	2.21E+03	
	tsw37	15.7	2.21E+03	
	tsw38	15.5	2.17E+03	
	tsw39	6.7	2.17E+03	
CH	ch1	15.7	1.48E+03	1510.6
	ch2	19.3	1.52E+03	
	ch3	19.3	1.52E+03	
	ch4	19.3	1.52E+03	
	ch5	19.3	1.52E+03	
	ch6	18.0	1.52E+03	
PP	pp4	9.7	1.48E+03	1554.9
	pp3	19.1	1.48E+03	
	pp2	17.4	1.83E+03	
	pp1	34.5	1.48E+03	

Source: [a]SNL 2008 [DIRS 184748], Table 6-6.

Table L-41. Unsaturated Zone Layer Distribution Coefficients

Species	Layer	Type of Uncertainty Distribution	Coefficients Describing Distribution (Kd: mL/g)
U	TSW	Cumulative	(Kd value, probability) (0, 0) (0.2, 0.5) (3.0, 1.0)
	CHV	Cumulative	(Kd value, probability) (0, 0) (0.2, 0.5) (3.0, 1.0)
	CHZ	Cumulative	(Kd value, probability) (0, 0) (0.5, 0.5) (30.0, 1.0)
	PP	Cumulative	(Kd value, probability) (0, 0) (0.2, 0.5) (3.0, 1.0)
Np	TSW	Cumulative	(Kd value, probability) (0, 0) (1.0, 0.5) (3.0, 1.0)
	CHV	Cumulative	(Kd value, probability) (0, 0) (1.0, 0.5) (3.0, 1.0)
	CHZ	Cumulative	(Kd value, probability) (0, 0) (0.5, 0.5) (6.0, 1.0)
	PP	Cumulative	(Kd value, probability) (0, 0) (1.0, 0.5) (3.0, 1.0)
Pu	TSW	Cumulative	(Kd value, probability) (10.0, 0) (100.0, 0.5) (200.0, 1.0)
	CHV	Cumulative	(Kd value, probability) (10.0, 0) (100.0, 0.5) (200.0, 1.0)
	CHZ	Cumulative	(Kd value, probability) (10.0, 0) (100.0, 0.5) (200.0, 1.0)
	PP	Cumulative	(Kd value, probability) (10.0, 0) (100.0, 0.5) (200.0, 1.0)
Pa	TSW	Truncated Normal	Range = 1,000 - 10,000, μ = 5500 σ = 1500
	CHV	Truncated Normal	Range = 1,000 - 10,000, μ = 5500 σ = 1500
	CHZ	Truncated Normal	Range = 1,000 - 10,000, μ = 5500 σ = 1500
	PP	Truncated Normal	Range = 1,000 - 10,000, μ = 5500 σ = 1500
Cs	TSW	Cumulative	(Kd value, probability) (0.0, 0) (2.0, 0.5) (100.0, 1.0)
	CHV	Cumulative	(Kd value, probability) (0.0, 0) (2.0, 0.5) (100.0, 1.0)
	CHZ	Cumulative	(Kd value, probability) (425.0, 0) (5,000.0, 0.5) (20,000.0, 1.0)
	PP	Cumulative	(Kd value, probability) (0.0, 0) (2.0, 0.5) (100.0, 1.0)
Sr	TSW	Uniform	Range = 0 - 50
	CHV	Uniform	Range = 0 - 50
	CHZ	Uniform	Range = 50 - 2,000
	PP	Uniform	Range = 0 - 50
Th	TSW	Uniform	Range = 1,000 - 10,000
	CHV	Uniform	Range = 1,000 - 10,000
	CHZ	Uniform	Range = 1,000 - 30,000
	PP	Uniform	Range = 1,000 - 10,000
Se[1]	TSW	Truncated Normal	Range = 0 - 25, μ = 8.6 σ = 7.9
	CHV	Truncated Normal	Range = 0 - 25, μ = 8.6 σ = 7.9
	CHZ	Truncated Normal	Range = 1 - 35, μ = 14.3 σ = 7.9
	PP	Truncated Normal	Range = 0 - 25, μ = 8.6 σ = 7.9
Sn[1]	TSW	Log Uniform	Range = 100 - 5,000
	CHV	Log Uniform	Range = 100 - 5,000
	CHZ	Log Uniform	Range = 100 - 5,000
	PP	Log Uniform	Range = 100 - 5,000

Sources: DTN: LA0408AM831341.001_R0 [DIRS 171584] except for those noted by [1], then DTN: LB0701PAKDSESN.001_R0 [DIRS 179299].

Table L-42. Average Specific Discharge in Flow Path Segments

HAVO	Average Specific Discharge (m/year)		
	0-5 km	5-13 km	13-18 km
0.05	0.354	0.408	2.56
1.00	0.459	0.486	0.769
5.00	0.409	0.544	5.98
20.00	0.555	0.500	5.93

Source: DTN: SN0702PASZFTMA.002_R1 [DIRS 183471].

Table L-43. Saturated Zone Horizontal Anisotropy

Horizontal Anisotropy	Cumulative Probability
0.05	0
0.2	0.0042
0.4	0.0168
0.6	0.0379
0.8	0.0674
1.0	0.1
5.0	0.6
8.0	0.744
11.0	0.856
14.0	0.936
17.0	0.984
20.0	1

Source: DTN: SN0302T0502203.001_R0 [DIRS 163563].

Table L-44. Saturated Zone Specific Discharge Multiplier

Log-10 of Specific Discharge Multiplier	Cumulative Probability
-0.951	0
-0.506	0.05
-0.394	0.1
-0.208	0.25
0.208	0.75
0.394	0.9
0.506	0.95
0.951	1

Source: Modified from *Saturated Zone Flow and Transport Model Abstraction* (SNL 2007 [DIRS 183750], Tables 6-7[a] and 6-8). The following updated or new parameters are from Table 6-7[a]: GWSPD, FISVO, FPLANW, Kd_Pu_Col, Kd_Cs_Col, Kd_Sn_Col, Kd_Sn_Vo, Kd_Sn_Al, Kd_Se_Vo, Kd_Sn_Al, and Correlation matrix for K_d sampling in the SZ. Parameters NVF26 and NVF11 are new names for Parameters NVF19 and NVF7 in Table 6-8. Only the names are changed. The rest of the parameters are from Table 6-8.

Table L-45. Saturated Zone Flowing Interval Porosity

Log-10 of Flowing Interval Porosity	Cumulative Probability
-5	0
-4	0.05
-3	0.5
-2	0.8
-1	1

Source: DTN: SN0310T0502103.009_R0 [DIRS 168763].

Table L-46. Saturated Zone Distribution Coefficients in mL/g

Species	Unit	Distribution Type and Parameters	
Np[a]	Fractured Volcanic	Cumulative	
		Value	Probability
		0.00	0.00
		0.99	0.05
		1.83	0.90
		6.00	1.00
	Alluvium	Cumulative	
		Value	Probability
		1.80	0.00
		4.00	0.05
		8.70	0.95
		13.00	1.00
Sn[b]	Fractured Volcanic	Log-Uniform	
		Min.	10^2
		Max.	10^5
	Alluvium	Log-Uniform	
		Min.	10^2
		Max.	10^5
U[a]	Fractured Volcanic	Cumulative	
		Value	Probability
		0.00	0.00
		5.39	0.05
		8.16	0.95
		20.00	1.00
	Alluvium	Cumulative	
		Value	Probability
		1.70	0.00
		2.90	0.05
		6.30	0.95
		8.90	1.00
Cs[a]	Fractured Volcanic	Cumulative	
		Value	Probability
		100.00	0.00
		3,000.59	0.05
		6,782.92	1.00
	Alluvium	Truncated Normal	
		μ	728
		σ	464
		Min.	100
		Max.	1,000
Pa[c]	Fractured Volcanic	Truncated Normal	
		μ	5,500
		σ	1,500
		Min.	1,000
		Max.	10,000
	Alluvium	Truncated Normal	
		μ	5,500
		σ	1,500
		Min.	1,000
		Max.	10,000
Th[c]	Fractured Volcanic	Truncated Normal	
		μ	5,500
		σ	1,500
		Min.	-3σ
		Max.	$+3\sigma$
	Alluvium	Truncated Normal	
		μ	5,500
		σ	1,500
		Min.	-3σ
		Max.	$+3\sigma$

Table L-46. Saturated Zone Distribution Coefficients in mL/g (Continued)

Species	Unit	Distribution Type and Parameters		Species	Unit	Distribution Type and Parameters	
Pu[d]	Fractured Volcanic	Cumulative		Se[b]	Fractured Volcanic	Truncated Normal	
		Value	Probability			μ	14
		10.00	0.00			σ	11
		89.90	0.25			Min.	1
		129.87	0.95			Max.	50
		300.00	1.00		Alluvium	Truncated Normal	
	Alluvium	Normal[b]				μ	14
		μ	100			σ	11
		σ	15			Min.	1
						Max.	50

Sources: [a]DTN: SN0310T0502103.009_R0 [DIRS 168763]
[b]DTN: LA702AM150304.001_R5 [DIRS 184763]
[c]*Site-Scale Saturated Zone Transport* (SNL 2007 [DIRS 177392], Table A-4.
[d]DTN: SN0310T0502103.009_R0 [DIRS 168763] - Beta distribution in source; used mean and standard deviation in normal

Table L-47. Groundwater Biosphere Dose Conversion Factors for the Present-Day Climate

Cumulative Probability	Biosphere Dose Conversion Factor (Sv/yr per Bq/m^3)							
	Ac-227	C-14	Cl-36	Cs-135	I-129	Np-237	Pa-231	Pb-210
0%	4.08E-07	7.18E-10	1.28E-09	3.10E-09	8.59E-08	1.06E-07	6.58E-07	1.63E-06
5%	6.23E-07	8.30E-10	1.88E-09	4.97E-09	9.37E-08	1.43E-07	1.20E-06	1.82E-06
10%	7.07E-07	8.78E-10	2.14E-09	5.80E-09	9.69E-08	1.66E-07	1.38E-06	1.90E-06
15%	7.93E-07	9.33E-10	2.41E-09	6.68E-09	1.00E-07	1.81E-07	1.50E-06	1.95E-06
20%	8.59E-07	9.96E-10	2.65E-09	7.38E-09	1.02E-07	1.92E-07	1.63E-06	2.00E-06
25%	9.27E-07	1.04E-09	2.96E-09	7.99E-09	1.04E-07	2.05E-07	1.73E-06	2.06E-06
30%	9.78E-07	1.09E-09	3.22E-09	8.72E-09	1.07E-07	2.17E-07	1.85E-06	2.12E-06
35%	1.03E-06	1.16E-09	3.61E-09	9.35E-09	1.09E-07	2.26E-07	1.96E-06	2.17E-06
40%	1.09E-06	1.22E-09	4.03E-09	1.02E-08	1.11E-07	2.37E-07	2.04E-06	2.23E-06
45%	1.15E-06	1.28E-09	4.42E-09	1.10E-08	1.14E-07	2.49E-07	2.14E-06	2.29E-06
50%	1.21E-06	1.36E-09	4.86E-09	1.17E-08	1.17E-07	2.58E-07	2.26E-06	2.38E-06
55%	1.27E-06	1.44E-09	5.72E-09	1.26E-08	1.20E-07	2.69E-07	2.36E-06	2.49E-06
60%	1.32E-06	1.54E-09	6.31E-09	1.36E-08	1.24E-07	2.80E-07	2.45E-06	2.56E-06
65%	1.40E-06	1.68E-09	6.99E-09	1.45E-08	1.28E-07	2.93E-07	2.58E-06	2.67E-06
70%	1.47E-06	1.86E-09	7.74E-09	1.58E-08	1.33E-07	3.06E-07	2.71E-06	2.82E-06
75%	1.57E-06	2.04E-09	8.63E-09	1.73E-08	1.37E-07	3.22E-07	2.88E-06	2.99E-06
80%	1.68E-06	2.36E-09	1.02E-08	1.93E-08	1.43E-07	3.43E-07	3.09E-06	3.16E-06
85%	1.82E-06	2.71E-09	1.19E-08	2.24E-08	1.53E-07	3.73E-07	3.35E-06	3.46E-06
90%	2.07E-06	3.28E-09	1.54E-08	2.69E-08	1.66E-07	4.07E-07	3.78E-06	4.01E-06
95%	2.30E-06	5.11E-09	2.29E-08	3.46E-08	1.90E-07	4.52E-07	4.44E-06	5.22E-06
100%	4.32E-06	2.56E-08	3.00E-07	8.48E-08	1.13E-06	8.05E-07	8.56E-06	1.30E-05

Cumulative Probability	Biosphere Dose Conversion Factor (Sv/yr per Bq/m^3)							
	Pu-239	Pu-240	Pu-242	Ra-226	Ra-228	Se-79	Sn-126	Tc-99
0%	3.49E-07	3.47E-07	3.31E-07	8.79E-07	6.14E-07	3.62E-09	8.92E-08	5.28E-10
5%	5.20E-07	5.19E-07	4.94E-07	1.46E-06	7.12E-07	5.02E-09	1.57E-07	6.01E-10
10%	5.85E-07	5.84E-07	5.56E-07	1.67E-06	7.43E-07	5.68E-09	1.89E-07	6.29E-10
15%	6.35E-07	6.35E-07	6.03E-07	1.85E-06	7.66E-07	6.19E-09	2.15E-07	6.53E-10
20%	6.70E-07	6.69E-07	6.36E-07	2.08E-06	7.83E-07	6.64E-09	2.35E-07	6.77E-10
25%	7.06E-07	7.05E-07	6.71E-07	2.23E-06	8.01E-07	7.14E-09	2.58E-07	6.99E-10
30%	7.43E-07	7.41E-07	7.06E-07	2.41E-06	8.23E-07	7.65E-09	2.75E-07	7.26E-10
35%	7.82E-07	7.81E-07	7.43E-07	2.59E-06	8.38E-07	8.31E-09	2.93E-07	7.57E-10
40%	8.29E-07	8.25E-07	7.88E-07	2.76E-06	8.53E-07	8.89E-09	3.17E-07	7.82E-10
45%	8.62E-07	8.61E-07	8.18E-07	2.98E-06	8.67E-07	9.66E-09	3.44E-07	8.15E-10
50%	9.01E-07	8.99E-07	8.57E-07	3.21E-06	8.80E-07	1.02E-08	3.74E-07	8.51E-10
55%	9.38E-07	9.34E-07	8.92E-07	3.46E-06	9.02E-07	1.12E-08	4.07E-07	8.85E-10
60%	9.75E-07	9.72E-07	9.26E-07	3.74E-06	9.24E-07	1.24E-08	4.36E-07	9.29E-10
65%	1.02E-06	1.02E-06	9.69E-07	4.02E-06	9.42E-07	1.37E-08	4.70E-07	9.82E-10
70%	1.08E-06	1.07E-06	1.03E-06	4.35E-06	9.60E-07	1.58E-08	5.08E-07	1.05E-09
75%	1.14E-06	1.14E-06	1.08E-06	4.75E-06	9.86E-07	1.89E-08	5.50E-07	1.13E-09
80%	1.19E-06	1.19E-06	1.13E-06	5.23E-06	1.01E-06	2.27E-08	6.20E-07	1.24E-09

Table L-47. Groundwater Biosphere Dose Conversion Factors for the Present-Day Climate (Continued)

Cumulative Probability	Biosphere Dose Conversion Factor (Sv/yr per Bq/m^3)							
	Pu-239	Pu-240	Pu-242	Ra-226	Ra-228	Se-79	Sn-126	Tc-99
85%	1.27E-06	1.27E-06	1.21E-06	5.85E-06	1.05E-06	2.92E-08	6.84E-07	1.42E-09
90%	1.38E-06	1.38E-06	1.31E-06	6.57E-06	1.09E-06	4.11E-08	7.61E-07	1.79E-09
95%	1.61E-06	1.61E-06	1.53E-06	7.64E-06	1.16E-06	6.75E-08	8.76E-07	2.41E-09
100%	2.93E-06	2.90E-06	2.79E-06	1.75E-05	1.53E-06	1.51E-06	1.68E-06	2.85E-08

Cumulative Probability	Biosphere Dose Conversion Factor (Sv/yr per Bq/m^3)								
	Th-228	Th-229	Th-230	Th-232	U-233	U-234	U-235	U-236	U-238
0%	1.38E-07	7.43E-07	2.74E-07	5.05E-07	4.13E-08	3.96E-08	3.91E-08	3.75E-08	3.85E-08
5%	1.95E-07	1.32E-06	5.30E-07	8.97E-07	5.14E-08	4.90E-08	4.93E-08	4.61E-08	4.70E-08
10%	2.16E-07	1.49E-06	6.13E-07	1.05E-06	5.58E-08	5.30E-08	5.44E-08	5.00E-08	5.11E-08
15%	2.33E-07	1.64E-06	6.76E-07	1.16E-06	6.00E-08	5.66E-08	6.01E-08	5.33E-08	5.49E-08
20%	2.44E-07	1.75E-06	7.33E-07	1.24E-06	6.41E-08	6.02E-08	6.40E-08	5.66E-08	5.82E-08
25%	2.55E-07	1.88E-06	7.88E-07	1.31E-06	6.68E-08	6.27E-08	6.67E-08	5.88E-08	6.04E-08
30%	2.64E-07	2.00E-06	8.29E-07	1.39E-06	6.97E-08	6.57E-08	7.03E-08	6.17E-08	6.26E-08
35%	2.75E-07	2.09E-06	8.70E-07	1.48E-06	7.23E-08	6.77E-08	7.47E-08	6.35E-08	6.51E-08
40%	2.87E-07	2.19E-06	9.20E-07	1.56E-06	7.50E-08	7.03E-08	7.78E-08	6.60E-08	6.75E-08
45%	2.96E-07	2.28E-06	9.62E-07	1.64E-06	7.79E-08	7.26E-08	8.16E-08	6.81E-08	6.99E-08
50%	3.06E-07	2.37E-06	1.01E-06	1.73E-06	8.09E-08	7.45E-08	8.53E-08	7.00E-08	7.24E-08
55%	3.19E-07	2.48E-06	1.04E-06	1.84E-06	8.46E-08	7.79E-08	8.93E-08	7.31E-08	7.50E-08
60%	3.27E-07	2.61E-06	1.10E-06	1.92E-06	8.87E-08	8.21E-08	9.41E-08	7.68E-08	7.85E-08
65%	3.39E-07	2.73E-06	1.15E-06	2.02E-06	9.31E-08	8.55E-08	9.98E-08	8.01E-08	8.21E-08
70%	3.50E-07	2.89E-06	1.23E-06	2.12E-06	9.87E-08	8.93E-08	1.06E-07	8.36E-08	8.71E-08
75%	3.63E-07	3.05E-06	1.30E-06	2.24E-06	1.05E-07	9.52E-08	1.15E-07	8.89E-08	9.14E-08
80%	3.80E-07	3.28E-06	1.38E-06	2.41E-06	1.12E-07	1.01E-07	1.22E-07	9.39E-08	9.73E-08
85%	3.94E-07	3.52E-06	1.50E-06	2.62E-06	1.21E-07	1.08E-07	1.32E-07	1.01E-07	1.04E-07
90%	4.15E-07	3.94E-06	1.64E-06	2.83E-06	1.33E-07	1.17E-07	1.43E-07	1.09E-07	1.11E-07
95%	4.70E-07	4.58E-06	1.91E-06	3.22E-06	1.52E-07	1.35E-07	1.65E-07	1.25E-07	1.29E-07
100%	8.02E-07	8.05E-06	3.27E-06	5.26E-06	3.13E-07	2.20E-07	2.97E-07	2.02E-07	2.07E-07

Source: DTN: MO0702PAGBDCFS.001_R0 [DIRS 179327].

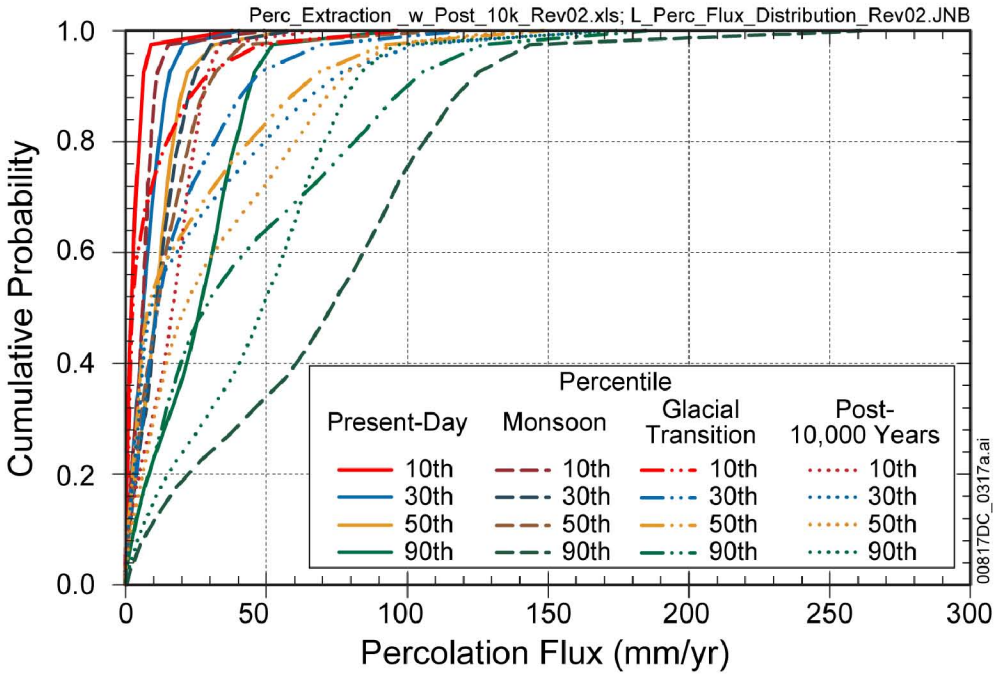

Source: DTN: SN0703PAEBSPCE.006_R2 [DIRS 181571].

Figure L-1. Percolation Flux over the Repository Area

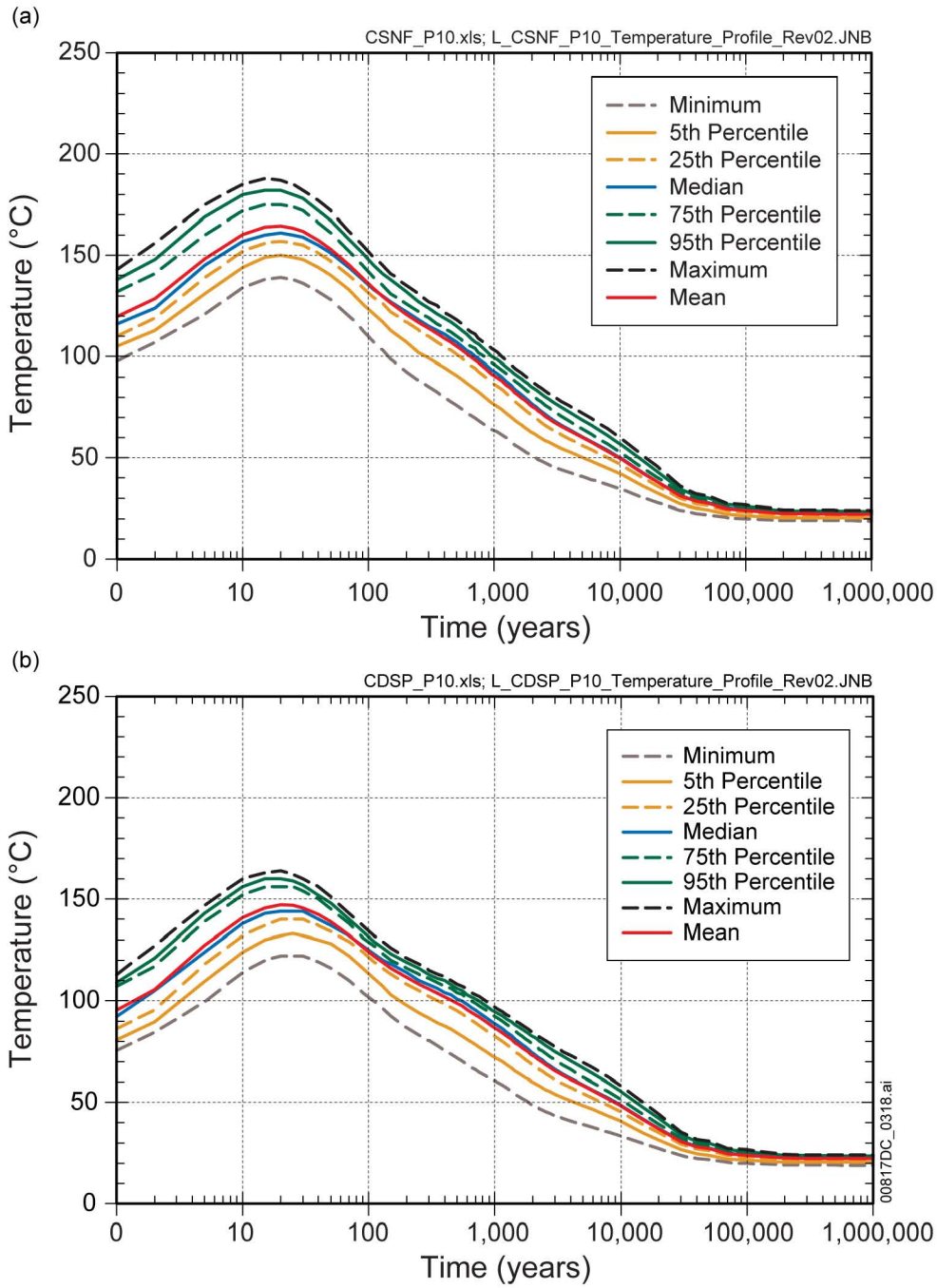

Source: Corroborative DTN: MO0708SIMPLIFI.000 [DIRS 182980].

Figure L-2. CSNF and Defense HLW Waste Package Surface Temperatures, 10th Percentile Infiltration Scenario, Medium Thermal Conductivity

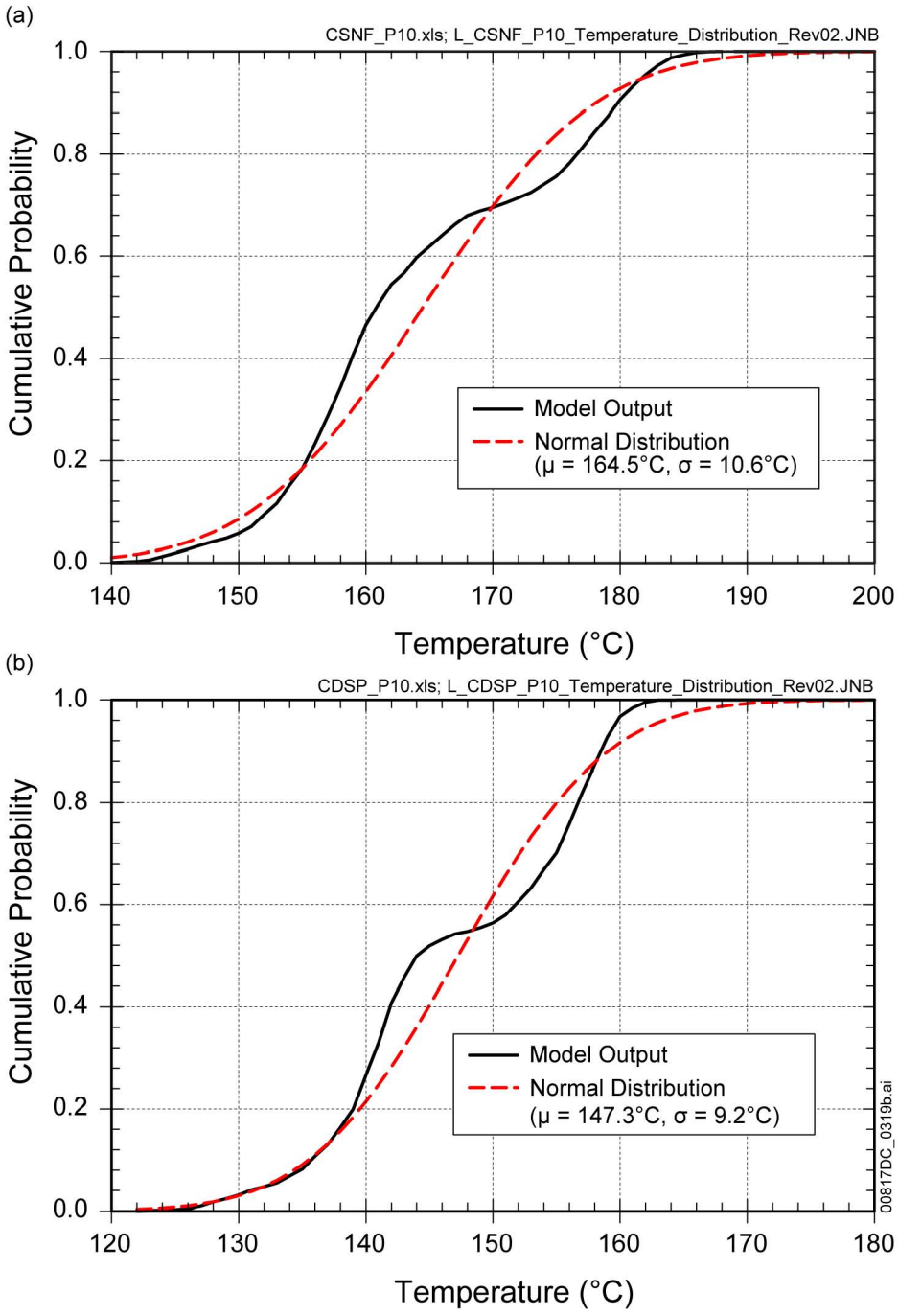

Source: Corroborative DTN: MO0708SIMPLIFI.000 [DIRS 182980].

Figure L-3. CSNF and Defense HLW Peak Waste Package Surface Temperature Distribution, 10th Percentile Infiltration Scenario, Medium Thermal Conductivity

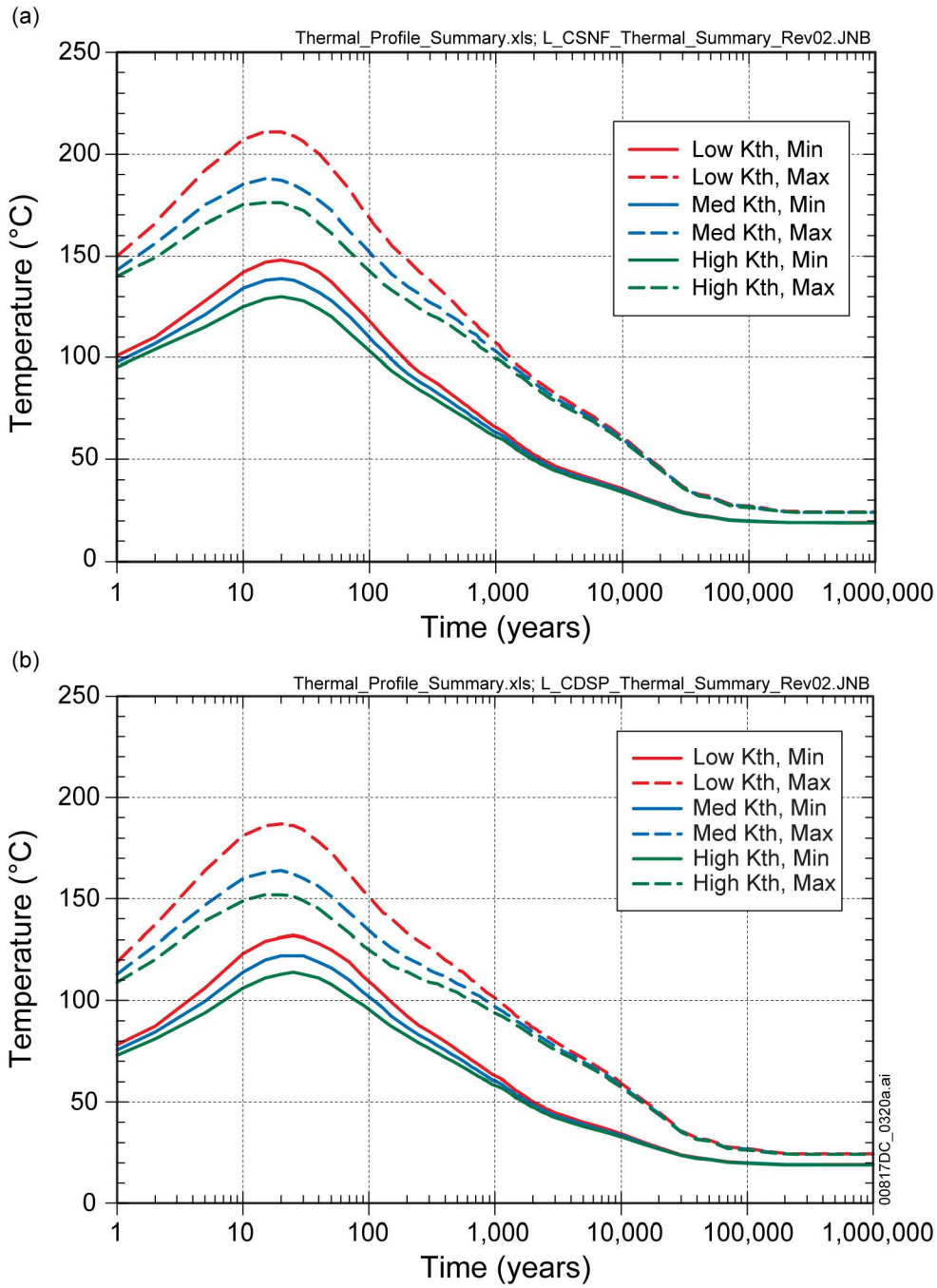

Source: Corroborative DTN: MO0708SIMPLIFI.000 [DIRS 182980].

Figure L-4. CSNF and Defense HLW Waste Package Surface Temperature Range, 10th Percentile Infiltration Scenario

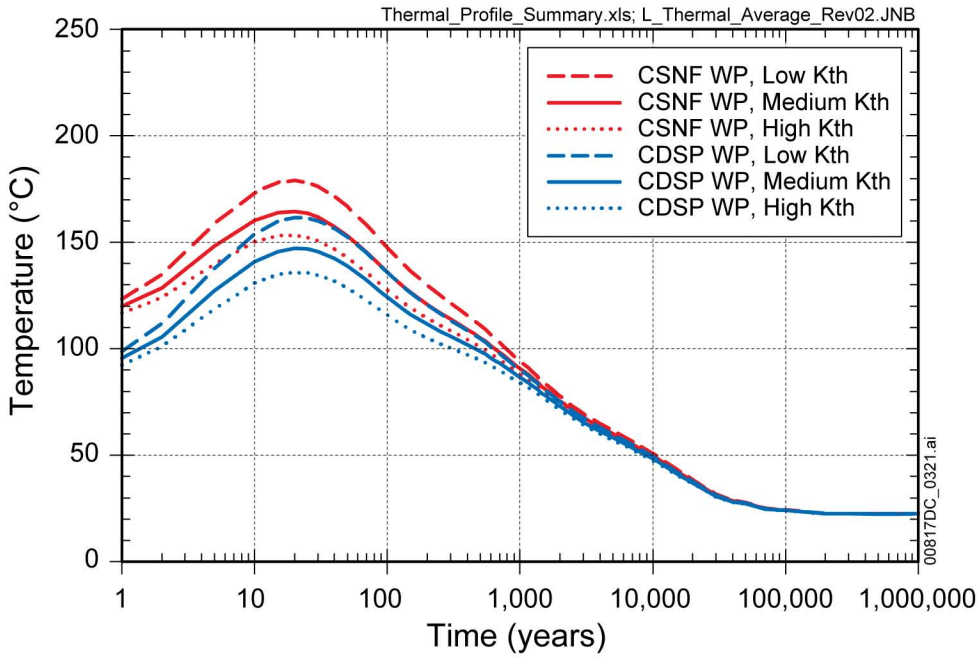

Source: Corroborative DTN: MO0708SIMPLIFI.000 [DIRS 182980].

Figure L-5. Average CSNF and Defense HLW Peak Waste Package Surface Temperature, 10th Percentile Infiltration Scenario

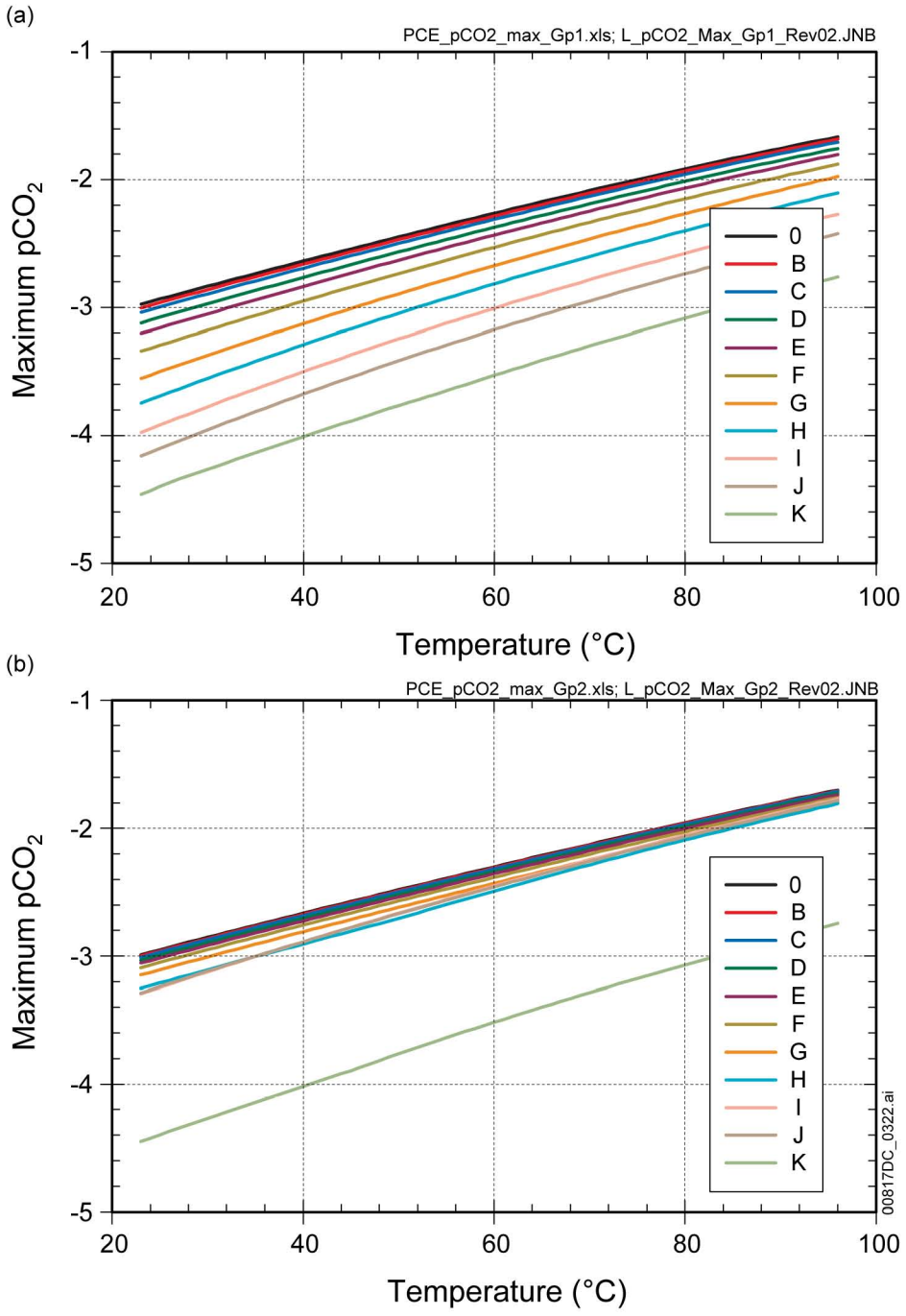

Source: DTN: SN0701PAEBSPCE.002_R0 [DIRS 179425].

NOTES: The lines represent different values of a water-rock interaction parameter.

Figure L-6. Maximum CO_2 Partial Pressure: (a) Group 1 Starting Water, (b) Group 2 Starting Water, (c) Group 3 Starting Water, and (d) Group 4 Starting Water

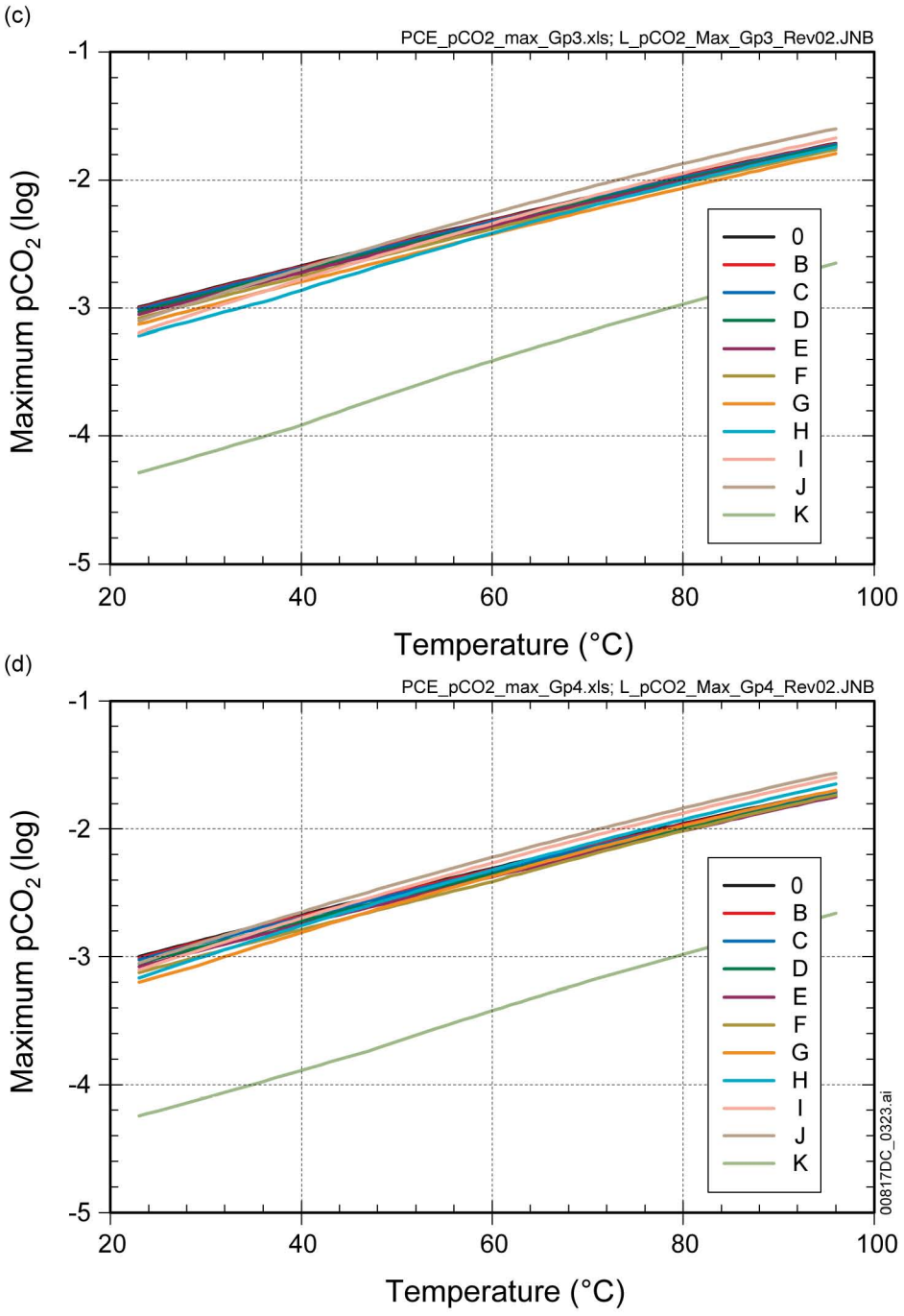

Source: DTN: SN0701PAEBSPCE.002_R0 [DIRS 179425].

NOTES: The lines represent different values of a water-rock interaction parameter.

Figure L-6. Maximum CO_2 Partial Pressure: (a) Group 1 Starting Water, (b) Group 2 Starting Water, (c) Group 3 Starting Water, and (d) Group 4 Starting Water (Continued)

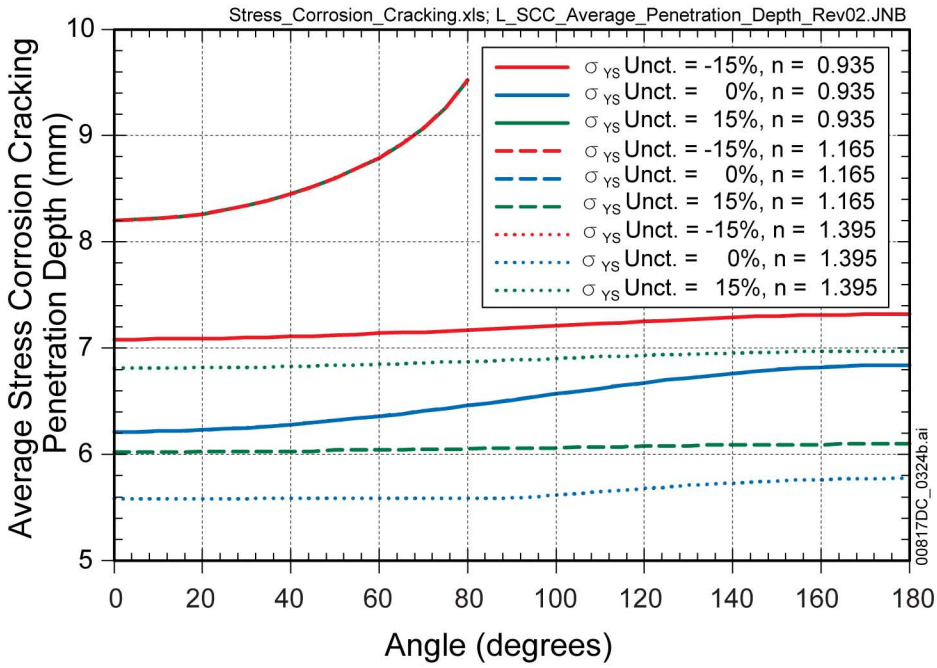

Source: Corroborative DTN: MO0708SIMPLIFI.000 [DIRS 182980].

Figure L-7. Depth Where Stress Corrosion Cracks Can Initiate and Propagate Along the Circumference of the Waste Package Outer Lid Closure Weld Region

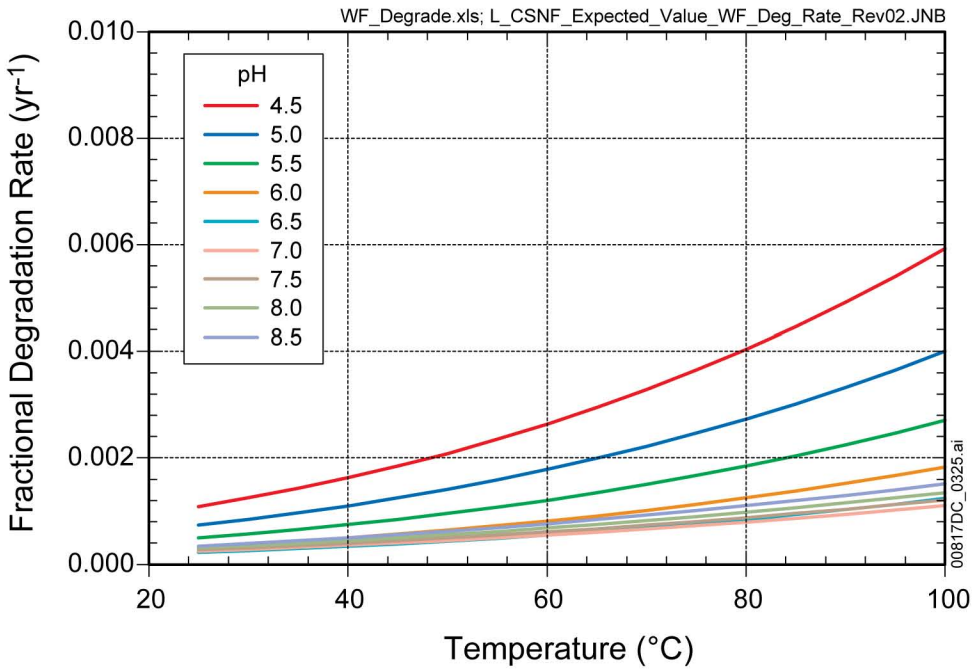

Source: Corroborative DTN: MO0708SIMPLIFI.000 [DIRS 182980].

Figure L-8. CSNF Waste Form Degradation for Expected Value Coefficients with Varying pH

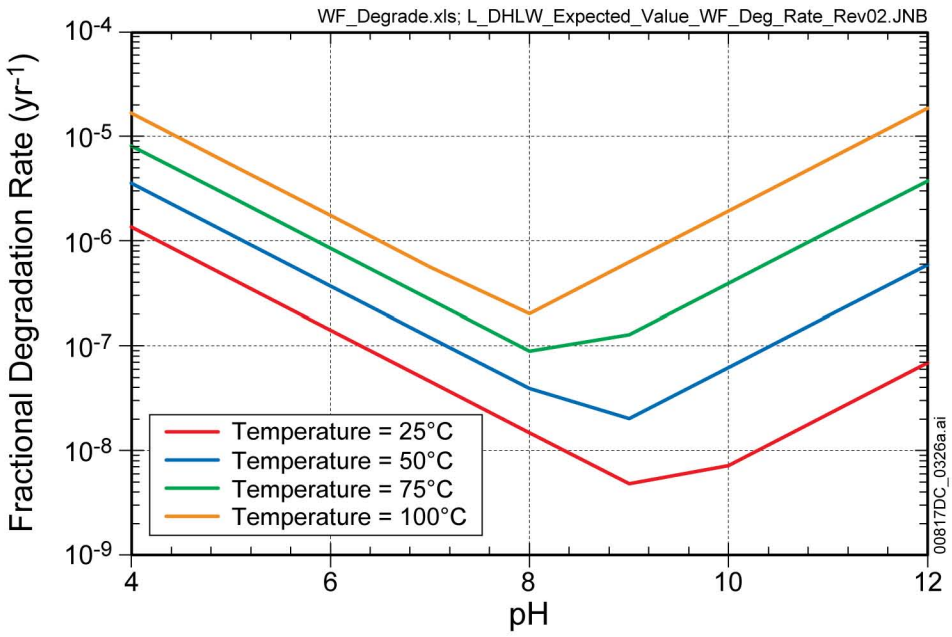

Source: Corroborative DTN: MO0708SIMPLIFI.000 [DIRS 182980].

Figure L-9. Defense HLW Waste Form Degradation for Expected Value Coefficients at Different Temperatures

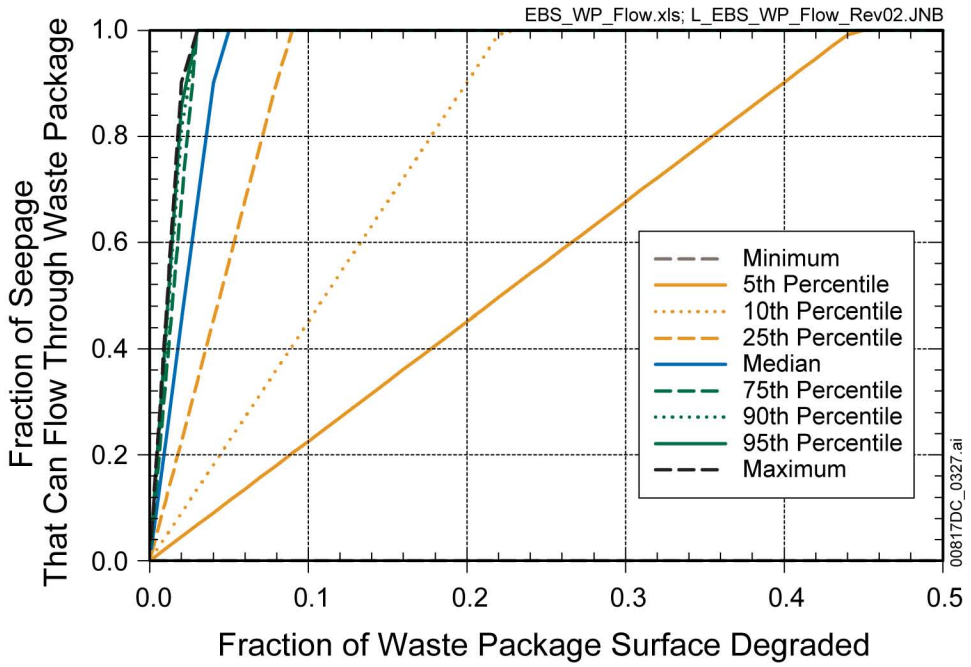

Source: Corroborative DTN: MO0708SIMPLIFI.000 [DIRS 182980].

Figure L-10. Fraction of Seepage that Can Enter a Waste Package with General Corrosion Breaches

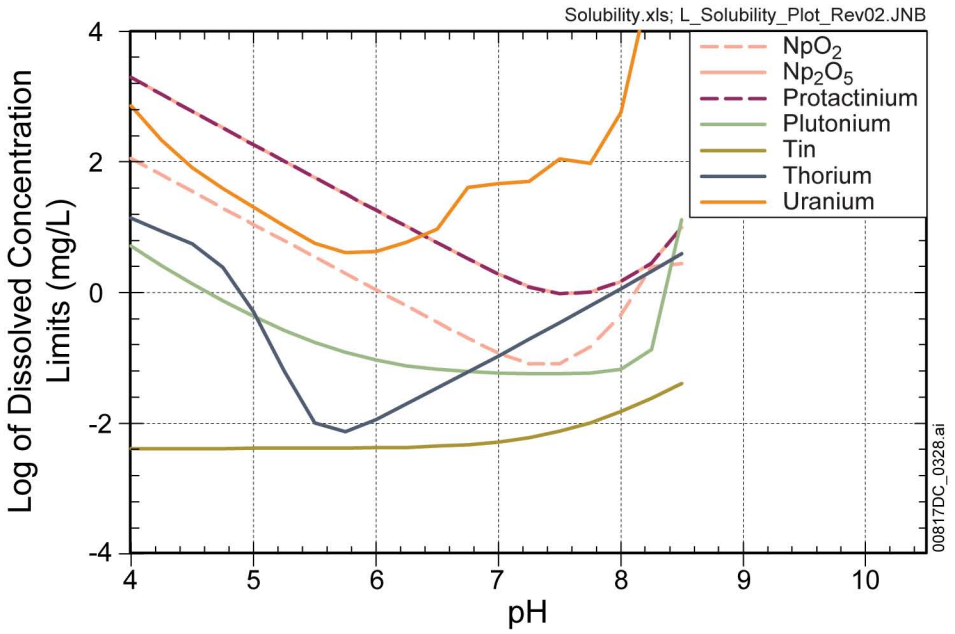

Source: Corroborative DTN: MO0708SIMPLIFI.000 [DIRS 182980].

Figure L-11. Dissolved Concentration Limits

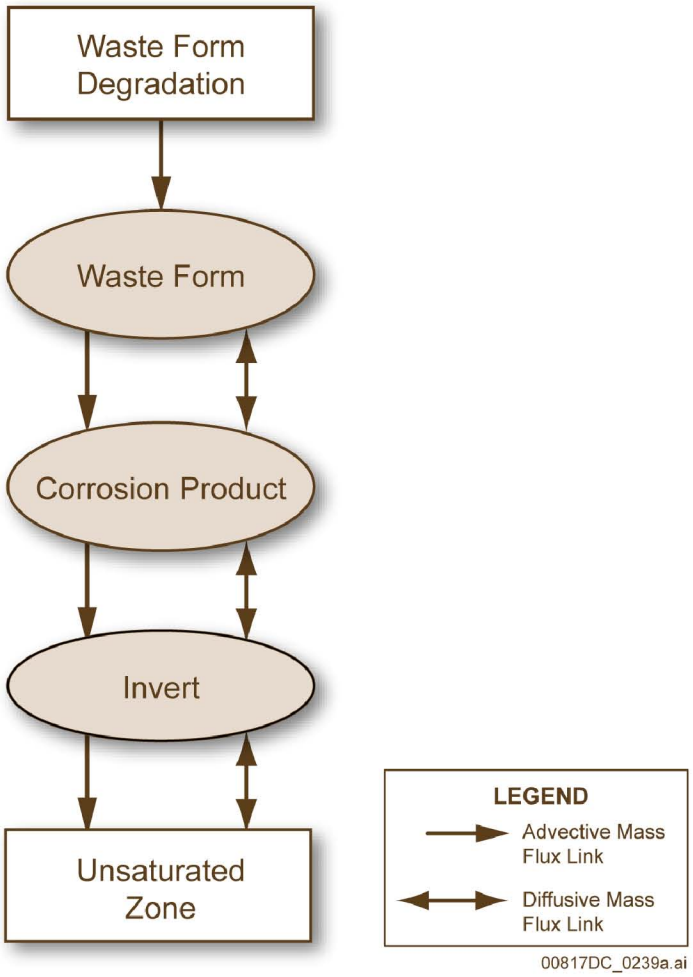

Figure L-12. General Schematic Diagram of a Single EBS Radionuclide Transport Network in Simplified TSPA

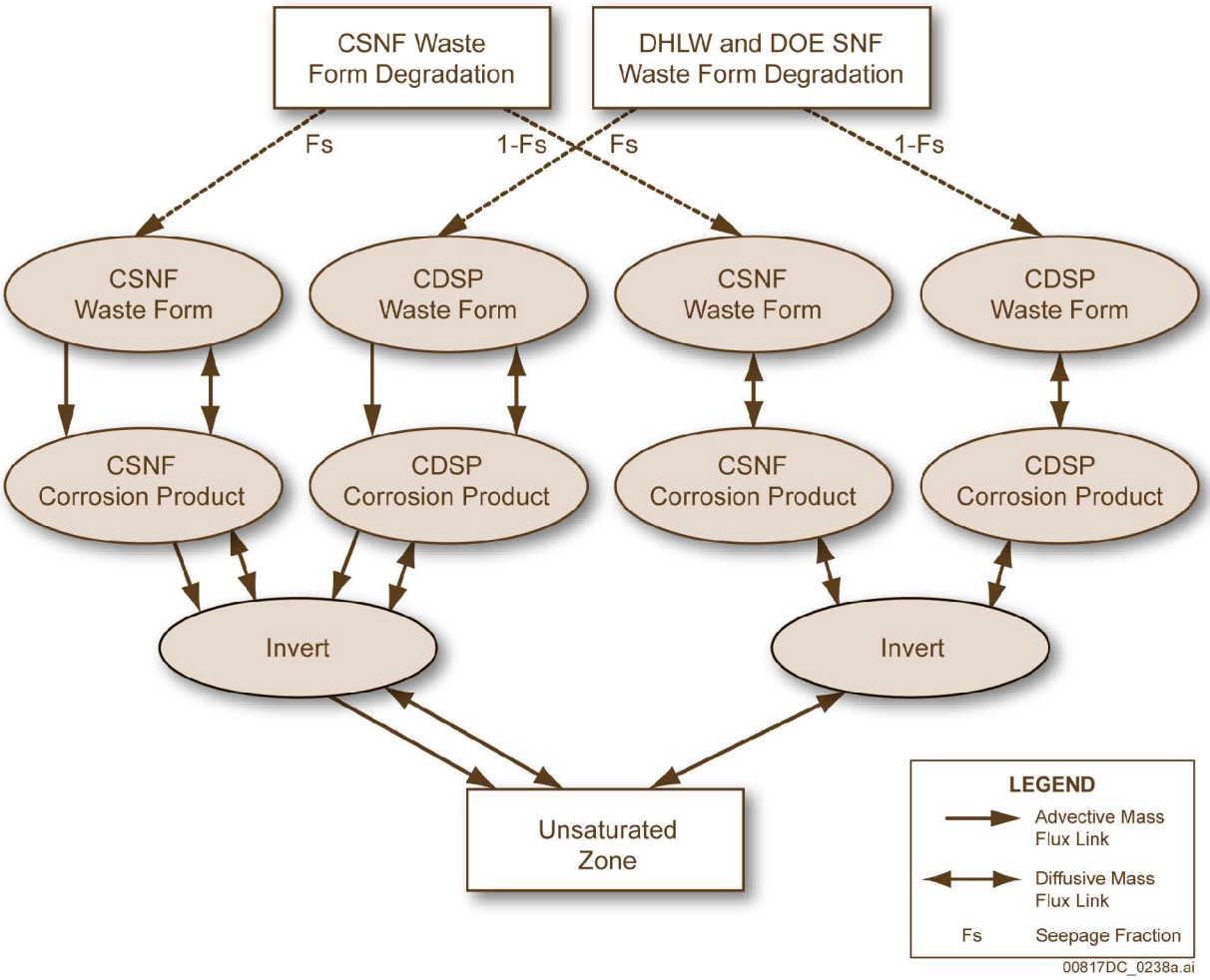

Figure L-13. General Schematic Diagram of a Single EBS Radionuclide Transport Network Used in the Simplified TSPA

APPENDIX M

COMPARISON WITH ELECTRIC POWER RESEARCH INSTITUTE MODEL

M1. INTRODUCTION

This appendix presents a comparison of the Total System Performance Assessment for the License Application (TSPA-LA) Model and the TSPA of the proposed high-level waste repository at Yucca Mountain conducted by the Electric Power Research Institute (EPRI). The purpose of the comparison of the Yucca Mountain TSPA conducted by EPRI with the TSPA-LA Model is to provide a potential unique independent means of TSPA-LA Model validation. The EPRI TSPA Analysis was developed by an independent organization, based on independently developed methodology and its own total systems performance code, the Integrated Multiple Assumptions and Release Code (IMARC). Input into IMARC is generally derived from the model and/or analyses reports developed for the TSPA-LA. Because the input to the EPRI TSPA Analysis corresponds to an earlier version of the TSPA model, an exact comparison between the results from the EPRI TSPA Analysis and the TSPA-LA Model is not possible. Nevertheless, the overall features of the dose curves can be compared and, together with evaluating the apparent differences, provide a validation of the general methodology and strategy used in the TSPA-LA Model.

M1.1 APPROACH

The approach for the comparison includes discussion of the rationale and objectives of EPRI's TSPA efforts and review of the development and status of EPRI's TSPA IMARC, which serves as the basis for the comparison with the TSPA-LA Model that is implemented in GoldSim. The focus of the comparison is on the Nominal Scenario Class for which specific model parameters of both models are examined in greater detail. EPRI has been conducting independent assessments of the total system performance of the candidate radioactive waste repository at Yucca Mountain, Nevada, since 1989 (Kozak and Kessler 2005 [DIRS 178580]). The objective of the EPRI's TSPA Analysis is to provide an independent third-party assessment of key technical and scientific issues associated with the proposed geologic repository at Yucca Mountain and to ensure that adequate information exists to support resolution of those issues that have the potential to significantly impact any Yucca Mountain regulatory activities.

M1.2 IMARC OVERVIEW

The development of EPRI's TSPA IMARC has followed the evolution of Yucca Mountain regulations, disposal system design, and conceptual understanding of the proposed repository. IMARC is intended to permit an independent probabilistic evaluation of the performance of the proposed Yucca Mountain Repository. The EPRI TSPA approach is guided by the principal U.S. Nuclear Regulatory Commission (NRC) regulations, which are consistent with a reasonable expectation philosophy as opposed to a most conservative philosophy.

The IMARC solves the equations for transport of radionuclides in groundwater for an abstracted concept of the behavior of Yucca Mountain. The overall conceptual approach of the IMARC and the basic elements of the analysis method are similar to the TSPA-LA approach depicted on Figure 6.1.5-9. The differences between the implementation in IMARC and that in the TSPA-LA Model are in the details of the implementation and the specifics of the assumptions, models, parameters, and couplings used.

The different scenarios thus far considered in the IMARC TSPA include:

- Nominal scenario
- Igneous scenario, distinguishing an igneous intrusive and an igneous extrusive scenario
- Seismic scenario.

The evolution of the IMARC and associated evaluation of the proposed Yucca Mountain Repository has been reported in a series of EPRI reports. The most recent comprehensive description of the IMARC, designated as Version 8, has been reported in a final report dated May 2005 (Kozak and Kessler 2005 [DIRS 178580]). More recent updates and implementations in the IMARC Version 9 were reported in November 2005 (Apted and Ross 2005 [DIRS 182229]). The most recent documentations include various analyses related to Yucca Mountain, such as a progress report on *Effects of Seismicity and Rockfall on Long-Term Performance of the Yucca Mountain Repository* (Apted and Kessler 2005 [DIRS 182228]), a final report in November 2006 on the effects of multiple seismic events (Apted 2006 [DIRS 182227]), and a December 2006 progress report (Apted et al., 2006 [DIRS 182231]). Accordingly, the EPRI TSPA does not account for the most recent updates of analysis and/or model reports, which are incorporated in the TSPA-LA Model.

M2. TSPA CONCEPTUAL MODEL DESIGN

The overall conceptual approach of the EPRI TSPA Analysis and the model components implemented in the IMARC follows the TSPA-LA approach and model components for the Nominal Scenario Class depicted on Figure 6.1.5-9.

M2.1 FEATURES, EVENTS, AND PROCESSES AND SCENARIO DEVELOPMENT

For the nominal and igneous scenarios, EPRI lists the following features, events, and processes (FEPs) that correspond to the *System Performance Assessment-License Application Features, Events, and Processes* (BSC 2005 [DIRS 173800], Section 3.1 and Appendix E):

- Present-day climate and future climate variation affecting rainfall and human behavior (variation in use of surface and groundwater and agricultural practices).

- Rainfall and temperatures for the different climate states affect infiltration into the upper saturated zone (SZ).

- Lateral redistribution of infiltrating groundwater due to heterogeneous fracture and matrix properties in the upper part of the unsaturated zone (UZ).

- The amount of water percolating into the drifts is a function of the lateral distribution of infiltrating groundwater above the drifts, capillary effects at the drift walls, or, for the igneous scenario, the hydrologic characteristic of the cooled magma.

- Some of the groundwater seeping into the drift may drip onto the drip shields (DSs), which prevents water from dripping onto the underlying waste packages (WPs); if the DSs fail, water will drip onto the underlying WPs.

- DS failure mechanisms considered include improper emplacement, seismic rockfall processes, and general corrosion and hydride embrittlement.
- WPs prevent humid air and groundwater from penetrating into the WP and from releasing gaseous, dissolved, or colloidal radionuclides. If WPs fail, water may condensate from either humid air or dripping groundwater.
- WP failure mechanisms considered include seismic, rockfall, and various corrosion processes. For the igneous intrusion scenario, a high temperature effect on failure is considered.
- Cladding surrounding the spent fuel, which prevents water from contacting the waste form, can fail by various mechanisms, including initial failures at emplacement, creep, localized corrosion, and hydride embrittlement.
- Seepage entering the failed WP and cladding may absorb radionuclides released from the waste form. The release of radionuclides is controlled by waste-form degradation, seepage rates, solubility limits, and diffusion.
- The released radionuclides are transported from the failed WPs through the lower area of the drift and into the lower UZ, which is governed largely by fracture/matrix interaction and radionuclide sorption.
- The radionuclides are then transported through the SZ to a far-field point 18 km downstream, where it is assumed to be taken up by the reasonably maximally exposed individual (RMEI). According to RMEI behavior, assumptions stipulated by the applicable regulations determine the committed radiological dose to the RMEI.
- For the igneous intrusion scenario, the repository functions according to the nominal scenario but includes the additional FEPs associated with igneous intrusion events (Apted and Kessler 2005 [DIRS 182327], Section 8).
- Magma intrudes via a basaltic dike and enters the drift at a slow rate, which does not affect the mechanical integrity of the DS away from the dike.
- The hot magma contacts WPs and spent fuel, cools, and solidifies rapidly.
- Indirect thermal and chemical effects may be propagated along the drift farther than the magma itself intrudes.
- The magma, and any radionuclide released into it from failed WPs, is not released via an intrusive pathway but remains available for release to groundwater.
- The far-field groundwater flow system returns to its undisturbed condition after a localized (tens of meters) and brief disruption (tens of years).
- The near-field rock surrounding the intrusion zone requires on the order of 1,000 years to resaturate before groundwater can begin flowing into the drift.

For the igneous extrusive scenario, EPRI concluded that it is very unlikely that WPs will be breached by the magma during the active eruption period or that radioactive material will be released from the repository as a result of a volcanic event (EPRI 2004 [DIRS 171915]). As a result, the igneous extrusive scenario was not implemented in the IMARC model.

The FEPs associated with multiple seismic events that could affect the repository performance include (Apted 2006 [DIRS 182227]):

- Vibratory ground motion damaging the engineered barrier system (EBS) components
- Seismically induced collapse of open drifts damaging the EBS
- Potential stress corrosion cracking (SCC) due to static load from accumulated drift collapse rock.

The potential effects of fault displacement induced by seismic events are considered to be mitigatable through drift construction and appropriate WP emplacement practice and are not considered in the EPRI TSPA Analysis (Apted and Kessler 2005 [DIRS 182228]).

M2.2 TREATMENT OF UNCERTAINTY

IMARC uses the logic tree analysis methodology for quantifying the impacts of model and parameter uncertainty in the TSPA calculations. Logic tree analysis is particularly useful for uncertainty propagation when parameter and/or model uncertainty is described using a limited number of probable states (e.g., high, medium, low values) and their likelihoods (Kozak and Kessler 2005 [DIRS 178580], Figure 2-3). Logic trees (also known as probability trees) combine individual scenarios resulting from uncertain discrete events and/or parameter states. As such, they may be recognized as a special case of decision trees containing only chance nodes but no decision nodes.

The logic tree is ordered such that independent effects are placed to the upstream (left) side, and dependent effects are organized to the downstream (right) side. Each branch is assigned a probability, conditional on the values of the previous branches leading to that node. All possibilities must be considered in building the logic tree such that probabilities for branches originating from each node sum to one.

Consider a simple groundwater contaminant transport modeling problem involving two uncertain inputs—source concentration (s) and groundwater velocity (v). Uncertainty in the source node is represented by two values, s1 and s2, with probabilities P1 and P2, respectively. Uncertainty in the velocity node is also represented by two values, v1 and v2. These values have conditional probabilities ranging from P3 to P6, depending on which branch of the source node they are attached. Each path from the root to an end branch (or terminal node) of the tree represents a feasible scenario. The four feasible scenarios for this system can be enumerated as: (s1,v1), (s1,v2), (s2,v1), and (s2,v2). The probability of each scenario is the product of conditional probabilities of the branches along that path.

The logic tree thus organizes various parameter (model) combinations and their probabilities. Given this information, the computation of the consequence for each of the discrete

combinations is a straightforward task. The results can be organized in terms of a table or graph of sorted discrete outcomes versus the corresponding summed probabilities. Such a risk profile is equivalent to a cumulative distribution of model output generated via Monte Carlo simulation by GoldSim.

M2.3 MODEL STRUCTURE AND IMPLEMENTATION

The IMARC solves for transport of radionuclides in groundwater for an abstracted concept of the behavior of the Yucca Mountain Repository. The different model components represented in the TSPA-LA (Figure 6.1.3-1) are incorporated into the EPRI TSPA Analysis as look-up tables, failure distribution curves, and numerical submodels. IMARC includes three major numerical submodels describing: (1) near-field radionuclide release and transport, (2) UZ flow and transport beneath the repository, and (3) SZ flow and transport.

The UZ above the repository is represented by look-up tables providing the fraction of the repository with active groundwater flow where the groundwater flux is controlled by net infiltration rates into the upper UZ which, in turn, depends on the climate state. EPRI considers three climate states represented by step changes in infiltration rates (EPRI 2002 [DIRS 158069]). Uncertainties in the amount of net infiltration that depend on rainfall and temperature for the different climate states are included in a look-up table of low, moderate, and high net infiltration.

Degradation of WPs and DSs is represented by failure distribution curves, which were generated by Monte Carlo simulations of models describing various failure mechanisms, implemented in EPRI's TSPA code (EPRI 2002 [DIRS 158069]) and in its successor EBSCOM code (Apted and Kessler 2005 [DIRS 182228]). Input to these Monte Carlo simulations included uncertainty distributions of model parameters describing different degradation mechanisms for DSs, WPs, and cladding.

A near-field model comprises all the components inside the drift, which includes the DS, WP, cladding, waste form, pedestal, and invert. The release of radionuclides from the near field is computed using the COMPASS (Compartment Model for Partially Saturated Repository Source Terms) code (Kozak and Kessler 2005 [DIRS 178580]). Releases from the repository are only assumed to occur after the thermal pulse has significantly dissipated. Thermal effects are neglected in the model for the nominal scenario, because it is assumed that there will be little to no liquid water present to facilitate radionuclide mobilization and movement until temperatures have decreased to near the boiling point of water. For the igneous intrusion scenario, thermal effects on the failure mechanisms of DSs, WPs, and cladding and on in-drift groundwater flow behavior are taken into account.

The hydrologic behavior of the near field is represented by two zones, representing dripping and non-dripping conditions, for which different cumulative probability curves of failure versus time are computed for DSs, WPs, and cladding. Additional inputs to the near-field model include: seepage rates into drifts, as a function of time and climate conditions; near-field transport parameters, including dimensions, sorption coefficients, and solubility limits; densities; and porosities in the near-field materials; and diffusion/advection distances to the nearest flowing fracture.

The combined computed radionuclide release rates from both dripping and non-dripping zones are used as boundary conditions for the UZ.

The UZ is represented by the second numerical submodel embedded within the IMARC. The submodel simulates flow and transport through the natural barriers of the UZ beneath the repository horizon. Flow and transport through the UZ is treated as one-dimensional, down vertically, into different geologic horizons. At the base of the UZ, the flux of radionuclides exiting the UZ is used as a time series input to the SZ code.

The SZ is represented by the third numerical submodel embedded within the IMARC. This submodel simulates flow and transport through the natural barriers of the SZ. The SZ code has a specified upstream flow rate, and a uniform infiltration rate is added to the upper surface of the computation region such that the groundwater flow velocity increases along the transport path length.

The SZ model consists of two segments: (1) the first representing fractured tuff extending from beneath the repository to 15 km downgradient, and (2) the second, representing the alluvium extending from 15 km downgradient to the location of the RMEI 18 km downgradient.

The UZ and SZ models communicate with the remainder of IMARC by the transfer of radionuclides from the near field and to the biosphere. All other parameters needed for the UZ and SZ models are unique to this part of the code making them, to a large extent, stand-alone calculations.

The resulting fluxes of radionuclide in the groundwater at 18 km are assumed to enter the biosphere via groundwater used by the RMEI. These radionuclide fluxes in the groundwater are adjusted to concentrations based on the residential water usage of 3,000 acre-feet per year (3.7×10^6 m^3/yr) according to the requirements of 10 CFR 63.332(a)(3) [DIRS 180319]. These concentrations are then multiplied by the radionuclide-specific biosphere dose conversion factor (BDCF) for the RMEI to produce the dose to the RMEI for individual radionuclides at a given time of output concentration. These individual radionuclide doses are then summed to produce the total dose to the RMEI as a function of time.

M2.4 OVERALL COMPARISON OF EPRI TSPA ANALYSIS AND TSPA-LA MODEL

Overall, the EPRI TSPA Analysis accounts for the same model components and considers the same FEPs as the TSPA-LA Model. The EPRI model implementation is a more simplified abstraction of the relevant processes and uncertainty in model parameters. EPRI uses the logic tree approach and cumulative distributions of failure curves of different EBS components. Even though these distributions were derived from Monte Carlo simulations, uncertainty parameters were not sampled in the EPRI model but, instead, used mean parameter values as input in IMARC.

The main differences in model components include:

- The EPRI Analysis considers a single infiltration domain distinguishing wet and dry conditions, compared to five infiltration bins having different infiltration rates and UZ properties in the TSPA-LA Model.

- EPRI only considers the inventory of spent nuclear fuel (SNF) in commercial spent nuclear fuel (CSNF) packages compared to the TSPA-LA Model, which includes U.S. Department of Energy spent nuclear fuel (DSNF) and high-level radioactive waste (HLW) in DSNF WPs.

- EPRI accounts for the gradual cladding failure following WP failure, whereby the TSPA-LA takes no cladding credit.

- The radionuclide inventory used in the EPRI TSPA Analysis is based on that given in *Initial Radionuclides Inventories* (SNL 2007 [DIRS 180472], Table 7-1), which is superseded by SNL 2007 [DIRS 180472], Table 7-1[a], and considers only 12 radionuclides; whereas the TSPA-LA Model considers 26 radionuclides, including ^{135}Cs and ^{79}Se.

M3. TSPA NOMINAL SCENARIO COMPARISON

M3.1 UNSATURATED FLOW

In the EPRI TSPA Analysis, groundwater flow in the UZ above the repository is represented in a simplified manner by a set of lumped parameters describing:

- Time history of infiltration rate
- Flow focusing factor
- Fraction of the repository that is wet.

All three parameters are represented in the logic tree as uncertain parameters, described in Section M2.2. EPRI considers three climate states corresponding to step changes in infiltration rates (EPRI 2002 [DIRS 158069]):

- Greenhouse period (0 to 1,000 years)
- Interglacial period (1,000 to 2,000 years) similar to present-day climate
- Full glacial period (2,000 to one million years).

Uncertainties in the amount of net infiltration that depend on rainfall and temperature for the different climate states are included in a look-up table of low, moderate, and high net infiltration. In the logic tree, the low infiltration rate is assigned a branch probability of 0.05, the moderate 0.9, and the high 0.05. For each climate state, values of low, moderate, and high net infiltration rate were averaged across the entire repository shown in Table M-1. In the most recent IMARC Version 9, the infiltration rates for the period after 10,000 years were based on an infiltration range of 19 to 64 mm/yr with a mean of 32 mm/yr as specified in NRC Proposed Rule 10 CFR 63.342(c)(2) [DIRS 178394]).

The IMARC implementation of the SZ also considers infiltration beyond the footprint of the repository along the 18 km distance to the location of the RMEI. However, the infiltration rate over the water table of the SZ beyond the repository does not vary with climate states but is fixed to a constant rate. Similarly, the groundwater flow rate in the SZ upstream of the repository is fixed to a steady-state value, resulting in steady-state flow conditions and constant water table

depth. This prescribed infiltration at the water table of the SZ along the flow path results in continuous dilution of radionuclide release from the UZ beneath the repository.

In the TSPA-LA Model, the UZ flow above the repository is simulated by the Site-Scale UZ Flow Process Model described in Section 6.1.4.1. This process model simulated three-dimensional, dual permeability, steady-state flow conditions and generated 16 three-dimensional flow fields for 10th percentile, 30th percentile, 50th percentile, and 90th percentile infiltration boundary condition scenarios and four different climate states within each infiltration scenario. Four climate states are used in the TSPA LA Model: (1) present-day climate for the first 550 years after repository closure; 600 years after emplacement; (2) monsoon climate for the period 550 to 1,950 years after repository closure; (3) glacial-transition climate for the period 1,950 to 10,000 years after repository closure; and (4) post-10,000-years climate, for the period 10,000 to the modeling time frame of 1,000,000 years after repository closure (Section 1, Regulatory Framework).

The 16 flow fields and UZ hydrologic properties generated by the Site-Scale UZ Flow Process Model are used by the Multiscale Thermohydrologic Model (MSTHM) process model (SNL 2007 [DIRS 181383]) for the development of EBS environment thermo-hydrologic (TH) conditions and are accessed directly by the UZ Transport Submodel (SNL 2008 [DIRS 184748], Sections 6 and 8). The four infiltration scenarios are sampled in the TSPA-LA Model once per realization based on the probability weighting factors, shown in Table M-2. Overall infiltration rates for the different climate states used in the EPRI TSPA Analysis (Table M-1) compare reasonably well with the weighted mean infiltration rates used in TSPA-LA Model (Table M-2).

In the IMARC model, heterogeneity within the fractured tuff is described by the flow focusing factor, which is also represented in the logic tree as an uncertain parameter. For the branch of focused flow, the infiltration rate is increased by a factor of four over 25 percent of the area of the repository, but is set to zero for the remaining 75 percent of the repository. The probability for the branch with focused flow is 0.135 and for the branch without focused flow is 0.865.

Estimates of seepage rates into the drifts and seepage fractions used in the EPRI TSPA were based on TSPA-SR analyses, described by uncertain parameters representing a base-case seepage and a high seepage rate, with probabilities of 0.96 and 0.04, respectively (Table M-3a) (Kozak and Kessler 2005 [DIRS 178580], Table 3-2). A comparison of the seepage rates relative to infiltration rates shown in Table M-3a with those used in the TSPA-LA Model summarized in Table M-3b indicates that the seepage rates used in the EPRI TSPA are higher than those in the TSPA-LA Model (Figure 7.7.3-1(a)). A comparison of the seepage fraction given in Table M-3a with those given in the TSPA-LA analysis (Table M-3b) indicates that the seepage fractions used in the EPRI TSPA Analysis are lower than those in the TSPA-LA Model for the corresponding infiltration rate (Figure 7.7.3-1(b)), The 96% probability base-seepage case and 4% probability high-seepage case in the EPRI TSPA Analysis indicate seepage conditions only at infiltration rates greater than 60 mm/yr and 2.4 mm/yr, respectively (Table M-3a). The TSPA-LA Model indicates seepage conditions for the 10% percentile infiltration scenario at infiltration rates of 3.7 mm/yr (Table M-3b). Even though the seepage rates in the EPRI TSPA Analysis are higher, the lower seepage fractions contribute to the lower estimated dose calculated by the EPRI TSPA Analysis as compared to the dose calculated by the TSPA-LA Model.

M3.2 ENGINEERED BARRIER SYSTEM ENVIRONMENT

The EPRI TSPA Analysis neglects thermal effects on water flow, release, and migration of radionuclides for the nominal scenario. It is assumed that there is little to no liquid water present to facilitate radionuclide mobilization and migration until temperatures have decreased to near the local boiling point of water. However, failure distributions generated for each of the three main EBS components (i.e., DS, WP, and cladding) do take into account thermal history within the drift and drift stability due to thermal stresses, described in Section M3.3.

In the TSPA-LA Model, the EBS TH Environment Submodel implements the EBS TH abstraction, which is provided by the MSTHM described in detail in Section 6.1.4.2. The MSTHM subdivides the repository footprint into subdomains and computes temperatures and relative humidity for the WP and associated DS, average drift wall temperature, average invert temperature, average invert saturation, and average invert flux in each subdomain. These TH responses are used as input to the Drift Seepage and Drift Condensation submodels, the WP and DS Degradation model components, the EBS Chemical Environment model, the EBS Flow Submodel, the Waste Form Degradation and Mobilization model component, and the EBS Transport Submodel.

M3.3 WASTE PACKAGE AND DRIP SHIELD DEGRADATION

Waste form degradation and mobilization is computed as part of the near-field radionuclide release and transport submodel EBSCOM in the IMARC. The EBSCOM code uses Monte Carlo simulations to take into account uncertainty and variability of various input parameters in the abstracted corrosion models. These models are used to compute failure curves of various engineered barrier components, which include the DS, WP shell, WP outer closure lid weld, and WP middle closure lid weld. In addition to temperature evolution, the chemical environment associated with the different seepage water bins that was updated and described in *Engineered Barrier System: Physical and Chemical Environmental Model* (SNL 2007 [DIRS 177412]) is the principal parameter for the various corrosion processes. The different corrosion processes include:

For DS:

- Initial failure due to undetected manufacturing defect or emplacement error
- General corrosion (main failure mechanism)
- Hydrogen-induced cracking (low probability).

For the WP in the nominal scenario:

- Initial failure due to undetected manufacturing defect
- General corrosion and microbially influenced corrosion (MIC) (main failure mechanism
- Localized corrosion (low probability)
- SCC (for the outer and middle WP closure lids).

In addition to the conditions for the nominal scenario, different versions of the EBSCOM code incorporate the additional effects of seismic events and igneous events, respectively.

The TSPA-LA Model considers five degradation processes, which include: general corrosion, MIC, SCC, early failure, and localized corrosion, which correspond largely to those listed above for the EPRI TSPA Analysis. The implementation of the abstracted degradation modes are described in Section 6.3.5. The TSPA-LA Model uses the WAPDEG software to model general corrosion, MIC, and SCC. Early failure of WPs is directly implemented in GoldSim, accounting for manufacturing and material defects, including defects due to improper heat treatment that augment corrosion processes and result in early failures. WP degradation considers general corrosion, microbially enhanced corrosion, and SCC. In addition, localized corrosion is implemented within the TSPA-LA Model using a submodel (Figure 6.3.5-2), which is only considered for WP degradation. For DS degradation only general corrosion is considered. Overall, TSPA-LA and EPRI consider the same degradation processes, except for localized corrosion that was considered low probability in the EPRI TSPA. Early WP failure in the TSPA-LA Model was defined by a Poisson distribution, which gave a failure distribution and the number of realizations having at least one WP failure, whereby early failure mechanisms applicable for DSs were determined to have no consequence on DS performance and were therefore excluded in TSPA-LA (Section 6.3.5.1.2). In the EPRI TSPA Analysis, early failure of both the DS and WP is considered.

In the EPRI TSPA Analysis, the computed failure distributions curves for the nominal scenario for the DS and for the WP are shown on Figure 4-5 in EPRI (Apted and Ross 2005 [DIRS 182229]). In comparison, the mean WP failure curve for the TSPA-LA nominal scenario (Figure 7.7.3-2) indicates a later failure onset but a steeper curve, where 6,256 WPs failed after one million years.

M3.4 WASTE FORM DEGRADATION AND MOBILIZATION

Waste form degradation and mobilization is computed as part of the near-field radionuclide release and transport submodel COMPASS in IMARC, which includes the Engineered Barrier System Flow and Transport, described in Section M3.5 (Table 7.7.3-1). The COMPASS Near-Field Model consists of different components and solves mass transfer across these compartments, which includes: waste, corrosion product, pallet/basalt, invert, near-field rock matrix and fracture, and farfield rock (Kozak and Kessler 2005 [DIRS 178580], Figure 5-1). In addition, the COMPASS model considers diversion of seepage water entering the drift and flowing into the invert, thereby bypassing the waste.

The waste that contains the radionuclide inventory degrades after water contact following WP and cladding failure. Radionuclides dissolve into water congruently with the waste form degradation rate. Uncertainty in waste form degradation rates is accounted for in the logic tree analysis, using alteration times of 1,000 years; 3,000 years; and 5,000 years and associated probabilities (Kozak and Kessler 2005 [DIRS 178580], Figure 2-3). The EPRI TSPA accounts for gradual cladding failure whereby the fraction of radionuclides in the gap and grain-boundaries of the spent fuel dissolve instantaneously into water.

For specific radionuclides bound in the waste form, the release of radionuclides in water is constrained by solubility limits. The ranges in solubility limits used in TSPA-LA and in the EPRI TSPA Analysis are summarized in Table M-4. In the EPRI TSPA Analysis, the uncertainty in the solubility limits represented by low, moderate, and high values is linked to the

probabilities for the alteration times of the waste form degradation (Kozak and Kessler 2005 [DIRS 178580], Figure 2-3).

The EPRI TSPA Analysis only considers CSNF WPs and the associated inventory, whereby the inventory is based on that given in *Initial Radionuclides Inventories* (SNL 2007 [DIRS 180472], Table 7-1). Furthermore, the EPRI TSPA considers only 12 radionuclides, which were identified to have a significant contribution to total dose. The inventory used in the EPRI TSPA Analysis, in comparison with that used in the current TSPA-LA Model (Table M-5), indicates that the total inventory per WP compares well with that for CSNF in the TSPA-LA Model. The inventory for DSNF and HLW, in a WP that is not considered in the EPRI TSPA, amounts to about 12.5 percent of the inventory in a CSNF WP. The EPRI TSPA accounts for 8,160 CSNF WPs, whereas the TSPA-LA Model considered 8,203 CSNF WPs and 3,413 CDSP WPs containing DSNF and HLW.

The implementation of waste form degradation and mobilization in the TSPA-LA Model is described in detail in Section 6.3.7. The Waste Form Degradation and Mobilization Model Component of the TSPA-LA Model evaluates cladding failure and calculates the rate of degradation for CSNF, DSNF, and HLW forms. Given the radionuclide inventory of the different wastes, the submodel calculates solubilities of radioactive elements (given the solubility limits) and colloidal concentrations of radionuclides in a failed WP and the invert, accounting for the in-package chemistry and drift geochemical environment. The computed solubilities and colloidal concentrations of radionuclides serve as inputs to the EBS Transport Submodel.

M3.5 ENGINEERED BARRIER SYSTEM FLOW AND TRANSPORT

In the COMPASS model, radionuclides released from the waste form are transported by diffusion and advection through the corrosion product, pallet/basalt, invert, and near-field rock fractures and rock matrix (diffusion only) to the far-field rock (Kozak and Kessler 2005 [DIRS 178580], Figure 5-1). The compartments are assumed to be partially saturated, forming a continuous water pathway, and water flows through the near-field fractures only in wet conditions. For wet conditions (release dominated by advective transport), a saturation of 0.01 is assumed inside the WP and the near-field rock fracture saturation is set to 0.05. For dry conditions (release only by diffusion, no advective transport), a saturation of 0.001 is assumed inside the WP and the minimum saturation in the fractures is set to 0.002. The COMPASS model did not consider colloid-facilitated transport of certain radionuclides. The EPRI's assessment of the potential for colloid-facilitated transport indicated that "colloids will not be present at high enough concentrations to be significant," "colloid suspensions will not be stable over necessary time and space scales," and that "colloids will be appreciably filtered, both in the near-field and in the SZ."

The computed radionuclide release rates from the far-field rock is then used as the boundary condition for the UZ submodel, simulating radionuclide transport in the UZ below the repository.

In the TSPA-LA, the EBS is represented by a series of domains, representing the waste form, the corrosion products, the invert, and the EBS-UZ interface, which is described in detail in Section 6.3.8. Radionuclide transport through each domain occurs by advection and diffusion. Diffusion is the primary transport mechanism when the water flow into the WP is negligibly

small. Advection is the primary mechanism when there is appreciable flow through the WP. In general, the treatment of transport through the EBS is similar between the EPRI TSPA Analysis and TSPA-LA Model. However, the TSPA-LA EBS flow and transport model is more complex in incorporating DSNF and HLW, diffusive and advective transport through corrosion cracks and patches, respectively, in the WP, and considering the transport of reversibly and irreversibly sorbed radionuclides on ironhydroxide colloids and waste-form colloids.

M3.6 UNSATURATED ZONE TRANSPORT

In the EPRI TSPA, flow and transport in the UZ below the repository is simulated by the UZ-code represented by several one-dimensional vertical columns approximating spatial variations of repository releases and different lengths corresponding to spatial and temporal variations in the water table. The vertical discretization distinguishes the main UZ layers below the repository, which include: Tsw-35, TSv-5, CHnv-5, and CHnz-6.

The model accounts for variations in saturations associated with variations in permeability, capillary pressure, porosity, and fracture spacing for both fractures and matrix in each geologic layer. Unsaturated flow and transport of radionuclides is downward only. The one-dimensional columns account for coupled matrix-fracture interaction, representing either a single-porosity, single-permeability, or double-porosity/double-permeability medium. Radionuclide transport accounts for dispersion, decay, diffusion, and sorption, which is parameterized for the different layers and columns. Uncertainty in sorption in the UZ is represented in the logic tree approach as retardation (Kozak and Kessler 2005 [DIRS 178580], Figure 2-3), which also includes sorption in the SZ. In the EPRI TSPA Analysis, sorption coefficients are defined for specific radionuclides for volcanic rocks in the UZ and SZ and for the alluvium in the SZ. Only for neptunium is uncertainty in sorption coefficients considered for individual layers, which is represented as low, median, and high values in the logic-tree analysis.

The UZ Transport Submodel of the TSPA-LA Model computes the transport from the EBS through the UZ to the SZ, which is simulated by the Finite Element Heat and Mass (Model) (FEHM) external code, which is linked to GoldSim. The details of the UZ Transport Submodel are described in Section 6.3.9. Input to FEHM is given by transport parameters and associated uncertainties as well as by the rate of radionuclide mass release from the waste emplacement drifts. Processes affecting transport of dissolved or colloidal-bound radionuclides through the UZ include advection, diffusion, sorption, hydrodynamic dispersion, and radioactive decay and ingrowth. Colloids are transported through the UZ primarily in the fractures due to size exclusion, and diffusion into the rock matrix is limited owing to low values of diffusion coefficients.

The main mechanisms for retardation of radionuclides are through sorption. A comparison of the Kd values used in the EPRI TSPA Analysis and in the TSPA-LA Model is given in Table M-6. Median Kd values for plutonium and thorium are lower in the EPRI TSPA compared to the median values in the TSPA-LA Model, whereas the Kd value for neptunium and uranium are greater.

M3.7 SATURATED ZONE TRANSPORT

The SZ submodel in the EPRI TSPA Analysis (SZ code) consists of two segments representing the fractured tuff (15 km downgradient) and the subsequent alluvial segment (5 km), which extends 2 km beyond the location of the RMEI. The SZ was initially implemented using a three-dimensional rectangular model geometry for simulating linear mass transport in a steady-state groundwater flow field. For transport simulations, the model considers steady-state groundwater flow in the fracture only. A more simplified two-dimensional, vertically integrated aquifer model produced similar results and was ultimately used as the SZ submodel in the TSPA Model.

Boundary conditions for the transport simulation include prescribed mass fluxes from the UZ model along the footprint of the repository, and infiltration (head-dependent flux boundary condition) is prescribed along the entire water table. Similar to the UZ model, transport is affected by fracture flow and sorption in the tuff and in the alluvium. Uncertainty in the Kd values in the SZ is included in the logic-tree analysis that is combined with the UZ Kds (Kozak and Kessler 2005 [DIRS 178580], Figure 2-3).

For the TSPA-LA Model, the SZ transport was abstracted from an external three-dimensional SZ model to calculate flow and transport of individual radionuclides through the SZ to the regulatory boundary 18 km downgradient from the repository. A detailed description of the model abstraction is given in Section 6.3.10. The results of the three-dimensional transport model were put in the form of unit-source radionuclide breakthrough curves, which are combined with time-varying radionuclide sources from the UZ to compute the radionuclide transport to the regulatory boundary. In addition, a one-dimensional SZ Transport Submodel is implemented in the TSPA-LA Model to calculate radionuclide daughter products. Similar to the UZ zone, sorption is the main mechanism for retardation of radionuclides in the SZ. A comparison of the sorption coefficients between those used in the EPRI TSPA Analysis and those used in TSPA-LA is presented in Table M-7. In general, median Kd values are similar in the EPRI TSPA and TSPA-LA Model for both fractured volcanic rocks and alluvium.

M3.8 BIOSPHERE

The conversion of radionuclide concentration to dose is through the BDCFs for the RMEI living approximately 18 km downstream of the repository. For this, a representative volume of 3,000 acre-feet for consumption by the RMEI is assumed. The BDCFs used in the EPRI TSPA Analysis and those used in the TSPA-LA are compared in Table M-8. Overall, the EPRI BDCFs are higher than those used in the TSPA-LA, which would result in higher doses in the EPRI TSPA for the same concentration.

M3.9 MEAN ANNUAL DOSE COMPARISON – NOMINAL CASE

The computed mean radionuclide doses for the EPRI nominal scenario are shown on Figure 5-10 in Apted and Ross (2005 [DIRS 182229]). In comparison, the results of the computed mean doses for the TSPA-LA combined Nominal and Waste Package Early Failure Modeling Cases are shown on Figure 7.7.3-3. The results indicate a similar pattern for the nominal scenario characterized by a significant increase in dose after 100,000 years. The early failure dose is

represented by the dose increase after about 1,000 years in the TSPA-LA Model (Figure 7.7.3-3), which is somewhat delayed in the EPRI TSPA Analysis (Apted and Ross 2005 [DIRS 182229], Figure 5-10). Overall, the mean annual dose in the EPRI TSPA is about 2.E-2 mrem/yr compared to about 4.E-1 mrem/yr in the TSPA-LA Model at one million years. The main contributor to total dose at late time is ^{129}I in both cases.

The differences between the EPRI TSPA Analysis and the TSPA-LA Model dose results can be accounted for by differences in:

- Seepage fraction and seepage rates through the repository
- Early failure representation and failure curves of the EBS components
- Inventory, both in terms of waste type and individual radionuclides
- Solubility limits and sorption characteristics in the UZ and SZ.

Seepage rates used in the EPRI TSPA are higher than the corresponding rates used in the TSPA-LA Model (Figure 7.7.3-1(a)). The seepage rates in the EPRI TSPA are based on previous analysis and/or model report results. The lower seepage fraction values for the EPRI TSPA Analysis (Figure 7.7.3-1(b)) results in a lower number of packages being subjected to seepage conditions. This causes a delay in radionuclide release from the EBS and a corresponding lower estimate of total dose compared to the dose calculated by the TSPA-LA Model.

The EPRI TSPA Analysis only accounts for CSNF waste and considers failure of DSs, WPs, and cladding, whereas the TSPA-LA Model accounts for CSNF, DSNF, and HLW, but does not take credit for cladding of CSNF WPs. Consequently, the overall dose release in the EPRI TSPA Analysis is delayed both during the early failure scenario and for the nominal scenario. The WP failure curves in the EPRI TSPA Analysis indicate that only about 5,300 CSNF WPs failed after one million years, whereas the TSPA-LA Model results indicate that on average about 6,256 WPs failed after one-million years, even though the onset of WP failure for the nominal scenario is later (Figure 7.7.3-2) compared to that in the EPRI TSPA Analysis (Apted and Ross 2005 [DIRS 182229], Figure 4-5).

The total CSNF radionuclide inventory used in the EPRI TSPA Analysis is about 10 percent less than the combined inventory for all CSNF and CDSP WPs (Table M-4). During early failure, C-14 is shown to contribute significantly to total dose in the TSPA-LA Model, which is not considered in the EPRI TSPA. At late time, the dominant radionuclides contributing to total dose include ^{129}I, ^{99}Tc, ^{135}Cs, and ^{79}Se in the TSPA-LA Model. The dominant radionuclides in the EPRI TSPA Analysis include ^{129}I followed by ^{237}Np, ^{233}U, and ^{229}Th. However, the EPRI does not consider ^{135}Cs and ^{79}Se.

Solubility limits used in the EPRI TSPA Analysis are significantly lower for neptunium, plutonium, and thorium compared to the range assigned in the TSPA-LA Model. On the other hand, sorption characteristics used in the EPRI TSPA Analysis for the UZ are significantly lower for uranium and plutonium compared to those in the TSPA-LA Model. However, this does not affect ^{129}I, ^{99}Tc, and ^{135}Cs, which represent the main contributors to total dose in the TSPA-LA Model.

In general, the main features of the dose release curves for the nominal scenario compare reasonably well with the TSPA-LA Model. The differences can be related mostly to differences in seepage and in different implementation of the inventory and EBS failure characteristics. This is primarily due to the fact that the EPRI TSPA did not use the most recent analysis and/or model report results.

Table M-1. Net Infiltration Rates (mm/yr) used in the Integrated Multiple Assumptions and Release Code Event Tree Branches for Infiltration

	Scenario			
	Low	Med	High	Weighted Avg. Infiltration (mm/yr)
Greenhouse	1.1	11	19	10.905
Interglacial	1.1	7.2	13.81	7.2255
Full Glacial Maximum	6.8	20	22.12	19.446
Weighting Factor	0.05	0.9	0.05	
Post-10,000 yr	19	32	64	32.95

Source: Kozak and Kessler 2005 [DIRS 178580], Table 3-1.

Table M-2. Infiltration Rates (mm/yr) used in TSPA-LA

	Flux Map Percentile				Weighted Avg. Infiltration (mm/yr)
	10th percentile	30th percentile	50th percentile	90th percentile	
Present-Day	3.7	9.4	13.4	31.4	7.84033
Monsoon	7.2	14.8	17.8	85.1	14.77822
Glacial-Transition	10.8	23.8	32.5	63.4	19.54301
Post-10,000 Year	19.8	36.3	47.1	56.8	29.08325
Weighting Factor	0.6191	0.1568	0.1645	0.0596	

Sources: *Abstraction of Drift Seepage* (SNL 2007 [DIRS 181244], Table 6-5[a]) and DTN: LB0701PAWFINFM.001_R0 [DIRS 179283].

Table M-3a. Seepage Fraction and Flow Rate as a Function of Infiltration Rate

	Base-Seepage Case (Probability 0.96)		High-Seepage Case (Probability 0.04)	
Infiltration Rate* (mm/yr)	Fraction	Flow Rate (m^3/yr)	Fraction	Flow Rate (m^3/y)
2.4	0	0	0	0
5	0	0	0.083	0.086
14.6	0	0	0.083	0.401
60	0	0	0.31	0.701
73.2	0.054	0.365	0.376	0.788
213	0.054	4.24	0.452	4.24

Source: Kozak and Kessler 2005 [DIRS 178580].

*The infiltration rate immediately above the repository horizon.

Table M-3b. Summary Statistics for Probabilistic Seepage Evaluation (Intact Drifts)

Summary Statistics for Probabilistic Seepage Evaluation (Intact Drifts)				
	10 Percentile Infiltration Scenario			
	Seepage Rate (kg/yr/WP)	Seepage Rate (m^3/yr/WP)*	Seepage Fraction (%)	Infiltration Rate (mm/yr)**
Present Day	1.2	0.0012	7.6	3.7
Monsoon	4.6	0.0046	13.4	7.2
Glacial Transition	14.4	0.0144	17.0	10.8
	30 Percentile Infiltration Scenario			
	Seepage Rate (kg/yr/WP)	Seepage Rate (m^3/yr/WP)*	Seepage Fraction (%)	Infiltration Rate (mm/yr)**
Present Day	8.1	0.0081	16.7	9.4
Monsoon	20.5	0.0205	22.8	14.8
Glacial Transition	54.0	0.0540	29.5	23.8
	50 Percentile Infiltration Scenario			
	Seepage Rate (kg/yr/WP)	Seepage Rate (m^3/yr/WP)*	Seepage Fraction (%)	Infiltration Rate (mm/yr)**
Present Day	16.5	0.0165	21.6	13.4
Monsoon	30.4	0.0304	25.4	17.8
Glacial Transition	98.4	0.0984	33.9	32.5
	90 Percentile Infiltration Scenario			
	Seepage Rate (kg/yr/WP)	Seepage Rate (m^3/yr/WP)*	Seepage Fraction (%)	Infiltration Rate (mm/yr)**
Present Day	82.9	0.0829	34.9	31.4
Monsoon	470.8	0.4708	52.6	85.1
Glacial Transition	297.1	0.2971	46.1	63.4
	Post-10,000-Year Period			
	Seepage Rate (kg/yr/WP)	Seepage Rate (m^3/yr/WP)*	Seepage Fraction (%)	Infiltration Rate (mm/yr)**
Flow Field 1	35.2	0.0352	27.3	19.8
Flow Field 2	119.8	0.1198	35.5	36.3
Flow Field 3	178.3	0.1783	40.9	47.1
Flow Field 4	237.2	0.2372	45.2	56.8

Source: Modified from SNL 2007 [DIRS 181244], Table 6-6[a]

* SeepageRate(m^3/yr/WP) is calculated by dividing the SeepageRate(kg/yr/WP) by 1,000 kg/m^3, which is the assumed water density.

** Source: SNL 2007 [DIRS 181244], Tables 6-5[a]

Table M-4. Comparison of Solubility Limits used in TSPA-LA and EPRI

	Base-10 Logarithm of the Dissolved Concentration Limit (mg/L)						
	TSPA-LA[1]				EPRI[2]		
	Min.	Max.	Min. Range	Max. Range	median	min	max
NpO_2	-1.090	2.050	-2.890	3.850	-2.998	-4.002	-2.002
Np_2O_5	-0.019	3.290	-2.419	5.690			
Pa	-0.019	3.290	-4.440	3.239	-0.159		
Pu	-1.240	1.110	-4.240	4.110	-2.703	-4.701	-0.701
Th	-2.130	1.140	-4.230	3.240	-3.163	-4.701	-1.701
Sn	-2.390	-1.390	-3.740	-0.040			
U	0.611	2.860	-0.889	4.360	0.830	0.639486	1.690
U	1.510	4.780	0.010	6.280			
U1	0.611	4.780	-0.889	6.280			
I	No solubility limit				5.003		
Tc	No solubility limit				5.037		

Sources: [1] Modified from DTN: MO0702PADISCON.001_R0 [DIRS 179358], Table L-25.
[2] Modified from Kozak and Kessler 2005 [DIRS 178580], Table 5-2.

Table M-5. Inventory used in EPRI Model (Based on SNL 2007) and in TSPA-LA Model

Inventory used in EPRI Model[1]				Inventory used in TSPA-LA Model[2]			
	CSNF	CSNF			CSNF	DSNF	HLW
Element	mol/WP	grams/WP		Element	grams/WP	grams/WP	grams/WP
Ac-227	1.1013E-08	2.5000E-06		Ac-227	2.470E-06	1.219E-03	1.907E-04
Am-241	3.4357E+01	8.2800E+03		Am-241	8.180E+03	2.183E+02	3.749E+01
Am-243	5.1852E+00	1.2600E+03		Am-243	1.245E+03	6.733E+00	5.748E-01
C-14	9.7857E-02	1.3700E+00		C-14	1.353E+00	1.808E+00	0.000E+00
Cl-36	9.0833E-02	3.2700E+00		Cl-36	3.231E+00	4.235E+00	0.000E+00
Cm-245	7.2245E-02	1.7700E+01		Cm-245	1.749E+01	9.251E-02	5.425E-02
Cs-135	3.2667E+01	4.4100E+03		Cs-135	4.357E+03	9.739E+01	1.271E+02
Cs-137	4.3577E+01	5.9700E+03		Cs-137	5.898E+03	9.718E+01	3.021E+02
I-129	***1.3566E+01***	***1.7500E+03***		I-129	1.729E+03	3.564E+01	7.268E+01
Np-237	***1.9536E+01***	***4.6300E+03***		Np-237	4.574E+03	8.144E+01	9.948E+01
Pa-231	4.0173E-05	9.2800E-03		Pa-231	9.168E-03	2.143E+00	1.529E+00
Pb-210	0.0000E+00	0.0000E+00		Pb-210	0.000E+00	3.351E-07	3.399E-10
Pu-238	6.4706E+00	1.5400E+03		Pu-238	1.521E+03	1.249E+01	3.906E+01
Pu-239	***1.8285E+02***	***4.3701E+04***		Pu-239	4.317E+04	2.214E+03	5.582E+02
Pu-240	***8.6667E+01***	***2.0800E+04***		Pu-240	2.055E+04	4.346E+02	4.615E+01
Pu-241	1.1162E+01	2.6900E+03		Pu-241	2.658E+03	2.925E+01	1.216E+00
Pu-242	2.2066E+01	5.3400E+03		Pu-242	5.276E+03	3.016E+01	3.887E+00
Ra-226	0.0000E+00	0.0000E+00		Ra-226	0.000E+00	4.570E-05	2.423E-05
Ra-228	0.0000E+00	0.0000E+00		Ra-228	0.000E+00	1.513E-05	5.997E-06
Se-79	5.3671E-01	4.2400E+01		Se-79	4.189E+01	6.824E+00	7.010E+00
Sn-126	3.7222E+00	4.6900E+02		Sn-126	4.633E+02	9.404E+00	1.704E+01
Sr-90	2.8000E+01	2.5200E+03		Sr-90	2.490E+03	5.220E+01	1.741E+02
Tc-99	***7.7172E+01***	***7.6400E+03***		Tc-99	7.548E+03	1.584E+02	1.013E+03
Th-229	***0.0000E+00***	***0.0000E+00***		Th-229	0.000E+00	3.239E-01	3.298E-03
Th-230	***6.6957E-04***	***1.5400E-01***		Th-230	1.521E-01	1.178E-01	8.115E-04
Th-232	0.0000E+00	0.0000E+00		Th-232	0.000E+00	2.173E+04	2.975E+04
U-232	4.4397E-05	1.0300E-02		U-232	1.018E-02	1.280E+00	4.081E-04
U-233	***2.5021E-04***	***5.8299E-02***		U-233	5.760E-02	5.382E+02	1.944E+01
U-234	***7.5641E+00***	***1.7700E+03***		U-234	1.749E+03	4.732E+02	2.330E+01
U-235	***2.6979E+02***	***6.3401E+04***		U-235	6.264E+04	2.508E+04	1.409E+03
U-236	***1.6483E+02***	***3.8900E+04***		U-236	3.843E+04	1.249E+03	5.987E+01
U-238	***3.3277E+04***	***7.9199E+06***		U-238	7.824E+06	6.845E+05	2.367E+05
Total EPRI		***8.1025E+06***		Total	8.0370E+06	7.3702E+05	2.7050E+05
Total/WP	3.4287E+04	8.1351E+06					
No. of Waste Packages:		**8160**		No. of Waste Packages:	8213		3416
(bold: radionuclides used in EPRI model)							
Total/Repository		6.612E+7			6.601E+7		3442E+9

Sources: [1] SNL 2007 [DIRS 180472], Table 7-1 (EPRI) and Table 7-1[a] (TSPA-LA Model).

[2] DTN: MO0702PASTREAM.001_R0 [DIRS 179925].

[3] Radionuclide inventory given [mol/WP] in Apted et. al., 2006 [DIRS 182231] Table 5-29.

Table M-6. Unsaturated Zone Layer Distribution Coefficients

	EPRI[1]	TSPA-LA[2]
	Median Kd	Median Kd
Radionuclide	[mL/g]	[mL/g]
I	0	0
Tc	0	0
C	0	0
Np	1.5	0.5 - 1.0
U	1	0.2 – 0.5
Am	400	5,500
Pa	500	5,500
Cs	4	2 – 5,000
Se	2	8.6 - 14.3
Pu	50	70 - 100
Sr	18	25 – 1,025
Th	2,500	5,500 – 15,500

Sources: [1] Modified from Apted and Ross 2005 [DIRS 182229], Table 5-4.
[2] Modified Table 6.3.9-2: DTN: LA0408AM831341.001_R0 [DIRS 171584] and DTN: LB0701PAKDSESN.001_R0 [DIRS 179299].

Table M-7. Saturated Zone Layer Distribution Coefficients

	EPRI Median Kd[1]		TSPA-LA Median Kd[2]	
	Volcanics	Alluvium	Volcanics	Alluvium
	[mL/g]	[mL/g]	[mL/g]	[mL/g]
Np	1.50E+00	3.30E+00	1.43E+00	6.35E+00
U	5.00E+00	2.20E+00	6.78E+00	4.60E+00
Th	2.50E+03	2.50E+03	5.50E+03	5.50E+03
Pu	7.50E+01	7.50E+00	1.04E+02	1.00E+02

Sources: [1] Modified from Apted and Ross 2005 [DIRS 182229],Table 5-5.
[2] Modified from Table L-46, Source: DTN: SN0310T0502103.009_R0 [DIRS 168763] and LA0702AM150304.001_R5 [DIRS 184763].

Table M-8. BDCFs used in EPRI Model

	EPRI-BDCF[1]	TSPA-LA: Mean BDCF[2]
Radionuclide	Sv/yr per Bq/m^3	Sv/yr per Bq/m^3
TC-99	3.3724E-09	1.68E-09
I-129	1.1505E-06	1.48E-07
Np-237	1.7793E-06	2.79E-07
U-233	6.9646E-07	9.20E-08
TH-229	3.0884E-05	2.62E-06
PU-239	6.1914E-06	9.74E-07
U-235	3.9934E-07	9.59E-08
U-238	3.7177E-07	7.94E-08
U-234	3.8870E-07	8.27E-08
Th-230	5.3621E-05	1.10E-06
PU-240	5.4570E-06	9.71E-07
U-236	3.1861E-07	7.73E-08

Source: [1] Modified from Apted and Kessler 2005 [DIRS 182228], Table 5-7.
[2] Modified from Table L-42, Source: DTN: MO0702PAGBDCFS.001_R0 [DIRS 179327].

INTENTIONALLY LEFT BLANK

APPENDIX N
DERIVATION OF IMPLEMENTING EQUATIONS FOR WASTE PACKAGE PARSING AND AVERAGE DAMAGE AREA

N1. DERIVATION OF IMPLEMENTING EQUATIONS FOR WASTE PACKAGE PARSING AND AVERAGE DAMAGE AREA

In the Total System Performance Assessment for the License Application (TSPA-LA) Model, the failure properties of a group of waste packages (WPs) are assigned to the entire group of failed WPs. If the group of WPs contains WPs failing by different mechanisms, average failure properties are applied for all of the failed WPs in the group. In general, averaging WP failure properties can lead to unintended model responses, such as overestimating the opening area on a failed WP. Therefore, to mitigate unintended model responses introduced by averaging WP failure properties for WPs with very different properties, it is desirable to define the WP groups based on WP failure properties. This appendix describes the calculations implemented in the TSPA-LA Model that divide the entire set of WPs into smaller WP groups.

WP damage mechanisms and dripping conditions are the two characteristics that define the WP groups implemented in the TSPA-LA Model. As discussed in Section 6.1.5, the TSPA-LA Model divides that total number of emplaced WPs into five percolation subregions and two fuel types. For modeling purposes, each of these 10 WP groups, is then further divided into three smaller groups based on WP damage mechanism and dripping conditions. Therefore, the TSPA-LA Model includes calculations for 30 different WP groups each time the model is exercised.

The implementing equations defining the WP groups are discussed first for the Nominal Scenario Class. Following the discussion of the Nominal Scenario Class, the adjustments necessary to accommodate the other scenario classes are described.

N2. NOMINAL SCENARIO CLASS

This section of the text describes the derivation for the number of WPs in each WP group and the average WP damage area for a WP group, modeled in the Nominal Scenario Class. In the Nominal Scenario Class there are two major mechanisms for WP damage:

1. Stress corrosion cracking (SCC) coupled with general corrosion
2. Localized corrosion coupled with general corrosion

Early failure of the WP, seismic-induced WP damage, and igneous intrusion WP damage are excluded from the Nominal Scenario Class, but are captured in separate modeling cases.

WP failure and damage area resulting from the first damage mechanism listed above, SCC coupled with general corrosion, is calculated as a function of time using the software code WAPDEG V4.07 (STN: 10000-4.07-00 [DIRS 161240] and STN: 10000-4.07-01 [DIRS 181064]). WAPDEG V4.07 calculates the fraction of the WPs that are failed by either SCC or general corrosion. WAPDEG V4.07 also calculates the average number of SCCs on a failed WP and the average number of general corrosion patches on a failed WP. Coupled with the area of each opening and the total surface area of the WP, the dynamically linked libraries (DLL) output can be used to calculate the fraction of the WP surface area damaged by SCC and/or general corrosion.

WP failure resulting from the second damage mechanism listed above, localized corrosion coupled with general corrosion, is calculated as a function of time using the TSPA-LA Localized Corrosion Initiation Submodel, a separate GoldSim analysis that is described in Section 6.3.5.2.3. WP damage area from localized corrosion is implemented in the TSPA-LA Model as a fixed damage area once localized corrosion failure occurs. The TSPA-LA Localized Corrosion Initiation Submodel calculates the fraction of WPs that are failed by localized corrosion coupled with general corrosion as a function of time. The results are stored as external files and read into the TSPA-LA Model using the software code PassTable1D_LA V2.0 (STN: 11142-2.0-00 [DIRS 181051]). Two different localized corrosion mechanisms, termed LC1 and LC2, are considered in the equations derived below. As derived below, the WP damage area from each localized corrosion mechanism does not need to be the same amount. The TSPA-LA Model only considers crown seepage localized corrosion from one mechanism, but the capability to consider a second mechanism is retained in the model. These two mechanisms could represent crown seepage localized corrosion resulting separately from early and late failed drip shields (DS). Because the damage area from each localized corrosion mechanism is treated as a fixed value, the mechanism for localized corrosion damage is not relevant to the equations derived below.

In order to derive general equations that can be used to determine the average properties of the WP group, certain simplifications are modeled.

1. The WP surface area damage by localized corrosion is instantly damaged when a localized corrosion penetration occurs on a WP. The damage area per WP is a fixed value for each localized corrosion mechanism considered.

2. SCC and general corrosion failures develop independently from localized corrosion on different areas of the WP. Furthermore, an area that is previously damaged by localized corrosion or SCC/general corrosion is not also subject to SCC/general corrosion or localized corrosion until the entire WP surface area is damaged. This simplification allows WP damage area due to multiple damage mechanisms to be additive on a WP. Thus, if localized corrosion occurs on one patch and general corrosion occurs on one patch, the two patch openings will not be at the same location on the WP. This simplification maximizes the opening area on a WP.

Considering the discussion presented above, there are seven types of damage areas that are possible in the TSPA-LA Model from these two sources. Figure N-1 graphically depicts the definition of these seven areas. The seven areas, as identified on Figure N-1, are:

A. SCC and general corrosion damage without any localized corrosion damage
B. SCC and general corrosion damage with LC2 damage and without LC1 damage
C. SCC and general corrosion damage with LC1 damage and without LC2 damage
D. SCC and general corrosion damage with both LC1 and LC2 damage
E. LC1 and LC2 damage without SCC or general corrosion damage
F. LC2 damage without LC1 damage or SCC and general corrosion damage
G. LC1 damage without LC2 damage or SCC and general corrosion damage.

Furthermore, if all WPs eventually fail by the SCC and general corrosion mechanism, then damage types E, F, and G become null sets.

It should be noted that the derivations of the functions defined below are valid for any damage mode and should not be limited to SCC/general corrosion and localized corrosion conditions.

The following variables are identified as inputs in the calculations that are coupled together to assess WP damage area on a group of failed WPs for the Nominal Scenario Class. These input values and time histories are considered in the derivation of the damage area equation for each of the seven damage types discussed above. Additional definitions are presented in the derivation discussion.

$f_{fail,WAPDEG}(t)$ The fraction of the total number of WPs that are failed by SCC or general corrosion processes as a function of time.

$f_{dam,SCC,WAPDEG}(t)$ The average fraction of the WP surface area damaged by SCC as a function of time on a WP failed by SCC or general corrosion.

$f_{dam,patch,WAPDEG}(t)$ The average fraction of the WP surface area damaged by general corrosion patches as a function of time on a WP failed by SCC or general corrosion.

$f_{fail,LC1}(t)$ The fraction of the total number of WPs that are failed by localized corrosion mechanism #1 as a function of time.

$f_{dam,LC1}(t)$ The average fraction of the WP surface area damaged by localized corrosion patches as a function of time on a WP that is failed by localized corrosion mechanism #1.

$f_{fail,LC2}(t)$ The fraction of the total number of WPs that are failed by localized corrosion mechanism #2 as a function of time.

$f_{dam,LC2}(t)$ The average fraction of the WP surface area damaged by localized corrosion patches as a function of time on a WP that is failed by localized corrosion mechanism #2.

f^{tmax} The fraction of damage or failure evaluated at the end of the simulated duration.

$f^{C,tmax}$ The complement to the fraction of damage or failure evaluated at the end of the simulated duration.

N_{Total} The total number of WPs distributed between the seven groups including WPs that do not fail by any damage mechanism in the simulated duration

For consideration in the TSPA-LA Model, WP damage areas will be derived for seven WP damage mechanisms, or combinations of damage mechanisms. Failure fractions for each of the seven damage mechanisms are identified as f_A, f_B, f_C, f_D, f_E, f_F, and f_G, where the subscript is consistent with the regions described below and depicted on Figure N-1. These calculations

become part of the WP parsing calculations in the TSPA-LA Model. These calculations are used to determine the size of each WP group in the Nominal Scenario Class. For classification purposes, the fraction of the total WPs assigned to each of the seven WP failure groups is determined by the damage state of the WPs at the simulated duration. Thus, all WPs assigned to WP Group D have an end state combining SCC coupled with general corrosion damage, LC1 damage, and LC2 damage.

Applying the principals of inclusion and exclusion, at the end of the simulated duration, the fraction of WPs that are damaged by SCC/general corrosion only, without localized corrosion from damage mechanisms #1 or #2 is:

$$f_A = f_{fail,WAPDEG}^{t\max} \cap f_{fail,LC1}^{C,t\max} \cap f_{fail,LC2}^{C,t\max} \quad \text{(Eq. N-1)}$$

where $f_{fail,LC1}^{C,t\max}$ and $f_{fail,LC2}^{C,t\max}$ define the complement to the fraction of WPs that are failed by localized corrosion mechanism #1 and localized corrosion mechanism #2, respectively. The complement fractions define the fraction of WPs that are not failed by the mechanism indicated.

At the end of the simulated duration, the fraction of WPs that are damaged by SCC/general corrosion and also have damage from LC2 but not any damage from LC1 is:

$$f_B = f_{fail,WAPDEG}^{t\max} \cap f_{fail,LC1}^{C,t\max} \cap f_{fail,LC2}^{t\max}. \quad \text{(Eq. N-2)}$$

At the end of the simulated duration, the fraction of WPs that are damaged by SCC/general corrosion and also have damage from LC1 but not any damage from LC2 is:

$$f_C = f_{fail,WAPDEG}^{t\max} \cap f_{fail,LC1}^{t\max} \cap f_{fail,LC2}^{C,t\max}. \quad \text{(Eq. N-3)}$$

At the end of the simulated duration, the fraction of WPs that are damaged by SCC/general corrosion and also have damage from LC1 and LC2 is:

$$f_D = f_{fail,WAPDEG}^{t\max} \cap f_{fail,LC1}^{t\max} \cap f_{fail,LC2}^{t\max}. \quad \text{(Eq. N-4)}$$

At the end of the simulated duration, the fraction of WPs that are damaged by LC1 and LC2, but have no SCC/general corrosion damage is:

$$f_E = f_{fail,WAPDEG}^{C,t\max} \cap f_{fail,LC1}^{t\max} \cap f_{fail,LC2}^{t\max} \quad \text{(Eq. N-5)}$$

where $f_{fail,WAPDEG}^{C,t\max}$ defines the compliment to the fraction of WPs that are failed SCC and/or general corrosion.

At the end of the simulated duration, the fraction of WPs that are damaged by LC2 only is:

$$f_F = f_{fail,WAPDEG}^{C,t\max} \cap f_{fail,LC1}^{C,t\max} \cap f_{fail,LC2}^{t\max} \quad \text{(Eq. N-6)}$$

At the end of the simulated duration, the fraction of WPs that are damaged by LC1 only is:

$$f_G = f_{fail,WAPDEG}^{C,t\max} \cap f_{fail,LC1}^{t\max} \cap f_{fail,LC2}^{C,t\max} \quad \text{(Eq. N-7)}$$

Using the simplification that the SCC, general corrosion, and localized corrosion damage are independent events, the fraction of WPs failing by the intersection of two or more mechanisms is equal to the product of the individual failure fractions ($f_i \cap f_j = f_i f_j$). Furthermore, the definition of a complement is

$$f_i^C = 1 - f_i \quad \text{(Eq. N-8)}$$

Therefore, the above equations can be rewritten as

$$f_A = f_{fail,WAPDEG}^{t\max} \times (1 - f_{fail,LC1}^{t\max}) \times (1 - f_{fail,LC2}^{t\max}) \quad \text{(Eq. N-9)}$$

$$f_B = f_{fail,WAPDEG}^{t\max} \times (1 - f_{fail,LC1}^{t\max}) \times f_{fail,LC2}^{t\max} \quad \text{(Eq. N-10)}$$

$$f_C = f_{fail,WAPDEG}^{t\max} \times f_{fail,LC1}^{t\max} \times (1 - f_{fail,LC2}^{t\max}) \quad \text{(Eq. N-11)}$$

$$f_D = f_{fail,WAPDEG}^{t\max} \times f_{fail,LC2}^{t\max} \times f_{fail,LC1}^{t\max} \quad \text{(Eq. N-12)}$$

$$f_E = (1 - f_{fail,WAPDEG}^{t\max}) \times f_{fail,LC2}^{t\max} \times f_{fail,LC1}^{t\max} \quad \text{(Eq. N-13)}$$

$$f_F = (1 - f_{fail,WAPDEG}^{t\max}) \times (1 - f_{fail,LC1}^{t\max}) \times f_{fail,LC2}^{t\max} \quad \text{(Eq. N-14)}$$

$$f_G = (1 - f_{fail,WAPDEG}^{t\max}) \times f_{fail,LC1}^{t\max} \times (1 - f_{fail,LC2}^{t\max}) \quad \text{(Eq. N-15)}$$

The number of WPs damaged by each of the seven mechanisms at the end of the simulated duration is equal to the product of the failure fraction and the total number of WPs to be modeled, N_{Total}. If a WP does not fail by one of these modes in the simulated duration, then it is not considered in the average damage calculations. For this reason, it is necessary to normalize the WP failure fractions so that the equations only represent the WPs that will be damaged by the applicable mechanism in the simulated duration. Normalizing the failure fractions is done by dividing the time-dependent failure fraction by its final value.

Once the number of WPs in each of the seven WP groups is determined, the average fraction of WP surface area damaged on the failed WPs in each group is then determined.

For Group A, the average damage fraction on the failed WPs is calculated by the WAPDEG DLL:

$$f_{dam,A}(t) = f_{dam,WAPDEG}(t) = f_{dam,SCC,WAPDEG}(t) + f_{dam,patch,WAPDEG}(t). \quad \text{(Eq. N-16)}$$

For Groups F and G, the average damage fraction on the failed WPs is equal to the fixed values:

$$f_{dam,F}(t) = f_{dam,LC2} \quad \text{(Eq. N-17)}$$

$$f_{dam,G}(t) = f_{dam,LC1}. \quad \text{(Eq. N-18)}$$

When determining the average damage area for a WP that will fail by a combination of two or more mechanisms, the damage area for the group needs to be applied as an average to the entire group. Given that SCC and general corrosion damage may not occur at the same time as localized corrosion, but given that eventually both will occur for the group, the average area needs to consider the timing at which the damage occurs. For simplification, LC1 and/or LC2 damage to a WP occurs instantly once LC1 and/or LC2 failures have occurred. In the equations derived below, the total surface area damaged by one mechanism or a combination of mechanisms cannot exceed the total WP surface area; therefore, damage fractions are limited to the value 1.

For Group B, which has damage due to SCC/general corrosion and LC2 combined, the average damage area for the group considers the total damage area from the damage mechanisms and then divides the total damage area by the number of failed WPs in the group. The parts are:

B1. WPs with SCC/general corrosion only damage prior to LC2 damage
B2. WPs with LC2 damage only prior to SCC/general corrosion damage
B3. WPs with both LC2 damage and SCC/general corrosion damage.

The failure fractions defined previously are the time-dependent failure fractions of all WPs that are failed by a specified mechanism. Because Group B only contains WPs that will fail by SCC/general corrosion and LC2 combined, the failure fractions applied in these equations should only consider those WPs that will fail by both mechanisms and thus each failure fraction must have a final value of one. Therefore, the SCC/general corrosion and LC2 failure fractions are both normalized by the final failure fraction.

$$f^{norm}_{fail,WAPDEG}(t) = \frac{f_{fail,WAPDEG}(t)}{f^{t\max}_{fail,WAPDEG}} \quad \text{(Eq. N-19)}$$

$$f^{norm}_{fail,LC2}(t) = \frac{f_{fail,LC2}(t)}{f^{t\max}_{fail,LC2}}. \quad \text{(Eq. N-20)}$$

Eventually WPs in Group B with SCC/general corrosion only damage prior to LC2 damage (B1) and WPs with LC2 damage only prior to SCC/general corrosion damage (B2) will eventually become WPs with both LC2 damage and SCC/general corrosion damage (B3). However, as time elapses, the number of B1 WPs, B2 WPs, and B3 WPs changes according to the time histories of the applicable failure fractions. Prior to this time, the average damage on a B1 WP is the SCC/general corrosion damage fraction, but the average Group B damage fraction is the weighted average of B1, B2, and B3 damage fractions. When calculating the average damage area to all Group B WPs, the damage area contribution from B1 WPs to the Group B total as a

function of time is the product of the fraction of WP surface area damaged by SCC/general corrosion and the fraction of WPs in Group B with only SCC/general corrosion damage.

$$f_{dam,B1}(t) = f_{dam,WAPDEG}(t) \times f^{norm}_{fail,WAPDEG}(t) \times (1 - f^{norm}_{fail,LC2}(t)) \quad \text{(Eq. N-21)}$$

The damage area contribution from B2 WPs to the Group B total as a function of time is the product of the fraction of WP surface area damaged by LC2 and the fraction of WPs in Group B with only LC2 damage.

$$f_{dam,B2}(t) = f_{dam,LC2} \times f^{norm}_{fail,LC2}(t) \times (1 - f^{norm}_{fail,WAPDEG}(t)) \quad \text{(Eq. N-22)}$$

The damage area contribution from B3 WPs to the Group B total as a function of time is the product of the fraction of WP surface area damaged by SCC/general corrosion and LC2 and the fraction of WPs in Group B with both SCC/corrosion and LC2 damage.

$$f_{dam,B3}(t) = \min[1, f_{dam,LC2} + f_{dam,WAPDEG}(t)] \times f^{norm}_{fail,LC2}(t) \times f^{norm}_{fail,WAPDEG}(t) \quad \text{(Eq. N-23)}$$

The average damage for Group B WPs is then the sum of the products of the number of WP in each subgroup and the damage area for the subgroup divided by the total number of Group B WPs that are failed as a function of time. Expressed as fractions, the equation simplifies to:

$$f_{dam,B}(t) = \min\left(1, \frac{[f_{dam,LC2} \times f^{norm}_{fail,LC2}(t) + f_{dam,WAPDEG}(t) \times f^{norm}_{fail,WAPDEG}(t)]}{f^{norm}_{fail,LC2}(t) + f^{norm}_{fail,WAPDEG}(t) - f^{norm}_{fail,LC2}(t) \times f^{norm}_{fail,WAPDEG}(t)}\right) \quad \text{(Eq. N-24)}$$

Analogous equations can be derived for the Group C WPs but the equations will be the same as those in Equations N-19 through N-24, replacing LC2 fractions with LC1 equivalents. Likewise, analogous equations can be derived for the Group E WPs but the equations will be the same as those in Equations N-19 through N-24, replacing SCC/general corrosion fractions and with LC1 equivalents.

For Group D, which at the end of the simulation has damage due to SCC/general corrosion and LC1 and LC2 combined, the average damage area for the group as a function of time considers the total damage area from the damage mechanisms and then divides the total damage area by the number of failed WPs in the group. The parts are:

D1. WPs with SCC/general corrosion only damage prior to LC1 and LC2 damage
D2. WPs with LC1 damage only prior to SCC/general corrosion and LC2 damage
D3. WPs with LC1 and SCC/general corrosion damage only prior to LC2 damage
D4. WPs with LC1 and LC2 damage only prior to SCC/general corrosion damage
D5. WPs with LC2 damage only prior to SCC/general corrosion and LC1 damage
D6. WPs with LC2 and SCC/general corrosion damage only prior to LC1 damage
D7. WPs with SCC/general corrosion and LC1 and LC2 damage.

Because Group D only contains WPs that will fail by SCC/general corrosion and localized corrosion combined and the failure fractions are defined for all WPs, the failure fractions are normalized by the value at the end of the simulation. The SCC/general corrosion and localized

corrosion failure fractions are normalized. Equations N-19, N-20, and N-25 are the normalization equations.

$$f_{fail,LC1}^{norm}(t) = \frac{f_{fail,LC1}(t)}{f_{fail,LC1}^{t\max}} \quad \text{(Eq. N-25)}$$

The damage contribution from D1 WPs to Group D total as a function of time is the product of the fraction of WP surface area damaged by SCC/general corrosion and the fraction of WPs in Group D with only SCC/general corrosion damage.

$$f_{dam,D1}(t) = f_{dam,WAPDEG}(t) \times f_{fail,WAPDEG}^{norm}(t) \times [(1 - f_{fail,LC1}^{norm}(t)) \times (1 - f_{fail,LC2}^{norm}(t))] \quad \text{(Eq. N-26)}$$

The damage contribution from D2 WPs to Group D total as a function of time is the product of the fraction of WP surface area damaged by LC1 and the fraction of WPs in Group D with only LC1 damage.

$$f_{dam,D2}(t) = f_{dam,LC1} \times f_{fail,LC1}^{norm}(t) \times [(1 - f_{fail,WAPDEG}^{norm}(t)) \times (1 - f_{fail,LC2}^{norm}(t))] \quad \text{(Eq. N-27)}$$

The damage contribution from D3 WPs to Group D total as a function of time is the product of the fraction of WP surface area damaged by LC1 and SCC/general corrosion and the fraction of WPs in Group D with only LC1 and SCC/general corrosion damage.

$$f_{dam,D3}(t) = \min[1, f_{dam,WAPDEG}(t) + f_{dam,LC1}] \times f_{fail,LC1}^{norm}(t) \times f_{fail,WAPDEG}^{norm}(t) \times (1 - f_{fail,LC2}^{norm}(t)) \quad \text{(Eq. N-28)}$$

The damage contribution from D4 WPs to Group D total as a function of time is the product of the fraction of WP surface area damaged by LC1 and LC2 and the fraction of WPs in Group D with only LC1 and LC2 damage.

$$f_{dam,D4}(t) = \min[1, f_{dam,LC1}(t) + f_{dam,LC2}] \times f_{fail,LC1}^{norm}(t) \times f_{fail,LC2}^{norm}(t) \times (1 - f_{fail,WAPDEG}^{norm}(t)) \quad \text{(Eq. N-29)}$$

The damage contribution from D5 WPs to Group D total as a function of time is calculated using Equation N-27 with the LC1 and LC2 inputs reversed.

The damage contribution from D6 WPs to Group D total as a function of time is calculated using Equation N-28 with the LC1 and LC2 inputs reversed.

The damage contribution from D7 WPs to Group D total as a function of time is the product of the fraction of WP surface area damaged by LC1, LC2, and SCC/general corrosion and the fraction of WPs in Group D with LC1, LC2, and SCC/general corrosion damage.

$$f_{dam,D7}(t) = \min[1, f_{dam,LC1} + f_{dam,LC2} + f_{dam,WAPDEG}(t)] \times f^{norm}_{fail,LC1}(t) \times f^{norm}_{fail,LC2}(t) \times f^{norm}_{fail,WAPDEG}(t) \quad \text{(Eq. N-30)}$$

The average damage for Group D WPs is then

$$f_{dam,D}(t) = \min\left(1, \frac{\begin{array}{l}[f_{dam,D1}(t) + f_{dam,D2}(t) + f_{dam,D3}(t) + f_{dam,D4}(t) + \\ f_{dam,D5}(t) + f_{dam,D6}(t) + f_{dam,D7}(t)]\end{array}}{\begin{array}{l}f^{norm}_{fail,LC1}(t) + f^{norm}_{fail,LC2}(t) + f^{norm}_{fail,WAPDEG}(t) - \\ f^{norm}_{fail,LC2}(t) \times f^{norm}_{fail,WAPDEG}(t) - \\ f^{norm}_{fail,LC1}(t) \times f^{norm}_{fail,WAPDEG}(t) - f^{norm}_{fail,LC1}(t) \times f^{norm}_{fail,LC2}(t) + \\ f^{norm}_{fail,LC1}(t) \times f^{norm}_{fail,LC2}(t) \times f^{norm}_{fail,WAPDEG}(t)\end{array}}\right) \quad \text{(Eq. N-31)}$$

N3. WP PARSING

For the Nominal Scenario Class, the emplaced number of WP are first binned by fuel type and percolation subregion (see Section 6.3.2) before assigning WPs to one of the seven groups described above. There are two fuel types and five percolation subregions for a total of 10 WP subgroups. These 10 subgroups are then further divided into three groups each for a total of 30 WP groups. Equations N-1 through N-31 are applicable to each of the 10 subgroups. A subset of these equations applies to the smaller set of three WP groups within each of the 10 subgroups. The first of these three groups contains the subset of WPs that are not exposed to drift seepage. According to the Drift Seepage Abstraction (see Section 6.3.3), a certain fraction of WPs within each percolation subregion are in locations that are not susceptible to drift seepage. Because the WPs in this group are not susceptible to localized corrosion, the failed WPs in this group belong to Group A described above. The second of these three groups contains the subset of WPs that are subject to drift seepage, but are not susceptible to localized corrosion as a result of exposure to corrosive seepage water. These WPs are the subset of WPs in a dripping location that do not have the environmental conditions (e.g., pH, temperature, DS failure, etc.) that initiate localized corrosion when the WP is exposed to the seepage water. Like the non-seeping group, the WPs in this group are not susceptible to localized corrosion and the failed WPs in this group also belong to Group A described above. The third group contains the subset of WPs that are subject to drift seepage and are also susceptible to localized corrosion following exposure to seepage water. Because the WPs in this group are susceptible to localized corrosion, the failed WPs in this group belong to groups B through G described above.

To determine the number of WPs that populate each of the 30 WP groups, the group of WPs that comprise the first and second subsets are the WPs in Group A. These WPs have no localized corrosion. For the first group, the non-seeping group, the number of WPs of each fuel type in each percolation subregion is the product of the number of WPs of each fuel type in each percolation subregion assigned to Group A and the fraction of WPs that are not exposed to drift seepage. The number of WPs in the second group, the seeping group without localized corrosion, is the balance of the Group A WPs and is the product of the number of WPs of each fuel type in each percolation subregion, the number of WPs in Group A, and the fraction of WPs that are exposed to drift seepage. For the third group, the seeping group with localized corrosion, the number of WPs of each fuel type in each percolation subregion is the number of WPs of each fuel type in each percolation subregion assigned to Groups B through G ($=N_{TOTAL}*(f_B+f_C+f_D+f_E+f_F+f_G)$, where N_{TOTAL} is the number of WPs of a specified fuel type in a specified percolation subregion).

Within the TSPA-LA Model, for WPs modeled in the third WP group, those WPs that incur localized corrosion damage by either localized corrosion mechanism, an average damage area is determined for the WP group. The average damage area is the sum of the products of the fraction of damage on each WP of type B, C, D, E, F, or G, above, and the fraction of WPs failed that belong to each WP type B, C, D, E, F, or G divided by the sum of the fraction of WPs failed that belong to each WP type B, C, D, E, F, or G

$$f_{dam}^{avg,LC}(t) = \frac{\sum_{i=B}^{G} f_{dam,i}(t) \times f_{fail,i}(t)}{\sum_{i=B}^{G} f_{fail,i}(t)} \quad \text{(Eq. N-32)}$$

Where $f_{fail,i}(t)$ defines the fraction of WP belonging to each of the six applicable groups that are failed as a function of time. These fractions are calculated using a time-dependent form of Equation N-10 through Equation N-15. The time-dependent form replaces the value at the end of the simulation, f^{tmax}, with the equivalent value for the current time.

N4. DISRUPTIVE EVENTS

When seismic or igneous event(s) are considered, Equations N-1 though N-32 need to be updated to reflect the additional damage caused by the event(s). In the Igneous Intrusion Modeling Case of the Igneous Scenario Class, all of the WPs in a group will be subjected to the same igneous damage area because the igneous intrusion events cause all of the WPs to fail at the time of the event, and the amount of damage to the WP is the entire WP surface area (Section 6.5.1). Thus, when computing an average damage area for each WP group, the amount of damage to a WP from the igneous intrusion event is additive to any prior damage caused by nominal processes. Similarly, in the Seismic Scenario Class, all WPs in a group will be subjected to the same seismic damage area because the events cause all WPs to fail at the time of the event and the amount of seismic damage is calculated as an average damage for all failed WPs. Thus, when computing an average damage area for each WP group, the amount of damage to a WP from each seismic event is additive to any prior damage caused by nominal processes or seismic events.

For the Igneous Intrusion Modeling Case of the Igneous Scenario Class, all of the WPs are impacted and the damage area becomes unity for all modeled WPs (Section 6.5.1). Therefore, there is no need to consider WP damage area averaging for this case. Prior to the igneous intrusion event, the average WP damage area is calculated under nominal repository conditions.

When seismic consequences are considered, the equations for the average WP damage fraction need to be updated to reflect additional damage caused by the seismic event. For the Seismic Scenario Class, the equations derived below are applicable to both modeling cases of the Seismic Scenario Class presented in Sections 6.6.1 and 6.6.2. The mechanism of damage, vibratory ground motion, or fault displacement, is irrelevant to the derivation of the equations provided that the appropriate failure fraction and damage fractions are applied. In addition, when considering the average of a group of WPs, the average damage area may not increase by the amount of the seismic damage because WPs that are already fully failed will not be subjected to additional damage and thus the contribution of damage from these WPs will not increase following an event.

The revised equations considering the consequences of a seismic event are presented below.

Adding in seismic consequences affects all Group A, F, and G WPs similarly. If the fraction of seismic failed WPs is $f_{fail,seismic}(t)$ and the amount of seismic damage is $f_{dam,seismic}(t)$, then Equation N-16 is modified as follows:

$$f_{dam,A}(t) = \min[1, f_{dam,WAPDEG}(t) + f_{dam,seismic}(t)] \quad \text{(Eq. N-33)}$$

Since all WPs are failed following the seismic event, but localized corrosion failures may not be completed by the time of the seismic event, there may be seismic-damaged WPs with and without localized corrosion. The average damage area considers the fraction of WPs that have localized corrosion damage and Equations N-17 and N-18 are modified as follows:

$$f_{dam,F}(t) = f^{norm}_{fail,LC2}(t) \times \min[1, f_{dam,seismic}(t) + f_{dam,LC2}] + (1 - f^{norm}_{fail,LC2}(t)) \times f_{dam,seismic}(t) \quad \text{(Eq. N-34)}$$

$$f_{dam,G}(t) = if^{norm}_{fail,LC1}(t) \times \min[1, f_{dam,seismic}(t) + f_{dam,LC1}] + (1 - f^{norm}_{fail,LC1}(t)) \times f_{dam,seismic}(t) \quad \text{(Eq. N-35)}$$

With the added constraint that the seismic and SCC/general corrosion damage cannot exceed total surface area of the failed WPs, Equation N-21 can then be rewritten as:

$$f_{dam,seismic,B1}(t) = \min[1, f_{dam,seismic}(t) + f_{dam,WAPDEG}(t)] \times f^{norm}_{fail,WAPDEG}(t) \times (1 - f^{norm}_{fail,LC2}(t)) \quad \text{(Eq. N-36)}$$

Similarly, with the added constraint that the seismic and localized corrosion damage cannot exceed total surface area of the failed WPs, the Equation N-22 can then be rewritten as:

$$f_{dam,seismic,B2}(t) = \min[1, f_{dam,seismic}(t) + f_{dam,LC2}] \times f^{norm}_{fail,LC2}(t) \times (1 - f^{norm}_{fail,WAPDEG}(t)) \quad \text{(Eq. N-37)}$$

It follows then that, with the added constraint that the seismic and SCC/general corrosion and localized corrosion damage cannot exceed total surface area of the failed WPs, the Equation N-23 can then be rewritten as:

$$f_{dam,B3}(t) = \min[1, f_{dam,seismic}(t) + f_{dam,LC2} + f_{dam,WAPDEG}(t)] \times f^{norm}_{fail,LC2}(t) \times f^{norm}_{fail,WAPDEG}(t) \quad \text{(Eq. N-38)}$$

The localized corrosion failure fractions do not need to be adjusted to accommodate the seismic consequence. Localized corrosion continues to propagate at the calculated rate and additional WP damage should be considered at the same rate. Therefore, Equation N-24 does not need to be modified to include seismic consequences. Because the seismic event fails all WPs of the same fuel type simultaneously, (see Sections 6.6.1 and 6.6.2), the denominator in Equation N-24 becomes unity at the time of the seismic event and the result will be based on the damage area for all WPs in the group at the time of the event. Under seismic conditions that cause the failure fraction output by the WAPDEG DLL to become unity at the time of the event, Equation N-37 becomes zero at the time of the event and the damage area calculated by Equation N-24 becomes the sum of the seismic damage and SCC/general corrosion damage weighted by the fraction of non-localized corrosion damaged WPs and the seismic damage and SCC/general corrosion damage and localized corrosion damage weighted by the fraction of localized corrosion damaged WPs,

$$f_{dam,B}(t) = \min\left(\begin{array}{l} 1, \{\min[1, f_{dam,seismic}(t) + f_{dam,WAPDEG}(t)] \times (1 - f^{norm}_{fail,LC2}(t)) + \\ \min[1, f_{dam,seismic}(t) + f_{dam,LC2} + f_{dam,WAPDEG}(t)] \times f^{norm}_{fail,LC2}(t)\} \end{array}\right) \quad \text{(Eq. N-39)}$$

Analogous equations can be derived for the Group C WPs but the equations will be the same as those in Equations N-36 through N-39, replacing LC2 fractions with LC1 equivalents. Similarly, analogous equations can be derived for the Group E WPs but the equations will be the same as those in Equations N-36 through N-39, replacing SCC/general corrosion fractions with LC1 equivalents.

Similar to the discussion presented for Group B WPs, Group D equations are modified to account for seismic activity by adding seismic damage fractions to the damage area calculation in each of the seven Group D calculations (Equations N-26 through N-30) to yield the following modified forms:

$$f_{dam,D1}(t) = \min[1, f_{dam,seismic}(t) + f_{dam,WAPDEG}(t)] \times f^{norm}_{fail,WAPDEG}(t) \times [1 - f^{norm}_{fail,LC2}(t) - f^{norm}_{fail,LC1}(t) + f^{norm}_{fail,LC2}(t) \times f^{norm}_{fail,LC1}(t)] \quad \text{(Eq. N-40)}$$

$$f_{dam,D2}(t) = \min[1, f_{dam,seismic}(t) + f_{dam,LC1}] \times f^{norm}_{fail,LC1}(t) \times [1 - f^{norm}_{fail,WAPDEG}(t) - f^{norm}_{fail,LC2}(t) + f^{norm}_{fail,WAPDEG}(t) \times f^{norm}_{fail,LC2}(t)] \quad \text{(Eq. N-41)}$$

$$f_{dam,D3}(t) = \min[1, f_{dam,seismic}(t) + f_{dam,WAPDEG}(t) + f_{dam,LC1}] \times f^{norm}_{fail,LC1}(t) \times f^{norm}_{fail,WAPDEG}(t) \times (1 - f^{norm}_{fail,LC2}(t)) \quad \text{(Eq. N-42)}$$

$$f_{dam,D4}(t) = \min[1, f_{dam,seismic}(t) + f_{dam,LC1}(t) + f_{dam,LC2}] \times f^{norm}_{fail,LC1}(t) \times f^{norm}_{fail,LC2}(t) \times (1 - f^{norm}_{fail,WAPDEG}(t)) \quad \text{(Eq. N-43)}$$

$$f_{dam,D5}(t) = \min[1, f_{dam,seismic}(t) + f_{dam,LC2}] \times f^{norm}_{fail,LC2}(t) \times [1 - f^{norm}_{fail,WAPDEG}(t) - f^{norm}_{fail,LC1}(t) + f^{norm}_{fail,WAPDEG}(t) \times f^{norm}_{fail,LC1}(t)] \quad \text{(Eq. N-44)}$$

$$f_{dam,D6}(t) = \min[1, f_{dam,seismic}(t) + f_{dam,WAPDEG}(t) + f_{dam,LC2}] \times f^{norm}_{fail,LC2}(t) \times f^{norm}_{fail,WAPDEG}(t) \times (1 - f^{norm}_{fail,LC1}(t)) \quad \text{(Eq. N-45)}$$

$$f_{dam,D7}(t) = \min[1, f_{dam,seismic}(t) + f_{dam,LC1} + f_{dam,LC2} + f_{dam,WAPDEG}(t)] \times f^{norm}_{fail,LC1}(t) \times f^{norm}_{fail,LC2}(t) \times f^{norm}_{fail,WAPDEG}(t) \quad \text{(Eq. N-46)}$$

Because the failure fraction output by the WAPDEG DLL becomes unity at the time of the seismic event, the denominator in Equation N-31 becomes unity at the time of the seismic event and the calculated average will be based on the damage area for all WPs in the group at the time of the event. Under seismic conditions that cause the WP failure fraction to become unity at the time of the event, Equations N-41, N-43, and N-44 become zero at the time of the event and the damage area calculated by Equation N-31 becomes the sum of the seismic damage and SCC/general corrosion damage weighted by the fraction of non-localized corrosion damaged WPs and the seismic damage and SCC/general corrosion damage and localized corrosion damage weighted by the fraction of SCC/general corrosion and localized corrosion damaged WPs for each localized corrosion mechanism.

$$\begin{aligned} f_{dam,D}(t) = \; & \min[1, f_{dam,seismic}(t) + f_{dam,WAPDEG}(t)] \times (1 - f^{norm}_{fail,LC2}(t))(1 - f^{norm}_{fail,LC1}(t)) + \\ & \min[1, f_{dam,seismic}(t) + f_{dam,WAPDEG}(t) + f_{dam,LC1}] \times f^{norm}_{fail,LC1}(t) \times (1 - f^{norm}_{fail,LC2}(t)) + \\ & \min[1, f_{dam,seismic}(t) + f_{dam,WAPDEG}(t) + f_{dam,LC2}] \times f^{norm}_{fail,LC2}(t) \times (1 - f^{norm}_{fail,LC1}(t)) + \\ & \min[1, f_{dam,seismic}(t) + f_{dam,LC1} + f_{dam,LC2} + f_{dam,WAPDEG}(t)] \times f^{norm}_{fail,LC1}(t) \times f^{norm}_{fail,LC2}(t) \end{aligned} \quad \text{(Eq. N-47)}$$

Seismic event damage is additive to the WP damage caused by localized corrosion in WP groups E, F, and G.

To account for WPs damaged by the seismic event before other damage mechanisms cause damage, the average damage must be set equal to the seismic damage fraction if the damage by SCC/general corrosion and /or localized corrosion is not incurred before the seismic event.

The calculations described above are necessary to determine the average patch damage on the failed WPs. The seismic crack damage is added to SCC damage when the two occur simultaneously and is tracked separately.

Similar to the Nominal Scenario Class, for WPs modeled in the third WP group, those WPs that incur localized corrosion damage by either localized corrosion mechanism, an average damage area is determined for the WP group. The average damage area is the sum of the products of the fraction of damage on each WP of type B, C, D, E, F, or G, above, and the fraction of WPs failed that belong to each WP type B, C, D, E, F, or G, above divided by the sum of the fraction of WPs failed that belong to each WP type B, C, D, E, F, or G (Equation N-32).

For the Seismic Fault Displacement Modeling Case, which includes fault failed WPs with and without localized corrosion, the average damage will be the average calculated by Equation N-32 weighted by the fraction of failed WPs with localized corrosion damage plus the fraction of damage on WPs that do not get localized corrosion damage times the fraction of fault damaged WPs that do not get localized corrosion.

$$f_{dam}^{avg,seismic-FD}(t) =$$
$$\min[1, f_{dam,seismic}(t) + f_{dam}^{avg,LC}(t)] \times (f_{fail,LC1}(t) + f_{fail,LC2}(t) - f_{fail,LC1}(t) \times f_{fail,LC2}(t)) \quad \text{(Eq. N-48)}$$
$$+ f_{dam,seismic}(t) \times (1 - (f_{fail,LC1}(t) + f_{fail,LC2}(t) - f_{fail,LC1}(t) \times f_{fail,LC2}(t)))$$

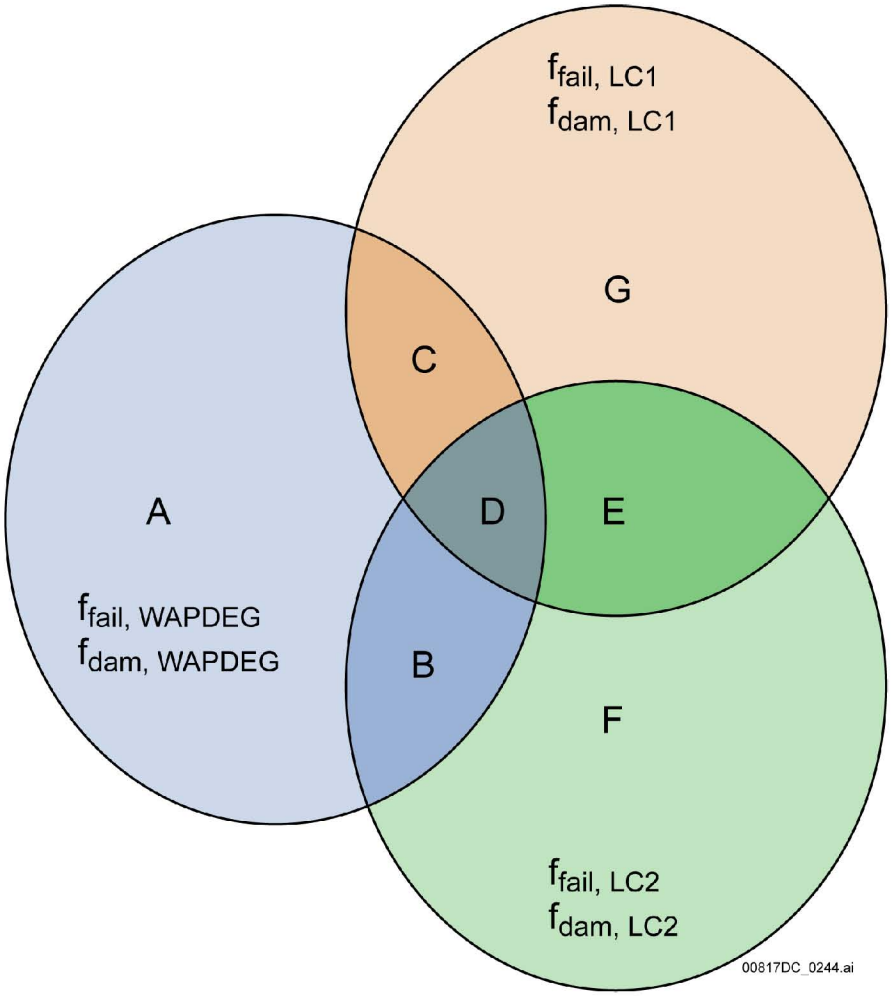

Figure N-1. Venn diagram of overlapping damage modes

INTENTIONALLY LEFT BLANK

APPENDIX O
LOCALIZED CORROSION INITIATION UNCERTAINTY ANALYSIS

O1. INTRODUCTION

This appendix presents the Localized Corrosion Initiation Uncertainty Analysis, which implements the Localized Corrosion Initiation Submodel described in Section 6.3.5.2. The original Localized Corrosion Initiation Model is developed in *General Corrosion and Localized Corrosion of Waste Package Outer Barrier* (SNL 2007 [DIRS 178519], Sections 6.4.4, 6.4.4.3.1, and 6.4.4.5). The effects of localized corrosion are not directly included and calculated in the TSPA-LA Model. The results of the Localized Corrosion Initiation Uncertainty Analysis are used to support screening arguments that localized corrosion initiation can occur only with a low probability and only at a few locations in the repository.

The Localized Corrosion Initiation Uncertainty Analysis uses only a subset of the TSPA-LA Model. Specifically, it is an Engineered Barrier System (EBS) only model in which the unsaturated zone (UZ), saturated zone (SZ), biosphere, and results portions of the TSPA-LA Model have been removed. Also, the EBS has been simplified so that only seepage, thermal hydrology, drift-wall condensation, and chemistry are calculated. The epistemic sampling is identical to the TSPA-LA Model. Also, the aleatory submodels, including the seismic model, are identical. However, the Localized Corrosion Initiation Uncertainty Analysis does not use the representative package for each percolation subregion, but instead it calculates conditions at each of the 3,264 thermal-hydrologic (TH) nodes in the repository. This gives the spatial variability that is necessary to evaluate whether localized corrosion initiates throughout the repository.

The uncertainty analysis in this appendix calculates the chemical conditions on the waste package (WP) surface to determine if the conditions for localized corrosion initiation can exist. If the drip shield (DS) is intact, localized corrosion initiation cannot occur because seepage does not contact the WP surface. However, if the DS is breached or if the DS is assumed to not perform as intended, then the chemistry on the WP surface may allow localized corrosion to initiate. This Localized Corrosion Initiation Uncertainty Analysis assumes that the DS is failed and does not keep seepage water from contacting the WP. The results and conclusions of this analysis can then be used qualitatively in the TSPA-LA Model for any cases in which the DS does not perform as intended.

As will be discussed in more detail later, the conditions for localized corrosion initiation do not exist anywhere in the repository beyond 12,000 years after closure because temperatures decrease and chemical conditions become less aggressive. The average fraction of WPs on which localized corrosion may potentially initiate peaks at about 0.08 in the first few hundred years after closure when the repository is hot, and highly evaporative conditions exist on the WP surface. After 5,000 years, the fraction decreases to below 10^{-3}. Because the probability of localized corrosion initiation is small, the effect on dose would also be low.

O2. MODEL ABSTRACTION

As discussed in Section 6.3.5.2, the Localized Corrosion Initiation Submodel stipulates that localized corrosion of the WP outer surface initiates when the open-circuit potential, or corrosion potential (E_{corr}), is equal to or greater than the critical threshold potential ($E_{critical}$); that is, when $\Delta E = E_{critical} - E_{corr} \leq 0$. This Localized Corrosion Initiation Uncertainty Analysis uses $\Delta E \leq 0$ as the condition necessary for localized corrosion to initiate. For the TSPA-LA Model, the Localized Corrosion Initiation Abstraction uses the crevice repassivation potential (E_{rcrev}) as the critical potential. The crevice repassivation potential for crevice corrosion on the WP outer surface is defined in terms of WP surface temperature and chemical conditions as follows:

$$E_{critical} = E_{rcrev} = a_o + a_1 T + a_2 \ln[Cl^-] + a_3 \frac{[NO_3^-]}{[Cl^-]} + a_4 T[Cl^-] + \varepsilon_{rcrev} \qquad \text{(Eq. O-1)}$$

where a_o, a_1, a_2, a_3, and a_4 are regression constants, T is the WP outer barrier surface temperature (°C), $[NO_3^-]$ is the nitrate ion molality (moles/kg water), and $[Cl^-]$ is the chloride ion molality (moles/kg water). The error term, ε_{rcrev}, represents data variance not explained by the fitting procedure and is modeled by a normal distribution with a mean of 0 mV versus the saturated silver chloride electrode and a standard deviation (SD) of 45.055 mV versus saturated silver chloride electrode. The Localized Corrosion Initiation Abstraction stipulates that the calculated value of E_{rcrev} be constrained to the ±2 SD prediction intervals of the unconstrained model.

The long-term steady-state corrosion potential, E_{corr}, for the WP outer surface is expressed as:

$$E_{corr} = c_o + c_1 T + c_2 pH + c_3 \frac{[NO_3^-]}{[Cl^-]} + c_4 T \frac{[NO_3^-]}{[Cl^-]} + c_5 pH \frac{[NO_3^-]}{[Cl^-]} + c_6 pH \ln[Cl^-] + \varepsilon_{corr} \qquad \text{(Eq. O-2)}$$

where c_o, c_1, c_2, c_3, c_4, c_5, and c_6 are coefficients of the parameters, pH is the calculated Pitzer pH, and the other parameters are as previously defined. The error term, ε_{corr}, is a term representing data variance not explained by the fitting procedure and has a normal distribution with a mean of zero mV versus saturated silver chloride electrode, and an SD of 85.265 mV versus saturated silver chloride electrode. The units of the coefficients should be consistent with E_{corr} having units of mV. The calculated value of E_{rcrev} should also be constrained to the ±2 SD prediction intervals of the unconstrained model.

The thermal hydrology, seepage, and chemistry submodels used in the Localized Corrosion Initiation Uncertainty Analysis differ from those in the TSPA-LA Model in that they are applied at the individual WP level. Seepage and drift wall condensation are important because localized corrosion initiation requires seepage or condensation to bring corrosive chemicals to the WP surface. The seepage calculation in the Localized Corrosion Initiation Uncertainty Analysis is similar to the TSPA-LA Model. The main difference is that the seepage calculation is implemented directly in the Localized Corrosion Initiation GoldSim model instead of as a linked external program. Also, rather than calculating the average seepage rate and seepage fraction for the percolation subregion, the seepage calculation in this Localized Corrosion Initiation Uncertainty Analysis determines the seepage rate at each WP location. The seepage calculation

includes the same seismic effects as the TSPA-LA Model. The drift-wall condensation is calculated as part of the analysis. Driftwall condensation is independent of seepage and can also bring water and chemicals to the surface of the WP. Drift wall condensation is especially important for co-disposed (CDSP) WPs during Stage 2 when all CDSP WPs are assumed to have drift-wall condensation.

The Localized Corrosion Initiation Uncertainty Analysis uses a similar chemistry submodel (Section 6.3.4.3.2) as the TSPA-LA Model, accessing the same 396 chemical composition look-up tables. However, rather than calculating the *pH* and ionic strength in the invert, the chemistry submodel calculates the *pH*, $[Cl^-]$, and $[NO_3^-]$ on the WP surface

The thermal-hydrology submodel is similar to the TSPA-LA Model (Section 6.3.2) and determines the temperature and relative humidity on the WP surface. The effects on the temperature and relative humidity from rubble are included as in the TSPA-LA Model. The main difference is in how the individual locations in the repository are modeled. The repository is divided into percolation subregions, or bins with a total of 3,264 multi-scale thermal hydrology nodes in all of the bins. Bin 1 has 163 nodes, bin 2 has 817 nodes, bin 3 has 1,300 nodes, bin 4 has 820 nodes, and bin 5 has 164 nodes. These nodes do not correspond exactly to the actual WP locations. The TSPA-LA Model represents each bin with a representative WP (Section 6.3.2). Unlike in the TSPA-LA Model, this Localized Corrosion Initiation Uncertainty Analysis represents the uncertainty in the thermal hydrology submodel by modeling two CDSP WPs and six commercial spent nuclear fuel (CSNF) WPs at each of the 3,264 nodes.

In summary, the Localized Corrosion Initiation Submodel samples the epistemic parameters for the 300 realizations just like the TSPA-LA Model. At each node within each bin for every realization, a specific CSNF WP and CDSP WP is chosen from the thermal-hydrology files. The model determines the thermal conditions and the relative humidity conditions for the WPs. Then, at every timestep, the model determines the chemical conditions on the WP surface. The model determines whether or not seepage is occurring on the WP, assuming that the DS does not keep water off of the WP. Finally, the model outputs the total number of nodes in each bin with $\Delta E \leq 0$ as a function of time. This total number of nodes is further post-processed to determine the fraction of nodes within each bin that have conditions favorable for the initiation of localized corrosion. Ultimately, the results of this Localized Corrosion Initiation Uncertainty Analysis are used in qualitative arguments in the TSPA-LA.

O3. RESULTS

The Localized Corrosion Initiation Uncertainty Analysis calculates the ΔE at each WP location in the repository for 300 epistemic realizations. The DS is assumed to allow water to contact the WP surface. The main result of the Localized Corrosion Initiation Uncertainty Analysis shown on Figure O-1 is the fraction of nodes for each WP type in each bin that have $\Delta E \leq 0$, indicating localized corrosion could initiate on the WP surface. Each figure shows 300 curves, one for each of 300 realizations of the epistemic parameters. Each curve displays the fraction of locations within the percolation bin at which localized corrosion could potentially occur, if a WP of the appropriate type were present at these locations. Statistics (mean, median, and 95th and 5th percentiles) are shown for the distribution of these 300 curves. In addition, one realization (Realization 142) is identified for further analysis. The curves for each realization end at the last

time at which localized corrosion could occur at any location. The plots of statistics end at the time when no realization has localized corrosion at any location. All of the plots end at 12,000-years, indicating conditions for WP localized corrosion initiation do not occur in the repository beyond 12,000 years.

In general, bins 3, 4, and 5 have higher fractions of localized corrosion because they have more locations with seepage. The climate changes at 2,000 years and 10,000 years are evident as small kinks in the mean curves. These kinks are due to more WPs having seepage in the glacial transition climate and the post-10,000-year climate. Before about 1,000 years, the CDSP WPs have a higher fraction of locations with potential localized corrosion initiation. This is due solely to the Stage 2 drift-wall condensation at every CDSP WP location. After Stage 2 ends at around 1,000-years, drift seepage dominates over drift-wall condensation and CSNF WPs have a higher incidence of localized corrosion initiation mainly because CSNF WPs have higher temperatures than CDSP WPs. Also, shown on Figure O-1 is the dominant effect of the single epistemic realization number 142, which is the only realization to have any nodes with localized corrosion after a few thousand years.

Figure O-2 shows the average fraction of WPs that could potentially experience localized corrosion, computed by multiplying each of the mean curves on Figure O-1 by its respective bin fraction (0.05, 0.25, 0.40, 0.25, and 0.05) and its WP type fraction (3416/11629 for CDSP WP and 8213/11629 for CSNF WP). There are more CSNF WPs and they are hotter so they have a higher incidence of potential localized corrosion than CDSP WPs. Thus, CSNF WPs comprise a larger fraction of the total number of WPs that could experience localized corrosion. The repository total curve shows the mean fraction of WPs with potential for localized corrosion for the entire repository.

As mentioned previously, only realization 142 has conditions favorable for localized corrosion initiation persisting beyond a few thousand years. This persistence is due to the combination of uncertain parameters in this realization. The coefficients in Equation O-1 and Equation O-2 are correlated within each equation, but the uncertainty terms and the coefficients are not correlated between the two equations. This allows for sampling large negative values for a_o and ε_{rcrev}, and large positive values for c_o and ε_{corr}. Also, the algorithm for applying uncertainty in the chemistry model essentially fixes the $[Cl^-]/[NO_3^-]$ ratio as an epistemic parameter (Section 6.3.4.3.2). These two features of this analysis imply that seven of the epistemic uncertain parameters essentially combine to give a constant value for each realization.

$$\text{Constant value} = \left(a_o + a_3 \frac{[NO_3^-]}{[Cl^-]} + \varepsilon_{rcrev} \right) - \left(c_o + c_3 \frac{[NO_3^-]}{[Cl^-]} + \varepsilon_{corr} \right) \qquad \text{(Eq. O-3)}$$

The combined value of the uncertain parameters in Equation O-3 for realization 142 is -936 mV, which is the tenth lowest of the 300 realizations. This large negative value means that the other conditions must change dramatically for the ΔE to become positive. Specifically, the temperature must cool down significantly and the $[Cl^-]$ and $[NO_3^-]$ must both become smaller. It takes a long time in realization 142 to overcome the large negative value indicated by Equation O-3.

The time histories of the chemical conditions and ΔE at every node for every realization cannot reasonably be shown. However, the time histories of the mean of all the nodes in a single bin can be shown. The values for the CSNF WPs in bin 3 are shown to represent the range of values for ΔE, with Realization 142 highlighted. Figure O-3 shows the value of ΔE, averaged over all of the 1,300 nodes for this bin. Notice that the mean ΔE for realization 142 is the last to go above zero. As mentioned previously, the large negative value for the parameters shown in Equation O-3 keeps ΔE low. The highest curves on Figure O-3, which have large positive values for the parameters in Equation 3, are never close to zero. Thus, localized corrosion never occurs in these realizations.

O4. IMPLEMENTATION IN TSPA-LA MODEL

Localized corrosion affects only those modeling cases in which the drip shield (DS) could fail to function within 12,000 years. The events and processes that could lead to DS failure include general corrosion of the DS, igneous intrusions, and seismic events. Section 6.3.5.2.3 discusses each of the modeling cases and indicates that localized corrosion is not modeled directly in any of the cases because of the low incidence of initiation within the first 10,000 years. This Localized Corrosion Initiation Uncertainty Analysis supports the low incidence argument.

INTENTIONALLY LEFT BLANK

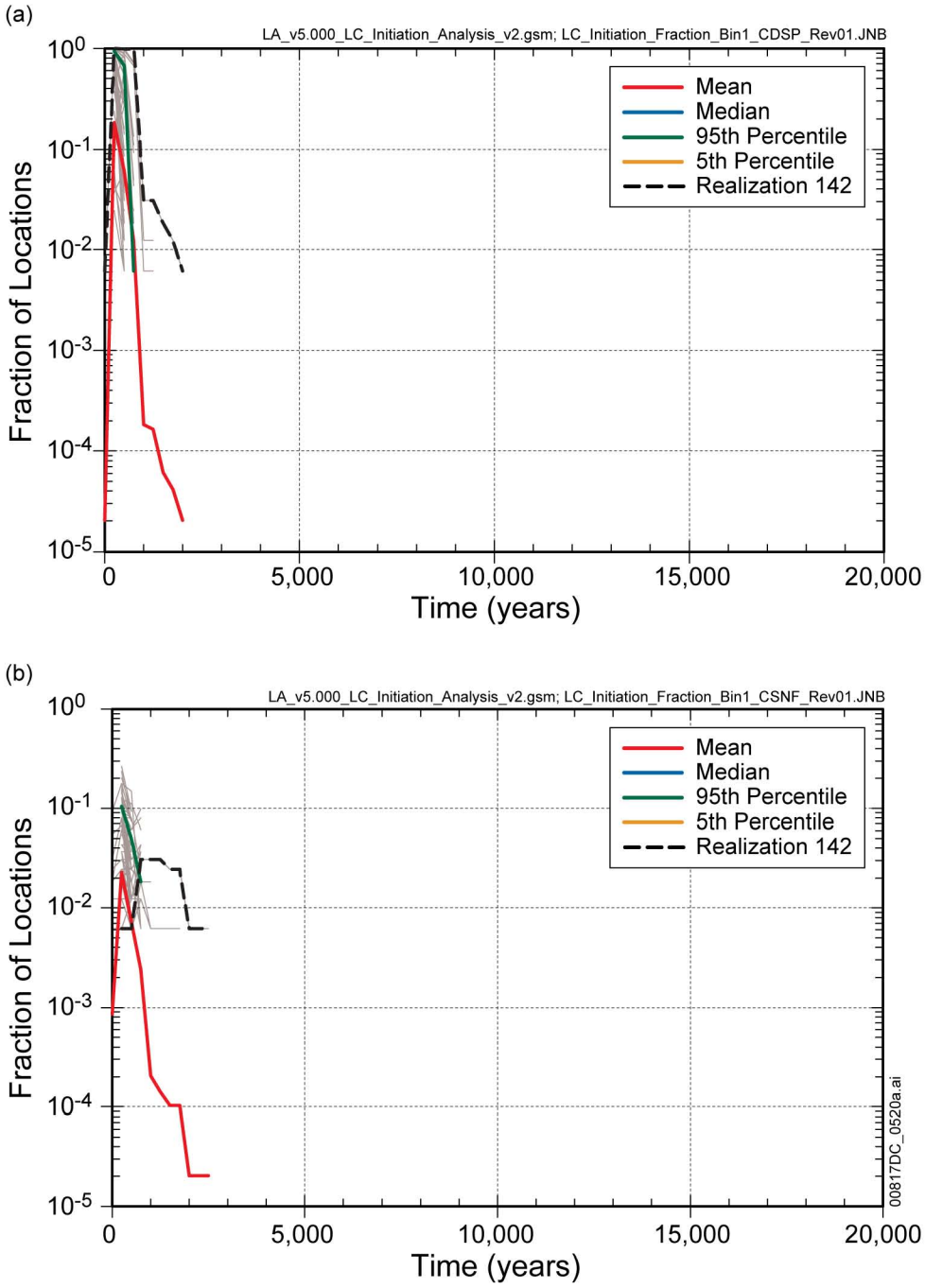

Source: Output DTN: MO0709TSPALOCO.000 [DIRS 182994].

Figure O-1. Fraction of Locations with the Potential for Localized Corrosion Initiation: (a) Bin1, CDSP; (b) Bin1, CSNF; (c) Bin2, CDSP; (d) Bin2, CSNF; (e) Bin3, CDSP; (f) Bin3, CSNF; (g) Bin4, CDSP; (h) Bin4, CSNF; (i) Bin5, CDSP; and (j) Bin5, CSNF

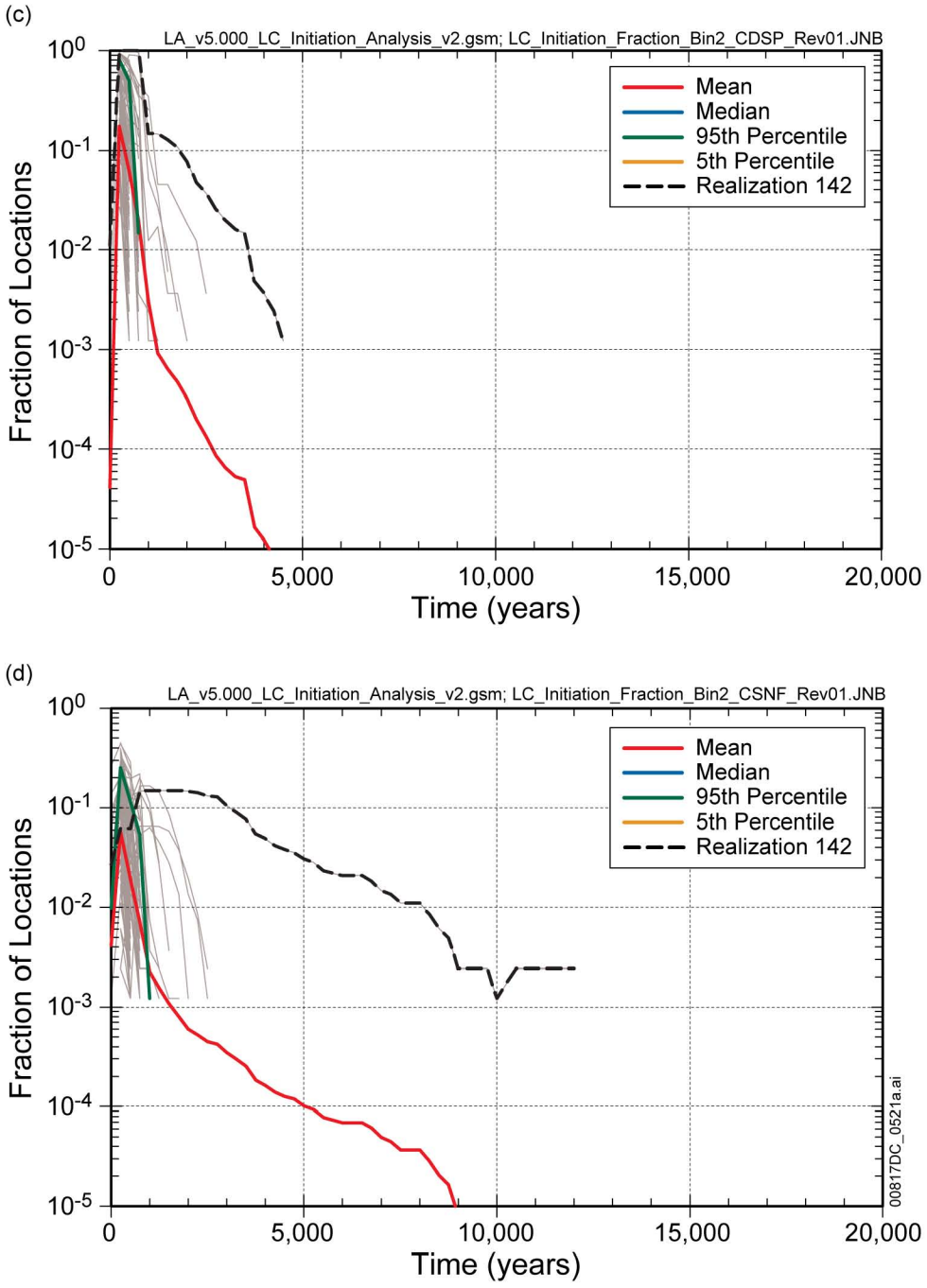

Source: Output DTN: MO0709TSPALOCO.000 [DIRS 182994].

Figure O-1. Fraction of Locations with the Potential for Localized Corrosion Initiation: (a) Bin1, CDSP; (b) Bin1, CSNF; (c) Bin2, CDSP; (d) Bin2, CSNF; (e) Bin3, CDSP; (f) Bin3, CSNF; (g) Bin4, CDSP; (h) Bin4, CSNF; (i) Bin5, CDSP; and (j) Bin5, CSNF (continued)

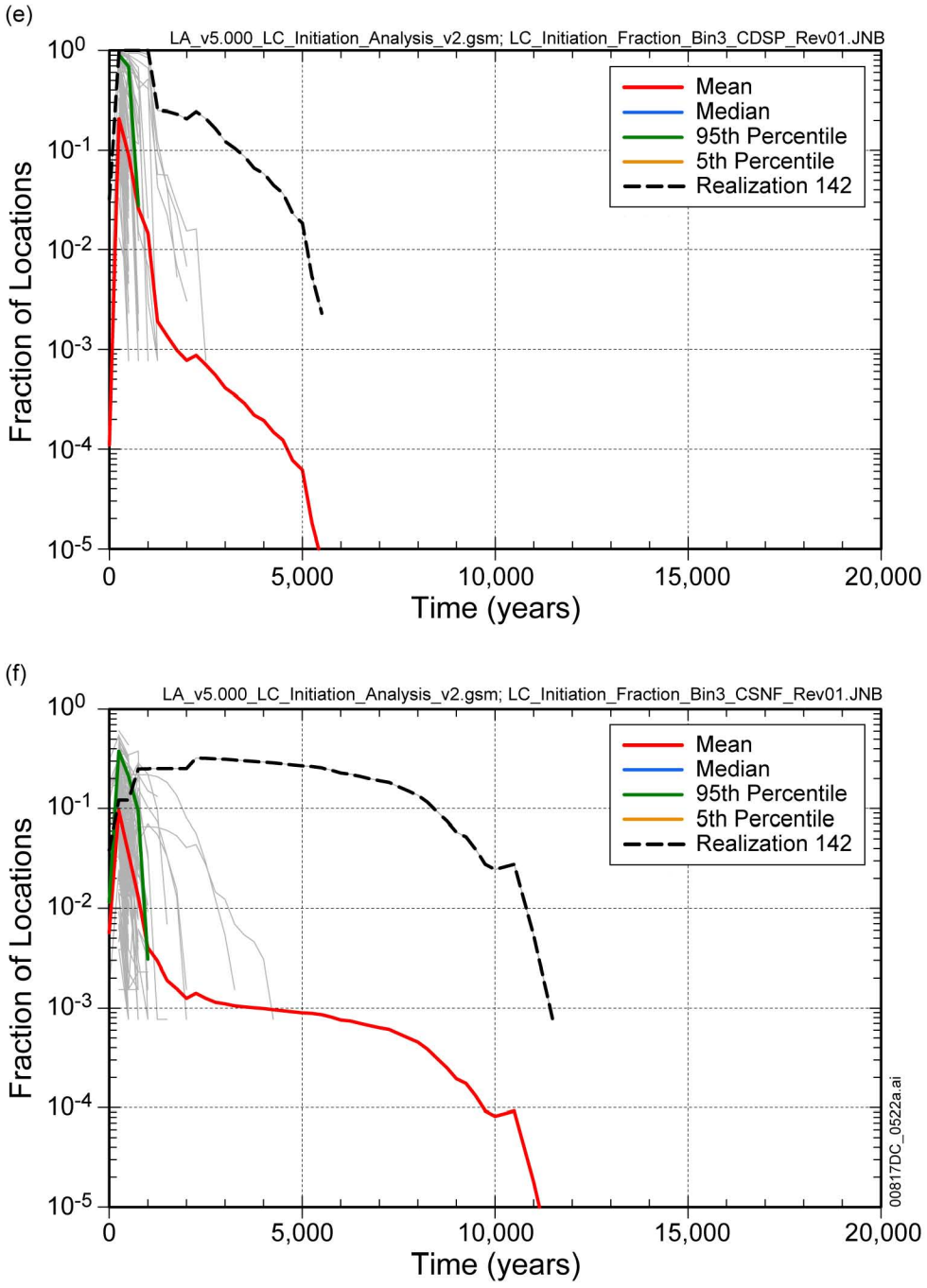

Source: Output DTN: MO0709TSPALOCO.000 [DIRS 182994].

Figure O-1. Fraction of Locations with the Potential for Localized Corrosion Initiation: (a) Bin1, CDSP; (b) Bin1, CSNF; (c) Bin2, CDSP; (d) Bin2, CSNF; (e) Bin3, CDSP; (f) Bin3, CSNF; (g) Bin4, CDSP; (h) Bin4, CSNF; (i) Bin5, CDSP; and (j) Bin5, CSNF (continued)

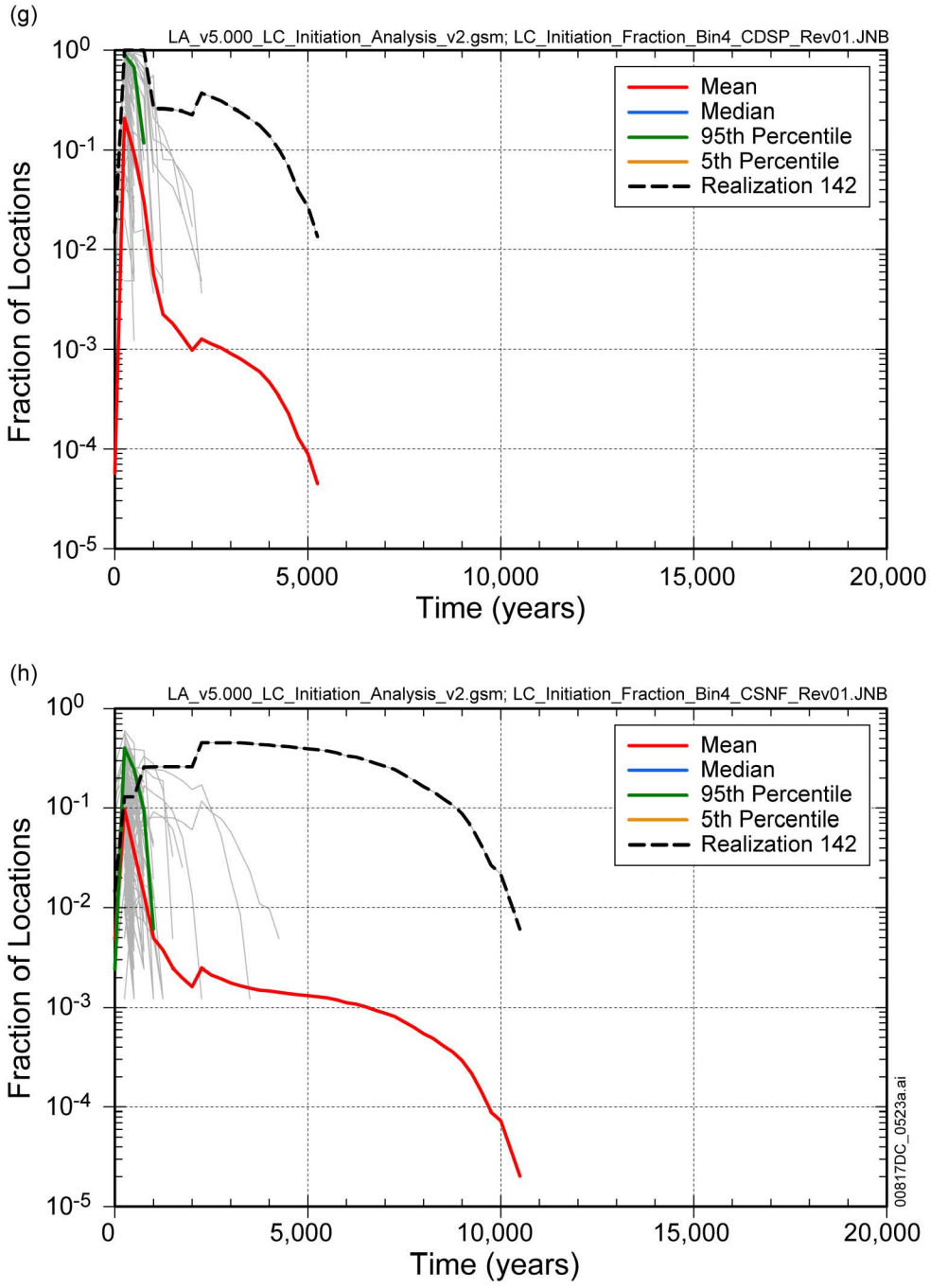

Source: Output DTN: MO0709TSPALOCO.000 [DIRS 182994].

Figure O-1. Fraction of Locations with the Potential for Localized Corrosion Initiation: (a) Bin1, CDSP; (b) Bin1, CSNF; (c) Bin2, CDSP; (d) Bin2, CSNF; (e) Bin3, CDSP; (f) Bin3, CSNF; (g) Bin4, CDSP; (h) Bin4, CSNF; (i) Bin5, CDSP; and (j) Bin5, CSNF (continued)

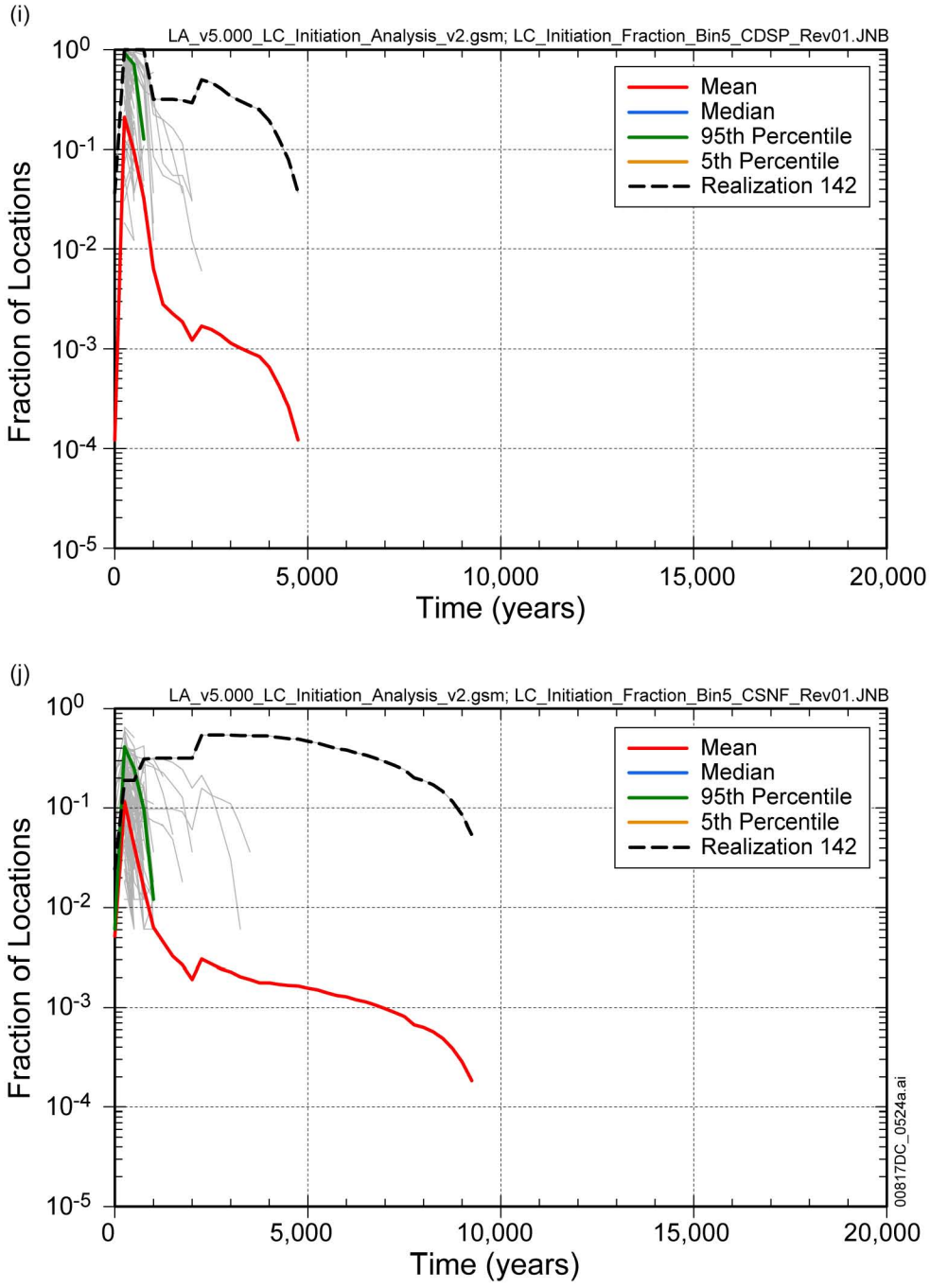

Source: Output DTN: MO0709TSPALOCO.000 [DIRS 182994].

Figure O-1. Fraction of Locations with the Potential for Localized Corrosion Initiation: (a) Bin1, CDSP; (b) Bin1, CSNF; (c) Bin2, CDSP; (d) Bin2, CSNF; (e) Bin3, CDSP; (f) Bin3, CSNF; (g) Bin4, CDSP; (h) Bin4, CSNF; (i) Bin5, CDSP; and (j) Bin5, CSNF (continued)

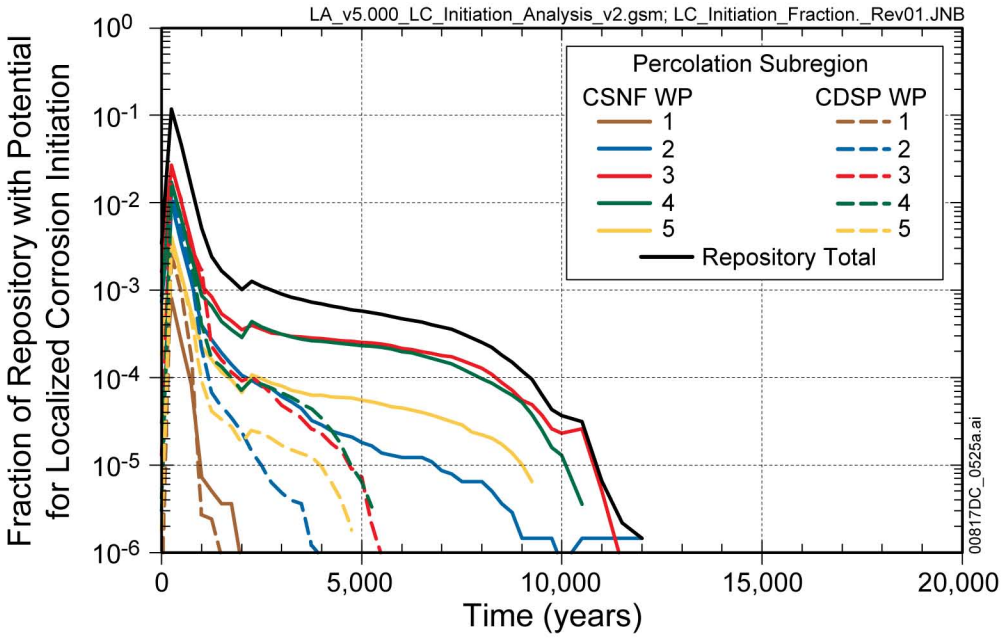

Source: Output DTN: MO0709TSPALOCO.000 [DIRS 182994].

Figure O-2. Fraction of Locations in Each Percolation Subregion with the Potential for Localized Corrosion Initiation

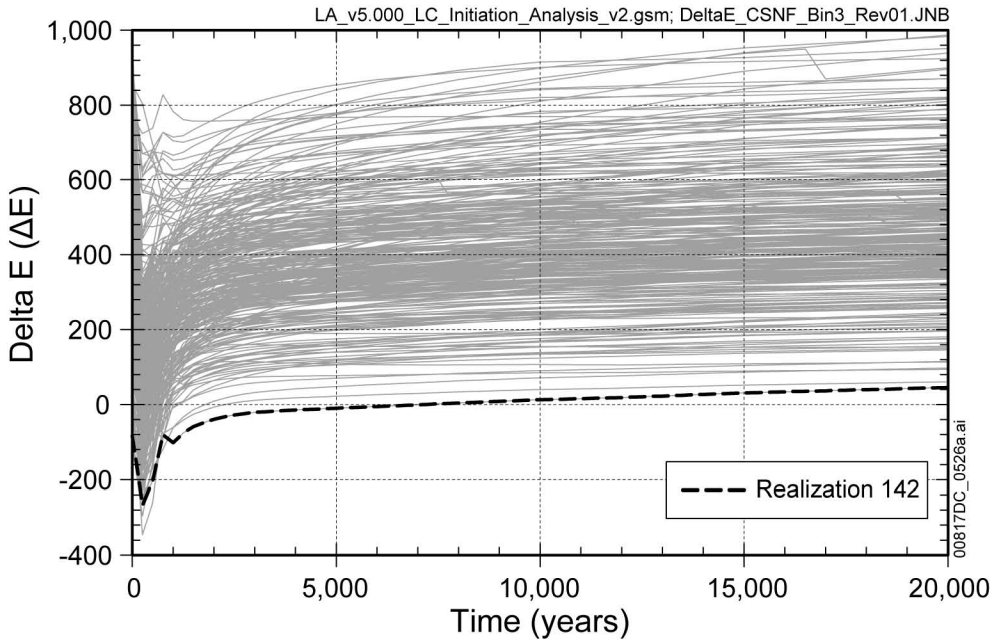

Source: Output DTN: MO0709TSPALOCO.000 [DIRS 182994].

Figure O-3. Average Delta E for Percolation Subregion 3, CSNF, for 300 Epistemic Realizations

INTENTIONALLY LEFT BLANK

APPENDIX P
IMPACT ASSESSMENTS

P1. INTRODUCTION

The post-model development activities following the completion of the TSPA-LA Model (Version 5.0) identified several issues related to errors in implementation, identification of undocumented conservatisms, and updates to parameter values. These issues are addressed here as per the review criteria outlined in Sections 2.1.4 and 2.3.5.2.1 of the *Technical Work Plan for: Total System Performance Assessment FY 07-08 Activities* (SNL 2008 [DIRS 184920]). In addition, this appendix includes an evaluation of the sensitivity of mean annual dose with respect to a fixed igneous event frequency (Section P.14), which is not documented elsewhere. Not all identified issues that are evaluated fall in the category of errors, as some of the issues are presented to only evaluate the degree of conservatism from the modeling choices made during the model development phase.

P2. INVENTORY AND SEEPAGE FRACTION

P2.1 ISSUE

Inventory for ^{36}Cl, ^{79}Se, and ^{126}Sn was omitted in the 10,000-year simulation modeling cases and thus not included in the dose calculations. In addition, the seepage fractions applied for the 10,000-year simulations are based on the post-10,000-year climate.

P2.2 ISSUE DESCRIPTION

The inventories for ^{36}Cl, ^{79}Se, and ^{126}Sn were zeroed out in the 10,000-year simulations but were included for the 1,000,000-year simulations. As a result, the mean annual dose is under predicted for the 10,000-year simulations in all modeling cases except for Volcanic Eruption Modeling Case, where the radionuclide inventories are correct.

The seepage fractions for the 10,000-year simulations are based on the post-10,000-year climate instead of the glacial-transition climate, which could lead to small error in estimating the number of waste packages (WPs) in the dripping environment.

P2.3 IMPACT ASSESSMENT

The impact from these errors is anticipated to be negligible to the mean annual dose because: (a) the three omitted radionuclides do not significantly contribute to the total dose at 10,000 years as determined based on the 1,000,000-year simulations, where the inventory of these radionuclides were included (Figures 8.2-2, 8.2-4b, 8.2-6b, 8.2-8b, 8.2-12b, and 8.2-14b); (b) the change in seepage fraction based on the glacial-transition climate versus the post-10,000-year climate is estimated to be small, leading to a small decrease in the number of waste packages (WPs) assigned to the dripping environment.

The impact evaluation was conducted by correcting the two errors and running the modeling cases for the 10,000-year time period. The impact evaluation for each modeling case is provided in detail below:

<u>Waste Package Early Failure (EF) Modeling Case</u>

The mean annual dose for the impact evaluation case is compared to the base case on Figure P-1a. The impact evaluation case shows a small increase (<10 percent) in the mean annual dose for small time periods due to inclusion of the inventory of the three radionuclides. Note that ^{36}Cl and ^{79}Se are among the top six dose contributors in the first 10,000 years (Figure P-1b). The effect of reduction in seepage fraction by 22.5 percent for the impact evaluation case (Table P-1) is not discernable as the drip shield (DS) remains intact throughout the simulation and the transport out of the WP is still diffusive. Thus, even though there is lesser probability of WP being placed in the dripping environment (based on seepage fraction) the diffusive mass release out of the WP would not change appreciably and any small perturbations due to change in boundary conditions in the engineered barrier system (EBS) would be overshadowed by the dispersion effects in the unsaturated zone (UZ) and saturated zone (SZ). The expected dose calculations are not affected from change in seepage fraction (Equation 6.1.2-13), as the dose is summed over both dripping and non-dripping environments.

Drip Shield Early Failure (EF) Modeling Case

The mean annual dose for the impact evaluation case is compared to the base case on Figure P-2a. The impact evaluation case shows a small decrease in the mean annual dose even though the three radionuclides are included (Figure P-2b). The mean annual dose is typically lower by about 22 percent in the impact evaluation case. This is due to the reduction in the seepage fraction since the total seepage fraction also changed by about 22 percent in the impact evaluation case (see total of last column in Table P-1). Note that there is no localized corrosion-related early failure modeled for WP in a non-dripping environment and, thus, the only release in this modeling case is from the localized corrosion of WPs in a dripping environment. Consequently, the seepage fraction is used as a weighting factor in the expected dose calculations as shown by Equation 6.1.2-14, and thus has a linear effect on the mean annual dose.

Seismic Fault Displacement (FD) Modeling Case

The mean annual dose for the impact evaluation case is compared to the base case on Figure P-3a. The impact evaluation case shows a small decrease (of about 5 percent) in the mean annual dose even though the three radionuclides are included (Figure P-3b). The contribution of the three added radionuclides is less than 2 percent to the mean annual dose. This increase is offset by a larger decrease due to the change in the seepage fraction where the percolation subregion weighted average seepage fraction reduced by about 10 percent in the impact evaluation case (Table P-2). As a result, the number of WPs that are exposed to the seepage are reduced, leading to lower advective mass flux. The mean annual dose does not reduce in proportion to the reduction in seepage fraction (as was the case for the Drip Shield EF Modeling Case) because the water flux through the WP is scaled down by the fractional breach area while the breach area is small. In such cases, the release is dominated by diffusion out of the WP and thus the overall effect on the mean annual dose from reduction in seepage fraction is non-linear.

Seismic Ground Motion (GM) Modeling Case

The mean annual dose for the impact evaluation case is compared to the base case on Figure P-4a. The mean annual dose for the impact evaluation case shows a gradual increase with time from about 1 percent at 500 years to over 7 percent by 10,000 years. This is primarily due

to the dose contribution from the three included radionuclides whose dose is also increasing with time (Figure P-4b). Specifically, ^{36}Cl and ^{79}Se are the fourth and fifth largest dose contributors with a contribution of about 10 percent to the total dose.

Because the DSs remain intact and the WP breaches are only stress corrosion cracks in this modeling case, releases from the WP are diffusive and insensitive to the seepage fraction. Therefore, even though the effect on seepage fraction is appreciable for this modeling case, with the average (area weighted) reduction of over 55 percent (Table P-3), the dose is not significantly influenced. The seepage fraction reduction is greater compared to other modeling cases because the base-case calculations have the effect of drift degradation included that occur past 10,000 years (up to 1,000,000 years), which leads to a greater number of locations undergoing seepage. The impact evaluation case is not affected by this, as drift degradation from seismic activity in the first 10,000 years is not considered (Section 7.3.2.6.1.3), and thus the seepage fraction is the same as for the nominal conditions (as shown in Table P-1). So even though there are fewer WPs being placed in the dripping environment (based on seepage fraction) the overall diffusive mass releases out of the WPs is not appreciably affected due to the presence of small crack areas, although the boundary concentrations in the invert may have changed. Any small perturbations due to changes in boundary conditions in the EBS are likely to be overshadowed by the dispersion effects in the UZ and SZ. Thus, mean annual dose is only affected by the added radionuclides.

Igneous Intrusion Modeling Case

The mean annual dose for the impact evaluation case is compared to the base case on Figure P-5a. The mean annual dose for the impact evaluation case is marginally higher (by <4 percent) compared to the base case. The contribution of the three included radionuclides to the mean annual dose is negligibly small (Figure P-5b).

The seepage fraction effect is not seen in this modeling case, as all WPs see percolation flux following the igneous intrusion. There is no nominal corrosion-related WP failure prior to the igneous event in the 10,000-year simulation and, thus, the seepage fraction correction has no effect prior to the igneous event. The marginal increase in the mean annual dose is likely related to the inclusion of the three radionuclides.

P3. WASTE PACKAGE DAMAGE FROM SEISMIC EVENTS

P3.1 ISSUE

Conservative treatment of WP damage from seismic events following the first breach due to nominal corrosion processes.

P3.2 ISSUE DESCRIPTION

The probability of seismic damage is provided for two end-member states of the WP—one with intact internals and one with fully degraded internals. In the base case, once any WP is breached by a nominal process in a given percolation subregion (e.g., from first occurrence of stress corrosion cracks located on the outer lids) the probability of seismic damage is switched from the intact internals abstraction to the fully degraded internals abstraction, which increases the chance

of seismic damage occurring while the DS is intact. This probability is then applied to all the WPs in the given percolation subregion, which is conservative, as most of the WPs have not yet failed by the nominal processes and should be using the intact internals damage probability. As a result, most WPs fail earlier and acquire greater damage area than expected.

P3.3 IMPACT ASSESSMENT

The impact of this conservative implementation is anticipated to vary with time, as it only occurs in situations where the breach from nominal corrosion occurs earlier than the seismic damage event. Since nominal breaches do not occur in the first 10,000 years, the seismic modeling cases that are run for the 10,000-year compliance duration are not affected. The only modeling case where this has an effect is in the Seismic GM Modeling Case run for the 1,000,000-year simulation duration. Even in this case, the CDSP WPs are generally not impacted because the seismic damage is likely to occur earlier than the nominal corrosion failure: the nominal corrosion failures from stress corrosion cracks do not occur until after 100,000 years while the probability of seismic damage on CDSP WPs has a mean value of around 0.36 in 100,000 years (output DTN: MO0709TSPAWPDS.000 [DIRS 183170]). In contrast, the probability of commercial spent nuclear fuel (CSNF) WPs failing from seismic events is low, with a mean value of around 0.006 in 100,000 years (output DTN: MO0709TSPAWPDS.000 [DIRS 183170]), and thus the nominal corrosion failures are likely to cause the first damage for CSNF WPs. Consequently, the impact of this conservative treatment in likely to occur only for CSNF WPs.

The nominal corrosion failures for CSNF WPs do not start until after 100,000 years and only about 5 percent of realizations would have initiated CSNF WP failures by 200,000 years. Thus, the impact of the conservative treatment of applying degraded internals abstraction following nominal corrosion failure is likely to occur past 100,000 years and likely to last for up to about 400,000 years as by then the majority of the realizations (about 50 percent) would have had some WP failures by nominal corrosion, irrespective of the seismic damage. In the period between 100,000 and 400,000 years, the conservatism is likely to have the maximum impact between 200,000 years and 300,000 years. This is because in this time period the DSs are intact and thus any nominal corrosion failure of any WP in a given percolation subregion would lead to usage of seismic damage abstraction for the "degraded internals under intact DS" for all WPs in the percolation subregion. Since the probability of damage is fairly high from this abstraction (Figure 6.6-10b and Figure 6.6-10c) there is a good chance of failing the WPs and thereby releasing the radionuclides. Following DS failures (typically past 250,000 years), the probability of damage decreases as the WP is likely to be surrounded by rubble and the seismic damage abstraction for the WP with "degraded internals surrounded by rubble" is used (Figure 6.6-15a and Figure 6.6-15b).

Because the seismic damage is likely to cause stress corrosion cracking (SCC), the breach area on the WP would be very small initially, and then grow with each seismic-damage event, but the overall area would still remain small compared to the WP surface area, and thus the release rate out of the WP would be limited. Since non-sorbing radionuclides such as ^{99}Tc and ^{129}I are the major dose contributors and since the WP release would be diffusive (as no advection can occur through the stress corrosion cracks) the breach area along with the number of failed WPs would predominantly control the mass release. The impact of the current implementation is likely to

cause the mean annual dose to be significantly higher in the timeframe of 200,000 and 300,000 years compared to the case where the conservatism is removed. The impact is anticipated to be small at later times.

P4. OUTER BARRIER FAILURE FLAG IN SEISMIC MODEL

P4.1 ISSUE

WP outer barrier failure flag is triggered when the inside-out corrosion of the WP is initiated in the Seismic GM Modeling Case, which could be earlier than the actual breach time from seismic damage or nominal corrosion.

P4.2 ISSUE DESCRIPTION

The inside-out corrosion initiation time for the WP is approximated by pre-calculating the breach time from a seismic event using a conservative calculation and then passing this time to Waste Package Degradation Model (WAPDEG). But this time is also used, by error, to trigger the WP outer barrier failure flag which could be much earlier than the appearance of the first actual breach (crack or patch opening area). Since the downstream waste form and transport submodels use this flag to initiate the waste form degradation and transport processes inside the WP they get started earlier than intended. Once the WP breach occurs (either by nominal corrosion or by seismic damage) the release rates could be higher than expected due to build-up of mass in solution prior to the breach.

P4.3 IMPACT ASSESSMENT

The impact of this error is anticipated to be negligibly small, as most realizations would have either a nominal corrosion failure or seismic event failure before the pre-calculated inside-out corrosion initiation time. Thus, in most realizations, the outer barrier failure flag trigger time and the first breach times will occur simultaneously leading to correct calculations. This is because even though the pre-calculated inside-out corrosion initiation times are based on conservative calculations, they still lead to initiation times, in most realizations, that are either later than the actual breach times from nominal corrosion failures or at the same time as the breach time calculated from the actual seismic calculations.

For CDSP WPs, only about 14 percent of realizations have inside-out corrosion initiation times earlier than the actual seismic damage time, while for CSNF WPs only about one percent of realizations have inside-out corrosion initiation times earlier than the actual seismic damage time (output DTN: MO0709TSPAWPDS.000 [DIRS 183170], file v5.000_GS_9.60.100_StandAlone_9krlz.gsm in folder Seismic_9k_Rlz). Even in these realizations, the time difference between the outer barrier failure flag trigger time and the actual breach time may not always be large, as the nominal corrosion is accelerated from the initiation of inside-out corrosion leading to rapid failure.

It should be noted that in these few realizations, even though the outer barrier failure is triggered earlier and waste form degradation processes and transport processes inside the WP start, there is no mass release from the WP until the WP is truly breached. So the mass release time to the UZ and SZ is unchanged. Since the breach area is small due to the presence of only stress corrosion

cracks, the diffusive releases out of the WP would be controlled by the breach area rather than by the concentration gradient. Thus, the release rates would be small and the mass would be depleted slowly. The overall effect of the error on the mean annual dose is likely to be negligibly small.

P5. INVERT CHEMISTRY

P5.1 ISSUE

In-package chemistry applied in the invert after the DS is failed without considering flow through the WP.

P5.2 ISSUE DESCRIPTION

Currently the in-package chemistry computed for the corrosion products domain is applied to the invert after the DS is failed, without considering whether there is flow through the WP or not. The direction provided by *Engineered Barrier System: Physical and Chemical Environment* (EBS P&CE) (SNL 2007 [DIRS 177412], Table 6.15-1) was to only apply the in-package chemistry from the corrosion products domain of the WP to the invert when there was flow through the WP after the DS is failed. In all other cases, the chemistry equilibrated to the invert temperature, relative humidity, and Pco_2 as described by the EBS P&CE model was supposed to be applied.

P5.3 IMPACT ASSESSMENT

The impact on the mean annual dose from this error is anticipated to be negligible, as this error would only occur in situations where the DS has failed while the WP only has SCC opening areas (leading to no flow through the WP). This situation is only possible in the Nominal Modeling Case and in the Seismic GM Modeling Case. But even in these cases, because the DS failure is not expected until past 200,000 years, any releases prior to DS failure are not impacted. Furthermore, past 200,000 years, benign chemical conditions are anticipated in both the WP and invert due to near-ambient temperatures, and, thus, the difference in the in-package chemistry (from the corrosion products domain) and the chemistry calculated from the EBS P&CE model will be small. In addition, the two radionuclides that control the mean annual dose for the majority of the simulated time period beyond 200,000 years, in both modeling cases are ^{99}Tc and ^{129}I, which are not affected by the chemistry. Once the general corrosion patches appear and the flow through the WP initiates, the calculations become correct once again.

Because of the above arguments, this error is anticipated to have negligible impact on the mean annual dose.

P6. WELD VOLUME

P6.1 ISSUE

Incorrect weld volume is used in computing the probability of manufacturing defects as a factor of π was omitted from the WP circumference calculation.

P6.2 ISSUE DESCRIPTION

The weld volume is an input to the CWD software (STN: 10363-2.0-00 [DIRS 162809]) that is used to compute the cumulative probability of a manufacturing defect conditional on the probability for the non-detection of weld defects. The calculated value is then used as an input in the WAPDEG code for calculating the time of WP failure from SCC or by general corrosion.

The Poisson intensity parameter for the average number of defects per closure weld is given by

$$\lambda = DF \cdot V \cdot \lambda_c \cdot \frac{\lambda_s \cdot H(t)}{(1 - \exp(-\lambda_s \cdot t))} \quad \text{(Eq. P-1)}$$

where,

DF is the fraction of defects capable of propagation;

V is the weld volume;

λ_c is the Poisson intensity before detection;

λ_s is the parameter for a truncated (at the weld thickness) exponential distribution for weld sizes before detection;

t is weld thickness; and

H(t) is the conditional probability that the defect is not detected.

Inspection of the above equation shows that correcting the weld volume (V) by a factor of π will also increase the value of λ by a factor of π (about 3.14).

Based on the Poisson intensity parameter, the CWD software returns a value of q, the probability of one or more defects per closure lid weld, as:

$$q = 1 - \exp(-\lambda) \approx \lambda \quad \text{for } \lambda << 1 \quad \text{(Eq. P-2)}$$

P6.3 IMPACT ASSESSMENT

This error impacts only those modeling cases where nominal corrosion processes are considered. Thus, only the Nominal Modeling Case and the Seismic GM Modeling Case are likely to be affected. In order to evaluate the impact on the value of q (the probability of one or more defects per closure lid weld), a standalone model that was derived from the base case and uses the same random seed (and hence the same sampling) was run for the 300 realizations to sample epistemic uncertainties. This was run twice, once with the uncorrected (original) weld volume and then once with the corrected weld volume, for both CDSP and CSNF WPs. The distribution of q (from 300 realizations) was compared for the two cases and it was found that the probabilities increased by about a factor of three for the impact evaluation case, indicating approximately three times more probability of having one or more defects per closure lid weld (per WP).

The mean probability of one or more defects per closure weld lid per CDSP WP increased from about 1.2×10^{-4} to 3.8×10^{-4} and that for the CSNF WP increased from about 1.1×10^{-4} to

3.4×10^{-4} (output DTN: MO0709TSPALAMO.000 [DIRS 182981]. For either WP type, the expected number of weld flaws per WP is significantly smaller than one. On the other hand, there are about six incipient cracks per patch expected on the closure lid patches (Section 6.3.5.1.2), which would lead to about 252 cracks per CDSP WP and about 228 cracks per CSNF WP. Because the main contribution to WP failure due to cracking comes from the presence and growth of incipient cracks and not weld flaws, the error in the weld volume is estimated to have negligible impact on the diffusive area, however it is possible that the first breach time could be earlier in some WPs due to occurrence of cracks from weld flaws. The overall impact on the mean annual dose is anticipated to be negligible.

P7. CRACK FAILURE OPENING

P7.1 ISSUE

The nominal crack failure opening area incorrectly calculated once the elapsed time is greater than the seismic damage time.

P7.2 ISSUE DESCRIPTION

After a seismic event that causes damage, the opening area calculation per failed WP from nominal stress corrosion cracks is incorrectly divided by the cumulative fraction of first crack failures on the WP. This results in an overestimation of the opening area as the cumulative fraction is small (<<1) early on and increases gradually to unity.

P7.3 IMPACT ASSESSMENT

The error can only impact the Seismic GM Modeling Case and would appear only after WP has undergone seismic damage. Note that prior to the seismic damage the calculated nominal crack area is calculated correctly. Because the total opening area from cracks per failed WP that occurs as a consequence of seismic damage (vibratory ground motion) is at least an order of magnitude greater than the area from the nominal SCC, correcting the error is not going to affect the transport area for diffusion calculations. The mean damaged areas for CSNF and CDSP WP are shown on Figures 6.6-12 and 6.6-13 under intact DS.

Because of the above arguments, this error is anticipated to show no to negligible impact on the mean annual dose for the Seismic GM Modeling Case.

P8. DEGRADATION START TIME

P8.1 ISSUE

Degradation processes inside the WP could start before the breach from an igneous event under certain aleatory configurations of specified igneous event times. This is not consistent with the treatment in other modeling cases.

P8.2 ISSUE DESCRIPTION

Two calculations for the igneous event time are currently made in the model. One is based on randomly sampling the event time (from a log-uniform distribution) to be used for the unified sampling case (no separation of aleatory and epistemic uncertainty) and the other is based on specifying the event time to be used in the compliance calculations (by separation of aleatory and epistemic uncertainty). An error occurs in connection with the WAPDEG subroutine as the sampled event time is passed to WAPDEG even when the event time is specified. This could result in failing all WPs in realizations where the sampled event time is prior to the specified event time. As a result, the degradation processes inside the WP could be triggered earlier than the actual event. The breach area, however, is calculated correctly and is based on the breach occurring either from the specified event time or from the nominal corrosion processes. In cases where nominal corrosion has not breached the WP, the breach area remains zero prior to the specified event time.

P8.3 IMPACT ASSESSMENT

This error only occurs in the Igneous Intrusion Modeling Case and is anticipated to have negligible impact on the mean annual dose. This is because all waste forms are modeled to degrade instantaneously after the igneous intrusion and thus starting the degradation processes inside the WP prior to the specified igneous event is likely to have negligible impact.

In realizations where the sampled event time is earlier than the specified event time and where the nominal corrosion processes could cause the WP to breach prior to the specified event time, the calculations would not be correct, as it would over predict the number of failed WPs. But such situations are only possible in very few realizations and unlikely to occur before 200,000 years, as in most realizations the breach from nominal corrosion processes typically do not occur prior to this time. The impact on mean annual dose is likely to be negligible.

P9. THRESHOLD RUBBLE VOLUME

P9.1 ISSUE

Threshold rubble volume (per drift length) that is used for determining when the nonlithophysal drifts undergo collapse is incorrect. It is currently using the value of 5 m^3/m while the correct value is 0.5 m^3/m.

P9.2 ISSUE DESCRIPTION

The threshold rubble volume (per drift length) is used to calculate the time when the drifts in the nonlithophysal locations should be considered collapsed for the purpose of determining the degraded-drift seepage flux. A similar calculation is done for the lithophysal locations but the threshold rubble volume is calculated correctly for the lithophysal locations.

P9.3 IMPACT ASSESSMENT

This error only occurs in the Seismic GM Modeling Case that is run for the 1,000,000-year duration, where the rubble volume resulting from multiple seismic events is calculated inside the

drift. For other modeling cases in the Seismic Scenario Class, the rubble volume is specified and is always greater than the threshold value of 5 m^3/m. Thus, reducing the threshold is not going to affect the outcome.

In the Seismic GM Modeling Case, the drift rubble calculations for the lithophysal zones are used in the nonlithophysal zones for the DS fragility calculations based on the rockfall loads. This is a conservative treatment, as the rockfall volume from the lithophysal zones is greater than that for the nonlithophysal zones (Figure 6.6-7) leading to greater probability of DS failure. Thus, this error does not affect the DS failure times in the nonlithophysal zones.

The threshold rubble volume for the nonlithophysal drift is used in the seepage calculations (for the percolation subregion) to determine when the seepage flux should be changed from the intact drift seepage value to the degraded drift seepage value. Nominal seepage values are used under intact drift conditions but after drift collapse the percolation flux at the base of the PTn is used for the nonlithophysal locations. This switch to percolation flux would occur earlier due to lowering of the threshold rubble volume. But the effects are likely to be very small, as only about 16 percent of the repository is in the nonlithophysal zone. For the five percolation subregions (from 1 to 5), the nonlithophysal fraction is 0.32, 0.24, 0.17, 0.04, and 0.11, respectively. The greatest change in seepage flux is likely to occur in percolation subregion 1, but because it only occupies 5 percent of the repository area the contribution to the overall mass release from the EBS is negligibly small. The actual change in the seepage flux is estimated to be relatively small in all percolation subregions, leading to negligible impact on the mean annual dose.

P10. UNINTENDED CORRELATION OF UNCERTAIN PARAMETERS

P10.1 ISSUE

Base-case TSPA-LA Model contains an inadvertent perfect correlation between two uncertainty parameters: WRIP_beta_rand_a and PCE_Delta_pCO2_a.

P10.2 ISSUE DESCRIPTION

The WRIP_beta_rand_a uncertainty parameter is used to sample a probability value (uniform between 0 and 1) such that when the Water-Rock Interaction Parameter is sampled from a beta distribution at every timestep, it samples from the same probability level in a given realization. The water-rock interaction parameter is used in the P&CE calculations for computing the appropriate invert chemistry.

The PCE_Delta_pCO2_a uncertainty parameter (uniform between -1 and 1) is used in scaling the ambient P_{CO2} in the drift between the minimum and maximum values to compute the drift P_{CO2}.

These two parameters got inadvertently correlated when one of the stochastic elements that was initially created was copied into another submodel to create the other stochastic element, thereby retaining the same local random seed.

P10.3 IMPACT ASSESSMENT

The two uncertainties, generally affect different abstractions, one in terms of water-rock interaction and the other in terms of drift P_{CO2} calculations. However, there is some indirect interaction between the two parameters. The maximum P_{CO2} value that is used in calculating the final drift P_{CO2} is a function of the water-rock interaction parameter. Even though some relationship, if any, may be present, the effect of this correlation on downstream calculations is likely to be weak. This is because: (a) the WRIP_beta_rand_a is used to only determine the probability value and not the actual value of the water-rock interaction parameter, which itself could vary at each timestep due to changes in the mean and standard deviations (SD); and (b) the calculations for the drift P_{CO2} and invert chemistry are further modified by considering other uncertainties, thus diluting the already-weak interaction. As a result, the unintentional correlation is likely to have negligible impact on the mean annual dose.

P11. UNCERTAINTY IN URANIUM SOLUBILITY

P11.1 ISSUE

The uncertainty associated with fluoride concentration in calculating the uranium solubility for the CSNF WPs is incorrectly calculated in the Igneous Intrusion Modeling Case.

P11.2 ISSUE DESCRIPTION

The GoldSim selector elements U_Eps_2_Hi_IStr and U_Norm_Hi_IStr calculate the uncertainty associated from variations in fluoride concentration (ε2 and N) in the uranium solubility for CSNF waste form domain (CSNF Cell 1) and for the CSNF corrosion products domain (CSNF Cell 2) (see Section 6.3.7.5.2). The values that are used under certain sets of P_{CO2} and pH conditions were mistakenly set to their CDSP counterparts. The correct values should be set to U_Eps_2_Boltwoodite_CSNF_High and U_Boltwoodite_CSNF_High_N, respectively, instead of U_Eps_2_Boltwoodite_CDSP_High and U_Boltwoodite_CDSP_High_N. In addition, the value of the third switch in the selector U_Norm_Hi_IStr was mistakenly set to U_Boltwoodite_Glass_Low_N. The correct value should be U_Schoepite_CSNF_High_N.

P11.3 IMPACT ASSESSMENT

This error only affects the uranium solubility calculation for the Igneous Intrusion Modeling Case. The duration of the error is likely to be small, as these calculations are only incorrect under high ionic strength conditions (I>0.2 mol/kg), which would last for only a short duration in the simulation due to dilution from flow through the WP. Furthermore, even under limited duration high ionic strength conditions, the calculation is only incorrect when the Na-Boltwoodite solubility is used, which is only applicable under limited P_{CO2} and pH conditions.

Because of the small probability of the error and its short duration, its effect is not likely to have an impact on the total mass transported out to the UZ and SZ. As presented on Figure 8.2-8 and discussed in Section 8.2.3.1, uranium is not a major contributor to the mean annual dose in the Igneous Intrusion Modeling Case and thus the effect of this error, if any, will be negligibly small.

P12. IONIC STRENGTH FOR HIGH-LEVEL WASTE GLASS DOMAIN

P12.1 ISSUE

During model calculations, for conditions where there is flow through the WP (exceeding a threshold of 0.1 L/yr), the ionic strength for the high-level waste (HLW) glass domain is always determined for flowing conditions, while it should be selecting the minimum between the ionic strength calculations for the flowing conditions and non-flowing conditions as described in *In-Package Chemistry Abstraction* (SNL 2007 [DIRS 180506], Section 6.10.9.1[a]).

P12.2 ISSUE DESCRIPTION

Two ionic strength abstractions are implemented in TSPA that are applicable to HLW waste form subdomain (CDSP Cell 1a): one that is based on relative humidity when there is no flow through the WP (referred as vapor influx case), and the other that is based on the flow rates and the time since WP failure (referred as liquid influx case). For conditions when there is no flow through the WP or where the flow through the WP is less than the threshold of 0.1 L/yr, the vapor influx based calculations are to be used. For flowing conditions, (equaling or exceeding threshold of 0.1 L/yr), the ionic strength should be based on choosing the minimum value after evaluating the ionic strength from both abstractions (SNL 2007 [DIRS 180506], Section 6.10.9.1[a]). The implementation error occurs in the latter case, where the ionic strength calculated for the liquid influx case is always used without evaluating the minimum.

P12.3 IMPACT ASSESSMENT

The implementation error is only applicable to ionic strength calculations in the HLW waste form subdomain of the EBS Transport Model and does not affect the ionic strength calculations for the downstream transport subdomains. Furthermore, it is only an issue when there is flow through the WP that equals or exceeds the threshold of 0.1 L/yr. But even here, for the majority of the time, the calculations would be correct, as under flowing conditions it is most likely that the minimum ionic strength would be calculated from the liquid influx-based abstractions rather than from the vapor influx-based abstraction. Thus the error, even if it occurs, would only occur for very short duration.

The most likely ionic strength for the liquid influx case typically ranges from 0.001 to about 0.1 mol/kg (see Table 6.3.7-11), while that for the vapor influx case typically ranges from about 0.13 mol/kg at relative humidity of 99.8 percent (a reasonable high value in the simulation) to 2.6 mol/kg at relative humidity of 95 percent (a reasonable low value at the start of transport) (Table 6.3.7-9 and Equation 6.3.7-1). The range of most likely ionic strength value for the liquid influx case is lower than that for the vapor influx case. However, because of the uncertainties that are computed independently for the two abstractions, the final values could either increased or decreased somewhat and thus there is a small chance that the current calculation may not be correct. But the duration of this condition is likely to be small, if it occurs, because the ionic strength typically decreases with increasing flow rates.

The ionic strength is used in the solubility model to determine the applicable uncertainty range and in the colloid-facilitated transport model to determine the colloid stability. Both models are unlikely to be affected for the most part, as they are only sensitive to variations across certain

ionic strength boundaries: the primary uncertainty in solubility model (ε_1) is affected when ionic strength goes above 1 mol/kg, while the colloid stability is typically affected above 0.1 mol/kg. Crossing these boundaries by taking the minimum from the vapor influx and liquid influx abstraction is unlikely. The overall effect on the mean annual dose is likely to be negligibly small, if any.

P13. EFFECT ON SEEPAGE FROM WASTE PACKAGE LENGTH CHANGE

P13.1 ISSUE

The seepage abstraction for the TSPA-LA Model uses an average WP length (including gap spacing) of 5.1 m. However, the average length of a WP (including gap spacing) should be about 5.6 m (DTN: MO0702PASTREAM.001_R0 [DIRS 179925]).

P13.2 ISSUE DESCRIPTION

The average WP length used in the seepage abstraction is 5.0 m (SNL 2007 [DIRS 181244], Table 4.1-1), which was the rounded length of the 44-BWR and 21-PWR WPs considered in previous designs. This length formed the basis for defining the model domain length used in the Seepage Model for Performance Assessment seepage simulations (BSC 2004 [DIRS 167652]). In other words, the Seepage Model for Performance Assessment model results, such as seepage rate or seepage percentage, represent the seepage conditions predicted for a drift section comprising one 5.0-m-long WP plus the 0.1-m gap spacing between WPs. With the introduction of the transportation, aging, and disposal (TAD) canisters for commercial spent nuclear fuel (CSNF), which are about 5.85-m long each (SNL 2007 [DIRS 179394], Table 4-3), the average length of all WPs plus gap increases to about 5.614 m (DTN: MO0702PASTREAM.001_R0 [DIRS 179925]).

P13.3 IMPACT ASSESSMENT

The Seepage Model for Performance Assessment provides the mean and SD of the distribution of seepage rates (kg/WP/yr) over a large range of capillary strengths, permeabilities and percolation fluxes. The seepage dynamically linked library (DLL) used in the TSPA-LA Model uses these rates, along with percolation fields, thermal histories at each WP location, and sampled values for mean capillary strength and mean permeability, to determine seepage rates (kg/WP/yr) at each location and time in each realization, and computes the seepage fraction (fraction of WP locations at which seepage occurs) at each time in each realization.

The Seepage Model for Performance Assessment is a three-dimensional continuum representation of a fractured rock system used to calculate drift seepage at Yucca Mountain. The three-dimensional calculational domain for the model is 10-m high, 4-m wide, and 2.4384-m long (BSC 2004 [DIRS 167652], Figure 6-1). This domain takes advantage of model symmetry and spatial correlation lengths to represent a system based on a drift diameter of 5.5 m and a WP length of 5.1 m with a smaller domain. Rock above and around the drift is also represented in the model. Because the model uses a no-flow vertical boundary along the drift axis, and also only represents a part of the WP length, seepage rates from the model are scaled up by a factor of

4.183, which represents the ratio between the considered drift area (5.5 m × 5.1 m) and the modeled drift area ((5.5 m / 2)*2.4384 m).

The seepage rates for an average WP length of 5.614 m can be estimated by scaling the Seepage Model for Performance Assessment results for an average WP length of 5.0 m. As noted in *The Seepage Model for PA Including Drift Collapse* (BSC 2004 [DIRS 167652]), the limited size of the calculational domain was chosen to allow for the use of a fine mesh at the same refinement as the SCM, while containing a reasonable number of cells that would not make the computational time too long. The cell dimensions in the vertical plane perpendicular to the drift axis are 0.1 m by 0.1 m and cell lengths parallel to the drift axes are about 0.3 m each (Section 6.3.1 of [DIRS 167652]). The vertical boundaries, perpendicular to the drift axis and along the drift centerline are appropriate due to symmetry. The main issue for a heterogeneous system is the domain length versus spatial correlation length (Section 6.3.1 of [DIRS 167652]). The lengths of the flow domain in the direction of the drift axis (2.4384 m) and normal to the drift axis (4 m) are 8 times and 13 times the spatial correlation length (0.3 m), respectively. Since the length of the flow domain in the direction of the drift axis is 8 times the correlation length, the no flow boundaries perpendicular to the drift axis are considered appropriate, and should not have significant effect on flow results. Because the no-flow boundaries have little effect on flow results, the model adequately represents any WP length longer than the model dimensions along the drift axis, as long as the results are scaled by the ratio of the chosen WP length to the modeled WP length. Thus, seepage rates for an average WP length of 5.614 m can be estimated by scaling the Seepage Model for Performance Assessment results for an average WP length of 5.0 m. This scaling would increase the mean and SD of the distribution proportionally (by a factor of 5.614 / 5.1 = 1.10).

The seepage fraction is computed in the Seepage DLL as the fraction of locations at which seepage exceeds the threshold of 0.1 kg/WP/yr. Since seepage rates increase when the average WP length is increased, the seepage fraction may also increase, because the seepage rate at some locations may increase from just less than the threshold to greater than the threshold. Current TSPA-LA software does not support a numerical evaluation of the degree to which the seepage fraction may increase when average WP length increases. However, sensitivity analyses conducted in *Abstraction of Drift Seepage* (SNL 2007 [DIRS 181244]) provide some insight into the degree that seepage fraction may change.

Abstraction of Drift Seepage (SNL 2007 [DIRS 181244], Section 6.8.2) reports the results of a sensitivity analysis that varied the distribution of the flow-focusing factor. The flow-focusing factor increases (or decreases) the local percolation flux to account for variability in flow at the scale of a few drift diameters. The distribution of flow focusing conserves the total water volume in the model domain; if percolation flux is increased at one location, this increase is offset by a corresponding decrease at other locations. The base distribution of flow focusing ranges between approximately 0.1 and 5 (SNL 2007 [DIRS 181244], Section 6.6.5.2.3), which introduces significant variability in local percolation flux. Sensitivity case 6a computes seepage results when the flow focusing was fixed at a constant value of 1 (no adjustment to local percolation flux) rather than sampled from the base distribution. This sensitivity case illustrates the effect on seepage fraction of increasing percolation flux at locations that have small fluxes. Because these locations are also the locations at which seepage is likely to be small, the effect on seepage fraction of increasing percolation flux at these locations is similar to the effect of

increasing the seepage flux at these locations. *Abstraction of Drift Seepage* (SNL 2007 [DIRS 181244], Table 6-12[a]) shows that using a constant value of 1 for the flow-focusing factor increases the seepage fraction by less than 3 percent over the first three climate states. Therefore, it is expected that the seepage fraction would not increase substantially by increasing the average WP length by 10 percent.

Because seepage rates increase proportionally with increased WP length, and seepage fraction is not anticipated to increase substantially, the net effect of increasing WP length on annual dose is to increase seepage rates in a percolation bin by approximately 10 percent. As demonstrated in Section P.17, annual dose may increase in proportion to relatively small changes in seepage rates. Therefore, the overall effect of increasing the average WP length used in the seepage abstraction is minor.

P14. IGNEOUS EVENT PROBABILITY

P14.1 ISSUE

Evaluate the effect on mean annual dose from the Igneous Intrusion and Volcanic Eruption Modeling Cases with the probability of the igneous event set to 10^{-7} per year. Note that this is purely a sensitivity analysis and not due to any error in the implementation.

P14.2 ISSUE DESCRIPTION

Since the impact assessment involves changing only the igneous event frequency, the mean annual dose can be calculated using EXDOC_LA V2.0 [DIRS 182102] software by applying a constant igneous event probability (λ_I) of 10^{-7} per year instead of sampling 300 values from a cumulative distribution function (CDF) (ranging from 1.38×10^{-11} to 7.76×10^{-7} per year) for the base case.

For the Igneous Intrusion Modeling Case, the expected annual dose is given by Equation 6.1.2-16, which is reproduced here:

$$\overline{D}_{II}(\tau|\mathbf{e}_i) = \int_0^{\tau} D_{II}(\tau|[1,t],\mathbf{e}_i)\lambda_{I,i}\,dt \qquad \text{(Eq. 6.1.2-16)}$$

In this sensitivity analysis, $\lambda_{I,i}$ is set to 10^{-7} per year for all 300 $\mathbf{e}_i$.

For the volcanic eruption case the expected annual dose is given by Equation 6.1.2-18, which is reproduced here:

$$\overline{D}(\tau|\mathbf{e}_i) = pE\,\lambda_{I,i}\,\overline{N}_{IE}\,\overline{F}\int_{U_{IE}}\left[\int_0^{\tau} D_{IE}(\tau|[1,t,1,\mathbf{u}],\mathbf{e}_i)\,dt\right] d_U(\mathbf{u})\,dU \qquad \text{(Eq. 6.1.2-18)}$$

where,

pE is the probability that an igneous event includes one or more eruptive conduits that intersects waste (= 8.314×10^{-2})

$\lambda_{I,i}$ is the frequency of igneous events for realization $\mathbf{e}_i$

$\overline{N}_{IE}$ is the mean number of WPs affected by an eruptive conduit

$\overline{F}$ is the mean fraction of WP content ejected into the atmosphere.

In this sensitivity analysis, because $\lambda_{I,i}$ is set to 10^{-7} per year the $pE \times \lambda_{I,i}$ is set to a constant value of 8.314×10^{-9} for all 300 $\mathbf{e}_i$. The value of pE is calculated by multiplying the probability of an eruption, given that a dike intersects the repository (= 0.28 [Section 6.5.2]) by the probability of one or more WPs hit by conduits originating from the dike (1-0.703 = 0.297 [Table 6.5-3]).

The calculations are done for the 10,000-year and 1,000,000-year simulations for both modeling cases.

P14.3 IMPACT ASSESSMENT

The comparison of the mean annual dose for the sensitivity analyses with the base case are shown on Figures P-6 and P-7. The mean annual dose increased by a factor of about six (ranging from 4.12 to 6.96 over the timesteps for the four cases), when the probability of the igneous event was set to 10^{-7} per year. This linear increase is expected, as the igneous event probability of 10^{-7} per year is about six times the mean of the distribution of $\lambda_{I,i}$ for the base case (mean value of approximately 1.67×10^{-8} per year).

P15. LONGITUDINAL DISPERSIVITY IN 1-D SZ TRANSPORT MODEL

P15.1 ISSUE

The epistemic uncertainty distribution for longitudinal dispersivity that is used in the 1-D SZ Flow and Transport Model, which is implemented using the pipe pathways, produces unrealistically large values of dispersivity in some realizations that are not supported by the scientific literature. This effect is primarily due to the unbounded log-normal distribution that is used to define the uncertainty in longitudinal dispersivity.

P15.2 ISSUE DESCRIPTION

The log-normal distribution for the longitudinal dispersivity (α_L), implemented in the 1-D SZ Flow and Transport Model for the base case, is unbounded with Mean [$\log_{10}(\alpha_L)$] = 2.0 and SD [$\log_{10}(\alpha_L)$] = 0.75. The sampled value is further adjusted by increasing it by one order of magnitude as it leads to better agreement between the SZ 1-D Transport Model and SZ Site-Scale (3-D) Transport Model results. As a result, sometimes the final values calculated become larger than are physically possible. For example, the largest value computed is 370 km, which is greater than 15 times the length scale of approximately 20 km for flowpaths in the SZ and well beyond any reasonable value tabulated in the literature.

P15.3 IMPACT ASSESSMENT

The 1-D SZ transport model is used to compute the dose for the listed radionuclides that are also shown by decay chain: $^{235}U \rightarrow {}^{231}Pa$, $^{233}U \rightarrow {}^{229}Th$, $^{230}Th \rightarrow {}^{226}Ra$, and ^{232}Th. The dose from ^{227}Ac and ^{228}Ra is calculated by assuming secular equilibrium with ^{231}Pa and ^{232}Th, respectively. In the base cases, transport of all these radionuclides are affected by the unrealistically high longitudinal dispersivity as it leads to earlier arrival of the mass and higher initial concentrations at the RMEI leading to higher early dose. Of the radionuclides taken from the 1-D SZ transport model, none are important to the mean annual dose in any of the modeling cases for the 10,000-year simulations. Thus, all modeling cases run for 10,000 years will be negligibly impacted.

For the 1,000,000-year simulations, the only significant dose contributor modeled using the 1-D SZ transport model is ^{226}Ra. It is important in those modeling cases where there is rapid transport of ^{226}Ra (along with its parent radionuclides) through the WP to the UZ and SZ without much decay. ^{226}Ra is the top dose contributor in the Igneous Intrusion Modeling Case for the majority of the simulation (Figure 8.2-5b). It is second highest dose contributor in the Seismic FD Modeling Case (Figure 8.2-14b) and second or third highest for the two Early Failure Modeling Cases (Figures 8.2-4b and 8.2-6b). Bounding the longitudinal dispersivity at the upper end is likely to have the greatest effect on the Igneous Intrusion Modeling Case as ^{226}Ra is the highest dose contributor. However, even here, the impact on mean annual dose would be relatively small because only a few realizations (epistemic vectors) have the unrealistically high longitudinal dispersivity values, while most realizations have the values within the physical range. ^{226}Ra has a relatively short half-life of 1,600 years compared to the transport times through the SZ (SNL 2008 [DIRS 183750], Figure 6-14[a]). Thus, most of the mass that is released from the WP and UZ will be decayed while being transported through the SZ pipe pathways, even accounting for the high dispersivity values.

To evaluate the impact of using unrealistically high longitudinal dispersivity, the log-normal distribution was truncated at the upper end at two SDs from the geometric mean and the sampled value was directly used without adjusting it further. The upper bound was provided by the subject matter expert (DTN: SN0710PASZFTMA.003_R0 [DIRS 183485]) bearing in mind that the two SD upper bound would cover about 98 percent of the area under the standard normal curve. As a result, the maximum value possible is 3.16 km, which is considered reasonable for the transport distances in the SZ. The impact of the updated dispersivity range was evaluated for the Igneous Intrusion Modeling Case, where maximum effect is likely to be seen. Note that only 26 percent of the realizations in the base case have longitudinal dispersivity values greater than the maximum value of 3.16 km, and thus the impact is likely to be small. A comparison of the mean annual dose for the base case and the impact evaluation case is shown on Figure P-8. The mean annual dose from the impact evaluation case shows a reduction of about 25 percent to 30 percent for the majority of the simulation. Figure P-9 shows the effect on ^{226}Ra dose where the reduction is over 60 percent, with greater percentage reduction (over 80 percent) prior to 200,000 years. The effect is somewhat non-linear on ^{226}Ra dose compared to the number of realizations that are impacted, because almost all of the ^{226}Ra release out of the SZ in the impact evaluation case comes from decay of ^{234}U to ^{230}Th, which decays to ^{226}Ra while being transported through the pipe pathways. Because ^{230}Th has a much larger K_d in the SZ (ranging from 1,000 to 10,000 mL/g) compared to ^{226}Ra (ranging from 100 to 1,000 mL/g) (Table 6.3.10-2) and has much larger half-life (about 75,400 years), the transport of ^{230}Th (and to

some extent ^{234}U) through the 1-D SZ transport model ultimately controls the ^{226}Ra dose (Figure P-9). The major radionuclides contributing to the mean annual dose are shown on Figure P-10 for the impact evaluation case. Here, the ^{226}Ra dose contribution drops, as anticipated, from being the top contributor to the third highest contributor, with ^{242}Pu and ^{237}Np becoming the two highest contributors. The overall impact on the mean annual dose is relatively small with a reduction of 25 percent to 30 percent.

P16. GLASS DEGRADATION RATE

P16.1 ISSUE

The HLW glass degradation rate calculation for the Igneous Intrusion Modeling Case uses the degradation model that was developed for nominal conditions instead of applying an instantaneous degradation, as described in Section 5.3.1.

P16.2 ISSUE DESCRIPTION

The HLW glass degradation rate for the Igneous Intrusion Modeling Case uses the glass degradation model that is applicable for nominal conditions (valid up to 300°C) and computes the dissolution rate by holding the temperature at a maximum value of 300°C for all times while the WP temperature from igneous intrusion is greater than 300°C. The intended rate should have been an arbitrarily chosen high value (>>1 per year) that results in instantaneous degradation of HLW glass, following an igneous event.

P16.3 IMPACT ASSESSMENT

Two glass dissolution rate calculations are made at every timestep in the HLW glass degradation model, one for an acidic solution and the other for an alkaline solution and then the higher rate is selected for the given timestep. However, when the temperatures are above 100°C, the in-package pH is set to 10 and the dissolution rate for alkaline solution is used. The equation for dissolution rate calculation is presented by Equation 6.3.7-8, which is reproduced here:

$$rate_G = k_E 10^{\eta \bullet pH} \exp(-E_a / RT) \qquad \text{(Eq. 6.3.7-8)}$$

where

$rate_G$ = absolute HLW glass dissolution rate ($g/m^2/d$)

k_E = rate coefficient ($g/m^2/d$)

η = pH dependence coefficient (dimensionless)

E_a = effective activation energy (kJ/mol)

R = universal gas constant (8.14E-03 kJ/mol/K)

T = temperature (K).

The parameter values for k_E, η, and E_a are presented in Table 6.3.7-32. For the alkaline solution, the mean value for k_E is 11,585 $g/m^2/day$, while η and E_a are constant values of 0.49 and 69 kJ/mol, respectively.

The calculated dissolution rate is converted into a fractional degradation rate by multiplying with the specific surface area of glass (fixed value of 2.7×10^{-3} m^2/kg) and by the glass exposure factor that accounts for the higher effective surface area of the glass log resulting from cracking of the HLW glass after it is poured into the canister (mean value of 8.3).

Since the WP temperature is set at a maximum value of 300°C for times when the calculated temperature from igneous intrusion is above it, and since the pH is set at 10 while the WP temperatures are above 100°C, the mean fractional degradation rate following the igneous event time can be calculated using the mean values of the uncertain parameters. The mean fractional degradation rate is calculated to be about 3.9 per year. This results in instantaneous degradation of the HLW glass (for all practical purposes) on an average. Considering the lower bound (most likely values) of the uncertain distributions (k_E = 28.2 $g/m^2/day$ and glass exposure factor = 4) results in fractional degradation of 0.0045 per year. This results in degrading almost all of the HLW glass in about 200 years, which is less than one time-step length in the TSPA simulations for the 1,000,000-year calculations and thus instantaneous for all practical purposes.

Since the HLW glass degradation is nearly instantaneous even by using the degradation model developed for the nominal conditions, there is no impact anticipated on the mean annual dose even by explicitly modeling instantaneous degradation following the igneous event. Furthermore, since CSNF is degraded instantaneously following the igneous event and because it holds most of the total radionuclide mass in the repository, the dose contribution from CSNF releases is likely to control the mean annual dose. Any small changes in the degradation rate for HLW glass are unlikely to have an impact on the mean annual dose.

P17. SEEPAGE FLUX AFTER DRIFT COLLAPSE

P17.1 ISSUE

The seepage flux in the lithophysal zones following the drift collapse may be under predicted in some realizations due to error in estimating the bounding values.

P17.2 ISSUE DESCRIPTION

The seepage flux (a volumetric flux) for the lithophysal zones following the drift collapse is doubled compared to the intact drift seepage flux, based on the assumption of doubling the drift diameter following the drift collapse in the lithophysal zones. This value is then compared to the theoretical maximum, which is calculated by multiplying the percolation flux with the plan area equal to drift diameter times the WP length of 5.1 m. If the calculated seepage flux exceeds the theoretical maximum, the maximum value is taken. However, the plan area for calculating the theoretical maximum flux is not doubled following the drift collapse. This results in under predicting the maximum flux, which may in turn result in under predicting the seepage flux following the drift collapse. The seepage fractions are not affected as the number of repository locations that see seepage at the end of simulation remain unchanged even after drift collapse.

P17.3 IMPACT ASSESSMENT

The error is anticipated to only have an impact on the Seismic GM and Seismic FD Modeling Cases as drift collapse occurs in only those modeling cases. There is no impact on the 10,000 year Seismic GM Modeling Case, as drift collapse is not considered. In the 1,000,000-year Seismic GM Modeling Case, the impact of the error is estimated to be small, as the transport through the WP is only diffusive for the majority of the simulation due to the presence of stress corrosion cracks. Only after enough general corrosion patches appear on the WP would the advective flux be significant. But since the average number of patches on the failed WP is less than 1 percent by 700,000 years, the start of advective flux is not likely to have an appreciable impact on dose. Furthermore, the diffusive flux is expected to remain the dominant transport process even later than 700,000 years until large number of patches have formed. The impact of this error is likely to be negligibly small on the mean annual dose.

For the Seismic FD Modeling Case, complete drift collapse occurs following the seismic event and based on the breach area all of the seepage flux could go through the WP. The amount of increase in seepage flux from this error and its impact on mean annual dose is evaluated by running a 300-realization case, where the epistemic and aleatory uncertainties are sampled per realization (in a unified manner for computational convenience), and then comparing the output from the Seepage DLL for the impact evaluation case with the uncorrected case (called base case). The results indicate that the mean seepage flux increases, as anticipated, for the impact evaluation case for all percolation subregions (Table P-4) in proportion to the lithophysal rock fraction in the percolation subregion. The area weighted increase in mean seepage flux at 1,000,000 years is about 22 percent. The mean seepage flux for percolation subregion 3 (the largest percolation subregion) is compared for the two case (Figure P-11). The comparison shows that the increase in seepage rate is fairly constant (around 20 percent) for the majority of the simulated time but increases slightly with increasing seepage rates. Since the area weighted mean seepage flux increased by about 22 percent at 1,000,000 years, it is anticipated that the advective flux of radionuclides, whose concentration remains at the solubility limits, would also increase by about the same amount. The mean annual dose comparison for the two cases is presented on Figure P-12. It shows an increase of about 20 percent. This is because ^{242}Pu is the major dose-controlling radionuclide and its concentration is solubility-controlled in the EBS and hence its dose increases by about 20 percent (Figure P-12). For radionuclides that do not have

solubility limits, the increased seepage flux would have negligible impact on the mass flux. The overall impact on mean annual dose is relatively small.

P18. UNSTABLE IRON OXYHYDROXIDE COLLOIDS

P18.1 ISSUE

Minimum iron oxyhydroxide colloid concentration is being applied even under stable conditions due to error in calculating the ionic strength threshold for colloid stability calculations.

P18.2 ISSUE DESCRIPTION

The iron oxyhydroxide (or steel degradation) colloid concentration for the EBS Transport Model is determined by first evaluating the stability of colloids under given pH and ionic strength conditions at each timestep as shown on Figure 6.3.7-11d. If the ionic strength is less than the ionic strength threshold (for a given pH), the iron oxyhydroxide colloids are considered to be stable and the colloid concentration is sampled from a distribution (Table 6.3.7-65). However, if the ionic strength is higher than the ionic strength threshold, a constant minimum value of 1×10^{-6} mg/L is applied. The equation for computing the ionic strength threshold for the pH between 4.5 and 8.4 is shown by Equation 6.3.7-18, which is reproduced here:

$$I_{threshold} = -0.013 \times pH + 0.11 \qquad \text{(Eq. 6.3.7-18)}$$

The coefficient term of -0.013 is incorrectly entered as -0.13 in the database. As a result of this error, the ionic strength threshold becomes negative over the pH range of 4.5 to 8.4 leading to unstable iron oxyhydroxide colloids, thus under predicting the colloid concentration, which is set to a minimum value of 1×10^{-6} mg/L.

P18.3 IMPACT ASSESSMENT

The error is expected to have a negligible impact on the mean annual dose for all modeling cases. This is because in the modeling cases where there is no flow through the WP, the ionic strength is likely to be greater than the maximum threshold of about 0.05 mol/kg for iron oxyhydroxide colloids (Figure 6.3.7-11d). The most likely in-package ionic strength for the vapor-influx case, based on Equation 6.3.7-1 and Table 6.3.7-9, ranges from about 0.13 mol/kg at relative humidity of 99.8 percent (a reasonable high value in the simulation) to 2.6 mol/kg at relative humidity of 95 percent (lower bound for initiating transport). Even considering the uncertainty, which could reduce the ionic strength by half, the values are still likely to be greater than the threshold value of about 0.05 mol/kg, leading to continued instability of the iron oxyhydroxide colloids, irrespective of the error.

In the modeling cases, where the flow through the WP exceeds 0.1 L/yr such that in-package chemistry is determined by liquid-influx case, the ionic strength values are likely to be less than the ionic strength threshold (at a given pH) for the majority of the realizations leading to under prediction of colloid concentrations. But since iron oxyhydroxide colloid concentrations are relatively small even under stable conditions (mean value of about 1.5 mg/L from the stainless steel degradation; Table 6.3.7-65) the majority of the transport is likely to be in the dissolved state leading to negligible impact on the mean annual dose. Since the Igneous Intrusion

Modeling Case has the highest dose contribution among the modeling cases where there is flow through the WP, such as the FD Modeling Case and Drip Shield EF Modeling Case (compare Figures 8.2-5, 8.2-8, and 8.2-14), the impact of the error is evaluated for this modeling case.

The impact is evaluated by running a 300-realization simulation, where the epistemic and aleatory uncertainties are sampled per realization (in a unified manner for computational convenience), and then the mean annual dose is compared to the uncorrected case (called base case), which is also run in a similar fashion. As shown on Figure P-13, the impact on mean annual dose is negligible, even though the dose contribution from plutonium that is irreversibly sorbed on the colloids has increased. This is because the dissolved plutonium controls the mean annual dose. The impact of the correction is greater for the ^{242}Pu mass compared to ^{239}Pu mass that is irreversibly associated with the colloids. This is because the majority of the ^{239}Pu mass irreversibly associated with colloids is due to contribution from the mass irreversibly associated (embedded) with HLW glass waste form colloids as compared to the mass that is irreversibly associated with the iron oxyhydroxide colloids. In contrast, ^{242}Pu mass in the HLW glass inventory is negligibly small (compared to ^{239}Pu mass) and thus ^{242}Pu that is irreversibly associated with the iron oxyhydroxide colloids dominates over ^{242}Pu mass irreversibly associated with the HLW glass waste form colloids, leading to greater change as a result of the correction. The overall impact on the mean annual dose is negligibly small.

P19. DOE SPENT NUCLEAR FUEL MASS RELEASE

P19.1 ISSUE

In the Igneous Intrusion Modeling Case, the number of WPs assigned for computing the DOE spent nuclear fuel (DSNF) mass in the non-dripping environments are not correctly calculated following the igneous event.

P19.2 ISSUE DESCRIPTION

Following the igneous event, the number of WPs assigned to the non-dripping environment is incorrectly set to be the same as the number of WPs assigned to the dripping environment. As a result, the DSNF mass available for release is incorrectly computed based on the explicit calculations performed using the discrete change element in GoldSim. There is no effect on the CSNF or HLW mass calculations, as the GoldSim Source element is used leading to a static number of WPs that are determined at the start of the simulation.

P19.3 IMPACT ASSESSMENT

The impact of the error on the Igneous Intrusion Modeling Case is likely to be negligibly small, as total DSNF inventory itself represents a small part of the total inventory in the repository (based on information in Tables 6.3.7-5 and 6.3.7-1). But since the error is restricted to only non-dripping environments, the impact would be even smaller. Table P-1 (second column) shows the seepage fraction that is applied prior to the igneous event, and based on that, the majority of the WPs would fall into the non-dripping environment. After the igneous event, due to the error, the number of WPs assigned to the non-dripping environment, are set to be the same as those for the dripping environment, resulting in a decrease of the number WPs in the non-dripping environment, thus under-representing the DSNF mass. The decrease in the number

of WPs for non-dripping environments would vary by each percolation subregion, but the weighted average reduction (weighted by the area of each percolation subregion) would be about 31 percent. Considering that the weighted non-dripping area prior to the igneous event is about 60 percent, thus the maximum under estimation in total mass out of the EBS would be about 19 percent (= 0.31 × 0.6). In actuality, the under estimation would be even smaller, as different radionuclides would be affected differently based on the proportion of their mass in the DSNF inventory compared to the HLW and CSNF inventory. Since the major dose contributors for this modeling case are expected to be ^{99}Tc, ^{239}Pu, ^{242}Pu, and ^{237}Np (Figure P-10), and because contribution of DSNF inventory is less than 2 percent of the total inventory for these radionuclides, the impact of the error is likely to be negligible.

P20. GOLDSIM SOFTWARE ERROR

P20.1 ISSUE

Incorrect mass amounts could be calculated by the Source and Pipe elements (special GoldSim elements) in the Contaminant Transport module of GoldSim software when decay chains have feedback loops.

P20.2 ISSUE DESCRIPTION

In the TSPA-LA Model, the decay chain feedback loops are utilized in the EBS transport-related cell pathways to model kinetic sorption-desorption processes (with both forward and backward rate constants) in the WP. Since the Source elements are used in the EBS transport submodel and the Pipe elements are used in the UZ and SZ transport submodels, the calculated mass fluxes could be affected by the error. Note that the Volcanic Eruption Modeling Case is not affected by this error as the transport calculations are done through external DLLs.

P20.3 IMPACT ASSESSMENT

Since the error was discovered, the software vendor (GoldSim Technology Group) has corrected the software problem and released a service pack update (GoldSim Version 9.60 Service Pack 3). To evaluate the impact of the error, all modeling cases (except for the Volcanic Eruption Modeling Case) were rerun with the corrected software by simulating 300 realizations, where the epistemic and aleatory uncertainties are sampled per realization (in a unified manner for computational convenience). The results, which are summarized in Table P-5, indicate minor dose differentials on a per realization basis, with up to a ±5 percent change. The impact on mean annual dose is likely to be even smaller over most of the simulated duration. For the purpose of illustration, the impact on mean annual dose for the Seismic GM Modeling Case and the Igneous Intrusion Modeling Case (the two cases with highest mean annual dose for the 1,000,000-year simulation duration) are shown on Figures P-14 and P-15. In these figures, the base case refers to the uncorrected case while the impact evaluation case refers to the case where the error has been corrected. In both modeling cases, the mean annual dose remains practically unchanged. The impact of this error is categorized to be small for all modeling cases.

P21. UNSATURATED ZONE TRANSPORT THROUGH FAULT ZONE

P21.1 ISSUE

Transport through the fault zones of the UZ transport model could be delayed for some radionuclides that are generated from the decay of the parents and whose sorption properties differ widely from their parents. Note that this issue has been documented in Condition Report (CR) 11572.

P21.2 ISSUE DESCRIPTION

The conceptual model for the transport of dissolved or reversibly sorbed radionuclides through the UZ fault zones is different from the remainder of the UZ in two aspects: (1) the fault zones utilize a dual-permeability transport model that considers advection and dispersion without any fracture-matrix diffusive interaction, and (2) the sorption in the fault zones is simulated for both the fracture and the matrix continuum. The manner in which the particle-tracker subroutine for transport in the fault zones is implemented may sometimes cause an unexpected delay in the transport of daughter species. The delay is caused by the fact that when a parent species particle decays to a daughter species particle within a given grid-block cell, the effect of the change in sorption coefficient is not manifested until the daughter species particle enters the next cell. In other words, the sorption coefficient for the parent species is continuously applied to the daughter species while the daughter species resides in the cell where it was generated. This could sometimes result in a significant delay of the daughter species if the sorption coefficient of the parent species were to be much greater. This delay could affect the transport of species, such as ^{237}Np and ^{226}Ra, whose respective parents, ^{241}Am and ^{230}Th, have much greater sorption coefficients (Table 6.3.9-2). The effects on transport are likely to be small for those daughter species whose sorption coefficients are not very different from their parents and would result in faster transport for those daughter species whose sorption coefficients are greater than those of the parents, which is conservative.

P21.3 IMPACT ASSESSMENT

The impact on the mean annual dose from this error is anticipated to be small as only about 7 percent of the repository nodes in the UZ transport model are considered as fault nodes (39 fault nodes out of 560 nodes) and, thus, a small fraction of the total mass released from the EBS will be passed through the faults. Furthermore, it should be noted that the anomalous behavior occurs only for those daughter species that are generated from the decay of the parents in the fault-zone cell while they reside in that cell. Correct sorption coefficients are applied to the daughter species once they move into a different cell or when they are injected directly in the fault zones.

To evaluate the impact of the error, the Seismic GM Modeling Case and the Igneous Intrusion Modeling Case, the two cases with the highest mean annual dose for the 1,000,000-year simulation duration, were rerun for 300 realizations such that the epistemic and aleatory uncertainties are sampled per realization in a unified manner for computational convenience. For the impact evaluation, the transport characteristics of the fault zones were modified so that the conceptual model for transport through the fault pathways is made similar to the rest of the UZ transport model, thus allowing for the fracture-matrix diffusive interaction and no sorption in the

fracture continuum of the fault zones. This is an acceptable alternative conceptualization besides being somewhat conservative. In this approach, the sorption properties of the daughter species are applied correctly while they reside in the cell where they were generated.

The mean annual dose comparison plots for the Seismic GM Modeling Case and the Igneous Intrusion Modeling Case are shown on Figures P-16 and P-18. The mean annual dose remains practically unchanged with a small increase (< 5 percent) for the impact evaluation case in the majority of the simulation. Among the major dose contributing radionuclides, the dose for ^{226}Ra and ^{237}Np is affected, as anticipated (Figures P-17 and P-19). The overall impact of the error on the mean annual dose for all modeling cases is categorized to be small (< 5 percent).

The sensitivity analyses of radionuclide transport presented in Appendix K are also unlikely to be affected including those analyses that investigate the uncertainty in transport of ^{239}Pu and ^{237}Np through the UZ. This is because (a) the mass transported through the UZ fault nodes represents a small fraction of the total mass transported through the UZ, and (b) the mass of ^{239}Pu and ^{237}Np entering the UZ fault nodes from EBS is likely to be much higher than that produced in the UZ fault nodes from the decay of their parents, ^{243}Am and ^{241}Am, respectively, due to small initial mass of ^{243}Am in the emplaced inventory and fast decay rates of ^{241}Am compared to slow transport through the EBS due to sorption.

P22. OTHER MINOR IMPLEMENTATION ERRORS

P22.1 ISSUE

Other minor implementation errors that have been discovered since running the compliance case are grouped and addressed here.

P22.2 ISSUE DESCRIPTION

The implementation errors whose effects are unlikely to have any impact on the dose are grouped together and addressed in Table P-6. They are unlikely to affect the radionuclide releases appreciably in our judgment but are documented for future correction.

P23. SUPERFICIAL CHANGES

P23.1 ISSUE

Several suggested changes to the model file structure are tracked in a model status log.

P23.2 ISSUE DESCRIPTION

Several nice-to-have changes are proposed in the model status log that will make the TSPA Model file more transparent and consistent with the conceived code architecture.

P23.3 IMPACT ASSESSMENT

There is no impact from these as these are only superficial (cosmetic) changes and do not affect the calculations.

P24. SUMMARY

The issues presented in this appendix are summarized in Table P-7 with their anticipated impact on the mean annual dose for the modeling cases discussed in the preceding sections. Since most of the issues evaluated are estimated to have negligible to small impact (except for the issue discussed in Section P3), the combined effect of correcting the errors is expected to be small as well on the mean annual dose for all modeling cases. The impact of the issue discussed in Section P3 is estimated to cause appreciable decrease in the mean annual dose for some period of time (typically between 200,000 and 300,000 years) in only the Seismic GM Modeling Case for the 1,000,000-year duration. In none of the issues evaluated does the mean annual dose increase appreciably (by a factor of two or more) above the base-case results presented in Section 8. In fact, in most cases, it decreases. Thus, the confidence in the base-case results as an estimator of the mean annual dose to the reasonably maximally exposed individual (RMEI) can be maintained, and the validation activities performed on the base-case results remain applicable.

Table P-1. Comparison of Mean Seepage Fraction for Various Percolation Subregions for Nominal Conditions

Percolation Subregion	Seepage Fraction – Base Case	Seepage Fraction – Impact Analysis	Percent Change from Base Case	Percolation Subregion Weighting	Percent Weighted Change in Seepage Fraction
1	0.125	0.088	-29.0	0.05	1.45
2	0.340	0.230	-32.1	0.25	8.03
3	0.437	0.329	-24.6	0.4	9.85
4	0.436	0.384	-11.7	0.25	2.93
5	0.494	0.466	-5.54	0.05	0.27
Total					22.53

Source: Output DTNs: MO0709TSPAREGS.000 [DIRS 182976] – for base case; MO0709TSPALAMO.000 [DIRS 182981] – for impact analysis.

Table P-2. Comparison of Mean Seepage Fraction for Various Percolation Subregions for Seismic Fault Displacement Modeling Case

Percolation Subregion	Seepage Fraction – Base Case	Seepage Fraction – Impact Analysis	Percent Change from Base Case	Percolation Subregion Weighting	Percent Weighted Change in Seepage Fraction
1	0.467	0.431	-7.78	0.05	0.389
2	0.649	0.558	-14.08	0.25	3.52
3	0.719	0.636	-11.59	0.4	4.64
4	0.704	0.661	-6.06	0.25	1.52
5	0.751	0.734	-2.38	0.05	0.12
Total					10.18

Source: Output DTNs: MO0709TSPAREGS.000 [DIRS 182976] – for base case; MO0709TSPALAMO.000 [DIRS 182981] – for impact analysis.

Table P-3. Comparison of Mean Seepage Fraction for Various Percolation Subregions for the Seismic Ground Motion Modeling Case

Percolation Subregion	Seepage Fraction – Base Case	Seepage Fraction – Impact Analysis	Percent Change from Base Case	Percolation Subregion Weighting	Percent Weighted Change in Seepage Fraction
1	0.464	0.088	-81.0	0.05	4.05
2	0.647	0.230	-64.4	0.25	16.1
3	0.718	0.329	-54.2	0.4	21.7
4	0.704	0.384	-45.4	0.25	11.4
5	0.752	0.466	-38.0	0.05	1.9
Total					55.1

Source: Output DTNs: MO0709TSPAREGS.000 [DIRS 182976] – for base case; MO0709TSPALAMO.000 [DIRS 182981] – for impact analysis.

Table P-4. Comparison of Mean Seepage Flux (m^3/yr) at 1,000,000 years for Various Percolation Subregions for the Seismic Ground Motion Modeling Case

Percolation Subregion	Seepage Flux – Base Case	Seepage Flux – Impact Analysis	Percent Change from Base Case	Percolation Subregion Weighting	Percent Weighted Change in Seepage Flux
1	0.096	0.098	1.76	0.05	0.09
2	0.350	0.400	14.3	0.25	3.58
3	0.523	0.635	21.3	0.4	8.53
4	0.547	0.723	32.2	0.25	8.06
5	0.748	0.964	28.8	0.05	1.44
Total					21.7

Source: Output DTN: MO0709TSPALAMO.000 [DIRS 182981].

Table P-5. Quantitative Evaluation of the Impact of GoldSim Software Error on Various Modeling Cases Based on Dose

Number	Modeling Case	Duration (years)	Percent Realizations with a Dose Change (%)	Typical Difference (for at least 90% of realization) (%)
1	Nominal	10,000	0	0
2	Nominal	1,000,000	97	±3
3	EF DS	10,000	28	±3
4	EF DS	1,000,000	87	±0.5
5	EF WP	10,000	2.3	0
6	EF WP	1,000,000	43	±2
7	Igneous	10,000	93	±2.2
8	Igneous	1,000,000	100	±5
9	Seismic GM	10,000	7.3 (88 showed zero dose)	±1
10	Seismic GM	1,000,000	96	±4
11	Seismic FD	10,000	21	±1.3
12	Seismic FD	1,000,000	93	±3
13	Human Intrusion	1,000,000	99	-5.2 to +1

Source: Output DTN: MO0709TSPALAMO.000 [DIRS 182981].

Table P-6. Discussion of Other Minor Implementation Errors

	ISSUE DESCRIPTION	ANTICIPATED IMPACT
1	Drift-wall condensation incorrectly turned off in the non-dripping environments.	This error should have negligible or no impact in all modeling cases. Because drift-wall condensation occurs for at most 2,000 years (Section 6.3.3.2.3) and because the DS remains intact throughout this period in all modeling cases except Drip Shield EF Modeling Case, the release from any failed WP should be negligibly impacted. In the Drip Shield EF Modeling Case since the WP is always modeled to be located in the dripping environment (Section 6.4.1.3), there should be no impact.
2	Inconsistent half-lives applied to ^{79}Se and ^{126}Sn for calculations performed using GoldSim elements and those used by the UZ and SZ transport models implemented through DLLs.	The ^{79}Se half life in GoldSim is set at 290,000 years while that in the UZ and SZ transport model is set at 295,000 years. The ^{126}Sn half life in GoldSim is set at 230,000 years while that in the UZ and SZ transport model is set at 250,000 years. These inconsistencies are minor, as they occur only in the second significant digit. Since the dose contribution from ^{79}Se and ^{126}Sn is at least an order of magnitude lower than some of the other radionuclides (see Figures P-1 to P-5), the impact on the mean annual dose would be negligible.
3	In the calculations to determine the time of first seismic damage to the WP, the abstraction for WP failure under intact DS is considered while the DS is intact. This calculation should not be used after either the DS plate or DS framework has failed. However, this calculation ignores the DS framework failure and only considers the DS plate failure to determine whether to use this abstraction or not.	It should be noted that this error only affects the 1,000,000-year Seismic GM Modeling Case because the DS remains intact in the 10,000-year modeling case. Since the DS framework failure (average failure time of 100,000 years) occurs earlier than the DS plate failure (average failure time of 250,000 years), there is a possibility of predicting the WP failure time earlier than intended in the time duration where the DS framework has failed but the DS plate is intact. This error may have an impact on estimating first failure time for only CDSP WPs as the probability of WP failure under intact DS is generally greater than the probability of failure under failed DS that is surrounded by rubble. Even here, the probability of occurrence of this error is small as the DS framework lasts up to 100,000 years on an average, during which time CDSP WPs that are likely to fail from seismic damage would have failed in majority of the realizations (~70%). For CSNF WPs there is no impact anticipated, as the probability of failure under intact DS is much smaller than the probability of failure under the failed DS that is surrounded by rubble. As a result, this error is likely to have only a negligible impact on the mean annual dose.
4	The calculation for the time of first seismic damage may be incorrect if the WP damage is from the first seismic event.	This error only appears when the first seismic event causes the damage to the WP or leads to rockfall. Since seismic events occur on an average of every 2,330 years (inverse of specified annual rate of 4.287×10^{-4} yr^{-1}), only those realizations would be impacted where the WP damage or rockfall occurs within 2,330 years (on an average). There are only five such realizations in the 9,000 realization seismic ground motion base case where the damage should have occurred from the first seismic event but did not occur due to the error. The impact of this error is negligible. No other modeling cases are affected.

Table P-6. Discussion of Other Minor Implementation Errors (Continued)

	ISSUE DESCRIPTION	ANTICIPATED IMPACT
5	The HLW glass derived waste form colloid concentrations are overestimated under conditions when the waste form colloids are unstable.	This error occurs only when the conditions are unstable for the generation of glass waste form colloids. Since the maximum concentration of HLW glass waste form colloids, under stable conditions, is itself small (maximum of 2 mg/L and a mean of 0.3 mg/L) the mass transported on colloids will be negligibly small compared to that transported in the dissolved phase. Thus, this overestimation would have negligible impact on the mean annual dose. Furthermore, the unstable conditions generally occur when the ionic strength is greater than 0.4 mol/kg, which are typical while there is no flow through the WP. Since the transport mechanism is diffusion when there is no flow and because the diffusion coefficient of colloids is much smaller compared to the dissolved species (by at least two orders) no appreciable mass can be carried by the colloids.
6	The element that integrates the mass released from the WP in the Human Intrusion Scenario integrates the mass flux rate computed for the previous timestep over the next timestep using the next timestep length. It should instead integrate the mass flux rate computed for the given timestep over that timestep length.	This error would only have an impact when the timestep length is changing as the integrated mass would change. Since the intrusion time is set at 200,000 years in the Human Intrusion Scenario and because there is no change made in the timestep length for the remaining simulation duration, the calculations are not affected. The only impact is one timestep delay in passing the mass to the UZ borehole pathway while the dose magnitudes remain unaffected. Since this is a highly stylized modeling case, with a selected intrusion time, the one timestep delay is not important to the overall system results and does not affect the dose values.
7	The implemented range of two uncertain parameters used in determining the number of monolayers of adsorbed water for corrosion products as part of the EBS Transport submodel is different from their intended ranges.	The stochastic elements FHH_Isotherm_k_CP_a and FHH_Isotherm_s_CP_a are sampled to determine the value for parameters *k* and *s* that are used in the water adsorption isotherm for corrosion products to determine the number of sorbed layers of water (Section 6.3.4.3.2 of the *EBS Radionuclide Transport Abstraction*, SNL 2007 [DIRS 177407]), which is eventually used in computing the saturation under conditions when there is no flow through the WP. The uniform distribution ranges used, as specified in the DTN: SN0703PAEBSRTA.001_R3 [DIRS 183217] (modified from Table 8.2-4 of the *EBS Radionuclide Transport Abstraction*, SNL 2007 [DIRS 177407]) are: FHH_Isotherm_k_CP_a: 1.048 – 1.370 FHH_Isotherm_s_CP_a: 1.525 – 1.852 The correct ranges, as intended in Section 6.3.4.3.2 of the *EBS Radionuclide Transport Abstraction*, (SNL 2007 [DIRS 177407]) are: FHH_Isotherm_k_CP_a: 1.030 – 1.326 FHH_Isotherm_s_CP_a: 1.493 – 1.799 The difference in the two ranges is small compared to their uncertainty ranges and thus the effect on calculating the number of monolayers of adsorbed water and saturation of corrosion products is likely to be negligible, leading to negligible impact on the mean annual dose.

Table P-6. Discussion of Other Minor Implementation Errors (Continued)

	ISSUE DESCRIPTION	ANTICIPATED IMPACT
8	The K_d range for sorption of Np on the Uranium mineral colloids in the EBS is not correct.	The K_d range for sorption of Np on the uranium colloids is given by a log-uniform distribution ranging from 10 to 500 mL/g (Table 6.3.7-64). The lower bound value of 10 mL/g was incorrectly set to 1 mL/g during the implementation. The impact of this reduction in the lower bound is anticipated to be negligible as the Np mass carried by the uranium colloids is likely to be small (even with the corrected values) compared to the mass carried by other colloid types and in the dissolved phase. Considering the mean uranium colloid concentration of about 6 mg/l (based on cumulative distribution function given in Table 6.3.7-64) and the maximum Np K_d of 500 mL/g, and multiplying the two would lead to a value of about 3×10^{-3}, which represents the ratio of Np mass on the uranium colloids to the mass in the dissolved phase in given water volume. This indicates that the predominant mechanism for Np transport is in the dissolved phase. The impact of this error is anticipated to be negligible, if any, on the mean annual dose.
9	In the Human Intrusion Modeling Case, the mass irreversibly associated with colloids that is released to the SZ is not partitioned into the fast transport fraction and the slow transport fraction.	In the Human Intrusion Modeling Case, the mass irreversibly associated with the waste form colloids (referred as "Ic") and the iron oxyhydroxide colloids (referred as "If") from the WP and passed through the UZ borehole needs to be combined together and repartitioned based on the fast fraction, before passing the mass to SZ. This needs to be done in such a way that only a small fraction (0.00168) travels unretarded (fast) while the rest of the mass travels with some retardation (slowly). The impact of this error is anticipated to be small as the relative contribution from fast and slow traveling mass fraction cannot be fully differentiated due to large timesteps employed in the TSPA-LA Model past 200,000 years (when the human intrusion is modeled). Thus, even though the relative contribution of Ic and If species could vary, the combined mass flux from the mass irreversibly associated with colloids is not anticipated to change. As a result, the impact on the mean annual dose is anticipated to be negligible.
10	In the UZ transport model, the correct minimum value for the selenium K_d for vitric rock units was supposed to be 0 mL/g. However, the minimum value after natural log transformation was set to 0, which is equivalent to K_d of 1 mL/g.	The impact of this error is anticipated to be negligible as the mean K_d value remains largely unchanged (reduced by 0.8%) when the minimum value is corrected. Furthermore, ^{79}Se is not a large contributor to dose.
11	For the UZ transport model, the uranium K_d for zeolitic rock unit has an error at probability level of 1. It was incorrectly set to 20 mL/g instead of 30 mL/g.	The impact of this error is anticipated to be negligible as the mean K_d value would change from 5.25 mL/g to 7.75 mL/g. This small increase is unlikely to affect the transport of uranium through the UZ. Furthermore, the current error is conservative as it leads to lowering the uranium K_d in the UZ matrix.

Table P-6. Discussion of Other Minor Implementation Errors (Continued)

	ISSUE DESCRIPTION	ANTICIPATED IMPACT
12	The concentration limit for plutonium and americium mass irreversibly sorbed on the iron oxyhydroxide colloids in the invert is incorrectly based on the stability criteria for the waste form domain instead of the corrosion products domain.	The error would only have an impact if the irreversible colloid concentration in the invert is nearing the concentration limit in the invert, which is an unlikely condition due to fast transport rates out of the invert compared to the incoming transport rate. Even if the conditions conducive to error occur, they would remain for a short time period compared to the simulation time. The impact of this error is expected to be negligible on the mean annual dose.
13	The time-dependent increase in the diffusive area from nominal corrosion of the WP outer barrier should be removed from the stylized Human Intrusion Modeling Case.	Ignoring the time-dependent increase in diffusive area from nominal corrosion processes (by either SCC or general corrosion patches) on the WP for the Human Intrusion Modeling Case is unlikely to affect the diffusive release out of the WP as only about 5% of the realizations would have some SCC failures by 200,000 years, the time when the human intrusion event is modeled. Following the event, the patch area equal to the drill stem area is applied to the WP for both diffusive and advective release. The patch area applied is large enough to cause large diffusive releases. Since the general corrosion patches do not occur until very late times (>400,000 years), any small increases in diffusive area from SCCs is unlikely to affect the diffusive flux. The impact of this error is likely to be negligibly small on the mean annual dose.
14	In calculating the first damage time for the WP due to seismic ground motion, the possibility of failure from puncture was not considered.	The first damage time calculations only evaluate the failures caused by seismic-induced SCCs or by nominal corrosion processes (nominal SCC or general corrosion). However, there is a small probability that punctures could occur earlier under certain conditions. The conditions, for puncture failure require that the DSs have failed and the WPs are surrounded by rubble. Under these conditions the probability of puncture varies as a function of PGV, but the probabilities remain low even at high PGVs (Figure 6.6-17). First failures from puncture damage are only likely to occur late in time when the WP has a reduced thickness (Figure 7.3.2-15). The number of realizations where puncture occurs before seismic-induced SCCs would be small since there is a higher probability of damage from seismic-induced SCCs (Figure 6.6-15). Note that this error only occurs in the Seismic GM Modeling Case run for 1,000,000 years. There is no effect on the Seismic GM Modeling Case run for 10,000 years as the conditions conducive to puncture do not occur. Analysis of a stand-alone model for WP degradation that includes both nominal and seismic degradation processes (output DTN: MO0709TSPAWPDS.000 [DIRS 183170]; file v5.000_GS_9.60.100_StandAlone_9krlz.gsm in folder Seismic_9k_Rlz) showed that 63 out of 9,000 realizations could have first damage from punctures. The impact of this on the mean annual dose is likely to be negligible as only 0.7% of the realizations would be affected and the effects are likely to be late (after the DSs are failed and the WPs have thinned).

Table P-6. Discussion of Other Minor Implementation Errors (Continued)

	ISSUE DESCRIPTION	ANTICIPATED IMPACT
15	The temperature and relative humidity modifications may be incorrectly applied after rubble fills the drifts as a result of degradation due to seismic ground motion.	The percolation subregion representative temperature and relative humidity time histories under nominal conditions (from MSTHM abstraction) are modified once the drifts become filled with rubble as a result of drift degradation from seismic ground motion. These modifications (deltas) are applied by adding to or subtracting from the representative temperature and relative humidity datasets. Twelve possible delta combinations, from four infiltration scenarios over three host-rock thermal conductivity cases (Section 6.3.2.2), are considered in the TSPA-LA Model for each percolation subregion and for each fuel type. However, in order to limit the computational burden, only eight delta combinations are actually calculated: six delta combinations for CSNF and two delta combinations for HLW. The six delta combinations for CSNF are then mapped to 12 possible delta combinations for the CSNF fuel type in each percolation subregion. Similarly, the two delta combinations for HLW are then mapped to 12 possible delta combinations for the HLW fuel type (CDSP WP) for each percolation subregion. Due to an implementation error, some of the combinations are incorrectly matched and the data are incorrectly read from the look-up tables. This could sometimes result in incorrect modifications of representative temperature and relative humidity time histories for the given percolation subregion and a given fuel type. In addition, some of the data sets used in the modification of temperatures (called temperature deltas) have been entered in a sequence that is different compared to the relative humidity deltas resulting in internal inconsistency once the modifications are made. Note that the error is only possible in the two modeling cases in which rubble fills the drifts, the Seismic GM Modeling Case run for 1,000,000 years and the Seismic FD Modeling Case. The impact of this error on the mean annual dose for either modeling case is likely to be negligible as the variation in the delta among various combinations is small. Thus, even though incorrect values may be applied, they would not result in any appreciable deviations from the corrected time history profiles. Furthermore, the magnitude of the modification is itself small relative to the actual temperature and relative humidity values even at the maximum initial values (the magnitudes of the deltas decrease with time). As a result, the downstream models affecting radionuclide transport are unlikely to be appreciably impacted by this error. The impact of the error on localized corrosion initiation is also evaluated based on the Localized Corrosion Initiation Uncertainty Analysis described in Appendix O. The five realizations (out of 300) that have early rubble fill times (within 12,000 years) all have conditions that are not conducive to localized corrosion initiation, even accounting for slightly incorrect temperature and relative humidity. One realization (Realization 142), which has conditions favorable for localized corrosion until 12,000 years, has a rubble fill time greater than 100,000 years, by which time localized corrosion is not favored. It is concluded that there is no impact of this error on the localized corrosion initiation.

Table P-6. Discussion of Other Minor Implementation Errors (Continued)

	ISSUE DESCRIPTION	ANTICIPATED IMPACT
16	Drift-wall condensation flux is being applied even after the igneous intrusive event, when the drifts are all assumed to be filled with magma.	The drift-wall condensation model is applicable only under nominal conditions and does not apply once the drifts are degraded from seismic ground motion or filled with magma following the igneous intrusion. However, it is being incorrectly applied even after the igneous intrusion. The impact of the error is restricted to the first 2,000 years only because the drift-wall condensation can only occur in the first 2,000 years (Section 6.3.3.2.3). As a result, the water flux through the WP could be higher than the percolation flux leading to increased advective mass flux of radionuclides for realizations when the igneous intrusion occurs within the first 2,000 years. But because the probability of having an igneous event in the first 2,000 years is negligibly small (mean value of 3.3×10^{-5}) the effect on expected dose of this additional mass flux is small. The impact of the error is evaluated to be negligible.

Table P-6. Discussion of Other Minor Implementation Errors (Continued)

	ISSUE DESCRIPTION	ANTICIPATED IMPACT
17	The WP temperatures could sometimes fall below the lower range of validity of the abstractions provided for computing in-package chemistry, HLW glass degradation rate, and dissolved concentration limits in the TSPA-LA Model.	An assessment of the range of validity shows that most of the validity ranges specified for the process models and abstractions included in the TSPA-LA Model are honored (see output DTN: MO0709TSPALAMO.000 [DIRS 182981]). However for three submodels (discussed below) that are included in the 1,000,000-year performance calculations the representative WP temperatures could fall below the lower limit specified by the abstractions; the minimum waste package temperature noted in the TSPA-LA Model is about 17°C for the 1,000,000 year simulation period. The lower temperature limit for the range of applicability of the In-Package Chemistry Abstraction (SNL 2007 [DIRS 180506]) is 25°C. Without an alternate implementation for low temperature conditions, the TSPA-LA Model applies the In-Package Chemistry Abstraction at temperatures below 25°C. Given that the In-Package Chemistry Abstraction for pH and ionic strength includes uncertainty to account for higher temperatures, the application of abstraction at lower temperatures is anticipated to produce results that are within the range of uncertainty captured in the abstractions for pH and ionic strength. The lower temperature limit for the range of applicability of the HLW Glass Waste Form Degradation Abstraction (BSC 2004 [DIRS 169988]) is 20°C. Without an alternate implementation for low temperature conditions, the TSPA-LA Model applies the HLW glass waste form degradation rate model at temperatures below 20°C. The lower temperature limit was determined by the ranges considered in the experimental results used to validate the rate model (BSC 2004 [DIRS 169988], Section 7.3) which showed that the Arrhenius relationship for glass degradation rate is maintained between 20°C and 90°C. This relationship is not anticipated to change between 17°C and 20°C and therefore unlikely to have any effect on mass transport calculations. The lower temperature limit for the range of applicability of the Dissolved Concentration Limits Abstraction (SNL 2007 [DIRS 177418]) is 25°C. Without an alternate implementation for low temperature conditions, the TSPA-LA Model applies the Dissolved Concentration Limits Abstraction at temperatures below 25°C. Because actinides have retrograde solubility (SNL 2007 [DIRS 177418], Section 6.3.3.3), it is possible that dissolved concentration limits below 25°C could be higher than those implemented in the TSPA-LA Model. But because the Dissolved Concentration Limits Abstraction includes additional uncertainty to account for differences in temperature conditions (SNL 2007 [DIRS 177418], Section 6.3.3), it is anticipated that any small effects from extrapolation would produce results that are within the range of uncertainty captured in the abstractions for dissolved concentration limits. For the 10,000 year simulations the temperatures remain within the range of validity.

Table P-6. Discussion of Other Minor Implementation Errors (Continued)

	ISSUE DESCRIPTION	ANTICIPATED IMPACT
18	Drift-wall condensation flow only occurs in the non-lithophysal regions of the repository.	The drift wall condensation abstraction states that drift wall condensation should cease after the drift has collapsed. Drift collapse is only modeled in the Seismic Scenario Class. In the Seismic Scenario Class, drift collapse occurs in the lithophysal regions of the repository; thus the fraction of WPs that are exposed to drift wall condensation is limited to the fraction of WPs in the non-lithophysal region. However, this limit was not properly implemented in the TSPA-LA Model. As a result, in all but the Igneous Intrusion modeling case, drift wall condensation was limited to the fraction of WPs in the nonlithophysal region and therefore was underestimated in the TSPA-LA Model. Because drift wall condensation only increases the flux in the repository for the first 2,000 years, the dose impact can only occur in the modeling cases that fail WPs in the first 2,000 years and have radionuclide transport in the first 2,000 years. The implementation is correct for the Seismic Ground Motion and Seismic Fault Displacement modeling cases and the Igneous Intrusion Modeling Case. The Nominal Scenario Class and Human Intrusion Scenario do not have failures in the first 2,000 years and thus are not affected. The EF WP modeling case does have WP failures in the first 2,000 years, but the DS remains intact so any additional condensation flux is not anticipated to change transport out of the EF WP. The flux through a failed WP in the EF DS modeling case could be increased by drift wall condensation. As a result, WP releases could also be increased, leading to a higher expected dose in the EF DS modeling case. Contributing less than 2.5% to the total mean dose, the EF DS modeling case is not a significant contributor to the total dose from the repository. The impact of the error is evaluated to be negligible.

Table P-7. Impact Assessment Summary Table

Issue/Section No.	Issue Description	Anticipated Impact
P2.	Inventory for ^{36}Cl, ^{79}Se, and ^{126}Sn was omitted in the 10,000-year simulation modeling cases and the seepage fractions applied for the 10,000-year simulations are based on the post-10,000-year climate.	Negligible
P3.	Conservative treatment of WP damage from seismic events following the first breach due to nominal corrosion processes.	Significant between 200,000 and 300,000 years
P4.	WP outer barrier failure flag is triggered when the inside-out corrosion of the WP is initiated in the Seismic GM Modeling Case, which could be earlier than the actual breach time.	Negligible
P5.	In-package chemistry applied in the invert after the DS is failed without considering flow through the WP.	Negligible
P6.	Incorrect weld volume is used in computing the probability of manufacturing defects.	Negligible
P7.	Nominal crack failure opening area incorrectly calculated once the elapsed time is greater than the seismic damage time.	Negligible
P8.	Degradation processes inside the WP could start before the breach from an igneous event under certain aleatory configuration of specified igneous event times.	Negligible
P9.	Threshold rubble volume (per drift length) that is used for determining when the non-lithophysal drifts undergo collapse is incorrect. It is currently using the value of 5 m^3/m while the correct value is 0.5 m^3/m.	Negligible
P10.	Unintended perfect correlation between two uncertainty parameters: WRIP_beta_rand_a and PCE_Delta_pCO2_a.	Negligible
P11.	The uncertainty associated with fluoride concentration in calculating the uranium solubility for the CSNF WPs is incorrectly calculated in the Igneous Intrusion Modeling Case.	Negligible
P12.	The ionic strength for the HLW glass domain, for conditions where there is flow through the WP always chooses the ionic strength determined for flowing conditions.	Negligible
P13.	The seepage abstraction uses an average WP length (including gap spacing) of 5.1 m. However, the average length of a WP (including gap spacing) should be about 5.6 m.	Small (≤10%)
P14.	Evaluate the mean annual dose from the Igneous Intrusion and Volcanic Eruption Modeling Cases with the probability of the igneous event set to 10^{-7} per year. Note that this is purely a sensitivity analysis and not due to any error in the implementation.	None
P15.	The distribution for longitudinal dispersivity that is sampled produces unrealistically large values in the 1-D SZ flow and transport model.	Small (<30%)
P16.	The HLW glass degradation rate calculation for the Igneous Intrusion Modeling Case uses the degradation model that was developed for nominal conditions instead of applying an instantaneous degradation	Negligible
P17.	The seepage flux in the lithophysal zones following the drift collapse may be under predicted in some realizations due to error in estimating the bounding values.	Small (~20%)
P18.	Minimum iron oxyhydroxide colloid concentration is being applied even under stable conditions due to error in calculating the ionic strength threshold for colloid stability calculations.	Negligible
P19.	In the Igneous Intrusion Modeling Case, the number of WPs assigned for computing the DSNF mass in the non-dripping environments are not correctly calculated following the igneous event.	Small (<6%)

Table P-7. Impact Assessment Summary Table (Continued)

Issue/Section No.	Issue Description	Anticipated Impact
P20.	GoldSim software error where incorrect masses could be calculated by the Source and Pipe elements (special GoldSim elements) when decay chains have feedback loops.	Small (<5%)
P21.	Delay in transport for some radionuclides through the fault zones in the UZ transport model.	Small (<5%)
P22.	Other minor implementation errors that have been discovered since running the compliance case are grouped and addressed (Table P-6).	Negligible
P23.	Several suggested changes to the model file structure are tracked in a model status log.	None

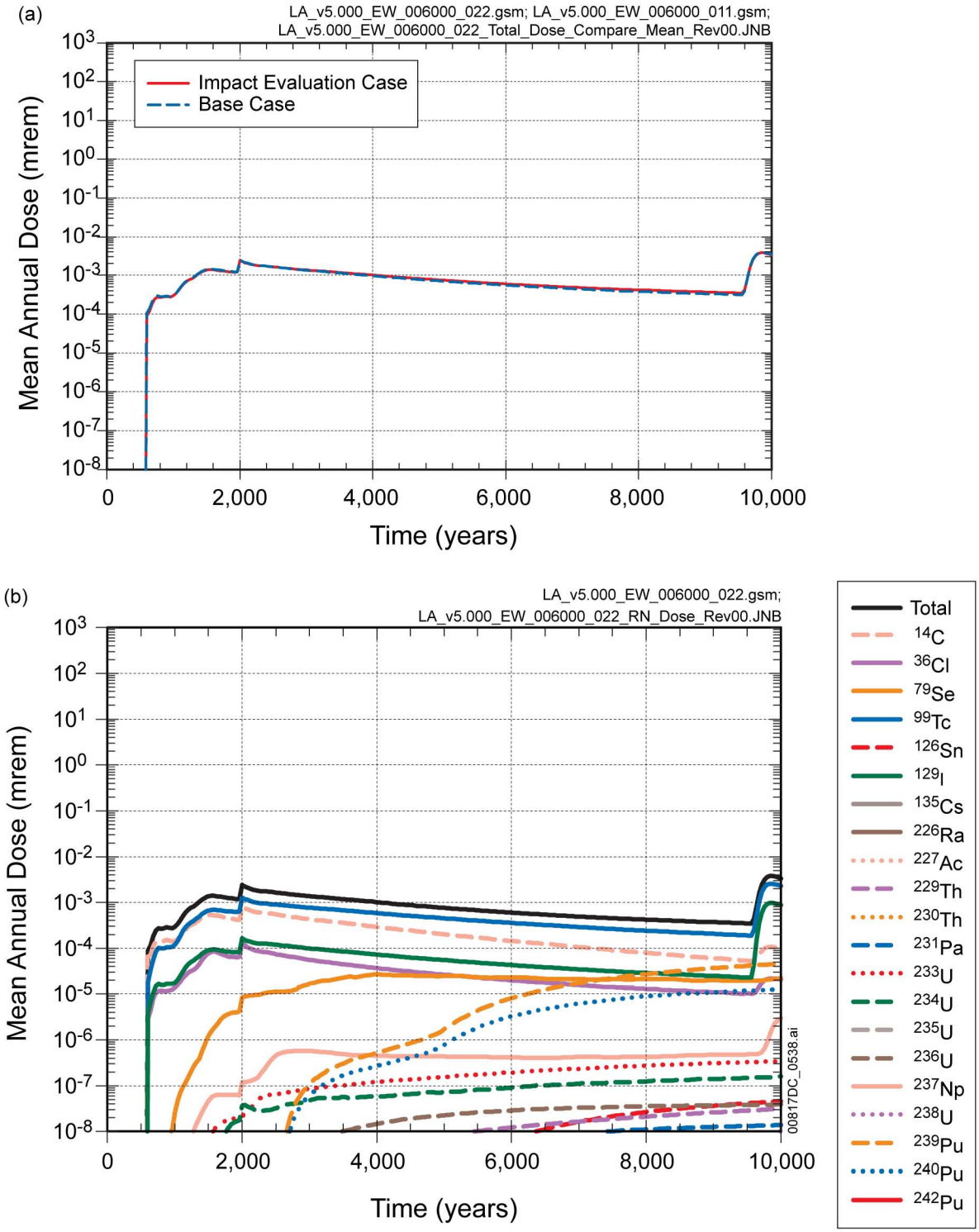

Source: Output DTNs: MO0709TSPALAMO.000 [DIRS 182981]; and MO0709TSPAREGS.000 [DIRS 182976].

Figure P-1. (a) Comparison of the Mean Annual Dose for the Impact Evaluation Case with the Base Case for the Waste Package EF Modeling Case and (b) Major Radionuclide Dose Contributors for the Corrected Case

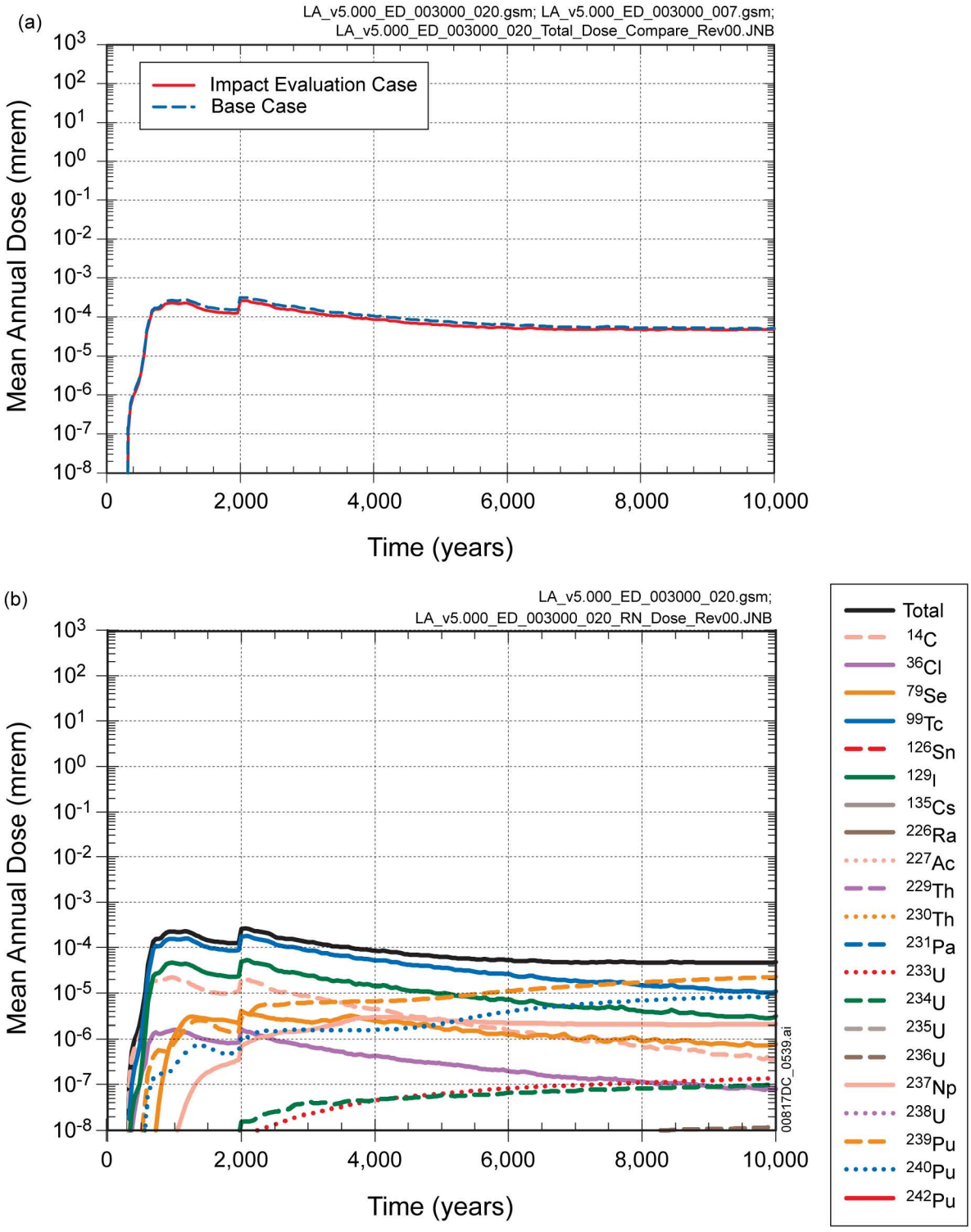

Source: Output DTNs: MO0709TSPALAMO.000 [DIRS 182981]; and MO0709TSPAREGS.000 [DIRS 182976].

Figure P-2. (a) Comparison of the Mean Annual Dose for the Impact Evaluation Case with the Base Case for the Drip Shield EF Modeling Case and (b) Major Radionuclide Dose Contributors for the Corrected Case

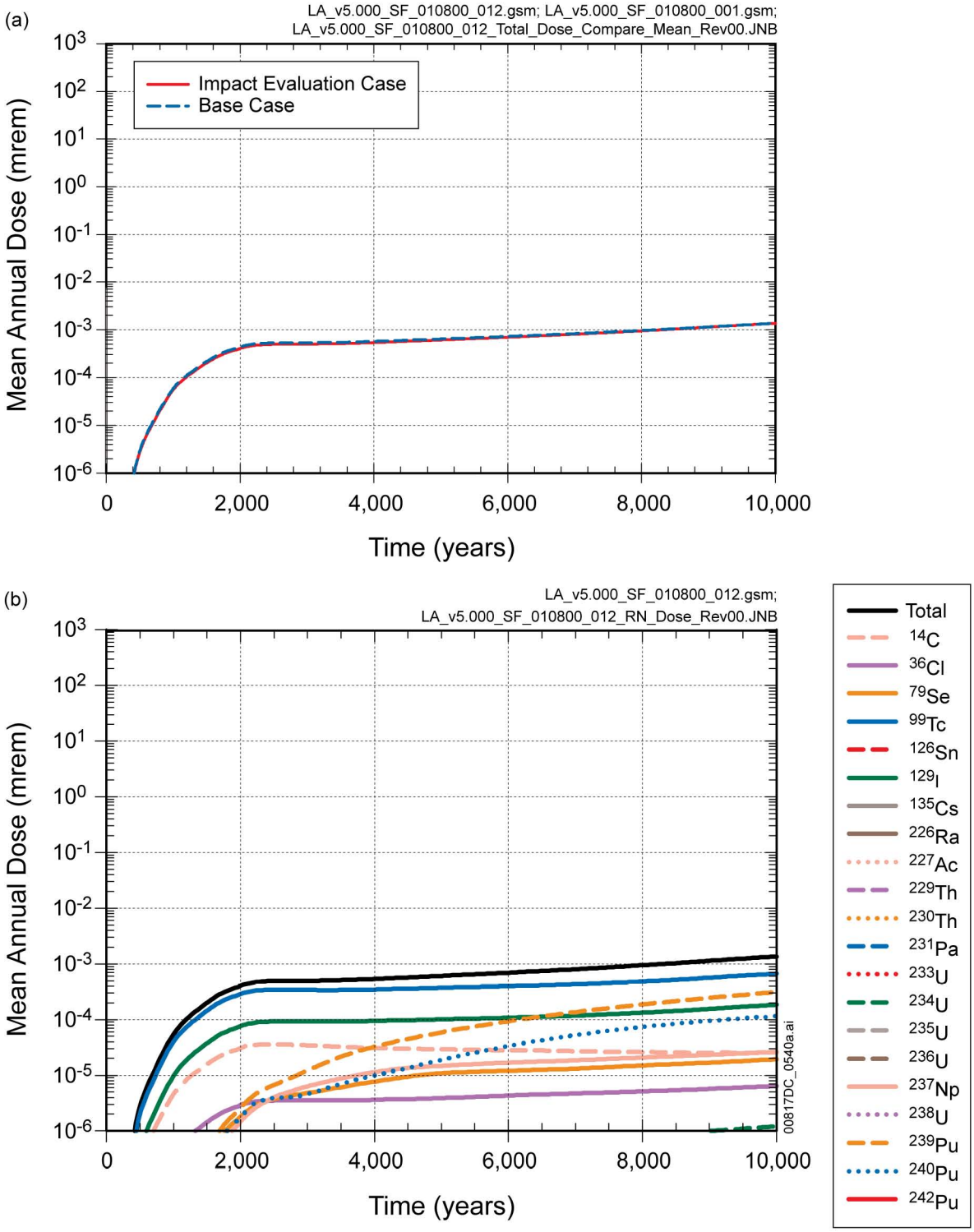

Source: Output DTNs: MO0709TSPALAMO.000 [DIRS 182981]; and MO0709TSPAREGS.000 [DIRS 182976].

Figure P-3. (a) Comparison of the Mean Annual Dose for the Impact Evaluation Case with the Base Case for the Seismic FD Modeling Case and (b) Major Radionuclide Dose Contributors for the Corrected Case

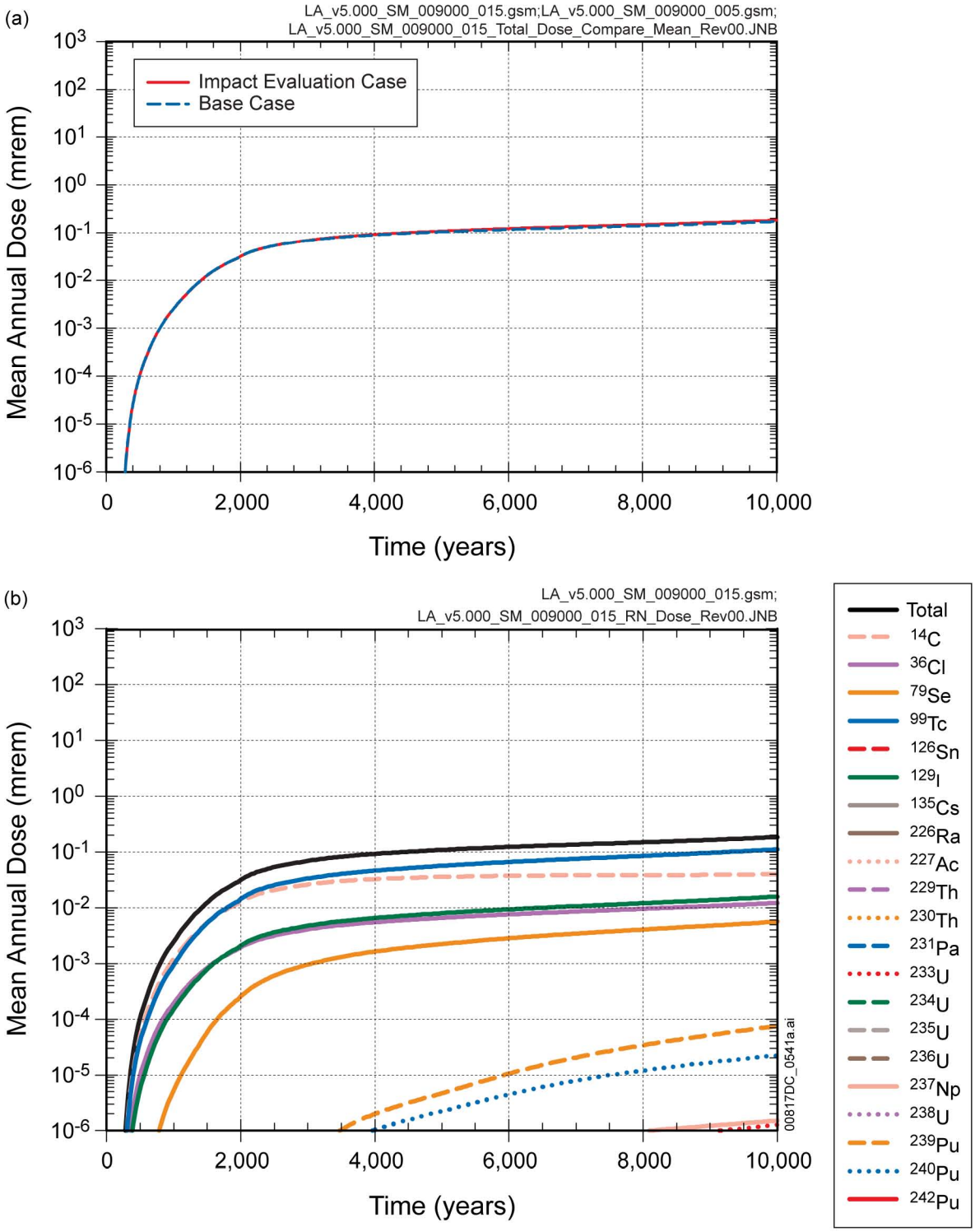

Source: Output DTNs: MO0709TSPALAMO.000 [DIRS 182981]; and MO0709TSPAREGS.000 [DIRS 182976].

Figure P-4. (a) Comparison of the Mean Annual Dose for the Impact Evaluation Case with the Base Case for the Seismic GM Modeling Case and (b) Major Radionuclide Dose Contributors for the Corrected Case

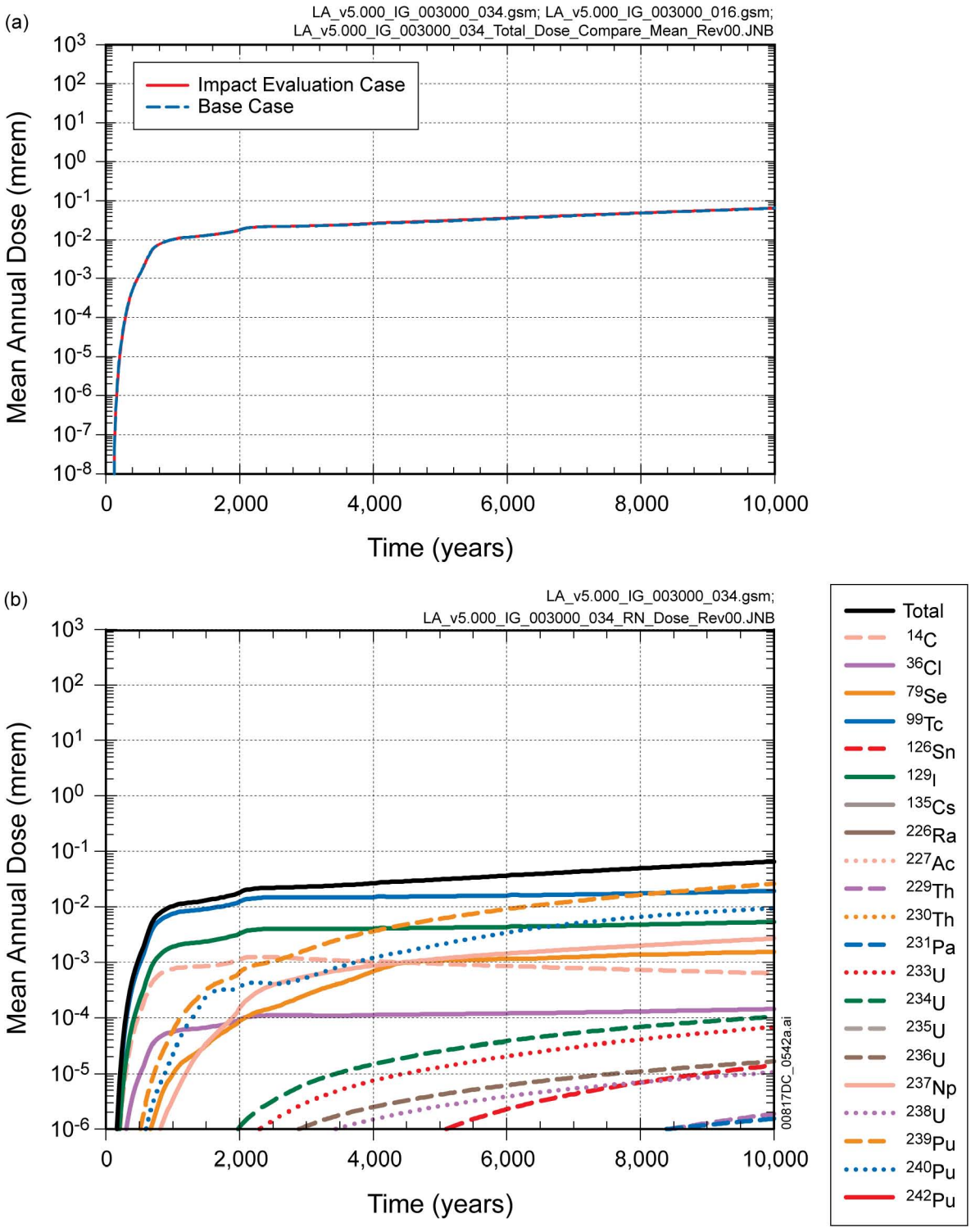

Source: Output DTNs: MO0709TSPALAMO.000 [DIRS 182981]; and MO0709TSPAREGS.000 [DIRS 182976].

Figure P-5. (a) Comparison of the Mean Annual Dose for the Impact Evaluation Case with the Base Case for the Igneous Intrusion Modeling Case and (b) Major Radionuclide Dose Contributors for the Corrected Case

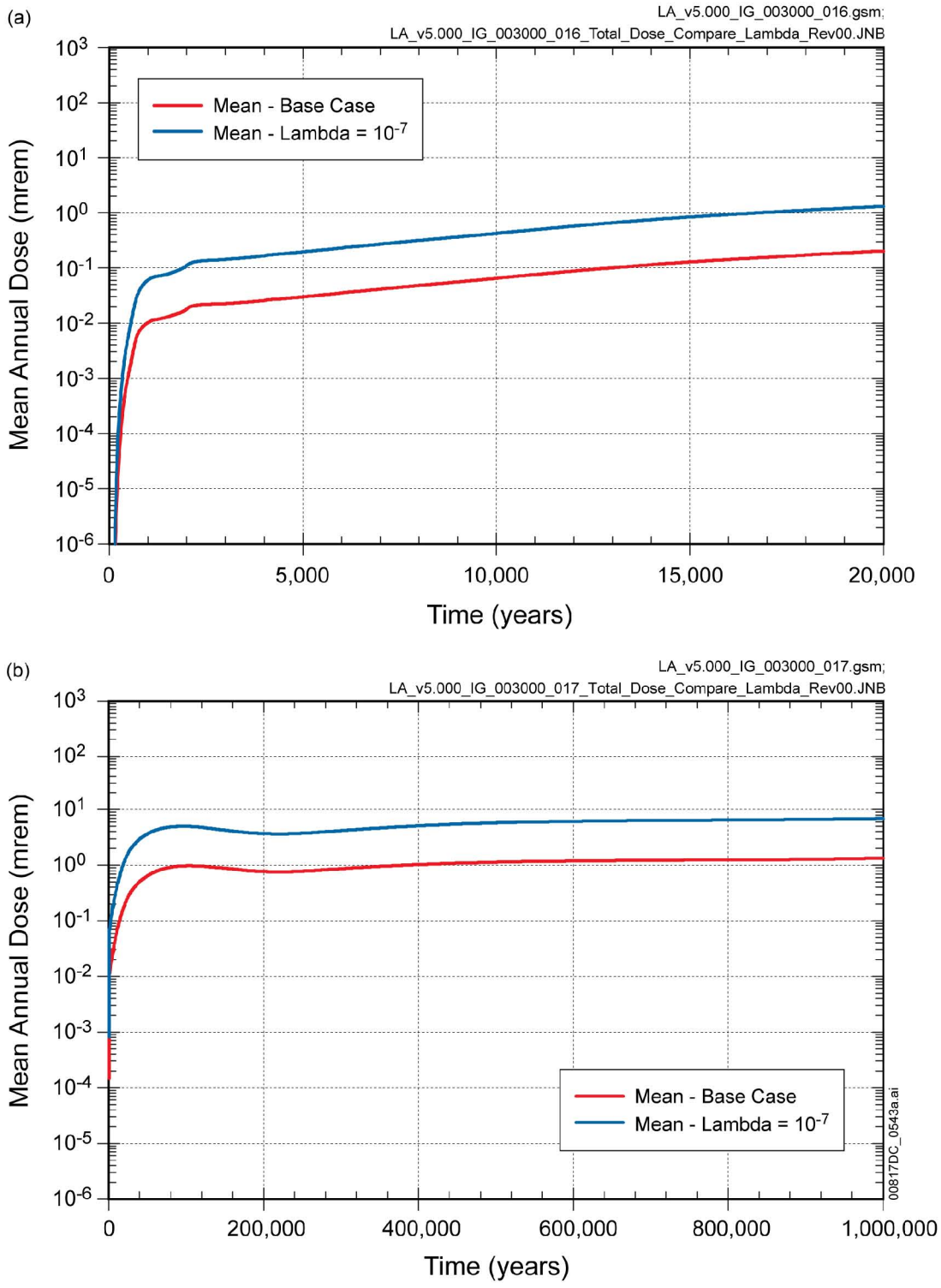

Source: Output DTNs: MO0709TSPALAMO.000 [DIRS 182981]; and MO0709TSPAREGS.000 [DIRS 182976].

Figure P-6. Mean Annual Dose for the Igneous Intrusion Modeling Case: Base Case and Probability of the Igneous Event set to 10^{-7} per year for (a) 20,000 Years and (b) 1,000,000 Years

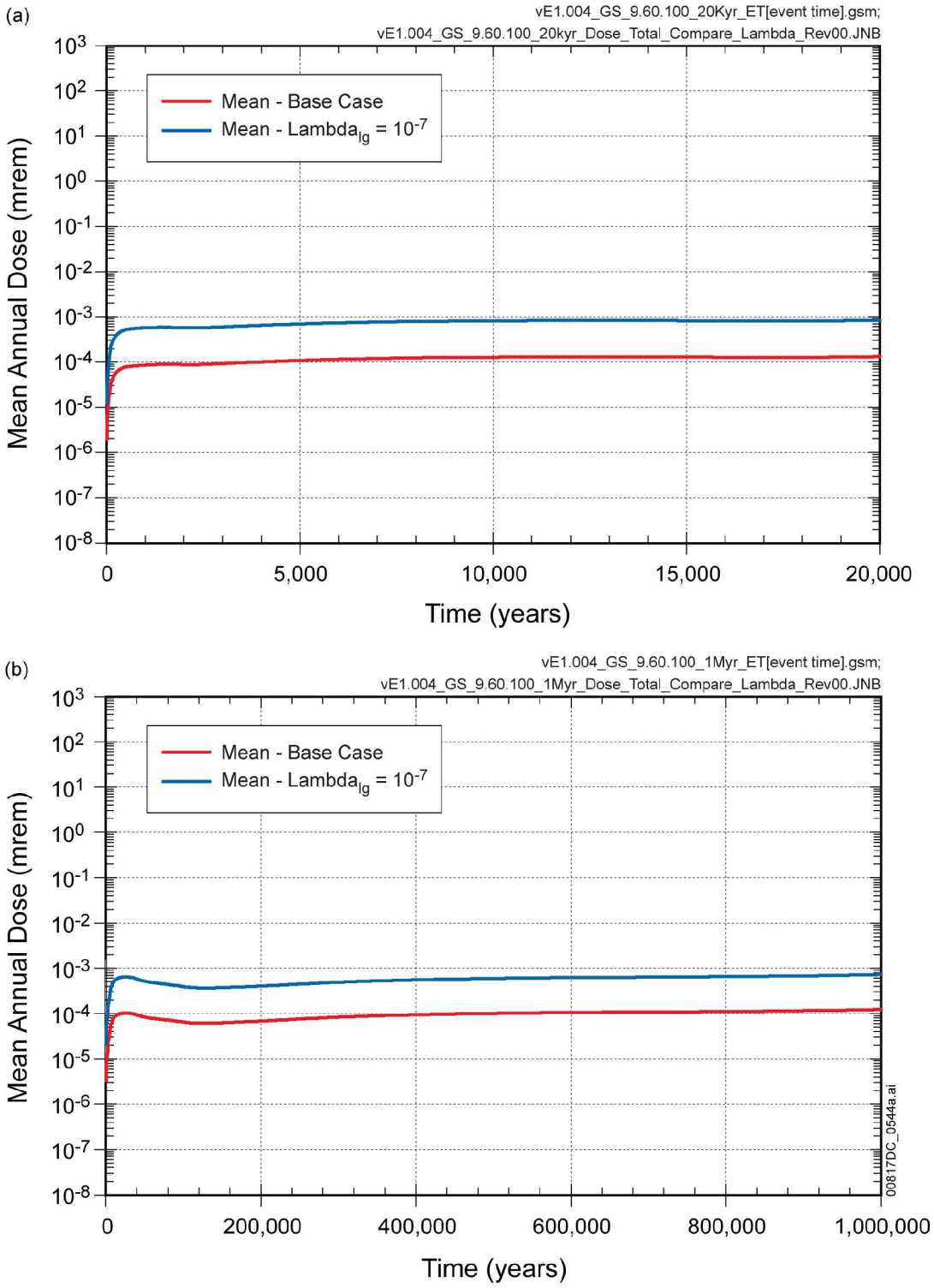

Source: Output DTNs: MO0709TSPALAMO.000 [DIRS 182981]; MO0709TSPAREGS.000 [DIRS 182976].

Figure P-7. Mean Annual Dose for the Volcanic Eruption Modeling Case: Base Case and Probability of the Igneous Event set to 10^{-7} per year for (a) 20,000 Years and (b) 1,000,000 Years

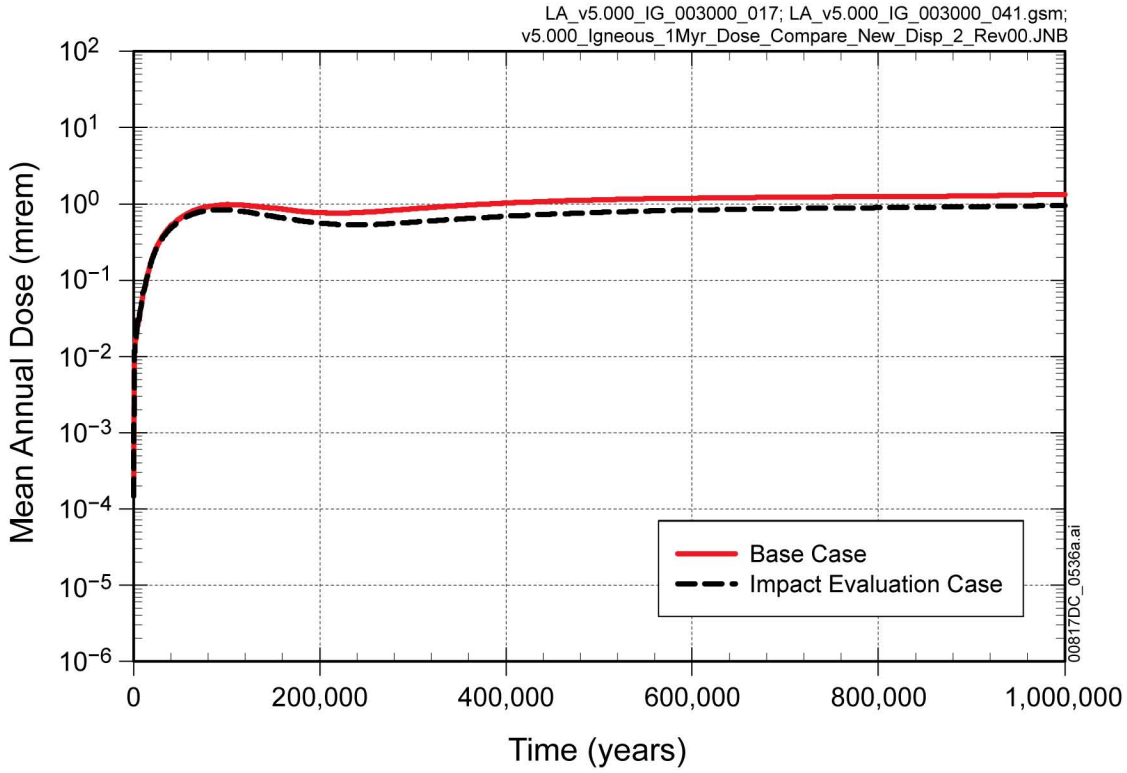

Source: Output DTNs: MO0709TSPALAMO.000 [DIRS 182981]; and MO0709TSPAREGS.000 [DIRS 182976].

Figure P-8. Mean Annual Dose Comparison for the Base Case and the Impact Evaluation Case with Updated Longitudinal Dispersivity for the Igneous Intrusion Modeling Case

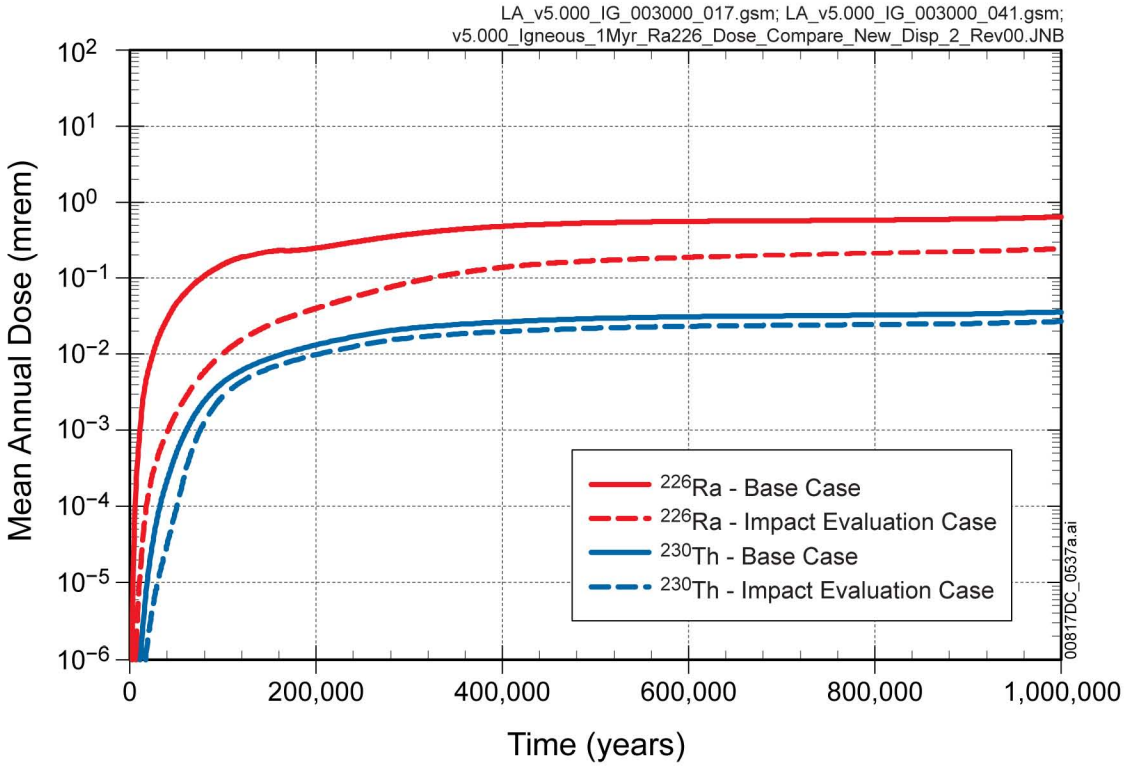

Source: Output DTNs: MO0709TSPALAMO.000 [DIRS 182981]; and MO0709TSPAREGS.000 [DIRS 182976].

Figure P-9. Comparison of Mean Annual Dose Contribution from ^{226}Ra and ^{230}Th for the Base Case and the Impact Evaluation Case with Updated Longitudinal Dispersivity for the Igneous Intrusion Modeling Case

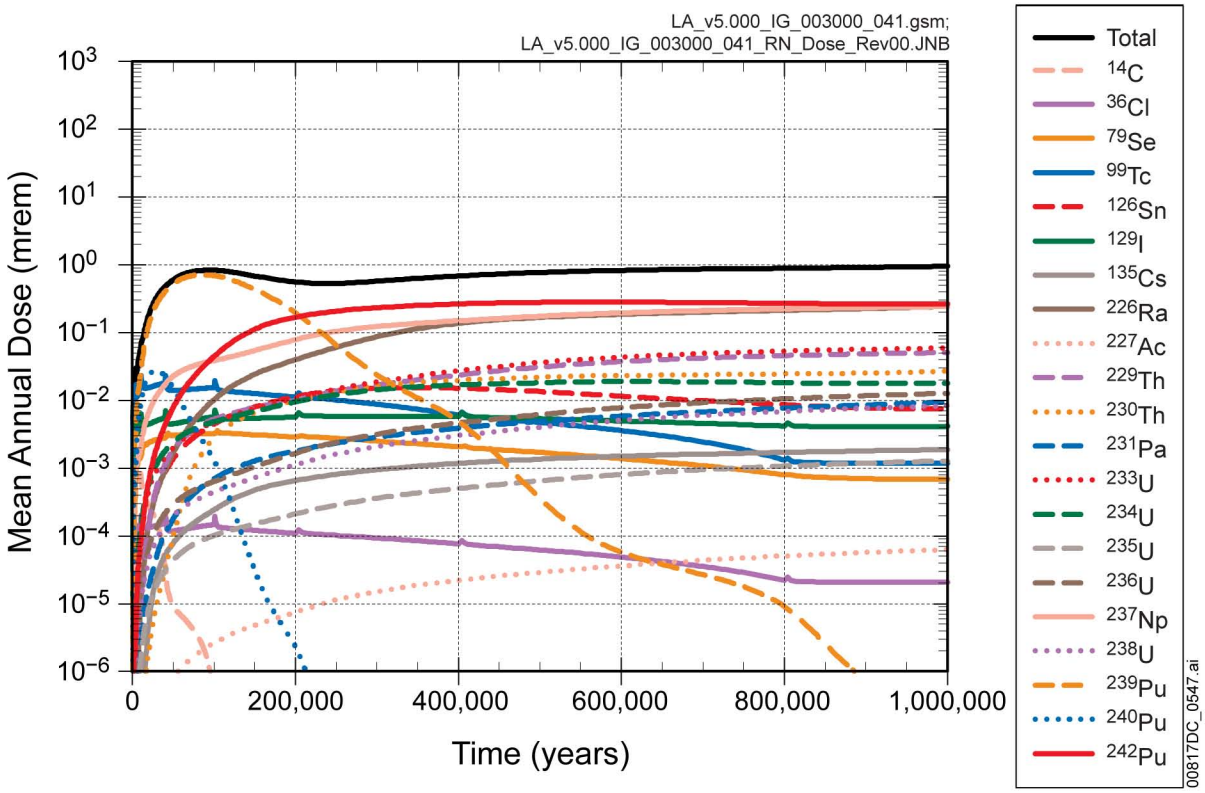

Source: Output DTN: MO0709TSPALAMO.000 [DIRS 182981].

Figure P-10. Major Radionuclide Dose Contributors for the Impact Evaluation Case with Updated Longitudinal Dispersivity for the Igneous Intrusion Modeling Case

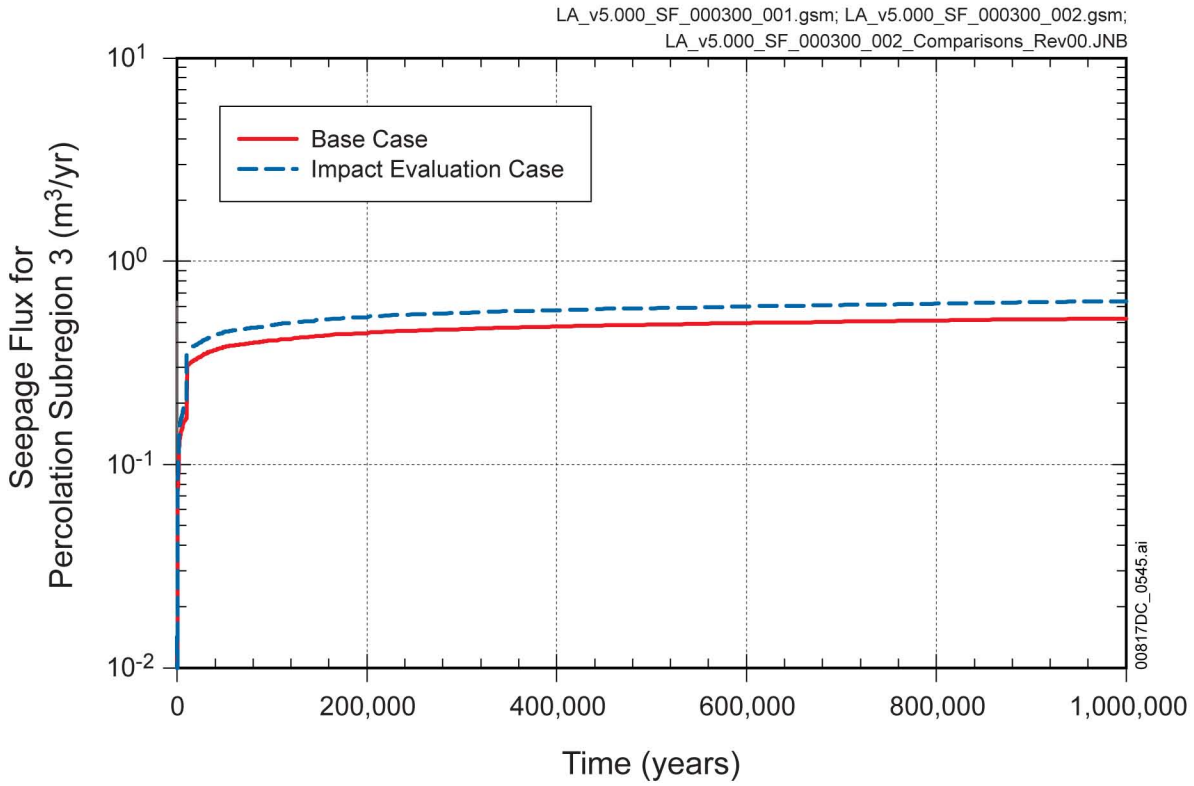

Source: Output DTN: MO0709TSPALAMO.000 [DIRS 182981].

Figure P-11. Mean Seepage Flux Comparison for Percolation Subregion 3 for the Base Case and the Impact Evaluation Case for the Seismic FD Modeling Case

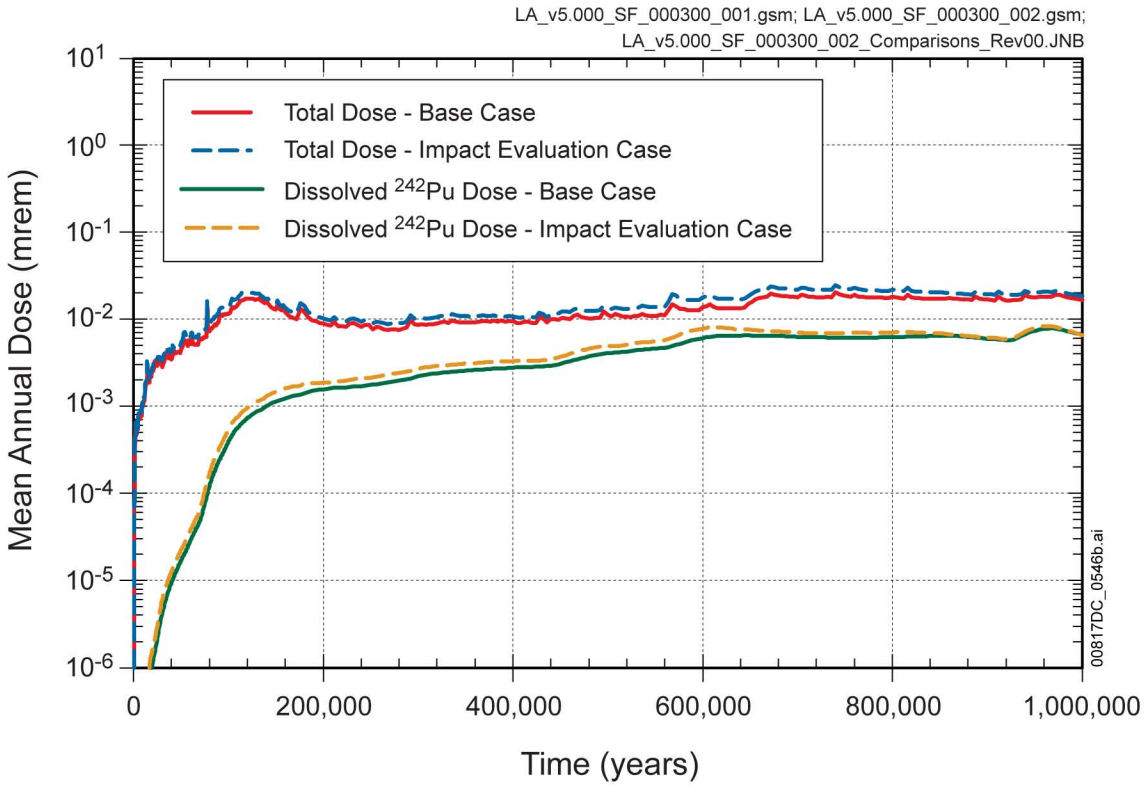

Source: Output DTN: MO0709TSPALAMO.000 [DIRS 182981].

Figure P-12. Mean Annual Dose Comparisons for the Base Case and the Impact Evaluation Case for the Seismic FD Modeling Case

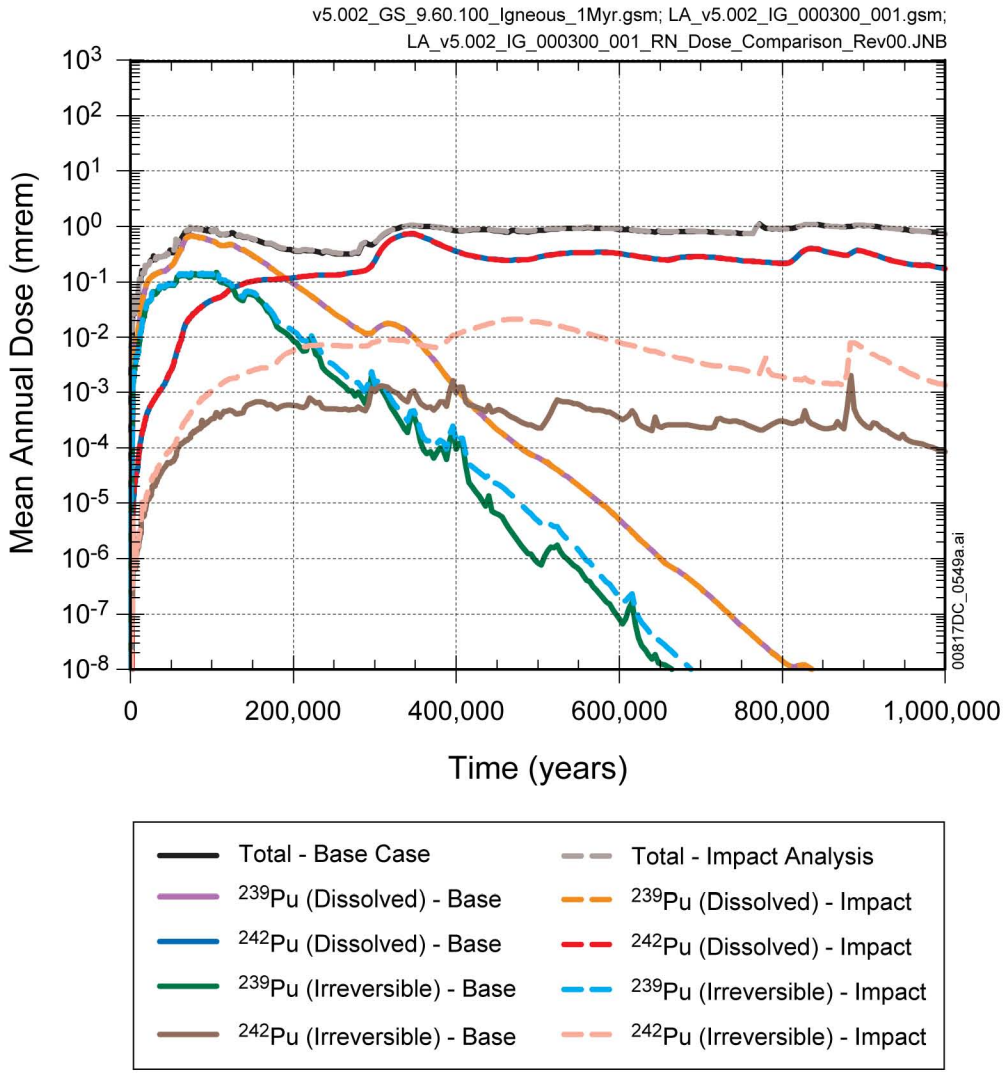

Source: Output DTN: MO0709TSPALAMO.000 [DIRS 182981].

Figure P-13. Mean Annual Dose Comparisons for the Base Case and the Impact Evaluation Case for the Igneous Intrusion Modeling Case

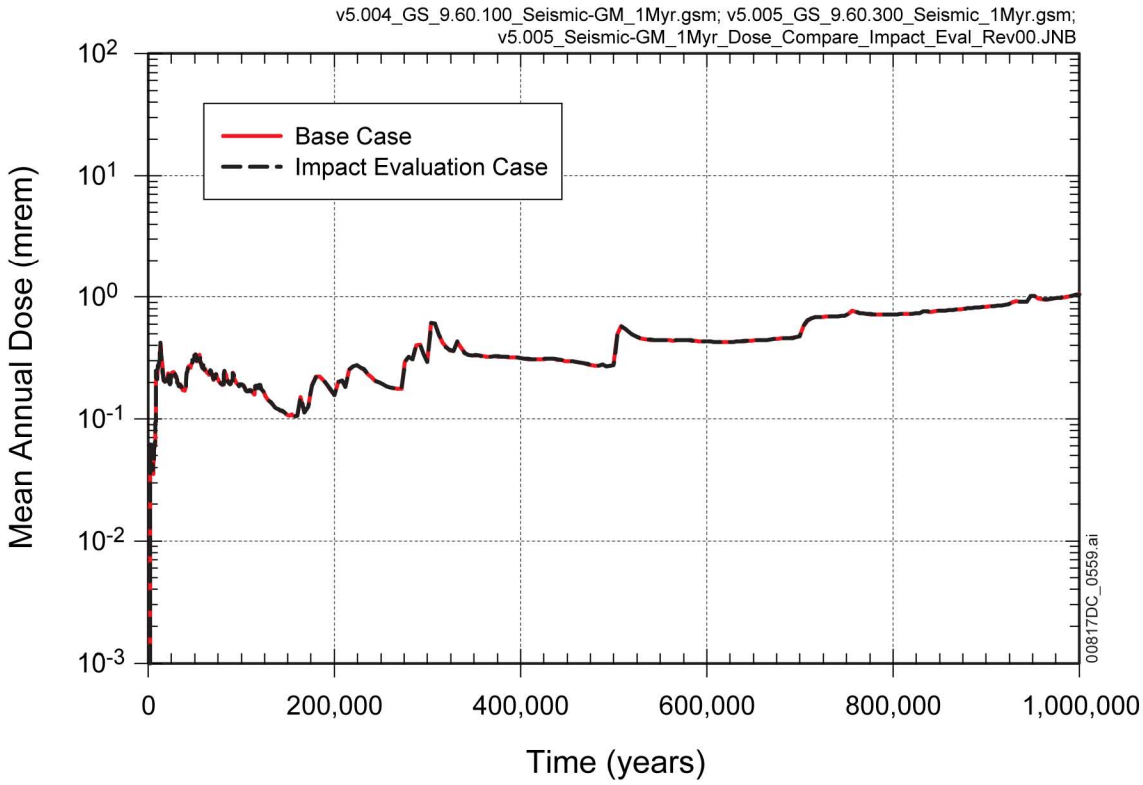

Source: Output DTN: MO0709TSPALAMO.000 [DIRS 182981].

Figure P-14. Mean Annual Dose Comparisons for the Base Case and the Impact Evaluation Case for the Seismic Ground Motion Modeling Case to Evaluate the Impact of the GoldSim Solver Error

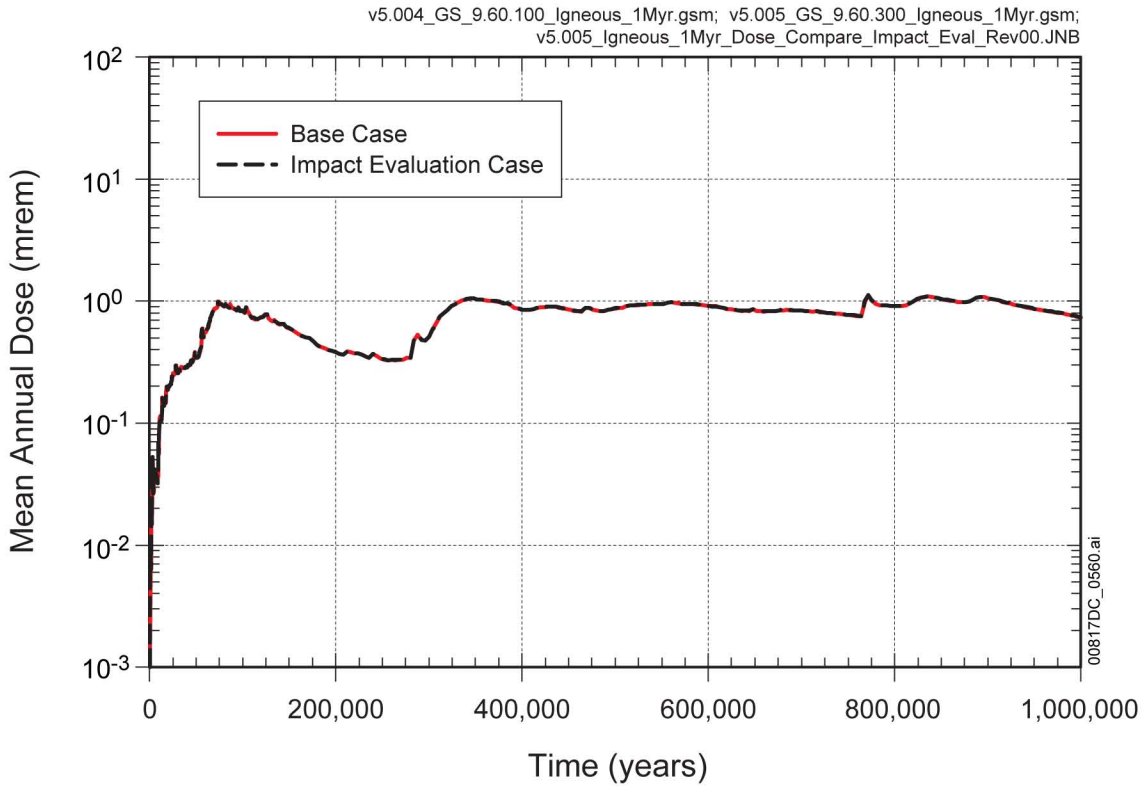

Source: Output DTN: MO0709TSPALAMO.000 [DIRS 182981].

Figure P-15. Mean Annual Dose Comparisons for the Base Case and the Impact Evaluation Case for the Igneous Intrusion Modeling Case to Evaluate the Impact of the GoldSim Solver Error

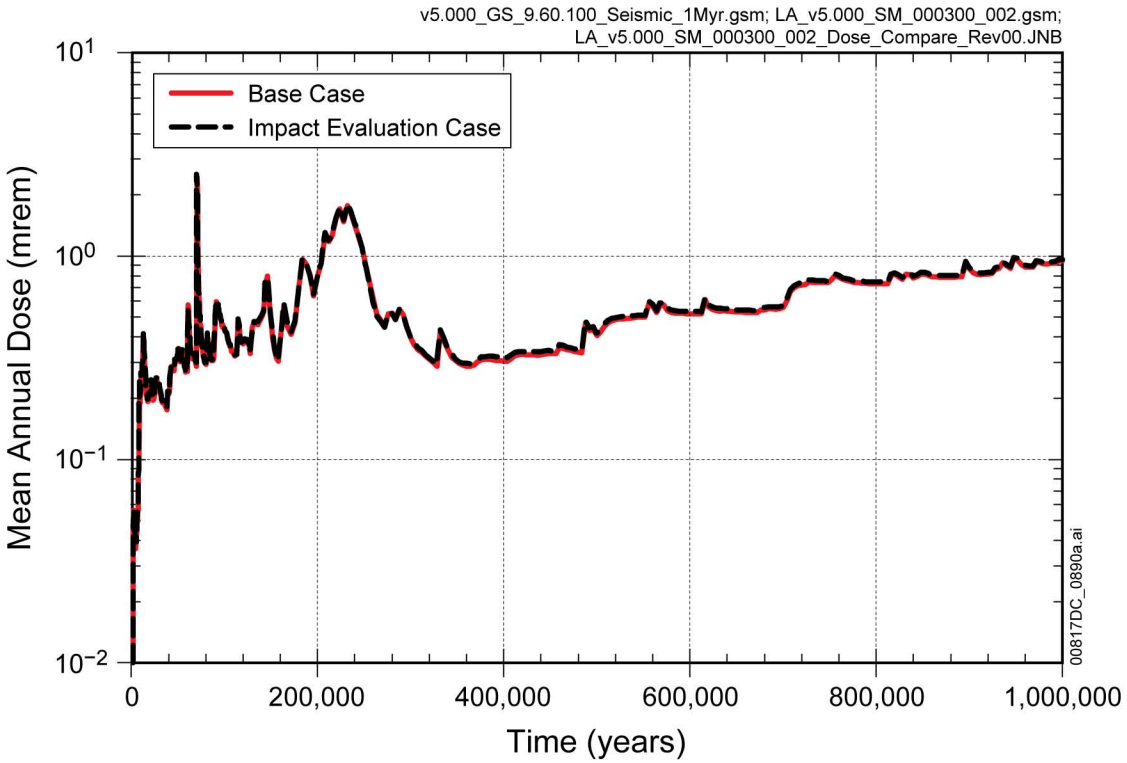

Source: Output DTN: MO0709TSPALAMO.000 [DIRS 182981].

Figure P-16. Mean Annual Dose Comparisons for the Base Case and the Impact Evaluation Case for the Seismic GM Modeling Case to Evaluate the Impact of UZ Transport Delay of some Radionuclides through the Fault Zones

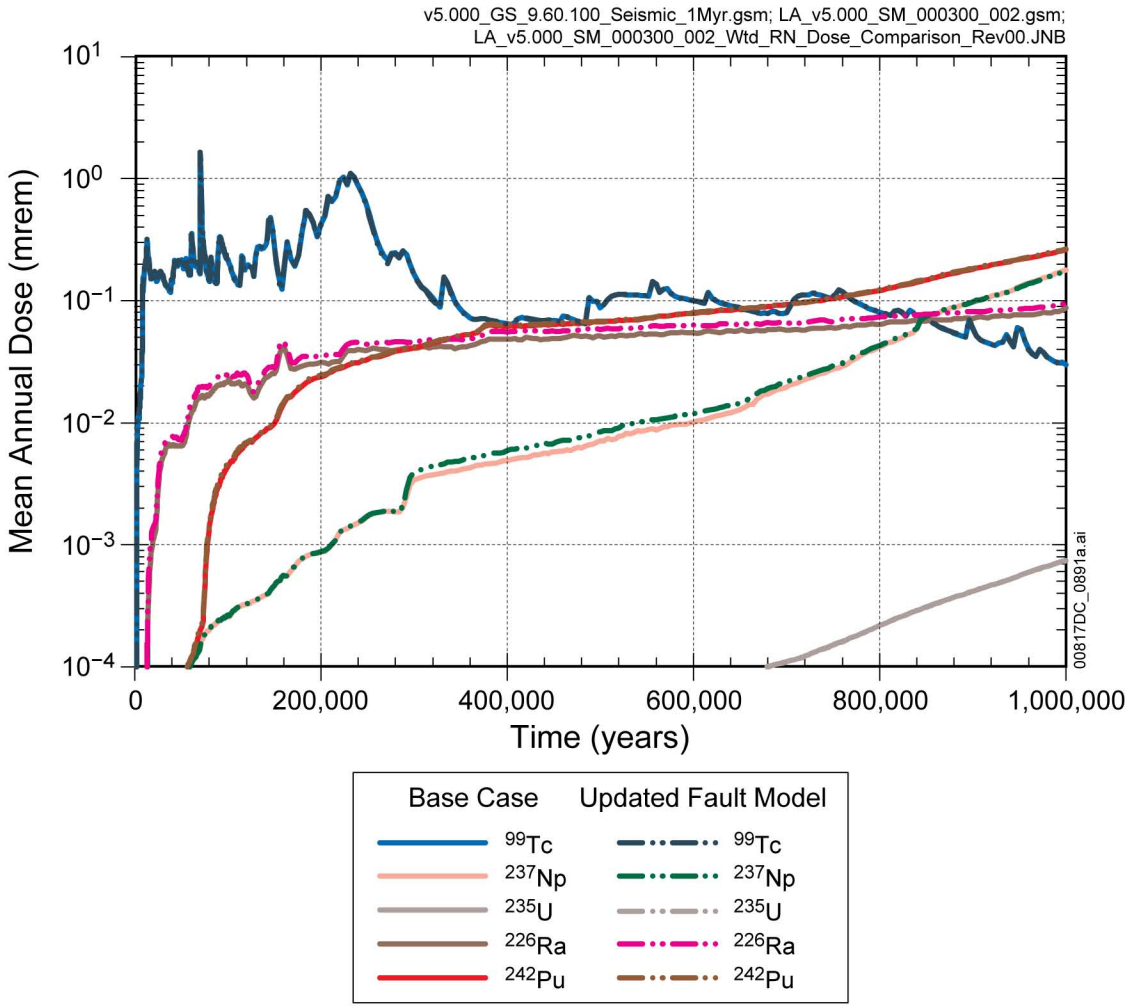

Source: Output DTN: MO0709TSPALAMO.000 [DIRS 182981].

Figure P-17. Mean Annual Dose Comparisons of Major Radionuclides for the Base Case and the Impact Evaluation Case for the Seismic Ground Motion Modeling Case to Evaluate the Impact of Unsaturated Zone Transport Error through the Fault Zones

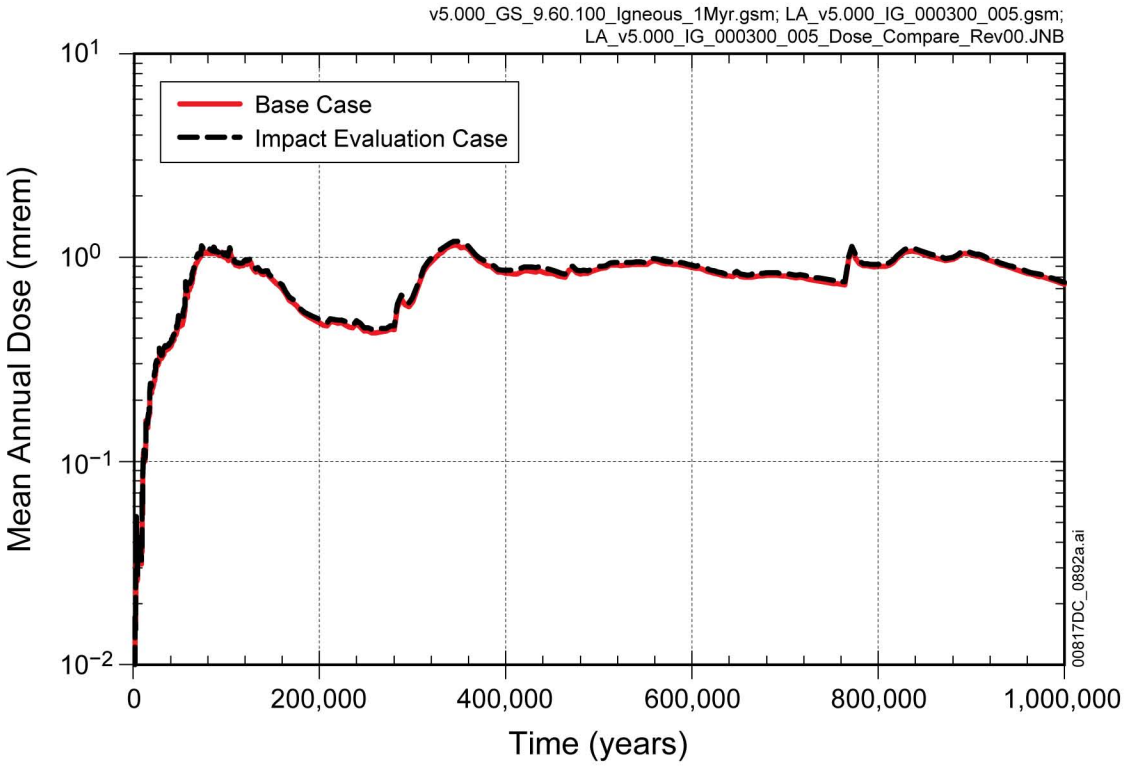

Source: Output DTN: MO0709TSPALAMO.000 [DIRS 182981].

Figure P-18. Mean Annual Dose Comparisons for the Base Case and the Impact Evaluation Case for the Igneous Intrusion Modeling Case to Evaluate the Impact of Unsaturated Zone Transport Error through the Fault Zones

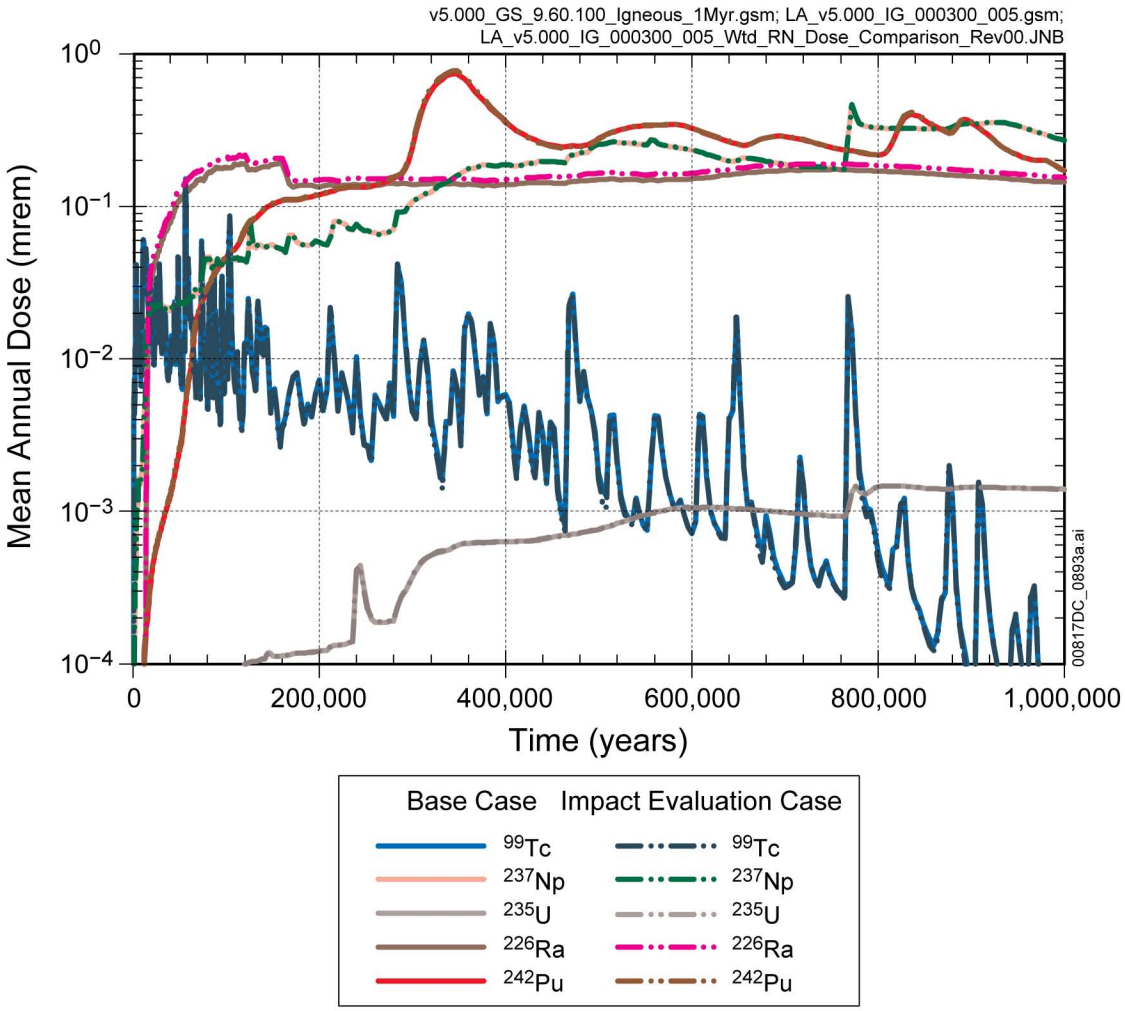

Source: Output DTN: MO0709TSPALAMO.000 [DIRS 182981].

Figure P-19. Mean Annual Dose Comparisons of Major Radionuclides for the Base Case and the Impact Evaluation Case for the Igneous Intrusion Modeling Case to Evaluate the Impact of Unsaturated Zone Transport Error through the Fault Zones

INTENTIONALLY LEFT BLANK

QA: QA

MDL-WIS-PA-000005 REV 00 AD 01

March 2008

Total System Performance Assessment Model/Analysis for the License Application Addendum 01

Volume I

Prepared for:
U.S. Department of Energy
Office of Civilian Radioactive Waste Management
Office of Repository Development
1551 Hillshire Drive
Las Vegas, Nevada 89134-6321

Prepared by:
Sandia National Laboratories
OCRWM Lead Laboratory for Repository Systems
1180 Town Center Drive
Las Vegas, Nevada 89144

Under Contract Number
DE-AC04-94AL85000

DISCLAIMER

This report was prepared as an account of work sponsored by an agency of the United States Government. Neither the United States Government nor any agency thereof, nor any of their employees, nor any of their contractors, subcontractors or their employees, makes any warranty, express or implied, or assumes any legal liability or responsibility for the accuracy, completeness, or any third party's use or the results of such use of any information, apparatus, product, or process disclosed, or represents that its use would not infringe privately owned rights. Reference herein to any specific commercial product, process, or service by trade name, trademark, manufacturer, or otherwise, does not necessarily constitute or imply its endorsement, recommendation, or favoring by the United States Government or any agency thereof or its contractors or subcontractors. The views and opinions of authors expressed herein do not necessarily state or reflect those of the United States Government or any agency thereof.

Addendum Cover Page

Complete only applicable items.

QA: QA

1. Total Pages: ~794

2. Addendum to (Title):

Total System Performance Assessment Model/Analysis for the License Application: Addendum

3. DI (including Revision and Addendum No.):

MDL-WIS-PA-000005 REV 00 AD 01

	Printed Name	Signature	Date
4. Originator	Patrick D. Mattie - Lead		3-11-08
5. Independent Technical Reviewer	Mel Marietta		3/11/2008
6. Checker	Robert Zimmerman - Lead		3/11/2008
7. QCS/QA Reviewer	John Devers - Lead		03/11/08
8. Responsible Manager/ Lead	Jerry McNeish		3/11/08.
9. Responsible Manager	M. Kathryn Knowles - PASI Manager		3/11/08

10. Remarks

Change History

11. Revision and Addendum No.	12. Description of Change
Rev.00 AD 01	This addendum presents updated analyses for the TSPA-LA Rev 00 and any changes to the parent document necessary to document these updated analyses. The updated analyses include updates to direct inputs of the TSPA-LA. In addition, issues identified in Appendix P of the parent document are addressed here per the review criteria outlined in Sections 2.1.4 and 2.3.5.2.1 of the *Technical Work Plan for: Total System Performance Assessment FY 07-08 Activities* (SNL 2008 [DIRS 184920]).

INTENTIONALLY LEFT BLANK

CONTENTS

Page

ES1[a] SCOPE ..... ES-1[a]
ES1.1[a] Introduction ..... ES-1[a]
ES2[a] TOTAL SYSTEM PERFORMANCE ASSESSMENT METHODOLOGY ..... ES-2[a]
ES3[a] TSPA-LA MODEL DEVELOPMENT PROCESS ..... ES-3[a]
ES3.1[a] Features, Events, and Processes Analysis ..... ES-3[a]
ES3.2[a] Development of the Scenario Classes ..... ES-3[a]
ES3.3[a] Incorporation of Uncertainty ..... ES-3[a]
ES3.4[a] Natural and Engineered Model Components ..... ES-4[a]
ES3.5[a] Alternative Conceptual Models ..... ES-4[a]
ES3.6[a] Configuration Management for the TSPA-LA Model ..... ES-4[a]
ES4[a] YUCCA MOUNTAIN SITE DESCRIPTION ..... ES-4[a]
ES4.1[a] Physiographic Setting and Topography ..... ES-4[a]
ES4.2[a] Climate ..... ES-4[a]
ES4.3[a] Geology ..... ES-4[a]
ES4.4[a] Regional Tectonic Setting ..... ES-4[a]
ES5[a] THE REPOSITORY SUBSURFACE FACILITY AND ENGINEERED BARRIER SYSTEM ..... ES-4[a]
ES6[a] NATURAL AND ENGINEERED BARRIERS ..... ES-4[a]
ES7[a] GENERAL DESCRIPTION OF THE TSPA-LA MODEL ..... ES-5[a]
ES8[a] VERIFICATION/VALIDATION OF THE TOTAL SYSTEM PERFORMANCE ASSESSMENT MODEL ..... ES-5[a]
ES8.1[a] Verification and Validation Strategy ..... ES-5[a]
ES8.2[a] Computer Code and Input Verification ..... ES-5[a]
ES8.3[a] Stability Testing ..... ES-6[a]
ES8.4[a] Uncertainty Characterization Reviews ..... ES-7[a]
ES8.5[a] Surrogate Waste Form Validation ..... ES-7[a]
ES8.6[a] Corroboration of Abstraction Model Results with Validated Process Models ..... ES-7[a]
ES8.7[a] Auxiliary Analyses ..... ES-7[a]
ES8.8[a] Confidence Building: Natural Analogues ..... ES-9[a]
ES8.9[a] Summary of Technical Reviews ..... ES-9[a]
ES9[a] SYSTEM PERFORMANCE ANALYSES ..... ES-9[a]
ES9.1[a] Total Mean Annual Dose to the Reasonably Maximally Exposed Individual for the Repository System ..... ES-10[a]
ES9.2[a] Results of the Scenario Class Modeling Case Simulations ..... ES-10[a]
ES9.2.1[a] Nominal Scenario Class Modeling Case ..... ES-11[a]
ES9.2.2[a] Early Failure Scenario Class Modeling Cases ..... ES-11[a]
ES9.2.3[a] Igneous Scenario Class Modeling Cases ..... ES-12[a]
ES9.2.4[a] Seismic Scenario Class Modeling Cases ..... ES-13[a]
ES9.2.5[a] Total Mean Annual Dose to the Reasonably Maximally Exposed Individual for the Repository System ..... ES-15[a]

CONTENTS (Continued)

Page

ES9.3[a] Comparison of Annual Dose with Postclosure Individual and Groundwater Protection Standards ..... ES-15[a]
ES9.3.1[a] Individual Protection Standard ..... ES-15[a]
ES9.3.2[a] Groundwater Protection Standard ..... ES-17[a]
ES9.4[a] Human Intrusion Scenario ..... ES-17[a]
ES10[a] SUMMARY OF THE RESULTS OF THE TSPA-LA MODEL ..... ES-18[a]

CONTENTS (Continued)

Page

1[a]. PURPOSE ..... 1-1[a]
- 1.1[a] INTRODUCTION ..... 1-1[a]
  - 1.1.1[a] Governing Regulations ..... 1-1[a]
  - 1.1.2[a] Total System Performance Assessment Methodology ..... 1-1[a]
  - 1.1.3[a] Treatment of Uncertainty ..... 1-2[a]
- 1.2[a] TSPA-LA MODEL DEVELOPMENT PROCESS ..... 1-2[a]
- 1.3[a] YUCCA MOUNTAIN SITE DESCRIPTION ..... 1-2[a]
- 1.4[a] DESIGN OF YUCCA MOUNTAIN REPOSITORY SUBSURFACE FACILITIES ..... 1-2[a]
- 1.5[a] GENERAL DESCRIPTION OF THE TSPA-LA MODEL ..... 1-2[a]
- 1.6[a] CONCEPTUAL DESCRIPTION OF PROCESSES RELEVANT TO AN EVALUATION OF POSTCLOSURE PERFORMANCE IN THE ABSENCE OF DISRUPTIVE EVENTS ..... 1-2[a]
- 1.7[a] CONCEPTUAL DESCRIPTION OF PROCESSES RELEVANT TO AN EVALUATION OF POSTCLOSURE PERFORMANCE AFTER THE OCCURRENCE OF DISRUPTIVE EVENTS ..... 1-2[a]
- 1.8[a] CONSERVATISMS AND LIMITATIONS RELATED TO THE TSPA-LA MODEL ..... 1-2[a]
  - 1.8.1[a] Conservatisms Incorporated in the TSPA-LA Model ..... 1-2[a]
  - 1.8.2[a] Limitations of the TSPA-LA Model ..... 1-2[a]
- 1.9[a] DESCRIPTION OF THE TOTAL SYSTEM PERFORMANCE ASSESSMENT MODEL/ANALYSIS FOR THE LICENSE APPLICATION ..... 1-5[a]
- 1.10[a] DOCUMENT ORGANIZATION ..... 1-5[a]
  - 1.10.1[a] Volume I[a] ..... 1-5[a]
  - 1.10.2[a] Volume II[a] ..... 1-6[a]
  - 1.10.3[a] Volume III[a] ..... 1-8[a]

2[a]. QUALITY ASSURANCE ..... 2-1[a]
- 2.1[a] CONFIGURATION MANAGEMENT ..... 2-1[a]

3[a]. USE OF SOFTWARE ..... 3-1[a]
- 3.1[a] INTRODUCTION ..... 3-1[a]
- 3.2[a] ASHPLUME_DLL_LA ..... 3-1[a]
- 3.3[a] CWD ..... 3-1[a]
- 3.4[a] EXDOC_LA ..... 3-1[a]
- 3.5[a] FAR ..... 3-1[a]
- 3.6[a] FEHM ..... 3-1[a]
- 3.7[a] GETTHK_LA ..... 3-1[a]
- 3.8[a] GOLDSIM ..... 3-1[a]
  - 3.8.1[a] Description of Software ..... 3-2[a]
  - 3.8.2[a] Relationship to the TSPA-LA Model ..... 3-2[a]

CONTENTS (Continued)

Page

3.8.3[a] Software Documentation ..... 3-2[a]
3.8.4[a] Range of Validation ..... 3-2[a]
3.9[a] INTERPZDLL_LA ..... 3-2[a]
3.10[a] MFCP_LA ..... 3-2[a]
3.11[a] MKTABLE AND MKTABLE_LA ..... 3-2[a]
3.12[a] MVIEW ..... 3-2[a]
3.13[a] PASSTABLE1D_LA ..... 3-3[a]
3.14[a] PASSTABLE3D_LA ..... 3-3[a]
3.15[a] PREWAP_LA ..... 3-3[a]
3.16[a] SCCD ..... 3-3[a]
3.17[a] SEEPAGEDLL_LA ..... 3-3[a]
3.18[a] SOILEXP_LA ..... 3-3[a]
3.19[a] SZ_CONVOLUTE ..... 3-3[a]
3.20[a] TSPA_INPUT_DB ..... 3-3[a]
3.21[a] WAPDEG ..... 3-3[a]
3.22[a] CORROBORATIVE SOFTWARE USED ..... 3-3[a]

4[a]. INPUTS ..... 4-1[a]
4.1[a] DIRECT INPUTS ..... 4-1[a]
4.2[a] TSPA-LA MODEL-GENERATED PARAMETERS ..... 4-1[a]
4.3[a] PARAMETER ENTRY FORMS ..... 4-1[a]
4.4[a] TRACEABILITY OF INPUTS ..... 4-1[a]
4.5[a] CRITERIA ..... 4-1[a]
4.6[a] CODES AND STANDARDS ..... 4-1[a]
4.7[a] TSPA INPUT DATABASE ..... 4-1[a]

5[a]. ASSUMPTIONS ..... 5-1[a]
5.1[a] NOMINAL SCENARIO CLASS ..... 5-1[a]
5.2[a] EARLY FAILURE SCENARIO CLASS ..... 5-1[a]
5.3[a] IGNEOUS SCENARIO CLASS ..... 5-1[a]
5.4[a] SEISMIC SCENARIO CLASS ..... 5-1[a]
5.5[a] HUMAN INTRUSION SCENARIO ..... 5-1[a]

6[a]. TSPA-LA MODEL DESCRIPTION ..... 6-1[a]
6.1[a] CONCEPTUAL DESIGN ..... 6-1[a]
6.1.1[a] Features, Events, and Processes Screening and Scenario Development ..... 6-1[a]
6.1.2[a] Calculation of Dose for the TSPA-LA Model ..... 6-1[a]
6.1.3[a] Treatment of Uncertainty in the TSPA-LA Model ..... 6-3[a]
6.1.4[a] TSPA-LA Model Structure and Design ..... 6-3[a]
6.1.5[a] TSPA-LA Model File Architecture ..... 6-7[a]
6.2[a] ALTERNATIVE CONCEPTUAL MODELS ..... 6-13[a]
6.3[a] TSPA-LA MODEL FOR THE NOMINAL SCENARIO CLASS ..... 6-13[a]

CONTENTS (Continued)

Page

6.3.1[a] Mountain-Scale Unsaturated Zone Flow ..... 6-13[a]
6.3.2[a] Engineered Barrier System Thermal-Hydrologic Environment ..... 6-13[a]
6.3.3[a] Drift-Scale Unsaturated Zone Flow ..... 6-17[a]
6.3.4[a] Engineered Barrier System Chemical Environment ..... 6-17[a]
6.3.5[a] Waste Package and Drip Shield Degradation ..... 6-18[a]
6.3.6[a] Engineered Barrier System Flow ..... 6-19[a]
6.3.7[a] Waste Form Degradation and Mobilization ..... 6-23[a]
6.3.8[a] Engineered Barrier System Transport ..... 6-31[a]
6.3.9[a] Unsaturated Zone Transport ..... 6-35[a]
6.3.10[a] Saturated Zone Flow and Transport Model Component ..... 6-41[a]
6.3.11[a] Biosphere ..... 6-49[a]
6.4[a] TSPA-LA MODEL FOR THE EARLY FAILURE SCENARIO CLASS ..... 6-49[a]
6.5[a] TSPA-LA MODEL FOR THE IGNEOUS SCENARIO CLASS ..... 6-49[a]
6.6[a] TSPA-LA MODEL FOR THE SEISMIC SCENARIO CLASS ..... 6-49[a]
6.6.1[a] TSPA-LA Model Components and Submodels for the Seismic Scenario Class ..... 6-49[a]
6.6.2[a] Interaction of Seismic Scenario Class Submodels with other TSPA-LA Submodels ..... 6-53[a]
6.6.3[a] Model Component Consistency and Conservatisms in Assumptions and Parameters ..... 6-54[a]
6.6.4[a] Alternative Conceptual Model(s) for Seismic Scenario Modeling Cases ..... 6-54[a]
6.7[a] TSPA-LA MODEL FOR THE HUMAN INTRUSION SCENARIO ..... 6-59[a]

INTENTIONALLY LEFT BLANK

FIGURES

Page

ES-12[a]. Topographic Map of the Yucca Mountain Site Showing Differences in Slope Characteristics North and South of Drill Hole Wash ..... FES-1[a]
ES-40[a]. Total Expected Annual Dose for 10,000 Years after Repository Closure ..... FES-2[a]
ES-41[a]. Total Expected Annual Dose for 1,000,000 Years after Repository Closure ..... FES-3[a]
ES-42[a]. Contribution of Individual Radionuclides to Total Mean Annual Dose for 10,000 Years after Repository Closure ..... FES-4[a]
ES-43[a]. Contribution of Individual Radionuclides to Total Mean Annual Dose for 1,000,000 Years after Repository Closure ..... FES-5[a]
ES-44[a]. Annual Dose for the Nominal Scenario Class Modeling Case for the Post-10,000-Year Period ..... FES-6[a]
ES-45[a]. Mean Annual Dose Contributions from Major Radionuclides for the Nominal Scenario Class Modeling Case for the Post-10,000-Year Period ..... FES-7[a]
ES-46[a]. Expected Annual Dose for the Drip Shield Early Failure Modeling Case for (a) the First 10,000 Years after Repository Closure and (b) Post-10,000-Year Period ..... FES-8[a]
ES-47[a]. Mean Annual Dose Contributions from Major Radionuclides for the Drip Shield Early Failure Modeling Case for (a) the First 10,000 Years after Repository Closure and (b) Post-10,000-Year Period ..... FES-9[a]
ES-48[a]. Expected Annual Dose for the Waste Package Early Failure Modeling Case for (a) the First 10,000 Years after Repository Closure and (b) Post-10,000-Year Period ..... FES-10[a]
ES-49[a]. Mean Annual Dose Contributions from Major Radionuclides for the Waste Package Early Failure Modeling Case for (a) the First 10,000 Years after Repository Closure and (b) Post-10,000-Year Period ..... FES-11[a]
ES-50[a]. Expected Annual Dose for the Igneous Intrusion Modeling Case for (a) 10,000 Years after Repository Closure and (b) Post-10,000-Year Period ..... FES-12[a]
ES-51[a]. Mean Annual Dose Contributions from Major Radionuclides for the Igneous Intrusion Modeling Case for (a) the First 10,000 Years after Repository Closure and (b) Post-10,000-Year Period ..... FES-13[a]
ES-54[a]. Expected Annual Dose for the Seismic Ground Motion Modeling Case for (a) 10,000 Years after Repository Closure and (b) Post-10,000-Year Period ..... FES-14[a]
ES-55[a]. Mean Annual Dose Contributions from Major Radionuclides for the Seismic Ground Motion Modeling Case for (a) the First 10,000 Years after Repository Closure and (b) Post-10,000-Year Period ..... FES-15[a]
ES-56[a]. Expected Annual Dose for the Seismic Fault Displacement Modeling Case for (a) 10,000 Years after Repository Closure and (b) Post-10,000-Year Period ..... FES-16[a]
ES-57[a]. Mean Annual Dose Contributions from Major Radionuclides for the Seismic Fault Displacement Modeling Case for (a) 10,000 Years after Repository Closure and (b) Post-10,000-Year Period ..... FES-17[a]

FIGURES (Continued)

Page

ES-58[a]. Total Mean Annual Dose and Median Annual Doses for Each Modeling Case for (a) 10,000 Years after Repository Closure and (b) Post-10,000-Year Period ..... FES-18[a]
ES-59[a]. Combined ^{226}Ra and ^{228}Ra Activity Concentrations, Excluding Natural Background, for Likely Features, Events, and Processes Using Nominal, Early Failure, and Seismic Ground Motion Damage Processes ..... FES-19[a]
ES-60[a]. Combined Activity Concentrations of All Alpha Emitters (including ^{226}Ra but without radon and uranium isotopes), Excluding Natural Background, for Likely Features, Events, and Processes Using Nominal, Early Failure, and Seismic Ground Motion Damage Processes ..... FES-20[a]
ES-61[a]. Mean Annual Drinking Water Dose from Combined Beta and Photon Emitters for Likely Features, Events, and Processes using the Nominal, Early Failure, and Seismic Ground Motion Damage Processes ..... FES-21[a]
ES-62[a]. Expected Annual Individual Dose at the RMEI Location from a Human Intrusion 200,000 Years after Repository Closure ..... FES-22[a]

3-2[a]. TSPA-LA Software Architecture ..... 3-9[a]

6.1.4-5[a]. Information Transfer between the Submodels of the TSPA-LA Volcanic Eruption Modeling Case ..... 6-5[a]

6.3.2-7[a]. Repository Percolation Subregions Used in the TSPA-LA Model (based upon the 10th percentile infiltration scenario, glacial-transition period) ..... 6-15[a]
6.3.6-3[a]. Illustrative Cross Section of a Typical Emplacement Drift ..... 6-21[a]
6.3.10-8[a]. Radionuclide Decay Chains Considered in Saturated Zone Transport Calculations ..... 6-47[a]

6.6-13[a]. Quadratic Fit for Mean Damaged Area on a CDSP WP under an Intact Drip Shield: (a) 23-mm WP Outer Barrier with Intact Internals, (b) 23-mm WP Outer Barrier with Degraded Internals, and (c) 17-mm WP Outer Barrier with Degraded Internals ..... 6-57[a]

TABLES

ES-1[a]. Top-Ranking Uncertainty Importance Parameters ..... ES-16[a]

3-1[a]. TSPA-LA Model Software Codes ..... 3-5[a]
3-8[a]. GoldSim Software Documents for Version 9.60.300 (STN: 10344-9.60-30) ..... 3-7[a]

4-1[a]. Direct Inputs ..... 4-3[a]
4-2[a]. Additional TSPA-LA Model Generated Data Tracking Numbers Referenced by Parameter Entry Forms ..... 4-5[a]

6.1.5-1[a]. Location of Implementation Description in the GoldSim TSPA-LA Model File ..... 6-9[a]

6.3.7-6[a]. Disposition of Radionuclides for Groundwater Release Modeling Cases: Nominal, Igneous Intrusion, and Seismic ..... 6-25[a]
6.3.7-64[a]. Parameters for TSPA-LA Spent Nuclear Fuel Waste Form Reversible Colloid Abstraction ..... 6-29[a]
6.3.8-4[a]. Sampled Model Inputs Used in the EBS Radionuclide Transport Abstraction ..... 6-33[a]
6.3.9-1[a]. Radionuclide Half-Life and Daughter Products Used in the TSPA-LA Addendum ..... 6-39[a]
6.3.10-8[a]. Radionuclide Species Mass Passed to the Biosphere Submodel ..... 6-45[a]

6.6-3[a]. Seismic Ground Motion and Fault Displacement Modeling Cases Using Pre-Specified Parameters ..... 6-55[a]

INTENTIONALLY LEFT BLANK

EXECUTIVE SUMMARY

This addendum to the Executive Summary in *Total System Performance Assessment Model/Analysis for the License Application* (hereafter referred to as the parent document), contains changes in the form of corrections and insertions for clarity. The addendum to the Executive Summary consists of a combination of supplemental information and revised TSPA-LA Model results for the postclosure performance demonstrations in revisions to plots, tables, and discussions found in the parent document. The organization of the sections and subsections is the same as found in the parent document Section, figure, and table numbers referred to in the text with [a] indicate sections of this addendum with revised information, while those without [a] refer to the unrevised section, figure, and table numbers in the parent document. Each section designated as no change means the reader should refer to the parent document for the content of that section. In some cases, portions of the Executive Summary are restated from the parent document for clarity. This addendum to the Executive Summary is intended to be used in conjunction with the Executive Summary in the parent document.

ES1[a] SCOPE

This addendum provides minor corrections as well as an update of the results of the Total System Performance Assessment for the License Application (TSPA-LA) presented in *Total System Performance Assessment Model/Analysis for the License Application*. The updated TSPA-LA Model results address the issues identified and described in Appendix P of the parent document. The issues were identified during analysis, checking, and review activities. These issues, documented in Appendix P of the parent document, were primarily related to minor inaccuracies in model implementation and identification of undocumented or unintended conservatisms or non-conservatisms. TSPA-LA Model v5.005 incorporates changes to TSPA-LA Model v5.000, the source for results in the parent document, and TSPA-LA Model v5.005 was used to provide the analyses presented in this addendum. Appendix P[a] of this addendum includes tables that summarize the issues that were addressed in the development of TSPA-LA Model v5.005. Tables P-6[a] and P-7[a] discuss the changes to TSPA-LA Model v.5005 in response to the issues identified in Appendix P of the parent document. Table P-6[a] summarizes the TSPA-LA Model implementation issues and Table P-7[a] summarizes the impact assessments as a result of the changes to the TSPA-LA Model. The additional analyses presented in this addendum were developed according to the review criteria outlined in *Technical Work Plan for: Total System Performance Assessment FY 07-08 Activities* (SNL 2008 [DIRS 184920], Sections 2.1.4 and 2.3.5.2.1).

ES1.1[a] Introduction

The performance requirements discussed in Section ES1.1[a] are restated from the parent document in order to provide clarity in the subsequent presentation.

Among the regulatory mandates of U.S. Nuclear Regulatory Commission (NRC) Proposed Rule 10 CFR Part 63 ([DIRS 178394] and [DIRS 180319]) is the requirement to demonstrate, by means of a probabilistic assessment, that there is a reasonable expectation of meeting the requirements of 10 CFR 63 Subpart L (DIRS 180319] regarding waste isolation after closure of the repository (NRC Proposed Rule 10 CFR 63.303, unrevised, [DIRS 180319]) according to the

performance measures given in NRC Proposed Rule 10 CFR 63.303(a) and (b) [DIRS 178394]. NRC Proposed Rule 10 CFR Part 63 ([DIRS 178394] and [DIRS 180319]) sets standards for individual protection and for protection of groundwater. The Individual Protection Standard after Permanent Closure applies to the first 10,000 years following repository closure (10 CFR 63.311(a)(1) [DIRS 178394]), and 10 CFR 63.311(a)(2) [DIRS 178394] specifies the individual protection standard from 10,000 years to the period of geologic stability, defined as one million years after disposal (10 CFR 63.302 [DIRS 178394]).

Figure ES-1 shows the Yucca Mountain area and the entrance to the underground facilities, which will become part of the repository after a license to construct the repository is granted. Figure ES-2 shows a timeline of the major legislative and regulatory actions bearing on the Yucca Mountain Project from 1980 to the present.

In particular, the TSPA-LA Model calculates estimates of the:

a. Annual doses to the reasonably maximally exposed individual (RMEI) from releases from the undisturbed Yucca Mountain disposal system (NRC Proposed Rule 10 CFR 63.311 [DIRS 178394], Individual Protection Standard after Permanent Closure), subject to the performance measures in NRC Proposed Rule 10 CFR 63.303 [DIRS 178394]

b. Annual doses to the RMEI from releases from the Yucca Mountain disposal system resulting from human intrusion (NRC Proposed Rule 10 CFR 63.321 [DIRS 178394], Individual Protection Standard for Human Intrusion), excluding very low probability events after 10,000 years per NRC Proposed Rule 10 CFR 63.342(b) [DIRS 178394]

c. Levels of radioactivity (NRC Proposed Rule 10 CFR 63.331 [DIRS 180319], Separate Standards for Protection of Groundwater) in the representative annual volume of groundwater of 3,000 acre-feet (NRC Proposed Rule 10 CFR 63.332(a)(3) [DIRS 180319])

d. Annual doses to the RMEI for early drip shield (DS) and waste package (WP) failures, the two failure modes that meet the low probability of occurrence requirement of NRC Proposed Rule 10 CFR 63.342(a) [DIRS 178394]

e. Mean annual doses to the RMEI for all scenario classes considered for 10,000 years after repository closure (NRC Proposed Rule 10 CFR 63.342(c)(1) [DIRS 178394])

f. Median annual doses to the RMEI for all scenario classes considered (NRC Proposed Rule 10 CFR 63.342(c)(1) [DIRS 178394]) after 10,000 years but within the period of geologic stability.

ES2[a] TOTAL SYSTEM PERFORMANCE ASSESSMENT METHODOLOGY

The general TSPA process adopted by the U.S. Department of Energy (DOE) follows the methodology described by the NRC (Eisenberg et al. 1999 [DIRS 155354], Section 1 and Appendix A). Over time, the methodology has been developed and enhanced by critical reviews

conducted by various national and international organizations. In addition, DOE has adopted the methodology developed by Cranwell et al. (1990 [DIRS 101234], Sections 2 and 3) to arrive at scenarios for use in evaluating the Yucca Mountain repository. Figure ES-4 shows the major steps in the Performance Assessment (PA) process. Previous PAs and related supplemental analyses were conducted to meet various DOE milestones that followed the publication of the Nuclear Waste Policy Amendments Act of 1987, Public Law No. 100-203 [DIRS 100016]. The Yucca Mountain PAs have been iterative, with each succeeding PA building on and extending the scope and results of the previous PAs. The successive PAs incorporate both an improved understanding of the processes affecting performance, and additional field observations and measurements, laboratory experiments and analyses, and better identification and quantification of the parameters used in the PA analyses. Figure ES-5 illustrates the evolution of the PA iterations for the Yucca Mountain Project and identifies the corresponding TSPAs. The most recent TSPA documents were *Total System Performance Assessment for the Site Recommendation* (TSPA-SR) (CRWMS M&O 2000 [DIRS 143665]) and the application of the TSPA-SR Model in *Total System Performance Assessment – Analyses for Disposal of Commercial and DOE Waste Inventories at Yucca Mountain – Input to Final Environmental Impact Statement and Site Suitability Evaluation* (Williams 2001 [DIRS 157307]). The TSPA-LA Model is built on the foundation of those earlier PAs and has been enhanced by updated analyses of the processes affecting Yucca Mountain and the design elements of the repository, including a comprehensive consideration of the features, events and processes (FEPs) that are relevant to repository system performance.

ES3[a] TSPA-LA MODEL DEVELOPMENT PROCESS

No change.

ES3.1[a] Features, Events, and Processes Analysis

No change.

ES3.2[a] Development of the Scenario Classes

The TSPA-LA approach focuses on a set of scenario classes that are distinguished by initiating events. The Nominal Scenario Class includes all possible future outcomes except those initiated by early failure of the DSs or WPs, igneous or seismic activity, and inadvertent human intrusion into the repository. The Early Failure Scenario Class addresses FEPs that describe the potential for DS and WP early failure in the absence of igneous or seismic events. The early failure scenarios include DSs and WPs that fail prematurely. The Igneous Scenario Class includes all possible future outcomes initiated by igneous activity. The Seismic Scenario Class includes all possible future outcomes initiated by seismic activity. In addition to the analyses of the scenario classes, the TSPA-LA Model also simulates a Human Intrusion Scenario according to the scenario description and criteria in 10 CFR 63.322 [DIRS 180319].

ES3.3[a] Incorporation of Uncertainty

No change.

ES3.4[a] Natural and Engineered Model Components

No change.

ES3.5[a] Alternative Conceptual Models

No change.

ES3.6[a] Configuration Management for the TSPA-LA Model

No change.

ES4[a] YUCCA MOUNTAIN SITE DESCRIPTION

No change.

ES4.1[a] Physiographic Setting and Topography

There is no change to the text of ES4.1. However, the caption for Figure ES-12 in the parent document has been corrected and is included as Figure ES-12[a] of this addendum.

ES4.2[a] Climate

No change

ES4.3[a] Geology

No change.

ES4.4[a] Regional Tectonic Setting

The overall tectonic setting of the Great Basin physiographic province, including Yucca Mountain, is extensional, and generally consisting of fault-bounded basins and mountain ranges that have been modified by volcanic activity during the past 15 million years. Typically, the faults in the Great Basin include normal and strike-slip faults that reflect the extensional deformation caused by plate tectonic interactions in the western portion of the North American continent. The structural geology of Yucca Mountain and its vicinity is generally characterized by north-trending normal faults with displacement down to the west (Figures ES-14 and ES-15). Some of the faults on Figure ES-14 show evidence of Quaternary activity (i.e., activity within the last 1.8 million years).

ES5[a] THE REPOSITORY SUBSURFACE FACILITY AND ENGINEERED BARRIER SYSTEM

No change.

ES6[a] NATURAL AND ENGINEERED BARRIERS

No change.

ES7[a] GENERAL DESCRIPTION OF THE TSPA-LA MODEL

No change.

ES8[a] VERIFICATION/VALIDATION OF THE TOTAL SYSTEM PERFORMANCE ASSESSMENT MODEL

SCI-PRO-006, *Models*, Section 6.3, was utilized to support verification and validation of the TSPA-LA Model, providing confidence that the TSPA-LA Model adequately represents the physical processes in the repository system and properly transfers outputs between the TSPA-LA Model modules and submodels. In preparing this addendum, each validation activity utilized for TSPA-LA Model v5.000 was reviewed to determine which activities were affected by changes made between TSPA-LA Model v5.000 and v5.005. Where validation activities could potentially be affected by these model changes, the affected validation activities were repeated using v5.005 to verify that model changes did not adversely affect the overall validation of the TSPA-LA Model. Additional verification and validation results beyond those presented in the parent document are also provided to further enhance confidence in the TSPA-LA Model. This section summarizes revised or additional validation activities that were conducted for TSPA-LA Model v5.005 and are documented in this addendum. The following subsections include any changes to the Executive Summary in the parent document.

ES8.1[a] Verification and Validation Strategy

No change.

ES8.2[a] Computer Code and Input Verification

The following model verification activities are described in the parent document and/or were revised and included in this addendum and demonstrate that incorporation of information and submodels from other sources into the TSPA-LA Model has not altered the validity of the information, the submodels, or both:

- The TSPA-LA Model software, GoldSim, was qualified and placed under the control of Software Configuration Management per IM-PRO-003.
- Outputs from DLLs from other sources, including analysis/model reports and data tracking numbers, were correctly replicated in the TSPA-LA Model.
- Analysis of the verification of the range of applicability of submodels and model components was performed.
- Outputs from DLLs calculated within the TSPA-LA Model were found to be within established acceptance criteria.
- Individual submodels were validated in their respective analysis/model reports.
- Results from submodels within the TSPA-LA Model were compared to results contained in analysis/model reports and were found to agree within selected acceptance criteria.

- Feeds from one submodel to another submodel were found to be correctly transferred, and the values used were determined to be appropriate for the intended use of the receiving submodel (Section 7.2.6[a]).

- Inputs from the TSPA Input Database were verified to correspond with source data.

Computer codes and input reverification presented in Section 7.2[a] include: (1) reverification of a revised version of the GoldSim software (GoldSim V9.60.300, STN: 10344-9.60-03 [DIRS 184387]) used in all updated TSPA-LA Model results reported in this addendum; (2) verification testing for the Human Intrusion Submodel, testing that was inadvertently omitted from the parent document (Section 7.2.4.1.12[a]); and (3) a summary of an assessment of the range of validity for all TSPA-LA Model submodels that was inadvertently omitted from the parent document (Section 7.2.6[a]).

The activities in Section 7.2 of the parent document and the additional work presented in Section 7.2[a] of this addendum demonstrate that the system software for TSPA-LA Model v5.005 is appropriate and valid, that input is correct and verified, that the internal transfer of information within TSPA-LA Model v5.005 is correct and within the valid range of successive submodels, and that submodels are valid per their respective source analysis/model reports. Therefore, incorporation of information and submodels from other sources into TSPA-LA Model v5.005 has not altered the validity of the information or the submodels, or both, as demonstrated in the parent document for TSPA-LA Model v5.000.

ES8.3[a] Stability Testing

Section 7.3.1 of the parent document presents analyses that demonstrate the statistical stability of the total mean annual dose (summed over all modeling cases) and the mean annual dose for each modeling case for TSPA-LA Model v5.000. Section 7.3.1[a] compares uncertainty and sensitivity analyses generated by TSPA-LA Model v5.000 and TSPA-LA Model v5.005 and concludes that the results from TSPA-LA Model v5.005 are also statistically stable. An additional illustration of the stability of the estimate of the total mean annual dose for TSPA-LA Model v5.005, using a bootstrap sampling procedure to generate confidence intervals, is presented for results for both the 10,000-year and 1,000,000-year time periods. This addendum confirms the numerical accuracy of the expected annual dose calculations for the Seismic Fault Displacement Modeling Case.

This addendum also includes an update to the evaluation of temporal stability of the TSPA-LA Model for both the Nominal Modeling Case and the Human Intrusion Modeling Case. A reevaluation of the temporal stability of the Human Intrusion Modeling Case was necessary due to the change in the timestepping system used for the Human Intrusion Modeling Case in TSPA-LA Model v5.005. The simulations were conducted by reducing the TSPA-LA Model timestep size to examine sensitivity to timestep duration. The annual dose from the TSPA-LA Model calculations with different timestep durations were compared graphically to determine the effect of changing the timestep durations. The approach and results of this analysis are provided in Section 7.3.3 of the parent document. The results of this analysis show a better resolution using the revised timestep durations than previously documented in the parent document. The

test results for the Human Intrusion Modeling Case confirm that its timestep system was adequate.

Section 7.3.3.7[a] presents a revised evaluation of the temporal stability of the TSPA-LA Model Nominal Modeling Case. The temporal discretization used to determine general corrosion rates is influential to the annual dose resulting from nominal corrosion processes. The nominal modeling case simulation was conducted with shorter timesteps for the calculation of the crack growth rate, which removes the jumps in the number of WP failures by stress corrosion cracking (SCC), which in turn is reflected in the expected annual dose curves for the alternative timestepping. However, the similarity in statistics for expected annual dose for the two timestep durations indicates that the Nominal Modeling Case is sufficiently stable with respect to temporal discretization.

Section 7.3.2[a] demonstrates that the calculation of expected annual dose is sufficiently accurate for each TSPA-LA Model modeling case.

ES8.4[a] Uncertainty Characterization Reviews

No change.

ES8.5[a] Surrogate Waste Form Validation

Section 7.5.3[a] presents a reevaluation of the adequacy of using commercial spent nuclear fuel (CSNF) as a surrogate for naval spent nuclear fuel (NSNF) using TSPA-LA Model v5.005. The analyses presented in Section 7.5 of the parent document and Section 7.5[a] of this addendum show that the use of a surrogate to represent NSNF is appropriate. The analyses show that mean annual dose from NSNF is bounded by the mean annual dose calculated for the Zircaloy-clad CSNF surrogate.

ES8.6[a] Corroboration of Abstraction Model Results with Validated Process Models

No change.

ES8.7[a] Auxiliary Analyses

The auxiliary analyses presented in the parent document were updated with a reevaluation of the corroboration of the TSPA-LA Model results documented in the parent document with auxiliary analyses (Section 7.7[a]). These additional verification and validation activities further enhance confidence in the TSPA-LA Model.

Single-Realization Analyses

The single realization analyses presented in the parent document and in Section 7.7.1[a] comprise a comprehensive explanation of how the transport of key radionuclides is affected by coupling various submodel components of the engineered barrier system (EBS), unsaturated zone (UZ), and saturated zone (SZ) domains in the TSPA-LA Model, following WP failure under varying physical-chemical-thermal-mechanical conditions. These results provide confidence that these model components are working as expected and the aggregate TSPA-LA

Model results (in terms of dose) are consistent with the model components. Examination and explanation of key aspects affecting radionuclide releases demonstrate that the TSPA-LA Model is functioning as intended and that the submodels are coupled correctly and provide system-level results. The revised analyses in this addendum provide confidence that TSPA-LA Model v5.005 is functioning as designed and helps confirm the validation of the model.

The parent document includes single realization analyses of four modeling cases: (1) Waste Package EF Modeling Case, (2) Drip Shield EF Modeling Case, (3) Igneous Intrusion Modeling Case, and (4) Seismic Ground Motion (GM) Modeling Case (1,000,000 years). The revised analyses using TSPA-LA Model v5.005 include additional analyses of outlier realizations in Section 7.7.1[a]. Three additional modeling cases: (1) Nominal Modeling Case, (2) Human Intrusion Modeling Case, and (3) Seismic GM Modeling Case (10,000 years), are included in this addendum. The results confirm that the changes from TSPA-LA Model v5.000 to TSPA-LA Model v5.005 support the demonstration of model validation and add to the confidence in the TSPA-LA Model results.

Comparison with Simplified TSPA Analysis

A comparison of the TSPA-LA Model results to a stand-alone Simplified TSPA Analysis was conducted and documented in Section 7.7.2 and Appendix L of the parent document. Section 7.7.2 of the parent document provides the comparative results for the individual modeling cases for the Simplified TSPA Analysis and the TSPA-LA Model, including the minor differences in the prominence of certain radionuclides and in the mean annual doses calculated by the two approaches. Section 7.7.2[a] provides a comparison of the updated results presented in this addendum with the Simplified TSPA Analysis in the parent document.

Section 7.7.2[a] compares the TSPA-LA Model v5.005 results to the Simplified TSPA Analysis and corroborates the conclusions presented in the parent document.

Comparison with Electric Power Research Institute TSPA Analysis

This addendum describes a limited comparison of the Electric Power Research Institute (EPRI) TSPA Analysis results with those of TSPA-LA Model v5.005. The similarities and differences between the EPRI TSPA Analysis and TSPA-LA Model v5.000 are discussed in Section 7.7.3 of the parent document. Appendix M of the parent document provides additional information.

The results documented in Section 7.7.3[a] confirm the general similarities as well as the differences between the results from the EPRI TSPA Analysis and those of the TSPA-LA Model as described in Section 7.7.3 of the parent document.

Performance Margin Analysis

A comparison of TSPA-LA Model v5.005 results with the Performance Margin Analysis (PMA) confirms the quantitative evaluation of the differences in repository performance due to significant explicit and implicit conservatisms embedded in the TSPA-LA Model subcomponents as documented in Section 7.7.4 and Appendix C of the parent document. The conservatisms were evaluated to (1) confirm that they are conservative with respect to the mean annual dose calculated by the TSPA-LA Model; (2) quantify the extent to which TSPA-LA Model v5.005

and the PMA, individually and collectively, overestimate the projected annual dose; and (3) assess whether or not the evaluated conservatisms introduced any inappropriate risk dilution in the TSPA-LA Model results presented in support of the LA. Section 7.7.4 of the parent document describes the approach and results of the PMA, and Appendix C provides additional supporting material. The results show that the margin evaluated in the PMA, as documented in the parent document, is indeed conservative with respect to the total system performance measures (e.g., maximum mean annual dose); the largest doses calculated in the PMA for 10,000 years and 1,000,000 years are lower than the doses used in the compliance demonstration presented in Section 8[a] of this addendum. The additional analyses confirm that the largest calculated PMA mean annual doses are lower by over an order of magnitude and a factor of two over the largest mean annual dose relative to the TSPA-LA Model (Section 8[a]) for the time periods of 10,000 years and 1,000,000 years, respectively. Further, this PMA confirms that the significant conservatisms did not introduce risk dilution in the TSPA-LA results, as demonstrated by the absence of higher maximum mean annual doses in the comparison of the projected total mean annual dose for the PMA relative to TSPA-LA Model v5.005. The differences in the relative contributions to the total mean annual dose from each of the modeling cases evaluated with the PMA and the TSPA-LA Model indicate that having fewer conservative assumptions in the PMA than in these TSPA-LA model components provides a performance margin in the projected annual dose predictions presented in Section 8 of the parent document and Section 8[a] of this addendum.

ES8.8[a] Confidence Building: Natural Analogues

No change.

ES8.9[a] Summary of Technical Reviews

Technical reviews of PA models form an important part of model validation. During the past decade, the Yucca Mountain Project has developed successive TSPA models as well as accompanying input process models, all of which have been subject to technical reviews by external experts as part of their validation. Each milestone PA for the Yucca Mountain repository was subject to external reviews. The Total System Performance Assessment for the Viability Assessment was the subject of a peer review as described in Section 7.9.1. An International Review Team conducted an evaluation of the TSPA-SR, and the accompanying TSPA-SR performance assessment model. Appendix E summarizes the 27 comments provided by the International Review Team review of the TSPA-SR Model. The responses to those comments were addressed and implemented as appropriate into the TSPA-LA Model and its supporting documents. An Independent Validation Review Team (IVRT) reviewed a draft version of the TSPA-LA Model and the accompanying IVRT report provided comments as described in Section 7.9. The comments from the IVRT technical review of the draft TSPA-LA Model were addressed, and the TSPA-LA Model incorporates the material contained in the responses to those comments.

ES9[a] SYSTEM PERFORMANCE ANALYSES

The revisions found in the following subsections of Section ES9[a] contain primarily references to updated figures and revised estimates for the magnitude and timing of estimates of the

maximum mean annual dose, radionuclides of importance, revised results of the uncertainty/sensitivity analyses, and other information derived from the revised simulations of modeling cases using TSPA-LA Model v5.005. Except for one correction to a reference to proposed 10 CFR Part 63 and clarification of the language relating to meeting the proposed 10 CFR Part 63 performance standards, the text in this section is largely the same as that in the parent document.

The TSPA-LA Model was used to conduct a PA of the Yucca Mountain repository system. The analyses provide mean and median annual dose to the RMEI for the first 10,000 years after repository closure and for the period of geologic stability (one million years) specified in NRC Proposed Rule 10 CFR 63.302 [DIRS 178394]. The TSPA-LA Model evaluated modeling cases representing nominal conditions, early DS and WP failures, and disruptive events. The TSPA-LA Model analyses also address both the individual and groundwater protection standards of NRC Proposed Rule 10 CFR 63.311 [DIRS 178394] and 10 CFR 63.331 ([DIRS 180319], Table 1), respectively.

The analyses account for uncertainties in the representations of FEPs that could affect the annual dose. The PA analyses address the effect of alternative parameters, submodels, and approaches to FEPs. The calculations are probabilistic in the sense that the results are for multiple realizations, carried out using sampled values from the probability distributions for the values of the uncertain model parameters.

ES9.1[a] Total Mean Annual Dose to the Reasonably Maximally Exposed Individual for the Repository System

Figure ES-40[a] displays the total expected annual dose for the first 10,000 years after repository closure, and the calculated results indicate that the greatest mean annual dose for this period is less than 0.24 millirem. Figure ES-41[a] displays the total expected annual dose for the postclosure period from 10,000 to one million years after repository closure, and the calculated results indicate that the greatest median annual dose for this period is less than 0.96 millirem. These total expected annual dose values represent the sum of the expected dose calculations for the four scenario classes considered for the TSPA-LA Model. Figures ES-40[a] and ES-41[a] show the distribution of the expected annual doses and, thus, display the uncertainty in the total expected annual dose resulting from epistemic uncertainty about the repository system.

Figure ES-42[a] shows the radionuclides that contribute most to the estimate of mean annual dose, and indicates that ^{99}Tc, ^{14}C, ^{129}I, and ^{239}Pu dominate the estimated mean annual dose during the first 10,000 years after repository closure. In a similar manner, Figure ES-43[a] shows that ^{239}Pu, ^{99}Tc, and ^{129}I generally dominate the mean annual dose for the first 100,000 years of the postclosure period, and that ^{242}Pu, ^{237}Np, ^{129}I, and ^{226}Ra generally dominate the mean annual dose for the postclosure period from 100,000 to one million years.

ES9.2[a] Results of the Scenario Class Modeling Case Simulations

Following are descriptions of the results provided by the scenario class modeling cases used to simulate repository performance. Figures ES-44[a] through ES-51[a] and ES-54[a] through ES-57[a] present the expected annual dose calculated for the individual modeling cases. Figures ES-52 and ES-53 for the Volcanic Eruption Modeling Case are unchanged from those in

the parent document. The following sections describe, by modeling case, the results of the scenario class modeling case simulations.

ES9.2.1[a] Nominal Scenario Class Modeling Case

The results of this modeling case show no annual dose to the RMEI in the first 10,000 years. The earliest occurrence of dose is around 21,000 years. The projections of WP breaches exhibit a few realizations with a SCC crack penetrating the WP outer barrier well before 100,000 years. In particular, one crack penetration occurred in less than 10,000 years in one WP in one realization because a combination of sampled values for SCC in the closure-lid weld resulted in a large initial crack length and a high crack propagation velocity (Section 8.2.1). Because infiltration rates and temperatures vary across the repository footprint, the time of occurrence of the continuous thin film of adsorbed water required to begin diffusive radionuclide transport also varies, delaying radionuclide releases until after 10,000 years. The bulk of the WP failures (by nominal SCC) would occur after 100,000 years, and the DSs would begin to fail by general corrosion at approximately 260,000 years. Figure ES-44[a] shows the estimated maximum mean and median annual doses for the postclosure period from 10,000 to one million years, and the calculated results indicate that the values would be 0.55 and 0.28 millirem, respectively. Figure ES-45[a] shows the radionuclides that dominate the estimate of mean annual dose for the Nominal Scenario Class Modeling Case. The main contributors to mean annual dose would be the highly soluble and mobile radionuclides ^{129}I and ^{99}Tc.

ES9.2.2[a] Early Failure Scenario Class Modeling Cases

The Early Failure Scenario Class Modeling Cases include FEPs that relate to early WP and DS failure due to manufacturing, material defects, or pre-emplacement operations that would include improper heat treatment. Radionuclide mobilization and transport for the Early Failure Scenario Class is similar to the Nominal Scenario Class, but differs from the Nominal Scenario Class in that the Early Failure Scenario Class considers only WPs affected by early DS and WP failures.

ES9.2.2.1[a] Drip Shield Early Failure Modeling Case

The defective DSs were modeled as being failed at the time of repository closure, and WPs underlying any failed DSs and exposed to seepage are conservatively considered as failed. Figure ES-46[a] shows the expected annual dose histories for the first 10,000 years after closure and the postclosure period from 10,000 to one million years. The expected annual doses account for aleatory uncertainty about the number of early failed DSs, types of WPs under failed DSs, and their locations in the repository. The mean, median, and 5th and 95th percentile curves in this plot show the uncertainty in the expected annual dose due to epistemic uncertainty from incomplete knowledge of the behavior of the repository system. The calculations for the first 10,000 years indicate a projected mean annual dose of approximately 2.8×10^{-4} millirem at 2,000 years after repository closure. The calculated mean annual dose then decreases steadily and is less than 1.5×10^{-4} millirem during the postclosure period from 10,000 to one million years.

Figure ES-47a[a] shows that the radionuclides contributing most to the total mean annual dose during the first 2,000 years after repository closure are soluble and mobile radionuclides, in

particular ^{99}Tc, ^{129}I, and ^{14}C. During the postclosure period from 10,000 to one million years, Figure ES-47b[a] shows that ^{239}Pu dominated the mean annual dose for the first 200,000 years, and ^{242}Pu and ^{237}Np dominate the mean annual dose up to one million years.

ES9.2.2.2[a] Waste Package Early Failure Modeling Case

The WPs are assumed to be failed at the time of repository closure. However, intact DSs overlying early failed WPs will degrade by general corrosion after repository closure. Figure ES-48[a] shows the expected annual dose histories for the first 10,000 years after repository closure and for the postclosure period from 10,000 to one million years. The expected annual dose accounts for aleatory uncertainty about the number of early failed WPs, types of early failed WPs, and their locations in the repository. The mean, median, and 5th and 95th percentile curves on Figures ES-48a[a] and ES-48b[a] reflect the epistemic uncertainty in the expected annual dose.

Figure ES-48a[a] shows the estimated mean annual dose. The maximum mean annual dose occurs between 9,000 and 10,000 years and its value is 3.7×10^{-3} millirem. The mean annual dose during the first 10,000 years postclosure results from early failed co-disposed (CDSP) WPs. The relative humidity in the CDSP WP emplacement locations tend to be higher and forms an aqueous layer suitable for radionuclide diffusion earlier than in the CSNF WPs. Because the CDSP WPs contain DOE SNF and the TSPA-LA Model does not take credit for the canister, cladding, or fuel matrix, diffusive transport of radionuclides can start as soon as the humidity in the breached CDSP WPs is greater than 95 percent (Section 8.2.2.2). The increase in mean annual dose at about 9,800 years postclosure, as shown on Figure ES-48a[a], is due to the beginning of diffusive transport from early-failed CSNF WPs. Figure ES-48b[a] shows the estimated mean and median annual doses; the calculated results indicate that the maximum values are 2.1×10^{-2} and 6.1×10^{-3} millirem, respectively, before 15,000 years, and the doses gradually decrease thereafter until about 250,000 years postclosure. At about 250,000 years postclosure, the DSs begin to fail from general corrosion, and the expected annual dose increases during the period from 300,000 to 400,000 years postclosure because of advective transport of radionuclides through failed WPs.

Figure ES-49a[a] shows that in the first 10,000 years after closure, the more soluble and mobile radionuclides, ^{99}Tc, ^{129}I, and ^{14}C, dominate the estimate of mean annual dose. Figure ES-49b[a] shows that during the postclosure period from 10,000 to one million years, ^{239}Pu, ^{242}Pu, ^{237}Np, and ^{226}Ra dominate the expected mean annual dose.

ES9.2.3[a] Igneous Scenario Class Modeling Cases

The Igneous Scenario Class addresses the set of FEPs that describe igneous events that could affect repository performance. The Igneous Scenario Class is represented by: (1) the Igneous Intrusion Modeling Case that represents a magmatic dike that intrudes into the repository causing subsequent release of radionuclides to the groundwater in the UZ, and (2) the Volcanic Eruption Modeling Case that represents a hypothetical volcanic eruption from a volcanic conduit that passes through the repository and emerges at the land surface with the release of radionuclides to the atmosphere.

ES9.2.3.1[a] Igneous Intrusion Modeling Case

After a magmatic dike intersects the repository, radionuclide release and transport away from the repository would be similar to the Nominal Modeling Case. All of the DSs and WPs would be damaged, exposing the waste forms to percolating groundwater with subsequent degradation, radionuclide mobilization, and transport through the UZ to the SZ. The Igneous Intrusion Modeling Case considers that the remnants of the DSs, WPs, or cladding do not divert any water from the waste.

Figure ES-50[a] shows the distribution of calculated expected annual dose histories, one for each sample element, where each dose history accounts for aleatory uncertainty in igneous intrusions, such as the number of future events and the time at which they may occur. The mean, median, and 5th and 95th percentile curves on Figure ES-50[a] indicate epistemic uncertainty in expected annual dose resulting from incomplete knowledge of the behavior of the physical system during and after the disruptive event. The maximum calculated mean annual dose for the first 10,000 years postclosure is 6.6×10^{-2} millirem, occurring at the end of the 10,000-year period. The maximum projected median annual dose during the postclosure period from 10,000 to one million years is estimated to be 0.32 millirem, and the maximum value occurs at the end of the one-million year period.

Figure ES-51a[a] shows that ^{99}Tc and ^{129}I dominate the estimate of the expected mean annual dose for the first 4,000 years, and ^{239}Pu, ^{99}Tc, and ^{240}Pu dominate the estimate of the mean annual dose for the first 10,000 years postclosure. Figure ES-51b[a] shows that ^{239}Pu dominates the estimate of the mean annual dose for the first 100,000 years, and ^{242}Pu, ^{226}Ra, and ^{237}Np dominate the expected mean annual dose for the postclosure period from 10,000 to one million years.

ES9.2.3.2[a] Volcanic Eruption Modeling Case

No change.

ES9.2.4[a] Seismic Scenario Class Modeling Cases

The Seismic Scenario Class represents the direct effects of vibratory ground motion and fault displacement associated with seismic activity affecting repository performance. The Seismic Scenario Class modeling cases include seismic-related changes in seepage, the performance of WPs and DSs, and flow in the EBS. The Seismic Scenario Class is represented by the Seismic GM Modeling Case and the Seismic Fault Displacement (FD) Modeling Case.

ES9.2.4.1[a] Seismic Ground Motion Modeling Case

The Seismic GM Modeling Case considers the possible failures of DSs and WPs due to mechanical damage associated with seismic vibratory ground motion, including: accumulation of rockfall on DSs, collapse of the DS framework, SCC of WPs, and rupture or puncture of WPs. Figure ES-54[a] presents calculated expected annual dose histories for the Seismic GM Modeling Case for the first 10,000 years after closure and the postclosure period from 10,000 to one million years. The distribution of the expected annual dose takes into account aleatory

uncertainty associated with the number of seismic ground motion events, the time and magnitude of each event, and the effects of each event on WPs, DSs, and the emplacement drifts.

The mean, median, and 5th and 95th percentiles of the distribution of the expected annual dose shown on Figure ES-54[a] reflect epistemic uncertainty due to incomplete knowledge of the behavior of the repository system during and after seismic events. Figure ES-54[a] shows the mean annual dose for the first 10,000 years after closure, and the calculated results indicate that the maximum value is 0.17 millirem. The maximum median annual dose for the postclosure period from 10,000 to one million years was calculated to be 0.37 millirem. The plot of the expected annual doses shown on Figure ES-54a[a] was developed using a quadrature method to numerically integrate over the aleatory uncertainty for the first 10,000 years after repository closure. Alternatively, the realizations contributing to Figure ES-54b[a] were calculated using a Monte Carlo method to numerically integrate over aleatory uncertainty for the postclosure period from 10,000 to one million years.

The results on Figure ES-55a[a] show that ^{99}Tc, ^{14}C, ^{129}I, and ^{36}Cl dominate the estimate of the mean for the first 10,000 years after closure. Figure ES-55b[a] shows that radionuclides ^{99}Tc, ^{129}I, ^{242}Pu, and ^{237}Np dominate the calculated expected mean annual dose during most of the postclosure period from 100,000 to one million years, with ^{242}Pu and ^{237}Np increasingly prominent after 800,000 years postclosure. Because of radioactive decay, the expected mean annual dose due to ^{14}C decreases to insignificant levels within the first 100,000 years postclosure. The CDSP WPs would be the primary WPs damaged during the first 10,000 years after closure because the CSNF WPs are more failure resistant. The CSNF WPs will be more robust than CDSP WPs because they include two inner stainless-steel vessels instead of one. Although the CSNF WPs have an inner vessel and lid similar to the CDSP WPs, the CSNF WPs are placed in an outer, tightly fitting stainless-steel transportation, aging, and disposal canister. In contrast, the CDSP WPs contain several smaller waste-containing canisters that do not fit as tightly and could move more freely under the influence of ground motion. The predominant mechanism that would cause damage to both CDSP and CSNF WPs is SCC, which would result in diffusive releases of radionuclides.

ES9.2.4.2[a] Seismic Fault Displacement Modeling Case

The Seismic FD Modeling Case includes disruption of WPs and DSs by the displacement of faults. Figure ES-56[a] shows the expected annual dose histories for the Seismic FD Modeling Case for the first 10,000 years after closure and for the postclosure period from 10,000 to one million years. The expected annual dose accounts for aleatory uncertainty about the number, type, and locations of disrupted DSs and WPs. The mean, median, and 5th and 95th percentile curves on Figure ES-56[a] show uncertainty in the distribution of expected annual dose, due to epistemic uncertainty regarding the behavior of the repository system during and after fault displacement events. These figures show the maximum mean annual dose for the first 10,000 years after closure; the calculated results indicate that the maximum mean annual value is 1.5×10^{-3} millirem. The maximum median projected dose for the postclosure period from 10,000 to one million years is calculated to be 1.1×10^{-2} millirem.

Figure ES-57a[a] shows that ^{99}Tc and ^{129}I dominate the dose for the first 5,000 years after closure, and ^{99}Tc and ^{239}Pu dominate the dose between 5,000 and 10,000 years after closure.

Figure ES-57b[a] shows that ^{239}Pu dominates the mean annual dose up to 200,000 years postclosure, and ^{242}Pu, ^{237}Np, and ^{226}Ra dominate the mean annual dose for the remainder of the postclosure period from 200,000 to one million years.

ES9.2.5[a] Total Mean Annual Dose to the Reasonably Maximally Exposed Individual for the Repository System

Figure ES-58[a] shows the contribution to the total mean annual dose histories for the Drip Shield Early Failure (EF), Waste Package EF, Igneous Intrusion, Volcanic Eruption, Seismic GM, and Seismic FD Modeling Cases. Figure ES-58[a] shows that the Seismic GM and Igneous Intrusion Modeling Cases provide the largest contributions to the total mean annual dose for the postclosure period from 10,000 to one million years. The Seismic GM Modeling Case includes general corrosion processes for the postclosure period from 10,000 to one million years. Figure ES-58[a] shows that the events that most affect the total mean annual dose are seismic ground motion, igneous intrusions, and WP failure due to general corrosion.

ES9.3[a] Comparison of Annual Dose with Postclosure Individual and Groundwater Protection Standards

ES9.3.1[a] Individual Protection Standard

The results provided by the TSPA-LA Model include calculations of the total mean annual dose to the RMEI in any year during the next 10,000 years after repository closure (NRC Proposed Rule 10 CFR 63.303(a) [DIRS 178394]) and the total median annual dose to the RMEI in any year from 10,000 years after repository closure through the period of geologic stability (NRC Proposed Rule 10 CFR 63.303(b) [DIRS 178394]). According to NRC Proposed Rule 10 CFR 63.311 [DIRS 178394], the postclosure individual protection standard is 15 millirem up to 10,000 years postclosure, and 350 millirem after 10,000 years, but within the period of geologic stability (one million years). The TSPA-LA Model results, shown on Figures ES-40[a] and ES-41[a], which refer to distribution of total expected annual dose, show that the maximum projected total mean and total median annual doses to the RMEI are estimated to be about 0.24 millirem (Figure ES-40[a]) and 0.96 millirem (Figure ES-41[a]), respectively. These results demonstrate that the total mean annual dose to the RMEI in any year during the next 10,000 years after repository closure is less than the individual protection standard of 15 millirem per NRC Proposed Rule 10 CFR 63.311(a)(1) [DIRS 178394]. In addition, the highest projected dose values, mean or median, throughout the period of geologic stability are more than two orders of magnitude below the individual protection limit of 350 millirem per 10 CFR 63.311(a)(2) [DIRS 178394].

Uncertainty/Sensitivity Results

For different time frames in the analysis, different epistemic parameters emerge as important to the overall uncertainty in the results. Table ES-1[a] lists summary results of the sensitivity analysis. The important parameters listed on Table ES-1[a] are as follows:

- *IGRATE.* This parameter is the probability of an igneous event expressed as the annual frequency of an intersection of the repository by a volcanic dike. Uncertainty in this

parameter arises from epistemic uncertainty about igneous activity that may affect the repository.

- *SCCTHRP*. This parameter is the residual stress threshold for the Alloy 22 WP outer barrier, expressed as a percentage of the yield strength. If the residual stress in the WP outer barrier exceeded this threshold value, stress corrosion cracks could form, which could allow radionuclides to migrate from the WP. The primary causes of residual stresses in the WP outer barrier would be high peak-ground-velocity seismic ground motions, which may cause impacts from WP to WP, from WP to emplacement pallet, and from WP to DS. These impacts could cause dynamic loads that could dent the WP, resulting in structural deformation with residual stresses that could make the material susceptible to SCC.

- *SZGWSPDM*. This SZ flow and transport parameter is the logarithm of the scale factor for the groundwater specific discharge multiplier, which accounts for the epistemic uncertainty in the discharge flow rate used to compute advective radionuclide transport. This uncertainty parameter is applied to all of the climate states. Values for this parameter are sampled from an empirical cumulative distribution function; the technical basis for that distribution is documented in *Saturated Zone Flow and Transport Model Abstraction* (SNL 2008 [DIRS 183750], Section 6.5.2.1).

- *WDGCA22*. This parameter relates to the temperature dependence of the Alloy 22 WP outer barrier general corrosion rate. This uncertainty parameter determines the magnitude of this temperature dependence and directly influences the short-term and long-term general corrosion rates of the Alloy 22. Larger values of *WDGCA22* result in earlier, higher general corrosion rates during the thermal period, and lower long-term corrosion rates when the repository temperatures are near the ambient *in situ* temperature.

The parameters in Table ES-1[a] that most affect the total uncertainty in the TSPA-LA Model are factors that govern degradation of the WPs, the occurrence of damage from seismic events, and the frequency with which igneous intrusions occur.

Table ES-1[a]. Top Ranking Uncertainty Importance Parameters

Time After Closure (years)	Two Most Important Parameters	
3,000	SCCTHRP	IGRATE
5,000	SCCTHRP	IGRATE
10,000	SCCTHRP	IGRATE
125,000	IGRATE	*SZGWSPDM*
250,000	IGRATE	*SZGWSPDM*
500,000	IGRATE	WDGCA22
1,000,000	IGRATE	WDGCA22

Sources: Appendix K[a], Figure K8.1-2[a] and Figure K8.2-2[a]; output DTN: MO0801TSPAMVAC.000 [DIRS 185080].

ES9.3.2[a] Groundwater Protection Standard

The separate standards for protection of groundwater in NRC Proposed Rule 10 CFR 63.331 ([DIRS 180319], Table 1) stipulate that the releases of radionuclides in groundwater at the location of the RMEI should not cause the level of radioactivity in the representative water volume of 3,000 acre-feet of water (10 CFR 63.332(a)(3) [DIRS 180319]) to exceed the groundwater protection standards. The regulation does not require that evaluation of the groundwater protection standards include very unlikely events (NRC Proposed Rule 10 CFR 63.342(b) and (c)(1) [DIRS 178394]).

Figures ES-59[a], ES-60[a], and ES-61[a] show the projections for the performance measures of the separate standards for protection of groundwater in the representative volume of 3,000 acre-ft of water. Figure ES-59[a] shows the projections of the combined ^{226}Ra and ^{228}Ra activity concentrations, excluding natural background. Figure ES-60[a] shows the combined activity concentrations of all alpha emitters (including ^{226}Ra but without radon and uranium isotopes), excluding natural background. Figure ES-61[a] shows the dose from beta-and photon-emitting radionuclides in the groundwater at the location of the RMEI, expressed in terms of annual dose to the whole body or any organ of a human receptor resulting from drinking two liters of this water per day. The TSPA-LA Model results show that the projected releases from the repository will meet the NRC separate standards for protection of groundwater in NRC Proposed Rule 10 CFR 63.331 ([DIRS 180319], Table 1).

ES9.4[a] Human Intrusion Scenario

The TSPA-LA Model was used to simulate a Human Intrusion Scenario in order to address the second requirement of the human intrusion standard (10 CFR 63.321(b) [DIRS 178394]). To calculate dose for all environmental pathways per 10 CFR 63.321(c) [DIRS 178394], the TSPA-LA Model used a probabilistic approach analogous to that used to evaluate conformance with the individual protection and groundwater protection standards.

The estimates of WP degradation suggest that, using current technology, a degraded WP could not be penetrated by drilling before about 200,000 years postclosure. Consequently, the analysis considered the effects of a drilling intrusion at 200,000 years. Figure ES-62[a] shows the expected annual dose that could result from a drilling intrusion 200,000 years after repository closure. The expected annual dose accounts for aleatory uncertainty about the type of WP intersected by the drill and location of the intersected WP. The mean, median, and 5th and 95th percentiles of the distribution of expected annual dose reflect epistemic uncertainty due to incomplete knowledge of the behavior of the physical system during and after the drilling intrusion.

The values on Figure ES-62[a] represent the dose from a single WP and are not combinations of releases from other WPs that may fail due to other processes. The mean and median annual doses from human intrusion are estimated to be less than 0.014 millirem. These results indicate that releases from a human intrusion would result in doses well below the human intrusion individual protection standard of 350 millirem annual individual dose to the RMEI during the postclosure period from 200,000 to one million years.

ES10[a] SUMMARY OF THE RESULTS OF THE TSPA-LA MODEL

The TSPA-LA Model was applied to the assessment of total system performance of the Yucca Mountain repository based on FEPs that could affect total system performance. The TSPA-LA analyses incorporate uncertainty in input data and submodel performance and use the validated TSPA-LA Model.

The TSPA-LA Model simulation/analysis periods cover 10,000 years after repository closure and from 10,000 years to the one-million-year period of geologic stability (NRC Proposed Rule 10 CFR 63.302 [DIRS 178394]). The 10,000-year simulations were extended an additional 10,000 years to assess whether or not the trends present at the end of 10,000 years continued beyond that time. The results of the analyses showed that the period between 10,000 years to 20,000 years after repository closure did not display any significant changes to the trends observed from 0 to 10,000 years, providing confidence in the conclusions regarding the 10,000-year period.

The TSPA-LA Model results demonstrate that the projected maximum mean dose to the RMEI in any year during the next 10,000 years after repository closure is less than the individual protection standard after permanent closure in NRC Proposed Rule 10 CFR 63.311(a)(1) [DIRS 178394], which describes the limits on radionuclides in the representative volume. The TSPA-LA Model analyses also indicate the performance of the repository system provides significant protection to groundwater. The results show that concentrations in the groundwater are likely to be well below the separate standards for the protection of groundwater in NRC Proposed Rule 10 CFR 63.331 ([DIRS 180319], Table 1). The results suggest the mean annual drinking water dose to any organ and to the whole body from beta- and photon-emitting radionuclides is likely to be well below the separate standards for the protection of groundwater.

The physiographic setting, topography, climate, area geology, and soil characteristics at the site of the Yucca Mountain repository are favorable for restricting the amount of infiltration of precipitation into the subsurface. The reduced infiltration along with rock characteristics, ambient and perturbed subsurface environmental conditions, and the geometry of emplacement drifts will further limit the amount of liquid water available to enter the drifts. Features of the waste form and other components of the EBS, together with limitations due to the solubility of radionculides and the subsurface geology and hydrology, will limit the release, rate of release, and transport of radionuclides to the SZ beneath the repository. Only a small fraction of the radionuclide inventory is projected to be released from the EBS, move down through the UZ beneath the repository, and enter the SZ. Sorption and diffusion of radionuclides into the UZ will further reduce the concentrations of radionuclides entering the SZ. After the migrating radionuclides enter the SZ, the TSPA-LA Model results indicate that the characteristics of the rock, soil, and the hydrologic and geochemical environmental factors in the SZ will combine to retard radionuclide transport and reduce the rate of radionuclide transport to the accessible environment. Including igneous and seismic phenomena, the TSPA-LA Model analysis indicates that the repository will, with a high degree of confidence, perform in a manner that protects the natural environment and future human populations in the area.

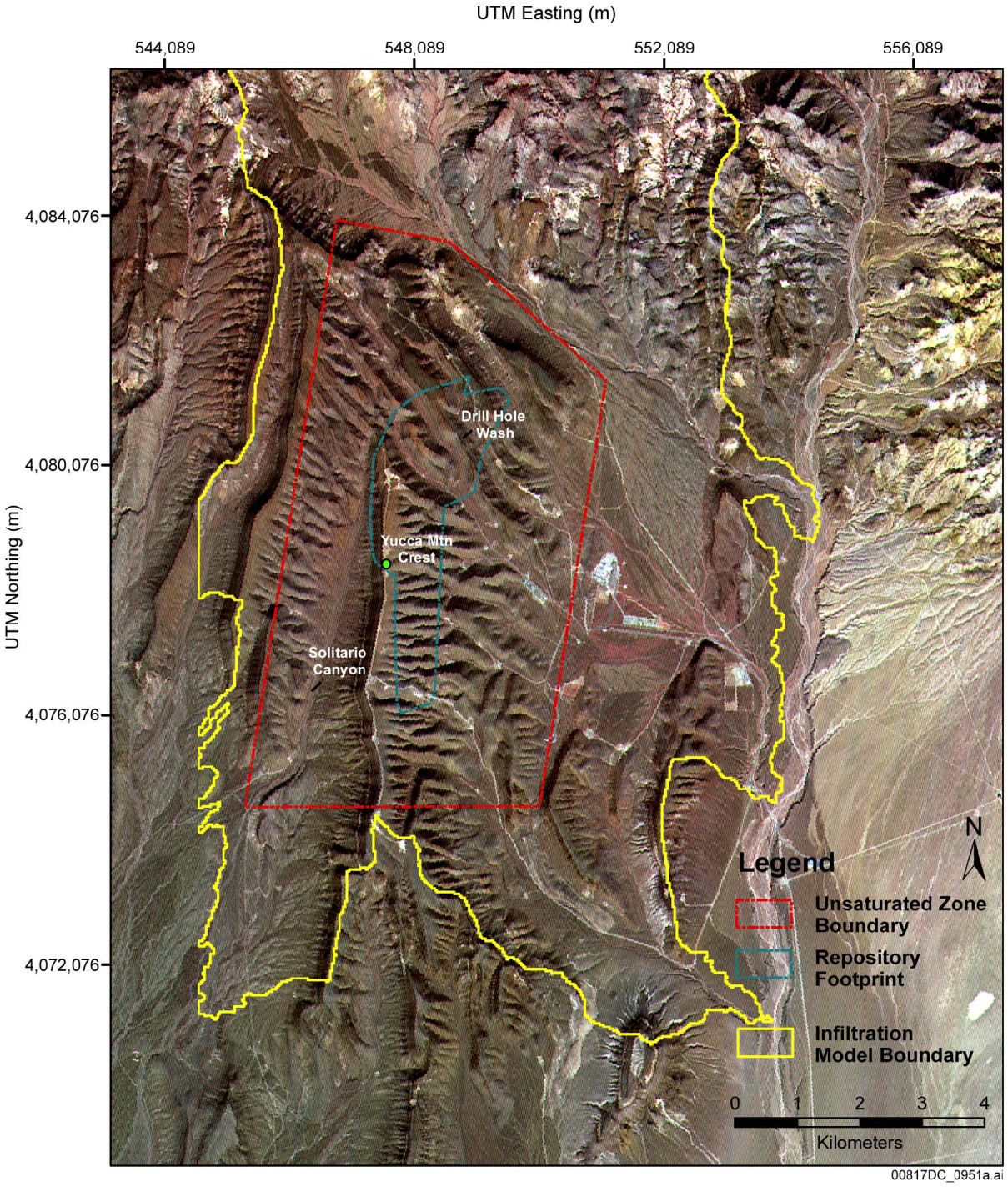

Source: Modified from SNL 2007 [DIRS 182145], Figure 6.5.2.1-1[a].

NOTE: The model boundary is the same as the 1999 unsaturated zone flow model domain of the TSPA-SR.

Figure ES-12[a]. Topographic Map of the Yucca Mountain Site Showing Differences in Slope Characteristics North and South of Drill Hole Wash

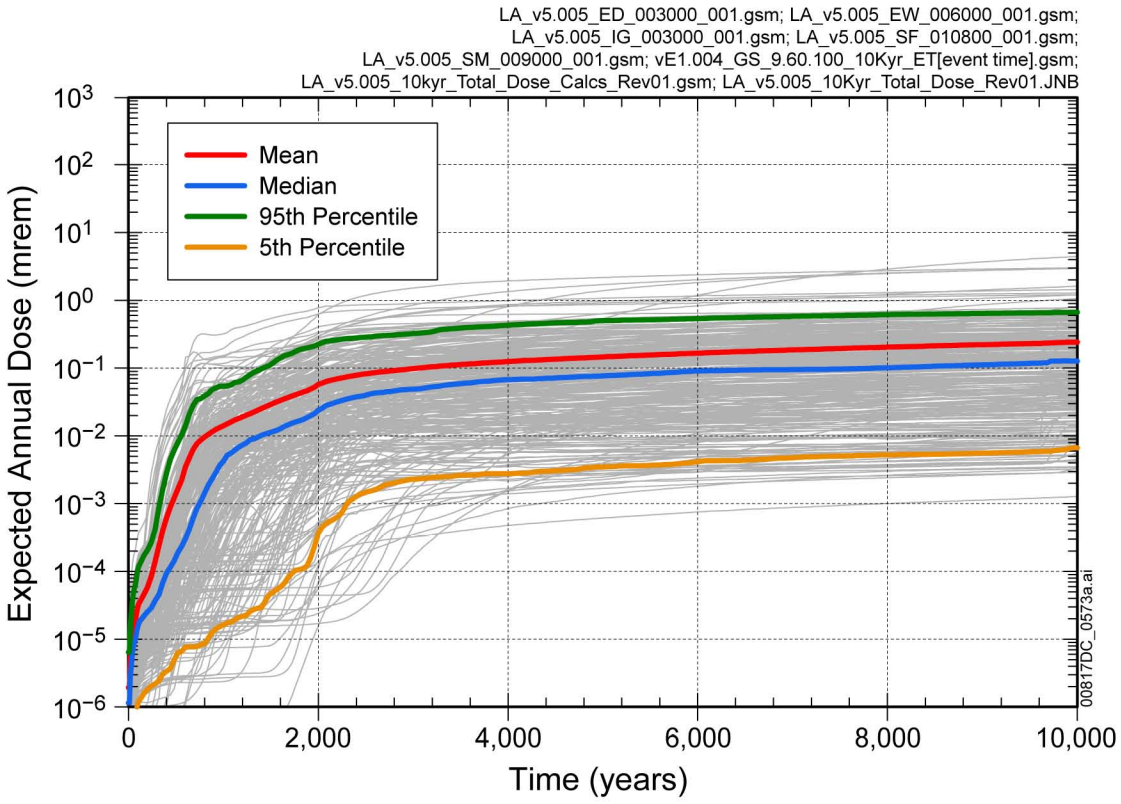

Source: Output DTNs: MO0710ADTSPAWO.000 [DIRS 183752]; MO0710PLOTSFIG.000 [DIRS 185207]; and MO0709TSPAREGS.000 [DIRS 182976].

Figure ES-40[a]. Total Expected Annual Dose for 10,000 Years after Repository Closure

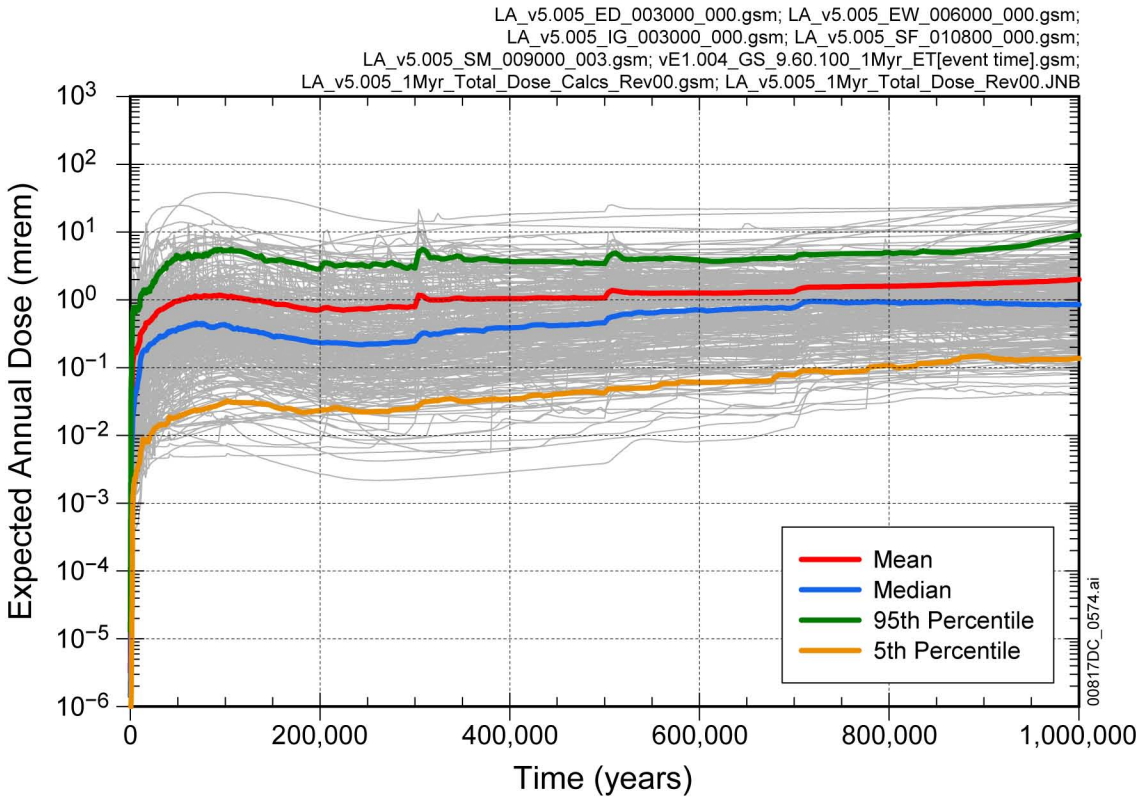

Source: Output DTNs: MO0710ADTSPAWO.000 [DIRS 183752]; MO0710PLOTSFIG.000 [DIRS 185207]; and MO0709TSPAREGS.000 [DIRS 182976].

Figure ES-41[a]. Total Expected Annual Dose for 1,000,000 Years after Repository Closure

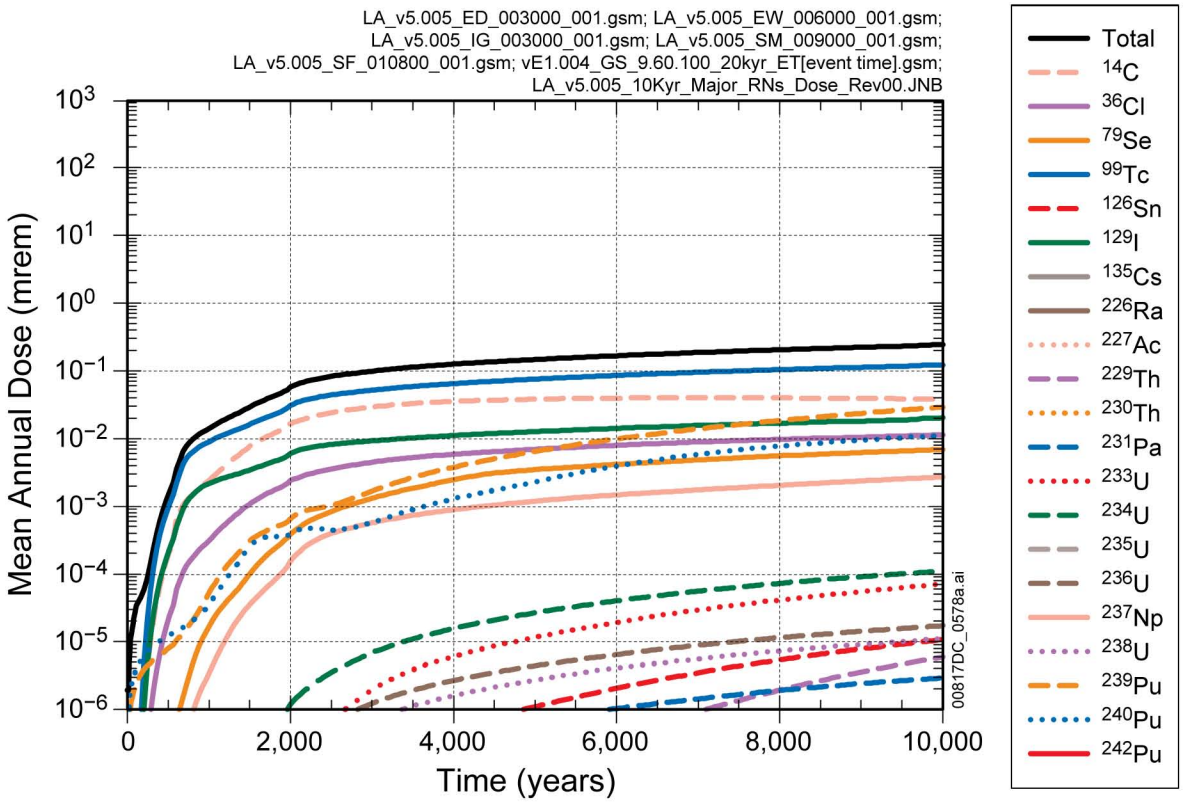

Source: Output DTNs: MO0710ADTSPAWO.000 [DIRS 183752]; MO0710PLOTSFIG.000 [DIRS 185207]; and MO0709TSPAREGS.000 [DIRS 182976].

Figure ES-42[a]. Contribution of Individual Radionuclides to Total Mean Annual Dose for 10,000 Years after Repository Closure

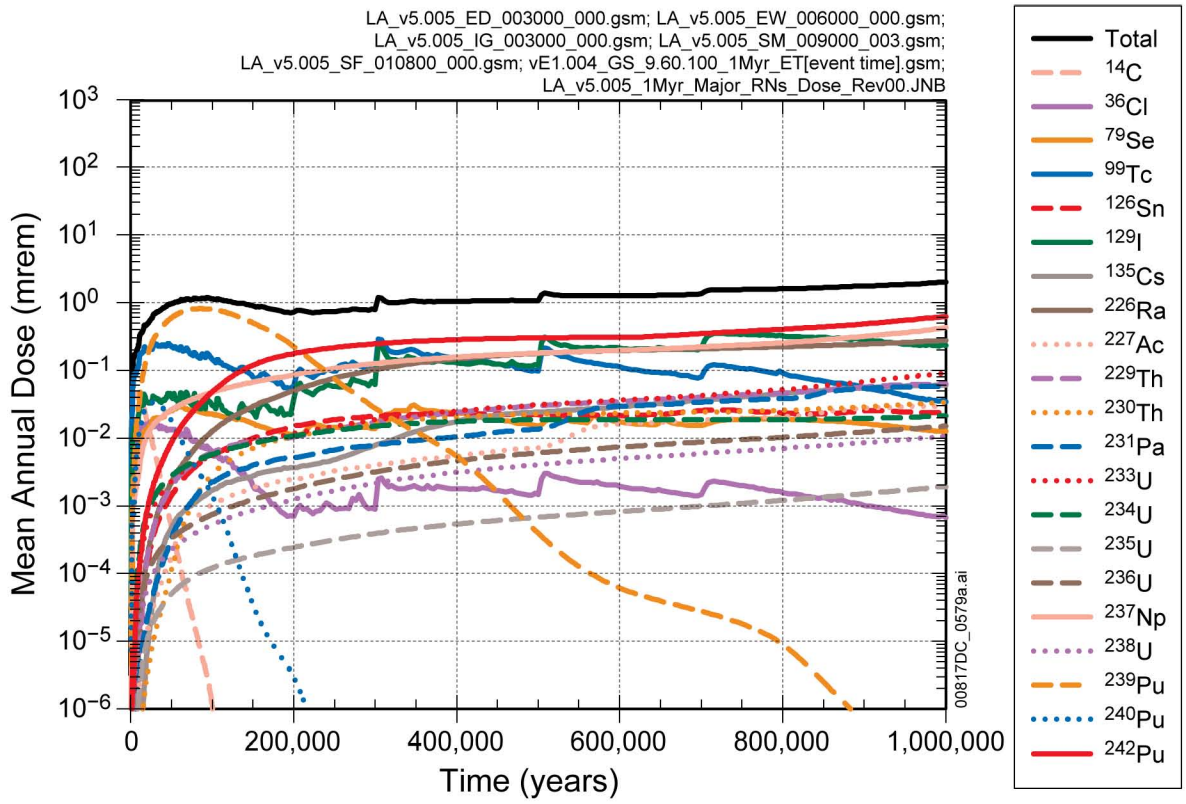

Source: Output DTNs: MO0710ADTSPAWO.000 [DIRS 183752]; MO0710PLOTSFIG.000 [DIRS 185207]; and MO0709TSPAREGS.000 [DIRS 182976].

Figure ES-43[a]. Contribution of Individual Radionuclides to Total Mean Annual Dose for 1,000,000 Years after Repository Closure

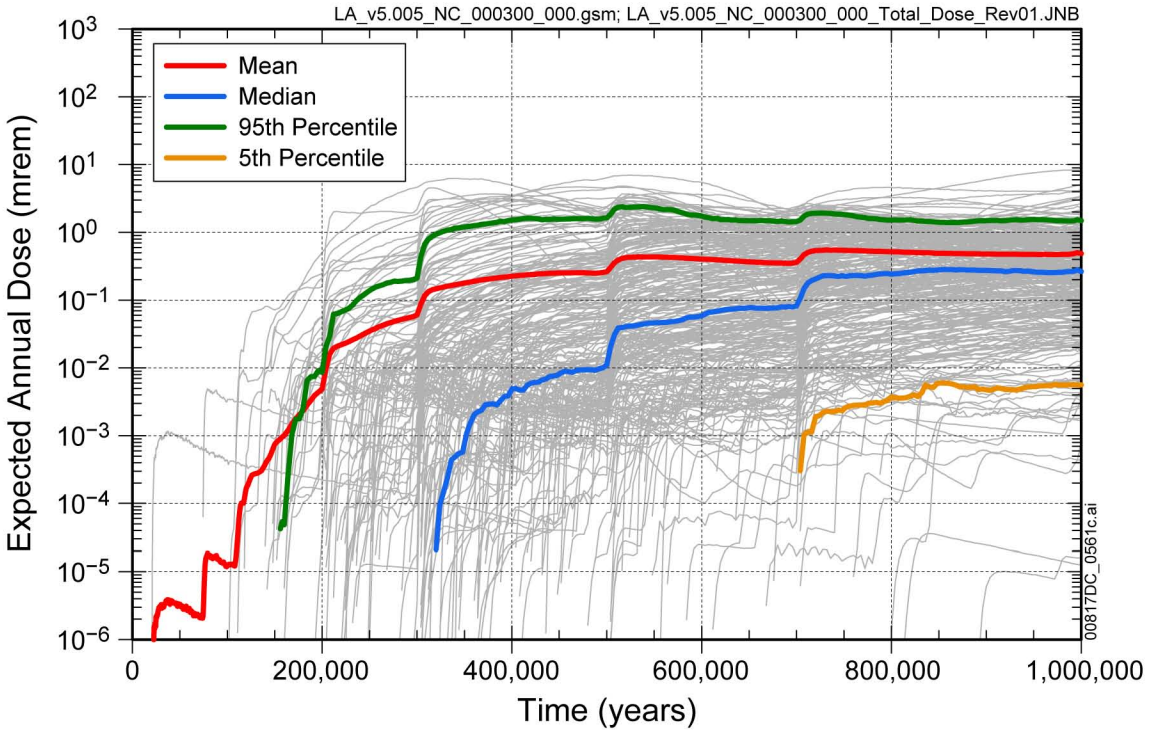

Source: Output DTNs: MO0710ADTSPAWO.000 [DIRS 183752]; and MO0710PLOTSFIG.000 [DIRS 185207].

Figure ES-44[a]. Annual Dose for the Nominal Scenario Class Modeling Case for the Post-10,000-Year Period

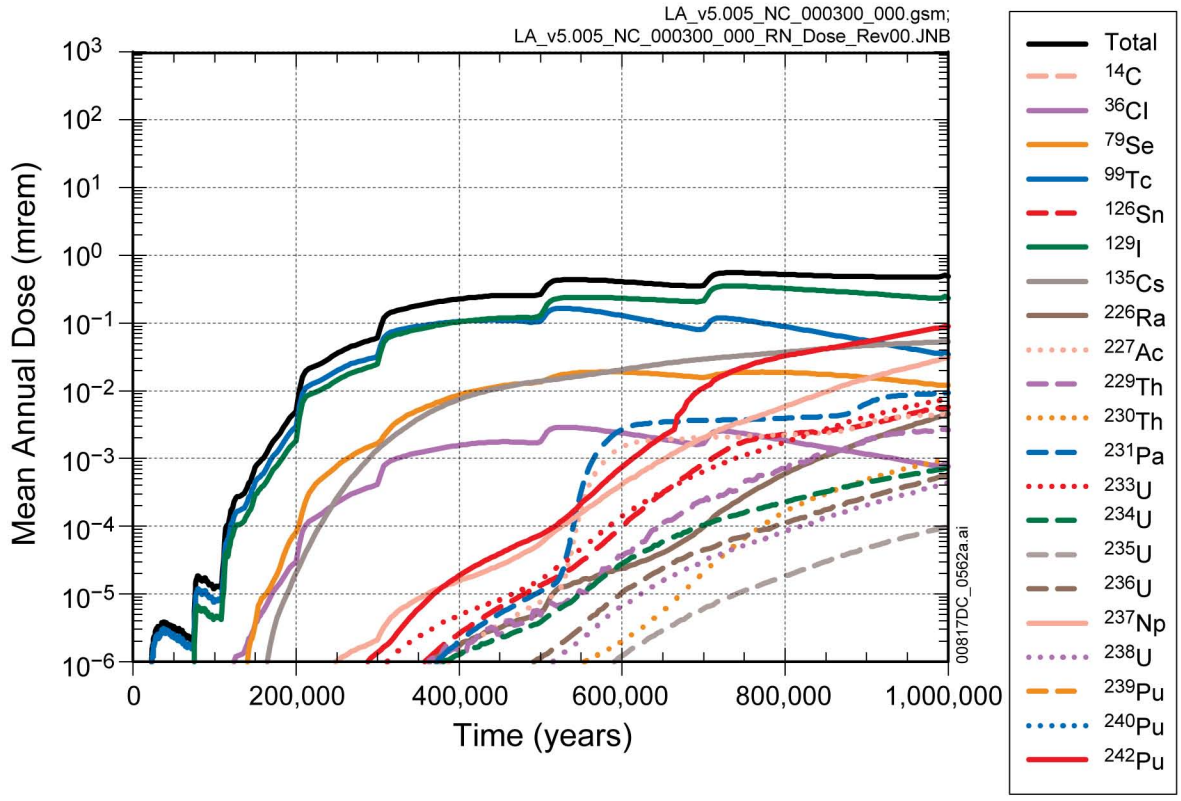

Source: Output DTNs: MO0710ADTSPAWO.000 [DIRS 183752]; and MO0710PLOTSFIG.000 [DIRS 185207].

Figure ES-45[a]. Mean Annual Dose Contributions from Major Radionuclides for the Nominal Scenario Class Modeling Case for the Post-10,000-Year Period

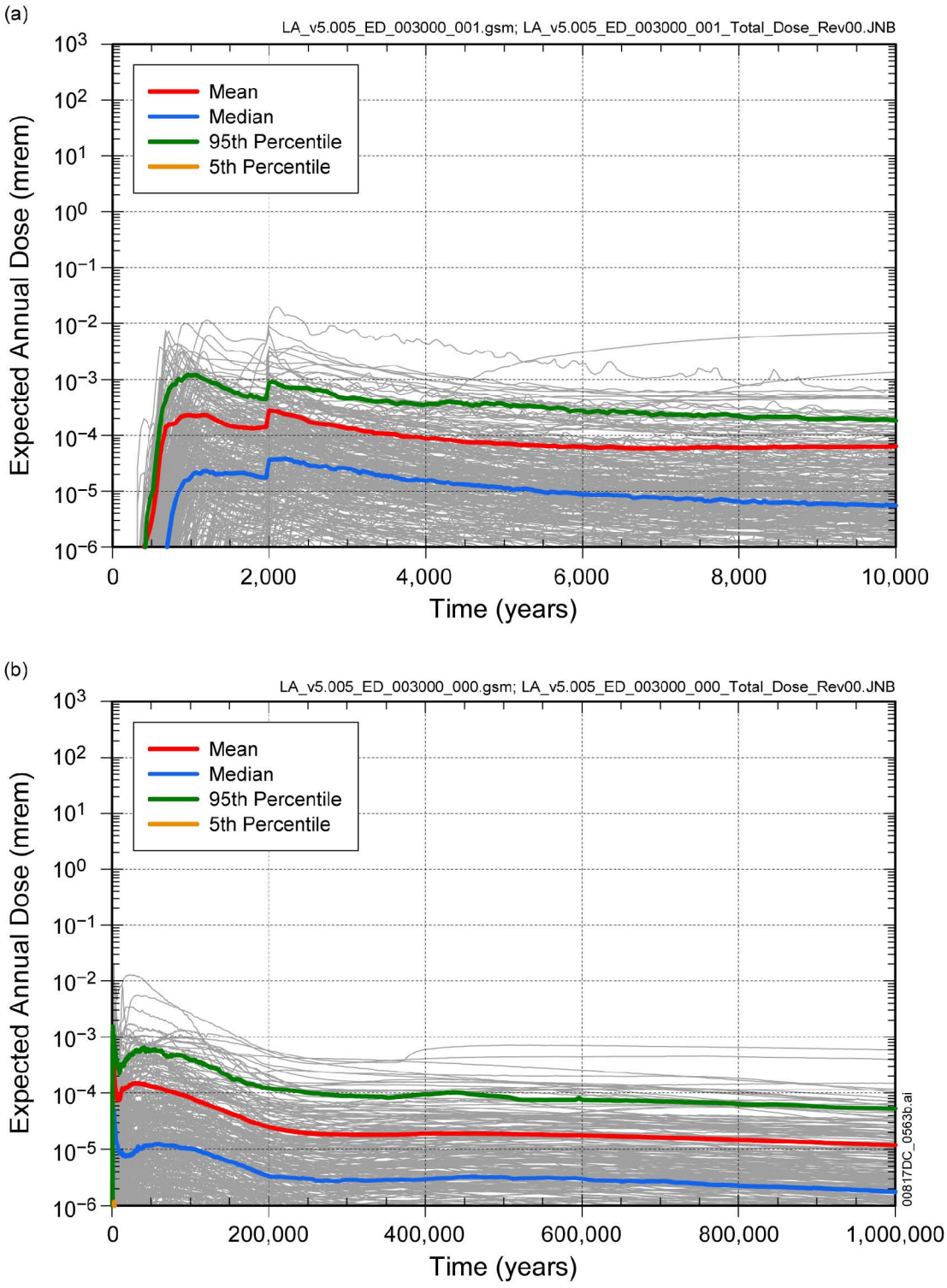

Source: Output DTNs: MO0710ADTSPAWO.000 [DIRS 183752]; and MO0710PLOTSFIG.000 [DIRS 185207].

Figure ES-46[a]. Expected Annual Dose for the Drip Shield Early Failure Modeling Case for (a) the First 10,000 Years after Repository Closure and (b) Post-10,000-Year Period

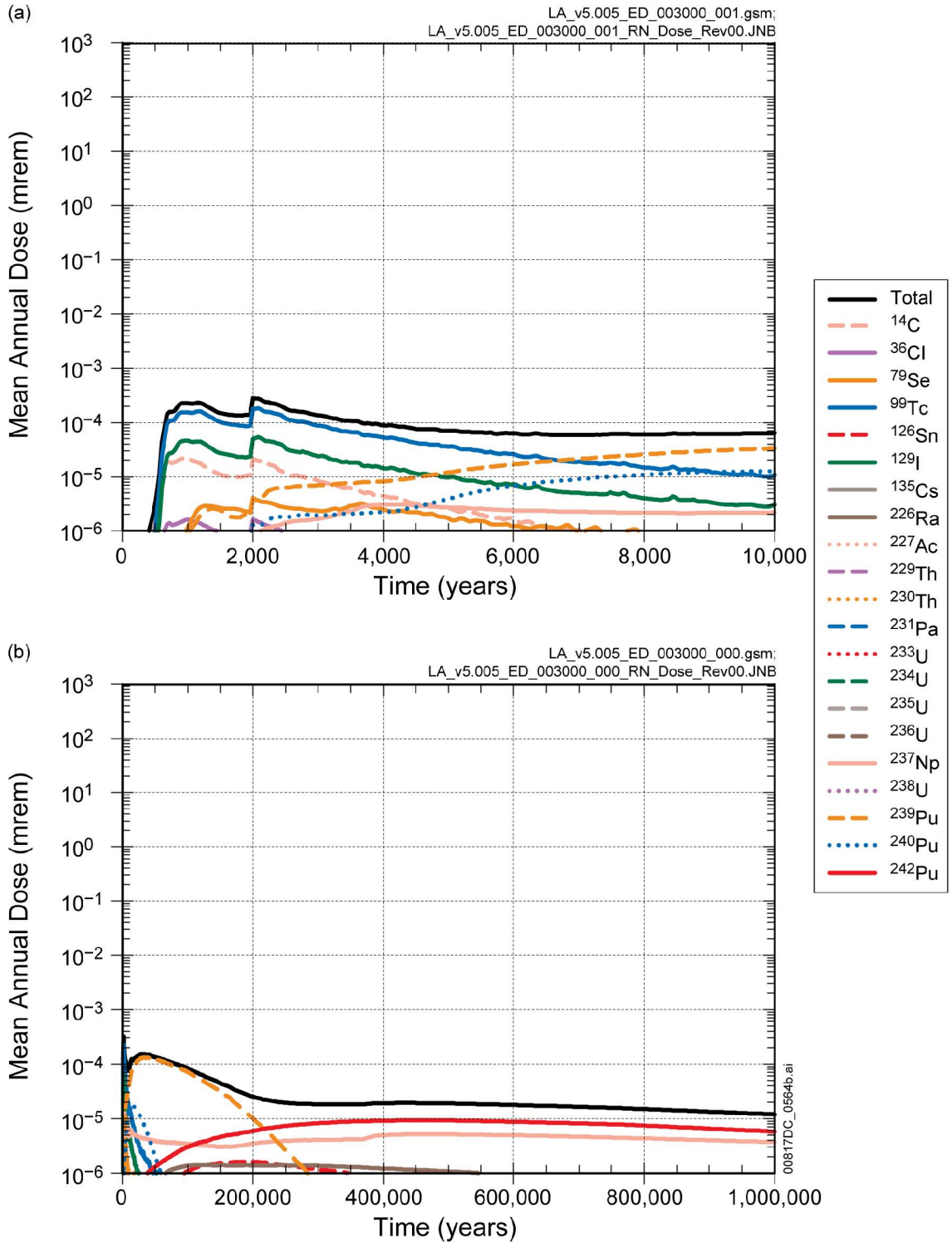

Source: Output DTNs: MO0710ADTSPAWO.000 [DIRS 183752]; and MO0710PLOTSFIG.000 [DIRS 185207].

Figure ES-47[a]. Mean Annual Dose Contributions from Major Radionuclides for the Drip Shield Early Failure Modeling Case for (a) the First 10,000 Years after Repository Closure and (b) Post-10,000-Year Period

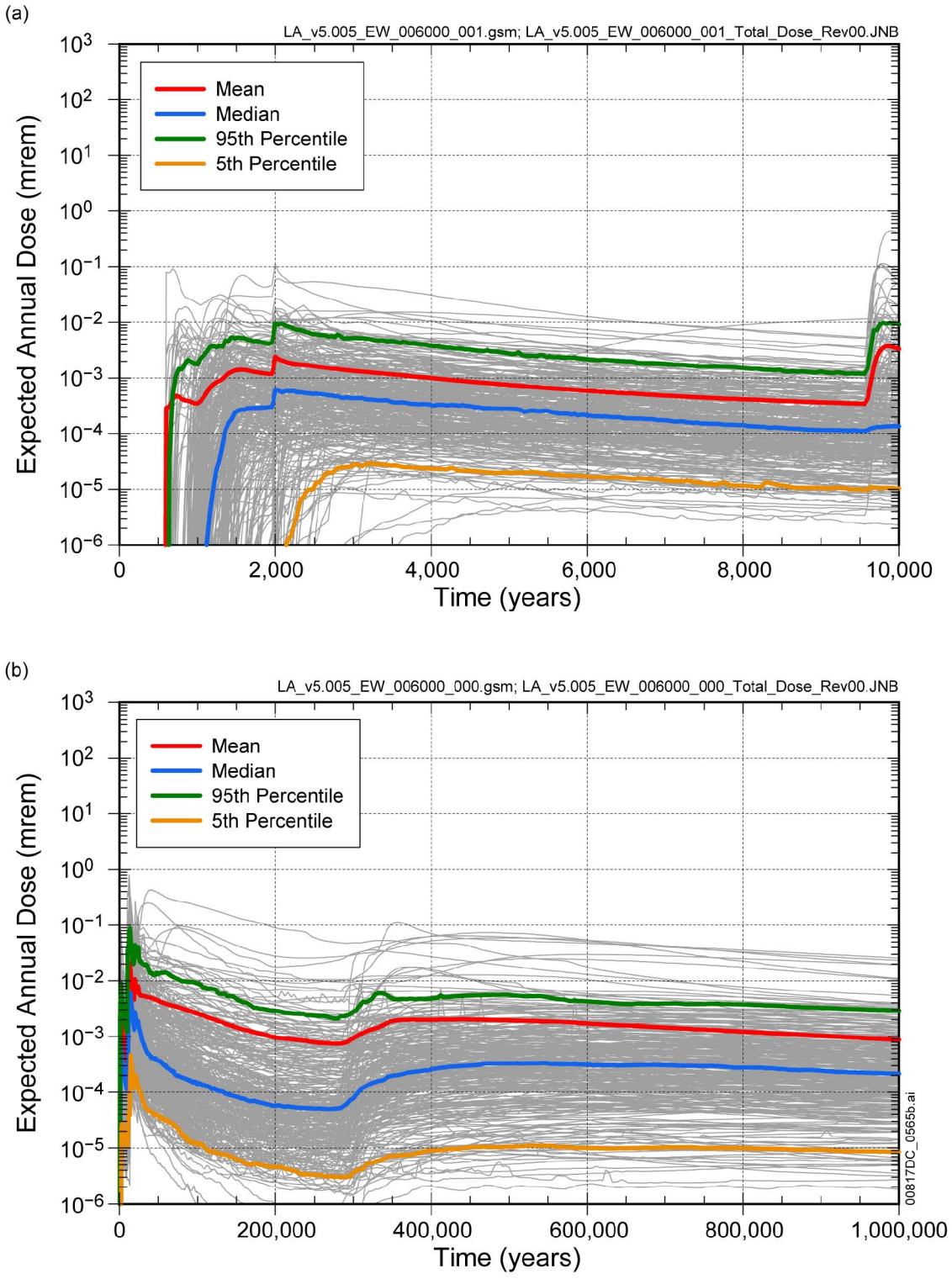

Source: Output DTNs: MO0710ADTSPAWO.000 [DIRS 183752]; and MO0710PLOTSFIG.000 [DIRS 185207].

Figure ES-48[a]. Expected Annual Dose for the Waste Package Early Failure Modeling Case for (a) the First 10,000 Years after Repository Closure and (b) Post-10,000-Year Period

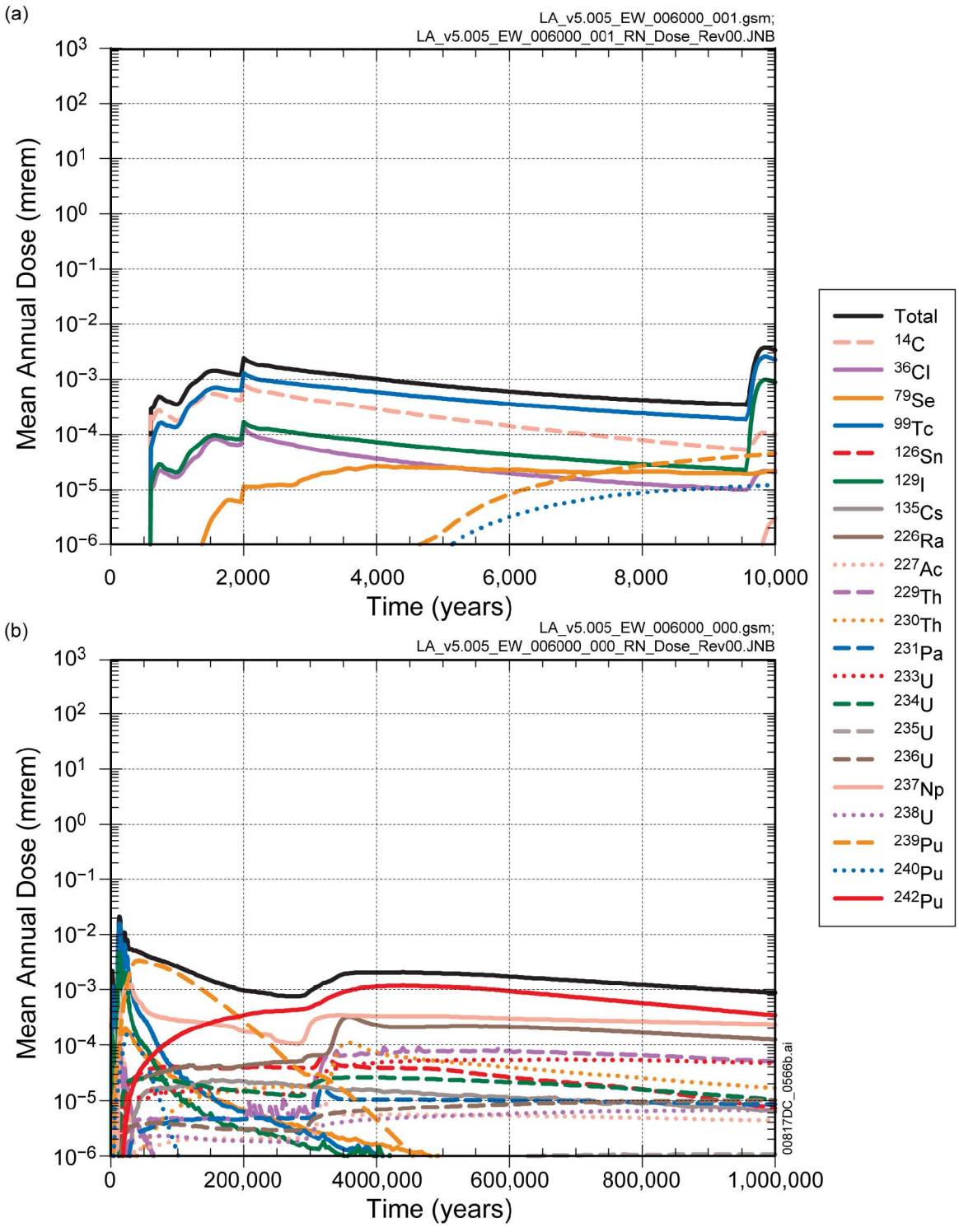

Source: Output DTNs: MO0710ADTSPAWO.000 [DIRS 183752]; and MO0710PLOTSFIG.000 [DIRS 185207].

Figure ES-49[a]. Mean Annual Dose Contributions from Major Radionuclides for the Waste Package Early Failure Modeling Case for (a) the First 10,000 Years after Repository Closure and (b) Post-10,000-Year Period

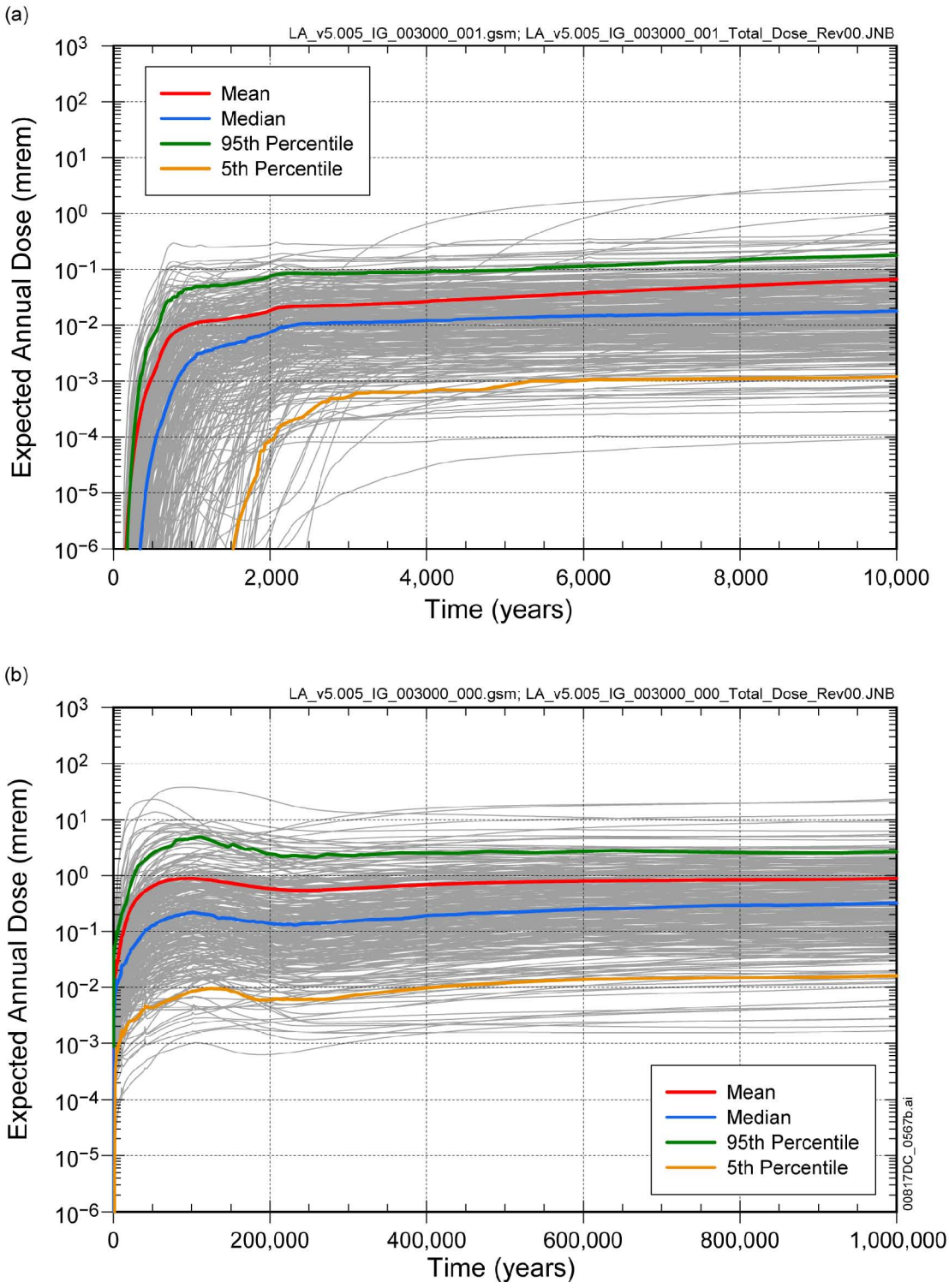

Source: Output DTNs: MO0710ADTSPAWO.000 [DIRS 183752]; and MO0710PLOTSFIG.000 [DIRS 185207].

Figure ES-50[a]. Expected Annual Dose for the Igneous Intrusion Modeling Case for (a) 10,000 Years after Repository Closure and (b) Post-10,000-Year Period

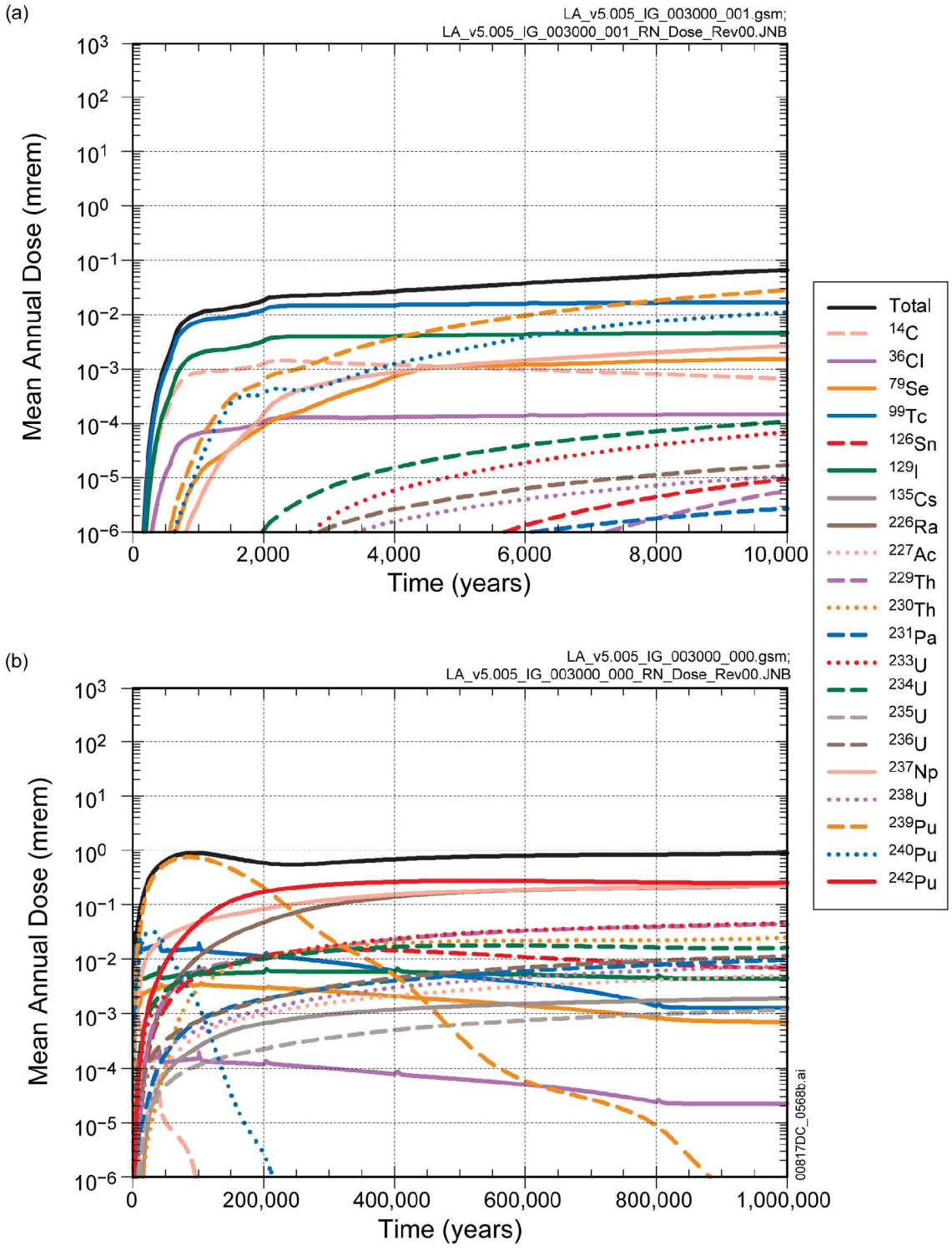

Source: Output DTNs: MO0710ADTSPAWO.000 [DIRS 183752]; and MO0710PLOTSFIG.000 [DIRS 185207].

Figure ES-51[a]. Mean Annual Dose Contributions from Major Radionuclides for the Igneous Intrusion Modeling Case for (a) the First 10,000 Years after Repository Closure and (b) Post-10,000-Year Period

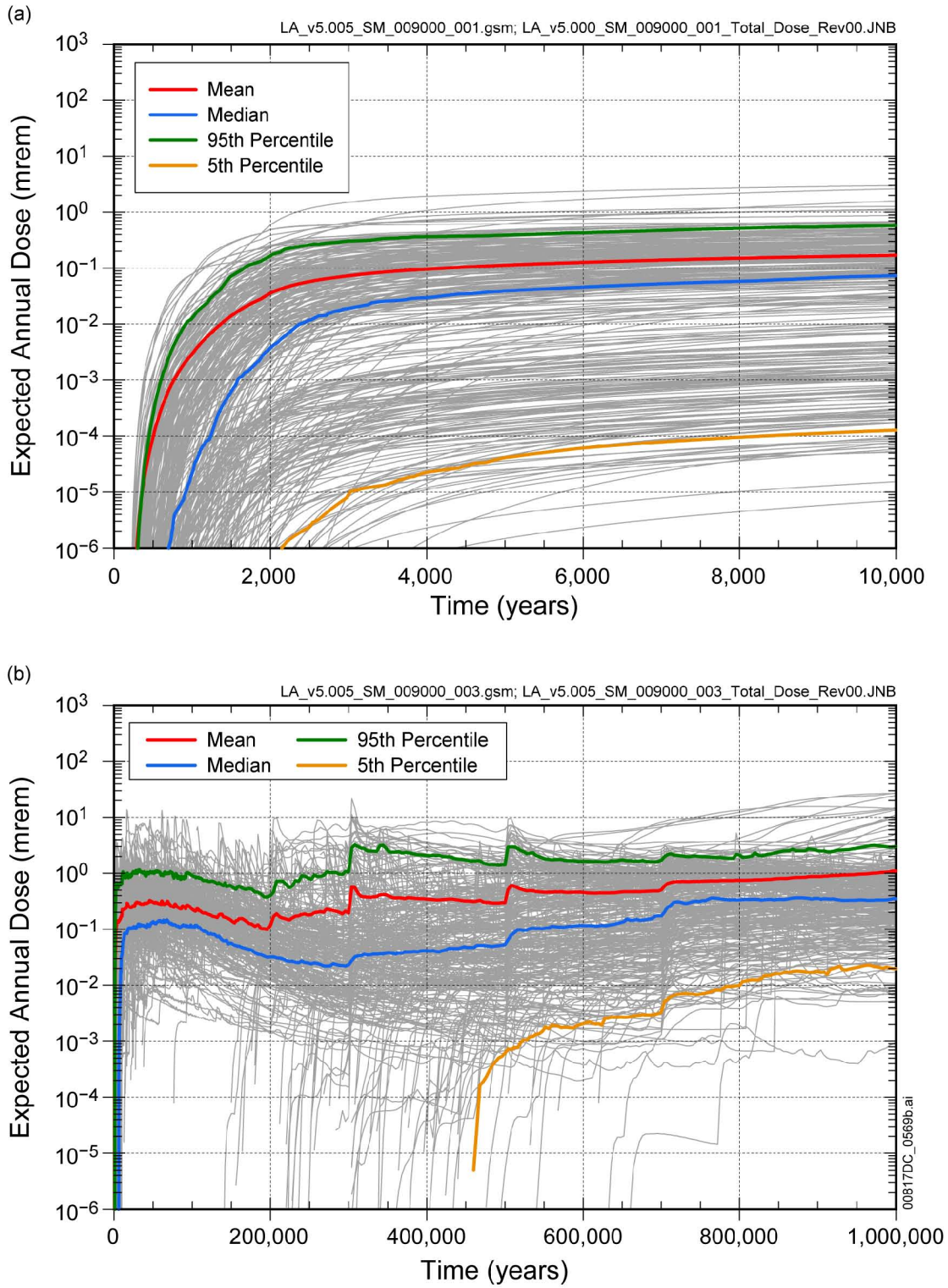

Source: Output DTNs: MO0710ADTSPAWO.000 [DIRS 183752]; and MO0710PLOTSFIG.000 [DIRS 185207].

Figure ES-54[a]. Expected Annual Dose for the Seismic Ground Motion Modeling Case for (a) 10,000 Years after Repository Closure and (b) Post-10,000-Year Period

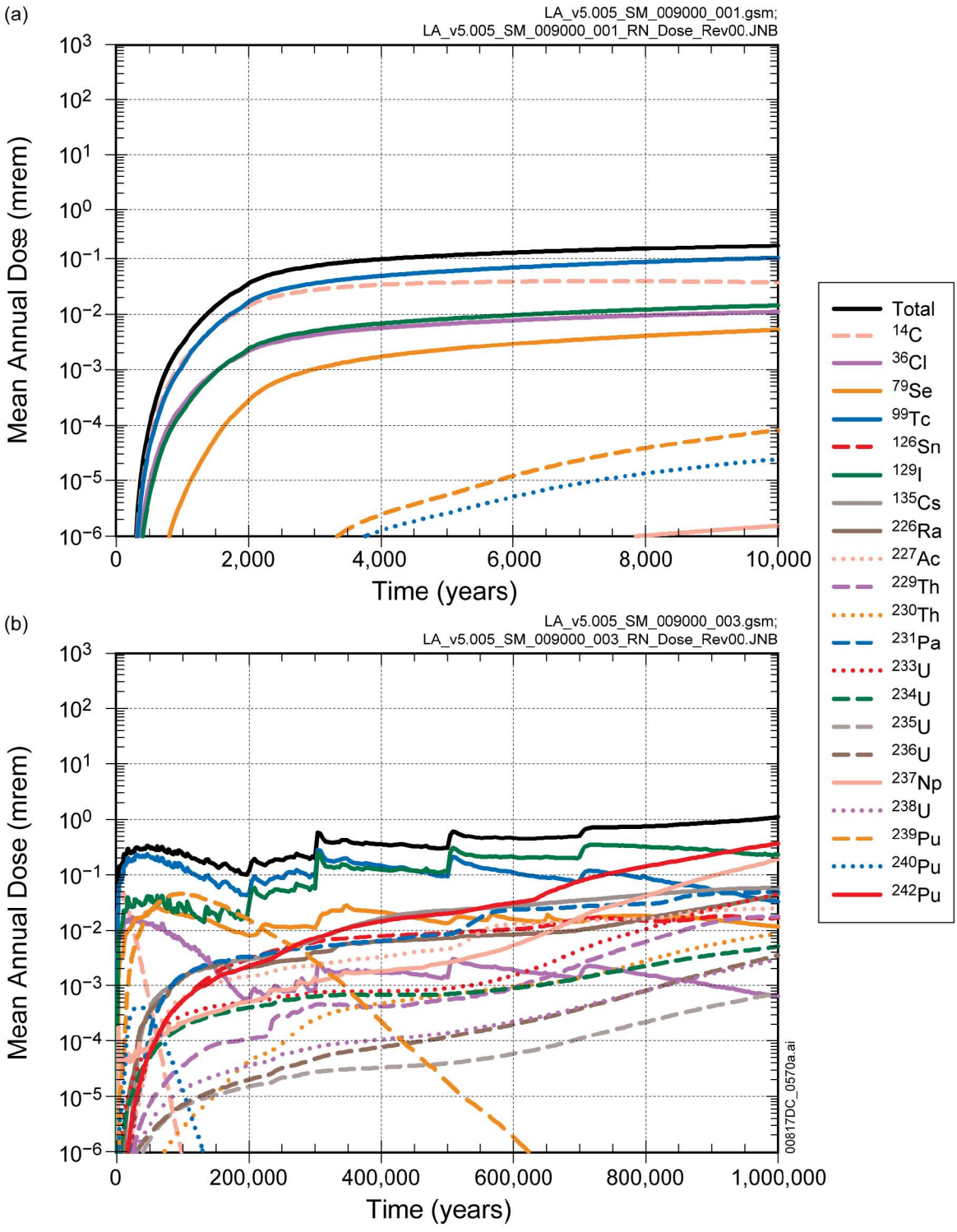

Source: Output DTNs: MO0710ADTSPAWO.000 [DIRS 183752]; and MO0710PLOTSFIG.000 [DIRS 185207].

Figure ES-55[a]. Mean Annual Dose Contributions from Major Radionuclides for the Seismic Ground Motion Modeling Case for (a) the First 10,000 Years after Repository Closure and (b) Post-10,000-Year Period

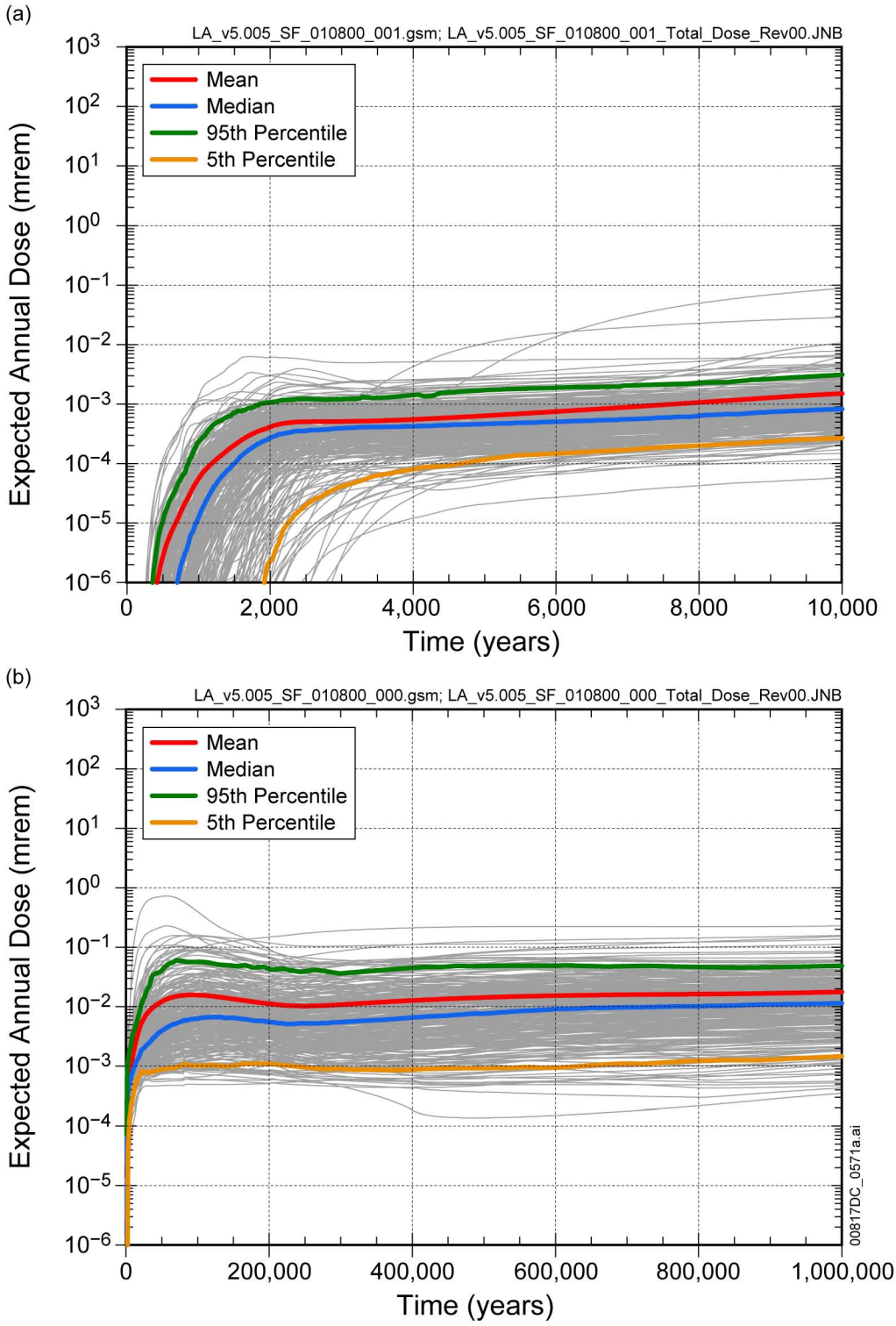

Source: Output DTNs: MO0710ADTSPAWO.000 [DIRS 183752]; and MO0710PLOTSFIG.000 [DIRS 185207].

Figure ES-56[a]. Expected Annual Dose for the Seismic Fault Displacement Modeling Case for (a) 10,000 Years after Repository Closure and (b) Post-10,000-Year Period

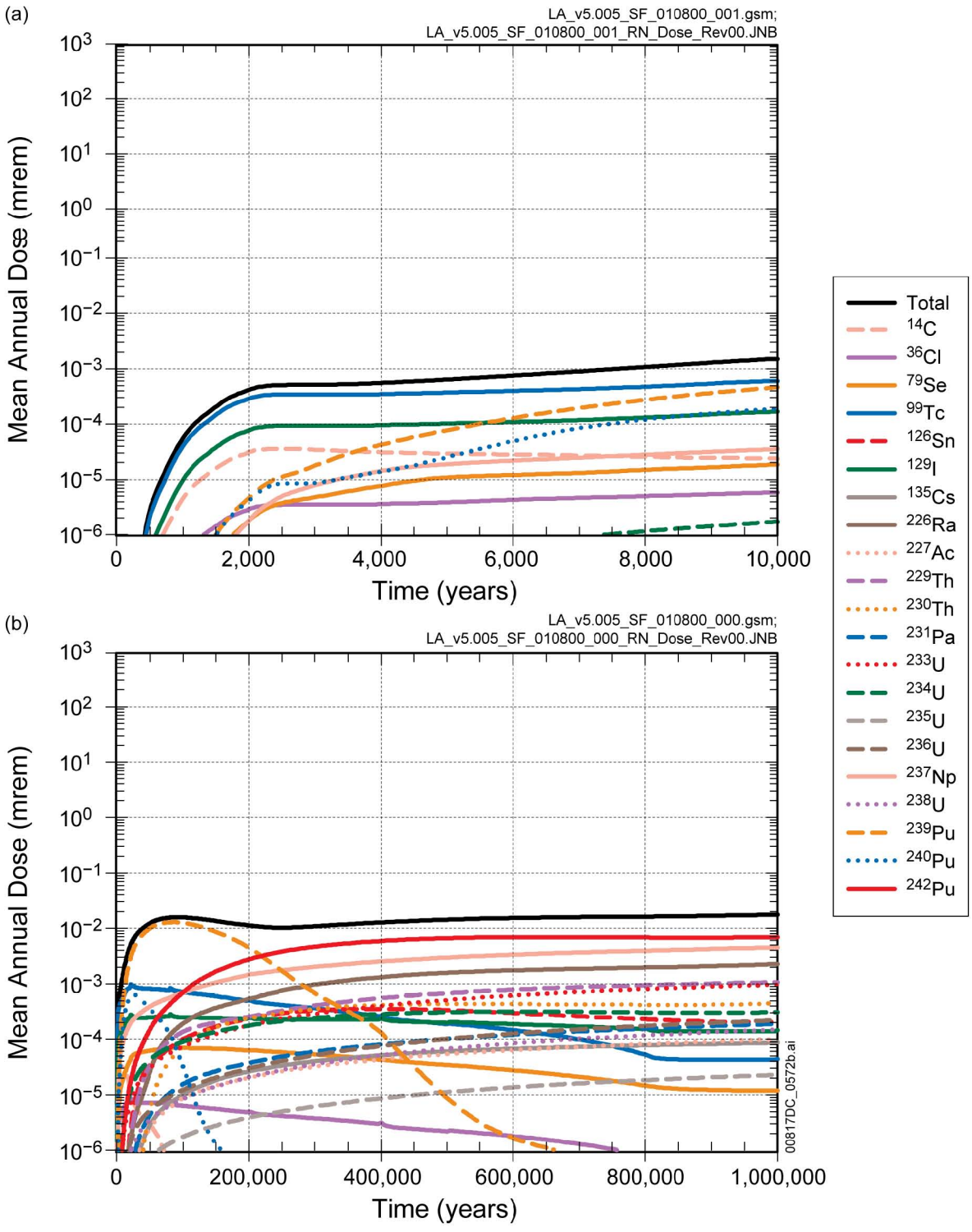

Source: Output DTNs: MO0710ADTSPAWO.000 [DIRS 183752]; and MO0710PLOTSFIG.000 [DIRS 185207].

Figure ES-57[a]. Mean Annual Dose Contributions from Major Radionuclides for the Seismic Fault Displacement Modeling Case for (a) 10,000 Years after Repository Closure and (b) Post-10,000-Year Period

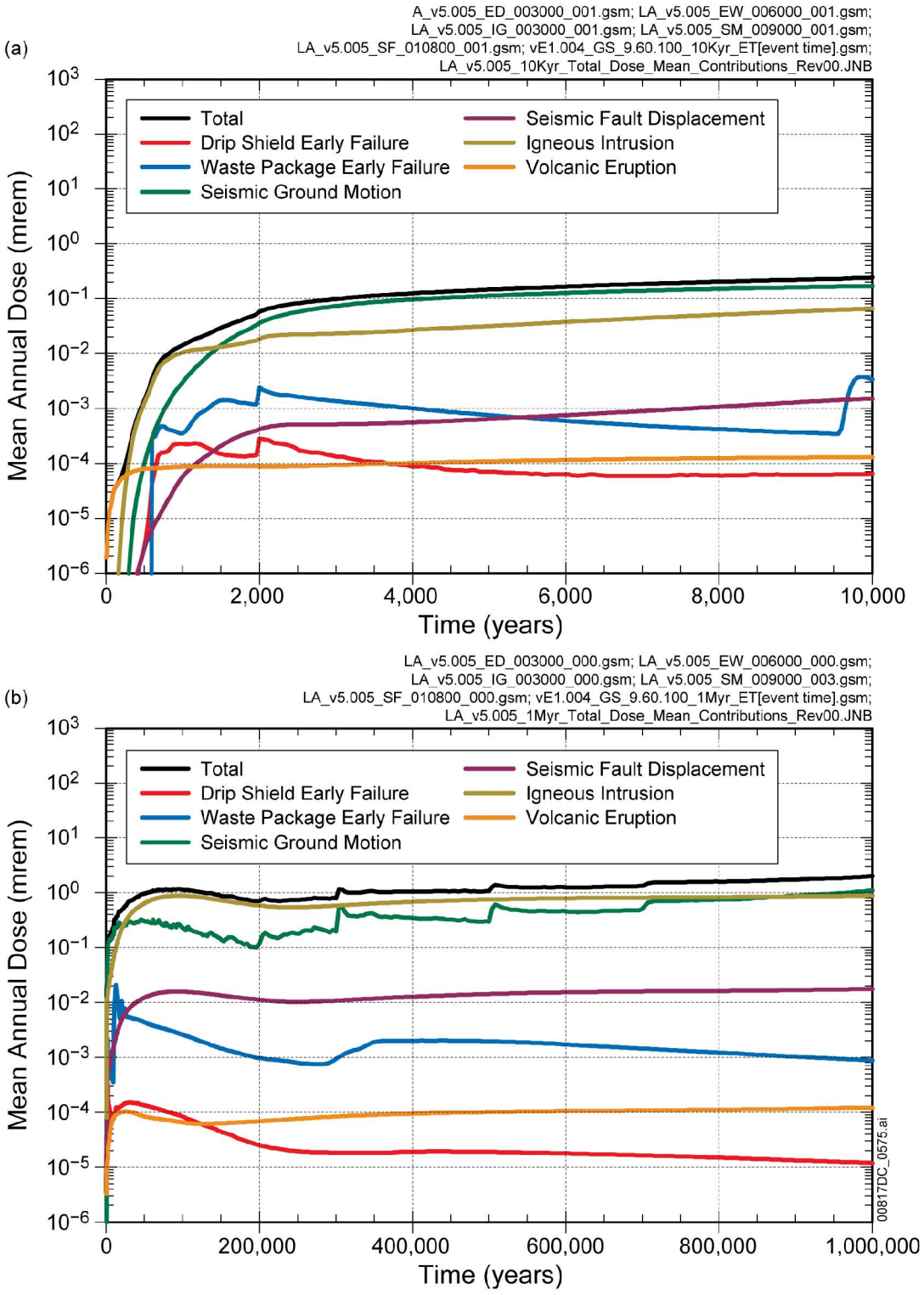

Source: Output DTNs: MO0710ADTSPAWO.000 [DIRS 183752]; and MO0709TSPAREGS.000 [DIRS 182976].

Figure ES-58[a]. Total Mean Annual Dose and Median Annual Doses for Each Modeling Case for (a) 10,000 Years after Repository Closure and (b) Post-10,000-Year Period

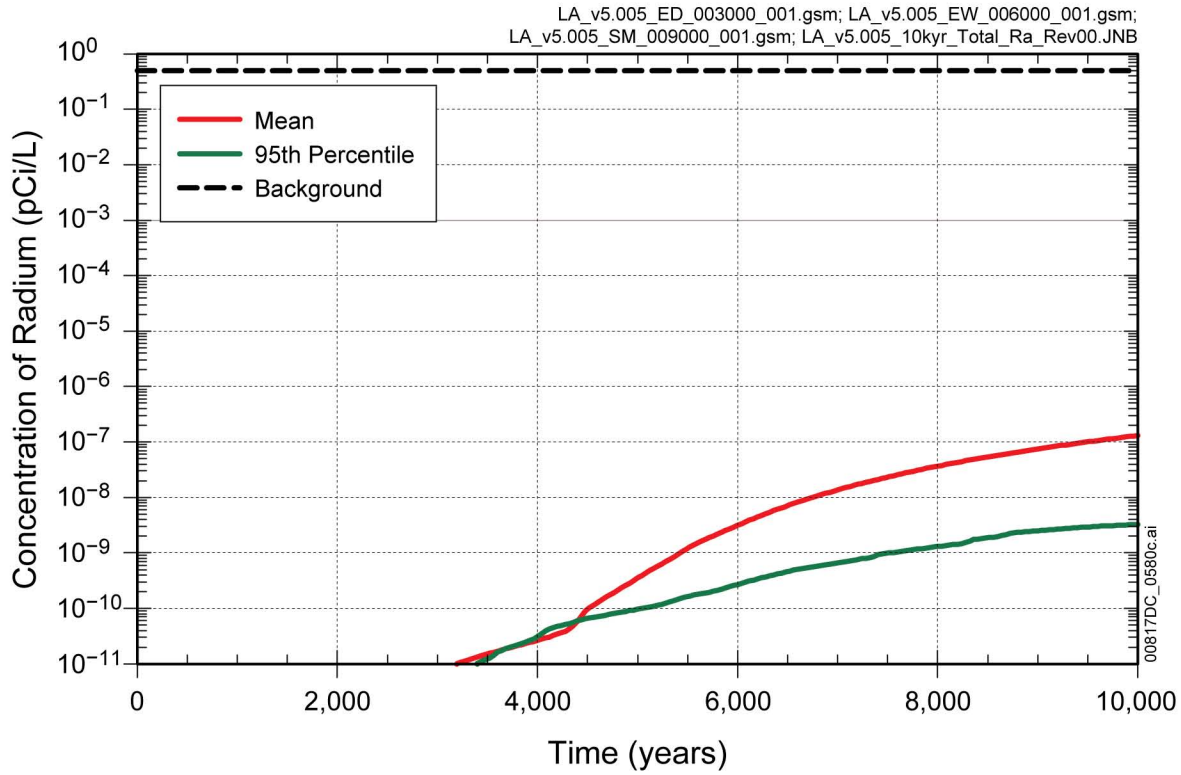

Source: Output DTNs: MO0710ADTSPAWO.000 [DIRS 183752]; and MO0710PLOTSFIG.000 [DIRS 185207].

Figure ES-59[a]. Combined ^{226}Ra and ^{228}Ra Activity Concentrations, Excluding Natural Background, for Likely Features, Events, and Processes Using Nominal, Early Failure, and Seismic Ground Motion Damage Processes

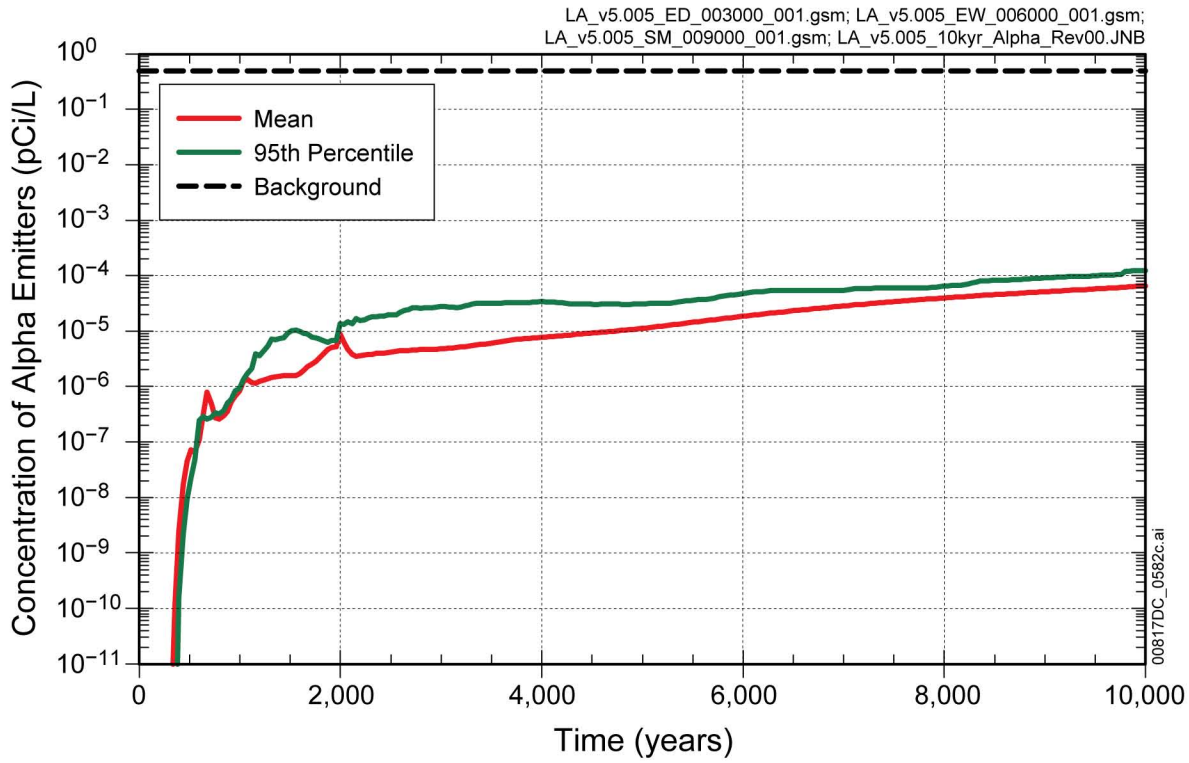

Source: Output DTNs: MO0710ADTSPAWO.000 [DIRS 183752]; and MO0710PLOTSFIG.000 [DIRS 185207].

Figure ES-60[a]. Combined Activity Concentrations of All Alpha Emitters (including ^{226}Ra but without radon and uranium isotopes), Excluding Natural Background, for Likely Features, Events, and Processes Using Nominal, Early Failure, and Seismic Ground Motion Damage Processes

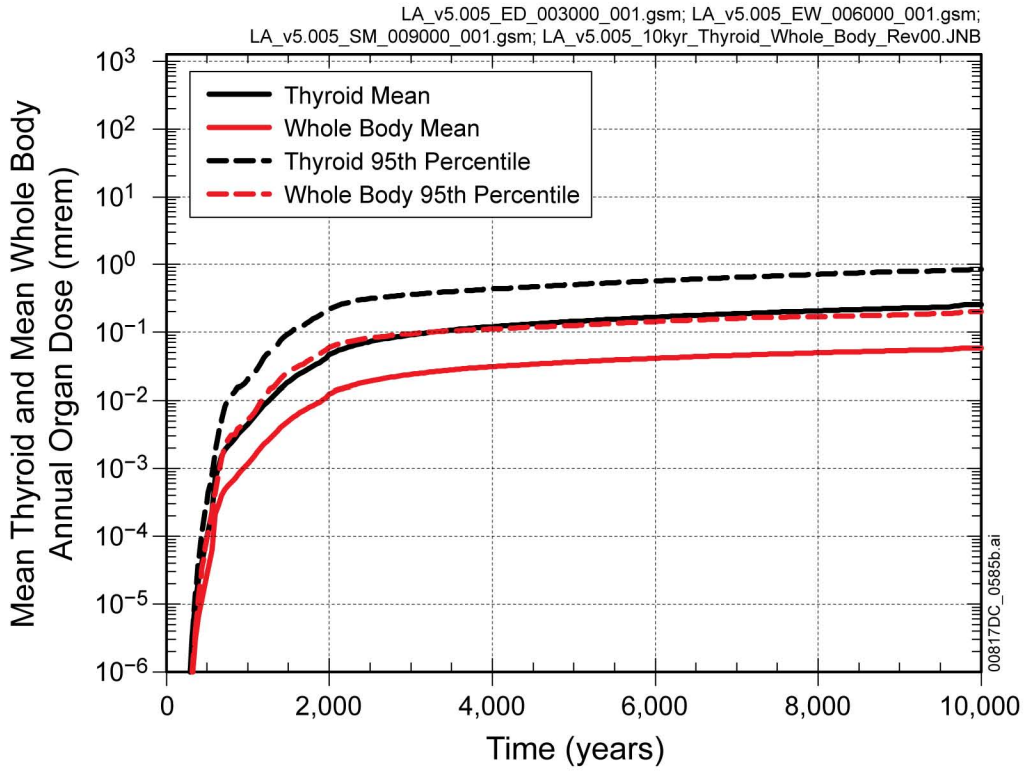

Source: Output DTNs: MO0710ADTSPAWO.000 [DIRS 183752]; and MO0710PLOTSFIG.000 [DIRS 185207].

Figure ES-61[a]. Mean Annual Drinking Water Dose from Combined Beta and Photon Emitters for Likely Features, Events, and Processes using the Nominal, Early Failure, and Seismic Ground Motion Damage Processes

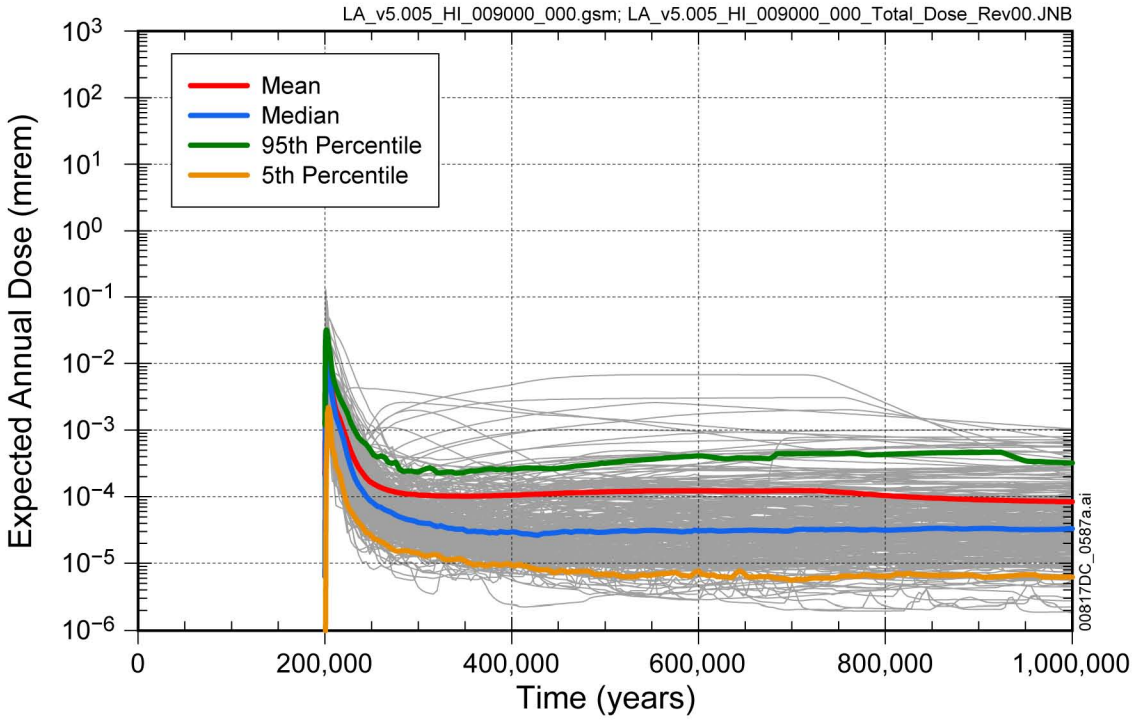

Source: Output DTNs: MO0710ADTSPAWO.000 [DIRS 183752]; and MO0710PLOTSFIG.000 [DIRS 185207].

Figure ES-62[a]. Expected Annual Individual Dose at the RMEI Location from a Human Intrusion 200,000 Years after Repository Closure

1[a]. PURPOSE

1.1[a] INTRODUCTION

This addendum updates the results of the Total System Performance Assessment for the License Application (TSPA-LA) Model presented in *Total System Performance Assessment Model/Analysis for the License Application* (the parent document). The updated results from TSPA-LA Model v5.005 incorporated changes to a supporting document, *Saturated Zone Flow and Transport Model Abstraction* (SNL 2008 [DIRS 183750]), amended after TSPA-LA Model v5.000 results in the parent document were completed. In addition, this addendum presents TSPA-LA results that address the issues identified and described in Appendix P. The issues were identified during detailed analysis, checking, and review activities. These issues were primarily related to minor inaccuracies in model implementation and identification of undocumented or unintended conservatisms or non-conservatisms. Appendix P[a] of this addendum includes updated tables (Tables P-6[a] and P-7[a]) that summarize the changes made in the TSPA-LA Model to address these issues. These additional analyses are presented in this addendum according to the review criteria outlined in *Technical Work Plan for: Total System Performance Assessment FY 07-08 Activities* (SNL 2008 [DIRS 184920], Sections 2.1.4 and 2.3.5.2.1).

For clarity, the general outline of the parent document is preserved in this addendum. In sections without any changes relative to the parent document, the text from the parent document is not repeated. Instead, the corresponding section in this addendum simply indicates that there are no changes, implicitly referring the reader to the same section of the parent document. Documentation provided in this addendum consists of a combination of supplemental and revised information. Section, figure, or table numbers cited in the text with [a] refer to this addendum, while those without it refer to the section, figure, or table number in the parent document. Section 1.10[a] lists the updates and additions to the parent document by section, which are included in this addendum.

The figures presented in this addendum, primarily reference output data tracking numbers (DTNs) containing data generated by the TSPA-LA Model. These output DTNs are described in Appendix B[a] and Appendix B of the parent document. Figure B-3[a] shows the relationship among the output DTNs referenced in this addendum and the output DTNs described in Appendix B of the parent document. Electronic copies of the figures generated for this addendum from TSPA-LA Model output are found in the output DTN: MO0710PLOTSFIG.000 [DIRS 185207] along with supporting documentation.

1.1.1[a] Governing Regulations

No change.

1.1.2[a] Total System Performance Assessment Methodology

No change.

1.1.3[a] Treatment of Uncertainty

No change.

1.2[a] TSPA-LA MODEL DEVELOPMENT PROCESS

No change.

1.3[a] YUCCA MOUNTAIN SITE DESCRIPTION

No change.

1.4[a] DESIGN OF YUCCA MOUNTAIN REPOSITORY SUBSURFACE FACILITIES

No change.

1.5[a] GENERAL DESCRIPTION OF THE TSPA-LA MODEL

No change.

1.6[a] CONCEPTUAL DESCRIPTION OF PROCESSES RELEVANT TO AN EVALUATION OF POSTCLOSURE PERFORMANCE IN THE ABSENCE OF DISRUPTIVE EVENTS

No change.

1.7[a] CONCEPTUAL DESCRIPTION OF PROCESSES RELEVANT TO AN EVALUATION OF POSTCLOSURE PERFORMANCE AFTER THE OCCURRENCE OF DISRUPTIVE EVENTS

No change.

1.8[a] CONSERVATISMS AND LIMITATIONS RELATED TO THE TSPA-LA MODEL

Section 1.8.2.5[a] addresses condition reports that have changed or are new since the parent document.

1.8.1[a] Conservatisms Incorporated in the TSPA-LA Model

No change.

1.8.2[a] Limitations of the TSPA-LA Model

Section 1.8.2.5[a] addresses condition reports that have changed or are new since the parent document.

1.8.2.1[a] Software Limitations

No change.

1.8.2.2[a] Computational Limitations

No change.

1.8.2.3[a] Data Limitations

No change.

1.8.2.4[a] Process Model Limitations

No change.

1.8.2.5[a] Condition Reports

The *Total System Performance Assessment Model/Analysis for the License Application,* Addendum 01, addresses the issues raised in the following condition reports (CRs) (cutoff date for inclusion: March 07, 2008):

- *Condition Report 11152* (Updates for draft Supplemental Environmental Impact Statement [SEIS]-TSPA)—CR 11152 identifies several issues in the TSPA-LA Model relating to the SEIS. The issues identified in the TSPA-LA Model log as described in the condition report have been addressed as documented in Appendix P[a].

- *Condition Report 11382* (Office of Chief Scientist)—CR 11382 identifies the following expectations of the Office of Chief Scientist: (1) provide an addendum to the *Total System Performance Assessment Model/Analysis for the License Application* to address issues identified in the development of the TSPA-LA Model, and (2) address the proposed changes to the regulations governing the preparation of the TSPA-LA Model in this addendum. The second item is documented in Section 1.1.1, Governing Regulations.

- *Condition Report 11655* (Addenda Planning Documentation)—CR-11655 concerns the issue that the current Technical Work Plan does not address the need for the scope of Addendum 01, and there is no documentation in the records package for the analyses or in the supplemental records package for the Technical Work Plan. However, this condition does not exist for this addendum. The planning for Addendum 01 is found in *Technical Work Plan for: Total System Performance FY 07-08 Activities* (SNL 2008 [DIRS 184920], Section 2.3.5.3). Although the word addendum does not appear, the content of Addendum 01 is planned to document additional analyses and associated changes, based on identified needs, in accordance with the review criteria described in *Technical Work Plan for: Total System Performance FY 07-08 Activities* (SNL 2008 [DIRS 184920], Sections 2.1.4 and 2.3.5.2.1). The additional analyses do not require any changes to the planning document and there is no impact to the TSPA-LA or this addendum.

- *Condition Report 11715* (Inconsistency in the Development of Water Table Temperature)—CR 11715 identifies the water table temperatures that are used in the evaluation of unsaturated zone (UZ) flow uncertainty and the impact on the weighting factors for UZ flow uncertainty cases used in the TSPA-LA Model. Despite the inconsistency in the development of the water table temperature boundary condition, the impact on the weighting factors used in the TSPA-LA Model is expected to be small.

- *Condition Report 11728* (Typographical Error in Table 4-1)—CR 11728 identifies that the DTN SN0701PAWPHIT1.001_R2 [DIRS 182961] addressed on lines 58 and 59 of Table 4-1 of the parent document was incorrectly identified as SN0701PAWPHIT.001_R2 [DIRS 182961]. This issue is corrected in Table 4-1[a].

- *Condition Report 11755* (EBS Radionuclide Transport Abstraction Typographical Error)—This condition report identifies that Table 8.2-4 in the EBS Radionuclide Transport Abstraction contains two parameter values for use in the water adsorption isotherm for corrosion products that are not the same as the output values in DTN: SN0703PAEBSTRA.001_R3 [DIRS 183217] or the values developed in the *EBS Radionuclide Transport Abstraction* (SNL 2007 [DIRS 177407], Section 6.3.4.3.2). The values on Table 8.2-4 are found in the output DTN file: SN0703PAEBSTRA.001-RTA Input Tables.Doc and were used in TSPA-LA Rev. 00 (Parameter Entry Form [PEF] 59). The correct values are found in the same DTN file: Corrosion Products Composite Isotherm 7-19-2007.xls as identified in the DTN readme file. This CR was discovered during the development of the TSPA-LA Rev 00 Addendum 01 and was corrected and verified during checking of the TSPA Input Database (PEF 203). The correct inputs were used to develop the TSPA-LA Addendum outputs.

- *Condition Report 11756* (Draft Data in DTN)—This condition report identifies output DTN: MO0708FREQCALC.000 [DIRS 183006] found in this addendum as containing files with content marked as DRAFT. Specifically, the DTN contains files named FreqDamageTAD.pdf and FreqRupture.pdf with headers on these documents indicating that they are DRAFT. The documentation issues raised in this CR do not involve the quality of the information; therefore, they are judged to have no impact on this addendum.

- *Condition Report 11759* (pdf of TSPA-LA)—The initial pdf file submitted to records for the TSPA-LA Rev00 inadvertently omitted two subsections, included some nonessential text regarding hidden headings, and appeared to have misnumbered pages in Appendix C. The first two items have been corrected and a new pdf has been submitted to records. It has been determined the third item (Appendix C page numbering) is not an issue as all pages were included and, therefore, does not impact the document. The documentation issues raised in this CR do not involve the quality of information and have no impact on this addendum. No further action is required.

- *Condition Report 11816* (Invert Thickness Change not in EBS RTA)—The range used for the TSPA parameter Diff_Path_Length_Invert_Top_a is based on an earlier outdated invert configuration. The diffusive path length from the WP outer barrier to the mid-point of the invert is treated as an epistemic uncertain parameter

(Diff_Path_Length_Invert_Top_a in Table 6.3.8-4 of the parent document) in the TSPA-LA Model. The updated average invert thickness would cause the diffusive path length used in the TSPA-LA Model to range from 0.47m to 1.41m. Because the diffusive path length parameter used in the TSPA-LA Model is based on a smaller value, the TSPA-LA Model conservatively overestimates diffusive releases from a breached WP to the invert relative to releases that would be obtained sampling an updated diffusive path length range. Therefore, not using the updated range is likely to have a negligible effect on the overall releases from the EBS calculated by the TSPA-LA Model. The issue raised in this CR has been determined to have no impact on this addendum.

1.9[a] DESCRIPTION OF THE TOTAL SYSTEM PERFORMANCE ASSESSMENT MODEL/ANALYSIS FOR THE LICENSE APPLICATION

No change.

1.10[a] DOCUMENT ORGANIZATION

The TSPA-LA parent document is organized in three volumes. This addendum follows the same organizational structure as the parent document. Only sections wherein additional information or results are presented are provided in this addendum. The information found in Volumes I[a], II[a], and III[a] of this addendum, along with the parent document, provides cross referencing that allows investigation of the structure and operation of the TSPA-LA Model files used to perform performance assessment calculations documented herein.

1.10.1[a] Volume I[a]

Volume I[a] of this addendum provides a description of the additional information required to document the TSPA-LA Model that was used for the analyses documented in this addendum. This includes information regarding direct inputs, parameters, and submodel descriptions as required to describe the TSPA-LA Model calculations and trace the sources of the TSPA-LA Model's direct inputs. Volume I[a] also contains appropriate references to source information. Volume I of the parent document should be used in conjunction with the information provided in this addendum.

Section 1[a]: **Purpose**—Section 1[a] provides no additional information with respect to the features, events, and processes that led to the development of the scenario classes used in analyzing the performance of the repository system; the regulatory framework for the TSPA-LA Model; the overview of the natural and engineered barriers in the repository system, including site-description information, descriptions of the elements of the engineered barrier system (EBS), processes affecting water movement through the UZ and saturated zone (SZ), and descriptions of the model components; and a general description of the architecture of the TSPA-LA Model. All of these topics are discussed in the parent document and apply to the analyses presented in this addendum.

Section 2[a]: **Quality Assurance**—Section 2 of the parent document describes the applicable quality assurance procedures of *Quality Assurance Requirements and Description* (DOE 2007

[DIRS 182051]), along with descriptions and references to the methods used for the electronic management of information. There is no additional information provided in this addendum.

Section 3[a]: **Use of Software**—Section 3 of the parent document lists and describes the software used in the development of the TSPA-LA Model. For the analyses presented in this addendum, only additional software or changes in the software used for the model results presented in the parent document are listed in Section 3[a].

Section 4[a]: **Inputs**—Section 4[a] identifies the additional direct inputs used in the TSPA-LA Model results presented in this addendum, either by direct tabulations included in this document or through linkage to the appropriate sections of the GoldSim model file or TSPA-LA Model database. Section 4 of the parent document should be used in conjunction with the data provided in Section 4[a] of this addendum.

Section 5[a]: **Assumptions**—Section 5 of the parent document lists the assumptions directly used to perform the TSPA-LA Model analyses along with their basis. Section 5[a] includes no additional assumptions for the TSPA-LA Model results documented in this addendum.

Section 6[a]: **Model Description**—Section 6 of the parent document describes the TSPA-LA Model representation of the repository system, presents the scenario classes being analyzed, describes the modeling cases used to analyze the scenario classes, and provides references to the applicable sections of the TSPA-LA Model, the GoldSim model file, and supporting analyses. Section 6 of the parent document also includes detailed descriptions of the conceptual models, mathematical formulations, implementations of the submodels in the TSPA-LA Model, conservatisms, and alternate conceptual models. Section 6[a] provides additional information consisting of typographical corrections, omissions, or descriptions of changes or additions to the conceptual models, mathematical formulations, implementations of the submodels for the TSPA-LA Model, conservatisms, and alternate conceptual models necessary to document the additional analyses presented in this addendum. Section 6 of the parent document should be used in conjunction with the data provided in Section 6[a] of this addendum.

1.10.2[a] Volume II[a]

Volume II[a] contains the supplemental information supporting the TSPA-LA Model validation.

Section 7[a]: **Validation**—Section 7 of the parent document describes the validation of the TSPA-LA Model as required by Section 6.3 of SCI-PRO-006, *Models*. The model validation of the TSPA-LA Model is consistent with the intended use of the TSPA-LA Model and the required level of confidence. In addition, the TSPA-LA Model validation results presented in this addendum are consistent with the intended use of the TSPA-LA Model. Additional model validation results documented in Volume II of this addendum are presented to confirm that the TSPA-LA Model validation has been maintained for v5.005 as well as to enhance the overall level of confidence in the TSPA-LA Model.

- Computer code and input re-verification (Section 7.2[a]) including:
  - Verification testing for the Human Intrusion Submodel inadvertently omitted from the parent document (Section 7.2.4.1.12[a])
  - Summary of an assessment of the range of validity for all TSPA-LA Model submodels inadvertently omitted from the parent document (Section 7.2.6[a])
- Demonstration of Model Stability (Section 7.3[a])
  - Comparison between TSPA-LA Model v5.000 and v5.005 expected dose results (Section 7.3.1[a])
  - Reevaluation of the statistical stability of TSPA-LA Model v5.005 results (Section 7.3.1[a])
  - Confirmation of numerical accuracy of expected dose results for the Seismic Fault Displacement (FD) Modeling Case (Section 7.3.2.7[a])
  - Reevaluation of the temporal stability testing for the Human Intrusion Modeling Case as the result of a change to the time step size for this modeling case (Section 7.3.3.6[a])
  - Evaluation of the temporal stability of the Nominal Modeling Case (Section 7.3.3.7[a])
- Surrogate Waste Form Validation (Section 7.5[a])
  - Reevaluation of the adequacy of using commercial spent nuclear fuel (CSNF) as a surrogate for naval spent nuclear fuel (NSNF) using TSPA-LA Model v5.005 (Section 7.5.3[a])
- Reevaluation of the corroboration of the TSPA-LA Model results documented in the parent document with auxiliary analyses (Section 7.7[a]), including:
  - Updated analyses of single realizations for the Early Failure Scenario Class, the Igneous Intrusion Modeling Case, and the Seismic Ground Motion (GM) Modeling Case for 1,000,000 years, including additional analyses of outlier realizations (Section 7.7.1[a])
  - Additional analyses of single realizations including: (1) the Nominal Scenario Class (Section 7.7.1.5[a]), (2) a Seismic GM Modeling Case for 10,000 years (Section 7.7.1.7[a]), and (3) the Human Intrusion Scenario (Section 7.7.1.6[a])
  - Updated evaluation with a Simplified TSPA Analysis (Section 7.7.2[a])
  - Updated evaluation with the Electric Power Research Institute (EPRI) Analysis (Section 7.7.3[a])

– Reevaluation of a comparison of results from the Performance Margin Analysis (Section 7.7.4[a]).

1.10.3[a] Volume III[a]

This volume contains the updated results for the TSPA-LA Model. These are detailed below.

Section 8[a]: **Analyses**—Section 8 of the parent document includes conclusions of the analyses as required by SCI-PRO-006. Section 8[a] of this addendum contains the updated results for the TSPA-LA Model performance analyses evaluating the postclosure performance of the repository and its compliance with U.S. Nuclear Regulatory Commission (NRC) Proposed Rule 10 CFR 63.113 [DIRS 180319] and the performance measures defined in proposed 10 CFR 63.303 [DIRS 178394] for the individual protection standard after permanent closure in proposed 10 CFR 63.311(a)(1) and (2) [DIRS 178394], the individual protection standard for human intrusion in 10 CFR 63.321(a)(1) and (2) [DIRS 178394], and the separate standards for protection of groundwater in 10 CFR 63.331, Table 1 [DIRS 180319]. The probabilistic analyses account for uncertainty and address features, events, and processes that could affect total system performance. Volume III[a] presents the updated results of analyses and calculations in the following areas:

- Comparison of TSPA-LA Model analyses with the performance measures defined in proposed 10 CFR 63.303 [DIRS 178394] for the individual protection standard after permanent closure in proposed 10 CFR 63.311(a)(1) and (2) [DIRS 178394], the individual protection standard for human intrusion in 10 CFR 63.321(a)(1) and (2) [DIRS 178394], and the separate standards for protection of groundwater in 10 CFR 63.331, Table 1 [DIRS 180319]

- System and subsystem performance analyses for the Nominal Scenario Class, including the Nominal Modeling Case; the Early Failure Scenario Class, including the Drip Shield Early Failure (EF) and Waste Package EF Modeling Cases; the Igneous Scenario Class, including both Igneous Intrusion and Volcanic Eruption Modeling Cases; and the Seismic Scenario Class, including the Seismic GM and FD Modeling Cases

- Analyses of the capabilities and importance of the upper and lower natural barriers and the EBS that have been identified as contributing to repository performance.

The results presented in this addendum represent an iterative process that reflects a rigorous model verification and implementation cycle.

Section 9[a]: **Inputs and References**—Section 9[a] provides additional sources of inputs, software, DTNs, and cited references.

Appendices

A. Acronyms and Abbreviations—No changes from the parent document.

B[a]. Data Tracking Numbers for the TSPA-LA Model—Appendix B[a] describes the contents of the output DTNs for the analyses presented in this addendum.

C[a]. Performance Margin Analysis—Appendix C[a] includes an update to Table C9-1 presented in the parent document; issue and impact assessments were not previously documented for the Performance Margin Analysis.

D[a]. Parameter Listing—Appendix D[a] refers to the TSPA Input Database, which contains a listing of all the additional parameters used to conduct the analyses presented in this addendum and the source(s) for each parameter. It also directs the reader to the appropriate sections in this document (Section 4[a] and Appendix K[a]) for further information on the addendum parameters.

E. Response to Review Comments from the International Review Team—No changes from the parent document.

F. Dynamically Linked Libraries Description and Feeds—No changes from the parent document.

G. Wiring Diagrams for Model Information Feeds—No changes from the parent document.

H[a]. Yucca Mountain Review Plan Acceptance Criteria—Appendix H[a] includes minor changes from the parent document to reference the proposed rule.

I[a]. Features, Events, and Processes Mapped to TSPA-LA Model—Appendix I[a] updates selected descriptions in Table I-2 from the parent document.

J[a]. Conceptual Structure of TSPA-LA—This addendum presents additional supplemental material in Appendix J[a], Section J3[a], which provides an overview of the underlying concepts used in the TSPA-LA Model that are described in Appendix J of the parent document.

K[a]. Uncertainty and Sensitivity Analysis Results—Appendix K[a] presents the distributions of results for each modeling case (uncertainty analyses) and identifies the uncertain parameters that predominantly contribute to the uncertainty in each modeling cases' results (sensitivity analyses) for the analyses presented in this addendum.

L. Simplified TSPA—No changes from the parent document.

M[a]. Comparison with Electric Power Research Institute Analysis—Minor changes from the parent document are incorporated to rectify a mistaken reference to supporting documentation.

N. Derivation of Implementing Equations for Waste Package Parsing and Average Damage Area—No changes from the parent document.

O. Localized Corrosion Initiation Uncertainty Analysis—No changes from the parent document.

P[a]. Impact Assessments—Appendix P[a] includes updates to Tables P-6 and P-7 in the parent document indicating the issues that have been addressed in the updated results. In addition, Appendix P[a] includes a modification to the issue description and analysis of the expected impact documented in Section P13 of the parent document.

2[a]. QUALITY ASSURANCE

2.1[a] CONFIGURATION MANAGEMENT

No change.

INTENTIONALLY LEFT BLANK

3[a]. USE OF SOFTWARE

3.1[a] INTRODUCTION

Section 3 of the parent document describes the software used in the development of the TSPA-LA Model. For the analyses presented in this addendum, only additional software or changes in the software used for the model results presented in the parent document are listed in Section 3[a]. In addition, Table 3-1 has been revised with the additional software and is included as Table 3-1[a] of this addendum. In addition, Figure 3-2 of the parent document incorrectly identified the surface infiltration external process model. Therefore, the figure has been updated and is included as Figure 3-2[a] of this addendum.

3.2[a] ASHPLUME_DLL_LA

No change.

3.3[a] CWD

No change.

3.4[a] EXDOC_LA

No change.

3.5[a] FAR

No change.

3.6[a] FEHM

No change.

3.7[a] GETTHK_LA

No change.

3.8[a] GOLDSIM

A software problem report (SPR013420071203 [DIRS 184391]) was submitted for GoldSim version 9.60.100 (STN: 10344-9.60-01 [DIRS 181903]) as a result of errors in radionuclide ingrowth calculations for the source term elements (Appendix P[a], Table P-7[a], Item P20). A new service pack, GoldSim version 9.60.300 (STN: 10344-9.60-03 [DIRS 184387]) was issued to address the problem. The GoldSim service pack problem report is included in the software problem report (SPR013420071203 [DIRS 184391]). An impact assessment was conducted by comparing results obtained using GoldSim version 9.60.300 with results from GoldSim version 9.60.100. The software errors resulted in an insignificant impact to the TSPA-LA results documented in the parent document (Appendix P, Section P20). Analyses presented in this addendum use the updated software (GoldSim version 9.60.300).

3.8.1[a] Description of Software

No change.

3.8.2[a] Relationship to the TSPA-LA Model

GoldSim version 9.60.100 [DIRS 181903] was used for the TSPA-LA Model development and validation and analysis cases (v5.000) as documented in Section 3.8 of the parent document. GoldSim version 9.60.300 [DIRS 184387] was used for the TSPA-LA Model development and validation and analysis cases (v5.005) documented in this addendum.

A controlled version of GoldSim version 9.60.300 was used prior to a qualified version as allowed by SCI-PRO-006. After qualification, GoldSim version 9.60.300 was obtained from Software Configuration Management in accordance with the governing procedure, IM-PRO-003, *Software Management,* and installed. The GoldSim version 9.60.300 installation package documents the confirmation that the controlled version of GoldSim version 9.60.300 is identical to the qualified version of GoldSim version 9.60.300 obtained from Software Configuration Management.

3.8.3[a] Software Documentation

Table 3-8[a] is modified to list the additional software documents pertaining to GoldSim version 9.60.300 [DIRS 184387].

3.8.4[a] Range of Validation

The range of validation for the versions of GoldSim listed in Section 3.8.2[a] is defined by the documented functionality (i.e., requirements) and range(s) of acceptable inputs. The requirements are located in the respective requirements documents listed in Table 3-8[a]. The range(s) of acceptable inputs is discussed in the respective design and user documents listed in Table 3-8[a].

3.9[a] INTERPZDLL_LA

No change.

3.10[a] MFCP_LA

No change.

3.11[a] MKTABLE AND MKTABLE_LA

No change.

3.12[a] MVIEW

No change.

3.13[a] PASSTABLE1D_LA

No change.

3.14[a] PASSTABLE3D_LA

No change.

3.15[a] PREWAP_LA

No change.

3.16[a] SCCD

No change.

3.17[a] SEEPAGEDLL_LA

No change.

3.18[a] SOILEXP_LA

No change.

3.19[a] SZ_CONVOLUTE

No change.

3.20[a] TSPA_INPUT_DB

No change.

3.21[a] WAPDEG

No change.

3.22[a] CORROBORATIVE SOFTWARE USED

No change.

INTENTIONALLY LEFT BLANK

Table 3-1[a]. TSPA-LA Model Software Codes

Code	Version	Software Tracking Number	Operating System	DIRS Number
ASHPLUME_DLL_LA[a1]	2.0	STN: 11117-2.0-00	Windows 2000	DIRS 181034
ASHPLUME_DLL_LA[a2 a3]	2.1	STN: 11117-2.1-00	Windows 2000	DIRS 181035
ASHPLUME_DLL_LA[a2 a3]	2.1	STN: 11117-2.1-01	Windows 2003	DIRS 180147
CWD[a2 a3]	2.0	STN: 10363-2.0-00	Windows 2000	DIRS 162809
CWD[a2 a3]	2.0	STN: 10363-2.0-01	Windows 2003	DIRS 181037
EXDOC_LA[b1]	2.0	STN: 11193-2.0-00	Windows 2000 Windows 2003 Windows XP	DIRS 182102
FAR [a1]	1.1	STN: 11190-1.1-00	Windows 2000 Windows 2003	DIRS 180002
FAR [a2]	1.2	STN: 11190-1.2-00	Windows 2000 Windows 2003	DIRS 182225
FEHM[a1]	2.23	STN: 10086-2.23-00	Windows 2000	DIRS 173139
FEHM[a2 a3]	2.24-01	STN: 10086-2.24-01-00	Windows 2000 Windows 2003 Windows XP	DIRS 179419
GetThk_LA [a2 a3]	1.0	STN: 11229-1.0-00	Windows 2000 Windows 2003	DIRS 181040
GoldSim[a1]	9.60	STN: 10344-9.60-00	Windows 2000 Windows 2003 Windows XP	DIRS 180224
GoldSim[a2]	9.60.100	STN: 10344-9.60-01	Windows 2000 Windows 2003 Windows XP	DIRS 181903
GoldSim[a3]	9.60.300	STN: 10344-9.60-03	Windows 2000 Windows 2003 Windows XP	DIRS 184387
InterpZdll_LA [a2 a3]	1.0	STN: 11107-1.0-00	Windows 2000	DIRS 167885
InterpZdll_LA [a2 a3]	1.0	STN: 11107-1.0-01	Windows 2003	DIRS 181043
MFCP_LA[a2 a3]	1.0	STN: 11071-1.0-00	Windows 2000	DIRS 167884
MFCP_LA[a2 a3]	1.0	STN: 11071-1.0-01	Windows 2003	DIRS 181045
MkTable[a1]	1.00	STN: 10505-1.00-00	Windows 2000	DIRS 174528
MkTable_LA[a2 a3]	1.0	STN: 11217-1.0-00	Windows 2000	DIRS 181047
MkTable_LA[a2 a3]	1.0	STN: 11217-1.0-01	Windows 2003	DIRS 181048
MView[b1]	4.0	STN: 10072-4.0-01	Windows XP	DIRS 181049
PassTable1D_LA[a1]	1.0	STN: 11142-1.0-00	Windows 2000	DIRS 169130
PassTable1D_LA[a1]	1.0	STN: 11142-1.0-01	Windows 2003	DIRS 181050
PassTable1D_LA[a2 a3]	2.0	STN: 11142-2.0-00	Windows 2000 Windows 2003	DIRS 181051
PassTable3D_LA[a1]	1.0	STN: 11143-1.0-00	Windows 2000	DIRS 168980

Table 3-1[a]. TSPA-LA Model Software Codes (Continued)

Code	Version	Software Tracking Number	Operating System	DIRS Number
PassTable3D_LA[a1]	1.0	STN: 11143-1.0-01	Windows 2003	DIRS 181052
PassTable3D_LA [a2 a3]	2.0	STN: 11143-2.0-00	Windows 2000 Windows 2003	DIRS 182556
PREWAP_LA[b1]	1.1	STN: 10939-1.1-00	Windows 2000	DIRS 181053
SCCD[a2 a3]	2.01	STN: 10343-2.01-00	Windows 2000	DIRS 181157
SCCD[a2 a3]	2.01	STN: 10343-2.01-01	Windows 2003	DIRS 181054
SEEPAGEDLL_LA[a1]	1.2	STN: 11076-1.2-00	Windows 2000	DIRS 173435
SEEPAGEDLL_LA[a2 a3]	1.3	STN: 11076-1.3-00	Windows 2000	DIRS 180318
SEEPAGEDLL_LA[a2 a3]	1.3	STN: 11076-1.3-01	Windows 2003	DIRS 181058
SoilExp_LA [a1]	1.0	STN: 10933-1.0-00	Windows 2000	DIRS 167883
SZ_Convolute[a1]	3.0	STN: 10207-3.0-00	Windows 2000	DIRS 164180
SZ_Convolute[a2 a3]	3.10.01	STN: 10207-3.10.01-00	Windows 2000/ Windows 2003	DIRS 181060
TSPA_Input_DB[a2 a3]	2.2	STN: 10931-2.2-00	Windows 2000	DIRS 181061
TSPA_Input_DB[a2 a3]	2.2	STN: 10931-2.2-01	Windows 2003	DIRS 181062
WAPDEG[a2 a3]	4.07	STN: 10000-4.07-00	Windows 2000	DIRS 181774
WAPDEG[a2 a3]	4.07	STN: 10000-4.07-01	Windows 2003	DIRS 181064

[a1] Codes are used only for the TSPA-LA Model development (See note below).

[a2] Codes used in the TSPA-LA Model that are used for the TSPA-LA Model development (See note below) and to develop results and conclusions in Section 8 of the parent document.

[a3] Codes used in the TSPA-LA Model that are used for the TSPA-LA Model development (See note below) and to develop results and conclusions in Section 8[a] of this addendum.

[b1] Code is a pre- or post-processor that does not require GoldSim to run codes that are used for the TSPA-LA Model development (See NOTE below) and to develop results and conclusions in Section 8.

NOTE: TSPA-LA Model development should not be confused with model development as described in SCI-PRO-006. TSPA-LA Model development is merely a phrase to represent the draft model versions (i.e., v4.001 to v4.047) that were created before finalizing the model (e.g., v5.000) presented in the parent document and v5.001 to v5.004 that were created before finalizing the model v5.005 presented in this addendum. The draft model versions, v4.001 to v4.047, were submitted as part of the records package for the parent document. The draft model versions, v5.001 to v5.004, are to be submitted as part of the records package for this addendum. All software codes used for the results presented in this document are on the software baseline.

Table 3-8[a]. GoldSim Software Documents for Version 9.60.300 (STN: 10344-9.60-30)

Version 9.60.300, Windows 2000, Windows 2003, and Windows XP (STN: 10344-9.60-03)			
Description	**Document ID**	**DIRS Number**	**Tracking Number**
Requirements Document (RD)	10344-RD-9.60-00	181106	MOL.20070416.0330
Design Document (DD)	10344-DD-9.60-01	181107	MOL.20070416.0338
User Information Document (UID)	10344-UID-9.60-00	181108	MOL.20070416.0339
User's Guide, GoldSim Probabilistic Simulation Environment, v9.60	NA	181727	TIC: 259221
Software Validation Report (SVR)	10344-SVR-9.60-03-WIN2000	185016	MOL.20080125.0059
Software Validation Report (SVR)	10344-SVR-9.60-03-WIN2003	185017	MOL.20080125.0061
Software Validation Report (SVR)	10344-SVR-9.60-03-WINXP	185018	MOL.20080125.0057

INTENTIONALLY LEFT BLANK

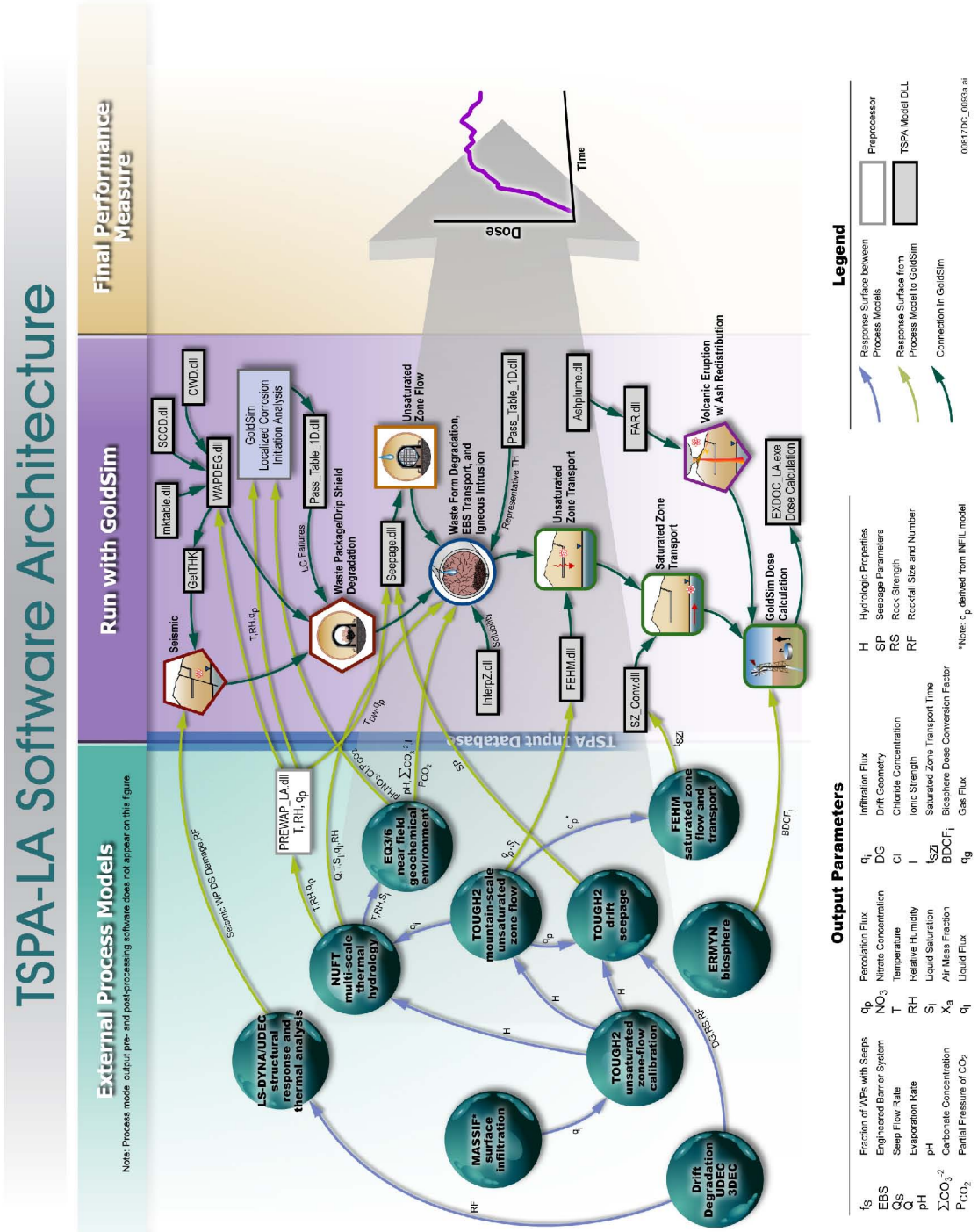

Figure 3-2[a]. TSPA-LA Software Architecture

INTENTIONALLY LEFT BLANK

4[a]. INPUTS

4.1[a] DIRECT INPUTS

Direct inputs are those parameters whose values are used by the TSPA-LA Model to compute the results presented in this document. This information is stored in the TSPA Input Database and is described in Section 4.7 of the parent document. Table 4-1 lists the direct input required for the analyses in the parent document. Table 4-1[a] of this addendum lists the additional direct input required for the analyses documented in this addendum and associates it with a reference source and a PEF number (see Section 4.3 of the parent document for an overview of PEFs).

The direct inputs listed in Table 4-1[a], except where noted, reflect parameter values that were corrected in TSPA-LA Model v5.005, rather than new direct inputs to the TSPA-LA Model, and are therefore cited in Section 6 of the parent document. The discussions presented in Section 6 of the parent document for these parameters remain unchanged. Line items starting with #129 represent new direct input and are cited in Section 6[a] of this addendum. All other references in Table 4-1 of the parent document remain unchanged.

4.2[a] TSPA-LA MODEL-GENERATED PARAMETERS

The TSPA-LA Model requires the generation of many parameters (often incorporated into large data files) that are created by preprocessing methods (i.e., created prior to running the TSPA-LA Model). These parameters are captured in output DTNs along with explanations for how they were generated. The use of output DTNs in the TSPA-LA Model is described at various locations in the parent document. PEFs that reference new output DTNs generated to support the analyses documented in this addendum are listed in Table 4-2[a].

4.3[a] PARAMETER ENTRY FORMS

No change.

4.4[a] TRACEABILITY OF INPUTS

No change.

4.5[a] CRITERIA

No change.

4.6[a] CODES AND STANDARDS

No change.

4.7[a] TSPA INPUT DATABASE

No change.

INTENTIONALLY LEFT BLANK

Table 4-1[a]. Direct Inputs

Line #	Document _ID	Reference _Document	Document DIRS	DTN	DTN DIRS	PEF
14 [a]	ANL-EBS-MD-000033 Rev 06	*Engineered Barrier System: Physical and Chemical Environment*	NA	SN0701PAEBSPCE.001_R1	180523	214
58 [a] 59 [a]	ANL-MGR-GS-000003	*Number of Waste Packages Hit by Igneous Events*	NA	SN0701PAWPHIT1.001_R2	182961	30, 61
66 [a]	ANL-WIS-MD-000010 Rev 06	*Dissolved Concentration Limits of Elements with Radioactive Isotopes*	NA	MO0702PAFLUORI.000_R1	181219	215
70 [a]	ANL-WIS-MD-000020 Rev 01 AD01	*Initial Radionuclide Inventories*	NA	SN0310T0505503.004_R0	168761	202
73 [a]	ANL-WIS-PA-000001 Rev 03	*EBS Radionuclide Transport Abstraction*	NA	SN0703PAEBSRTA.001_R3	183217	203
79 [a]	MDL-EBS-PA-000004 Rev 03	*Waste Form and In-Drift Colloids-Associated Radionuclide Concentrations: Abstraction and Summary*	NA	MO0701PACSNFCP.000_R1	180439	213
82 [a]	MDL-EBS-PA-000004 Rev 03	*Waste Form and In-Drift Colloids-Associated Radionuclide Concentrations: Abstraction and Summary*	NA	MO0701PAIRONCO.000_R1	180440	219
101 [a]	MDL-NBS-HS-000008 Rev 02 AD01	*Radionuclide Transport Models Under Ambient Conditions*	NA	LA0408AM831341.001_R0	171584	217, 218
103 [a]	MDL-NBS-HS-000008 Rev 02 AD01	*Radionuclide Transport Models Under Ambient Conditions*	NA	LB0701PAKDSESN.001_R0	179299	216, 218
105 [a]	MDL-NBS-HS-000019 Rev 01 AD01	*Abstraction of Drift Seepage*	NA	LB0702PASEEP02.001_R1	181635	201
108 [a] 109 [a]	MDL-NBS-HS-000020 Rev 02 AD02	*Particle Tracking Model and Abstraction of Transport Processes*	NA	LA0701PANS02BR.003_R2	180497	218
110 [a] 111 [a]	MDL-NBS-HS-000020 Rev 02 AD02	*Particle Tracking Model and Abstraction of Transport Processes*	NA	LA0702PANS02BR.001_R1	180322	207
113 [a]	MDL-NBS-HS-000008 Rev 02 AD01	*Radionuclide Transport Models Under Ambient Conditions*	NA	LB0702PAUZMTDF.001_R1	180776	218
115 [a]	MDL-NBS-HS-000020 Rev 02 AD02	*Particle Tracking Model and Abstraction of Transport Processes*	NA	MO0704PAFEHMBR.001_R3	184647	202

Table 4-1[a]. Direct Inputs (Continued)

Line #	Document _ID	Reference _Document	Document DIRS	DTN	DTN DIRS	PEF
129 [b]	MDL-NBS-HS-000021 Rev 03 AD02	*Saturated Zone Flow and Transport Model Abstraction*	NA	SN0710PASZFTMA.003_R0	183485	205, 209
130 [b]	ANL-WIS-MD-000020 Rev 01 AD01	*Initial Radionuclide Inventories*	NA	MO0702PASTREAM.001_R0	179925	202
131 [b]	ANL-WIS-MD-000006 Rev 02	*Radionuclide Screening*	177424	NA	NA	210
132 [c]	ANL-EBS-MD-000003 Rev 03	*General Corrosion and Localized Corrosion of Waste Package Outer Barrier*	178519	NA	NA	212

NOTES: [a] The direct inputs indicated reflect parameter values that were corrected in TSPA-LA Model v5.005, rather than new direct inputs to the TSPA-LA Model and are therefore cited in Section 6 of the parent document. Line item numbers from Table 4-1 of the parent report are listed for these items.

[b] New direct inputs are numbered starting with line 129 to 131 and are cited in Section 6[a] of this addendum.

[c] Line item 132 is a new line item that captures direct input inadvertently omitted from Table 4-1 of the parent document and cited in Section 6.3.5.1.2, Equation 6.3.5-4, in the parent document.

NA–Not applicable. Either the reference document or the DTN listed is the origin for the direct input as indicated.

Table 4-2[a]. Additional TSPA-LA Model Generated Data Tracking Numbers Referenced by Parameter Entry Forms

Line #	Document ID	Document Title	Document DIRS	OUTPUT DTN	DTN DIRS	PEF
1	MDL-WIS-PA-000005 REV00 AD01	*Total System Performance Assessment Model/Analysis for the License Application*	NA	MO0711GENERINP.000	183937	200, 202, 204, 206, 208, 210, 211, 214, 216, 218
2	MDL-WIS-PA-000005 REV00 AD01	*Total System Performance Assessment Model/Analysis for the License Application*	NA	MO0707UZKDCORR.000	183003	218
3	MDL-WIS-PA-000005 REV00 AD01	*Total System Performance Assessment Model/Analysis for the License Application*	NA	MO0708TSPAGENT.000	183000	202
4	MDL-WIS-PA-000005 REV00 AD01	*Total System Performance Assessment Model/Analysis for the License Application*	NA	MO0707EMPDECAY.000	182995	202

NOTE: See Appendix B in the parent document and Appendix B[a] of this addendum for a complete listing of all DTNs that support the TSPA-LA Model.

INTENTIONALLY LEFT BLANK

5[a]. ASSUMPTIONS

5.1[a] NOMINAL SCENARIO CLASS

No change.

5.2[a] EARLY FAILURE SCENARIO CLASS

No change.

5.3[a] IGNEOUS SCENARIO CLASS

No change.

5.4[a] SEISMIC SCENARIO CLASS

No change.

5.5[a] HUMAN INTRUSION SCENARIO

No change.

INTENTIONALLY LEFT BLANK

6[a]. TSPA-LA MODEL DESCRIPTION

The primary goals of Section 6 of the parent document are to describe how model components and the associated submodels (illustrated on Figure 6-1 of the parent document) are integrated in the TSPA-LA Model and how the TSPA-LA Model is implemented in order to estimate the dose incurred by a reasonably maximally exposed individual due to radionuclide releases in the Nominal, Early Failure, Igneous, and Seismic Scenario Classes, and the Human Intrusion Scenario. The contents of Section 6 in large part remain unchanged from the parent document. The focus of Section 6.3 of the parent document is on the TSPA-LA Model components and submodels and includes a discussion of their implementation. Section 6.3[a] documents the changes to conceptual models and implementation required for the addendum analyses.

In addition, it should be noted that in the parent document the terms "dripping environment" and "non-dripping environment" were used interchangeably with "seeping environment" and "non-seeping environment." The waste package (WP) groups are determined by the fraction of WP locations that are exposed to drift seepage (Section 6.1.5.3 of parent document), not drift seepage and/or drift-wall condensation. WP locations in a non-seeping environment may be exposed to dripping as a result of drift-wall condensation. When reading the parent document the term "dripping environment" should be replaced with the term "seeping environment" and the term "non-dripping environment" should be replaced with the term "non-seeping environment."

6.1[a] CONCEPTUAL DESIGN

No change.

6.1.1[a] Features, Events, and Processes Screening and Scenario Development

No change.

6.1.2[a] Calculation of Dose for the TSPA-LA Model

This section of the parent document outlines the calculation of total mean annual dose and total median annual dose using the scenario classes defined in Section 6.1.1 of the parent document. Specifically, Section 6.1.2.4 of the parent document describes calculations for each of the individual modeling cases used in the TSPA-LA Model. Section 6.1.2.4.2 has been updated to include additional information inadvertently omitted from the parent document which is relevant to the calculations for the expected annual dose for the Early Failure Modeling Cases. Section 6.1.2.4.2[a] in this addendum contains the additional information which should be used in conjunction with the documentation provided in the parent document. Appendix J of the parent document presents formal derivations for calculation of total mean annual dose and total median annual dose and the calculations performed for each modeling case. Appendix J[a] includes additional supplemental background discussion about the conceptual structure of the TSPA-LA Model calculations.

6.1.2.1[a] Description of Uncertainty

No change.

6.1.2.2[a] Calculation of Total Mean Annual Dose

No change.

6.1.2.3[a] Screening of Scenario Classes

No change.

6.1.2.4[a] Calculation of Expected Annual Dose for the Modeling Cases

Section 6.1.2.4.2[a] includes additional information inadvertently omitted from the parent document which is relevant to the calculations for the expected annual dose for the Early Failure Modeling Cases.

6.1.2.4.1[a] Nominal Scenario Class

No change.

6.1.2.4.2[a] Early Failure Scenario Class

The calculation of expected annual dose for the Waste Package and Drip Shield EF Modeling Case is defined in Equation 6.1.2-13 and Equation 6.1.2-14 of the parent document. In both the Waste Package EF and Drip Shield EF Modeling Cases, aleatory uncertainty in the location of the early failed WP within its assigned percolation bin is implicitly considered by assigning the mass released from the WP uniformly across the bin. The uniform mass release is implemented by distributing the mass released by the WP equally to all the UZ particle tracking model's repository release nodes (Section 6.3.9.3) associated with the specific percolation bin. The definitions of $D_{EW}\left(\tau\left|[1,r,s,t],\mathbf{e}_i\right.\right)$ and $D_{ED}\left(\tau\left|[1,r,s,t],\mathbf{e}_i\right.\right)$ are modified accordingly:

$D_{EW}\left(\tau\left|[1,r,s,t],\mathbf{e}_i\right.\right)$ is the dose at time τ that results from early failure of one WP of type r in percolation bin s with seeping ($t=1$) or non-seeping conditions ($t=0$), where release from the WP is distributed uniformly over the UZ repository release nodes for percolation bins. This quantity is calculated using the GoldSim component of the TSPA-LA Model.

and,

$D_{ED}\left(\tau\left|[1,r,s,t],\mathbf{e}_i\right.\right)$ is the dose at time τ that results from early failure of one drip shield (DS) over a WP of type r in percolation bin s with seeping ($t=1$) or non-seeping conditions ($t=0$), where release from the WP is distributed uniformly over the UZ repository release nodes for percolation bin s. This quantity is calculated using the GoldSim component of the TSPA-LA Model.

6.1.2.4.3[a] Igneous Scenario Class

No change.

6.1.2.4.4[a] Seismic Scenario Class

No change.

6.1.2.5[a] Calculation of Expected Annual Dose for the Human Intrusion Modeling Case

No change.

6.1.3[a] Treatment of Uncertainty in the TSPA-LA Model

No change.

6.1.4[a] TSPA-LA Model Structure and Design

This section in the parent document provides an overview of how model components and submodels are connected within the TSPA-LA Model and how information flows between them. The primary focus of this section is on the description of the TSPA-LA Model for the Nominal Scenario Class. This addendum contains an update that incorporates additional information about the TSPA-LA Model structure and information flow documented in Section 6.1.4.2 of the parent document. In addition, Figure 6.1.4-5 from the parent document has been revised to correct an error in the original figure and is included as Figure 6.1.4-5[a].

6.1.4.1[a] Mountain-Scale Unsaturated Zone Flow

No change.

6.1.4.2[a] Engineered Barrier System Thermal-Hydrologic Environment

In the parent document, the fourth bullet of Output 3, Information Transfer from the EBS TH Environment Submodel to the Drift Seepage and Drift Wall Condensation Submodels, omitted the transfer of information pertaining to drift-wall condensation Stage 2 and Stage 3 start times. This addendum includes the correction for this omission.

Output 3—The following outputs are passed from the EBS TH Environment Submodel (Section 6.3.2) to the Drift Seepage and Drift Wall Condensation Submodel (Section 6.3.3):

- For each of the five percolation subregions (Section 6.3.2):
  - The percolation flux at the base of the PTn for each infiltration scenario and climate at each multiscale thermohydrologic model subdomain location (Drift Seepage Submodel)
  - The average percolation flux at the base of the PTn for each infiltration scenario and climate (Drift Wall Condensation Submodel)
  - The drift-wall temperature surrounding each of the eight WPs (two co-disposed [CDSP] WPs and six CSNF WPs) at each subdomain location (Drift Seepage Submodel)

- Time-dependent temperature for the drift wall and WP for the representative CDSP WP and the representative CSNF WP, including the time that these temperatures drop to 96°C (Drift Wall Condensation Submodel)

- The fraction of lithophysal unit at each location.

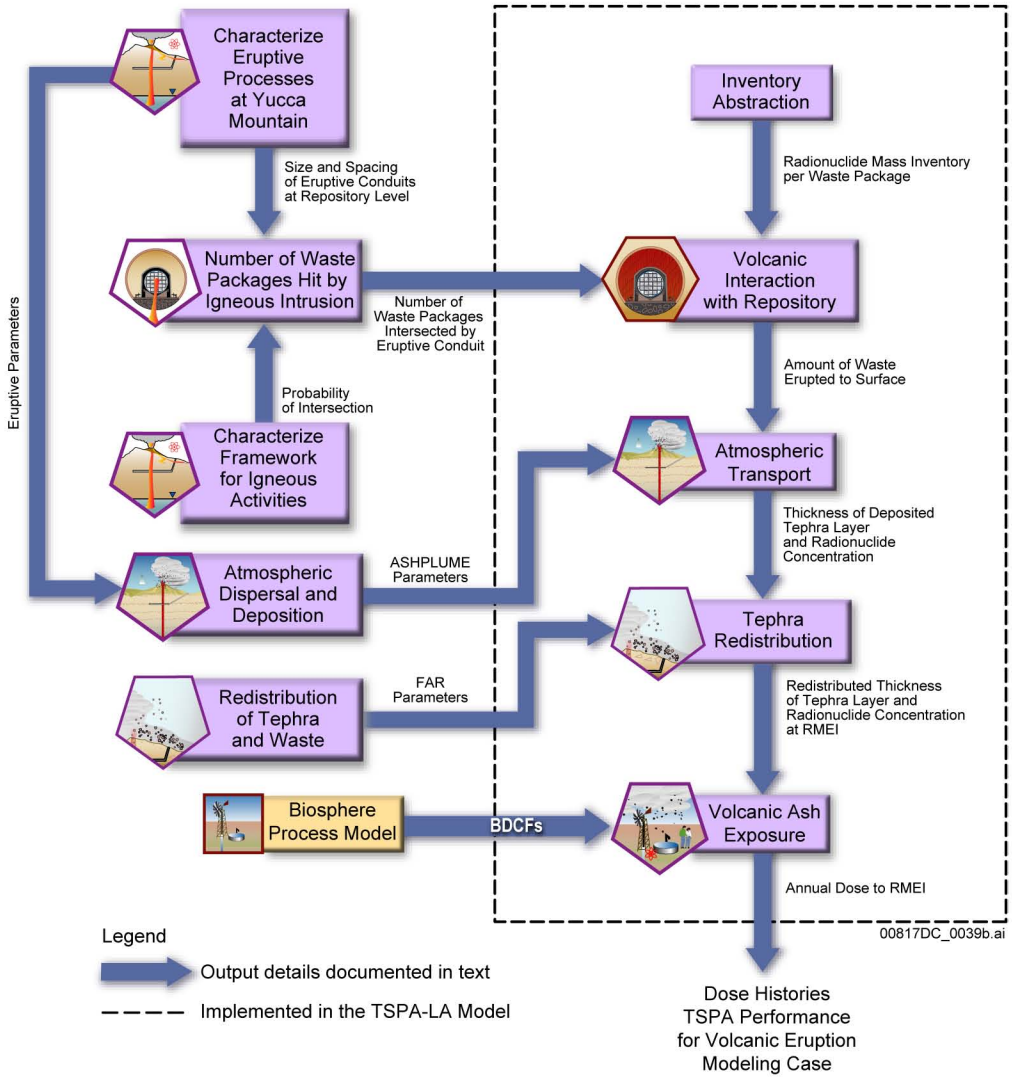

Figure 6.1.4-5[a]. Information Transfer between the Submodels of the TSPA-LA Volcanic Eruption Modeling Case

INTENTIONALLY LEFT BLANK

6.1.5[a] TSPA-LA Model File Architecture

In addition to the issues that have been addressed in the updated TSPA-LA Model v5.005 model file for this addendum, an additional cosmetic change was made to TSPA-LA Model v5.005. This change was the reorganization of the elements within the model, primarily adding clarity and traceability. As a result, some model pathways identified in Table 6.1.5-1 have changed. Table 6.1.5-1[a] provides an updated summary of the locations of submodel documentation within the GoldSim model file.

INTENTIONALLY LEFT BLANK

Table 6.1.5-1[a]. Location of Implementation Description in the GoldSim TSPA-LA Model File

Submodel	Documentation Location(s)
Epistemic Parameters GoldSim Submodel	\Epistemic_Uncertainty\Epistemic_Params
Aleatory Parameters and Dynamic Calculations GoldSim Submodel	\Time_Zero\Aleatory_Params
EBS GoldSim Submodel	\Time_Zero\EBS_PS_Loop\EBS_PSE_Loop\EBS_Submodel
Natural System below the Repository	\TSPA_Model
Climate	Epistemic: NA Aleatory: NA EBS: \Global_Inputs_and_Calcs\Global_UZ_Flow\Climate Other: \TSPA_Model\UZ_Flow\Climate
Infiltration	Epistemic: \Input_Params_Epistemic\Epistemic_Params_UZ_Flow\Uncertain_Params_Infiltration Aleatory: NA EBS: \Time_Zero\EBS_PS_Loop\Static_Calcs_PS_Loop\Static_Calcs_UZ_Flow\Infiltration \Global_Inputs_and_Calcs\Global_UZ_Flow\Infiltration
Drift Seepage	Epistemic: \Input_Params_Epistemic\Epistemic_Params_UZ_Flow\Input_Params_Seepage_Uncert \Input_Params_Epistemic\Epistemic_Params_UZ_Flow\Uncertain_Params_Seepage Aleatory: NA EBS: \Time_Zero\EBS_PS_Loop\Static_Calcs_PS_Loop\Static_Calcs_UZ_Flow\Drift_Seepage \Global_Inputs_and_Calcs\Global_UZ_Flow\Drift_Seepage
Drift Wall Condensation	Epistemic: \Input_Params_Epistemic\Epistemic_Params_UZ_Flow\Uncertain_Params_DWC Aleatory: NA EBS: \Global_Inputs_and_Calcs\Global_UZ_Flow\Drift_Wall_Condensation
EBS TH Environment	Epistemic: \Input_Params_Epistemic\Epistemic_Params_EBS_Environ\Uncertain_Params_TH Aleatory: NA EBS: \Global_Inputs_and_Calcs\Global_EBS_Environ\ThermoHydrology
WP and DS Degradation	Epistemic: \Input_Params_Epistemic\Epistemic_Params_WP_DS_Deg Aleatory: \Model_Calcs_Aleatory\Aleatory_Calcs_WP_DS_Deg EBS: \Time_Zero\EBS_PS_Loop\Static_Calcs_PS_Loop\Static_Calcs_WP_DS_Deg \Global_Inputs_and_Calcs\Global_WP_DS_Deg\Global_IWPD
Localized Corrosion	Epistemic: \Input_Params_Epistemic\Epistemic_Params_WP_DS_Deg Aleatory: NA EBS: \Time_Zero\EBS_PS_Loop\Static_Calcs_PS_Loop\Static_Calcs_WP_DS_Deg \Global_Inputs_and_Calcs\Global_WP_DS_Deg\Global_LC

Table 6.1.5-1[a]. Location of Implementation Description in the GoldSim TSPA Model File (Continued)

Submodel	Documentation Location(s)
Radionuclide Inventory	Epistemic: \Input_Params_Epistemic\Epistemic_Params_WF_Deg_Mob\Uncertain_Params_RN_Inventory Aleatory: NA EBS: \Global_Inputs_and_Calcs\Global_WF_Deg_Mob\RN_Inventory
In-Package Chemistry	Epistemic: \Input_Params_Epistemic\Epistemic_Params_WF_Deg_Mob\Uncertain_Params_InPkg_Chem Aleatory: NA EBS: \Global_Inputs_and_Calcs\Global_WF_Deg_Mob\In_Package_Chemistry
Waste Form Degradation	Epistemic: \Input_Params_Epistemic\Epistemic_Params_WF_Deg_Mob\Uncertain_Params_CSNF_WF Aleatory: NA EBS: \Global_Inputs_and_Calcs\Global_WF_Deg_Mob\WF_Degradation\CSNF_WF_Dissolution
	Epistemic: \Input_Params_Epistemic\Epistemic_Params_WF_Deg_Mob\Uncertain_Params_HLW_WF Aleatory: NA EBS: \Global_Inputs_and_Calcs\Global_WF_Deg_Mob\WF_Degradation\Input_Params_HLW_WF
	Epistemic: NA Aleatory: NA EBS: \Global_Inputs_and_Calcs\Global_WF_Deg_Mob\WF_Degradation\Input_Params_DSNF_WF
EBS Chemical Environment	Epistemic: \Input_Params_Epistemic\Epistemic_Params_EBS_Environ\Uncertain_Params_EBS_CE Aleatory: \Input_Params_Aleatory\Input_Params_EBS_Environ\Input_Params_EBS_CE EBS: \Global_Inputs_and_Calcs\Global_EBS_Environ\EBS_Chemical_Environment
Dissolved Concentration Limits	Epistemic: \Input_Params_Epistemic\Epistemic_Params_WF_Deg_Mob\Uncertain_Params_Solubility Aleatory: NA EBS: \Global_Inputs_and_Calcs\Global_WF_Deg_Mob\Global_Solubility
EBS Colloids	Epistemic: \Input_Params_Epistemic\Epistemic_Params_EBS_F_and_T\Uncertain_Params_Colloids Aleatory: NA EBS: \Global_Inputs_and_Calcs\Global_EBS_F_and_T\Model_Input_EBS_Transport\Input_Params_Colloids

Table 6.1.5-1[a]. Location of Implementation Description in the GoldSim TSPA Model File (Continued)

Submodel	Documentation Location(s)
EBS Flow	Epistemic: \Input_Params_Epistemic\Epistemic_Params_EBS_F_and_T\Uncertain_Params_Flux_Split Aleatory: NA EBS: \Global_Inputs_and_Calcs\Global_EBS_F_and_T\Model_Feeds_EBS_Flow
EBS Transport	Epistemic: \Input_Params_Epistemic\Epistemic_Params_EBS_F_and_T Aleatory: NA EBS: \Global_Inputs_and_Calcs\Global_EBS_F_and_T\Model_Input_EBS_Transport
EBS-UZ Interface	Epistemic: \Input_Params_Epistemic\Epistemic_Params_EBS_F_and_T\Uncertain_Params_EBS_UZ_Trans Aleatory: NA EBS: \Global_Inputs_and_Calcs\Global_EBS_F_and_T\EBS_UZ_Transport_Inputs
UZ Transport	Epistemic: \Input_Params_Epistemic\Epistemic_Params_UZ_Transport Aleatory: NA Other: \TSPA_Model\UZ_Transport
SZ Flow and Transport	Epistemic: \Input_Params_Epistemic\Epistemic_Params_SZ_Transport Aleatory: NA Other: \TSPA_Model\SZ_Transport
Biosphere	Epistemic: \Input_Params_Epistemic\Epistemic_Params_Biosphere Aleatory: NA Other: \TSPA_Model\Biosphere
Early Failure Scenario Class	Epistemic: \Input_Params_Epistemic\Epistemic_Params_Events\Epistemic_Parameters_EF Aleatory: \Input_Params_Aleatory\Aleatory_Params_Events\Aleatory_Params_EF EBS: \Time_Zero\EBS_PS_Loop\Static_Calcs_PS_Loop\Static_Calcs_Events\Static_Calcs_EF \Global_Inputs_and_Calcs\Global_Events\Global_EF
Igneous Scenario Class	Epistemic: \Input_Params_Epistemic\Epistemic_Params_Events\Epistemic_Params_Igneous_Intr Aleatory: \Input_Params_Aleatory\Aleatory_Params_Events\Aleatory_Params_Igneous_Intr EBS: \Time_Zero\EBS_PS_Loop\Static_Calcs_PS_Loop\Static_Calcs_Events\Igneous_Intrusion \Global_Inputs_and_Calcs\Global_Events\Igneous_Scenario
	Epistemic: \Model_Uncertainties\EU Aleatory: \Model_Uncertainties\AU EBS: \Eruptive_Model

Table 6.1.5-1[a]. Location of Implementation Description in the GoldSim TSPA Model File (Continued)

Submodel	Documentation Location(s)
Seismic Scenario Class	Epistemic: \Input_Params_Epistemic\Epistemic_Params_Events\Epistemic_Params_Seismic Aleatory: \Input_Params_Aleatory\Aleatory_Params_Events\Input_Params_Seismic_Uncert \Input_Params_Aleatory\Aleatory_Params_Events\Input_Params_Seismic_FD_Uncert EBS: \Time_Zero\EBS_PS_Loop\Static_Calcs_PS_Loop\Static_Calcs_Events\Seismic_Scenario_Class \Time_Zero\EBS_PS_Loop\Static_Calcs_PS_Loop\Static_Calcs_Events\Seismic_Fault_Displacement \Global_Inputs_and_Calcs\Global_Events\Seismic_Scenario
Human Intrusion Scenario	Epistemic: NA Aleatory: \Input_Params_Aleatory\Aleatory_Params_Events\Aleatory_Params_HI EBS: \Time_Zero\EBS_PS_Loop\Static_Calcs_PS_Loop\Static_Calcs_Events\Human_Intrusion_Events \Global_Inputs_and_Calcs\Global_Events\Human_Intrusion Other: \TSPA_Model\UZ_Transport\UZ_Transport_Calculations\HI_Borehole_Transport

6.2[a] ALTERNATIVE CONCEPTUAL MODELS

No change.

6.3[a] TSPA-LA MODEL FOR THE NOMINAL SCENARIO CLASS

This section presents an updated description of the Nominal Scenario Class in support of the analyses of the TSPA-LA Model presented in this addendum (output DTN: MO0710ADTSPAWI.000 [DIRS 183751]). This addendum describes only additions or changes to the conceptual models, model abstractions, and implementation of these abstractions in the TSPA-LA Model that were necessary to support the analyses presented in this addendum. It also provides a description of amendments to the following subsections of the parent document:

- Section 6.3.2, Engineered Barrier System Thermal-Hydrologic Environment
- Section 6.3.3, Drift-Scale Unsaturated Zone Flow
- Section 6.3.7, Waste Form Degradation and Mobilization
- Section 6.3.8, Engineered Barrier System Transport
- Section 6.3.9, Unsaturated Zone Transport
- Section 6.3.10, Saturated Zone Flow and Transport Model Component.

The focus of this section is on the updated TSPA-LA Model components and submodels and their implementation for the Nominal Scenario Class.

6.3.1[a] Mountain-Scale Unsaturated Zone Flow

No change.

6.3.2[a] Engineered Barrier System Thermal-Hydrologic Environment

Section 6.3.2.3[a] includes supplemental material to be used in conjunction with the discussion documented in Section 6.3.2.3 of the parent document. The material was inadvertently omitted from Section 6.3.2.3 of the parent document and does not reflect a change in the EBS Thermal-Hydrologic (TH) Environment conceptual model, abstraction, or implementation in the TSPA-LA Model. In addition, the caption for Figure 6.3.2-7 in the parent document has been corrected and is included as Figure 6.3.2-7[a] of this addendum.

6.3.2.1[a] Conceptual Model

No change.

6.3.2.2[a] Model Abstraction

No change.

6.3.2.3[a] TSPA-LA Model Implementation

Section 6.3.2.3[a] has been modified to include an additional sentence that clarifies the details of the EBS TH Environment Submodel implementation in the TSPA-LA Model.

The following text should be added to the third paragraph of Section 6.3.2.3 of the parent document:

The ten representative TH histories applied to the WP groups in the TSPA-LA Model closely matched the median history of a large group of waste packages that, as modeled, included the effects of percolation, dry out, and rewetting of the host rock above the repository. As such, the history is expected to be representative of a WP whether it is exposed to seepage or not.

6.3.2.4[a] Model Component Consistency and Conservatism in Assumptions and Parameters

No change.

6.3.2.5[a] Alternative Conceptual Model(s) for the Engineered Barrier System Thermal-Hydrologic Environment

No change.

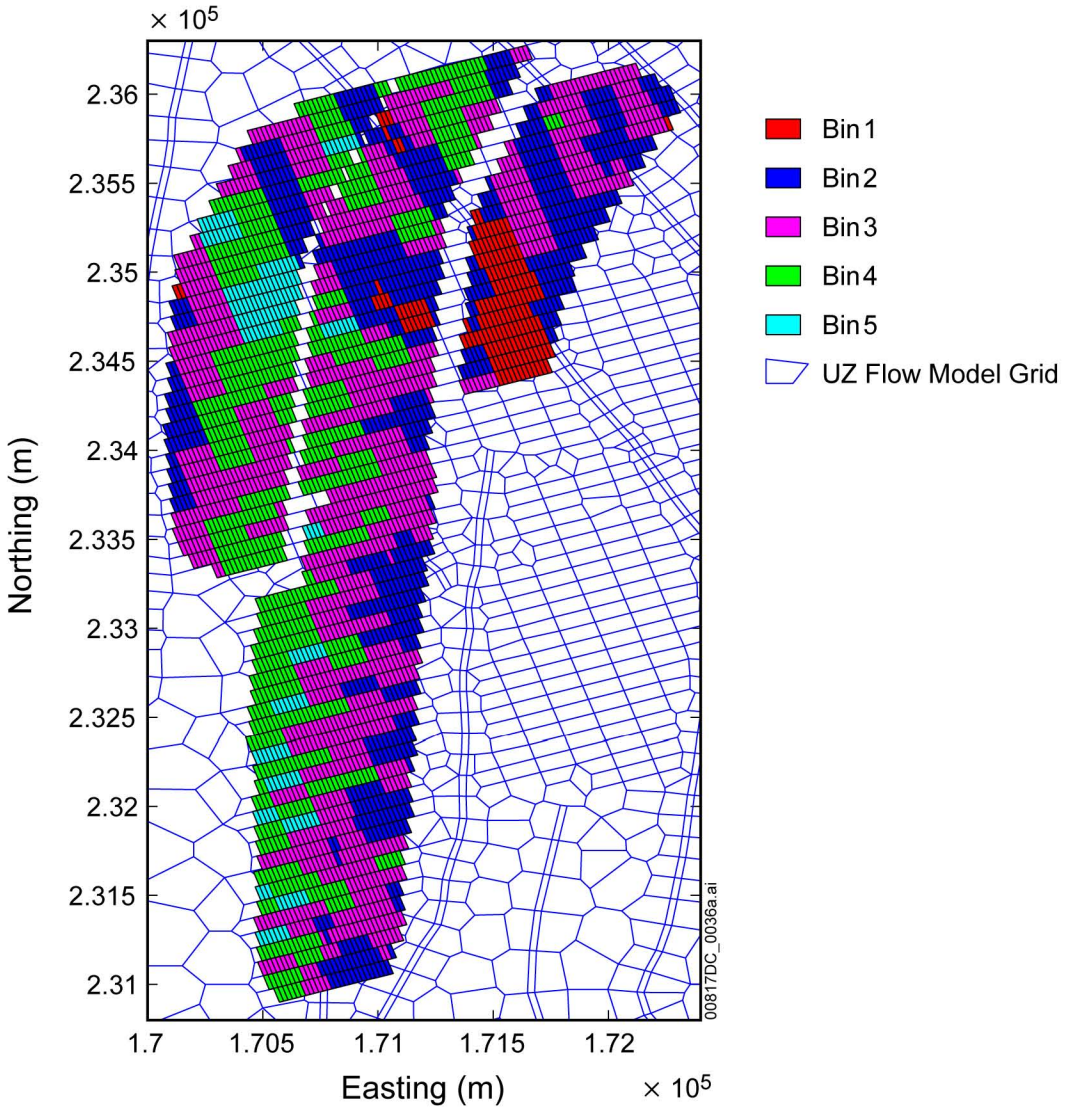

Source: SNL 2007 [DIRS 181383], Figure VIII-1[a].

Figure 6.3.2-7[a]. Repository Percolation Subregions Used in the TSPA-LA Model (based upon the 10th percentile infiltration scenario, glacial-transition period)

INTENTIONALLY LEFT BLANK

6.3.3[a] Drift-Scale Unsaturated Zone Flow

The analyses documented in this addendum include an update of the seepage fraction for the 10,000-year regulatory time period from that used in the analyses documented in the parent document (Appendix P, Section P2, of the parent document). The following text details the amendments to the Drift-Scale Unsaturated Zone Flow Submodel implementation in support of the analyses documented in this addendum.

6.3.3.1.1[a] Conceptual Model

No change.

6.3.3.1.2[a] TSPA-LA Model Abstraction

No change.

6.3.3.1.3[a] TSPA-LA Model Implementation

The TSPA-LA Model implementation of drift seepage is primarily accomplished through the use of an external dynamically linked library. Drift-seepage submodel calculations in the TSPA-LA Model are conducted by the SEEPAGEDLL_LA (STN: 11076-1.3-01 [DIRS 181058]). Section 6.3.3.1.3 of the parent document describes the drift-seepage implementation in detail. The calculation of the seepage rates is comprised of two main steps: (1) evaluate ambient seepage rate from seepage look-up tables, and (2) adjust ambient seepage rate for thermal and drift degradation effects. This approach remains unchanged in the analyses documented in this addendum. The calculation of the seepage fraction for the addendum is determined as outlined in Step 3 below and differs slightly from that of the parent document.

Step 3: Determination of Seepage Fraction for the TSPA-LA Addendum Analyses

For the analyses documented in this addendum, the seepage fractions for the 10,000-year simulations are based on the glacial-transition climate. The seepage fraction is the fraction of WPs, by type, in a percolation subregion that experiences seepage in a given realization. Although the projections of the expected annual dose to the reasonably maximally exposed individual that are compared to the 10,000-year Individual Protection Standard (NRC Proposed Rule 10 CFR 63.311 [DIRS 178394]) in Section 8.2[a] are extracted from the 20,000-year simulations, the seepage fraction is determined as the fraction of WPs that experiences seepage at any time during the first 10,000 years, instead of over the entire 20,000-year period as calculated in the parent document. The seepage fraction is calculated, as described in Section 6.3.3.1.3 of the parent document, by using a threshold seepage rate of 0.1 kg/yr per WP. WPs with seepage at any time are in a seep environment, and those without seepage are in a non-seep environment as evaluated during the 10,000-year regulatory period. The seepage fractions used for the additional analyses documented in this addendum for the 1,000,000-year simulations are identical to those described in the parent document.

6.3.4[a] Engineered Barrier System Chemical Environment

No change.

6.3.5[a] Waste Package and Drip Shield Degradation

Section 6.3.5.1.3[a] includes supplemental material that should be used in conjunction with the discussion documented in Section 6.3.5.1.3 of the parent document. The material was inadvertently omitted from Section 6.3.5.1.3 of the parent document and does not reflect a change in the WP and DS degradation conceptual model, abstraction, or implementation in the TSPA-LA Model.

6.3.5.1[a] Waste Package and Drip Shield Degradation

Section 6.3.5.1.3[a] has been modified to include an additional paragraph that details the implementation for both incipient and weld flaw crack penetration in a closure-lid patch for WPs in the TSPA-LA Model.

6.3.5.1.1[a] Conceptual Model

No change.

6.3.5.1.2[a] Abstraction of Waste Package and Drip Shield Degradation

No Change.

6.3.5.1.3[a] Implementation in the TSPA-LA Model

The following paragraph should follow the last paragraph in this section of the parent document and be used to supplement the material presented in parent document Section 6.3.5.1.3, under the subheading WP and DS Degradation Submodel Output.

WP and DS Degradation Submodel Output

Stress corrosion cracking can be initiated on an outer barrier closure-lid patch as the result of incipient cracks and weld flaws (Section 6.3.5.1.2 of the parent document). The incipient cracks are present on all lid patches (six cracks per patch with an initial length of 0.05 mm) (Section 6.3.5.1.2 of the parent document). Weld flaws are far less frequent (Equation 6.3.5-12 of the parent document). For a given patch, all incipient cracks grow at the same rate so they penetrate at the same time. The WAPDEG V4.07 (STN: 10000-4.07-00 [DIRS 181774] and STN: 10000-4.07-01 [DIRS 181064]) software tracks only one crack per patch so that the output for the crack area is scaled up by a factor of six to account for the true density of incipient cracks. If the first crack penetration on a closure-lid patch is due to a weld flaw then the scale up is conservative because the probability of 2 or more weld flaws per patch is very small (Equation 6.3.5-12 of the parent document).

6.3.5.2[a] Localized Corrosion on the Waste Package Outer Surface

No change.

6.3.5.3[a] Model Component Consistency and Conservatism in Assumptions and Parameters

No change.

6.3.5.4[a] Alternative Conceptual Model(s) for Waste Package and Drip Shield Degradation

No change.

6.3.6[a] Engineered Barrier System Flow

Figure 6.3.6-3[a] has been revised from the parent document to illustrate a representation of a typical emplacement drift according to the current design.

INTENTIONALLY LEFT BLANK

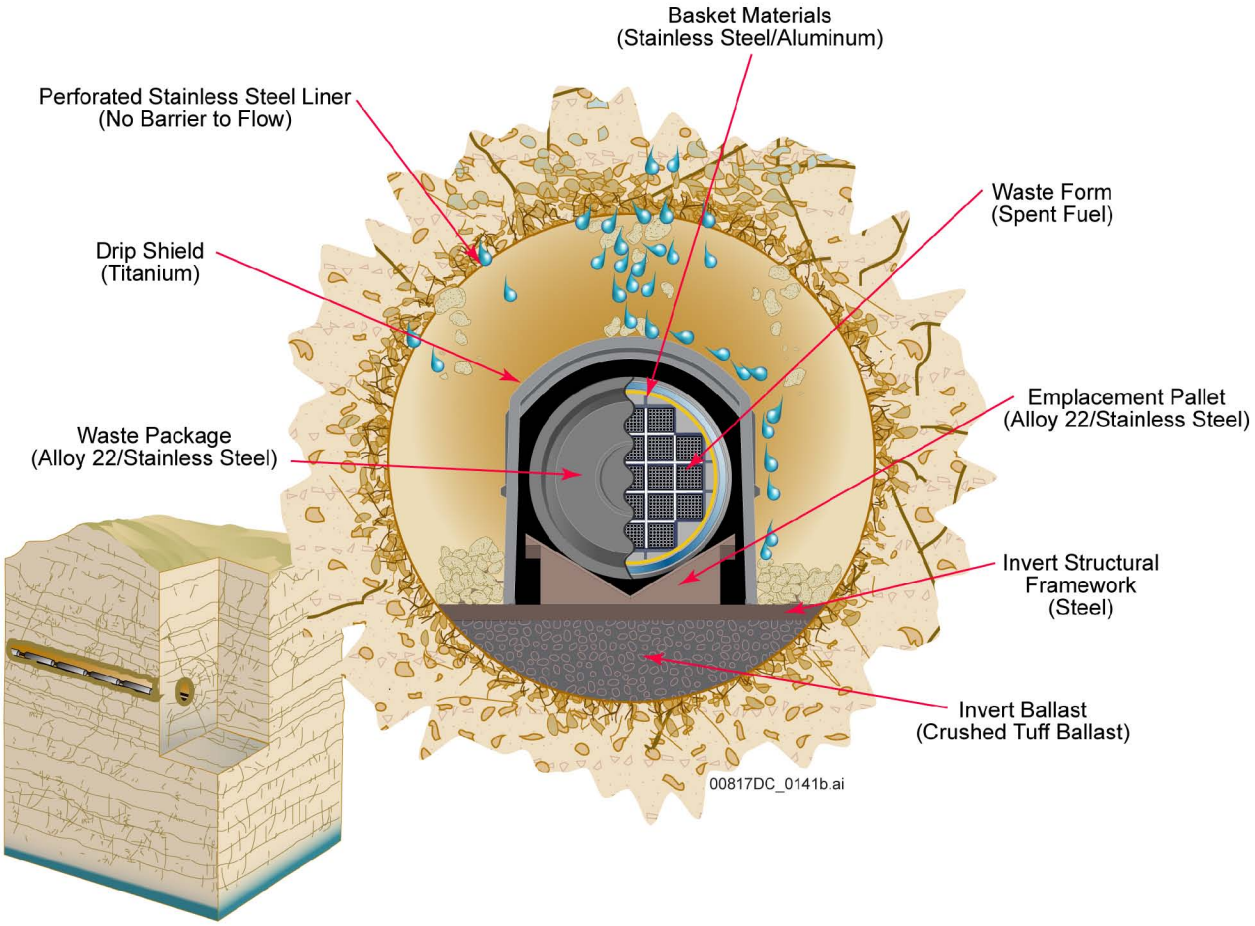

Figure 6.3.6-3[a]. Illustrative Cross Section of a Typical Emplacement Drift

INTENTIONALLY LEFT BLANK

6.3.7[a] Waste Form Degradation and Mobilization

Table 6.3.7-6[a] contains an update to the summary of the treatment of each radionuclide within the SZ Transport Submodel (Section 6.3.10[a]) and the Biosphere Submodel (Section 6.3.11) for the groundwater release modeling cases. In addition, Table 6.3.7-64[a] contains an update to correct the distribution coefficient for reversible sorption of neptunium onto uranophane colloids, incorrectly implemented as 1 to 5×10^2 (Appendix P[a], Table P-6[a], Item 8).

INTENTIONALLY LEFT BLANK

Table 6.3.7-6[a]. Disposition of Radionuclides for Groundwater Release Modeling Cases: Nominal, Igneous Intrusion, and Seismic

Radionuclide (Table 6.3.7-2)	Disposition in Waste Form, EBS, and UZ TSPA-LA Model Components (Section 6.3.7)	Disposition in 3-D UZ FEHM Submodel[a] (Section 6.3.9)	Disposition in SZ Submodels (3-D SZ_Convolute and 1-D Pipe)[b] (Section 6.3.10 and 6.3.10[a])	Disposition in Biosphere (Section 6.3.11)
^{227}Ac	Not transported	Not transported	Not transported	Dose from 3-D and 1-D[c], assuming secular equilibrium with ^{231}Pa
^{241}Am	Transport embedded colloid $^{241}Am_{emb}$ (decay to ^{237}Np) Transport irreversible FeO colloid $^{241}Am_{FeO}$ (decay to ^{237}Np) Transport reversible colloid and solute (decay to ^{237}Np)	Transport slow irreversible colloid $^{241}Am_{irs}$ (decay to ^{237}Np) Transport fast irreversible colloid $^{241}Am_{irf}$ (decay to ^{237}Np) Transport reversible colloid and solute (decay to ^{237}Np)	3-D transport of americium/plutonium slow irreversible colloid [SZ BTC 6] 3-D transport of americium/plutonium fast irreversible colloid [SZ BTC 10] 3-D transport of americium /thorium/protactinium reversible colloid and solute [SZ BTC 2]	Dose from 3-D[g]
^{243}Am	Transport embedded colloid $^{243}Am_{emb}$ (decay to $^{239}Pu_{emb}$) Transport irreversible FeO colloid $^{243}Am_{FeO}$ (decay to $^{239}Pu_{FeO}$) Transport reversible colloid and solute (decay to ^{239}Pu)	Transport slow irreversible colloid $^{243}Am_{irs}$ (decay to $^{239}Pu_{irs}$) Transport fast irreversible colloid $^{243}Am_{irf}$ (decay to $^{239}Pu_{irf}$) Transport reversible colloid and solute (decay to ^{239}Pu)	3-D transport of americium/plutonium slow irreversible colloid [SZ BTC 6] 3-D transport of americium/plutonium fast irreversible colloid [SZ BTC 10] 3-D transport of americium/ thorium/protactinium reversible colloid and solute [SZ BTC 2]	Dose from 3-D
^{14}C	Transport solute	Transport solute	3-D transport of nonsorbing solute [SZ BTC 1]	Dose from 3-D
^{36}Cl	Transport solute	Transport solute	3-D transport of nonsorbing solute [SZ BTC 1]	Dose from 3-D
^{245}Cm[d]	Not transported (decay to ^{241}Pu)	Not transported	Not transported	Dose not computed
^{135}Cs	Transport reversible colloid and solute	Transport reversible colloid and solute	3-D transport of cesium reversible colloid and solute [SZ BTC3]	Dose from 3-D
^{137}Cs	Transport reversible colloid and solute	Transport reversible colloid and solute	3-D transport of cesium reversible colloid and solute [SZ BTC 3]	Dose from 3-D[e]
^{129}I	Transport solute	Transport solute	3-D transport of nonsorbing solute [SZ BTC 1]	Dose from 3-D
^{237}Np	Transport reversible colloid and solute (decay to ^{233}U)	Transport solute (decay to ^{233}U)	3-D transport of neptunium solute [SZ BTC 5], boosted[f] by $^{241}Am_{irs}$, $^{241}Am_{irf}$, and $^{241}Am_{rev/sol}$	Dose from 3-D

Table 6.3.7-6[a]. Disposition of Radionuclides for Groundwater Release Modeling Cases: Nominal, Igneous Intrusion, and Seismic (Continued)

Radionuclide (Table 6.3.7-2)	Disposition in Waste Form, EBS, and UZ TSPA-LA Model Components (Section 6.3.7)	Disposition in 3-D UZ FEHM Submodel[a] (Section 6.3.9)	Disposition in SZ Submodels (3-D SZ_Convolute and 1-D Pipe)[b] (Section 6.3.10 and 6.3.10[a])	Disposition in Biosphere (Section 6.3.11)
^{231}Pa	Transport reversible colloid and solute (decay to ^{227}Ac)	Transport reversible colloid and solute (simple decay)	3-D transport of reversible colloid and solute (decay to ^{227}Ac) [SZ BTC 2] 1-D transport only the mass created by ingrowth from ^{235}U decay	Dose from 3-D and 1-D
^{210}Pb[g]	Not explicitly included	Not explicitly included	Not explicitly included	Dose included with ^{226}Ra BDCF[e]
^{238}Pu	Transport embedded colloid $^{238}Pu_{emb}$ (decay to ^{234}U) Transport irreversible FeO colloid $^{238}Pu_{FeO}$ (decay to ^{234}U) Transport reversible colloid and solute (decay to ^{234}U)	Transport slow irreversible colloid $^{238}Pu_{irs}$ (decay to ^{234}U) Transport fast irreversible colloid $^{238}Pu_{irf}$ (decay to ^{234}U) Transport reversible colloid and solute (decay to ^{234}U)	3-D transport of americium/plutonium slow irreversible colloid [SZ BTC 6] 3-D transport of americium/plutonium fast irreversible colloid [SZ BTC 10] 3-D transport of plutonium reversible colloid [SZ-BTC 4]	Dose from 3-D[g]
^{239}Pu	Transport embedded colloid $^{239}Pu_{emb}$ (decay to ^{235}U) Transport irreversible FeO colloid $^{239}Pu_{FeO}$ (decay to ^{235}U) Transport reversible colloid and solute (decay to ^{235}U)	Transport slow irreversible colloid $^{239}Pu_{irs}$ (decay to ^{235}U) Transport fast irreversible colloid $^{239}Pu_{irf}$ (decay to ^{235}U) Transport reversible colloid and solute (decay to ^{235}U)	3-D transport of americium/plutonium slow irreversible colloid [SZ BTC 6], boosted[c] by $^{243}Am_{irs}$ 3-D transport of americium/plutonium fast irreversible colloid [SZ BTC 10], boosted[c] by $^{243}Am_{irf}$ 3-D transport of plutonium reversible colloid [SZ BTC 4], boosted[c] by $^{243}Am_{rev/sol}$	Dose from 3-D
^{240}Pu	Transport embedded colloid Pu_{emb} (decay to ^{236}U) Transport irreversible FeO colloid $^{240}Pu_{FeO}$ (decay to ^{236}U) Transport reversible colloid and solute (decay to ^{236}U)	Transport slow irreversible colloid $^{240}Pu_{irs}$ (decay to ^{236}U) Transport fast irreversible colloid $^{240}Pu_{irf}$ (decay to ^{236}U) Transport reversible colloid and solute (decay to ^{236}U)	3-D transport of americium/plutonium slow irreversible colloid [SZ BTC 6] 3-D transport of americium/plutonium fast irreversible colloid [SZ BTC 10] 3-D transport of plutonium reversible colloid [SZ BTC 4]	Dose from 3-D
^{241}Pu[d]	Not transported (decay to ^{241}Am)	Not transported	Not transported	Dose not computed

Table 6.3.7-6[a]. Disposition of Radionuclides for Groundwater Release Modeling Cases: Nominal, Igneous Intrusion, and Seismic (Continued)

Radionuclide (Table 6.3.7-2)	Disposition in Waste Form, EBS, and UZ TSPA-LA Model Components (Section 6.3.7)	Disposition in 3-D UZ FEHM Submodel[a] (Section 6.3.9)	Disposition in SZ Submodels (3-D SZ_Convolute and 1-D Pipe)[b] (Section 6.3.10 and 6.3.10[a])	Disposition in Biosphere (Section 6.3.11)
^{242}Pu	Transport embedded colloid $^{242}Pu_{emb}$ (decay to ^{238}U) Transport irreversible FeO colloid $^{242}Pu_{FeO}$ (decay to ^{238}U) Transport reversible colloid and solute (decay to ^{238}U)	Transport slow irreversible colloid $^{242}Pu_{irs}$ (decay to ^{238}U) Transport fast irreversible colloid $^{242}Pu_{irf}$ (decay to ^{238}U) Transport reversible colloid and solute (decay to ^{238}U)	3-D transport of americium/plutonium slow irreversible colloid [SZ BTC 6] 3-D transport of americium/plutonium fast irreversible colloid [SZ BTC 10] 3-D transport of plutonium reversible colloid and solute [SZ BTC 4]	Dose from 3-D[f]
^{226}Ra	Transport reversible colloid and solute (simple decay)	Transport solute (simple decay)	3-D transport of solute (simple decay) [SZ BTC 7] 1-D transport only the mass created by ingrowth from ^{230}Th decay	Dose from 3-D and 1-D[f]
^{228}Ra	Not transported	Not transported	Not transported	Dose from3-D and 1-D[f]; assuming secular equilibrium with ^{232}Th
^{79}Se	Transport solute	Transport solute	3-D transport of nonsorbing solute [SZ BTC 11]	Dose from 3-D
^{126}Sn	Transport reversible colloid and solute	Transport reversible colloid and solute	3-D transport of tin reversible colloid and solute [SZ BTC 12]	Dose from 3-D
^{90}Sr	Transport solute	Transport solute	3-D transport of strontium solute [SZ BTC 8]	Dose from 3-D[g]
^{99}Tc	Transport solute	Transport solute	3-D transport of nonsorbing solute [SZ BTC 1]	Dose from 3-D
^{229}Th	Transport reversible colloid and solute (simple decay)	Transport reversible colloid and solute (simple decay)	3-D transport of reversible colloid and solute (simple decay) [SZ BTC 2] 1-D transport only the mass created by ingrowth from ^{233}U decay	Dose from 3-D and 1-D
^{230}Th	Transport reversible colloid and solute (decay to ^{226}Ra)	Transport reversible colloid and solute (decay to ^{226}Ra)	1-D transport of reversible colloid and solute (decay to ^{226}Ra) [SZ BTC 2]	Dose from 1-D[f]
^{232}Th	Transport reversible colloid and solute (decay to ^{228}Ra)	Transport reversible colloid and solute (simple decay)	3-D transport of reversible colloid and solute (decay to ^{228}Ra) [SZ BTC 2] 1-D transport only the mass created by ingrowth from ^{236}U decay	Dose from 3-D and 1-D[f]
^{232}U	Transport reversible colloid and solute	Transport solute	3-D transport of ^{232}U solute [SZ BTC 9]	Dose from 3-D

Table 6.3.7-6[a]. Disposition of Radionuclides for Groundwater Release Modeling Cases: Nominal, Igneous Intrusion, and Seismic (Continued)

Radionuclide (Table 6.3.7-2)	Disposition in Waste Form, EBS, and UZ TSPA-LA Model Components (Section 6.3.7)	Disposition in 3-D UZ FEHM Submodel[a] (Section 6.3.9)	Disposition in SZ Submodels (3-D SZ_Convolute and 1-D Pipe)[b] (Section 6.3.10 and 6.3.10[a])	Disposition in Biosphere (Section 6.3.11)
^{233}U	Transport reversible colloid and solute (decay to ^{229}Th)	Transport solute (decay to ^{229}Th)	1-D transport of solute (decay to thorium) [SZ BTC 9]	Dose from 1-D
^{234}U	Transport reversible colloid and solute (decay to ^{230}Th)	Transport solute (decay to ^{230}Th)	3-D transport of ^{234}U solute, [SZ BTC 9], boosted[c] by ^{238}U, $^{238}Pu_{irs}$, $^{238}Pu_{irf}$, and $^{238}Pu_{rev/sol}$	Dose from 3-D
^{235}U	Transport reversible colloid and solute (decay to ^{231}Pa)	Transport solute (decay to ^{231}Pa)	1-D transport of solute (decay to ^{231}Pa) [SZ BTC 9]	Dose from 1-D[f]
^{236}U	Transport reversible colloid and solute (decay to ^{232}Th)	Transport solute (decay to ^{232}Th)	3-D transport of ^{236}U solute [SZ BTC 9], boosted[c] by $^{240}Pu_{irs}$, $^{240}Pu_{irf}$, and $^{240}Pu_{rev/sol}$	Dose from 3-D
^{238}U	Transport reversible colloid and solute (decay to ^{234}U)	Transport solute (decay to ^{234}U)	3-D transport of ^{238}U solute [SZ BTC 9], boosted[c] by $^{242}Pu_{irs}$, $^{242}Pu_{irf}$, and $^{242}Pu_{rev/sol}$	Dose from 3-D

NOTE: [a] Plutonium and americium isotopes are transported irreversibly on two different colloid types in the EBS: iron oxyhydroxide colloids (e.g., see $^{239}Pu_{FeO}$ in the above table) and waste form colloids (e.g., see $^{239}Pu_{emb}$ in the above table). However, at the EBS-UZ interface, the plutonium or americium mass associated with these two types of colloids is combined (effectively losing or ignoring the mineral specificity) and then resplit into slow-transport and fast-transport irreversible colloids in the natural system (e.g., see $^{239}Pu_{irs}$ and $^{239}Pu_{irf}$ in the above table). Thus, the specific radionuclides in GoldSim, designated "Ic" and "If", are used differently in the EBS versus the natural system—in the EBS "Ic" stands for plutonium and americium mass transported in "embedded" colloids (i.e., the plutonium and americium mass is embedded in the mineral matrix of these colloid particles), and "If" stands for plutonium and americium mass sorbed irreversibly onto iron oxyhydroxide colloids, whereas in the UZ (Section 6.3.9) and SZ (Section 6.3.10), "Ic" stands for plutonium and americium mass transported irreversibly on slow colloids, and "If" stands for plutonium or americium mass transported irreversibly on fast colloids.

[b] Saturated Zone Breakthrough Curve and the associated number refers to the "Radionuclide Group Number" listed in the first column of Table 6.3.10-1 (Section 6.3.10).

[c] Boosting of a daughter (e.g., ^{239}Pu) means that the injected mass of the daughter over any timestep at the UZ-SZ interface is increased by the maximum decay (over the remaining simulation time) of the designated parent (e.g., ^{243}Am).

[d] ^{245}Cm and ^{241}Pu were recommended for inclusion in the TSPA-LA in *Radionuclide Screening* (SNL 2007 [DIRS 177424], Section 6.6.2 and Table 6-9) only to ensure that the effect of their decay on the inventories of ^{241}Am and ^{237}Np are included in the model. They are not recommended for transport or dose consequences.

[e] Though ^{210}Pb is not tracked, it is assumed to be in secular equilibrium with ^{226}Ra; that is, the biosphere dose conversion (BDCF) used for ^{226}Ra is the summation of the BDCFs provided for ^{226}Ra and ^{210}Pb.

[f] Doses only calculated for 1,000,000-year simulations (SNL 2007 [DIRS 177424], Table 6-9).

[g] Doses only calculated for 10,000-year simulations (SNL 2007 [DIRS 177424], Table 6-9).

SZ BTC = Saturated Zone Breakthrough Curve.

Table 6.3.7-64[a]. Parameters for TSPA-LA Spent Nuclear Fuel Waste Form Reversible Colloid Abstraction

TSPA-LA Parameter Name	Model Abstraction Symbol	Description	Units	Distribution Type	Distribution Specification	
Conc_Col_U_Sampled_a	$m_{coll,Uranophane,sampled}$	Expected mass of uranophane colloids per unit volume or mass of water.	mg/L	Cumulative Distribution Function	Prob Level	Value
					0	1×10^{-3}
					0.5	1×10^{-1}
					0.75	1×10^{0}
					0.90	1×10^{1}
					0.98	5×10^{1}
					1	2×10^{2}
Conc_Col_U_Min	$m_{coll,Uranophane,min}$	Lowest observed or expected mass of uranophane colloids per unit volume or mass of water.	mg/L	Single Value	1×10^{-6}	
U_pH_lo	None	Lower limit of pH range for U colloid stability data.	None	Single Value	4	
U_pH_hi	None	Upper limit of pH range for U colloid stability data.	None	Single Value	9	
Coeff_pH_Sq_U	None	Coefficient of pH squared term for fit of ionic strength threshold for U colloid stability.	None	Single Value	−0.008	
Coeff_pH_U	None	Coefficient of pH term for fit of ionic strength threshold for U colloid stability.	None	Single Value	0.14	
Coeff_inter_U	None	Coefficient of intercept term for fit of ionic strength threshold for U colloid stability.	None	Single Value	0.4	
Kd_Pu_Rev_U_Col_a	$K_{d,Pucoll,uranophane}$	Distribution coefficient for reversible sorption of plutonium onto uranophane colloids.	mL/g	Log Uniform	5×10^{0} to 1×10^{4}	
Kd_Am_Rev_U_Col_a	$K_{d,Amcoll,uranophane}$	Distribution coefficient for reversible sorption of americium onto uranophane colloids.	mL/g	Log Uniform	5×10^{0} to 1×10^{4}	
Kd_Th_Rev_U_Col_a	$K_{d,Thcoll,uranophane}$	Distribution coefficient for reversible sorption of thorium onto uranophane colloids.	mL/g	Log Uniform	5×10^{0} to 1×10^{4}	

Table 6.3.7-64[a]. Parameters for TSPA-LA SNF Waste Form Reversible Colloid Abstraction (Continued)

TSPA-LA Parameter Name	Model Abstraction Symbol	Description	Units	Distribution Type	Distribution Specification
Kd_Pa_Rev_U_Col_a	$K_{d,Pacoll,uranophane}$	Distribution coefficient for reversible sorption of Pa onto uranophane colloids.	mL/g	Log Uniform	5×10^{0} to 1×10^{4}
Kd_Cs_Rev_U_Col_a	$K_{d,Cscoll,uranophane}$	Distribution coefficient for reversible sorption of cesium onto uranophane colloids.	mL/g	Log Uniform	1×10^{1} to 1×10^{3}
Kd_Np_Rev_U_Col_a	$K_{d,Npcoll,uranophane}$	Distribution coefficient for reversible sorption of neptunium onto uranophane colloids.	mL/g	Log Uniform	1×10^{1} to 5×10^{2}
Kd_Ra_Rev_U_Col_a	$K_{d,Racoll,uranophane}$	Distribution coefficient for reversible sorption of radium onto uranophane colloids.	mL/g	Log Uniform	1×10^{1} to 1×10^{3}
Kd_Sn_Rev_U_Col_a	$K_{d,Sncoll,uranophane}$	Distribution coefficient for reversible sorption of tin onto uranophane colloids.	mL/g	Log Uniform	1×10^{0} to 1×10^{2}
Specific_SA_U_Col	$S_{A,\ uranophane,\ coll}$	Specific surface area for uranophane.	m^2/g	Single Value	30
U_Site_Density	$N_{S,uranophane,\ coll}$	Site density for uranophane particle colloid.	Sites/ nm^2	Single Value	2

Source: DTN: MO0701PACSNFCP.000_R1 [DIRS 180439], File: DTN_SNF_REV03.doc.

NOTE: Condition report 11424 describes the errata in the source documents.

6.3.8[a] Engineered Barrier System Transport

Table 6.3.8-4 of the parent document was updated (Table 6.3.8-4[a]) to reflect the update to the TSPA-LA Model for the adsorption isotherm parameter *k* and parameter *s* for corrosion products incorrectly implemented (Appendix P[a], Table P-6[a], Item 7).

INTENTIONALLY LEFT BLANK

Table 6.3.8-4[a]. Sampled Model Inputs Used in the EBS Radionuclide Transport Abstraction

Input Name	Input Description	Range	Distribution
Invert_Diff_Coeff_Uncert_a	Invert diffusion coefficient uncertainty	Range: $10^{\mu\pm3\sigma}$ (dimensionless) Mean: $\mu = 0.033$ Std. Dev. $\sigma = 0.218$	Truncated Normal
SS_Corrosion_Rate_a	Stainless steel corrosion rate	0.01 – 0.51 μm/yr Mean = 0.267 μm/yr Std. Dev. = 0.209 μm/yr	Truncated Lognormal
CS_Corrosion_Rate_a	Carbon steel corrosion rate	25 – 135 μm/yr Mean = 78.5 μm/yr Std. Dev. = 25.0 μm/yr	Truncated Lognormal
DS_Flux_Uncertainty_a	Drip shield flux-splitting uncertainty factor	0 – 0.85 (dimensionless)	Uniform
WP_Flux_Uncertainty_a	Waste package flux-splitting uncertainty factor	0 – 2.41 (dimensionless)	Uniform
Diameter_Colloid_a	Diameter of colloid particle	50 – 300 nm	Uniform
Goethite_SA_a	Specific surface area of goethite (FeOOH)	14.7 – 110 m^2/g Mean = 51.42 m^2/g Std. Dev. = 30.09 m^2/g	Lognormal (Truncated)
HFO_SA_a	Specific surface area of HFO	68 – 600 m^2/g Mean = 275.6 m^2/g Std. Dev. = 113.4 m^2/g	Lognormal (Truncated)
NiO_SA_a	Specific surface area of NiO	1 – 30 m^2/g	Uniform
Cr2O3_SA_a	Specific surface area of Cr_2O_3	1 – 20 m^2/g	Uniform
Relative_Abundance_Goethite_a	Mass fraction of iron oxides (goethite and HFO) that is goethite	0.45 – 0.80 (fraction)	Uniform
FHH_Isotherm_k_CP_a_5003[a]	FHH adsorption isotherm parameter *k* for corrosion products	1.030 – 1.326 (dimensionless)	Uniform
FHH_Isotherm_s_CP_a_5003[a]	FHH adsorption isotherm parameter *s* for corrosion products	1.493 – 1.799 (dimensionless)	Uniform
CSNF_Rind_SA_a	Specific surface area of CSNF rind	0.5 – 60 m^2/g	Uniform
Density_CSNF_Rind_a	Density of CSNF rind	5,600 – 11,500 kg m^{-3}	Uniform
Porosity_Rind_CSNF_a	Porosity of CSNF rind	0.05 – 0.3 (fraction)	Uniform
FHH_Isotherm_k_CSNF_Rind_a	FHH adsorption isotherm parameter *k* for CSNF rind	1.606 – 8.215 (dimensionless)	Uniform
FHH_Isotherm_s_CSNF_Rind_a	FHH adsorption isotherm parameter *s* for CSNF rind	1.656 – 3.038 (dimensionless)	Uniform
HLWG_Rind_SA_a	Specific surface area of high-level radioactive water glass (HLWG) rind	10 – 38 m^2/g	Uniform
Diameter_Colloid_a	Colloid particle diameter	50 – 300 nm	Uniform
Gamma_AFM_a	Active fracture model gamma parameter DTN: LA0701PANS02BR.003_R2 [DIRS 180497], Readme File	0.2 – 0.6	Uniform

Table 6.3.8-4[a]. Sampled Model Inputs Used in the EBS Radionuclide Transport Abstraction (Continued)

Input Name	Input Description	Range	Distribution
EBS_UZ_Flux_Sat_PS1 EBS_UZ_Flux_Sat_PS2 EBS_UZ_Flux_Sat_PS3 EBS_UZ_Flux_Sat_PS4 EBS_UZ_Flux_Sat_PS5	Unsaturated zone fracture saturation DTN: LA0701PANS02BR.003_R2 [DIRS 180497]. This includes the average fracture and matrix percolation fluxes and saturations for both glacial transition and post-10,000-year periods. There are a total of five percolation subregions.	Average values for the five percolation subregions based on the average of repository nodes in each percolation subregion.	2-D Table; see Table 6.3.8-5
pH_Cell2_Regression_Error_a	Error term added to the surface complexation based pH calculation in the corrosion products domain.	Mean: $\mu = 0$; Std. Dev. $\sigma = 0.32$ Truncated at ± 2 Std. Dev.	Truncated Normal
Diff_Path_Length_Invert_Top_a	Diffusive path length from waste package outer corrosion barrier (OCB) to mid-point of invert.	0.30 – 1.24 m	Uniform

Sources: Modified from DTN: SN0703PAEBSRTA.001_R3 [DIRS 183217], Files: SN0703PAEBSRTA.001_RTA Input Tables.doc and Corrosion Products Composite Isotherm 7-19-2007.xls.

NOTES: [a] Condition Report 11755 documents this error which is being addressed in this Addendum.

6.3.9[a] Unsaturated Zone Transport

The analyses documented in this addendum include a change to Table 6.3.9-1[a] that reflects the radionuclide half-lives documented in the parent document (Appendix P[a], Table P-6[a], Item 2). In addition input errors discovered during the checking of the TSPA Input Database have been corrected and are documented in Table P-6[a], Item 10 and Item 11. Section 6.3.9.4[a] contains an expanded discussion of the consistency of assumptions for UZ Transport Properties. The following text details the amendments to the UZ Transport Submodel implementation in support of the analyses documented in this addendum.

6.3.9.1[a] Conceptual Model

No change.

6.3.9.2[a] TSPA-LA Model Abstraction

To ensure consistency among the EBS Transport Submodel, UZ Transport Submodel, and SZ Transport Submodel, the radionuclide half-lives used in the UZ Transport Submodel were changed to the values listed in Table 6.3.9-1[a] (DTN: MO0702PASTREAM.001_R0 [DIRS 179925]) for the analyses presented in this addendum.

6.3.9.3[a] TSPA LA Model Implementation

No change.

6.3.9.4[a] Model Component Consistency and Conservatism in Assumptions and Parameters

An expanded discussion of the UZ Transport Properties consistency of assumptions is included in Section 6.3.9.4.1[a]. This discussion is a more detailed documentation of the consistency in UZ Transport Properties and is provided as a replacement to the material included in Section 6.3.9.4.1 of the parent document. The remainder of Section 6.3.9.4 included in the parent document remains unchanged.

6.3.9.4.1[a] Consistency of Assumptions

UZ Transport Properties—In the Unsaturated Zone Transport Submodel, the calibrated values of parameters used to develop the pre-generated flow fields do not explicitly match the values used to generate the matrix-diffusion parameters. In general, the parameters used to describe flow and transport are the same (SNL 2008 [DIRS 184748], Sections 6.5.5.4[a], 6.5.7, and A.4[a]; SNL 2007 [DIRS 184614], Section 6.1.5; and SNL 2007 [DIRS 179545]). An exception is the range of values of the active fracture model parameter γ as discussed in *Particle Tracking Model and Abstraction of Transport Processes* (SNL 2008 [DIRS 184748], Section 6.5.6 [a]).

The matrix-diffusion process implemented in the Unsaturated Zone Transport Submodel is sensitive to various physical parameters that are also used to define the UZ flow fields. Because the matrix-diffusion process may be very sensitive to these parameters, it is important to propagate the uncertainties in parameter values into the Unsaturated Zone Transport Submodel.

There are several UZ flow-related parameters used by the radionuclide transport model. Parameters used directly are: matrix porosity, fracture porosity, fracture spacing (the inverse of fracture frequency), and the active fracture model parameter γ. These parameters are deterministic in the UZ Flow Model.

Several matrix hydrologic parameters are also used indirectly to develop mean values of tortuosity (SNL 2008 [DIRS 184748], Section A.2[a]) using a correlation between matrix effective permeability and water content for tortuosity (matrix diffusion) (Equation 6.3.9-1). The matrix parameters used to determine tortuosity are: porosity, residual saturation, capillary strength (van Genuchten α), pore size distribution index (van Genuchten m), and permeability (SNL 2008 [DIRS 184748], Section A.2[a]). Deterministic values are used to compute mean tortuosity values for each of three rock categories; tortuosity is then sampled based on the uncertainty in the tortuosity correlation associated with differences between diffusion coefficient values predicted by Equation 6.3.9-1 and measured values (SNL 2008 [DIRS 184748], Section A.4[a]).

Effect on the TSPA Model—A study presented in *UZ Flow Models and Submodels* (BSC 2004 [DIRS 169861], Section 6.8.1) indicates that the Site-Scale UZ Flow Model is relatively insensitive to changes in the value of the active fracture model parameter γ. In the steady-state site-scale UZ Flow Model, the active fracture model parameter γ influences the partitioning of water flow between the fractures and rock matrix. The conclusion of the study noted that for the flow model, changing the values of active fracture model parameter γ will have only a small effect on matrix liquid saturations, water potentials, and average percolation fluxes. This may also indicate that γ values, estimated based on flow calibrations, may not be well constrained, and the application of a greater uncertainty for transport calculations is valid. Note, the *UZ Flow Models and Submodels* referenced above is a historical document that was revised to incorporate new infiltration data (SNL 2007 [DIRS 184614). Several sensitivity analyses presented in the historical version, which are still valid despite changes in the infiltration data, were not repeated or discussed in the current version but are needed for this discussion.

The aperture values used in the UZ Transport Model are generated from fracture porosity and fracture frequency (the inverse of fracture spacing) values. In general, the large permeability contrast between the fractures and rock matrix (SNL 2007 [DIRS 184614], Appendix B) indicates that the rock matrix will not contribute significantly to the flow process (minimizing the influence of fracture spacing), and matrix diffusion will be the dominant process controlling mass retardation in the rock matrix. In addition, fracture porosities are important in defining the transient matrix-diffusion process in the UZ Transport Model. However, as storage terms in the site-scale UZ Flow Model, they do not influence results of the steady-state model. It should also be noted that fracture permeabilities and van Genuchten α parameters are related to fracture apertures (BSC 2004 [DIRS 170038], Section 6.1.2). A sensitivity study on flow model parameters showed relatively small differences between base-case flow fields and flow fields generated by changing fracture permeabilities and van Genuchten α parameters (BSC 2005 [DIRS 174116], Section 6.3). Studies presented in *Particle Tracking Model and Abstraction of Transport Processes* (SNL 2008 [DIRS 184748], Sections 6.6.3 and 6.6.4) also showed that transport in the UZ is generally less sensitive to changes in flow parameters than to changes in the transport properties. The analyses showed that the transport results were insensitive to the van Genuchten α parameter. Transport results showed greater sensitivity to changes in fracture

permeability compared to that of the van Genuchten α parameter, but as noted, the changes were relatively small.

The mean values for tortuosity used in the UZ Transport Submodel are based on the deterministic values of porosity, residual saturation, capillary strength (van Genuchten α), pore size distribution index (van Genuchten m), and permeability used in the 10th percentile infiltration scenario for the UZ Site-Scale Flow Model present-day, monsoon, glacial-transition, and post-10,000-year simulations. The 10th percentile infiltration scenario is the most commonly sampled infiltration scenario (62 percent of the time). Additionally, it can be shown that tortuosity values generated using deterministic parameters from the other infiltration scenarios differ only slightly from the values used in the TSPA-LA Model. The uncertainty in tortuosity values considered in the transport calculations is the uncertainty in the correlation between the tortuosity and fracture permeability and porosity and, therefore, is only pertinent to the transport calculations.

6.3.9.5[a] Alternative Conceptual Model(s) for Unsaturated Zone Transport

No change.

INTENTIONALLY LEFT BLANK

Table 6.3.9-1[a]. Radionuclide Half-Life and Daughter Products Used in the TSPA-LA Addendum

No.	Species	Half Life (years)	Daughter Index
1	^{14}C	5.72×10^{3}	NA
2	^{135}Cs (rev)	2.30×10^{6}	NA
3	^{137}Cs (rev)	3.01×10^{1}	NA
4	^{129}I	1.57×10^{7}	NA
5	^{90}Sr	2.88×10^{1}	NA
6	^{99}Tc	2.13×10^{5}	NA
7	^{243}Am (rev)	7.37×10^{3}	10
8	$^{243}Am^{lc}$	7.37×10^{3}	11
9	$^{243}Am^{lf}$	7.37×10^{3}	12
10	^{239}Pu (rev)	2.41×10^{4}	13
11	$^{239}Pu^{lc}$	2.41×10^{4}	13
12	$^{239}Pu^{lf}$	2.41×10^{4}	13
13	^{235}U	7.04×10^{8}	14
14	^{231}Pa (rev)	3.28×10^{4}	NA
15	^{241}Am (rev)	4.33×10^{2}	18
16	$^{241}Am^{lc}$	4.33×10^{2}	18
17	$^{241}Am^{lf}$	4.33×10^{2}	18
18	^{237}Np	2.14×10^{6}	19
19	^{233}U	1.59×10^{5}	20
20	^{229}Th (rev)	7.30×10^{3}	NA
21	^{240}Pu (rev)	6.56×10^{3}	24
22	$^{240}Pu^{lc}$	6.56×10^{3}	24
23	$^{240}Pu^{lf}$	6.56×10^{3}	24
24	^{236}U	2.34×10^{7}	25
25	^{232}Th (rev)	1.40×10^{10}	NA
26	^{232}U	6.98×10^{1}	NA
27	^{242}Pu (rev)	3.75×10^{5}	33
28	$^{242}Pu^{lc}$	3.75×10^{5}	33
29	$^{242}Pu^{lf}$	3.75×10^{5}	33
30	^{238}Pu (rev)	8.77×10^{1}	34
31	$^{238}Pu^{lc}$	8.77×10^{1}	34
32	$^{238}Pu^{lf}$	8.77×10^{1}	34
33	^{238}U	4.47×10^{9}	34
34	^{234}U	2.46×10^{5}	35
35	^{230}Th (rev)	7.54×10^{4}	36
36	^{226}Ra	1.60×10^{3}	NA
37	^{36}Cl	3.01×10^{5}	NA
38	^{79}Se	2.90×10^{5} (2.95×10^{5})[a]	NA
39	^{126}Sn (rev)	2.30×10^{5} (2.50×10^{5})[a]	NA

Source: DTN: MO0702PASTREAM.001_R0 [DIRS 179925], File: DTN-Inventory-Rev00.xls.

NOTES: rev = reversible colloids.

Daughter Index lists the radionuclide species number of the daughters produced for decay-chain species.

[a] Denotes the half-life value used in the analyses documented in the parent document.

INTENTIONALLY LEFT BLANK

6.3.10[a] Saturated Zone Flow and Transport Model Component

The analyses documented in this addendum include changes necessary to reflect the most recent addendum to *Saturated Zone Flow and Transport Model Abstraction* (SNL 2008 [DIRS 183750]). The discussions below supplement the material presented in Section 6.3.10 of the parent document, noting differences between the 3-D and 1-D SZ Flow and Transport Abstractions used in the analyses documented in this addendum.

6.3.10.1[a] Conceptual Model

No change.

6.3.10.2[a] TSPA-LA Model Abstraction

As documented in the parent document, two abstractions of the SZ Flow and Transport Model Component were implemented in the TSPA-LA Model: (1) the 3-D SZ Flow and Transport Abstraction Model, which uses a convolution integral technique to combine radionuclide breakthrough curves with time-varying radionuclide sources from the UZ to quantify radionuclide transport to the accessible environment, and (2) the 1-D SZ Flow and Transport Abstraction implemented directly in the TSPA-LA Model to calculate radioactive decay, ingrowth, and transport for specified radionuclide chains. These analyses incorporate amendments to both the 3-D and 1-D SZ Transport Model Abstractions, as documented in *Saturated Zone Flow and Transport Model Abstraction* (SNL 2008 [DIRS 183750] and DTN: SN0710PASZFTMA.003_R0 [DIRS 183485]). The following sections detail the amendments to the SZ Transport Submodel abstraction and implementation in support of the analyses documented in this addendum.

3-D SZ Flow and Transport Abstraction—The three-dimensional SZ flow and transport process modeling, described in *Saturated Zone Site-Scale Flow Model* (SNL 2007 [DIRS 177391]) and *Site-Scale Saturated Zone Transport* (SNL 2008 [DIRS 184806]), forms the technical basis for the 3-D SZ Flow and Transport Abstraction, as documented in the parent document for the TSPA-LA Model. The analyses documented within this addendum utilize the same abstraction documented in the parent document (SNL 2008 [DIRS 183750], Section 6.3.1[a]). The 3-D SZ Flow and Transport Abstraction used for the analyses presented in this addendum differs from the parent document (DTNs: SN0702PASZFTMA.002_R1 [DIRS 183471], File: Test_SZ_Sampled_Vectors_Latest.txt, and SN0702PASZFTMA.001 [DIRS 179504], File: output_to_TSPA-dir.zip) only in the updated half-life values for ^{79}Se and ^{126}Sn, reflecting a revision to the source data for the radionuclide half-lives (DTN: MO0702PASTREAM.001_R0 [DIRS 179925], File: DTN-Inventory-Rev00.xls).

1-D SZ Flow and Transport Abstraction—Because the ingrowth of radionuclides is not explicitly included in the 3-D SZ Flow and Transport Abstraction, a 1-D SZ Flow and Transport Abstraction is used to account for the decay and ingrowth of radionuclide daughter products for the four decay chains shown on Figure 6.3.10-8[a]. The updated 1-D SZ Flow and Transport Abstraction (DTN: SN0710PASZFTMA.003_R0 [DIRS 183485], File: Compliance_Sampling_with_LDISP_Changes_Truncated.txt) includes the same uncertain input parameters as the 3-D SZ Flow and Transport Abstraction. With one exception, these input parameters are

identical to those documented in Table 6.3.10-2 of the parent document. However, the longitudinal dispersivity that is used in the 1-D SZ Flow and Transport Model for the analyses documented in the parent document has an unbounded lognormal distribution that defines the epistemic uncertainty in longitudinal dispersivity (Table 6.3.10-2). The sampled value is further adjusted by increasing it by one order of magnitude (SNL 2008 [DIRS 183750], Section 6.5.1.2[a]). As documented in Section P15 of the parent document, the values calculated for the longitudinal dispersivity could become larger than are physically possible. The analyses documented in this addendum include an amended distribution for longitudinal dispersivity values used in the 1-D SZ Flow and Transport Abstraction (DTN: SN0710PASZFTMA.003_R0 [DIRS 183485], File: Compliance_Sampling_with_LDISP_Changes_Truncated.txt). The normal distribution for the logarithm of the longitudinal dispersivity (α_L), implemented in the 1-D SZ Flow and Transport Model for the analyses documented in this addendum, was truncated at the upper end at two standard deviations from the mean, and the sampled value was used directly without further adjustment (DTN: SN0710PASZFTMA.003_R0 [DIRS 183485], File: Readme.txt).

6.3.10.3[a] TSPA-LA Model Implementation

For the analyses documented in this addendum, the 1-D SZ Flow and Transport Abstraction is used to account for the ingrowth of the second-, third-, or fourth-generation daughters: ^{235}U, ^{231}Pa, ^{227}Ac, ^{233}U, ^{229}Th, ^{232}Th, ^{228}Ra, ^{230}Th, and ^{226}Ra. The exception is ^{234}U, which is second generation in one chain and first generation in another chain. The radionuclide mass input to the 1-D SZ Flow and Transport Abstraction comes from the UZ Transport Submodel. As documented in the parent document, this mass is fed to both the 1-D and 3-D SZ Flow and Transport Abstractions. The radionuclide mass for all species is tracked in both the 1-D and 3-D SZ Flow and Transport Abstractions. As a response to the issue identified in Section P15 of the parent document and for the analyses documented in this addendum, no mass is passed from the UZ Transport Submodel to the 1-D SZ Flow and Transport Abstraction for the following radionuclides: ^{231}Pa, ^{229}Th, ^{232}Th, and ^{226}Ra. The radionuclide mass exiting each submodel (3-D and 1-D) is then screened such that, for the biosphere calculation, only the mass from the 1-D SZ Flow and Transport Abstraction is used for the second-generation daughter species ^{235}U, ^{233}U, and ^{230}Th. In addition, for the biosphere calculations, the mass of the daughter products ^{231}Pa, ^{229}Th, ^{232}Th, and ^{226}Ra created along the transport pathway due to decay of their parent species from the 1-D SZ Flow and Transport Submodel is summed with the mass from the 3-D SZ Flow and Transport Submodel. The 3-D SZ Flow and Transport Submodel is used to transport the radionuclide mass that is passed from the UZ Transport Submodel. For these four species, no mass is passed from the UZ Transport Submodel to the 1-D SZ Flow and Transport Submodel, so the output from the 1-D SZ Flow and Transport Submodel contains only the mass of the daughter products. All the other radionuclide biosphere calculations utilize the output from the 3-D SZ Flow and Transport Abstraction. The disposition of SZ submodel mass is shown in Table 6.3.10-8[a].

Even though they are accounted for in the 3-D SZ Flow and Transport Abstraction, the parents of the second-generation daughters are also transported in the 1-D SZ Flow and Transport Abstraction. The parents are included in the 1-D SZ Flow and Transport Abstraction to account for the in growth of the second-generation daughters.

6.3.10.4[a] Model Component Consistency and Conservatism in Assumptions and Parameters

No change.

6.3.10.5[a] Alternative Conceptual Model(s) for Saturated Zone Flow and Transport

No change.

INTENTIONALLY LEFT BLANK

Table 6.3.10-8[a]. Radionuclide Species Mass Passed to the Biosphere Submodel

Radionuclide Group		3-D SZ Flow and Transport Submodel	1-D SZ Flow and Transport Submodel
Fission Products		^{14}C, ^{36}Cl, ^{79}Se, ^{90}Sr, ^{99}Tc, ^{126}Sn, ^{129}I, ^{135}Cs, ^{137}Cs, ^{232}U	None
Actinide Decay Chains	Actinium Series	^{243}Am, ^{239}Pu, ^{231}Pa	^{235}U, ^{231}Pa[a]
	Neptunium Series	^{241}Am, ^{237}Np, ^{229}Th	^{233}U, ^{229}Th[a]
	Thorium Series	^{240}Pu, ^{236}U, ^{232}Th	^{232}Th[a]
	Uranium Series	^{242}Pu, ^{238}U, ^{238}Pu, ^{234}U, ^{226}Ra	^{230}Th, ^{226}Ra[a]

[a] Denotes only the radionuclide mass produced as a result of ingrowth (e.g., only the daughter product mass is counted for these species).

INTENTIONALLY LEFT BLANK

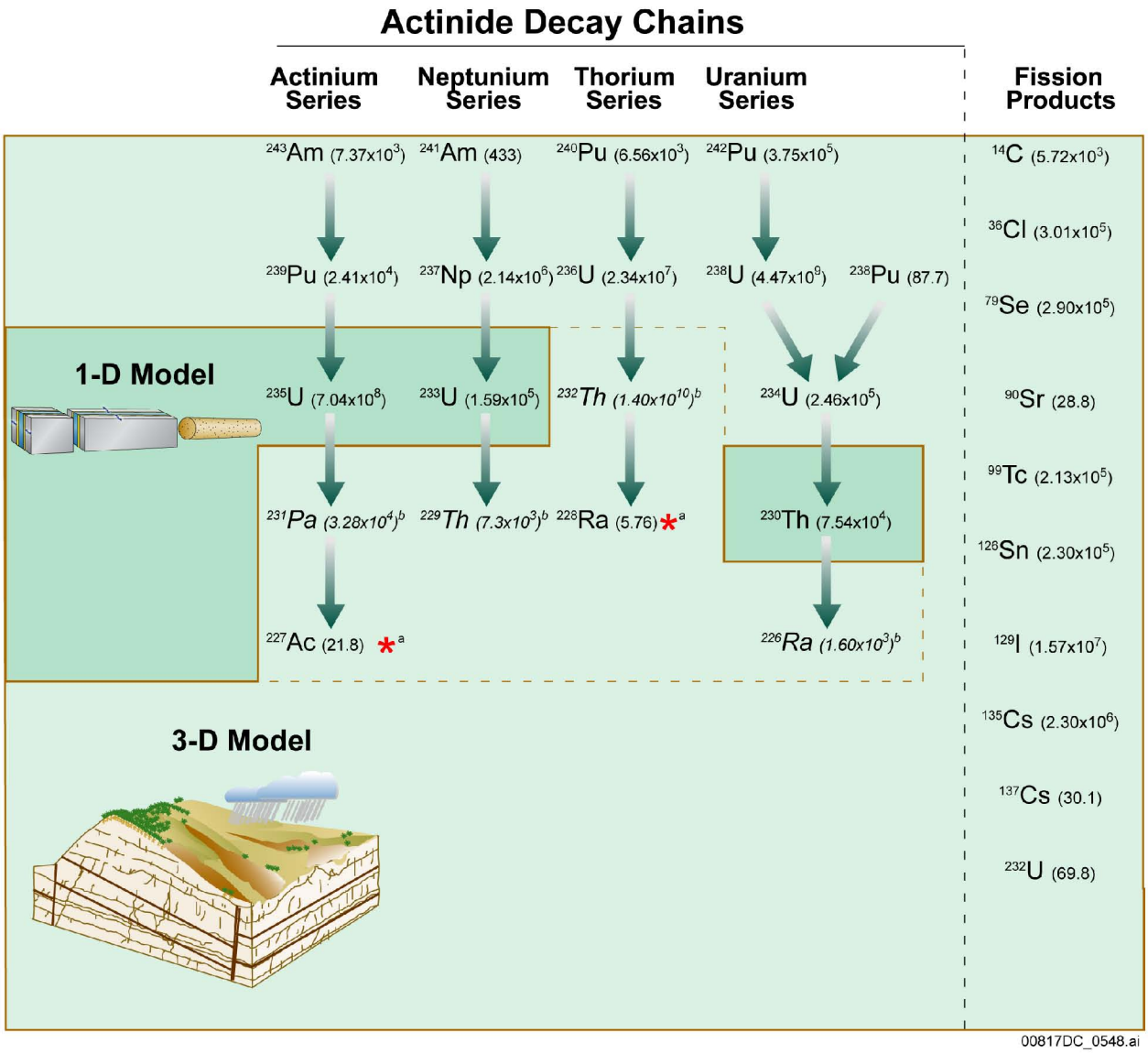

* Mass of RN calculated by assuming secular equilibrium with parent RN

(2.3×10^6) Half-life of RN indicated in parentheses (years)

Sources: DTNs: MO0702PASTREAM.001_R0 [DIRS 179925], File: DTN-Inventory-Rev00.xls; and SN0710PASZFTMA.003_R0 [DIRS 183485], File: Radionuclides_1D_3D.doc.

NOTES: The (a) denotes half-life values used in the 1-D Transport Model taken from DTN: MO0702PASTREAM.001_R0 [DIRS 179925]; (b) denotes the mass created by ingrowth from actinide decay in the 1-D SZ Flow and Transport Abstraction for ^{231}Pa, ^{229}Th, ^{232}Th, and ^{226}Ra are added to the radionuclide mass for these species from the 3-D SZ Transport model, the combined mass is used as the input to the Biosphere Submodel calculations (Section 6.3.10.3[a]).

The Biosphere Submodel calculations use the mass released from the SZ 1-D Transport Model for radionuclides ^{235}U, ^{233}U, and ^{230}Th as indicated by the shaded areas. The Biosphere Submodel calculations use the mass released from the 3-D SZ Flow and Transport Abstraction for all other radionuclides (see Section 6.3.10[a] for details).

Figure 6.3.10-8[a]. Radionuclide Decay Chains Considered in Saturated Zone Transport Calculations

INTENTIONALLY LEFT BLANK

6.3.11[a] Biosphere

No change.

6.4[a] TSPA-LA MODEL FOR THE EARLY FAILURE SCENARIO CLASS

No change.

6.5[a] TSPA-LA MODEL FOR THE IGNEOUS SCENARIO CLASS

No change.

6.6[a] TSPA-LA MODEL FOR THE SEISMIC SCENARIO CLASS

The analyses documented in this addendum include changes necessary to reflect the removal of a non-physical and conservative treatment of WP damage from seismic events following the first breach due to nominal corrosion processes as documented in Appendix P of the parent document, specifically Section P3. In addition, issues identified on Table P-6 of the parent document, Items 3, 4, and 14, have been addressed in TSPA-LA Model v5.005 (see Appendix P[a] for a list of the issues addressed in this addendum). Sections 6.6.1.3.7[a] and 6.6.1.3.8[a] outline the modifications necessary for the revised treatment of WP damage from seismic events used in TSPA-LA Model v5.005. In addition, the caption for Figure 6.6-13 in the parent document has been revised and is included as Figure 6.6-13[a]. Section 6.6.2.4[a] contains an update to two paragraphs that incorrectly documented the implementation of the Localized Corrosion Submodel for the Seismic Scenario Class.

6.6.1[a] TSPA-LA Model Components and Submodels for the Seismic Scenario Class

The subsections included in this addendum outline only the model implementation descriptions that have changed from those presented in the parent document.

6.6.1.1[a] Conceptual Model for Seismic Response of the Engineered Barrier System

No change.

6.6.1.2[a] Abstraction Model for Seismic Response of the Engineered Barrier System

No change.

6.6.1.3[a] Implementation in the TSPA-LA Model

Sections 6.6.1.3.1, 6.6.1.3.7, and 6.6.1.3.8 of the parent document have been updated to provide corrected descriptions and to reflect model changes for TSPA-LA Model v5.005.

6.6.1.3.1[a] TSPA-LA Modeling Cases

The aleatory parameter set used to calculate mean annual dose in the Seismic GM Modeling Case for 10,000 years was not reported correctly in the parent document. Table 6.6-3[a] shows

the correct values for this modeling case. These corrections are described in the following paragraph.

Seismic GM Modeling Case

For each element in the Latin hypercube sample, the expected annual dose history is calculated by Equation 6.1.2-22 of the parent document, using the annual dose histories computed for each element of the Latin hypercube sample. The integral in Equation 6.1.2-22 of the parent document accounts for the uncertainty in the number of seismic events, the time of each event, and the damaged area. Table 6.6-3[a] summarizes these parameters for the Seismic GM Modeling Case (10,000 years), including the correct time for the first seismic event (200 years) and one additional CDSP damage fraction of 0.0001, which was inadvertently omitted from the parent document.

6.6.1.3.2[a] Seismic Event Time and Magnitude Calculations for the 1,000,000-Year Ground Motion Case

No change.

6.6.1.3.3[a] Methodology for Damage Abstraction Implementation

No change.

6.6.1.3.4[a] Implementation of Rockfall for the 1,000,000-Year Ground Motion Case

No change.

6.6.1.3.5[a] Implementation of Drip Shield Plate and Framework Damage from Ground Motion

No change.

6.6.1.3.6[a] Implementation of Waste Package Rupture and Puncture from Ground Motion

No change.

6.6.1.3.7[a] Implementation of Waste Package Stress Corrosion Cracking Damage from Ground Motion

The probability of seismic damage is provided for two end-member states of the WP—one with intact internals and one with fully degraded internals. In TSPA-LA Model v5.000, once any WP is breached by a nominal process in a given percolation subregion (e.g., from first occurrence of stress corrosion cracks located on the outer lids), the probability of seismic damage is switched from the intact internals abstraction to the fully degraded internals abstraction for all WPs in a given percolation subregion. This implementation selection increases the chance of seismic damage occurring while the DS is intact, which is conservative, as most of the WPs have not yet failed by the nominal processes and should be using the intact internals damage probability

(as documented in Appendix P, Section P3, of the parent document). In TSPA-LA Model v5.005, documented in this addendum, the implementation has been modified as outlined below to track the fraction of packages with degraded internals (e.g., WPs that have been breached) and apply the seismic WP damage proportionally over each repository percolation subregion. The description of the implementation for the probability of WP damage for both end-member states and the calculation of WP damage area, as presented in Section 6.6.1.3.7 of the parent document, remains unchanged.

The abstractions for the probability of WP damage and for the conditional damaged area are functions of whether or not the WP internals are degraded. The internals are considered non-degraded until an intact package is breached by a seismic event or nominal corrosion process. If WP failure, due to nominal corrosion processes, occurs before the first seismic damage event, the calculation of probability of seismic damage is switched from the intact internals abstraction to the fully degraded internals abstraction, which increases the chance of seismic damage occurring. Damage from seismic events is accumulated and applied only to those WPs that are failed. When either a seismic event occurs that is large enough to damage all the WPs (including those that have not failed) or all of the WPs have been breached by nominal corrosion processes, the accumulated seismic damage area is applied to all WPs in the percolation subregion.

6.6.1.3.8[a] Waste Package Thickness Calculations

In Section 6.6.1.3.8 of the parent document, the abstraction for the probability of damage for CSNF WPs surrounded by rubble used results for a 17-mm WP outer corrosion barrier (OCB) thickness to obtain a conservative estimate of the probability of first failure time of a CSNF WP surrounded by rubble. The same approximation is used for CDSP WPs if the WP damage does not occur before DS failure. The 17-mm abstraction was applied to determine the time of first failure for a WP surrounded by rubble regardless of the time-dependent thickness of the WPs in TSPA-LA Model v5.000. In TSPA-LA Model v5.005, this conservatism is no longer applied. The first damage time to WPs surrounded by rubble is calculated using both the 17-mm and 23-mm thickness abstractions. In addition, in TSPA-LA Model v5.000, WP puncture was omitted as a mechanism contributing to the time of first WP failure because of the low probability of puncture occurring (Appendix P of the parent document, Table P-6, Item 14). In TSPA-LA Model v5.005, this omission has been corrected as outlined in the paragraphs below.

WPs and overlying DSs are partitioned among the five percolation subregions according to the partitioning described in Section 6.3.2.2.1. In the Seismic GM Modeling Case, the calculations for the probability of damage and damaged area are a function of WP OCB thickness, which depends on the general corrosion rate of Alloy 22. The general corrosion calculation depends on temperature, and other parameters that vary at the percolation subregion level and with fuel type (Section 6.3.5.1.2). Therefore, the time-dependent WP OCB thickness will be different for each of the five percolation subregions and for each of the two fuel types.

The general corrosion rate of the Titanium Grade 7 DSs is given by a distribution that is independent of percolation subregion parameters and will be the same for all DSs (Section 6.3.5.1.2).

The abstractions for WP degradation used in the Seismic GM Modeling Case require the spatially-averaged thickness of the WP OCB as a function of time. This calculation is done as part of the WP and DS Degradation Submodel calculations. The WAPDEG V4.07 software is run 10 times, once for each percolation subregion and fuel type, to produce a time history of WP thickness. This calculation is done separately from the calculation of WP breach used to feed the EBS Flow and Transport Model Component (Sections 6.3.6 and 6.3.8) for nominal corrosion processes. The general corrosion rate used for the feed to the Seismic GM Modeling Cases is done with an average rate rather than an extreme patch approximation to the general corrosion rate discussed in Section 6.3.5.1.2. The method discussed in Section 6.3.5.1.2 used the highest of four sampled corrosion rates (from the two-parameter Weibull distribution) to analyze general corrosion of the WP patch. For the purposes of the seismic abstractions, the average of the four sampled corrosion rates was used to generate the general corrosion rate fed to the WAPDEG V4.07 software (output DTN: MO0707WPDRIPSD.000 [DIRS 183005]). The GetThk_LA V1.0 (STN: 11229-1.0-00 [DIRS 181040]) software was used to post-process the thickness file output by the WAPDEG V4.07 software and generate a one-dimensional table of mean WP OCB thickness versus time. This mean thickness is a spatially-averaged WP OCB thickness over all the WPs in a particular percolation subregion for each fuel type.

Since the nominal corrosion processes calculated by the WAPDEG V4.07 software calculations are included in the Seismic GM Modeling Case, the calculations must account for inside-out corrosion that occurs after a seismic event has damaged a WP. The mean time of the first seismic event that causes WP damage is an input to the WAPDEG V4.07 calculations. However, the WAPDEG V4.07 calculations are done at the beginning of the simulation, before any seismic calculations are done. Therefore, a separate *a priori* calculation of the time that WPs are first damaged by a seismic event is carried out.

The calculation of the first damage time is performed *a priori* in the Aleatory Parameters and Dynamic Calculations GoldSim Submodel. The calculation generates a history of seismic events and evaluates whether or not each event causes WPs to fail. The time of the event that causes the first failure for each fuel type and percolation subregion is recorded as an output of the calculation. The calculation considers whether the WPs are under an intact DS or are surrounded by rubble. If the WPs are surrounded by rubble, the calculations evaluate whether or not stress corrosion crack damage or punctures occur.

CSNF and CDSP WPs are considered to have intact internals before the first seismic damage event and the probability of damage for WPs with intact internals under intact DSs is not a function of WP thickness (Figures 6.6-10 and 6.6-11; and DTN: MO0703PASEISDA.002_R4 [DIRS 183156], Tables 1-4 and 1-6). However, for CSNF WPs, damage is not likely to occur before DS failure. Therefore, for CSNF WPs, the abstraction for the probability of damage for WPs surrounded by rubble is dependent on the thickness of the WPs (Figure 6.6-15; and DTN: MO0703PASEISDA.002_R4 [DIRS 183156], Table 1-8). For each percolation subregion and fuel type, time histories for the average WP thickness under nominal conditions are generated when the Nominal Scenario Class is performed. These histories are used to determine the time of first WP damage in the Seismic Scenario Class when the DS plates have failed and the WP is surrounded by rubble.

6.6.2[a] Interaction of Seismic Scenario Class Submodels with other TSPA-LA Submodels

In the parent document, Section 6.6.2.4, Waste Package Localized Corrosion Initiation Submodel for Seismic Disruption, the title of this subsection was misleading and the first and second paragraphs contained incorrect information concerning the environmental conditions that can support initiation of localized corrosion. In addition, Section 6.6.2.4 of the parent document omitted a cross-reference to the supporting localized corrosion initiation analyses documented in Appendix O of the parent document. Section 6.6.2.4[a] of this addendum, now titled Waste Package Localized Corrosion Initiation Submodel Implementation for Seismic Disruption, includes the corrected version of only the first two paragraphs of Section 6.6.2.4. These paragraphs should be used in replacement of the first two paragraphs included in Section 6.6.2.4 of the parent document. These changes are strictly due to the documentation and do not represent any model changes from TSPA-LA Model v5.000. The conclusions and analyses presented in the parent document remain unchanged.

6.6.2.1[a] Drift Seepage Submodel and Drift Wall Condensation Submodel Modification for Seismic Disruption

No change.

6.6.2.2[a] Engineered Barrier System Thermal-Hydrologic Environment Submodel Modification for Seismic Disruption

No change.

6.6.2.3[a] Waste Package and Drip Shield Degradation Submodel Modifications for Seismic Disruption

No change.

6.6.2.4[a] Waste Package Localized Corrosion Initiation Submodel Implementation for Seismic Disruption

The Seismic Scenario Class does not include the potential effect of crown-seepage initiated localized corrosion on the WP outer surface. Although crown-seepage induced localized corrosion is possible for both the Seismic GM and FD Modeling Cases, a stand-alone localized corrosion initiation analysis has been carried out to determine if the environmental conditions required for localized corrosion initiation are present only for approximately 12,000 years after repository closure (Figure O-2 of the parent document). Beyond this time, the chemistry of the seepage water is benign, and localized corrosion no longer occurs (Section O3 of the parent document). This stand-alone analysis is documented in Section 6.3.5.2. The temperature, pH, chloride-ion concentration, and nitrate-ion concentration in aqueous solutions on the WP outer surface are the primary factors that determine the potential for initiating localized corrosion. In addition, localized corrosion can only occur if crown seepage water contacts the WP outer surface (i.e., if the DS is failed).

In the Seismic GM Modeling Case simulations, there is a low probability (Figure 7.3.2-16 of the parent document) of DS plate failure occurring before 12,000 years. Section 7.3.2.6.1.3.2 of the parent document discusses the justification for not considering localized corrosion due to these early DS failures. In the Seismic FD Modeling Case simulations, DSs can be failed at early times where environmental conditions are suitable for localized corrosion initiation. However, it is assumed that the added damage due to the fault displacement is sufficient to account for the effects of localized corrosion. This assumption has been verified by simulation runs showing that the dose is insensitive to increasing the fraction of the damaged area beyond 1/3 of the WP cross-sectional area (Section 7.3.2.7 and Figure 7.3.2-25 of the parent document).

6.6.3[a] Model Component Consistency and Conservatisms in Assumptions and Parameters

No change.

6.6.4[a] Alternative Conceptual Model(s) for Seismic Scenario Modeling Cases

No change.

Table 6.6-3[a]. Seismic Ground Motion and Fault Displacement Modeling Cases Using Pre-Specified Parameters

Modeling Case	Seismic Event Time (yr)	CSNF WP Damage Fraction (fraction of WP surface area)	CDSP WP Damage Fraction (fraction of WP surface area)	Number of Failed CSNF WPs	Number of Failed CDSP WPs	Rubble Volume Accumulated (m^3/m)	Rubble Fill Time (yr)	DS Damage Fraction (fraction of WP surface area)
Seismic 1M year FD Case[a]	1,000 20,000 80,000 200,000 400,000 800,000	0.028 0.056 0.084	0.0335 0.067 0.101	0 100	100 0	120	Seismic Event Time	1.0
Seismic 10k year FD Case[b]	200 800 2,000 4,000 8,000 18,000	0.028 0.056 0.084	0.0335 0.067 0.101	0 100	100 0	120	Seismic Event Time	1.0
Seismic 10k year GM Case[c]	200 1,000 3,000 6,000 12,000 18,000	0	1.00×10^{-7} 1.00×10^{-6} 0.00001 0.0001 0.001	0	3416	0	2,000,000	0.0
Seismic 1M yr GM Case	Section 6.6.1.3.1	Section 6.6.1.3.4	Section 6.6.1.3.4	Section 6.6.1.3.4	Section 6.6.1.3.4	Section 6.6.1.3.2	Section 6.6.1.3.2	Section 6.6.1.3.3

Source: [a] Output DTN: MO0708TSPAGENT.000 [DIRS 183000], folder: PL-TSPA-DTN-9 (PEF 126)
[b] Output DTN: MO0708TSPAGENT.000 [DIRS 183000], folder: PL-TSPA-DTN-8 (PEF 125)
[c] Output DTN: MO0708TSPAGENT.000 [DIRS 183000], folder: PL-TSPA-DTN-7 (PEF 124)

NOTE: For each modeling case run defined above, the model cycles through all possible combinations of the aleatory parameters one realization at a time, holding the epistemic sample number constant. For the Seismic FD Case (1,000,000 years) and the Seismic FD Case (10,000 years), there are 108 possible combinations of aleatory parameters. For the Seismic GM Case (10,000 years) there are 30 possible combinations of aleatory parameters.

INTENTIONALLY LEFT BLANK

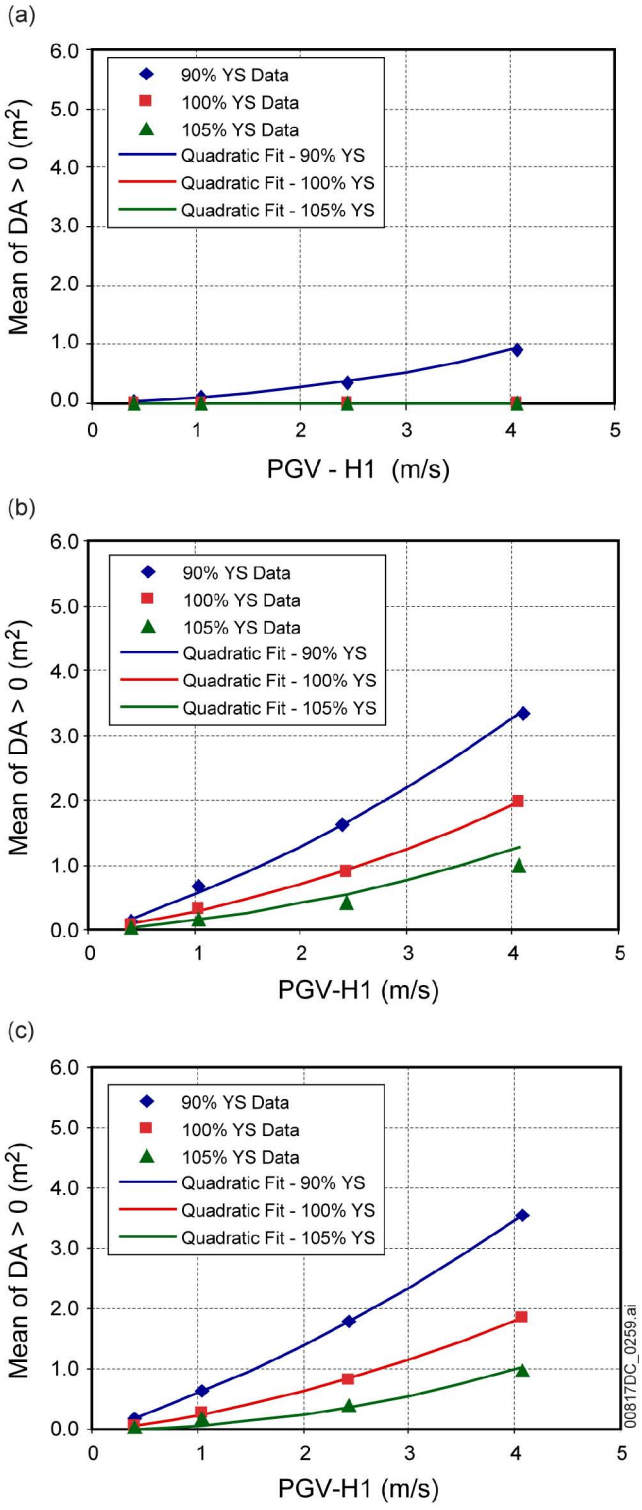

Source: DTN: MO0703PASDSTAT.001_R3 [DIRS 183148], CDSP *Kinematic Damage Abstraction 23-mm Intact.xls, Dependence on RST, CDSP Kinematic Damage Abstraction 23-mm Degraded.xls, Dependence on RST*, and *CDSP Kinematic Damage Abstraction 17-mm Degraded.xls, Dependence on RST*.

Figure 6.6-13[a]. Quadratic Fit for Mean Damaged Area on a CDSP WP under an Intact Drip Shield: (a) 23-mm WP Outer Barrier with Intact Internals, (b) 23-mm WP Outer Barrier with Degraded Internals, and (c) 17-mm WP Outer Barrier with Degraded Internals

INTENTIONALLY LEFT BLANK

6.7[a] TSPA-LA MODEL FOR THE HUMAN INTRUSION SCENARIO

No change.

INTENTIONALLY LEFT BLANK

QA: QA

MDL-WIS-PA-000005 REV 00 AD 01

March 2008

Total System Performance Assessment Model/Analysis for the License Application Addendum 01

Volume II

Prepared for:
U.S. Department of Energy
Office of Civilian Radioactive Waste Management
Office of Repository Development
1551 Hillshire Drive
Las Vegas, Nevada 89134-6321

Prepared by:
Sandia National Laboratories
OCRWM Lead Laboratory for Repository Systems
1180 Town Center Drive
Las Vegas, Nevada 89144

Under Contract Number
DE-AC04-94AL85000

DISCLAIMER

This report was prepared as an account of work sponsored by an agency of the United States Government. Neither the United States Government nor any agency thereof, nor any of their employees, nor any of their contractors, subcontractors or their employees, makes any warranty, express or implied, or assumes any legal liability or responsibility for the accuracy, completeness, or any third party's use or the results of such use of any information, apparatus, product, or process disclosed, or represents that its use would not infringe privately owned rights. Reference herein to any specific commercial product, process, or service by trade name, trademark, manufacturer, or otherwise, does not necessarily constitute or imply its endorsement, recommendation, or favoring by the United States Government or any agency thereof or its contractors or subcontractors. The views and opinions of authors expressed herein do not necessarily state or reflect those of the United States Government or any agency thereof.

CONTENTS

Page

7[a]. MODEL VALIDATION AND CONFIDENCE BUILDING ..... 7-1[a]
7.1[a] MODEL VALIDATION STRATEGY ..... 7-3[a]
7.2[a] COMPUTER CODE AND INPUT VERIFICATION ..... 7-13[a]
7.2.1[a] Selection and Verification of the Integrated System Software: GoldSim ..... 7-13[a]
7.2.2[a] Verification of Dynamically Linked Libraries as Single Modules and in an Integrated System ..... 7-13[a]
7.2.3[a] Verification of Inputs in Total System Performance Assessment Input Database ..... 7-13[a]
7.2.4[a] Verification of Single Model Components ..... 7-14[a]
7.2.5[a] Verification of Coupling among Submodels and Model Components ..... 7-17[a]
7.2.6[a] Verification of Range of Applicability of Submodels and Model Components ..... 7-17[a]
7.3[a] MODEL STABILITY ..... 7-18[a]
7.3.1[a] Statistical Stability ..... 7-18[a]
7.3.2[a] Numerical Accuracy of Expected Annual Dose ..... 7-31[a]
7.3.3[a] Temporal Stability ..... 7-33[a]
7.3.4[a] Analyses of Spatial Discretization ..... 7-39[a]
7.3.5[a] Stability of FEHM Particle Tracking Model ..... 7-39[a]
7.4[a] UNCERTAINTY AND VARIABILITY CHARACTERIZATION REVIEWS ..... 7-39[a]
7.5[a] SURROGATE WASTE FORM VALIDATION ..... 7-39[a]
7.5.1[a] Methodology ..... 7-39[a]
7.5.2[a] Spent Fuel Categories and Representation in Model ..... 7-39[a]
7.5.3[a] Naval Spent Fuel, Category 1 ..... 7-39[a]
7.5.4[a] U.S. Department of Energy Spent Fuel, Categories 2 through 11 ..... 7-42[a]
7.5.5[a] Selected Sensitivity Analyses ..... 7-42[a]
7.5.6[a] Summary of Results for U.S. Department of Energy Spent Fuel ..... 7-42[a]
7.6[a] CORROBORATION OF ABSTRACTION MODEL RESULTS WITH VALIDATED PROCESS MODELS ..... 7-42[a]
7.7[a] CORROBORATION OF RESULTS WITH AUXILIARY ANALYSES ..... 7-42[a]
7.7.1[a] Analyses of Single Realizations ..... 7-43[a]
7.7.2[a] Comparison with Simplified TSPA Analysis ..... 7-84[a]
7.7.3[a] Comparison with Electric Power Research Institute Analysis ..... 7-86[a]
7.7.4[a] Performance Margin Analysis ..... 7-88[a]
7.8[a] NATURAL ANALOGUES ..... 7-90[a]
7.9[a] TECHNICAL REVIEWS SUMMARY ..... 7-91[a]
7.10[a] SUMMARY OF MODEL CONFIDENCE BUILDING ..... 7-91[a]

CONTENTS (Continued)

Page

7.10.1[a] Validation Strategy ..... 7-91[a]
7.10.2[a] Code and Input Verification ..... 7-91[a]
7.10.3[a] Model Stability Testing ..... 7-91[a]
7.10.4[a] Uncertainty Characterization Review and Sensitvity Analyses ..... 7-93[a]
7.10.5[a] Surrogate Waste Form Validation ..... 7-93[a]
7.10.6[a] Corroboration of Abstraction Results with Validated Process Models ..... 7-93[a]
7.10.7[a] Corroboration of Results with Auxiliary Analyses ..... 7-93[a]
7.10.8[a] Corroboration of Results with Natural Analogues ..... 7-95[a]
7.10.9[a] Technical Reviews Summary ..... 7-95[a]
7.10.10[a] Conclusions ..... 7-95[a]

FIGURES

Page

7.2-17[a]. Cumulative Releases of ^{129}I, ^{237}Np, and ^{233}U from the Human Intrusion Borehole Based on Simulations Considering and not Considering Matrix Diffusion ..... F7.2-1[a]

7.3.1-14[a]. Stability of Human Intrusion Scenario: (a) Comparison of Expected Annual Dose for Three Replicates and (b) Confidence Interval around Mean Annual Dose ..... F7.3-1[a]

7.3.1-17[a]. Expected Annual Dose for 1,000,000 Years for the Nominal Modeling Case from (a) TSPA-LA Model v5.000 and (b) TSPA-LA Model v5.005 ..... F7.3-2[a]

7.3.1-18[a]. Comparison of Statistics for Expected Annual Dose in the Nominal Modeling Case between TSPA-LA Model v5.000 and TSPA-LA Model v5.005 ..... F7.3-3[a]

7.3.1-19[a]. Comparison of Expected Annual Dose for Individual Sample Elements in the Nominal Modeling Case between TSPA-LA Model v5.000 and TSPA-LA Model v5.005 at (a) 400,000; (b) 600,000; (c) 800,000; and (d) 1,000,000 Years ..... F7.3-4[a]

7.3.1-20[a]. Comparison of Statistics for Expected Annual Dose over 20,000 Years in the Drip Shield Early Failure Modeling Case between TSPA-LA Model v5.000 and TSPA-LA Model v5.005 ..... F7.3-5[a]

7.3.1-21[a]. Comparison of Statistics for Expected Annual Dose over 1,000,000 Years in the Drip Shield Early Failure Modeling Case between TSPA-LA Model v5.000 and TSPA-LA Model v5.005 ..... F7.3-6[a]

7.3.1-22[a]. Comparison of Expected Annual Dose for Individual Sample Elements in the Drip Shield Early Failure Modeling Case between TSPA-LA Model v5.000 and TSPA-LA Model v5.005 at (a) 1,000; (b) 3,000; (c) 5,000; and (d) 10,000 Years ..... F7.3-7[a]

7.3.1-23[a]. Comparison of Expected Annual Dose for Individual Sample Elements in the Drip Shield Early Failure Modeling Case between TSPA-LA Model v5.000 and TSPA-LA Model v5.005 at (a) 100,000; (b) 200,000; (c) 600,000; and (d) 1,000,000 Years ..... F7.3-8[a]

7.3.1-24[a]. Comparison of Statistics for Expected Annual Dose over 20,000 Years in the Waste Package Early Failure Modeling Case between TSPA-LA Model v5.000 and TSPA-LA Model v5.005 ..... F7.3-9[a]

7.3.1-25[a]. Comparison of Statistics for Expected Annual Dose over 1,000,000 Years in the Waste Package Early Failure Modeling Case between TSPA-LA Model v5.000 and TSPA-LA Model v5.005 ..... F7.3-10[a]

7.3.1-26[a]. Comparison of Expected Annual Dose for Individual Sample Elements in the Waste Package Early Failure Modeling Case between TSPA-LA Model v5.000 and TSPA-LA Model v5.005 at (a) 1,000; (b) 3,000; (c) 5,000; and (d) 10,000 Years ..... F7.3-11[a]

FIGURES (Continued)

Page

7.3.1-27[a]. Comparison of Expected Annual Dose for Individual Sample Elements in the Waste Package Early Failure Modeling Case between TSPA-LA Model v5.000 and TSPA-LA Model v5.005 at (a) 100,000; (b) 200,000; (c) 600,000; and (d) 1,000,000 Years ..... F7.3-12[a]

7.3.1-28[a]. Comparison of Statistics for Expected Annual Dose over 20,000 Years in the Igneous Intrusion Modeling Case between TSPA-LA Model v5.000 and TSPA-LA Model v5.005 ..... F7.3-13[a]

7.3.1-29[a]. Comparison of Statistics for Expected Annual Dose over 1,000,000 Years in the Igneous Intrusion Modeling Case between TSPA-LA Model v5.000 and TSPA-LA Model v5.005 ..... F7.3-14[a]

7.3.1-30[a]. Comparison of Expected Annual Dose for Individual Sample Elements in the Igneous Intrusion Modeling Case between TSPA-LA Model v5.000 and TSPA-LA Model v5.005 at (a) 1,000; (b) 3,000; (c) 5,000; and (d) 10,000 Years ..... F7.3-15[a]

7.3.1-31[a]. Comparison of Expected Annual Dose for Individual Sample Elements in the Igneous Intrusion Modeling Case between TSPA-LA Model v5.000 and TSPA-LA Model v5.005 at (a) 100,000; (b) 200,000; (c) 600,000; and (d) 1,000,000 Years ..... F7.3-16[a]

7.3.1-32[a]. Comparison of Statistics for Expected Annual Dose over 20,000 Years in the Seismic Ground Motion Modeling Case between TSPA-LA Model v5.000 and TSPA-LA Model v5.005 ..... F7.3-17[a]

7.3.1-33[a]. Comparison of Expected Annual Dose for Individual Sample Elements in the Seismic Ground Motion Modeling Case between TSPA-LA Model v5.000 and TSPA-LA Model v5.005 at (a) 1,000; (b) 3,000; (c) 5,000; and (d) 10,000 Years ..... F7.3-18[a]

7.3.1-34[a]. Expected Annual Dose for 1,000,000 Years for the Seismic Ground Motion Modeling Case from (a) TSPA-LA Model v5.000 and (b) TSPA-LA Model v5.005 ..... F7.3-19[a]

7.3.1-35[a]. Comparison of Statistics for Expected Annual Dose over 1,000,000 Years in the Seismic Ground Motion Modeling Case between TSPA-LA Model v5.000 and TSPA-LA Model v5.005 ..... F7.3-20[a]

7.3.1-36[a]. Comparison of Expected Annual Dose for Individual Sample Elements in the Seismic Ground Motion Modeling Case between TSPA-LA Model v5.000 and TSPA-LA Model v5.005 at (a) 100,000; (b) 200,000; (c) 600,000; and (d) 1,000,000 Years ..... F7.3-21[a]

7.3.1-37[a]. Comparison of Statistics for Expected Annual Dose over 20,000 Years in the Seismic Fault Displacement Modeling Case between TSPA-LA Model v5.000 and TSPA-LA Model v5.005 ..... F7.3-22[a]

7.3.1-38[a]. Comparison of Statistics for Expected Annual Dose over 1,000,000 Years in the Seismic Fault Displacement Modeling Case between TSPA-LA Model v5.000 and TSPA-LA Model v5.005 ..... F7.3-23[a]

FIGURES (Continued)

Page

7.3.1-39[a]. Comparison of Expected Annual Dose for Individual Sample Elements in the Seismic Fault Displacement Modeling Case between TSPA-LA Model v5.000 and TSPA-LA Model v5.005 at (a) 1,000; (b) 3,000; (c) 5,000; and (d) 10,000 Years ..... F7.3-24[a]

7.3.1-40[a]. Comparison of Expected Annual Dose for Individual Sample Elements in the Seismic Fault Displacement Modeling Case between TSPA-LA Model v5.000 and TSPA-LA Model v5.005 at (a) 100,000; (b) 200,000; (c) 600,000; and (d) 1,000,000 Years ..... F7.3-25[a]

7.3.1-41[a]. Total Expected Annual Dose for 10,000 Years from (a) TSPA-LA Model v5.000 and (b) TSPA-LA Model v5.005 ..... F7.3-26[a]

7.3.1-42[a]. Comparison of Statistics for Total Expected Annual Dose over 20,000 Years between TSPA-LA Model v5.000 and TSPA-LA Model v5.005 ..... F7.3-27[a]

7.3.1-43[a]. Comparison of Total Expected Annual Dose for Individual Sample Elements between TSPA-LA Model v5.000 and TSPA-LA Model v5.005 at (a) 1,000; (b) 3,000; (c) 5,000; and (d) 10,000 Years ..... F7.3-28[a]

7.3.1-44[a]. Total Expected Annual Dose for 1,000,000 Years from (a) TSPA-LA Model v5.000 and (b) TSPA-LA Model v5.005 ..... F7.3-29[a]

7.3.1-45[a]. Comparison of Statistics for Total Expected Annual Dose over 1,000,000 Years between TSPA-LA Model v5.000 and TSPA-LA Model v5.005 ..... F7.3-30[a]

7.3.1-46[a]. Comparison of Total Expected Annual Dose for Individual Sample Elements between TSPA-LA Model v5.000 and TSPA-LA Model v5.005 at (a) 100,000; (b) 200,000; (c) 600,000; and (d) 1,000,000 Years ..... F7.3-31[a]

7.3.1-47[a]. Confidence Interval for Total Mean Annual Dose for 20,000 Years for (a) TSPA-LA Model v5.000 and (b) TSPA-LA Model v5.005 Computed with the Bootstrap Technique ..... F7.3-32[a]

7.3.1-48[a]. Confidence Interval for Total Mean Annual Dose for 1,000,000 Years for (a) TSPA-LA Model v5.000 and (b) TSPA-LA Model v5.005 Computed with the Bootstrap Technique ..... F7.3-33[a]

7.3.3-10[a]. Expected Annual Dose from a Human Intrusion at 200,000 Years for Two Timestep Schemes ..... F7.3-34[a]

7.3.3-11[a]. Detail of Expected Annual Dose from a Human Intrusion at 200,000 Years for Two Timestep Schemes ..... F7.3-35[a]

7.3.3-12[a]. Expected Annual Dose for 1,000,000 Years for the Nominal Modeling Case from (a) TSPA-LA Model v5.005 and (b) Alternative Timestep Scheme ..... F7.3-36[a]

7.3.3-13[a]. Expected Annual Dose Statistics for 1,000,000 Years for the Nominal Modeling Case Using Two Timestep Schemes ..... F7.3-37[a]

FIGURES (Continued)

Page

7.5-4[a]. Comparison of Mean Annual Dose for a Single CSNF WP and a Single Waste Package with a Naval Source Term for the Drip Shield Early Failure Modeling Case ..... F7.5-1[a]

7.5-5[a]. Comparison of Mean Annual Dose for a Single CSNF WP and Single WP with a Naval Source Term for the Igneous Intrusion Modeling Case ..... F7.5-2[a]

7.7.1-1[a]. Expected Annual Dose from 300 Epistemic Vectors, Along with their Quantiles and Expected Dose from Epistemic Vector 281 for the Waste Package Early Failure Modeling Case for 1,000,000 Years after Repository Closure: (a) Linear Time and (b) Log Time ..... F7.7-1[a]

7.7.1-2[a]. Annual Dose from Realizations 5601 through 5620 of the Waste Package Early Failure Modeling Case for 1,000,000 Years after Repository Closure ..... F7.7-2[a]

7.7.1-3[a]. Major Radionuclide Contributors to Mean Annual Dose for the Waste Package Early Failure Modeling Case for 1,000,000 Years after Repository Closure ..... F7.7-3[a]

7.7.1-4[a]. Major Radionuclide Contributors to Annual Dose for Realization 5608 of the Waste Package Early Failure Modeling Case for 1,000,000 Years after Repository Closure ..... F7.7-4[a]

7.7.1-5[a]. (a) Release Rates of Technetium from the Waste Form, EBS, Unsaturated Zone, and Saturated Zone for Realization 5608 and (b) Saturated Zone Breakthrough Curves of Technetium and Plutonium for Epistemic Uncertainty Vector 281 of the Waste Package Early Failure Modeling Case for 1,000,000 Years after Repository Closure ..... F7.7-5[a]

7.7.1-6[a]. (a) Release Rates and (b) Concentration of ^{239}Pu for Realization 5608 of the Waste Package Early Failure Modeling Case for 1,000,000 Years after Repository Closure ..... F7.7-6[a]

7.7.1-7[a]. (a) Dissolved Concentrations of Plutonium in the CSNF Waste Form Domain for Realization 5608 and (b) CSNF Waste Form Domain Chemistry for Realization 5608 of the Waste Package Early Failure Modeling Case for 1,000,000 Years after Repository Closure ..... F7.7-7[a]

7.7.1-8[a]. Corrosion Product Sorption Coefficients (K_ds) and In-package pH for Realization 5608 of the Waste Package Early Failure Modeling Case for 1,000,000 Years after Repository Closure ..... F7.7-8[a]

7.7.1-9[a]. (a) Release Rates and (b) Concentration of ^{242}Pu for Realization 5608 of the Waste Package Early Failure Modeling Case for 1,000,000 Years after Repository Closure ..... F7.7-9[a]

7.7.1-10[a]. Major Radionuclide Contributors to Annual Dose for Realization 5618 of the Waste Package Early Failure Modeling Case for 1,000,000 Years after Repository Closure ..... F7.7-10[a]

FIGURES (Continued)

Page

7.7.1-11[a]. Cumulative Release from HLW and DSNF Waste Forms for Realization 5618 of the Waste Package Early Failure Modeling Case for 1,000,000 Years after Repository Closure ..... F7.7-11[a]

7.7.1-12[a]. Release Rates of ^{99}Tc from the Waste Form, Invert, Unsaturated Zone, and Saturated Zone for Realization 5618 of the Waste Package Early Failure Modeling Case for 1,000,000 Years after Repository Closure ..... F7.7-12[a]

7.7.1-13[a]. (a) Release Rates and (b) Concentration of ^{239}Pu for Realization 5618 of the Waste Package Early Failure Modeling Case for 1,000,000 Years after Repository Closure ..... F7.7-13[a]

7.7.1-14[a]. (a) Dissolved Concentrations of Plutonium in the High-Level Radioactive Waste Domain and (b) DSNF Waste Form Domain Chemistry for Realization 5618 of the Waste Package Early Failure Modeling Case for 1,000,000 Years after Repository Closure ..... F7.7-14[a]

7.7.1-15[a]. (a) Release Rates and (b) Concentration of ^{242}Pu for Realization 5618 of the Waste Package Early Failure Modeling Case for 1,000,000 Years after Repository Closure ..... F7.7-15[a]

7.7.1-16[a]. Expected Annual Dose from 300 Epistemic Uncertainty Vectors, Along with their Quantiles and Expected Dose from Epistemic Uncertainty Vector 247 for the Waste Package Early Failure Modeling Case for 1,000,000 Years after Repository Closure: (a) Linear Time and (b) Log Time ..... F7.7-16[a]

7.7.1-17[a]. Annual Dose from Realizations 4921 through 4940 of the Waste Package Early Failure Modeling Case for 1,000,000 Years after Repository Closure ..... F7.7-17[a]

7.7.1-18[a]. Major Radionuclide Dose Contributors for Realization (a) 4930 and (b) 4940 of the Waste Package Early Failure Modeling Case for 1,000,000 Years after Repository Closure ..... F7.7-18[a]

7.7.1-19[a]. Saturated Zone Breakthrough Curves for Epistemic Uncertainty Vector 247 of the Waste Package Early Failure Modeling Case for 1,000,000 Years after Repository Closure ..... F7.7-19[a]

7.7.1-20[a]. Concentration of (a) ^{239}Pu and (b) ^{242}Pu for Realization 4930 of the Waste Package Early Failure Modeling Case for 1,000,000 Years after Repository Closure ..... F7.7-20[a]

7.7.1-21[a]. Expected Annual Dose from 300 Epistemic Uncertainty Vectors, Along with their Quantiles and Expected Dose from Epistemic Uncertainty Vector 228 for the Drip Shield Early Failure Modeling Case for 1,000,000 Years after Repository Closure ..... F7.7-21[a]

7.7.1-22[a]. Major Radionuclide Contributors to Mean Annual Dose for the Drip Shield Early Failure Modeling Case for 1,000,000 Years after Repository Closure ..... F7.7-22[a]

7.7.1-23[a]. Annual Dose for Ten Aleatory Uncertainty Realizations (Vectors) for the Epistemic Uncertainty Vector 228 of the Drip Shield Early Failure Modeling Case for 1,000,000 Years after Repository Closure ..... F7.7-23[a]

FIGURES (Continued)

Page

7.7.1-24[a]. (a)Annual Dose along with Major Radionuclide Dose Contributors and (b) Contribution of ^{239}Pu and ^{242}Pu (Aqueous and Associated Irreversibly with Colloids) for Realization 2278 of the Drip Shield Early Failure Modeling Case for 1,000,000 Years after Repository Closure ..... F7.7-24[a]

7.7.1-25[a]. EBS Release Rates of ^{99}Tc Along with Waste Package Temperatures for the Two Selected Realizations (2273 and 2278) of the Drip Shield Early Failure Modeling Case for 1,000,000 Years after Repository Closure ..... F7.7-25[a]

7.7.1-26[a]. Flow Rate Incident on the Waste Package Showing the Effects of Drift Wall Condensation and Climate Change for the Two Selected Realizations (2273 and 2278) of the Drip Shield Early Failure Modeling Case for 1,000,000 Years after Repository Closure ..... F7.7-26[a]

7.7.1-27[a]. Fraction of CSNF and HLW Glass Waste Form Degraded for the Two Selected Realizations (2273 and 2278) of the Drip Shield Early Failure Modeling Case for 1,000,000 Years after Repository Closure ..... F7.7-27[a]

7.7.1-28[a]. Fraction of EBS Mass Flux Released into Unsaturated Zone Fractures for Selected Radionuclides for Realization 2278 of the Drip Shield Early Failure Modeling Case for 1,000,000 Years after Repository Closure ..... F7.7-28[a]

7.7.1-29[a]. Cumulative Mass Release of ^{99}Tc and ^{242}Pu from the EBS, Unsaturated Zone, and Saturated Zone for Realization 2278 of the Drip Shield Early Failure Modeling Case for 1,000,000 Years after Repository Closure ..... F7.7-29[a]

7.7.1-30[a]. Expected Annual Dose and Epistemic Uncertainty Vector 244 for the Drip Shield Early Failure Modeling Case for 1,000,000 Years after Repository Closure ..... F7.7-30[a]

7.7.1-31[a]. Ten Aleatory Uncertainty Vectors for the Epistemic Uncertainty Vector 244 of the Drip Shield Early Failure Modeling Case for 1,000,000 Years after Repository Closure ..... F7.7-31[a]

7.7.1-32[a]. Major Radionuclide Dose Contributors to Annual Dose for Realization 2433 of the Drip Shield Early Failure Modeling Case for 1,000,000 Years after Repository Closure ..... F7.7-32[a]

7.7.1-33[a]. Seepage Fraction Statistics and Seepage Fraction for Realization 2433 for the Drip Shield Early Failure Modeling Case for 1,000,000 Years after Repository Closure ..... F7.7-33[a]

7.7.1-34[a]. Seepage Rate Statistics and Seepage Rate for Realization 2433 for the Drip Shield Early Failure Modeling Case for 1,000,000 Years after Repository Closure ..... F7.7-34[a]

7.7.1-35[a]. Saturated Zone Breakthrough Curves for Plutonium and Neptunium for All Four Saturated Zone Regions for Realization 2433 of the Drip Shield Early Failure Modeling Case for 1,000,000 Years after Repository Closure ..... F7.7-35[a]

FIGURES (Continued)

Page

7.7.1-36[a]. Major Radionuclide Contributors to Mean Annual Dose for the Igneous Intrusion Modeling Case for 1,000,000 Years after Repository Closure ..... F7.7-36[a]

7.7.1-37[a]. Expected Annual Dose from the 300 Epistemic Uncertainty Vectors Along with their Quantiles and Expected Dose from Epistemic Uncertainty Vector 286 for the Igneous Intrusion Modeling Case for 1,000,000 Years after Repository Closure ..... F7.7-37[a]

7.7.1-38[a]. Annual Dose for Realizations 2851 through 2860 (representing Epistemic Uncertainty Vector 286) along with Selected Realization 2855 of the Igneous Intrusion Modeling Case for 1,000,000 Years after Repository Closure ..... F7.7-38[a]

7.7.1-39[a]. Major Radionuclide Dose Contributors to Annual Dose for Realization 2855 of the Igneous Intrusion Modeling Case for 1,000,000 Years after Repository Closure ..... F7.7-39[a]

7.7.1-40[a]. Dissolved Concentrations and Solubility Limits of Neptunium, Plutonium, Uranium, and Radium in the CSNF Waste Form Domain for Percolation Subregion 3 Seeping Environment for Realization 2855 of the Igneous Intrusion Modeling Case for 1,000,000 Years after Repository Closure ..... F7.7-40[a]

7.7.1-41[a]. In-Package pH and Pco_2 in the Waste Form Domain for Percolation Subregion 3 Seeping Environment for Realization 2855 of the Igneous Intrusion Modeling Case for 1,000,000 Years after Repository Closure ..... F7.7-41[a]

7.7.1-42[a]. Release Rate of Major Radionuclides from all Waste Packages for Realization 2855 of the Igneous Intrusion Modeling Case for 1,000,000 Years after Repository Closure ..... F7.7-42[a]

7.7.1-43[a]. Advective and Diffusive Release Rates of Major Radionuclides (Dissolved and Reversibly Associated with Colloids) from the CSNF WPs for Realization 2855 of the Igneous Intrusion Modeling Case for 1,000,000 Years after Repository Closure ..... F7.7-43[a]

7.7.1-44[a]. Total Dissolved Concentrations and Solubility Limits of Neptunium, Plutonium, Uranium, and Radium in the Corrosion Products Domain of CSNF WPs Located in Percolation Subregion 3 Seeping Environment for Realization 2855 of the Igneous Intrusion Modeling Case for 1,000,000 Years after Repository Closure ..... F7.7-44[a]

7.7.1-45[a]. Cumulative Releases of: (a) ^{237}Np, (b) ^{234}U, (c) ^{242}Pu (Dissolved and Reversibly Associated with Colloids), and (d) ^{226}Ra from the EBS, Unsaturated Zone, and Saturated Zone for Realization 2855 of the Igneous Intrusion Modeling Case for 1,000,000 Years after Repository Closure ..... F7.7-45[a]

7.7.1-46[a]. Concentrations of Major Radionuclides (Dissolved and Reversibly Associated with Colloids) at the RMEI Location for Realization 2855 of the Igneous Intrusion Modeling Case for 1,000,000 Years after Repository Closure ..... F7.7-47[a]

FIGURES (Continued)

Page

7.7.1-47[a]. Expected Annual Dose from the 300 Epistemic Uncertainty Vectors along with their Quantiles and Expected Dose from Epistemic Uncertainty Vector 20 for the Igneous Intrusion Modeling Case for 1,000,000 Years after Repository Closure ..... F7.7-48[a]

7.7.1-48[a]. Annual Dose from the Ten Aleatory Vectors Associated with the Epistemic Uncertainty Vector 20 for the Igneous Intrusion Modeling Case for 1,000,000 Years after Repository Closure ..... F7.7-49[a]

7.7.1-49[a]. Major Radionuclide Dose Contributors to Annual Dose for Realization 191 of the Igneous Intrusion Modeling Case for 1,000,000 Years after Repository Closure ..... F7.7-50[a]

7.7.1-50[a]. Climate Status and Water Flux for Realization 191 of the Igneous Intrusion Modeling Case for 1,000,000 Years after Repository Closure ..... F7.7-51[a]

7.7.1-51[a]. Solubility and Dissolved Concentrations of Plutonium and Uranium within the CSNF Domain for Realization 191 of the Igneous Intrusion Modeling Case for 1,000,000 Years after Repository Closure ..... F7.7-52[a]

7.7.1-52[a]. Expected Annual Dose from the 300 Epistemic Uncertainty Vectors Along With their Quantiles and Expected Dose from Epistemic Uncertainty Vector 155 for the Seismic Ground Motion Modeling Case for 1,000,000 Years after Repository Closure ..... F7.7-53[a]

7.7.1-53[a]. Annual Dose from the Thirty Aleatory Vectors (Seismic Event Sequences) Associated with the Epistemic Uncertainty Vector 155 for the Seismic Ground Motion Modeling Case for 1,000,000 Years after Repository Closure ..... F7.7-54[a]

7.7.1-54[a]. Annual Dose along with Major Radionuclide Dose Contributors for Realization 4641 of the Seismic Ground Motion Modeling Case for 1,000,000 Years after Repository Closure ..... F7.7-55[a]

7.7.1-55[a]. Number of Seismic Events and the Peak Ground Velocities for Realization 4641 of the Seismic Ground Motion Modeling Case for 1,000,000 Years after Repository Closure ..... F7.7-56[a]

7.7.1-56[a]. Failure Fraction for the Drip Shield Plate and Framework and the Fraction of the Collapsed Drift Filled with Rubble (Lithophysal Zone) for Realization 4641 of the Seismic Ground Motion Modeling Case for 1,000,000 Years after Repository Closure ..... F7.7-57[a]

7.7.1-57[a]. CDSP WP Failure for Each Percolation Subregion for Both Seeping and Non-Seeping Environments for Realization 4641 of the Seismic Ground Motion Modeling Case for 1,000,000 Years after Repository Closure ..... F7.7-58[a]

7.7.1-58[a]. CSNF WP Failure for Each Percolation Subregion for Both Seeping and Non-Seeping Environments for Realization 4641 of the Seismic Ground Motion Modeling Case for 1,000,000 Years after Repository Closure ..... F7.7-59[a]

FIGURES (Continued)

Page

7.7.1-59[a]. CDSP WP Opening Area after Failure from Cracks and Patches for Percolation Subregion 3 for Realization 4641 of the Seismic Ground Motion Modeling Case for 1,000,000 Years after Repository Closure ... F7.7-60[a]

7.7.1-60[a]. CSNF WP Opening Area after Failure from Cracks and Patches for Percolation Subregion 3 for Realization 4641 of the Seismic Ground Motion Modeling Case for 1,000,000 Years after Repository Closure ... F7.7-61[a]

7.7.1-61[a]. Average Waste Package Outer Barrier Thicknesses and Waste Package Failure Fractions for Percolation Subregion 3 for Realization 4641 of the Seismic Ground Motion Modeling Case for 1,000,000 Years after Repository Closure ... F7.7-62[a]

7.7.1-62[a]. Diffusive Release Rates of: (a) ^{99}Tc and (b) ^{242}Pu (Dissolved and Reversibly Associated with Colloids) from CDSP WPs from each Percolation Subregion for Realization 4641 of the Seismic Ground Motion Modeling Case for 1,000,000 Years after Repository Closure ... F7.7-63[a]

7.7.1-63[a]. Dissolved Concentration of ^{242}Pu in the Corrosion Products Domain Compared to the Sorbed Concentration on Corrosion Products for CDSP WPs for Percolation Subregion 3 Seeping Environment for Realization 4641 of the Seismic Ground Motion Modeling Case for 1,000,000 Years after Repository Closure ... F7.7-64[a]

7.7.1-64[a]. Diffusive Release Rates of (a) ^{99}Tc and (b) ^{242}Pu (Dissolved and Reversibly Associated with Colloids) from CSNF WPs from each Percolation Subregion for Realization 4641 of the Seismic Ground Motion Modeling Case for 1,000,000 Years after Repository Closure ... F7.7-65[a]

7.7.1-65[a]. Comparison of ^{242}Pu Cumulative Mass Released from the Inventory, Mass Sorbed on Corrosion Products, and the Dissolved Concentration in the Corrosion Products Domain for CSNF WPs for Percolation Subregion 3 Seeping Environment for Realization 4641 of the Seismic Ground Motion Modeling Case for 1,000,000 Years after Repository Closure ... F7.7-66[a]

7.7.1-66[a]. pH and Ionic Strength Profiles in the Corrosion Products Domain for CSNF WPs for Percolation Subregion 3 Seeping Environment for Realization 4641 of the Seismic Ground Motion Modeling Case for 1,000,000 Years after Repository Closure ... F7.7-67[a]

7.7.1-67[a]. Concentration of ^{242}Pu in the CSNF and CDSP WPs (Corrosion Products Domain) for Percolation Subregion 3 Seeping Environment for Realization 4641 of the Seismic Ground Motion Modeling Case for 1,000,000 Years after Repository Closure ... F7.7-68[a]

7.7.1-68[a]. Concentration of Various Colloids in the CSNF and CDSP WPs (Corrosion Products Domain) for Percolation Subregion 3 Seeping Environment for Realization 4641 of the Seismic Ground Motion Modeling Case for 1,000,000 Years after Repository Closure ... F7.7-69[a]

7.7.1-69[a]. EBS Release Rates from CSNF and CDSP WPs (All Percolation Subregions) for Realization 4641 of the Seismic Ground Motion Modeling Case for 1,000,000 Years after Repository Closure ... F7.7-70[a]

FIGURES (Continued)

Page

7.7.1-70[a]. Fraction of ^{242}Pu Mass Going to Unsaturated Zone Fractures at the Repository Horizon for Realization 4641 of the Seismic Ground Motion Modeling Case for 1,000,000 Years after Repository Closure ... F7.7-71[a]

7.7.1-71[a]. Cumulative Mass Release of ^{99}Tc and ^{242}Pu from the EBS, Unsaturated Zone, and Saturated Zone for Realization 4641 of the Seismic Ground Motion Modeling Case for 1,000,000 Years after Repository Closure ... F7.7-72[a]

7.7.1-72[a]. Comparison of Saturated Zone Breakthrough Curves for ^{99}Tc and ^{242}Pu for All Four Saturated Zone Source Regions for Realization 4641 of the Seismic Ground Motion Modeling Case for 1,000,000 Years after Repository Closure ... F7.7-73[a]

7.7.1-73[a]. Saturated Zone Release at the Location of the RMEI of ^{99}Tc and ^{242}Pu for Realization 4641 of the Seismic Ground Motion Modeling Case for 1,000,000 Years after Repository Closure ... F7.7-74[a]

7.7.1-74[a]. Expected Annual Dose from 300 Epistemic Uncertainty Vectors, Along with their Quantiles for the Nominal Modeling Case for 1,000,000 Years after Repository Closure in (a) Linear Time and (b) Log Time ... F7.7-75[a]

7.7.1-75[a]. Contribution of Individual Radionuclides to Mean Annual Dose for the Nominal Modeling Case for 1,000,000 Years after Repository Closure ... F7.7-76[a]

7.7.1-76[a]. Expected Annual Dose from 300 Epistemic Uncertainty Vectors, Along with their Quantiles and Expected Dose from Epistemic Uncertainty Vector 286 for the Nominal Modeling Case for 1,000,000 Years after Repository Closure ... F7.7-77[a]

7.7.1-77[a]. Contribution of Individual Radionuclides to Expected Annual Dose for Realization 286 of the Nominal Modeling Case for 1,000,000 Years after Repository Closure ... F7.7-78[a]

7.7.1-78[a]. Expected Number of (a) CDSP WP Failures and (b) CSNF WP Failures by Percolation Subregion for Realization 286 of the Nominal Modeling Case for 1,000,000 Years after Repository Closure ... F7.7-79[a]

7.7.1-79[a]. Average Failure Area for (a) CDSP WPs and (b) CSNF WPs by Percolation Subregion for Realization 286 of the Nominal Modeling Case for 1,000,000 Years after Repository Closure ... F7.7-80[a]

7.7.1-80[a]. Release Rates of ^{129}I from the Waste Form, Waste Package, Invert, Unsaturated Zone, and Saturated Zone for Realization 286 of the Nominal Modeling Case for 1,000,000 Years after Repository Closure ... F7.7-81[a]

7.7.1-81[a]. Release Rates of ^{79}Se from the Waste Form, Waste Package, Invert, Unsaturated Zone, and Saturated Zone for Realization 286 of the Nominal Modeling Case for 1,000,000 Years after Repository Closure ... F7.7-82[a]

FIGURES (Continued)

Page

7.7.1-82[a]. Release Rates of ^{135}Cs from the Waste Form, Waste Package, Invert, Unsaturated Zone, and Saturated Zone for Realization 286 of the Nominal Modeling Case for 1,000,000 Years after Repository Closure ..... F7.7-83[a]

7.7.1-83[a]. Release Rates of ^{242}Pu (Dissolved and Reversibly Associated with Colloids) from the Waste Form, Waste Package, Invert, Unsaturated Zone, and Saturated Zone for Realization 286 of the Nominal Modeling Case for 1,000,000 Years after Repository Closure ..... F7.7-84[a]

7.7.1-84[a]. Diffusive and Advective Release Rates of ^{129}I from the CDSP and CSNF Waste Packages for Realization 286 of the Nominal Modeling Case for 1,000,000 Years after Repository Closure ..... F7.7-85[a]

7.7.1-85[a]. Diffusive and Advective Release Rates of ^{242}Pu (Dissolved and Reversibly Associated with Colloids) from the CDSP and CSNF Waste Packages for Realization 286 of the Nominal Modeling Case for 1,000,000 Years after Repository Closure ..... F7.7-86[a]

7.7.1-86[a]. Fraction of ^{129}I Mass Going to Unsaturated Zone Fractures at the Repository Horizon for Realization 286 of the Nominal Modeling Case for 1,000,000 Years after Repository Closure ..... F7.7-87[a]

7.7.1-87[a]. Fraction of ^{242}Pu Mass Going to Unsaturated Zone Fractures at the Repository Horizon for Realization 286 of the Nominal Modeling Case for 1,000,000 Years after Repository Closure ..... F7.7-88[a]

7.7.1-88[a]. Expected Annual Dose for Aqueous ^{242}Pu and Slow and Fast Fractions of Irreversibly Sorbed Colloidal ^{242}Pu for Realization 286 of the Nominal Modeling Case for 1,000,000 Years after Repository Closure ..... F7.7-89[a]

7.7.1-89[a]. Expected Annual Dose from the 300 Epistemic Uncertainty Vectors along with their Quantiles and Expected Dose from Epistemic Uncertainty Vector 85 for the Nominal Modeling Case for 1,000,000 Years after Repository Closure ..... F7.7-90[a]

7.7.1-90[a]. Contribution of Individual Radionuclides to Expected Annual Dose of Realization 85 of the Nominal Modeling Case for 1,000,000 Years after Repository Closure ..... F7.7-91[a]

7.7.1-91[a]. (a) Release Rates of ^{242}Pu (Dissolved and Reversibly Associated with Colloids) from the Waste Form, Waste Package, Invert, Unsaturated Zone, and Saturated Zone, and (b) CSNF WP Failure History for Realization 85 of the Nominal Modeling Case for 1,000,000 Years after Repository Closure ..... F7.7-92[a]

7.7.1-92[a]. Expected Annual Dose from the 300 Epistemic Uncertainty Vectors along with their Quantiles and Expected Dose from Epistemic Uncertainty Vector 277 for the Human Intrusion Modeling Case for 1,000,000 Years after Repository Closure ..... F7.7-93[a]

7.7.1-93[a]. Annual Dose from the Thirty Aleatory Vectors Associated with the Epistemic Uncertainty Vector 277 for the Human Intrusion Modeling Case for 1,000,000 Years after Repository Closure ..... F7.7-94[a]

FIGURES (Continued)

Page

7.7.1-94[a]. Annual Dose along with Major Radionuclide Dose Contributors for Realization 8309 of the Human Intrusion Modeling Case for 1,000,000 Years after Repository Closure ..... F7.7-95[a]

7.7.1-95[a]. Cumulative Release of ^{99}Tc and ^{242}Pu from the Inventory for Percolation Subregion 4 for Realization 8309 of the Human Intrusion Modeling Case for 1,000,000 Years after Repository Closure ..... F7.7-96[a]

7.7.1-96[a]. Advective and Diffusive Release Rates of ^{99}Tc from Waste Form and Corrosion Products Domain for failed CSNF WPs for Realization 8309 of the Human Intrusion Modeling Case for 1,000,000 Years after Repository Closure ..... F7.7-97[a]

7.7.1-97[a]. Advective and Diffusive Release Rates of ^{242}Pu (Aqueous) from Waste Form and Corrosion Products Domain and ^{242}Pu (Irreversibly Sorbed on Iron Oxyhydroxide Colloids) from Corrosion Products Domain for failed CSNF WPs for Realization 8309 of the Human Intrusion Modeling Case for 1,000,000 Years after Repository Closure ..... F7.7-98[a]

7.7.1-98[a]. Dissolved Concentration of ^{242}Pu in the Waste Form and Corrosion Products Domain, the Plutonium Solubility in Respective Domains, and Concentration of ^{242}Pu Irreversibly Sorbed on Iron Oxyhydroxide Colloids for Realization 8309 of the Human Intrusion Modeling Case for 1,000,000 Years after Repository Closure ..... F7.7-99[a]

7.7.1-99[a]. Comparison of ^{99}Tc Release from Waste Package, Unsaturated Zone Borehole, and Saturated Zone for Realization 8309 of the Human Intrusion Modeling Case for 1,000,000 Years after Repository Closure ..... F7.7-100[a]

7.7.1-100[a]. Comparison of ^{242}Pu (Dissolved and Reversibly Associated with Colloids) Release from Waste Package, Unsaturated Zone Borehole, and Saturated Zone for Realization 8309 of the Human Intrusion Modeling Case for 1,000,000 Years after Repository Closure ..... F7.7-101[a]

7.7.1-101[a]. Cumulative Release Comparison of ^{99}Tc, ^{242}Pu (Aqueous), and ^{242}Pu (Irreversibly Sorbed on Colloids) from Waste Package, Unsaturated Zone Borehole, and Saturated Zone for Realization 8309 of the Human Intrusion Modeling Case for 1,000,000 Years after Repository Closure ..... F7.7-102[a]

7.7.1-102[a]. Saturated Zone Release Rates to the Biosphere for ^{99}Tc, ^{242}Pu (Aqueous), ^{242}Pu (Irreversibly Sorbed on Colloids that Travel Slowly due to Retardation), and ^{242}Pu (Irreversibly Sorbed on Colloids that Travel Fast due to no Retardation) for Realization 8309 of the Human Intrusion Modeling Case for 1,000,000 Years after Repository Closure ..... F7.7-103[a]

7.7.1-103[a]. Expected Annual Dose from the 300 Epistemic Uncertainty Vectors along with their Quantiles and Expected Dose from Epistemic Uncertainty Vector 181 for the Human Intrusion Modeling Case for 1,000,000 Years after Repository Closure ..... F7.7-104[a]

FIGURES (Continued)

Page

7.7.1-104[a]. Annual Dose from the Thirty Aleatory Vectors Associated with the Epistemic Uncertainty Vector 181 for the Human Intrusion Modeling Case for 1,000,000 Years after Repository Closure ..... F7.7-105[a]

7.7.1-105[a]. Annual Dose along with Major Radionuclide Dose Contributors for Realization 5415 of the Human Intrusion Modeling Case for 1,000,000 Years after Repository Closure ..... F7.7-106[a]

7.7.1-106[a]. Dissolved Concentration of ^{242}Pu in the Waste Form and Corrosion Products Domains, the Plutonium Solubility in Respective Domains, and Concentration of ^{242}Pu Irreversibly Sorbed on Iron Oxyhydroxide Colloids for Realization 5415 of the Human Intrusion Modeling Case for 1,000,000 Years after Repository Closure ..... F7.7-107[a]

7.7.1-107[a]. Expected Annual Dose from the 300 Epistemic Uncertainty Vectors along with their Quantiles and Expected Dose from Epistemic Uncertainty Vector 155 for the Seismic Ground Motion Modeling Case for 10,000 Years after Repository Closure ..... F7.7-108[a]

7.7.1-108[a]. Annual Dose from the Thirty Aleatory Vectors Associated with the Epistemic Uncertainty Vector 155 for the Seismic Ground Motion Modeling Case for 10,000 Years after Repository Closure ..... F7.7-109[a]

7.7.1-109[a]. Annual Dose along with Major Radionuclide Dose Contributors for Realization 4628 of the Seismic Ground Motion Modeling Case for 10,000 Years after Repository Closure ..... F7.7-110[a]

7.7.1-110[a]. CDSP WP Failure History in all Five Percolation Subregions for Both Seeping and Non-Seeping Environments for Realization 4628 of the Seismic Ground Motion Modeling Case for 10,000 Years after Repository Closure ..... F7.7-111[a]

7.7.1-111[a]. Diffusive Release Rates of ^{99}Tc from CDSP WPs from each Percolation Subregion for Realization 4628 of the Seismic Ground Motion Modeling Case for 10,000 Years after Repository Closure ..... F7.7-112[a]

7.7.1-112[a]. Diffusive Release Rates of ^{79}Se from CDSP WPs from each Percolation Subregion for Realization 4628 of the Seismic Ground Motion Modeling Case for 10,000 Years after Repository Closure ..... F7.7-113[a]

7.7.1-113[a]. Mass Flux of ^{99}Tc from the EBS for Percolation Subregion 3 (Seeping and Non-Seeping Environments) for Realization 4628 of the Seismic Ground Motion Modeling Case for 10,000 Years after Repository Closure ..... F7.7-114[a]

7.7.1-114[a]. Comparison of Dissolved Concentration of ^{99}Tc from the Various EBS Transport Domains and Fraction of HLW Degraded for CDSP Percolation Subregion 3, Non-Seeping Environment for Realization 4628 of the Seismic Ground Motion Modeling Case for 10,000 Years after Repository Closure ..... F7.7-115[a]

7.7.1-115[a]. Comparison of Diffusive Releases of ^{99}Tc from the Various EBS Transport Domains for CDSP Percolation Subregion 3, Non-Seeping Environment for Realization 4628 of the Seismic Ground Motion Modeling Case for 10,000 Years after Repository Closure ..... F7.7-116[a]

FIGURES (Continued)

Page

7.7.1-116[a]. Fraction of ^{99}Tc Mass Going to Unsaturated Zone Fractures as Compared to the Unsaturated Zone Matrix at the Repository Horizon for Realization 4628 of the Seismic Ground Motion Modeling Case for 10,000 Years after Repository Closure ..... F7.7-117[a]

7.7.1-117[a]. Fraction of ^{79}Se Mass Going to Unsaturated Zone Fractures as Compared to the Unsaturated Zone Matrix at the Repository Horizon for Realization 4628 of the Seismic Ground Motion Modeling Case for 10,000 Years after Repository Closure ..... F7.7-118[a]

7.7.1-118[a]. Cumulative Release of ^{99}Tc from Various Model Domains for Realization 4628 of the Seismic Ground Motion Modeling Case for 10,000 Years after Repository Closure ..... F7.7-119[a]

7.7.1-119[a]. Cumulative Release of ^{79}Se from Various Model Domains for Realization 4628 of the Seismic Ground Motion Modeling Case for 10,000 Years after Repository Closure ..... F7.7-120[a]

7.7.1-120[a]. Comparison of Saturated Zone Breakthrough Curves for ^{99}Tc and ^{79}Se for All Four Saturated Zone Regions for Realization 4628 of the Seismic Ground Motion Modeling Case for 10,000 Years after Repository Closure ..... F7.7-121[a]

7.7.1-121[a]. Saturated Zone Release to the Biosphere for ^{99}Tc and ^{79}Se for Realization 4628 of the Seismic Ground Motion Modeling Case for 10,000 Years after Repository Closure ..... F7.7-122[a]

7.7.2-3[a]. Time-Slice Comparison of the Simplified TSPA Analysis Results against the TSPA-LA Model Results for the Waste Package Early Failure Modeling Case ..... F7.7-123[a]

7.7.2-6[a]. Time-Slice Comparison of the Simplified TSPA Analysis Results against the TSPA-LA Model Results for the Nominal Modeling Case ..... F7.7-124[a]

7.7.2-9[a]. Time-Slice Comparison of the Simplified TSPA Analysis Results against the TSPA-LA Model Results for the Seismic Ground Motion Modeling Case ..... F7.7-125[a]

7.7.2-12[a]. Time-Slice Comparison of the Simplified TSPA Analysis Results against the TSPA-LA Model Results for the Igneous Intrusion Modeling Case ..... F7.7-126[a]

7.7.3-2[a]. TSPA-LA Nominal Scenario Class Mean Failure Curves for the Drip Shield and Waste Package ..... F7.7-127[a]

7.7.3-3[a]. TSPA-LA Mean Annual Dose for Major Radionuclides for the Combined Early Failure and Nominal Scenario Classes ..... F7.7-128[a]

7.7.4-7[a]. Comparison of Total Mean Annual Dose for TSPA-LA Model Version 5.000, Version 5.005, and the Performance Margin Analysis for: (a) 10,000 Years and (b) 1,000,000 Years after Repository Closure ..... F7.7-129[a]

TABLES

7.1-1[a]. TSPA-LA Model v5.005 Validation Analyses ..... 7-5[a]

7.3.1-1[a]. Uncertainty Distribution Changes for TSPA-LA Model v5.005 ..... 7-29[a]

7.3.3-2[a]. Revised Timestep Schemes used in Temporal Stability Analysis ..... 7-37[a]

INTENTIONALLY LEFT BLANK

7[a]. MODEL VALIDATION AND CONFIDENCE BUILDING

One distinguishing characteristic of validating and building confidence in the Total System Performance Assessment for the License Application (TSPA-LA) Model is the iterative nature of the process. The results presented in this addendum were generated with an updated version of the TSPA-LA Model, v5.005, and address issues that were identified during detailed post-development analysis, checking, and review of the TSPA-LA Model v5.000 results described in the parent document. The issues were primarily related to inaccuracies in model implementation and identification of unintended conservatisms as documented in Appendix P of the parent document. Changes were made to the TSPA-LA Model to address the issues presented in Appendix P of the parent document and to address unintended conservatisms in the TSPA-LA Model, as indicated in Appendix P[a] of this addendum. Appendix P[a] of this addendum includes updated tables that summarize the issues that have been addressed in the TSPA-LA Model v5.005.

Appendix P of the parent document describes the identified issues and errors, and assesses their anticipated impacts. The overall impacts on mean annual dose were projected to be "negligible" or "small" with one issue assessed as "significant" in a specified timeframe. These projected impacts were based on the understanding of the TSPA-LA Model v5.000 results during post-development analysis and review activities. As described below and listed in Tables P-6[a] and P-7[a], the projected impacts were confirmed in the TSPA-LA Model v5.005 results, indicating that the v5.000 results were well understood. The validation portion of the model documentation in the parent document was judged adequate for the intended purpose of TSPA-LA Model performance analyses in evaluating the postclosure performance of the repository and its compliance with U.S. Nuclear Regulatory Commission Proposed Rule 10 CFR 63.113 [DIRS 180319] and the performance measures defined in proposed 10 CFR 63.303 [DIRS 178394] for the individual protection standard after permanent closure in proposed 10 CFR 63.311a(1) and (2) [DIRS 178394], the individual protection standard for human intrusion in 10 CFR 63.321(a)(1) and (2) [DIRS 178394], and the separate standards for protection of groundwater in 10 CFR 63.331 [DIRS 180319], Table 1. The next iteration of the evaluation is the subject of this addendum. Confidence has been enhanced because the process has proceeded to identify, describe, and fix issues and errors during development of a thorough understanding of the results. However, it is still necessary to re-assess the adequacy of the validation portion of the model documentation of the parent document and update activities if necessary. Thus, in preparing this addendum, each validation activity for TSPA-LA Model v5.000 was reviewed to determine which activities were affected by changes made between TSPA-LA Model v5.000 and v5.005. Where validation activities could potentially be affected by model changes, these validation activities were repeated using v5.005 to verify that model changes did not adversely affect the overall validation of the TSPA-LA Model. Additional verification and validation results beyond those presented in the parent document are also provided to further enhance confidence in the TSPA-LA Model. The following validation activities were conducted for TSPA-LA Model v5.005 and are documented in this addendum:

- Computer code and input re-verification (Section 7.2[a]) including:
  - Verification testing for the Human Intrusion Submodel inadvertently omitted from the parent document (Section 7.2.4.1.12[a])

  - Summary of an assessment of the range of validity for all TSPA-LA Model submodels inadvertently omitted from the parent document (Section 7.2.6[a])

- Demonstration of Model Stability (Section 7.3[a])
  - Comparison between TSPA-LA Model v5.000 and v5.005 expected dose results (Section 7.3.1[a])
  - Reevaluation of the statistical stability of TSPA-LA Model v5.005 results (Section 7.3.1[a])
  - Confirmation of numerical accuracy of expected dose results for the Seismic Fault Displacement Modeling Case (Section 7.3.2.7[a])
  - Reevaluation of the temporal stability testing for the Human Intrusion Modeling Case as the result of a change to the timestep size for this modeling case (Section 7.3.3.6[a])
  - Evaluation of the temporal stability of the Nominal Modeling Case (Section 7.3.3.7[a])
- Surrogate Waste Form Validation (Section 7.5[a])
  - Reevaluation of the adequacy of using commercial spent nuclear fuel (CSNF) as a surrogate for naval spent nuclear fuel (NSNF) using TSPA-LA Model v5.005 (Section 7.5.3[a])
- Reevaluation of the corroboration of the TSPA-LA Model results documented in the parent document with auxiliary analyses (Section 7.7[a]), including:
  - Updated analyses of single realizations for the Early Failure Scenario Class, the Igneous Intrusion Modeling Case, and the Seismic Ground Motion (GM) Modeling Case for 1,000,000 years, including additional analyses of outlier realizations (Section 7.7.1[a])
  - Additional analyses of single realizations including: (1) the Nominal Scenario Class (Section 7.7.1.5[a]), (2) a Seismic GM Modeling Case for 10,000 years (Section 7.7.1.7[a]), and (3) the Human Intrusion Scenario (Section 7.7.1.6[a])
  - Updated evaluation with a Simplified TSPA Analysis (Section 7.7.2[a])
  - Updated evaluation with the Electric Power Research Institute (EPRI) Analysis (Section 7.7.3[a])
  - Reevaluation of a comparison of results from the Performance Margin Analysis (PMA) (Section 7.7.4[a]).

These additional verification and validation activities are presented to further enhance confidence in the TSPA-LA Model. Table 7.1-1[a] includes the verification and validation analyses presented in this addendum as well as those documented in the parent document. The analyses presented in this addendum confirm that TSPA-LA Model v5.005 is within the range of validation previously documented in the parent document.

7.1[a] MODEL VALIDATION STRATEGY

Table 7.1-1 of the parent document has been revised to include the verification and validation analyses presented in this addendum. Table 7.1-1[a] includes cross-references for the model validation analyses documented in Section 7 of the parent document and Section 7[a] of this addendum.

INTENTIONALLY LEFT BLANK

Table 7.1-1[a]. TSPA-LA Model v5.005 Validation Analyses

Activity Category/Subcategory	Purpose	Activity Description	Document Section
During–Development Validation Activities (Technical Work Plan Validation (SNL 2008 [DIRS 184920], Section 2.3.5.1))			
Computer Code and Input Verification			
Model Testing and Verification	Testing of software that is the basis for the TSPA-LA Model.	Verify GoldSim software, version 9.60.100 (STN: 10344-9.60-01 [DIRS 181903]) and 9.60.300 (STN: 10344-9.60-03 [DIRS 184387]).	7.2.1 and 7.2.1[a]
	Checking to determine whether the correct input parameters are used.	Verify input parameters.	7.2.3 and 7.2.3[a]
	Test cases to determine whether the model is working correctly, saving appropriate results, interfacing with DLLs, feeding the correct information among model components, and not exceeding the applicable range of model components.	Includes verification of DLLs, submodels, model components, and coupling among submodels and model components; and comparison with other models (e.g., stand-alone models from analysis model reports). In addition, the verification of coupling among submodels and model components includes subsystem analyses of annual release across model interfaces, drift-wall condensation, and localized corrosion initiation.	7.2.2, 7.2.4, 7.2.4[a], 7.2.5, 7.2.6[a]; Tables 7.2-1 and 7.2-2
Model Stability Testing			
Statistical Stability of Mean Annual Dose	Determine confidence interval around total mean annual dose and mean annual dose for each modeling case using three replicates.	TSPA-LA Model v5.000: Generate total mean annual dose and mean annual dose for each modeling case using three replicates with different random seeds. Determine a confidence interval around the estimate of the overall mean with a t-test. TSPA-LA Model v5.005: Determine stability by comparison with results from TSPA-LA Model v5.000. Determine a confidence interval around the estimate of the overall mean with a bootstrap procedure.	7.3.1, 7.3.1[a]
Numerical Accuracy of Expected Annual Dose Calculation – Igneous Scenario Class	Demonstrate accuracy of calculation of expected annual dose for the modeling cases of the Igneous Scenario Class.	For the Igneous Intrusion Modeling Case, demonstrate accuracy of the quadrature integration technique by increasing the discretization used in the integral. Increase the number of specified event times from 10 to 50. Calculate expected annual dose for five epistemic realizations for both 10,000 and 1,000,000 years. For the Volcanic Eruption Modeling Case for 10,000 years, demonstrate accuracy of the combined Monte Carlo and quadrature integration techniques by increasing the sample size used in the Monte Carlo integration and the discretization used in the quadrature integration. Calculate expected annual dose for 10,000 years for five epistemic realizations, increasing the aleatory LHS sample size from 40 to 120, and the number of specified event times from 10 to 20. Conclusions for 10,000 years apply to the 1,000,000 year calculations.	7.3.2

Table 7.1-1[a]. TSPA-LA Model v5.005 Validation Analyses (Continued)

Activity Category/Subcategory	Purpose	Activity Description	Document Section
Numerical Accuracy of Expected Annual Dose Calculation – Seismic Scenario Class	Demonstrate accuracy of calculation of expected annual dose for the modeling cases of the Seismic Scenario Class.	For the Seismic GM Modeling Case for 1,000,000 years, demonstrate the accuracy of the Monte Carlo integration technique by means of increased sample size. Repeat Replicate 1 (300 epistemic realizations) with a different aleatory seed to generate a second set of 9,000 dose histories (30 independent aleatory samples for each epistemic realization). Pool the two sets of 9,000 dose histories and generate expected annual dose based on the pooled set of 60 independent aleatory samples per epistemic realization, and compare to expected annual dose for the base case of 30 independent aleatory samples per epistemic realization. For the Seismic GM Modeling Case for 10,000 years, demonstrate accuracy of the quadrature integration technique by increasing the discretization used in each integral. Increase the number of specified event times from 6 to 12 and the number of specified damage levels from 5 to 8. Calculate expected annual dose for 5 epistemic realizations. For the Seismic FD Modeling Case, demonstrate accuracy of the quadrature integration technique by increasing the discretization used in each integral. Increase the number of specified event times from 6 to 12 and the number of specified damaged areas from 3 to 6. Calculate expected annual dose for 5 epistemic realizations for both 10,000 and 1,000,000 years.	7.3.2 and 7.3.2[a]
Justification of Simplifications for the Seismic GM Modeling Case for 10,000 Years	For the Seismic GM Modeling Case for 10,000 years, demonstrate that simplifications of the Seismic Consequences Abstraction used in the calculation of expected annual dose are reasonable.	Estimate the effect on mean annual dose of drip shield plate rupture and of framework failure. Estimate the effect on mean annual dose of accounting for rockfall effects on temperature and seepage entering the drift. Estimate the contribution to mean annual dose from WP rupture and puncture. Estimate the contribution to mean annual dose from damage to CSNF WPs.	7.3.2
Temporal Stability	Demonstrate stability of expected annual dose for temporal discretization in GoldSim.	Comparison of expected annual dose histories for five epistemic vectors for the following modeling cases: Waste Package EF; Seismic GM (10,000 years); Igneous Intrusion (10,000 and 1,000,000 years); and Drip Shield EF (10,000 years). Compare expected annual dose histories for different temporal discretizations. Assess the temporal stability for the Nominal Modeling Case (1,000,000 years). Assess the temporal stability for the Human Intrusion Modeling Case.	7.3.3 and 7.3.3[a]; Table 7.3.3-2[a]

Table 7.1-1[a]. TSPA-LA Model v5.005 Validation Analyses (Continued)

Activity Category/Subcategory	Purpose	Activity Description	Document Section
Spatial Discretization	Evaluate the impact due to the spatial discretizations inherited by the TSPA-LA Model from the supporting natural and engineered-barrier process models.	Evaluate the appropriateness of use of the inherited spatial discretization schemes of the process model abstractions that feed the TSPA-LA Model. These abstractions include the process models: Mountain-Scale UZ Flow, EBS TH Environment, UZ Transport, and SZ Flow and Transport abstractions.	7.3.4.1
	Evaluate the impact due to the spatial discretizations created within the TSPA-LA Model.	Describe the spatial discretization of the repository on the basis of percolation subregions and the binning of the percolation subregions by quantiles (0.0 to 0.05, 0.05 to 0.3, 0.3 to 0.7, 0.7 to 0.95, and 0.95 to 1.0).	7.3.4.2
		Demonstrate the appropriateness and validity of using the representative TH histories as inputs to the EBS Thermal-Hydrologic Environments Submodel of the TSPA-LA Model, as opposed to using the comprehensive data set available from the MSTHM.	7.3.4.3
Stability of UZ Transport Modeling for the Igneous Intrusion Modeling Case	Evaluate the stability of results in reference to the maximum number of particles allowed per species for the Igneous Intrusion Modeling Case for 10,000 years.	Analyze the differences in UZ releases of ^{99}Tc, ^{233}U, ^{234}U, ^{237}Np, and ^{239}Pu, and in cumulative dose for three cases (500,000; 750,000; and 900,000 particles).	7.3.5
Stability of UZ Transport Modeling for the Seismic GM Modeling Case	Evaluate the stability of results in reference to the maximum number of particles allowed per species for the Seismic GM Modeling Case for 10,000 years.	Analyze the differences in UZ releases of ^{99}Tc, ^{233}U, ^{234}U, ^{237}Np, and ^{239}Pu and in cumulative dose for three cases (500,000; 750,000; and 900,000 particles.).	7.3.5
Stability of UZ Transport Modeling for the Drip Shield EF Modeling Case	Evaluate the stability of results in reference to the maximum number of particles allowed per species for the Drip Shield EF Modeling Case for 1,000,000 years.	Analyze the differences in UZ releases of ^{99}Tc, ^{233}U, ^{234}U, ^{237}Np, and ^{239}Pu, and in cumulative dose for three cases (500,000; 750,000; and 900,000 particles).	7.3.5
Uncertainty Characterization Reviews			
Ranking of Scenario Classes	Prioritize scenario classes of higher significance to dose.	Develop a risk-based ranking of TSPA-LA scenario classes and modeling cases in order to focus the uncertainty characterization reviews of the most important component model abstractions.	7.4.2
Key Uncertain Parameters	Identify the key uncertain parameters that are important to dose.	Select the key uncertain parameters that are important to dose in the Seismic, Igneous, and Nominal Modeling Cases for characterization review based on both importance rankings from past TSPA scoping studies and recommendations provided by model abstraction developers and experienced TSPA analysts.	7.4.3

Table 7.1-1[a]. TSPA-LA Model v5.005 Validation Analyses (Continued)

Activity Category/Subcategory	Purpose	Activity Description	Document Section
Uncertainty-Characterization Review Findings and their Implementation	Review uncertainty characterization and address findings.	Perform uncertainty characterization of the selected key parameters impacting dose for the Seismic, Igneous, and Nominal Modeling Cases and implement corrective actions for observed deficiencies.	7.4.4
Surrogate Waste Form Validation			
Spent Fuel Categories	Comparison of naval surrogate fuel to naval fuel (Category 1).	Perform probabilistic runs to compare the naval surrogate (Zircaloy-clad commercial fuel) with naval fuel for Nominal, Igneous Intrusion, and Volcanic Eruption Modeling Cases.	7.5.3 and 7.5.3[a]
	Comparison of the DOE surrogate fuel to each DOE spent fuel category (Category 2 through Category 11).	Perform probabilistic run using Drip Shield EF Modeling Case to compare the DOE surrogate with plutonium/uranium alloy spent fuel (Category 2), plutonium/uranium-carbide spent fuel (Category 3), mixed-oxide spent fuel (Category 4), uranium/thorium-carbide spent fuel (Category 5), uranium/thorium-oxide spent fuel (Category 6), uranium-metal spent fuel (Category 7), uranium-oxide spent fuel (Category 8), aluminum-based spent fuel (Category 9), miscellaneous spent fuel (Category 10) for two inventories, and uranium-zirconium hydride spent fuel (Category 11).	7.5.4
Selected Sensitivity Analyses	Justification of the DOE surrogate dissolution model.	Perform probabilistic comparison of fuel degradation models for Category 2 through Category 11 and air alteration rates for Category 5 and Category 7.	7.5.5
	Justification of the DOE surrogate dissolution model.	Perform comparison of uranium-metal dissolution model, uranium-metal dissolution model with air alteration, and instantaneous dissolution (Category 7). Perform similar comparison for the uranium/thorium-carbide dissolution model (Category 5).	7.5.5
	Effects of fuel surface area and free inventory and uncertainty of radionuclide inventory.	Perform probabilistic comparison of uranium-metal nominal surface area with bounding surface area and free inventory and comparison of nominal inventory with the bounding inventory (Category 7).	7.5.5
	Uncertainty in number of WPs.	Perform probabilistic comparison of aluminum-based spent fuel for nominal and bounding number of WPs (Category 9).	7.5.5
	Comparison of radionuclides that contribute to annual dose from surrogate DOE spent fuel, HLW, uranium-metal spent fuel (Category 7), uranium/thorium-carbide spent fuel (Category 5), and uranium/thorium-oxide spent fuel (Category 6).	Analyze plots of key radionuclides that contribute to total annual dose for the DOE surrogate spent fuel only, HLW only, Category 7 only, Category 5 only, and Category 6 only.	7.5.6

Table 7.1-1[a]. TSPA-LA Model v5.005 Validation Analyses (Continued)

Activity Category/Subcategory	Purpose	Activity Description	Document Section
	Justification of the DOE surrogate fuel.	Compare of the weighted sum of Category 2 through Category 11 spent fuel with a single WP of the DOE surrogate spent fuel.	7.5.5
Post–Development Validation Activities (Technical Work Plan Validation (SNL 2008 [DIRS 184920], Section 2.3.5.2))			
Corroboration of Direct Input Abstraction Results with Validated Process Models			
Corroboration of Abstraction Results with Underlying Process Models	Evaluate consistency of the abstraction results with the underlying validated key natural system environment models.	Perform quantitative and qualitative evaluation of how well the direct input abstraction results corroborate with the underlying validated key natural system environment models. Provide the evidence that builds confidence in the direct inputs.	7.6.4.1
	Evaluate consistency of the abstraction results with the underlying validated key engineered barrier system models.	Perform quantitative and qualitative evaluation of how well direct input abstraction results corroborate the underlying validated key EBS models. Provide the evidence that builds confidence in the direct inputs.	7.6.4.2
	Evaluate consistency of the abstraction results with the underlying validated key drip shield, WP, and waste form degradation and mobilization models.	Perform quantitative and qualitative evaluation of how well the direct input abstraction results corroborate the underlying validated key drip shield, WP, and waste form degradation and mobilization models. Provide the evidence that builds confidence in the direct inputs.	7.6.4.3
	Evaluate consistency of the abstraction results with the underlying validated key disruptive events models.	Perform quantitative and qualitative evaluation of how well the direct input abstraction results corroborate the underlying validated key seismic and igneous disruptive events models. Provide the evidence that builds confidence in the direct inputs.	7.6.4.4
	Evaluate consistency of the abstraction results with the underlying validated biosphere model.	Provide the evidences that build confidence in the direct inputs from the biosphere model to the TSPA-LA Model.	7.6.4.5
Corroboration of Results with Auxiliary Analyses			
Analysis of Single Realizations	Evaluate a realization that contributes significantly to mean annual dose for the Early Failure Modeling Cases.	Select a realization each from the Waste Package EF Modeling Case and Drip Shield EF Modeling Case and analyze it to examine how the transport of key radionuclides is affected by coupling various components of the EBS, UZ, and SZ domains following the WP failure under varying physical-chemical-thermal-mechanical conditions. Also select an outlier realization and examine it to understand what leads to the extreme dose.	7.7.1 and 7.7.1[a]

Table 7.1-1[a]. TSPA-LA Model v5.005 Validation Analyses (Continued)

Activity Category/Subcategory	Purpose	Activity Description	Document Section
	Evaluate a realization that contributes significantly to mean annual dose for the Igneous Intrusion Modeling Case.	Select a realization from the Igneous Intrusion Modeling Case and analyze it to examine how the transport of key radionuclides is affected by coupling various components of the EBS, UZ, and SZ domains following the waste package failure under varying physical-chemical-thermal-mechanical conditions. Also select an outlier realization and examine it to understand what leads to the extreme dose.	7.7.1 and 7.7.1[a]
	Evaluate a realization that contributes significantly to mean annual dose for the Seismic GM Modeling Case.	Select a realization from the Seismic GM Modeling Case and analyze it to examine how the transport of key radionuclides is affected by coupling various components of the EBS, UZ, and SZ domains following the WP failure under varying physical-chemical-thermal-mechanical conditions. Both the 1,000,000-year and 10,000-year modeling cases were examined.	7.7.1 and 7.7.1[a]
	Evaluate a realization that contributes significantly to mean annual dose for the Nominal Modeling Case.	Select a realization from the Nominal Modeling Case and analyze it to examine how the transport of key radionuclides is affected by coupling various components of the EBS, UZ, and SZ domains. Also evaluate statistical outlier for this modeling case. Also select an outlier realization and examine it to understand what leads to the extreme dose.	7.7.1[a]
	Evaluate a realization that contributes significantly to mean annual dose for the Human Intrusion Modeling Case.	Select a realization from the Human Intrusion Modeling Case and analyze it to examine how the transport of key radionuclides is affected by coupling various components of the EBS, UZ borehole, and SZ domains following the human intrusion event. Also select an outlier realization and examine it to understand what leads to the extreme dose.	7.7.1[a]
Comparison with Other Simple Models	Compare the TSPA-LA Model component results with a simplified analysis.	Perform a Simplified TSPA Analysis and compare the results with those of the TSPA-LA Model.	7.7.2 and 7.7.2[a]
	Compare with the Energy and Power Research Institute (EPRI) TSPA Analysis.	Develop a comparison of the approach and results of the TSPA independently conducted by EPRI using its code IMARC for the postclosure performance of the Yucca Mountain repository.	7.7.3 and 7.7.3[a]

Table 7.1-1[a]. TSPA-LA Model v5.005 Validation Analyses (Continued)

Activity Category/Subcategory	Purpose	Activity Description	Document Section
Performance Margin Analyses	Provide objective evidence for assessing performance margin and degree of conservatism or non conservatism in the TSPA-LA Model.	Conduct several auxiliary analyses (see Section 7.7.4 of the parent document for a list) utilizing revisions to selected component models in the TSPA-LA Model, including conceptual or uncertainty alternatives, to assess the performance margin in the TSPA-LA Model and to evaluate whether the TSPA-LA Model dose is underestimated. The analyses include both individual component revisions as well as a combined analysis that incorporates all of the selected component revisions.	7.7.4 and 7.7.4[a]
Corroboration of Results with Natural Analogues			
Cerro Negro	Validation of ASHPLUME for the Volcanic Eruption Modeling Case.	Comparison Cerro Negro ash-fall measurements with the results from ASHPLUME.	7.8.1
Peña Blanca, Nopal I Uranium Deposit	Validation of the UZ and SZ Transport Model.	Evaluation of geochemical data collected from rock and water samples with respect to distance from the Nopal I ore deposit.	7.8.2
Independent Technical Reviews Performed in Preparation of the TSPA-LA Model			
TSPA-VA Peer Review	Evaluate the TSPA-VA methodology and prediction of the future behavior of the total system.	Performed peer review of the TSPA-VA and the supporting process models. The review was conducted by an independent group of external experts from 1997 to 1999.	7.9.1
TSPA-SR Peer Review	Evaluation of the TSPA-SR for methodology and ability to meet the needs for SR and future LA compliance.	Performed peer review of the TSPA-SR and selected supporting documents to evaluate the approach used in the performance assessment, and how well the TSPA-SR and the future TSPA-LA Model needs were addressed. The review was conducted by an international panel of experts managed by the OECD/NEA in 2002.	7.9.2
Draft TSPA-LA Technical Review	Evaluate the earlier draft iterations of the TSPA-LA Model as they were being drafted as to the degree of validation of the model for its intended purpose.	Perform technical review on the evaluation of the degree to which the draft TSPA-LA Model was valid for its intended purpose for the 10,000-year compliance period for which the model was prepared. The review was conducted by a team of experts during 2004, 2005, and early part of 2006.	7.9.3

INTENTIONALLY LEFT BLANK

7.2[a] COMPUTER CODE AND INPUT VERIFICATION

7.2.1[a] Selection and Verification of the Integrated System Software: GoldSim

A revised version of the GoldSim software (GoldSim V9.60.300, STN: 10344-9.60-03 [DIRS 184387]) was used in all updated TSPA-LA Model results reported in this addendum. Information about GoldSim is discussed in Section 7.2.1 of the parent document.

The revised version of GoldSim was qualified in accordance with IM-PRO-004, *Qualification of Software*. The updated software was obtained from Software Configuration Management in accordance with IM-PRO-003, *Software Management*, and was installed in accordance with installation test instructions listed in *User Information Document for: GoldSim Version 9.60* (DOE 2007 [DIRS 181108], Section 3.1). GoldSim was used to develop the analyses for the TSPA-LA Model within the limitations and the range of verification guidance presented in Appendix G of the *User's Guide, GoldSim Probabilistic Simulation Environment, Version 9.60* (GoldSim Technology Group 2007 [DIRS 181727]). Additional information regarding the GoldSim software is discussed in Section 3.8 of the parent document, Section 3.8[a] of this addendum, and in the documents listed in Table 3-8[a].

7.2.2[a] Verification of Dynamically Linked Libraries as Single Modules and in an Integrated System

No change.

7.2.3[a] Verification of Inputs in Total System Performance Assessment Input Database

Parameters used in the analyses presented in this addendum are documented in the TSPA Input Database described in Section 4.7 of the parent document, with additional detail provided in Section 7.2.3 of the parent document. Each TSPA-LA Model simulation described in this addendum accesses the TSPA Input Database in order to obtain values for each model's parameters from sources listed in Table 4-1 of the parent document and Table 4-1[a] of this addendum. Parameter values are maintained as originally entered, without transformation or post-processing, and are manually entered into the database (this is described in more detail in Section 7.2.3 of the parent document). Figure 4-3 of the parent document shows the structural framework of the TSPA Input Database, which is described in Section 4.7 of the parent document.

The value of every parameter is checked and verified before using it for a performance-assessment analysis. Any discovered errors are documented in the TSPA-LA Model Log; corrected values are entered into the database and, if determined to be necessary by an impact analysis (e.g., Appendix P of the parent document), the impacted calculations are performed again. The parameter verification is documented on the Parameter Verification Form (Section 4.7 of the parent document). Only users with access to the TSPA-LA Model's controlled-access input database can verify parameter values. The verification process includes recording the checker's name, along with the date and time, in order to identify the last user who changed any parameter categories. Strict control of access and documentation increases confidence in the security, integrity, and traceability of information entered into, or downloaded from, the TSPA Input Database. In this same way, the TSPA Input Database was verified with

the new information (listed in Table 4-1[a]) that supports the analyses documented in this addendum.

7.2.4[a] Verification of Single Model Components

The TSPA-LA Model is composed primarily of submodels derived from abstraction models that are documented in analysis and/or model reports. Verification and validation activities used to improve confidence in numerical models implemented in the TSPA-LA Model are described in Section 7.2.4 of the parent document. As discussed in Section 7.2.4 of the parent document, the approach to verification is to compare TSPA-LA Model file results with results of stand-alone implementations reported in analysis and/or model reports or validation test reports, where applicable. Additional verification activities that were not included in the parent document are presented in Section 7.2.4.1.12[a] of this addendum. These additional verification activities were conducted only for the Human Intrusion Modeling Case. Verification tests of input and submodels specific to the Human Intrusion Modeling Case included verifying inputs in the TSPA database, verifying the submodels (such as the borehole pipe model), and verifying proper coupling among submodels.

7.2.4.1[a] Verification Results

The results of the submodel implementation verification activities are presented in Sections 7.2.4.1.1 through 7.2.4.1.11 of the parent document. These apply to TSPA-LA Model v5.005 without change. One additional verification of the Human Intrusion Submodel is provided in Section 7.2.4.1.12[a] of this addendum. This verification activity consists of verifying Human Intrusion Submodel inputs in the TSPA-LA Model database, verifying selected Human Intrusion Submodels (such as the borehole pipe model), and verifying proper coupling among Human Intrusion Submodels. The results of the verification of the Human Intrusion Submodel (output DTN: MO0801TSPAMVAC.000 [DIRS 185080]) are discussed in Section 7.2.4.1.12[a].

7.2.4.1.1[a] Drift Seepage

No change.

7.2.4.1.2[a] Drift Wall Condensation Submodel Verification

No change.

7.2.4.1.3[a] Engineered Barrier System Chemical Environment

No change.

7.2.4.1.4[a] Waste Package and Drip Shield Degradation

No change.

7.2.4.1.5[a] Waste Form Degradation and Mobilization

No change.

7.2.4.1.6[a] Engineered Barrier System Transport

No change.

7.2.4.1.7[a] Unsaturated Zone Transport

No change.

7.2.4.1.8[a] Saturated Zone Flow and Transport

No change.

7.2.4.1.9[a] Biosphere

No change.

7.2.4.1.10[a] Igneous Scenario Class Modeling Cases

No change.

7.2.4.1.11[a] Seismic Scenario Class Modeling Cases

No change.

7.2.4.1.12[a] Human Intrusion Scenario

Verification of the Human Intrusion Scenario focuses on an alternate implementation of the UZ Transport Submodel where the radionuclide transport from the engineered barrier system (EBS) to the saturated zone (SZ) is confined to a borehole penetrating the waste package (WP) and extending through the unsaturated zone (UZ) to the SZ. A simplified deterministic analysis was performed in order to verify the implementation of the Human Intrusion Submodel. The verification test utilized one Latin hypercube sample (LHS) vector for the epistemic and aleatory parameter values. Beginning at 200,000 years into the simulation, the source term for the realization was redefined as a single release into the EBS of one gram of the non-sorbing radionuclide ^{129}I and one gram of the sorbing radionuclide ^{237}Np. The rest of the radionuclide inventory was set to zero for the simulation. This allowed a comparison of the simple mass release from the EBS to the mass leaving the borehole at the water-table. A specific percolation rate of 25 mm/yr was assigned for the simulation and was used to check that both the EBS and the borehole-pipe element were using the same rate (as specified in the model implementation, Section 6.7.3.2 of the parent document) and to approximate the time needed for the cumulative mass release from the borehole to reach 0.5 grams for a simulation without considering matrix diffusion. Two simulations were performed: the first allowed for matrix diffusion into the surrounding rock matrix and the second did not consider matrix diffusion. The selected realization is number 8,309 (out of 9,000 total realizations) and represents epistemic vector 277 and aleatory vector 29 (output DTN: MO0710ADTSPAWO.000 [DIRS 183752]). The aleatory vector 29 is defined as a CSNF WP release from a WP located in percolation subregion 4.

The source term was implemented by adding the radionuclide mass for ^{129}I and ^{237}Np to the CSNF interface cell representing the WP outer corrosion barrier (OCB) during the 250-year

timestep beginning 200,000 years into the simulation. To ensure that most of the mass would reach the borehole rapidly, no diffusion was allowed from the interface cell back to the upstream cell representing the corrosion products domain. The selected percolation rate was implemented by changing the input value for the percolation rate for the borehole to 25 mm/yr for any CNSF WP release from a WP located in percolation subregion 4. As part of this verification, simulation results were examined to make sure that the CSNF EBS seepage feed (model parameter *Seepage_Flux_Feed_EBS*) was set to 0.00081 m^3/year, the product of the borehole area (0.0324 m^2), and the percolation rate of 25 mm/yr. The outflow rate from the borehole pipe element was also checked and was given to be 2.56674 x 10^{-11} m^3/s (0.00081 m^3/year).

For both simulations, 99.99 percent of the ^{129}I and 99.98 percent of the ^{237}Np are released from the EBS into the borehole in the first timestep. Also, ^{233}U produced by decay of ^{237}Np is released from the EBS. The results for the borehole release to the SZ from the two simulations are presented on Figure 7.2-17[a]. For the simulation with matrix diffusion considered, it can be seen on Figure 7.2-17[a] that the total release of ^{129}I from the borehole is very close to the applied EBS mass release of one gram (0.9999 grams). Because of decay, the total release of ^{237}Np is only 0.9785 g. When the product of the mass release of ^{233}U, its daughter product from the borehole and the ratio of the atomic weights of ^{237}Np and ^{233}U, is added to the ^{237}Np release the total release increases to 0.9970 g. Note that a very small amount (3.539 x 10^{-7} g) of ^{229}Th, ^{233}U's daughter product, is also produced. For ^{129}I, there is a short delay of the mass release associated with the diffusion of mass between the fracture and rock matrix. This delay is approximately 1,250 years as defined by the 0.5 gram breakthrough level in the cumulative results. For ^{237}Np, the delay is approximately 64,000 years. Note that the matrix retardation for ^{237}Np in this simulation is 47.8, which is close to 51.2, the ratio of the breakthrough time of ^{237}Np to that of ^{129}I, which has a retardation coefficient of 1.0.

As shown on Figure 7.2-17[a], for the simulation without matrix diffusion, most of the ^{129}I and ^{237}Np mass leaving the EBS has exited the borehole within one timestep (250 years). Based on the volumetric rate of water entering the borehole (0.00081 m^3/year), the fracture area of 0.0004211 m^2 within the borehole cross-section and the fracture saturation of 0.0253, over the 190 m borehole length (Section 6.7.3.2 of the parent document) the advective transport velocity in the fracture, is approximately 76 m/year, which translates into an advective transport time of 2.5 years. A comparison of the time between the mass application and the time of the 0.5 gram breakthrough level in the cumulative mass release curve, with a transport time of 2.5 years, is not possible because of the coarseness of the simulation timesteps. By the end of the timestep starting at 200,000 years, 99.04 percent of ^{129}I and 99.03 percent of ^{237}Np have exited the borehole. This release pattern is consistent with a very short transport time through the borehole when matrix diffusion is not considered.

The analysis presented above verifies that the UZ Transport Submodel for the Human Intrusion Scenario is implemented correctly. This verification test for the submodel specific to the Human Intrusion Modeling Case, combined with the verification of the TSPA-LA Model's submodels documented in the parent document, are used to assert that the Human Intrusion Scenario is verified.

7.2.5[a] Verification of Coupling among Submodels and Model Components

No change.

7.2.6[a] Verification of Range of Applicability of Submodels and Model Components

A discussion of the verification of the range of applicability of submodels and model components is provided in Section 7.2.6 of the parent document. An assessment of the range of validity for all TSPA-LA Model submodels (output DTN: MO0709TSPALAMO.000 [DIRS 182981]) was conducted over the specified range of validity. The summary results of this assessment were inadvertently left out of Section 7.2.6 of the parent report. The summary results of this verification assessment are documented below. The records that document the implementation and checking of the TSPA-LA Model are located in the relevant records package.

During the development of the TSPA-LA Model, fatal error encounters and flag setting conditions signaling an out-of-range condition did occur. In many cases, when an out-of-range condition occurred, the provided abstractions were revised to preclude the occurrence of the out-of-range condition. The abstractions were revised to: (1) constrain the calculated values by removing undue uncertainty that could broaden the calculated results, (2) expand the range of validity of the abstraction, or (3) provide additional guidance on how to handle out-of-range conditions. However, an assessment of the range of validity for all TSPA-LA Model submodels (output DTN: MO0709TSPALAMO.000 [DIRS 182981]) revealed that for the 1,000,000-year performance runs, three submodels of the Waste Form Degradation and Mobilization Model Component were applied below the lower temperature limit in the specified range of validity. For the 10,000-year simulations, the temperatures remain within the range of validity.

In the 1,000,000-year performance runs, WPs return to ambient temperatures in the modeled duration. The ambient temperature from the EBS TH Environment Submodel (Section 6.3.2) can be as low as 17°C. The lower temperature limit for the In-Package Chemistry Abstraction (SNL 2007 [DIRS 180506], Section 1[a]) and the Dissolved Concentration Limits Abstraction (SNL 2007 [DIRS 177418], Section 6.3.3.3) is 25°C. The lower temperature limit for the HLW Glass Waste Form Degradation Abstraction is 20°C (BSC 2004 [DIRS 169988], Section 1.2). As discussed below, the application of these three submodels below the stated range of applicability is not expected to have a significant affect on the EBS release calculations; therefore, the TSPA-LA Model applies the provided abstractions below the lower temperature limits without further modifications.

The lower temperature limit for the range of applicability of the In-Package Chemistry Abstraction is 25°C. The pH and ionic strength abstractions were developed for conditions at 25°C, but there is no explicit temperature dependence in the abstractions for pH and ionic strength within the waste form domain. Through the use of sensitivity studies and conservative modeling choices, the effects of temperature were determined to be negligible and the range of applicability was extended up to temperatures of 100°C (SNL 2007 [DIRS 180506], Section 6.6[a] and 8.1[a]). Because of the pH buffering capacity in the waste form cells results in a high degree of confidence in the minimum and maximum pH at 25°C (SNL 2007 [DIRS 180506], Section 6.10.8.1[a]) and because sensitivity studies reveal that temperature has a

negligible effect on ionic strength (SNL 2007 [DIRS 180506], Section 6.6.6 and 6.6[a]), the application of pH and ionic strength abstractions developed at 25°C to temperatures as low as 17°C is not anticipated to produce results that are outside the range of uncertainty captured in the abstractions for pH and ionic strength.

The lower temperature limit for the range of applicability of the Dissolved Concentration Limits Abstraction is 25°C. Because actinides in carbonate systems, such as those that will prevail in the EBS, have retrograde solubility, abstractions for the solubility of actinides were developed for conditions at 25°C and include additional uncertainty to expand the temperatures range of applicability up to 100°C, but there is no explicit temperature dependence in the abstractions for actinide solubility in the EBS (SNL 2007 [DIRS 177418], Section 6.3.3.3). The TSPA-LA Model applies the Dissolved Concentration Limits Abstraction at temperatures below 25°C. Because actinides have retrograde solubility, it is possible that dissolved concentration limits below 25°C could be higher than those implemented in the TSPA-LA Model. But because the Dissolved Concentration Limits Abstraction includes additional uncertainty to account for differences in temperature conditions (SNL 2007 [DIRS 177418], Section 6.3.3), it is anticipated that dissolved concentration limits at lower temperatures would be within the range of uncertainty captured in the Dissolved Concentration Limits Abstraction. Radium solubility is higher at higher temperatures and the abstraction developed at 100°C is conservatively applied to all temperatures below 100°C.

The lower temperature limit for the range of applicability of the HLW Glass Waste Form Degradation Abstraction is 20°C. The HLW Glass Waste Form Degradation Abstraction has explicit temperature dependence in the rate expression and below 20°C, the TSPA-LA Model applies the applicable temperature in the rate expression. The lower temperature limit of the HLW Glass Waste Form Degradation Abstraction was determined by the ranges considered in the experimental results used to validate the rate model (BSC 2004 [DIRS 169988], Section 7.3), which showed that the Arrhenius relationship for glass degradation rate is maintained between 20°C and 90°C. This relationship is not anticipated to change between 17°C and 20°C. Therefore, applying the rate model at 17°C to high-level radioactive waste (HLW) glass that is still intact within the waste form domain when the WP temperatures drop below 20°C, is not expected to have any effect on mass transport calculations.

7.3[a] MODEL STABILITY

7.3.1[a] Statistical Stability

As outlined in Section 7.3 of the parent document, the calculated total mean annual dose is an expected value over epistemic and aleatory uncertainties of estimates of annual dose (Equation 7.3-1 of the parent document). The expectation of annual dose over aleatory uncertainty is evaluated first, the result of which is called (for brevity) 'expected annual dose'. The accuracy of the integral over aleatory uncertainty is discussed in Section 7.3.2 of the parent document. The integral of expected annual dose over epistemic uncertainty is referred to as the mean annual dose and is evaluated numerically by using a Monte Carlo technique. The mean annual dose is statistically stable if the sample size employed in the Monte Carlo technique produces an adequate estimate of the mean annual dose.

Section 7.3.1 of the parent document presents analyses that demonstrate the statistical stability of the total mean annual dose (summed over all modeling cases) and the mean annual dose for each modeling case for TSPA-LA Model v5.000. This section compares uncertainty and sensitivity analyses generated by TSPA-LA Model v5.000 and TSPA-LA Model v5.005 and concludes that the results from TSPA-LA Model v5.005 are also statistically stable. Additionally, this section describes the bootstrap sampling procedure (Davison and Kuonen 2002 [DIRS 184463]) used in this addendum to compute confidence intervals for the total mean annual dose for TSPA-LA Model v5.005. Confidence intervals are presented for both 20,000 years (Figure 7.3.1-47[a]) and 1,000,000 years (Figure 7.3.1-48[a]).

7.3.1.1[a] Replicated Sampling Procedure (Procedure for Demonstrating Stability)

No change.

7.3.1.2[a] Stability Analysis Results for Modeling Cases

Human Intrusion Modeling Case—Because of the error involving the timesteps used in the Human Intrusion Modeling Case (Appendix P, Table P-6, Item 6 of the parent document), coarseness of the temporal stability analysis for TSPA-LA Model v5.000 (Section 7.3.1.2), and absence of sensitivity analysis results for the Human Intrusion Modeling Case in the parent document, the statistical stability of the Human Intrusion Modeling Case is demonstrated in this addendum by repeating the replicated sampling procedure. Figure 7.3.1-14a[a] shows the mean annual dose for each of the three replicates of the Human Intrusion Modeling Case, along with the median and the 5th and 95th percentiles of the distribution of the expected annual dose. Figure 7.3.1-14b[a] displays the confidence interval for this modeling case. The high degree of similarity among replicates and the very narrow confidence interval indicates that the mean annual dose for this modeling case is estimated accurately, and the sample size of 300 is adequate.

7.3.1.3[a] Stability Analysis Results for Total Mean Annual Dose

No change.

7.3.1.4[a] Conclusion

No change.

7.3.1.5[a] Statistical Stability of Model Results

As discussed in Section 7.3.1 of the parent document, a replicated sampling procedure provides an effective approach to estimating the potential sampling error in quantities derived from Latin hypercube sampling (Iman 1982 [DIRS 146012]). With this procedure, the LHS is repeatedly generated with different random seeds. Each LHS is used to produce an estimate of the mean annual dose. The ensemble of estimates of the mean annual dose is used to compute an overall mean and standard error. Confidence intervals for the mean annual dose are estimated by means of the *t*-distribution. Appendix J, Section J4.10, of the parent document provides details on the replicated sampling procedure and the application of the *t*-distribution. The analysis presented in the parent document concludes that the LHS size of 300 is sufficient to produce a statistically stable estimate of the total mean annual dose and of the mean annual dose for each modeling

case. The confidence intervals provide a quantitative assessment of the accuracy of the estimates of total mean annual dose and mean annual dose for each modeling case.

Section 4[a] identifies additional direct inputs used in generating the TSPA-LA Model results presented in this addendum. Appendix P[a] lists the changes and corrections made to the TSPA-LA Model in updating from v5.000 to v5.005. Model changes summarized in Appendix P[a] are relatively minor in that the features, events, and processes (FEPs) that determine radionuclide releases from the repository remain constant in the TSPA-LA Model (also see Appendix P of the parent document). Moreover, the LHSs used to generate results from the two models are nearly identical. Table 7.3.1-1[a] summarizes the differences in the sampled parameters in the two LHSs. Both LHSs are of the same size (300) and, with three exceptions, the pairing of sampled values is the same in each LHS. The technique chosen to correct the distributions for FHH_Isotherm_k_CP_a and FHH_Isotherm_s_CP_a resulted in new orderings of the sampled values for these parameters, and the removal of an unintended correlation between WRIP_beta_rand_a and PCE_Delta_pCO2_a (Table K3-2) resulted in a new ordering for the sampled values for WRIP_beta_rand_a. As a consequence, the two LHSs differ in the pairing of the sampled values for these three parameters with the sampled values of the other parameters. Because the changes are relatively minor and both model versions use nearly identical LHSs, the replicated sampling procedure is not repeated with TSPA-LA Model v5.005, except for the Human Intrusion Modeling Case (Section 7.3.1.2[a]). Instead, results from TSPA-LA Model v5.000 are compared to results from TSPA-LA Model v5.005 to demonstrate the statistical stability of results from TSPA-LA Model v5.005.

7.3.1.5.1[a] Expected Annual Dose for Nominal Modeling Case

Figure 7.3.1-17[a] shows the distribution of expected annual dose for 1,000,000 years and statistics for this distribution for the Nominal Modeling Case for (a) TSPA-LA Model v5.000 and (b) TSPA-LA Model v5.005. The general trends and the range of uncertainty in expected annual dose are similar for both models. Because of the correction of the error in computing the weld volume (Appendix P, Section P6, of the parent document), weld flaws are roughly three times more likely to occur in the results from TSPA-LA Model v5.005 than in the results from TSPA-LA Model v5.000. Consequently, weld failures occur earlier in the TSPA-LA Model v5.005 results, as is evident in the few realizations showing expected dose prior to 100,000 years. Despite the earlier occurrence of WP failures in the results from TSPA-LA Model v5.005, Figure 7.3.1-18[a] shows that the statistics for the distribution of expected annual dose are similar for both models, and the scatterplots in Figure 7.3.1-19[a] illustrate (at the selected times) that the expected annual dose is the same for most epistemic sample elements. Expected annual dose increases in TSPA-LA Model v5.005 results after 600,000 years for a few sample elements are due to the corrections to models for waste form and iron oxyhydroxide colloids (Appendix P, Section P18, and Table P-6, Items 5 and 12 of the parent document). Comparison of Figure K4.5-2a of the parent document and Figure K4.5-2a[a] demonstrates that the uncertain inputs that predominately determine uncertainty in expected annual dose are almost identical for both model versions. Because (1) model changes are relatively minor, (2) both models use nearly identical LHSs of the same size, (3) model results show close agreement in both the magnitude and range of uncertainty of expected annual dose, (4) the uncertain inputs that predominately determine uncertainty in expected annual dose are identical for both versions, and (5) TSPA-LA Model v5.000 produces a statistically stable estimate of mean annual dose

(demonstrated in Section 7.3.1.2 of the parent document), it is reasonable to conclude that the sample size used in TSPA-LA Model v5.005 produces a statistically stable estimate of mean annual dose for the Nominal Modeling Case.

7.3.1.5.2[a] Expected Annual Dose for Drip Shield Early Failure Modeling Case

Figure 7.3.1-20[a] and Figure 7.3.1-21[a] show statistics for the distribution of expected annual dose for 20,000 years and 1,000,000 years, respectively, for the Drip Shield Early Failure (EF) Modeling Case. The corresponding distributions for expected annual dose from TSPA-LA Model v5.000 and TSPA-LA Model v5.005 are shown on Figure 8.2-3 of the parent document and Figure 8.2-3[a], respectively. The general trends and the range of uncertainty in expected annual dose are similar for both models. The small but general reduction in expected annual dose for TSPA-LA Model v5.005 results for 20,000 years (Figures 7.3.1-20[a] and 7.3.1-22[a]) is due to the change in the calculation of the seepage fraction (Appendix P, Section P2). Figure 7.3.1-22[a] and Figure 7.3.1-23[a] show that, for most sample elements, the expected annual dose is similar in both model versions. The increase in expected annual dose in TSPA-LA Model v5.005 results for a few sample elements is due to the corrections to models for waste form and iron oxyhydroxide colloids (Appendix P, Section P18, and Table P-6, Items 5 and 12 of the parent document). In particular, the outlying value of expected annual dose at 1,000 years is due to a contribution to expected annual dose from ^{241}Am sorbed to iron oxyhydroxide colloids, which transports relatively rapidly through the natural barriers. For most sample elements, ^{241}Am contributes negligibly to expected annual dose in both model versions. The decrease in expected annual dose in TSPA-LA Model v5.005 results for a few sample elements in Figure 7.3.1-23[a] is due to the change in longitudinal dispersivity, which reduces the contribution to expected annual dose of ^{226}Ra (Appendix P, Section P15 of the parent document). Despite these differences, Figure 7.3.1-22[a] and Figure 7.3.1-23[a] demonstrate that the distribution of expected annual dose is similar for both model versions.

The comparison of Figure K5.7.1-2a of the parent document and Figure K5.7.1-2a[a] demonstrates that the uncertain inputs that predominately determine uncertainty in expected annual dose before 10,000 years are almost identical for both model versions; the comparison of Figure K5.7.1-4a and Figure K5.7.1-4a[a] shows the same conclusion after 10,000 years. Moreover, Section 7.7.1.2 and Section 7.7.1.2[a] demonstrate that the processes affecting radionuclide releases are essentially unchanged from TSPA-LA Model v5.000. It is reasonable to conclude that the sample size used in TSPA-LA Model v5.005 produces a statistically stable estimate of mean annual dose for the Drip Shield EF Modeling Case because (1) model changes are relatively minor, (2) both models use nearly identical LHSs of the same size, (3) model results show close agreement in both the magnitude and range of uncertainty of expected annual dose, (4) the uncertain inputs that predominately determine uncertainty in expected annual dose are identical for both versions, and (5) TSPA-LA Model v5.000 produces a statistically stable estimate of mean annual dose (demonstrated in Section 7.3.1.2 of the parent document).

7.3.1.5.3[a] Expected Annual Dose for Waste Package Early Failure Modeling Case

Figure 7.3.1-24[a] and Figure 7.3.1-25[a] show statistics for the distribution of expected annual dose for 20,000 years and 1,000,000 years, respectively, for the Waste Package EF Modeling Case. The corresponding distributions for expected annual dose from TSPA-LA Model v5.000

and TSPA-LA Model v5.005 are shown on Figure 8.2-5 of the parent document and Figure 8.2-5[a], respectively. The general trends and the range of uncertainty in expected annual dose are similar for both models. Expected annual dose between about 10,000 years and 14,000 years is generally smaller in TSPA-LA Model v5.005 results as shown in Figure 7.3.1-24[a] due to corrections in the calculations for the seepage fraction (Appendix P, Section P2). This item is addressed by TSPA-LA Model v5.005 in Section 6.3.3[a]. Figure 7.3.1-26[a] and Figure 7.3.1-27[a] show that the expected annual dose is the same for most epistemic sample elements. The decrease in expected annual dose (Figure 7.3.1-27[a]) in TSPA-LA Model v5.005 results for a few sample elements is due to the change in longitudinal dispersivity, which reduces the contribution to expected annual dose of ^{226}Ra (Appendix P, Section P15 of the parent document). The comparison of Figure K5.7.2-2a of the parent document and Figure K5.7.2-2a[a] demonstrates that the uncertain inputs that predominately determine uncertainty in expected annual dose before 10,000 years are identical for both model versions; the comparison of Figure K5.7.2-4a of the parent document and Figure K5.7.2-4a[a] shows the same conclusion after 10,000 years. Moreover, Section 7.7.1.1 of the parent document and Section 7.7.1.1[a] demonstrate that the processes affecting radionuclide releases are essentially unchanged from TSPA-LA Model v5.000. Because of these similarities, and because TSPA-LA Model v5.000 produces a statistically stable estimate of mean annual dose for the Waste Package EF Modeling Case (as demonstrated in Section 7.3.1.2 of the parent document), it is reasonable to conclude that the sample size used in TSPA-LA Model v5.005 produces a statistically stable estimate of mean annual dose for the Waste Package EF Modeling Case.

7.3.1.5.4[a] Expected Annual Dose for Igneous Intrusion Modeling Case

Figure 7.3.1-28[a] and Figure 7.3.1-29[a] show statistics for the distribution of expected annual dose for 20,000 years and 1,000,000 years, respectively, for the Igneous Intrusion Modeling Case. The corresponding distributions for expected annual dose from TSPA-LA Model v5.000 and TSPA-LA Model v5.005 are shown on Figure 8.2-7 of the parent document and Figure 8.2-7[a], respectively. The general trends and the range of uncertainty in expected annual dose are similar for both models, although the expected annual dose is generally reduced in magnitude after 10,000 years in the results from TSPA-LA Model v5.005. This reduction is a consequence of the corrected distribution for the longitudinal dispersivity (LDISP in Table K3-2), as described in Appendix P, Section P15 of the parent document. Figure 7.3.1-30[a] and Figure 7.3.1-31[a] show that, for most epistemic sample elements, the expected annual dose is the same for both models. However, prior to 3,000 years, for a few epistemic sample elements the expected annual dose is much higher in the results from TSPA-LA Model v5.005, due to the corrections to models for iron oxyhydroxide colloids (Appendix P, Section P18, and Table P-6, Items 5 and 12 of the parent document). In particular, the outlying values of expected annual dose at 1,000 years are due to contributions to the expected annual dose from ^{241}Am sorbed to iron oxyhydroxide colloids, which transport relatively rapidly through the natural barriers. For most sample elements, ^{241}Am contributes negligibly to expected annual dose in either model version. At 100,000 years, the outlying values of expected annual dose in TSPA-LA Model v5.005 results are due to contributions to expected annual dose from ^{239}Pu sorbed to iron oxyhydroxide colloids, which were not observed in the results from TSPA-LA Model v5.000 due to the errors affecting iron oxyhydroxide colloids. Additionally, after 100,000 years, the expected annual dose for most epistemic sample elements is somewhat less in the results from TSPA-LA Model v5.005; for a few sample

elements, the expected annual dose is much lower than in the results from TSPA-LA Model v5.000. The reduction in expected annual dose is attributable to the reduction in the contribution of ^{226}Ra (compare Figure 8.2-8b of the parent document and Figure 8.2-8b[a]), which in turn results from the corrected distribution for the longitudinal dispersivity (Appendix P, Section P15 of the parent document).

The comparison of Figure K6.7.1-2a of the parent document and Figure K6.7.1-2a[a] demonstrates that the uncertain inputs that predominately determine uncertainty in expected annual dose before 10,000 years are the same for both model versions; the comparison of Figure K6.7.2-2a of the parent document and Figure K6.7.2-2a[a] shows the same conclusion after 10,000 years. Moreover, Section 7.7.1.3 of the parent document and Section 7.7.1.3[a] demonstrate that the processes affecting radionuclide releases are essentially unchanged from TSPA-LA Model v5.000. Because of these similarities, and because TSPA-LA Model v5.000 produces a statistically stable estimate of mean annual dose for the Igneous Intrusion Modeling Case (as demonstrated in Section 7.3.1.2 of the parent document), it is reasonable to conclude that the sample size used in TSPA-LA Model v5.005 produces a statistically stable estimate of mean annual dose for the Igneous Intrusion Modeling Case.

7.3.1.5.5[a] Expected Annual Dose for Volcanic Eruption Modeling Case

No changes to the TSPA-LA Model affected the evaluation of the Volcanic Eruption Modeling Case. Therefore, the results for this modeling case are not different from those reported in the parent document.

7.3.1.5.6[a] Expected Annual Dose for Seismic Ground Motion Modeling Case

Figure 7.3.1-32[a] shows statistics for the distribution of expected annual dose for 20,000 years for the Seismic GM Modeling Case. The corresponding distributions for expected annual dose from TSPA-LA Model v5.000 and TSPA-LA Model v5.005 are shown in Figure 8.2-11a of the parent document and Figure 8.2-11a[a], respectively. The general trends and the range of uncertainty in expected annual dose are similar for both models. Figure 7.3.1-33[a] shows that expected annual dose is essentially unchanged for all epistemic sample elements. The high degree of similarity in the 20,000-year results from both model versions can be attributed to the simplifications to the seismic damage abstractions for this modeling case (Section 7.3.2.6 of the parent document) and to the dominant contribution of ^{99}Tc to expected annual dose for this modeling case (Figure 8.2-12a of the parent document and Figure 8.2-12a[a]). The changes to the seismic damage models summarized in Appendix P[a] do not affect the 20,000-year results because of the simplifications to the seismic damage abstractions (Section 7.3.2.6 of the parent document), and few of the errors detailed in Appendix P have any effect on the mobilization or transport of ^{99}Tc. The comparison of Figure K7.7.1-2a of the parent document and Figure K7.7.1-2a[a] shows that the uncertain model inputs that are important contributors to the uncertainty in expected annual dose for the Seismic GM Modeling Case before 10,000 years are the same for both model versions. Because of these similarities, and because TSPA-LA Model v5.000 produces a statistically stable estimate of mean annual dose for the Seismic GM Modeling Case (as demonstrated in Section 7.3.1.2 of the parent document), it is reasonable to conclude that the sample size used in TSPA-LA Model v5.005 produces a statistically stable estimate of mean annual dose for the Seismic GM Modeling Case for 20,000 years.

Figure 7.3.1-34[a] shows the distribution of expected annual dose for 1,000,000 years and statistics for this distribution for the Seismic GM Modeling Case for (a) TSPA-LA Model v5.000 and (b) TSPA-LA Model v5.005. Due primarily to improving upon the conservative treatment of synergisms between seismic events and nominal corrosion processes (Appendix P, Section P3 of the parent document), in many sample elements fewer CSNF WPs experience seismic damage in the results from TSPA-LA Model v5.005 (shown by a comparison of Figure 8.1-5b of the parent document and Figure 8.1-5b[a]), which in turn results in the reduction in magnitude of expected annual dose before about 300,000 years. Because seismic damage occurs to fewer CSNF WPs, these WPs remain intact until compromised by nominal corrosion processes, which are relatively unchanged (see discussion of Nominal Modeling Case results in Section 7.3.1.5.1[a]). Thus, after 300,000 years, the general trends in expected dose are more representative of the expected dose due to nominal corrosion processes (compare Figure 7.3.1-34b[a] to Figure 7.3.1-17[a]). Statistics for the distribution of expected annual dose for the Seismic GM Modeling Case for 1,000,000 years are shown on Figure 7.3.1-35[a]; Figure 7.3.1-36[a] shows comparisons of expected annual dose for each sample element at selected times. These figures illustrate the general reduction in expected annual dose due to improving the treatment of synergisms between seismic damage and nominal corrosion processes. However, for a few sample elements, expected annual dose is higher at 600,000 years (Figure 7.3.1-36c[a]) and 1,000,000 years (Figure 7.3.1-36d[a]) in the results from TSPA-LA Model v5.005. For these sample elements, increases in expected annual dose are observed at these times because WPs are less likely to be breached by earlier seismic events, which in turn means that more of the waste inventory is contained in the EBS until later times, when WPs are breached due to general corrosion. In addition, the corrections to the calculation of stability of iron oxyhydroxide colloid can lead to larger plutonium releases for those sample elements in which general corrosion failures occur prior to 1,000,000 years.

Despite the differences evident in expected annual dose, Figure 7.3.1-35[a] shows that the range of uncertainty in expected annual dose is similar for both model versions. The comparison of Figure K7.7.2-2a of the parent document and Figure K7.7.2-2a[a] shows that the uncertain model inputs that are important contributors to the uncertainty in expected annual dose for the Seismic GM Modeling Case for 1,000,000 years are generally the same for both model versions. Section 7.7.1.4 of the parent document and Section 7.7.1.4[a] demonstrate that, once WP failure has occurred, the subsequent processes affecting radionuclide releases are essentially unchanged from TSPA-LA Model v5.000. Because of these similarities, and because TSPA-LA Model v5.000 produces a statistically stable estimate of mean annual dose for the Seismic GM Modeling Case (as demonstrated in Section 7.3.1.2 of the parent document), it is reasonable to conclude that the sample size used in TSPA-LA Model v5.005 produces a statistically stable estimate of mean annual dose for the Seismic GM Modeling Case for 1,000,000 years.

7.3.1.5.7[a] Expected Annual Dose for Seismic Fault Displacement Modeling Case

Figure 7.3.1-37[a] and Figure 7.3.1-38[a] show statistics for the distribution of expected annual dose for 20,000 years and 1,000,000 years, respectively, for the Seismic Fault Displacement (FD) Modeling Case. The corresponding distributions for expected annual dose from TSPA-LA Model v5.000 and TSPA-LA Model v5.005 are shown on Figure 8.2-13 of the parent document and Figure 8.2-13[a], respectively. The general trends and the range of uncertainty in expected annual dose are similar for both models. Figure 7.3.1-39[a] and Figure 7.3.1-40[a] show that, for

most epistemic sample elements, the expected annual dose is the same for both models. However, prior to 3,000 years, for a few epistemic sample elements the expected annual dose is much higher in the results from TSPA-LA Model v5.005, due to the corrections to models for iron oxyhydroxide colloids (Appendix P, Section P18, and Table P-6, Items 5 and 12 of the parent document). Additionally, after 100,000 years, the expected annual dose for a few sample elements is much lower than in the results from TSPA-LA Model v5.000 due to the corrected distribution for the longitudinal dispersivity (Appendix P, Section P15 of the parent document). The comparison of Figure K7.8.1-2a of the parent document and Figure K7.8.1-2a[a] demonstrates that the uncertain inputs that predominately determine uncertainty in expected annual dose before 10,000 years are similar for both model versions; the comparison of Figure K7.8.2-2a of the parent document and Figure K7.8.2-2a[a] shows the same conclusion after 10,000 years. Moreover, because the processes that determine radionuclide releases following a fault displacement are similar to those investigated for the early failure modeling cases (i.e., advection and diffusion), and these processes are essentially the same in the Early Failure Modeling Cases for both model versions (as demonstrated by Sections 7.7.1.1 and 7.7.1.2 of the parent document and 7.7.1.1[a], and 7.7.1.2[a]), it is reasonable to conclude that the processes affecting radionuclide releases in the Seismic FD Modeling Case are essentially unchanged from TSPA-LA Model v5.000. Because of the similarities in model results, and because TSPA-LA Model v5.000 produces a statistically stable estimate of mean annual dose for the Seismic FD Modeling Case (as demonstrated in Section 7.3.1.2 of the parent document), it is reasonable to conclude that the sample size used in TSPA-LA Model v5.005 produces a statistically stable estimate of mean annual dose for the Seismic FD Modeling Case.

7.3.1.5.8[a] Total Mean Annual Dose for 20,000 Years

Figure 7.3.1-41[a] shows the distribution of total expected annual dose for 10,000 years and statistics for this distribution for (a) TSPA-LA Model v5.000 and (b) TSPA-LA Model v5.005. The general trends and the range of uncertainty in total expected annual dose are the same for both models. Figure 7.3.1-42[a] shows that the statistics for the distribution of total expected annual dose are similar for both models, and the scatterplots in Figure 7.3.1-43[a] illustrate (at the selected times) that the total expected annual dose is the same for most epistemic sample elements. The similarity in total expected annual dose from both model versions is due primarily to the similarity in expected annual dose from the Seismic GM Modeling Case (Section 7.3.1.5.6[a]) because this case is the dominant contributor to the total expected annual dose in both model versions (compare Figure 8.1-3 of the parent document to Figure 8.1-3[a]). The comparison of Figure K8.1-2a of the parent document and Figure K8.1-2a[a] demonstrates that the uncertain inputs that predominately determine uncertainty in total expected annual dose are the same for both versions. The comparison of Figure 8.1-3a of the parent document and Figure 8.1-3a[a] shows that the contribution of each modeling case to total mean annual dose is unchanged. Finally, Section 7.7.1[a] demonstrates that processes affecting radionuclide releases in each modeling case are essentially unchanged from TSPA-LA Model v5.000. In summary, it is reasonable to conclude that the sample size used in TSPA-LA Model v5.005 produces a statistically stable estimate of total mean annual dose for 20,000 years because (1) model changes are relatively minor, (2) both models use nearly identical LHSs of the same size, (3) model results show close agreement in both the magnitude and range of uncertainty of total expected annual dose, (4) the uncertain inputs that predominately determine uncertainty in total expected annual dose are identical for both versions, (5) the contribution of each modeling case

to total mean annual dose is unchanged, (6) important processes affecting radionuclide releases are unchanged, and (7) TSPA-LA Model v5.000 produces a statistically stable estimate of total mean annual dose (demonstrated in Section 7.3.1 of the parent document).

7.3.1.5.9[a] Total Mean Annual Dose for 1,000,000 Years

Figure 7.3.1-44[a] shows the distribution of total expected annual dose for 1,000,000 years and statistics for this distribution for (a) TSPA-LA Model v5.000 and (b) TSPA-LA Model v5.005. Figure 7.3.1-44[a] shows some differences in the general trend in total expected annual dose between the two sets of model results. The comparison of Figure 8.1-3b of the parent document and Figure 8.1-3b[a] shows that the differences in the trends in dose history result from changes that affect the Seismic GM Modeling Case. Specifically, as discussed in Section 7.3.1.5.6[a], improving upon the conservative treatment of synergisms between seismic events and nominal corrosion processes (Appendix P, Section P3, of the parent document) results in changes in total mean annual dose between about 100,000 years and 600,000 years. The range of uncertainty in total expected annual dose is compared for the two sets of model results in Figure 7.3.1-45[a]. Before 600,000 years, the reduction in the magnitude of the mean, median, 5th and 95th percentiles for total expected annual dose is due to the reduction in CSNF WP damage in the Seismic GM Modeling Case in the TSPA-LA Model v5.005. After 600,000 years, the reduction in magnitude of the mean of total expected annual dose is due to the corrected distribution for the longitudinal dispersivity (documented in Section 6.3.10[a] of this addendum), which results in a general reduction in the expected annual dose for the Igneous Intrusion Modeling Case (Section 7.3.1.5.4[a]). However, the range of uncertainty in total expected annual dose is generally the same for the two sets of model results.

Figure 7.3.1-46[a] illustrates (at the selected times) that the total expected annual dose is similar for many epistemic sample elements. Figure 7.3.1-46b[a] shows the reduction in the total expected annual dose at 200,000 years, which was noted in the comparison in the uncertainty in the total expected annual dose discussed above. The comparison of Figure K8.2-2a and Figure K8.2-2a[a] demonstrates that the uncertain inputs that predominately determine uncertainty in total expected annual dose after 10,000 years are the same for both versions. Finally, Section 7.7.1[a] demonstrates that processes affecting radionuclide releases in each modeling case are essentially unchanged from TSPA-LA Model v5.000.

In summary, although there are significant differences in the total expected annual dose between approximately 100,000 to 300,000 years, the important processes affecting radionuclide releases remain unchanged, and (1) model changes to the TSPA-LA Model v5.005 are relatively minor, (2) both models use nearly identical LHSs of the same size, (3) the uncertain inputs that predominately determine uncertainty in total expected annual dose are the same for both versions, (4) model results are similar in both the magnitude and range of uncertainty of total expected annual dose over the majority of the simulation, and (5) the relative contributions of each modeling case to total mean annual dose is unchanged. Since the TSPA-LA Model v5.000 produces a statistically stable estimate of total mean annual dose (demonstrated in Section 7.3.1 of the parent document), it is reasonable to conclude that the sample size used in TSPA-LA Model v5.005 produces a statistically stable estimate of total mean annual dose for 1,000,000 years.

7.3.1.6[a] Procedure for Computing Confidence Intervals

To provide a quantitative assessment of the accuracy of the estimate of total mean annual dose for TSPA-LA Model v5.005, a bootstrap sampling procedure is used to generate confidence intervals. Bootstrap simulation is a numerical procedure for estimating confidence intervals for statistics of interest. Given a sample of size *n*, the general approach in bootstrap simulation is to: (1) assume that the sample is an adequate approximation of the underlying distribution; (2) perform *r* replications of the set of values by randomly selecting, with replacement, *n* values from the sample; and (3) calculate *r* values for the statistic of interest. Davison and Kuonen (2002 [DIRS 184463]) provide an outline of the bootstrap procedure. The underlying assumption that the sample is an adequate approximation of the underlying distribution is justified because (1) the assumption has already been justified for TSPA-LA Model v5.000, as demonstrated by the stability analysis presented in Section 7.3.1 of the parent document; (2) TSPA-LA Model v5.005 produces results with uncertainty ranges similar to those observed for the TSPA-LA Model v5.000 results; and (3) uncertain inputs that dominate uncertainty in total expected annual dose are generally the same for TSPA-LA Model v5.000 and TSPA-LA Model v5.005.

Figure 7.3.1-47[a] displays the confidence interval for total mean annual dose for a simulation of 20,000 years, computed by using the bootstrap technique for both versions of the TSPA-LA Model. The upper and lower confidence bounds displayed on Figure 7.3.1-47[a] are the 97.5 percentile and 2.5 percentile, respectively, for the sampling distribution of total mean annual dose. Figure 7.3.1-47[a] shows that, with a probability 0.975, the true mean is estimated to lie more than an order of magnitude below the individual protection standard of 15 mrem for 10,000 years after permanent closure as specified in 10 CFR 63.311(a)(1) [DIRS 178394]. The narrowness of the confidence interval (less than ±0.2 mrem/yr) over the 20,000-year simulation and the relatively large separation between the confidence interval and the regulatory limit relative to the width of the confidence interval indicates that total mean annual dose for this modeling case is estimated with sufficient accuracy. The corresponding confidence interval for TSPA-LA Model v5.000 (Replicate 1) is shown for comparison.

Figure 7.3.1-48[a] shows the confidence interval for total mean annual dose for 1,000,000 years. Again, the upper and lower confidence bounds displayed on Figure 7.3.1-48[a] are the 97.5 percentile and 2.5 percentile, respectively, for the sampling distribution of total mean annual dose. Similar to the 20,000-year simulation, the narrowness of the confidence interval (less than ±0.5 mrem/yr) over the 1,000,000-year simulation and the separation between the confidence interval and the regulatory standard of 350 mrem specified in U.S. Nuclear Regulatory Commission Proposed Rule 10 CFR 63.311(a)(2) [DIRS 178394]) indicates that total mean annual dose for this modeling case is estimated with sufficient accuracy.

7.3.1.7[a] Conclusion

In Section 7.3.1 of the parent document, statistical stability of the total mean annual dose was evaluated by means of a replicated sampling procedure. The comparison of three estimates of total mean annual dose and the associated distributions of uncertainty in expected annual dose showed that the three independent LHS replicates produced statistically similar values of the total mean annual dose, as well as similar distributions of uncertainty in expected annual dose. The analysis concluded that the results of TSPA-LA Model v5.000 are statistically stable.

Statistical stability of the total mean annual dose presented in this addendum was evaluated by means of comparisons between TSPA-LA Model v5.000 and TSPA-LA Model v5.005 and results from these models, for all except the Human Intrusion Modeling Case. The relatively few changes between the models, and the similarities evident in the results of the models, support the conclusion that because the results of TSPA-LA Model v5.000 are demonstrated to be statistically stable, the results of TSPA-LA Model v5.005 are also statistically stable. Confidence intervals are computed for TSPA-LA Model v5.005 using a bootstrap procedure. The replicated sampling procedure was repeated for the Human Intrusion Modeling Case to demonstrate statistical stability.

Table 7.3.1-1[a]. Uncertainty Distribution Changes for TSPA-LA Model v5.005

Parameter Listing (Table K3-2)	TSPA-LA Model Description	TSPA-LA Model v5.000	TSPA-LA Model v5.005
LDISP	Section 6.3.10.2, Section 6.3.10.2[a], Table 6.3.10-2	Normal: (Log_{10}-transformed) Mean: 2.0 m Standard Deviation: 0.75 m	Truncated Normal: (Log_{10}-transformed) Mean: 2.0 m Standard Deviation: 0.75 m Maximum 2 Standard Deviation
FHH_Isotherm_k_CP_a	Table 6.3.8-4[a], Table P-6, 7	Uniform (1.048 to 1.370)	Uniform (1.030 to 1.326)
FHH_Isotherm_s_CP_a	Table 6.3.8-4[a], Table P-6, 7	Uniform (1.525 to 1.852)	Uniform (1.493 to 1.799)
KdU_Zeo_a	Section 6.3.9.2, Section 6.3.9.3, Table 6.3.9-2, Table P-6, 11	Piecewise Uniform (0 to 20 mL/g)	Piecewise Uniform (0 to 30 mL/g)
KdSe_Vit_a	Section 6.3.9.2, Section 6.3.9.3, Table 6.3.9-2, Table P-6, 10	Truncated log normal (1 to 25 mL/g)	Truncated lognormal (0 to 25 mL/g)
Kd_Np_Rev_U_Col_a	Section 6.3.7.6.2, Section 6.3.7.6.3, Table 6.3.7-64, Table 6.3.7-64[a], Table P-6, 8	Log Uniform (1 to 500 mL/g)	Log Uniform (10 to 500 mL/g)

INTENTIONALLY LEFT BLANK

7.3.2[a] Numerical Accuracy of Expected Annual Dose

No change.

7.3.2.1[a] Nominal Modeling Case

No change.

7.3.2.2[a] Waste Package Early Failure Modeling Case

No change.

7.3.2.3[a] Drip Shield Early Failure Modeling Case

No change.

7.3.2.4[a] Igneous Intrusion Modeling Case

No change.

7.3.2.5[a] Volcanic Eruption Modeling Case

No change.

7.3.2.6[a] Seismic Ground Motion Modeling Case

No change.

7.3.2.6.1[a] Seismic Ground Motion Modeling Case for 10,000 Years

No change.

7.3.2.6.1.1[a] Accuracy of Expected Annual Dose Calculations

No change.

7.3.2.6.1.2[a] Additivity in Annual Dose from Multiple Seismic Events

This section has been edited for clarity and replaces the corresponding section in the parent document.

As noted in Section 6.1.2.4.4 of the parent document, Equation 6.1.2-22 is based on the assumption that the annual dose from two or more events causing cumulative damage to WPs is reasonably approximated by the sum of the annual doses from the events modeled independently. Figure 7.3.2-12 of the parent document illustrates the change in annual dose at 10,000 years due to changes in damage fraction, after an event at 100 years, for epistemic realization 1. The change in annual dose is proportional to changes in damage fraction up to the damage fraction of about 10^{-5}. Beyond the damage fraction of 10^{-5}, annual dose does not increase proportionally with increasing damage fraction. Thus, when two or more seismic events cause cumulative damage fraction exceeding 10^{-5}, the additivity assumption results in an overestimate of the annual dose resulting from seismic events. The dose resulting from a single event causing

damage fraction exceeding 10^{-5} is not overestimated since this quantity is computed by interpolation between the level curves shown on Figure 7.3.2-9 of the parent document.

To estimate the degree of conservatism incurred by this additivity assumption, expected annual dose from one seismic event was calculated by evaluating the first integral term in Equation 6.1.2-22:

$$\bar{D}_{SG}\left(\tau\left|1,\mathbf{e}_i\right.\right)=\int_0^{\tau}\left(\lambda_1\left(\mathbf{e}_i\right)e^{-\lambda_1(\mathbf{e}_i)t}\left(\int_{A_{\min}}^{A_{\max}}D_{SG}\left(\tau\left|\left[1,t,A\right],\mathbf{e}_i\right.\right)d_{A1}\left(A\left|\mathbf{e}_i\right.\right)dA\right)\right)dt \qquad \text{(Eq. 7.3.2-1[a])}$$

The integral displayed in Equation 7.3.2-1[a] computes the expected annual dose from the first seismic event that damages co-disposed (CDSP) WPs. The second integral in Equation 6.1.2-22 computes the additional expected annual dose from the second and subsequent seismic events. Figure 7.3.2-13 of the parent document shows the expected annual dose from the first damaging seismic event; Figure 7.3.2-14 of the parent document shows the expected annual dose from all damaging seismic events for all 300 epistemic realizations. The comparison of the expected annual dose from the first damaging event to the expected annual dose from all damaging events shows that the second and subsequent damaging events add somewhat to the magnitude of the expected annual dose but do not change the magnitude or range of uncertainty to any great extent. Consequently, the additivity assumption, while conservative, does not result in a significant overestimate of the expected annual dose.

7.3.2.6.1.3[a] Simplifications to the Seismic Consequences Abstraction

No change.

7.3.2.6.2[a] Seismic Ground Motion Modeling Case for 1,000,000 Years

No change.

7.3.2.7[a] Seismic Fault Displacement Modeling Case

The analysis presented in the parent document showed the expected annual dose for the Seismic Fault Displacement Modeling Case is estimated with sufficient accuracy. However, the analysis showed the calculation's accuracy could be improved by further discretization of the aleatory variables. In particular, Figure 7.3.2-26 (of the parent document) compares the expected annual dose for five epistemic realizations for a base case of aleatory discretization and an expanded case; the expected annual dose generally increased by approximately 30 percent in the expanded case. To determine whether further refinement in aleatory discretization would lead to additional increases in expected annual dose, a second expanded case was formed and expected annual dose was evaluated. In this second expansion case the number of times of fault displacement events was increased from 6 to 23 and the number of damage areas was again increased from 3 to 5. The results did not show further increase in expected annual dose (output DTN: MO0801TSPAADSA.000 [DIRS 185078], file *LA_v5.000_SF_010800_10k_Dose_Compare_Rev01.JNB*), confirming the assessment that expected annual dose is computed with sufficient numerical accuracy.

7.3.2.8[a] Human Intrusion Modeling Case

No change.

7.3.3[a] Temporal Stability

This material supplements the corresponding section in the parent document.

Another issue related to the stability of the TSPA-LA Model results is temporal discretization of the model. In order to calculate transport of radionuclides, the TSPA-LA Model numerically solves partial differential equations in various submodels (e.g., FEHM for UZ transport) and model abstractions (e.g., SZ 3-D transport). The numerical solution involves computations with discrete timesteps which is referred to as temporal discretization. Temporal discretization may affect the accuracy of the solution of the differential equations and, thereby, affect the results of the TSPA-LA Model. Several different TSPA-LA Model runs were documented in Section 7.3.3 of the parent document that evaluated the potential for variability in model output due to timestep size. These analyses demonstrated that the output of the TSPA-LA Model is not significantly affected by refining the temporal discretization and concluded that the temporal discretization used in the TSPA-LA Model is adequate. Included in Section 7.3.3.6[a] of this addendum is an update to the temporal stability for the Human Intrusion Modeling Case necessitated by the correction of an error documented in Appendix P, Table P-6, Item 6, of the parent document. In addition, a temporal stability assessment of the Nominal Modeling Case has been added as Section 7.3.3.7[a] of this addendum.

7.3.3.1[a] Selection of Modeling Cases

No change.

7.3.3.2[a] Methodology

No change.

7.3.3.3[a] Waste Package Early Failure Modeling Case

No change.

7.3.3.4[a] Igneous Intrusion Modeling Case

No change.

7.3.3.5[a] Seismic Ground Motion Modeling Case

No change.

7.3.3.6[a] Human Intrusion Modeling Case

In the Human Intrusion Modeling Case, a single stylized intrusion occurs at 200,000 years. Annual dose is computed by the GoldSim component of the TSPA-LA Model for each combination of a sampled intrusion location (characterized by WP type, percolation rate and entry point into the SZ) and epistemic realization. For each epistemic realization, the ensemble

of dose histories is averaged to compute expected dose, as described by Equation 6.1.2-26 in Section 6.1.2.5 of the parent document. At the time of the intrusion, percolation begins to flow through the waste and transport the radionuclides down the borehole to the SZ. Thus, the dose following an intrusion has a large initial value that decreases rapidly as radionuclide inventory is depleted or decays.

To complete a comprehensive analysis of temporal stability for the TSPA-LA Model, an additional analysis is presented in this addendum for the Human Intrusion Scenario, which includes the correction of a timestep error documented in Appendix P, Table P-6, Item 6, of the parent document. In the parent document, temporal stability for the Human Intrusion Modeling Case was judged to be adequate, despite the presence of the timestep error and the coarseness of the temporal resolution of expected dose (see Figures 7.3.3-10 and 7.3.3-11 of the parent report). Because of the correction of the timestep error and the coarseness evident in the parent document, the base timestep scheme for the Human Intrusion Modeling Case was revised to that shown in Table 7.3.3-2[a], and temporal stability was re-assessed for TSPA-LA Model v5.005. Figure 7.3.3-10[a] compares the base-case timestep results with the alternative timestep scheme for the 1,000,000 Year simulation period. Figure 7.3.3-11[a] focuses on the dose immediately after the intrusion (out to 220,000 years only) and shows that the base-case timestep size in TSPA-LA Model v5.005 provides results that are nearly identical to the alternate timestep scheme. The similarity in expected annual dose for the two timestep schemes confirms that the Human Intrusion Modeling Case is stable with respect to temporal discretization.

7.3.3.7[a] Nominal Modeling Case

The Nominal Modeling Case estimates the annual dose resulting from WP failures from nominal corrosion processes (i.e., general corrosion, microbial influenced corrosion, stress corrosion cracking [SCC]), as well as the effects of general corrosion of DS materials (Section 6.3.5 of the parent document). The number and type of WP failures at each point in time is estimated by the use of several software packages, as described in Section 6.3.5.1.3 of the parent document; the radionuclide transport and dose resulting from this sequence of failures is estimated by the GoldSim component of the TSPA-LA Model, as described in Section 6.1.2.4.1 of the parent document.

The time of failure of a WP depends on the temperature-dependent general corrosion rates applied to the WP, which change over time as temperature changes. Thus, the temporal discretization, which defines when the value of the general corrosion rate will be updated, is influential to the annual dose resulting from nominal corrosion processes.

In the base case, the coarse timestep discretization beyond 200,000 years used to calculate general corrosion was taken from the thermal hydrology histories. The temperature and relative humidity data did not fluctuate significantly once ambient conditions within the repository were reestablished and a coarse timestep discretization was selected to represent the data. The general corrosion calculations used the same timestep discretization. In the temporal stability study, the timestep discretization used by the general corrosion calculations was refined by updating the timestep scheme in the thermal hydrology history files. The number of data points was increased from 68 in the base case to 279 in the temporal stability run. The timesteps for the base case are found in the files with an .ou extension within output DTN: MO0710ADTSPAWO.000

([DIRS 183752], Input_File_Set_064.zip) and the timesteps for the alternative time scheme are in the files with an .ou extension within output DTN: MO0801TSPAWPDS.000 ([DIRS 185077], Replacement_Input_File_Set_25.zip). The GoldSim timestep schedule was not altered for this analysis. The new timestep discretization was selected so that the maximum timestep size used in the general corrosion calculations was 10,000 years. The timestep schedule maintained the timestep scheme previously used for the first 750 years. From 200 years up until 1000 years, the timestep size was 50 years. From 1,000 years to 10,000 years the timestep size was 100 years, compared to a maximum 2,000 year timestep over this time period in the base case. From 10,000 years to 20,000 years the timestep size was 500 years, compared to a maximum 5,000 year timestep over this time period in the base case. From 20,000 years to 50,000 years the timestep size was 1000 years, compared to a maximum 10,000 year timestep over this time period in the base case. From 50,000 years to 75,000 years the timestep size was 2500 years, compared to a maximum 20,000 year timestep over this time period in the base case. From 75,000 years to 100,000 years the timestep size was 5000 years, compared to a maximum 30,000 year timestep over this time period in the base case. Beyond 100,000 years the timestep size was 10,000 years until the last time point at 999,950 years, compared to a maximum 300,000 year timestep over this time period in the base case.

Figure 7.3.3-12[a] compares the base-case timestep results with the alternative timestep scheme for the 1,000,000 year simulation period. The few realizations with expected annual dose before 200,000 years appear similar for either timestep scheme. However, in the base case, the coarse timesteps used after 200,000 years result in observable jumps in expected annual dose at 200,000; 300,000; 500,000 and 700,000 years. At these timesteps, the number of WP failures (from SCC) calculated by the WP degradation code WAPDEG V4.07 (STN: 10000-4.07-01 [DIRS 181064]) increases sharply. The stress corrosion crack growth rate is given by a power law function of stress intensity factor and repassivation slope n (Equation 6.3.5-14 of the parent document). The stress intensity factor is evaluated at the beginning of each WAPDEG timestep and is a function of the crack depth that drives the crack propagation. The large timesteps taken past 100,000 years combined with the sensitivity of the crack growth rate to the stress intensity factor, which is raised to the power 4n, where n has a mean value of 1.165 (SNL 2007 [DIRS 181953], Table 8-15), can cause dramatic changes in the crack growth rate at each timestep. As a result, the crack growth rate can change from a small value for the timestep in which the crack initiates to a much larger value at the beginning of the next timestep, resulting in almost immediate penetration of many cracks and WP failures. Use of shorter timesteps in the alternative scheme improves the calculation of the crack growth rate, which removes the jumps in the number of WP failures by SCC, which in turn is reflected in the expected annual dose curves for the alternative scheme. The increase in expected annual dose from using the increased number of timesteps in the alternative time scheme is due to an increase in the number of WP failures calculated by the WAPDEG code. Between the two cases, the number of WP failures were approximately the same midway between each large timestep used in the base case (output DTN: MO0801TSPAWPDS.000 [DIRS 185077], file: LA_v5.005_NC_000300_006_Dose_Assessment.doc), but the base case underestimated the number of WP failures in the second half of the WAPDEG timestep. The WAPDEG code applies an average penetration depth over an entire timestep to determine the general corrosion and stress corrosion consequences for each timestep. Applied as an average, the calculated results for a large timestep are overestimated in the beginning of the timestep and underestimated at the end of the timestep. Thus, because the TSPA-LA Model ends at the end of a WAPDEG timestep, the number of failures is underestimated at the end of the realization.

Figure 7.3.3-13[a] compares statistics on expected annual dose for the base-case and the alternative timestep scheme. The comparison shows that both the magnitude of expected annual dose and the range of uncertainty in expected annual dose are similar for both timestep schemes. This similarity in statistics for expected annual dose for the two timestep schemes indicates that the Nominal Modeling Case is sufficiently stable with respect to temporal discretization and that any underestimation in dose due to the large WAPDEG timesteps taken in the base case is not significant.

The timestep scheme for the base case model was selected for computational efficiency. In the base case calculations, the WAPDEG calculations accounted for about 40 to 50 percent of the simulation time. In the sensitivity study, the WAPDEG calculation time increased by a factor of four, doubling the run time. Because the TSPA-LA Model results were judged to be sufficiently stable with respect to temporal discretization and because improving the smoothness of the expected annual dose curves would involve significant additional calculation time, the base case timestep scheme was used in the TSPA-LA Model for the Nominal Modeling Case.

Table 7.3.3-2[a]. Revised Timestep Schemes used in Temporal Stability Analysis

Modeling Case	Base-Case Timestep Scheme (v5.000)	Base-Case Timestep Scheme (v5.005)	First Alternate Timestep Scheme
Human Intrusion (intrusion occurs at 200,000 yr)	250 yr from 0 to 10k yr 500 yr from 10k to 100k yr 1,000 yr from 100k to 120k yr 2,000 yr from 120k to 160k yr 4,000 yr from 160k to 1M yr	250 yr from 0 to 10k yr 500 yr from 10k to 100k yr 1,000 yr from 100k to 120k yr 2,000 yr from 120k to 158k yr 4,000 yr from 158k to 198k yr 250 yr from 198k to 204k yr 1,000 yr from 204k to 212k yr 4,000 yr from 212k to 1M yr	250 yr from 0 to 10k yr 500 yr from 10k to 100k yr 1,000 yr from 100k to 120k yr 2,000 yr from 120k to 158k yr 4,000 yr from 158k to 198k yr 40 yr from 198k to 204k yr 400 yr from 204k to 212k yr 4,000 yr from 212k to 1M yr

Source: Output DTNs: MO0709TSPAREGS.000 [DIRS 182976], File: V5.000_HI_009000_002.gsm (for Base Case v5.000); MO0710ADTSPAWO.000 [DIRS 183752], File: v5.005_HI_009000_000.gsm, (for Base Case v5.005); and MO0801TSPAADSA.000 [DIRS 185078], File: v5.005_HI_009000_001.gsm, (for Alternate).

INTENTIONALLY LEFT BLANK

7.3.4[a] Analyses of Spatial Discretization

No change.

7.3.5[a] Stability of FEHM Particle Tracking Model

No change.

7.4[a] UNCERTAINTY AND VARIABILITY CHARACTERIZATION REVIEWS

No change.

7.5[a] SURROGATE WASTE FORM VALIDATION

This material supplements the corresponding material in the parent document.

The purpose of the analyses documented in Section 7.5 of the parent document is to show that the surrogate representation of naval spent fuel (Category 1 DOE spent nuclear fuel [DSNF]) and the DSNF surrogate, the average of DSNF Categories 2 through 11, are appropriate. The averaging of Categories 2 through 11 is related to the spatial averaging that is analyzed in Section 7.3.4 of the parent document.

The updated analyses presented in this addendum were conducted to confirm that Zircaloy-clad CSNF adequately represents Category 1 DSNF in TSPA-LA Model v5.005. Category 1 DSNF, naval spent fuel in the TSPA-LA Model, is represented as Zircaloy-clad CSNF. Section 7.5.3[a] discusses the analyses using TSPA-LA Model v5.005 where the naval source term replaced the CSNF source term for the Drip Shield EF and Igneous Intrusion Modeling Cases.

7.5.1[a] Methodology

No change.

7.5.2[a] Spent Fuel Categories and Representation in Model

No change.

7.5.3[a] Naval Spent Fuel, Category 1

Analyses were performed to confirm the adequacy of the use of CSNF as a surrogate for NSNF. These analyses are outlined in Table 7.5-5 of the parent document. The analyses were conducted for simulations of 10,000 years, and a qualitative argument for the extension of the results beyond 10,000 years is also presented. For this addendum, TSPA-LA Model v5.005 was exercised explicitly using NSNF inventories in place of the CSNF inventory. The dose results from these cases were compared to demonstrate that CSNF inventory bounds the NSNF inventory.

7.5.3.1[a] Comparison of the Naval Spent Nuclear Fuel and Commercial Spent Nuclear Fuel Inventories for 10,000 Years and 1,000,000 Years

No change.

7.5.3.2[a] Disposition of Commercial Spent Nuclear Fuel as a Surrogate for Naval Spent Nuclear Fuel for the Early Failure Modeling Cases

NSNF was analyzed using inventories, or source terms, supplied by the Navy for radionuclides that are available for release from naval spent fuel. The source terms are based on a hypothetically failed WP of naval spent fuel for the Drip Shield EF and Igneous Intrusion Modeling Cases. These source terms were provided by the Naval Nuclear Propulsion Program (McKenzie 2007 [DIRS 182657]). The analyses of naval spent fuel are special cases developed to compare CSNF and naval spent fuel for the Drip Shield EF and Igneous Intrusion Modeling Cases. For these analyses, the NSNF source term (radionuclides available for release within a failed WP) was modeled in a failed CSNF WP, and the radionuclides were then subject to all of the transport processes that are applied to dissolved CSNF (e.g., solubility, sorption, and chemistry along the transport pathway from dissolved CSNF to the reasonably maximally exposed individual [RMEI]) in the TSPA-LA Model.

In the modeled repository, there are 8,213 WPs of CSNF, 417 of which represent naval spent fuel (SNL 2007 [DIRS 180472], Table 6-2[a]). The TSPA-LA Model does not explicitly include naval spent fuel but bounds its behavior with 417 CSNF WPs that represent naval spent fuel. The special case analyses in this section were conducted to demonstrate that the annual dose from naval spent fuel is bounded by the annual dose from CSNF.

For the validation of CSNF as a surrogate for naval spent fuel for the non-disruptive event cases, the Drip Shield EF Modeling Case was chosen over the Waste Package EF Modeling Case because of the following considerations. First, the transport of radionuclides within the EBS for the Drip Shield EF Modeling Case is advection dominated with some diffusion. The transport of radionuclides within the EBS for the Waste Package EF Modeling Case is diffusion dominated since the drip shield (DS) stays intact. The Waste Package EF Modeling Case would produce lower radionuclide doses compared to the Drip Shield EF Modeling Case and, therefore, can be considered a subset of the Drip Shield EF Modeling Case for the NSNF analysis. In addition, in the TSPA-LA Model, the Waste Package EF Modeling Case applies not only a temperature threshold to transport, but a relative humidity threshold to transport radionuclides from the waste form to the WP OCB. Since the naval source term is a release from a failed WP, it is implemented in the TSPA-LA Model by applying the release to the WP transport cell and, therefore, bypasses the relative humidity threshold for transport from the waste form transport cell. The result of using the Waste Package EF Modeling Case for the analysis would be an early release of radionuclides to the accessible environment for the naval source term, which would be inconsistent with a later release of radionuclides for the CSNF source term. The delay in release from the waste form to the WP OCB due to the relative humidity threshold for transport is not implemented in the Drip Shield EF Modeling Case. Therefore, for the Drip Shield EF Modeling Case, the timing of the release of radionuclides to the accessible environment from a failed WP with a CSNF source term is more consistent with the timing of the release from a failed WP where the naval source term has been substituted for the CSNF source term in the WP transport cell.

For the Drip Shield EF Modeling Case, a single DS failure was forced to occur at the first timestep of the simulation. Two simulations using TSPA-LA Model v5.005 were run: one for a single CSNF WP and one for a single WP where the naval source term replaced the CSNF source term. The simulations were run for 10,000 years and used a unified sampling of epistemic and aleatory uncertainty over 300 model realizations. The results, in terms of a mean annual dose over the unified sampling of epistemic and aleatory uncertainty, are shown on Figure 7.5-4[a]. As noted in the results documented in the parent document, the results of this analysis show that over a 10,000-year period, the dose associated with the naval source term is less than that of the CSNF source term. At 10,000 years, the mean annual dose from a failed WP with a naval source term is over two orders of magnitude lower than the mean annual dose for a failed CSNF WP, confirming the appropriateness of the use of a CSNF WP as a surrogate for a naval WP.

7.5.3.3[a] Disposition of Commercial Spent Nuclear Fuel as a Surrogate for Naval Spent Nuclear Fuel for the Igneous Intrusion Modeling Case

A similar analysis conducted for the Igneous Intrusion Modeling Case is used to confirm the appropriateness of the use of CSNF as a surrogate for NSNF. For both the CSNF and naval source term stylized analysis, the time of the igneous intrusion was forced to occur at a specified timestep, and a single WP was failed. Using TSPA-LA Model v5.005, simulations were run for 10,000 years and used a unified sampling of epistemic and aleatory uncertainty over 300 model realizations. The results, in terms of a mean annual dose over the unified sampling of epistemic and aleatory uncertainty, are shown on Figure 7.5-5[a]. As was the case for the Drip Shield EF Modeling Case, the results for the Igneous Intrusion Modeling Case show that for a 10,000-year period, the dose associated with the naval source term is less than that of the CSNF source term, again justifying the use of a CSNF WP as a surrogate for a naval WP.

7.5.3.4[a] Disposition of Commercial Spent Nuclear Fuel as a Surrogate for Naval Spent Nuclear Fuel for the Volcanic Eruption Modeling Case

No change.

7.5.3.5[a] Disposition of Commercial Spent Nuclear Fuel as a Surrogate for Naval Spent Nuclear Fuel for the Human Intrusion Modeling Case

No change.

7.5.3.6[a] Disposition of Commercial Spent Nuclear Fuel as a Surrogate for Naval Spent Nuclear Fuel for the Nominal Modeling Case

Note, minor reference change from the parent document.

The use of CSNF as a surrogate for NSNF for the first 10,000 years of the Nominal Modeling Case is justified because there are no WP failures during this time period, and because the naval WP is more robust than the commercial WP. The 1,000,000 year Nominal Modeling Case is a stylized case (see Section 8.2.1 of the parent document) where the WP fails by SCC and general corrosion sometime after the first 10,000 years. These effects are accounted for in the 1,000,000 year Seismic GM Modeling Case. The use of CSNF as a surrogate for NSNF for the 1,000,000 year Nominal Modeling Case is justified because of the NSNF is adequately represented by

CSNF in the early failure cases, and again because the naval WP is more robust than the commercial WP.

7.5.3.7[a] Disposition of Commercial Spent Nuclear Fuel as a Surrogate for Naval Spent Nuclear Fuel for the Seismic Modeling Cases.

No change.

7.5.4[a] U.S. Department of Energy Spent Fuel, Categories 2 through 11

No change.

7.5.5[a] Selected Sensitivity Analyses

No change.

7.5.6[a] Summary of Results for U.S. Department of Energy Spent Fuel

The additional analyses presented in this section of the addendum confirm that comparing naval spent fuel with Zircaloy-clad CSNF demonstrates that CSNF bounds the results of naval spent fuel for both non-disruptive (Drip Shield EF) and disruptive event (Igneous Intrusion) modeling cases. Additional analyses performed by the Naval Nuclear Propulsion Project as documented in Section 7.5.3.7 of the parent document confirm the use of CSNF as a surrogate for naval spent fuel for the seismic scenarios (Gisch 2004 [DIRS 171782]). Representing naval spent fuel by CSNF as its surrogate in the TSPA-LA Model adequately bounds the behavior of naval spent fuel (Section 7.5.3[a]).

No additional analyses were conducted for the remaining categories of DSNF.

7.6[a] CORROBORATION OF ABSTRACTION MODEL RESULTS WITH VALIDATED PROCESS MODELS

No change.

7.7[a] CORROBORATION OF RESULTS WITH AUXILIARY ANALYSES

The auxiliary analyses are an important aspect of determining whether the TSPA-LA Model is yielding reasonable results (e.g., that the model is producing the results that would be expected). To supplement the results presented in Section 7.7 of the parent document, the following auxiliary analyses were performed using TSPA-LA Model v5.005 and documented in this addendum: (1) single realization analysis of various modeling cases, including additional analyses for outlier realizations; (2) comparison of the results of the TSPA-LA Model with a Simplified TSPA Analysis (Section 7.7.2[a]); (3) comparison of the results of the TSPA-LA Model with the TSPA independently developed by EPRI (Section 7.7.3[a]); and (4) PMA (Section 7.7.4[a]). A summary of the additional auxiliary analyses included in this addendum is provided below.

7.7.1[a] Analyses of Single Realizations

Analyses of single realizations provide insight into the coupling of various submodel processes within the TSPA-LA Model. The analyses presented in Section 7.7.1 of the parent document and Section 7.7.1[a] of this addendum include an in-depth explanation about how the transport of key radionuclides is affected by coupling various components of the EBS, UZ, and SZ domains following WP failure under a variety of physical, chemical, thermal, and mechanical conditions. The insight gained provides assurance that the various submodel processes are working as expected and, in turn, helps provide confidence in the TSPA-LA Model.

The single realization analyses presented in this addendum evaluate seven modeling cases that are used to cover the range of WP failure mechanisms considered in the TSPA-LA Model and highlight various processes affecting and controlling radionuclide releases under a variety of conditions. The seven modeling cases are: (1) Waste Package EF Modeling Case (Section 7.7.1.1[a]), (2) Drip Shield EF Modeling Case (Section 7.7.1.2[a]), (3) Igneous Intrusion Modeling Case (Section 7.7.1.3[a]), (4) Seismic GM Modeling Case (Section 7.7.1.4[a]), (5) Nominal Modeling Case (Section 7.7.1.5[a]), (6) Human Intrusion Modeling Case (Section 7.7.1.6[a]), and (7) Seismic GM Modeling Case for the 10,000-year duration (Section 7.7.1.7[a]). The durations for all modeling cases, except where noted, was 1,000,000-years.

The methodology for calculating expected annual dose (i.e., the expectation of annual dose over aleatory uncertainty) for the various modeling cases is described in Section 6.1.2 of the parent document, which discusses how to differentiate epistemic uncertainty from aleatory uncertainty in the TSPA-LA Model. Although the treatment of aleatory uncertainty varies with each modeling case, the general methodology for selecting a realization for detailed analysis is similar for all seven modeling cases described in this section. First, an epistemic uncertainty vector is chosen from the set of epistemic uncertainty vectors. The two primary criteria for selecting a particular epistemic uncertainty vector are that (1) the *functional form* (shape) of the expected annual dose (for the chosen epistemic vector) is similar to that of the mean annual dose (computed by taking expectation over all epistemic uncertainty vectors) and (2) the *magnitude* of the expected annual dose for the chosen epistemic vector is similar or higher than the mean annual dose over the time period of interest. These criteria are intended to help select epistemic uncertainty vectors that highlight processes of most interest for each modeling case. Since the expected annual dose for an epistemic vector is calculated by taking the expectation over aleatory uncertainty, each expected annual dose is further broken down in order to select the realization(s) representing individual aleatory uncertainty vectors. An aleatory vector is chosen by comparing its dose contribution to other aleatory vectors in the set and that which best describes the behavior of the expected annual dose for the epistemic vector over the time period of interest. For the Igneous Intrusion, Human Intrusion, Nominal, and the two Seismic GM Modeling Cases, one GoldSim realization, representing a unique combination of epistemic and aleatory uncertainties, is chosen for detailed analyses. For the Waste Package EF and Drip Shield EF Modeling Cases, two GoldSim realizations, representing two aleatory uncertainty vectors (corresponding to CSNF and CDSP WP locations) for a given epistemic uncertainty vector, are selected to adequately describe the expected annual dose for the chosen epistemic uncertainty vector. More details about how a specific single realization was selected for analysis are presented in each subsection.

In addition to the detailed explanation of results from the chosen realization (representing a typical epistemic and aleatory vector), an outlier realization is analyzed for selected modeling cases. The realization is chosen in such a way that the expected dose is one of the highest for the period of interest. The motivation for analyzing an outlier realization is to understand the combination of parameters or submodels that lead to the large expected dose, because the mean annual dose is influenced more by an outlier realization than by any other realization.

The analysis for the outlier realization is limited to highlighting the primary reasons for its high dose and contrasting them to the results presented for the typical realization. The outlier realization analysis for a given modeling case is presented at the end of the section where the detailed single realization analysis for the same modeling case is described. The outlier realization analysis is conducted for all modeling cases except for the two Seismic GM Modeling Cases because the epistemic vector chosen for the detailed analysis in the two Seismic GM Modeling Cases also has large expected dose.

All single realization analyses discussed below are carried out by running the single realizations using GoldSim software (GoldSim v9.60.300, STN: 10344 9.60-03 [DIRS 184387]). However, the results of the expected annual doses are based on calculations performed by using EXDOC_LA software (EXDOC_LA V2.0, STN: 11193-2.0-00 [DIRS 182102]) with proper weighting of scenario-specific probabilities and expectations over aleatory and epistemic uncertainties.

7.7.1.1[a] Waste Package Early Failure Modeling Case

This section presents analyses of two realizations selected from the 6,000 realization base-case run performed for calculating expected annual dose from the Waste Package EF Modeling Case (GoldSim filename: LA_v5.005_EW_006000_000.gsm; output DTN: MO0710ADTSPAWO.000 [DIRS 183752]). The distribution of expected annual dose, along with the mean and various quantiles, is shown on a linear time scale (Figure 7.7.1-1a[a]) and on a log-time scale (Figure 7.7.1-1b[a]), the latter to more clearly illustrate the variation in dose at early times. The 300 displayed expected annual dose histories correspond to 300 epistemic uncertainty vectors. Each expected annual dose history is calculated as a weighted average of twenty aleatory uncertainty vectors (Equation 6.1.2-13 of the parent document). The twenty aleatory uncertainties are derived by considering the five spatial percolation subregions, two environments (seeping and non-seeping environments) for each percolation subregion, and two WP types for each environment (Section 6.1.2.4 of the parent document). Early failure of one WP is modeled for each of the aleatory vectors. Epistemic vector 281 is chosen for detailed analysis since it has an expected annual dose curve similar to the mean (Figure 7.7.1-1[a]). The twenty aleatory uncertainty vectors corresponding to epistemic vector 281 are GoldSim realization numbers 5601 through 5620 (Figure 7.7.1-2[a]).

The mean annual dose from this modeling case has several peaks (Figure 7.7.1-1b[a]). The first broad peak between 1,000 and 10,000 years is due to contributions from CDSP WPs, predominantly, as the relative humidity in the CDSP WPs in the various percolation subregions exceeds 95 percent and diffusive transport begins (Section 5.1.4 of the parent document). A second set of dose peaks between 10,000 and 30,000 years reflects dose contributions from CSNF WPs when the relative humidity inside CSNF WPs in the various percolation subregions

rises above 95 percent. The last broad dose peak occurs after the DSs fail (between approximately 250,000 and 300,000 years) and water flux through the WPs starts.

The radionuclides that contribute most to the mean annual dose are shown on Figure 7.7.1-3[a]. ^{99}Tc and ^{129}I are the top dose contributors at the peak of the mean annual dose, which occurs around 12,500 years. Beyond about 30,000 years, ^{239}Pu and ^{242}Pu are the major dose contributors. In the sections that follow, the transport characteristics of ^{99}Tc are discussed as an example of all highly soluble, weakly, or negligibly sorbing radionuclides. ^{239}Pu and ^{242}Pu provide examples of sparingly soluble, strongly sorbing radionuclides.

In order to investigate peaks in the mean annual dose curve, it was necessary to inspect two GoldSim realizations (representing two aleatory uncertainty vectors for the same epistemic uncertainty vector). One realization corresponds to an early CSNF WP failure, whereas the second corresponds to an early CDSP WP failure. Each affects expected annual dose at different times. Realization 5608 is chosen to represent the early failure of a CSNF WP, while realization 5618 is chosen to represent the early failure of a CDSP WP. These two realizations were chosen because both exhibit early failure of CSNF and CDSP WPs within percolation Subregion 3, which represents about 40 percent of the total repository area. Also, both represent a seeping environment, where releases are typically greater than from a non-seeping environment. The annual doses from these two realizations are highlighted on Figure 7.7.1-2[a], along with 18 other realizations representing aleatory uncertainty vectors for epistemic vector 281. These two realizations are examined more closely in the sections that follow.

Early Failure CSNF Package—Realization 5608

Figure 7.7.1-4[a] shows the annual dose attributable to 21 radionuclides for realization 5608 (GoldSim filename: LA_v5.005_EW_006000_002.gsm; output DTN: MO0801TSPAMVAC.000 [DIRS 185080]). Two radionuclides, ^{99}Tc and ^{129}I, dominate the first sharp peak in dose at 12,000 years. There is a broad peak due to ^{239}Pu between 20,000 and 100,000 years and a much broader peak after the DS fails at 292,000 years, due primarily to ^{242}Pu and ^{237}Np. At no time do radionuclides irreversibly attached to colloids contribute significantly to dose.

The peak dose (12,000 years) is due to the almost pulse-like releases of ^{99}Tc and ^{129}I from CSNF packages; these two radionuclides are transported essentially without retardation through the EBS, UZ, and SZ. In the Waste Package EF Modeling Case, the CSNF matrix is modeled to degrade instantaneously when the WP is breached and the temperature is above 100°C (Section 6.3.7.4.1.3 of the parent document). However, releases of radionuclides cannot occur until there is a continuous film of water within the WP to support diffusive transport, which is modeled to occur once the relative humidity rises above the threshold of 95 percent in the absence of flow. In realization 5608, the relative humidity exceeds 95 percent at 11,500 years, causing releases by diffusive transport to start. All of the highly soluble radionuclides (such as technetium and iodine) that are part of the CSNF inventory dissolve into the available water volume, establishing a large concentration gradient between the waste form domain and invert. This gradient drives diffusion and rapidly depletes the mass in the waste form domain. Figure 7.7.1-5[a] shows the technetium release rate from the waste form, invert (EBS), UZ, and SZ for realization 5608. The initial pulse-like release from the waste form is attenuated only slightly by transport through the WP corrosion products domain and the invert domain. As

indicated on Figure 7.7.1-5a[a], these two curves virtually coincide. The release rate is somewhat attenuated in the UZ and SZ due to hydrodynamic dispersion, which is caused by fracture-matrix interactions in the volcanic rock units and transport through alluvium. Figure 7.7.1-5b[a] shows the SZ breakthrough curves for technetium, reversibly attached plutonium, and irreversibly attached plutonium. The median SZ travel times for technetium for epistemic vector 281 range from 30 to 60 years over the four SZ regions. The small but sharp increase in the SZ release rate around 164,000 years (Figure 7.7.1-5a[a]) is due to a small step change in the SZ breakthrough curve from Source Region 2 reflecting coarse time discretization, rather than a physical process, which when convolved with the UZ release leads to such behavior.

In contrast to technetium, plutonium has a propensity to sorb strongly to most surfaces and also form a sparingly soluble solid, which results in entirely different geochemical behavior from that of the more soluble and weakly sorbing radionuclides like ^{99}Tc. Unlike technetium, which exhibits a large pulse-like release, the release of plutonium from the waste form rises to a value below that of technetium and remains relatively constant for a long time (Figure 7.7.1-6a[a]). This plutonium release characteristic reflects the fact that dissolved plutonium concentrations are solubility limited, whereas technetium concentrations are limited by the waste form degradation rates and transport rates. As a result, a considerable mass of plutonium released from the degraded waste form reprecipitates within the waste form domain. Figure 7.7.1-7a[a] shows dissolved plutonium concentrations within the CSNF waste form domain. All isotopes contribute to their dissolved elemental concentrations in proportion to their mass in the waste form cell; therefore, ^{239}Pu dominates plutonium concentrations at early times and ^{242}Pu dominates at later times (after most ^{239}Pu has decayed). The mass of plutonium modeled as having precipitated in the waste form domain remains there as a solid (PuO_2) throughout the one-million-year simulation in realization 5608. The decrease in plutonium solubility observed around 292,000 years (Figure 7.7.1-7a[a]) is due to a change in the in-package chemistry from initiation of flow (about 0.14 m^3/yr) through the WP following the failure of the DS. This initiation of flow causes the in-package chemistry to be calculated based on the evaluation of both the vapor influx and liquid influx (Section 6.3.7.2.1 of the parent document), which results in the change in pH and ionic strength (Figure 7.7.1-7b[a]) and thereby the plutonium solubility. Note that CSNF colloids remain unstable throughout the simulation even though pH and ionic strength change (Figure 6.3.7-11b of the parent document), so the concentration of plutonium irreversibly associated with CSNF colloids remains minimal as seen on Figure 7.7.1-6b[a].

Besides solubility, sorption onto WP corrosion products controls the plutonium concentration and releases from the WP. The effect of sorption on the plutonium concentration within the WP corrosion products can be seen on Figure 7.7.1-6b[a], where there is an initial spike in the concentration which then decreases due to sorption. The spike results from the initial calculation of small K_d on corrosion products as minimum initial values for the radionuclide concentrations are used by the surface-complexation based competitive sorption model to calculate the sorption coefficients. Once the radionuclide concentrations rise above the minimum values, the K_ds adjust to higher values in the next timestep (Figure 7.7.1-8[a]). The low initial K_d allows a pulse of radionuclides, most notably ^{239}Pu and ^{243}Am, to be released through the WP corrosion products and sorbed onto the invert before significant K_ds are calculated in the corrosion products. This is a model limitation due to the explicit-in-time solution method for the competitive sorption calculations. However, the current implementation is adequate because it

causes only a minor over-prediction of the ^{239}Pu release to the invert in a single timestep. Because of decay of ^{243}Am to ^{239}Pu, the dissolved concentration of ^{239}Pu in the WP corrosion products is calculated to exceed that in the waste form domain. In the subsequent timesteps, the establishment of higher K_ds causes the WP corrosion products domain ^{239}Pu concentration to drop below that of the waste form domain and then below that of the invert. As a result, there is backward diffusion from the invert into the WP corrosion products (represented by a negative release rate on Figure 7.7.1-6a[a]). Advective transport through the invert depletes the mass and eventually drops the concentration in the invert below that in the WP corrosion products and positive release from the WP to the invert is reinstated. The diffusion gradient between the invert and the UZ remains positive, however, resulting in continuous down-gradient releases (Figure 7.7.1-6a[a]). The release rates decrease in the UZ and further in the SZ, due to dispersion, sorption, and radioactive decay during transport. The SZ breakthrough curves for reversibly attached plutonium and irreversibly attached plutonium show median travel times of 16,000 to 39,000 years and 11,000 to 12,000 years, respectively (Figure 7.7.1-5b[a]). The small concentration of ^{239}Pu irreversibly attached to CSNF colloids in the waste form domain (Figure 7.7.1-6b[a]) shows that colloidal transport of ^{239}Pu is not important in this realization.

The release rate of ^{242}Pu (Figure 7.7.1-9a[a]) correlates well with its dissolved concentrations (Figure 7.7.1-9b[a]). The share of ^{242}Pu relative to the elemental solubility increases with time as mentioned earlier, so its concentration and release rate also increases. Release from the WP corrosion product domain is significantly reduced due to sorption onto the WP corrosion products. Unlike ^{239}Pu where the concentration in the WP corrosion products domain exceeded that in the waste form domain in the initial timestep due to ingrowth from decay of ^{243}Am (at 11,500 years), ^{242}Pu is not the daughter of a significant short-lived parent, and the concentration in the WP corrosion products domain remains below that of the waste form domain. At 292,000 years, the DS breaches so water flux through the WP starts and causes a sharp increase in the release rate from the WP.

Early Failure Co-Disposed Package—Realization 5618

Figure 7.7.1-10[a] shows the contributions to annual dose by the major radionuclides for realization 5618 (GoldSim filename: LA_v5.005_EW_006000_003.gsm; output DTN: MO0801TSPAMVAC.000 [DIRS 185080]). Three radionuclides, ^{14}C, ^{99}Tc, and ^{129}I, dominate the first peak, which starts around 1,000 years when the relative humidity of the CDSP WP rises above 95 percent. Although the CDSP WP is failed at the start of the simulation, only the DSNF is assumed to degrade instantaneously; whereas, the CDSP HLW glass degrades according to its temperature- and pH-dependent degradation rate (BSC 2004 [DIRS 169988], Section 8.1). Relative contributions from degradation of DSNF and HLW glass to combined waste form release for selected radionuclides is shown on Figure 7.7.1-11[a]. Radionuclides released from degraded DSNF are evident at the end of the first timestep (250-year duration), with a gradual rise in the cumulative release as the HLW glass degrades. The line for ^{14}C is flat because there is no ^{14}C inventory in the HLW glass. The slow degradation of HLW glass leads to a gradual release of ^{99}Tc from the HLW waste form domain (Figure 7.7.1-12[a]) compared to that from the CSNF waste form (Figure 7.7.1-5[a]). The lower inventory of ^{99}Tc within DSNF compared to that within CSNF (on a per-package basis; Table 6.3.7-5 of the parent document) results in a lower initial release rate. Once again a small but observable lowering and delay of the release rate peak occurs in the UZ and SZ (Figure 7.7.1-12[a]).

Figure 7.7.1-13a[a] shows the release rates of ^{239}Pu from the different domains. Figure 7.7.1-13b[a] shows the concentration of ^{239}Pu in each successive domain of the EBS transport model: HLW glass, DSNF, WP corrosion products, and invert. Each domain has a distinct chemistry and solubility control on plutonium concentration. Most plutonium is precipitated in both the HLW glass domain and the DSNF domain at the outset of the simulation but is depleted first in the DSNF domain by about 4,000 years. After that time, the concentration of plutonium in the DSNF domain is controlled by transport from the upstream HLW cell. Kinetic sorption and desorption processes, that are modeled in the WP corrosion products domain, control the concentration of plutonium and maintain it at the solubility limit. As diffusive release continues to the invert, the plutonium mass is depleted from the corrosion products domain and by 75,000 years, the dissolved concentrations cannot be maintained at the solubility limits leading to its gradual decline. This reduction in corrosion product domain concentration increases the concentration gradient between the HLW and WP corrosion products domains and increases the release rate from the waste form domain (Figure 7.7.1-13a[a]). Plutonium within the HLW glass waste-form domain is depleted after 176,000 years (Figure 7.7.1-14a[a]), and total plutonium release rate from the waste form domain drops to zero (Figure 7.7.1-13a[a]). In addition to the dissolved concentrations, Figure 7.7.1-13b[a] also shows the concentrations of ^{239}Pu irreversibly attached to glass waste form colloids. The ionic strength in the waste form domain (Figure 7.7.1-14b[a]) remains above the threshold for stable glass waste form colloid (Figure 6.3.7-11a of the parent document) until about 45,000 years, at which time stable colloids form. However, the concentration of ^{239}Pu irreversibly attached to waste form colloids remains orders of magnitude below the dissolved ^{239}Pu concentration. The net result is that the colloidal release of ^{239}Pu is not significant in realization 5618.

The release rate characteristics of ^{242}Pu from the various domains for the CDSP packages (Figure 7.7.1-15a[a]) are similar to those of ^{239}Pu (Figure 7.7.1-13a[a]), except that, due to its longer half-life (375,000 years), ^{242}Pu does not decay as quickly and later-time releases are significant. Just like ^{239}Pu, ^{242}Pu becomes depleted in the DSNF domain at 4,000 years, but the concentration in the WP corrosion products domain remains steady due to sorption and desorption. Early in the simulation, the concentration of ^{242}Pu in the HLW waste form domain is low since the elemental concentration is dominated by the more abundant isotopes, ^{239}Pu and ^{240}Pu (Figure 7.7.1-14a[a]). As ^{239}Pu and ^{240}Pu decay, the concentration of ^{242}Pu increases, maintaining the dissolved concentration of total plutonium at the solubility limit (of about 0.0085 mg/L between 100,000 years and 280,000 years). At around 176,000 years the plutonium becomes depleted within the HLW waste form domain and the ^{239}Pu and ^{242}Pu concentrations drop (Figures 7.7.1-14a[a] and 7.7.1-15b[a]). As a result, the diffusion gradient from the WP corrosion products domain to the upstream waste form domain reverses, leading to increasing down-gradient release (represented by a positive release rate) and depletion of the mass in the waste form domain. Once the mass of plutonium has been depleted, the dissolved concentration of plutonium in the waste form domain decreases and plutonium once again diffuses from the WP corrosion products domain to the waste form domain (represented by a negative release rate on Figure 7.7.1-15b[a]). Initially, release of ^{242}Pu irreversibly attached to glass waste form colloids is low; however, after the DS fails, ^{242}Pu release increases due to advective release from the WP. This is the only significant release of colloidal radionuclides for this modeling case, with the release rate of irreversibly attached plutonium nearly equal to that of dissolved plutonium.

Waste Package Early Failure Modeling Case: Outlier

For the purpose of analyzing an outlier realization, epistemic vector 247 was chosen as shown on Figure 7.7.1-16[a]. Figure 7.7.1-17[a] shows the 20 aleatory realizations that are associated with epistemic vector 247 and correspond to GoldSim realizations 4921 through 4940. Two realizations (realization 4930 and 4940) are highlighted as they represent the highest unweighted dose for an early failed CSNF WP and a CDSP WP, respectively. The major radionuclide dose contributors for realizations 4930 and 4940 are shown on Figure 7.7.1-18[a]. The annual dose contributions from various aleatory vectors for the outlier epistemic vector 247 (Figure 7.7.1-17[a]) show the same general features as those shown for epistemic vector 281 discussed previously (Figure 7.7.1-2[a]): broad peaks between 1,000 and 10,000 years due to the contribution of ^{99}Tc from early failed CDSP WP; a series of peaks between 10,000 and 30,000 years representing contribution of ^{99}Tc from early failed CSNF packages located in various percolation subregions, where relative humidity increases above 95 percent threshold level at different times ; and peaks due to ^{239}Pu and ^{242}Pu that occur after ^{99}Tc peaks. Despite these similarities, the dose magnitudes are quite different among the two epistemic vectors: the magnitude of ^{99}Tc dose is an order of magnitude higher for epistemic vector 247 and up to two orders of magnitude higher for ^{242}Pu dose. Although all uncertain parameters are sampled separately among the two epistemic vectors, a comparison analysis reveals that these differences stem primarily from the sampled value of the probability of WP early failure with some contribution from differences in the solubility of plutonium in the WP and the SZ breakthrough curve for plutonium.

The probability of early failure of a WP (the pW_i term of Equation 6.1.2-13 of the parent document, equivalent to GoldSim parameter UNC_WP_EF_conv_from_ln) is the weighting term used by EXDOC when computing the expected dose for an epistemic vector. This term is about an order of magnitude higher for epistemic vector 247 (sampled value of 4.6×10^{-3} representing 99.98 percentile of the distribution) compared to that of epistemic vector 281 (sampled value of 3.3×10^{-4} representing 94.77 percentile of the distribution) and is responsible mostly for the outlier behavior of epistemic vector 247. The unweighted annual doses from 20 GoldSim realizations for these two vectors are quite similar as shown on Figures 7.7.1-2[a] and 7.7.1-17[a], underlining the importance of the weighting factor in determining the expected dose.

Figure 7.7.1-19[a] shows the SZ breakthrough curves for epistemic vector 247. The median travel time for dissolved and reversibly sorbed plutonium (denoted as aqueous) ranges from 49,000 to 110,000 years, which is significantly longer than for epistemic vector 281 with median travel times of 16,000 to 39,000 (Figure 7.7.1-5b[a]). This explains the delay in the ^{239}Pu peak in epistemic vector 247 compared to that in epistemic vector 281.

The mean plutonium solubilities within each EBS transport domain depends on the domain chemistry, but the sampled parameters Pu_Eps_1_low_a and Pu_Eps_1_high_a add uncertainty to the mean value thereby influencing the plutonium solubility throughout the EBS for both the CSNF and CDSP WPs. These parameters are above the 97th percentile for epistemic vector 247, but near the 50th percentile for epistemic vector 281, which causes an order of magnitude increase in the solubilities for epistemic vector 247. This is reflected in the higher concentrations within the waste form and WP seen on Figure 7.7.1-20a[a] compared to Figure 7.7.1-6b[a] and at early times on Figure 7.7.1-20b[a] versus 7.7.1-9b[a]. With the higher plutonium concentrations,

release is greater for epistemic vector 247. Unlike epistemic vector 281, ^{242}Pu becomes depleted within the WP.

7.7.1.2[a] Drip Shield Early Failure Modeling Case

This section presents an analysis of two out of the 3,000 realizations selected from the realization base-case run performed for calculating the expected annual dose from the Drip Shield EF Modeling Case (GoldSim filename: LA_v5.005_ED_003000_000.gsm; output DTN: MO0710ADTSPAWO.000 [DIRS 183752]). The 3,000 realizations in GoldSim represent 300 epistemic uncertainty vectors where each epistemic vector is used for 10 aleatory uncertainty vectors.

In the stylized Drip Shield EF Modeling Case, a single CSNF or CDSP WP is modeled in a seeping environment under a DS that is assumed to be completely failed (breached) at the start of the simulation. Furthermore, the WP is assumed to fail completely from localized corrosion at the onset of drift seepage when the in-drift temperatures are still hot.

The expected annual dose from all 300 epistemic vectors, along with the statistics on the distribution of expected annual dose, is shown on Figure 7.7.1-21[a]. Figure 7.7.1-22[a] shows the major radionuclides that contribute to the mean annual dose. There is an early peak due to ^{99}Tc and ^{129}I, whereas ^{239}Pu , ^{242}Pu, and ^{237}Np are the top contributors later on. Epistemic vector 228 was chosen for further analysis because it has a shape similar to the mean annual dose curve and has a higher dose than the mean annual dose curve for the simulated duration (Figure 7.7.1-21[a]).

The expected annual dose from epistemic vector 228 is calculated as a weighted average of annual dose for ten aleatory vectors (Equation 6.1.2-14 of the parent document). The ten aleatory vectors that correspond to epistemic vector 228 are GoldSim realizations 2271 to 2280, and their unweighted annual dose histories are shown on Figure 7.7.1-23[a]. The ten aleatory vectors represent only the dripping environments in five percolation subregions for both CSNF and CDSP WP types. As outlined in Equation 6.1.2-14 of the parent document, the dose from each realization is then multiplied by the probability of early DS failure, the fraction of waste type, the seepage fraction, and the percolation bin fraction, the latter being equal to the number of WPs in the percolation subregion divided by the total number of WPs in the repository. These weighted doses are then summed to derive the expected annual dose for epistemic vector 228, shown on Figure 7.7.1-21[a]. GoldSim realizations 2273 and 2278 are highlighted on Figure 7.7.1-23[a] to show the relative difference in unweighted dose behavior between a CSNF WP type (realization 2273) and CDSP WP type (realization 2278) located in the same percolation subregion (percolation subregion 3). Both realizations are considered for further analysis in this section (GoldSim filenames: LA_v5.005_ED_003000_002.gsm and LA_v5.005_ED_003000_003.gsm; output DTN: MO0801TSPAMVAC.000 [DIRS 185080]). The major radionuclides contributing to dose for realization 2278 are shown on Figure 7.7.1-24[a], and they are similar to the major dose contributors for the mean annual dose (Figure 7.7.1-22[a]). The early part of the dose curve is dominated by ^{99}Tc, the middle part is dominated by ^{239}Pu, and the latest part is dominated by ^{242}Pu (after ^{239}Pu has decayed). ^{79}Se is also important early on since no solubility-controlling solid for selenium is included in the TSPA-LA Model and it is retarded only moderately during transport (^{79}Se shows spiky behavior

later on due to the particle tracking algorithm used in the UZ transport model to track mass (Section 6.3.9 of the parent document)). The major radionuclides contributing to dose for realization 2273 are similar to the ones shown for realization 2278 and thus are not shown separately.

During the first 5,000 years, annual dose is dominated by the unretarded or weakly retarded species that have no solubility constraints, such as ^{99}Tc, ^{79}Se, and ^{14}C. After 5,000 years, and until about 250,000 years, ^{239}Pu dominates dose (Figure 7.7.1-24a[a]). As shown on Figure 7.7.1-24b[a], the dose from ^{239}Pu is a combination of dissolved plutonium and plutonium that is irreversibly sorbed onto colloids. The dose from ^{239}Pu irreversibly associated with the slow traveling fraction of colloids is comparable to the dose from dissolved ^{239}Pu. At later times (after about 300,000 years), ^{242}Pu is the dominant contributor to dose, as was demonstrated for the Waste Package EF Modeling Case discussed previously (Section 7.7.1.1[a]). Here again, the dose from ^{242}Pu is a combination of dissolved and irreversibly sorbed colloidal plutonium (Figure 7.7.1-24b[a]). Unlike the Waste Package EF Modeling Case, releases from the WP in this Drip Shield EF Modeling Case are mainly advective with low ionic strengths, so that colloidal transport becomes important early on.

The transport behaviors described above and depicted on Figure 7.7.1-24[a] are expected because ^{99}Tc, ^{79}Se, and ^{14}C are transported as solutes with little or no retardation in the engineered barrier and natural systems. Despite their similar transport properties and travel times to the biosphere, these three radionuclides exhibit variations in terms of dose due to differences in the initial inventory, decay rates, and biosphere dose conversion factors (BDCFs) for each of the radionuclides. In contrast to ^{99}Tc, ^{79}Se, and ^{14}C, the transport of ^{239}Pu is strongly affected by retardation in the EBS, UZ, and SZ. This retardation is caused by reversible sorption onto WP corrosion products and invert material (crushed tuff) in the EBS and on the rock matrix in the UZ and SZ. Almost all the ^{239}Pu that is associated irreversibly with colloids (embedded in HLW glass waste form colloids) is transported faster than dissolved ^{239}Pu due to a lesser degree of fracture matrix interaction in the UZ and SZ, so that colloidal ^{239}Pu contributes more significantly to dose earlier than dissolved ^{239}Pu.

Releases from Engineered Barrier System—The release of ^{99}Tc out of the EBS occurs around 500 years for the CDSP WP and around 750 years for the CSNF WP, even though the WP fails early at the start of the simulation (Figure 7.7.1-25[a]). This delay is due to the effects of temperature since no transport (diffusive or advective) is allowed as long as temperatures remain above the boiling point of water (100°C). Figure 7.7.1-25[a] shows that the temperature within a CDSP WP does not fall below 100°C until approximately 400 years after closure and, for CSNF WPs, the temperature does not fall below 100°C until after approximately 600 years. [Note that the radionuclide transport related calculations start as soon as the WP temperatures drop below 100°C but the release rate information is not available as an output until the end of the user specified timestep. For the first 10,000 years of simulation in this modeling case, the selected timestep size is 250 years.]

A number of processes in both the WP and invert influence the release of radionuclides from the EBS. Figure 7.7.1-25[a] shows the mass flux of ^{99}Tc out of the EBS into the UZ from both CSNF and CDSP WPs (from realizations 2273 and 2278, respectively). The ^{99}Tc release curve for the CDSP WP starts around 500 years and initially decreases as drift-wall condensation flux

changes from Stage 2 to Stage 3 (discussed next). Technetium is released instantaneously from the CSNF WPs, dropping off rapidly on this log-log plot.

Figure 7.7.1-26[a] shows water flow rate into WPs as a function of time for CDSP and CSNF WPs. The initially high flow rate for the CDSP WP occurs during Stage 2 drift-wall condensation; that is, for those times between when the temperature at the first location in a drift drops below boiling and when the temperature at the last location drops below boiling (Section 6.3.3.2 of the parent document). Flow into the CDSP WP becomes equal to the seepage rate after 500 years, when Stage 2 ends. The CSNF package shows low initial seepage because there is no Stage 2 drift-wall condensation for the hotter CSNF WP.

Figure 7.7.1-26[a] also shows how seepage into each WP increases with each change in climate state because of corresponding increases in the percolation rate. Changes in climate occur around 600 years; 2,000 years; and 10,000 years; and each change in a climate state is marked by an instantaneous change in seepage rates through the EBS (Figure 7.7.1-26[a]). The small increase in seepage rates at about 2,000 years is in response to a change in climate state from monsoonal to glacial-transition. A considerably larger increase in seepage rate occurs around 10,000 years in response to the change in climate from glacial-transition to the post-10,000 year climate state with its higher percolation and higher seepage rate.

The fractions of each waste form that have degraded for CDSP and CSNF packages are shown on Figure 7.7.1-27[a]. The CSNF waste form is completely degraded when the WP fails at the start of the simulation because the temperature exceeds 100°C, and CSNF degradation is modeled as being instantaneous above this temperature. Although not shown on Figure 7.7.1-27[a], the same is true for DSNF, which is assumed to degrade instantaneously upon WP breach at all temperatures. On the other hand, HLW glass in the CDSP package (Figure 7.7.1-27[a]) degrades according to the modeled degradation rate, which declines gradually as WP temperature decreases until all of the HLW glass has degraded by about 10,000 years (in this realization).

Unsaturated Zone—After their releases from the EBS, radionuclides enter the UZ and are partitioned among the UZ fractures and matrix. Most radionuclide mass released from the EBS is partitioned into the UZ fractures because the DS is failed and the WP is in the seeping environment of the given percolation subregion, so that most of the transport is by advection. Figure 7.7.1-28[a] shows the fraction of mass released to the UZ fractures for selected radionuclides from a CDSP WP located in seeping environment of percolation subregion 3. The ^{239}Pu mass in dissolved state and reversibly associated with colloids (denoted as aqueous) is differentiated from the mass irreversibly associated with slow traveling colloids, which is not in equilibrium with the mass in solution. Figure 7.7.1-28[a] shows that, at a minimum, 80 percent of the mass flux enters the UZ fractures but more commonly (at later times, especially beyond 10,000 years) greater than 95 percent of the mass flux is partitioned into the UZ fractures. The spikes down to zero (near the end of the simulation) are due to numerical approximations in the partitioning algorithm when essentially all of the ^{239}Pu has decayed and the actual release is approximately zero. Because of fast transport times in the UZ fractures, there is little delay in the first arrival of radionuclide mass at the SZ, as shown on Figure 7.7.1-29[a]. Almost all of the ^{99}Tc mass released from the EBS is also released out of the UZ in a short time and the cumulative release curves virtually overlay each other. However, only about 62 percent of the

^{242}Pu mass released from the EBS is released out of the UZ by 1,000,000 years. This reduction in the mass of ^{242}Pu released from UZ is attributed to the diffusive interaction between UZ fracture and matrix continuum with sorption in the matrix that leads to reduced mass transport through the UZ, particularly for the repository release nodes located in the southern part of the UZ transport domain (SNL 2008 [DIRS 184748], Figure D.2-5[b]).

Saturated Zone—Transport of ^{99}Tc through the SZ is relatively fast because it does not sorb to the SZ volcanic and alluvium units and almost all of the mass released out of the UZ is released from the SZ without any appreciable delay (Figure 7.7.1-29[a]). Transport of ^{242}Pu in the SZ shows a small delay over the simulated time period despite the potential to be retarded considerably from sorption onto the volcanic and alluvium units. This is because, in this realization, one of the fastest SZ breakthrough curves is sampled (out of a set of 200 breakthrough curves) for transport of plutonium with a median travel time of less than 10,000 years (SNL 2008 [DIRS 183750], Figure 6-9[a]). Almost all of the ^{242}Pu mass released out of the UZ is released from the SZ by the end of the simulated time period.

Drip Shield Early Failure Modeling Case: Outlier

For the purpose of analyzing an outlier realization, epistemic vector 244 was chosen as shown on Figure 7.7.1-30[a] because it has the highest annual dose from about 5,000 years to beyond 100,000 years for this Drip Shield EF Modeling Case. As discussed previously, each of the 300 curves shown on Figure 7.7.1-30[a] is a combination of ten aleatory vectors representing seeping environments in five percolation subregions for both CSNF and CDSP WP types. The unweighted annual dose from each of the ten aleatory vectors is multiplied by the corresponding probability of early DS failure, the WP type, the seepage fraction, and the percolation bin fraction, and then summed over aleatory vectors to derive the expected annual dose for the curve shown (Equation 6.1.2-14 of the parent document). Figure 7.7.1-31[a] shows the unweighted annual dose for the ten aleatory vectors corresponding to GoldSim realizations 2431 to 2440 for epistemic vector 244. Realization 2433 for the CSNF WP type is chosen for further analysis as it has a higher annual dose compared to a CDSP WP (e.g., realization 2438).

The major radionuclide dose contributors for realization 2433 are shown on Figure 7.7.1-32[a]. For the most part, the main contributors are similar to those in realizations 2273 and 2278 previously discussed. The major dose contributing radionuclide is ^{99}Tc before 1,000 years as it is not solubility limited and transports unretarded through the EBS, UZ, and SZ. The dose from ^{99}Tc decreases quickly as its inventory is depleted following waste form degradation. ^{237}Np is the major contributor at 2,000 years and also beyond 200,000 years. The peak around 5,000 years is due to the slow traveling fraction of colloids with irreversibly sorbed ^{243}Am and ^{239}Pu. From 6,000 years to 200,000 years, a combination of dissolved and reversibly sorbed ^{239}Pu mass on colloids (denoted as aqueous) and irreversibly sorbed ^{239}Pu mass on colloids dominate the dose.

Although all uncertain parameters are sampled separately for each epistemic vector, a comparison analysis reveals that for epistemic vector 244, the high dose for radionuclides of interest stem primarily from the sampling of iron oxyhydroxide colloid concentration and the solubility uncertainties. The concentration of iron oxyhydroxide colloids from corrosion of stainless steel inside the WP is determined by the epistemic uncertain parameter,

Conc_Col_FeOx_SS_Sampled_a. This parameter has a sampled value of about 5.1 mg/L in realization 2433, which is at the 92nd percentile. For comparison, the value of this parameter in realization 2273 described earlier is about 0.076 mg/L, which is at the 45th percentile.

The solubility limits of both neptunium and plutonium are high in realization 2433. Equation 6.3.7-13a of the parent document shows the importance of ε_1 (the term accounting for thermodynamic uncertainty) in determining the solubility for neptunium and plutonium. Both neptunium and plutonium have high sampled values of ε_1 in realization 2433. As discussed in Section 6.3.7, neptunium solubility is controlled by NpO_2 when stainless steel is present in the WP and by Np_2O_5 after the stainless steel is gone. The sampled value of ε_1 for NpO_2 is at the 90th percentile and the sampled value of ε_1 for Np_2O_5 is at the 99.7th percentile. Np_2O_5 has a higher base solubility than NpO_2 so there is a jump in dose when the solubility controlling phase changes just after 200,000 years (Figure 7.7.1-32[a]). Plutonium also has an extremely high value of ε_1 as it is sampled at the 99th percentile in realization 2433. These high values of ε_1 for neptunium and plutonium mean high solubility limits in the WP.

Seepage fraction (that is used to determine fraction of WPs in a seeping environment) and seepage rate are both important parameters in the Drip Shield EF Modeling Case. Figure 7.7.1-33[a] presents the seepage fraction statistics of the Drip Shield EF Modeling Case run for 6,000 realizations along with the seepage fraction for realization 2433. The seepage fraction for realization 2433 is only slightly below the mean and median seepage fraction indicating that seepage fraction is not the reason for the high doses in this realization. Figure 7.7.1-34[a] presents the seepage rate statistics along with the seepage rate for realization 2433. The seepage rate for realization 2433 is above the mean past 2,000 years and at the 95th percentile beyond 10,000 years. This high seepage rate in this realization, when combined with a greater concentration of iron oxyhydroxide colloids and higher solubility limits for neptunium and plutonium, results in high advective release from EBS and a larger dose.

In addition to the higher release from the EBS, fast breakthrough curves in the SZ are sampled for neptunium and plutonium. Figure 7.7.1-35[a] shows the SZ breakthrough curves for neptunium and plutonium for the four SZ regions for realization 2433. These curves, particularly for Region 1, can be compared to the 200 possible breakthrough curves for Region 1 used in the SZ model that are shown in *Saturated Zone Flow and Transport Model Abstraction* (SNL 2008 [DIRS 183750], Figures 6-9[a] and 6-11[a]). The breakthrough curves for both neptunium and plutonium in realization 2433 appear to be in the fastest 5 to 10 percent of the 200 breakthrough curves. The short travel time in the SZ results in little decay in the natural system so the high EBS releases contribute to high dose.

7.7.1.3[a] Igneous Intrusion Modeling Case

This section presents analyses of two single realizations selected from among the 3,000 realization base-case runs used to calculate the expected annual dose from the Igneous Intrusion Modeling Case for a one-million-year simulation (GoldSim filename: LA_v5.005_IG_003000_000.gsm; output DTN: MO0710ADTSPAWO.000 [DIRS 183752]). The 3,000 realizations are the combination of 300 epistemic uncertainty vectors and ten aleatory uncertainty vectors that specify the times of igneous intrusion events. In other words, each realization of this modeling case has one igneous intrusion event occurring at a specified time

with one given epistemic vector. The duration of the simulation for this modeling case is 1,000,000 years. The reader is referred to Sections 6.1.2 and 6.1.3 of the parent document for a discussion of how aleatory and epistemic uncertainties are treated and how expected annual dose is calculated for the Igneous Intrusion Modeling Case. Sections 6.5.1 of the parent document and 6.5.1[a] of this addendum provide details about the conceptual model, model abstraction, and TSPA-LA Model implementations for the Igneous Intrusion Modeling Case.

All WPs and DSs are assumed to have failed completely due to the igneous intrusion event so that the capabilities of both WP and DS to act as barriers to water flow are ignored. In addition, before the time of intrusion, only nominal corrosion is assumed for this modeling case, such that WPs could be breached by either SCC or by general corrosion and, thereby, subject radionuclides to potential release.

The mean annual dose and predominant radionuclides that contribute to it are shown for the base case on Figure 7.7.1-36[a]. This figure shows that the mean annual dose increases rapidly for the first 100,000 years to about 0.9 mrem, then decreases slightly to the value of 0.54 mrem at around 250,000 years, and then increases gradually for the remaining 750,000 years to a maximum of 0.89 mrem. The radionuclide that dominates dose early on (for the first 200,000 years) is ^{239}Pu, with its contribution decreasing as it undergoes radioactive decay. While the contribution from ^{239}Pu decreases, the contributions from ^{226}Ra, ^{242}Pu, and ^{237}Np increase. At around 200,000 years, ^{242}Pu overtakes ^{239}Pu as the radionuclide that dominates dose. Beyond 250,000 years, ^{226}Ra, ^{242}Pu, and ^{237}Np together account for more than two-thirds of the mean annual mean dose.

Expected annual dose from all 300 epistemic vectors is shown on Figure 7.7.1-37[a]. The expected annual dose of epistemic vector 286 is similar to the mean annual dose, which is why this epistemic vector was chosen for selecting the single realization used in the following analysis. Figure 7.7.1-38[a] presents the annual dose for the ten aleatory vectors that are associated with epistemic vector 286 and are represented by GoldSim realizations 2851 through 2860. Among these, GoldSim realization 2855, which has an igneous event occurring at 10,000 years, is chosen for the single realization analysis because its contribution to dose starts early. The model for GoldSim realization 2855 was run twice in order to first save information for all the percolation subregions and then to specifically save EBS cell-pathway details related to percolation subregion 3 under a seeping environment (GoldSim filenames: LA_v5.005_IG_003000_003.gsm and LA_v5.005_IG_003000_004.gsm; output DTN: MO0801TSPAMVAC.000 [DIRS 185080]).

This analysis of realization 2855 focuses on the four major contributors to dose mentioned above (^{239}Pu, ^{226}Ra, ^{242}Pu, and ^{237}Np) plus ^{234}U, whose transport behavior largely dominates the transport behavior of the decay product ^{226}Ra. Note that the annual dose for realization 2855 decreases slowly (Figure 7.7.1-38[a]), which differs somewhat from the late-time trend of expected annual dose for epistemic vector 286 (Figure 7.7.1-37[a]). This difference is due to the fact that the expected annual dose includes contributions from additional aleatory vectors with later igneous events.

Figure 7.7.1-39[a] shows the time history of total annual dose (summed over all radionuclides) along with the contributions to annual dose from the five radionuclides selected for the analysis

for realization 2855. A spike in total annual dose (~1,000 mrem) is noticeable immediately after the igneous intrusion event at 10,000 years. This spike is dominated by highly mobile radionuclides, primarily ^{99}Tc, ^{129}I, ^{14}C, and ^{36}Cl (none of which are shown on Figure 7.7.1-39[a]). Dose contributions from these four radionuclides decrease by about two orders of magnitude or more over the 10,000 years following the igneous event, so that by about 20,000 years after repository closure they contribute less than about 10 percent of the total annual dose (in this realization). For this reason, these four radionuclides are not analyzed in further detail in this section.

While dose contributions from these (and other) highly mobile radionuclides decrease, dose contributions from the four actinide radionuclides, ^{239}Pu, ^{237}Np, ^{234}U, and ^{242}Pu, increase until their contributions to total annual dose levels off between 28,000 and 130,000 years. After this, total annual dose decreases gradually for the duration of the simulation.

Igneous Intrusion—For GoldSim realization 2855, the igneous intrusion occurs at 10,000 years. The igneous intrusion fails all CSNF and CDSP WPs (total of 11,629 WPs) as well as the DSs. None of the WPs and DSs have failed by nominal corrosion processes prior to this event. Following the igneous intrusion, all WPs and waste forms experience high temperatures (peak expected temperature is 1,150°C) because of the heat of the magma. The high temperatures result in degrading all of CSNF instantaneously, oxidizing the UO_2 to U_3O_8, and making all non-uranium radionuclides available for release. Furthermore, because U_3O_8 has a high specific surface area (BSC 2004 [DIRS 169987], Section 6.2.2.2), the dissolution of U_3O_8 is also essentially instantaneous once contacted by water. The high temperature also results in rapid degradation of HLW glass. Five hundred years after the igneous event (i.e., a single timestep in the simulation during this time) WP temperature is calculated to have dropped to 52°C.

The various EBS environments affect waste form degradation and radionuclide mobilization differently for the Igneous Intrusion Modeling Case (discussed in Section 6.5.1.1.2 of the parent document) as compared to the Nominal Scenario Class (Section 6.3.4 of the parent document).

EBS Releases—The high degradation rates of CSNF and HLW allow the near-immediate release of their corresponding radionuclide inventories into solution. Because of solubility constraints, some radionuclides precipitate within the waste form domain of the EBS transport model. Following the igneous event, dissolved concentrations of neptunium, plutonium, and uranium from the CSNF waste form domain reach and are maintained at their solubility limits (Figure 7.7.1-40[a]). The solution (water) remains saturated with neptunium for about 40,000 years after the intrusion event while it is saturated with plutonium for about 200,000 years. The solution remains saturated with uranium throughout the simulation, owing to its large inventory. Dissolved radium concentrations, however, remain below the solubility limit in the CSNF waste form domain throughout the simulation. The dissolved concentration of radium increases early and is followed by a gradual decrease, due to the decay-chain ingrowth from ^{234}U (half-life = 246,000 yr) and subsequent decay of ^{226}Ra (half-life = 1,600 yr). The dissolved concentrations of neptunium and plutonium decrease rapidly once their precipitated solids have dissolved. As a result, their subsequent releases are not solubility controlled.

Gradual decreases in uranium, neptunium, and plutonium solubility limits (between 10,000 and 170,000 years) are caused by the gradual shift of pH towards neutral and a decrease of P_{CO_2} over

that period (Figure 7.7.1-41[a]). The sharp increase in the solubility limit for neptunium at 172,000 years (Figure 7.7.1-40[a]) occurs because the solubility controlling phase is changed from NpO_2 to Np_2O_5 following complete degradation of all steel that can act as a reductant (i.e., an electron donor) inside the waste form domain (Section 6.3.7.5 of the parent document for further discussion).

As discussed in Section 6.5.1.1.1 of the parent document, every WP and DS is rendered incapable of protecting its contents after an igneous intrusion event. As a result, high seepage fluxes flow through each WP, and these fluxes are set equal to the local percolation flux after an igneous intrusion (Section 6.5.1 of the parent document) and range from 0.18 to 3.54 m^3/yr. This leads to rapid releases of radionuclides from the WPs once the temperature drops below the boiling point of water (Figure 7.7.1-42[a]). Note that two types of mass release rates for ^{239}Pu and ^{242}Pu are presented in Figure 7.7.1-42[a]: (a) the release rate of mass dissolved and reversibly sorbed on colloids (denoted as aqueous) and (b) the release rate that also includes the mass irreversibly associated with the colloids (denoted as total). Among the four radionuclides for this analysis, ^{237}Np exhibits the highest release rate (approximately 550 g/yr), and its release rate decreases gradually as its inventory is depleted and its concentration declines. Releases of ^{242}Pu, ^{234}U, and ^{226}Ra have trends similar to that of ^{237}Np, whereas the release of ^{239}Pu decreases rapidly because of its relatively short half-life (2.41×10^4 years). Figure 7.7.1-42[a] also shows that most (greater than 90 percent) of ^{239}Pu and ^{242}Pu is transported as dissolved and reversibly sorbed on colloids, with the rest being transported irreversibly sorbed on colloids. For this reason, the irreversibly sorbed colloidal component of plutonium is not discussed in the rest of this analysis and the release rates of ^{239}Pu and ^{242}Pu referred hereafter only include the mass dissolved and reversibly sorbed on colloids.

Figure 7.7.1-43[a] shows the advective and diffusive release rates of major radionuclides from CSNF WPs. It shows that advection is the major transport mechanism for radionuclides released from WPs for the Igneous Intrusion Modeling Case. Diffusion contributes less than one percent of the total release from WPs except for ^{242}Pu at late time. Comparing Figure 7.7.1-43[a] with Figure 7.7.1-42[a] reveals that CSNF WPs are the dominant source for those major radionuclides.

Figure 7.7.1-44[a] presents the dissolved concentrations of neptunium, uranium, plutonium, and radium and their solubilities in the CSNF corrosion products domain for percolation subregion 3 under seeping environment. It shows that in the corrosion products domain, neptunium and plutonium concentrations maintain at their solubilities for a longer time than in the waste form domain (Figure 7.7.1-40[a]). However, unlike in the waste form domain, uranium concentration does not reach its solubility limit. Similar to the waste form domain, radium concentration does not reach its solubility limit. Moreover, dissolved concentrations of neptunium and plutonium decrease at slower rates than in the waste form domain because the corrosion products in the corrosion products domain gradually release neptunium and plutonium that had been sorbed onto corrosion product solids. The solubility controlled releases of ^{237}Np and ^{239}Pu are responsible for the 'plateau' in total dose between 28,000 and 130,000 years (Figure 7.7.1-39[a]).

Changes in radium solubility at 57,500 and 340,000 years are due to pH changes that cause the model to switch between two values of the radium solubility limit (Section 6.3.7.5.2 of the parent document). Changes in uranium solubility at those times also reflect changes in pH that cause

the model to switch between dissolved uranium concentrations being controlled by Na-boltwoodite solubility and schoepite solubility (Section 6.3.7.5.2 and Tables 6.3.7-56 and 6.3.7-57 of the parent document).

Natural System—Cumulative releases of ^{237}Np, ^{242}Pu, ^{234}U, and ^{226}Ra from the EBS, UZ, and SZ are presented in Figure 7.7.1-45[a]. Figure 7.7.1-45a[a] shows a small delay for ^{237}Np from the UZ and SZ of 500 years each (i.e., one timestep for each zone). This small delay is due to the fast transport predominately along the fracture pathways, with limited diffusion into the surrounding matrix. At the end of the simulation, 99 percent of neptunium that had been released from the EBS has migrated through the UZ, and 96 percent of that has migrated through the SZ. In other words, the UZ and SZ provide relatively minor retardation for ^{237}Np in this realization of the Igneous Intrusion Modeling Case. This is attributed to the relatively small K_d values assigned to neptunium. Similarly, ^{234}U is not substantially retarded by the UZ and SZ on Figure 7.7.1-45b[a]. The figure shows that the cumulative release of ^{234}U from the SZ after 330,000 years is higher than that from the EBS. This is not a numerical error but is caused by 'inventory boosting' performed at the UZ-SZ interface for transport through the SZ (Section 6.3.10.3 of the parent document).

Cumulative release of ^{242}Pu shown on Figure 7.7.1-45c[a] illustrates the relative influences that the UZ and SZ have on delaying plutonium release. The UZ delays plutonium release for a few thousand years, whereas plutonium release is delayed for more than 10,000 years by the SZ. At the end of the simulation, about 24 percent of ^{242}Pu that had been released from the EBS remains in the UZ, and 29 percent of ^{242}Pu that had been released from the UZ remains in the SZ. The UZ and SZ both retard ^{242}Pu significantly. This is attributed to the sorption of plutonium in the SZ volcanic matrix (as a result of fracture-matrix interactions) and alluvium.

The cumulative release history for ^{226}Ra is presented on Figure 7.7.1-45d[a], which indicates that a large fraction of ^{226}Ra released from the EBS does not exit the SZ. If radioactive decay and decay-chain ingrowth is ignored, then by 1,000,000 years, only 25 percent of ^{226}Ra that had been released from the EBS would have migrated through the UZ, and less than 0.1 percent of ^{226}Ra that had been released from the UZ would have migrated through the SZ. This substantial reduction in the mass of ^{226}Ra is caused by the high K_d values assigned to radium in the UZ and SZ (Tables 6.3.9-2 and 6.3.10-2 of the parent document) that serve to retard ^{226}Ra transport through the UZ and SZ. When this delay is combined with the short half-life of ^{226}Ra (1,600 years; Figure 6.3.7-4 of the parent document) it results in a significant decrease in the cumulative release from the SZ.

As pointed out previously, Figure 7.7.1-39[a] shows that the annual dose curve has a plateau that appears between 28,000 and 130,000 years. This plateau corresponds to the SZ groundwater concentration plateau of ^{237}Np and ^{239}Pu at the RMEI location for the same duration as shown on Figure 7.7.1-46[a]. The concentration plateaus correspond to the solubility controlled releases of neptunium and plutonium from the corrosion products domain shown on Figure 7.7.1-44[a]. Note that the SZ groundwater concentrations shown on Figure 7.7.1-46[a] are obtained by dividing the annual releases of radionuclides from the SZ by the 3,000 acre-ft/yr annual water usage, as per the regulatory requirements. Although the SZ groundwater concentration of ^{237}Np is higher than that of ^{239}Pu, the latter has a higher concentration dose conversion factor. As a result, ^{239}Pu dose is higher than ^{237}Np dose.

Figure 7.7.1-46[a] shows that for the first 500,000 years, the ^{234}U concentration increases with time and then decreases; so does the ^{226}Ra concentration. This suggests that ^{226}Ra concentration is largely controlled by ^{234}U concentration since the former is a decay product of the latter.

Igneous Intrusion Modeling Case: Outlier

For the purpose of analyzing an outlier realization for the Igneous Intrusion Modeling Case, epistemic vector 20 was chosen as shown on Figure 7.7.1-47[a] because it has the highest annual dose from about 50,000 years to about 300,000 years. Figure 7.7.1-48[a] shows the unweighted annual dose from 10 aleatory vectors, equivalent to GoldSim realizations 191 through 200, for epistemic vector 20. GoldSim realization 191 was chosen for further study, and the results are compared with GoldSim realization 2855 described earlier. In realization 191, the igneous event time is specified at 250 years and thereby occurs much earlier than for realization 2855, where it is specified at 10,000 years. Figure 7.7.1-49[a] shows the time history of annual dose and the contributions to annual dose from the selected radionuclides for realization 191. Four spikes in the total annual dose can be seen, with three prior to 10,000 years and the fourth being a broad peak past 10,000 years. The first spike (annual dose magnitude of about 1,100 mrem) occurs shortly after the igneous intrusion. This spike is caused by mobile radionuclides that travel unretarded through the engineered barrier and natural barrier system, such as ^{99}Tc, ^{129}I, and ^{14}C. The second spike (annual dose magnitude of about 400 mrem) occurs at 2,250 years shortly after a climate change from the monsoon to the glacial-transition climate. As shown in Figure 7.7.1-50[a], water flux through WPs increases due to the climate change, which causes higher advective releases and annual dose. The second spike is also caused by mobile radionuclides, such as ^{99}Tc, ^{129}I, and ^{14}C.

The third spike (annual dose magnitude of about 900 mrem) occurs at 4,500 years. Dose contribution from ^{79}Se dominants this spike. Selenium is moderately retarded in the UZ and SZ, as it has moderate K_d values in the UZ and SZ (Tables 6.3.9-2 and 6.3.10-2 of the parent document). ^{79}Se is not a major dose contributor in realization 2855 analyzed previously, nor in the base case (Figures 7.7.1-39[a] and 7.7.1-36[a]). Further analysis reveals that the sampled BDCF for ^{79}Se in realization 191 is 123 times higher than that in realization 2855 (a sampled value of 2.73 (mrem/yr)/(pCi/l) versus 2.22×10^{-2} (mrem/yr)/(pCi/l)). This is the primary reason for high ^{79}Se dose in realization 191.

The fourth spike (annual dose magnitude of about 6,900 mrem) occurs around 50,000 years with ^{239}Pu as the dominant radionuclide and the peak dose is about ten times higher than that in realization 2855 (Figure 7.7.1-39[a]). This is attributed to the higher solubility of plutonium in this realization, which is calculated to be about 0.105 mg/L in the CSNF waste form domain (Figure 7.7.1-51[a] compared to a value of about 0.005 mg/L for realization 2855 (Figure 7.7.1-40[a]). This difference (a factor of 21) is mainly caused by the difference in the sampled thermodynamic uncertainty values (the term ε_1 in Equation 6.3.7-13a of the parent document) for plutonium solubility (equivalent to GoldSim uncertain parameter Pu_Eps_1_low_a). In realization 191, the log of thermodynamic uncertainty is sampled to be 1.218 (at 96th percentile of the distribution), while for realization 2855, the sampled log value is -0.3428 (at 30th percentile of the distribution). The difference results in an increase in plutonium solubility by a factor of 36. Since there are other factors that modify the solubility, the actual

difference in plutonium solubility is smaller (21 times) than the difference in the sampled thermodynamic uncertainty.

The increase in ^{239}Pu dose after 10,000 years is due to climate change at 10,000 years leading to increased flow rate through the WP (Figure 7.7.1-50[a]) and faster travel times through the UZ and SZ. Annual dose contribution from ^{239}Pu decreases with time after 50,000 years, as the mass is depleted from the inventory and undergoes radioactive decay. Figure 7.7.1-51[a] shows that in the CSNF waste form domain, plutonium release is under solubility control until 156,000 years, while uranium release is under solubility control until 344,000 years. At later times, past 200,000 years, ^{242}Pu, ^{237}Np, ^{234}U, and ^{226}Ra overtake ^{239}Pu as the major dose contributors and show behavior similar to that of realization 2855.

7.7.1.4[a] Seismic Ground Motion Modeling Case for One Million Years

This section presents an analysis of a single realization from the 9,000 realization base-case run performed for calculating the expected dose from the Seismic GM Modeling Case (GoldSim filename: LA_v5.005_SM_009000_003.gsm; output DTN: MO0710ADTSPAWO.000 [DIRS 183752]) for the one-million-year long simulation. The expected annual dose is presented on Figure 7.7.1-52[a], where each of the 300 realizations represents expected annual dose for one epistemic uncertainty vector. The expected annual dose for each epistemic uncertainty vector is generated by taking an expectation over a sample of 30 aleatory uncertainty vectors. More details about the computational methodology is provided in Sections 6.1.2.4.4 and 7.3.2.6.2 of the parent document. A single epistemic vector is selected for further analysis in such a manner that the expected annual dose is broadly representative of the modeling case and similar in behavior to the mean annual dose curve (Figure 7.7.1-52[a]). A separate outlier realization analysis is not included for 1,000,000 year Seismic GM Modeling Case because the epistemic vector chosen for the detailed analysis has an expected annual dose near or above the 95th percentile and could be considered an outlier realization.

Epistemic uncertainty vector 155 is selected for further analysis. The thirty corresponding aleatory vectors (sampling sequences) are represented by GoldSim realizations 4621 through 4650 (Figure 7.7.1-53[a]). Of these, the aleatory vector 21 (sampling sequence 21), which is equivalent to GoldSim realization 4641, is selected for detailed analysis (solid red curve on Figure 7.7.1-53[a]). The GoldSim file for realization 4641 was run twice: first to save information for all the percolation subregions and then to specifically save details of the EBS cell pathway related to percolation subregion 3 for the seeping environment (GoldSim filenames: LA_v5.005_SM_009000_004.gsm and LA_v5.005_SM_009000_005.gsm; output DTN: MO0801TSPAMVAC.000 [DIRS 185080]).

The annual dose from realization 4641 is presented on Figure 7.7.1-54[a], along with contributions to dose from individual radionuclides. The annual dose profile shows four major peaks, two of which occur before 100,000 years and the other two around 300,000 years and 500,000 years. Prior to 500,000 years, the radionuclides that dominate dose are ^{99}Tc, ^{129}I, ^{79}Se, ^{239}Pu, and ^{242}Pu, after which dose is predominantly from ^{242}Pu, with minor contributions from ^{135}Cs and ^{237}Np. The annual dose increases steadily after 700,000 years. There is no dose prior to 24,500 years.

Seismic events are modeled as a Poisson process and are generated randomly at the specified rate of 4.287×10^{-4} yr^{-1} (equal to the difference between maximum annual exceedance frequency of 4.287×10^{-4} yr^{-1} and the minimum annual exceedance frequency of 1×10^{-8} yr^{-1}) (Section 6.6.1.3.2 of the parent document). Over the course of any simulation, several seismic events can occur with an average value of 429 total events (computed by multiplying the specified rate of the Poisson process, 4.287×10^{-4} yr^{-1}, by the simulation time period of one million years). For realization 4641, a total of 460 seismic events occur over the simulated duration (Figure 7.7.1-55[a]). The horizontal component of the peak ground velocity (PGV) corresponding to each seismic event (also shown on Figure 7.7.1-55[a]) is calculated from the mean bounded seismic hazard curve (Section 6.6 of the parent document) by uniformly sampling the annual exceedance frequency between the minimum and maximum values for each event.

The probability of damage from an event is calculated separately for the CDSP and CSNF packages due to the inclusion of a transportation, aging, and disposal canister in the CSNF packages, which increases their structural strength. Though the response surfaces for the probability of damage are different for CDSP and CSNF packages, they are both functions of the PGV and the residual stress threshold (RST) of Alloy 22. The PGV value varies with each seismic event (as shown on Figure 7.7.1-55[a]), whereas the RST of Alloy 22 is treated as an epistemic uncertainty and held constant over the realization. The RST can vary uniformly from 90 percent to 105 percent of the yield strength, and the value of 91.92 percent for epistemic vector 155 indicates a sample from the lower end of the distribution. A lower RST value typically results in a greater probability of damage to the WP during a given seismic event; however, the actual damage depends on a number of other conditions, such as whether the WP has intact internals or degraded internals, whether the DS framework and plate are intact or not, and whether the WP is covered by rubble or not. Each of these conditions is determined separately.

Based on the DS plate and framework fragility analysis (Section 6.6.1.3.5 of the parent document), which is a function of DS plate and framework thicknesses at the time of the event; the fraction of the drift filled by rubble (in lithophysal zones) at event time; and the PGV of the event, the DS framework is not calculated to fail until 90,485 years and the DS plate does not fail until 267,465 years (Figure 7.7.1-56[a]). (The failure times are taken from calculations done in GoldSim filenames: LA_v5.005_SM_009000_004.gsm and LA_v5.005_SM_009000_005.gsm; output DTN: MO0801TSPAMVAC.000 [DIRS 185080].) At the time of DS plate failure, the fraction of drift filled by rubble is still less than half (about 0.43). Note that the failure time of the DS from rubble fill (due to seismic events) is computed to be much earlier than the expected DS failure time from general corrosion only, which is computed to occur around 307,000 years.

The time of initial damage to the WP due to a seismic event is determined separately for CDSP and CSNF WPs (Section 6.6.1.3.8 of the parent document) and is calculated as the earliest of the following three failure times:

1. The time of initial damage to the intact WP moving freely beneath the intact DS. The probability of damage is based on intact WP-internals abstraction by assuming a 23-mm thickness of the WP OCB and is a function of PGV and RST.

2. The time of initial damage to the WP surrounded by rubble after the DS (either framework or plate) is failed. The probability of damage is based on the damage abstraction for the degraded WP internals surrounded by rubble and is a function of PGV, RST, and WP OCB thickness.

3. The time of initial damage to the WP by puncture after the DS plate is failed. The probability of damage is a function of PGV and WP OCB thickness.

For a CDSP WP, initial damage is caused by the seismic event at about 24,100 years, which is calculated from the damage abstraction for the intact WP moving freely beneath the intact DS. (The failure times are taken from calculations done in GoldSim filenames: LA_v5.005_SM_009000_004.gsm and LA_v5.005_SM_009000_005.gsm; output DTN: MO0801TSPAMVAC.000 [DIRS 185080].) The DS failure times are much later than the CDSP WP failure times. The PGV of the seismic event is about 0.7 m/s, and the probability of damage is computed to be about 0.22 for the sampled RST of 91.92 percent, based on results presented on Figure 6.6-11a of the parent document. To determine if damage occurs, the probability of damage is compared to a random number generated by sampling a uniform distribution between 0 and 1 for each seismic event; if the probability of damage exceeds the random number, the WP is calculated to be damaged. At the event time of about 24,100 years, the random number is 0.15 and so the CDSP WP is considered to be damaged. All CDSP WPs fail at this time, as there is no spatial variability for seismic damage (ignoring the small variation in WP thicknesses across various percolation subregions). The number of CDSP WPs failing in each percolation subregion for both seeping and non-seeping environments is shown on Figure 7.7.1-57[a].

For CSNF WPs, the first damage from a seismic event is calculated to be past the simulation time period. This is possible since the probability of a CSNF WP getting damaged directly from a seismic event is extremely small (Figure 6.6-10a of the parent document). Therefore, in this realization, CSNF WP breaches from SCC caused by nominal processes occur much earlier than breaches due to seismic damage within the simulated time period (Figure 7.7.1-58[a]). The breach times calculated by WAPDEG differ for each percolation subregion due to variability in corrosion processes and thermal profiles for the WP. The time of the first breach of CSNF WPs in the various percolation subregions is as follows: 188,000 years in percolation subregion 1; 168,000 years in percolation subregion 2; and around 204,000 years in percolation subregions 3, 4, and 5. Failure of additional CSNF WPs from nominal processes occur based on the WAPDEG calculated WP failure history for each percolation subregion. The CSNF WP failure time history for each percolation subregion, for both seeping and non-seeping environments, is shown on Figure 7.7.1-58[a]. Noticeable jumps in the number of failed WPs around 300,000 years and 500,000 years reflect coarse time discretization used by WAPDEG at late simulation time periods.

In order to compute the representative WP damaged area for a given percolation subregion for performing radionuclide transport calculations, a conservative approach is adopted when the WP failures first occur due to nominal processes and fail over time. Following the first WP failure, the WP damage abstraction for degraded internals is used and any damage from subsequent seismic events is added to the previous damaged area for the representative WP. This time varying cumulative damage area computed for the first failed WP is then applied to other WPs in

the percolation subregion once they fail by either nominal processes or seismic ground motion, thereby maximizing the area for radionuclide transport. Since all CDSP WPs simultaneously fail around 24,100 years from seismic damage, the damaged area of a WP increases from zero to an initial small area due to the first appearance of cracks. It then increases from subsequent seismic events that cause damage but remains relatively small, as shown for percolation subregion 3 (Figure 7.7.1-59[a]). The initial damage area increases sharply past 49,000 years, followed by a few more increases from events that cause damage. After failure of the DS plate (around 268,000 years), the WP is assumed to be surrounded by rubble, and the probability of damage decreases considerably, leading to no additional damage from subsequent seismic events—until the seismic event that occurs at about 850,000 years. However, past 200,000 years there are small, gradual increases in the opening area due to continuing SCC from nominal processes. Beyond 500,000 years, patches from general corrosion processes start to appear and the total opening area increases rapidly. The breach area history for the CSNF WPs is similar to that for CDSP WPs, except for the start time which is much later, as shown for the percolation subregion 3 on Figure 7.7.1-60[a]. Following the first stress corrosion crack failure from nominal processes around 204,000 years, the opening area increases discretely (from further SCC) as a result of subsequent seismic damages, although there is some small gradual increase in the opening area due to continuing SCC from nominal processes. Nevertheless, the breach area remains relatively small until general corrosion patches appear after about 600,000 years.

Calculations of the seismically damaged area that use the degraded internals abstraction are based on the thickness of the WP OCB (Figures 6.6-10 to 6.6-17 of the parent document), in addition to the sampled PGV and the RST value. Two end-member seismic-damage abstractions are generally used in the TSPA-LA Model. One is based on the 23-mm OCB thickness applied if the OCB thickness is greater than or equal to 23 mm. The second abstraction is based on the 17-mm OCB thickness applied if the OCB thickness is less than or equal to 17 mm (this happens rarely and typically near the end of the simulated time period). For OCB thicknesses between 23 mm and 17 mm, the damage is based on the linear interpolation between the two end-member damage abstractions. Inside-out corrosion of the OCB begins once the WP is breached, which accelerates thinning of the WP OCB and makes it more susceptible to both seismic damage and general corrosion patches. Profiles of mean thicknesses of WP OCB for both CDSP and CSNF WPs in percolation subregion 3 are shown on Figure 7.7.1-61[a], along with WP failure fractions. The initial thicknesses of both types of WP are the same but diverge due to the initiation of inside-out corrosion of all CDSP WPs following seismic damage around 24,100 years. On the other hand, the CSNF WPs do not begin to fail until after 200,000 years, and they typically fail over an extended period. Thus, failed CSNF WPs are, on average, thicker than failed CDSP WPs, making CSNF WPs less susceptible to seismic damage and general corrosion induced patch failures compared to CDSP WPs. This is the primary reason for the smaller opening area and longer time taken for patches to appear on CSNF WPs (Figure 7.7.1-60[a]) compared to CDSP WPs (Figure 7.7.1-59[a]).

Because general corrosion patches on the WPs (either CSNF or CDSP) do not appear until 500,000 years or later, all mass released from failed WPs until that time is by diffusion through stress corrosion cracks (because no advective water flow is allowed through stress corrosion cracks). ^{99}Tc is a major dose contributor, and its diffusive mass flux out of CDSP WPs for various percolation subregions is shown on Figure 7.7.1-62a[a]. Note that the relative magnitude of release rates among percolation subregions is proportional to the number of failed WPs in

each percolation subregion (Figure 7.7.1-57[a]). Releases of ^{99}Tc start when WPs are first damaged (around 24,100 years), then decrease over the next approximately 25,000 years as steady-state conditions are established. Release rates increase again around 49,500 years due to a sharp increase (about 30 fold) in the WP damage area (Figure 7.7.1-59[a]). Even though most of the HLW glass waste form has degraded by 40,000 years, including all of DSNF mass, not until about 55,000 years is most of the ^{99}Tc mass released from the WP. This delay reflects the role of small cracks in reducing the rate of release, despite the lack of a solubility controlling solid for ^{99}Tc and large concentration gradients across the WP.

In contrast, the diffusive mass flux of ^{242}Pu (a major dose contributor past 500,000 years) out of the failed CDSP WPs remains relatively constant (Figure 7.7.1-62b[a]). The release rate follows the WP OCB area opening curve, an indication that diffusive release of plutonium is proportional to the total WP opening area (Figure 7.7.1-59[a]). The slow relative release of ^{242}Pu is maintained throughout the simulation for a variety of reasons, including (a) longer half-life of ^{242}Pu (~ 375,000 years) compared to that of ^{99}Tc (210,000 years), (b) the dissolved concentration inside the waste form domain is limited by the solubility controlling mineral phase (Section 6.3.7.5 of the parent document) so that not all of the degraded mass is available for release, (c) sorption of ^{242}Pu in the corrosion products domain retards its transport and reduces the concentration gradient for diffusive flux, and (d) small diffusive areas associated with the WP OCB reduce the mass flux. Of these four factors, most important is sorption onto corrosion products. For example, in percolation subregion 3 for the seeping environment, 1,055 CDSP WPs fail around 24,100 years. Total initial ^{242}Pu mass in the CDSP inventory (combined HLW and DSNF masses) is approximately 38.65 g/pkg (grams per CDSP package) (from Table 6.3.7-5 of the parent document, with an adjustment based on uncertainty in the inventory). By using the decay rate of 1.85×10^{-6} yr^{-1}, the maximum mass of ^{242}Pu at the time of WP breach would be about 36.97 g/pkg, and about 35.31 g/pkg at 49,000 years, when breach area increases (Figure 7.7.1-59[a]). Based on the results of the transport calculation, the mass of ^{242}Pu sorbed onto corrosion products at 49,000 years is about 35.30 g/pkg, which accounts for just about all of the available mass. The mass is slowly released by desorption from corrosion products into the solution, thereby controlling both dissolved concentration (Figure 7.7.1-63[a]) and diffusive flux. Note that a mechanistic competitive sorption model that considers kinetic sorption and desorption is implemented for plutonium in the corrosion products domain (Section 6.3.8 of the parent document). As a result, variations in ^{242}Pu concentration within the corrosion products domain are moderated, even though upstream concentrations (in the waste form domain) can vary over a larger range based on time-varying degradation rates and solubility limits.

The diffusive flux of ^{99}Tc and ^{242}Pu from all five percolation subregions for CSNF WPs is shown on Figure 7.7.1-64a[a] and Figure 7.7.1-64b[a]. The release from percolation subregion 2 precedes releases from other percolation subregions (as expected) because CSNF WPs fail in percolation subregion 2 first (Figure 7.7.1-58[a]). Figure 7.7.1-60[a] shows the evolution of the CSNF WP OCB opening area for percolation subregion 3 in a seeping environment. The ^{99}Tc diffusive releases from CSNF WPs are sustained for a much longer time than are releases from CDSP WPs (compare Figure 7.7.1-64a[a] to Figure 7.7.1-62a[a]) due to the more gradual failure of CSNF WPs as shown on Figure 7.7.1-58[a]. However, once all CSNF WPs in a given percolation subregion have failed by nominal SCC (typically by about 550,000 years) and almost all of the CSNF waste form has degraded, the ^{99}Tc mass is depleted relatively quickly out of the WP, but still takes over 10,000 years to be fully released (equivalent to fewer than three model

timesteps at such late times). Compared to ^{99}Tc release, diffusive release of ^{242}Pu is more gradual and follows the breach area curve rather than the CSNF WP failure curve. The increase in diffusive releases after 800,000 years is caused by the patch opening that significantly increases the total WP breach area (Figure 7.7.1-60[a]) while the continued release of ^{242}Pu from CSNF WPs is maintained by sorption-desorption reactions with corrosion products. Figure 7.7.1-65[a] shows the example for percolation subregion 3 for the seeping environment, where most of the ^{242}Pu mass released from the inventory is sorbed on the corrosion products and then is gradually released by desorption, thereby controlling the dissolved concentration and diffusive release out of the WP (note that the curve showing the mass sorbed on corrosion products also includes the effects of radioactive decay).

The time histories for pH and ionic strength in the corrosion products domain for percolation subregion 3 for the seeping environment are shown on Figure 7.7.1-66[a]. The first sharp decline in ionic strength occurs around 380,000 years because that is the time when rubble completely fills the drift (a consequence of multiple seismic events, as shown on Figure 7.7.1-56[a]). At that time, the differential temperature and relative humidity time histories for high thermal conductivity rubble is imposed, leading to a small increase in relative humidity from 0.9956 to 0.9984. Since this increase in relative humidity corresponds to an equivalent increase in activity of water, it causes an appreciable decrease in ionic strength, indicating its high degree of sensitivity to relative humidity under vapor influx conditions (see Section 6.3.7.2.2 of the parent document for details on ionic strength abstraction). The second decline in ionic strength that occurs around 712,000 years is caused by water flowing through the WP after general corrosion patches have formed and exceeded a threshold of 0.1 L/yr, thereby leading to a change in the In-Package Chemistry Submodel (Section 6.3.7.2 of the parent document) from calculations based on vapor influx to calculations based on liquid influx. Despite the changes in ionic strength over the course of the simulation, pH in the corrosion products domain remains nearly constant as a result of buffering by surface complexation reactions.

Figure 7.7.1-67[a] compares (a) the concentration of ^{242}Pu that is associated reversibly and irreversibly with colloids to (b) the dissolved concentration in the WP (corrosion products domain) for both CDSP and CSNF WPs for the seeping environment in percolation subregion 3. The concentration of dissolved and reversibly sorbed ^{242}Pu mass on colloids (denoted as aqueous) overlays the dissolved concentration, indicating that the mass of ^{242}Pu reversibly associated with colloids is negligible. The concentration of various colloid types over time for both CDSP and CSNF WPs are shown on Figure 7.7.1-68[a]. Different types of colloids become stable at different times based on their stability relationships as illustrated on Figure 6.3.7-11 of the parent document. CSNF waste form colloids remain unstable throughout the simulation and therefore maintain a constant minimum concentration. The HLW glass waste form colloids become stable first, followed by uranium colloids while there is no advection through the WP and ionic strength remains relatively high. Following the opening of general corrosion patches and advent of advective flow, groundwater colloids and iron oxyhydroxide colloids become stable primarily because of the appreciable decrease in ionic strength (for example, as shown in Figure 7.7.1-66[a] for CSNF WP).

Both reversible and irreversible sorption of plutonium is modeled on HLW glass waste form colloids while only irreversible sorption is modeled on the iron oxyhydroxide colloids and CSNF

waste form colloids. Only reversible sorption of plutonium is modeled on the groundwater colloids and uranium colloids. The sampled plutonium K_d for HLW glass waste form colloids and groundwater colloids (both represented by smectite mineralogy) is about 1,700 mL/g, and the sampled plutonium K_d for uranium colloids is about 247 mL/g. Due to the combination of small colloid concentrations and relatively small sampled K_d for plutonium, the plutonium mass reversibly associated with colloids remains negligibly small compared to the mass in the dissolved state (Figure 7.7.1-67[a]). The concentration of ^{242}Pu irreversibly associated with HLW glass waste form colloids and iron oxyhydroxide colloids becomes significant at various times as shown on (Figure 7.7.1-67[a]).

Total EBS releases (i.e., summed over all percolation subregions) of ^{99}Tc and ^{242}Pu in the dissolved state, dissolved and reversibly associated with colloids (denoted as aqueous), and irreversibly sorbed on colloids for both CSNF and CDSP WPs are shown on Figure 7.7.1-69[a]. (The EBS release of ^{242}Pu mass irreversibly sorbed on CSNF waste form colloids is not shown as it is negligible due to the instability of those colloids.) The mass release of ^{99}Tc and ^{242}Pu (total) from CSNF WPs exceeds that released from CDSP WPs due to the greater number of CSNF WPs and larger inventory on a per package basis (Tables 6.3.7-1 and 6.3.7-5 of the parent document). It is interesting to note that, until the patches appear and advection starts, most of the ^{242}Pu mass released from the WP is in the dissolved state and very little is irreversibly associated with colloids (Figure 7.7.1-69[a]), even though the concentration of ^{242}Pu irreversibly associated with colloids is higher than the dissolved concentration in the WP (as shown by the example on Figure 7.7.1-67[a]). This is because prior to the opening of patches, since only diffusive release can occur through the WP, the colloid facilitated transport is limited by the diffusion coefficient of colloids, which is computed to be about 700 times smaller than that for the dissolved plutonium based on the sampled colloid particle diameter (SNL 2007 [DIRS 177407], Section 6.3.4.4). Once advection through the WP starts the transport of mass irreversibly associated with colloids becomes important.

The majority of the mass (combined for CSNF and CDSP WPs) that is passed from the EBS to the UZ at the repository horizon goes into fracture nodes in the UZ, rather than into the matrix nodes as shown on Figure 7.7.1-70[a] for ^{242}Pu. This is because the majority of the WPs in a given percolation subregion (except for percolation subregion 1) are in the seeping environment where drift seepage that flows out through the invert carries the mass advectively through the fractures, even though most of the mass is diffusing out of the WP. For percolation subregion 1, the fraction of mass going into the fractures is initially relatively small (about 0.4) but increases (to approximately 0.9) around 81,500 years. This behavior is due to the change in seepage flux, which remains relatively small (about 0.005 m^3/yr) until around 81,500 years and then increases to about 0.08 m^3/yr. This is because at this time, the nonlithophysal locations are considered to be collapsed from drift degradation based on the drift seepage model abstraction, resulting in the seepage flux for such locations to change from the non-collapsed drift seepage to the percolation flux (Section 6.3.3.1.2 of the parent document). The effect of this change is greatest for percolation subregion 1 because, compared to other percolation subregions, it has (a) the smallest ambient seepage rates prior to the drift collapse and (b) the highest fraction of nonlithophysal locations (about 32 percent).

The cumulative mass releases from EBS, UZ, and SZ are compared on Figure 7.7.1-71[a] for ^{99}Tc, ^{242}Pu (dissolved and reversibly sorbed on colloids; denoted as aqueous), and ^{242}Pu

(irreversibly sorbed on all colloids). The transport characteristics are quite different for ^{99}Tc and ^{242}Pu in the UZ and SZ domains as ^{99}Tc is transported without retardation; whereas ^{242}Pu (aqueous) experiences considerable retardation due to sorption onto the tuff matrix and alluvium (Table 6.3.9.2 and Table 6.3.10.2 of the parent document). Little retardation is apparent in the UZ and SZ domains for ^{242}Pu irreversibly sorbed onto colloids because the diffusive interaction between fractures and matrix continua for mass irreversibly sorbed onto colloids is not modeled and, once the mass is placed in the fracture continuum, it tends to stay there. Although a small fraction (0.00168) of irreversible mass associated with colloids travels unretarded through the UZ and SZ (designated as the 'fast fraction'; Section 6.3.8.3 of the parent document), almost all irreversible mass on colloids undergoes some retardation due to interaction between colloid particles and fracture surfaces. Despite this interaction, the mass irreversibly associated with colloids travels quickly through the UZ and SZ. As shown on Figure 7.7.1-71[a], almost all the mass released from the EBS, for both ^{99}Tc and ^{242}Pu (irreversibly sorbed onto colloids), is also released at the SZ model boundary within a relatively short period compared to the simulation time of 1,000,000 years. In contrast, the mass of ^{242}Pu (aqueous) released from the UZ and SZ model boundaries at the end of the simulation is appreciably smaller than that released from the EBS, indicating significant retardation (about 65 percent is released out of the UZ while only 31 percent is released out of the SZ). Since most of the mass is passed to the fracture nodes of the UZ, it diffuses from the fracture continuum into the matrix continuum due to fracture-matrix interaction in the UZ, with some mass also being transported into the matrix by advection due to lateral flow. Even though the free water diffusion coefficients in the UZ (as in EBS) vary by species (Table 6.3.9-3 of the parent document), the difference between ^{99}Tc and ^{242}Pu (aqueous) is relatively small (differ by a factor of 1.5) and can be ignored for most practical purposes. Thus, both ^{99}Tc and ^{242}Pu (aqueous) are equally likely to diffuse (assuming equal concentrations) from the fracture continuum into the matrix continuum. Because of sorption of ^{242}Pu in the UZ matrix, the concentration gradient between fracture and matrix is higher for ^{242}Pu than for ^{99}Tc, leading to greater diffusive flux of ^{242}Pu into the matrix and smaller cumulative release at the UZ-SZ boundary.

In the SZ domain, the mass released from each of the four UZ regions is passed to the corresponding SZ region. In each SZ region, a location is randomly selected as the starting point for transport and is manifested through sampling one of the 200 pre-generated SZ breakthrough curves for a given species (Section 6.3.10.2 of the parent document). Due to their different transport characteristics through volcanic units and alluvium, separate sets of breakthrough curves are available for ^{99}Tc, ^{242}Pu (dissolved and reversibly sorbed on colloids; denoted as aqueous), ^{242}Pu (fast traveling fraction irreversibly associated with colloids), and ^{242}Pu (slow traveling fraction irreversibly associated with colloids). The breakthrough curves are pre-generated as an impulse response function to a unit pulse and are convolved with the incoming UZ mass flux by using the convolution integral approach to produce the SZ mass flux at the location of the RMEI.

In this realization, SZ breakthrough curve number 122 was selected, and the breakthrough times of ^{99}Tc, ^{242}Pu (dissolved and reversibly sorbed on colloids; denoted as aqueous), and ^{242}Pu (slow traveling fraction irreversibly associated with colloids) are compared for all four zones on Figure 7.7.1-72[a]. The breakthrough curves for ^{242}Pu (fast traveling fraction irreversible on colloids) are not presented as very little mass is transported by them. The breakthrough of ^{99}Tc from all four SZ regions is much earlier than that for ^{242}Pu (aqueous) and for ^{242}Pu (slow

traveling fraction irreversible on colloids), with almost half of the mass input recovered after a few hundred years of travel in the SZ for ^{99}Tc compared to almost 100,000 years of travel time required for ^{242}Pu (aqueous) and 10,000 years of travel time required for ^{242}Pu (slow traveling fraction irreversible on colloids). However, the long tail noticeable in the breakthrough curve for ^{99}Tc for the remaining half of its input mass results from longitudinal and transverse dispersion in the volcanic units and alluvium due to fracture-matrix diffusive interactions in the dual porosity volcanic domain of the SZ transport model. The ^{242}Pu (aqueous) breakthrough is further impacted by sorption in both the volcanic matrix and alluvium. For SZ breakthrough curve 122, the initially sampled plutonium K_d for volcanic matrix units is approximately 120 mL/g, and the initially sampled plutonium K_d for the alluvium is 107 mL/g (SNL 2008 [DIRS 183750], Table A-1[b]). Both are modified in order to calculate effective K_d values but nevertheless result in considerable retardation. Nearly all the plutonium (>0.999 fraction) is transported in the dissolved phase, with a small fraction (<0.001) being transported via reversible sorption on the groundwater colloids. This is because the groundwater colloid concentration sampled is about 0.11 mg/L and the K_d for plutonium on the colloid is sampled to be about 6,560 mL/g, which when multiplied together, provides the fraction of the mass associated with colloids versus that transported in dissolved state. This fraction is equal to about 0.000722.

The release rates out of the SZ for ^{99}Tc, ^{242}Pu (dissolved and reversibly sorbed on colloids; denoted as aqueous), and ^{242}Pu (irreversibly associated with colloids for both fast and slow traveling fractions) are shown on Figure 7.7.1-73[a] for realization 4641, and all three essentially follow their release rates out of the EBS when combined over CDSP and CSNF WPs (Figure 7.7.1-69[a]). The SZ releases are converted into annual dose by taking the annual releases out of the SZ for each radionuclide, dissolving them in the 3,000 acre-ft of water (annual usage at RMEI as defined by the regulation) to compute the mass concentrations, converting the mass concentration into concentration of radioactivity (in curies per liter of water), and then multiplying with the corresponding BDCFs computed for the modern-interglacial climate (present-day climate). The end result of this calculation is shown on Figure 7.7.1-54[a].

7.7.1.5[a] Nominal Modeling Case

This section presents an analysis of a single realization out of the 300 realization base-case run performed for calculating the expected annual dose from the Nominal Scenario Class (GoldSim filename: LA_v5.005_NC_000300_000.gsm; output DTN: MO0710ADTSPAWO.000 [DIRS 183752]). The Nominal Scenario Class consists of a single modeling case that represents a set of possible repository futures from which are excluded (1) disruptive events and (2) early failures of DSs and WPs. Moreover, the Nominal Modeling Case serves as a 'reference system state' from which all other modeling cases are developed (Section 8.2.1 of parent document). The distribution of expected annual dose for 300 epistemic vectors that also implicitly account for aleatory uncertainties (such as time, location, and degree of damage to each WP) is shown on Figures 7.7.1-74a[a] (linear time) and 7.7.1-74b[a] (log time). Details about the calculation of the expected annual dose for this modeling case are described in Section 6.1.2.4.1 of the parent document.

The major radionuclides contributing to mean annual dose for this modeling case are shown on Figure 7.7.1-75[a]. Long-lived, highly-soluble, and mobile radionuclides, such as ^{99}Tc and ^{129}I, are the dominant dose contributors for most of the simulation, whereas long-lived,

sparingly-soluble, and strongly-sorbing radionuclides, such as ^{242}Pu, ^{135}Cs, and ^{237}Np become important dose contributors at later times when contributions from ^{99}Tc have declined.

Two minor peaks in the mean annual dose are apparent early on, at around 40,000 and 80,000 years (Figures 7.7.1-74[a]). These are the result of WPs failing by SCC from two realizations (out of the total of 300 realizations). After about 100,000 years, the mean annual dose steadily increases as a result of gradual WP failures. Step-wise increases in the mean annual dose noticeable around 200,000; 300,000; 500,000; and 700,000 years are due to increases in the number of WP failures (from SCC) calculated by the waste package degradation code WAPDEG V4.07 (STN:10000-4.07-01 [DIRS 181064]). WAPDEG calculates the corrosion rates at the timesteps provided in the WP thermal history input files from the multiscale thermohydrologic model (MSTHM) Abstraction (Section 6.3.2.3 of the parent document). The thermal history files have coarse temporal resolution past 100,000 years (due to small changes at late time periods) leading to evaluation of temperature at 200,000; 300,000; 500,000, 700,000; and 1,000,000 years. The stress corrosion crack growth rate is given by a power law function of stress intensity factor and repassivation slope n (Equation 6.3.5-14 of the parent document). The stress intensity factor is evaluated at the beginning of each WAPDEG timestep and is a function of the crack depth that drives the crack propagation. The large timesteps taken past 100,000 years combined with the sensitivity of the crack growth rate to the stress intensity factor, which is raised to the power $4n$, where n has a mean value of 1.165 (SNL 2007 [DIRS 181953], Table 8-15), can cause dramatic changes in the crack growth rate at each timestep. As a result, the crack growth rate can change from a small value for the timestep in which the crack initiates to a much larger value at the beginning of the next timestep, resulting in almost immediate penetration of many cracks and failure of WPs. An assessment of this temporal discretization for the Nominal Modeling Case is presented in Section 7.3.3.7[a].

Nominal Modeling Case—Realization 286

A single epistemic vector is selected for further analysis in such a manner that the expected annual dose is broadly representative of the modeling case and similar in behavior to the mean annual dose. Epistemic vector 286 is chosen for further analysis (Figure 7.7.1-76[a]), which is equivalent to GoldSim realization 286 (GoldSim filename: LA_v5.005_NC_000300_001.gsm; output DTN: MO0801TSPAMVAC.000 [DIRS 185080]).

Figure 7.7.1-77[a] shows the major radionuclides that contribute to the annual dose for realization 286 of the Nominal Modeling Case. Of these, ^{99}Tc and ^{129}I are the primary contributors with relatively minor contributions from ^{36}Cl, ^{79}Se, and ^{135}Cs. Between 250,000 and 300,000 years, the annual dose for realization 286 exhibits local step increases that result from a single CDSP WP failure in the non-seeping environment of percolation subregion 2 and two CDSP WP failures in the seeping environment of percolation subregion 2. All three CDSP WP failures are caused by SCC failure on the outer lids prior to the DS failure, which occurs at 304,000 years.

The three significant step increases in the annual dose at 300,000; 500,000; and 700,000 years for realization 286 (Figure 7.7.1-77[a]) result from the coarse time discretization employed in WAPDEG V4.07 software leading to increased WP failures from SCC shortly following those times. A more detailed explanation of the effect of large timesteps on crack propagation is

provided through an example calculation at the 500,000 and 700,000 year timesteps for percolation subregion 1, based on the sampled epistemic parameters for realization 286. The discussion will focus on incipient crack growth since they occur on every lid patch. Cracks due to weld flaws are ignored as they are much less frequent and are present on only a few WP lids in a given realization (Section 6.3.5.1.2 of the parent document). Incipient cracks initiate (nucleate) when general corrosion has penetrated to the depth at which the stress profile exceeds the threshold stress (critical depth). For realization 286 the threshold stress is sampled to be about 329 MPa (from a uniform distribution between 315.9 and 368.55 MPa; Table 6.3.5-3 of the parent document). Using the output table of stress versus depth generated by the SCCD V2.01 software (STN: 10343-2.01-01 [DIRS 181054]), evaluating at an angle of π radians (one of the five choices of angles), the critical depth is found to be approximately 6.5 mm (see file *WDStressO.fil* located in the output DTN: MO0801TSPAMVAC.000 [DIRS 185080] in the path: LA_v5.005_NC_000300_001 (Nominal Single)\ Additional_Information\ Supplemental_Work_for_Analysis\ WAPDEG_out_files_from_PS1ND_only_run). To initiate the stress corrosion cracks by 500,000 years (equivalent to thinning the WP OCB by 6.5 mm), the general corrosion rate is calculated to be around 13 nm/year (ignoring the temperature effects). This value is within the uncertainty range of general corrosion rate (Figure 6.3.5-6 of the parent document), which typically ranges from 2 to 15 nm/year over a cumulative probability range of 0.1 to 0.9 for the medium uncertainty curve selected in realization 286. Using the output table of stress intensity factor versus depth generated by SCCD V2.01 software at an angle of π radians, the stress intensity factor at 6.5 mm is found to be approximately 10.3 (MPa($\sqrt{m}$)) (see file *WDKISCCO.fil* located in the output DTN: MO0801TSPAMVAC.000 [DIRS 185080] in the path: LA_v5.005_NC_000300_001 (Nominal Single)\ Additional_Information\Supplemental_Work_for_Analysis\WAPDEG_out_files_from_PS1ND_ only_run). The crack growth rate is then calculated from Equation 6.3.5-14 of the parent document to be 0.000005 mm/year (using the sampled value of 3.03×10^{-11} for A and 1.29 for n). This rate when applied over the 200,000 year timestep (from 500,000 years to 700,000 years) would result in a crack growth of 1 mm. At 700,000 years (beginning of new timestep) the stress intensity factor is re-evaluated based on the new crack depth, which is the sum of the critical depth at 500,000 years (6.5 mm), the crack growth over 200,000 year period (1 mm), and the additional general corrosion thinning over 200,000 year period (2.6 mm using a general corrosion rate of 13 nm/year). The new stress intensity factor, evaluated at the current depth of 10.1 mm, would be approximately 39.4 (MPa($\sqrt{m}$)), which results in a crack growth rate of roughly 0.0054 mm/year and penetration of WP OCB (for remaining thickness of about 14.9 mm) in about 2,800 years after the start of the timestep. This calculation illustrates that the crack growth rates when recomputed over large time periods result in significant increase which in turn cause complete crack penetrations to occur shortly after the beginning of a new timestep leading to failure of large number of WPs.

Figures 7.7.1-78a[a] and 7.7.1-78b[a] illustrate the number and timing of WP failures within each percolation subregion for CDSP and CSNF WPs. These WP failures occur in both the non-seeping and seeping environments of each percolation subregion. Since there are about 2.4 times more CSNF WPs compared to CDSP WPs in the repository (8,213 CSNF WPs versus 3,416 CDSP WPs), relatively more CSNF WPs fail over the simulated duration. By the end of the simulation at 1,000,000 years, a total of 7,716 CSNF WPs have failed compared to a total of 3,227 failed CDSP WPs. The average WP failure area (breached area) time history for various

percolation subregions for CDSP and CSNF WPs are shown on Figures 7.7.1-79a[a] and 7.7.1-79b[a]. The breached area in all percolation subregions remains small throughout the simulation because WP failure is primarily from SCC. Only percolation subregion 1 for CSNF WPs has a (single) patch failure within the simulated time frame, which occurs past 950,000 years, leading to a small increase in area but even then the average breach area remains relatively small as the SCC failure area averaged over all failed WPs remains greater than the single patch failure area averaged over all the failed WPs. Thus, because only SCC failures occur on most WPs for the majority of the simulation, advective releases are negligible and radionuclides are primarily transported by diffusion out of the WP.

The rates at which ^{129}I, ^{79}Se, ^{135}Cs, and ^{242}Pu (dissolved and reversibly sorbed on colloids) are released over all percolation subregions from the EBS (as shown for waste form, WP, and invert), UZ, and SZ are shown on Figure 7.7.1-80[a] (for ^{129}I), Figure 7.7.1-81[a] (for ^{79}Se), Figure 7.7.1-82[a] (for ^{135}Cs), and Figure 7.7.1-83[a] (for ^{242}Pu). For ^{129}I and ^{79}Se, the curves that represent these release rates generally lie close to each other, which is indicative of each radionuclide being transported as a solute with little to no retardation through the engineered barrier and natural systems. The transport of ^{135}Cs (as solute and reversibly sorbed on the colloids) exhibits the same behavior through the EBS and the UZ but has significant retardation through the SZ. For ^{242}Pu (dissolved and reversibly sorbed on colloids), the mass released from the waste form is large relative to the mass released from the WP, invert, UZ, and SZ. This behavior reflects retardation due to sorption onto corrosion products inside the WP.

Figure 7.7.1-84[a] and Figure 7.7.1-85[a] compare the advective and diffusive releases of ^{129}I and ^{242}Pu (dissolved and reversibly sorbed on colloids) from all failed WPs in all percolation subregions. There is no advective release from CDSP WPs as there is no general corrosion patch failure. However, because there is corrosion patch failure for CSNF WPs in percolation subregion 1 past 950,000 years, there is some advective release, but it is still negligible compared to diffusive release. The advective release for ^{242}Pu (dissolved and reversibly sorbed on colloids) is not shown as it is below the cut-off scale for the plot. The step increase in diffusive releases coincides with the step increases in WP failures, but beside the step changes, the diffusive release remains steady for ^{129}I and shows gradual increase for ^{242}Pu that is dissolved and reversibly sorbed on colloids. This is attributed to the relatively steady rate of WP failures between the step changes (Figure 7.7.1-78[a]). Thus, although more WPs are failing with time, the rate of WP failure remains relatively steady, thereby maintaining steady releases of ^{129}I even after accounting for large diffusive flux due to high concentration gradient. The release of ^{242}Pu, in contrast, in addition to being similarly affected by the rate of WP failure, is also impacted by relatively low aqueous solubility and sorption on the corrosion products inside the WP, which reduce the concentration gradient. Combined with a small breach area per package (Figure 7.7.1-79[a]), these factors cause ^{242}Pu to be released slowly from each failed WP. As a result, as more WPs fail through time, the ^{242}Pu release rate increases gradually. Releases from CSNF WPs dominate that of CDSP WPs because (a) comparatively more CSNF WPs are failed and (b) there is comparatively larger inventory for the radionuclides of interest on a per package basis in a CSNF WP. Note that results for ^{99}Tc, ^{36}Cl, and ^{79}Se are not shown separately as they demonstrate similar transport characteristics as ^{129}I.

As previously shown on Figures 7.7.1-80[a] through 7.7.1-83[a], the release rates of ^{129}I are quite different from those for ^{242}Pu but are generally similar to ^{99}Tc, ^{36}Cl, and ^{79}Se. ^{129}I is transported

as an unretarded species through the EBS, UZ and SZ, and nearly all of the mass released from the waste form travels quickly through the EBS (WP and invert), UZ, and SZ. The mass fraction of ^{129}I passed to the UZ matrix and fracture continuum from the EBS at the repository level is shown on Figure 7.7.1-86[a]. The fraction of mass released to UZ fracture increases from percolation subregion 1 to 5, in proportion to the seepage fraction assigned to various percolation subregions (Section 6.3.3.1.3 of the parent document). The seepage fraction determines the fraction of WPs assigned to the seeping environment versus the non-seeping environment within a percolation subregion. Since ^{129}I is neither sorbed nor limited by solubility, the diffusive mass release from the WP remains largely a function of waste form degradation rate and concentration inside the WP. The change in the WP to invert concentration gradient between non-seeping environment and seeping environment due to flow through the invert has limited effect on the diffusive releases of ^{129}I per failed WP. Thus the fraction of ^{129}I mass passed to UZ fracture for a given percolation subregion is proportional to the number of failed WPs in a seeping environment compared to the non-seeping environment and thus directly related to the seepage fraction, which increases from percolation subregion 1 to 5. [Note: Although no water is modeled to flow advectively through the WPs due to the presence of stress corrosion cracks, the in-drift seepage in the seeping environments flows around the WPs (and DSs) to the invert and, thus, the diffusive releases out of the WP are carried primarily by advection from the invert into UZ fracture continuum with less mass release into the matrix continuum. In the non-seeping environment the transport through the invert is primarily by diffusion into the matrix continuum due to large effective diffusive area of the matrix continuum (Section 6.3.8.3 of the parent document).]

The mass fraction of ^{242}Pu (dissolved and reversibly sorbed on colloids) passed to the UZ matrix and fracture continuum from the EBS at the repository level is shown on Figure 7.7.1-87[a]. In contrast to the mass fraction of ^{129}I, a relatively larger fraction of ^{242}Pu is passed into the fractures, indicating a disproportionately larger contribution from WPs located in the seeping environments compared to the non-seeping environment. This is because highly sorbed species such as ^{242}Pu have a lower concentration in the WP than a nonsorbing species such as ^{129}I, and the diffusive flux is primarily controlled by concentration gradient between the WP and the invert. In the seeping environment the flow through the invert causes the concentration gradient to increase (due to reduction in distance to the effective zero concentration boundary from the WP) leading to disproportionately larger diffusive mass flux from the seeping environment than the non-seeping environment per failed WP. As a result, most of the ^{242}Pu mass released in a given percolation subregion is from the contribution of WPs in the seeping environment that are released to the UZ fracture continuum.

Transport through the SZ for each radionuclide is governed by sampling a breakthrough curve from 200 pre-generated breakthrough curves applicable to each radionuclide. The breakthrough curves are abstractions of more complex SZ flow and transport modeling studies. Each epistemic realization randomly samples a number from 1 to 200, and that sampled number represents the set of species-specific breakthrough curves to be used in that particular realization. For realization 286, breakthrough curve set 33 is selected. Solute transport of ^{129}I and ^{79}Se in the SZ is relatively quick due to no retardation modeled for ^{129}I and limited retardation for ^{79}Se (sampled K_d of about 8.3 mL/g and 6.7 mL/g in the SZ volcanic matrix and alluvium, respectively) as shown by release rates for SZ when compared to UZ in Figures 7.7.1-80[a] and 7.7.1-81[a]. In contrast, dissolved ^{242}Pu (with sampled K_d of about 84 mL/g for SZ volcanic

matrix and 87 mL/g for SZ alluvium) and, to a much greater extent, dissolved ^{135}Cs (with sampled K_d of about 5986 mL/g for SZ volcanic matrix and 563 mL/g for SZ alluvium) undergo sorption while being transported through the SZ and hence are retarded (Figures 7.7.1-83[a] and 7.7.1-82[a]).

^{242}Pu is one of the radionuclide species that is transported both dissolved and reversibly sorbed on colloids and irreversibly associated with fast traveling and slow traveling fraction of colloids. Figure 7.7.1-88[a] shows the contribution to the mean annual dose of ^{242}Pu (dissolved and reversibly sorbed on colloids; denoted as aqueous) and associated irreversibly with colloids (for both traveling fast and slow). While colloidal ^{242}Pu exists as a species in the natural system, its contribution to the mean annual dose is very small and the majority of the dose is from the dissolved ^{242}Pu.

Nominal Modeling Case: Outlier

For the purpose of analyzing an outlier realization for the Nominal Modeling Case, epistemic vector 85 (equivalent to GoldSim realization 85) was chosen as shown on Figure 7.7.1-89[a] because it has the highest annual dose at 1,000,000 years. As shown on Figure 7.7.1-90[a], ^{242}Pu is the major radionuclide contributor to the dose past 700,000 years. The release rates for ^{242}Pu from the waste form, WP, invert, UZ, and SZ are shown on Figure 7.7.1-91a[a]. For realization 85, the release of ^{242}Pu from the waste form starts earlier and occurs within a shorter time frame leading to an order of magnitude higher release rates compared to the gradual release for realization 286 (Figure 7.7.1-83[a]) that occurs over extended time periods. This difference in waste form release rate stems primarily from the difference in WP failure rates due to SCC on the outer lids of the WP from nominal processes. As shown on Figure 7.7.1-91b[a] for realization 85, the CSNF WP failure in all percolation subregions starts past 160,000 years and by about 500,000 years, all WPs are failed. In comparison, for realization 286, the CSNF WP failures (Figure 7.7.1-78b[a]) occur over a longer time frame starting around 300,000 years and continuing until the end of simulation at 1,000,000 years.

For realization 85, the peak release of ^{242}Pu from waste form occurs around 300,000 years. But due to sorption of plutonium on the corrosion products inside the WP, significant retardation of ^{242}Pu occurs inside the WP, and the peak release out of the WP is delayed until around 900,000 years indicating long residence times inside the WP on the order of 500,000 to 600,000 years. Because the WP release rates control the release behavior out of the UZ and SZ (Figure 7.7.1-91a[a]), it indicates that sorption and resulting retardation is the primary control on annual dose. The release rate of ^{242}Pu for realization 286 shows similar behavior (Figure 7.7.1-83[a]) as the sorption inside the WP reduces the release rate. However, because the peak waste form release does not occur until around 800,000 years, the peak release from the WP is not seen within the simulated time period as it is anticipated that the peak releases from the WP would be delayed by 500,000 to 600,000 years.

Thus, due to a combination of earlier WP failure start times and faster failure rate, the mass released from the waste form is also mostly released from the WP within the simulated time period. This results in a higher annual dose magnitude for realization 85.

7.7.1.6[a] Human Intrusion Modeling Case

This section presents an analysis of a single realization from the 9,000 realization base-case run performed for calculating the expected dose for the Human Intrusion Modeling Case for the 1,000,000-year simulation duration (Base Case GoldSim Run filename: LA_v5.005_HI_009000_000.gsm; output DTN: MO0710ADTSPAWO.000 [DIRS 183752]). The expected annual dose is presented in Figure 7.7.1-92[a], where each of the 300 realizations represents expected annual dose for one epistemic uncertainty vector. The expected annual dose for each epistemic uncertainty vector is generated by taking an expectation over a sample of 30 aleatory uncertainty vectors (for more details on the computational methodology, refer to Section 6.1.2.5 of the parent document). A single epistemic vector is selected for further analysis such that its expected annual dose is broadly representative of the modeling case and similar in behavior to the mean annual dose curve (Figure 7.7.1-92[a]).

The epistemic uncertainty vector 277 is selected for further analysis. The 30 corresponding aleatory sampling vectors for the selected epistemic vector correspond to GoldSim realizations 8281 through 8310 (Figure 7.7.1-93[a]). The annual dose from the 30 aleatory vectors falls into two groups: (1) the group with higher dose represents those realizations in which a CSNF WP is selected, and (2) the group with lower dose represents those realizations in which a CDSP WP is selected. The specific realization selected for further analysis is GoldSim realization 8309 (Figure 7.7.1-93[a]), which is chosen from the first group (representing releases from a CSNF WP). Realization 8309 represents aleatory uncertainty vector 29, in which the CSNF WP breached from a human intrusion event is located in percolation subregion 4 of the EBS and where the mass from the UZ borehole is passed to SZ source region 1 (GoldSim filename: LA_v5.005_HI_009000_002.gsm; output DTN: MO0801TSPAMVAC.000 [DIRS 185080]).

In the stylized Human Intrusion Modeling Case, a borehole pathway is modeled as being drilled directly through a single DS and WP vertically down to the water table. The time of this intrusion, which is assumed to result from exploratory drilling for ground water, is fixed at 200,000 years. Once the WP is breached, the waste form degrades by nominal degradation processes and the radionuclides are transported from the WP under nominal conditions to the vertical UZ borehole pathway, such that the mass is released at the water table for transport through the SZ to the RMEI at the regulatory boundary. The vertical borehole pathway is modeled as being 190 meters in length and conceptualized as a dual-porosity medium consisting of a discrete vertical fracture surrounded by matrix consisting of rubble from partial collapse of the borehole. The fracture is assumed to be open so that the water that flows in the borehole moves through the fracture pathway. Also, the radionuclide mass released from the WP (by diffusion and advection) is passed to the fracture pathway where it undergoes vertical advection within the fracture and lateral diffusion into the surrounding matrix due to fracture-matrix interaction. No retardation of colloids or solute is modeled on the fracture surface although species-dependent sorption coefficients are applied in the matrix (for additional details, refer to Section 6.7 of the parent document).

The major radionuclides contributing to annual dose for realization 8309 are shown on Figure 7.7.1-94[a], along with the total annual dose. ^{99}Tc and ^{129}I are the early major dose contributors (before 300,000 years), following the WP breach at 200,000 years, whereas ^{242}Pu becomes the dominant dose contributing radionuclide later on (with minor contribution from

^{237}Np, ^{135}Cs, ^{79}Se, and ^{233}U). The early contribution to dose from ^{99}Tc and ^{129}I occurs because they travel unretarded through the WP, UZ borehole pathway, and SZ. By contrast, ^{242}Pu, ^{237}Np, ^{135}Cs, and ^{233}U are retarded in these transport pathways to varying degrees and therefore contribute to dose much later. Because ^{99}Tc and ^{242}Pu are the dominant radionuclides with very different transport properties, they have been chosen for further analysis.

The cumulative mass release of ^{99}Tc and ^{242}Pu from the waste form inventory following the failure of one CSNF WP is shown on Figure 7.7.1-95[a]. The waste form starts degrading following the breach at 200,000 years, and due to the relatively slow CSNF degradation rate (about 6.9×10^{-5} yr^{-1}), it is almost fully (0.99 fraction) degraded by 268,000 years. The rate at which ^{99}Tc is released from the waste form domain and the corrosion products domain of the WPs is shown on Figure 7.7.1-96[a]. Because the dissolved concentration of ^{99}Tc is not limited by a solubility controlling solid, the mass of ^{99}Tc released from the degrading waste form is quickly transported out of the WPs by advection and diffusion. In this realization, the volumetric water flux through the WP (and going to the UZ borehole) is calculated to be about 8.7×10^{-4} m^3/yr (which is equivalent to the calculated percolation rate of about 26.9 mm/yr for the drilled borehole cross-sectional area of 0.0324 m^2 [Table 6.7-5 of the parent document]). Diffusive releases are higher than advective releases through the WP (in both waste form and corrosion products domains) because of the implementation of a zero concentration boundary just outside the WPs to maximize the concentration gradient. Almost all of the ^{99}Tc mass is released by about 300,000 years, as indicated by the negligibly small release rates past this time period (Figure 7.7.1-96[a]). The waste form degradation primarily controls the release of ^{99}Tc out of the WPs. After the ^{99}Tc mass is made available for transport, it is released out of the WPs without appreciable delay.

The ^{242}Pu mass release from the waste form domain and the corrosion products domain of the WP are shown on Figure 7.7.1-97[a]. ^{242}Pu is modeled as being transported both as dissolved and reversibly sorbed on colloids (denoted as aqueous) and as irreversibly sorbed onto iron oxyhydroxide colloids and waste form colloids. Note that CSNF waste form colloids remain unstable throughout the simulation (and are set to a minimum defined concentration) so they contribute negligibly to the total mass released, whereas iron oxyhydroxide colloids remain unstable for a short period, until about 220,000 years, and contribute to the mass release afterwards. The diffusive release of ^{242}Pu (dissolved and reversibly sorbed on colloids) exceeds advective releases as most of the ^{242}Pu mass remains in dissolved state, with very little being reversibly sorbed onto groundwater and uranium mineral colloids. However, the mass that is irreversibly sorbed on the iron oxyhydroxide colloids is predominantly transported by advection (Figure 7.7.1-97[a]) due to the small diffusion coefficient of colloids. The concentration of ^{242}Pu that is dissolved, and that which is irreversibly sorbed onto iron oxyhydroxide colloids, are both shown on Figure 7.7.1-98[a] for the waste form domain and the corrosion products domain. The dissolved concentration in the waste form domain is limited by the solubility of plutonium dioxide (PuO_2) in the waste form domain for several hundred thousand years following the breach. Because the solubility of PuO_2 is low, most ^{242}Pu mass from the degraded waste form is precipitated early in the waste form domain. Plutonium is gradually depleted from the waste form domain by diffusion and advection, and not until 748,000 years is enough mass depleted to cause the plutonium concentration inside the waste form domain to drop below the solubility limit. The dissolved concentration of ^{242}Pu in the corrosion products domain remains small initially, as ^{242}Pu is sorbed onto corrosion products whose mass increases over time from

degradation of steel. By 320,000 years, all of the steel in the corrosion products domain is degraded, and the maximum sorption capacity for the corrosion products domain is reached. As ^{242}Pu continues to be transported from the waste form domain to the corrosion products domain, the dissolved concentration of ^{242}Pu in the corrosion products domain starts to build up after 320,000 years, reaching the solubility limit in that domain, which is maintained until all ^{242}Pu mass has been depleted in the waste form domain and the concentration of ^{242}Pu drops at 748,000 years (Figure 7.7.1-98[a]). The concentration of ^{242}Pu in the corrosion products domain after this time is maintained by ^{242}Pu mass desorbing from the corrosion products. The concentration of ^{242}Pu that is irreversibly sorbed onto iron oxyhydroxide colloids also keeps increasing until about 748,000 years and then declines slowly as iron oxyhydroxide colloids are transported out, predominantly by advection (Figure 7.7.1-97[a]). Because the concentration of ^{242}Pu irreversibly sorbed onto iron oxyhydroxide colloids is not limited by solubility, it exceeds the dissolved concentration within a short period. Nevertheless, because the diffusion coefficient of colloids is calculated to be much smaller than the diffusion coefficient of dissolved plutonium (by a factor of about 700), the diffusive mass flux of ^{242}Pu (aqueous), which is mostly dissolved mass, exceeds the advective mass flux of ^{242}Pu irreversibly sorbed onto iron oxyhydroxide colloids (Figure 7.7.1-97[a]).

The mass released from the WP is passed into the UZ borehole that consists of dual porosity fracture and matrix media. The borehole is modeled using the GoldSim pipe element pathway, where only 1-D transport is considered. All of the mass released from the WP is placed in the fracture where it advects vertically downwards and diffuses laterally into the surrounding matrix medium. The volumetric flux of water applied to the fracture pathway is the same as that applied to the WP (about 8.7×10^{-4} m^3/yr; equivalent to the percolation rate of about 26.9 mm/yr), which results in an average linear velocity of about 82 m/yr through the fracture medium, considering the fracture plan area of 4.2×10^{-4} m^2, fracture saturation of 0.025, and no infill material in the fracture. Thus, for a species where fracture-matrix interaction is ignored, the travel time through the borehole length of 190 m should be less than 3 years.

The mass release of ^{99}Tc from the borehole virtually overlays the mass release from the WP (Figure 7.7.1-99[a]), indicating negligible delay. This is expected as no retardation is modeled for ^{99}Tc. Although fracture-matrix interaction could cause a minor delay in the ^{99}Tc breakthrough time, those effects are not apparent because of large timesteps taken past 204,000 years. The long tail in the ^{99}Tc release past 300,000 years, after most of the mass has been released, results from fracture-matrix interaction in the SZ where the mass is released back into the fractures from the matrix. The release rate from the SZ is comparable with that of the WP and UZ borehole releases early on, indicating fast transport through the SZ.

The release rates for the dissolved and reversibly sorbed ^{242}Pu (denoted as aqueous) from the WP, UZ borehole, and SZ are shown on Figure 7.7.1-100[a]. The release rates out of the borehole are considerably smaller than the incoming release rates from the WP. This is attributed to retardation in the matrix once the mass diffuses into the matrix from the fractures. The K_d for plutonium in the matrix is sampled to be about 115 mL/g (0.115 m^3/kg), which results in an effective retardation of about 1,550 (using the matrix bulk density of 1,980 kg/m^3 and matrix water content of 0.15). Because of the sorption, the dissolved concentration of ^{242}Pu in the matrix medium is reduced, thereby increasing the diffusive gradient (and diffusive flux) from the fracture to the matrix, thus limiting the mass available for advective transport through the

fracture. The release rates out of the SZ are lower than that for the UZ borehole due to further retardation in the SZ volcanic and alluvium units.

The cumulative mass releases from the WP, UZ borehole, and SZ for the ^{99}Tc, ^{242}Pu (aqueous), and ^{242}Pu (irreversibly sorbed on colloids) is shown on Figure 7.7.1-101[a]. The cumulative releases of ^{99}Tc out of WP, UZ, and SZ virtually overlay, indicating negligible retardation. Similarly, negligible retardation is indicated for ^{242}Pu (irreversibly sorbed on colloids) as the cumulative releases out of WP, UZ, and SZ virtually overlap. The fracture-matrix diffusive interaction for the mass irreversibly sorbed on colloids is not modeled in the UZ borehole and the SZ pathway due to the small diffusion coefficient of colloids. Thus, the mass of ^{242}Pu irreversibly sorbed on colloids that is introduced into the UZ borehole fracture stays in the fracture and is advected out quickly. In the SZ, some retardation of the colloids due to interaction with the fracture surfaces is modeled but the affects are not apparent due to the large timesteps taken. In contrast, the cumulative mass released from the UZ borehole for ^{242}Pu (aqueous) indicates that at the end of the simulation (one-million years), only a negligibly small fraction (<0.004) of the mass released from the WP is released out of the UZ borehole and, of the mass released from the UZ borehole, only about half is released out of the SZ. It is interesting to note that even though ^{242}Pu (aqueous) release is higher out of the WP compared to the release of irreversibly sorbed ^{242}Pu mass on colloids, due to retardation of ^{242}Pu (aqueous) in the UZ borehole, the release of ^{242}Pu irreversibly sorbed on colloids becomes relatively larger out of the UZ borehole.

The ^{242}Pu mass irreversibly sorbed on colloids coming out of the UZ borehole is partitioned into a fast traveling fraction and a slow traveling fraction before being passed to the SZ. Almost all of the ^{242}Pu mass irreversibly sorbed (99.8 percent) travels as a slow fraction in the SZ with some retardation of the colloid particles in the volcanic units and alluvium while the remaining travels unretarded as a fast fraction. All of the mass from the UZ borehole is passed into the SZ Source Region 1, consistent with the sampled aleatory uncertainty in this realization.

The mass release out of the SZ for ^{99}Tc, ^{242}Pu (aqueous), ^{242}Pu (irreversible on colloids traveling slowly), and ^{242}Pu (irreversible on colloids traveling fast) is shown on Figure 7.7.1-102[a]. The long tail in the ^{99}Tc release past 300,000 years, after most of the mass has been released, results from fracture-matrix interaction in the SZ where the mass is released back into the fractures from the matrix. Following the depletion of ^{99}Tc mass, the release rates from the slow traveling fraction of ^{242}Pu mass irreversibly sorbed on colloids becomes dominant.

The SZ releases are converted into annual dose by taking the annual releases out of the SZ for each radionuclide, dissolving them in the 3,000 acre-ft of water (annual usage at RMEI as defined by the regulation) to compute the mass concentrations, converting the mass concentration into a concentration of radioactivity (in curies per liter of water), and then multiplying with the corresponding BDCFs computed for the modern-interglacial climate (present-day climate). The end result of this is Figure 7.7.1-94[a], where dose for total ^{242}Pu (combined for mass in dissolved state, reversibly associated with colloids, and irreversibly associated with colloids) is shown.

Human Intrusion Modeling Case: Outlier

For the purpose of analyzing an outlier realization for the Human Intrusion Modeling Case, epistemic vector 181 was chosen as shown in Figure 7.7.1-103[a] because it has the highest annual dose between 300,000 and 800,000 years. Figure 7.7.1-104[a] displays the annual dose from 30 aleatory vectors associated with epistemic vector 181. The aleatory vector 15 (equivalent to GoldSim realization 5415) is chosen for further analysis due to its high dose. In this realization a CSNF WP, located in percolation subregion 3, is breached by the human intrusion and the mass is released through the UZ borehole pathway to the SZ source region 3.

The major dose contributing radionuclides for realization 5415 are shown in Figure 7.7.1-105[a]. Of these, the relative dose contribution from ^{242}Pu is by far the highest from 300,000 years until the end of the simulation. Although ^{242}Pu is also the dominant dose contributing radionuclide for realization 8309 described earlier (Figure 7.1.1-94[a]), its dose contribution relative to other radionuclides is much higher in realization 5415.

Figure 7.7.1-106[a] compares the dissolved ^{242}Pu concentrations in the waste form and corrosion product domains along with the plutonium solubilities in the respective domains for realization 5415. Although plutonium solubilities and dissolved concentrations are similar to those for realization 8309, the concentrations of ^{242}Pu associated irreversibly with iron oxyhydroxide colloids in the corrosion products domain is significantly higher. This is due to sampling higher iron oxyhydroxide colloid concentration (GoldSim epistemic uncertainty parameter Conc_Col_FeOx_SS_Sampled_a). For realization 5415, colloid concentration is sampled at 20.49 mg/L (at 98 percentile of the distribution) compared to a sampled value of 0.23 mg/L (at 64 percentile) for realization 8309. This two orders of magnitude difference in iron oxyhydroxide colloid concentration is proportional to the concentration of ^{242}Pu associated irreversibly with iron oxyhydroxide colloids. This is the main reason for the outlier behavior observed at later times for this realization as the irreversibly sorbed mass is transported through the UZ and SZ. The volumetric flux through the WP and UZ borehole in realization 5415 ($= 7.6 \times 10^{-4}$ m^3/yr) is similar to that for realization 8309 ($= 8.7 \times 10^{-4}$ m^3/yr).

7.7.1.7[a] Seismic Ground Motion Modeling Case for 10,000 Years

This section presents an analysis of a single realization from the 9,000 realization base-case run performed for calculating the expected dose for the Seismic GM Modeling Case for the 10,000-year simulation duration (GoldSim filename: LA_v5.005_SM_009000_001.gsm; output DTN: MO0710ADTSPAWO.000 [DIRS 183752]). The expected annual dose is presented on Figure 7.7.1-107[a], where each of the 300 realizations represent expected annual dose for an epistemic uncertainty vector. The expected annual dose for each epistemic uncertainty vector is generated by taking an expectation over a sample of 30 aleatory uncertainty vectors that specify both the time of the seismic damage and the fractional damaged area of the WP.

The computational methodology for dose from the 10,000-year Seismic GM Modeling Case is different from that of the one-million-year case. Unlike the latter, where the sequence of seismic events are generated randomly and the damaged area of the WP is determined based on the computed PGV along with other parameters, the former is based on determining the dose response by specifying the WP damage time and the damaged area. This dose response function

is used by Equation 6.1.2-22 of the parent document to compute the expected dose by taking the expectation over various damage areas and damage times. Because of this computational requirement, for each epistemic vector, the dose response functions for 30 aleatory uncertainty vectors are considered by specifying six discrete damage times (at 200; 1,000; 3,000; 6,000; 12,000; and 18,000 years) over each of the five fractional WP damage areas (10^{-7}, 10^{-6}, 10^{-5}, 10^{-4}, and 10^{-3}) (Table 6.6-3[a]). In addition, the consequences of seismic ground motion events are approximated by examining only the occurrence of SCC damage to CDSP WPs under intact DS without considering rockfall and without considering the effects of corrosion processes in thinning the WP OCB and DS. As a result, only diffusive releases from the CDSP WPs can occur. Furthermore, because the drift degradation is not considered, the thermal-hydrologic processes in the EBS remain the same as under nominal condition. For more details on the computational methodology, refer to Sections 6.1.2.4.4 and 7.3.2.6.1 of the parent document.

A single epistemic vector (out of a sample size of 300 epistemic vectors) is selected for further analysis in such a manner that the expected annual dose is broadly representative of the modeling case and similar in behavior to the mean annual dose curve. After consideration, epistemic vector 155 is chosen for further evaluation (Figure 7.7.1-107[a]). The thirty corresponding aleatory vectors (sampled for the given epistemic vector) are represented by GoldSim realizations 4621 through 4650 (Figure 7.7.1-108[a]). Of these, the eighth aleatory vector, which is equivalent to GoldSim realization 4628, is selected for further analysis (dashed red curve). In this aleatory vector, the seismic damage time is specified at 1,000 years and the fractional damaged area of the CDSP WP is specified at 10^{-5}. The GoldSim file for realization 4628 is run twice to first save information for all the percolation subregions and then to specifically save EBS cell-pathway details related to percolation subregion 3 for the non-seeping environment (GoldSim filenames: LA_v5.005_SM_009000_008.gsm and LA_v5.005_SM_009000_009.gsm; output DTN: MO0801TSPAMVAC.000 [DIRS 185080]).

The total annual dose from realization 4628 is presented on Figure 7.7.1-109[a] along with the individual dose from major dose contributing radionuclides. The dominant radionuclides are ^{99}Tc, ^{129}I, ^{14}C, ^{36}Cl, and ^{79}Se, with negligible contributions from remaining radionuclides. The annual dose increases rapidly following the WP damaging event at 1,000 years, reaching a maximum around 2,000 years and then declining gradually with time as the radionuclide mass is depleted. The bump noticeable around 2,000 years is a result of climate change from monsoonal to glacial-transition climate that occurs at 1,950 years. The dose behavior for ^{99}Tc, ^{129}I, ^{14}C, and ^{36}Cl is observed to be nearly identical to each other and results from their similar transport characteristics through the EBS, UZ, and SZ as these radionuclides are transported without any solubility control and without undergoing any sorption. The relative differences in dose among them are primarily due to their different masses in the inventory, decay rates, and BDCFs. The transport of ^{79}Se is somewhat different from the rest as ^{79}Se is retarded in the UZ and SZ despite having no solubility controlling mineral phase. Hence, for the purpose of describing the transport behavior of major dose contributing radionuclides, only ^{99}Tc (the highest dose contributor among radionuclides that have similar transport characteristics) and ^{79}Se are considered in the following discussion.

All CDSP WPs in all five percolation subregions fail at 1,000 years in this realization. The number of packages in a given percolation subregion is proportional to the repository area occupied by that percolation subregion. As a result, 40 percent of the WPs belong to percolation

subregion 3, 25 percent each to percolation subregions 2 and 4, and 5 percent each to percolation subregions 1 and 5. In each percolation subregion, the number of WPs is further distributed among seeping and non-seeping environments based on the seepage fraction for that percolation subregion. The number of failed CDSP WPs for all percolation subregions distinguished by seeping and non-seeping environments is shown on Figure 7.7.1-110[a]. Note that for a given percolation subregion, most of the WPs fall in the non-seeping environment due to small calculated seepage fraction. For example, the seepage fraction for percolation subregion 3 is about 0.33, so only 33 percent of the WPs assigned to percolation subregion 3 belong to the seeping environment, the remaining (67 percent) belong to the non-seeping environment. The seepage fraction for a given percolation subregion remains constant over the simulation duration and is based on the determination of fraction of seeping locations at 10,000 years in the given percolation subregion.

Since the DSs remains intact and only SCC on the CDSP WP surface due to vibratory ground motion is modeled, no advective transport of radionuclides can occur through the WP. The only release mechanism out of the WP is by diffusion along the diffusive pathways inside the WP and through the cracks on the WP OCB to the invert. Since the fractional damage area to the WP OCB, in this realization, is specified to be 10^{-5}, it is equivalent to the diffusive area of 3.26×10^{-4} m^2 (note that the outer surface area of the CDSP WP is set to be 32.6 m^2), which is applied only over the WP OCB thickness (computed to be 0.0301 m, the distance from outside the inner vessel to the outside of the OCB). Inside the WP the diffusive areas and diffusive lengths for the discretized transport domains are different and are described in Section 6.3.8 of the parent document.

The diffusive releases of ^{99}Tc from the failed CDSP WPs for various percolation subregions (combined over seeping and non-seeping environments) are shown on Figure 7.7.1-111[a]. The diffusive release for percolation subregion 3 is the highest, as expected, due to greatest number of failed WPs among various percolation subregions. Although the number of failed WPs is the same among percolation subregions 2 and 4 and among percolation subregions 1 and 5, the relative peak releases are different because of higher seepage fractions for percolation subregion 4 (compared to 2) and 5 (compared to 1), leading to greater proportion of WPs being placed in a seeping environment. Diffusive release from a WP placed in a seeping environment, compared to a non-seeping environment, tends to be higher due to changed boundary conditions as drift seepage water flows through the invert and removes the mass. This has the effect of moving the zero concentration boundary closer to the WP, thereby increasing the concentration gradient from the WP to the invert. The diffusive releases of ^{79}Se from failed CDSP WPs for various percolation subregions are similarly affected as ^{99}Tc (Figure 7.7.1-112[a]). The magnitudes, however, are much smaller for ^{79}Se due primarily to lower inventory mass per failed CDSP WP (about 12.5 g) compared to ^{99}Tc (of about 960 g per failed CDSP WP), thus leading to lower concentrations in the WP and lower diffusive gradient. In addition, the free water diffusion coefficients among the two radionuclides are slightly different (^{99}Tc has a free water diffusion coefficient of 1.95×10^{-9} m^2/s while that for ^{79}Se is 1.04×10^{-9} m^2/s), which could also cause minor differences in release.

Within percolation subregion 3, the diffusive and advective mass fluxes of ^{99}Tc from the EBS are compared on Figure 7.7.1-113[a] for the seeping and non-seeping environments. Even though the releases from the WP are only diffusive, because of flow in the invert, the advective flux

from EBS is greater in the seeping environment. For the non-seeping environment, the diffusive flux from EBS is greater than the advective flux that results from imbibition flow in the invert. Since the total mass flux for the non-seeping environment is greater than that for the seeping environment for percolation subregion 3 (due to larger number of failed WPs in the non-seeping environment), the results for the non-seeping environment are analyzed in more detail.

The dissolved concentrations of ^{99}Tc out of the various transport domains in the EBS are shown in Figure 7.7.1-114[a]. The concentrations in the HLW and DSNF waste form subdomains and in the majority of the corrosion products domain overlap as a result of fast transport of ^{99}Tc inside the WP due to the large diffusive areas modeled. As shown on Figure 7.7.1-114[a], the HLW glass is almost completely degraded by about 4,000 years. However, the ^{99}Tc mass in the waste form and corrosion products domain is not fully depleted and the concentration declines gradually. This is attributed to the small diffusive area of 3.26×10^{-4} m^2 applied to the transport cell representing the OCB thickness of 0.031 m within the corrosion products domain. This small diffusive area reduces the diffusive conductance across the WP OCB cell pathway and thus exerts a strong influence on the mass transport and concentrations in the surrounding cells that are part of the EBS transport finite difference network (Section 6.3.8 of the parent document). As a result, the concentration in the WP OCB cell is considerably reduced compared to the upstream waste form cells. The diffusive mass flux of ^{99}Tc across various cell pathways is compared on Figure 7.7.1-115[a], which shows the reduction in diffusive flux across the WP OCB, thereby causing retention of appreciable mass in the WP for thousands of years following the breach. The diffusive release out of the upstream cell representing the corrosion products domain (except WP OCB cell) virtually overlaps that of the downstream WP OCB cell due to harmonic averaging of the cell properties for computing the diffusive conductance between the adjoining cells (see Equation 6.3.8-28 of the parent document). Since the diffusive area of the downstream WP OCB cell (3.26×10^{-4} m^2) is orders of magnitude smaller than that of the upstream cell (29.7 m^2; Section 6.3.8.2.3 of the parent document), the diffusive conductance between the two cells (within a finite difference network of cells) is controlled by the WP OCB cell.

The initial sharp increase in concentration noticeable on Figure 7.7.1-114[a] is due to the delayed onset of transport following the breach at 1,000 years as the relative humidity remains below the threshold value of 95 percent (required to initiate transport) until 1,080 years. As a result, almost 80 years of HLW mass is accumulated from degradation prior to the onset of release. Similarly, because all of the DSNF mass is degraded instantaneously following the WP breach, it is also all available for release after 1,080 years. The characteristics of diffusive release and concentrations for ^{79}Se (not shown) are similar to that for ^{99}Tc, except for the magnitudes, and also show the strong influence of reduced diffusive area of the WP OCB in controlling the mass flux out of the WP.

The mass released from the EBS (for each percolation subregion summed over the seeping and non-seeping environments) is passed to the UZ by partitioning the mass into the fracture and matrix nodes of the UZ transport model at the repository horizon. The fraction of ^{99}Tc and ^{79}Se mass that is passed to the fractures is shown on Figures 7.7.1-116[a] and 7.7.1-117[a]. In almost all percolation subregions (except for percolation subregion 1), the mass fraction going into the fracture (compared to the matrix) is greater than 0.5 initially following the breach and then reduces rapidly. This is because initially the mass flux from the seeping environment is greater

than the non-seeping environment (due to increased concentration gradient between the WP and invert due to flow through the invert), which is predominantly passed into the UZ fracture continuum. Eventually, the mass contribution from the non-seeping environment increases (since more WPs are failed in the non-seeping environment) and more mass diffuses into the UZ matrix continuum due to the larger effective diffusive area connection between the matrix and the invert. After 4,000 years, steady state conditions are established once the HLW waste form is fully degraded and the release is controlled by the small diffusive area through the WP OCB. Among various percolation subregions, the fraction of mass released into the fracture is proportional to the seepage fraction. Thus, percolation subregion 5 (seepage fraction of 0.44) has relatively greater mass going into the fractures than percolation subregion 1 (seepage fraction of 0.16). As a result, the sharp increase noticed around 2,000 years due to climate change is most pronounced in percolation subregion 5 and least in percolation subregion 1.

The cumulative release over all percolation subregions from various transport domains from the engineered and natural barrier systems are shown on Figure 7.7.1-118[a] for ^{99}Tc and Figure 7.7.1-119[a] for ^{79}Se. For ^{99}Tc, considerable delay in release occurs out of the WP compared to the release out of the waste form due to the small diffusive area in the WP OCB. Marginal delay is noticed in the invert early on (as shown by EBS release) due to transient conditions as the concentrations build up in the invert. After a few thousand years, the mass released from the EBS matches that released from the WP indicating the limited barrier capability of the invert for a non-sorbing radionuclide with no solubility control. The cumulative release curve for the UZ indicates considerable delay compared to the release from the EBS. This is attributed to the majority of the mass entering the UZ in the matrix nodes and undergoing slower transport. Due to fracture-matrix interaction, the mass that is released into the matrix continuum is transferred into the fracture continuum and quickly carried out via advection. Thus, although most of the mass enters the UZ through matrix nodes, most of it is released out of the fracture nodes at the UZ-SZ interface over the simulated time period. Despite this, only about 75 percent of the mass released from the EBS is released out of the UZ by 10,000 years, indicating appreciable UZ barrier capability in delaying the mass release once the mass enters the matrix. Some delay in the SZ is also observed due to the effects of longitudinal dispersion and fracture-matrix diffusive interaction; however, by 10,000 years, about 90 percent of the mass released from the UZ is released out of the SZ model boundary. The breakthrough curves for ^{99}Tc in the SZ for all four regions are shown on Figure 7.7.1-120[a]. The breakthrough occurs quickly and, by 200 years following the mass input, almost half the mass gets released out of the SZ. The long tail that extends for thousands of years indicates a high degree of dispersion due to the fracture-matrix interaction as the mass that initially diffused into the SZ matrix moves back into the fracture and is eventually transported out.

The cumulative releases for ^{79}Se (Figure 7.7.1-119[a]) show similar behavior to ^{99}Tc for the release from the waste form, WP, and EBS. Due to the small diffusive area in the WP OCB, the release out of the WP is delayed and magnitude is reduced compared to the release out of the waste-form domain. However, in contrast to ^{99}Tc, the transport of ^{79}Se is significantly retarded in the UZ and SZ. This is because of reversible sorption of ^{79}Se in the UZ and SZ volcanic matrix and SZ alluvium. The sampled K_d for the UZ tuff matrix is about 9.3 mL/g (for zeolitic units), 7.4 mL/g (for devitrified units), and 4 mL/g (for vitric units). The sampled K_d for the SZ matrix in the volcanic units is about 16.4 mL/g and that for the SZ alluvium is about 13.4 mL/g. The SZ alluvium K_d is further modified by multiplying by the ratio of effective porosity (sampled value of 0.22) to the total porosity (0.3), thus leading to the effective SZ alluvium K_d of 9.8 mL/g. In the UZ matrix, even with small sampled K_d values, the retardation is significant as the concentration gradient from the matrix to the fracture is further reduced due to sorption in the matrix. By 10,000 years, only about 41 percent of the total mass released from the EBS is released out of the UZ. In the SZ, the delay is even more pronounced as only about 20 percent of the mass that enters from UZ is released out of the SZ model boundary by 10,000 years. Figure 7.7.1-120[a] shows the breakthrough curves from the four SZ regions indicating significant retardation for ^{79}Se, with median delay of around 20,000 years. Compared to the transport of unretarded species such as ^{99}Tc, the effective retardation factor of ^{79}Se in the SZ, for this realization, is about 100 (based on the ratio of median travel times of ^{79}Se to ^{99}Tc).

The release rates out of the SZ model boundary for ^{99}Tc and ^{79}Se are shown on Figure 7.7.1-121[a] for realization 4628. The SZ releases are converted into annual dose by taking the annual releases out of the SZ for each radionuclide, dissolving them in the 3,000 acre-ft of water (annual usage at RMEI as defined by the regulation) to compute the mass concentrations, converting the mass concentration into concentration of radioactivity (in curies per liter of water), and then multiplying with the corresponding BDCFs computed for the modern-interglacial climate (present-day climate). The end result of this is Figure 7.7.1-109[a].

7.7.1.8[a] Summary of Single-Realization Analyses

The single-realization analyses of the seven modeling cases described above provide useful insights into interactions among several submodels under a variety of thermal, mechanical, chemical, and physical conditions in and around the repository. These analyses assist in understanding the coupling among the EBS, UZ, and SZ transport models when calculating annual dose to the RMEI in a given realization. Within each transport model domain, the interaction of various submodels (and their abstractions) under a given set of physicochemical conditions is described in detail, providing confidence that the submodels are coupled as intended and that their behaviors can be explained in a logical manner, leading to the dose calculations. In addition to explaining the interaction of submodels, the transport behaviors of major dose contributing radionuclides are also described and highlighted in the various modeling cases. For some modeling cases, outlier realization analysis is presented to highlight various processes or weighting factors that exert control on the magnitude of dose. In all cases, early releases following WP breach are dominated by non-sorbing and solubility-unlimited radionuclides, such as ^{99}Tc and ^{129}I, whereas later releases are dominated by longer-lived, solubility-limited radionuclides that tend to sorb more strongly, such as ^{242}Pu, ^{237}Np, and ^{239}Pu.

7.7.2[a] Comparison with Simplified TSPA Analysis

A Simplified Analysis has been developed to evaluate repository performance utilizing simplified representations of the mathematical equations that describe radionuclide mass transfer rates. This analysis, called Simplified TSPA Analysis, is described in detail in Appendix L of the parent document. The analysis results are compared to the TSPA-LA Model results to generally corroborate the maximum dose levels. The Simplified TSPA Analysis has its bases in the process- and abstraction-level modeling captured in supporting analysis and model reports. Thus, it represents the same conceptualization of the repository system and its underlying technical bases to those of the TSPA-LA Model. However, detailed analysis, checking, and review activities identified an unintended inconsistency between the distribution coefficients (K_d) used for the TSW units in the UZ used in the simplified analysis (Appendix L of parent document) and those used in the TSPA-LA Model that was not previously documented in the parent document. The UZ K_d distributions are set to the values for vitrified tuff in the simplified analysis (Appendix L of the parent document). These values are consistent with vitrified tuffs at the base of the TSW but inconsistent with the TSW units between the repository and the basal units, which make up much of the TSW below the repository, and are comprised of devitrified tuffs. The K_d distributions for vitrified and devitrified tuff are similar for all radionuclides excluding ^{126}Sn and ^{135}Cs, which show significant differences (Table 6.3.9-2 and Table L-41 of the parent document). Since ^{126}Sn and ^{135}Cs are minor contributors to dose (Section 8.1[a]) despite the differences in the K_d distributions, the basic results of the two models (i.e., dose over time and contribution to dose of dominant radionuclides) can be compared for individual modeling cases.

Models of the degradation of the engineered barriers were developed for the nominal, seismic ground motion, and igneous intrusion conditions. This was done to allow for comparisons with the modeling cases evaluated with the TSPA-LA Model. The Simplified TSPA Analysis is a different system level mathematical model, and the results can be used to generally corroborate the TSPA-LA Model v5.005 maximum dose.

7.7.2.1[a] Waste Package Early Failure Modeling Case

In the Simplified TSPA Analysis, a 500 realization simulation of the Waste Package EF Modeling Case was conducted over a 1,000,000-year period. A comparison of the Simplified TSPA Analysis results considering all realizations and the TSPA-LA Model results using v5.005 for this modeling case at 200,000 years; 400,000 years; 600,000 years; 800,000 years; and 1,000,000 years following repository closure is shown on Figure 7.7.2-3[a]. This comparison is identical to the results documented in Section 7.7.2.1 of the parent document and shows that the Simplified TSPA Analysis results in annual doses that are similar in magnitude to, but higher than, those of the TSPA-LA Model.

7.7.2.2[a] Nominal Modeling Case

The Nominal Modeling Case accounts for the WPs that fail under nominally expected conditions because of general corrosion and SCC and for the DSs that fail under nominally expected conditions because of general corrosion.

Figure 7.7.2-6[a] shows a comparison of the mean annual dose between the two models. The difference in the time that SCC begins between the Simplified TSPA Analysis and the TSPA-LA Model results in the difference in the annual dose histories. In a sense, the annual dose from the Simplified TSPA Analysis is translated outward in time by a few hundred thousand years.

This comparison is identical to the results documented in Section 7.7.2.2 of the parent document and shows that the general trend in the annual dose between the two models is very similar and the peak mean annual dose calculated using the Simplified TSPA Analysis is within approximately half of an order of magnitude as that calculated by the TSPA-LA Model.

7.7.2.3[a] Seismic Ground Motion Modeling Case

The Seismic GM Modeling Case evaluates repository performance for those WPs that fail due to the ground motion damage associated with the seismic event. This case begins with the Nominal Modeling Case discussed above and includes the effect of seismic events over a 1,000,000-year period. In the Simplified TSPA Analysis, the occurrence of seismic events is modeled using the approach presented in Section L2.1 of the parent document. The effects of seismic events on rockfall/drift degradation and seepage are modeled as presented in Sections L2.2 and L2.5 of the parent document, respectively. The effects of seismic ground motion on the performance of the DS and WP is modeled as presented in Sections L2.7.2 and L2.8.3 of the parent document, respectively.

The mean annual dose results for the Simplified TSPA Analysis are similar to those from the TSPA-LA Model. Figure 7.7.2-9[a] shows a comparison of the Simplified TSPA Analysis results and the TSPA-LA Model results for the Seismic GM Modeling Case at 200,000 years; 400,000 years; 600,000 years; 800,000 years; and 1,000,000 years following repository closure. There is generally a positive trend in the annual dose for the TSPA-LA Model results whereas the Simplified TSPA Analysis is variable with time. The two models show a similar peak mean annual dose; the Simplified TSPA Analysis is within approximately half an order of magnitude lower as that calculated by the TSPA-LA Model. However, the earlier peak dose in the Simplified TSPA Analysis reflects the differences in the sampling technique used in the Simplified TSPA Analysis and the lower rate of general corrosion results in 40 percent of the realizations having no WP failures over the 1,000,000-year simulation period, as documented in Section 7.7.2.3 of the parent document. Another notable difference occurs at 200,000 years. Figure 7.7.2-9[a] shows a significant reduction between the TSPA-LA Model v5.005 results and the Simplified TSPA Analysis. This is a result of differences between version 5.000 and 5.005 of the TSPA-LA Model as discussed in Section 7.3.1.5.6[a] of this addendum. Overall, for all other time periods the comparison presented in this addendum is nearly identical to the comparison of results documented in Section 7.7.2.3 of the parent document.

7.7.2.4[a] Igneous Intrusion Modeling Case

The Igneous Intrusion Modeling Case evaluates repository performance for the disruptive event where a volcanic dike intersects the repository. In the Simplified TSPA Analysis, a 1,000,000-year simulation was conducted where a single igneous intrusion event was assumed to randomly occur over the simulation period in each of 500 realizations. All WPs are assumed to be completely failed when the event occurs.

The mean annual dose results for the Simplified TSPA Analysis are similar to those from the TSPA-LA Model. Figure 7.7.2-12[a] shows a comparison of the Simplified TSPA Analysis results and the TSPA-LA Model v5.005 results for this modeling case at 200,000 years; 400,000 years; 600,000 years; 800,000 years; and 1,000,000 years following repository closure. There is generally a positive trend in the annual dose for the TSPA-LA Model results whereas the Simplified TSPA Analysis is variable with time. The results of the Simplified TSPA Analysis are similar in magnitude as those generated by the TSPA-LA Model with the Simplified TSPA Analysis yielding slightly higher mean annual doses. The comparison presented in this addendum differs slightly from the comparison of results documented in Section 7.7.2.4 of the parent document in that the results presented using version 5.005 of the TSPA-LA Model are generally lower that version 5.000 over all time periods after approximately 100,000 years. This difference can be attributed to the corrected distribution for the SZ longitudinal dispersivity as documented in Section 7.3.1.5.4[a] of this addendum.

7.7.3[a] Comparison with Electric Power Research Institute Analysis

No change.

7.7.3.1[a] Introduction and Purpose

This section gives a brief confirmation of the comparison between the EPRI TSPA Analysis and the TSPA-LA Model using v5.005 results. The purpose of this comparison is to confirm a summary presented in Section 7.7.3 of the parent document. The previous analysis showed the EPRI TSPA Analysis compared reasonably well with the TSPA-LA Model, and differences can be related to the different treatment of seepage, inventory, and EBS failure characteristics.

Section 7.7.3 of the parent document presents a comparison between the EPRI TSPA Analysis and the TSPA-LA Model considering the overall features of the dose history curves, together with evaluating the apparent differences between the two models. It is not necessary to reproduce that discussion in this addendum as the summary and conclusions will not change. Rather, only a brief comparison of the mean annual dose results using v5.005 is presented as confirmation of the comparison between the EPRI TSPA Analysis and the TSPA-LA Model.

7.7.3.2[a] Overview of the TSPA Models

No change.

7.7.3.3[a] Unsaturated Zone Flow

No change.

7.7.3.4[a] Engineered Barrier System Environment

No change.

7.7.3.5[a] Waste Package and Drip Shield Degradation

The EBS Corrosion Model is used in the EPRI TSPA Analysis to compute failure distributions for different components of the EBS, which comprise three versions for the nominal, seismic and

igneous scenarios. The EBS Corrosion Model accounts for various failure mechanisms and uncertain parameters that are sampled using Monte Carlo simulations to produce mean failure distribution curves for the DS, WP, and cladding. These mean failure distribution curves are used as input in the near-field model, which is described in greater detail in Appendix M. The current TSPA-LA Model does not take credit for cladding; that is, radionuclides can be released as soon as the WP starts to fail. The EPRI TSPA Analysis accounts for cladding failure for dripping and non-dripping conditions following WP failure.

In the EPRI TSPA Analysis, the computed failure distribution curves for the nominal scenario for the WP are shown on Figure 5-7 in Apted and Ross (2005 [DIRS 182229]), indicating onset of WP failures before 100,000 years. The EPRI TSPA Analysis only considers 8,160 CSNF WPs, of which 5,304 WPs fail after 1,000,000 years (Senger 2008 [DIRS 185124]). In the TSPA-LA Nominal Scenario Class, the probabilistic projections of WP breaches exhibit a few realizations with a SCC occurring before 100,000 years (Section 8.2.1[a]). However, as Figure 7.7.3-2[a] indicates, the bulk of the WP failure occurs after about 200,000 years with 6,256 WPs failed after 1,000,000 years.

As a confirmation of the comparison presented in Section 7.7.3.5 of the parent document, the mean WP and DS failure curves for the TSPA-LA Nominal Scenario Class are shown on Figure 7.7.3-2[a] using TSPA-LA Model v5.005. These results are identical to those presented on Figure 7.7.3-2 of the parent document.

7.7.3.6[a] Waste Form Degradation and Mobilization

No change.

7.7.3.7[a] Engineered Barrier System Flow and Transport

No change.

7.7.3.8[a] Unsaturated Zone Transport

No change.

7.7.3.9[a] Saturated Zone Transport

No change.

7.7.3.10[a] Biosphere

No change.

7.7.3.11[a] Mean Annual Dose Comparison—Nominal Case

The computed mean radionuclide doses for the EPRI nominal scenario is given on Figure 5-10 in Apted and Ross (2005 [DIRS 182229]). In comparison, the results from TSPA-LA Model v5.005 for the computed mean annual doses for the combined Nominal Scenario Modeling Case and the Waste Package EF Modeling Case are shown on Figure 7.7.3-3[a]. The results presented in this addendum are identical to the comparison of results documented in Section 7.7.3.11 of the parent document. These results corroborate the detailed analysis of the

comparison presented in Section 7.7.3.11 of the parent document. In general, the results presented in this addendum confirm the main features of the dose release curves for the EPRI nominal scenario compares reasonably well with the TSPA-LA Model. The differences can be related mostly to differences in seepage and in the different implementation of the inventory and EBS failure characteristics. This is partly due to the fact that the EPRI TSPA Analysis uses earlier analysis and/or model report results.

7.7.4[a] Performance Margin Analysis

The PMA calculations presented in Section 7.7.4 and Appendix C of the parent document paralleled those of the TSPA-LA Model (Section 8) but focused on scrutinizing the impact of select conservatisms embedded in the TSPA-LA Model components and submodels (utilized by the modeling cases to calculate annual doses). The PMA is intended to estimate the cumulative impact of the conservatisms in the TSPA-LA Model and, thereby, indicate the potential performance margin embedded in the TSPA-LA Model's dose-risk projections. Thus, the PMA is an important validation activity supporting the TSPA-LA Model. The PMA evaluates and confirms the conservative nature of the TSPA-LA Model and it provides confidence that there are no non-conservatism remaining in the analysis. The results included in this addendum are used to update the conclusions of the PMA presented in the parent document.

7.7.4.1[a] Projections of the TSPA-LA Performance Margin

The objective of the PMA is to quantitatively evaluate the impact of the major explicit and implicit conservatisms in the TSPA-LA Model. This section provides a comparison of the total dose calculated by TSPA-LA Model v5.000, TSPA-LA Model v5.005, and the PMA presented in Appendix C of the parent document. This comparison confirms the conclusion of the analysis presented in Section 7.7.4.1 of the parent document.

Performance Margin in the Total Mean Annual Dose for 10,000 Years Postclosure

A comparison of the total mean annual dose history for the PMA and the TSPA-LA Model is shown on Figure 7.7.4-7a[a]. Figure 7.7.4-7a[a] shows that there is essentially no difference that exists between the mean annual dose estimates calculated by the two TSPA-LA Model versions for the first 10,000 years postclosure. Figure 7.7.4-7a[a] also shows that the following general observations about the performance margin projections for the first 10,000 years postclosure are the same as presented in Section 7.7.4 of the parent document:

- The PMA total mean annual doses are generally lower by nearly an order of magnitude over the first 10,000 years compared with the total mean annual dose from the TSPA-LA Model.
- The peak PMA total mean annual doses calculated over 10,000 years are lower by over an order of magnitude over the largest total mean annual dose from the TSPA-LA Model.
- Total mean annual doses calculated for 10,000 years are dominated by projected releases for the Igneous Intrusion Modeling Case (Appendix C, Figure C7-7, of the parent document).

Performance Margin in the Total Mean Annual Dose after 10,000 Years through the Period of Geologic Stability

A comparison of the total mean annual dose history for the PMA and the TSPA-LA Model is shown on Figure 7.7.4-7b[a]. For the 1,000,000-year simulation, the mean annual dose calculated by using TSPA-LA Model v5.005 is noticeably lower than TSPA-LA Model v5.000 from an approximate period of 120,000 years through about 300,000 years after postclosure (Figure 7.7.4-7b[a]). From this comparison plot, the following general observations can be drawn about the PMA out to 1,000,000 years postclosure:

- The PMA total mean annual doses are generally lower by nearly an order of magnitude over the first 100,000 years instead of 200,000 years as documented in the parent document and compared with the total mean annual dose from the TSPA-LA Model.

- The peak PMA total mean annual doses calculated over 1,000,000 years are lower by a factor of two over the largest total mean annual dose from the TSPA-LA Model as documented in the parent document.

The differences between the PMA results presented in the parent document to those in this addendum can be related mostly to an update to the implementation of the Seismic Ground Motion damage abstraction, as documented in Section P3 of Appendix P in the parent document. The probability of seismic damage is provided for two end-member states of the WP—one with intact internals and one with fully degraded internals. In TSPA-LA Model v5.000, once any WP is breached by a nominal process in a given percolation subregion (e.g., from first occurrence of stress corrosion cracks located on the outer lids), the probability of seismic damage is switched from the intact internals abstraction to the fully degraded internals abstraction, which increases the chance of seismic damage occurring while the DS is intact. This probability is then applied to all the WPs in the given percolation subregion, which is conservative, as most of the WPs have not yet failed by the nominal processes and should be using the intact internals damage probability. As a result, CSNF WPs fail earlier (Figure 8.1-5b of the parent document), beginning at approximately 150,000 years postclosure, and acquire greater damage area than expected, between approximately 200,000 and 300,000 years postclosure. The removal of this conservative implementation for seismic ground motion damage from v5.000 to v5.005 of the TSPA-LA Model results in fewer WPs damaged during a seismic event between approximately 200,000 and 300,000 years postclosure (Figure 8.1-5b[a]). This difference accounts for the smaller performance margin observed from approximately 200,000 to 300,000 years postclosure between the PMA and TSPA-LA Model v5.005 results presented in this addendum.

Scenario Specific Insights about the Performance Margin

Additional important insights about the performance margin can be gained by disaggregating the total mean annual dose into the total mean annual dose curves for the individual modeling cases and conducting a systematic evaluation of the effects of the changes incorporated into the PMA. This detailed analysis is included in Appendix C of the parent document; however, one notable change is documented in this addendum.

A comparison between the observations listed above for the PMA and the TSPA-LA Model results yields some notable differences. With regards to TSPA-LA Model v5.000 results, the Seismic GM Modeling Case dominates the total mean annual dose for the 10,000-year time period; whereas for 1,000,000 years, the Seismic GM and Igneous Intrusion Modeling Cases are the dominant contributors to the total mean annual dose to the RMEI (Figure 8.1-3, Section 8.1.1.2, of the parent document). However, in TSPA-LA Model v5.005 results while the Seismic GM Modeling Case still dominates the total mean annual dose for the 10,000-year time period, over the 1,000,000-year period the Igneous Intrusion Modeling Case dominates the total mean annual dose until approximately 700,000 years postclosure when the Seismic GM and Igneous Intrusion Modeling Cases contribute nearly equally to the total mean annual dose (Section 8.1.1.2[a]). In the PMA results, the Igneous Intrusion Modeling Case dominates the total mean annual dose for the time period of 10,000 years (Figure C7-7f of the parent document). For the time period after 10,000 years and through the period of geologic stability, the Igneous Intrusion Modeling Case dominates the total mean annual dose with a small contribution from the Seismic GM Modeling Case beginning around 225,000 years (Figure C7-8f of the parent document). These differences are primarily due to a lower incidence of WP failure (Appendix C6.8 and C7.2) and a reduction in the seismic induced WP SCC crack damage in the PMA Model (Appendix C6.8 and C7.2). The remaining cases combined have a negligible contribution for both the PMA and TSPA-LA Model total mean annual dose results.

7.7.4.2[a] Summary of the TSPA-LA Performance Margin

The results in this addendum confirm that the specified objectives of the PMA are met as follows:

1. The PMA results confirm that submodel conservatisms propagated through the TSPA-LA Model are also conservative with respect to the total system performance measures (e.g., total mean annual dose).

2. Relative to the TSPA-LA Model results, the peak PMA total mean annual dose is lower by over an order of magnitude for the 10,000-year time period and lower by a factor of two for the time period after 10,000 years.

3. The evaluated conservatisms did not introduce any inappropriate risk dilution in the TSPA Model results presented in support of the LA. This was demonstrated by the absence of higher peak mean annual doses relative to the TSPA-LA Model for the PMA results for both the probabilistic projections of the total dose histories and the projected total mean dose.

The assessment of the potential performance margin embedded in the TSPA-LA Model results is presented in detail in Appendix C of the parent document.

7.8[a] NATURAL ANALOGUES

No change.

7.9[a] TECHNICAL REVIEWS SUMMARY

No change.

7.10[a] SUMMARY OF MODEL CONFIDENCE BUILDING

The purpose of Section 7.10[a] is to summarize the additional validation activities documented in this addendum. Concluding remarks are presented in Section 7.10.10[a].

7.10.1[a] Validation Strategy

No change.

7.10.2[a] Code and Input Verification

For the results presented in this addendum, additional code and input verification testing was documented, including: (1) verification of the integrated system software (GoldSim) that is the software platform for the TSPA-LA Model used in this addendum, and (2) verification of model inputs from the TSPA Input Database. GoldSim V9.60.300 (STN: 10344-9.60-03 [DIRS 184387]) was qualified per IM-PRO-004. Additional submodels used in the Human Intrusion Scenario were verified. Coupling between the Human Intrusion submodels was examined by verifying that the information generated by one submodel is fed correctly to successive submodels and that this information does not exceed the applicable range of the successive submodel. The code and input verification was conducted to provide additional confidence in the software and the input used in the TSPA-LA Model and to comply with the requirements of SCI-PRO-006 *Models*, Section 6.3.2. In other words, these activities were conducted to verify that the computer codes and model inputs that originated from an outside source (analysis and/or model reports), or generated internally within the TSPA-LA Model, are implemented correctly.

The activities in Section 7.2 of the parent document and the additional work presented in Section 7.2[a] of this addendum demonstrate that the system software for TSPA-LA Model v5.005 is appropriate and valid, that input is correct and verified, that the internal transfer of information within the model is correct and within the valid range of successive submodels, and that submodels are valid per their respective source analysis and/or model reports. In other words, incorporation of information and submodels from other sources into TSPA-LA Model v5.005 has not altered the validity of the information or the submodels or both as demonstrated in the parent document for TSPA-LA Model v5.000.

7.10.3[a] Model Stability Testing

Demonstration of stability of TSPA-LA Model v5.005 is essential to validation and confidence building of the model results. As discussed in Section 7.3 of the parent document, the TSPA-LA Model computes mean annual dose in four steps: (1) selection of values for epistemic parameters and aleatory uncertainties; (2) numerically solving a complex, coupled system of differential equations describing radionuclide decay, flow, transport, and other physical processes; (3) integration over aleatory uncertainty, carried out either by quadrature or Monte Carlo techniques; and (4) integration over epistemic uncertainty, conducted by a Monte Carlo

technique. Section 7.3 of the parent document discusses the details of how the stability of the TSPA-LA Model is verified through implementation of the four steps during the TSPA-LA Model computations. TSPA-LA Model stability verification involved five different analyses: (1) statistical stability of mean annual dose, (2) numerical accuracy of expected annual dose, (3) temporal stability, (4) spatial stability, and (5) stability of a FEHM particle tracking model. A summary of each of these stability tests and their results obtained from them are provided in Section 7.10.3 of the parent document. Two additional analyses were presented in this addendum, one for statistical stability and one for temporal stability.

Statistical Stability

The TSPA-LA Model v5.005 changes are minor, the same LHS size (300) was used for TSPA-LA Model v5.000, and the uncertainty in total expected annual dose is driven by the same uncertain inputs. Thus, it is reasonable to conclude that TSPA-LA Model v5.005 also produces a statistically stable estimate of the total mean annual dose based upon the evaluation of the statistical stability presented in the parent document. However, an additional illustration of the accuracy of the estimate of the total mean annual dose for TSPA-LA Model v5.005, using a bootstrap sampling procedure to generate confidence intervals, is presented.

Numerical Accuracy of Expected Annual Dose

No change.

Temporal Stability

This addendum includes an update to the evaluation of temporal stability of the TSPA-LA Model Human Intrusion Scenario. This update was necessary due to the change in the timestepping scheme used in the Human Intrusion Scenario in TSPA-LA Model v5.005. The simulations were conducted by reducing the TSPA-LA Model timestep size to examine the timestep size sensitivity. The annual dose from the TSPA-LA Model calculations with different timestep sizes were compared graphically to determine the effect of refining the timesteps. The details of the approach and results are provided in Section 7.3.3 of the parent document. The results of this analysis show a better resolution using the base-case timestep scheme than previously documented in the parent document. The test results for the Human Intrusion Modeling Case confirm that the timestep scheme used for dose calculation in this modeling case is adequate.

In addition, a new evaluation of the temporal stability of the TSPA-LA Model Nominal Modeling Case is presented in Section 7.3.3.7[a]. The temporal discretization used to determine general corrosion rates is influential to the annual dose resulting from nominal corrosion processes. Simulation was conducted with shorter timesteps for the calculation of the crack growth rate, which removes the jumps in the number of WP failures by SCC, which in turn is reflected in the expected annual dose curves for the alternative scheme. However, this similarity in statistics for expected annual dose for the two timestep schemes indicates that the Nominal Modeling Case is sufficiently stable with respect to temporal discretization.

Spatial Stability

No change.

Stability of FEHM Particle Tracking Model

No change.

7.10.4[a] Uncertainty Characterization Review and Sensitivity Analyses

No change.

7.10.5[a] Surrogate Waste Form Validation

The analyses presented in Section 7.5 of the parent document and Section 7.5[a] of this addendum show that the use of surrogates to represent naval spent fuel is appropriate. Both analyses of NSNF show that mean annual dose from NSNF is bounded by that from the Zircaloy-clad CSNF surrogate.

7.10.6[a] Corroboration of Abstraction Results with Validated Process Models

No change.

7.10.7[a] Corroboration of Results with Auxiliary Analyses

The auxiliary analyses are an important aspect of determining whether the TSPA-LA Model is yielding reasonable results (e.g., that the model is producing the results that would be expected). Additional discussions of the results for some of the verification and validation testing activities presented in Section 7.7 of the parent document are presented in Section 7.7[a] for four different sets of auxiliary analyses: (1) single realization analysis (Section 7.7.1[a]), (2) updated comparison of the results of TSPA-LA Model v5.005 with a Simplified TSPA Analysis (Section 7.7.2[a]), (3) updated comparison of the results of TSPA-LA Model v5.005 with the TSPA independently developed by EPRI (Section 7.7.3[a]), and (4) updated PMA comparison to TSPA-LA Model v5.005 (Section 7.7.4[a]). A summary of the additional discussion included in this addendum is provided below.

Single Realization Analysis

The single realization analyses presented in the parent document and in Section 7.7.1[a] of this addendum comprise a comprehensive explanation detailing how the transport of key radionuclides is affected by coupling various submodels of the EBS, UZ, and SZ domains in the TSPA Model, following the WP failure under varying physical-chemical-thermal-mechanical conditions, and providing confidence that these model components are working as expected and the aggregate TSPA-LA Model results (in terms of dose) are reflective of the model components. Through examination and explanation of key aspects affecting the release of radionuclides, it is demonstrated that the TSPA-LA Model is functioning as intended and that the submodels are coupled correctly to yield the system level results. Repeating these analyses in this addendum

provides confidence that TSPA-LA Model v5.005 is functioning as designed and helps confirm the validation of the model.

The parent document includes single realization analyses of four modeling cases: (1) Waste Package EF Modeling Case (Section 7.7.1.1), (2) Drip Shield EF Modeling Case (Section 7.7.1.2), (3) Igneous Intrusion Modeling Case (Section 7.7.1.3), and (4) Seismic GM Modeling Case (1,000,000 years) (Section 7.7.1.4). Details of the analyses and ensuing results are repeated in this addendum and discussed in Sections 7.7.1.1[a] through 7.7.1.4[a]. Three additional modeling cases: (1) Nominal Modeling Case (Section 7.7.1.5), (2) Human Intrusion Modeling Case (Section 7.7.1.6), and (3) Seismic GM Modeling Case (10,000 years) (Section 7.7.1.7) are included in this addendum. The results confirm that the changes from TSPA-LA Model v5.000 to TSPA-LA Model v5.005 had little impact on the results presented using v5.000 and, therefore, support the demonstration of model validation and add to the confidence in the TSPA-LA Model results.

Comparison with Simplified TSPA Analysis

A comparison of the TSPA-LA Model results to a stand-alone Simplified TSPA Analysis was conducted and documented in Section 7.7.2 and Appendix L of the parent document. Section 7.7.2 of the parent document provides a detailed discussion on the comparative results for the individual modeling cases for the Simplified TSPA Analysis and the TSPA-LA Model, including the minor differences in the prominence of certain radionuclides and mean annual doses calculated by the two approaches. A comparison of the updated results presented in this addendum with the Simplified TSPA Analysis was provided in Section 7.7.2[a].

The results presented in Section 7.7.2[a] comparing the TSPA-LA Model v5.005 results and the Simplified TSPA Analysis corroborate the conclusions presented in the parent report.

Comparison with EPRI TSPA Analysis

A limited comparison of the EPRI TSPA Analysis results with those of TSPA-LA Model v5.005 is documented in this addendum. Detail of the similarities and differences between the EPRI TSPA Analysis and TSPA-LA Model v5.000 is discussed in Section 7.7.3 of the parent document with additional detail provided in Appendix M of the parent document.

The results documented in Section 7.7.3[a] identify the general similarities as well as the differences between the results from the two models detailed in Section 7.7.3 of the parent document.

Performance Margin Analysis

A comparison of TSPA-LA Model v5.005 results with the PMA was conducted to confirm the quantitative evaluation of the differences in repository performance due to significant explicit and implicit conservatisms embedded in the TSPA-LA Model submodels documented in Section 7.7.4 and Appendix C of the parent document. The conservatisms were evaluated to (1) confirm that they are conservative with respect to the mean annual dose of the TSPA-LA Model; (2) quantify the extent to which they, individually and collectively, overestimate the projected annual dose; and (3) assess that the evaluated conservatisms did not introduce any inappropriate

risk dilution in the TSPA-LA Model results presented in support of the LA. The details of approach and results of the PMA are presented in Section 7.7.4 of the parent document with additional supporting material in Appendix C of the parent document. Summarizing here, the results show that the margin evaluated in the PMA as documented in the parent document are indeed conservative with respect to the total system performance measures (e.g., peak mean annual dose) as the largest doses calculated in the PMA for 10,000 years and 1,000,000 years are lower than the doses used in the compliance demonstration presented in Section 8[a] of this addendum. The additional analyses confirm that the largest calculated PMA mean annual doses are lower by over an order of magnitude and a factor of two over the largest mean annual dose relative to the TSPA-LA Model (Section 8[a]) for the time periods of 10,000 years and 1,000,000 years, respectively. Further, this PMA confirms that the significant conservatisms did not introduce risk dilution in the TSPA-LA Model results, as demonstrated by the absence of higher peak doses in the comparison of the projected total mean annual dose for the PMA relative to TSPA-LA Model v5.005. The differences in the relative contributions to the total mean annual dose from each of the scenario modeling cases between the PMA and the TSPA-LA Model indicate that the reduction in the selected conservative assumptions embedded in these TSPA-LA Model components provides a performance margin in the projected annual dose predictions presented in Section 8 of the parent document and Section 8[a] of this addendum.

7.10.8[a] Corroboration of Results with Natural Analogues

No change.

7.10.9[a] Technical Reviews Summary

No change.

7.10.10[a] Conclusions

The comparison of TSPA-LA Model v5.005 results to the validation activities that were presented in the parent document were conducted to verify that modifications to parameter values and submodel implementations detailed in Sections 4[a] and 6[a] of this addendum did not adversely affect the overall validation of the TSPA-LA Model. Additionally, only the validation and confidence building activities presented in the parent document that may have been affected by the changes from v5.000 to v5.005 have been updated in this addendum. Section 7[a] also includes additional discussion of the results for some of the verification and validation testing activities presented in the parent document that are used to enhance confidence in the TSPA-LA Model results. All results presented in this section utilized TSPA-LA Model v5.005 and confirmed that the updated model is within the range of validation previously documented in the parent document.

Changes were made to the TSPA-LA Model to address the issues presented in Appendix P of the parent document and to address unintended conservatisms in the TSPA-LA Model, as indicated in Appendix P[a] of this addendum. As documented in Appendix P of the parent document, and confirmed in the updated validation activities presented in this addendum, only Section P3 identified an issue in the TSPA-LA Model v5.000 that had the potential to significantly change the total expected annual dose results (Appendix P of the parent document). Although the

TSPA-LA Model v5.005 expected annual dose results confirm a significant decrease over the time period between approximately 100,000 to 300,000 years, the activities presented in Section 7 of the parent document, and the additional results documented in Section 7[a] of this addendum, confirm: (1) the GoldSim code functions as intended; (2) inputs were accurately implemented in the TSPA-LA Model; (3) the TSPA-LA Model is numerically, temporally, and spatially stable; and (4) the resultant dose calculations are appropriate for their intended use.

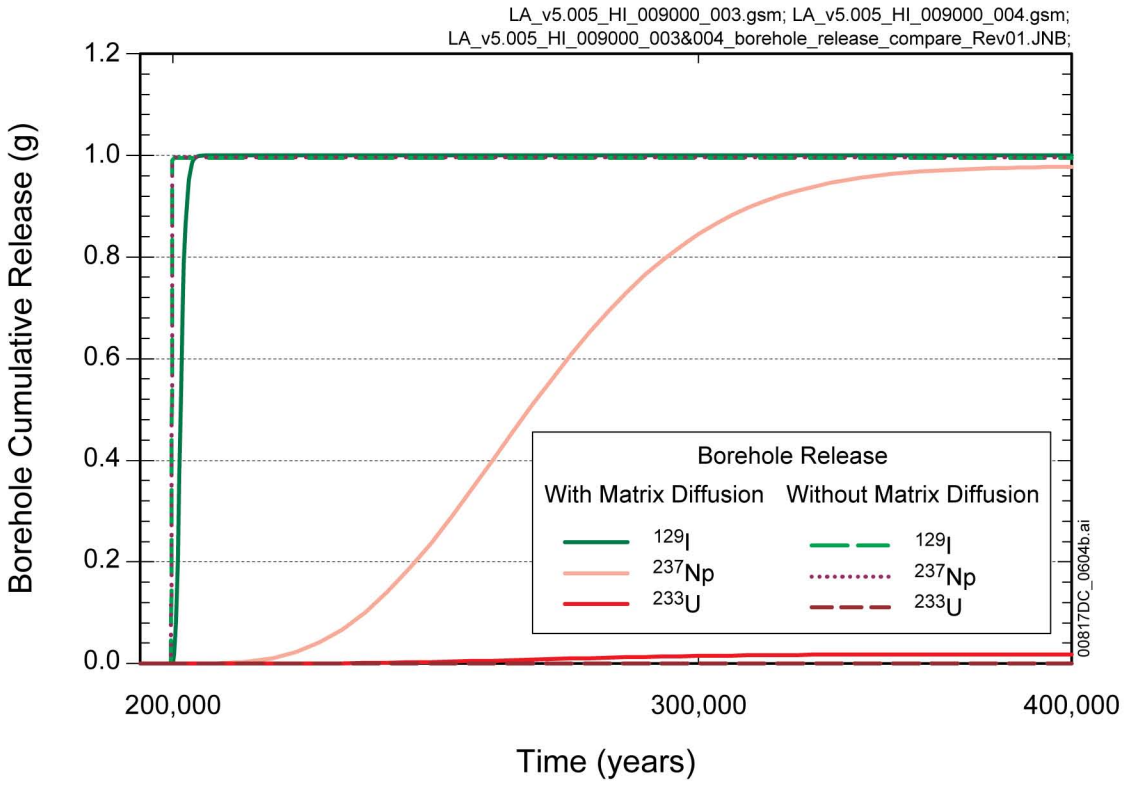

Source: Output DTN: MO0801TSPAMVAC.000 [DIRS 185080].

Figure 7.2-17[a]. Cumulative Releases of ^{129}I, ^{237}Np, and ^{233}U from the Human Intrusion Borehole Based on Simulations Considering and not Considering Matrix Diffusion

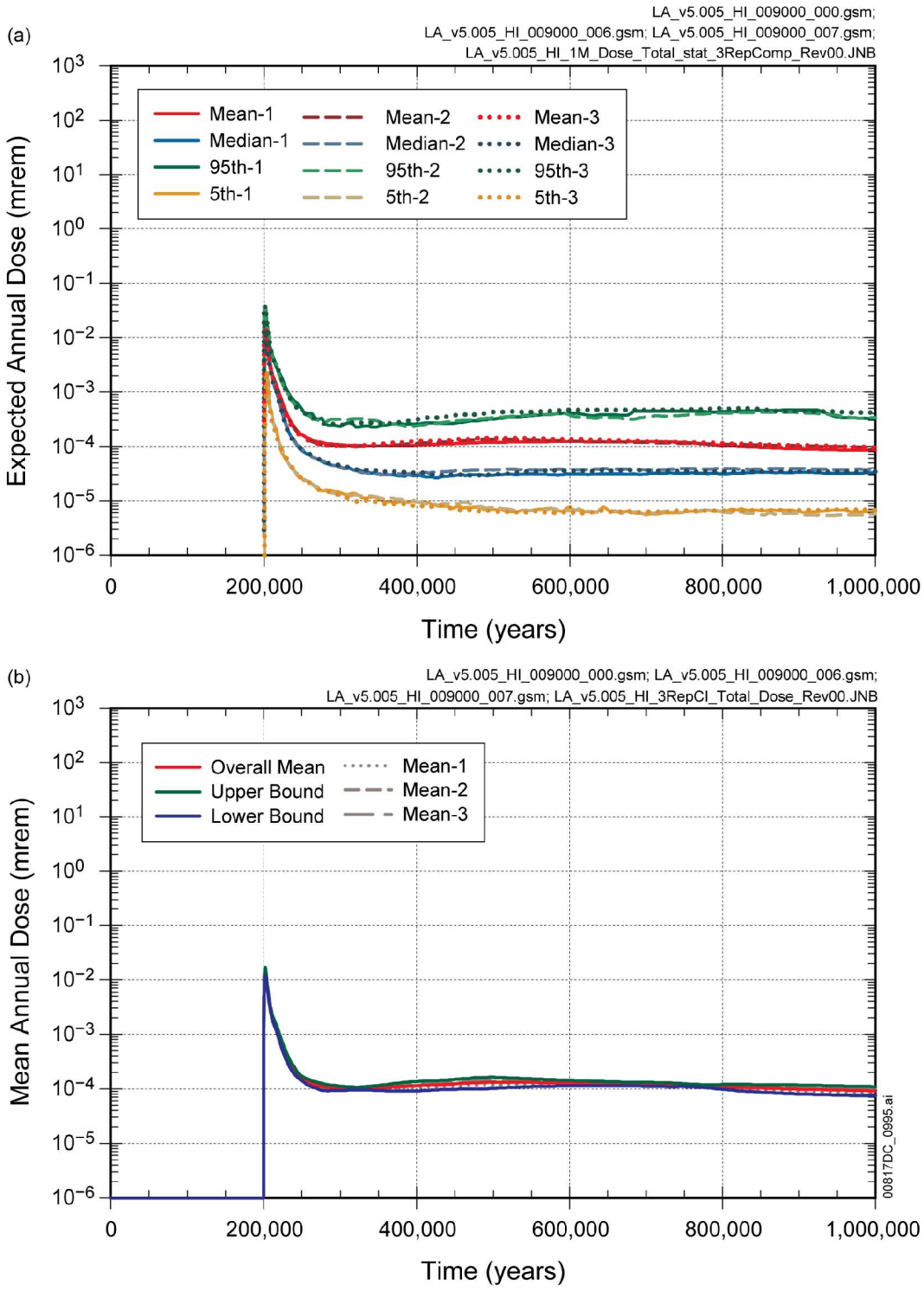

Source: Output DTNs: MO0710ADTSPAWO.000 [DIRS 183752]; and MO0801TSPAADSA.000 [DIRS 185078].

Figure 7.3.1-14[a]. Stability of Human Intrusion Scenario: (a) Comparison of Expected Annual Dose for Three Replicates and (b) Confidence Interval around Mean Annual Dose

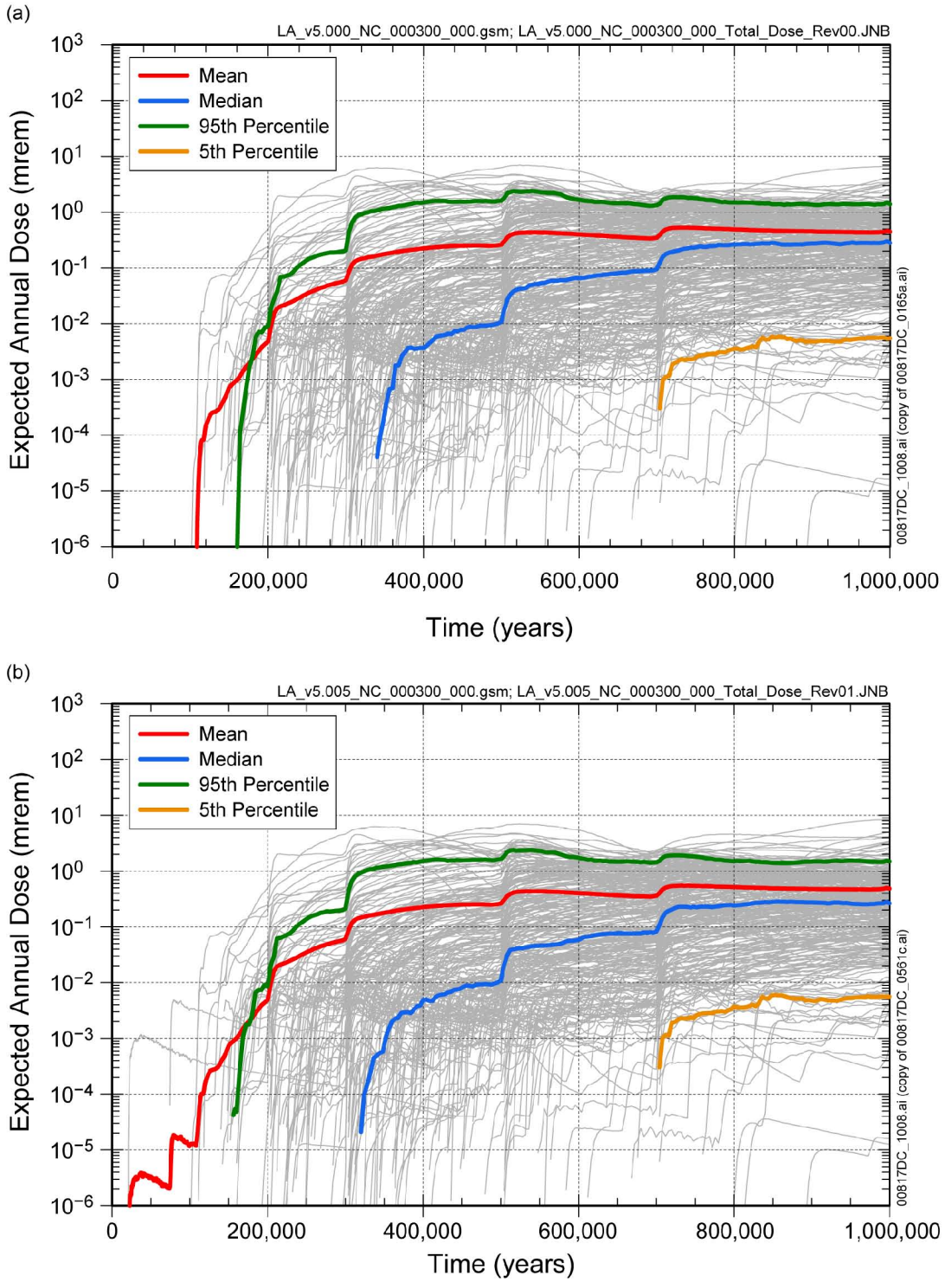

Source: Output DTNs: MO0709TSPAREGS.000 [DIRS 182976]; and MO0710ADTSPAWO.000 [DIRS 183752].

Figure 7.3.1-17[a]. Expected Annual Dose for 1,000,000 Years for the Nominal Modeling Case from (a) TSPA-LA Model v5.000 and (b) TSPA-LA Model v5.005

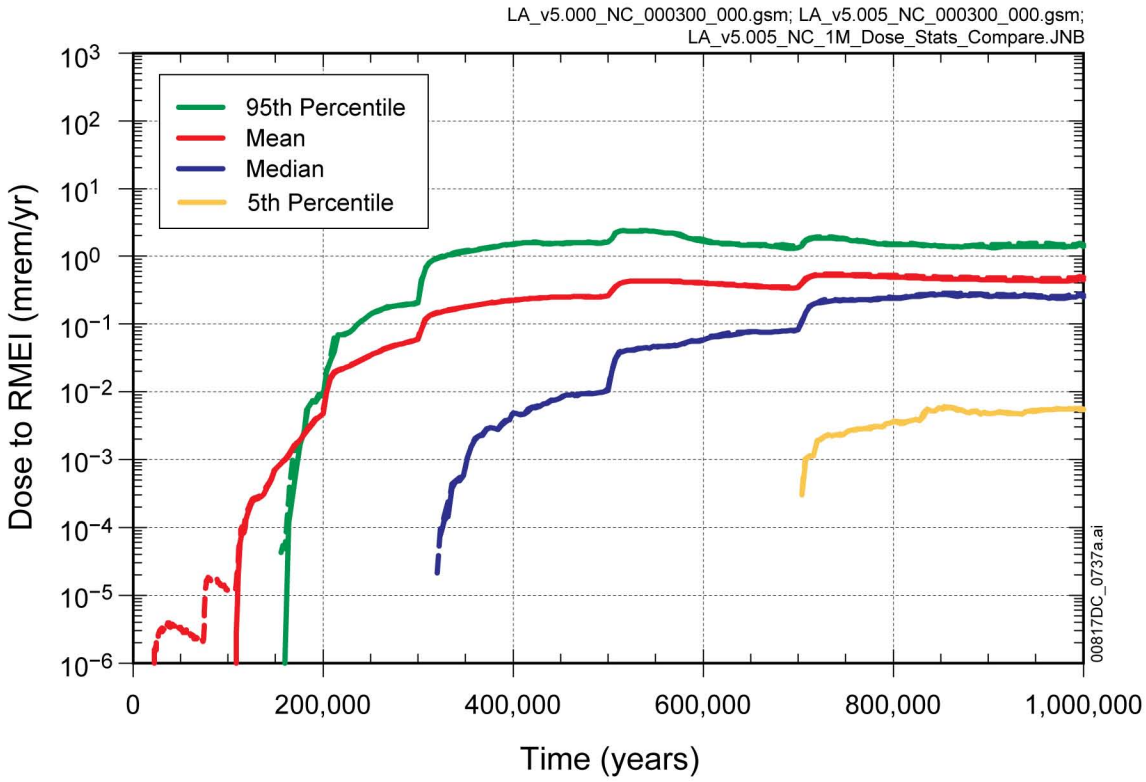

Source: Output DTNs: MO0710ADTSPAWO.000 [DIRS 183752]; and MO0709TSPAREGS.000 [DIRS 182976].

NOTE: Solid lines indicate TSPA-LA Model v5.000 and dashed lines indicate TSPA-LA Model v5.005.

Figure 7.3.1-18[a]. Comparison of Statistics for Expected Annual Dose in the Nominal Modeling Case between TSPA-LA Model v5.000 and TSPA-LA Model v5.005

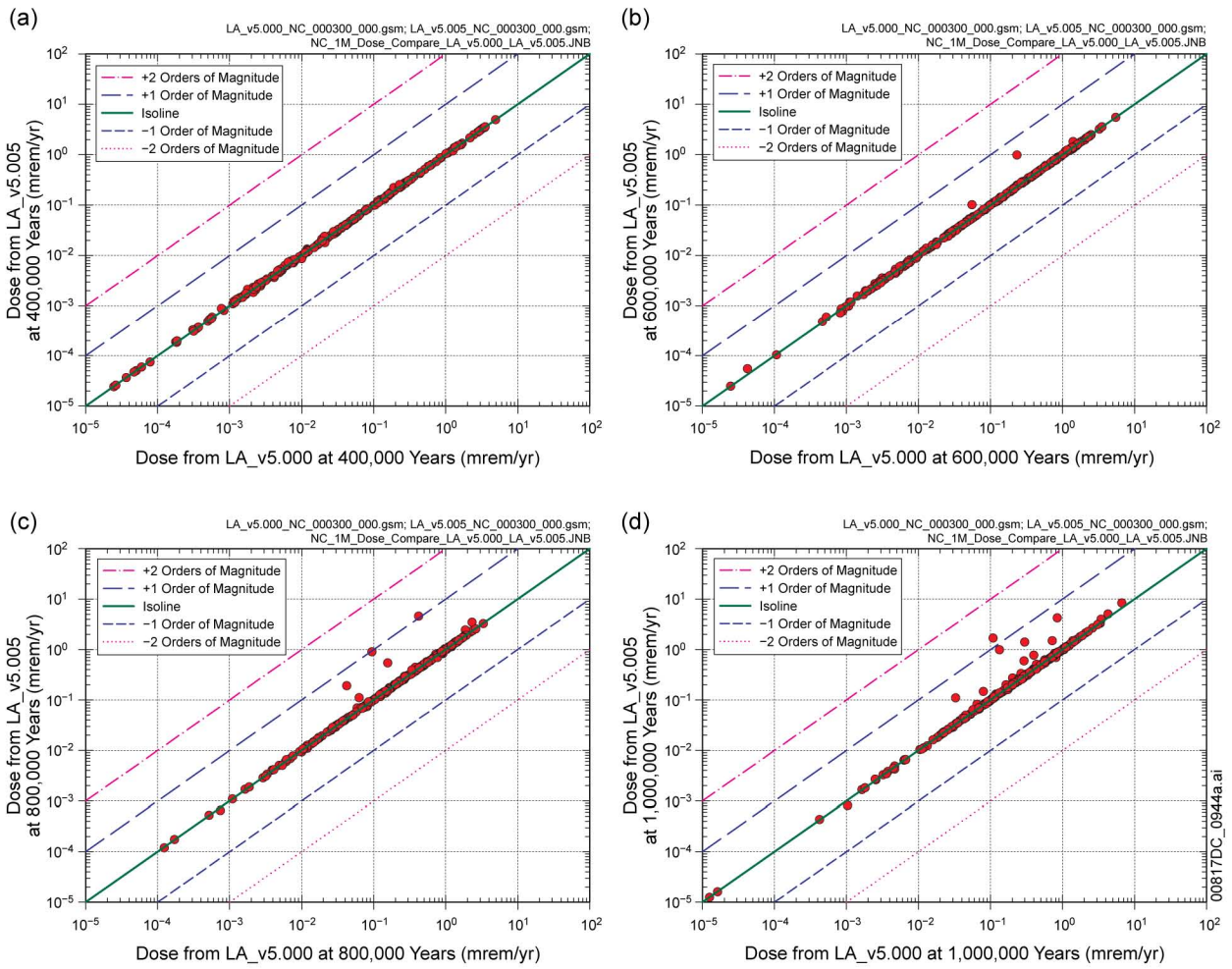

Source: Output DTNs: MO0710ADTSPAWO.000 [DIRS 183752]; and MO0709TSPAREGS.000 [DIRS 182976].

Figure 7.3.1-19[a]. Comparison of Expected Annual Dose for Individual Sample Elements in the Nominal Modeling Case between TSPA-LA Model v5.000 and TSPA-LA Model v5.005 at (a) 400,000; (b) 600,000; (c) 800,000; and (d) 1,000,000 Years

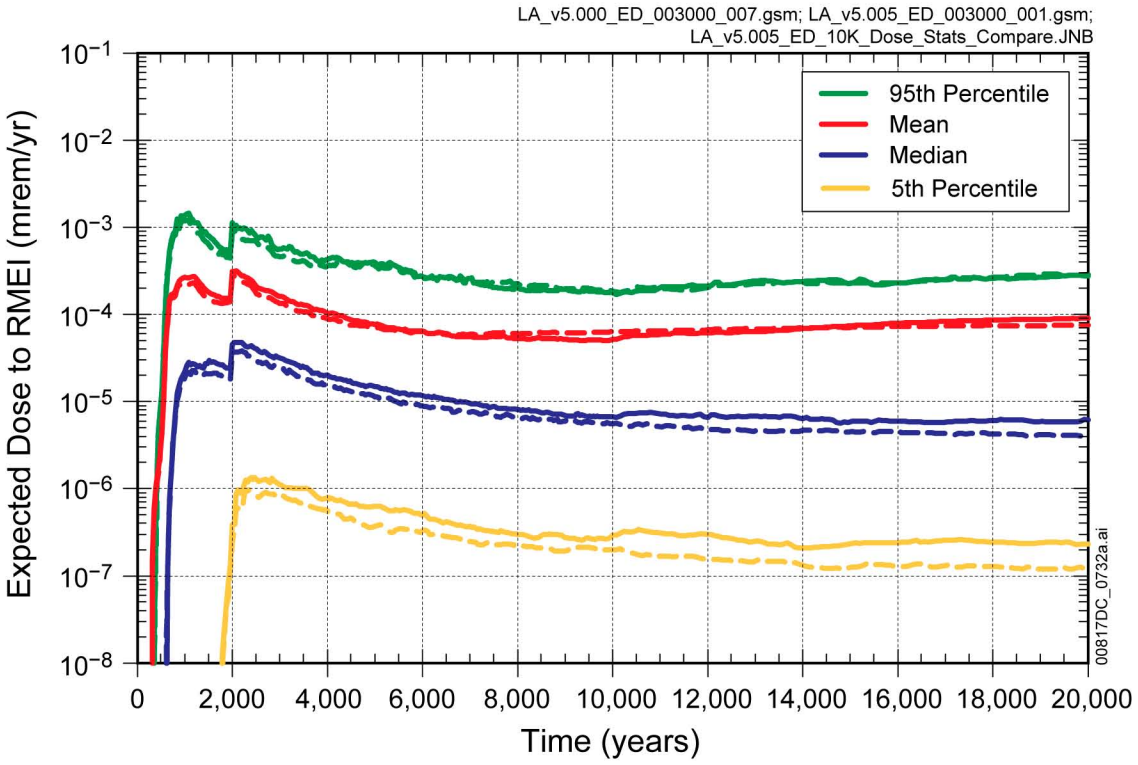

Source: Output DTNs: MO0710ADTSPAWO.000 [DIRS 183752]; and MO0709TSPAREGS.000 [DIRS 182976].

NOTE: Solid lines indicate TSPA-LA Model v5.000 and dashed lines indicate TSPA-LA Model v5.005.

Figure 7.3.1-20[a]. Comparison of Statistics for Expected Annual Dose over 20,000 Years in the Drip Shield Early Failure Modeling Case between TSPA-LA Model v5.000 and TSPA-LA Model v5.005

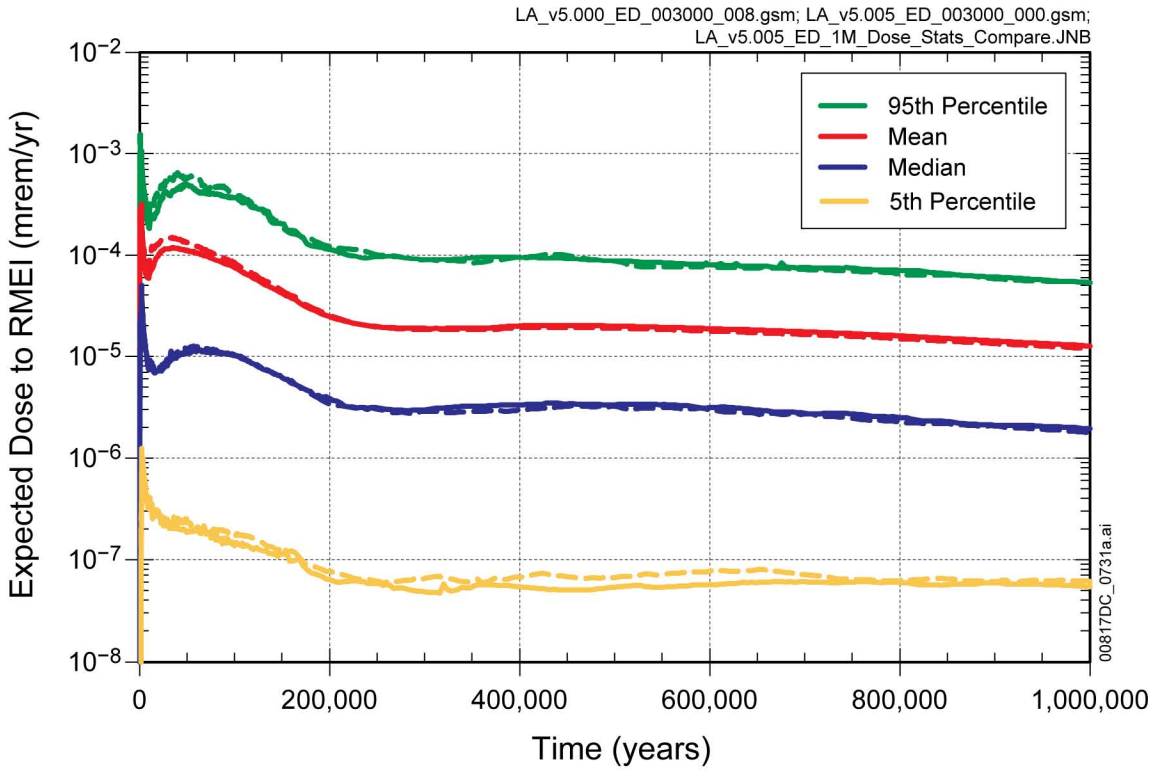

Source: Output DTNs: MO0710ADTSPAWO.000 [DIRS 183752]; and MO0709TSPAREGS.000 [DIRS 182976].

NOTE: Solid lines indicate TSPA-LA Model v5.000 and dashed lines indicate TSPA-LA Model v5.005.

Figure 7.3.1-21[a]. Comparison of Statistics for Expected Annual Dose over 1,000,000 Years in the Drip Shield Early Failure Modeling Case between TSPA-LA Model v5.000 and TSPA-LA Model v5.005

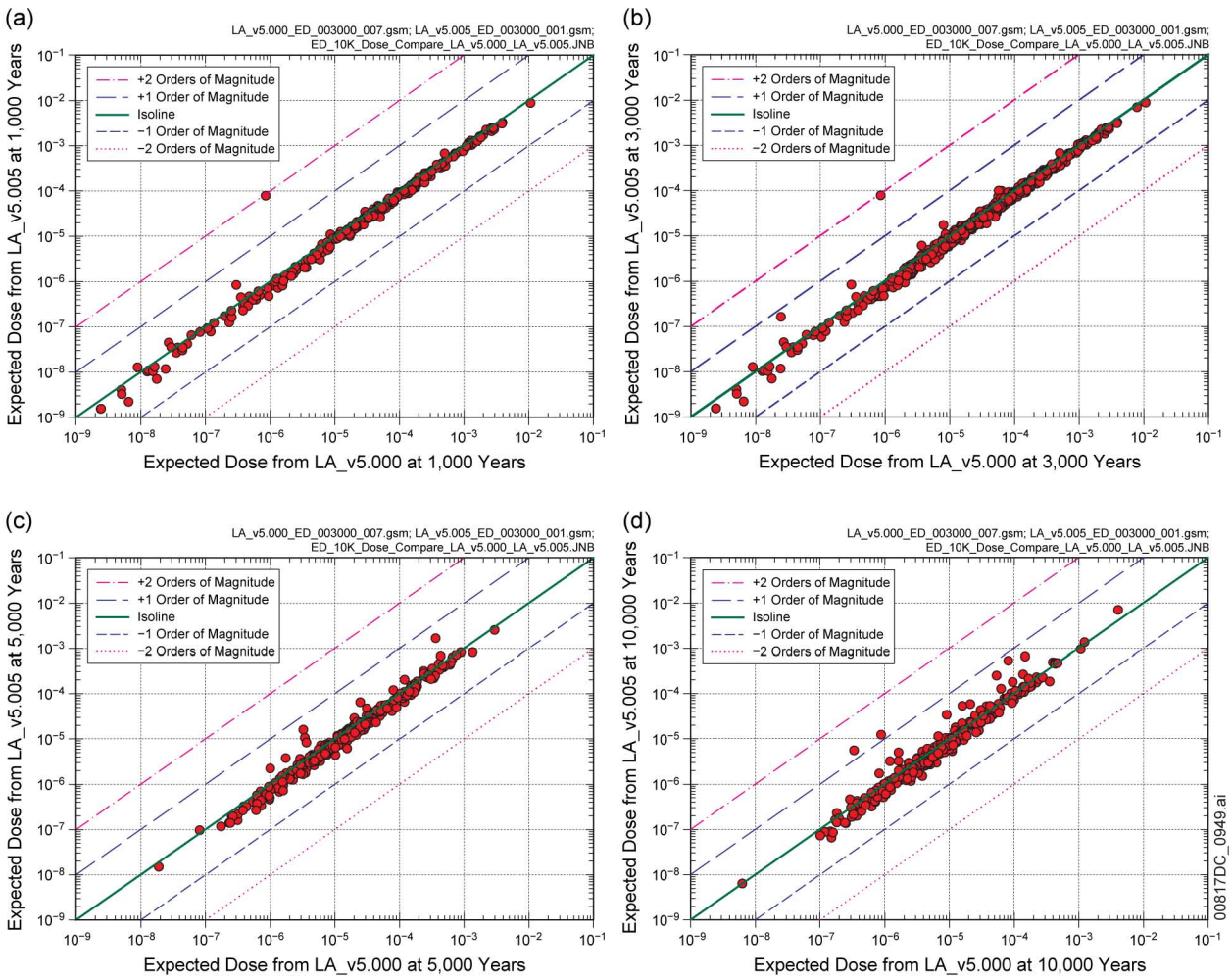

Source: Output DTNs: MO0710ADTSPAWO.000 [DIRS 183752]; and MO0709TSPAREGS.000 [DIRS 182976].

Figure 7.3.1-22[a]. Comparison of Expected Annual Dose for Individual Sample Elements in the Drip Shield Early Failure Modeling Case between TSPA-LA Model v5.000 and TSPA-LA Model v5.005 at (a) 1,000; (b) 3,000; (c) 5,000; and (d) 10,000 Years

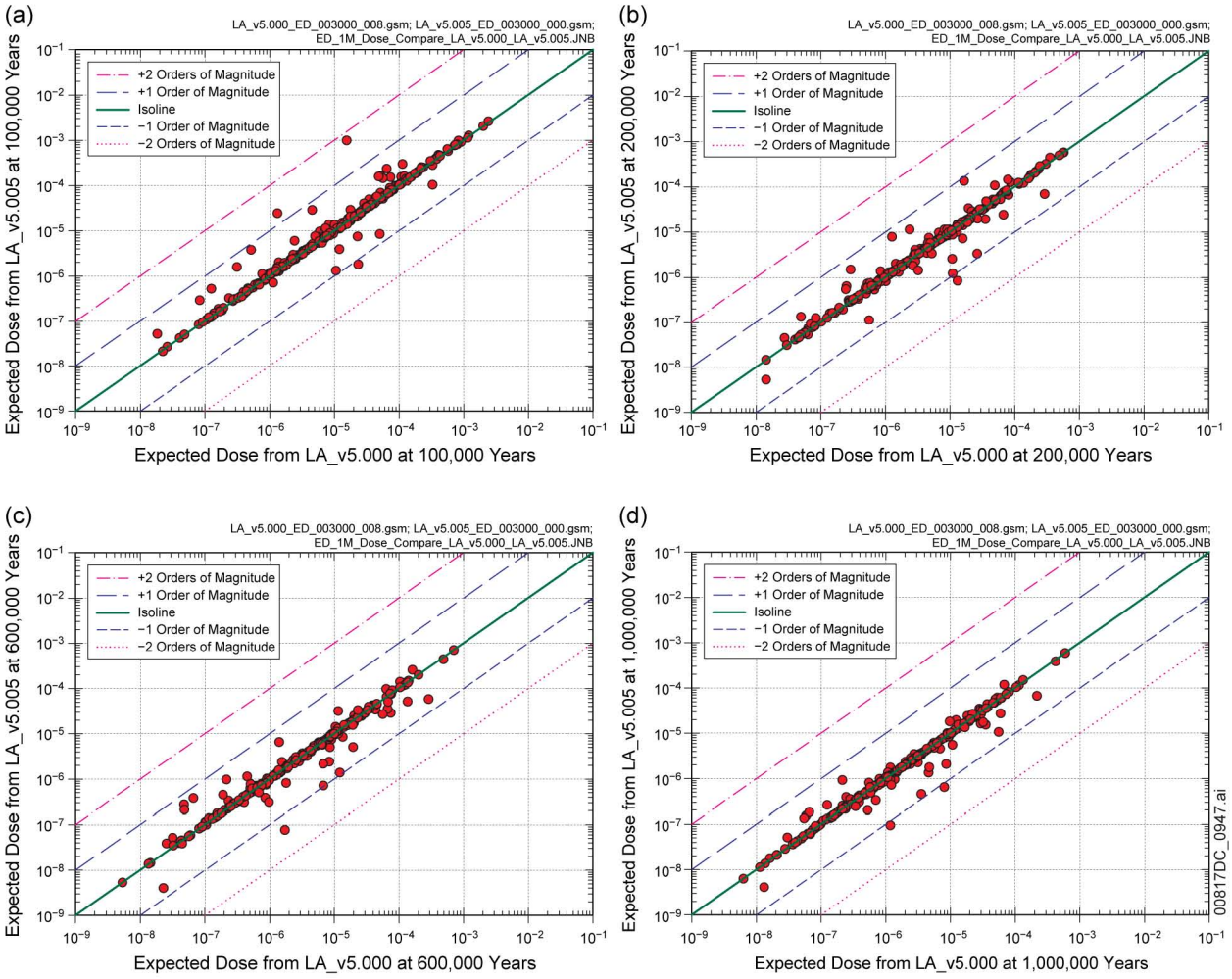

Source: Output DTNs: MO0710ADTSPAWO.000 [DIRS 183752]; and MO0709TSPAREGS.000 [DIRS 182976].

Figure 7.3.1-23[a]. Comparison of Expected Annual Dose for Individual Sample Elements in the Drip Shield Early Failure Modeling Case between TSPA-LA Model v5.000 and TSPA-LA Model v5.005 at (a) 100,000; (b) 200,000; (c) 600,000; and (d) 1,000,000 Years

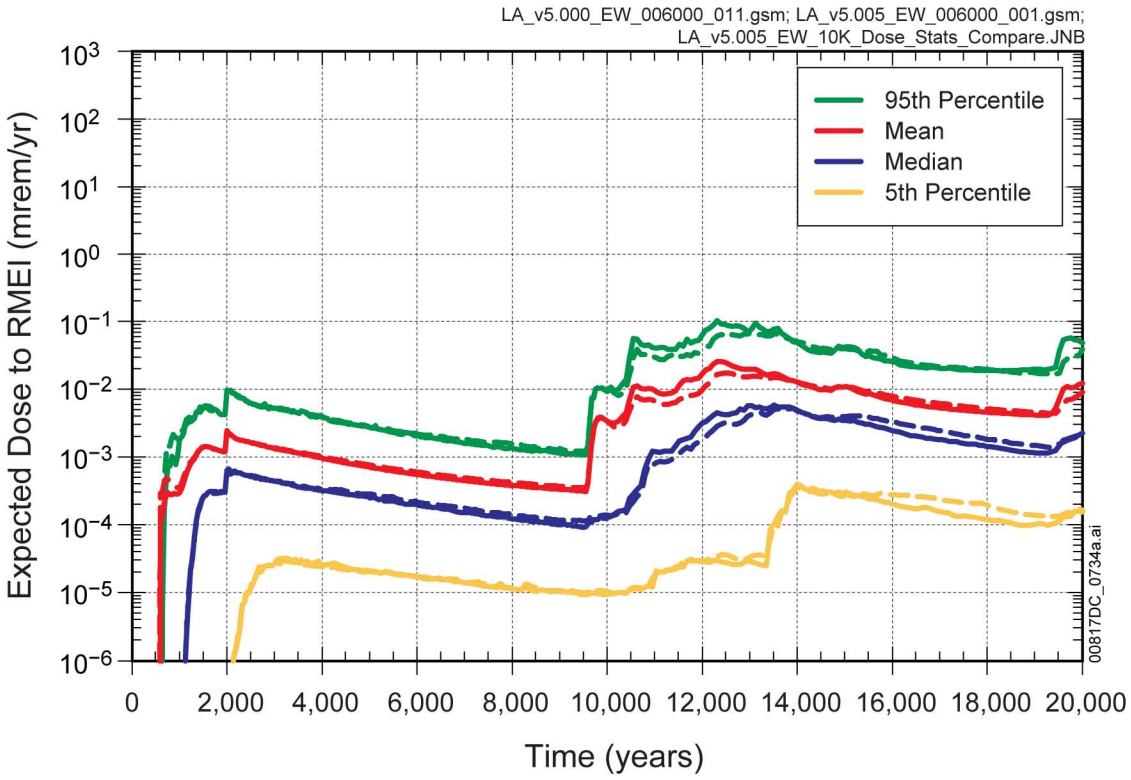

Source: Output DTNs: MO0710ADTSPAWO.000 [DIRS 183752]; and MO0709TSPAREGS.000 [DIRS 182976].

NOTE: Solid lines indicate TSPA-LA Model v5.000 and dashed lines indicate TSPA-LA Model v5.005.

Figure 7.3.1-24[a]. Comparison of Statistics for Expected Annual Dose over 20,000 Years in the Waste Package Early Failure Modeling Case between TSPA-LA Model v5.000 and TSPA-LA Model v5.005

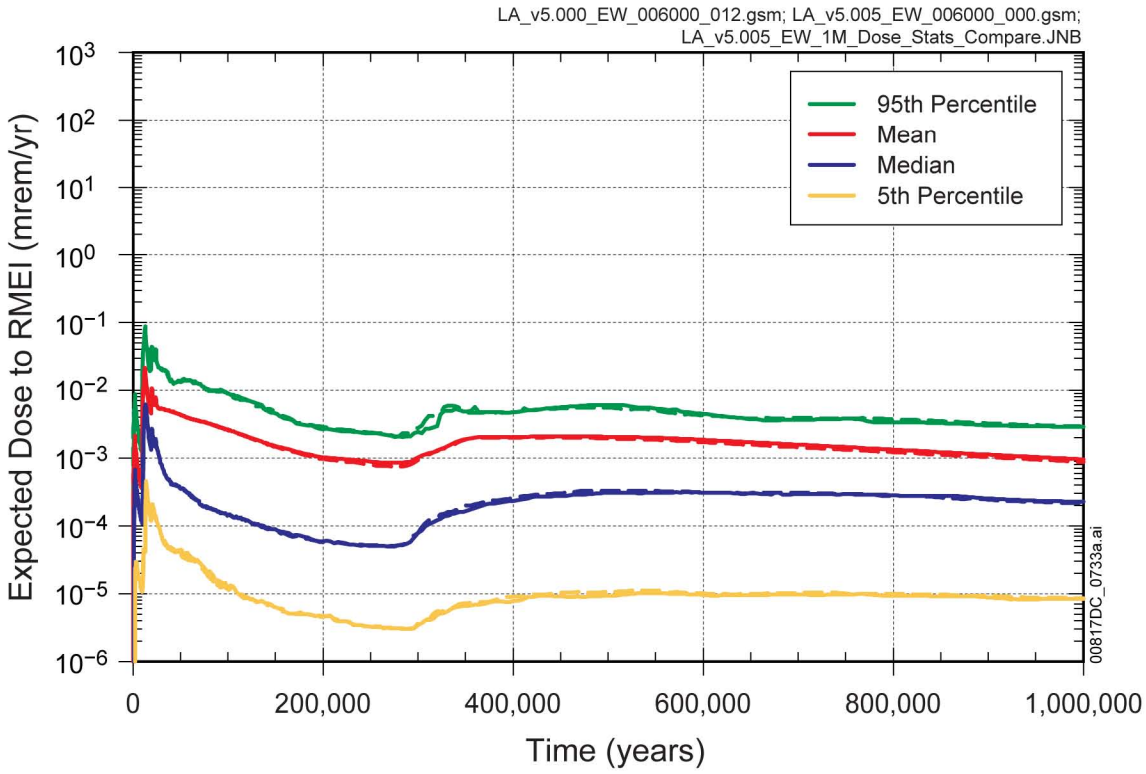

Source: Output DTNs: MO0710ADTSPAWO.000 [DIRS 183752]; and MO0709TSPAREGS.000 [DIRS 182976].

NOTE: Solid lines indicate TSPA-LA Model v5.000 and dashed lines indicate TSPA-LA Model v5.005.

Figure 7.3.1-25[a]. Comparison of Statistics for Expected Annual Dose over 1,000,000 Years in the Waste Package Early Failure Modeling Case between TSPA-LA Model v5.000 and TSPA-LA Model v5.005

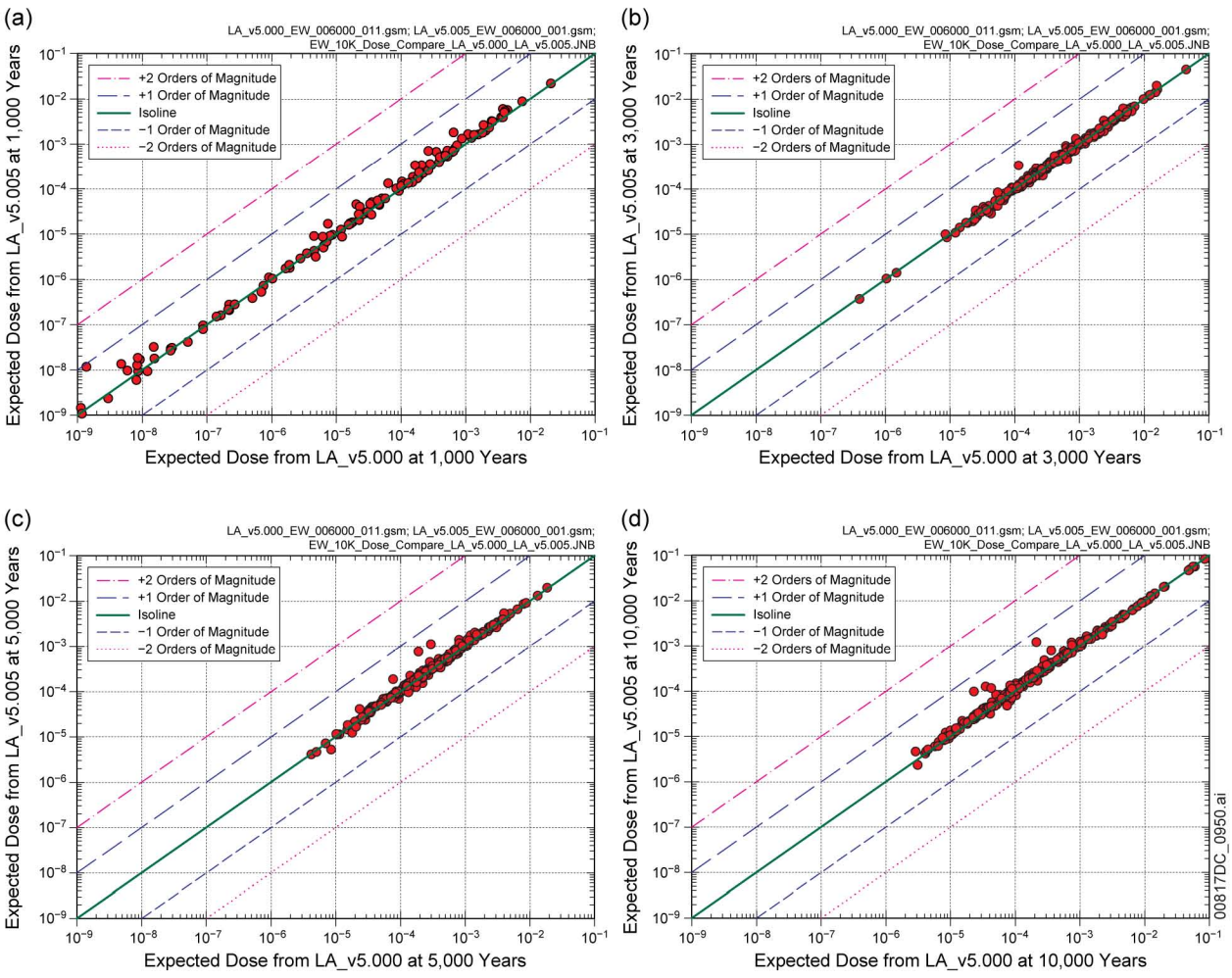

Source: Output DTNs: MO0710ADTSPAWO.000 [DIRS 183752]; and MO0709TSPAREGS.000 [DIRS 182976].

Figure 7.3.1-26[a]. Comparison of Expected Annual Dose for Individual Sample Elements in the Waste Package Early Failure Modeling Case between TSPA-LA Model v5.000 and TSPA-LA Model v5.005 at (a) 1,000; (b) 3,000; (c) 5,000; and (d) 10,000 Years

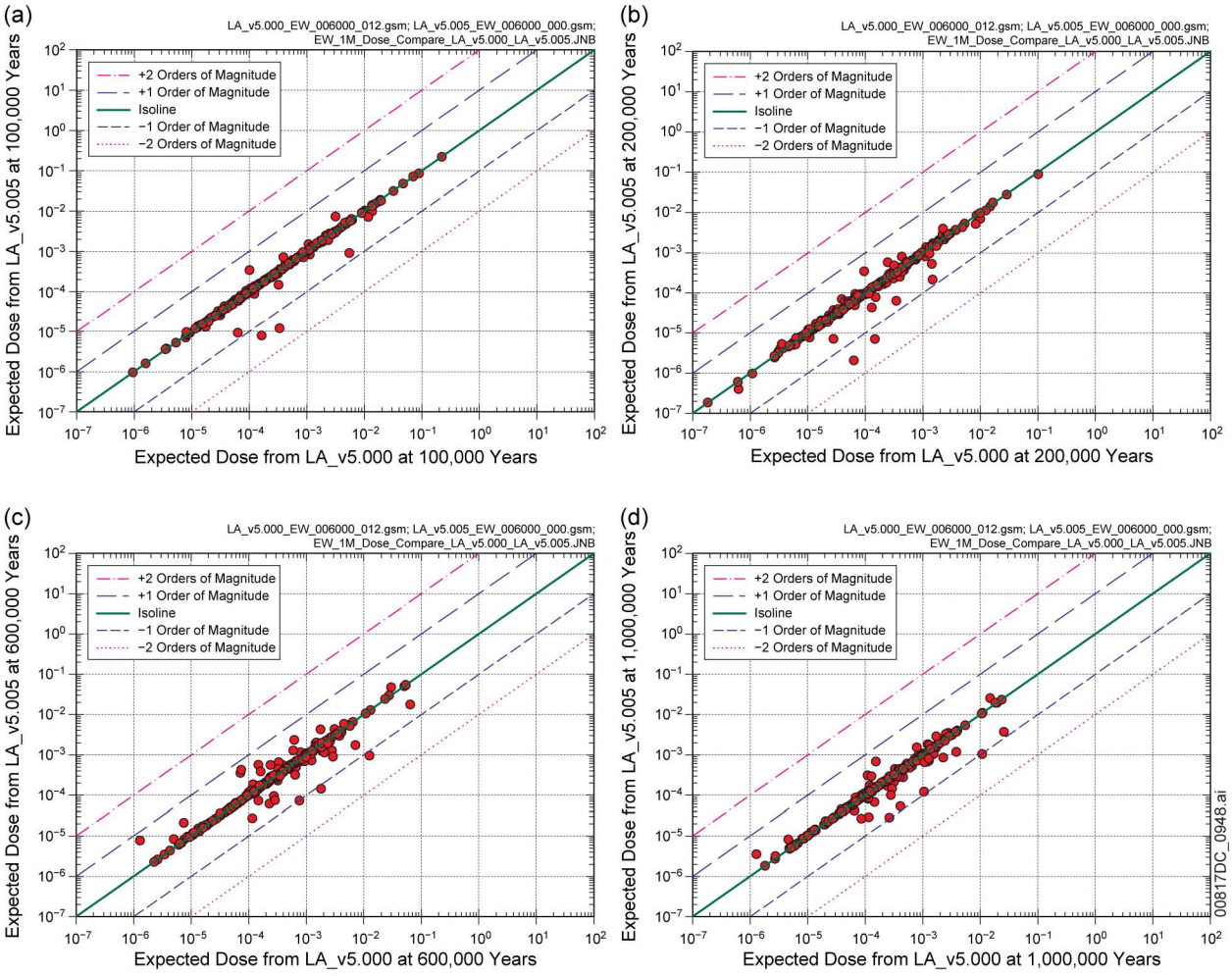

Source: Output DTNs: MO0710ADTSPAWO.000 [DIRS 183752]; and MO0709TSPAREGS.000 [DIRS 182976].

Figure 7.3.1-27[a]. Comparison of Expected Annual Dose for Individual Sample Elements in the Waste Package Early Failure Modeling Case between TSPA-LA Model v5.000 and TSPA-LA Model v5.005 at (a) 100,000; (b) 200,000; (c) 600,000; and (d) 1,000,000 Years

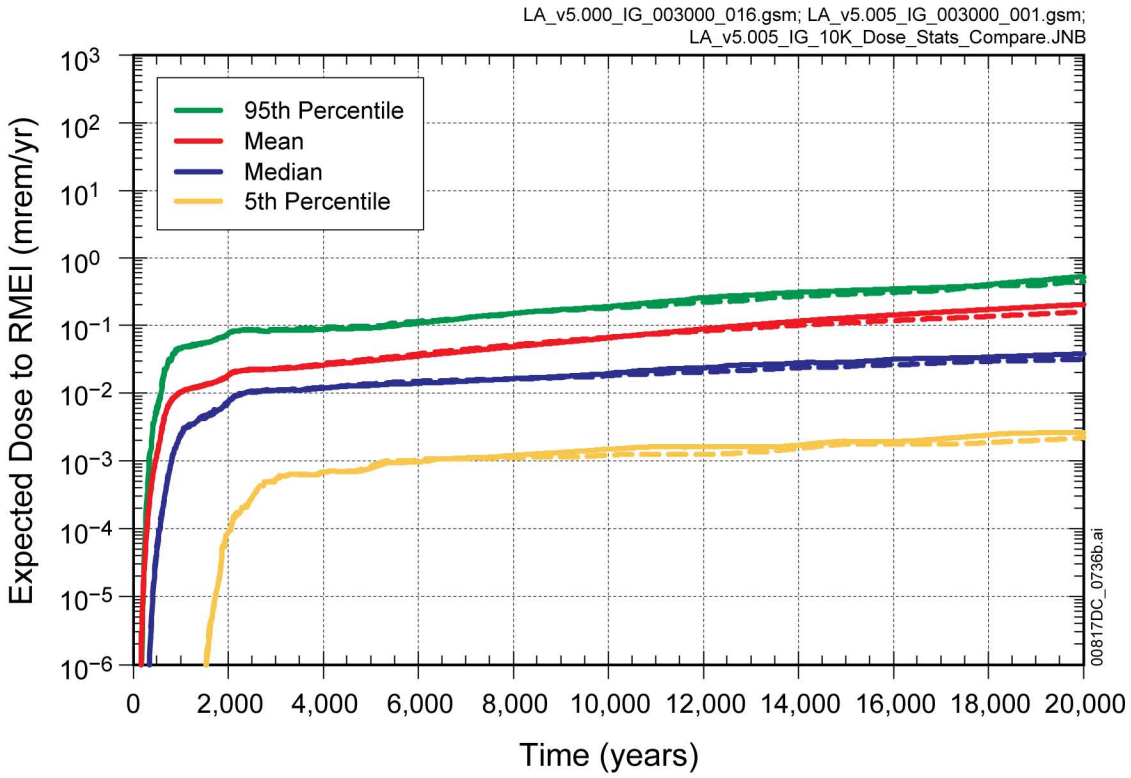

Source: Output DTNs: MO0710ADTSPAWO.000 [DIRS 183752]; and MO0709TSPAREGS.000 [DIRS 182976].

NOTE: Solid lines indicate TSPA-LA Model v5.000 and dashed lines indicate TSPA-LA Model v5.005.

Figure 7.3.1-28[a]. Comparison of Statistics for Expected Annual Dose over 20,000 Years in the Igneous Intrusion Modeling Case between TSPA-LA Model v5.000 and TSPA-LA Model v5.005

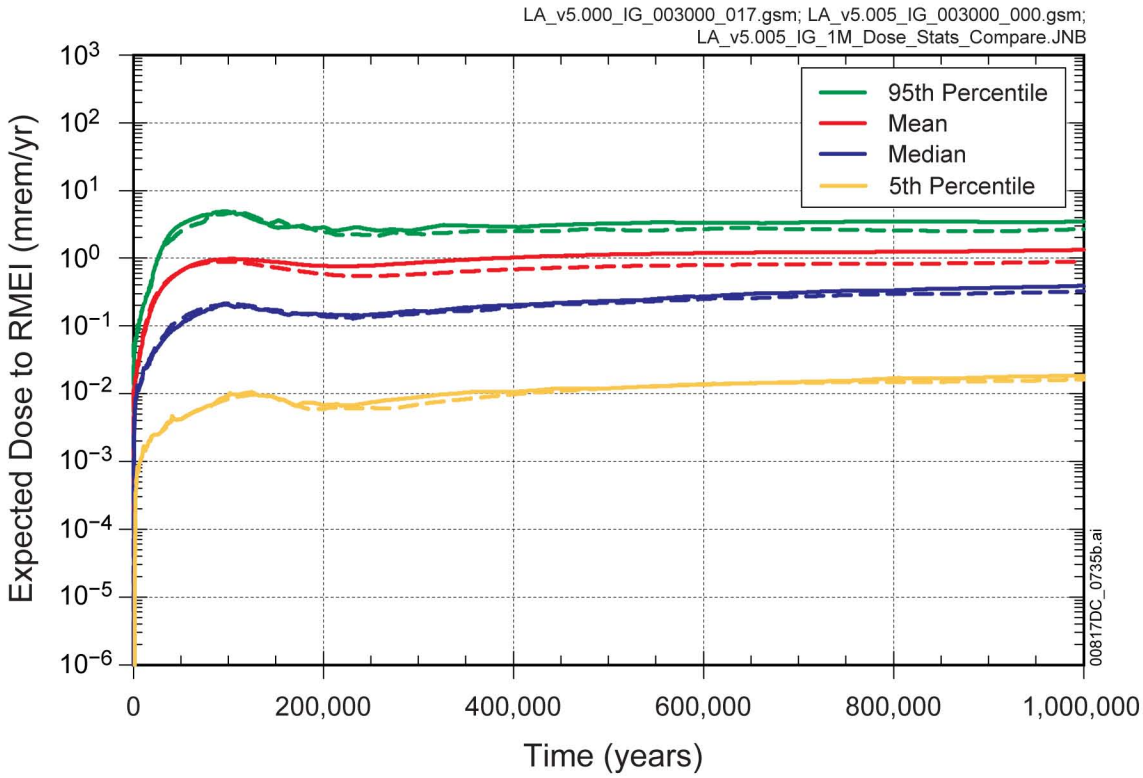

Source: Output DTNs: MO0710ADTSPAWO.000 [DIRS 183752]; and MO0709TSPAREGS.000 [DIRS 182976].

NOTE: Solid lines indicate TSPA-LA Model v5.000 and dashed lines indicate TSPA-LA Model v5.005.

Figure 7.3.1-29[a]. Comparison of Statistics for Expected Annual Dose over 1,000,000 Years in the Igneous Intrusion Modeling Case between TSPA-LA Model v5.000 and TSPA-LA Model v5.005

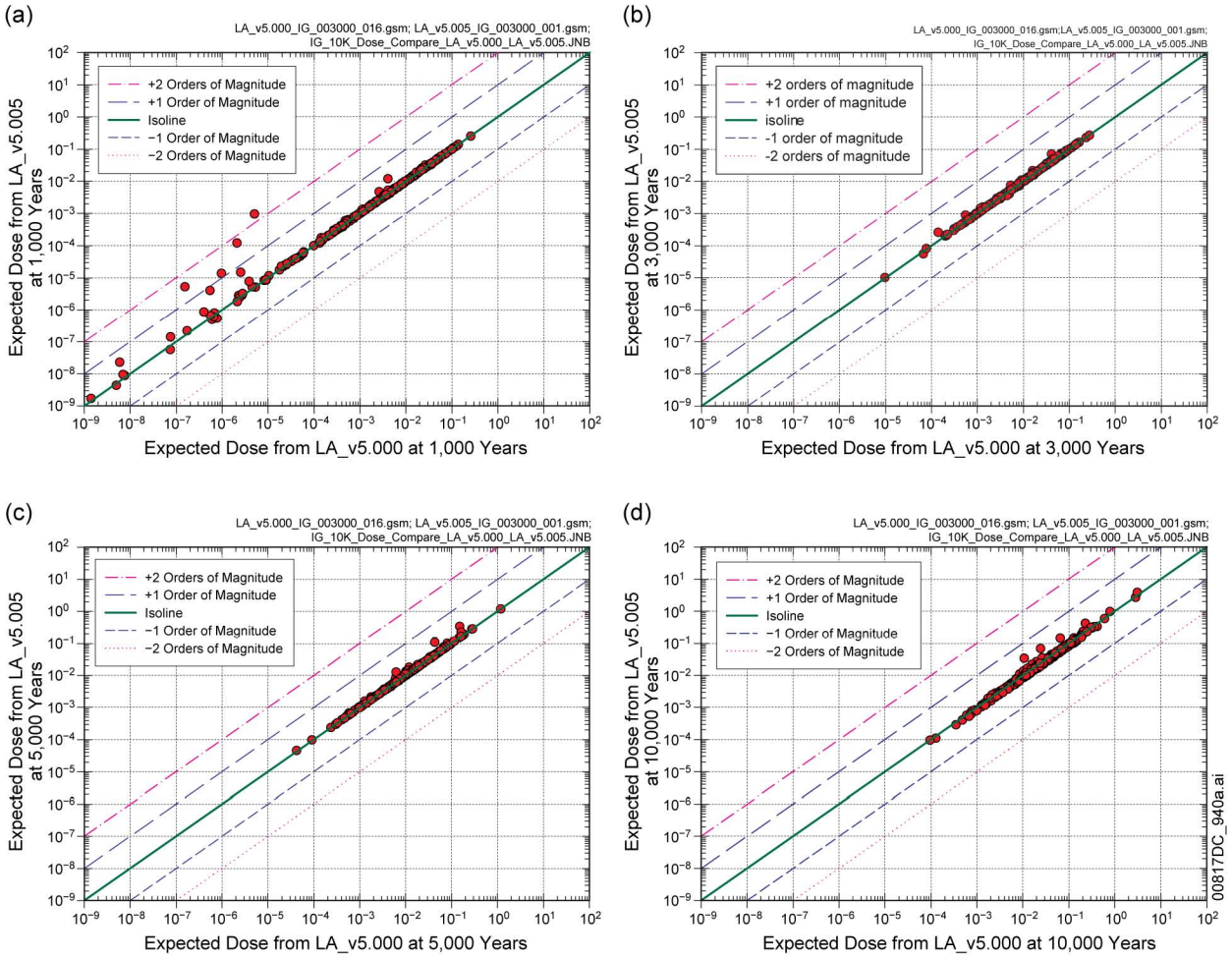

Source: Output DTNs: MO0710ADTSPAWO.000 [DIRS 183752]; and MO0709TSPAREGS.000 [DIRS 182976].

Figure 7.3.1-30[a]. Comparison of Expected Annual Dose for Individual Sample Elements in the Igneous Intrusion Modeling Case between TSPA-LA Model v5.000 and TSPA-LA Model v5.005 at (a) 1,000; (b) 3,000; (c) 5,000; and (d) 10,000 Years

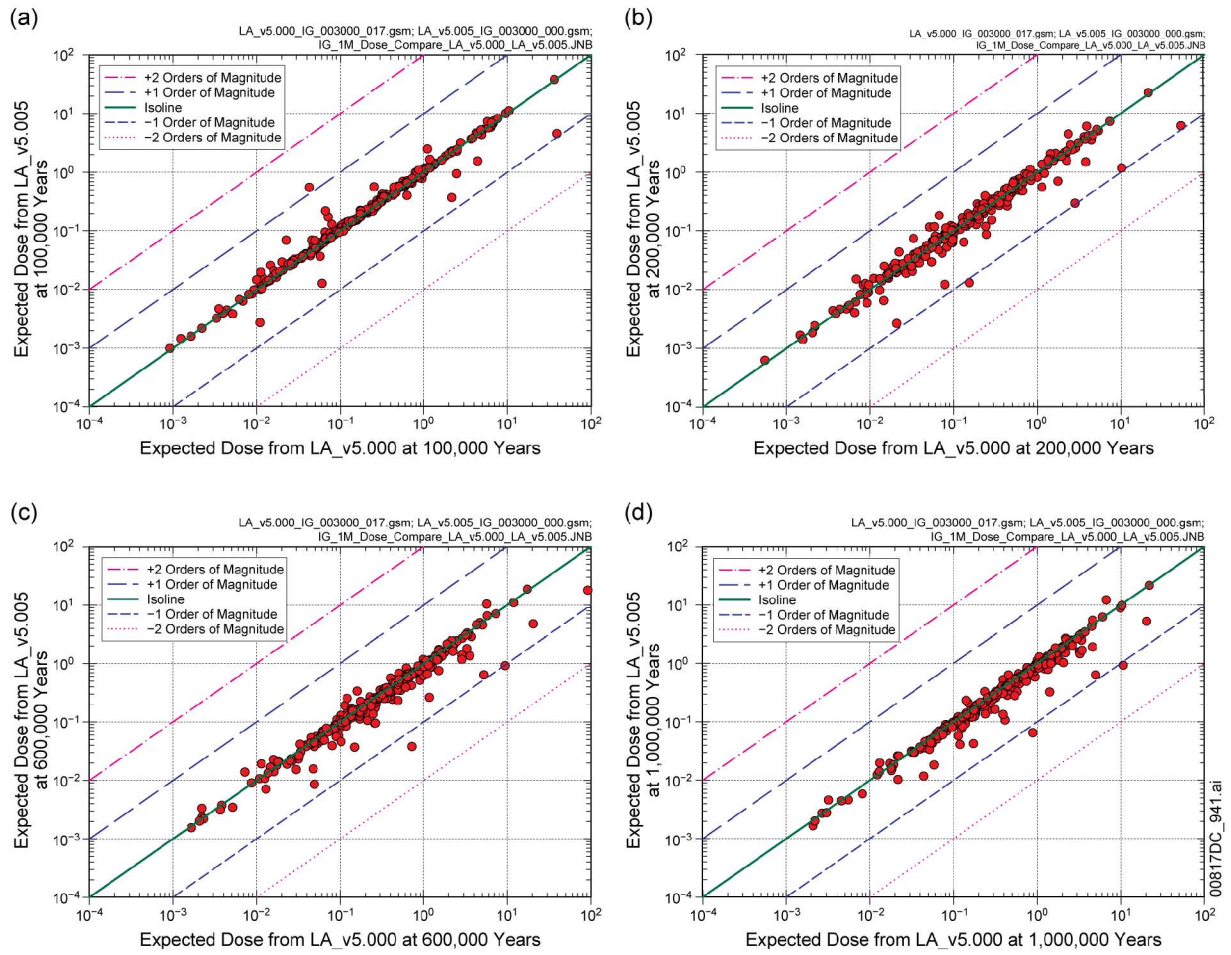

Source: Output DTNs: MO0710ADTSPAWO.000 [DIRS 183752]; and MO0709TSPAREGS.000 [DIRS 182976].

Figure 7.3.1-31[a]. Comparison of Expected Annual Dose for Individual Sample Elements in the Igneous Intrusion Modeling Case between TSPA-LA Model v5.000 and TSPA-LA Model v5.005 at (a) 100,000; (b) 200,000; (c) 600,000; and (d) 1,000,000 Years

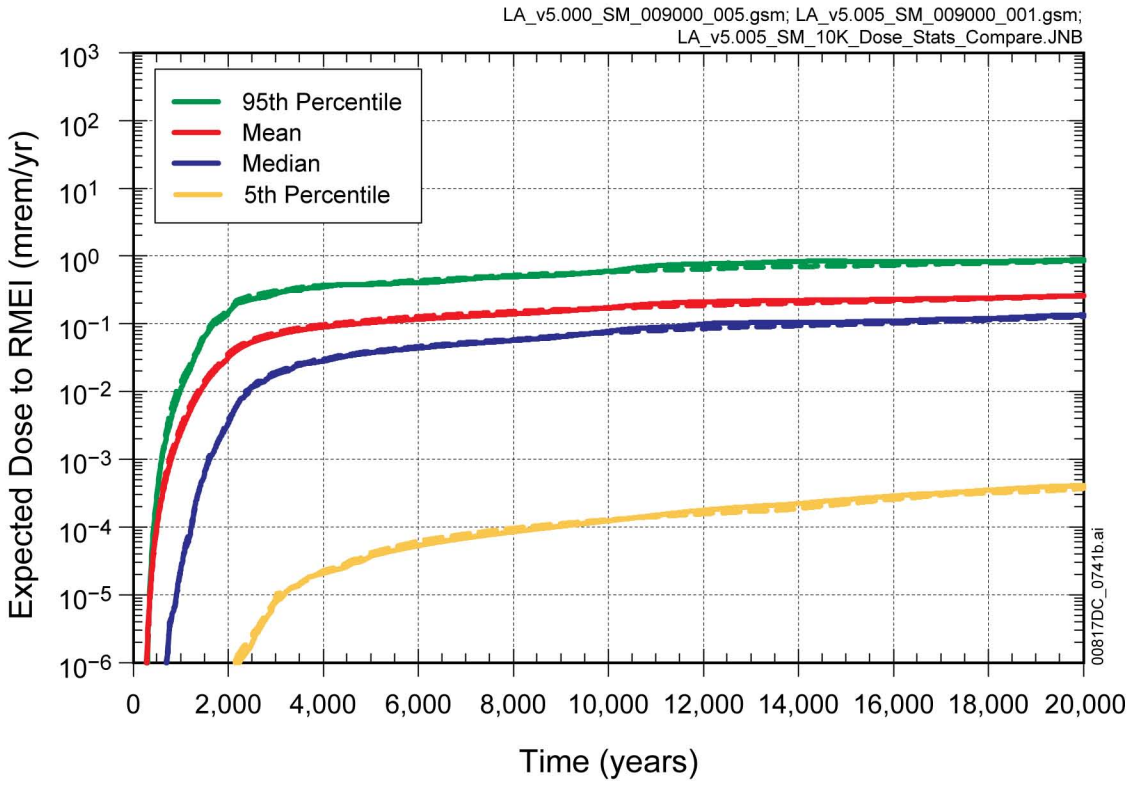

Source: Output DTNs: MO0710ADTSPAWO.000 [DIRS 183752]; and MO0709TSPAREGS.000 [DIRS 182976].

NOTE: Solid lines indicate TSPA-LA Model v5.000 and dashed lines indicate TSPA-LA Model v5.005.

Figure 7.3.1-32[a]. Comparison of Statistics for Expected Annual Dose over 20,000 Years in the Seismic Ground Motion Modeling Case between TSPA-LA Model v5.000 and TSPA-LA Model v5.005

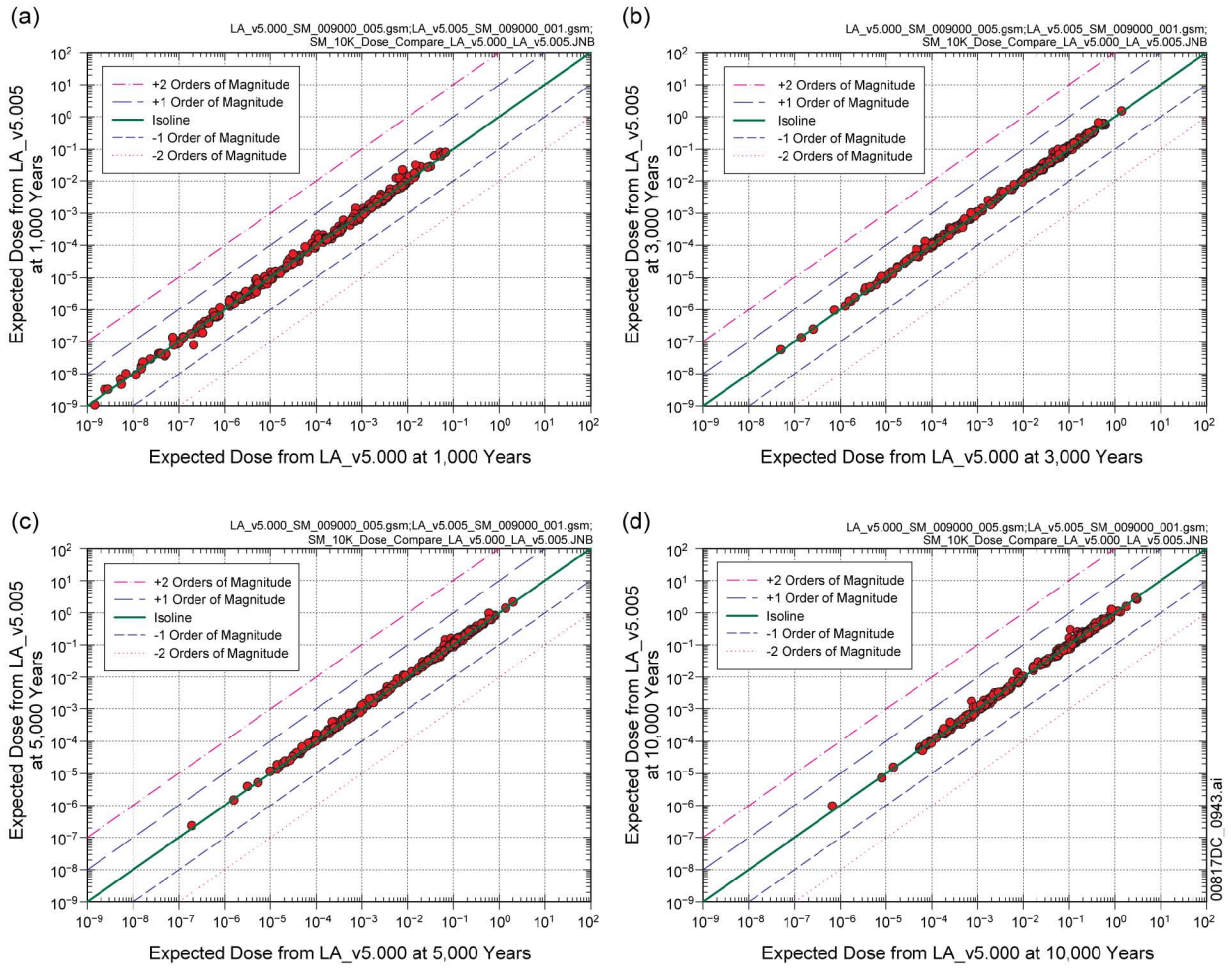

Source: Output DTNs: MO0710ADTSPAWO.000 [DIRS 183752]; and MO0709TSPAREGS.000 [DIRS 182976].

Figure 7.3.1-33[a]. Comparison of Expected Annual Dose for Individual Sample Elements in the Seismic Ground Motion Modeling Case between TSPA-LA Model v5.000 and TSPA-LA Model v5.005 at (a) 1,000; (b) 3,000; (c) 5,000; and (d) 10,000 Years

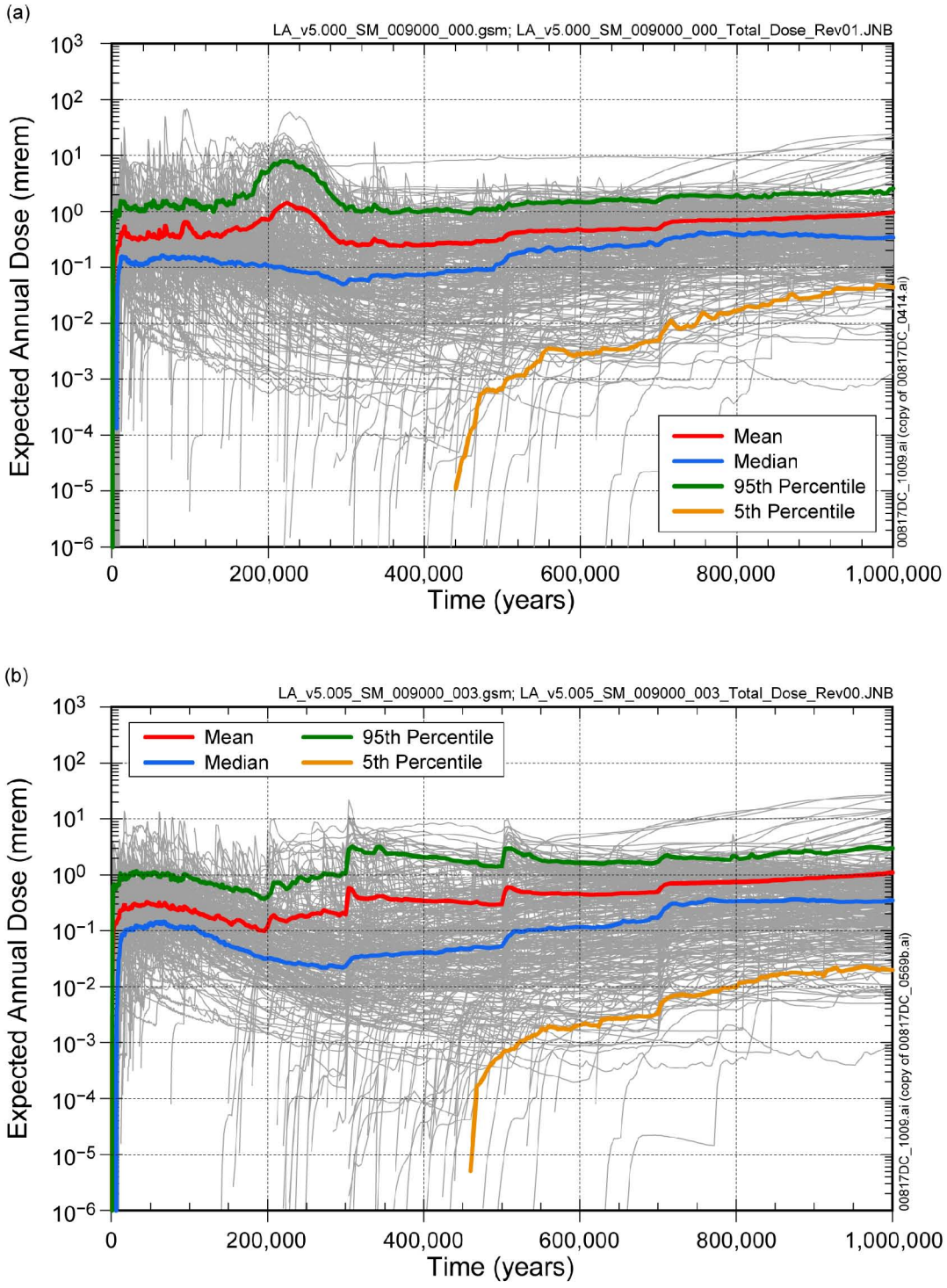

Source: Output DTNs: MO0709TSPAREGS.000 [DIRS 182976]; and MO0710ADTSPAWO.000 [DIRS 183752].

Figure 7.3.1-34[a]. Expected Annual Dose for 1,000,000 Years for the Seismic Ground Motion Modeling Case from (a) TSPA-LA Model v5.000 and (b) TSPA-LA Model v5.005

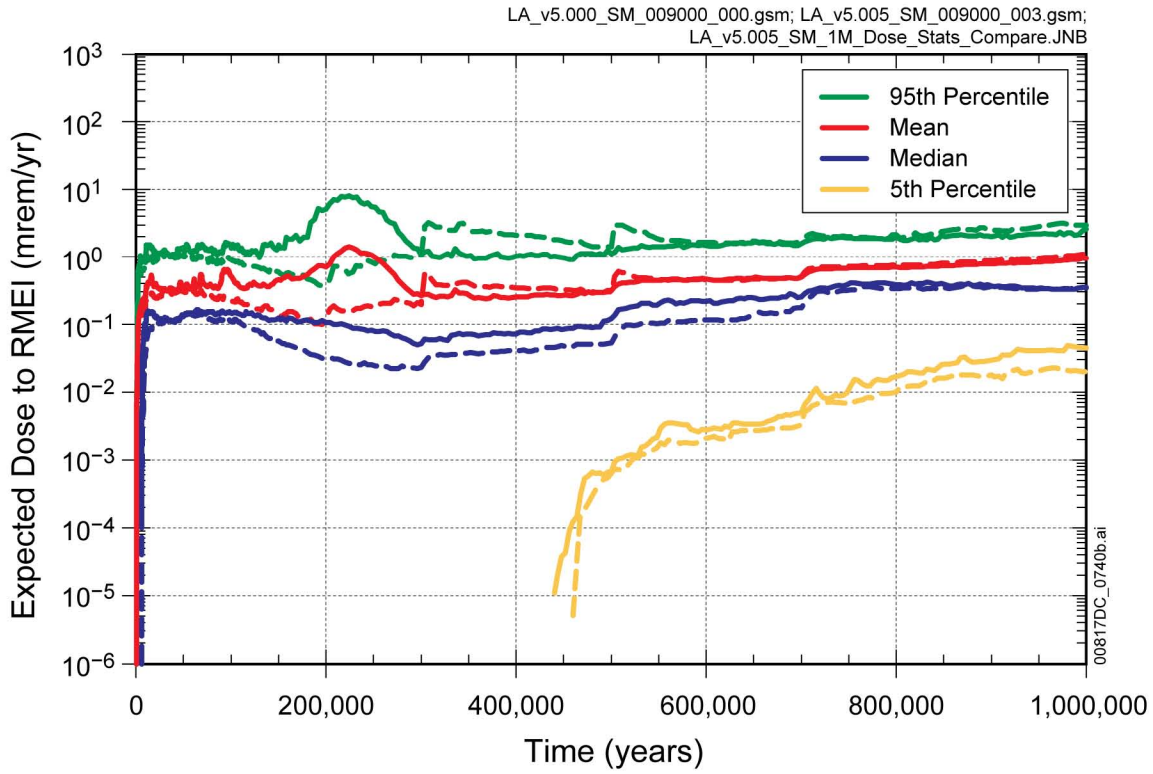

Source: Output DTNs: MO0710ADTSPAWO.000 [DIRS 183752]; and MO0709TSPAREGS.000 [DIRS 182976].

NOTE: Solid lines indicate TSPA-LA Model v5.000 and dashed lines indicate TSPA-LA Model v5.005.

Figure 7.3.1-35[a]. Comparison of Statistics for Expected Annual Dose over 1,000,000 Years in the Seismic Ground Motion Modeling Case between TSPA-LA Model v5.000 and TSPA-LA Model v5.005

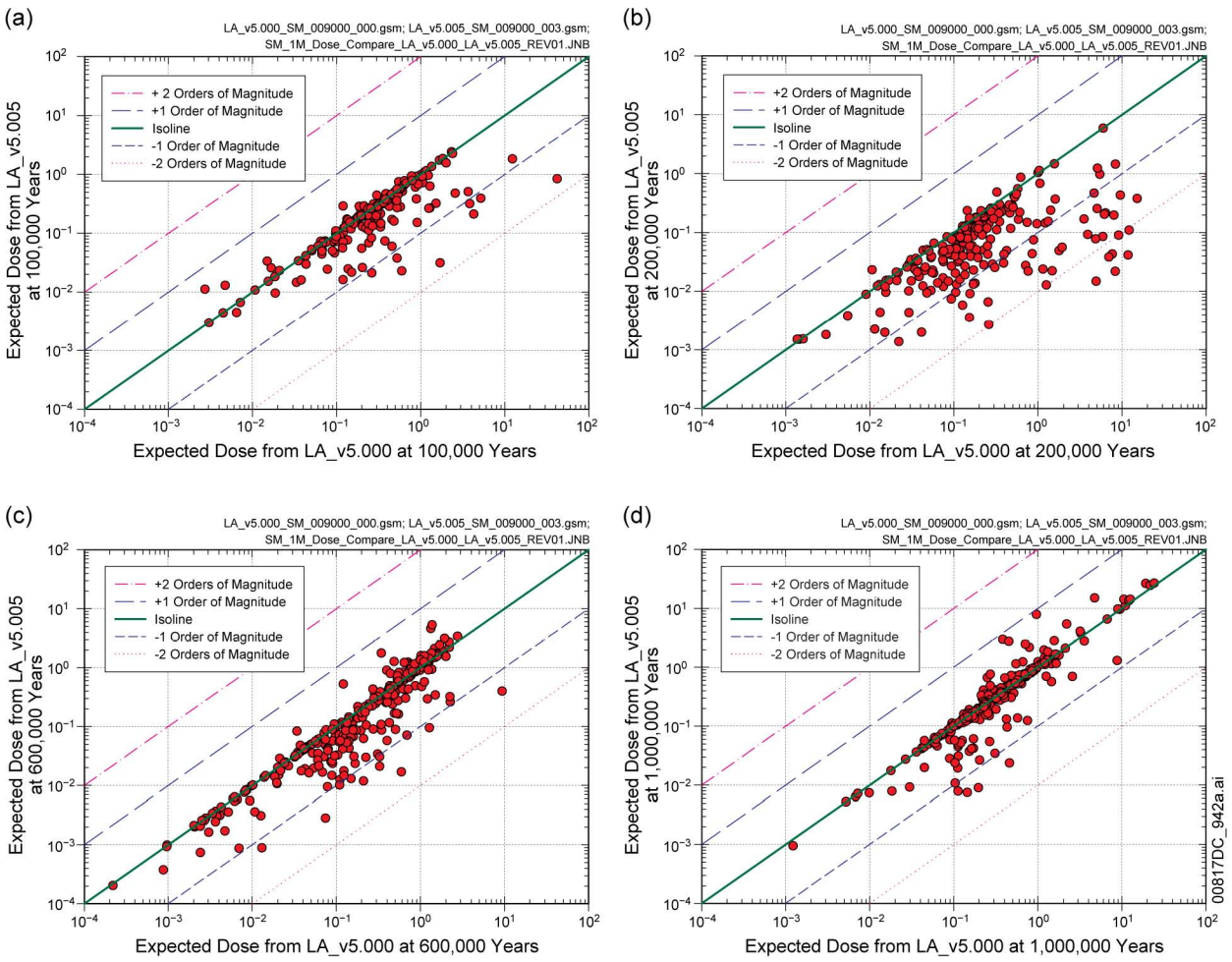

Source: Output DTNs: MO0710ADTSPAWO.000 [DIRS 183752]; and MO0709TSPAREGS.000 [DIRS 182976].

Figure 7.3.1-36[a]. Comparison of Expected Annual Dose for Individual Sample Elements in the Seismic Ground Motion Modeling Case between TSPA-LA Model v5.000 and TSPA-LA Model v5.005 at (a) 100,000; (b) 200,000; (c) 600,000; and (d) 1,000,000 Years

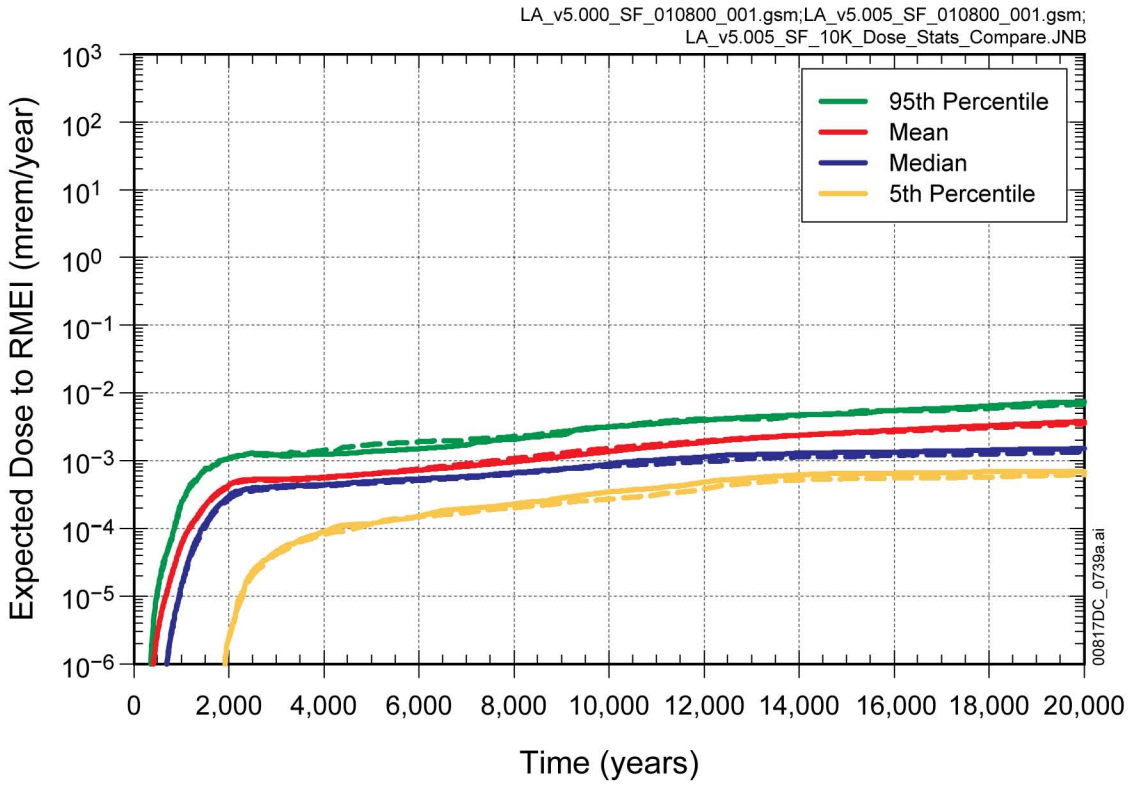

Source: Output DTNs: MO0710ADTSPAWO.000 [DIRS 183752]; and MO0709TSPAREGS.000 [DIRS 182976].

NOTE: Solid lines indicate TSPA-LA Model v5.000 and dashed lines indicate TSPA-LA Model v5.005.

Figure 7.3.1-37[a]. Comparison of Statistics for Expected Annual Dose over 20,000 Years in the Seismic Fault Displacement Modeling Case between TSPA-LA Model v5.000 and TSPA-LA Model v5.005

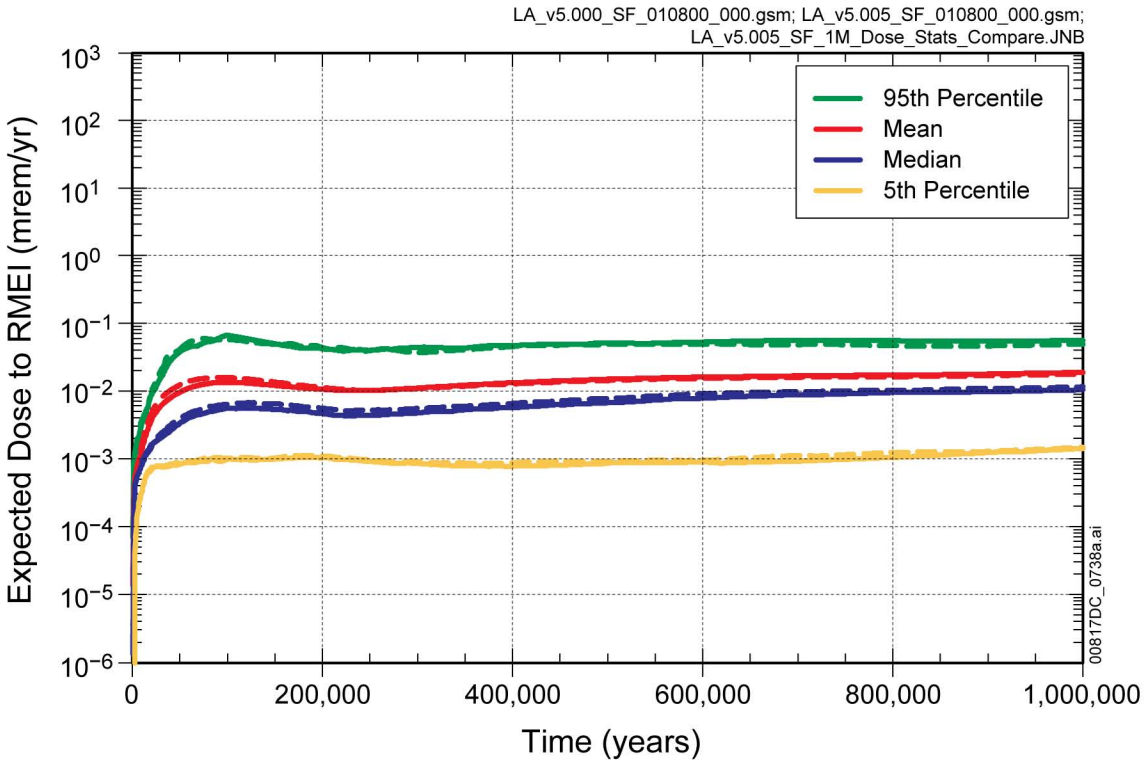

Source: Output DTNs: MO0710ADTSPAWO.000 [DIRS 183752]; and MO0709TSPAREGS.000 [DIRS 182976].

NOTE: Solid lines indicate TSPA-LA Model v5.000 and dashed lines indicate TSPA-LA Model v5.005.

Figure 7.3.1-38[a]. Comparison of Statistics for Expected Annual Dose over 1,000,000 Years in the Seismic Fault Displacement Modeling Case between TSPA-LA Model v5.000 and TSPA-LA Model v5.005

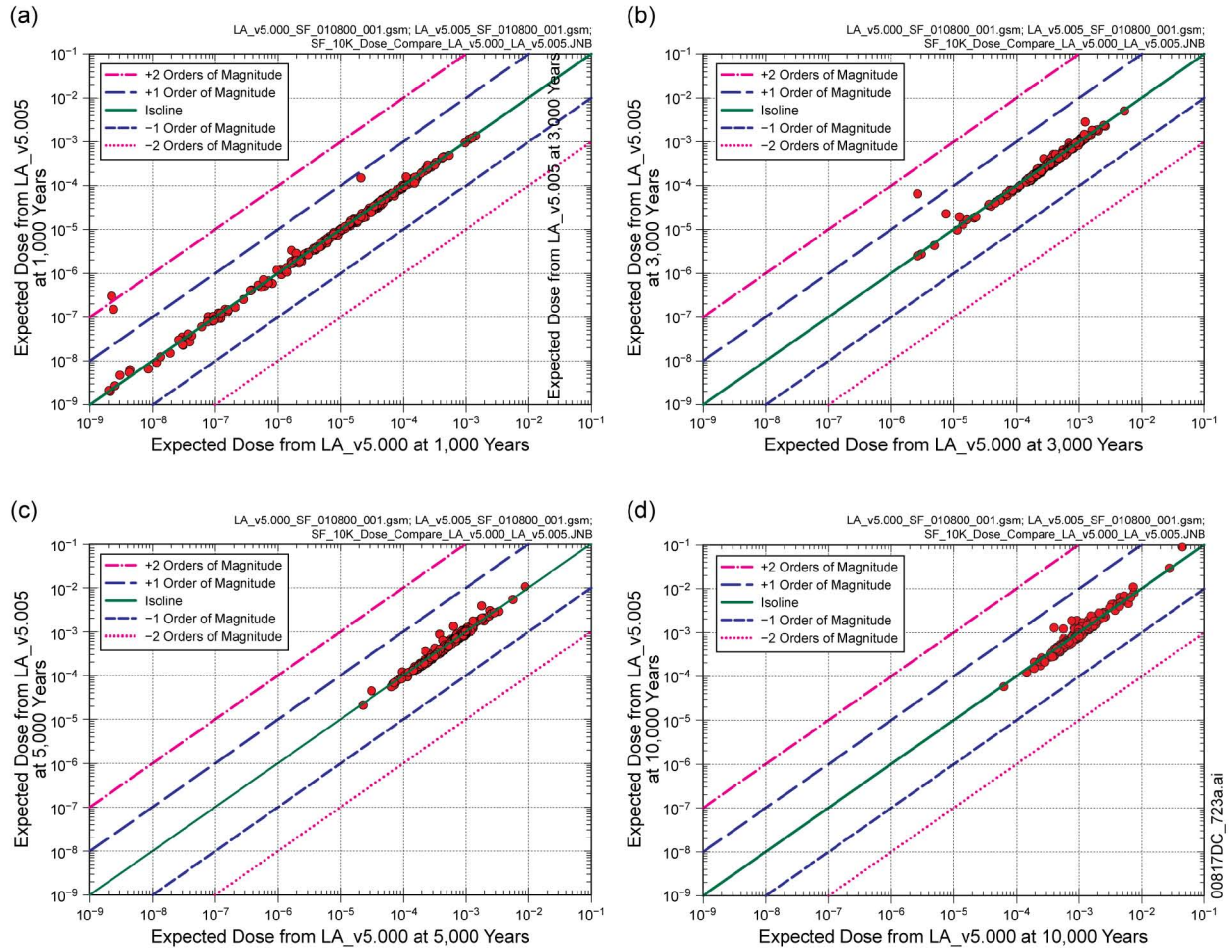

Source: Output DTNs: MO0710ADTSPAWO.000 [DIRS 183752]; and MO0709TSPAREGS.000 [DIRS 182976].

Figure 7.3.1-39[a]. Comparison of Expected Annual Dose for Individual Sample Elements in the Seismic Fault Displacement Modeling Case between TSPA-LA Model v5.000 and TSPA-LA Model v5.005 at (a) 1,000; (b) 3,000; (c) 5,000; and (d) 10,000 Years

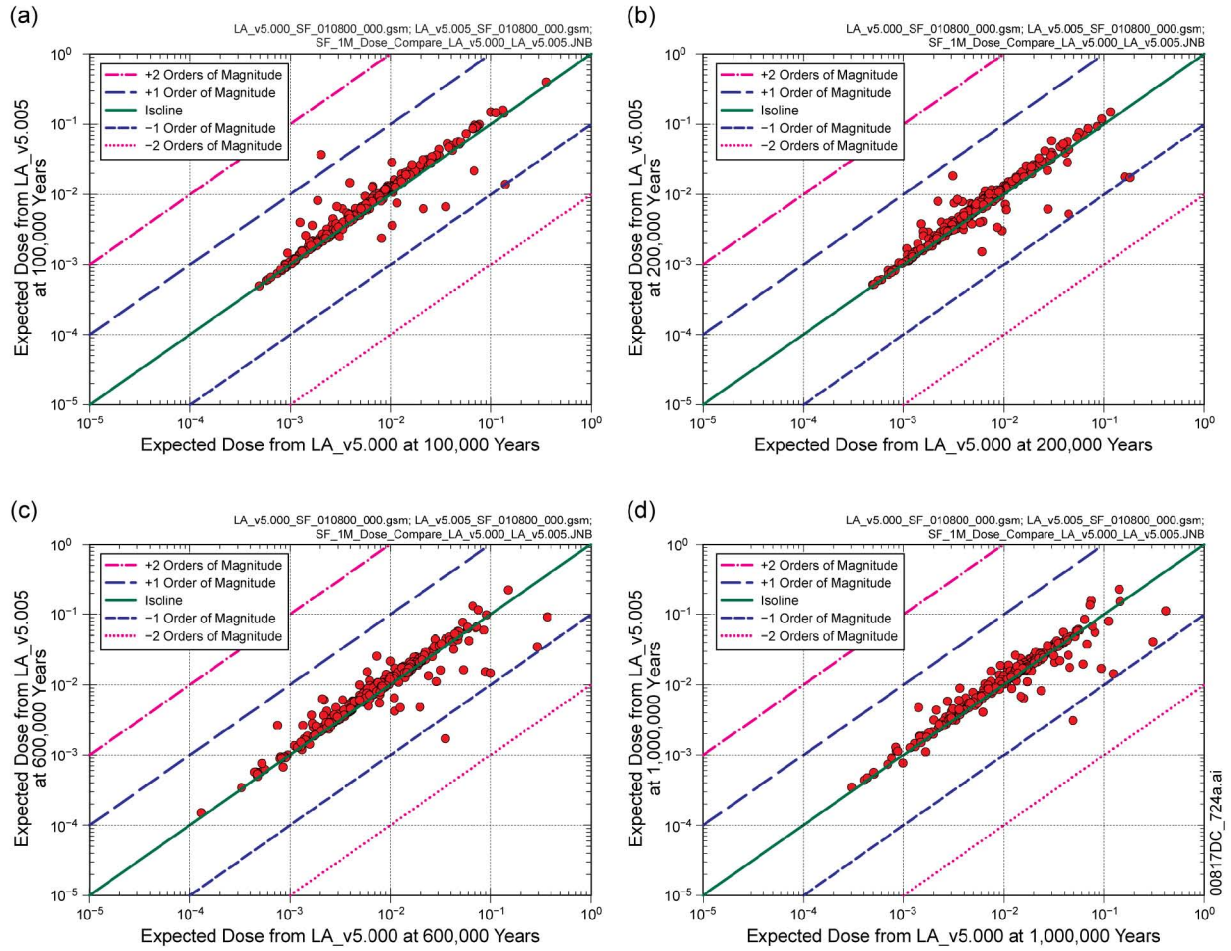

Source: Output DTNs: MO0710ADTSPAWO.000 [DIRS 183752]; and MO0709TSPAREGS.000 [DIRS 182976].

Figure 7.3.1-40[a]. Comparison of Expected Annual Dose for Individual Sample Elements in the Seismic Fault Displacement Modeling Case between TSPA-LA Model v5.000 and TSPA-LA Model v5.005 at (a) 100,000; (b) 200,000; (c) 600,000; and (d) 1,000,000 Years

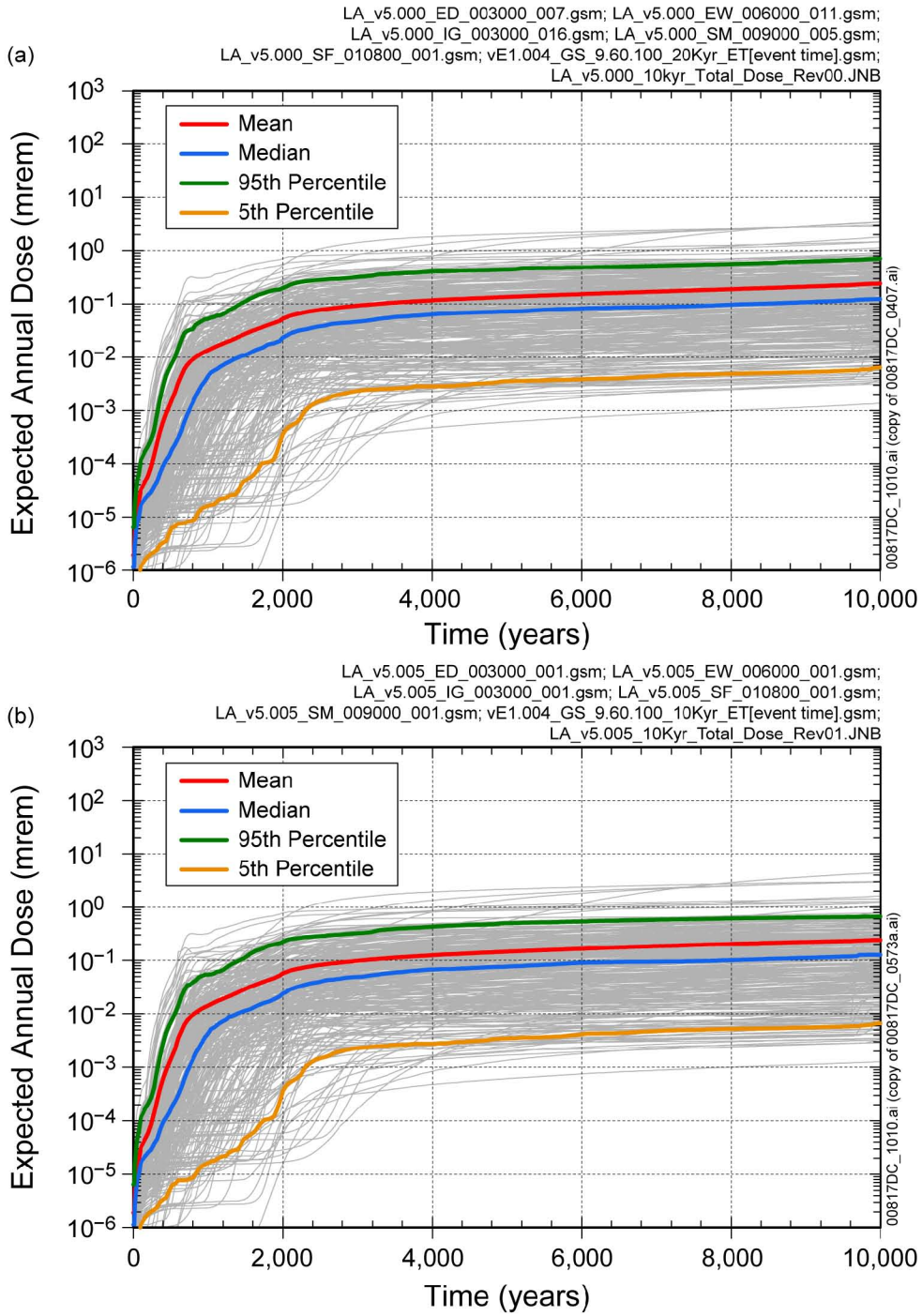

Source: Output DTNs: MO0709TSPAREGS.000 [DIRS 182976]; and MO0710ADTSPAWO.000 [DIRS 183752].

Figure 7.3.1-41[a]. Total Expected Annual Dose for 10,000 Years from (a) TSPA-LA Model v5.000 and (b) TSPA-LA Model v5.005

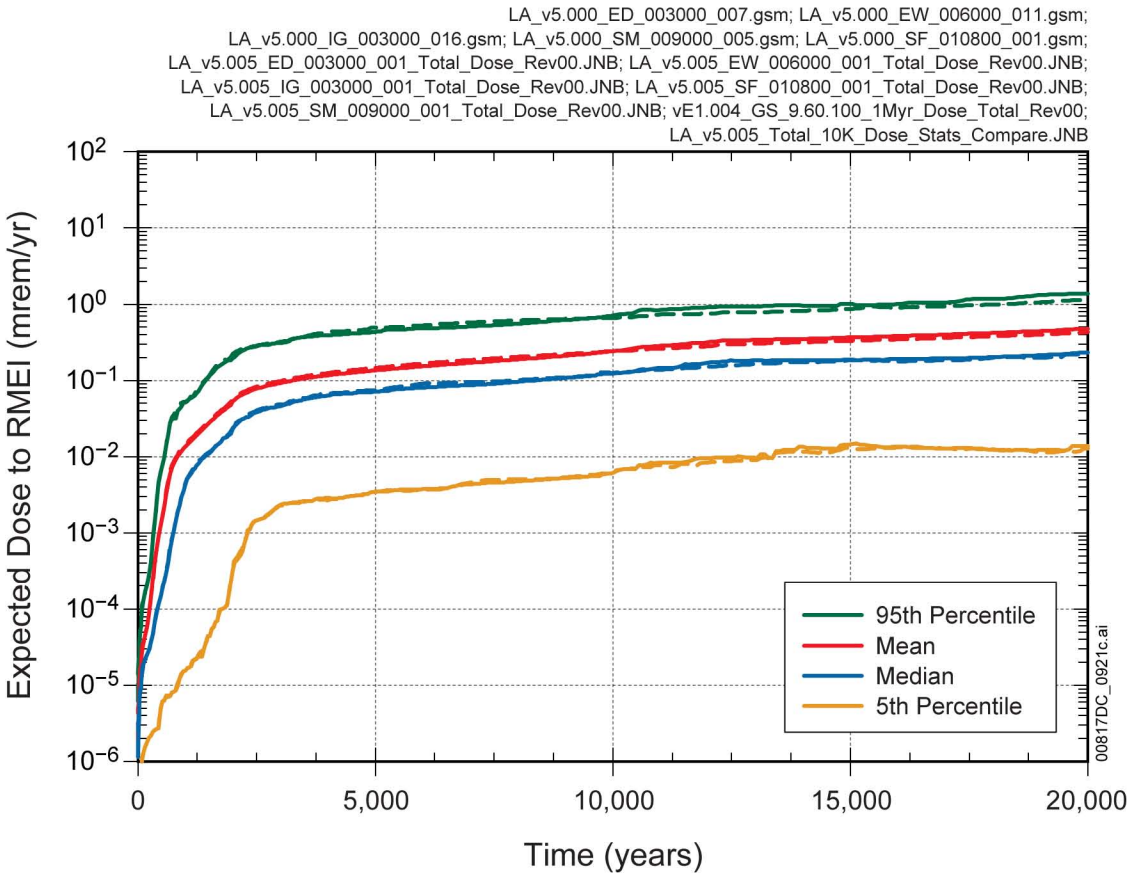

Source: Output DTNs: MO0710ADTSPAWO.000 [DIRS 183752]; and MO0709TSPAREGS.000 [DIRS 182976].

NOTE: Solid lines indicate TSPA-LA Model v5.000 and dashed lines indicate TSPA-LA Model v5.005.

Figure 7.3.1-42[a]. Comparison of Statistics for Total Expected Annual Dose over 20,000 Years between TSPA-LA Model v5.000 and TSPA-LA Model v5.005

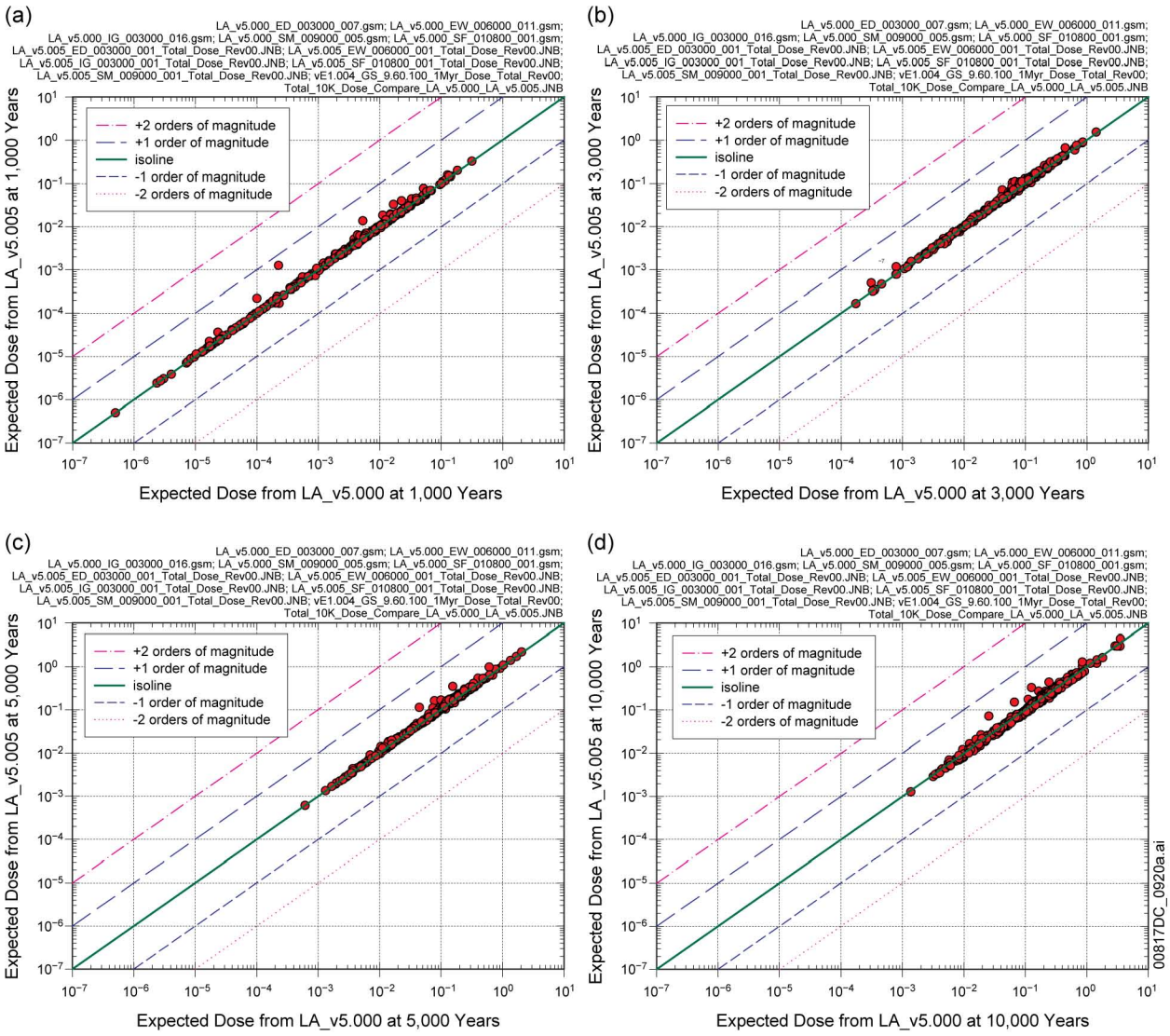

Source: Output DTNs: MO0710ADTSPAWO.000 [DIRS 183752]; and MO0709TSPAREGS.000 [DIRS 182976].

Figure 7.3.1-43[a]. Comparison of Total Expected Annual Dose for Individual Sample Elements between TSPA-LA Model v5.000 and TSPA-LA Model v5.005 at (a) 1,000; (b) 3,000; (c) 5,000; and (d) 10,000 Years

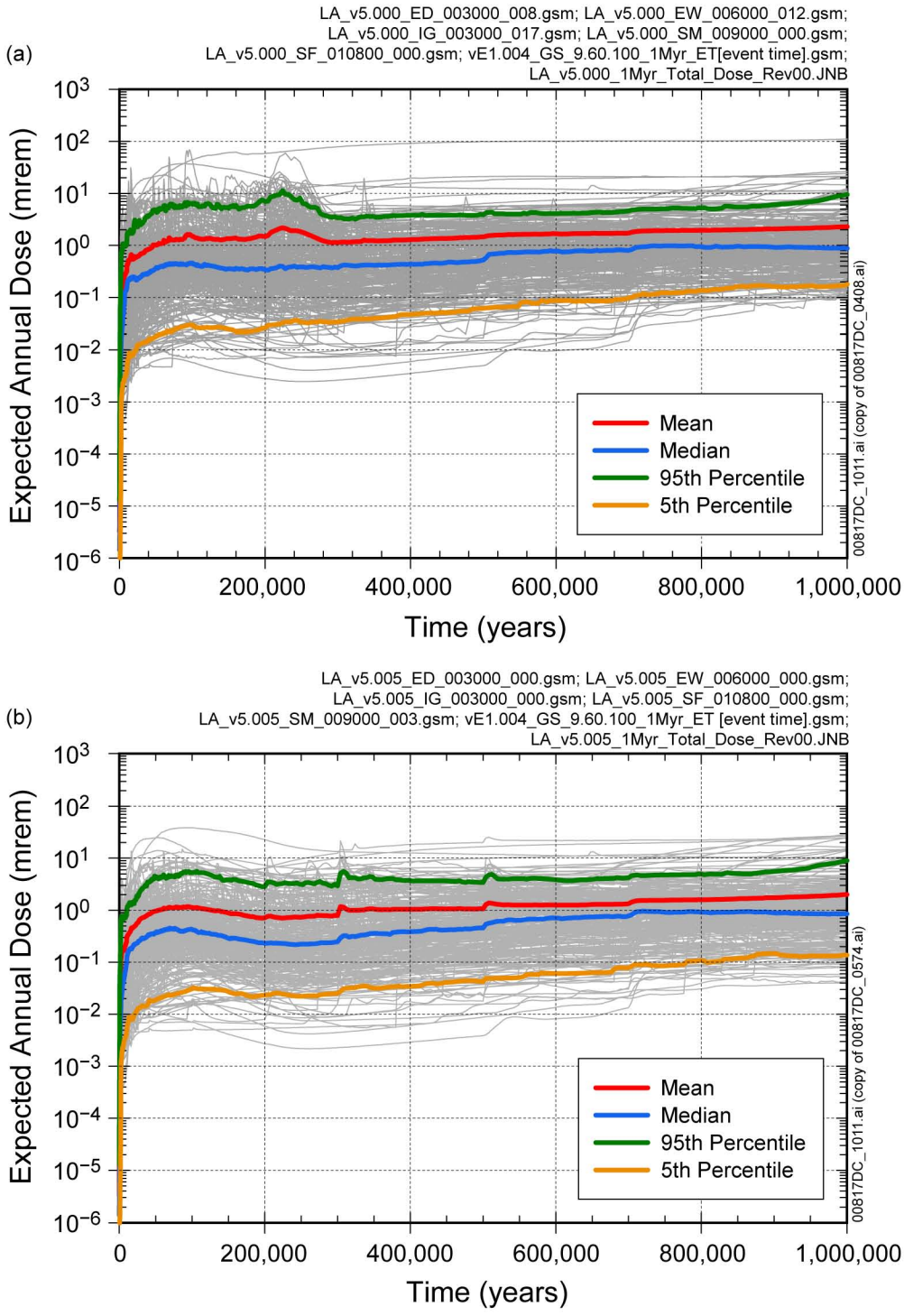

Source: Output DTNs: MO0709TSPAREGS.000 [DIRS 182976]; and MO0710ADTSPAWO.000 [DIRS 183752].

Figure 7.3.1-44[a]. Total Expected Annual Dose for 1,000,000 Years from (a) TSPA-LA Model v5.000 and (b) TSPA-LA Model v5.005

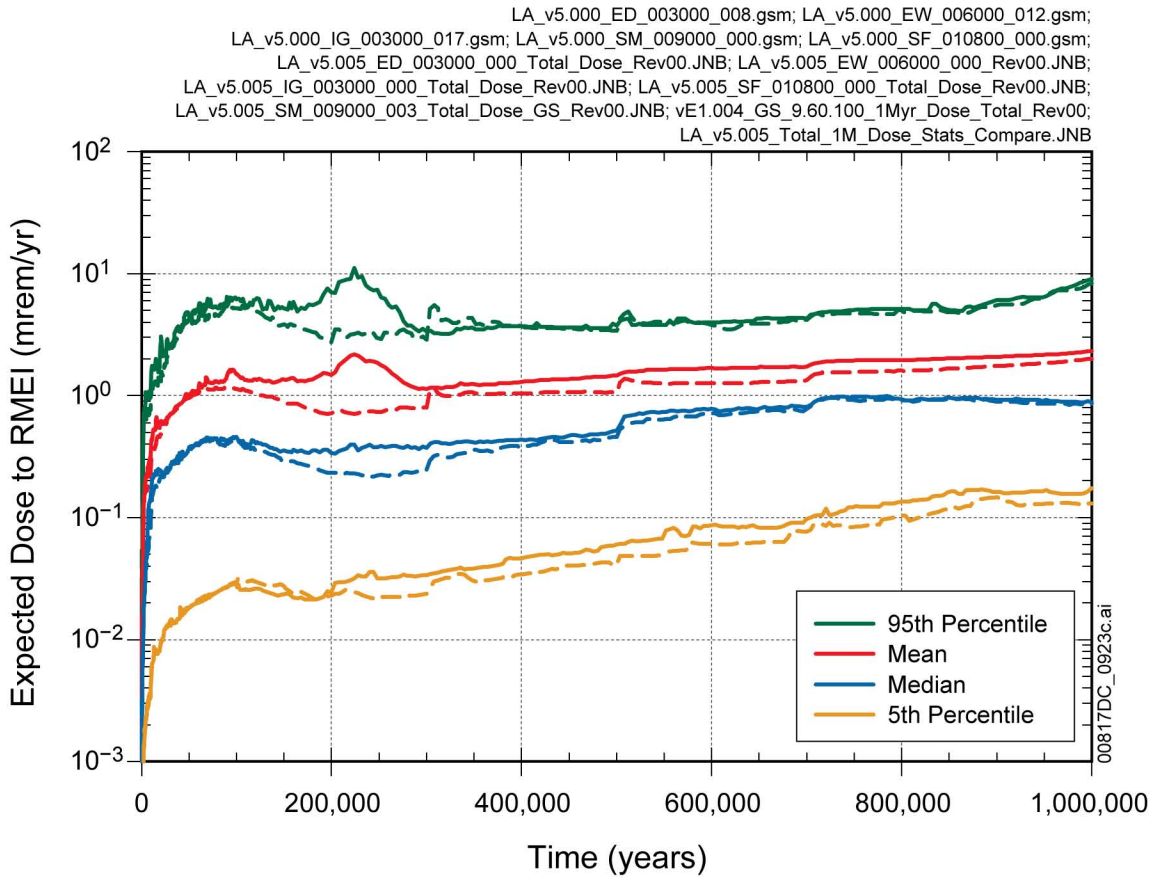

Source: Output DTNs: MO0710ADTSPAWO.000 [DIRS 183752]; and MO0709TSPAREGS.000 [DIRS 182976].

NOTE: Solid lines indicate TSPA-LA Model v5.000 and dashed lines indicate TSPA-LA Model v5.005.

Figure 7.3.1-45[a]. Comparison of Statistics for Total Expected Annual Dose over 1,000,000 Years between TSPA-LA Model v5.000 and TSPA-LA Model v5.005

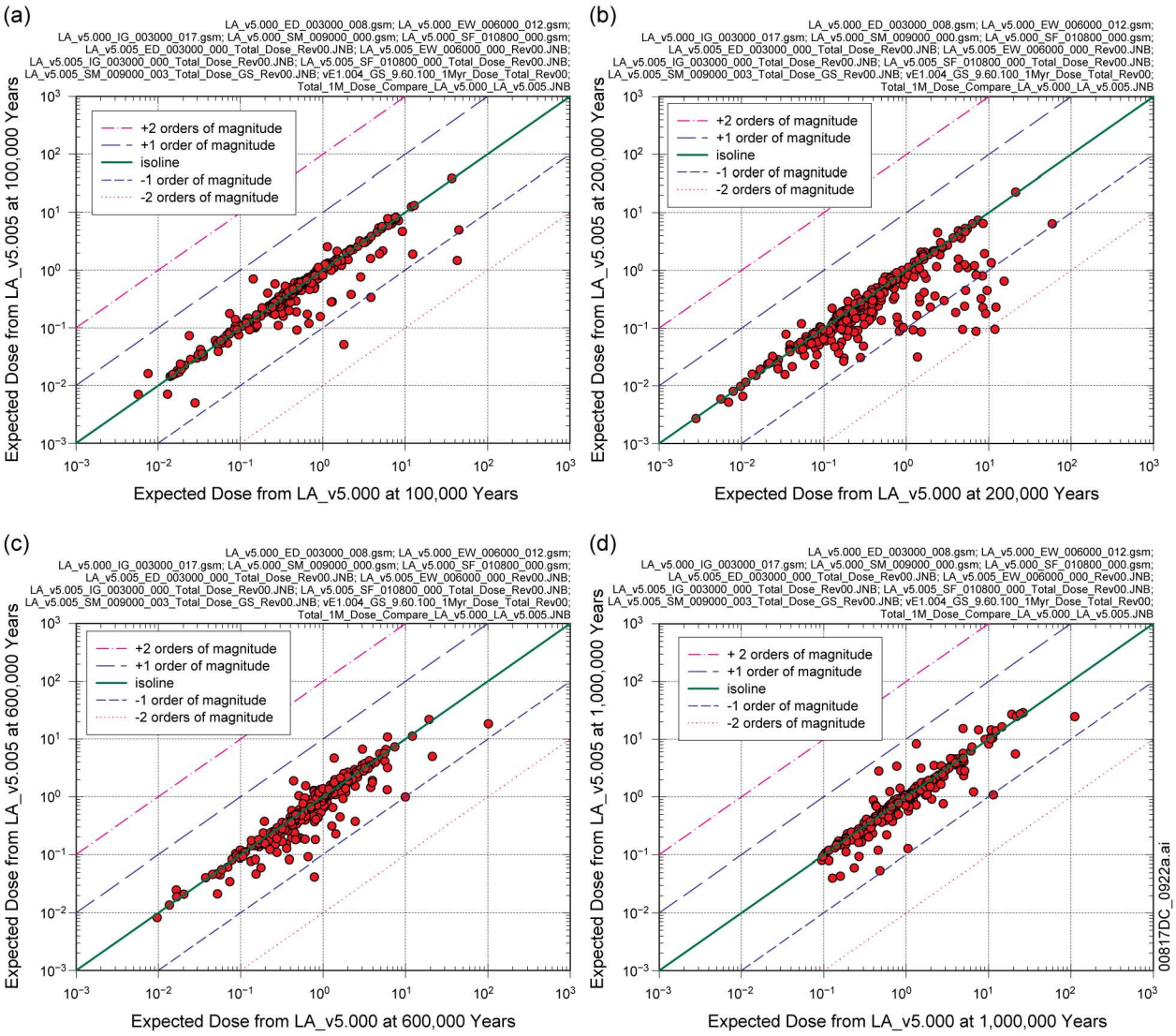

Source: Output DTNs: MO0710ADTSPAWO.000 [DIRS 183752]; and MO0709TSPAREGS.000 [DIRS 182976].

Figure 7.3.1-46[a]. Comparison of Total Expected Annual Dose for Individual Sample Elements between TSPA-LA Model v5.000 and TSPA-LA Model v5.005 at (a) 100,000; (b) 200,000; (c) 600,000; and (d) 1,000,000 Years

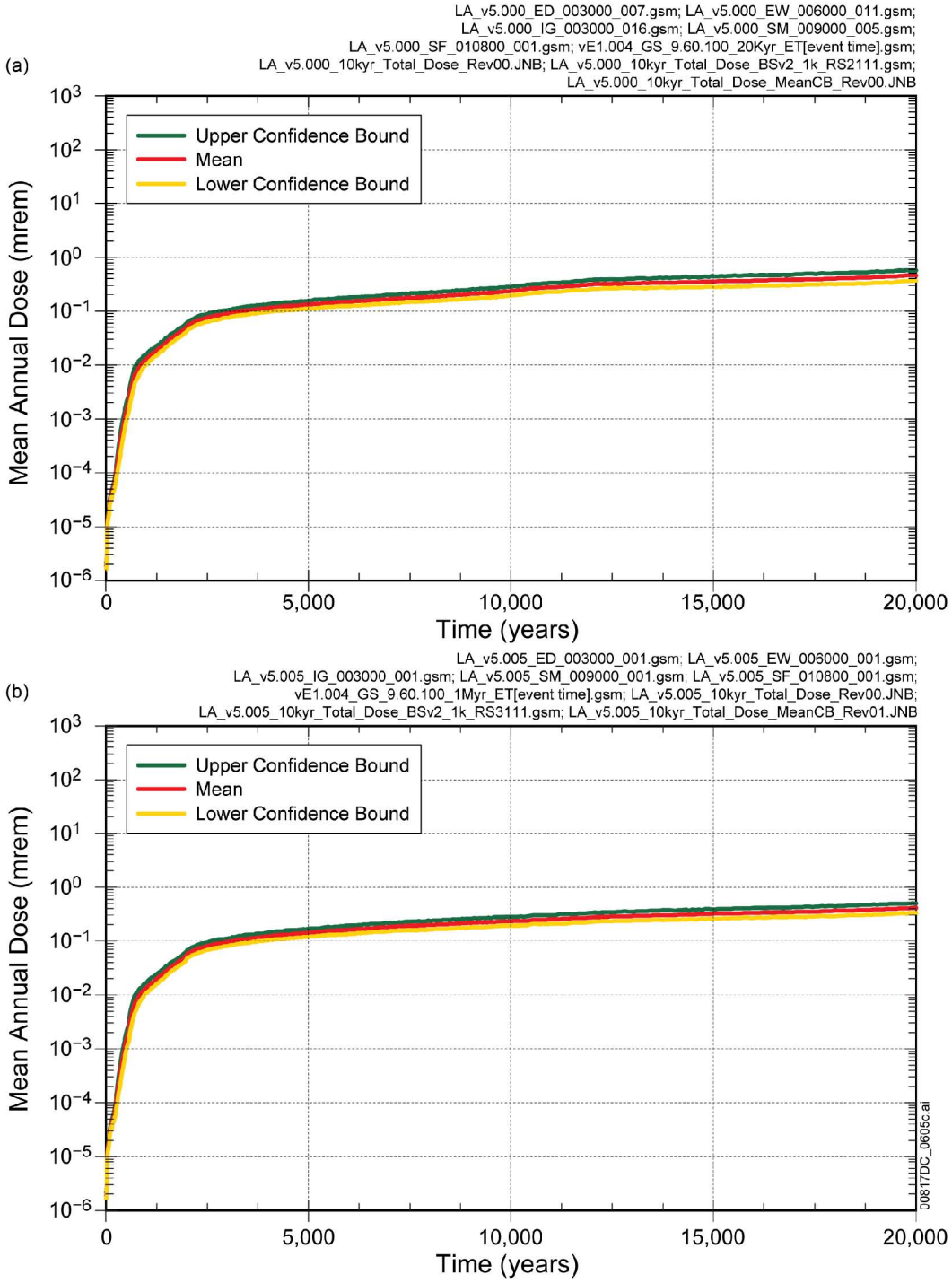

Source: Output DTN: MO0801TSPAADSA.000 [DIRS 185078].

Figure 7.3.1-47[a]. Confidence Interval for Total Mean Annual Dose for 20,000 Years for (a) TSPA-LA Model v5.000 and (b) TSPA-LA Model v5.005 Computed with the Bootstrap Technique

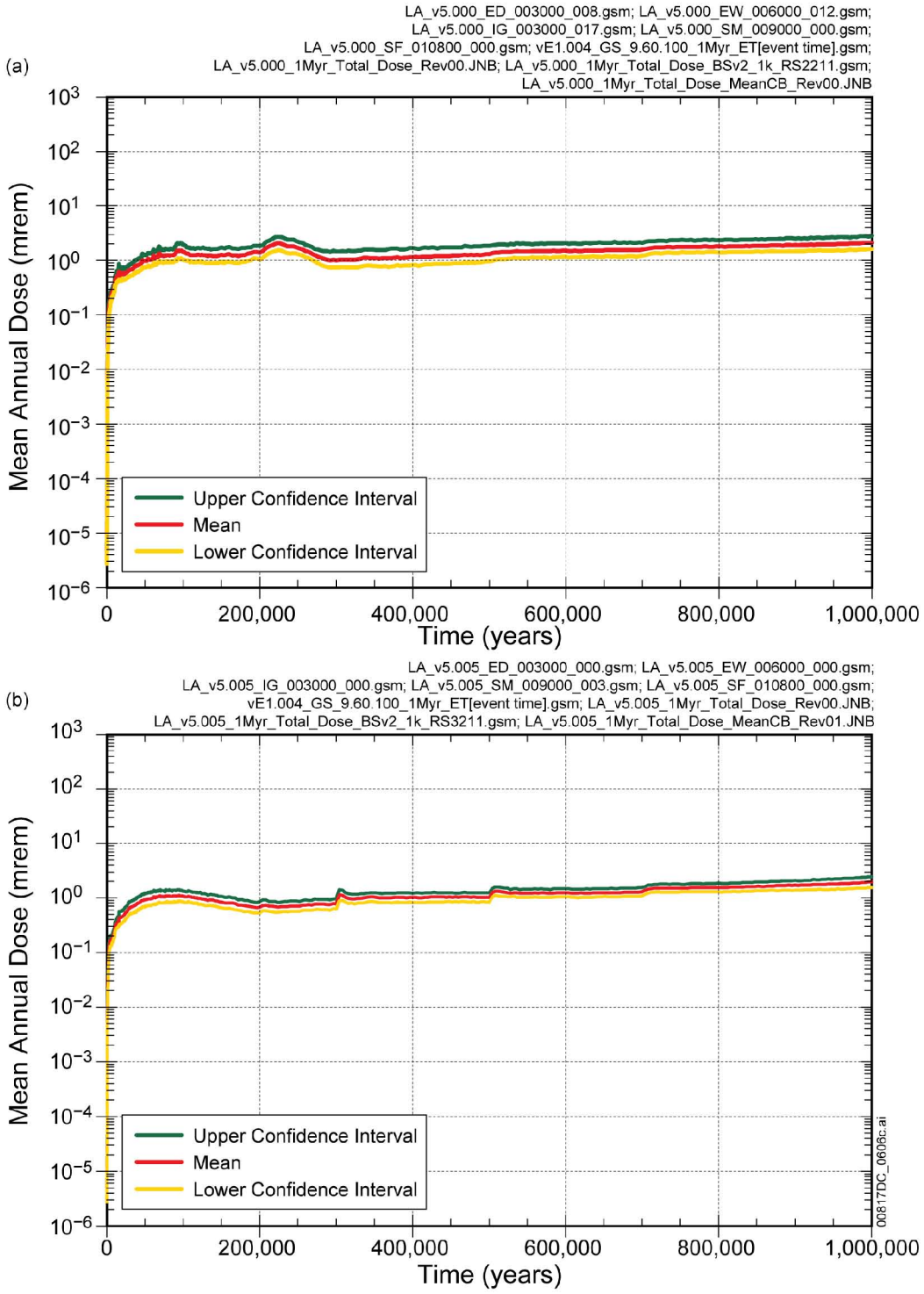

Source: Output DTN: MO0801TSPAADSA.000 [DIRS 185078].

Figure 7.3.1-48[a]. Confidence Interval for Total Mean Annual Dose for 1,000,000 Years for (a) TSPA-LA Model v5.000 and (b) TSPA-LA Model v5.005 Computed with the Bootstrap Technique

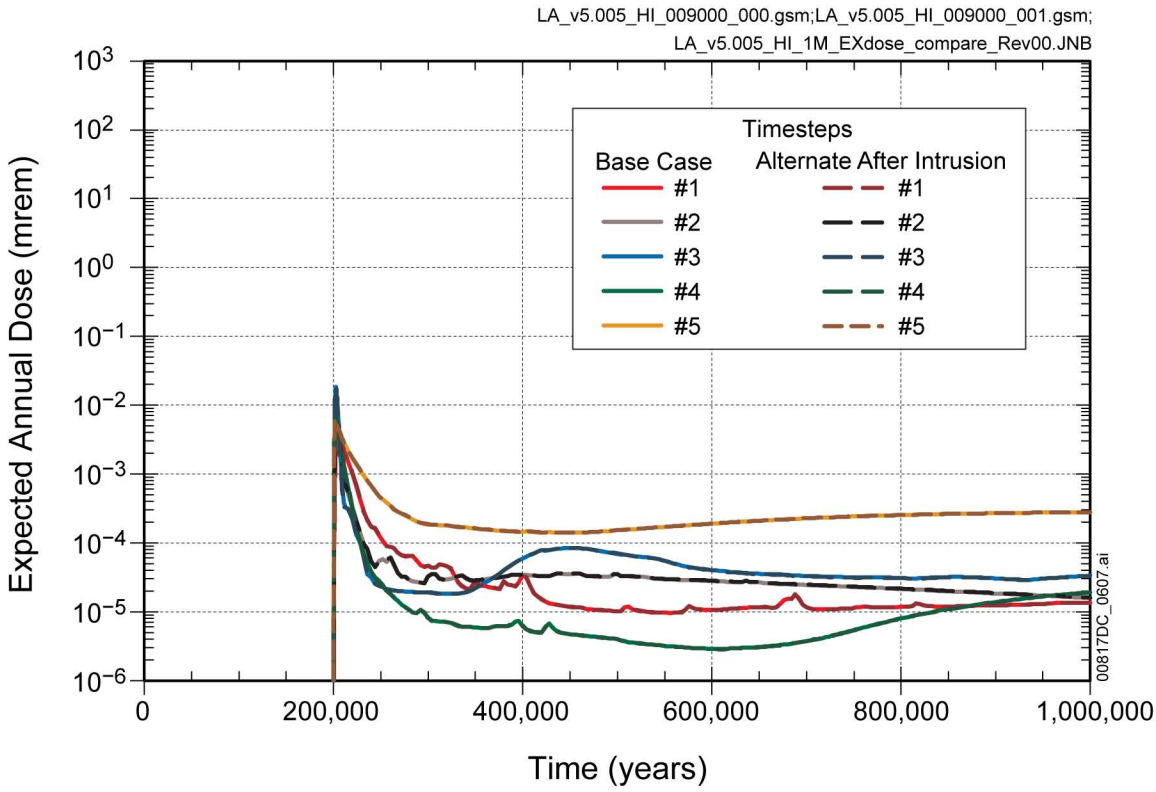

Source: Output DTNs: MO0710ADTSPAWO.000, File: v5.005_HI_009000_000 [DIRS 183752], for Base Case; and MO0801TSPAADSA.000, File: v5.005_HI_009000_001 [DIRS 185078], for Alternates.

Figure 7.3.3-10[a]. Expected Annual Dose from a Human Intrusion at 200,000 Years for Two Timestep Schemes

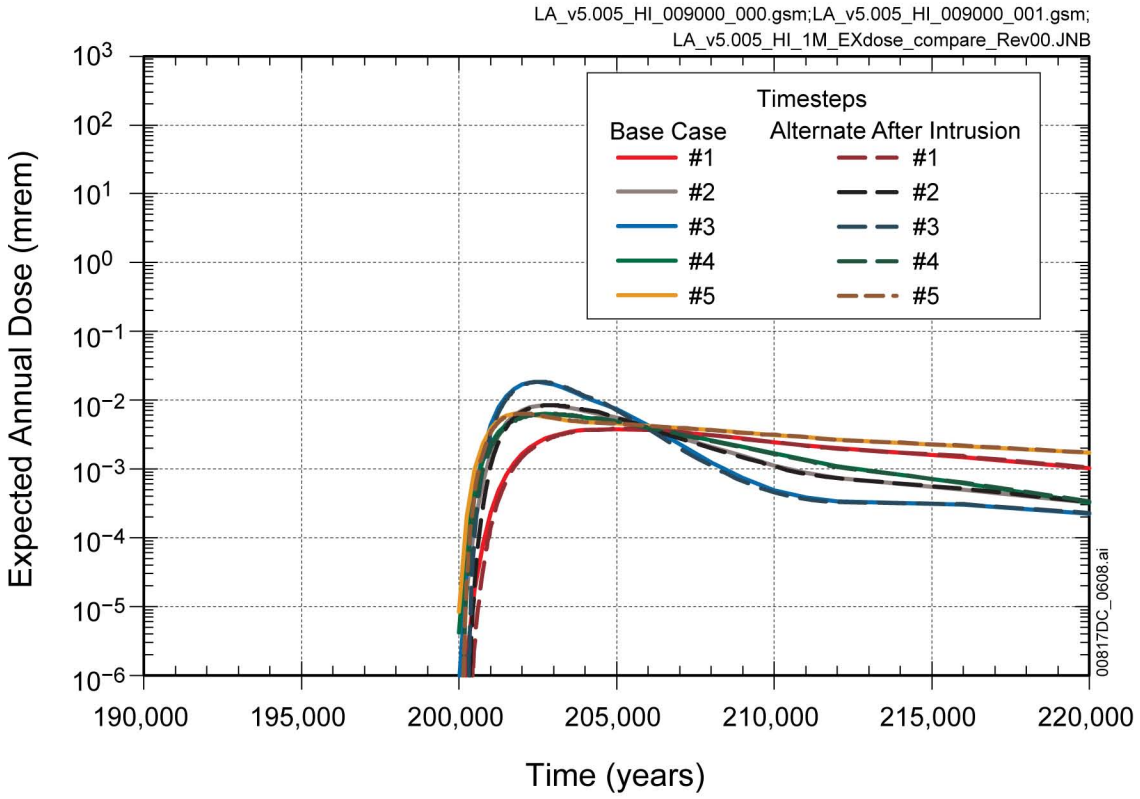

Source: Output DTNs: MO0710ADTSPAWO.000, File: v5.005_HI_009000_000 [DIRS 183752], for Base Case; and MO0801TSPAADSA.000, File: v5.005_HI_009000_001 [DIRS 185078], for Alternates.

Figure 7.3.3-11[a]. Detail of Expected Annual Dose from a Human Intrusion at 200,000 Years for Two Timestep Schemes

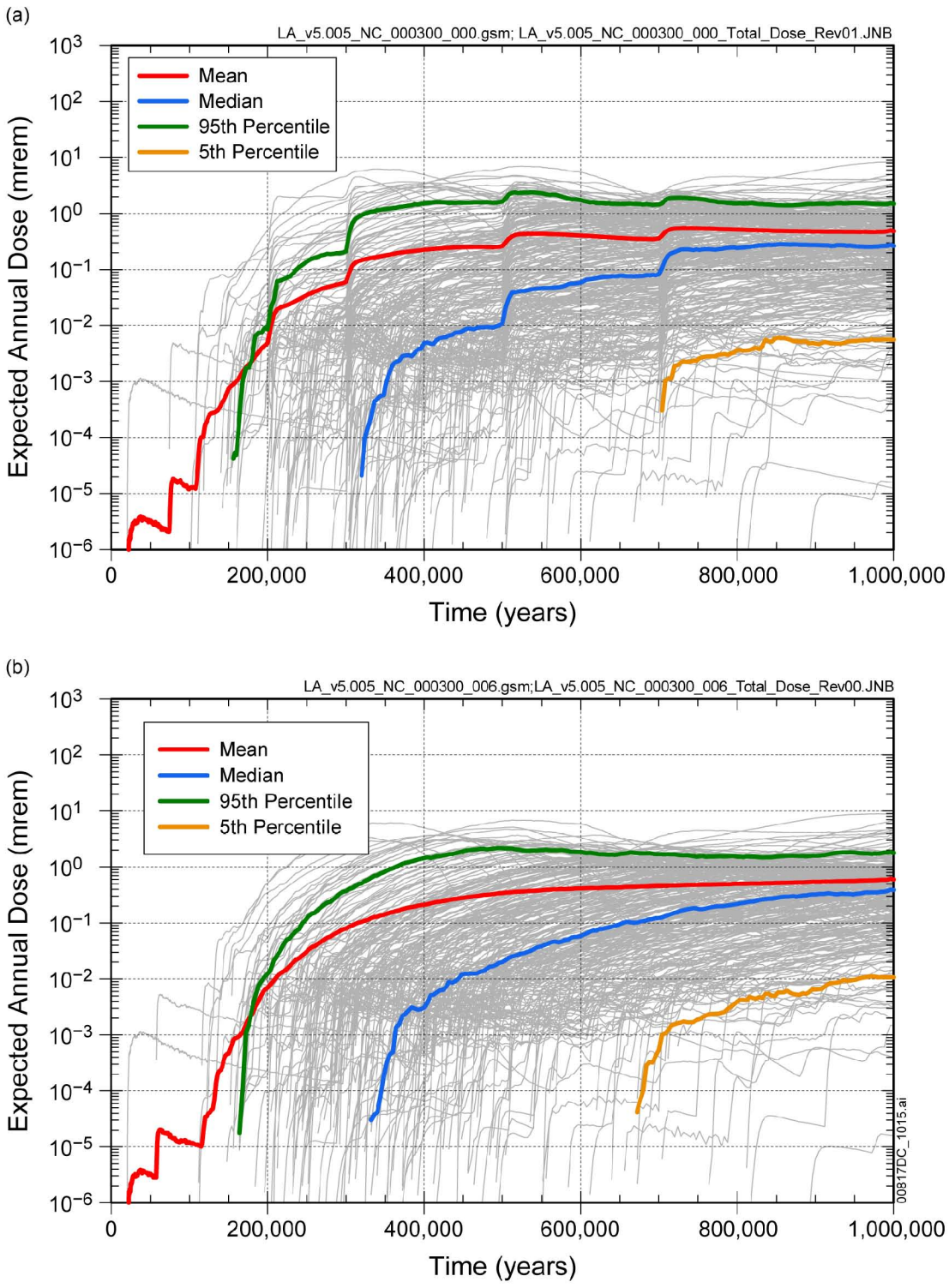

Source: Output DTNs: MO0710ADTSPAWO.000 [DIRS 183752]; and MO0801TSPAWPDS.000 [DIRS 185077].

Figure 7.3.3-12[a]. Expected Annual Dose for 1,000,000 Years for the Nominal Modeling Case from (a) TSPA-LA Model v5.005 and (b) Alternative Timestep Scheme

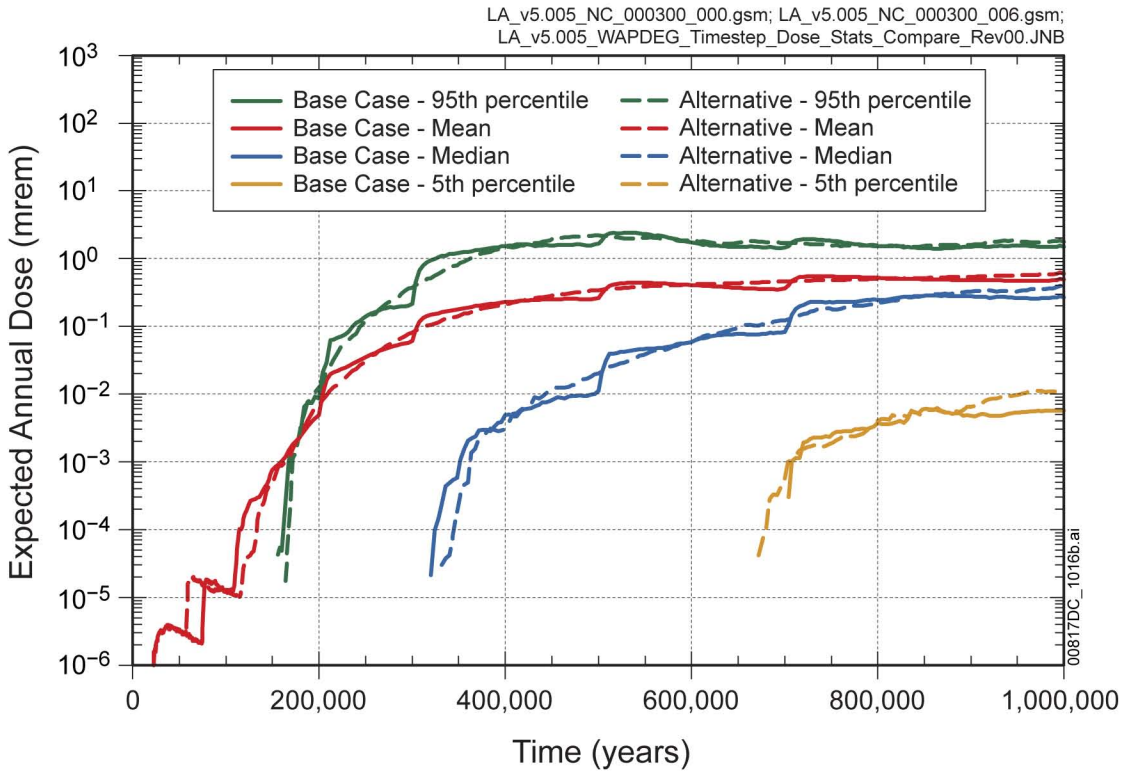

Source: Output DTNs: MO0801TSPAWPDS.000 [DIRS 185077].

Figure 7.3.3-13[a]. Expected Annual Dose Statistics for 1,000,000 Years for the Nominal Modeling Case Using Two Timestep Schemes

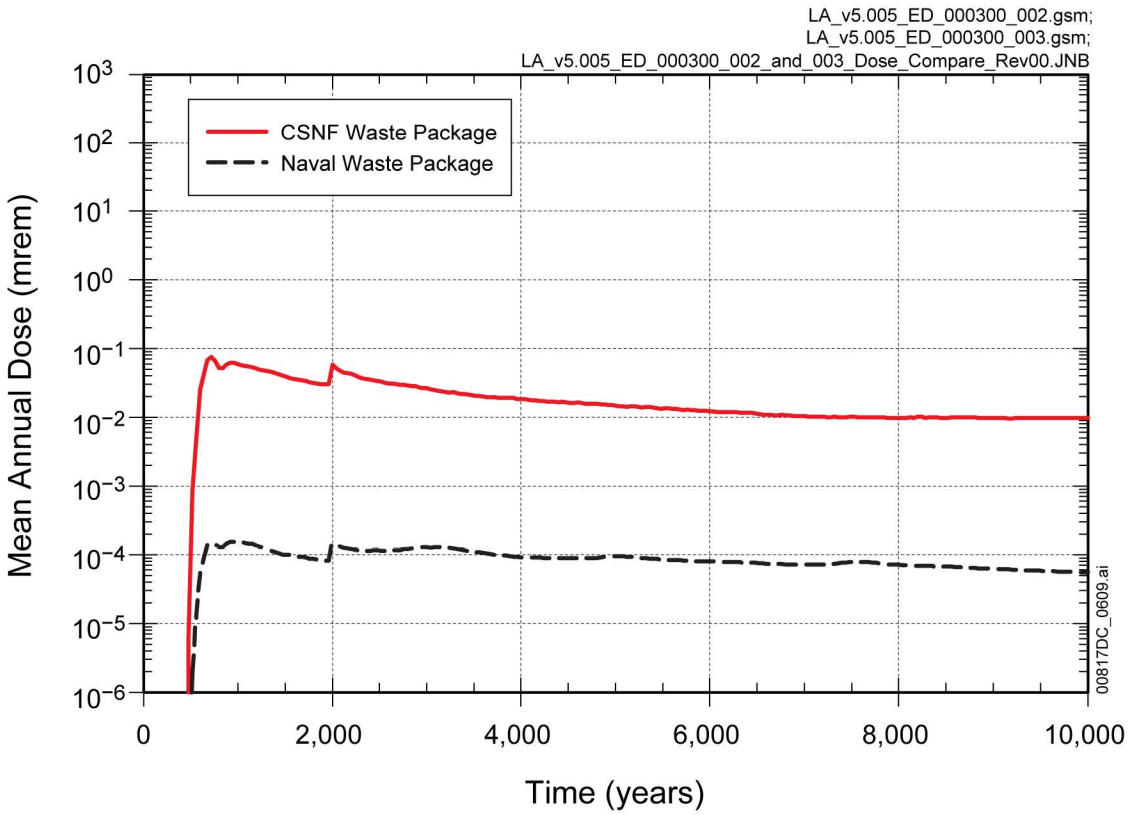

Source: Output DTN: MO0801TSPANSNF.000 [DIRS 184619].

Figure 7.5-4[a]. Comparison of Mean Annual Dose for a Single CSNF WP and a Single Waste Package with a Naval Source Term for the Drip Shield Early Failure Modeling Case

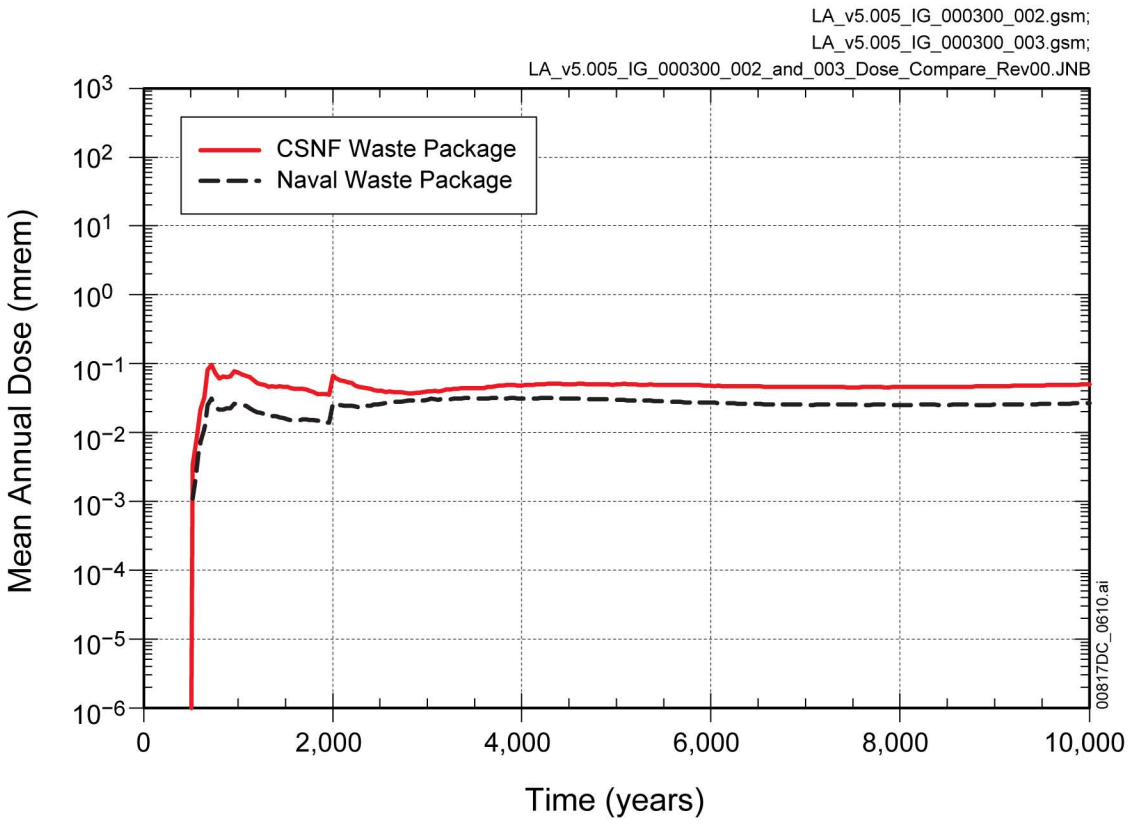

Source: Output DTN: MO0801TSPANSNF.000 [DIRS 184619].

Figure 7.5-5[a]. Comparison of Mean Annual Dose for a Single CSNF WP and Single WP with a Naval Source Term for the Igneous Intrusion Modeling Case

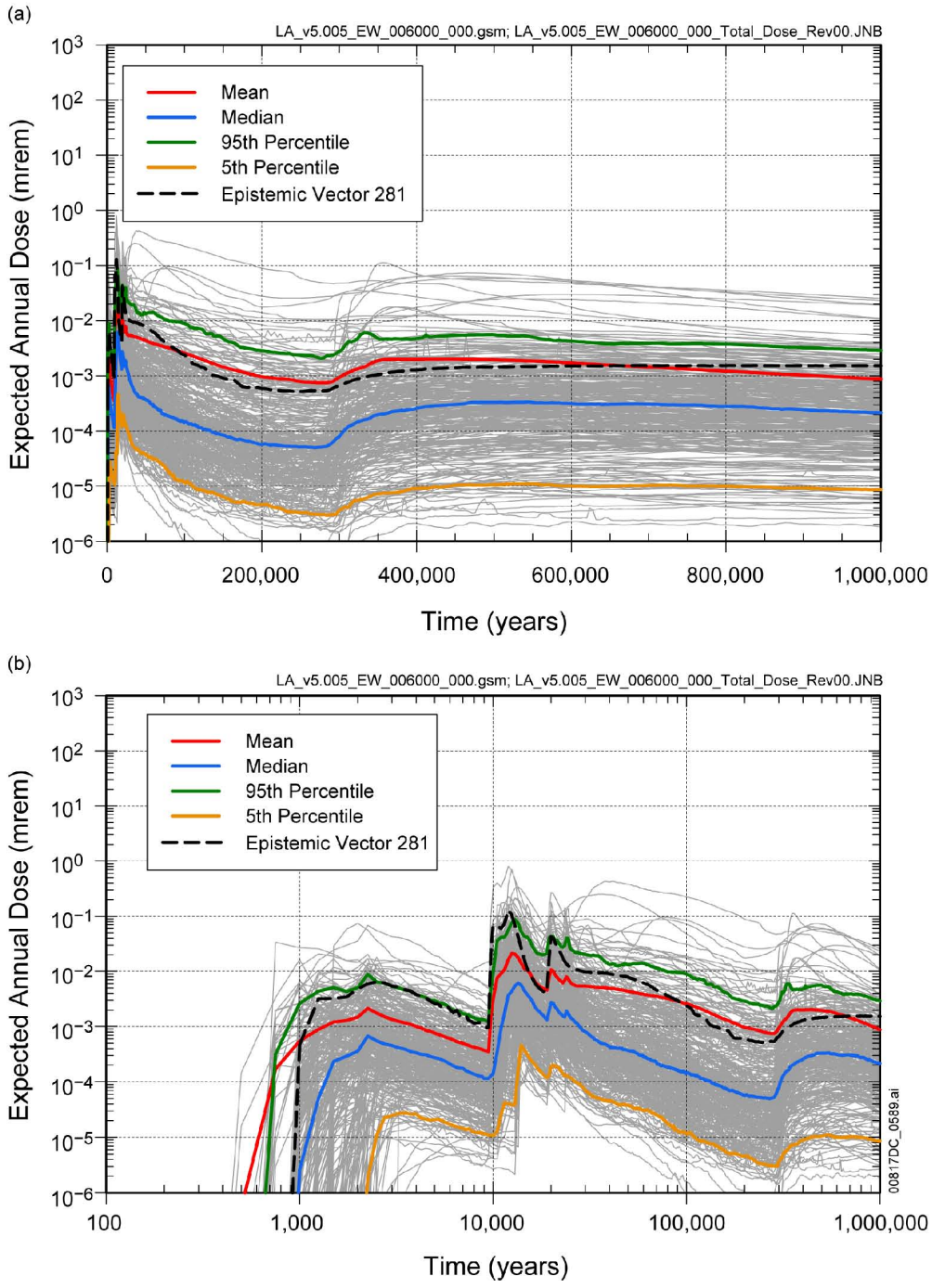

Source: Output DTN: MO0710ADTSPAWO.000 [DIRS 183752].

Figure 7.7.1-1[a]. Expected Annual Dose from 300 Epistemic Vectors, Along with their Quantiles and Expected Dose from Epistemic Vector 281 for the Waste Package Early Failure Modeling Case for 1,000,000 Years after Repository Closure: (a) Linear Time and (b) Log Time

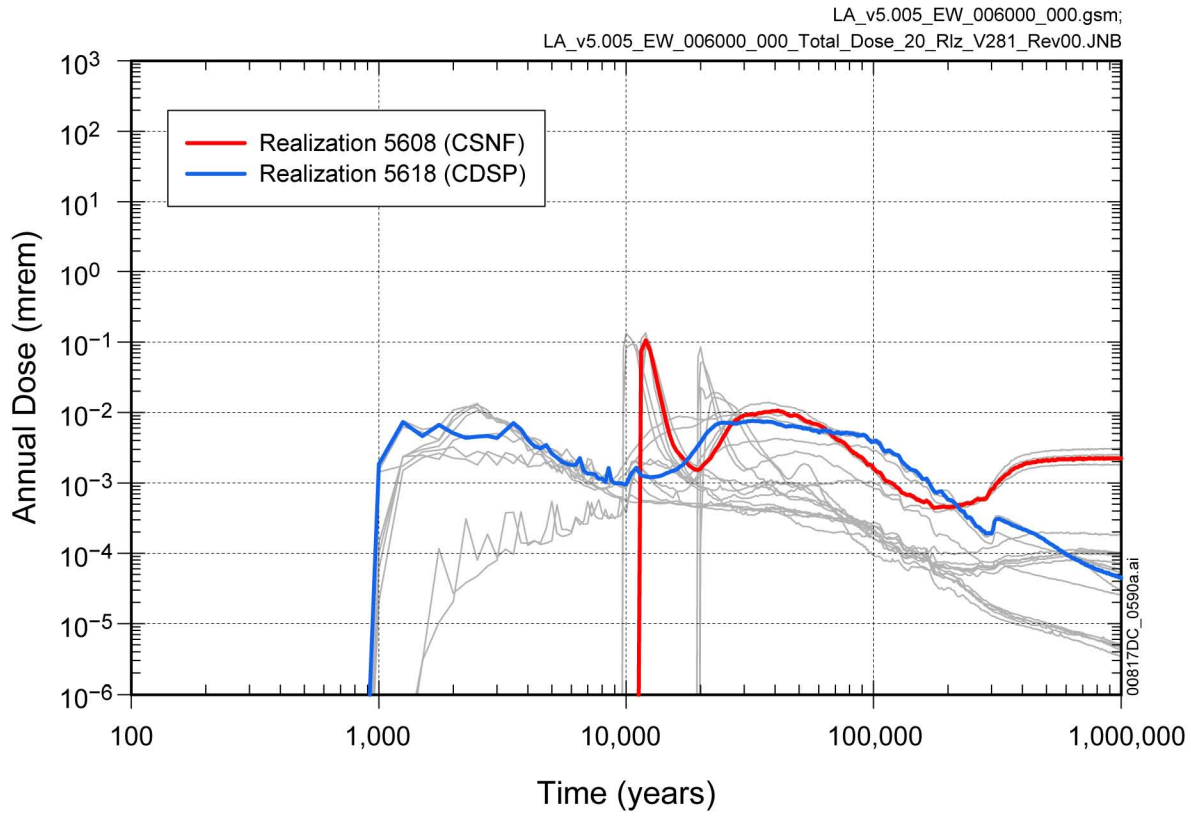

Source: Output DTN: MO0710ADTSPAWO.000 [DIRS 183752].

Figure 7.7.1-2[a]. Annual Dose from Realizations 5601 through 5620 of the Waste Package Early Failure Modeling Case for 1,000,000 Years after Repository Closure

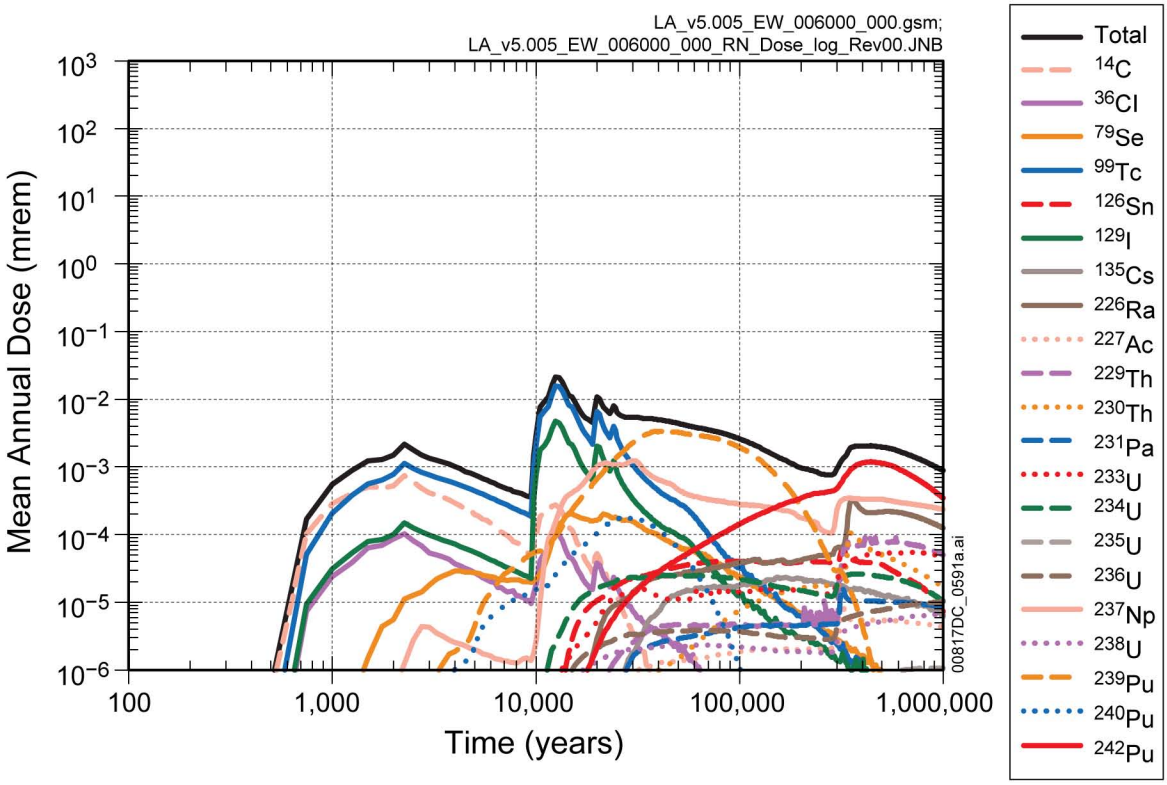

Source: Output DTN: MO0710ADTSPAWO.000 [DIRS 183752].

Figure 7.7.1-3[a]. Major Radionuclide Contributors to Mean Annual Dose for the Waste Package Early Failure Modeling Case for 1,000,000 Years after Repository Closure

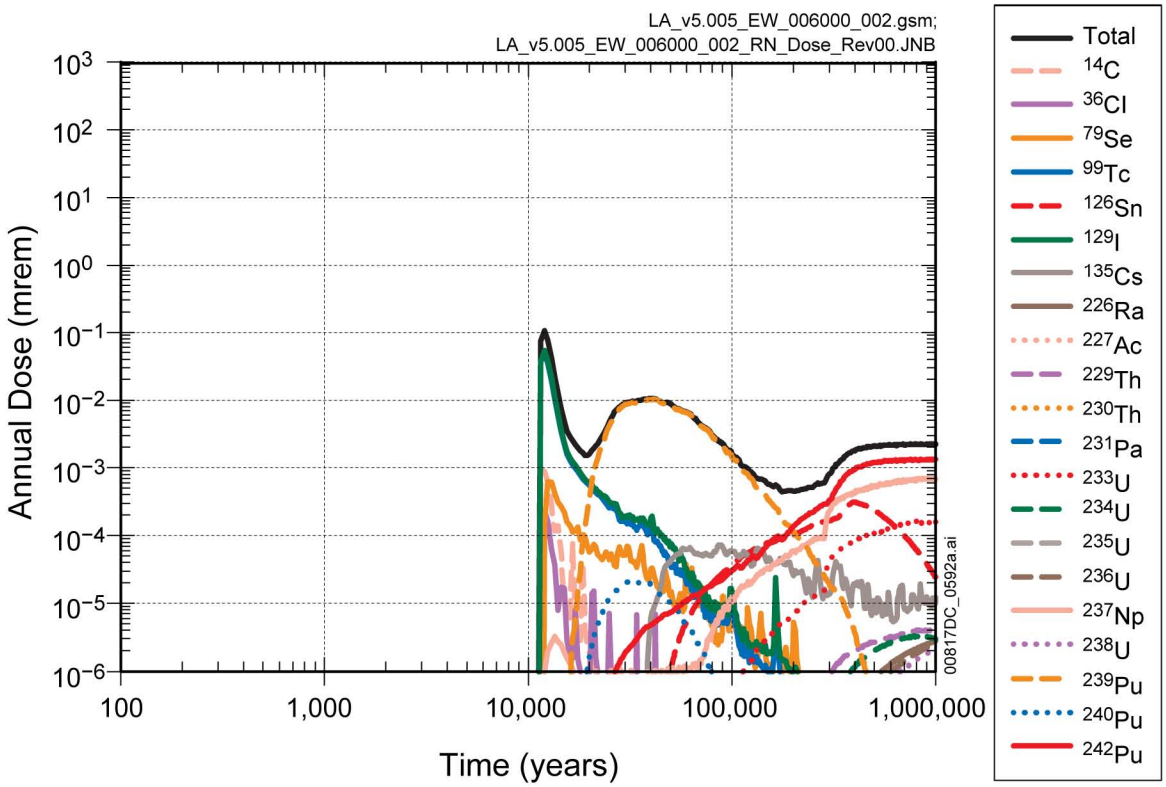

Source: Output DTN: MO0801TSPAMVAC.000 [DIRS 185080].

Figure 7.7.1-4[a]. Major Radionuclide Contributors to Annual Dose for Realization 5608 of the Waste Package Early Failure Modeling Case for 1,000,000 Years after Repository Closure

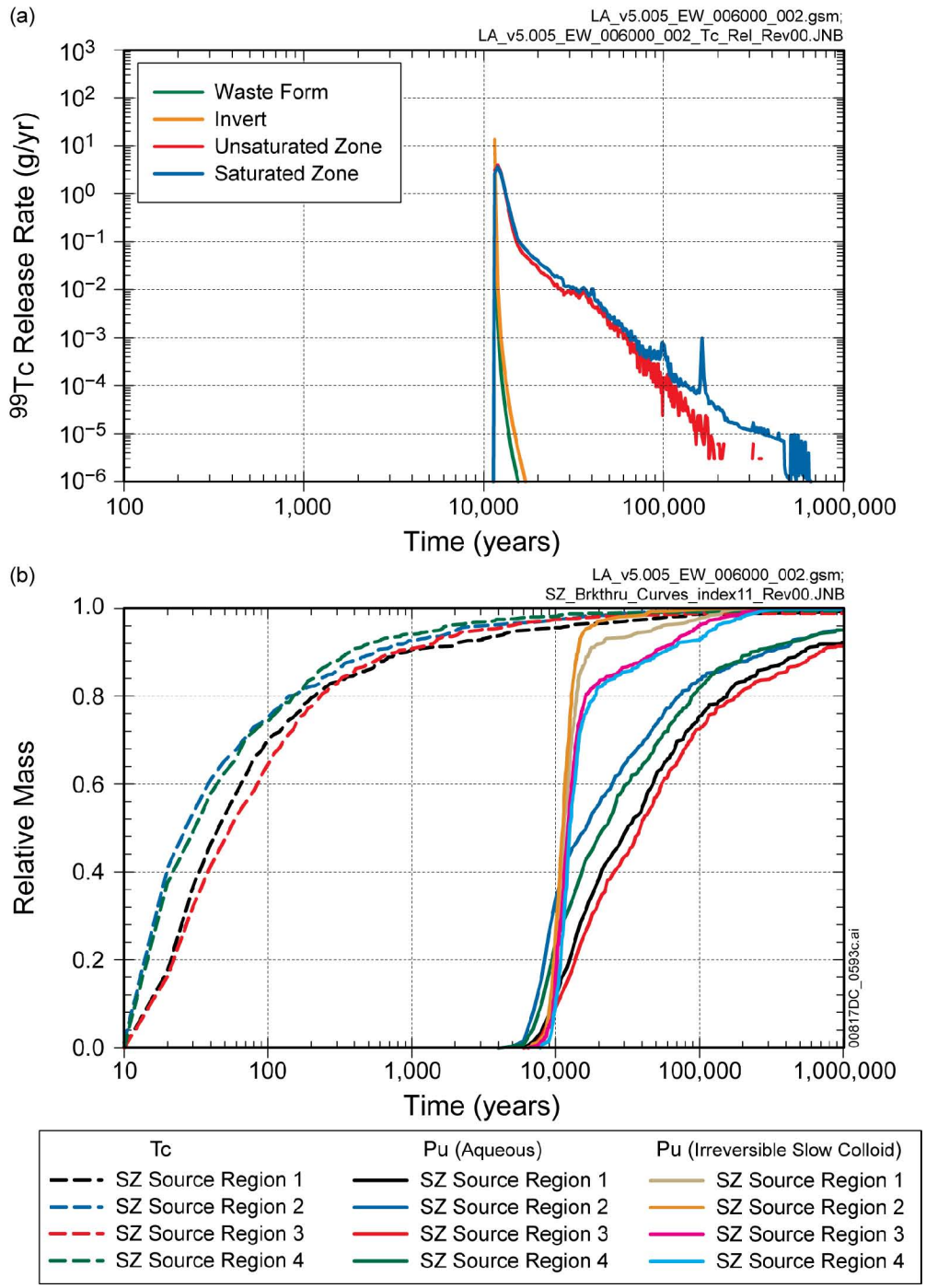

Source: Output DTN: MO0801TSPAMVAC.000 [DIRS 185080].

NOTE: In the (b) plot, the mass of plutonium dissolved and reversibly associated with colloids is denoted as aqueous.

Figure 7.7.1-5[a]. (a) Release Rates of Technetium from the Waste Form, EBS, Unsaturated Zone, and Saturated Zone for Realization 5608 and (b) Saturated Zone Breakthrough Curves of Technetium and Plutonium for Epistemic Uncertainty Vector 281 of the Waste Package Early Failure Modeling Case for 1,000,000 Years after Repository Closure

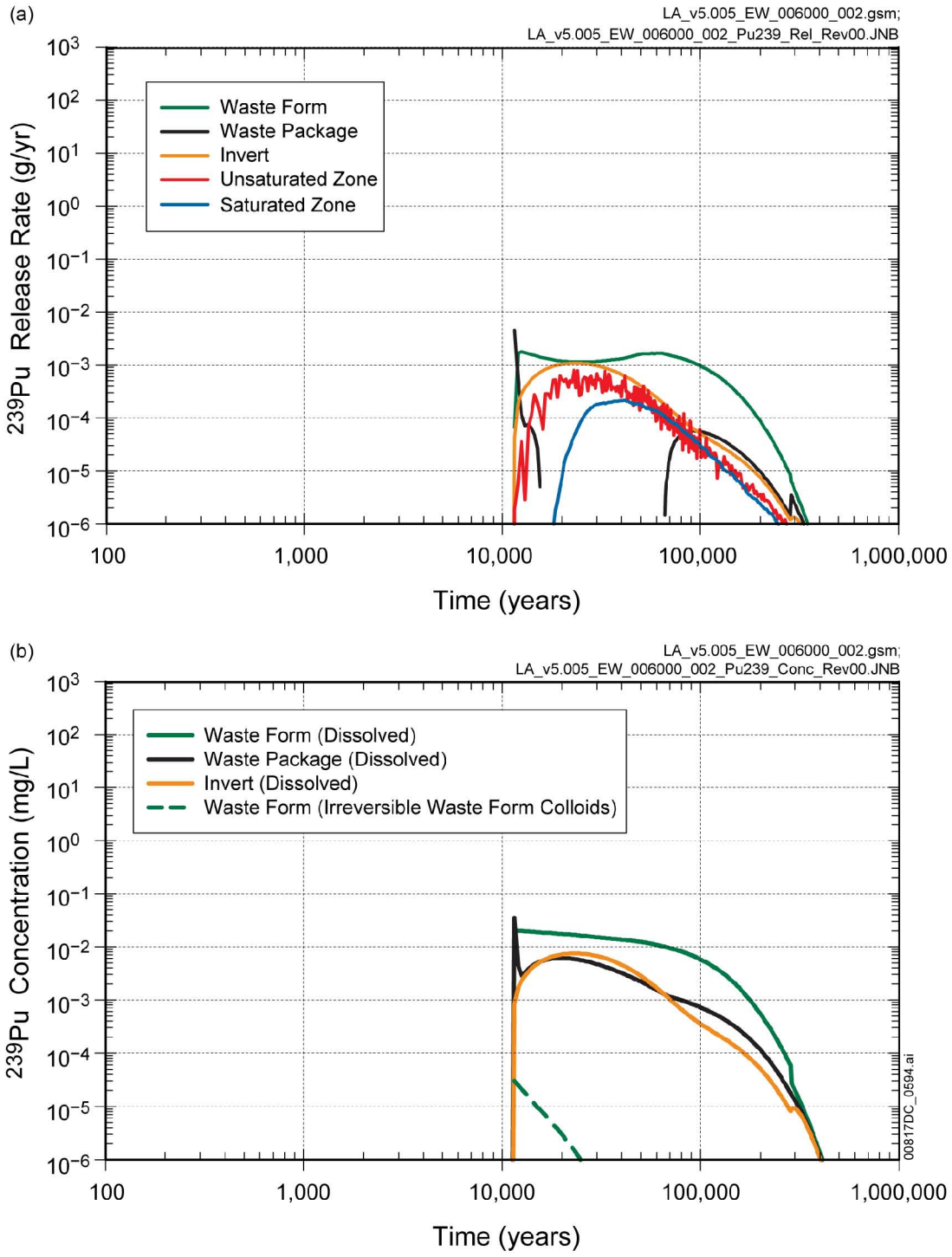

Source: Output DTN: MO0801TSPAMVAC.000 [DIRS 185080].

NOTE: In the (a) plot, the release rate does not include the mass released as irreversibly associated with colloids.

Figure 7.7.1-6[a]. (a) Release Rates and (b) Concentration of ^{239}Pu for Realization 5608 of the Waste Package Early Failure Modeling Case for 1,000,000 Years after Repository Closure

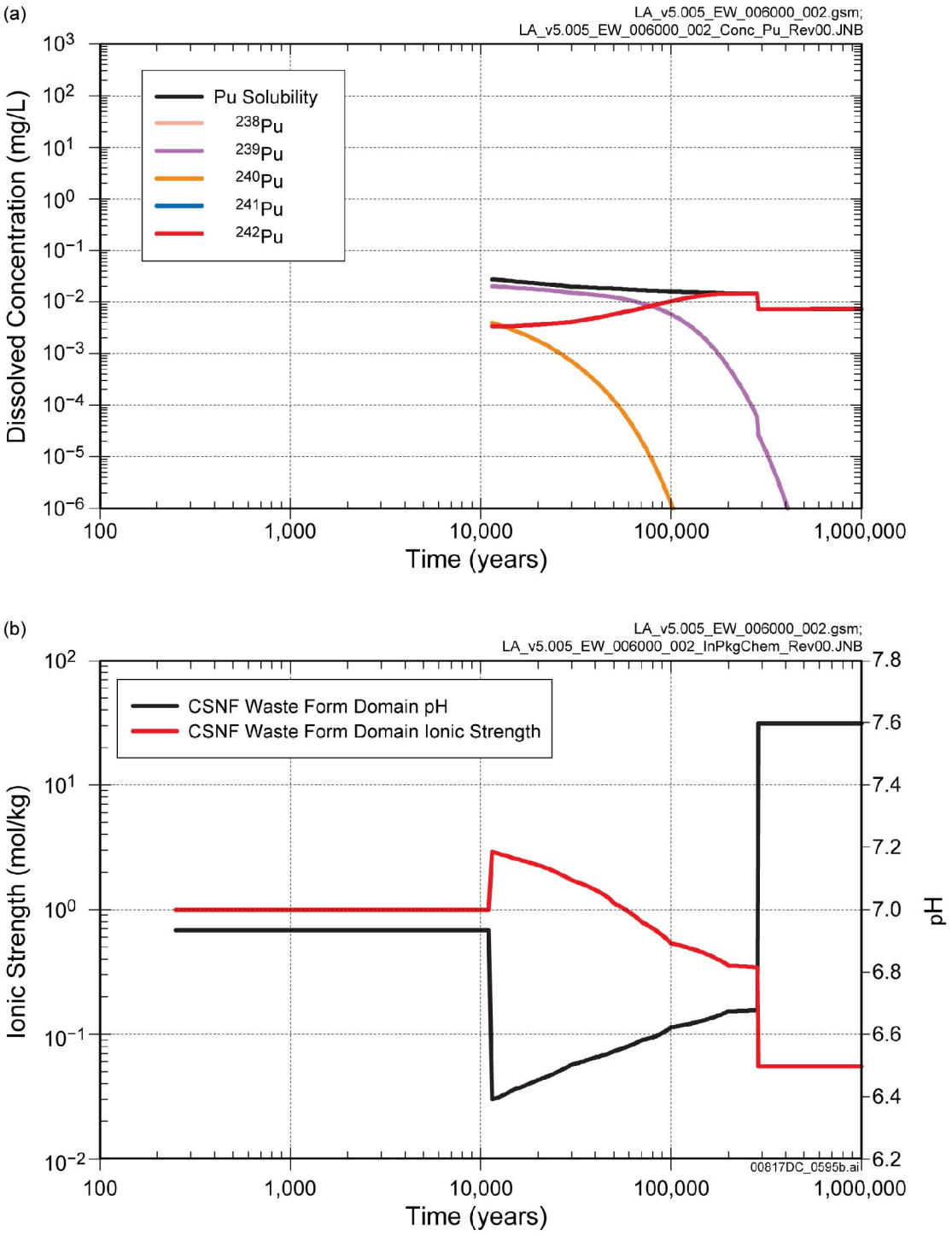

Source: Output DTN: MO0801TSPAMVAC.000 [DIRS 185080].

Figure 7.7.1-7[a]. (a) Dissolved Concentrations of Plutonium in the CSNF Waste Form Domain for Realization 5608 and (b) CSNF Waste Form Domain Chemistry for Realization 5608 of the Waste Package Early Failure Modeling Case for 1,000,000 Years after Repository Closure

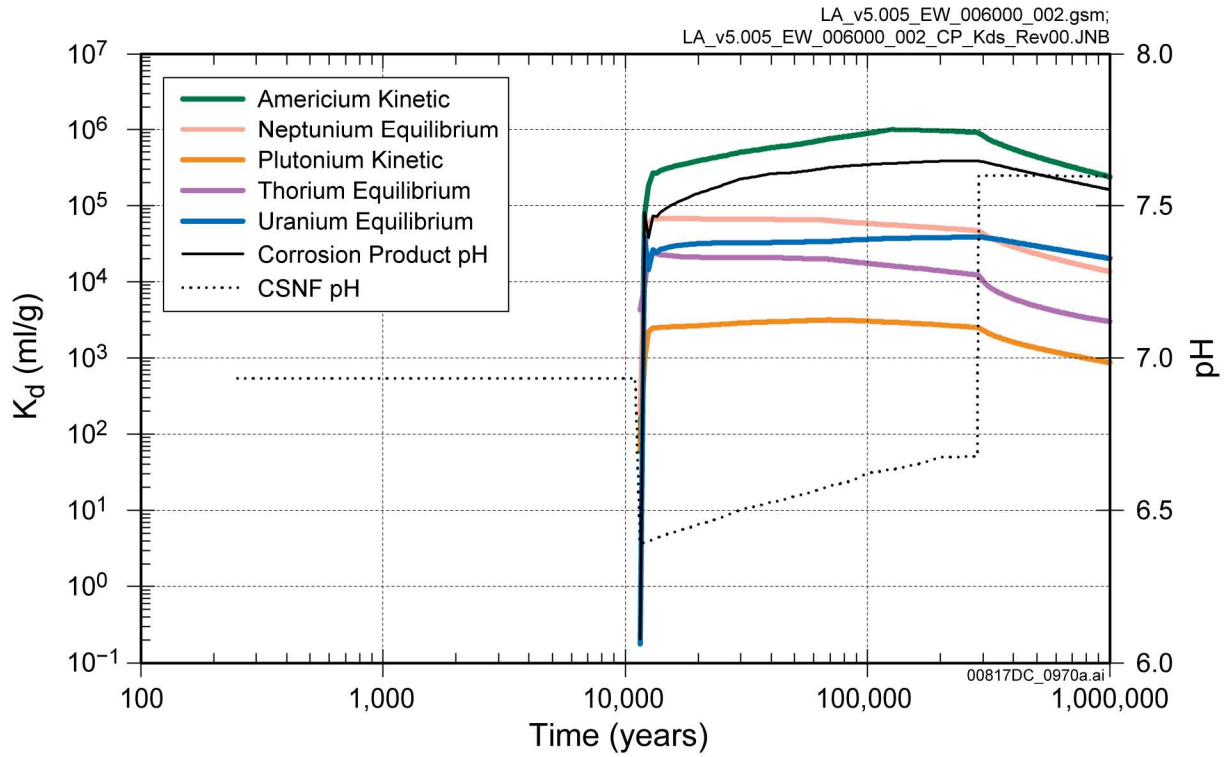

Source: Output DTN: MO0801TSPAMVAC.000 [DIRS 185080].

Figure 7.7.1-8[a]. Corrosion Product Sorption Coefficients (K_ds) and In-package pH for Realization 5608 of the Waste Package Early Failure Modeling Case for 1,000,000 Years after Repository Closure

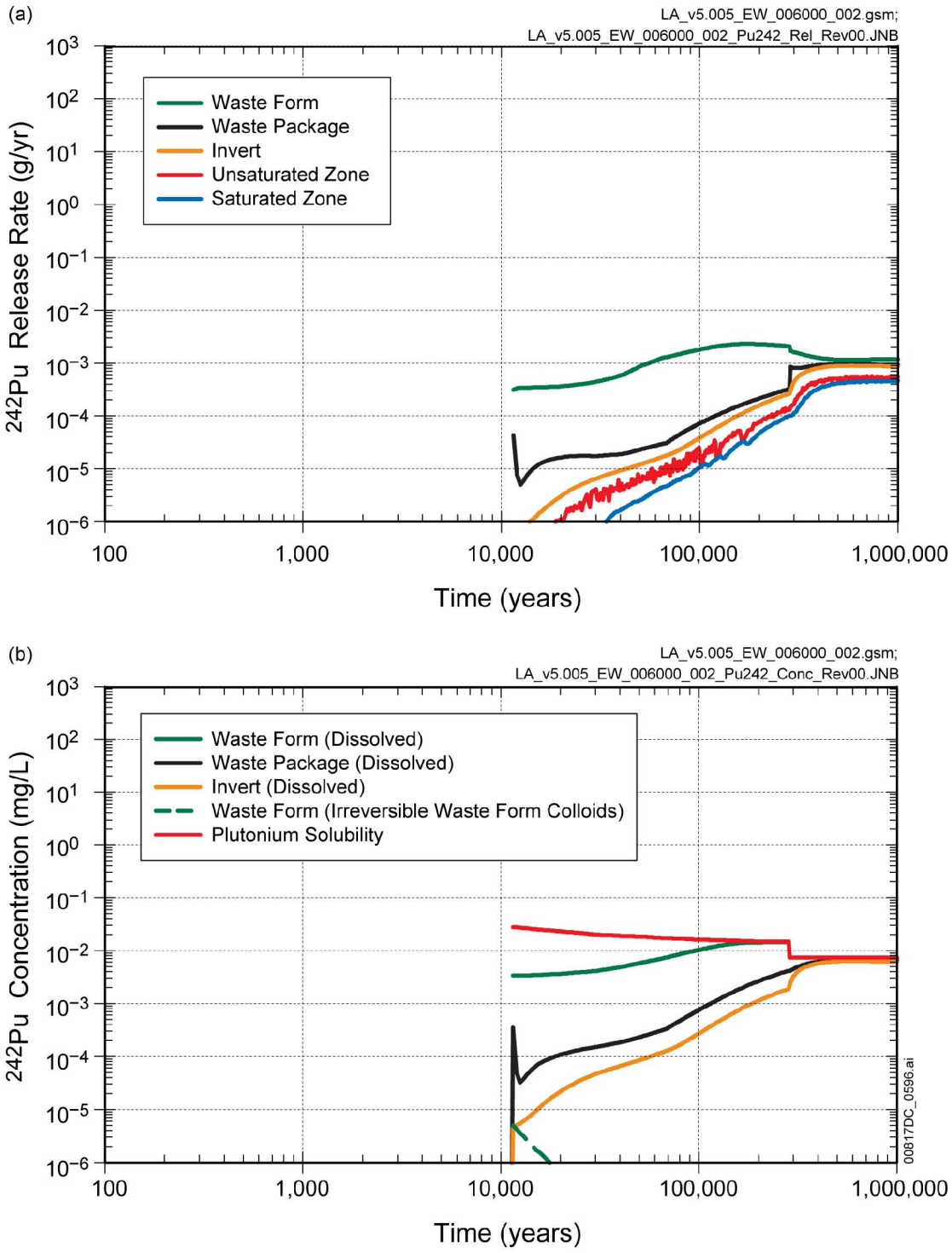

Source: Output DTN: MO0801TSPAMVAC.000 [DIRS 185080].

NOTE: In the (a) plot, the release rate does not include the mass released as irreversibly associated with colloids.

Figure 7.7.1-9[a]. (a) Release Rates and (b) Concentration of ^{242}Pu for Realization 5608 of the Waste Package Early Failure Modeling Case for 1,000,000 Years after Repository Closure

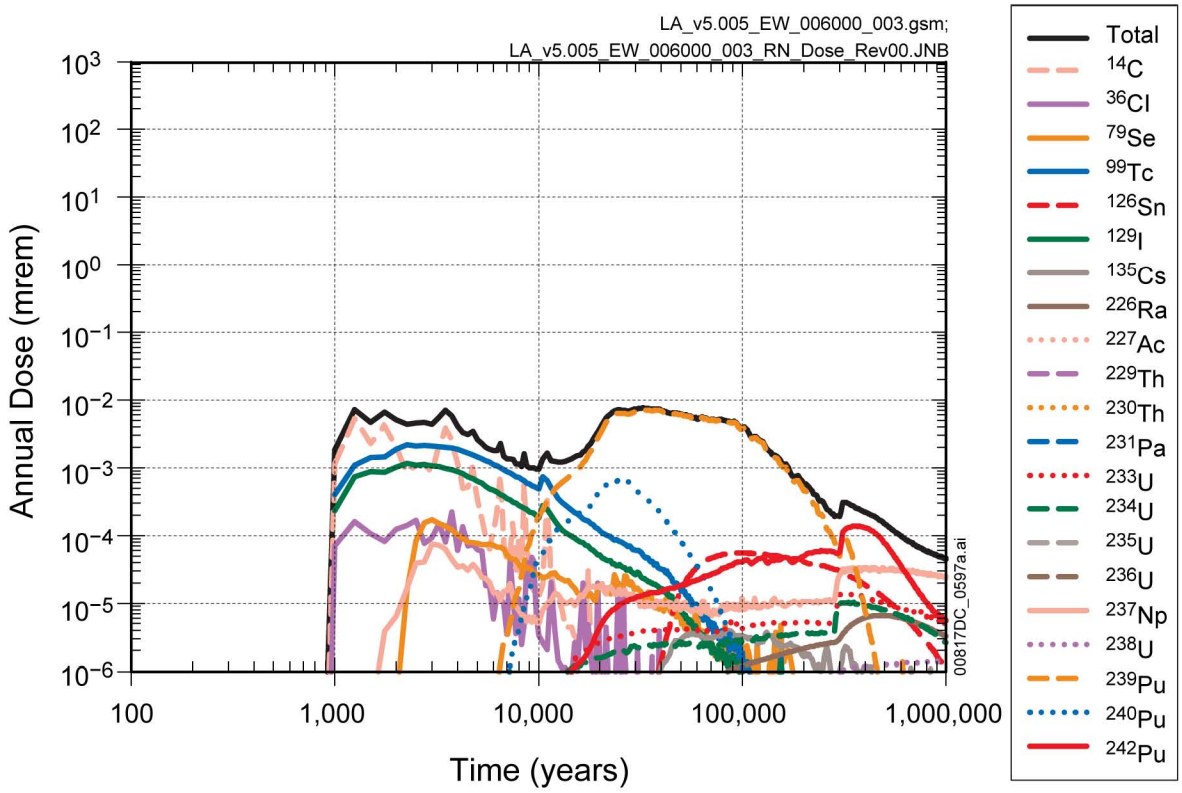

Source: Output DTN: MO0801TSPAMVAC.000 [DIRS 185080].

Figure 7.7.1-10[a]. Major Radionuclide Contributors to Annual Dose for Realization 5618 of the Waste Package Early Failure Modeling Case for 1,000,000 Years after Repository Closure

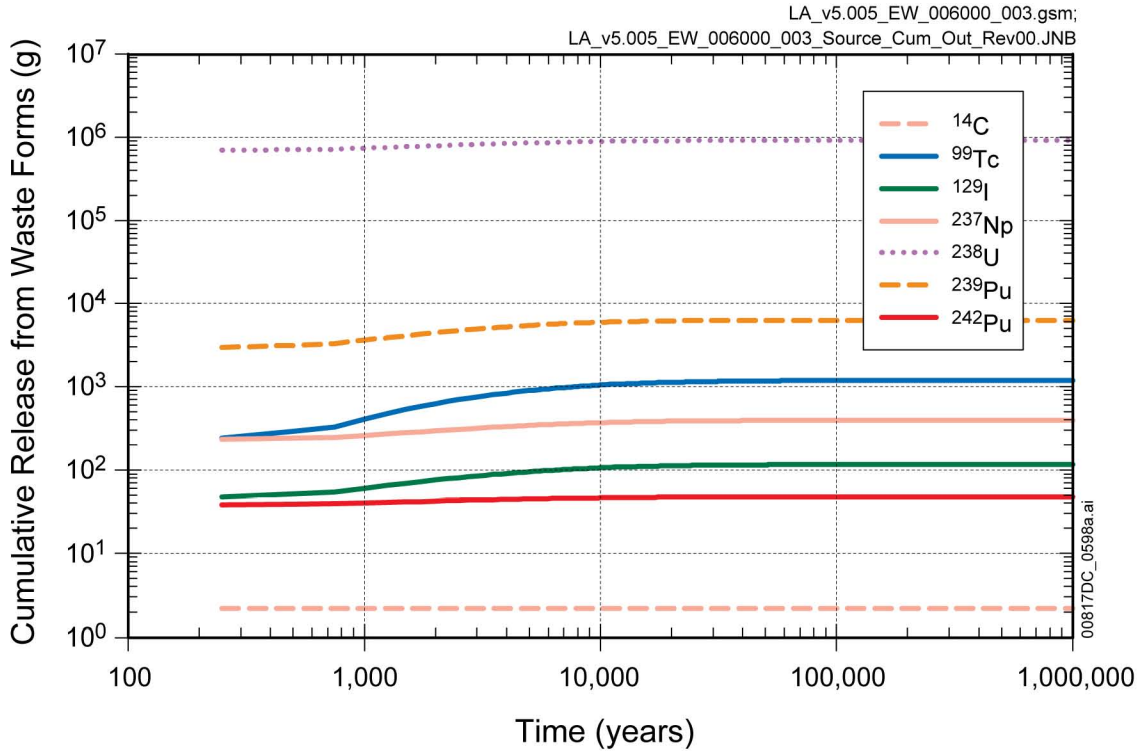

Source: Output DTN: MO0801TSPAMVAC.000 [DIRS 185080].

Figure 7.7.1-11[a]. Cumulative Release from HLW and DSNF Waste Forms for Realization 5618 of the Waste Package Early Failure Modeling Case for 1,000,000 Years after Repository Closure

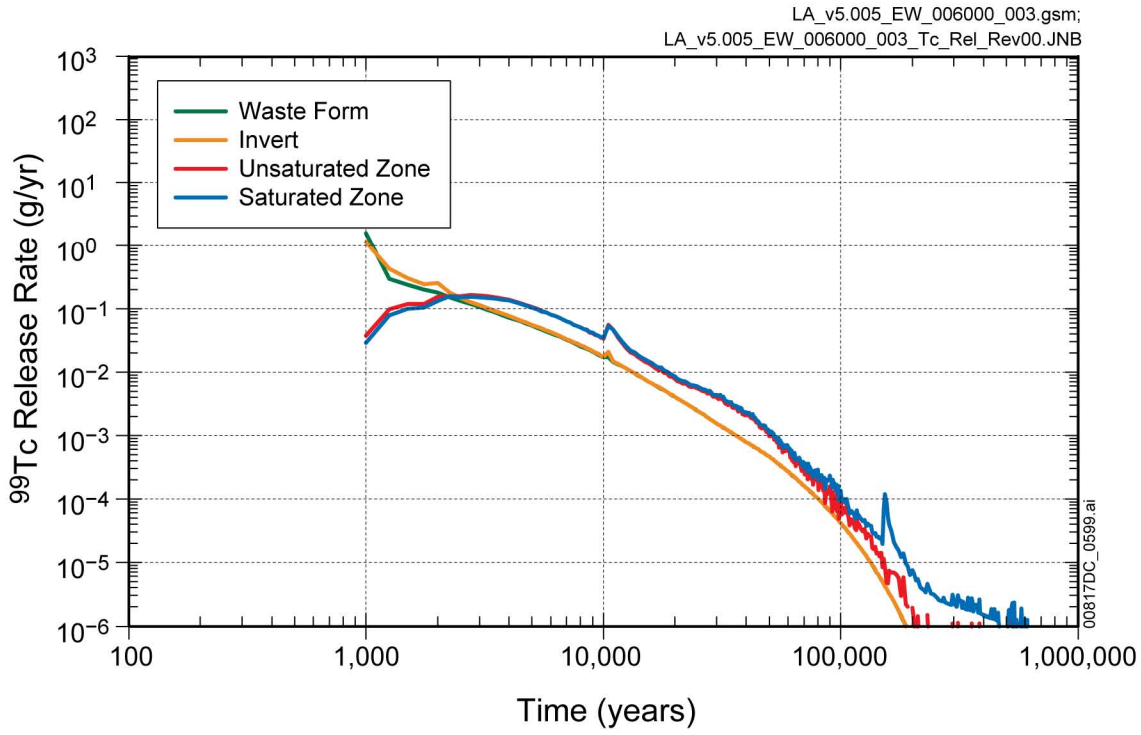

Source: Output DTN: MO0801TSPAMVAC.000 [DIRS 185080].

Figure 7.7.1-12[a]. Release Rates of ^{99}Tc from the Waste Form, Invert, Unsaturated Zone, and Saturated Zone for Realization 5618 of the Waste Package Early Failure Modeling Case for 1,000,000 Years after Repository Closure

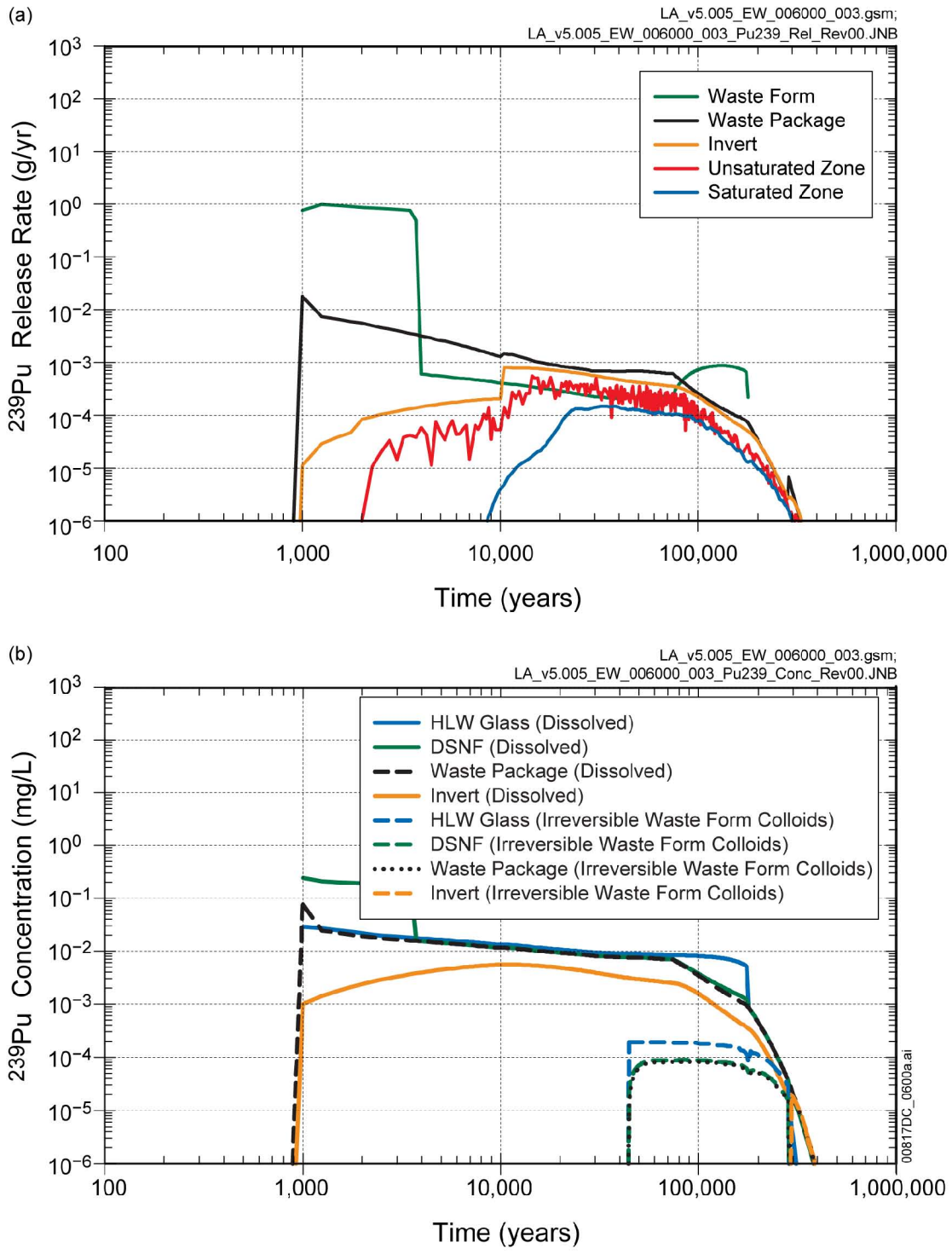

Source: Output DTN: MO0801TSPAMVAC.000 [DIRS 185080].

NOTE: In the (a) plot, the release rate does not include the mass released as irreversibly associated with colloids.

Figure 7.7.1-13[a]. (a) Release Rates and (b) Concentration of ^{239}Pu for Realization 5618 of the Waste Package Early Failure Modeling Case for 1,000,000 Years after Repository Closure

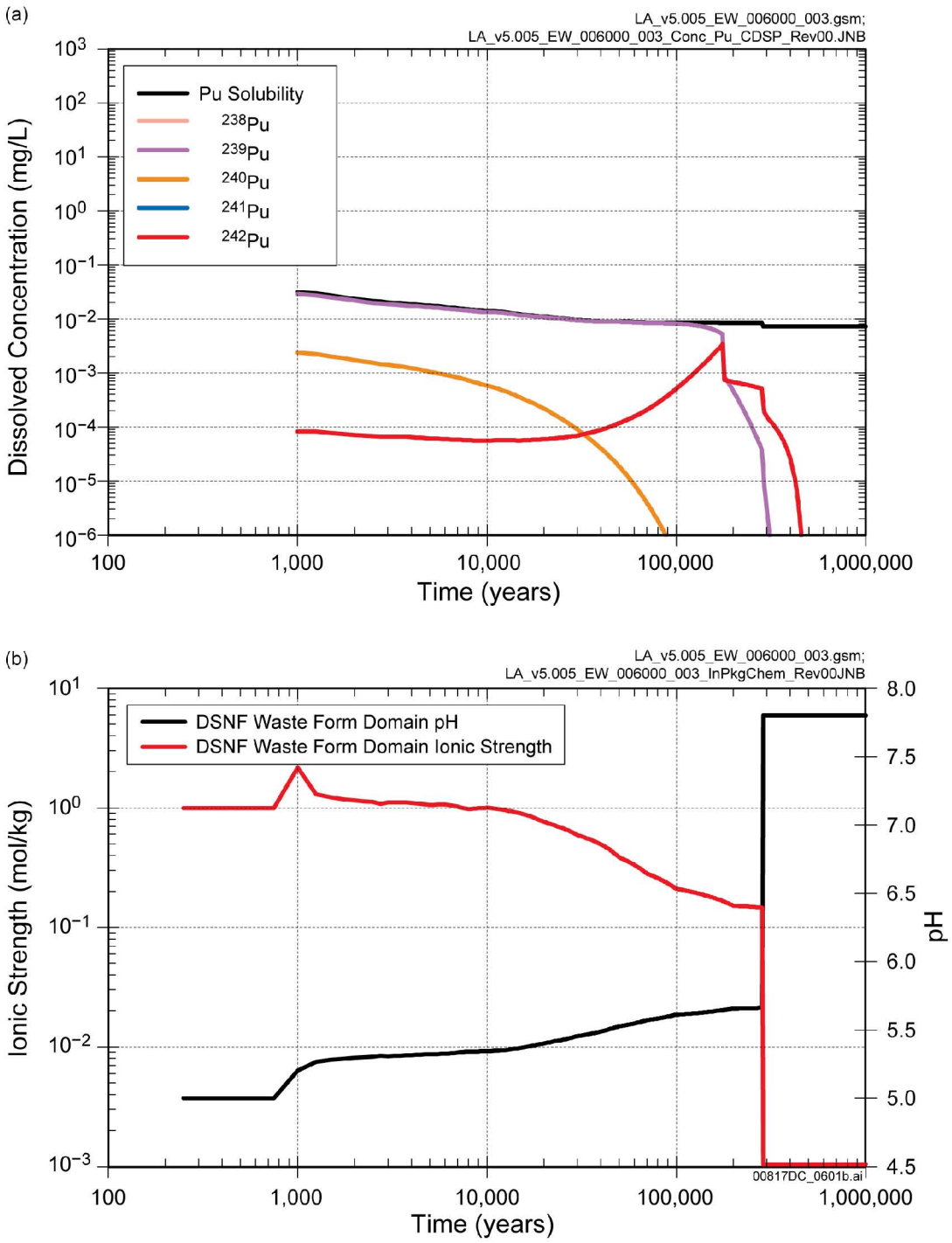

Source: Output DTN: MO0801TSPAMVAC.000 [DIRS 185080].

Figure 7.7.1-14[a]. (a) Dissolved Concentrations of Plutonium in the High-Level Radioactive Waste Domain and (b) DSNF Waste Form Domain Chemistry for Realization 5618 of the Waste Package Early Failure Modeling Case for 1,000,000 Years after Repository Closure

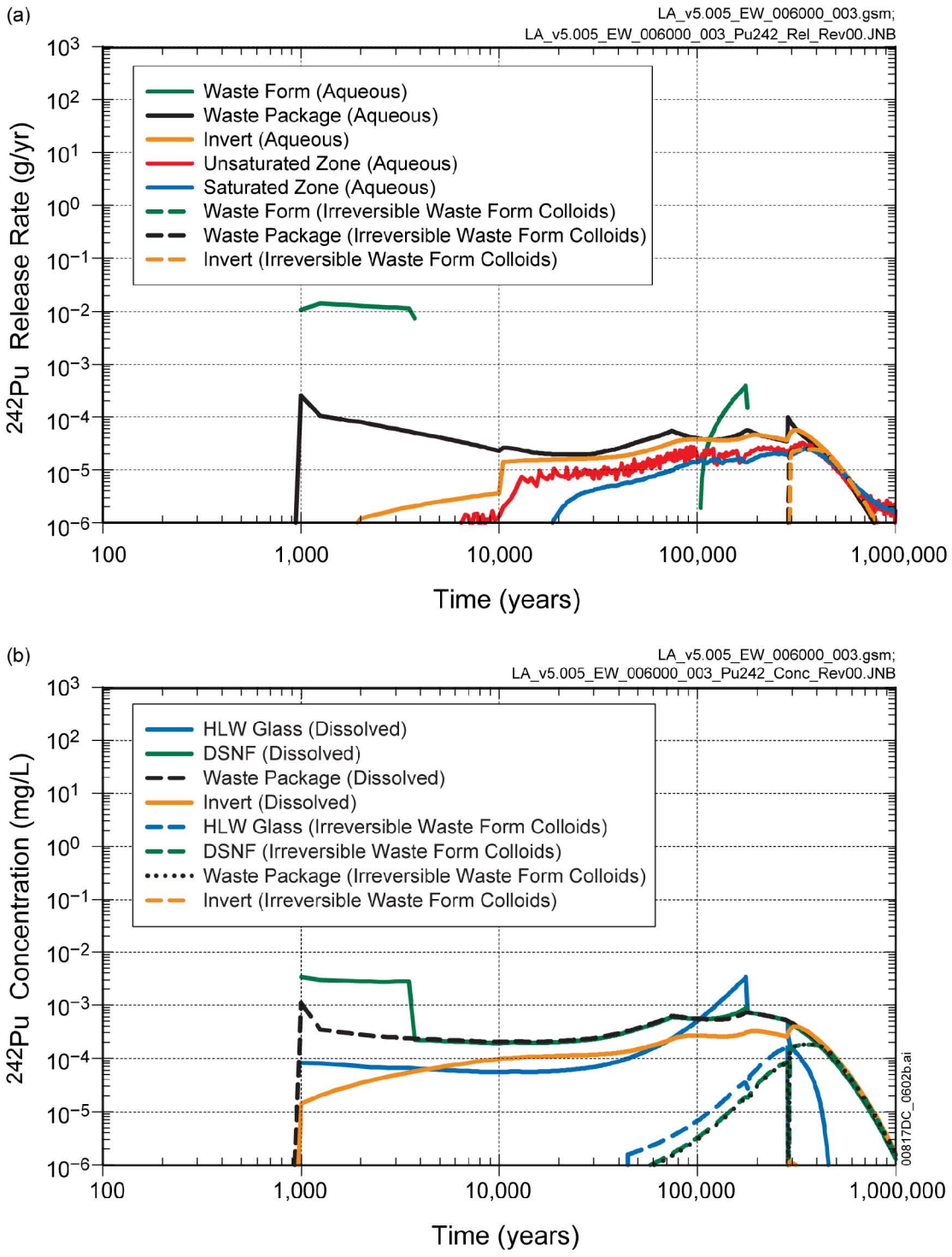

Source: Output DTN: MO0801TSPAMVAC.000 [DIRS 185080].

NOTE: In the (a) plot, plutonium dissolved and reversibly associated with colloids is denoted as aqueous.

Figure 7.7.1-15[a]. (a) Release Rates and (b) Concentration of ^{242}Pu for Realization 5618 of the Waste Package Early Failure Modeling Case for 1,000,000 Years after Repository Closure

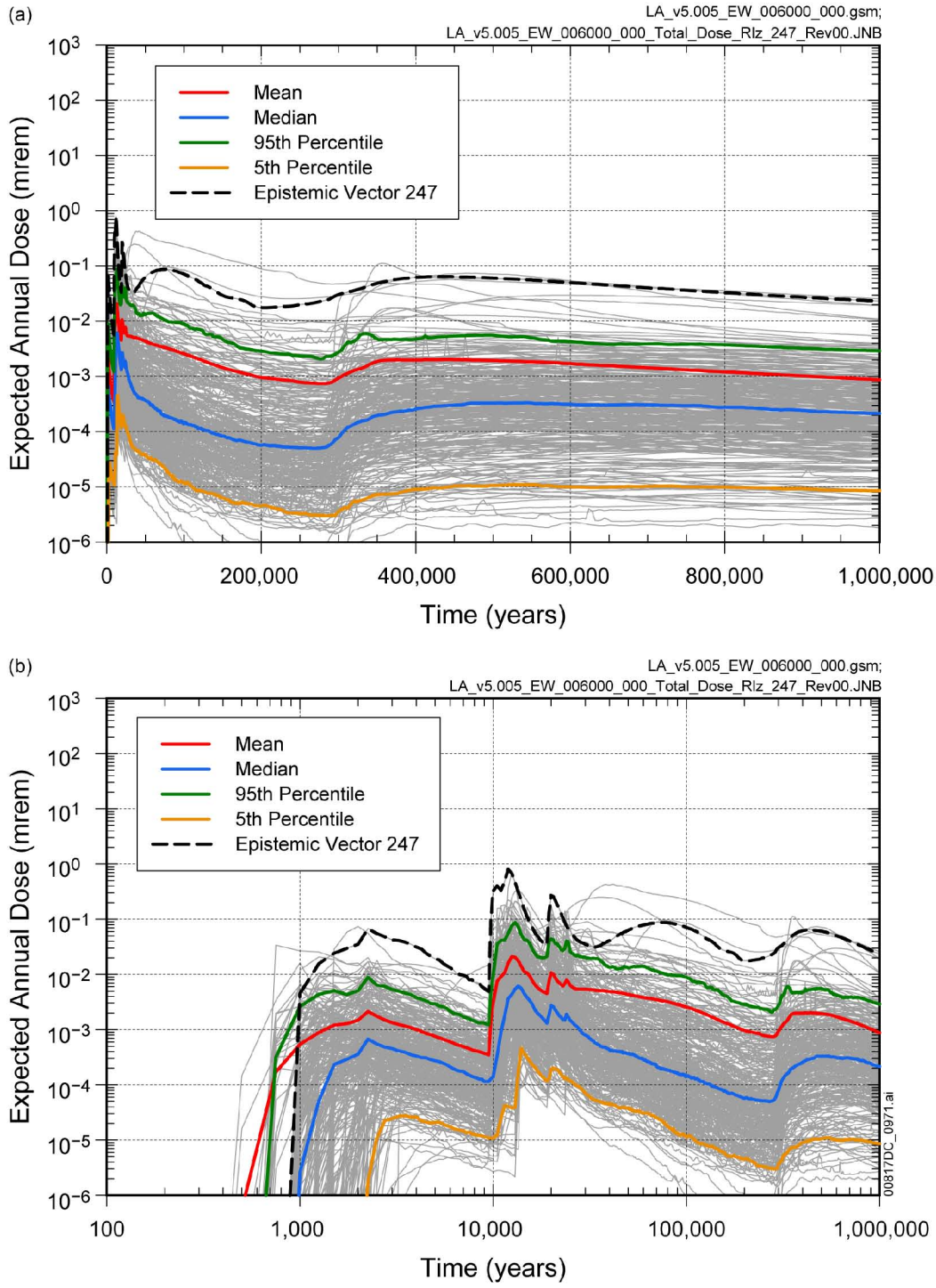

Source: Output DTN: MO0710ADTSPAWO.000 [DIRS 183752].

Figure 7.7.1-16[a]. Expected Annual Dose from 300 Epistemic Uncertainty Vectors, Along with their Quantiles and Expected Dose from Epistemic Uncertainty Vector 247 for the Waste Package Early Failure Modeling Case for 1,000,000 Years after Repository Closure: (a) Linear Time and (b) Log Time

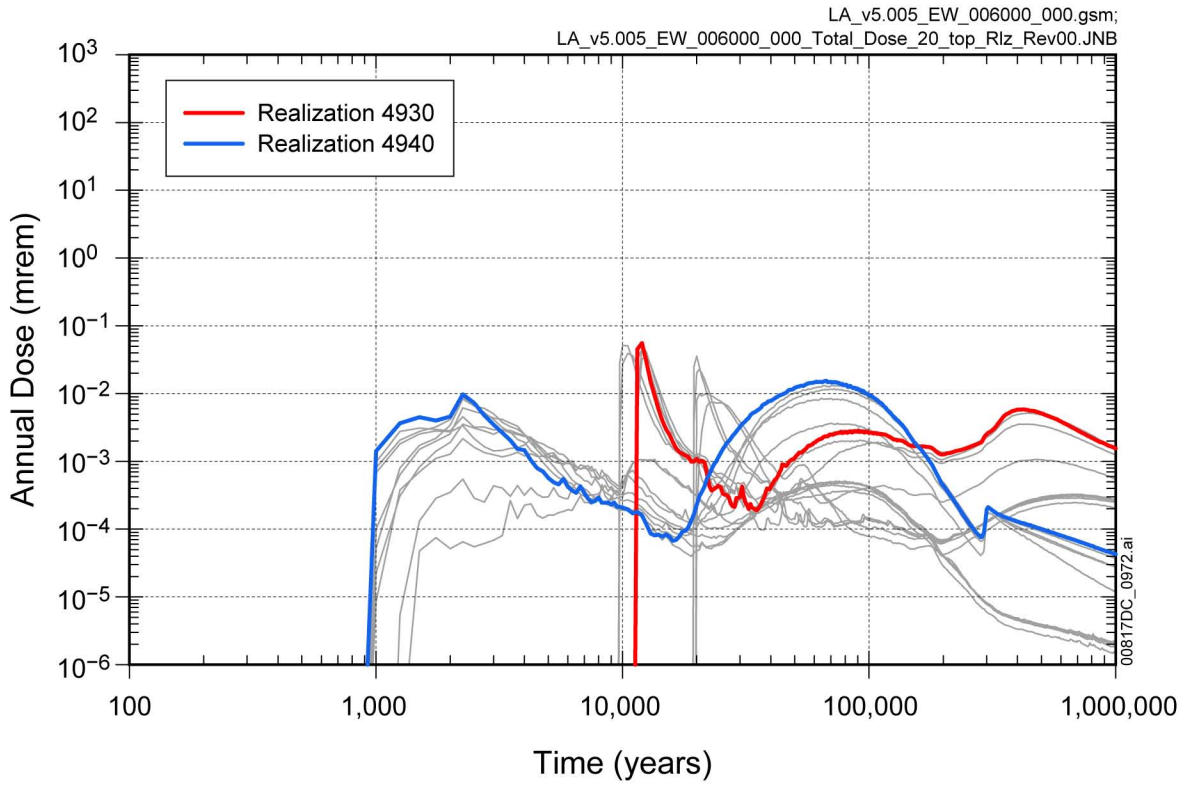

Source: Output DTN: MO0710ADTSPAWO.000 [DIRS 183752].

Figure 7.7.1-17[a]. Annual Dose from Realizations 4921 through 4940 of the Waste Package Early Failure Modeling Case for 1,000,000 Years after Repository Closure

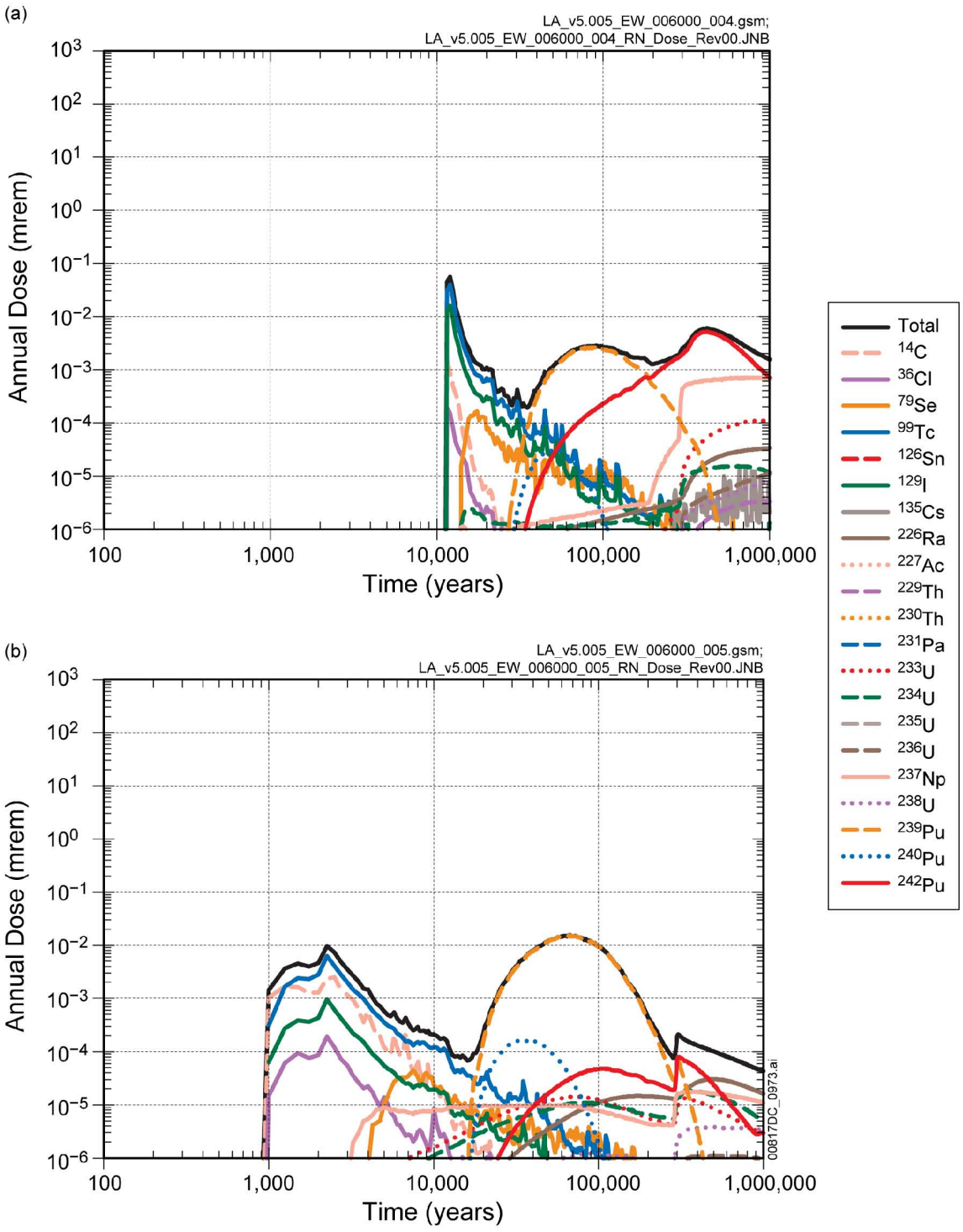

Source: Output DTN: MO0801TSPAMVAC.000 [DIRS 185080].

Figure 7.7.1-18[a]. Major Radionuclide Dose Contributors for Realization (a) 4930 and (b) 4940 of the Waste Package Early Failure Modeling Case for 1,000,000 Years after Repository Closure

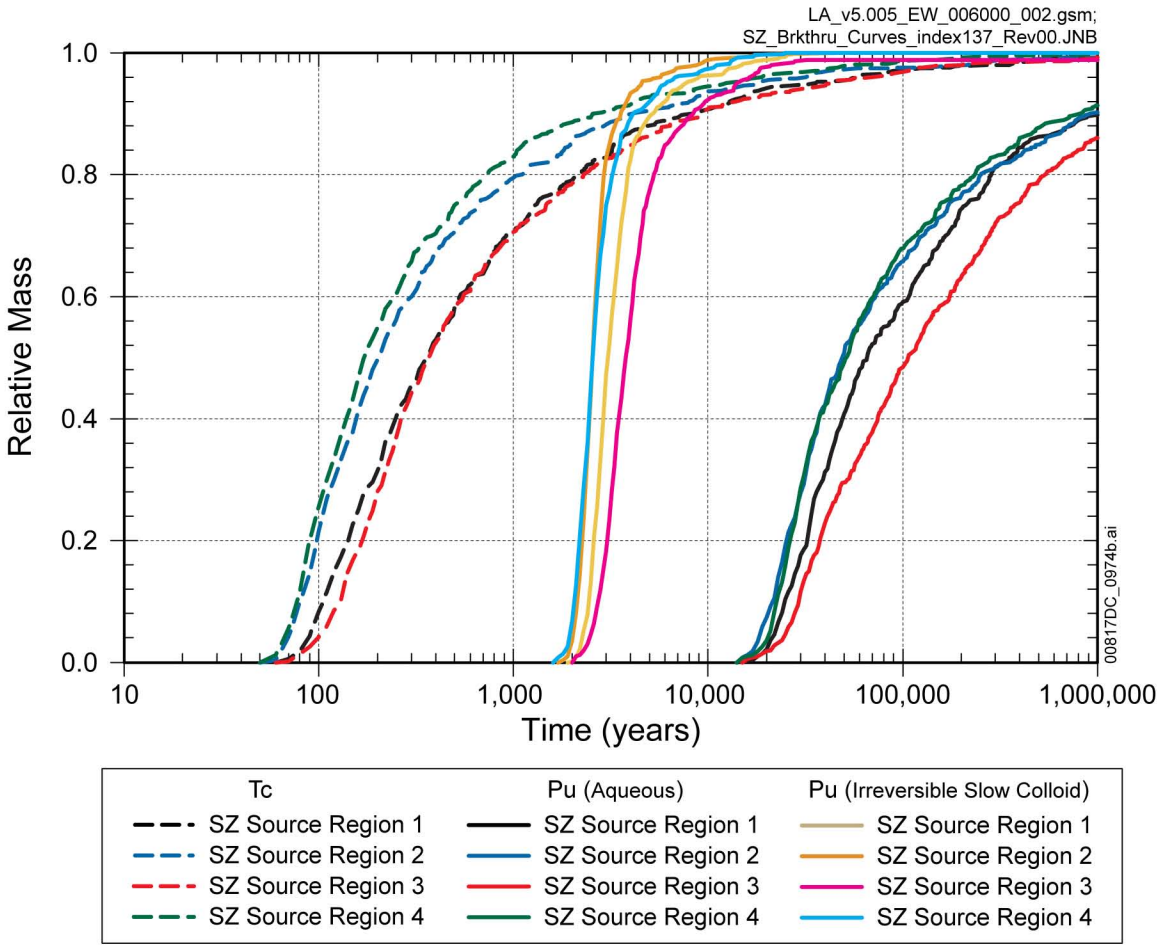

Source: Output DTN: MO0801TSPAMVAC.000 [DIRS 185080].

NOTE: Plutonium dissolved and reversibly associated with colloids is denoted as aqueous.

Figure 7.7.1-19[a]. Saturated Zone Breakthrough Curves for Epistemic Uncertainty Vector 247 of the Waste Package Early Failure Modeling Case for 1,000,000 Years after Repository Closure

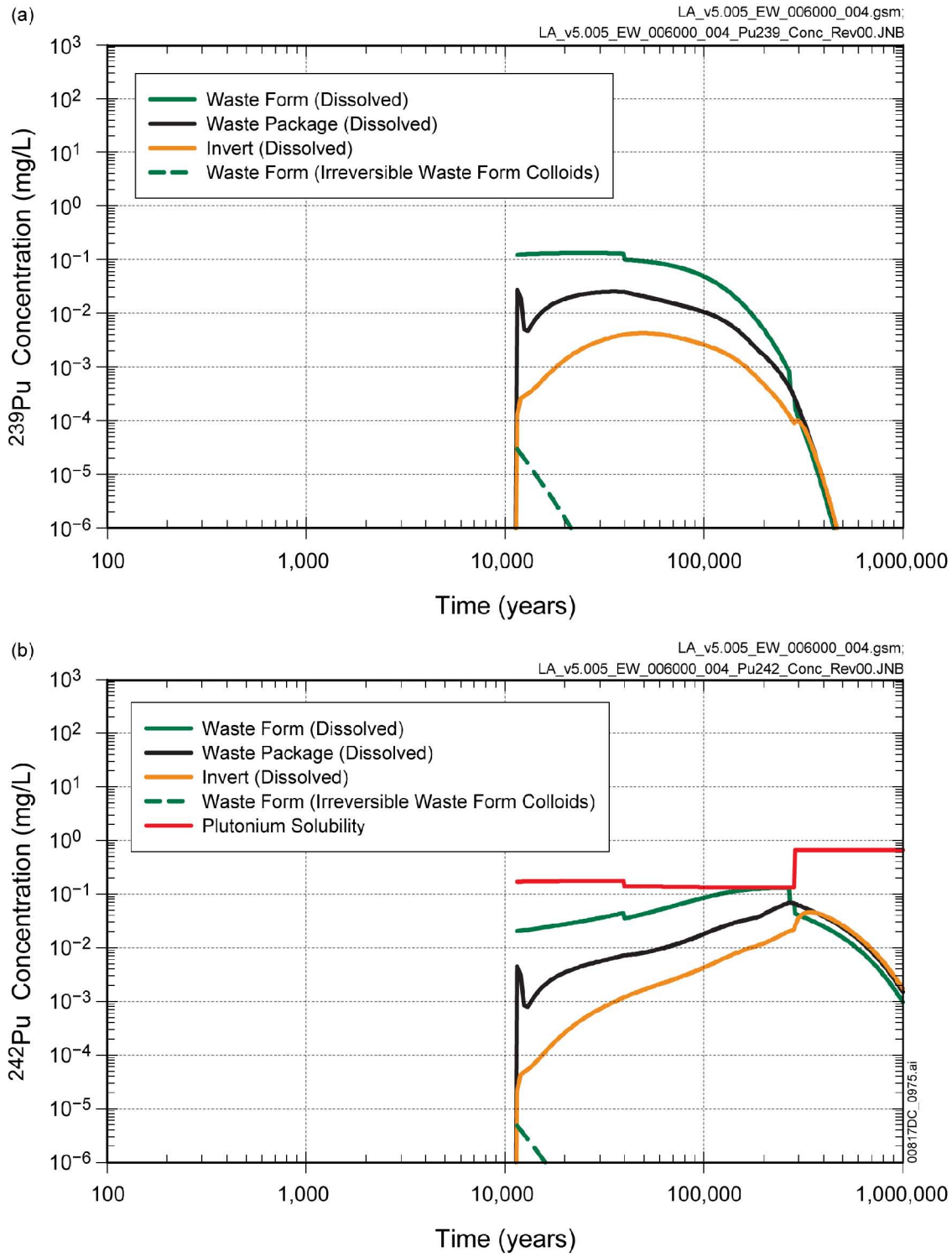

Source: Output DTN: MO0801TSPAMVAC.000 [DIRS 185080].

Figure 7.7.1-20[a]. Concentration of (a) ^{239}Pu and (b) ^{242}Pu for Realization 4930 of the Waste Package Early Failure Modeling Case for 1,000,000 Years after Repository Closure

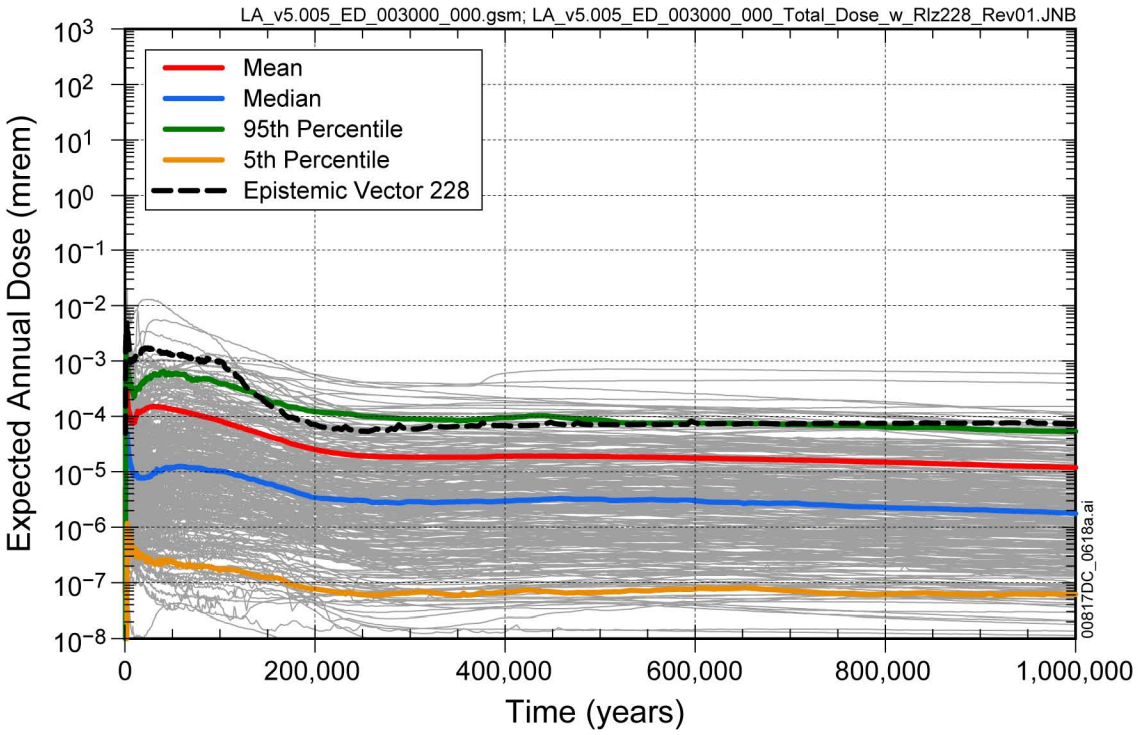

Source: Output DTN: MO0710ADTSPAWO.000 [DIRS 183752].

Figure 7.7.1-21[a]. Expected Annual Dose from 300 Epistemic Uncertainty Vectors, Along with their Quantiles and Expected Dose from Epistemic Uncertainty Vector 228 for the Drip Shield Early Failure Modeling Case for 1,000,000 Years after Repository Closure

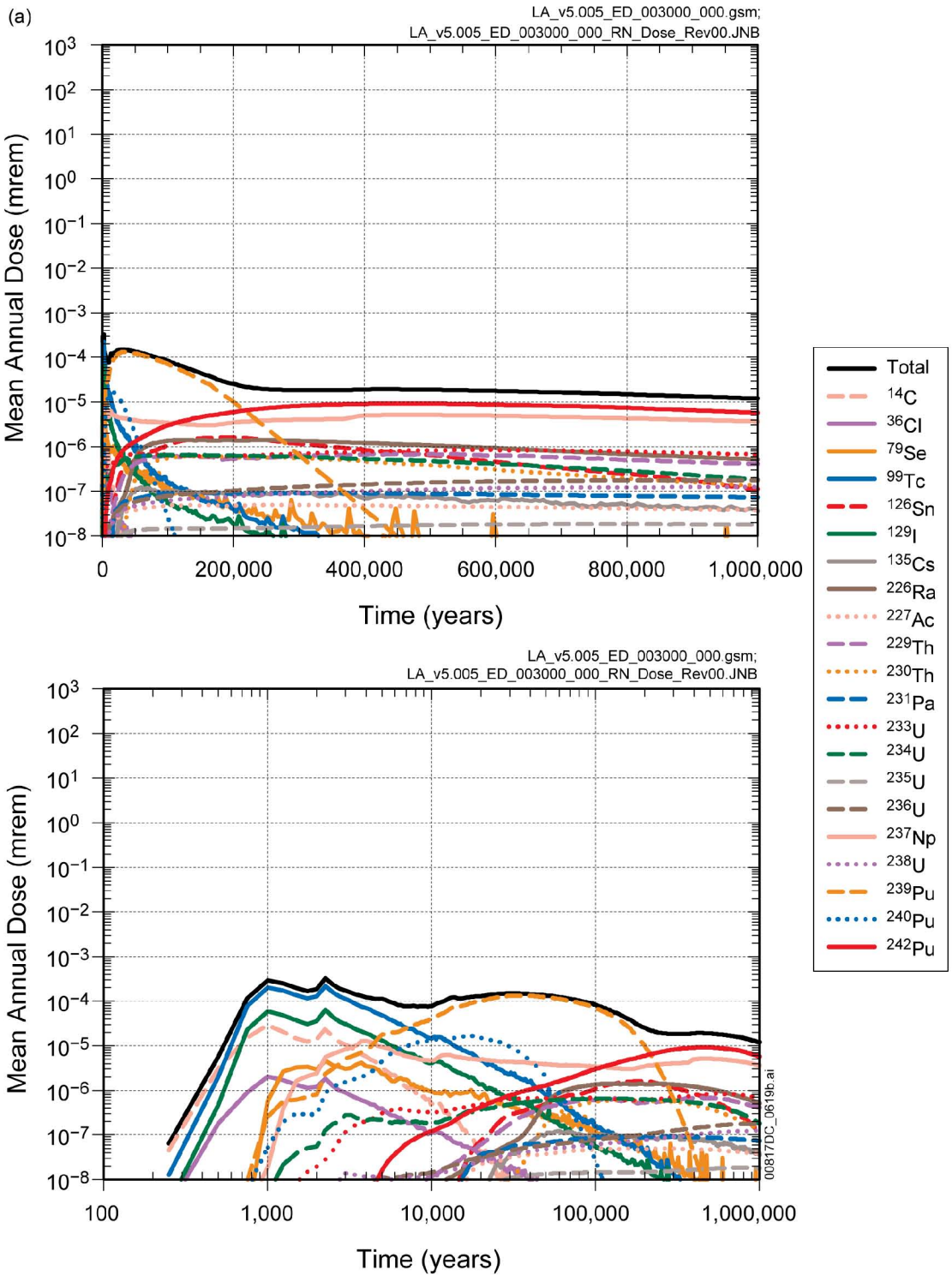

Source: Output DTN: MO0710ADTSPAWO.000 [DIRS 183752].

Figure 7.7.1-22[a]. Major Radionuclide Contributors to Mean Annual Dose for the Drip Shield Early Failure Modeling Case for 1,000,000 Years after Repository Closure

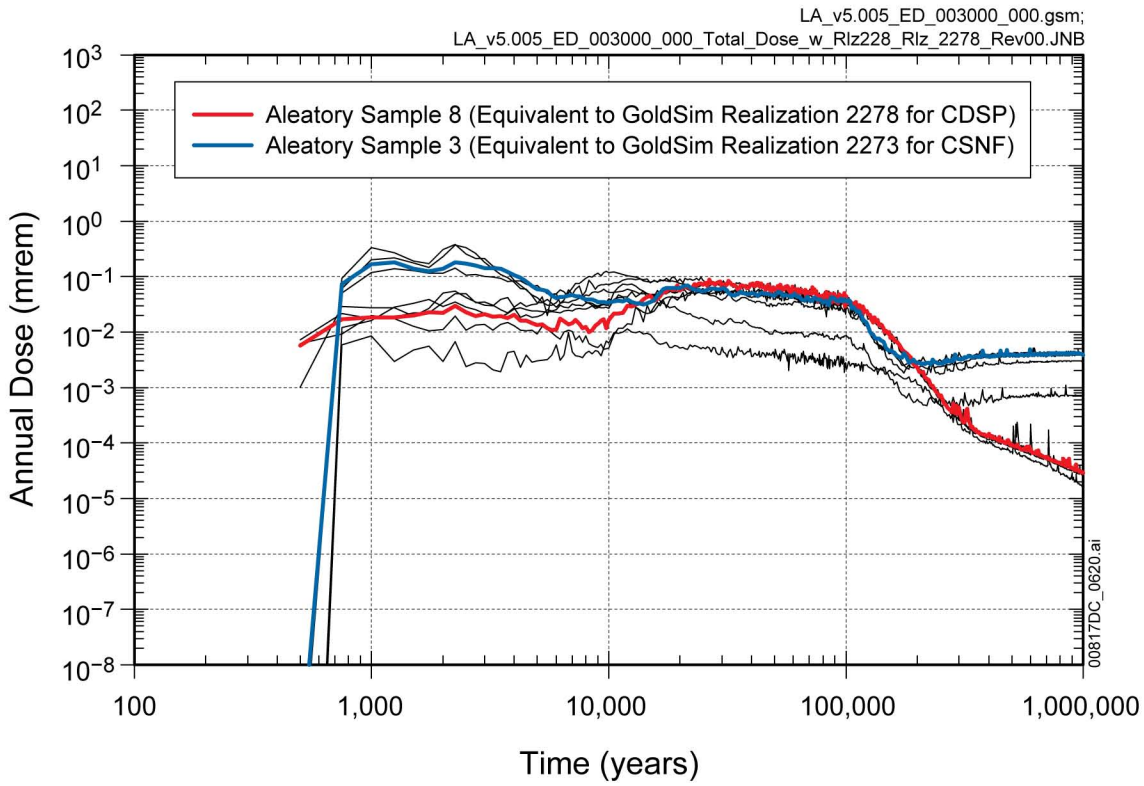

Source: Output DTN: MO0710ADTSPAWO.000 [DIRS 183752].

Figure 7.7.1-23[a]. Annual Dose for Ten Aleatory Uncertainty Realizations (Vectors) for the Epistemic Uncertainty Vector 228 of the Drip Shield Early Failure Modeling Case for 1,000,000 Years after Repository Closure

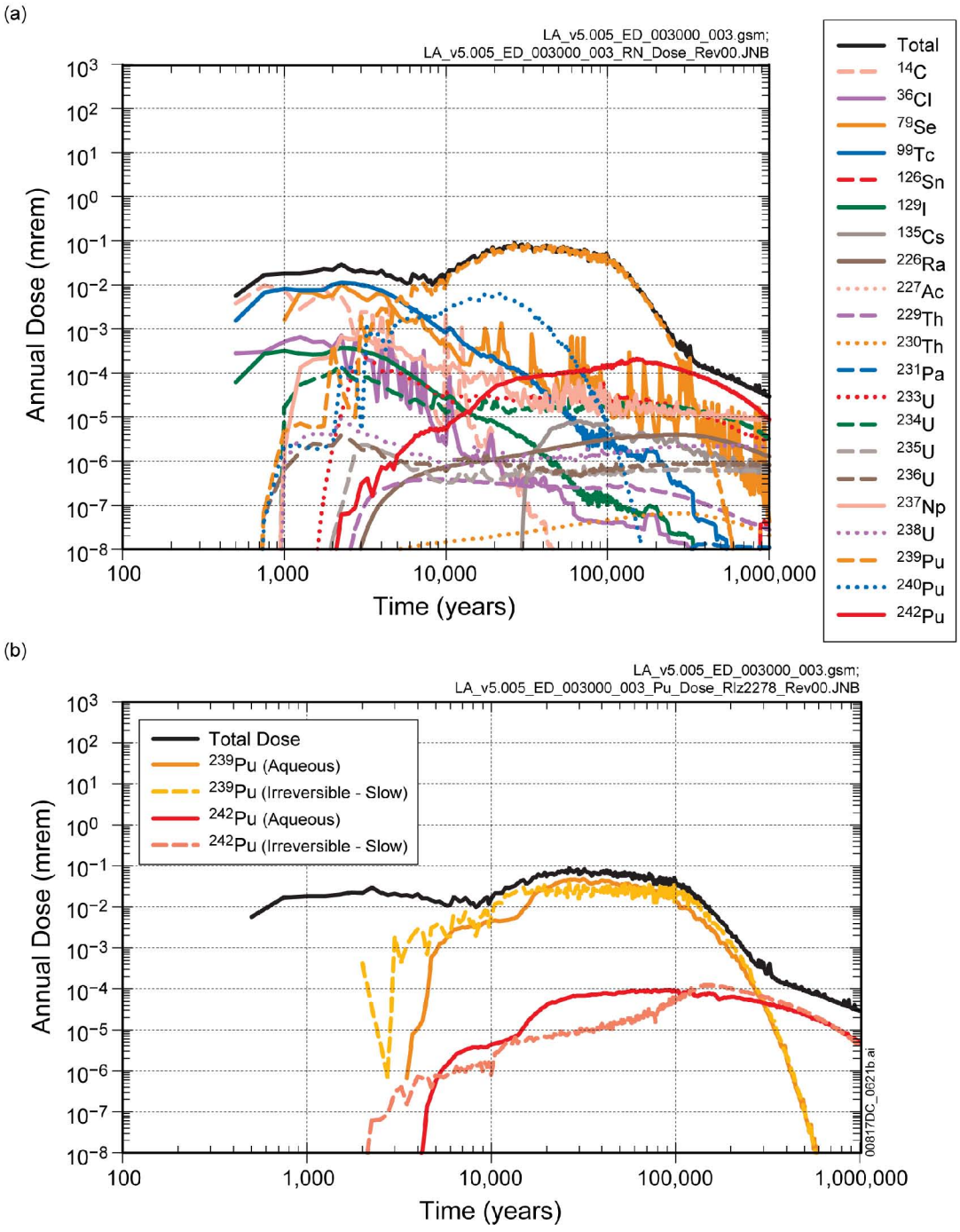

Source: Output DTN: MO0801TSPAMVAC.000 [DIRS 185080].

NOTE: Plutonium dissolved and reversibly associated with colloids is denoted as aqueous.

Figure 7.7.1-24[a]. (a) Annual Dose along with Major Radionuclide Dose Contributors and (b) Contribution of ^{239}Pu and ^{242}Pu (Aqueous and Associated Irreversibly with Colloids) for Realization 2278 of the Drip Shield Early Failure Modeling Case for 1,000,000 Years after Repository Closure

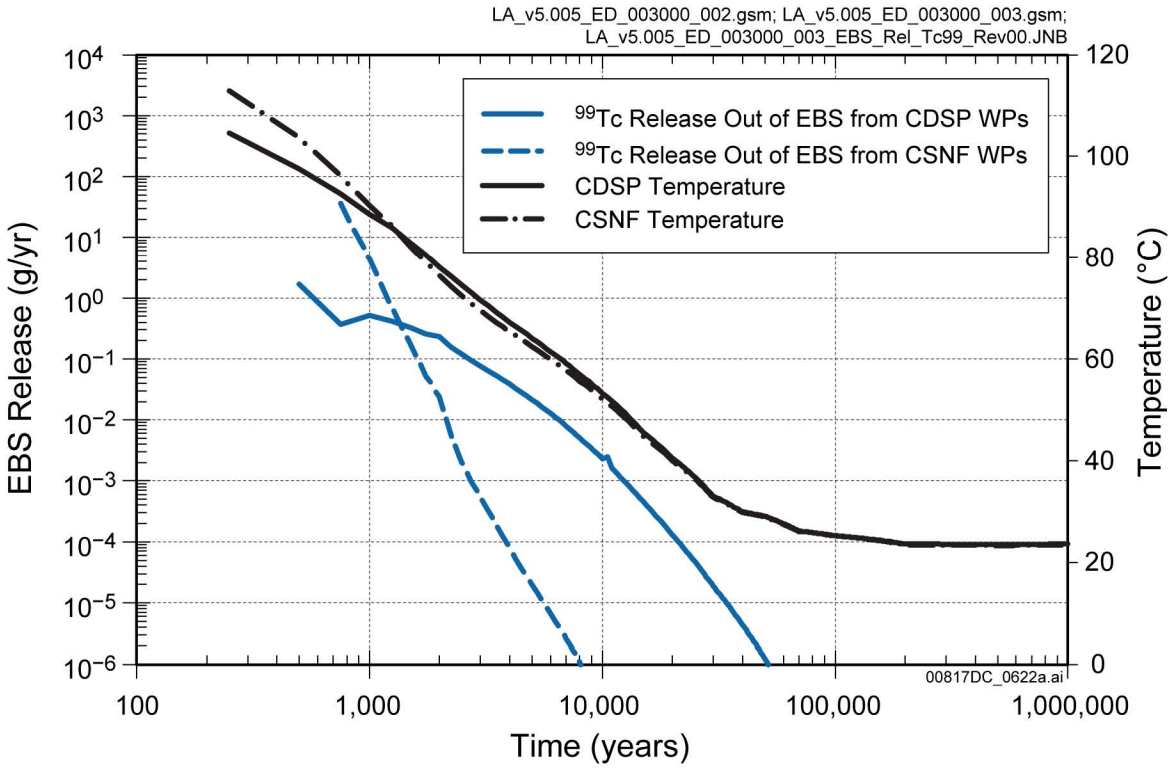

Source: Output DTN: MO0801TSPAMVAC.000 [DIRS 185080].

Figure 7.7.1-25[a]. EBS Release Rates of ^{99}Tc Along with Waste Package Temperatures for the Two Selected Realizations (2273 and 2278) of the Drip Shield Early Failure Modeling Case for 1,000,000 Years after Repository Closure

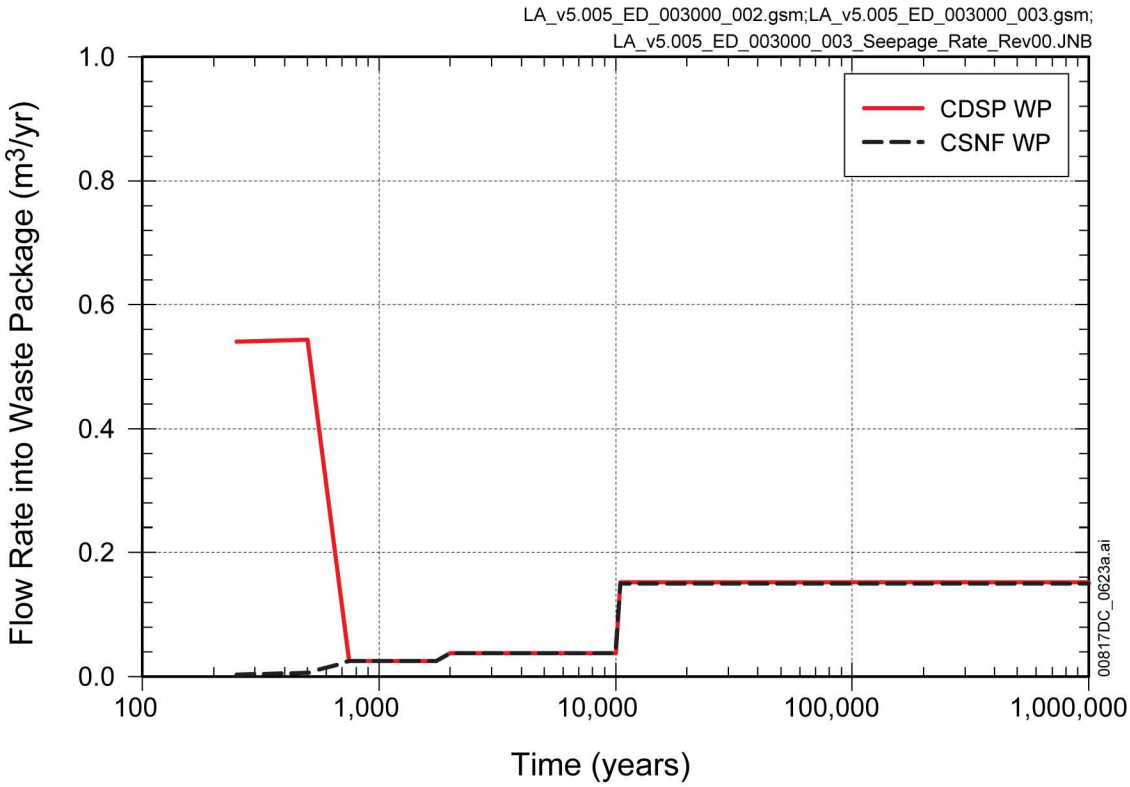

Source: Output DTN: MO0801TSPAMVAC.000 [DIRS 185080].

Figure 7.7.1-26[a]. Flow Rate Incident on the Waste Package Showing the Effects of Drift Wall Condensation and Climate Change for the Two Selected Realizations (2273 and 2278) of the Drip Shield Early Failure Modeling Case for 1,000,000 Years after Repository Closure

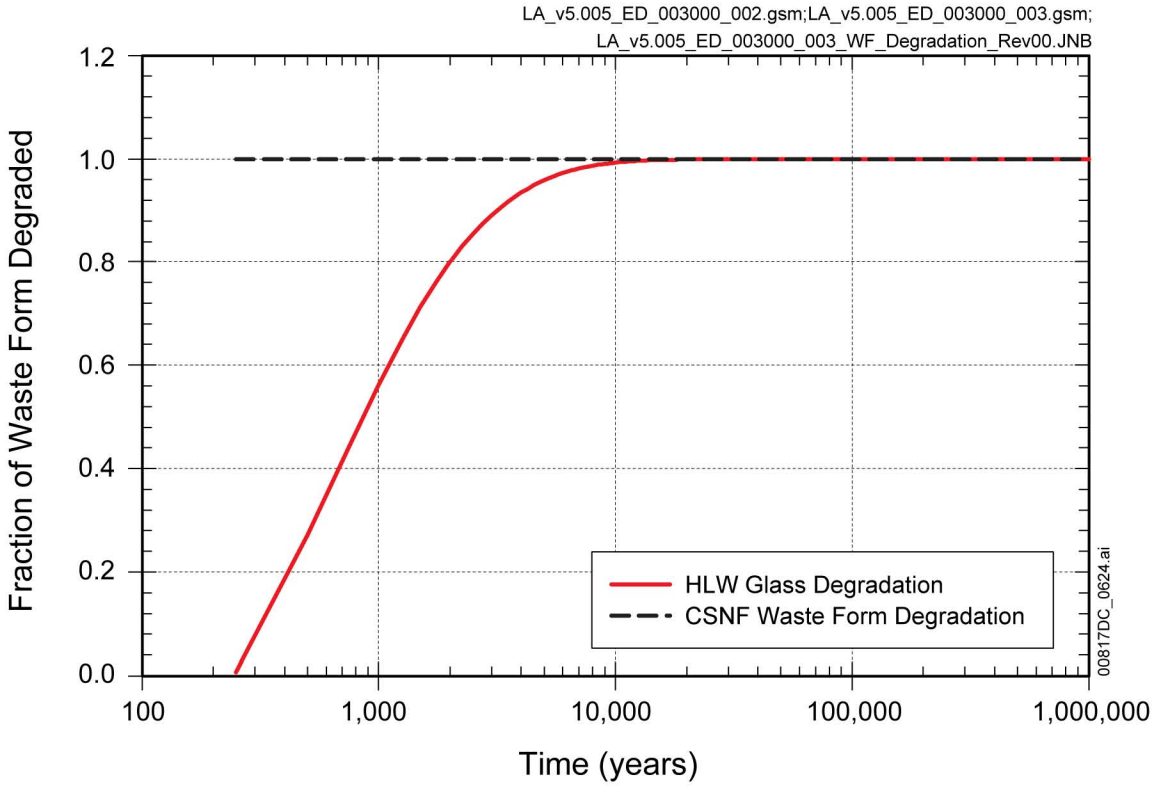

Source: Output DTN: MO0801TSPAMVAC.000 [DIRS 185080].

Figure 7.7.1-27[a]. Fraction of CSNF and HLW Glass Waste Form Degraded for the Two Selected Realizations (2273 and 2278) of the Drip Shield Early Failure Modeling Case for 1,000,000 Years after Repository Closure

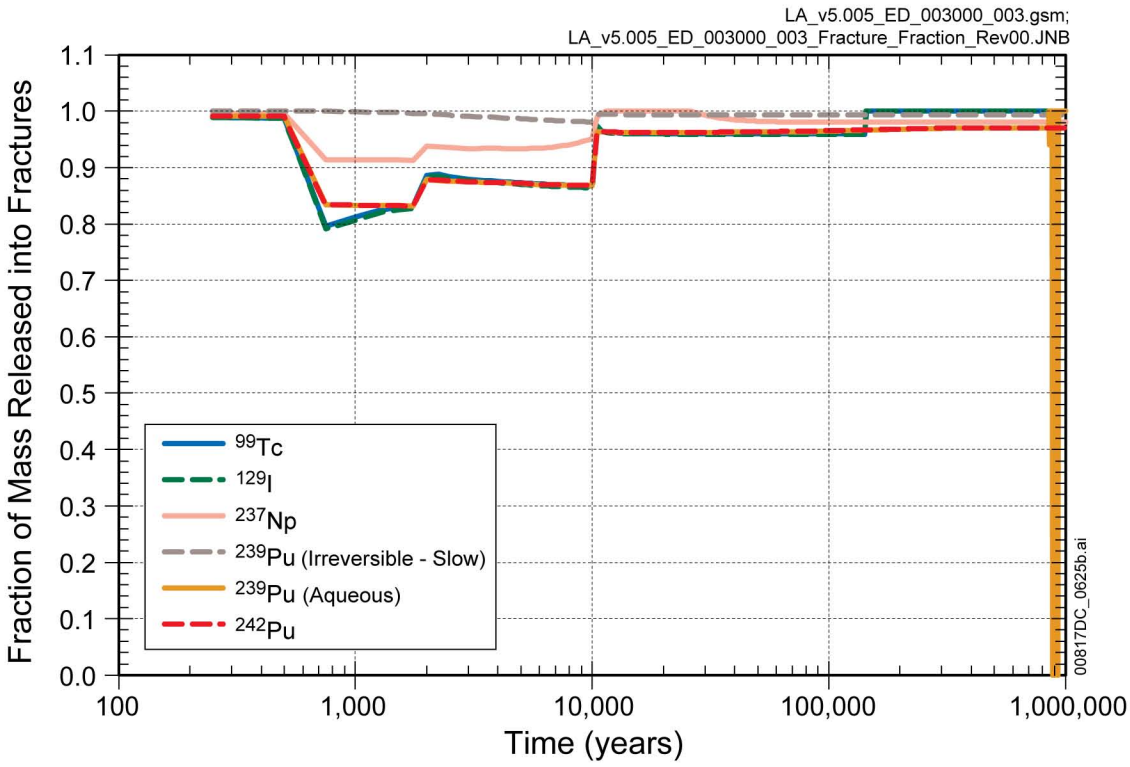

Source: Output DTN: MO0801TSPAMVAC.000 [DIRS 185080].

NOTES: GoldSim realization 2278 represents a CDSP WP in percolation subregion 3. Plutonium dissolved and reversibly associated with colloids is denoted as aqueous.

Figure 7.7.1-28[a]. Fraction of EBS Mass Flux Released into Unsaturated Zone Fractures for Selected Radionuclides for Realization 2278 of the Drip Shield Early Failure Modeling Case for 1,000,000 Years after Repository Closure

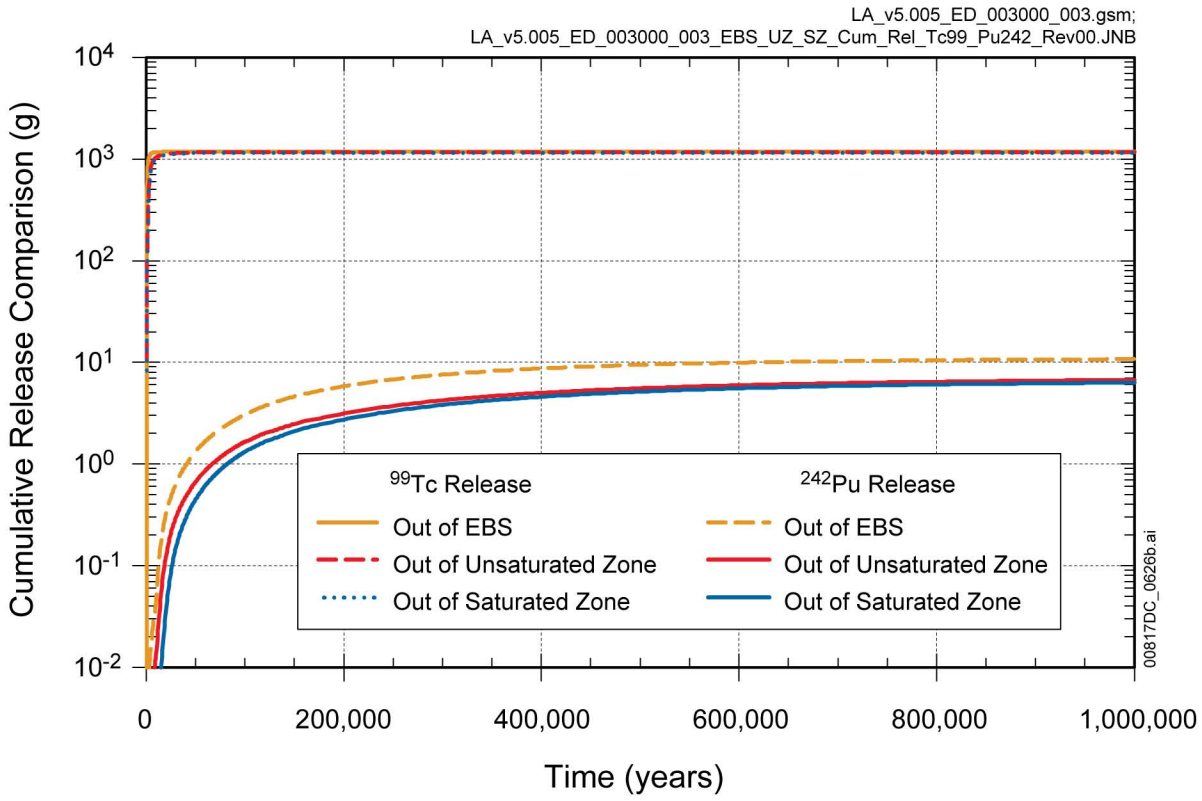

Source: Output DTN: MO0801TSPAMVAC.000 [DIRS 185080].

NOTE: For ^{242}Pu, the release includes the mass released in the dissolved state and reversibly associated with colloids.

Figure 7.7.1-29[a]. Cumulative Mass Release of ^{99}Tc and ^{242}Pu from the EBS, Unsaturated Zone, and Saturated Zone for Realization 2278 of the Drip Shield Early Failure Modeling Case for 1,000,000 Years after Repository Closure

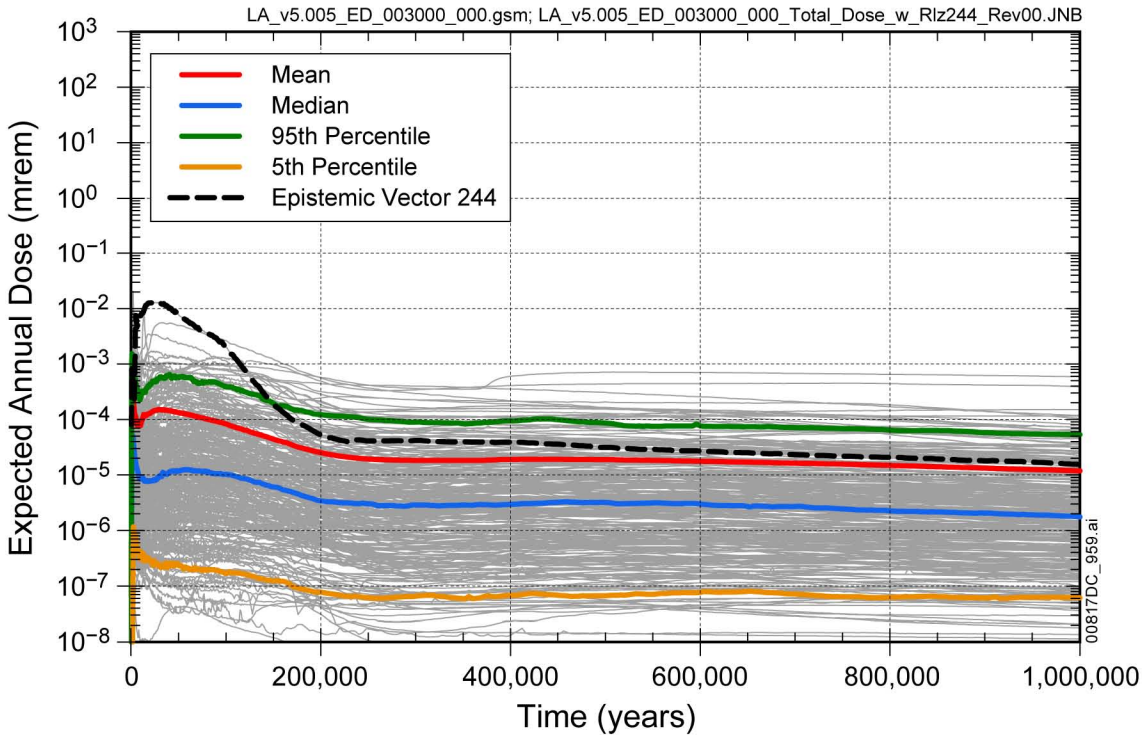

Source: Output DTN: MO0710ADTSPAWO.000 [DIRS 183752].

Figure 7.7.1-30[a]. Expected Annual Dose and Epistemic Uncertainty Vector 244 for the Drip Shield Early Failure Modeling Case for 1,000,000 Years after Repository Closure

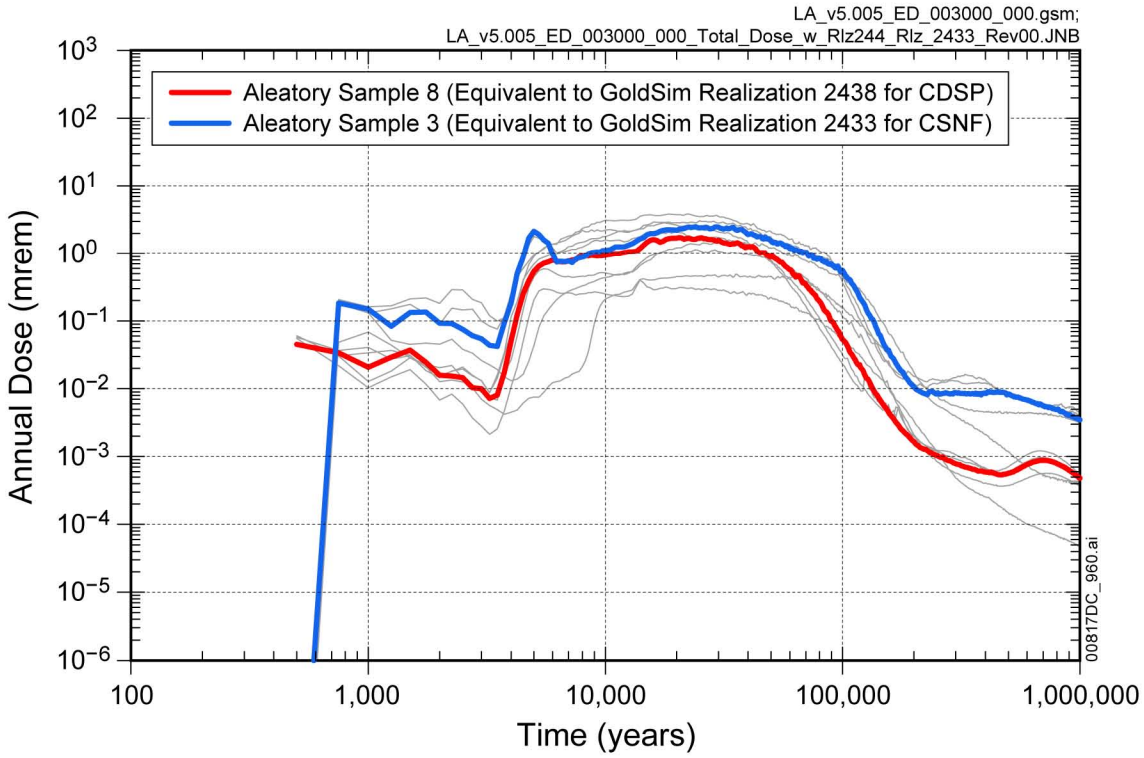

Source: Output DTN: MO0710ADTSPAWO.000 [DIRS 183752].

Figure 7.7.1-31[a]. Ten Aleatory Uncertainty Vectors for the Epistemic Uncertainty Vector 244 of the Drip Shield Early Failure Modeling Case for 1,000,000 Years after Repository Closure

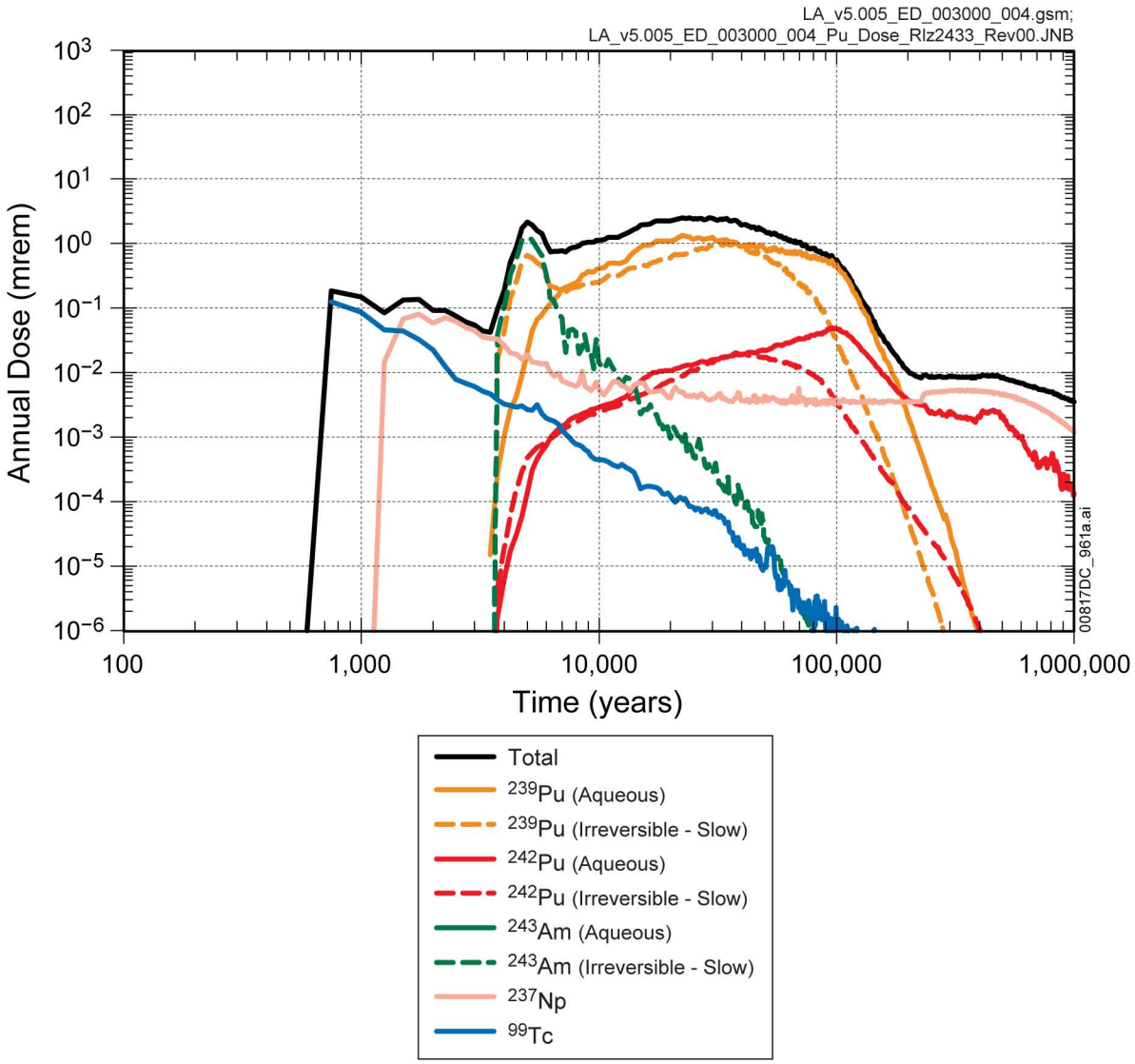

Source: Output DTN: MO0801TSPAMVAC.000 [DIRS 185080].

NOTE: Radionuclides dissolved and reversibly associated with colloids are denoted as aqueous.

Figure 7.7.1-32[a]. Major Radionuclide Dose Contributors to Annual Dose for Realization 2433 of the Drip Shield Early Failure Modeling Case for 1,000,000 Years after Repository Closure

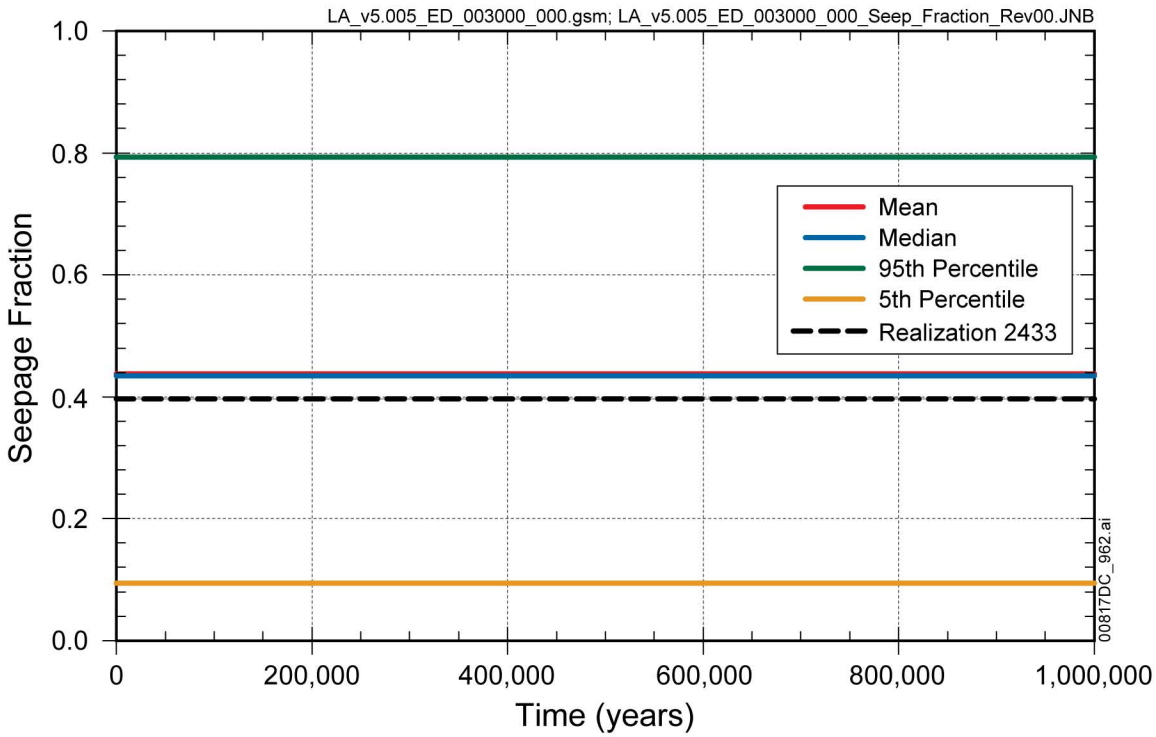

Source: Output DTN: MO0710ADTSPAWO.000 [DIRS 183752].

Figure 7.7.1-33[a]. Seepage Fraction Statistics and Seepage Fraction for Realization 2433 for the Drip Shield Early Failure Modeling Case for 1,000,000 Years after Repository Closure

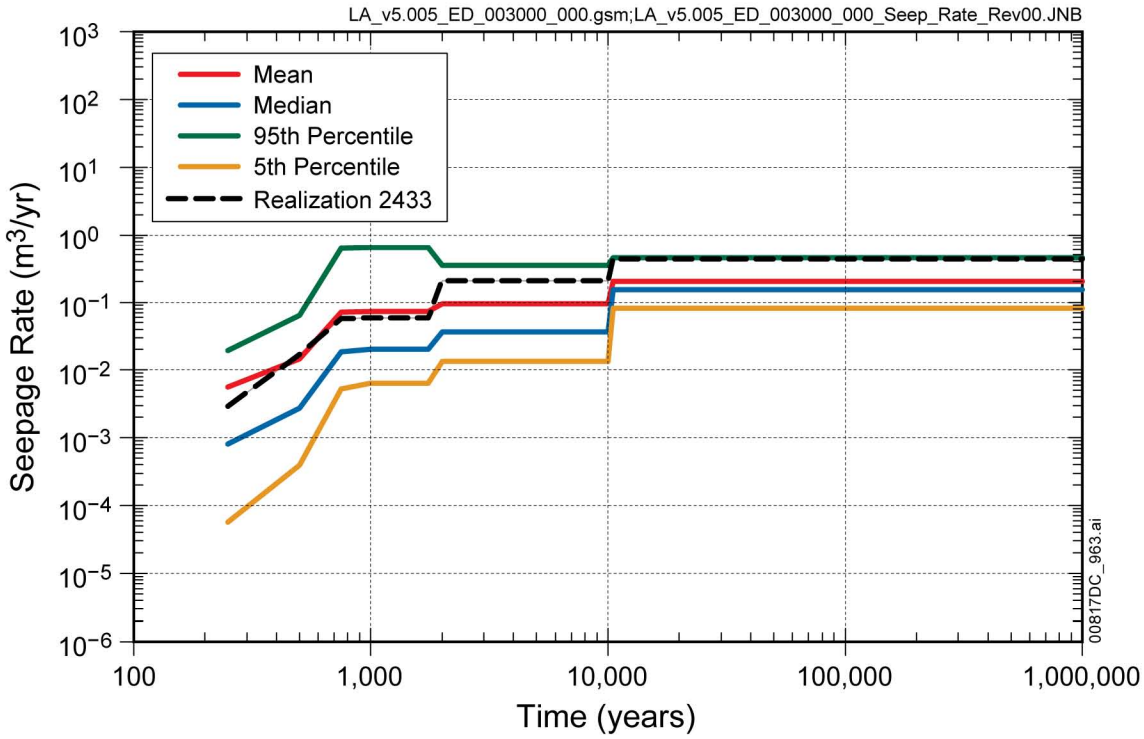

Source: Output DTN: MO0710ADTSPAWO.000 [DIRS 183752].

Figure 7.7.1-34[a]. Seepage Rate Statistics and Seepage Rate for Realization 2433 for the Drip Shield Early Failure Modeling Case for 1,000,000 Years after Repository Closure

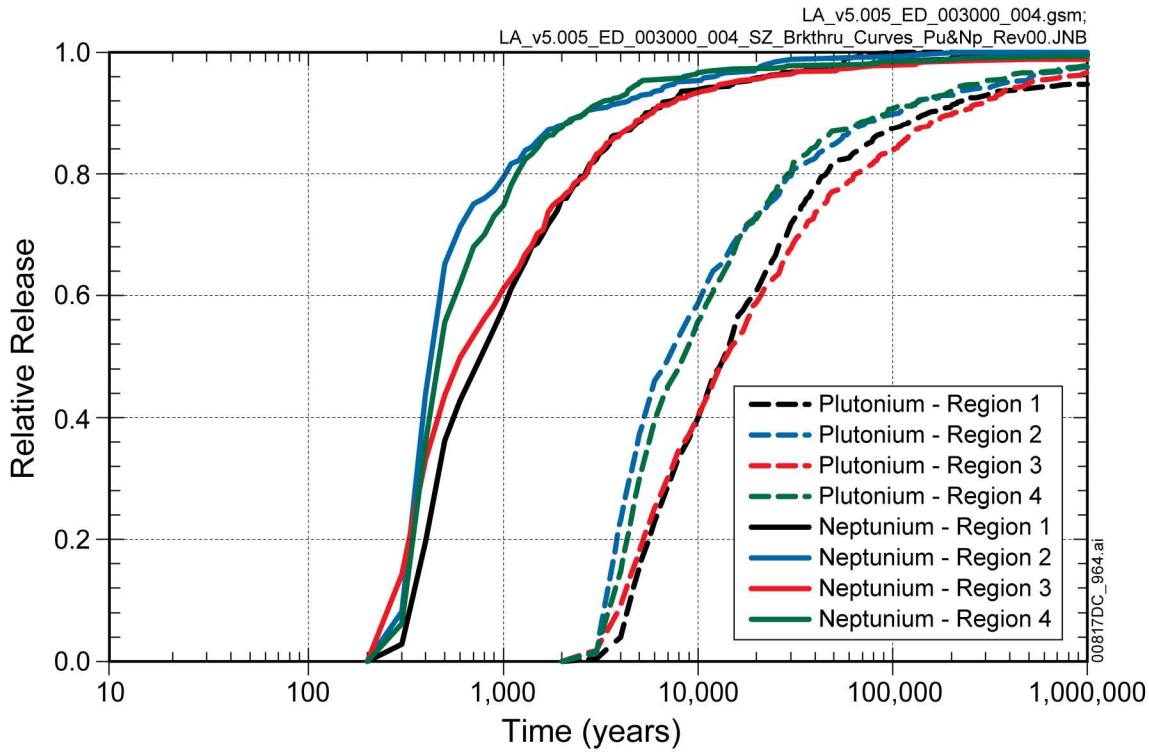

Source: Output DTN: MO0801TSPAMVAC.000 [DIRS 185080].

NOTE: For plutonium, release includes the mass released in the dissolved state and reversibly associated with colloids.

Figure 7.7.1-35[a]. Saturated Zone Breakthrough Curves for Plutonium and Neptunium for All Four Saturated Zone Regions for Realization 2433 of the Drip Shield Early Failure Modeling Case for 1,000,000 Years after Repository Closure

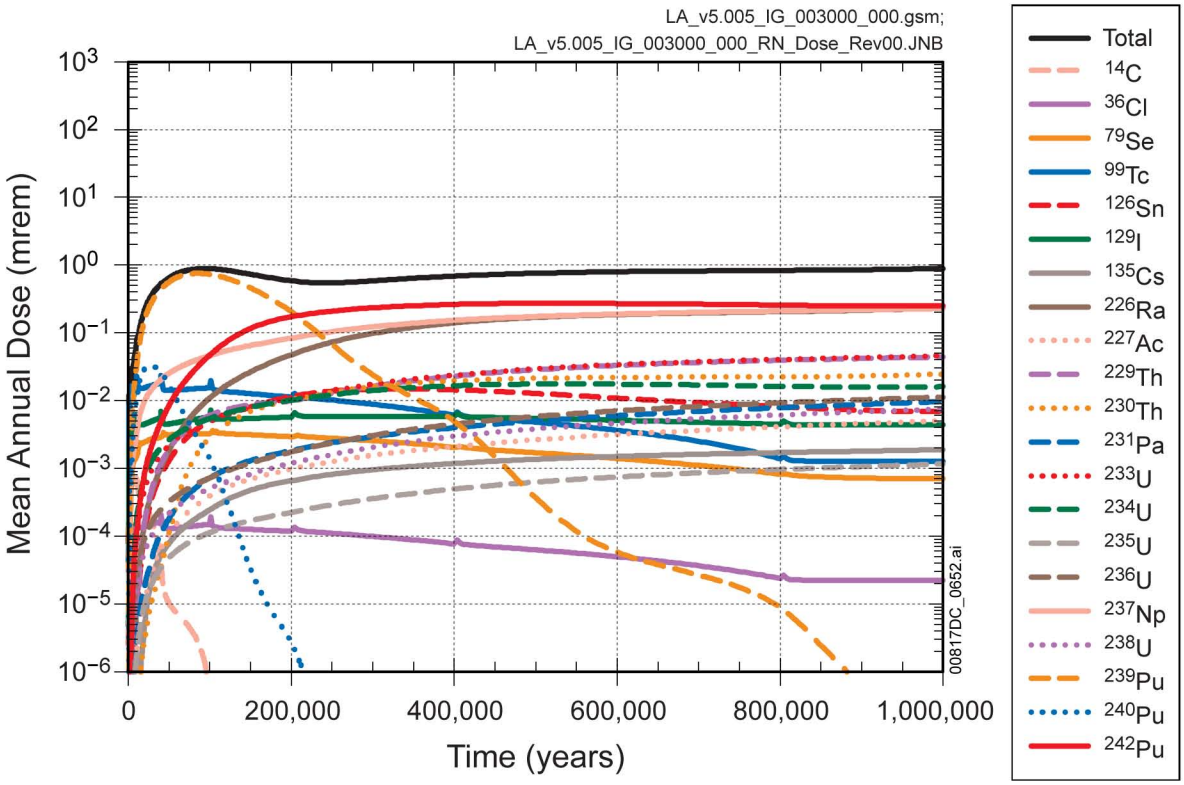

Source: Output DTN: MO0710ADTSPAWO.000 [DIRS 183752].

Figure 7.7.1-36[a]. Major Radionuclide Contributors to Mean Annual Dose for the Igneous Intrusion Modeling Case for 1,000,000 Years after Repository Closure

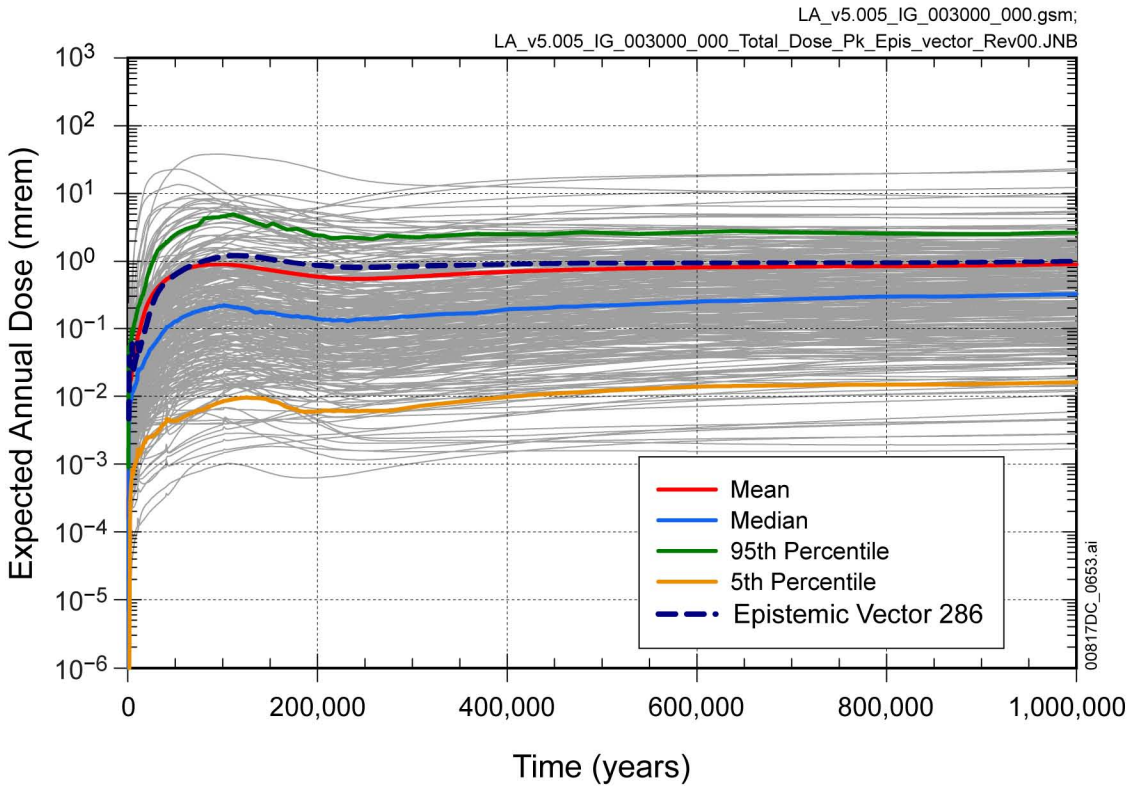

Source: Output DTN: MO0710ADTSPAWO.000 [DIRS 183752].

Figure 7.7.1-37[a]. Expected Annual Dose from the 300 Epistemic Uncertainty Vectors Along with their Quantiles and Expected Dose from Epistemic Uncertainty Vector 286 for the Igneous Intrusion Modeling Case for 1,000,000 Years after Repository Closure

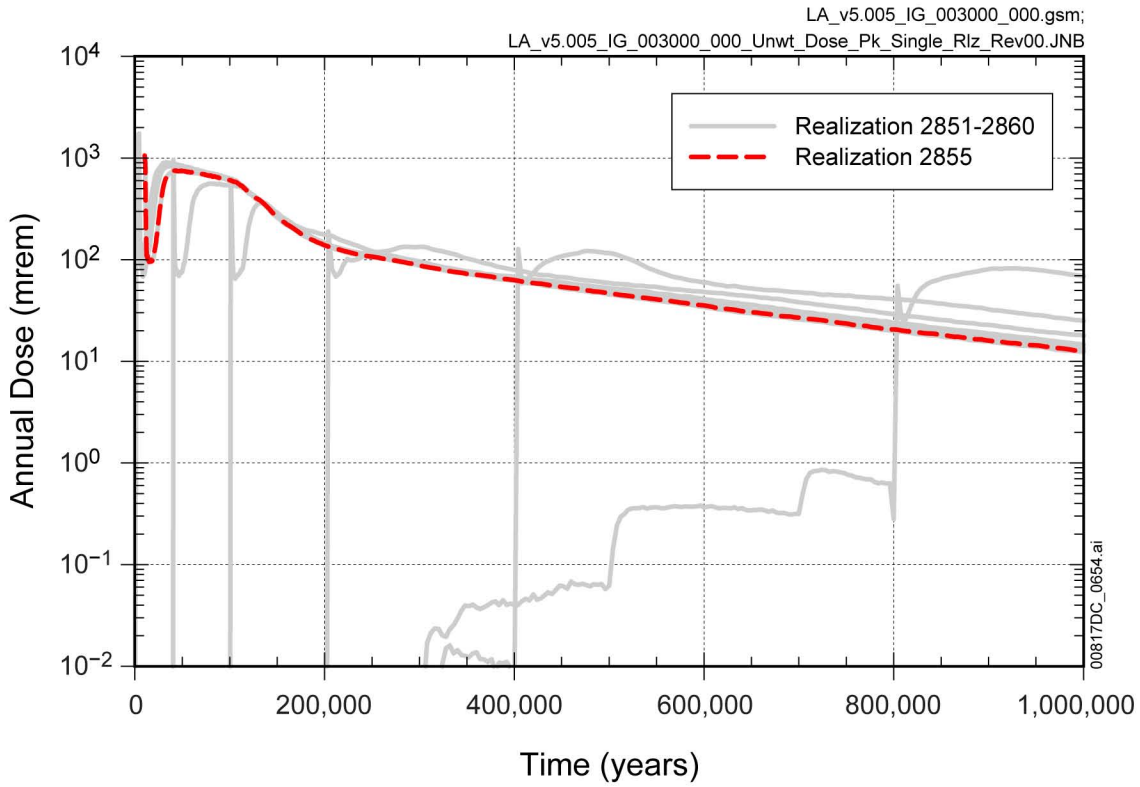

Source: Output DTN: MO0710ADTSPAWO.000 [DIRS 183752].

Figure 7.7.1-38[a]. Annual Dose for Realizations 2851 through 2860 (representing Epistemic Uncertainty Vector 286) along with Selected Realization 2855 of the Igneous Intrusion Modeling Case for 1,000,000 Years after Repository Closure

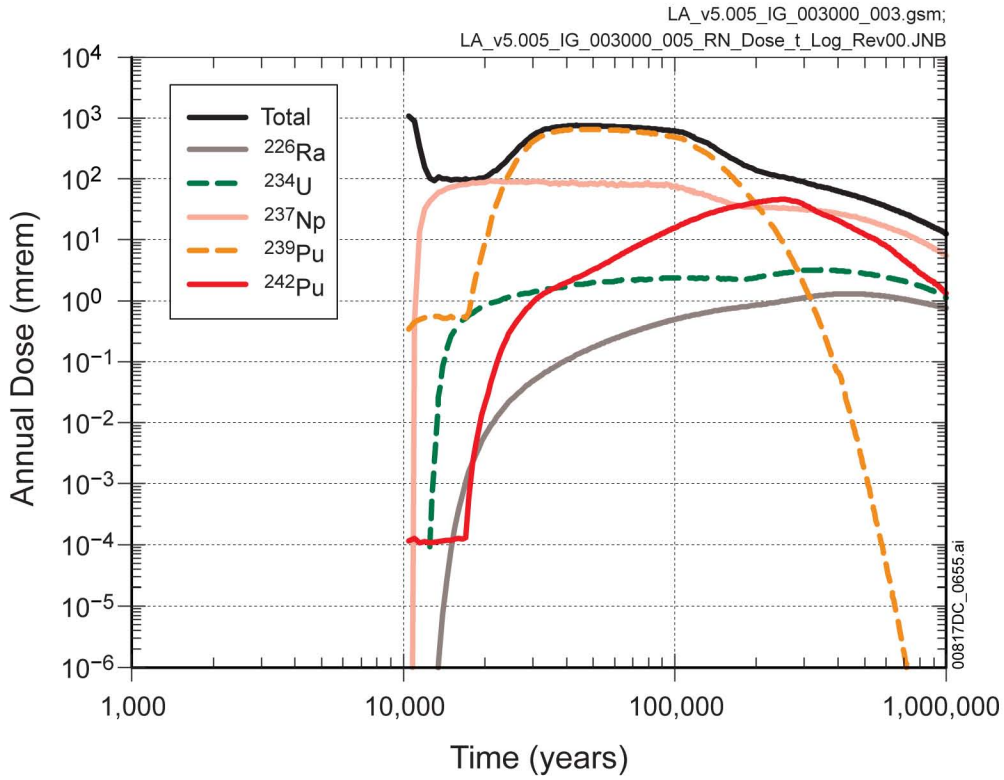

Source: Output DTN: MO0801TSPAMVAC.000 [DIRS 185080].

Figure 7.7.1-39[a]. Major Radionuclide Dose Contributors to Annual Dose for Realization 2855 of the Igneous Intrusion Modeling Case for 1,000,000 Years after Repository Closure

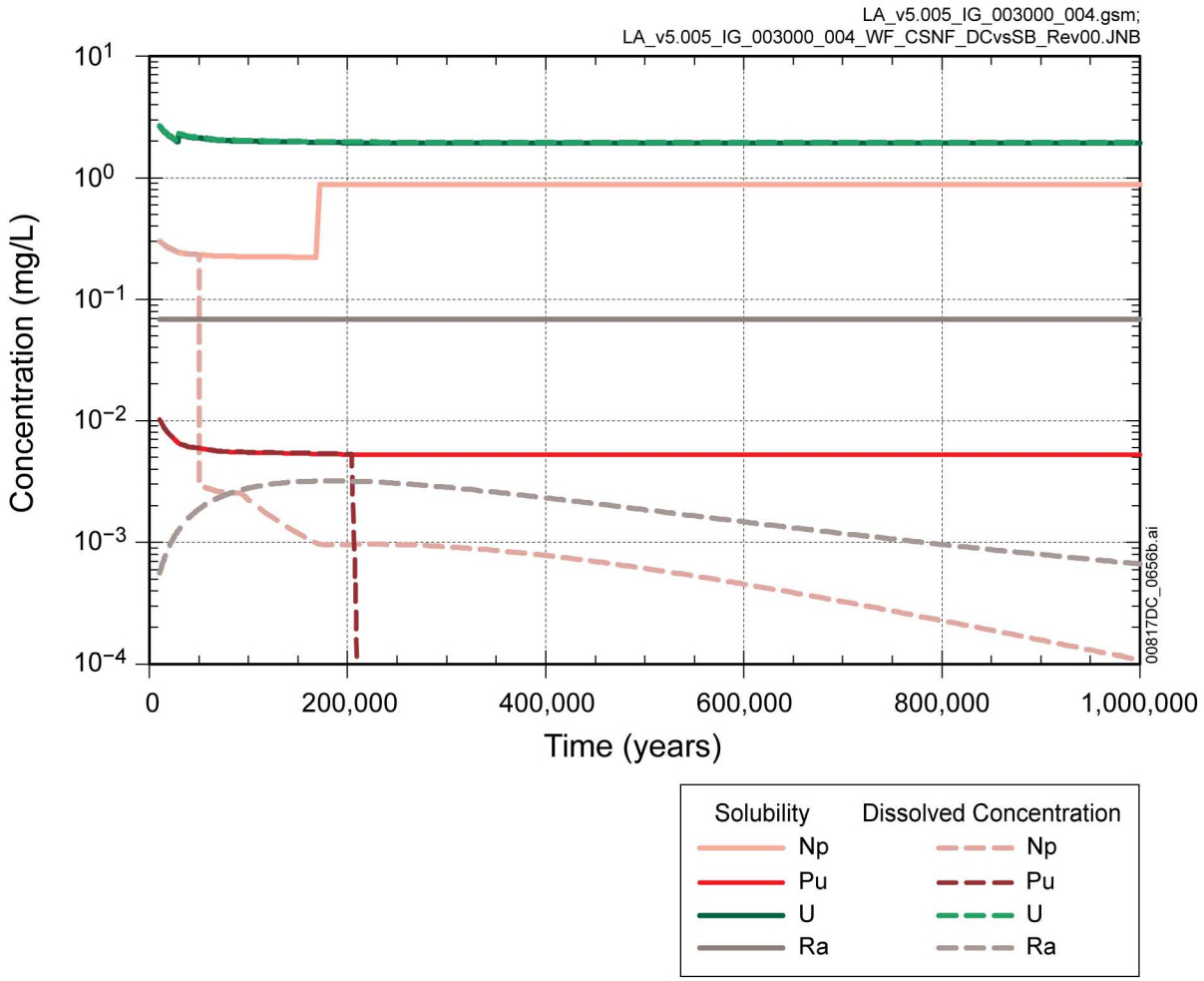

Source: Output DTN: MO0801TSPAMVAC.000 [DIRS 185080].

Figure 7.7.1-40[a]. Dissolved Concentrations and Solubility Limits of Neptunium, Plutonium, Uranium, and Radium in the CSNF Waste Form Domain for Percolation Subregion 3 Seeping Environment for Realization 2855 of the Igneous Intrusion Modeling Case for 1,000,000 Years after Repository Closure

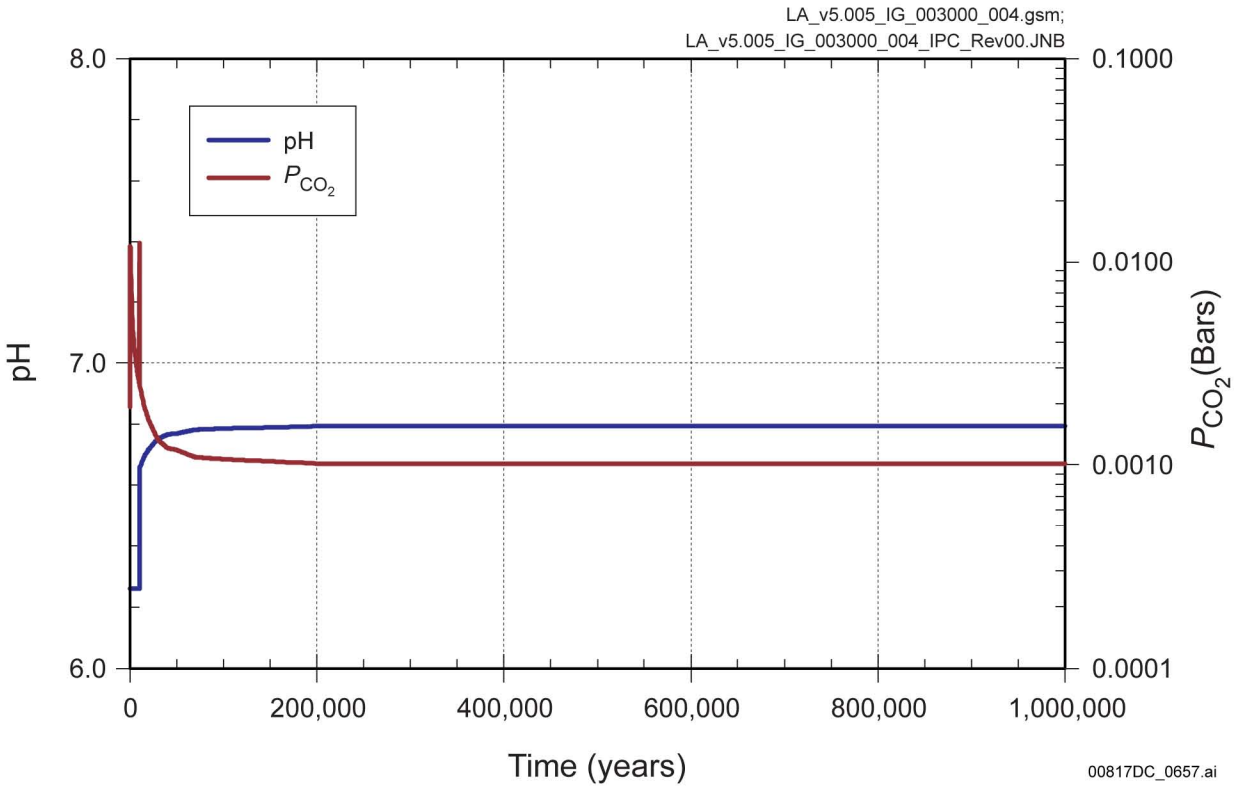

Source: Output DTN: MO0801TSPAMVAC.000 [DIRS 185080].

Figure 7.7.1-41[a]. In-Package pH and Pco_2 in the Waste Form Domain for Percolation Subregion 3 Seeping Environment for Realization 2855 of the Igneous Intrusion Modeling Case for 1,000,000 Years after Repository Closure

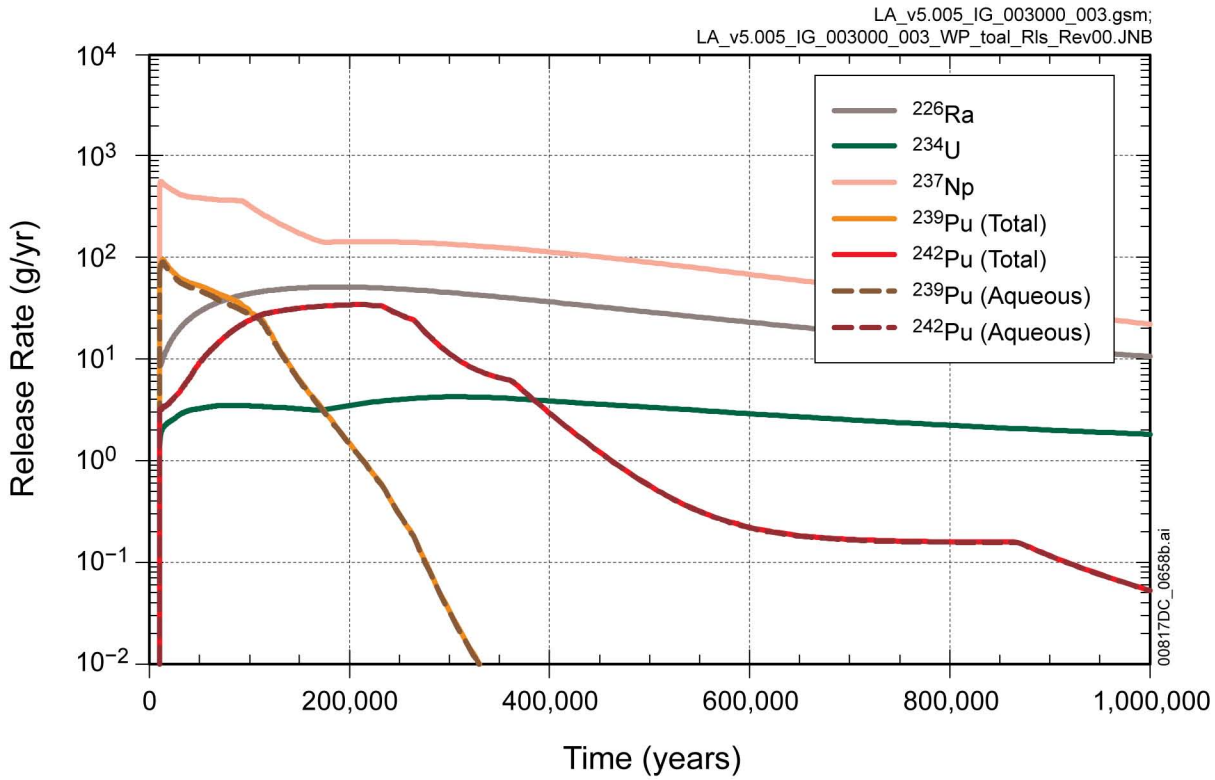

Source: Output DTN: MO0801TSPAMVAC.000 [DIRS 185080].

NOTE: Plutonium dissolved and reversibly associated with colloids is denoted as aqueous.

Figure 7.7.1-42[a]. Release Rate of Major Radionuclides from all Waste Packages for Realization 2855 of the Igneous Intrusion Modeling Case for 1,000,000 Years after Repository Closure

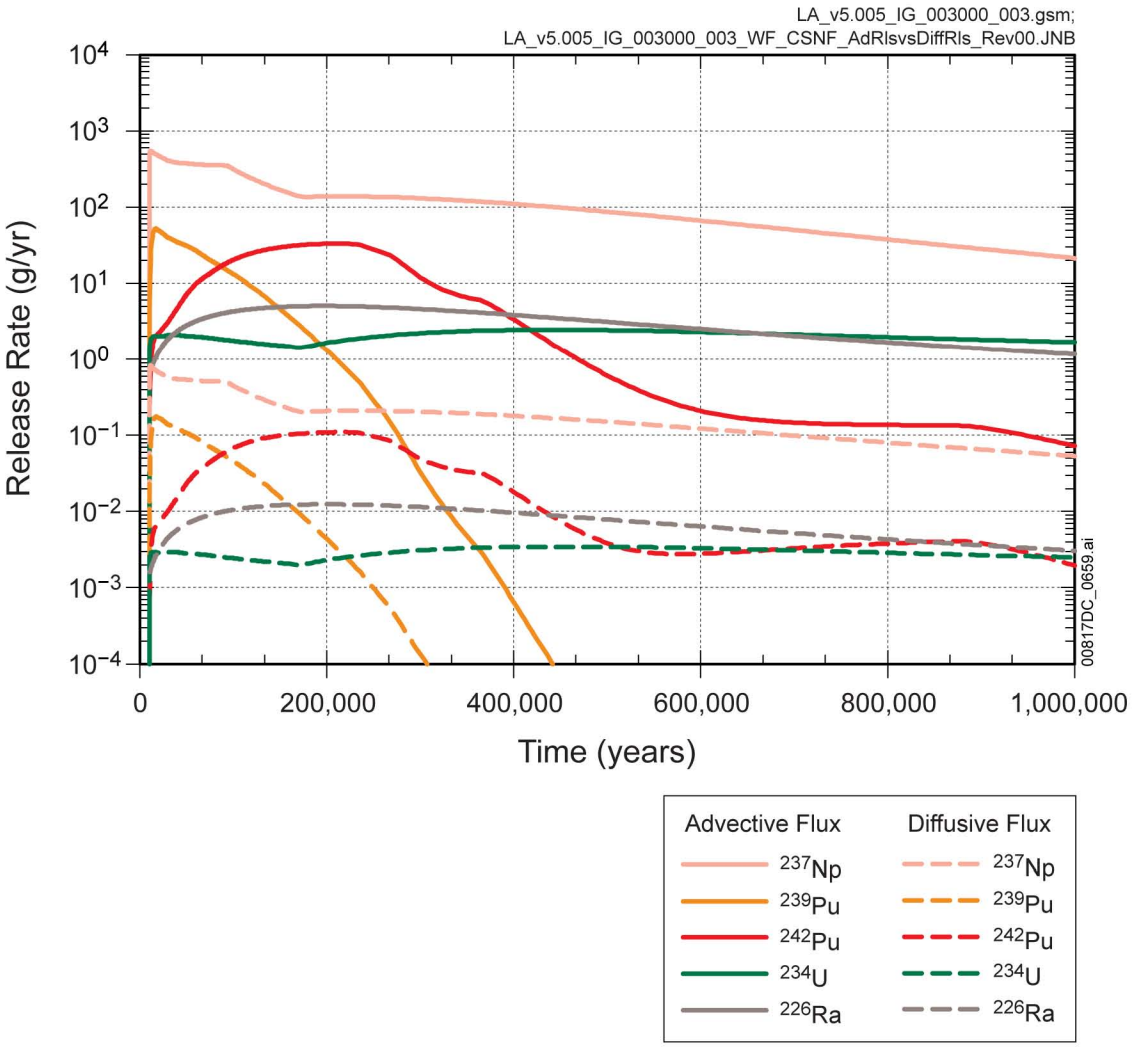

Source: Output DTN: MO0801TSPAMVAC.000 [DIRS 185080].

Figure 7.7.1-43[a]. Advective and Diffusive Release Rates of Major Radionuclides (Dissolved and Reversibly Associated with Colloids) from the CSNF WPs for Realization 2855 of the Igneous Intrusion Modeling Case for 1,000,000 Years after Repository Closure

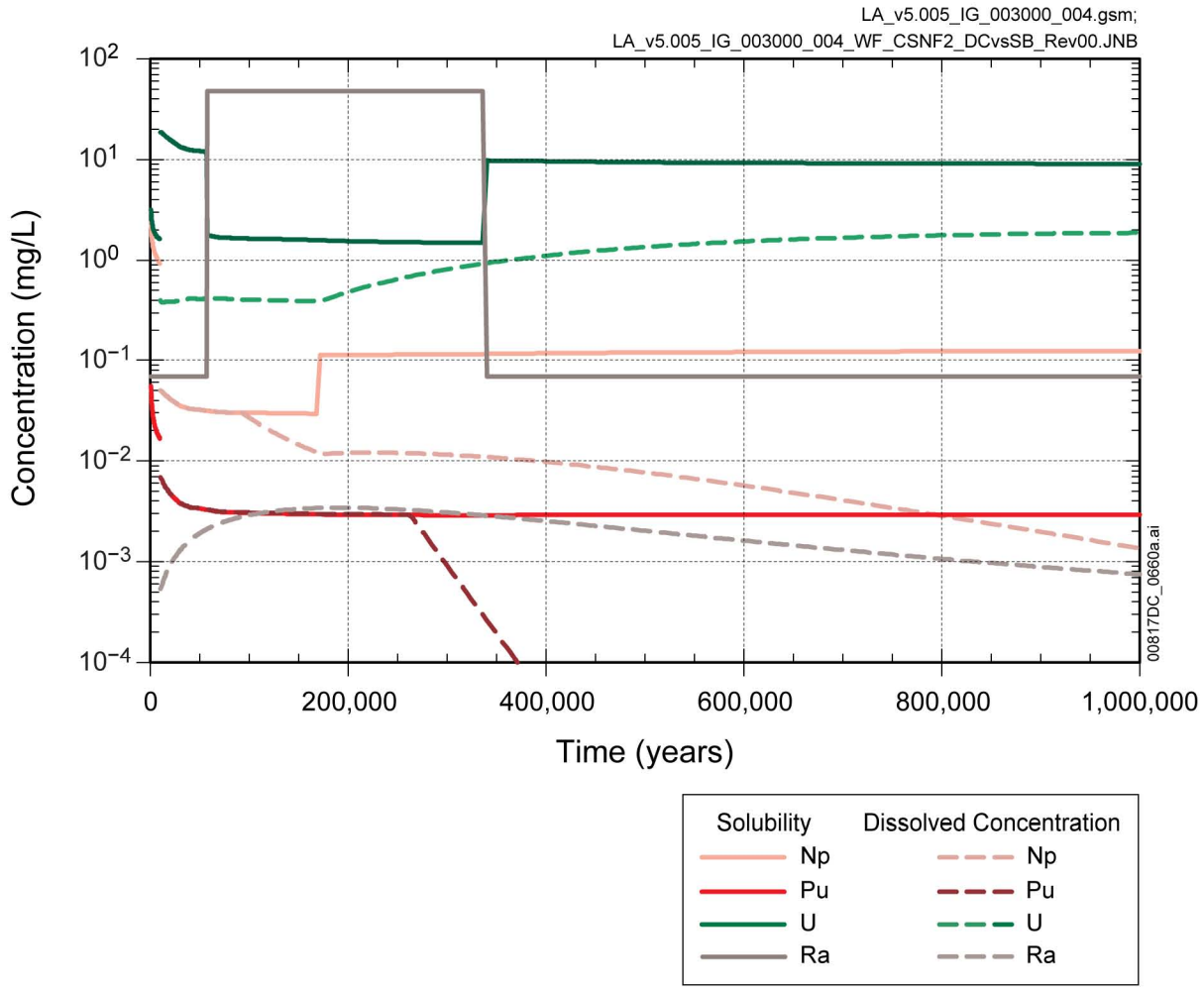

Source: Output DTN: MO0801TSPAMVAC.000 [DIRS 185080].

Figure 7.7.1-44[a]. Total Dissolved Concentrations and Solubility Limits of Neptunium, Plutonium, Uranium, and Radium in the Corrosion Products Domain of CSNF WPs Located in Percolation Subregion 3 Seeping Environment for Realization 2855 of the Igneous Intrusion Modeling Case for 1,000,000 Years after Repository Closure

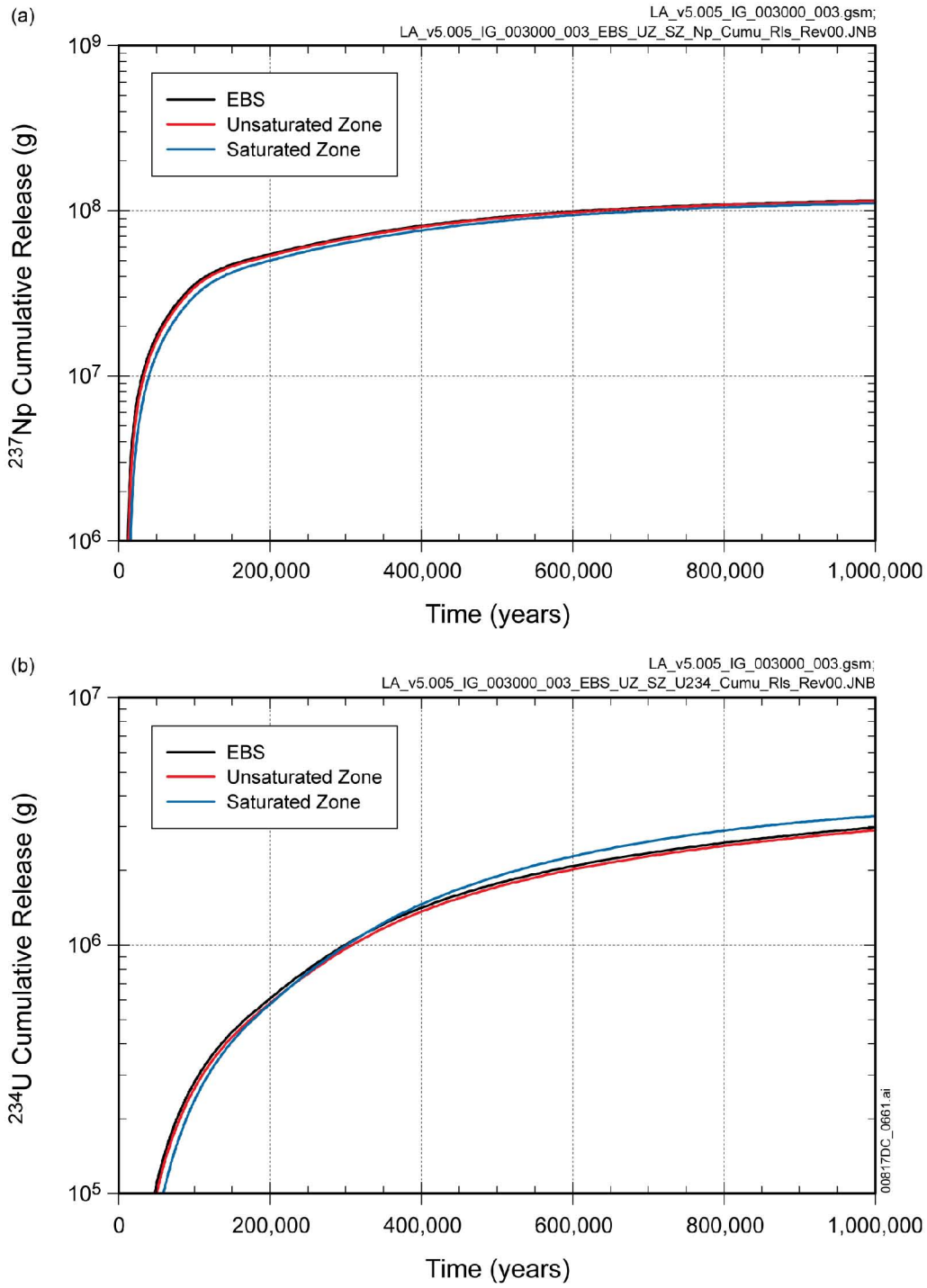

Source: Output DTN: MO0801TSPAMVAC.000 [DIRS 185080].

Figure 7.7.1-45[a]. Cumulative Releases of: (a) ^{237}Np, (b) ^{234}U, (c) ^{242}Pu (Dissolved and Reversibly Associated with Colloids), and (d) ^{226}Ra from the EBS, Unsaturated Zone, and Saturated Zone for Realization 2855 of the Igneous Intrusion Modeling Case for 1,000,000 Years after Repository Closure

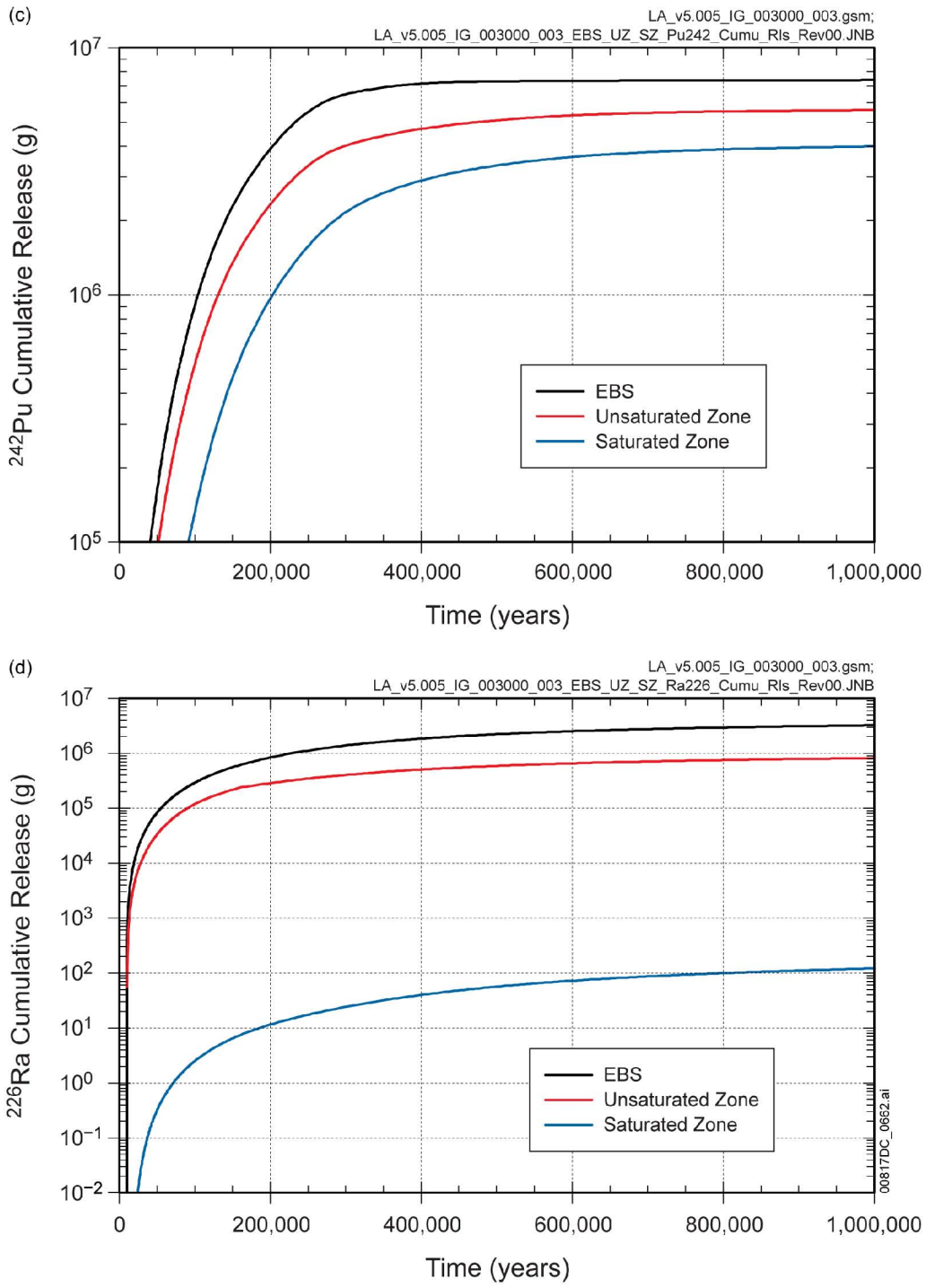

Source: Output DTN: MO0801TSPAMVAC.000 [DIRS 185080].

Figure 7.7.1-45[a]. Cumulative Releases of: (a) ^{237}Np, (b) ^{234}U, (c) ^{242}Pu (Dissolved and Reversibly Associated with Colloids), and (d) ^{226}Ra from the EBS, Unsaturated Zone, and Saturated Zone for Realization 2855 of the Igneous Intrusion Modeling Case for 1,000,000 Years after Repository Closure (Continued)

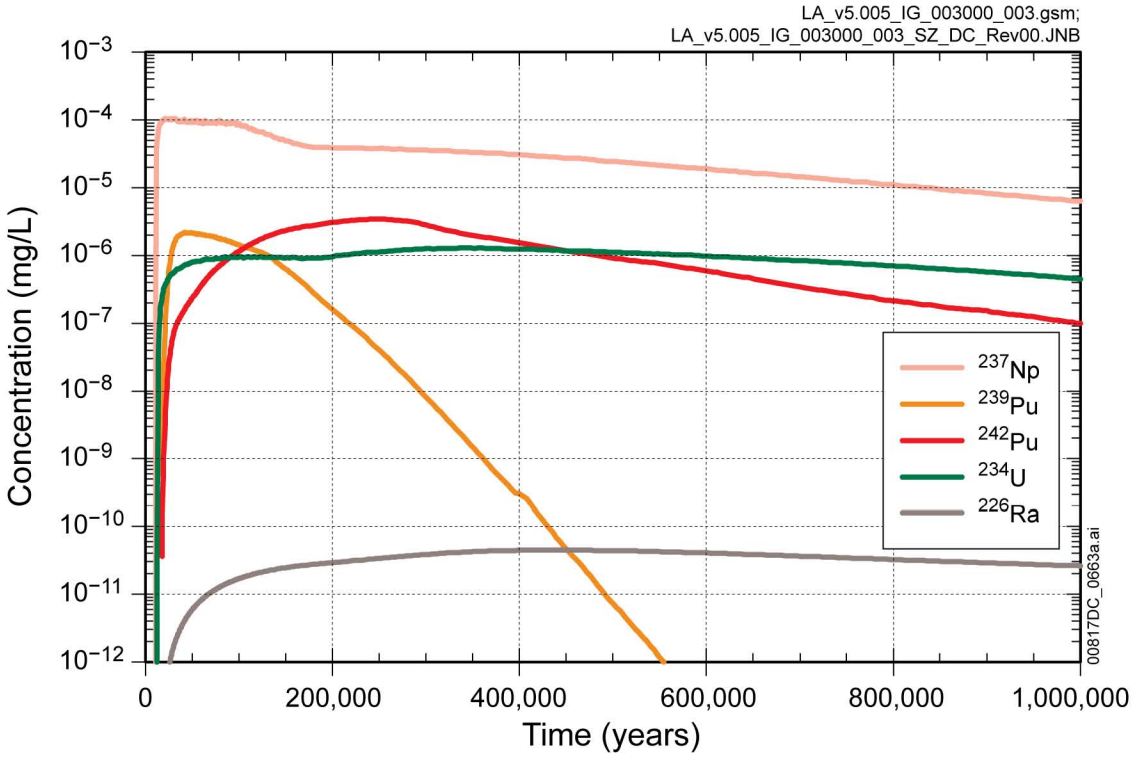

Source: Output DTN: MO0801TSPAMVAC.000 [DIRS 185080].

NOTE: The saturated zone concentrations shown on this figure are obtained by dividing the annual releases of radionuclides from the saturated zone by the 3,000 acre-ft/yr annual water usage, as required by regulations.

Figure 7.7.1-46[a]. Concentrations of Major Radionuclides (Dissolved and Reversibly Associated with Colloids) at the RMEI Location for Realization 2855 of the Igneous Intrusion Modeling Case for 1,000,000 Years after Repository Closure

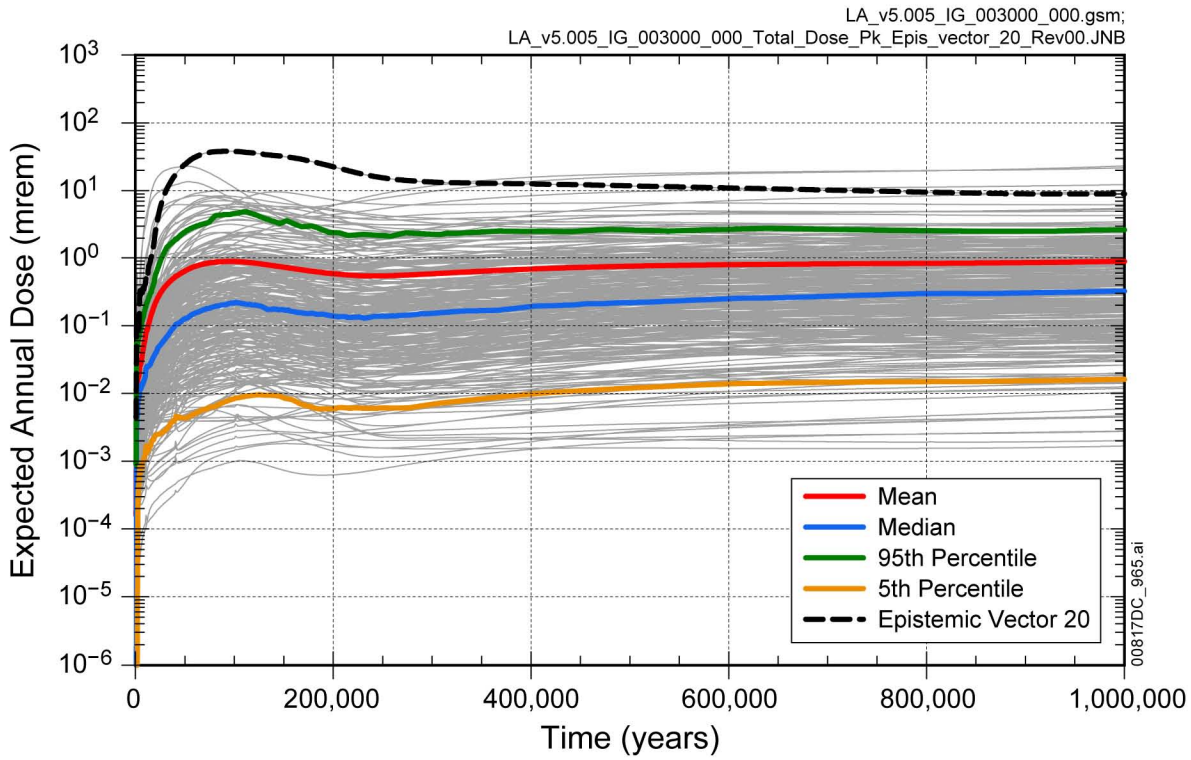

Source: Output DTN: MO0710ADTSPAWO.000 [DIRS 183752].

Figure 7.7.1-47[a]. Expected Annual Dose from the 300 Epistemic Uncertainty Vectors along with their Quantiles and Expected Dose from Epistemic Uncertainty Vector 20 for the Igneous Intrusion Modeling Case for 1,000,000 Years after Repository Closure

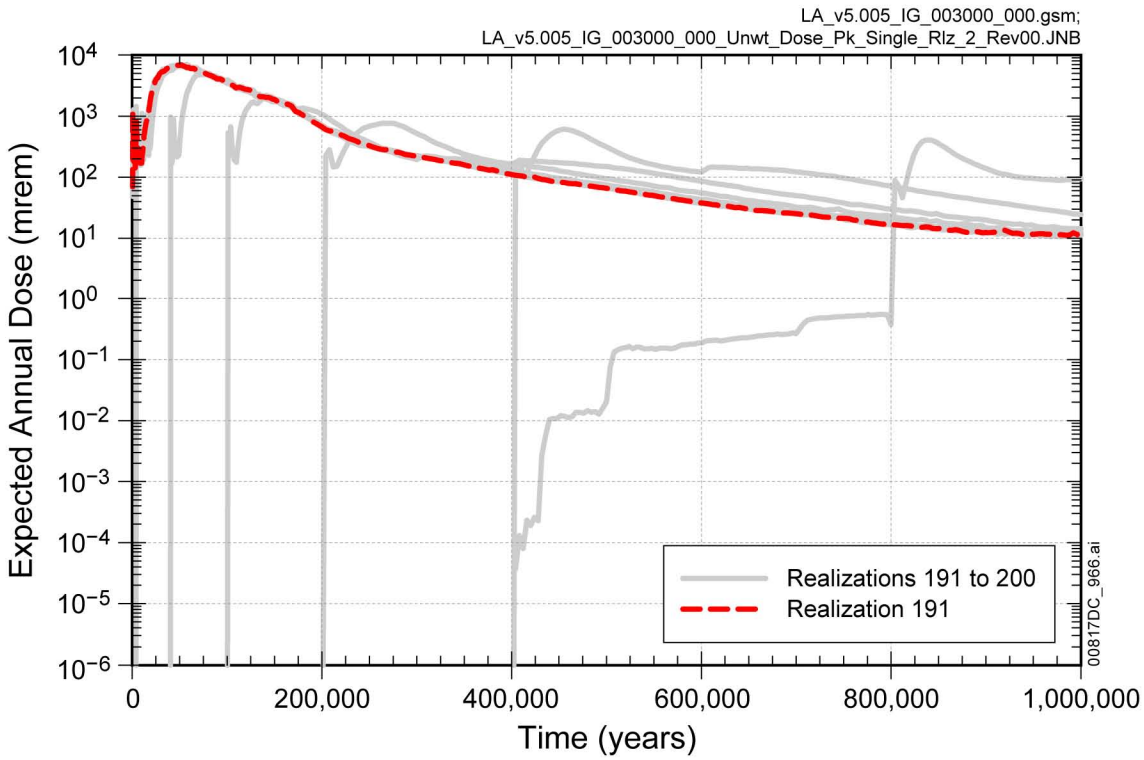

Source: Output DTN: MO0710ADTSPAWO.000 [DIRS 183752].

Figure 7.7.1-48[a]. Annual Dose from the Ten Aleatory Vectors Associated with the Epistemic Uncertainty Vector 20 for the Igneous Intrusion Modeling Case for 1,000,000 Years after Repository Closure

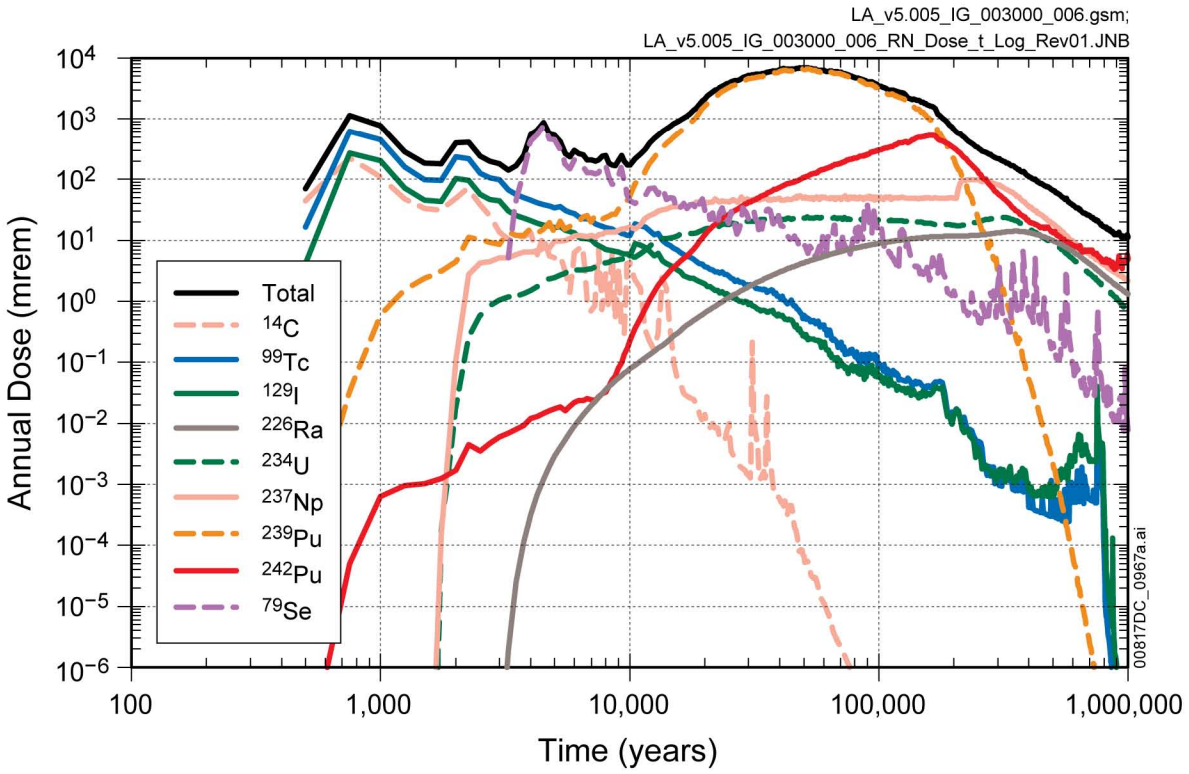

Source: Output DTN: MO0801TSPAMVAC.000 [DIRS 185080].

Figure 7.7.1-49[a]. Major Radionuclide Dose Contributors to Annual Dose for Realization 191 of the Igneous Intrusion Modeling Case for 1,000,000 Years after Repository Closure

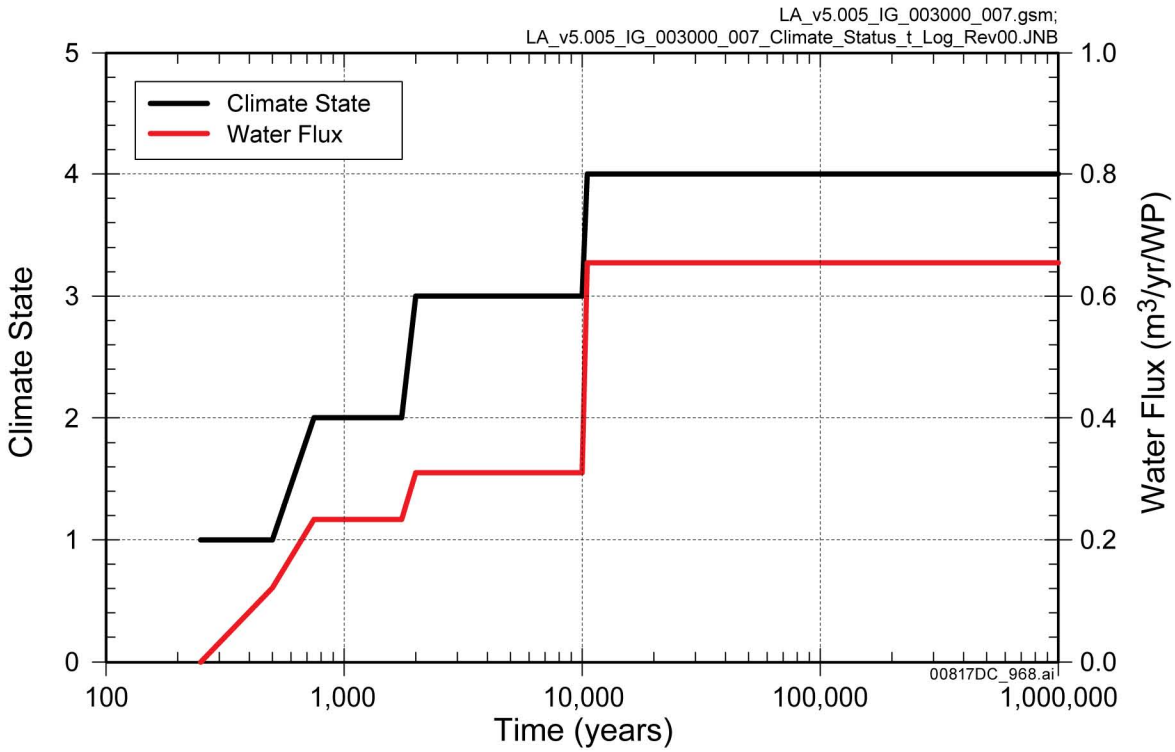

Source: Output DTN: MO0801TSPAMVAC.000 [DIRS 185080].

Figure 7.7.1-50[a]. Climate Status and Water Flux for Realization 191 of the Igneous Intrusion Modeling Case for 1,000,000 Years after Repository Closure

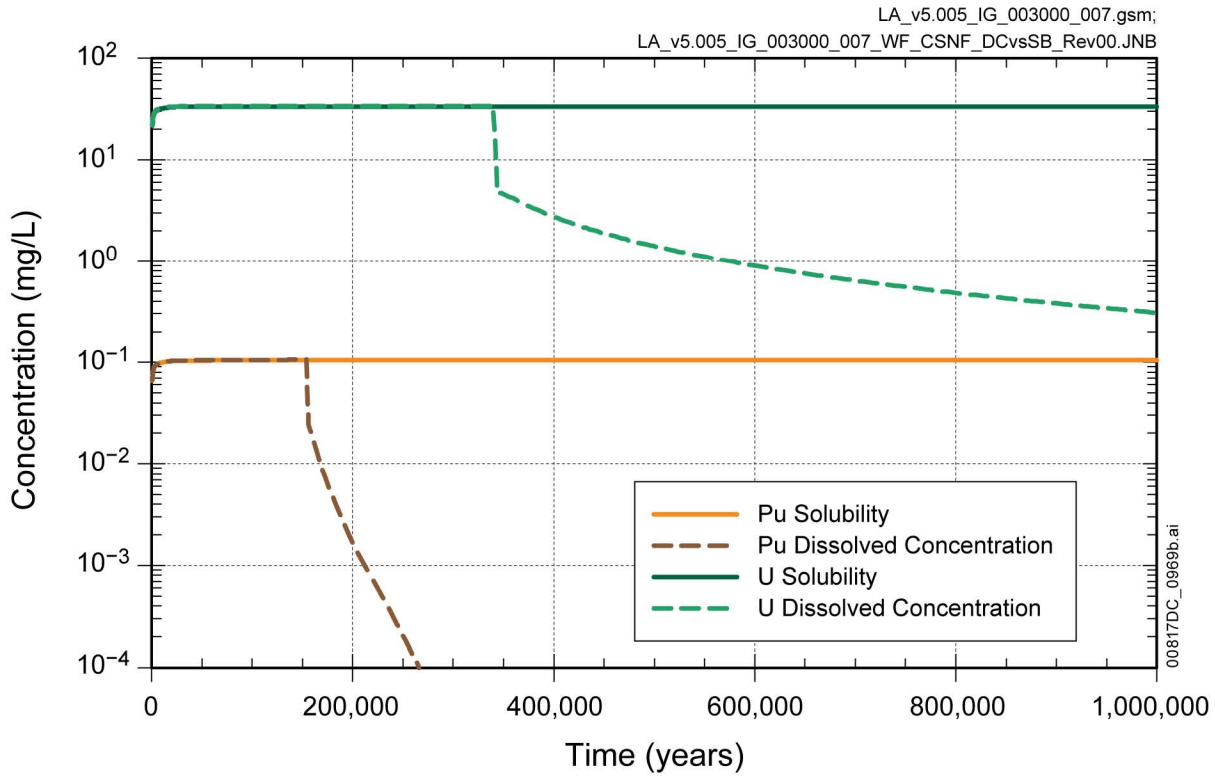

Source: Output DTN: MO0801TSPAMVAC.000 [DIRS 185080].

Figure 7.7.1-51[a]. Solubility and Dissolved Concentrations of Plutonium and Uranium within the CSNF Domain for Realization 191 of the Igneous Intrusion Modeling Case for 1,000,000 Years after Repository Closure

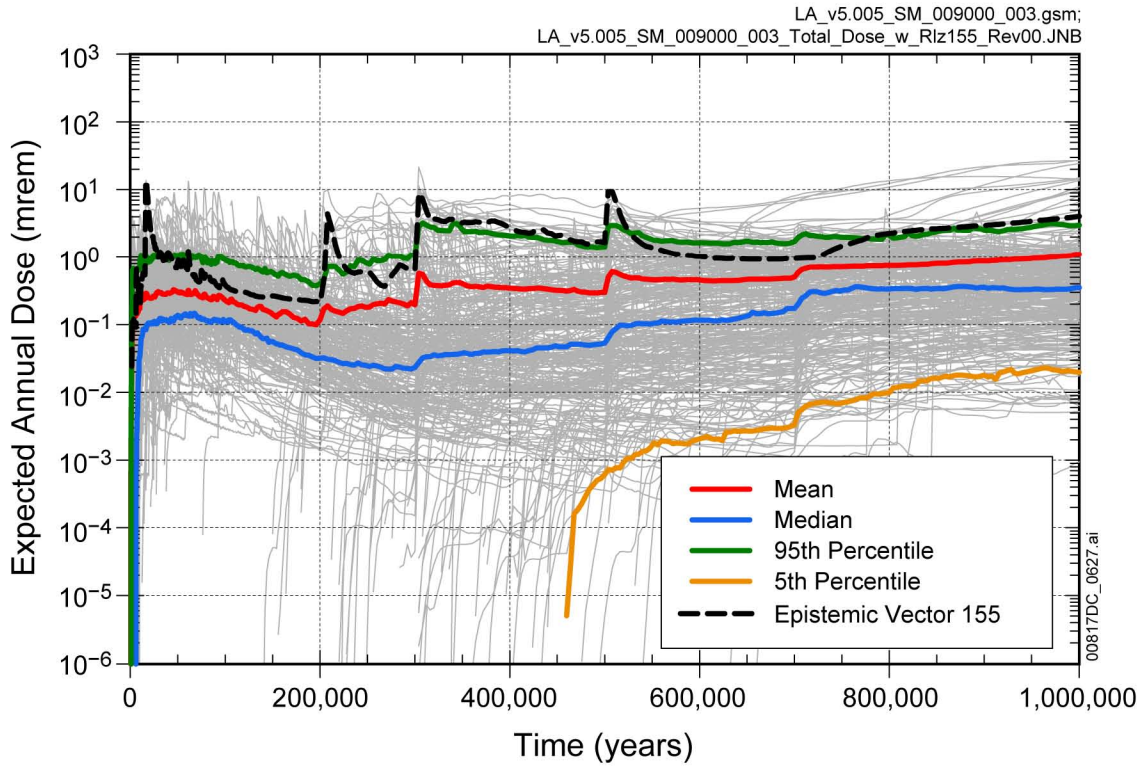

Source: Output DTN: MO0710ADTSPAWO.000 [DIRS 183752].

Figure 7.7.1-52[a]. Expected Annual Dose from the 300 Epistemic Uncertainty Vectors Along With their Quantiles and Expected Dose from Epistemic Uncertainty Vector 155 for the Seismic Ground Motion Modeling Case for 1,000,000 Years after Repository Closure

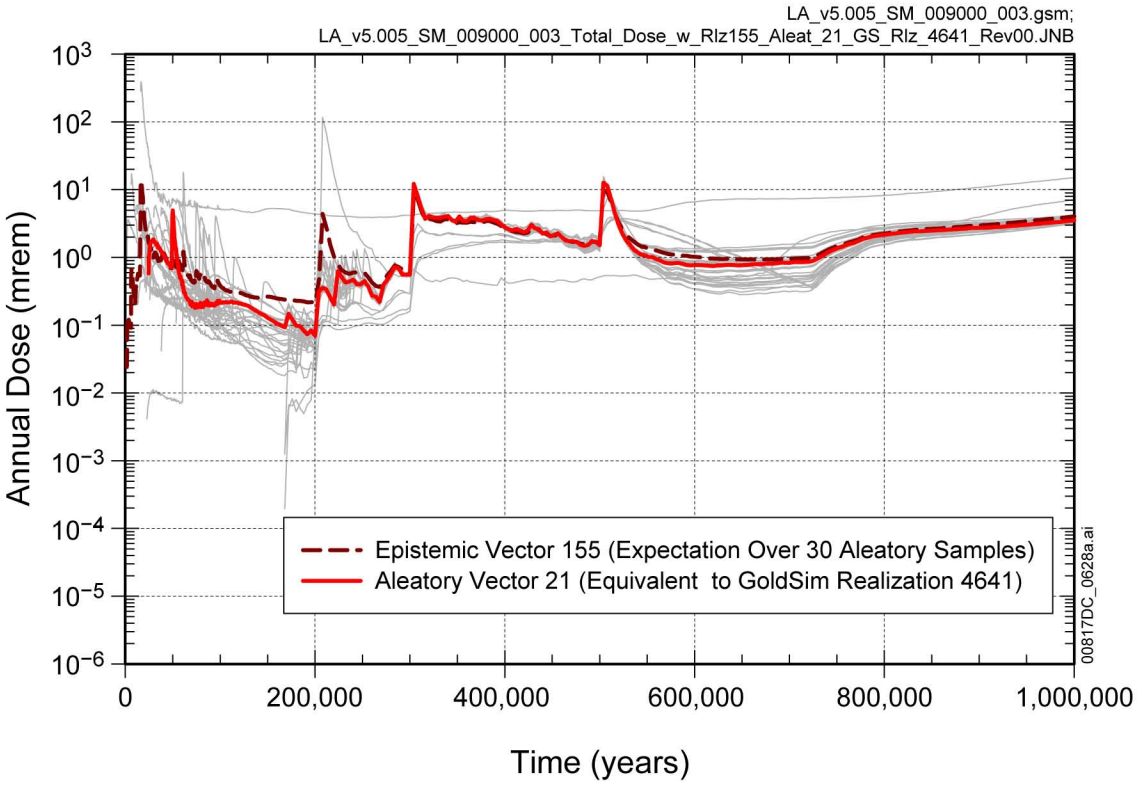

Source: Output DTN: MO0710ADTSPAWO.000 [DIRS 183752].

NOTES: The dashed line is the expected annual dose for epistemic uncertainty vector 155 by taking expectation over the thirty aleatory vectors. The solid red line is the annual dose from aleatory vector 21, which is equivalent to GoldSim realization 4641.

Figure 7.7.1-53[a]. Annual Dose from the Thirty Aleatory Vectors (Seismic Event Sequences) Associated with the Epistemic Uncertainty Vector 155 for the Seismic Ground Motion Modeling Case for 1,000,000 Years after Repository Closure

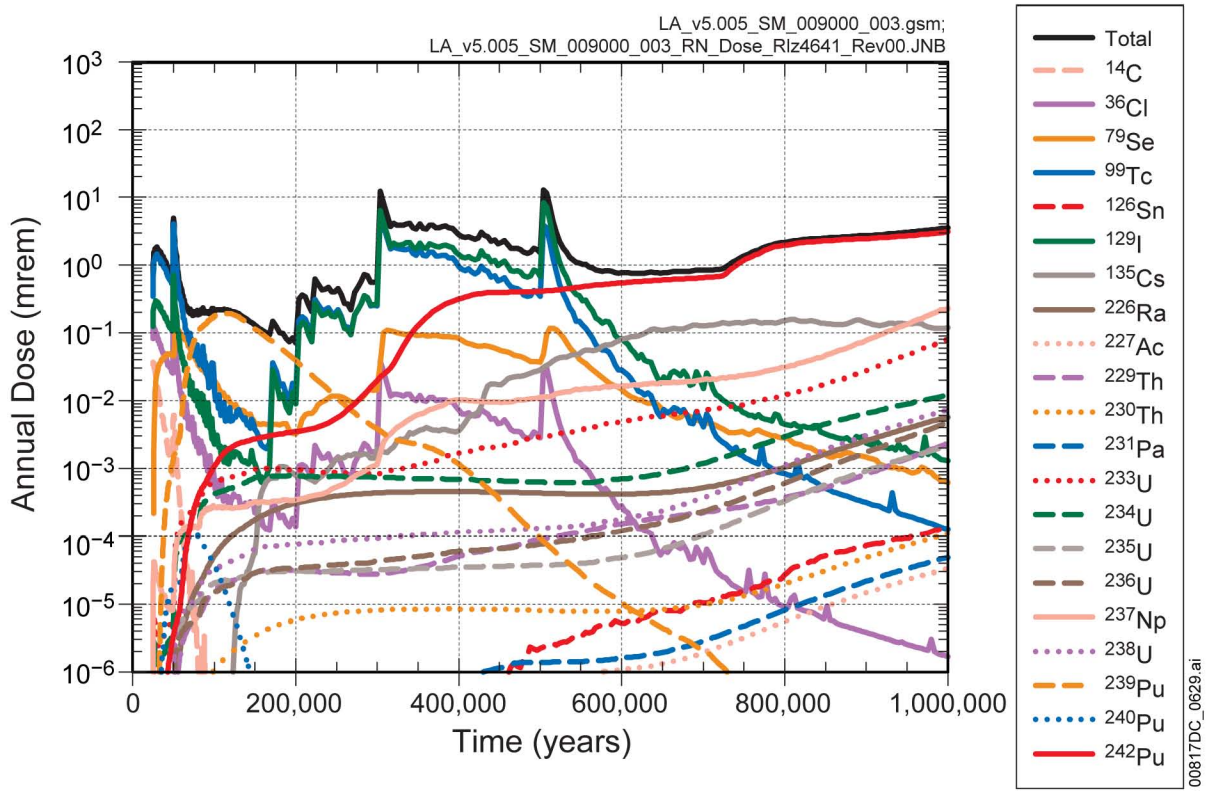

Source: Output DTN: MO0710ADTSPAWO.000 [DIRS 183752].

Figure 7.7.1-54[a]. Annual Dose along with Major Radionuclide Dose Contributors for Realization 4641 of the Seismic Ground Motion Modeling Case for 1,000,000 Years after Repository Closure

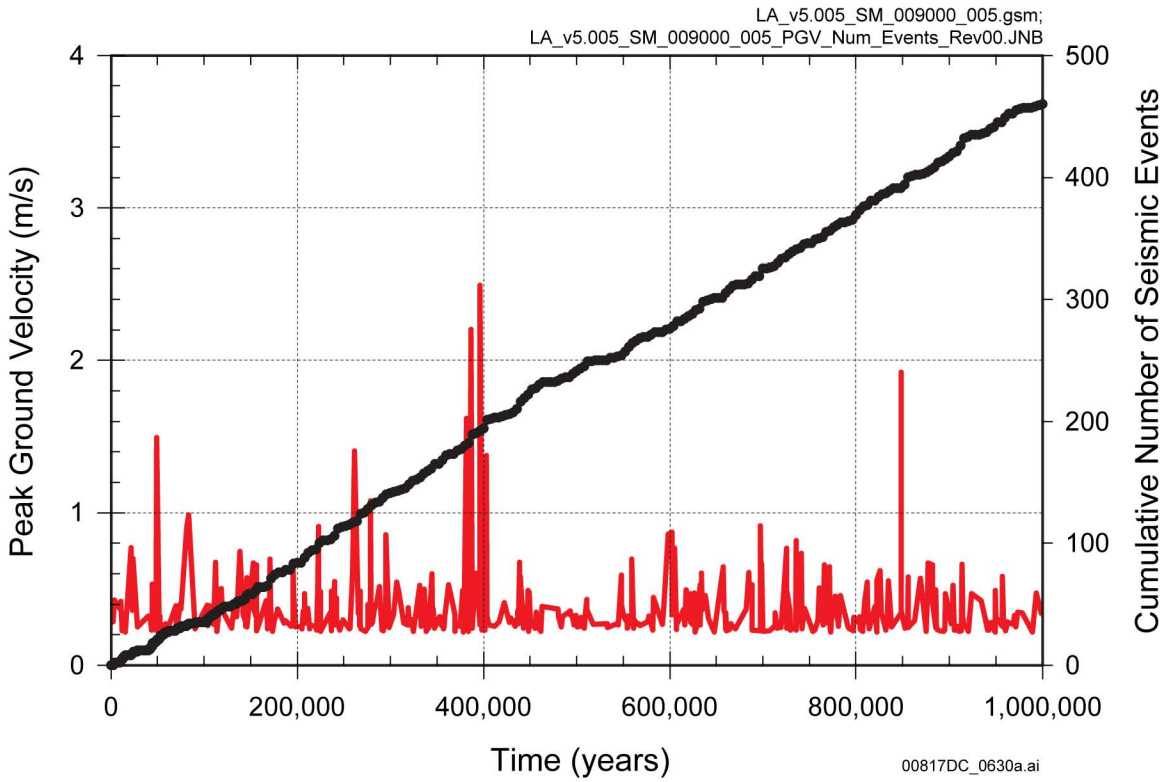

Source: Output DTN: MO0801TSPAMVAC.000 [DIRS 185080].

Figure 7.7.1-55[a]. Number of Seismic Events and the Peak Ground Velocities for Realization 4641 of the Seismic Ground Motion Modeling Case for 1,000,000 Years after Repository Closure

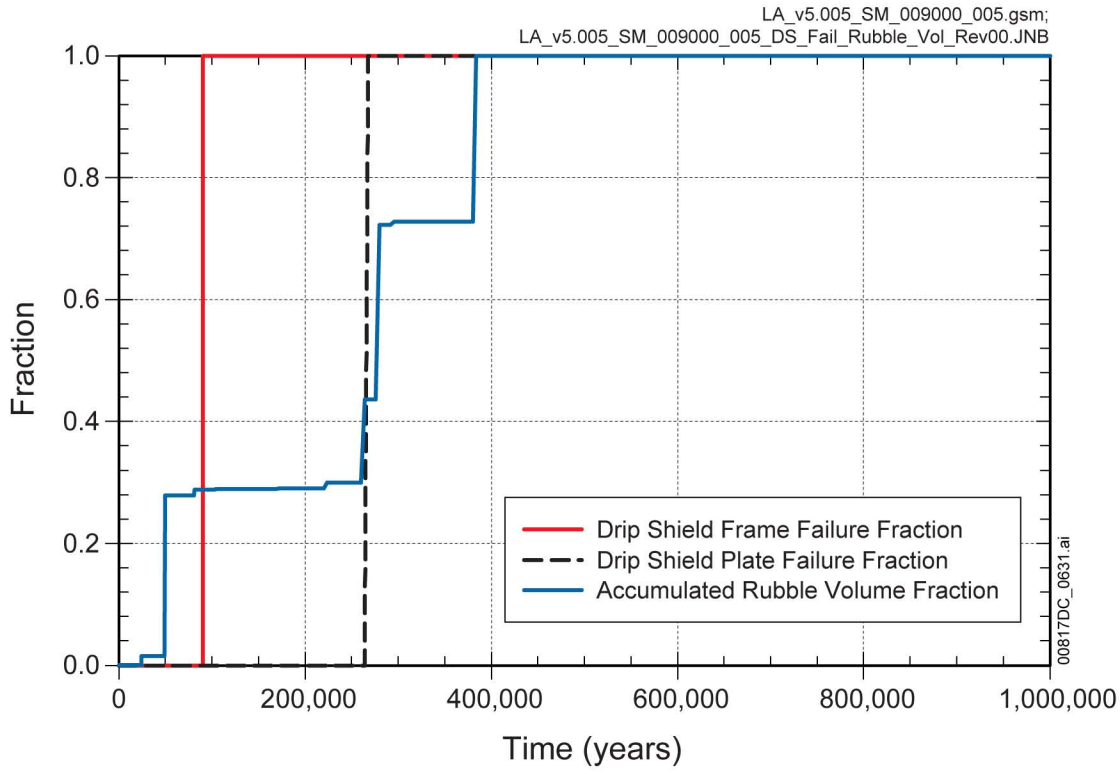

Source: Output DTN: MO0801TSPAMVAC.000 [DIRS 185080].

Figure 7.7.1-56[a]. Failure Fraction for the Drip Shield Plate and Framework and the Fraction of the Collapsed Drift Filled with Rubble (Lithophysal Zone) for Realization 4641 of the Seismic Ground Motion Modeling Case for 1,000,000 Years after Repository Closure

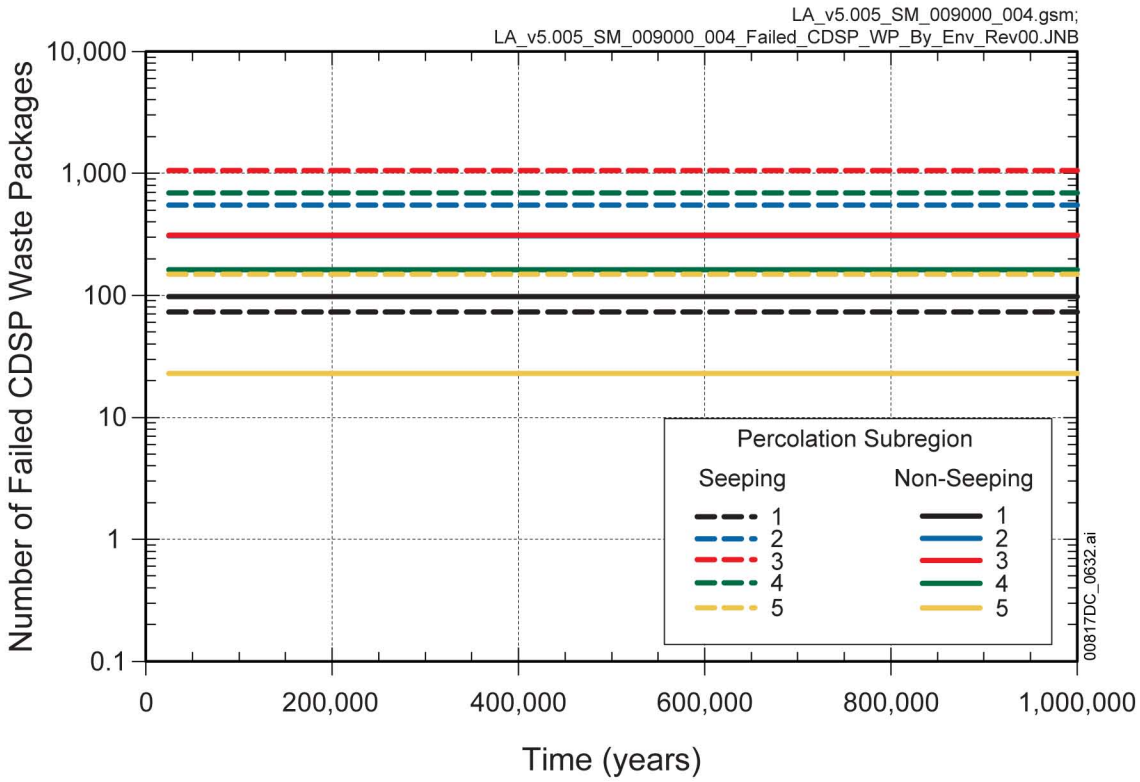

Source: Output DTN: MO0801TSPAMVAC.000 [DIRS 185080].

Figure 7.7.1-57[a]. CDSP WP Failure for Each Percolation Subregion for Both Seeping and Non-Seeping Environments for Realization 4641 of the Seismic Ground Motion Modeling Case for 1,000,000 Years after Repository Closure

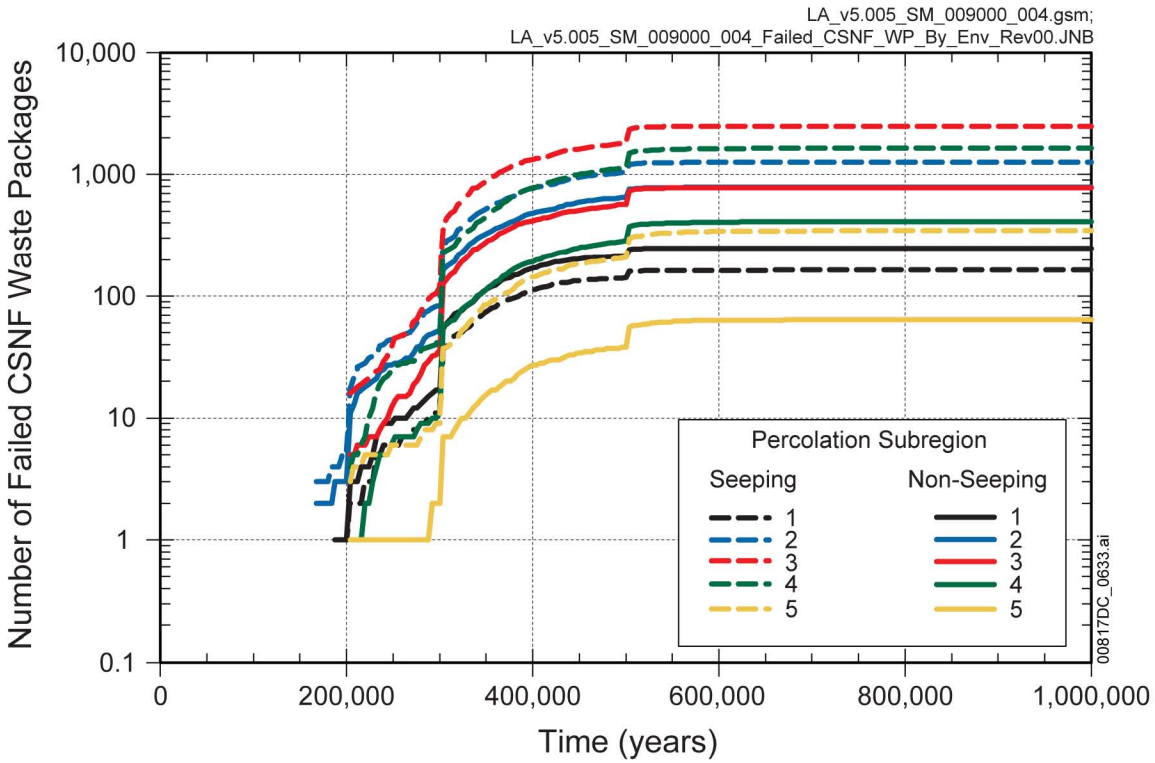

Source: Output DTN: MO0801TSPAMVAC.000 [DIRS 185080].

Figure 7.7.1-58[a]. CSNF WP Failure for Each Percolation Subregion for Both Seeping and Non-Seeping Environments for Realization 4641 of the Seismic Ground Motion Modeling Case for 1,000,000 Years after Repository Closure

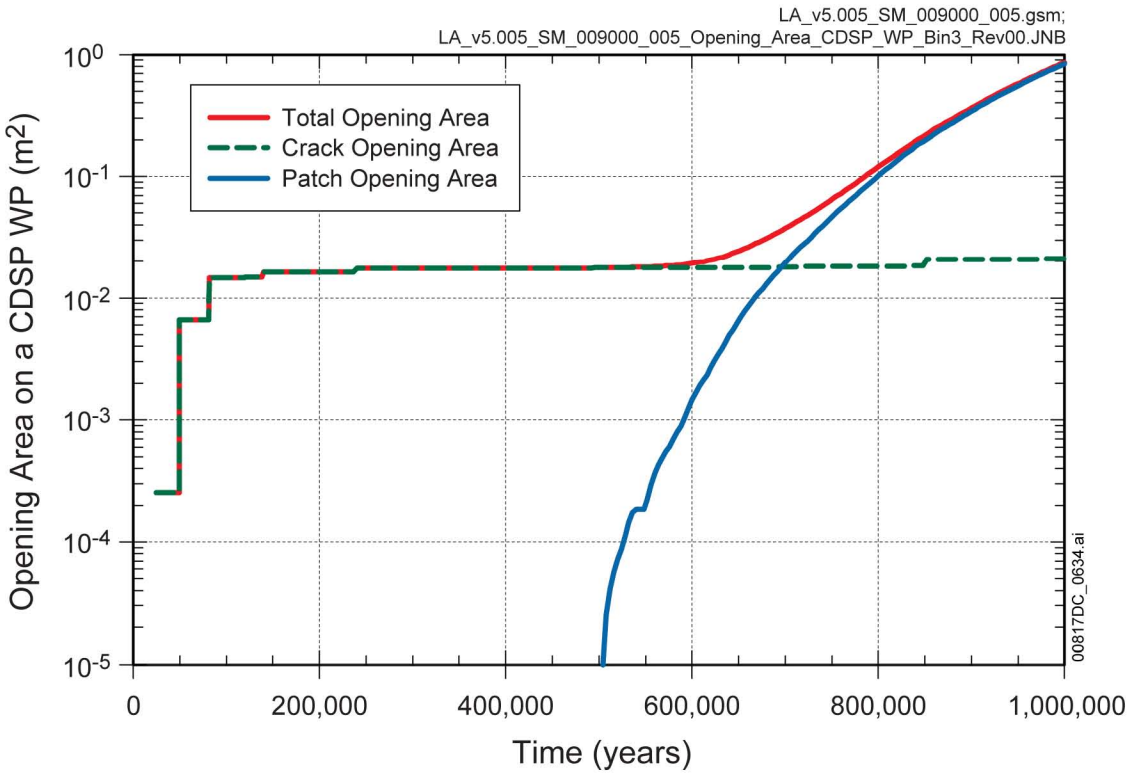

Source: Output DTN: MO0801TSPAMVAC.000 [DIRS 185080].

Figure 7.7.1-59[a]. CDSP WP Opening Area after Failure from Cracks and Patches for Percolation Subregion 3 for Realization 4641 of the Seismic Ground Motion Modeling Case for 1,000,000 Years after Repository Closure

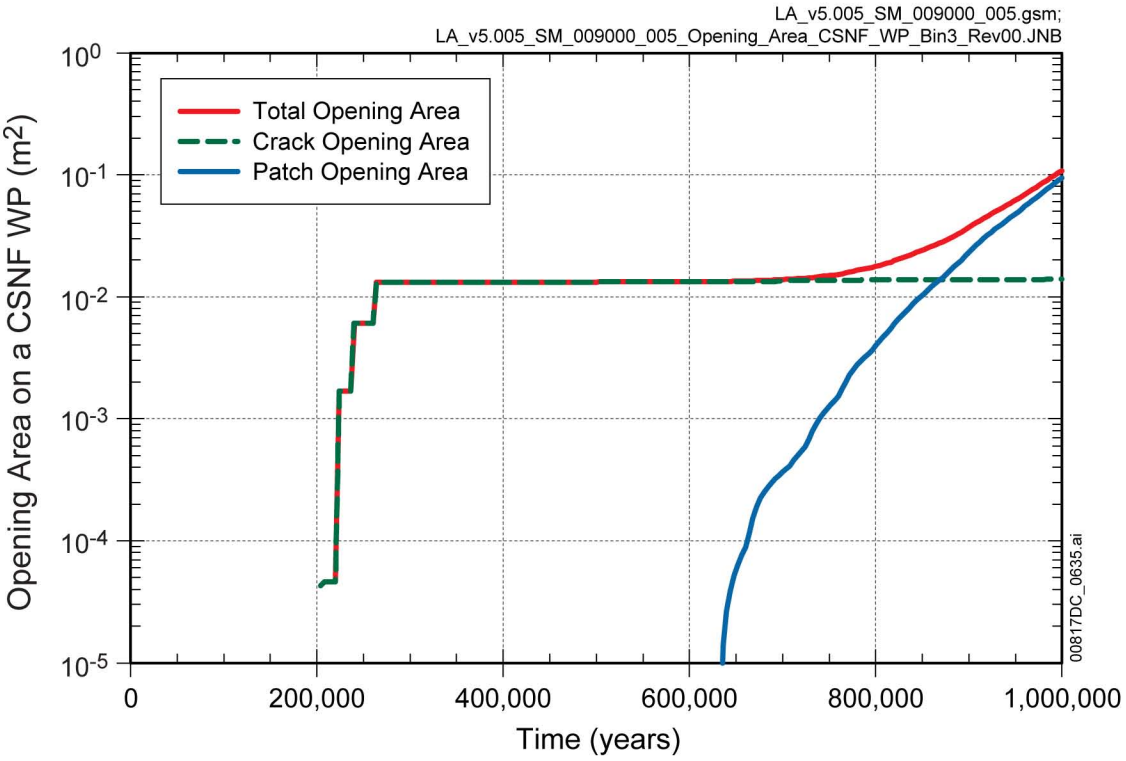

Source: Output DTN: MO0801TSPAMVAC.000 [DIRS 185080].

Figure 7.7.1-60[a]. CSNF WP Opening Area after Failure from Cracks and Patches for Percolation Subregion 3 for Realization 4641 of the Seismic Ground Motion Modeling Case for 1,000,000 Years after Repository Closure

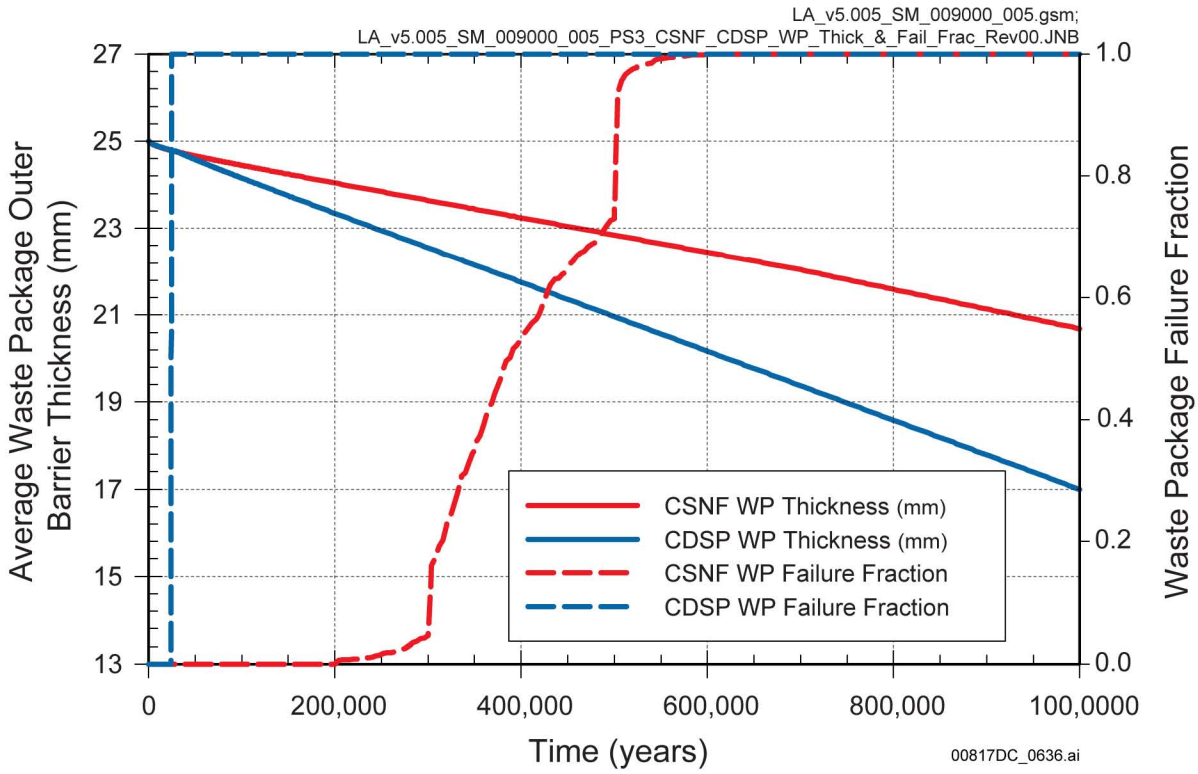

Source: Output DTN: MO0801TSPAMVAC.000 [DIRS 185080].

Figure 7.7.1-61[a]. Average Waste Package Outer Barrier Thicknesses and Waste Package Failure Fractions for Percolation Subregion 3 for Realization 4641 of the Seismic Ground Motion Modeling Case for 1,000,000 Years after Repository Closure

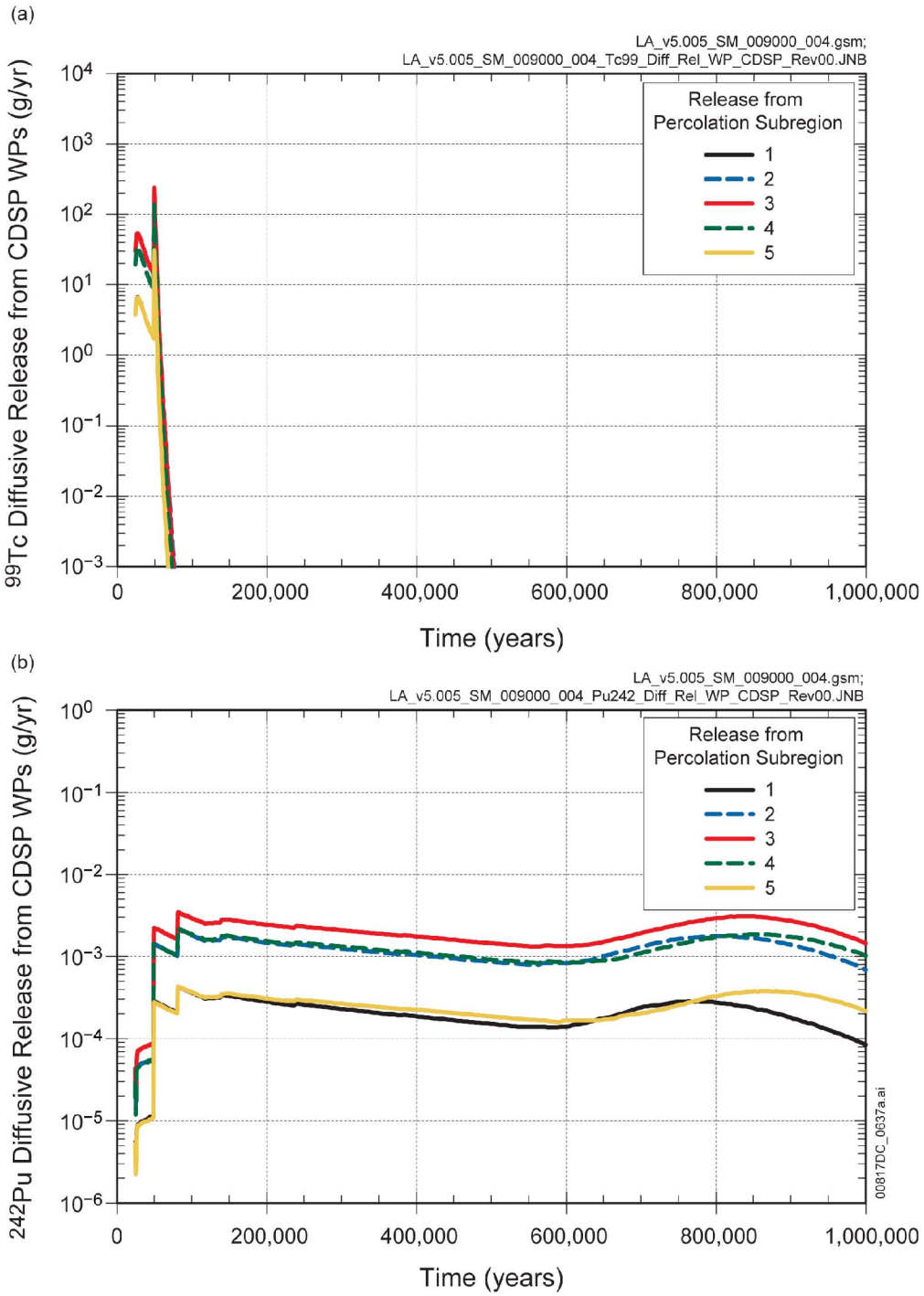

Source: Output DTN: MO0801TSPAMVAC.000 [DIRS 185080].

Figure 7.7.1-62[a]. Diffusive Release Rates of: (a) ^{99}Tc and (b) ^{242}Pu (Dissolved and Reversibly Associated with Colloids) from CDSP WPs from each Percolation Subregion for Realization 4641 of the Seismic Ground Motion Modeling Case for 1,000,000 Years after Repository Closure

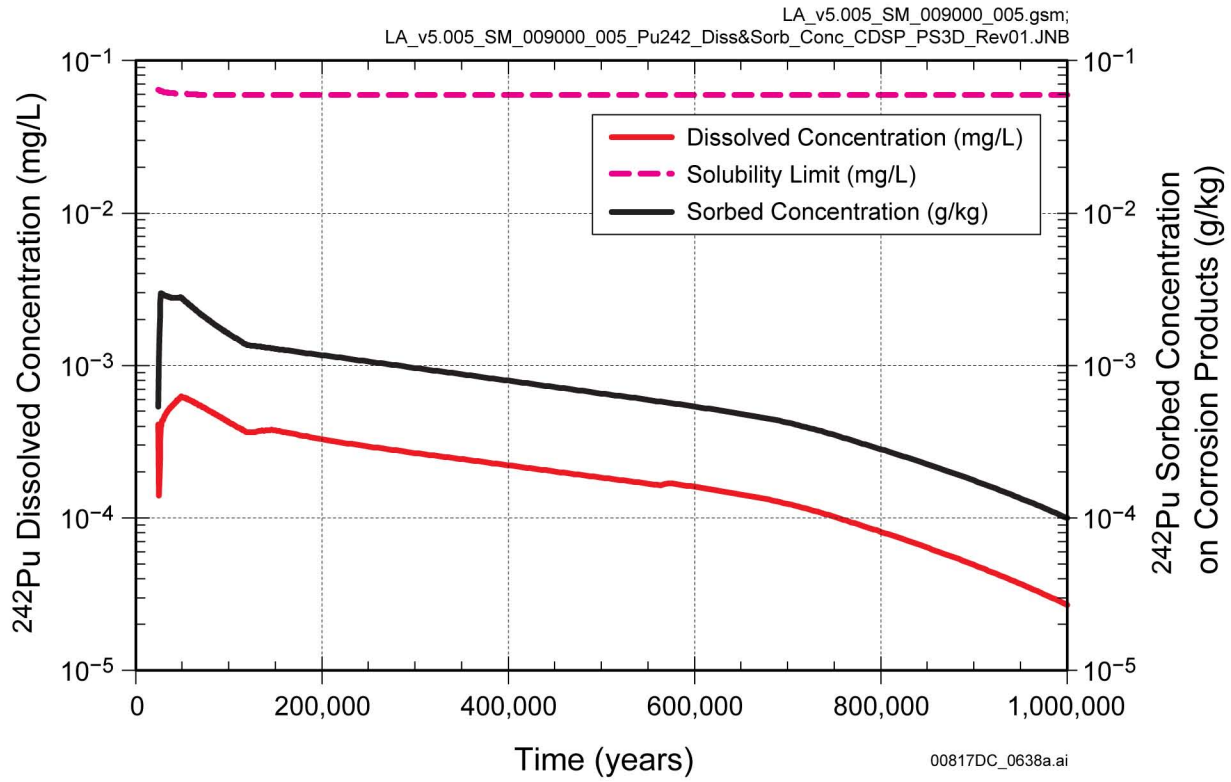

Source: Output DTN: MO0801TSPAMVAC.000 [DIRS 185080].

Figure 7.7.1-63[a]. Dissolved Concentration of ^{242}Pu in the Corrosion Products Domain Compared to the Sorbed Concentration on Corrosion Products for CDSP WPs for Percolation Subregion 3 Seeping Environment for Realization 4641 of the Seismic Ground Motion Modeling Case for 1,000,000 Years after Repository Closure

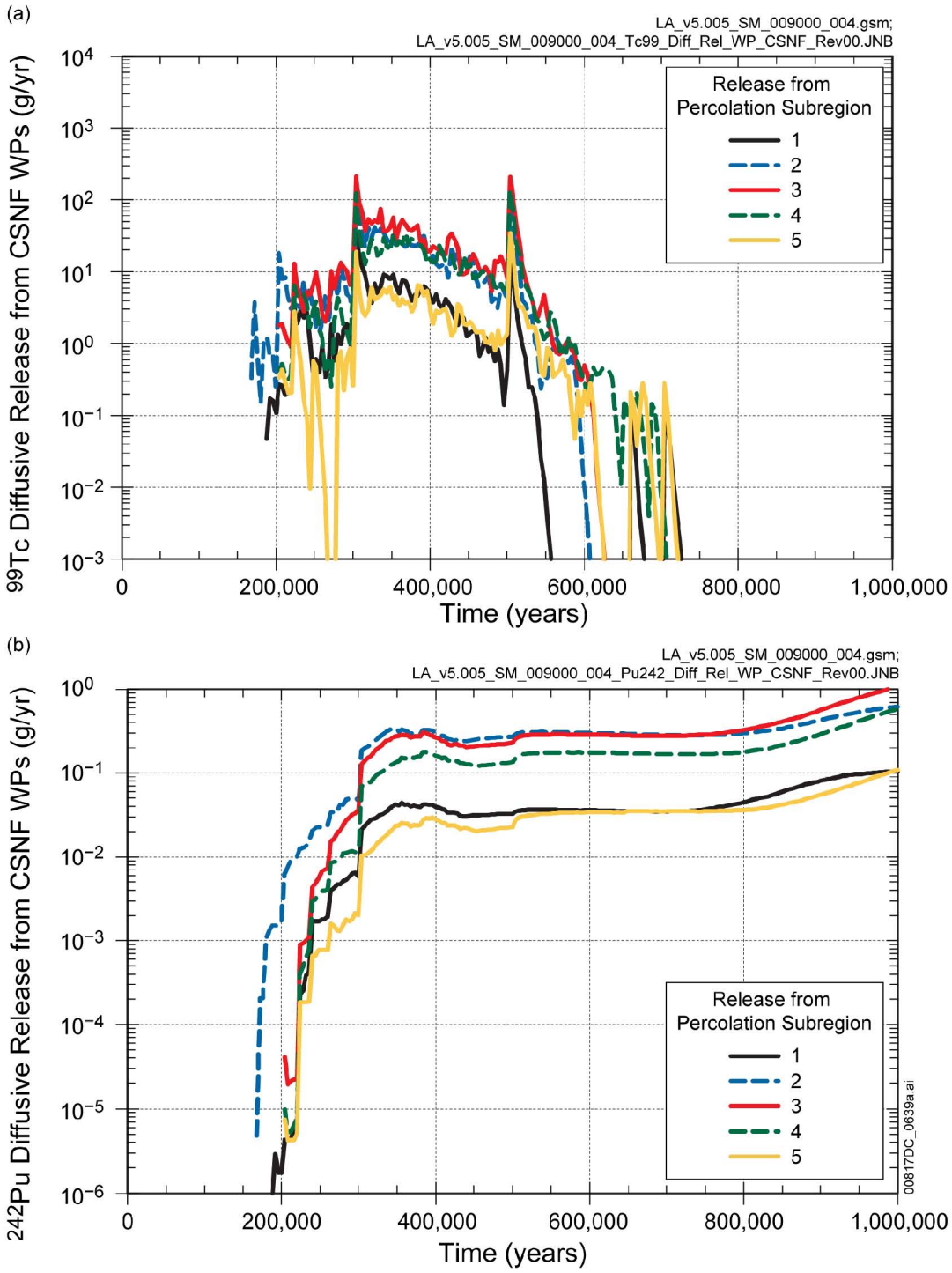

Source: Output DTN: MO0801TSPAMVAC.000 [DIRS 185080].

Figure 7.7.1-64[a]. Diffusive Release Rates of (a) ^{99}Tc and (b) ^{242}Pu (Dissolved and Reversibly Associated with Colloids) from CSNF WPs from each Percolation Subregion for Realization 4641 of the Seismic Ground Motion Modeling Case for 1,000,000 Years after Repository Closure

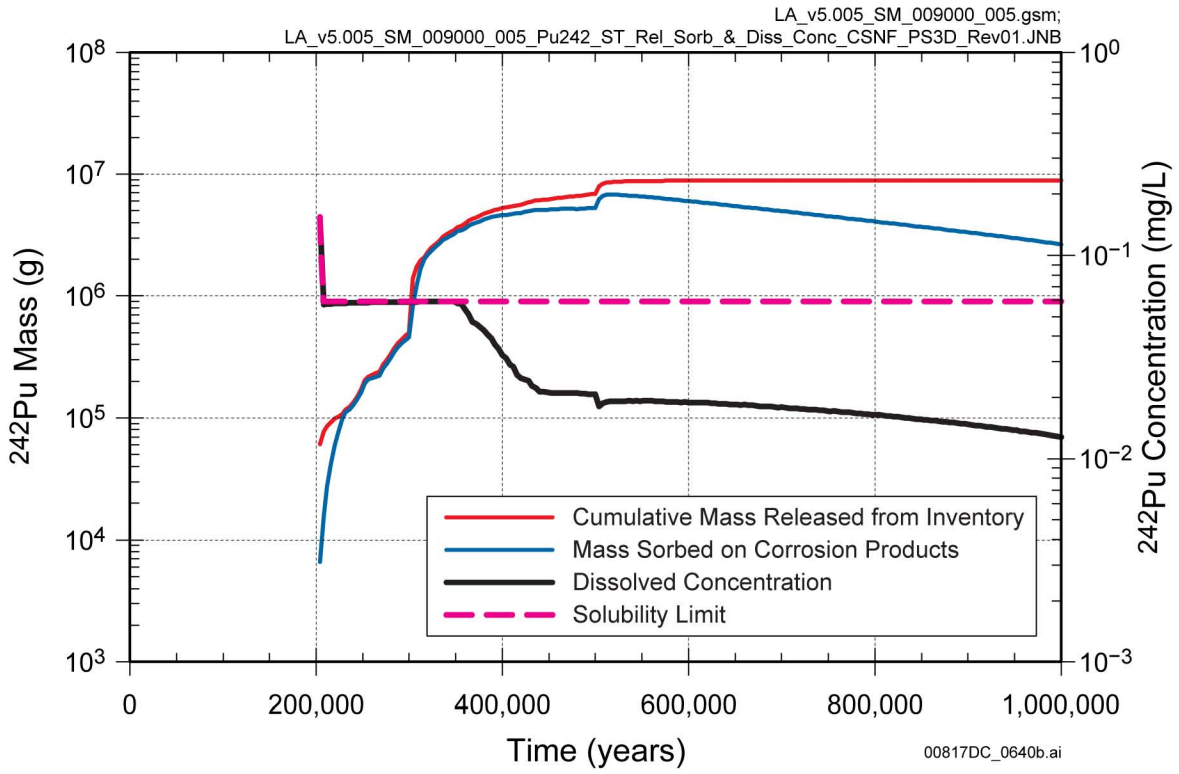

Source: Output DTN: MO0801TSPAMVAC.000 [DIRS 185080].

Figure 7.7.1-65[a]. Comparison of ^{242}Pu Cumulative Mass Released from the Inventory, Mass Sorbed on Corrosion Products, and the Dissolved Concentration in the Corrosion Products Domain for CSNF WPs for Percolation Subregion 3 Seeping Environment for Realization 4641 of the Seismic Ground Motion Modeling Case for 1,000,000 Years after Repository Closure

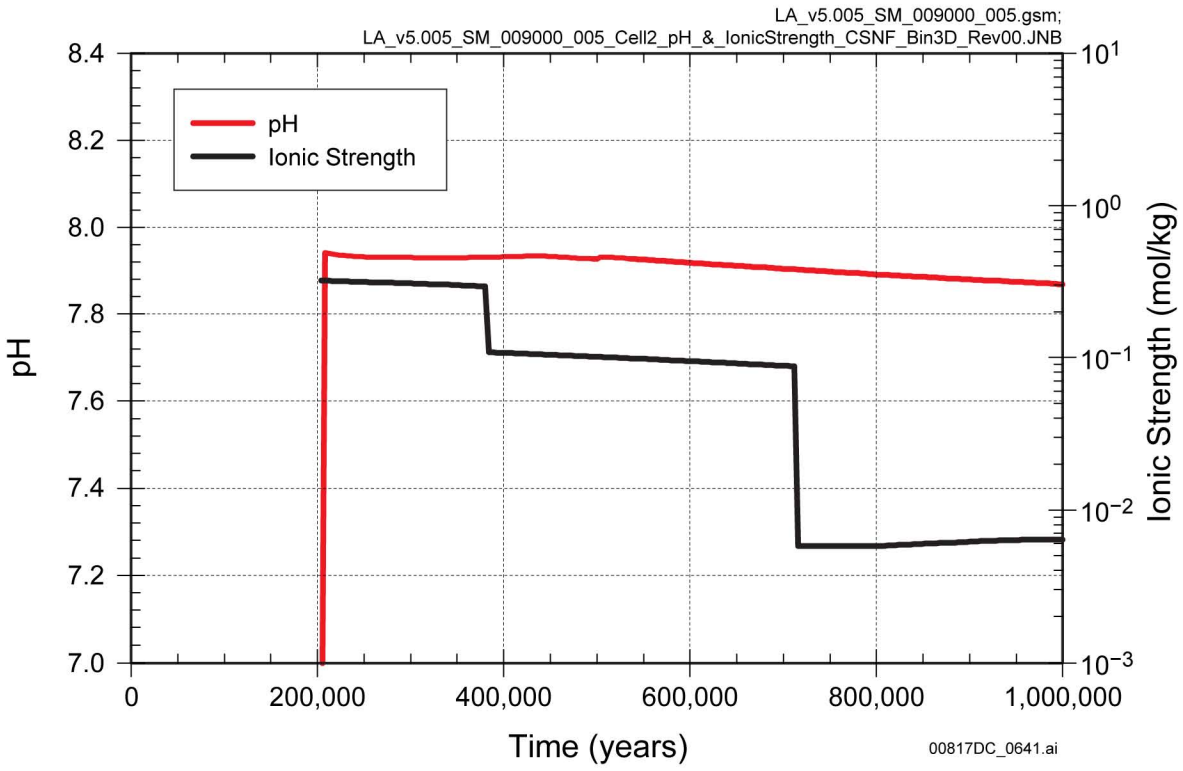

Source: Output DTN: MO0801TSPAMVAC.000 [DIRS 185080].

Figure 7.7.1-66[a]. pH and Ionic Strength Profiles in the Corrosion Products Domain for CSNF WPs for Percolation Subregion 3, Seeping Environment for Realization 4641 of the Seismic Ground Motion Modeling Case for 1,000,000 Years after Repository Closure

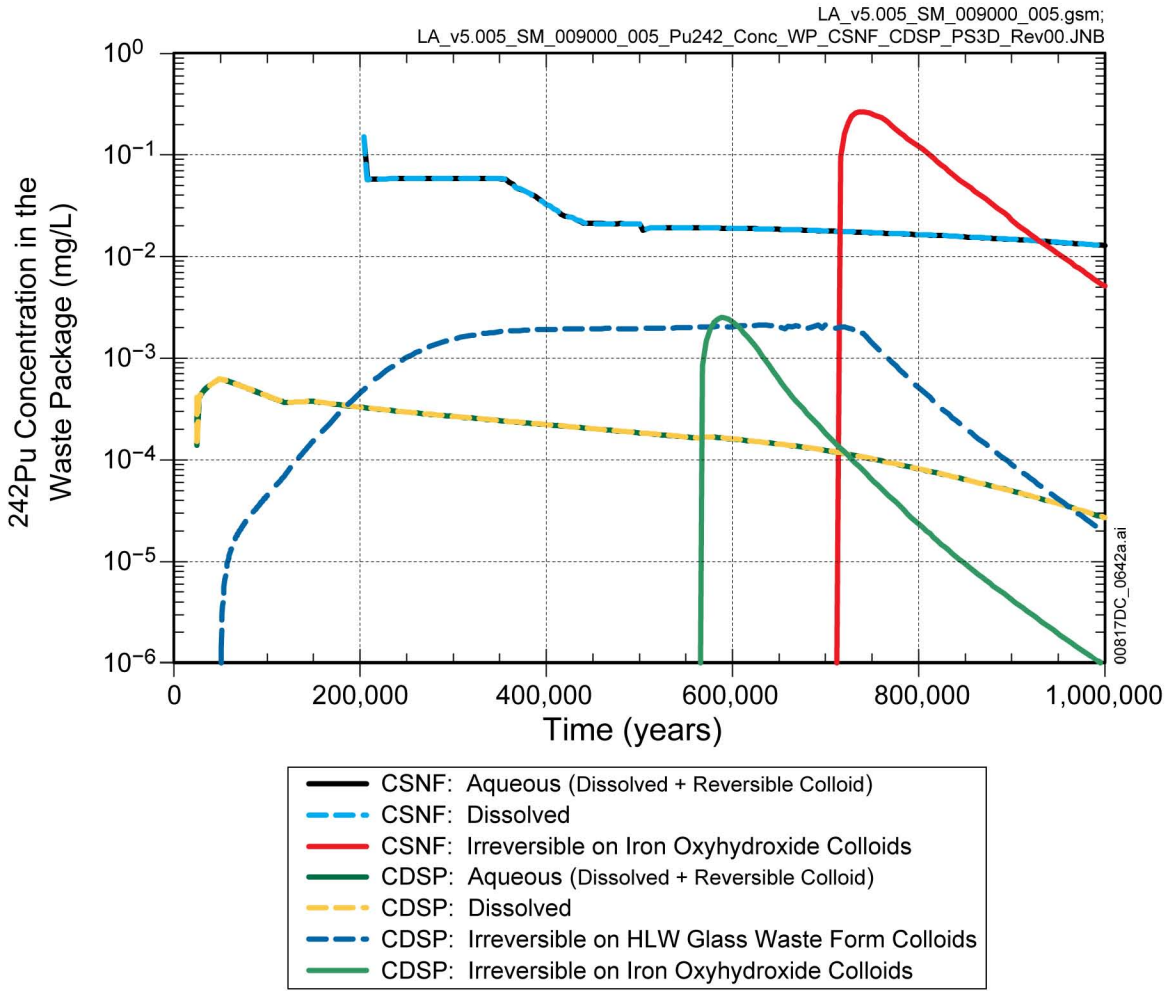

Source: Output DTN: MO0801TSPAMVAC.000 [DIRS 185080].

Figure 7.7.1-67[a]. Concentration of ^{242}Pu in the CSNF and CDSP WPs (Corrosion Products Domain) for Percolation Subregion 3 Seeping Environment for Realization 4641 of the Seismic Ground Motion Modeling Case for 1,000,000 Years after Repository Closure

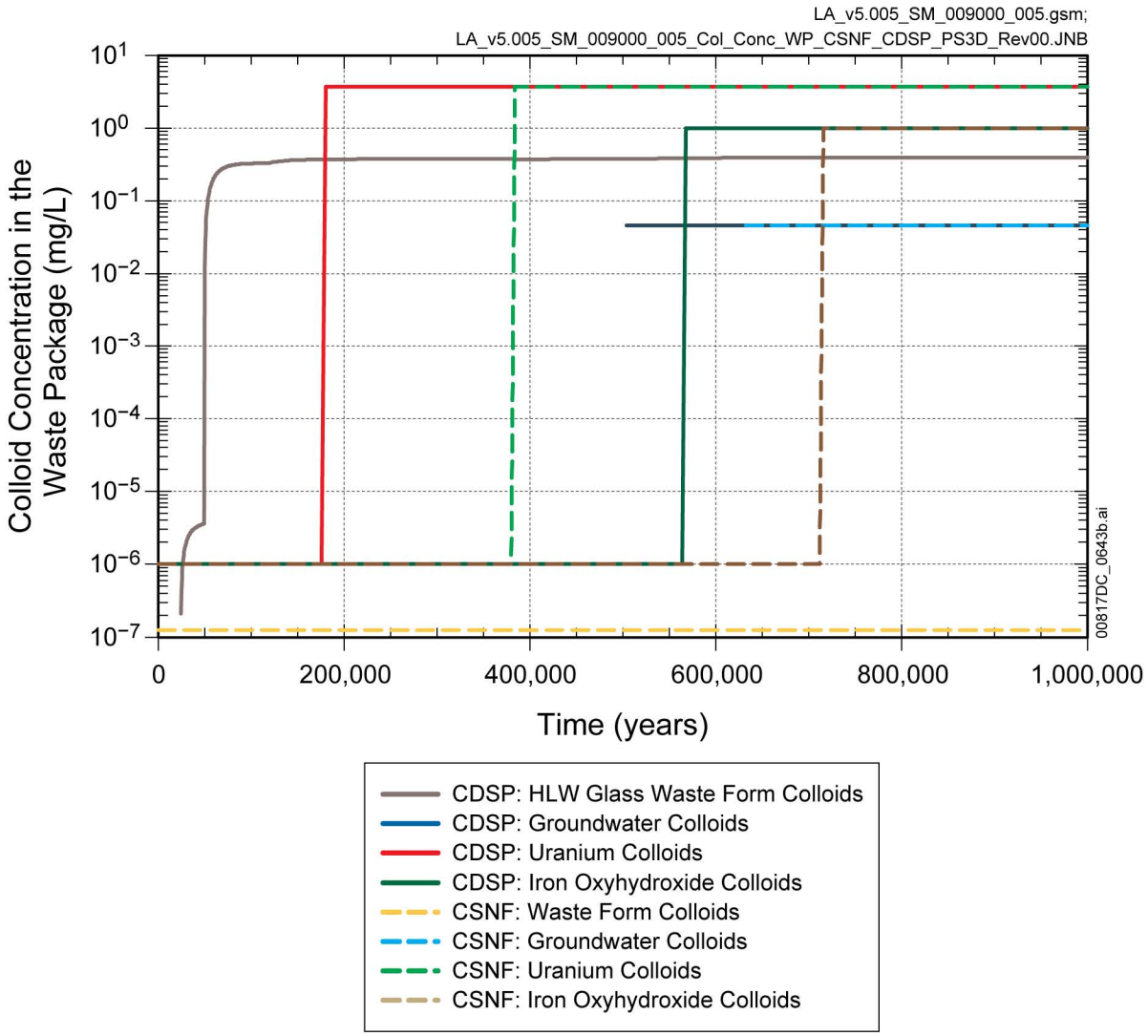

Source: Output DTN: MO0801TSPAMVAC.000 [DIRS 185080].

Figure 7.7.1-68[a]. Concentration of Various Colloids in the CSNF and CDSP WPs (Corrosion Products Domain) for Percolation Subregion 3 Seeping Environment for Realization 4641 of the Seismic Ground Motion Modeling Case for 1,000,000 Years after Repository Closure

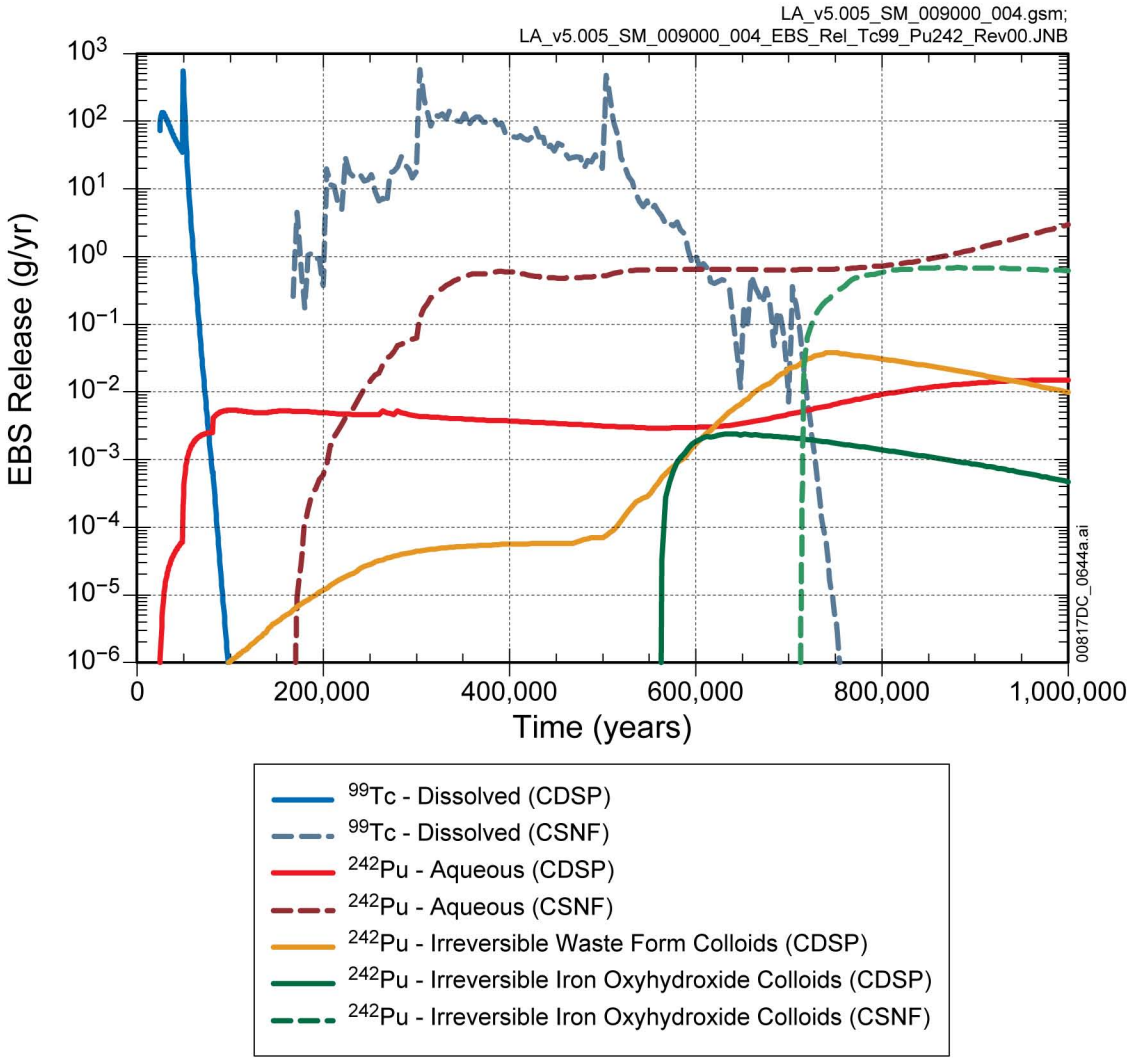

Source: Output DTN: MO0801TSPAMVAC.000 [DIRS 185080].

NOTE: Plutonium dissolved and reversibly associated with colloids is denoted as aqueous.

Figure 7.7.1-69[a]. EBS Release Rates from CSNF and CDSP WPs (All Percolation Subregions) for Realization 4641 of the Seismic Ground Motion Modeling Case for 1,000,000 Years after Repository Closure

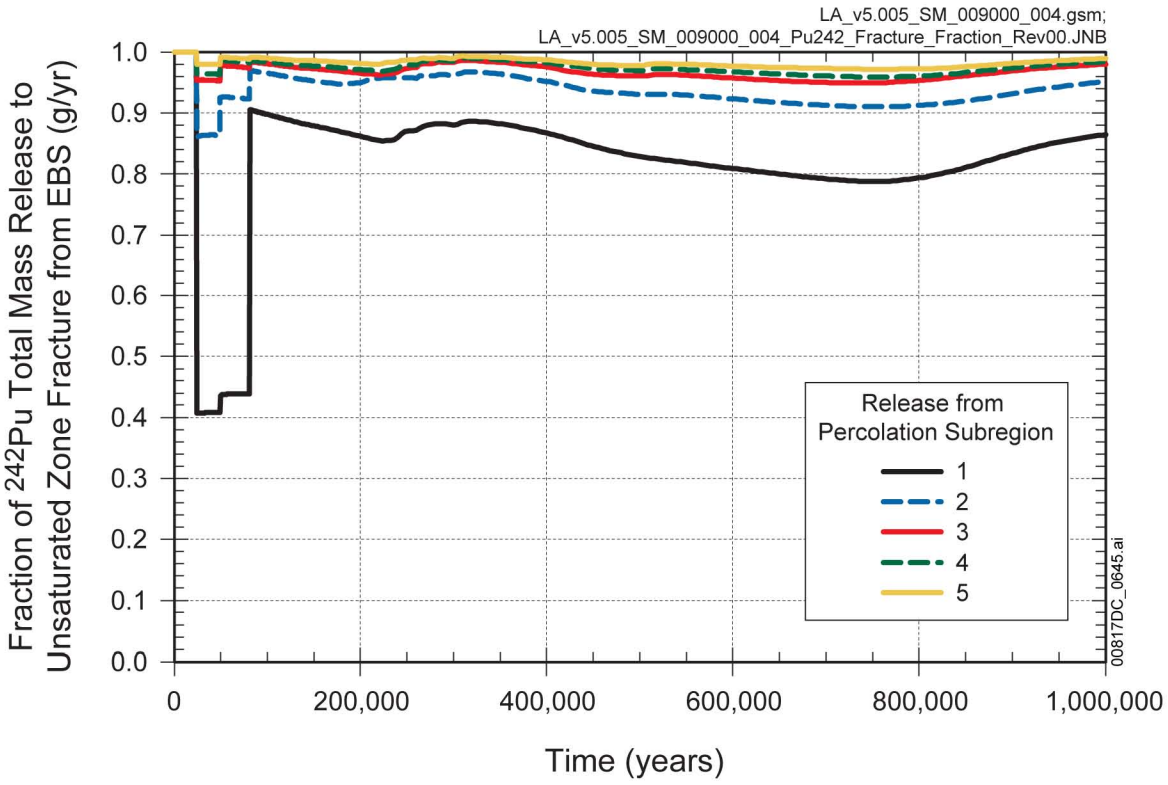

Source: Output DTN: MO0801TSPAMVAC.000 [DIRS 185080].

Figure 7.7.1-70[a]. Fraction of ^{242}Pu Mass Going to Unsaturated Zone Fractures at the Repository Horizon for Realization 4641 of the Seismic Ground Motion Modeling Case for 1,000,000 Years after Repository Closure

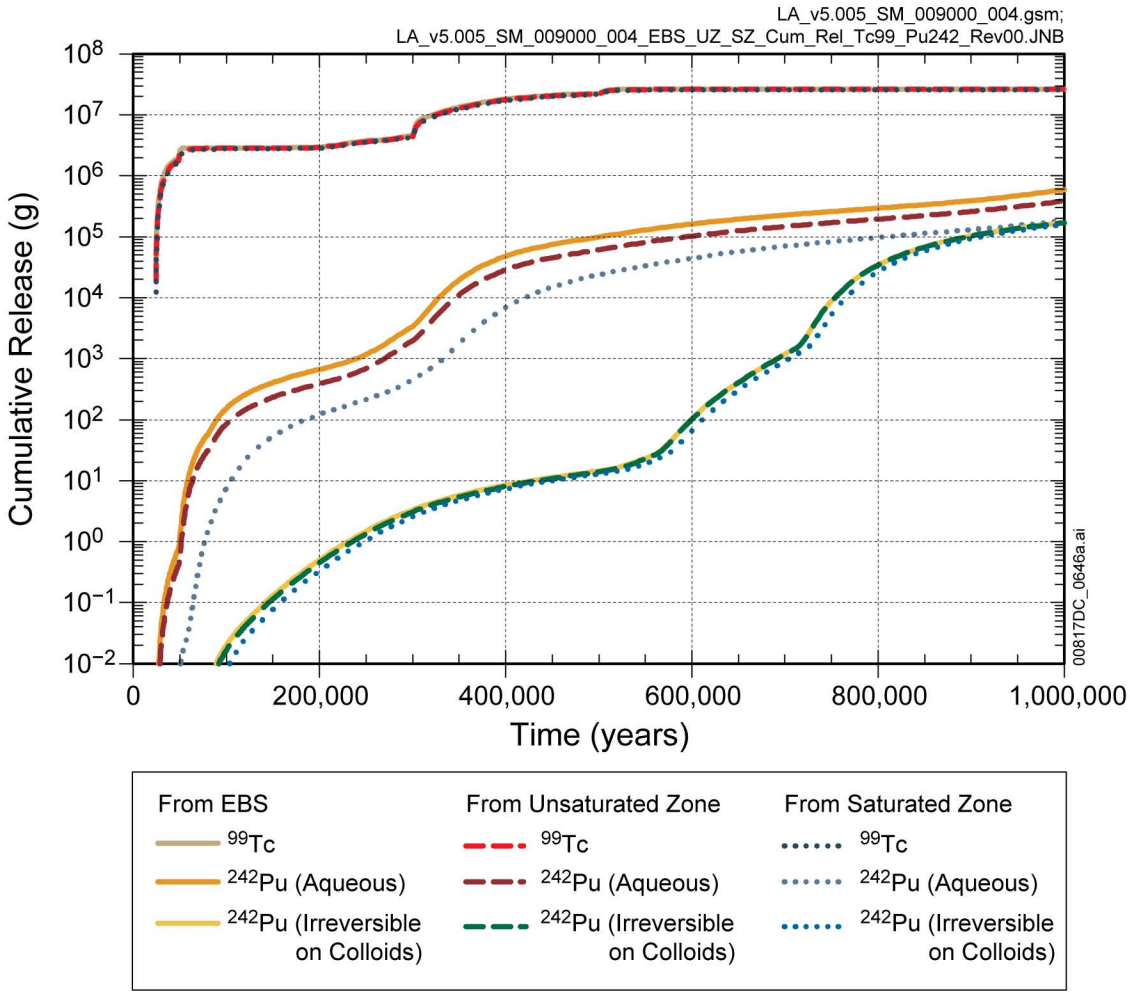

Source: Output DTN: MO0801TSPAMVAC.000 [DIRS 185080].

NOTE: Plutonium dissolved and reversibly associated with colloids is denoted as aqueous.

Figure 7.7.1-71[a]. Cumulative Mass Release of ^{99}Tc and ^{242}Pu from the EBS, Unsaturated Zone, and Saturated Zone for Realization 4641 of the Seismic Ground Motion Modeling Case for 1,000,000 Years after Repository Closure

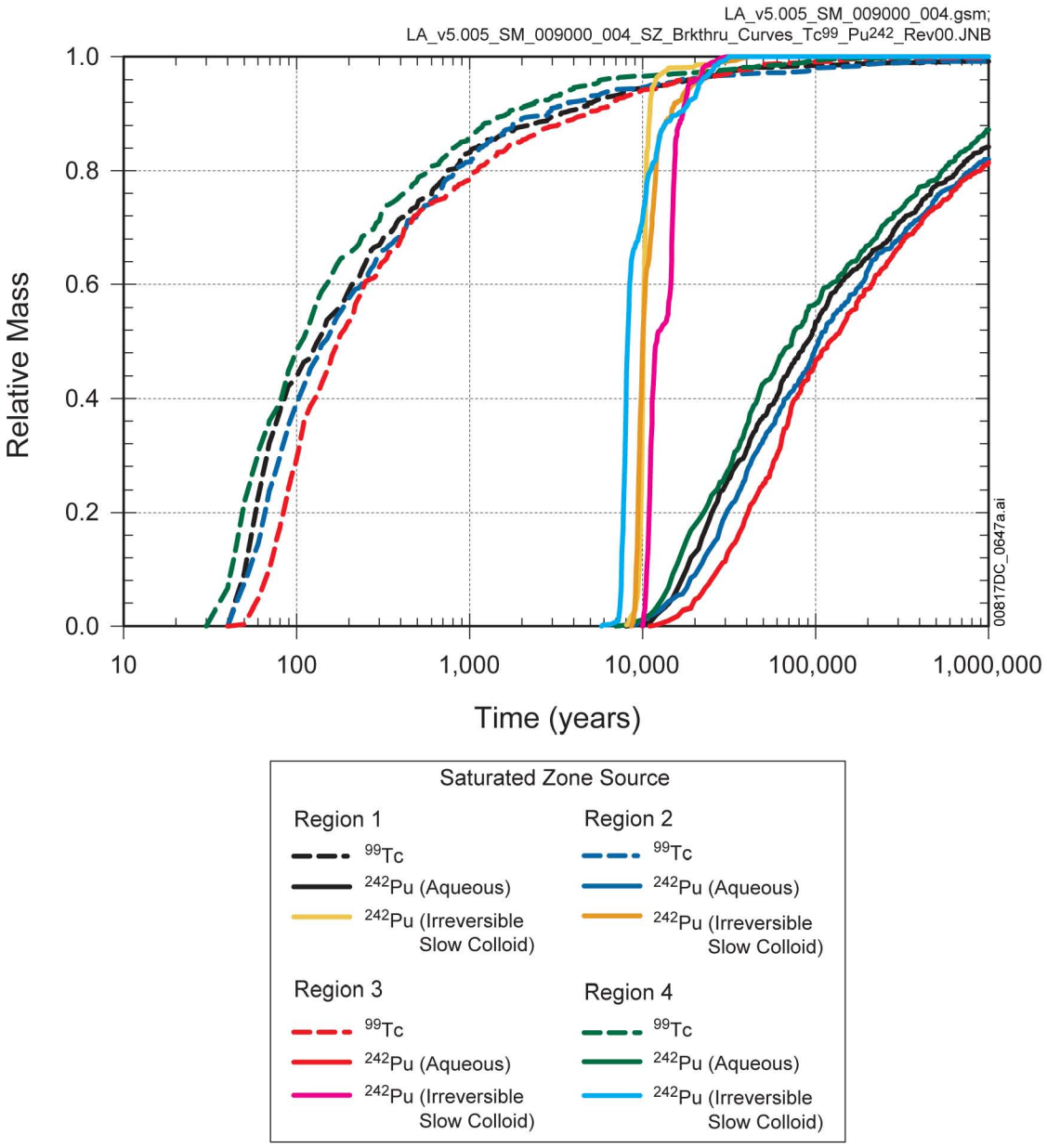

Source: Output DTN: MO0801TSPAMVAC.000 [DIRS 185080].

NOTES: The SZ breakthrough curve #122 is used in realization 4641. Plutonium dissolved and reversibly associated with colloids are denoted as aqueous.

Figure 7.7.1-72[a]. Comparison of Saturated Zone Breakthrough Curves for ^{99}Tc and ^{242}Pu for All Four Saturated Zone Source Regions for Realization 4641 of the Seismic Ground Motion Modeling Case for 1,000,000 Years after Repository Closure

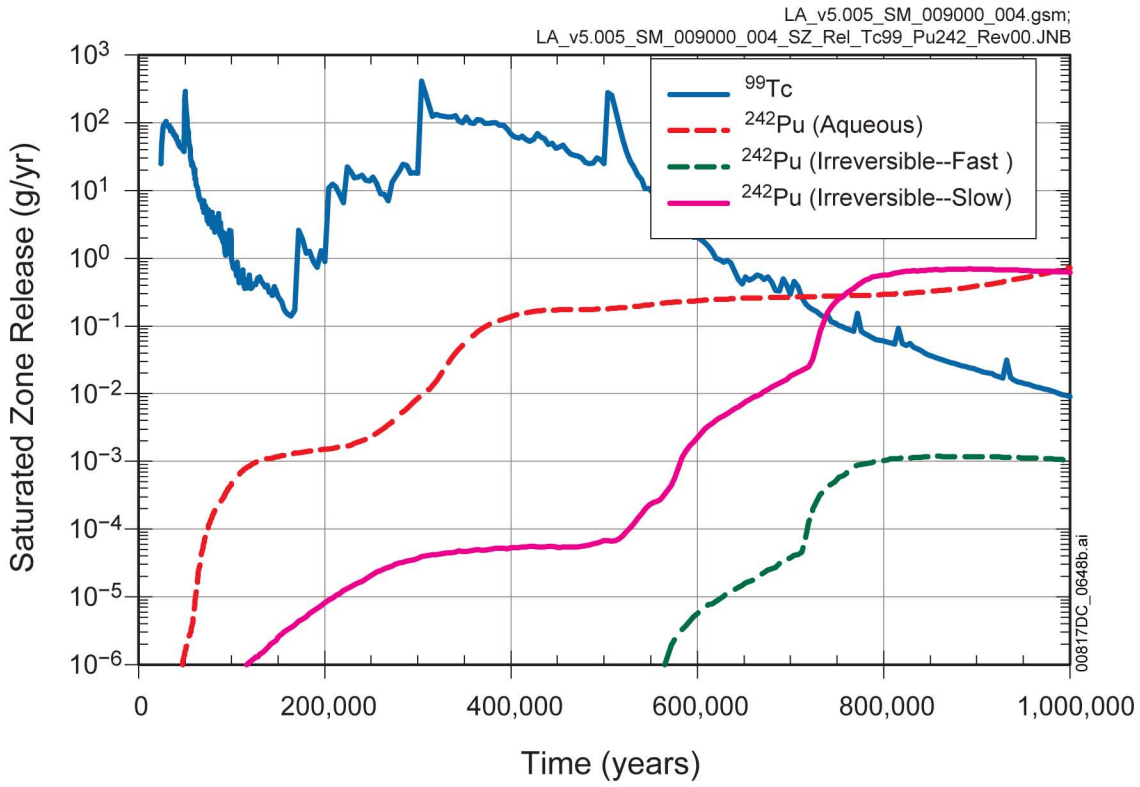

Source: Output DTN: MO0801TSPAMVAC.000 [DIRS 185080].

NOTE: Plutonium dissolved and reversibly associated with colloids is denoted as aqueous.

Figure 7.7.1-73[a]. Saturated Zone Release at the Location of the RMEI of ^{99}Tc and ^{242}Pu for Realization 4641 of the Seismic Ground Motion Modeling Case for 1,000,000 Years after Repository Closure

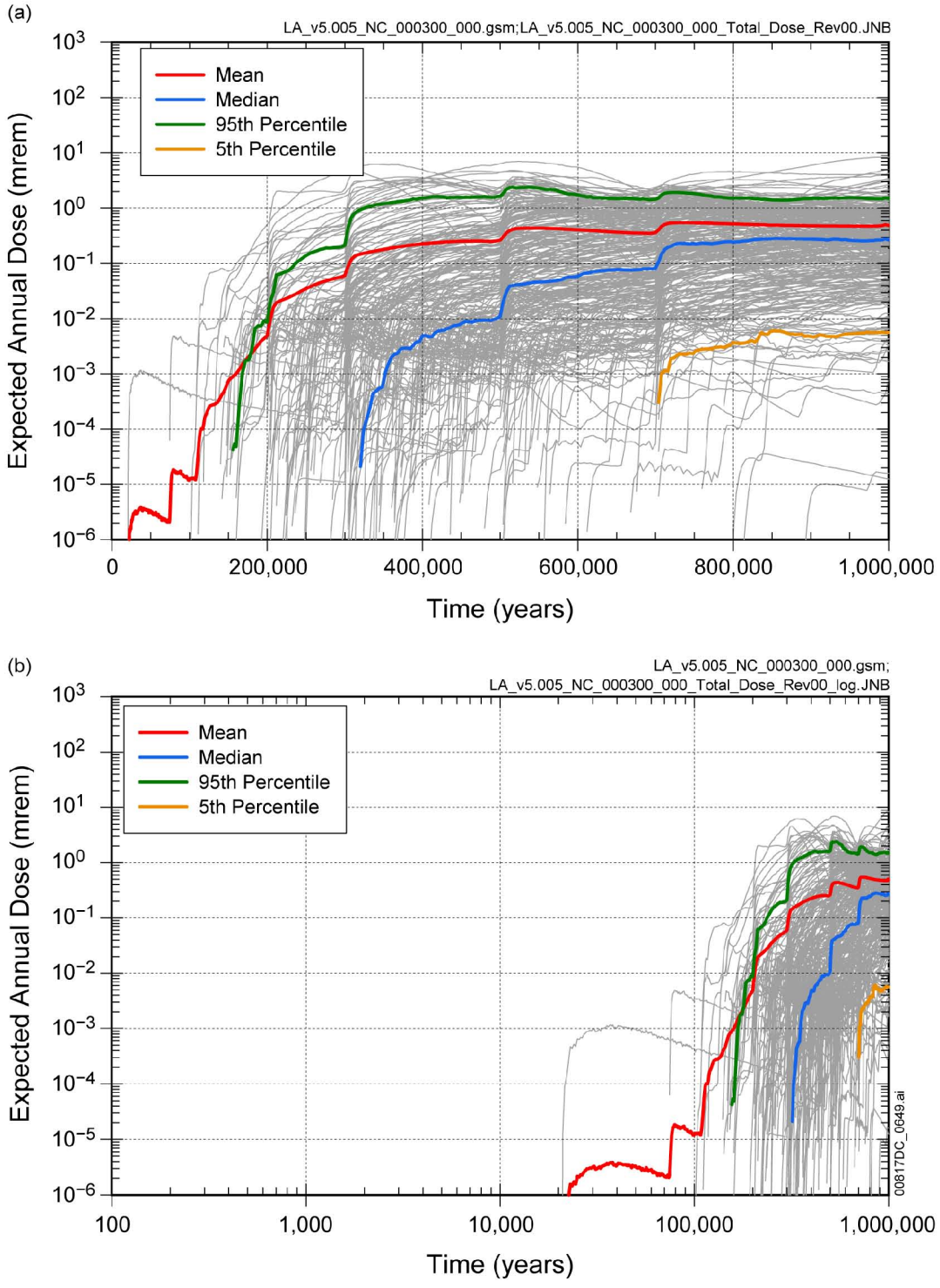

Source: Output DTN: MO0710ADTSPAWO.000 [DIRS 183752].

Figure 7.7.1-74[a]. Expected Annual Dose from 300 Epistemic Uncertainty Vectors, Along with their Quantiles for the Nominal Modeling Case for 1,000,000 Years after Repository Closure in (a) Linear Time and (b) Log Time

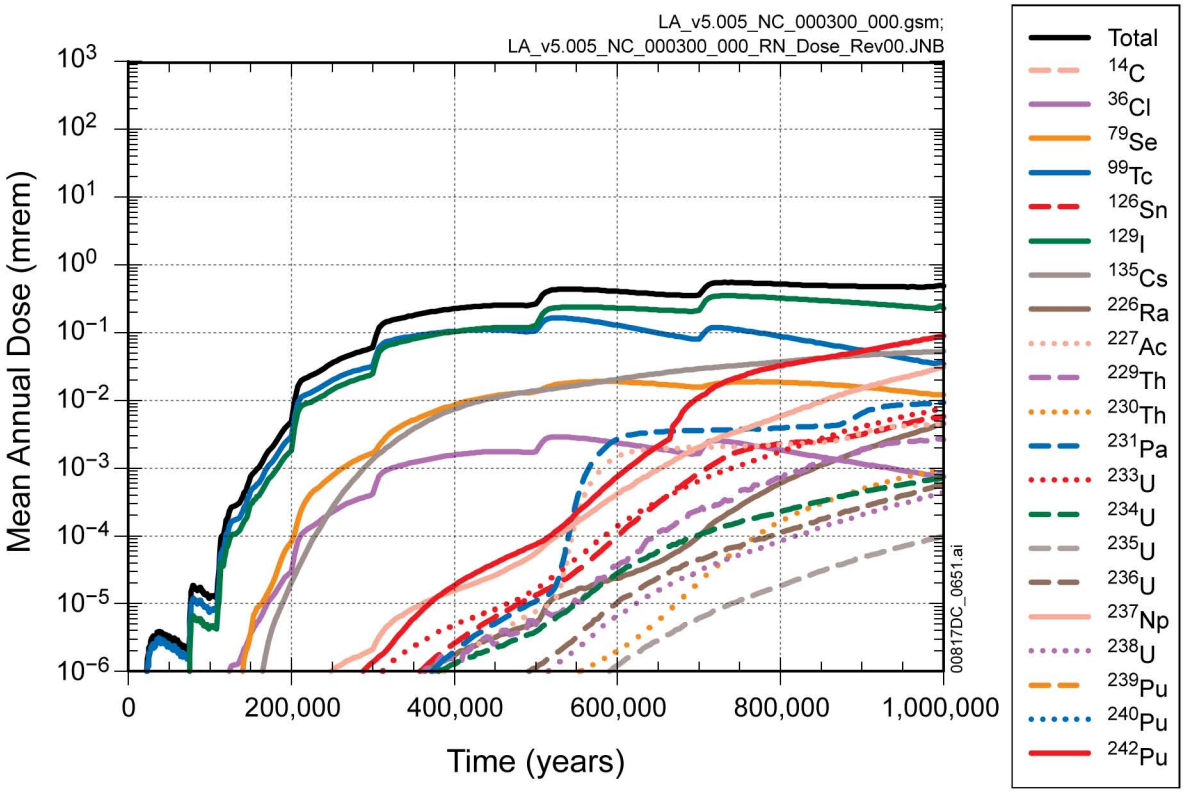

Source: Output DTN: MO0710ADTSPAWO.000 [DIRS 183752].

Figure 7.7.1-75[a]. Contribution of Individual Radionuclides to Mean Annual Dose for the Nominal Modeling Case for 1,000,000 Years after Repository Closure

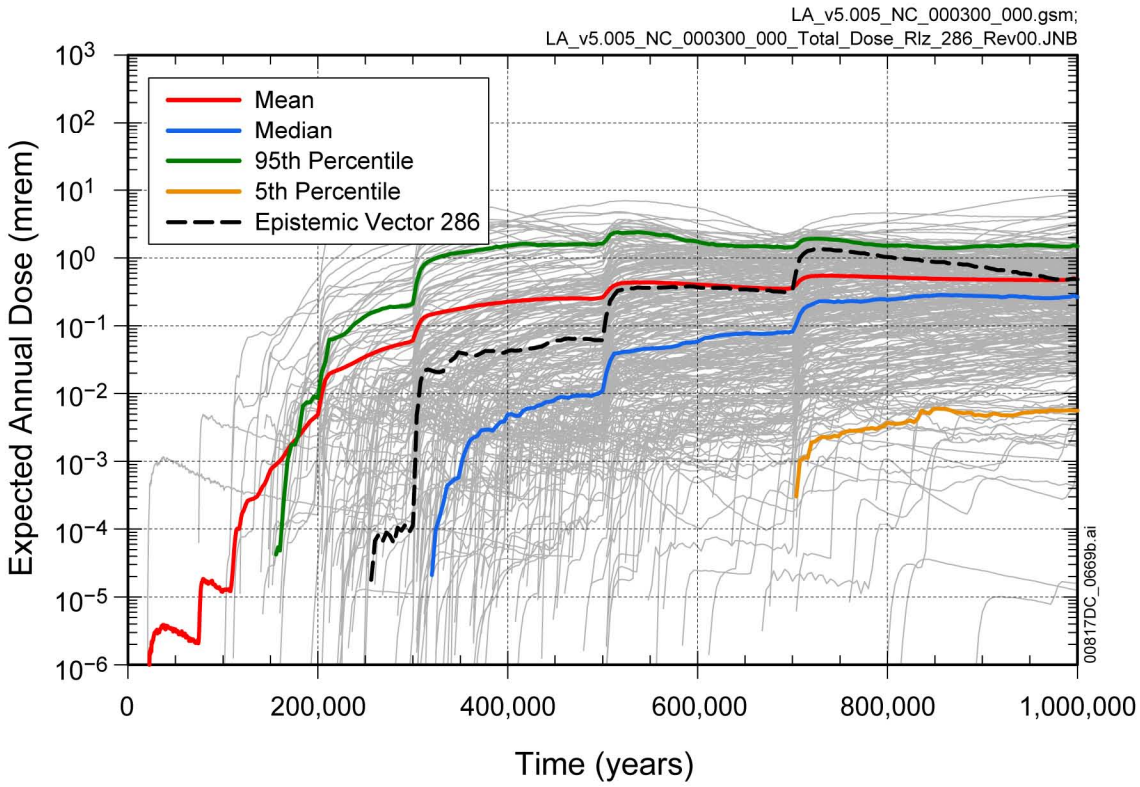

Source: Output DTN: MO0710ADTSPAWO.000 [DIRS 183752].

Figure 7.7.1-76[a]. Expected Annual Dose from 300 Epistemic Uncertainty Vectors, Along with their Quantiles and Expected Dose from Epistemic Uncertainty Vector 286 for the Nominal Modeling Case for 1,000,000 Years after Repository Closure

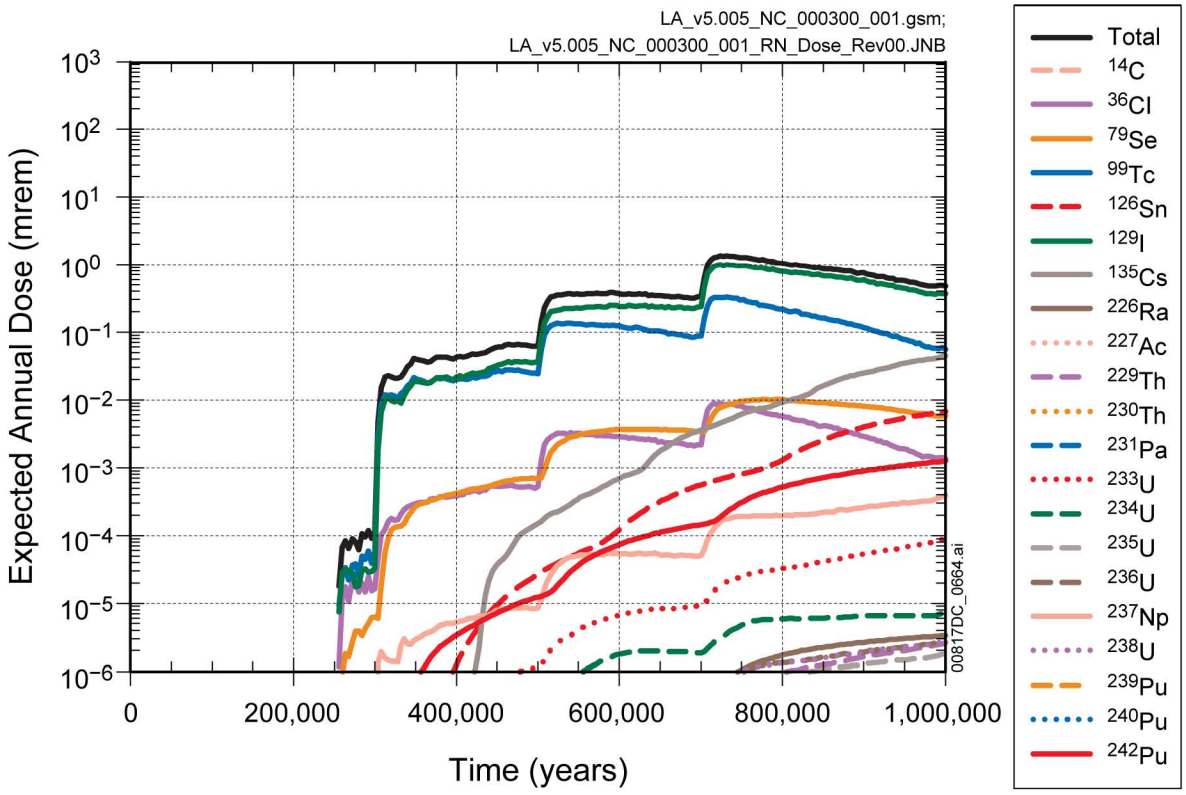

Source: Output DTN: MO0801TSPAMVAC.000 [DIRS 185080].

Figure 7.7.1-77[a]. Contribution of Individual Radionuclides to Expected Annual Dose for Realization 286 of the Nominal Modeling Case for 1,000,000 Years after Repository Closure

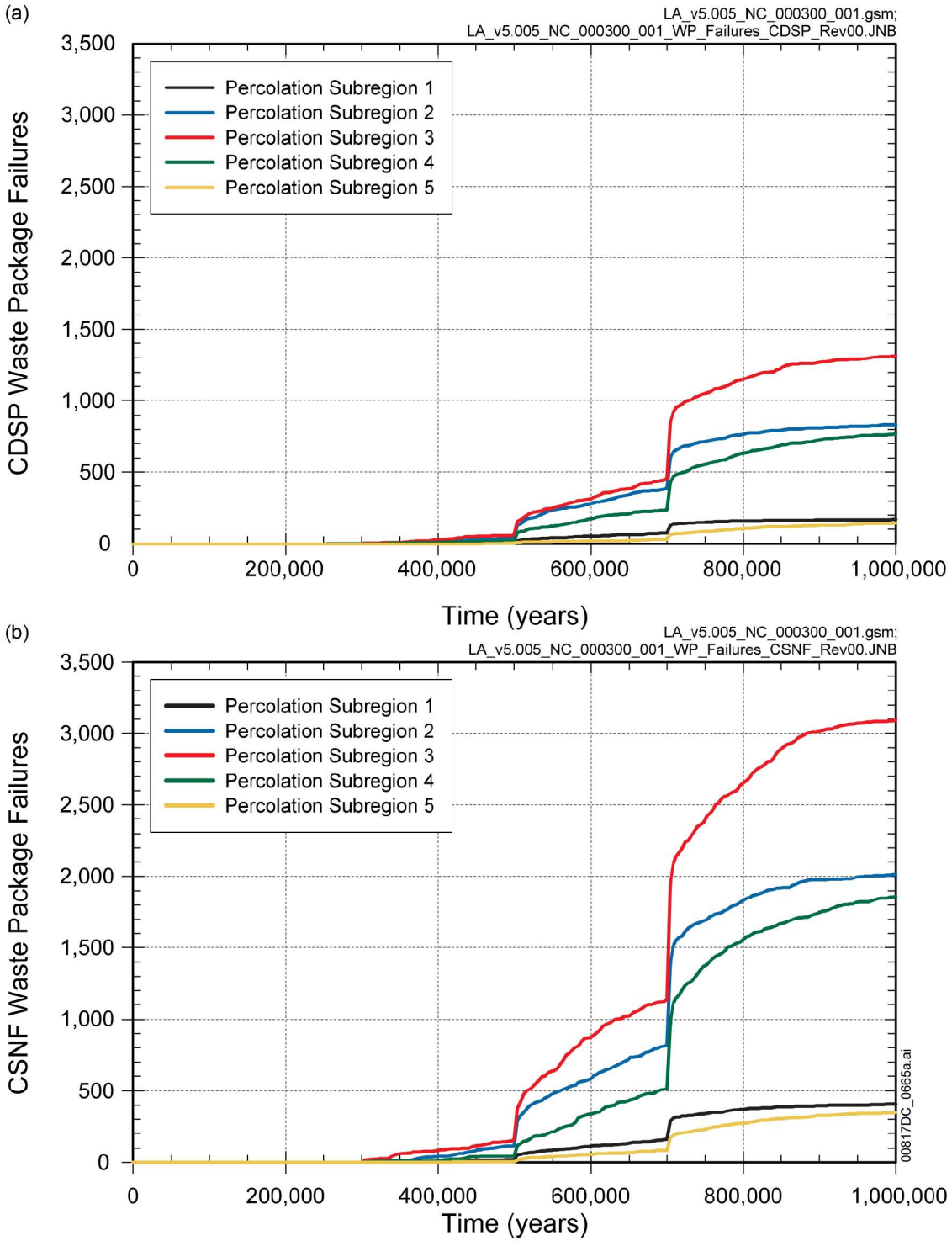

Source: Output DTN: MO0801TSPAMVAC.000 [DIRS 185080].

Figure 7.7.1-78[a]. Expected Number of (a) CDSP WP Failures and (b) CSNF WP Failures by Percolation Subregion for Realization 286 of the Nominal Modeling Case for 1,000,000 Years after Repository Closure

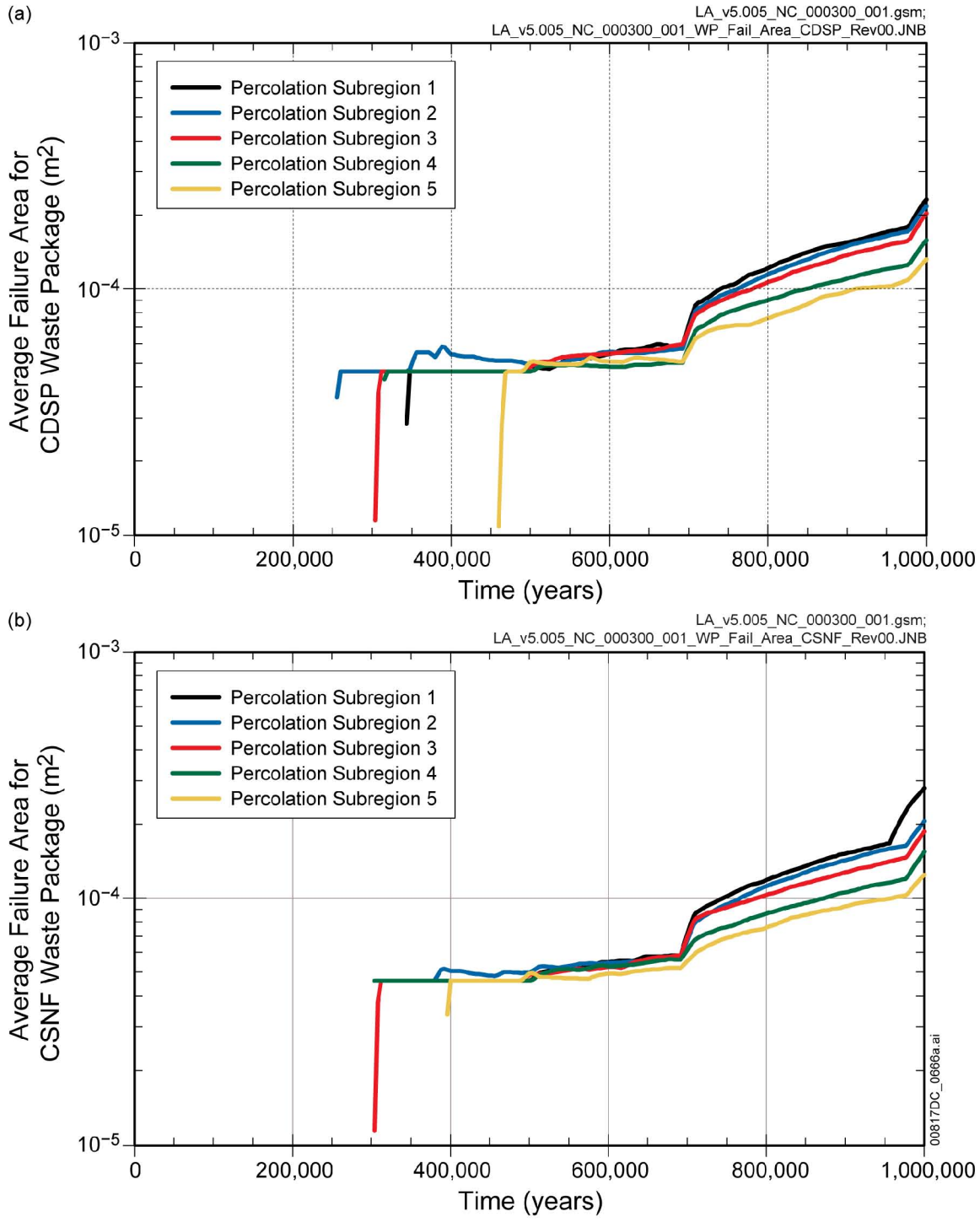

Source: Output DTN: MO0801TSPAMVAC.000 [DIRS 185080].

Figure 7.7.1-79[a]. Average Failure Area for (a) CDSP WPs and (b) CSNF WPs by Percolation Subregion for Realization 286 of the Nominal Modeling Case for 1,000,000 Years after Repository Closure

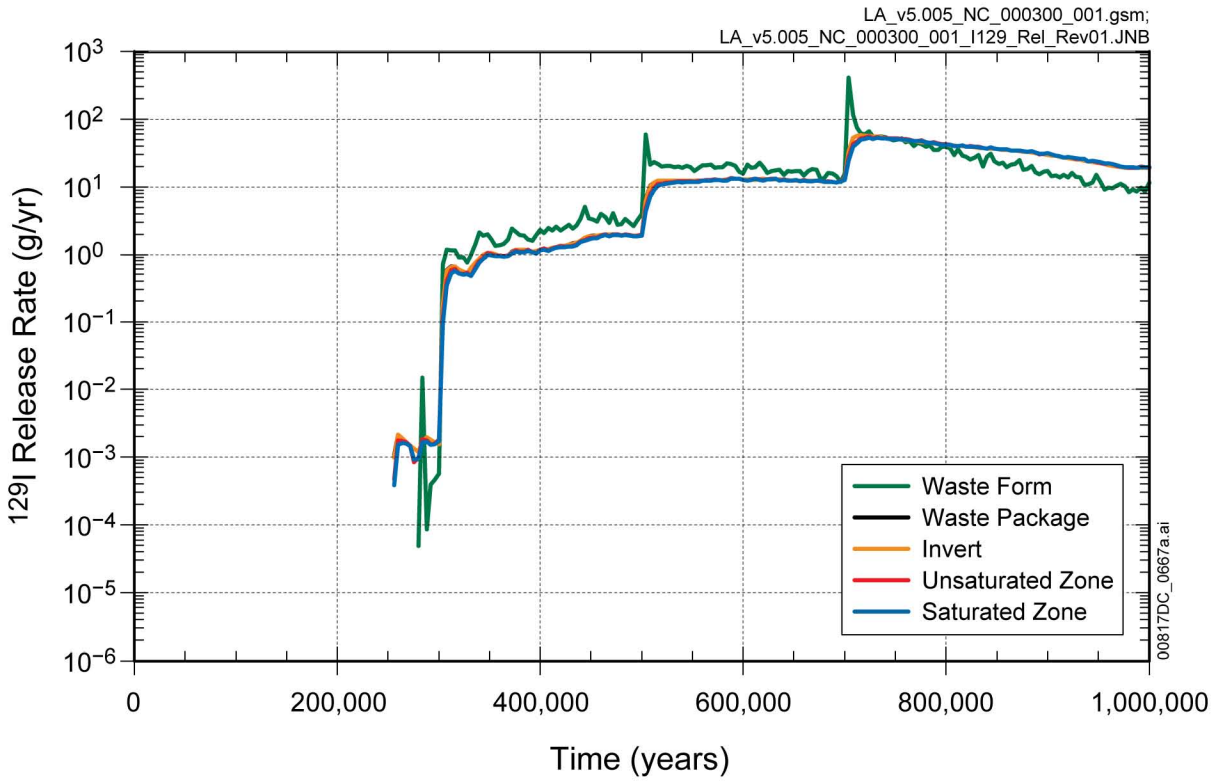

Source: Output DTN: MO0801TSPAMVAC.000 [DIRS 185080].

Figure 7.7.1-80[a]. Release Rates of ^{129}I from the Waste Form, Waste Package, Invert, Unsaturated Zone, and Saturated Zone for Realization 286 of the Nominal Modeling Case for 1,000,000 Years after Repository Closure

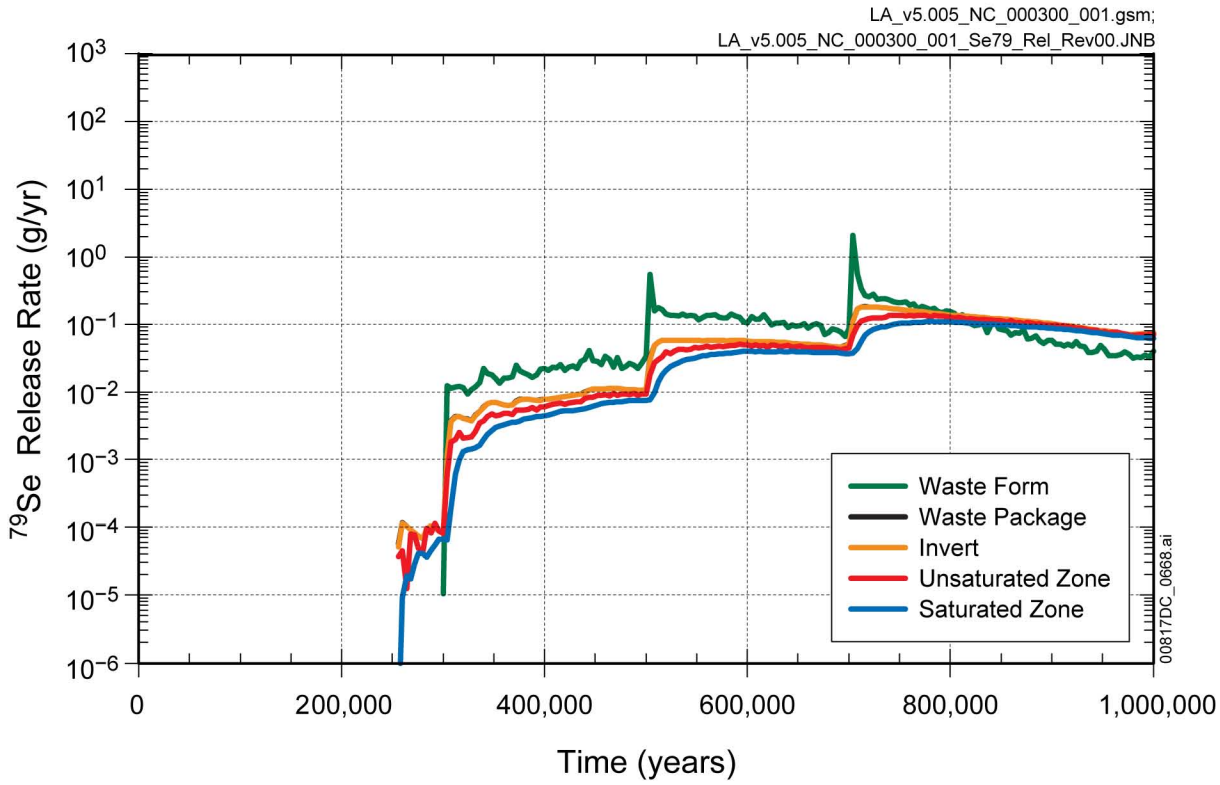

Source: Output DTN: MO0801TSPAMVAC.000 [DIRS 185080].

Figure 7.7.1-81[a]. Release Rates of ^{79}Se from the Waste Form, Waste Package, Invert, Unsaturated Zone, and Saturated Zone for Realization 286 of the Nominal Modeling Case for 1,000,000 Years after Repository Closure

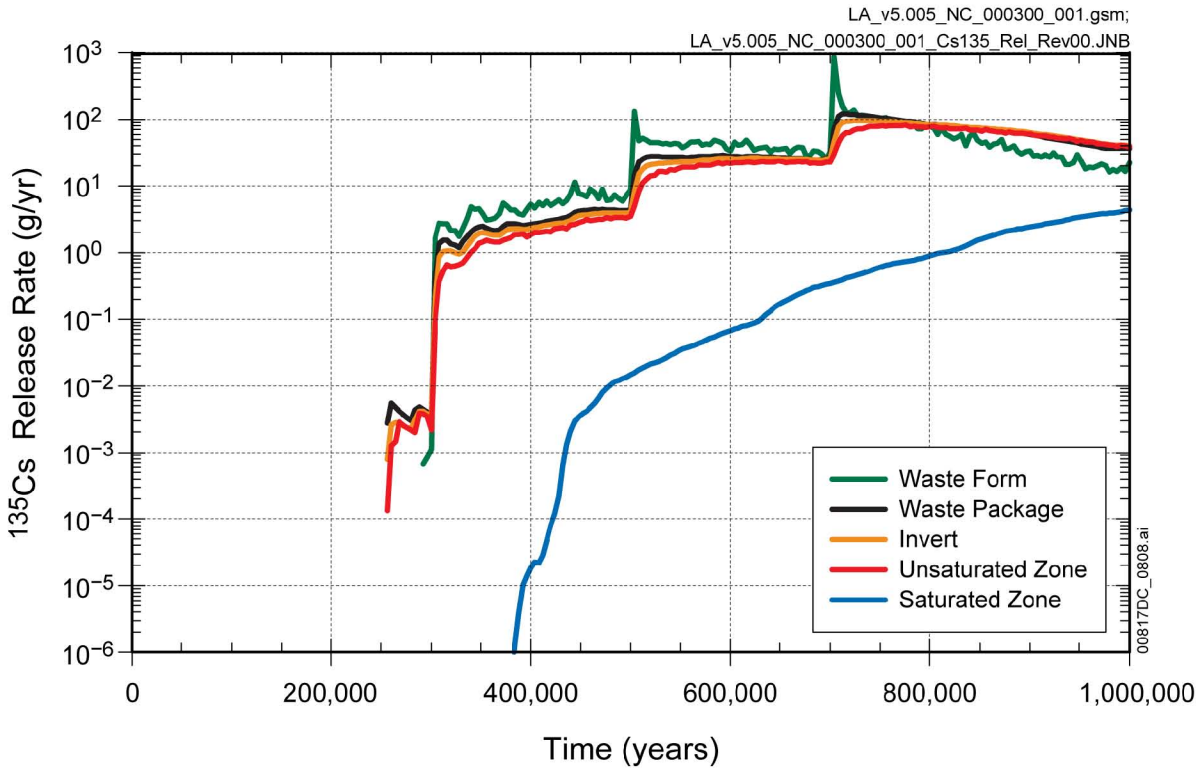

Source: Output DTN: MO0801TSPAMVAC.000 [DIRS 185080].

Figure 7.7.1-82[a]. Release Rates of ^{135}Cs from the Waste Form, Waste Package, Invert, Unsaturated Zone, and Saturated Zone for Realization 286 of the Nominal Modeling Case for 1,000,000 Years after Repository Closure

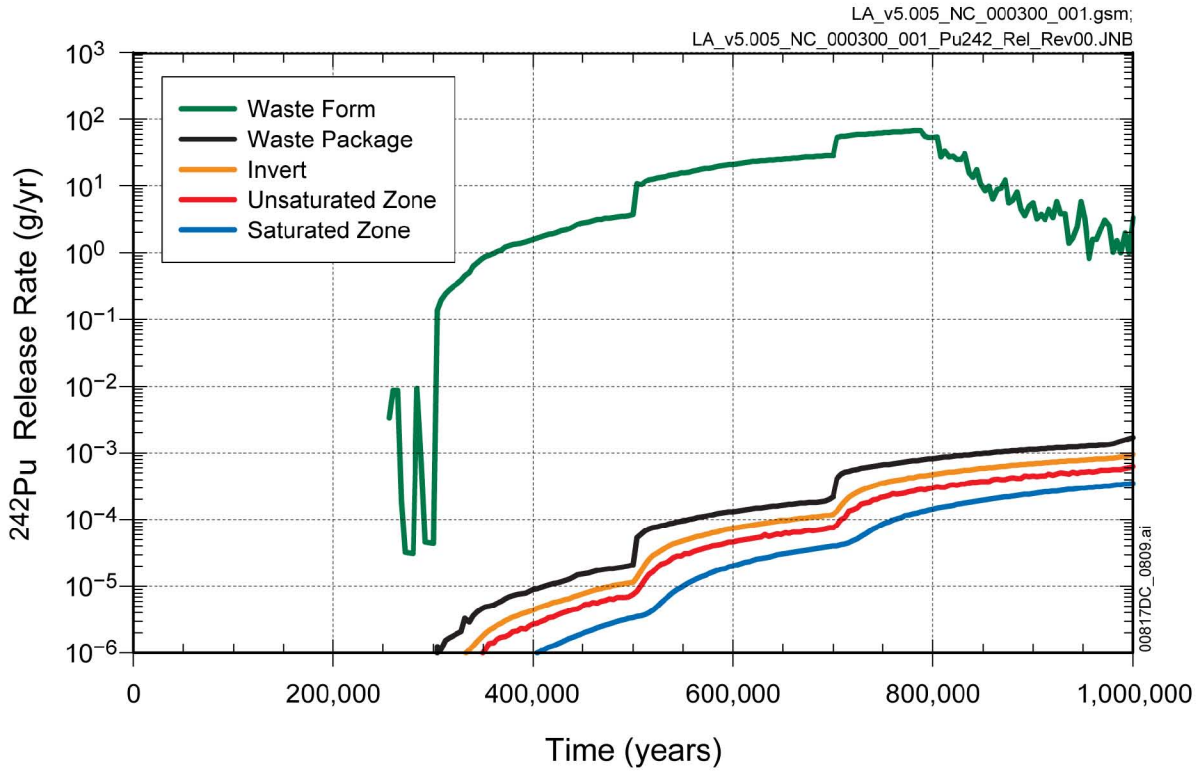

Source: Output DTN: MO0801TSPAMVAC.000 [DIRS 185080].

Figure 7.7.1-83[a]. Release Rates of ^{242}Pu (Dissolved and Reversibly Associated with Colloids) from the Waste Form, Waste Package, Invert, Unsaturated Zone, and Saturated Zone for Realization 286 of the Nominal Modeling Case for 1,000,000 Years after Repository Closure

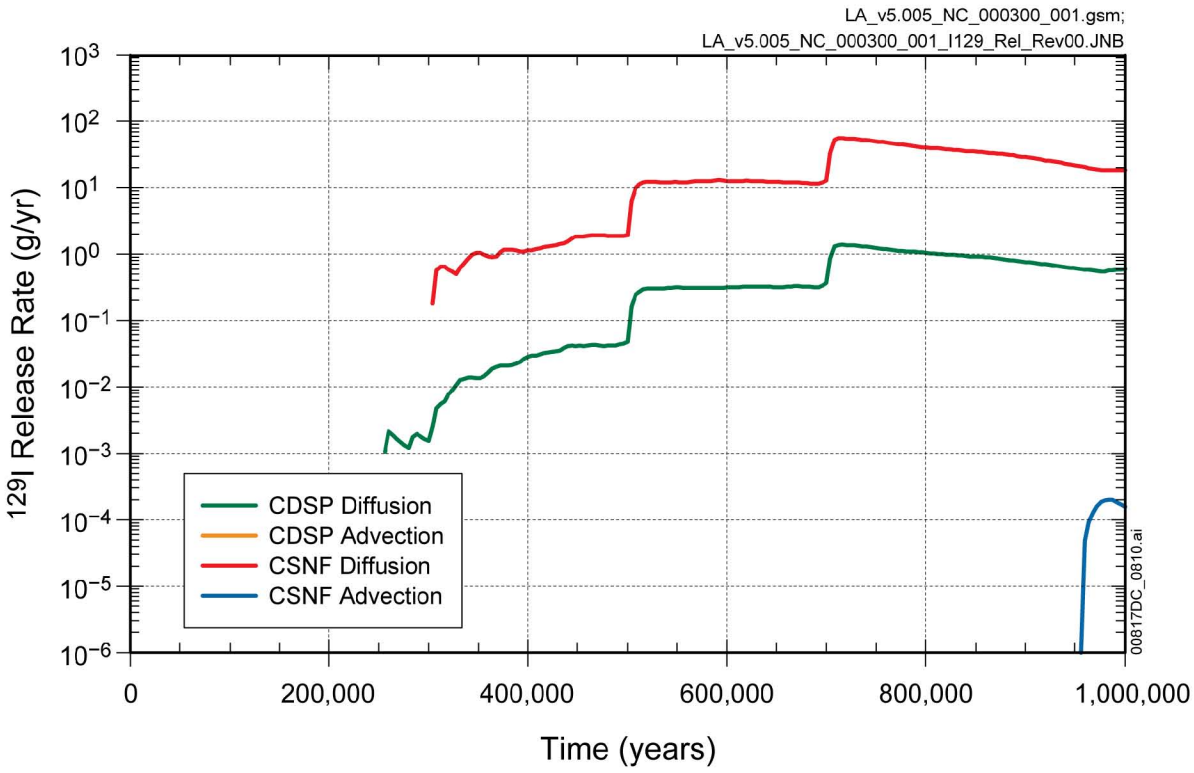

Source: Output DTN: MO0801TSPAMVAC.000 [DIRS 185080].

Figure 7.7.1-84[a]. Diffusive and Advective Release Rates of ^{129}I from the CDSP and CSNF Waste Packages for Realization 286 of the Nominal Modeling Case for 1,000,000 Years after Repository Closure

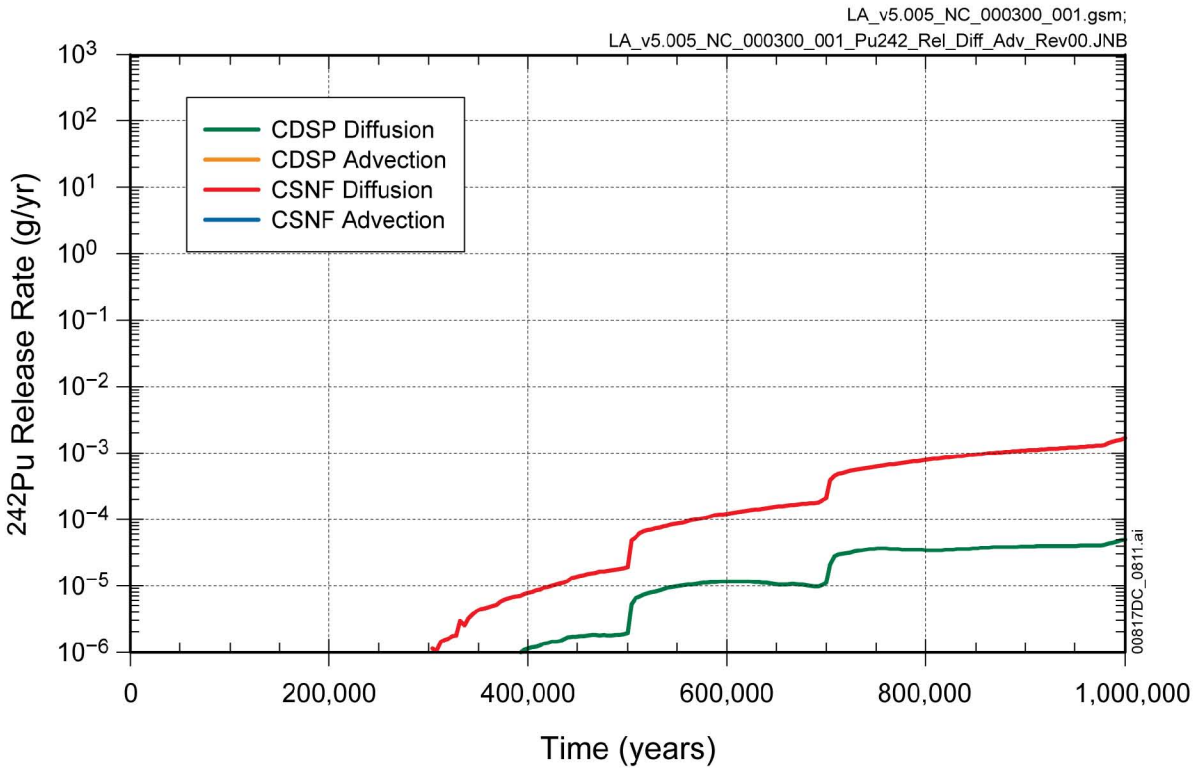

Source: Output DTN: MO0801TSPAMVAC.000 [DIRS 185080].

Figure 7.7.1-85[a]. Diffusive and Advective Release Rates of ^{242}Pu (Dissolved and Reversibly Associated with Colloids) from the CDSP and CSNF Waste Packages for Realization 286 of the Nominal Modeling Case for 1,000,000 Years after Repository Closure

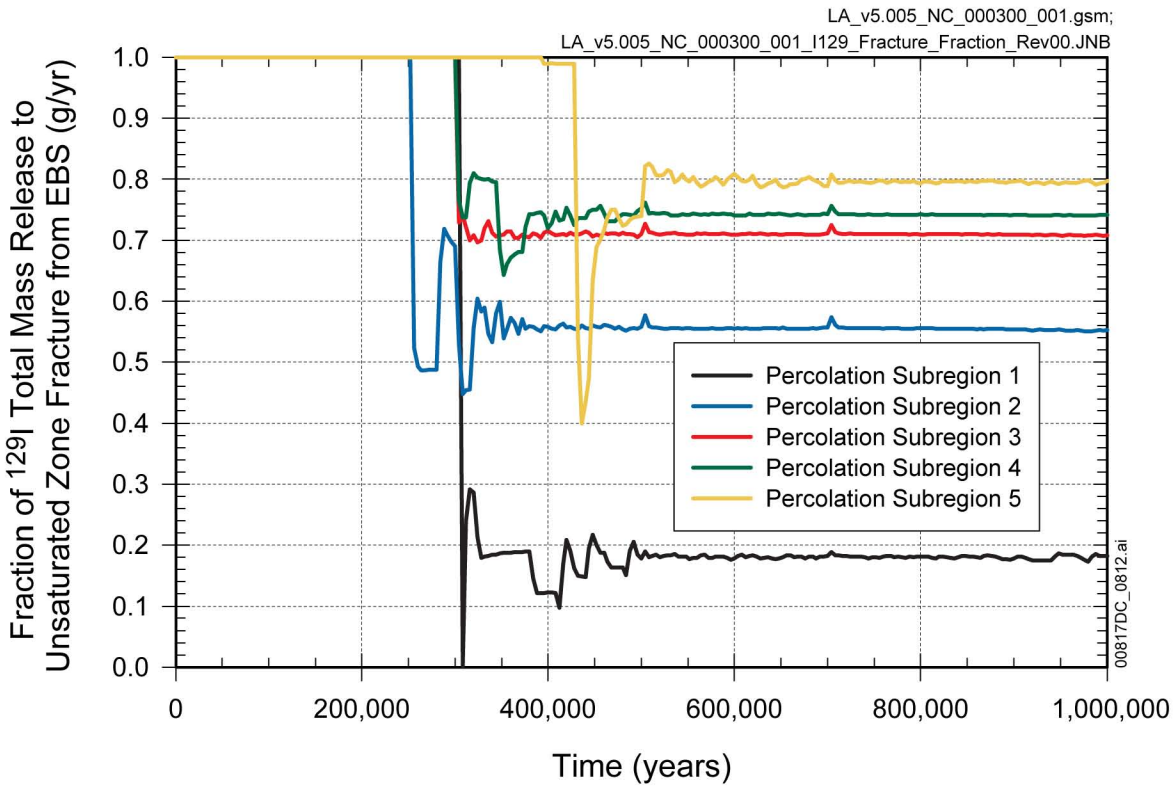

Source: Output DTN: MO0801TSPAMVAC.000 [DIRS 185080].

Figure 7.7.1-86[a]. Fraction of ^{129}I Mass Going to Unsaturated Zone Fractures at the Repository Horizon for Realization 286 of the Nominal Modeling Case for 1,000,000 Years after Repository Closure

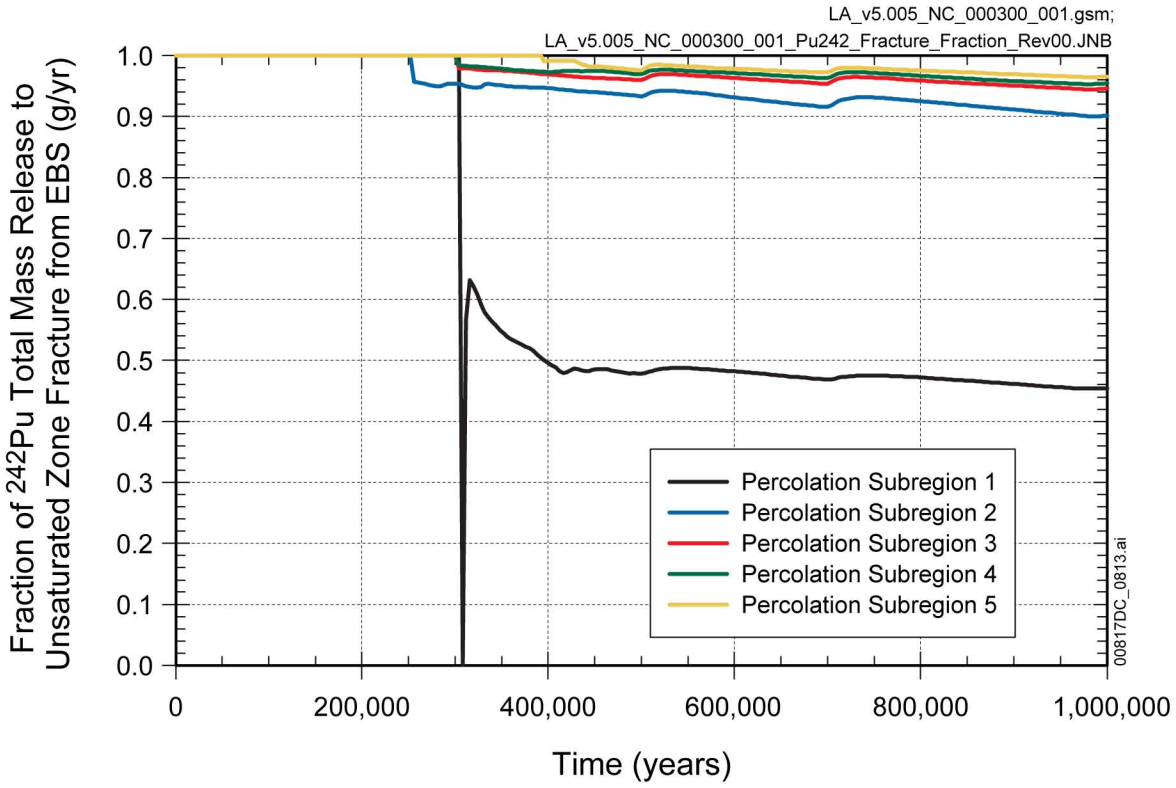

Source: Output DTN: MO0801TSPAMVAC.000 [DIRS 185080].

Figure 7.7.1-87[a]. Fraction of ^{242}Pu Mass Going to Unsaturated Zone Fractures at the Repository Horizon for Realization 286 of the Nominal Modeling Case for 1,000,000 Years after Repository Closure

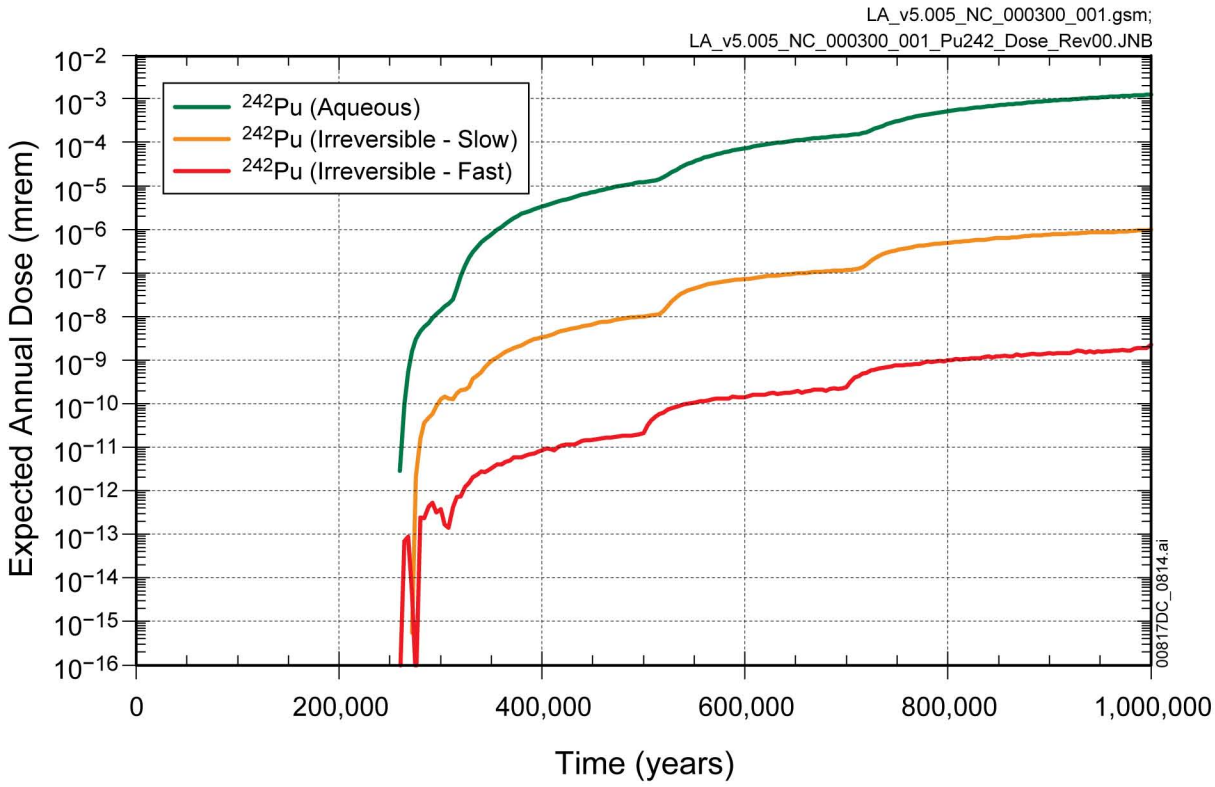

Source: Output DTN: MO0801TSPAMVAC.000 [DIRS 185080].

NOTE: Plutonium dissolved and reversibly associated with colloids is denoted as aqueous.

Figure 7.7.1-88[a]. Expected Annual Dose for Aqueous ^{242}Pu and Slow and Fast Fractions of Irreversibly Sorbed Colloidal ^{242}Pu for Realization 286 of the Nominal Modeling Case for 1,000,000 Years after Repository Closure

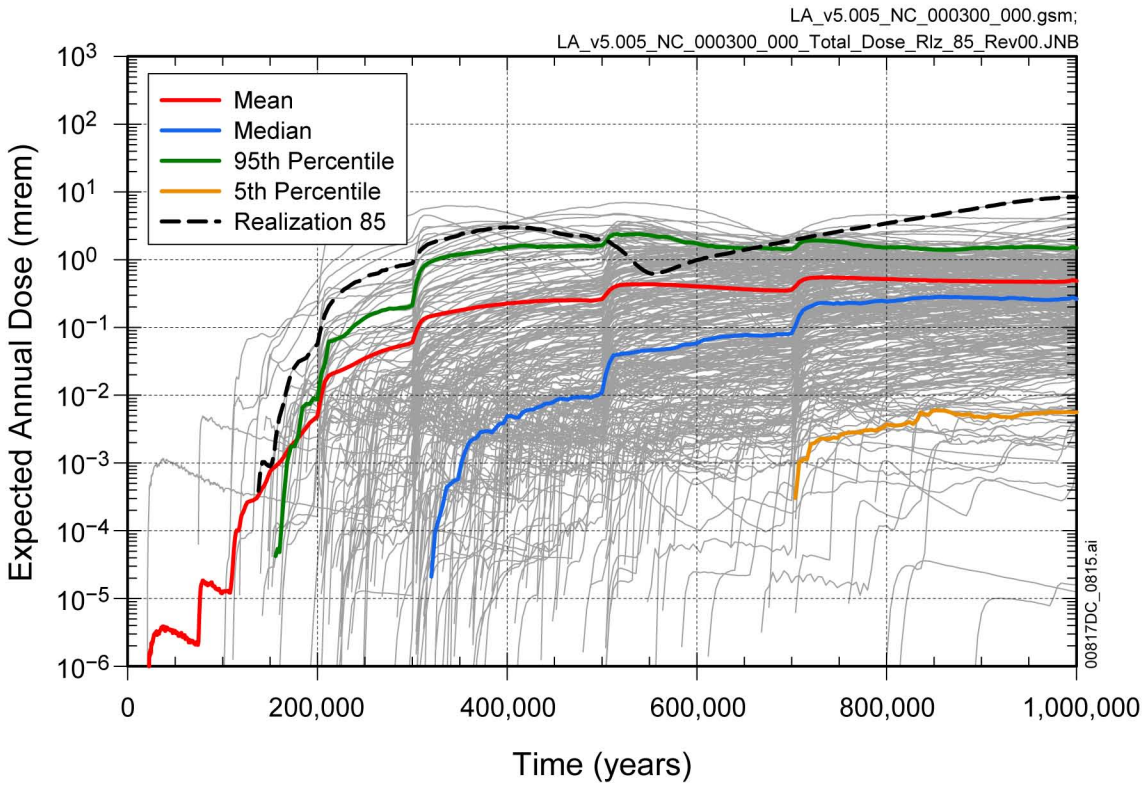

Source: Output DTN: MO0710ADTSPAWO.000 [DIRS 183752].

Figure 7.7.1-89[a]. Expected Annual Dose from the 300 Epistemic Uncertainty Vectors along with their Quantiles and Expected Dose from Epistemic Uncertainty Vector 85 for the Nominal Modeling Case for 1,000,000 Years after Repository Closure

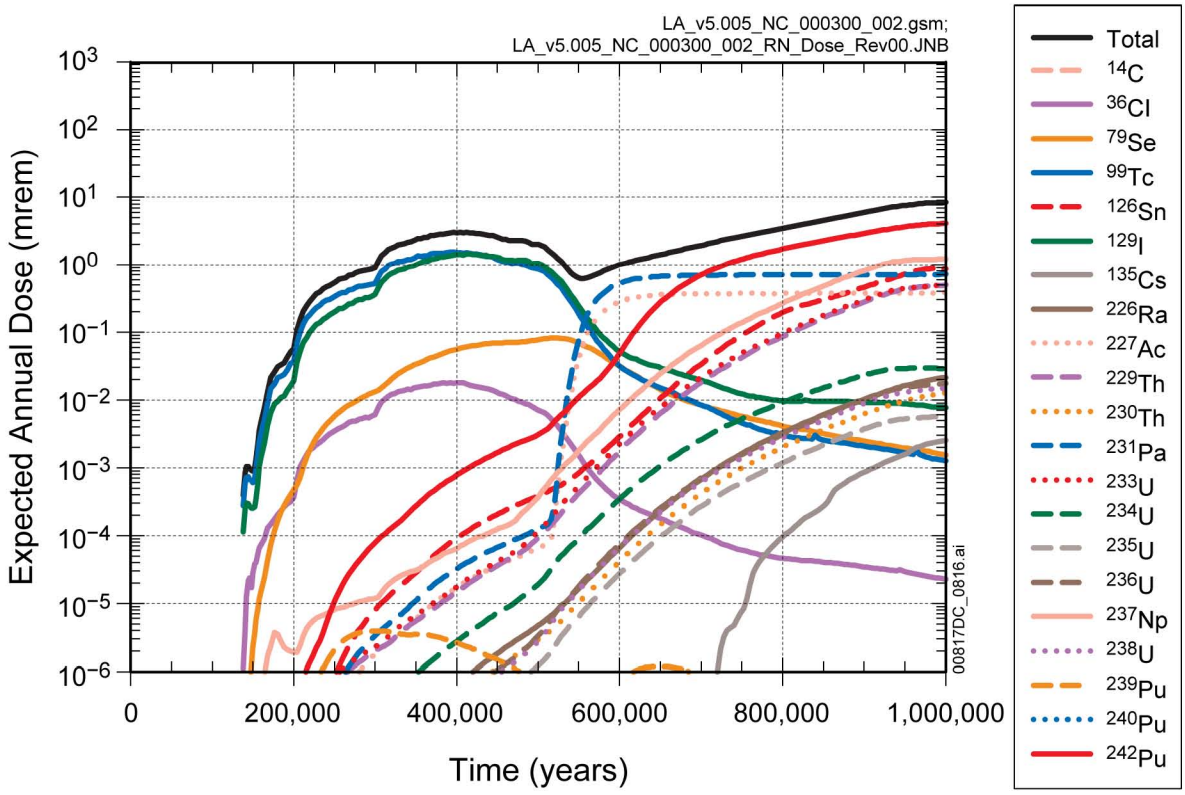

Source: Output DTN: MO0801TSPAMVAC.000 [DIRS 185080].

Figure 7.7.1-90[a]. Contribution of Individual Radionuclides to Expected Annual Dose of Realization 85 of the Nominal Modeling Case for 1,000,000 Years after Repository Closure

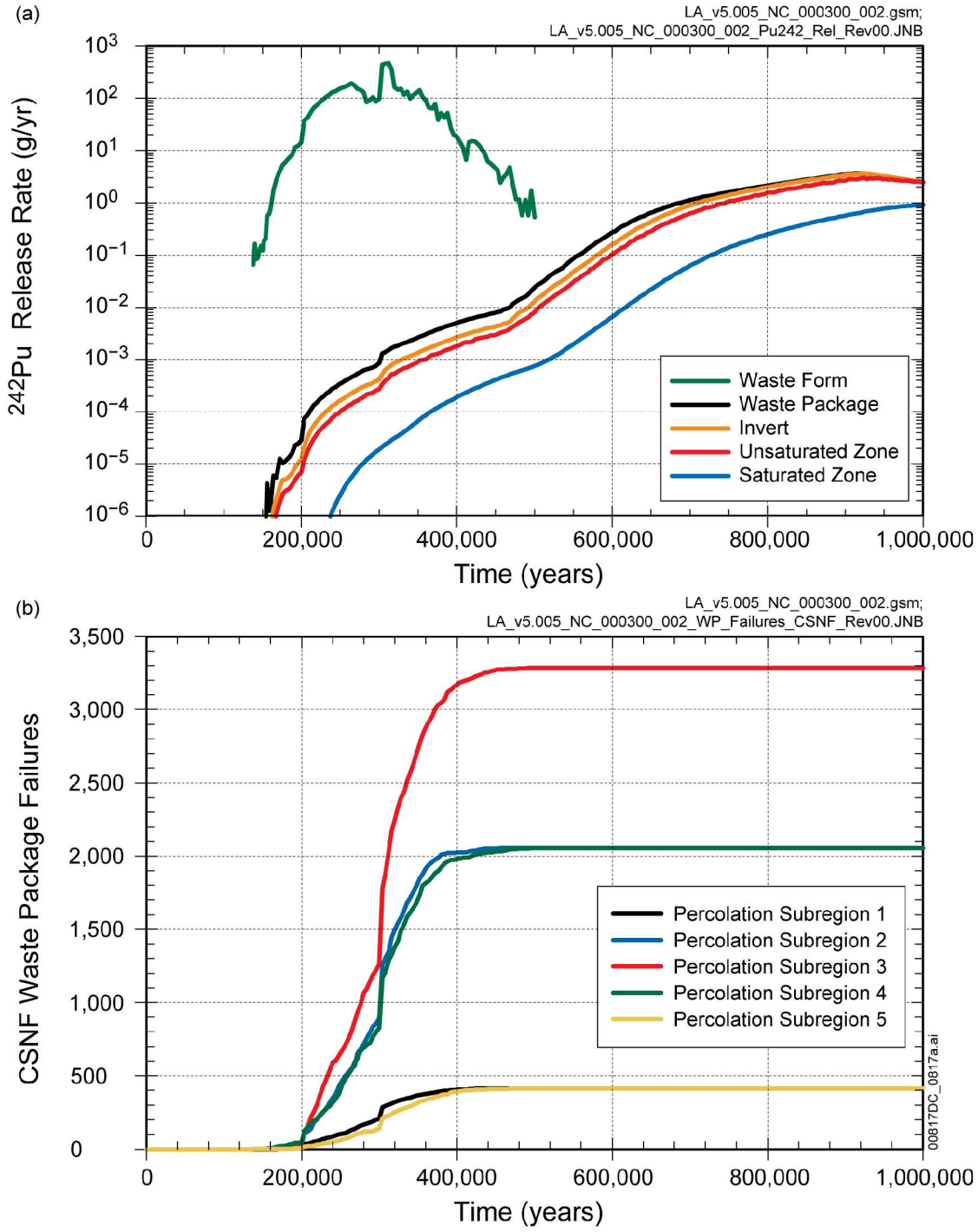

Source: Output DTN: MO0801TSPAMVAC.000 [DIRS 185080].

Figure 7.7.1-91[a]. (a) Release Rates of ^{242}Pu (Dissolved and Reversibly Associated with Colloids) from the Waste Form, Waste Package, Invert, Unsaturated Zone, and Saturated Zone, and (b) CSNF WP Failure History for Realization 85 of the Nominal Modeling Case for 1,000,000 Years after Repository Closure

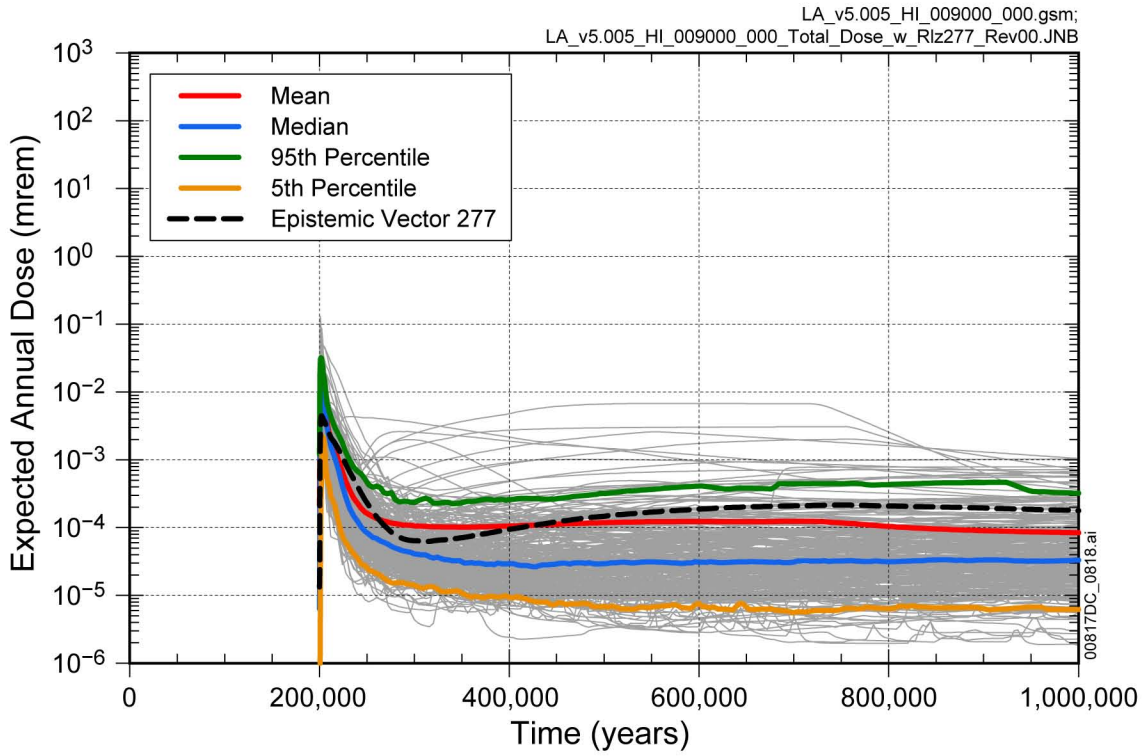

Source: Output DTN: MO0710ADTSPAWO.000 [DIRS 183752].

Figure 7.7.1-92[a]. Expected Annual Dose from the 300 Epistemic Uncertainty Vectors along with their Quantiles and Expected Dose from Epistemic Uncertainty Vector 277 for the Human Intrusion Modeling Case for 1,000,000 Years after Repository Closure

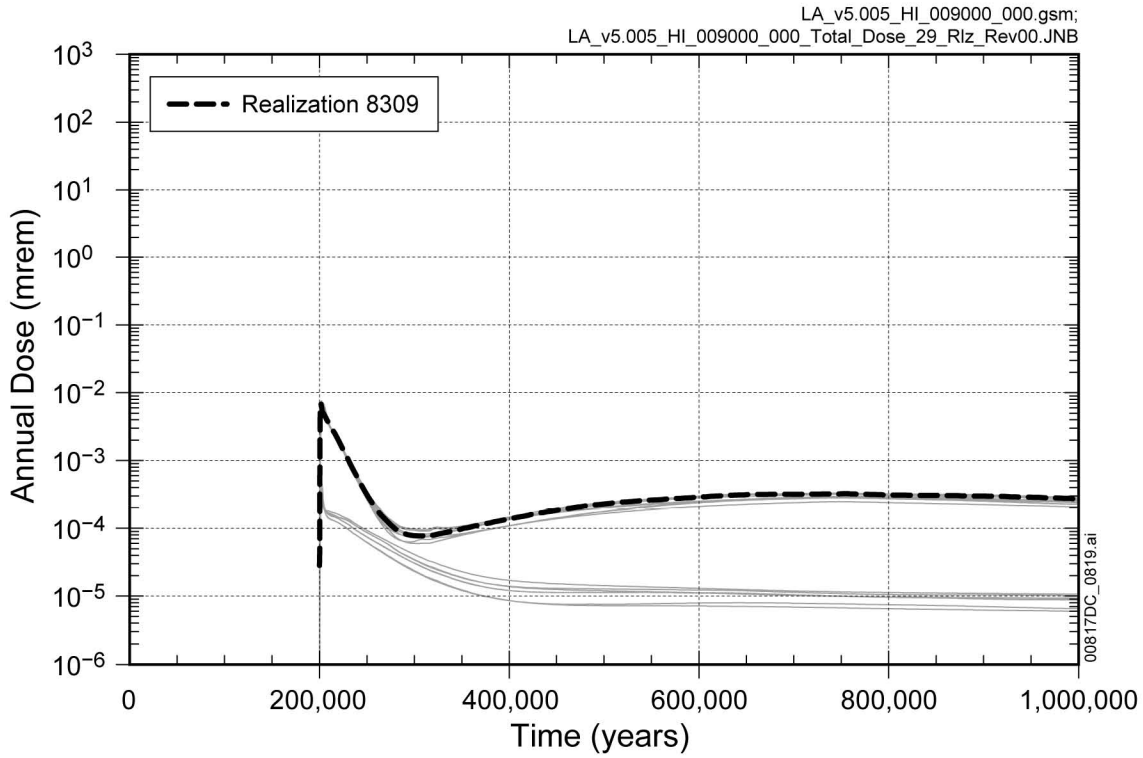

Source: Output DTN: MO0710ADTSPAWO.000 [DIRS 183752].

NOTE: The dashed line is the annual dose from aleatory vector 29, which is equivalent to GoldSim realization 8309.

Figure 7.7.1-93[a]. Annual Dose from the Thirty Aleatory Vectors Associated with the Epistemic Uncertainty Vector 277 for the Human Intrusion Modeling Case for 1,000,000 Years after Repository Closure

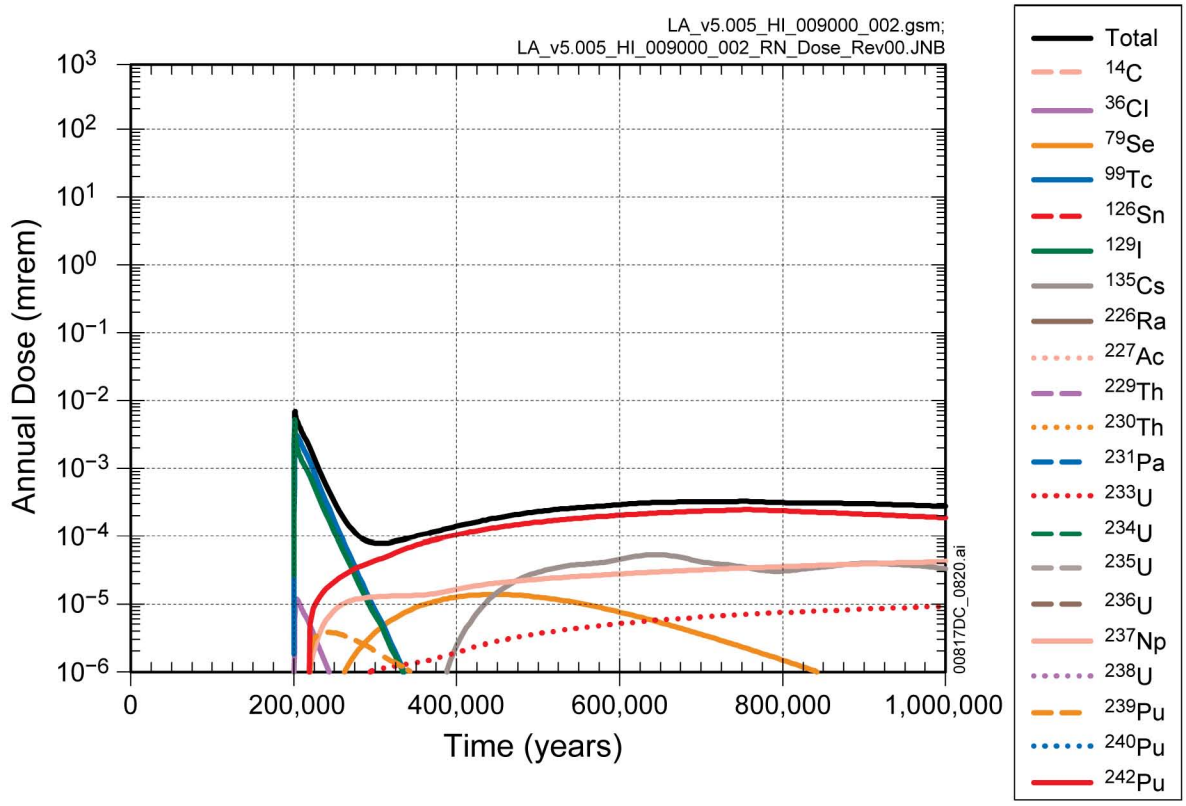

Source: Output DTN: MO0801TSPAMVAC.000 [DIRS 185080].

Figure 7.7.1-94[a]. Annual Dose along with Major Radionuclide Dose Contributors for Realization 8309 of the Human Intrusion Modeling Case for 1,000,000 Years after Repository Closure

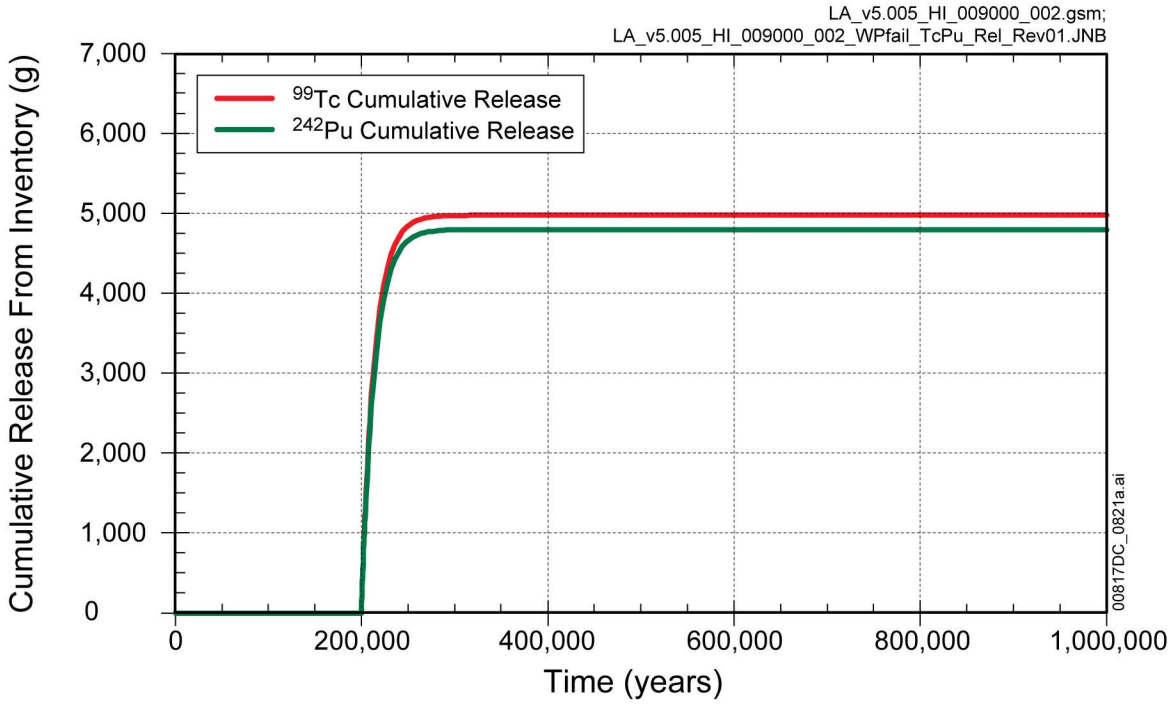

Source: Output DTN: MO0801TSPAMVAC.000 [DIRS 185080].

Figure 7.7.1-95[a]. Cumulative Release of ^{99}Tc and ^{242}Pu from the Inventory for Percolation Subregion 4 for Realization 8309 of the Human Intrusion Modeling Case for 1,000,000 Years after Repository Closure

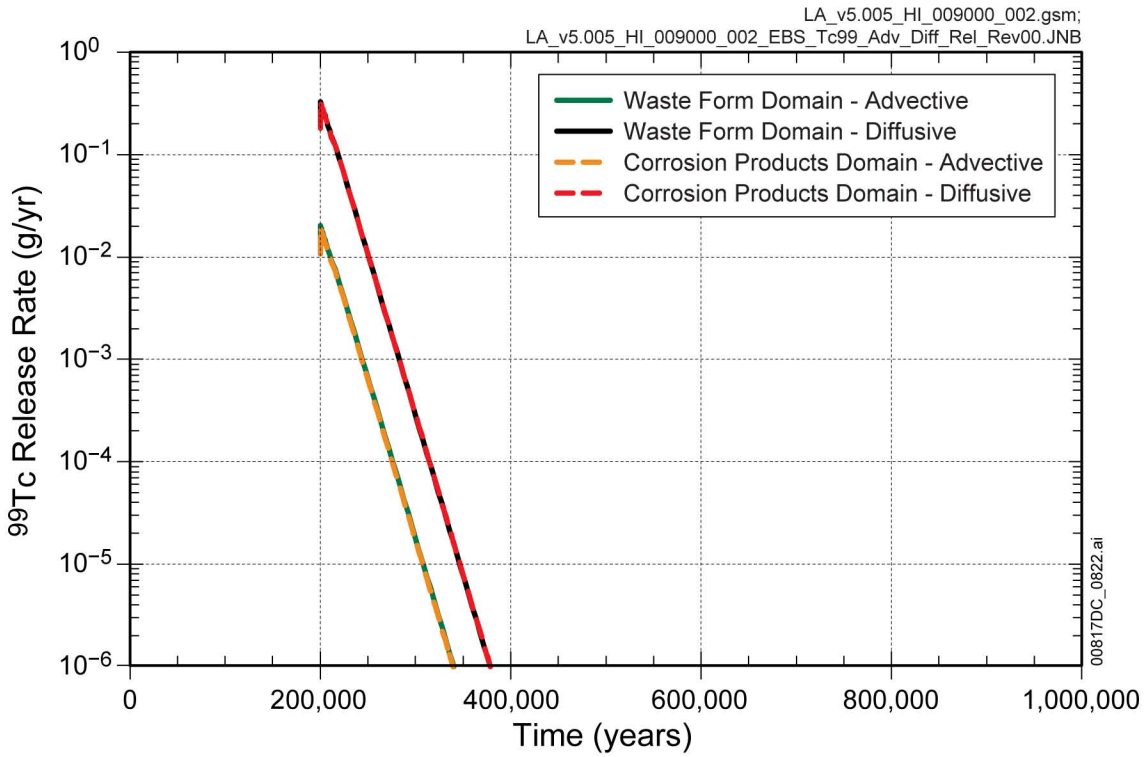

Source: Output DTN: MO0801TSPAMVAC.000 [DIRS 185080].

Figure 7.7.1-96[a]. Advective and Diffusive Release Rates of ^{99}Tc from Waste Form and Corrosion Products Domain for failed CSNF WPs for Realization 8309 of the Human Intrusion Modeling Case for 1,000,000 Years after Repository Closure

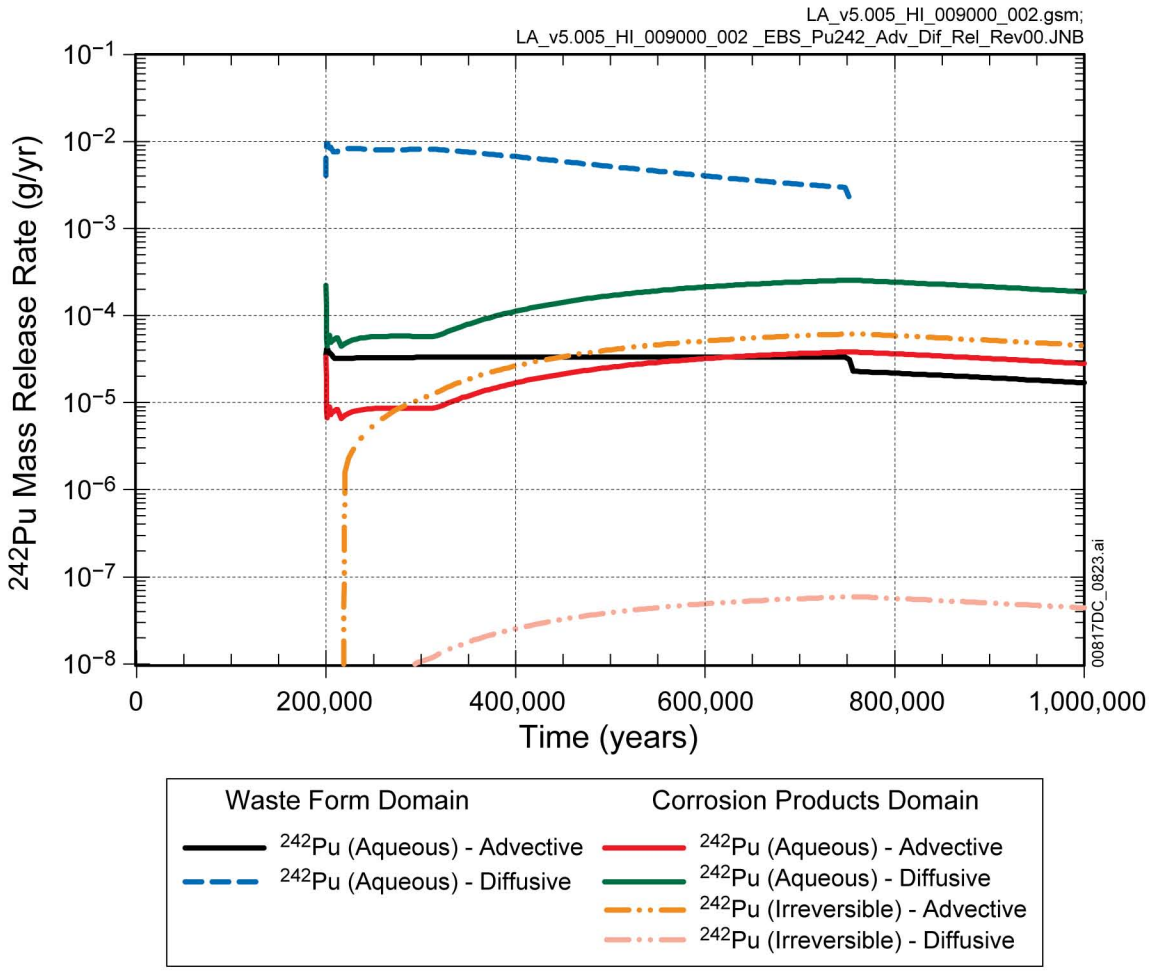

Source: Output DTN: MO0801TSPAMVAC.000 [DIRS 185080].

NOTE: Plutonium dissolved and reversibly associated with colloids is denoted as aqueous.

Figure 7.7.1-97[a]. Advective and Diffusive Release Rates of ^{242}Pu (Aqueous) from Waste Form and Corrosion Products Domain and ^{242}Pu (Irreversibly Sorbed on Iron Oxyhydroxide Colloids) from Corrosion Products Domain for failed CSNF WPs for Realization 8309 of the Human Intrusion Modeling Case for 1,000,000 Years after Repository Closure

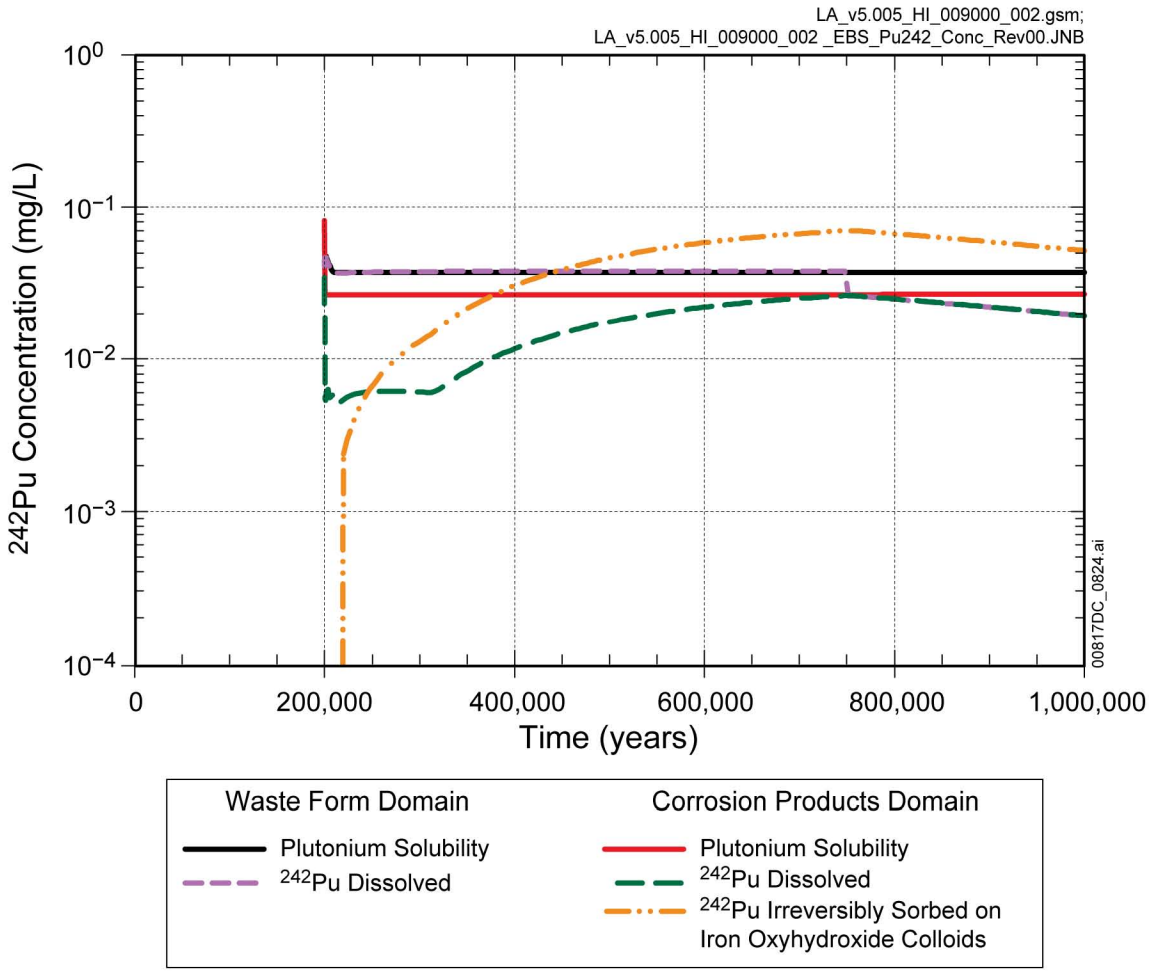

Source: Output DTN: MO0801TSPAMVAC.000 [DIRS 185080].

Figure 7.7.1-98[a]. Dissolved Concentration of ^{242}Pu in the Waste Form and Corrosion Products Domain, the Plutonium Solubility in Respective Domains, and Concentration of ^{242}Pu Irreversibly Sorbed on Iron Oxyhydroxide Colloids for Realization 8309 of the Human Intrusion Modeling Case for 1,000,000 Years after Repository Closure

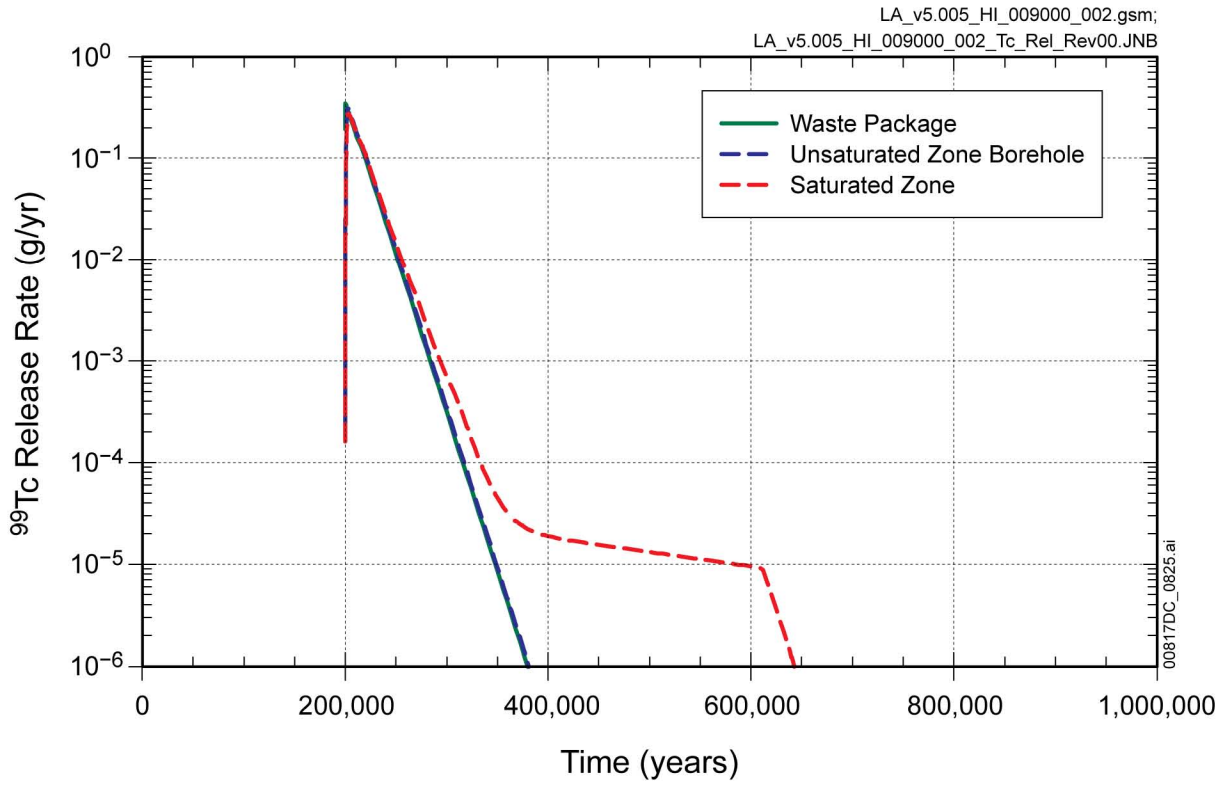

Source: Output DTN: MO0801TSPAMVAC.000 [DIRS 185080].

Figure 7.7.1-99[a]. Comparison of ^{99}Tc Release from Waste Package, Unsaturated Zone Borehole, and Saturated Zone for Realization 8309 of the Human Intrusion Modeling Case for 1,000,000 Years after Repository Closure

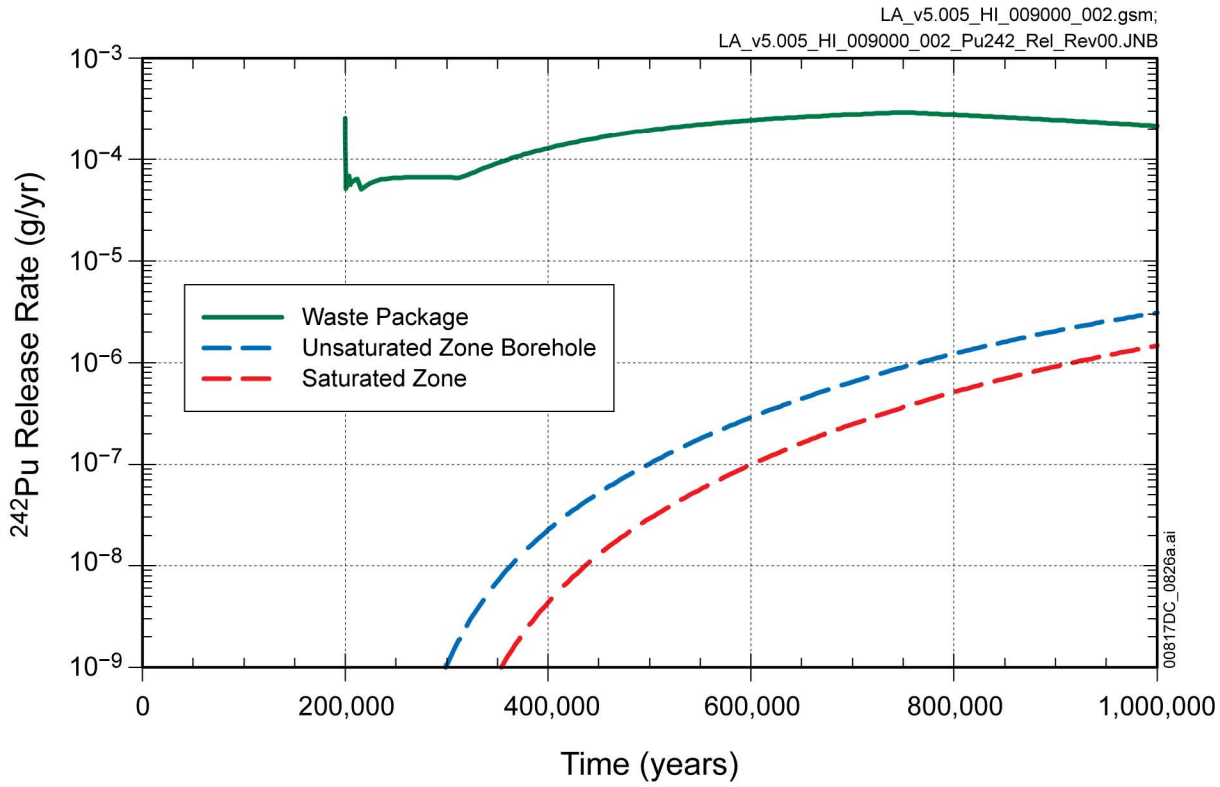

Source: Output DTN: MO0801TSPAMVAC.000 [DIRS 185080].

Figure 7.7.1-100[a]. Comparison of ^{242}Pu (Dissolved and Reversibly Associated with Colloids) Release from Waste Package, Unsaturated Zone Borehole, and Saturated Zone for Realization 8309 of the Human Intrusion Modeling Case for 1,000,000 Years after Repository Closure

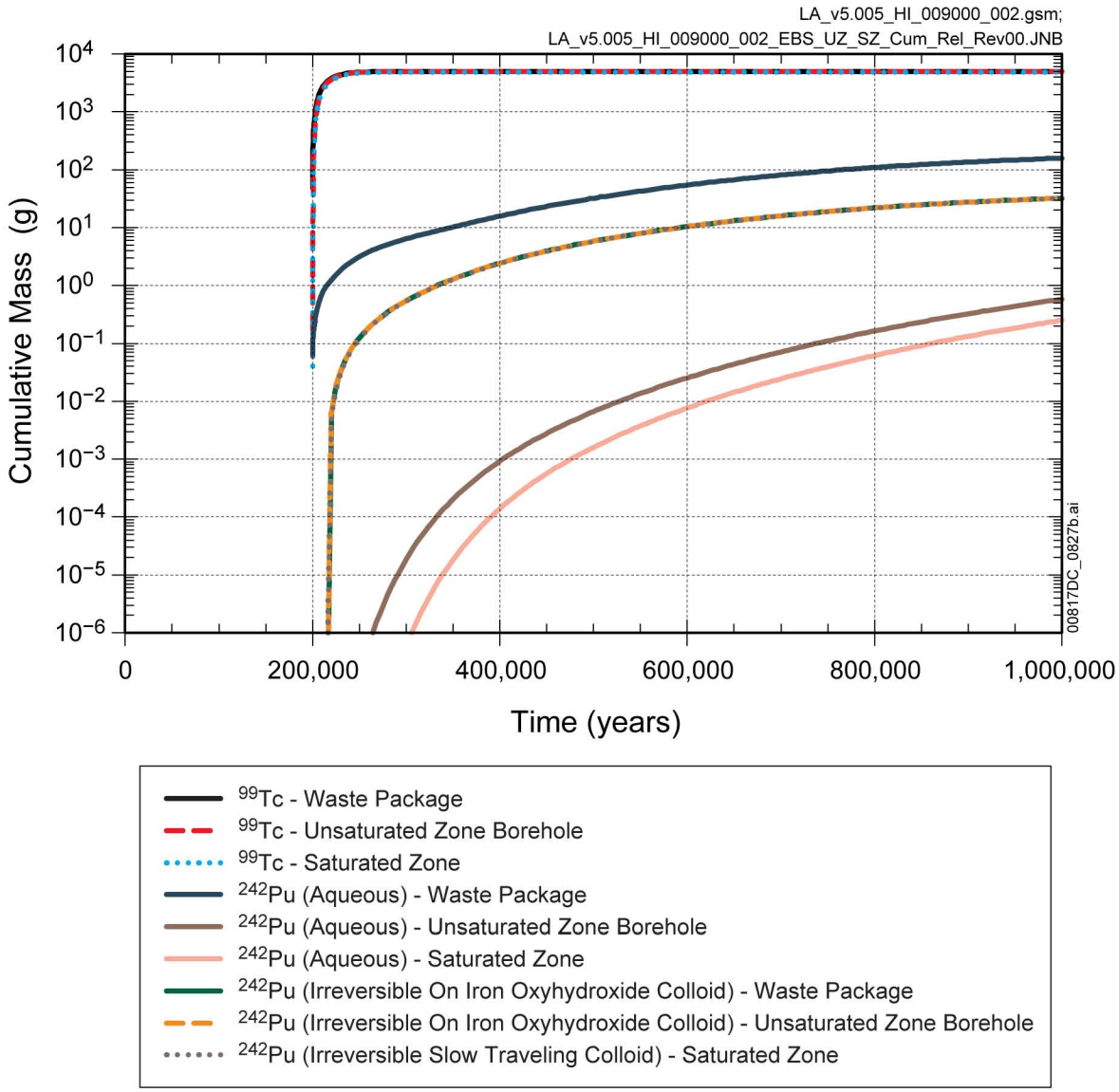

Source: Output DTN: MO0801TSPAMVAC.000 [DIRS 185080].

NOTE: Plutonium dissolved and reversibly associated with colloids is denoted as aqueous.

Figure 7.7.1-101[a]. Cumulative Release Comparison of ^{99}Tc, ^{242}Pu (Aqueous), and ^{242}Pu (Irreversibly Sorbed on Colloids) from Waste Package, Unsaturated Zone Borehole, and Saturated Zone for Realization 8309 of the Human Intrusion Modeling Case for 1,000,000 Years after Repository Closure

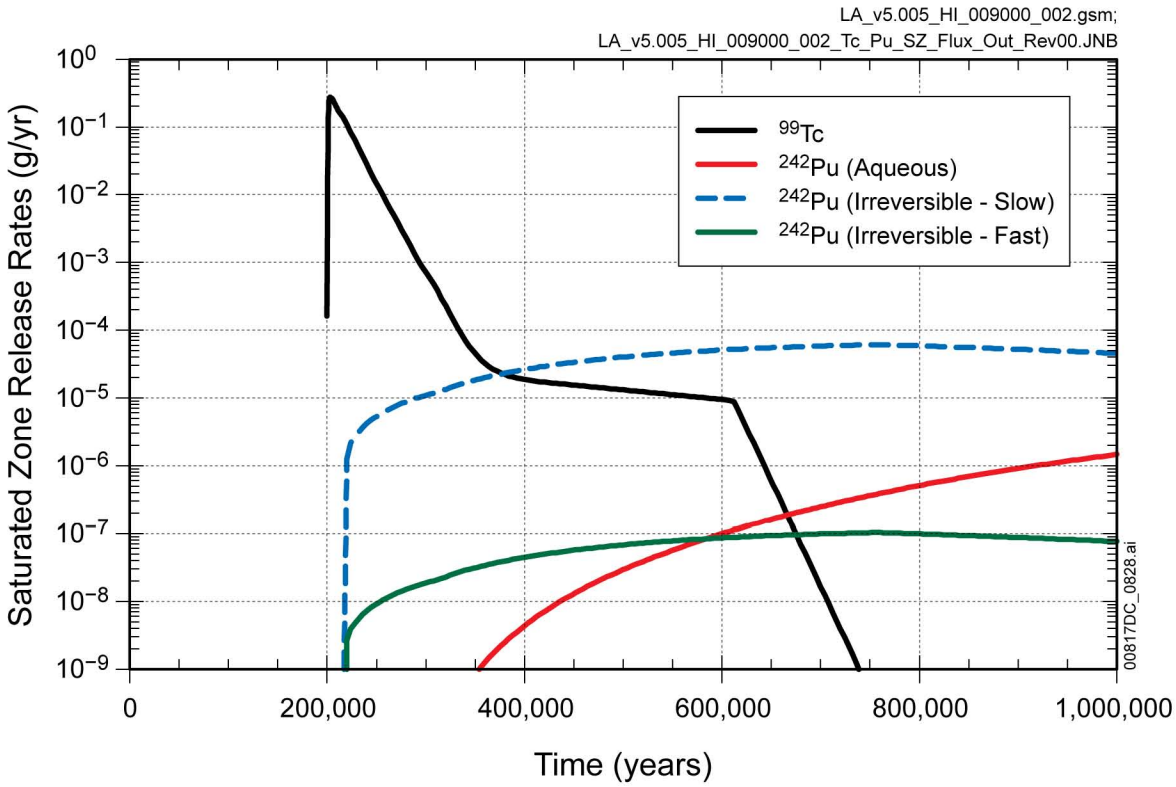

Source: Output DTN: MO0801TSPAMVAC.000 [DIRS 185080].

NOTE: Plutonium dissolved and reversibly associated with colloids is denoted as aqueous.

Figure 7.7.1-102[a]. Saturated Zone Release Rates to the Biosphere for ^{99}Tc, ^{242}Pu (Aqueous), ^{242}Pu (Irreversibly Sorbed on Colloids that Travel Slowly due to Retardation), and ^{242}Pu (Irreversibly Sorbed on Colloids that Travel Fast due to no Retardation) for Realization 8309 of the Human Intrusion Modeling Case for 1,000,000 Years after Repository Closure

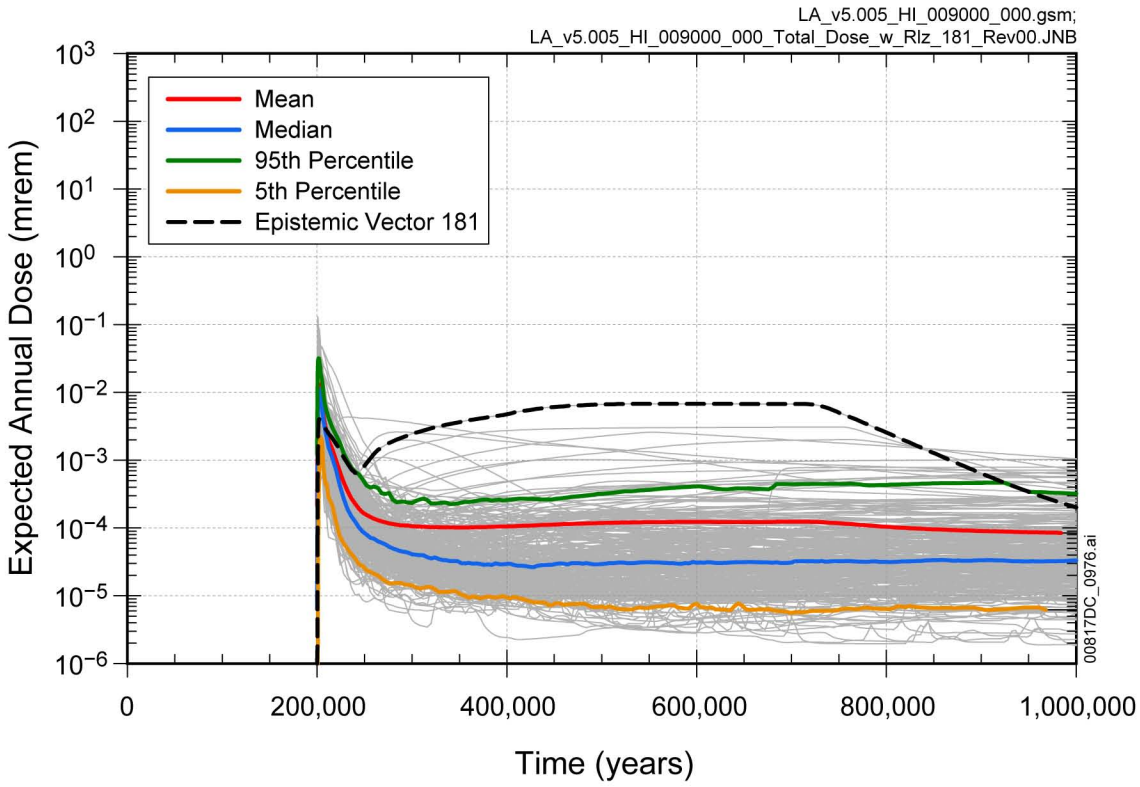

Source: Output DTN: MO0710ADTSPAWO.000 [DIRS 183752].

Figure 7.7.1-103[a]. Expected Annual Dose from the 300 Epistemic Uncertainty Vectors along with their Quantiles and Expected Dose from Epistemic Uncertainty Vector 181 for the Human Intrusion Modeling Case for 1,000,000 Years after Repository Closure

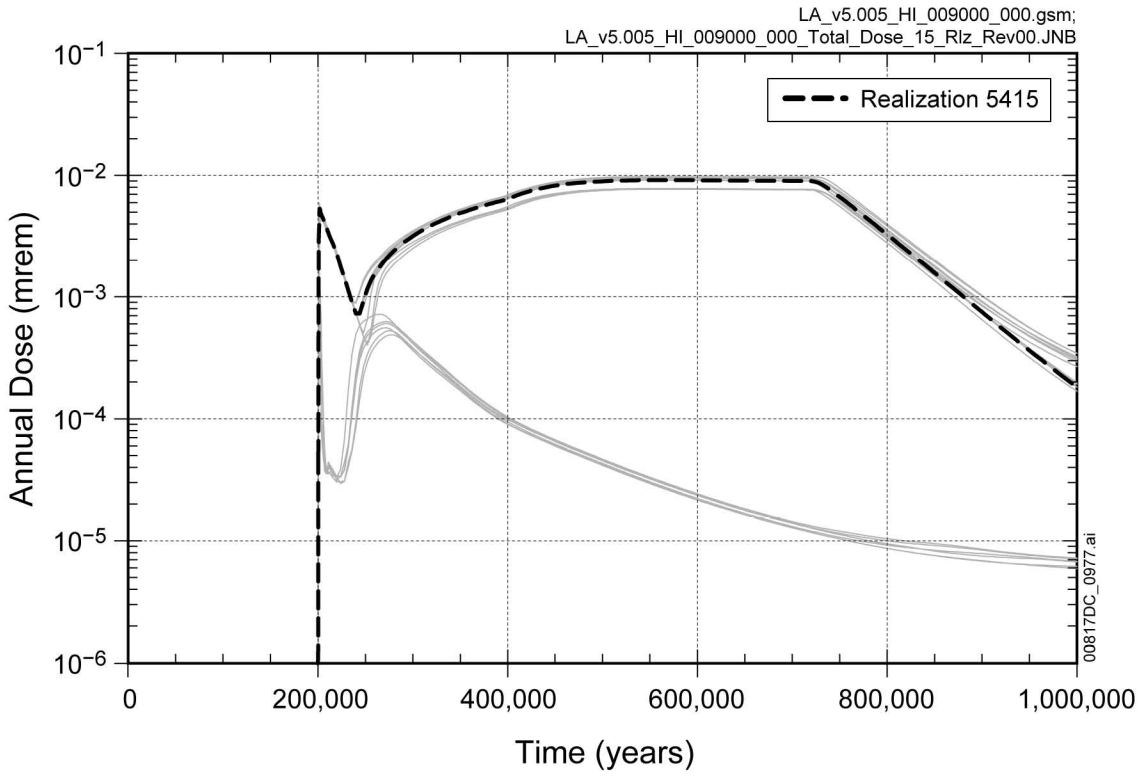

Source: Output DTN: MO0710ADTSPAWO.000 [DIRS 183752].

Figure 7.7.1-104[a]. Annual Dose from the Thirty Aleatory Vectors Associated with the Epistemic Uncertainty Vector 181 for the Human Intrusion Modeling Case for 1,000,000 Years after Repository Closure

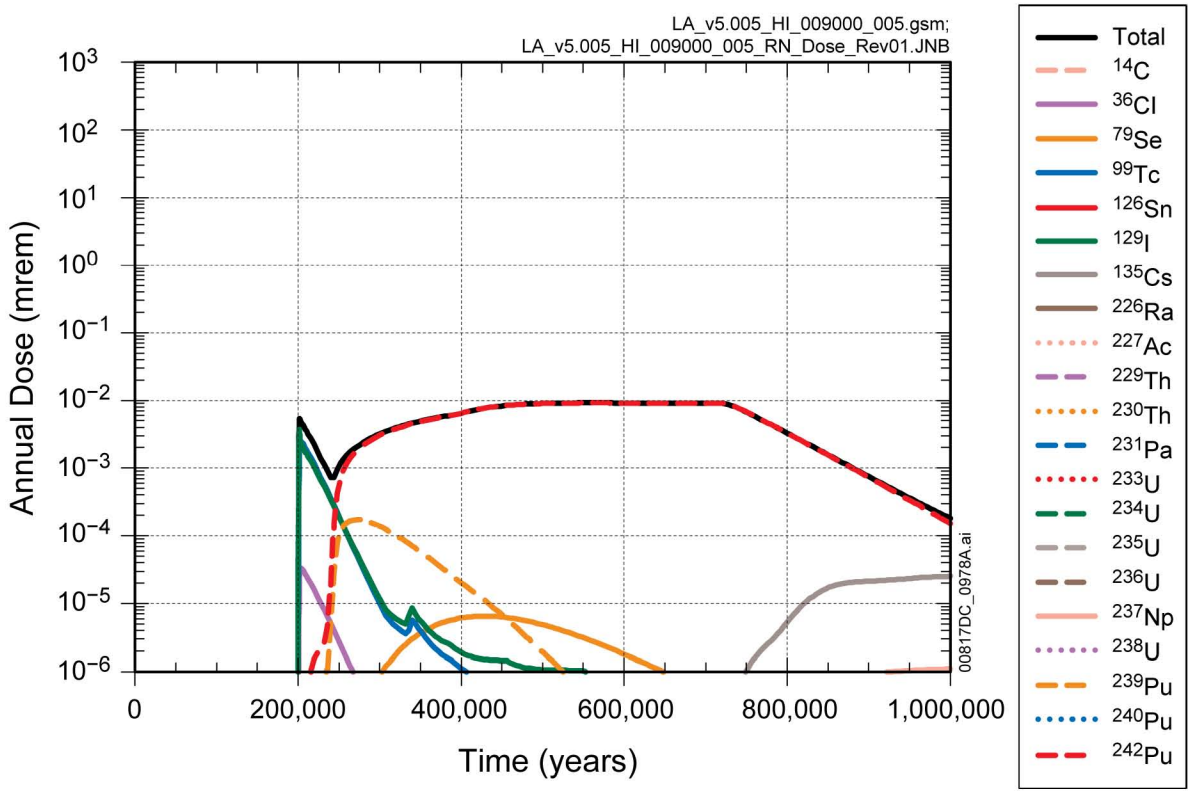

Source: Output DTN: MO0801TSPAMVAC.000 [DIRS 185080].

Figure 7.7.1-105[a]. Annual Dose along with Major Radionuclide Dose Contributors for Realization 5415 of the Human Intrusion Modeling Case for 1,000,000 Years after Repository Closure

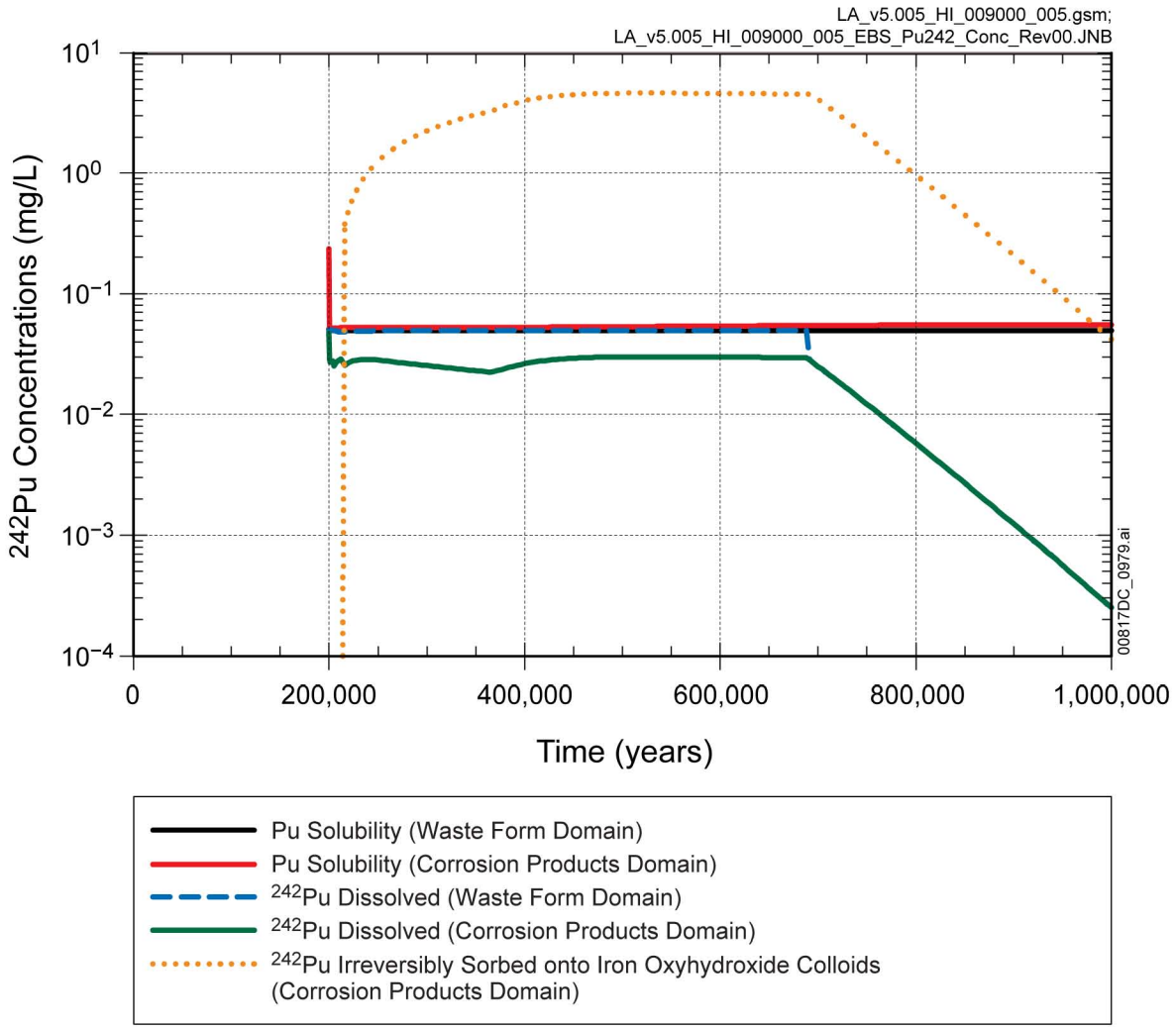

Source: Output DTN: MO0801TSPAMVAC.000 [DIRS 185080].

Figure 7.7.1-106[a]. Dissolved Concentration of ^{242}Pu in the Waste Form and Corrosion Products Domains, the Plutonium Solubility in Respective Domains, and Concentration of ^{242}Pu Irreversibly Sorbed on Iron Oxyhydroxide Colloids for Realization 5415 of the Human Intrusion Modeling Case for 1,000,000 Years after Repository Closure

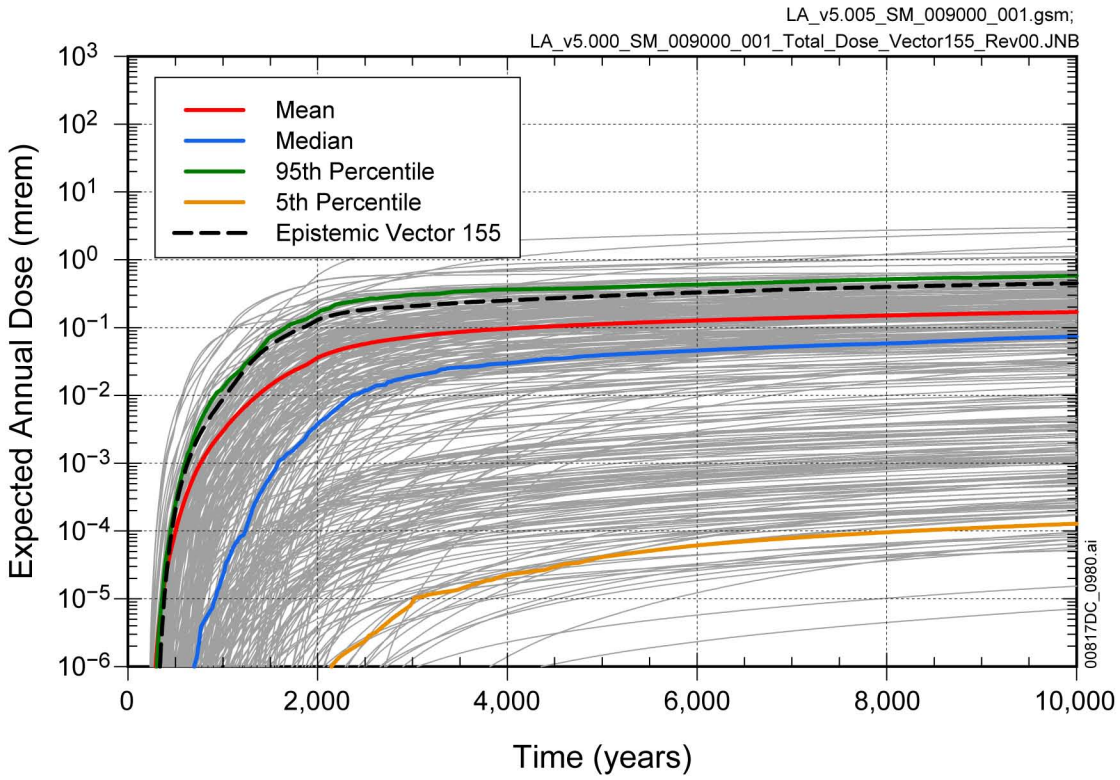

Source: Output DTN: MO0710ADTSPAWO.000 [DIRS 183752].

Figure 7.7.1-107[a]. Expected Annual Dose from the 300 Epistemic Uncertainty Vectors along with their Quantiles and Expected Dose from Epistemic Uncertainty Vector 155 for the Seismic Ground Motion Modeling Case for 10,000 Years after Repository Closure

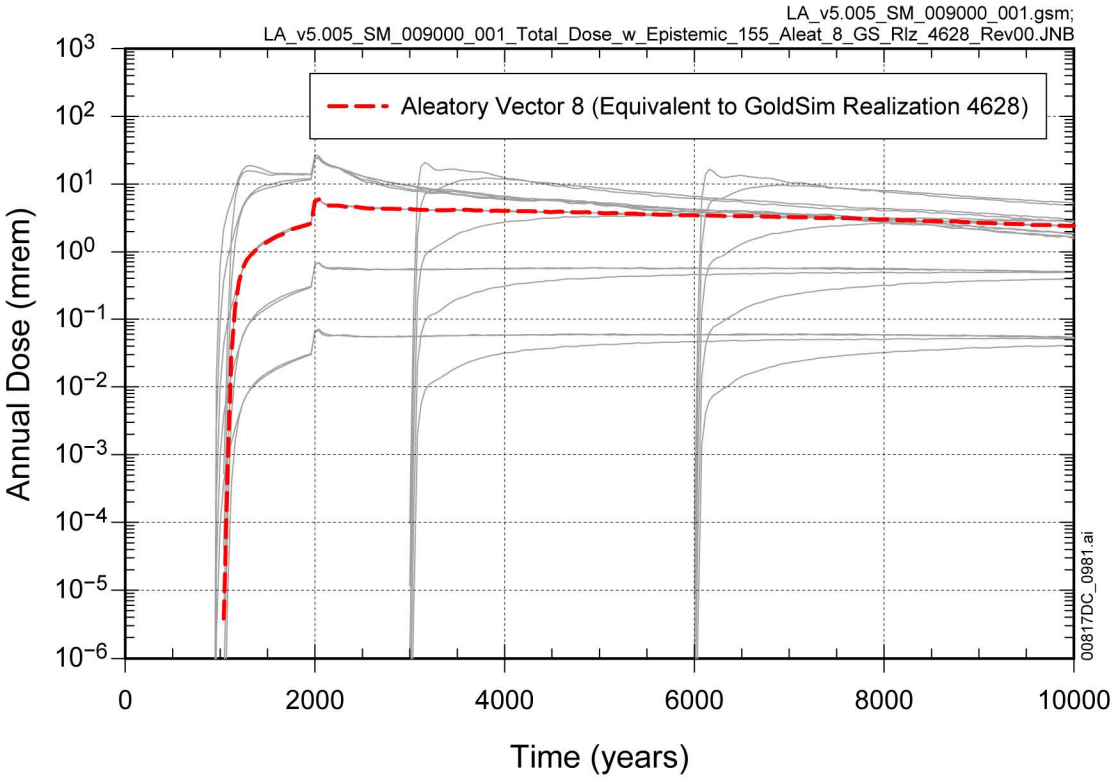

Source: Output DTN: MO0710ADTSPAWO.000 [DIRS 183752].

Figure 7.7.1-108[a]. Annual Dose from the Thirty Aleatory Vectors Associated with the Epistemic Uncertainty Vector 155 for the Seismic Ground Motion Modeling Case for 10,000 Years after Repository Closure

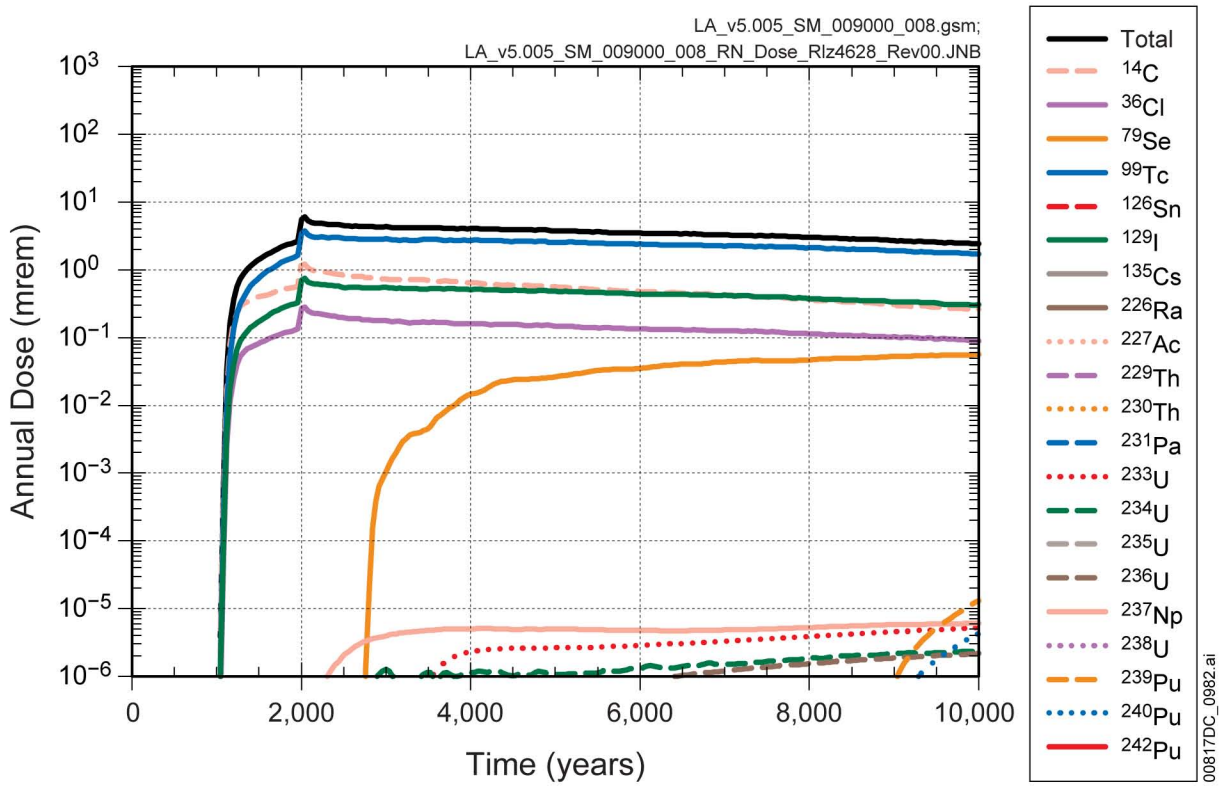

Source: Output DTN: MO0801TSPAMVAC.000 [DIRS 185080].

Figure 7.7.1-109[a]. Annual Dose along with Major Radionuclide Dose Contributors for Realization 4628 of the Seismic Ground Motion Modeling Case for 10,000 Years after Repository Closure

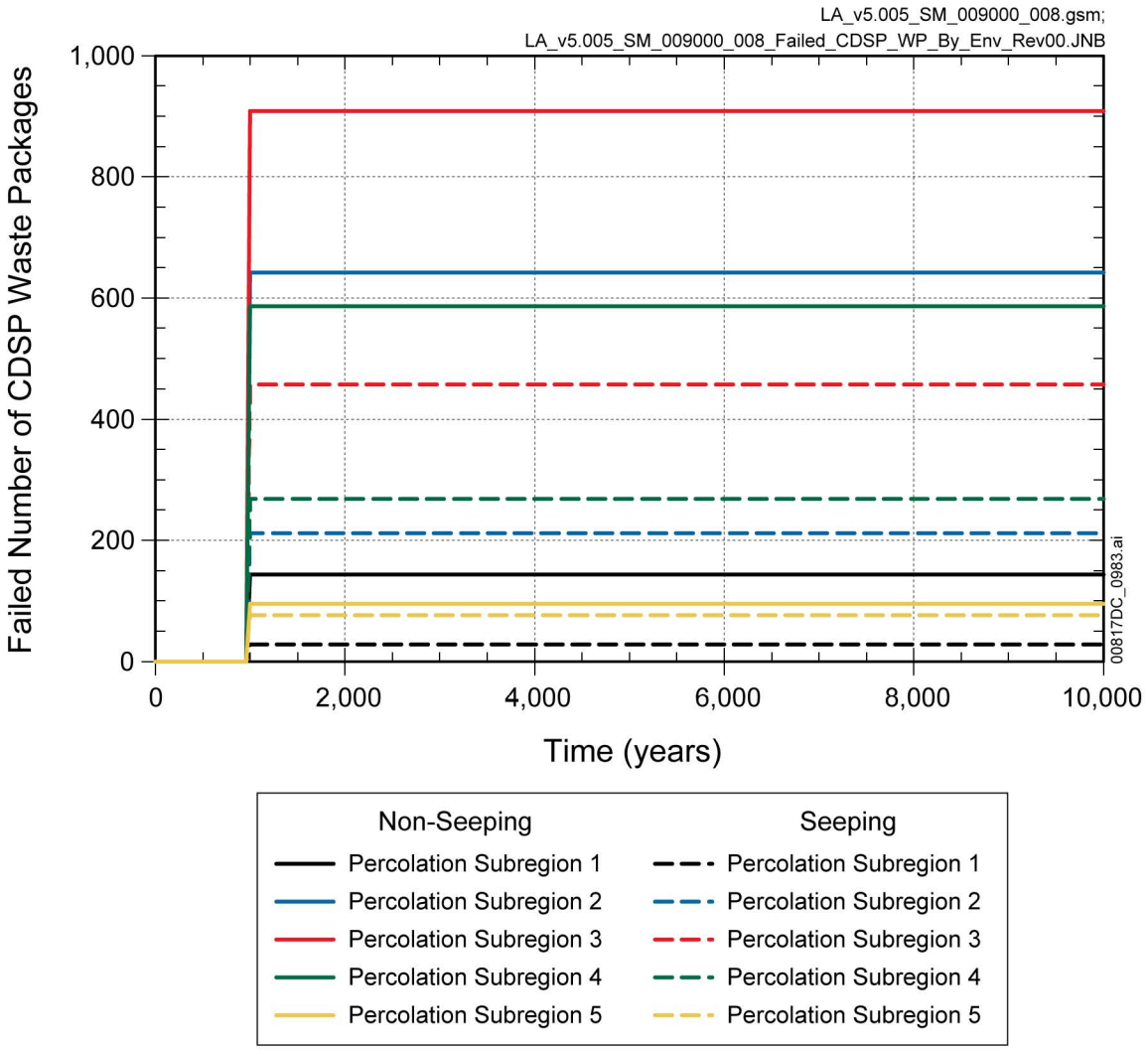

Source: Output DTN: MO0801TSPAMVAC.000 [DIRS 185080].

Figure 7.7.1-110[a]. CDSP WP Failure History in all Five Percolation Subregions for Both Seeping and Non-Seeping Environments for Realization 4628 of the Seismic Ground Motion Modeling Case for 10,000 Years after Repository Closure

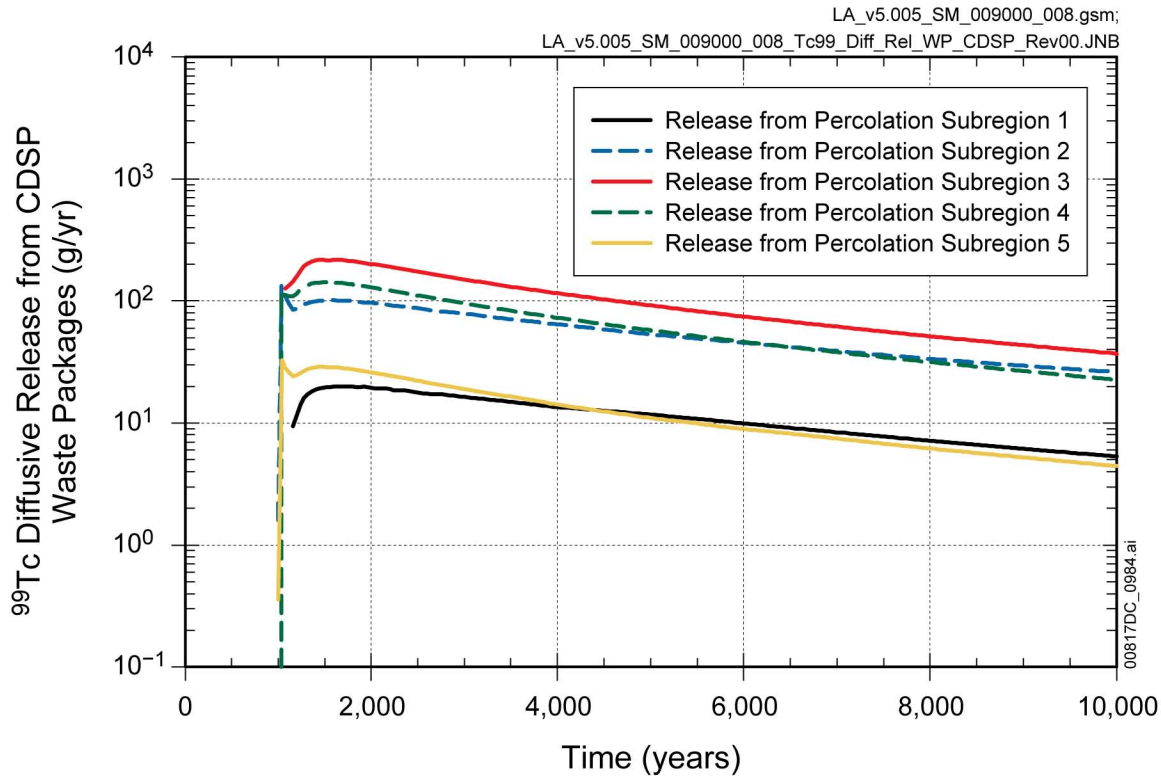

Source: Output DTN: MO0801TSPAMVAC.000 [DIRS 185080].

Figure 7.7.1-111[a]. Diffusive Release Rates of ^{99}Tc from CDSP WPs from each Percolation Subregion for Realization 4628 of the Seismic Ground Motion Modeling Case for 10,000 Years after Repository Closure

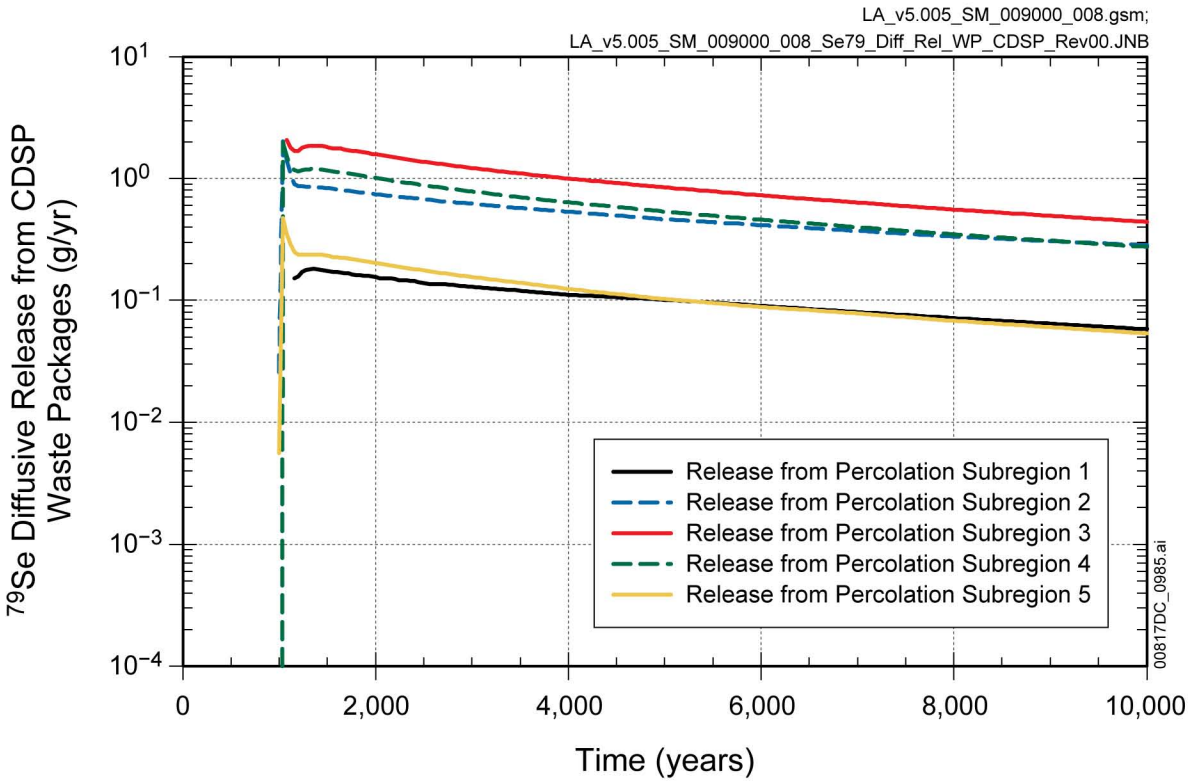

Source: Output DTN: MO0801TSPAMVAC.000 [DIRS 185080].

Figure 7.7.1-112[a]. Diffusive Release Rates of ^{79}Se from CDSP WPs from each Percolation Subregion for Realization 4628 of the Seismic Ground Motion Modeling Case for 10,000 Years after Repository Closure

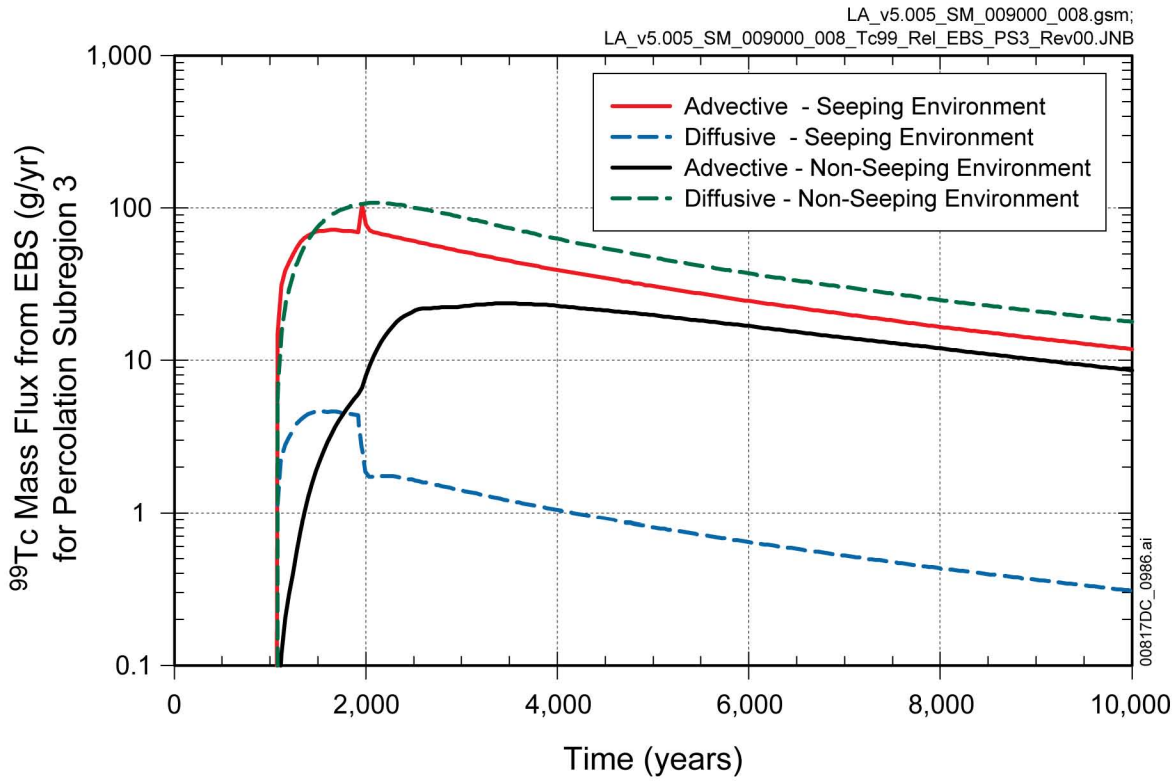

Source: Output DTN: MO0801TSPAMVAC.000 [DIRS 185080].

Figure 7.7.1-113[a]. Mass Flux of ^{99}Tc from the EBS for Percolation Subregion 3 (Seeping and Non-Seeping Environments) for Realization 4628 of the Seismic Ground Motion Modeling Case for 10,000 Years after Repository Closure

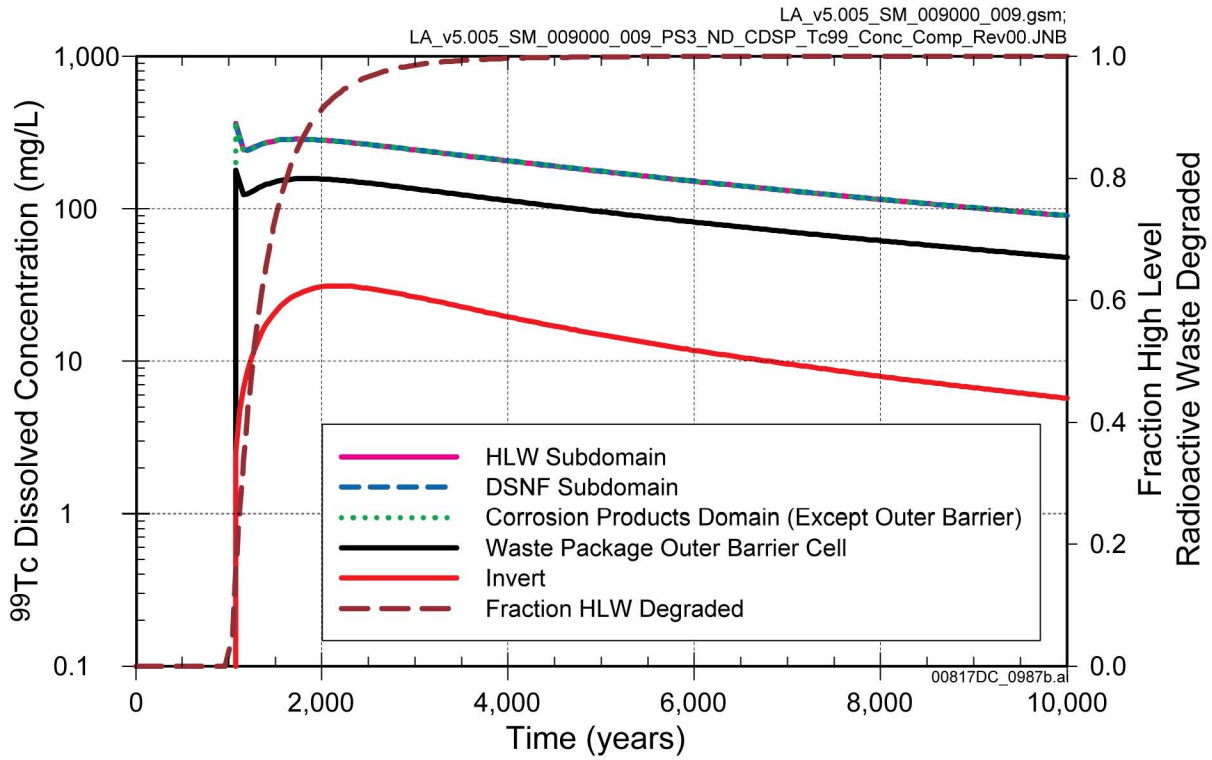

Source: Output DTN: MO0801TSPAMVAC.000 [DIRS 185080].

Figure 7.7.1-114[a]. Comparison of Dissolved Concentration of ^{99}Tc from the Various EBS Transport Domains and Fraction of HLW Degraded for CDSP Percolation Subregion 3, Non-Seeping Environment for Realization 4628 of the Seismic Ground Motion Modeling Case for 10,000 Years after Repository Closure

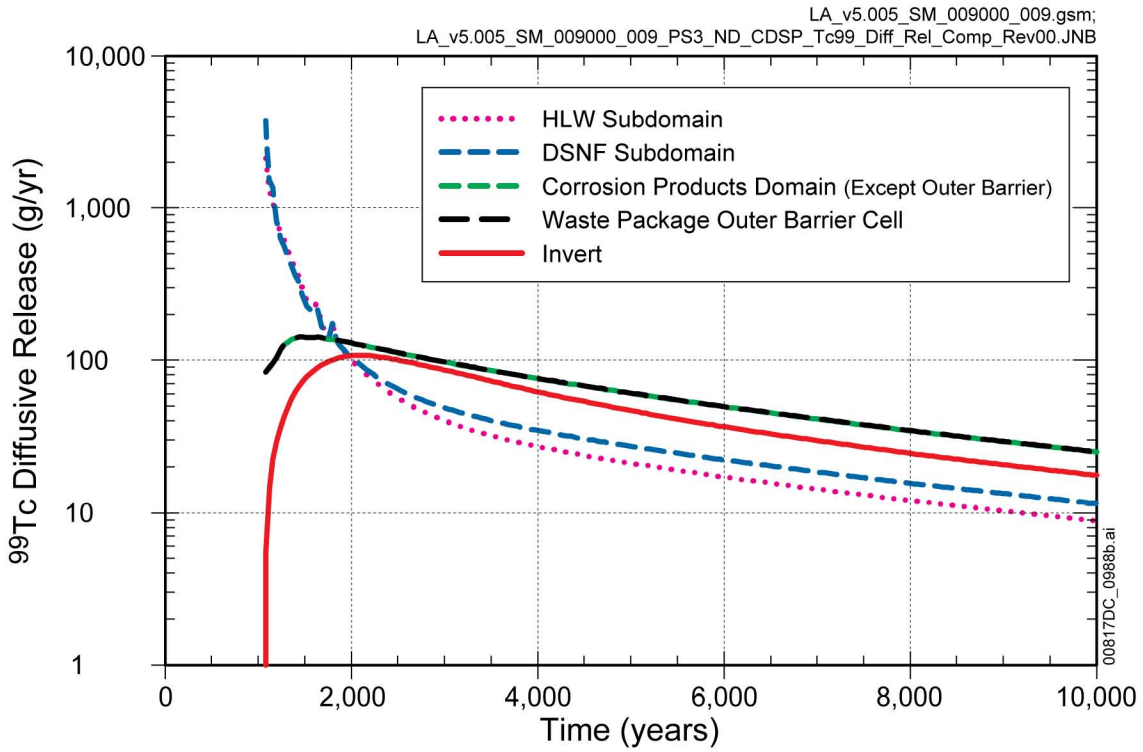

Source: Output DTN: MO0801TSPAMVAC.000 [DIRS 185080].

Figure 7.7.1-115[a]. Comparison of Diffusive Releases of ^{99}Tc from the Various EBS Transport Domains for CDSP Percolation Subregion 3 Non-Seeping Environment for Realization 4628 of the Seismic Ground Motion Modeling Case for 10,000 Years after Repository Closure

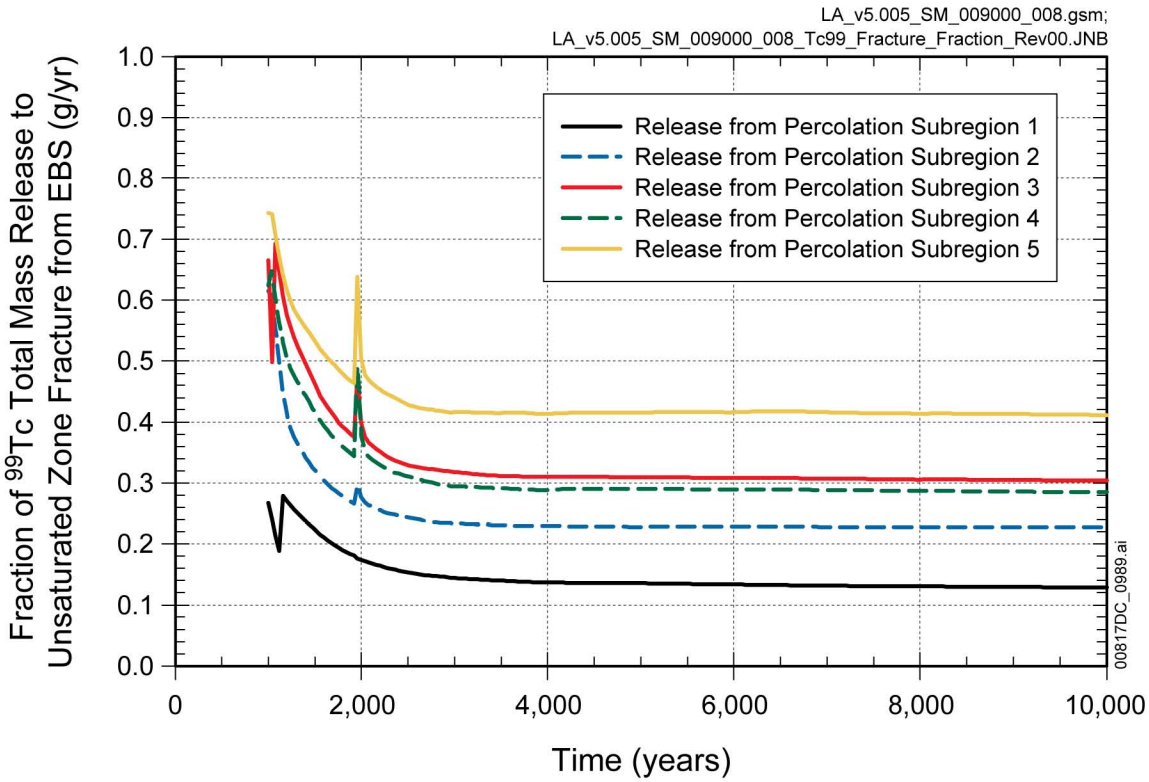

Source: Output DTN: MO0801TSPAMVAC.000 [DIRS 185080].

Figure 7.7.1-116[a]. Fraction of ^{99}Tc Mass Going to Unsaturated Zone Fractures as Compared to the Unsaturated Zone Matrix at the Repository Horizon for Realization 4628 of the Seismic Ground Motion Modeling Case for 10,000 Years after Repository Closure

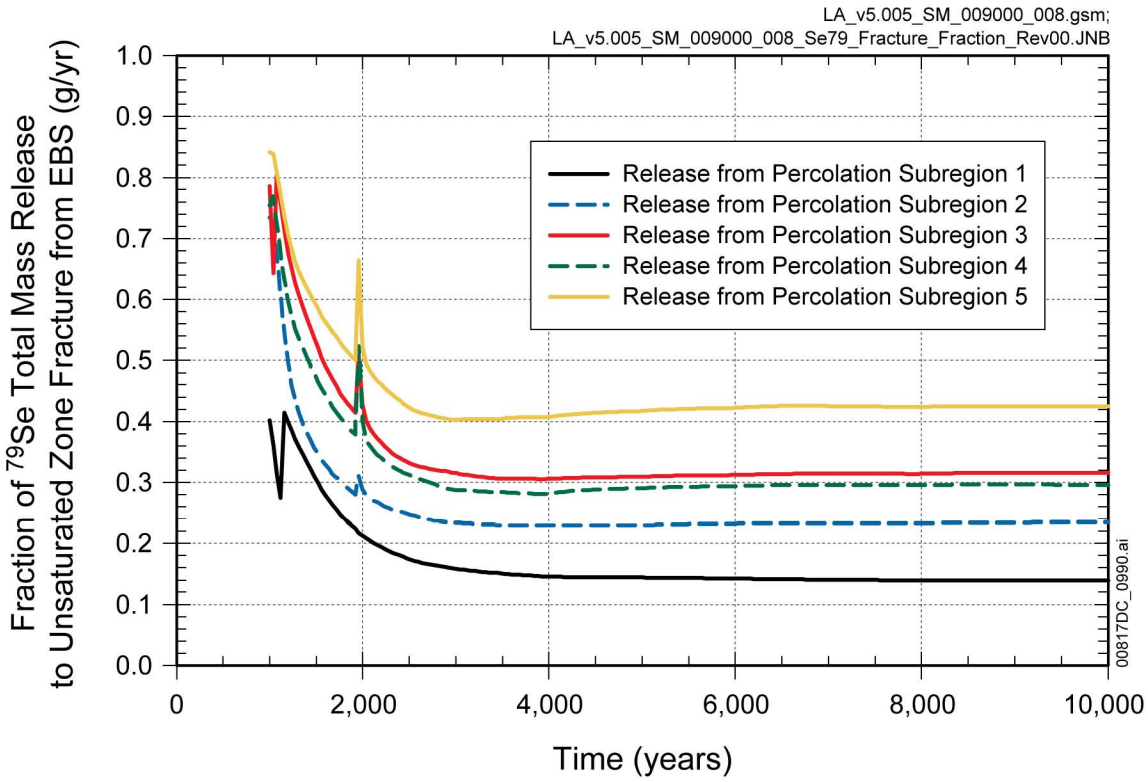

Source: Output DTN: MO0801TSPAMVAC.000 [DIRS 185080].

Figure 7.7.1-117[a]. Fraction of ^{79}Se Mass Going to Unsaturated Zone Fractures as Compared to the Unsaturated Zone Matrix at the Repository Horizon for Realization 4628 of the Seismic Ground Motion Modeling Case for 10,000 Years after Repository Closure

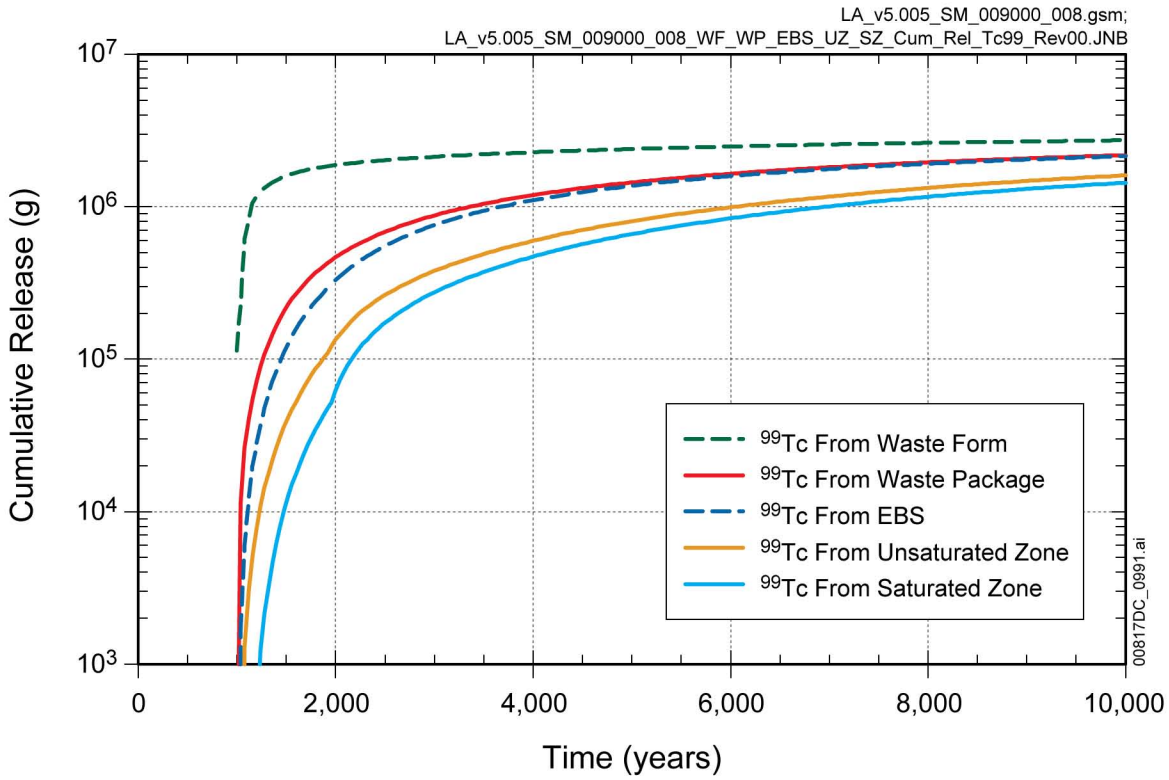

Source: Output DTN: MO0801TSPAMVAC.000 [DIRS 185080].

Figure 7.7.1-118[a]. Cumulative Release of ^{99}Tc from Various Model Domains for Realization 4628 of the Seismic Ground Motion Modeling Case for 10,000 Years after Repository Closure

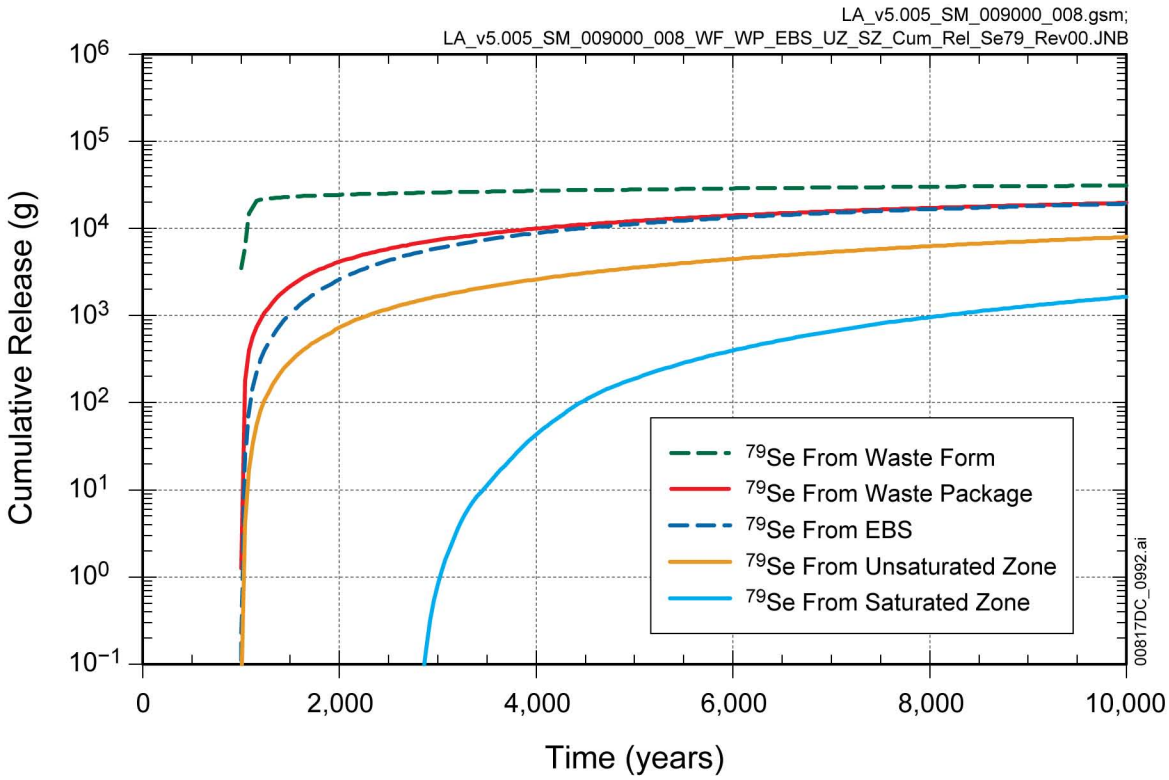

Source: Output DTN: MO0801TSPAMVAC.000 [DIRS 185080].

Figure 7.7.1-119[a]. Cumulative Release of ^{79}Se from Various Model Domains for Realization 4628 of the Seismic Ground Motion Modeling Case for 10,000 Years after Repository Closure

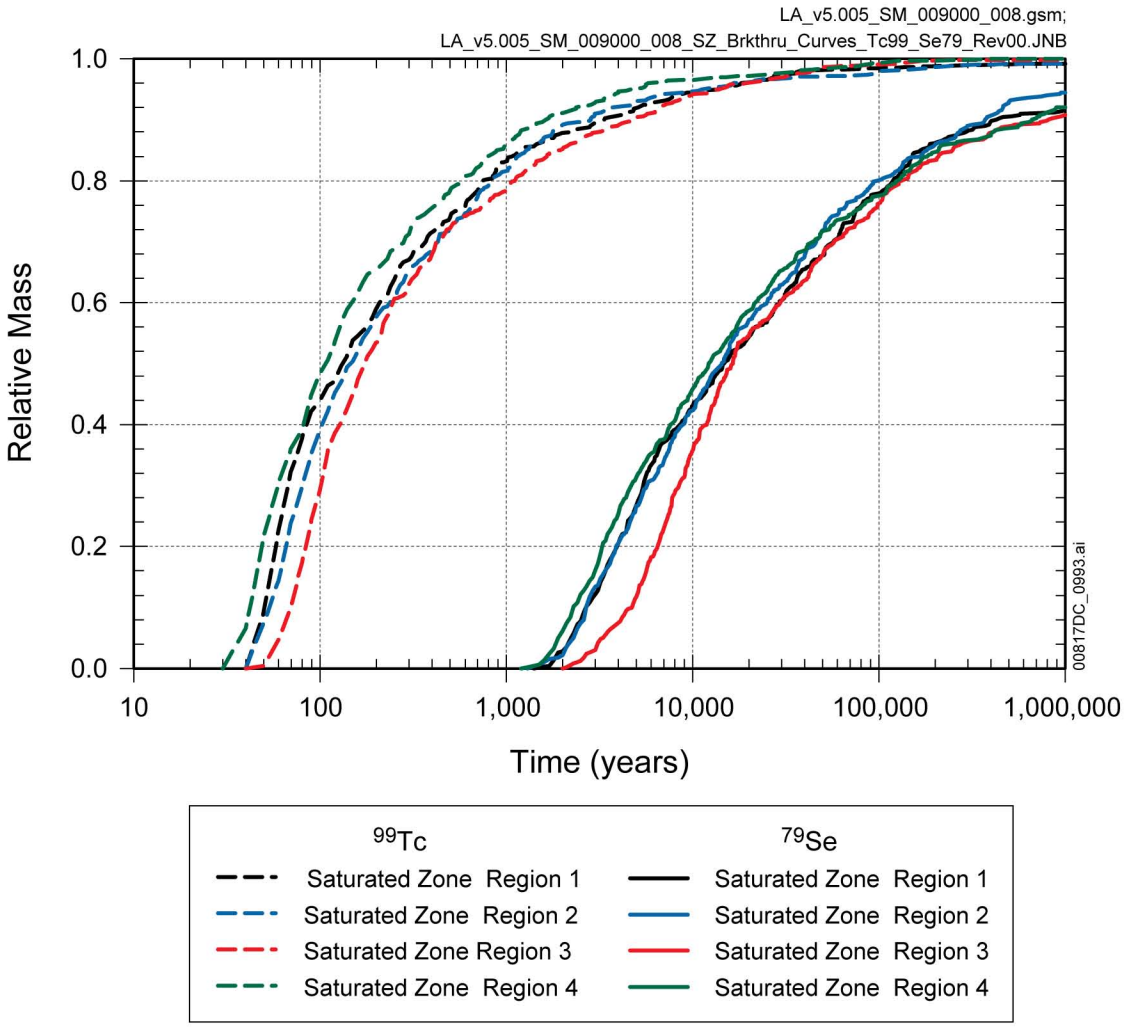

Source: Output DTN: MO0801TSPAMVAC.000 [DIRS 185080].

NOTES: The SZ Breakthrough Curve #122 is used in realization 4628.

Figure 7.7.1-120[a]. Comparison of Saturated Zone Breakthrough Curves for ^{99}Tc and ^{79}Se for All Four Saturated Zone Regions for Realization 4628 of the Seismic Ground Motion Modeling Case for 10,000 Years after Repository Closure

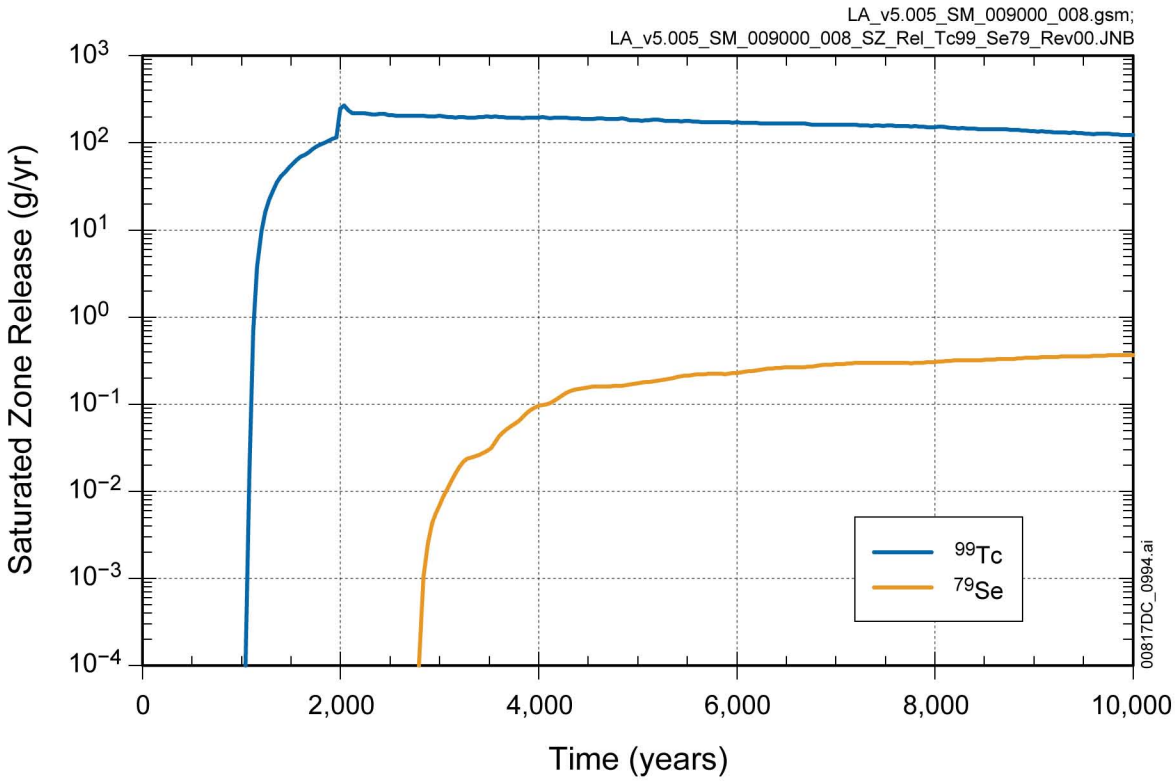

Source: Output DTN: MO0801TSPAMVAC.000 [DIRS 185080].

Figure 7.7.1-121[a]. Saturated Zone Release to the Biosphere for ^{99}Tc and ^{79}Se for Realization 4628 of the Seismic Ground Motion Modeling Case for 10,000 Years after Repository Closure

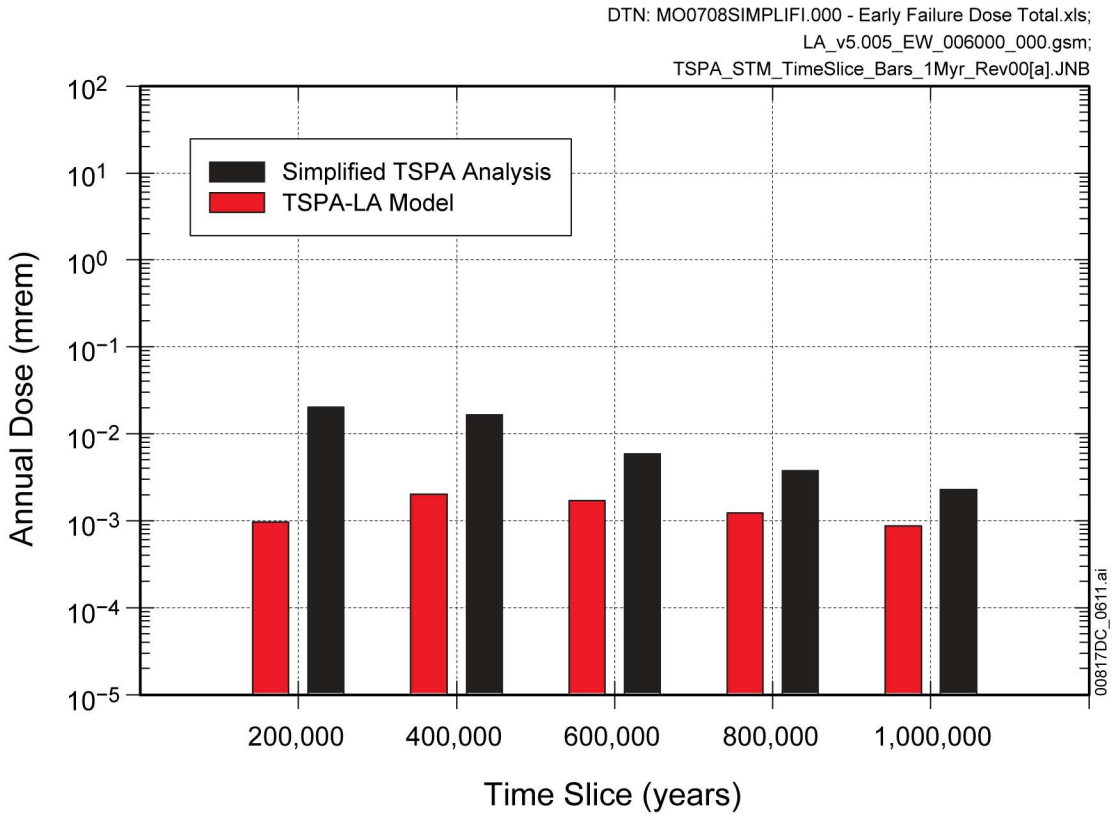

Source: Output DTN: MO0710ADTSPAWO.000 [DIRS 183752]; and Corroborative DTN: MO0708SIMPLIFI.000 [DIRS 182980].

Figure 7.7.2-3[a]. Time-Slice Comparison of the Simplified TSPA Analysis Results against the TSPA-LA Model Results for the Waste Package Early Failure Modeling Case

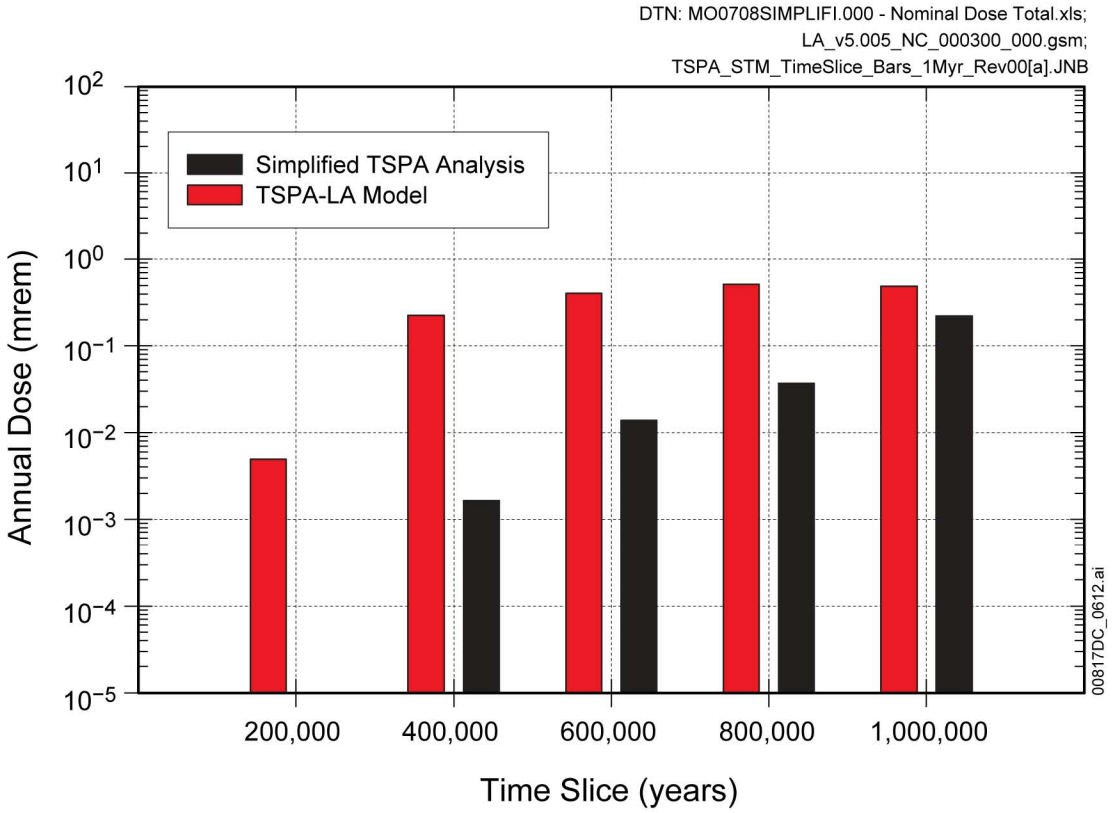

Source: Output DTN: MO0710ADTSPAWO.000 [DIRS 183752]; and Corroborative DTN: MO0708SIMPLIFI.000 [DIRS 182980].

Figure 7.7.2-6[a]. Time-Slice Comparison of the Simplified TSPA Analysis Results against the TSPA-LA Model Results for the Nominal Modeling Case

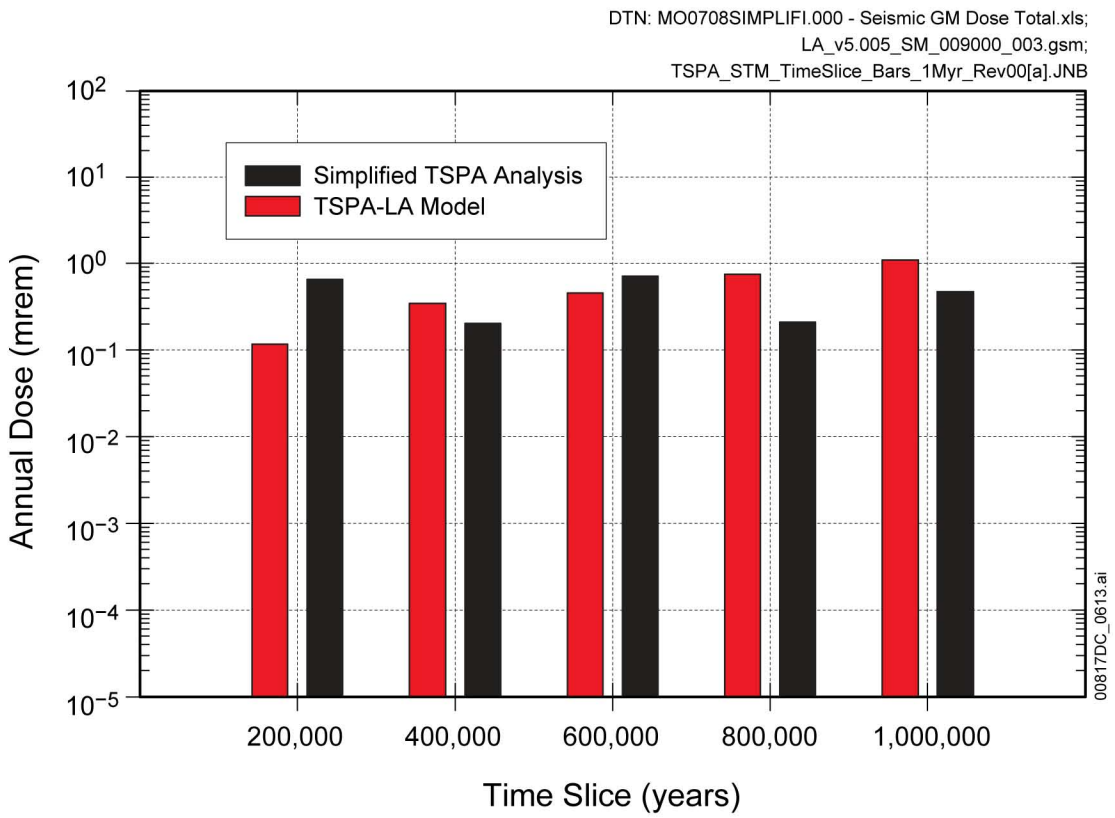

Source: Output DTN: MO0710ADTSPAWO.000 [DIRS 183752]; and Corroborative DTN: MO0708SIMPLIFI.000 [DIRS 182980].

Figure 7.7.2-9[a]. Time-Slice Comparison of the Simplified TSPA Analysis Results against the TSPA-LA Model Results for the Seismic Ground Motion Modeling Case

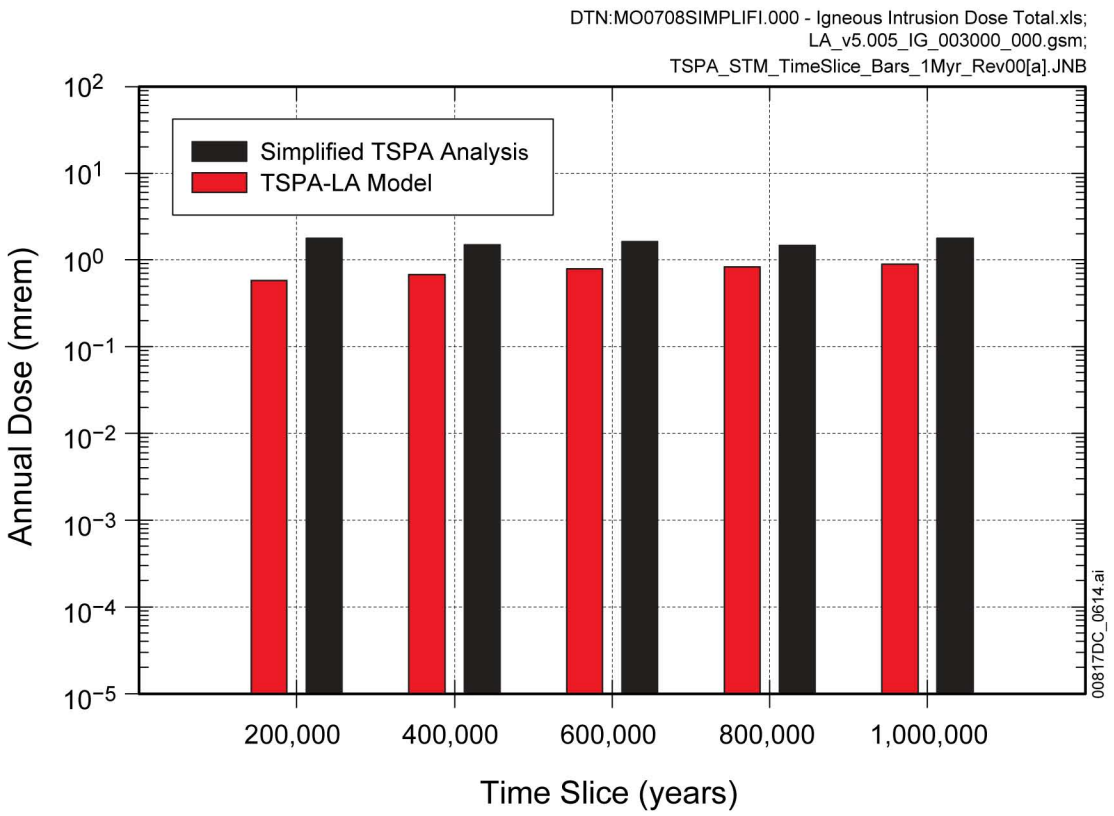

Source: Output DTN: MO0710ADTSPAWO.000 [DIRS 183752]; and Corroborative DTN: MO0708SIMPLIFI.000 [DIRS 182980].

Figure 7.7.2-12[a]. Time-Slice Comparison of the Simplified TSPA Analysis Results against the TSPA-LA Model Results for the Igneous Intrusion Modeling Case

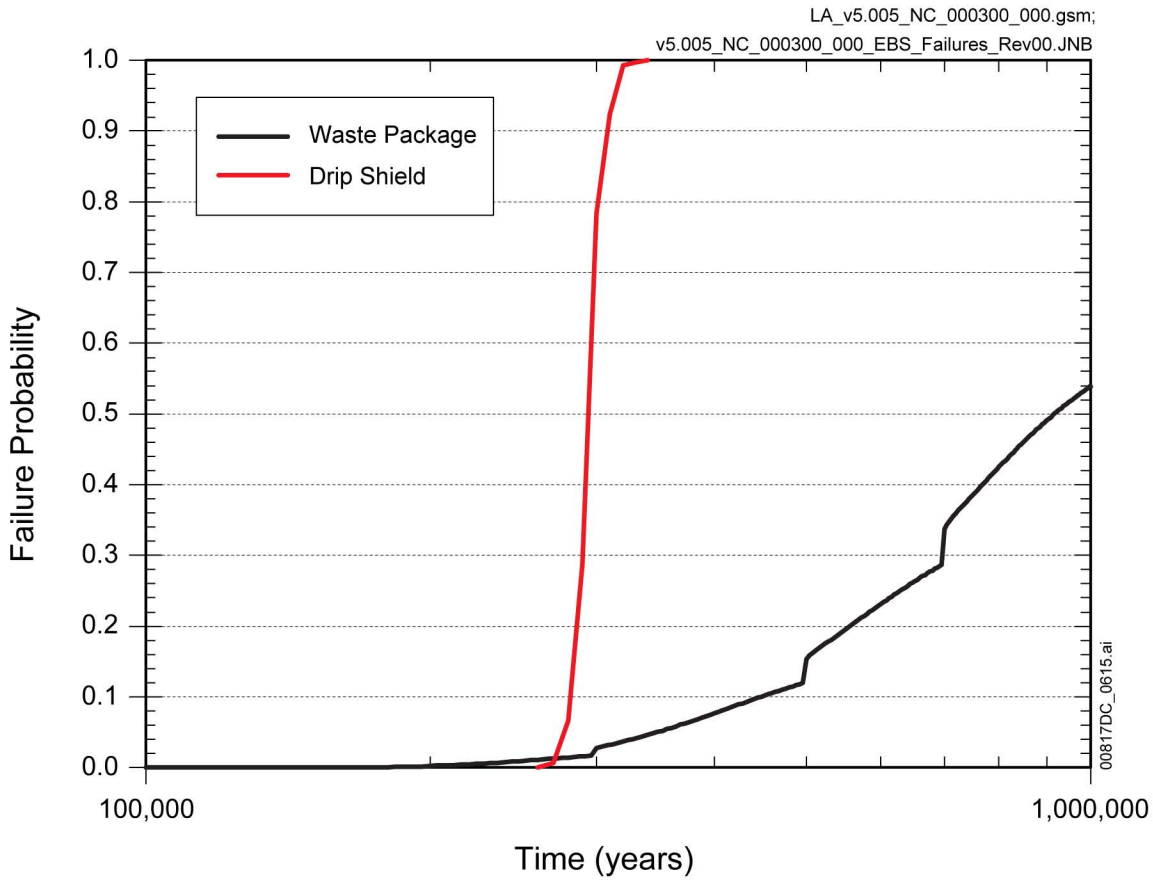

Source: Output DTN: MO0710ADTSPAWO.000 [DIRS 183752].

Figure 7.7.3-2[a]. TSPA-LA Nominal Scenario Class Mean Failure Curves for the Drip Shield and Waste Package

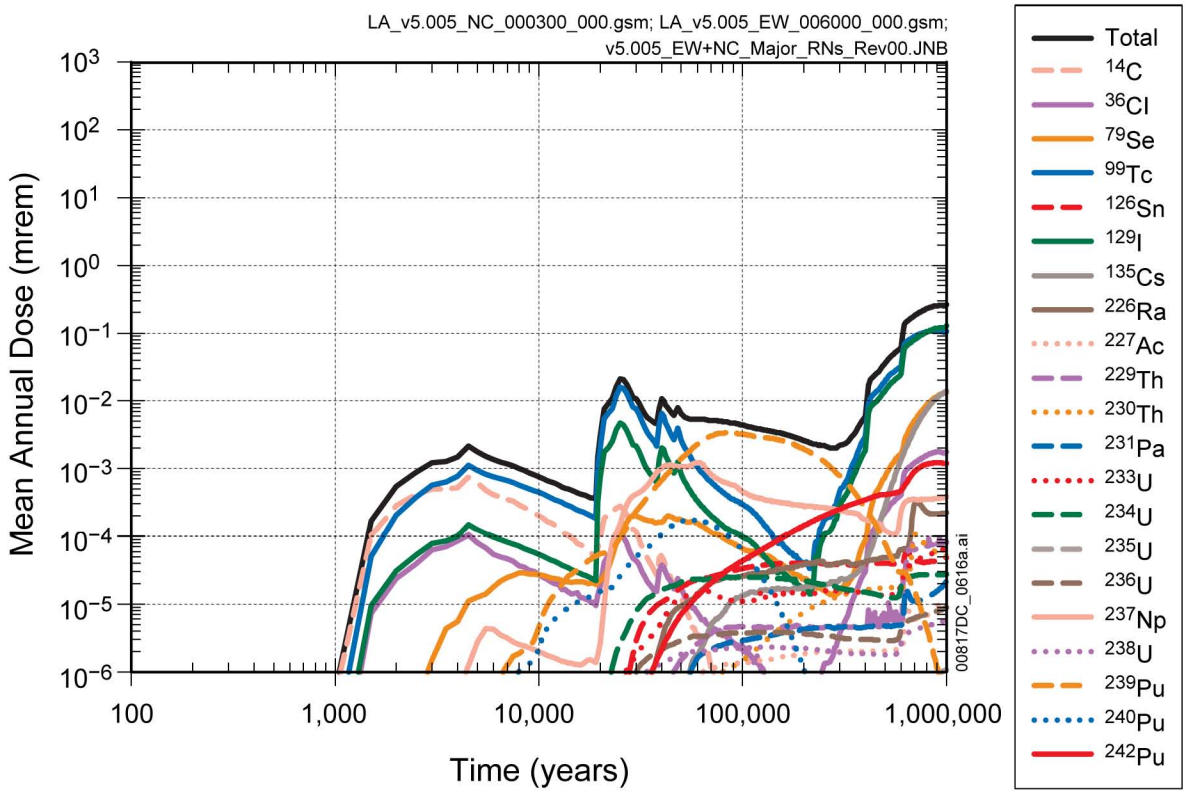

Source: Output DTN: MO0710ADTSPAWO.000 [DIRS 183752].

Figure 7.7.3-3[a]. TSPA-LA Mean Annual Dose for Major Radionuclides for the Combined Early Failure and Nominal Scenario Classes

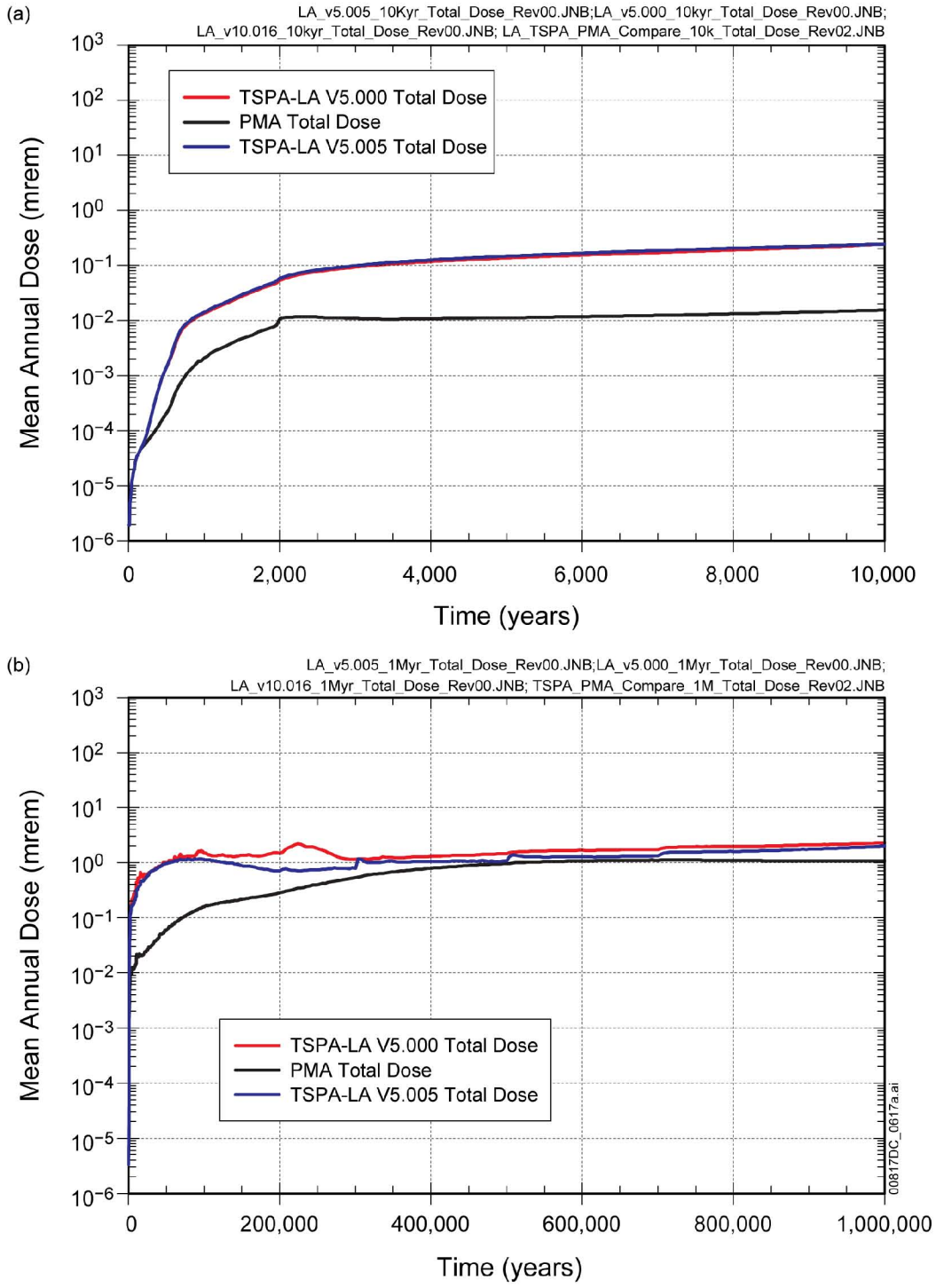

Source: Output DTN: MO0710PLOTSFIG.000 [DIRS 185207]; and Corroborative DTN: MO0709MARGANAL.000 [DIRS 182978].

Figure 7.7.4-7[a]. Comparison of Total Mean Annual Dose for TSPA-LA Model Version 5.000, Version 5.005, and the Performance Margin Analysis for: (a) 10,000 Years and (b) 1,000,000 Years after Repository Closure

INTENTIONALLY LEFT BLANK

QA: QA

MDL-WIS-PA-000005 REV 00 AD 01

March 2008

Total System Performance Assessment Model/Analysis for the License Application Addendum 01

Volume III

Prepared for:
U.S. Department of Energy
Office of Civilian Radioactive Waste Management
Office of Repository Development
1551 Hillshire Drive
Las Vegas, Nevada 89134-6321

Prepared by:
Sandia National Laboratories
OCRWM Lead Laboratory for Repository Systems
1180 Town Center Drive
Las Vegas, Nevada 89144

Under Contract Number
DE-AC04-94AL85000

DISCLAIMER

This report was prepared as an account of work sponsored by an agency of the United States Government. Neither the United States Government nor any agency thereof, nor any of their employees, nor any of their contractors, subcontractors or their employees, makes any warranty, express or implied, or assumes any legal liability or responsibility for the accuracy, completeness, or any third party's use or the results of such use of any information, apparatus, product, or process disclosed, or represents that its use would not infringe privately owned rights. Reference herein to any specific commercial product, process, or service by trade name, trademark, manufacturer, or otherwise, does not necessarily constitute or imply its endorsement, recommendation, or favoring by the United States Government or any agency thereof or its contractors or subcontractors. The views and opinions of authors expressed herein do not necessarily state or reflect those of the United States Government or any agency thereof.

CONTENTS

Page

8[a]. POSTCLOSURE PERFORMANCE DEMONSTRATION ..... 8-1[a]
8.1[a] CONFORMANCE WITH RADIATION PROTECTION STANDARDS ..... 8-2[a]
8.1.1[a] Individual Protection Standard ..... 8-3[a]
8.1.2[a] Groundwater Protection ..... 8-14[a]
8.1.3[a] Human Intrusion Protection ..... 8-21[a]
8.2[a] PROJECTIONS FOR INDIVIDUAL MODELING CASES ..... 8-27[a]
8.2.1[a] Nominal Modeling Case ..... 8-27[a]
8.2.2[a] Early Failure Scenario Class Modeling Cases ..... 8-29[a]
8.2.3[a] Igneous Scenario Class Modeling Cases ..... 8-32[a]
8.2.4[a] Seismic Scenario Class Modeling Cases ..... 8-34[a]
8.3[a] DESCRIPTION OF MULTIPLE BARRIER CAPABILITY ..... 8-39[a]
8.3.1[a] Radionuclides Selected to Demonstrate Multiple Barrier Capability ..... 8-39[a]
8.3.2[a] Identification of Barriers for Yucca Mountain Repository ..... 8-39[a]
8.3.3[a] Demonstration of Multiple Barrier Capability ..... 8-40[a]
8.4[a] VALIDITY AND DEFENSIBILITY OF PERFORMANCE DEMONSTRATION ..... 8-85[a]
8.4.1[a] Validation of TSPA Model and Component Models ..... 8-85[a]
8.4.2[a] Verification and Validation of TSPA Software and Input Data ..... 8-85[a]
8.4.3[a] Uncertainty Characterization Reviews ..... 8-85[a]
8.4.4[a] Corroboration of TSPA-LA Results ..... 8-85[a]
8.4.5[a] Peer Reviews of YMP TSPA Methodology ..... 8-85[a]

9[a]. INPUTS AND REFERENCES ..... 9-1[a]
9.1[a] DOCUMENTS CITED ..... 9-1[a]
9.2[a] CODES, STANDARDS, REGULATIONS, AND PROCEDURES ..... 9-9[a]
9.3[a] SOFTWARE CODES ..... 9-9[a]
9.4[a] SOURCE DATA LISTED BY DATA TRACKING NUMBER ..... 9-11[a]

APPENDIX B[a] DATA TRACKING NUMBERS FOR THE TSPA-LA MODEL ..... B-1[a]
APPENDIX C[a] PERFORMANCE MARGIN ANALYSIS ..... C-1[a]
APPENDIX D[a] PARAMETER LISTING ..... D-1[a]
APPENDIX H[a] YUCCA MOUNTAIN REVIEW PLAN ACCEPTANCE CRITERIA ..... H-1[a]
APPENDIX I[a] FEATURES, EVENTS, AND PROCESSES MAPPED TO TSPA-LA MODEL ..... I-1[a]
APPENDIX J[a] CONCEPTUAL STRUCTURE OF TSPA-LA ..... J-1[a]
APPENDIX K[a] UNCERTAINTY AND SENSITIVITY ANALYSIS RESULTS ..... K-1[a]
APPENDIX M[a] COMPARISON WITH ELECTRIC POWER RESEARCH INSTITUTE ANALYSIS ..... M-1[a]
APPENDIX P[a] IMPACT ASSESSMENTS ..... P-1[a]

INTENTIONALLY LEFT BLANK

FIGURES

Page

8.1-1[a]. Distribution of Total Expected Annual Dose for 10,000 Years after Repository Closure....F8.1-1[a]

8.1-2[a]. Distribution of Total Expected Annual Dose for 1,000,000 Years after Closure....F8.1-2[a]

8.1-3[a]. Relative Contributions of Modeling Cases to Total Mean Annual Dose for (a) 10,000 Years and (b) 1,000,000 Years after Repository Closure....F8.1-3[a]

8.1-4[a]. Histogram of the Time of Drip Shield Failure for the Nominal and Seismic Ground Motion Modeling Cases....F8.1-4[a]

8.1-5[a]. Fraction of (a) CDSP Waste Packages and (b) CSNF Waste Packages Failed by Seismic Damage as a Function of Time....F8.1-5[a]

8.1-6[a]. Contribution of Individual Radionuclides to Total Mean Annual Dose for 10,000 Years after Repository Closure....F8.1-6[a]

8.1-7[a]. Contribution of Individual Radionuclides to Total Mean Annual Dose for 1,000,000 Years after Repository Closure....F8.1-7[a]

8.1-9[a]. Summary Statistics for Activity Concentrations of Total Radium (^{226}Ra and ^{228}Ra) in Groundwater, Excluding Natural Background, for 10,000 Years after Repository Closure....F8.1-8[a]

8.1-10[a]. Contributions of the Modeling Cases to the Mean Combined ^{226}Ra and ^{228}Ra Activity Concentration in Groundwater, Excluding Natural Background, for 10,000 Years after Repository Closure....F8.1-9[a]

8.1-11[a]. Summary Statistics for Activity Concentration of Gross Alpha and ^{226}Ra (Excluding Radon and Uranium) in Groundwater for 10,000 Years after Repository Closure....F8.1-10[a]

8.1-12[a]. Contributions of the Modeling Cases to the Mean Gross Alpha Activity Concentrations (Including ^{226}Ra but Excluding Radon and Uranium) in Groundwater for 10,000 Years after Repository Closure....F8.1-11[a]

8.1-13[a]. Mean Annual Dose from Beta-Photon Dose for All Organs, Including the Whole Body for (a) 10,000 Years after Repository Closure and (b) Detail for 8,000 to 10,000 Years after Repository Closure....F8.1-12[a]

8.1-14[a]. Summary Statistics for Annual Drinking Water Doses for Combined Beta and Photon Emitting Radionuclides for 10,000 Years after Repository Closure....F8.1-13[a]

8.1-15[a]. Contributions of Modeling Cases to the (a) Whole Body Dose and (b) Thyroid for 10,000 Years after Repository Closure....F8.1-14[a]

8.1-16[a]. Distribution of Expected Annual Doses for the Human Intrusion Scenario for 1,000,000 Years after Repository Closure with Drilling Event at 200,000 Years....F8.1-15[a]

8.1-17[a]. Contribution of Individual Radionuclides to Mean Annual Dose for the Human Intrusion Scenario for 1,000,000 Years after Repository Closure....F8.1-16[a]

FIGURES (Continued)

Page

8.2-1[a]. Distributions of Expected Annual Dose for the Nominal Modeling Case for 1,000,000 Years after Repository Closure ..... F8.2-1[a]

8.2-2[a]. Contribution of Individual Radionuclides to Mean Annual Dose for the Nominal Modeling Case for 1,000,000 Years after Repository Closure ..... F8.2-2[a]

8.2-3[a]. Distributions of Expected Annual Dose for the Drip Shield Early Failure Modeling Case for (a) 10,000 Years and (b) 1,000,000 Years after Repository Closure ..... F8.2-3[a]

8.2-4[a]. Contribution of Individual Radionuclides to Mean Annual Dose for Drip Shield Early Failure Modeling Case for (a) 10,000 Years and (b) 1,000,000 Years after Repository Closure ..... F8.2-4[a]

8.2-5[a]. Distributions of Expected Annual Dose for Waste Package Early Failure Modeling Case for (a) 10,000 Years and (b) 1,000,000 Years after Repository Closure ..... F8.2-5[a]

8.2-6[a]. Contribution of Individual Radionuclides to Mean Annual Dose for Waste Package Early Failure Modeling Case for (a) 10,000 Years and (b) 1,000,000 Years after Repository Closure ..... F8.2-6[a]

8.2-7[a]. Distributions of Expected Annual Dose for the Igneous Intrusion Modeling Case for (a) 10,000 Years and (b) 1,000,000 Years after Repository Closure ..... F8.2-7[a]

8.2-8[a]. Contribution of Individual Radionuclides to Mean Annual Dose for the Igneous Intrusion Modeling Case for (a) 10,000 Years and (b) ,000,000 Years after Repository Closure ..... F8.2-8[a]

8.2-11[a]. Distributions of Expected Annual Dose for the Seismic Ground Motion Modeling Case for (a) 10,000 Years and (b) 1,000,000 Years after Repository Closure ..... F8.2-9[a]

8.2-12[a]. Contribution of Individual Radionuclides to Mean Annual Dose for the Seismic Ground Motion Modeling Case for (a) 10,000 Years and (b) 1,000,000 Years after Repository Closure ..... F8.2-10[a]

8.2-13[a]. Distributions of Expected Annual Dose for the Seismic Fault Displacement Modeling Case for (a) 10,000 Years and (b) 1,000,000 Years after Repository Closure ..... F8.2-11[a]

8.2-14[a]. Contribution of Individual Radionuclides to Mean Annual Dose for the Seismic Fault Displacement Modeling Case for (a) 10,000 Years and (b) 1,000,000 Years after Repository Closure ..... F8.2-12[a]

8.3-1[a]. Mean Radionuclide Activities for Total Repository Inventory as a Function of Time for (a) 10,000 Years and (b) 1,000,000 Years after Repository Closure ..... F8.3-1[a]

8.3-2[a]. Mean Radionuclide Contributions to Total Inventory as a Function of Time for (a) 10,000 Years and (b) 1,000,000 Years after Repository Closure ..... F8.3-2[a]

8.3-3[a]. Upper Natural Barrier Capability to Prevent or Substantially Reduce the Rate of Water Movement to the Waste for the Mean

FIGURES (Continued)

Page

Spatially-Averaged (a) Annual Precipitation, Net Infiltration, and Post-10,000-Year Percolation Rates and (b) Drift Seepage Fluxes for the Combined Nominal/Early Failure Modeling Case and the Seismic Ground Motion Modeling Case – 1,000,000-Year Period ..... F8.3-3[a]

8.3-4[a]. Probability of Drip Shield Failure by General Corrosion for the Nominal Modeling Case Based on 300 Epistemic Realizations of Drip Shield General Corrosion Rates ..... F8.3-4[a]

8.3-5[a]. Summary Statistics for Fraction of Waste Packages Breached for (a) CSNF Waste Packages and (b) CDSP Waste Packages for the Nominal Modeling Case as a Function of Time ..... F8.3-5[a]

8.3-6[a]. Summary Statistics for Fraction of CSNF Waste Packages (a) reached by Stress Corrosion Cracking and (b) Breached by General Corrosion Patches for the Nominal Modeling Case as a Function of Time ..... F8.3-6[a]

8.3-7[a]. Cumulative Distribution Functions of Drip Shield Failure Time for (a) Distributions of Failure Time for 300 Epistemic Sample Elements and (b) Distribution of Expected (Over Aleatory) Failure Time with Confidence Interval for the Seismic Ground Motion Modeling Case ..... F8.3-7[a]

8.3-8[a]. Summary Statistics for Expected Fraction of CSNF WPs (a) Breached by Seismic and Nominal Processes and (b) Breached by Seismic Processes Only; and CDSP WPs (c) Breached by Seismic and Nominal Processes and (d) Breached by Seismic Processes Only for the Seismic Ground Motion Modeling Case as a Function of Time ..... F8.3-8[a]

8.3-9[a]. Summary Statistics for Average Fraction of CSNF Waste Package Surface Breached by Cracks per Breached Waste Package for (a) the Seismic Ground Motion Modeling Case and (b) the Nominal Modeling Case as a Function of Time ..... F8.3-10[a]

8.3-10[a]. Summary Statistics for Fraction of CDSP Waste Package Surface Breached by Cracks per Breached Waste Package for (a) the Seismic Ground Motion Modeling Case and (b) the Nominal Modeling Case as a Function of Time ..... F8.3-11[a]

8.3-11[a]. Summary Statistics for Fraction of CSNF Waste Package Surface Breached by Patches per Breached Waste Package for (a) the Seismic Ground Motion Modeling Case and (b) the Nominal Modeling Case as a Function of Time ..... F8.3-12[a]

8.3-12[a]. Summary Statistics for Fraction of CDSP WP Surface Breached by Patches per Breached Waste Package for (a) the Seismic Ground Motion Modeling Case and (b) the Nominal Modeling Case as a Function of Time ..... F8.3-13[a]

8.3-13[a]. Mean Activity Released from the Engineered Barrier System for the Combined Nominal/Early Failure Modeling Case for (a) 10,000 Years after Repository Closure and (b) Post-10,000-Years after Repository Closure ..... F8.3-14[a]

FIGURES (Continued)

Page

8.3-14[a]. Uncertainty in Activity of ^{99}Tc Released from the Engineered Barrier System for the Combined Nominal/Early Failure Modeling Case for (a) 10,000 Years and (b) 1,000,000 Years after Repository Closure.....F8.3-15[a]

8.3-15[a]. Uncertainty in Activity of ^{239}Pu Released from the Engineered Barrier System for the Combined Nominal/Early Failure Modeling Case for (a) 10,000 Years and (b) 1,000,000 Years after Repository Closure.....F8.3-16[a]

8.3-16[a]. Mean Activity Released from the Engineered Barrier System for the Seismic Ground Motion Modeling Case for (a) 10,000 Years and (b) 1,000,000 Years after Repository Closure.....F8.3-17[a]

8.3-17[a]. Uncertainty in Activity of ^{99}Tc Released from the Engineered Barrier System for the Seismic Ground Motion Modeling Case for (a) 10,000 Years and (b) 1,000,000 Years after Repository Closure.....F8.3-18[a]

8.3-18[a]. Uncertainty in Activity of ^{237}Np Released from the Engineered Barrier System for the Seismic Ground Motion Modeling Case for (a) 10,000 Years and (b) 1,000,000 Years after Repository Closure.....F8.3-19[a]

8.3-19[a]. Uncertainty in Activity of ^{234}U Released from the Engineered Barrier System for the Seismic Ground Motion Modeling Case for (a) 10,000 Years and (b) 1,000,000 Years after Repository Closure.....F8.3-20[a]

8.3-20[a]. Uncertainty in Activity of ^{226}Ra Released from the Engineered Barrier System for the Seismic Ground Motion Modeling Case for (a) 10,000 Years and (b) 1,000,000 Years after Repository Closure.....F8.3-21[a]

8.3-21[a]. Uncertainty in Activity of ^{239}Pu Released from the Engineered Barrier System for the Seismic Ground Motion Modeling Case for (a) 10,000 Years and (b) 1,000,000 Years after Repository Closure.....F8.3-22[a]

8.3-22[a]. Uncertainty in Activity of ^{242}Pu Released from the Engineered Barrier System for the Seismic Ground Motion Modeling Case for (a) 10,000 Years and (b) 1,000,000 Years after Repository Closure.....F8.3-23[a]

8.3-23[a]. Mean Activity Released from the (a) Saturated Zone and (b) Engineered Barrier System for the Combined Nominal/Early Failure Modeling Case for 10,000 Years after Repository Closure.....F8.3-24[a]

8.3-24[a]. Mean Activity Released from the (a) Saturated Zone and (b) Engineered Barrier System for the Combined Nominal/Early Failure Modeling Case for 1,000,000 Years after Repository Closure.....F8.3-25[a]

8.3-25[a]. Mean Activity Released from the (a) Saturated Zone and (b) Engineered Barrier System for the Seismic Ground Motion Modeling Case for 10,000 Years after Repository Closure.....F8.3-26[a]

8.3-26[a]. Mean Activity Released from the (a) Saturated Zone and (b) Engineered Barrier System for the Seismic Ground Motion Modeling Case for 1,000,000 Years after Repository Closure.....F8.3-27[a]

8.3-27[a]. Uncertainty in Activity of ^{99}Tc Released from the Saturated Zone for the Seismic Ground Motion Modeling Case for (a) 10,000 Years and (b) 1,000,000 Years after Repository Closure.....F8.3-28[a]

FIGURES (Continued)

Page

8.3-28[a]. Uncertainty in Activity of ^{237}Np Released from the Saturated Zone for the Seismic Ground Motion Modeling Case for (a) 10,000 Years and (b) 1,000,000 Years after Repository Closure ..... F8.3-29[a]

8.3-29[a]. Uncertainty in Activity of ^{234}U Released from the Saturated Zone for the Seismic Ground Motion Modeling Case for (a) 10,000 Years and (b) 1,000,000 Years after Repository Closure ..... F8.3-30[a]

8.3-30[a]. Uncertainty in Activity of ^{226}Ra Released from the Saturated Zone for the Seismic Ground Motion Modeling Case for (a) 10,000 Years and (b) 1,000,000 Years after Repository Closure ..... F8.3-31[a]

8.3-31[a]. Uncertainty in Activity of ^{239}Pu Released from the Saturated Zone for the Seismic Ground Motion Modeling Case for (a) 10,000 Years and (b) 1,000,000 Years after Repository Closure ..... F8.3-32[a]

8.3-32[a]. Uncertainty in Activity of ^{242}Pu Released from the Saturated Zone for the Seismic Ground Motion Modeling Case for (a) 10,000 Years and (b) 1,000,000 Years after Repository Closure ..... F8.3-33[a]

B-3[a]. Road Map of TSPA-LA Model v5.005 Data Tracking Numbers ..... B-5[a]

K4.5-1[a]. Dose to RMEI (*DOSTOT*, mrem/yr) for all radioactive species under nominal conditions obtained with version 5.005 of the TSPA-LA Model: (a) *DOSTOT* for all (i.e., 300) sample elements, (b) *DOSTOT* for first 50 sample elements, (c) PRCCs for *DOSTOT* for [0; 1,000,000 yr], and (d) PRCCs for *DOSTOT* for [200,000; 1,000,000 yr] ..... FK-1[a]

K4.5-2[a]. Stepwise rank regression analyses and selected scatterplots for dose to RMEI (*DOSTOT*, mrem/yr) for all radioactive species under nominal conditions obtained with version 5.005 of the TSPA-LA Model: (a) regressions for *DOSTOT* at 400,000, 600,000, and 800,000 years, and (b,c,d) scatterplots for *DOSTOT* at 600,000 years ..... FK-2[a]

K5.7.1-1[a]. Expected dose to RMEI (*EXPDOSE*, mrem/yr) over [0, 20,000 yr] for all radioactive species resulting from early DS failure obtained with version 5.005 of the TSPA-LA Model: (a) *EXPDOSE* for all (i.e., 300) sample elements, (b) *EXPDOSE* for first 50 sample elements, and (c) PRCCs for *EXPDOSE* ..... FK-3[a]

K5.7.1-2[a]. Stepwise rank regression analyses and selected scatterplots for expected dose to RMEI (*EXPDOSE*, mrem/yr) over [0, 20,000 yr] for all radioactive species resulting from early DS failure obtained with version 5.005 of the TSPA-LA Model: (a) regressions for *EXPDOSE* at 3,000, 5,000, and 10,000 years, and (b,c,d) scatterplots for *EXPDOSE* at 10,000 years ..... FK-4[a]

K5.7.1-3[a]. Expected dose to RMEI (*EXPDOSE*, mrem/yr) over [0, 1,000,000 yr] for all radioactive species resulting from early DS failure obtained with version 5.005 of the TSPA-LA Model: (a) *EXPDOSE* for all

FIGURES (Continued)

Page

(i.e., 300) sample elements, (b) *EXPDOSE* for first 50 sample elements, and (c) PRCCs for *EXPDOSE* ..... FK-5[a]

K5.7.1-4[a]. Stepwise rank regression analyses and selected scatterplots for expected dose to RMEI (*EXPDOSE*, mrem/yr) over [0, 1,000,000 yr] for all radioactive species resulting from early DS failure obtained with version 5.005 of the TSPA-LA Model: (a) regressions for *EXPDOSE* at 50,000, 200,000, and 500,000 years, and (b,c,d) scatterplots for *EXPDOSE* at 500,000 years ..... FK-6[a]

K5.7.2-1[a]. Expected dose to RMEI (*EXPDOSE*, mrem/yr) over [0, 20,000 yr] for all radioactive species resulting from early WP failure obtained with version 5.005 of the TSPA-LA Model: (a) *EXPDOSE* for all (i.e., 300) sample elements, (b) *EXPDOSE* for first 50 sample elements, and (c) PRCCs for *EXPDOSE* ..... FK-7[a]

K5.7.2-2[a]. Stepwise rank regression analyses and selected scatterplots for expected dose to RMEI (*EXPDOSE*, mrem/yr) over [0, 20,000 yr] for all radioactive species resulting from early WP failure obtained with version 5.005 of the TSPA-LA Model: (a) regressions for *EXPDOSE* at 3,000, 5,000, and 10,000 years, and (b,c,d) scatterplots for *EXPDOSE* at 10,000 years..... FK-8[a]

K5.7.2-3[a]. Expected dose to RMEI (*EXPDOSE*, mrem/yr) over [0, 1,000,000 yr] for all radioactive species resulting from early WP failure obtained with version 5.005 of the TSPA-LA Model: (a) *EXPDOSE* for all (i.e., 300) sample elements, (b) *EXPDOSE* for first 50 sample elements, and (c) PRCCs for *EXPDOSE* ..... FK-9[a]

K5.7.2-4[a]. Stepwise rank regression analyses and selected scatterplots for expected dose to RMEI (*EXPDOSE*, mrem/yr) over [0, 1,000,000 yr] for all radioactive species resulting from early WP failure obtained with version 5.005 of the TSPA-LA Model: (a) regressions for *EXPDOSE* at 50,000, 200,000, and 500,000 years, and (b,c,d) scatterplots for *EXPDOSE* at 500,000 years..... FK-10[a]

K6.3.2-5[a]. Time-dependent release rates (*ESU234*, g/yr) and cumulative (i.e., integrated) releases (*ESU234C*, g) over 1,000,000 years for the movement of dissolved ^{234}U from the EBS to the UZ resulting from an igneous intrusive event at 250 years that destroys all WPs in the repository obtained with version 5.005 of the TSPA-LA Model: (a,b) *ESU234* and *ESU234C* for all (i.e., 300) sample elements, (c,d) *ESU234* and *ESU234C* for first 50 sample elements, and (e,f) PRCCs for *ESU234* and *ESU234C* ..... FK-11[a]

K6.3.2-6[a]. Stepwise rank regression analyses and selected scatterplots for time-dependent release rates (*ESU234*, g/yr) and cumulative (i.e., integrated) releases (*ESU234C*, g) for the movement of dissolved ^{234}U from the EBS to the UZ resulting from an igneous intrusive event at 250 years that destroys all WPs in the repository obtained with

FIGURES (Continued)

Page

version 5.005 of the TSPA-LA Model: (a,b) regressions for *ESU234* and *ESU234C* at 50,000, 200,000, and 500,000 years, and (c-h) scatterplots for *ESU234* and *ESU234C* at 500,000 years ..... FK-12[a]

K6.3.2-7[a]. Time-dependent release rates (*ESTH230*, g/yr) and cumulative (i.e., integrated) releases (*ESTH230C*, g) over 1,000,000 years for the movement of dissolved ^{230}Th from the EBS to the UZ resulting from an igneous intrusive event at 250 years that destroys all WPs in the repository obtained with version 5.005 of the TSPA-LA Model: (a,b) *ESTH230* and *ESTH230C* for all (i.e., 300) sample elements, (c,d) *ESTH230* and *ESTH230C* for first 50 sample elements, and (e,f) PRCCs for *ESTH230* and *ESTH230C* ..... FK-14[a]

K6.3.2-8[a]. Stepwise rank regression analyses and selected scatterplots for time-dependent release rates (*ESTH230*, g/yr) and cumulative (i.e., integrated) releases (*ESTH230C*, g) for the movement of dissolved ^{230}Th from the EBS to the UZ resulting from an igneous intrusive event at 250 years that destroys all WPs in the repository obtained with version 5.005 of the TSPA-LA Model: (a,b) regressions for *ESTH230* and *ESTH230C* at 50,000, 200,000, and 500,000 years, and (c-h) scatterplots for *ESTH230* and *ESTH230C* at 200,000 years ..... FK-15[a]

K6.3.2-9[a]. Time-dependent release rates (*ESRA226*, g/yr) and cumulative (i.e., integrated) releases (*ESRA226C*, g) over 1,000,000 years for the movement of dissolved ^{226}Ra from the EBS to the UZ resulting from an igneous intrusive event at 250 years that destroys all WPs in the repository obtained with version 5.005 of the TSPA-LA Model: (a,b) *ESRA226* and *ESRA226C* for all (i.e., 300) sample elements, (c,d) *ESRA226* and *ESRA226C* for first 50 sample elements, and (e,f) PRCCs for *ESRA226* and *ESRA226C* ..... FK-17[a]

K6.3.2-10[a]. Stepwise rank regression analyses and selected scatterplots for time-dependent release rates (*ESRA226*, g/yr) and cumulative (i.e., integrated) releases (*ESRA226C*, g) for the movement of dissolved ^{226}Ra from the EBS to the UZ resulting from an igneous intrusive event at 250 years that destroys all WPs in the repository obtained with version 5.005 of the TSPA-LA Model: (a,b) regressions for *ESRA226* and *ESRA226C* at 50,000, 200,000, and 500,000 years, and (c-h) scatterplots for *ESRA226* and *ESRA226C* at 50,000 years..... FK-18[a]

K6.4.2-1[a]. Time-dependent release rates (*UZU234*, g/yr) and cumulative (i.e., integrated) releases (*UZU234C*, g) over 1,000,000 years for the movement of dissolved ^{234}U from the UZ to the SZ resulting from an igneous intrusive event at 250 years that destroys all WPs in the repository obtained with version 5.005 of the TSPA-LA Model: (a,b) *UZU234* and *UZU234C* for all (i.e., 300) sample elements, (c,d) *UZU234* and *UZU234C* for first 50 sample elements, and (e,f) PRCCs for *UZU234* and *UZU234C* ..... FK-20[a]

FIGURES (Continued)

Page

K6.4.2-2[a]. Stepwise rank regression analyses and selected scatterplots for time-dependent release rates (*UZU234*, g/yr) and cumulative (i.e., integrated) releases (*UZU234C*, g) for the movement of dissolved ^{234}U from the UZ to the SZ resulting from an igneous intrusive event at 250 years that destroys all WPs in the repository obtained with version 5.005 of the TSPA-LA Model: (a,b) regressions for *UZU234* and *UZU234C* at 50,000, 200,000, and 500,000 years, and (c-h) scatterplots for *UZU234* and *UZU234C* at 500,000 years ..... FK-21[a]

K.6.4.2-3[a]. Comparison of cumulative releases of dissolved ^{234}U into the UZ (*ESU234C*, g) and out of the UZ (*UZU234C*, g) obtained with version 5.005 of the TSPA-LA Model at (a) 50,000, (b) 100,000, (c) 200,000, and (d) 600,000 years for an igneous intrusive event at 250 years that destroys all WPs in the repository ..... FK-23[a]

K6.4.2-4[a]. Time-dependent release rates (*UZTH230*, g/yr) and cumulative (i.e., integrated) releases (*UZTH230C*, g) over 1,000,000 years for the movement of dissolved ^{230}Th from the UZ to the SZ resulting from an igneous intrusive event at 250 years that destroys all WPs in the repository obtained with version 5.005 of the TSPA-LA Model: (a,b) *UZTH230* and *UZTH230C* for all (i.e., 300) sample elements, (c,d) *UZTH230* and *UZTH230C* for first 50 sample elements, and (e,f) PRCCs for *UZTH230* and *UZTH230C* ..... FK-24[a]

K6.4.2-5[a]. Stepwise rank regression analyses and selected scatterplots for time-dependent release rates (*UZTH230*, g/yr) and cumulative (i.e., integrated) releases (*UZTH230C*, g) for the movement of dissolved ^{230}Th from the UZ to the SZ resulting from an igneous intrusive event at 250 years that destroys all WPs in the repository obtained with version 5.005 of the TSPA-LA Model: (a,b) regressions for *UZTH230* and *UZTH230C* at 50,000, 200,000, and 500,000 years, and (c-h) scatterplots for *UZTH230* and *UZTH230C* at 200,000 years..... FK-25[a]

K.6.4.2-6[a]. Comparison of cumulative releases of dissolved ^{230}Th into the UZ (*ESTH230C*, g) and out of the UZ (*UZTH230C*, g) obtained with version 5.005 of the TSPA-LA Model at (a) 50,000, (b) 100,000, (c) 200,000, and (d) 600,000 years for an igneous intrusive event at 250 years that destroys all WPs in the repository ..... FK-27[a]

K6.4.2-7[a]. Time-dependent release rates (*UZRA226*, g/yr) and cumulative (i.e., integrated) releases (*UZRA226C*, g) over 1,000,000 years for the movement of dissolved ^{226}Ra from the UZ to the SZ resulting from an igneous intrusive event at 250 years that destroys all WPs in the repository obtained with version 5.005 of the TSPA-LA Model: (a,b) *UZRA226* and *UZRA226C* for all (i.e., 300) sample elements, (c,d) *UZRA226* and *UZRA226C* for first 50 sample elements, and (e,f) PRCCs for *UZRA226* and *UZRA226C* ..... FK-28[a]

FIGURES (Continued)

Page

K6.4.2-8[a]. Stepwise rank regression analyses and selected scatterplots for time-dependent release rates (*UZRA226*, g/yr) and cumulative (i.e., integrated) releases (*UZRA226C*, g) for the movement of dissolved ^{226}Ra from the UZ to the SZ resulting from an igneous intrusive event at 250 years that destroys all WPs in the repository obtained with version 5.005 of the TSPA-LA Model: (a,b) regressions for *UZRA226* and *UZRA226C* at 50,000, 200,000, and 500,000 years, and (c-h) scatterplots for *UZRA226* and *UZRA226C* at 50,000 years ..... FK-29[a]

K.6.4.2-9[a]. Comparison of cumulative releases of dissolved ^{226}Ra into the UZ (*UZRA226C*, g) and out of the UZ (*UZRA226C*, g) obtained with version 5.005 of the TSPA-LA Model at (a) 50,000, (b) 100,000, (c) 200,000, and (d) 600,000 years for an igneous intrusive event at 250 years that destroys all WPs in the repository ..... FK-31[a]

K6.5.2-5[a]. Time-dependent release rates (*SZU234*, g/yr) and cumulative (i.e., integrated) releases (*SZU234C*, g) over 1,000,000 years for the movement of dissolved ^{234}U across a subsurface plane at the location of the RMEI resulting from an igneous intrusive event at 250 years that destroys all WPs in the repository obtained with version 5.005 of the TSPA-LA Model: (a,b) *SZU234* and *SZU234C* for all (i.e., 300) sample elements, (c,d) *SZU234* and *SZU234C* for first 50 sample elements, and (e,f) PRCCs for *SZU234* and *SZU234C*..... FK-32[a]

K6.5.2-6[a]. Stepwise rank regression analyses and selected scatterplots for time-dependent release rates (*SZU234*, g/yr) and cumulative (i.e., integrated) releases (*SZU234C*, g) for the movement of dissolved ^{234}U across a subsurface plane at the location of the RMEI resulting from an igneous intrusive event at 250 years that destroys all WPs in the repository obtained with version 5.005 of the TSPA-LA Model: (a,b) regressions for *SZU234* and *SZU234C* at 50,000, 200,000, and 500,000 years, and (c-h) scatterplots for *SZU234* and *SZU234C* at 500,000 years ..... FK-33[a]

K.6.5.2-7[a]. Comparison of cumulative releases of dissolved ^{234}U into the SZ (*UZU234C*, g) and across a subsurface plane at the location of the RMEI (*SZU234C*, g) obtained with version 5.005 of the TSPA-LA Model at (a) 50,000, (b) 100,000, (c) 200,000, and (d) 600,000 years for an igneous intrusive event at 250 years that destroys all WPs in the repository ..... FK-35[a]

K6.5.2-8[a]. Time-dependent release rates (*SZTH230*, g/yr) and cumulative (i.e., integrated) releases (*SZTH230C*, g) over 1,000,000 years for the movement of dissolved ^{230}Th across a subsurface plane at the location of the RMEI resulting from an igneous intrusive event at 250 years that destroys all WPs in the repository obtained with version 5.005 of the TSPA-LA Model: (a,b) *SZTH230* and *SZTH230C* for all (i.e., 300)

FIGURES (Continued)

Page

sample elements, (c,d) *SZTH230* and *SZTH230C* for first 50 sample elements, and (e,f) PRCCs for *SZTH230* and *SZTH230C* ..... FK-36[a]

K6.5.2-9[a]. Stepwise rank regression analyses and selected scatterplots for time-dependent release rates (*SZTH230*, g/yr) and cumulative (i.e., integrated) releases (*SZTH230C*, g) for the movement of dissolved ^{230}Th across a subsurface plane at the location of the RMEI resulting from an igneous intrusive event at 250 years that destroys all WPs in the repository obtained with version 5.005 of the TSPA-LA Model: (a,b) regressions for *SZTH230* and *SZTH230C* at 50,000, 200,00, and 500,000 years, and (c-h) scatterplots for *SZTH230* and *SZTH230C* at 500,000 years ..... FK-37[a]

K.6.5.2-10[a]. Comparison of cumulative releases of dissolved ^{230}Th into the SZ (*UZTH230C*, g) and across a subsurface plane at the location of the RMEI (*SZTH230C*, g) obtained with version 5.005 of the TSPA-LA Model at (a) 50,000, (b) 100,000, (c) 200,000, and (d) 600,000 years for an igneous intrusive event at 250 years that destroys all WPs in the repository ..... FK-39[a]

K6.5.2-11[a]. Time-dependent release rates (*SZRA226*, g/yr) and cumulative (i.e., integrated) releases (*SZRA226C*, g) over 1,000,000 years for the movement of dissolved ^{226}Ra across a subsurface plane at the location of the RMEI resulting from an igneous intrusive event at 250 years that destroys all WPs in the repository obtained with version 5.005 of the TSPA-LA Model: (a,b) *SZRA226* and *SZRA226C* for all (i.e., 300) sample elements, (c,d) *SZRA226* and *SZRA226C* for first 50 sample elements, and (e,f) PRCCs for *SZRA226* and *SZRA226C* ..... FK-40[a]

K6.5.2-12[a]. Stepwise rank regression analyses and selected scatterplots for time-dependent release rates (*SZRA226*, g/yr) and cumulative (i.e., integrated) releases (*SZRA226C*, g) for the movement of dissolved ^{226}Ra across a subsurface plane at the location of the RMEI resulting from an igneous intrusive event at 250 years that destroys all WPs in the repository obtained with version 5.005 of the TSPA-LA Model: (a,b) regressions for *SZRA226* and *SZRA226C* at 50,000, 200,000, and 500,000 years, and (c-h) scatterplots for *SZRA226* and *SZRA226C* at 50,000 years ..... FK-41[a]

K.6.5.2-13[a]. Comparison of cumulative releases of dissolved ^{226}Ra into the SZ (*UZRA226C*, g) and across a subsurface plane at the location of the RMEI (*SZRA226C*, g) obtained with version 5.005 of the TSPA-LA Model at (a) 50,000, (b) 100,000, (c) 200,000, and (d) 600,000 years for an igneous intrusive event at 250 years that destroys all WPs in the repository ..... FK-43[a]

K.6.6.2-5[a]. Time-dependent dose to the RMEI (*DOU234*, mrem/yr) over 1,000,000 years for the movement of dissolved ^{234}U across a subsurface plane at the location of the RMEI resulting from an igneous

FIGURES (Continued)

Page

intrusive event at 250 years that destroys all WPs in the repository obtained with version 5.005 of the TSPA-LA Model: (a) *DOU234* for all (i.e., 300) sample elements, (b) *DOU234* for first 50 sample elements, and (c) PRCCs for *DOU234* ..... FK-44[a]

K.6.6.2-6[a]. Stepwise rank regression analyses and selected scatterplots for time-dependent dose to the RMEI (*DOU234*, mrem/yr) for the movement of dissolved ^{234}U across a subsurface plane at the location of the RMEI (*SZU234*, g/yr) resulting from an igneous intrusive event at 250 years that destroys all WPs in the repository obtained with version 5.005 of the TSPA-LA Model: (a) regressions for *DOU234* at 50,000, 200,000, and 500,000 years, (b,c,d) scatterplots for *DOU234* at 500,000 years, and (e) scatterplot comparing *SZU234* and *DOU234* at 500,000 years ..... FK-45[a]

K.6.6.2-7[a]. Time-dependent dose to the RMEI (*DOTH230*, mrem/yr) over 1,000,000 years for the movement of dissolved ^{230}Th across a subsurface plane at the location of the RMEI resulting from an igneous intrusive event at 250 years that destroys all WPs in the repository obtained with version 5.005 of the TSPA-LA Model: a) *DOTH230* for all (i.e., 300) sample elements, (b) *DOTH230* for first 50 sample elements, and (c) PRCCs for *DOTH230* ..... FK-46[a]

K.6.6.2-8[a]. Stepwise rank regression analyses and selected scatterplots for time-dependent dose to the RMEI (*DOTH230*, mrem/yr) for the movement of dissolved ^{230}Th across a subsurface plane at the location of the RMEI (*SZTH230*, g/yr) resulting from an igneous intrusive event at 250 years that destroys all WPs in the repository obtained with version 5.005 of the TSPA-LA Model: (a) regressions for *DOTH230* at 50,000, 200,000, and 500,000 years, (b,c,d) scatterplots for *DOTH230* at 500,000 years, and (e) scatterplot comparing *SZTH230* and *DOTH230* at 500,000 years ..... FK-47[a]

K.6.6.2-9[a]. Time-dependent dose to the RMEI (*DORA226*, mrem/yr) over 1,000,000 years for the movement of dissolved ^{226}Ra across a subsurface plane at the location of the RMEI resulting from an igneous intrusive event at 250 years that destroys all WPs in the repository obtained with version 5.005 of the TSPA-LA Model: (a) *DORA226* for all (i.e., 300) sample elements, (b) *DORA226* for first 50 sample elements, and (c) PRCCs for *DORA226* ..... FK-48[a]

K.6.6.2-10[a]. Stepwise rank regression analyses and selected scatterplots for time-dependent dose to the RMEI (*DORA226*, mrem/yr) for the movement of dissolved ^{226}Ra across a subsurface plane at the location of the RMEI (*SZRA226*, g/yr) resulting from an igneous intrusive event at 250 years that destroys all WPs in the repository obtained with version 5.005 of the TSPA-LA Model: (a) regressions for *DORA226* at 50,000, 200,000, and 500,000 years, (b,c,d) scatterplots for

FIGURES (Continued)

Page

DORA226 at 50,000 years, and (e) scatterplot comparing *SZRA226* and *DORA226* at 50,000 years ..... FK-49[a]

K6.7.1-1[a]. Expected dose to RMEI (*EXPDOSE*, mrem/yr) over [0, 20,000 yr] for all radioactive species resulting from igneous intrusion obtained with version 5.005 of the TSPA-LA Model: (a) *EXPDOSE* for all (i.e., 300) sample elements, (b) *EXPDOSE* for first 50 sample elements, and (c) PRCCs for *EXPDOSE* ..... FK-50[a]

K6.7.1-2[a]. Stepwise rank regression analyses and selected scatterplots for expected dose to RMEI (*EXPDOSE*, mrem/yr) over [0, 20,000 yr] for all radioactive species resulting from igneous intrusion obtained with version 5.005 of the TSPA-LA Model: (a) regressions for *EXPDOSE* at 3,000, 5,000, and 10,000 years, and (b,c,d) scatterplots for *EXPDOSE* at 10,000 years ..... FK-51[a]

K.6.7.2-1[a]. Expected dose to RMEI (*EXPDOSE*, mrem/yr) over [0, 1,000,000 yr] for all radioactive species resulting from igneous intrusion obtained with version 5.005 of the TSPA-LA Model: (a) *EXPDOSE* for all (i.e., 300) sample elements, (b) *EXPDOSE* for first 50 sample elements, and (c) PRCCs for *EXPDOSE* ..... FK-52[a]

K.6.7.2-2[a]. Stepwise rank regression analyses and selected scatterplots for expected dose to RMEI (*EXPDOSE*, mrem/yr) over [0, 1,000,000 yr] for all radioactive species resulting from igneous intrusion obtained with version 5.005 of the TSPA-LA Model: (a) regressions for *EXPDOSE* at 50,000, 200,000, and 500,000 years, and (b,c,d) scatterplots for *EXPDOSE* at 500,000 years ..... FK-53[a]

K7.7.1-1[a]. Expected dose to RMEI (*EXPDOSE*, mrem/yr) over [0, 20,000 yr] for all radioactive species resulting from seismic ground motion obtained with version 5.005 of the TSPA-LA Model: (a) *EXPDOSE* for all (i.e., 300) sample elements, (b) *EXPDOSE* for first 50 sample elements, and (c) PRCCs for *EXPDOSE* ..... FK-54[a]

K7.7.1-2[a]. Stepwise rank regression analyses and selected scatterplots for expected dose to RMEI (*EXPDOSE*, mrem/yr) over [0, 20,000 yr] for all radioactive species resulting from seismic ground motion obtained with version 5.005 of the TSPA-LA Model: (a) regressions for *EXPDOSE* at 3,000, 5,000, and 10,000 years, and (b,c,d) scatterplots for *EXPDOSE* at 10,000 years ..... FK-55[a]

K7.7.2-1[a]. Expected dose to RMEI (*EXPDOSE*, mrem/yr) over [0, 1,000,000 yr] for all radioactive species resulting from seismic ground motion obtained with version 5.005 of the TSPA-LA Model: (a) *EXPDOSE* for all (i.e., 300) sample elements, (b) *EXPDOSE* for first 50 sample elements, and (c) PRCCs for *EXPDOSE* ..... FK-56[a]

K7.7.2-2[a]. Stepwise rank regression analyses and selected scatterplots for expected dose to RMEI (*EXPDOSE*, mrem/yr) over [0, 1,000,000 yr]

FIGURES (Continued)

Page

for all radioactive species resulting from seismic ground motion obtained with version 5.005 of the TSPA-LA Model: (a) regressions for *EXPDOSE* at 50,000, 200,000, and 500,000 years, and (b,c,d) scatterplots for *EXPDOSE* at 500,000 years ..... FK-57[a]

K7.8.1-1[a]. Expected dose to RMEI (*EXPDOSE*, mrem/yr) over [0, 20,000 yr] for all radioactive species resulting from seismic fault displacement: (a) *EXPDOSE* for all (i.e., 300) sample elements, (b) *EXPDOSE* for first 50 sample elements, and (c) PRCCs for *EXPDOSE* ..... FK-58[a]

K7.8.1-2[a]. Stepwise rank regression analyses and selected scatterplots for expected dose to RMEI (*EXPDOSE*, mrem/yr) over [0, 20,000 yr] for all radioactive species resulting from seismic fault displacement: (a) regressions for *EXPDOSE* at 3,000, 5,000, and 10,000 years, and (b,c,d) scatterplots for *EXPDOSE* at 10,000 years ..... FK-59[a]

K7.8.2-1[a]. Expected dose to RMEI (*EXPDOSE*, mrem/yr) over [0, 1,000,000 yr] for all radioactive species resulting from seismic fault displacement: (a) *EXPDOSE* for all (i.e., 300) sample elements, (b) *EXPDOSE* for first 50 sample elements, and (c) PRCCs for *EXPDOSE* ..... FK-60[a]

K7.8.2-2[a]. Stepwise rank regression analyses and selected scatterplots for expected dose to RMEI (*EXPDOSE*, mrem/yr) over [0, 1,000,000 yr] for all radioactive species resulting from seismic fault displacement: (a) regressions for *EXPDOSE* at 50,000, 200,000, and 500,000 years, and (b,c,d) scatterplots for *EXPDOSE* at 500,000 years ..... FK-61[a]

K8.1-1[a]. Expected dose to RMEI (*EXPDOSE*, mrem/yr) over [0, 20,000 yr] for all scenario classes obtained with version 5.005 of the TSPA-LA Model: (a) *EXPDOSE* for all (i.e., 300) sample elements, (b) *EXPDOSE* for first 50 sample elements, and (c) PRCCs for *EXPDOSE* .. FK-62[a]

K8.1-2[a]. Stepwise rank regression analyses and selected scatterplots for expected dose to RMEI (*EXPDOSE*, mrem/yr) over [0, 20,000 yr] for all scenario classes obtained with version 5.005 of the TSPA-LA Model: (a) regressions for *EXPDOSE* at 3,000, 5,000, and 10,000 years, and (b,c,d) scatterplots for *EXPDOSE* at 10,000 years ..... FK-63[a]

K8.2-1[a]. Expected dose to RMEI (*EXPDOSE*, mrem/yr) over [0, 1,000,000 yr] for all scenario classes obtained with version 5.005 of the TSPA-LA Model: (a) *EXPDOSE* for all (i.e., 300) sample elements, (b) *EXPDOSE* for first 50 sample elements, and (c) PRCCs for *EXPDOSE* .. FK-64[a]

K8.2-2[a]. Stepwise rank regression analyses and selected scatterplots for expected dose to RMEI (*EXPDOSE*, mrem/yr) over [0, 1,000,000 yr] for all scenario classes obtained with version 5.005 of the TSPA-LA Model: (a) regressions for *EXPDOSE* at 50,000, 200,000, and 500,000 years, and (b,c,d) scatterplots for *EXPDOSE* at 500,000 years ..... FK-65[a]

FIGURES (Continued)

		Page
K10-1[a].	Expected dose to RMEI (*EXPDOSE*, mrem/yr) over [200,000, 220,000 yr] resulting from human intrusion at 200,000 years obtained with version 5.005 of the TSPA-LA Model: (a) *EXPDOSE* for all (i.e., 300) sample elements, (b) *EXPDOSE* for first 50 sample elements, and (c) PRCCs for *EXPDOSE*	FK-66[a]
K10-2[a].	Stepwise rank regression analyses and selected scatterplots for expected dose to RMEI (*EXPDOSE*, mrem/yr) over [200,000, 220,000 yr] resulting from human intrusion at 200,000 years obtained with version 5.005 of the TSPA-LA Model: (a) regressions for *EXPDOSE* at 201,000, 203,000, and 205,000 years, (b,c,d) scatterplots for *EXPDOSE* at 201,000 years, and (e,f,g) scatterplots for *EXPDOSE* at 205,000 years	FK-67[a]
K10-3[a].	Expected dose to RMEI (*EXPDOSE*, mrem/yr) over [220,000, 1,000,000 yr] resulting from human intrusion at 200,000 years obtained with version 5.005 of the TSPA-LA Model: (a) *EXPDOSE* for all (i.e., 300) sample elements, (b) *EXPDOSE* for first 50 sample elements, and (c) PRCCs for *EXPDOSE*.	FK-69[a]
K10-4[a].	Stepwise rank regression analyses and selected scatterplots for expected dose to RMEI (*EXPDOSE*, mrem/yr) over [220,000, 1,000,000 yr] resulting from human intrusion at 200,000 years obtained with version 5.005 of the TSPA-LA Model: (a) regressions for *EXPDOSE* at 240,000, 500,000, and 760,000 years, and (b,c,d,e) scatterplots for *EXPDOSE* at 500,000 years	FK-70[a]
K10-5[a].	Comparison of expected dose to RMEI (*EXPDOSE*, mrem/yr) over [200,000, 1,000,000 yr] resulting from human intrusion at 200,000 years obtained with versions 5.000 and 5.005 of the TSPA-LA Model at (a) 201,000, (b) 205,000, (c) 500,000, and (d) 1,000,000 years	FK-71[a]
K10-6[a].	Comparison of summary curves (i.e., mean and 0.05, 0.5, and 0.95 quantile) for expected dose to RMEI (*EXPDOSE*, mrem/yr) over [200,000, 1,000,000 yr] resulting from human intrusion at 200,000 years obtained with versions 5.000 and 5.005 of the TSPA-LA Model	FK-72[a]
P-20[a].	Expected Annual Dose versus Average Seepage Fraction for the Nominal Modeling Case for 1,000,000 Years after Repository Closure	FP-23[a]
P-21[a].	Expected Annual Dose versus Average Seepage Fraction for the Seismic Ground Motion Modeling Case for (a) 10,000 Years and (b) 1,000,000 Years after Repository Closure	FP-24[a]

TABLES

8.1-1[a]. Performance Demonstration Results for Individual Protection Standard ..... 8-25[a]
8.1-2[a]. Performance Demonstration Results for the Separate Standards for the Protection of Groundwater ..... 8-25[a]
8.1-3[a]. Performance Demonstration Results for the Individual Protection Standard for Human Intrusion ..... 8-25[a]
8.1-4[a]. Uncertainty in Projections of Maximum Total Mean and Median Annual Dose (mrem) for the Individual Protection Standard ..... 8-26[a]
8.1-5[a]. Inventories and Biosphere Dose Conversion Factors for Radionuclides Important to Total Mean Annual Dose for 10,000 Years ..... 8-26[a]
8.1-6[a]. Uncertainty Importance Ranking as a Function of Time for Four Key TSPA-LA Model Parameters ..... 8-26[a]

8.3-2[a]. Seepage Fractions for CDSP and CSNF Waste Packages for Combined Nominal/Early Failure Modeling Case for Glacial-Transition Climate, 2,000 to 10,000 Years ..... 8-81[a]
8.3-3[a]. Seepage Fractions for CDSP and CSNF Waste Packages for Combined Nominal/Early Failure Modeling Case for Post-10,000-Year Period ..... 8-81[a]
8.3-4[a]. Seepage Fractions for CDSP and CSNF Waste Packages for Seismic Ground Motion Modeling Case for Glacial-Transition Climate, 2,000 to 10,000 Years ..... 8-82[a]
8.3-5[a]. Seepage Fractions for CDSP and CSNF Waste Packages for Seismic Ground Motion Modeling Case for Post-10,000-Year Period ..... 8-82[a]
8.3-6[a]. Drift Wall Condensation for CSNF Waste Packages for Stage 2 and Stage 3 Condensation ..... 8-83[a]
8.3-7[a]. Drift Wall Condensation for CDSP Waste Packages for Stage 2 and Stage 3 Condensation ..... 8-84[a]
8.3-8[a]. Mean Seepage Rates for Waste Packages during Stage 2 and Stage 3 Condensation ..... 8-84[a]

C9-1[a]. Impact Assessment Summary Table ..... C-3[a]

H-1[a]. Applicable Regulatory Requirements of 10 CFR Part 63 and NUREG-1804 Acceptance Criteria Addressed in this Document ..... H-3[a]

I-2[a]. Model Implementation for Included Features, Events, and Processes ..... I-3[a]

K9-1[a]. Summary of Selected Sensitivity Analysis Results ..... K-35[a]

P-6[a]. Discussion of Other Minor Implementation Errors ..... P-11[a]
P-7[a]. Impact Assessment Summary Table ..... P-20[a]

INTENTIONALLY LEFT BLANK

8[a]. POSTCLOSURE PERFORMANCE DEMONSTRATION

Section 8[a] of this addendum contains the updated results for the Total System Performance Assessment for the License Application (TSPA-LA) Model performance analyses used for evaluating the postclosure performance of the repository and its compliance with U.S. Nuclear Regulatory Commission (NRC) Proposed Rule 10 CFR 63.113 [DIRS 180319] and the performance measures defined in proposed 10 CFR 63.303 [DIRS 178394] for the individual protection standard after permanent closure in proposed 10 CFR 63.311(a)(1) and (2) [DIRS 178394], the individual protection standard for human intrusion in 10 CFR 63.321(a)(1) and (2) [DIRS 178394], and the separate standards for protection of groundwater in 10 CFR 63.331 ([DIRS 180319], Table 1). The probabilistic TSPA-LA analyses account for uncertainty and address features, events and processes (FEPs) that could affect total system performance. Volume III presents the updated results of analyses and calculations in the following areas:

- Comparison of TSPA-LA Model analyses with the performance measures defined in proposed 10 CFR 63.303 [DIRS 178394] for the individual protection standard after permanent closure in 10 CFR 63.311(a)(1) and (2) [DIRS 178394], the individual protection standard for human intrusion in 10 CFR 63.321(a)(1) and (2) [DIRS 178394], and the separate standards for protection of groundwater in 10 CFR 63.331 ([DIRS 180319], Table 1)

- System and subsystem performance analyses for the Nominal Scenario Class, including the Nominal Modeling Case; the Early Failure Scenario Class, including the Drip Shield Early Failure (EF) and Waste Package EF Modeling Cases; the Igneous Scenario Class, including Igneous Intrusion Modeling Case; and the Seismic Scenario Class, including the Seismic Ground Motion (GM) and Fault Displacement (FD) Modeling Cases

- Analyses of the capabilities and importance of the upper and lower natural barriers and the engineered barrier system (EBS) that have been identified as contributing to repository performance.

The results presented in this addendum represent an iterative process that reflects a rigorous model verification and implementation cycle.

As used in this addendum, the designator "no change" means that the reader should refer to the original text for that section or subsection of the parent TSPA-LA document. Documentation provided in this addendum consists of a combination of supplemental and revised information for the postclosure performance demonstration. In the case of revised information, the documentation presents the revised plots, tables, and discussion of the revised TSPA-LA results. The organization of the sections and subsections parallel those of the parent document. Also, section numbers, figure numbers and table numbers cited in the text with [a] refer to this addendum, while those without it refer to the section, figure or table number in the parent document. It should be noted, that some of the important aspects of the performance requirements are restated from the parent document. The material from the parent document is reproduced in this addendum to provide clarity in the presentation.

The primary output DTNs are presented in Section 8 of the parent document and in Section 8[a] of this addendum. However, for a complete listing of the output DTNs associated with the parent document and this addendum, see Appendix B and Appendix B[a].

8.1[a] CONFORMANCE WITH RADIATION PROTECTION STANDARDS

The U.S. Environmental Protection Agency (EPA) and NRC regulations for a high-level radioactive waste (HLW) repository at Yucca Mountain require that the U.S. Department of Energy (DOE) demonstrate a reasonable expectation of compliance with the applicable radiation protection standards. The proposed EPA regulation, 40 CFR Part 197 (2005 [DIRS 175755]), establishes three separate and distinct radiation protection standards for the Yucca Mountain repository. As the licensing agency, the NRC adopted the following three radiation protection standards:

- Individual Protection Standard after Permanent Closure (10 CFR 63.311 [DIRS 178394]), which considers the required characteristics of the reasonably maximally exposed individual (RMEI) as described in 10 CFR 63.312 [DIRS 180319].
- Individual Protection Standard for Human Intrusion (10 CFR 63.321 [DIRS 178394]) according to the Human Intrusion Scenario described in 10 CFR 63.322 [DIRS 180319].
- Separate Standards for Protection of Ground Water (10 CFR 63.331 [DIRS 180319]) using the representative volume specified in 10 CFR 63.332 [DIRS 180319].

The EPA and NRC proposed regulations for Individual Protection and Human Intrusion establish standards for annual doses to the RMEI corresponding to: (1) the time period of 10,000 years after closure, and (2) the time period after 10,000 years but within the period of geologic stability, defined as 1,000,000 years in 10 CFR 63.302 [DIRS 178394]. In contrast, the Separate Standards for Protection of Ground Water sets limits for annual dose and activity concentrations (i.e., radionuclide activity per unit volume) for only the 10,000-year period following repository closure. For the purpose of making performance projections for these time periods, the characteristics of the RMEI are defined in 10 CFR 63.312 [DIRS 180319], and the RMEI is taken to reside approximately 18 km (11 mi) downgradient of the repository (66 FR 55732 [DIRS 156671], III Public Comments and Responses, 3.5, p. 55750).

Detailed probabilistic projections developed for this postclosure performance demonstration are presented and explained in the subsequent sections. Tables 8.1-1[a] through 8.1-3[a] present tabulations of the maximum of total mean and median annual doses and mean activity concentrations for direct comparisons with the three radiation protection standards. The times at which the maximum total annual doses occur are also shown in Tables 8.1-1[a]. To highlight the spread in the computed distribution of expected annual doses, additional statistics are presented in Table 8.1-4[a] to better clarify the comparison with the limits of the Individual Protection Standard. Comparisons of these updated results with the results reported in the parent document are provided in Sections 8.1.1[a], 8.1.2[a], and 8.1.3[a] as part of the discussion for each radiation protection standard.

As shown in the tabular comparisons, the numerical limits prescribed in all three standards are met, with the maximum total annual doses and activity concentrations falling well below the

limits. These numerical comparisons, however, represent only a part of the postclosure performance demonstration and many detailed calculations and graphical outputs are presented in Section 8.2[a] to elucidate the comparisons with the regulatory requirements. For the purpose of explaining the basis for a reasonable expectation of compliance, the performance demonstration for each radiation protection standard addresses the following fundamental questions regarding the TSPA of the repository and the projections of the regulatory metrics:

1. What scenario classes are considered to make performance projections, and what contribution does each scenario class make to the performance metrics?

2. What events, processes, or site characteristics modeled in the scenario classes are most important to the projections of each performance metric?

3. What barrier attributes and/or characteristics are most influential in reducing the radionuclide release rates, rate of water, or radionuclide movement?

4. What radionuclides in the nuclear waste inventory contribute the most to the annual doses and why?

5. Which uncertain input variables are most dominant in determining the uncertainty in the projected performance metrics and why?

In addition, the effect on the performance assessment of the conservatisms incorporated into the TSPA-LA Model is summarized in Section 7.7.4[a]; Section 8.4[a] summarizes the activities performed to ensure that the TSPA-LA Model and the results obtained from the model are technically sound and defensible.

The next sections describe and explain the projections that constitute the postclosure performance demonstration for the three radiation protection standards. Section 8.1.1[a] summarizes the results relevant to the Individual Protection Standard after permanent closure, Section 8.1.2[a] presents the results relevant to the Standards for the Protection of Groundwater, and Section 8.1.3[a] addresses the Individual Protection Standard for Human Intrusion. The exposure models and conversion factors used to calculate annual dose and activity concentrations in groundwater are summarized in the Biosphere Submodel description (Section 6.3.11). Conversion factors for dose to the RMEI are calculated for two general exposure scenarios, namely, groundwater and volcanic ash (SNL 2007 [DIRS 177399], Section 6.1.3).

8.1.1[a] Individual Protection Standard

No change.

8.1.1.1[a] Scenario Classes Considered and Calculation of Total Annual Doses

No change.

8.1.1.2[a] Projected Annual Doses and Major Observations

Projections of postclosure performance for comparison with the Individual Protection Standard were developed using the Monte Carlo simulation methodology, which is described in

Appendix J of the parent document. This methodology incorporates aleatory and epistemic uncertainties into the projections in two separate computational loops: (1) an outer loop that samples probability distributions for model parameters with epistemic uncertainty using the Latin hypercube sampling technique (Helton and Davis 2002 [DIRS 163475]), and (2) an inner loop that evaluates expected annual dose for each epistemic sample element by integrating over probability distributions that represent aleatory uncertainties. The methodology produces an ensemble of expected annual dose histories for each scenario class, which are then combined to obtain an ensemble of total expected annual doses. This is described by Equation 8.1.1-1 of the parent document, using the separate terms $\bar{D}_N(\tau \mid \mathbf{e})$ and $\bar{D}_S(\tau \mid \mathbf{e})$ for 10,000-year results and including the combined term $\bar{D}_N(\tau \mid \mathbf{e}) + \bar{D}_S(\tau \mid \mathbf{e})$ for post-10,000-year results.

The expected annual dose histories for the RMEI are generally plotted in the form of a multi-realization plot. The mean and median values of this ensemble of total expected annual doses are termed the total mean annual dose and total median annual dose, respectively, and are the performance metrics for comparison with the Individual Protection Standard. The revised projections of postclosure performance for the 10,000-year and 1,000,000-year compliance periods were developed using TSPA-LA Model v5.005, and the results are shown on Figure 8.1-1[a] and Figure 8.1-2[a]; the plots in these figures show the multi-realization dose histories and include curves for the mean, median, 5th and 95th percentiles. For 10,000 years after closure, the maximum total mean and median annual doses to the RMEI are estimated to be about 0.24 mrem and 0.13 mrem, respectively, well below the individual protection limit of 15 mrem. Similarly, for the post-10,000-year period over the period of geologic stability, the maximum total mean and median annual doses to the RMEI are estimated to be about 2.0 mrem and 0.96 mrem, respectively. The projected maximum total median annual dose for the post-10,000 year time period is well below the proposed individual protection limit of 350 mrem.

In the parent document, results from TSPA-LA Model v5.000 showed the maximum total mean annual doses to the RMEI for 10,000 years of 0.24 mrem, and maximum total median annual doses to the RMEI for 1,000,000 years of 0.99 mrem. Thus, the corrections and changes to the TSPA-LA Model from v5.000 to v5.005 (detailed in Appendix P[a]) result in only minor changes to these performance metrics. Additional comparison of the maximum total annual doses between the two model versions is provided in Sections 7.3.1.5.8[a] and 7.3.1.5.9[a].

Contribution to Total Annual Doses by Modeling Case

To show the relative contribution of each of the four scenario classes to total mean annual dose, the total mean annual dose is disaggregated into the mean annual dose histories for the individual modeling cases. The four scenario classes include Nominal, Early Failure, Igneous, and Seismic. As described in the parent document, the Nominal Scenario Class (Section 6.3) is composed of one modeling case, while Early Failure (Section 6.4), Igneous (Section 6.5), and Seismic (Section 6.6) Scenario Classes each have two modeling cases. The Early Failure Scenario Class consists of the Drip Shield and Waste Package EF Modeling Cases. The Igneous Scenario Class is composed of Igneous Intrusion and Volcanic Eruption Modeling Cases. Finally, the Seismic Scenario Class is made up of the Seismic GM and Seismic FD Modeling Cases.

Projections of the expected annual doses to the RMEI for each of these modeling cases are shown on Figure 8.1-3[a]. These annual dose history curves demonstrate that:

- Total mean annual doses for both the 10,000-year and post-10,000-year compliance periods are dominated by contributions from the Seismic GM and Igneous Intrusion Modeling Cases, which are on the order of 10^{-1} mrem for the 10,000-year period and 1 mrem for the post-10,000-year compliance period.

- Mean annual doses for the Waste Package EF and Seismic FD Modeling Cases are relatively small and are estimated to be on the order of 10^{-2} mrem or less for both the 10,000-year and post-10,000-year time periods.

- Mean annual doses projected for Drip Shield EF and Volcanic Eruption Modeling Cases are on the order of 10^{-3} mrem or less for both the 10,000-year and post-10,000-year time periods.

For each modeling case, the expected annual dose at a time τ can be conceptualized as the sum (over all possible events represented by a modeling case) of the annual dose at time τ from each event weighted by the probability of each event's occurrence (Section 6.1.2.4 of the parent document). Thus, the relative influence on total mean annual dose of each modeling case stems from one or both of the factors involved: the dose resulting from an event and the probability of an event's occurrence.

For the 10,000-year period after closure, the Seismic GM Modeling Case (Section 6.6.1 of the parent document) provides the majority of the total mean annual dose, with a smaller contribution from the Igneous Intrusion Modeling Case (Section 6.5.1 of the parent document). The Seismic GM Modeling Case estimates the expected annual dose resulting from the occurrence of seismic ground motion events that could damage waste packages (WPs). The dominant effect of ground motion events in the first 10,000-years after repository closure is stress-corrosion cracks of co-disposed (CDSP) WPs (Section 7.3.2.6.1.3). Within 10,000 years, the probability of a seismic event that results in damage to CDSP WPs ranges between 0 and 0.2 with a mean value of 0.07 (output DTN: MO0708CDSPSEIS.000 [DIRS 183007], *FreqDamageCDSP_v5.pdf*). This probability depends on the sampled value for the parameter *SCCTHRP* (residual stress threshold [RST] for stress corrosion cracking [SCC] nucleation of Alloy 22 as a percentage of yield strength; see Section 8.1.1.6[a]). The dose resulting from a damaging seismic event includes releases from all 3,416 CDSP WPs (Section 6.6.1.2.2.2 of the parent document). However, the ensuant radionuclide releases are moderated by the relatively small damaged area on each of the WPs (Figure 6.6-13a of the parent document), which limits the radionuclide release rates from the WPs (Section 6.3.8.1 of the parent document). Appendix J, Figure J8.3-1 of the parent document, illustrates the distribution of annual doses that are projected after the occurrence of a seismic ground motion event.

In contrast, the mean probability of an igneous event is estimated to be $1.69 \times 10^{-4} = (1.69 \times 10^{-8}\ /\text{yr}) \times (10^{4}\ \text{yr})$ (Table 6.5-2 of the parent document) much less than the probability of occurrence of a seismic event. The annual dose that results after an igneous event (Appendix J, Figure J7.2-1 of the parent document) is much larger than the annual dose from a seismic ground motion event, because: (1) an igneous intrusion affects all WPs (Section 6.5.1.1

of the parent document) and (2) after the intrusion, neither the drip shields (DSs) nor the WPs present any barrier to radionuclide mobilization and transport. However, as illustrated by the curves on Figure 8.1-3a[a], the lower probability of occurrence of an igneous event offsets the larger annual dose from an igneous event, which explains why the expected annual dose from igneous events is less than that from seismic ground motion events.

For the post-10,000-year time period, the Igneous Intrusion Modeling Case (Section 6.5.1 of the parent document) dominates the total mean annual dose history for about 725,000 years. After that time and up to 1,000,000 years, the Igneous Intrusion and Seismic GM Modeling Cases contribute almost equally to the total mean annual dose. The probability of an igneous event remains below 0.02 before 1,000,000 years. However, as discussed in Section 8.2.4.1[a], for the post-10,000-year period, the Seismic GM Modeling Case includes the combined effects of seismic events and nominal corrosion processes on all DSs and WPs in the repository. Additional discussion of the occurrence of damage to DSs and WPs from corrosion and seismic events is provided in Section 8.3.3.2[a] and in Section 8.1.1.3[a], respectively.

The remaining four modeling cases (i.e., Drip Shield EF, Waste Package EF, Seismic FD, and Volcanic Eruption) address events that occur with varying probabilities but result in radionuclide releases from only a small number of WPs. Fault displacement events, for example, are estimated to occur with annual frequencies in the range of 10^{-7} yr^{-1}, and involve on average at most a few tens of WPs (Table 6.6-1 of the parent document). The probability that at least one WP experiences an early failure is 0.442 (Section 8.2.2 of the parent document), while the expected number of early failed WPs (given that at least one early failure occurs) is estimated to be 2.46 (Section 8.2.2 of the parent document) out of 11,629 WPs (3,416 CDSPs and 8,213 CSNFs). The probability of at least one or more DS early failures is 0.017 (Section 8.2.2), and the expected number of early failed DSs (given that at least one early failure occurs) is only 1.09 (Section 8.2.2 of the parent document). Potential volcanic eruptions occur within 10,000 years with a mean probability of $(0.083) \times (1.69 \times 10^{-8}/yr) \times (10^{4}\ yr) = 1.4 \times 10^{-6}$ (Appendix J, Section J7.5 of the parent document) and are projected to induce releases from seven WPs or less (Table 6.5-3 of the parent document). Additional discussion and explanation of the results for each modeling case is presented in Section 8.2[a].

8.1.1.3[a] Disruptive Events Important to Postclosure Performance

As noted in Section 8.1.1.2[a], the most important events potentially affecting releases from the WPs were found to be seismic ground motion and igneous intrusion (i.e., a magmatic dike rising through the earth's crust and intersecting the repository). Based on the FEPs screening process, the seismic and igneous events only affect the EBS. In the case of seismic or vibratory ground motion, it is possible that extensive damage and failure of the WPs and DSs could be caused by a single extreme ground motion event. More commonly, however, damage would accumulate from a sequence of small to moderate vibratory ground motions over a period of time (Section 6.6.1.2.2.2 of the parent document). However, not all WPs that experience small to moderate ground motion events are breached. In contrast, a potential igneous intrusion into the repository area is assumed to cause complete failure of all WPs and DSs in a single discrete event (Section 6.5.1.1 of the parent document).

Vibratory ground motion events can cause damage to WPs, in the form of stress corrosion cracks, ruptures or punctures of the WP outer corrosion barrier (OCB) (Section 6.6.1.1.2 of the parent document) whereas for the DS, failure occurs as the result of loading from seismic induced rock fall. In the first 10,000 years after repository closure, the primary damage caused by ground motion events is stress corrosion cracks of CDSP WPs (Section 7.3.2.6.1.3 of the parent document). The probability of a seismic event that results in damage to CDSP WPs has a mean value of about 0.07 (based on λD_CDSPi23 = 7.484 $\times 10^{-6}$ yr^{-1} for 10,000 years), with a maximum value of about 0.2 (based on λD_CDSPi23r90 = 2.181 $\times 10^{-5}$ yr^{-1} for 10,000 years) (output DTN: MO0708CDSPSEIS.000 [DIRS 183007], FreqDamageCDSP_v5.pdf). The probability of seismic induced DS failure before 10,000 years is approximately 1.8×10^{-4} (DTN: MO0712PBANLNWP.000 [DIRS 184664], Lith Probability of DS Failure.pdf). Rupture and puncture of WPs are not considered because the probability that these events occur within 10,000 years is low enough and the consequence in terms of expected annual dose to the RMEI has been shown to be small enough that the contribution to the expected annual dose for the Seismic GM Modeling Case from these events is also low (Section 7.3.2.6.1.3). For this reason, the projections of mean annual dose from seismic ground motion events before 10,000 years is approximated by considering only SCC damage to CDSP WPs.

For the time period out to 1,000,000 years, seismic ground motion events have a variety of effects on the DSs and WPs. Ground motion events can lead to drift degradation and rockfall accumulation on the DS (Section 6.6.1.1 of the parent document). Subsequent failure of the DS can occur as a result of dynamic loading and deformation and/or by static loading due to accumulated rockfall. The ability of the DS to withstand the dynamic and static loading diminishes with time because general corrosion reduces the thickness of the titanium DS plate and framework. Ultimately, the DSs will fail as a result of load-induced buckling or rupture. A histogram of the time of DS plate failure for the Seismic GM Modeling Case is shown on Figure 8.1-4[a]; DS failure times for the Nominal Modeling Case (described in Section 6.3.5 of the parent document), in which DS plate failure occurs only due to general corrosion, are also shown for the purposes of comparison. As shown, the projected times of DS plate failure for the Seismic GM Modeling case are largely distributed between 100,000 years and about 300,000 years. In contrast, for the Nominal Modeling Case, DS plate failure times are distributed between 270,000 years and 340,000 years. A cumulative distribution function (CDF) for DS failure times is presented later in Section 8.3.3.2[a], along with discussion of the uncertainty in the time of DS failure. These updated histograms of DS plate failure times are nearly identical to those presented in the parent document.

As presented in Section 6.6 of the parent document, seismically induced damage of the WPs is most likely to occur from deformation or denting of the WP OCB. These localized areas of deformation or denting develop residual stresses that are susceptible to SCC. Rupture of a WP could potentially occur as a result of kinematic loading caused by package-to-pallet and/or package-to-package impacts, and a severely deformed OCB may be punctured by the sharp edges of fractured or partly degraded internal components. Generally, seismic crack damage is more likely to occur than either rupture or puncture, and CDSP WPs are more likely to be damaged than are CSNF WPs. Figure 8.1-5[a] shows summary statistics for the distribution of the probability of occurrence of seismic damage to (a) CDSP WPs and (b) CSNF WPs, estimated as the fraction of aleatory samples (futures) in which seismic damage occurs to all WPs, for each epistemic sample element. The probability of occurrence of seismic damage to CSNF WP is

zero at and below the 5th percentile (Figure 8.1-5b[a]). The distribution summarized on Figure 8.1-5a[a] results from epistemic uncertainty in the RST for Alloy 22 (*SCCTHRP*, RST for SCC nucleation of Alloy 22 as a percentage of yield strength; see Section 8.1.1.6[a]); the spread between the quantiles indicates the strong dependence of the occurrence of seismic damage on this uncertain parameter. Section 8.1.1.6[a] provides a summary of sensitivity analyses that further illustrate this dependence.

Figure 8.1-5[a] illustrates that CSNF WPs are far less likely to be damaged by seismic events than are CDSP WPs, due to the use of the transportation, aging, and disposal (TAD) canister for CSNF, which enhances the structural integrity of these WPs. Finally, the probability that seismic events have damaged CDSP WPs increases until around 200,000 years, when DSs fail, after which only slight increases are observed. While the DSs are intact, WP damage from seismic events is determined by abstractions in which the WPs move freely beneath the DSs. In contrast, after DS failure, rubble is assumed to surround the WPs (Section 6.6.1.2.2.1 of the parent document), resulting in a significant reduction in the probabilities of damage from seismic events (output DTN: MO0708FREQCALC.000 [DIRS 183006], compare files: *Rubble_Damage.pdf* and DTN: MO0708CDSPSEIS.000 [DIRS 183007] *FreqDamageCDSP_v5.pdf*). The effects of seismic events on EBS components are described and explained in more detail in Section 8.3.3.2[a]. The revised projections of expected fraction of WPs breached by SCC are shown on Figure 8.1-5[a]; these plots reflect the corrections made to address implementation errors in two model abstractions (Appendix P, Table P-7, issues P3 and P4 in the parent document).

8.1.1.4[a] Multiple Barrier Processes that Contribute to Postclosure Performance

Many of the multiple barrier processes that are important to postclosure performance have been identified in previous TSPAs of the Yucca Mountain repository (Williams 2001 [DIRS 157307]). The modeling studies conducted in support of this TSPA-LA have provided additional insights and understanding, particularly with regard to individual features of natural and engineered barriers. Some of the fundamental barrier processes and characteristics that are typically influential in determining how well the system of multiple barriers isolates (i.e., contains and confines) the nuclear waste are:

- Net infiltration into the unsaturated zone (UZ) (Section 6.3.1 of the parent document) and seepage into the drifts (Section 6.3.3 of the parent document)
- Mechanical strength and corrosion rates of the WPs and DSs (Section 6.3.5 of the parent document)
- Solubilities for key radionuclides such as neptunium, uranium, and plutonium (Section 6.3.7 of the parent document)
- Radionuclide sorption onto corrosion products inside the WPs (Section 6.3.8 of the parent document)

- Diffusion-limited radionuclide releases from failed WPs (Section 6.3.8 of the parent document)

- Sorption and matrix diffusion properties of the UZ and saturated zone (SZ) underlying the repository (Sections 6.3.9 and 6.3.10 of the parent document).

With regard to infiltration and seepage, these attributes are important because they determine: (1) fraction of WPs and DSs in seeping and non-seeping environments, and (2) water flow into a failed WP and the ensuant mobilization and release of radionuclides. The strength properties of the WP OCB (i.e., Alloy 22 [UNS N06022]) and DS plate (i.e., Titanium Grade 7) and frame (i.e., Titanium Grade 29) determine their capability to withstand dynamic and static loads induced by vibratory ground motion (Section 6.6.1.2 of the parent document). General corrosion and SCC are important processes affecting WP structural integrity because they progressively reduce metal barrier thickness over a period of time. The general corrosion rate of the WP OCB is temperature-dependent, which makes the WP surface temperature an important factor. The importance of radionuclide solubilities is derived from the fact that they limit the release rates from the WPs. Solubilities of such radionuclides as neptunium, uranium, and plutonium are particularly important because they have relatively large initial inventories and produce radionuclide species that have very long half-lives. Corrosion of the WP internals produces metal oxides that provide sorption sites for a variety of fission products and actinide elements (Section 6.3.8 of the parent document). Diffusional release of radionuclides from a failed WP is a function of the breach geometry (e.g., cracks and patches) and effectively limits the rate of release to the natural barrier. The sorption properties of the volcanic tuff and alluvium layers in the UZ and SZ influence the rate of subsurface migration to the RMEI location.

Analyses of single realizations from the TSPA-LA Model (presented in Section 7.7.1[a]) illustrate these important processes and their role in isolating the nuclear waste. Although these analyses are conducted on individual modeling cases, the results for modeling cases that are important to total mean annual dose (Figure 8.1-3[a]) provide useful insights into processes and their relationships with dose outcomes. For example, the single realization analyses of the Seismic GM Modeling Case for 10,000 years (Section 7.7.1.7[a]) provide insights about impacts on repository performance for 10,000 years after closure; whereas the analyses of the Igneous Intrusion Modeling Case (Section 7.7.1.3[a]) and Seismic GM Modeling Case for 1,000,000 years (Section 7.7.1.4[a]) illustrate processes that dominate performance over 1,000,000 years. Additional discussion and interpretation of the simulation results for each of these modeling cases is provided in Section 8.2[a]. Section 8.3.3[a] provides further insight into the processes important within each of the three primary barriers.

8.1.1.5[a] Radionuclides Important to Postclosure Performance

In general, the radionuclides in the nuclear waste that dominate the calculation of annual doses typically have one or more of the following characteristics: (1) large initial inventories in the nuclear waste, (2) moderate to high solubilities, (3) very long half-lives (e.g., $\geq 10^5$ years), and (4) low to non-sorbing properties. The radionuclides that become important to dose also depend on the time frame considered (i.e., 10,000 years or 1,000,000 years after closure), because of the effect of radionuclide decay on the activity concentrations. Ingrowth of radionuclides via chain decay (Figure 6.3.7-4 of the parent document) can also be an important process that determines

the role and importance of actinide elements in the actinium, uranium, neptunium, and thorium series. For groundwater releases, the basic transport processes of advection, dispersion, matrix diffusion, and sorption play an important role, as illustrated in the analyses documented in Section 7.7.1[a]. Moreover, the specific modes (e.g., dissolved and colloidal phases) of transport can also be important; the modes analyzed for each radionuclide are listed in Table 6.3.7-6[a].

The contributions of the individual radionuclides to the maximum total mean annual dose are shown on Figures 8.1-6[a] and 8.1-7[a] for 10,000 years and post-10,000 years, respectively. The relative contribution of each radionuclide is determined by its mass in the initial inventory, the intrinsic properties of each radionuclide, as well as the relative importance of the events (i.e., seismic and igneous), which lead to release of radionuclides. The radionuclide half-lives quoted in the following discussion can be found in Table 6.3.9-1[a].

Important Radionuclides for 10,000-Year Performance Projection—The total mean annual dose curves for individual radionuclides on Figure 8.1-6[a] show that the principal contributors to the total mean annual dose, ranked from highest to lowest, are: ^{99}Tc (half-life 2.13×10^5 yrs), ^{14}C (half-life 5.72×10^3 yrs), ^{239}Pu (half-life 2.41×10^4 yrs), and ^{129}I (half-life 1.57×10^7 yrs). Collectively, these four radionuclides account for about 87 percent of the maximum of the total mean annual dose, which occurs at 10,000 years postclosure. The dominant contributor is ^{99}Tc, which accounts for about 51 percent of the total. Other radionuclides, notably ^{36}Cl, ^{240}Pu, ^{79}Se, and ^{237}Np, make up the remaining 13 percent of the total mean annual dose.

The fission products, ^{99}Tc and ^{129}I, and the activation product, ^{14}C, collectively represent about 75 percent of the total mean annual dose. These three radionuclides are important because they are very soluble in water, do not sorb in earth materials, and in the case of ^{99}Tc and ^{129}I have very long half-lives relative to the 10,000-year time frame. Because technetium, iodine, and carbon radionuclides are very soluble, their release rates from the nuclear waste are limited only by: (1) the waste form degradation rates, (2) rate and extent of water saturation inside WPs, and (3) mass transport mechanisms (i.e., diffusion and/or advection) out of the WPs. The non-sorbing property is important because these radionuclides are transported from the EBS, through the natural barrier, and to the RMEI at the rate at which the groundwater naturally travels (i.e., no delay by chemical retardation). The relatively long half-lives of ^{99}Tc and ^{129}I, compared to 10,000 years, means that decay would not appreciably reduce their activity level.

The rate of transport of radionuclides from WPs depends on the nature and extent of damage to DSs and WPs resulting from disruptive events, the most important of which are seismic ground motion and igneous intrusion events. Before 10,000 years, roughly 70 percent of the total mean annual dose is attributable to the mean annual dose for the Seismic GM Modeling Case (Figure 8.1-3[a]), which in turn consists almost entirely of the highly soluble radionuclides ^{99}Tc, ^{14}C, ^{129}I, ^{36}Cl, and ^{79}Se (Figure 8.2-12a[a]). The predominant damage caused by vibratory ground motion is SCC of CDSP WPs (Section 7.3.2.6.1.3 of the parent document), which permits diffusion of radionuclides from WPs but not advection. In these circumstances, highly soluble radionuclides are more readily transported from the damaged WPs than are solubility-limited radionuclides such as plutonium.

The dominance of ^{99}Tc, compared to ^{14}C and ^{129}I, largely stems from its WP inventory (Table 8.1-5[a]) and the fact that the predominant damage caused by vibratory ground motion is

SCC of CDSP WPs (Section 7.3.2.6.1.3 of the parent document). In CDSP WPs, the total of ^{99}Tc inventory on a curie per package basis is about 1,000 times that of ^{129}I and about 2.5 times that of ^{14}C. Although ^{14}C has a larger biosphere dose conversion factor (BDCF) (Table 8.1-5[a]) than ^{99}Tc and ^{129}I, it also has a relatively short half-life (5,715 years) and will experience some decay in transport. Thus, due to the larger inventory of ^{99}Tc and it's very long half-life (2.13×10^5), it is reasonable and consistent that ^{99}Tc would have greater influence than ^{14}C and ^{129}I on total mean annual dose to the RMEI.

In contrast, the Igneous Intrusion Modeling Case contributes roughly 30 percent of the total mean annual dose before 10,000 years (Figure 8.1-3[a]). The highly soluble, non-sorbing radionuclides, ^{99}Tc, ^{14}C, and ^{129}I, are important to the mean annual dose for this modeling case (Figure 8.2-8a[a]) for the first 4,000 years. However, after 8,000 years, ^{239}Pu becomes the dominant radionuclide with ^{99}Tc, ^{240}Pu, and ^{129}I contributing to mean annual dose from igneous intrusions. Because an igneous intrusion causes complete failure of all DSs and WPs at the time of the event, radionuclides are transported from the WPs by advection as well as diffusion, resulting in the emerging importance of ^{239}Pu. The time that ^{239}Pu becomes important is determined by the processes that govern the mobilization and transport of this radionuclide. The mean annual dose between 4,000 and 6,000 years shows both ^{239}Pu and ^{240}Pu emerging as dominant dose contributors (Figure 8.2-8a[a]). The comparison of Figure 8.2-8a[a] to Figure 8.1-6[a] shows that the contribution of ^{239}Pu to total mean annual dose at 10,000 years is due to its contribution to mean annual dose from the Igneous Intrusion Modeling Case. Thus, although the actinide ^{239}Pu has a relatively large initial inventory (Table 6.3.7-5 of the parent document), its contribution to total mean annual dose is limited due to the low probability of an event that can lead to its release, as well as the hydrologic and chemical processes that determine the rate of plutonium transport through the EBS and lower natural barrier. Additional discussion of these processes is provided in Sections 6.3.7 through 6.3.10 of the parent document.

Important Radionuclides for Post-10,000-Year Performance Projection—Figure 8.1-7[a] shows the mean annual dose for individual radionuclides for 1,000,000 years after repository closure. Between 10,000 years and 20,000 years, the dominant radionuclides are the same as those listed for the 10,000-year performance projection, namely, ^{99}Tc, ^{14}C, ^{239}Pu, and ^{129}I; however, ^{239}Pu becomes increasingly important with time. Between about 20,000 years until 200,000 years, the radionuclides with largest contributions to total mean annual dose are ^{239}Pu and ^{99}Tc, with ^{242}Pu (half-life 3.75×10^5 yrs) overtaking ^{99}Tc around 150,000 years. Beyond 200,000 years, ^{242}Pu is the largest contributor, with secondary contributions from ^{99}Tc, ^{129}I, ^{237}Np (half-life 2.14×10^6 yrs), and ^{226}Ra (half-life 1,600 yrs). The maximum of the total mean annual dose occurs at 1,000,000 years; the radionuclides contributing to total mean annual dose, ranked from highest to lowest, are: ^{242}Pu, ^{237}Np, ^{226}Ra, and ^{129}I. These four radionuclides account for about 77 percent of the total. The actinides ^{242}Pu and ^{237}Np together represent about 52 percent of the total annual dose with ^{226}Ra and ^{129}I contributing about 25 percent.

At 1,000,000 years, the primary difference between the projections presented in this addendum (TSPA-LA Model v5.005) and the original projections documented in the parent document (TSPA-LA Model v5.000) is that ^{226}Ra is ranked third in the addendum projections instead of first for the post-10,000-year compliance period. This change is attributed to the correction to longitudinal dispersivity distribution, which is described in Appendix P, Section P15, of the

parent document. The explanation for persistence of the ^{226}Ra at 1,000,000 years is due to chain decay, which is described in the parent document.

The persistent importance of ^{99}Tc and ^{129}I to total mean annual dose throughout the 1,000,000-year time period is derived from their contributions to mean annual dose in the Seismic GM Modeling Case (Figure 8.2-12b[a]). This modeling case includes the combined effects of seismic events and nominal corrosion processes on all DSs and WPs in the repository. Because of the relatively low probability that seismic events have damaged all WPs (Figure 8.1-5[a]), it is likely that some WPs remain intact until failure occurs by nominal corrosion processes, most commonly as SCC of lid welds. As the intact WPs fail, additional quantities of ^{99}Tc and ^{129}I are released from the EBS, which results in continual releases of these radionuclides from the repository system throughout the 1,000,000 period. Additional discussion of the Seismic GM Modeling Case is provided in Section 8.2.4.1[a].

Beyond 20,000 years, two plutonium species, ^{239}Pu and ^{242}Pu, are the dominant contributors to total mean annual dose, with ^{242}Pu supplanting ^{239}Pu at about 200,000 years due to radioactive decay of the latter. The contribution of these two plutonium species to total mean annual dose is due primarily to their importance in the Igneous Intrusion Modeling Case (Figure 8.2-8b[a]), where these two species comprise the dominant contributors to mean annual dose. In the Seismic GM Modeling Case, these radionuclides are minor contributors to mean annual dose until about 600,000 years, when WPs begin to fail by general corrosion. After general corrosion failures begin, seepage waters can flow through WPs with general corrosion failures, thereby increasing the quantity of plutonium released from the EBS and into the lower natural barrier. The processes that govern the mobilization and transport of plutonium are discussed in Sections 6.3.7 through 6.3.10 of the parent document.

Plutonium from degraded waste forms can be transported through the EBS either in dissolved phase, as well as sorbed reversibly or irreversibly to colloids. Plutonium releases from the EBS are moderated by sorption onto the corrosion products inside the WP (Section 6.3.8). Plutonium species are transported through groundwater in dissolved phase and reversible colloids, as well as fast (i.e., not retarded by matrix diffusion or attachment/detachment process) and slow irreversible colloids (Table 6.3.7-6), with a broad range of transport times in the SZ. Detailed probabilistic simulations of plutonium transport through the SZ in dissolved phase and as reversible colloids, neglecting effects of decay, indicate median transport times ranging from 3,000 years to greater than 1,000,000 years, with a median among all realizations of about 95,000 years (SNL 2008 [DIRS 183750], Table 6-10[a]). Simulations for the fast irreversible plutonium colloids show transport times ranging from 10 years to about 1,800 years, with a median among all realizations of about 60 years (SNL 2008 [DIRS 183750], Table 6-10[a]). However, the fast irreversible colloids represent less than one percent of all irreversible colloids (BSC 2004 [DIRS 170006], Section 6.6, Table 6-4). In contrast, for slow irreversible colloids, transport times range from 100 years to about 500,000 years, with a median among all realizations of about 4,500 years (SNL 2008 [DIRS 183750], Table 6-10[a]). The TSPA-LA Model projections indicate that the dissolved phase and reversible colloids account for the larger fraction of the contribution of plutonium to total mean annual dose.

In contrast, neptunium has higher solubilities than plutonium (compare Table 6.3.7-35 and Table 6.3.7-36 to Table 6.3.7-37 of the parent document) and travels relatively more rapidly

through the SZ; transport simulations for neptunium (neglecting effects of decay) indicate median transport times ranging from 100 years to 455,000 years, with a median among all realizations of about 3,700 years (SNL 2008 [DIRS 183750], Table 6-10[a]). However, neptunium is more retarded by sorption to corrosion products inside the WPs than is plutonium (Figure 7.7.1-8[a]), thus limiting the rate of release of neptunium from the EBS as compared to plutonium. Transport of radium is discussed in Section 8.1.2.1[a] with the presentation of results for the Groundwater Protection Standard.

8.1.1.6[a] Model Parameters Influencing Uncertainty in Expected Annual Doses

Uncertainty and sensitivity analyses were conducted to identify the TSPA-LA Model parameters that were most influential in determining the spread in the total expected annual dose projections (Appendix K[a], Section K8[a]). Those analyses identify four model parameters as having the largest influence on the overall uncertainty in the expected annual doses to the RMEI. These four parameters are: (1) occurrence rate of igneous events, *IGRATE*; (2) RST for Alloy 22, *SCCTHRP*; (3) temperature dependence parameter for Alloy 22 general corrosion rate, *WDGCA22*; and (4) the SZ ground water specific discharge, *SZGWSPDM*. The importance ranking of these four model parameters varies with time, which is illustrated in Table 8.1-6[a]. Appendix K[a], Figure K8.1-2[a], provides information for times prior to 20,000 years, and Figure K8.2-2[a] provides information for times after 20,000 years. These model parameters are described below; Table K3-1 of the parent document provides additional details and references for each parameter. These results are very similar to that presented in the parent document.

IGRATE—This parameter is the estimated annual frequency of an igneous dike intersecting the repository, which is characterized as an epistemic uncertain quantity. The annual frequency of an igneous event intersecting the repository ranges from approximately 7.4×10^{-10}/yr to 5.5×10^{-8}/yr for the 5th and 95th percentiles, respectively, with a mean annual frequency of 1.7×10^{-8}/yr (Table 6.5-2 of the parent document). In a given epistemic realization, the annual frequency of an igneous event is sampled from the CDF for *IGRATE*, and is used to determine the probability that an igneous event occurs.

SCCTHRP—This parameter is the RST for the Alloy-22 WP OCB, which is represented as an epistemically uncertain value. When the residual stress in the OCB of a WP exceeds this threshold, then SCC is presumed to occur. As explained in Section 6.3.5, residual stresses in the WP OCB result primarily from seismic ground motions that cause impacts between WPs and other WPs, emplacement pallets, or DSs; these impacts could potentially cause dynamic loads that dent the OCB, which could result in creation of residual stresses. The uncertainty in this model parameter is represented using a uniform distribution.

WDGCA22—This parameter relates to the temperature dependence for the general corrosion rate of the Alloy 22 WP OCB, which is characterized as an epistemically uncertain quantity. As explained in Section 6.3.5, this parameter determines the magnitude of this temperature dependence and directly influences the short-term and long-term general corrosion rates of the Alloy 22. Larger values of this parameter correspond to higher general corrosion rates while WP temperatures are above 60°C, and to lower general corrosion rates when WP temperatures are below 60°C. This parameter is sampled from a truncated normal distribution.

SZGWSPDM—This SZ flow and transport parameter is the logarithm of the scale factor for the groundwater specific discharge multiplier. The parameter accounts for the epistemic uncertainty in the discharge flow rate, which is used to compute advective radionuclide transport. As explained in Section 6.3.10, this uncertainty parameter is applied to all of the climate states. Values for this parameter are sampled from an empirical CDF; the technical basis for that distribution is documented in *Saturated Zone Flow and Transport Model* (SNL 2008 [DIRS 183750], Section 6.5.2.1).

More detailed discussion of the importance of these and other model parameters is given in Appendix K[a], Section K8[a].

8.1.2[a] Groundwater Protection

No change.

8.1.2.1[a] Projections for Combined ^{226}Ra and ^{228}Ra

The performance demonstration for this first metric of the Separate Standards for the Protection of Groundwater is based on the combined activity concentration for ^{226}Ra and ^{228}Ra (NRC Proposed Rule 10 CFR 63.331 [DIRS 180319], Table 1). The revised probabilistic projections of the activity concentrations are presented on Figure 8.1-9[a]. The curves shown in this figure include the estimated background level, projected mean, and 95th percentile activity concentrations of combined radium species; both the mean and 95th percentile curves exclude background. From these plots, the maximum mean groundwater concentration of combined radium at the RMEI location is estimated to be about 1.3×10^{-7} pCi/L, or less than 10^{-6} pCi/L. This maximum mean activity concentration is well below the 5 pCi/L limit specified in 10 CFR 63.331 ([DIRS 180319], Table 1). This maximum activity concentration is about one order of magnitude lower than the projection presented in the parent document. This difference is primarily due to the change to the uncertainty distribution for longitudinal mass dispersivity; the description of this change is documented in Section 6.3.10.2[a].

Figure 8.1-10[a] shows the contributions of the modeling cases to the projected mean of combined radium activity concentration in groundwater, excluding natural background, for 10,000 years after closure (with the natural background level included in the graph). From the curves in this figure, it is evident that the mean of the combined radium concentration is dominated by the contribution from the Waste Package EF Modeling Case (Section 6.4.2) until 4,500 years, after which the contribution from the Seismic GM Modeling Case dominates. At 10,000 years, when the mean radium concentration obtains its maximum value, roughly 90 percent of the mean radium concentration is attributable to the Seismic GM Modeling Case. The contributions to the mean radium concentration from each modeling case parallel the importance of these modeling cases to the total mean annual dose (Section 8.1.1.2[a]). In particular, the Seismic GM Modeling Case is the dominant contributor to mean radium concentrations because this modeling case represents the potential radionuclide releases from many WPs that may be damaged by seismic events, whereas the early failure modeling cases represent radionuclide releases from the relatively few WPs that may be affected by early failures of either DSs or WPs. In both the Seismic GM and Waste Package EF Modeling Cases, radionuclide transport from the WP occurs primarily by diffusion. In contrast, early failure of DSs allows seepage waters to flow through the underlying WPs (Section 6.4.1.3 of the parent

document), which could result in greater quantity of radionuclides mobilized from each affected WPs. However, this potential for greater releases is offset by the lower expected number of affected WPs, resulting in a relatively minor contribution to the mean radium concentration from the Drip Shield EF Modeling Case.

The fundamental reasons for the very low mean radium concentrations at the RMEI location are: the relatively short half-lives of the two radium isotopes compared to their transport times in the lower natural barrier; the limited release of thorium (a parent of radium) from the EBS; and the lengthy transport time of thorium in the lower natural barrier. Both ^{228}Ra and ^{226}Ra are discussed below.

^{228}Ra Activity Concentration—The chemical and nuclear properties of ^{228}Ra, together with its very small inventory, largely explain its small contribution to the total radium activity concentrations. The radionuclide radium sorbs very strongly in the geologic media (Tables 6.3.9-2 and 6.3.10-2 of the parent document), resulting in very long transport times for ^{228}Ra through the lower natural barrier. Travel times for radium through the SZ alone are predominantly greater than 10,000 years (SNL 2008 [DIRS 183750], Figure 6-14[a]). However, if radium was released from WPs into the lower natural barrier, and if one postulates an unlikely hypothetical pathway with a very fast transport time, for example, of 500 years, then ^{228}Ra, with a half-life of 5.8 years, would still experience about 86 half-lives of decay before reaching the RMEI location. This would reduce its activity by a factor of $(1/2)^{86} \sim 10^{-26}$. The initial total inventory of ^{228}Ra is almost entirely in the CDSP WPs (Table 6.3.7-5 of the parent document). The total activity of ^{228}Ra can be estimated by multiplying its initial activity per WP with the total number of CDSP WPs (Table 6.3.7-1) ($(2.39 \times 10^{-3}$ Ci/pkg from DOE spent nuclear fuel [DSNF] + 3.27×10^{-3} Ci/pkg from HLW) × 3416 pkg = 19.3 Ci). After 86 half-lives of decay, the original quantity of ^{228}Ra would be reduced to about 2×10^{-13} pCi. After mixing this activity in the representative volume of 3,000 acre-ft, the ^{228}Ra activity concentration in the groundwater would be undetectable.

^{228}Ra could also potentially reach the RMEI location via transport of its precursor ^{232}Th and subsequent ingrowth. The relevant part of the decay chain is:

$$^{232}\text{Th (half-life } 1.4 \times 10^{10} \text{ years)} \rightarrow {}^{228}\text{Ra}$$

Because of its extraordinarily long half-life, the ^{232}Th is for all practical purposes a stable element for time periods of 10,000 years. For this reason, it is conservatively assumed that ^{228}Ra and ^{232}Th are in secular equilibrium. The total initial activity of ^{232}Th is about the same as that of ^{228}Ra, about 20 Ci (Table 6.3.7-5 of the parent document). However, in the Seismic GM Modeling Case, transport of thorium from the EBS to the lower natural barrier is significantly constrained by (1) the relatively small damaged area on WP surfaces with stress corrosion cracks, which limits the quantity of water available to dissolve thorium; (2) sorption of thorium onto stationary iron oxyhydroxide corrosion products within the WP; and (3) diffusion of thorium through the WP OCB. For other radionuclides (i.e., uranium and plutonium) affected by these same processes, the mean mass of these radionuclides released from the EBS over 10,000 years is only a minute fraction of the inventory (Figure 8.3-19a[a] for uranium, and Figure 8.3-21a[a] for plutonium). Once in the lower natural barrier, thorium is retarded more by sorption in the geologic media than is radium (Tables 6.3.9-2 and 6.3.10-2 of the parent

document). Simulations of thorium transport through the SZ show that (neglecting effects of decay) the median transport times (through the SZ) for thorium range from about 1,000 years to over 1,000,000 years, with the 50th percentile of the median transport times among all realizations being greater than 1,000,000 years (SNL 2008 [DIRS 183750], Table 6-10[a]).

Thus, due to the short half-life of ^{228}Ra, the processes constraining the release of its parent, ^{232}Th, from the EBS, and the long travel time of thorium through the lower natural barrier, it is reasonable to expect the activity concentrations for ^{228}Ra to show effectively undetectable levels for 10,000 years after disposal.

^{226}Ra Activity Concentration—The explanation for the projected low ^{226}Ra activity concentrations is similar to that for ^{228}Ra. More specifically, ^{226}Ra is initially present in the nuclear waste, and it may also be produced as a result of the decay of uranium and thorium (Figure 6.3.7-4). The relevant part of that decay chain consists of the following:

$$^{234}\text{U (half-life 246,000 yrs)} \rightarrow {}^{230}\text{Th (half-life 75,400 yrs)} \rightarrow {}^{226}\text{Ra (half-life 1,600 yrs).}$$

This decay chain is significant because it means that, even after ^{226}Ra depletes its initial inventory, it will be continuously replenished so long as there is a source of ^{230}Th and ^{234}U. While both ^{226}Ra and ^{230}Th have relatively small initial inventories in the nuclear waste, the precursor ^{234}U has a significant initial inventory. Also, the large contrast in half-lives between ^{226}Ra and ^{230}Th means that ^{226}Ra will ultimately reach a state of secular equilibrium with ^{230}Th. Similarly, after ^{230}Th depletes its initial inventory, its activity will be in secular equilibrium with its precursor ^{234}U. The net effect is that ^{226}Ra will persist in the waste form for potentially millions of years.

In the Seismic GM Modeling Case, only a minute fraction of the radium present in the WP is released from the EBS (Figure 8.3-20a[a]). Radium that is released from the EBS is unlikely to reach the RMEI location in any significant quantity. As mentioned above, radium exhibits high sorption in the unsaturated tuff layers, particularly in the Zeolitic and devitrified tuff (Table 6.3.9-2 of the parent document), as well as in the volcanic units and alluvium of the SZ (Table 6.3.10-2 of the parent document). These sorption properties have the effect of greatly slowing the ^{226}Ra rate of migration through the lower natural barrier, to the extent that the activity concentrations of ^{226}Ra would diminish by simple decay before reaching the RMEI location. The breakthrough curves for radium transport through the SZ are reproduced on Figure 8.1-8; additional information is provided in *Saturated Zone Flow and Transport Model Abstraction* (SNL 2008 [DIRS 183750], Figure 6-14[a]). It is important to note that the breakthrough curves shown on Figure 8.1-8 do not account for decay during transport; rather, the decay is accounted for when the time-dependent releases of ^{226}Ra from the UZ are computed (SNL 2008 [DIRS 183750], Section 6.5). Figure 8.1-8 shows that (neglecting effects of decay) the majority of the ^{226}Ra transport times at the RMEI location are much greater than 10,000 years; more specifically, for individual realizations the median transport times (i.e., the times when relative mass equals 0.5 on the upper plot on Figure 8.1-8 of the parent document) in the SZ range from 18,000 years to more than 1,000,000 years (SNL 2008 [DIRS 183750], Table 6-10[a]). The 50th percentile of the median ^{226}Ra transport times among all realizations is estimated to be about 731,000 years (SNL 2008 [DIRS 183750], Table 6-10[a]). Due to the magnitude of these transport times, ^{226}Ra would experience from about 11 to more than

600 half-lives of decay before reaching the RMEI, thus reducing the activity concentration by factors $(1/2)^{11}$ to $(1/2)^{600}$. These decay factors suggest that any ^{226}Ra released from the EBS would contribute negligibly to radium activity concentrations at the RMEI location.

^{226}Ra could also potentially reach the RMEI location via transport of ^{230}Th and ^{234}U. Release of uranium from the EBS is constrained by the same processes described in the previous section for thorium. Due to the relatively long transport times for thorium (median greater than 1,000,000 years, see previous section) compared to the half-life of ^{230}Th (75,400 years), any ^{230}Th entering the SZ will likely experience significant decay before exiting the SZ. Any ^{226}Ra produced in the SZ will be subject to chemical sorption in the geologic media, as discussed, and will also likely decay. Because of these factors, it is reasonable to expect insignificant levels of ^{226}Ra activity at the RMEI location from transport and decay of its precursors.

Figure 8.3-30a[a] shows that for the Seismic GM Modeling Case at 10,000 years, the repository system retains all but a minute fraction (mean of 10^{-10}) of all ^{226}Ra in the initial inventory or produced by chain decay over 10,000 years. This performance is due to the relatively short half-life of ^{226}Ra compared to its transport time in the SZ, the processes constraining the release of ^{234}U and ^{230}Th from the EBS, and the long travel time of thorium through the lower natural barrier. Thus, it is reasonable to expect the activity concentrations for ^{226}Ra to show effectively undetectable levels for 10,000 years after disposal.

Uncertainty in Radium Activity Concentrations—The combined activity concentration for ^{226}Ra and ^{228}Ra are computed probabilistically using the TSPA-LA Model described in Section 6.0. Conceptually, a combined ^{226}Ra and ^{228}Ra activity concentration is computed for each combination of an epistemic sample element with values for aleatory parameters; an overall mean activity concentration is determined analogous to the computation of total mean dose to the RMEI (Section 8.1.1.1), although the calculation of mean activity concentration considers only a subset of the scenario classes. Thus, in principle, the calculation of a combined ^{226}Ra and ^{228}Ra activity concentration yields an ensemble of expected activity concentrations (where the expectation averages over aleatory uncertainty), and the relationship between epistemically uncertain variables and expected activity concentrations can be explored through sensitivity analyses.

However, for most epistemic sample elements, the expected activity concentration is effectively zero. Only a few sample elements yield numerically meaningful values, which can be observed by noting that the mean activity concentration at 10,000 years is greater than the 95th percentile (Figure 8.1-9[a]). Consequently, no sensitivity analyses are conducted for the expected activity concentration. The uncertain variables most likely to influence the uncertainty in activity concentration are those that determine the occurrence and extent of failure of WPs and the rate of radium and thorium transport through the SZ. The most important of these variables are the RST for Alloy 22 (*SCCTHRP*), which is important in the Seismic GM Modeling Case (Section 8.2.4.1[a]), the probability of early failure of WPs (*PROBWPEF*) which is important in the Waste Package EF Modeling Case (Section 8.2.2.2[a]), and the logarithm of the scale factor for the SZ groundwater specific discharge (*SZGWSPDM*). Additionally, sensitivity analyses of the movement of ^{234}U, ^{230}Th, and ^{226}Ra through the EBS and lower natural barrier are presented in Appendix K[a], Section K.6, for the Igneous Intrusion Modeling Case. Although the Igneous Scenario Class is not considered in the calculation of mean activity concentration, results of

these analyses are informative about the influence of uncertain variables on the transport of these radionuclides. Additional discussion of the capability of the EBS and lower natural barrier to retain these radionuclides is presented in Section 8.3.3.2[a] and Section 8.3.3.3[a].

In summary, the projections for the mean activity concentrations of combined radium demonstrate with a high level of confidence that the projected level of radioactivity in a representative volume of groundwater would not exceed the numerical limit of 5 pCi/L for the combined ^{226}Ra and ^{228}Ra for the separate standards for the Protection of Groundwater (10 CFR 63.331 [DIRS 180319], Table 1).

8.1.2.2[a] Projections for Gross Alpha Activity Concentration

The performance demonstration for this metric of the Groundwater Protection Standard is based on a calculation of the mean of the gross alpha activity concentration, including ^{226}Ra but excluding ^{222}Rn and the uranium species (10 CFR 63.331 [DIRS 180319]). The TSPA Biosphere Component Model, documented in DTN: MO0702PAGWPROS.001_R0 [DIRS 179328], identifies 15 primary radionuclides that have one or more alpha emitters in their decay chain to the next tracked radionuclide. The specific alpha emitting radionuclides considered in estimating the gross alpha activity concentrations are:

- ^{210}Pb (half-life 22.3 years)
- ^{226}Ra (half-life 1,600 years)
- ^{227}Ac (half-life 21.8 years)
- ^{228}Th (half-life 1.913 years)
- ^{229}Th (half-life 7,300 years)
- ^{230}Th (half-life 75,400 years)
- ^{232}Th (half-life 1.4×10^{10} years)
- ^{231}Pa (half-life 32,800 years)
- ^{237}Np (half-life 2.14×10^{6} years)
- ^{238}Pu (half-life 87.7 years)
- ^{239}Pu (half-life 24,100 years)
- ^{240}Pu (half-life 6,560 years)
- ^{242}Pu (half-life 3.75×10^{5} years)
- ^{241}Am (half-life 433 years)
- ^{243}Am (half-life 7,370 years).

In the calculation for gross alpha, the concentration of ^{210}Pb is not calculated in the TSPA-LA Model instead one alpha particle for ^{210}Pb has been added to that for ^{226}Ra resulting in a total of four alpha particles for ^{226}Ra Likewise, four alpha particles for ^{228}Th have been added to ^{232}Th resulting in a total of five alpha particles for ^{232}Th.

The revised probabilistic projections for gross alpha activity concentrations over the 10,000-year time period are shown on Figure 8.1-11[a]; the activity concentration for gross alpha was calculated based on the annual mass flux of the alpha emitting radionuclides across the boundary of the accessible environment and collected in the representative groundwater volume of 3,000 acre-ft/yr. The plot in this figure shows curves for the mean and 95th percentile for gross alpha activity concentration as well as the background concentration. From the plot, the

maximum of the mean activity concentration is estimated to be 6.70×10^{-5} pCi/L (excluding background), or effectively less than 10^{-4} pCi/L. This maximum value is well below the 10 CFR 63.331 ([DIRS 180319], Table 1) limit for gross alpha activity of 15 pCi/L. This revised projection is higher than the maximum activity concentration documented in the parent document by about 26 percent. This increase in projected activity concentration is due to the correction of several of the errors documented in Appendix P of the parent document; in particular, correction of the error involving iron oxyhydroxide colloid concentrations (Appendix P, Table P-7, item P18) affects the release of americium in the Drip Shield EF Modeling Case (Section 7.3.1.5.2[a]).

Figure 8.1-12[a] shows the contributions of the individual modeling cases to the mean curve for the gross alpha activity, for 10,000 years after closure (with the background level shown in the graph). Figure 8.1-12[a] shows that the mean gross alpha activity concentration is dominated by the Drip Shield EF Modeling Case until approximately 7,000 years postclosure. From 7,000 to 8,000 years, the Waste Package EF, the Drip Shield EF, and Seismic GM Modeling Case contribute approximately equally to the projected gross alpha activity concentration. Over the remaining 2,000 years, the releases from the Seismic GM modeling case become the dominant factor in the projected gross alpha activity concentration.

The primary radionuclides contributing to the mean gross alpha are solubility controlled species. The advective water flux through the WPs in the Drip Shield EF Modeling Case accounts for the early dominance of this modeling case. Both the Waste Package EF and Seismic GM Modeling Cases have intact DSs and therefore exhibit only diffusive releases from the WPs. The diffusive release mechanism in these two cases, combined with the solubility control and sorption of the alpha emitting radionuclides, accounts for the delay in their contributions to the projected gross alpha activity concentration history. Additional discussion of these modeling cases, including discussion of important radionuclides and uncertain variables, is provided in Section 8.2[a].

In summary, the projections for the mean activity concentrations of gross alpha demonstrate with a high level of confidence that the level of radioactivity in a representative volume of groundwater would not exceed the numerical limit of 15 pCi/L for the gross alpha activity (including ^{226}Ra but excluding radon and uranium isotopes) for the Separate Standards for the Protection of Groundwater (10 CFR 63.331 [DIRS 180319], Table 1).

8.1.2.3[a] Projections for Combined Beta- and Photon-Emitting Radionuclides

The performance demonstration for this metric of the Separate Standards for Protection of Groundwater is based on combined beta- and photon-emitting radionuclides; both the primary beta emitters and any daughter products that decay by beta-emission are considered. The annual doses from exposure to beta-photon emitters are quantified in terms of both whole body and organ dose. The TSPA Biosphere Component Model documented in the *Biosphere Model Report* (SNL 2007 [DIRS 177399], Table 6.15-2), identifies a total of 19 primary radionuclides that are used to compute this groundwater protection metric.

Some of the more prominent beta emitters are: ^{14}C, ^{36}Cl, ^{79}Se, ^{90}Sr, ^{99}Tc, ^{129}I, ^{135}Cs, and ^{137}Cs. Of this set, only ^{90}Sr and ^{137}Cs have short half-lives (~ 30 years) relative to the 10,000-year time period. Some of the beta-photon emitters are daughter products of alpha and beta emitters (SNL 2007 [DIRS 177399], Table 6.15-2) such as ^{137m}Ba (half-life 2.55 m), ^{228}Ac (half-life

6.15 h), ^{212}Pb (10.64 h), and ^{208}Tl (half-life 3.05 m). Because these radioisotopes have half-lives ranging from minutes to several hours, they are not included in radionuclide transport calculations; however, the associated conversion factors are included in the calculation of the beta-photon dose (SNL 2007 [DIRS 177399], Section 6.15.1.2). The projections of annual doses for beta-photon emitting radionuclides are evaluated as a function of the release rates from the repository, in-growth, and groundwater transport to the accessible environment.

The revised mean annual doses to the major organs and whole body are shown on Figure 8.1-13[a] for the 10,000-year compliance period. Mean annual doses are calculated by summing the expected annual doses from each beta- and photon-emitting radionuclide and averaging over all epistemic sample elements, analogous to the calculation of total mean annual dose for the Individual Protection Standard (Section 8.1.1.1[a]). As shown on Figure 8.1-13b[a], the mean annual dose curves for the thyroid and lower large intestine overlay one another; the maximum mean annual dose for the thyroid is estimated to be 0.26 mrem and for the lower large intestine about 0.25 mrem. These maximum doses from beta-photon emitters are well below the 10 CFR 63.331 ([DIRS 180319], Table 1) limit of less than or equal to 4 mrem. The mean annual doses for the thyroid and whole body are higher than the original results presented in the parent document by 35 and 38 percent respectively, due primarily to the inclusion of ^{36}Cl and ^{79}Se in the revised calculations (Appendix P[a], Table P-7[a], item P2). Plots of the revised projected mean and 95th percentile curves are shown on Figure 8.1-14[a], which illustrate the uncertainties in the whole body and thyroid annual dose curves.

As can be seen on Figure 8.1-15[a], the largest contributions to mean annual doses to the thyroid and whole body are attributable to the Seismic GM Modeling Case. The dominance of this modeling case for the mean annual doses to the thyroid and whole body is similar to its dominance in the total mean annual dose to the RMEI, and is explained by the fact that the Seismic GM Modeling Case represents a larger expected number of breached WPs and therefore larger radionuclide releases (Section 8.1.1.2[a]). The important radionuclides for these performance metrics are similar to those for the Seismic GM Modeling Case (Section 8.2.4.1[a]). In particular, dose to the thyroid is largely attributable to ^{129}I; while, ^{99}Tc contributes primarily to the alimentary tract organs, with the lower large intestine and the stomach receiving the highest doses (EPA 2002 [DIRS 175544], CD-ROM, ingestion dose coefficients for ^{99}Tc and ^{129}I). Whole body dose is calculated as a weighted sum of doses to the individual organs. In this calculation, the alimentary tract organs, in particular the colon (lower large intestine) and the stomach, have large tissue weighting factors relative to other organs (proposed 40 CFR Part 197 (70 FR 49014 [DIRS 177357], Appendix A, Table A.2)). The ingestion of ^{99}Tc largely contributes to the dose to these organs (EPA 2002 [DIRS 175544], CD-ROM, ingestion dose coefficient for ^{99}Tc). Thus, most of the whole body dose can be attributed to the dose from ^{99}Tc to the lower large intestine and the stomach, and to the dose from ^{129}I to the thyroid.

Because the largest contributions to the mean annual doses to the thyroid and whole body are attributable to the Seismic GM Modeling Case and result from two radionuclides that are important to the mean annual dose to the RMEI for this modeling case, the uncertain inputs important to uncertainty in organ and whole body doses are the same as those important to the mean annual dose to the RMEI. Specifically, the most important uncertain input is the RST for the Alloy-22 WP OCB (*SCCTHRP*), which largely determines the probability of WP failure from

seismic events. Additional discussion of important uncertain inputs for the Seismic GM Modeling Case is provided in Section 8.2.4.1[a].

In summary, the projections of mean annual beta-photon dose demonstrate with a high level of confidence that the annual doses to the whole body or any organ would not exceed the numerical limit of 4 mrem for groundwater protection for the combined beta- and photon-emitting doses for the separate standards for the Protection of Groundwater (10 CFR 63.331 [DIRS 180319], Table 1).

8.1.3[a] Human Intrusion Protection

No change.

8.1.3.1[a] Determination of Earliest Time for Drilling Intrusion

No change.

8.1.3.2[a] Projections of Annual Doses for Human Intrusion

To address the requirements of the Individual Protection Standard for Human Intrusion (10 CFR 63.321 [DIRS 178394]), a probabilistic TSPA methodology, analogous to that used to demonstrate performance with the Individual Protection Standard after Permanent Closure and the Separate Standards for Protection of Groundwater, was used to make projections of the annual dose following a human intrusion. The calculations of expected annual dose account for only the radionuclides released into groundwater as a consequence of the intrusion, as specified in 10 CFR 63.322(f and g) [DIRS 180319]. Based on the analysis described in Section 8.1.3.1 of the parent document, the earliest time after disposal for the drilling intrusion was taken to be 200,000 years.

As described in Section 6.1.2.5 of the parent document, a separate scenario, the Human Intrusion Scenario, is used to estimate projections of annual dose resulting from a human intrusion. This scenario considers aleatory uncertainty in the type of WP assumed to be penetrated and the location of the penetration, both within the repository footprint and in the underlying SZ. For each epistemic sample element, expected annual dose is computed by averaging over these aleatory uncertainties.

The revised probabilistic projections of expected annual dose for the Human Intrusion Scenario are presented on Figure 8.1-16[a]. The plots show the curves for the mean, median, and 5th and 95th percentiles of the distribution of expected annual doses for the period of geologic stability. The maximum of the mean annual dose to the RMEI occurs within a few thousand years after the intrusion. The maximum values of the mean and median are projected to be less than 0.013 mrem and 0.011 mrem, respectively, well below the regulatory limit of 350 mrem (10 CFR 63.321(b)(2) [DIRS 178394]). The maximum of the median annual dose, which occurs about 2500 years after the intrusion, is about 70 percent higher than the results presented in the parent document. This change is the result of correcting several implementation errors affecting this modeling case (Appendix P[a], Table P-6[a], items 6, 9, and 13) and of refining the temporal discretization for this modeling case (Section 7.3.3.6[a]). The spread of values about the median annual dose is reflected in the 5th and 95th percentiles, which are approximately

1.24×10^{-3} mrem and 2.86×10^{-2} mrem, respectively, at the time when the median achieves its maximum value.

The contribution of individual radionuclides to the total mean annual dose for the Human Intrusion Scenario for 1,000,000 years after repository closure is shown on Figure 8.1-17[a]. The Human Intrusion Modeling Case conservatively assumes that the intruded WP is intact until the intrusion. Following the intrusion, the long-lived fission products that are highly soluble and non-sorbing, such as ^{99}Tc (half-life 2.13×10^5 yrs) and ^{129}I (half-life 1.57×10^7 yrs), dominate the annual dose for about 50,000 years after the intrusion while the waste form is degrading, and account for about 99 percent of the maximum median annual dose. After ^{99}Tc and ^{129}I inventory is depleted, the long-term dose to the RMEI occurs from long-lived radionuclides that undergo sorption, primarily ^{242}Pu (half-life 3.75×10^5 yrs) with secondary contributions from ^{135}Cs (half-life 2.3×10^6 yrs), and ^{237}Np (half-life 2.14×10^6 yrs). The annual dose from radionuclides that are not solubility limited, such as ^{99}Tc, ^{129}I, and ^{135}Cs, is similar to those in the Waste Package EF Modeling Case because the expected number of early failed waste packages is approximately equal to 1 (Section 6.4.2.2 of the parent document) and the releases for these radionuclides out of the WP are primarily diffusive. (Note that in the Waste Package EF Modeling Case, most of the mass for these radionuclides is released prior to DS failure and thus remains primarily diffusive.) It is not feasible to compare the magnitude of ^{242}Pu dose between the two modeling cases due to differences in transport through the EBS and UZ. For example, following DS failure in the Waste Package EF Modeling Case, the advective releases of ^{242}Pu dominate over diffusive releases, which is not the case in the Human Intrusion Modeling Case where the diffusive releases remain dominant for the simulated time period (Section 7.7.1.6[a]). In addition, more retardation of dissolved ^{242}Pu mass occurs in the Human Intrusion Modeling Case due to matrix diffusion along UZ borehole pathway (Section 7.7.1.6[a]).

Sensitivity analyses of the expected annual dose to the RMEI resulting from a human intrusion are presented in Appendix K[a], Section K10[a]. Due to the highly transient nature of the pulse of ^{99}Tc and ^{129}I, sensitivity analyses are performed within a few thousand years of the intrusion (Figures K10-1[a] and K10-2[a]) as well as many thousands of years after the intrusion (Figures K10-3[a] and K10-4[a]). The uncertain inputs that influence the uncertainty in expected annual dose during the initial pulse of ^{99}Tc and ^{129}I are those that influence (1) the time of arrival of the pulse (i.e., *SZGWSPDM* (logarithm of scale factor that characterizes uncertainty in groundwater specific discharge) and *INFIL* (pointer variable for determining infiltration condition)), (2) the effect of these radionuclides on the RMEI (i.e., *MICTC99* (BDCF for technetium)) and (3) the total mass of these radionuclides in the nuclear waste (i.e., *CSNFMASS* (uncertainty in radionuclide content of CSNF)). After the initial pulse of ^{99}Tc and ^{129}I, sensitivity analyses identify several variables with influence on the uncertainty in the long-term expected annual dose, although the analyses do not produce regression models with large R^2 values (Figure K10-4a[a]). These variables are primarily related to the mobilization of plutonium from the waste, and to the rate of plutonium transport through the lower natural barrier. Additional discussion is provided in Appendix K[a], Section K10[a].

In summary, these projections demonstrate with a high level of confidence that the mean annual doses to the RMEI would be well below the limits for the Individual Protection Standard for Human Intrusion (10 CFR 63.321 [DIRS 178394]). Moreover, the projections indicate that the system of multiple barriers would be sufficiently robust and resilient to limit annual doses for the prescribed Human Intrusion Scenario.

INTENTIONALLY LEFT BLANK

Table 8.1-1[a]. Performance Demonstration Results for Individual Protection Standard

Time After Closure (yrs)	Maximum Total Mean Annual Dose (mrem)	Time of Maximum Total Mean Annual Dose (yr)	Maximum Total Median Annual Dose (mrem)	Time of Maximum Total Median Annual Dose (yr)	Limit for Annual Dose (mrem)
10,000	0.24	10,000	0.13	~ 9,900	15 (mean)
1,000,000	2.00	1,000,000	0.96	~ 720,000	350 (median)

Source: Output DTN: MO0710PLOTSFIG.000 [DIRS 185207],
Files: LA_v5.005_10kyr_Total_Dose_Calcs_Rev01.gsm and LA_v5.005_1Myr_Total_Dose_Calcs_Rev00.gsm.
Numerical Limits from 10 CFR 63.311(a) [DIRS 178394]

Table 8.1-2[a]. Performance Demonstration Results for the Separate Standards for the Protection of Groundwater

Type of Limit	Maximum of Mean Activity Concentration or Annual Dose	Natural Background Level	Limit for Activity Concentration or Annual Dose
Combined ^{226}Ra and ^{228}Ra	$<10^{-6}$ pCi/L	0.5 pCi/L	5 pCi/L
Gross Alpha Activity	$<10^{-4}$ pCi/L	0.5 pCi/L	15 pCi/L
Dose from Combined Beta & Photon Emitting Radionuclides	Whole Body ~ 0.06 mrem Thyroid ~ 0.26 mrem	Background level excluded in regulatory requirement	4 mrem

Source: Output DTN: MO0710PLOTSFIG.000 [DIRS 185207],
Files: LA_v5.005_10k_Ra_Mean_Contributions_Rev00.JNB, LA_v5.005_10Kyr_Alpha_Mean_Contributions_Rev00.JNB, and LA_v5.005_10kyr_Thyroid_Whole_Body_Rev00.JNB.
Numerical Limits from 10 CFR 63.331 [DIRS 180319]

Table 8.1-3[a]. Performance Demonstration Results for the Individual Protection Standard for Human Intrusion

Time After Closure (yrs)	Projected Maximum Annual Dose (mrem)	Limit for Annual Dose (mrem)
10,000	0	15 (mean)
1,000,000	0.01 (median)	350 (median)

Source: Output DTN: MO0710ADTSPAWO.000 [DIRS 185207],
File: LA_v5.005_HI_009000_000.gsm.
Numerical Limits from 10 CFR 63.321(b) [DIRS 178394]

Table 8.1-4[a]. Uncertainty in Projections of Maximum Total Mean and Median Annual Dose (mrem) for the Individual Protection Standard

Time After Closure (yrs)	Total Mean Annual Dose	Total Median Annual Dose	5th Percentile Total Expected Annual Dose	95th Percentile Total Expected Annual Dose
10,000	0.24	0.13	6.67×10^{-3}	0.67
720,000	1.55	0.96	0.09	4.62
1,000,000	2.00	0.86	0.14	9.06

Source: Output DTN: MO0710PLOTSFIG.000 [DIRS 185207], Files: LA_v5.005_10kyr_Total_Dose_Calcs_Rev01.gsm and LA_v5.005_1Myr_Total_Dose_Calcs_Rev00.gsm.

Table 8.1-5[a]. Inventories and Biosphere Dose Conversion Factors for Radionuclides Important to Total Mean Annual Dose for 10,000 Years

Radionuclide	Radionuclide Activity (Ci per Waste Package)			Mean BDCF (Sv/yr) / (Bq / m^3)
	CSNF	CDSP-DSNF	CDSP-HLW	
^{99}Tc	1.30×10^{2}	2.69	17.2	1.12×10^{-9}
^{14}C	6.09	7.98	0.00	1.93×10^{-9}
^{129}I	3.12×10^{-1}	6.30×10^{-3}	1.29×10^{-2}	1.29×10^{-7}

Sources: Table 6.3.7-5 and SNL 2007 [DIRS 177399], Table 6.11-12.

NOTE: Activity is estimated at time of closure and does not include uncertainty in waste inventory (Section 6.3.7.1.2).

Table 8.1-6[a]. Uncertainty Importance Ranking as a Function of Time for Four Key TSPA-LA Model Parameters

Time After Closure (yrs)	Two Most Important Parameters	
3,000	*SCCTHRP*	*IGRATE*
5,000	*SCCTHRP*	*IGRATE*
10,000	*SCCTHRP*	*IGRATE*
125,000	*IGRATE*	*SZGWSPDM*
250,000	*IGRATE*	*SZGWSPDM*
500,000	*IGRATE*	*WDGCA22*
1,000,000	*IGRATE*	*WDGCA22*

Sources: Appendix K[a], Figure K8.1-2[a] and Figure K8.2-2[a]; and output DTN: MO0801TSPAMVAC.000 [DIRS 185080]

NOTE: *IGRATE* = occurrence rate of igneous events

SCCTHRP = RST for Alloy 22

SZGWSPDM = logarithm of scale factor for SZ groundwater-specific discharge

WDGCA22 = temperature dependence parameter for Alloy 22 general corrosion rate

8.2[a] PROJECTIONS FOR INDIVIDUAL MODELING CASES

This section presents the probabilistic projections for the set of modeling cases used in developing the performance demonstration for the Individual Protection Standard After Permanent Closure (10 CFR 63.311 [DIRS 178394]). A subset of these modeling cases was also used for the performance demonstration for the Separate Standards for the Protection of Groundwater (NRC Proposed Rule 10 CFR 63.331, Table 1 [DIRS 180319]) (Section 8.2.1[a]). Six modeling cases are presented and explained, including: (1) Nominal (Section 6.3), (2) Waste Package EF (Section 6.4.2), (3) Drip Shield EF (Section 6.4.1), (4) Igneous Intrusion (Section 6.5.1), (5) Seismic GM (Section 6.6.1), and (6) Seismic FD (Section 6.6.1). Because the changes from TSPA-LA Model v5.000 to v5.005 only affect the analysis of the groundwater pathway, the Volcanic Eruption Modeling Case was not recalculated. Thus, the discussion presented for the Igneous Scenario Class, Section 8.2.3[a], only addresses the results of the Igneous Intrusion Modeling Case. These analyses are presented supplemental to the analyses documented in Section 8.2 of the parent document.

As noted in Section 8.1.1.2[a], the revised projections of total mean annual doses to the RMEI are largely dominated by two modeling cases: (1) Seismic GM and (2) Igneous Intrusion—as shown on Figure 8.1-3[a]. This observation is consistent with the original projections in the parent document. For the 10,000-year period, the Seismic GM Modeling Case contributed about 70 percent and the Igneous Intrusion Modeling Case contributed about 27 percent of the maximum of the total mean annual dose (i.e., 0.24 mrem). In contrast, for the post-10,000-year period, the Igneous Intrusion Modeling Case is the primary contributor with the Seismic GM Modeling Case increasing in importance as the second highest contributor to the total mean and median annual doses until approximately 750,000 years after closure. After approximately 750,000 years postclosure, the Seismic GM and Igneous Intrusion Modeling Cases contributed almost equally to the maximum median of the total annual dose (i.e., 0.96 mrem) for the post-10,000 year period.

8.2.1[a] Nominal Modeling Case

The revised projections for the Nominal Modeling Case (Section 6.3) are shown on Figure 8.2-1[a]. There is no annual dose to the REMI in the first 10,000 years, with earliest occurrence of dose around 21,000 years. In the parent document, there were no doses until about 120,000 years after closure. This change in projected doses is due to correcting the implementation error documented in Appendix P, Section P6, of the parent document. That section of the parent document describes the implementation error in the weld volume calculation, which caused an underestimation of the volume for stress corrosion cracks. Correcting this error increased the median probability of SCC occurring by a factor of about 3 for both the CDSP and CSNF WPs (Appendix P, Section P6 of the parent document). As a result, the probabilistic projections of WP breaches now exhibit a few realizations with a SCC crack penetrating the WP OCB well before 100,000 years. In particular, crack penetration occurred in less than 10,000 years in one WP in one realization because of a combination of sampled values for SCC in the closure-lid weld resulting in large initial crack length and high crack propagation velocity (output DTN: MO0801TSPAWPDS.000 [DIRS 185077] files: LA_v5.005_NC_000300_005_Conceptual_Description.doc, v5.005_rlz_182_initial_crack_length_estimate.xls]). Further comparison of the TSPA-LA Model v5.005 results to the

TSPA-LA Model v5.000 results for the Nominal Modeling Case is provided in Section 7.3.1.5.1[a].

The revised maximum mean and median annual doses for the post-10,000-year period are 0.55 mrem and 0.28 mrem, respectively. The maximum mean and median annual doses to the RMEI occur at about 730,000 and 850,000 years, respectively. The two radionuclides dominating the maximum annual dose are the very soluble, long-lived, and mobile radionuclide species ^{129}I and ^{99}Tc. Other second order contributors to this maximum dose value are ^{135}Cs, ^{242}Pu, ^{79}Se, and ^{237}Np (Figure 8.2-2[a]).

As discussed in Section 6.1.2.4, expected annual dose from WPs in the Nominal Modeling Case is computed directly by the GoldSim component of the TSPA-LA Model. Aleatory uncertainty in the time and location of WP breaches, as well as the degree of damage to each WP, is implicitly accounted for in the averaging performed by the WAPDEG software and in the partitioning of WPs into representative groups (Appendix N of the parent document). The expected dose histories on Figure 8.2-1[a] are the result of a succession of three phases for releases from WPs. First, a few WP breaches may occur early, which generally consist of SCC occurring in the WP OCB closure lid welds. SCC may initiate in the lid welds once general corrosion processes have removed the layer of compressive stress produced by low plasticity burnishing (Section 6.3.5.1.2). No releases are observed before about 20,000 years after repository closure (Figure 7.7.1-74b[a]). Because infiltration rates and temperatures vary across the repository footprint, the time at which a continuous thin film of adsorbed water required for diffusive radionuclide transport begins also varies (Section 6.3.8.1 of the parent document). The second phase begins at approximately 200,000 years and dominates until roughly 800,000 years, at which time SCC breaches in the WP lid welds have occurred in most realizations (Figure 8.3-6a[a]). The third phase starts around 500,000 years when WPs begin to fail by general corrosion (i.e., begin to have patch openings in the WP OCB (Figure 8.3-6b[a])). When patch openings occur, seepage waters can flow through the waste, generally resulting in larger releases of radionuclides. However, general corrosion patch penetrations occur in only a minority of WPs, and in a few realizations. Section 7.7.1.5[a] provides additional analyses of individual realizations in the Nominal Modeling Case. Finally, the step-wise increases in the annual dose curves at around 200,000 years, 300,000 years, 500,000 years and 700,000 years are due to immediate increases in the number of WP failures from SCC. These immediate increases in WP failure are caused by the coarse temporal discretization used by WAPDEG V4.07 past 100,000 years (Section 7.3.3.7[a]).

Appendix K[a] presents sensitivity analyses that determine the contribution to the uncertainty in expected annual dose that derives from individual uncertain inputs. These analyses identify the temperature dependence parameter for the Alloy 22 general corrosion rate, *WDGCA22*, as the uncertain input that largely explains the uncertainty in the expected annual dose for the Nominal Modeling Case (Figure K4.5-1[a] and Figure K4.5-2[a]). Higher values of *WDGCA22* lead to lower general corrosion rates throughout most of the 1,000,000-year performance period. In turn, lower general corrosion rates lead to later WP failures by SCC, and to fewer WP failures by general corrosion. Several other uncertain inputs, such as the deviation from median yield strength range for the WP outer lid, *WDZOLID*, are identified as having additional, lesser effects. The effects of these other inputs are discussed in Appendix K[a], Section K4.5[a].

Sensitivity analyses for intermediate model outputs, such as the number of failed WPs, environmental and chemical conditions within the EBS, and the movement of an important radionuclide (^{237}Np), are presented in Appendix K, Section K4. Although these analyses are performed using results from TSPA-LA Model v5.000, the conclusions of these analyses also apply to results from TSPA-LA Model v5.005, due to the similarity in the results for the two model versions (Section 7.3.1.5.1[a]).

8.2.2[a] Early Failure Scenario Class Modeling Cases

No change.

8.2.2.1[a] Drip Shield Early Failure Modeling Case

Revised projections for the Drip Shield EF Modeling Case (Section 6.4.1) are shown on Figure 8.2-3[a] for both the (a) 10,000-year period after closure and (b) post-10,000 year time period. The expected annual dose to the RMEI for the first 10,000 years shows a maximum mean value of about 2.8×10^{-4} mrem and maximum median of 3.8×10^{-5} mrem; these maximum values occur at approximately 2,000 years and 2,200 years, respectively. Comparing these revised maximum doses with those reported in the parent document, the differences are very small. The only observable difference between the original and revised projections is that the 5th percentile curve in the revised results is slightly below 10^{-6} mrem level and thus does not appear on Figure 8.2-3[a]. Similarly, the maximum doses for the post-10,000-year period are also nearly identical to the original results in the parent document, including the timing of the maximums. Further comparison of the results of this modeling case is provided in Section 7.3.1.5.2[a].

The primary radionuclides that contribute to the mean annual dose for the Drip Shield EF Modeling Case are shown on Figure 8.2-4[a]. In the first 4,000 years after repository closure, three soluble and mobile radionuclides dominate dose; these radionuclides are ^{99}Tc, ^{129}I, and ^{14}C. Between 4,000 and 7,000 years the contribution of ^{239}Pu becomes increasingly important. After 7,000 years, ^{239}Pu is the dominant contributor. The mean annual dose from ^{239}Pu continues to increase from 7,000 years until about 40,000, creating a secondary peak in the mean annual dose curve of about 1.5×10^{-4} mrem. The ^{239}Pu continues to dominate but its contribution declines until about 200,000 years, at which point ^{242}Pu and ^{237}Np become dominant. This pattern of dominant radionuclides and timing of the maximums are nearly identical to those discussed in Section 8.2.2.1 of the parent document.

As discussed in Section 6.1.2.4, expected annual dose from early-failed DSs is computed as a weighted average of the dose resulting from early failure of DSs overlying CDSP and CSNF WPs that may occur in different percolation subregions. Additional discussion of the processes important in determining radionuclide releases from early-failed DSs is provided in the analyses of single realizations (Section 7.7.1.2[a]).

Appendix K[a] presents sensitivity analyses that determine the contribution to the uncertainty in expected annual dose that derives from individual uncertain inputs. These analyses identify the probability for undetected defects in DSs, *PROBDSEF*, as the uncertain input that for the most part explains the uncertainty in the expected annual dose for the Drip Shield EF Modeling Case (Figure K5.7.1-1[a] and Figure K5.7.1-2[a] for 20,000 years; and Figure K5.7.1-3[a] and Figure K5.7.1-4[a] for 1,000,000 years). Higher values of *PROBDSEF* lead to a greater

expected number of early-failed DSs, which in turn exposes a larger number of WPs to seepage waters. At early times, other uncertain inputs that determine the extent and rate of seepage are identified as having lesser effects, namely, *SEEPUNC* (uncertainty factor accounting for small-scale heterogeneity in fracture permeability) and *SEEPPRM* (logarithm of mean fracture permeability in the lithophysal rock units). At later times, *INFIL* (pointer variable for determining infiltration condition) is also important. The effects of these and other inputs are discussed in Appendix K[a], Section K5.7.1[a].

Sensitivity analyses for intermediate model outputs, such as the movement of several important radionuclides (^{239}Pu, ^{237}Np, and ^{99}Tc) through the repository system, are presented in Appendix K, Section K5. Although these analyses are performed using results from TSPA-LA Model v5.000, the conclusions of these analyses also apply to results from TSPA-LA Model v5.005, due to the similarity in the results for the two model versions (Section 7.3.1.5.2[a]).

8.2.2.2[a] Waste Package Early Failure Modeling Case

Revised projections for the Waste Package EF Modeling Case (Section 6.4.2) are shown on Figure 8.2-5[a] for both the (a) 10,000-year period after closure and (b) post-10,000 years. For the first 10,000 years after repository closure, the maximum mean and median annual doses are estimated to be about 3.7×10^{-3} mrem and 6.2×10^{-4} mrem; the maximum values occur between 9,000 to 10,000 years for the mean and at 2,000 years for the median. These maximum dose values are slightly higher than those reported in the parent document. The higher doses are attributed to the correction for ^{36}Cl, ^{79}Se, and ^{126}Sn, which were omitted in the analyses for the parent document; the effect of the error is documented in Appendix P, Section P2.1, of the parent document. For the post-10,000-year period, the maximum mean and median annual doses reach levels of approximately 2.1×10^{-2} mrem and 6.1×10^{-3} mrem, respectively. The maximum mean annual dose occurs at about 12,500 years, while the maximum median annual dose occurs at about 13,500 years. The dose curves gradually decline until about 250,000 years, then increase slightly as a result of the timing of nominal failures of the DSs. When the DSs fail due to general corrosion and seepage waters begin to flow through the failed WPs, advective flow through the WPs will result in additional radionuclide mobilization and transport. By the end of the 1,000,000-year period, the projected mean annual dose falls below 10^{-3} mrem. These patterns and trends are nearly identical to those documented in Section 8.2.2.2 of the parent document. Further comparison of the results of this modeling case is provided in Section 7.3.1.5.3[a].

The major radionuclides that contribute to the mean annual dose for the Waste Package EF Modeling Case are shown on Figure 8.2-6[a]. In the first 10,000 years postclosure, soluble and mobile radionuclides, in particular ^{99}Tc, ^{14}C, and ^{129}I, dominate the estimate of mean annual dose. In the post-10,000-year period, the maximum mean annual dose is dominated by ^{99}Tc, ^{129}I, and ^{239}Pu until approximately 50,000 years, then ^{239}Pu dominates up to about 200,000 years; thereafter, ^{242}Pu, ^{226}Ra, and ^{237}Np are the primary contributors to the maximum mean annual dose. This pattern of dominant radionuclides is identical to that documented in Section 8.2.2.2 of the parent document.

As discussed in Section 6.1.2.4, expected annual dose from early-failed WPs is computed as a weighted average of the dose resulting from early failures of CDSP and CSNF WPs that may occur in different percolation subregions and that may or may not experience seepage. The

expected dose histories on Figure 8.2-5[a] are the result of a succession of four phases for releases from early-failed WPs. During the first phase, no releases are observed before about 500 years after repository closure, because WP temperatures are high enough during the first few hundred years after repository closure that insufficient water is present in the failed WPs to allow diffusive transport of radionuclides. The second phase starts when CDSP WPs begin to cool sufficiently to allow diffusion of radionuclides from the waste to the invert. Between about 500 years and 2000 years, radionuclide concentrations begin to be observed in the groundwater at the RMEI location.

The third phase begins when CSNF WPs begin to cool sufficiently that radionuclides begin to diffuse from these WPs. The initiation of release from these WPs causes the sharp increase in expected annual dose indicated on Figure 8.2-5[a] just prior to 10,000 years; additional detail is shown on Figure 7.7.1-1[a]. Because CSNF WP temperatures vary spatially in the repository, diffusive releases from these WPs begin at different times, resulting in the sequence of increases in expected annual dose. The third phase lasts until about 300,000 years, when the DSs fail due to general corrosion, and seepage waters begin to flow through the failed WPs. These advective flows result in additional radionuclide mobilization and transport, as shown by the increase in expected dose around 300,000 years. Further information about the important processes that result in radionuclide releases from early-failed WPs is provided in the analysis of single realizations in Section 7.7.1.1[a].

Appendix K[a] presents sensitivity analyses that determine the contribution to the uncertainty in expected annual dose that derives from individual uncertain inputs. These analyses identify the probability for undetected defects in WPs, *PROBWPEF*, as the uncertain input that predominately explains the uncertainty in the expected annual dose for the Waste Package EF Modeling Case (Figure K5.7.2-1[a] and Figure K5.7.2-2[a] for 20,000 years, and Figure K5.7.2-3[a] and Figure K5.7.2-4[a] for 1,000,000 years). Higher values of *PROBWPEF* lead to a greater expected number of early-failed WPs. Other uncertain inputs are identified as having lesser effects on expected annual dose, depending on the time after repository closure. In particular, at early times, the analysis identifies *INFIL* (pointer variable for determining infiltration condition) and *THERMCON* (selector variable for host-rock thermal conductivity) as important, because these variables significantly influence the time at which humidity in the WP allows diffusion to begin. Before DS failure at 300,000 years, the analysis indicates an effect from *ISCSNS* (pointer variable that determines ionic strength for CSNF under vapor influx conditions) because this variable affects the solubility of many radionuclides. After DS failure, the analysis identifies as important several variables that determine the rate of water flow through the WPs (*INFIL*, *SEEPPRM* (logarithm of mean fracture permeability in the lithophysal rock units), and *SEEPUNC* (uncertainty factor accounting for small-scale heterogeneity in fracture permeability)) as well as variables that determine the solubility of plutonium (*EP1LOWPU* (logarithm of scale factor used to characterize uncertainty in plutonium solubility)) and uranium (*EP1LOWNU* (logarithm of scale factor used to characterize uncertainty in uranium solubility)). The effects of these and other inputs are discussed in Appendix K[a], Section K5.7.2[a].

Sensitivity analyses for intermediate model outputs, such as the movement of several important radionuclides (^{239}Pu, ^{237}Np, and ^{99}Tc) through the repository system, are presented in Appendix K, Section K5. Although these analyses are performed using results from TSPA-LA

Model v5.000, the conclusions of these analyses also apply to results from TSPA-LA Model v5.005 due to the similarity in the results for the two model versions (Section 7.3.1.5.3[a]).

8.2.3[a] Igneous Scenario Class Modeling Cases

As described in Section 6.5 of the parent document, the Igneous Scenario Class consists of two modeling cases: (1) the Igneous Intrusion Modeling Case that represents the interaction of a hypothetical magmatic dike with the repository and ensuant release of radionuclides to the groundwater pathway, and (2) the Volcanic Eruption Modeling Case that represents a hypothetical volcanic eruption at the land surface and the release of radionuclides to the atmospheric pathway. Because the changes from TSPA-LA Model v5.000 to v5.005 only affect the analysis of the groundwater pathway, the Volcanic Eruption Modeling Case was not recalculated. Thus, the discussion below only addresses the results of the Igneous Intrusion Modeling Case.

8.2.3.1[a] Igneous Intrusion Modeling Case

The revised projections of expected annual dose for the Igneous Intrusion Modeling Case (Section 6.5.1) are shown on Figure 8.2-7[a] for both the (a) 10,000-year period after closure and (b) post-10,000 years time period. For the first 10,000 years after repository closure, the maximum mean and median annual doses are estimated to be about 6.6×10^{-2} mrem and 1.8×10^{-2} mrem; both maximum values occur at the end of the 10,000 time period. These values are comparable with those documented in the parent document. For the post-10,000-year period, the maximum mean and median annual doses are estimated to be about 0.89 mrem and 0.32 mrem, respectively; both the maximum annual doses occur at 1,000,000 years. These maximum values are lower but comparable to those presented in Section 8.2.3.1 of the parent document. Further comparison of the results of this modeling case is provided in Section 7.3.1.5.4[a].

The radionuclides that contribute most to the mean annual dose are shown on Figure 8.2-8[a]. Figure 8.2-8a[a] shows that radionuclides ^{99}Tc and ^{129}I dominate the estimate of the mean for the first 4,000 years, and ^{239}Pu and ^{99}Tc dominate the estimate of the mean for the remainder of the 10,000 years postclosure period with a significant contribution from ^{240}Pu starting from about 6,000 years. Figure 8.2-8b[a] shows that ^{239}Pu, which is transported both in dissolved and colloidal form, dominates the maximum mean annual dose for the first 200,000 years and radionuclides ^{242}Pu, ^{237}Np, and ^{226}Ra dominate the estimate of the mean for the remainder of the post-10,000-year time period. These patterns of radionuclide dominance are identical to those documented in Section 8.2.3.1 of the parent document.

As discussed in Section 6.1.2.4, the expected annual dose at time τ is computed as the sum of the contributions to dose from all possible preceding igneous events, where the dose from each event is weighted by the probability of the event's occurrence. The results of this expectation can be seen in the different shapes of the individual radionuclide mean dose curves on Figure 8.2-8b[a]. The ^{129}I dose curve is relatively flat and stable for the entire 1,000,000-year period (and essentially unaffected by radioactive decay because of its long half-life), whereas the dose curves for actinides with long half-lives, such as ^{235}U, ^{238}U, and ^{237}Np (and their decay products) are steadily increasing. These two differing behaviors are a result of the Poisson nature of igneous activity at the repository in which the probability of an igneous event increases linearly through

time at the annual occurrence rate, with a mean of 1.7×10^{-8} yr^{-1}. The steadily increasing probability of occurrence of an igneous event, combined with: (1) nearly instantaneous release of a highly soluble, non-sorbing radionuclide such as ^{129}I, and (2) nearly constant continuous release of a solubility-limited, sorbing radionuclide such as ^{237}Np, results in a relatively constant mean annual dose for the instantaneous release radionuclide (^{129}I) and an approximately linearly increasing mean annual dose for the constant release radionuclide (^{237}Np). The mean annual dose curve for ^{129}I is not perfectly flat through time, as would be expected for a Poisson process, but rather begins to show a decreasing tendency in mean annual dose beginning between 200,000 and 400,000 years after repository closure because, as mentioned in Section 6.1.4.2 of the parent document, nominal corrosion processes are not included in the igneous intrusion modeling case to avoid double-counting the inventory in the calculation of total dose. Consequently, ^{129}I that is released from the WPs due to nominal SCC and general corrosion patches is not included in the calculation of expected annual dose due to igneous intrusions, which results in lower expected annual dose at later times.

Section 7.7.1.3[a] presents analyses of individual realizations of expected annual dose, and illustrates the computation of expected annual dose from the results of simulations of single igneous intrusion events. The analyses presented in Section 7.7.1.3[a] also describe processes that determine the release of radionuclides after an intrusion, and the movement of these radionuclides through the barriers of the repository. Analyses are presented for a realization for which the expected annual dose is similar to the mean annual dose, and for a realization that has the largest value of expected annual dose, and hence significantly influences the mean annual dose.

Appendix K[a] presents sensitivity analyses that determine the contribution to the uncertainty in expected annual dose that derives from individual uncertain inputs. These analyses identify the frequency of occurrence of igneous events, *IGRATE*, as the uncertain input that primarily explains the uncertainty in the expected annual dose for the Igneous Intrusion Modeling Case (Figure K6.7.1-1[a] and Figure K6.7.1-2[a] for 20,000 years, and Figure K6.7.2-1[a] and Figure K6.7.2-2[a] for 1,000,000 years). Higher values of *IGRATE* lead to a greater probability of occurrence of igneous events. The strong and consistent correlation between uncertainty in expected annual dose and *IGRATE* also indicates that the uncertainty in dose resulting from igneous intrusions does not change significantly over time. Other uncertain inputs are identified as having lesser effects on expected annual dose. In particular, the analysis identifies *SZGWSPDM* (logarithm of scale factor that characterizes uncertainty in groundwater specific discharge) and *INFIL* (pointer variable for determining infiltration condition), because these variables significantly influence the rate of water flow through the natural barriers and hence influence the rate of radionuclide transport. Also, before 10,000 years, the analysis identifies the BDCF for technetium (*MICTC99*) as important because ^{99}Tc is a large contributor to dose before 10,000 years. Similarly after 10,000 years, the variable *EPILOWPU* (logarithm of scale factor used to characterize uncertainty in plutonium solubility) is important because plutonium is the dominant contributor to dose after 10,000 years. The effects of these and other inputs are discussed in Appendix K[a], Section K6.7.1[a] and Section K6.7.2[a].

Sensitivity analyses for intermediate model outputs, such as the movement of several important radionuclides (^{239}Pu, ^{237}Np, and ^{99}Tc) through the repository system, are presented in Appendix K, Section K6. Although these analyses are performed using results from TSPA-LA

Model v5.000, the conclusions of these analyses also apply to results from TSPA-LA Model v5.005 due to the similarity in the results for the two model versions (Section 7.3.1.5.4[a]).

8.2.3.2[a] Volcanic Eruption Modeling Case

No change.

8.2.4[a] Seismic Scenario Class Modeling Cases

As described in Section 6.6 of the parent document, the Seismic Scenario Class consists of two modeling cases: (1) Seismic GM Modeling Case and (2) Seismic FD Modeling Case. The following sections present and explain the revised projections for these two modeling cases.

8.2.4.1[a] Seismic Ground Motion Modeling Case

Summary of Results—The expected annual dose for the Seismic GM Modeling Case is shown on Figure 8.2-11[a]; plots are presented for both the (a) 10,000-year period and (b) post-10,000-year period. The projections of annual dose take into account aleatory uncertainty associated with characteristics of future events, such as number of events, times of events, and the event's peak ground velocity. The mean, median, and 5th and 95th percentile curves on Figure 8.2-11[a] show uncertainty in the value of the expected annual dose, taking into account epistemic uncertainty associated with incomplete knowledge of the behavior of the physical system during and after the disruptive event. The maximum mean and median annual dose for the 10,000 year period are about 0.17 mrem and 0.07 mrem, respectively; both the maximum annual doses occur at the end of the 10,000 year time period. For the post-10,000-year period, the maximum mean and median annual doses are 1.1 mrem and 0.37 mrem, respectively; the maximum annual doses occur at 1,000,000 years and at 875,000 years, respectively. The maximum values for the 10,000 year time period are slightly lower but comparable to those documented in the parent document; however, those for the post-10,000 year period are lower by about 50 percent. The occurrence and timing of intermediate maximums in the dose curves are also different. These differences are largely attributed to the implementation correction documented in Appendix P, Sections P3 and P4, of the parent document. Further comparison of the results of this modeling case is provided in Section 7.3.1.5.6[a].

The radionuclides that contribute most to the estimate of mean annual dose are presented on Figure 8.2-12[a]. The mean dose curves on Figure 8.2-12a[a] illustrate that four radionuclides, ^{99}Tc, ^{14}C, ^{129}I, and ^{36}Cl, contribute the most to the maximum mean annual dose for the 10,000-year time period. One of these species, ^{36}Cl, was not listed in the parent document as important due to an implementation error, as documented in Appendix P, Section P2, of the parent document. As can be seen from Figure 8.2-12b[a], the dominant radionuclides for the post-10,000 years are ^{99}Tc, ^{129}I, ^{242}Pu, and ^{237}Np. Two dominant radionuclide species, ^{226}Ra and ^{79}Se, listed in the parent document do not significantly influence the expected annual dose results presented in this addendum. The reduction of the importance of these two radionuclides in the analyses presented in this addendum can be attributed to correction for the longitudinal dispersivity used in the SZ Flow and Transport Submodel documented in Section 6.3.10[a] and Appendix P, Section P15, of the parent document.

Expected Annual Dose for 10,000 Years—As summarized in Section 6.1.2.4, for the first 10,000 years after repository closure, the expected annual dose at time τ is computed as the sum of the contributions to dose from all possible preceding seismic ground motion events, where the dose from each event is weighted by the probability of the event's occurrence. The integration-based procedure used to calculate expected annual dose results in the relatively smooth results evident on Figure 8.2-11a[a]. Section 7.7.1.7[a] presents analyses of an individual realization of expected annual dose for the 10,000-year period. Appendix J, Figure J8.3-3, illustrates the computation of expected annual dose from the results of simulations of single seismic events, using the simplifications to the seismic damage abstractions that are justified in Section 7.3.2.6.1.

The analyses presented in Section 7.7.1.7[a] also describe processes that determine the release of radionuclides after a damaging seismic event in the first 10,000 years, and the movement of these radionuclides through the barriers of the repository. Analyses are presented for a realization for which the expected annual dose is relatively large, and thus has a significant influence on the mean annual dose. The analyses focus on two radionuclides (^{99}Tc and ^{79}Se) that are representative of radionuclides important to the expected annual dose for this modeling case. These radionuclides are dominant contributors to the expected annual dose because they are highly soluble and thus diffuse relatively rapidly through SCC in the WP OCB, and they transport relatively rapidly through the UZ and SZ.

Appendix K[a] presents sensitivity analyses that determine the contribution to the uncertainty in expected annual dose that derives from individual uncertain inputs. These analyses identify the RST for Alloy 22, *SCCTHRP*, as the uncertain input that predominately explains the uncertainty in the expected annual dose for the Seismic GM Modeling Case for 10,000 years (Figure K7.7.1-1[a] and Figure K7.7.1-2[a]). Lower values of *SCCTHRP* lead to a greater probability of damage occurring from seismic events, which in turn increases the expected value of the dose resulting from seismic events. Aside from *SCCTHRP*, other uncertain inputs are identified as having lesser effects on expected annual dose, although the correlations with these other inputs are not strong. At 10,000 years, the analysis identifies the BDCF for technetium (*MICTC99*) as important because ^{99}Tc is the largest contributor to dose at 10,000 years. Other variables with minor contributions to uncertainty include *DSNFMASS* (scale factor characterizing uncertainty in radionuclide content of DSNF) and *HLWDRACD* (effective rate coefficient for the dissolution of HLW glass), because of the effect these variables have on the mass of ^{99}Tc and its release from the waste form. The effects of these and other inputs are discussed in Appendix K[a], Section K7.7.1[a].

Sensitivity analyses for intermediate model outputs, such as the movement of several important radionuclides (^{239}Pu, ^{237}Np, and ^{99}Tc) through the repository system, are presented in Appendix K, Section K7.3 of the parent document. Although these analyses are performed using results from TSPA-LA Model v5.000, the conclusions of these analyses also apply to results from TSPA-LA Model v5.005 due to the similarity in the results for the two model versions (Sections 7.3.1.5.6[a], and 7.3.1.5.8[a]).

Expected Annual Dose for 1,000,000 Years—For the time period out to 1,000,000 years after repository closure, the expected annual dose at time τ is computed by a Monte Carlo simulation employing the full detail of the seismic consequences abstraction. As explained in Section 6.1.2.4, this numerical treatment is used due to the complexity of the seismic

consequences abstraction and the necessity to combine nominal corrosion processes with the effects of seismic ground motion events in this modeling case. The use of the Monte Carlo technique produces relatively noisy results as shown on Figure 8.2-11b[a]. Appendix J, Figure J8.4-1, illustrates the computation of expected annual dose from the results of simulations of single seismic events for a few epistemic sample elements, and the variability in annual dose that can result from aleatory uncertainty in the seismic events and from epistemic uncertainty in the model inputs.

The expected dose histories shown on Figure 8.2-11b[a] display two phases for the occurrence of damage to WPs. First, prior to DS failure at roughly 200,000 years (Figure 8.1-4[a]), WPs experience damage primarily from seismic events. Moreover, CDSP WPs are damaged far more frequently than are CSNF WPs (compare Figure 8.3-8a[a] for CSNF WPs and Figure 8.3-8c[a] for CDSP WPs). However, as indicated by Appendix K[a], Figure K7.7.2-2[a], the occurrence of damage to WPs in the first 200,000 years is strongly affected by the uncertainty in the RST for Alloy 22 (*SCCTHRP*). In particular, in sample elements with a large value of *SCCTHRP*, the probability of damage to CDSP WPs can be quite small (output DTN: MO0708CDSPSEIS.000 [DIRS 183007], *FreqDamageCDSP_v5.pdf*).

A second phase begins when the DS fails and the drifts are conceptualized to be filled with rubble. The presence of rubble significantly reduces the probability of further damage to WPs from seismic events (output DTN: MO0708FREQCALC.000 [DIRS 183006], *Rubble_Damage.pdf*). After DS failure, nominal corrosion processes are generally the cause of further damage to WPs, first as SCC failures of lid welds, and at much later times, as patch openings caused by general corrosion. As a consequence, at later times, the expected dose from the combination of nominal corrosion processes and seismic ground motion events (Figure 8.2-11b[a]) resembles the expected dose for the Nominal Modeling Case (Figure 8.2-1[a]). The step-wise increases in the annual dose curves at around 200,000 years, 300,000 years, 500,000 years and 700,000 years are due to immediate increases in the number of WP failures from SCC. These immediate increases in WP failure are caused by the coarse temporal discretization used by WAPDEG v4.07 past 100,000 years (Section 7.3.3.7[a]). Additional discussion of these failures is provided with the Nominal Modeling Case in Section 8.2.1[a].

Section 7.7.1.4[a] presents an analysis of a single realization of expected annual dose for the post-10,000-year period, and illustrates the progression of damage to EBS components as seismic events occur, as well as the effects of nominal corrosion processes on EBS components. Figures 8.3-7[a] through 8.3-12[a] summarize the performance of DS and WP components of the EBS subjected to ground motion and nominal corrosion processes; these results should be contrasted with Figures 8.3-4[a] through 8.3-6[a], which summarize the effects of only the nominal corrosion processes on EBS components.

Appendix K[a] presents sensitivity analyses that determine the contribution to the uncertainty in expected annual dose that derives from individual uncertain inputs. At early times, before DS failure, these analyses identify the RST for Alloy 22, *SCCTHRP*, as the uncertain input that predominantly explains the uncertainty in the expected annual dose (Figure K7.7.2-1[a] and Figure K7.7.2-2[a]). At later times, the temperature dependence parameter for Alloy 22 general corrosion rate, *WDGCA22*, is dominant. Beyond *SCCTHRP* and *WDGCA22*, the analysis identifies a number of other variables with minor contributions to uncertainty in expected annual

dose. However, the lack of smoothness in the expected annual dose results due to the use of the Monte Carlo method inhibits the sensitivity analysis' resolution of the importance of these minor contributors. In addition, the use of the Monte Carlo method precludes sensitivity analyses for intermediate model outputs, such as the movement of several important radionuclides (^{239}Pu, ^{237}Np, and ^{99}Tc) through the repository system, as explained in Appendix K[a], Section K7.7.2[a].

8.2.4.2[a] Seismic Fault Displacement Modeling Case

The revised projections of expected mean annual dose for the Seismic FD Modeling Case are shown on Figure 8.2-13[a]; the figure shows plots for both the (a) 10,000-year period and (b) post-10,000-year period. The expected annual dose takes into account aleatory uncertainty associated with characteristics associated with the number, type and location of DSs and WPs disrupted. The mean, median, and 5th and 95th percentile curves on Figure 8.2-13[a] show uncertainty in the value of the expected annual dose, taking into account epistemic uncertainty associated with incomplete knowledge of the behavior of the physical system during and after the disruptive event. For the 10,000-year postclosure period, the revised maximum mean annual dose is about 1.5×10^{-3} mrem, which is slightly lower than the original projection of 1.8×10^{-3} mrem. Similarly, for the post-10,000-year period, the revised maximum median annual dose is about 1.1×10^{-2} mrem, whereas the original projection was 1.5×10^{-2} mrem. Further comparison of the results of this modeling case is provided in Section 7.3.1.5.7[a].

The individual radionuclide contributions to mean annual dose are shown in the results presented on Figure 8.2-14[a] for both the 10,000-year and post-10,000-year period after closure. The plot for the 10,000-year period (Figure 8.2-14a[a]) shows that ^{99}Tc and ^{129}I dominate the dose for approximately the first 5,000 years after closure and ^{99}Tc and ^{239}Pu dominate the dose for the subsequent 5,000 years. Figure 8.2-14b[a] shows that ^{239}Pu dominates the mean annual dose for the post-10,000-year time period until approximately 200,000 years postclosure. After approximately 200,000 years and until 1,000,000 years postclosure, the radionuclides contributing most to the mean annual dose are ^{242}Pu, ^{237}Np, and ^{226}Ra. These patterns of radionuclide contribution and dominance are identical to those documented in Section 8.2.4.2 of the parent document.

Analyses of single realizations from the Seismic FD Modeling Case are not presented in Section 7.7.1, because this modeling case is a relatively low contributor to the total expected dose (Figure 8.1-3[a]), and because the processes important to radionuclide releases are examined in the analyses for the Waste Package EF Modeling Case (Section 7.7.1.1[a]) and Drip Shield EF Modeling Case (7.7.1.2[a]). The expected annual dose at time τ is computed as the sum of the contributions to dose from all possible preceding fault displacement events, where the dose from each event is weighted by the probability of the event's occurrence (Section 6.1.2.4). As indicated by Equation 6.1.2-25, each realization of expected annual dose is implicitly averaged over the aleatory uncertainty in the number, type and location of WPs damaged by fault displacement. Specifically, the GoldSim component of the TSPA-LA Model computes the dose resulting from fault displacement damage to 100 WPs of each type distributed proportionally among the percolation subregions, and within each subregion, into either seeping or non-seeping conditions. The EXDOC component (EXDOC_LA V2.0, STN: 11193-2.0-00 [DIRS 182102]) of the TSPA-LA Model computes expected annual dose by scaling these results to the expected number of WPs of each type. This implementation is chosen for numerical efficiency. Because

of this implementation, each annual dose history computed by the GoldSim component involves WPs placed in both seeping and non-seeping conditions. Therefore, the analyses presented in Section 7.7.1.2[a] for the Drip Shield EF Modeling Case provide insight into the processes important to radionuclide releases from WPs affected by fault displacement that are in seeping conditions. Similarly, the analyses presented in Section 7.7.1.1[a] for the Waste Package EF Modeling Case provide insight into the processes important to radionuclide releases from WPs affected by fault displacement that are in non-seeping conditions.

Appendix K[a] presents sensitivity analyses that determine the contribution to the uncertainty in expected annual dose that derives from individual uncertain inputs. These analyses identify several variables with moderate influence on the uncertainty in the expected annual dose for the Seismic FD Modeling Case (Figure K7.8.1-1[a] and Figure K7.8.1-2[a] for 10,000 years; and Figure K7.8.2-1[a] and Figure K7.8.2-2[a] for 1,000,000 years). For the first 10,000 years after repository closure, the uncertain inputs with the strongest influence on the uncertainty in expected annual dose are variables that influence the rate of water flow and the dose from ^{99}Tc. In particular, the analysis identifies *SZGWSPDM* (logarithm of scale factor that characterizes uncertainty in groundwater specific discharge) and *INFIL* (pointer variable for determining infiltration condition) as important, because these variables significantly influence the rate of water flow through the natural barriers and, hence, influence the rate of radionuclide transport. Also, before 10,000 years, the analysis identifies the BDCF for technetium (*MICTC99*) as important because ^{99}Tc is a large contributor to dose before 10,000 years. However, the regression model (Figure 7.8.1-2a[a]) that results from considering these three variables explains only part of the uncertainty in expected annual dose; a number of other uncertain inputs are identified as having lesser effects and incrementally improving the regression model.

After 10,000 years, the uncertain inputs with the strongest influence on the uncertainty in expected annual dose are variables that influence the rate of water flow, along with uncertainty in plutonium solubility. In particular, the analysis again identifies the variables *SZGWSPDM* and *INFIL*, along with *WPFLUX* (WP flux splitting factor) and *SEEPPRM* (logarithm of mean fracture permeability in the lithophysal rock units) as important due to the effects that these variables have on water flow through the EBS and natural barriers. Also, the variable *EPILOWPU* (logarithm of scale factor used to characterize uncertainty in plutonium solubility) is important because plutonium is the dominant contributor to dose after 10,000 years. However, the regression model (Figure K7.8.2-2a[a]) that results from considering these variables explains only part of the uncertainty in expected annual dose; a number of other uncertain inputs are identified as having lesser effects and incrementally improving the regression model.

Sensitivity analyses for intermediate model outputs, such as the movement of radionuclides through the repository system, are not presented for the Seismic FD Modeling Case. Insight into the processes important to radionuclide movement can be obtained from the analyses of radionuclide movement for early failure modeling cases, presented in Appendix K, Section K5. Although these analyses are performed using results from TSPA-LA Model v5.000, the conclusions of these analyses also apply to results from TSPA-LA Model v5.005 due to the similarity in the results for the two model versions (Section 7.3.1.5.7[a]).

8.3[a] DESCRIPTION OF MULTIPLE BARRIER CAPABILITY

As shown on Figure 8-1 of the parent document, the repository system is composed of three primary barriers that include: (1) upper natural barrier (Section 8.3.2.1), (2) engineered barrier system (EBS) (Section 8.3.2.2), and (3) lower natural barrier (Section 8.3.2.3). In this section, both qualitative and quantitative descriptions are presented to explain the performance capabilities of the multiple barriers. As used here, barrier capability is defined as the extent to which a barrier performs its functions. Barrier functions are two-fold: (1) prevent or substantially reduce the water from contacting the waste, and (2) prevent or substantially reduce the release of radionuclides from the repository to the accessible environment.

The analyses presented in this section are intended to address the NRC requirements of 10 CFR 63.115 [DIRS 180319] for multiple barriers. Section 8.3.3[a] of this addendum has been added to the material presented in the parent document. Section 8.3.3[a] contains a quantitative discussion of the capabilities of the individual barriers. This section should be utilized with the material in Section 8.3 of the parent document to provide a complete discussion of the performance characteristics and capabilities of the individual barriers.

8.3.1[a] Radionuclides Selected to Demonstrate Multiple Barrier Capability

As described in Section 8.3.1 of the parent document, twelve radionuclides were selected for analysis in the demonstration of barrier capability. The radionuclides were grouped into the five categories shown below (descriptions slightly modified from parent document):

1. Large initial inventory and short half-life: ^{137}Cs, ^{90}Sr, ^{241}Am, and ^{240}Pu
2. Highly soluble, non-sorbing, long half-life, and major contributor to dose: ^{99}Tc
3. Solubility limited, moderately to strongly sorbing, long half-life, transported in dissolved and colloidal phases, and important contributor to dose: ^{239}Pu and ^{242}Pu
4. Moderately soluble, weakly sorbing in the lower natural barrier, very long half-life, and transported in dissolved phase: ^{237}Np and ^{234}U
5. Strongly sorbed, and contributes to or is produced by decay chain ingrowth: ^{243}Am, ^{230}Th, and ^{226}Ra.

These twelve radionuclides represent a broad range of radioactive decay properties, geochemical behavior, BDCFs, and transport characteristics in geologic media. Because of these diverse properties, these twelve radionuclides provide a means of examining the performance characteristics of the natural and engineered barriers. The inventory decay histories for these twelve radionuclides are shown on Figure 8.3-1[a] for the two compliance periods (i.e., 10,000 years and post-10,000 years); Figure 8.3-2[a] shows the fraction of total activity attributed to each radionuclide.

8.3.2[a] Identification of Barriers for Yucca Mountain Repository

No change.

8.3.2.1[a] Upper Natural Barrier

No change.

8.3.2.2[a] Engineered Barrier System

No change.

8.3.2.3[a] Lower Natural Barrier

No change.

8.3.3[a] Demonstration of Multiple Barrier Capability

While the applicable NRC regulation (10 CFR 63.115 [DIRS 180319]) does not require performance analyses of individual barriers, a model-based demonstration of barrier capability was considered central to explaining and supporting the compliance demonstrations presented earlier in Section 8.1 of the parent document, as well as the revised results in Section 8.1[a]. In the case of the upper natural barrier, the performance characteristics have been analyzed using detailed process-level models (SNL 2007 [DIRS 182145] and SNL 2007 [DIRS 184614]). Performance analyses of the EBS and the lower natural barrier, however, were conducted using the TSPA-LA Model, which is described in Section 6 of the parent document.

In this section, TSPA-LA Model simulation results are presented that provide insights to the intrinsic characteristics of individual barriers that would contribute significantly to the isolation (i.e., containment and confinement) of the nuclear waste. Probabilistic projections for fundamental barrier performance and characteristics are presented that clearly illustrate effectiveness of three principal barriers. As described in Section 8.3 of the parent document, two demonstration modeling cases are used to quantify the capability for the three primary barriers. These demonstration modeling cases are: (1) combined Nominal/Early Failure Modeling Case (representative of the absence of disruptive events), and (2) Seismic GM Modeling Case (representative of the presence of disruptive events). With regard to the combined Nominal/Early Failure Modeling Case, the early failures include both DSs and WPs (Section 6.4.1 and 6.4.2 of the parent report). Because nominal corrosion processes alter the response of the engineered barrier components to seismic events, nominal corrosion processes are also included in the Seismic GM Modeling Case calculation.

8.3.3.1[a] Upper Natural Barrier

The hydrologic effectiveness of the Yucca Mountain upper natural barrier has been evaluated in recent modeling studies of: (1) net infiltration through the surficial soil, (2) three-dimensional flow and deep percolation, and (3) local flow processes determining drift seepage. The recent study of net infiltration (SNL 2008 [DIRS 182145]) provided boundary conditions for the study of three-dimensional (3-D) flow (SNL 2007 [DIRS 184614]) in the unsaturated tuff unit overlying the repository. Based on the UZ flow fields, probabilistic analyses of drift seepage were conducted to study the processes determining drift seepage and to project drift seepage for intact and collapsed drift conditions (SNL 2007 [DIRS 181244]). Collectively, these flow modeling studies and projections provide the basis to describe how well the upper natural barrier

prevents or substantially reduces the rate of water flow through the UZ and to the repository. The effectiveness of the upper natural barrier is described using the following three relative metrics:

1. Net infiltration into the bedrock as a percentage of precipitation rate for the 10,000-year compliance period

2. Spatially averaged drift seepage rate as a percentage of percolation flux (percolation rates are prescribed for the post-10,000-year compliance period in NRC Proposed Rule 10 CFR 63.342(c)(2) [DIRS 178394])

3. Seepage fraction for each percolation subregion for the 10,000-year and post-10,000-year compliance periods.

The first barrier capability metric provides a quantitative demonstration of the effectiveness of the topography and surficial soils. The second and third metrics focus on the effectiveness of the UZ tuff units above and inclusive of the repository horizon. The quantification of these relative metrics is presented for each of the three climate states (BSC 2004 [DIRS 170002], Section 7.1) of the 10,000-year compliance period, namely: (1) present-day (from 0 to 600 years), (2) monsoon (from 600 to 2,000 years), and (3) glacial-transition (from 2,000 to 10,000 years). For the post-10,000-year period, net infiltration and precipitation are not used because the percolation rates are prescribed in NRC Proposed Rule 10 CFR 63.342(c)(2) [DIRS 178394].

In the case of the first metric, net infiltration is the same for the two demonstration modeling cases because the barrier function of surficial soils is independent of the repository conditions. In contrast, the drift seepage (i.e., flow of liquid water into a drift per unit of time per unit area) and seepage fractions (i.e., ratio of WPs experiencing seepage to all WPs in a percolation subregion) are direct functions of hydrologic, thermal, drift degradation, and other repository conditions that depend on modeling cases; thus, these two metrics will have different values for the combined Nominal/Early Failure and Seismic GM Modeling Cases.

Basis for Net Infiltration Metric—To ensure a defensible basis for estimates of net infiltration (i.e., water flux across the soil/bed rock interface), a technical work plan (BSC 2006 [DIRS 177492]) was developed for independent evaluations of the available field data, software, and documentation. Those evaluations confirmed that the field data and supporting information used for the TSPA-LA conformed to appropriate quality assurance requirements. In addition, a new infiltration model, Mass Accounting System for Soil Infiltration and Flow (MASSIF) (SNL 2008 [DIRS 182145], Section 6.5.7), was developed and validated in accordance with SCI-PRO-006, *Models*. This new model of infiltration processes was used to develop projections of net infiltration into the bedrock. These projections were compared with published estimates of net infiltration and recharge efficiencies for other Nevada hydrographic areas/subareas (SNL 2008 [DIRS 182145], Section 7.2.1.2[a] and Figure 7.2.1.2-2[a]). The full technical basis for the model and revised assessment of net infiltration at Yucca Mountain is documented in *Simulation of Net Infiltration for Present-Day and Potential Future Climates* (SNL 2008 [DIRS 182145]). The estimates of precipitation and other meteorological data used are documented in *Data Analysis for Infiltration Modeling: Extracted Weather Station Data*

Used to Represent Present-Day and Potential Future Climate Conditions in the Vicinity of Yucca Mountain (SNL 2006 [DIRS 177081]).

Basis for Drift Seepage Metric—The scientific basis for the projections of three-dimensional UZ flow fields, deep percolation flow, and drift seepage are the end products of more than a decade of studies, including field testing and data collection. The modeling studies have been largely conducted using the well established TOUGH2 family of codes (i.e., TOUGH2 (STN: 10007-1.6-01 [DIRS 161491]), T2R3D (STN: 10006-1.4-00 [DIRS 146654]), and TOUGHREACT (STN: 10396-3.0-00 [DIRS 161256])), which have been subjected to a rigorous validation process using a wide variety of field data from the Yucca Mountain site. More specifically, the UZ flow model and submodels have been tested and corroborated using: (1) water-potential data from the Enhanced Characterization of Repository Block; (2) chloride data from the Exploratory Studies Facility (ESF), Enhanced Characterization of Repository Block, and boreholes; (3) perched water data and pneumatic data from boreholes; (4) carbon-14 data from gas samples; (5) strontium concentrations; and (6) calcite coating (SNL 2007 [DIRS 184614]). Most of the results of the model validation and corroboration studies are published in refereed scientific journals. The full technical basis for the deep percolation flow models and drift seepage is documented in *UZ Flow Models and Submodels* (SNL 2007 [DIRS 184614]) and *Abstraction of Drift Seepage* (SNL 2007 [DIRS 181244]).

Basis for Drift Seepage Fraction Metric—The TSPA-LA Model utilizes an abstraction of UZ flow to determine the percolation flux at the top of the repository horizon. Drift seepage flux is then computed as a function of the local percolation flux (defined as the percolation flux times the flow focusing factor), host rock permeability, and capillary strength (Figure 6.3.3-5 of the parent document). The drift seepage flux calculation is also adjusted to account for drift degradation and a thermal-hydrologic (TH) environment. The seepage fraction is calculated as the ratio of WPs experiencing seepage to all WPs in a percolation subregion; seepage fractions are determined for each WP type. Percolation subregions are described in Section 6.3.2.2.1 of the parent document. The abstractions of drift seepage and seepage fraction are explained in Section 6.3.3 of the parent document; the abstraction of the TH environment is described in Section 6.3.2 of the parent document. The modeling studies and technical basis for these abstractions are documented in *Multiscale Thermohydrologic Model* (SNL 2007 [DIRS 181383]) and *Abstraction of Drift Seepage* (SNL 2007 [DIRS 181244]).

8.3.3.1.1[a] Capability of Upper Natural Barrier to Prevent or Reduce Movement of Water to the Waste

Net Infiltration as Percentage of Annual Precipitation—Net infiltration as a percentage of climate dependent annual precipitation is the metric used to provide insights to the effectiveness of the surficial soils and topography to prevent or reduce the rate of water flow into the UZ. In addition, examining the partitioning of precipitation into the various water balance components (i.e., change in water storage in soil, run-off, evapotranspiration, and sublimation) is also useful in explaining the factors controlling net infiltration. The focus here is on the three climate states in the first 10,000 years (Section 6.3.1 of the parent document), namely, the present-day climate defined as occurring for 600 years; monsoon climate defined as occurring from 600 years to 2,000 years; and the glacial-transition which is defined to occur from 2,000 years to 10,000 years.

The following estimates of mean net infiltration rate as a percentage of mean precipitation rate for each climate state are taken from Tables 6.5.7.4-1 through 6.5.7.4-3 of the recent infiltration study (SNL 2008 [DIRS 182145]), namely:

- Present-day climate: $\overline{I} \sim 8.02\%$ of $\overline{P}$
- Monsoon climate: $\overline{I} \sim 8.69\%$ of $\overline{P}$
- Glacial-transition climate: $\overline{I} \sim 10.38\%$ of $\overline{P}$

where $\overline{I}$ is the mean net infiltration rate as a percentage of $\overline{P}$, the mean precipitation rate. Ranges of net infiltration for the four infiltration scenarios (defined by the 10th, 30th, 50th, and 90th percentiles of spatially averaged infiltration, see Section 6.3.1 of the parent document) can be summarized as follows. Estimated average present-day net infiltration ranges from less than 3 percent of precipitation for the drier 10th percentile infiltration scenario to about 13 percent of precipitation for the 90th percentile infiltration scenario (SNL 2008 [DIRS 182145], Table 6.5.7.1-3). For the monsoon climate, average net infiltration rate estimates for the 10th to 90th percentile infiltration scenarios range from about 3 percent to 17 percent of precipitation (SNL 2008 [DIRS 182145], Table 6.5.7.2-3). For the glacial-transition climate, the average net infiltration rate estimates for the 10th to 90th percentile infiltration scenarios range from about 5 percent to 16 percent of precipitation (SNL 2008 [DIRS 182145], Table 6.5.7.3-3). Note that the ratios of net infiltration to precipitation presented above are averaged over the entire infiltration model domain, not over the repository footprint area.

Water balance components tabulated in *Simulation of Net Infiltration for Present-Day and Potential Future Climates* (SNL 2008 [DIRS 182145]) show that the process of evapotranspiration (i.e., transfer of moisture from soil to the atmosphere by evaporation and transpiration from plants) alone accounts for most of the reduction in infiltration into the surficial soils; this reduction ranges from 85 to 88 percent of the mean precipitation rate (SNL 2008 [DIRS 182145], Tables 6.5.7.4-1 through 6.5.7.4-3). The remainder of the reduction is accounted for by the change in storage of moisture in the soil and surface runoff. The infiltration study contains comparisons with published estimates for other Nevada hydrographic areas/subareas (SNL 2008 [DIRS 182145], Section 7.2.1.2[a] and Figure 7.2.1.2-2[a]).

Seepage Rate as Percentage of Local Percolation Rate—Water entering the UZ as net infiltration from precipitation at the land surface affects the overall hydrological and thermal-hydrological (TH) conditions within the Yucca Mountain UZ. Net infiltration is the ultimate source of percolation through the UZ. Water percolating downward through the UZ is the source for seepage into the drifts. Multi-dimensional modeling of water flow in the UZ rock layers suggests that average percolation flux flowing to the repository footprint is within a few percent of the net infiltration rate (SNL 2007 [DIRS 184614], Section 6.1.4). This means that lateral flow in the Paint Brush non-welded (PTn) tuff, flow focusing in faults in the northern part of the repository, and perched water zones collectively have a small effect on reducing the local percolation rate at the top of the repository horizon. Of the water flow (percolation) arriving at the repository horizon, however, only a small portion results in drift seepage. The reduction from percolation to seepage is the result of two natural processes that divert flow around and away from the emplacement drift; these processes (SNL 2007 [DIRS 181244], Section 6.1.4) are referred to as: (1) the vaporization barrier effect during the thermal period, and (2) the capillary

barrier effect after the thermal period. While the vaporization barrier effect persists for a short time relative to the compliance periods, the capillary barrier effect persists through the period of geologic stability.

The surface soil and topography, the surficial bedrock, and the TSw unit will combine to substantially reduce movement of water from the surface of Yucca Mountain into the emplacement drifts. The combination of reduced infiltration into Yucca Mountain, effects of heat during the thermal period, and capillary barrier effects in the TSw unit, results in a seepage flux that will be substantially reduced from the precipitation flux at the surface. The magnitude of this reduction is shown on Figure 8.3-3[a]. The top figure (a) illustrates the effectiveness of surficial soils and topography in preventing or reducing the rate of water flow into the UZ. The bottom figure (b) illustrates the effectiveness of decay heat and capillary diversion in limiting water movement into the drifts. On Figure 8.3-3a[a], mean spatially-averaged annual precipitation and net infiltration rates are plotted for each of the three climate states in the 10,000-year compliance period. Net infiltration rates are shown to range from approximately 5 percent of precipitation during the present-day climate to over 7 percent of precipitation during the glacial-transition climate. For the post-10,000-year period, the effects of infiltration are implicitly included in the TSPA-LA Model by using the distribution for deep percolation rate as specified in NRC Proposed Rule 10 CFR 63.342(c)(2) (70 FR 53313 [DIRS 178394]), namely, a log-uniform distribution with a range of 13 to 64 mm/yr. The mean value of deep percolation from this distribution, 32 mm/yr, is shown on Figure 8.3-3a[a].

Three mean spatially-averaged drift seepage flux curves are shown on Figure 8.3-3b[a]. The top curve denoted by the dashed line represents a zero-diversion seepage flux that would result if capillary and thermal effects at the drift wall were neglected. This volumetric seepage flux is obtained by applying the average net infiltration flux to the projected area of an intact emplacement drift segment that is 5.1 m long by 5.5 m wide. This zero-diversion seepage flux is compared to the TSPA-calculated seepage fluxes for the two demonstration modeling cases (i.e., the combined Nominal/Early Failure Modeling Case and the Seismic GM Modeling Case) to illustrate the effectiveness of the UZ barrier in limiting the movement of water into the drifts. Note that the average net infiltration flux and, thus, zero-diversion seepage flux used here, is based on a spatial averaging over the entire infiltration model domain. Therefore, the zero-diversion seepage flux is only a representative approximation of the average flux that would occur within the repository footprint.

In contrast, the TSPA-calculated seepage fluxes are based on the percolation flux within the repository footprint. The nominal seepage flux curve shows that seepage varies in the early part of the thermal period when temperatures above 100°C are achieved; as temperatures gradually decrease to lower values, seepage fluxes into the drift increase. The estimate shows that for the 10,000-year compliance period, on average, 2 to 11 percent of the zero-diversion seepage flux occurs as seepage into the drifts. The mean seepage flux for the post-10,000-year period is about 0.095 m^3/yr or about 11 percent of the zero-diversion seepage flux.

The seepage curve for the Seismic GM Modeling Case is discussed next. For the first 10,000 years, the mean seepage flux curve is almost identical to the mean curve for the combined Nominal/Early Failure Modeling Case. This similarity occurs because seismic events of sufficient magnitude that cause drift degradation are unlikely to occur in this time period. The

likelihood of seismic events is described by the mean seismic hazard curve (Figure 6.6-6 of the parent document), which shows that exceedance frequencies on the order of 10^{-4} yr^{-1} correspond to relatively small amplitude vibratory ground motions that are unlikely to result in rockfall (Section 6.6.1.2.1 of the parent document). The drift degradation aspect is based on the simulations of rockfall resulting from seismic ground motion events, which are shown on Figure 7.3.2-19 of the parent document. This figure indicates that for most realizations, drift degradation, quantified in terms of mean rubble volume per meter of drift length (i.e., seismic induced rockfall), is less than 5 m^3/m and 0.5 m^3/m for both the lithophysal and nonlithophysal rock zones, respectively, for the first 10,000 years. The lithophysal rock zones encompass approximately 80 to 85 percent of the emplacement drifts in the repository (Section 6.6.1.2.2). As described in Section 6.3.3.1.3, a mean rubble volume of less than or equal to the 5 m^3/m of drift length for lithophysal rock zone or 0.5 m^3/m for nonlithophysal rock zone indicates that the emplacement drifts are essentially intact and, thus, the seepage rates are determined by nominal flow processes in the repository horizon. Consequently, the values of the seepage rate metric are about the same as those for the combined Nominal/Early Failure Modeling Case.

For the post-10,000-year time period, the Seismic GM Modeling Case seepage rates on Figure 8.3-3b[a] are significantly different from the seepage rates for the combined Nominal/Early Failure Modeling Case. These differences are due to a greater degree of drift degradation and, at late times, to drift collapse in lithophysal rock (i.e., lithophysal rubble volume 60 m^3/m or greater). In nonlithophysal rock, once rockfall has accumulated to an amount of 0.5 m^3/m, capillary diversion is no longer considered, and the seepage rate is set to the percolation rate in the TSPA-LA Model. The spatially averaged mean seepage rates for the Seismic GM Modeling Case increase with time and are larger than those for the combined Nominal/Early Failure Modeling Case. The mean drift seepage rates for the Seismic GM Modeling Case range from 0.109 m^3/yr just after 10,000 years to about 0.434 m^3/yr at 1,000,000 years. For these same two times, the seepage rates, as a percentage of the mean zero diversion seepage rate calculated using the NRC prescribed local percolation rate, are about 12 percent and 48 percent, respectively. Although the effectiveness of capillary diversion is reduced from that of the combined Nominal/Early Failure Modeling Case, it is still substantial in the Seismic GM Modeling Case.

Seepage Fractions for Percolation Subregions—Drift seepage rates are expected to vary spatially over the length of the emplacement drifts. This means that emplacement drifts can exhibit both seeping and non-seeping environments (Section 6.3.3.1.1). In the TSPA-LA Model, this spatial variability is quantified by the seepage fraction. The seepage fraction is the ratio of the number of WPs experiencing seepage to the total WPs in a percolation subregion; separate values are computed for CDSP and CSNF WPs. Distributions of seepage fraction have been computed for each climate and for the five percolation subregions that represent the repository footprint. The calculations were performed using a three-dimensional flow model (BSC 2004 [DIRS 167652]) and a probabilistic approach (SNL 2007 [DIRS 181244], Section 6.5); implementation of the abstraction in the TSPA-LA Model is described in Section 6.3.3.2.2. Seepage fractions for all five percolation regions are provided in Tables 8.3-2[a] through Table 8.3-4[a]. Unlike seepage rates, which vary with time, seepage fractions are constant values that are based on the percolation flux at the end of the simulation period (either 10,000 years or one million years).

For the combined Nominal/Early Failure Modeling Case, statistics for the distributions of the seepage fraction are tabulated in Table 8.3-2[a] for glacial-transition climate (2,000 to 10,000 years) and in Table 8.3-3[a] for post-10,000-year deep percolation rates. The statistics consist of mean and 5th and 95th percentiles for each WP type (i.e., CDSP and CSNF). As can be noted from Table 8.3-3[a], for the post-10,000 year period the mean seepage fraction in percolation subregion 3 is ~ 0.44 for the CDSP and CSNF WP locations. Percolation subregion 5, which represents about 5 percent of the repository footprint, has the highest mean seepage fraction of ~ 0.49 for both CDSP and CSNF WPs. Averaging over the entire repository footprint, the mean seepage fractions for both CDSP and CSNF WPs are ~ 0.4; this indicates that, on average, in the post-10,000-year period, about 60 percent of the emplacement locations in the repository have non-seeping environments for the combined Nominal/Early Failure Modeling Case.

For the Seismic GM Modeling Case, the seepage fraction statistics are tabulated in Table 8.3-4[a] for glacial-transition climate (2,000 to 10,000 years) and Table 8.3-5[a] for post-10,000 year deep percolation rates. As can be noted from Table 8.3-5[a], for the post-10,000 year period the mean seepage fraction in percolation subregion 3 is about 0.72 for both CDSP and CSNF WPs. Percolation subregion 5, which represents about 5 percent of the repository footprint, has the highest mean seepage fractions of ~ 0.75 for both the CDSP and CSNF WP locations. The mean seepage fraction for the overall repository footprint is ~ 0.7 for both CDSP and CSNF WP locations. This indicates that for the post-10,000-year period, about 30 percent of the emplacement locations in the repository are in non-seeping environments for the Seismic GM Modeling Case. It is important to note that the calculations of mean seepage fractions for the Seismic GM Modeling Case account for effects of drift degradation and collapse, which reduce the flow diversion by the capillary barrier (BSC 2004 [DIRS 167652], Section 6.6.3). This is the reason that the seepage fractions are higher than those for the combined Nominal/Early Failure Modeling Case.

8.3.3.2[a] Engineered Barrier System

The basic role of the EBS is to provide long-term containment and to prevent and delay the release of radionuclides into the lower natural barrier. The EBS achieves this design intent by ensuring two important barrier functions: (1) preventing or substantially reducing the amount of seepage water and drift wall condensation that contacts the waste, and (2) preventing or substantially reducing the rate of release of radionuclides from the EBS to the lower natural barrier. The first barrier function is provided by the emplacement drift, DS, and WP OCB (Figure 6.3.6-4), whereas the second function is provided by the various waste forms, the WP OCB, corrosion products from WP internals, and the crushed tuff in the invert. The TSPA-LA Model was used to demonstrate EBS barrier capability; as described in Section 6.1.1, excluded features, events and processes are not considered in this demonstration.

Drip Shield and Waste Package Performance Metrics—To provide a basis for assessing the capability of the EBS to achieve the first barrier function, projections for three barrier capability metrics were developed for the DSs and WPs. The first metric is the DS failure time profile, which is quantified in terms of a cumulative probability distribution function (CDF) for failure time of the DS plates (Titanium Grade 7). DS failure is defined as a hole or opening through the 15-mm thick DS plate; breach of the plate by SCC cracks is not considered as a DS failure

because a crack-damaged DS will still prevent seepage water from contacting the underlying WP. The second capability metric is the WP breach time profile, which is defined as a penetration of the OCB (Alloy 22 [UNS N06022]) by either cracks or patch openings. In the combined Nominal/Early Failure Modeling Case, WP breaches include crack breaches due to SCC of the closure lid welds and patch breaches of the WP OCB due to general corrosion penetrations. In the Seismic GM Modeling Case, crack breaches include seismically-induced SCC of the WP OCB as well as SCC of the closure lid welds; patch breaches include seismically-induced rupture and puncture, in addition to general corrosion penetrations. In addition, a third metric, the capability of the EBS system to retain radionuclides, addresses the performance of the EBS as a whole.

Insights to potential WP breach modes were developed by examining the breach characteristics underlying these metrics for each of the two demonstration modeling cases. For the combined Nominal/Early Failure Modeling Case, the following two WP breach characteristics (Section 6.3.5) were calculated and are presented:

1. Fraction of WPs breached by general corrosion (i.e., patch penetration) as a function of time

2. Fraction of WPs breached by cracks (i.e., nominal process SCC in closure welds) as a function of time.

The following three WP breach characteristics (Section 6.6 of the parent document) for the Seismic GM Modeling Case are presented and discussed:

1. Fraction of WPs breached by nominal and seismic ground motion processes as a function of time

2. Fraction of WP surface area breached by nominal and seismic ground-motion induced SCC cracks per breached WP as a function of time

3. Fraction of WP surface area breached by patches resulting from general corrosion and seismic induced puncture and rupture failure mechanisms per breached WP as a function of time.

In the following discussion, WP performance is generally presented in terms of mean barrier capability metrics and breach characteristics. To illustrate uncertainty in these metrics and characteristics, quantiles (median, 5th, and 95th percentiles) are also shown. It is important to note that the TSPA-LA Model computes WP degradation metrics and breach characteristics for each of five percolation subregions that represent the repository footprint. The graphical results presented in the following sections for the WPs were computed as a weighted average combining all of the five percolation regions to arrive at a representation for the entire repository.

An assessment of the EBS capability as a whole to achieve the second barrier function was developed based on probabilistic projections of mean radionuclide activity (in curies) released from the EBS as a function of time. This barrier capability metric is calculated using the inventory balance equation:

$$\bar{R}_{EBS,k}(\tau \mid \mathbf{e}) = \bar{A}_{T,k}(\tau \mid \mathbf{e}) - \left(\bar{A}_{WP,k}(\tau \mid \mathbf{e}) + \bar{A}_{I,k}(\tau \mid \mathbf{e})\right) \qquad \text{(Eq. 8.3.3-1[a])}$$

where $\bar{R}_{EBS,k}(\tau \mid \mathbf{e})$ is the expected (average over aleatory uncertainty) activity (Ci) of radionuclide *k* released from the EBS; $\bar{A}_{T,k}(\tau \mid \mathbf{e})$ is the expected activity (Ci) of radionuclide *k* in the inventory disposed in the geologic repository (initial inventory decayed through time); $\bar{A}_{WP,k}(\tau \mid \mathbf{e})$ is the expected activity (Ci) of radionuclide *k* retained in the WPs (including the activity still in undegraded waste forms); and $\bar{A}_{I,k}(\tau \mid \mathbf{e})$ is the expected activity (Ci) of radionuclide *k* retained in the invert. The term τ is time, and $\mathbf{e}$ is the set of epistemically uncertain parameters, which are sampled in the Monte Carlo simulation (output DTN: MO0701PLOTSFIG.000 [DIRS 185207], file: *Calculation of expected activity Seismic GMD 10K.doc*). The activity quantities, $\bar{A}_{T,k}(\tau \mid \mathbf{e})$, $\bar{A}_{WP,k}(\tau \mid \mathbf{e})$, and $\bar{A}_{I,k}(\tau \mid \mathbf{e})$, are obtained from the Monte Carlo simulation performed with the TSPA-LA Model.

Basis for Engineered Barrier System Barrier Capability Projections—The conceptual models and mathematical basis for DS and WP degradation can be found in Section 6.3.5. An important aspect to note is that the DS degradation abstraction does not implement spatial variability for general corrosion rates. This means that all DSs in the repository fail in unison at the failure time determined by the general corrosion model and the DS fragility abstraction (Section 6.6.1.2.2.1 of the parent document). The uncertain parameters for DS general corrosion are derived from laboratory data for general corrosion of the Titanium Grade 7 samples and are documented in *General Corrosion and Localized Corrosion of the Drip Shield* (SNL 2007 [DIRS 180778]). Similarly, the experimental basis for the WP degradation models and parameters can be found in *General Corrosion and Localized Corrosion of Waste Package Outer Barrier* (SNL 2007 [DIRS 178519]) and *Stress Corrosion Cracking of Waste Package Outer Barrier and Drip Shield Materials* (SNL 2007 [DIRS 181953]).

Probabilistic projections for DS failure and WP breach time profiles were developed to provide insight into barrier capability (output DTN: MO0801TSPAWPDS.000 [DIRS 185077]). These projections used an optimized version of the TSPA-LA Model v5.005 that excludes all transport calculations to efficiently calculate DS and WP failure under nominal and seismic conditions for the purpose of presenting projections of DS and WP performance. The optimized version of the TSPA-LA Model uses the same Monte Carlo simulation approach as the full TSPA-LA Model, which incorporates aleatory and epistemic uncertainties by means of two separate computational loops:

1. An outer calculation loop that samples values from probability distributions for parameters with epistemic uncertainty using the Latin hypercube sampling technique (Helton and Davis 2002 [DIRS 163475])

2. An inner loop that samples, for each epistemic set, values from probability distributions of parameters describing aleatory uncertainty (i.e., randomness) in the occurrence of events.

The optimized version of the TSPA-LA Model uses the same samples for aleatory and epistemic uncertainty as are used to produce the TSPA-LA Model results shown in Section 8.1[a] and Section 8.2[a].

For the combined Nominal/Early Failure Modeling Case, the probabilistic analysis of DS capability (output DTN: MO0801TSPAWPDS.000 [DIRS 185077], file: v5.005_NC_000300.gsm) included general corrosion of the DS plates; other DS corrosion mechanisms such as localized corrosion have been screened out (Section 6.3.5.1 and Table 6.3.5-1). As described in Section 6.3.5, the degradation of the topside of the DS plate is based on a corrosion rate model for an aggressive water chemistry environment (i.e., elevated fluoride concentration), whereas the underside surface degradation is based on a corrosion rate model for water chemistry representative of a benign environment. For the WPs, WAPDEG was applied to analyze WP degradation, taking into account the following processes: general corrosion, microbially influenced corrosion, and SCC in the closure-lid weld region. Localized corrosion of the WPs was analyzed with a standalone model using GoldSim (external to WAPDEG) and was shown not to impact the combined Nominal/Early Failure Modeling Case or the Seismic GM Modeling Case (Section 6.3.5.2.3).

As described in Section 6.4 of the parent document, a DS or WP early failure is characterized as a through wall penetration of a WP or DS caused by manufacturing or handling-induced defects that occurs prior to or at the time of repository closure. In the case of the early DS failure, the penetration of the DS plate is assumed to represent complete failure of the DS. In addition, if an early-failed DS is located in a seeping environment, it is assumed that the underlying WP is completely degraded by localized corrosion processes. In the case of early WP failure, it is assumed that the entire surface of the WP is completely degraded. The probabilities of early failure of a randomly selected DS or WP are sampled from lognormal distributions (Sections 6.4.1.3 and 6.4.2.3).

For the Seismic GM Modeling Case (Section 6.6), analysis of the seismic impacts to the DS and WP degradation was performed by first applying WAPDEG to simulate the nominal corrosion processes, then transferring the calculation results to GoldSim to evaluate damage and breaches caused by vibratory ground motion. Details of the associated model implementation are discussed in Sections 6.6.1.3 and 6.6.2.3 of the parent document.

8.3.3.2.1[a] Engineered Barrier System Capability to Prevent or Reduce Movement of Water to the Waste

The DSs serve as the first engineered feature that prevents seepage and drift wall condensation water from contacting the WPs and thereby the waste forms. The DSs would maintain this barrier function until the 15-mm thick DS plates are fully penetrated by general corrosion or ruptured as a result of seismic events. As explained in Section 6.3.5.1.1, Table 6.3.5-1, localized corrosion of DS plates has been screened out (DTN: MO0706SPAFEPLA.001_R1 [DIRS 185200], FEP 2.1.03.03.0B). The DS capability to achieve the first barrier function is demonstrated considering both nominal general corrosion of the plate (topside and underside surfaces) and seismic induced loading (dynamic and static) causing plate failure (rupture).

The WPs serve as the second feature that prevents water from contacting the waste forms. The WP barrier capability is demonstrated by considering breaches attributed to:

- Nominal corrosion degradation conditions: SCC of the closure-lid weld region (Figure 6.3.5-7) and general corrosion of the WP OCB.

- Seismic ground motion conditions: seismic-induced SCC, rupture, and puncture of the WP OCB, combined with breaches due to nominal corrosion processes. The seismic-induced SCC of the WP OCB is attributed to a local residual stress exceeding a residual tensile stress threshold for SCC initiation and is conceptualized as a tightly spaced network of stress corrosion cracks (Section 6.6.1.1.2). Note that the DS and WP capability analysis results for these conditions also include degradation by the nominal corrosion mechanisms.

It is important to note that the process of liquid water flow through the stress corrosion cracks in the WP OCB has been screened out (Section 6.3.6.1 and DTN: MO0706SPAFEPLA.001_R1 [DIRS 185200], FEP 2.1.03.10.0A). Consequently, liquid seepage water would not contact the waste form until a patch penetration develops in the WP OCB. The significance of SCC to EBS capability to achieve the second barrier function is addressed in Section 8.3.3.2.2[a].

The following sections present results for each performance metric for the EBS capability to prevent or reduce movement of water to the waste, as well as characteristics for breaches of WPs, namely:

- DS failure time for nominal conditions
- WP breach time for nominal conditions
- WP breach characteristics for nominal conditions
- DS failure time for seismic ground motion conditions
- WP breach time for seismic ground motion conditions
- WP breach characteristics for seismic ground motion conditions.

Drip Shield Failure Time Profile for Nominal Conditions—A failure time profile for the DSs was developed via a probabilistic projection of the general corrosion degradation of the DS plates as a function of time. For this performance metric, DS failure under nominal conditions is defined as complete penetration of the DS plate by general corrosion (Section 6.3.5). Degradation of the DS framework is also considered and used in the seismic damage abstraction. However, analyses indicate that DS framework failure does not alter the capability of the DS plates to deflect seepage away from the WPs (Section 6.6.1.2.2.1).

Because spatial variability in DS general corrosion rates is not represented in the TSPA-LA Model (Section 6.3.5.1.2), the distribution of the DS failure times simplifies to a single CDF, representing the uncertainty in the failure time for all the DSs in the repository. To calculate the CDF for DS plate failure times, the WAPDEG software was run with a total of 300 epistemic realizations. Each realization is based on one sampled general corrosion rate for each of the topside and underside plate surfaces from their respective distribution (Table 6.3.5-3).

The epistemic uncertainty in the general corrosion rates for the topside and underside surfaces are represented by CDFs (SNL 2007 [DIRS 180778], Section 8.1[a]) developed from laboratory data. The corrosion rate CDF for the topside is for aggressive corrosion conditions, while the CDF for the underside is for benign corrosion conditions. The distribution of DS plate failure times is shown on Figure 8.3-4[a]. Uncertainty in failure time is dominated by the uncertainty in the general corrosion rate for the topside (Appendix K, Section K4.2, of the parent document); this is because the corrosion rate on the topside of the DS is much greater than that on the underside. The CDF for DS plate failure times has a median value of approximately 290,000 years. A histogram of this failure time profile is presented in Section 8.1[a] (Figure 8.1-4[a]), which shows the majority of the Monte Carlo realizations with DS plate failure times ranging from 270,000 to 340,000 years.

Waste Package Breach Time Profiles for Nominal Conditions—Breach time profiles for the WPs for the Nominal Modeling Case were developed via a probabilistic projection of the breaches consisting of cracks in the closure lid-weld region of the WP OCB (Section 6.3.5.1.1) and corrosion patch penetrations of the WP OCB (Section 6.3.5.1.1). Projections were made for both the CDSP and CSNF WPs over the entire repository. To calculate the breach time profile as a function of time, a total of 300 epistemic realizations were run. Spatial variability in the degradation processes is modeled by the WAPDEG software. Temporal variability in the degradation processes is represented by the temperature-dependent general corrosion rate of the WP OCB (Section 6.3.5.1.2). The breach time profiles for both types of WPs are summarized by the fraction of WPs breached as a function of time, shown on Figure 8.3-5[a]; these plots show curves corresponding to the mean, median, and 5th and 95th percentiles.

Comparing the plots on Figures 8.3-5a[a] and 8.3-5b[a], it is evident that the CDSP and CSNF WP breach time profiles for nominal conditions are very similar. This similarity is explained by the fact that the two WP types have common design characteristics (e.g., OCB material [Alloy 22], OCB thickness [25 mm], and closure-lid weld stress mitigation method [i.e., low plasticity burnishing] for the closure weld surface (Section 6.3.5.1)). A small difference in breach-time profiles is expected because the two WP types have different temperature histories (i.e., CSNF WPs have higher thermal output and therefore a hotter outer surface than the CDSP WPs (SNL 2007 [DIRS 181383], Figure 6.3-82[a])), which affects general corrosion rates. In addition, because the CSNF and CDSP WPs have different nominal diameters and therefore different closure-lid weld volumes, different values for the associated SCC-model parameters for the closure-lid weld region are expected to introduce small differences in the SCC crack breach time profiles for the WPs. Based on the 95th percentile curves, CDSP and CSNF WPs breaches are likely to begin occurring after approximately 170,000 years. The mean curves for both WP types show that approximately 54 percent of the WPs could be breached at one million years as a result of SCC crack penetration and general corrosion patch penetration.

Waste Package Breach Characteristics for Nominal Conditions—To better understand the degree of degradation of the WPs under nominal corrosion conditions in the repository, the model results were analyzed to quantify the fraction of CDSP and CSNF WPs: (1) breached by SCC as a function of time, and (2) breached by general corrosion patches as a function of time. Under nominal conditions, SCC occurs in the closure-lid weld region of the WP OCB and general corrosion occurs over the entire WP OCB surface, including the closure weld region. Additional breach characteristics were calculated to estimate the expected fraction of WP surface

area breached by crack and patch penetrations as a function of time, per breached WP. Because the breach profiles for CDSP and CSNF WPs are very similar, only the nominal corrosion breach characteristics for the CSNF WP are discussed herein. Figure 8.3-6[a] shows the projected fraction of CSNF WPs breached as a function of time, which illustrates the initiation and timing of the two breach modes.

From the 95th percentile curve on Figure 8.3-6a[a], breach of CSNF WPs by SCC becomes more likely to occur after approximately 170,000 years. At the end of the one-million-year period, the mean fraction of the WPs with at least one SCC crack breach is 0.54, or 54 percent of the CSNF WPs in the repository. This result also means that almost half of the CSNF WPs would not be breached by SCC cracks within one million years. Comparing these results with those for the first breach-time profile of CSNF WPs (Figure 8.3-5[a]) confirms that the initial breach of the WPs would be by SCC. It is important to reiterate that the cracks induced by SCC are highly tortuous, tight hairline cracks (SNL 2007 [DIRS 181953], Section 6.7.1). Because of these typical tight hairline crack properties, plus sealing the cracks by corrosion products and mineral precipitates, no water in a liquid phase would flow into the WPs and contact the waste forms; however, diffusion of water vapor through cracks and into the WPs is accounted for in the TSPA-LA Model.

Based on the 95th percentile curve on Figure 8.3-6b[a], the CSNF WP is unlikely to be breached by a general corrosion patch penetration before about 560,000 years. By one million years, the mean fraction of the CSNF WPs with at least one patch breach is approximately 0.09 or 9 percent. This suggests that about 90 percent of the CSNF WPs in the repository would not exhibit general corrosion patch penetrations before one million years. It is important to note that the curves for the 5th percentile and median are absent from Figure 8.3-6b[a] due to the large number of realizations with no patch penetration by general corrosion (i.e., zero occurrences) within one million years.

Drip Shield Failure Time Profile for Seismic Ground Motion Conditions—The mechanical strength properties of the DS plates (i.e., Titanium Grade 7) and framework (i.e., Titanium Grade 29) were specifically selected to perform their barrier function in the seismic environment of the Yucca Mountain site. However, over the very long time periods specified in the NRC regulation, the combination of dynamic loads induced by vibratory ground motion, static loads associated with drift degradation and rubble accumulation, and plate thinning due to general corrosion would ultimately cause failures of the DSs. As outlined in Section 6.6.1.1.2 of the parent document, vibratory ground motion can cause DS plates to:

1. Rupture when the local strain exceeds the ultimate tensile strain
2. Degrade by induced high residual tensile stress resulting in SCC breach.

DS plate failure by large rock block impact in the nonlithophysal zones has been screened out based on low consequence (Section 6.6.1.2.2.1 and DTN: MO0706SPAFEPLA.001_R1 [DIRS 185200], FEP 1.2.03.02.0B). In the lithophysal units, the accumulation of rubble from multiple seismic events and the dynamic motion during a seismic event can generate SCC damaged areas on DSs. Because advective flow through stress corrosion cracks in DSs sealed by corrosion products and mineral precipitates has been screened out (DTN: MO0706SPAFEPLA.001_R1 [DIRS 185200], FEP 2.1.03.10.0B), the DS damage due to SCC is

not included in the TSPA-LA Model. In addition to being affected by dynamic and static loads, the DS plates are subjected to degradation by general corrosion. Failure of the DS framework occurs as a result of buckling that would be caused by the combined processes of general corrosion of the framework and seismic-induced loads. Buckling of the framework does not alter the capability of the DS plates to divert seepage away from the WPs (Section 6.6.1.2.2.1); however, the framework failure does affect the susceptibility of the underlying WPs to seismic damage from subsequent ground motion events because it inhibits the free motion of the underlying WPs and then of the emplacement pallets.

The DS plate failure time profile for seismic ground motion conditions was computed by the TSPA-LA Model using a total of 300 epistemic realizations, with 30 aleatory realizations to represent random sequences of future seismic events for each epistemic realization. The epistemic and aleatory sampled elements are the same as those used to generate results for the Seismic GM Modeling Case for post-10,000 years (Section 8.2.4.1[a]). The failure (rupture) time profile for the DS plates is described by the CDFs presented on Figure 8.3-7[a]. The plot on Figure 8.3-7a[a] shows three types of curves: (1) the set of 300 CDFs constructed from the 30 aleatory realizations for each of the 300 epistemic realizations, (2) the best estimate CDF for DS failure time, and (3) the expected (averaged over epistemic uncertainty) CDF of DS plate failure times. Figure 8.3-7b[a] shows the CDF of expected (averaged over aleatory uncertainty) DS plate failure times, along with the 95 percent confidence interval.

As used here, the best estimate CDF is defined as an unbiased estimate of the CDF based on all the simulation outcomes for the DS plate failure times. Based on this definition, the CDF is constructed directly from all 9,000 realizations (300 epistemic and 30 aleatory) simulated by the TSPA-LA Model; this CDF includes both aleatory uncertainty (randomness) and epistemic uncertainty (uncertainty in knowledge). The best estimate CDF on Figure 8.3-7a[a] has the following statistics: (1) median of ~255,000 years, (2) 5th percentile of 191,000 years, and (3) 95th percentile of ~280,000 years. The long leading tail of the CDF indicates that very few DS plate failures occur before 100,000 years. In fact, only about 50 out of the 9,000 realizations exhibit DS plate failures before 100,000 years; this means that there is approximately a 0.55 percent chance of DS plate failure occurring at or before 100,000 years by seismic events. DS plate failures before 100,000 years are the result of low probability high magnitude seismic events. The probability of DS plate failures increases gradually after 100,000 years as thinning of the DS plate progresses by general corrosion. At about 200,000 years, the DS plate is projected to have thinned to about one-third of its original thickness or ~5 mm (assuming a mean corrosion rate of ~51 nm/yr; DTN: SN0704PADSGCMT.001_R2 [DIRS 182122]), making it much more susceptible to failure. From the best estimate CDF, the average probability of DS plate failure on or before 200,000 years is approximately 6×10^{-2}; after about 300,000 years, the probability of the DS plate failures is effectively one.

The set of 300 CDFs on Figure 8.3-7a[a] is presented to illustrate the range of uncertainty about the best estimate CDF. Each CDF represents the uncertainty introduced by parameters with aleatory uncertainty (e.g., timing of seismic event) and is conditional on the set of parameter values (e.g., general corrosion rates for topside and underside DS plate surfaces) sampled for the given epistemic realization. The spread among the CDFs gives an estimate of uncertainty in DS plate failures associated with epistemically uncertain parameters. The expected CDF highlights the influence of aleatory uncertainties. The expected CDF, which is computed by averaging over

the epistemic uncertainty, represents what should be on average the randomness in the time of DS plate failure. As can be noted from the plot, it is very close to the best estimate CDF except in the tails of the distribution.

The influence of epistemic uncertainty on DS plate failure times is highlighted by the CDF of expected DS plate failure times, which is shown on Figure 8.3-7b[a]. In this case, the CDF was constructed by averaging over the aleatory uncertainty to obtain an expected DS plate failure time for each epistemic realization, then ranking the 300 expected DS plate failure times as a CDF. Recognizing that the accuracy of this CDF is based on only 30 aleatory realizations, the 0.95 confidence interval was computed and plotted on Figure 8.3-7b[a]; this confidence interval provides an estimate of the accuracy of each estimate of expected DS plate failure time.

Waste Package Breach Time Profile for Seismic Ground Motion Conditions—The mechanical design of the CDSP and CSNF WPs, as well as the corrosion properties of the WP OCB material (i.e., Alloy 22), were specifically selected so the WP would perform its barrier function for a wide range of seismic events and corrosion conditions at the Yucca Mountain site. However, over very long time periods, the combination of dynamic impacts and stress and corrosion processes would ultimately cause breaches in the WP OCB. As outlined in Section 6.6.1.1.2, vibratory ground motion can potentially cause WP damage and breaches of the following types:

1. Breaches of the WP OCB caused by SCC (crack penetration)

2. Rupture of the WP OCB as a result of local strain exceeding the ultimate tensile strain (note that rupture can only occur after the WP internals have degraded following an earlier breach in the OCB)

3. Puncture of the WP OCB as a result of rockfall and sharp corners or edges from degraded WP internals.

With regard to the latter two breach modes, rupture can occur while the DSs are intact; puncture can occur after DS failure. In the Seismic Ground Motion Damage Submodel (Section 6.6.1), it is assumed that the WP internals degrade as structural elements when the WP OCB is breached (typically by SCC); this degradation of internals has the effect of making the WPs more susceptible to seismic damage by subsequent events. The cumulative effects from multiple seismic events are analyzed for the time period of one million years.

The statistics on the expected fraction of breached CSNF WPs as a function of time are shown on Figure 8.3-8a[a] for the nominal and seismic processes combined and for the seismic processes only on Figure 8.3-8b[a]. The same statistics for CDSP WPs breached are shown on Figure 8.3-8c[a] and Figure 8.3-8d[a] for the nominal and seismic processes combined, and the seismic processes only, respectively. The mean of the expected fraction of WPs breached under seismic conditions at 200,000 years is projected to be approximately 0.007 for the CSNF WPs (Figure 8.3-8a[a]) and 0.37 for the CDSP WPs (Figure 8.3-8c[a]). In each realization (i.e., combination of epistemic and aleatory sample elements), the fraction of breached WPs, $F_{b,WP}\left(\tau \mid \mathbf{a},\mathbf{e}\right)$, is recorded for each WP type (WP) within each percolation subregion (b) as a function of time (τ). This fraction is determined by:

$$F_{b,WP}(\tau \mid \mathbf{a}, \mathbf{e}) = \min\left[1, fN_{b,WP}(\tau \mid \mathbf{e}) + fS_{b,WP}(\tau \mid \mathbf{a}, \mathbf{e})\right] \qquad \text{(Eq. 8.3.3-2[a])}$$

where $fN_{b,WP}(\tau \mid \mathbf{e})$ is the fraction of WPs of type *WP* within percolation subregion *b* failed by nominal corrosion processes, and $fS_{b,WP}(\tau \mid \mathbf{a}, \mathbf{e})$ is the fraction failed due to seismic events. Because a seismic event affects all WPs within a percolation subregion, $fS_{b,WP}(\tau \mid \mathbf{a}, \mathbf{e})$ can only have the values 0 or 1. The expected fraction of breached WPs, $\bar{F}_{b,WP}(\tau \mid \mathbf{e})$, is estimated for each epistemic sample element as the average of $F_{b,WP}(\tau \mid \mathbf{a}, \mathbf{e})$ over the aleatory sample elements. Thus, before any seismic damage occurs, the expected fraction of breached WPs is equal to the fraction of WPs with nominal corrosion damage. However, in the absence of nominal corrosion damage, $\bar{F}_{b,WP}(\tau \mid \mathbf{e})$ can be viewed as an estimate of the probability that seismic damage has occurred.

At early times before about 200,000 years, breaches of the WPs are primarily due to seismic processes only. Therefore, the expected fraction can be interpreted as a probability that a damaging seismic event has occurred. As shown on Figure 8.3-8b[a], the 95th percentile curve transitions from an expected fraction of 0 to 3.3×10^{-2} (which is 1/30) at approximately 61,000 years for CSNF WPs. That is, for 5 percent of the 300 epistemic realizations, the probability of failure due to seismic processes only before 61,000 years is at least 1/30. For 95 percent of the realizations, this probability is lower than 1/30 (note that the probability of 1/30 is linked to the fact that 30 futures are generated to represent aleatory uncertainty). This same level of confidence is reached for CDSP WPs as early as 500 years indicating that CDSP WPs are much less resistant to seismic damage and that damage is likely to occur much earlier.

As can be noted by comparing Figures 8.3-8b[a] and 8.3-8d[a], the CSNF WPs are far less likely to be breached by seismic events than the CDSP WPs. The higher resistance to seismic damage of the CSNF WPs versus the CDSP WPs is explained by the enhanced structural response capability (i.e., damping) contributed by the massive TAD canister in the CSNF WPs (Section 6.6). For both CDSP and CSNF WPs, however, the initial breaches consist of SCC or rupture induced by seismic damage while breaches at very late times are dominated by nominal general corrosion processes. For purposes of comparison, note that for nominal conditions the initial breaches of the CSNF and CDSP WPs are likely to begin occurring, as shown by the 95th percentile curves after approximately 170,000 years (Figure 8.3-5a[a] and Figure 8.3-5b[a]); these breaches are due to the nominal process SCC in the closure-lid weld region.

Waste Package Breach Characteristics for Seismic Ground Motion Conditions—To develop a quantitative description of the extent of seismic damage to the CDSP and CSNF WPs, probabilistic projections for two breach characteristics were developed: (1) fraction of the WP OCB surface area breached by cracks, and (2) fraction of WP OCB surface area breached by patches. To provide a comparative basis, the two breach characteristics (fraction of WP OCB surface area breached by cracks and by patches) were also computed for the nominal conditions (i.e., in the absence of disruptive events).

The fraction of surface area breached by SCC cracks (i.e., crack area fraction) per breached (crack or patch) CSNF package is shown on Figure 8.3-9[a]. The probabilistic projection for the

Seismic GM Modeling Case is shown on Figure 8.3-9a[a] and for the Nominal Modeling Case on Figure 8.3-9b[a]. Focusing on the plot for the Seismic GM Modeling Case (Figure 8.3-9a[a]), the initial slope of the mean curve indicates that the seismic induced SCC would predominately occur within the first 250,000 years. After about 250,000 years, the slope of the mean curve is much smaller, due to a significant reduction in the probability of further seismic damage. This decrease in the probability of further seismic damage is attributed to the failure of DS plates from seismic induced drift degradation, which progressively fills the emplacement drift with rubble. The accumulation of rubble around the WPs after DS failure, in turn, reduces the probability of damage by dynamic impacts (e.g., WP to pallet impacts).

In terms of the mean crack-breach characteristic for seismic conditions, the peak mean crack-area fraction for the CSNF WP occurs at one million years and is approximately 4.3×10^{-5}. In contrast, the peak mean crack-area fraction for nominal conditions at one million years from Figure 8.3-9b[a] is 6.5×10^{-6}. The slope of the mean curve on Figure 8.3-9b[a] indicates a steady but gradual progression of additional crack breaches in the closure-lid weld region of the WP OCB. In the closure-weld region, additional SCC cracks can initiate over time as general corrosion removes the stress-mitigated layer of the OCB (SNL 2007 [DIRS 181953], Section 8.4.2.1).

The average crack-breach area fraction per breached WP for the CDSP WPs is presented on Figure 8.3-10[a]. The probabilistic projection for the Seismic GM Modeling Case is shown on Figure 8.3-10a[a] and for the Nominal Modeling Case on Figure 8.3-10b[a]. The mean curve for the Seismic GM Modeling Case shows a very rapid rise in the crack-breach area fraction in the first 50,000 years, then gradually transitions to a near horizontal line after about 250,000 years. The near horizontal line again reflects a sharp decrease in the probability of further seismic damage. The timing of this decrease corresponds to the time frame when the DS plates fail (Figure 8.3-7a[a]) and the emplacement drifts are being filled by rubble. The peak mean crack-breach area fraction estimated from Figure 8.3-10a[a] occurs at one million years and is approximately 2.1×10^{-4}. This estimate of a CDSP WP crack-breach open area is almost five times greater than that for a CSNF WP. The greater crack-breach open area for CDSP WPs reflects a greater accumulation of seismic damage, due to the lower resistance to seismic damage for the CDSP WPs (Section 6.6.1.1.2). Focusing on the peak mean crack-breach area fraction for nominal conditions (Figure 8.3-10b[a]), the largest mean value is 7.1×10^{-6}.

The average fraction of surface area breached by patches (i.e., patch area fraction) per breached (crack or patch) CSNF WP is shown on Figure 8.3-11[a] for the Seismic GM Modeling Case and the Nominal Modeling Case. It is important to clarify that patch breaches in the Seismic GM Modeling Case (Figure 8.3-11a[a]) include general corrosion penetrations, ruptures, and punctures of the WP OCB, whereas the patch breaches in the Nominal Modeling Case (Figure 8.3-11b[a]) include only general corrosion penetrations. Comparison of the mean curves for breaches by cracks (Figure 8.3-9[a]) and by patches (Figure 8.3-11[a]), shows that breaches by cracks are more likely to occur than patch breaches. The 5th percentile and median are absent from Figure 8.3-11[a] because of the large number of realizations with no patch breaches.

As can be noted on Figure 8.3-11a[a], the mean curve for the CSNF WP OCB average patch-breach area fraction begins abruptly at approximately 240,000 years. This abrupt increase results from the first occurrence of rupture or puncture in the Seismic GM Modeling Case. Due

to the low probability of seismic events that cause crack damage to CSNF WPs (Section 7.3.2.6.1.3.7 of the parent document), which is a prerequisite for rupture of CSNF WP, as well as the low probability of seismic events that induce ruptures or punctures in the WP OCB (Sections 7.3.2.6.1.3.5 and 7.3.2.6.1.3.6 of the parent document), ruptures and punctures occur in only a few realizations. Accordingly, until about 480,000 years, the mean curve remains relatively flat, because it is determined by the few realizations in which ruptures or punctures occur. After 480,000 years, the mean curve ascends gradually, corresponding to an increasing likelihood that general corrosion penetrations have occurred. The timing of the initiation of the general corrosion patch penetrations is consistent with the mean curve for the nominal conditions shown on Figure 8.3-11b[a]. At the end of one million years, the patch-breach area fraction attributed to seismic conditions is about 2.6×10^{-3}, whereas for nominal conditions, shown on Figure 8.3-11b[a], it is about 2.4×10^{-3}. The similarity between the expected average seismic and nominal patch-breach area fractions indicates that the majority of patch penetrations of the CSNF WP OCB are caused by general corrosion.

Summary statistics for the expected average fraction of CDSP WP surface area breached by patches (i.e., patch area fraction) per breached (crack or patch) CDSP WP are shown on Figure 8.3-12a[a] for the Seismic GM Modeling Case and Figure 8.3-12b[a] for the Nominal Modeling Case. The mean curve for the average patch-breach area fraction for the Seismic GM Modeling Case shows a sharp increase beginning at about 14,000 years and then gradually increases until about 480,000 years. Similar to the results for CSNF WPs, this part of the mean curve is determined by a few realizations in which ruptures and/or punctures occur. Because CDSP WPs are more likely to be damaged by seismic events (Figure 8.3-8c[a]), it is also more likely that CDSP WPs could be ruptured, as evident in the earlier occurrence of patch breaches for CDSP WPs (Figure 8.3-12a[a]) as compared to CSNF WPs (Figure 8.3-11a[a]). At about 480,000 years, general corrosion begins to penetrate the CDSP WP OCB (Figure 8.3-12b[a]). At the end of one million years, the patch-breach area fraction attributed to seismic conditions is about 4.5×10^{-3}, whereas for nominal conditions, shown on Figure 8.3-12b[a], it is about 2.4×10^{-3}. The larger patch-breach area fraction for CDSP WPs for seismic conditions (as compared to nominal conditions) results because damage to CDSP WPs is relatively likely to occur (Figure 8.3-8d[a]). When SCC occurs, the WP OCB begins to corrode from the inside out, effectively doubling the rate of thinning of the WP OCB (Figure 7.7.1-61[a]), and thus increasing the likelihood of general corrosion patch penetrations before one million years. In addition, the WP internals degrade after seismic damage, and thus the early occurrence of SCC increases the probability that ruptures may occur.

Summary of the Capability of the Engineered Barrier System to Prevent or Substantially Reduce Water Contacting the Waste—The capability of the EBS to prevent or limit the movement of water and prevent contact between water and waste depends on the integrity of the DSs and WPs. The performance demonstration for the EBS indicates the DSs remain intact for hundreds of thousands of years and protect the WPs from seepage. Moreover, the majority of WPs remain intact for tens of thousands to hundreds of thousands of years, thus only a fraction of the emplaced waste will be exposed to water during this period.

For the combined Nominal/Early Failure Modeling Case, with early-failed DSs notwithstanding, the performance demonstration projects a distribution of DS plate failure times (Figure 8.3-4[a]) with a median of approximately 290,000 years, with DS plate failure times generally ranging

from 270,000 to 340,000 years (Figure 8.3-4[a]). For the Seismic GM Modeling Case, the best estimate distribution of DS failure times (Figure 8.3-7a[a]) has a median of about 255,000 years, with the average probability of DS failure at or before 200,000 years being approximately 0.06.

With regards to WP performance capability, the projected distributions for the mean fraction of WPs (CDSP and CSNF) breached (Figure 8.3-5[a]) for the Nominal Modeling Case show that at 500,000 years, about 15 percent of WPs would have breaches and at one million years about 54 percent of WPs would be breached. For the Seismic GM Modeling Case, the mean of the expected fraction of WPs breached at 200,000 years is projected to be approximately 0.007 for the CSNF WPs (Figure 8.3-8a[a]) and 0.37 for the CDSP WPs (Figure 8.3-8c[a]). After 200,000 years, nominal corrosion processes start to dominate the expected fraction of breached WPs for the Seismic GM Modeling Case. These performance metrics show that the DSs and WPs together substantially reduce the contact of water with the emplaced waste for hundreds of thousands of years.

8.3.3.2.2[a] Engineered Barrier System Capability to Prevent or Reduce the Rate of Radionuclide Releases

The EBS prevents or substantially reduces the release rate of radionuclides from the waste and prevents or substantially reduces the rate of movement of radionuclides from the repository to the accessible environment. The EBS performs these functions by (1) preventing or substantially reducing the contact of water with the waste, (2) reducing the rate of release due to the slow alteration of the waste and by limited water flux into the WPs, and (3) reducing the rate of radionuclide transport from the waste form to the lower natural barrier. This section summarizes how the different processes contribute to the EBS functions, then presents results demonstrating the EBS capability to prevent or reduce radionuclide releases for undisturbed (combined Nominal/Early Failure Modeling Case) and disturbed (Seismic GM Modeling Case) conditions.

WPs can be breached through general corrosion, through seismic damage, or by early failure. In the latter case, the WPs are assumed to provide no protection from the drift environment starting at the time of repository closure. After WPs are breached, spent nuclear fuel assemblies and HLW canisters will be exposed to the drift environment including air, water vapor, and possibly dripping water. The WP exterior will be subjected to advective seepage flow only if seepage is dripping at the WP location and the DS fails—possibly due to early failure, seismic ground motion, or general corrosion of the DS. Seismic-induced rupture or puncture of the WP as well as general corrosion of the WP can provide pathways for advective flux of water into a breached WP. Stress corrosion cracks will not permit advective flux of water into the WPs; stress corrosion cracks will, however, permit the transfer of oxygen and water vapor by diffusion into the WPs.

Radionuclide transport out of the EBS and into the UZ is dependent on several processes. The processes discussed below are described in detail in Section 6.3.7 and Section 6.3.8 of the parent document. After a WP is breached, radionuclides are not available for release and transport until the following processes have occurred:

- Oxygen and water (liquid water or water vapor) enter a WP enabling degradation of the waste form and formation of a liquid pathway for radionuclide transport. At and above

the boiling point of water in the repository, a liquid pathway is assumed not to exist, and no transport of radionuclides takes place. When only water vapor enters a WP, no transport takes place until a continuous water film is formed on the internal components. This condition occurs when the WP temperature falls below 100°C and the relative humidity in these WPs reaches 95 percent.

- The fuel cladding or HLW canister degrade and fail. (Note: The barrier capability provided by the intact cladding and canisters is not accounted for in the TSPA-LA Model.)

- The solid waste form degrades. This process provides the rate at which the radionuclides are made available for mobilization and release.

- Radionuclides are mobilized into aqueous solution, aqueous colloidal suspension, or gaseous phase. (Note: Gaseous transport is not included in the TSPA-LA Model because it is not a significant release mode (DTN: MO0706SPAFEPLA.001_R1 [DIRS 185200], FEP 2.1.12.06.0A).)

Once water and oxygen are available within a breached WP, corrosion products from degradation of steel internal components would form. In CSNF WPs, these steel components include the fuel basket guides, the TAD canister, and the inner vessel. In CDSP WPs, these steel components include the central support tube and divider assembly and the inner vessel. The TAD canister shield plug (15 in. thick) in CSNF WPs and the inner lid (9 in. thick) in CDSP WPs are not included as contributing to corrosion products available for sorption because the large mass of these components is localized at one end of the WP and therefore should not appreciably affect transport throughout the rest of the WP (SNL 2007 [DIRS 177407], Section 6.5.2.1.1.2 and Section 6.5.2.1.2).

Mobile radionuclides are transported out of the breached WPs and through the EBS to the UZ. Transport out of the breached WPs can occur by advection, when there is a liquid flux through the WPs, and by diffusion through continuous liquid pathways in the WPs, including thin films of adsorbed water. As noted above, a continuous thin film cannot form until the WP temperature falls below 100°C and the relative humidity interior to the WPs reaches 95 percent. Diffusive transport through WP corrosion products depends on the water saturation, porosity, temperature, and relative humidity in the WPs. In the TSPA-LA Model, it is assumed that temperature and relative humidity in the WPs are equal to the temperature and relative humidity on the WP outer surfaces. The two transport processes (diffusion and advection) are each a function of the type of penetration through the DSs and WPs and the local seepage conditions. Diffusion can occur through stress corrosion cracks or through general corrosion patches in the WP both with and without liquid flux through the WPs. Advection is not considered through stress corrosion cracks or through corrosion patches in the absence of seepage flux.

The corrosion products from the WP internal components have the potential to strongly sorb actinides. The process of radionuclide sorption onto the WP corrosion products and invert ballast material (crushed tuff) is beneficial to performance because this process can retain radionuclides in the EBS and delay release to the UZ. Because the WP corrosion products are in intimate contact or directly in the flow or diffusion path of the radionuclide source inside the

WPs, retardation by corrosion products inside the WPs will occur. However, note that because corrosion products from the structural steel members of the invert are more localized and not necessarily in any flow path from the WPs, sorption onto corrosion products in the invert is not represented in the TSPA-LA Model.

The volume of liquid water that could contact a WP is the sum of the dripping seepage and any condensation that may occur on the drift wall. The volume of dripping seepage is quantified by the abstraction for drift seepage (Section 6.3.3.1 of the parent document); results from this abstraction are discussed in Section 8.3.3.1.1[a]. The occurrence and volume of condensation are quantified by the Drift Wall Condensation Submodel (Section 6.3.3.2 of the parent report), and results are summarized here.

Within the emplacement drifts, water evaporated from the emplacement drift walls and invert is transported primarily by natural convection from warmer to cooler areas, where it condenses on cooler surfaces such as the drift wall. The rates of evaporation and condensation, as well as the rate of water vapor transport in the emplacement drift, determine the extent of condensation. In-drift condensation is evaluated with the in-drift condensation model (Section 6.3.3.2). This model provides the TSPA-LA Model with both the probability and magnitude of condensation on the drift wall during cool-down. The TSPA-LA Model treats the flow of drift-wall condensation as a source of liquid water to be added to the liquid water entering the drift as seepage. The TSPA-LA Model uses this combined liquid-water source term in the EBS flow and chemical environment calculations.

The in-drift condensation model defines three stages for the occurrence of condensation. Stage 1 is when the drift wall temperature is above the boiling temperature of water at all locations in the drifts. No condensation occurs during Stage 1. Stage 2 is for times between when the first location in a drift drops below the boiling temperature and the last location drops below the boiling temperature. Stage 3 occurs after all WPs (and thus the drift wall) drop below the boiling temperature. Drift-wall condensation results are presented in Tables 8.3-6[a] and 8.3-7[a]. Results in Table 8.3-6[a] show that drift-wall condensation does not occur on CSNF WPs during Stage 2 and that there is a small probability a negligible condensation rate will occur during Stage 3 on a very small fraction of CSNF WPs. Results in Table 8.3-7[a] show that a significant drift-wall condensation rate (approximately 0.5 m^3/yr) will occur on all CDSP WPs (probability of one and mean WP fraction of one) during Stage 2 for approximately 1,000 years. For comparison, mean seepage rates at 1,500 years are presented in Table 8.3-8[a]. During Stage 3, which lasts until about 2,000 years after closure, the probability of condensation decreases dramatically and the condensation rates are negligible. Drift-wall condensation ceases after 2,000 years for both CSNF and CDSP WPs.

The impact of condensation water on the barrier capability of CDSP WPs is not significant because DSs do not fail to perform their water diversion function during the time condensation will occur. Thus, in the TSPA-LA Model condensation water is diverted around the CDSP WPs except possibly in the case of a very small number of early DS failures or in the unlikely event of DS failure by fault displacement.

Activity Releases from the Engineered Barrier System for Combined Early Drip Shield Failure, Early Waste Package Failure, and Nominal Processes

The aspects of EBS performance that determine the release of radionuclides as modeled in the TSPA-LA Model for the combined Nominal/Early Failure Modeling Case can be summarized as follows:

- Nominal processes cause only a single WP breach (output DTN: MO0710ADTSPAWO.000 [DIRS 183752], LA_v5.005_NC_000300_000.gsm) within the 0- to 10,000-year time interval over all the epistemic samples (Section 8.2.1[a]); WP breach is due to SCC of the closure-lid weld.

- Prior to 170,000 years, radionuclide releases from the EBS are determined by processes related to early DS failure and early WP failure.

- After 170,000 years, radionuclide releases from the EBS are determined primarily by processes related to the failure of WPs from nominal processes.

- DS failure for nominal conditions is defined as a complete breach of the DS plate by general corrosion (Section 6.3.5.1). DS failure times are distributed between 270,000 and 340,000 years (Figure 8.1-4[a]).

- The probability of one or more WP early failures is 0.442 (Section 8.2.2). The expected number of WP early failures is 1.09 (Section 8.2.2).

- The probability of one or more DS early failures is 0.0166 (Section 8.2.2). The expected number of DS early failures is 0.018 (Section 8.2.2).

- Early DS failure is assumed to result in WP failure only if the failed DS is located in a seeping environment; otherwise, there is no WP failure and, hence, no radionuclide release. Water flows into the failed WPs as soon as the WP temperature falls below 100°C and advective transport occurs immediately (Section 6.4.1.3).

- Early WP failure results in releases of radionuclides only by diffusion prior to DS failure by general corrosion. After DS failure, advective transport can occur if the WP is experiencing dripping conditions.

- By about 340,000 years, all DSs have failed and the number of WPs breached by nominal corrosion processes steadily increases (Section 8.3.3.2[a]). As a result, radionuclide releases due to nominal corrosion processes also tend to increase with time (Figure 8.2-1[a]).

- The TSPA-LA Model represents 11,629 WPs (8,213 CSNF WPs and 3,416 CDSP WPs) (Table 6.3.7-1). In CDSP WPs, HLW contains most of the ^{99}Tc with an average initial inventory of 1.01×10^3 g (17.2 Ci) per CDSP WP. In contrast, the DSNF component of waste in a CDSP WP contains 1.58×10^2 g (2.69 Ci) of ^{99}Tc. The amount of ^{99}Tc

contained in the CSNF waste is substantially greater at 7.55×10^3 g (130 Ci) per CSNF WP (Section 6.3.7.1, Table 6.3.7-3, and Table 6.3.7-5).

- At 10,000 years, there is a sharp increase in radionuclide releases (Figure 8.2-6a[a]) resulting from the early failure of CSNF WPs. Diffusive transport from early failed CSNF WPs begins between 9,000 years and 14,000 years, whereas diffusive transport from early failed CDSP WPs begins between 500 years and 3,000 years (Section 7.7.1.1[a]). CSNF WPs are hotter than CDSP WPs (SNL 2007 [DIRS 181383], Section 6.3.5, Figure 6.3-53), with the result that releases from CSNF WPs are delayed until both the WP temperature falls below 100°C and the relative humidity interior to these packages reaches 95 percent, at which time a continuous thin film of adsorbed water required for diffusive radionuclide transport is assumed to be present (Section 6.3.8.1). Because infiltration rates and temperatures vary across the repository footprint, the time at which a continuous thin film of adsorbed water required for diffusive radionuclide transport begins also varies (Section 6.3.8.1).

- Because ^{99}Tc is assumed to have no solubility limit and to be non-sorbing (Section 6.3.7.5), released technetium moves very rapidly from the EBS to the UZ. The EBS release characteristics of ^{99}Tc are representative of other highly soluble and non-sorbing radionuclides such as ^{129}I.

- Because the Waste Package Early Failure Modeling Case is the most dominant case in the first few thousand years for the combined Nominal/Early Failure Modeling Case, ^{239}Pu is not an important contributor to expected dose over this time period (Figure 8.2-4a[a] and Figure 8.2-6a[a]). Much of the mobilized plutonium sorbs onto stationary corrosion products and its subsequent release depends on the rates of desorption (Section 6.3.8), which results in the slow but steady release of ^{239}Pu from the WP. (Appendix K of the parent document, Figure K5.3.3-4 and Figure K5.3.5-4 illustrate release of dissolved ^{239}Pu from the EBS for early failure of one CDSP WP and one CSNF WP, respectively).

- The initial release of ^{239}Pu from the EBS is primarily from DSNF waste forms, which are conservatively assumed to immediately degrade when a CDSP WP is breached (Section 6.3.7.4.2). The releases of ^{239}Pu later in the first 10,000 years are primarily from HLW, which degrades relatively slowly over time. Releases of ^{239}Pu from CSNF WPs are delayed until diffusive transport begins after about 9,000 years (Section 7.7.1.1[a]).

Figure 8.3-13[a] compares the mean total activity of all radionuclides remaining after decay of the initial inventory to the mean total activity of all radionuclides released from the EBS for the combined Nominal/Early Failure Modeling Case for both compliance periods. The plots indicate that under nominal conditions, including early failure of DSs and WPs, only a small fraction (less than 3.9×10^{-7}) of the activity in the total radionuclide inventory would be released from the EBS in 10,000 years. After one million years, the mean total release would be about 7 percent of the inventory.

Figure 8.3-13[a] indicates that for both the first 10,000 year time period and the post-10,000-year time period, of the 12 radionuclides selected for analysis, ^{99}Tc is the most significant contributor to mean activity release from the EBS, comprising most of the mean total activity released, even though ^{99}Tc provides less than one percent of the total activity 1,000 years after closure (Figure 8.3-1a[a]). The contribution for the other radionuclides selected is much less. In the case of plutonium species, the plots on Figure 8.3-13[a] show the activity of radionuclides transported irreversibly sorbed to colloids (designated by the superscript I) and the total activity of the mass in dissolved phase, and reversibly and irreversibly associated with colloids (designated by the superscript T). For americium, only the total activity is plotted because the colloidal phase is small compared to the dissolved phase.

The release of ^{99}Tc during the first 10,000 years (Figure 8.3-13a[a]) is primarily due to diffusive releases from early failure of WPs and, to a lesser extent, advective releases from early DS failure and concomitant WP failure. Nominal WP degradation processes are not likely to cause WP failures prior to about 170,000 years after closure (Figure 8.3-5[a], as shown by the 95th percentile curve). As a result, average releases from the EBS prior to 170,000 years are determined by processes related to early DS failure and early WP failure. The expected number of early failed WPs is about sixty times greater than the expected number of early failed DSs. In addition, early DS failure is assumed to result in WP failure only if the early failed DS is experiencing seeping conditions. Otherwise, there is no WP failure and, hence, no radionuclide release. Under nominal conditions, approximately 69 percent of the WP locations in the repository have non-seeping conditions (Table 8.3-2[a]); therefore, only about 31 percent of early failed DSs result in failure of the underlying WP. Thus, on average, the number of early failed WPs is about one hundred times greater than the number of failed WPs associated with early-failed DSs. Hence, releases due to early WP failure tend to be substantially greater than releases due to early DS failure.

Furthermore, of those WPs that become breached, radionuclide releases during the first 10,000 years are primarily from the cooler CDSP WPs. As noted above, CSNF WPs are hotter than the CDSP WPs (SNL 2007 [DIRS 181383], Section 6.3.5) with the result that releases from early failed CSNF WPs are delayed until after 9,000 years; whereas releases from early failed CDSP WPs are delayed until after 500 years to allow formation of a continuous thin film of adsorbed water, which is required to initiate diffusive radionuclide transport (Section 6.3.8.1). The initiation of transport from CSNF WPs is illustrated on Figure 8.3-13b[a] by the sharp increases in radionuclide releases at around 10,000 years.

Figure 8.3-1[a] indicates that radionuclides such as ^{90}Sr, ^{137}Cs, and ^{241}Am dominate the total inventory activity at the earliest times. Figure 8.3-13a[a] shows that these radionuclides are released in small amounts from the EBS from early failure of CDSP WPs and/or DSs, and experience only moderate sorption and negligible delay during transport out of the EBS (Section 6.3.7 and Section 6.3.8). Due to the short half-lives of ^{90}Sr and ^{137}Cs, these radionuclides are secondary contributors to the mean total activity releases from the EBS for only a few hundred years. Because of the longer half-life of ^{241}Am, this radionuclide is a secondary contributor to the mean total activity releases until about 2,000 years. A second peak in activity releases of ^{241}Am occurs just after 10,000 years, caused by releases from early failed CSNF WPs (Figure 8.3-13b[a]).

From about 2,000 to 10,000 years, ^{239}Pu and ^{240}Pu are important contributors to mean total activity released. These two radionuclides dominate the total inventory at 10,000 years with ^{239}Pu and ^{240}Pu contributing 52 percent and 40 percent of the mean total activity, respectively (Figure 8.3-1[a]). ^{239}Pu and ^{242}Pu are less mobile solutes that reversibly sorb to stationary corrosion products in the WPs, which reduces releases from the WPs. On Figure 8.3-13[a], the activity releases of ^{239}Pu and ^{242}Pu are shown as totals (denoted by $^{239}Pu^{T}$ and $^{242}Pu^{T}$) of the mass in dissolved phase and the mass sorbed on colloids (reversibly and irreversibly); the activity releases of ^{239}Pu and ^{242}Pu irreversibly sorbed on colloids (only) are denoted by $^{239}Pu^{I}$ and $^{242}Pu^{I}$. The comparison shows that the irreversible colloids contribute only about 1 percent of the mean activity releases of these radionuclides.

The relatively small value of mean total activity release from the EBS after 10,000 years and prior to about 170,000 years (Figure 8.3-13b[a]) is explained by the absence of DS failure (except for early failures) and the limited number of WP failures prior to 170,000 years. As noted above and described in Section 8.3.3.2.1[a], DS failure times range from 270,000 to 340,000 years. In addition, SCC penetrations of the WP closure-lid welds are unlikely to occur before approximately 170,000 years (as shown by the 95th percentile curves on Figure 8.3-9b[a] and Figure 8.3-10b[a]). As SCC penetrations occur, releases from the WPs and EBS increase, as illustrated by the increase in releases of ^{99}Tc at around 170,000 years (Figure 8.3-13b[a]). The amount of activity released from the EBS by moderately soluble and weakly to moderately sorbing radionuclides in the lower natural barrier system (Categories 3 and 4, Section 8.3.1[a]), such as ^{237}Np, ^{242}Pu, and ^{234}U, increases after 200,000 years as well, but substantial increases are not observed until general corrosion failures of WPs begin to occur at about 600,000 years (as shown by the 95th percentile curves; Figures 8.3-11b[a] and 8.3-12b[a]) and subsequent advective releases become significant. However, these releases remain small compared to ^{99}Tc throughout the one-million-year period.

As discussed above, the performance of the EBS in preventing or substantially reducing the rate of radionuclide release to the lower natural barrier is a function of several features and uncertain processes in the EBS. The degree of degradation of the WP is uncertain, spatially variable, and controls the amount and rate of water that may enter the WP and potentially allow degradation of the waste forms. The thermal and chemical environment is also uncertain and spatially variable and affects the degradation rate and characteristics of the waste forms and, more importantly, affects the solubility of the radionuclides in the aqueous phase, as well as the stability of colloids to which radionuclides may be attached. The rate of release is affected by the advective and diffusive transport pathways out of the WPs and through the invert. The transport pathways through the EBS are generally diffusive and their properties are treated as uncertain. Solubility limits significantly control the rate of radionuclide diffusion as they define the concentration gradient through which radionuclides may diffuse. Solubility limits are treated as uncertain except for those radionuclides that are not solubility limited, such as ^{99}Tc (Section 6.3.7.5). Finally, the sorption of radionuclides onto stationary corrosion products from the degraded WPs and internal structural supports is treated as uncertain and affects the release of those radionuclides that are highly sorbed on iron substrates.

To illustrate the resulting uncertainty associated with the release of radionuclide activity (in curies) from the EBS, radionuclide-specific release plots for ^{99}Tc and ^{239}Pu are presented on Figures 8.3-14[a] and 8.3-15[a] for the combined Nominal/Early Failure Modeling Case and both

the first 10,000 year time period and the post-10,000 year time period. Shown on each plot are the mean total inventory for that radionuclide along with the mean release curve and 5th and 95th percentile release curves. These plots illustrate that the mean release is affected by the range of the values of the uncertain parameters used in the analysis as summarized above. As illustrated, the mean release is typically close to the 95th percentile of the uncertain results indicating that the mean release is determined by a relatively few realizations with comparatively large releases. The uncertainty in ^{99}Tc and ^{239}Pu releases prior to 200,000 years is dominated by uncertain parameters that determine the number of early failure WPs and DSs, the degradation rates of HLW glass and CSNF, and the diffusive transport of ^{99}Tc and ^{239}Pu from the waste form to the WP outer barrier (Appendix K, Section K5.3 of the parent document). In addition, uncertainty in the release of ^{239}Pu is also influenced by uncertain parameters that determine the solubility of plutonium and sorption of ^{239}Pu onto stationary corrosion products.

Activity Releases from Engineered Barrier System Due to Seismic Ground Motion Damage of Engineered Barrier System Components

Many of the aspects of EBS performance under nominal and early failure conditions summarized in the preceding discussion are relevant to the Seismic GM Modeling Case. The following factors indicate EBS performance for the Seismic GM Modeling Case:

- Prior to about 170,000 years, radionuclide releases from the EBS are determined by processes related to vibratory ground motion-induced WP failures. The mean release from these processes is significantly greater than the mean release from the combined Nominal/Early Failure Modeling Case (Figure 8.3-13[a] and Figure 8.3-16[a]).

- Between 170,000 to 600,000 years, radionuclide releases from the EBS are determined by contributions from both nominal and vibratory ground motion-induced DS and WP failures (Figure 8.3-8[a]).

- After about 600,000 years, radionuclide releases from the EBS are determined primarily by processes related to the failure of WPs from nominal general corrosion processes (Figure 8.3-6[a]).

- Seismically-induced SCC of the CSNF WPs is not likely to occur before approximately 61,000 years (Figure 8.3-9a[a]), whereas breaches of CDSP WPs may occur much earlier (Figure 8.3-10a[a]). For purposes of comparison, based on the 95th percentile, nominal corrosion breaches of the CSNF and CDSP WPs are not likely to occur before about 170,000 years (Figure 8.3-6a[a]); these breaches, however, are due to nominal process SCC in the closure-lid weld region.

- DS failures by combined seismically-induced rupture and general corrosion are largely distributed between about 40,000 and 300,000 years (Figure 8.3-7[a]) as compared to DS failures by general corrosion alone (under nominal conditions), which are distributed from about 270,000 to 340,000 years (Figure 8.3-4[a]).

- Vibratory ground motion-induced drift collapse during the post-10,000-year period causes the mean seepage fraction to increase to 70 percent as compared to the mean value of 40 percent in the Nominal Modeling Case (Table 8.3-5[a] and Table 8.3-3[a]).

- Much of the mobilized plutonium sorbs onto stationary corrosion products, and its subsequent release depends on the rates of desorption from the corrosion products (Section 6.3.8 of the parent document and Figures 7.7.1-6[a] and 7.7.1-8[a]). ^{242}Pu is a key contributor to expected dose late in the post-10,000-year period (Section 8.1.1.5[a] and Figure 8.2-12[a]).

The EBS capability to prevent or reduce the release of radionuclides in the presence of seismic damage is shown on Figure 8.3-16[a] for both compliance periods.

In the Seismic GM Modeling Case, the CDSP WPs are much more likely to be damaged during 10,000 years after closure (Figure 8.3-8[a]) because the CSNF WPs are much stronger and more failure resistant (Section 7.3.2.6.1). The CSNF WPs include two inner stainless-steel vessels instead of one: namely, an inner vessel and its lid that is similar to the CDSP WPs and an additional stainless-steel TAD canister (SNL 2007 [DIRS 179394], Table 4-3). During the first 10,000 years after closure, the predominant mechanism that causes damage to CDSP WPs is SCC by vibratory ground motion-induced residual stresses in the WP OCB (Figure 8.3-10[a]). The DSs remain intact for seismic events occurring in the first 10,000 years (Figure 8.3-7[a]). As a result, dripping seepage cannot contact the WPs. Therefore, water enters the WP only by vapor diffusion through the cracks in the WP OCB. As CDSP WPs cool and the DSNF and HLW degrade, water films form on WP internals, permitting the diffusive transport of radionuclides through the small cracks and into the invert (Section 6.3.8). Comparing estimates of EBS release of ^{99}Tc shown on Figure 8.3-13[a] with Figure 8.3-16[a] indicates a reduction in EBS capability to retain ^{99}Tc by a factor of about 70 as compared to the combined Nominal/Early Failure Modeling Case. However, the comparison still indicates substantial and similar EBS capability during 10,000 years after closure for the less mobile radionuclides.

Estimates of the EBS release shown on Figure 8.3-16b[a] indicate a reduction in the EBS capability to retain ^{99}Tc by a factor of about 140 at 100,000 years as compared to the combined Nominal/Early Failure Modeling Case. There is also a reduction in EBS capability by a factor of between 4 and 10 for less mobile radionuclides at 100,000 years and one million years, including ^{226}Ra, ^{242}Pu, and ^{237}Np, which are key contributors to dose during the post-10,000-year period. Note that the activity of these radionuclides increases substantially after about 600,000 years when failure of the WPs by general corrosion processes begin to occur. By one million years, the total activity released in both the Seismic GM Modeling Case and the combined Nominal/Early Failure Modeling Case is approximately the same (Figures 8.3-13b[a] and 8.3-16b[a]), indicating that the overall reduction in barrier capability in each case, in terms of total activity released (Figure 8.3-1[a]), is about a factor of 10 after one million years.

The performance of the EBS in preventing or substantially reducing the rate of radionuclide release to the lower natural barrier as a result of combined seismic ground motion-induced degradation and nominal degradation processes is a function of several features and uncertain processes in the EBS. Similar to the combined Nominal/Early Failure Modeling Case, the degree of degradation of the WP controls the amount and rate of water that may enter the WP

and potentially allow degradation of the waste form. The degree of WP degradation is highly uncertain and spatially variable and is significantly influenced by the magnitude and timing of seismic ground motions that are also uncertain. After about 600,000 years (Figure 8.3-11[a]), radionuclide releases from the EBS begin to be determined primarily by processes related to the failure of WPs from nominal processes. Again thermal, chemical, waste-form degradation, and transport processes determine the radionuclide releases from the EBS once WPs are breached. The uncertainty in these processes contributes uncertainty to the projected radionuclide releases from the EBS.

To illustrate the uncertainty associated with the release of radionuclide activity from the EBS, radionuclide-specific release plots for selected radionuclides are presented on Figures 8.3-17[a] to 8.3-22[a] for Seismic GM Modeling Case (which includes degradation processes by nominal general corrosion processes):

- Figure 8.3-17[a]: ^{99}Tc
- Figure 8.3-18[a]: ^{237}Np
- Figure 8.3-19[a]: ^{234}U
- Figure 8.3-20[a]: ^{226}Ra
- Figure 8.3-21[a]: ^{239}Pu
- Figure 8.3-22[a]: ^{242}Pu.

The results in these figures are expected releases (averaged over the aleatory uncertainties) and thus largely reflect the influence of epistemic uncertainties. This series of plots is presented to illustrate the impact of uncertainties on the projections of the EBS radionuclide releases. As can be noted from these plots, the EBS releases for all six radionuclides corresponding to the 95th percentile are consistently close to the corresponding mean release curves but are distant from the 5th percentile curves. This demonstrates that the mean releases are determined by expected releases for a relatively small number of epistemic sample elements for which the expected releases are comparatively large.

8.3.3.3[a] Lower Natural Barrier

As noted earlier, the lower natural barrier component (Section 8.3.2.3) of the repository system includes: (1) the UZ below the repository horizon, and (2) the SZ below the repository that extends downgradient from the repository footprint to the accessible environment. The role of the lower natural barrier is to prevent or substantially reduce the rate of movement of radionuclides from the repository to the accessible environment. The lower natural barrier performs this role through the intrinsic site characteristics that are directly reflected by such factors and processes as:

- Slow advective water transport
- Matrix diffusion and sorption of dissolved phase radionuclides
- Dispersion/dilution of dissolved and colloidal phase radionuclides
- Reversible filtration of colloids that have irreversibly sorbed radionuclides.

These intrinsic site characteristics along with radioactive decay properties of individual radionuclides determine the projected capability of the lower natural barrier. Insights to the

overall effectiveness of the lower natural barrier were developed via probabilistic projections. The projections were generated using the TSPA-LA Model to simulate the evolution of releases from the repository and ensuant radionuclide transport through the UZ and SZ and radionuclide activity at the accessible environment boundary.

To ensure that the capability of the lower natural barrier was examined for a range of release conditions, two demonstration modeling cases were selected:

1. Combined Nominal/Early Failures
2. Seismic GM, including nominal corrosion processes.

The combined Nominal/Early Failure Modeling Case provides insight to barrier capability to reduce radionuclide movement for conditions of early releases from a few early-failed WPs and late releases (e.g., from general corrosion patch penetrations after ~ 400,000 years) from a large number of WPs. The Seismic GM Modeling Case examines the lower natural barrier's capability to reduce radionuclide movement for conditions of releases distributed over both the 10,000-year and post-10,000-year time periods. As described in Section 8.3.3.2[a], the radionuclide releases computed for the Seismic GM Modeling Case occur from a variety of breach modes (e.g., seismic induced SCC cracking, rupture/puncture, and general corrosion patches).

To provide a metric of barrier effectiveness, the activity (in curies) of each radionuclide released from the UZ and SZ was computed using the TSPA-LA Model and the balance equations:

$$\bar{R}_{UZ,k}(t \mid \mathbf{e}) = \bar{A}_{T,k}(t \mid \mathbf{e}) - \left(\bar{A}_{WP,k}(t \mid \mathbf{e}) + \bar{A}_{I,k}(t \mid \mathbf{e}) + \bar{A}_{UZ,k}(t \mid \mathbf{e})\right) \quad \text{(Eq. 8.3.3-3[a])}$$

$$\bar{R}_{SZ,k}(t \mid \mathbf{e}) = \bar{A}_{T,k}(t \mid \mathbf{e}) - \left(\bar{A}_{WP,k}(t \mid \mathbf{e}) + \bar{A}_{I,k}(t \mid \mathbf{e}) + \bar{A}_{UZ,k}(t \mid \mathbf{e}) + \bar{A}_{SZ,k}(t \mid \mathbf{e})\right) \quad \text{(Eq. 8.3.3-4[a])}$$

where $\bar{R}_{UZ,k}(t \mid \mathbf{e})$ and $\bar{R}_{SZ,k}(t \mid \mathbf{e})$ are the expected activities (in curies) of releases of radionuclide k from the UZ and SZ, respectively. The term $\bar{A}_{T,k}(t \mid \mathbf{e})$ is the expected total activity of radionuclide k in the inventory (initial inventory decayed through time); $\bar{A}_{WP,k}(t \mid \mathbf{e})$ is the expected activity of radionuclide k in a WP (including the activity in undegraded waste forms); $\bar{A}_{I,k}(t \mid \mathbf{e})$ is the expected activity of radionuclide k in the invert; $\bar{A}_{UZ,k}(t \mid \mathbf{e})$ is the expected activity of radionuclide k in the UZ; and $\bar{A}_{SZ,k}(t \mid \mathbf{e})$ is the expected activity of radionuclide k in the SZ.

The means of the quantities $\bar{R}_{UZ,k}(t \mid \mathbf{e})$ and $\bar{R}_{SZ,k}(t \mid \mathbf{e})$ are denoted by $\bar{\bar{R}}_{UZ,k}(t)$ and $\bar{\bar{R}}_{SZ,k}(t)$, respectively, and are compared with the mean EBS releases, $\bar{\bar{R}}_{EBS,k}(t)$, to provide an indication of barrier capability. The mean percent reduction ($\overline{\overline{PR}}$) in activity achieved by the UZ alone and by the lower natural barrier as a whole is estimated from the equations:

$$\overline{\overline{PR}}_{UZ,k} = \left(1 - \left[\bar{\bar{R}}_{UZ,k} \Big/ \bar{\bar{R}}_{EBS,k}\right]\right) \times 100 \quad \text{(Eq. 8.3.3-5[a])}$$

$$\overline{\overline{PR}}_{LNB,k} = \left(1 - \left[\overline{\overline{R}}_{SZ,k} / \overline{\overline{R}}_{EBS,k}\right]\right) \times 100 \qquad \text{(Eq. 8.3.3-6[a])}$$

where $\overline{\overline{R}}_{EBS,k}$, $\overline{\overline{R}}_{UZ,k}$, and $\overline{\overline{R}}_{SZ,k}$ are the peak values (at any time) of the mean activity release of radionuclide *k* within the time period under consideration (i.e., time 0 to 10,000 years and 10,000 years to 1,000,000 years). The calculations of $\overline{\overline{PR}}_{UZ,k}$ and $\overline{\overline{PR}}_{LNB,k}$, which are presented below, can be found in output DTN: MO0701PLOTSFIG.000 ([DIRS 185207], *Releases from UZ & SZ updated.xls*).

In the special case of decay chain radionuclides, the quantities $\overline{R}_{UZ,k}(t \mid \mathbf{e})$ and $\overline{R}_{SZ,k}(t \mid \mathbf{e})$ are typically dominated by ingrowth rather than transport of the individual species. This is the case for ^{230}Th and ^{226}Ra; their activities in the lower natural barrier are generally in secular equilibrium with their respective precursors according to the simple decay chain:

^{234}U (half-life 240,000 yrs) → ^{230}Th (half-life 77,000 yrs) → ^{226}Ra (half-life 1,600 years).

Both ^{230}Th and ^{226}Ra move through the lower natural barrier at significantly slower rates than their precursor ^{234}U (SNL 2008 [DIRS 183750], Table 6.10[a]). As a result, their activities are primarily determined by the chain decay process as opposed to by groundwater transport of their individual species. As documented in Section 6.3.7 of the parent document and Sections 6.3.9[a] and 6.3.10[a], the radionuclide half-life values used in the EBS, UZ, and SZ submodels are from DTN: MO0702PASTREAM.001_R0 [DIRS 179925]. The following discussion uses these half-life values (Table 6.3.9-1[a]).

Basis for Lower Natural Barrier Capability Projections—The conceptual models and mathematical basis for the UZ and SZ transport can be found in Sections 6.3.9 and 6.3.10; those sections also describe the implementation of the UZ and SZ abstractions in the overall TSPA-LA Model. The simulation methodology and abstractions of dissolved and colloidal phase transport are documented in: (1) *Particle Tracking Model and Abstraction of Transport Processes* (SNL 2008 [DIRS 184748]), which describes the UZ transport simulation model; (2) *Site-Scale Saturated Zone Transport* (SNL 2008 [DIRS 184806]); and (3) *Saturated Zone Flow and Transport Model Abstraction* (SNL 2008 [DIRS 183750]), which collectively describe the SZ transport simulation model. The experimental data used to characterize UZ and SZ transport model parameters are documented in *Radionuclide Transport Models Under Ambient Conditions* (SNL 2007 [DIRS 177396]).

The TSPA-LA Model uses a Monte Carlo simulation methodology that incorporates aleatory and epistemic uncertainties into the projections. For the combined Nominal/Early Failure Modeling Case, the epistemic loop performs 300 realizations. For the Seismic GM Modeling Case, the probabilistic projections are based on 9,000 realizations consisting of 300 epistemic and 30 aleatory realizations. The aleatory and epistemic sample elements are the same as those used in the analyses presented in Section 8.3.3.2[a].

8.3.3.3.1[a] Capability of Lower Natural Barrier to Prevent or Substantially Reduce the Rate of Radionuclide Movement

A demonstration of lower natural barrier capability was developed using the TSPA-LA Model to simulate radionuclide movement from the EBS through the combined UZ and SZ groundwater path. The UZ portion includes the Topopah Springs welded (TSw) and Calico Hills nonwelded (CHn) tuffs of the Crater Flat Group. Within the repository footprint, the present-day water table varies from around 730 m to 850 m above mean sea level (BSC 2004 [DIRS 169855], Figure 6.2). For wetter climates such as the monsoon and glacial-transition climates, a water table rise up to 120 m for the wetter climate reduces the length of the UZ transport path (Section 6.3.9). The SZ flow path, which extends 18 km from below the repository footprint to the accessible environment boundary, is composed of volcanic units and alluvium (Section 6.3.10). The projected groundwater transport pathway is southeast from the repository site, transitioning to a southerly direction towards the designated accessible environment boundary in the Amargosa Desert. The first 12 to 14 km of the SZ flow path is in fractured volcanic rocks; the remainder of the 18-km flow path is composed of alluvium. The model components of the TSPA-LA Model account for transport in fractured-porous media and are based on: (1) a dual-continuum approach for the UZ (Section 6.3.9.2), and (2) a dual-porosity approach for the fractured volcanic units and an equivalent-continuum approach for the alluvium in the SZ (SNL 2008 [DIRS 183750], Section 6.3.1).

Probabilistic projections of radionuclide releases for the 12 representative radionuclides selected in Section 8.3.1[a] are used to compute the radionuclide releases (in Ci) (from Equation 8.3.3-3[a] and Equation 8.3.3-4[a]) and mean activity reductions (from Equation 8.3.3-5[a] and Equation 8.3.3-6[a]). The radionuclides considered are: ^{137}Cs, ^{90}Sr, ^{241}Am, ^{240}Pu, ^{99}Tc, ^{239}Pu, ^{242}Pu, ^{237}Np, ^{234}U, ^{243}Am, ^{230}Th, and ^{226}Ra. Of these 12 radionuclides, five are transported in the dissolved phase and reversibly and irreversibly sorbed to colloids, namely: ^{241}Am, ^{240}Pu, ^{239}Pu, ^{242}Pu, and ^{243}Am. The calculations of radionuclide release reductions are based on the total activity of these radionuclides, designated with superscript T; it is noteworthy to mention that the activity releases for these five radionuclides are dominated by the dissolved phase activities.

Barrier Capability for Combined Nominal/Early Failure Modeling Case—The aim of this performance demonstration is to estimate the natural barrier capability for a broad range of undisturbed conditions (i.e., in the absence of disruptive events). As will be shown, the early failures of DSs and WPs produce relatively low mean releases starting immediately at repository closure and persisting for the simulated time period of 1,000,000 years. Added to these releases are radionuclides released due to DS and WP failure by nominal processes that mainly occur in the post-10,000-year period (Section 8.3.3.2.1[a]); these failures ultimately lead to relatively large advective radionuclide releases from a large number of WPs.

Projections of Barrier Capability for 10,000 Years after Closure—The projected mean activity releases from the lower natural barrier, specifically $\overline{\overline{R}}_{SZ,k}(t)$, are shown on Figure 8.3-23[a] for the combined Nominal/Early Failure Modeling Case; this figure also shows the corresponding plot for the projected releases from the EBS for 10,000 years after closure (Figure 8.3-23b[a]). At 10,000 years, the mean of total activity released from the SZ (summed

over all radionuclides) is approximately 6 Ci, compared to the mean total activity released from the EBS of about 15 Ci and the mean total activity in the inventory of about 4×10^7 Ci. ^{99}Tc comprises most of the mean total release from the EBS. Figure 8.3-23[a] indicates an overall reduction in activity release due to the lower natural barrier of about 60 percent, although the reduction varies widely for individual radionuclides, as discussed next.

As shown on Figure 8.3-23b[a], the shapes of the curves for various radionuclides released from the EBS vary as a function of time. The variation in shape provides insights into the capability of the EBS to prevent or reduce the rate of movement of radionuclides from the repository to the lower natural barrier and how this capability changes with time. The slope of the activity release curve for a given radionuclide changes with time and typically starts with a positive slope that gradually decreases to zero prior to becoming negative. This shape is attributed to the interplay of the release rate of a radionuclide from the EBS (or mass retention rate in the EBS) compared to its radioactive decay rate. As shown in Equation 8.3.3-1[a], the activity release of a given radionuclide from the EBS is computed by taking the difference between the activity of the emplaced inventory and that retained in the EBS. The positive slope in the activity release curve indicates that the rate of mass release from the EBS is greater than the effective rate of decay of the emplaced mass, where the effective rate of decay accounts for any ingrowth from decay of a parent radionuclide. A positive slope typically occurs when the release rate out of the EBS is large. When the slope is zero, the release rate from the EBS is the same as the effective decay rate; a negative slope occurs when mass is released from the EBS slower than the effective rate of decay. This is typically the case when the EBS release rate becomes negligible and the slope of the activity release curve approaches the rate of change corresponding to the effective decay rate.

In comparing the peak mean activity radionuclide releases for the large initial inventory group (Section 8.3.1[a]): ^{137}Cs (transported as a solute and reversibly sorbed on colloids); ^{90}Sr (transported as a solute); ^{241}Am (transported as a solute and reversibly and irreversibly sorbed on colloids); and ^{240}Pu (transported as a solute and reversibly and irreversibly sorbed on colloids); the calculations of $\overline{\overline{PR}}_{LNB,k}$ indicate that the lower natural barrier effectively accounts for the following reductions in the activity released from the EBS:

- ^{137}Cs (half-life 30.1 yrs): ~100 percent reduction (from ~40 μCi to ~0 μCi)
- ^{90}Sr (half-life 28.8 yrs): ~100 percent reduction (from ~7 μCi to ~0 μCi)
- ^{241}Am (half-life 433 yrs): ~99.9 percent reduction (from ~3 mCi to ~4 μCi)
- ^{240}Pu (half-life 6,560 yrs): ~99.5 percent reduction (from ~17 mCi to ~80 μCi).

The barrier effectiveness of the UZ is supported by detailed particle tracking calculations (SNL 2008 [DIRS 184748], Sections 6.6.2.1[a], [b], and 6.6.2.2[a], [b]) that indicate mean water transport times (to the water table) from the southern part of the repository on the order of 400 years or longer, which means that any mass of ^{137}Cs and ^{90}Sr released in the southern part of the repository would experience more than 10 half-lives of decay before reaching the water table. Mean transport times from northern repository locations, however, are shorter because of the predominance of flow through fractures. In addition, calculations for the SZ (SNL 2008 [DIRS 183750], Table 6-10[a]) indicate median radionuclide transport times ranging from 42,000 years to greater than 1,000,000 years for cesium species and from 9,000 years to greater

than 1,000,000 years for strontium species (SNL 2008 [DIRS 183750], Table 6-10[a]). In the case of ^{241}Am and ^{240}Pu, reductions in radionuclide activity released are primarily the result of retardation effects arising from a combination of (1) mean seepage fractions that are less than 0.5 (Table 8.3-2[a]), indicating that (on average) more than half of the mass released from the EBS diffuses into the matrix of the UZ; (2) sorption of dissolved phase radionuclides, reversible exchanges from dissolved to colloidal phases, and reversible colloidal filtration; and (3) radionuclide decay occurring during transport through the lower natural barrier.

For ^{99}Tc (half-life 2.13 × 10^5 yrs), $\overline{\overline{PR}}_{LNB,k}$ indicates a reduction of about 62 percent within 10,000 years (~14 Ci to ~5.3 Ci), with the UZ accounting for about three quarters of this reduction. The level of activity reduction of this non-sorbing radionuclide indicates a significant degree of transport through the rock matrix occurring during the first 10,000 years. This effectiveness of the lower natural barrier is due to the interplay of radionuclide transport through the invert and rock matrix, matrix diffusion between fractures and matrix of the UZ, and matrix diffusion in the volcanic units of the SZ in combination with transport time in the SZ. Median transport time for technetium through the SZ is estimated to range from 10 years to about 22,000 years, which means that the capability of the SZ to reduce the rate of movement would be limited for the 10,000-year compliance period. These release characteristics for other highly soluble and non-sorbing radionuclides with long half-lives, such as ^{129}I, are expected to be similar to those of ^{99}Tc.

Regarding projections of $\overline{\overline{PR}}_{LNB,k}$ for radionuclides in the category of low to moderate solubility, low sorption, and long half-life, such as ^{239}Pu, ^{242}Pu, ^{237}Np, and ^{234}U, the reductions in peak mean activities released are estimated to be:

- ^{239}Pu (half-life 2.41 × 10^4 yrs): ~99.6 percent reduction (from ~60 mCi to ~0.3 mCi)
- ^{242}Pu (half-life 3.75 × 10^5 yrs): ~99.1 percent reduction (from ~62 µCi to ~0.5 µCi)
- ^{237}Np (half-life 2.14 × 10^6 yrs): ~78 percent reduction (from ~0.3 mCi to ~77 µCi)
- ^{234}U (half-life 2.46 × 10^5 yrs): ~89 percent reduction (from ~0.1 mCi to ~16 µCi).

With the half-lives of these radionuclides being much greater than 10,000 years, the projected reductions in the activity are primarily attributed to delay in the subsurface transport produced by: (1) the combined processes of matrix diffusion and sorption in the UZ, and (2) matrix diffusion and sorption in volcanic units and sorption in the alluvium of the SZ. With regard to ^{239}Pu and ^{242}Pu, the percent reductions are nearly the same because they have the same sorption properties.

For ^{243}Am, ^{230}Th, and ^{226}Ra, the projected reductions in peak mean activity achieved by the lower natural barrier within 10,000 years after closure are estimated to be:

- ^{243}Am (half-life 7,370 yrs): ~99.8 percent reduction (from ~2 mCi to ~4 µCi)
- ^{230}Th (half-life 7.54 × 10^4 yrs): ~99.4 percent reduction (from ~76 µCi to ~0.5 µCi)
- ^{226}Ra (half-life 1,600 yrs): ~99.9 percent reduction (from ~0.6 mCi to ~0.3 µCi).

More than half of the projected activity reductions in the lower natural barrier are achieved by the UZ. These large reductions occur due to very strong sorption in both the zeolitic and

devitrified tuff layers (Table 6.3.9-2) of the UZ, as well as in the volcanic units and alluvium (Table 6.3.10-2) of the SZ.

Projections of Barrier Capability for Post-10,000 Years after Closure—The plot for the projected mean activity released from the lower natural barrier for the combined Nominal/Early Failure Modeling Case is shown on Figure 8.3-24[a]. Also shown on this figure, is the corresponding projection for mean activity released from the EBS. The peak mean total activity released from the SZ (summed over all radionuclides) is approximately 2.8×10^4 Ci at 800,000 years, compared to the peak mean total activity released from the EBS of about 4×10^4 Ci at 900,000 years. ^{99}Tc comprises most of the mean total release from the EBS. Figure 8.3-24[a] indicates an overall reduction (peak to peak) in activity releases due to the lower natural barrier of about 30 percent.

Of the four radionuclides in the large inventory group (i.e., ^{137}Cs, ^{90}Sr, ^{241}Am, and ^{240}Pu), the inventories for ^{137}Cs and ^{90}Sr are essentially depleted by radioactive decay by 1,000 years (e.g., more than 30 half-lives of decay) after closure (Figure 8.3-1[a]). As a result, there would be no releases of these radionuclides from the EBS or SZ in the post-10,000-year period. In the case of ^{241}Am and ^{240}Pu, however, their total repository inventories are still substantial at 10,000 years (i.e., approximately 1.4×10^4 Ci for ^{241}Am and 1.6×10^7 Ci for ^{240}Pu) (Figure 8.3-1[a]) . Consequently, releases of these radionuclides occur until about 150,000 years.

The calculations of $\overline{\overline{PR}}_{LNB,k}$ for the post-10,000-year period show the following reductions in the peak mean activity of ^{241}Am and ^{240}Pu:

- ^{241}Am (half-life 433 yrs): ~100 percent reduction (from ~0.2 mCi to ~0 mCi)
- ^{240}Pu (half-life 6,560 yrs): ~98 percent reduction (from ~60 mCi to ~1 mCi).

These activity reductions are similar to those projected for the 10,000-year period. Moreover, most of the ^{241}Am activity reduction is accounted for by the UZ portion of the lower natural barrier. In the case of ^{240}Pu, the UZ accounts for about 50 percent of the reduction.

For ^{99}Tc (half-life 2.13×10^5 yrs), the lower natural barrier achieves a reduction of about 5 percent (from $\sim 2.8 \times 10^4$ Ci to $\sim 2.6 \times 10^4$ Ci) at 1,000,000 years. This reduction is predominantly the result of matrix diffusion in the rock layers of the UZ and the volcanic units of the SZ. This activity reduction is considerably smaller than the reductions projected for the 10,000-year period; however, this is due to the fact that the technetium released from the EBS in the first 10,000-year period may not have been released from the SZ within 10,000 years. Note that for ^{99}Tc, the travel time ranges between 10 and 22,190 years within the SZ with a median travel time of 230 years (SNL 2008 [DIRS 183750], Table 6-10[a]). Regarding projections of $\overline{\overline{PR}}_{LNB,k}$ for radionuclides in the category of low to moderate solubility, low sorption, and long half-life, such as ^{239}Pu, ^{242}Pu, ^{237}Np, and ^{234}U, the reductions in peak mean activities released are lower than those for the 10,000-year period. The projected percent reductions are:

- ^{239}Pu (half-life 2.41×10^4 yrs): ~90 percent reduction (from ~0.8 Ci to ~0.08 Ci)
- ^{242}Pu (half-life 3.75×10^5 yrs): ~66 percent reduction (from ~44 Ci to ~15 Ci)

- ^{237}Np (half-life 2.14 × 10^6 yrs): ~23 percent reduction (from ~16 Ci to ~13 Ci)
- ^{234}U (half-life 2.46 × 10^5 yrs): ~32 percent reduction (from ~1.5 Ci to ~1 Ci).

With regard to ^{239}Pu and ^{242}Pu, the percent reductions are distinct because of the effects of radioactive decay and ^{239}Pu having a small half-life compared to the 1,000,000-year time period. The UZ accounts for almost half of the reduction in ^{239}Pu and ^{242}Pu activities. In contrast, the UZ accounts for only about one-third of the reduction in ^{237}Np and ^{234}U activities.

In the case of ^{243}Am, ^{230}Th, and ^{226}Ra, the projected reductions achieved by the lower natural barrier are comparable to those for the 10,000-year period. They are estimated to be:

- ^{243}Am (half-life 7,370 yrs): ~99.6 percent reduction (from ~0.2 Ci to ~0.7 mCi)
- ^{230}Th (half-life 7.54 × 10^4 yrs): ~85 percent reduction (from ~4.5 Ci to ~0.7 Ci)
- ^{226}Ra (half-life 1,600 yrs): ~97.6 percent reduction (from ~28 Ci to ~0.7 Ci).

The UZ portion of the lower natural barrier accounts for about 40 percent of the ^{230}Th activity reduction and about 80 percent of the activity reduction for $^{243}Am^T$ and ^{226}Ra.

Barrier Capability for Seismic Ground Motion Modeling Case—The intent of this demonstration modeling case is to examine the capability of the lower natural barrier under conditions of EBS releases attributed to vibratory ground motion events (i.e., disruptive events). The Seismic GM Modeling Case is particularly relevant because it was shown to be important to projections for the Individual Protection Standard (Section 8.1.1.2[a]). In this demonstration modeling case, damage and failure of the DSs and WPs occur as a result of vibratory ground motion and nominal corrosion processes. Moreover, the WP breach modes are quite varied, including seismic-induced SCC, rupture and puncture, as well as general corrosion penetration of the WP OCB and SCC of the closure-lid welds. These breach modes ultimately lead to a broad range of slow diffusive and fast advective releases to the lower natural barrier.

Projections of Barrier Capability for 10,000 Years after Closure—The projected mean activity released from the lower natural barrier is shown on Figure 8.3-25[a]; also shown on this figure is the corresponding plot for the projected releases from the EBS for 10,000 years after closure. At 10,000 years, the mean of total activity released from the SZ (summed over all radionuclides) is approximately 540 Ci, compared to the mean total activity released from the EBS of about 1,200 Ci and the mean total activity in the inventory of about 4 × 10^7 Ci. ^{99}Tc comprises most of the mean total release from the EBS. Figure 8.3-25[a] indicates an overall reduction in activity releases due to the lower natural barrier of about 55 percent, although the reduction varies widely for individual radionuclides, as discussed next.

In comparing the peak mean activity radionuclide releases for the large initial inventory group (Section 8.3.1[a]): ^{137}Cs (transported as a solute and reversibly sorbed on colloids); ^{90}Sr (transported solute); $^{241}Am^T$ (transported as a solute and reversibly and irreversibly sorbed on colloids); and $^{240}Pu^T$ (transported as a solute and reversibly and irreversibly sorbed on colloids); the calculations of $\overline{\overline{PR}}_{LNB,k}$ indicate that the lower natural barrier effectively accounts for the following reductions in the peak mean activity:

- ^{137}Cs (half-life 30.1 yrs): ~100 percent reduction (from ~0.6 μCi to ~0 μCi)

- ^{90}Sr (half-life 28.8 yrs): ~100 percent reduction (from ~0.03 µCi to ~0 µCi)
- ^{241}Am (half-life 433 yrs): ~100 percent reduction (from ~73 µCi to ~0 µCi)
- ^{240}Pu (half-life 6,560 yrs): ~99.6 percent reduction (from ~15 mCi to ~55 µCi).

These percent reductions are almost identical to those estimated for the combined Nominal/Early Failure Modeling Case. Also similar is the fact that the UZ accounts for very significant reductions (e.g., 80 to 88 percent) of ^{137}Cs, ^{90}Sr, and ^{241}Am activities. It is worth noting that although the percent reductions are similar, the EBS releases for the Seismic Ground Motion are much higher than those for the combined Nominal/Early Failure Modeling Case (Figure 8.3-23[a]).

The mean activity reduction projected for ^{99}Tc (half-life 2.13 × 10^5 yrs) for the first 10,000 years is approximately 55 percent (from 941 Ci to 427 Ci), with more than half of the reduction provided by the UZ (output DTN: MO0710PLOTSFIG.000 [DIRS 185207], *Releases from UZ & SZ Updated.xls*). This level of activity reduction for ^{99}Tc is similar to that for the combined Nominal/Early Failure Modeling Case, but the curies released in the Seismic Modeling Case are much higher.

The percent reductions projected for ^{239}Pu, ^{242}Pu, ^{237}Np, and ^{234}U for the lower natural barrier are as follows:

- ^{239}Pu (half-life 2.41 × 10^4 yrs): ~99.6 percent reduction (from ~48 mCi to ~0.2 mCi)
- ^{242}Pu (half-life 3.75 × 10^5 yrs): ~99.6 percent reduction (from ~49 µCi to ~0.2 µCi)
- ^{237}Np (half-life 2.14 × 10^6 yrs): ~81 percent reduction (from ~0.1 mCi to ~20 µCi)
- ^{234}U (half-life 2.46 × 10^5 yrs): ~93 percent reduction (from ~0.3 mCi to ~22 µCi).

These percent reductions are very similar to those projected for the combined Nominal/Early Failure Modeling Case.

Finally, for ^{243}Am, ^{230}Th, and ^{226}Ra, the projected reductions are estimated to be:

- ^{243}Am (half-life 7,370 yrs): ~100 percent reduction (from ~10 µCi to ~0 µCi)
- ^{230}Th (half-life 7.54 × 10^4 yrs): ~96.2 percent reduction (from ~11 µCi to ~0.4 µCi)
- ^{226}Ra (half-life 1,600 yrs): ~100 percent reduction (from ~30 mCi to ~0.6 µCi).

These percent reductions are also very similar to those projected for the combined Nominal/Early Failure Modeling Case.

Projections of Barrier Capability for Post-10,000 Years after Closure—The plot for the projected mean activity released from the lower natural barrier is shown on Figure 8.3-26[a]; this figure also shows the corresponding projection for mean activity released from the EBS. The peak mean total activity released from the SZ (summed over all radionuclides) is approximately 3 × 10^4 Ci at 800,000 years; compared to the peak mean total activity released from the EBS of about 5 × 10^4 Ci at 800,000 years. ^{99}Tc comprises most of the mean total release from the EBS. Figure 8.3-26[a] indicates an overall reduction (peak to peak) in activity releases due to the lower natural barrier of about 40 percent.

Of the four radionuclides in the large inventory group (i.e., ^{137}Cs, ^{90}Sr, ^{241}Am, and ^{240}Pu), the inventories for ^{137}Cs and ^{90}Sr are essentially depleted by radioactive decay by 1,000 years (e.g., more than 30 half-lives of decay) after closure (Figure 8.3-1[a]). As a result, there would be no releases of these radionuclides from the EBS or SZ in the post-10,000-year period. In the case of ^{241}Am and ^{240}Pu, however, their total repository inventories are still substantial and estimated to be approximately 1.4×10^4 Ci for ^{241}Am and 1.6×10^7 Ci for ^{240}Pu remaining in the repository at 10,000 years after closure.

For the post-10,000-year period, the calculations of $\overline{\overline{PR}}_{LNB,k}$ show the following reductions in the peak mean activity of ^{241}Am and ^{240}Pu:

- ^{241}Am (half-life 433 yrs): ~100 percent reduction (from ~3 μCi to ~0 μCi)
- ^{240}Pu (half-life 6,560 yrs): ~97 percent reduction (from ~0.1 Ci to ~4 mCi).

The UZ accounts for about half of the ^{241}Am activity reductions and nearly all of the ^{240}Pu activity reductions. These reductions are very similar to those estimated for the combined Nominal/Early Failure Modeling Case for the post-10,000-year period.

For ^{99}Tc (half-life 2.13×10^5 yrs), the lower natural barrier is projected to achieve a reduction of about 5 percent (from ~3.3×10^4 Ci to ~3.1×10^4 Ci) at 1,000,000 years. This level of barrier effectiveness is similar to the reduction estimated for the combined Nominal/Early Failure Modeling Case for the post-10,000-year period.

Regarding projections for radionuclides in the category of low-to-moderate solubility; low sorption in the UZ and SZ; and long half-life, such as ^{239}Pu, ^{242}Pu, ^{237}Np, and ^{234}U; the reductions in peak mean activities released are less than those for the 10,000-year period. The projected percent reductions are:

- ^{239}Pu (half-life 2.41×10^4 yrs): ~88 percent reduction (from ~11 Ci to ~1.4 Ci)
- ^{242}Pu (half-life 3.75×10^5 yrs): ~70 percent reduction (from ~200 Ci to ~62 Ci)
- ^{237}Np (half-life 2.14×10^6 yrs): ~20 percent reduction (from ~100 Ci to ~81 Ci)
- ^{234}U (half-life 2.46×10^5 yrs): ~25 percent reduction (from ~14 Ci to ~10 Ci).

The UZ accounts for roughly half of the reductions in ^{239}Pu and ^{242}Pu activity; whereas for ^{237}Np and ^{234}U, it only accounts for about one-quarter of the reductions (output DTN: MO0710PLOTSFIG.000 [DIRS 185207], *Releases from UZ & SZ Updated.xls*). These reductions are very similiar and consistent with those projected for the combined Nominal/Early Failure Modeling Case for the post-10,000-year time period.

In the case of the radionuclides ^{243}Am, ^{230}Th, and ^{226}Ra, the projected reductions are comparable to those shown earlier for the combined Nominal/Early Failure Modeling Case for the post-10,000-year period. The reductions are estimated to be:

- ^{243}Am (half-life 7,370 yrs): ~99.8 percent reduction (from ~3 mCi to ~8 μCi)
- ^{230}Th (half-life 7.54×10^4 yrs): ~89 percent reduction (from ~71 Ci to ~8 Ci)
- ^{226}Ra (half-life 1,600 yrs): ~97 percent reduction (from ~260 Ci to ~8 Ci).

For these three radionuclides, the UZ accounts for one-half or more of the activity reductions (output DTN: MO0710PLOTSFIG.000 [DIRS 185207], *Releases from UZ & SZ Updated.xls*). Again, these reductions are consistent with those projected for the combined Nominal/Early Failure Modeling Case and post-10,000-year time period.

Uncertainty in Projections of Lower Natural Barrier Capability—Uncertainty in the projections of lower natural barrier capability is influenced by uncertainties in of the models for flow and transport processes. The TSPA-LA Model accounts for these epistemic uncertainties by using probabilistic representations of the input parameters in the component models for UZ flow, UZ transport, SZ flow, and SZ transport. In the case of UZ flow and transport (Section 6.3.9), the parameters of primary importance include (1) sorption coefficients for various radionuclides, (2) matrix diffusion coefficient, and (3) infiltration scenario. Important parameters related to groundwater flow (or advection) in the SZ (Section 6.3.10) are: (1) groundwater specific discharge, (2) flowing interval porosity, (3) alluvium effective porosity, and (4) horizontal anisotropy. The process of matrix diffusion is dependent on flowing interval spacing, effective diffusion coefficient, and matrix porosity. The process of radionuclide sorption on the fractured and porous media is a function of the sorption coefficients, bulk density and porosity for various radionuclides, and geologic media. Tables presented in Sections 6.3.9 and 6.3.10 summarize the values and uncertainty distributions for all parameters used in the UZ and SZ transport simulations.

To illustrate the uncertainty associated with the release of radionuclide activity from the lower natural barrier, radionuclide-specific release plots for selected radionuclides are presented on Figures 8.3-27[a] to 8.3-32[a] for combined nominal and seismic ground motion-induced degradation processes:

- Figure 8.3-27[a]: ^{99}Tc
- Figure 8.3-28[a]: ^{237}Np
- Figure 8.3-29[a]: ^{234}U
- Figure 8.3-30[a]: ^{226}Ra
- Figure 8.3-31[a]: ^{239}Pu
- Figure 8.3-32[a]: ^{242}Pu.

The results in these figures are expected releases (averaged over the aleatory uncertainties) and thus largely reflect the impact of epistemic uncertainties. These plots are presented to illustrate the impact of uncertainties on the projections of the lower natural barrier radionuclide releases. As can be noted from these plots, the lower natural barrier releases for all six radionuclides corresponding to the 95th percentile are consistently close to the corresponding mean release curves but are distant from the 5th percentile curves. The aleatory and epistemic sample elements are the same as those used in the analyses presented in Section 8.3.3.2[a].

8.3.3.4[a] Summary of Barrier Capability Demonstration

As illustrated on Figure 8-1 of the parent document, the multiple barriers of the Yucca Mountain repository system consist of three primary barriers: (1) upper natural barrier, (2) EBS, and (3) lower natural barrier. The upper natural barrier consists of the topography and surficial soils of the mountain, the unsaturated tuff units above the repository, and rock strata in which the

repository is constructed. The EBS includes the emplacement drifts, WPs, DSs, waste forms, cladding (associated with the CSNF, DSNF, and naval SNF), pallets, and the drift invert; no credit is taken, however, for cladding performance. The lower natural barrier below the repository includes the unsaturated rock layers beneath the repository as well as the volcanic rock units and the alluvium in the SZ, which extends from the repository site to the designated accessible environment boundary. Collectively, these three barriers function to:

1. Prevent or substantially reduce the rate of movement of water or radionuclides from the repository to the accessible environment, and

2. Prevent or substantially reduce the release of radionuclides from the repository.

Probabilistic projections for two demonstration modeling cases were developed to quantify the capability for the three primary barriers. These two demonstration modeling cases are: (1) combined Nominal/Early Failure Modeling Case (representative of the absence of disruptive events), and (2) Seismic GM Modeling Case (representative of the presence of disruptive events).

Upper Natural Barrier—Barrier capability analyses demonstrate that topography and surficial soils substantially reduce the net infiltration into the underlying UZ rock layers above the repository. For climate states projected for the first 10,000 years after closure, the topography and surficial soils prevent on average about 90 percent or more of the precipitation from entering the underlying UZ rock layers. More specifically, the mean net infiltration rate ($\overline{I}$) as a percentage of precipitation rate ($\overline{P}$) for each climate state is estimated to be: (1) present-day climate: $\overline{I} \sim 8.0$ percent of $\overline{P}$; (2) monsoon climate: $\overline{I} \sim 8.7$ percent of $\overline{P}$; and (3) glacial-transition climate: $\overline{I} \sim 10.4$ percent of $\overline{P}$.

Of the water ultimately reaching the repository horizon (i.e., Topopah Springs welded [TSw]), only a fraction of the local percolation would enter the emplacement drifts as a result of the capillary barrier effect. This capillary barrier effect diverts ambient water flow around the emplacement drifts (Section 6.3.1.1). Taking this effect into account, the mean drift seepage ($\overline{S}$) is less than 11 percent of mean annual percolation rate for intact drifts, and is less than 12 to 48 percent for degraded drifts, varying with the extent of drift degradation.

These seepage rate reductions indicate that very small fractions of the precipitation and ensuant net infiltration would enter the emplacement drifts.

Engineered Barrier System—The EBS prevents or substantially reduces the release rate of radionuclides from the waste forms and prevents or substantially reduces the rate of movement of radionuclides from the repository to the accessible environment. It performs these functions by virtue of the materials and design of the emplacement drifts, DSs, WPs and waste forms, and WP internals. In addition, the EBS provides for chemical and TH environments that lead to low solubilities for the radionuclides that make up the greatest fraction of the inventory activity. Finally, the EBS environments are such that radionuclide transport from the waste to the UZ is limited to a small fraction of the available inventory (less than 3×10^{-3} percent in 10,000 years and 5 percent in 1 million years), even in the case of seismic-induced mechanical degradation.

Lower Natural Barrier—Projections of barrier capability demonstrate that for large initial inventory, soluble, and short half-life radionuclides, such as ^{137}Cs and ^{90}Sr, the mean activity released from the EBS would be reduced by 100 percent (i.e., they are highly unlikely to reach the accessible environment). For radionuclides with longer half-lives such as ^{241}Am and ^{240}Pu, the mean activity released would be reduced by 97 to 100 percent by the natural barrier. For radionuclides of low to moderate solubility, weak to strong sorption, and long half life, such as ^{237}Np, ^{242}Pu, and ^{239}Pu, mean activity released from the EBS would be reduced by 80 percent to 100 percent before reaching the accessible environment during the 10,000-year period and by 20 percent to 88 percent during the post-10,000-year period. In terms of total mean activity, the lower natural barrier reduces the total mean activity released (primarily due to highly soluble, long half-life, non-sorbing ^{99}Tc) from the EBS by 55 percent for the 10,000-year period, and 5 percent for post-10,000-year period, respectively. These reductions of EBS releases would be achieved by the combination of lower natural barrier processes, including slow advective water transport, matrix diffusion and sorption of dissolved phase radionuclides, dispersion/dilution of dissolved and colloidal phase radionuclides, and reversible filtration of colloidal phase radionuclides, as well as radioactive decay.

The demonstration of barrier capability for the EBS and lower natural barrier was developed using the TSPA-LA Model. The values of the parameters used in the TSPA-LA Model are the same as those used in the demonstration of compliance with the individual and groundwater protection standards presented in Section 8.1[a]. Although uncertainty exists in the parameters and models of the relevant processes that affect the assessment of barrier capability, this uncertainty has been appropriately addressed in the assessments. In summary, these barrier capability projections demonstrate that the multiple barriers increase the confidence that the postclosure performance objectives specified in NRC Proposed Rule 10 CFR 63.113(b) and (c) [DIRS 180319] would be achieved.

INTENTIONALLY LEFT BLANK

Table 8.3-2[a]. Seepage Fractions for CDSP and CSNF Waste Packages for Combined Nominal/Early Failure Modeling Case for Glacial-Transition Climate, 2,000 to 10,000 Years

Percolation Subregion		Seepage Fraction for CDSP Waste Packages			Seepage Fraction for CSNF Waste Packages		
Subregion Index	Quantile Range	5th Percentile	Mean	95th Percentile	5th Percentile	Mean	95th Percentile
1	$p < 0.05$	0.0031	0.0881	0.2764	0.0020	0.0887	0.2823
2	$0.05 \le p < 0.30$	0.0261	0.2292	0.5782	0.0217	0.2308	0.5780
3	$0.30 \le p < 0.70$	0.0448	0.3306	0.7395	0.0455	0.3294	0.7439
4	$0.70 \le p < 0.95$	0.0453	0.3846	0.7955	0.0431	0.3848	0.7998
5	$p \ge 0.95$	0.0880	0.4656	0.8447	0.0870	0.4666	0.8386
Repository Average		0.0441	0.3134	0.6898	0.0424	0.3134	0.6950

Source: Output DTN: MO0710PLOTSFIGS.000 [DIRS 185207], file: LA_v5.005_NC_000300_004_Seepage_Fraction.xls.

NOTE: The repository average values are based on weighted averages for each realization using the percolation subregion quantile ranges.

Table 8.3-3[a]. Seepage Fractions for CDSP and CSNF Waste Packages for Combined Nominal/Early Failure Modeling Case for Post-10,000-Year Period

Percolation Subregion		Seepage Fraction for CDSP Waste Packages			Seepage Fraction for CSNF Waste Packages		
Subregion Index	Quantile Range	5th Percentile	Mean	95th Percentile	5th Percentile	Mean	95th Percentile
1	$p < 0.05$	0.0092	0.1251	0.3166	0.0082	0.1251	0.3121
2	$0.05 \le p < 0.30$	0.0623	0.3393	0.6525	0.0617	0.3402	0.6555
3	$0.30 \le p < 0.70$	0.0933	0.4382	0.8072	0.0949	0.4369	0.7943
4	$0.70 \le p < 0.95$	0.0626	0.4365	0.8464	0.0606	0.4364	0.8439
5	$p \ge 0.95$	0.0941	0.4935	0.8872	0.0934	0.4944	0.8802
Repository Average		0.0750	0.4001	0.7483	0.0784	0.3999	0.7449

Source: Output DTN: MO0710PLOTSFIGS.000 [DIRS 185207], file: LA_v5.005_NC_000300_000_Seepage_Fraction.xls.

NOTE: The repository average values are based on weighted averages for each realization using the percolation subregion quantile ranges.

Table 8.3-4[a]. Seepage Fractions for CDSP and CSNF Waste Packages for Seismic Ground Motion Modeling Case for Glacial-Transition Climate, 2,000 to 10,000 Years

Percolation Subregion		Seepage Fraction for CDSP Waste Packages			Seepage Fraction for CSNF Waste Packages		
Subregion Index	Quantile Range	5th Percentile	Mean	95th Percentile	5th Percentile	Mean	95th Percentile
1	$p < 0.05$	0.0031	0.0881	0.2764	0.002	0.0887	0.2823
2	$0.05 \le p < 0.30$	0.0261	0.2292	0.5782	0.0217	0.2308	0.578
3	$0.30 \le p < 0.70$	0.0448	0.3306	0.7395	0.0455	0.3294	0.7439
4	$0.70 \le p < 0.95$	0.0453	0.3846	0.7955	0.0431	0.3848	0.7998
5	$p \ge 0.95$	0.088	0.4656	0.8447	0.087	0.4666	0.8386
Repository Average		0.0441	0.3134	0.6898	0.0424	0.3134	0.6950

Source: Output DTN: MO0710PLOTSFIGS.000 [DIRS 185207], file: LA_v5.005_SM_009000_001_Seepage_Fraction.xls.

NOTE: The repository average values are based on weighted averages for each realization using the percolation subregion quantile ranges.

Table 8.3-5[a]. Seepage Fractions for CDSP and CSNF Waste Packages for Seismic Ground Motion Modeling Case for Post-10,000-Year Period

Percolation Subregion		Seepage Fraction for CDSP Waste Packages			Seepage Fraction for CSNF Waste Packages		
Subregion Index	Quantile Range	5th Percentile	Mean	95th Percentile	5th Percentile	Mean	95th Percentile
1	$p < 0.05$	0.3252	0.4666	0.6965	0.3231	0.4673	0.6923
2	$0.05 \le p < 0.30$	0.3077	0.6484	0.9164	0.3089	0.6491	0.9173
3	$0.30 \le p < 0.70$	0.309	0.7196	0.9725	0.3114	0.7193	0.975
4	$0.70 \le p < 0.95$	0.231	0.7051	0.9793	0.226	0.7041	0.9803
5	$p \ge 0.95$	0.3076	0.7525	0.9878	0.3107	0.7518	0.9869
Repository Average		0.2909	0.6871	0.9450	0.2912	0.6870	0.9465

Source: Output DTN: MO0710PLOTSFIGS.000 [DIRS 185207], file: LA_v5.005_SM_009000_003_Seepage_Fraction.xls.

NOTE: The repository average values are based on weighted averages for each realization using the percolation subregion quantile ranges.

Table 8.3-6[a]. Drift Wall Condensation for CSNF Waste Packages for Stage 2 and Stage 3 Condensation

Percolation Subregion	CSNF Waste Packages							
	Stage 2				Stage 3			
	Probability	Mean WP Fraction	Mean Flux (m^3/yr)	Mean Duration	Probability at 1,500 Years	Mean WP Fraction	Mean Flux (m^3/yr) at 1,500 Years	Mean Duration
1	0	0	0	NA	0.020	0.020	7.50E-05	750 to 2,000 years
2	0	0	0	NA	0.023	0.023	6.74E-05	750 to 2,000 years
3	0	0	0	NA	0.020	0.020	7.94E-05	750 to 2,000 years
4	0	0	0	NA	0.0067	0.0067	6.95E-06	750 to 2,000 years
5	0	0	0	NA	0.010	0.010	4.78E-05	750 to 2,000 years

Source: Output DTN: MO0801TSPAMVAC.000 [DIRS 185080], file: *condensation_rates_and_fractions.xls.*

NOTE: Drift-wall condensation fraction and flux are the same for both the combined Nominal/Early Failure and Seismic Ground Motion Modeling Cases.

Table 8.3-7[a]. Drift Wall Condensation for CDSP Waste Packages for Stage 2 and Stage 3 Condensation

Percolation Subregion	CDSP Waste Packages							
	Stage 2				Stage 3			
	Probability	Mean WP Fraction	Mean Flux (m^3/yr)	Mean Duration	Probability at 1,500 Years	Mean WP Fraction	Mean Flux (m^3/yr) at 1,500 Years	Mean Duration
1	1	1	0.54	0 to 1,000 years	0.020	0.020	6.78E-05	750 to 2,000 years
2	1	1	0.54	0 to 1,000 years	0.017	0.017	5.97E-05	750 to 2,000 years
3	1	1	0.54	0 to 1,000 years	0.017	0.017	7.16E-05	750 to 2,000 years
4	1	1	0.54	0 to 1,000 years	0.0033	0.0033	6.00E-06	750 to 2,000 years
5	1	1	0.54	0 to 1,000 years	0.010	0.010	4.32E-05	750 to 2,000 years

Source: Output DTN: MO0801TSPAMVAC.000 [DIRS 185080], file: *condensation_rates_and_fractions.xls.*

NOTE: Drift-wall condensation fraction and flux are the same for both the combined Nominal/Early Failure and Seismic Ground Motion Modeling Cases.

Table 8.3-8[a]. Mean Seepage Rates for Waste Packages during Stage 2 and Stage 3 Condensation

Percolation Subregion		Mean Seepage Rates (m^3/yr) 0 to 2,000 years (Seepage at 1,500 years)	
Subregion Index	Quantile Range	CNSF Waste Packages	CDSP Waste Packages
1	$p < 0.05$	0.011176	0.011055
2	$0.05 \le p < 0.30$	0.051718	0.051666
3	$0.30 \le p < 0.70$	0.073576	0.073266
4	$0.70 \le p < 0.95$	0.080291	0.079843
5	$p \ge 0.95$	0.11245	0.11025
Repository Average		0.068614	0.068249

Source: Output DTN: MO0801TSPAMVAC.000 [DIRS 185080], file: *condensation_rates_and_fractions.xls*.

NOTES: Mean seepage flux is the same for both the Nominal/Early Failure and Seismic Ground Motion Modeling Cases over the first 2,000 years.

The repository average values are weighted averages using the percolation subregion quantile ranges.

8.4[a] VALIDITY AND DEFENSIBILITY OF PERFORMANCE DEMONSTRATION

The validation activities are presented in Section 7 of the parent document and an additional set of analyses are presented in Section 7[a] of this addendum. Any additions to the description of the TSPA-LA Model presented in Section 6 of the parent document are presented in Section 6[a]. The technical basis for the component models and TSPA input database is documented in supporting model reports. The parent document and supporting documentation were prepared in a manner that would ensure the technical basis is auditable and traceable so as to facilitate the licensing review.

The issuance of this addendum reflects the TSPA methodology defined in the parent document, which specifies:

- Continued scrutiny of the conceptual and mathematical models through internal and external peer reviews
- Further development and testing of TSPA component models and submodels
- Statistical analysis of data and development of improved characterizations of uncertainty.

In this addendum, the issues identified in Appendix P of the parent document have been addressed, the rationale for their use explained, and their impact on postclosure performance metrics evaluated.

This section provides a summary of the specific YMP technical and programmatic activities conducted to ensure that the DOE postclosure performance demonstration is suitable to support the LA for the nuclear waste repository at Yucca Mountain. This section has not changed and applies to the work presented in this addendum.

8.4.1[a] Validation of TSPA Model and Component Models

No change.

8.4.2[a] Verification and Validation of TSPA Software and Input Data

No change.

8.4.3[a] Uncertainty Characterization Reviews

No change.

8.4.4[a] Corroboration of TSPA-LA Results

No change.

8.4.5[a] Peer Reviews of YMP TSPA Methodology

No change.

INTENTIONALLY LEFT BLANK

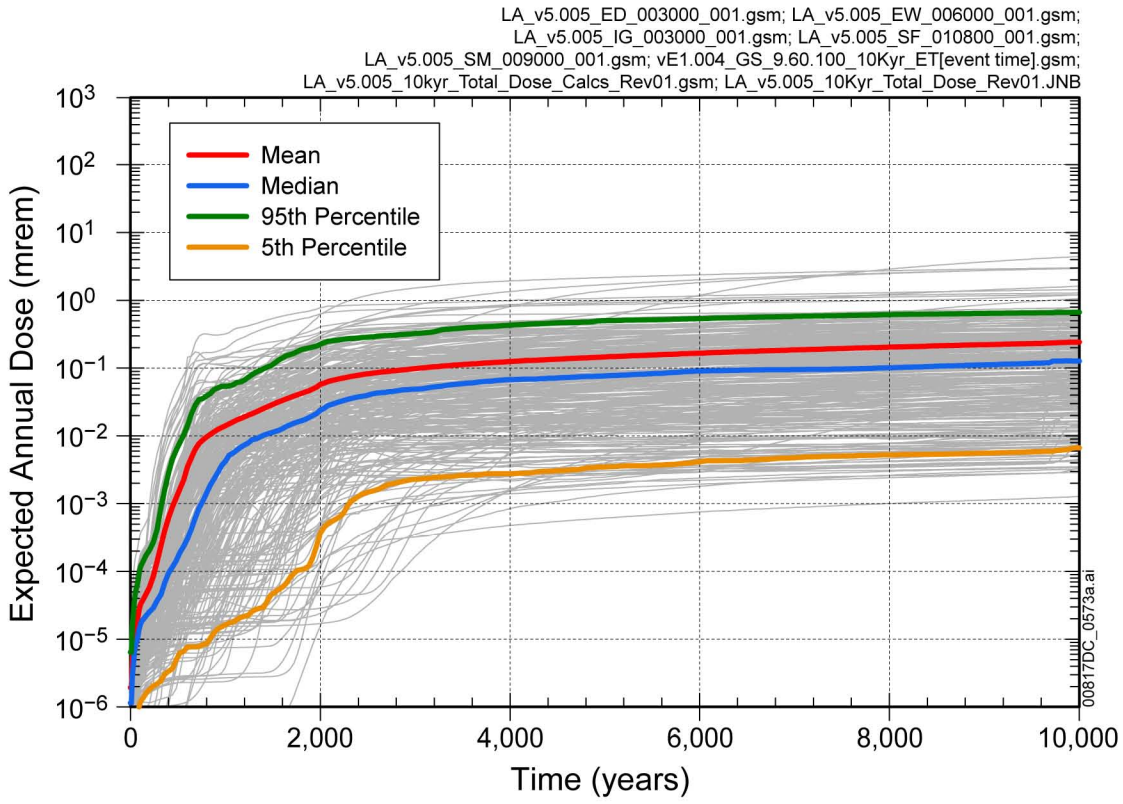

Source: Output DTNs: MO0710ADTSPAWO.000 [DIRS 183752]; MO0710PLOTSFIG.000 [DIRS 185207]; and MO0709TSPAREGS.000 [DIRS 182976].

Figure 8.1-1[a]. Distribution of Total Expected Annual Dose for 10,000 Years after Repository Closure

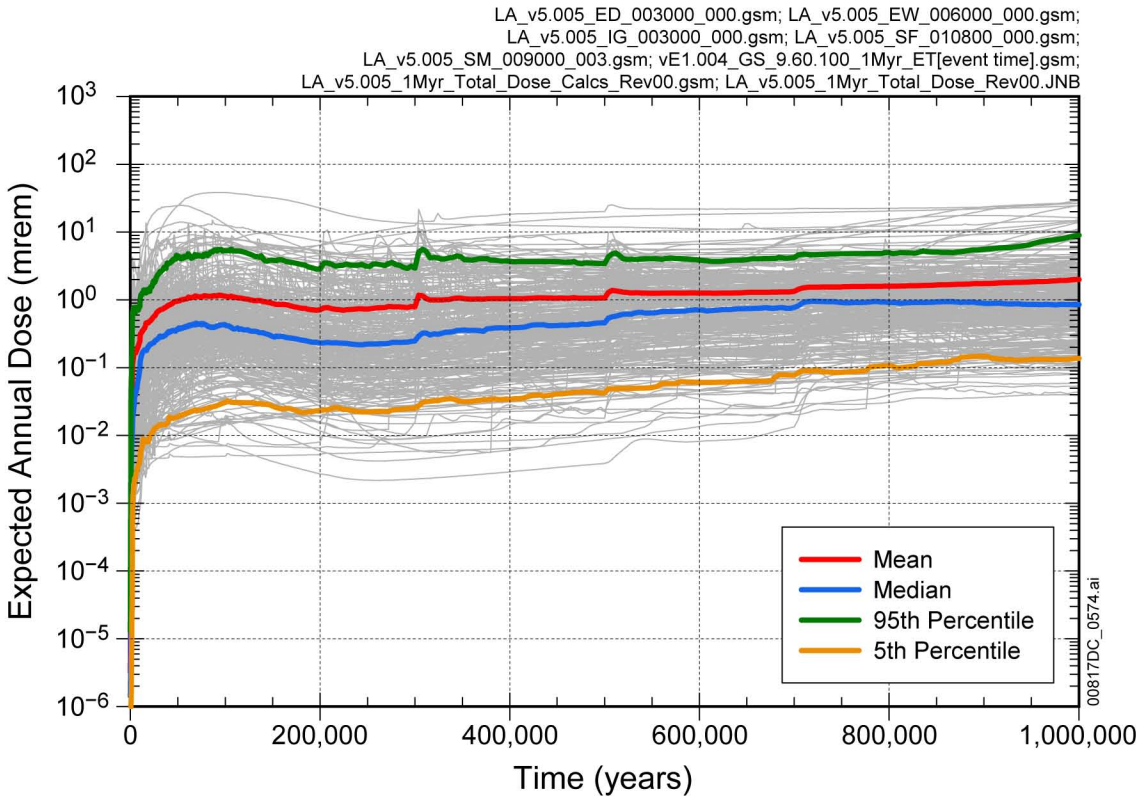

Source: Output DTNs: MO0710ADTSPAWO.000 [DIRS 183752]; MO0710PLOTSFIG.000 [DIRS 185207]; and MO0709TSPAREGS.000 [DIRS 182976].

Figure 8.1-2[a]. Distribution of Total Expected Annual Dose for 1,000,000 Years after Closure

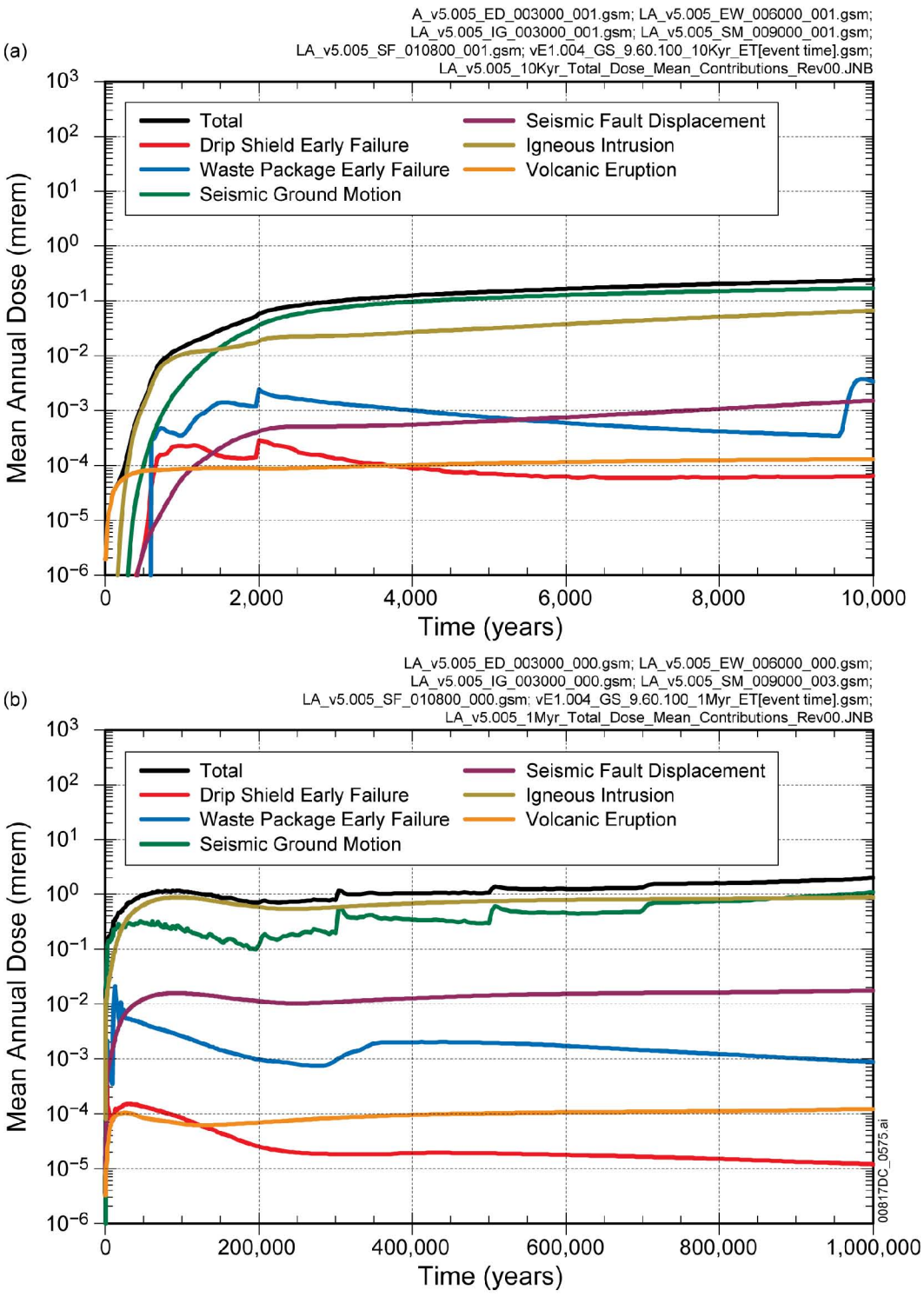

Source: Output DTNs: MO0710ADTSPAWO.000 [DIRS 183752]; and MO0709TSPAREGS.000 [DIRS 182976].

Figure 8.1-3[a]. Relative Contributions of Modeling Cases to Total Mean Annual Dose for (a) 10,000 Years and (b) 1,000,000 Years after Repository Closure

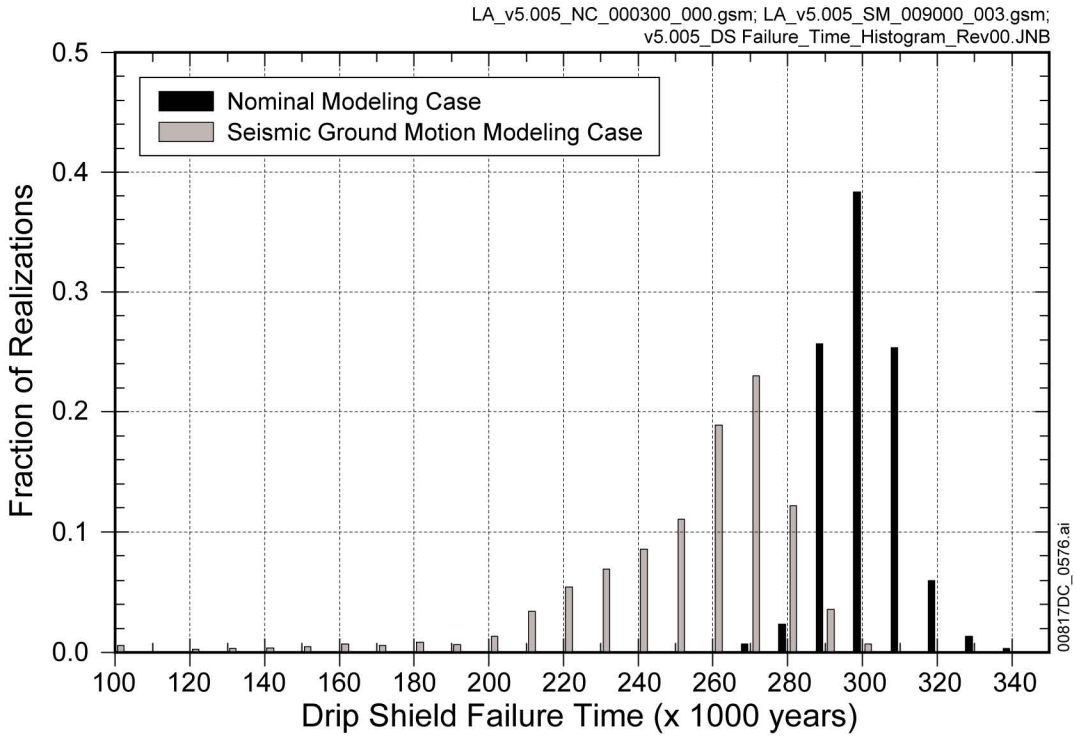

Source: Output DTN: MO0710ADTSPAWO.000 [DIRS 183752].

NOTE: Nominal failures are due to general corrosion. Seismic ground motion failures are caused by the combined effects of general corrosion, vibratory ground motion, and rockfall.

Figure 8.1-4[a]. Histogram of the Time of Drip Shield Failure for the Nominal and Seismic Ground Motion Modeling Cases

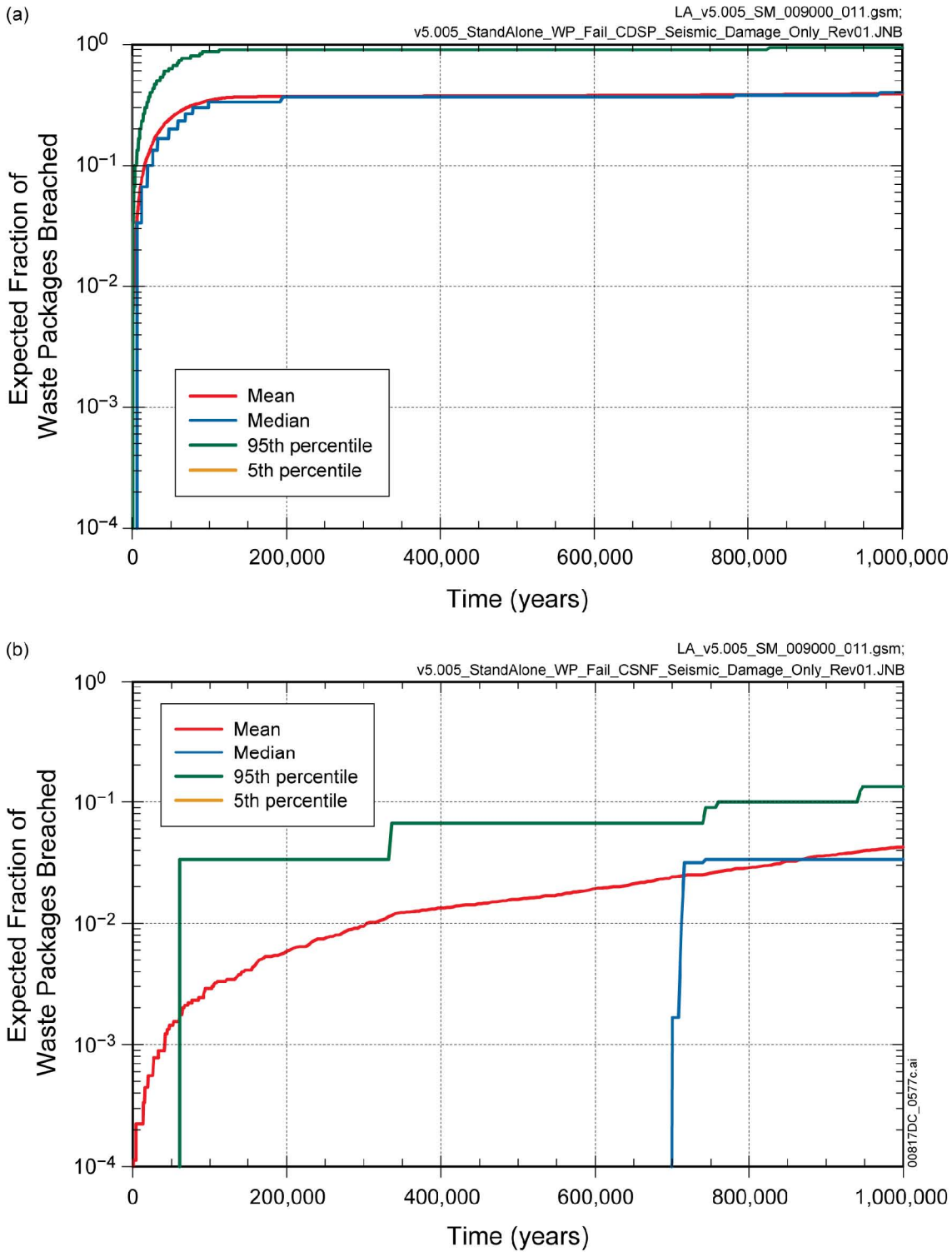

Source: Output DTN: MO0801TSPAWPDS.000 [DIRS 185077].

Figure 8.1-5[a]. Fraction of (a) CDSP Waste Packages and (b) CSNF Waste Packages Failed by Seismic Damage as a Function of Time

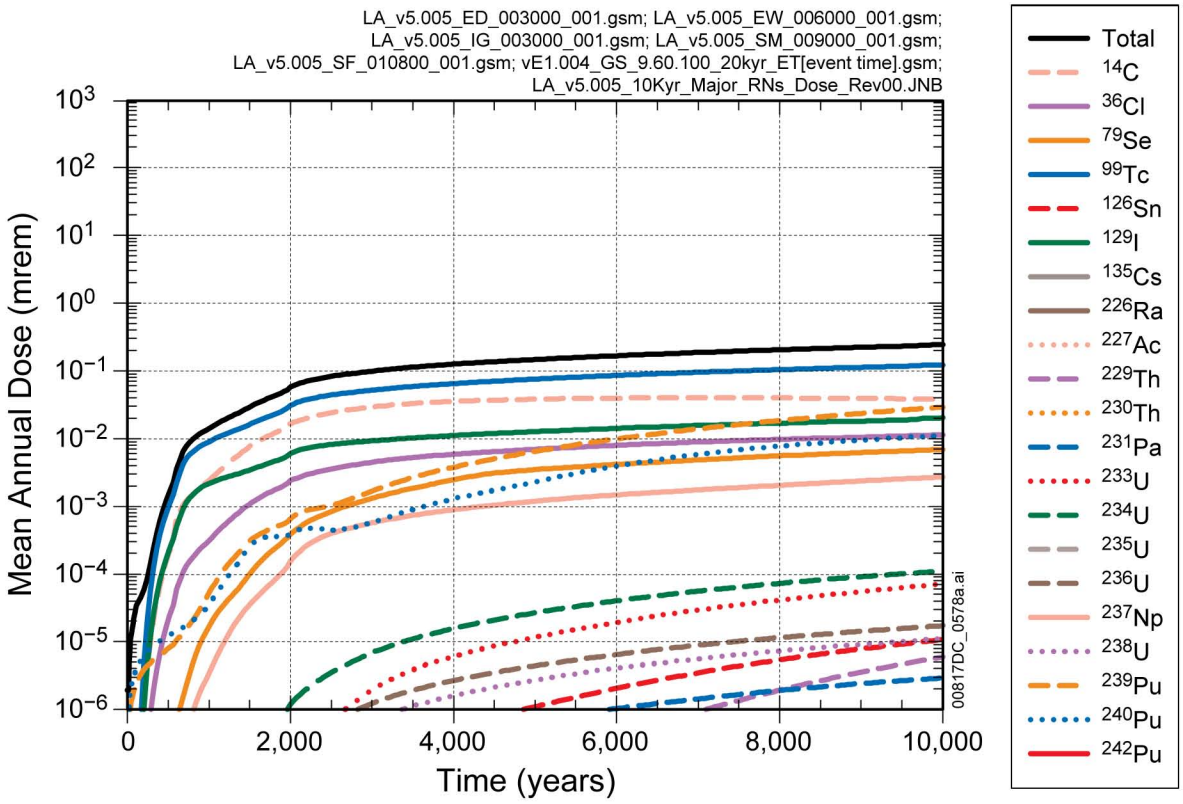

Source: Output DTNs: MO0710ADTSPAWO.000 [DIRS 183752]; MO0710PLOTSFIG.000 [DIRS 185207]; and MO0709TSPAREGS.000 [DIRS 182976].

Figure 8.1-6[a]. Contribution of Individual Radionuclides to Total Mean Annual Dose for 10,000 Years after Repository Closure

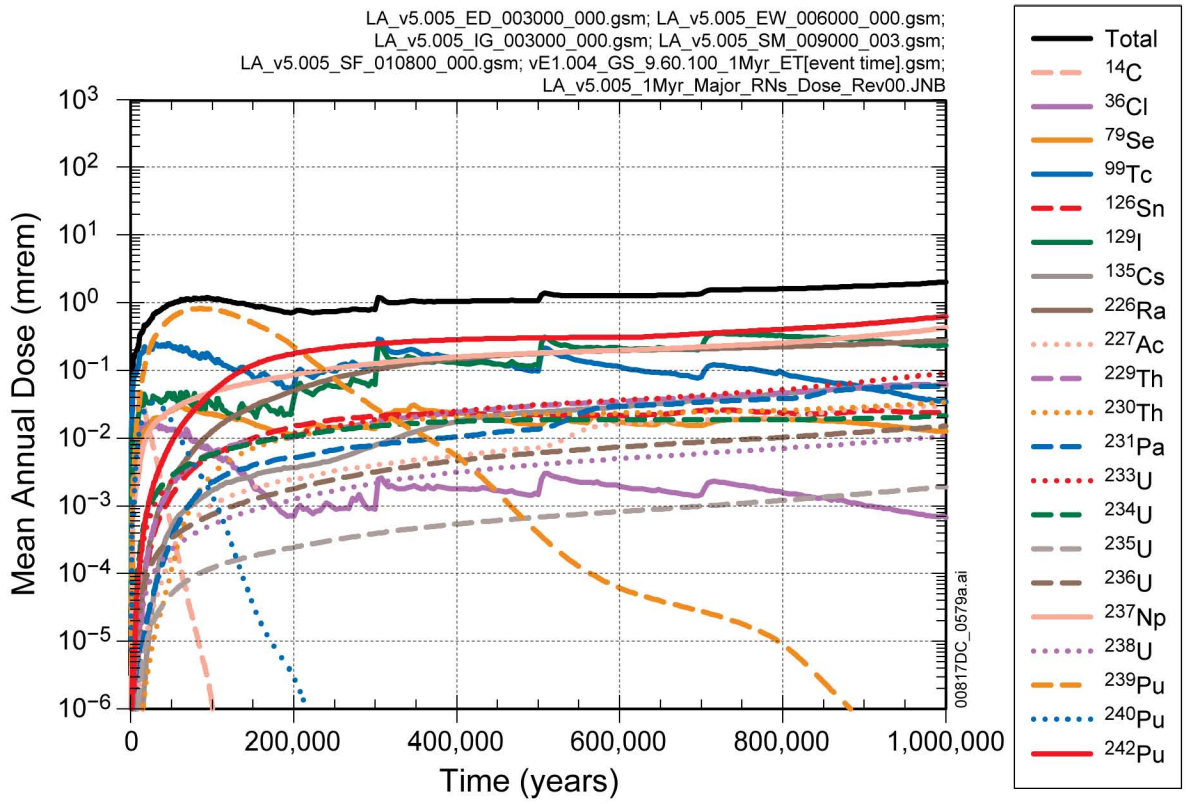

Source: Output DTNs: MO0710ADTSPAWO.000 [DIRS 183752]; MO0710PLOTSFIG.000 [DIRS 185207]; and MO0709TSPAREGS.000 [DIRS 182976].

Figure 8.1-7[a]. Contribution of Individual Radionuclides to Total Mean Annual Dose for 1,000,000 Years after Repository Closure

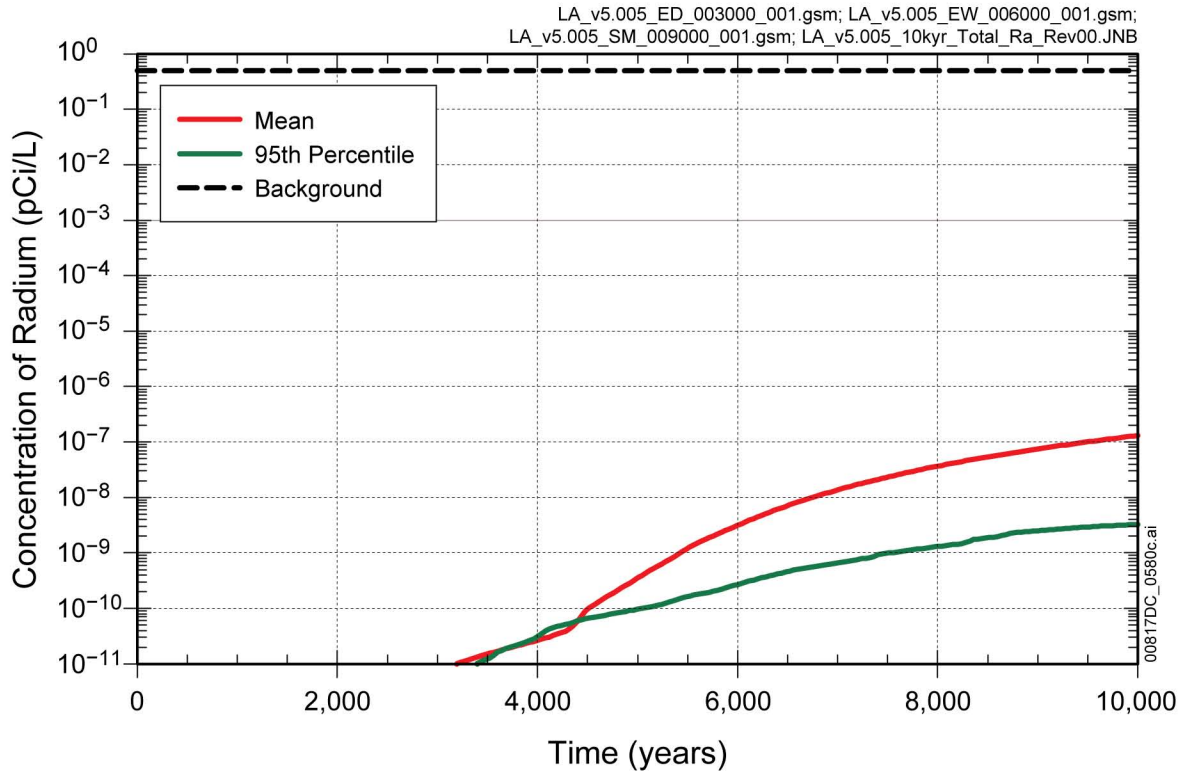

Source: Output DTNs: MO0710ADTSPAWO.000 [DIRS 183752]; and MO0710PLOTSFIG.000 [DIRS 185207].

Figure 8.1-9[a]. Summary Statistics for Activity Concentrations of Total Radium (^{226}Ra and ^{228}Ra) in Groundwater, Excluding Natural Background, for 10,000 Years after Repository Closure

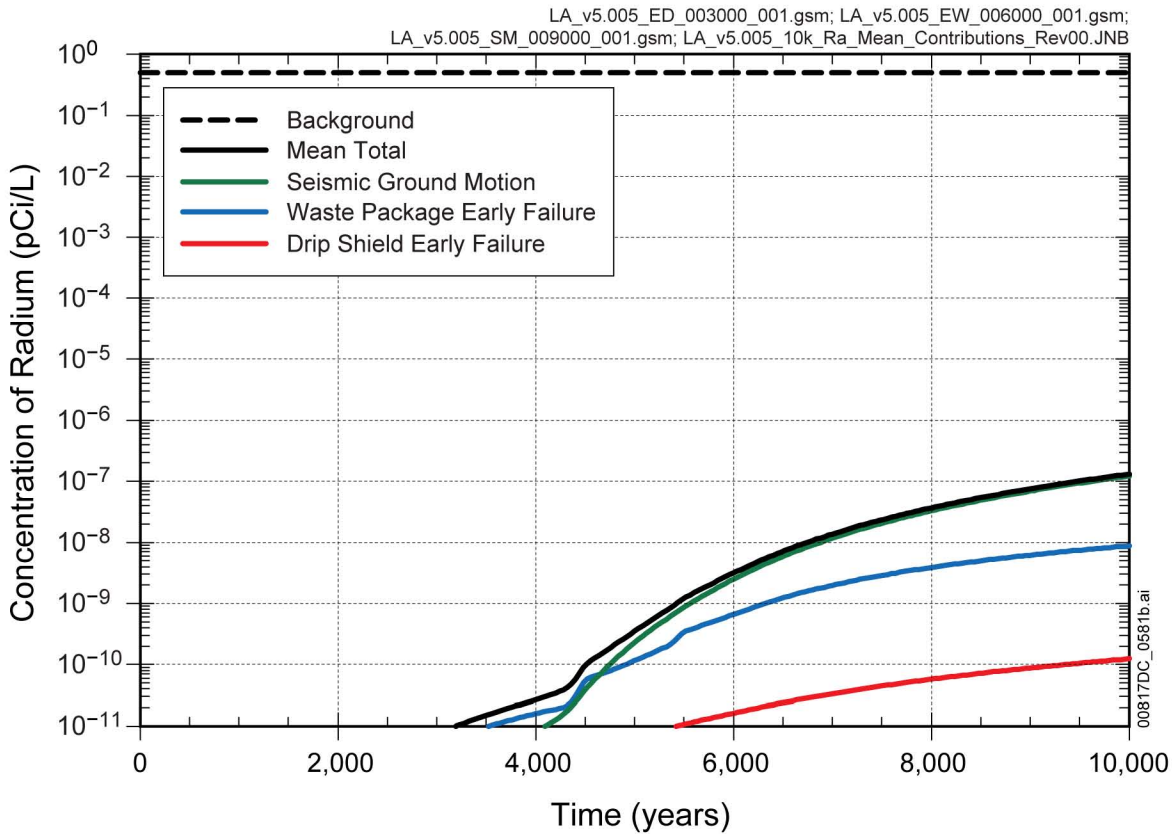

Source: Output DTNs: MO0710ADTSPAWO.000 [DIRS 183752]; and MO0710PLOTSFIG.000 [DIRS 185207].

Figure 8.1-10[a]. Contributions of the Modeling Cases to the Mean Combined ^{226}Ra and ^{228}Ra Activity Concentration in Groundwater, Excluding Natural Background, for 10,000 Years after Repository Closure

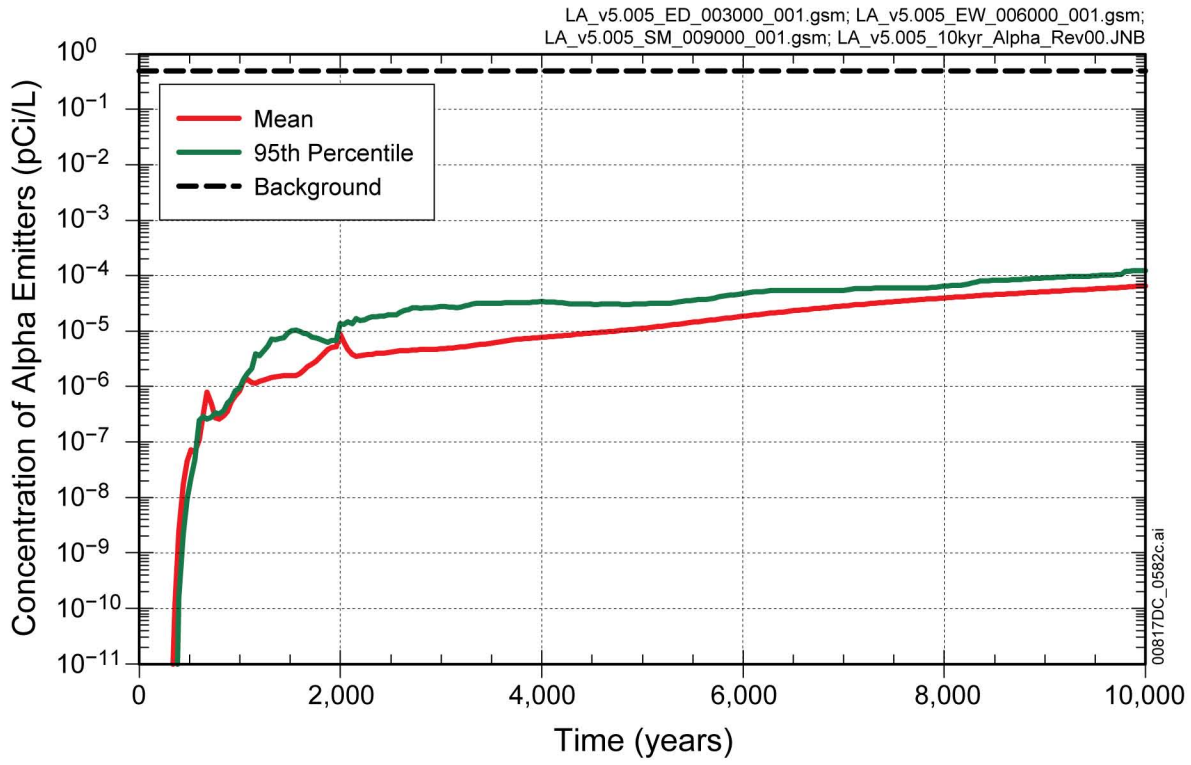

Source: Output DTNs: MO0710ADTSPAWO.000 [DIRS 183752]; and MO0710PLOTSFIG.000 [DIRS 185207].

Figure 8.1-11[a]. Summary Statistics for Activity Concentration of Gross Alpha and ^{226}Ra (Excluding Radon and Uranium) in Groundwater for 10,000 Years after Repository Closure

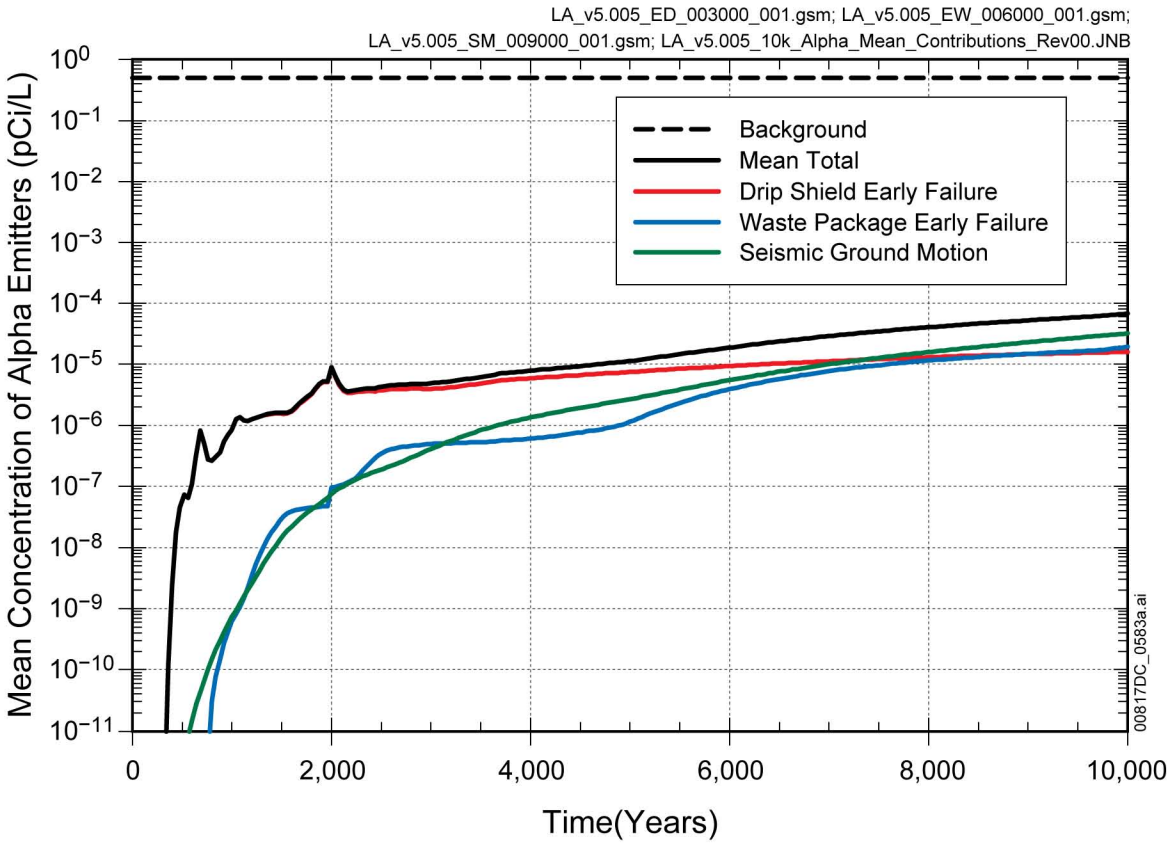

Source: Output DTNs: MO0710ADTSPAWO.000 [DIRS 183752]; and MO0710PLOTSFIG.000 [DIRS 185207].

Figure 8.1-12[a]. Contributions of the Modeling Cases to the Mean Gross Alpha Activity Concentrations (Including ^{226}Ra but Excluding Radon and Uranium) in Groundwater for 10,000 Years after Repository Closure

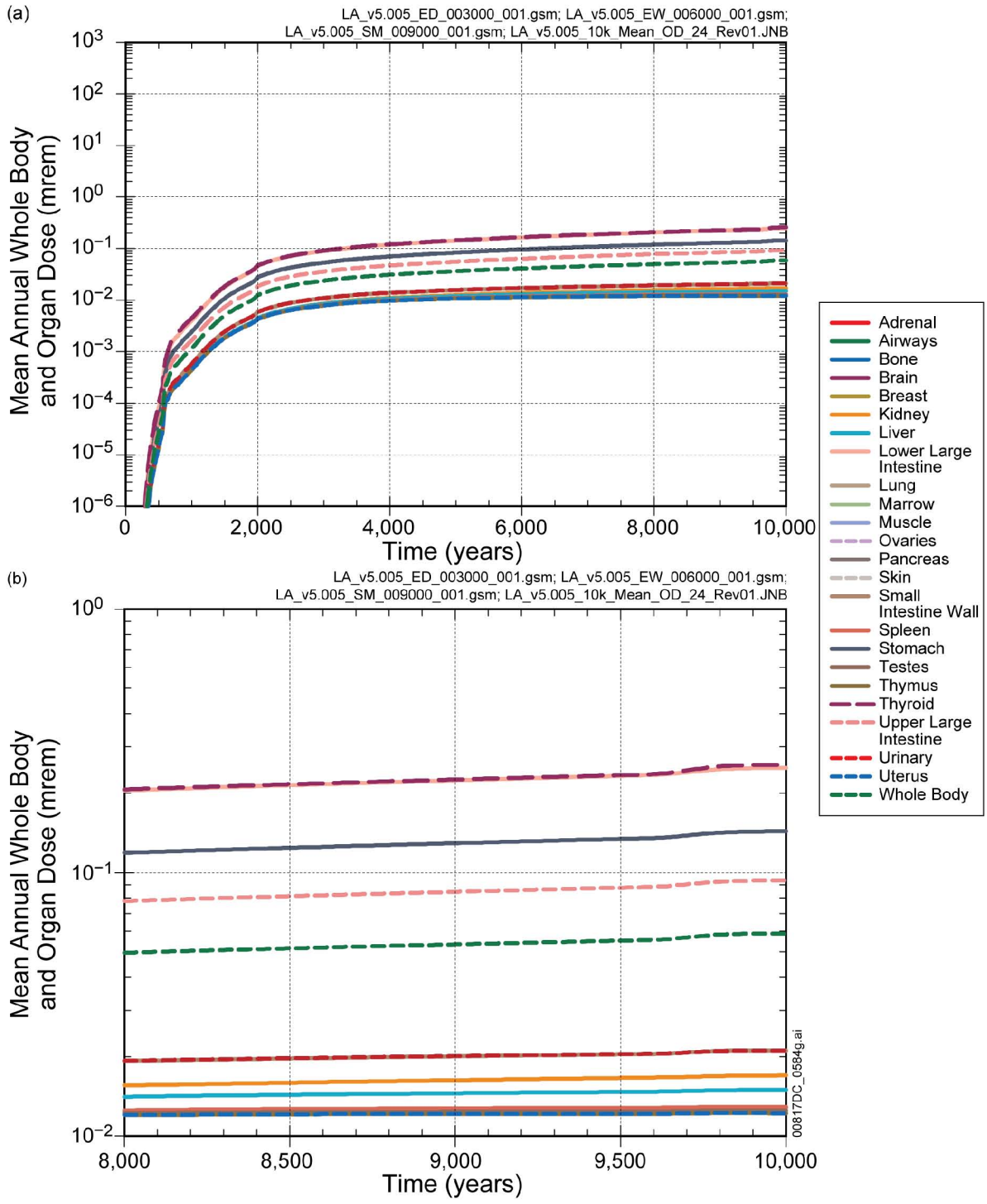

Source: Output DTNs: MO0710ADTSPAWO.000 [DIRS 183752]; and MO0710PLOTSFIG.000 [DIRS 185207].

NOTE: There are 24 dose histories in the plot: 23 organs and one for the whole body.

Figure 8.1-13[a]. Mean Annual Dose from Beta-Photon Dose for All Organs, Including the Whole Body for (a) 10,000 Years after Repository Closure and (b) Detail for 8,000 to 10,000 Years after Repository Closure

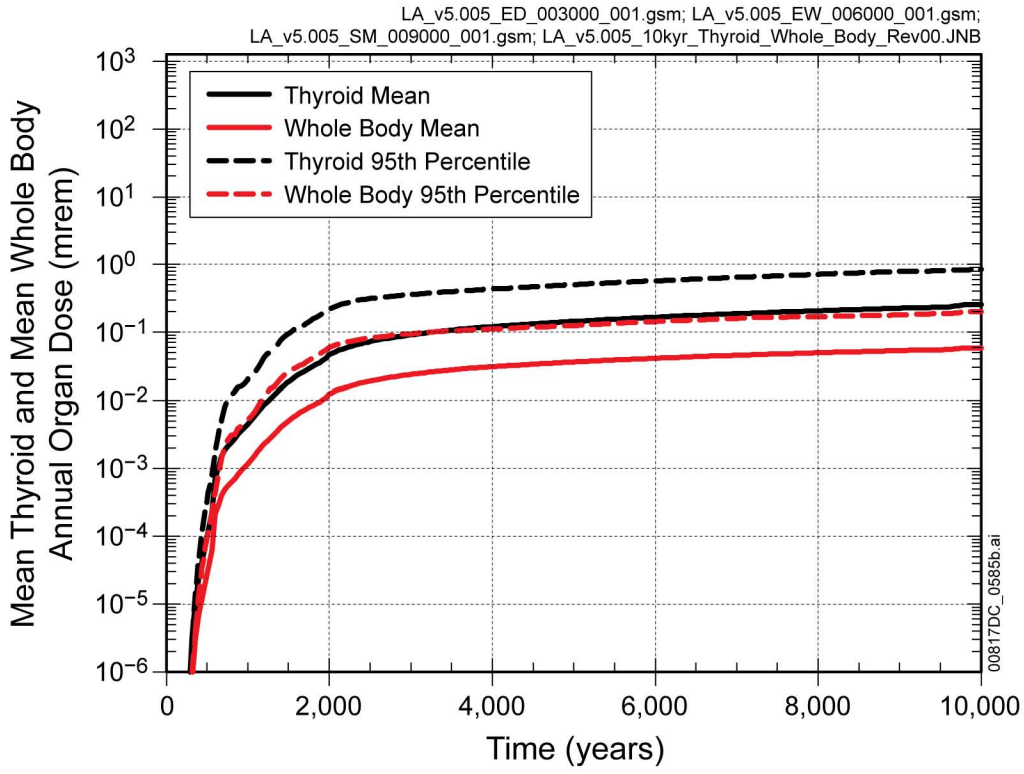

Source: Output DTNs: MO0710ADTSPAWO.000 [DIRS 183752]; and MO0710PLOTSFIG.000 [DIRS 185207].

Figure 8.1-14[a]. Summary Statistics for Annual Drinking Water Doses for Combined Beta and Photon Emitting Radionuclides for 10,000 Years after Repository Closure

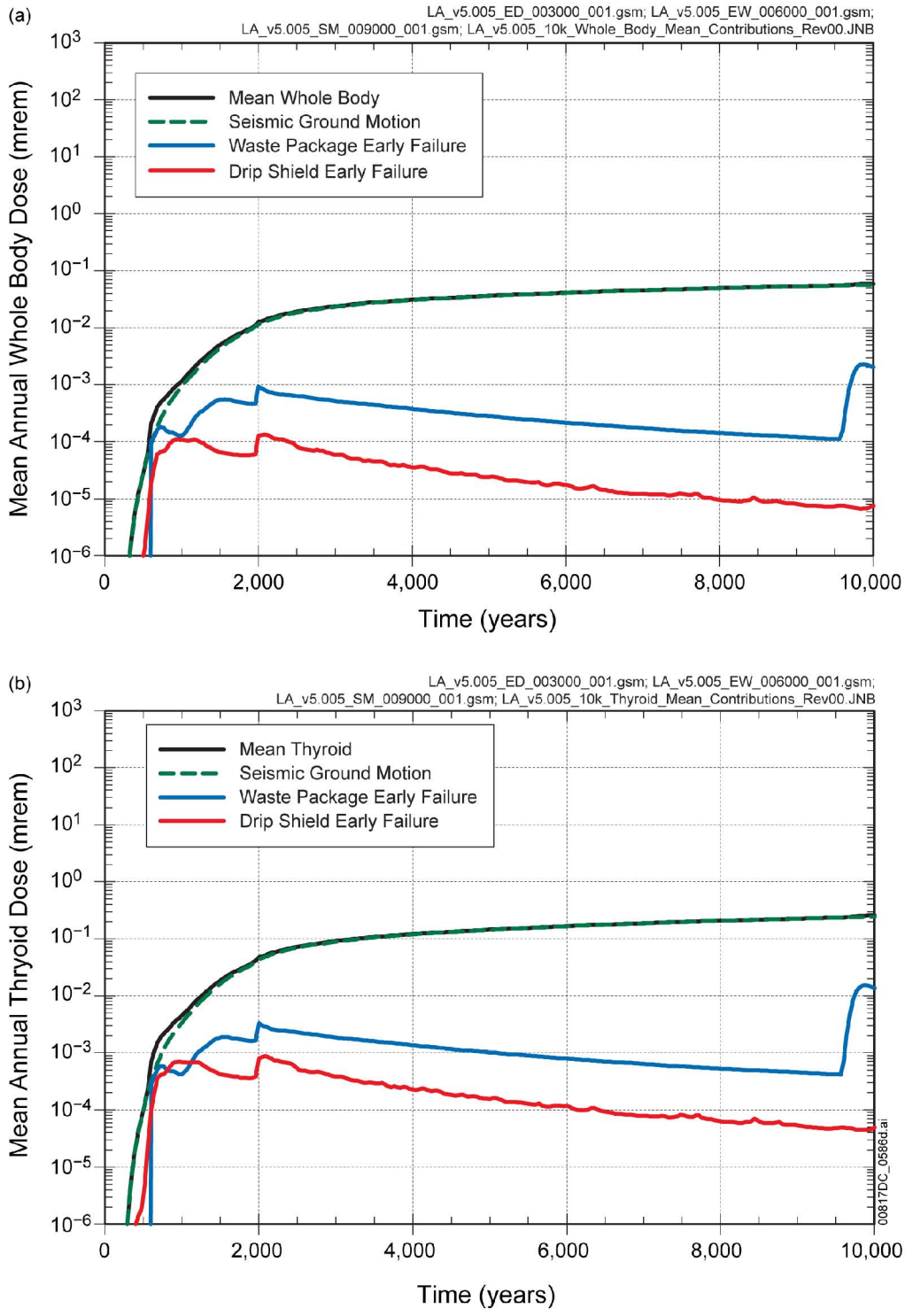

Source: Output DTNs: MO0710ADTSPAWO.000 [DIRS 183752]; and MO0710PLOTSFIG.000 [DIRS 185207].

Figure 8.1-15[a]. Contributions of Modeling Cases to the (a) Whole Body Dose and (b) Thyroid for 10,000 Years after Repository Closure

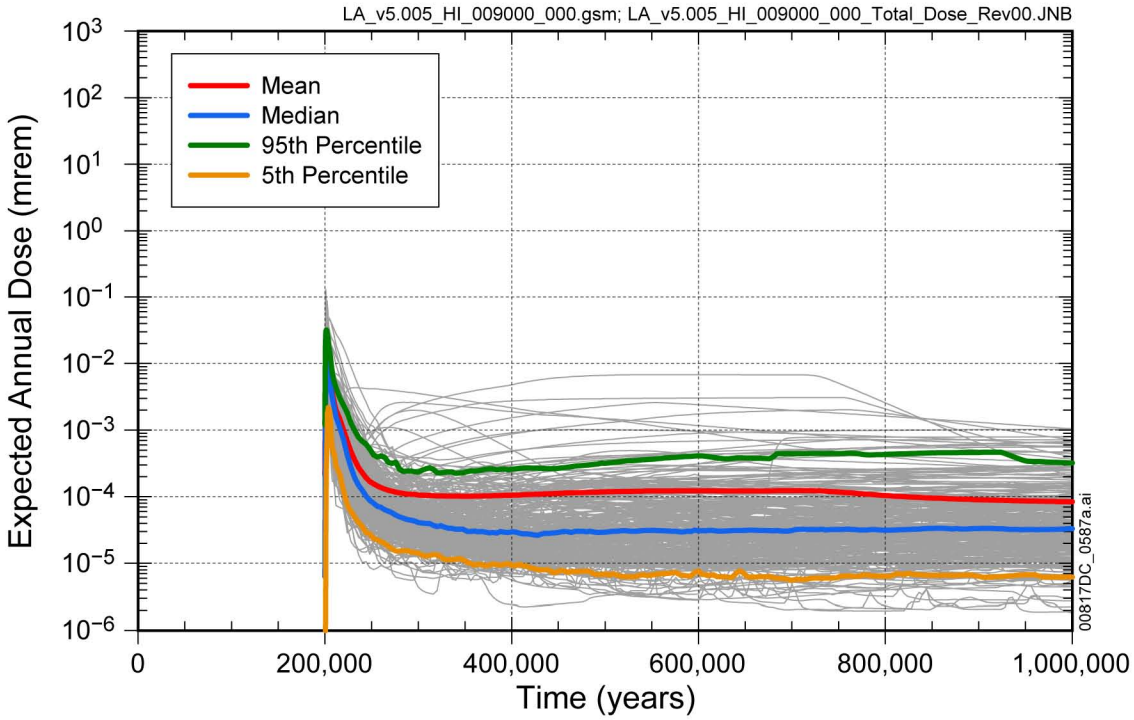

Source: Output DTNs: MO0710ADTSPAWO.000 [DIRS 183752]; and MO0710PLOTSFIG.000 [DIRS 185207].

Figure 8.1-16[a]. Distribution of Expected Annual Doses for the Human Intrusion Scenario for 1,000,000 Years after Repository Closure with Drilling Event at 200,000 Years

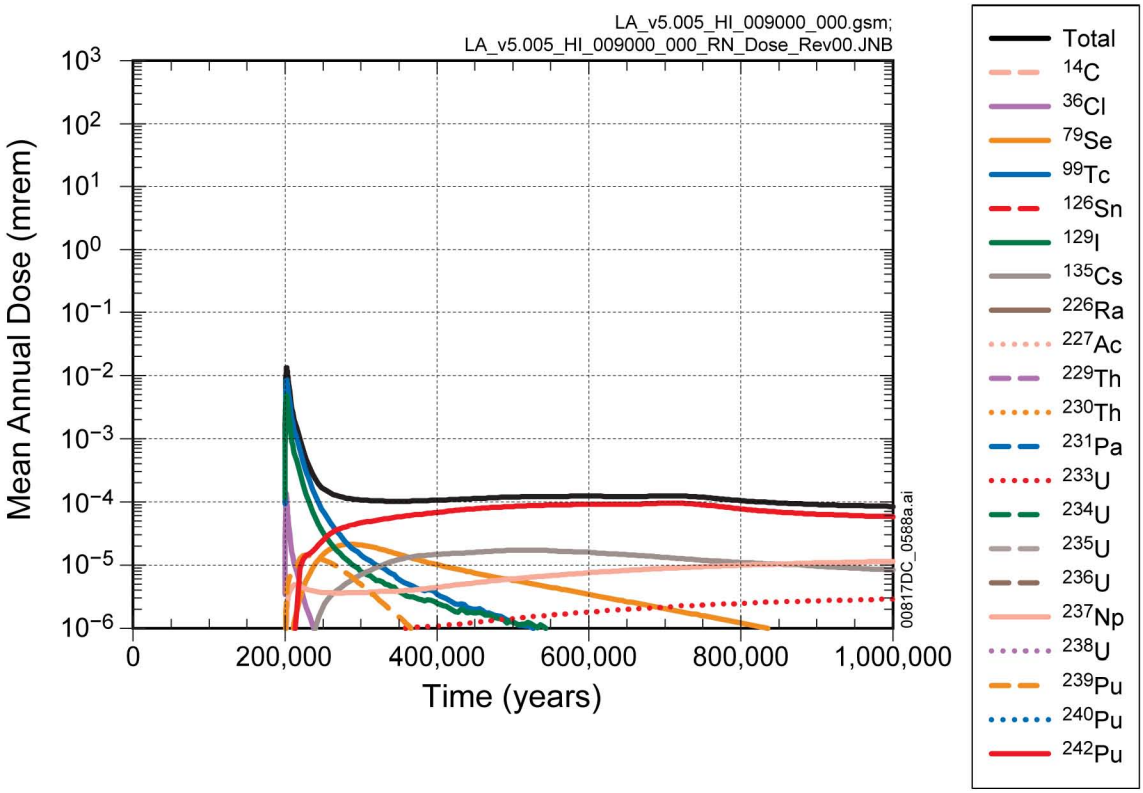

Source: Output DTN: MO0710ADTSPAWO.000 [DIRS 183752].

Figure 8.1-17[a]. Contribution of Individual Radionuclides to Mean Annual Dose for the Human Intrusion Scenario for 1,000,000 Years after Repository Closure

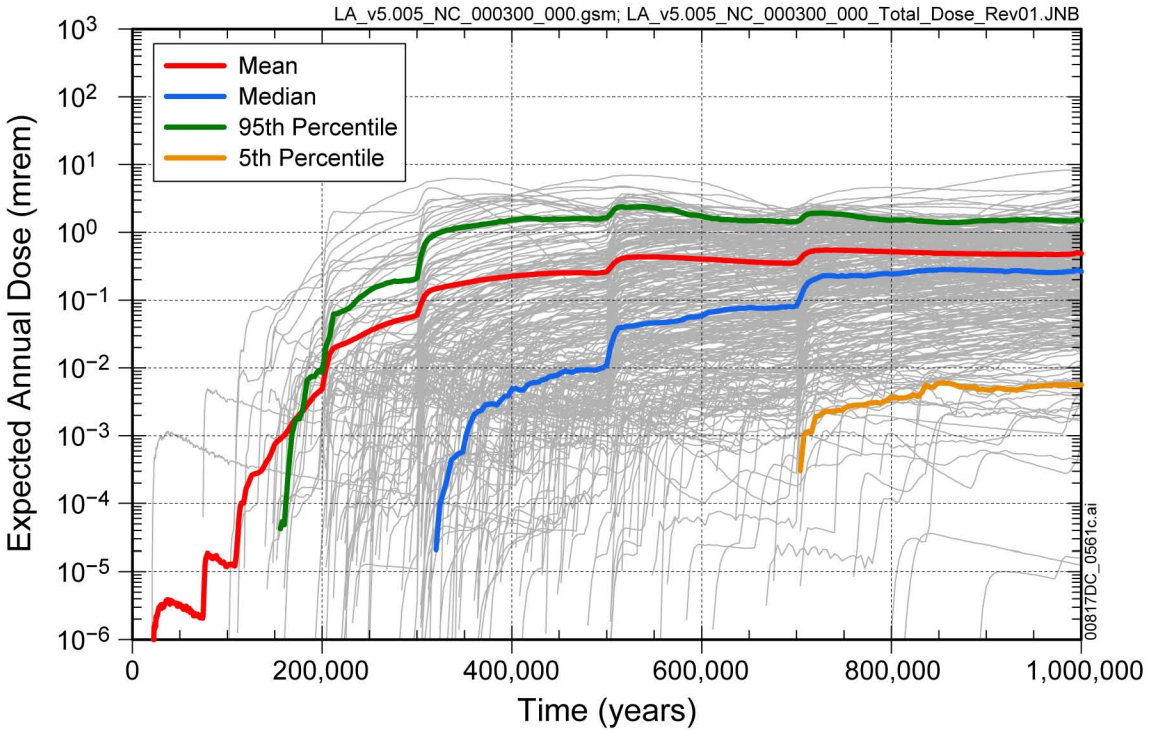

Source: Output DTNs: MO0710ADTSPAWO.000 [DIRS 183752]; and MO0710PLOTSFIG.000 [DIRS 185207].

Figure 8.2-1[a]. Distributions of Expected Annual Dose for the Nominal Modeling Case for 1,000,000 Years after Repository Closure

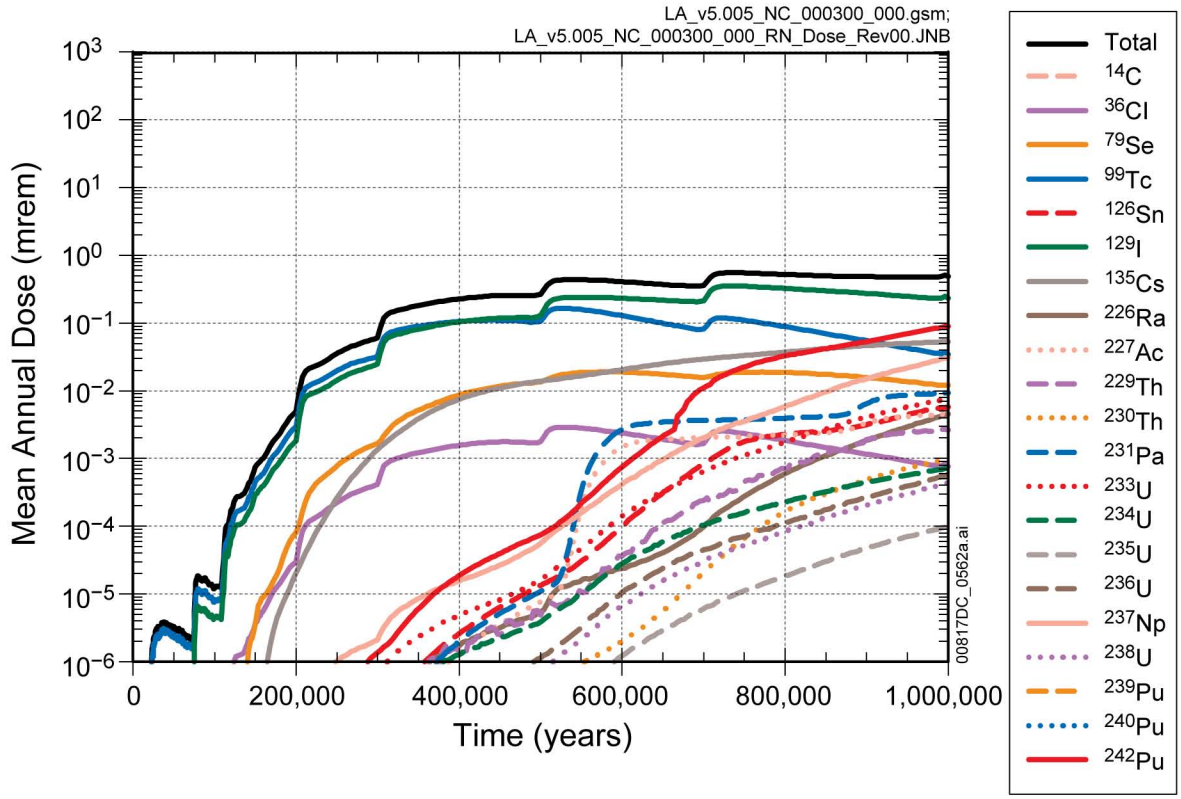

Source: Output DTNs: MO0710ADTSPAWO.000 [DIRS 183752]; and MO0710PLOTSFIG.000 [DIRS 185207].

Figure 8.2-2[a]. Contribution of Individual Radionuclides to Mean Annual Dose for the Nominal Modeling Case for 1,000,000 Years after Repository Closure

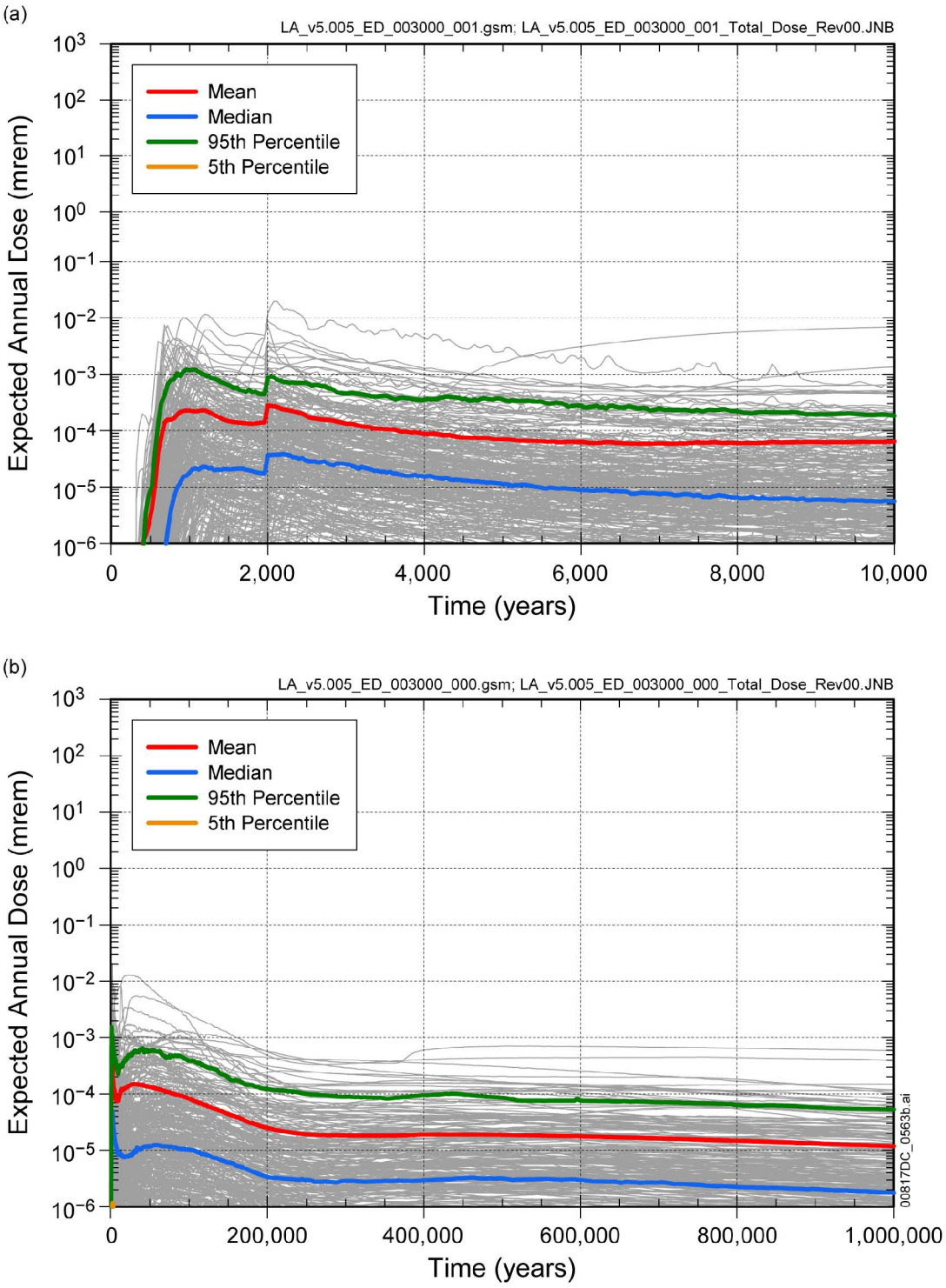

Source: Output DTNs: MO0710ADTSPAWO.000 [DIRS 183752]; and MO0710PLOTSFIG.000 [DIRS 185207].

Figure 8.2-3[a]. Distributions of Expected Annual Dose for the Drip Shield Early Failure Modeling Case for (a) 10,000 Years and (b) 1,000,000 Years after Repository Closure

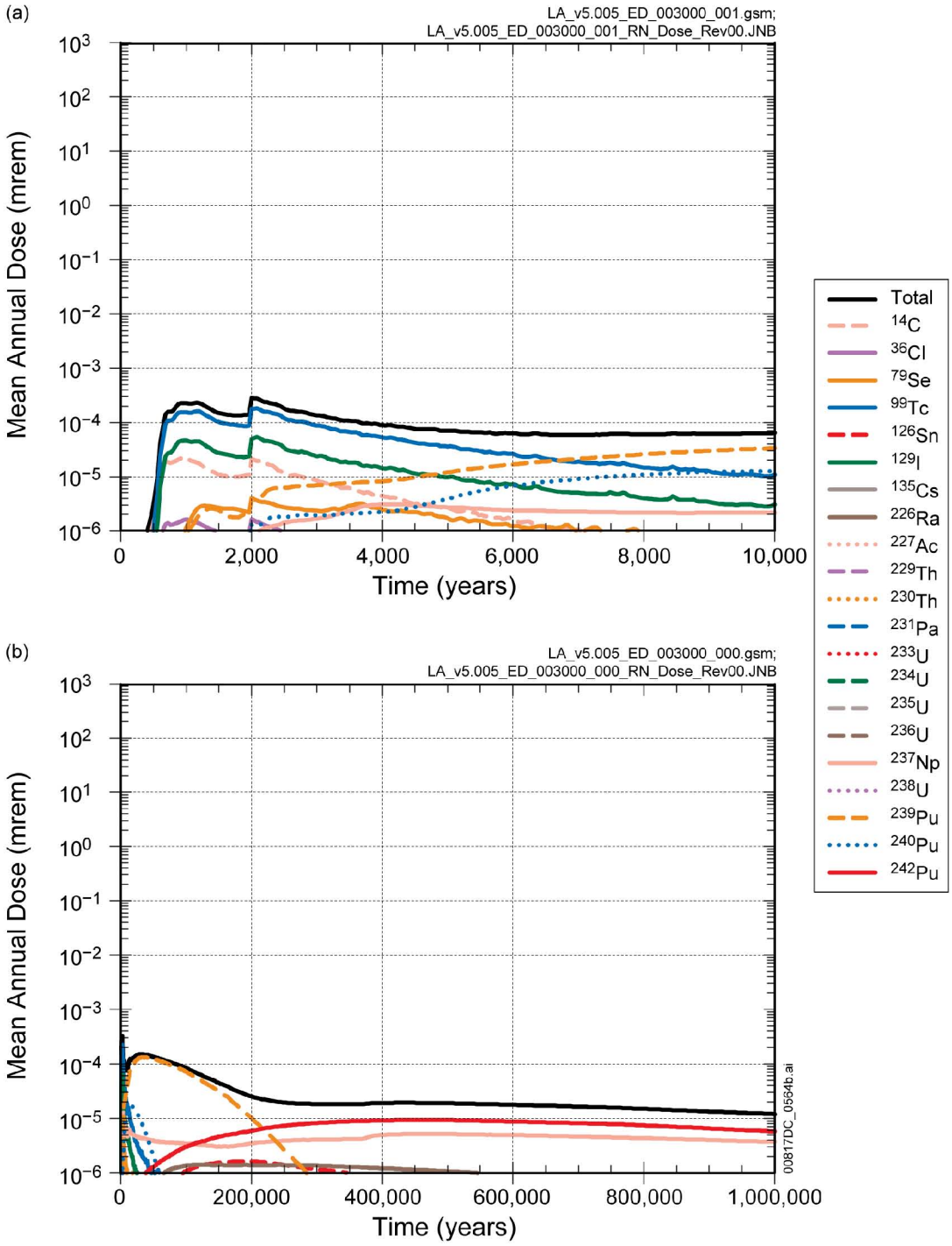

Source: Output DTNs: MO0710ADTSPAWO.000 [DIRS 183752]; and MO0710PLOTSFIG.000 [DIRS 185207].

Figure 8.2-4[a]. Contribution of Individual Radionuclides to Mean Annual Dose for Drip Shield Early Failure Modeling Case for (a) 10,000 Years and (b) 1,000,000 Years after Repository Closure

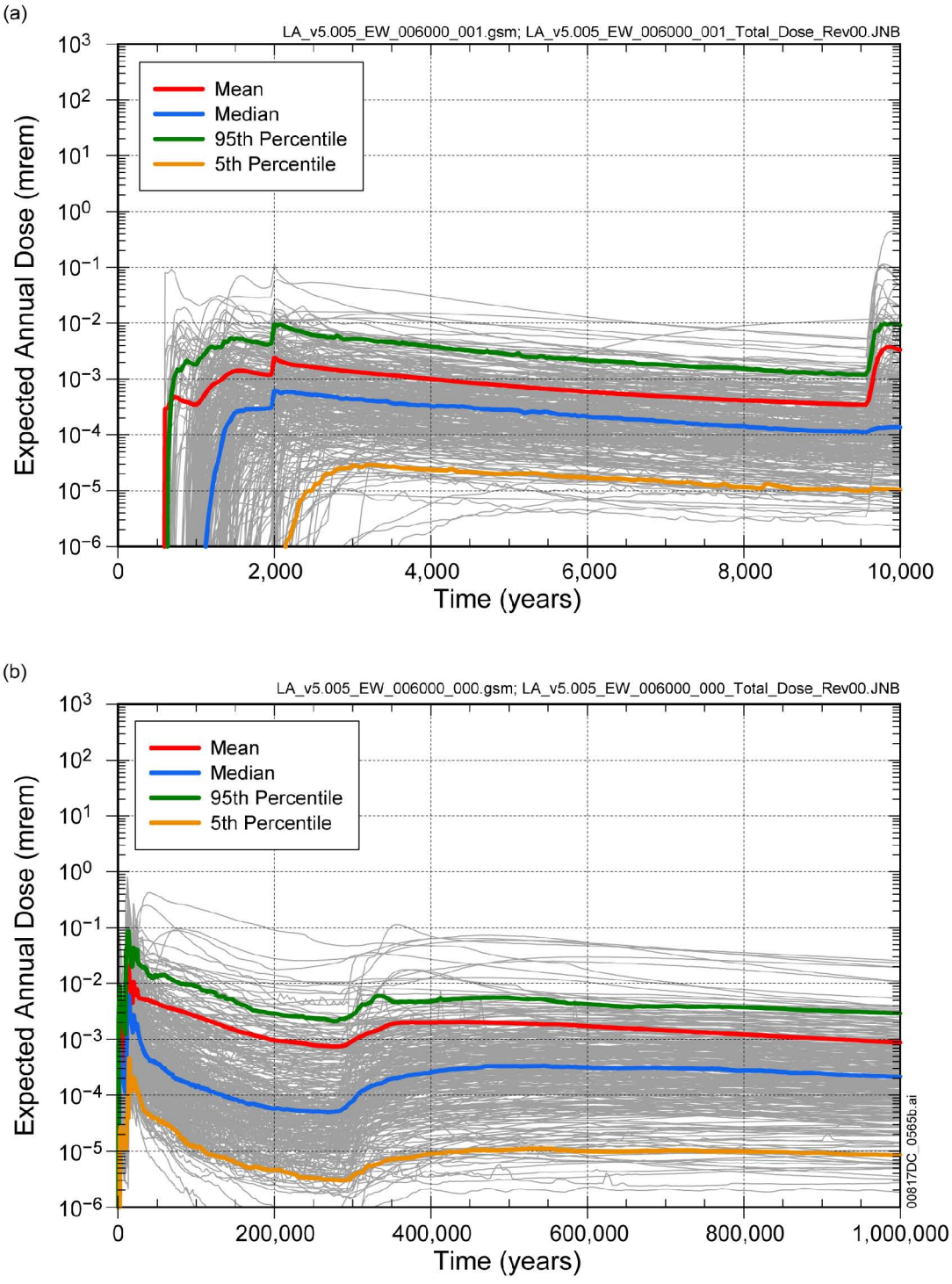

Source: Output DTNs: MO0710ADTSPAWO.000 [DIRS 183752]; and MO0710PLOTSFIG.000 [DIRS 185207].

Figure 8.2-5[a]. Distributions of Expected Annual Dose for Waste Package Early Failure Modeling Case for (a) 10,000 Years and (b) 1,000,000 Years after Repository Closure

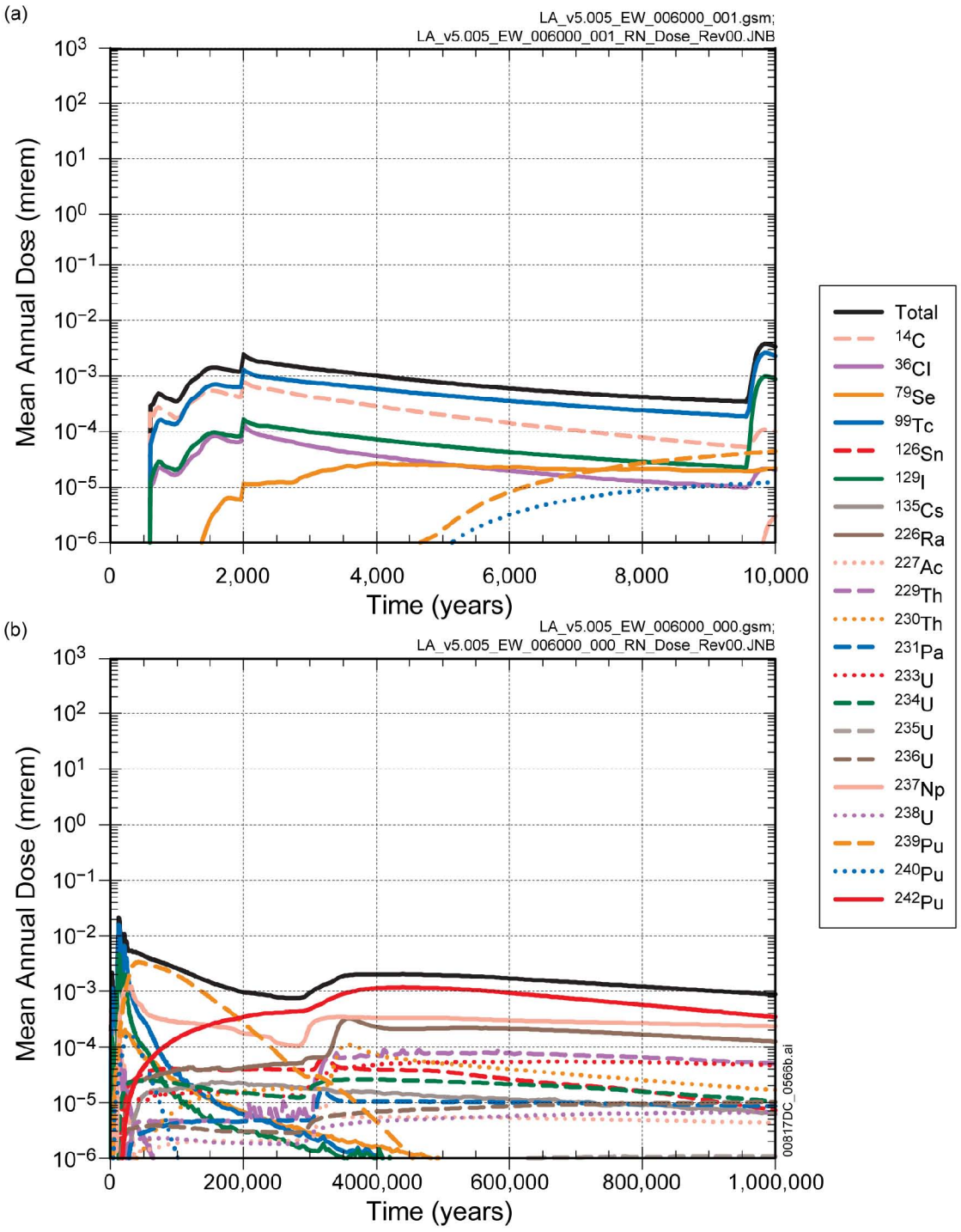

Source: Output DTNs: MO0710ADTSPAWO.000 [DIRS 183752]; and MO0710PLOTSFIG.000 [DIRS 185207].

Figure 8.2-6[a]. Contribution of Individual Radionuclides to Mean Annual Dose for Waste Package Early Failure Modeling Case for (a) 10,000 Years and (b) 1,000,000 Years after Repository Closure

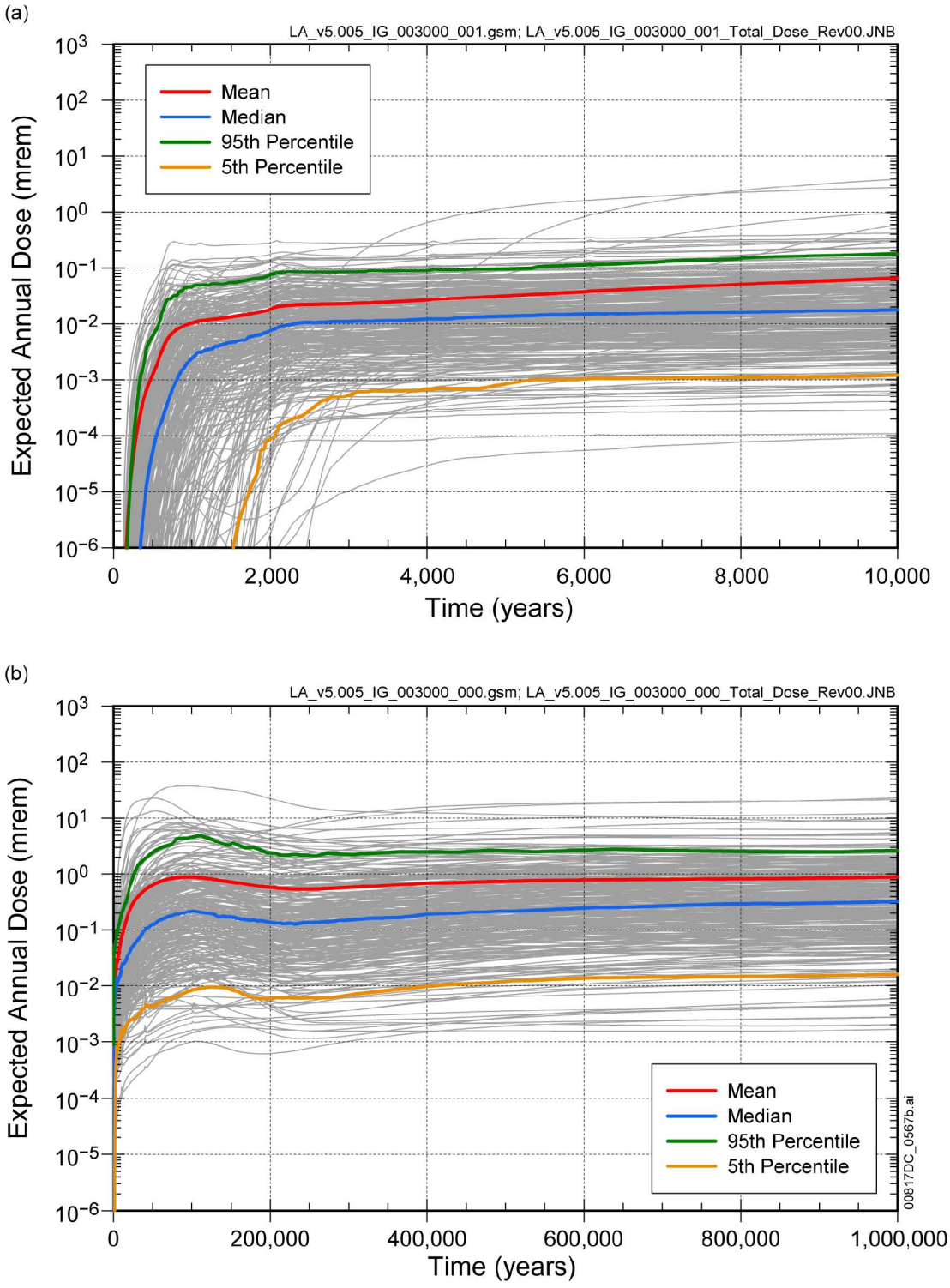

Source: Output DTNs: MO0710ADTSPAWO.000 [DIRS 183752]; and MO0710PLOTSFIG.000 [DIRS 185207].

Figure 8.2-7[a]. Distributions of Expected Annual Dose for the Igneous Intrusion Modeling Case for (a) 10,000 Years and (b) 1,000,000 Years after Repository Closure

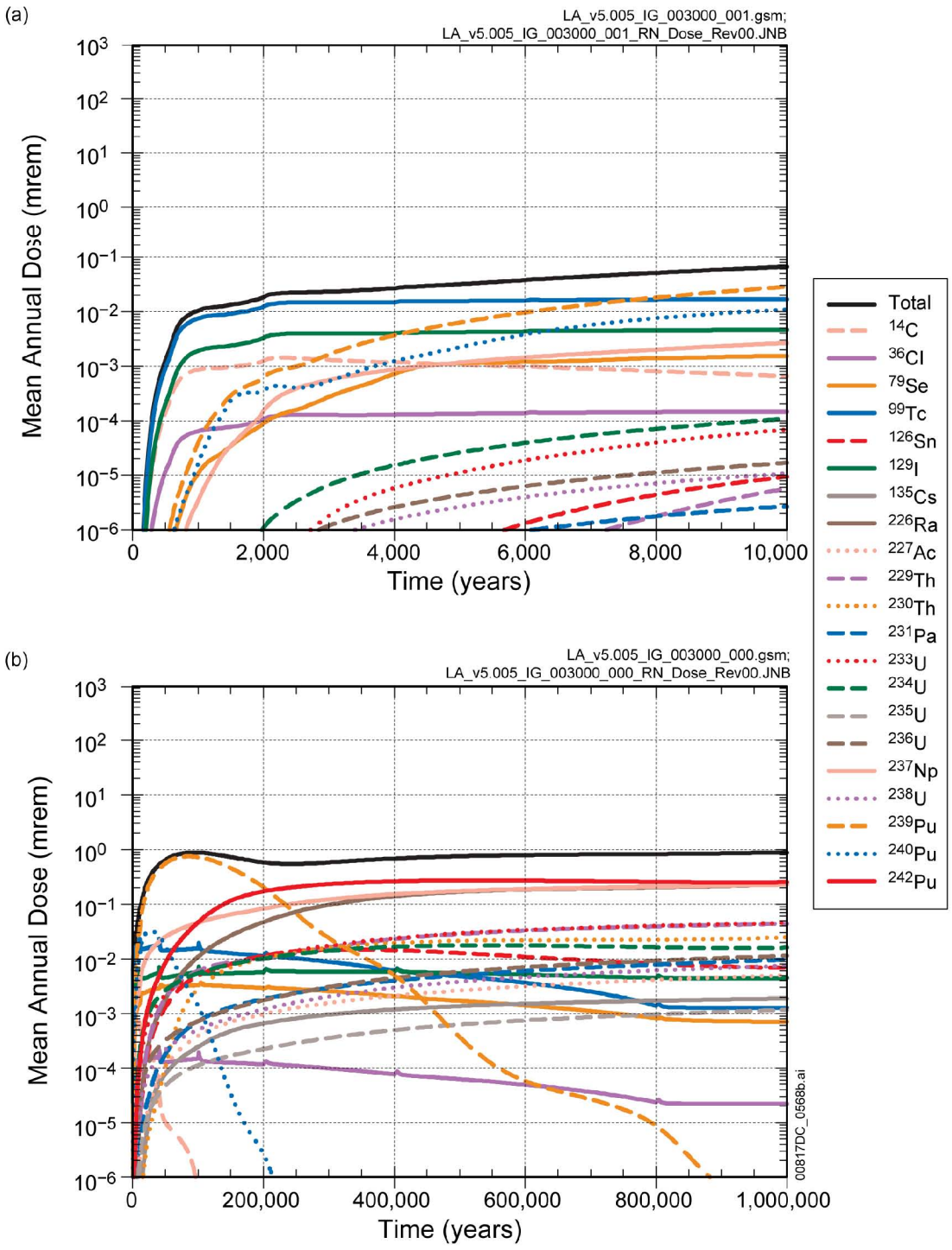

Source: Output DTNs: MO0710ADTSPAWO.000 [DIRS 183752]; and MO0710PLOTSFIG.000 [DIRS 185207].

Figure 8.2-8[a]. Contribution of Individual Radionuclides to Mean Annual Dose for the Igneous Intrusion Modeling Case for (a) 10,000 Years and (b) 1,000,000 Years after Repository Closure

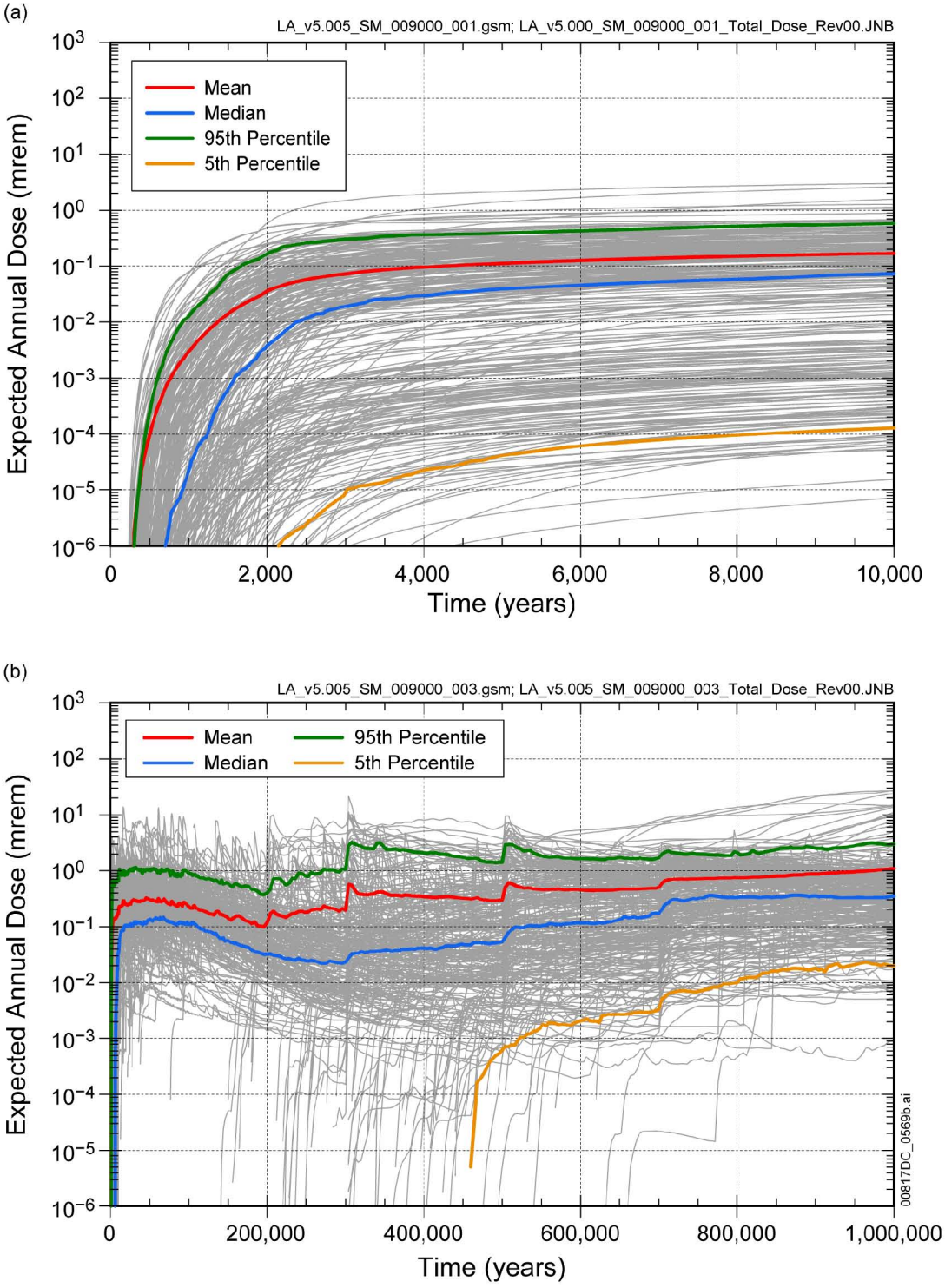

Source: Output DTNs: MO0710ADTSPAWO.000 [DIRS 183752]; and MO0710PLOTSFIG.000 [DIRS 185207].

Figure 8.2-11[a]. Distributions of Expected Annual Dose for the Seismic Ground Motion Modeling Case for (a) 10,000 Years and (b) 1,000,000 Years after Repository Closure

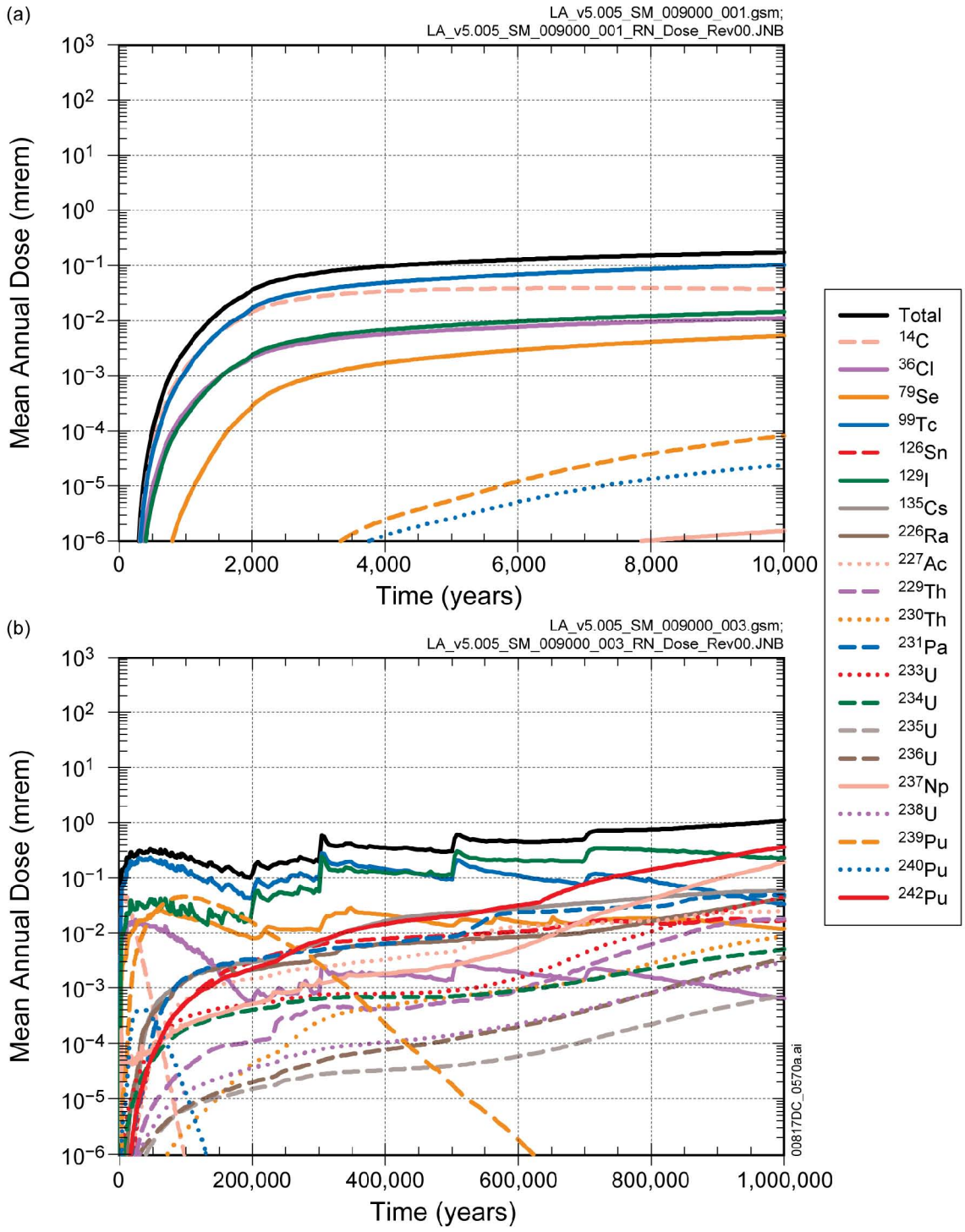

Source: Output DTNs: MO0710ADTSPAWO.000 [DIRS 183752]; and MO0710PLOTSFIG.000 [DIRS 185207].

Figure 8.2-12[a]. Contribution of Individual Radionuclides to Mean Annual Dose for the Seismic Ground Motion Modeling Case for (a) 10,000 Years and (b) 1,000,000 Years after Repository Closure

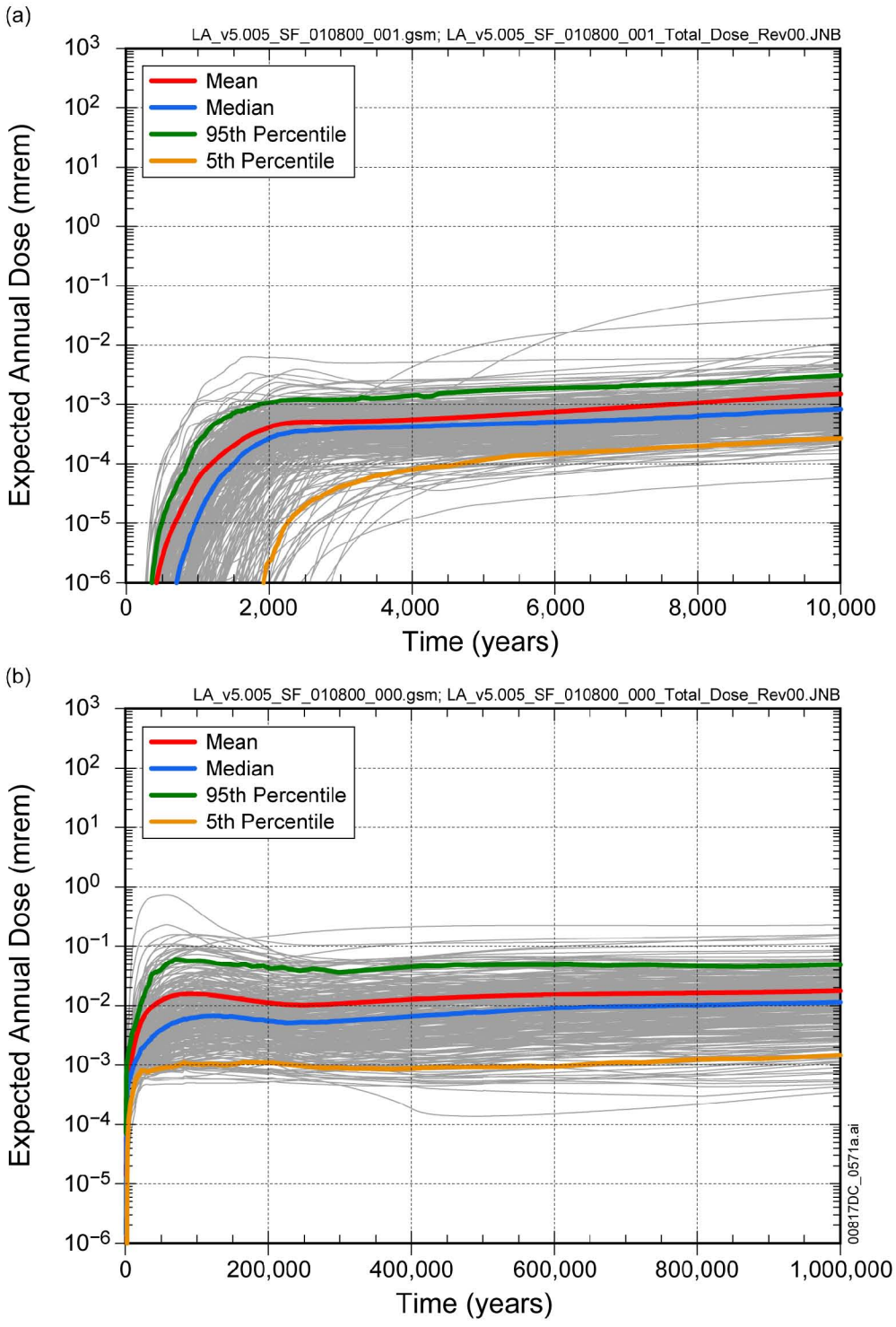

Source: Output DTNs: MO0710ADTSPAWO.000 [DIRS 183752]; and MO0710PLOTSFIG.000 [DIRS 185207].

Figure 8.2-13[a]. Distributions of Expected Annual Dose for the Seismic Fault Displacement Modeling Case for (a) 10,000 Years and (b) 1,000,000 Years after Repository Closure

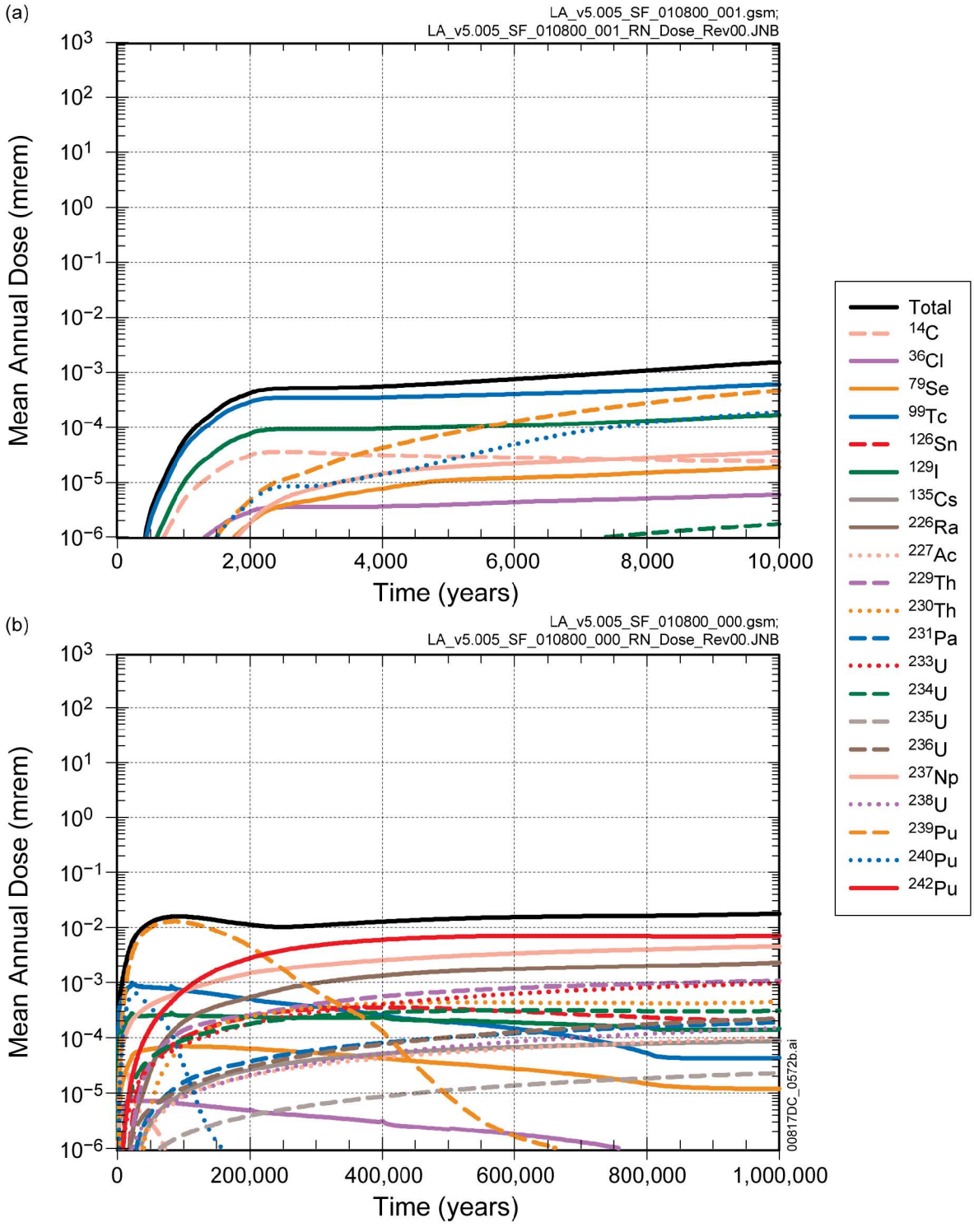

Source: Output DTNs: MO0710ADTSPAWO.000 [DIRS 183752]; and MO0710PLOTSFIG.000 [DIRS 185207].

Figure 8.2-14[a]. Contribution of Individual Radionuclides to Mean Annual Dose for the Seismic Fault Displacement Modeling Case for (a) 10,000 Years and (b) 1,000,000 Years after Repository Closure

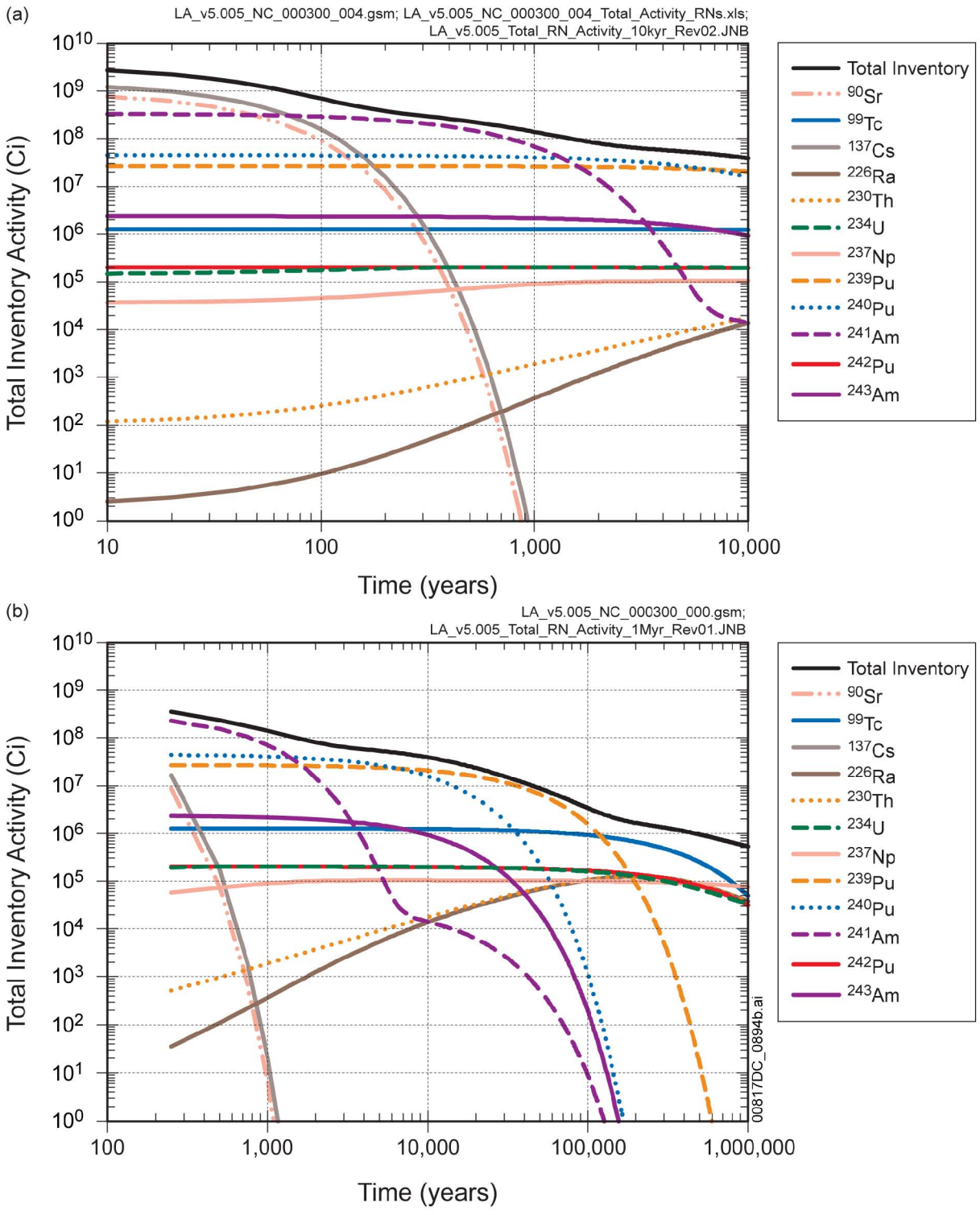

Source: Output DTNs: MO0710ADTSPAWO.000 [DIRS 183752]; and MO0710PLOTSFIG.000 [DIRS 185207].

Figure 8.3-1[a]. Mean Radionuclide Activities for Total Repository Inventory as a Function of Time for (a) 10,000 Years and (b) 1,000,000 Years after Repository Closure

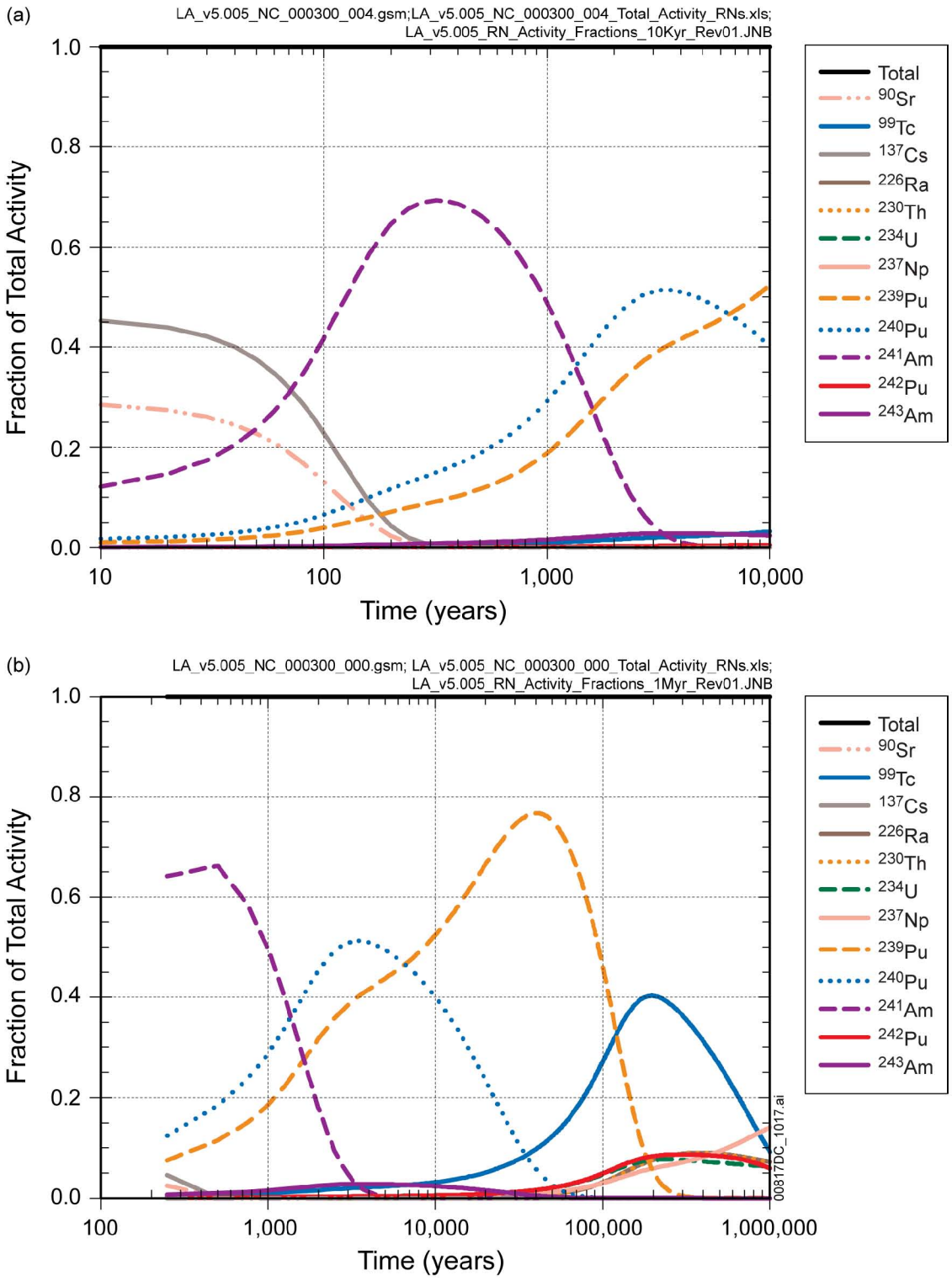

Source: Output DTNs: MO0710ADTSPAWO.000 [DIRS 183752]; and MO0710PLOTSFIG.000 [DIRS 185207].

Figure 8.3-2[a]. Mean Radionuclide Contributions to Total Inventory as a Function of Time for (a) 10,000 Years and (b) 1,000,000 Years after Repository Closure

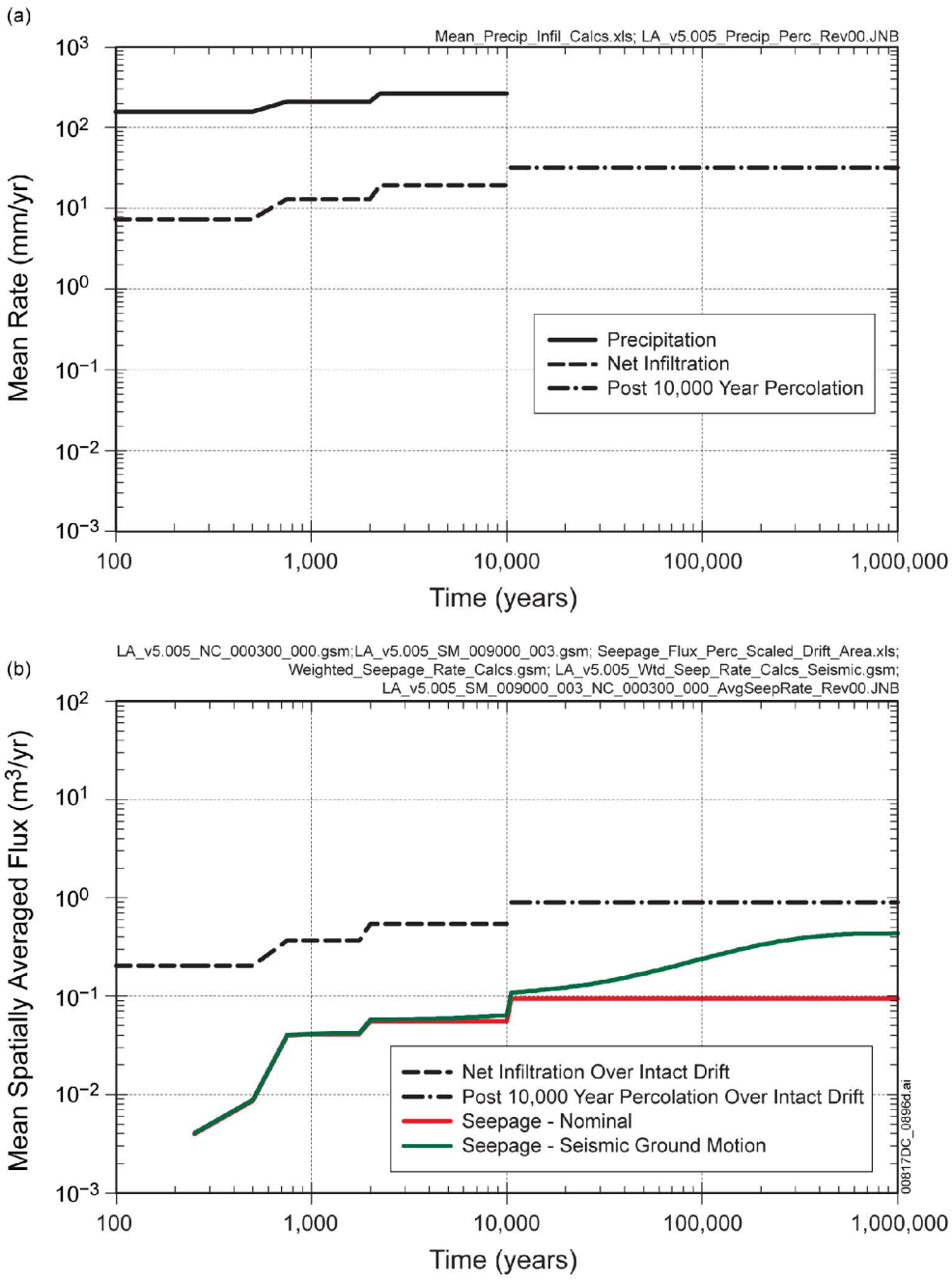

Source: SNL 2007 [DIRS 182145], Tables 6.5.7.1-3, 6.5.7.2-3, and 6.5.7.3-3; NRC Proposed Rule 10 CFR 63.342(c)(2) [DIRS 178394]; and Output DTNs: MO0710ADTSPAWO.000 [DIRS 183752]; MO0710PLOTSFIG.000 [DIRS 185207].

NOTE: For comparison to seepage, volumetric fluxes (m^3/yr) of infiltration and post-10,000 year percolation are calculated by multiplying the net infiltration and post-10,000 year percolation rates by the plan area over an intact drift (m^2).

Figure 8.3-3[a]. Upper Natural Barrier Capability to Prevent or Substantially Reduce the Rate of Water Movement to the Waste for the Mean Spatially-Averaged (a) Annual Precipitation, Net Infiltration, and Post-10,000-Year Percolation Rates and (b) Drift Seepage Fluxes for the Combined Nominal/Early Failure Modeling Case and the Seismic Ground Motion Modeling Case – 1,000,000-Year Period

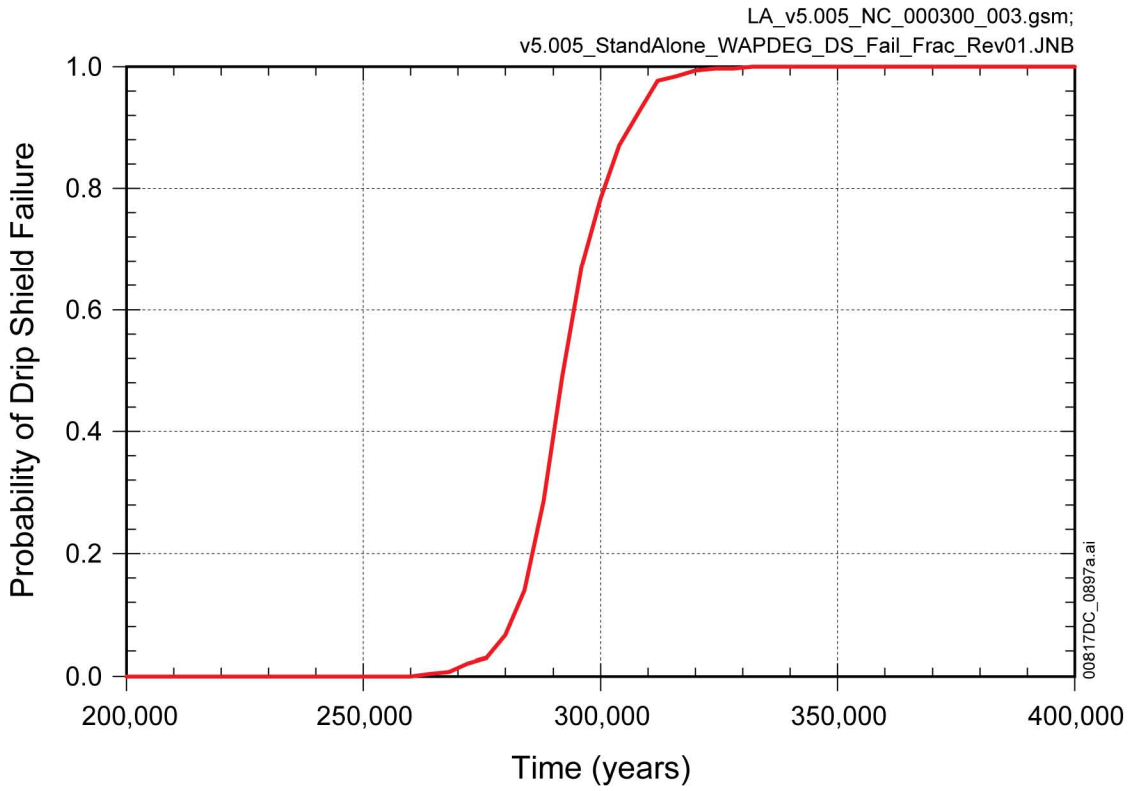

Source: Output DTNs: MO0801TSPAWPDS.000 [DIRS 185077]; and MO0710PLOTSFIG.000 [DIRS 185207].

Figure 8.3-4[a]. Probability of Drip Shield Failure by General Corrosion for the Nominal Modeling Case Based on 300 Epistemic Realizations of Drip Shield General Corrosion Rates

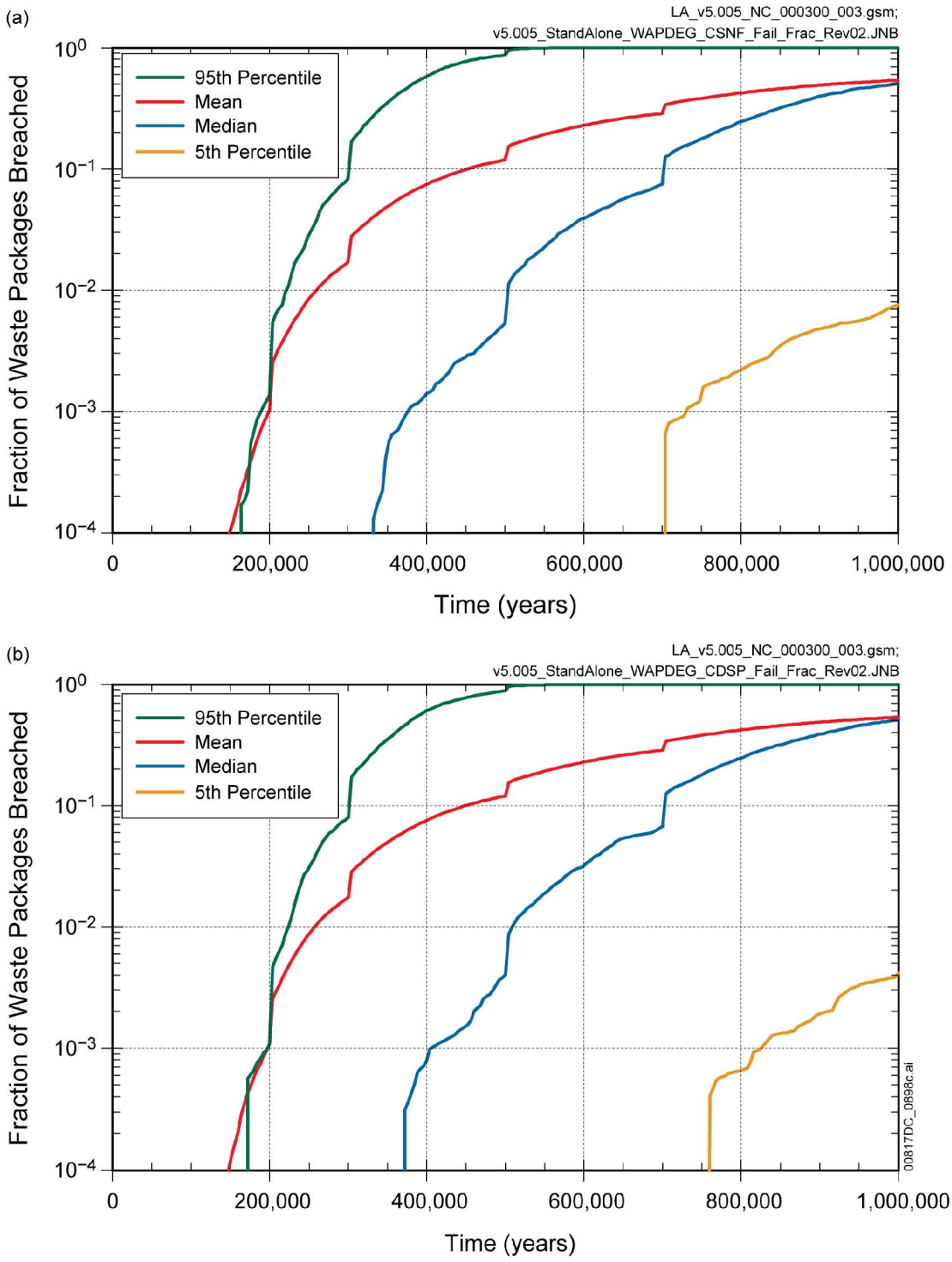

Source: Output DTN: MO0801TSPAWPDS.000 [DIRS 185077].

Figure 8.3-5[a]. Summary Statistics for Fraction of Waste Packages Breached for (a) CSNF Waste Packages and (b) CDSP Waste Packages for the Nominal Modeling Case as a Function of Time

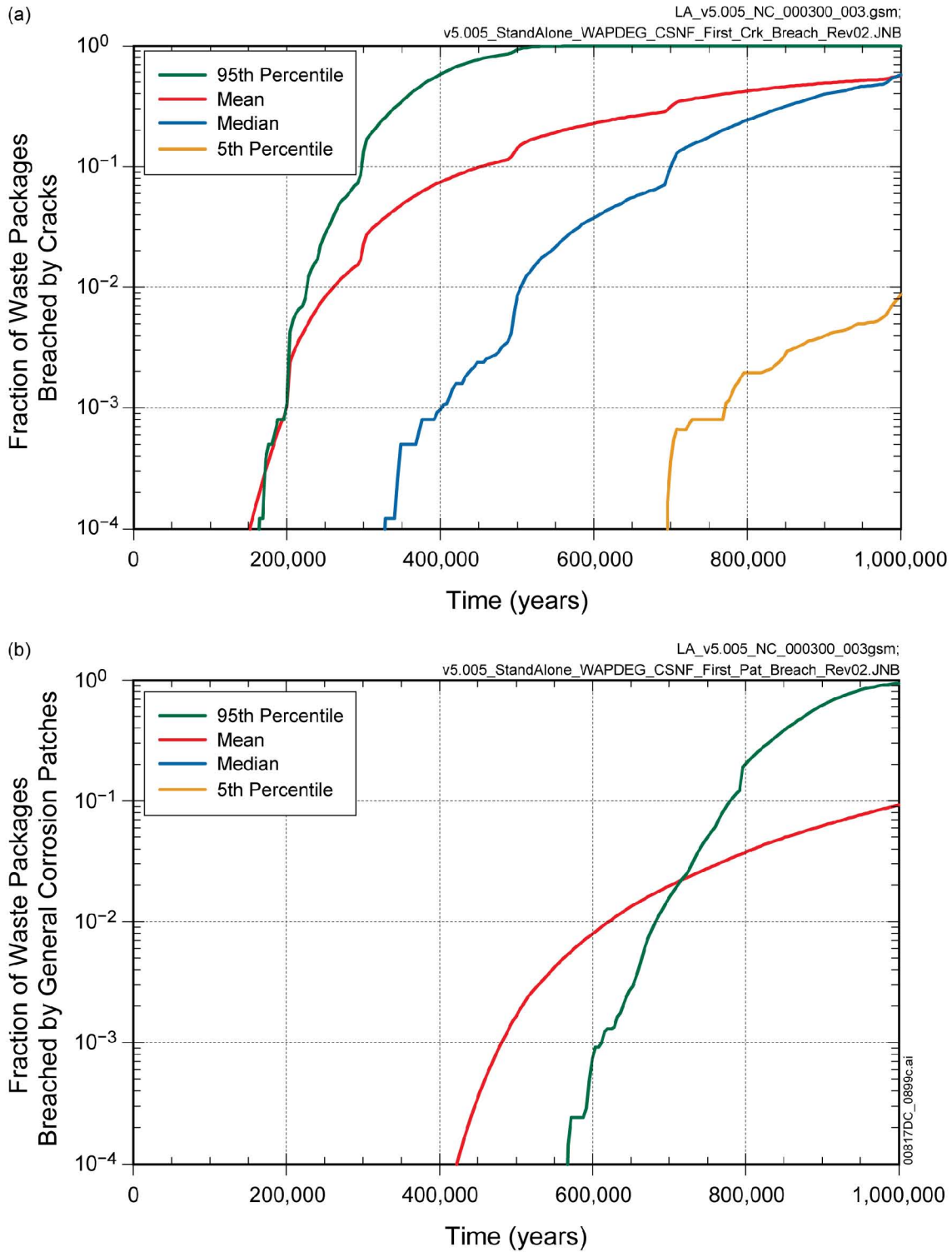

Source: Output DTN: MO0801TSPAWPDS.000 [DIRS 185077].

Figure 8.3-6[a]. Summary Statistics for Fraction of CSNF Waste Packages (a) Breached by Stress Corrosion Cracking and (b) Breached by General Corrosion Patches for the Nominal Modeling Case as a Function of Time

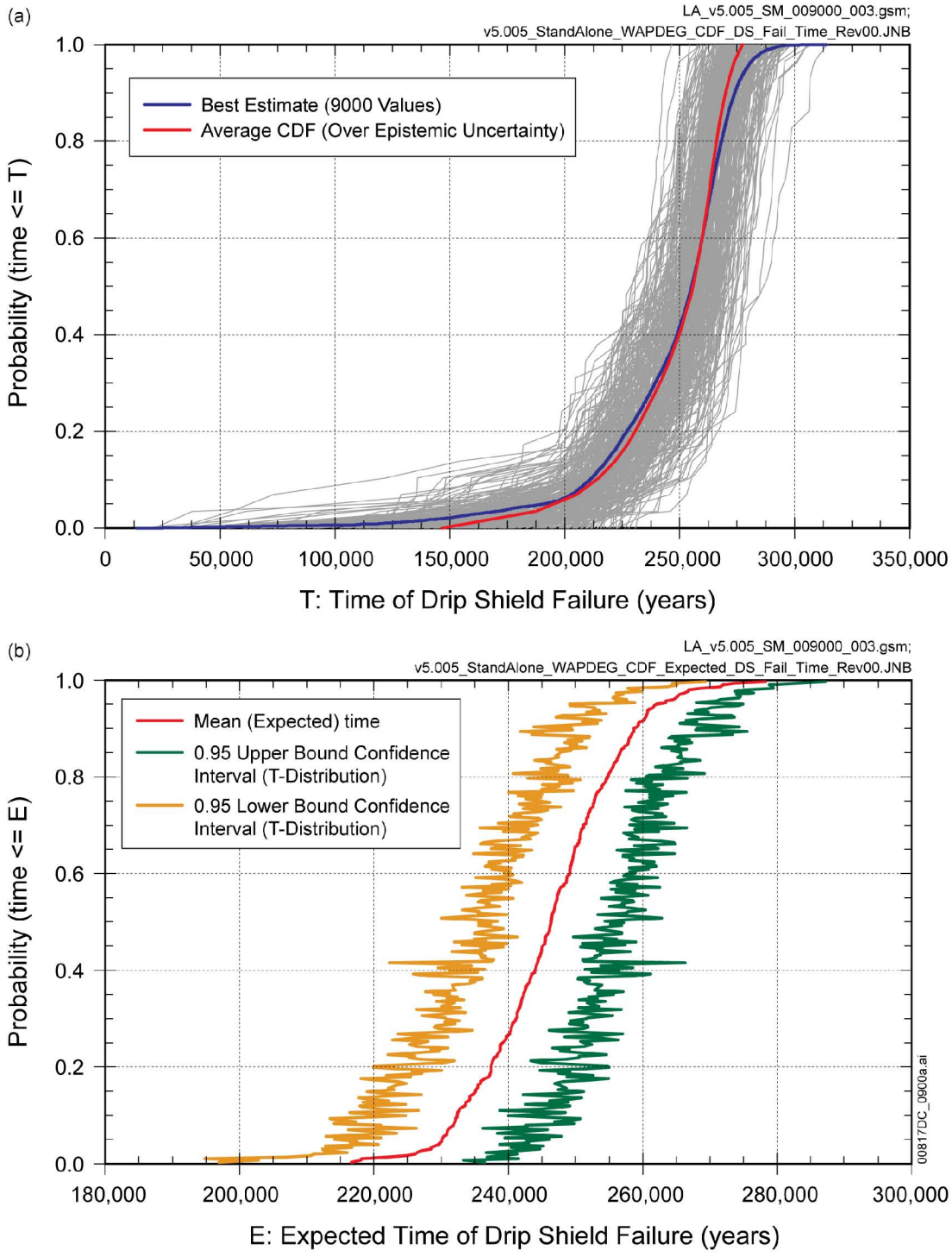

Source: Output DTN: MO0710ADTSPAWO.000 [DIRS 183752].

Figure 8.3-7[a]. Cumulative Distribution Functions of Drip Shield Failure Time for (a) Distributions of Failure Time for 300 Epistemic Sample Elements and (b) Distribution of Expected (Over Aleatory) Failure Time with Confidence Interval for the Seismic Ground Motion Modeling Case

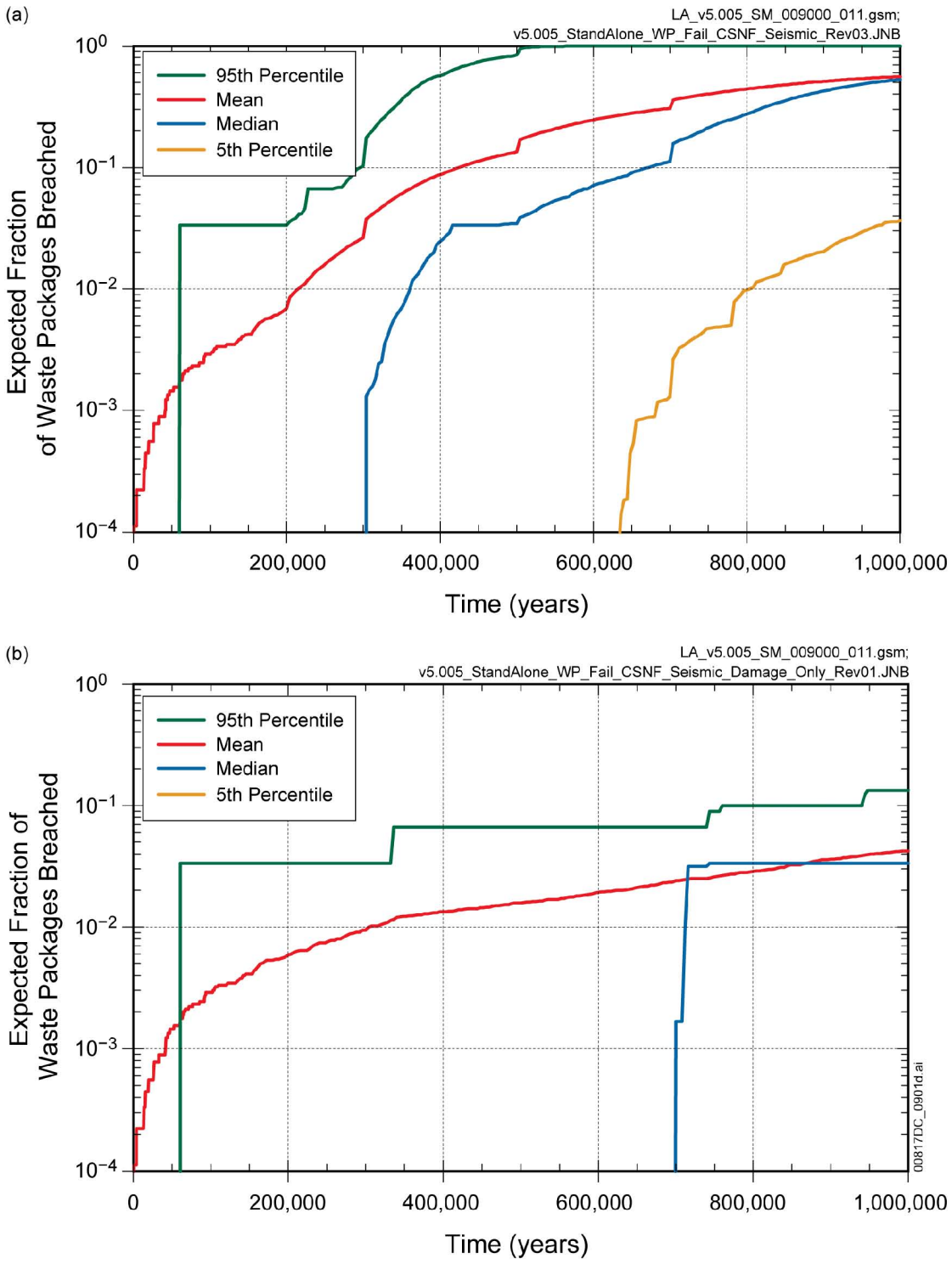

Source: Output DTN: MO0801TSPAWPDS.000 [DIRS 185077].

Figure 8.3-8[a]. Summary Statistics for Expected Fraction of CSNF WPs (a) Breached by Seismic and Nominal Processes and (b) Breached by Seismic Processes Only; and CDSP WPs (c) Breached by Seismic and Nominal Processes and (d) Breached by Seismic Processes Only for the Seismic Ground Motion Modeling Case as a Function of Time

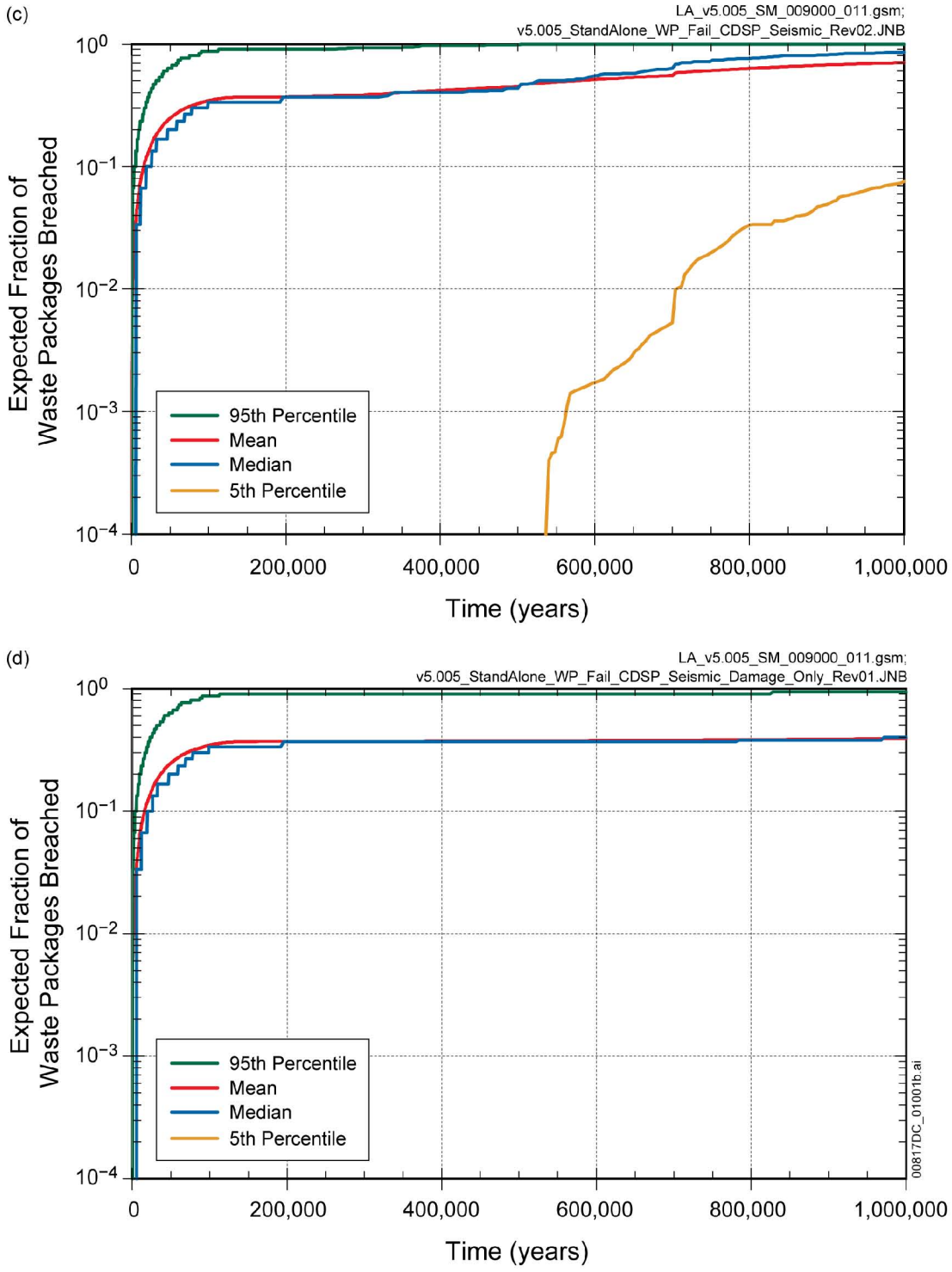

Source: Output DTN: MO0801TSPAWPDS.000 [DIRS 185077].

Figure 8.3-8[a]. Summary Statistics for Expected Fraction of CSNF WPs (a) Breached by Seismic and Nominal Processes and (b) Breached by Seismic Processes Only; and CDSP WPs (c) Breached by Seismic and Nominal Processes and (d) Breached by Seismic Processes Only for the Seismic Ground Motion Modeling Case as a Function of Time (continued)

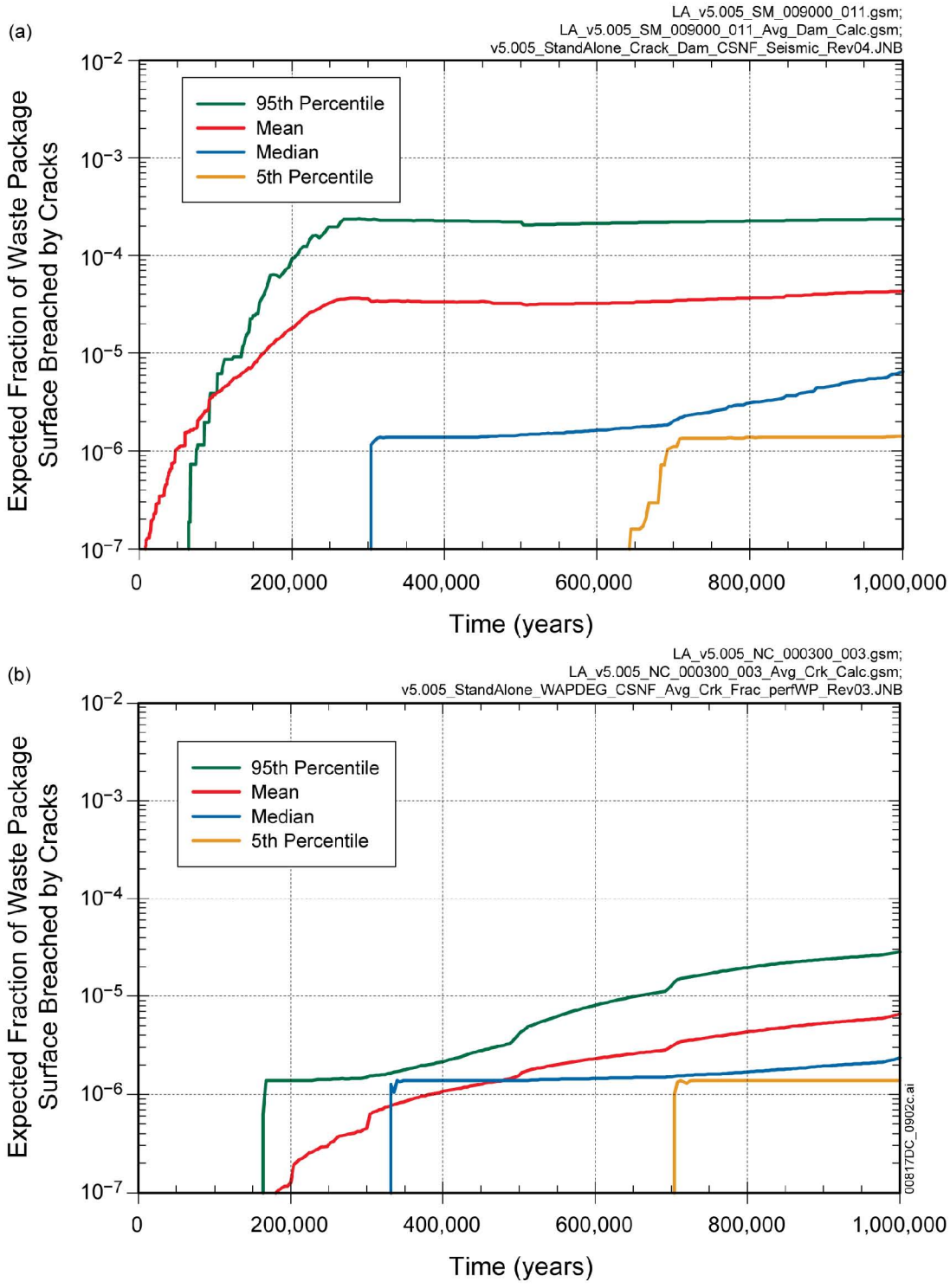

Source: Output DTN: MO0801TSPAWPDS.000 [DIRS 185077].

Figure 8.3-9[a]. Summary Statistics for Average Fraction of CSNF Waste Package Surface Breached by Cracks per Breached Waste Package for (a) the Seismic Ground Motion Modeling Case and (b) the Nominal Modeling Case as a Function of Time

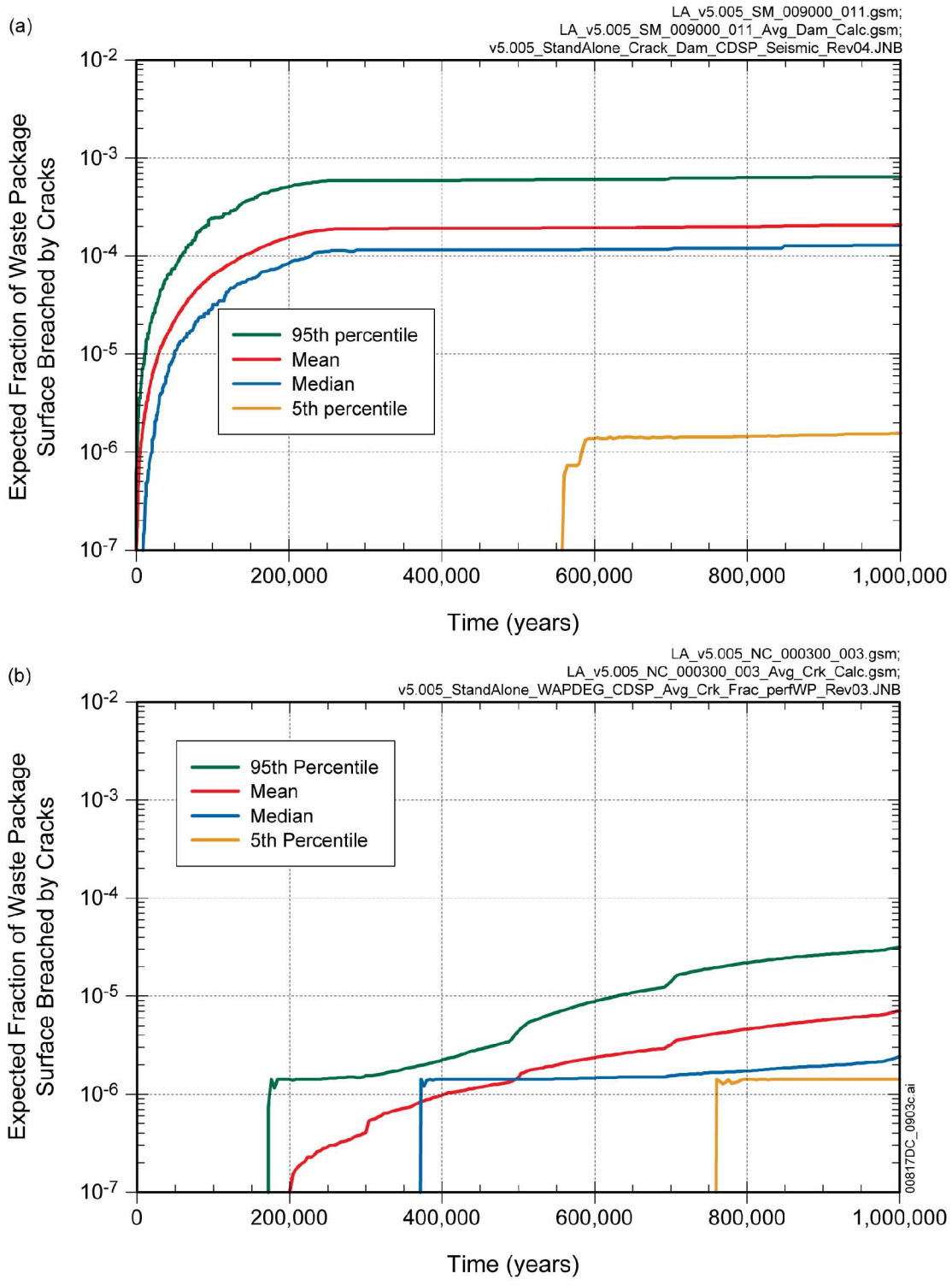

Source: Output DTN: MO0801TSPAWPDS.000 [DIRS 185077].

Figure 8.3-10[a]. Summary Statistics for Fraction of CDSP Waste Package Surface Breached by Cracks per Breached Waste Package for (a) the Seismic Ground Motion Modeling Case and (b) the Nominal Modeling Case as a Function of Time

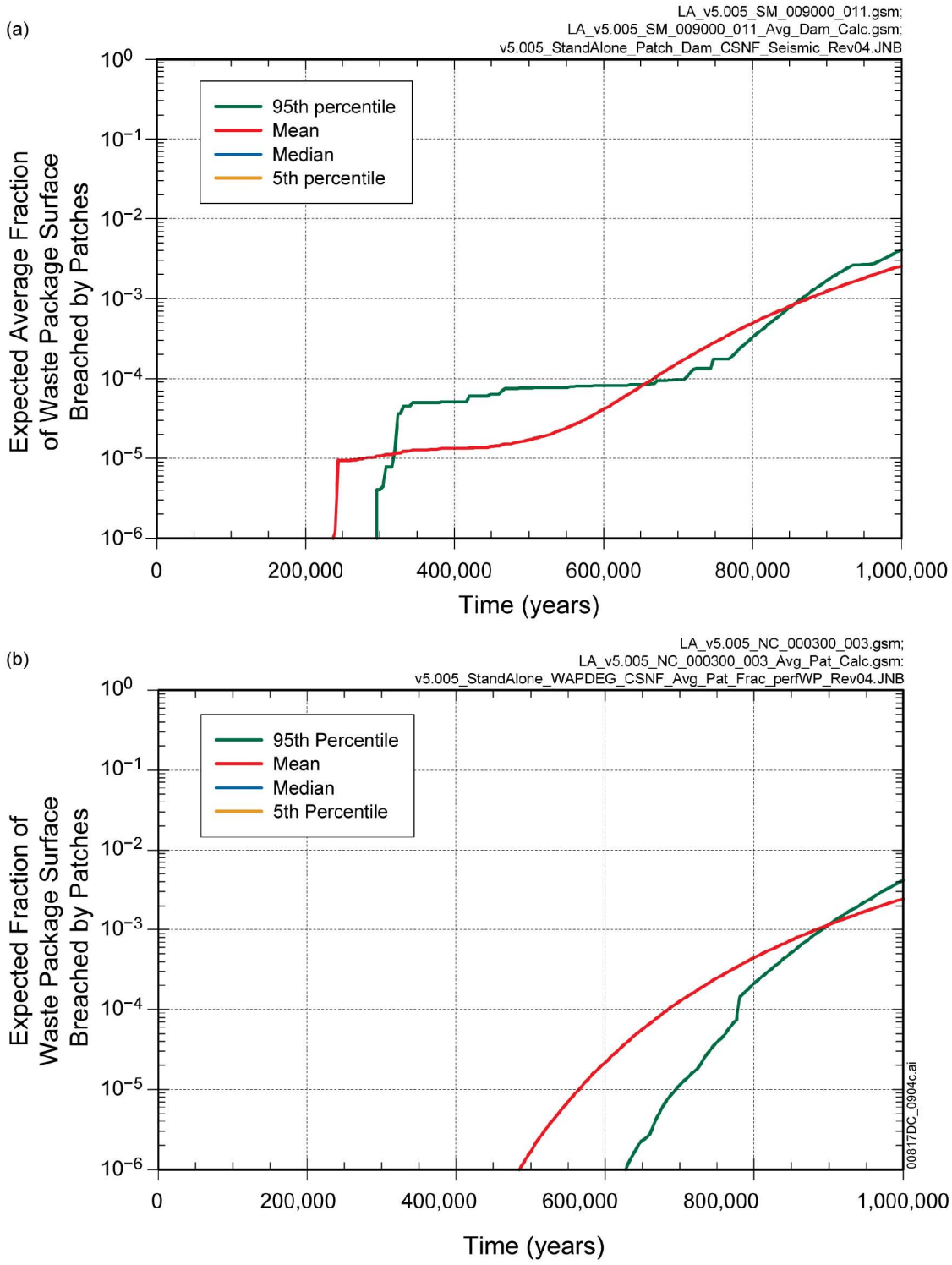

Source: Output DTN: MO0801TSPAWPDS.000 [DIRS 185077].

Figure 8.3-11[a]. Summary Statistics for Fraction of CSNF Waste Package Surface Breached by Patches per Breached Waste Package for (a) the Seismic Ground Motion Modeling Case and (b) the Nominal Modeling Case as a Function of Time

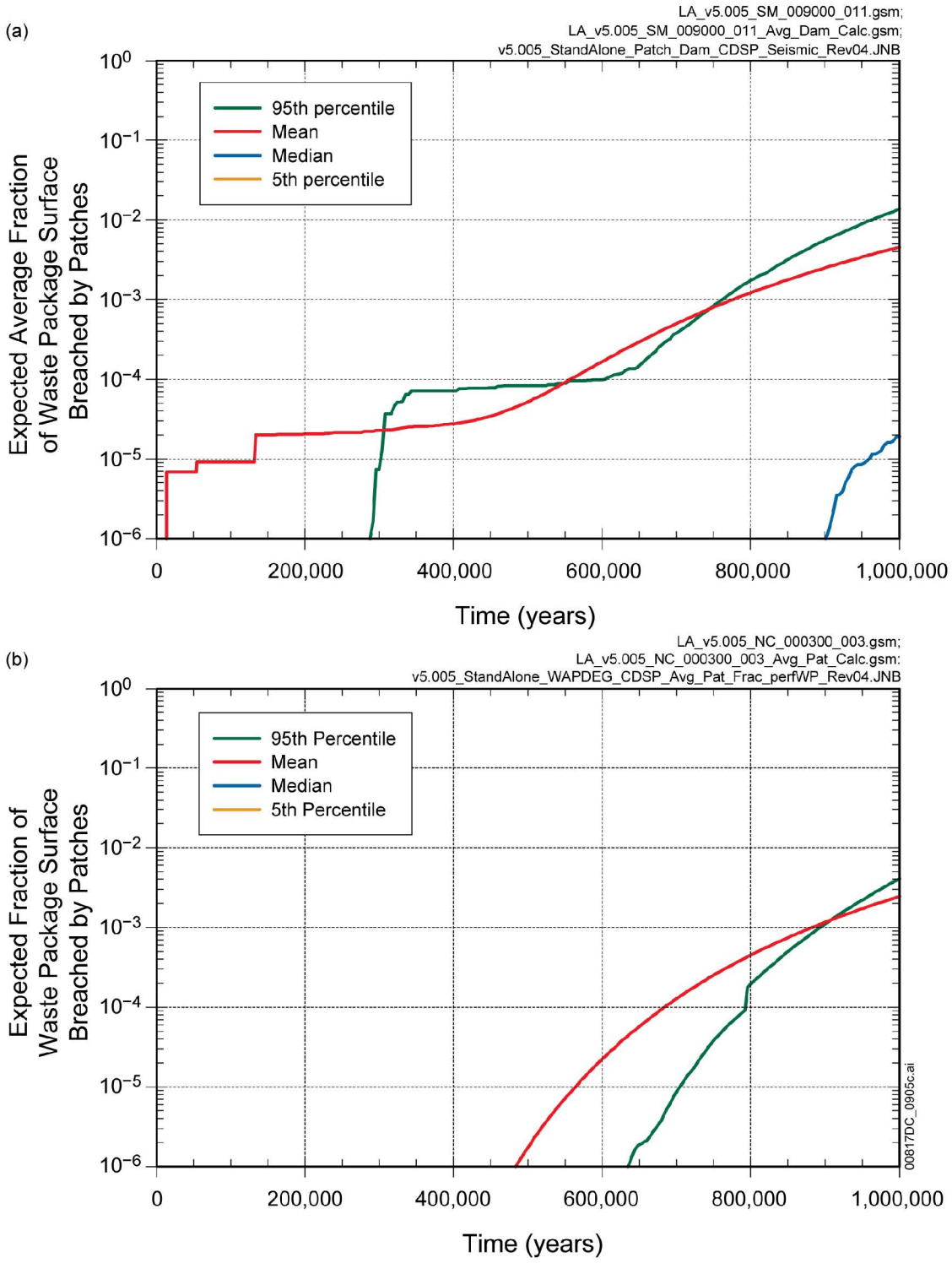

Source: Output DTN: MO0801TSPAWPDS.000 [DIRS 185077].

Figure 8.3-12[a]. Summary Statistics for Fraction of CDSP WP Surface Breached by Patches per Breached Waste Package for (a) the Seismic Ground Motion Modeling Case and (b) the Nominal Modeling Case as a Function of Time

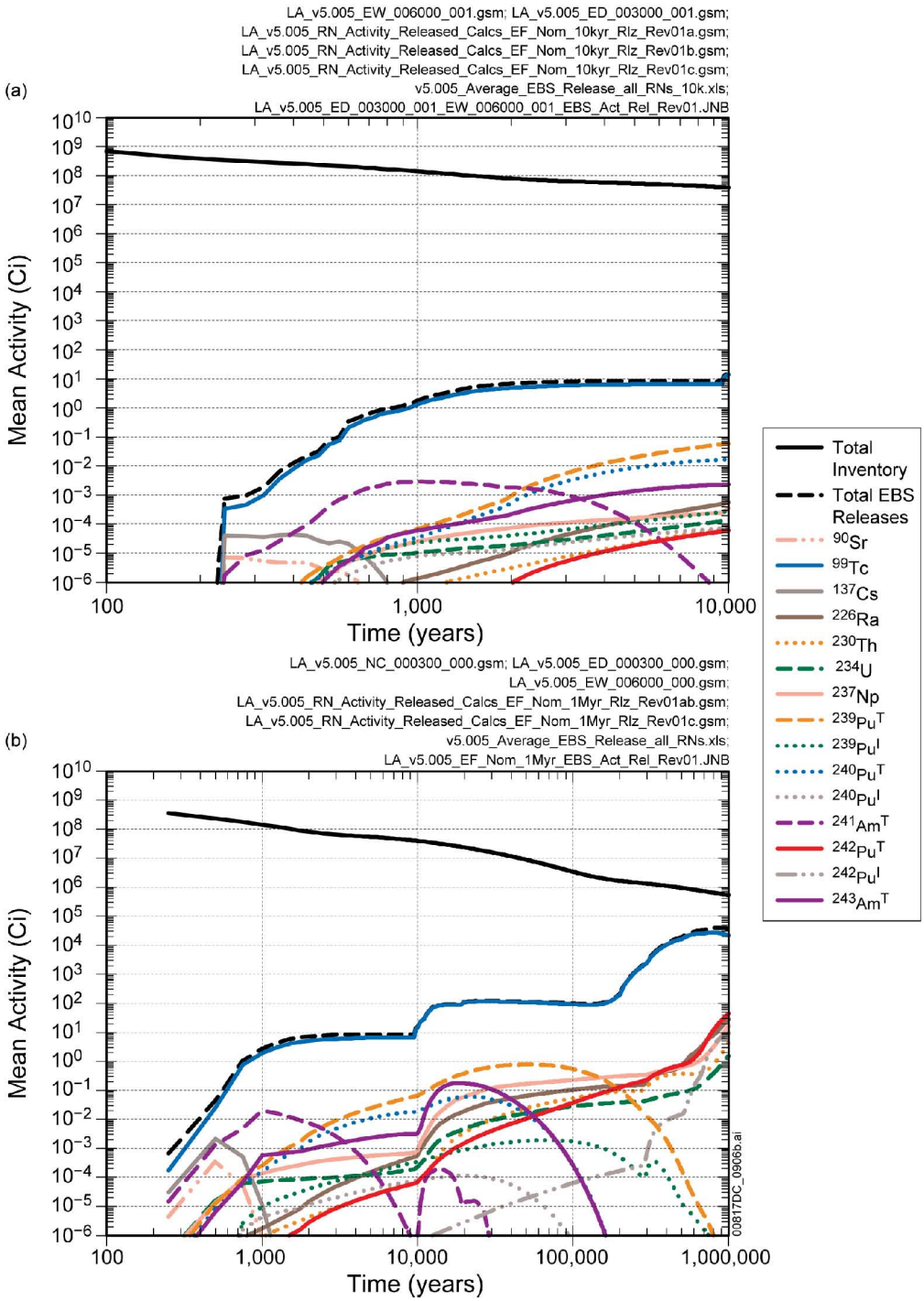

Source: Output DTNs: MO0710ADTSPAWO.000 [DIRS 183752]; and MO0710PLOTSFIG.000 [DIRS 185207].

NOTE: Total inventory indicates the repository total activity as a function of time and is included for comparison to the activity released.

Figure 8.3-13[a]. Mean Activity Released from the Engineered Barrier System for the Combined Nominal/Early Failure Modeling Case for (a) 10,000 Years after Repository Closure and (b) Post-10,000-Years after Repository Closure

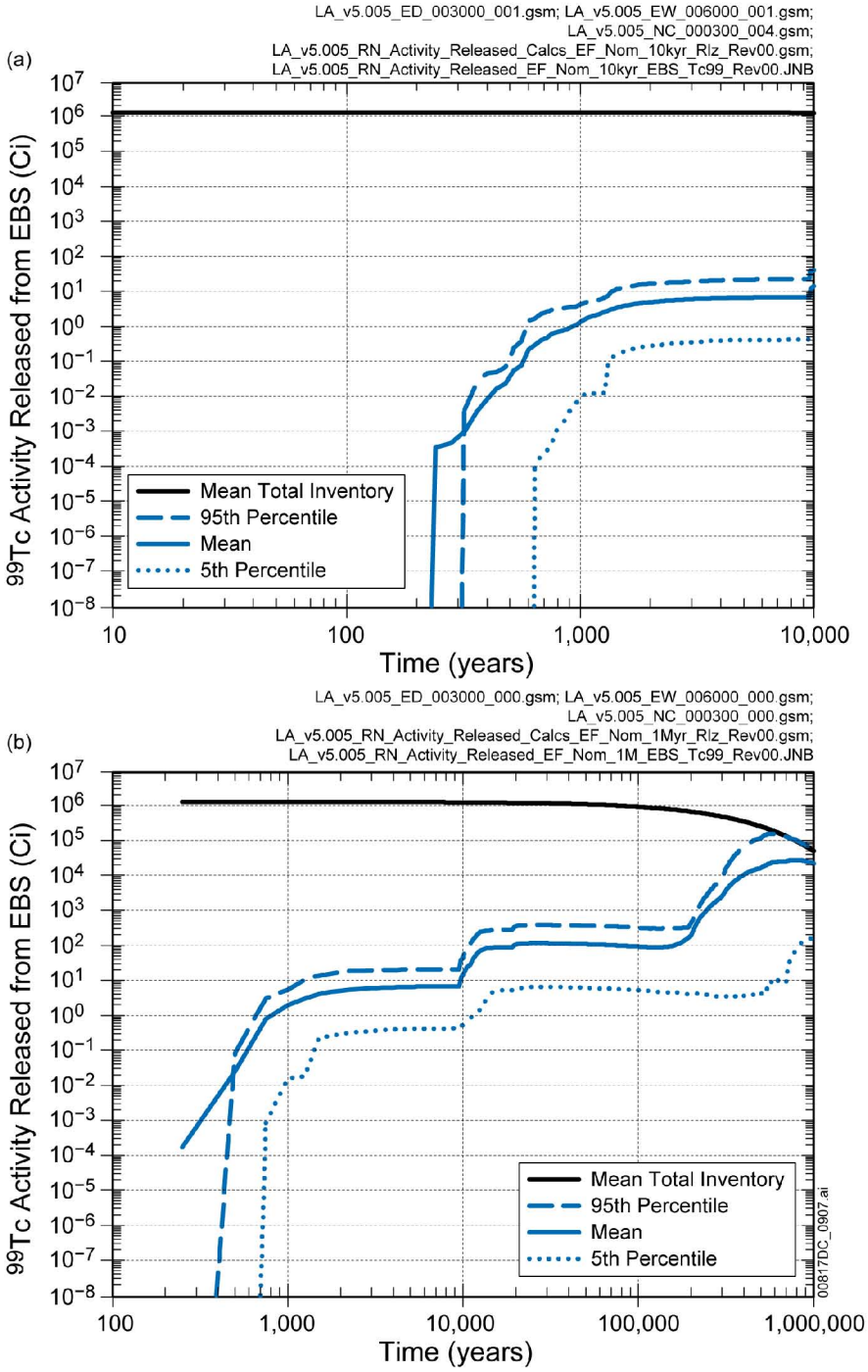

Source: Output DTNs: MO0710ADTSPAWO.000 [DIRS 183752]; and MO0710PLOTSFIG.000 [DIRS 185207].

NOTE: Mean total inventory indicates the repository total ^{99}Tc activity as a function of time and is included for comparison to the activity released.

Figure 8.3-14[a]. Uncertainty in Activity of ^{99}Tc Released from the Engineered Barrier System for the Combined Nominal/Early Failure Modeling Case for (a) 10,000 Years and (b) 1,000,000 Years after Repository Closure

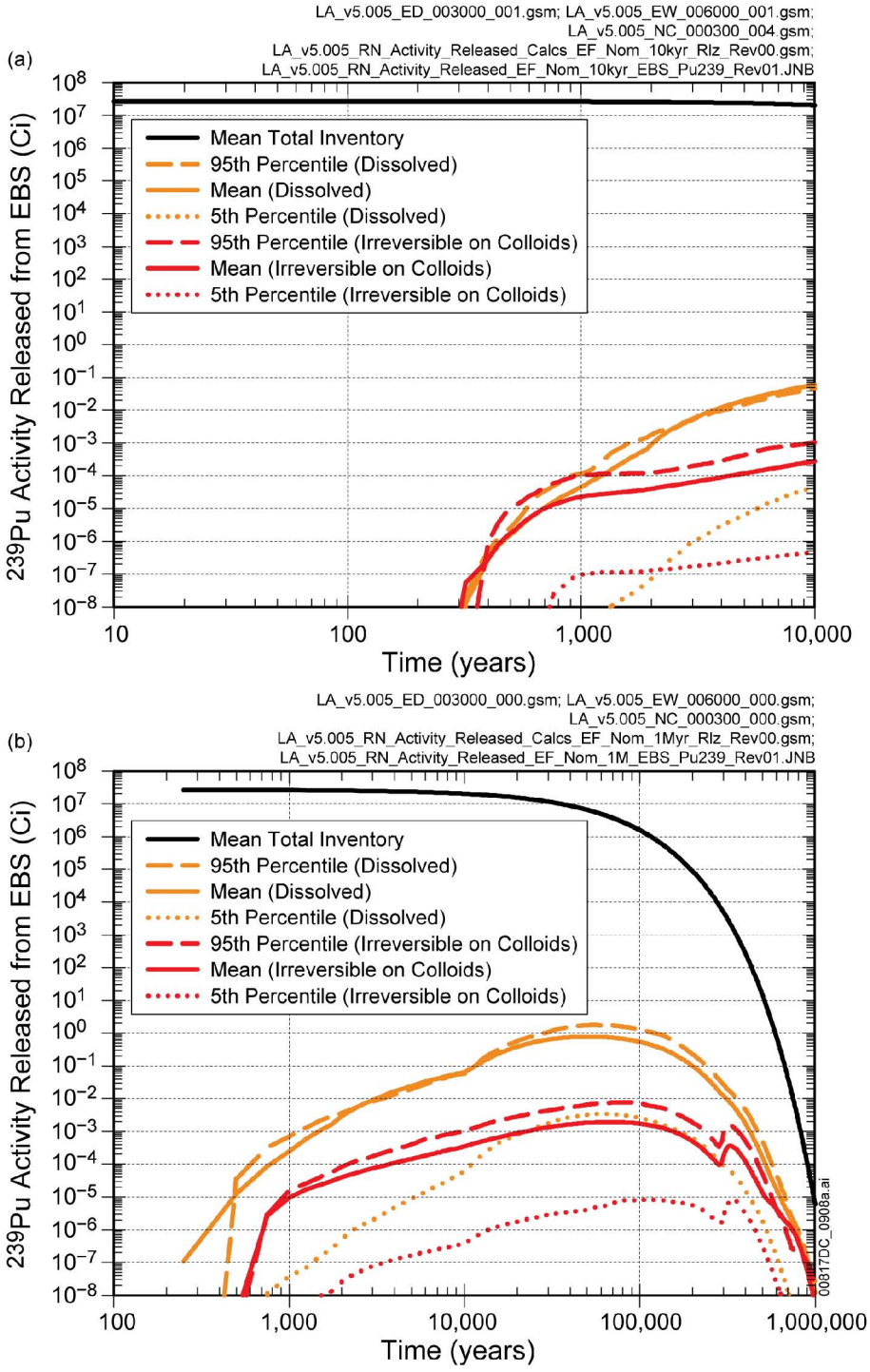

Source: Output DTNs: MO0710ADTSPAWO.000 [DIRS 183752]; and MO0710PLOTSFIG.000 [DIRS 185207].

NOTE: Mean total inventory indicates the repository total ^{239}Pu activity as a function of time and is included for comparison to the activity released.

Figure 8.3-15[a]. Uncertainty in Activity of ^{239}Pu Released from the Engineered Barrier System for the Combined Nominal/Early Failure Modeling Case for (a) 10,000 Years and (b) 1,000,000 Years after Repository Closure

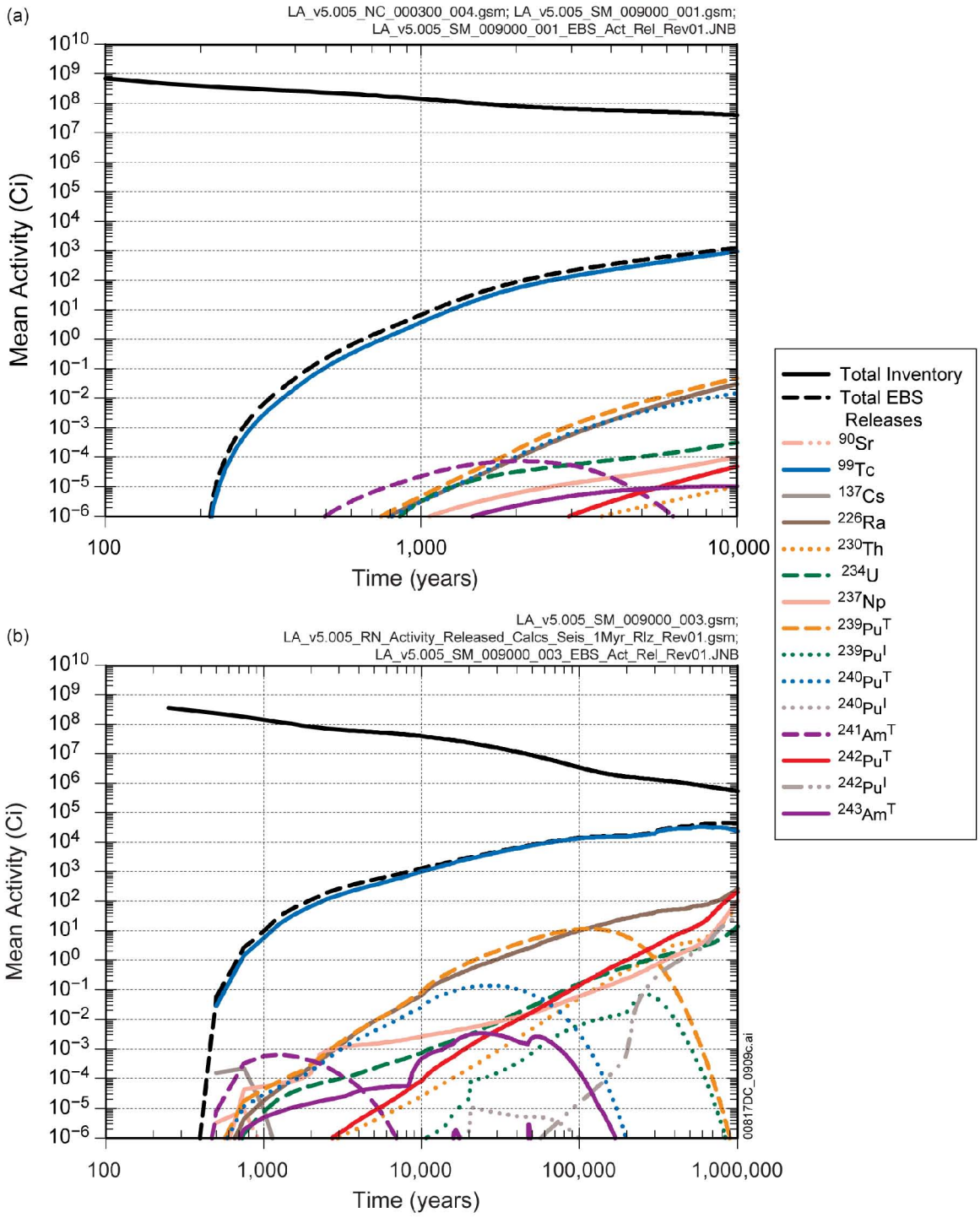

Source: Output DTNs: MO0710ADTSPAWO.000 [DIRS 183752]; and MO0710PLOTSFIG.000 [DIRS 185207].

NOTE: Total inventory indicates the repository total activity as a function of time and is included for comparison to the activity released.

Figure 8.3-16[a]. Mean Activity Released from the Engineered Barrier System for the Seismic Ground Motion Modeling Case for (a) 10,000 Years and (b) 1,000,000 Years after Repository Closure

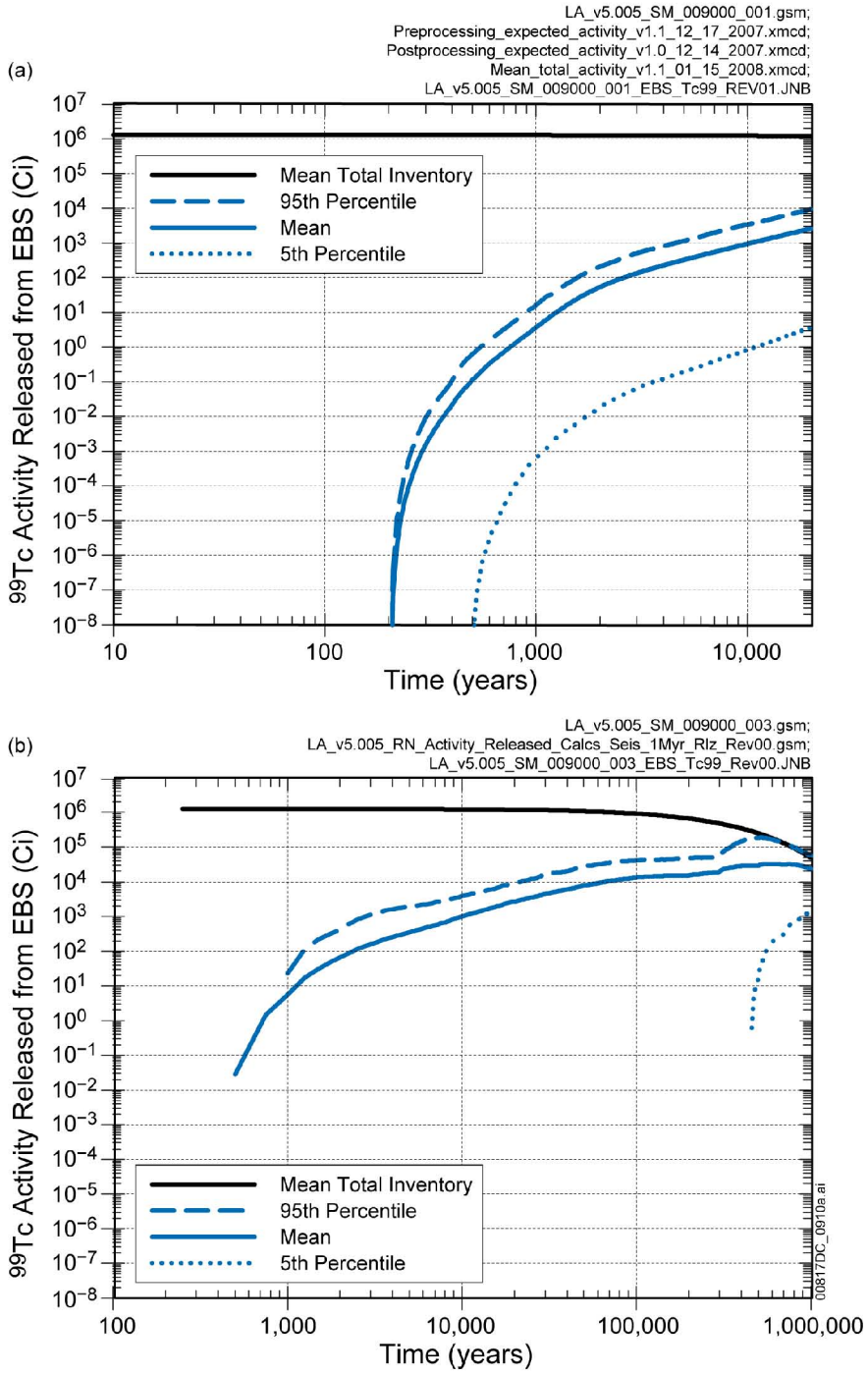

Source: Output DTNs: MO0710ADTSPAWO.000 [DIRS 183752]; and MO0710PLOTSFIG.000 [DIRS 185207].

NOTE: Mean total inventory indicates the repository total ^{99}Tc activity as a function of time and is included for comparison to the activity released.

Figure 8.3-17[a]. Uncertainty in Activity of ^{99}Tc Released from the Engineered Barrier System for the Seismic Ground Motion Modeling Case for (a) 10,000 Years and (b) 1,000,000 Years after Repository Closure

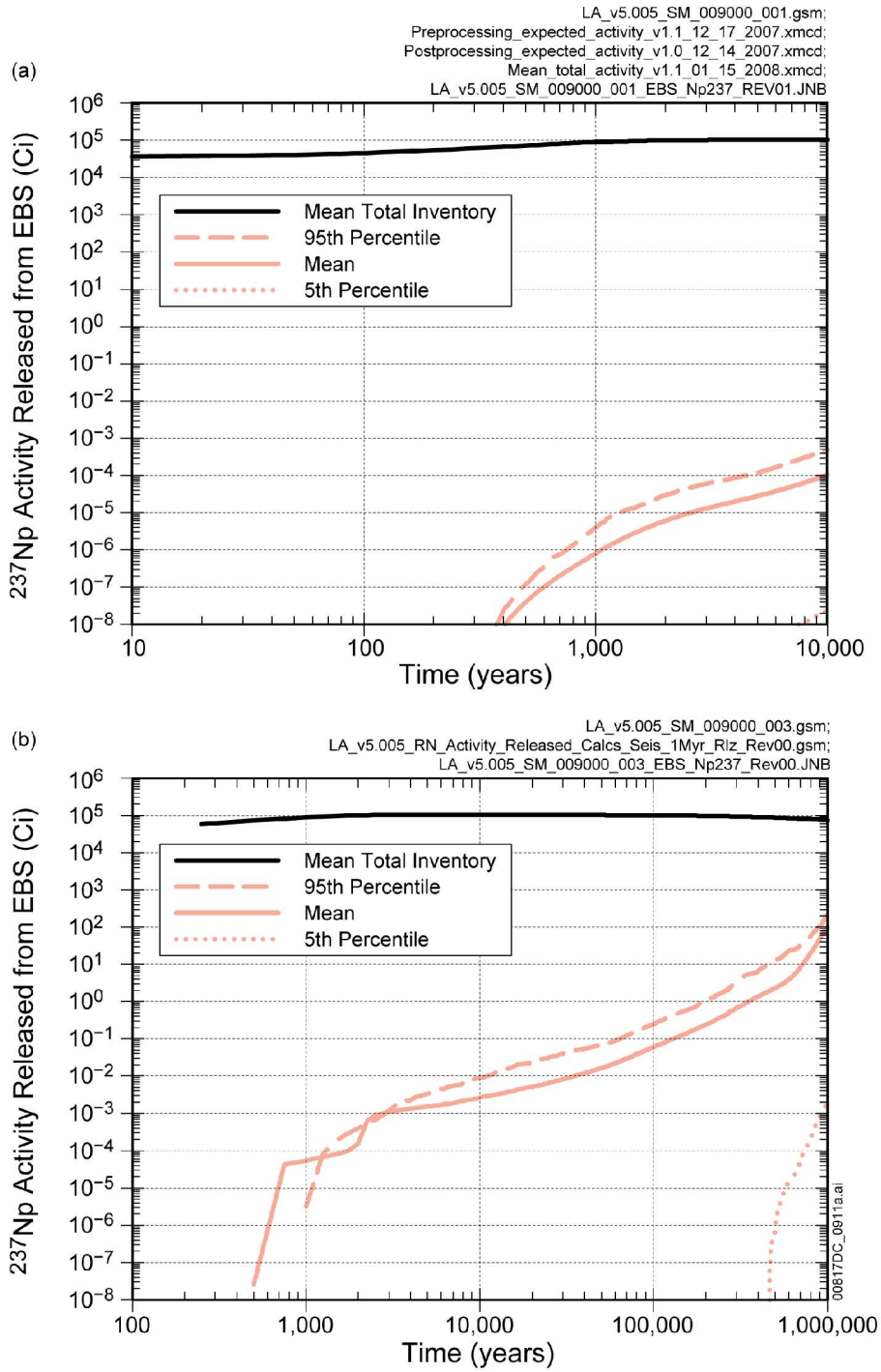

Source: Output DTNs: MO0710ADTSPAWO.000 [DIRS 183752]; and MO0710PLOTSFIG.000 [DIRS 185207].

NOTE: Mean total inventory indicates the repository total ^{237}Np activity as a function of time and is included for comparison to the activity released.

Figure 8.3-18[a]. Uncertainty in Activity of ^{237}Np Released from the Engineered Barrier System for the Seismic Ground Motion Modeling Case for (a) 10,000 Years and (b) 1,000,000 Years after Repository Closure

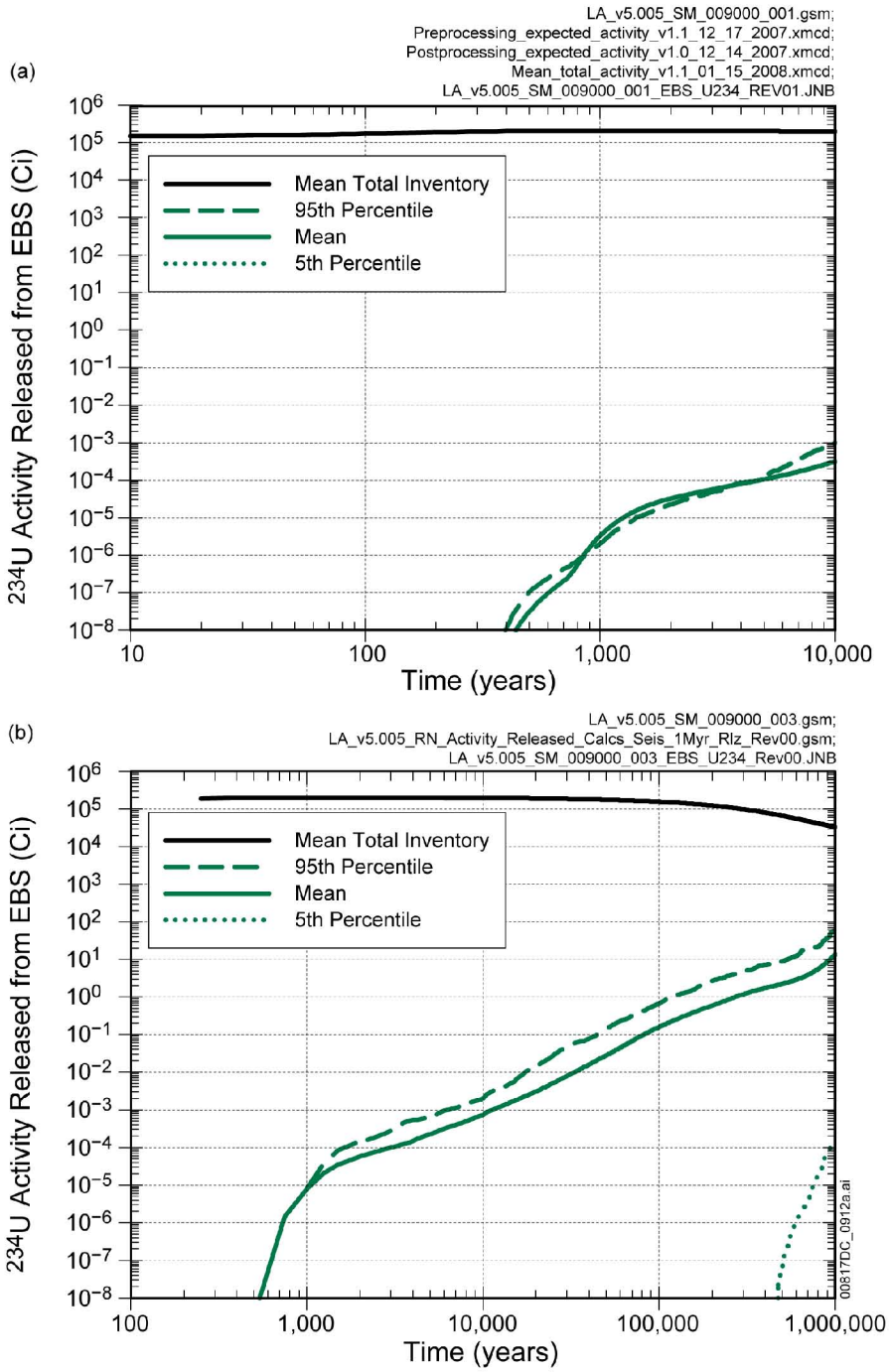

Source: Output DTNs: MO0710ADTSPAWO.000 [DIRS 183752]; and MO0710PLOTSFIG.000 [DIRS 185207].

NOTE: Mean total inventory indicates the repository total ^{234}U activity as a function of time and is included for comparison to the activity released.

Figure 8.3-19[a]. Uncertainty in Activity of ^{234}U Released from the Engineered Barrier System for the Seismic Ground Motion Modeling Case for (a) 10,000 Years and (b) 1,000,000 Years after Repository Closure

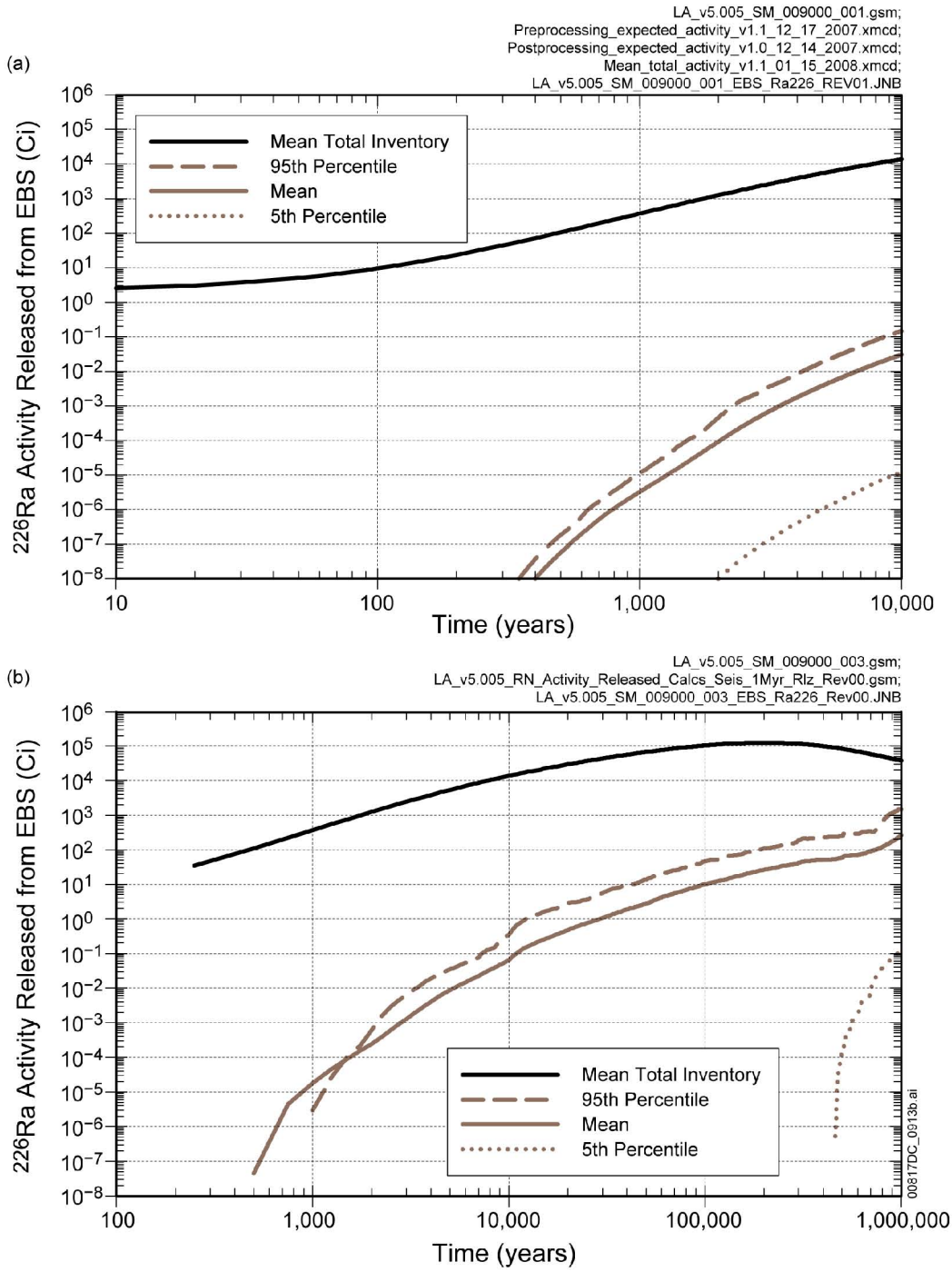

Source: Output DTNs: MO0710ADTSPAWO.000 [DIRS 183752]; and MO0710PLOTSFIG.000 [DIRS 185207].

NOTE: Mean total inventory indicates the repository total ^{226}Ra activity as a function of time and is included for comparison to the activity released.

Figure 8.3-20[a]. Uncertainty in Activity of ^{226}Ra Released from the Engineered Barrier System for the Seismic Ground Motion Modeling Case for (a) 10,000 Years and (b) 1,000,000 Years after Repository Closure

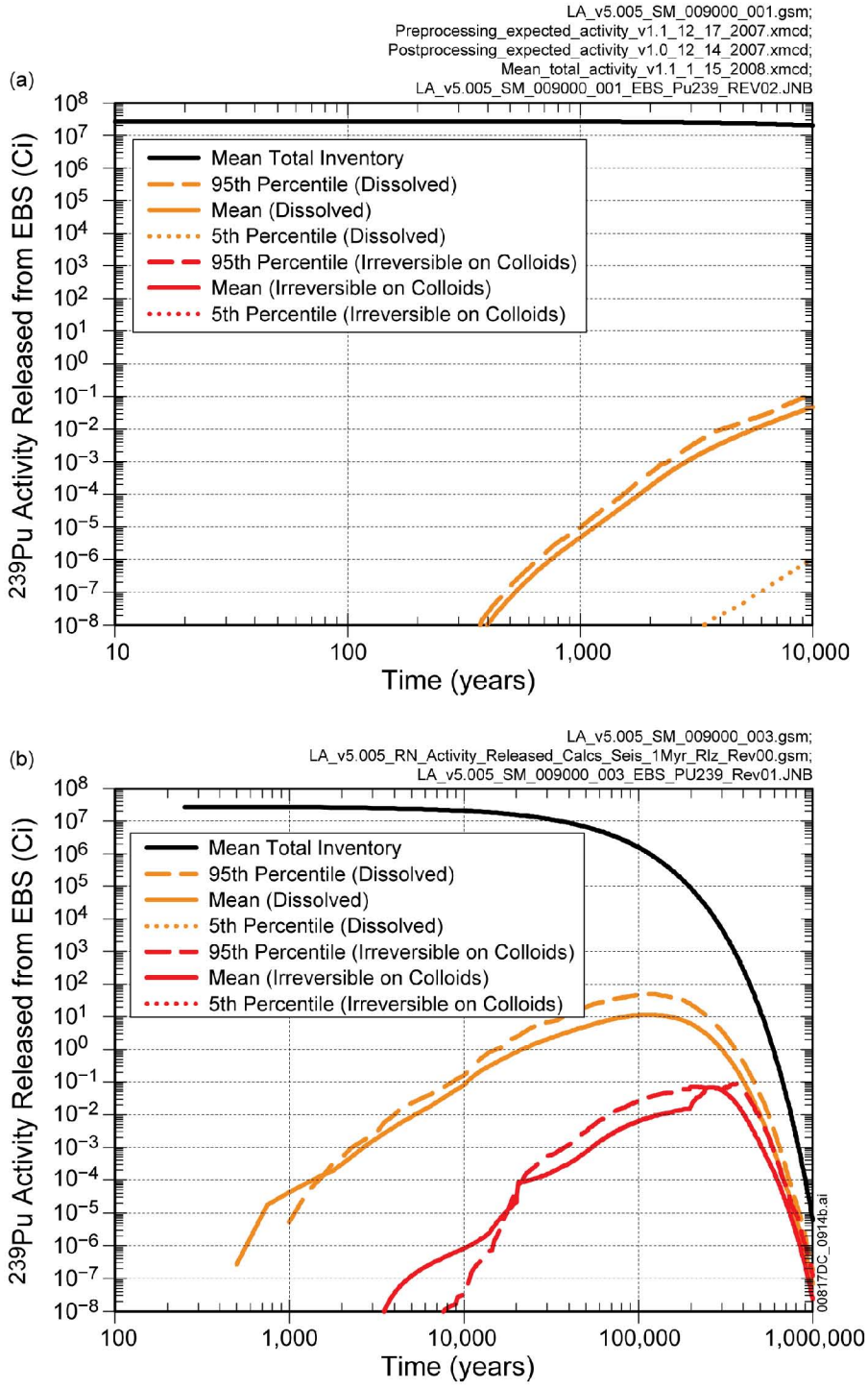

Source: Output DTNs: MO0710ADTSPAWO.000 [DIRS 183752]; and MO0710PLOTSFIG.000 [DIRS 185207].

NOTE: Mean total inventory indicates the repository total ^{239}Pu activity as a function of time and is included for comparison to the activity released.

Figure 8.3-21[a]. Uncertainty in Activity of ^{239}Pu Released from the Engineered Barrier System for the Seismic Ground Motion Modeling Case for (a) 10,000 Years and (b) 1,000,000 Years after Repository Closure

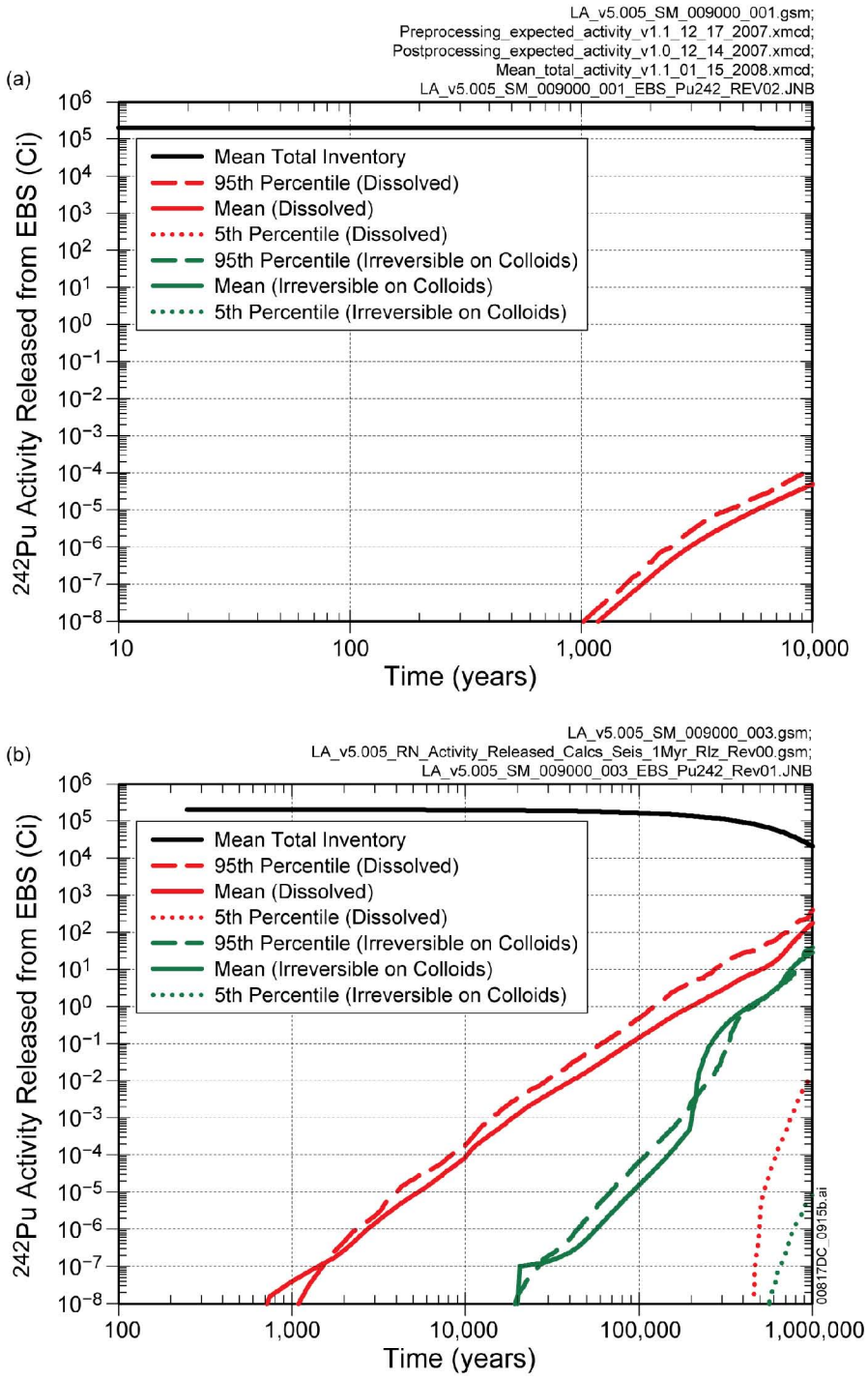

Source: Output DTNs: MO0710ADTSPAWO.000 [DIRS 183752]; and MO0710PLOTSFIG.000 [DIRS 185207].

NOTE: Mean total inventory indicates the repository total ^{242}Pu activity as a function of time and is included for comparison to the activity released.

Figure 8.3-22[a]. Uncertainty in Activity of ^{242}Pu Released from the Engineered Barrier System for the Seismic Ground Motion Modeling Case for (a) 10,000 Years and (b) 1,000,000 Years after Repository Closure

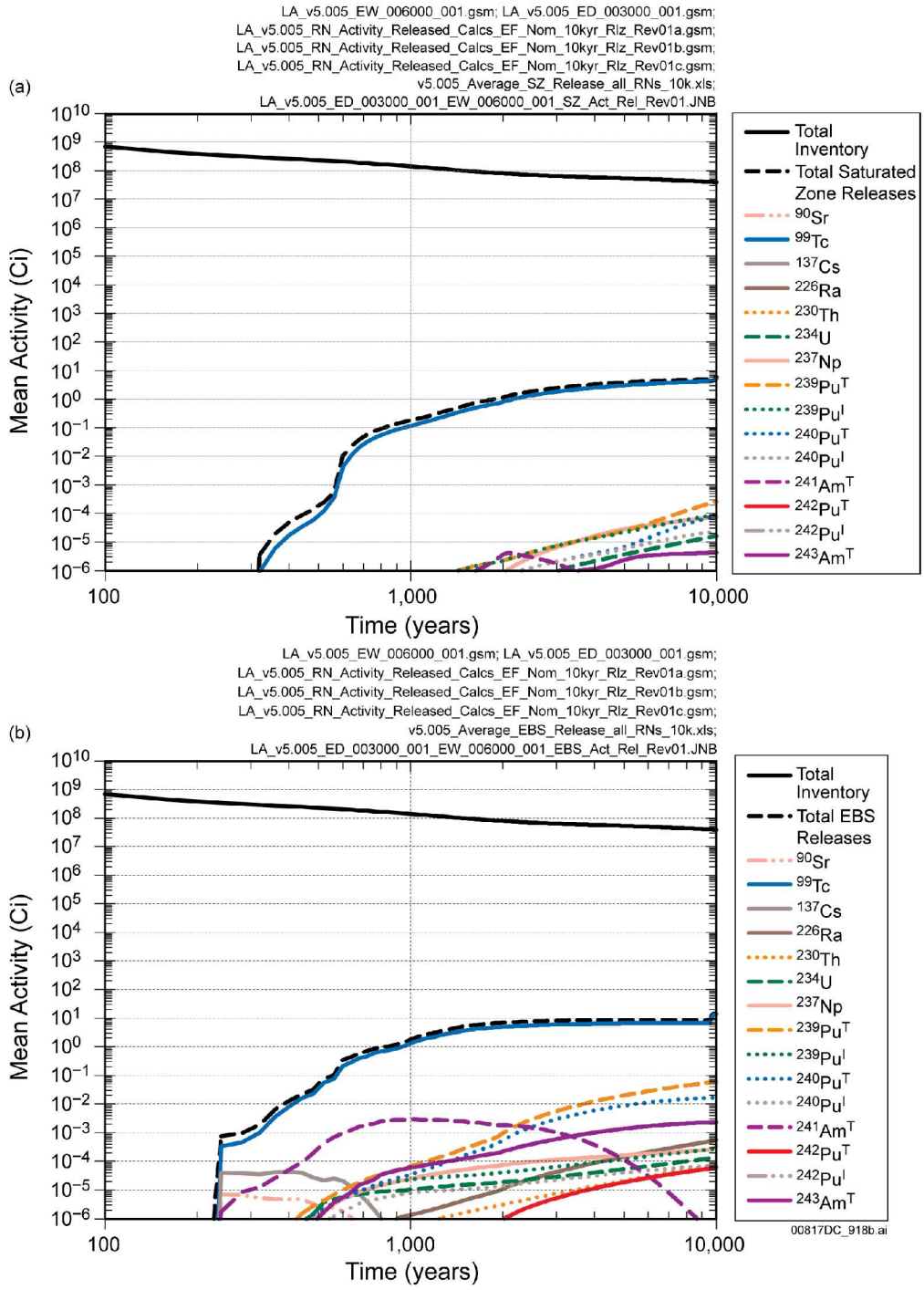

Source: Output DTNs: MO0710ADTSPAWO.000 [DIRS 183752]; and MO0710PLOTSFIG.000 [DIRS 185207].

NOTE: Total inventory indicates the repository total activity as a function of time and is included for comparison to the activity released.

Figure 8.3-23[a]. Mean Activity Released from the (a) Saturated Zone and (b) Engineered Barrier System for the Combined Nominal/Early Failure Modeling Case for 10,000 Years after Repository Closure

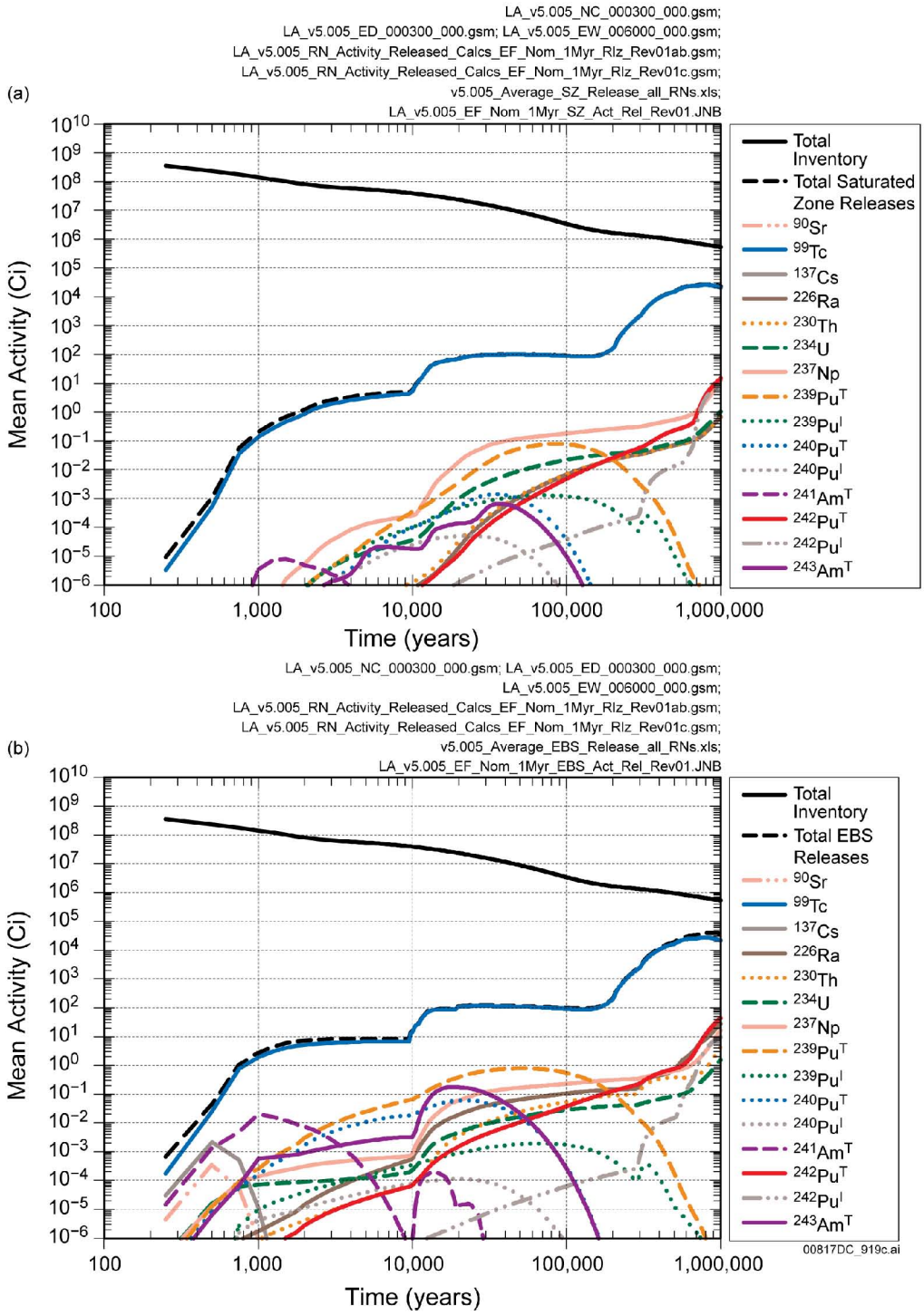

Source: Output DTNs: MO0710ADTSPAWO.000 [DIRS 183752]; and MO0710PLOTSFIG.000 [DIRS 185207].

NOTE: Total inventory indicates the repository total activity as a function of time and is included for comparison to the activity released.

Figure 8.3-24[a]. Mean Activity Released from the (a) Saturated Zone and (b) Engineered Barrier System for the Combined Nominal/Early Failure Modeling Case for 1,000,000 Years after Repository Closure

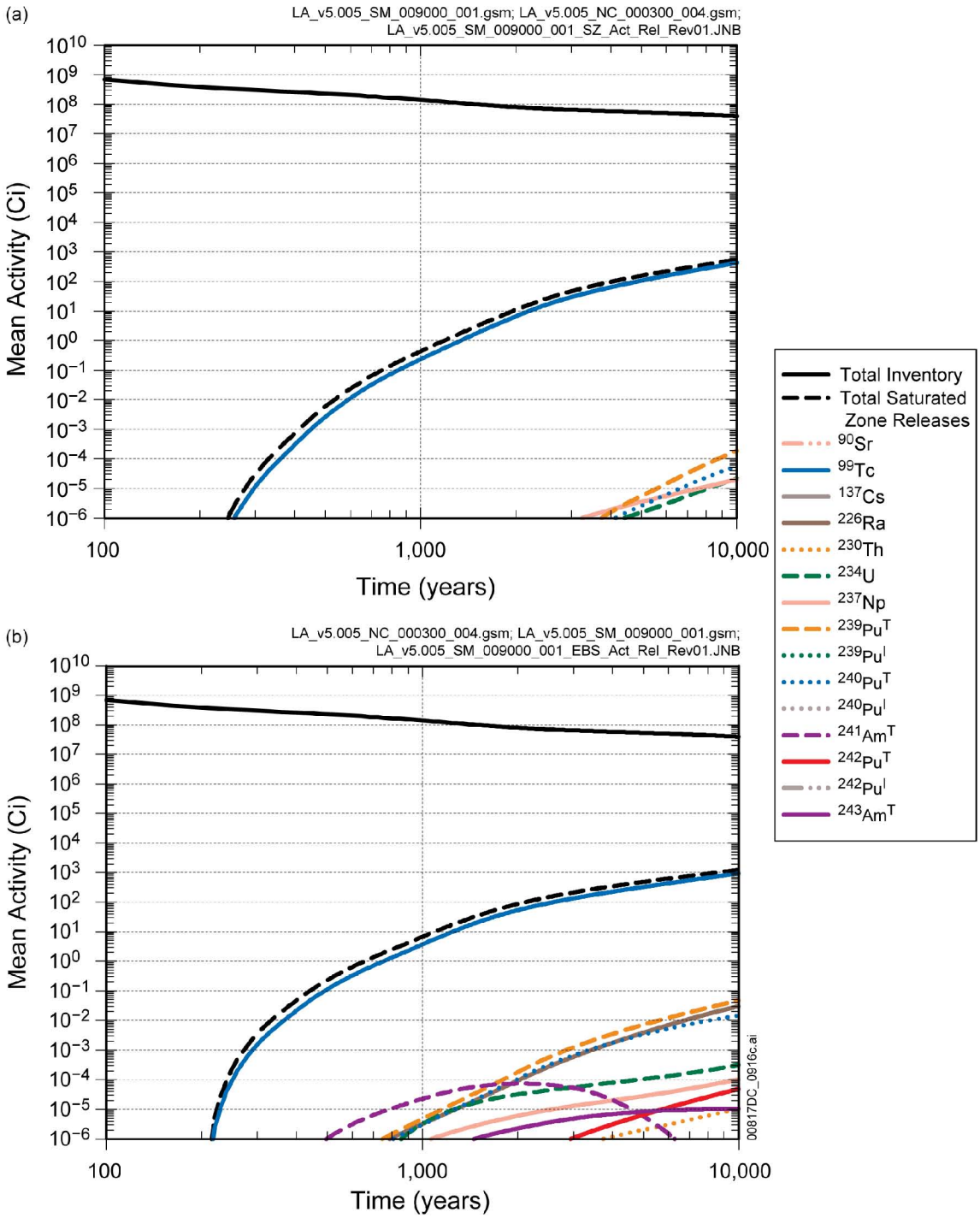

Source: Output DTNs: MO0710ADTSPAWO.000 [DIRS 183752]; and MO0710PLOTSFIG.000 [DIRS 185207].

NOTE: Total inventory indicates the repository total activity as a function of time and is included for comparison to the activity released.

Figure 8.3-25[a]. Mean Activity Released from the (a) Saturated Zone and (b) Engineered Barrier System for the Seismic Ground Motion Modeling Case for 10,000 Years after Repository Closure

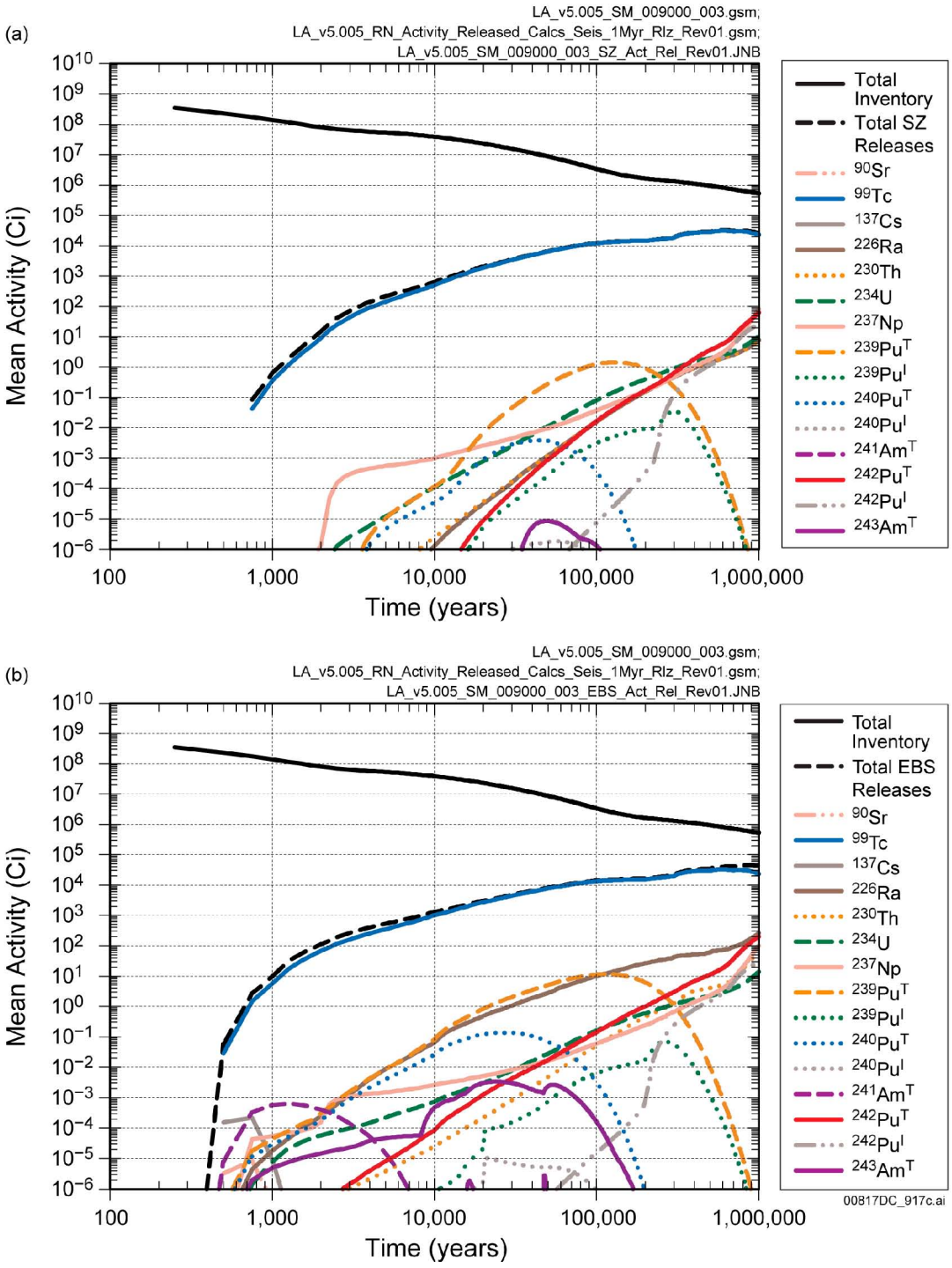

Source: Output DTNs: MO0710ADTSPAWO.000 [DIRS 183752]; and MO0710PLOTSFIG.000 [DIRS 185207].

NOTE: Total inventory indicates the repository total activity as a function of time and is included for comparison to the activity released.

Figure 8.3-26[a]. Mean Activity Released from the (a) Saturated Zone and (b) Engineered Barrier System for the Seismic Ground Motion Modeling Case for 1,000,000 Years after Repository Closure

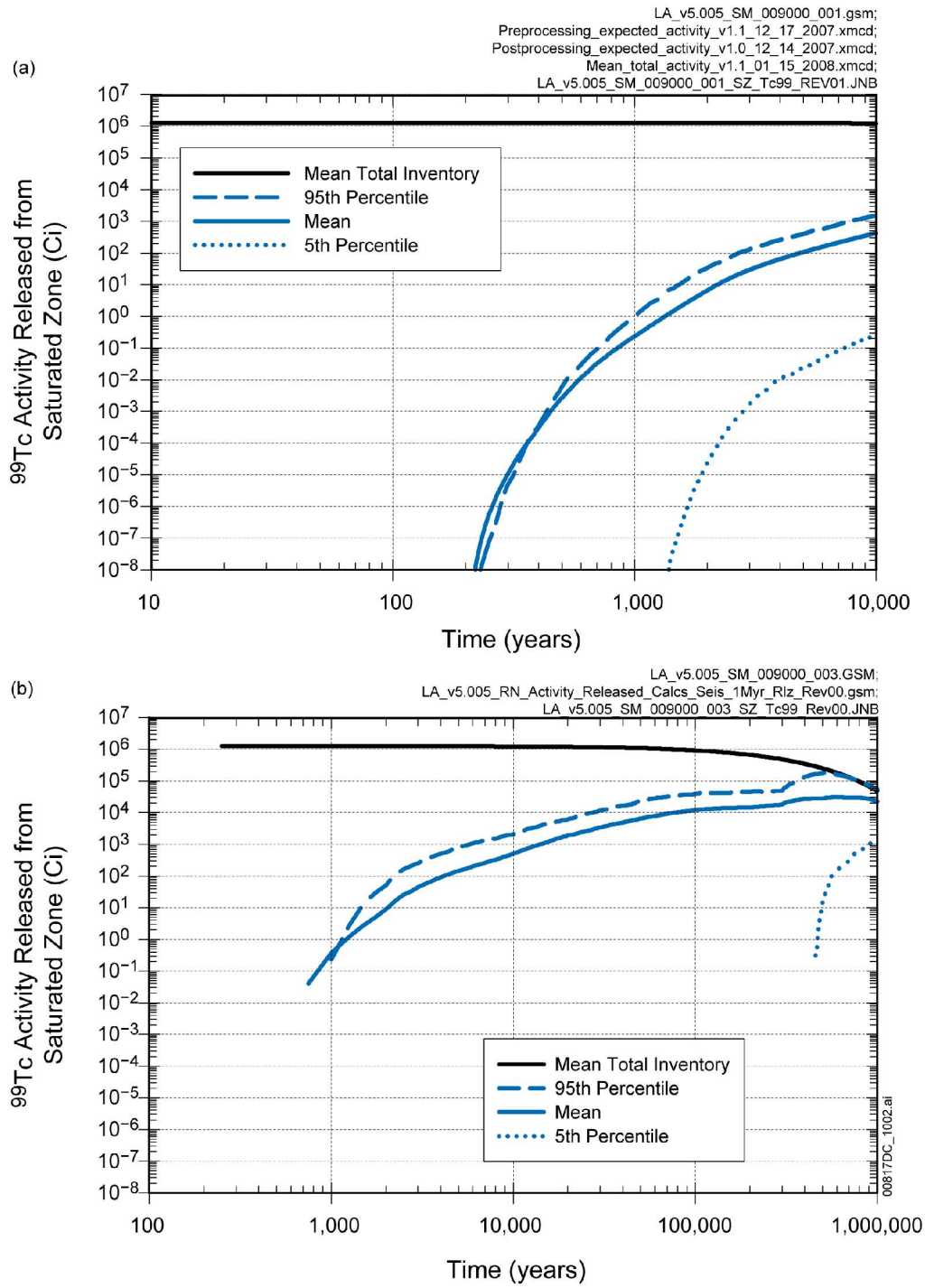

Source: Output DTN: MO0710ADTSPAWO.000 [DIRS 183752].

NOTE: Mean total inventory indicates the repository total ^{99}Tc activity as a function of time and is included for comparison to the activity released.

Figure 8.3-27[a]. Uncertainty in Activity of ^{99}Tc Released from the Saturated Zone for the Seismic Ground Motion Modeling Case for (a) 10,000 Years and (b) 1,000,000 Years after Repository Closure

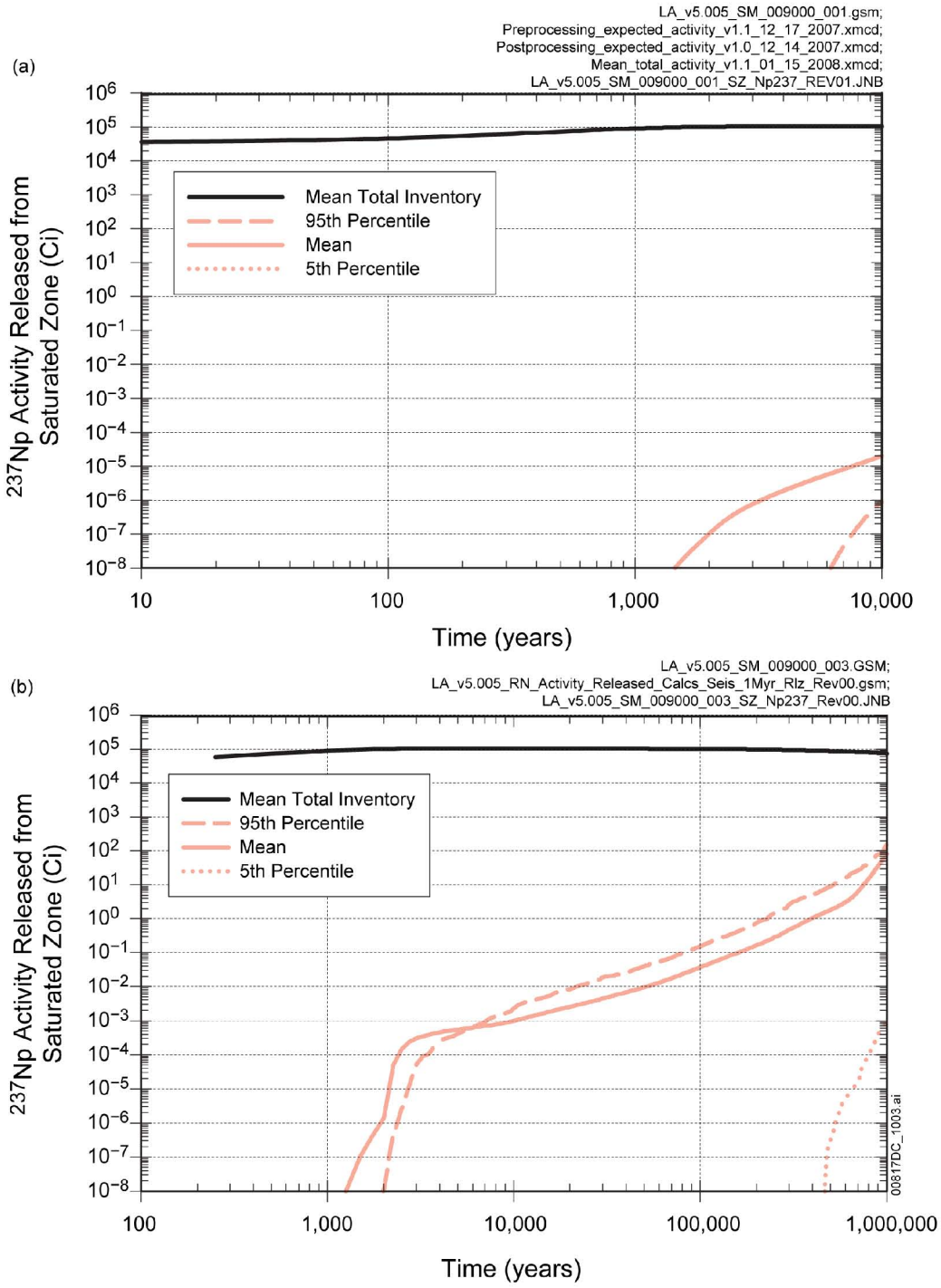

Source: Output DTN: MO0710ADTSPAWO.000 [DIRS 183752].

NOTE: Mean total inventory indicates the repository total ^{237}Np activity as a function of time and is included for comparison to the activity released.

Figure 8.3-28[a]. Uncertainty in Activity of ^{237}Np Released from the Saturated Zone for the Seismic Ground Motion Modeling Case for (a) 10,000 Years and (b) 1,000,000 Years after Repository Closure

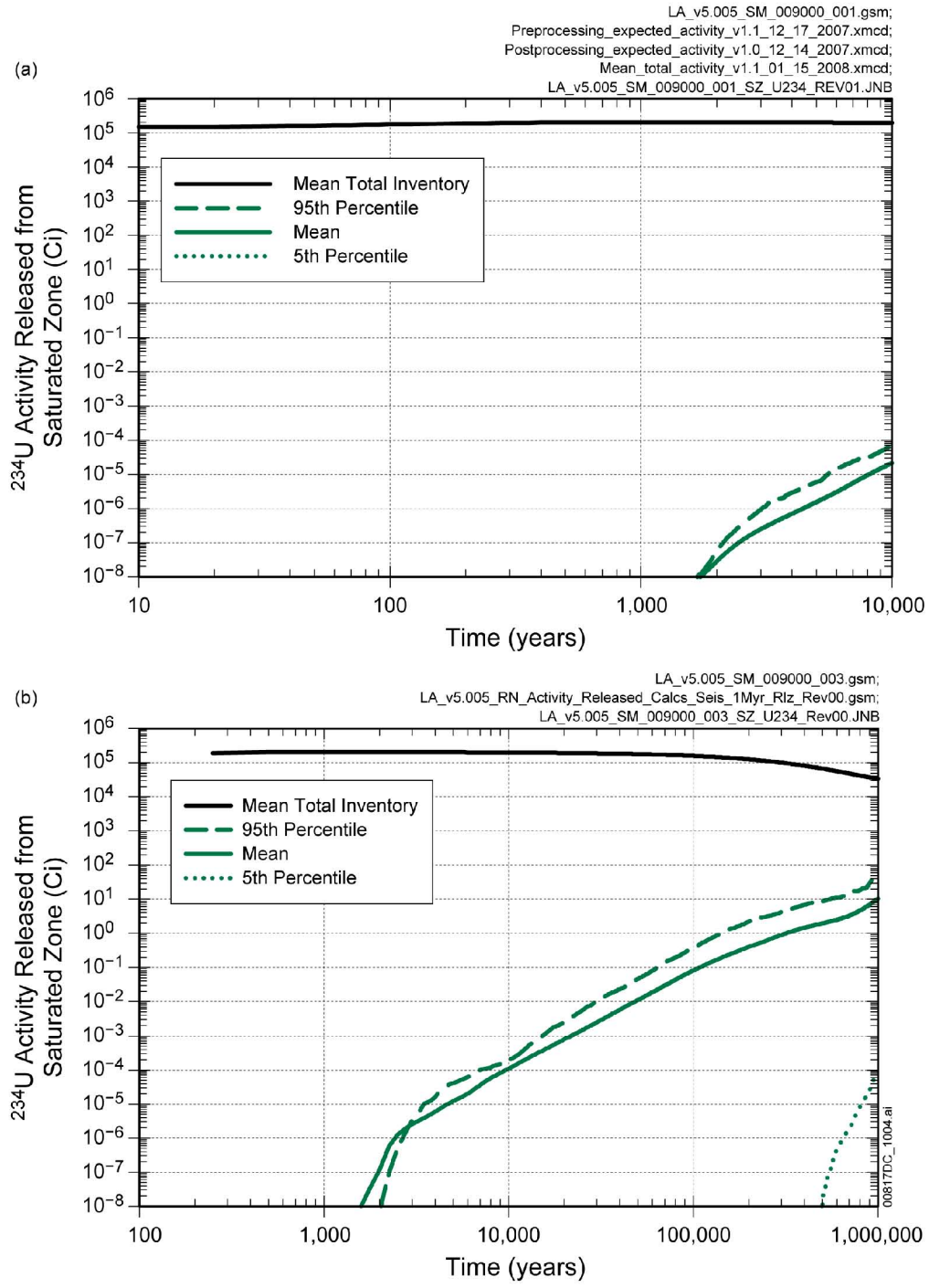

Source: Output DTN: MO0710ADTSPAWO.000 [DIRS 183752].

NOTE: Mean total inventory indicates the repository total ^{234}U activity as a function of time and is included for comparison to the activity released.

Figure 8.3-29[a]. Uncertainty in Activity of ^{234}U Released from the Saturated Zone for the Seismic Ground Motion Modeling Case for (a) 10,000 Years and (b) 1,000,000 Years after Repository Closure

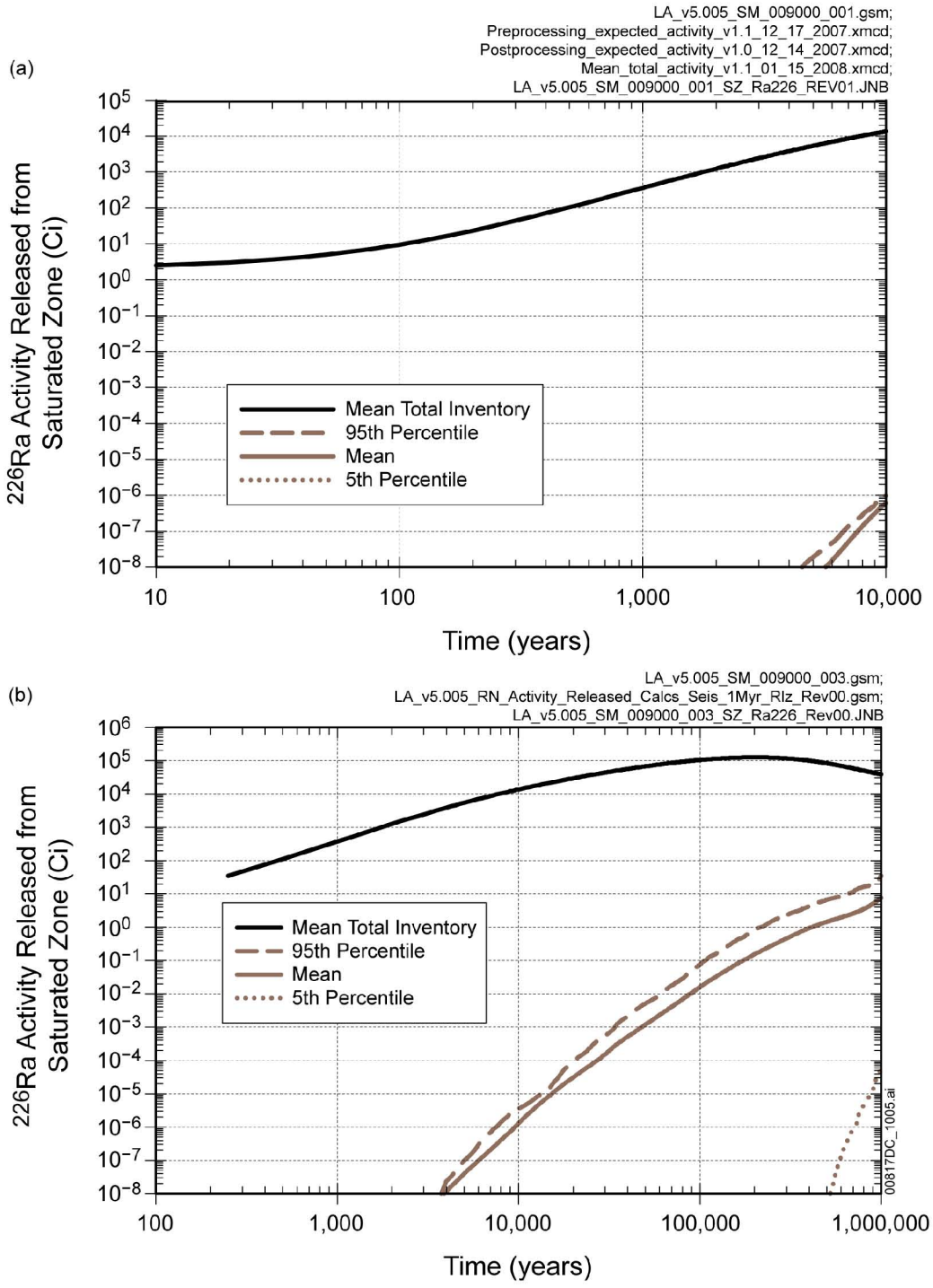

Source: Output DTN: MO0710ADTSPAWO.000 [DIRS 183752].

NOTE: Mean total inventory indicates the repository total ^{226}Ra activity as a function of time and is included for comparison to the activity released.

Figure 8.3-30[a]. Uncertainty in Activity of ^{226}Ra Released from the Saturated Zone for the Seismic Ground Motion Modeling Case for (a) 10,000 Years and (b) 1,000,000 Years after Repository Closure

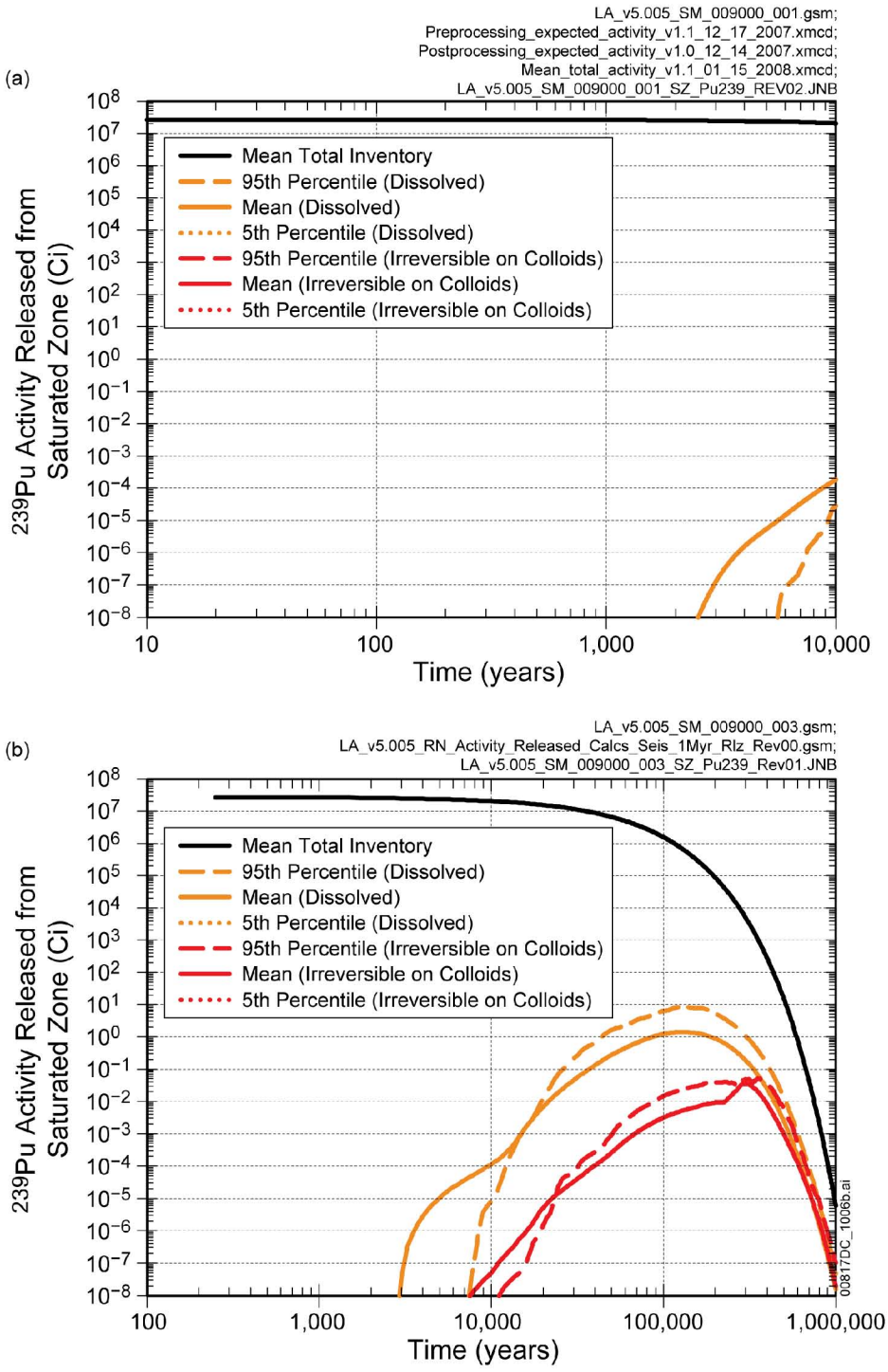

Source: Output DTN: MO0710ADTSPAWO.000 [DIRS 183752].

NOTE: Mean total inventory indicates the repository total ^{239}Pu activity as a function of time and is included for comparison to the activity released.

Figure 8.3-31[a]. Uncertainty in Activity of ^{239}Pu Released from the Saturated Zone for the Seismic Ground Motion Modeling Case for (a) 10,000 Years and (b) 1,000,000 Years after Repository Closure

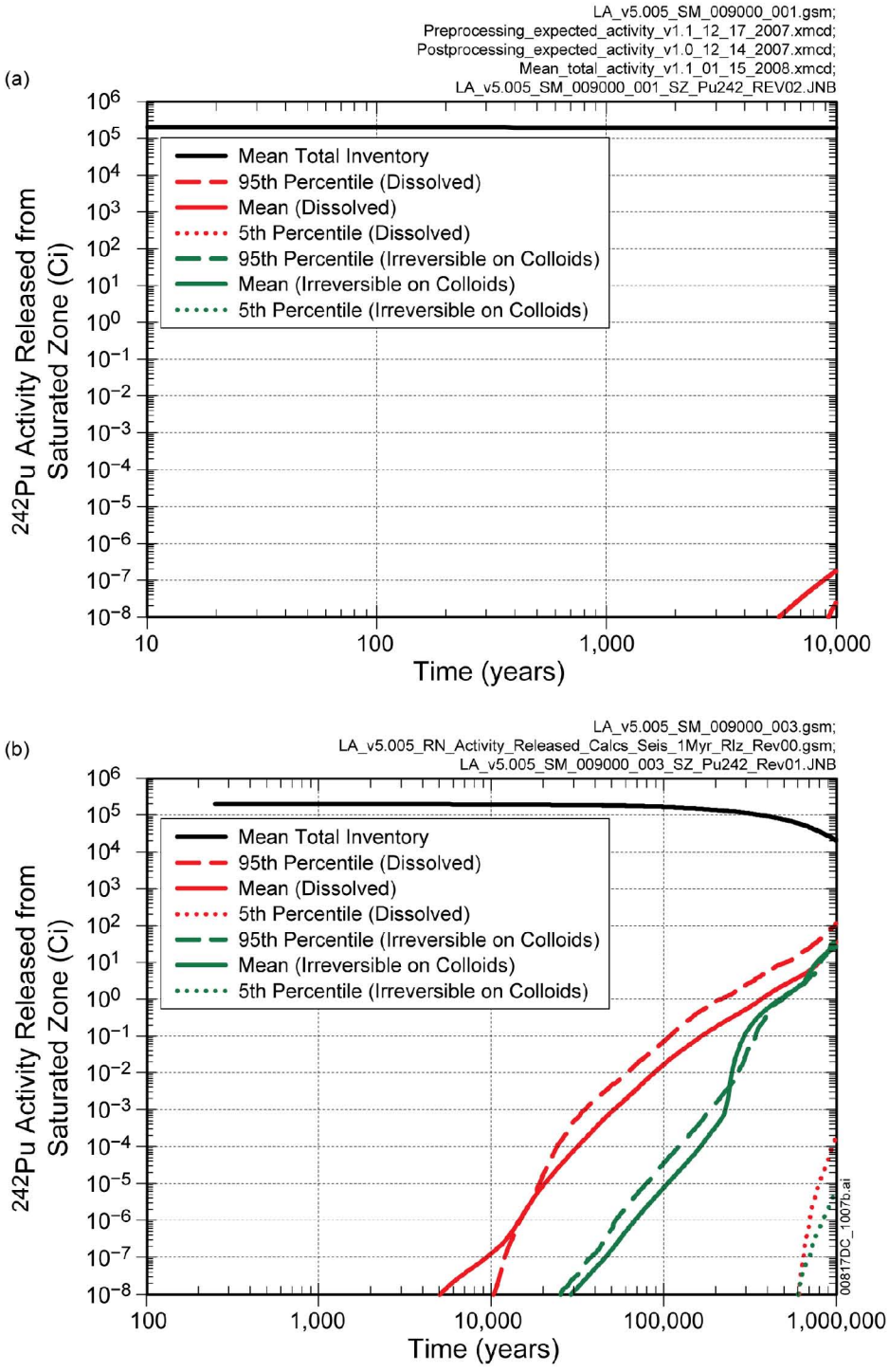

Source: Output DTN: MO0710ADTSPAWO.000 [DIRS 183752].

NOTE: Mean total inventory indicates the repository total ^{242}Pu activity as a function of time and is included for comparison to the activity released.

Figure 8.3-32[a]. Uncertainty in Activity of ^{242}Pu Released from the Saturated Zone for the Seismic Ground Motion Modeling Case for (a) 10,000 Years and (b) 1,000,000 Years after Repository Closure

INTENTIONALLY LEFT BLANK

9[a]. INPUTS AND REFERENCES

9.1[a] DOCUMENTS CITED

182229 Apted, M. and Ross, A. 2005. Program on Technology Innovation: Evaluation of a Spent Fuel Repository at Yucca Mountain, Nevada, 2005 Progress Report. EPRI TR 1010074. Palo Alto, California: Electric Power Research Institute. TIC: 259561.

185068 Breeding, R.J.; Helton, J.C.; Murfin, W.B.; Smith, L.N.; Johnson, J.D.; Jow, H.-N.; and Shiver, A.W. 1992. "The NUREG-1150 Probabilistic Risk Assessment for the Surry Nuclear Power Station." *Nuclear Engineering and Design, 135,* 29-59. [New York, New York]: North-Holland. ACC: 260059.

107727 Breeding, R.J.; Helton, J.C.; Gorham, E.D.; and Harper, F.T. 1992. "Summary Description of the Methods Used in the Probabilistic Risk Assessments for NUREG-1150." *Nuclear Engineering and Design, 135,* 1-27. New York, New York: Elsevier. TIC: 246312.

185069 Brown, T.D.; Breeding, R.J.; Helton, J.C.; Jow, H.N.; Higgins, S.J.; and Shiver, A.W. 1992. "The NUREG-1150 Probabilistic Risk Assessment for the Grand Gulf Nuclear Station." *Nuclear Engineering and Design, 135,* 117-137. [New York, New York]: North-Holland. TIC: 260060.

170038 BSC (Bechtel SAIC Company) 2004. *Analysis of Hydrologic Properties Data.* ANL-NBS-HS-000042 REV 00. Las Vegas, Nevada: Bechtel SAIC Company. ACC: DOC.20041005.0004; DOC.20050815.0003.

169987 BSC 2004. *CSNF Waste Form Degradation: Summary Abstraction.* ANL-EBS-MD-000015 REV 02. Las Vegas, Nevada: Bechtel SAIC Company. ACC: DOC.20040908.0001; DOC.20050620.0004.

169988 BSC 2004. Defense HLW Glass Degradation Model. ANL-EBS-MD-000016 REV 02. Las Vegas, Nevada: Bechtel SAIC Company. ACC: DOC.20041020.0015; DOC.20050922.0002.

170002 BSC 2004. *Future Climate Analysis.* ANL-NBS-GS-000008 REV 01. Las Vegas, Nevada: Bechtel SAIC Company. ACC: DOC.20040908.0005.

170006 BSC 2004. *Saturated Zone Colloid Transport.* ANL-NBS-HS-000031 REV 02. Las Vegas, Nevada: Bechtel SAIC Company. ACC: DOC.20041008.0007; DOC.20051215.0005.

167652 BSC 2004. *Seepage Model for PA Including Drift Collapse.* MDL-NBS-HS-000002 REV 03. Las Vegas, Nevada: Bechtel SAIC Company. ACC: DOC.20040922.0008; DOC.20051205.0001.

169861 BSC 2004. *UZ Flow Models and Submodels.* MDL-NBS-HS-000006 REV 02. Las Vegas, Nevada: Bechtel SAIC Company. ACC: DOC.20041101.0004; DOC.20050629.0003.

169855 BSC (Bechtel SAIC Company) 2004. *Development of Numerical Grids for UZ Flow and Transport Modeling.* ANL-NBS-HS-000015 REV 02. Las Vegas, Nevada: Bechtel SAIC Company. ACC: DOC.20040901.0001.

173433 BSC (Bechtel SAIC Company) 2005. *EBS Radionuclide Transport Abstraction.* ANL-WIS-PA-000001 REV 02. Las Vegas, Nevada: Bechtel SAIC Company. ACC: DOC.20050825.0008.

174116 BSC 2005. *Parameter Sensitivity Analysis for Unsaturated Zone Flow.* ANL-NBS-HS-000049 REV 00. Las Vegas, Nevada: Bechtel SAIC Company. ACC: DOC.20050808.0005; DOC.20060329.0020.

177492 BSC 2006. *Technical Work Plan for: Infiltration Model Assessment, Revision, and Analyses of Downstream Impacts.* TWP-NBS-HS-000012 REV 02. Las Vegas, Nevada: Bechtel SAIC Company. ACC: DOC.20060831.0006.

184391 BSC 2007. *Software Problem Report, GoldSim Version 9.60.100. Software Tracking Number: 10344-9.60-01.* SPR013420071203. Las Vegas, Nevada: Bechtel SAIC Company. ACC: MOL.20080122.0108.

185064 Campbell, J.E.; Dillon, R.T.; Tierney, M.S.; Davis, H.T.; McGrath, P.E.; Pearson, F.J., Jr.; Shaw, H.R.; Helton J.C.; and Donath, F.A. 1978. *Risk Methodology for Geologic Disposal of Radioactive Waste: Interim Report.* NUREG/CR-0458. Washington, D.C.: U.S. Nuclear Regulatory Commission. ACC: HQS.19880517.2632.

185066 Cranwell, R.M.; Campbell, J.E.; Helton, J.C.; Iman, R.L.; Longsine, D.E.; Ortiz, N.R.; Runkle, G.E.; and Shortencarier, M.J. 1987. *Risk Methodology for Geologic Disposal of Radioactive Waste: Final Report.* NUREG/CR-2452. Washington, D.C.: U.S. Nuclear Regulatory Commission. ACC: NNA.19910123.0035.

101234 Cranwell, R.M.; Guzowski, R.V.; Campbell, J.E.; and Ortiz, N.R. 1990. *Risk Methodology for Geologic Disposal of Radioactive Waste, Scenario Selection Procedure.* NUREG/CR-1667. Washington, D.C.: U.S. Nuclear Regulatory Commission. ACC: NNA.19900611.0073.

143665 CRWMS M&O 2000. *Total System Performance Assessment for the Site Recommendation.* TDR-WIS-PA-000001 REV 00. Las Vegas, Nevada: CRWMS M&O. ACC: MOL.20001005.0282.

184463 Davison, A.C. and Kuonen, D. 2002. "An Introduction to the Bootstrap with Applications in R." *Statistical Computing & Statistical Graphics Newsletter, 13,* (1), 6-11. Alexandria, Virginia: American Statistical Association. TIC: 259980.

181107 DOE (U.S. Department of Energy) 2007. *Design Document for: GoldSim v9.60.* Document ID: 10344-DD-9.60-01. Las Vegas, Nevada: U.S. Department of Energy, Office of Repository Development. ACC: MOL.20070416.0338.

182051 DOE 2007. *Quality Assurance Requirements and Description.* DOE/RW-0333P, Rev. 19. Washington, D. C.: U.S. Department of Energy, Office of Civilian Radioactive Waste Management. ACC: DOC.20070717.0006.

181106 DOE 2007. *Requirements Document for: GoldSim v9.60.* Document ID: 10344-RD-9.60-00. Las Vegas, Nevada: U.S. Department of Energy, Office of Repository Development. ACC: MOL.20070416.0330.

181108 DOE 2007. *User Information Document for: GoldSim Version 9.60.* Document ID: 10344-UID-9.60-00. Las Vegas, Nevada: U.S. Department of Energy, Office of Repository Development. ACC: MOL.20070416.0339.

185016 DOE 2008. *Software Validation Report for: GoldSim Version 9.60.300 on Windows 2000*. Document ID: 10344-SVR-9.60-03-WIN2000. Las Vegas, Nevada: U.S. Department of Energy, Office of Repository Development. ACC: MOL.20080125.0059.

185017 DOE 2008. *Software Validation Report for: GoldSim Version 9.60.300 on Windows Server 2003*. Document ID: 10344-SVR-9.60-03-WIN2003. Las Vegas, Nevada: U.S. Department of Energy, Office of Repository Development. ACC: MOL.20080125.0061.

185018 DOE 2008. *Software Validation Report for: GoldSim Version 9.60.300 on Windows XP*. Document ID: 10344-SVR-9.60-03-WINXP. Las Vegas, Nevada: U.S. Department of Energy, Office of Repository Development. ACC: MOL.20080125.0057.

100975 DOE 1996. *Title 40 CFR Part 191 Compliance Certification Application for the Waste Isolation Pilot Plant.* DOE/CAO-1996-2184. Twenty-one volumes. Carlsbad, New Mexico: U.S. Department of Energy, Carlsbad Area Office. TIC: 240511.

155354 Eisenberg, N.A.; Lee, M.P.; Federline, M.V.; Wingefors, S.; Andersson, J.; Norrby, S.; Sagar, B.; and Wittmeyer, G.W. 1999. *Regulatory Perspectives on Model Validation in High-Level Radioactive Waste Management Programs: A Joint NRC/SKI White Paper.* NUREG-1636. Washington, D.C.: U.S. Nuclear Regulatory Commission. TIC: 246310.

171782 Gisch, R.G. 2004. Postclosure Source Term Information for Naval Spent Fuel with Attachment Entitled "NNPP Postclosure Source Term Discussion for Seismic Disruptive Event Scenario". Letter from R.G. Gisch (DOE) to W.J. Arthur, III (DOE/ORD), September 2, 2004, 09130043151, NA:FA:KAKenney U#04-02635, with attachment. ACC: MOL.20040922.0363.

181727 GoldSim Technology Group 2007. *User's Guide, GoldSim Probabilistic Simulation Environment.* Version 9.60. Two volumes. Issaquah, Washington: GoldSim Technology Group. TIC: 259221.

185070 Gregory, J.J.; Breeding, R.J.; Helton, J.C.; Murfin, W.B.; Higgins, S.J.; and Shiver, A.W. 1992. "The NUREG-1150 Probabilistic Risk Assessment for the Sequoyah Nuclear Plant." *Nuclear Engineering and Design, 135,* 95-115. [New York, New York]: North-Holland. TIC: 260061.

170558 Helton, J.C. 2003. "Mathematical and Numerical Approaches in Performance Assessment for Radioactive Waste Disposal: Dealing with Uncertainty." Chapter 12 of *Modelling Radioactivity in the Environment.* Scott, E.M., ed. Radioactivity in the Environment. New York, New York: Elsevier. TIC: 256241.

100452 Helton, J.C. 1993. "Uncertainty and Sensitivity Analysis Techniques for Use in Performance Assessment for Radioactive Waste Disposal." *Reliability Engineering and System Safety, 42,* (2-3), 327-367. Barking, Essex, England: Elsevier. TIC: 237878.

107739 Helton, J.C. 1994. "Treatment of Uncertainty in Performance Assessments for Complex Systems." *Risk Analysis, 14,* (4), 483-511. New York, New York: Plenum Press. TIC: 245848.

107496 Helton, J.C. 1997. "Uncertainty and Sensitivity Analysis in the Presence of Stochastic and Subjective Uncertainty." *Journal of Statistical Computation and Simulation, 57,* (1-4), 3-76. New York, New York: Gordon and Breach Science Publishers. TIC: 245958.

184402 Helton, J.C. and Breeding, R.J. 1993. "Calculation of Reactor Accident Safety Goals." *Reliability Engineering and System Safety, 39,* 129-158. [New York, New York]: Elsevier. TIC: 259936.

163475 Helton, J.C. and Davis, F.J. 2002. Latin Hypercube Sampling and the Propagation of Uncertainty in Analyses of Complex Systems. SAND2001-0417. Albuquerque, New Mexico: Sandia National Laboratories. TIC: 254367.

170518 Helton, J.C. and Davis, F.J. 2003. "Latin Hypercube Sampling and the Propagation of Uncertainty in Analyses of Complex Systems." *Reliability Engineering & System Safety, 81,* ([1]), 23-69. [New York, New York]: Elsevier. TIC: 256239.

171759 Helton, J.C. and Marietta, M.G. 2000. "The 1996 Performance Assessment for the Waste Isolation Pilot Plant." *Reliability Engineering and System Safety, 69,* 1-3. [New York, New York]: Elsevier. TIC: 256585.

185072 Helton, J.C. and Sallaberry, C.J. 2007. *Illustration of Sampling-Based Approaches to the Calculation of Expected Dose in Performance Assessments for the Proposed High Level Radioactive Waste Repository at Yucca Mountain, Nevada.* SAND2007-1353. Albuquerque, New Mexico: Sandia National Laboratories. ACC: LLR.20080221.0240.

183873 Helton, J.C.; Johnson, J.D.; Sallaberry, C.J.; and Storlie, C.B. 2006. "Survey of Sampling-Based Methods for Uncertainty and Sensitivity Analysis." *Reliability Engineering and System Safety, 91,* 1175-1209. [New York, New York]: Elsevier. TIC: 259831.

146012 Iman, R.L. 1982. "Statistical Methods for Including Uncertainties Associated with the Geologic Isolation of Radioactive Waste Which Allow for a Comparison with Licensing Criteria." Proceedings of the Symposium on Uncertainties Associated with the Regulation of the Geologic Disposal of High-Level Radioactive Waste, Gatlinburg, Tennessee, March 9-13, 1981. Kocher, D.C., ed. NUREG/CP-0022. Pages145-157. Washington, D.C.: U.S. Nuclear Regulatory Commission. TIC: 213069.

165064 Iman, R.L. and Conover, W.J. 1982. *Sensitivity Analysis Techniques: Self-Teaching Curriculum.* NUREG/CR-2350. Washington, D.C.: U.S. Nuclear Regulatory Commission. ACC: HQS.19880517.2724.

185067 Iman, R.L. and Helton, J.C. 1985. *A Comparison of Uncertainty and Sensitivity Analysis Techniques for Computer Models.* NUREG/CR-3904. Washington, D.C.: U.S. Nuclear Regulatory Commission. ACC: NNA.19890907.0001.

124198 Iman, R.L.; Conover, W.J.; and Campbell, J.E. 1980. *Risk Methodology for Geologic Disposal of Radioactive Waste: Small Sample Sensitivity Analysis Techniques for Computer Models, with an Application to Risk Assessment.* NUREG/CR-1397. Washington, D.C.: U.S. Nuclear Regulatory Commission. TIC: 211289.

159559 Iman, R.L.; Helton, J.C.; and Campbell, J.E. 1978. *Risk Methodology for Geologic Disposal of Radioactive Waste: Sensitivity Analysis Techniques.* NUREG/CR-0394. Washington, D.C.: U.S. Nuclear Regulatory Commission. TIC: 208076.

100557 Kaplan, S. and Garrick, B.J. 1981. "On the Quantitative Definition of Risk." *Risk Analysis, 1,* (1), 11-27. New York, New York: Plenum Press. TIC: 241205.

107800 Lewis, H.W.; Budnitz, R.J.; Kouts, H.J.C.; Loewenstein, W.B.; Rowe, W.D.; von Hippel, F.; and Zachariasen, F. 1978. *Risk Assessment Review Group Report to the U.S. Nuclear Regulatory Commission.* NUREG/CR-0400. Washington, D.C.: U.S. Regulatory Commission. TIC: 206094.

127905 McKay, M.D.; Beckman, R.J.; and Conover, W.J. 1979. "A Comparison of Three Methods for Selecting Values of Input Variables in the Analysis of Output from a Computer Code." *Technometrics, 21,* (2), 239-245. Alexandria, Virginia: American Statistical Association. TIC: 221741.

182657 McKenzie, J.M. 2007. Postclosure Radionuclide Release Source Term for Representative Naval SNF Waste Package - Igneous Intrusive and Nominal/Early Failure Scenarios. Letter from J.M. McKenzie to E.F. Sproat, III, August 22, 2007, NR:RA:GFHOLDEN U#07-03303, with enclosure. ACC: LLR.20070823.0027.

107798 NRC (U.S. Nuclear Regulatory Commission) 1990. *Severe Accident Risks: An Assessment for Five U.S. Nuclear Power Plants.* NUREG-1150. Washington, D.C.: U.S. Nuclear Regulatory Commission. TIC: 214826.

163274 NRC 2003. *Yucca Mountain Review Plan, Final Report.* NUREG-1804, Rev. 2. Washington, D.C.: U.S. Nuclear Regulatory Commission, Office of Nuclear Material Safety and Safeguards. TIC: 254568.

107799 NRC 1975. *Reactor Safety Study: An Assessment of Accident Risks in U.S. Commercial Nuclear Power Plants.* WASH-1400. Washington, D.C.: U.S. Nuclear Regulatory Commission. TIC: 236923.

107814 Payne, A.C., Jr. 1992. *Analysis of the LaSalle Unit 2 Nuclear Power Plant: Risk Methods Integration and Evaluation Program (RMIEP).* NUREG/CR-4832. Washington, D.C.: U.S. Nuclear Regulatory Commission. TIC: 246147.

185071 Payne, A.C., Jr.; Breeding, R.J.; Helton, J.C.; Smith, L.N.; Johnson, J.D.; Jow, H.-N.; and Shiver, A.W. 1992. "The NUREG-1150 Probabilistic Risk Assessment for the Peach Bottom Atomic Power Station." *Nuclear Engineering and Design, 135,* 61-94. [New York, New York]: North-Holland. TIC: 260062.

107812 PLG (Pickard, Lowe, and Garrick) 1982. *Indian Point Probabilistic Safety Study.* Irvine, California: Pickard, Lowe, and Garrick. TIC: 247144.

185063 PLG 1983. *Seabrook Station Probabilistic Safety Assessment.* Irvine, California: Pickard, Lowe and Garrick. TIC: 255977.

145383 Rechard, R.P. 1999. "Historical Relationship Between Performance Assessment for Radioactive Waste Disposal and Other Types of Risk Assessment." *Risk Analysis, 19,* (5), 763-807. New York, New York: Kluwer Academic / Plenum Publishers. TIC: 246972.

185124 Senger, R. 2008. "Re: Appendix M, TSPA-LA Addendum [Corroborative Data]." E-mail from R. Senger to K. Brooks, February 27, 2008. ACC: LLR.20080227.0161.

177081 SNL (Sandia National Laboratories) 2006. *Data Analysis for Infiltration Modeling: Extracted Weather Station Data Used to Represent Present-Day and Potential Future Climate Conditions in the Vicinity of Yucca Mountain.* ANL-MGR-MD-000015 REV 00. Las Vegas, Nevada: Sandia National Laboratories. ACC: DOC.20070109.0002.

181244 SNL 2007. *Abstraction of Drift Seepage.* MDL-NBS-HS-000019 REV 01 ADD 01. Las Vegas, Nevada: Sandia National Laboratories. ACC: DOC.20070807.0001.

177399 SNL 2007. *Biosphere Model Report.* MDL-MGR-MD-000001 REV 02. Las Vegas, Nevada: Sandia National Laboratories. ACC: DOC.20070830.0007.

179545 SNL 2007. *Calibrated Unsaturated Zone Properties.* ANL-NBS-HS-000058 REV 00. Las Vegas, Nevada: Sandia National Laboratories. ACC: DOC.20070530.0013.

177418 SNL 2007. *Dissolved Concentration Limits of Elements with Radioactive Isotopes.* ANL-WIS-MD-000010 REV 06. Las Vegas, Nevada: Sandia National Laboratory. ACC: DOC.20070918.0010.

177407 SNL 2007. *EBS Radionuclide Transport Abstraction.* ANL-WIS-PA-000001 REV 03. Las Vegas, Nevada: Sandia National Laboratories. ACC: DOC.20071004.0001.

180778 SNL 2007. *General Corrosion and Localized Corrosion of the Drip Shield.* ANL-EBS-MD-000004 REV 02 ADD 01. Las Vegas, Nevada: Sandia National Laboratories. ACC: DOC.20060427.0002; DOC.20070807.0004; DOC.20071003.0019.

178519 SNL 2007. *General Corrosion and Localized Corrosion of Waste Package Outer Barrier.* ANL-EBS-MD-000003 REV 03. Las Vegas, Nevada: Sandia National Laboratories. ACC: DOC.20070730.0003; DOC.20070807.0007.

180506 SNL 2007. *In-Package Chemistry Abstraction.* ANL-EBS-MD-000037 REV 04 ADD 01. Las Vegas, Nevada: Sandia National Laboratories. ACC: DOC.20070816.0004.

180472 SNL 2007. *Initial Radionuclide Inventories.* ANL-WIS-MD-000020 REV 01 ADD 01. Las Vegas, Nevada: Sandia National Laboratories. ACC: DOC.20050927.0005; DOC.20070801.0001.

181383 SNL 2007. *Multiscale Thermohydrologic Model.* ANL-EBS-MD-000049 REV 03 ADD 01. Las Vegas, Nevada: Sandia National Laboratories. ACC: DOC.20070831.0003.

177424 SNL 2007. *Radionuclide Screening.* ANL-WIS-MD-000006 REV 02. Las Vegas, Nevada: Sandia National Laboratories. ACC: DOC.20070326.0003.

177396 SNL 2007. *Radionuclide Transport Models Under Ambient Conditions.* MDL-NBS-HS-000008 REV 02 ADD 01. Las Vegas, Nevada: Sandia National Laboratories. ACC: DOC.20050823.0003; DOC.20070718.0003.

177391 SNL 2007. *Saturated Zone Site-Scale Flow Model.* MDL-NBS-HS-000011 REV 03. Las Vegas, Nevada: Sandia National Laboratories. ACC: DOC.20070626.0004; DOC.20071001.0013.

176828 SNL 2007. *Seismic Consequence Abstraction.* MDL-WIS-PA-000003 REV 03. Las Vegas, Nevada: Sandia National Laboratories. ACC: DOC.20070928.0011.

181953 SNL 2007. *Stress Corrosion Cracking of Waste Package Outer Barrier and Drip Shield Materials.* ANL-EBS-MD-000005 REV 04. Las Vegas, Nevada: Sandia National Laboratories. ACC: DOC.20070913.0001.

179394 SNL 2007. *Total System Performance Assessment Data Input Package for Requirements Analysis for Transportation Aging and Disposal Canister and Related Waste Package Physical Attributes Basis for Performance Assessment.* TDR-TDIP-ES-000006 REV 00. Las Vegas, Nevada: Sandia National Laboratories. ACC: DOC.20070918.0005.

179354 SNL (Sandia National Laboratories) 2007. *Total System Performance Assessment Data Input Package for Requirements Analysis for Engineered Barrier System In-Drift Configuration.* TDR-TDIP-ES-000010 REV 00. Las Vegas, Nevada: Sandia National Laboratories. ACC: DOC.20070921.0008.

184614 SNL 2007. *UZ Flow Models and Submodels.* MDL-NBS-HS-000006 REV 03 AD 01. Las Vegas, Nevada: Sandia National Laboratories. ACC: DOC.20080108.0003; DOC.20080114.0001.

184748 SNL 2008. *Particle Tracking Model and Abstraction of Transport Processes.* MDL-NBS-HS-000020 REV 02 AD 02. Las Vegas, Nevada: Sandia National Laboratories. ACC: DOC.20080129.0008.

183750 SNL 2008. *Saturated Zone Flow and Transport Model Abstraction.* MDL-NBS-HS-000021 REV 03 AD 02. Las Vegas, Nevada: Sandia National Laboratories. ACC: DOC.20080107.0006.

182145 SNL 2007. *Simulation of Net Infiltration for Present-Day and Potential Future Climates.* MDL-NBS-HS-000023 REV 01 AD 01. Las Vegas, Nevada: Sandia National Laboratories.

184806 SNL 2008. *Site-Scale Saturated Zone Transport.* MDL-NBS-HS-000010 REV 03 AD 01. Las Vegas, Nevada: Sandia National Laboratories. ACC: DOC.20080121.0003.

184920 SNL 2008. *Technical Work Plan for: Total System Performance Assessment FY 07-08 Activities.* TWP-MGR-PA-000045 REV 01 ICN 02. Las Vegas, Nevada: Sandia National Laboratories. ACC: DOC.20080131.0048.

157307 Williams, N.H. 2001. "Contract No. DE-AC08-01RW12101 – Total System Performance Assessment – Analyses for Disposal of Commercial and DOE Waste Inventories at Yucca Mountain – Input to Final Environmental Impact Statement and Site Suitability Evaluation REV 00 ICN 02." Letter from N.H. Williams (BSC) to J.R. Summerson (DOE/YMSCO), December 11, 2001, RWA:cs-1204010670, with enclosure. ACC: MOL.20011213.0056.

9.2[a] CODES, STANDARDS, REGULATIONS, AND PROCEDURES

175755 40 CFR 197. 2005. Protection of Environment: Public Health and Environmental Radiation Protection Standards for Yucca Mountain, Nevada. ACC: MOL.20051121.0084.

156671 66 FR 55732. Disposal of High-Level Radioactive Wastes in a Proposed Geologic Repository at Yucca Mountain, NV, Final Rule. 10 CFR Parts 2, 19, 20, 21, 30, 40, 51, 60, 61, 63, 70, 72, 73, and 75. ACC: MOL.20050324.0102; MOL.20050418.0124.

177357 70 FR 49014. Public Health and Environmental Radiation Protection Standards for Yucca Mountain, NV. Internet Accessible.

178394 70 FR 53313. Implementation of a Dose Standard After 10,000 Years. Internet Accessible.

180319 CFR 63. 2007. Energy: Disposal of High-Level Radioactive Wastes in a Geologic Repository at Yucca Mountain, Nevada. Internet Accessible.

175544 EPA (U.S. Environmental Protection Agency) 2002. Federal Guidance Report 13, CD Supplement, Cancer Risk Coefficients for Environmental Exposure to Radionuclides, EPA. EPA-402-C-99-001, Rev. 1. [Washington, D.C.]: U.S. Environmental Protection Agency. ACC: MOL.20051013.0016.

100016 Nuclear Waste Policy Amendments Act of 1987. Public Law No. 100-203, 101 Stat. 1330. TIC: 223717.

9.3[a] SOFTWARE CODES

181034 ASHPLUME_DLL_LA V. 2.0. 2003. WINDOWS 2000. STN: 11117-2.0-00.

181035 ASHPLUME_DLL_LA V. 2.1. 2006. WinDOWS 2000/XP. STN: 11117-2.1-00.

180147 ASHPLUME_DLL_LA V. 2.1. 2007. WINDOWS 2003. STN: 11117-2.1-01.

162809 CWD V. 2.0. 2003. WINDOWS 2000. STN: 10363-2.0-00.

181037 CWD V. 2.0. 2007. WINDOWS 2003. STN: 10363-2.0-01.

182102 EXDOC_LA V. 2.0. 2007. WINDOWS XP, WINDOWS 2000 & WINDOWS 2003. STN: 11193-2.0-00.

180002 FAR V. 1.1. 2007. WINDOWS 2000 & 2003. STN: 11190-1.1-00.

182225 FAR V. 1.2. 2007. WINDOWS 2000 & WINDOWS 2003. STN: 11190-1.2-00.

173139 FEHM V. 2.23. 2005. WINDOWS 2000. STN: 10086-2.23-00.

179419 FEHM V. 2.24-01. 2007. WIN2003, 2000, & XP, Red Hat Linux 2.4.21, OS 5.9. STN: 10086-2.24-01-00.

181040 GetThk_LA V. 1.0. 2006. WINDOWS 2000 & WINDOWS 2003. STN: 11229-1.0-00.

180224 GoldSim V. 9.60. 2007. WINDOWS 2000, WINDOWS XP, WINDOWS 2003. STN: 10344-9.60-00.

181903 Goldsim V. 9.60.100. 2007. WIN 2000, 2003, XP. STN: 10344-9.60-01.

184387 Goldsim V. 9.60.300. 2007. WIN 2000, 2003, XP. STN: 10344-9.60-03.

167885 InterpZdll_LA V. 1.0. 2004. WINDOWS 2000. STN: 11107-1.0-00.

181043 InterpZdll_LA V. 1.0. 2007. WINDOWS 2003. STN: 11107-1.0-01.

167884 MFCP_LA V. 1.0. 2003. WINDOWS 2000. STN: 11071-1.0-00.

181045 MFCP_LA V. 1.0. 2006. WINDOWS 2003. STN: 11071-1.0-01.

174528 MkTable V. 1.00. 2003. WINDOWS 2000. STN: 10505-1.00-00.

181047 Mkable_LA V. 1.0. 2006. WINDOWS 2000. STN: 11217-1.0-00.

181048 MkTable_LA V. 1.0. 2007. WINDOWS 2003. STN: 11217-1.0-01.

181049 MView V. 4.0. 2007. WINDOWS XP. STN: 10072-4.0-01.

169130 PassTable1D_LA V. 1.0. 2004. WINDOWS 2000. STN: 11142-1.0-00.

181050 PassTable1D_LA V. 1.0. 2006. WINDOWS 2003. STN: 11142-1.0-01.

181051 PassTable1D_LA V. 2.0. 2007. WINDOWS 2000 & WINDOWS 2003. STN: 11142-2.0-00.

168980 PassTable3D_LA V. 1.0. 2004. WINDOWS 2000. STN: 11143-1.0-00.

181052 PassTable3D_LA V. 1.0. 2007. WINDOWS 2003. STN: 11143-1.0-01.

182556 PassTable3D_LA V. 2.0. 2007. WINDOWS 2000 & WINDOWS 2003. STN: 11143-2.0-00.

181157 SCCD V. 2.01. 2003. WINDOWS 2000. STN: 10343-2.01-00.

181054 SCCD V. 2.01. 2007. WINDOWS 2003. STN: 10343-2.01-01.

173435 SEEPAGEDLL_LA V. 1.2. 2005. WINDOWS 2000. STN: 11076-1.2-00.

180318 SEEPAGEDLL_LA V. 1.3. 2006. WINDOWS 2000. STN: 11076-1.3-00.

181053 PREWAP_LA V. 1.1. 2006. WINDOWS 2000. STN: 10939-1.1-00.

181058 SEEPAGEDLL_LA V. 1.3. 2007. WINDOWS 2003. STN: 11076-1.3-01.

164180 Software Code: SZ_Convolute V. 3.0. 2003. PC, Windows 2000. 10207-3.0-00.

161256 Software Code: TOUGHREACT V. 3.0. 2002. DEC ALPHA/OSF1 V5.1, DEC ALPHA/OSF1 V5.0, Sun UltraSparc/Sun OS 5.5.1, PC/Linux Redhat 7.2. STN: 10396-3.0-00.

167883 Soilexp_LA V. 1.0. 2004. WINDOWS 2000. STN: 10933-1.0-00.

181060 SZ_CONVOLUTE V. 3.10.01. 2007. WINDOWS 2000 & WINDOWS 2003. STN: 10207-3.10.01-00.

146654 T2R3D V. 1.4. 1999. UNIX, WINDOWS 95/98NT 4.0. STN: 10006-1.4-00.

161491 TOUGH2 V. 1.6. 2003. DOS Emulation (win95/98), SUN OS 5.5.1., OSF1 V4.0. STN: 10007-1.6-01.

181061 TSPA_Input_DB V. 2.2. 2006. WINDOWS 2000. STN: 10931-2.2-00.

181062 TSPA_Input_DB V. 2.2. 2006. WINDOWS 2003. STN: 10931-2.2-01.

181774 WAPDEG V. 4.07. 2003. Windows 2000. STN: 10000-4.07-00.

181064 WAPDEG V. 4.07. 2007. WINDOWS SERVER 2003. STN: 10000-4.07-01.

9.4[a] SOURCE DATA LISTED BY DATA TRACKING NUMBER

171584 LA0408AM831341.001. Unsaturated Zone Distribution Coefficients (Kds) for U, Np, Pu, Am, Pa, Cs, Sr, Ra, and Th. Submittal date: 08/24/2004.

180497 LA0701PANS02BR.003. UZ Transport Parameters. Submittal date: 04/23/2007.

180322 LA0702PANS02BR.001. Repository and Water Table Bins. Submittal date: 04/16/2007.

179299 LB0701PAKDSESN.001. Unsaturated Zone Sorption Coefficients for Selenium and Tin. Submittal date: 01/31/2007.

181635 LB0702PASEEP02.001. Seepage Abstraction for Degraded Drifts. Submittal date: 06/29/2007.

180776 LB0702PAUZMTDF.001. Unsaturated Zone Matrix Diffusion Coefficients. Submittal date: 05/10/2007.

180439 MO0701PACSNFCP.000. CSNF Colloid Parameters. Submittal date: 04/17/2007.

180440 MO0701PAIRONCO.000. Colloidal Iron Corrosion Products Parameters. Submittal date: 04/17/2007.

181219 MO0702PAFLUORI.000. Fluoride Uncertainty Associated with Dissolved Concentration Limits. Submittal date: 06/01/2007.

179328 MO0702PAGWPROS.001. Groundwater Protection Standards Conversion Factors. Submittal date: 02/06/2007.

179925 MO0702PASTREAM.001. Waste Stream Composition and Thermal Decay Histories for LA. Submittal date: 02/15/2007.

183148 MO0703PASDSTAT.001. Statistical Analyses for Seismic Damage Abstractions. Submittal date: 09/21/2007.

183156 MO0703PASEISDA.002. Seismic Damage Abstractions for TSPA Compliance Case. Submittal date: 09/21/2007.

184647 MO0704PAFEHMBR.001. FEHM Model and Input. Submittal date: 01/10/2008.

185200 MO0706SPAFEPLA.001. FY 2007 LA FEP List and Screening. Submittal date: 03/05/2008.

184664 MO0712PBANLNWP.000. Probabilistic Analysis of Navy Waste Packages. Submittal date: 12/13/2007.

168761 SN0310T0505503.004. Initial Radionuclide Inventories for TSPA-LA. Submittal date: 10/27/2003.

180523 SN0701PAEBSPCE.001. PCE TDIP Potential Seepage Water Chemistry Lookup Tables. Submittal date: 04/25/2007.

182961 SN0701PAWPHIT1.001. Number of Waste Packages Hit by Igneous Events. Submittal date: 09/13/2007.

179504 SN0702PASZFTMA.001. Saturated Zone Flow and Transport Model Abstraction. Submittal date: 02/06/2007

183471 SN0702PASZFTMA.002. Saturated Zone 1-D Transport Model. Submittal date: 10/15/2007.

183217 SN0703PAEBSRTA.001. Inputs Used in the Engineered Barrier System (EBS) Radionuclide Transport Abstraction. Submittal date: 09/28/2007.

182122 SN0704PADSGCMT.001. Drip Shield General Corrosion Models Based on 2.5-Year Titanium Grade 7 Corrosion Rates. Submittal date: 07/24/2007.

183485 SN0710PASZFTMA.003. Updated Saturated Zone 1-D Transport Model. Submittal date: 10/10/2007.

INTENTIONALLY LEFT BLANK

APPENDIX B[a]
DATA TRACKING NUMBERS FOR THE TSPA-LA MODEL

B1[a] INTRODUCTION

Appendix B of the parent document describes the interrelationships among the Total System Performance Assessment for the License Application (TSPA-LA) Model output data tracking numbers (DTNs) for the TSPA-LA Model. Additional output generated as a result of the analysis presented in this addendum is described in Appendix B[a]. Figure B-3[a] shows the information flow among the output DTNs submitted to the Technical Data Management System for the analyses documented in this addendum.

The following sections contain brief descriptions of the contents of the DTNs. The respective ReadMe.doc file located in each DTN provides more detailed information on the contents of each DTN. Figure B-3[a] provides an overview of the relationships between the DTNs.

B2[a] DESCRIPTIONS OF THE DATA TRACKING NUMBERS

The following text supports Figure B-3[a]. Figures B-1 and B-2 in the parent document remain unchanged and are documented in Appendix B, Section B.2, of the parent document.

B2.1[a] MODEL DEVELOPMENT RECORDS PACKAGE

This records package documents each of the model changes that were generated since v5.000 of the Model. This records package contains v5.001 through v5.005 of the Groundwater Model. All model versions generally follow the same folder content. For example, the content for a typical folder would contain a Master Folder and the specific case folders that were appropriate at that stage of model development. Each Master Folder generally contains the following:

- One or more change approval forms
- Change checklist
- Implementation checklist
- Conceptual checklist
- Conceptual description
- GoldSim model file
- GoldSim version report
- Additional information directory (optional).

This records package feeds output DTN: MO0710ADTSPAWO.000_R0 [DIRS 183752], which utilizes the final version of the Groundwater Model (v5.005).

B2.2[a] PLOTS AND FIGURES FOR THE TSPA-LA ADDENDUM (V5.005): OUTPUT DTN: MO0710PLOTSFIG.000_R1 [DIRS 185207]

Reference Figure B-3[a], Block 4—This DTN contains electronic copies of the plots and any post-processing files for all of the plots generated for this document. The plots were generated using SigmaPlot 2002 for Windows Version 8.0, (www.sigmaplot.com). Each figure generated for this document includes header information listing the file name(s) which contain the output data used in the plot (generally a GoldSim file with the file extension .gsm) which can be found in the source DTN listed for the plot. The plot header information contains the file name(s) of the SigmaPlot (file extension .JNB) and any post-processing files used to generate the plot which

can be found in this DTN. In addition, any checklists used for checking of the plots are also included.

B2.3[a] TSPA-LA ADDENDUM PARAMETER SENSITIVITY ANALYSIS: OUTPUT DTN: MO0801TSPAPRSA.000_R0 [DIRS 184620]

Reference Figure B-3[a], Block 6—This DTN contains analyses to evaluate the significant uncertain parameters in the TSPA-LA Groundwater Models that are documented in output DTN: MO0710ADTSPAWO.000_R0 [DIRS 183752].

B2.4[a] TSPA-LA ADDENDUM, REPRESENTATION OF (GW V5.005) NAVAL SPENT NUCLEAR FUEL: OUTPUT DTN: MO0801TSPANSNF.000_R0 [DIRS 184619]

Reference Figure B-3[a], Block 5—This DTN contains the TSPA-LA Model cases, including checking documentation, that were run to evaluate the representation of naval spent nuclear fuel in the TSPA-LA Model as discussed in Section 7.5.3[a].

B2.5[a] TSPA-LA ADDENDUM GROUNDWATER MODEL (V5.005) AND ERUPTIVE MODEL (V1.004) WITH FINAL DOCUMENTATION: OUTPUT DTN: MO0710ADTSPAWI.000_R0 [DIRS 183751]

Reference Figure B-3[a], Block 10—This is the version of the TSPA-LA Groundwater Model (v5.005) and Eruptive Model (v1.004) that is used to generate the GoldSim Player Files that support the TSPA-LA. The difference between the GoldSim files in this DTN versus output DTN: MO0710ADTSPAWO.000_R0 [DIRS 183752] is that this DTN contains the master file for v5.005 and for v1.004. These master files have been modified to update the explanatory text. The explanatory text that is in output DTN: MO0710ADTSPAWO.000_R0 [DIRS 183752] is not as detailed as the explanatory text included in this DTN. The enclosed master files have not been run; therefore, there are no results in this DTN. The value in providing an input file without the output is that the files can be opened on most current model personal computers. The value in adding the documentation is that an interested party can read the embedded text to obtain an overview of how the model is constructed. Also included is a data only copy of the TSPA Input Database. The value of the data-only version of the TSPA Input Database is that an interested party can review the input parameters to quickly determine the numerical value of a parameter as well as the product that the value is documented within. In most cases, the product is an output DTN from a model and/or analysis report.

B2.6[a] TSPA GENERATED INPUTS AND POST-PROCESSED INPUTS: OUTPUT DTN: MO0711GENERINP.000_R0 [DIRS 183937]

Reference Figure B-3[a], Block 2—This DTN contains inputs that fall into two categories: (1) TSPA-LA Model-generated inputs and (2) post-processed inputs. The TSPA-LA Model generated inputs do not have any external inputs used to create the input values. Post-processed inputs have external inputs supplied by supporting analysis and/or model reports. These external inputs must be post-processed for use in the TSPA-LA Model.

B2.7[a] TSPA-LA ADDENDUM GROUNDWATER MODELING CASES (V5.005) WITHOUT FINAL DOCUMENTATION (USED FOR REGULATORY COMPLIANCE): OUTPUT DTN: MO0710ADTSPAWO.000_R0 [DIRS 183752]

Reference Figure B-3[a], Block 3—This is the version of the Groundwater Model (v5.005) that is used for Regulatory Compliance presented in Section 8[a]. This DTN contains all the modeling cases and supporting checking documentation.

B2.8[a] TSPA-LA ADDENDUM, WASTE PACKAGE AND DRIP SHIELD DEGRADATION ANALYSIS: OUTPUT DTN: MO0801TSPAWPDS.000_R1 [DIRS 185077]

Reference Figure B-3[a], Block 9—This DTN contains the TSPA-LA Waste Package (WP) and Drip Shield (DS) degradation stand alone analysis documented in Section 8.3[a].

B2.9[a] TSPA-LA MODEL (GROUNDWATER) USED FOR REGULATORY COMPLIANCE STABILITY ANALYSIS: OUTPUT DTN: MO0801TSPAADSA.000_R1 [DIRS 185078]

Reference Figure B-3[a], Block 7—This DTN contains the GoldSim runs confirming that the TSPA-LA Model is statistically stable as discussed in Section 7.3.1[a].

B2.10[a] TSPA-LA ADDENDUM, MODEL VALIDATION AND ANALYSES CASES: OUTPUT DTN: MO0801TSPAMVAC.000_R1 [DIRS 185080]

Reference Figure B-3[a], Block 8—This DTN contains GoldSim files addressing the following subjects that support model validation:

- Single Realizations (discussed in Section 7.7.1[a])
- Accuracy of Expected Dose (discussed in Section 7.3.2[a])
- Validation of the Number of Human Intrusion Scenario Timesteps (discussed in Section 7.3.3[a]).

B2.11[a] TSPA-LA ADDENDUM, SEEPAGE RESULTS FROM THE TSPA-LA MODEL: OUTPUT DTN: MO0705TSPASEEP.000_R1 [DIRS 183008]

Reference Figure B-3[a], Block 11—This DTN contains the extracted seepage rates and seepage fractions. The results are taken from model development v5.005_GS_9.60.300 of the TSPA-LA Model for one-million years for the Seismic Fault Displacement and Igneous Intrusion Modeling Cases.

INTENTIONALLY LEFT BLANK

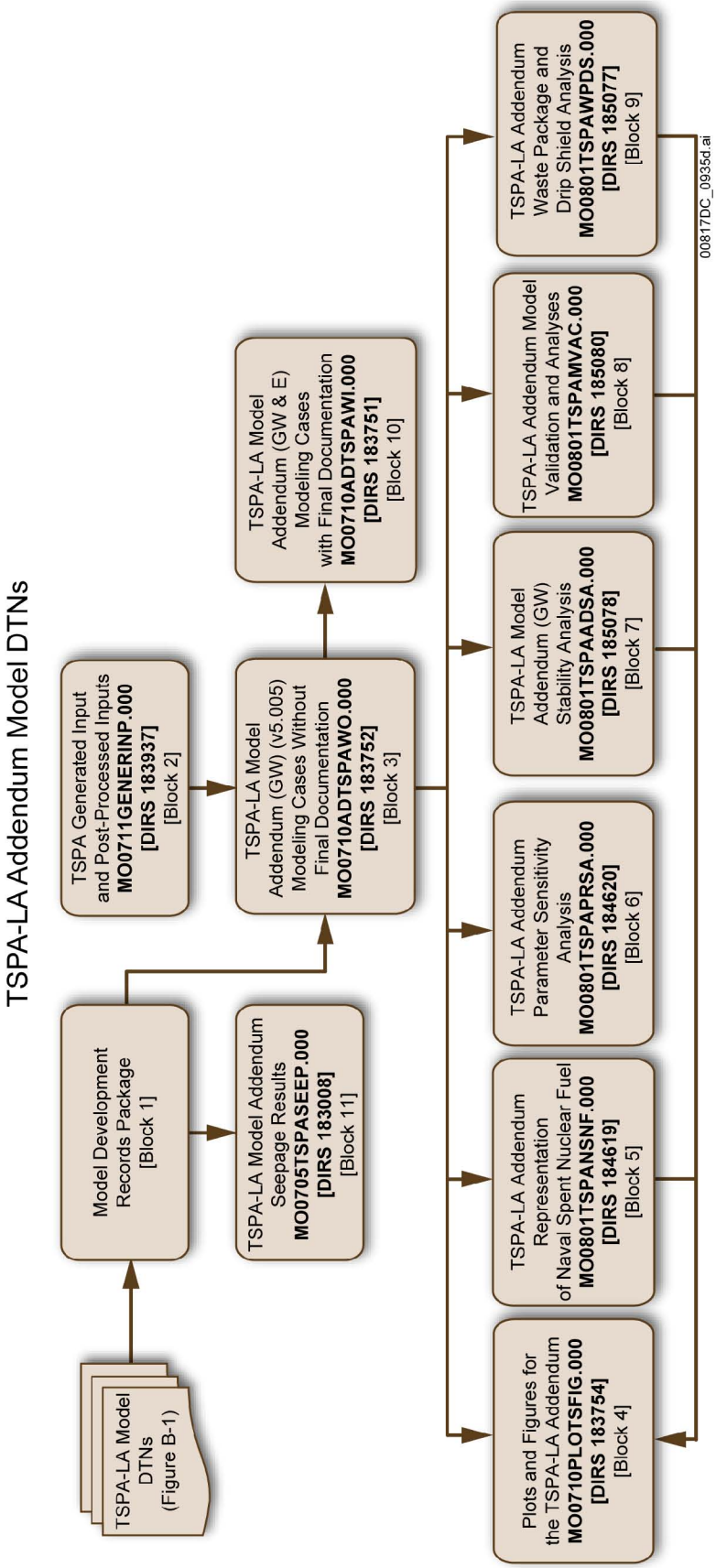

Figure B-3[a]. Road Map of TSPA-LA Model v5.005 Data Tracking Numbers

INTENTIONALLY LEFT BLANK

APPENDIX C[a]
PERFORMANCE MARGIN ANALYSIS

C1[a] PURPOSE AND OBJECTIVE

Appendix C of the parent document includes the analyses and results supporting the Performance Margin Analysis (PMA). This addendum documents an additional impact analysis of a single issue identified in the performance margin model implementation that was not previously documented in Section C9 of the parent document. Table C9-1 of the parent document is included as Table C9-1[a] of this addendum. The items numbered 1 through 14 in the table are repeated from the parent document, only the last item (item #15) has been added in this addendum.

C2[a] QUALITY ASSURANCE

No change.

C3[a] USE OF SOFTWARE

No change.

C4[a] INPUTS

No change.

C5[a] ASSUMPTIONS

No change.

C6[a] PERFORMANCE MARGIN ANALYSIS DESCRIPTION

No change, except for the following subsection, C6.3.1[a].

C6.1[a] METHODOLOGY

No change.

C6.2[a] DRIFT-SCALE UNSATURATED ZONE FLOW

No change.

C6.3[a] WASTE PACKAGE AND DRIP SHIELD DEGRADATION

No change.

C6.3.1[a] CONCEPTUAL MODEL

The following paragraphs are edited to correct the value for the WP surface area, and replace the corresponding paragraphs in the parent document.

Localized Corrosion WP Failure Area

Localized corrosion is a phenomenon in which corrosion progresses at discrete sites or in a non-uniform manner (SNL 2007 [DIRS 178519], Section 6.4.4). The area of the Alloy 22 WP outer barrier that is contacted by seepage is potentially subject to localized corrosion (SNL 2007 [DIRS 178519], Sections 6.3.5 and 6.4.4.8.3). In the TSPA-LA Model, it is assumed the maximum available area for localized corrosion (i.e., the area of the WP wetted by seepage) is the area of the WP damaged by localized corrosion (SNL 2007 [DIRS 178519], Section 6.3.5.2.2). Therefore, the entire surface area of the WP is removed as a barrier to water inflow and transport of radionuclides from a localized corrosion damaged WP.

In the PMA, the results of an ACM are used to establish a minimum WP area subject to crevice corrosion processes from localized corrosion (SNL 2007 [DIRS 178519], Section 6.4.4.8.3). The ACM considers a minimum WP creviced surface area based on the WP-to-emplacement pallet contact area (SNL 2007 [DIRS 178519], Sections 6.4.4.8.3). The calculated minimum WP-pallet contact area is 1.924×104 mm^2 (SNL 2007 [DIRS 178519], Section 6.4.4.8.3). Therefore, the minimum creviced area is about 0.05 percent of the cylindrical WP surface area of 33 m^2 for the transportation, aging, and disposal (TAD) canister-bearing WP configuration. The maximum available area for localized corrosion is the area of the WP wetted by seepage. In the absence of specific information regarding local environments on the WP, for the PMA the area of the WP failed by localized corrosion was assumed to have a log-uniform distribution that was sampled between the range of the entire WP surface area that is exposed to seepage (100 percent) and the calculated ACM minimum of 0.05 percent of the WP surface area (SNL 2007 [DIRS 178519], Section 6.4.4.8.3).

C7[a] RESULTS

No change.

C7.1[a] PERFORMANCE MARGIN IN TOTAL ANNUAL DOSE PREDICTIONS

No change.

C7.2[a] PERFORMANCE MARGIN ANALYSIS—MODELING CASE RESULTS

No change.

C7.3[a] KEY FACTORS AFFECTING THE PERFORMANCE MARGIN

No change.

C8[a] SUMMARY

No change.

C9[a] IMPACT ANALYSIS

Table C9-1 has been updated to include one additional issue (#15) identified during completion of the addendum.

Table C9-1[a]. Impact Assessment Summary Table

	ISSUE DESCRIPTION	IMPACT ASSESSMENT
1	Fifteen of the sixteen UZ_Params_Multi_PMA tables, input files to FEHM DLL (version 2.25), need to be populated at run time according to the model simulation specific settings.	This issue does not impact the TSPA-LA PMA dose calculation which uses the appropriate updated UZ_Params file for 300 epistemic realizations. The UZ_Params_Multi files, tables of sampled values of epistemically uncertain parameters, are only used when the PMA model is run with the compliance implementation of the unsaturated zone.
2	The 4 external FEHM .mptr input files for the EF 10k and 1Myr cases need to be updated to point to the correct UZ_Params_Multi_PMA file to use.	This modification only impacts EF EXDOC PMA simulations that turn the PMA UZ implementation off (i.e., compliance UZ implementation is used). This feature was not used for the PMA dose calculations, but was intended for future sensitivity analyses. This change needs to occur in conjunction with populating the UZ_Params_Mult files identified in issue #1. This issue does not have any impact on dose results.
3	The selector containing the logic for the determination of the CDSP WP Seismic first damage time is incorrectly set.	The first switch in the selector element, Seismic_1st_Dam_Time_CDSP is incorrectly set to suppress any seismic events. The correct setting should select the EXDOC table, Seismic_Time_A1_Spec, which specifies the sampling configuration for the Seismic GM 10,000-year simulation. This issue, which only applies to the 10,000-year Seismic GM simulation, was corrected prior to running the model, and therefore has no impact on dose.
4	UZ tortuosity parameters, UZ_Tortuosity_RG2_a and UZ_Tortuosity_RG3_a were incorrectly set (v10.002) (err#-case# 001-10.002 needs to change to 002-10.002)	The UZ tortuosity parameters should Correct settings: min(1.0,(10^(UZDC_Mean_RG2+UZDC_STN_RG2*UZDC_SD_RG2))) The expression for UZ_Tortuosity_RG3_a should be min(1.0,(10^(UZDC_Mean_RG3+UZDC_STN_RG3*UZDC_SD_RG3))) This error should have negligible or no impact in all modeling cases.
5	The IWPD submodel selector elements for the timing of the first Igneous or Seismic event are incorrectly set to supress events until 400,000 years. To correct this, the first two switches in the selector elements, Event_Time_Feed_IWPD_CDSP and Event_Time_Feed_IWPD_CSNF need to be deleted. (err#-case# 002-10.016)	This issue is scenario specific to the Igneous, Seismic FD, and Seismic GM 10,000-year simulations, as well as the Seismic FD 1, 000,000 year simulations. The model file for each of the affected cases was corrected prior to running the file, and therefore does not impact the dose calculations.
6	ExDoc type runs for both 1Myr EF cases are run with the PMA cladding failure submodel calculations turned on. (err#-case# 003-10.016)	This is not an error and is not applicable to the impact evaluation.
7	The RH threshold for the fluoride ion calculation is incorrect in nineteen of the tables.	Most of these incorrect values were not used in the actual simulations because these values, both the incorrect and the corrected ones, are low (<0.65). At such low RH, the temperatures in the drift will be still high (> 96°C) and there will be no seepage water dripping. For the other incorrect values, the differences between the incorrect and the correct ones are small (<0.012). Therefore, the impact on dose is expected to be negligible.

Table C9-1[a]. Impact Assessment Summary Table (Continued)

	ISSUE DESCRIPTION	IMPACT ASSESSMENT
8	The PMA early failure scenarios distribute the EBS mass released to the UZ nodes unevenly within a given percolation subregion.	Although the EBS mass released to the UZ nodes is distributed unevenly within a given percolation subregion in each realization, the even distribution is captured by calculating the annual mean dose from 300 realizations sampling uncertainty uniformly. Therefore no dose impact is expected.
9	Certain parameters within the model were not connected to the PMA database.	The PMA simulations use the correct values for the parameters listed below, and therefore this issue does not affect the dose calculations. The parameters that need to be linked to the PMA database include, FPLRZN, FPLRZS, FPLRZE, FPVO_PMA, Rf1-Rf10, Kd_Np_RZ, Kd_Np_RZ, SZ_Block_Length, SZ_Block_Thickness, Viscosity_water_T, Sat_Vap_Density_Outside_WP, Water_Vap_Diff_Coeff, Water_Vap_Diff_Cond, Air_Entry_Potential, Sat_Vap_Density_Inside_WP, Osmotic_Coeff, pH_eq
10	Certain parameters within the model were not locked on to the PMA database. GoldSim allows you to "lock onto" the file that is being referenced by a file element. When you lock onto a file (by checking the Lock onto this file option in the File element dialog), the following additional information regarding the referenced file is saved with the element: File and path name; Date the file was created; Date the file was last modified; File size; and CRC signature. Once you have locked onto a file, this information is displayed in a tool-tip when you hold your cursor over the filename in the dialog.	The PMA simulations used the correct files because they were downloaded from the controlled PMA database when the model was run, and therefore this issue does not affect the dose calculations.
11	The pH regression equation contains incorrect coefficients.	The coefficients in the regression for pH_eq need to be corrected. The value of 7.2625 should be rounded to 7.3. The value of 0.00185 has an extra zero and should also be rounded to 0.02. pH_eq is the pH where the acid and the alkaline dissolution rates cross over, and this pH weakly depends on temperature. For the most part of repository time period, the resulting difference in pH_eq due to the error is less than one unit, which is within the uncertainty range of predicted in-package pH values. Therefore, the impact on annual dose is expected to be negligible.

Table C9-1[a]. Impact Assessment Summary Table (Continued)

	ISSUE DESCRIPTION	IMPACT ASSESSMENT
12	There are incorrect values in some of the tables used in the in-package chemistry calculations.	Some of the inputs in the PMA database for the lookup tables named: IPC_XXX_pH_Rsw_YY_Z_LUT (where XXX = CSNF, DHLW, or MCO; YY = 15, 2, 3, or 4; and Z = A-I) has some rows with erroneous data. The DTN that supplied the tables had some independent variables that were duplicated in multiple rows. GoldSim could not read tables with these duplicate independent variables. The DTN supplier indicated that it was acceptable to average these rows together. The error occurred because the analyst who averaged these rows failed to expand out each cell to display the maximum number of significant figures. Therefore some rows were rounded together that did not need to be. No impacts to the dose results are expected. More information is provided in PEF 500. The PEF has a Roadmap to the TSPA-produced DTN that holds the modified lookup tables. This DTN now has two file sets: Uncorrected and Corrected. To correct this error, replace the PMA database entries with the tables in the Corrected folder.
13	The parameter specifying the value of Np Carbonate Eps is incorrect.	The input in the PMA database for parameter "Np_Carbonate_PMA_Eps" is not correct. It should be a triangular distribution with a=-0.5 and b=0 and c=0.5 rather than a truncated normal distribution. The truncated normal distribution is equally well justified. No impacts to the dose results are expected.
14	In determining whether the drift chemical environment is benign or aggressive for drip shield general corrosion, 5 mM dissolved fluoride concentration is used instead of 0.5 mM as suggested in C6.3.1.	The value of 5 mM is justifiable because this value is close to the middle point of the fluoride concentration interval within which the corrosion rate starts to increase at the lower bound (0.5 mM) and then levels off at the upper bound (5 mM). Furthermore, this error only affects one out four initial seepage waters used in the model and this effect will diminish as the seepage water composition returns to the ambient conditions after the thermal event. Therefore, the impact of this error is negligible.

Table C9-1[a]. Impact Assessment Summary Table (Continued)

	ISSUE DESCRIPTION	IMPACT ASSESSMENT
15	The Water Balance submodel incorrectly calculates: 1) the stainless steel degradation rate for Co-disposed (CDSP) WPs . 2) the average stainless steel degradation rate 3) the stainless steel degradation rate by treating all corrosion products as degraded stainless steel	1) The expression for the degradation rate in the CDSP portion of the model should be divided by the number of packages failed to obtain a per-package degradation rate. Otherwise, the rate is too high which keeps the water saturation low and ionic strength high until the steel is gone. Low water saturation may reduce the diffusive release from the waste form. High ionic strength tends to increase radionuclide solubility because of out-of-bound conditions. The overall effect is anticipated to be small because CSNF WPs usually dominate the dose. The early failed scenarios are not affected because they fail only one WP. 2) The stainless steel degradation rate is based on the difference between the volume of corrosion products times the number of failed packages at the current timestep and the previous timestep. However, the corrosion products volume is already an average so this technique is unnecessary. This results in small overestimation of the stainless steel degradation rate when the number of failed WPs increases with time, such as in the Nominal Modeling Case run for the 1,000,000 year duration. The overall effect on dose is anticipated to be small because the water saturation inside the WP would not be greatly affected by this overestimation. 3) The stainless steel degradation rate uses a conversion factor for calculating the volume of corrosion products per kilogram of stainless steel. However, some of the corrosion products in the CDSP WPs are formed from the degradation of carbon steel, which should use a different conversion factor. The effect is anticipated to be small because the conversion factors would be approximately the same.

APPENDIX D[a]
PARAMETER LISTING

D1[a] INTRODUCTION

The Total System Performance Assessment (TSPA) Input Database was updated and includes the parameters used in both TSPA-LA Model v5.000 (documented in the parent document) and TSPA-LA Model v5.005 (documented in this addendum). The details of this database are described in Section 4.7 of the parent document and Section 4[a] of this addendum. Parameter Entry Form series 200 numbers, listed in Tables 4-1[a] and 4-2[a], contain the additional TSPA-LA Model v5.005 parameters. Additionally, Appendix K of the parent report contains two tables that describe the significant uncertain parameters (Tables K.3-1 and K.3-2).

INTENTIONALLY LEFT BLANK

APPENDIX H[a]
YUCCA MOUNTAIN REVIEW PLAN ACCEPTANCE CRITERIA

H1[a] EVALUATION OF THE TOTAL SYSTEM PERFORMANCE ASSESSMENT FOR THE LICENSE APPLICATION MODEL DOCUMENT AGAINST REGULATORY REQUIREMENTS

Appendix H[a] includes minor editorial changes from the text included in the parent document when referencing the proposed rule. The supplemental information presented in this addendum should be used to clarify these issues.

H1.1[a] EVALUATION AGAINST 10 CFR 63.113(a); 10 CFR 63.115(a); AND 10 CFR 63.115(b)

No change.

H1.2[a] EVALUATION AGAINST 10 CFR 63.113(b)

No change.

H1.3[a] EVALUATION AGAINST 10 CFR 63.113(c)

Acceptance Criterion 1 and 2 below have been revised slightly from the parent document with some minor updates to the references. The bulk of the information presented is the same as in the parent document.

Acceptance Criterion 1–An Adequate Demonstration is Provided that the Expected Concentration of Combined ^{226}Ra and ^{228}Ra, Expected Concentration of Specified Alpha-Emitting Radionuclides, and Expected Whole Body or Organ–Specific Doses from any Photon– or Beta–Emitting Radionuclides at Any Year During the Compliance Period Do Not Exceed the Separate Standards for Protection of Groundwater—Section 8.1.2 presents the results of analyses addressing the separate standards for protection of groundwater in 10 CFR 63.331 [DIRS 180319], Table 1. In particular, Section 8.1.2 shows the estimate of groundwater radioactivity for the representative volume of groundwater that includes combined ^{226}Ra and ^{228}Ra, gross alpha activity (including due to ^{226}Ra, but excluding that due to radon and uranium), and combined beta- and photon-emitting radionuclides. Sections 6.3 and 8.1.2 discuss the methods, assumptions, models, and data used in calculating these estimates. Sections 6.3 and 8.1.2 show that these estimates are consistent with the repository performance assessment calculations for likely processes and events that may occur after disposal, and that the calculations are supported by an adequate technical basis. Therefore, the material in Sections 6.3 and 8.1.2 provides information useful in evaluating Acceptance Criterion 1.

Acceptance Criterion 2–The Methods and Assumptions Used to Determine the Position of the Representative Volume of Groundwater are Credible and Consistent, and the Representative Volume of Groundwater Includes the Highest Concentration Level in the Plume of Contamination in the Accessible Environment—Section 6.3.10 discusses the methods and assumptions for determination of groundwater concentrations in the representative volume that is located along the radionuclide migration path from the repository at Yucca Mountain to the accessible environment. Section 8.1.2 provides results and a detailed evaluation of the concentrations in the context of the groundwater concentration standards (10 CFR 63.331 [DIRS 180319], Table 1). In the TSPA-LA Model, a conservative approach is used in which

radionuclide concentrations are estimated by assuming the entire annual release from the repository system is discharged into the representative volume, located 18 km from the repository (66 FR 55732 [DIRS 156671], III Public Comments and Responses, 3.5, p. 55750). Therefore, the estimated radionuclide concentrations provide an upper bound to the groundwater concentrations needed to assess the groundwater protection requirements. This approach eliminates the need to specify the dimensions of the representative volume or the water usage by the reasonably maximally exposed individual (RMEI) (Section 1.1.1) (10 CFR 63.332(a)(3) [DIRS 180319]). The information provided in Sections 6.3.10 and 8.1.2 therefore, supports evaluation of Acceptance Criterion 2 by the U.S. Nuclear Regulatory Commission (NRC).

Acceptance Criterion 3–The Methods and Assumptions Used to Calculate the Physical Dimensions of the Representative Volume of Groundwater are Credible and Consistent—No changes.

H1.4[a] EVALUATION AGAINST 10 CFR 63.113(d)

Acceptance Criterion 1–Evaluation of the Time of an Intrusion Event—No change.

Acceptance Criterion 2–Evaluation of an Intrusion Event Demonstrates That the Annual Dose to the Reasonably Maximally Exposed Individual in Any Year During the Compliance Period Is Acceptable—Sections 6.7 and 8.1.3 discuss how the TSPA-LA Model addresses the Human Intrusion Scenario, the implementation, and how the resultant RMEI dose complies with the requirement of this acceptance criterion. Section 6.7.3 specifically discusses implementation of the TSPA-LA Model for human intrusion separately from the overall TSPA, and is consistent with the requirements for performance assessments, as specified in NRC Proposed rule 10 CFR 63.114 [DIRS 178394]. Section 6.7 analyzes a postulated human intrusion event with characteristics as defined in 10 CFR 63.322 [DIRS 180319], and excludes the consideration of unlikely natural features, events, or processes (10 CFR 63.342(b) [DIRS 178394]) (Section 6.7.2.2). Sections 6.7.3 and 6.7.4 show that many of the nominal abstractions, process models, and parameters values are used in the analysis of the TSPA-LA Human Intrusion Scenario, and therefore, many of the implementation provisions in Section 6.3 apply to the Human Intrusion Modeling Case. In addition, the numerical values in the Individual Protection Standard in NRC Proposed Rule 10 CFR 63.311(a) [DIRS 178394] are identical to the numerical values of the Individual Protection Standard for Human Intrusion in NRC Proposed Rule 10 CFR 63.321(b) [DIRS 178394]. Section 7.3 provides information regarding the fact that a sufficient number of realizations have been run using the TSPA-LA Model, to ensure that the results of the calculations are statistically stable. Section 8.1.3 discusses the overall system performance analyses and presents the resulting annual dose curves for the Human Intrusion Scenario. The information provided in Sections 6.7 and 8.1 supports confirmation that the repository system meets performance objectives specified in 10 CFR 63.321 [DIRS 178394] for a human intrusion into the repository.

Acceptance Criterion 3—The Total System Performance Assessment Code Provides a Credible Representation of the Intrusion Event—No change.

Table H-1[a]. Applicable Regulatory Requirements of 10 CFR Part 63 and NUREG-1804 Acceptance Criteria Addressed in this Document

Applicable Sections of 10 CFR Part 63	Associated Section of NUREG-1804 Acceptance Criterion	NUREG-1804 Acceptance Criterion		Section of Report Addressing NUREG-1804 Acceptance Subcriterion
		Criterion	Subcriterion	
10 CFR 63.113(b) [DIRS 180319] and 10 CFR 63.311 [DIRS 178394]	2.2.1.4.1.3 Demonstration of Compliance with Postclosure Individual Protection Standard	1. Scenario Classes	1. Scenario class screening	6.1.2
			2. Combining mean annual dose from scenario classes	6.1.2 and 8.1.1.1
		2. Mean Annual Doses	1. Number of realizations	7.3
			2. Uncertainty in mean annual dose	6.1.3 and 8.1.1.2
			3. Performance of components and subsystems	8.2 – 8.4
			4. Comparison with individual protection standard (10 CFR 63.311 [DIRS 178394])	8.1.1.2
		3. Credible TSPA-LA Model	1. Consistency of assumptions	5, 6.3 to 6.6
			2. Model verification	7.2
			3. Uncertainty analysis	6.1.3 and 7.4
			4. Parameter sampling	6.1.3
10 CFR 63.113(c) [DIRS 180319], 10 CFR 63.331 [DIRS 180319], Table 1, and 10 CFR 63.332 [DIRS 180319]	2.2.1.4.3.3 Demonstration of Compliance with Groundwater Protection Standards	1. Groundwater Protection Standards	1. Compliance with concentration and dose standards	8.1.2.1 to 8.1.2.2, and 8.1.2.3
			2. Methods and assumptions	8.1.2
			3. Comparison with groundwater protection standards (10 CFR 63.331 [DIRS 180319], Table 1)	8.1.2
		2. Position of Representative Volume	1. Along radionuclide migration path	6.3.10
			2. Method of locating position	6.3.10
			3. Highest concentration	6.3.10
		3. Dimensions of Representative Volume	1. Specifications on representative volume	8.1.2
			2. Method to determine dimensions	6.3.10 and 8.1.2
			3. Consistency with water usage	8.1.2 and 6.3.11

Table H-1[a]. Applicable Regulatory Requirements of 10 CFR Part 63 and NUREG-1804 Acceptance Criteria Addressed in this Document (Continued)

Applicable Sections of 10 CFR Part 63	Associated Section of NUREG-1804 Acceptance Criterion	NUREG-1804 Acceptance Criterion		Section of Report Addressing NUREG-1804 Acceptance Subcriterion
		Criterion	Subcriterion	
10 CFR 63.113(d) [DIRS 180319], 10 CFR 63.321 [DIRS 178394], and 10 CFR 63.322 [DIRS 180319]	2.2.1.4.2 Demonstration of Compliance with the Human Intrusion Standard	1. Evaluation of the Time of a Human Intrusion Event	1. The technical basis and associated analyses adequately support the selection of the time of occurrence of a human intrusion, as specified in 10 CFR 63.321 [DIRS 178394].	6.7.2
		2. Evaluation of an Intrusion Event Demonstrates That the Annual Dose to the RMEI in Any Year During the Compliance Period Is Acceptable	1. The TSPA for the Human Intrusion Scenario is performed separately from the overall TSPA, and meets the requirements for performance assessments, specified in 10 CFR 63.114 [DIRS 178394].	6.7.3 and 6.7.4
			2. The TSPA for the Human Intrusion Scenario is identical to the TSPA for individual protection, except that it assumes the occurrence of a postulated human intrusion event with characteristics, as defined in 10 CFR 63.322 [DIRS 180319] and excludes the consideration of unlikely natural features, events, or processes in 10 CFR 63.342(b) [DIRS 178394].	6.7.2.2, 6.7.3, and 6.7.4
			3. A sufficient number of realizations have been run using the TSPA code, to ensure that the results of the calculations are statistically stable.	8.1.1.2 and 7.3
			4. The estimated repository performance is reasonable and consistent with the analysis of overall repository performance, and with the characteristics of the postulated Human Intrusion Scenario.	8.1.3.2
			5. The annual dose curve for limited human intrusion confirms that the repository system meets performance objectives, specified in 10 CFR 63.321 [DIRS 178394], for limited human intrusion events.	8.1.3.2

Table H-1[a]. Applicable Regulatory Requirements of 10 CFR Part 63 and NUREG-1804 Acceptance Criteria Addressed in this Document (Continued)

Applicable Sections of 10 CFR Part 63	Associated Section of NUREG-1804 Acceptance Criterion	NUREG-1804 Acceptance Criterion		Section of Report Addressing NUREG-1804 Acceptance Subcriterion
		Criterion	Subcriterion	
		3. The TSPA Code Provides a Credible Representation of a Human Intrusion Event.	1. Assumptions made on the method of transport from a breached waste package within the TSPA for evaluating the postulated intrusion event are consistent among different modules of the code. The use of assumptions and parameter values that differ among modules of the code is adequately documented.	5, 6.7.1 to 6.7.5, and 7.7
			2. The TSPA code for evaluating human intrusion is properly verified, such that there is confidence that the code is modeling the physical processes in the repository system in a manner that is consistent with the characteristics of the postulated intrusion event. The transfer of data between modules of the code is conducted properly.	7.2
			3. The estimate of uncertainty in the performance assessment results is consistent with the uncertainties considered in the characteristics of the postulated intrusion event, and with model and parameter uncertainty.	8.1.3, 6.7.3 ,6.1.3, and 7.4
			4. The sampling method used in the TSPA ensures that sampled parameters of the postulated intrusion event have been sampled across their ranges of uncertainty.	6.1.3, 6.7, and 7.4

Sources: 10 CFR Part 63 [DIRS 178394 and DIRS 180319]; NUREG-1804 (NRC 2003 [DIRS 163274]).

INTENTIONALLY LEFT BLANK

APPENDIX I[a]
FEATURES, EVENTS, AND PROCESSES MAPPED TO TSPA-LA MODEL

I1[a] INTRODUCTION

Appendix I[a] contains a revision to selected descriptions listed in Table I-2 of the parent document. One new description for the EBS Thermal Hydrologic Environment Submodel is included in Table I-2[a]. Only the table entries that have been revised are included in the updated Table I-2[a] included in this addendum. The corrected table entries should be substituted into the original table presented in Appendix I of the parent document.

INTENTIONALLY LEFT BLANK

Table I-2[a]. Model Implementation for Included Features, Events, and Processes

Submodel Implemented in the TSPA-LA Model and Section Number	Path in GoldSim Model File	FEPs Included in the Submodel	TSPA Inclusion Explanation	Performance Assessment Standard[a]	TSPA-LA Model Implementation
EBS TH Environment Submodel 6.3.2	Epistemic: \Input_Params_Epistemic\Epistemic_Params_EBS_Environ\Uncertain_Params_TH EBS: \Global_Inputs_and_Calcs\Global_EBS_Environ\EBS_Environment\ThermoHydrology	2.1.06.06.0A Effects of drip shield on flow	The effects of a drip shield on flow is included in the Multiscale Thermohydrologic Model (MSTHM) by predicting the temperature of the in-drift environment both inside and outside the intact drip shield. Water fluxes in the invert are influenced by temperature and capillary pressure processes. The thermal effects on flow are assessed by multiple MSTHM process model simulations. These simulations are used to develop the MSTHM Abstraction implemented in the TSPA-LA Model.	10 CFR 63.311 10 CFR 63.331 10 CFR 63.321	MA
WP and DS Degradation Submodel 6.3.5	Epistemic: \Input_Params_Epistemic\Epistemic_Params_WP_DS_Deg\ Aleatory: \Model_Calcs_Aleatory\Aleatory_Calcs_WP_DS_Deg EBS: \Time_Zero\EBS_PS_Loop\Static_Calcs_PS_Loop\Static_Calcs_WP_DS_Deg \Global_Inputs_and_Calcs\Global_WP_DS_Deg\Global_IWPD	2.1.03.05.0A Microbially influenced corrosion of waste packages	Microbially influenced corrosion is modeled in the TSPA-LA Model as an enhancement factor uniformly distributed between 1 and 2 due to uncertainty. The factor is applied to the entire waste package outer barrier general corrosion rate when the relative humidity at the waste package outer corrosion barrier surface is above a threshold value represented by, and sampled from, a uniform distribution ranging from 75 percent to 90 percent.	10 CFR 63.311 10 CFR 63.331	DLL

Table I-2[a] Model Implementation for Included Features, Events, and Processes (Continued)

Submodel Implemented in the TSPA-LA Model and Section Number	Path in GoldSim Model File	FEPs Included in the Submodel	TSPA Inclusion Explanation	Performance Assessment Standard[a]	TSPA-LA Model Implementation
Biosphere Submodel 6.3.11	Epistemic: \Input_Params_Epistemic\Epistemic_Params_Biosphere Other: \TSPA_Model\Biosphere	2.4.01.00.0A Human characteristics (physiology, metabolism)	Metabolic and physiologic considerations consistent with present knowledge of adults, as per 10 CFR 63.312(e) [DIRS 180319], were used in the development of parameter distributions for the external exposure, inhalation, and ingestion submodels. Therefore, this feature, event, or process (FEP) is included in the biosphere component of the TSPA-LA Model through the use of groundwater exposure scenario biosphere dose conversion factors (BDCFs) that are direct inputs to the TSPA-LA for the scenario classes involving radionuclide release to the groundwater, and through the use of the conversion factors for demonstrating compliance with the groundwater protection standards. The annual doses are calculated as the product of radionuclide concentration in groundwater and the BDCFs or conversion factors.	10 CFR 63.311 10 CFR 63.321 10 CFR 63.331	MA

[a] 10 CFR 63.311 Individual Protection (70 FR 53313 [DIRS 178394]).
10 CFR 63.331 Groundwater Protection (10 CFR 63 [DIRS 180319]).
10 CFR 63.321 Human Intrusion (70 FR 53313 [DIRS 178394]).

APPENDIX J[a]
CONCEPTUAL STRUCTURE OF TSPA-LA

J1[a] INTRODUCTION

Appendix J of the parent document includes detailed documentation of the TSPA-LA Model conceptual structure. This addendum includes additional supplemental material in Section J3[a] that presents an overview of the underlying concepts used in the TSPA-LA Model, which are described in Appendix J of the parent document. The supplemental material provided in Section J3[a] of this addendum should be reviewed in conjunction with Appendix J included with the parent document.

J2[a] REQUIREMENTS UNDERLYING CONCEPTUAL STRUCTURE OF TSPA-LA

No change.

J3[a] TUTORIAL ON PROBABILITY, UNCERTAINTY AND THE STRUCTURE OF PERFORMANCE ASSESSMENTS

The conceptual and computational design of the TSPA-LA is based on standard concepts underlying risk assessments for complex systems. An overview of the evolution and development of these concepts is provided in Rechard (1999 [DIRS 145383]).

A natural starting place in a discussion of the antecedents to the TSPA-LA conceptual and computational design is the Reactor Safety Study, which was initiated by the Atomic Energy Commission to study the risk from commercial nuclear power plants and completed by the NRC (1975 [DIRS 107799]). This was a landmark study and constituted the largest systematic risk analysis ever performed at the time of its completion. The primary emphasis of this study was on aleatory uncertainty in the sense of the universe of possible accidents that could occur at a commercial nuclear power plant.

After the completion of the Reactor Safety Study, the NRC commissioned a review of the study that is now commonly referred to as the Lewis Report (Lewis et al. 1978 [DIRS 107800]). This report was highly complimentary of the Reactor Safety Study but had one notable criticism. This criticism was that the Reactor Safety Study had not appropriately assessed and presented the uncertainty in its results. Here, the uncertainty being referred to was of a state of knowledge or epistemic character.

The Reactor Safety Study was highly influential and set the stage for a number of the following risk assessments (e.g., PLG 1983 [DIRS 185063]; PLG 1982 [DIRS 107812]). It was out of this work that the Kaplan/Garrick ordered triple representation for risk emerged (Kaplan and Garrick 1981 [DIRS 100557]). Conceptually, the TSPA-LA can be cast in the context of this representation for risk. However, for computational reasons the TSPA-LA uses a continuous integral-based version of the original ordered triple representation for risk. It was also during this period that Latin hypercube sampling was introduced for use in uncertainty and sensitivity analyses for computationally demanding models (McKay et al. 1979 [DIRS 127905]).

After the publication of the Reactor Safety Study, the NRC initiated the development of a risk assessment methodology at Sandia National Laboratories for the disposal of radioactive waste (Campbell et al. 1978 [DIRS 185064]; Cranwell et al. 1987 [DIRS 185066]). As a result of the

Lewis Committee's report on the importance of the treatment of (epistemic) uncertainty, the appropriate treatment of such uncertainty was given high importance in the methodology development at Sandia (Iman and Conover 1982 [DIRS 165064]; Iman et al. 1980 [DIRS 124198]; and Iman et al. 1978 [DIRS 159559]).

The early work on uncertainty and sensitivity analysis in the preceding project significantly influenced later analyses for complex systems. In particular, it formed the basis for the treatment of uncertainty in the NRC's MELCOR project to develop a new suite of models for reactor accidents (Iman and Helton 1985 [DIRS 185067]), the NRC's reassessment of the risk from commercial nuclear power plants (i.e., the NUREG-1150 analyses) (Breeding et al. 1992 [DIRS 107727]; Breeding et al. 1992 [DIRS 185068]; Brown et al. 1992 [DIRS 185069]; Gregory et al. 1992 [DIRS 185070]; Helton and Breeding 1993 [DIRS 184402]; Payne et al. 1992 [DIRS 185071]; and NRC 1990 [DIRS 107798]), the NRC's Risk Methods Integration and Evaluation Program (Payne 1992 [DIRS 107814]), and the U.S. Department of Energy's (DOE's) successful compliance certification application to the U.S. Environmental Protection Agency (EPA) for the Waste Isolation Pilot Plant (Helton and Marietta 2000 [DIRS 171759]; and DOE 1996 [DIRS 100975]). The basic ideas underlying the treatment of uncertainty and the performance of associated sensitivity analyses in the preceding analyses are summarized in a number of review articles (Helton 1993 [DIRS 100452]; Helton 1994 [DIRS 107739]; Helton 1997 [DIRS 107496]; Helton 2003 [DIRS 170558]; Helton and Davis 2003 [DIRS 170518]; and Helton et al. 2006 [DIRS 183873]).

The conceptual organization of the TSPA-LA is the same as the conceptual organization of the NRC's NUREG-1150 analyses and the DOE's analysis for the Waste Isolation Pilot Plant. Of course, the details of the analyses are different because different facilities, and hence different processes and models, are involved. However, the analyses are the same conceptually and have a structure of the form described in Helton (2003 [DIRS 170558]). Further, all of these analyses use uncertainty and sensitivity analysis procedures of the form described in Helton and Davis (2003 [DIRS 170518]) and Helton et al. (2006 [DIRS 183873]). Thus, the TSPA-LA has an overall conceptual structure that has been successfully used in several preceding and important analyses. A detailed illustration of the conceptual ideas that underlie the calculation of expected dose to the reasonably RMEI in the TSPA-LA is presented in Helton and Sallaberry (2007 [DIRS 185072]).

J4[a] CONCEPTUAL STRUCTURE OF TSPA-LA

No change.

J5[a] NOMINAL SCENARIO CLASS

No change.

J6[a] EARLY FAILURE SCENARIO CLASSES

No change.

J7[a] IGNEOUS SCENARIO CLASSES

No change.

J8[a] SEISMIC SCENARIO CLASSES

No change.

J9[a] EXPECTED DOSE FROM ALL SCENARIO CLASSES

No change.

J10[a] JUSTIFICATION FOR ANALYSIS DECOMPOSITION

No change.

J11[a] HUMAN INTRUSION SCENARIO

No change.

INTENTIONALLY LEFT BLANK

APPENDIX K[a]
UNCERTAINTY AND SENSITIVITY ANALYSIS RESULTS

K1[a] INTRODUCTION

No change.

K2[a] UNCERTAINTY AND SENSITIVITY ANALYSIS PROCEDURES

No change.

K3[a] INDEPENDENT AND DEPENDENT VARIABLES

No change.

K4[a] NOMINAL SCENARIO CLASS

No change.

K4.1[a] Nominal Scenario Class: Summary

No change.

K4.2[a] Nominal Scenario Class: Drip Shield (DS) and Waste Package (WP) Failure

No change.

K4.3[a] Nominal Scenario Class: Engineered Barrier System (EBS) Conditions

No change.

K4.4[a] Nominal Scenario Class: Release Results Engineered Barrier System (EBS), Unsaturated Zone (UZ) and Saturated Zone (SZ)

No change.

K4.5[a] Nominal Scenario Class: Dose to Reasonably Maximally Exposed Individual (RMEI)

No substantive changes in the uncertainty and sensitivity analyses for dose to the RMEI (*DOSTOT*, mrem/yr) over the time interval [0, 1,000,000 yr] resulting from nominal conditions were observed (i.e., compare the results in Figures K4.5-1 and K4.5-2 with the results in Figures K4.5-1[a] and K4.5-2[a]). Additional comparisons are presented in Figures 7.3.1-18[a] and 7.3.1-19[a] and are discussed in Section 7.3.1.5.1[a].

For reader convenience, the following discussion of the expected dose results in Figures K4.5-1[a] and K4.5-2[a] is provided. This discussion updates Section K4.5 from the parent report.

The uncertainty and sensitivity analyses for total dose to the RMEI (*DOSTOT*, mrem/yr) are summarized in Figures K4.5-1[a] and K4.5-2[a]. Nonzero values for *DOSTOT* begin as early as 20,000 yr as a result of WP failure and then show a general tendency to increase

(Figure K4.5-1a,b[a]). However, some dose curves and especially some of the curves with the largest values for *DOSTOT*, change from increasing to decreasing at some point in time. This change results from inventory depletion, and hence decreasing or terminating releases, for highly mobile species such as ^{99}Tc and ^{129}I. All curves remain below 10 mrem/yr.

The PRCCs in Figure K4.5-1c[a] indicate that the uncertainty in *DOSTOT* is dominated by *WDGCA22* (temperature dependence coefficient associated with the general corrosion rate for Alloy 22, K), with *DOSTOT* tending to decrease as *WDGCA22* increases. This effect results because the general corrosion rate for Alloy 22 decreases as *WDGCA22* increases. Smaller effects are indicated for *SCCTHR* (stress corrosion cracking threshold, MPa), *WDZOLID* (scale factor used to incorporate uncertainty into the stress intensity factor for closure-lid weld), *THERMCON* (host rock thermal conductivity level), *WDNSCC* (stress corrosion cracking growth rate exponent), and *CPUCOLWF* (concentration of irreversibly attached plutonium on stable glass/waste form colloids, mol/L). The variables *SCCTHR*, *WDZOLID*, *THERMCON* and *WDNSCC* affect *DOSTOT* through their effects on WP failure. Specifically, increasing *SCCTHR* increases the stress level at which stress corrosion cracking initiates and thus reduces failures at the closure-lid weld; increasing *WDZOLID* increases the stress at the closure lid and thus increases failures at the closure-lid weld; increasing *THERMCON* tends to lower WP temperatures and thus reduce the rate of corrosion; and increasing *WDNSCC* tends to increase the threshold stress intensity factor, which determines the threshold stress at which stress corrosion cracks propagate, and thus reduces failures at the closure-lid weld. The indicated effects of *CPUCOLWF* are small and possibly spurious.

The PRCCs in Figure K4.5-1d[a] are for [200,000; 1,000,000 years] rather than for [0; 1,000,000 years] as is the case for the PRCCs in Figure K4.5-1c[a]. The only substantive difference is the selection of *INFRCTC* (initial release fraction for ^{99}Tc in a CSNF WP) as the last variable in the analysis for [200,000; 1,000,000 years]; in contrast *CPUCOLWF* is selected as the last variable in the analysis for [0; 1,000,000 years]. The PRCCs presented originally in Figure K4.5-1c are for [0; 1,000,000 years]; however, the written discussion of the PRCC results in Section K4.5 is for PRCCs obtained for [200,000; 1,000,000 years]. As a result, the effects of *INFRCTC* are discussed in Section K4.5 although a PRCC for *INFRCTC* does not appear in Figure K4.5-1c. The effects for *INFRCTC* discussed in Section K4.5 can be seen in Figure K4.5-1d[a].

More detailed sensitivity analysis results for *DOSTOT* are provided by the regression results in Figure K4.5-2a[a]. Specifically, *WDGCA22* is the dominant variable with R^2 values of 0.78, 0.85 and 0.63 at 400,000 yr, 600,000 yr and 800,000 yr, respectively. Actually, the indicated R^2 values tend to under represent the effect of *WDGCA22* because of the nonlinear relationship between *WDGCA22* and *DOSTOT* that can be seen in Figure K4.5-2b,c,d of Appendix K and is more apparent in Figure K4.5-3 of Appendix K. Specifically, large values of *WDGCA22* result in small values for *DOSTOT* at late times because of limited WP failure and hence limited radionuclide releases, and small values of *WDGCA22* also result in small values for *DOSTOT* at late times because of extensive, early WP failure and the resultant reduction in radionuclide inventory by late times.

In addition to *WDGCA22*, the regressions in Figure K4.5-2a[a] indicate small effects for the following variables that affect WP failure: *WDZOLID*, *THERMCON*, *INFIL* (infiltration level), *SCCTHR*, *WDNSCC*, and *WDGCUA22* (pointer variable used to select the distribution of base

corrosion rates of Alloy 22 at 60°C over the patches on the WPs). The effects of *WDZOLID*, *THERMCON*, *SCCTHR* and *WDNSCC* have already been discussed in conjunction with Figure K4.5-1c[a]. Like *THERMCON*, the negative effect associated with *INFIL* probably results because increased values for *INFIL* result in lower WP temperatures and thus lower rates of corrosion. The variable *WDGCUA22* has a small positive effect on the uncertainty in *DOSTOT*. Specifically, *WDGCUA22* is a pointer variable used to select from three uncertain distributions that derive from both the uncertainty in a base corrosion rate for Alloy 22 at 60°C and the uncertainty that exists in the prediction of small scale variability in chemical and physical conditions across patches used in the modeling of WP degradation. Increasing *WDGCUA22* results in higher overall corrosion rates and thus higher values for *DOSTOT*. The dominance of *WDGCA22* with respect to the uncertainty associated with *DOSTOT* can be seen in the scatterplot in Figure K4.5-2b[a].

The regressions in Figure K4.5-2a[a] also indicate very small effects of several variables related to physical processes. However, the effects of these variables are minor given the much larger effects of variables related to WP failure and, in particular, the dominant effect of *WDGCA22* on WP failure.

K5[a] EARLY FAILURE SCENARIO CLASSES

No change.

K5.1[a] Early Failure Scenario Classes: Summary

No change.

K5.2[a] Early Failure Scenario Classes: Engineered Barrier System (EBS) Conditions

No change.

K5.3[a] Early Failure Scenario Classes: Release from Engineered Barrier System (EBS)

No change.

K5.4[a] Early Failure Scenario Classes: Release from Unsaturated Zone (UZ)

No change.

K5.5[a] Early Failure Scenario Classes: Release from Saturated Zone (SZ)

No change.

K5.6[a] Early Failure Scenario Classes: Dose to Reasonably Maximally Exposed Individual (RMEI)

No change.

K5.7[a] Early Failure Scenario Classes: Expected Dose to Reasonably Maximally Exposed Individual (RMEI)

No change.

K5.7.1[a] Early Failure Scenario Classes: Expected Dose to Reasonably Maximally Exposed Individual (RMEI) from Early Drip Shield (DS) Failure

Expected Dose to RMEI over [0, 20,000 yr]: *EXPDOSE*. The uncertainty and sensitivity analyses for expected dose to the RMEI (*EXPDOSE*, mrem/yr) over the time interval [0, 20,000 yr] resulting from early DS failure are summarized in Figures K5.7.1-1[a] and K5.7.1-2[a]. Specifically, Figures K5.7.1-1[a] and K5.7.1-2[a] have the same structure as Figures K5.7.1-1 and K5.7.1-2 but present results calculated with version 5.005 of the TSPA-LA Model rather than with version 5.000 used in the calculation of the results in Figures K5.7.1-1 and K5.7.1-2. A comparison of the results in Figures K5.7.1-1a[a] and K5.7.1-1a obtained with the two versions of the TSPA-LA Model is provided in Figures 7.3.1-20[a] and 7.3.1-22[a]; discussion of the differences in the results is provided in Section 7.3.1.5.2[a]. As examination of Figures 7.3.1-20[a] and 7.3.1-22[a] shows, there is little difference in the values for *EXPDOSE* obtained with the two versions of the TSPA-LA Model. Consistent with this comparison, there is also little difference in the sensitivity analysis results presented in Figures K5.7.1-1c and K5.7.1-2 for version 5.000 and the corresponding results presented in Figures K5.7.1-1c[a] and K5.7.1-2[a] for version 5.005. As a result, the discussion presented in Section K5.7.1 for *EXPDOSE* over the time interval [0, 20,000 yr] resulting from early DS failure for results obtained with version 5.000 of the TSPA-LA Model also applies to the results obtained with version 5.005 of the TSPA-LA Model. For this reason, no additional discussion is provided.

For reader convenience, the following discussion of the expected dose results in Figures K5.7.1-1[a] and K5.7.1-2[a] is provided. This discussion updates the corresponding material in Section K5.7.1 from the parent report.

The uncertainty and sensitivity analyses for expected dose to the RMEI (*EXPDOSE*, mrem/yr) over the time interval [0, 20,000 years] resulting from early DS failure are summarized in Figures K5.7.1-1[a] and K5.7.1-2[a]. There are sharp peaks in *EXPDOSE* prior to 1000 yr resulting from the release of ^{99}Tc. At the time of these peaks, maximum values for *EXPDOSE* are in the vicinity of 0.01 mrem/yr, although the values for most sample elements are considerably smaller (Figure K5.7.1-1a,b[a]). After the early peaks, *EXPDOSE* has values in a range from 10^{-7} to 10^{-3} mrem/yr.

The PRCCs in Figure K5.7.1-1c[a] indicate that the uncertainty in *EXPDOSE* is dominated by *PROBDSEF* (probability that a randomly selected DS will experience an early failure), with the value for *EXPDOSE* increasing as *PROBDSEF* increases. This effect results because increasing *PROBDSEF* increases the expected number of DSs that experience early failure and hence increases *EXPDOSE*.

In addition to *PROBDSEF*, smaller effects are indicated for *SZFIPOVO* (flowing interval porosity in the volcanic unit of the SZ), *SZGWSPDM* (groundwater specific discharge multiplier; as sampled, *SZGWSPDM* is actually the logarithm of the indicated multiplier), *SEEPUNC*

(pointer variable used to determine local seepage rates), *INFIL* (infiltration level), and *THERMCON* (host rock thermal conductivity level) (Figure K5.7.1-1c[a]). A negative effect is indicated for *SZFIPOVO* at early times (i.e., prior to 3000 yr), with this effect then going to zero. This effect results because increasing *SZFIPOVO* increases the time required for the initial releases of mobile species such as ^{99}Tc to reach the location of the RMEI. The positive effect associated with *SZGWSPDM* results from increasing the flow velocity in the SZ, which in turn moves radioactive species more rapidly to the location of the RMEI. This effect is especially pronounced at early times (i.e., prior to 2000 yr) because increasing *SZGWSPDM* decreases the time of first arrival of radioactive species at the location of the RMEI. Both *INFIL* and *THERMCON* have small positive effects on *EXPDOSE* at early times (i.e., prior to 3000 yr). These effects are possibly related to the influence of these variables on repository temperature and hence the time at which release from the EBS can begin. Specifically, increasing *INFIL* and *THERMCON* tends to reduce EBS temperatures and thus reduce the time at which releases from the EBS can begin. After 3000 yr, *THERMCON* has no effect on *EXPDOSE*; however, *INFIL* continues to have a small effect, probably resulting from increased water flow through the EBS and UZ that results as *INFIL* increases in value.

More detailed sensitivity analyses for *EXPDOSE* are provided by the regression analyses in Figure K5.7.1-2a[a]. The dominant effect of *PROBDSEF* on the uncertainty in *EXPDOSE* is indicated by R^2 values of 0.70, 0.71 and 0.63 for the regressions containing only *PROBDSEF* at 3000, 5000 and 10,000 yr. After *PROBDSEF*, the most important variable is *SEEPUNC*. However the incremental effect associated with *SEEPUNC* is small as the R^2 values for the regression models containing both *PROBDSEF* and *SEEPUNC* are 0.77 and 0.78 at 3000 and 5000 yr, respectively.

After *PROBDSEF* and *SEEPUNC*, smaller effects are indicated for a number of variables (Figure K5.7.1-2a[a]). For example, the following additional variables are indicated as affecting *EXPDOSE* at 10,000 yr: *INFIL*, *SEEPPRM* (mean fracture permeability in lithophysal rock units, m^2; as sampled, *SEEPPRM* is actually the logarithm of the indicated permeability), *ALPHAL* (capillary strength parameter in lithophysal rock units), *SZCOLRAL* (colloid retardation factor in alluvial unit of SZ, dimensionless; as sampled, *SZCOLRAL* is actually the logarithm of the indicated retardation factor), *MICPU239* (dose conversion factor for ^{239}Pu for modern interglacial climate, (rem/yr)/(pCi/L)), *CPUCOLWF* (concentration of irreversibly attached plutonium on stable glass/waste form colloids, mol/L), *SEEPPRMN* (mean fracture permeability in nonlithophysal rock units, m^2; as sampled, *SEEPPRMN* is actually the logarithm of the indicated permeability), *RHMU0* (scale factor used to represent uncertainty in chloride concentration in drift waters for relative humidities in the range [0, 0.2]; as sampled, *RHMU0* is actually the logarithm of the indicated scale factor), *SMECSA* (specific surfaces area for smectite colloids, m^2/g), *SZGWSPDM* (groundwater specific discharge multiplier; as sampled, *SZGWSPDM* is actually the logarithm of the indicated multiplier), *UZFAG4* (fracture aperture for Group 4 rock units in UZ), and *EP1LOWPU* (scale factor used to incorporate uncertainty into plutonium solubility under low ionic strength conditions; as sampled, *EP1LOWPU* is actually the logarithm of the indicated scale factor). Specifically, the positive effects associated with *INFIL* and *SEEPUNC* result from increasing water flux through the EBS; the negative effects associated with *SEEPPRM*, *SEEPPRMN* and *ALPHAL* result from increasing water diversion around the EBS; the negative effect associated with *SZCOLRAL* results from increasing colloid

retardation in the SZ; the positive effect associated with *MICPU239* results from increasing the received dose for a given exposure to ^{239}Pu (and possibly other radionuclides due to positive correlations that exist between uncertain dose factors); the positive effect associated with *CPUCOLWF* results from increasing the amount of plutonium attached to colloids; and the remaining variables have very small effects that may be real or may be spurious.

The dominant effect of *PROBDSEF* is readily apparent in the scatterplot in Figure K5.7.1-2b[a]. Further, the smaller effects of *INFIL* and *SEEPUNC* can be seen in the scatterplots in Figure K5.7.1-2b,c[a].

Two of the variables identified in the analysis with PRCCs (i.e., *SZFIPOVO*, *THERMCON*) in Figure K5.7.1-1c[a] do not appear in the regressions in Figure K5.7.1-2a[a]. However, the times at which these variables have identifiable effects on *EXPDOSE* in Figure K5.7.1-1c[a] are not the times at which the regressions in Figure K5.7.1-2a[a] are performed.

Expected Dose to RMEI over [0, 1,000,000 yr]: *EXPDOSE*. The uncertainty and sensitivity analyses for expected dose to the RMEI (*EXPDOSE*, mrem/yr) over the time interval [0, 1,000,000 yr] resulting from early DS failure are summarized in Figures K5.7.1-3[a] and K5.7.1-4[a]. Specifically, Figures K5.7.1-3[a] and K5.7.1-4[a] have the same structure as Figures K5.7.1-3 and K5.7.1-4 but present results calculated with version 5.005 of the TSPA-LA Model rather than with version 5.000 used in the calculation of the results in Figures K5.7.1-3 and K5.7.1-4. A comparison of the results in Figures K5.7.1-3a[a] and K5.7.1-3a obtained with the two versions of the TSPA-LA Model is provided in Figures 7.3.1-21[a] and 7.3.1-23[a]; discussion of the differences in the results is provided in Section 7.3.1.5.2[a]. As examination of Figures 7.3.1-21[a] and 7.3.1-23[a] shows, there is little difference in the values for *EXPDOSE* obtained with the two versions of the TSPA-LA Model. Consistent with this comparison, there is also little difference in the sensitivity analysis results presented in Figures K5.7.1-3c and K5.7.1-4 for version 5.000 and the corresponding results presented in Figures K5.7.1-3c[a] and K5.7.1-4[a] for version 5.005. As a result, the discussion presented in Section K5.7.1 for *EXPDOSE* over the time interval [0, 1,000,000 yr] resulting from early DS failure for results obtained with version 5.000 of the TSPA-LA Model also applies to the results obtained with version 5.005 of the TSPA-LA Model. For this reason, no additional discussion is provided.

For reader convenience, the following discussion of the expected dose results in Figures K5.7.1-3[a] and K5.7.1-4[a] is provided. This discussion updates the corresponding material in Section K5.7.1 from the parent report.

The uncertainty and sensitivity analyses for expected dose to the RMEI (*EXPDOSE*, mrem/yr) over the time interval [0, 1,000,000 years] resulting from early DS failure are summarized in Figures K5.7.1-3[a] and K5.7.1-4[a]. The time dependent results for *EXPDOSE* tend to decrease until about 200,000 yr and then level off (Figure K5.7.1-3-a,b[a]). This decrease is due to the decay of ^{239}Pu, which has a half life of 24,100 yr, and is the largest contributor to expected dose before 200,000 yr (Figure 8.2-4[a]). The values for *EXPDOSE* are bounded above by 0.01 mrem/yr and, after 200,000 yr, by 0.001 mrem/yr.

The sensitivity analyses for the time interval [0, 1,000,000 yr] are similar to those for the time interval [0, 20,000 yr]. Specifically, the sensitivity analysis with PRCCs for [0, 1,000,000 yr] in

Figure K5.7.1-3c[a] identifies the following variables as influencing the uncertainty in *EXPDOSE*: *PROBDSEF* (probability that a randomly selected DS will experience an early failure), *SEEPPRM* (mean fracture permeability in lithophysal rock units, m^2; as sampled, *SEEPPRM* is actually the logarithm of the indicated permeability), *INFIL* (infiltration level), *SZFIPOVO* (flowing interval porosity in the volcanic unit of the SZ), *SZGWSPDM* (groundwater specific discharge multiplier; as sampled, *SZGWSPDM* is actually the logarithm of the indicated multiplier), and *SEEPUNC* (pointer variable used to determine local seepage rates). Similarly, the sensitivity analysis with PRCCs for [0, 20,000 yr] in Figure K5.7.1-1c[a] identifies the following variables as influencing the uncertainty in *EXPDOSE*: *PROBDSEF*, *SZFIPOVO*, *SZGWSPDM*, *SEEPUNC*, *INFIL*, and *THERMCON* (host rock thermal conductivity level). For both time periods, *PROBDSEF* is the dominant contributor to the uncertainty in *EXPDOSE*, with the other variables making much smaller contributions to the uncertainty in *EXPDOSE*. The PRCC plots are constrained to contain a maximum of 6 variables. As a result, the slight differences in the variables shown in Figures K5.7.1-1c[a] and K5.7.1-3c[a] result from slight variations in the importance of individual variables over the time intervals under consideration.

More detailed sensitivity analyses for the time interval [0, 1,000,000 yr] are provided by the regressions in Figure K5.7.1-4a[a]. Similar to the regressions for [0, 20,000 yr] in Figure K5.7.1-2a[a], the dominant variable is *PROBDSEF*. Specifically, the dominant effect of *PROBDSEF* on the uncertainty in *EXPDOSE* is indicated by R^2 values of 0.47, 0.55 and 0.52 for the regressions containing only *PROBDSEF* at 50,000, 200,000 and 500,000 yr. These values are lower than the corresponding R^2 values of 0.70, 0.71 and 0.63 obtained in the analyses in Figure K5.7.1-2a[a] at 3000, 5000 and 10,000 yr, which suggests that more variables are having small effects on the uncertainty in *EXPDOSE* at later times than is the case for the first 20,000 yr. This is borne out by the large number of variables indicated as having small effects on *EXPDOSE* in the regression analyses in Figure K5.7.1-4a[a]. After *PROBDSEF*, the next most important variable in the three regressions is either *SZGWSPDM* or *INFIL*, with *EXPDOSE* tending to increase as *INFIL* increases as a result of increased water flow through the EBS and UZ and also to increase as *SZGWSPDM* increases as a result of increased water flow in the SZ. Together, the first two selected variables result in regressions with R^2 values of 0.55, 0.63 and 0.63 at 50,000, 200,000 and 500,000 yr.

After the first two variables, the three regressions select a subset of *INFIL*, *SEEPPRM*, *SZGWSPDM*, *EP1LOWPU* (scale factor used to incorporate uncertainty into plutonium solubility under low ionic strength conditions; as sampled, *EP1LOWPU* is actually the logarithm of the indicated scale factor), and *SEEPUNC* as the next three variables to add to the regression models (Figure K5.7.1-4a[a]). Addition of these three variables brings the R^2 values up to 0.73, 0.77 and 0.75 at 50,000, 200,000 and 500,000 yr. As previously discussed, *INFIL* has positive effect on *EXPDOSE* as a result of increasing water flow through the EBS and UZ; *SEEPPRM* has a negative effect on *EXPDOSE* as a result of increasing water flow around the EBS and thus reducing water flow through the EBS; *EP1LOWPU* has a positive effect on *EXPDOSE* as a result of increasing the solubility of plutonium in the EBS; *SZGWSPDM* has a positive effect on *EXPDOSE* as a result of speeding up flow in the SZ; and *SEEPUNC* has a positive effect on *EXPDOSE* as a result of increasing water flow through the EBS.

After the first five variables, the regressions at 50,000, 200,000 and 500,000 yr add 8, 11 and 11 additional variables, respectively, and produce models with R^2 values of 0.82, 0.86 and 0.87 (Figure K5.7.1-4a[a]). Thus, as noted earlier, a large number of variables are having small effects on the uncertainty in *EXPDOSE* at later times.

The dominant effect of *PROBDSEF* on the uncertainty in *EXPDOSE* can also been seen in the scatterplot in Figure K5.7.1-4b[a]. In contrast, the much smaller effects of *INFIL* and *SEEPPRM* on the uncertainty in *EXPDOSE* can been in the scatterplots in Figure K5.7.1-4c,d[a].

K5.7.2[a] Early Failure Scenario Classes: Expected Dose to Reasonably Maximally Exposed Individual (RMEI) from Early Waste Package (WP) Failure

Expected Dose to RMEI over [0, 20,000 yr]: *EXPDOSE*. The uncertainty and sensitivity analyses for expected dose to the RMEI (*EXPDOSE*, mrem/yr) over the time interval [0, 20,000 yr] resulting from early WP failure are summarized in Figures K5.7.2-1[a] and K5.7.2-2[a]. Specifically, Figures K5.7.2-1[a] and K5.7.2-2[a] have the same structure as Figures K5.7.2-1 and K5.7.2-2 but present results calculated with version 5.005 of the TSPA-LA Model rather than with version 5.000 used in the calculation of the results in Figures K5.7.2-1 and K5.7.2-2. A comparison of the results in Figures K5.7.2-1a[a] and K5.7.2-1a obtained with the two versions of the TSPA-LA Model is provided in Figures 7.3.1-24[a] and 7.3.1-26[a]; discussion of the differences in the results is provided in Section 7.3.1.5.3[a]. As examination of Figures 7.3.1-24[a] and 7.3.1-26[a] shows, there is little difference in the values for *EXPDOSE* obtained with the two versions of the TSPA-LA Model. Consistent with this comparison, there is also little difference in the sensitivity analysis results presented in Figures K5.7.2-1c and K5.7.2-2 for version 5.000 and the corresponding results presented in Figures K5.7.2-1c[a] and K5.7.2-2[a] for version 5.005. As a result, the discussion presented in Section K5.7.2 for *EXPDOSE* over the time interval [0, 20,000 yr] resulting from early WP failure for results obtained with version 5.000 of the TSPA-LA Model also applies to the results obtained with version 5.005 of the TSPA-LA Model. For this reason, no additional discussion is provided.

For reader convenience, the following discussion of the expected dose results in Figures K5.7.2-1[a] and K5.7.2-2[a] is provided. This discussion updates the corresponding material in Section K5.7.2 from the parent report.

The uncertainty and sensitivity analyses for expected dose to the RMEI (*EXPDOSE*, mrem/yr) over the time interval [0, 20,000 yr] resulting from early WP failure are summarized in Figures K5.7.2-1[a] and K5.7.2-2[a]. There are sharp peaks in *EXPDOSE* between 1000 and 2000 yr resulting from the release of ^{99}Tc from the failure of CDSP WPs (Figure K5.7.2-1a,b[a]). At the time of these peaks, maximum values for *EXPDOSE* are in the vicinity of 0.1 mrem/yr, although the values for most sample elements are considerably smaller. After these initial early peaks, *EXPDOSE* has values in a range from approximately 10^{-5} to 10^{-2} mrem/yr until a time of about 10,000 yr.

Between approximately 9000 and 14,000 yr, there are sharp jumps in the values for *EXPDOSE* (Figure K5.7.2-1a,b[a]). These jumps result from the arrival of radionuclide releases at the location of the RMEI that result from the failure of CSNF WPs. The CSNF WPs are hotter than the CDSP WPs, with the result that releases from CSNF WPs are delayed until both the WP

temperature falls below 100°C and the relative humidity interior to these packages reaches 95 percent, at which time diffusive transport begins. The jumps in *EXPDOSE* correspond to the arrival of ^{99}Tc at the location of the RMEI (Figure 8.2-6a[a]). After these jumps, the values for *EXPDOSE* again decrease as the pulse of ^{99}Tc passes.

This bimodal behavior of *EXPDOSE* with different peaks for the two waste types does not occur for early DS failure (compare Figures K5.7.1-1a,b[a] and K5.7.2-1a,b[a]). Early DS failure is assumed to result in WP failure only if the failed DS is experiencing seepage; otherwise, there is no WP failure and hence no radionuclide release. Because all failed WPs are in seepage environments, water flows into every failed WP as soon as WP temperature falls below 100°C and advective transport occurs immediately, with the result that there is little temporal variability in the start of radionuclide releases from the EBS for different WP types.

The PRCCs in Figure K5.7.2-1c[a] indicate that the uncertainty in *EXPDOSE* is dominated by *PROBWPEF* (probability that a randomly selected WP will experience an early failure), with the value for *EXPDOSE* increasing as *PROBWPEF* increases. This effect results because increasing *PROBWPEF* increases the expected number of WPs that experience early failure and hence increases *EXPDOSE*. The PRCCs for *PROBWPEF* decrease in value over the period from approximately 9000 to 14,000 yr because of the noise introduced into the analysis as a result of the pulse releases arriving from the failed CSNF WPs.

In addition to *PROBWPEF*, smaller effects are indicated for *SZFIPOVO* (flowing interval porosity in the volcanic unit of the SZ), *THERMCON* (host rock thermal conductivity level), *INFIL* (infiltration level), *SZGWSPDM* (groundwater specific discharge multiplier; as sampled, *SZGWSPDM* is actually the logarithm of the indicated multiplier), and *DSNFMASS* (scale factor used to characterize uncertainty in the amount of DSNF contained in CDSP WPs) (Figure K5.7.2-1c[a]). The effects of *SZFIPOVO*, *INFIL*, and *SZGWSPDM* are the same as previously discussed in conjunction with Figure K5.7.1-1c[a]. The effect of *THERMCON* is similar, although more pronounced. Increasing *THERMCON* leads to lower drift temperatures and earlier arrival of seepage waters, and thus to earlier beginning of diffusive transport. This effect is evident in the positive correlation between *THERMCON* and *EXPDOSE* between 0 yr and 1500 yr. However, between 2500 yr and 9500 yr, the correlation becomes negative. This change in correlation results from the effect of temperature on waste form degradation. Increasing temperature increases the dissolution rate of the HLW in CDSP WPs (BSC 2004 [DIRS 169988], Section 6.5.2.1). Consequently, as *THERMCON* increases, temperatures decrease and HLW degradation slows, resulting in less radionuclides available for mobilization and transport, and in turn reducing *EXPDOSE*. This pattern repeats for the CSNF waste, which starts diffusive transport at about 9500 yr. The positive effect associated with *DSNFMASS* results from increasing the amount of ^{99}Tc in CDSP WPs and hence the dose from ^{99}Tc that results from the failure of these WPs.

More detailed sensitivity analyses for *EXPDOSE* are provided by the regression analyses in Figure K5.7.2-2a[a]. The dominant effect of *PROBWPEF* on the uncertainty in *EXPDOSE* is indicated by R^2 values of 0.62, 0.77 and 0.47 for the regressions containing only *PROBWPEF* at 3000, 5000 and 10,000 yr.

As for the PRCCs for *PROBWPEF* in Figure K5.7.2-1c[a], the R^2 value for the regression at 10,000 years decreases in value as a result of the noise introduced into the analysis by the pulse releases arriving from the failed CSNF WPs over the period from approximately 9000 to 14,000 yr. Because of this noise, the final regression model at 10,000 has an R^2 value of 0.71; in contrast, the analyses at 3000 and 5000 yr have final R^2 values of 0.80 and 0.89. However, a clearer view of what is driving the uncertainty in *EXPDOSE* at 10,000 yr is provided by the scatterplots in Figure K5.7.2-2b,c,d[a]. Specifically, the uncertainty in *EXPDOSE* is still clearly dominated by *PROBWPEF* (Figure K5.7.2-2b[a]), with smaller contributions to this uncertainty from *INFIL* (Figure K5.7.2-2c[a]) and *THERMCON* (Figure K5.7.2-2d[a]). The scatterplot for *PROBWPEF* (Figure K5.7-2b[a]) shows an interesting pattern in that it contains two separate populations of points that each increase monotonically with *PROBWPEF*. The upper population of points consists of realizations in which the CSNF WPs in one or more percolation bins have begun diffusive transport (relative humidity interior to the WP exceeds 95 percent) by 10,000 yr. Because infiltration rates and temperatures vary between percolation bins, the time at which diffusive transport begins also varies, with most CSNF WPs beginning diffusive transport between 9000 yr and 14,000 yr, whereas CDSP WPs begin diffusive transport between 500 yr and 3000 yr. The differences are also apparent in Figure K5.7.2-1a[a] as two jumps in expected dose corresponding to the occurrence of dose from each of the two WP types.

Figure K5.7.2-2c[a] indicates that the expected dose at 10,000 yr decreases as *INFIL* increases. As *INFIL* increases, percolation rates tend to increase in most percolation bins, leading to earlier arrival of seepage into a drift. Because increased infiltration also leads to lower temperatures, and at lower drift temperatures, the difference in relative humidity on WPs of different temperatures becomes more pronounced, increasing infiltration results in the counter-intuitive effect that the warmer WPs (CSNF WPs) have lower relative humidity at higher values of infiltration. These lower values of relative humidity are less likely to permit diffusive transport, which in turn yields a negative relationship between *INFIL* and expected dose at 10,000 years. The relationship between infiltration, temperature and relative humidity is described and documented in Multiscale Thermohydrologic Model (SNL 2007 [DIRS 181383]).

Figure K5.7.2-2c[a] indicates that expected dose at 10,000 yr slightly increases as *THERMCON* increases. This correlation is valid at 10,000 yr because at this time CSNF WPs are just beginning diffusive transport, so the correlation indicates the positive relationship between *THERMCON* and *EXPDOSE* described above. If the correlation were to be performed at later times, after transport has begun, the relationship between *THERMCON* and *EXPDOSE* would be reversed, because at these times *THERMCON* is affecting waste degradation rates, as described above.

In contrast, more informative results are given by the regression analyses at 3000 and 5000 years without the added need to examine scatterplots (Figure K5.7.2-2a[a]). Specifically, both indicated regressions select the following four variables after *PROBWPEF*: *MICTC99* (dose conversion factor for ^{99}Tc for modern interglacial climate, (rem/yr)/(pCi/L)), *MICC14* (dose conversion factor for ^{14}C for modern interglacial climate, (rem/yr)/(pCi/L)), *DSNFMASS*, and *UZFAG8* (fracture aperture for Group 8 rock units in UZ). Increasing *MICTC99* and *MICC14* has a positive effect on *EXPDOSE* that results from increasing the received dose for a given exposure level; increasing *DSNFMASS* has a positive effect on *EXPDOSE* that results from increasing the amount of radionuclides in CDSP WPs and hence the dose that results from the

failure of these WPs; and increasing *UZFAG8* has a negative effect on *EXPDOSE* that results from decreasing the proportion of radionuclides moving through fractures in the UZ. Specifically, increasing *UZFAG8* increases the proportion of the interface area between the EBS and the UZ that consists of fractures, which increases the mass of radionuclides that diffuse into fractures in the UZ, where radionuclide movement is relatively rapid, and decreases the mass of radionuclides that diffuse into the surrounding rock matrix, where radionuclide movement is slower. Collectively, the inclusion of *MICTC99*, *MICC14*, *DSNFMASS* and *UZFAG8* increases the R^2 values for the two regressions to 0.74 and 0.86. After *MICTC99*, *MICC14*, *DSNFMASS* and *UZFAG8*, the regressions add an additional six and eight variables, respectively, that have small effects and result in final models that have R^2 values of 0.80 and 0.89. The regression models at 3000 yr tend to have smaller R^2 values than the regression models at 5000 yr because of the noise introduced by the arrival of the ^{99}Tc releases (i.e., compare the smoothness of the time-dependent releases at 3000 and 5000 yr in Figure K5.7.2-2a,b[a]).

Expected Dose to RMEI over [0, 1,000,000 yr]: *EXPDOSE*. The uncertainty and sensitivity analyses for expected dose to the RMEI (*EXPDOSE*, mrem/yr) over the time interval [0, 1,000,000 yr] resulting from early WP failure are summarized in Figures K5.7.2-3[a] and K5.7.2-4[a]. Specifically, Figures K5.7.2-3[a] and K5.7.2-4[a] have the same structure as Figures K5.7.2-3 and K5.7.2-4 but present results calculated with version 5.005 of the TSPA-LA Model rather than with version 5.000 used in the calculation of the results in Figures K5.7.2-3 and K5.7.2-4. A comparison of the results in Figures K5.7.2-3a[a] and K5.7.2-3[a] obtained with the two versions of the TSPA-LA Model is provided in Figures 7.3.1-25[a] and 7.3.1-27[a]; discussion of the differences in the results is provided in Section 7.3.1.5.3[a]. As examination of Figures 7.3.1-25[a] and 7.3.1-27[a] shows, there is little difference in the values for *EXPDOSE* obtained with the two versions of the TSPA-LA Model. Consistent with this comparison, there is also little difference in the sensitivity analysis results presented in Figures K5.7.2-3c and K5.7.2-4 for version 5.000 and the corresponding results presented in Figures K5.7.2-3c[a] and K5.7.2-4[a] for version 5.005. As a result, the discussion presented in Section K5.7.2 for *EXPDOSE* over the time interval [0, 1,000,000 yr] resulting from early WP failure for results obtained with version 5.000 of the TSPA-LA Model also applies to the results obtained with version 5.005 of the TSPA-LA Model. For this reason, no additional discussion is provided.

For reader convenience, the following discussion of the expected dose results in Figures K5.7.2-3[a] and K5.7.2-4[a] is provided. This discussion updates the corresponding material in Section K5.7.2 from the parent report.

The uncertainty and sensitivity analyses for expected dose to the RMEI (*EXPDOSE*, mrem/yr) over the time interval [0, 1,000,000 yr] resulting from early WP failure are summarized in Figures K5.7.2-3[a] and K5.7.2-4[a].

Except for a few sample elements, the values for *EXPDOSE* fall between 10^{-6} and 0.1 mrem/yr for the 0 to 1,000,000 yr time interval (Figure K5.7.2-3a[a]). For most sample elements, the values for *EXPDOSE* monotonically decrease until about 300,000 yr, at which time they show a sharp increase in value as the result of the failure of the DSs from general corrosion (Figure 8.1-4[a]). This failure allows seeping water to directly contact the failed WPs, and as a consequence, produces larger radionuclide releases from the failed WPs.

The single most important variable with respect to the uncertainty in *EXPDOSE* is *PROBWPEF* (probability that a randomly selected WP will experience an early failure), with the value for *EXPDOSE* increasing as *PROBWPEF* increases. This effect results because increasing *PROBWPEF* increases the expected number of WPs that experience early failure and hence increases *EXPDOSE* (Figures K5.7.2-3c[a] and K5.7.2-4a[a]). The positive effect of *PROBWPEF* can be seen in the scatterplot in Figure K5.7.2-4b[a].

Prior to 300,000 yr, *ISCSNS* (pointer variable used to determine ionic strength in CSNF cell under vapor influx conditions) and *SZGWSPDM* (groundwater specific discharge multiplier; as sampled, *SZGWSPDM* is actually the logarithm of the indicated multiplier) also have significant positive effects on the uncertainty in *EXPDOSE* (Figures K5.7.2-3c[a] and K5.7.2-4a[a]). These effects result because increasing *ISCSNS* increases plutonium solubility, and increasing *SZGWSPDM* increases water flow in the SZ. After 300,000 yr, *INFIL* (infiltration level) is indicated as having a positive effect on *EXPDOSE* (Figures K5.7.2-3c[a] and K5.7.2-4a[a]). This effect results because increasing *INFIL* increases water flow in the EBS and UZ. After *PROBWPEF*, *ISCSNS*, *SZGWSPDM* and *INFIL*, the analyses identify a number of additional variables that have small effects on *EXPDOSE*.

K5.7.3[a] Early Failure Scenario Classes: Expected Dose to Reasonably Maximally Exposed Individual (RMEI) from Both Early Drip Shield (DS) Failure and Early Waste Package (WP) Failure

No change.

K5.7.4[a] Early Failure Scenario Classes: Expected Dose to Reasonably Maximally Exposed Individual (RMEI) from Early Drip Shield (DS) Failure, Early Waste Package (WP) Failure, and Nominal Processes

No change.

K6[a] IGNEOUS SCENARIO CLASSES

No change.

K6.1[a] Igneous Scenario Classes: Summary

No change.

K6.2[a] Igneous Intrusive Scenario Classes: Engineered Barrier System (EBS) Conditions over the Time Interval [0, 1,000,000 yr] for an Event at 250 years

No change.

K6.3[a] Igneous Intrusive Scenario Classes: Release from Engineered Barrier System (EBS)

No change.

K6.3.1[a] Igneous Intrusive Scenario Classes: Release from Engineered Barrier System (EBS) over the Time Interval [0, 20,000 yr] for an Event at 10 years

No change.

K6.3.2[a] Igneous Intrusive Scenario Classes: Release from Engineered Barrier System (EBS) over the Time Interval [0, 1,000,000 yr] for an Event at 250 years

Results from TSPA-LA Model v5.000 determined that ^{226}Ra was the dominant contributor to the expected (mean) dose to the RMEI for the Igneous Intrusive Scenario Class (Figure 8.2-8). However, analysis determined that the contribution to expected (mean) dose from ^{226}Ra was due to an unconstrained distribution describing the uncertainty in longitudinal dispersivity (LDISP in Table K3-1), (see Appendix P, Section P15). For TSPA-LA Model v5.005, the uncertainty distribution for longitudinal dispersivity was constrained so that values sampled from this distribution would be physically meaningful (Section 6.3.10.2[a]). Because of this change, and because of the importance of ^{226}Ra to expected (mean) dose, additional sensitivity analyses are presented for the transport of radionuclides in the decay chain for ^{226}Ra, namely ^{234}U, ^{230}Th and ^{226}Ra, for the Igneous Intrusive Scenario Class.

Movement of Dissolved ^{234}U: *ESU234* and *ESU234C*. The uncertainty and sensitivity analyses for the time-dependent release rates (*ESU234*, g/yr) and cumulative releases (*ESU234C*, g) over the time interval [0, 1,000,000 yr] for the movement of dissolved ^{234}U from the EBS to the UZ resulting from an igneous intrusive event at 250 years that destroys all WPs in the repository are summarized in Figures K6.3.2-5[a] and K6.3.2-6[a].

The dominant contributors to the uncertainty in *ESU234* and *ESU234C* are *EP1LOWOU* (scale factor used to incorporate uncertainty into uranium solubility under low ionic strength conditions after an igneous intrusive event; as sampled, *EP1LOWOU* is actually the logarithm of the indicated scale factor), *GOESITED* (density of sorption sites on goethite, sites/nm^2), and *INFIL* (infiltration level) (Figures K6.3.2-5e,f[a] and K6.3.2-6a,b[a]). The variables *EP1LOWOU* and *INFIL* have positive effects on *ESU234* and *ESU234C* because increasing *EP1LOWOU* increases uranium solubility and increasing *INFIL* increases water flow through the EBS. In contrast, increasing *GOESITED* has a negative effect on *ESU234* and *ESU234C* as a result of increasing the sorption of uranium onto corrosion products. All the regression models select *EP1LOWOU* and *INFIL* as the first two variables and have R^2 values between 0.48 and 0.64 with the inclusion of these two variables (Figure K6.3.2-6a,b[a]).

In addition to *EP1LOWOU, GOESITED* and *INFIL*, generally smaller but significant effects are also indicated for *PHCSS* (pointer variable used to determine pH in CSNF cell 1 under liquid influx conditions), *CORRATSS* (corrosion rate for stainless steel, μm/yr), and *HFOSA* (surface area for hydrous ferrous oxide, m^2/g) (Figures K6.3.2-5e,f[a] and K6.3.2-6a,b[a]). The positive effect associated with *PHCSS* results because increasing *PHCSS* increases uranium solubility, and the negative effects associated with *CORRATSS* and *HFOSA* result because increasing these variables increases uranium sorption on corrosion products. The effect on *ESU234* associated with *CORRATSS* varies with time, because while stainless steel is corroding, corrosion products are increasing and the sorption of uranium on the corrosion products reduces the release rate of uranium. However, once corrosion of stainless steel has ceased (roughly at 200,000 yr),

additional corrosion materials are not subsequently produced, so the release rate of uranium is controlled by factors other than the rate at which the corrosion products are generated.

The effects of *EP1LOWOU, GOESITED, INFIL* and *PHCSS* on *ESU234* and *ESU234C* can be seen in the scatterplots in Figure K6.3.2-6 c,d,e,f,g,h[a]. In particular, the dominant positive effect of *EP1LOWPU* is apparent in Figure K6.3.2-6 c,f[a].

A number of additional variables that have small effects on *ESU234* and *ESU234C* are also identified at the latter stages of the stepwise regressions in Figure K6.3.2-6a,b[a]. The final regression models in Figure K6.3.2-6a,b[a] have R^2 values between 0.75 and 0.81. Thus, most of the uncertainty in *ESU234* and *ESU234C* is being accounted for.

Movement of ^{230}Th: *ESTH230* and *ESTH230C*. The uncertainty and sensitivity analyses for the time-dependent release rates (*ESTH230*, g/yr) and cumulative releases (*ESTH230C*, g) over the time interval [0, 1,000,000 yr] for the movement of dissolved and reversible attached ^{230}Th from the EBS to the UZ resulting from an igneous intrusive event at 250 years that destroys all WPs in the repository are summarized in Figures K6.3.2-7[a] and K6.3.2-8[a].

The dominant contributors to the uncertainty in *ESTH230* and *ESTH230C* are *INFIL* (infiltration level), *COLGW* (concentration of groundwater colloids when colloids are stable, mg/L), *KDTHSMEC* (distribution coefficient for reversible sorption of thorium to waste form, i.e., smectite, colloids, mL/g), *PHCSS* (pointer variable used to determine pH in CSNF cell 1 under liquid influx conditions), *EP1LOWTH* (scale factor used to incorporate uncertainty into thorium solubility at an ionic strength below 1 molal; as sampled, *EP1LOWTH* is actually the logarithm of the indicated scale factor), and *UZKDTHDT* (sorption coefficient for thorium in devitrified tuff units of UZ, mL/g; also used as sorption coefficient for thorium in ballast in EBS) (Figures K6.3.2-7e,f[a] and K6.3.2-8a,b[a]). The variables *INFIL, COLGW, KDTHSMEC, PHCSS* and *EP1LOWTH* have positive effects on *ESTH230* and *ESTH230C* because (1) increasing *INFIL* increases water flow through the EBS, (2) increasing *COLGW* and *KDTHSMEC* increases the amount of thorium sorbed to colloids, and (3) increasing *PHCSS* and *EP1LOWTH* increases the solubility of thorium. In contrast, increasing *UZKDTHDT* has a negative effect on *ESTH230* and *ESTH230C* as a result of increasing the sorption of uranium onto the ballast used in the EBS.

In addition to *INFIL, COLGW, KDTHSMEC, PHCSS, EP1LOWTH* and *UZKDTHDT*, the stepwise regression analyses identify several additional variables that have small effects on *ESTH230* and *ESTH230C* (Figure K6.3.2-8a,b[a]). The final regression models contain from 9 to 12 variables and have R^2 values between 0.64 and 0.72. To some extent, the regression models are probably being challenged by the difficulty of capturing effects that derive from the decay of ^{234}U to ^{230}Th, as well as relationships between concentrations of radionuclides proscribed by the regression model for surface complexation and sorption onto corrosion products (SNL 2007 [DIRS 177407], Section 6.5.2.4). In particular, the positive influence of *EP1LOWOU* (scale factor used to incorporate uncertainty into uranium solubility under low ionic strength conditions after an igneous intrusive event; as sampled, *EP1LOWOU* is actually the logarithm of the indicated scale factor) on *ESTH230* and *ESTH230C* (Figure K6.3.2-8a,b[a]) results from both the decay of ^{234}U to ^{230}Th, as well as the negative relationship between the

concentration of dissolved uranium and the concentration of thorium sorbed to corrosion products (SNL 2007 [DIRS 177407], Table 6.5-14).

Overall, the three dominant variables are *INFIL, COLGW* and *KDTHSMEC*. The positive effects associated with these variables can be seen in the scatterplots in Figure K6.3.2-8c,d,e,f,g,h[a]).

The PRCCs for *COLGW* are somewhat larger than the PRCCs for *INFIL*. In contrast, all the stepwise regression analyses except one select *INFIL* first and then *COLGW*. This slight inconsistency possibly results because there is a rank correlation of 0.078 between *INFIL* and *COLGW* in the sample in use. In addition, both *INFIL* and *COLGW* have rank correlations with other variables that are as high as 0.18 in absolute value. It is possible that some of these correlations could also be affecting the PRCCs in Figure K6.3.2-7e,f[a]; also, the fact that *INFIL* is a discrete variable with only four levels could be affecting the analysis. However, as is evident from the scatterplots in Figure K6.3.2-8ac,d,f,g[a]), both *ESTH230* and *ESTH230C* tend to increase as *INFIL* and *COLGW* increase.

Movement of Dissolved ^{226}Ra: *ESRA226* and *ESRA226C*. The uncertainty and sensitivity analyses for the time-dependent release rates (*ESRA226*, g/yr) and cumulative releases (*ESRA226C*, g) over the time interval [0, 1,000,000 yr] for the movement of dissolved ^{226}Ra from the EBS to the UZ resulting from an igneous intrusive event at 250 years that destroys all WPs in the repository are summarized in Figures K6.3.2-9[a] and K6.3.2-10[a].

The dominant contributors to the uncertainty in *ESRA226* and *ESRA226C* are *UZKDCSDT* (sorption coefficient for cesium and radium in devitrified tuff units of UZ, mL/g; also used as sorption coefficient for cesium and radium in ballast in EBS), *INFIL* (infiltration level), and *COLGW* (concentration of groundwater colloids when colloids are stable, mg/L) (Figures K6.3.2-9e,f[a] and K6.3.2-10a,b[a]). The negative effects associated with *UZKDCSDT* and *COLGW* result because (i) increasing *UZKDCSDT* increases the sorption of ^{226}Ra to ballast material in the EBS and thus increases the loss of ^{226}Ra in the EBS as the result of decay and (ii) increasing *COLGW* increases the removal of ^{230}Th attached to colloids from the EBS and thus reduces the production of ^{226}Ra from the decay of ^{230}Th. The positive effect associated with *INFIL* results from increasing water flow through the EBS.

Similarly to *COLGW*, the negative effects on *ESRA226* and *ESRA226C* associated with *KDTHSMEC* (distribution coefficient for reversible sorption of thorium to waste form, i.e., smectite, colloids, mL/g), *PHCSS* (pointer variable used to determine pH in CSNF cell 1 under liquid influx conditions), and *EP1LOWOU* (scale factor used to incorporate uncertainty into uranium solubility under low ionic strength conditions after an igneous intrusive event; as sampled, *EP1LOWOU* is actually the logarithm of the indicated scale factor) result from increasing the removal of the parent and grandparent of ^{226}Ra from the EBS. Specifically, increasing *KDTHSMEC* increases the removal of ^{230}Th attached to waste form colloids; increasing *PHCSS* increases the solubility of uranium, thorium and radium; and increasing *EP1LOWOU* increases the solubility of uranium. In contrast, *CSNFMASS* (scale factor used to characterize uncertainty in amount of CSNF in CSNF WPs), *DSNFMASS* (scale factor used to characterize uncertainty in amount of DSNF in DSNF WPs), and *GOESITED* (density of sorption sites on goethite, sites/nm^2) have positive effects on *ESRA226* and *ESRA226C* because

(i) increasing *CSNFMASS* and *DSNFMASS* increases the amount of waste in the repository and (ii) increasing *GOESITED* increases the amount of ^{234}U and ^{230}Th retained in the EBS.

Overall, the three dominant variables are *UZKDCSDT*, *INFIL* and *COLGW*. The effects associated with these variables can be seen in the scatterplots in Figure K6.3.2-10c,d,e,f,g,h[a]. Of the three, *UZKDCSDT* is clearly the most influential variable.

K6.4[a] Igneous Intrusive Scenario Classes: Release from Unsaturated Zone (UZ)

No change.

K6.4.1[a] Igneous Intrusive Scenario Classes: Release from Unsaturated Zone (UZ) over the Time Interval [0, 20,000 yr] for an Event at 10 years

No change.

K6.4.2[a] Igneous Intrusive Scenario Classes: Release from Unsaturated Zone (UZ) over the Time Interval [0, 1,000,000 yr] for an Event at 250 years

Movement of Dissolved ^{234}U: *UZU234* and *UZU234C*. The uncertainty and sensitivity analyses for the time-dependent release rates (*UZU234*, g/yr) and cumulative releases (*UZU234C*, g) over the time interval [0, 1,000,000 yr] for the movement of dissolved ^{234}U from the UZ to the SZ resulting from an igneous intrusive event at 250 years that destroys all WPs in the repository are summarized in Figures K6.4.2-1[a] and K6.4.2-2[a]. Further, a comparison of the movement of ^{234}U into and out of the UZ is presented in Figure K6.4.2-3[a]. As shown by the results in Figure K6.4.2-3[a], the movement of ^{234}U into the UZ (i.e., *ESU234C*) is effectively the same as the movement of ^{234}U out of the UZ (i.e., *UZU234C*) for the time scales under consideration. Because of this behavior, the uncertainty and sensitivity analysis results in Figures K6.4.2-1[a] and K6.4.2-2[a] for the release of ^{234}U from the UZ to the SZ are essentially the same as the results in Figures K6.3.2-5[a] and K6.3.2-6[a] for the release of ^{234}U from the EBS to the UZ. As a result, the discussion of the results in Figures K6.3.2-5[a] and K6.3.2-6[a] also applies to the results in Figures K6.4.2-1[a] and K6.4.2-2[a].

Movement of Dissolved ^{230}Th: *UZTH230* and *UZTH230C*. The uncertainty and sensitivity analyses for the time-dependent release rates (*UZTH230*, g/yr) and cumulative releases (*UZTH230C*, g) over the time interval [0, 1,000,000 yr] for the movement of dissolved ^{230}Th from the UZ to the SZ resulting from an igneous intrusive event at 250 years that destroys all WPs in the repository are summarized in Figures K6.4.2-4[a] and K6.4.2-5[a]. Further, a comparison of the movement of ^{230}Th into and out of the UZ is presented in Figure K6.4.2-6[a]. As shown by the results in Figure K6.4.2-6[a], the movement of ^{230}Th into the UZ (i.e., *ESU234C*) is related to the movement of ^{230}Th out of the UZ (i.e., *UZU234C*) by a constant fractional shift for the time scales under consideration; specifically, the ratio *UZTH230C* to *ESTH230C* is approximately 0.5 for the results in Figure K6.4.2-6[a]. The reduction occurs primarily because of the spatial variability in UZ transport, specifically, ^{230}Th released into the UZ under the northern part of the repository transits through the UZ relatively rapidly, whereas ^{230}Th released into the UZ under the southern part of the repository is very unlikely to ever leave the UZ (SNL 2008 [DIRS 184748], Figure 6.6.2-7[b]). Because the ratio of *UZTH230C* to

ESTH230C is essentially constant, the uncertainty and sensitivity analysis results in Figures K6.4.2-4[a] and K6.4.2-5[a] for the release of ^{230}Th from the UZ to the SZ are essentially the same as the results in Figures K6.3.2-7[a] and K6.3.2-8[a] for the release of ^{230}Th from the EBS to the UZ. This similarity is particularly evident when the stepwise regression analyses in Figures K6.3.2-8a,b[a] and K6.4.2-5[a] are compared. As a result, the discussion of the results in Figures K6.3.2-7[a] and K6.3.2-8[a] also applies to the results in Figures K6.4.2-4[a] and K6.4.2-5[a].

Movement of Dissolved ^{226}Ra: *UZRA226* and *UZRA226C*. The uncertainty and sensitivity analyses for the time-dependent release rates (*UZRA226*, g/yr) and cumulative releases (*UZRA226C*, g) over the time interval [0, 1,000,000 yr] for the movement of dissolved ^{226}Ra from the UZ to the SZ resulting from an igneous intrusive event at 250 years that destroys all WPs in the repository are summarized in Figures K6.4.2-7[a] and K6.4.2-8[a]. Further, a comparison of the movement of ^{226}Ra into and out of the UZ is presented in Figure K6.4.2-9[a]. As shown by the results in Figure K6.4.2-9[a], the UZ has noticeable effect on the movement of ^{226}Ra from the EBS to the SZ; specifically, the releases of ^{226}Ra out of the UZ are smaller than the releases into the UZ for most sample elements.

The dominant variables affecting the uncertainty in *UZRA226* and *UZRA226C* are *UZKDCSDT* (sorption coefficient for cesium and radium in devitrified tuff units of UZ, mL/g; also used as sorption coefficient for cesium and radium in ballast in EBS), *INFIL* (infiltration level), *UZFAG8* (fracture aperture for Group 8 rock unit in UZ, m), and *UZTORRG3* (tortuosity for Group 3 rock unit in UZ) (Figures K6.4.2-7e,f[a] and K6.4.2-8a,b[a]). The negative effects associated with *UZKDCSDT* and *UZTORRG3* result because (1) increasing *UZKDCSDT* increases the retardation of ^{226}Ra in the EBS and the UZ and (2) increasing *UZTORRG3* increases the complexity of the transport path in the UZ. The positive effects associated with *INFIL* and *UZFAG8* result because (1) increasing *INFIL* increases water flow in both the EBS and UZ and (2) increasing *UZFAG8* increases the amount of ^{226}Ra transported by flow in fractures.

After *UZKDCSDT*, *INFIL*, *UZFAG8* and *UZTORRG3*, the regression analyses identify several additional variables that have small effects on *UZRA226* and *UZRA226C* (Figure K6.4.2-8a,b[a]). Specifically, positive effects are identified for *CSNFMASS* (scale factor used to characterize uncertainty in amount of CSNF in CSNF WPs), *COLGW* (concentration of groundwater colloids when colloids are stable, mg/L), *KDTHSMEC* (distribution coefficient for reversible sorption of thorium to waste form, i.e., smectite, colloids, mL/g), and *UZKDTHDT* (sorption coefficient for thorium in devitrified tuff units of UZ, mL/g; also used as sorption coefficient for thorium in ballast in EBS). These effects result because (1) increasing *CSNFMASS* increases the amount of waste in the repository, (2) increasing *COLGW* and *KDTHSMEC* increases the amount of ^{230}Th that enters the UZ and thus increases the amount of ^{226}Ra that can be produced by decay in the UZ, and (3) increasing *UZKDTHDT* increases the retention of ^{230}Th in the UZ and thus increases the amount of ^{226}Ra that can be produced by decay in the UZ. A negative effect is indicated for *EP1LOWOU* (scale factor used to incorporate uncertainty into uranium solubility under low ionic strength conditions after an igneous intrusive event; as sampled, *EP1LOWOU* is actually the logarithm of the indicated scale factor) and results from the role of *EP1LOWOU* in mobilizing ^{234}U in the EBS and thus reducing the

production of ^{226}Ra by the decay of ^{230}Th in the EBS and UZ. Very small effects are indicated for several additional variables.

Scatterplots showing the negative effect of *UZKDCSDT* and the positive effects of *INFIL* and *UZFAG8* are presented in Figure K6.4.2-8c,d,e,f,g,h[a].

K6.5[a] Igneous Intrusive Scenario Classes: Release from Saturated Zone (SZ)

No change.

K6.5.1[a] Igneous Intrusive Scenario Classes: Release from Saturated Zone (SZ) over the Time Interval [0, 20,000 yr] for an Event at 10 years

No change.

K6.5.2[a] Igneous Intrusive Scenario Classes: Release from Saturated Zone (SZ) over the Time Interval [0, 1,000,000 yr] for an Event at 250 years

Movement of Dissolved ^{234}U: *SZU234* and *SZU234C*. The uncertainty and sensitivity analyses for the time-dependent release rates (*SZU234*, g/yr) and cumulative releases (*SZU234C*, g) over the time interval [0, 1,000,000 yr] for the movement of dissolved ^{234}U across a subsurface plane at the location of the RMEI resulting from an igneous intrusive event at 250 years that destroys all WPs in the repository are summarized in Figures K6.5.2-5[a] and K6.5.2-6[a]. Further, a comparison of the movement of ^{234}U into and out of the SZ is presented in Figure K6.5.2-7[a]. As shown by the results in Figure K6.5.2-7[a], the SZ has a noticeable effect on the movement of ^{234}U in the SZ over the 50,000-yr time period (Figure K6.5.2-7a[a]). However, with increasing time, much of the ^{234}U released into the SZ exits the SZ at the location of the RMEI (Figure K6.5.2-7b,c,d[a]). Also, decay of ^{238}U produces ^{234}U within the SZ as can be observed in Figure K6.5.2-7d[a]. Although the half-life of ^{238}U is very long (4.47×10^9 yr), the mass of ^{238}U in the inventory is thousands of times greater than the mass of ^{234}U (SNL 2007 [DIRS 180472], Table 7-2[a]), thus decay of ^{238}U over 600,000 yr can produce enough ^{234}U that the additional mass of ^{234}U can be observed in Figure K6.5.2-7d[a].

The dominant variables affecting *SZU234* and *SZU234C* are *EP1LOWOU* (scale factor used to incorporate uncertainty into uranium solubility under low ionic strength conditions after an igneous intrusive event; as sampled, *EP1LOWOU* is actually the logarithm of the indicated scale factor), *INFIL* (infiltration level), *GOESITED* (density of sorption sites on goethite, sites/nm^2), *PHCSS* (pointer variable used to determine pH in CSNF cell 1 under liquid influx conditions), and *SZGWSPDM* (groundwater specific discharge multiplier; as sampled, *SZGWSPDM* is actually the logarithm of the indicated multiplier) (Figures K6.5.2-5e,f[a] and K6.5.2-6a,b[a]). The positive effects associated with *EP1LOWOU*, *INFIL* and *PHCSS* and the negative effect associated with *GOESITED* result from the previously discussed effects of these variables on the release of ^{234}U from the EBS. The positive effect associated with *SZGWSPDM* results from increasing water flow in the SZ. Smaller effects are indicated for a number of additional variables.

The dominant effect of *EP1LOWOU* and the lesser effects of *INFIL* and *GOESITED* can be seen in the scatterplots in Figure K6.5.2-6c,d,e,f,g,h[a].

Movement of Dissolved ^{230}Th: *SZTH230* and *SZTH230C*. The uncertainty and sensitivity analyses for the time-dependent release rates (*SZTH230*, g/yr) and cumulative releases (*SZTH230C*, g) over the time interval [0, 1,000,000 yr] for the movement of dissolved ^{230}Th across a subsurface plane at the location of the RMEI resulting from an igneous intrusive event at 250 years that destroys all WPs in the repository are summarized in Figures K6.5.2-8[a] and K6.5.2-9[a]. Further, a comparison of the movement of ^{234}U into and out of the SZ is presented in Figure K6.5.2-10[a]. As shown by the results in Figure K6.5.2-10[a], the SZ has a noticeable effect on the movement of ^{230}Th from the UZ to the location of the RMEI; specifically, the releases of ^{230}Th out of the SZ at the location of the RMEI are much smaller than the releases into the SZ for most sample elements.

The dominant variables affecting *SZTH230* and *SZTH230C* are *SZCONCOL* (concentration of colloids in ground water, g/mL; as sampled, *SZCONCOL* is actually the logarithm of the indicated concentration), *EP1LOWOU* (scale factor used to incorporate uncertainty into uranium solubility under low ionic strength conditions after an igneous intrusive event; as sampled, *EP1LOWOU* is actually the logarithm of the indicated scale factor), *SZKDAMCO* (sorption coefficient for reversible sorption of americium, thorium and protactinium onto ground water colloids, mL/g), *INFIL* (infiltration level), *SZGWSPDM* (groundwater specific discharge multiplier; as sampled, *SZGWSPDM* is actually the logarithm of the indicated multiplier), and *GOESITED* (density of sorption sites on goethite, sites/nm^2) (Figures K6.5.2-8e,f[a] and K6.5.2-9a,b[a]).

The positive effects associated with *SZCONCOL* and *SZKDAMCO* result from increasing the amount of ^{230}Th transported on colloids. The interaction of *SZCONCOL* and *SZKDAMCO* in affecting *SZTH230* and *SZTH230C* can be seen in the scatterplots in Figure K6.5.2-9c,e,f,h[a]. The positive effects associated with *EP1LOWOU* and *INFIL* result from increasing the release of ^{234}U from the EBS and increasing water flow in the EBS and UZ, respectively. The positive effect associated with *SZGWSPDM* results from increasing water flow in the SZ. The negative effect associated with *GOESITED* results from reducing the release of ^{234}U and ^{230}Th from the EBS. Smaller effects are indicated for a number of additional variables.

Movement of Dissolved ^{226}Ra: *SZRA226* and *SZRA226C*. The uncertainty and sensitivity analyses for the time-dependent release rates (*SZRA226*, g/yr) and cumulative releases (*SZRA226C*, g) over the time interval [0, 1,000,000 yr] for the movement of dissolved ^{226}Ra across a subsurface plane at the location of the RMEI resulting from an igneous intrusive event at 250 years that destroys all WPs in the repository are summarized in Figures K6.5.2-11[a] and K6.5.2-12[a]. Further, a comparison of the movement of ^{226}Ra into and out of the SZ is presented in Figure K6.5.2-13[a]. As shown by the results in Figure K6.5.2-13[a], the SZ has a large effect on the movement of ^{226}Ra from the UZ to the location of the RMEI.

Overall, the two most important variables affecting *SZRA226* and *SZRA226C* are *EP1LOWOU* (scale factor used to incorporate uncertainty into uranium solubility under low ionic strength conditions after an igneous intrusive event; as sampled, *EP1LOWOU* is actually the logarithm of the indicated scale factor) and *SZGWSPDM* (groundwater specific discharge multiplier; as sampled, *SZGWSPDM* is actually the logarithm of the indicated multiplier) (Figures K6.5.2-11e,f[a] and K6.5.2-12a,b[a]). The positive effects associated with *EP1LOWOU* and *SZGWSPDM* result because increasing *EP1LOWOU* increases the release of ^{234}U from the

EBS and increasing *SZGWSPDM* increases water flow in the SZ. The positive effects of *EP1LOWOU* and *SZGWSPDM* can be seen in the scatterplots in Figure K6.5.2-12c,d,f,g[a]. In addition to *EP1LOWOU* and *SZGWSPDM*, a number of additional variables have smaller effects on *SZRA226* and *SZRA226C* (Figures K6.5.2-11e,f[a] and K6.5.2-12a,b[a]).

K6.6[a] Igneous Intrusive Scenario Classes: Dose to Reasonably Maximally Exposed Individual (RMEI)

No change.

K6.6.1[a] Igneous Intrusive Scenario Classes: Dose to Reasonably Maximally Exposed Individual (RMEI) over the Time Interval [0, 20,000 yr] for an Event at 10 years

No change.

K6.6.2[a] Igneous Intrusive Scenario Classes: Dose to Reasonably Maximally Exposed Individual (RMEI) over the Time Interval [0, 1,000,000 yr] for an Event at 250 years

Dose to RMEI from Dissolved ^{234}U: *DOU234*. The uncertainty and sensitivity analyses for dose to the RMEI (*DOU234*, mrem/yr) over the time interval [0, 1,000,000 yr] for the movement of dissolved ^{234}U across a subsurface plane at the location of the RMEI resulting from an igneous intrusive event at 250 years that destroys all WPs in the repository are summarized in Figures K6.6.2-5[a] and K6.6.2-6[a].

The uncertainty in *DOU234* is determined primarily by the uncertainty in *SZU234* (Figure K6.6.2-6e[a]). As a result, the analyses in Figures K6.6.2-5[a] and K6.6.2-6[a] for *DOU234* are essentially the same as the analyses in Figures K6.5.2-5[a] and K6.5.2-6[a] for *SZU234*. The only substantive difference is the appearance of *MICU234* (dose conversion factor for ^{234}U for modern interglacial climate (rem/yr)/(pCi/L)) in the analyses for *DOU234* in Figures K6.6.2-5[a] and K6.6.2-6[a]. The positive effect associated with *MICU234* results from increasing the dose that derives from a unit intake of ^{234}U.

Dose to RMEI from Dissolved ^{230}Th: *DOTH230*. The uncertainty and sensitivity analyses for dose to the RMEI (*DOTH230*, mrem/yr) over the time interval [0, 1,000,000 yr] for the movement of dissolved ^{230}Th across a subsurface plane at the location of the RMEI resulting from an igneous intrusive event at 250 years that destroys all WPs in the repository are summarized in Figures K6.6.2-7[a] and K6.6.2-8[a].

The uncertainty in *DOTH230* is determined primarily by the uncertainty in *SZTH230* (Figure K6.6.2-8e[a]). As a result, the analyses in Figures K6.6.2-7[a] and K6.6.2-8[a] for *DOTH230* are essentially the same as the analyses in Figures K6.5.2-8[a] and K6.5.2-9[a] for *SZTH230*. The only minor difference is the appearance of *MICTH229* (dose conversion factor for ^{229}Th for modern interglacial climate (rem/yr)/(pCi/L)) in the analyses for *DOTH230* in Figure K6.6.2-8a[a]. The positive effect associated with *MICTH229* results from increasing the dose that derives from a unit intake of ^{230}Th.

Dose to RMEI from Dissolved ^{226}Ra: *DORA226*. The uncertainty and sensitivity analyses for dose to the RMEI (*DORA226*, mrem/yr) over the time interval [0, 1,000,000 yr] for the movement of dissolved ^{226}Ra across a subsurface plane at the location of the RMEI resulting from an igneous intrusive event at 250 years that destroys all WPs in the repository are summarized in Figures K6.6.2-9[a] and K6.6.2-10[a].

The uncertainty in *DORA226* is determined primarily by the uncertainty in *SZRA226* (Figure K6.6.2-10e[a]). As a result, the analyses in Figures K6.6.2-9[a] and K6.6.2-10[a] for *DORA226* are essentially the same as the analyses in Figures K6.5.2-11[a] and K6.5.2-12[a] for *SZRA226*. The only minor difference is the appearance of *MICRA226* (dose conversion factor for ^{226}Ra for modern interglacial climate (rem/yr)/(pCi/L)) in the analyses for *DORA226* in Figure K6.6.2-10a[a]. The positive effect associated with *MICRA229* results from increasing the dose that derives from a unit intake of ^{226}Ra.

K6.7[a] Igneous Intrusive Scenario Classes: Expected Dose (*EXPDOSE*) to Reasonably Maximally Exposed Individual (RMEI)

No change.

K6.7.1[a] Igneous Intrusive Scenario Classes: Expected Dose (*EXPDOSE*) to Reasonably Maximally Exposed Individual (RMEI) over [0, 20,000 yr]

No substantive changes in the uncertainty and sensitivity analyses for expected dose to the RMEI (*EXPDOSE*, mrem/yr) over the time interval [0, 20,000 yr] resulting from igneous intrusion were observed (i.e., compare the results in Figures K6.7.1-1 and K6.7.1-2 with the results in Figures K6.7.1-1[a] and K6.7.1-2[a]). Additional comparisons are presented in Figures 7.3.1-28[a] and 7.3.1-30[a]; discussion of the differences in the results is provided in Section 7.3.1.5.4[a].

K6.7.2[a] Igneous Intrusive Scenario Classes: Expected Dose (*EXPDOSE*) to Reasonably Maximally Exposed Individual (RMEI) over [0, 1,000,000 yr]

No substantive changes in the uncertainty and sensitivity analyses for expected dose to the RMEI (*EXPDOSE*, mrem/yr) over the time interval [0, 1,000,000 yr] resulting from igneous intrusion were observed (i.e., compare the results in Figures K6.7.2-1 and K6.7.2-2 with the results in Figures K6.7.2-1[a] and K6.7.2-2[a]. Additional comparisons are presented in Figures 7.3.1-29[a] and 7.3.1-31[a]; discussion of the differences in the results is provided in Section 7.3.1.5.4[a].

K6.8[a] Igneous Eruptive Scenario Classes: Expected Dose (*EXPDOSE*) to Reasonably Maximally Exposed Individual (RMEI)

No change.

K6.8.1[a] Igneous Eruptive Scenario Classes: Expected Dose (*EXPDOSE*) to Reasonably Maximally Exposed Individual (RMEI) over [0, 20,000 yr]

No change.

K6.8.2[a] Igneous Eruptive Scenario Classes: Expected Dose (*EXPDOSE*) to Reasonably Maximally Exposed Individual (RMEI) over [0, 1,000,000 yr]

No change.

K7[a] SEISMIC SCENARIO CLASSES

No change.

K7.1[a] Seismic Scenario Classes: Summary

No change.

K7.2[a] Seismic Ground Motion Scenario Classes: Engineered Barrier System (EBS) Conditions over the Time Interval [0, 20,000 yr]

No change.

K7.3[a] Seismic Ground Motion Scenario Classes: Release from Engineered Barrier System (EBS) over the Time Interval [0, 20,000 yr]

No change.

K7.4[a] Seismic Ground Motion Scenario Classes: Release from Unsaturated Zone (UZ) over the Time Interval [0, 20,000 yr]

No change.

K7.5[a] Seismic Ground Motion Scenario Classes: Release from Saturated Zone (SZ) over the Time Interval [0, 20,000 yr]

No change.

K7.6[a] Seismic Ground Motion Scenario Classes: Dose to Reasonably Maximally Exposed Individual (RMEI) over the Time Interval [0, 20,000 yr]

No change.

K7.7[a] Seismic Ground Motion Scenario Classes: Expected Dose to Reasonably Maximally Exposed Individual (RMEI)

K7.7.1[a] Seismic Ground Motion Scenario Classes: Expected Dose (*EXPDOSE*) to Reasonably Maximally Exposed Individual (RMEI) over the Time Interval [0, 20,000 yr]

No substantive changes in the uncertainty and sensitivity analyses for expected dose to the RMEI (*EXPDOSE*, mrem/yr) over the time interval [0, 20,000 yr] resulting from seismic ground motion were observed (i.e., compare the results in Figures K7.7.1-1 and K7.7.1-2 with the results in Figures K7.7.1-1[a] and K7.7.1-2[a]). Additional comparisons are presented in

Figures 7.3.1-32[a] and 7.3.1-33[a]; discussion of these comparisons is provided in Section 7.3.1.5.6[a].

For reader convenience, the following discussion of the expected dose results in Figures K7.7.1-1[a] and K7.7.1-2[a] is provided. This discussion updates the corresponding material in Section K7.7.1 from the parent report.

The uncertainty and sensitivity analyses for expected dose to the RMEI (*EXPDOSE*, mrem/yr) over the time interval [0, 20,000 yr] resulting from seismic ground motion events are summarized in Figures K7.7.1-1[a] and K7.7.1-2[a]. After the earliest arrival of released radionuclides at the location of the RMEI, *EXPDOSE* increases monotonically with time (Figure K7.7-1a,b[a]). At 10,000 yr, the value for *EXPDOSE* falls between 10^{-4} and 1 mrem/yr for most sample elements, with a few sample elements having values for *EXPDOSE* between 1 and 10 mrem/yr. Due to the use of the quadrature-based methods rather than Monte Carlo methods to evaluate expected dose to the RMEI over the time interval [0, 20,000 yr] (see Equations J8.3-8 and J8.3-13), the expected dose results in Figure 7.7.1-1a,b[a] are relatively smooth.

The PRCCs in Figure K7.7.1-1c[a] indicate that the uncertainty in *EXPDOSE* is dominated by residual stress threshold *SCCTHRP* (as sampled, *SCCTHRP* is a percent of a base value of 351 MPa and is related to the stress corrosion cracking threshold, *SCCTHR*, by *SCCTHRP* = (*SCCTHR* × 100)/(351 MPa)). The value for *EXPDOSE* decreases as *SCCTHRP* increases. This effect occurs because increasing *SCCTHRP* increases the stress required to initiate stress corrosion cracking and thus decreases the probability that a given seismic ground motion event will cause WP damage.

In addition to *SCCTHRP*, smaller effects are indicated for *SZGWSPDM* (groundwater specific discharge multiplier; as sampled, *SZGWSPDM* is actually the logarithm of the indicated multiplier), *SZFIPOVO* (flowing interval porosity in the volcanic unit of the SZ), *INFIL* (infiltration level), *DSNFMASS* (scale factor used to characterize uncertainty in the radionuclide content of DSNF contained in CDSP WPs), and *MICC14* (dose conversion factor for ^{14}C for modern interglacial climate, (rem/yr)/(pCi/L)) (Figure K7.7.1-1c[a]). The variables *SZGWSPDM*, *DSNFMASS* and *MICC14* have positive effects on *EXPDOSE*, with these effects resulting because (1) increasing *SZGWSPDM* increases water flow in the SZ, (2) increasing *DSNFMASS* increases the amount of radionuclides in CDSP WPs and hence the dose from the failure of these WPs, and (3) increasing *MICC14* increases the received dose from ^{14}C for a given exposure level. The variables *SZFIPOVO* and *INFIL* have effects at early times, but limited effects at later times. The negative effect for *SZFIPOVO* results from slowing water flow in the SZ and thus delaying the initial arrival of radionuclides at the location of the RMEI. In contrast, the positive effect for *INFIL* results from accelerating the initial arrival of radionuclides at the location of the RMEI; specifically, increased values for *INFIL* result (1) in cooler conditions in the EBS, which contributes to earlier radionuclide releases, and (2) in more water flux in the EBS and UZ, which contributes to more rapid radionuclide movement. Owing to the nature of the integration process that defines *EXPDOSE*, the indicated effects associated with *SZFIPOVO* and *INFIL* decrease with increasing time.

More detailed sensitivity analyses for *EXPDOSE* are provided by the regression analyses in Figure K7.7.1-2a[a]. The dominant effect of *SCCTHRP* on the uncertainty in *EXPDOSE* is indicated by R^2 values of 0.81, 0.86 and 0.88 for the regressions containing only *SCCTHRP* at 3000, 5000 and 10,000 yr. After *SCCTHRP*, the regressions select a large number of variables that have small effects on *EXPDOSE*. For example, the regression at 3000 yr then selects *SZGWSPDM*, *INFIL* and *MICTC99* (dose conversion factor for ^{99}Tc for modern interglacial climate, (rem/yr)/(pCi/L)) and produces a model with an R^2 value of 0.87; the regression at 5,000 yr then selects *MICTC99*, *DSNFMASS* and *MICC14* and produces a model with an R^2 value of 0.90; and the regression at 10,000 yr then selects *MICTC99*, *DSNFMASS* and *HLWDRACD* (rate term for dissolution of HLW glass in CDSP WPs under low pH conditions, g/m^2/d) and produces a model with an R^2 value of 0.91. After the first four variables, the regressions at 3000, 5000 and 10,000 yr select an additional 12, 11 and 12 variables, respectively, and produce final models with R^2 values of 0.92, 0.94 and 0.95. Thus, the uncertainty in *EXPDOSE* is dominated by *SCCTHRP*, with small contributions to this uncertainty by many additional variables.

The doses that are integrated to obtain *EXPDOSE* arise primarily from ^{99}Tc (Figure 8.2-12(a) and Figure J8.3-8). The importance of ^{99}Tc to *EXPDOSE* is also evident in the regression results at 10,000 yr (Figure K7.7.1-2a[a]). Specifically, the three variables selected immediately after *SCCTHRP* (i.e., *MICTC99*, *DSNFMASS* and *HLWDRACD*) are variables that affect the dose received from ^{99}Tc. Specifically, increasing *MICTC99* increases the dose received from a fixed concentration of ^{99}Tc in groundwater; increasing *DSNFMASS* increases the mass of ^{99}Tc present to be released from the CDSP WPs; and increasing *HLWDRACD* increases the rate at which ^{99}Tc is released from the glass waste form.

The dominant effect of *SCCTHRP* on the uncertainty in *EXPDOSE* can be seen in the scatterplot in Figure K7.7.1-2b[a]. The much smaller effects associated with *MICTC99* and *DSNFMASS* can be seen in the scatterplots in Figure K7.7.1-2c,d[a].

It is important to recognize that the results in Figures K7.7.1-1[a] and K7.7.1-2[a] reflect the sensitivity of *EXPDOSE* to the parameters that are treated as being uncertain in the TSPA-LA Model. Some important parameters and model inputs are not treated as being uncertain, but are instead represented by conservative, fixed values or by assumptions. The sensitivity of *EXPDOSE* to these parameters can be discussed qualitatively but cannot be quantified. For example, the results in Figures K7.7.1-1[a] and K7.7.1-2[a] were generated with a fixed value for the seismic hazard curve, estimated as the mean of a distribution of possible seismic hazard curves. This mean seismic hazard curve underlies the probabilistic weightings of the seismic events that give rise to *EXPDOSE* through an integration process (Section 6.1.2.4.4). Significant uncertainty is associated with the definition of the mean seismic hazard curve (SNL 2007 [DIRS 176828], Section 6.4.1). If the uncertainty associated with the seismic hazard curve was incorporated into the analysis, it is likely that this uncertainty would have a significant effect on the uncertainty associated with *EXPDOSE*. Including this uncertainty in the TSPA-LA Model would likely improve the estimated repository performance, because the mean seismic hazard curve typically lies above the 80th percentile of the distribution of seismic hazard curves. Including the uncertainty in the seismic hazard curve would reduce the frequency of damaging seismic events in most realizations, which would reduce releases from the repository and

improve repository performance. Thus, the use of the mean seismic hazard curve results in conservative estimates of repository performance.

K7.7.2[a] Seismic Ground Motion Scenario Classes: Expected Dose (*EXPDOSE*) to Reasonably Maximally Exposed Individual (RMEI) over the Time Interval [0, 1,000,000 yr]

The results obtained with version 5.005 of the TSPA-LA Model in the uncertainty analyses for expected dose to the RMEI (*EXPDOSE*, mrem/yr) over the time interval [0, 1,000,000 yr] resulting from seismic ground motion tend to be somewhat smaller than the results obtained with version 5.000 of the TSPA-LA Model (i.e., compare the results in Figures K7.7.2-1 and K7.7.2-2 with the results in Figures K7.7.2-1[a] and K7.7.2-2[a]. Additional comparisons are presented in Figures 7.3.1-35[a] and 7.3.1-36[a]; discussion of the differences in the results is provided in Section 7.3.1.5.6[a]. However, there is a large amount of variability in the comparisons across sample elements, with (1) version 5.005 producing smaller results for some sample elements, (2) version 5.000 producing smaller results for some sample elements, and (3) both versions producing similar results for some sample elements (Figures K7.3.1-35[a] and 7.3.1-36[a]). The major cause for the difference in the results from both model versions is the change to the models for estimating damage from seismic events, as described in Appendix P, Section P3, with other minor effects from the other errors described in Appendix P. To some extent, this variability is also influenced by the use of only 30 futures in the estimation of *EXPDOSE* for each sample element. The sensitivity analyses tended to agree on the two most important variables but showed considerable disagreement on less important variables. The differences in sensitivity analysis results are due to the differences between the model versions, primarily to the time and extent of seismic damage (Appendix P, Section P3), and secondarily to the processes by which radionuclide transport occurs.

For reader convenience, the following discussion of the expected dose results in Figures K7.7.2-1[a] and K7.7.2-2[a] is provided. This discussion updates the corresponding material in Section K7.7.2 from the parent report.

The uncertainty and sensitivity analyses for expected dose to the RMEI (*EXPDOSE*, mrem/yr) over the time interval [0, 1,000,000 yr] resulting from seismic ground motion are summarized in Figures K7.7.2-1[a] and K7.7.2-2[a].

The time-dependent values for *EXPDOSE* for the 1,000,000-yr period in Figure K7.7.2-1a,b[a] are much choppier than the values for the 20,000 yr time period in Figure K7.7.1-1a,b[a]. This difference results from the numerical procedures used over 20,000-yr and 1,000,000-yr, respectively, to evaluate the integrals that define *EXPDOSE*. Because the effects of the seismic ground motion events are relatively well behaved for the 20,000-yr time period, it is possible to use a quadrature procedure to evaluate *EXPDOSE* for this time period. This results in the relatively smooth time-dependent values for *EXPDOSE* in Figure K7.7.1-1a,b[a]. In contrast, the effects of seismic ground motion events are much more complex for the 1,000,000-yr time period. As a result of this complexity, it is not possible to use a quadrature procedure to evaluate the defining integral for *EXPDOSE* over this longer time period. Instead, it was necessary to use a sampling-based (i.e., Monte Carlo) integration procedure to evaluate the defining integral for *EXPDOSE*. Specifically, thirty 1,000,000-yr futures involving seismic ground motion events

were randomly sampled for each LHS element and then the 30 time-dependent dose results associated with these futures were vertically averaged at each point in time to produce the estimated time-dependent value for *EXPDOSE* for each sample element (Appendix J, Figures J8.4-1 and J8.4-2). Because individual seismic ground motion events are discrete occurrences that initiate radionuclide releases that ultimately lead to doses to the RMEI, the time dependent doses associated with individual futures and their vertical averages to produce expected doses for individual LHS elements tend to be choppy. In addition, the progression of nominal processes and the occurrence of resultant DS and WP failures contribute to the complexity of the 1,000,000-yr dose calculations. The individual curves in Figure K7.7.2-1a,b would eventually converge to smooth curves if a sufficiently large number of futures was sampled for each LHS element, or if an appropriate kernel smoother was used on the time-dependent results for each LHS element. However, despite the lack of smoothness in the results presented in Figure 7.7.2-1a,b[a], the distribution of expected annual doses (*EXPDOSE*) is shown to be statistically stable (Section 7.3.1) by means of a replicated sampling procedure (Section J4.10). In addition, confidence intervals are computed that show that the mean annual dose is estimated with sufficient accuracy (Section 7.3.1). The stability of the results from TSPA-LA Model v5.005 is discussed in Section 7.3.1.5[a].

Most values for *EXPDOSE* in Figure K7.7.2-1a,b[a] are less than 10 mrem/yr, with a few values between 10 and 100 mrem/yr. The sharp peaks in *EXPDOSE* in Figure K7.7.2-1a,b[a] are associated with peaks that derive from single seismic ground motion events sampled in a single future. The peaks in *EXPDOSE* would be reduced if the sampling-based approximations to the integrals defining *EXPDOSE* were more fully converged.

Although the results in Figure K7.7.2-1a,b[a] are choppy, insights can be gained from a careful examination. In particular, Figure K7.7.2-1b[a] is more informative than Figure K7.7.2-1a[a] because the time-dependent values for *EXPDOSE* for individual LHS elements are more distinct. Overall, after an initial peak, there is a tendency for *EXPDOSE* to decrease up to about 200,000 yr, with this decrease resulting from the depletion of soluble radionuclides (i.e. ^{99}Tc and ^{129}I) in WPs with seismic damage (Figure 8.2-12[a]. In this time period, the values of *EXPDOSE* derive from the occurrence of seismic ground motion events as the failure of WPs from nominal processes does not begin until about 200,000 yr. The dominance of seismic ground motion events is indicated by the importance of the residual stress threshold *SCCTHRP* (as sampled, *SCCTHRP* is a percent of a base value of 351 MPa and is related to the stress corrosion cracking threshold, *SCCTHR*, by *SCCTHRP* = (*SCCTHR* × 100)/(351 MPa)); specifically, the PRCCs in Figure K7.7.2-1c[a] indicate that *SCCTHRP* dominates the uncertainty in *EXPDOSE* out to approximately 200,000 yr. This result is also indicated by the regression for *EXPDOSE* at 50,000 yr in Figure K7.7.2-2a [a], where *SCCTHRP* is the first variable selected in the analysis with an R^2 value of 0.71.

Beyond 200,000 years, corrosion processes become important to *EXPDOSE* as WPs that have not been damaged by seismic events begin to fail by SCC of lid welds (Section 8.2.1[a]). Consistent with this, the PRCCs in Figure K7.7.2-1c[a] indicate that the uncertainty in *EXPDOSE* becomes dominated by *WDGCA22* (temperature dependence coefficient associated with the general corrosion rate for Alloy 22, K). Specifically, *WDGCA22* corresponds to a coefficient used to alter the general corrosion rate for Alloy 22 as function of temperature, with the Alloy 22 corrosion rate decreasing as *WDGCA22* increases. As indicated in

Figures K4.2-2e,f and K4.5-1c[a], *WDGCA22* is the dominant variable with respect to the uncertainty associated with the failure of WPs from nominal processes. After 400,000 yr, the values for *EXPDOSE* tend to increase and beyond 700,000 years are somewhat smoother than at earlier times (Figure K7.7.2-1a,b[a]). This smoothness results from an increasing dominance of nominal corrosion processes in the values for *EXPDOSE*.

In addition to *SCCTHRP* and *WDGCA22*, the PRCCs in Figure K7.7.2-1c[a] indicate effects for several additional variables. However, the effects are small and the PRCCs are very choppy as a result of the choppiness in the values for *EXPDOSE*. Smoother results for *EXPDOSE* would result in smoother values for the PRCCs in Figure K7.7.2-1c[a].

More detailed sensitivity analyses for *EXPDOSE* are provided by the regression analyses in Figure K7.7.2-2a[a]. Specifically, *SCCTHRP* is the dominant contributor to the uncertainty in *EXPDOSE* at 50,000 yr; *SCCTHRP* is the dominant contributor to the uncertainty in *EXPDOSE* at 200,000 yr with a contribution from *WDGCA22*; and *WDGCA22* is the dominant contributor to the uncertainty in *EXPDOSE* at 500,000 yr with a contribution from *SCCTHRP*. The individual regressions then add several additional variables that have small effects on *EXPDOSE*. The final regression models 50,000, 200,000 and 500,000 yr have R^2 values of 0.77, 0.62 and 0.76, which are not particularly high due in part to the choppiness of the values for *EXPDOSE* (Figure K7.7.2-1a,b[a]) and in part to the large number of processes that affect *EXPDOSE* for the 1,000,000 yr seismic ground motion calculation.

For perspective, the scatterplots in Figure K7.7.2-2b,c,d[a] show the effects of *WDGCA22*, *SCCTHRP* and *WDNSCC* (stress corrosion cracking growth rate exponent) at 500,000 yr. The negative effects of *WDGCA22* and *SCCTHRP* can be easily seen in the scatterplots in Figure K7.7.2-2b,c[a]. The negative effect for *WDNSCC* is more subtle but still discernable in the scatterplot in Figure K7.7.2-2d[a].

As previously indicated in conjunction with Figures K7.7.1-1[a] and K7.7.1-2[a] for the 20,000-year time period, it is important to recognize that the results in Figures K7.7.2-1[a] and K7.7.2-2[a] reflect the sensitivity of *EXPDOSE* for the 1,000,000-yr time period to those parameters that are treated as being uncertain in the TSPA-LA Model. Some important parameters and model inputs are not treated as being uncertain, but are instead represented by conservative, fixed values or by assumptions. The sensitivity of *EXPDOSE* to these parameters can be discussed qualitatively but cannot be quantified. In particular, significant uncertainty is associated with the definition of the seismic hazard curve that underlies the occurrence of seismic events and the effects of seismic events. If the uncertainty associated with the seismic hazard curve was incorporated into the analysis, it is likely that this uncertainty would have a significant effect on the uncertainty associated with *EXPDOSE*.

K7.8[a] Seismic Fault Displacement Scenario Classes: Expected Dose (*EXPDOSE*) to Reasonably Maximally Exposed Individual (RMEI)

No change.

K7.8.1[a] Seismic Fault Displacement Scenario Classes: Expected Dose (*EXPDOSE*) to Reasonably Maximally Exposed Individual (RMEI) over the Time Interval [0, 20,000 yr]

No substantive changes in the uncertainty and sensitivity analyses for expected dose to the RMEI (*EXPDOSE*, mrem/yr) over the time interval [0, 20,000 yr] resulting from fault displacement were observed (i.e., compare the results in Figures K7.8.1-1 and K7.8.1-2 with the results in Figures K7.8.1-1[a] and K7.8.1-2[a]). Additional comparisons are presented in Figures 7.3.1-37[a] and 7.3.1-39[a]; discussion of the differences in the results is provided in Section 7.3.1.5.7[a].

K7.8.2[a] Seismic Fault Displacement Scenario Classes: Expected Dose (*EXPDOSE*) to Reasonably Maximally Exposed Individual (RMEI) over the Time Interval [0, 1,000,000 yr]

No substantive changes in the uncertainty and sensitivity analyses for expected dose to the RMEI (*EXPDOSE*, mrem/yr) over the time interval [0, 1,000,000 yr] resulting from fault displacement were observed (i.e., compare the results in Figures K7.8.2-1 and K7.8.2-2 with the results in Figures K7.8.2-1[a] and K7.8.2-2[a]). Additional comparisons are presented in Figures 7.3.1-38[a] and 7.3.1-40[a]; discussion of the differences in the results is provided in Section 7.3.1.5.7[a].

K8[a] ALL SCENARIO CLASSES: EXPECTED DOSE (*EXPDOSE*) TO REASONABLY MAXIMALLY EXPOSED INDIVIDUAL (RMEI)

No change.

K8.1[a] All Scenario Classes: Expected Dose (*EXPDOSE*) to Reasonably Maximally Exposed Individual (RMEI) over the Time Interval [0, 20,000 yr]

No substantive changes in the uncertainty and sensitivity analyses for expected dose to the RMEI (*EXPDOSE*, mrem/yr) over the time interval [0, 20,000 yr] resulting from all scenario classes were observed (i.e., compare the results in Figures K8.1-1 and K8.1-2 with the results in Figures K8.1-1[a] and K8.1-2[a]). The similarity in expected dose to the RMEI results from the similarity in the results of the Seismic Ground Motion Scenario Class. Additional comparisons are presented in Figures 7.3.1-42[a] and 7.3.1-43[a] and discussed in Section 7.3.1.5.8[a].

For reader convenience, the following discussion of the expected dose results in Figures K8.1-1[a] and K8.1-2[a] is provided. This discussion updates the corresponding material in Section K8.1 from the parent report.

The uncertainty and sensitivity analyses for expected dose to the RMEI (*EXPDOSE*, mrem/yr) over the time interval [0, 20,000 yr] resulting from all scenario classes are summarized in Figures K8.1-1[a] and K8.1-2[a]. Initial transport to the location of the RMEI takes up to 2000 yr; after the earliest possible arrival time for released radionuclides at the location of the RMEI, *EXPDOSE* increases monotonically with time (Figure K8.1-1a,b[a]). At 10,000 yr, the value for *EXPDOSE* falls between 10^{-3} and 4 mrem/yr. As indicated by Figure 8.1-3a[a], the expected dose to the RMEI from all scenario classes is predominantly determined by the

expected dose to the RMEI resulting from seismic ground motion and igneous intrusion. However, for some sample elements, minor effects from early WP failures can be observed in Figure K8.1-1b[a], where the initiation of transport from CNSF WPs after 9000 yr produces spikes in the expected dose. In turn, these spikes result in minor variability in the PRCCs (Figure K8.1-1c[a]).

The PRCCs in Figure K8.1-1c[a] indicate that the four most important variables with respect to the uncertainty in *EXPDOSE* over the time interval [0, 20,000 yr] are *SCCTHRP* (residual stress threshold; as sampled, *SCCTHRP* is a percent of a base value of 351 MPa and is related to the stress corrosion cracking threshold, *SCCTHR*, by *SCCTHRP* = (*SCCTHR* × 100)/(351 MPa)), *IGRATE* (rate of occurrence of igneous intrusive events, yr^{-1}), *SZGWSPDM* (groundwater specific discharge multiplier; as sampled, *SZGWSPDM* is actually the logarithm of the indicated multiplier), and *MICC14* (dose conversion factor for ^{14}C for modern interglacial climate, (rem/yr)/(pCi/L)). The negative effect associated with *SCCTHRP* results because increasing *SCCTHRP* results in WPs being more resistant to seismic ground motion damage; the positive effect associated with *IGRATE* results because increasing *IGRATE* increases the probability of occurrence for igneous events; the positive effect associated with *SZGWSPDM* results because increasing *SZGWSPDM* increases water flow in the SZ; and the positive effect associated with *MICC14* results from increasing the dose that results from a given exposure to ^{14}C (and probably other radionuclides as a result of positive correlations involving dose factors). As indicated by the size of the PRCCs, *SCCTHRP* is the most important of these four variables.

After *SCCTHRP*, *IGRATE*, *SZGWSPDM* and *MICC14*, smaller effects are indicated for *SZFIPOVO* (flowing interval porosity in the volcanic unit of the SZ) and *INFIL* (infiltration level) (Figure K8.1-1c[a]) before about 5,000 years. The negative effect associated with *SZFIPOVO* at early times results from initially slowing the movement of radioactive species in the SZ, and the positive effect associated with *INFIL* results from its role in both speeding the cooling of the repository and increasing water flow in the EBS and UZ.

More detailed sensitivity analyses for *EXPDOSE* are provided by the regression analyses and associated scatterplots in Figure K8.1-2[a]. Overall, the dominant variable with respect to the uncertainty in *EXPDOSE* is *SCCTHRP*. Specifically, the regressions containing only *SCCTHRP* have R^2 values of 0.55, 0.66 and 0.69 at 3000, 5000 and 10,000 yr, respectively (Figure K8.1-2a[a]). After *SCCTHRP*, the next variable selected in all regressions is *IGRATE*, with the inclusion of *IGRATE* raising the cumulative R^2 values to 0.62, 0.71 and 0.73. Thus, the effect of *IGRATE* on *EXPDOSE* is not as great as the effect of *SCCTHRP*. In consistency with the analysis with PRCCs, *SZGWSPDM* is then the third variable selected in the three regressions analyses. The negative effect associated with *SCCTHRP* and the positive effects associated with *IGRATE* and *SZGWSPDM* can be seen in the scatterplots in Figure K8.1-2a,b,c[a]. After *SCCTHRP*, *IGRATE* and *SZGWSPDM*, the regressions select a number of additional variables that have small effects on *EXPDOSE*. The final regression models have R^2 values of 0.81, 0.85 and 0.82, which indicates that they are reasonably successful in accounting for the uncertainty in *EXPDOSE*. However, as is always the case, some of the variables selected at the ends of individual regression analyses that have very small effects on cumulative R^2 values may be spurious.

It is important to recognize that the results in Figures K8.1-1[a] and K8.1-2[a] reflect the sensitivity of *EXPDOSE* for the 20,000-yr time period to those parameters that are treated as being uncertain in the TSPA-LA Model. Where parameters and model inputs are not treated as being uncertain, but are instead represented by conservative, fixed values or by assumptions, the sensitivity of *EXPDOSE* to these parameters can be discussed qualitatively but cannot be quantified. For example, significant uncertainty is associated with the definition of the seismic hazard curve that underlies the occurrence of seismic events and the effects of seismic events. If the uncertainty associated with the seismic hazard curve was incorporated into the analysis, it is likely that this uncertainty would have an effect on the uncertainty associated with *EXPDOSE*.

K8.2[a] All Scenario Classes: Expected Dose (*EXPDOSE*) to Reasonably Maximally Exposed Individual (RMEI) over the Time Interval [0, 1,000,000 yr]

Because of the changes to the Seismic Ground Motion Scenario Class (Appendix P, Section P3), and the importance of this scenario class to the total expected dose (Figure 8.1-3[a]), the changes to the Seismic Ground Motion Scenario Class affect the uncertainty and sensitivity analyses for expected dose to the RMEI (*EXPDOSE*, mrem/yr) over the time interval [0, 1,000,000 yr]. As discussed in Section K7.7.2[a], the change to the models for estimating damage from seismic events, as described in Appendix P, Section P3, alters the relationships between input and output variables. The most significant effect of the model changes is to flatten the peak in the expected (mean) dose that occurs around 230,000 years (compare Figure 8.1-2 and Figure 8.1-2[a]). As a consequence, the input variables identified as important at 200,000 yr and at 252,000 yr are different for the two model versions. However, at earlier and at later times, the sensitivity analyses for both model versions agree on the three most important variables but showed considerable disagreement on less important variables (i.e., compare the results in Figures K8.2-1 and K8.2-2 with the results in Figures K8.2-1[a] and K8.2-2[a]). Additional comparisons are presented in Figures 7.3.1-45[a] and 7.3.1-46[a] and discussed in Section 7.3.1.5.9[a].

For reader convenience, the following discussion of the expected dose results in Figures K8.2-1[a] and K8.2-2[a] is provided. This discussion updates the corresponding material in Section K8.2 from the parent report.

The uncertainty and sensitivity analyses for expected dose to the RMEI (*EXPDOSE*, mrem/yr) over the time interval [0, 1,000,000 yr] resulting from all scenario classes are summarized in Figures K8.2-1[a] and K8.2-2[a]. As indicated by Figure 8.1-3b[a], the expected dose to the RMEI from all scenario classes is predominantly determined by the expected dose to the RMEI resulting from seismic ground motion and from igneous intrusion.

The time-dependent values for *EXPDOSE* appear somewhat choppy as a result of the sampling-based effects of nominal processes and seismic ground motion events (Figure K7.7.2-1[a]). Smoother results could be obtained by using a larger sample of aleatory futures for seismic ground motion events or possibly a more sophisticated integration procedure for the incorporation of such events. However, because the distribution of *EXPDOSE* has been shown to be statistically stable (Section 7.3.1.3 and Section 7.3.1.5.9[a]), improved convergence or use of a better integration procedure would produce smoother estimates of expected dose, but

would not produce results that differ substantially from those shown in Figure K8.2-1[a]. The values for *EXPDOSE* fall in a range from 10^{-4} to 40 mrem/yr.

The PRCCs in Figure K8.2-1c[a] indicate that the three most important variables with respect to the uncertainty in *EXPDOSE* are *SCCTHRP* (residual stress threshold; as sampled, *SCCTHRP* is a percent of a base value of 351 MPa and is related to the stress corrosion cracking threshold, *SCCTHR*, by *SCCTHRP* = (*SCCTHR* × 100)/(351 MPa)), *IGRATE* (rate of occurrence of igneous intrusive events, yr^{-1}), *SZGWSPDM* (groundwater specific discharge multiplier; as sampled, *SZGWSPDM* is actually the logarithm of the indicated multiplier), and *WDGCA22* (temperature dependence coefficient associated with the general corrosion rate for Alloy 22, K). The negative effect associated with *SCCTHRP* results because increasing *SCCTHRP* increases the resistance of WPs to seismic ground motion damage; the positive effect associated with *IGRATE* results because increasing *IGRATE* increases the probability of occurrence for igneous events; the positive effect associated with *SZGWSPDM* results because increasing *SZGWSPDM* increases water flow in the SZ; and the negative effect associated with *WDGCA22* results from its role in slowing the rate of general corrosion of Alloy 22, which in turn delays and reduces WP failures due to both seismic ground motion events and general corrosion.

Smaller effects are indicated for *SZFIPOVO* (flowing interval porosity in the volcanic unit of the SZ) and *EP1LOWPU* (scale factor used to incorporate uncertainty into plutonium solubility under low ionic strength conditions; as sampled, *EP1LOWPU* is actually the logarithm of the indicated scale factor). The negative effect of *SZFIPOVO* only occurs at very early times (Figure K8.1-1c[a]) and results from increasing the time required for an initial radionuclide release into the SZ to reach the RMEI. The positive effect of *EP1LOWPU* results from increasing the amount of dissolved plutonium that is released from the EBS.

More detailed sensitivity analysis results are provided by the regression analyses and associated scatterplots in Figure K8.2-2[a]. At 50,000 yr, the most important variable is *SCCTHRP*, which results in a single-variable regression model with an R^2 value of 0.27. At 200,000 and 500,000 yr, the most important variable is *IGRATE*, which results in single-variable regression models with R^2 values of 0.38 and 0.29. Further, *IGRATE* is the second variable selected at 50,000 yr. After these initial selections, the stepwise analyses continue and construct models with 9, 16 and 13 variables and corresponding R^2 values of 0.67, 0.74 and 0.70. Thus, a large number of variables are affecting uncertainty in *EXPDOSE* over 1,000,000 yr with no single variable dominating this uncertainty. For perspective, the effects of *IGRATE*, *WDGCA22* and *SZGWSPDM* on *EXPDOSE* at 500,000 yr can be seen in the scatterplots in Figure K8.2-2b,c,d[a].

As previously indicated in conjunction with Figures K8.1-1[a] and K8.1-2[a] for the 20,000-yr time period, it is important to recognize that the results in Figures K8.2-1[a] and K8.2-2[a] reflect the sensitivity of *EXPDOSE* for the 1,000,000 yr time period to those parameters that are treated as being uncertain in the TSPA-LA Model. Some important parameters and model inputs are not treated as being uncertain, but are instead represented by conservative, fixed values or by assumptions. In particular, if the uncertainty associated with the seismic hazard curve was incorporated into the analysis, it is likely that this uncertainty would have an effect on the uncertainty associated with *EXPDOSE*.

K9[a] SUMMARY

This addendum updates uncertainty and sensitivity analyses for expected dose to the RMEI reported in Appendix K with results obtained from TSPA-LA Model v5.005. In addition, for the Igneous Intrusion Scenario Classes, this addendum reports new uncertainty and sensitivity analyses for the movement of ^{234}U, ^{230}Th, and ^{226}Ra out of the EBS, UZ and SZ, as well as dose to the RMEI for these radionuclides. Comparison of the results of the uncertainty and sensitivity analyses for the two TSPA-LA Model versions shows that the two models produce similar results, although some differences in results can be observed for the Seismic Ground Motion Scenario Class, and for a few sample elements in most scenario classes. Due to the similarity evident in the results from the two models, the analyses presented in Appendix K for the movement of representative radionuclides (^{239}Pu, ^{237}Np, and ^{99}Tc) are not repeated; conclusions from these analyses apply equally to TSPA-LA Model v5.005.

Table K9-1[a] summarizes sensitivity analysis results for total expected dose and expected dose by scenario class by listing the key uncertain inputs identified by the analysis, using results from TSPA-LA Model v5.005. The key uncertain inputs in Table K9-1[a] are listed in decreasing order of importance with the first listed input having the most effect on the output quantity. The key uncertain inputs are identified on the basis of sensitivity analysis results at roughly the time the mean of the output variable achieves its maximum value. Table K9-1[a] and Table K9-1 generally show the same key uncertain inputs for each scenario class, but there are exceptions. The changes to the Seismic Ground Motion Scenario Class for TSPA-LA Model v5.005 caused the maximum of the expected (mean) dose for this scenario class as well as for total expected (mean) dose to move from 230,000 yr to 1,000,000 yr. Consequently, the key uncertain inputs for these two output variables are different. Additionally, the third or fourth uncertain inputs for some scenario classes have changed due to other corrections to the TSPA-LA Model.

Generally, the uncertain inputs that predominantly determine uncertainty in expected dose for each scenario class are those inputs that describe the occurrence and extent of failure of EBS components. This conclusion is the same for both model versions. For the Seismic Ground Motion Scenario Class, the key uncertain input at early times is *SCCTHRP* (residual stress threshold; as sampled, *SCCTHRP* is a percent of a base value of 351 MPa and is related to the stress corrosion cracking threshold, *SCCTHR*, by $SCCTHRP = (SCCTHR \times 100)/(351\ MPa)$), which essentially determines the probability of damage to CDSP or CSNF WPs for each seismic event. At later times, because the Seismic Ground Motion Scenario Class is combined with the Nominal Scenario Class, the key uncertain input is *WDGCA22* (temperature dependence coefficient associated with general corrosion rate for Alloy 22, K), which essentially determines the uncertainty in the time and extent of general corrosion failures (both by stress-corrosion cracking and by patches). For the Igneous Intrusive Scenario Class, the key uncertain input is *IGRATE* (rate of occurrence of igneous intrusive events, yr^{-1}). For the Nominal Scenario Class the key uncertain input is *WDGCA22* (temperature dependence coefficient associated with general corrosion rate for Alloy 22, K), which essentially determines the uncertainty in the time and extent of general corrosion failures (both by SCC and by patches). For the Early Failure Scenario Classes key uncertain inputs are *PROBWPEF* (probability that a randomly selected WP will experience an early failure) and *PROBDSEF* (probability that a randomly selected DS will experience an early failure). For the Igneous Eruptive Scenario Class the key uncertain input is *IGERATE* (rate of occurrence of volcanic eruption events, yr^{-1}). For the Seismic Fault

Displacement Modeling Case, no single input emerged as predominant. Rather, the analysis identified several uncertain inputs with moderately monotonic effects on the expected dose for the scenario class.

INTENTIONALLY LEFT BLANK

Table K9-1[a]. Summary of Selected Sensitivity Analysis Results

Scenario Class	TSPA-LA Model Output (time of maximum mean value)	Key Uncertain Inputs[a]
Total System	Total expected dose 0 to 10,000 years (10,000 years)	• Residual stress threshold for SCC (*SCCTHRP*) • Frequency of occurrence of igneous events (*IGRATE*) • Logarithm of scale factor in ground water specific discharge (*SZGWSPDM*)
	Total expected dose 10,000 to 1,000,000 years (1,000,000 years)	• Frequency of occurrence of igneous events (*IGRATE*) • General corrosion rate (Alloy 22) temperature dependence (*WDGCA22*) • Logarithm of scale factor in ground water specific discharge (*SZGWSPDM*)
Nominal	Expected dose resulting from corrosion processes (720,000 years)	• General corrosion rate (Alloy 22) temperature dependence (*WDGCA22*) • Deviation from median yield strength range for outer lid (*WDZOLID*)
Early Failure Drip Shield	Expected dose resulting from early failure of drip shields over 20,000 years (2,000 years)	• Probability of early failure per drip shield (*PROBDSEF*) • Uncertainty factor accounting for small-scale heterogeneity in fracture permeability (*SEEPUNC*) • Logarithm of mean fracture permeability in lithophysal rock units (*SEEPRM*)
Early Failure Waste Package	Expected dose resulting from early failure of waste packages over 20,000 years (12,000 years)	• Probability of early failure per waste package (*PROBWPEF*) • Pointer variable for infiltration scenario (*INFIL*) • Selector for host-rock thermal conductivity scenario (*THERMCON*)
Igneous Intrusive	Expected dose resulting from igneous intrusion over 20,000 years (20,000 years)	• Frequency of occurrence of igneous events (*IGRATE*) • Logarithm of scale factor in ground water specific discharge (*SZGWSPDM*) • Pointer variable for infiltration scenario (*INFIL*)
	Expected dose resulting from igneous intrusion over 1,000,000 years (1,000,000 years)	• Frequency of occurrence of igneous events (*IGRATE*) • Logarithm of scale factor in ground water specific discharge (*SZGWSPDM*) • Pointer variable for infiltration scenario (*INFIL*)
Igneous Eruptive	Expected dose resulting from volcanic eruption over 20,000 years (20,000 years)	• Frequency of occurrence of volcanic eruptions (*IGERATE*) • Pointer variable for long-term inhalation dose conversation factors for exposure to volcanic ash (*INHLTPV*) • Diffusivity of radionuclides in divides (*DDIVIDE*)
	Expected dose resulting from volcanic eruption over 1,000,000 years (1,000,000 years)	• Frequency of occurrence of volcanic eruptions (*IGERATE*) • Depth of soil within which radionuclides affect the biosphere (*BTILLAGE*)

Table K9-1[a]. Summary of Selected Sensitivity Analysis Results (Continued)

Scenario Class	TSPA-LA Model Output (time of maximum mean value)	Key Uncertain Inputs[a]
Seismic Ground Motion	Expected dose resulting from seismic ground motion over 20,000 years (20,000 years)	• Residual stress threshold for SCC (*SCCTHRP*)
	Expected dose resulting from combination of seismic ground motion and corrosion processes over 1,000,000 years (1,000,000 years)	• General corrosion rate (Alloy 22) temperature dependence (*WDGCA22*) • Residual stress threshold (*SCCTHRP*)
Seismic Fault Displacement	Expected dose resulting from fault displacement over 20,000 years (20,000 years)	• Groundwater biosphere dose conversion factor for ^{99}Tc (*MICTC99*) • Pointer variable for infiltration scenario (*INFIL*) • Logarithm of scale factor in ground water specific discharge (*SZGWSPDM*) • Selector variable determining the collapsed drift rubble thermal conductivity (*DTDRHUNC*)
	Expected dose resulting from fault displacement over 1,000,000 years (1,000,000 years)	• Pointer variable for infiltration scenario (*INFIL*) • Logarithm of scale factor for uncertainty in plutonium solubility at ionic strength below 1 molal (*EP1LOWPU*) • Logarithm of scale factor in ground water specific discharge (*SZGWSPDM*) • Waste package flux splitting factor (*WPFLUX*)

[a] Name (in parentheses) is the variable name used in the sensitivity analyses (see Table K3-1).

K10[a] HUMAN INTRUSION SCENARIO

Uncertainty and sensitivity analysis results for human intrusion at 200,000 yr are presented in two sets. The first set is for expected dose to the RMEI (*EXPDOSE*, mrem/yr) over the time period [200,000, 220,000 yr] (Figures K10-1[a] and K10-2[a]); the second set is for expected dose to the RMEI (*EXPDOSE*, mrem/yr) over the time period [220,000, 1,000,000 yr] (Figures K10-3[a] and K10-4[a]). This division is made because of the rapid changes in *EXPDOSE* that occur in the first 20,000 yr after a drilling intrusion. This analysis is reported separately from the other scenario classes because the human intrusion results are calculated for comparison with the human intrusion standard. In contrast, the preceding analyses for expected dose to the RMEI are calculated for comparison with the individual protection standard.

As examination of Figure K10-1a,b[a] shows, *EXPDOSE* increases rapidly for the first 1000 to 2000 yr after a drilling intrusion at 200,000 yr and then decreases monotonically out to 220,000 yr. The individual sample elements produce peak values for *EXPDOSE* between approximately 0.003 and 0.1 mrem/yr; at 220,000 yr the values for *EXPDOSE* are between 0.00006 and 0.02 mrem/yr. The monotonic decrease in *EXPDOSE* can be seen in Figure K10-3a,b[a] to continue out to approximately 400,000 yr; beyond 400,000 yr, *EXPDOSE* remains approximately constant with a slight tendency to increase.

For the time period [200,000, 300,000 yr], ^{99}Tc and ^{129}I are the dominant radionuclides contributing to *EXPDOSE*; for the time period [300,000, 1,000,000 yr], ^{242}Pu is the dominant radionuclide contributing to *EXPDOSE* (Figure 8.1-17[a]).

Sensitivity analysis results for the [200,000, 220,000 yr] time period are presented in Figures K10-1c[a] and K10-2b,c,d,e,f,g[a]. As indicated by the PRCCs in Figure K10-1c[a], the most important variables affecting *EXPDOSE* for the first 5000 yr after the intrusion are *INFIL* (infiltration level), *CSSPECSA* (effective specific surface area of CSNF waste, m^2/mg; as sampled, *CSSPECSA* is actually the logarithm of the indicated surface area), *SZGWSPDM* (groundwater specific discharge multiplier; as sampled, *SZGWSPDM* is actually the logarithm of the indicated multiplier), *SZFIPOVO* (flowing interval porosity in the volcanic unit of the SZ), *MICTC99* (dose conversion factor for ^{99}Tc for modern interglacial climate, (rem/yr)/(pCi/L)), and *EBSDIFCF* (scale factor used to represent uncertainty in EBS diffusion coefficient; as sampled, *EBSDIFCF* is actually the logarithm of the indicated scale factor). For the first 5000 yr after the intrusion, *INFIL*, *CSSPECSA*, *SZGWSPDM*, *MICTC99* and *EBSDIFCF* have positive effects on *EXPDOSE*, and *SZFIPOVO* has a negative effect on *EXPDOSE*. These effects result because (1) increasing *INFIL* increases water flow in the EBS and UZ, (2) increasing *CSSPECSA* increases the release of radionuclides from degrading CSNF waste, (3) increasing *SZGWSPDM* increases water movement in the SZ, (4) increasing *MICTC99* increases the dose received from a unit concentration of ^{99}Tc in groundwater, and (5) increasing *EBSDIFCF* increases the release of radionuclides from the EBS. In contrast, increasing *SZFIPOVO* has an early negative effect on *EXPDOSE* as a result of increasing the volume of water involved in radionuclide transport in the SZ; however, this dilution effect is short lived and quickly ceases as more radionuclides enter the SZ.

After approximately 5000 yr, *INFIL*, *CSSPECSA*, *SZGWSPDM* and *EBSDIFCF* have a negative effect on *EXPDOSE* (Figure K10-1c[a]). This reversal in effects results from the high mobility

of ^{99}Tc and ^{129}I, which are the dominant radionuclides contributing to *EXPDOSE* prior to 300,000 yr. Because of this mobility, variables that increase the release of ^{99}Tc and ^{129}I at early times (i.e., in the first 5000 yr after intrusion) also decrease the releases of ^{99}Tc and ^{129}I at later times. As a result, *INFIL*, *CSSPECSA*, *SZGWSPDM* and *EBSDIFCF* have a positive effect on *EXPDOSE* in the first 5000 yr after intrusion and a negative effect on *EXPDOSE* at later times. In contrast, *MICTC99* continues to have a positive effect on *EXPDOSE* with increasing time.

More detailed analyses for *EXPDOSE* for the time period [200,000, 205,000 yr] are provided by the stepwise regression analyses and scatterplots in Figure K10-2[a]. As examination of the regression analyses and associated scatterplots shows, many individual variables affect *EXPDOSE* with no single variable having a dominant effect on the uncertainty in *EXPDOSE*. Further, many variables having small effects and possibly some complex interactions between variables and the radionuclides that they affect, results in regression models with small R^2 values (i.e., 0.75, 0.53 and 0.41).

As indicated by the PRCCS in Figure K10-3c[a], the most important variables affecting *EXPDOSE* after approximately 300,000 yr are *SZGWSPDM*, *GOESITED* (density of sorption sites on goethite, sites/nm^2), *COLFEOSS* (iron oxide colloid concentration when degraded stainless steel is present but no degrading carbon steel is present, mg/L), *EP1LOWPU* (scale factor used to incorporate uncertainty into plutonium solubility under low ionic strength conditions; as sampled, *EP1LOWPU* is actually the logarithm of the indicated scale factor), and *SZFISPVO* (flowing interval spacing in volcanic unit of SZ, m). The variables *SZGWSPDM*, *COLFEOSS*, *EP1LOWPU* and *SZFISPVO* have positive effects on *EXPDOSE*; in contrast, *GOESITED* has a negative effect. The positive effects associated with *SZGWSPDM*, *COLFEOSS*, *EP1LOWPU* and *SZFISPVO* result because (1) increasing *SZGWSPDM* increases water flow in the SZ, (2) increasing *COLFEOSS* increases the attachment of radionuclides to mobile colloids, (3) increasing *EP1LOWPU* increases the solubility of plutonium, and (4) increasing *SZFISPVO* decreases the diffusion of radionuclides from fractures in the volcanic unit of the SZ into the surrounding rock matrix. The negative effect associated with *GOESITED* results from increasing the sorption of radionuclides onto corrosion products in the EBS.

More detailed analyses for *EXPDOSE* for the time period [220,000, 1,000,000 yr] are provided by the stepwise regression analyses and scatterplots in Figure K10-4[a]. As examination of the regression analyses and associated scatterplots shows, many individual variables affect *EXPDOSE* with no single variable having a dominant effect on the uncertainty in *EXPDOSE*. Further, many variables having small effects and possibly some complex interactions between variables and the radionuclides that they affect is resulting in regression models with small R^2 values (i.e., 0.50, 0.55, and 0.63).

Comparisons of results for *EXPDOSE* resulting from human intrusion at 200,000 yr obtained with versions 5.000 and 5.005 of the TSPA-LA Model are presented in Figures K10-5[a] and K10-6[a].

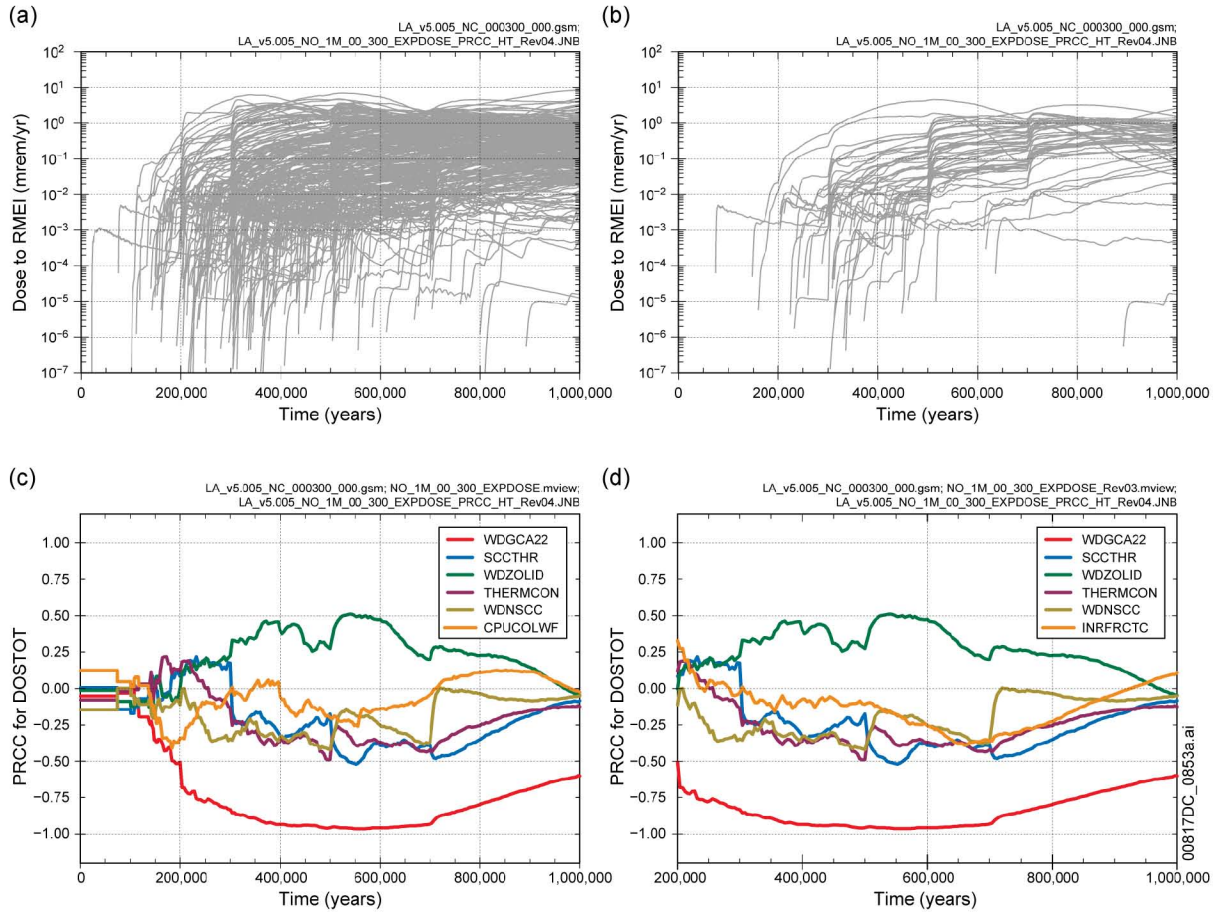

Source: Output DTNs: MO0710ADTSPAWO.000 [DIRS 183752]; and MO0710PLOTSFIG.000 [DIRS 185207].

Figure K4.5-1[a]. Dose to RMEI (*DOSTOT*, mrem/yr) for all radioactive species under nominal conditions obtained with version 5.005 of the TSPA-LA Model: (a) *DOSTOT* for all (i.e., 300) sample elements, (b) *DOSTOT* for first 50 sample elements, (c) PRCCs for *DOSTOT* for [0; 1,000,000 yr], and (d) PRCCs for *DOSTOT* for [200,000; 1,000,000 yr]

(a)

	DOSTOT: 400,000 Years			DOSTOT: 600,000 Years			DOSTOT: 800,000 Years		
Step[a]	Variable[b]	R^{2c}	SRRC[d]	Variable	R^2	SRRC	Variable	R^2	SRRC
1	WDGCA22	0.78	−0.90	WDGCA22	0.85	−0.94	WDGCA22	0.63	−0.80
2	WDZOLID	0.81	0.16	WDZOLID	0.87	0.14	WDZOLID	0.65	0.16
3	WDNSCC	0.82	−0.12	THERMCON	0.88	−0.10	MICI129	0.67	0.13
4	THERMCON	0.83	−0.13	INFIL	0.89	−0.10	SCCTHR	0.68	−0.10
5	INFIL	0.84	−0.10	SCCTHR	0.90	−0.09			
6	SCCTHR	0.85	−0.09	WDNSCC	0.91	−0.08			
7	WDGCUA22	0.85	0.07	CORRATSS	0.91	−0.07			
8	WDLCRATE	0.86	0.06	WDGCUA22	0.92	0.08			
9				MICTC99	0.92	0.07			
10				DTDRHUNC	0.92	0.04			
11				CSNFMASS	0.92	0.04			

a: Steps in stepwise rank regression analysis
b: Variables listed in order of selection in stepwise regression
c: Cumulative R^2 value with entry of each variable into regression model
d: Standardized rank regression coefficients (SRRCs) in final regression model

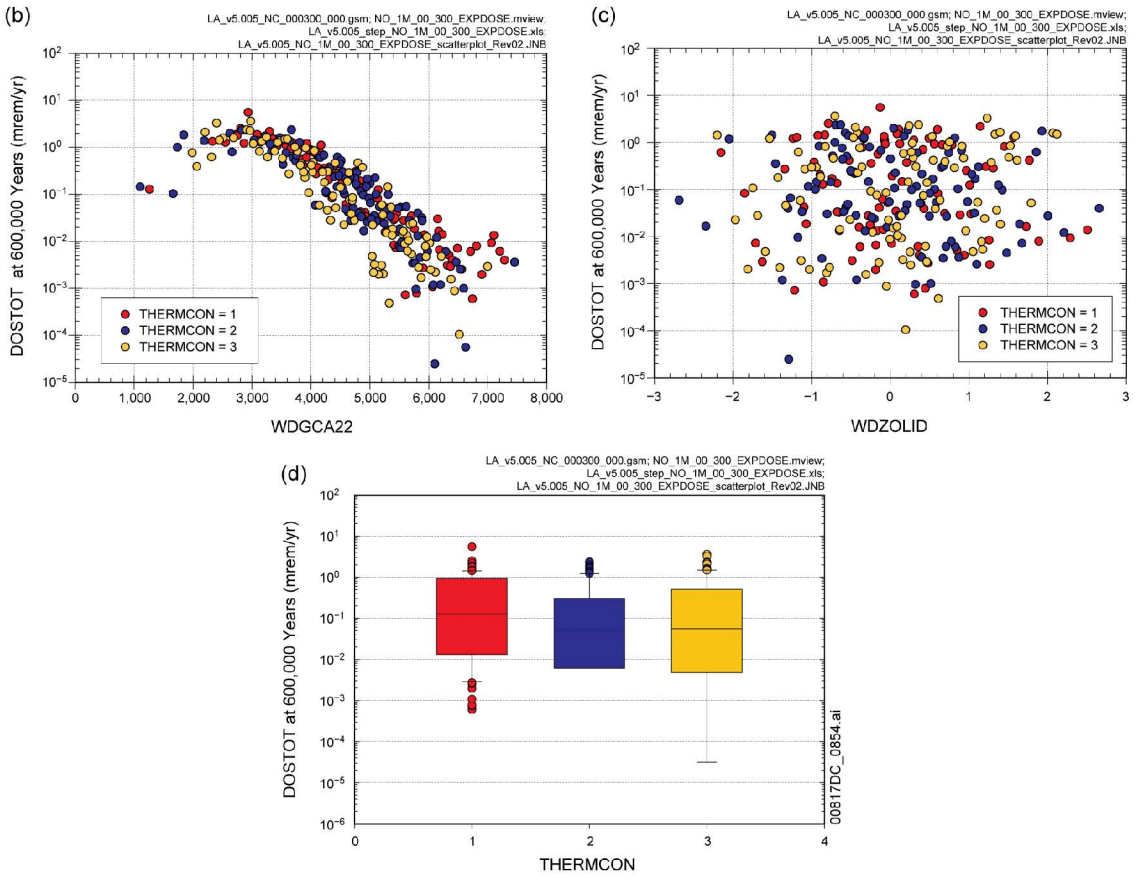

Source: Output DTNs: MO0710ADTSPAWO.000 [DIRS 183752]; and MO0710PLOTSFIG.000 [DIRS 185207].

NOTE: In (d), the box extends from 0.25 to 0.75 quantile; lower and upper bar and whisker extend to 0.1 and 0.9 quantile, respectively; dots represent values outside 0.1 to 0.9 quantile range; median indicated by light horizontal line.

Figure K4.5-2[a]. Stepwise rank regression analyses and selected scatterplots for dose to RMEI (*DOSTOT*, mrem/yr) for all radioactive species under nominal conditions obtained with version 5.005 of the TSPA-LA Model: (a) regressions for *DOSTOT* at 400,000, 600,000, and 800,000 years, and (b,c,d) scatterplots for *DOSTOT* at 600,000 years

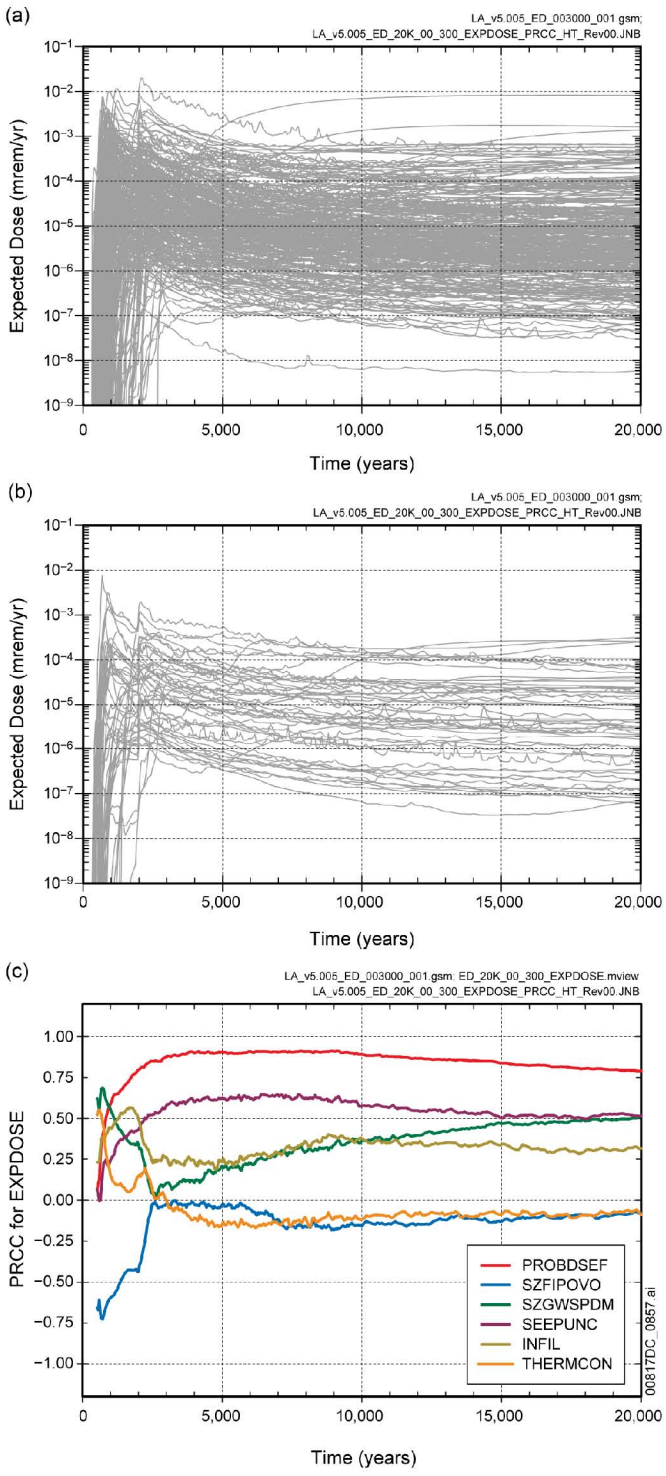

Source: Output DTNs: MO0710ADTSPAWO.000 [DIRS 183752]; and MO0710PLOTSFIG.000 [DIRS 185207].

Figure K5.7.1-1[a]. Expected dose to RMEI (*EXPDOSE*, mrem/yr) over [0, 20,000 yr] for all radioactive species resulting from early DS failure obtained with version 5.005 of the TSPA-LA Model: (a) *EXPDOSE* for all (i.e., 300) sample elements, (b) *EXPDOSE* for first 50 sample elements, and (c) PRCCs for *EXPDOSE*

(a)

	EXPDOSE: 3,000 Years			EXPDOSE: 5,000 Years			EXPDOSE: 10,000 Years		
Step[a]	Variable[b]	R^{2c}	SRRC[d]	Variable	R^2	SRRC	Variable	R^2	SRRC
1	PROBDSEF	0.70	0.80	PROBDSEF	0.71	0.81	PROBDSEF	0.63	0.79
2	SEEPUNC	0.77	0.24	SEEPUNC	0.78	0.24	INFIL	0.69	0.23
3	SEEPPRM	0.81	−0.22	SEEPPRM	0.81	−0.19	SEEPUNC	0.73	0.23
4	MICTC99	0.83	0.15	INFIL	0.83	0.13	SEEPPRM	0.77	−0.21
5	INFIL	0.85	0.12	MICTC99	0.84	0.09	ALPHAL	0.79	−0.13
6	ALPHAL	0.86	−0.08	ALPHAL	0.85	−0.11	SZCOLRAL	0.80	−0.12
7	MICNP237	0.87	0.07	MICNP237	0.86	0.09	MICPU239	0.81	0.09
8	CSNFMASS	0.87	0.07				CPUCOLWF	0.82	0.08
9	GP4NO3	0.87	0.07				SEEPPRMN	0.82	−0.08
10							RHMU0	0.83	0.08
11							SMECSA	0.83	0.08
12							SZGWSPDM	0.84	0.07
13							UZFAG4	0.84	−0.07
14							EP1LOWPU	0.85	0.06

a: Steps in stepwise rank regression analysis
b: Variables listed in order of selection in stepwise regression
c: Cumulative R^2 value with entry of each variable into regression model
d: Standardized rank regression coefficients (SRRCs) in final regression model

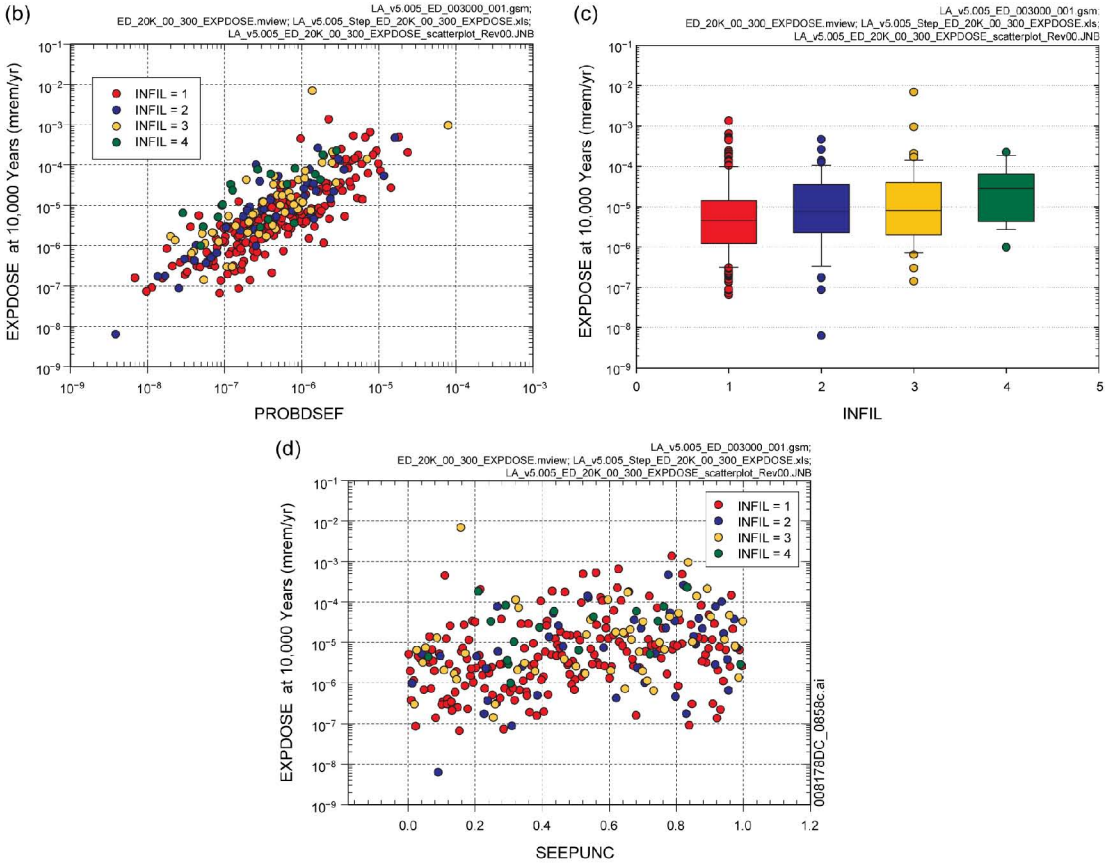

Source: Output DTNs: MO0710ADTSPAWO.000 [DIRS 183752]; and MO0710PLOTSFIG.000 [DIRS 185207].

NOTE: In (c), the box extends from 0.25 to 0.75 quantile; lower and upper bar and whisker extend to 0.1 and 0.9 quantile, respectively; dots represent values outside 0.1 to 0.9 quantile range; median indicated by light horizontal line.

Figure K5.7.1-2[a]. Stepwise rank regression analyses and selected scatterplots for expected dose to RMEI (*EXPDOSE*, mrem/yr) over [0, 20,000 yr] for all radioactive species resulting from early DS failure obtained with version 5.005 of the TSPA-LA Model: (a) regressions for *EXPDOSE* at 3,000, 5,000, and 10,000 years, and (b,c,d) scatterplots for *EXPDOSE* at 10,000 years

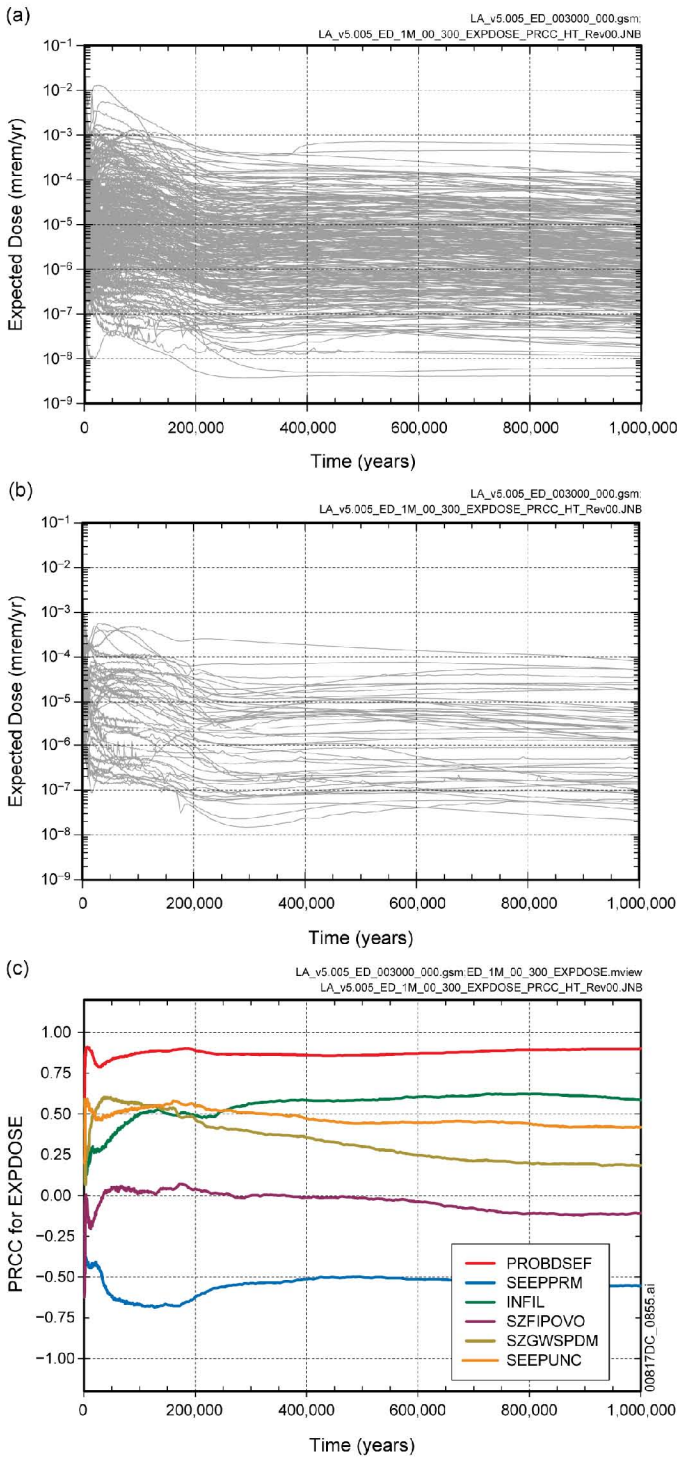

Source: Output DTNs: MO0710ADTSPAWO.000 [DIRS 183752]; and MO0710PLOTSFIG.000 [DIRS 185207].

Figure K5.7.1-3[a]. Expected dose to RMEI (*EXPDOSE*, mrem/yr) over [0, 1,000,000 yr] for all radioactive species resulting from early DS failure obtained with version 5.005 of the TSPA-LA Model: (a) *EXPDOSE* for all (i.e., 300) sample elements, (b) *EXPDOSE* for first 50 sample elements, and (c) PRCCs for *EXPDOSE*

(a)

	EXPDOSE: 50,000 Years			EXPDOSE: 200,000 Years			EXPDOSE: 500,000 Years		
Step[a]	Variable[b]	R^{2c}	SRRC[d]	Variable	R^2	SRRC	Variable	R^2	SRRC
1	PROBDSEF	0.47	0.71	PROBDSEF	0.55	0.76	PROBDSEF	0.52	0.73
2	SZGWSPDM	0.55	0.29	INFIL	0.63	0.26	INFIL	0.63	0.31
3	INFIL	0.64	0.28	SEEPPRM	0.68	−0.23	SEEPPRM	0.68	−0.21
4	SEEPPRM	0.69	−0.26	SZGWSPDM	0.72	0.21	EP1LOWPU	0.71	0.18
5	EP1LOWPU	0.73	0.20	SEEPUNC	0.77	0.23	SEEPUNC	0.75	0.20
6	SEEPUNC	0.77	0.20	EP1LOWPU	0.79	0.15	SZGWSPDM	0.78	0.15
7	MICPU239	0.78	0.10	MICPU239	0.80	0.13	GOESITED	0.79	−0.12
8	SEEPPRMN	0.78	−0.08	GOESITED	0.82	−0.11	MICPU239	0.81	0.11
9	SZCOLRAL	0.79	−0.10	SEEPPRMN	0.82	−0.07	PHCSS	0.82	0.11
10	PHCSS	0.80	−0.08	HFOSA	0.83	−0.09	SEEPPRMN	0.82	−0.08
11	SZDIFCVO	0.81	−0.10	SZFISPVO	0.84	0.10	EP1LOWNU	0.83	0.11
12	SZFISPVO	0.81	0.10	SZDIFCVO	0.84	−0.09	ALPHAL	0.84	−0.10
13	ALPHAL	0.82	−0.07	ALPHAL	0.85	−0.09	UZFAG4	0.85	−0.07
14				EP1LOWNU	0.85	0.08	SZFISPVO	0.85	0.10
15				SZCONCOL	0.86	0.07	SZDIFCVO	0.86	−0.09
16				SZCOLRVO	0.86	0.06	HFOSA	0.87	−0.08

a: Steps in stepwise rank regression analysis
b: Variables listed in order of selection in stepwise regression
c: Cumulative R^2 value with entry of each variable into regression model
d: Standardized rank regression coefficients (SRRCs) in final regression model

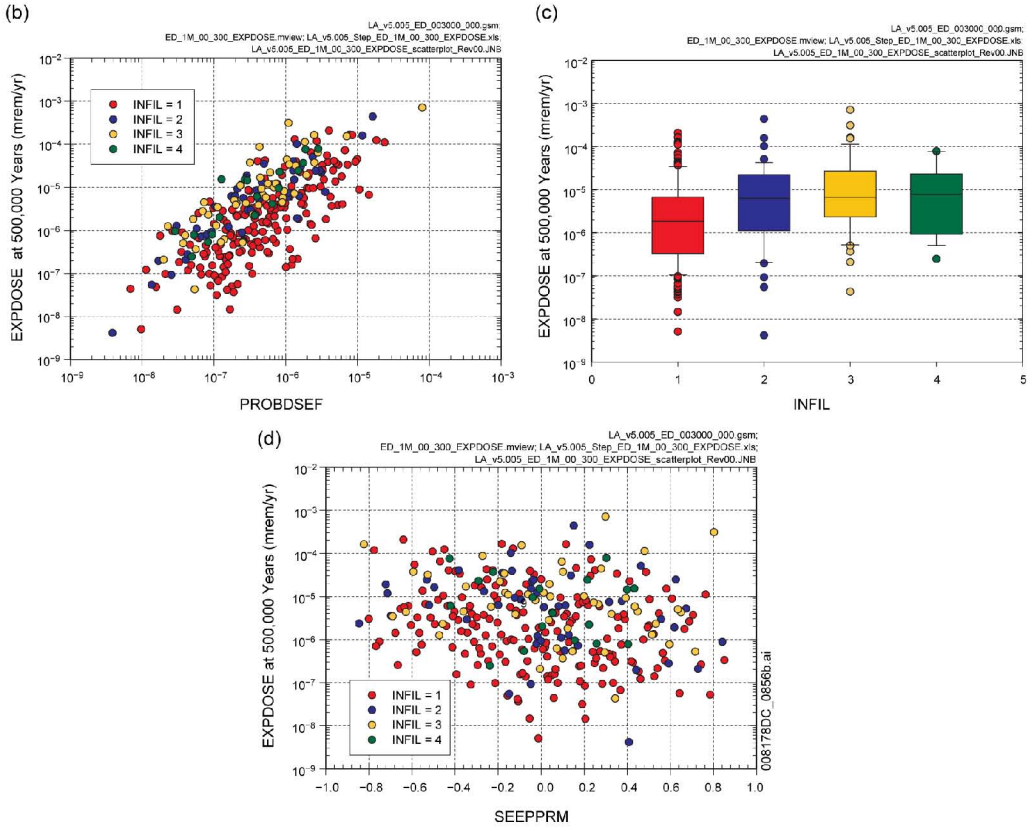

Source: Output DTNs: MO0710ADTSPAWO.000 [DIRS 183752]; and MO0710PLOTSFIG.000 [DIRS 185207].

NOTE: In (c), the box extends from 0.25 to 0.75 quantile; lower and upper bar and whisker extend to 0.1 and 0.9 quantile, respectively; dots represent values outside 0.1 to 0.9 quantile range; median indicated by light horizontal line.

Figure K5.7.1-4[a]. Stepwise rank regression analyses and selected scatterplots for expected dose to RMEI (*EXPDOSE*, mrem/yr) over [0, 1,000,000 yr] for all radioactive species resulting from early DS failure obtained with version 5.005 of the TSPA-LA Model: (a) regressions for *EXPDOSE* at 50,000, 200,000, and 500,000 years, and (b,c,d) scatterplots for *EXPDOSE* at 500,000 years

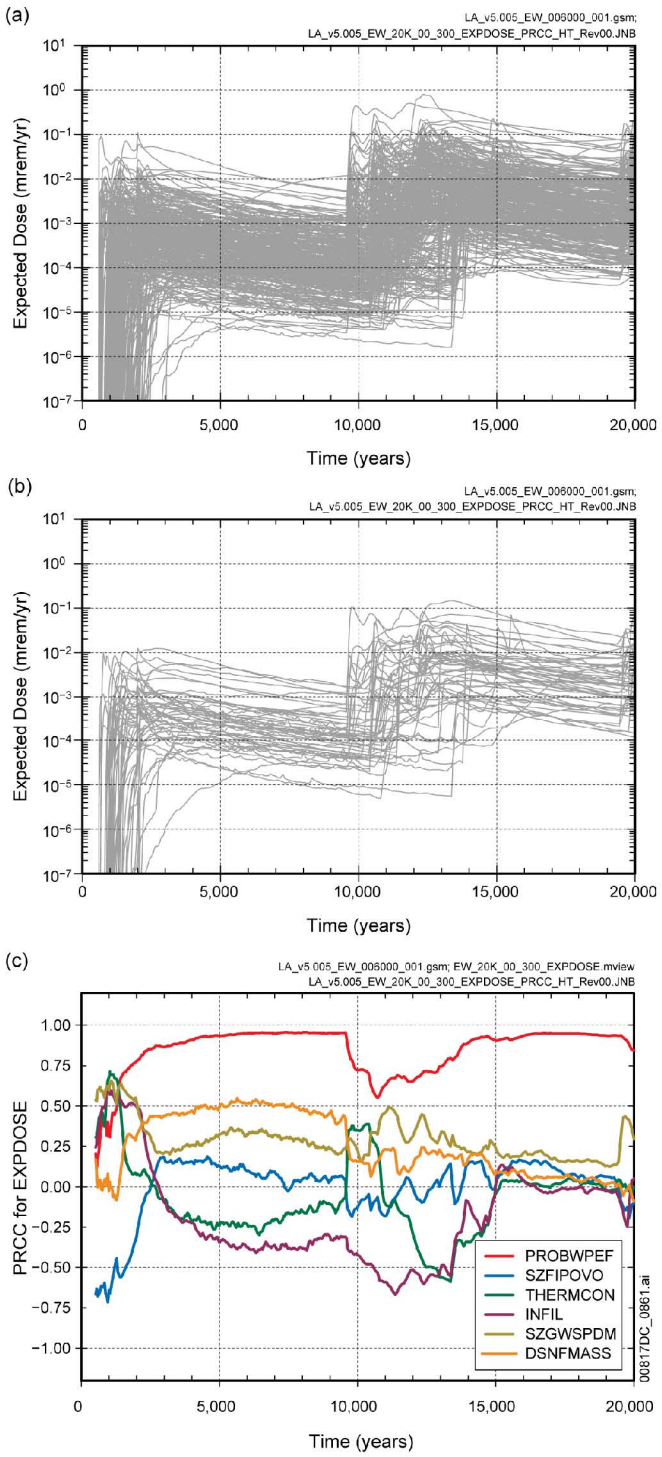

Source: Output DTNs: MO0710ADTSPAWO.000 [DIRS 183752]; and MO0710PLOTSFIG.000 [DIRS 185207].

Figure K5.7.2-1[a]. Expected dose to RMEI (*EXPDOSE*, mrem/yr) over [0, 20,000 yr] for all radioactive species resulting from early WP failure obtained with version 5.005 of the TSPA-LA Model: (a) *EXPDOSE* for all (i.e., 300) sample elements, (b) *EXPDOSE* for first 50 sample elements, and (c) PRCCs for *EXPDOSE*

(a)

	EXPDOSE: 3,000 Years			EXPDOSE: 5,000 Years			EXPDOSE: 10,000 Years		
Step[a]	Variable[b]	R^{2c}	SRRC[d]	Variable	R^2	SRRC	Variable	R^2	SRRC
1	PROBWPEF	0.62	0.76	PROBWPEF	0.77	0.86	PROBWPEF	0.47	0.69
2	MICTC99	0.67	0.22	MICTC99	0.81	0.16	INFIL	0.57	−0.30
3	MICC14	0.70	0.16	DSNFMASS	0.83	0.18	THERMCON	0.64	0.26
4	DSNFMASS	0.72	0.17	MICC14	0.85	0.14	MICCI36	0.66	0.10
5	UZFAG8	0.74	−0.13	UZFAG8	0.86	−0.10	EP1LOWPU	0.67	0.10
6	SZFISPVO	0.75	0.13	HLWDRACD	0.87	0.08	MICTC99	0.68	0.12
7	HLWDRACD	0.76	0.09	INFIL	0.87	−0.09	SZSREG1Y	0.69	−0.10
8	UZTORRG3	0.77	0.11	HLWDRALK	0.88	0.06	DSNFMASS	0.69	0.09
9	SZGWSPDM	0.78	0.10	MICNP237	0.88	0.07	SEEPPRM	0.70	0.09
10	SZDIFCVO	0.79	−0.08	THERMCON	0.88	−0.06	KDSNCOL	0.71	0.09
11	UZGAM	0.80	−0.08	PH2DHLNS	0.89	−0.06			
12				UZGAM	0.89	−0.06			
13				RHMUN65	0.89	−0.05			

a: Steps in stepwise rank regression analysis
b: Variables listed in order of selection in stepwise regression
c: Cumulative R^2 value with entry of each variable into regression model
d: Standardized rank regression coefficients (SRRCs) in final regression model

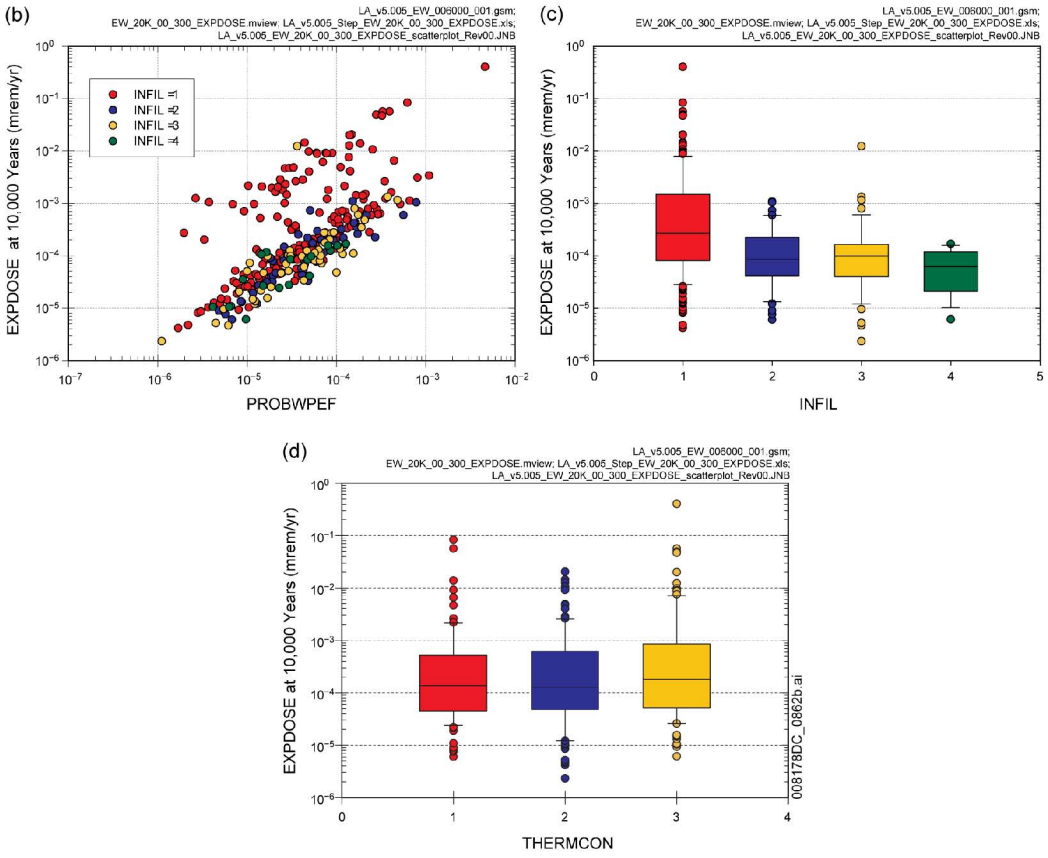

Source: Output DTNs: MO0710ADTSPAWO.000 [DIRS 183752]; and MO0710PLOTSFIG.000 [DIRS 185207].

NOTE: In (c,d), the box extends from 0.25 to 0.75 quantile; lower and upper bar and whisker extend to 0.1 and 0.9 quantile, respectively; dots represent values outside 0.1 to 0.9 quantile range; median indicated by light horizontal line.

Figure K5.7.2-2[a]. Stepwise rank regression analyses and selected scatterplots for expected dose to RMEI (*EXPDOSE*, mrem/yr) over [0, 20,000 yr] for all radioactive species resulting from early WP failure obtained with version 5.005 of the TSPA-LA Model: (a) regressions for *EXPDOSE* at 3,000, 5,000, and 10,000 years, and (b,c,d) scatterplots for *EXPDOSE* at 10,000 years

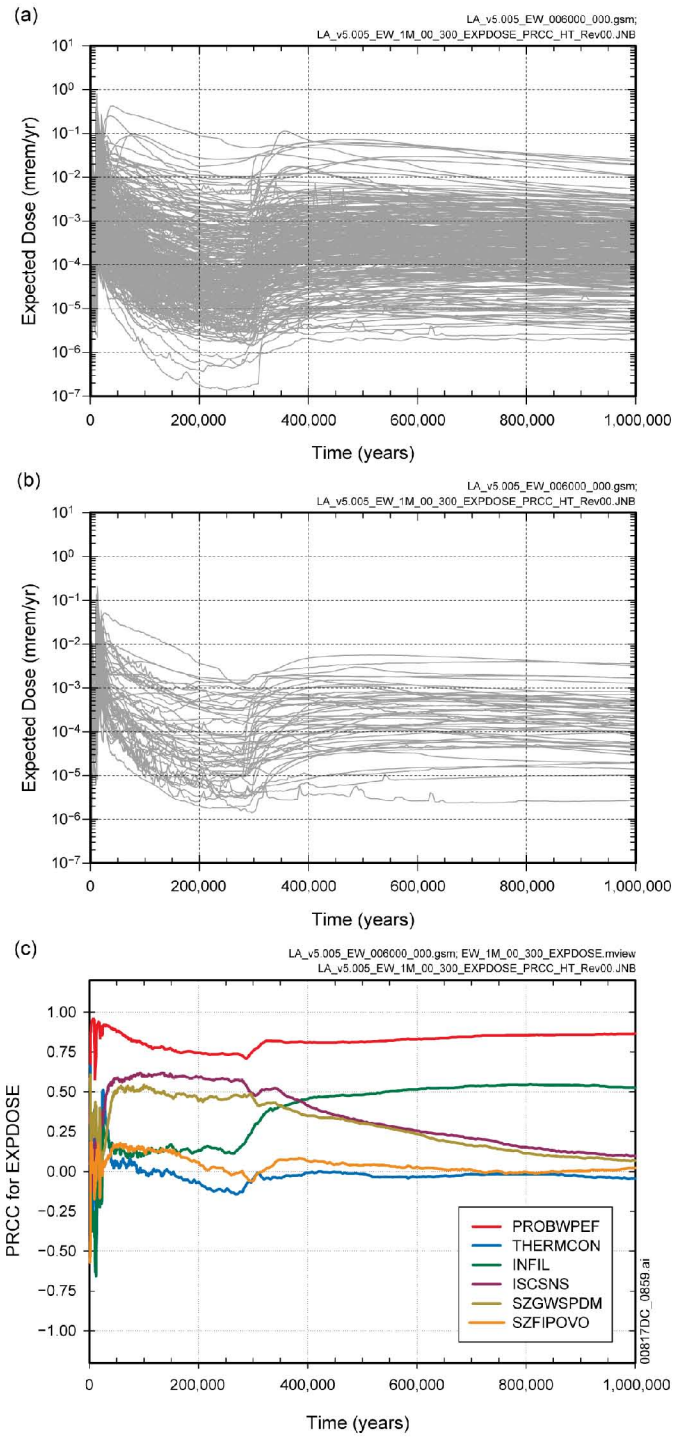

Source: Output DTNs: MO0710ADTSPAWO.000 [DIRS 183752]; and MO0710PLOTSFIG.000 [DIRS 185207].

Figure K5.7.2-3[a]. Expected dose to RMEI (*EXPDOSE*, mrem/yr) over [0, 1,000,000 yr] for all radioactive species resulting from early WP failure obtained with version 5.005 of the TSPA-LA Model: (a) *EXPDOSE* for all (i.e., 300) sample elements, (b) *EXPDOSE* for first 50 sample elements, and (c) PRCCs for *EXPDOSE*

(a)

	EXPDOSE: 50,000 Years			EXPDOSE: 200,000 Years			EXPDOSE: 500,000 Years		
Step[a]	Variable[b]	R^{2c}	SRRC[d]	Variable	R^2	SRRC	Variable	R^2	SRRC
1	PROBWPEF	0.60	0.79	PROBWPEF	0.37	0.62	PROBWPEF	0.39	0.70
2	ISCSNS	0.66	0.25	ISCSNS	0.50	0.38	INFIL	0.51	0.31
3	SZGWSPDM	0.72	0.22	SZGWSPDM	0.56	0.24	EP1LOWPU	0.55	0.20
4	EP1LOWPU	0.74	0.14	EP1LOWPU	0.58	0.15	SEEPPRM	0.59	−0.22
5	MICNP237	0.75	0.10	SZFISPVO	0.60	0.17	SZGWSPDM	0.62	0.17
6	SZFISPVO	0.75	0.08	SZDIFCVO	0.61	−0.14	SEEPUNC	0.65	0.19
7	SZKDSRAL	0.76	0.09	IGRATE	0.63	0.10	EP1LOWNU	0.67	0.17
8	COLU	0.77	0.08	SEEPPRM	0.64	−0.11	ALPHAL	0.69	−0.14
9				SEEPUNC	0.65	0.10	SZFISPVO	0.71	0.15
10				RHMU20	0.66	0.10	GOESITED	0.73	−0.14
11							HFOSA	0.74	−0.12
12							MICPU239	0.75	0.11
13							SZDIFCVO	0.76	−0.10
14							SEEPPRMN	0.77	−0.09
15							ISCSNS	0.77	0.09
16							HFOSITED	0.78	−0.08

a: Steps in stepwise rank regression analysis
b: Variables listed in order of selection in stepwise regression
c: Cumulative R^2 value with entry of each variable into regression model
d: Standardized rank regression coefficients (SRRCs) in final regression model

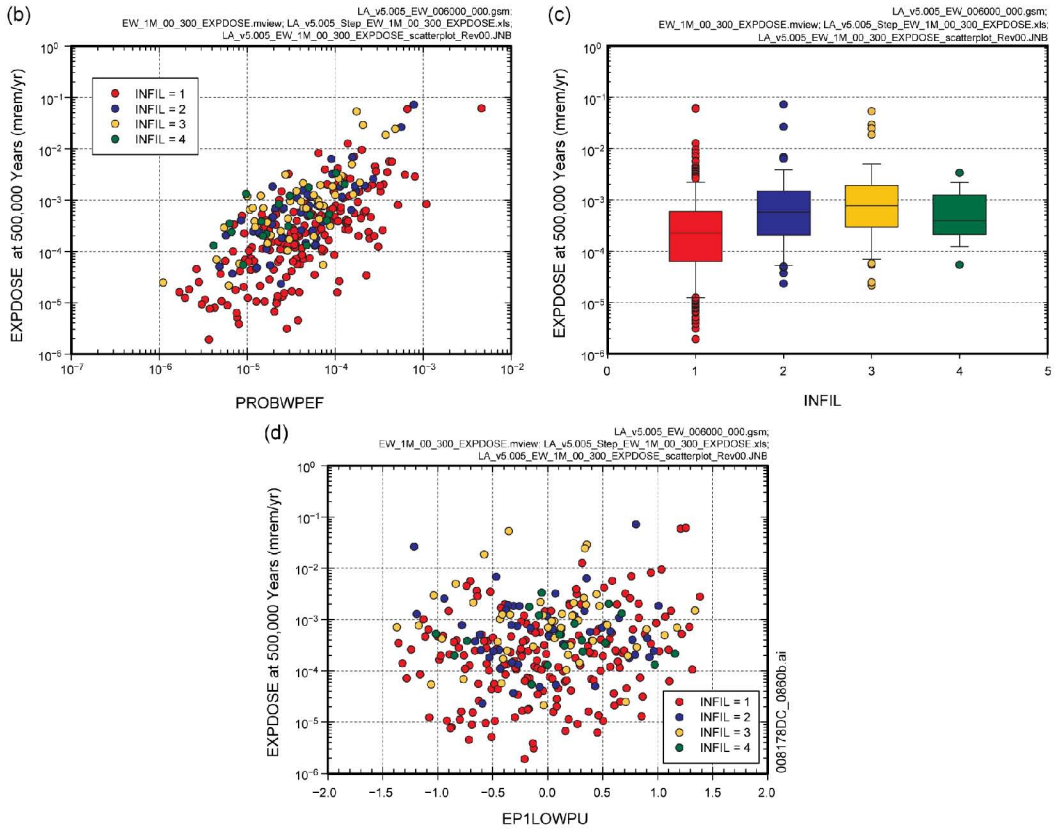

Source: Output DTNs: MO0710ADTSPAWO.000 [DIRS 183752]; and MO0710PLOTSFIG.000 [DIRS 185207].

NOTE: In (c), the box extends from 0.25 to 0.75 quantile; lower and upper bar and whisker extend to 0.1 and 0.9 quantile, respectively; dots represent values outside 0.1 to 0.9 quantile range; median indicated by light horizontal line.

Figure K5.7.2-4[a]. Stepwise rank regression analyses and selected scatterplots for expected dose to RMEI (*EXPDOSE*, mrem/yr) over [0, 1,000,000 yr] for all radioactive species resulting from early WP failure obtained with version 5.005 of the TSPA-LA Model: (a) regressions for *EXPDOSE* at 50,000, 200,000, and 500,000 years, and (b,c,d) scatterplots for *EXPDOSE* at 500,000 years

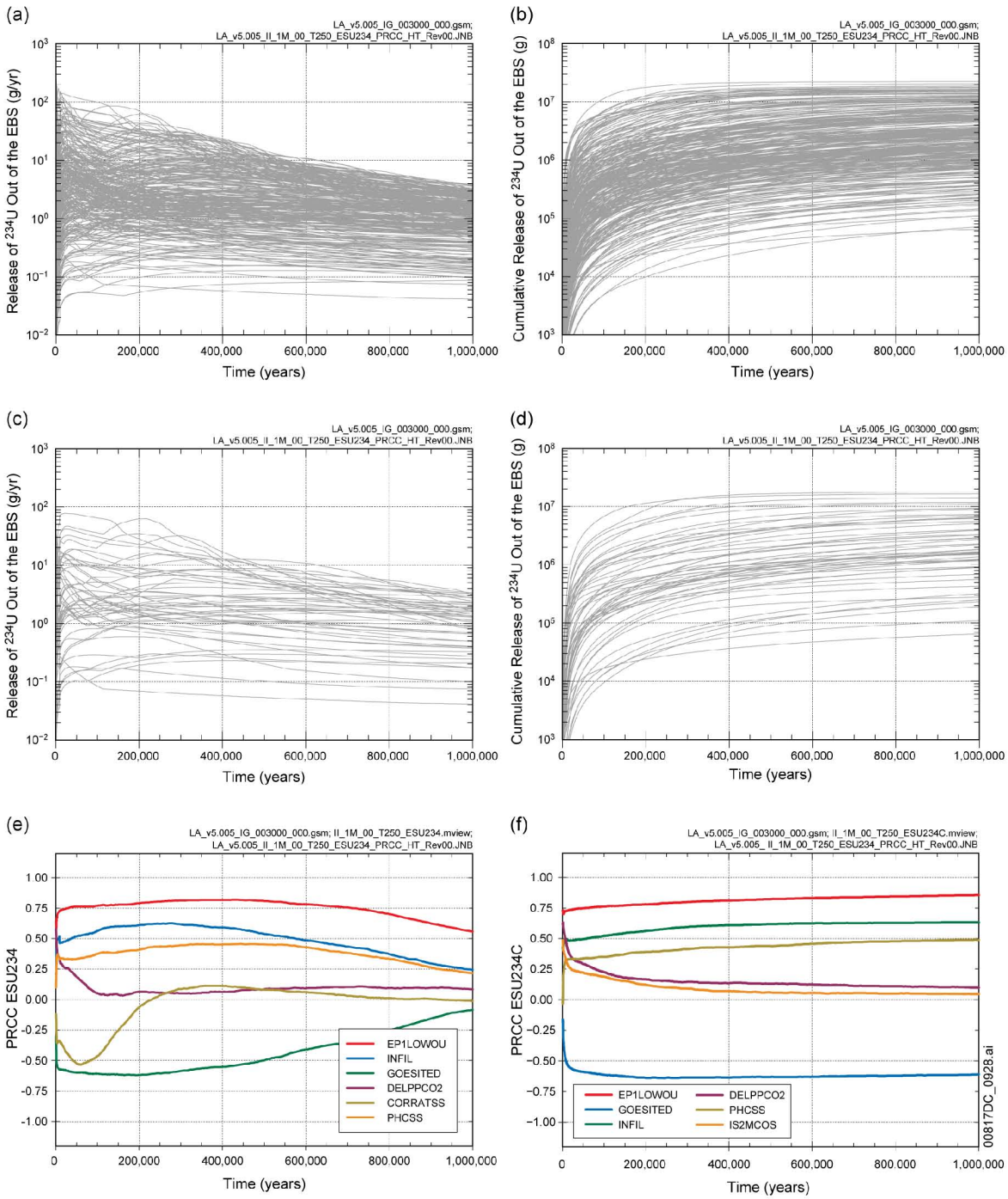

Source: Output DTNs: MO0801TSPAPRSA.000 [DIRS 184620]; and MO0710PLOTSFIG.000 [DIRS 185207].

Figure K6.3.2-5[a]. Time-dependent release rates (*ESU234*, g/yr) and cumulative (i.e., integrated) releases (*ESU234C*, g) over 1,000,000 years for the movement of dissolved ^{234}U from the EBS to the UZ resulting from an igneous intrusive event at 250 years that destroys all WPs in the repository obtained with version 5.005 of the TSPA-LA Model: (a,b) *ESU234* and *ESU234C* for all (i.e., 300) sample elements, (c,d) *ESU234* and *ESU234C* for first 50 sample elements, and (e,f) PRCCs for *ESU234* and *ESU234C*

(a)

	ESU234: 50,000 Years			ESU234: 200,000 Years			ESU234: 500,000 Years		
Step[a]	Variable[b]	R^2 [c]	SRRC[d]	Variable	R^2	SRRC	Variable	R^2	SRRC
1	EP1LOWOU	0.38	0.56	EP1LOWOU	0.41	0.60	EP1LOWOU	0.49	0.68
2	INFIL	0.49	0.33	INFIL	0.58	0.39	INFIL	0.64	0.38
3	GOESITED	0.57	−0.29	GOESITED	0.66	−0.32	PHCSS	0.69	0.22
4	CORRATSS	0.64	−0.30	HFOSA	0.70	−0.20	GOESITED	0.73	−0.23
5	HFOSA	0.67	−0.19	PHCSS	0.73	0.19	HFOSA	0.75	−0.14
6	GOERELAB	0.69	0.12	DSNFMASS	0.75	0.12	CSNFMASS	0.77	0.13
7	DSNFMASS	0.71	0.12	GOERELAB	0.76	0.13	GOERELAB	0.78	0.12
8	PHCSS	0.72	0.16	GOESA	0.77	−0.09	WDLCRATE	0.79	−0.11
9	IS2MCOS	0.74	0.13	CSNFMASS	0.77	0.08	PROBWPEF	0.80	0.09
10	CSNFMASS	0.75	0.12	HFOSITED	0.78	−0.08			
11	KDPUCOL	0.76	0.09	IS2MCONS	0.79	0.07			
12	GOESA	0.77	−0.08	WDDSGC29	0.79	0.08			
13	DELPPCO2	0.76	0.08						

(b)

	ESU234C: 50,000 Years			ESU234C: 200,000 Years			ESU234C: 500,000 Years		
Step[a]	Variable[b]	R^2 [c]	SRRC[d]	Variable	R^2	SRRC	Variable	R^2	SRRC
1	EP1LOWOU	0.37	0.56	EP1LOWOU	0.40	0.58	EP1LOWOU	0.45	0.62
2	INFIL	0.48	0.34	INFIL	0.53	0.36	INFIL	0.61	0.38
3	GOESITED	0.55	−0.29	GOESITED	0.62	−0.30	GOESITED	0.68	−0.29
4	CORRATSS	0.60	−0.25	HFOSA	0.65	−0.19	HFOSA	0.72	−0.20
5	PHCSS	0.63	0.19	CORRATSS	0.68	−0.21	PHCSS	0.75	0.21
6	IS2MCOS	0.65	0.16	PHCSS	0.71	0.18	GOERELAB	0.77	0.13
7	HFOSA	0.67	−0.17	DSNFMASS	0.73	0.12	DSNFMASS	0.78	0.10
8	DELPPCO2	0.69	0.12	GOERELAB	0.74	0.13	GOESA	0.79	−0.08
9	CSNFMASS	0.70	0.14	GOESA	0.75	−0.09	CSNFMASS	0.80	0.11
10	GOERELAB	0.71	0.11	KDPUCOL	0.76	0.09	KDPUCOL	0.80	0.08
11	GOESA	0.72	−0.09	CSNFMASS	0.77	0.10	CORRATSS	0.81	−0.08
12	DSNFMASS	0.73	0.09	IS2MCOS	0.78	0.09	HFOSITED	0.81	−0.07
13	CPUPERCS	0.74	−0.08						
14	RHMUN40	0.75	−0.08						
15	KDPUCOL	0.75	0.08						

00817DC_0929a.ai

a: Steps in stepwise rank regression analysis
b: Variables listed in order of selection in stepwise regression
c: Cumulative R^2 value with entry of each variable into regression model
d: Standardized rank regression coefficients (SRRCs) in final regression model

Source: Output DTNs: MO0801TSPAPRSA.000 [DIRS 184620]; and MO0710PLOTSFIG.000 [DIRS 185207].

Figure K6.3.2-6[a]. Stepwise rank regression analyses and selected scatterplots for time-dependent release rates (*ESU234*, g/yr) and cumulative (i.e., integrated) releases (*ESU234C*, g) for the movement of dissolved ^{234}U from the EBS to the UZ resulting from an igneous intrusive event at 250 years that destroys all WPs in the repository obtained with version 5.005 of the TSPA-LA Model: (a,b) regressions for *ESU234* and *ESU234C* at 50,000, 200,000, and 500,000 years, and (c-h) scatterplots for *ESU234* and *ESU234C* at 500,000 years

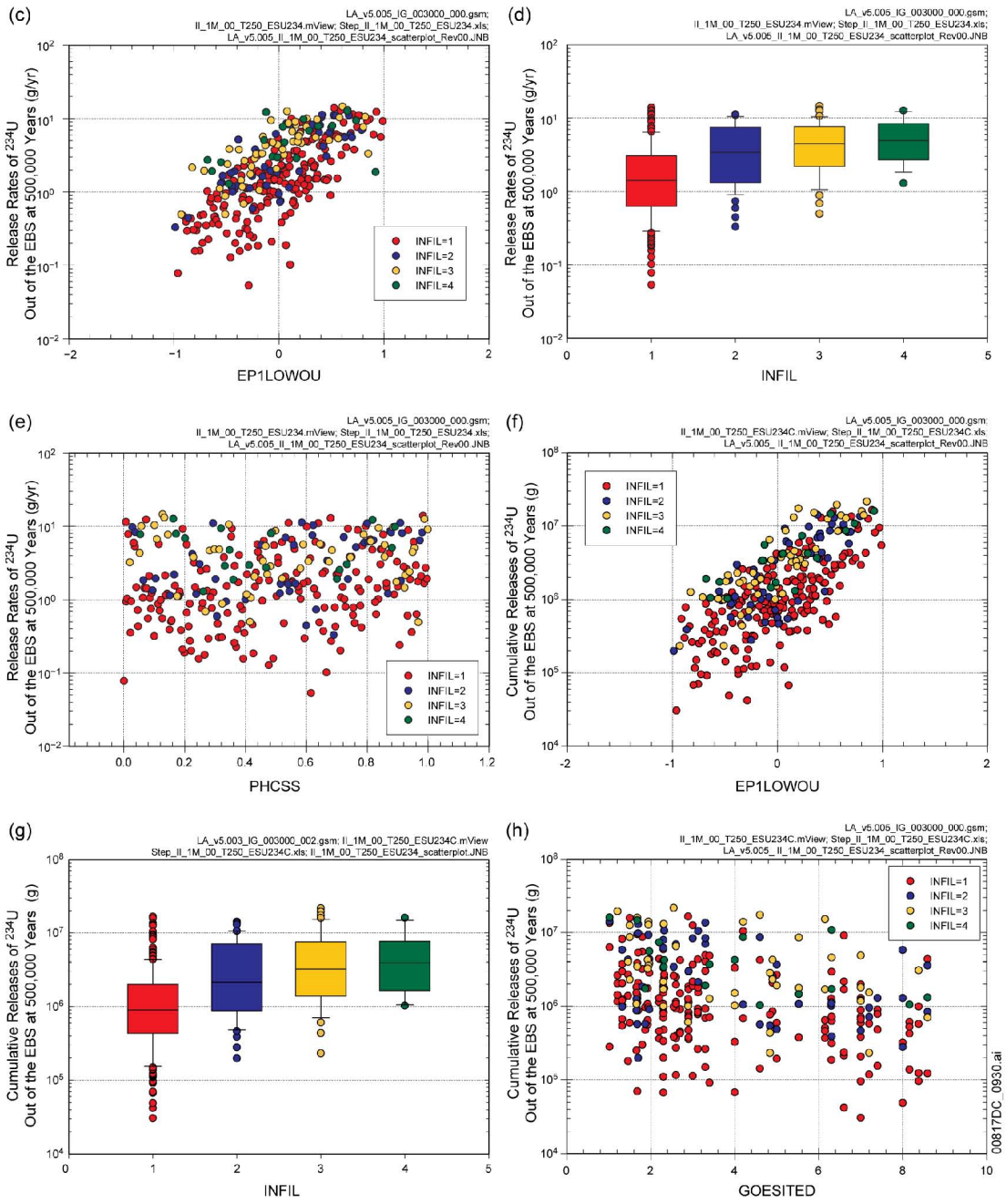

Source: Output DTNs: MO0801TSPAPRSA.000 [DIRS 184620]; and MO0710PLOTSFIG.000 [DIRS 185207].

NOTE: In (d,g), the box extends from 0.25 to 0.75 quantile; lower and upper bar and whisker extend to 0.1 and 0.9 quantile, respectively; dots represent values outside 0.1 to 0.9 quantile range; median indicated by light horizontal line.

Figure K6.3.2-6[a]. Stepwise rank regression analyses and selected scatterplots for time-dependent release rates (*ESU234*, g/yr) and cumulative (i.e., integrated) releases (*ESU234C*, g) for the movement of dissolved ^{234}U from the EBS to the UZ resulting from an igneous intrusive event at 250 years that destroys all WPs in the repository obtained with version 5.005 of the TSPA-LA Model: (a,b) regressions for *ESU234* and *ESU234C* at 50,000, 200,000, and 500,000 years, and (c-h) scatterplots for *ESU234* and *ESU234C* at 500,000 years (continued)

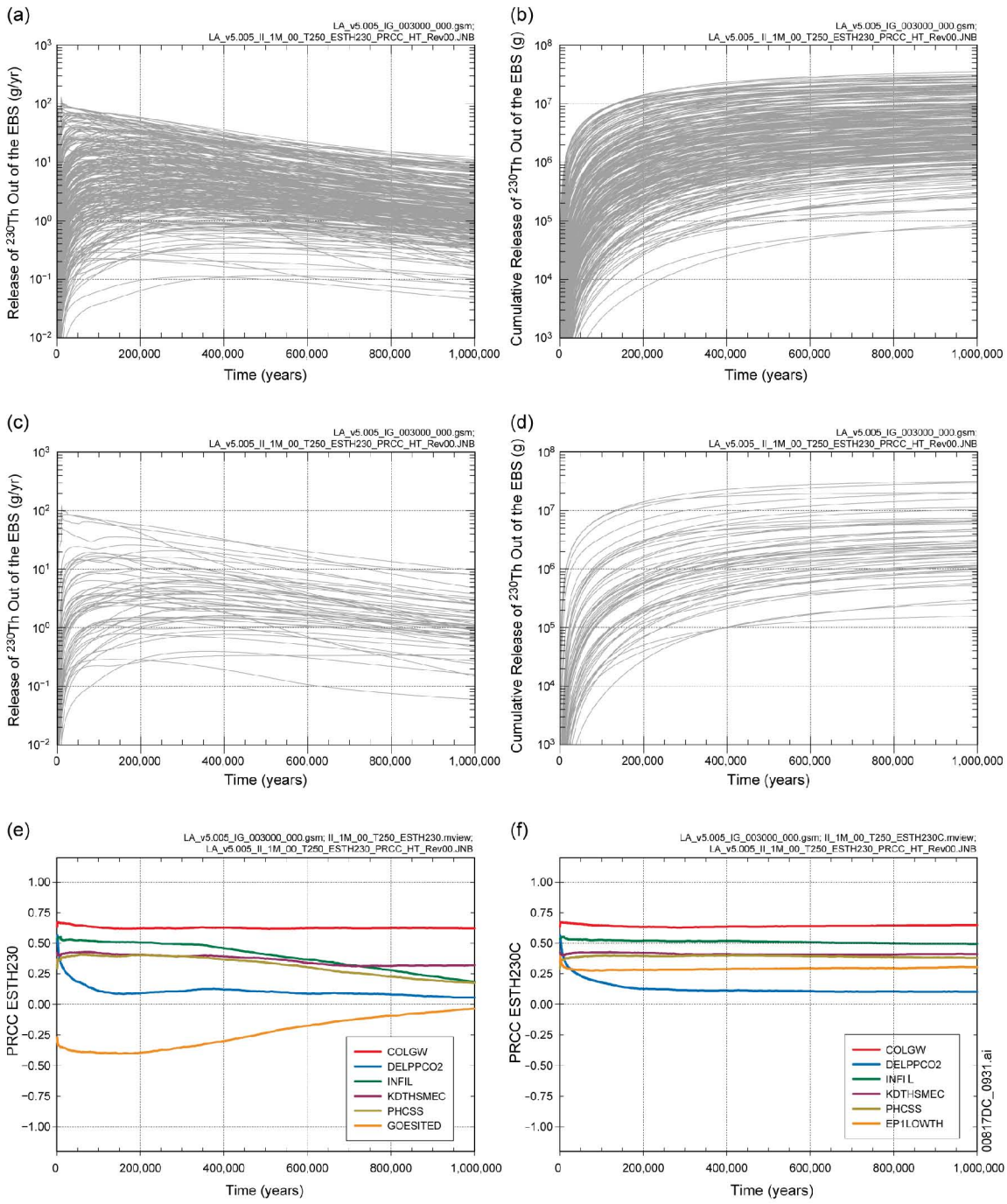

Source: Output DTNs: MO0801TSPAPRSA.000 [DIRS 184620]; and MO0710PLOTSFIG.000 [DIRS 185207].

Figure K6.3.2-7[a]. Time-dependent release rates (*ESTH230*, g/yr) and cumulative (i.e., integrated) releases (*ESTH230C*, g) over 1,000,000 years for the movement of dissolved ^{230}Th from the EBS to the UZ resulting from an igneous intrusive event at 250 years that destroys all WPs in the repository obtained with version 5.005 of the TSPA-LA Model: (a,b) *ESTH230* and *ESTH230C* for all (i.e., 300) sample elements, (c,d) *ESTH230* and *ESTH230C* for first 50 sample elements, and (e,f) PRCCs for *ESTH230* and *ESTH230C*

(a)

	ESTH230: 50,000 Years			ESTH230: 200,000 Years			ESTH230: 500,000 Years		
Step[a]	Variable[b]	$R^{2\,c}$	SRRC[d]	Variable	R^2	SRRC	Variable	R^2	SRRC
1	INFIL	0.24	0.43	INFIL	0.25	0.43	COLGW	0.23	0.45
2	COLGW	0.42	0.43	COLGW	0.41	0.42	INFIL	0.38	0.36
3	KDTHSMEC	0.51	0.27	KDTHSMEC	0.51	0.29	KDTHSMEC	0.49	0.30
4	PHCSS	0.55	0.24	PHCSS	0.56	0.24	PHCSS	0.52	0.21
5	EP1LOWTH	0.59	0.22	EP1LOWTH	0.59	0.21	EP1LOWTH	0.56	0.21
6	UZKDTHDT	0.62	−0.20	EP1LOWOU	0.62	0.15	UZKDTHDT	0.59	−0.17
7	CORRATSS	0.66	−0.17	UZKDTHDT	0.65	−0.17	CSNFMASS	0.61	0.15
8	GOESITED	0.68	−0.13	GOESITED	0.67	−0.17	HFOSA	0.62	−0.11
9	EP1LOWOU	0.69	0.12	HFOSA	0.68	−0.12	FHHISSCP	0.63	0.10
10	HLWMASS	0.70	0.10	GOESA	0.69	−0.09	GOESITED	0.64	−0.10
11							RUBMAXL	0.65	0.09

(b)

	ESTH230C: 50,000 Years			ESTH230C: 200,000 Years			ESTH230C: 500,000 Years		
Step[a]	Variable[b]	$R^{2\,c}$	SRRC[d]	Variable	R^2	SRRC	Variable	R^2	SRRC
1	INFIL	0.24	0.43	INFIL	0.25	0.44	INFIL	0.25	0.43
2	COLGW	0.43	0.45	COLGW	0.42	0.43	COLGW	0.43	0.43
3	KDTHSMEC	0.51	0.27	KDTHSMEC	0.51	0.29	KDTHSMEC	0.52	0.28
4	PHCSS	0.56	0.24	PHCSS	0.56	0.23	PHCSS	0.57	0.22
5	EP1LOWTH	0.60	0.22	EP1LOWTH	0.60	0.22	EP1LOWTH	0.61	0.21
6	UZKDTHDT	0.63	−0.22	UZKDTHDT	0.62	−0.18	UZKDTHDT	0.63	−0.17
7	CORRATSS	0.66	−0.16	EP1LOWOU	0.65	0.14	EP1LOWOU	0.66	0.14
8	GOESITED	0.68	−0.13	CORRATSS	0.67	−0.13	GOESITED	0.67	−0.15
9	EP1LOWOU	0.69	0.12	GOESITED	0.69	−0.15	HFOSA	0.69	−0.12
10	DELPPCO2	0.70	0.12	HFOSA	0.69	−0.10			
11	HLWMASS	0.71	0.10	HLWMASS	0.70	0.09			
12	HFOSA	0.72	−0.09						

00817DC_0932a.ai

a: Steps in stepwise rank regression analysis
b: Variables listed in order of selection in stepwise regression
c: Cumulative R^2 value with entry of each variable into regression model
d: Standardized rank regression coefficients (SRRCs) in final regression model

Source: Output DTNs: MO0801TSPAPRSA.000 [DIRS 184620]; and MO0710PLOTSFIG.000 [DIRS 185207].

Figure K6.3.2-8[a]. Stepwise rank regression analyses and selected scatterplots for time-dependent release rates (*ESTH230*, g/yr) and cumulative (i.e., integrated) releases (*ESTH230C*, g) for the movement of dissolved ^{230}Th from the EBS to the UZ resulting from an igneous intrusive event at 250 years that destroys all WPs in the repository obtained with version 5.005 of the TSPA-LA Model: (a,b) regressions for *ESTH230* and *ESTH230C* at 50,000, 200,000, and 500,000 years, and (c-h) scatterplots for *ESTH230* and *ESTH230C* at 200,000 years

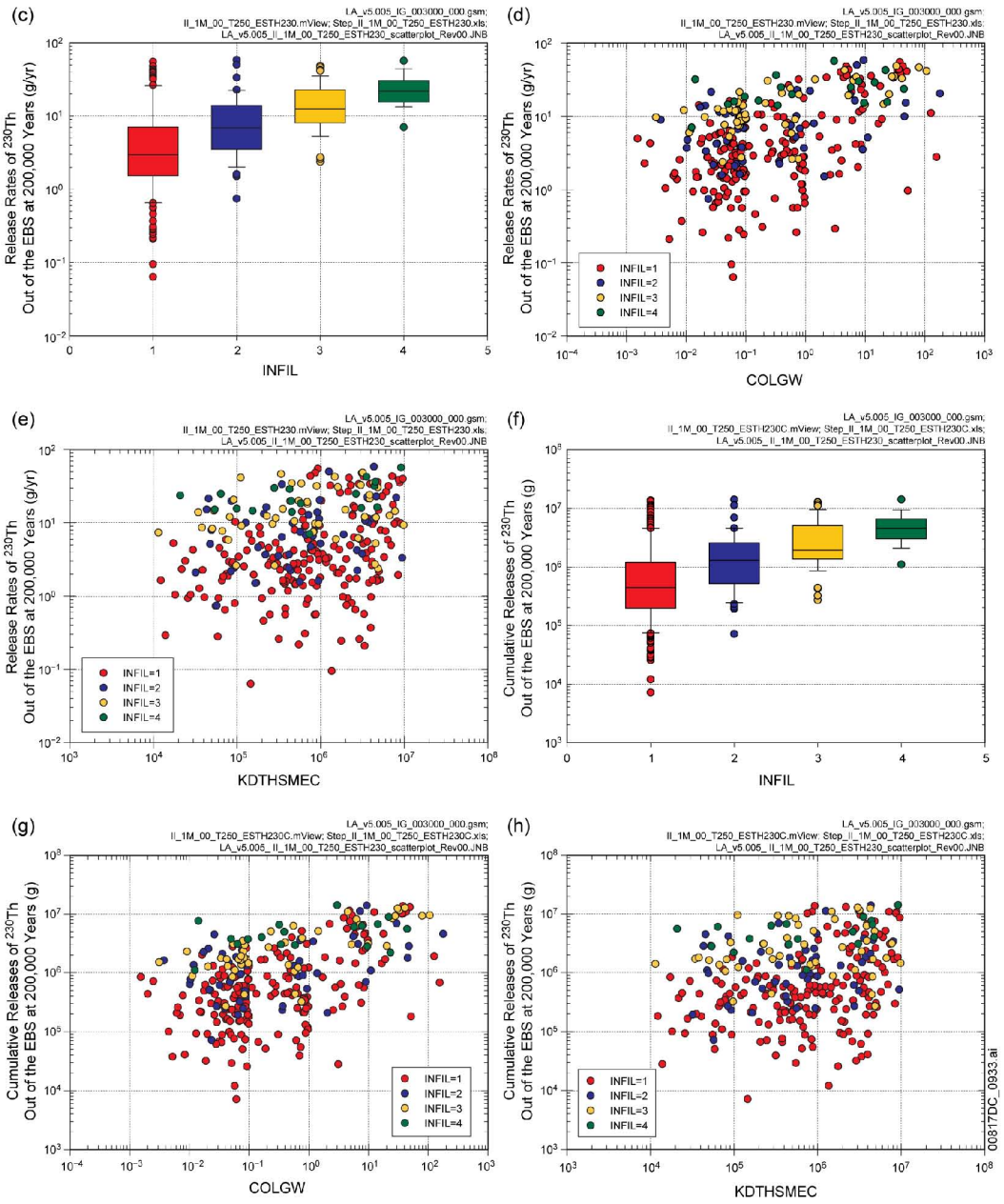

Source: Output DTNs: MO0801TSPAPRSA.000 [DIRS 184620]; and MO0710PLOTSFIG.000 [DIRS 185207].

NOTE: In (c,f), the box extends from 0.25 to 0.75 quantile; lower and upper bar and whisker extend to 0.1 and 0.9 quantile, respectively; dots represent values outside 0.1 to 0.9 quantile range; median indicated by light horizontal line.

Figure K6.3.2-8[a]. Stepwise rank regression analyses and selected scatterplots for time-dependent release rates (*ESTH230*, g/yr) and cumulative (i.e., integrated) releases (*ESTH230C*, g) for the movement of dissolved ^{230}Th from the EBS to the UZ resulting from an igneous intrusive event at 250 years that destroys all WPs in the repository obtained with version 5.005 of the TSPA-LA Model: (a,b) regressions for *ESTH230* and *ESTH230C* at 50,000, 200,000, and 500,000 years, and (c-h) scatterplots for *ESTH230* and *ESTH230C* at 200,000 years (continued)

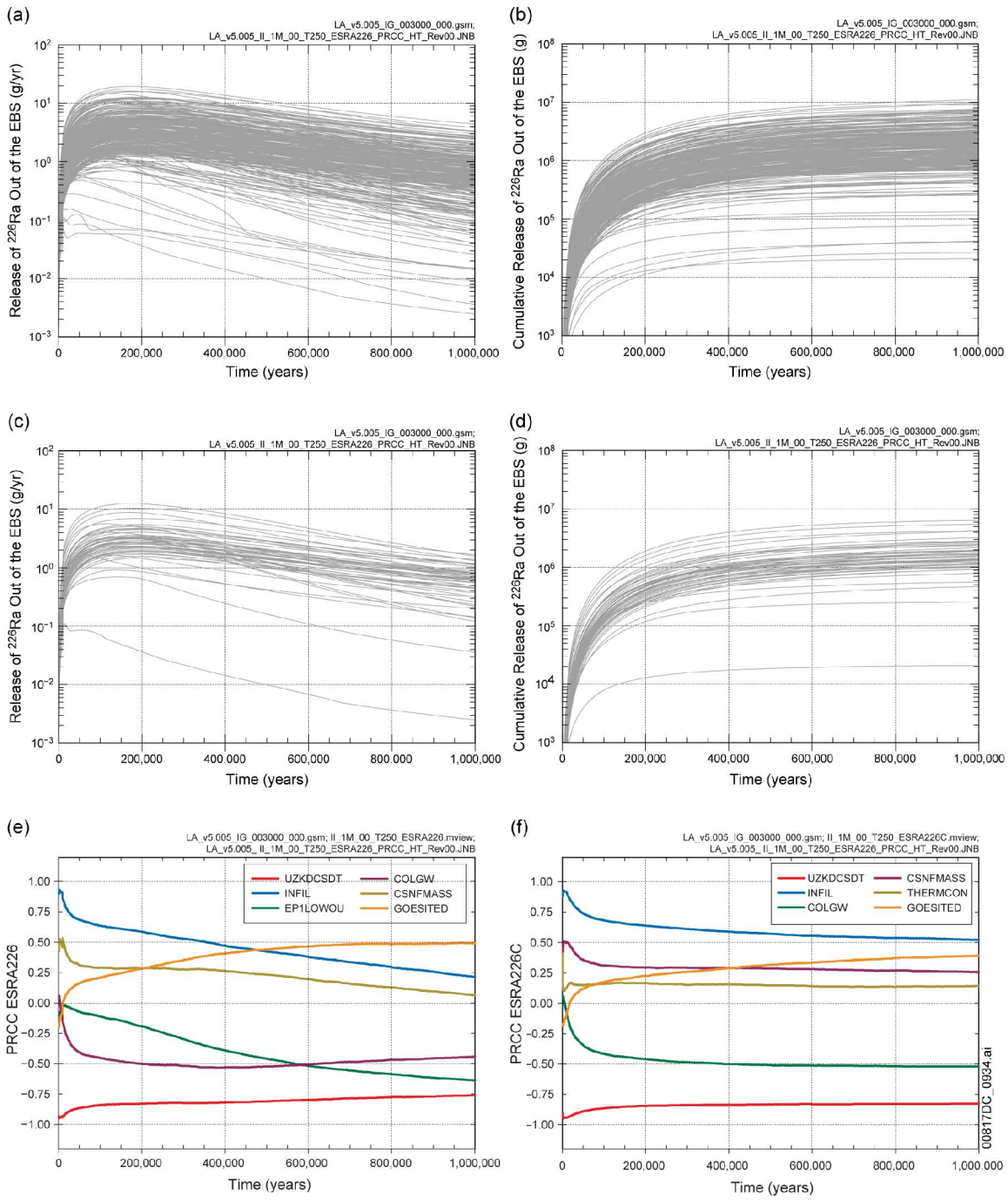

Source: Output DTNs: MO0801TSPAPRSA.000 [DIRS 184620]; and MO0710PLOTSFIG.000 [DIRS 185207].

Figure K6.3.2-9[a] Time-dependent release rates (*ESRA226*, g/yr) and cumulative (i.e., integrated) releases (*ESRA226C*, g) over 1,000,000 years for the movement of dissolved ^{226}Ra from the EBS to the UZ resulting from an igneous intrusive event at 250 years that destroys all WPs in the repository obtained with version 5.005 of the TSPA-LA Model: (a,b) *ESRA226* and *ESRA226C* for all (i.e., 300) sample elements, (c,d) *ESRA226* and *ESRA226C* for first 50 sample elements, and (e,f) PRCCs for *ESRA226* and *ESRA226C*

(a)

	ESRA226: 50,000 Years			ESRA226: 200,000 Years			ESRA226: 500,000 Years		
Step[a]	Variable[b]	R^{2c}	SRRC[d]	Variable	R^2	SRRC	Variable	R^2	SRRC
1	UZKDCSDT	0.54	−0.76	UZKDCSDT	0.50	−0.73	UZKDCSDT	0.46	−0.68
2	INFIL	0.71	0.42	INFIL	0.59	0.30	EP1LOWOU	0.53	−0.29
3	COLGW	0.75	−0.21	COLGW	0.66	−0.27	COLGW	0.59	−0.28
4	CSNFMASS	0.78	0.17	CSNFMASS	0.68	0.16	KDTHSMEC	0.62	−0.16
5	KDTHSMEC	0.79	−0.12	EP1LOWOU	0.70	−0.16	INFIL	0.64	0.15
6	EP1LOWOU	0.80	−0.09	KDTHSMEC	0.72	−0.16	PHCSS	0.67	−0.13
7	KDNPSMEC	0.80	0.09	PHCSS	0.73	−0.09	GOESITED	0.69	0.14
8	DSNFMASS	0.81	0.09	DSNFMASS	0.73	0.09	CSNFMASS	0.70	0.13
9				KDNPSMEC	0.74	0.09			

(b)

	ESRA226C: 50,000 Years			ESRA226C: 200,000 Years			ESRA226C: 500,000 Years		
Step[a]	Variable[b]	R^{2c}	SRRC[d]	Variable	R^2	SRRC	Variable	R^2	SRRC
1	UZKDCSDT	0.56	−0.78	UZKDCSDT	0.52	−0.75	UZKDCSDT	0.51	−0.73
2	INFIL	0.77	0.45	INFIL	0.65	0.36	INFIL	0.58	0.28
3	COLGW	0.80	−0.18	COLGW	0.70	−0.25	COLGW	0.65	−0.27
4	CSNFMASS	0.82	0.17	CSNFMASS	0.73	0.17	EP1LOWOU	0.67	−0.18
5	KDTHSMEC	0.83	−0.10	KDTHSMEC	0.74	−0.14	CSNFMASS	0.70	0.16
6	DSNFMASS	0.84	0.08	EP1LOWOU	0.75	−0.12	KDTHSMEC	0.72	−0.15
7	KDNPSMEC	0.84	0.08	KDNPSMEC	0.76	0.10	PHCSS	0.73	−0.09
8	EP1LOWOU	0.85	−0.08	DSNFMASS	0.77	0.09	GOESITED	0.74	0.09
9	CPUPERCS	0.85	0.06				KDNPSMEC	0.74	0.09
10							DSNFMASS	0.75	0.08

00817DC_0936a.ai

a: Steps in stepwise rank regression analysis
b: Variables listed in order of selection in stepwise regression
c: Cumulative R^2 value with entry of each variable into regression model
d: Standardized rank regression coefficients (SRRCs) in final regression model

Source: Output DTNs: MO0801TSPAPRSA.000 [DIRS 184620]; and MO0710PLOTSFIG.000 [DIRS 185207].

Figure K6.3.2-10[a]. Stepwise rank regression analyses and selected scatterplots for time-dependent release rates (*ESRA226*, g/yr) and cumulative (i.e., integrated) releases (*ESRA226C*, g) for the movement of dissolved ^{226}Ra from the EBS to the UZ resulting from an igneous intrusive event at 250 years that destroys all WPs in the repository obtained with version 5.005 of the TSPA-LA Model: (a,b) regressions for *ESRA226* and *ESRA226C* at 50,000, 200,000, and 500,000 years, and (c-h) scatterplots for *ESRA226* and *ESRA226C* at 50,000 years

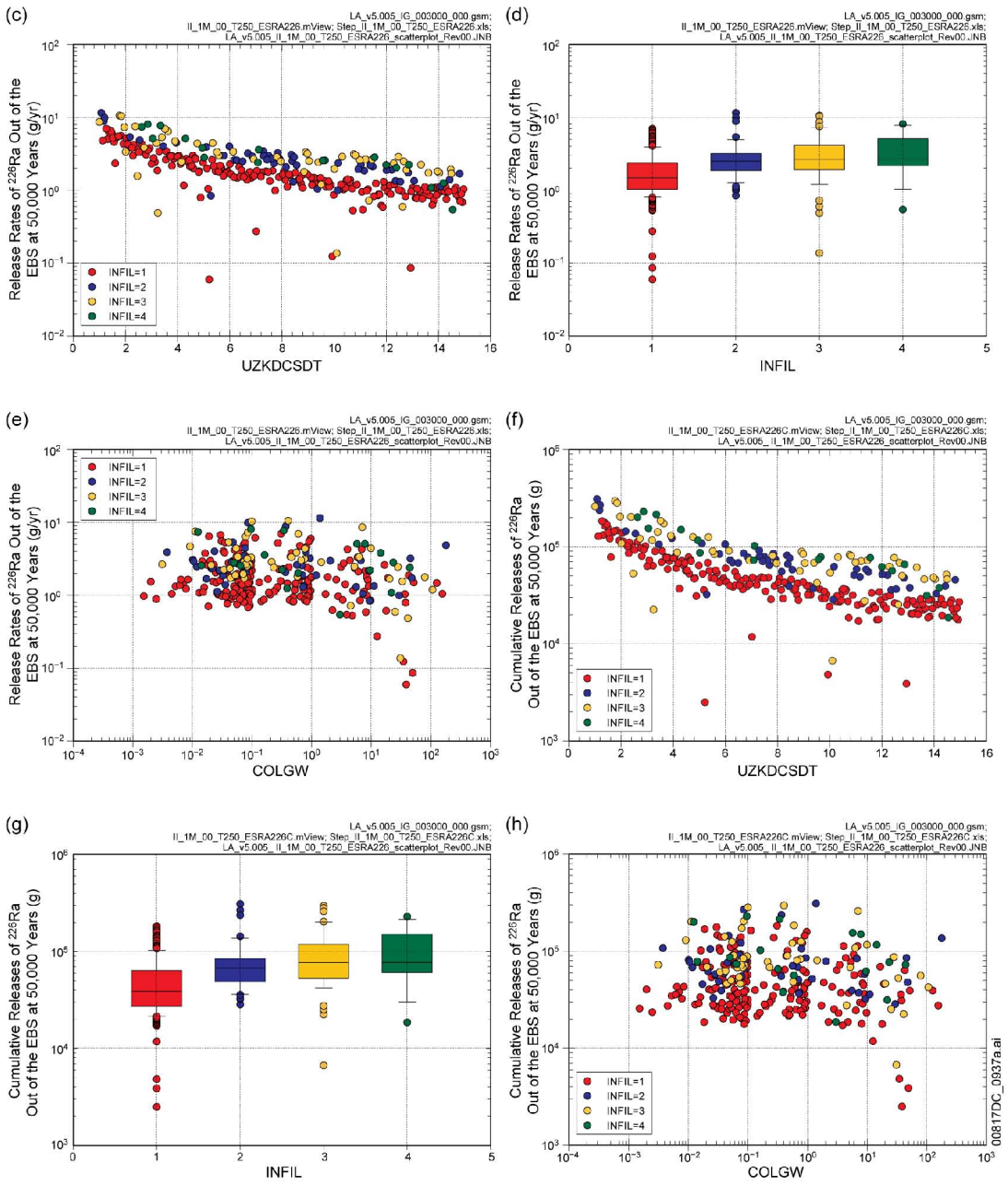

Source: Output DTNs: MO0801TSPAPRSA.000 [DIRS 184620]; and MO0710PLOTSFIG.000 [DIRS 185207].

NOTE: In (d,g), the box extends from 0.25 to 0.75 quantile; lower and upper bar and whisker extend to 0.1 and 0.9 quantile, respectively; dots represent values outside 0.1 to 0.9 quantile range; median indicated by light horizontal line.

Figure K6.3.2-10[a]. Stepwise rank regression analyses and selected scatterplots for time-dependent release rates (*ESRA226*, g/yr) and cumulative (i.e., integrated) releases (*ESRA226C*, g) for the movement of dissolved ^{226}Ra from the EBS to the UZ resulting from an igneous intrusive event at 250 years that destroys all WPs in the repository obtained with version 5.005 of the TSPA-LA Model: (a,b) regressions for *ESRA226* and *ESRA226C* at 50,000, 200,000, and 500,000 years, and (c-h) scatterplots for *ESRA226* and *ESRA226C* at 50,000 years (continued)

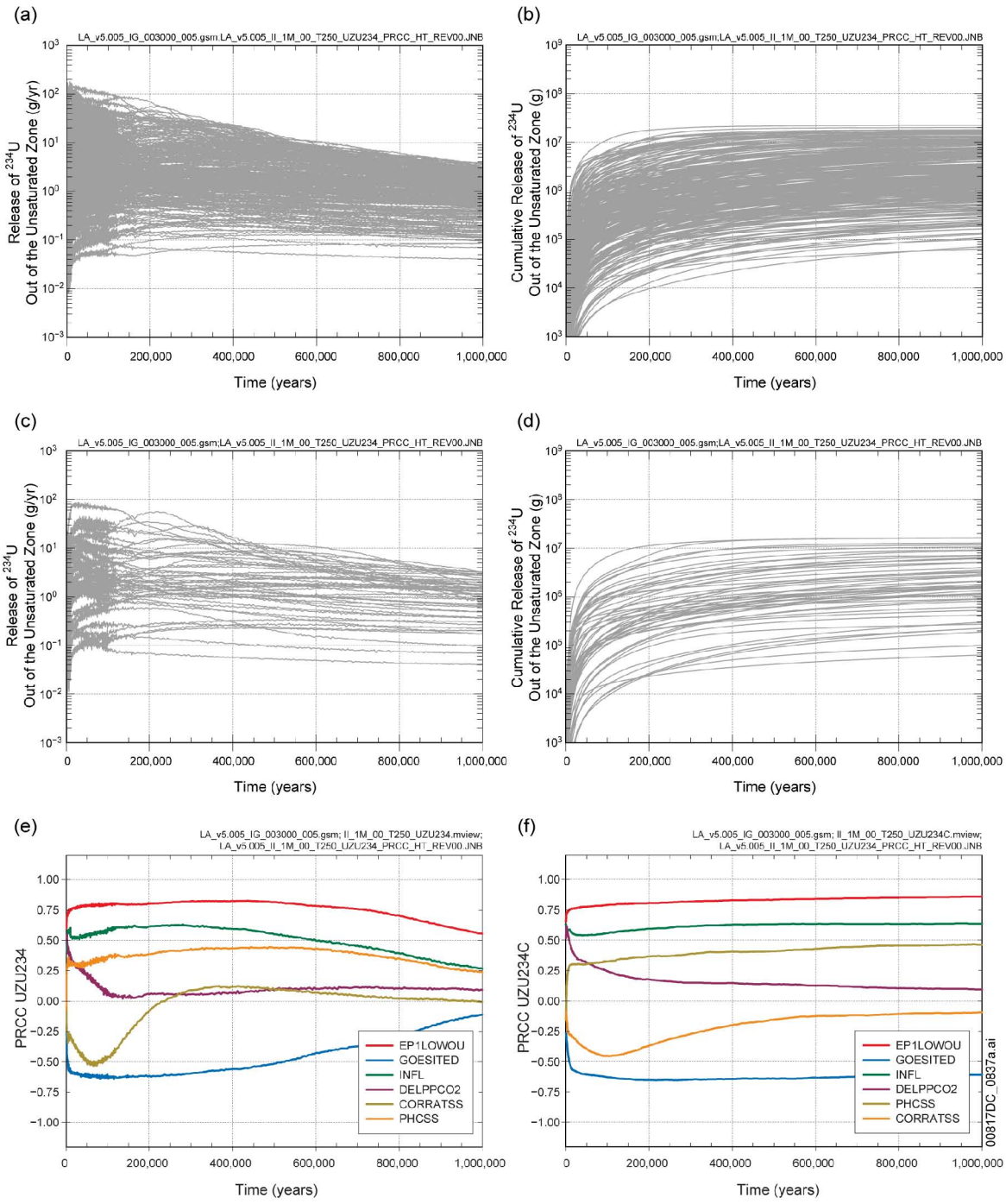

Source: Output DTNs: MO0801TSPAPRSA.000 [DIRS 184620]; and MO0710PLOTSFIG.000 [DIRS 185207].

Figure K6.4.2-1[a]. Time-dependent release rates (*UZU234*, g/yr) and cumulative (i.e., integrated) releases (*UZU234C*, g) over 1,000,000 years for the movement of dissolved ^{234}U from the UZ to the SZ resulting from an igneous intrusive event at 250 years that destroys all WPs in the repository obtained with version 5.005 of the TSPA-LA Model: (a,b) *UZU234* and *UZU234C* for all (i.e., 300) sample elements, (c,d) *UZU234* and *UZU234C* for first 50 sample elements, and (e,f) PRCCs for *UZU234* and *UZU234C*

(a)

	UZU234: 50,000 Years			UZU234: 200,000 Years			UZU234: 500,000 Years		
Step[a]	Variable[b]	R^{2c}	SRRC[d]	Variable	R^2	SRRC	Variable	R^2	SRRC
1	EP1LOWOU	0.38	0.57	EP1LOWOU	0.41	0.60	EP1LOWOU	0.49	0.68
2	INFIL	0.49	0.34	INFIL	0.58	0.40	INFIL	0.64	0.38
3	GOESITED	0.58	-0.29	GOESITED	0.66	-0.31	PHCSS	0.69	0.22
4	CORRATSS	0.65	-0.29	HFOSA	0.70	-0.21	GOESITED	0.73	-0.23
5	HFOSA	0.67	-0.18	PHCSS	0.73	0.20	HFOSA	0.75	-0.14
6	GORELAB	0.70	0.13	DSNFMASS	0.75	0.12	GORELAB	0.77	0.12
7	DSNFMASS	0.71	0.12	GORELAB	0.76	0.13	CSNFMASS	0.78	0.13
8	PHCSS	0.73	0.16	GOESA	0.77	-0.09	WDLCRATE	0.79	-0.11
9	IS2MCOS	0.74	0.12	CSNFMASS	0.77	0.08	PROBWPEF	0.80	0.09
10	CSNFMASS	0.75	0.11	HFOSITED	0.78	-0.08			
11	KDPUCOL	0.76	0.10	KDPUCOL	0.78	0.08			
12	DELPPCO2	0.77	0.09	UZFAG4	0.79	-0.08			
13	GOESA	0.77	-0.08						
14	UZFAG4	0.78	-0.07						

(b)

	UZU234C: 50,000 Years			UZU234C: 200,000 Years			UZU234C: 500,000 Years		
Step[a]	Variable[b]	R^{2c}	SRRC[d]	Variable	R^2	SRRC	Variable	R^2	SRRC
1	EP1LOWOU	0.36	0.56	EP1LOWOU	0.39	0.59	EP1LOWOU	0.45	0.62
2	INFIL	0.48	0.36	INFIL	0.54	0.37	INFIL	0.61	0.39
3	GOESITED	0.56	-0.28	GOESITED	0.62	-0.30	GOESITED	0.69	-0.29
4	CORRATSS	0.61	-0.24	CORRATSS	0.66	-0.21	HFOSA	0.72	-0.20
5	PHCSS	0.63	0.19	HFOSA	0.69	-0.20	PHCSS	0.75	0.21
6	IS2MCOS	0.65	0.15	PHCSS	0.71	0.19	GORELAB	0.77	0.14
7	HFOSA	0.68	-0.17	DSNFMASS	0.73	0.12	DSNFMASS	0.78	0.10
8	DELPPCO2	0.69	0.13	GORELAB	0.75	0.13	GOESA	0.79	-0.08
9	GORELAB	0.71	0.12	GOESA	0.76	-0.09	CSNFMASS	0.80	0.10
10	CSNFMASS	0.72	0.13	IS2MCOS	0.77	0.09	CORRATSS	0.80	-0.08
11	GOESA	0.73	-0.08	CSNFMASS	0.77	0.10	KDPUCOL	0.81	0.09
12	DSNFMASS	0.74	0.09	KDPUCOL	0.78	0.09	UZFAG4	0.81	-0.08
13	CPUPERCS	0.75	-0.08	UZFAG4	0.79	-0.08	HFOSITED	0.82	-0.07
14	RHMUN40	0.75	-0.10	DELPPCO2	0.79	0.07			
15	UZFAG4	0.76	-0.09						
16	KDPUCOL	0.77	0.09						

00817DC_0838c.ai

a: Steps in stepwise rank regression analysis
b: Variables listed in order of selection in stepwise regression
c: Cumulative R^2 value with entry of each variable into regression model
d: Standardized rank regression coefficients (SRRCs) in final regression model

Source: Output DTNs: MO0801TSPAPRSA.000 [DIRS 184620]; and MO0710PLOTSFIG.000 [DIRS 185207].

Figure K6.4.2-2[a]. Stepwise rank regression analyses and selected scatterplots for time-dependent release rates (*UZU234*, g/yr) and cumulative (i.e., integrated) releases (*UZU234C*, g) for the movement of dissolved ^{234}U from the UZ to the SZ resulting from an igneous intrusive event at 250 years that destroys all WPs in the repository obtained with version 5.005 of the TSPA-LA Model: (a,b) regressions for *UZU234* and *UZU234C* at 50,000, 200,000, and 500,000 years, and (c-h) scatterplots for *UZU234* and *UZU234C* at 500,000 years

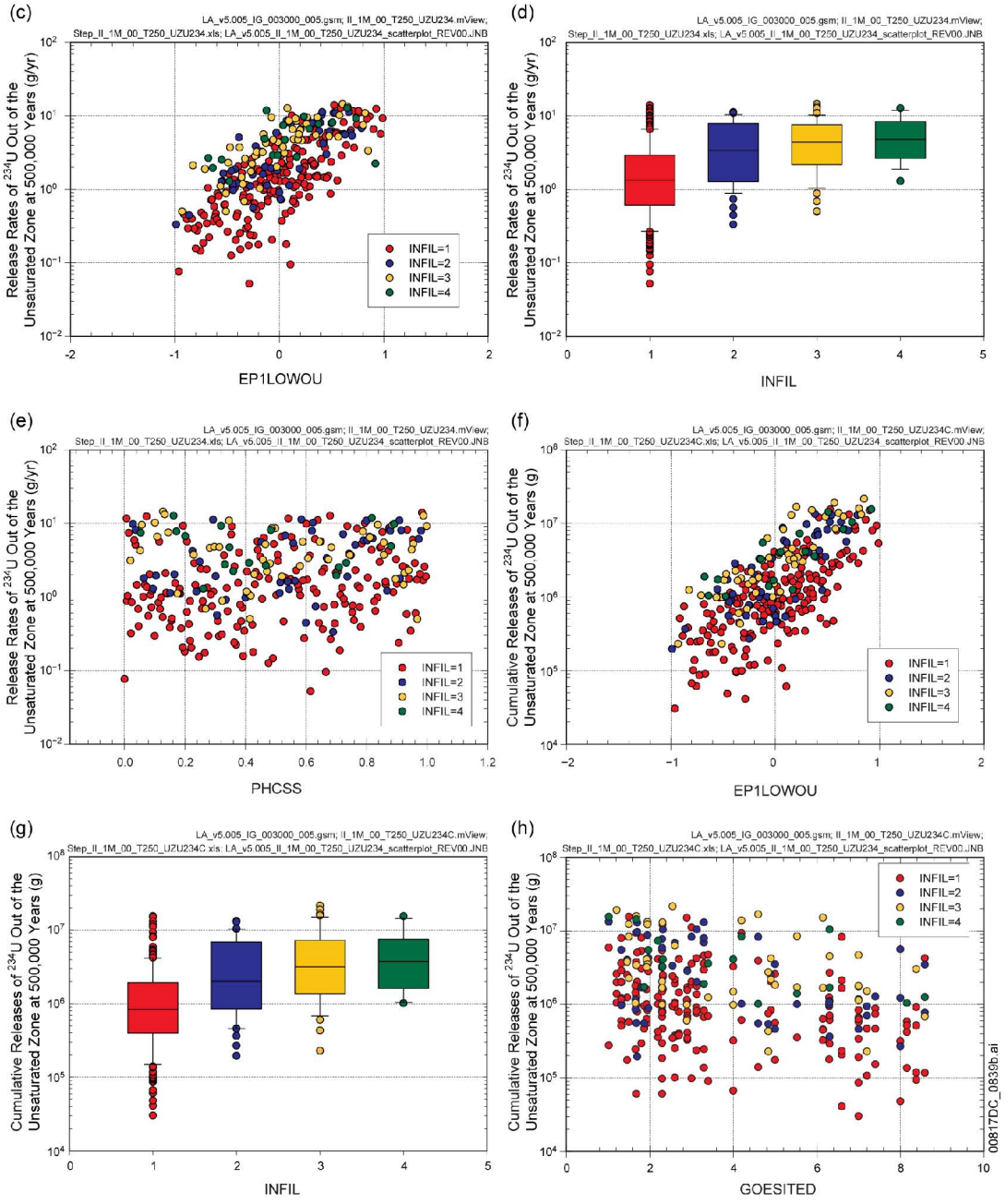

Source: Output DTNs: MO0801TSPAPRSA.000 [DIRS 184620]; and MO0710PLOTSFIG.000 [DIRS 185207].

NOTE: In (d,g), the box extends from 0.25 to 0.75 quantile; lower and upper bar and whisker extend to 0.1 and 0.9 quantile, respectively; dots represent values outside 0.1 to 0.9 quantile range; median indicated by light horizontal line.

Figure K6.4.2-2[a]. Stepwise rank regression analyses and selected scatterplots for time-dependent release rates (*UZU234*, g/yr) and cumulative (i.e., integrated) releases (*UZU234C*, g) for the movement of dissolved ^{234}U from the UZ to the SZ resulting from an igneous intrusive event at 250 years that destroys all WPs in the repository obtained with version 5.005 of the TSPA-LA Model: (a,b) regressions for *UZU234* and *UZU234C* at 50,000, 200,000, and 500,000 years, and (c-h) scatterplots for *UZU234* and *UZU234C* at 500,000 years (continued)

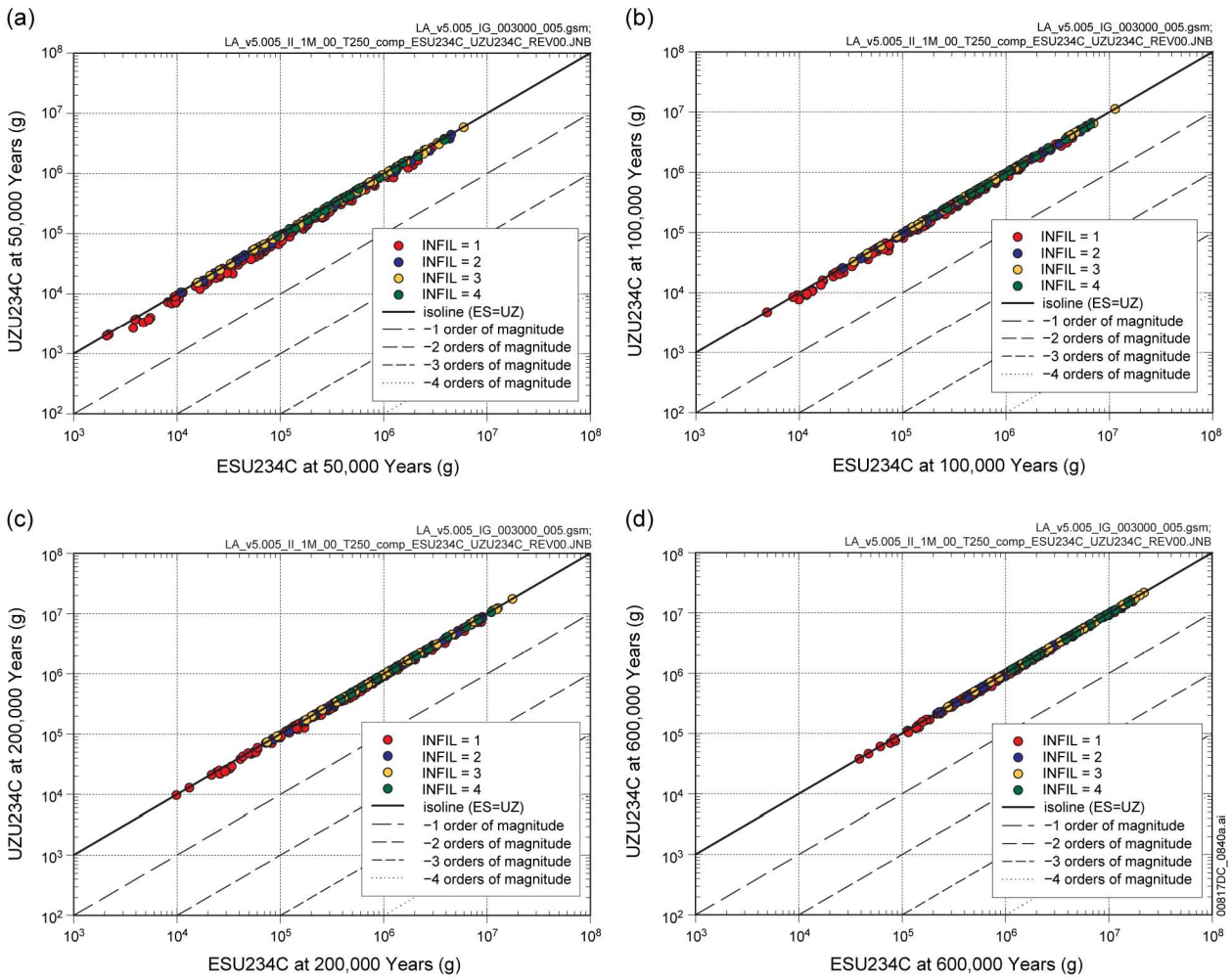

Source: Output DTNs: MO0801TSPAPRSA.000 [DIRS 184620]; and MO0710PLOTSFIG.000 [DIRS 185207].

Figure K.6.4.2-3[a]. Comparison of cumulative releases of dissolved ^{234}U into the UZ (*ESU234C*, g) and out of the UZ (*UZU234C*, g) obtained with version 5.005 of the TSPA-LA Model at (a) 50,000, (b) 100,000, (c) 200,000, and (d) 600,000 years for an igneous intrusive event at 250 years that destroys all WPs in the repository

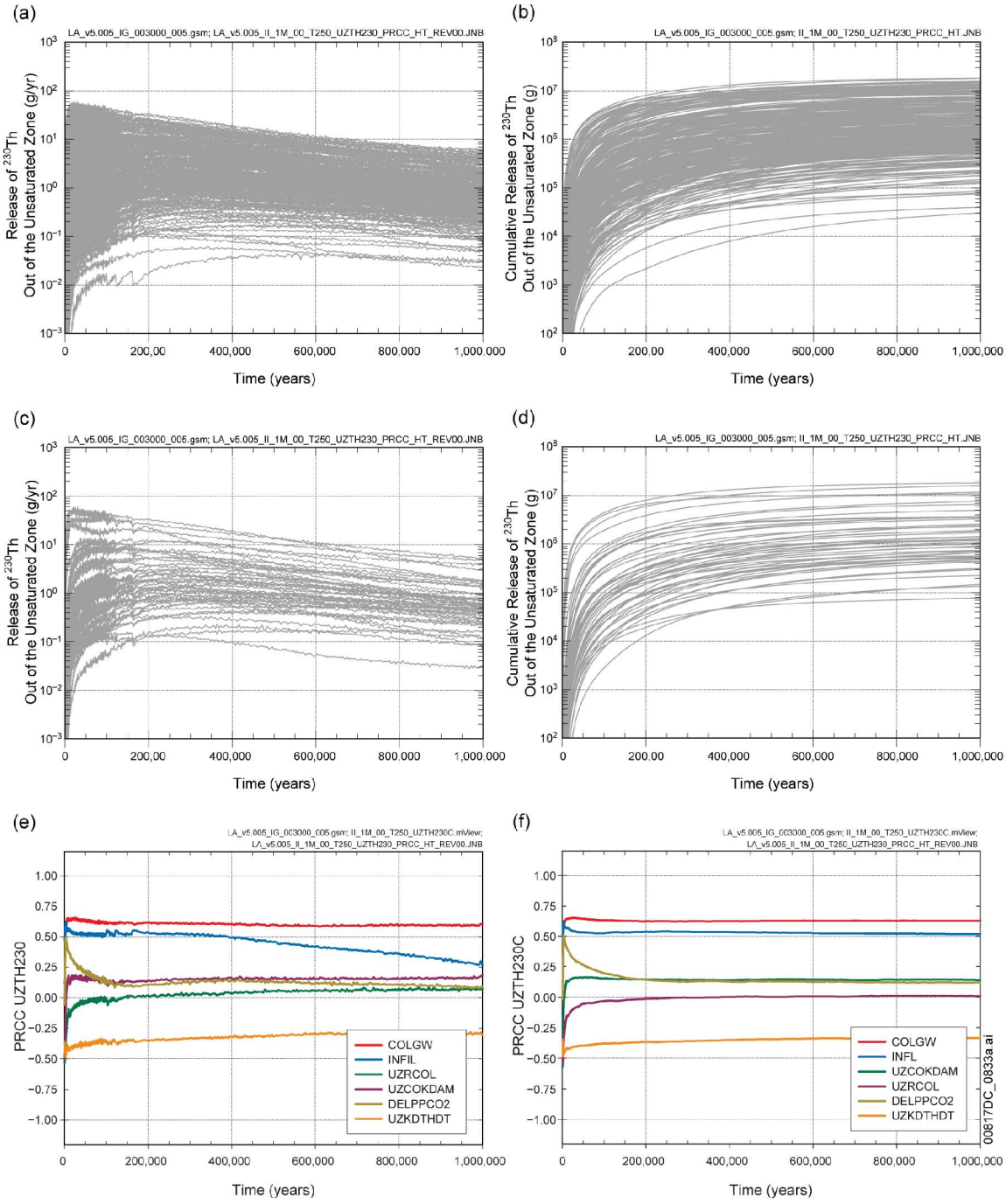

Source: Output DTNs: MO0801TSPAPRSA.000 [DIRS 184620]; and MO0710PLOTSFIG.000 [DIRS 185207].

Figure K6.4.2-4[a]. Time-dependent release rates (*UZTH230*, g/yr) and cumulative (i.e., integrated) releases (*UZTH230C*, g) over 1,000,000 years for the movement of dissolved ^{230}Th from the UZ to the SZ resulting from an igneous intrusive event at 250 years that destroys all WPs in the repository obtained with version 5.005 of the TSPA-LA Model: (a,b) *UZTH230* and *UZTH230C* for all (i.e., 300) sample elements, (c,d) *UZTH230* and *UZTH230C* for first 50 sample elements, and (e,f) PRCCs for *UZTH230* and *UZTH230C*

(a)

	UZTH230: 50,000 Years			UZTH230: 200,000 Years			UZTH230: 500,000 Years		
Step[a]	Variable[b]	R^{2} [c]	SRRC[d]	Variable	R^2	SRRC	Variable	R^2	SRRC
1	INFIL	0.25	0.44	INFIL	0.27	0.46	COLGW	0.22	0.43
2	COLGW	0.42	0.44	COLGW	0.43	0.41	INFIL	0.40	0.39
3	KDTHSMEC	0.51	0.28	KDTHSMEC	0.52	0.29	KDTHSMEC	0.50	0.29
4	PHCSS	0.55	0.24	PHCSS	0.57	0.23	UZKDTHDT	0.54	-0.20
5	UZKDTHDT	0.60	-0.23	EP1LOWTH	0.60	0.21	PHCSS	0.58	0.20
6	EP1LOWTH	0.63	0.22	UZKDTHDT	0.63	-0.19	EP1LOWTH	0.61	0.20
7	CORRATSS	0.66	-0.15	EP1LOWOU	0.66	0.15	CSNFMASS	0.63	0.12
8	EP1LOWOU	0.68	0.13	GOESITED	0.68	-0.17	HFOSA	0.64	-0.12
9	GOESITED	0.69	-0.14	HFOSA	0.70	-0.13	GOESITED	0.65	-0.12
10	HLWMASS	0.70	0.10	GOESA	0.70	-0.09	UZFAG1	0.66	-0.09
11	DELPPCO2	0.71	0.10	HLWMASS	0.71	0.09	EP2HICAM	0.67	0.09

(b)

	UZTH230C: 50,000 Years			UZTH230C: 200,000 Years			UZTH230C: 500,000 Years		
Step[a]	Variable[b]	R^{2} [c]	SRRC[d]	Variable	R^2	SRRC	Variable	R^2	SRRC
1	INFIL	0.25	0.44	INFIL	0.27	0.46	INFIL	0.27	0.46
2	COLGW	0.44	0.45	COLGW	0.43	0.42	COLGW	0.44	0.43
3	KDTHSMEC	0.52	0.27	KDTHSMEC	0.52	0.28	KDTHSMEC	0.53	0.30
4	UZKDTHDT	0.57	-0.24	PHCSS	0.57	0.22	PHCSS	0.58	0.22
5	PHCSS	0.61	0.23	EP1LOWTH	0.60	0.21	EP1LOWTH	0.61	0.21
6	EP1LOWTH	0.65	0.22	UZKDTHDT	0.64	-0.20	UZKDTHDT	0.65	-0.20
7	CORRATSS	0.67	-0.15	GOESITED	0.66	-0.15	EP1LOWOU	0.67	0.14
8	GOESITED	0.69	-0.13	EP1LOWOU	0.68	0.13	GOESITED	0.69	-0.15
9	EP1LOWOU	0.70	0.11	CORRATSS	0.70	-0.13	HFOSA	0.70	-0.12
10	DELPPCO2	0.71	0.13	HFOSA	0.71	-0.10	HLWMASS	0.71	0.09
11	HLWMASS	0.72	0.10	HLWMASS	0.71	0.09	GOESA	0.72	-0.09
12	HFOSA	0.73	-0.10				DSCRACKA	0.72	-0.08

00817DC_0834c.ai

a: Steps in stepwise rank regression analysis
b: Variables listed in order of selection in stepwise regression
c: Cumulative R^2 value with entry of each variable into regression model
d: Standardized rank regression coefficients (SRRCs) in final regression model

Source: Output DTNs: MO0801TSPAPRSA.000 [DIRS 184620]; and MO0710PLOTSFIG.000 [DIRS 185207].

Figure K6.4.2-5[a]. Stepwise rank regression analyses and selected scatterplots for time-dependent release rates (*UZTH230*, g/yr) and cumulative (i.e., integrated) releases (*UZTH230C*, g) for the movement of dissolved ^{230}Th from the UZ to the SZ resulting from an igneous intrusive event at 250 years that destroys all WPs in the repository obtained with version 5.005 of the TSPA-LA Model: (a,b) regressions for *UZTH230* and *UZTH230C* at 50,000, 200,000, and 500,000 years, and (c-h) scatterplots for *UZTH230* and *UZTH230C* at 200,000 years

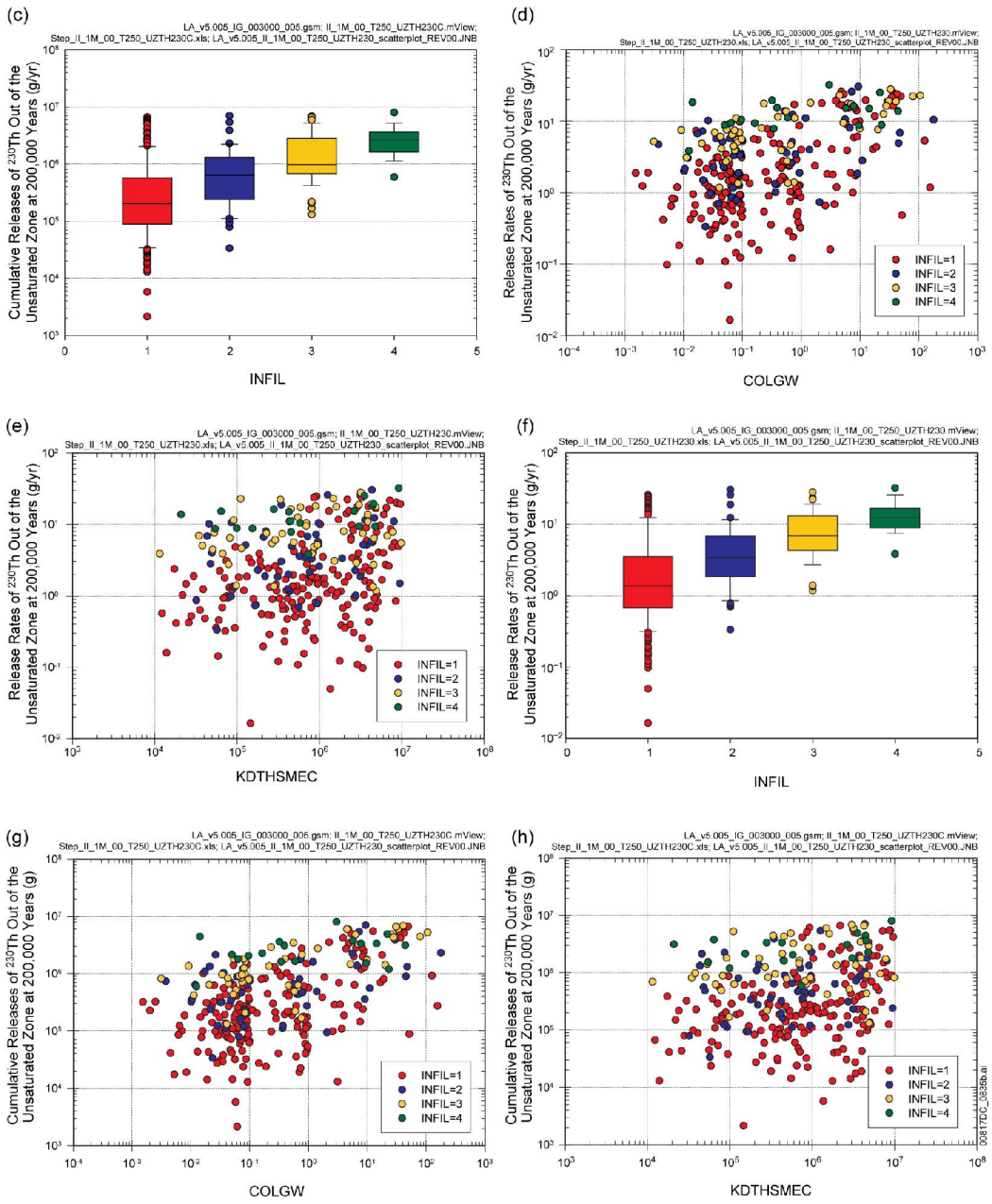

Source: Output DTNs: MO0801TSPAPRSA.000 [DIRS 184620]; and MO0710PLOTSFIG.000 [DIRS 185207].

NOTE: In (c,f), the box extends from 0.25 to 0.75 quantile; lower and upper bar and whisker extend to 0.1 and 0.9 quantile, respectively; dots represent values outside 0.1 to 0.9 quantile range; median indicated by light horizontal line.

Figure K6.4.2-5[a]. Stepwise rank regression analyses and selected scatterplots for time-dependent release rates (*UZTH230*, g/yr) and cumulative (i.e., integrated) releases (*UZTH230C*, g) for the movement of dissolved ^{230}Th from the UZ to the SZ resulting from an igneous intrusive event at 250 years that destroys all WPs in the repository obtained with version 5.005 of the TSPA-LA Model: (a,b) regressions for *UZTH230* and *UZTH230C* at 50,000, 200,000, and 500,000 years, and (c-h) scatterplots for *UZTH230* and *UZTH230C* at 200,000 years (continued)

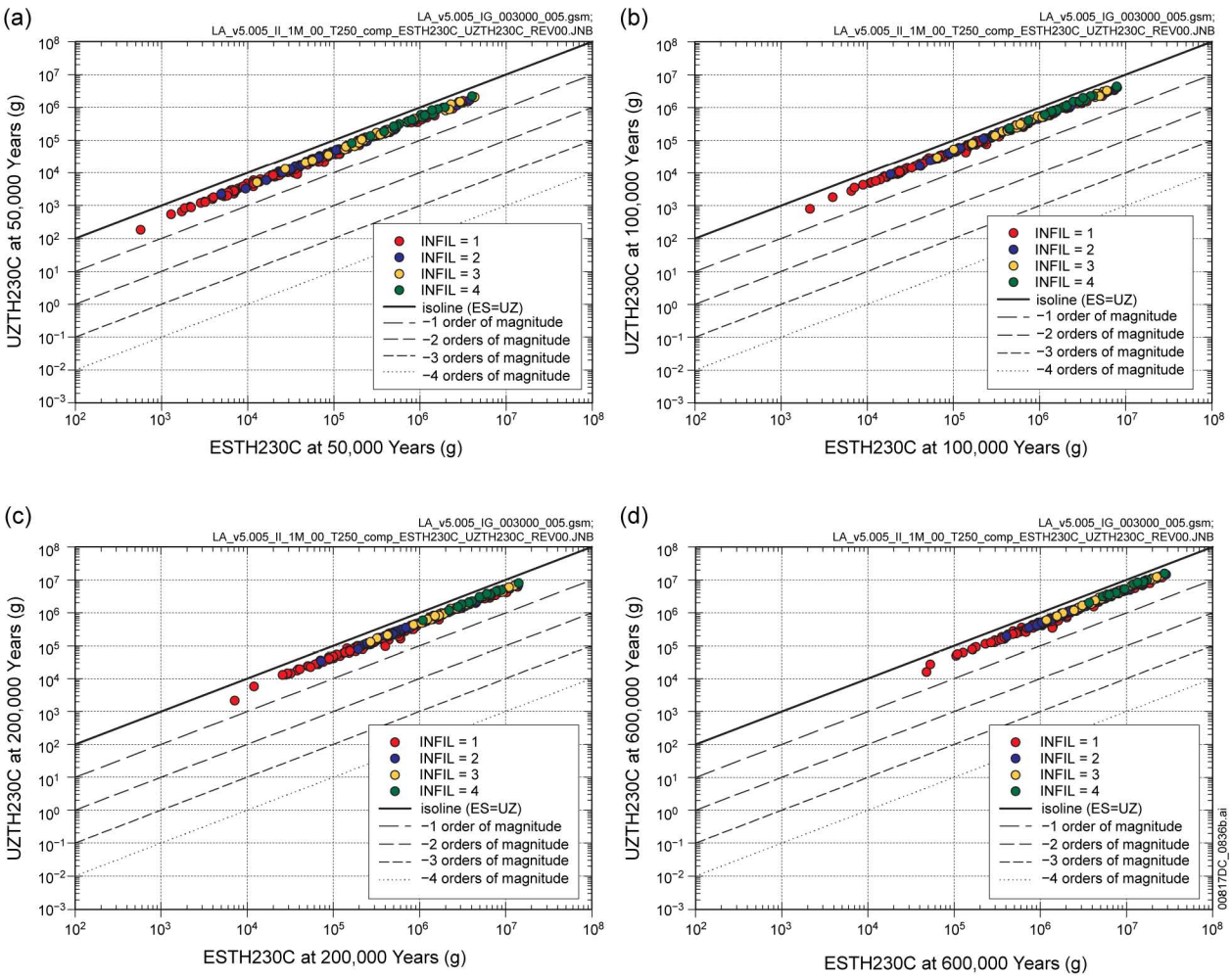

Source: Output DTNs: MO0801TSPAPRSA.000 [DIRS 184620]; and MO0710PLOTSFIG.000 [DIRS 185207].

Figure K.6.4.2-6[a]. Comparison of cumulative releases of dissolved ^{230}Th into the UZ (*ESTH230C*, g) and out of the UZ (*UZTH230C*, g) obtained with version 5.005 of the TSPA-LA Model at (a) 50,000, (b) 100,000, (c) 200,000, and (d) 600,000 years for an igneous intrusive event at 250 years that destroys all WPs in the repository

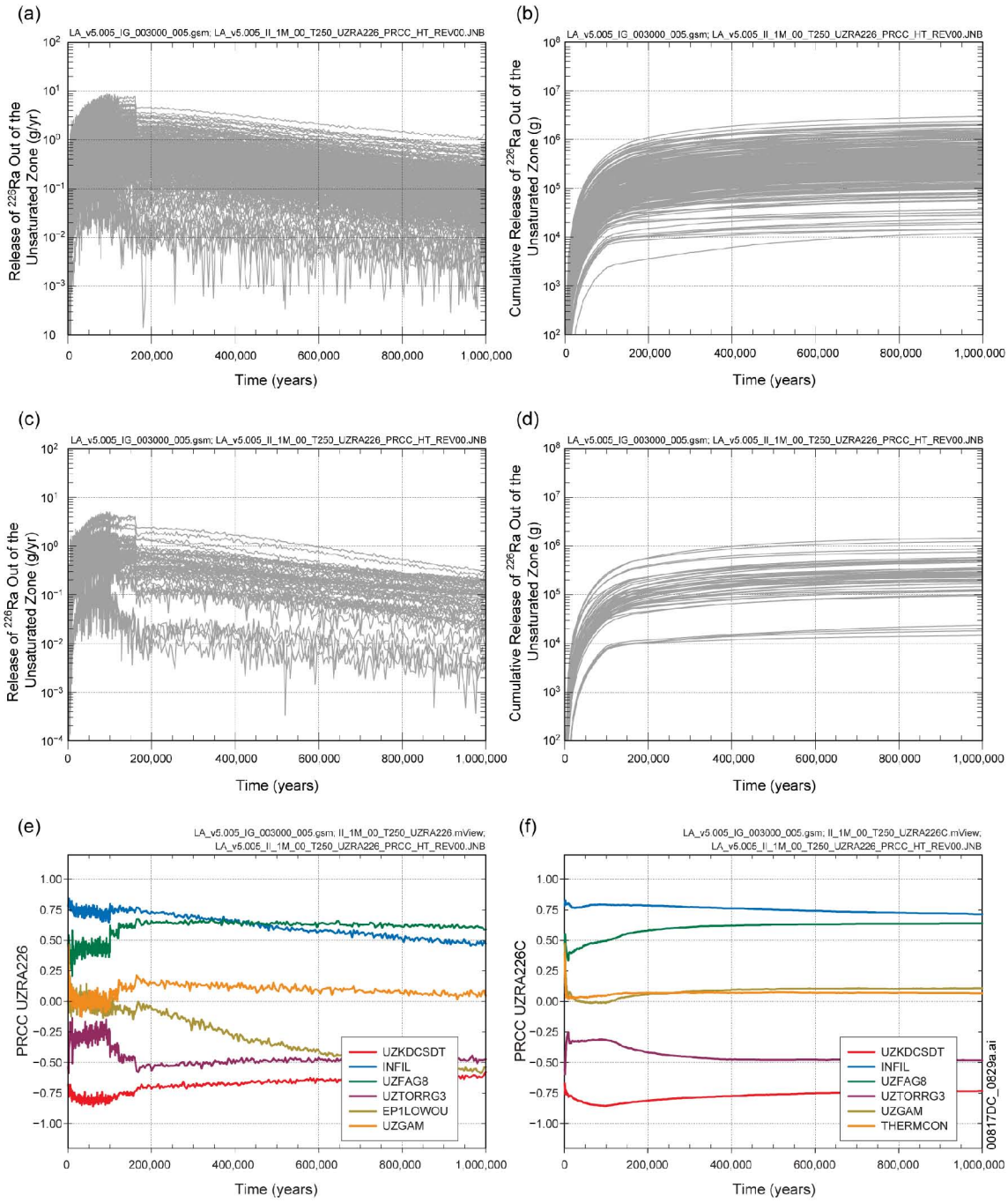

Source: Output DTNs: MO0801TSPAPRSA.000 [DIRS 184620]; and MO0710PLOTSFIG.000 [DIRS 185207].

Figure K6.4.2-7[a]. Time-dependent release rates (*UZRA226*, g/yr) and cumulative (i.e., integrated) releases (*UZRA226C*, g) over 1,000,000 years for the movement of dissolved ^{226}Ra from the UZ to the SZ resulting from an igneous intrusive event at 250 years that destroys all WPs in the repository obtained with version 5.005 of the TSPA-LA Model: (a,b) *UZRA226* and *UZRA226C* for all (i.e., 300) sample elements, (c,d) *UZRA226* and *UZRA226C* for first 50 sample elements, and (e,f) PRCCs for *UZRA226* and *UZRA226C*

(a)

	UZRA226: 50,000 Years			UZRA226: 200,000 Years			UZRA226: 500,000 Years		
Step[a]	Variable[b]	R^{2} [c]	SRRC[d]	Variable	R^2	SRRC	Variable	R^2	SRRC
1	UZKDCSDT	0.41	−0.64	INFIL	0.27	0.52	UZKDCSDT	0.24	−0.47
2	INFIL	0.72	0.54	UZKDCSDT	0.52	−0.48	UZFAG8	0.41	0.42
3	UZFAG8	0.76	0.20	UZFAG8	0.67	0.38	INFIL	0.56	0.39
4	CSNFMASS	0.78	0.15	UZTORRG3	0.77	−0.33	UZTORRG3	0.64	−0.32
5	UZTORRG3	0.80	−0.14	CSNFMASS	0.78	0.13	EP1LOWOU	0.68	−0.22
6	KDNPSMEC	0.80	0.08	COLGW	0.79	0.09	CSNFMASS	0.70	0.13
7	KDAMSMEC	0.81	−0.08	UZGAM	0.80	0.07	UZKDTHDT	0.71	0.11
8	KDNPCOL	0.81	0.07	UZKDTHDT	0.80	0.08			
9				EP1LOWOU	0.81	−0.07			

(b)

	UZRA226C: 50,000 Years			UZRA226C: 200,000 Years			UZRA226C: 500,000 Years		
Step[a]	Variable[b]	R^{2} [c]	SRRC[d]	Variable	R^2	SRRC	Variable	R^2	SRRC
1	UZKDCSDT	0.40	−0.63	UZKDCSDT	0.38	−0.61	UZKDCSDT	0.31	−0.55
2	INFIL	0.73	0.56	INFIL	0.69	0.55	INFIL	0.59	0.53
3	UZFAG8	0.77	0.18	UZFAG8	0.77	0.28	UZFAG8	0.71	0.35
4	UZTORRG3	0.79	−0.16	UZTORRG3	0.81	−0.22	UZTORRG3	0.77	−0.27
5	CSNFMASS	0.81	0.15	CSNFMASS	0.83	0.14	CSNFMASS	0.79	0.15
6	COLGW	0.83	0.13	UZKDTHDT	0.83	0.06	EP1LOWOU	0.80	−0.10
7	KDTHSMEC	0.84	0.09				UZKDTHDT	0.81	0.08
8	GOESITED	0.84	−0.06						

00817DC_0830b.ai

a: Steps in stepwise rank regression analysis
b: Variables listed in order of selection in stepwise regression
c: Cumulative R^2 value with entry of each variable into regression model
d: Standardized rank regression coefficients (SRRCs) in final regression model

Source: Output DTNs: MO0801TSPAPRSA.000 [DIRS 184620]; and MO0710PLOTSFIG.000 [DIRS 185207].

Figure K6.4.2-8[a]. Stepwise rank regression analyses and selected scatterplots for time-dependent release rates (*UZRA226*, g/yr) and cumulative (i.e., integrated) releases (*UZRA226C*, g) for the movement of dissolved ^{226}Ra from the UZ to the SZ resulting from an igneous intrusive event at 250 years that destroys all WPs in the repository obtained with version 5.005 of the TSPA-LA Model: (a,b) regressions for *UZRA226* and *UZRA226C* at 50,000, 200,000, and 500,000 years, and (c-h) scatterplots for *UZRA226* and *UZRA226C* at 50,000 years

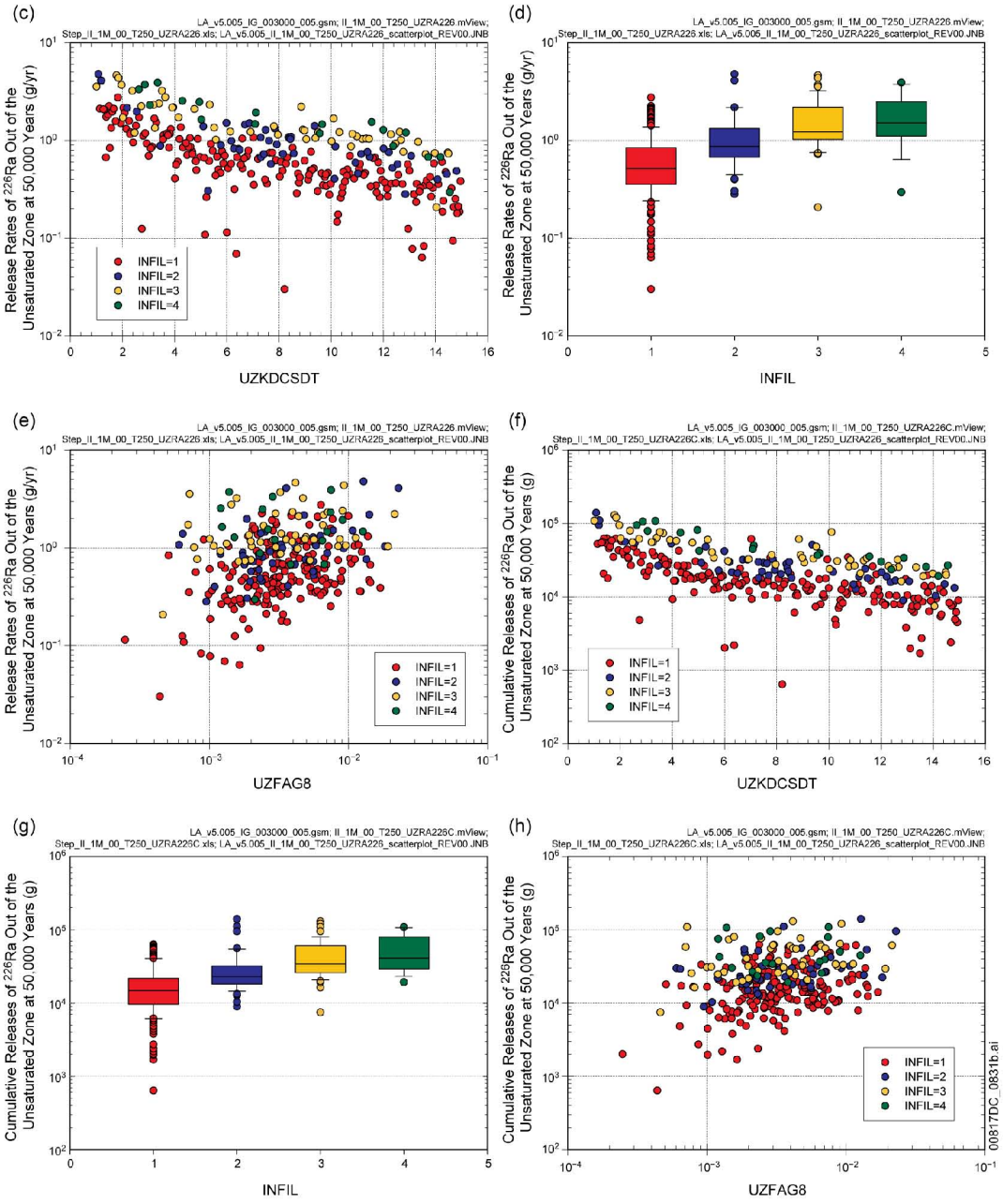

Source: Output DTNs: MO0801TSPAPRSA.000 [DIRS 184620]; and MO0710PLOTSFIG.000 [DIRS 185207].

NOTE: In (d,g), the box extends from 0.25 to 0.75 quantile; lower and upper bar and whisker extend to 0.1 and 0.9 quantile, respectively; dots represent values outside 0.1 to 0.9 quantile range; median indicated by light horizontal line.

Figure K6.4.2-8[a]. Stepwise rank regression analyses and selected scatterplots for time-dependent release rates (*UZRA226*, g/yr) and cumulative (i.e., integrated) releases (*UZRA226C*, g) for the movement of dissolved ^{226}Ra from the UZ to the SZ resulting from an igneous intrusive event at 250 years that destroys all WPs in the repository obtained with version 5.005 of the TSPA-LA Model: (a,b) regressions for *UZRA226* and *UZRA226C* at 50,000, 200,000, and 500,000 years, and (c-h) scatterplots for *UZRA226* and *UZRA226C* at 50,000 years (continued)

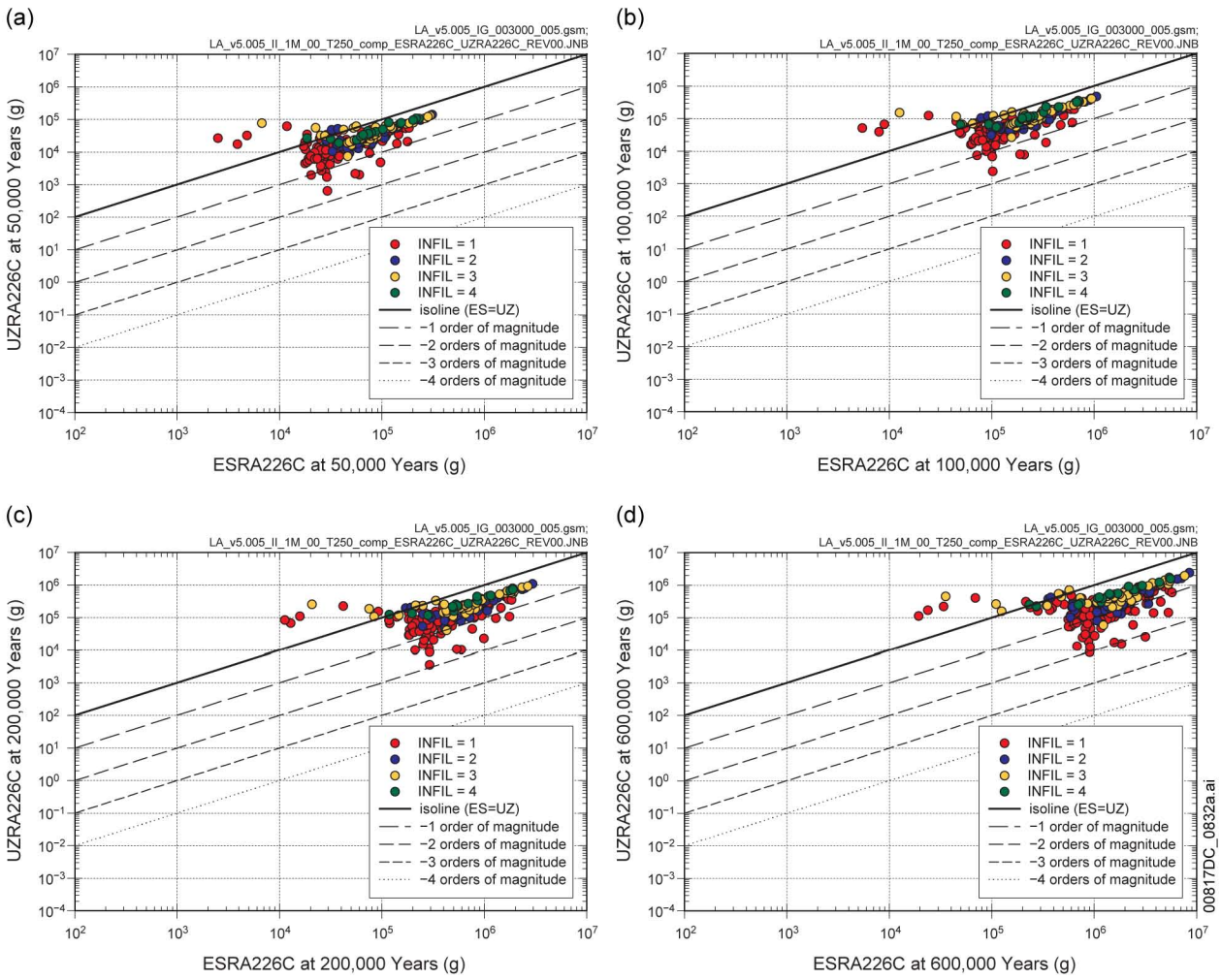

Source: Output DTNs: MO0801TSPAPRSA.000 [DIRS 184620]; and MO0710PLOTSFIG.000 [DIRS 185207].

Figure K.6.4.2-9[a]. Comparison of cumulative releases of dissolved ^{226}Ra into the UZ (*UZRA226C*, g) and out of the UZ (*UZRA226C*, g) obtained with version 5.005 of the TSPA-LA Model at (a) 50,000, (b) 100,000, (c) 200,000, and (d) 600,000 years for an igneous intrusive event at 250 years that destroys all WPs in the repository

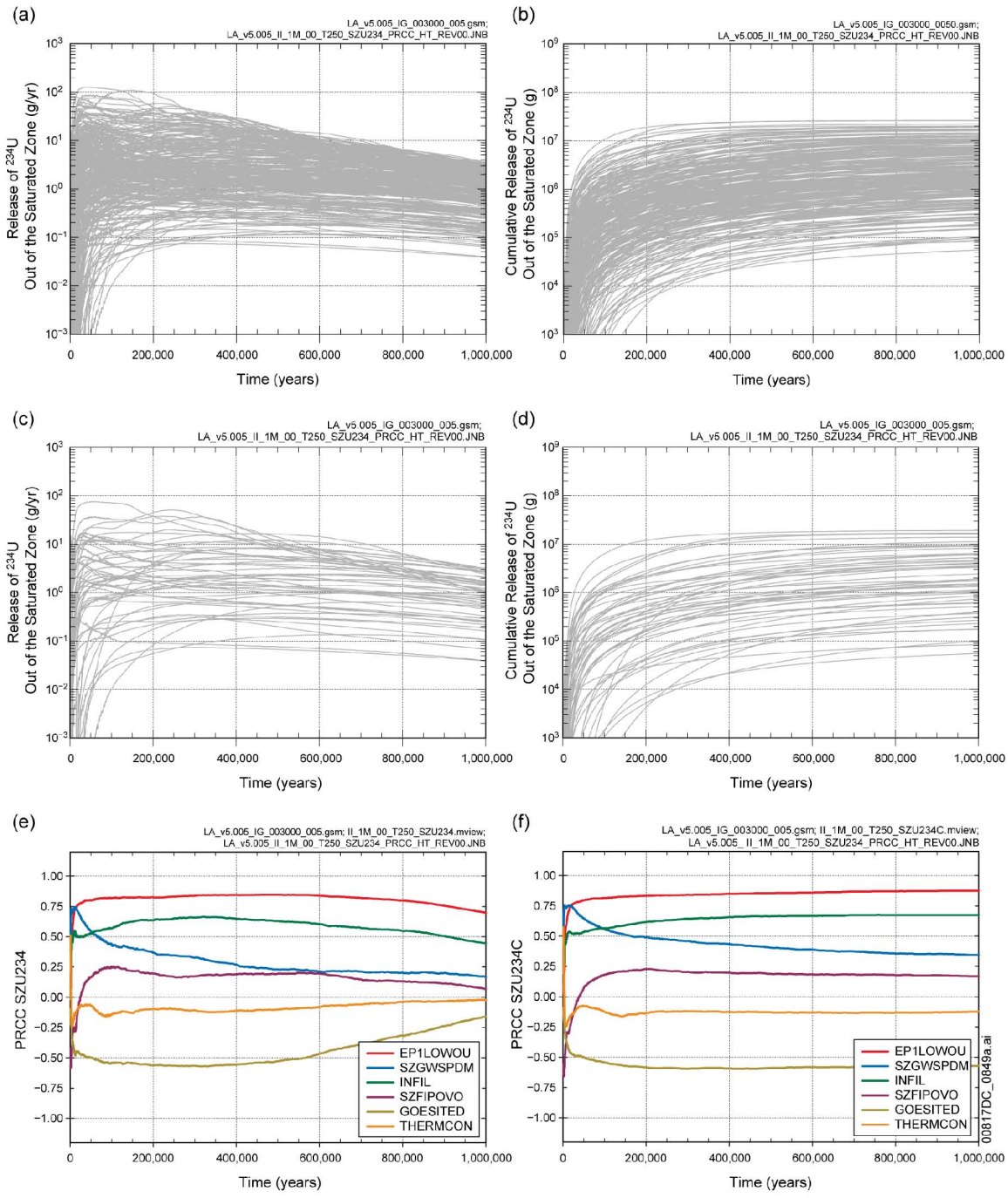

Source: Output DTNs: MO0801TSPAPRSA.000 [DIRS 184620]; and MO0710PLOTSFIG.000 [DIRS 185207].

Figure K6.5.2-5[a]. Time-dependent release rates (*SZU234*, g/yr) and cumulative (i.e., integrated) releases (*SZU234C*, g) over 1,000,000 years for the movement of dissolved ^{234}U across a subsurface plane at the location of the RMEI resulting from an igneous intrusive event at 250 years that destroys all WPs in the repository obtained with version 5.005 of the TSPA-LA Model: (a,b) *SZU234* and *SZU234C* for all (i.e., 300) sample elements, (c,d) *SZU234* and *SZU234C* for first 50 sample elements, and (e,f) PRCCs for *SZU234* and *SZU234C*

(a)

	SZU234: 50,000 Years			SZU234: 200,000 Years			SZU234: 500,000 Years		
Step[a]	Variable[b]	R^{2c}	SRRC[d]	Variable	R^2	SRRC	Variable	R^2	SRRC
1	EP1LOWOU	0.30	0.53	EP1LOWOU	0.37	0.58	EP1LOWOU	0.46	0.65
2	INFIL	0.42	0.36	INFIL	0.54	0.41	INFIL	0.64	0.41
3	SZGWSPDM	0.49	0.29	GOESITED	0.62	−0.27	PHCSS	0.69	0.21
4	GOESITED	0.55	−0.22	PHCSS	0.65	0.20	GOESITED	0.73	−0.25
5	CORRATSS	0.59	−0.22	SZGWSPDM	0.68	0.19	HFOSA	0.75	−0.13
6	PHCSS	0.62	0.17	HFOSA	0.71	−0.17	SZGWSPDM	0.77	0.12
7	IS2MCOS	0.64	0.15	GOERELAB	0.72	0.12	CSNFMASS	0.78	0.13
8	CSNFMASS	0.66	0.14	CORRATSS	0.73	−0.11	GOERELAB	0.79	0.11
9	SZDIFCVO	0.68	−0.15	CSNFMASS	0.74	0.12	WDLCRATE	0.80	−0.10
10	SZFISPVO	0.70	0.13	KDPUSMEC	0.75	0.10	SZLODISP	0.81	−0.08
11	KDPUSMEC	0.71	0.12	CSCORRAT	0.76	0.09	UZFAG1	0.81	−0.07
12	GOERELAB	0.72	0.11	KDPUCOL	0.77	0.09	SZSREG2X	0.82	0.07
13	HFOSA	0.73	−0.12	UZFAG4	0.77	−0.08			
14	CSWFA4AC	0.73	−0.10	WDDEFCNT	0.78	−0.08			
15	DELPPCO2	0.74	0.09						
16	SZSREG1X	0.75	−0.09						

(b)

	SZU234C: 50,000 Years			SZU234C: 200,000 Years			SZU234C: 500,000 Years		
Step[a]	Variable[b]	R^{2c}	SRRC[d]	Variable	R^2	SRRC	Variable	R^2	SRRC
1	EP1LOWOU	0.26	0.51	EP1LOWOU	0.34	0.56	EP1LOWOU	0.41	0.61
2	INFIL	0.38	0.35	INFIL	0.48	0.37	INFIL	0.58	0.39
3	SZGWSPDM	0.49	0.35	GOESITED	0.56	−0.26	GOESITED	0.65	−0.26
4	GOESITED	0.55	−0.20	SZGWSPDM	0.61	0.24	PHCSS	0.69	0.21
5	SZDIFCVO	0.58	−0.18	CORRATSS	0.64	−0.21	SZGWSPDM	0.72	0.19
6	SZFISPVO	0.61	0.17	PHCSS	0.67	0.18	HFOSA	0.74	−0.16
7	CORRATSS	0.64	−0.19	HFOSA	0.69	−0.14	GOERELAB	0.75	0.12
8	PHCSS	0.66	0.16	GOERELAB	0.70	0.11	CSNFMASS	0.76	0.11
9	IS2MCOS	0.68	0.17	SZFISPVO	0.72	0.13	CORRATSS	0.77	−0.10
10	CSNFMASS	0.70	0.12	SZDIFCVO	0.73	−0.13	KDPUSMEC	0.78	0.09
11	KDPUSMEC	0.71	0.11	CSNFMASS	0.74	0.11	CSCORRAT	0.79	0.08
12	DELPPCO2	0.72	0.11	IS2MCOS	0.76	0.09	KDPUCOL	0.80	0.09
13	HFOSA	0.72	−0.10	KDPUSMEC	0.77	0.10	SZDIFCVO	0.80	−0.09
14	DSCRACKA	0.73	−0.10	KDPUCOL	0.77	0.09	SZFISPVO	0.81	0.10
15	CSWFA4AC	0.74	−0.09	UZFAG4	0.78	−0.09	UZFAG4	0.81	−0.07
16	GOERELAB	0.75	0.09	DSNFMASS	0.79	0.08	DSNFMASS	0.82	0.07

00817DC_0850a.ai

a: Steps in stepwise rank regression analysis
b: Variables listed in order of selection in stepwise regression
c: Cumulative R^2 value with entry of each variable into regression model
d: Standardized rank regression coefficients (SRRCs) in final regression model

Source: Output DTNs: MO0801TSPAPRSA.000 [DIRS 184620]; and MO0710PLOTSFIG.000 [DIRS 185207].

Figure K6.5.2-6[a]. Stepwise rank regression analyses and selected scatterplots for time-dependent release rates (*SZU234*, g/yr) and cumulative (i.e., integrated) releases (*SZU234C*, g) for the movement of dissolved ^{234}U across a subsurface plane at the location of the RMEI resulting from an igneous intrusive event at 250 years that destroys all WPs in the repository obtained with version 5.005 of the TSPA-LA Model: (a,b) regressions for *SZU234* and *SZU234C* at 50,000, 200,000, and 500,000 years, and (c-h) scatterplots for *SZU234* and *SZU234C* at 500,000 years

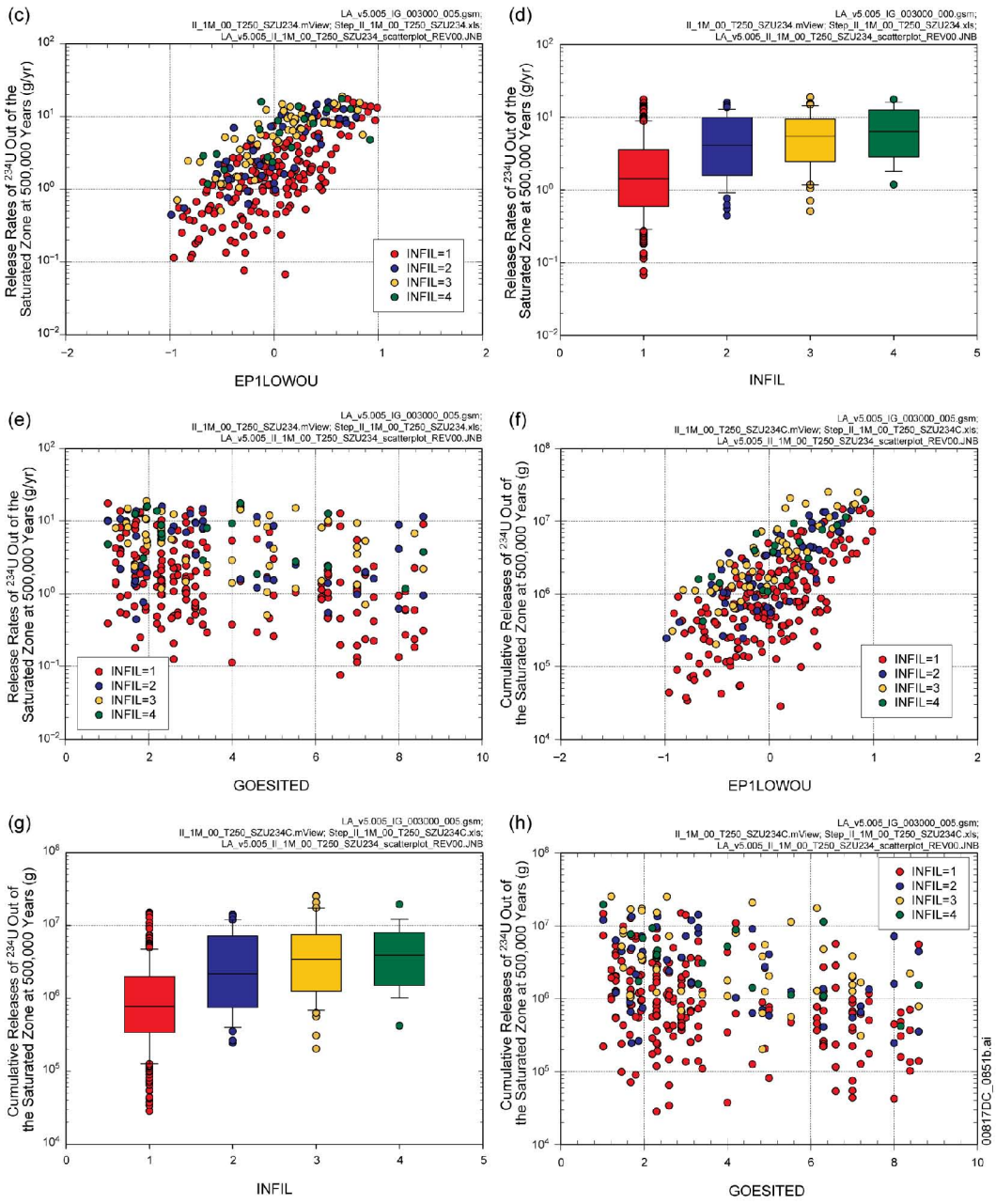

Source: Output DTNs: MO0801TSPAPRSA.000 [DIRS 184620]; and MO0710PLOTSFIG.000 [DIRS 185207].

NOTE: In (d,g), the box extends from 0.25 to 0.75 quantile; lower and upper bar and whisker extend to 0.1 and 0.9 quantile, respectively; dots represent values outside 0.1 to 0.9 quantile range; median indicated by light horizontal line.

Figure K6.5.2-6[a]. Stepwise rank regression analyses and selected scatterplots for time-dependent release rates (*SZU234*, g/yr) and cumulative (i.e., integrated) releases (*SZU234C*, g) for the movement of dissolved ^{234}U across a subsurface plane at the location of the RMEI resulting from an igneous intrusive event at 250 years that destroys all WPs in the repository obtained with version 5.005 of the TSPA-LA Model: (a,b) regressions for *SZU234* and *SZU234C* at 50,000, 200,000, and 500,000 years, and (c-h) scatterplots for *SZU234* and *SZU234C* at 500,000 years (continued)

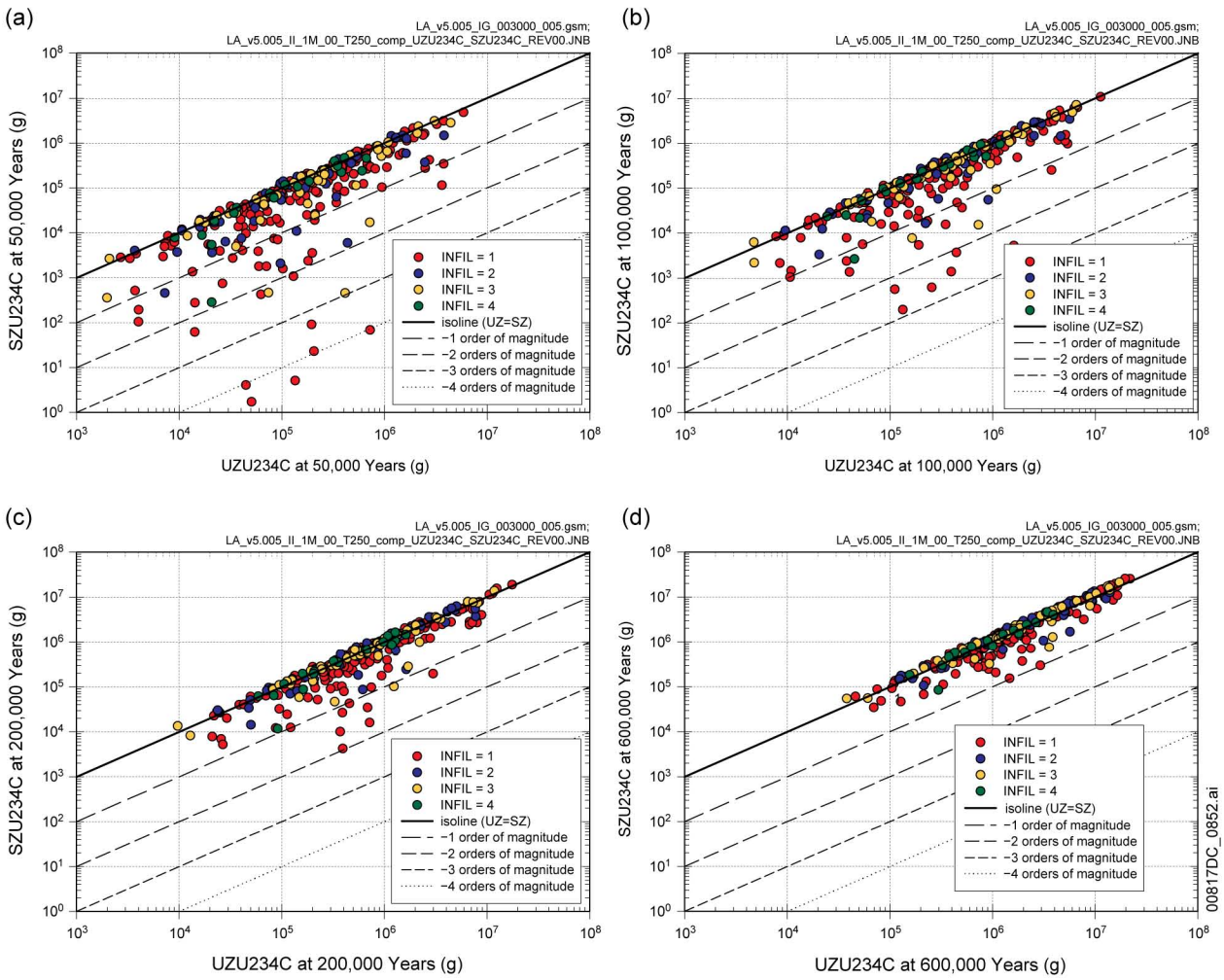

Source: Output DTNs: MO0801TSPAPRSA.000 [DIRS 184620]; and MO0710PLOTSFIG.000 [DIRS 185207].

Figure K.6.5.2-7[a]. Comparison of cumulative releases of dissolved ^{234}U into the SZ (*UZU234C*, g) and across a subsurface plane at the location of the RMEI (*SZU234C*, g) obtained with version 5.005 of the TSPA-LA Model at (a) 50,000, (b) 100,000, (c) 200,000, and (d) 600,000 years for an igneous intrusive event at 250 years that destroys all WPs in the repository

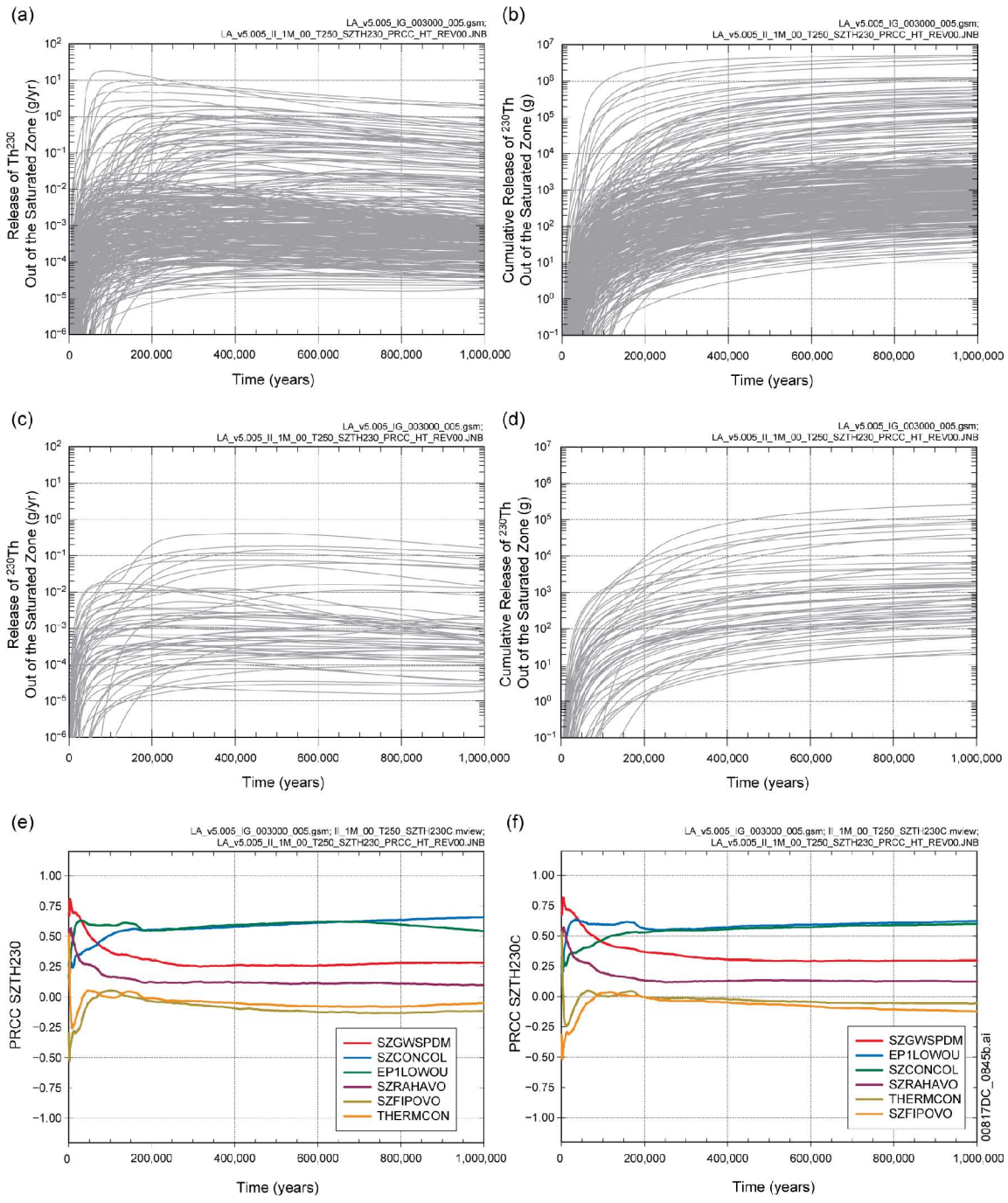

Source: Output DTNs: MO0801TSPAPRSA.000 [DIRS 184620]; and MO0710PLOTSFIG.000 [DIRS 185207].

Figure K6.5.2-8[a]. Time-dependent release rates (*SZTH230*, g/yr) and cumulative (i.e., integrated) releases (*SZTH230C*, g) over 1,000,000 years for the movement of dissolved ^{230}Th across a subsurface plane at the location of the RMEI resulting from an igneous intrusive event at 250 years that destroys all WPs in the repository obtained with version 5.005 of the TSPA-LA Model: (a,b) *SZTH230* and *SZTH230C* for all (i.e., 300) sample elements, (c,d) *SZTH230* and *SZTH230C* for first 50 sample elements, and (e,f) PRCCs for *SZTH230* and *SZTH230C*

(a)

	SZTH230: 50,000 Years			SZTH230: 200,000 Years			SZTH230: 500,000 Years		
Step[a]	Variable[b]	R^2 [c]	SRRC[d]	Variable	R^2	SRRC	Variable	R^2	SRRC
1	EP1LOWOU	0.17	0.40	SZCONCOL	0.19	0.45	SZCONCOL	0.20	0.46
2	SZCONCOL	0.33	0.39	EP1LOWOU	0.37	0.38	EP1LOWOU	0.40	0.40
3	SZGWSPDM	0.45	0.36	SZKDAMCO	0.43	0.23	SZKDAMCO	0.48	0.26
4	INFIL	0.52	0.29	INFIL	0.49	0.27	INFIL	0.54	0.24
5	GOESITED	0.57	−0.20	GOESITED	0.54	−0.23	SZGWSPDM	0.57	0.20
6	SZKDAMCO	0.60	0.17	SZGWSPDM	0.58	0.23	GOESITED	0.60	−0.19
7	SZDIFCVO	0.62	−0.12	KDPUSMEC	0.60	0.14	SZKDAMAL	0.61	−0.13
8	CSWFA4AC	0.63	−0.11	CORRATSS	0.62	−0.15	SZKDUAL	0.63	0.13
9	KDPUSMEC	0.64	0.11	RHMUNO65	0.63	−0.11	HFOSA	0.65	−0.11
10	CORRATSS	0.65	−0.13	HFOSA	0.65	−0.14	PHCSS	0.66	0.10
11	CSNFMASS	0.66	0.13	SZKDSNAL	0.66	−0.15	CSNFMASS	0.67	0.10
12	IS2MCOS	0.67	0.12	SZKDSEAL	0.67	0.11	KDPUSMEC	0.67	0.10
13	PHCSS	0.68	0.12	SZSREG2X	0.68	0.10	WDGCUA22	0.68	0.09
14				RHMU20	0.69	0.10			
15				HLWDRALK	0.70	0.09			
16				IS2MCONS	0.70	0.09			

(b)

	SZTH230C: 50,000 Years			SZTH230C: 200,000 Years			SZTH230C: 500,000 Years		
Step[a]	Variable[b]	R^2 [c]	SRRC[d]	Variable	R^2	SRRC	Variable	R^2	SRRC
1	EP1LOWOU	0.16	0.40	SZCONCOL	0.19	0.44	SZCONCOL	0.19	0.46
2	SZCONCOL	0.30	0.34	EP1LOWOU	0.37	0.39	EP1LOWOU	0.39	0.40
3	SZGWSPDM	0.46	0.41	SZGWSPDM	0.44	0.28	SZKDAMCO	0.46	0.27
4	INFIL	0.53	0.29	INFIL	0.50	0.27	INFIL	0.52	0.24
5	GOESITED	0.58	−0.19	SZKDAMCO	0.55	0.24	SZGWSPDM	0.57	0.22
6	SZKDAMCO	0.60	0.15	GOESITED	0.60	−0.20	GOESITED	0.61	−0.21
7	SZDIFCVO	0.62	−0.16	CORRATSS	0.62	−0.20	KDPUSMEC	0.62	0.12
8	SZFISPVO	0.64	0.10	KDPUSMEC	0.64	0.12	HFOSA	0.64	−0.12
9	CSWFA4AC	0.65	−0.11	RHMUNO65	0.65	−0.09	SZKDSNAL	0.65	−0.16
10	DSCRACKA	0.66	−0.09	CSWFA4AC	0.66	−0.09	SZKDNPAL	0.66	0.11
11	PHCSS	0.67	0.12	PHCSS	0.68	0.13	PHCSS	0.67	0.11
12	CORRATSS	0.68	−0.12	PROBWPEF	0.69	0.10	CSNFMASS	0.68	0.11
13	IS2MCOS	0.69	0.12	CSCORRAT	0.70	0.11	CORRATSS	0.69	−0.10
14	CSNFMASS	0.70	0.11	CSNFMASS	0.70	0.12			
15	KDPUSMEC	0.71	0.10	SZKDSNAL	0.71	−0.10			
16	SZFIPOVO	0.72	−0.09						

00817DC_0846b.ai

a: Steps in stepwise rank regression analysis
b: Variables listed in order of selection in stepwise regression
c: Cumulative R^2 value with entry of each variable into regression model
d: Standardized rank regression coefficients (SRRCs) in final regression model

Source: Output DTNs: MO0801TSPAPRSA.000 [DIRS 184620]; and MO0710PLOTSFIG.000 [DIRS 185207].

Figure K6.5.2-9[a]. Stepwise rank regression analyses and selected scatterplots for time-dependent release rates (*SZTH230*, g/yr) and cumulative (i.e., integrated) releases (*SZTH230C*, g) for the movement of dissolved ^{230}Th across a subsurface plane at the location of the RMEI resulting from an igneous intrusive event at 250 years that destroys all WPs in the repository obtained with version 5.005 of the TSPA-LA Model: (a,b) regressions for *SZTH230* and *SZTH230C* at 50,000, 200,000, and 500,000 years, and (c-h) scatterplots for *SZTH230* and *SZTH230C* at 500,000 years

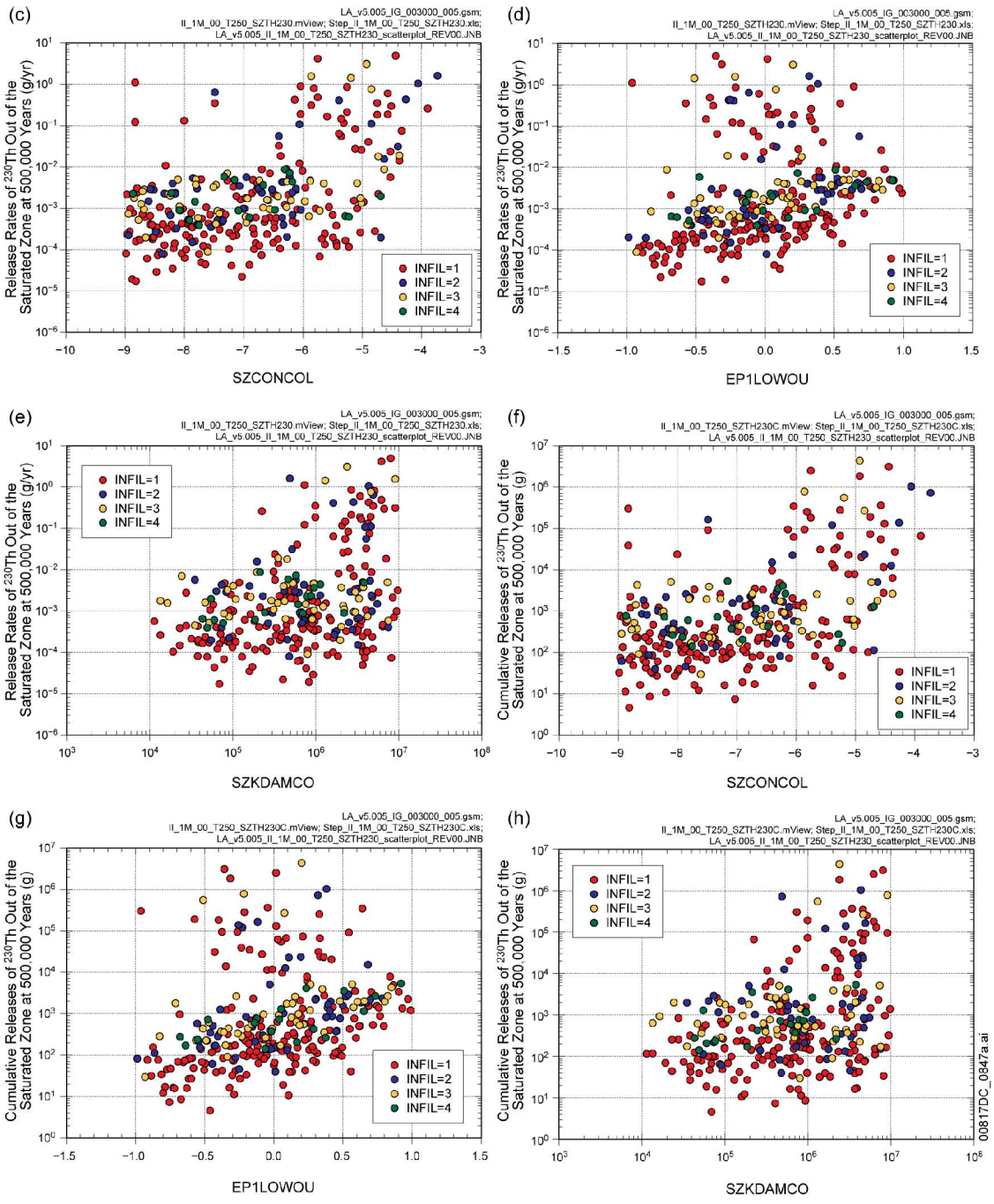

Source: Output DTNs: MO0801TSPAPRSA.000 [DIRS 184620]; and MO0710PLOTSFIG.000 [DIRS 185207].

Figure K6.5.2-9[a]. Stepwise rank regression analyses and selected scatterplots for time-dependent release rates (*SZTH230*, g/yr) and cumulative (i.e., integrated) releases (*SZTH230C*, g) for the movement of dissolved ^{230}Th across a subsurface plane at the location of the RMEI resulting from an igneous intrusive event at 250 years that destroys all WPs in the repository obtained with version 5.005 of the TSPA-LA Model: (a,b) regressions for *SZTH230* and *SZTH230C* at 50,000, 200,000, and 500,000 years, and (c-h) scatterplots for *SZTH230* and *SZTH230C* at 500,000 years (continued)

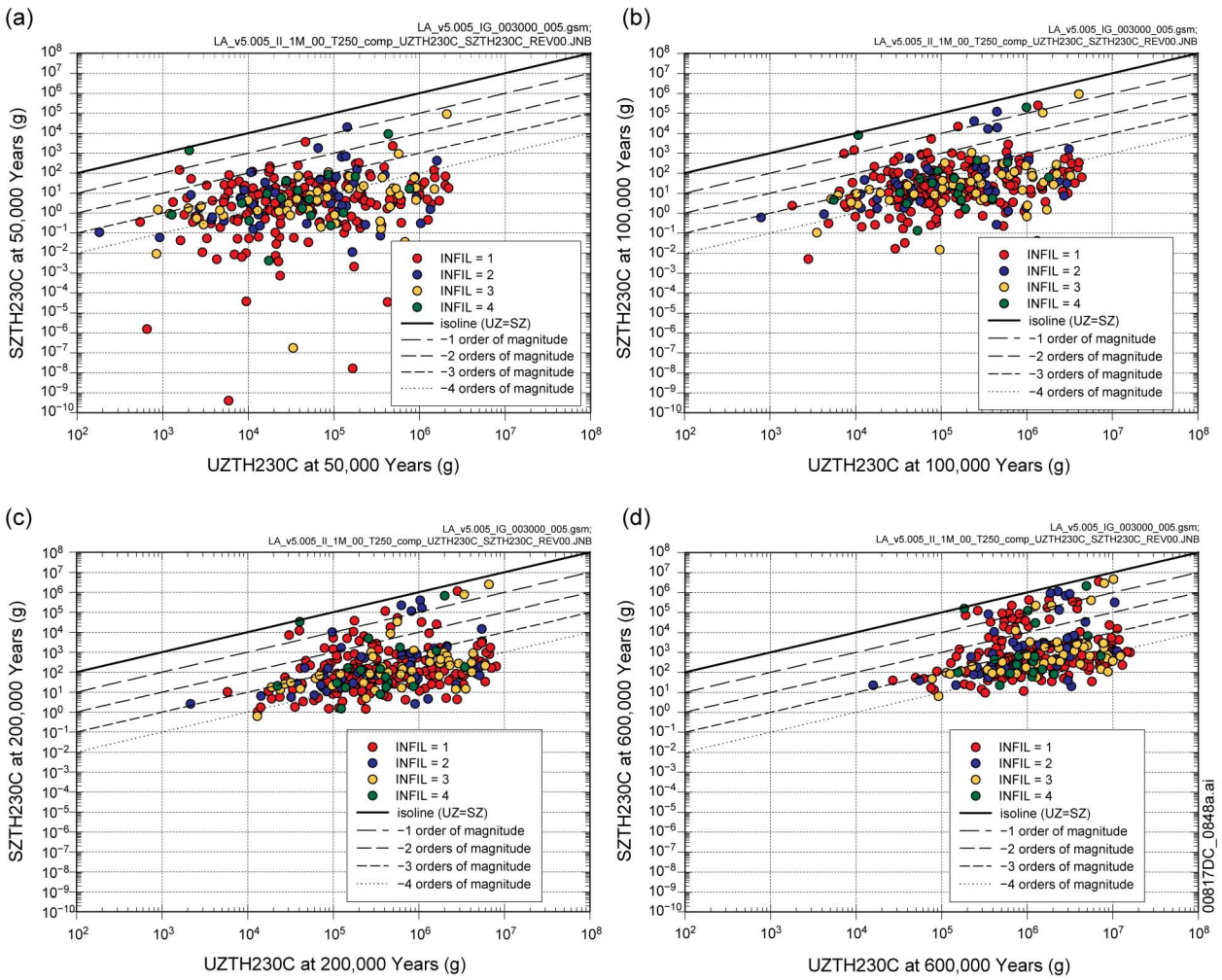

Source: Output DTNs: MO0801TSPAPRSA.000 [DIRS 184620]; and MO0710PLOTSFIG.000 [DIRS 185207].

Figure K.6.5.2-10[a]. Comparison of cumulative releases of dissolved ^{230}Th into the SZ (*UZTH230C*, g) and across a subsurface plane at the location of the RMEI (*SZTH230C*, g) obtained with version 5.005 of the TSPA-LA Model at (a) 50,000, (b) 100,000, (c) 200,000, and (d) 600,000 years for an igneous intrusive event at 250 years that destroys all WPs in the repository

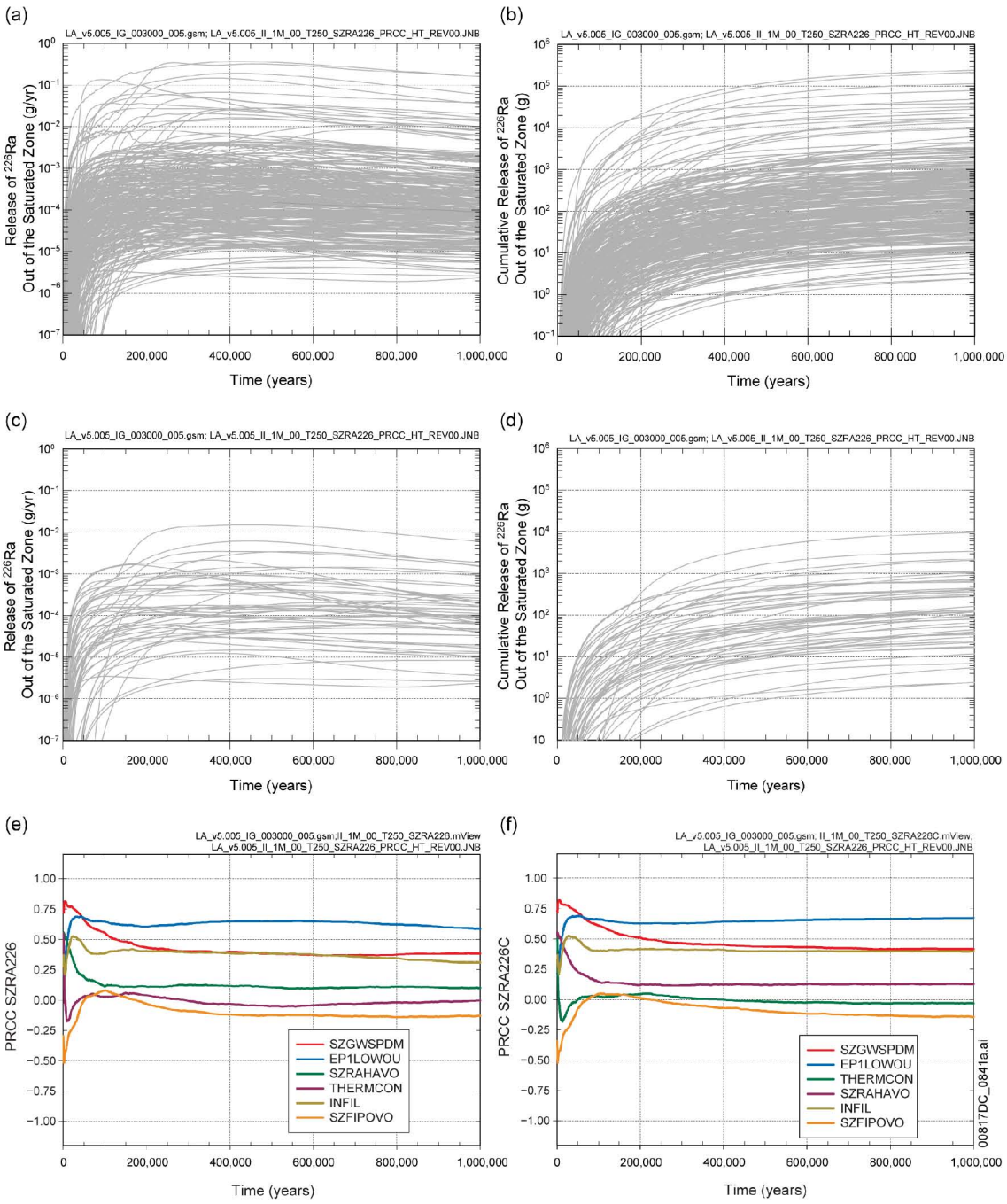

Source: Output DTNs: MO0801TSPAPRSA.000 [DIRS 184620]; and MO0710PLOTSFIG.000 [DIRS 185207].

Figure K6.5.2-11[a]. Time-dependent release rates (*SZRA226*, g/yr) and cumulative (i.e., integrated) releases (*SZRA226C*, g) over 1,000,000 years for the movement of dissolved ^{226}Ra across a subsurface plane at the location of the RMEI resulting from an igneous intrusive event at 250 years that destroys all WPs in the repository obtained with version 5.005 of the TSPA-LA Model: (a,b) *SZRA226* and *SZRA226C* for all (i.e., 300) sample elements, (c,d) *SZRA226* and *SZRA226C* for first 50 sample elements, and (e,f) PRCCs for *SZRA226* and *SZRA226C*

(a)

	SZRA226: 50,000 Years			SZRA226: 200,000 Years			SZRA226: 500,000 Years		
Step[a]	Variable[b]	R^2 [c]	SRRC[d]	Variable	R^2	SRRC	Variable	R^2	SRRC
1	SZGWSPDM	0.22	0.48	EP1LOWOU	0.19	0.43	EP1LOWOU	0.21	0.45
2	EP1LOWOU	0.40	0.43	SZGWSPDM	0.28	0.34	SZCONCOL	0.37	0.27
3	INFIL	0.48	0.32	INFIL	0.41	0.26	SZGWSPDM	0.45	0.27
4	GOESITED	0.52	−0.20	GOESITED	0.47	−0.26	INFIL	0.49	0.22
5	SZKDRAAL	0.56	−0.21	SZCONCOL	0.52	0.20	SZKDAMCO	0.53	0.20
6	CORRATSS	0.58	−0.15	HFOSA	0.55	−0.16	GOESITED	0.56	−0.21
7	PHCSS	0.60	0.13	SZKDAMCO	0.57	0.13	PHCSS	0.59	0.14
8	IS2MCOS	0.61	0.13	PHCSS	0.59	0.15	HFOSA	0.61	−0.15
9	CSNFMASS	0.63	0.12	CORRATSS	0.61	−0.15	SZKDUAL	0.62	0.13
10	KDPUSMEC	0.65	0.16	KDPUSMEC	0.63	0.12	SZKDRAAL	0.63	−0.28
11	UZFAG4	0.66	−0.10	UZFAG4	0.64	−0.12			
12	THERMCON	0.67	0.11	HLWDRALK	0.65	0.11			
13	HFOSA	0.67	−0.09	SZKDRAAL	0.66	−0.27			
14	SZRAHAVO	0.68	0.11						
15	DSCRACKA	0.69	−0.09						
16	SZDIFCVO	0.70	−0.09						

(b)

	SZRA226C: 50,000 Years			SZRA226C: 200,000 Years			SZRA226C: 500,000 Years		
Step[a]	Variable[b]	R^2 [c]	SRRC[d]	Variable	R^2	SRRC	Variable	R^2	SRRC
1	SZGWSPDM	0.25	0.50	EP1LOWOU	0.19	0.43	EP1LOWOU	0.21	0.46
2	EP1LOWOU	0.42	0.40	SZGWSPDM	0.31	0.39	SZGWSPDM	0.31	0.29
3	INFIL	0.51	0.32	INFIL	0.37	0.26	SZKDCSAL	0.37	−0.25
4	GOESITED	0.54	−0.16	GOESITED	0.43	−0.25	SZCONCOL	0.45	0.23
5	SZKDRAAL	0.58	−0.20	SZKDRAAL	0.50	−0.25	INFIL	0.50	0.23
6	KDPUSMEC	0.59	0.13	SZCONCOL	0.54	0.19	GOESITED	0.54	−0.22
7	SZDIFCVO	0.61	−0.15	CORRATSS	0.58	−0.19	SZKDAMCO	0.58	0.18
8	SZRAHAVO	0.63	0.13	PHCSS	0.60	0.16	HFOSA	0.60	−0.16
9	SZFISPVO	0.64	0.13	HFOSA	0.62	−0.14	PHCSS	0.62	0.15
10	CORRATSS	0.66	−0.16	KDPUSMEC	0.64	0.13	SZRAHAVO	0.64	0.10
11	IS2MCOS	0.67	0.13	UZFAG4	0.65	−0.12	KDPUSMEC	0.65	0.10
12	PHCSS	0.69	0.12	HLWDRALK	0.66	0.10	UZFAG4	0.65	−0.11
13	CSNFMASS	0.70	0.11	SZKDAMCO	0.67	0.11	UZCOKDPU	0.66	0.09
14	SZFIPOVO	0.71	−0.10	CSCORRAT	0.68	0.09			
15	DSCRACKA	0.72	−0.10						
16	THERMCON	0.73	0.10						

008178DC_0842a.ai

a: Steps in stepwise rank regression analysis
b: Variables listed in order of selection in stepwise regression
c: Cumulative R^2 value with entry of each variable into regression model
d: Standardized rank regression coefficients (SRRCs) in final regression model

Source: Output DTNs: MO0801TSPAPRSA.000 [DIRS 184620]; and MO0710PLOTSFIG.000 [DIRS 185207].

Figure K6.5.2-12[a]. Stepwise rank regression analyses and selected scatterplots for time-dependent release rates (*SZRA226*, g/yr) and cumulative (i.e., integrated) releases (*SZRA226C*, g) for the movement of dissolved ^{226}Ra across a subsurface plane at the location of the RMEI resulting from an igneous intrusive event at 250 years that destroys all WPs in the repository obtained with version 5.005 of the TSPA-LA Model: (a,b) regressions for *SZRA226* and *SZRA226C* at 50,000, 200,000, and 500,000 years, and (c-h) scatterplots for *SZRA226* and *SZRA226C* at 50,000 years

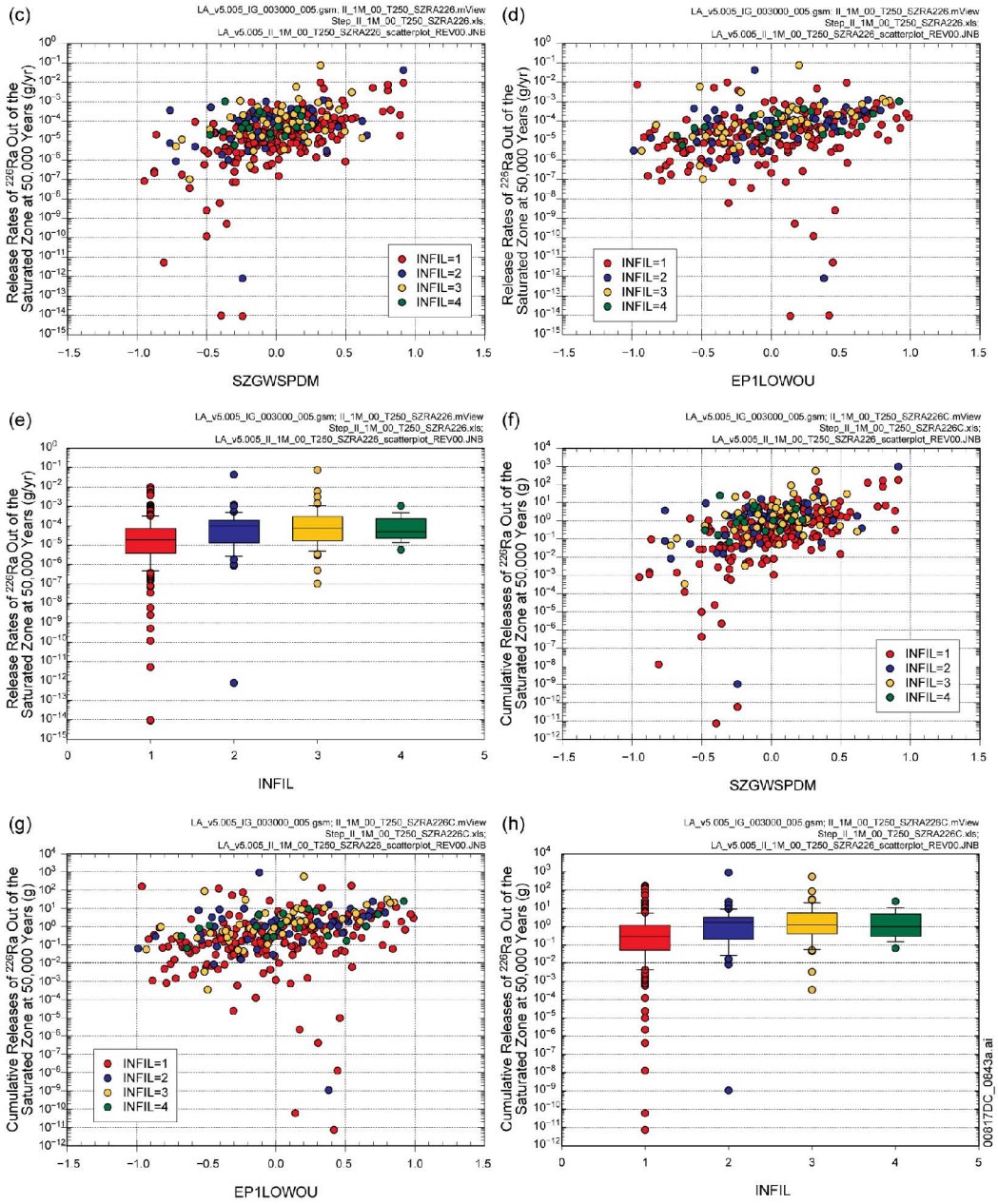

Source: Output DTNs: MO0801TSPAPRSA.000 [DIRS 184620]; and MO0710PLOTSFIG.000 [DIRS 185207].

NOTE: In (e,h), the box extends from 0.25 to 0.75 quantile; lower and upper bar and whisker extend to 0.1 and 0.9 quantile, respectively; dots represent values outside 0.1 to 0.9 quantile range; median indicated by light horizontal line.

Figure K6.5.2-12[a]. Stepwise rank regression analyses and selected scatterplots for time-dependent release rates (*SZRA226*, g/yr) and cumulative (i.e., integrated) releases (*SZRA226C*, g) for the movement of dissolved ^{226}Ra across a subsurface plane at the location of the RMEI resulting from an igneous intrusive event at 250 years that destroys all WPs in the repository obtained with version 5.005 of the TSPA-LA Model: (a,b) regressions for *SZRA226* and *SZRA226C* at 50,000, 200,000, and 500,000 years, and (c-h) scatterplots for *SZRA226* and *SZRA226C* at 50,000 years (continued)

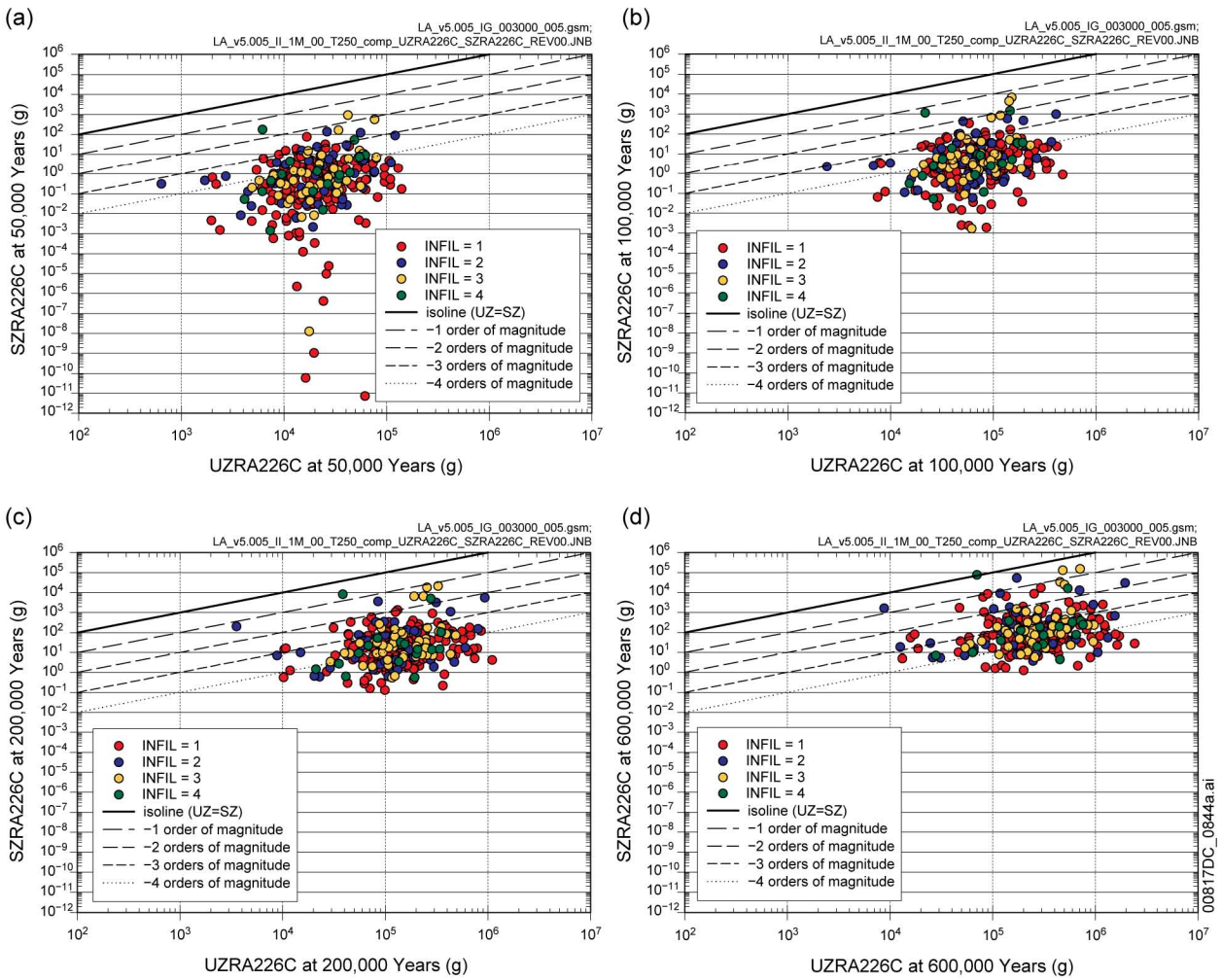

Source: Output DTNs: MO0801TSPAPRSA.000 [DIRS 184620]; and MO0710PLOTSFIG.000 [DIRS 185207].

Figure K.6.5.2-13[a]. Comparison of cumulative releases of dissolved ^{226}Ra into the SZ (*UZRA226C*, g) and across a subsurface plane at the location of the RMEI (*SZRA226C*, g) obtained with version 5.005 of the TSPA-LA Model at (a) 50,000, (b) 100,000, (c) 200,000, and (d) 600,000 years for an igneous intrusive event at 250 years that destroys all WPs in the repository

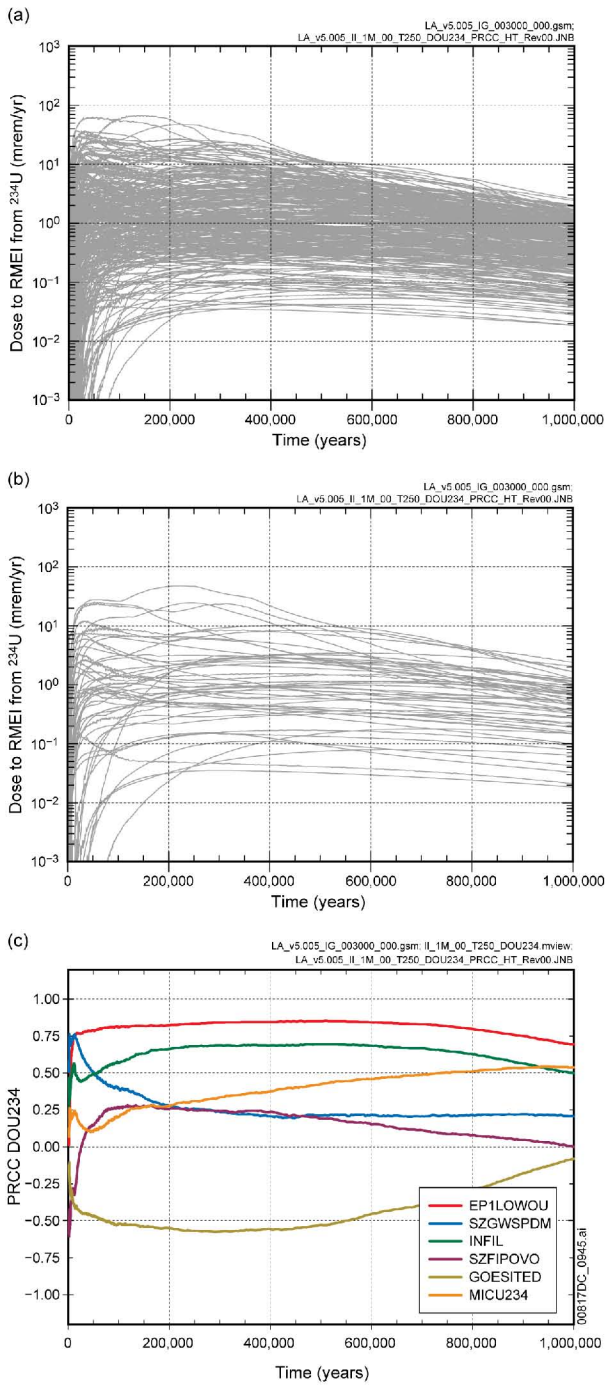

Source: Output DTNs: MO0801TSPAPRSA.000 [DIRS 184620]; and MO0710PLOTSFIG.000 [DIRS 185207].

Figure K.6.6.2-5[a]. Time-dependent dose to the RMEI (*DOU234*, mrem/yr) over 1,000,000 years for the movement of dissolved ^{234}U across a subsurface plane at the location of the RMEI resulting from an igneous intrusive event at 250 years that destroys all WPs in the repository obtained with version 5.005 of the TSPA-LA Model: (a) *DOU234* for all (i.e., 300) sample elements, (b) *DOU234* for first 50 sample elements, and (c) PRCCs for *DOU234*

(a)

	DOU234: 50,000 Years			DOU234: 200,000 Years			DOU234: 500,000 Years		
Step[a]	Variable[b]	R^{2c}	SRRC[d]	Variable	R^2	SRRC	Variable	R^2	SRRC
1	EP1LOWOU	0.27	0.49	EP1LOWOU	0.35	0.57	EP1LOWOU	0.42	0.64
2	INFIL	0.40	0.36	INFIL	0.54	0.41	INFIL	0.61	0.40
3	SZGWSPDM	0.48	0.28	GOESITED	0.61	−0.26	MICU234	0.66	0.25
4	GOESITED	0.55	−0.21	MICU234	0.65	0.17	GOESITED	0.71	−0.24
5	CORRATSS	0.59	−0.23	PHCSS	0.68	0.19	PHCSS	0.75	0.19
6	PHCSS	0.61	0.16	SZGWSPDM	0.70	0.18	HFOSA	0.77	−0.13
7	IS2MCOS	0.64	0.12	HFOSA	0.72	−0.15	SZGWSPDM	0.78	0.12
8	CSNFMASS	0.66	0.14	GOERELAB	0.74	0.11	GOERELAB	0.79	0.11
9	SZDIFCVO	0.67	−0.15	KDPUSMEC	0.75	0.10	CSNFMASS	0.80	0.10
10	SZFISPVO	0.69	0.12	UZFAG4	0.75	−0.09	MICTC99	0.81	−0.08
11	MICU234	0.70	0.11	CORRATSS	0.76	−0.10	WDLCRATE	0.81	−0.09
12	KDPUSMEC	0.71	0.10	CSCORRAT	0.77	0.09	SZSREG2X		
13	GOERELAB	0.72	0.10	DSNFMASS	0.78	0.07			
14	WDDEFCNT	0.73	−0.09	CSNFMASS	0.78	0.10			
15	INRFRCCS	0.73	−0.09	KDPUCOL	0.79	0.09			
16	KDPUCOL	0.74	0.09	WDDEFCNT	0.80	−0.08			

a: Steps in stepwise rank regression analysis
b: Variables listed in order of selection in stepwise regression
c: Cumulative R^2 value with entry of each variable into regression model
d: Standardized rank regression coefficients (SRRCs) in final regression model

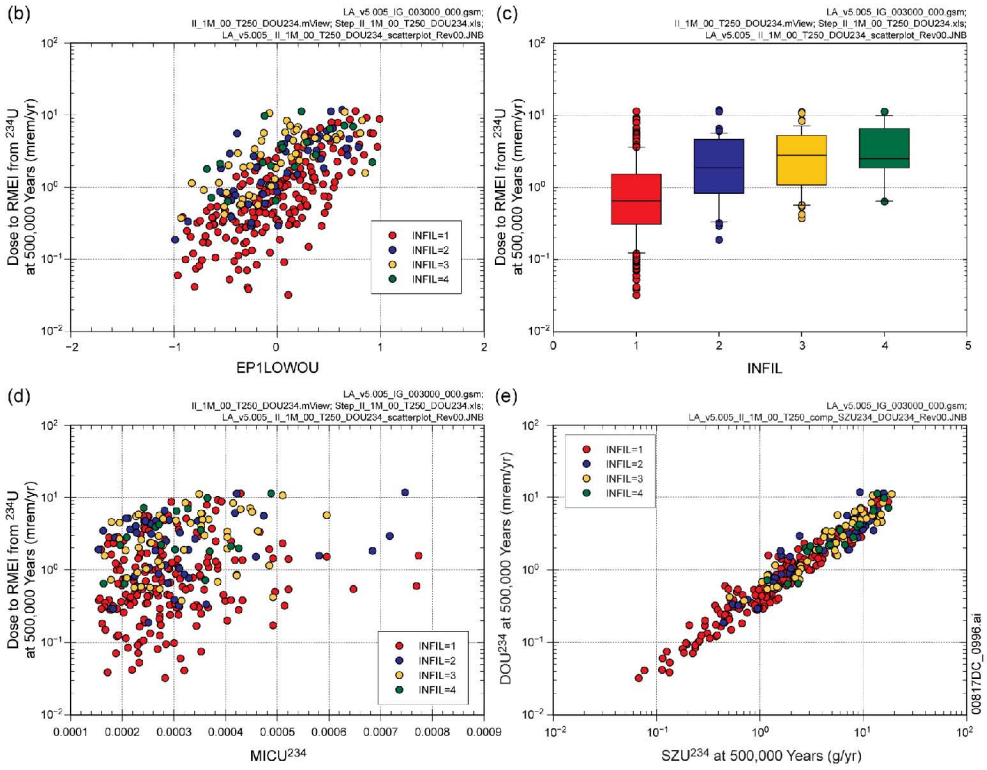

Source: Output DTNs: MO0801TSPAPRSA.000 [DIRS 184620]; and MO0710PLOTSFIG.000 [DIRS 185207].

NOTE: In (c), the box extends from 0.25 to 0.75 quantile; lower and upper bar and whisker extend to 0.1 and 0.9 quantile, respectively; dots represent values outside 0.1 to 0.9 quantile range; median indicated by light horizontal line.

Figure K.6.6.2-6[a]. Stepwise rank regression analyses and selected scatterplots for time-dependent dose to the RMEI (*DOU234*, mrem/yr) for the movement of dissolved ^{234}U across a subsurface plane at the location of the RMEI (*SZU234*, g/yr) resulting from an igneous intrusive event at 250 years that destroys all WPs in the repository obtained with version 5.005 of the TSPA-LA Model: (a) regressions for *DOU234* at 50,000, 200,000, and 500,000 years, (b,c,d) scatterplots for *DOU234* at 500,000 years, and (e) scatterplot comparing *SZU234* and *DOU234* at 500,000 years

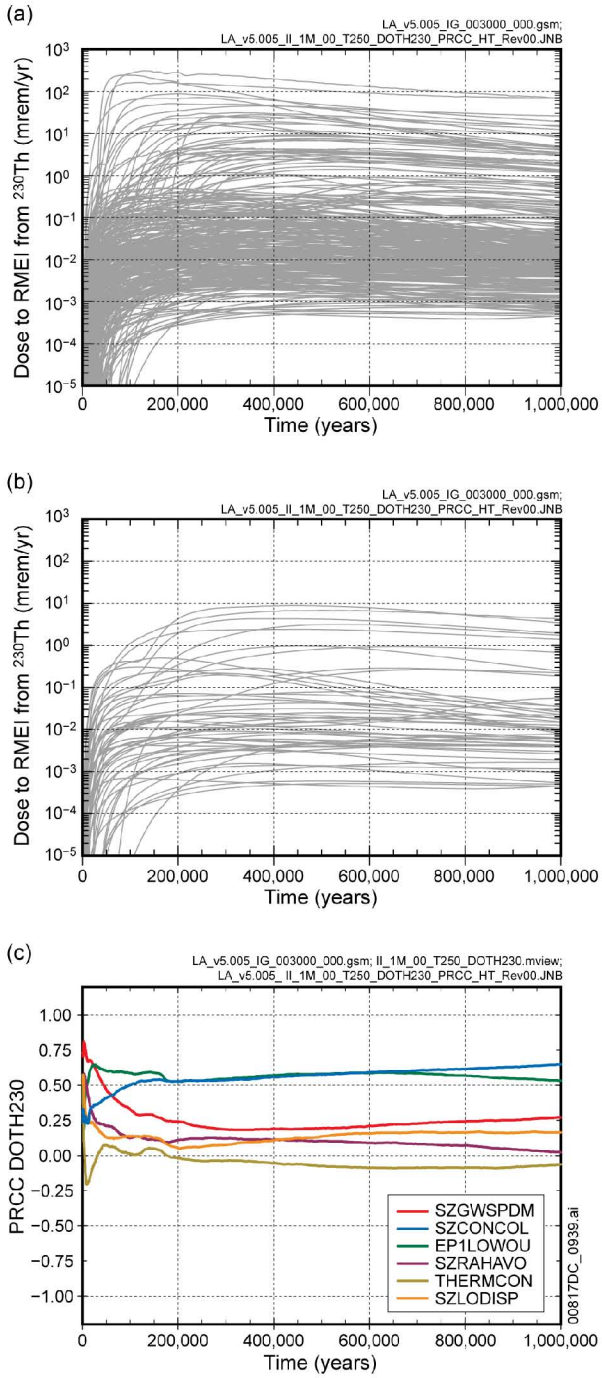

Source: Output DTNs: MO0801TSPAPRSA.000 [DIRS 184620]; and MO0710PLOTSFIG.000 [DIRS 185207].

Figure K.6.6.2-7[a]. Time-dependent dose to the RMEI (*DOTH230*, mrem/yr) over 1,000,000 years for the movement of dissolved ^{230}Th across a subsurface plane at the location of the RMEI resulting from an igneous intrusive event at 250 years that destroys all WPs in the repository obtained with version 5.005 of the TSPA-LA Model: a) *DOTH230* for all (i.e., 300) sample elements, (b) *DOTH230* for first 50 sample elements, and (c) PRCCs for *DOTH230*

(a)

	DOTH230: 50,000 Years			DOTH230: 200,000 Years			DOTH230: 500,000 Years		
Step[a]	Variable[b]	R^{2c}	SRRC[d]	Variable	R^2	SRRC	Variable	R^2	SRRC
1	EP1LOWOU	0.16	0.41	SZCONCOL	0.19	0.45	SZCONCOL	0.20	0.46
2	SZCONCOL	0.31	0.38	EP1LOWOU	0.36	0.37	EP1LOWOU	0.39	0.39
3	SZGWSPDM	0.42	0.35	SZKDAMCO	0.42	0.25	SZKDAMCO	0.46	0.26
4	INFIL	0.50	0.29	INFIL	0.48	0.26	INFIL	0.52	0.22
5	GOESITED	0.55	−0.20	GOESITED	0.52	−0.21	SZGWSPDM	0.55	0.19
6	MICTH229	0.59	0.17	SZGWSPDM	0.56	0.21	GOESITED	0.58	−0.17
7	SZKDAMCO	0.61	0.17	MICTH229	0.59	0.16	MICTH229	0.60	0.17
8	SZDIFCVO	0.63	−0.12	CORRATSS	0.61	−0.16	PHCSS	0.62	0.12
9	CSWFA4AC	0.64	−0.11	KDPUSMEC	0.63	0.13	SZKDAMAL	0.63	−0.15
10	KDPUSMEC	0.65	0.11	PHCSS	0.64	0.11	HFOSA	0.64	−0.10
11	PHCSS	0.66	0.13	CSNFMASS	0.65	0.11	SZKDUAL	0.65	0.12
12	CORRATSS	0.67	−0.13	SZKDSNAL	0.66	−0.16	CSNFMASS	0.66	0.10
13	CSNFMASS	0.69	0.13	HFOSA	0.67	−0.11	WDGCUA22	0.67	0.09
14	IS2MCOS	0.70	0.12	SZKDNPAL	0.68	0.11			
15				SZSREG2X	0.69	0.09			

a: Steps in stepwise rank regression analysis
b: Variables listed in order of selection in stepwise regression
c: Cumulative R^2 value with entry of each variable into regression model
d: Standardized rank regression coefficients (SRRCs) in final regression model

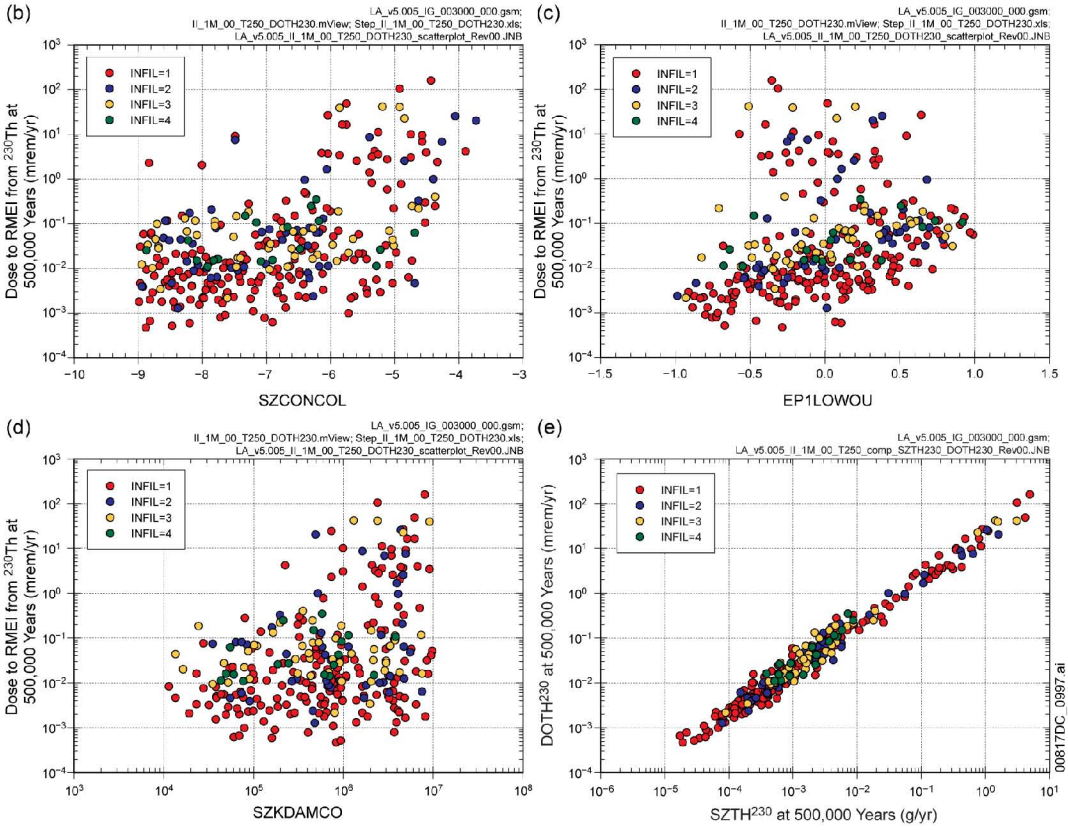

Source: Output DTNs: MO0801TSPAPRSA.000 [DIRS 184620]; and MO0710PLOTSFIG.000 [DIRS 185207].

Figure K.6.6.2-8[a]. Stepwise rank regression analyses and selected scatterplots for time-dependent dose to the RMEI (*DOTH230*, mrem/yr) for the movement of dissolved ^{230}Th across a subsurface plane at the location of the RMEI (*SZTH230*, g/yr) resulting from an igneous intrusive event at 250 years that destroys all WPs in the repository obtained with version 5.005 of the TSPA-LA Model: (a) regressions for *DOTH230* at 50,000, 200,000, and 500,000 years, (b,c,d) scatterplots for *DOTH230* at 500,000 years, and (e) scatterplot comparing *SZTH230* and *DOTH230* at 500,000 years

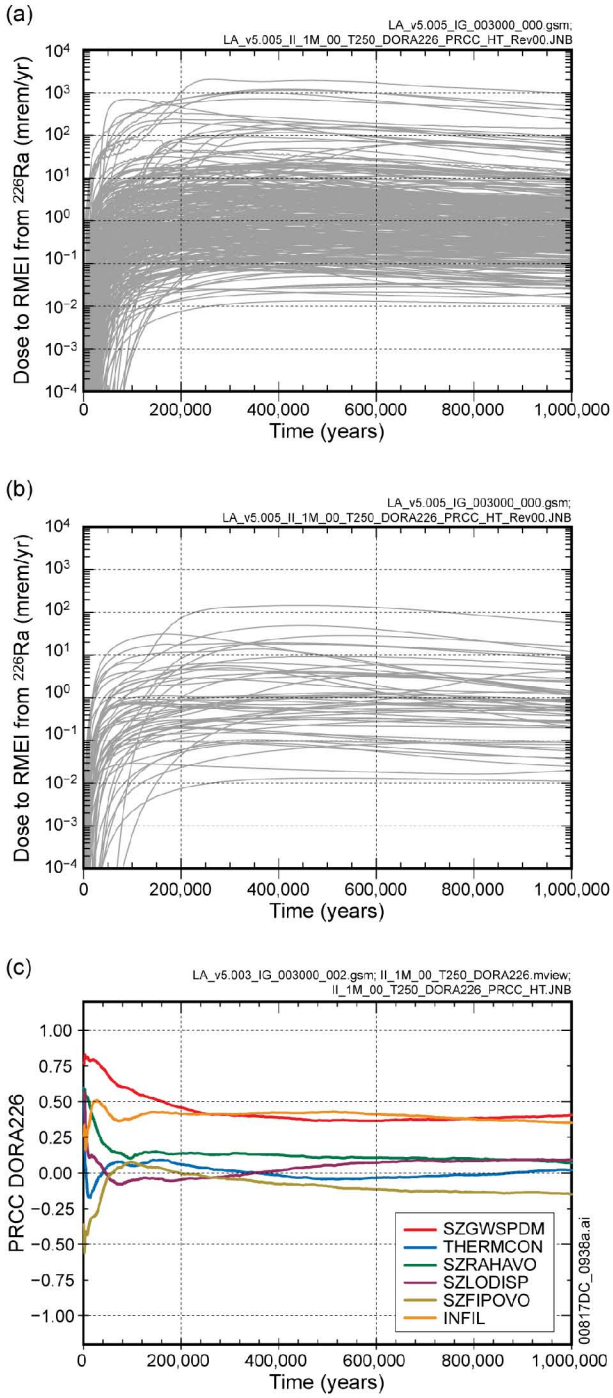

Source: Output DTNs: MO0801TSPAPRSA.000 [DIRS 184620]; and MO0710PLOTSFIG.000 [DIRS 185207].

Figure K.6.6.2-9[a]. Time-dependent dose to the RMEI (*DORA226*, mrem/yr) over 1,000,000 years for the movement of dissolved ^{226}Ra across a subsurface plane at the location of the RMEI resulting from an igneous intrusive event at 250 years that destroys all WPs in the repository obtained with version 5.005 of the TSPA-LA Model: (a) *DORA226* for all (i.e., 300) sample elements, (b) *DORA226* for first 50 sample elements, and (c) PRCCs for *DORA226*

(a)

	DORA226: 50,000 Years			DORA226: 200,000 Years			DORA226: 500,000 Years		
Step[a]	Variable[b]	R^2 [c]	SRRC[d]	Variable	R^2	SRRC	Variable	R^2	SRRC
1	SZGWSPDM	0.21	0.50	EP1LOWOU	0.19	0.43	EP1LOWOU	0.21	0.44
2	EP1LOWOU	0.39	0.43	SZKDCSAL	0.28	−0.24	SZKDCSAL	0.30	−0.26
3	INFIL	0.47	0.32	SZGWSPDM	0.34	0.32	SZCONCOL	0.36	0.25
4	GOESITED	0.51	−0.19	INFIL	0.40	0.25	SZGWSPDM	0.43	0.24
5	SZKDRAAL	0.55	−0.20	MICRA226	0.45	0.24	INFIL	0.47	0.22
6	MICRA226	0.58	0.17	GOESITED	0.51	−0.23	MICRA226	0.51	0.20
7	KDPUSMEC	0.60	0.16	SZCONCOL	0.55	0.20	SZKDAMCO	0.55	0.19
8	UZFAG4	0.62	−0.11	HFOSA	0.58	−0.15	GOESITED	0.57	−0.19
9	PHCSS	0.64	0.14	PHCSS	0.60	0.16	PHCSS	0.60	0.14
10	CORRATSS	0.65	−0.15	SZKDAMCO	0.62	0.13	HFOSA	0.62	−0.15
11	IS2MCOS	0.66	0.14	CORRATSS	0.64	−0.12	SZKDUAL	0.63	0.10
12	CSNFMASS	0.68	0.11	KDPUSMEC	0.65	0.11	SZRAHAVO	0.64	0.10
13	SZCONCOL	0.69	0.09	UZFAG4	0.66	−0.12			
14	HFOSA	0.70	−0.09	HLWDRALK	0.67	0.11			
15	THERMCON	0.70	0.09	SZKDSNAL	0.68	−0.10			
16				SZDENAL	0.68	−0.09			

a: Steps in stepwise rank regression analysis
b: Variables listed in order of selection in stepwise regression
c: Cumulative R^2 value with entry of each variable into regression model
d: Standardized rank regression coefficients (SRRCs) in final regression model

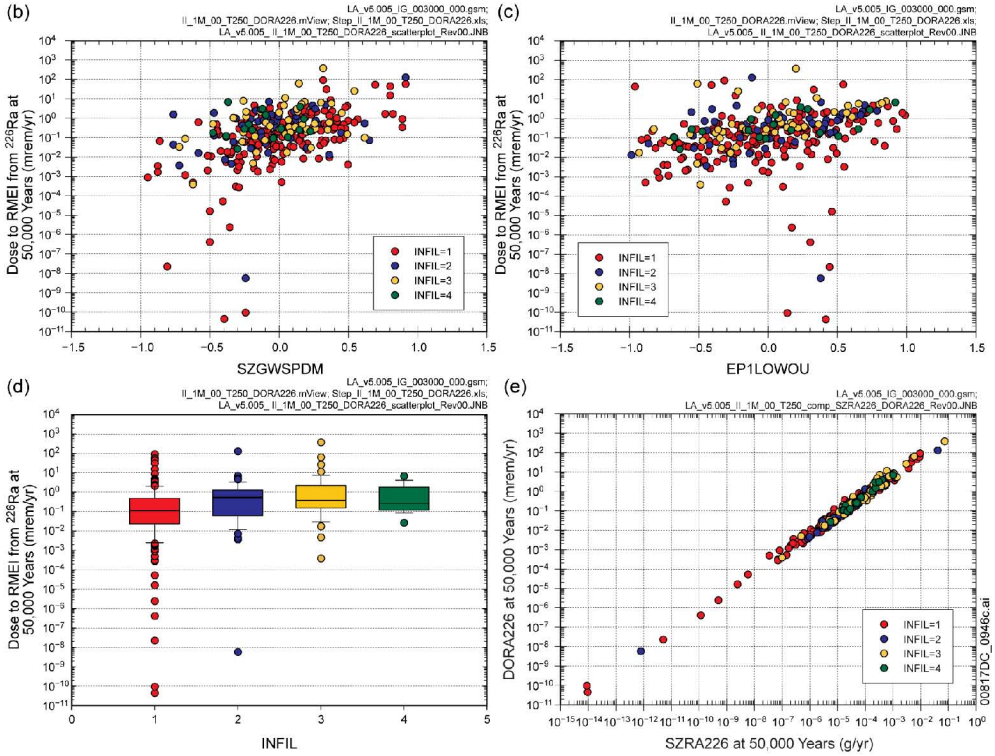

Source: Output DTNs: MO0801TSPAPRSA.000 [DIRS 184620]; and MO0710PLOTSFIG.000 [DIRS 185207].

NOTE: In (d), the box extends from 0.25 to 0.75 quantile; lower and upper bar and whisker extend to 0.1 and 0.9 quantile, respectively; dots represent values outside 0.1 to 0.9 quantile range; median indicated by light horizontal line.

Figure K.6.6.2-10[a]. Stepwise rank regression analyses and selected scatterplots for time-dependent dose to the RMEI (*DORA226*, mrem/yr) for the movement of dissolved ^{226}Ra across a subsurface plane at the location of the RMEI (*SZRA226*, g/yr) resulting from an igneous intrusive event at 250 years that destroys all WPs in the repository obtained with version 5.005 of the TSPA-LA Model: (a) regressions for *DORA226* at 50,000, 200,000, and 500,000 years, (b,c,d) scatterplots for *DORA226* at 50,000 years, and (e) scatterplot comparing *SZRA226* and *DORA226* at 50,000 years

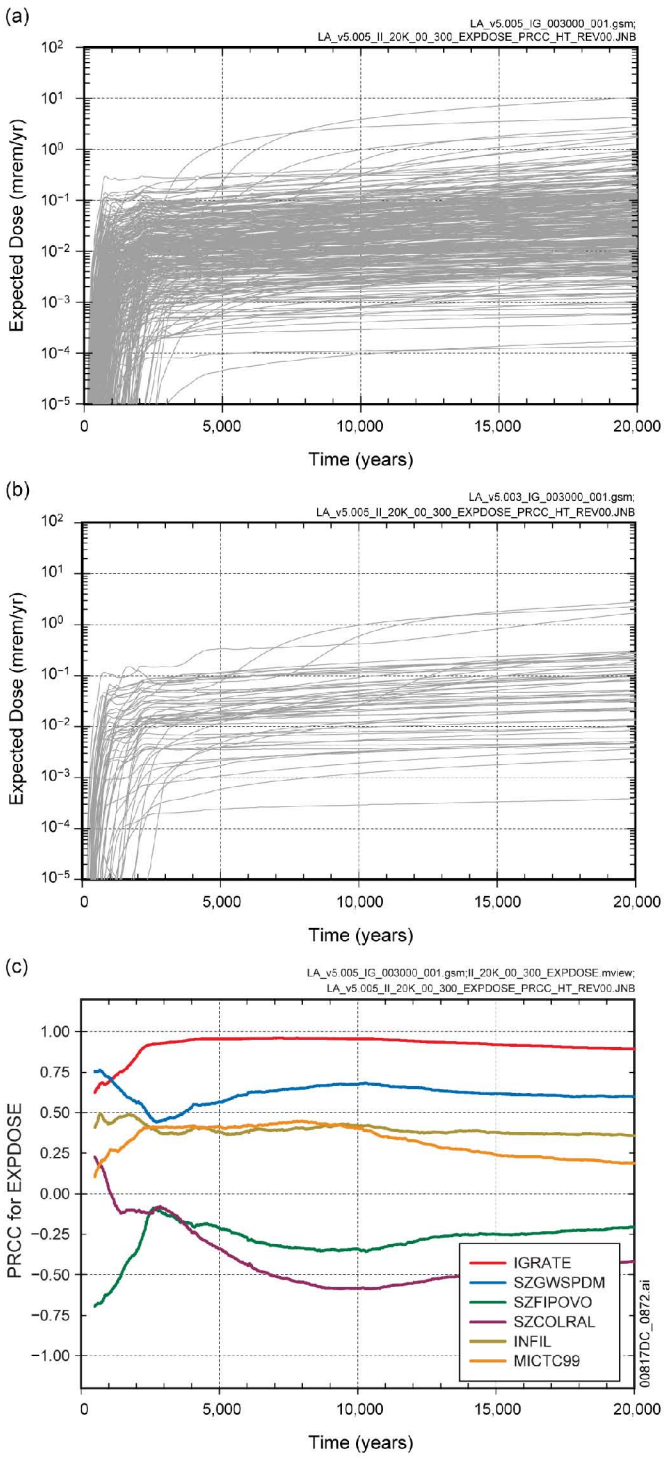

Source: Output DTNs: MO0710ADTSPAWO.000 [DIRS 183752]; and MO0710PLOTSFIG.000 [DIRS 185207].

Figure K6.7.1-1[a]. Expected dose to RMEI (*EXPDOSE*, mrem/yr) over [0, 20,000 yr] for all radioactive species resulting from igneous intrusion obtained with version 5.005 of the TSPA-LA Model: (a) *EXPDOSE* for all (i.e., 300) sample elements, (b) *EXPDOSE* for first 50 sample elements, and (c) PRCCs for *EXPDOSE*

(a)

	3,000 Years			5,000 Years			10,000 Years		
Step[a]	Variable[b]	R^{2} [c]	SRRC[d]	Variable	R^{2}	SRRC	Variable	R^{2}	SRRC
1	IGRATE	0.74	0.88	IGRATE	0.80	0.90	IGRATE	0.76	0.87
2	SZGWSPDM	0.79	0.22	SZGWSPDM	0.84	0.19	SZGWSPDM	0.81	0.22
3	INFIL	0.82	0.16	MICTC99	0.86	0.13	INFIL	0.83	0.15
4	MICTC99	0.85	0.15	INFIL	0.89	0.16	MICTC99	0.85	0.09
5	SZFISPVO	0.87	0.13	SZFISPVO	0.90	0.07	SZCOLRAL	0.86	−0.13
6	CSNFMASS	0.87	0.09	MICC14	0.90	0.09	CPUCOLWF	0.87	0.10
7	SZDIFCVO	0.88	−0.09	CSNFMASS	0.91	0.08	SZFIPOVO	0.88	−0.08
8	MICC14	0.89	0.08	MICNP237	0.91	0.08	MICNP237	0.89	0.10
9	MICNP237	0.89	0.08	SZFIPOVO	0.92	−0.07	SZFISPVO	0.89	0.08
10	SZCOLRVO	0.89	−0.06	SZCOLRAL	0.92	−0.06	ISCSS	0.90	−0.06
11	SZFIPOVO	0.90	−0.06	SZCOLRVO	0.92	−0.06	SZDENAL	0.90	−0.06
12	SZSREG3Y	0.90	−0.06	SMECSA	0.92	0.05	EP1LOWNU	0.90	0.06
13	ISCSNS	0.90	0.05	PHCSNS	0.93	−0.04	KDRASMEC	0.91	0.07
14							EP1NPO2	0.91	0.06
15							WPFLUX	0.91	0.05

a: Steps in stepwise rank regression analysis
b: Variables listed in order of selection in stepwise regression
c: Cumulative R^2 value with entry of each variable into regression model
d: Standardized rank regression coefficients (SRRCs) in final regression model

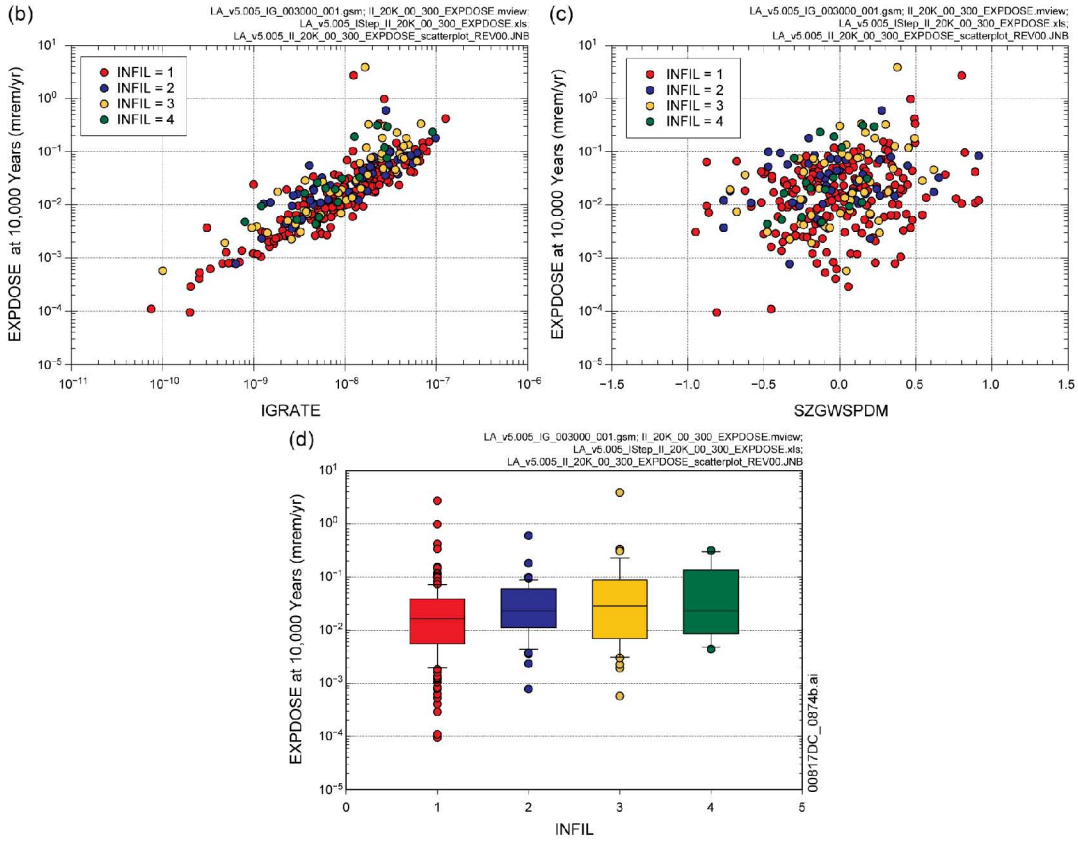

Source: Output DTNs: MO0710ADTSPAWO.000 [DIRS 183752]; and MO0710PLOTSFIG.000 [DIRS 185207].

NOTE: In (d), the box extends from 0.25 to 0.75 quantile; lower and upper bar and whisker extend to 0.1 and 0.9 quantile, respectively; dots represent values outside 0.1 to 0.9 quantile range; median indicated by light horizontal line.

Figure K6.7.1-2[a]. Stepwise rank regression analyses and selected scatterplots for expected dose to RMEI (*EXPDOSE*, mrem/yr) over [0, 20,000 yr] for all radioactive species resulting from igneous intrusion obtained with version 5.005 of the TSPA-LA Model: (a) regressions for *EXPDOSE* at 3,000, 5,000, and 10,000 years, and (b,c,d) scatterplots for *EXPDOSE* at 10,000 years

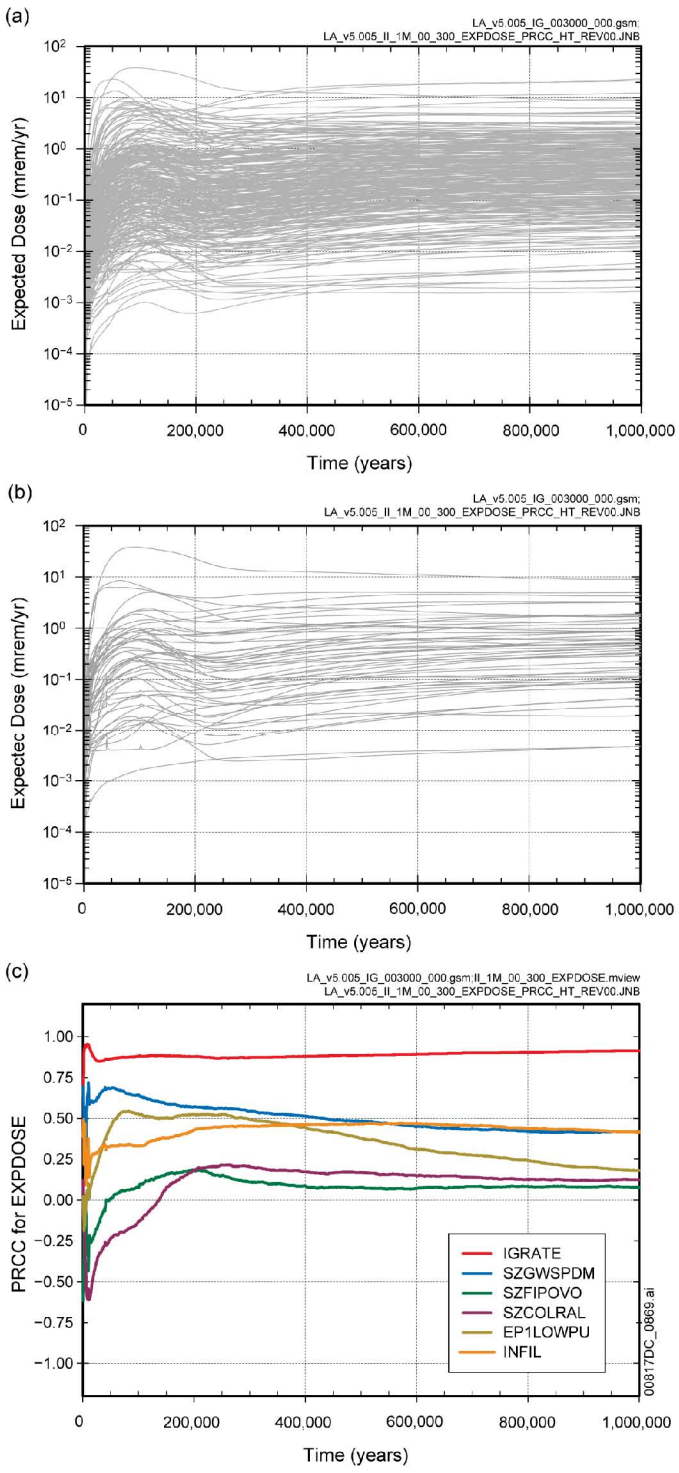

Source: Output DTNs: MO0710ADTSPAWO.000 [DIRS 183752]; and MO0710PLOTSFIG.000 [DIRS 185207].

Figure K.6.7.2-1[a]. Expected dose to RMEI (*EXPDOSE*, mrem/yr) over [0, 1,000,000 yr] for all radioactive species resulting from igneous intrusion obtained with version 5.005 of the TSPA-LA Model: (a) *EXPDOSE* for all (i.e., 300) sample elements, (b) *EXPDOSE* for first 50 sample elements, and (c) PRCCs for *EXPDOSE*

(a)

	EXPDOSE: 50,000 Years			EXPDOSE: 200,000 Years			EXPDOSE: 500,000 Years		
Step[a]	Variable[b]	R^2 [c]	SRRC[d]	Variable	R^2	SRRC	Variable	R^2	SRRC
1	IGRATE	0.53	0.72	IGRATE	0.57	0.75	IGRATE	0.62	0.79
2	SZGWSPDM	0.69	0.39	SZGWSPDM	0.67	0.30	SZGWSPDM	0.68	0.25
3	EP1LOWPU	0.74	0.20	EP1LOWPU	0.72	0.20	INFIL	0.73	0.19
4	INFIL	0.77	0.16	INFIL	0.75	0.19	EP1LOWPU	0.75	0.16
5	EP1NPO2	0.78	0.11	SZFISPVO	0.77	0.16	GOESITED	0.78	−0.15
6	MICNP237	0.79	0.11	GOESITED	0.79	−0.12	EP1LOWNU	0.79	0.14
7	CPUCOLWF	0.80	0.13	EP1NPO2	0.81	0.11	SZFISPVO	0.80	0.13
8	SZFISPVO	0.81	0.11	CORRATSS	0.82	−0.06	MICPU239	0.82	0.13
9	SZCOLRAL	0.82	−0.10	HFOSA	0.83	−0.09	SZCONCOL	0.83	0.10
10	KDRASMEC	0.83	0.08	EP1LOWNU	0.83	0.09	HFOSA	0.84	−0.08
11				SZDIFCVO	0.84	−0.09	UZFAG4	0.84	−0.08
12				SZCONCOL	0.85	0.08	SZDIFCVO	0.85	−0.07
13				PHCSS	0.85	−0.07	CSWFA0AK	0.85	−0.07
14				SZKDAMCO	0.85	0.06	SZKDAMCO	0.85	0.07
15				SCHOBOLT	0.86	0.07	SZSREG1X	0.86	0.07
16				MICNP237	0.86	0.11			

a: Steps in stepwise rank regression analysis
b: Variables listed in order of selection in stepwise regression
c: Cumulative R^2 value with entry of each variable into regression model
d: Standardized rank regression coefficients (SRRCs) in final regression model

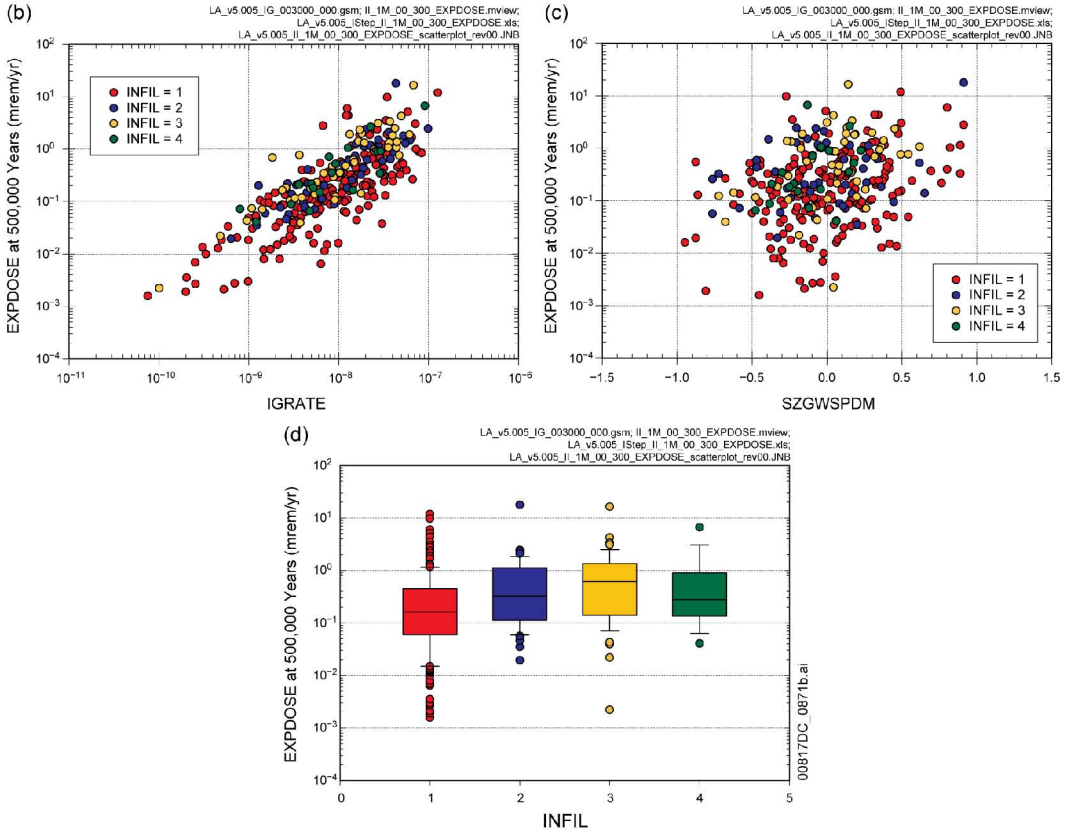

Source: Output DTNs: MO0710ADTSPAWO.000 [DIRS 183752]; and MO0710PLOTSFIG.000 [DIRS 185207].

NOTE: In (d), the box extends from 0.25 to 0.75 quantile; lower and upper bar and whisker extend to 0.1 and 0.9 quantile, respectively; dots represent values outside 0.1 to 0.9 quantile range; median indicated by light horizontal line.

Figure K.6.7.2-2[a]. Stepwise rank regression analyses and selected scatterplots for expected dose to RMEI (*EXPDOSE*, mrem/yr) over [0, 1,000,000 yr] for all radioactive species resulting from igneous intrusion obtained with version 5.005 of the TSPA-LA Model: (a) regressions for *EXPDOSE* at 50,000, 200,000, and 500,000 years, and (b,c,d) scatterplots for *EXPDOSE* at 500,000 years

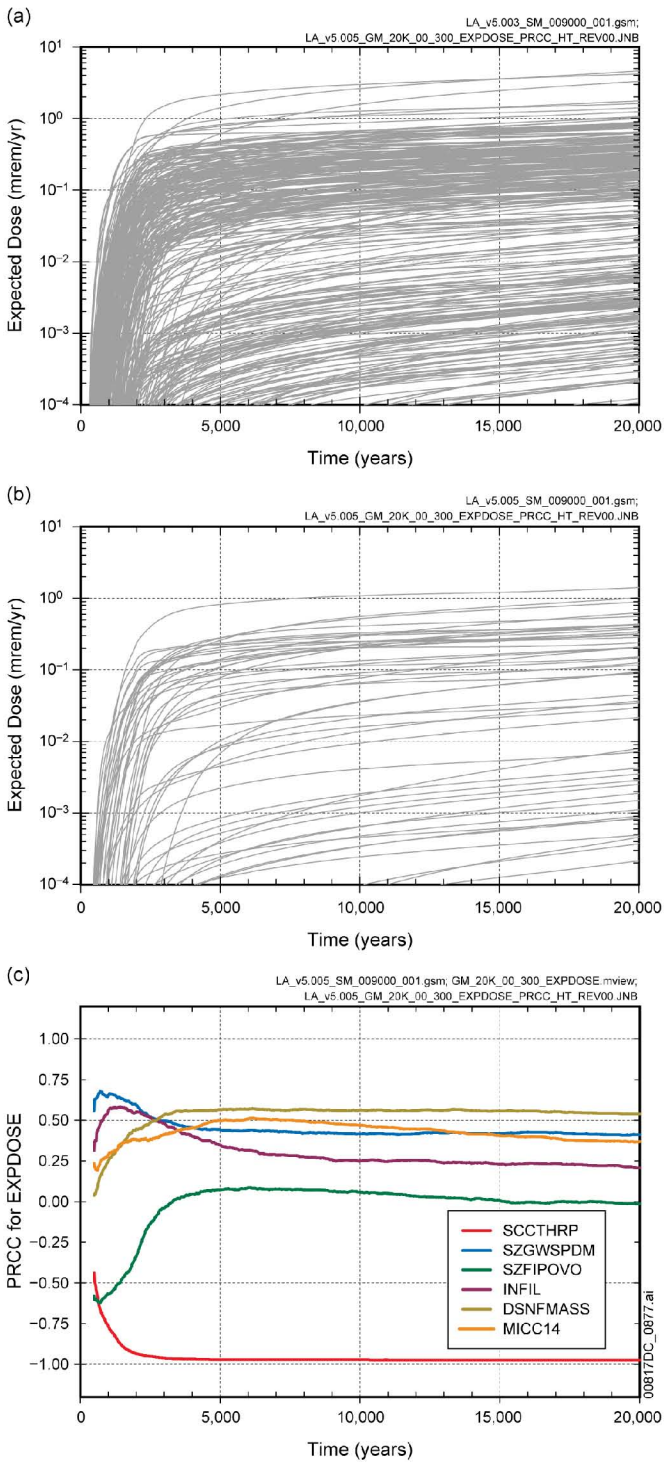

Source: Output DTNs: MO0710ADTSPAWO.000 [DIRS 183752]; and MO0710PLOTSFIG.000 [DIRS 185207].

Figure K7.7.1-1[a]. Expected dose to RMEI (*EXPDOSE*, mrem/yr) over [0, 20,000 yr] for all radioactive species resulting from seismic ground motion obtained with version 5.005 of the TSPA-LA Model: (a) *EXPDOSE* for all (i.e., 300) sample elements, (b) *EXPDOSE* for first 50 sample elements, and (c) PRCCs for *EXPDOSE*

(a)

	3,000 Years			5,000 Years			10,000 Years		
Step[a]	Variable[b]	R^2 [c]	SRRC[d]	Variable	R^2	SRRC	Variable	R^2	SRRC
1	SCCTHRP	0.81	−0.87	SCCTHRP	0.86	−0.91	SCCTHRP	0.88	−0.93
2	SZGWSPDM	0.83	0.16	MICTC99	0.88	0.10	MICTC99	0.90	0.12
3	INFIL	0.85	0.13	DSNFMASS	0.89	0.14	DSNFMASS	0.91	0.14
4	MICTC99	0.87	0.10	SZGWSPDM	0.90	0.11	HLWDRACD	0.91	0.08
5	DSNFMASS	0.88	0.13	MICC14	0.90	0.10	MICC14	0.92	0.08
6	SZFISPVO	0.88	0.10	INFIL	0.91	0.07	WDCRCDEN	0.93	0.09
7	MICC14	0.89	0.10	WDCRCDEN	0.92	0.09	SZGWSPDM	0.93	0.07
8	WDCRCDEN	0.90	0.08	HLWDRACD	0.92	0.06	PH2DHLNS	0.93	−0.06
9	SZDIFCVO	0.90	−0.06	SZFISPVO	0.93	0.06	WFDEGEXF	0.94	0.07
10	UZFAG8	0.91	−0.06	UZFAG8	0.93	−0.07	INFIL	0.94	0.04
11	SEEPUNC	0.91	0.07	SEEPUNC	0.93	0.05	UZFAG8	0.94	−0.06
12	UZTORRG3	0.91	0.05	UZTORRG3	0.94	0.05	HLWDRALK	0.94	0.04
13	HLWDRACD	0.91	0.05	KDUSMEC	0.94	0.04	SZFISPVO	0.94	0.04
14	KDUSMEC	0.92	0.05	HLWDRALK	0.94	0.05	WDGCUA22	0.95	−0.04
15	GOESA	0.92	0.05	WFDEGEXF	0.94	0.05	UZGAM	0.95	−0.04
16	SZSREG4X	0.92	−0.05				SEEPUNC	0.95	0.04

a: Steps in stepwise rank regression analysis
b: Variables listed in order of selection in stepwise regression
c: Cumulative R^2 value with entry of each variable into regression model
d: Standardized rank regression coefficients (SRRCs) in final regression model

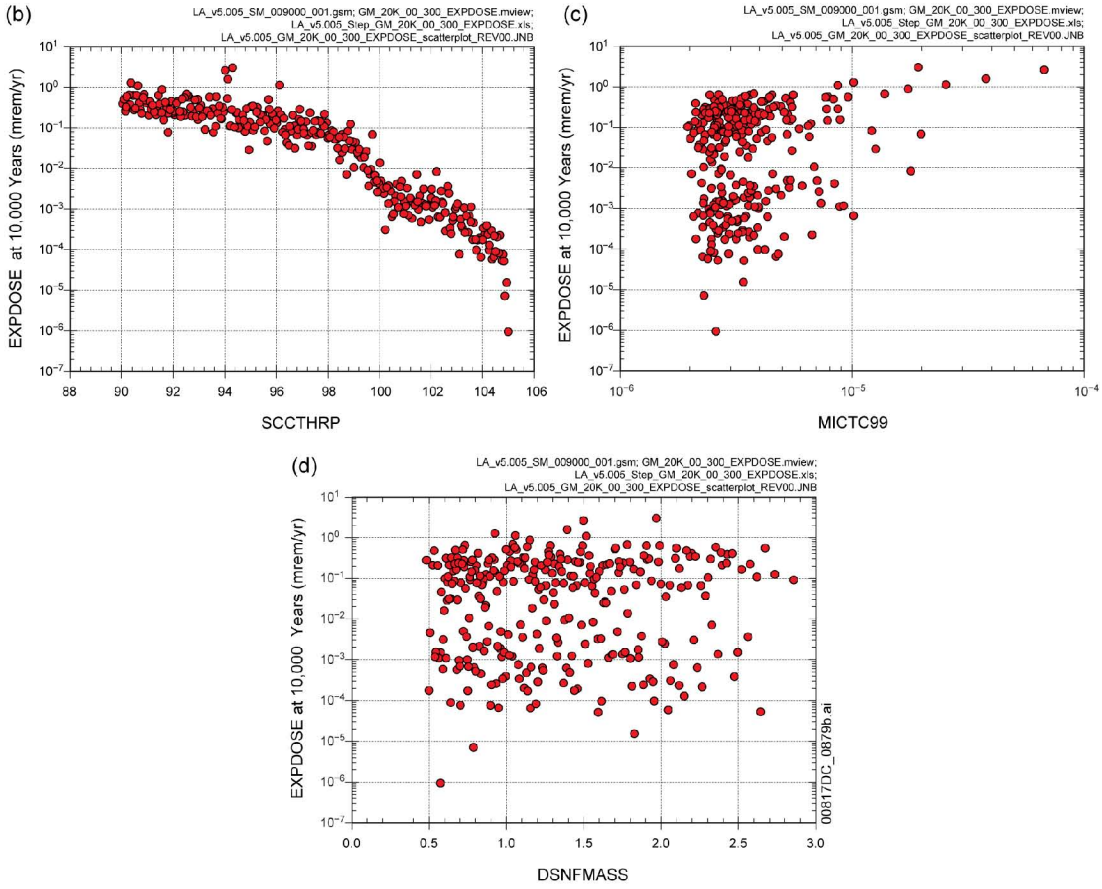

Source: Output DTNs: MO0710ADTSPAWO.000 [DIRS 183752]; and MO0710PLOTSFIG.000 [DIRS 185207].

Figure K7.7.1-2[a]. Stepwise rank regression analyses and selected scatterplots for expected dose to RMEI (*EXPDOSE*, mrem/yr) over [0, 20,000 yr] for all radioactive species resulting from seismic ground motion obtained with version 5.005 of the TSPA-LA Model: (a) regressions for *EXPDOSE* at 3,000, 5,000, and 10,000 years, and (b,c,d) scatterplots for *EXPDOSE* at 10,000 years

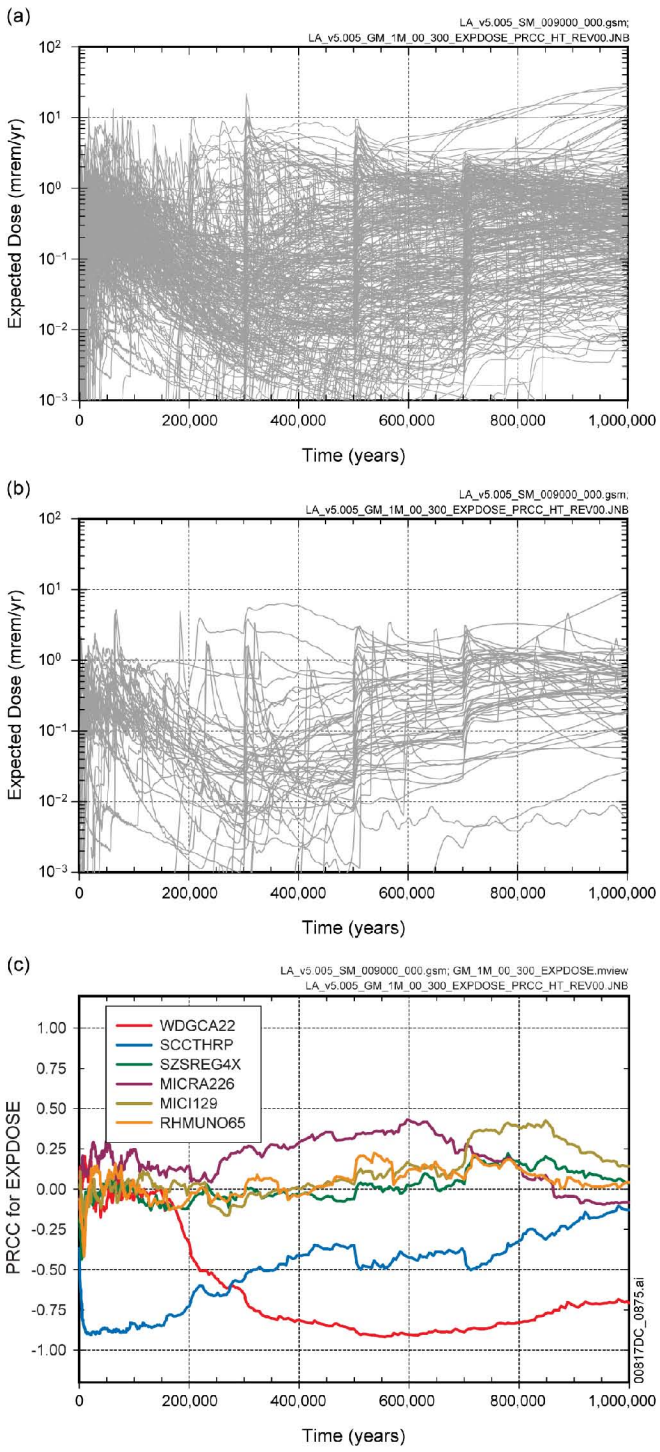

Source: Output DTNs: MO0710ADTSPAWO.000 [DIRS 183752]; and MO0710PLOTSFIG.000 [DIRS 185207].

Figure K7.7.2-1[a]. Expected dose to RMEI (*EXPDOSE*, mrem/yr) over [0, 1,000,000 yr] for all radioactive species resulting from seismic ground motion obtained with version 5.005 of the TSPA-LA Model: (a) *EXPDOSE* for all (i.e., 300) sample elements, (b) *EXPDOSE* for first 50 sample elements, and (c) PRCCs for *EXPDOSE*

(a)

	50,000 Years			200,000 Years			500,000 Years		
Step[a]	Variable[b]	R^{2} [c]	SRRC[d]	Variable	R^2	SRRC	Variable	R^2	SRRC
1	SCCTHRP	0.71	−0.85	SCCTHRP	0.54	−0.72	WDGCA22	0.62	−0.77
2	MICTC99	0.72	0.09	WDDSGC29	0.58	−0.18	SCCTHRP	0.71	−0.28
3	HLWDRACD	0.73	0.10	WDGCA22	0.60	−0.14	WDNSCC	0.72	−0.12
4	DSNFMASS	0.74	0.11	DSNFMASS	0.61	0.11	SZPORSAL	0.73	0.08
5	SZLODISP	0.75	−0.10	CSNFMASS	0.62	0.10	SZGWSPDM	0.73	0.11
6	SZKDSEVO	0.76	−0.09				SZCONCOL	0.74	0.09
7	CPUPERCS	0.77	0.09				EP1LOWNU	0.75	0.10
8							UZFAG4	0.76	−0.08

a: Steps in stepwise rank regression analysis
b: Variables listed in order of selection in stepwise regression
c: Cumulative R^2 value with entry of each variable into regression model
d: Standardized rank regression coefficients (SRRCs) in final regression model

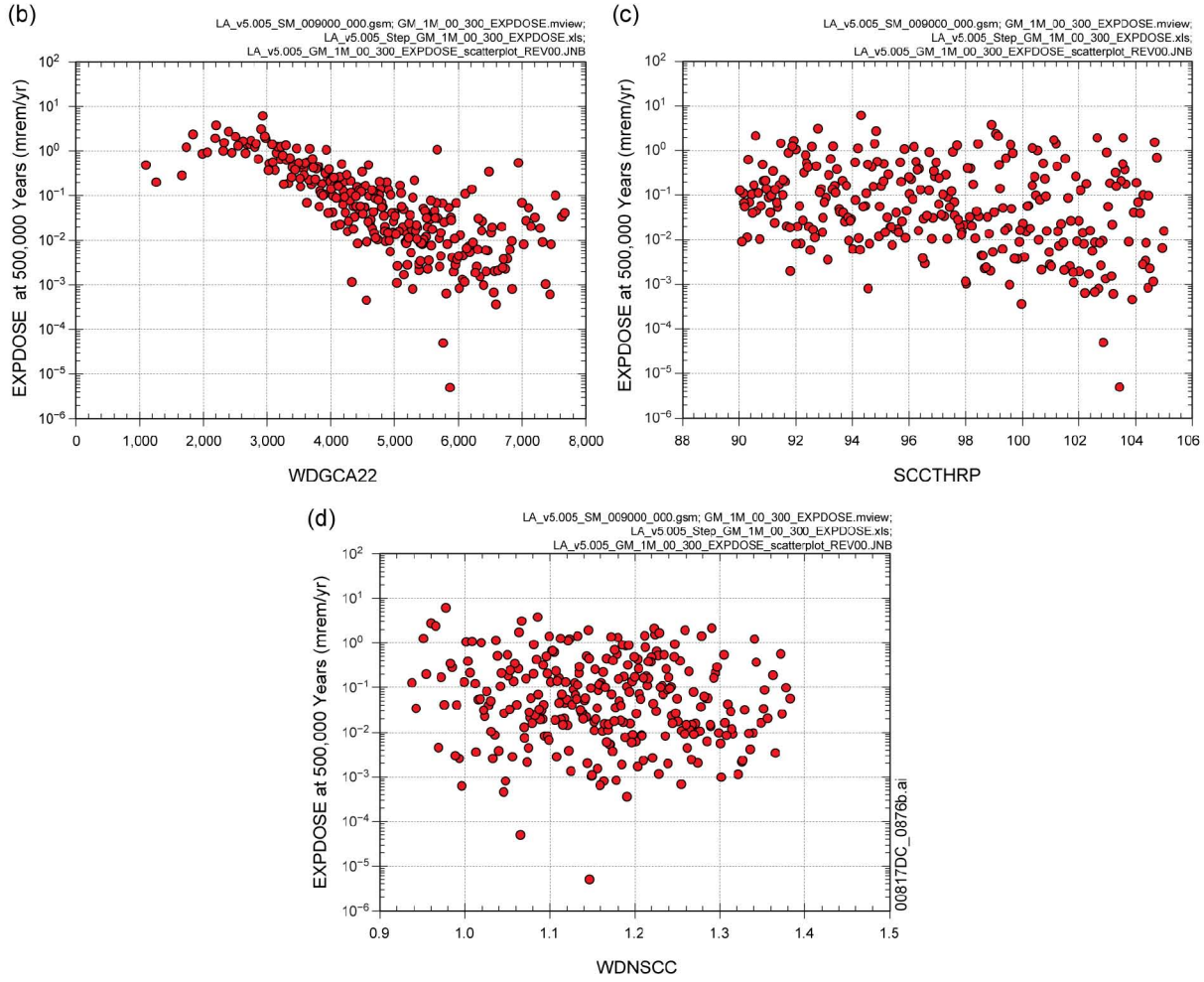

Source: Output DTNs: MO0710ADTSPAWO.000 [DIRS 183752]; and MO0710PLOTSFIG.000 [DIRS 185207].

Figure K7.7.2-2[a]. Stepwise rank regression analyses and selected scatterplots for expected dose to RMEI (*EXPDOSE*, mrem/yr) over [0, 1,000,000 yr] for all radioactive species resulting from seismic ground motion obtained with version 5.005 of the TSPA-LA Model: (a) regressions for *EXPDOSE* at 50,000, 200,000, and 500,000 years, and (b,c,d) scatterplots for *EXPDOSE* at 500,000 years

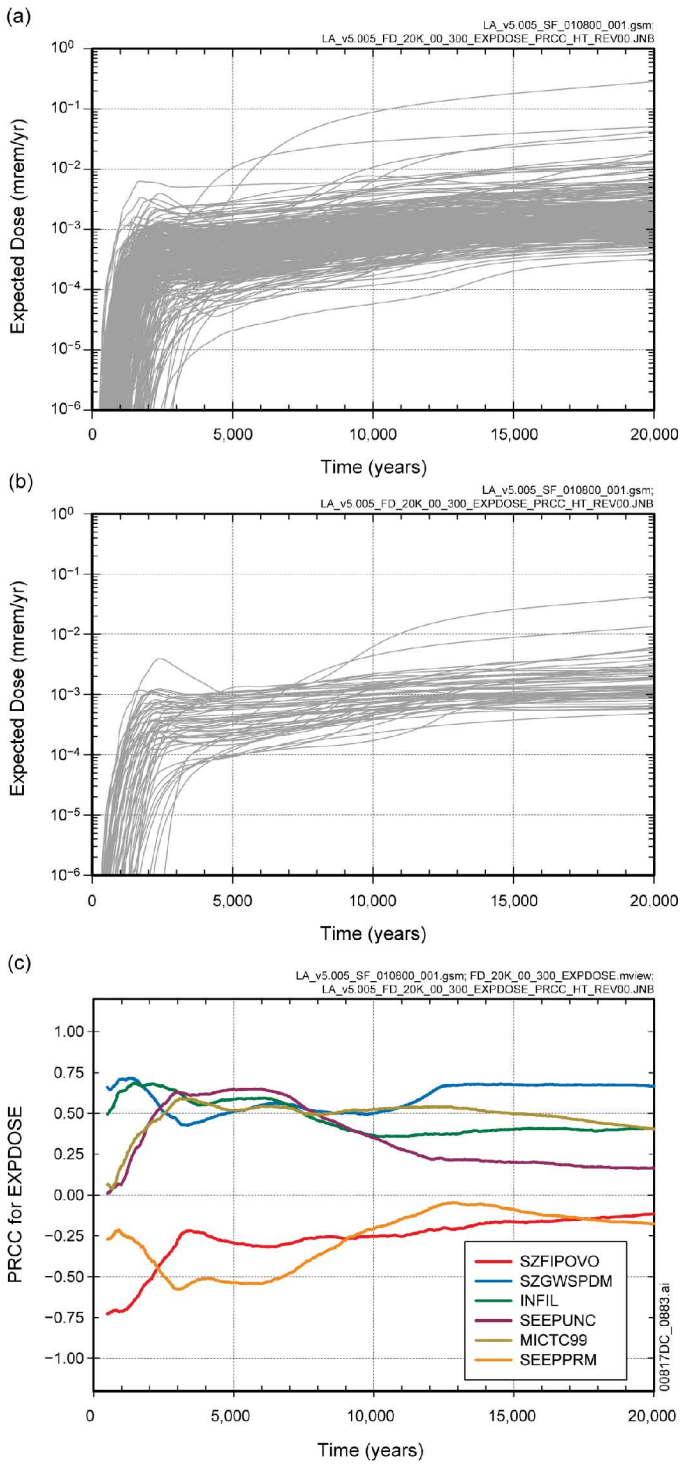

Source: Output DTNs: MO0710ADTSPAWO.000 [DIRS 183752]; and MO0710PLOTSFIG.000 [DIRS 185207].

Figure K7.8.1-1[a]. Expected dose to RMEI (*EXPDOSE*, mrem/yr) over [0, 20,000 yr] for all radioactive species resulting from seismic fault displacement: (a) *EXPDOSE* for all (i.e., 300) sample elements, (b) *EXPDOSE* for first 50 sample elements, and (c) PRCCs for *EXPDOS*

(a)

	3,000 years			5,000 years			10,000 years		
Step[a]	Variable[b]	R^2[c]	SRRC[d]	Variable	R^2	SRRC	Variable	R^2	SRRC
1	INFIL	0.18	0.45	INFIL	0.19	0.44	MICTC99	0.15	0.36
2	MICTC99	0.31	0.32	MICTC99	0.32	0.34	INFIL	0.27	0.35
3	SZGWSPDM	0.40	0.31	SEEPPRM	0.42	-0.31	SZGWSPDM	0.37	0.33
4	SEEPPRM	0.49	-0.29	SZGWSPDM	0.49	0.29	DTDRHUNC	0.45	0.26
5	SEEPUNC	0.57	0.30	SEEPUNC	0.57	0.31	SEEPPRM	0.49	-0.16
6	CSSPECSA	0.62	0.22	CSSPECSA	0.62	0.21	SZCOLRAL	0.52	-0.19
7	SZFISPVO	0.66	0.22	SZFISPVO	0.65	0.18	SZFISPVO	0.55	0.18
8	CSNFMASS	0.68	0.15	ALPHAL	0.67	-0.16	SZFIPOVO	0.56	-0.14
9	MICC14	0.69	0.14	CSNFMASS	0.68	0.18	CSNFMASS	0.58	0.13
10	SZDIFCVO	0.71	-0.14	MICC14	0.70	0.12	SZDIFCVO	0.59	-0.13
11	ALPHAL	0.73	-0.14	SZCOLRAL	0.71	-0.14	MICAM243	0.61	0.13
12	MICSE79	0.74	0.09	SZFIPOVO	0.72	-0.12	CSSPECSA	0.62	0.13
13	SZFIPOVO	0.74	-0.10	SZCOLRVO	0.73	-0.12	CSWFA4AC	0.63	0.12
14	SZCOLRVO	0.75	-0.08	MICSN126	0.74	0.10	KDUSMEC	0.64	0.11
15	THERMCON	0.76	-0.08	SZDIFCVO	0.75	-0.10			
16				CSWFA4AC	0.76	0.09			

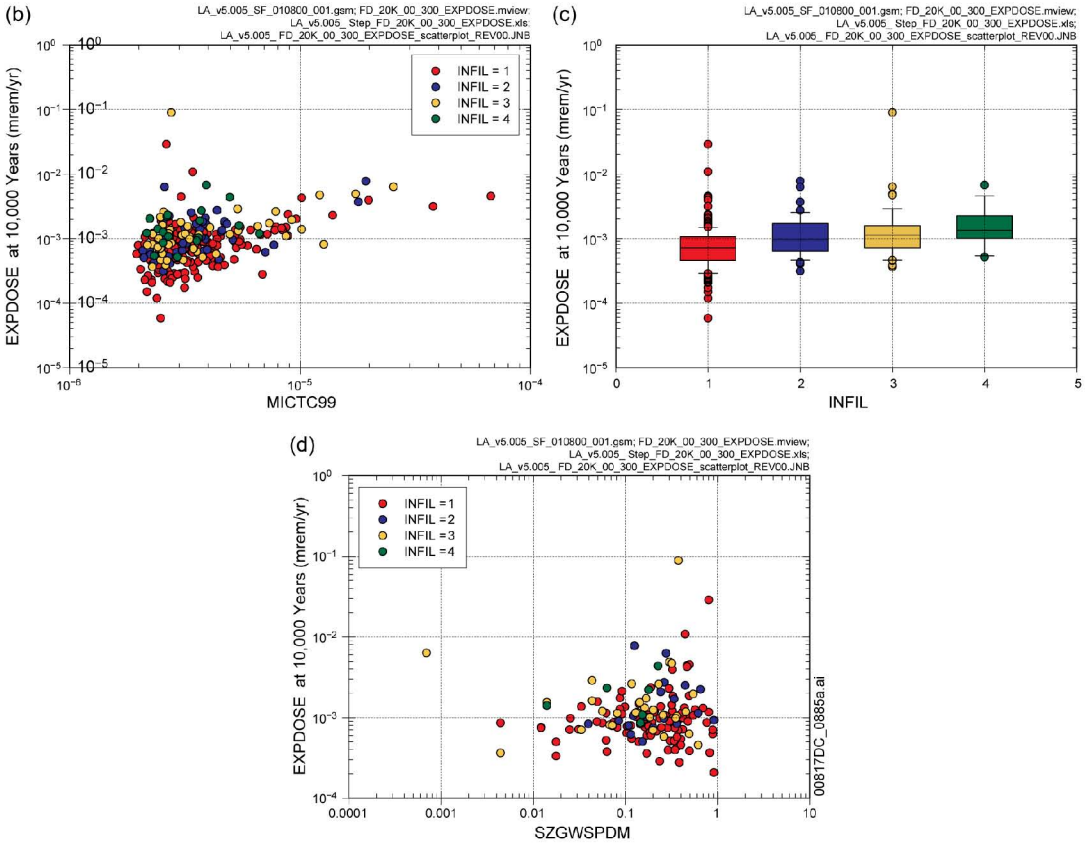

Source: Output DTNs: MO0710ADTSPAWO.000 [DIRS 183752]; and MO0710PLOTSFIG.000 [DIRS 185207].

NOTE: In (c), the box extends from 0.25 to 0.75 quantile; lower and upper bar and whisker extend to 0.1 and 0.9 quantile, respectively; dots represent values outside 0.1 to 0.9 quantile range; median indicated by light horizontal line.

Figure K7.8.1-2[a]. Stepwise rank regression analyses and selected scatterplots for expected dose to RMEI (*EXPDOSE*, mrem/yr) over [0, 20,000 yr] for all radioactive species resulting from seismic fault displacement: (a) regressions for *EXPDOSE* at 3,000, 5,000, and 10,000 years, and (b,c,d) scatterplots for *EXPDOSE* at 10,000 years

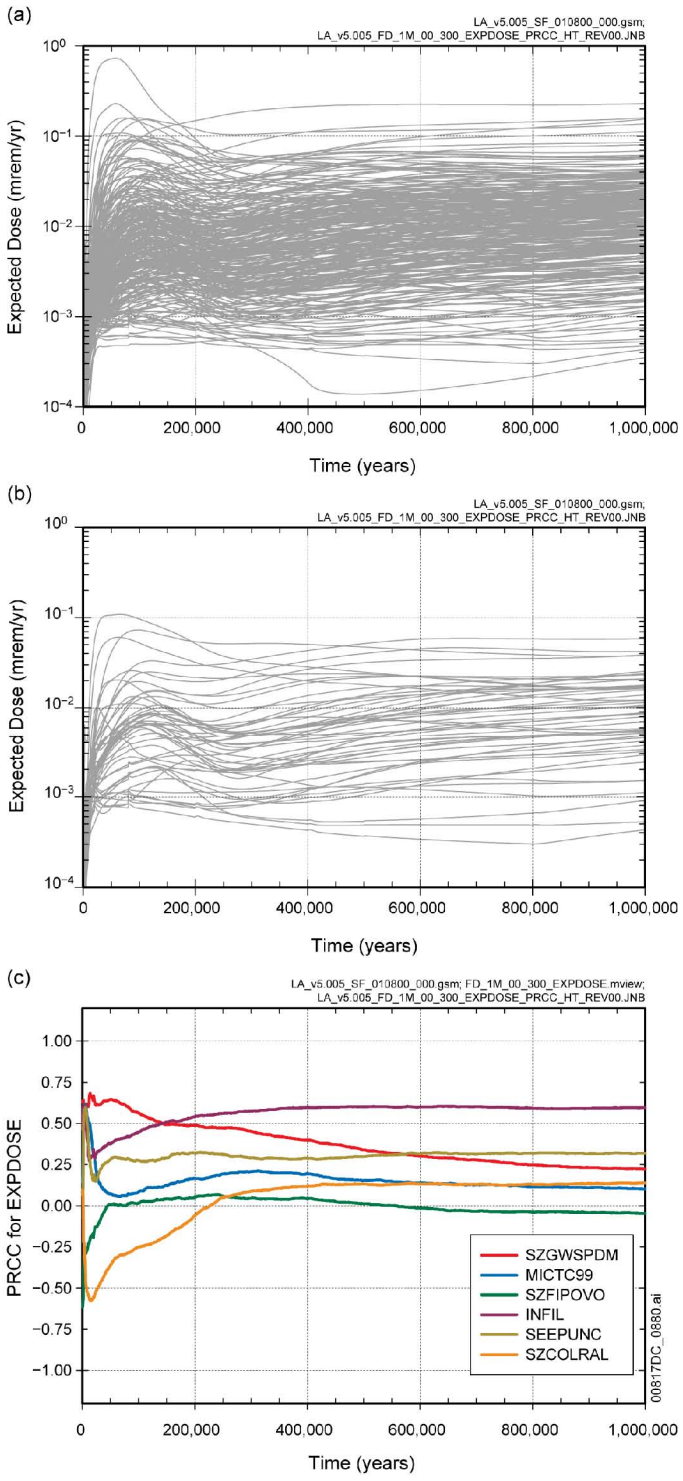

Source: Output DTNs: MO0710ADTSPAWO.000 [DIRS 183752]; and MO0710PLOTSFIG.000 [DIRS 185207].

Figure K7.8.2-1[a]. Expected dose to RMEI (*EXPDOSE*, mrem/yr) over [0, 1,000,000 yr] for all radioactive species resulting from seismic fault displacement: (a) *EXPDOSE* for all (i.e., 300) sample elements, (b) *EXPDOSE* for first 50 sample elements, and (c) PRCCs for *EXPDOS*

(a)

	50,000 years			200,000 years			500,000 years		
Step[a]	Variable[b]	R^2[c]	SRRC[d]	Variable	R^2	SRRC	Variable	R^2	SRRC
1	SZGWSPDM	0.25	0.51	INFIL	0.15	0.37	INFIL	0.18	0.40
2	INFIL	0.37	0.31	SZGWSPDM	0.29	0.40	EP1LOWPU	0.29	0.33
3	WPFLUX	0.43	0.22	WPFLUX	0.37	0.28	SZGWSPDM	0.38	0.36
4	EP1LOWPU	0.48	0.21	EP1LOWPU	0.44	0.28	WPFLUX	0.43	0.25
5	SEEPPRM	0.52	−0.19	SEEPPRM	0.48	−0.22	GOESITED	0.48	−0.18
6	MICNP237	0.55	0.18	SZFISPVO	0.55	0.19	SEEPPRM	0.52	−0.20
7	CPUCOLWF	0.57	0.17	SEEPUNC	0.57	0.17	MICPU239	0.54	0.19
8	SZCOLRAL	0.60	−0.15	CORRATSS	0.59	−0.10	SEEPUNC	0.57	0.17
9	SZFISPVO	0.62	0.16	EP1NPO2	0.60	0.11	SZFISPVO	0.60	0.17
10	SEEPUNC	0.63	0.12	SZCONCOL	0.62	0.11	SZCONCOL	0.62	0.14
11	PHCSS	0.65	−0.12	EP1LOWNU	0.63	0.12	EP1LOWNU	0.64	0.18
12	HFOSA	0.66	−0.11	SZDIFCVO	0.64	−0.11	UZFAG4	0.67	−0.15
13	RUBMAXL	0.67	−0.10	SZKDAMCO	0.65	0.10	HFOSA	0.68	−0.11
14	PH2MCONS	0.67	−0.09	GOESITED	0.66	−0.11	SZDIFCVO	0.69	−0.12
15				MICPU239	0.67	0.19	KDPUSMEC	0.70	0.10
16				UZFAG4	0.68	−0.11	SZWBNDAL	0.71	−0.10

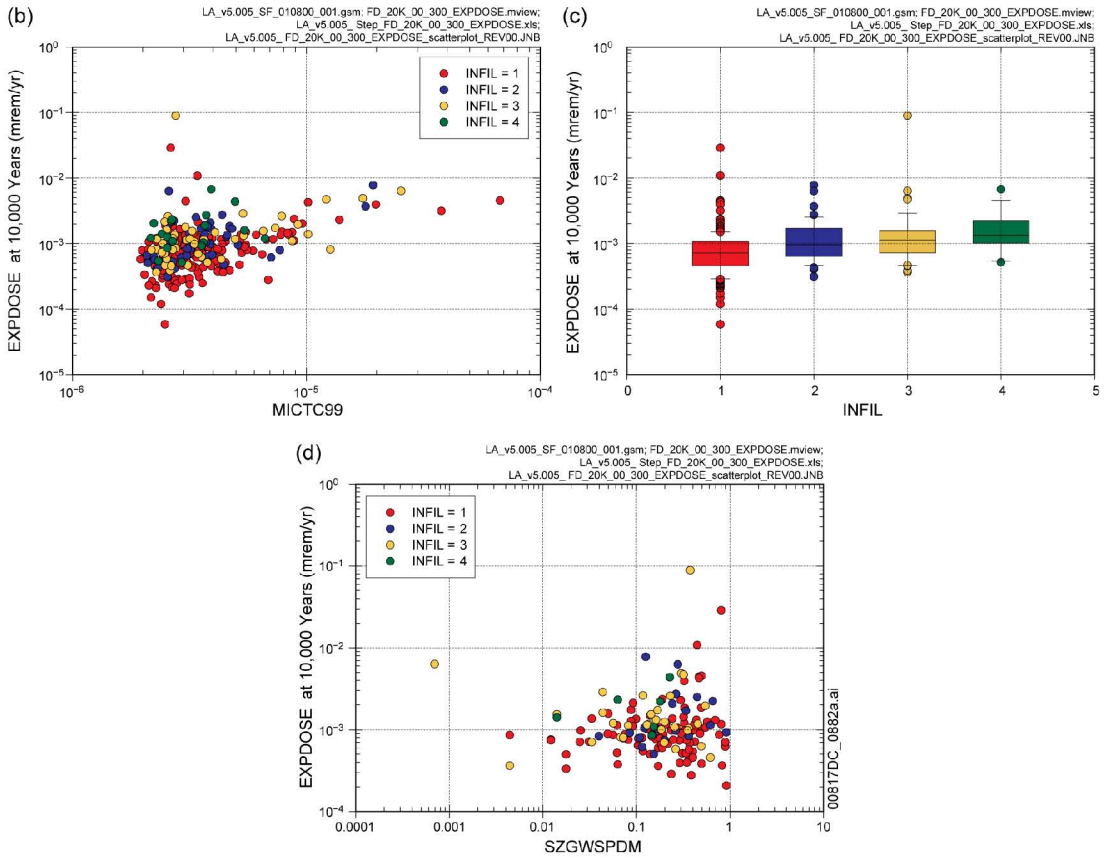

Source: Output DTNs: MO0710ADTSPAWO.000 [DIRS 183752]; and MO0710PLOTSFIG.000 [DIRS 185207].

NOTE: In (c), the box extends from 0.25 to 0.75 quantile; lower and upper bar and whisker extend to 0.1 and 0.9 quantile, respectively; dots represent values outside 0.1 to 0.9 quantile range; median indicated by light horizontal line.

Figure K7.8.2-2[a]. Stepwise rank regression analyses and selected scatterplots for expected dose to RMEI (*EXPDOSE*, mrem/yr) over [0, 1,000,000 yr] for all radioactive species resulting from seismic fault displacement: (a) regressions for *EXPDOSE* at 50,000, 200,000, and 500,000 years, and (b,c,d) scatterplots for *EXPDOSE* at 500,000 years

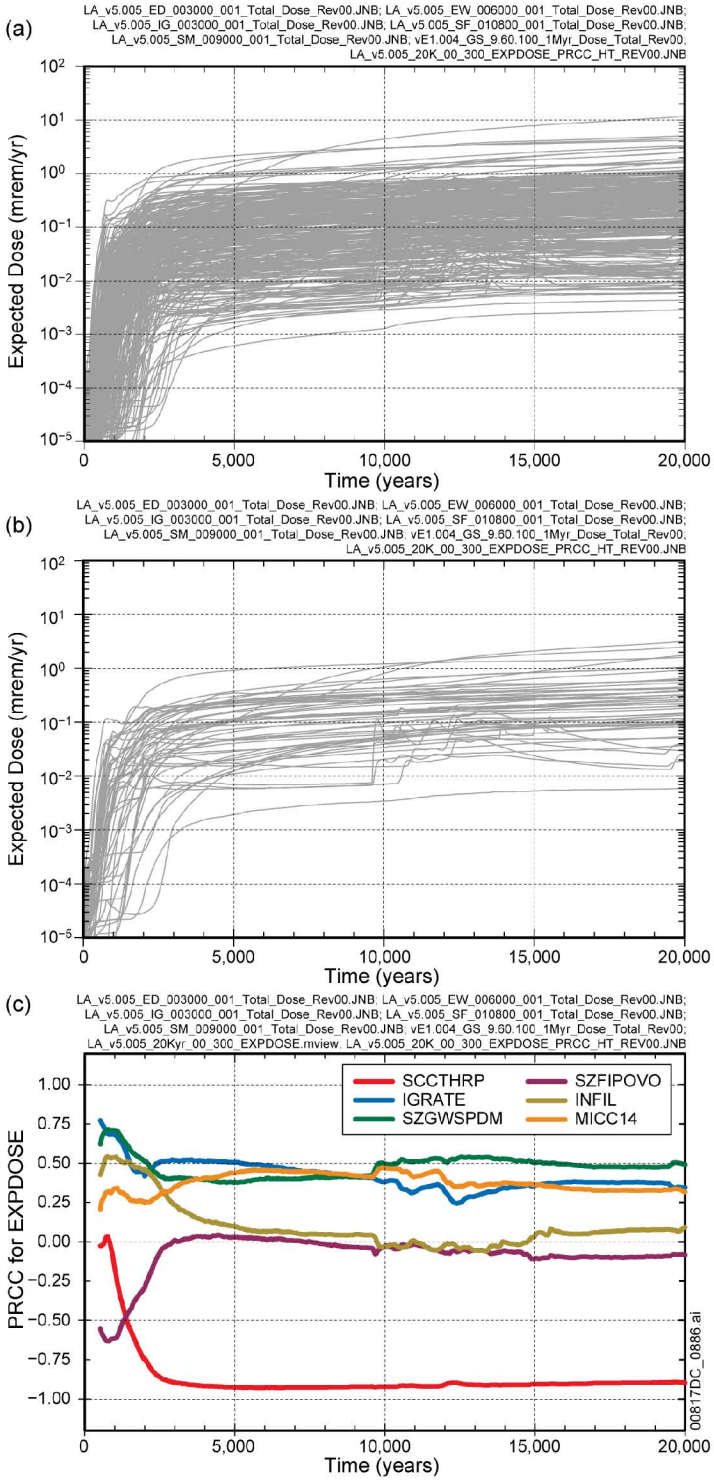

Source: Output DTNs: MO0710ADTSPAWO.000 [DIRS 183752]; and MO0710PLOTSFIG.000 [DIRS 185207].

Figure K8.1-1[a]. Expected dose to RMEI (*EXPDOSE*, mrem/yr) over [0, 20,000 yr] for all scenario classes obtained with version 5.005 of the TSPA-LA Model: (a) *EXPDOSE* for all (i.e., 300) sample elements, (b) *EXPDOSE* for first 50 sample elements, and (c) PRCCs for *EXPDOSE*

(a)

	3,000 Years			5,000 Years			10,000 Years		
Step[a]	Variable[b]	R^{2c}	SRRC[d]	Variable	R^2	SRRC	Variable	R^2	SRRC
1	SCCTHRP	0.55	−0.72	SCCTHRP	0.66	−0.79	SCCTHRP	0.69	−0.83
2	IGRATE	0.62	0.28	IGRATE	0.71	0.24	IGRATE	0.73	0.22
3	SZGWSPDM	0.67	0.21	SZGWSPDM	0.74	0.15	SZGWSPDM	0.76	0.16
4	INFIL	0.71	0.19	MICTC99	0.76	0.14	MICTC99	0.77	0.14
5	MICTC99	0.73	0.15	MICC14	0.78	0.12	WFDEGEXF	0.78	0.10
6	SZFISPVO	0.75	0.14	INFIL	0.79	0.11	MICC14	0.79	0.11
7	MICC14	0.76	0.12	DSNFMASS	0.80	0.11	UZGAM	0.80	−0.09
8	DSNFMASS	0.77	0.10	SZFISPVO	0.81	0.09	INFIL	0.81	0.09
9	UZFAG8	0.78	−0.10	UZFAG8	0.82	−0.10	CSWFA0AC	0.81	−0.07
10	UZGAM	0.79	−0.09	UZGAM	0.82	−0.10	UZKDSRDT	0.82	0.07
11	SZDIFCVO	0.79	−0.08	WFDEGEXF	0.83	0.10			
12	WFDEGEXF	0.80	0.08	WDCRCDEN	0.83	0.08			
13	KDUSMEC	0.80	0.08	WDZOLID	0.84	−0.07			
14	MICPA231	0.81	−0.08	WDGCUA22	0.84	0.07			
15				BCKRA226	0.85	−0.06			

a: Steps in stepwise rank regression analysis
b: Variables listed in order of selection in stepwise regression
c: Cumulative R^2 value with entry of each variable into regression model
d: Standardized rank regression coefficients (SRRCs) in final regression model

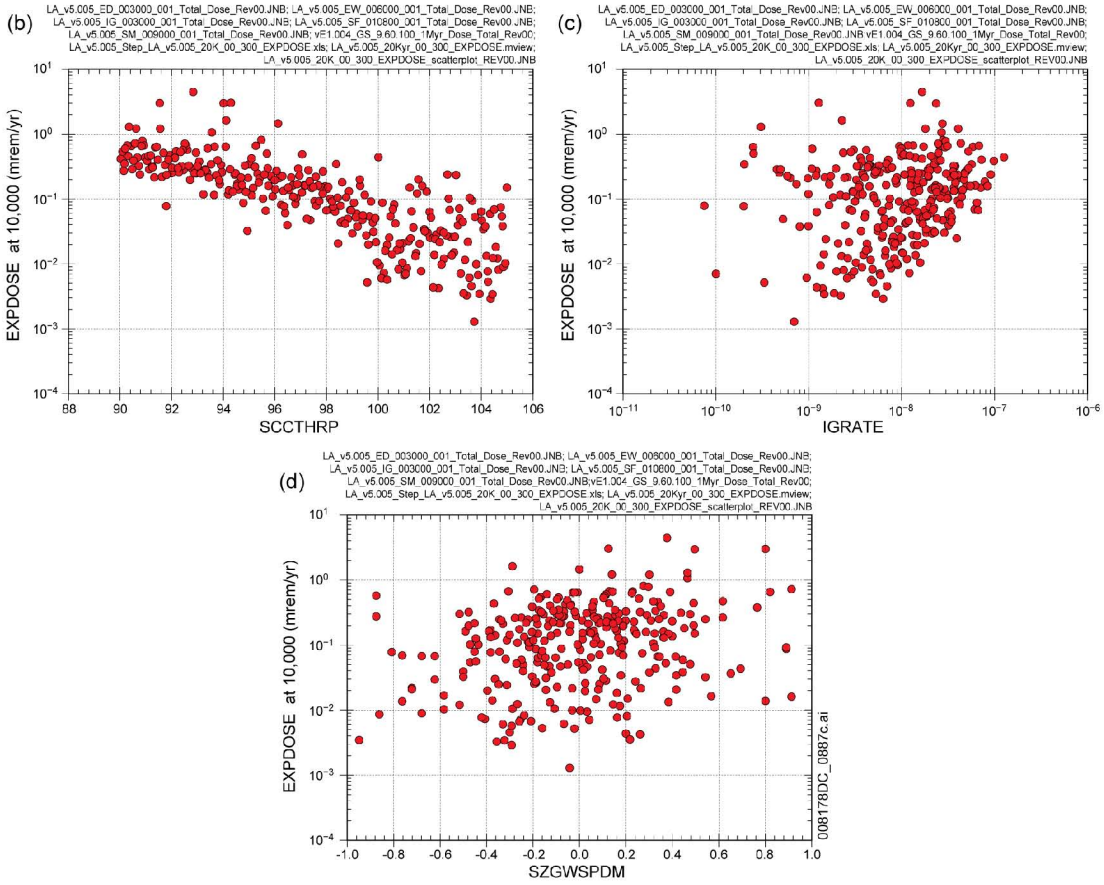

Source: Output DTNs: MO0710ADTSPAWO.000 [DIRS 183752]; and MO0710PLOTSFIG.000 [DIRS 185207].

Figure K8.1-2[a]. Stepwise rank regression analyses and selected scatterplots for expected dose to RMEI (*EXPDOSE*, mrem/yr) over [0, 20,000 yr] for all scenario classes obtained with version 5.005 of the TSPA-LA Model: (a) regressions for *EXPDOSE* at 3,000, 5,000, and 10,000 years, and (b,c,d) scatterplots for *EXPDOSE* at 10,000 years

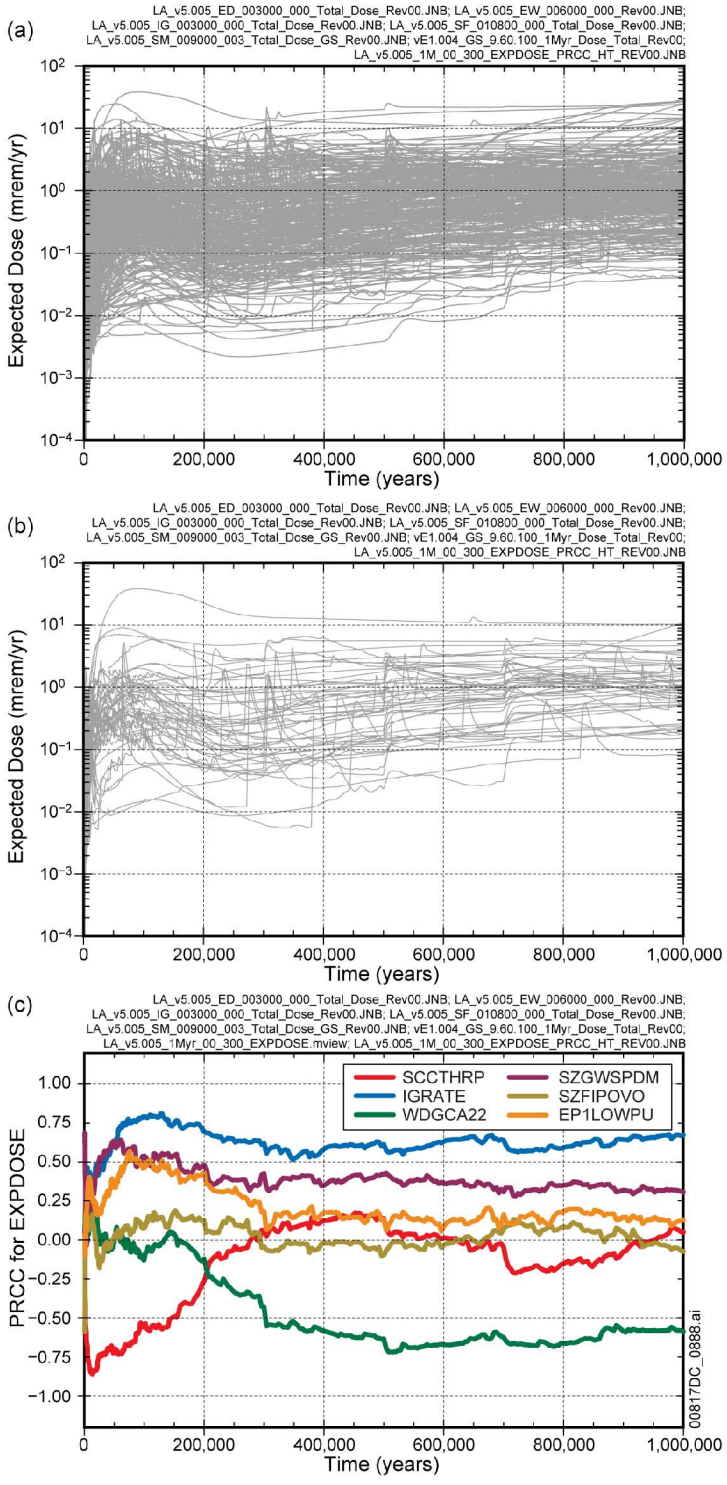

Source: Output DTNs: MO0710ADTSPAWO.000 [DIRS 183752]; and MO0710PLOTSFIG.000 [DIRS 185207].

Figure K8.2-1[a]. Expected dose to RMEI (*EXPDOSE*, mrem/yr) over [0, 1,000,000 yr] for all scenario classes obtained with version 5.005 of the TSPA-LA Model: (a) *EXPDOSE* for all (i.e., 300) sample elements, (b) *EXPDOSE* for first 50 sample elements, and (c) PRCCs for *EXPDOSE*

(a)

	EXPDOSE: 50,000 Years			EXPDOSE: 200,000 Years			EXPDOSE: 500,000 Years		
Step[a]	Variable[b]	R^{2c}	SRRC[d]	Variable	R^2	SRRC	Variable	R^2	SRRC
1	SCCTHRP	0.27	−0.48	IGRATE	0.38	0.61	IGRATE	0.29	0.54
2	IGRATE	0.43	0.41	SZGWSPDM	0.48	0.28	WDGCA22	0.46	−0.38
3	SZGWSPDM	0.55	0.33	EP1LOWPU	0.53	0.23	SZGWSPDM	0.53	0.24
4	EP1LOWPU	0.60	0.20	SCCTHRP	0.57	−0.21	EP1LOWNU	0.56	0.19
5	MICNP237	0.62	0.11	SZFISPVO	0.60	0.15	MICNP237	0.59	0.16
6	INFIL	0.63	0.13	INFIL	0.62	0.16	EP1L0WPU	0.61	0.17
7	EP1NPO2	0.65	0.13	EP1NPO2	0.64	0.14	SZCONCOL	0.64	0.15
8	MICTC99	0.66	0.11	GOESITED	0.66	−0.14	SZFISPVO	0.66	0.15
9	ALPHAL	0.67	0.10	MICSE79	0.68	0.09	INFIL	0.67	0.11
10				MICNP237	0.69	0.14	GOESITED	0.68	−0.10
11				EP1LOWNU	0.70	0.11	SZKDCSVO	0.69	−0.10
12				SZCONCOL	0.71	0.11	HFOSITED	0.69	−0.09
13				PHCSS	0.72	−0.11	SZDIFCVO	0.70	−0.09
14				HFOSA	0.73	−0.09			
15				SZDIFCVO	0.73	−0.09			
16				SEEPCOND	0.74	−0.09			

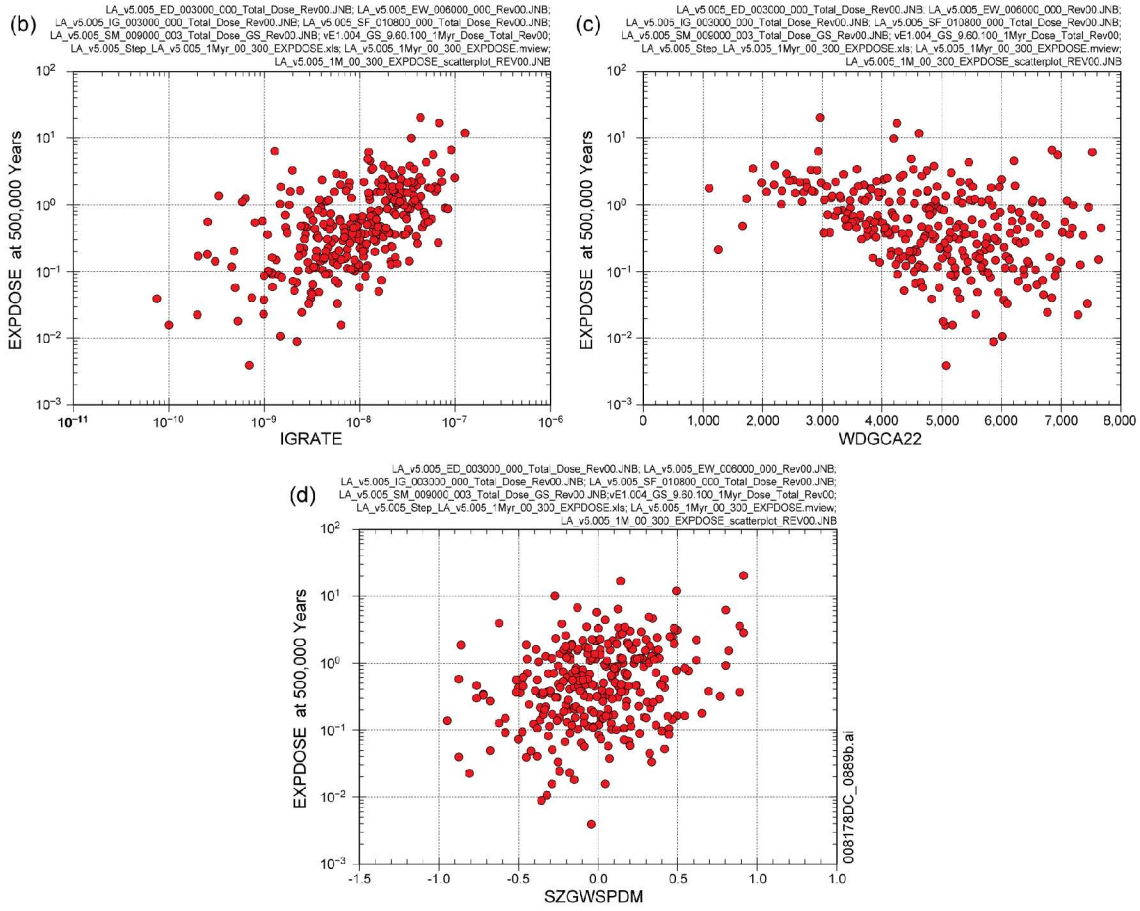

Source: Output DTNs: MO0710ADTSPAWO.000 [DIRS 183752]; and MO0710PLOTSFIG.000 [DIRS 185207].

Figure K8.2-2[a]. Stepwise rank regression analyses and selected scatterplots for expected dose to RMEI (*EXPDOSE*, mrem/yr) over [0, 1,000,000 yr] for all scenario classes obtained with version 5.005 of the TSPA-LA Model: (a) regressions for *EXPDOSE* at 50,000, 200,000, and 500,000 years, and (b,c,d) scatterplots for *EXPDOSE* at 500,000 years

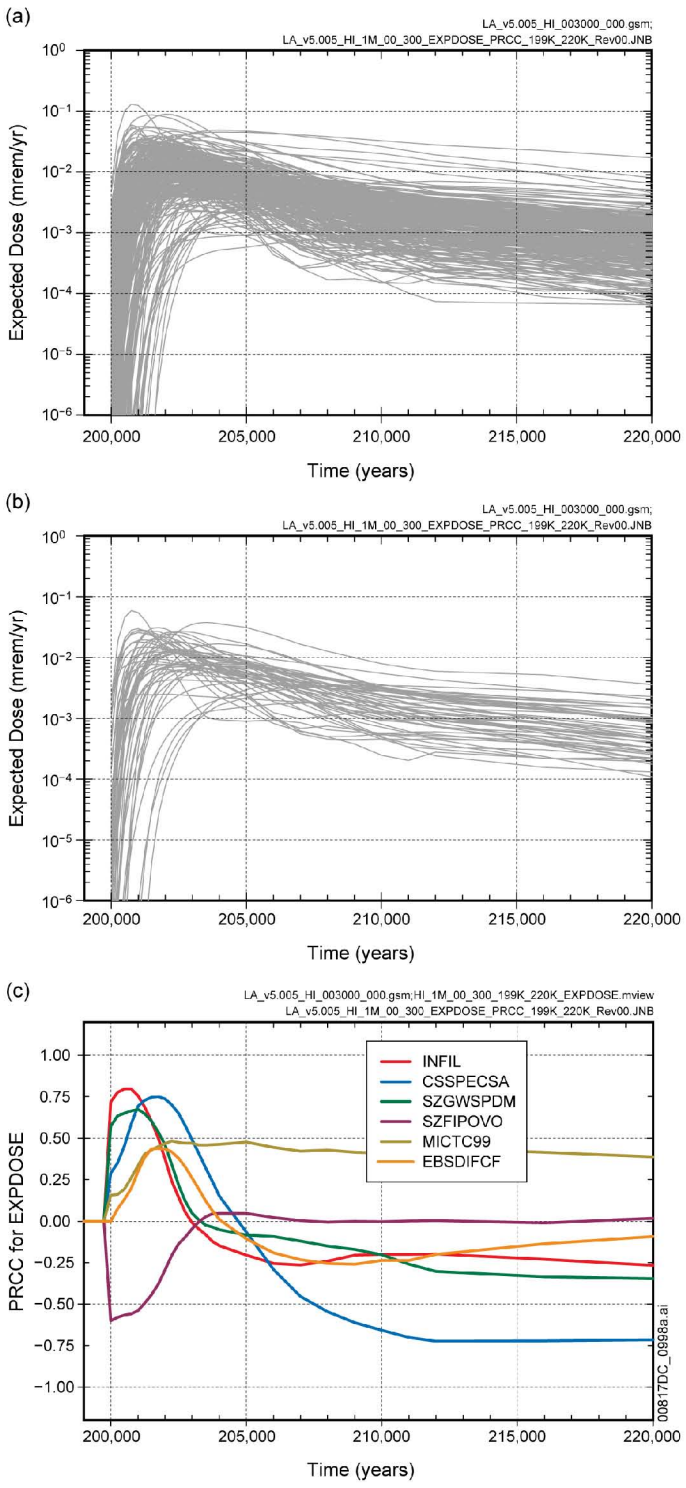

Source: Output DTNs: MO0710ADTSPAWO.000 [DIRS 183752]; and MO0710PLOTSFIG.000 [DIRS 185207].

Figure K10-1[a]. Expected dose to RMEI (*EXPDOSE*, mrem/yr) over [200,000, 220,000 yr] resulting from human intrusion at 200,000 years obtained with version 5.005 of the TSPA-LA Model: (a) *EXPDOSE* for all (i.e., 300) sample elements, (b) *EXPDOSE* for first 50 sample elements, and (c) PRCCs for *EXPDOSE*

	EXPDOSE: 201,000 Year			EXPDOSE: 203,000 Year			EXPDOSE: 205,000 Year		
Step[a]	Variable[b]	R^{2c}	SRRC[d]	Variable	R^2	SRRC	Variable	R^2	SRRC
1	SZGWSPDM	0.20	0.45	MICTC99	0.15	0.44	MICTC99	0.33	0.58
2	INFIL	0.40	0.48	CSSPECSA	0.33	0.44	CSNFMASS	0.38	0.22
3	CSSPECSA	0.54	0.41	SZFISPVO	0.40	0.26	INFIL	0.41	−0.18
4	SZFISPVO	0.61	0.28	SZGWSPDM	0.43	0.18			
5	SZFIPOVO	0.65	−0.20	CSNFMASS	0.47	0.19			
6	SZDIFCVO	0.68	−0.18	SZDIFCVO	0.50	−0.19			
7	MICTC99	0.70	0.14	INFIL	0.51	−0.13			
8	CSWFA4AC	0.71	0.11	CSRINDPO	0.53	−0.11			
9	PHCSS	0.72	−0.11						
10	EP1NP2O5	0.73	−0.10						
11	CSNFMASS	0.73	0.10						
12	SZPORSAL	0.74	0.09						
13	DIAMCOLL	0.75	0.08						

00817DC_0999.ai

a: Steps in stepwise rank regression analysis
b: Variables listed in order of selection in stepwise regression
c: Cumulative R^2 value with entry of each variable into regression model
d: Standardized rank regression coefficients (SRRCs) in final regression model

Source: Output DTNs: MO0710ADTSPAWO.000 [DIRS 183752]; and MO0710PLOTSFIG.000 [DIRS 185207].

Figure K10-2[a]. Stepwise rank regression analyses and selected scatterplots for expected dose to RMEI (*EXPDOSE*, mrem/yr) over [200,000, 220,000 yr] resulting from human intrusion at 200,000 years obtained with version 5.005 of the TSPA-LA Model: (a) regressions for *EXPDOSE* at 201,000, 203,000, and 205,000 years, (b,c,d) scatterplots for *EXPDOSE* at 201,000 years, and (e,f,g) scatterplots for *EXPDOSE* at 205,000 years

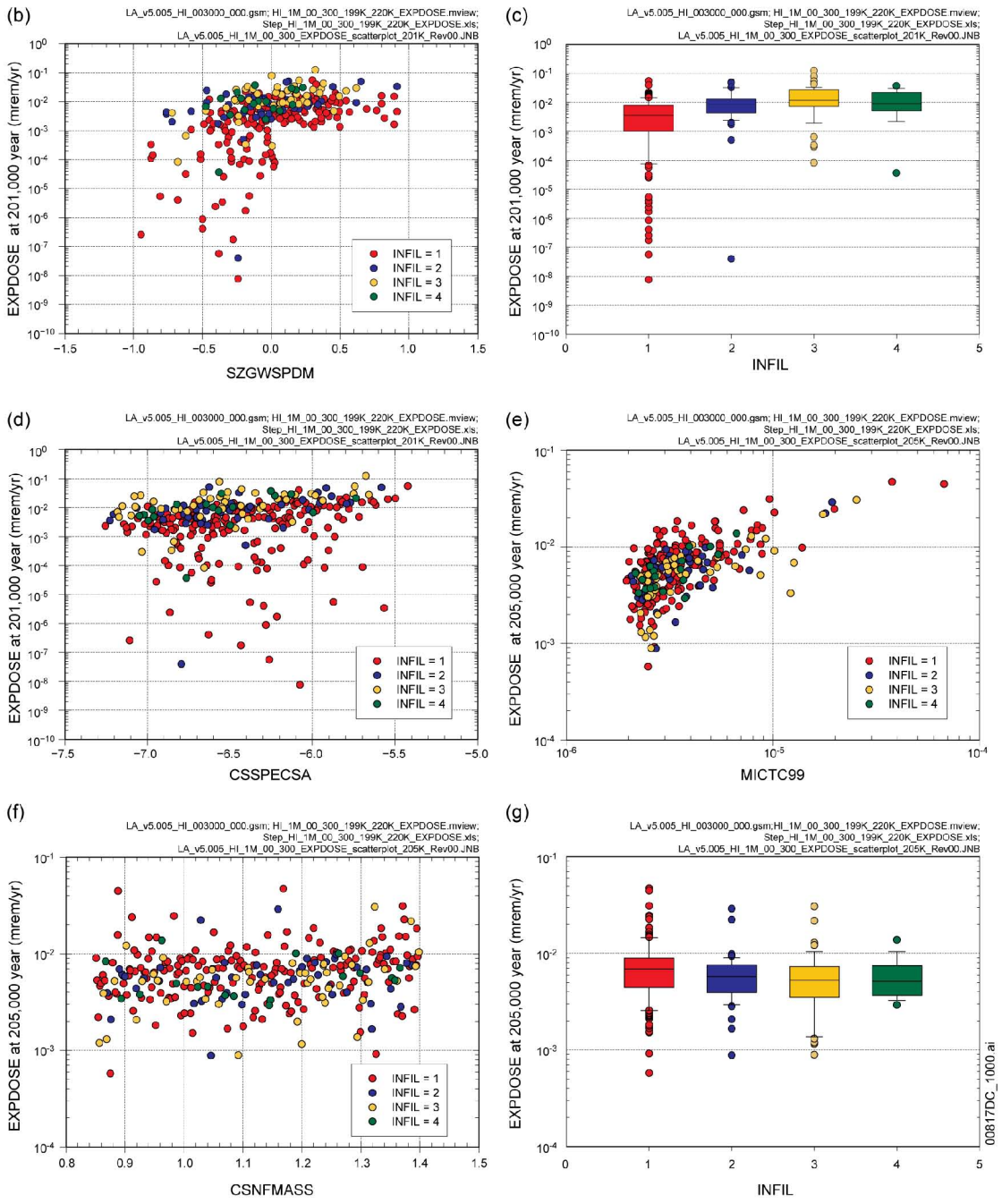

Source: Output DTNs: MO0710ADTSPAWO.000 [DIRS 183752]; and MO0710PLOTSFIG.000 [DIRS 185207].

NOTE: In (c, g), the box extends from 0.25 to 0.75 quantile; lower and upper bar and whisker extend to 0.1 and 0.9 quantile, respectively; dots represent values outside 0.1 to 0.9 quantile range; median indicated by light horizontal line.

Figure K10-2[a]. Stepwise rank regression analyses and selected scatterplots for expected dose to RMEI (*EXPDOSE*, mrem/yr) over [200,000, 220,000 yr] resulting from human intrusion at 200,000 years obtained with version 5.005 of the TSPA-LA Model: (a) regressions for *EXPDOSE* at 201,000, 203,000, and 205,000 years, (b,c,d) scatterplots for *EXPDOSE* at 201,000 years, and (e,f,g) scatterplots for *EXPDOSE* at 205,000 years (continued)

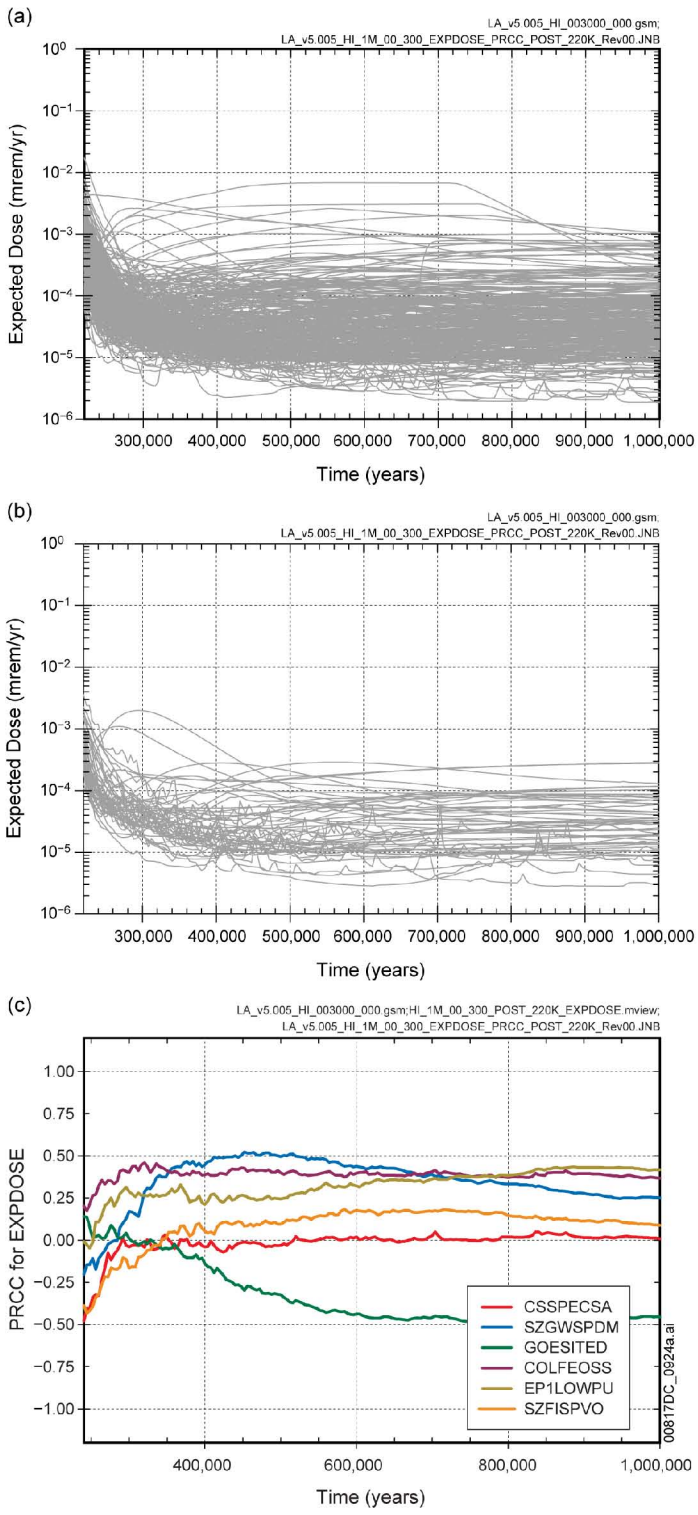

Source: Output DTNs: MO0710ADTSPAWO.000 [DIRS 183752]; and MO0710PLOTSFIG.000 [DIRS 185207].

Figure K10-3[a]. Expected dose to RMEI (*EXPDOSE*, mrem/yr) over [220,000, 1,000,000 yr] resulting from human intrusion at 200,000 years obtained with version 5.005 of the TSPA-LA Model: (a) *EXPDOSE* for all (i.e., 300) sample elements, (b) *EXPDOSE* for first 50 sample elements, and (c) PRCCs for *EXPDOSE*

(a)

	EXPDOSE: 240,000 Years			EXPDOSE: 500,000 Years			EXPDOSE: 760,000 Years		
Step[a]	Variable[b]	R^{2} [c]	SRRC[d]	Variable	R^{2}	SRRC	Variable	R^{2}	SRRC
1	CSSPECSA	0.20	−0.44	SZGWSPDM	0.15	0.37	GOESITED	0.10	−0.33
2	SZGWSPDM	0.29	−0.29	GOESITED	0.23	−0.27	SZGWSPDM	0.20	0.27
3	SZFISPVO	0.36	−0.34	ISCSS	0.29	−0.26	COLFEOSS	0.27	0.29
4	MICTC99	0.42	0.22	COLFEOSS	0.34	0.22	EP1LOWPU	0.34	0.23
5	SZDIFCVO	0.45	0.19	EP1LOWPU	0.39	0.22	ISCSS	0.39	−0.23
6	MICI129	0.46	0.14	HFOSA	0.43	−0.20	EP1LOWNU	0.44	0.18
7	UZKDCSDT	0.48	−0.12	EP1LOWNU	0.46	0.17	HFOSA	0.48	−0.20
8	CSNFMASS	0.49	0.12	MICCS135	0.48	0.14	MICCS135	0.51	0.17
9	ISCSS	0.50	−0.11	SZDIFCVO	0.49	−0.16	MICPU239	0.54	0.16
10				SZFISPVO	0.51	0.17	SZDIFCVO	0.55	−0.17
11				SZCOLRAL	0.53	−0.14	SZFISPVO	0.57	0.14
12				UZRCOL	0.54	0.12	HFOSITED	0.59	−0.15
13				HFOSITED	0.55	−0.11	WDGCUA22	0.60	0.12
14							SZSREG2Y	0.61	0.13
15							SZKDSRVO	0.62	−0.11
16							SZLODISP	0.63	−0.10

a: Steps in stepwise rank regression analysis
b: Variables listed in order of selection in stepwise regression
c: Cumulative R^{2} value with entry of each variable into regression model
d: Standardized rank regression coefficients (SRRCs) in final regression model

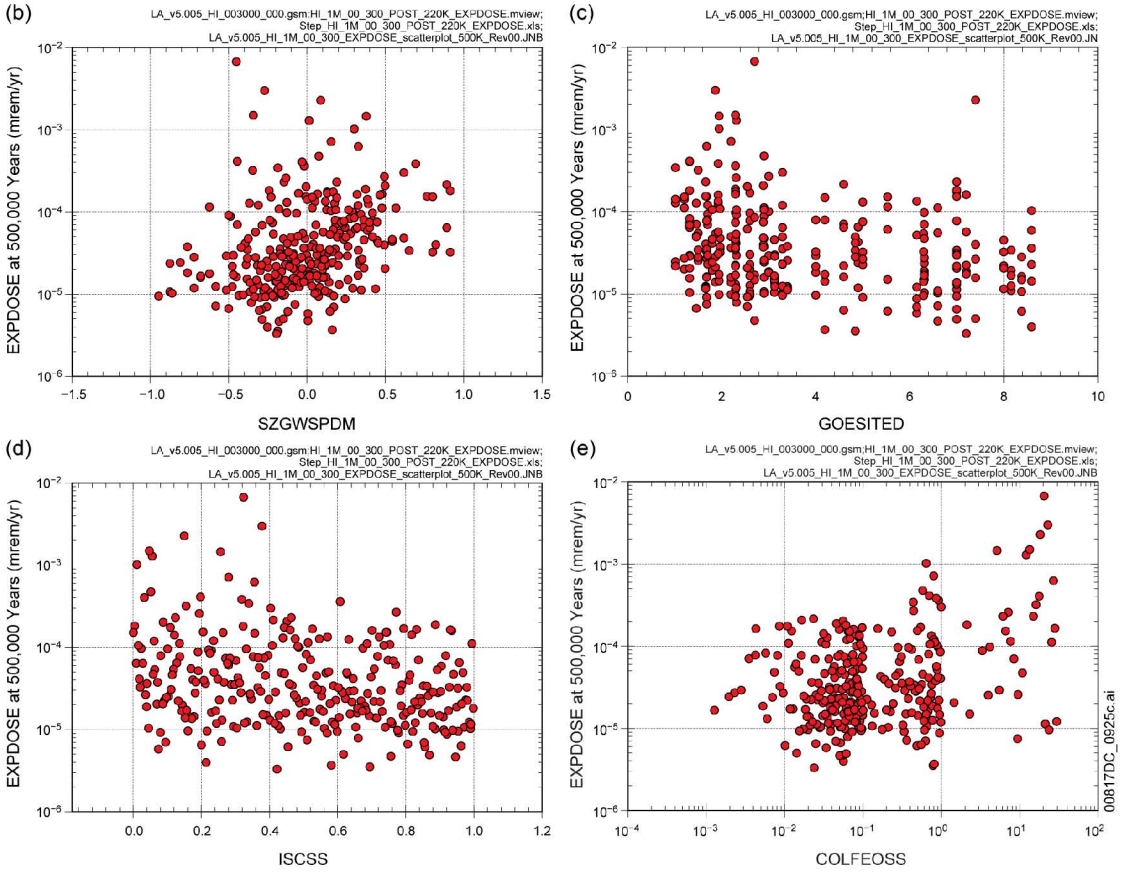

Source: Output DTNs: MO0710ADTSPAWO.000 [DIRS 183752]; and MO0710PLOTSFIG.000 [DIRS 185207].

Figure K10-4[a]. Stepwise rank regression analyses and selected scatterplots for expected dose to RMEI (*EXPDOSE*, mrem/yr) over [220,000, 1,000,000 yr] resulting from human intrusion at 200,000 years obtained with version 5.005 of the TSPA-LA Model: (a) regressions for *EXPDOSE* at 240,000, 500,000, and 760,000 years, and (b,c,d,e) scatterplots for *EXPDOSE* at 500,000 years

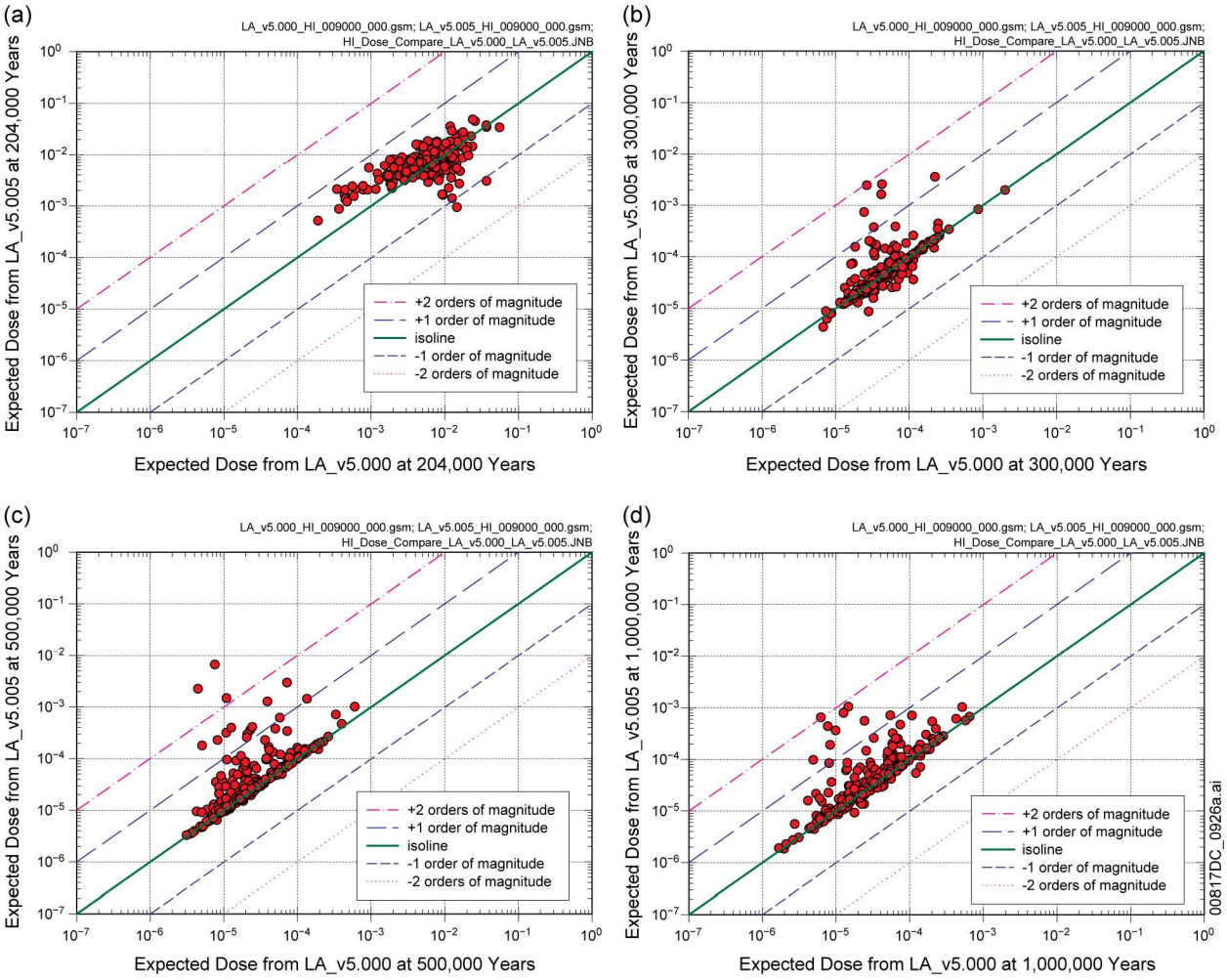

Source: Output DTNs: MO0710ADTSPAWO.000 [DIRS 183752]; and MO0710PLOTSFIG.000 [DIRS 185207].

Figure K10-5[a]. Comparison of expected dose to RMEI (*EXPDOSE*, mrem/yr) over [200,000, 1,000,000 yr] resulting from human intrusion at 200,000 years obtained with versions 5.000 and 5.005 of the TSPA-LA Model at (a) 201,000, (b) 205,000, (c) 500,000, and (d) 1,000,000 years

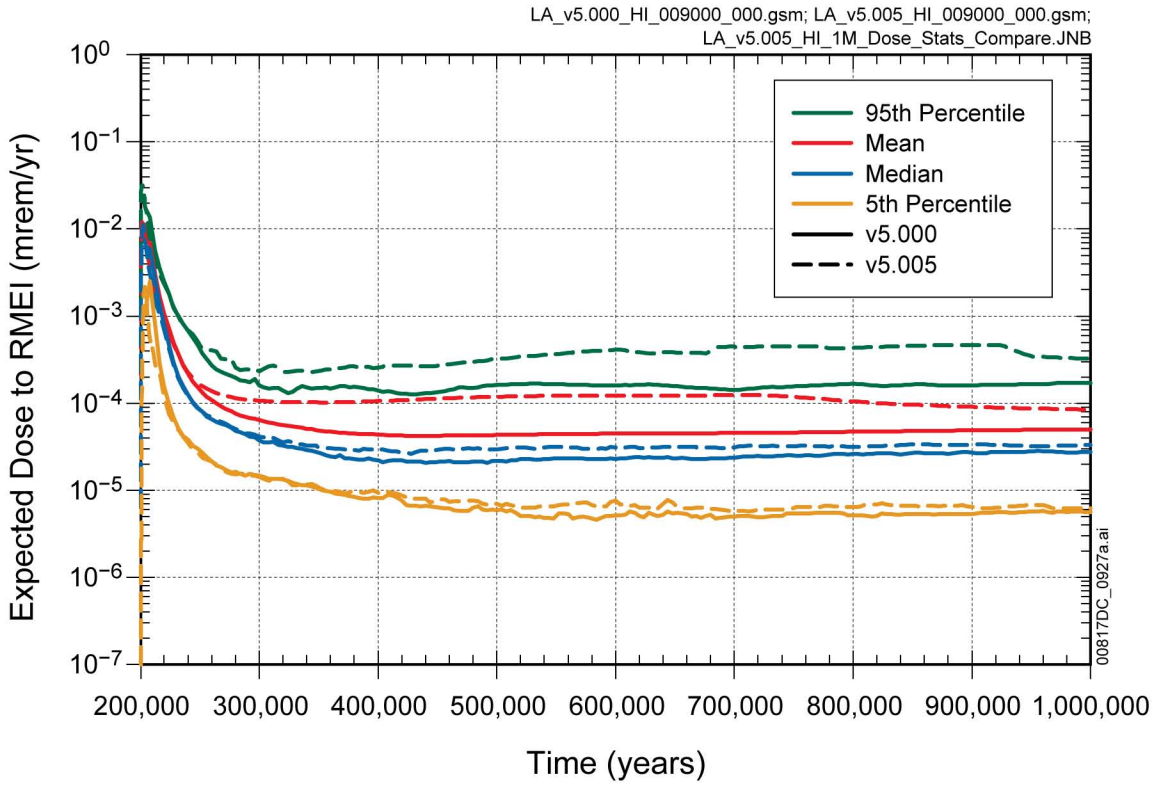

Source: Output DTNs: MO0710ADTSPAWO.000 [DIRS 183752]; and MO0710PLOTSFIG.000 [DIRS 185207].

Figure K10-6[a]. Comparison of summary curves (i.e., mean and 0.05, 0.5, and 0.95 quantile) for expected dose to RMEI (*EXPDOSE*, mrem/yr) over [200,000, 1,000,000 yr] resulting from human intrusion at 200,000 years obtained with versions 5.000 and 5.005 of the TSPA-LA Model

APPENDIX M[a]
COMPARISON WITH ELECTRIC POWER RESEARCH INSTITUTE ANALYSIS

M1[a] INTRODUCTION

Appendix M[a] contains a minor change from the parent document to correct a reference to supporting documentation. The last paragraph in Section M3.3 of the parent document has been updated to correct the reference and is included in Section M3.3[a] of this addendum. The corrected paragraph should be substituted into the discussion presented in Appendix M of the parent document.

M2[a] TSPA CONCEPTUAL MODEL DESIGN

No change.

M3[a] TSPA NOMINAL SCENARIO COMPARISON

No change.

M3.1[a] UNSATURATED FLOW

No change.

M3.2[a] ENGINEERED BARRIER SYSTEM ENVIRONMENT

No change.

M3.3[a] WASTE PACKAGE AND DRIP SHIELD DEGRADATION

In the Electric Power Research Institute (EPRI) TSPA, the computed failure distributions curves for the nominal scenario for the WP are shown on Figure 5-7 in Apted and Ross (2005 [DIRS 182229]), indicating onset of WP failures before 100,000 years. The EPRI TSPA Analysis only considers 8,160 CSNF WPs, of which 5,304 WPs fail after one million years (Senger 2008 [DIRS 185124]). In the TSPA-LA Nominal Scenario Class, the probabilistic projections of WP breaches exhibit a few realizations with a stress corrosion cracking penetrating crack occurring before 100,000 years (Section 8.2.1[a]). However, as Figure 7.7.3-2[a] indicates the bulk of the WP failures occur after about 200,000 years with 6,256 WPs failed by one million years.

INTENTIONALLY LEFT BLANK

APPENDIX P[a]
IMPACT ASSESSMENTS

P1[a] INTRODUCTION

The checking and review activities following the completion of the TSPA-LA Model (v5.000) identified several issues related to errors in implementation, identification of undocumented conservatisms, and updates to parameter values. A detailed discussion of these issues, including an evaluation of the expected impact to the mean annual dose, is included in Appendix P of the parent document. The impact assessment documented in Section P13.3 of the parent document has been updated and is included in Section P13[a] of this addendum. The remaining issue descriptions and impact analyses documented in the parent document are not repeated in this addendum.

The results described in this addendum were generated with TSPA-LA Model v5.005, an updated version of the TSPA-LA Model v5.000, unless otherwise indicated. TSPA-LA Model v5.005 addresses most of the items presented in Appendix P of the parent document; the items resolved in v5.005 are listed in Appendix P[a] of this addendum. The issues addressed in v5.005 are identified in two updated tables, Table P-6[a] and P-7[a]. These two tables comprise a summary of the changes between v5.000 and v5.005 of the TSPA-LA Model.

The discussion and impact assessment presented in Appendix P of the parent document for the remaining issues not addressed in v5.005 of the TSPA-LA Model, as indicated on Table P-7[a], are not repeated in this addendum, as the issue description and impact assessment (excluding Section P13, which is revised in this addendum) remain unchanged and apply equally to v5.005 of the TSPA-LA Model.

P2[a] INVENTORY AND SEEPAGE FRACTION

P2.1[a] ISSUE

Addressed in TSPA-LA Model v5.005.

P2.2[a] ISSUE DESCRIPTION

No change.

P2.3[a] IMPACT ASSESSMENT

No impact to TSPA-LA v5.005 results.

P3[a] WASTE PACKAGE DAMAGE FROM SEISMIC EVENTS

P3.1[a] ISSUE

Addressed in TSPA-LA Model v5.005.

P3.2[a] ISSUE DESCRIPTION

No change.

P3.3[a] IMPACT ASSESSMENT

No impact to TSPA-LA v5.005 results.

P4[a] OUTER BARRIER FAILURE FLAG IN SEISMIC MODEL

P4.1[a] ISSUE

Addressed in TSPA-LA Model v5.005.

P4.2[a] ISSUE DESCRIPTION

No change.

P4.3[a] IMPACT ASSESSMENT

No impact to TSPA-LA v5.005 results.

P5[a] INVERT CHEMISTRY

P5.1[a] ISSUE

Addressed in TSPA-LA Model v5.005.

P5.2[a] ISSUE DESCRIPTION

No change.

P5.3[a] IMPACT ASSESSMENT

No impact to TSPA-LA v5.005 results.

P6[a] WELD VOLUME

P6.1[a] ISSUE

Addressed in TSPA-LA Model v5.005.

P6.2[a] ISSUE DESCRIPTION

No change.

P6.3[a] IMPACT ASSESSMENT

No impact to TSPA-LA v5.005 results.

P7[a] CRACK FAILURE OPENING

P7.1[a] ISSUE

Addressed in TSPA-LA Model v5.005.

P7.2[a] ISSUE DESCRIPTION

No change.

P7.3[a] IMPACT ASSESSMENT

No impact to TSPA-LA v5.005 results.

P8[a] DEGRADATION START TIME

P8.1[a] ISSUE

Addressed in TSPA-LA Model v5.005.

P8.2[a] ISSUE DESCRIPTION

No change.

P8.3[a] IMPACT ASSESSMENT

No impact to TSPA-LA v5.005 results.

P9[a] THRESHOLD RUBBLE VOLUME

P9.1[a] ISSUE

Addressed in TSPA-LA Model v5.005.

P9.2[a] ISSUE DESCRIPTION

No change.

P9.3[a] IMPACT ASSESSMENT

No impact to TSPA-LA v5.005 results.

P10[a] UNINTENDED CORRELATION OF UNCERTAIN PARAMETERS

P10.1[a] ISSUE

Addressed in TSPA-LA Model v5.005.

P10.2[a] ISSUE DESCRIPTION

No change.

P10.3[a] IMPACT ASSESSMENT

No impact to TSPA-LA v5.005 results.

P11[a] UNCERTAINTY IN URANIUM SOLUBILITY

P11.1[a] ISSUE

Addressed in TSPA-LA Model v5.005.

P11.2[a] ISSUE DESCRIPTION

No change.

P11.3[a] IMPACT ASSESSMENT

No impact to TSPA-LA v5.005 results.

P12[a] IONIC STRENGTH FOR HIGH-LEVEL WASTE GLASS DOMAIN

P12.1[a] ISSUE

Addressed in TSPA-LA Model v5.005.

P12.2[a] ISSUE DESCRIPTION

No change.

P12.3[a] IMPACT ASSESSMENT

No impact to TSPA-LA v5.005 results.

P13[a] EFFECT ON SEEPAGE FROM WASTE PACKAGE LENGTH CHANGE

The impact assessment documented in Section P13.3 of the parent document has been updated. Specifically, the last two paragraphs of the impact assessment have been revised, however, the entire section has been repeated and is included below in Section P13.3[a] of this addendum.

P13.1[a] ISSUE

No change.

P13.2[a] ISSUE DESCRIPTION

No change.

P13.3[a] IMPACT ASSESSMENT

The Seepage Model for Performance Assessment provides the mean and standard deviation of the distribution of seepage rates (kg/WP/yr) over a large range of capillary strengths, permeabilities, and percolation fluxes. The seepage dynamically linked library (DLL) used in the TSPA-LA Model uses these rates, along with percolation fields, thermal histories at each WP location, and sampled values for mean capillary strength and mean permeability, to determine seepage rates (kg/WP/yr) at each location and time in each realization, and computes the seepage fraction (fraction of WP locations at which seepage occurs) at each time in each realization.

The Seepage Model for Performance Assessment is a three-dimensional continuum representation of a fractured rock system used to calculate drift seepage at Yucca Mountain. The three-dimensional calculational domain for the model is 10-m high, 4-m wide, and 2.4384-m long (BSC 2004 [DIRS 167652], Figure 6-1). This domain takes advantage of model symmetry and spatial correlation lengths to represent a system based on a drift diameter of 5.5 m and a WP length of 5.1 m with a smaller domain. Rock above and around the drift is also represented in the model. Because the model uses a no-flow vertical boundary along the drift axis, and also only represents a part of the WP length, seepage rates from the model are scaled up by a factor of 4.183, which represents the ratio between the considered drift area (5.5 m × 5.1 m) and the modeled drift area ((5.5 m / 2)*2.4384 m).

The seepage rates for an average WP length of 5.614 m can be estimated by scaling the Seepage Model for Performance Assessment results for an average WP length of 5.0 m. As noted in *Seepage Model for PA Including Drift Collapse* (BSC 2004 [DIRS 167652]), the limited size of the calculational domain was chosen to allow for the use of a fine mesh at the same resolution as the Software Configuration Management, while containing a reasonable number of cells that would not make the computational time too long. The cell dimensions in the vertical plane perpendicular to the drift axis are 0.1 m by 0.1 m and cell lengths parallel to the drift axes are about 0.3 m each (BSC 2004 [DIRS 167652], Section 6.3.1). The vertical boundaries, perpendicular to the drift axis and along the drift centerline are appropriate due to symmetry. The main issue for a heterogeneous system is the domain length versus spatial correlation length (BSC 2004 [DIRS 167652], Section 6.3.1). The lengths of the flow domain in the direction of the drift axis (2.4384 m) and normal to the drift axis (4 m) are 8 times and 13 times the spatial correlation length (0.3 m), respectively. Since the length of the flow domain in the direction of the drift axis is 8 times the correlation length, the no flow boundaries perpendicular to the drift axis are considered appropriate, and should not have a significant effect on flow results. Because the no-flow boundaries have little effect on flow results, the model adequately represents any WP length longer than the model dimensions along the drift axis, as long as the results are scaled by the ratio of the chosen WP length to the modeled WP length. Thus, seepage rates for an average WP length of 5.614 m can be estimated by scaling the Seepage Model for Performance Assessment results for an average WP length of 5.0 m. This scaling would increase the mean and standard deviation of the distribution proportionally (by a factor of 5.614 / 5.1 = 1.10).

The seepage fraction is computed in the Seepage DLL as the fraction of locations at which seepage exceeds the threshold of 0.1 kg/WP/yr. Since seepage rates increase when the average WP length is increased, the seepage fraction may also increase, because the seepage rate at some locations may increase from just less than the threshold to greater than the threshold. Current

TSPA-LA software does not support a numerical evaluation of the degree to which the seepage fraction may increase when average WP length increases. To evaluate the potential impact on total dose associated with an increase in seepage fraction due to an increased WP length, the correlation between seepage fraction and expected annual dose was examined for the 1,000,000-year Nominal Modeling Case, the 10,000-year Seismic Ground Motion (GM) Modeling Case, and the 1,000,000-year Seismic GM Modeling Case. The 10,000-year Igneous Intrusion Modeling Case and the 1,000,000-year Igneous Intrusion Modeling Case which are also major contributors to dose were not examined because after an igneous event occurs, all WPs are evaluated in a seeping environment. For the three cases, scatter plots of expected annual doses versus seepage fraction at 10,000 or 1,000,000 years are presented along with the rank correlations of expected annual dose and seepage fraction at those times. As shown in Figure P-20[a], for the 1,000,000-year Nominal Modeling Case, negligible correlation between expected annual dose and seepage fraction at 1,000,000 years is seen. The rank correlation between expected annual dose and seepage fraction is 2.4×10^{-2}. Similarly, for the 10,000-year Seismic GM Case, negligible correlation between expected annual dose and seepage fraction at 10,000 years is seen (Figure P-21(a)[a]). The rank correlation between expected annual dose and seepage fraction, for the 10,000-year Seismic GM Case, is 4.65×10^{-2}. For the 1,000,000-year Seismic Ground Motion Case, negligible correlation between expected annual dose and seepage fraction at 1,000,000 years is seen (Figure P-21(b)[a]). The rank correlation between expected annual dose and seepage fraction, for the 1,000,000-year Seismic GM Case, is 1.17×10^{-2}. Based on the negligible correlation between expected annual dose and seepage fraction shown in these analyses, it is assumed that change in seepage fractions, associated with an increase in the waste package length to 5.614 m, will have little impact on total dose.

Because seepage rates increase proportionally with increased WP length, and seepage fraction is not anticipated to have a large impact on dose, the net effect of increasing WP length on annual dose is to increase seepage rates in a percolation bin by approximately 10 percent. As demonstrated in Section P17, annual dose may increase in proportion to changes in seepage rates for cases where the major dose-controlling radionuclide is solubility-controlled in the EBS. For radionuclides that do not have solubility limits, the increased seepage flux would have negligible impact on the mass flux. Therefore, the overall effect of increasing the average WP length used in the seepage abstraction by 10 percent would be minor.

P14[a] IGNEOUS EVENT PROBABILITY

P14.1[a] ISSUE

No change.

P14.2[a] ISSUE DESCRIPTION

No change.

P14.3[a] IMPACT ASSESSMENT

No change.

P15[a] LONGITUDINAL DISPERSIVITY IN 1-D SZ TRANSPORT MODEL

P15.1[a] ISSUE

Addressed in TSPA-LA Model v5.005.

P15.2[a] ISSUE DESCRIPTION

No change.

P15.3[a] IMPACT ASSESSMENT

No impact to TSPA-LA v5.005 results.

P16[a] GLASS DEGRADATION RATE

P16.1[a] ISSUE

Addressed in TSPA-LA Model v5.005.

P16.2[a] ISSUE DESCRIPTION

No change.

P16.3[a] IMPACT ASSESSMENT

No impact to TSPA-LA v5.005 results.

P17[a] SEEPAGE FLUX AFTER DRIFT COLLAPSE

P17.1[a] ISSUE

No change.

P17.2[a] ISSUE DESCRIPTION

No change.

P17.3[a] IMPACT ASSESSMENT

No change.

P18[a] UNSTABLE IRON OXYHYDROXIDE COLLOIDS

P18.1[a] ISSUE

Addressed in TSPA-LA Model v5.005.

P18.2[a] ISSUE DESCRIPTION

No change.

P18.3[a] IMPACT ASSESSMENT

No impact to TSPA-LA v5.005 results.

P19[a] DOE SPENT NUCLEAR FUEL MASS RELEASE

P19.1[a] ISSUE

Addressed in TSPA-LA Model v5.005.

P19.2[a] ISSUE DESCRIPTION

No change.

P19.3[a] IMPACT ASSESSMENT

No impact to TSPA-LA v5.005 results.

P20[a] GOLDSIM SOFTWARE ERROR

P20.1[a] ISSUE

Addressed in TSPA-LA Model v5.005.

P20.2[a] ISSUE DESCRIPTION

No change.

P20.3[a] IMPACT ASSESSMENT

No impact to TSPA-LA v5.005 results.

P21[a] UNSATURATED ZONE TRANSPORT THROUGH FAULT ZONE

P21.1[a] ISSUE

No change.

P21.2[a] ISSUE DESCRIPTION

No change.

P21.3[a] IMPACT ASSESSMENT

No change.

P22[a] OTHER MINOR IMPLEMENTATION ERRORS

P22.1[a] ISSUE

Addressed in Table P-6[a].

P22.2[a] ISSUE DESCRIPTION

No change.

P23[a] SUPERFICIAL CHANGES

P23.1[a] ISSUE

No change.

P23.2[a] ISSUE DESCRIPTION

No change.

P23.3[a] IMPACT ASSESSMENT

No change.

P24[a] SUMMARY

The issues addressed in TSPA-LA Model v5.005 which were presented in Appendix P of the parent document are summarized in Table P-7[a]. Since most of the issues evaluated had a negligible to small impact (except for the issue discussed in Section P3), the combined effect of correcting the issues was small for mean annual dose for all modeling cases (as documented in Section 7.3.1[a]). In none of the issues evaluated does the mean annual dose increase appreciably above the base-case results presented in Section 8 of the parent document, in fact, in most cases, it decreases (see Section 7[a] and Section 8[a] of this addendum). Thus, the impact assessments presented in Appendix P of the parent document were accurate and the validation activities performed on the results documented therein remain applicable.

INTENTIONALLY LEFT BLANK

Table P-6[a]. Discussion of Other Minor Implementation Errors

	ISSUE DESCRIPTION	ANTICIPATED IMPACT (V5.000)	ADDRESSED V5.005
1	Drift-wall condensation incorrectly turned off in the non-dripping environments.	This error should have negligible or no impact in all modeling cases. Because drift-wall condensation occurs for at most 2,000 years (Section 6.3.3.2.2) and because the DS remains intact throughout this period in all modeling cases except Drip Shield EF Modeling Case, the release from any failed WP should be negligibly impacted. In the Drip Shield EF Modeling Case since the WP is always modeled to be located in the dripping environment (Section 6.4.1.3), there should be no impact.	Yes – Drift wall condensation appropriately applied to the non-dripping environments.
2	Inconsistent half-lives especially for ^{79}Se and ^{126}Sn between those applied in GoldSim and those used by the UZ and SZ transport models implemented using DLLs.	The ^{79}Se half-life in GoldSim is set at 290,000 years while that in the UZ and SZ transport model is set at 295,000 years. The ^{126}Sn half-life in GoldSim is set at 230,000 years while that in the UZ and SZ transport model is set at 250,000 years. These inconsistencies are minor, as they occur only in the second significant digit. Since the dose contribution from ^{79}Se and ^{126}Sn is at least an order of magnitude lower than some of the other radionuclides (see Figures P-1 to P-5), the impact on the mean annual dose would be negligible.	Yes – EBS, Unsaturated Zone, and Saturated Zone submodels use the same half-life values.
3	In the calculations to determine the time of first seismic damage to the WP, the abstraction for WP failure under intact DS is considered while the DS is intact. This calculation should not be used after either the DS plate or DS framework has failed. However, this calculation ignores the DS framework failure and only considers the DS plate failure to determine whether to use this abstraction or not.	It should be noted that this error only affects the 1,000,000-year Seismic GM Modeling Case because the DS remains intact in the 10,000-year modeling case. Since the DS framework failure (average failure time of 100,000 years) occurs earlier than the DS plate failure (average failure time of 250,000 years), there is a possibility of predicting the WP failure time earlier than intended in the time duration where the DS framework has failed but the DS plate is intact. This error may have an impact on estimating first failure time for only CDSP WPs as the probability of WP failure under intact DS is generally greater than the probability of failure under failed DS that is surrounded by rubble. Even here, the probability of occurrence of this error is small, as the DS framework lasts up to 100,000 years on an average, during which time CDSP WPs that are likely to fail from seismic damage would have failed in a majority of the realizations (~70%). For CSNF WPs there is no impact anticipated, as the probability of failure under intact DS is much smaller than the probability of failure under the failed DS that is surrounded by rubble. As a result, this error is likely to have only a negligible impact on the mean annual dose.	Yes – Corrected to consider both the DS plate and framework failures.
4	The calculation for the time of first seismic damage may be incorrect if the WP damage is from the first seismic event.	This error only appears when the first seismic event causes the damage to the WP or leads to rockfall. Since seismic events occur on an average of every 2,330 years (inverse of specified annual rate of 4.287×10^{-4} yr^{-1}), only those realizations would be impacted where the WP damage or rockfall occurs within 2,330 years (on an average). There are only five such realizations in the 9,000 realization seismic ground motion base case where the damage should have occurred from the first seismic event but did not occur due to the error. The impact of this error is negligible. No other modeling cases are affected.	Yes – Calculation was corrected to accurately reflect the first seismic event.

Table P-6[a]. Discussion of Other Minor Implementation Errors (Continued)

	ISSUE DESCRIPTION	ANTICIPATED IMPACT (V5.000)	ADDRESSED V5.005
5	The HLW glass derived waste form colloid concentrations are overestimated under conditions when the waste form colloids are unstable.	This error occurs only when the conditions are unstable for the generation of glass waste form colloids. Since the maximum concentration of HLW glass waste form colloids, under stable conditions, is itself small (maximum of 2 mg/L and a mean of 0.3 mg/L) the mass transported on colloids will be negligibly small compared to that transported in the dissolved phase. Thus, this overestimation would have negligible impact on the mean annual dose. Furthermore, the unstable conditions generally occur when the ionic strength is greater than 0.4 mol/kg, which is typical while there is no flow through the WP. Since the transport mechanism is diffusion when there is no flow and because the diffusion coefficient of colloids is much smaller compared to the dissolved species (by at least two orders) no appreciable mass can be carried by the colloids.	Yes – High-level radioactive waste glass colloid concentration calculation was corrected.
6	The element that integrates the mass released from the WP in the Human Intrusion Scenario integrates the mass flux rate computed for the previous timestep over the next timestep using the next timestep length. It should instead integrate the mass flux rate computed for the given timestep over that timestep length.	This error would only have an impact when the timestep length is changing as the integrated mass would change. Since the intrusion time is set at 200,000 years in the Human Intrusion Scenario and because there is no change made in the timestep length for the remaining simulation duration, the calculations are not affected. The only impact is one timestep delay in passing the mass to the UZ borehole pathway while the dose magnitudes remain unaffected. Since this is a highly stylized modeling case, with a selected intrusion time, the one timestep delay is not important to the overall system results and does not affect the dose values.	Yes – The calculation has been corrected to use the appropriate timestep length.

Table P-6[a]. Discussion of Other Minor Implementation Errors (Continued)

	ISSUE DESCRIPTION	ANTICIPATED IMPACT (V5.000)	ADDRESSED V5.005
7	The implemented range of two uncertain parameters used in determining the number of monolayers of adsorbed water for corrosion products as part of the EBS Transport submodel is different from their intended ranges.	The stochastic elements FHH_Isotherm_k_CP_a and FHH_Isotherm_s_CP_a are sampled to determine the value for parameters *k* and *s* that are used in the water adsorption isotherm for corrosion products to determine the number of sorbed layers of water (SNL 2007 [DIRS 177407], Section 6.3.4.3.2), which is eventually used in computing the saturation under conditions when there is no flow through the WP. The uniform distribution ranges used from *EBS Radionuclide Transport Abstraction*, (SNL 2007 [DIRS 177407], Table 8.2-4) are: FHH_Isotherm_k_CP_a: 1.048 – 1.370 FHH_Isotherm_s_CP_a: 1.525 – 1.852 The correct ranges, as intended in Section 6.3.4.3.2 of *EBS Radionuclide Transport Abstraction* (SNL 2007 [DIRS 177407]) are: FHH_Isotherm_k_CP_a: 1.030 – 1.326 FHH_Isotherm_s_CP_a: 1.493 – 1.799 The difference in the two ranges is small compared to their uncertainty ranges and thus the effect on calculating the number of monolayers of adsorbed water and saturation of corrosion products is likely to be negligible, leading to negligible impact on the mean annual dose.	Yes – Uncertainty distributions have been corrected.
8	The K_d range for sorption of Np on the Uranium mineral colloids in the EBS is not correct.	The K_d range for sorption of Np on the uranium colloids is given by a log-uniform distribution ranging from 10 to 500 mL/g (Table 6.3.7-64). The lower bound value of 10 mL/g was incorrectly set to 1 mL/g during the implementation. The impact of this reduction in the lower bound is anticipated to be negligible as the Np mass carried by the uranium colloids is likely to be small (even with the corrected values) compared to the mass carried by other colloid types and in the dissolved phase. Considering the mean uranium colloid concentration of about 6 mg/l (based on cumulative distribution function given in Table 6.3.7-64) and the maximum Np K_d of 500 mL/g, and multiplying the two would lead to a value of about 3×10^{-3}, which represents the ratio of Np mass on the uranium colloids to the mass in the dissolved phase in given water volume. This indicates that the predominant mechanism for Np transport is in the dissolved phase. The impact of this error is anticipated to be negligible, if any, on the mean annual dose.	Yes – K_d range for sorption of Np on the uranium colloids has been corrected.

Table P-6[a]. Discussion of Other Minor Implementation Errors (Continued)

	ISSUE DESCRIPTION	ANTICIPATED IMPACT (V5.000)	ADDRESSED V5.005
9	In the Human Intrusion Modeling Case, the mass irreversibly associated with colloids that is released to the SZ is not partitioned into the fast transport fraction and the slow transport fraction.	In the Human Intrusion Modeling Case, the mass irreversibly associated with the waste form colloids (referred as "Ic") and the iron oxyhydroxide colloids (referred as "If") from the WP and passed through the UZ borehole needs to be combined together and repartitioned based on the fast fraction, before passing the mass to the SZ. This needs to be done in such a way that only a small fraction (0.00168) travels unretarded (fast) while the rest of the mass travels with some retardation (slowly). The impact of this error is anticipated to be small as the relative contribution from the fast and slow traveling mass fractions cannot be fully differentiated due to large timesteps employed in the TSPA-LA Model past 200,000 years (when the human intrusion is modeled). Thus, even though the relative contribution of Ic and If species could vary, the combined mass flux from the mass irreversibly associated with colloids is not anticipated to change. As a result, the impact on the mean annual dose is anticipated to be negligible.	Yes – Human Intrusion Scenario Modeling Case was corrected to include a partitioning of the mass released to the SZ between fast and slow colloid fractions.
10	In the UZ transport model, the correct minimum value for the selenium K_d for vitric rock units was supposed to be 0 mL/g. However, the minimum value after natural log transformation was set to 0, which is equivalent to a K_d of 1 mL/g.	The impact of this error is anticipated to be negligible as the mean K_d value remains largely unchanged (reduced by 0.8%) when the minimum value is corrected. Furthermore, ^{79}Se is not a large contributor to dose.	Yes – The selenium K_d for vitric rock has been corrected.
11	For the UZ transport model, the uranium K_d for zeolitic rock unit has an error at probability level of 1. It was incorrectly set to 20 mL/g instead of 30 mL/g.	The impact of this error is anticipated to be negligible as the mean K_d value would change from 5.25 mL/g to 7.75 mL/g. This small increase is unlikely to affect the transport of uranium through the UZ. Furthermore, the current error is conservative as it leads to lowering the uranium K_d in the UZ matrix.	Yes – The uranium K_d for zeolitic rock has been corrected.
12	The concentration limit for plutonium and americium mass irreversibly sorbed on the iron oxyhydroxide colloids in the invert is incorrectly based on the stability criteria for the waste form domain instead of the corrosion products domain.	The error would only have an impact if the irreversible colloid concentration in the invert is nearing the concentration limit in the invert, which is an unlikely condition due to fast transport rates out of the invert compared to the incoming transport rate. Even if the conditions conducive to error occur, they would remain for a short time period compared to the simulation time. The impact of this error is expected to be negligible on the mean annual dose.	Yes – The calculation has been corrected to use the stability criteria in the corrosion products domain.

Table P-6[a]. Discussion of Other Minor Implementation Errors (Continued)

	ISSUE DESCRIPTION	ANTICIPATED IMPACT (V5.000)	ADDRESSED V5.005
13	The time-dependent increase in the diffusive area from nominal corrosion of the WP outer barrier should be removed from the stylized Human Intrusion Modeling Case.	Ignoring the time-dependent increase in diffusive area from nominal corrosion processes (by either SCC or general corrosion patches) on the WP for the Human Intrusion Modeling Case is unlikely to affect the diffusive release out of the WP as only about 5% of the realizations would have some SCC failures by 200,000 years, the time when the human intrusion event is modeled. Following the event, the patch area equal to the drill stem area is applied to the WP for both diffusive and advective release. The patch area applied is large enough to cause large diffusive releases. Since the general corrosion patches do not occur until very late times (>400,000 years), any small increases in diffusive area from SCCs is unlikely to affect the diffusive flux. The impact of this error is likely to be negligibly small on the mean annual dose.	Yes – The nominal corrosion processes have been removed from the diffusive area calculation in the Human Intrusion Scenario.
14	In calculating the first damage time for the WP due to seismic ground motion, the possibility of failure from puncture was not considered.	The first damage time calculations only evaluate the failures caused by seismic-induced SCCs or by nominal corrosion processes (nominal SCC or general corrosion). However, there is a small probability that punctures could occur earlier under certain conditions. The conditions for puncture failure require that the DSs have failed and the WPs are surrounded by rubble. Under these conditions the probability of puncture varies as a function of PGV, but the probabilities remain low even at high PGVs (Figure 6.6-17). First failures from puncture damage are only likely to occur late in time when the WP has a reduced thickness (Figure 7.3.2-15). The number of realizations where puncture occurs before seismic-induced SCCs would be small since there is a higher probability of damage from seismic-induced SCCs (Figure 6.6-15). Note that this error only occurs in the Seismic GM Modeling Case run for 1,000,000 years. There is no effect on the Seismic GM Modeling Case run for 10,000 years as the conditions conducive to puncture do not occur. Analysis of a stand-alone model for WP degradation that includes both nominal and seismic degradation processes (output DTN: MO0709TSPAWPDS.000 [DIRS 183170]; file v5.000_GS_9.60.100_StandAlone_9krlz.gsm in folder Seismic_9k_Rlz) showed that 63 out of 9,000 realizations could have first damage from punctures. The impact of this on the mean annual dose is likely to be negligible as only 0.7% of the realizations would be affected and the effects are likely to be late (after the DSs are failed and the WPs have thinned).	Yes – Corrected the first damage calculation to include puncture failures during a seismic event.

Table P-6[a]. Discussion of Other Minor Implementation Errors (Continued)

	ISSUE DESCRIPTION	ANTICIPATED IMPACT (V5.000)	ADDRESSED V5.005
15	The temperature and relative humidity modifications may be incorrectly applied after rubble fills the drifts as a result of degradation due to seismic ground motion.	The percolation subregion representative temperature and relative humidity time histories under nominal conditions (from MSTHM abstraction) are modified once the drifts become filled with rubble as a result of drift degradation from seismic ground motion. These modifications (deltas) are applied by adding to or subtracting from the representative temperature and relative humidity datasets. Twelve possible delta combinations, from four infiltration scenarios over three host-rock thermal conductivity cases (Section 6.3.2.2), are considered in the TSPA-LA Model for each percolation subregion and for each fuel type. However, in order to limit the computational burden, only eight delta combinations are actually calculated: six delta combinations for CSNF and two delta combinations for HLW. The six delta combinations for CSNF are then mapped to 12 possible delta combinations for the CSNF fuel type in each percolation subregion. Similarly, the two delta combinations for HLW are then mapped to 12 possible delta combinations for the HLW fuel type (CDSP WP) for each percolation subregion. Due to an implementation error, some of the combinations are incorrectly matched and the data are incorrectly read from the look-up tables. This could sometimes result in incorrect modifications of representative temperature and relative humidity time histories for the given percolation subregion and a given fuel type. In addition, some of the data sets used in the modification of temperatures (called temperature deltas) have been entered in a sequence that is different compared to the relative humidity deltas resulting in internal inconsistency once the modifications are made. Note that the error is only possible in the two modeling cases in which rubble fills the drifts, the Seismic GM Modeling Case run for 1,000,000 years and the Seismic FD Modeling Case. The impact of this error on the mean annual dose for either modeling case is likely to be negligible as the variation in the delta among various combinations is small. Thus, even though incorrect values may be applied, they would not result in any appreciable deviations from the corrected time history profiles. Furthermore, the magnitude of the modification is itself small relative to the actual temperature and relative humidity values even at the maximum initial values (the magnitudes of the deltas decrease with time). As a result, the downstream models affecting radionuclide transport are unlikely to be appreciably impacted by this error. The impact of the error on localized corrosion initiation is also evaluated based on the Localized Corrosion Initiation Uncertainty Analysis described in Appendix O. The five realizations (out of 300) that have early rubble fill times (within 12,000 years) all have conditions that are not conducive to localized corrosion initiation, even accounting for slightly incorrect temperature and relative humidity. One realization (realization 142), which has conditions favorable for localized corrosion until 12,000 years, has a rubble fill time greater than 100,000 years, by which time localized corrosion is not favored. It is concluded that there is no impact of this error on the localized corrosion initiation.	No – Impact summary as assessed for v5.000.

Table P-6[a]. Discussion of Other Minor Implementation Errors (Continued)

	ISSUE DESCRIPTION	ANTICIPATED IMPACT (V5.000)	ADDRESSED V5.005
16	Drift-wall condensation flux is being applied even after the igneous intrusive event, when the drifts are all assumed to be filled with magma.	The drift-wall condensation model is applicable only under nominal conditions and does not apply once the drifts are degraded from seismic ground motion or filled with magma following the igneous intrusion. However, it is being incorrectly applied even after the igneous intrusion. The impact of the error is restricted to the first 2,000 years only because the drift-wall condensation can only occur in the first 2,000 years (Section 6.3.3.2.2). As a result, the water flux through the WP could be higher than the percolation flux leading to increased advective mass flux of radionuclides for realizations when the igneous intrusion occurs within the first 2,000 years. But because the probability of having an igneous event in the first 2,000 years is negligibly small (mean value of 3.3×10^{-5}) the effect on expected dose of this additional mass flux is small. The impact of the error is evaluated to be negligible.	Yes – Drift wall condensation flux was turned off after an igneous intrusion event.

Table P-6[a]. Discussion of Other Minor Implementation Errors (Continued)

	ISSUE DESCRIPTION	ANTICIPATED IMPACT (V5.000)	ADDRESSED V5.005
17	The WP temperatures could sometimes fall below the lower range of validity of the abstractions provided for computing in-package chemistry, HLW glass degradation rate, and dissolved concentration limits in the TSPA-LA Model.	An assessment of the range of validity shows that most of the validity ranges specified for the process models and abstractions included in the TSPA-LA Model are honored (see output DTN: MO0709TSPALAMO.000 [DIRS 182981]). However for three submodels (discussed below) that are included in the 1,000,000-year performance calculations the representative WP temperatures could fall below the lower limit specified by the abstractions; the minimum waste package temperature noted in the TSPA-LA Model is about 17°C for the 1,000,000-year simulation period. The lower temperature limit for the range of applicability of the In-Package Chemistry Abstraction (SNL 2007 [DIRS 180506]) is 25°C. Without an alternate implementation for low temperature conditions, the TSPA-LA Model applies the In-Package Chemistry Abstraction at temperatures below 25°C. Given that the In-Package Chemistry Abstraction for pH and ionic strength includes uncertainty to account for higher temperatures, the application of abstraction at lower temperatures is anticipated to produce results that are within the range of uncertainty captured in the abstractions for pH and ionic strength. The lower temperature limit for the range of applicability of the HLW Glass Waste Form Degradation Abstraction (BSC 2004 [DIRS 169988]) is 20°C. Without an alternate implementation for low temperature conditions, the TSPA-LA Model applies the HLW glass waste form degradation rate model at temperatures below 20°C. The lower temperature limit was determined by the ranges considered in the experimental results used to validate the rate model (BSC 2004 [DIRS 169988], Section 7.3) which showed that the Arrhenius relationship for glass degradation rate is maintained between 20°C and 90°C. This relationship is not anticipated to change between 17°C and 20°C and therefore unlikely to have any effect on mass transport calculations. The lower temperature limit for the range of applicability of the Dissolved Concentration Limits Abstraction (SNL 2007 [DIRS 177418]) is 25°C. Without an alternate implementation for low temperature conditions, the TSPA-LA Model applies the Dissolved Concentration Limits Abstraction at temperatures below 25°C. Because actinides have retrograde solubility (SNL 2007 [DIRS 177418], Section 6.3.3.3), it is possible that dissolved concentration limits below 25°C could be higher than those implemented in the TSPA-LA Model. But because the Dissolved Concentration Limits Abstraction includes additional uncertainty to account for differences in temperature conditions (SNL 2007 [DIRS 177418], Section 6.3.3), it is anticipated that any small effects from extrapolation would produce results that are within the range of uncertainty captured in the abstractions for dissolved concentration limits. For the 10,000 year simulations the temperatures remain within the range of validity.	No – Impact summary as assessed for v5.000.

Table P-6[a]. Discussion of Other Minor Implementation Errors (Continued)

	ISSUE DESCRIPTION	ANTICIPATED IMPACT (V5.000)	ADDRESSED V5.005
18	Drift-wall condensation flow only occurs in the non-lithophysal regions of the repository.	The drift wall condensation abstraction states that drift wall condensation should cease after the drift has collapsed. Drift collapse is only modeled in the Seismic Scenario Class. In the Seismic Scenario Class, drift collapse occurs in the lithophysal regions of the repository; thus the fraction of WPs that are exposed to drift wall condensation is limited to the fraction of WPs in the non-lithophysal region. However, this limit was not properly implemented in the TSPA-LA Model. As a result, in all but the Igneous Intrusion modeling case, drift wall condensation was limited to the fraction of WPs in the nonlithophysal region and therefore was underestimated in the TSPA-LA Model. Because drift wall condensation only increases the flux in the repository for the first 2,000 years, the dose impact can only occur in the modeling cases that fail WPs in the first 2,000 years and have radionuclide transport in the first 2,000 years. The implementation is correct for the Seismic Ground Motion and Seismic Fault Displacement modeling cases and the Igneous Intrusion Modeling Case. The Nominal Scenario Class and Human Intrusion Scenario do not have failures in the first 2,000 years and thus are not affected. The EF WP modeling case does have WP failures in the first 2,000 years, but the DS remains intact so any additional condensation flux is not anticipated to change transport out of the EF WP. The flux through a failed WP in the EF DS modeling case could be increased by drift wall condensation. As a result, WP releases could also be increased, leading to a higher expected dose in the EF DS modeling case. Contributing less than 2.5% to the total mean dose, the EF DS modeling case is not a significant contributor to the total dose from the repository. The impact of the error is evaluated to be negligible.	No – Impact summary as assessed for v5.000.
19	Mass of iron oxyhydroxide colloids computed for Cell 1 is used in the preliminary forward rate constant calculation for americium in Cell 2 of the EBS Transport Submodel for CSNF WP.	A preliminary calculation to determine the forward rate constant for implementing kinetic sorption of americium on iron oxyhydroxide colloids and stationary corrosion products for CSNF WP incorrectly uses the mass of iron oxyhydroxide colloids from Cell 1 of the EBS Transport Submodel. It should instead use the mass of iron oxyhydroxide colloids from Cell 2 because the sorption calculation is relevant to Cell 2 (corrosion products domain) of the EBS transport submodel. The impact of this error is anticipated to be negligible because it is used only in the preliminary calculation of the forward rate constant for americium. It is considered a final value only if certain constraints are met based on the stability of iron oxyhydroxide colloids and flow rates. In no case can it result in forward rate constant value outside the experimentally determined range. Because the bulk forward reaction rates are generally large (compared to the time step size), any small changes in the forward rate constant are likely to have negligible impact on the bulk reaction rates and consequently on the mass kinetically sorbed. The overall impact of the error is anticipated to be negligible, if any.	No

Table P-7[a]. Impact Assessment Summary Table

Issue No.	Issue Description	Anticipated Impact	Addressed in v5.005
P2.	Inventory for ^{36}Cl, ^{79}Se, and ^{126}Sn was omitted in the 10,000-year simulation modeling cases and the seepage fractions applied for the 10,000-year simulations are based on the post-10,000-year climate.	Negligible	Yes – Added ^{36}Cl, ^{79}Se, and ^{126}Sn (which was inadvertently omitted in the 10,000-year simulation modeling cases) and modified the seepage calculations (Section 6.3.3.1.3[a]).
P3.	Conservative treatment of WP damage from seismic events following the first breach due to nominal corrosion processes.	Significant between 200,000 and 300,000 years	Yes – Modified seismic damage submodel to remove conservatism (Section 6.6.1.3[a]).
P4.	WP outer barrier failure flag is triggered when the inside-out corrosion of the WP is initiated in the Seismic GM Modeling Case, which could be earlier than the actual breach time.	Negligible	Yes – corrected model implementation to more accurately match breach time.
P5.	In-package chemistry applied in the invert after the DS is failed without considering flow through the WP.	Negligible	Yes – corrected model implementation to include flow through the WP.
P6.	Incorrect weld volume is used in computing the probability of manufacturing defects.	Negligible	Yes – corrected weld volume.
P7.	Nominal crack failure opening area incorrectly calculated once the elapsed time is greater than the seismic damage time.	Negligible	Yes – corrected model implementation.
P8.	Degradation processes inside the WP could start before the breach from an igneous event under certain aleatory configuration of specified igneous event times.	Negligible	Yes – corrected model implementation.
P9.	Threshold rubble volume (per drift length) that is used for determining when the non-lithophysal drifts undergo collapse is incorrect. It is currently using the value of 5 m^3/m while the correct value is 0.5 m^3/m.	Negligible	Yes –corrected value to 0.5 m^3/m.
P10.	Unintended perfect correlation between two uncertainty parameters: WRIP_beta_rand_a and PCE_Delta_pCO2_a.	Negligible	Yes – removed unintended correlation.
P11.	The uncertainty associated with fluoride concentration in calculating the uranium solubility for the CSNF WPs is incorrectly calculated in the Igneous Intrusion Modeling Case.	Negligible	Yes – corrected model implementation.
P12.	The ionic strength for the HLW glass domain for conditions where there is flow through the WP always chooses the ionic strength determined for flowing conditions.	Negligible	Yes – corrected model implementation to select ionic strength based on flow conditions.
P13.	The average WP length seepage abstraction uses an average WP length of 5.0 m. However, the average length of WPs should be 5.6 m.	Small (≤12%)	No – Small impact (≤12%)
P14.	Evaluate the mean annual dose from the Igneous Intrusion and Volcanic Eruption Modeling Cases with the probability of the igneous event set to 10^{-7} per year. Note that this is purely a sensitivity analysis and not due to any error in the implementation.	None	NA
P15.	The distribution for longitudinal dispersivity that is sampled produces unrealistically large values in the 1-D SZ flow and transport model.	Small (<30%)	Yes – changed the longitudinal dispersivity (Section 6.3.10[a]).

Table P-7[a]. Impact Assessment Summary Table (Continued)

Issue No.	Issue Description	Anticipated Impact	Addressed in v5.005
P16.	The HLW glass degradation rate calculation for the Igneous Intrusion Modeling Case uses the degradation model that was developed for nominal conditions instead of applying an instantaneous degradation	Negligible	Yes – corrected model implementation to include instantaneous degradation for the Igneous Intrusion Modeling Case.
P17.	The seepage flux in the lithophysal zones following the drift collapse may be under predicted in some realizations due to an error in estimating the bounding values.	Small (~20%)	Yes – corrected model implementation to include the degraded drift diameter of 11 m for estimating bounding values following drift collapse.
P18.	Minimum iron oxyhydroxide colloid concentration is being applied even under stable conditions due to error in calculating the ionic strength threshold for colloid stability calculations.	Negligible	Yes – corrected model implementation.
P19.	In the Igneous Intrusion Modeling Case, the number of WPs assigned for computing the DSNF mass in the non-dripping environments are not correctly calculated following the igneous event.	Small (<6%)	Yes – corrected model implementation.
P20.	GoldSim software error where incorrect masses could be calculated by the Source and Pipe elements (special GoldSim elements) when decay chains have feedback loops.	Small (<5%)	Yes – No impact.
P21.	Delay in transport for some radionuclides through the fault zones in the UZ transport model.	Small (<5%)	No. Small (<5%)
P22.	Other minor implementation errors that have been discovered since running the compliance case are grouped and addressed (Table P-6).	Negligible	See Table P-6[a]
P23.	Several suggested changes to the model file structure are tracked in a model status log.	None	Yes.

INTENTIONALLY LEFT BLANK

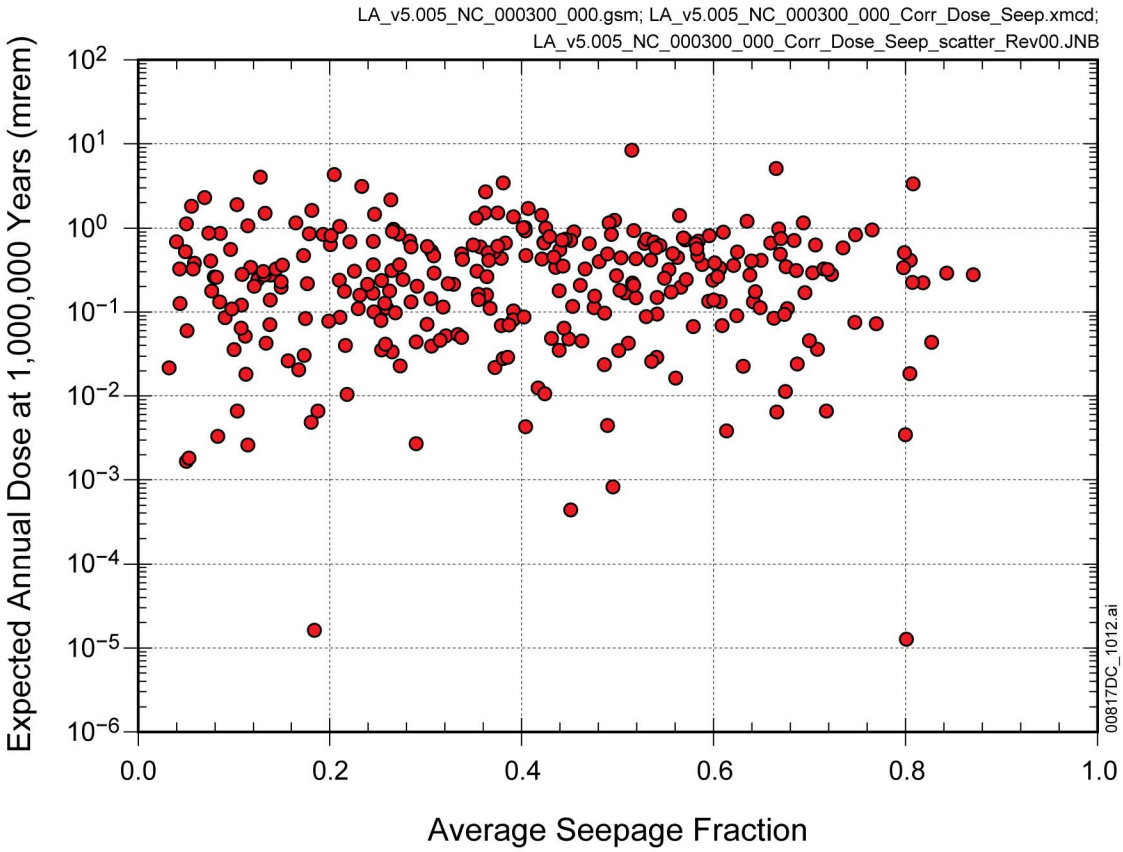

Source: Output DTN: MO0710ADTSPAWO.000 [DIRS 183752].

Figure P-20[a]. Expected Annual Dose versus Average Seepage Fraction for the Nominal Modeling Case for 1,000,000 Years after Repository Closure

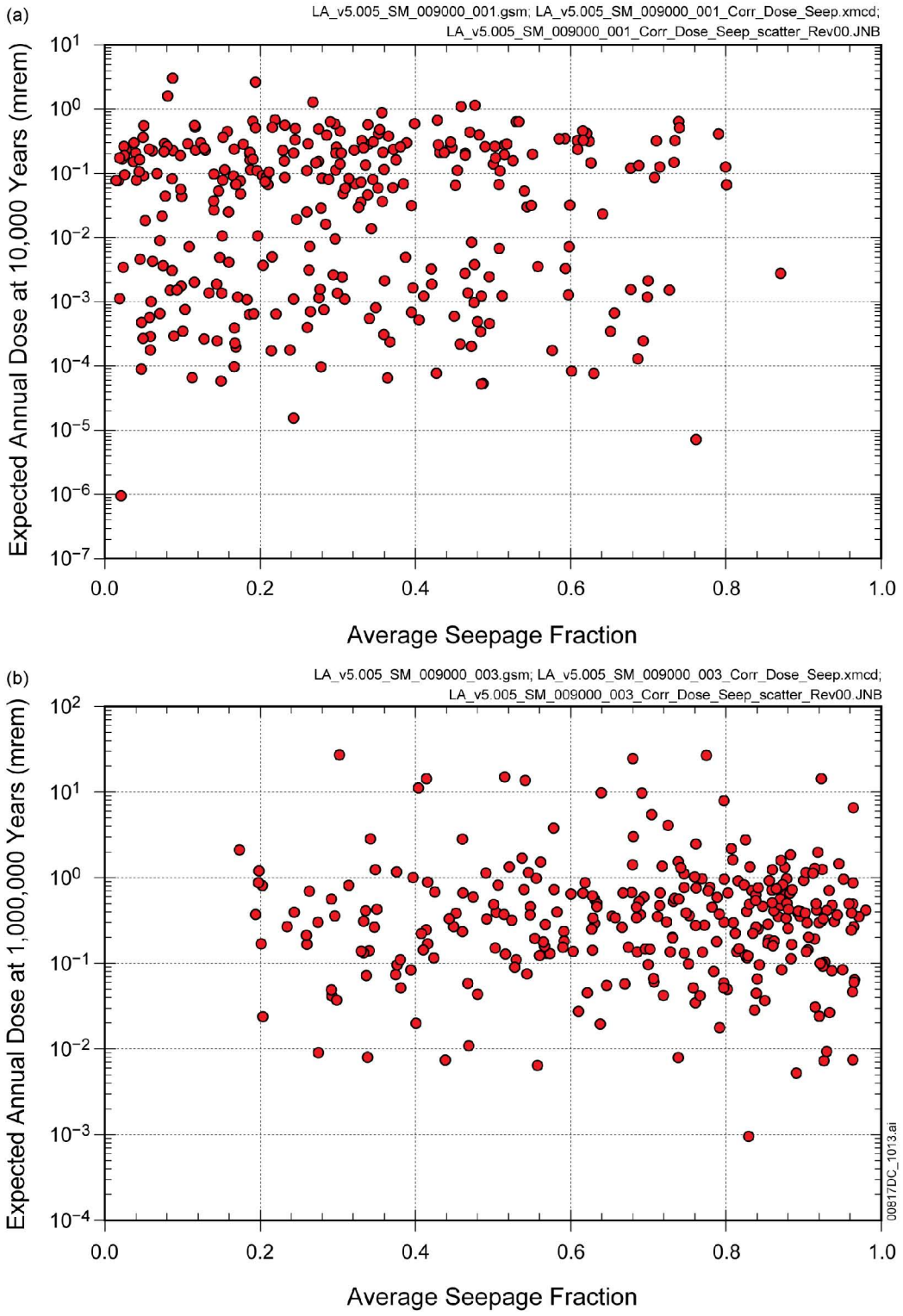

Source: Output DTN: MO0710ADTSPAWO.000 [DIRS 183752].

Figure P-21[a]. Expected Annual Dose versus Average Seepage Fraction for the Seismic Ground Motion Modeling Case for (a) 10,000 Years and (b) 1,000,000 Years after Repository Closure